INTERNATIONAL TABLES for CRYSTALLOGRAPHY

Volume

Mathematical, physical and chemical tables

Edited by E. Prince

Third edition

INTERNATIONAL TABLES FOR CRYSTALLOGRAPHY

International Tables for Crystallography

Volume A: *Space-Group Symmetry*
Editor Theo Hahn
First Edition 1983, Fifth Edition 2002

Volume B: *Reciprocal Space*
Editor U. Shmueli
First Edition 1993, Second Edition 2001

Volume C: *Mathematical, Physical and Chemical Tables*
Editor E. Prince
First Edition 1992, Third Edition 2004

Volume D: *Physical Properties of Crystals*
Editor A. Authier
First Edition 2003

Volume E: *Subperiodic Groups*
Editors V. Kopský and D. B. Litvin
First Edition 2002

Volume F: *Crystallography of Biological Macromolecules*
Editors Michael G. Rossmann and Eddy Arnold
First Edition 2001

Forthcoming volumes

Volume A1: *Symmetry Relations between Space Groups*
Editors H. Wondratschek and U. Müller

Volume G: *Definition and Exchange of Crystallographic Data*
Editors S. R. Hall and B. McMahon

INTERNATIONAL TABLES FOR CRYSTALLOGRAPHY

Volume C

MATHEMATICAL, PHYSICAL AND CHEMICAL TABLES

Edited by

E. PRINCE

Third Edition

Published for

THE INTERNATIONAL UNION OF CRYSTALLOGRAPHY

by

KLUWER ACADEMIC PUBLISHERS

DORDRECHT/BOSTON/LONDON

2004

A C.I.P. Catalogue record for this book
is available from the Library of Congress
ISBN 1-4020-1900-9 (acid-free paper)

Published by Kluwer Academic Publishers,
P.O. Box 17, 3300 AA Dordrecht, The Netherlands

Sold and distributed in North, Central and South America
by Kluwer Academic Publishers,
101 Philip Drive, Norwell, MA 02061, USA

In all other countries, sold and distributed
by Kluwer Academic Publishers,
P.O. Box 322, 3300 AH Dordrecht, The Netherlands

Technical Editors: S. E. King and N. J. Ashcroft

First published in 1992
Reprinted with corrections 1995
Second edition 1999
Third edition 2004

© International Union of Crystallography 1992, 1995, 1999, 2004

Short extracts may be
reproduced without formality, provided that the
source is acknowledged, but substantial portions
may not be reproduced by any process
without written permission from the
International Union of Crystallography

Printed in Denmark by P. J. Schmidt A/S

Contributing Authors

A. ALBINATI: Istituto Chimica Farmaceutica, Università di Milano, Viale Abruzzi 42, Milano 20131, Italy. [8.6]

N. G. ALEXANDROPOULOS: Department of Physics, University of Ioannina, PO Box 1186, Gr-45110 Ioannina, Greece. [7.4.3]

F. H. ALLEN: Cambridge Crystallographic Data Centre, 12 Union Road, Cambridge CB2 1EZ, England. [9.5, 9.6]

Y. AMEMIYA: Engineering Research Institute, Department of Applied Physics, Faculty of Engineering, University of Tokyo, 2-11-16 Yayoi, Bunkyo, Tokyo 113, Japan. [7.1.8]

I. S. ANDERSON: Institut Laue–Langevin, Avenue des Martyrs, BP 156X, F-38042 Grenoble CEDEX, France. [4.4.2]

U. W. ARNDT: MRC Laboratory of Molecular Biology, Hills Road, Cambridge CB2 2QH, England. [4.2.1, 7.1.6]

J. BARUCHEL: Experiment Division, ESRF, BP 220, F-38043 Grenoble CEDEX, France. [2.8]

P. J. BECKER: Ecole Centrale Paris, Centre de Recherche, Grand Voie des Vignes, F-92295 Châtenay Malabry CEDEX, France. [8.7]

G. BERGERHOFF: Institut für Anorganische Chemie der Universität Bonn, Gerhard-Domagkstrasse 1, D-53121 Bonn, Germany. [9.4]

P. T. BOGGS: Scientific Computing Division, National Institute of Standards and Technology, Gaithersburg, MD 20899, USA. [8.1]

L. BRAMMER: Department of Chemistry, University of Missouri–St Louis, 8001 Natural Bridge Road, St Louis, MO 63121-4499, USA. [9.5, 9.6]

K. BRANDENBURG: Institut für Anorganische Chemie der Universität Bonn, Gerhard-Domagkstrasse 1, D-53121 Bonn, Germany. [9.4]

P. J. BROWN: Institut Laue–Langevin, Avenue des Martyrs, BP 156X, F-38042 Grenoble CEDEX, France. [4.4.5, 6.1.2]

†B. BURAS [2.5.1, 7.1.5]

J. M. CARPENTER: Intense Pulsed Neutron Source, Building 360, Argonne National Laboratory, Argonne, IL 60439, USA. [4.4.1]

J. N. CHAPMAN: Department of Physics and Astronomy, University of Glasgow, Glasgow G12 8QQ, Scotland. [7.2]

P. CHIEUX: Institut Laue–Langevin, Avenue des Martyrs, BP 156X, F-38042 Grenoble CEDEX, France. [7.3]

J. CHIKAWA: Center for Advanced Science and Technology, Harima Science Park City, Kamigori-cho, Hyogo 678-12, Japan. [7.1.7, 7.1.8]

C. COLLIEX, Laboratoire Aimé Cotton, CNRS, Campus d'Orsay, Bâtiment 505, F-91405 Orsay CEDEX, France. [4.3.4]

D. M. COLLINS: Laboratory for the Structure of Matter, Code 6030, Naval Research Laboratory, Washington, DC 20375-5341, USA. [8.2]

P. CONVERT: Institut Laue–Langevin, Avenue des Martyrs, BP 156X, F-38042 Grenoble CEDEX, France. [7.3]

M. J. COOPER: Department of Physics, University of Warwick, Coventry CV4 7AL, England. [7.4.3]

P. COPPENS: 732 NSM Building, Department of Chemistry, State University of New York at Buffalo, Buffalo, NY 14260-3000, USA. [8.7]

J. M. COWLEY: Department of Physics and Astronomy, Arizona State University, Tempe, AZ 85287-1504, USA. [2.4.1, 4.3.1, 4.3.2, 4.3.8]

D. C. CREAGH: Division of Health, Design, and Science, University of Canberra, Canberra, ACT 2601, Australia. [4.2.3, 4.2.4, 4.2.5, 4.2.6, 10]

J. L. C. DAAMS: Materials Analysis Department, Philips Research Laboratories, Prof. Holstaan 4, 5656 AA Eindhoven, The Netherlands. [9.3]

W. I. F. DAVID: ISIS Science Division, Rutherford Appleton Laboratory, Chilton, Didcot, Oxfordshire OX11 0QX, England. [2.5.2]

†R. D. DESLATTES [4.2.2]

S. L. DUDAREV: Department of Materials, University of Oxford, Parks Road, Oxford OX1 3PH, England. [4.3.2]

S. ĎUROVIČ: Department of Theoretical Chemistry, Slovak Academy of Sciences, Dúbravská cesta, 842 36 Bratislava, Slovakia. [9.2.2]

L. W. FINGER: Geophysical Laboratory, Carnegie Institution of Washington, 5251 Broad Branch Road NW, Washington, DC 20015-1305, USA. [8.3]

M. FINK: Department of Physics, University of Texas at Austin, Austin, TX 78712, USA. [4.3.3]

W. FISCHER: Institut für Mineralogie, Petrologie und Kristallographie, Universität Marburg, Hans-Meerwein-Strasse, D-35032 Marburg, Germany. [9.1]

H. M. FLOWER: Department of Metallurgy, Imperial College, London SW7, England. [3.5]

A. G. FOX: Center for Materials Science and Engineering, Naval Postgraduate School, Monterey, CA 93943-5000, USA. [6.1.1]

J. R. FRYER: Department of Chemistry, University of Glasgow, Glasgow G12 8QQ, Scotland. [3.5]

E. GAŁDECKA: Institute of Low Temperature and Structure Research, Polish Academy of Sciences, PO Box 937, 50-950 Wrocław 2, Poland. [5.3]

L. GERWARD: Physics Department, Technical University of Denmark, DK-2800 Lyngby, Denmark. [2.5.1, 7.1.5]

J. GJØNNES: Department of Physics, University of Oslo, PO Box 1048, Blindern, N-0316 Oslo, Norway. [4.3.7, 8.8]

O. GLATTER: Institut für Physikalische Chemie, Universität Graz, Heinrichstrasse 28, A-8010 Graz, Austria. [2.6.1]

J. R. HELLIWELL: Department of Chemistry, University of Manchester, Manchester M13 9PL, England. [2.1, 2.2]

A. W. HEWAT: Institut Laue–Langevin, Avenue des Martyrs, BP 156X, F-38042 Grenoble CEDEX, France. [2.4.2]

R. L. HILDERBRANDT: Chemistry Division, Room 1055, The National Science Foundation, 4201 Wilson Blvd, Arlington, VA 22230, USA. [4.3.3]

A. HOWIE: Cavendish Laboratory, Madingley Road, Cambridge CB3 0HE, England [4.3.6.2]

H.-C. HU: China Institute of Atomic Energy, PO Box 275 (18), Beijing 102413, People's Republic of China [6.2]

J. H. HUBBELL: Room C314, Radiation Physics Building, National Institute of Standards and Technology, Gaithersburg, MD 20899, USA. [4.2.4]

P. INDELICATO: Laboratoire Kastler-Brossel, Case 74, Université Pierre et Marie Curie, 4 Place Jussieu, F-75252 Paris CEDEX 05, France. [4.2.2]

A. JANNER: Institute for Theoretical Physics, University of Nijmegen, Toernooiveld, NL-6525 ED Nijmegen, The Netherlands. [9.8]

T. JANSSEN: Institute for Theoretical Physics, University of Nijmegen, Toernooiveld, NL-6525 ED Nijmegen, The Netherlands. [9.8]

† Deceased.

† Deceased.

CONTRIBUTING AUTHORS

A. W. S. JOHNSON: Centre for Microscopy and Microanalysis, University of Western Australia, Nedlands, WA 6009, Australia. [5.4.1]

J. D. JORGENSEN: Materials Science Division, Building 223, Argonne National Laboratory, Argonne, IL 60439, USA. [2.5.2]

V. L. KAREN: NIST Center for Neutron Research, National Institute of Standards and Technology, Gaithersburg, MD 20899, USA. [9.7]

E. G. KESSLER JR: Atomic Physics Division, National Institute of Standards and Technology, Gaithersburg, MD 20899, USA. [4.2.2]

E. KOCH: Institut für Mineralogie, Petrologie und Kristallographie, Universität Marburg, Hans-Meerwein-Strasse, D-35032 Marburg, Germany. [1.1, 1.2, 1.3, 9.1]

J. H. KONNERT: Laboratory for the Structure of Matter, Code 6030, Naval Research Laboratory, Washington, DC 20375-5000, USA. [8.3]

P. KRISHNA: Rajghat Education Center, Krishnamurti Foundation India, Rajghat Fort, Varanasi 221001, India. [9.2.1]

G. LANDER: ITU, European Commission, Postfach 2340, D-76125 Karlsruhe, Germany. [4.4.1]

A. R. LANG: H. H. Wills Physics Laboratory, University of Bristol, Tyndall Avenue, Bristol BS8 1TL, England. [2.7]

J. I. LANGFORD: School of Physics & Astronomy, University of Birmingham, Birmingham B15 2TT, England. [2.3, 5.2, 6.2, 7.1.2]

†E. S. LARSEN JR. [3.3]

P. F. LINDLEY: ESRF, Avenue des Martyrs, BP 220, F-38043 Grenoble CEDEX, France. [3.1, 3.2.1, 3.2.3, 3.4]

E. LINDROTH, Department of Atomic Physics, Stockholm University, S-104 05 Stockholm, Sweden. [4.2.2]

† H. LIPSON. [6.2]

A. LOOIJENGA-VOS: Roland Holstlaan 908, NL-2624 JK Delft, The Netherlands. [9.8]

D. F. LYNCH: CSIRO Division of Materials Science & Technology, Private Bag 33, Rosebank MDC, Clayton, Victoria 3169, Australia. [4.3.6.1]

C. F. MAJKRZAK: NIST Center for Neutron Research, National Institute of Standards and Technology, Gaithersburg, MD 20899, USA. [2.9]

S. MARTINEZ-CARRERA: San Ernesto, 6-Esc. 3, 28002 Madrid, Spain. [10]

†E. N. MASLEN. [6.1.1, 6.3]

R. P. MAY: Institut Laue–Langevin, Avenue des Martyrs, BP 156X, F-38042 Grenoble CEDEX, France. [2.6.2]

†R. MEYROWITZ. [3.3]

A. MIGHELL: NIST Center for Neutron Research, National Institute of Standards and Technology, Gaithersburg, MD 20899, USA. [9.7]

M. A. O'KEEFE: National Center for Electron Microscopy, Lawrence Berkeley National Laboratory MS-72, University of California, Berkeley, CA 94720, USA. [6.1.1]

A. OLSEN: Department of Physics, University of Oslo, PO Box 1048, N-0316 Blindern, Norway. [5.4.2]

A. G. ORPEN: School of Chemistry, University of Bristol, Bristol BS8 1TS, England. [9.5, 9.6]

D. PANDEY: Physics Department, Banaras Hindu University, Varanasi 221005, India. [9.2.1]

†W. PARRISH. [2.3, 5.2, 7.1.2, 7.1.3, 7.1.4]

L. M. PENG: Department of Electronics, Peking University, Beijing 100817, People's Republic of China. [4.3.2]

E. PRINCE: NIST Center for Neutron Research, National Institute of Standards and Technology, Gaithersburg, MD 20899, USA. [8.1, 8.2, 8.3, 8.4, 8.5]

R. PYNN: LANSCE, MS H805, Los Alamos National Laboratory, PO Box 1663, Los Alamos, NM 87545, USA. [4.4.3]

G. REN: Beijing Laboratory of Electron Microscopy, Chinese Academy of Sciences, PO Box 2724, Beijing 100080, People's Republic of China. [4.3.2]

F. M. RICHARDS: Department of Molecular Biophysics and Biochemistry, Yale University, 260 Whitney Ave, New Haven, CT 06520-8114, USA. [3.2.2]

J. R. RODGERS: National Research Council of Canada, Canada Institute for Scientific and Technical Information, Ottawa, Canada K1A 0S2. [9.3]

A. W. ROSS: Physics Department, The University of Texas at Austin, Austin, TX 78712, USA. [4.3.3]

J. M. ROWE: NIST Center for Neutron Research, National Institute of Standards and Technology, Gaithersburg, MD 20899, USA. [4.4.3]

T. M. SABINE: ANSTO, Private Mail Bag 1, Menai, NSW 2234, Australia. [6.4]

O. SCHÄRPF: Physik-Department E13, TU München, James-Franck-Strasse 1, D-85748 Garching, Germany. [4.4.2]

M. SCHLENKER: l'Institut National Polytechnique de Grenoble, Laboratoire Louis Néel du CNRS, BP 166, F-38042 Grenoble CEDEX 9, France. [2.8]

V. F. SEARS: Atomic Energy of Canada Limited, Chalk River Laboratories, Chalk River, Ontario, Canada K0J 1J0. [4.4.4]

G. S. SMITH: Manuel Lujan Jr Neutron Scattering Center, Los Alamos National Laboratory, Los Alamos, NM 87545, USA. [2.9]

V. H. SMITH JR: Department of Chemistry, Queen's University, Kingston, Ontario, Canada K7L 3N6. [4.3.3]

J. C. H. SPENCE: Department of Physics, Arizona State University, Tempe, AZ 85287, USA. [4.3.8]

C. H. SPIEGELMAN: Department of Statistics, Texas A&M University, College Station, TX 77843, USA. [8.4, 8.5]

J. W. STEEDS: H. H. Wills Physics Laboratory, University of Bristol, Tyndall Avenue, Bristol BS8 1TL, England. [4.3.7]

Z. SU: Digital Equipment Co., 129 Parker Street, PKO1/C22, Maynard, MA 01754-2122, USA. [8.7]

P. SUORTTI: Department of Physics, PO Box 9, University of Helsinki, FIN-00014 Helsinki, Finland. [7.4.4]

R. TAYLOR: Cambridge Crystallographic Data Centre, 12 Union Road, Cambridge CB2 1EZ, England. [9.5, 9.6]

N. J. TIGHE: 42 Lema Lane, Palm Coast, FL 32137-2417, USA. [3.5]

V. VALVODA: Department of Physics of Semiconductors, Faculty of Mathematics and Physics, Charles University, Ke Karlovu 5, 121 16 Praha 2, Czech Republic. [4.1]

P. VILLARS: Intermetallic Phases Databank, Postal Box 1, CH-6354 Vitznau, Switzerland. [9.3]

J. WANG: Department of Chemistry, Queen's University, Kingston, Ontario, Canada K7L 3N6. [4.3.3]

D. G. WATSON: Cambridge Crystallographic Data Centre, 12 Union Road, Cambridge CB2 1EZ, England. [9.5, 9.6]

M. J. WHELAN: Department of Materials, University of Oxford, Parks Road, Oxford OX1 3PH, England. [4.3.2]

B. T. M. WILLIS: Chemical Crystallography Laboratory, University of Oxford, 9 Parks Road, Oxford OX1 3PD, England. [2.5.2, 3.6, 4.4.6, 5.5, 6.1.3, 7.4.2, 8.6]

†A. J. C. WILSON. [1.4, 3.3, 5.1, 5.2, 7.5, 9.7]

†P. M. DE WOLFF. [7.1.1, 9.8]

†B. B. ZVYAGIN. [4.3.5]

† Deceased.

† Deceased.

Contents

PAGE

PREFACE (A. J. C. Wilson) .. xxxi

PREFACE TO THE THIRD EDITION (E. Prince) .. xxxi

PART 1: CRYSTAL GEOMETRY AND SYMMETRY .. 1

1.1. Summary of General Formulae (E. Koch) .. 2

1.1.1. General relations between direct and reciprocal lattices .. 2

1.1.1.1. Primitive crystallographic bases .. 2

1.1.1.2. Non-primitive crystallographic bases .. 3

Table 1.1.1.1. *Direct and reciprocal lattices described with respect to conventional basis systems* .. 3

1.1.2. Lattice vectors, point rows, and net planes .. 3

1.1.3. Angles in direct and reciprocal space .. 4

1.1.4. The Miller formulae .. 5

1.2. Application to the Crystal Systems (E. Koch) .. 6

1.2.1. Triclinic crystal system .. 6

1.2.2. Monoclinic crystal system .. 6

1.2.2.1. Setting with 'unique axis ***b***' .. 6

1.2.2.2. Setting with 'unique axis ***c***' .. 6

1.2.3. Orthorhombic crystal system .. 6

1.2.4. Tetragonal crystal system .. 7

Table 1.2.4.1. *Assignment of integers $s \leq 100$ to pairs h, k with $s = h^2 + k^2$* .. 7

1.2.5. Trigonal and hexagonal crystal system .. 7

1.2.5.1. Description referred to hexagonal axes .. 7

1.2.5.2. Description referred to rhombohedral axes .. 8

Table 1.2.5.1. *Assignment of integers $s \leq 100$ to pairs h, k with $s = h^2 + k^2 + hk$* .. 8

Table 1.2.5.2. *Assignment of integers $s_1 \leq 50$ to triplets h, k, l with $s_1 = h^2 + k^2 + l^2$ and to integers $s_2 = hk + hl + kl$* .. 8

1.2.6. Cubic crystal system .. 9

Table 1.2.6.1. *Assignment of integers $s \leq 100$ to triplets h, k, l with $s = h^2 + k^2 + l^2$* .. 9

1.3. Twinning (E. Koch) .. 10

1.3.1. General remarks .. 10

1.3.2. Twin lattices .. 10

1.3.2.1. Examples .. 11

Table 1.3.2.1. *Lattice planes and rows that are perpendicular to each other independently of the metrical parameters* .. 11

1.3.3. Implication of twinning in reciprocal space .. 12

1.3.4. Twinning by merohedry .. 12

Table 1.3.4.1. *Possible twin operations for twins by merohedry* .. 13

Table 1.3.4.2. *Simulated Laue classes, extinction symbols, simulated 'possible space groups', and possible true space groups for crystals twinned by merohedry (type 2)* .. 13

1.3.5. Calculation of the twin element .. 14

1.4. Arithmetic Crystal Classes and Symmorphic Space Groups (A. J. C. Wilson) .. 15

1.4.1. Arithmetic crystal classes .. 15

1.4.1.1. Arithmetic crystal classes in three dimensions .. 15

1.4.1.2. Arithmetic crystal classes in one, two and higher dimensions .. 16

Table 1.4.1.1. *The two-dimensional arithmetic crystal classes* .. 15

1.4.2. Classification of space groups .. 20

1.4.2.1. Symmorphic space groups .. 21

Table 1.4.2.1. *The three-dimensional space groups, arranged by arithmetic crystal class* .. 16

1.4.3. Effect of dispersion on diffraction symmetry .. 21
1.4.3.1. Symmetry of the Patterson function .. 21
1.4.3.2. 'Laue' symmetry .. 21
Table 1.4.3.1. *Arithmetic crystal classes classified by the number of space groups that they contain* .. 20
References .. 21

PART 2: DIFFRACTION GEOMETRY AND ITS PRACTICAL REALIZATION .. 23

2.1. Classification of Experimental Techniques (J. R. Helliwell) .. 24
Table 2.1.1. *Summary of main experimental techniques for structure analysis* .. 25

2.2. Single-Crystal X-ray Techniques (J. R. Helliwell) .. 26

2.2.1. Laue geometry .. 26
2.2.1.1. General .. 26
2.2.1.2. Crystal setting .. 27
2.2.1.3. Single-order and multiple-order reflections .. 27
2.2.1.4. Angular distribution of reflections in Laue diffraction .. 29
2.2.1.5. Gnomonic and stereographic transformations .. 29

2.2.2. Monochromatic methods .. 29
2.2.2.1. Monochromatic still exposure .. 30
2.2.2.2. Crystal setting .. 30

2.2.3. Rotation/oscillation geometry .. 31
2.2.3.1. General .. 31
2.2.3.2. Diffraction coordinates .. 31
2.2.3.3. Relationship of reciprocal-lattice coordinates to crystal system parameters .. 33
2.2.3.4. Maximum oscillation angle without spot overlap .. 33
2.2.3.5. Blind region .. 34
Table 2.2.3.1. *Glossary of symbols used to specify quantitites on diffraction patterns and in reciprocal space* 32

2.2.4. Weissenberg geometry .. 34
2.2.4.1. General .. 34
2.2.4.2. Recording of zero layer .. 34
2.2.4.3. Recording of upper layers .. 34

2.2.5. Precession geometry .. 35
2.2.5.1. General .. 35
2.2.5.2. Crystal setting .. 35
2.2.5.3. Recording of zero-layer photograph .. 35
2.2.5.4. Recording of upper-layer photographs .. 35
2.2.5.5. Recording of cone-axis photograph .. 36
Table 2.2.5.1. *The distance displacement (in mm) measured on the film versus angular setting error of the crystal for a screenless precession ($\bar{\mu} = 5^\circ$) setting photograph* .. 35

2.2.6. Diffractometry .. 36
2.2.6.1. General .. 36
2.2.6.2. Normal-beam equatorial geometry .. 36
2.2.6.3. Fixed $\chi = 45^\circ$ geometry with area detector .. 37

2.2.7. Practical realization of diffraction geometry: sources, optics, and detectors .. 37
2.2.7.1. General .. 37
2.2.7.2. Conventional X-ray sources: spectral character, crystal rocking curve, and spot size .. 37
2.2.7.3. Synchrotron X-ray sources .. 38
2.2.7.4. Geometric effects and distortions associated with area detectors .. 41

2.3. Powder and Related Techniques: X-ray Techniques (W. Parrish and J. I. Langford) .. 42

2.3.1. Focusing diffractometer geometries .. 43
2.3.1.1. Conventional reflection specimen, θ–2θ scan .. 44
2.3.1.1.1. Geometrical instrument parameters .. 44
2.3.1.1.2. Use of monochromators .. 46
2.3.1.1.3. Alignment and angular calibration .. 46
2.3.1.1.4. Instrument broadening and aberrations .. 47
2.3.1.1.5. Focal line and receiving-slit widths .. 48
2.3.1.1.6. Aberrations related to the specimen .. 48

2.3.1.1.7. Axial divergence .. 50
2.3.1.1.8. Combined aberrations .. 50
2.3.1.2. Transmission specimen, θ–2θ scan .. 50
2.3.1.3. Seemann–Bohlin method .. 52
2.3.1.4. Reflection specimen, θ–θ scan .. 53
2.3.1.5. Microdiffractometry .. 53
2.3.2. Parallel-beam geometries, synchrotron radiation .. 54
2.3.2.1. Monochromatic radiation, θ–2θ scan .. 55
2.3.2.2. Cylindrical specimen, 2θ scan .. 57
2.3.2.3. Grazing-incidence diffraction .. 58
2.3.2.4. High-resolution energy-dispersive diffraction .. 58
2.3.3. Specimen factors, angle, intensity, and profile-shape measurement .. 60
2.3.3.1. Specimen factors .. 60
2.3.3.1.1. Preferred orientation .. 60
2.3.3.1.2. Crystallite-size effects .. 62
2.3.3.2. Problems arising from the $K\alpha$ doublet .. 62
2.3.3.3. Use of peak or centroid for angle definition .. 63
2.3.3.4. Rate-meter/strip-chart recording .. 63
2.3.3.5. Computer-controlled automation .. 63
2.3.3.6. Counting statistics .. 64
2.3.3.7. Peak search .. 65
2.3.3.8. Profile fitting .. 66
2.3.3.9. Computer graphics for powder patterns .. 69
Table 2.3.3.1. *Preferred-orientation data for silicon* .. 61
Table 2.3.3.2. *R(Bragg) values obtained with different preferred-orientation formulae* .. 61
2.3.4. Powder cameras .. 70
2.3.4.1. Cylindrical cameras (Debye–Scherrer) .. 70
2.3.4.2. Focusing cameras (Guinier) .. 70
2.3.4.3. Miscellaneous camera types .. 71
2.3.5. Generation, modifications, and measurement of X-ray spectra .. 71
2.3.5.1. X-ray tubes .. 71
2.3.5.1.1. Stability .. 72
2.3.5.1.2. Spectral purity .. 72
2.3.5.1.3. Source intensity distribution and size .. 73
2.3.5.1.4. Air and window transmission .. 73
2.3.5.1.5. Intensity variation with take-off angle .. 74
2.3.5.2. X-ray spectra .. 74
2.3.5.2.1. Wavelength selection .. 75
2.3.5.3. Other X-ray sources .. 75
2.3.5.4. Methods for modifying the spectrum .. 75
2.3.5.4.1. Crystal monochromators .. 76
2.3.5.4.2. Single and balanced filters .. 78
Table 2.3.5.1. *X-ray tube maximum ratings* .. 72
Table 2.3.5.2. *β filters for common target elements* .. 78
Table 2.3.5.3. *Calculated thickness of balanced filters for common target elements* .. 79

2.4. Powder and Related Techniques: Electron and Neutron Techniques .. 80

2.4.1. Electron techniques (J. M. Cowley) .. 80
2.4.1.1. Powder-pattern geometry .. 80
2.4.1.2. Diffraction patterns in electron microscopes .. 80
2.4.1.3. Preferred orientations .. 80
2.4.1.4. Powder-pattern intensities .. 80
2.4.1.5. Crystal-size analysis .. 81
2.4.1.6. Unknown-phase identification: databases .. 81
2.4.2. Neutron techniques (A. W. Hewat) .. 82

2.5. Energy-Dispersive Techniques .. 84

2.5.1. Techniques for X-rays (B. Buras and L. Gerward) .. 84
2.5.1.1. Recording powder diffraction spectra .. 84

2.5.1.2. Incident X-ray beam .. 84
2.5.1.3. Resolution .. 85
2.5.1.4. Integrated intensity for powder sample .. 85
2.5.1.5. Corrections .. 86
2.5.1.6. The Rietveld method .. 86
2.5.1.7. Single-crystal diffraction .. 86
2.5.1.8. Applications .. 86
2.5.2. White-beam and time-of-flight neutron diffraction (J. D. Jorgensen, W. I. F. David, and B. T. M. Willis) .. 87
2.5.2.1. Neutron single-crystal Laue diffraction .. 87
2.5.2.2. Neutron time-of-flight powder diffraction .. 87

2.6. Small-Angle Techniques .. 89

2.6.1. X-ray techniques (O. Glatter) .. 89
2.6.1.1. Introduction .. 89
2.6.1.2. General principles .. 90
2.6.1.3. Monodisperse systems .. 91
2.6.1.3.1. Parameters of a particle .. 91
2.6.1.3.2. Shape and structure of particles .. 93
2.6.1.3.2.1. Homogeneous particles .. 93
2.6.1.3.2.2. Hollow and inhomogeneous particles .. 96
2.6.1.3.3. Interparticle interference, concentration effects .. 97
2.6.1.4. Polydisperse systems .. 99
2.6.1.5. Instrumentation .. 99
2.6.1.5.1. Small-angle cameras .. 99
2.6.1.5.2. Detectors .. 100
2.6.1.6. Data evaluation and interpretation .. 100
2.6.1.6.1. Primary data handling .. 100
2.6.1.6.2. Instrumental broadening – smearing .. 101
2.6.1.6.3. Smoothing, desmearing, and Fourier transformation .. 101
2.6.1.6.4. Direct structure analysis .. 103
2.6.1.6.5. Interpretation of results .. 103
2.6.1.7. Simulations and model calculations .. 103
2.6.1.7.1. Simulations .. 103
2.6.1.7.2. Model calculation .. 104
2.6.1.7.3. Calculation of scattering intensities .. 104
2.6.1.7.4. Method of finite elements .. 104
2.6.1.7.5. Calculation of distance-distribution functions .. 104
2.6.1.8. Suggestions for further reading .. 104
Table 2.6.1.1. *Formulae for the various parameters for h and m scales* .. 92
2.6.2. Neutron techniques (R. May) .. 105
2.6.2.1. Relation of X-ray and neutron small-angle scattering .. 105
2.6.2.1.1. Wavelength .. 105
2.6.2.1.2. Geometry .. 106
2.6.2.1.3. Correction of wavelength, slit, and detector-element effects .. 106
2.6.2.2. Isotopic composition of the sample .. 106
2.6.2.2.1. Contrast variation .. 107
2.6.2.2.2. Specific isotopic labelling .. 107
2.6.2.3. Magnetic properties of the neutron .. 107
2.6.2.3.1. Spin-contrast variation .. 108
2.6.2.4. Long wavelengths .. 108
2.6.2.5. Sample environment .. 108
2.6.2.6. Incoherent scattering .. 108
2.6.2.6.1. Absolute scaling .. 108
2.6.2.6.2. Detector-response correction .. 109
2.6.2.6.3. Estimation of the incoherent scattering level .. 109
2.6.2.6.4. Inner surface area .. 109
2.6.2.7. Single-particle scattering .. 110
2.6.2.7.1. Particle shape .. 110
2.6.2.7.2. Particle mass .. 110

2.6.2.7.3. Real-space considerations .. 110
2.6.2.7.4. Particle-size distribution .. 111
2.6.2.7.5. Model fitting .. 111
2.6.2.7.6. Label triangulation .. 111
2.6.2.7.7. Triplet isotropic replacement .. 111
2.6.2.8. Dense systems .. 112

2.7. Topography (A. R. Lang) .. 113

2.7.1. Principles .. 113

2.7.2. Single-crystal techniques .. 114
2.7.2.1. Reflection topographs .. 114
2.7.2.2. Transmission topographs .. 115

2.7.3. Double-crystal topography .. 117

2.7.4. Developments with synchrotron radiation .. 119
2.7.4.1. White-radiation topography .. 119
2.7.4.2. Incident-beam monochromatization .. 120
Table 2.7.4.1. *Monolithic monochromator for plane-wave synchrotron-radiation topography* .. 121

2.7.5. Some special techniques .. 121
2.7.5.1. Moiré topography .. 121
2.7.5.2. Real-time viewing of topograph images .. 122

2.8. Neutron Diffraction Topography (M. Schlenker and J. Baruchel) .. 124

2.8.1. Introduction .. 124

2.8.2. Implementation .. 124

2.8.3. Application to investigations of heavy crystals .. 124

2.8.4. Investigation of magnetic domains and magnetic phase transitions .. 124

2.9. Neutron Reflectometry (G. S. Smith and C. F. Majkrzak) .. 126

2.9.1. Introduction .. 126

2.9.2. Theory of elastic specular neutron reflection .. 126

2.9.3. Polarized neutron reflectivity .. 127

2.9.4. Surface roughness .. 128

2.9.5. Experimental methodology .. 128

2.9.6. Resolution in real space .. 129

2.9.7. Applications of neutron reflectometry .. 129
2.9.7.1. Self-diffusion .. 129
2.9.7.2. Magnetic multilayers .. 130
2.9.7.3. Hydrogenous materials .. 130

References .. 130

PART 3: PREPARATION AND EXAMINATION OF SPECIMENS .. 147

3.1. Preparation, Selection, and Investigation of Specimens (P. F. Lindley) .. 148

3.1.1. Crystallization .. 148
3.1.1.1. Introduction .. 148
3.1.1.2. Crystal growth .. 148
3.1.1.3. Methods of growing crystals .. 148
3.1.1.4. Factors affecting the solubility of biological macromolecules .. 148
3.1.1.5. Screening procedures for the crystallization of biological macromolecules .. 150
3.1.1.6. Automated protein crystallization .. 150
3.1.1.7. Membrane proteins .. 150
Table 3.1.1.1. *Survey of crystallization techniques suitable for the crystallization of low-molecular-weight organic compounds for X-ray crystallography* .. 149
Table 3.1.1.2. *Commonly used ionic and organic precipitants* .. 150
Table 3.1.1.3. *Crystallization matrix parameters for sparse-matrix sampling* .. 151
Table 3.1.1.4. *Reservoir solutions for sparse-matrix sampling* .. 152

3.1.2. Selection of single crystals .. 151
3.1.2.1. Introduction .. 151
3.1.2.2. Size, shape, and quality .. 151
3.1.2.3. Optical examination .. 154
3.1.2.4. Twinning .. 155
Table 3.1.2.1. *Use of crystal properties for selection and preliminary study of crystals; morphological, optical, and mechanical properties* .. 153

3.2. Determination of the Density of Solids .. 156

3.2.1. Introduction (P. F. Lindley) .. 156
3.2.1.1. General precautions .. 156
3.2.2. Description and discussion of techniques (F. M. Richards) .. 156
3.2.2.1. Gradient tube .. 156
3.2.2.1.1. Technique .. 156
3.2.2.1.2. Suitable substances for columns .. 157
3.2.2.1.3. Sensitivity .. 158
3.2.2.2. Flotation method .. 158
3.2.2.3. Pycnometry .. 158
3.2.2.4. Method of Archimedes .. 158
3.2.2.5. Immersion microbalance .. 158
3.2.2.6. Volumenometry .. 158
3.2.2.7. Other procedures .. 158
Table 3.2.2.1. *Possible substances for use as gradient-column components* .. 157
3.2.3. Biological macromolecules (P. F. Lindley) .. 159
Table 3.2.3.1. *Typical calculations of the values of V_M and V_{solv} for proteins* .. 159

3.3. Measurement of Refractive Index (E. S. Larsen Jr, R. Meyrowitz, and A. J. C. Wilson) .. 160

3.3.1. Introduction .. 160
3.3.2. Media for general use .. 160
Table 3.3.2.1. *Immersion media for general use in the measurement of index of refraction* .. 160
3.3.3. High-index media .. 160
3.3.4. Media for organic substances .. 161
Table 3.3.4.1. *Aqueous solutions for use as immersion media for organic crystals* .. 160
Table 3.3.4.2. *Organic immersion media for use with organic crystals of low solubility* .. 160

3.4. Mounting and Setting of Specimens for X-ray Crystallographic Studies (P. F. Lindley) .. 162

3.4.1. Mounting of specimens .. 162
3.4.1.1. Introduction .. 162
3.4.1.2. Polycrystalline specimens .. 162
3.4.1.2.1. General .. 162
3.4.1.2.2. Non-ambient conditions .. 162
3.4.1.3. Single crystals (small molecules) .. 163
3.4.1.3.1. General .. 163
3.4.1.3.2. Non-ambient conditions .. 164
3.4.1.4. Single crystals of biological macromolecules at ambient temperatures .. 165
3.4.1.5. Cryogenic studies of biological macromolecules .. 166
3.4.1.5.1. Radiation damage .. 166
3.4.1.5.2. Cryoprotectants .. 166
3.4.1.5.3. Crystal mounting and cooling .. 166
3.4.1.5.4. Cooling devices .. 167
3.4.1.5.5. General .. 167
Table 3.4.1.1. *Single-crystal and powder mounting, capillary tubes and other containers* .. 163
Table 3.4.1.2. *Single-crystal mounting – adhesives* .. 164
Table 3.4.1.3. *Cryoprotectants commonly used for biological macromolecules* .. 166
3.4.2. Setting of single crystals by X-rays .. 167
3.4.2.1. Introduction .. 167
3.4.2.2. Preliminary considerations .. 168
3.4.2.3. Equatorial setting using a rotation camera .. 168

3.4.2.4. Precession geometry setting with moving-crystal methods .. 168
3.4.2.5. Setting and orientation with stationary-crystal methods .. 169
3.4.2.5.1. Laue images – white radiation .. 169
3.4.2.5.2. 'Still' images – monochromatic radiation .. 169
3.4.2.6. Setting and orientation for crystals with large unit cells using oscillation geometry .. 169
3.4.2.7. Diffractometer-setting considerations .. 170
3.4.2.8. Crystal setting and data-collection efficiency .. 170

3.5. Preparation of Specimens for Electron Diffraction and Electron Microscopy (N. J. Tighe, J. R. Fryer, and H. M. Flower) .. 171

3.5.1. Ceramics and rock minerals .. 171
3.5.1.1. Thin fragments, particles, and flakes .. 171
3.5.1.2. Thin-section preparation .. 171
3.5.1.3. Final thinning by argon-ion etching .. 172
3.5.1.4. Final thinning by chemical etching .. 173
3.5.1.5. Evaporated and sputtered thin films .. 173
Table 3.5.1.1. *Chemical etchants used for preparing thin foils from single-crystal ceramic materials* .. 173

3.5.2. Metals .. 173
3.5.2.1. Thin sections .. 174
3.5.2.2. Final thinning methods .. 174
3.5.2.3. Chemical and electrochemical thinning solutions .. 175

3.5.3. Polymers and organic specimens .. 176
3.5.3.1. Cast films .. 176
3.5.3.2. Sublimed films .. 176
3.5.3.3. Oriented solidification .. 176

3.6. Specimens for Neutron Diffraction (B. T. M. Willis) .. 177

References .. 177

PART 4: PRODUCTION AND PROPERTIES OF RADIATIONS .. 185

4.1. Radiations used in Crystallography (V. Valvoda) .. 186

4.1.1. Introduction .. 186

4.1.2. Electromagnetic waves and particles .. 186

4.1.3. Most frequently used radiations .. 187
Table 4.1.3.1. *Average diffraction properties of X-rays, electrons, and neutrons* .. 187

4.1.4. Special applications of X-rays, electrons, and neutrons .. 189
4.1.4.1. X-rays, synchrotron radiation, and γ-rays .. 189
4.1.4.2. Electrons .. 189
4.1.4.3. Neutrons .. 189

4.1.5. Other radiations .. 189
4.1.5.1. Atomic and molecular beams .. 189
4.1.5.2. Positrons and muons .. 189
4.1.5.3. Infrared, visible, and ultraviolet light .. 189
4.1.5.4. Radiofrequency and microwaves .. 190

4.2. X-rays .. 191

4.2.1. Generation of X-rays (U. W. Arndt) .. 191
4.2.1.1. The characteristic line spectrum .. 191
4.2.1.1.1. The intensity of characteristic lines .. 191
4.2.1.2. The continuous spectrum .. 192
4.2.1.3. X-ray tubes .. 193
4.2.1.3.1. Power dissipation in the anode .. 195
4.2.1.4. Radioactive X-ray sources .. 195
4.2.1.5. Synchrotron-radiation sources .. 196
4.2.1.6. Plasma X-ray sources .. 198
4.2.1.7. Other sources of X-rays .. 199
Table 4.2.1.1. *Correspondence between X-ray diagram levels and electron configurations* .. 191
Table 4.2.1.2. *Correspondence between IUPAC and Siegbahn notations for X-ray diagram lines* .. 191

Table 4.2.1.3. *Copper-target X-ray tubes and their loading* .. 194
Table 4.2.1.4. *Relative permissible loading for different target materials* .. 196
Table 4.2.1.5. *Radionuclides decaying wholly by electron capture, and yielding little or no γ-radiation* .. 196
Table 4.2.1.6. *Comparison of storage-ring synchrotron-radiation sources* .. 199
Table 4.2.1.7. *Intensity gain with storage rings over conventional sources* .. 200

4.2.2. X-ray wavelengths (R. D. Deslattes, E. G. Kessler Jr, P. Indelicato, and E. Lindroth) .. 200
4.2.2.1. Historical introduction .. 200
4.2.2.2. Known problems .. 201
4.2.2.3. Alternative strategies .. 201
4.2.2.4. The X-ray wavelength scales, old and new .. 201
4.2.2.5. *K*-series reference wavelengths .. 202
4.2.2.6. *L*-series reference wavelengths .. 202
4.2.2.7. Absorption-edge locations .. 202
4.2.2.8. Outline of the theoretical procedures .. 204
4.2.2.9. Evaluation of the uncorrelated energy with Dirac–Fock method .. 205
4.2.2.10. Correlation and Auger shifts .. 205
4.2.2.11. QED corrections .. 205
4.2.2.12. Structure and format of the summary tables .. 211
4.2.2.13. Availability of a more complete X-ray wavelength table .. 212
4.2.2.14. Connection with scales used in previous literature .. 212
Table 4.2.2.1. *K-series reference wavelengths* .. 203
Table 4.2.2.2. *Directly measured L-series reference wavelengths* .. 204
Table 4.2.2.3. *Directly measured and emission + binding energies K-absorption edges* .. 205
Table 4.2.2.4. *Wavelengths of K-emission lines and K-absorption edges* .. 206
Table 4.2.2.5. *Wavelengths of L-emission lines and L-absorption edges* .. 209
Table 4.2.2.6. *Wavelength conversion factors* .. 212

4.2.3. X-ray absorption spectra (D. C. Creagh) .. 213
4.2.3.1. Introduction .. 213
4.2.3.1.1. Definitions .. 213
4.2.3.1.2. Variation of X-ray attenuation coefficients with photon energy .. 213
4.2.3.1.3. Normal attenuation, XAFS, and XANES .. 213
4.2.3.2. Techniques for the measurement of X-ray attenuation coefficients .. 214
4.2.3.2.1. Experimental configurations .. 214
4.2.3.2.2. Specimen selection .. 215
4.2.3.2.3. Requirements for the absolute measurement of μ_l or (μ/ρ) .. 215
4.2.3.3. Normal attenuation coefficients .. 215
4.2.3.4. Attenuation coefficients in the neighbourhood of an absorption edge .. 216
4.2.3.4.1. XAFS .. 216
4.2.3.4.1.1. Theory .. 216
4.2.3.4.1.2. Techniques of data analysis .. 217
4.2.3.4.1.3. XAFS experiments .. 218
4.2.3.4.2. X-ray absorption near edge structure (XANES) .. 219
4.2.3.5. Comments .. 220
Table 4.2.3.1. *Some synchrotron-radiation facilities providing XAFS databases and analysis utilities* .. 219

4.2.4. X-ray absorption (or attenuation) coefficients (D. C. Creagh and J. H. Hubbell) .. 220
4.2.4.1. Introduction .. 220
4.2.4.2. Sources of information .. 221
4.2.4.2.1. Theoretical photo-effect data: σ_{pe} .. 221
4.2.4.2.2. Theoretical Rayleigh scattering data: σ_R .. 221
4.2.4.2.3. Theoretical Compton scattering data: σ_C .. 229
4.2.4.3. Comparison between theoretical and experimental data sets .. 229
4.2.4.4. Uncertainty in the data tables .. 229
Table 4.2.4.1. *Table of wavelengths and energies for the characteristic radiations used in Tables 4.2.4.2 and 4.2.4.3* .. 221
Table 4.2.4.2. *Total photon interaction cross section* .. 223
Table 4.2.4.3. *Mass attenuation coefficients* .. 230

4.2.5. Filters and monochromators (D. C. Creagh) .. 229
4.2.5.1. Introduction .. 229
4.2.5.2. Mirrors and capillaries .. 236

4.2.5.2.1. Mirrors .. 236
4.2.5.2.2. Capillaries .. 237
4.2.5.2.3. Quasi-Bragg reflectors .. 237
4.2.5.3. Filters .. 238
4.2.5.4. Monochromators .. 238
4.2.5.4.1. Crystal monochromators .. 238
4.2.5.4.2. Laboratory monochromator systems .. 239
4.2.5.4.3. Multiple-reflection monochromators for use with laboratory and synchrotron-radiation sources .. 239
4.2.5.4.4. Polarization .. 240

4.2.6. X-ray dispersion corrections (D. C. Creagh) .. 241

4.2.6.1. Definitions .. 242
4.2.6.1.1. Rayleigh scattering .. 242
4.2.6.1.2. Thomson scattering by a free electron .. 242
4.2.6.1.3. Elastic scattering from electrons bound to atoms: the atomic scattering factor, the atomic form factor, and the dispersion corrections .. 242
4.2.6.2. Theoretical approaches for the calculation of the dispersion corrections .. 243
4.2.6.2.1. The classical approach .. 243
4.2.6.2.2. Non-relativistic theories .. 244
4.2.6.2.3. Relativistic theories .. 245
4.2.6.2.3.1. Cromer and Liberman: relativistic dipole approach .. 245
4.2.6.2.3.2. The scattering matrix formalism .. 246
4.2.6.2.4. Intercomparison of theories .. 248
4.2.6.3. Modern experimental techniques .. 248
4.2.6.3.1. Determination of the real part of the dispersion correction: $f'(\omega, 0)$ .. 248
4.2.6.3.2. Determination of the real part of the dispersion correction: $f'(\omega, \mathbf{\Delta})$ .. 250
4.2.6.3.2.1. Measurements using the dynamical theory of X-ray diffraction .. 250
4.2.6.3.2.2. Friedel- and Bijvoet-pair techniques .. 251
4.2.6.3.3. Comparison of theory with experiment .. 251
4.2.6.3.3.1. Measurements in the high-energy limit $(\omega/\omega_\kappa \rightarrow 0)$ .. 251
4.2.6.3.3.2. Measurements in the vicinity of an absorption edge .. 252
4.2.6.3.3.3. Accuracy in the tables of dispersion corrections .. 253
4.2.6.3.3.4. Towards a tensor formalism .. 253
4.2.6.3.3.5. Summary .. 258
4.2.6.4. Table of wavelengths, energies, and linewidths used in compiling the tables of the dispersion corrections .. 258
4.2.6.5. Tables of the dispersion corrections for forward scattering, averaged polarization using the relativistic multipole approach .. 258
Table 4.2.6.1. *Values of E_{tot}/mc^2 listed as a function of atomic number Z* .. 246
Table 4.2.6.2(*a*). *Comparison between the S-matrix calculations of Kissel (1977) and the form-factor calculations of Cromer & Liberman (1970, 1981, 1983) and Creagh & McAuley for the noble gases and several common metals* .. 249
Table 4.2.6.2(*b*). *A comparison of the real part of the forward-scattering amplitudes computed using different theoretical approaches* .. 249
Table 4.2.6.3. *A comparison of the imaginary part of the forward-scattering amplitudes $f''(\omega, 0)$ computed using different theoretical approaches* .. 250
Table 4.2.6.4. *Comparison of measurements of the real part of the dispersion correction for LiF, Si, Al and Ge for characteristic wavelengths Ag $K\alpha_1$, Mo $K\alpha_1$ and Cu $K\alpha_1$ with theoretical predictions* .. 252
Table 4.2.6.5. *Comparison of measurements of $f'(\omega, 0)$ for C, Si and Cu for characteristic wavelengths Ag $K\alpha_1$, Mo $K\alpha_1$ and Cu $K\alpha_1$ with theoretical predictions* .. 253
Table 4.2.6.6. *Comparison of $f'(\omega_A, 0)$ for copper, nickel, zirconium, and niobium for theoretical and experimental data sets* .. 254
Table 4.2.6.7. *List of wavelengths, energies, and linewidths used in compiling the table of dispersion corrections* .. 254
Table 4.2.6.8. *Dispersion corrections for forward scattering* .. 255

4.3. Electron Diffraction .. 259

4.3.1. Scattering factors for the diffraction of electrons by crystalline solids (J. M. Cowley) .. 259

4.3.1.1. Elastic scattering from a perfect crystal .. 259
4.3.1.2. Atomic scattering factors .. 259
4.3.1.3. Approximations of restricted validity .. 260
4.3.1.4. Relativistic effects .. 260
4.3.1.5. Absorption effects .. 261
4.3.1.6. Tables of atomic scattering amplitudes for electrons .. 261
4.3.1.7. Use of Tables 4.3.1.1 and 4.3.1.2 .. 261
Table 4.3.1.1. *Atomic scattering amplitudes for electrons for neutral atoms* .. 263
Table 4.3.1.2. *Atomic scattering amplitudes for electrons for ionized atoms* .. 272

4.3.2. Parameterizations of electron atomic scattering factors (J. M. Cowley, L. M. Peng, G. Ren, S. L. Dudarev, and M. J. Whelan) .. 262
Table 4.3.2.1. *Parameters useful in electron diffraction as a function of accelerating voltage* .. 281
Table 4.3.2.2. *Elastic atomic scattering factors of electrons for neutral atoms and s up to 2.0 Å^{-1}* .. 282
Table 4.3.2.3. *Elastic atomic scattering factors of electrons for neutral atoms and s up to 6.0 Å^{-1}* .. 284

4.3.3. Complex scattering factors for the diffraction of electrons by gases (A. W. Ross, M. Fink, R. Hilderbrandt, J. Wang, and V. H. Smith Jr) .. 262
4.3.3.1. Introduction .. 262
4.3.3.2. Complex atomic scattering factors for electrons .. 262
4.3.3.2.1. Elastic scattering factors for atoms .. 262
4.3.3.2.2. Total inelastic scattering factors .. 389
4.3.3.2.3. Corrections for defects in the theory of atomic scattering .. 390
4.3.3.3. Molecular scattering factors for electrons .. 390
Table 4.3.3.1. *Partial wave elastic scattering factors for neutral atoms* .. 286
Table 4.3.3.2. *Inelastic scattering factors* .. 378

4.3.4. Electron energy-loss spectroscopy on solids (C. Colliex) .. 391
4.3.4.1. Definitions .. 391
4.3.4.1.1. Use of electron beams .. 391
4.3.4.1.2. Parameters involved in the description of a single inelastic scattering event .. 392
4.3.4.1.3. Problems associated with multiple scattering .. 392
4.3.4.1.4. Classification of the different types of excitations contained in an electron energy-loss spectrum .. 393
4.3.4.2. Instrumentation .. 394
4.3.4.2.1. General instrumental considerations .. 394
4.3.4.2.2. Spectrometers .. 395
4.3.4.2.3. Detection systems .. 397
4.3.4.3. Excitation spectrum of valence electrons .. 397
4.3.4.3.1. Volume plasmons .. 397
4.3.4.3.2. Dielectric description .. 399
4.3.4.3.3. Real solids .. 401
4.3.4.3.4. Surface plasmons .. 403
4.3.4.4. Excitation spectrum of core electrons .. 404
4.3.4.4.1. Definition and classification of core edges .. 404
4.3.4.4.2. Bethe theory for inelastic scattering by an isolated atom .. 406
4.3.4.4.3. Solid-state effects .. 408
4.3.4.4.4. Applications of core-loss spectroscopy .. 410
4.3.4.5. Conclusions .. 411
Table 4.3.4.1. *Different possibilities for using EELS information as a function of the different accessible parameters (**r**, θ, ΔE)* .. 394
Table 4.3.4.2. *Plasmon energies measured (and calculated) for a few simple metals* .. 397
Table 4.3.4.3. *Experimental and theoretical values for the coefficient α in the plasmon dispersion curve together with estimates of the cut-off wavevector* .. 398
Table 4.3.4.4. *Comparison of measured and calculated values for the halfwidth $\Delta E_{1/2}(0)$ of the plasmon line* .. 398

4.3.5. Oriented texture patterns (B. B. Zvyagin) .. 412
4.3.5.1. Texture patterns .. 412
4.3.5.2. Lattice plane oriented perpendicular to a direction (lamellar texture) .. 412
4.3.5.3. Lattice direction oriented parallel to a direction (fibre texture) .. 413
4.3.5.4. Applications to metals and organic materials .. 414

4.3.6. Computation of dynamical wave amplitudes .. 414

4.3.6.1. The multislice method (D. F. Lynch) .. 414
4.3.6.2. The Bloch-wave method (A. Howie) .. 415

4.3.7. Measurement of structure factors and determination of crystal thickness by electron diffraction (J. Gjønnes and J. W. Steeds) .. 416

4.3.8. Crystal structure determination by high-resolution electron microscopy (J. C. H. Spence and J. M. Cowley) 419

4.3.8.1. Introduction .. 419
4.3.8.2. Lattice-fringe images .. 421
4.3.8.3. Crystal structure images .. 422
4.3.8.4. Parameters affecting HREM images .. 424
4.3.8.5. Computing methods .. 425
4.3.8.6. Resolution and hyper-resolution .. 427
4.3.8.7. Alternative methods .. 427
4.3.8.8. Combined use of HREM and electron diffraction .. 428

4.4. Neutron Techniques .. 430

4.4.1. Production of neutrons (J. M. Carpenter and G. Lander) .. 430

4.4.2. Beam-definition devices (I. S. Anderson and O. Schärpf) .. 431

4.4.2.1. Introduction .. 431
4.4.2.2. Collimators .. 431
4.4.2.3. Crystal monochromators .. 432
4.4.2.4. Mirror reflection devices .. 435
4.4.2.4.1. Neutron guides .. 435
4.4.2.4.2. Focusing mirrors .. 436
4.4.2.4.3. Multilayers .. 436
4.4.2.4.4. Capillary optics .. 437
4.4.2.5. Filters .. 438
4.4.2.6. Polarizers .. 438
4.4.2.6.1. Single-crystal polarizers .. 438
4.4.2.6.2. Polarizing mirrors .. 440
4.4.2.6.3. Polarizing filters .. 440
4.4.2.6.4. Zeeman polarizer .. 442
4.4.2.7. Spin-orientation devices .. 442
4.4.2.7.1. Maintaining the direction of polarization .. 442
4.4.2.7.2. Rotation of the polarization direction .. 442
4.4.2.7.3. Flipping of the polarization direction .. 442
4.4.2.8. Mechanical choppers and selectors .. 443
Table 4.4.2.1. *Some important properties of materials used for neutron monochromator crystals* .. 433
Table 4.4.2.2. *Neutron scattering-length densities, Nb_{coh}, for some commonly used materials* .. 435
Table 4.4.2.3. *Characteristics of some typical elements and isotopes used as neutron filters* .. 439
Table 4.4.2.4. *Properties of polarizing crystal monochromators* .. 440
Table 4.4.2.5. *Scattering-length densities for some typical materials used for polarizing multilayers* .. 441

4.4.3. Resolution functions (R. Pynn and J. M. Rowe) .. 443

4.4.4. Scattering lengths for neutrons (V. F. Sears) .. 444

4.4.4.1. Scattering lengths .. 444
4.4.4.2. Scattering and absorption cross sections .. 452
4.4.4.3. Isotope effects .. 452
4.4.4.4. Correction for electromagnetic interactions .. 453
4.4.4.5. Measurement of scattering lengths .. 453
4.4.4.6. Compilation of scattering lengths and cross sections .. 453
Table 4.4.4.1. *Bound scattering lengths, b, and cross sections, σ, of the elements and their isotopes* .. 445

4.4.5. Magnetic form factors (P. J. Brown) .. 454

Table 4.4.5.1. *$\langle j_0 \rangle$ form factors for 3d transition elements and their ions* .. 454
Table 4.4.5.2. *$\langle j_0 \rangle$ form factors for 4d atoms and their ions* .. 455
Table 4.4.5.3. *$\langle j_0 \rangle$ form factors for rare-earth ions* .. 455
Table 4.4.5.4. *$\langle j_0 \rangle$ form factors for actinide ions* .. 455
Table 4.4.5.5. *$\langle j_2 \rangle$ form factors for 3d transition elements and their ions* .. 456
Table 4.4.5.6. *$\langle j_2 \rangle$ form factors for 4d atoms and their ions* .. 457
Table 4.4.5.7. *$\langle j_2 \rangle$ form factors for rare-earth ions* .. 457
Table 4.4.5.8. *$\langle j_2 \rangle$ form factors for actinide ions* .. 457
Table 4.4.5.9. *$\langle j_4 \rangle$ form factors for 3d atoms and their ions* .. 458

Table 4.4.5.10. $\langle j_4 \rangle$ *form factors for 4d atoms and their ions* .. 459
Table 4.4.5.11. $\langle j_4 \rangle$ *form factors for rare-earth ions* .. 459
Table 4.4.5.12. $\langle j_4 \rangle$ *form factors for actinide ions* .. 459
Table 4.4.5.13. $\langle j_6 \rangle$ *form factors for rare-earth ions* .. 460
Table 4.4.5.14. $\langle j_6 \rangle$ *form factors for actinide ions* .. 460

4.4.6. Absorption coefficients for neutrons (B. T. M. Willis) .. 461
Table 4.4.6.1. *Absorption of the elements for neutrons* .. 461

References .. 462

PART 5: DETERMINATION OF LATTICE PARAMETERS .. 489

5.1. Introduction (A. J. C. Wilson) .. 490

5.2. X-ray Diffraction Methods: Polycrystalline (W. Parrish, A. J. C. Wilson, and J. I. Langford) .. 491

5.2.1. Introduction .. 491
5.2.1.1. The techniques available .. 491
5.2.1.2. Errors and aberrations: general discussion .. 491
5.2.1.3. Errors of the Bragg angle .. 491
5.2.1.4. Bragg angle: operational definitions .. 491
Table 5.2.1.1. *Functions of the cell angles in equation (5.2.1.3) for the possible unit cells* .. 492

5.2.2. Wavelength and related problems .. 492
5.2.2.1. Errors and uncertainties in wavelength .. 492
5.2.2.2. Refraction .. 492
5.2.2.3. Statistical fluctuations .. 492

5.2.3. Geometrical and physical aberrations .. 493
5.2.3.1. Aberrations .. 493
5.2.3.2. Extrapolation, graphical and analytical .. 493

5.2.4. Angle-dispersive diffractometer methods: conventional sources .. 495
Table 5.2.4.1. *Centroid displacement* $\langle \Delta\theta/\theta \rangle$ *and variance W of certain aberrations of an angle-dispersive diffractometer* .. 494

5.2.5. Angle-dispersive diffractometer methods: synchrotron sources .. 495

5.2.6. Whole-pattern methods .. 496

5.2.7. Energy-dispersive techniques .. 496
Table 5.2.7.1. *Centroid displacement* $\langle \Delta E/E \rangle$ *and variance W of certain aberrations of an energy-dispersive diffractometer* .. 497

5.2.8. Camera methods .. 497
Table 5.2.8.1. *Some geometrical aberrations in the Debye–Scherrer method* .. 498

5.2.9. Testing for remanent systematic error .. 498

5.2.10. Powder-diffraction standards .. 498
Table 5.2.10.1. *NIST values for silicon standards* .. 499
Table 5.2.10.2. *Reflection angles for tungsten, silver, and silicon* .. 499
Table 5.2.10.3. *Silicon standard reflection angles* .. 500
Table 5.2.10.4. *Silicon standard high reflection angles* .. 501
Table 5.2.10.5. *Tungsten reflection angles* .. 502
Table 5.2.10.6. *Fluorophlogopite standard reflection angles* .. 503
Table 5.2.10.7. *Silver behenate standard reflection angles* .. 503

5.2.11. Intensity standards .. 500
Table 5.2.11.1. *NIST intensity standards, SRM 674* .. 503

5.2.12. Instrumental line-profile-shape standards .. 501

5.2.13. Factors determining accuracy .. 501

5.3. X-ray Diffraction Methods: Single Crystal (E. Gałdecka) .. 505

5.3.1. Introduction .. 505
5.3.1.1. General remarks .. 505
5.3.1.2. Introduction to single-crystal methods .. 506

5.3.2. Photographic methods .. 508
5.3.2.1. Introduction .. 508

5.3.2.2. The Laue method .. 508
5.3.2.3. Moving-crystal methods .. 508
5.3.2.3.1. Rotating-crystal method .. 508
5.3.2.3.2. Moving-film methods .. 509
5.3.2.3.3. Combined methods .. 509
5.3.2.3.4. Accurate and precise lattice-parameter determinations .. 509
5.3.2.3.5. Photographic cameras for investigation of small lattice-parameter changes .. 510
5.3.2.4. The Kossel method and divergent-beam techniques .. 510
5.3.2.4.1. The principle .. 510
5.3.2.4.2. Review of methods of accurate lattice-parameter determination .. 512
5.3.2.4.3. Accuracy and precision .. 515
5.3.2.4.4. Applications .. 515
5.3.3. Methods with counter recording .. 516
5.3.3.1. Introduction .. 516
5.3.3.2. Standard diffractometers .. 516
5.3.3.2.1. Four-circle diffractometer .. 516
5.3.3.2.2. Two-circle diffractometer .. 517
5.3.3.3. Data processing and optimization of the experiment .. 517
5.3.3.3.1. Models of the diffraction profile .. 517
5.3.3.3.2. Precision and accuracy of the Bragg-angle determination; optimization of the experiment 519
5.3.3.4. One-crystal spectrometers .. 521
5.3.3.4.1. General characteristics .. 521
5.3.3.4.2. Development of methods based on an asymmetric arrangement and their applications .. 521
5.3.3.4.3. The Bond method .. 522
5.3.3.4.3.1. Description of the method .. 522
5.3.3.4.3.2. Systematic errors .. 523
5.3.3.4.3.3. Development of the Bond method and its applications .. 524
5.3.3.4.3.4. Advantages and disadvantages of the Bond method .. 526
5.3.3.5. Limitations of traditional methods .. 526
5.3.3.6. Multiple-diffraction methods .. 526
5.3.3.7. Multiple-crystal – pseudo-non-dispersive techniques .. 528
5.3.3.7.1. Double-crystal spectrometers .. 528
5.3.3.7.2. Triple-crystal spectrometers .. 530
5.3.3.7.3. Multiple-beam methods .. 531
5.3.3.7.4. Combined methods .. 531
5.3.3.8. Optical and X-ray interferometry – a non-dispersive technique .. 533
5.3.3.9. Lattice-parameter and wavelength standards .. 534
5.3.4. Final remarks .. 534

5.4. Electron-Diffraction Methods .. 537
5.4.1. Determination of cell parameters from single-crystal patterns (A. W. S. Johnson) .. 537
5.4.1.1. Introduction .. 537
5.4.1.2. Zero-zone analysis .. 538
5.4.1.3. Non-zero-zone analysis .. 538
Table 5.4.1.1. *Unit-cell information available for photographic recording* .. 537
5.4.2. Kikuchi and HOLZ techniques (A. Olsen) .. 538

5.5. Neutron Methods (B. T. M. Willis) .. 541
References .. 541

PART 6: INTERPRETATION OF DIFFRACTED INTENSITIES .. 553

6.1. Intensity of Diffracted Intensities .. 554
6.1.1. X-ray scattering (E. N. Maslen, A. G. Fox, and M. A. O'Keefe) .. 554
6.1.1.1. Coherent (Rayleigh) scattering .. 554
6.1.1.2. Incoherent (Compton) scattering .. 554
6.1.1.3. Atomic scattering factor .. 554
6.1.1.3.1. Scattering-factor interpolation .. 565

6.1.1.4. Generalized scattering factors .. 565
6.1.1.5. The temperature factor .. 584
6.1.1.6. The generalized temperature factor .. 585
6.1.1.6.1. Gram–Charlier series .. 586
6.1.1.6.2. Fourier-invariant expansions .. 586
6.1.1.6.3. Cumulant expansion .. 588
6.1.1.6.4. Curvilinear density functions .. 588
6.1.1.6.5. Model-based curvilinear density functions .. 589
6.1.1.6.6. The quasi-Gaussian approximation for curvilinear motion .. 590
6.1.1.7. Structure factor .. 590
6.1.1.8. Reflecting power of a crystal .. 590
Table 6.1.1.1. *Mean atomic scattering factors in electrons for free atoms* .. 555
Table 6.1.1.2. *Spherical bonded hydrogen-atom scattering factors* .. 565
Table 6.1.1.3. *Mean atomic scattering factors in electrons for chemically significant ions* .. 566
Table 6.1.1.4. *Coefficients for analytical approximation to the scattering factors of Tables 6.1.1.1 and 6.1.1.3* 578
Table 6.1.1.5. *Coefficients for analytical approximation to the scattering factors of Table 6.1.1.1 for the range* $2.0 < (\sin\theta)/\lambda < 6.0\ \text{Å}^{-1}$ .. 581
Table 6.1.1.6. *Angle dependence of multipole functions* .. 583
Table 6.1.1.7. *Indices allowed by the site symmetry for the real form of the spherical harmonics* $Y_{lmp(\theta,\varphi)}$ .. 584
Table 6.1.1.8. *Cubic harmonics* $K_{lj}(\theta,\varphi)$ *for cubic site symmetries* .. 585
Table 6.1.1.9. $f_{nl}(\alpha, S) = \int_0^\infty r^n exp(-\alpha r) j_l(Sr) dr$ .. 586
Table 6.1.1.10. *Indices nmp allowed by the site symmetry for the functions* $H_n(z)\Phi_{mp}(\varphi)$ .. 586
Table 6.1.1.11. *Indices* n_x, n_y, n_z *allowed for the basis functions* $H_{n_x}(Ax)H_{n_y}(By)H_{n_z}(Cz)$ .. 587
6.1.2. Magnetic scattering of neutrons (P. J. Brown) .. 590
6.1.2.1. Glossary of symbols .. 590
6.1.2.2. General formulae for the magnetic cross section .. 591
6.1.2.3. Calculation of magnetic structure factors and cross sections .. 591
6.1.2.4. The magnetic form factor .. 592
6.1.2.5. The scattering cross section for polarized neutrons .. 592
6.1.2.6. Rotation of the polarization of the scattered neutrons .. 593
6.1.3. Nuclear scattering of neutrons (B. T. M. Willis) .. 593
6.1.3.1. Glossary of symbols .. 593
6.1.3.2. Scattering by a single nucleus .. 593
6.1.3.3. Scattering by a single atom .. 594
6.1.3.4. Scattering by a single crystal .. 594
6.2. Trigonometric Intensity Factors (H. Lipson, J. I. Langford and H.-C. Hu) .. 596
6.2.1. Expressions for intensity of diffraction .. 596
Table 6.2.1.1. *Summary of formulae for integrated powers of reflection* .. 597
6.2.2. The polarization factor .. 596
6.2.3. The angular-velocity factor .. 596
6.2.4. The Lorentz factor .. 596
6.2.5. Special factors in the powder method .. 596
6.2.6. Some remarks about the integrated reflection power ratio formulae for single-crystal slabs .. 598
6.2.7. Other factors .. 598
6.3. X-ray Absorption (E. N. Maslen) .. 599
6.3.1. Linear absorption coefficient .. 599
6.3.1.1. True or photoelectric absorption .. 599
6.3.1.2. Scattering .. 599
6.3.1.3. Extinction .. 599
6.3.1.4. Attenuation (mass absorption) coefficients .. 600
6.3.2. Dispersion .. 600
6.3.3. Absorption corrections .. 600
6.3.3.1. Special cases .. 600
6.3.3.2. Cylinders and spheres .. 600
6.3.3.3. Analytical method for crystals with regular faces .. 604
6.3.3.4. Gaussian integration .. 606

6.3.3.5. Empirical methods .. 607
6.3.3.6. Measuring crystals for absorption .. 608
Table 6.3.3.1. *Transmission coefficients* .. 601
Table 6.3.3.2. *Values of A* for cylinders* .. 602
Table 6.3.3.3. *Values of A* for spheres* .. 602
Table 6.3.3.4. *Values of (1/A*)(dA*/dμR) for spheres* .. 603
Table 6.3.3.5. *Coefficients for interpolation of A* and $\bar{T}$* .. 603

6.4. The Flow of Radiation in a Real Crystal (T. M. Sabine) .. 609

6.4.1. Introduction .. 609

6.4.2. The model of a real crystal .. 609

6.4.3. Primary and secondary extinction .. 609

6.4.4. Radiation flow .. 610

6.4.5. Primary extinction .. 610

6.4.6. The finite crystal .. 610

6.4.7. Angular variation of *E* .. 610

6.4.8. The value of *x* .. 610

6.4.9. Secondary extinction .. 611

6.4.10. The extinction factor .. 611
6.4.10.1. The correlated block model .. 611
6.4.10.2. The uncorrelated block model .. 611

6.4.11. Polarization .. 611

6.4.12. Anisotropy .. 612

6.4.13. Asymptotic behaviour of the integrated intensity .. 612
6.4.13.1. Non-absorbing crystal, strong primary extinction .. 612
6.4.13.2. Non-absorbing crystal, strong secondary extinction .. 612
6.4.13.3. The absorbing crystal .. 612

6.4.14. Relationship with the dynamical theory .. 612

6.4.15. Definitions .. 612

References .. 613

PART 7: MEASUREMENT OF INTENSITIES .. 617

7.1. Detectors for X-rays .. 618

7.1.1. Photographic film (P. M. de Wolff) .. 618
7.1.1.1. Visual estimation .. 618
7.1.1.2. Densitometry .. 618

7.1.2. Geiger counters (W. Parrish and J. I. Langford) .. 618

7.1.3. Proportional counters (W. Parrish) .. 619
7.1.3.1. The detector system .. 619
7.1.3.2. Proportional counters .. 619
7.1.3.3. Position-sensitive detectors .. 619
7.1.3.4. Resolution, discriminination, efficiency .. 619

7.1.4. Scintillation and solid-state detectors (W. Parrish) .. 619
7.1.4.1. Scintillation counters .. 619
7.1.4.2. Solid-state detectors .. 620
7.1.4.3. Energy resolution and pulse-amplitude discrimination .. 620
7.1.4.4. Quantum-counting efficiency and linearity .. 621
7.1.4.5. Escape peaks .. 622

7.1.5. Energy-dispersive detectors (B. Buras and L. Gerward) .. 622

7.1.6. Position-sensitive detectors (U. W. Arndt) .. 623
7.1.6.1. Choice of detector .. 623
7.1.6.1.1. Detection efficiency .. 624
7.1.6.1.2. Linearity of response .. 624
7.1.6.1.3. Dynamic range .. 625

7.1.6.1.4. Spatial resolution .. 625
7.1.6.1.5. Uniformity of response .. 625
7.1.6.1.6. Spatial distortion .. 625
7.1.6.1.7. Energy discrimination .. 625
7.1.6.1.8. Suitability for dynamic measurements .. 626
7.1.6.1.9. Stability .. 626
7.1.6.1.10. Size and weight .. 626
7.1.6.2. Gas-filled counters .. 626
7.1.6.2.1. Localization of the detected photon .. 627
7.1.6.2.2. Parallel-plate counters .. 627
7.1.6.2.3. Current ionization PSD's .. 628
7.1.6.3. Semiconductor detectors .. 629
7.1.6.3.1. X-ray-sensitive semiconductor PSD's .. 629
7.1.6.3.2. Light-sensitive semiconductor PSD's .. 630
7.1.6.3.3. Electron-sensitive PSD's .. 630
7.1.6.4. Devices with an X-ray-sensitive photocathode .. 630
7.1.6.5. Television area detectors with external phosphor .. 630
7.1.6.5.1. X-ray phosphors .. 631
7.1.6.5.2. Light coupling .. 632
7.1.6.5.3. Image intensifiers .. 632
7.1.6.5.4. TV camera tubes .. 632
7.1.6.6. Some applications .. 632
Table 7.1.6.1. *The importance of some detector properties for different X-ray patterns* .. 624
Table 7.1.6.2. *X-ray phosphors* .. 631
7.1.7. X-ray-sensitive TV cameras (J. Chikawa) .. 633
7.1.7.1. Signal-to-noise ratio .. 633
7.1.7.2. Imaging system .. 634
7.1.7.3. Image processing .. 635
7.1.8. Storage phosphors (Y. Amemiya and J. Chikawa) .. 635

7.2. Detectors for Electrons (J. N. Chapman) .. 639

7.2.1. Introduction .. 639
7.2.2. Characterization of detectors .. 639
7.2.3. Parallel detectors .. 640
7.2.3.1. Fluorescent screens .. 640
7.2.3.2. Photographic emulsions .. 640
7.2.3.3. Detector systems based on an electron-tube device .. 641
7.2.3.4. Electronic detection systems based on solid-state devices .. 641
7.2.3.5. Imaging plates .. 641
7.2.4. Serial detectors .. 642
7.2.4.1. Faraday cage .. 642
7.2.4.2. Scintillation detectors .. 642
7.2.4.3. Semiconductor detectors .. 642
7.2.5. Conclusions .. 643

7.3. Thermal Neutron Detection (P. Convert and P. Chieux) .. 644

7.3.1. Introduction .. 644
7.3.2. Neutron capture .. 644
Table 7.3.2.1. *Neutron capture reactions used in neutron detection* .. 645
7.3.3. Neutron detection processes .. 644
7.3.3.1. Detection *via* gas converter and gas ionization: the gas detector .. 644
7.3.3.2. Detection *via* solid converter and gas ionization: the foil detector .. 645
7.3.3.3. Detection *via* scintillation .. 645
7.3.3.4. Films .. 646
Table 7.3.3.1. *Commonly used detection processes* .. 646
Table 7.3.3.2. *A few examples of gas-detector characteristics* .. 646
7.3.4. Electronic aspects of neutron detection .. 648
7.3.4.1. The electronic chain .. 648

7.3.4.2. Controls and adjustments of the electronics .. 648
7.3.5. Typical detection systems .. 649
7.3.5.1. Single detectors .. 649
7.3.5.2. Position-sensitive detectors .. 649
7.3.5.3. Banks of detectors .. 650
Table 7.3.5.1. *Characteristics of some PSDs* .. 651
7.3.6. Characteristics of detection systems .. 651
7.3.7. Corrections to the intensity measurements depending on the detection system .. 652
7.3.7.1. Single detector .. 652
7.3.7.2. Banks of detectors .. 652
7.3.7.3. Position-sensitive detectors .. 652
7.4. Correction of Systematic Errors .. 653
7.4.1. Absorption .. 653
7.4.2. Thermal diffuse scattering (B. T. M. Willis) .. 653
7.4.2.1. Glossary of symbols .. 653
7.4.2.2. TDS correction factor for X-rays (single crystals) .. 654
7.4.2.2.1. Evaluation of $J(\mathbf{q})$ .. 654
7.4.2.2.2. Calculation of α .. 655
7.4.2.3. TDS correction factor for thermal neutrons (single crystals) .. 656
7.4.2.4. Correction factor for powders .. 657
7.4.3. Compton scattering (N. G. Alexandropoulos and M. J. Cooper) .. 657
7.4.3.1. Introduction .. 657
7.4.3.2. Non-relativistic calculations of the incoherent scattering cross section .. 657
7.4.3.2.1. Semi-classical radiation theory .. 657
7.4.3.2.2. Thomas–Fermi model .. 659
7.4.3.2.3. Exact calculations .. 659
7.4.3.3. Relativistic treatment of incoherent scattering .. 659
7.4.3.4. Plasmon, Raman, and resonant Raman scattering .. 660
7.4.3.5. Magnetic scattering .. 661
Table 7.4.3.1. *The energy transfer in the Compton scattering process for selected X-ray energies* .. 657
Table 7.4.3.2. *The incoherent scattering function for elements up to Z = 55* .. 658
Table 7.4.3.3. *Compton scattering of Mo Kα X-radiation through 170° from 2s electrons* .. 659
7.4.4. White radiation and other sources of backgound (P. Suortti) .. 661
7.4.4.1. Introduction .. 661
7.4.4.2. Incident beam and sample .. 661
7.4.4.3. Detecting system .. 663
7.4.4.4. Powder diffraction .. 664
7.5. Statistical Fluctuations (A. J. C. Wilson) .. 666
7.5.1. Distributions of intensities of diffraction .. 666
7.5.2. Counting modes .. 666
7.5.3. Fixed-time counting .. 666
7.5.4. Fixed-count timing .. 667
7.5.5. Complicating phenomena .. 667
7.5.5.1. Dead time .. 667
7.5.5.2. Voltage fluctuations .. 667
7.5.6. Treatment of measured-as-negative (and other weak) intensities .. 667
7.5.7. Optimization of counting times .. 667
References .. 668
PART 8: REFINEMENT OF STRUCTURAL PARAMETERS .. 677
8.1. Least Squares (E. Prince and P. T. Boggs) .. 678
8.1.1. Definitions .. 678
8.1.1.1. Linear algebra .. 678
8.1.1.2. Statistics .. 679

8.1.2. Principles of least squares .. 680

8.1.3. Implementation of linear least squares .. 681

8.1.3.1. Use of the QR factorization .. 681
8.1.3.2. The normal equations .. 682
8.1.3.3. Conditioning .. 682

8.1.4. Methods for nonlinear least squares .. 682

8.1.4.1. The Gauss–Newton algorithm .. 683
8.1.4.2. Trust-region methods – the Levenberg–Marquardt algorithm .. 683
8.1.4.3. Quasi-Newton, or secant, methods .. 683
8.1.4.4. Stopping rules .. 684
8.1.4.5. Recommendations .. 685

8.1.5. Numerical methods for large-scale problems .. 685

8.1.5.1. Methods for sparse matrices .. 685
8.1.5.2. Conjugate-gradient methods .. 686

8.1.6. Orthogonal distance regression .. 687

8.1.7. Software for least-squares calculations .. 688

8.2. Other Refinement Methods (E. Prince and D. M. Collins) .. 689

8.2.1. Maximum-likelihood methods .. 689

8.2.2. Robust/resistant methods .. 689

8.2.3. Entropy maximization .. 691

8.2.3.1. Introduction .. 691
8.2.3.2. Some examples .. 691

8.3. Constraints and Restraints in Refinement (E. Prince, L. W. Finger, and J. H. Konnert) .. 693

8.3.1. Constrained models .. 693

8.3.1.1. Lagrange undetermined multipliers .. 693
8.3.1.2. Direct application of constraints .. 693
Table 8.3.1.1. *Symmetry conditions for second-cumulant tensors* .. 695

8.3.2. Stereochemically restrained least-squares refinement .. 698

8.3.2.1. Stereochemical constraints as observational equations .. 698
Table 8.3.2.1. *Coordinates of atoms in standard groups appearing in polypeptides and proteins* .. 699
Table 8.3.2.2. *Ideal values for distances, torsion angles, etc. for a glycine–alanine dipeptide with a trans peptide bond* .. 700
Table 8.3.2.3. *Typical values of standard deviations for use in determining weights in restrained refinement of protein structures* .. 701

8.4. Statistical Significance Tests (E. Prince and C. H. Spiegelman) .. 702

8.4.1. The χ^2 distribution .. 702
Table 8.4.1.1. *Values of χ^2/ν for which the c.d.f. $\Psi(\chi_2, \nu)$ has the values given in the column headings, for various values of ν* .. 703

8.4.2. The *F* distribution .. 703
Table 8.4.2.1. *Values of the F ratio for which the c.d.f. $\Psi(F, \nu_1, \nu_2)$ has the value 0.95, for various choices of ν_1 and ν_2* .. 704

8.4.3. Comparison of different models .. 704
Table 8.4.3.1. *Values of t for which the c.d.f. $\Psi(t, \nu)$ has the values given in the column headings, for various values of ν* .. 704

8.4.4. Influence of individual data points .. 705

8.5. Detection and Treatment of Systematic Error (E. Prince and C. H. Spiegleman) .. 707

8.5.1. Accuracy .. 707

8.5.2. Lack of fit .. 707

8.5.3. Influential data points .. 708

8.5.4. Plausibility of results .. 709

8.6. The Rietveld Method (A. Albinati and B. T. M. Willis) .. 710

8.6.1. Basic theory .. 710

8.6.2. Problems with the Rietveld method .. 711

8.6.2.1. Indexing .. 711
8.6.2.2. Peak-shape function (PSF) .. 711
8.6.2.3. Background .. 711
8.6.2.4. Preferred orientation and texture .. 712
8.6.2.5. Statistical validity .. 712

8.7. Analysis of Charge and Spin Densities (P. Coppens, Z. Su, and P. J. Becker) .. 713

8.7.1. Outline of this chapter .. 713

8.7.2. Electron densities and the *n*-particle wavefunction .. 713

8.7.3. Charge densities .. 714

8.7.3.1. Introduction .. 714
8.7.3.2. Modelling of the charge density .. 714
8.7.3.3. Physical constraints .. 715

8.7.3.3.1. Electroneutrality constraint .. 715
8.7.3.3.2. Cusp constraint .. 715
8.7.3.3.3. Radial constraint .. 715
8.7.3.3.4. Hellmann–Feynman constraint .. 715

8.7.3.4. Electrostatic moments and the potential due to a charge distribution .. 716

8.7.3.4.1. Moments of a charge distribution .. 716

8.7.3.4.1.1. Moments as a function of the atomic multipole expansion .. 716
8.7.3.4.1.2. Molecular moments based on the deformation density .. 717
8.7.3.4.1.3. The effect of an origin shift on the outer moments .. 717
8.7.3.4.1.4. Total moments as a sum over the pseudoatom moments .. 718
8.7.3.4.1.5. Electrostatic moments of a subvolume of space by Fourier summation .. 718

8.7.3.4.2. The electrostatic potential .. 718

8.7.3.4.2.1. The electrostatic potential and its derivatives .. 718
8.7.3.4.2.2. Electrostatic potential outside a charge distribution .. 720
8.7.3.4.2.3. Evaluation of the electrostatic functions in direct space .. 720

8.7.3.4.3. Electrostatic functions of crystals by modified Fourier summation .. 720
8.7.3.4.4. The total energy of a crystal as a function of the electron density .. 721

8.7.3.5. Quantitative comparison with theory .. 721
8.7.3.6. Occupancies of transition-metal valence orbitals from multipole coefficients .. 722
8.7.3.7. Thermal smearing of theoretical densities .. 723

8.7.3.7.1. General considerations .. 723
8.7.3.7.2. Reciprocal-space averaging over external vibrations .. 723

8.7.3.8. Uncertainties in experimental electron densities .. 724
8.7.3.9. Uncertainties in derived functions .. 725

Table 8.7.3.1. *Definition of difference density functions* .. 714
Table 8.7.3.2. *Expressions for the shape factors S for a parallelepiped with edges δ_x, δ_y, and δ_z* .. 719
Table 8.7.3.3. *The matrix M^{-1} relating d-orbital occupancies P_{ij} to multipole populations P_{lm}* .. 722
Table 8.7.3.4. *Orbital–multipole relations for square-planar complexes (point group D_{4h})* .. 723
Table 8.7.3.5. *Orbital–multipole relations for trigonal complexes* .. 723

8.7.4. Spin densities .. 725

8.7.4.1. Introduction .. 725
8.7.4.2. Magnetization densities from neutron magnetic elastic scattering .. 725
8.7.4.3. Magnetization densities and spin densities .. 726

8.7.4.3.1. Spin-only density at zero temperature .. 726
8.7.4.3.2. Thermally averaged spin-only magnetization density .. 726
8.7.4.3.3. Spin density for an assembly of localized systems .. 727
8.7.4.3.4. Orbital magnetization density .. 727

8.7.4.4. Probing spin densities by neutron elastic scattering .. 727

8.7.4.4.1. Introduction .. 727
8.7.4.4.2. Unpolarized neutron scattering .. 728
8.7.4.4.3. Polarized neutron scattering .. 728

8.7.4.4.4. Polarized neutron scattering of centrosymmetric crystals .. 728
8.7.4.4.5. Polarized neutron scattering in the noncentrosymmetric case .. 728
8.7.4.4.6. Effect of extinction .. 728
8.7.4.4.7. Error analysis .. 729
8.7.4.5. Modelling the spin density .. 729
8.7.4.5.1. Atom-centred expansion .. 729
8.7.4.5.1.1. Spherical-atom model .. 729
8.7.4.5.1.2. Crystal-field approximation .. 729
8.7.4.5.1.3. Scaling of the spin density .. 730
8.7.4.5.2. General multipolar expansion .. 730
8.7.4.5.3. Other types of model .. 730
8.7.4.6. Orbital contribution to the magnetic scattering .. 730
8.7.4.6.1. The dipolar approximation .. 731
8.7.4.6.2. Beyond the dipolar approximation .. 731
8.7.4.6.3. Electronic structure of rare-earth elements .. 731
8.7.4.7. Properties derivable from spin densities .. 731
8.7.4.7.1. Vector fields .. 732
8.7.4.7.2. Moments of the magnetization density .. 732
8.7.4.8. Comparison between theory and experiment .. 732
8.7.4.9. Combined charge- and spin-density analysis .. 732
8.7.4.10. Magnetic X-ray scattering separation between spin and orbital magnetism .. 733
8.7.4.10.1. Introduction .. 733
8.7.4.10.2. Magnetic X-ray structure factor as a function of photon polarization .. 733

8.8. Accurate Structure-Factor Determination with Electron Diffraction (J. Gjønnes) .. 735

References .. 738

PART 9: BASIC STRUCTURAL FEATURES .. 745

9.1. Sphere Packings and Packings of Ellipsoids (E. Koch and W. Fischer) .. 746

9.1.1. Sphere packings and packings of circles .. 746
9.1.1.1. Definitions .. 746
9.1.1.2. Homogeneous packings of circles .. 746
9.1.1.3. Homogeneous sphere packings .. 746
9.1.1.4. Applications .. 750
9.1.1.5. Interpenetrating sphere packings .. 751
Table 9.1.1.1. *Types of circle packings in the plane* .. 747
Table 9.1.1.2. *Examples for sphere packings with high contact numbers and high densities and with low contact numbers and low densities* .. 748
9.1.2. Packings of ellipses and ellipsoids .. 751

9.2. Layer Stacking .. 752

9.2.1. Layer stacking in close-packed structures (D. Pandey and P. Krishna) .. 752
9.2.1.1. Close packing of equal spheres .. 752
9.2.1.1.1. Close-packed layer .. 752
9.2.1.1.2. Close-packed structures .. 752
9.2.1.1.3. Notations for close-packed structures .. 752
9.2.1.2. Structure of compounds based on close-packed layer stackings .. 753
9.2.1.2.1. Voids in close packing .. 753
9.2.1.2.2. Structures of SiC and ZnS .. 753
9.2.1.2.3. Structure of CdI_2 .. 754
9.2.1.2.4. Structure of GaSe .. 754
9.2.1.3. Symmetry of close-packed layer stackings of equal spheres .. 755
9.2.1.4. Possible lattice types .. 755
9.2.1.5. Possible space groups .. 755
9.2.1.6. Crystallographic uses of Zhdanov symbols .. 756
9.2.1.7. Structure determination of close-packed layer stackings .. 756
9.2.1.7.1. General considerations .. 756
9.2.1.7.2. Determination of the lattice type .. 757

9.2.1.7.3. Determination of the identity period .. 757
9.2.1.7.4. Determination of the stacking sequence of layers .. 757
9.2.1.8. Stacking faults in close-packed structures .. 758
9.2.1.8.1. Structure determination of one-dimensionally disordered crystals .. 759
Table 9.2.1.1. *Common close-packed metallic structures* .. 753
Table 9.2.1.2. *List of SiC polytypes with known structures in order of increasing periodicity* .. 754
Table 9.2.1.3. *Intrinsic fault configurations in the 6H ($A_0B_1C_2A_3C_4B_5,\ldots$) structure* .. 758
Table 9.2.1.4. *Intrinsic fault configurations in the 9R ($A_0B_1A_2C_0A_1C_2B_0C_1B_2,\ldots$) structure* .. 759
9.2.2. Layer stacking in general polytypic structures (S. Ďurovič) .. 760
9.2.2.1. The notion of polytypism .. 760
9.2.2.2. Symmetry aspects of polytypism .. 761
9.2.2.2.1. Close packing of spheres .. 761
9.2.2.2.2. Polytype families and OD groupoid families .. 761
9.2.2.2.3. MDO polytypes .. 762
9.2.2.2.4. Some geometrical properties of OD structures .. 762
9.2.2.2.5. Diffraction pattern – structure analysis .. 763
9.2.2.2.6. The vicinity condition .. 763
9.2.2.2.7. Categories of OD structures .. 764
9.2.2.2.7.1. OD structures of equivalent layers .. 764
9.2.2.2.7.2. OD structures with more than one kind of layer .. 765
9.2.2.2.8. Desymmetrization of OD structures .. 765
9.2.2.2.9. Concluding remarks .. 766
9.2.2.3. Examples of some polytypic structures .. 766
9.2.2.3.1. Hydrous phyllosilicates .. 766
9.2.2.3.1.1. General geometry .. 767
9.2.2.3.1.2. Diffraction pattern and identification of individual polytypes .. 769
9.2.2.3.2. Stibivanite Sb_2VO_5 .. 769
9.2.2.3.3. γ-$Hg_3S_2Cl_2$ .. 771
9.2.2.3.4. Remarks for authors .. 772
9.2.2.4. List of some polytypic structures .. 772

9.3. Typical Interatomic Distances: Metals and Alloys (J. L. C. Daams, J. R. Rodgers, and P. Villars) .. 774

9.3.1. Glossary .. 777

9.4. Typical Interatomic Distances: Inorganic Compounds (G. Bergerhoff and K. Brandenburg) .. 778

9.4.1. Introduction .. 778
Table 9.4.1.1. *Atomic distances between halogens and main-group elements in their preferred oxidation states* .. 779
Table 9.4.1.2. *Atomic distances between halogens and main-group elements in their special oxidation states* 780
Table 9.4.1.3. *Atomic distances between halogens and transition metals* .. 781
Table 9.4.1.4. *Atomic distances between halogens and lanthanoids* .. 784
Table 9.4.1.5. *Atomic distances between halogens and actinoids* .. 785
Table 9.4.1.6. *Atomic distances between oxygen and main-group elements in their preferred oxidation states* 785
Table 9.4.1.7. *Atomic distances between oxygen and main-group elements in their special oxidation states* .. 786
Table 9.4.1.8. *Atomic distances between oxygen and transition elements in their preferred and special oxidation states* .. 786
Table 9.4.1.9. *Atomic distances between oxygen and lanthanoids* .. 787
Table 9.4.1.10. *Atomic distances between oxygen and actinoids* .. 788
Table 9.4.1.11. *Atomic distances in sulfides and thiometallates* .. 788
Table 9.4.1.12. *Contact distances between some negatively charged elements* .. 789
9.4.2. The retrieval system .. 778
9.4.3. Interpretation of frequency distributions .. 778

9.5. Typical Interatomic Distances: Organic Compounds (F. H. Allen, D. G. Watson, L. Brammer, A. G. Orpen, and R. Taylor) .. 790

9.5.1. Introduction .. 790
Table 9.5.1.1. *Average lengths for bonds involving the elements H, B, C, N, O, F, Si, P, S, Cl, As, Se, Br, Te and I* .. 796
9.5.2. Methodology .. 790

9.5.2.1. Selection of crystallographic data .. 790
9.5.2.2. Program system .. 790
9.5.2.3. Classification of bonds .. 791
9.5.2.4. Statistics .. 791

9.5.3. Content and arrangement of the table .. 791
9.5.3.1. Ordering of entries: the 'Bond' column .. 792
9.5.3.2. Definition of 'Substructure' .. 792
9.5.3.3. Use of the 'Note' column .. 793

9.5.4. Discussion .. 794

9.6. Typical Interatomic Distances: Organometallic Compounds and Coordination Complexes of the *d*- and *f*-Block Metals (A. G. Orpen, L. Brammer, F. H. Allen, D. G. Watson, and R. Taylor) .. 812

9.6.1. Introduction .. 812

9.6.2. Methodology .. 812
9.6.2.1. Selection of crystallographic data .. 812
9.6.2.2. Program system .. 813
9.6.2.3. Classification of bonds .. 813
9.6.2.4. Statistics .. 813

9.6.3. Content and arrangement of table of interatomic distances .. 814
9.6.3.1. The 'Bond' column .. 815
9.6.3.2. Definition of 'Substructure' .. 815
9.6.3.3. Use of the 'Note' column .. 817
9.6.3.4. Locating an entry in Table 9.6.3.3 .. 818
Table 9.6.3.1. *Ligand index* .. 814
Table 9.6.3.2. *Numbers of entries in Table 9.6.3.3* .. 817
Table 9.6.3.3. *Interatomic distances* .. 818

9.6.4. Discussion .. 818

9.7. The Space-Group Distribution of Molecular Organic Structures (A. J. C. Wilson, V. L. Karen, and A. Mighell) .. 897

9.7.1. *A priori* classifications of space groups .. 897
9.7.1.1. Kitajgorodskij's categories .. 897
9.7.1.2. Symmorphism and antimorphism .. 897
9.7.1.3. Comparison of Kitajgorodskij's and Wilson's classifications .. 899
9.7.1.4. Relation to structural classes .. 900
Table 9.7.1.1. *Kitajgorodskij's categorization of the triclinic, monoclinic and orthorhombic space groups* .. 898
Table 9.7.1.2. *Space groups arranged by arithmetic crystal class and degree of symmorphism* .. 899

9.7.2. Special positions of given symmetry .. 900
Table 9.7.2.1. *Statistics of the use of Wyckoff positions of specified symmetry $\mathcal{G}$ in the homomolecular organic crystals* .. 903

9.7.3. Empirical space-group frequencies .. 902

9.7.4. Use of molecular symmetry .. 902
9.7.4.1. Positions with symmetry $\bar{1}$ .. 902
9.7.4.2. Positions with symmetry $\bar{1}$ .. 902
9.7.4.3. Other symmetries .. 903
9.7.4.4. Positions with the full symmetry of the geometric class .. 903
Table 9.7.4.1. *Occurrence of molecules with specified point group in centred symmmorphic and other space groups* .. 905

9.7.5. Structural classes .. 904

9.7.6. A statistical model .. 904

9.7.7. Molecular packing .. 904
9.7.7.1. Relation to sphere packing .. 904
9.7.7.2. The hydrogen bond and the definition of the packing units .. 906

9.7.8. *A priori* predictions of molecular crystal structures .. 906

9.8. Incommensurate and Commensurate Modulated Structures (T. Janssen, A. Janner, A. Looijenga-Vos, and P. M. de Wolff) .. 907

9.8.1. Introduction .. 907

9.8.1.1. Modulated crystal structures .. 907
9.8.1.2. The basic ideas of higher-dimensional crystallography .. 908
9.8.1.3. The simple case of a displacively modulated crystal .. 909

9.8.1.3.1. The diffraction pattern .. 909
9.8.1.3.2. The symmetry .. 909

9.8.1.4. Basic symmetry considerations .. 910

9.8.1.4.1. Bravais classes of vector modules .. 910
9.8.1.4.2. Description in four dimensions .. 911
9.8.1.4.3. Four-dimensional crystallography .. 911
9.8.1.4.4. Generalized nomenclature .. 912
9.8.1.4.5. Four-dimensional space groups .. 912

9.8.1.5. Occupation modulation .. 913

9.8.2. Outline for a superspace-group determination .. 913

9.8.3. Introduction to the tables .. 915

9.8.3.1. Tables of Bravais lattices .. 915
9.8.3.2. Table for geometric and arithmetic crystal classes .. 916
9.8.3.3. Tables of superspace groups .. 916

9.8.3.3.1. Symmetry elements .. 916
9.8.3.3.2. Reflection conditions .. 921

9.8.3.4. Guide to the use of the tables .. 935
9.8.3.5. Examples .. 936
9.8.3.6. Ambiguities in the notation .. 936

Table 9.8.3.1(*a*). *(2 + 1)-Dimensional Bravais classes for incommensurate structures* .. 915
Table 9.8.3.1(*b*). *(2 + 2)-Dimensional Bravais classes for incommensurate structures* .. 916
Table 9.8.3.2(*a*). *(3 + 1)-Dimensional Bravais classes for incommensurate structures* .. 917
Table 9.8.3.2(*b*). *(3 + 1)-Dimensional Bravais classes for commensurate structures* .. 918
Table 9.8.3.3. *(3 + 1)-Dimensional point groups and arithmetic crystal classes* .. 919
Table 9.8.3.4(*a*). *(2 + 1)-Dimensional superspace groups* .. 920
Table 9.8.3.4(*b*). *(2 + 2)-Dimensional superspace groups* .. 921
Table 9.8.3.5. *(3 + 1)-Dimensional superspace groups* .. 922
Table 9.8.3.6. *Centring reflection conditions for (3 + 1)-dimensional Bravais classes* .. 935

9.8.4. Theoretical foundation .. 937

9.8.4.1. Lattices and metric .. 937
9.8.4.2. Point groups .. 938

9.8.4.2.1. Laue class .. 938
9.8.4.2.2. Geometric and arithmetic crystal classes .. 939

9.8.4.3. Systems and Bravais classes .. 939

9.8.4.3.1. Holohedry .. 939
9.8.4.3.2. Crystallographic systems .. 940
9.8.4.3.3. Bravais classes .. 940

9.8.4.4. Superspace groups .. 940

9.8.4.4.1. Symmetry elements .. 940
9.8.4.4.2. Equivalent positions and modulation relations .. 940
9.8.4.4.3. Structure factor .. 941

9.8.5. Generalizations .. 941

9.8.5.1. Incommensurate composite crystal structures .. 941
9.8.5.2. The incommensurate *versus* the commensurate case .. 942

References .. 945

PART 10: PRECAUTIONS AGAINST RADIATION INJURY (D. C. Creagh and S. Martinez-Carrera) .. 957

10.1. Introduction .. 958

10.1.1. Definitions .. 958

Table 10.1.1. *The relationship between SI and the earlier system of units* .. 958

Table 10.1.2. *Maximum primary-dose limit per quarter* .. 960
Table 10.1.3. *Quality factors (QF)* .. 960

10.1.2. Objectives of radiation protection .. 960

10.1.3. Responsibilities .. 960
10.1.3.1. General .. 960
10.1.3.2. The radiation safety officer .. 960
10.1.3.3. The worker .. 960
10.1.3.4. Primary-dose limits .. 961

10.2. Protection from Ionizing Radiation .. 962

10.2.1. General .. 962

10.2.2. Sealed sources and radiation-producing apparatus .. 962
10.2.2.1. Enclosed installations .. 962
10.2.2.2. Open installations .. 962
10.2.2.3. Sealed sources .. 962
10.2.2.4. X-ray diffraction and X-ray analysis apparatus .. 962
10.2.2.5. Particle accelerators .. 962

10.2.3. Ionizing-radiation protection – unsealed radioactive materials .. 963

10.3. Responsible Bodies .. 964

Table 10.3.1. *Regulatory authorities* .. 964

References .. 967

Author Index .. 968

Subject Index .. 984

Preface

BY A. J. C. WILSON

A new volume of the *International Tables for Crystallography* containing mathematical, physical and chemical tables was discussed by the Executive Committee of the International Union of Crystallography at least as early as August 1979. My own ideas about what has become Volume C began to develop in the course of the Executive Committee meeting held at the Ottawa Congress in August 1981. It was then conceived as an editorial condensation of the old volumes II, III and IV, with obsolete material deleted and tables easily reproduced on a pocket calculator reduced to a skeleton form or omitted altogether. However, it soon became obvious that advances since the old volumes were produced could not be satisfactorily accommodated within such a condensation, and that if Volume C were to be a worthy companion of Volume A (*Space-Group Symmetry*) and Volume B (*Reciprocal Space*) it would have to consist largely of new material.

Work on Volumes B and C began officially on 1 January 1983, and the general outlines of the volumes were circulated to the Executive Committee, the National Committees, and others interested. This circulation generated much constructive criticism and offers of help, particularly from several Commissions of the Union. The Chairmen of certain Commissions were particularly helpful in finding qualified contributors of specialist sections, and from time to time served as members of the Commission on *International Tables for Crystallography*. I often had occasion to lament the lack of a Commission on X-ray Diffraction. The revised outlines of the two volumes were approved by the Executive Committee during the Hamburg Congress in 1984.

For various reasons the publication of Volume C has taken longer than expected. A requirement that prospective contributors should be approved by the Executive Committee produced some delays, and more serious delays were caused by authors who failed to deliver their contributions by the agreed date – or at all. A decision was taken to include in this first edition only what was in the Editor's hands in January 1990, and since that date the timetable has been set by the printers. The present Volume is the result. Readers will find a few sections resulting from the original idea of editorial condensation from Volumes II, III and IV, and some sections from those volumes revised or rewritten by their original authors. Most of Volume C is entirely new.

I am indebted to many crystallographers for advice and encouragement, to the authors of contributions that arrived before the deadline, to the Chairmen of various Commissions for their help, and to the Technical Editor for his skill and good humour in dealing with much difficult material.

Preface to the third edition

BY E. PRINCE

This is the third edition of *International Tables for Crystallography* Volume C. The purpose of this volume is to provide the mathematical, physical and chemical information needed for experimental studies in structural crystallography. It covers all aspects of experimental techniques, using all three principal radiation types, from the selection and mounting of crystals and production of radiation, through data collection and analysis, to the interpretation of results. As such, it is an essential source of information for all workers using crystallographic techniques in physics, chemistry, metallurgy, earth sciences and molecular biology.

Volume C of *International Tables for Crystallography* is one of the many legacies to crystallographers of the late Professor A. J. C. Wilson, whose death on 1 July 1995 left the preparation of a revised and expanded second edition unfinished. When I was appointed as Professor Wilson's successor as Editor, I realised that although most of the material in the first edition was new, some had been carried over from Volumes II, III, and IV of the earlier series *International Tables for X-ray Crystallography* and had become outdated. Moreover, many of the topics covered were changing very rapidly, so needed to be brought up to date. In fact, by the time the second edition was published in 1999, more than half the chapters had been revised or updated and two completely new chapters, on reflectometry and neutron topography, had been included. The second edition of Volume C was also the first volume of *International Tables* to be produced entirely electronically.

The authors of the second edition were asked if they wished to submit revisions to their articles for this third edition in August 2001. All revisions were received within the following year. In total, 11 chapters have been revised, corrected or updated, and all known errors in the second edition have been corrected. I hope few new errors have been introduced. I thank all authors, especially those who have submitted revisions, and I particularly thank the Editorial staff in Chester for their continued dilligence.

1.1. Summary of general formulae

By E. Koch

In an ideal crystal structure, the arrangement of atoms is three-dimensionally periodic. This periodicity is usually described in terms of point lattices, vector lattices, and translation groups [*cf.* *IT* A (1983, Section 8.1.3)].

1.1.1. General relations between direct and reciprocal lattices

1.1.1.1. *Primitive crystallographic bases*

The vectors **a**, **b**, **c** form a primitive crystallographic basis of the vector lattice **L**, if each translation vector $\mathbf{t} \in \mathbf{L}$ may be expressed as

$$\mathbf{t} = u\mathbf{a} + v\mathbf{b} + w\mathbf{c}$$

with u, v, w being integers.

A primitive basis defines a primitive unit cell for a corresponding point lattice. Its volume V may be calculated as the mixed product (triple scalar product) of the three basis vectors:

$$\begin{aligned} V &= (\mathbf{abc}) = \mathbf{a} \times \mathbf{b} \cdot \mathbf{c} \\ &= \left[\begin{vmatrix} a^2 & ab\cos\gamma & ac\cos\beta \\ ab\cos\gamma & b^2 & bc\cos\alpha \\ ac\cos\beta & bc\cos\alpha & c^2 \end{vmatrix} \right]^{1/2} \\ &= abc[1 - \cos^2\alpha - \cos^2\beta - \cos^2\gamma \\ &\quad + 2\cos\alpha\cos\beta\cos\gamma]^{1/2} \\ &= 2abc\left[\sin\frac{\alpha+\beta+\gamma}{2} \sin\frac{-\alpha+\beta+\gamma}{2} \right. \\ &\quad \left. \times \sin\frac{\alpha-\beta+\gamma}{2} \sin\frac{\alpha+\beta-\gamma}{2} \right]^{1/2}. \end{aligned} \tag{1.1.1.1}$$

Here a, b and c designate the lengths of the three basis vectors and $\alpha = \mathbf{b} \wedge \mathbf{c}$, $\beta = \mathbf{c} \wedge \mathbf{a}$ and $\gamma = \mathbf{a} \wedge \mathbf{b}$ the angles between them.

Each vector lattice **L** and each primitive crystallographic basis **a**, **b**, **c** is uniquely related to a reciprocal vector lattice $\mathbf{L}^*$ and a primitive reciprocal basis $\mathbf{a}^*$, $\mathbf{b}^*$, $\mathbf{c}^*$:

$$\left.\begin{aligned} \mathbf{a}^* &= \frac{\mathbf{b}\times\mathbf{c}}{V} \quad \text{or} \quad \mathbf{a}^*\cdot\mathbf{b} = \mathbf{a}^*\cdot\mathbf{c} = 0, \quad \mathbf{a}^*\cdot\mathbf{a} = 1; \\ \mathbf{b}^* &= \frac{\mathbf{c}\times\mathbf{a}}{V} \quad \text{or} \quad \mathbf{b}^*\cdot\mathbf{a} = \mathbf{b}^*\cdot\mathbf{c} = 0, \quad \mathbf{b}^*\cdot\mathbf{b} = 1; \\ \mathbf{c}^* &= \frac{\mathbf{a}\times\mathbf{b}}{V} \quad \text{or} \quad \mathbf{c}^*\cdot\mathbf{a} = \mathbf{c}^*\cdot\mathbf{b} = 0, \quad \mathbf{c}^*\cdot\mathbf{c} = 1. \end{aligned}\right\} \tag{1.1.1.2}$$

$$\mathbf{L}^* = \{\mathbf{r}^* | \mathbf{r}^* = h\mathbf{a}^* + k\mathbf{b}^* + l\mathbf{c}^* \text{ and } h, k, l \text{ integers}\}.$$

The lengths a^*, b^* and c^* of the reciprocal basis vectors and the angles $\alpha^* = \mathbf{b}^* \wedge \mathbf{c}^*$, $\beta^* = \mathbf{c}^* \wedge \mathbf{a}^*$ and $\gamma^* = \mathbf{a}^* \wedge \mathbf{b}^*$ are given by:

$$\left.\begin{aligned} a^* &= \frac{bc\sin\alpha}{V}, \quad b^* = \frac{ac\sin\beta}{V}, \quad c^* = \frac{ab\sin\gamma}{V}, \\ \cos\alpha^* &= \frac{\cos\beta\cos\gamma - \cos\alpha}{\sin\beta\sin\gamma}, \\ \cos\beta^* &= \frac{\cos\alpha\cos\gamma - \cos\beta}{\sin\alpha\sin\gamma}, \\ \cos\gamma^* &= \frac{\cos\alpha\cos\beta - \cos\gamma}{\sin\alpha\sin\beta}. \end{aligned}\right\} \tag{1.1.1.3}$$

$\mathbf{a}^*$, $\mathbf{b}^*$, $\mathbf{c}^*$ define a primitive unit cell in a corresponding reciprocal point lattice. Its volume V^* may be expressed by analogy with V [equation (1.1.1.1)]:

$$\begin{aligned} V^* &= (\mathbf{a}^*\mathbf{b}^*\mathbf{c}^*) = \mathbf{a}^* \times \mathbf{b}^* \cdot \mathbf{c}^* \\ &= \left[\begin{vmatrix} a^{*2} & a^*b^*\cos\gamma^* & a^*c^*\cos\beta^* \\ a^*b^*\cos\gamma^* & b^{*2} & b^*c^*\cos\alpha^* \\ a^*c^*\cos\beta^* & b^*c^*\cos\alpha^* & c^{*2} \end{vmatrix} \right]^{1/2} \\ &= a^*b^*c^*[1 - \cos^2\alpha^* - \cos^2\beta^* - \cos^2\gamma^* \\ &\quad + 2\cos\alpha^*\cos\beta^*\cos\gamma^*]^{1/2} \\ &= 2a^*b^*c^*\left[\sin\frac{\alpha^*+\beta^*+\gamma^*}{2} \sin\frac{-\alpha^*+\beta^*+\gamma^*}{2} \right. \\ &\quad \left. \times \sin\frac{\alpha^*-\beta^*+\gamma^*}{2} \sin\frac{\alpha^*+\beta^*-\gamma^*}{2} \right]^{1/2}. \end{aligned} \tag{1.1.1.4}$$

In addition, the following equation holds:

$$VV^* = 1. \tag{1.1.1.5}$$

As all relations between direct and reciprocal lattices are symmetrical, one can calculate **a**, **b**, **c** from $\mathbf{a}^*$, $\mathbf{b}^*$, $\mathbf{c}^*$:

$$\mathbf{a} = \frac{\mathbf{b}^*\times\mathbf{c}^*}{V^*}, \quad \mathbf{b} = \frac{\mathbf{c}^*\times\mathbf{a}^*}{V^*}, \quad \mathbf{c} = \frac{\mathbf{a}^*\times\mathbf{b}^*}{V^*}, \tag{1.1.1.6}$$

$$\left.\begin{aligned} a &= \frac{b^*c^*\sin\alpha^*}{V^*}, \\ b &= \frac{a^*c^*\sin\beta^*}{V^*}, \\ c &= \frac{a^*b^*\sin\gamma^*}{V^*}, \\ \cos\alpha &= \frac{\cos\beta^*\cos\gamma^* - \cos\alpha^*}{\sin\beta^*\sin\gamma^*}, \\ \cos\beta &= \frac{\cos\alpha^*\cos\gamma^* - \cos\beta^*}{\sin\alpha^*\sin\gamma^*}, \\ \cos\gamma &= \frac{\cos\alpha^*\cos\beta^* - \cos\gamma^*}{\sin\alpha^*\sin\beta^*}. \end{aligned}\right\} \tag{1.1.1.7}$$

The unit-cell volumes V and V^* may also be obtained from:

$$\begin{aligned} V &= abc\sin\alpha^*\sin\beta\sin\gamma \\ &= abc\sin\alpha\sin\beta^*\sin\gamma \\ &= abc\sin\alpha\sin\beta\sin\gamma^*, \end{aligned} \tag{1.1.1.8}$$

Copyright © 2006 International Union of Crystallography

Table 1.1.1.1. *Direct and reciprocal lattices described with respect to conventional basis systems*

Direct lattice $\mathbf{a}_c, \mathbf{b}_c, \mathbf{c}_c$			Reciprocal lattice		
			$\mathbf{a}_c^*, \mathbf{b}_c^*, \mathbf{c}_c^*$		
Bravais letter	Centring vectors	Unit-cell volume V_c	Conditions for reciprocal-lattice vectors $h\mathbf{a}_c^* + k\mathbf{b}_c^* + l\mathbf{c}_c^*$	Unit-cell volume V_c^*	Bravais letter
A	$\frac{1}{2}\mathbf{b}_c + \frac{1}{2}\mathbf{c}_c$	$2V$	$k + l = 2n$	$\frac{1}{2}V^*$	A
B	$\frac{1}{2}\mathbf{a}_c + \frac{1}{2}\mathbf{c}_c$	$2V$	$h + l = 2n$	$\frac{1}{2}V^*$	B
C	$\frac{1}{2}\mathbf{a}_c + \frac{1}{2}\mathbf{b}_c$	$2V$	$h + k = 2n$	$\frac{1}{2}V^*$	C
I	$\frac{1}{2}\mathbf{a}_c + \frac{1}{2}\mathbf{b}_c + \frac{1}{2}\mathbf{c}_c$	$2V$	$h + k + l = 2n$	$\frac{1}{2}V^*$	F
F	$\frac{1}{2}\mathbf{a}_c + \frac{1}{2}\mathbf{b}_c$, $\frac{1}{2}\mathbf{a}_c + \frac{1}{2}\mathbf{c}_c$, $\frac{1}{2}\mathbf{b}_c + \frac{1}{2}\mathbf{c}_c$	$4V$	$h + k = 2n$, $h + l = 2n$, $k + l = 2n$	$\frac{1}{4}V^*$	I
R	$\frac{1}{3}\mathbf{a}_c + \frac{2}{3}\mathbf{b}_c + \frac{2}{3}\mathbf{c}_c$, $\frac{2}{3}\mathbf{a}_c + \frac{1}{3}\mathbf{b}_c + \frac{1}{3}\mathbf{c}_c$	$3V$	$-h + k + l = 3n$	$\frac{1}{3}V^*$	R

$$\begin{aligned} V^* &= a^*b^*c^* \sin\alpha \sin\beta^* \sin\gamma^* \\ &= a^*b^*c^* \sin\alpha^* \sin\beta \sin\gamma^* \\ &= a^*b^*c^* \sin\alpha^* \sin\beta^* \sin\gamma. \end{aligned} \tag{1.1.1.9}$$

1.1.1.2. *Non-primitive crystallographic bases*

For certain lattice types, it is usual in crystallography to refer to a 'conventional' crystallographic basis $\mathbf{a}_c, \mathbf{b}_c, \mathbf{c}_c$ instead of a primitive basis $\mathbf{a}, \mathbf{b}, \mathbf{c}$. In that case, $\mathbf{a}_c$, $\mathbf{b}_c$, and $\mathbf{c}_c$ with all their integral linear combinations are lattice vectors again, but there exist other lattice vectors $\mathbf{t} \in \mathbf{L}$,

$$\mathbf{t} = t_1\mathbf{a}_c + t_2\mathbf{b}_c + t_3\mathbf{c}_c,$$

with at least two of the coefficients t_1, t_2, t_3 being fractional.

Such a conventional basis defines a conventional or centred unit cell for a corresponding point lattice, the volume V_c of which may be calculated by analogy with V by substituting $\mathbf{a}_c, \mathbf{b}_c, \mathbf{c}_c$ for $\mathbf{a}, \mathbf{b}$, and $\mathbf{c}$ in (1.1.1.1).

If m designates the number of centring lattice vectors $\mathbf{t}$ with $0 \le t_1, t_2, t_3 < 1$, V_c may be expressed as a multiple of the primitive unit-cell volume V:

$$V_c = mV. \tag{1.1.1.10}$$

With the aid of equations (1.1.1.2) and (1.1.1.3), the reciprocal basis $\mathbf{a}_c^*, \mathbf{b}_c^*, \mathbf{c}_c^*$ may be derived from $\mathbf{a}_c, \mathbf{b}_c, \mathbf{c}_c$. Again, each reciprocal-lattice vector

$$\mathbf{r}^* = h\mathbf{a}_c^* + k\mathbf{b}_c^* + l\mathbf{c}_c^* \in \mathbf{L}^*$$

is an integral linear combination of the reciprocal basis vectors, but in contrast to the use of a primitive basis only certain triplets h, k, l refer to reciprocal-lattice vectors.

Equation (1.1.1.5) also relates V_c to V_c^*, the reciprocal cell volume referred to $\mathbf{a}_c^*, \mathbf{b}_c^*, \mathbf{c}_c^*$. From this it follows that

$$V_c^* = \frac{1}{m}V^*. \tag{1.1.1.11}$$

Table 1.1.1.1 contains detailed information on 'centred lattices' described with respect to conventional basis systems.

As a direct lattice and its corresponding reciprocal lattice do not necessarily belong to the same type of Bravais lattices [*IT* A (1987, Section 8.2.4)], the Bravais letter of $\mathbf{L}^*$ is given in the last column of Table 1.1.1.1. Except for *P* lattices, a conventionally chosen basis for $\mathbf{L}^*$ coincides neither with $\mathbf{a}^*, \mathbf{b}^*, \mathbf{c}^*$ nor with $\mathbf{a}_c^*, \mathbf{b}_c^*, \mathbf{c}_c^*$. This third basis, however, is not used in crystallography. The designation of scattering vectors and the indexing of Bragg reflections usually refers to $\mathbf{a}_c^*, \mathbf{b}_c^*, \mathbf{c}_c^*$.

If the differences with respect to the coefficients of direct- and reciprocal-lattice vectors are disregarded, all other relations discussed in Part 1 are equally true for primitive bases and for conventional bases.

1.1.2. Lattice vectors, point rows, and net planes

The length t of a vector $\mathbf{t} = u\mathbf{a} + v\mathbf{b} + w\mathbf{c}$ is given by

$$\begin{aligned} t^2 = {} & u^2\mathbf{a}^2 + v^2\mathbf{b}^2 + w^2\mathbf{c}^2 + 2uvab\cos\gamma \\ & + 2uwac\cos\beta + 2vwbc\cos\alpha. \end{aligned} \tag{1.1.2.1}$$

Accordingly, the length r^* of a reciprocal-lattice vector $\mathbf{r}^* = h\mathbf{a}^* + k\mathbf{b}^* + l\mathbf{c}^*$ may be calculated from

$$\begin{aligned} r^{*2} = {} & h^2a^{*2} + k^2b^{*2} + l^2c^{*2} + 2hka^*b^*\cos\gamma^* \\ & + 2hla^*c^*\cos\beta^* + 2klb^*c^*\cos\gamma^*. \end{aligned} \tag{1.1.2.2}$$

If the coefficients u, v, w of a vector $\mathbf{t} \in \mathbf{L}$ are coprime, $[uvw]$ symbolizes the direction parallel to $\mathbf{t}$. In particular, $[uvw]$ is used to designate a crystal edge, a zone axis, or a point row with that direction.

The integer coefficients h, k, l of a vector $\mathbf{r}^* \in \mathbf{L}^*$ are also the coordinates of a point of the corresponding reciprocal lattice and designate the Bragg reflection with scattering vector $\mathbf{r}^*$. If h, k, l are coprime, the direction parallel to $\mathbf{r}^*$ is symbolized by $[hkl]^*$.

Each vector $\mathbf{r}^*$ is perpendicular to a family of equidistant parallel nets within a corresponding direct point lattice. If the coefficients h, k, l of $\mathbf{r}^*$ are coprime, the symbol (hkl) describes that family of nets. The distance $d(hkl)$ between two neighbouring nets is given by

$$d(hkl) = r^{*-1}. \tag{1.1.2.3}$$

Parallel to such a family of nets, there may be a face or a cleavage plane of a crystal.

The net planes (hkl) obey the equation

$$hx + ky + lz = n \quad (n = \text{integer}). \tag{1.1.2.4}$$

Different values of n distinguish between the individual nets of the family; x, y, z are the coordinates of points on the net planes (not necessarily of lattice points). They are expressed in units a, b, and c, respectively.

Similarly, each vector $\mathbf{t} \in \mathbf{L}$ with coprime coefficients u, v, w is perpendicular to a family of equidistant parallel nets within a corresponding reciprocal point lattice. This family of nets may be symbolized $(uvw)^*$. The distance $d^*(uvw)$ between two neighbouring nets can be calculated from

$$d^*(uvw) = t^{-1}. \tag{1.1.2.5}$$

A layer line on a rotation pattern or a Weissenberg photograph with rotation axis $[uvw]$ corresponds to one such net of the family $(uvw)^*$ of the reciprocal lattice.

The nets $(uvw)^*$ obey the equation

$$uh + vk + wl = n \quad (n = \text{integer}). \tag{1.1.2.6}$$

Equations (1.1.2.6) and (1.1.2.4) are essentially the same, but may be interpreted differently. Again, n distinguishes between the individual nets out of the family $(uvw)^*$. h, k, l are the coordinates of the reciprocal-lattice points, expressed in units a^*, b^*, c^*, respectively.

A family of nets (hkl) and a point row with direction $[uvw]$ out of the same point lattice are parallel if and only if the following equation is satisfied:

$$hu + kv + lw = 0. \tag{1.1.2.7}$$

This equation is called the 'zone equation' because it must also hold if a face (hkl) of a crystal belongs to a zone $[uvw]$.

Two (non-parallel) nets $(h_1k_1l_1)$ and $(h_2k_2l_2)$ intersect in a point row with direction $[uvw]$ if the indices satisfy the condition

$$u : v : w = \begin{vmatrix} k_1 l_1 \\ k_2 l_2 \end{vmatrix} : \begin{vmatrix} l_1 h_1 \\ l_2 h_2 \end{vmatrix} : \begin{vmatrix} h_1 k_1 \\ h_2 k_2 \end{vmatrix}. \tag{1.1.2.8}$$

The same condition must be satisfied for a zone axis $[uvw]$ defined by the crystal faces $(h_1k_1l_1)$ and $(h_2k_2l_2)$.

Three nets $(h_1k_1l_1)$, $(h_2k_2l_2)$, and $(h_3k_3l_3)$ intersect in parallel rows, or three faces with these indices belong to one zone if

$$\begin{vmatrix} h_1 k_1 l_1 \\ h_2 k_2 l_2 \\ h_3 k_3 l_3 \end{vmatrix} = 0. \tag{1.1.2.9}$$

Two (non-parallel) point rows $[u_1v_1w_1]$ and $[u_2v_2w_2]$ in the direct lattice are parallel to a family of nets (hkl) if

$$h : k : l = \begin{vmatrix} v_1 w_1 \\ v_2 w_2 \end{vmatrix} : \begin{vmatrix} w_1 u_1 \\ w_2 u_2 \end{vmatrix} : \begin{vmatrix} u_1 v_1 \\ u_2 v_2 \end{vmatrix}. \tag{1.1.2.10}$$

The same condition holds for a face (hkl) belonging to two zones $[u_1v_1w_1]$ and $[u_2v_2w_2]$.

Three point rows $[u_1v_1w_1]$, $[u_2v_2w_2]$, and $[u_3v_3w_3]$ are parallel to a net (hkl), or three zones of a crystal with these indices have a common face (hkl) if

$$\begin{vmatrix} u_1 v_1 w_1 \\ u_2 v_2 w_2 \\ u_3 v_3 w_3 \end{vmatrix} = 0. \tag{1.1.2.11}$$

A net (hkl) is perpendicular to a point row $[uvw]$ if

$$\begin{aligned} &\frac{a}{h}(au + bv\cos\gamma + cw\cos\beta) \\ &\quad = \frac{b}{k}(au\cos\gamma + bv + cw\cos\alpha) \\ &\quad = \frac{c}{l}(au\cos\beta + bv\cos\alpha + cw). \end{aligned} \tag{1.1.2.12}$$

1.1.3. Angles in direct and reciprocal space

The angles between the normal of a crystal face and the basis vectors $\mathbf{a}, \mathbf{b}, \mathbf{c}$ are called the direction angles of that face. They may be calculated as angles between the corresponding reciprocal-lattice vector $\mathbf{r}^*$ and the basis vectors $\lambda = \mathbf{r}^* \wedge \mathbf{a}$, $\mu = \mathbf{r}^* \wedge \mathbf{b}$ and $\nu = \mathbf{r}^* \wedge \mathbf{c}$:

$$\left.\begin{aligned} \cos\lambda = \frac{h}{a}d(hkl), \quad \cos\mu = \frac{k}{b}d(hkl), \\ \cos\nu = \frac{l}{c}d(hkl). \end{aligned}\right\} \tag{1.1.3.1}$$

The three equations can be combined to give

$$\left.\begin{aligned} a : b : c = \frac{h}{\cos\lambda} : \frac{k}{\cos\mu} : \frac{l}{\cos\nu} \\ \text{or} \\ h : k : l = a\cos\lambda : b\cos\mu : c\cos\nu. \end{aligned}\right\} \tag{1.1.3.2}$$

The first formula gives the ratios between a, b, and c, if for any face of the crystal the indices (hkl) and the direction angles λ, μ, and ν are known. Once the axial ratios are known, the indices of any other face can be obtained from its direction angles by using the second formula.

Similarly, the angles between a direct-lattice vector $\mathbf{t}$ and the reciprocal basis vectors $\lambda^* = \mathbf{t} \wedge \mathbf{a}^*$, $\mu^* = \mathbf{t} \wedge \mathbf{b}^*$ and $\nu^* = \mathbf{t} \wedge \mathbf{c}^*$ are given by

$$\left.\begin{aligned} \cos\lambda^* = \frac{u}{a^*}d^*(uvw), \quad \cos\mu^* = \frac{v}{b^*}d^*(uvw), \\ \cos\nu^* = \frac{w}{c^*}d^*(uvw). \end{aligned}\right\} \tag{1.1.3.3}$$

The angle ψ between two direct-lattice vectors $\mathbf{t}_1$ and $\mathbf{t}_2$ or between two corresponding point rows $[u_1v_1w_1]$ and $[u_2v_2w_2]$ may be derived from the scalar product

$$\begin{aligned} \mathbf{t}_1 \cdot \mathbf{t}_2 = {} & u_1u_2a^2 + v_1v_2b^2 + w_1w_2c^2 + (u_1v_2 + u_2v_1)ab\cos\gamma \\ & + (u_1w_2 + u_2w_1)ac\cos\beta + (v_1w_2 + v_2w_1)bc\cos\alpha \end{aligned} \tag{1.1.3.4}$$

as

$$\cos\psi = \frac{\mathbf{t}_1 \cdot \mathbf{t}_2}{t_1 t_2}. \tag{1.1.3.5}$$

Analogously, the angle φ between two reciprocal-lattice vectors $\mathbf{r}_1^*$ and $\mathbf{r}_2^*$ or between two corresponding point rows $[h_1k_1l_1]^*$ and $[h_2k_2l_2]^*$ or between the normals of two corresponding crystal faces $(h_1k_1l_1)$ and $(h_2k_2l_2)$ may be calculated as

$$\cos\varphi = \frac{\mathbf{r}_1^* \cdot \mathbf{r}_2^*}{r_1 r_2} \tag{1.1.3.6}$$

with

$$\begin{aligned} \mathbf{r}_1^* \cdot \mathbf{r}_2^* = {} & h_1h_2a^{*2} + k_1k_2b^{*2} + l_1l_2c^{*2} \\ & + (h_1k_2 + h_2k_1)a^*b^*\cos\gamma^* \\ & + (h_1l_2 + h_2l_1)a^*c^*\cos\beta^* \\ & + (k_1l_2 + k_2l_1)b^*c^*\cos\alpha^*. \end{aligned} \tag{1.1.3.7}$$

Finally, the angle ω between a first direction $[uvw]$ of the direct lattice and a second direction $[hkl]$ of the reciprocal lattice may also be derived from the scalar product of the corresponding vectors $\mathbf{t}$ and $\mathbf{r}^*$.

$$\cos\omega = \frac{\mathbf{t}\cdot\mathbf{r}^*}{tr^*} = \frac{uh+vk+wl}{tr^*}. \qquad (1.1.3.8)$$

1.1.4. The Miller formulae

Consider four faces of a crystal that belong to the same zone in consecutive order: $(h_1k_1l_1)$, $(h_2k_2l_2)$, $(h_3k_3l_3)$, and $(h_4k_4l_4)$. The angles between the ith and the jth face normals are designated φ_{ij}. Then the Miller formulae relate the indices of these faces to the angles φ_{ij}:

$$\frac{\sin\varphi_{12}\sin\varphi_{43}}{\sin\varphi_{13}\sin\varphi_{42}} = \frac{u_{12}u_{43}}{u_{13}u_{42}} = \frac{v_{12}v_{43}}{v_{13}v_{42}} = \frac{w_{12}w_{43}}{w_{13}w_{42}} \qquad (1.1.4.1)$$

with

$$u_{ij} = \begin{vmatrix} k_i l_i \\ k_j l_j \end{vmatrix}, \quad v_{ij} = \begin{vmatrix} l_i h_i \\ l_j h_j \end{vmatrix}, \quad w_{ij} = \begin{vmatrix} h_i k_i \\ h_j k_j \end{vmatrix}.$$

If all angles between the face normals and also the indices for three of the faces are known, the indices of the fourth face may be calculated. Equation (1.1.4.1) cannot be used if two of the faces are parallel.

From the definition of u_{ij}, v_{ij}, and w_{ij}, it follows that all fractions in (1.1.4.1) are rational:

$$\frac{\sin\varphi_{12}\sin\varphi_{43}}{\sin\varphi_{13}\sin\varphi_{42}} = \frac{p}{q} \quad \text{with } p, q \text{ integers.}$$

Therefore, (1.1.4.1) may be rearranged to

$$p\cot\varphi_{12} - q\cot\varphi_{13} = (p-q)\cot\varphi_{14}. \qquad (1.1.4.2)$$

This equation allows the determination of one angle if two of the angles and the indices of all four faces are known.

1.2. Application to the crystal systems

By E. Koch

Information on the description and classification of Bravais lattices, their assignment to crystal systems, the choice of basis vectors for reduced or conventional basis systems, and on basis transformations is given in *IT* A (1983, Parts 5 and 9). In the following, for each crystal system, the metrical conditions for conventionally chosen basis systems and the possible Bravais types of lattices are listed. As some of the general formulae from Chapter 1.1 become simpler when not applied to a lattice with general (triclinic) metric, these simplified formulae are tabulated for all crystal systems (except triclinic).

Except for triclinic, monoclinic, and orthorhombic symmetry, tables are given that relate pairs h, k or triplets h, k, l of indices to certain sums s of products of these indices needed in equation (1.1.2.2). Such tables may be useful, for example, for indexing powder diffraction patterns.

1.2.1. Triclinic crystal system

No metrical conditions:	$a, b, c, \alpha, \beta, \gamma$ arbitrary
Bravais lattice type:	aP
Symmetry of lattice points:	$\bar{1}$

1.2.2. Monoclinic crystal system

Bravais lattice types:	mP, mS
Symmetry of lattice points	$2/m$

1.2.2.1. *Setting with 'unique axis* $\mathbf{b}$*'*

Metrical conditions:	a, b, c, β arbitrary; $\alpha = \gamma = 90^\circ$
Bravais lattice types:	mP, mC or mA or mI
Symmetry of lattice points:	$.2/m.$
Simplified formulae:	

$$V = (\mathbf{abc}) = \left[\begin{vmatrix} a^2 & 0 & ac\cos\beta \\ 0 & b^2 & 0 \\ ac\cos\beta & 0 & c^2 \end{vmatrix}\right]^{1/2} = abc\sin\beta, \tag{1.1.1.1a}$$

$$\left.\begin{aligned} a^* &= \frac{1}{a\sin\beta}, \quad b^* = \frac{1}{b}, \quad c^* = \frac{1}{c\sin\beta}, \\ \alpha^* &= \gamma^* = 90^\circ, \quad \beta^* = 180^\circ - \beta, \end{aligned}\right\} \tag{1.1.1.3a}$$

$$V^* = (\mathbf{a}^*\mathbf{b}^*\mathbf{c}^*) = \left[\begin{vmatrix} a^{*2} & 0 & a^*c^*\cos\beta^* \\ 0 & b^{*2} & 0 \\ a^*c^*\cos\beta^* & 0 & c^{*2} \end{vmatrix}\right]^{1/2} = a^*b^*c^*\sin\beta^*, \tag{1.1.1.4a}$$

$$\left.\begin{aligned} a &= \frac{1}{a^*\sin\beta^*}, \quad b = \frac{1}{b^*}, \quad c = \frac{1}{c^*\sin\beta^*}, \\ \alpha &= \gamma = 90^\circ, \quad \beta = 180^\circ - \beta^*, \end{aligned}\right\} \tag{1.1.1.7a}$$

$$t^2 = u^2a^2 + v^2b^2 + w^2c^2 + 2uwac\cos\beta, \tag{1.1.2.1a}$$

$$r^{*2} = h^2a^{*2} + k^2b^{*2} + l^2c^{*2} + 2hla^*c^*\cos\beta^*, \tag{1.1.2.2a}$$

$$\frac{a}{h}(au + cw\cos\beta) = \frac{b^2v}{k} = \frac{c}{l}(au\cos\beta + cw), \tag{1.1.2.12a}$$

$$\mathbf{t}_1 \cdot \mathbf{t}_2 = u_1u_2a^2 + v_1v_2b^2 + w_1w_2c^2 + (u_1w_2 + u_2w_1)ac\cos\beta, \tag{1.1.3.4a}$$

$$\mathbf{r}_1^* \cdot \mathbf{r}_2^* = h_1h_2a^{*2} + k_1k_2b^{*2} + l_1l_2c^{*2} + (h_1l_2 + h_2l_1)a^*c^*\cos\beta^*. \tag{1.1.3.7a}$$

1.2.2.2. *Setting with 'unique axis* $\mathbf{c}$*'*

Metrical conditions:	a, b, c, γ arbitrary; $\alpha = \beta = 90^\circ$
Bravais lattice types:	mP, mB or mA or mI
Symmetry of lattice points:	$..2/m$
Simplified formulae:	

$$V = (\mathbf{abc}) = \left[\begin{vmatrix} a^2 & ab\cos\gamma & 0 \\ ab\cos\gamma & b^2 & 0 \\ 0 & 0 & c^2 \end{vmatrix}\right]^{1/2} = abc\sin\gamma, \tag{1.1.1.1b}$$

$$\left.\begin{aligned} a^* &= \frac{1}{a\sin\gamma}, \quad b^* = \frac{1}{b\sin\gamma}, \quad c^* = \frac{1}{c}, \\ \alpha^* &= \beta^* = 90^\circ, \quad \gamma^* = 180^\circ - \gamma, \end{aligned}\right\} \tag{1.1.1.3b}$$

$$V^* = (\mathbf{a}^*\mathbf{b}^*\mathbf{c}^*) = \left[\begin{vmatrix} a^{*2} & a^*b^*\cos\gamma^* & 0 \\ a^*b^*\cos\gamma^* & b^{*2} & 0 \\ 0 & 0 & c^{*2} \end{vmatrix}\right]^{1/2} = a^*b^*c^*\sin\gamma^*, \tag{1.1.1.4b}$$

$$\left.\begin{aligned} a &= \frac{1}{a^*\sin\gamma^*}, \quad b = \frac{1}{b^*\sin\gamma^*}, \quad c = \frac{1}{c^*}, \\ \alpha &= \beta = 90^\circ, \quad \gamma = 180^\circ - \gamma^*, \end{aligned}\right\} \tag{1.1.1.7b}$$

$$t^2 = u^2a^2 + v^2b^2 + w^2c^2 + 2uvab\cos\gamma, \tag{1.1.2.1b}$$

$$r^{*2} = h^2a^{*2} + k^2b^{*2} + l^2c^{*2} + 2hka^*b^*\cos\gamma^*, \tag{1.1.2.2b}$$

$$\frac{a}{h}(au + bv\cos\gamma) = \frac{b}{k}(au\cos\gamma + bv) = \frac{c^2w}{l}, \tag{1.1.2.12b}$$

$$\mathbf{t}_1 \cdot \mathbf{t}_2 = u_1u_2a^2 + v_1v_2b^2 + w_1w_2c^2 + (u_1v_2 + u_2v_1)ab\cos\gamma, \tag{1.1.3.4b}$$

$$\mathbf{r}_1^* \cdot \mathbf{r}_2^* = h_1h_2a^{*2} + k_1k_2b^{*2} + l_1l_2c^{*2} + (h_1k_2 + h_2k_1)a^*b^*\cos\gamma^*. \tag{1.1.3.7b}$$

1.2.3. Orthorhombic crystal system

Metrical conditions:	a, b, c arbitrary; $\alpha = \beta = \gamma = 90^\circ$
Bravais lattice types:	oP, oS (oC, oA), oI, oF
Symmetry of lattice points:	mmm

Copyright © 2006 International Union of Crystallography

Simplified formulae:

$$V = (\mathbf{abc}) = \left[\begin{vmatrix} a^2 & 0 & 0 \\ 0 & b^2 & 0 \\ 0 & 0 & c^2 \end{vmatrix}\right]^{1/2} = abc, \qquad (1.1.1.1c)$$

$$a^* = \frac{1}{a}, \quad b^* = \frac{1}{b}, \quad c^* = \frac{1}{c}, \quad \alpha^* = \beta^* = \gamma^* = 90^\circ, \qquad (1.1.1.3c)$$

$$V^* = (\mathbf{a}^*\mathbf{b}^*\mathbf{c}^*) = \left[\begin{vmatrix} a^{*2} & 0 & 0 \\ 0 & b^{*2} & 0 \\ 0 & 0 & c^{*2} \end{vmatrix}\right]^{1/2} = a^*b^*c^* = a^{-1}b^{-1}c^{-1}, \qquad (1.1.1.4c)$$

$$a = \frac{1}{a^*}, \quad b = \frac{1}{b^*}, \quad c = \frac{1}{c^*}, \quad \alpha = \beta = \gamma = 90^\circ, \qquad (1.1.1.7c)$$

$$t^2 = u^2a^2 + v^2b^2 + w^2c^2, \qquad (1.1.2.1c)$$

$$r^{*2} = h^2a^{*2} + k^2b^{*2} + l^2w^{*2}, \qquad (1.1.2.2c)$$

$$\frac{a^2u}{h} = \frac{b^2v}{k} = \frac{c^2w}{l}, \qquad (1.1.2.12c)$$

$$\mathbf{t}_1 \cdot \mathbf{t}_2 = u_1u_2a^2 + v_1v_2b^2 + w_1w_2c^2, \qquad (1.1.3.4c)$$

$$\mathbf{r}_1^* \cdot \mathbf{r}_2^* = h_1h_2a^{*2} + k_1k_2b^{*2} + l_1l_2c^{*2}. \qquad (1.1.3.7c)$$

1.2.4. Tetragonal crystal system

Metrical conditions: $a = b$; c arbitrary; $\alpha = \beta = \gamma = 90^\circ$
Bravais lattice types: tP, tI
Symmetry of lattice points: $4/mmm$
Simplified formulae:

$$V = (\mathbf{abc}) = \left[\begin{vmatrix} a^2 & 0 & 0 \\ 0 & a^2 & 0 \\ 0 & 0 & c^2 \end{vmatrix}\right]^{1/2} = a^2c, \qquad (1.1.1.1d)$$

$$a^* = b^* = \frac{1}{a}, \quad c^* = \frac{1}{c}, \quad \alpha^* = \beta^* = \gamma^* = 90^\circ, \qquad (1.1.1.3d)$$

$$V^* = (\mathbf{a}^*\mathbf{b}^*\mathbf{c}^*) = \left[\begin{vmatrix} a^{*2} & 0 & 0 \\ 0 & a^{*2} & 0 \\ 0 & 0 & c^{*2} \end{vmatrix}\right]^{1/2} = a^{*2}c^* = a^{-2}c^{-1}, \qquad (1.1.1.4d)$$

$$a = b = \frac{1}{a^*}, \quad c = \frac{1}{c^*}, \quad \alpha = \beta = \gamma = 90^\circ, \qquad (1.1.1.7d)$$

$$t^2 = (u^2 + v^2)a^2 + w^2c^2, \qquad (1.1.2.1d)$$

$$r^{*2} = (h^2 + k^2)a^{*2} + l^2c^{*2} = sa^{*2} + l^2c^{*2} \qquad (1.1.2.2d)$$

with

$$s = h^2 + k^2.$$

For each value of $s \leq 100$, all corresponding pairs h, k are listed in Table 1.2.4.1.

Table 1.2.4.1. *Assignment of integers $s \leq 100$ to pairs h, k with $s = h^2 + k^2$*

Each pair h, k represents all eight pairs which result from permutation and different sign combinations.

s	h k	s	h k	s	h k
1	1 0	32	4 4	68	8 2
2	1 1	34	5 3	72	6 6
4	2 0	36	6 0	73	8 3
5	2 1	37	6 1	74	7 5
8	2 2	40	6 2	80	8 4
9	3 0	41	5 4	81	9 0
10	3 1	45	6 3	82	9 1
13	3 2	49	7 0	85	9 2
16	4 0	50	7 1		7 6
17	4 1		5 5	89	8 5
18	3 3	52	6 4	90	9 3
20	4 2	53	7 2	97	9 4
25	5 0	58	7 3	98	7 7
	4 3	61	6 5	100	10 0
26	5 1	64	8 0		8 6
29	5 2	65	8 1		
			7 4		

$$\frac{u}{h} = \frac{v}{k} = \frac{c^2w}{a^2l}, \qquad (1.1.2.12d)$$

$$\mathbf{t}_1 \cdot \mathbf{t}_2 = (u_1u_2 + v_1v_2)a^2 + w_1w_2c^2, \qquad (1.1.3.4d)$$

$$\mathbf{r}_1^* \cdot \mathbf{r}_2^* = (h_1h_2 + k_1k_2)a^{*2} + l_1l_2c^{*2}. \qquad (1.1.3.7d)$$

1.2.5. Trigonal and hexagonal crystal system

1.2.5.1. *Description referred to hexagonal axes*

Metrical conditions: $a = b$; c arbitrary; $\alpha = \beta = 90^\circ$; $\gamma = 120^\circ$
Bravais lattice types: hP, hR
Symmetry of lattice points: $6/mmm$ (hP), $\bar{3}m$ (hR)
Simplified formulae:

$$V = (\mathbf{abc}) = \left[\begin{vmatrix} a^2 & -\frac{1}{2}a^2 & 0 \\ -\frac{1}{2}a^2 & a^2 & 0 \\ 0 & 0 & c^2 \end{vmatrix}\right]^{1/2} = \tfrac{1}{2}\sqrt{3}\, a^2c, \qquad (1.1.1.1e)$$

$$\left.\begin{aligned} a^* = b^* = \tfrac{2}{3}\sqrt{3}\frac{1}{a}, \quad c^* = \frac{1}{c}, \\ \alpha^* = \beta^* = 90^\circ, \quad \gamma^* = 60^\circ, \end{aligned}\right\} \qquad (1.1.1.3e)$$

$$V^* = (\mathbf{a}^*\mathbf{b}^*\mathbf{c}^*) = \left[\begin{vmatrix} a^{*2} & \frac{1}{2}a^{*2} & 0 \\ \frac{1}{2}a^{*2} & a^{*2} & 0 \\ 0 & 0 & c^{*2} \end{vmatrix}\right]^{1/2} = \tfrac{1}{2}\sqrt{3}\, a^{*2}c^* = \tfrac{2}{3}\sqrt{3}\, a^{-2}c^{-1}, \qquad (1.1.1.4e)$$

$$a = b = \tfrac{2}{3}\sqrt{3}\frac{1}{a^*}, \quad c = \frac{1}{c^*}, \quad \alpha = \beta = 90^\circ, \quad \gamma = 120^\circ, \qquad (1.1.1.7e)$$

$$t^2 = (u^2 + v^2 - uv)a^2 + w^2c^2, \qquad (1.1.2.1e)$$

$$r^{*2} = (h^2 + k^2 + hk)a^{*2} + l^2c^{*2} = sa^{*2} + l^2c^{*2} \qquad (1.1.2.2e)$$

with

Table 1.2.5.1. *Assignment of integers $s \leq 100$ to pairs h, k with $s = h^2 + k^2 + hk$*

Each pair h, k represents in addition the pairs k, $-h-k$ and $-h-k$, h, the permutations of these three, and the six corresponding centrosymmetrical pairs.

s	h k	s	h k	s	h k
1	1 0	31	5 1	67	7 2
3	1 1	36	6 0	73	8 1
4	2 0	37	4 3	75	5 5
7	2 1	39	5 2	76	6 4
9	3 0	43	6 1	79	7 3
12	2 2	48	4 4	81	9 0
13	3 1	49	7 0	84	8 2
16	4 0		5 3	91	9 1
19	3 2	52	6 2		6 5
21	4 1	57	7 1	93	7 4
25	5 0	61	5 4	97	8 3
27	3 3	63	6 3	100	10 0
28	4 2	64	8 0		

$$s = h^2 + k^2 + hk.$$

For each value of $s \leq 100$, all corresponding pairs h, k are listed in Table 1.2.5.1.

$$\frac{2u - v}{2h} = \frac{2v - u}{2k} = \frac{c^2 w}{a^2 l}, \qquad (1.1.2.12e)$$

$$\mathbf{t}_1 \cdot \mathbf{t}_2 = (u_1 u_2 + v_1 v_2 - \tfrac{1}{2} u_1 v_2 - \tfrac{1}{2} u_2 v_1) a^2 + w_1 w_2 c^2, \quad (1.1.3.4e)$$

$$\mathbf{r}_1^* \cdot \mathbf{r}_2^* = (h_1 h_2 + k_1 k_2 + \tfrac{1}{2} h_1 k_2 + \tfrac{1}{2} h_2 k_1) a^{*2} + l_1 l_2 c^{*2}. \quad (1.1.3.7e)$$

1.2.5.2. *Description referred to rhombohedral axes*

Metrical conditions: $a = b = c$; $\alpha = \beta = \gamma$
Bravais lattice type: hR
Symmetry of lattice points: $\bar{3}m$
Simplified formulae:

$$\begin{aligned} V = (\mathbf{abc}) &= \left[\begin{vmatrix} a^2 & a^2\cos\alpha & a^2\cos\alpha \\ a^2\cos\alpha & a^2 & a^2\cos\alpha \\ a^2\cos\alpha & a^2\cos\alpha & a^2 \end{vmatrix} \right]^{1/2} \\ &= a^3[1 - 3\cos^2\alpha + 2\cos^3\alpha]^{1/2} \\ &= 2a^3 \left[\sin\tfrac{3}{2}\alpha \sin^3\frac{\alpha}{2} \right]^{1/2}, \end{aligned} \qquad (1.1.1.1f)$$

$$\left.\begin{aligned} \cos\frac{\alpha^*}{2} = \cos\frac{\beta^*}{2} = \cos\frac{\gamma^*}{2} &= \frac{1}{2\cos\alpha/2}, \\ a^* = b^* = c^* &= \frac{1}{a\sin\alpha\sin\alpha^*}, \end{aligned}\right\} \qquad (1.1.1.3f)$$

$$\begin{aligned} V^* = (\mathbf{a}^*\mathbf{b}^*\mathbf{c}^*) &= \left[\begin{vmatrix} a^{*2} & a^{*2}\cos\alpha^* & a^{*2}\cos\alpha^* \\ a^{*2}\cos\alpha^* & a^{*2} & a^{*2}\cos\alpha^* \\ a^{*2}\cos\alpha^* & a^{*2}\cos\alpha^* & a^{*2} \end{vmatrix} \right]^{1/2} \\ &= a^{*3}[1 - 3\cos^2\alpha^* + 2\cos^3\alpha^*]^{1/2} \\ &= 2a^{*3} \left[\sin\tfrac{3}{2}\alpha^* \sin^3\frac{\alpha^*}{2} \right]^{1/2}, \end{aligned} \qquad (1.1.1.4f)$$

Table 1.2.5.2. *Asssignment of integers $s_1 \leq 50$ to triplets h, k, l with $s_1 = h^2 + k^2 + l^2$ and to integers $s_2 = hk + hl + kl$*

Each triplet h, k, l represents all twelve triplets resulting from permutation and/or simultaneous change of all signs.

s_1	s_2	h	k	l	s_1	s_2	h	k	l	s_1	s_2	h	k	l
1	0	1	0	0	24	−12	−4	2	2	38	−19	−5	3	2
2	−1	−1	1	0		−4	4	−2	2		−11	−6	1	1
	1	1	1	0		20	4	2	2			5	−3	2
3	−1	−1	1	1	25	−12	−4	3	0		−1	6	−1	1
	3	1	1	1		0	5	0	0			5	3	−2
4	0	2	0	0		12	4	3	0		13	6	1	1
5	−2	−2	1	0	26	−13	−4	3	1		31	5	3	2
	2	2	1	0		−11	4	−3	1	40	−12	−6	2	0
6	−3	−2	1	1		−5	−5	1	0		12	6	2	0
	−1	2	−1	1		5	5	1	0	41	−20	−5	4	0
	5	2	1	1			4	3	−1		−16	−6	2	1
8	−4	−2	2	0		19	4	3	1			−4	4	3
	4	2	2	0	27	−9	−5	1	1		−8	6	−2	1
9	−4	−2	2	1			−3	3	3			4	4	−3
	0	3	0	0		−1	5	−1	1		4	6	2	−1
		2	2	−1		11	5	1	1		20	6	2	1
	8	2	2	1		27	3	3	3			5	4	0
10	−3	−3	1	0	29	−14	−4	3	2		40	4	4	3
	3	3	1	0		−10	−5	2	0	42	−21	−5	4	1
11	−5	−3	1	1			4	−3	2		−19	5	−4	1
	−1	3	−1	1		−2	4	3	−2		11	5	4	−1
	7	3	1	1		10	5	2	0		29	5	4	1
12	−4	−2	2	2		26	4	3	2	43	−21	−5	3	3
	12	2	2	2	30	−13	−5	2	1		−9	5	−3	3
13	−6	−3	2	0		−7	5	−2	1		39	5	3	3
	6	3	2	0		3	5	2	−1	44	−20	−6	2	2
14	−7	−3	2	1		17	5	2	1		−4	6	−2	2
	−5	3	−2	1	32	−16	−4	4	0		28	6	2	2
	1	3	2	−1		16	4	4	0	45	−22	−5	4	2
	11	3	2	1	33	−16	−5	2	2		−18	−6	3	0
16	0	4	0	0			−4	4	1			5	−4	2
17	−8	−3	2	2		−4	5	−2	2		2	5	4	−2
	−4	−4	1	0		8	4	4	−1		18	6	3	0
		3	−2	2		24	5	2	2		38	5	4	2
	4	4	1	0			4	4	1	46	−21	−6	3	1
	16	3	2	2	34	−15	−5	3	0		−15	6	−3	1
18	−9	−3	3	0			−4	3	3		9	6	3	−1
	−7	−4	1	1		−9	4	−3	3		27	6	3	1
	−1	4	−1	1		15	5	3	0	48	−16	−4	4	4
	9	4	1	1		33	4	3	3		48	4	4	4
		3	3	0	35	−17	−5	3	1	49	−24	−6	3	2
19	−9	−3	3	1		−13	5	−3	1		−12	6	−3	2
	3	3	3	−1		7	5	3	−1		0	7	0	0
	15	3	3	1		23	5	3	1			6	3	−2
20	−8	−4	2	0	36	−16	−4	4	2		36	6	3	2
	8	4	2	0		0	6	0	0	50	−25	−5	5	0
21	−10	−4	2	1			4	4	−2		−23	−5	4	3
	−6	4	−2	1		32	4	4	2		−17	5	−4	3
	2	4	2	−1	37	−6	−6	1	0		−7	−7	1	0
	14	4	2	1		6	6	1	0			5	4	−3
22	−9	−3	3	2							7	7	1	0
	−3	3	3	−2							25	5	5	0
	21	3	3	2							47	5	4	3

$$\left.\begin{aligned} \cos\frac{\alpha}{2} = \cos\frac{\beta}{2} = \cos\frac{\gamma}{2} &= \frac{1}{2\cos\alpha^*/2}, \\ a = b = c &= \frac{1}{a^*\sin\alpha^*\sin\alpha}, \end{aligned}\right\} \qquad (1.1.1.7f)$$

$$t^2 = (u^2 + v^2 + w^2)a^2 + 2(uv + uw + vw)a^2\cos\alpha, \quad (1.1.2.1f)$$

$$r^{*2} = (h^2 + k^2 + l^2)a^{*2} + 2(hk + hl + kl)a^{*2}\cos\alpha^* = s_1 a^{*2} + 2s_2 a^{*2}\cos\alpha^* \quad (1.1.2.2f)$$

with

$$s_1 = h^2 + k^2 + l^2 \quad \text{and} \quad s_2 = hk + hl + kl.$$

For each value of $s_1 \leq 50$, all corresponding values of s_2 and all triplets h, k, l are listed in Table 1.2.5.2.

$$\frac{u}{h} + \frac{v+w}{h}\cos\alpha = \frac{v}{k} + \frac{u+w}{k}\cos\alpha = \frac{w}{l} + \frac{u+v}{l}\cos\alpha, \quad (1.1.2.12f)$$

$$\mathbf{t}_1 \cdot \mathbf{t}_2 = (u_1u_2 + v_1v_2 + w_1w_2)a^2 + (u_1v_2 + u_2v_1 + u_1w_2 + u_2w_1 + v_1w_2 + v_2w_1)a^2\cos\alpha, \quad (1.1.3.4f)$$

$$\mathbf{r}_1^* \cdot \mathbf{r}_2^* = (h_1h_2 + k_1k_2 + l_1l_2)a^{*2} + (h_1k_2 + h_2k_1 + h_1l_2 + h_2l_1 + k_1l_2 + k_2l_1)a^{*2}\cos\alpha^*. \quad (1.1.3.7f)$$

1.2.6. Cubic crystal system

Metrical conditions: $a = b = c;\ \alpha = \beta = \gamma = 90^\circ$
Bravais lattice types: cP, cI, cF
Symmetry of lattice points: $m\bar{3}m$

Simplified formulae:

$$V = (\mathbf{abc}) = \left[\begin{vmatrix} a^2 & 0 & 0 \\ 0 & a^2 & 0 \\ 0 & 0 & a^2 \end{vmatrix}\right]^{1/2} = a^3, \quad (1.1.1.1g)$$

$$a^* = b^* = c^* = \frac{1}{a}, \quad \alpha^* = \beta^* = \gamma^* = 90^\circ, \quad (1.1.1.3g)$$

$$V^* = (\mathbf{a}^*\mathbf{b}^*\mathbf{c}^*) = \left[\begin{vmatrix} a^{*2} & 0 & 0 \\ 0 & a^{*2} & 0 \\ 0 & 0 & a^{*2} \end{vmatrix}\right]^{1/2} = a^{*3} = a^{-3}, \quad (1.1.1.4g)$$

$$a = b = c = \frac{1}{a^*}, \quad \alpha = \beta = \gamma = 90^\circ, \quad (1.1.1.7g)$$

$$t^2 = (u^2 + v^2 + w^2)a^2, \quad (1.1.2.1g)$$

$$r^{*2} = (h^2 + k^2 + l^2)a^{*2} = sa^{*2} \quad (1.1.2.2g)$$

with

$$s = h^2 + k^2 + l^2.$$

For each value of $s \leq 100$, all corresponding triplets h, k, l are listed in Table 1.2.6.1.

$$\frac{u}{h} = \frac{v}{k} = \frac{w}{l}, \quad (1.1.2.12g)$$

$$\mathbf{t}_1 \cdot \mathbf{t}_2 = (u_1u_2 + v_1v_2 + w_1w_2)a^2, \quad (1.1.3.4g)$$

$$\mathbf{r}_1^* \cdot \mathbf{r}_2^* = (h_1h_2 + k_1k_2 + l_1l_2)a^{*2}. \quad (1.1.3.7g)$$

Table 1.2.6.1. *Assignment of integers $s \leq 100$ to triplets h, k, l with $s = h^2 + k^2 + l^2$*

Each triplet represents all 48 triplets resulting from permutations and sign combinations.

s	$h\ k\ l$	s	$h\ k\ l$	s	$h\ k\ l$	s	$h\ k\ l$	s	$h\ k\ l$	s	$h\ k\ l$
1	1 0 0	25	5 0 0	42	5 4 1	59	7 3 1	74	8 3 1	88	6 6 4
2	1 1 0		4 3 0	43	5 3 3		5 5 3		7 5 0	89	9 2 2
3	1 1 1	26	5 1 0	44	6 2 2	61	6 5 0		7 4 3		8 5 0
4	2 0 0		4 3 1	45	6 3 0		6 4 3	75	7 5 1		8 4 3
5	2 1 0	27	5 1 1		5 4 2	62	7 3 2		5 5 5		7 6 2
6	2 1 1		3 3 3	46	6 3 1		6 5 1	76	6 6 2	90	9 3 0
8	2 2 0	29	5 2 0	48	4 4 4	64	8 0 0	77	8 3 2		8 5 1
9	3 0 0		4 3 2	49	7 0 0	65	8 1 0		6 5 4		7 5 4
	2 2 1	30	5 2 1		6 3 2		7 4 0	78	7 5 2	91	9 3 1
10	3 1 0	32	4 4 0	50	7 1 0		6 5 2	80	8 4 0	93	8 5 2
11	3 1 1	33	5 2 2		5 5 0	66	8 1 1	81	9 0 0	94	9 3 2
12	2 2 2		4 4 1		5 4 3		7 4 1		8 4 1		7 6 3
13	3 2 0	34	5 3 0	51	7 1 1		5 5 4		7 4 4	96	8 4 4
14	3 2 1		4 3 3		5 5 1	67	7 3 3		6 6 3	97	9 4 0
16	4 0 0	35	5 3 1	52	6 4 0	68	8 2 0	82	9 1 0		6 6 5
17	4 1 0	36	6 0 0	53	7 2 0		6 4 4		8 3 3	98	9 4 1
	3 2 2		4 4 2		6 4 1	69	8 2 1	83	9 1 1		8 5 3
18	4 1 1	37	6 1 0	54	7 2 1		7 4 2		7 5 3		7 7 0
	3 3 0	38	6 1 1		6 3 3	70	6 5 3	84	8 4 2	99	9 3 3
19	3 3 1		5 3 2		5 5 2	72	8 2 2	85	9 2 0		7 7 1
20	4 2 0	40	6 2 0	56	6 4 2		6 6 0		7 6 0		7 5 5
21	4 2 1	41	6 2 1	57	7 2 2	73	8 3 0	86	9 2 1	100	10 0 0
22	3 3 2		5 4 0		5 4 4		6 6 1		7 6 1		8 6 0
24	4 2 2		4 4 3	58	7 3 0				6 5 5		

International Tables for Crystallography (2006). Vol. C, Chapter 1.3, pp. 10–14.

1.3. Twinning

BY E. KOCH

1.3.1. General remarks

A twin consists of two or more single crystals of the same species but in different orientation, its *twin components*. They are intergrown in such a way that at least some of their lattice directions are parallel. The *twin law* describes the geometrical relation between the twin components. It specifies a symmetry operation, the *twin operation*, that brings one of the twin components into parallel orientation with the other. The corresponding symmetry element is called the *twin element*.

There are several kinds of twin laws:

(1) *Reflection twins*. Two twin components are related by reflection through a net plane (*hkl*), the *twin plane*. All lattice vectors parallel to (*hkl*), *i.e.* a complete lattice plane, coincide for both twin components, and their crystal faces (*hkl*) [and ($\bar{h}\bar{k}\bar{l}$)] are parallel. As a consequence, their corresponding zone axes parallel to (*hkl*) also coincide.

A twin plane cannot run parallel to a mirror or glide plane of the crystal structure, *i.e.* it cannot run parallel to a mirror plane of the point group of the crystal, because in that case both twin components would have the same orientation.

It must be noted that the vector normal to a twin plane need not have rational indices nor be parallel to a lattice vector.

(2) *Rotation twins*. The twin components can be brought into parallel orientation by a rotation about an axis, the *twin axis*. Two cases may be distinguished:

(i) Most frequently, the twin axis runs parallel to a lattice vector with components u, v, w. Then the lattice row [*uvw*] coincides for all twin components, *i.e.* they have the common zone axis [*uvw*]. Usually, the twin axis is a twofold axis, and all corresponding crystal faces of the two twin components belonging to that zone are parallel. Less frequently, a three-, four-, or sixfold rotation occurs as the twin operation.

A twin axis cannot run parallel to a (screw-) rotation axis of the crystal structure which induces the same rotation angle, *i.e.* it cannot be parallel to such a rotation axis of the point group of the crystal. For example, a twofold twin axis cannot be parallel to a twofold, fourfold, or sixfold axis, but it may run parallel to a threefold axis; a twin axis with rotation angle 60, 90, or 120°, however, may be parallel to a twofold axis.

(ii) In some cases, the direction of the twin axis is not rational, but the twofold twin axis runs perpendicular to a lattice row (zone axis) [*uvw*] and parallel to a net plane (crystal face) (*hkl*) that belongs to that zone. Then the lattices of the twin components coincide only in one lattice row parallel to [*uvw*], and [*uvw*] is the common zone axis of both twin components. The crystal faces (*hkl*) and ($\bar{h}\bar{k}\bar{l}$) are parallel for both components, but the other faces of the zone [*uvw*] are not.

Neither in case (i) nor in case (ii) does the plane perpendicular to the twin axis need to be a lattice plane. Therefore, in general, it cannot be described by Miller indices.

(3) *Inversion twins*. The twin components are related by inversion through a centre of symmetry, the *twin centre*. Only noncentrosymmetrical crystals can form such twins. As all corresponding lattice vectors of the two twin components are antiparallel, their entire vector lattices coincide. As a consequence, all corresponding zone axes and crystal faces of the twin components are parallel.

In many cases, there does not exist a unique twin law, but a twin may be described equally well by more than one twin law. (*a*) If the crystal structure of the twin components contains an evenfold rotation or screw-rotation axis, an inversion twin cannot be distinguished from a reflection twin with twin plane perpendicular to that axis. (*b*) If the crystal structure contains a mirror or a glide plane, an inversion twin cannot be distinguished from a rotation twin with a twofold twin axis perpendicular to that plane. (*c*) If for a centrosymmetrical crystal structure the normal of a twin plane runs parallel to a lattice vector or a twin axis runs perpendicular to a net plane, the twin may be described equally well as a reflection twin or as a rotation twin.

The twin components are grown together in a surface called *composition surface*, *twin interface* or *twin boundary*. In most cases, the composition surfaces are low-energy surfaces with good structural fit. For a reflection twin, it is usually a plane parallel to the twin plane. The composition surface of a rotation twin may either be a plane parallel to the twin axis or be a non-planar surface with irregular shape.

If more than two components are twinned according to the same law, the twin is called a *repeated twin* or a *multiple twin*. If all the twin boundaries are parallel planes, it is a *polysynthetic twin*, otherwise it is called a *cyclic twin*. If the twin components are related to each other by more than one twin law, the shape and the mutual arrangement of the twin domains may be very irregular.

With respect to the formation process, one may distinguish between *growth twins*, *transformation twins*, and *mechanical* (*deformation, glide*) *twins*. Transformation twins result from phase transitions, *e.g.* of ferroelectric or ferromagnetic crystals. The corresponding twin domains are usually small and the number of such domains is high. Mechanical twinning is due to mechanical stress and may often be described in terms of shear of the crystal structure. This includes ferroelasticity.

Twins are observable by, for example, macroscopic or microscopic observation of re-entrant angles between crystal faces, by etching, by means of different extinction positions for the twin components between cross polarizers of a polarization microscope, by different rotation angles of the plane of polarization of a beam of plane-polarized light passing through the components of a twin showing optical activity, by a splitting of part of the X-ray diffraction spots (except for twins by merohedry), by means of domain contrast or boundary contrast in an X-ray topogram, or by investigation with a transmission electron microscope.

The phenomenon of twinning has frequently been described and discussed in the literature and it is impossible, therefore, to give a complete list of references. Further details may be learned, *e.g.* from a review article by Cahn (1954) or from appropriate textbooks. A comprehensive survey of X-ray topography of twinned crystals is given by Klapper (1987). The following papers are related to twinning by merohedry or pseudo-merohedry: Catti & Ferraris (1976), Grimmer (1984, 1989*a*,*b*), Grimmer & Warrington (1985), Donnay & Donnay (1974), Le Page, Donnay & Donnay (1984), Hahn (1981, 1984), Klapper, Hahn & Chung (1987), Flack (1987).

1.3.2. Twin lattices

For reflection and rotation twins described in the last section, a special situation arises whenever there exists a lattice vector perpendicular to the twin plane or a lattice plane perpendicular to

Copyright © 2006 International Union of Crystallography

Table 1.3.2.1. *Lattice planes and rows that are perpendicular to each other independently of the metrical parameters*

Basis system	Lattice plane (*hkl*)	Lattice row [*uvw*]	Perpendicularity condition
Triclinic	–	–	–
Monoclinic (unique axis **b**)	(010)	[010]	–
Monoclinic (unique axis **c**)	(001)	[001]	–
Orthorhombic	(100) (010) (001)	[100] [010] [001]	– – –
Hexagonal/ trigonal	(*hk*0) (001)	[*uv*0] [001]	$u = 2h + k$, $v = h + 2k$ –
Rhombohedral	$(h, k, -h - k)$ (111)	$[u, v, -u - v]$ [111]	$u = h, v = k$ –
Tetragonal	(*hk*0) (001)	[*uv*0] [001]	$u = h, v = k$ –
Cubic	(*hkl*)	[*uvw*]	$u = h, v = k, w = l$

a rational twofold twin axis. Such a situation occurs systematically for all reflection and rotation twins with cubic symmetry and for certain twins with non-cubic symmetry (*cf.* Table 1.3.2.1). In addition, such a perpendicularity may occur occasionally if equation (1.1.2.12) is satisfied.

In the case of a noncentrosymmetric crystal structure, different twins result from a twin axis [*uvw*] with a perpendicular lattice plane (*hkl*), or from a twin plane (*hkl*) with a perpendicular lattice row [*uvw*]: the reflection twin consists of two enantiomorphous twin components whereas the rotation twin is built up from two crystals with the same handedness (*cf.*, for example, Brazil twins and Dauphiné twins of quartz). With respect to the first twin component, the lattice of the second component has the same orientation in both cases. For a centrosymmetrical crystal structure, both twin laws give rise to the same twin.

Whenever a twin plane or twin axis is perpendicular to a lattice vector or a net plane, respectively, the vector lattices of the twin components have a three-dimensional subset in common. This sublattice [derivative lattice, *cf. IT* A (1983, Chapter 13.2)] is called the *twin lattice*. It corresponds uniquely to the intersection group of the two translation groups referring to the twin components. The respective subgroup index i is called the *twin index*. It is equal to the ratio of the volumes of the primitive unit cells for the twin lattice and the crystal structure. If one subdivides the crystal lattice into nets parallel to the twin plane or perpendicular to the twin axis, each ith of these nets belongs to the common twin lattice of the two twin components (*cf.* Fig. 1.3.2.1). Important examples are cubic twins with [111] as twofold twin axis or (111) as twin plane and rhombohedral twins with [001] as twin axis or (001) as twin plane (hexagonal description). In all these cases, the twin index i equals 3.

For every twin lattice, its twin index i can be calculated from the Miller indices of the net plane (*hkl*) and the coprime coefficients u, v, w of the lattice vector $\mathbf{t}$ perpendicular to (*hkl*). Referred to a primitive lattice basis, i is simply related to the modulus of the scalar product j of the two vectors $\mathbf{r}^* = h\mathbf{a}^* + k\mathbf{b}^* + l\mathbf{c}^*$ and $\mathbf{t} = u\mathbf{a} + v\mathbf{b} + w\mathbf{c}$:

$$j = \mathbf{r}^* \cdot \mathbf{t} = hu + kv + lw,$$

$$i = \begin{cases} |j| & \text{for } j = 2n + 1 \\ |j|/2 & \text{for } j = 2n \end{cases} \qquad (n \text{ integer}).$$

The same procedure – but with modified coefficients – may be applied to a centred lattice described with respect to a conventionally chosen basis: The coprime Miller indices h, k, l that characterize the net plane have to be replaced by larger non-coprime indices h', k', l', if h, k, l do not refer to a (non-extinct) point of the reciprocal lattice. The integer coefficients u, v, w specifying the lattice vector perpendicular to (*hkl*) have to be replaced by smaller non-integer coefficients u', v', w', if the centred lattice contains such a vector in the direction [*uvw*].

1.3.2.1. *Examples*

(1) Cubic P lattice: [111] is perpendicular to (111).
$j = hu + kv + lw = 3$ odd
$i = |j| = 3$.

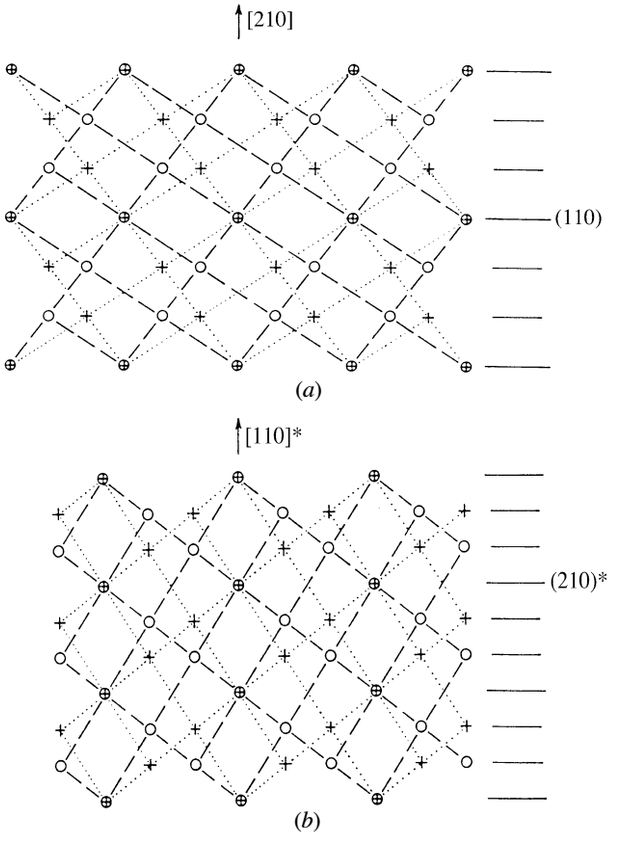

Fig. 1.3.2.1. (*a*) Projection of the lattices of the twin components of a monoclinic twinned crystal (unique axis **c**, $\gamma = 93°$) with twin index 3. The twin may be interpreted either as a rotation twin with twin axis [210] or as a reflection twin with twin plane (110). (*b*) Projection of the corresponding reciprocal lattices.

(2) Orthorhombic lattice with $b = \sqrt{3}a$: [310] is perpendicular to (110).

(i) *P* lattice (*cf.* Fig. 1.3.2.2):
$j = hu + kv + lw = 4$ even
$i = |j|/2 = 2$.

(ii) *C* lattice (*cf.* also Fig. 1.3.2.2):
Because of the *C* centring, [310] has to be replaced by $[\frac{3}{2}\frac{1}{2}0]$.
$j = hu' + kv' + lw' = 2$ even
$i = |j|/2 = 1$.

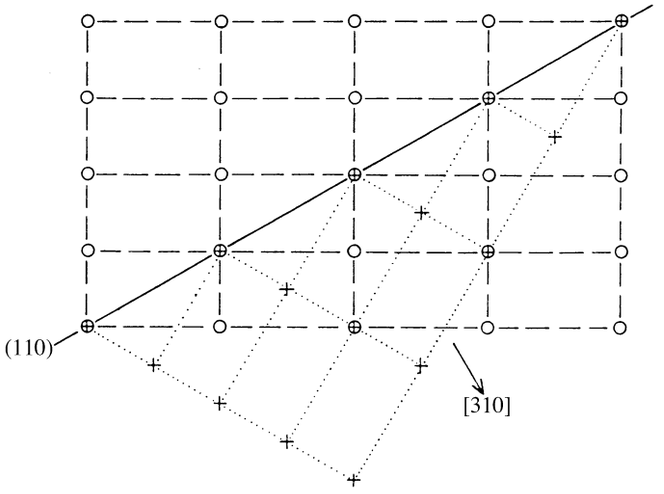

Fig. 1.3.2.2. Projection of the lattices of the twin components of an orthorhombic twinned crystal ($oP, b = \sqrt{3}a$) with twin index 2. The twin may be interpreted either as a rotation twin with twin axis [310] or as a reflection twin with twin plane (110). The figure shows, in addition, that twin index 1 results if the *oP* lattice is replaced by an *oC* lattice in this example (twinning by pseudomerohedry).

(3) Orthorhombic *C* lattice with $b = 2a$: [210] is perpendicular to (120) (*cf.* Fig. 1.3.2.3).
As (120) refers to an 'extinct reflection' of a *C* lattice, the triplet 240 has to be used in the calculation.
$j = h'u + k'v + l'w = 8$ even
$i = |j|/2 = 4$.

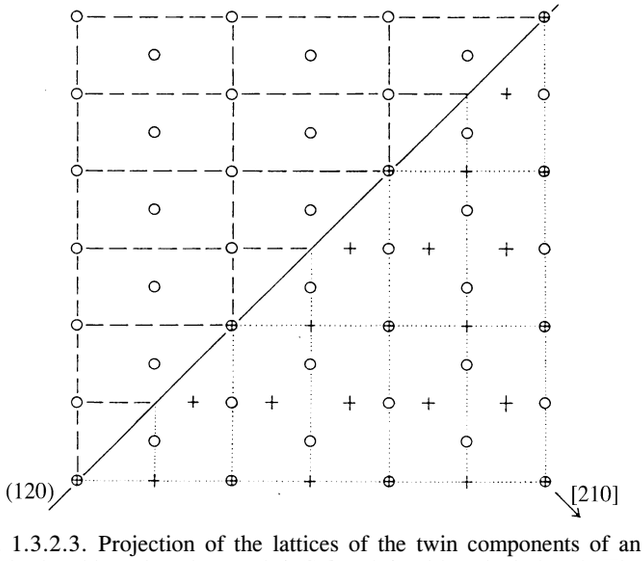

Fig. 1.3.2.3. Projection of the lattices of the twin components of an orthorhombic twinned crystal ($oC, b = 2a$) with twin index 4. The twin may be interpreted either as a rotation twin with twin axis [210] or as a reflection twin with twin plane (120).

(4) Rhombohedral lattice in hexagonal description with $c = \frac{1}{2}\sqrt{3}a$: $[\bar{1}1\bar{2}]$ is perpendicular to $(1\bar{1}1)$.
Because of the *R* centring, $[\bar{1}1\bar{2}]$ has to be replaced by $[\bar{\frac{1}{3}}\frac{1}{3}\bar{\frac{2}{3}}]$.
As $(1\bar{1}1)$ refers to an 'extinct reflection' of an *R* lattice, the triplet $1\bar{1}1$ has to be replaced by $3\bar{3}3$.
$j = h'u' + k'v' + l'w' = -4$ even
$i = |j|/2 = 2$.

1.3.3. Implication of twinning in reciprocal space

As shown above, the direct lattices of the components of any twin coincide in at least one row. The same is true for the corresponding reciprocal lattices. They coincide in all rows perpendicular to parallel net planes of the direct lattices.

For a reflection twin with twin plane (*hkl*), the reciprocal lattices of the twin components have only the lattice points with coefficients *nh*, *nk*, *nl* in common.

For a rotation twin with twofold twin axis [*uvw*], the reciprocal lattices of the twin components coincide in all points of the plane perpendicular to [*uvw*], *i.e.* in all points with coefficients *h*, *k*, *l* that fulfil the condition $hu + kv + lw = 0$.

For a rotation twin with irrational twin axis parallel to a net plane (*hkl*), only reciprocal-lattice points with coefficients *nh*, *nk*, *nl* are common to both twin components.

As the entire direct lattices of the two twin components coincide for an inversion twin, the same must be true for their reciprocal lattices.

For a reflection or rotation twin with a twin lattice of index *i*, the corresponding reciprocal lattices, too, have a sublattice with index *i* in common (*cf.* Fig. 1.3.2.1*b*). In analogy to direct space, the twin lattice in reciprocal space consists of each *i*th lattice plane parallel to the twin plane or perpendicular to the twin axis. If the twin index equals 1, the entire reciprocal lattices of the twin components coincide.

If for a reflection twin there exists only a lattice row [*uvw*] that is almost (but not exactly) perpendicular to the twin plane (*hkl*), then the lattices of the two twin components nearly coincide in a three-dimensional subset of lattice points. The corresponding misfit is described by the quantity ω, the *twin obliquity*. It is the angle between the lattice row [*uvw*] and the direction perpendicular to the twin plane (*hkl*). In an analogous way, the twin obliquity ω is defined for a rotation twin. If (*hkl*) is a net plane almost (but not exactly) perpendicular to the twin axis [*uvw*], then ω is the angle between [*uvw*] and the direction perpendicular to (*hkl*).

1.3.4. Twinning by merohedry

A twin is called a *twin by merohedry* if its twin operation belongs to the point group of its vector lattice, *i.e.* to the corresponding holohedry. As each lattice is centrosymmetric, an inversion twin is necessarily a twin by merohedry. Only crystals from merohedral (*i.e.* non-holohedral) point groups may form twins by merohedry; 159 out of the 230 types of space groups belong to merohedral point groups.

For a twin by merohedry, the vector lattices of all twin components coincide in direct *and* in reciprocal space. The twin index is 1. The maximal number of differently oriented twin components equals the subgroup index *m* of the point group of the crystal with respect to its holohedry.

Table 1.3.4.1 displays all possibilities for twinning by merohedry. For each holohedral point group (column 1), the types of Bravais lattices (column 2) and the corresponding merohedral point groups (column 3) are listed. Column 4 gives the subgroup index *m* of a merohedral point group in its

Table 1.3.4.1. *Possible twin operations for twins by merohedry*

m is the index of the point group in the corresponding holohedry; point groups allowing twins of type 2 are marked by an asterisk.

Holohedry	Bravais lattice	Point group	m	Possible twin operations
1	aP	1	2	$\bar{1}$
$2/m$	mP, mS	2 m	2 2	$\bar{1}$ $\bar{1}$
mmm	oP, oS, oI, oF	222 $mm2$	2 2	$\bar{1}$ $\bar{1}$
$4/mmm$	tP, tI	^{*4} $^*\bar{4}$ $^*4/m$ 422 $4mm$ $\bar{4}2m/\bar{4}m2$	4 4 2 2 2 2	$\bar{1}$, $.m.$, $.2.$ $\bar{1}$, $.m.$, $.2.$ $.m.$ $\bar{1}$ $\bar{1}$ $\bar{1}$
$\bar{3}m$	hR	^{*3} $^*\bar{3}$ 32 $3m$	4 2 2 2	$\bar{1}$, $.m$, $.2$ $.m$ $\bar{1}$ $\bar{1}$
$6/mmm$	hP	^{*3} $^*\bar{3}$ $^*321/312$ $^*3m1/31m$ $^*\bar{3}m1/\bar{3}1m$ ^{*6} $^*\bar{6}$ $^*6/m$ 622 $6mm$ $\bar{6}2m/\bar{6}m2$	8 4 4 4 2 4 4 2 2 2 2	$\bar{1}$, $.m.$, $.2.$, $m..$, $..m$, $2..$, $..2$ $.m.$, $m..$, $..m$ $\bar{1}$, $m..$, $..2/.2.$ $\bar{1}$, $m..$, $..m/.m.$ $m..$ $\bar{1}$, $.m.$, $.2.$ $\bar{1}$, $.m.$, $..m$ $.m.$ $\bar{1}$ $\bar{1}$ $\bar{1}$
$m\bar{3}m$	cP, cI, cF	^{*23} $^*m\bar{3}$ 432 $\bar{4}3m$	4 2 2 2	$\bar{1}$, $..m$, $..2$ $..m$ $\bar{1}$ $\bar{1}$

holohedry. Column 5 shows $m-1$ possible twin operations referring to the different twin components. These twin operations are not uniquely defined (except for point group 1), but may be chosen arbitrarily from the corresponding right coset of the crystal point group in its holohedry. It is always possible, however, to choose an inversion, a reflection, or a twofold rotation as twin operation.

A twin that is not a twin by merohedry as defined above but, because of metrical specialization, has a twin lattice with twin index 1 is called a *twin by pseudo-merohedry*.

Two kinds of twins by merohedry may be distinguished.

Type 1: The twin can be described as an inversion twin. Then, only two twin components exist and the twin operation belongs to the Laue class of the crystal. As a consequence, the reciprocal lattices of the twin components are superimposed so that coinciding lattice points refer to Bragg reflections with the same $|F|^2$ values as long as Friedel's law is valid. In that case, no differences with respect to symmetry, or to reflection conditions, or to relative intensities occur between two sets of Bragg

Table 1.3.4.2. *Simulated Laue classes, extinction symbols, simulated 'possible space groups', and possible true space groups for crystals twinned by merohedry (type 2)*

Twinned crystal			Single crystal
Simulated Laue class	Twin extinction symbol	Simulated 'possible space groups'	Possible true space groups
$4/mmm$	P---	$P422$, $P4mm$, $P\bar{4}2m$, $P\bar{4}m2$, $P4/mmm$	$P4$, $P\bar{4}$, $P4/m$
	$P4_2$--	$P4_222$	$P4_2$, $P4_2/m$
	$P4_1$--	$P4_122$, $P4_322$	$P4_1$, $P4_3$
	Pn--	$P4/nmm$	$P4/n$
	$P4_2/n$--	–	$P4_2/n$
	I---	$I422$, $I4mm$, $I\bar{4}2m$, $I\bar{4}m2$, $I4/mmm$	$I4$, $I\bar{4}$, $I4/m$
	$I4_1$--	$I4_122$	$I4_1$
	$I4_1/a$--	–	$I4_1/a$
$\bar{3}m1$	P---	$P321$, $P3m1$, $P\bar{3}m1$	$P3$, $P\bar{3}$
	$P3_1$--	$P3_121$, $P3_221$	$P3_1$, $P3_2$
$\bar{3}1m$	P---	$P312$, $P31m$, $P\bar{3}1m$	$P3$, $P\bar{3}$
	$P3_1$--	$P3_112$, $P3_212$	$P3_1$, $P3_2$
$\bar{3}m$	R--	$R32$, $R3m$, $R\bar{3}m$	$R3$, $R\bar{3}$
$6/m$	P---	$P6$, $P\bar{6}$, $P6/m$	$P3$, $P\bar{3}$
	$P6_2$--	$P6_2$, $P6_4$	$P3_1$, $P3_2$
$6/mmm$	P---	$P622$, $P6mm$, $P\bar{6}m2$, $P\bar{6}2m$, $P6/mmm$	$P3$, $P\bar{3}$, $P321$, $P312$, $P3m1$, $P31m$, $P\bar{3}m1$, $P\bar{3}1m$, $P6$, $P\bar{6}$, $P6/m$
	$P6_3$--	$P6_322$	$P6_3$, $P6_3/m$
	$P6_2$--	$P6_222$, $P6_422$	$P3_1$, $P3_2$, $P3_121$, $P3_221$, $P3_112$, $P3_212$, $P6_2$, $P6_4$
	$P6_1$--	$P6_122$, $P6_522$	$P6_1$, $P6_5$
	P--c	$P6_3mc$, $P\bar{6}2c$, $P6_3/mmc$	$P31c$, $P\bar{3}1c$
	P-c-	$P6_3cm$, $P\bar{6}c2$, $P6_3/mcm$	$P3c1$, $P\bar{3}c1$
$m\bar{3}m$	P---	$P432$, $P\bar{4}3m$, $Pm\bar{3}m$	$P23$, $Pm\bar{3}$
	$P4_2$--	$P4_232$	$P2_13$
	Pn--	$Pn\bar{3}m$	$Pn\bar{3}$
	I---	$I432$, $I\bar{4}3m$, $Im\bar{3}m$	$I23$, $I2_13$, $Im\bar{3}$
	Ia--	–	$Ia\bar{3}$
	F---	$F432$, $F\bar{4}3m$, $Fm\bar{3}m$	$F23$, $Fm\bar{3}$
	Fd--	$Fd\bar{3}m$	$Fd\bar{3}$
	$P2_1/a$, b--	–	$Pa\bar{3}$

intensities measured from a single crystal on the one hand and from a twin on the other hand (whether or not the twin components differ in their volumes). If anomalous scattering is observed *and* the twin components differ in size, the intensities of Bragg reflections are changed in comparison with the untwinned crystal but the symmetry of the diffraction pattern is unchanged. For equal volumes of the twin components, however, the diffraction pattern is centrosymmetric again. The occurrence of anomalous scattering does not produce additional difficulties for space-group determination. The change of the

Bragg intensities in comparison with the untwinned crystals, however, makes a structure determination more difficult.

Type 2: The twin operation does not belong to the Laue class of the crystal. Such twins can occur only in point groups marked by an asterisk in Table 1.3.4.1, *i.e.* in 55 out of the 159 types of space groups mentioned above. If the different twin components occur with equal volumes, the corresponding diffraction pattern shows enhanced symmetry. On the contrary, the reflection conditions are unchanged in comparison to those for a single crystal, except for $Pa\bar{3}$. As a consequence, for 51 out of the 55 space-group types, the derivation of 'possible space groups', as described in *IT* A (1983, Part 3), gives incorrect results. For $P4_2/n$, $I4_1/a$ and $Ia\bar{3}$, the combination of the simulated Laue class of the twin and the (unchanged) extinction symbol does not occur for single crystals. Therefore, the symmetry of these twins can be determined uniquely. In the case of $Pa\bar{3}$, the reflection conditions differ for the two twin components. [This is because the holohedry of $Pa\bar{3}$ is $m\bar{3}m$ whereas the Laue class of the Euclidean normalizer $Ia\bar{3}$ of $Pa\bar{3}$ is $m\bar{3}$; *cf. IT* A (1987, Part 15).] As a consequence, the reflection conditions for such a twinned crystal differ from all conditions that may be observed for single crystals (*hkl* cyclically permutable: $0kl$ only with $k = 2n$ *or* $l = 2n$; $00l$ only with $l = 2n$) and, therefore, the true symmetry can be identified without uncertainty.

In Table 1.3.4.2, all simulated Laue classes (column 1) are listed that may be observed for twins by merohedry of type 2. Column 2 shows the corresponding extinction symbols. The symbols of the simulated 'possible space groups' that follow from *IT* A (1983, Part 3) are gathered in column 3. The last column displays the symbols of those space groups which may be the true symmetry groups for twins by merohedry showing such diffraction patterns.

1.3.5. Calculation of the twin element

If the twin element cannot be recognized by direct macroscopic or microscopic inspection, it may be calculated as described below. Given are two analogous bases $\mathbf{a}$, $\mathbf{b}$, $\mathbf{c}$ and $\mathbf{a}'$, $\mathbf{b}'$, $\mathbf{c}'$ referring to the two twin components. If possible, both basis systems should be chosen with the same handedness. If no such bases exist, the twin is a reflection twin and one of the bases has to be replaced by its centrosymmetrical one, *e.g.* $\mathbf{a}'$, $\mathbf{b}'$, $\mathbf{c}'$ by $-\mathbf{a}'$, $-\mathbf{b}'$, $-\mathbf{c}'$. The relation between the two bases is described by

$$\mathbf{a}' = e_{11}\mathbf{a} + e_{12}\mathbf{b} + e_{13}\mathbf{c},$$
$$\mathbf{b}' = e_{21}\mathbf{a} + e_{22}\mathbf{b} + e_{23}\mathbf{c},$$
$$\mathbf{c}' = e_{31}\mathbf{a} + e_{32}\mathbf{b} + e_{33}\mathbf{c}.$$

The coefficients e_{ij} have to be obtained by measurement.

Basis $\mathbf{a}$, $\mathbf{b}$, $\mathbf{c}$ may be mapped onto $\mathbf{a}'$, $\mathbf{b}'$, $\mathbf{c}'$ by a pure rotation that brings $\mathbf{a}$ to $\mathbf{a}'$, $\mathbf{b}$ to $\mathbf{b}'$, and $\mathbf{c}$ to $\mathbf{c}'$. To derive the direction of the rotation axis, calculate the three vectors

$$\mathbf{a}_1 = \mathbf{a} + \mathbf{a}', \quad \mathbf{b}_1 = \mathbf{b} + \mathbf{b}', \quad \mathbf{c}_1 = \mathbf{c} + \mathbf{c}'.$$

$\mathbf{a}_1$, $\mathbf{b}_1$, $\mathbf{c}_1$ bisect the angles $\sigma_a = \mathbf{a} \wedge \mathbf{a}'$, $\sigma_b = \mathbf{b} \wedge \mathbf{b}'$, and $\sigma_c = \mathbf{c} \wedge \mathbf{c}'$, respectively. Calculate three further vectors of arbitrary length $\mathbf{a}_2, \mathbf{b}_2, \mathbf{c}_2$ which are perpendicular to the planes defined by $\mathbf{a}$ and $\mathbf{a}'$, $\mathbf{b}$ and $\mathbf{b}'$, and $\mathbf{c}$ and $\mathbf{c}'$, respectively, from the scalar products

$$\mathbf{a}_2 \cdot \mathbf{a} = \mathbf{a}_2 \cdot \mathbf{a}' = 0,$$
$$\mathbf{b}_2 \cdot \mathbf{b} = \mathbf{b}_2 \cdot \mathbf{b}' = 0,$$
$$\mathbf{c}_2 \cdot \mathbf{c} = \mathbf{c}_2 \cdot \mathbf{c}' = 0.$$

The plane defined by $\mathbf{a}_1$ and $\mathbf{a}_2$ is perpendicular to the plane defined by $\mathbf{a}$ and $\mathbf{a}'$ and bisects the angle $\mathbf{a} \wedge \mathbf{a}'$. Analogous planes refer to $\mathbf{b}_1$ and $\mathbf{b}_2$, and $\mathbf{c}_1$ and $\mathbf{c}_2$. Vectors $\mathbf{r}_a$, $\mathbf{r}_b$, and $\mathbf{r}_c$ lying within one of these planes may be described as linear combinations of $\mathbf{a}_1$ and $\mathbf{a}_2$, $\mathbf{b}_1$and $\mathbf{b}_2$, or $\mathbf{c}_1$ and $\mathbf{c}_2$, respectively:

$$\mathbf{r}_a = \lambda_a\mathbf{a}_1 + \mu_a\mathbf{a}_2,$$
$$\mathbf{r}_b = \lambda_b\mathbf{b}_1 + \mu_b\mathbf{b}_2,$$
$$\mathbf{r}_c = \lambda_c\mathbf{c}_1 + \mu_c\mathbf{c}_2.$$

The common intersection line of these three planes is parallel to the twin axis. It may be calculated by solving any of the three equations

$$\mathbf{r}_a = \mathbf{r}_b, \quad \mathbf{r}_a = \mathbf{r}_c, \quad \text{or} \quad \mathbf{r}_b = \mathbf{r}_c.$$

$\mathbf{r}_a = \mathbf{r}_b$: choose λ_a arbitrarily equal to 1.

$$\mathbf{a}_1 + \mu_a\mathbf{a}_2 = \lambda_b\mathbf{b}_1 + \mu_b\mathbf{b}_2.$$

Solve the inhomogeneous system of three equations that corresponds to this vector equation for the three variables μ_a, λ_b, and μ_b. Calculate the vector $\mathbf{r} = \mathbf{a}_1 + \mu_a\mathbf{a}_2$. Its components with respect to $\mathbf{a}$, $\mathbf{b}$, $\mathbf{c}$ describe the direction of the twin axis.

The angle τ of the twin rotation may then be calculated by

$$\sin\tfrac{1}{2}\tau = \frac{\sin\frac{1}{2}\sigma_a}{\sin\delta_a} = \frac{\sin\frac{1}{2}\sigma_b}{\sin\delta_b} = \frac{\sin\frac{1}{2}\sigma_c}{\sin\delta_c}$$

with $\delta_a = \mathbf{r} \wedge \mathbf{a}$, $\delta_b = \mathbf{r} \wedge \mathbf{b}$, $\delta_c = \mathbf{r} \wedge \mathbf{c}$.

If the basis $\mathbf{a}$, $\mathbf{b}$, $\mathbf{c}$ is orthogonal, τ may be obtained from

$$\cos\tau = \tfrac{1}{2}(\cos\sigma_a + \cos\sigma_b + \cos\sigma_c - 1).$$

If the coefficients of $\mathbf{r}$ are rational and τ equals 180°, then $\mathbf{r}$ describes the direction either of the twofold twin axis or of the normal of the twin plane. If $\mathbf{r}$ is rational and τ equals 60, 90 or 120°, $\mathbf{r}$ is parallel to the twin axis. If $\mathbf{r}$ is irrational, but τ equals 180° and there exists, in addition, a net plane perpendicular to $\mathbf{r}$, this net plane describes the twin plane.

If none of these conditions is fulfilled, one has to repeat the calculations with a differently chosen basis system for one of the twin components. The number of possibilities for this choice depends on the lattice symmetry. The following list gives all equivalent basis systems for all descriptions of Bravais lattices used in *IT* A (1983):

aP: $\mathbf{a}, \mathbf{b}, \mathbf{c}$;

mP, *mS* (unique axis **b**): $\mathbf{a}, \mathbf{b}, \mathbf{c}$; $-\mathbf{a}, \mathbf{b}, -\mathbf{c}$;

mP, *mS* (unique axis **c**): $\mathbf{a}, \mathbf{b}, \mathbf{c}$; $-\mathbf{a}, -\mathbf{b}, \mathbf{c}$;

oP, *oS*, *oI*, *oF*: $\mathbf{a}, \mathbf{b}, \mathbf{c}$; $-\mathbf{a}, -\mathbf{b}, \mathbf{c}$; $-\mathbf{a}, \mathbf{b}, -\mathbf{c}$; $\mathbf{a}, -\mathbf{b}, -\mathbf{c}$;

tP, *tI*: $\mathbf{a}, \mathbf{b}, \mathbf{c}$; $-\mathbf{a}, -\mathbf{b}, \mathbf{c}$; $-\mathbf{a}, \mathbf{b}, -\mathbf{c}$; $\mathbf{a}, -\mathbf{b}, -\mathbf{c}$;
$\mathbf{b}, -\mathbf{a}, \mathbf{c}$; $-\mathbf{b}, \mathbf{a}, \mathbf{c}$; $\mathbf{b}, \mathbf{a}, -\mathbf{c}$; $-\mathbf{b}, -\mathbf{a}, -\mathbf{c}$;

hP: $\mathbf{a}, \mathbf{b}, \mathbf{c}$; $\mathbf{b}, -\mathbf{a}-\mathbf{b}, \mathbf{c}$; $-\mathbf{a}-\mathbf{b}, \mathbf{a}, \mathbf{c}$; $\mathbf{b}, \mathbf{a}, -\mathbf{c}$;
$-\mathbf{a}-\mathbf{b}, \mathbf{b}, -\mathbf{c}$; $\mathbf{a}, -\mathbf{a}-\mathbf{b}, -\mathbf{c}$; $-\mathbf{a}, -\mathbf{b}, \mathbf{c}$; $-\mathbf{b}, \mathbf{a}+\mathbf{b}, \mathbf{c}$;
$\mathbf{a}+\mathbf{b}, -\mathbf{a}, \mathbf{c}$; $-\mathbf{b}, -\mathbf{a}, -\mathbf{c}$; $\mathbf{a}+\mathbf{b}, -\mathbf{b}, -\mathbf{c}$; $-\mathbf{a}, \mathbf{a}+\mathbf{b}, -\mathbf{c}$;

hR (hexagonal description): $\mathbf{a}, \mathbf{b}, \mathbf{c}$; $\mathbf{b}, -\mathbf{a}-\mathbf{b}, \mathbf{c}$;
$-\mathbf{a}-\mathbf{b}, \mathbf{a}, \mathbf{c}$; $\mathbf{b}, \mathbf{a}, -\mathbf{c}$; $-\mathbf{a}-\mathbf{b}, \mathbf{b}, -\mathbf{c}$; $\mathbf{a}, -\mathbf{a}-\mathbf{b}, -\mathbf{c}$;

hR (rhombohedral description): $\mathbf{a}, \mathbf{b}, \mathbf{c}$; $\mathbf{b}, \mathbf{c}, \mathbf{a}$; $\mathbf{c}, \mathbf{a}, \mathbf{b}$;
$-\mathbf{b}, -\mathbf{a}, -\mathbf{c}$; $-\mathbf{a}, -\mathbf{c}, -\mathbf{b}$; $-\mathbf{c}, -\mathbf{b}, -\mathbf{a}$;

cP, *cI*, *cF*: $\mathbf{a}, \mathbf{b}, \mathbf{c}$; $\mathbf{b}, \mathbf{c}, \mathbf{a}$; $\mathbf{c}, \mathbf{a}, \mathbf{b}$; $-\mathbf{a}, -\mathbf{b}, \mathbf{c}$;
$-\mathbf{b}, \mathbf{c}, -\mathbf{a}$; $\mathbf{c}, -\mathbf{a}, -\mathbf{b}$; $-\mathbf{a}, \mathbf{b}, -\mathbf{c}$; $\mathbf{b}, -\mathbf{c}, -\mathbf{a}$;
$-\mathbf{c}, -\mathbf{a}, \mathbf{b}$; $\mathbf{a}, -\mathbf{b}, -\mathbf{c}$; $-\mathbf{b}, -\mathbf{c}, \mathbf{a}$; $-\mathbf{c}, \mathbf{a}, -\mathbf{b}$;
$-\mathbf{b}, -\mathbf{a}, -\mathbf{c}$; $-\mathbf{a}, -\mathbf{c}, -\mathbf{b}$; $-\mathbf{c}, -\mathbf{b}, -\mathbf{a}$; $\mathbf{b}, \mathbf{a}, -\mathbf{c}$;
$\mathbf{a}, -\mathbf{c}, \mathbf{b}$; $-\mathbf{c}, \mathbf{b}, \mathbf{a}$; $\mathbf{b}, -\mathbf{a}, \mathbf{c}$; $-\mathbf{a}, \mathbf{c}, \mathbf{b}$; $\mathbf{c}, \mathbf{b}, -\mathbf{a}$;
$-\mathbf{b}, \mathbf{a}, \mathbf{c}$; $\mathbf{a}, \mathbf{c}, -\mathbf{b}$; $\mathbf{c}, -\mathbf{b}, \mathbf{a}$.

1.4. Arithmetic crystal classes and symmorphic space groups

By A. J. C. Wilson

1.4.1. Arithmetic crystal classes

Arithmetic crystal classes are of great importance in theoretical crystallography, and are treated from that point of view in Volume A of *International Tables for Crystallography* (Hahn, 1995, p. 719). They have, however, at least four applications in practical crystallography:

(1) in the classification of space groups (Section 1.4.2);

(2) in forming symbols for certain space groups in higher dimensions (see Chapter 9.8 and the references cited therein);

(3) in modelling the frequency of occurrence of space groups (see Chapter 9.7 and the references cited therein); and

(4) in establishing 'equivalent origins' (Wondratschek, 1995, p. 719).

The tabulation of arithmetic crystal classes in Volume A is incomplete, and the relation of the notation used in complete tabulations found elsewhere (for example, in Brown, Bülow, Neubüser, Wondratschek & Zassenhaus, 1978) to that of *International Tables* is not immediately obvious. Simple descriptions and complete enumerations of the arithmetic crystal classes in one, two and three dimensions are therefore given here.

1.4.1.1. *Arithmetic crystal classes in three dimensions*

The 32 geometric crystal classes and the 14 Bravais lattices are familiar in three-dimensional crystallography. The three-dimensional arithmetic crystal classes are easily derived in an elementary fashion by enumerating the compatible combinations of geometric crystal class and Bravais lattice; the symbol adopted by the International Union of Crystallography for an arithmetic crystal class is simply the juxtaposition of the symbol for the geometric crystal class and the symbol for the Bravais lattice (de Wolff *et al.*, 1985). For example, in the monoclinic system the geometric crystal classes are 2, m, and $2/m$, and the Bravais lattices are monoclinic P and monoclinic C. The six arithmetic crystal classes in the monoclinic system are thus $2P$, $2C$, mP, mC, $2/mP$, and $2/mC$. In certain cases (loosely, when the geometric crystal class and the Bravais lattice have unique directions that are not necessarily parallel), the crystal class and the lattice can be combined in two different orientations. The simplest example is the combination of the orthorhombic crystal class* mm with the end-centred lattice C. The intersection of the mirror planes of the crystal class defines one unique direction, the C centring of the lattice another. If these directions are placed parallel to one another, the arithmetic class $mm2C$ is obtained; if they are placed perpendicular to one another, a different arithmetic class† $2mmC$ is obtained. The other combinations exhibiting this phenomenon are lattice P with geometric classes 32, $3m$, $\bar{3}m$, $\bar{4}m$, and $\bar{6}m$. By consideration of all possible combinations of geometric class and lattice, one obtains the 73 arithmetic classes listed in Table 1.4.2.1.

* Here and in Chapter 9.7, it is convenient to use the 'short' symbols mm, 32, $3m$, $\bar{3}m$, $\bar{4}m$, and $\bar{6}m$ instead of $mm2$, 321, *etc.*, whenever it is desired to emphasize that no implication about orientation is intended.

† In the arithmetic crystal class $2mmC$, two conventions concerning the nomenclature of axes conflict. The first is that, if only one face of the Bravais lattice is centred, the c axis is chosen perpendicular to that face. The second is that, if there is one axis of symmetry uniquely different from any others, that axis is to be chosen as b in the monoclinic system and as c in the remaining systems. The second convention is usually regarded as the more important, and the 'standard setting' of $2mmC$ is $mm2A$. Both settings are listed in Table 1.4.2.1.

Table 1.4.1.1. *The two-dimensional arithmetic crystal classes*

	Crystal class			Space group	
		Arithmetic			
Crystal system	Geometric	Number	Symbol	Number	Symbol
Oblique	1	1	1p	1	$p1$
	2	2	2p	2	$p2$
Rectangular	m	3	mp	3	pm
				4	pg
		4	mc	5	cm
	2mm	5	2mmp	6	$p2mm$
				7	$p2mg$
				8	$p2gg$
		6	2mmc	9	$c2mm$
Square	4	7	4p	10	$p4$
	4mm	8	4mmp	11	$p4mm$
				12	$p4gm$
Hexagonal	3	9	3p	13	$p3$
	3m	10	3m1p	14	$p3m1$
		11	31mp	15	$p31m$
	6	12	6p	16	$p6$
	6mm	13	6mmp	17	$p6mm$

Copyright © 2006 International Union of Crystallography

1.4.1.2. *Arithmetic crystal classes in one, two and higher dimensions*

In one dimension, there are two geometric crystal classes, 1 and m, and a single Bravais lattice, $\not p$. Two arithmetic crystal classes result, $\not p$ and $m\not p$. In two dimensions, there are ten geometric crystal classes, and two Bravais lattices, p and c; 13 arithmetic crystal classes result. The two-dimensional geometric and arithmetic crystal classes are listed in Table 1.4.1.1.

The number of arithmetic crystal classes increases rapidly with increasing dimensionality; there are 710 (plus 70 enantiomorphs) in four dimensions (Brown, Bülow, Neubüser, Wondratschek & Zassenhaus, 1978), but those in dimensions higher than three are not needed in this volume.

Table 1.4.2.1. *The three-dimensional space groups, arranged by arithmetic crystal class; in a few geometric crystal classes this differs somewhat from the conventional numerical order; see International Tables Volume A, p. 728*

	Crystal class			Space group	
		Arithmetic			
Crystal system	Geometric	Number	Symbol	Number	Symbol
Triclinic	$\underline{1}$	1	$\underline{1}P$	1	$P\underline{1}$
	$\bar{1}$	2	$\bar{1}P$	2	$P\bar{1}$
Monoclinic	2	3	$2P$	3	$P2$
				4	$P2_1$
		4	$2C$	5	$C2$
	m	5	mP	6	Pm
				7	Pc
		6	mC	8	Cm
				9	Cc
	$2/m$	7	$2/mP$	10	$P2/m$
				11	$P2_1/m$
				13	$P2/c$
				14	$P2_1/c$
		8	$2/mC$	12	$C2/m$
				15	$C2/c$
Orthorhombic	222	9	$222P$	16	$P222$
				17	$P222_1$
				18	$P2_12_12$
				19	$P2_12_12_1$
		10	$222C$	20	$C222_1$
				21	$C222$
		11	$222F$	22	$F222$
		12	$222I$	23	$I222$
				24	$I2_12_12_1$
	mm	13	$mm2P$	25	$Pmm2$
				26	$Pmc2_1$
				27	$Pcc2$
				28	$Pma2$
				29	$Pca2_1$
				30	$Pnc2$
				31	$Pmn2_1$
				32	$Pba2$
				33	$Pna2_1$
				34	$Pnn2$
		14	$mm2C$	35	$Cmm2$
				36	$Cmc2_1$
				37	$Ccc2$
		15	$2mmC$ ($Amm2$)	38	$C2mm$ ($Amm2$)
				39	$C2me$ ($Aem2$)
				40	$C2cm$ ($Ama2$)
				41	$C2ce$ ($Aea2$)
		16	$mm2F$	42	$Fmm2$
				43	$Fdd2$
		17	$mm2I$	44	$Imm2$
				45	$Iba2$
				46	$Ima2$

Table 1.4.2.1. *Three-dimensional space groups (cont.)*

Crystal system	Crystal class			Space group	
	Geometric	Arithmetic			
		Number	Symbol	Number	Symbol
Orthorhombic (*cont.*)	*mmm*	18	*mmmP*	47	*Pmmm*
				48	*Pnnn*
				49	*Pccm*
				50	*Pban*
				51	*Pmma*
				52	*Pnna*
				53	*Pmna*
				54	*Pcca*
				55	*Pbam*
				56	*Pccn*
				57	*Pbcm*
				58	*Pnnm*
				59	*Pmmn*
				60	*Pbcn*
				61	*Pbca*
				62	*Pnma*
		19	*mmmC*	63	*Cmcm*
				64	*Cmce*
				65	*Cmmm*
				66	*Cccm*
				67	*Cmme*
				68	*Ccce*
		20	*mmmF*	69	*Fmmm*
				70	*Fddd*
		21	*mmmI*	71	*Immm*
				72	*Ibam*
				73	*Ibca*
				74	*Imma*
Tetragonal	4	22	4*P*	75	*P*4
				76	$P4_1$
				77	$P4_2$
				78	$P4_3$
		23	4*I*	79	*I*4
				80	$I4_1$
	$\bar{4}$	24	$\bar{4}P$	81	$P\bar{4}$
		25	$\bar{4}I$	82	$I\bar{4}$
	4/*m*	26	4/*mP*	83	*P*4/*m*
				84	$P4_2/m$
				85	*P*4/*n*
				86	$P4_2/n$
		27	4/*mI*	87	*I*4/*m*
				88	$I4_1/a$
	422	28	422*P*	89	*P*422
				90	$P42_12$
				91	$P4_122$
				92	$P4_12_12$
				93	$P4_222$
				94	$P4_22_12$
				95	$P4_322$
				96	$P4_32_12$
		29	422*I*	97	*I*422
				98	$I4_122$
	4*mm*	30	4*mmP*	99	*P*4*mm*
				100	*P*4*bm*
				101	$P4_2cm$
				102	$P4_2nm$
				103	*P*4*cc*
				104	*P*4*nc*
				105	$P4_2mc$
				106	$P4_2bc$
		31	4*mmI*	107	*I*4*mm*
				108	*I*4*cm*
				109	$I4_1md$
				110	$I4_1cd$

Table 1.4.2.1. *Three-dimensional space groups (cont.)*

Crystal system	Crystal class			Space group	
		Arithmetic			
	Geometric	Number	Symbol	Number	Symbol
Tetragonal (*cont.*)	$\bar{4}m$	32	$\bar{4}2mP$	111	$P\bar{4}2m$
				112	$P\bar{4}2c$
				113	$P\bar{4}2_1m$
				114	$P\bar{4}2_1c$
		33	$\bar{4}m2P$	115	$P\bar{4}m2$
				116	$P\bar{4}c2$
				117	$P\bar{4}b2$
				118	$P\bar{4}n2$
		34	$\bar{4}m2I$	119	$I\bar{4}m2$
				120	$I\bar{4}c2$
		35	$\bar{4}2mI$	121	$I\bar{4}2m$
				122	$I\bar{4}2d$
	$4/mmm$	36	$4/mmmP$	123	$P4/mmm$
				124	$P4/mcc$
				125	$P4/nbm$
				126	$P4/nnc$
				127	$P4/mbm$
				128	$P4/mnc$
				129	$P4/nmm$
				130	$P4/ncc$
				131	$P4_2/mmc$
				132	$P4_2/mcm$
				133	$P4_2/nbc$
				134	$P4_2/nnm$
				135	$P4_2/mbc$
				136	$P4_2/mnm$
				137	$P4_2/nmc$
				138	$P4_2/ncm$
		37	$4/mmmI$	139	$I4/mmm$
				140	$I4/mcm$
				141	$I4_1/amd$
				142	$I4_1/acd$
Trigonal	3	38	$3P$	143	$P3$
				144	$P3_1$
				145	$P3_2$
		39	$3R$	146	$R3$
	$\bar{3}$	40	$\bar{3}P$	147	$P\bar{3}$
		41	$\bar{3}R$	148	$R\bar{3}$
	32	42	$312P$	149	$P312$
				151	$P3_112$
				153	$P3_212$
		43	$321P$	150	$P321$
				152	$P3_121$
				154	$P3_221$
		44	$32R$	155	$R32$
	$3m$	45	$3m1P$	156	$P3m1$
				158	$P3c1$
		46	$31mP$	157	$P31m$
				159	$P31c$
		47	$3mR$	160	$R3m$
				161	$R3c$
	$\bar{3}m$	48	$\bar{3}1mP$	162	$P\bar{3}1m$
				163	$P\bar{3}1c$
		49	$\bar{3}m1P$	164	$P\bar{3}m1$
				165	$P\bar{3}c1$
		50	$\bar{3}mR$	166	$R\bar{3}m$
				167	$R\bar{3}c$

Table 1.4.2.1. *Three-dimensional space groups (cont.)*

Crystal system	Crystal class			Space group	
		Arithmetic			
	Geometric	Number	Symbol	Number	Symbol
Hexagonal	6	51	6*P*	168	*P*6
				169	$P6_1$
				170	$P6_5$
				171	$P6_2$
				172	$P6_4$
				173	$P6_3$
	$\bar{6}$	52	$\bar{6}P$	174	$P\bar{6}$
	6/*m*	53	6/*mP*	175	*P*6/*m*
				176	$P6_3/m$
	622	54	622*P*	177	*P*622
				178	$P6_122$
				179	$P6_522$
				180	$P6_222$
				181	$P6_422$
				182	$P6_322$
	6*mm*	55	6*mmP*	183	*P*6*mm*
				184	*P*6*cc*
				185	$P6_3cm$
				186	$P6_3mc$
	$\bar{6}m$	56	$\bar{6}m2P$	187	$P\bar{6}m2$
				188	$P\bar{6}c2$
		57	$\bar{6}2mP$	189	$P\bar{6}2m$
				190	$P\bar{6}2c$
	6/*mmm*	58	6/*mmmP*	191	*P*6/*mmm*
				192	*P*6/*mmc*
				193	$P6_3/mcm$
				194	$P6_3/mmc$
Cubic	23	59	23*P*	195	*P*23
				198	$P2_13$
		60	23*F*	196	*F*23
		61	23*I*	197	*I*23
				199	$I2_13$
	$m\bar{3}$	62	$m\bar{3}P$	200	$Pm\bar{3}$
				201	$Pn\bar{3}$
				205	$Pa\bar{3}$
		63	$m\bar{3}F$	202	$Fm\bar{3}$
				203	$Fd\bar{3}$
		64	$m\bar{3}I$	204	$Im\bar{3}$
				206	$Ia\bar{3}$
	432	65	432*P*	207	*P*432
				208	$P4_232$
				213	$P4_132$
				212	$P4_332$
		66	432*F*	209	*F*432
				210	$F4_132$
		67	432*I*	211	*I*432
				214	$I4_132$
	$\bar{4}3m$	68	$\bar{4}3mP$	215	$P\bar{4}3m$
				218	$P\bar{4}3n$
		69	$\bar{4}3mF$	216	$F\bar{4}3m$
				219	$F\bar{4}3c$
		70	$\bar{4}3mI$	217	$I\bar{4}3m$
				220	$I\bar{4}3d$
	$m\bar{3}m$	71	$m\bar{3}mP$	221	$Pm\bar{3}m$
				222	$Pn\bar{3}n$
				223	$Pm\bar{3}n$
				224	$Pn\bar{3}m$
		72	$m\bar{3}mF$	225	$Fm\bar{3}m$
				226	$Fm\bar{3}c$
				227	$Fd\bar{3}m$
				228	$Fd\bar{3}c$
		73	$m\bar{3}mI$	229	$Im\bar{3}m$
				230	$Ia\bar{3}d$

Table 1.4.3.1. *Arithmetic crystal classes classified by the number of space groups that they contain*

Number of space groups in the class	Symbols of the arithmetic crystal classes					
1	$1P$ $2C$ $222F$ $\bar{4}P$ $3R$ $\bar{6}P$ $23F$	$\bar{1}P$ $\bar{4}I$ $\bar{3}P$	$\bar{3}R$	$32R$		
2	$2P$ $222C$ $4I$ $3P^*$ $\bar{3}1mP$ $6/mP$ $\bar{2}3P$ $\bar{4}3mP$	mP $222I$ $4/mI$ $312P^*$ $\bar{3}m1P$ $\bar{6}m2P$ $\bar{2}3I$ $\bar{4}3mF$	mC $mm2F$ $422I$ $321P^*$ $\bar{3}mR$ $\bar{6}2mP$ $m\bar{3}F$ $\bar{4}3mI$	$2/mC$ $mmmF$ $\bar{4}m2I$ $3m1P$ $m\bar{3}I$ $m\bar{3}mI$	$\bar{4}2mI$ $31mP$ $432F$	$3mR$ $432I$
3	$mm2C$ $3P\dagger$ $4P^*$ $m\bar{3}P$	$mm2I$ $312P\dagger$ $432P^*$	$321P\dagger$			
4	$2/mP$ $222P$ $4P\dagger$ $6P^*$ $432P\dagger$	$2mmC$ $4/mP$ $622P^*$ $m\bar{3}mP$	$(= mm2A)$ $4mmI$ $6mmP$ $m\bar{3}mF$	$mmmI$ $\bar{4}2mP$ $6/mmmP$	$\bar{4}m2P$	$4/mmmI$
6	$mmmC$ $422P^*$ $6P\dagger$	 $622P\dagger$				
8	$422P\dagger$	$4mmP$				
10	$mm2P$					
16	$mmmP$ $4/mmmP$					

* Enantiomorphs combined. † Enantiomorphs distinguished.

1.4.2. Classification of space groups

Arithmetic crystal classes may be used to classify space groups on a scale somewhat finer than that given by the geometric crystal classes. Space groups are members of the same arithmetic crystal class if they belong to the same geometric crystal class, have the same Bravais lattice, and (when relevant) have the same orientation of the lattice relative to the point group. Each one-dimensional arithmetic crystal class contains a single space group, symbolized by $p1$ and pm, respectively. Most two-dimensional arithmetic crystal classes contain only a single space group; only $2mmp$ has as many as three.

The space groups belonging to each geometric and arithmetic crystal class in two and three dimensions are indicated in Tables 1.4.1.1 and 1.4.2.1, and some statistics for the three-dimensional classes are given in Table 1.4.3.1. 12 three-dimensional classes contain only a single space group, whereas two contain 16 each. Certain arithmetic crystal classes ($3P$, $312P$, $321P$, $422P$, $6P$, $622P$, $432P$) contain enantiomorphous pairs of space groups, so that the number of members of these classes depends on whether the enantiomorphs are combined or distinguished. Such classes occur twice in Table 1.4.3.1, marked with $*$ or †, respectively.

The space groups in Table 1.4.2.1 are listed in the order of the arithmetic crystal class to which they belong. It will be noticed that arrangement according to the conventional space-group numbering would separate members of the same arithmetic crystal class in the geometric classes $2/m$, $3m$, 23, $m\bar{3}$, 432, and $\bar{4}3m$. This point is discussed in detail in Volume A of *International Tables*, p. 728. The symbols of five space groups [$C2me$ ($Aem2$), $C2ce$ ($Aea2$), $Cmce$, $Cmme$, $Ccce$] have been conformed to those recommended in the fourth, revised edition of Volume A of *International Tables*.

1.4.2.1. *Symmorphic space groups*

The 73 space groups known as 'symmorphic' are in one-to-one correspondence with the arithmetic crystal classes, and their standard 'short' symbols (Bertaut, 1995) are obtained by interchanging the order of the geometric crystal class and the Bravais cell in the symbol for the arithmetic space group. In fact, conventional crystallographic symbolism did not distinguish between arithmetic crystal classes and symmorphic space groups until recently (de Wolff *et al.*, 1985); the symbol of the symmorphic group was used also for the arithmetic class.

This relationship between the symbols, and the equivalent rule-of-thumb *symmorphic space groups are those whose standard (short) symbols do not contain glide planes or screw axes*, reveal nothing fundamental about the nature of symmorphism; they are simply a consequence of the conventions governing the construction of symbols in *International Tables for Crystallography*.*

Although the *standard* symbols of the symmorphic space groups do not contain screw axes or glide planes, this is a result of the manner in which the space-group symbols have been devised. Most symmorphic space groups do in fact contain screw axes and/or glide planes. This is immediately obvious for the symmorphic space groups based on centred cells; *C*2 contains equal numbers of diad rotation axes and diad screw axes, and *Cm* contains equal numbers of reflection planes and glide planes. This is recognized in the 'extended' space-group symbols (Bertaut, 1995), but these are clumsy and not commonly used; those for *C*2 and *Cm* are $C1^{2}_{2_1}1$ and $C1^{m}_{a}1$, respectively. In the more symmetric crystal systems, even symmorphic space groups with primitive cells contain screw axes and/or glide planes; *P*422 ($P42^{2}_{2_1}$) contains many diad screw axes and *P*4/*mmm* ($P4/m2/m^{2/m}_{2_1/g}$) contains both screw axes and glide planes.

The balance of symmetry elements within the symmorphic space groups is discussed in more detail in Subsection 9.7.1.2.

1.4.3. Effect of dispersion on diffraction symmetry

In the absence of dispersion ('anomalous scattering'), the intensities of the reflections *hkl* and $\bar{h}\bar{k}\bar{l}$ are equal (Friedel's law), and statements about the symmetry of the weighted reciprocal lattice and quantities derived from it often rest on the tacit or explicit assumption of this law – the condition underlying it being forgotten. In particular, if dispersion is appreciable, the symmetry of the Patterson synthesis and the 'Laue' symmetry are altered.

1.4.3.1. *Symmetry of the Patterson function*

In Volume A of *International Tables*, the symmetry of the Patterson synthesis is derived in two stages. First, any glide planes and screw axes are replaced by mirror planes and the corresponding rotation axes, giving a symmorphic space group (Subsection 1.4.2.1). Second, a centre of symmetry is added. This second step involves the tacit assumption of Friedel's law, and should not be taken if any atomic scattering factors have appreciable imaginary components. In such cases, the symmetry of the Patterson synthesis will not be that of one of the 24 centrosymmetric symmorphic space groups, as given in Volume A, but will be that of the symmorphic space group belonging to the arithmetic crystal class to which the space group of the structure belongs. There are thus 73 possible Patterson symmetries.

An equivalent description of such symmetries, in terms of 73 of the 1651 dichromatic colour groups, has been given by Fischer & Knop (1987); see also Wilson (1993).

1.4.3.2. *'Laue' symmetry*

Similarly, the eleven conventional 'Laue' symmetries [*International Tables for Crystallography* (1995), Volume A, p. 40 and elsewhere] involve the explicit assumption of Friedel's law. If dispersion is appreciable, the 'Laue' symmetry may be that of any of the 32 point groups. The point group, in correct orientation, is obtained by dropping the Bravais-lattice symbol from the symbol of the arithmetic crystal class or of the Patterson symmetry.

---

* Three examples of informative definitions are:

1. The space group corresponding to the zero solution of the Frobenius congruences is called a symmorphic space group (Engel, 1986, p. 155).

2. A space group *F* is called *symmorphic* if one of its finite subgroups (and therefore an infinity of them) is of an order equal to the order of the point group R_r (Opechowski, 1986, p. 255).

3. A space group is called *symmorphic* if the coset representatives W_j can be chosen in such a way that they leave one common point fixed (Wondratschek, 1995, p. 717).

Even in context, these are pretty opaque.

References

1.1–1.3

Cahn, R. W. (1954). *Twinned crystals. Adv. Phys.* **3**, 363–445.

Catti, M. & Ferraris, G. (1976). *Twinning by merohedry and X-ray crystal structure determination. Acta Cryst.* A**32**, 163–165.

Donnay, G. & Donnay, J. D. H. (1974). *Classification of triperiodic twins. Can. Mineral.* **12**, 422–425.

Flack, H. D. (1987). *The derivation of twin laws for (pseudo-) merohedry by coset decomposition. Acta Cryst.* A**43**, 564–568.

Grimmer, H. (1984). *The generating function for coincidence site lattices in the cubic system. Acta Cryst.* A**40**, 108–112.

Grimmer, H. (1989*a*). *Systematic determination of coincidence orientations for all hexagonal lattices with axial ratios c/a in a given interval. Acta Cryst.* A**45**, 320–325.

Grimmer, H. (1989*b*). *Coincidence orientations of grains in rhombohedral materials. Acta Cryst.* A**45**, 505–523.

Grimmer, H. & Warrington, D. H. (1985). *Coincidence orientations of grains in hexagonal materials. J. Phys (Paris),* **46**, C4, 231–236.

Hahn, Th. (1981). *Meroedrische Zwillinge, Symmetrie, Domänen, Kristallstrukturbestimmung. Z. Kristallogr.* **156**, 114–115, and private communication.

Hahn, Th. (1984). *Twin domains and twin boundaries. Acta Cryst.* A**40**, C-117.

International Tables for Crystallography (1983). Vol. A. Dordrecht: Reidel.

International Tables for Crystallography (1987). Vol. A, second, revised ed. Dordrecht: Kluwer Academic Publishers.

Klapper, H. (1987). *X-ray topography of twinned crystals. Prog. Cryst. Growth Charact.* **14**, 367–401.

1.1–1.3 (*cont.*)

Klapper, H., Hahn, Th. & Chung, S. J. (1987). *Optical, pyroelectric and X-ray topographic studies of twin domains and twin boundaries in $KLiSO_4$. Acta Cryst.* B**43**, 147–159.

LePage, Y., Donnay, J. D. H. & Donnay, G. (1984). *Printing sets of structure factors for coping with orientation ambiguities and possible twinning by merohedry. Acta Cryst.* A**40**, 679–684.

1.4

Bertaut, E. F. (1995). *Synoptic tables of space-group symbols. Group–subgroup relations*. In *International tables for crystallography*, Vol. A, edited by Th. Hahn, pp. 50–68. Dordrecht: Kluwer Academic Publishers.

Brown, H., Bülow, R., Neubüser, J., Wondratschek, H. & Zassenhaus, H. (1978). *Crystallographic groups of four-dimensional space*. New York: Wiley.

Engel, P. (1986). *Geometric crystallography*. Dordrecht: Reidel. (Present distributor Kluwer Academic Publishers, Dordrecht.)

Fischer, K. F. & Knop, W. E. (1987). *Space groups for imaginary Patterson and for difference Patterson functions in the lambda technique. Z. Kristallogr.* **180**, 237-242.

Hahn, Th. (1995). Editor. *International tables for crystallography*, Vol. A. *Space-group symmetry*, fourth, revised, ed. Dordrecht: Kluwer Academic Publishers.

International Tables for Crystallography (1995). Vol. A. *Space-group symmetry,* fourth, revised ed., edited by Th. Hahn. Dordrecht: Kluwer Academic Publishers.

Opechowski, W. (1986). *Crystallographic and metacrystallographic groups*. Amsterdam: North Holland.

Wilson, A. J. C. (1993). *Laue and Patterson symmetry in the complex case. Z. Kristallogr.* **208**, 199–206.

Wolff, P. M. de, Belov, N. V., Bertaut, E. F., Buerger, M. J., Donnay, J. D. H., Fischer, W., Hahn, Th., Koptsik, V. A., Mackay, A. L., Wondratschek, H., Wilson, A. J. C. & Abrahams, S. C. (1985). *Nomenclature for crystal families, Bravais-lattice types and arithmetic classes. Acta Cryst.* A**41**, 278–280.

Wondratschek, H. (1995). *Introduction to space-group symmetry. International tables for crystallography*, Vol. A, edited by Th. Hahn, pp. 712–735. Dordrecht: Kluwer Academic Publishers.

International Tables for Crystallography (2006). Vol. C, Chapter 2.1, pp. 24–25.

2.1. Classification of experimental techniques

BY J. R. HELLIWELL

The diffraction of a wave of characteristic length, λ, by a crystal sample requires that λ is of the same order in size as the interatomic separation. Beams of X-rays, neutrons, and electrons can easily satisfy this requirement; for the latter two, the wavelength is determined by the de Broglie relationship $\lambda = h/p$, where h is Planck's constant and p is the momentum.

We can define 'diffraction geometry' as the description of the relationship between the beam and the sample orientation and the subsequent interception of the diffracted rays by a detector of given geometry and imaging properties. Each diffracted ray represents successful, constructive interference. The full stimulation of a reflection is achieved either by using a continuum of values of λ incident on the crystal, as used originally by Friedrich, Knipping & von Laue (1912) (the Laue method) or alternatively by using a monochromatic beam and rotation or precession of a crystal (moving-crystal methods) or a set of randomly oriented crystallites (the powder method).

The analysis of single-crystal reflection intensities allows the three-dimensional architecture of molecules to be determined. However, a single crystal cannot always be obtained. Diffraction from noncrystalline samples, *i.e.* fibres, amorphous materials or solutions, yields less detailed, but often very valuable, molecular information. Another method, surface diffraction, involves the determination of the organization of atoms deposited on the surface of a crystal substrate; a surface of perfectly repeating identical units, in identical environments, on such a substrate is sometimes referred to as a two-dimensional crystal. Ordered two-dimensional arrangements of proteins in membranes are studied by electron diffraction and, more recently, by undulator X-radiation. Another experimental probe of the structure of matter is EXAFS (extended X-ray absorption fine structure). This technique yields details of the *local* environment of a specific atom whose X-ray absorption edge is stimulated; the atom absorbs an X-ray photon and yields up a photoelectron, which can be scattered by neighbouring atoms. Interpretation of EXAFS therefore closely follows low-energy electron-diffraction (LEED) theory. All these methods (Table 2.1.1) can be called methods of structure analysis. Techniques for examining the perfection of crystals are also very important. Defects in crystals represent irregularities in the growth of a perfect crystalline array. There are many types of defect. The experimental technique of X-ray topography (Chapter 2.7) is used to image irregularities in a crystal lattice.

X-ray techniques have expanded in the 1970's and 1980's with the utilization of synchrotron radiation. The methods based on the use of neutrons and electrons have developed. Broadly speaking, the diffraction geometry is independent of the nature of the wave and depends only on its state, namely, the wavelength, λ, the spectral bandpass, $\delta\lambda/\lambda$, the convergence/divergence angles, and the beam direction. In what follows, the term monochromatic refers to the case where there is, practically speaking, a very small but finite wavelength spread. Similarly, the term polychromatic refers to the situation where the wavelength spread is of the same order as the mean wavelength. The technical means by which a given beam (of X-rays, neutrons or electrons) is conditioned vary, as do the means of detection. These methods are dealt with in the following pages as far as they relate to the geometry of diffraction.

In the previous version of *International Tables* (*IT* II, 1959, Part 4), various diffraction geometries were detailed and a variety of numerical tables were given. The numerical tables have mainly been dispensed with since the use of hand-held calculators and computers has rendered them obsolete.

Copyright © 2006 International Union of Crystallography

Table 2.1.1. *Summary of main experimental techniques for structure analysis*

Name of technique	Beam		Sample	Usual detectors
	Usual type	Spectrum		
(*A*) *Single crystal*				
Laue	X-ray or neutron	Polychromatic	Stationary single crystal	Film; image plate or storage phosphor; electronic area detector (*e.g.* CCD); for neutron case, detector sensitive to time-of-flight
Still	X-ray or neutron or electron	Monochromatic	Stationary single crystal	Film; image plate or storage phosphor; electronic area detector (*e.g.* MWPC, TV, CCD)
Rotation/oscillation	X-ray	Monochromatic	Single crystal rotating about a single axis (typical angular range per exposure 5–15° for small molecule; 1–2° for protein; 0.25–0.5° for virus)	Film; image plate or storage phosphor; electronic area detector (*e.g.* MWPC, TV, CCD)
Weissenberg	X-ray	Monochromatic	Single crystal rotating about a single axis (angular range $\geq 15^\circ$), coupled with detector translation	Film; image plate or storage phosphor
Precession	X-ray	Monochromatic	Single crystal (the normal to a reciprocal-lattice plane precesses about X-ray beam)	Flat film moving behind a screen coupled with crysal so as to be held parallel to a reciprocal-lattice plane
Diffractometry	X-ray or neutron	Monochromatic	Single crystal rotated over a small angular range	Single counter, linear detector or area detector
(*B*) *Polycrystalline powders*				
Monochromatic powder method	X-ray or neutron or electron	Monochromatic	Powder sample rotated to increase range of orientations presented to beam	Film or image plate; counter; 1D position-sensitive detector (linear or curved)
Energy-dispersive powder method	X-ray or neutron	Polychromatic	Powder sample	Energy-dispersive counter (for neutron case, detector sensitive to time-of-flight)
(*C*) *Fibres, solutions, surfaces, and membranes*				
Fibre method	X-ray or neutron	Monochromatic	Single fibre or a bundle of fibres; preferred orientation in a sample	Film or image plate; electronic area detector (*e.g.* MWPC or TV); records high-angle or low-angle diffraction data
Solution or 'small-angle method'	X-ray or neutron	Monochromatic	Dilute solutions of particles; crystalline defects	Counter or MWPC
Surface diffraction	Electron or X-ray	Monochromatic	Atoms deposited or adsorbed onto a substrate	Phosphor or counter
Membranes	Electron or X-ray	Monochromatic	Naturally occurring 2D ordered membrane protein	Film or image plate; CCD

Notes
(1) Monochromatic. Typical value of spectral spread, $\delta\lambda/\lambda$, on a conventional X-ray source; $K\alpha_1 - K\alpha_2$ line separation $\sim 2.5 \times 10^{-3}$, $K\alpha_1$ line width $\sim 10^{-4}$. On a synchrotron source a variable quantity dependent on type of monochromator; typical values $\sim 10^{-3}$ or $\sim 10^{-4}$ for the two common monochromator types (see Figs. 2.2.7.2 and 2.2.7.3, respectively).
(2) CCD = charge-coupled device; MWPC = multiwire proportional chamber detector; TV = television detector.
(3) Image plate is a trade name of Fuji. Storage phosphor is a trade name of Kodak.
(4) EXAFS can be performed on all types of sample whether crystalline or noncrystalline. It uses an X-ray beam that is tuned around an absorption edge and the transmitted intensity or the fluorescence emission is measured.

International Tables for Crystallography (2006). Vol. C, Chapter 2.2, pp. 26–41.

2.2. Single-crystal X-ray techniques

By J. R. Helliwell

In Chapter 2.1 *Classification of experimental techniques* there are given the various common approaches to the recording of X-ray crystallographic data, in different geometries, for crystal structure analysis. These are:

(*a*) Laue geometry;
(*b*) monochromatic still exposure;
(*c*) rotation/oscillation geometry;
(*d*) Weissenberg geometry;
(*e*) precession geometry;
(*f*) diffractometry.

The reasons for the choice of order are as follows. Laue geometry is dealt with first because it was historically the first to be used (Friedrich, Knipping & von Laue, 1912). In addition, the first step that should be carried out with a new crystal, at least of a small molecule, is to take a Laue photograph to make the first assessment of crystal quality. For macromolecules, the monochromatic still serves the same purpose. From consideration of the monochromatic still geometry, we can then describe the cases of single-axis rotation (rotation/oscillation method), single-axis rotation coupled with detector translation (Weissenberg method), crystal and detector precession (precession method), and finally three-axis goniostat and rotatable detector or area detector (diffractometry).

Method (*a*) uses a polychromatic beam of broad wavelength bandpass (*e.g.* $0.2 \leq \lambda \leq 2.5$ Å); if the bandwidth is restricted (*e.g.* to $\delta\lambda/\lambda = 0.2$), then it is sometimes referred to as narrow-bandpass Laue geometry. The remaining methods (*b*)–(*f*) use a monochromatic beam.

There are textbooks that concentrate on almost every geometry. References to these books are given in the respective sections in the following pages. However, in addition, there are several books that contain details of diffraction geometry. Blundell & Johnson (1976) describe the use of the various diffraction geometries with the examples taken from protein crystallography. There is an extensive discussion and many practical details to be found in the textbooks of Stout & Jensen (1968), Woolfson (1970, 1997), Glusker & Trueblood (1971, 1985), Vainshtein (1981), and McKie & McKie (1986), for example. A collection of early papers on the diffraction of X-rays by crystals involving, *inter alia*, experimental techniques and diffraction geometry, can be found in Bijvoet, Burgers & Hägg (1969, 1972). A collection of papers on, primarily, protein and virus crystal data collection *via* the rotation-film method and diffractometry can be found in Wyckoff, Hirs & Timasheff (1985). Synchrotron instrumentation, methods, and applications are dealt with in the books of Helliwell (1992) and Coppens (1992).

Quantitative X-ray crystal structure analysis usually involves methods (*c*), (*d*), and (*f*), although (*e*) has certainly been used. Electronic area detectors or image plates are extensively used now in all methods.

Traditionally, Laue photography has been used for crystal orientation, crystal symmetry, and mosaicity tests. Rapid recording of Laue patterns using synchrotron radiation, especially with protein crystals or with small crystals of small molecules, has led to an interest in the use of Laue geometry for quantitative structure analysis. Various fundamental objections made, especially by W. L. Bragg, to the use of Laue geometry have been shown not to be limiting.

The monochromatic still photograph is used for orientation setting and mosaicity tests, for protein or virus crystallography, and computer refinement of crystal orientation following initial crystal setting.

Precession photography allows the isolation of a specific zone or plane of reflections for which indexing can be performed by inspection, and systematic absences and symmetry are explored. From this, space-group assignment is made. The use of precession photography is usually avoided in small-molecule crystallography where auto-indexing methods are employed on a single-crystal diffractometer. In such a situation, the burden of data collection is not huge and symmetry elements can be determined after data collection. This is also now carried out on electronic area detectors in conjunction with auto-indexing principally at present for macromolecular crystallography but also for chemical crystallography.

In the following sections, the geometry of each method is dealt with in an idealized form. The practical realization of each geometry is then dealt with, including the geometric distortions introduced in the image by electronic area detectors. A separate section deals with the common means for beam conditioning, namely mirrors, monochromators, and filters. Sufficient detail is given to establish the magnitude of the wavelength range, spectral spreads, beam divergence and convergence angles, and detector effects. These values can then be utilized along with the formulae given for the calculation of spot bandwidth, spot size, and angular reflecting range.

2.2.1. Laue geometry

The main book dealing with Laue geometry is Amorós, Buerger & Amorós (1975). This should be used in conjunction with Henry, Lipson & Wooster (1951), or McKie & McKie (1986); see also Helliwell (1992, chapter 7). There is a synergy between synchrotron and neutron Laue diffraction developments (see Helliewell & Wilkinson, 1994).

2.2.1.1. *General*

The single crystal is bathed in a polychromatic beam of X-rays containing wavelengths between $\lambda_{\min}$ and $\lambda_{\max}$. A particular crystal plane will pick out a general wavelength λ for which constructive interference occurs and reflect according to Bragg's law

$$\lambda = 2d \sin\theta, \qquad (2.2.1.1)$$

where d is the interplanar spacing and θ is the angle of reflection. A sphere drawn with radius $1/\lambda$ and with the beam direction as diameter, passing through the origin of the reciprocal lattice (the point O in Fig. 2.2.1.1), will yield a reflection in the direction drawn from the centre of the sphere and out through the reciprocal-lattice point (relp) provided the relp in question lies on the surface of the sphere. This sphere is known as the Ewald sphere. Fig. 2.2.1.1 shows the Laue geometry, in which there exists a nest of Ewald spheres of radii between $1/\lambda_{\max}$ and $1/\lambda_{\min}$. An alternative convention is feasible whereby only a single Ewald sphere is drawn of radius 1 reciprocal-lattice unit (r.l.u.). Then each relp is no longer a point but a streak between $\lambda_{\min}/d$ and $\lambda_{\max}/d$ from the origin of reciprocal space (see McKie & McKie, 1986, p. 297). In the following discussions on the Laue approach, this notation is not followed. We use the nest of Ewald spheres of varying radii instead.

Copyright © 2006 International Union of Crystallography

Any relp (*hkl*) lying in the region of reciprocal space between the $1/\lambda_{max}$ and $1/\lambda_{min}$ Ewald spheres and the resolution sphere $1/d_{min}$ will diffract (the shaded area in Fig. 2.2.1.1). This region of reciprocal space is referred to as the accessible or stimulated region. Fig. 2.2.1.2 shows a predicted Laue pattern from a well aligned protein crystal. For a description of the indexing of a Laue photograph, see Bragg (1928, pp. 28, 29).

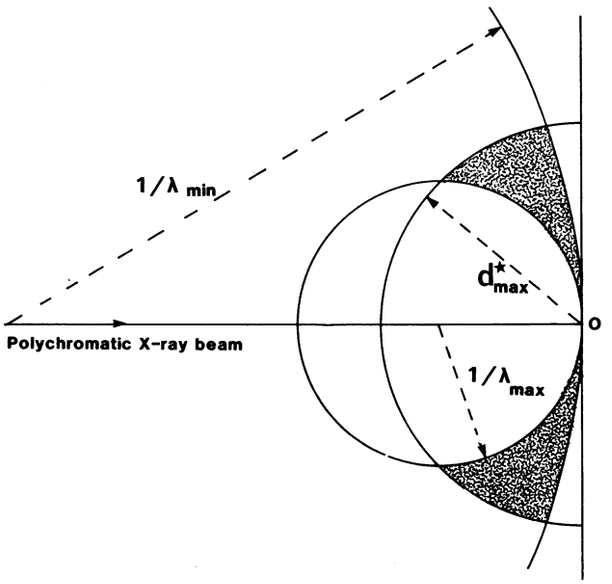

Fig. 2.2.1.1. Laue geometry. A polychromatic beam containing wavelengths λ_{min} to λ_{max} impinges on the crystal sample. The resolution sphere of radius $d^*_{max} = 1/d_{min}$ is drawn centred at O, the origin of reciprocal space. Any reciprocal-lattice point falling in the shaded region is stimulated. In this diagram, the radius of each Ewald sphere uses the convention $1/\lambda$.

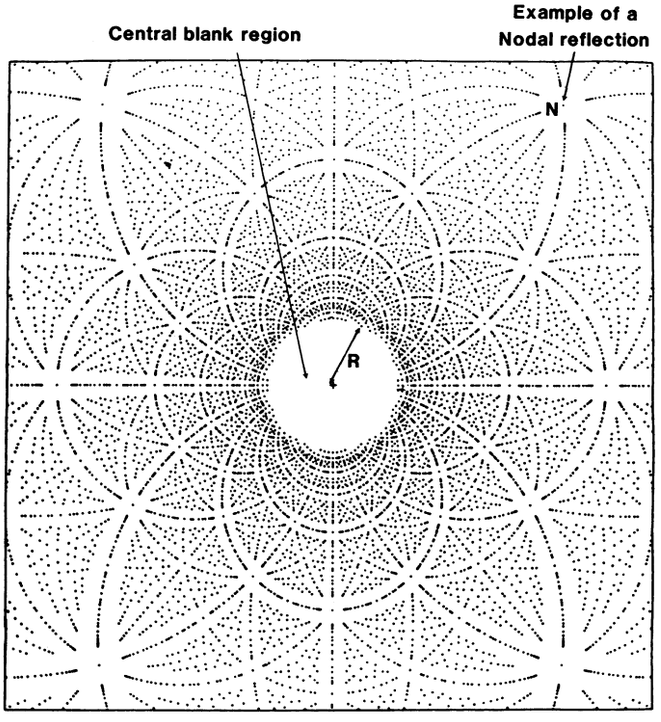

Fig. 2.2.1.2. A predicted Laue pattern of a protein crystal with a zone axis parallel to the incident, polychromatic X-ray beam. There is a pronounced blank region at the centre of the film (see Subsection 2.2.1.2). The spot marked *N* is one example of a nodal spot (see Subsection 2.2.1.4).

For a Laue spot at a given θ, only the ratio λ/d is determined, whether it is a single or a multiple relp component spot. If the unit-cell parameters are known from a monochromatic experiment, then a Laue spot at a given θ yields λ since d is then known. Conversely, precise unit-cell lengths cannot be determined from a Laue pattern alone; methods are, however, being developed to determine these (see Carr, Cruickshank & Harding, 1992).

The maximum Bragg angle θ_{max} is given by the equation

$$\theta_{max} = \sin^{-1}(\lambda_{max}/2d_{min}). \qquad (2.2.1.2)$$

2.2.1.2. *Crystal setting*

The main use of Laue photography has in the past been for adjustment of the crystal to a desired orientation. With small-molecule crystals, the number of diffraction spots on a monochromatic photograph from a stationary crystal is very small. With unfiltered, polychromatic radiation, many more spots are observed and so the Laue photograph serves to give a better idea of the crystal orientation and setting prior to precession photography. With protein crystals, the monochromatic still is used for this purpose before data collection *via* an area detector. This is because the number of diffraction spots is large on a monochromatic still and in a protein-crystal Laue photograph the stimulated spots from the *Bremsstrahlung* continuum are generally very weak. Synchrotron-radiation Laue photographs of protein crystals can be recorded with short exposure times. These patterns consist of a large number of diffraction spots.

Crystal setting *via* Laue photography usually involves trying to direct the X-ray beam along a zone axis. Angular mis-setting angles ε in the spindle and arc are easily calculated from the formula

$$\varepsilon = \tan^{-1}(\Delta/D), \qquad (2.2.1.3)$$

where Δ is the distance (resolved into vertical and horizontal) from the beam centre to the centre of a circle of spots defining a zone axis and D is the crystal-to-film distance.

After suitable angular correction to the sample orientation, the Laue photograph will show a pronounced blank region at the centre of the film (see Fig. 2.2.1.2). The radius of the blank region is determined by the minimum wavelength in the beam and the magnitude of the reciprocal-lattice spacing parallel to the X-ray beam (see Jeffery, 1958). For the case, for example, of the X-ray beam perpendicular to the a^*b^* plane, then

$$\lambda_{min} = c(1 - \cos 2\theta), \qquad (2.2.1.4a)$$

where

$$2\theta = \tan^{-1}(R/D) \qquad (2.2.1.4b)$$

and R is the radius of the blank region (see Fig. 2.2.1.2), and D is the crystal-to-flat-film distance. If λ_{min} is known then an approximate value of c, for example, can be estimated. The principal zone axes will give the largest radii for the central blank region.

2.2.1.3. *Single-order and multiple-order reflections*

In Laue geometry, several relp's can occur in a Laue spot or ray. The number of relp's in a given spot is called the multiplicity of the spot. The number of spots of a given multiplicity can be plotted as a histogram. This is known as the multiplicity distribution. The form of this distribution is dependent on the ratio $\lambda_{max}/\lambda_{min}$. The multiplicity distribution

in Laue diffraction is considered in detail by Cruickshank, Helliwell & Moffat (1987).

Any relp nh, nk, nl (n integer) will be stimulated by a wavelength λ/n since $d_{nhnknl} = d_{hkl}/n$, *i.e.*

$$\frac{\lambda}{n} = 2\frac{d_{hkl}}{n}\sin\theta. \qquad (2.2.1.5)$$

However, d_{nhnknl} must be $> d_{\min}$ as otherwise the reflection is beyond the sample resolution limit.

If h, k, l have no common integer divisor and if $2h$, $2k$, $2l$ is beyond the resolution limit, then the spot on the Laue diffraction photograph is a single-wavelength spot. The probability that h, k, l have no common integer divisor is

$$Q = \left[1-\frac{1}{2^3}\right]\left[1-\frac{1}{3^3}\right]\left[1-\frac{1}{5^3}\right]\ldots$$
$$= 0.832\ldots. \qquad (2.2.1.6)$$

Hence, for a relp where $d_{\min} < d_{hkl} < 2d_{\min}$ there is a very high probability (83.2%) that the Laue spot will be recorded as a single-wavelength spot. Since this region of reciprocal space corresponds to 87.5% (*i.e.* 7/8) of the volume of reciprocal space within the resolution sphere then $0.875 \times 0.832 = 72.8\%$ is the probability for a relp to be recorded in a single-wavelength spot. According to W. L. Bragg, all Laue spots should be multiple. He reasoned that for each h, k, l there will always be a $2h$, $2k$, $2l$ *etc*. lying within the same Laue spot. However, as the resolution limit is increased to accommodate this many more relp's are added, for which their hkl's have no common divisor.

The above discussion holds for infinite bandwidth. The effect of a more experimentally realistic bandwidth is to increase the proportion of single-wavelength spots.

The number of relp's within the resolution sphere is

$$\frac{4}{3}\frac{\pi d^{*3}_{\max}}{V^*}, \qquad (2.2.1.7)$$

where $d^*_{\max} = 1/d_{\min}$ and V^* is the reciprocal unit-cell volume.

The number of relp's within the wavelength band $\lambda_{\max}$ to $\lambda_{\min}$, for $\lambda_{\max} < 2/d^*_{\max}$, is (Moffat, Schildkamp, Bilderback & Volz, 1986)

$$\frac{\pi}{4}\frac{(\lambda_{\max}-\lambda_{\min})d^{*4}_{\max}}{V^*}. \qquad (2.2.1.8)$$

Note that the number of relp's stimulated in a 0.1 Å wavelength interval, for example between 0.1 and 0.2 Å, is the same as that between 1.1 and 1.2 Å, for example. A large number of relp's are stimulated at one orientation of the crystal sample.

The proportion of relp's within a sphere of small d^* (*i.e.* at low resolution) actually stimulated is small. In addition, the probability of them being single is zero in the infinite-band-width case and small in the finite-bandwidth case. However, Laue

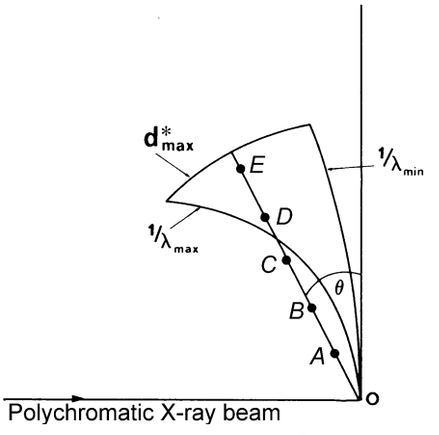

Fig. 2.2.1.3. A multiple component spot in Laue geometry. A ray of multiplicity 5 is shown as an example. The inner point A corresponds to d and a wavelength λ, the next point, B, is $d/2$ and wavelength $\lambda/2$. The outer point E corresponds to $d/5$ and $\lambda/5$. Rotation of the sample will either exclude inner points (at the $\lambda_{\max}$ surface) or outer points (at the $\lambda_{\min}$ surface) and so determine the recorded multiplicity.

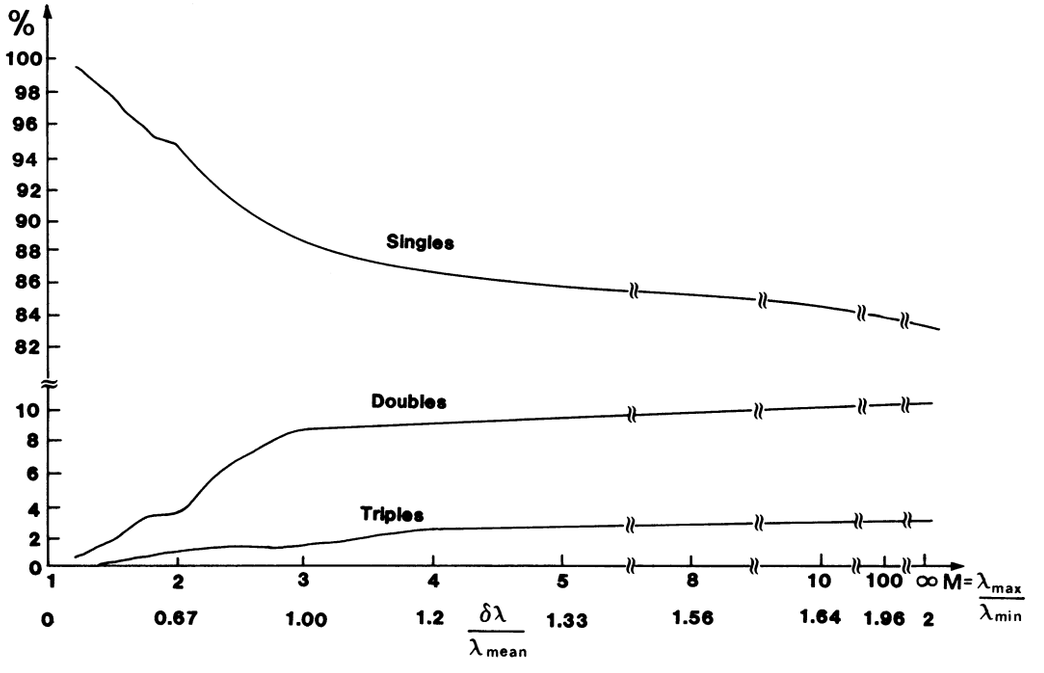

Fig. 2.2.1.4. The variation with $M = \lambda_{\max}/\lambda_{\min}$ of the proportions of relp's lying on single, double, and triple rays for the case $\lambda_{\max} < 2/d^*_{\max}$. From Cruickshank, Helliwell & Moffat (1987).

geometry is an efficient way of measuring a large number of relp's between d^*_{max} and $d^*_{max}/2$ as single-wavelength spots.

The above is a brief description of the overall multiplicity distribution. For a given relp, even of simple *hkl* values, lying on a ray of several relp's (multiples of *hkl*), a suitable choice of crystal orientation can yield a single-wavelength spot. Consider, for example, a spot of multiplicity 5. The outermost relp can be recorded at long wavelength with the inner relp's on the ray excluded since they need λ's greater than λ_{max} (Fig. 2.2.1.3). Alternatively, by rotating the sample, the innermost relp can be measured uniquely at short wavelength with the outer relp's excluded (they require λ's shorter than λ_{min}). Hence, in Laue geometry several orientations are needed to recover virtually all relp's as singles. The multiplicity distribution is shown in Fig. 2.2.1.4 as a function of $\lambda_{max}/\lambda_{min}$ (with the corresponding values of $\delta\lambda/\lambda_{mean}$).

2.2.1.4. *Angular distribution of reflections in Laue diffraction*

There is an interesting variation in the angular separations of Laue reflections that shows up in the spatial distributions of spots on a detector plane (Cruickshank, Helliwell & Moffat, 1991). There are two main aspects to this distribution, which are general and local. The general aspects refer to the diffraction pattern as a whole and the local aspects to reflections in a particular zone of diffraction spots.

The general features include the following. The spatial density of spots is everywhere proportional to $1/D^2$, where D is the crystal-to-detector distance, and to $1/V^*$, where V^* is the reciprocal-cell volume. There is also though a substantial variation in spatial density with diffraction angle θ; a prominent maximum occurs at

$$\theta_c = \sin^{-1}(\lambda_{min} d^*_{max}/2). \qquad (2.2.1.9)$$

Local aspects of these patterns particularly include the prominent conics on which Laue reflections lie. That is, the local spatial distribution is inherently one-dimensional in character. Between multiple reflections (nodals), there is always at least one single and therefore nodals have a larger angular separation from their nearest neighbours. The blank area around a nodal in a Laue pattern (Fig. 2.2.1.2) has been noted by Jeffery (1958). The smallest angular separations, and therefore spatially overlapped cases, are associated with single Laue reflections. Thus, the reflections involved in energy overlaps – the multiples – form a set largely distinct, except at short crystal-to-detector distances, from those involved in spatial overlaps, which are mostly singles (Helliwell, 1985).

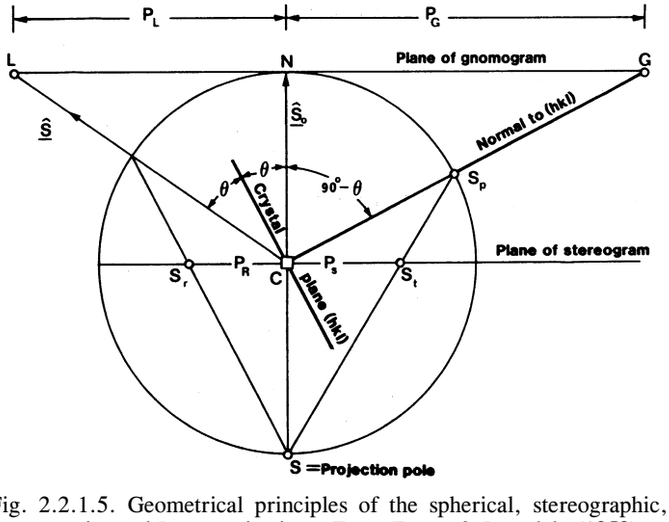

Fig. 2.2.1.5. Geometrical principles of the spherical, stereographic, gnomonic, and Laue projections. From Evans & Lonsdale (1959).

From a knowledge of the form of the angular distribution, it is possible, *e.g.* from the gaps bordering conics, to estimate d^*_{max} and λ_{min}. However, a development of this involving gnomonic projections can be even more effective (Cruickshank, Carr & Harding, 1992).

2.2.1.5. *Gnomonic and stereographic transformations*

A useful means of transformation of the flat-film Laue pattern is the gnomonic projection. This converts the pattern of spots lying on curved arcs to points lying on straight lines. The stereographic projection is also used. Fig. 2.2.1.5 shows the graphical relationships involved [taken from *International Tables*, Vol. II (Evans & Lonsdale, 1959)], for the case of a Laue pattern recorded on a plane film, between the incident-beam direction *SN*, which is perpendicular to a film plane and the Laue spot L and its spherical, stereographic, and gnomonic points S_p, S_t and G and the stereographic projection S_r of the reflected beams. If the radius of the sphere of projection is taken equal to D, the crystal-to-film distance, then the planes of the gnomonic projection and of the film coincide. The lines producing the various projection poles for any given crystal plane are coplanar with the incident and reflected beams. The transformation equations are

$$P_L = D\tan 2\theta \qquad (2.2.1.10)$$

$$P_G = D\cot\theta \qquad (2.2.1.11)$$

$$P_S = D\frac{\cos\theta}{(1+\sin\theta)} \qquad (2.2.1.12)$$

$$P_R = D\tan\theta. \qquad (2.2.1.13)$$

2.2.2. Monochromatic methods

In this section and those that follow, which deal with monochromatic methods, the convention is adopted that the Ewald sphere takes a radius of unity and the magnitude of the reciprocal-lattice vector is λ/d. This is not the convention used in the Laue section above.

Some historical remarks are useful first before progressing to discuss each monochromatic geometry in detail. The original rotation method (for example, see Bragg, 1949) involved a rotation of a perfectly aligned crystal of 360°. For reasons of relatively poor collimation of the X-ray beam, leading to spot-to-spot overlap, and background build-up, Bernal (1927) introduced the oscillation method whereby a repeated, limited, angular range was used to record one pattern and a whole series of contiguous ranges on different film exposures were collected to provide a large angular coverage overall. In a different solution to the same problem, Weissenberg (1924) utilized a layer-line screen to record only one layer line but allowed a full rotation of the crystal but now coupled to translation of the detector, thus avoiding spot-to-spot overlap. Again, several exposures were needed, involving one layer line collected on each exposure. The advent of synchrotron radiation with very high intensity allows small beam sizes at the sample to be practicable, thus simultaneously creating small diffraction spots and minimizing background scatter. The very fine collimation of the synchrotron beam keeps the diffraction-spot sizes small as they traverse their path to the detector plane.

The terminology used today for different methods is essentially the same as originally used except that the rotation method now tends to mean limited angular ranges (instead of 360°) per diffraction photograph/image. The Weissenberg method in its modern form now employed at a synchrotron is a screenless technique with limited angular range but still with detector translation coupled to crystal rotation.

2.2.2.1. *Monochromatic still exposure*

In a monochromatic still exposure, the crystal is held stationary and a near-zero wavelength-bandpass (*e.g.* $\delta\lambda/\lambda = 0.001$) beam impinges on it. For a small-molecule crystal, there are few diffraction spots. For a protein crystal, there are many (several hundred), because of the much denser reciprocal lattice. The actual number of stimulated relp's depends on the reciprocal-cell parameters, the size of the mosaic spread of the crystal, the angular beam divergence as well as the small, but finite, spectral spread, $\delta\lambda/\lambda$. Diffraction spots are only partially stimulated instead of fully integrated over wavelength, as in the Laue method, or over an angular rotation (the rocking width) in rotating-crystal monochromatic methods.

The diffraction spots lie on curved arcs where each curve corresponds to the intersection with a film of a cone. With a flat film the intersections are conic sections. The curved arcs are obviously recognizable for the protein crystal case where there are a large number of spots.

2.2.2.2. *Crystal setting*

Crystal setting follows the procedure given in Subsection 2.2.1.2 whereby angular mis-setting angles are given by equation (2.2.1.3). When viewed down a zone axis, the pattern on a flat film or electronic area detector has the appearance of a series of concentric circles. For example, with the beam parallel to $[00\bar{1}]$, the first circle corresponds to $l = 1$, the second to $l = 2$, *etc*. The radius of the first circle R is related to the interplanar spacing between the ($hk0$) and ($hk1$) planes, *i.e.* λ/c (in this example), through θ, by the formulae

$$\tan 2\theta = R/D; \quad \cos 2\theta = 1 - \lambda/c. \qquad (2.2.2.1)$$

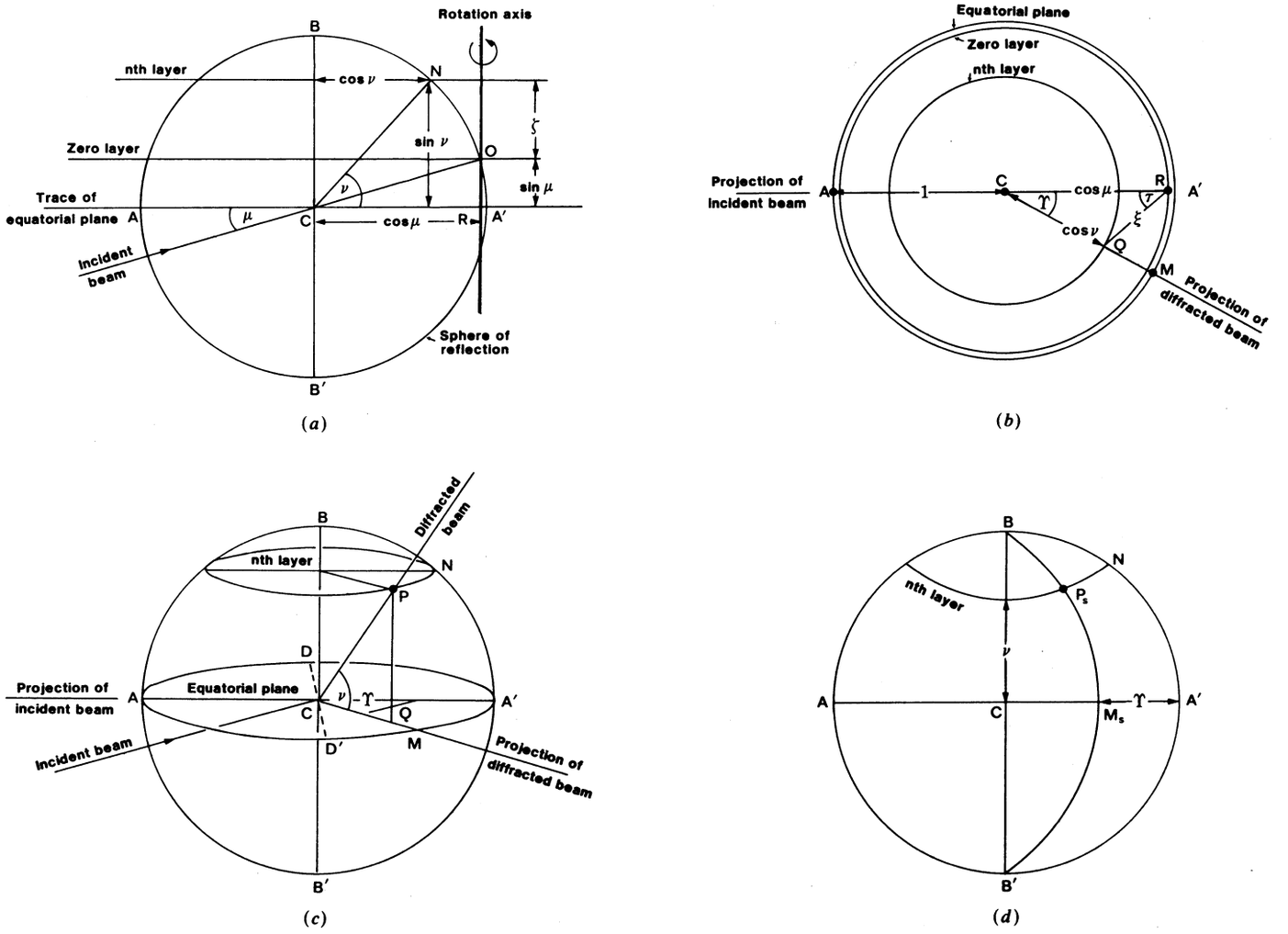

Fig. 2.2.3.1. (*a*) Elevation of the sphere of reflection. *O* is the origin of the reciprocal lattice. *C* is the centre of the Ewald sphere. The incident beam is shown in the plane. (*b*) Plan of the sphere of reflection. *R* is the projection of the rotation axis on the equatorial plane. (*c*) Perspective diagram. *P* is the relp in the reflection position with the cylindrical coordiantes ζ, ξ, φ. The angular coordinates of the diffracted beam are ν, Υ. (*d*) Stereogram to show the direction of the diffracted beam, ν, Υ, with DD', normal to the incident beam and in the equatorial plane, as the projection diameter. From Evans & Lonsdale (1959).

2.2.3. Rotation/oscillation geometry

The main modern book dealing with the rotation method is that of Arndt & Wonacott (1977).

2.2.3.1. *General*

The purpose of the monochromatic rotation method is to stimulate a reflection fully over its rocking width *via* an angular rotation. Different relp's are rotated successively into the reflecting position. The method, therefore, involves rotation of the sample about a single axis, and is used in conjunction with an area detector of some sort, *e.g.* film, electronic area detector or image plate. The use of a repeated rotation or oscillation, for a given exposure, is simply to average out any time-dependent changes in incident intensity or sample decay. The overall crystal rotation required to record the total accessible region of reciprocal space for a single crystal setting, and a detector picking up all the diffraction spots, is $180^\circ + 2\theta_{\max}$. If the crystal has additional symmetry, then a complete asymmetric unit of reciprocal space can be recorded within a smaller angle. There is a blind region close to the rotation axis; this is detailed in Subsection 2.2.3.5.

2.2.3.2. *Diffraction coordinates*

Figs. 2.2.3.1(*a*) to (*d*) are taken from *IT* II (1959, p. 176). They neatly summarize the geometrical principles of reflection, of a monochromatic beam, in the reciprocal lattice for the general case of an incident beam inclined at an angle (μ) to the equatorial plane. The diagrams are based on an Ewald sphere of unit radius.

With the nomenclature of Table 2.2.3.1:
Fig 2.2.3.1(*a*) gives

$$\sin\nu = \sin\mu + \zeta. \tag{2.2.3.1}$$

Fig. 2.2.3.1(*b*) gives, by the cosine rule,

$$\cos\Upsilon = \frac{\cos^2\nu + \cos^2\mu - \xi^2}{2\cos\nu\cos\mu} \tag{2.2.3.2}$$

and

$$\cos\tau = \frac{\cos^2\mu + \xi^2 - \cos^2\nu}{2\xi\cos\mu}, \tag{2.2.3.3}$$

and Figs. 2.2.3.1(*a*) and (*b*) give

$$\xi^2 + \zeta^2 = d^{*2} = 4\sin^2\theta. \tag{2.2.3.4}$$

The following special cases commonly occur:
(*a*) $\mu = 0$, normal-beam rotation method, then

$$\sin\nu = \zeta \tag{2.2.3.5}$$

and

$$\cos\Upsilon = \frac{2 - \xi^2 - \zeta^2}{2\sqrt{1-\zeta^2}}; \tag{2.2.3.6}$$

(*b*) $\mu = -\nu$, equi-inclination (relevant to Weissenberg upper-layer photography), then

$$\zeta = -2\sin\mu = 2\sin\nu \tag{2.2.3.7}$$

$$\cos\Upsilon = 1 - \frac{\xi^2}{2\cos^2\nu}; \tag{2.2.3.8}$$

(*c*) $\mu = +\nu$, anti-equi-inclination

$$\zeta = 0 \tag{2.2.3.9}$$

$$\cos\Upsilon = 1 - \frac{\zeta^2}{2\cos^2\nu}; \tag{2.2.3.10}$$

(*d*) $\nu = 0$, flat cone

$$\zeta = -\sin\mu \tag{2.2.3.11}$$

$$\cos\Upsilon = \frac{2 - \xi^2 - \zeta^2}{2\sqrt{1-\zeta^2}}. \tag{2.2.3.12}$$

In this section, we will concentrate on case (*a*), the normal-beam rotation method ($\mu = 0$). First, the case of a plane film or detector is considered.

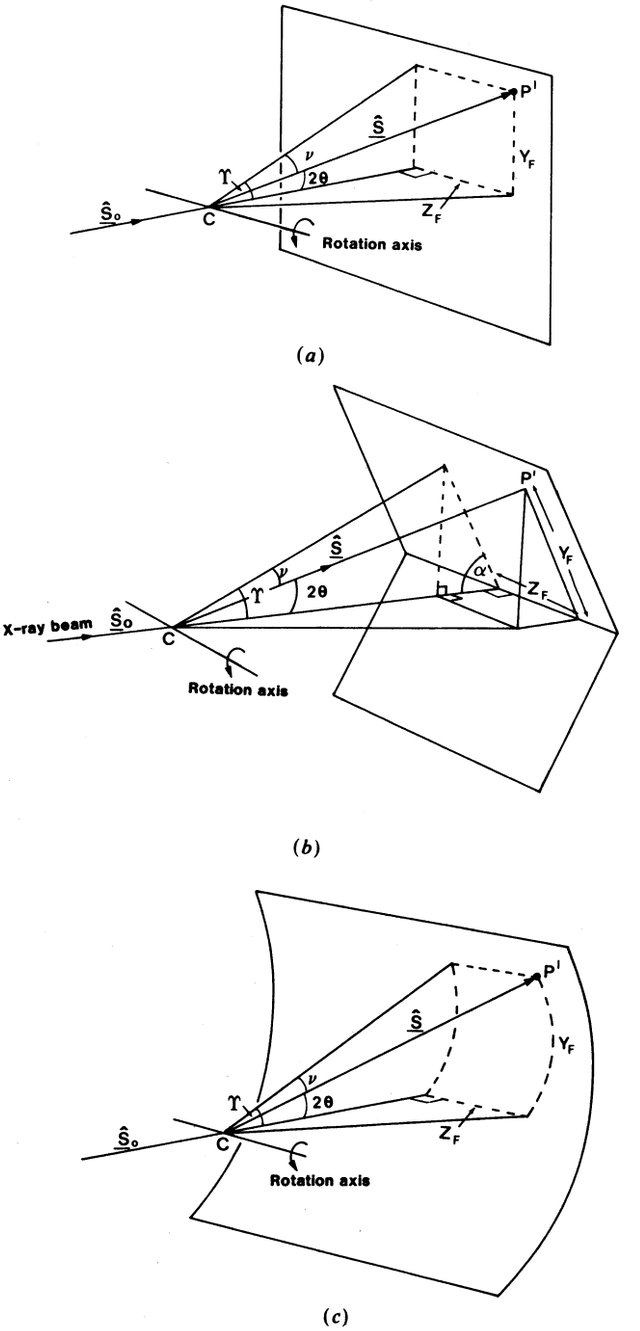

Fig. 2.2.3.2. Geometrical principles of recording the pattern on (*a*) a plane detector, (*b*) a *V*-shaped detector, (*c*) a cylindrical detector.

Table 2.2.3.1. *Glossary of symbols used to specify quantities on diffraction patterns and in reciprocal space*

θ	Bragg angle
2θ	Angle of deviation of the reflected beam with respect to the incident beam
$\hat{\mathbf{S}}_o$	Unit vector lying along the direction of the incident beam
$\hat{\mathbf{S}}$	Unit vector lying along the direction of the reflected beam
$\mathbf{s} = (\hat{\mathbf{S}} - \hat{\mathbf{S}}_o)$	The scattering vector of magnitude $2\sin\theta$. $\mathbf{s}$ is perpendicular to the bisector of the angle between $\hat{\mathbf{S}}_o$ and $\hat{\mathbf{S}}$. $\mathbf{s}$ is identical to the reciprocal-lattice vector $\mathbf{d}^*$ of magnitude λ/d, where d is the interplanar spacing, when $\mathbf{d}^*$ is in the diffraction condition. In this notation, the radius of the Ewald sphere is unity. This convention is adopted because it follows that in Volume II of *International Tables* (p. 175). Note that in Section 2.2.1 *Laue geometry* the alternative convention ($\|\mathbf{d}^*\| = 1/d$) is adopted whereby the radius of each Ewald sphere is $1/\lambda$. This allows a nest of Ewald spheres between $1/\lambda_{\max}$ and $1/\lambda_{\min}$ to be drawn
ζ	Coordinate of a point P in reciprocal space parallel to a rotation axis as the axis of cylindrical coordinates relative to the origin of reciprocal space
ξ	Radial coordinate of a point P in reciprocal space; that is, the radius of a cylinder having the rotation axis as axis
τ	The angular coordinate of P, measured as the angle between ξ and $\hat{\mathbf{S}}_o$ [see Fig. 2.2.3.1(*b*)]
φ	The angle of rotation from a defined datum orientation to bring a relp onto the Ewald sphere in the rotation method (see Fig. 2.2.3.3)
μ	The angle of inclination of $\hat{\mathbf{S}}_o$ to the equatorial plane
Υ	The angle between the projections of $\hat{\mathbf{S}}_o$ and $\hat{\mathbf{S}}$ onto the equatorial plane
ν	The angle of inclination of $\hat{\mathbf{S}}$ to the equatorial plane
ω, χ, φ	The crystal setting angles on the four-circle diffractometer (see Fig. 2.2.6.1). The φ used here is not the same as that in the rotation method (Fig. 2.2.3.3). This clash in using the same symbol twice is inevitable because of the widespread use of the rotation camera and four-circle diffractometer.

The equatorial plane is the plane normal to the rotation axis.

The notation now follows that of Arndt & Wonacott (1977) for the coordinates of a spot on the film or detector. Z_F is parallel to the rotation axis and ζ. Y_F is perpendicular to the rotation axis and the beam. *IT* II (1959, p. 177) follows the convention of y being parallel and x perpendicular to the rotation-axis direction, *i.e.* $(Y_F, Z_F) \equiv (x, y)$. The advantage of the (Y_F, Z_F) notation is that the x-axis direction is then the same as the X-ray beam direction.

The coordinates of a reflection on a flat film (Y_F, Z_F) are related to the cylindrical coordinates of a relp (ξ, ζ) [Fig. 2.2.3.2(*a*)] by

$$Y_F = D\tan\Upsilon \tag{2.2.3.13}$$

$$Z_F = D\sec\Upsilon\tan\nu, \tag{2.2.3.14}$$

which becomes

$$Z_F = 2D\zeta/(2 - \xi^2 - \zeta^2), \tag{2.2.3.15}$$

where D is the crystal-to-film distance.

For the case of a V-shaped cassette with the V axis parallel to the rotation axis and the film making an angle α to the beam direction [Fig. 2.2.3.2(*b*)], then

$$Y_F = D\tan\Upsilon/(\sin\alpha + \cos\alpha\tan\Upsilon) \tag{2.2.3.16}$$

$$Z_F = (D - Y_F\cos\alpha)\zeta/(1 - d^{*2}/2). \tag{2.2.3.17}$$

This situation also corresponds to the case of flat electronic area detector inclined to the incident beam in a similar way.

Note that Arndt & Wonacott (1977) use ν instead of α here. We use α and so follow *IT* II (1959). This avoids confusion with the ν of Table 2.2.3.1. D is the crystal to V distance. In the case of the V cassettes of Enraf–Nonius, α is 60°.

For the case of a cylindrical film or image plate where the axis of the cylinder is coincident with the rotation axis [Fig. 2.2.3.2(*c*)] then, for Υ in degrees,

$$Y_F = \frac{2\pi}{360}D\Upsilon \tag{2.2.3.18}$$

$$Z_F = D\tan\nu, \tag{2.2.3.19}$$

which becomes

$$Z_F = \frac{D\zeta}{\sqrt{(1 - \zeta^2)}}. \tag{2.2.3.20}$$

Here, D is the radius of curvature of the cylinder assuming that the crystal is at the centre of curvature.

In the three geometries mentioned here, detector-misalignment errors have to be considered. These are three orthogonal angular errors, translation of the origin, and error in the crystal-to-film distance.

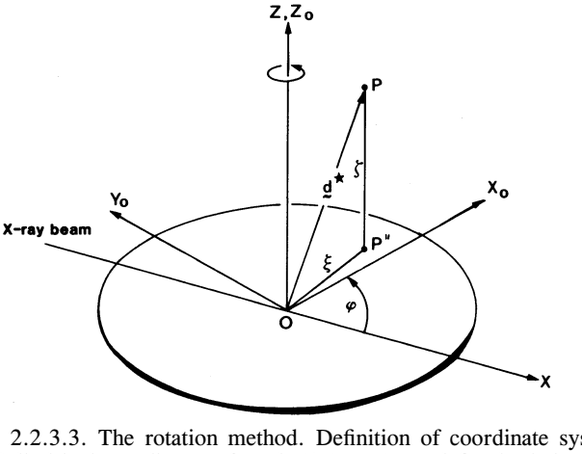

Fig. 2.2.3.3. The rotation method. Definition of coordinate systems. [Cylindrical coordinates of a relp P (ξ, ζ, φ) are defined relative to the axial system $X_0Y_0Z_0$ which rotates with the crystal.] The axial system XYZ is defined such that X is parallel to the incident beam and Z is coincident with the rotation axis. From Arndt & Wonacott (1977).

The coordinates Y_F and Z_F are related to film-scanner raster units *via* a scanner-rotation matrix and translation vector. This is necessary because the film is placed arbitrarily on the scanner drum. Details can be found in Rossmann (1985) or Arndt & Wonacott (1977).

2.2.3.3. *Relationship of reciprocal-lattice coordinates to crystal system parameters*

The reciprocal-lattice coordinates, $\zeta, \xi, \Upsilon, \nu$, *etc*. used earlier, refer to an axial system fixed to the crystal, $X_0Y_0Z_0$ of Fig. 2.2.3.3. Clearly, a given relp needs to be brought into the Ewald sphere by the rotation about the rotation axis. The treatment here follows Arndt & Wonacott (1977).

The rotation angle required, φ, is with respect to some reference 'zero-angle' direction and is determined by the particular crystal parameters. It is necessary to define a standard orientation of the crystal (*i.e.* datum) when $\varphi = 0^\circ$. If we define an axial system $X_0Y_0Z_0$ fixed to the crystal and a laboratory axis system XYZ with X parallel to the beam and Z coincident with the rotation axis then $\varphi = 0^\circ$ corresponds to these axial systems being coincident (Fig. 2.2.3.3).

The angle of the crystal at which a given relp diffracts is

$$\tan(\varphi/2) = \frac{2y_0 \pm (4y_0^2 + 4x_0^2 - d^{*4})^{1/2}}{(d^{*2} - 2x_0)}. \qquad (2.2.3.21)$$

The two solutions correspond to the two rotation angles at which the relp P cuts the sphere of reflection. Note that Y_F, Z_F (Subsection 2.2.3.2) are independent of φ.

The values of x_0 and y_0 are calculated from the particular crystal system parameters. The relationships between the coordinates x_0, y_0, z_0 and ξ and ζ are

$$\xi = (x_0^2 + y_0^2)^{1/2}, \qquad (2.2.3.22)$$

$$\zeta = z_0. \qquad (2.2.3.23)$$

$\mathbf{X}_0$ can be related to the crystal parameters by

$$\mathbf{X}_0 = \boldsymbol{A}\mathbf{h}. \qquad (2.2.3.24)$$

$\boldsymbol{A}$ is a crystal-orientation matrix defining the standard datum orientation of the crystal.

For example, if, by convention, $\mathbf{a}^*$ is chosen as parallel to the X-ray beam at $\varphi = 0^\circ$ and $\mathbf{c}$ is chosen as the rotation axis, then, for the general case,

$$\boldsymbol{A} = \begin{bmatrix} a^* & b^*\cos\gamma^* & c^*\cos\beta^* \\ 0 & b^*\sin\gamma^* & -c^*\sin\beta\cos\alpha \\ 0 & 0 & c^* \end{bmatrix}. \qquad (2.2.3.25)$$

If the crystal is mounted on the goniometer head differently from this then $\boldsymbol{A}$ can be modified by another matrix, $\boldsymbol{M}$, say, or the terms permuted. This exercise becomes clear if the reader takes an orthogonal case ($\alpha = \beta = \gamma = 90^\circ$). For the general case, see Higashi (1989).

The crystal will most likely be misaligned (slightly or grossly) from the ideal orientation. To correct for this, the misorientation matrices $\boldsymbol{\Phi}_x$, $\boldsymbol{\Phi}_y$, and $\boldsymbol{\Phi}_z$ are introduced, *i.e.*

$$\boldsymbol{\Phi}_x = \begin{bmatrix} 1 & 0 & 0 \\ 0 & \cos\Delta\varphi_x & -\sin\Delta\varphi_x \\ 0 & \sin\Delta\varphi_x & \cos\Delta\varphi_x \end{bmatrix} \qquad (2.2.3.26)$$

$$\boldsymbol{\Phi}_y = \begin{bmatrix} \cos\Delta\varphi_y & 0 & \sin\Delta\varphi_y \\ 0 & 1 & 0 \\ -\sin\Delta\varphi_y & 0 & \cos\Delta\varphi_y \end{bmatrix} \qquad (2.2.3.27)$$

$$\boldsymbol{\Phi}_z = \begin{bmatrix} \cos\Delta\varphi_z & -\sin\Delta\varphi_z & 0 \\ \sin\Delta\varphi_z & \cos\Delta\varphi_z & 0 \\ 0 & 0 & 1 \end{bmatrix}, \qquad (2.2.3.28)$$

where $\Delta\varphi_x$, $\Delta\varphi_y$, and $\Delta\varphi_z$ are angles around the X_0, Y_0, and Z_0 axes, respectively.

Hence, the relationship between $\mathbf{X}_0$ and $\mathbf{h}$ is

$$\boldsymbol{X}_0 = \boldsymbol{\Phi}_z\boldsymbol{\Phi}_y\boldsymbol{\Phi}_x\boldsymbol{M}\boldsymbol{A}\mathbf{h}. \qquad (2.2.3.29)$$

2.2.3.4. *Maximum oscillation angle without spot overlap*

For a given oscillation photograph, there is maximum value of the oscillation range, $\Delta\varphi$, that avoids overlapping of spots on a film. The overlap is most likely to occur in the region of the diffraction pattern perpendicular to the rotation axis and at the maximum Bragg angle. This is where relp's pass through the Ewald sphere with the greatest velocity. For such a separation between successive relp's of a^*, then the maximum allowable rotation angle to avoid spatial overlap is given by

$$\Delta\varphi_{\max} = \left[\frac{a^*}{d^*_{\max}} - \Delta\right], \qquad (2.2.3.30)$$

where Δ is the sample reflecting range (see Section 2.2.7). $\Delta\varphi_{\max}$ is a function of φ, even in the case of identical cell parameters. This is because it is necessary to consider, for a given orientation, the relevant reciprocal-lattice vector perpendicular to $d^*_{\max}$. In the case where the cell dimensions are quite different in magnitude (excluding the axis parallel to the rotation axis), then $\Delta\varphi_{\max}$ is a marked function of the orientation.

In rotation photography, as large an angle as possible is used up to $\Delta\varphi_{\max}$. This reduces the number of images that need to be processed and the number of partially stimulated reflections per image but at the expense of signal-to-noise ratio for individual spots, which accumulate more background since $\Delta < \Delta\varphi_{\max}$. In the case of a CCD detector system, $\Delta\varphi$ is chosen usually to be

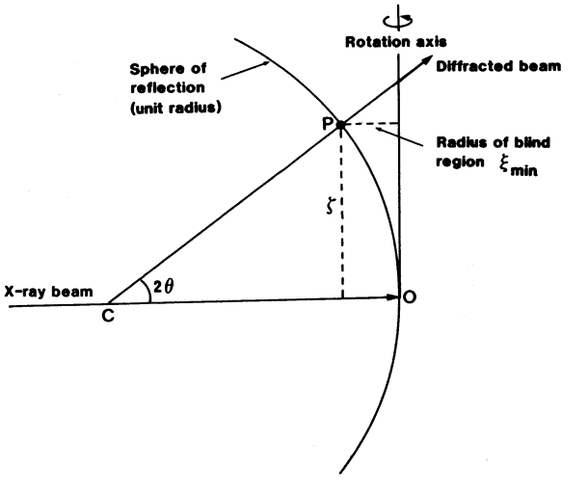

Fig. 2.2.3.4. The rotation method. The blind region associated with a single rotation axis. From Arndt & Wonacott (1977).

less than Δ so as to optimize the signal-to-noise ratio of the measurement and to sample the rocking-width profile.

The value of Δ, the crystal rocking width for a given *hkl*, depends on the reciprocal-lattice coordinates of the *hkl* relp (see Section 2.2.7). In the region close to the rotation axis, Δ is large.

In the introductory remarks to the monochromatic methods used, it has already been noted that originally the rotation method involved 360° rotations contributing to the diffraction image. Spot overlap led to loss of reflection data and encouraged Bernal and Weissenberg to devise improvements. With modern synchrotron techniques, the restriction on $\Delta\varphi_{\max}$ (equation 2.2.3.30) can be relaxed for special applications. For example, since the spot overlap that is to be avoided involves relp's from adjacent reciprocal-lattice planes, the different Miller indices *hkl* and $h + l$, k, l do lead in fact to a small difference in Bragg angle. With good enough collimation, a small spot size exists at the detector plane so that the two spots can be resolved. For a standard-sized detector, this is practical for low-resolution data recording. This can be a useful complement to the Laue method where the low-resolution data are rather sparsely stimulated and also tend to occur in multiple Laue spots. Alternatively, a much larger detector can be contemplated and even medium-resolution data can be recorded without major overlap problems. These techniques are useful in some time-resolved applications. For a discussion see Weisgerber & Helliwell (1993). For regular data collection, however, narrow angular ranges are still generally preferred so as to reduce the background noise in the diffraction images and also to avoid loss of any data because of spot overlap.

2.2.3.5. *Blind region*

In normal-beam geometry, any relp lying close to the rotation axis will not be stimulated at all. This situation is shown in Fig. 2.2.3.4. The blind region has a radius of

$$\xi_{\min} = d^*_{\max} \sin\theta_{\max} = \frac{\lambda^2}{2d^2_{\min}}, \qquad (2.2.3.31)$$

and is therefore strongly dependent on $d_{\min}$ but can be ameliorated by use of a short λ. Shorter λ makes the Ewald sphere have a larger radius, *i.e.* its surface moves closer to the rotation axis. At Cu $K\alpha$ for 2 Å resolution, approximately 5% of the data lie in the blind region according to this simple geometrical model. However, taking account of the rocking width Δ, a greater percentage of the data than this is not fully sampled except over very large angular ranges. The actual increase in the blind-region volume due to this effect is minimized by use of a collimated beam and a narrow spectral spread (*i.e.* finely monochromatized, synchrotron radiation) if the crystal is not too mosaic.

These effects are directly related to the Lorentz factor,

$$L = 1/(\sin^2 2\theta - \zeta^2)^{1/2}. \qquad (2.2.3.32)$$

It is inadvisable to measure a reflection intensity when L is large because different parts of a spot would need a different Lorentz factor.

The blind region can be filled in by a rotation about another axis. The total angular range that is needed to sample the blind region is $2\theta_{\max}$ in the absence of any symmetry or $\theta_{\max}$ in the case of *mm* symmetry (for example).

2.2.4. Weissenberg geometry

Weissenberg geometry (Weissenberg, 1924) is dealt with in the books by Buerger (1942) and Woolfson (1970), for example.

2.2.4.1. *General*

The conventional Weissenberg method uses a moving film in conjunction with the rotation of the crystal and a layer-line screen. This allows:

(*a*) A larger rotation range of the crystal to be used (say 200°), avoiding the problem of overlap of reflections (referred to in Subsection 2.2.3.4 on oscillation photography).

(*b*) Indexing of reflections on the photograph to be made by inspection.

The Weissenberg method is not widely used now. In small-molecule crystallography, quantitative data collection is usually performed by means of a diffractometer.

Weissenberg geometry has been revived as a method for macromolecular data collection (Sakabe, 1983, 1991), exploiting monochromatized synchrotron radiation and the image plate as detector. Here the method is used without a layer-line screen where the total rotation angle is limited to $\sim 15°$; this is a significant increase over the rotation method with a stationary film. The use of this effectively avoids the presence of partial reflections and reduces the total number of exposures required. Provided the Weissenberg camera has a large radius, the X-ray background accumulated over a single spot is actually not serious. This is because the X-ray background decreases approximately according to the inverse square of the distance from the crystal to the detector.

The following Subsections 2.2.4.2 and 2.2.4.3 describe the standard situation where a layer-line screen is used.

2.2.4.2. *Recording of zero layer*

Normal-beam geometry (*i.e.* the X-ray beam perpendicular to the rotation axis) is used to record zero-layer photographs. The film is held in a cylindrical cassette coaxial with the rotation axis. The centre of the gap in a screen is set to coincide with the zero-layer plane. The coordinate of a spot on the film measured parallel (Z_F) and perpendicular (Y_F) to the rotation axis is given by

$$Y_F = \frac{2\pi}{360} D\Upsilon \qquad (2.2.4.1)$$

$$Z_F = \varphi/f, \qquad (2.2.4.2)$$

where φ is the rotation angle of the crystal from its initial setting, f is the coupling constant, which is the ratio of the crystal rotation angle divided by the film cassette translation distance, in $^\circ\text{min}^{-1}$, and D is the camera radius. Generally, the values of f and D are $2^\circ\,\text{min}^{-1}$ and 28.65 mm, respectively.

2.2.4.3. *Recording of upper layers*

Upper-layer photographs are usually recorded in equi-inclination geometry [*i.e.* $\mu = -\nu$ in equations (2.2.3.7) and (2.2.3.8)]. The X-ray-beam direction is made coincident with the generator of the cone of the diffracted beam for the layer concerned, so that the incident and diffracted beams make equal angles (μ) with the equatorial plane, where

$$\mu = \sin^{-1}\zeta_n/2. \qquad (2.2.4.3)$$

The screen has to be moved by an amount

$$s\tan\mu, \qquad (2.2.4.4)$$

where s is the screen radius. If the cassette is held in the same position as the zero-layer photograph, then reflections produced by the same orientation of the crystal will be displaced

$$D\tan\mu \qquad (2.2.4.5)$$

Table 2.2.5.1. *The distance displacement (in mm) measured on the film versus angular setting error of the crystal for a screenless precession ($\bar{\mu} = 5°$) setting photograph*

Angular correction, ε, in degrees and minutes	Δ r.l.u	Distance displacement (mm) for three crystal-to-film distances		
		60 mm	75 mm	100 mm
0	0	0	0	0
15′	0.0175	1.1	1.3	1.8
30′	0.035	2.1	2.6	3.5
45′	0.0526	3.2	4.0	5.3
60′	0.070	4.2	5.3	7.0
1° 15′	0.087	5.2	6.5	8.7
1° 30′	0.105	6.3	7.9	10.5
1° 45′	0.123	7.4	9.2	12.3
2°	0.140	8.4	10.5	14.0

Alternatively, $\Delta = \delta/D \simeq \sin 4\varepsilon$ can be used if ε is small [from equation (2.2.5.1)].

Notes

(1) A value of $\bar{\mu}$ of 5° is assumed although there is a negligible variation in ε with $\bar{\mu}$ between 3° (typical for proteins) and 7° (typical for small molecules).

(2) Crystal-to-film distances on a precession camera are usually settable at the fixed distance $D = 60$, 75, and 100 mm.

(3) This table should be used in conjunction with Fig. 2.2.5.1.

(4) Values of ε are given in intervals of 5′ as this is convenient for various goniometer heads which usually have verniers in 5′, 6′ or 10′ units. The vernier on the spindle of the precession camera is often in 2′ units.

relative to the zero-layer photograph. This effect can be eliminated by initial translation of the cassette by $D \tan \mu$.

2.2.5. Precession geometry

The main book dealing with the precession method is that of Buerger (1964).

2.2.5.1. *General*

The precession method is used to record an undistorted representation of a single plane of relp's and their associated intensities. In order to achieve this, the crystal is carefully set so that the plane of relp's is perpendicular to the X-ray beam. The normal to this plane, the zone axis, is then precessed about the X-ray-beam axis. A layer-line screen allows only relp's of the plane of interest to pass through to the film. The motion of the crystal, screen, and film are coupled together to maintain the coplanarity of the film, screen, and zone.

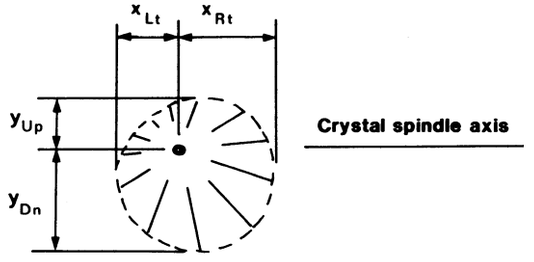

Fig. 2.2.5.1. The screenless precession setting photograph (schematic) and associated mis-setting angles for a typical orientation error when the crystal has been set previously by a monochromatic still or Laue.

2.2.5.2. *Crystal setting*

Setting of the crystal for one zone is carried out in two stages. First, a Laue photograph is used for small molecules or a monochromatic still for macromolecules to identify the required zone axis and place it parallel to the X-ray beam. This is done by adjustment to the camera-spindle angle and the goniometer-head arc in the horizontal plane. This procedure is usually accurate to a degree or so. Note that the vertical arc will only rotate the pattern around the X-ray beam. Second, a screenless precession photograph is taken using an angle of ~ 7–10° for small molecules or 2–3° for macromolecules. It is better to use unfiltered radiation, as then the edge of the zero-layer circle is easily visible. Let the difference of the distances from the centre of the pattern to the opposite edges of the trace in the direction of displacement be called $\delta = D\Delta$ so that for the horizontal goniometer-head arc and the dial: $\delta_{\rm arc} = x_{\rm Rt} - x_{\rm Lt}$ and $\delta_{\rm dial} = y_{\rm Up} - y_{\rm Dn}$ (Fig. 2.2.5.1). The corrections ε to the arc and camera spindle are given by

$$\Delta = \frac{\delta}{D} = \frac{\sin 4\varepsilon \cos \bar{\mu}}{\cos^2 2\varepsilon - \sin^2 \bar{\mu}} \text{ in r.l.u.,} \qquad (2.2.5.1)$$

where D is the crystal-to-film distance and $\bar{\mu}$ is the precession angle.

It is possible to measure δ to about 0.3 mm ($\delta = 1$ mm corresponds to 14′ error for $D = 60$ mm and $\bar{\mu} \simeq 7°$ [Table 2.2.5.1, based on *IT* II (1959, p. 200)].

2.2.5.3. *Recording of zero-layer photograph*

Before the zero-layer photograph is taken, an Nb filter (for Mo $K\alpha$) or an Ni filter (for Cu $K\alpha$) is introduced into the X-ray beam path and a screen is placed between the crystal and the film at a distance from the crystal of

$$s = r_s \cot \bar{\mu}, \qquad (2.2.5.2)$$

where r_s is the screen radius. Typical values of $\bar{\mu}$ would be 20° for a small molecule with Mo $K\alpha$ and 12–15° for a protein with Cu $K\alpha$. The annulus width in the screen is chosen usually as 2–3 mm for a small molecule and 1–2 mm for a macromolecule. A clutch slip allows the camera motor to be disengaged and the precession motion can be executed under hand control to check for fouling of the goniometer head, crystal, screen or film cassette; s and r_s need to be selected so as to avoid this happening. The zero-layer precession photograph produced has a radius of $2D \sin \bar{\mu}$ corresponding to a resolution limit $d_{\rm min} = \lambda/2 \sin \bar{\mu}$. The distance between spots A is related to the reciprocal-cell parameter a^* by the formula

$$a^* = \frac{A}{D}. \qquad (2.2.5.3)$$

2.2.5.4. *Recording of upper-layer photographs*

The recording of upper-layer photographs involves isolating the net of relp's at a distance from the zero layer of $\zeta_n = n\lambda/b$, where b is the case of the b axis antiparallel to the X-ray beam. In order to determine ζ_n, it is generally necessary to record a cone-axis photograph. If the cell parameters are known, then the camera settings for the upper-level photograph can be calculated directly without the need for a cone-axis photograph.

In the upper-layer precession photograph, the film is advanced towards the crystal by a distance

$$D\zeta_n \qquad (2.2.5.4)$$

and the screen is placed at a distance

$$s_n = r_s \cot \bar{\nu}_n = r_s \cot \cos^{-1}(\cos \bar{\mu} - \zeta_n). \quad (2.2.5.5)$$

The resulting upper-layer photograph has outer radius

$$D(\sin \bar{\nu}_n + \sin \bar{\mu}) \quad (2.2.5.6)$$

and an inner blind region of radius

$$D(\sin \bar{\nu}_n - \sin \bar{\mu}). \quad (2.2.5.7)$$

2.2.5.5. *Recording of cone-axis photograph*

A cone-axis photograph is recorded by placing a film enclosed in a light-tight envelope in the screen holder and using a small precession angle, *e.g.* 5° for a small molecule or 1° for a protein. The photograph has the appearance of concentric circles centred on the origin of reciprocal space, provided the crystal is perfectly aligned. The radius of each circle is

$$r_n = s \tan \bar{\nu}_n, \quad (2.2.5.8)$$

where

$$\cos \bar{\nu}_n = \cos \bar{\mu} - \zeta_n. \quad (2.2.5.9)$$

Hence, $\zeta_n = \cos \bar{\mu} - \cos \tan^{-1}(r_n/s)$.

2.2.6. Diffractometry

The main book dealing with single-crystal diffractometry is that of Arndt & Willis (1966). Hamilton (1974) gives a detailed treatment of angle settings for four-circle diffractometers. For details of area-detector diffractometry, see Howard, Nielsen & Xuong (1985) and Hamlin (1985).

2.2.6.1. *General*

In this section, we describe the following related diffractometer configurations:

(*a*) normal-beam equatorial geometry [ω, χ, φ option or ω, κ, φ (kappa) option];

(*b*) fixed $\chi = 45°$ geometry with area detector.

(*a*) is used with single-counter detectors. The kappa option is also used in the television area-detector system of Enraf–Nonius (the FAST). (*b*) is used with the multiwire proportional chamber, XENTRONICS, system. (FAST is a trade name of Enraf–Nonius; XENTRONICS is a trade name of Siemens.)

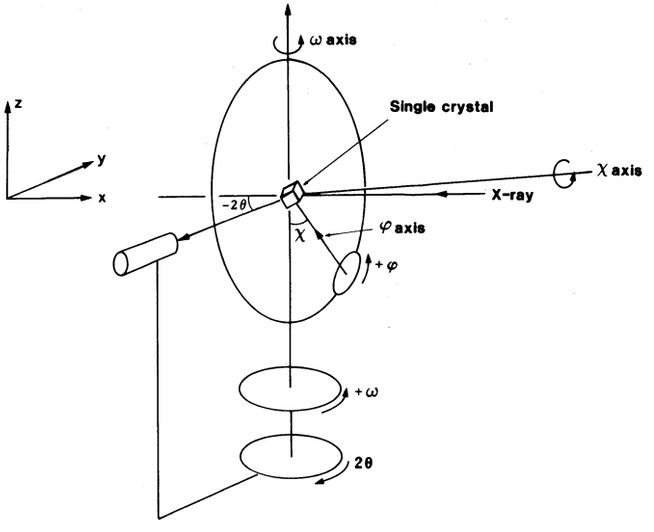

Fig. 2.2.6.1 Normal-beam equatorial geometry: the angles ω, χ, φ, 2θ are drawn in the convention of Hamilton (1974).

The purpose of the diffractometer goniostat is to bring a selected reflected beam into the detector aperture or a number of reflected beams onto an area detector of limited aperture (*i.e.* an aperture that does not intercept all the available diffraction spots at one setting of the area detector) [see Hamlin (1985, p. 431), for example].

Since the use of electronic area detectors is now increasingly common, the properties of these detectors that relate to the geometric prediction of spot position will be described later.

The single-counter diffractometer is primarily used for small-molecule crystallography. In macromolecular crystallography, many relp's are almost simultaneously in the diffraction condition. The single-counter diffractometer was extended to five separate counters [for a review, see Artymiuk & Phillips (1985)], then subsequently to a multi-element linear detector [for a review, see Wlodawer (1985)]. Area detectors offer an even larger aperture for simultaneous acquisition of reflections [Hamlin *et al.* (1981), and references therein].

Large-area on-line image-plate systems are now available commercially to crystallographers, whereby the problem of the limited aperture of electronic area detectors is circumvented and the need for a goniostat is relaxed so that a single axis of rotation can be used. Systems like the R-AXISIIc (Rigaku Corporation) and the MAR (MAR Research Systems) fall into this category, utilizing IP technology and an on-line scanner. A next generation of device beckons, involving CCD area detectors. These offer a much faster duty cycle and greater sensitivity than IP's. By tiling CCD's together, a larger-area device can be realized. However, it is likely that these will be used in conjunction with a three-axis goniostat again, except in special cases where a complete area coverage can be realized.

2.2.6.2. *Normal-beam equatorial geometry*

In normal-beam equatorial geometry (Fig. 2.2.6.1), the crystal is oriented specifically so as to bring the incident and reflected beams, for a given relp, into the equatorial plane. In this way, the detector is moved to intercept the reflected beam by a single rotation movement about a vertical axis (the 2θ axis). The value of θ is given by Bragg's law as $\sin^{-1}(d^*/2)$. In order to bring $\mathbf{d}^*$ into the equatorial plane (*i.e.* the Bragg plane into the meridional plane), suitable angular settings of a three-axis goniostat are necessary. The convention for the sign of the angles given in Fig. 2.2.6.1 is that of Hamilton (1974); his choice of sign of 2θ is adhered to despite the fact that it is left-handed, but in any case the signs of ω, χ, φ are standard right-handed. The

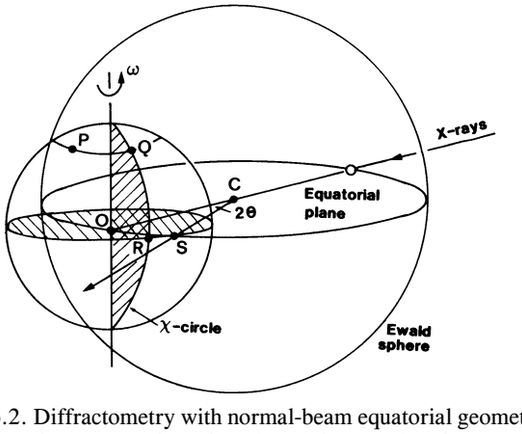

Fig. 2.2.6.2. Diffractometry with normal-beam equatorial geometry and angular motions ω, χ and φ. The relp at P is moved to Q *via* φ, from Q to R *via* χ, and R to S *via* ω. From Arndt & Willis (1966). In this specific example, the φ axis is parallel to the ω axis (*i.e.* $\chi = 0°$).

specific reciprocal-lattice point can be rotated from point P to point Q by the φ rotation, from Q to R *via* χ, and R to S *via* ω (see Fig. 2.2.6.2).

In the most commonly used setting, the χ plane bisects the incident and diffracted beams at the measuring position. Hence, the vector $\mathbf{d}^*$ lies in the χ plane at the measuring position. However, since it is possible for reflection to take place for any orientation of the reflecting plane rotated about $\mathbf{d}^*$, it is feasible therefore that $\mathbf{d}^*$ can make any arbitrary angle ε with the χ plane. It is conventional to refer to the azimuthal angle ψ of the reflecting plane as the angle of rotation about $\mathbf{d}^*$. It is possible with a ψ scan to keep the *hkl* reflection in the diffraction condition and so to measure the sample absorption surface by monitoring the variation in intensity of this reflection. This ψ scan is achieved by adjustment of the ω, χ, φ angles. When $\chi = \pm 90^\circ$, the ψ scan is simply a φ scan and ε is 0°.

The χ circle is a relatively bulky object whose thickness can inhibit the measurement of diffracted beams at high θ. Also, collision of the χ circle with the collimator or X-ray-tube housing has to be avoided. An alternative is the kappa goniostat geometry. In the kappa diffractometer [for a schematic picture, see Wyckoff (1985, p. 334)], the κ axis is inclined at 50° to the ω axis and can be rotated about the ω axis; the κ axis is an alternative to χ therefore. The φ axis is mounted on the κ axis. In this way, an unobstructed view of the sample is achieved.

2.2.6.3. *Fixed $\chi = 45^\circ$ geometry with area detector*

The geometry with fixed $\chi = 45^\circ$ was introduced by Nicolet and is now fairly common in the field. It consists of an ω axis, a φ axis, and χ fixed at 45°. The rotation axis is the ω axis. In this configuration, it is possible to sample a greater number of independent reflections per degree of rotation (Xuong, Nielsen, Hamlin & Anderson, 1985) because of the generally random nature of any symmetry axis.

An alternative method is to mount the crystal in a precise orientation and to use the φ axis to explore the blind region of the single rotation axis. It is feasible to place the capillary containing the sample in a vertically upright position *via* a 135° bracket mounted on the goniometer head. The bulk of the data is collected with the ω axis coincident with the capillary axis. This setting is beneficial to make the effect of capillary absorption symmetrical. At the end of this run, the blind region whose axis is coincident with the ω axis can be filled in by rotating around the φ axis by 180°. This renders the capillary axis horizontal and a different crystal axis vertical. Hence by rotation about this new crystal axis by $\pm\theta_{\max}$, the blind region can be sampled.

2.2.7. Practical realization of diffraction geometry: sources, optics, and detectors

2.2.7.1. *General*

The tools required for making the necessary measurement of reflection intensities include

(*a*) beam-conditioning items;
(*b*) crystal goniostat;
(*c*) detectors.

In this section, we describe the common configurations for defining precise states of the X-ray beam. The topic of detectors is dealt with in Part 7 (see especially Section 7.1.6). The impact of detector distortions on diffraction geometry is dealt with in Subsection 2.2.7.4.

Within the topic of beam conditioning the following subtopics are dealt with:

– collimation;
– monochromators;
– mirrors.

An exhaustive survey is not given, since a wide range of configurations is feasible. Instead, the commonest arrangements are covered. In addition, conventional X-ray sources are separated from synchrotron X-ray sources. The important difference in the treatment of the two types of source is that on the synchrotron the position and angle of the photon emission from the relativistic charged particles are correlated. One result of this, for example, is that after monochromatization of the synchrotron radiation (SR) the wavelength and angular direction of a photon are correlated.

The angular reflecting range and diffraction-spot size are determined by the physical state of the beam and the sample. *Hence, the idealized situation considered earlier of a point sample and zero-divergence beam will be relaxed.* Moreover, the effects of the detector-imaging characteristics are considered, *i.e.* obliquity, parallax, point-spread factor, and spatial distortions.

2.2.7.2. *Conventional X-ray sources: spectral character, crystal rocking curve, and spot size*

An extended discussion of instrumentation relating to conventional X-ray sources is given in Arndt & Willis (1966) and Arndt & Wonacott (1977). Witz (1969) has reviewed the use of monochromators for conventional X-ray sources.

It is generally the case that the $K\alpha$ line has been used for single-crystal data collection *via* monochromatic methods. The continuum *Bremsstrahlung* radiation is used for Laue photography at the stage of setting crystals.

The emission lines of interest consist of the $K\alpha_1$, $K\alpha_2$ doublet and the $K\beta$ line. The intrinsic spectral width of the $K\alpha_1$, or $K\alpha_2$ line is $\sim 10^{-4}$, their separation $(\delta\lambda/\lambda)$ is 2.5×10^{-3}, and they are of different relative intensity. The $K\beta$ line is eliminated either by use of a suitable metal filter or by a monochromator. A mosaic monochromator such as graphite passes the $K\alpha_1$, $K\alpha_2$ doublet in its entirety. The monochromator passes a certain, if small, component of a harmonic of the $K\alpha_1$, $K\alpha_2$ line extracted from the *Bremsstrahlung*. This latter effect only becomes important in circumstances where the *attenuated* main beam is used for calibration; the process of attenuation enhances the short-wavelength harmonic component to a significant degree. In diffraction experiments, this component is of negligible intensity. The polarization correction is different with and without a monochromator (see Chapter 6.2).

The effect of the doublet components of the $K\alpha$ emission is to cause a peak broadening at high angles. From Bragg's law, the following relationship holds for a given reflection:

$$\delta\theta = \frac{\delta\lambda}{\lambda}\tan\theta. \qquad (2.2.7.1)$$

For proteins where θ is relatively small, the effect of the $K\alpha_1$, $K\alpha_2$ separation is not significant. For small molecules, which diffract to higher resolution, this is a significant effect and has to be accounted for at high angles.

The width of the rocking curve of a crystal reflection is given by (Arndt & Willis, 1966)

$$\Delta = \left\{ \left[\frac{a+f}{s}\right] + \eta + \frac{\delta\lambda}{\lambda}\tan\theta \right\} \qquad (2.2.7.2)$$

when the crystal is fully bathed by the X-ray beam, where a is the crystal size, f the X-ray tube focus size (foreshortened), s the

distance between the X-ray tube focus and the crystal, and η the crystal mosaic spread (Fig. 2.2.7.1).

In the moving-crystal method, Δ is the minimum angle through which the crystal must be rotated, for a given reflection, so that every mosaic block can diffract radiation covering a fixed wavelength band $\delta\lambda$ from every point on the focal spot.

This angle Δ can be controlled to some extent, for the protein case, by collimation. For example, with a collimator entrance slit placed as close to the X-ray tube source and a collimator exit slit placed as close to the sample as possible, the value of $(a+f)/s$ can approximately be replaced by $(a'+f')/s'$, where f' is the entrance-slit size, a' is the exit-slit size, and s' the distance between them. Clearly, for $a' < a$, the whole crystal is no longer bathed by the X-ray beam. In fact, by simply inserting horizontal and vertical adjustable screws at the front and back of the collimator, adjustment to the horizontal and vertical divergence angles can be made. The spot size at the detector can be calculated approximately by multiplying the particular reflection rocking angle Δ by the distance from the sample to the spot on the detector. In the case of a single-counter diffractometer, tails on a diffraction spot can be eliminated by use of a detector collimator.

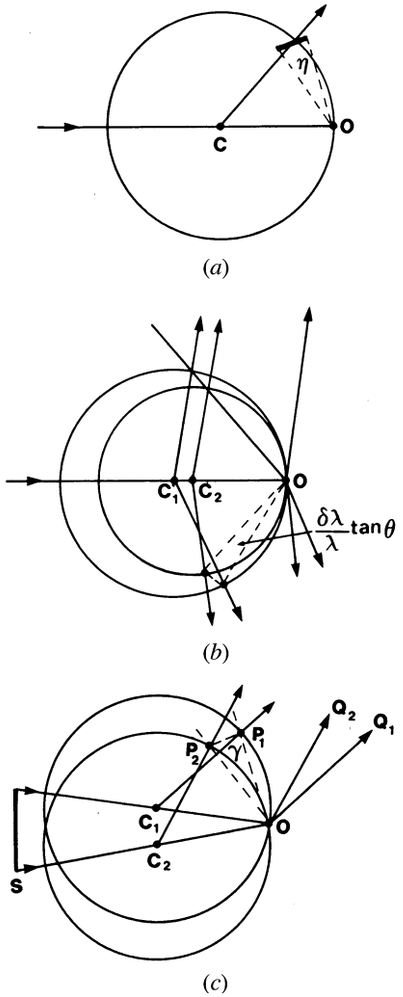

Fig. 2.2.7.1. Reflection rocking width for a conventional X-ray source. From Arndt & Wonacott (1977, p. 7). (*a*) Effect of sample mosaic spread. The relp is replaced by a spherical cap with a centre at the origin of reciprocal space where it subtends an angle η. (*b*) Effect of $(\delta\lambda/\lambda)_{\rm conv}$, the conventional source type spectral spread. (*c*) Effect of a beam divergence angle, γ. The overall reflection rocking width is a combination of these effects.

Spot-to-spot spatial resolution can be enhanced by use of focusing mirrors, which is especially important for large-protein and virus crystallography, where long cell axes occur. The effect is achieved by focusing the beam on the detector, thereby changing a divergence from the source into a convergence to the detector.

In the absence of absorption, at grazing angles, X-rays up to a certain critical energy are reflected. The critical angle θ_c is given by

$$\theta_c = \left[\frac{e^2}{mc^2}\frac{N}{\pi}\right]^{1/2}\lambda, \qquad (2.2.7.3)$$

where N is the number of free electrons per unit volume of the reflecting material. The higher the atomic number of a given material then the larger is θ_c for a given critical wavelength. The product of mirror aperture with reflectivity gives a figure of merit for the mirror as an efficient optical element.

The use of a pair of perpendicular curved mirrors set in the horizontal and vertical planes can focus the X-ray tube source to a small spot at the detector. The angle of the mirror to the incident beam is set to reject the $K\beta$ line (and shorter-wavelength *Bremsstrahlung*). Hence, spectral purity at the sample and diffraction spot size at the detector are improved simultaneously. There is some loss of intensity (and lengthening of exposure time) but the overall signal-to-noise ratio is improved. The primary reason for doing this, however, is to enhance spot-to-spot spatial resolution even with the penalty of the exposure time being lengthened. The rocking width of the sample is not affected in the case of 1:1 focusing (object distance = image distance). Typical values are tube focal-spot size, $f = 0.1$ mm, tube-to-mirror and mirror-to-sample distances ~ 200 mm, convergence angle 2 mrad, and focal-spot size at the detector ~ 0.3 mm.

To summarize, the configurations are

(*a*) beam collimator only;

(*b*) filter + beam collimator;

(*c*) filter + beam collimator + detector collimator (single-counter case);

(*d*) graphite monochromator + beam collimator;

(*e*) pair of focusing mirrors + exit-slit assembly;

(*f*) focusing germanium monochromator + perpendicular focusing mirror + exit-slit assembly.

(*a*) is for Laue mode; (*b*)–(*f*) are for monochromatic mode; (*f*) is a fairly recent development for conventional-source work.

2.2.7.3. *Synchrotron X-ray sources*

In the utilization of synchrotron X-radiation (SR), both Laue and monochromatic modes are important for data collection. The unique geometric and spectral properties of SR renders the treatment of diffraction geometry different from that for a conventional X-ray source. The properties of SR are dealt with in Subsection 4.2.1.5 and elsewhere; see Subject Index. Reviews of instrumentation, methods, and applications of synchrotron radiation in protein crystallography are given by Helliwell (1984, 1992).

(*a*) *Laue geometry: sources, optics, sample reflection bandwidth, and spot size*

Laue geometry involves the use of the fully polychromatic SR spectrum as transmitted through the beryllium window that is used to separate the apparatus from the machine vacuum. There is useful intensity down to a wavelength minimum of $\sim \lambda_c/5$, where λ_c is the critical wavelength of the magnet source. The maximum wavelength is typically ≥ 3 Å; however, if the crystal

is mounted in a capillary then the glass absorbs the wavelengths beyond ~ 2.6 Å.

The bandwidth can be limited somewhat under special circumstances. A reflecting mirror at grazing incidence can be used for two reasons. First, the minimum wavelength in the beam can be sharply defined to aid the accurate definition of the Laue-spot multiplicity. Second, the mirror can be used to focus the beam at the sample. The maximum-wavelength limit can be truncated by use of aluminium absorbers of varying thickness or by use of a transmission mirror (Lairson & Bilderback, 1992; Cassetta *et al.*, 1993).

The measured intensity of individual Laue diffraction spots depends on the wavelength at which they are stimulated. The problem of wavelength normalization is treated by a variety of methods. These include:

(*a*) use of a monochromatic reference data set;

(*b*) use of symmetry equivalents in the Laue data set recorded at different wavelengths;

(*c*) calibration with a standard sample such as a silicon crystal.

Each of these methods produces a 'λ-curve' describing the relative strength of spots measured at various wavelengths. The methods rely on the incident spectrum being smooth and stable with time. There are discontinuities in the 'λ-curve' at the bromine and silver *K*-absorption edges owing to the silver bromide in the photographic emulsion case. The λ-curve is therefore usually split up into wavelength regions, *i.e.* $\lambda_{\min}$ to 0.49 Å, 0.49 to 0.92 Å, and 0.92 Å to $\lambda_{\max}$. Other detector types have different discontinuities, depending on the material making up the X-ray absorbing medium. [The quantification of conventional-source Laue-diffraction data (Rabinovich & Lourie, 1987; Brooks & Moffat, 1991) requires the elimination of spots recorded near the emission-line wavelengths.]

The production and use of narrow-bandpass beams may be of interest, *e.g.* $\delta\lambda/\lambda \leq 0.2$. Such bandwidths can be produced by a combination of a reflection mirror used in tandem with a transmission mirror. Alternatively, an X-ray undulator of 10–100 periods ideally should yield a bandwidth behind a pinhole of $\delta\lambda/\lambda \simeq 0.1$–$0.01$. In these cases, wavelength normalization is more difficult because the actual spectrum over which a reflection is integrated is rapidly varying in intensity. The spot bandwidth is determined by the mosaic spread and horizontal beam divergence (since $\gamma_H > \gamma_V$) as

$$\left[\frac{\delta\lambda}{\lambda}\right] = (\eta + \gamma_H)\cot\theta, \tag{2.2.7.4}$$

where η = sample mosaic spread, assumed to be isotropic, γ_H = horizontal cross-fire angle, which in the absence of focusing is $(x_H + \sigma_H)/P$, where x_H is the horizontal sample size and σ_H the horizontal source size, and P is the sample to the tangent-point distance; and similarly for γ_V in the vertical direction. Generally, at SR sources, σ_H is greater than σ_V. When a focusing-mirror element is used, γ_H and/or γ_V are convergence angles determined by the focusing distances and the mirror aperture.

The size and shape of the diffraction spots vary across the film. The radial spot length is given by convolution of Gaussians as

$$(L_R^2 + L_c^2 \sec^2 2\theta)^{1/2} \tag{2.2.7.5}$$

and tangentially by

$$(L_T^2 + L_c^2)^{1/2}, \tag{2.2.7.6}$$

where L_c is the size of the X-ray beam (assumed circular) at the sample, and

$$L_R = D\sin(2\eta + \gamma_R)\sec^2 2\theta \tag{2.2.7.7}$$

$$L_T = D(2\eta + \gamma_T)\sin\theta\sec 2\theta, \tag{2.2.7.8}$$

and

$$\gamma_R = \gamma_V\cos\psi + \gamma_H\sin\psi \tag{2.2.7.9}$$

$$\gamma_T = \gamma_V\sin\psi + \gamma_H\cos\psi, \tag{2.2.7.10}$$

where ψ is the angle between the vertical direction and the radius vector to the spot (see Andrews, Hails, Harding & Cruickshank, 1987). For a crystal that is not too mosaic, the spot size is dominated by L_c. For a mosaic or radiation-damaged crystal, the main effect is a radial streaking arising from η, the sample mosaic spread.

(*b*) *Monochromatic SR beams: optical configurations and sample rocking width*

A wide variety of perfect-crystal monochromator configurations are possible and have been reviewed by various authors (Hart, 1971; Bonse, Materlik & Schröder, 1976; Hastings, 1977; Kohra, Ando, Matsushita & Hashizume, 1978). Since the reflectivity of perfect silicon and germanium is effectively 100%, multiple-reflection monochromators are feasible and permit the tailoring of the shape of the monochromator resolution function, harmonic rejection, and manipulation of the polarization state of the beam. Two basic designs are in common use. These are (*a*) the bent single-crystal monochromator of triangular shape (Lemonnier, Fourme, Rousseaux & Kahn, 1978) and (*b*) the double-crystal monochromator.

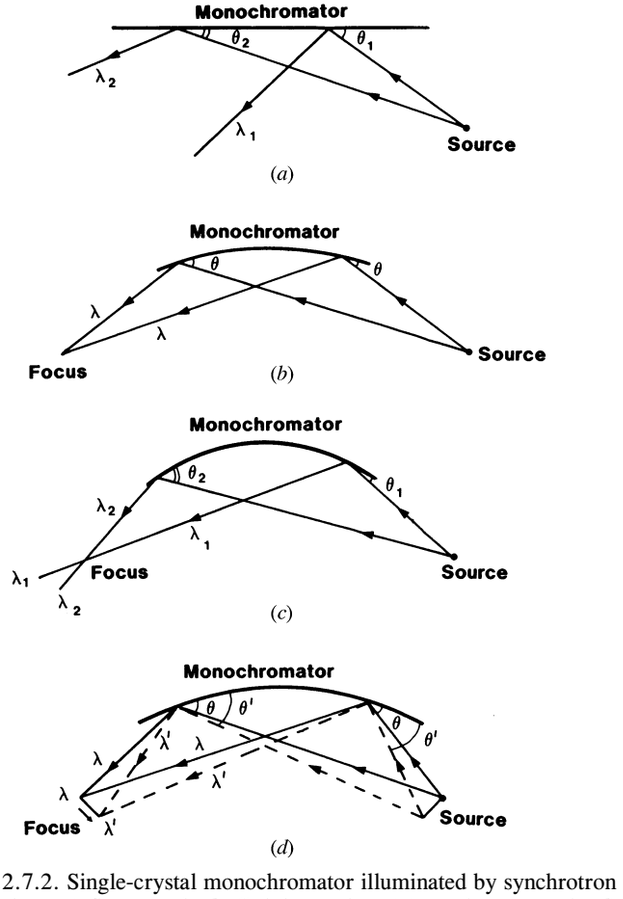

Fig. 2.2.7.2. Single-crystal monochromator illuminated by synchrotron radiation: (*a*) flat crystal, (*b*) Guinier setting, (*c*) overbent crystal, (*d*) effect of source size (shown at the Guinier setting for clarity). From Helliwell (1984).

In the case of the single-crystal monochromator, the actual curvature employed is very important in the diffraction geometry. For a point source and a flat monochromator crystal, there is a gradual change in the photon wavelength selected from the white beam as the length of the monochromator is traversed [Fig. 2.2.7.2(*a*)]. For a point source and a curved monochromator crystal, one specific curvature can compensate for this variation in incidence angle [Fig. 2.2.7.2(*b*)]. The reflected spectral bandwidth is then at a minimum; this setting is known as the 'Guinier position'. If the curvature of the monochromator crystal is increased further, a range of photon wavelengths, $(\delta\lambda/\lambda)_{\rm corr}$, is selected along its length so that the rays converging towards the focus have a correlation of photon wavelength and direction [Fig. 2.2.7.2(*c*)]. The effect of a finite source is to cause a change in incidence angle at the monochromator crystal, so that at the focus there is a photon-wavelength gradient across the width of the focus (for all curvatures) [Fig. 2.2.7.2(*d*)]. The use of a slit in the focal plane is akin to placing a slit at the tangent point to limit the source size.

The double-crystal monochromator with two parallel or nearly parallel perfect crystals of germanium or silicon is a common configuration. The advantage of this is that the outgoing monochromatic beam is parallel to the incoming beam, although it is slightly displaced vertically by an amount $2d\cos\theta$, where d is the perpendicular distance between the crystals and θ the monochromator Bragg angle. The monochromator can be rapidly tuned, since the diffractometer or camera need not be re-aligned significantly in a scan across an absorption edge. Between absorption edges, some vertical adjustment of the diffractometer is required. Since the rocking width of the fundamental is broader than the harmonic reflections, the strict parallelism of the pair of crystal planes can be relaxed, *i.e.* detuned so that the harmonic can be rejected with little loss of the fundamental intensity. The spectral spread in the reflected monochromatic beam is determined by the source divergence accepted by the monochromator, the angular size of the source, and the monochromator rocking width (see Fig. 2.2.7.3).

The double-crystal monochromator is often used with a toroid focusing mirror; the functions of monochromatization are then separated from the focusing (Hastings, Kincaid & Eisenberger, 1978).

The rocking width of a reflection depends on the horizontal and vertical beam divergences/convergences (after due account for collimation is taken) γ_H and γ_V, the spectral spreads $(\delta\lambda/\lambda)_{\rm conv}$ and $(\delta\lambda/\lambda)_{\rm corr}$, and the mosaic spread η. We assume that $\eta \gg \omega$, where ω is the angular broadening of a relp due to a finite sample. In the case of synchrotron radiation, γ_H and γ_V are usually widely asymmetric. On a conventional source, usually $\gamma_H \simeq \gamma_V$.

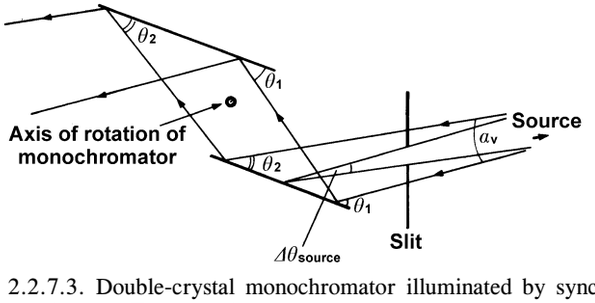

Fig. 2.2.7.3. Double-crystal monochromator illuminated by synchrotron radiation. The contributions of the source divergence α_V and angular source size $\Delta\theta_{\rm source}$ to the range of energies reflected by the monochromator are shown.

Two types of spectral spread occur with synchrotron and neutron sources. The term $(\delta\lambda/\lambda)_{\rm conv}$ is the spread that is passed down each incident ray in a divergent or convergent incident beam; the subscript refers to conventional source type. This is because it is similar to the $K\alpha_1$, $K\alpha_2$ line widths and separation. At the synchrotron, this component also exists and arises from the monochromator rocking width and finite-source-size effects. The term $(\delta\lambda/\lambda)_{\rm corr}$ is special to the synchrotron or neutron case. The subscript 'corr' refers to the fact that the ray direction can be correlated with the photon or neutron wavelength. Usually, an instrument is set to have $(\delta\lambda/\lambda)_{\rm corr} = 0$. In the most general case, for a $(\delta\lambda/\lambda)_{\rm corr}$ arising from the horizontal ray direction correlation with photon energy, and the case of a horizontal rotation axis, then the rocking width φ_R of an individual reflection is given by

$$\varphi_R = \left\{ L^2 \left[\left(\frac{\delta\lambda}{\lambda} \right)_{\rm corr} d^{*2} + \zeta\gamma_H \right]^2 + \gamma_V^2 \right\}^{1/2} + 2\varepsilon_s L, \quad (2.2.7.11)$$

where

$$\varepsilon_s = \frac{d^* \cos\theta}{2} \left[\eta + \left(\frac{\delta\lambda}{\lambda} \right)_{\rm conv} \tan\theta \right] \quad (2.2.7.12)$$

and L is the Lorentz factor $1/(\sin^2 2\theta - \zeta^2)^{1/2}$.

The Guinier setting of the instrument gives $(\delta\lambda/\lambda)_{\rm corr} = 0$. The equation for φ_R then reduces to

$$\varphi_R = L[(\zeta^2\gamma_H^2 + \gamma_V^2/L^2)^{1/2} + 2\varepsilon_s] \quad (2.2.7.13)$$

(from Greenhough & Helliwell, 1982). For example, for $\zeta = 0$, $\gamma_V = 0.2$ mrad (0.01°), $\theta = 15^\circ$, $(\delta\lambda/\lambda)_{\rm conv} = 1 \times 10^{-3}$ and $\eta = 0.8$ mrad (0.05°), then $\varphi_R = 0.08^\circ$. But φ_R increases as ζ increases [see Greenhough & Helliwell (1982, Table 5)].

In the rotation/oscillation method as applied to protein and virus crystals, a small angular range is used per exposure

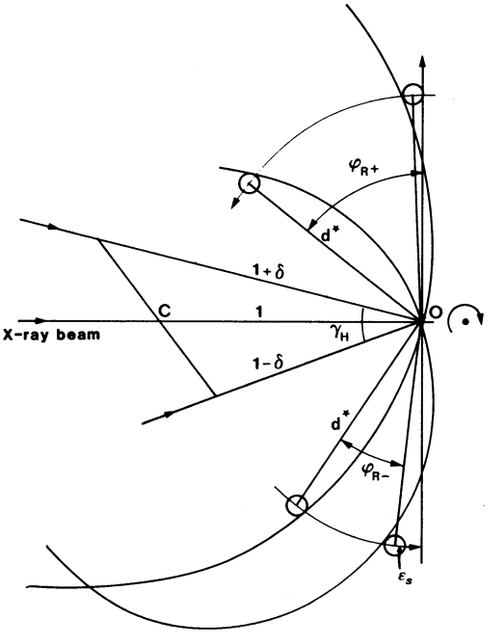

Fig. 2.2.7.4. The rocking width of an individual reflection for the case of Fig. 2.2.7.2(*c*) and a vertical rotation axis. φ_R is determined by the passage of a spherical volume of radius ε_s (determined by sample mosaicity and a conventional-source-type spectral spread) through a nest of Ewald spheres of radii set by $\delta = \frac{1}{2}[\delta\lambda/\lambda]_{\rm corr}$ and the horizontal convergence angle γ_H. From Greenhough & Helliwell (1982).

(Subsection 2.2.3.4). For example, $\Delta\varphi_{\max}$ may be 1.5° for a protein, and 0.4° or so for a virus. Many reflections will be only partially stimulated over the exposure. It is important, especially in the virus case, to predict the degree of penetration of the relp through the Ewald sphere. This is done by analysing the interaction of a spherical volume for a given relp with the Ewald sphere. The radius of this volume is given by

$$E \simeq \frac{\varphi_R}{2L} \qquad (2.2.7.14)$$

(Greenhough & Helliwell, 1982). For discussions, see Harrison, Winkler, Schutt & Durbin (1985) and Rossmann (1985).

In Fig. 2.2.7.4, the relevant parameters are shown. The diagram shows $(\delta\lambda/\lambda)_{\rm corr} = 2\delta$ in a plane, usually horizontal, with a perpendicular (vertical) rotation axis, whereas the formula for φ_R above is for a horizontal axis. This is purely for didactic reasons since the interrelationship of the components is then much clearer. For full details, see Greenhough & Helliwell (1982).

2.2.7.4. *Geometric effects and distortions associated with area detectors*

Electronic area detectors are real-time image-digitizing devices under computer control. The mechanism by which an X-ray photon is captured is different in the various devices available (*i.e.* gas chambers, television detectors, charge-coupled devices) and is different specifically from film or image plates. Arndt (1986 and Section 7.1.6) has reviewed the various devices available, their properties and performances. Section 7.1.8 deals with storage phosphors/image plates.

(*a*) *Obliquity*

In terms of the geometric reproduction of a diffraction-spot position, size, and shape, photographic film gives a virtually true image of the actual diffraction spot. This is because the emulsion is very thin and, even in the case of double-emulsion film, the thickness, g, is only ~ 0.2 mm. Hence, even for a diffracted ray inclined at $2\theta = 45°$ to the normal to the film plane, the 'parallax effect', $g\tan 2\theta$, is very small (see below for details of when this is serious). With film, the spot size is increased owing to oblique or non-normal incidence. The obliquity effect causes a beam, of width w, to be recorded as a spot of width

$$w' = w\sec 2\theta. \qquad (2.2.7.15)$$

For example, if $w = 0.5$ mm and $2\theta = 45°$, then w' is 0.7 mm. With an electronic area detector, obliquity effects are also present. In addition, the effects of parallax, point-spread factor, and spatial distortions have to be considered.

(*b*) *Parallax*

In the case of a one-atmosphere xenon-gas chamber of thickness $g = 10$ mm, the $g\tan 2\theta$ parallax effect is dramatic [see Hamlin (1985, p. 435)]. The wavelength of the beam has to be considered. If a λ of ~ 1 Å is used with such a chamber, the photons have a significant probability of fully traversing such a gap and parallax will be at its worst; the spot is elongated and the spot centre will be different from that predicted from the geometric centre of the diffracted beam. If a λ of 1.54 Å is used then the penetration depth is reduced and an effective g, *i.e.* $g_{\rm eff}$, of ~ 3 mm would be appropriate. The use of higher pressure in a chamber increases the photon-capture probability, thus reducing $g_{\rm eff}$ *pro rata*; at four atmospheres and $\lambda = 1.54$ Å, parallax is very small.

In general, we can take account of obliquity and parallax effects whereby the measured spot width, in the radial direction, is w'', where

$$w'' = w\sec 2\theta + g_{\rm eff}\tan 2\theta. \qquad (2.2.7.16)$$

As well as changing the spot size, the spot position, *i.e.* its centre, is also changed by both obliquity and parallax effects by $\frac{1}{2}(w'' - w)$. The spherical drift-chamber design eliminated the effects of parallax (Charpak, Demierre, Kahn, Santiard & Sauli, 1977). In the case of a phosphor-based television system, the X-rays are converted into visible light in a thin phosphor layer so that parallax is negligible.

(*c*) *Point-spread factor*

Even at normal incidence, there will be some spreading of the beam size. This is referred to as the point-spread factor, *i.e.* a single pencil ray of light results in a finite-sized spot. In the TV-detector and image-plate cases, the graininess of the phosphor and the system imaging the visible light contribute to the point-spread factor. In the case of a charge-coupled device (CCD) used in direct-detection mode, *i.e.* X-rays impinging directly on the silicon chip, the point-spread factor is negligible for a spot of typical size. For example, in Laue mode with a CCD used in this way, a 200 μm diameter spot normally incident on the device is not measurably broadened. The pixel size is ~ 25 μm. The size of such a device is small and it is used in this mode for looking at portions of a pattern.

(*d*) *Spatial distortions*

The spot position is affected by spatial distortions. These non-linear distortions of the predicted diffraction spot positions have to be calibrated for independently; in the worst situations, misindexing would occur if no account were taken of these effects. Calibration involves placing a geometric plate, containing a perfect array of holes, over the detector. The plate is illuminated, for example, with radiation from a radioactive source or scattered from an amorphous material at the sample position. The measured positions of each of the resulting 'spots' in detector space (units of pixels) can be related directly to the expected position (in mm). A 2D, non-linear, pixel-to-mm and mm-to-pixel correction curve or look-up table is thus established.

These are the special *geometric* effects associated with the use of electronic area detectors compared with photographic film or the image plate. We have not discussed non-uniformity of response of detectors since this does not affect the geometry. Calibration for non-uniformity of response is discussed in Section 7.1.6.

Acknowledgements

I am very grateful to various colleagues at the Universities of York and Manchester for their comments on the text of the first edition. However, special thanks go to Dr T. Higashi who commented extensively on the manuscript and found several errors. Any remaining errors are, of course, my own responsibility. Dr. F. C. Korber is thanked for his comments on the diffractometry section. Dr W. Parrish and Mrs E. J. Dodson are also thanked for discussions. Mrs Y. C. Cook is thanked for typing several versions of the manuscript and Mr A. B. Gebbie is thanked for drawing the diagrams. I am grateful to Miss Julie Holt for secretarial help in the production of the second edition.

International Tables for Crystallography (2006). Vol. C, Chapter 2.3, pp. 42–79.

2.3. Powder and related techniques: X-ray techniques

BY W. PARRISH AND J. I. LANGFORD

The X-ray diffraction powder method was developed independently by Debye & Scherrer (1916) and by Hull (1917, 1919) and hence is often named the Debye–Scherrer–Hull method. Their classic papers provide the basis for the powder diffraction method.

Debye and Scherrer made a 57 mm diameter cylindrical camera, used two films with each forming a half circle in contact with the camera wall, a light-tight cover, a primary-beam collimator, and a long black paper exit tube attached to the outside of the camera to avoid back scattering. (There were no radiation protection surveys in those days!) The powder specimen was 2 mm in diameter, 10 mm long and the exposure two hours. They worked out a method for determining the crystal structure from the powder diagrams, solved the structure of LiF using X-rays from Cu and Pt targets and found that a powder labelled 'amorphous silicon' was crystalline with the diamond structure.

Hull described many of the experimental factors. He apparently was the first to use a $K\beta$ filter and an intensifying screen; he enclosed the X-ray tube in a lead box, used both flat and cylindrical films, and measured the effect of X-ray tube voltage on the intensity of Mo $K\alpha$ radiation. He described the importance of using small particle sizes, specimen rotation, and the necessity for random orientation. He also worked out the methods for determining the crystal structure from the powder pattern and solved the structures of eight elements and diamond and graphite. Debye & Scherrer did not explicitly mention the use of the method for identification in their 1916 paper but Hull recognized its importance as shown by the title of his 1919 paper, *A new method of chemical analysis*, in which he wrote

> '... every crystalline substance gives a pattern; that the same substance always gives the same pattern; and that in a mixture of substances each produces its pattern independently of the others, so that the photograph obtained with a mixture is the superimposed sum of the photographs that would be obtained by exposing each of the components separately for the same length of time. This law applies quantitatively to the intensities of the lines, as well as to their positions, so that the method is capable of development as a quantitative analysis.'

In the late 1930's, compilations of X-ray powder data for minerals were published but the most important advance in the practical use of the powder method was made by Hanawalt & Rinn (1936) and Hanawalt, Rinn & Frevel (1938). Their detailed paper, entitled *Chemical analysis by X-ray diffraction*, contained tabulated d's and relative intensities of 1000 chemical substances. The editor wrote in the prologue

> 'Industrial and Engineering Chemistry considers itself fortunate in being able to present herewith a complete, new, workable system of analysis, for it is not often that this is possible in a single issue of any journal.'

They devised a scheme for pattern classification based on the d's of the three most intense lines in which the patterns were arranged in 77 groups, each of which contained 77 subgroups. The strongest line determined the group, the second strongest the subgroup, and the third the position within the subgroup. They used Mo $K\alpha$ radiation, 8 in radius quadrant cassettes and a direct comparison film intensity scale. These data formed the basis of the early ASTM (later JCPDS and now ICDD) powder diffraction file and made it possible to develop systematic methods of analysis.

A major advance in the powder method began in the early 1950's with the introduction of commercial high-resolution diffractometers which greatly expanded the use of the method (Parrish, 1949; Parrish, Hamacher & Lowitzsch, 1954). The replacement of film by the Geiger counter, and soon after by scintillation and proportional counters, made it possible to observe X-ray diffraction in real time and to make precision measurements of the intensities and profile shapes. The large space around the specimen permitted the design of various devices to vary the specimen temperature and apply stress as well as other experiments not possible in a powder camera. The much higher resolution, angular accuracy, and profile determination led to many advances in the interpretation and applications of the method. Powder diffraction began to be used in a large number of technical disciplines and thousands of papers have been published on material structure characterization in inorganic chemistry, mineralogy, metals and alloys, ceramics, polymers, and organic materials. The following is a partial list of the types of studies that are best performed by the powder method and are widely used:

- –identification of crystalline phases
- –qualitative and quantitative analysis of mixtures and minor constituents
- –distinction between crystalline and amorphous states and devitrification
- –following solid-state reactions
- –identification of solid solutions
- –isomorphism, polymorphism, and phase-diagram determination
- –lattice-parameter measurement and thermal expansion
- –preferred orientation
- –microstructure (crystallite size, strain, stacking faults, *etc*.) from profile broadening
- –*in situ* high-/low-temperature and high-pressure studies.

The introduction of computers for automation and data reduction and the use of synchrotron radiation are greatly expanding the information that can be obtained from the method. The determination and refinement of crystal structures from powder data are widely used for materials not available as single crystals.

The most comprehensive book on the powder method is that of Klug & Alexander (1974), which contains an extensive bibliography. Peiser, Rooksby & Wilson (1955) edited a book written by specialists on various powder methods (mainly cameras), interpretations, and results in various fields. Azároff & Buerger (1958) wrote a comprehensive description of the powder-camera method. Barrett & Massalski (1980), Taylor (1961), and Cullity (1978) wrote comprehensive texts on metallurgical applications. Warren (1969), Guinier (1956, 1963), and Schwartz & Cohen (1987) described the theory and application of powder methods to physical problems such as the use of Fourier methods to study deformed metals and alloys to separate crystallite size and microstrain profile broadening, stacking faults, order–disorder, amorphous structures, and temperature effects. A general description of the powder method is given by Lipson & Steeple (1970). A book on the powder method written by a number of authors (Bish & Post, 1989) contains detailed papers and long lists of references and describes recent developments including principles of powder

Copyright © 2006 International Union of Crystallography

diffraction (Reynolds, 1989), instrumentation, specimen preparation, profile fitting, synchrotron and neutron methods. A recent book by Jenkins & Snyder (1996) gives a useful comprehensive account of basic methods and practices in powder diffractometry.

Papers presented at international symposia on powder diffraction describe advances in the field (Block & Hubbard, 1980; *Australian Journal of Physics*, 1988; Bojarski & Bołd, 1979; Bish & Post, 1989; Prince & Stalick, 1992). Papers on the theory and new methods and applications are published in the *Journal of Applied Crystallography*. *Powder Diffraction* started in 1986 and contains powder data and papers on instrumentation and methods. Papers presented at the Annual Denver Conference on Applications of X-ray Analysis have been published yearly since 1957 as separate volumes entitled *Advances in X-Ray Analysis*, by Plenum Press. Volume 37 of the series was published in 1994. These volumes contain papers that are roughly equally divided between X-ray powder diffraction and fluorescence analysis. This extensive source describes many types of instrumentation, methods and applications. The *Norelco Reporter* has been published several times a year since 1954 and contains original articles and reprints of papers on powder diffraction, fluorescence analysis, and electron microscopy. There are other 'house journals' published by Rigaku, Siemens, and other X-ray companies. A history of the powder method in the USA was written by Parrish (1983).

The following description includes only the most frequently used methods. The divergent beam from X-ray tubes is best used with focusing geometries, and synchrotron radiation with parallel-beam optics.

2.3.1. Focusing diffractometer geometries

The critical elements in the basic geometries of the principal focusing diffractometers used with X-ray tubes are illustrated schematically in Fig. 2.3.1.1. The six arrangements are described below in paragraphs (*a*) to (*f*) corresponding to the subdivisions of Fig. 2.3.1.1. The most frequently used methods are illustrated in (*a*) and (*b*). The abbreviations used are *S*(*R*) for the specimen set for reflection, *S*(*T*) for a transmission specimen, and *M* refers to a focusing reflection monochromator. The letters are arranged in order of the beam direction. The detector rotates around the diffractometer axis at twice the speed of the specimen in the θ–2θ scanning used in (*a*) to (*e*). In the Seemann–Bohlin geometry (*S*-*B*), the specimen is stationary and the detector rotates around the focusing circle in scanning the pattern (*f*). The line focus of the X-ray tube is used in all cases.

The monochromator is either symmetrical, with the lattice planes parallel to the crystal surface, or asymmetric with the lattice planes inclined at a small angle to the surface to shorten one of the focal-length distances. Placing the monochromator in the diffracted beam has the important advantage of eliminating specimen fluorescence. It also simplifies shielding the detector if the specimen is radioactive. The monochromator in the incident beam reduces fluorescence and radiation damage to the specimen by removing the continuous X-ray spectrum. When the diffracted beam is defined by the receiving slit as in (*b*) and (*c*), highly oriented pyrolytic graphite (placed in front of the detector) is generally used to obtain high intensity. In the (*d*) and (*e*) geometries, a high-quality bent crystal such as silicon or quartz is necessary to achieve good focusing.

(*a*) *S*(*R*): The aperture of the incident divergent beam from the line focus of the X-ray tube *F* is limited by the entrance slit ES and the reflection from the specimen converges ('focuses') on the receiving slit RS. The intensity is determined by the ES and RS and the profile width is determined mainly by the RS width. The parallel slits PS in the incident and diffracted beams limit the axial divergence.

(*b*) *S*(*R*)/*M*: Same as (*a*) with the addition of the symmetrical monochromator (usually graphite) to record only the characteristic radiation. ES and RS have the same rôle as in (*a*), and only the incident PS are required.

(*c*) *M*/*S*(*R*): Using an incident-beam monochromator, the slit at *F*′ determines the effective source size and divergence of the beam striking the specimen, and *RS* limits the profile width.

(*d*) *S*(*T*)/*M*: The divergent incident beam continues to diverge after diffraction from the transmission specimen and the asymmetric monochromator focuses the beam on the detector.

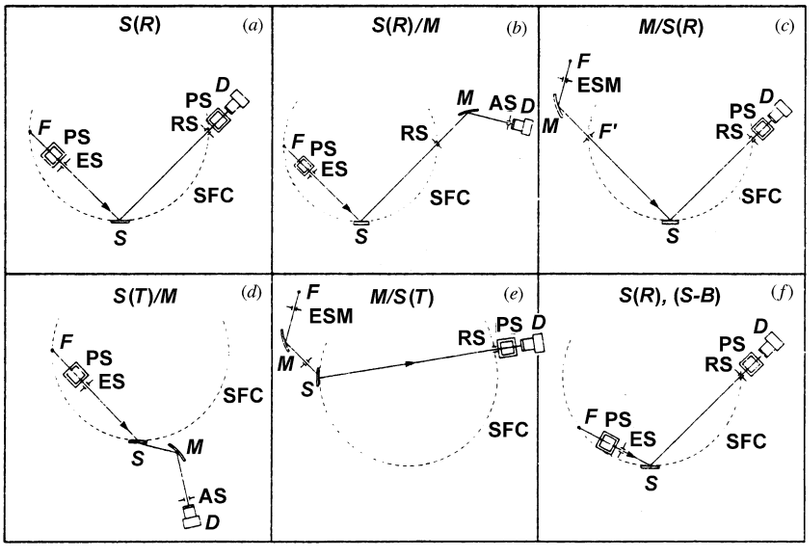

Fig. 2.3.1.1. Basic arrangements of focusing diffractometer methods. Simplified and not to scale; detailed drawings shown in later figures. (*a*)–(*e*) operate with θ–2θ scanning; (*f*) fixed specimen with detector scanning. *F* line focus of X-ray tube (normal to plane of drawings), *F*′ focus of incident-beam monochromator, PS parallel slits (to limit axial divergence), ES entrance (divergence) slit, ESM entrance slit for monochromator, *S* specimen, RS receiving slit, AS antiscatter slit, *D* detector, SFC specimen focusing circle, *M* focusing monochromator. Other symbols described in text.

M and *D* rotate around *S* in θ–2θ scanning and the profile width is determined by the monochromator. Only the forward-reflection region can be recorded.

(*e*) *M*/S(*T*): This is the diffractometer equivalent of the Guinier camera. A symmetric or asymmetric monochromator is used in the incident beam and the profile width is determined by the *RS*. The incident-beam divergence is limited by ESM.

(*f*) *S*(*R*),(*S*–*B*): The reflections are focused on a fixed-radius circle which measures 4θ. A linkage moves the detector around the focusing circle and always points it to the fixed specimen. The angular range is limited (normally 30–240°4θ) and can be changed by moving the specimen and diffractometer to different positions. The profile width is determined by ES and RS. The same geometry is used with an incident- or diffracted-beam focusing monochromator.

The interaction of the X-ray beam with the specimen varies in different geometries and this may have important consequences on the results, as will be described later. When a reflection specimen is used in θ–2θ or θ–θ scanning, only those crystallites whose lattice planes are oriented nearly parallel to the specimen surface can reflect (Fig. 2.3.1.2) (Parrish, 1974). A transmission specimen in θ–2θ scanning permits reflections only from planes nearly normal to the surface. In the *S*–*B* case, reflections can occur from planes inclined over a range of about 45° to the surface. Transmission specimens must, of course, be mounted on X-ray-transparent substrates. Jenkins (1989) has reviewed the instrumentation and experimental procedures.

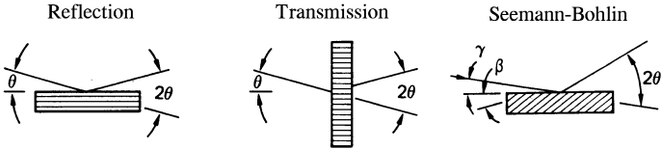

Fig. 2.3.1.2. Specimen orientation for three diffractometer geometries. With θ–2θ scanning, diffraction is possible only from planes nearly parallel to the reflection specimen surface (left), and from planes nearly normal to the transmission specimen surface (middle), and from planes inclined different amounts to the specimen surface in Seemann–Bohlin geometry (right).

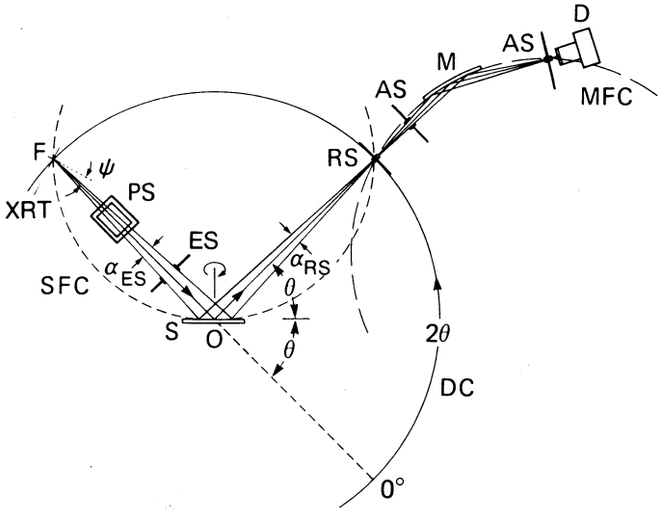

Fig. 2.3.1.3. X-ray optics in the focusing plane of a 'conventional' diffractometer with reflection specimen, diffracted-beam monochromator, and θ–2θ scanning: ψ take-off angle, DC diffractometer circle, MFC monochromator focusing circle, α_{ES} and α_{RS} entrance- and receiving-slit apertures, θ Bragg angle, 2θ reflection angle, *O* diffractometer and specimen rotation axis; other symbols listed in Fig. 2.3.1.1.

2.3.1.1. *Conventional reflection specimen, θ–2θ scan*

The reflection specimen with θ–2θ scanning in the focusing arrangement shown in Fig. 2.3.1.3 is the most widely used powder diffraction method. It is estimated that about 10 000 to 15 000 of these diffractometers have been sold since they were introduced in 1948, which makes it the most widely used X-ray crystallographic instrument. Some authors have called it the Bragg–Brentano parafocusing method (Bragg, 1921; Brentano, 1946), but the X-ray optics (described below) are significantly different from the methods and instruments described by these authors.

The X-ray tube spot focus was first used as the source and gave broad reflections. A narrow entrance slit improved the resolution but caused a large loss of intensity. Early diffractometers were described by LeGalley (1935), Lindemann & Trost (1940), and Bleeksma, Kloos & DiGiovanni (1948); see Parrish (1983). The use of the line focus with parallel slits to limit axial divergence was developed in the late 1940's and gave much higher resolution. A collection of papers by Parrish and co-workers (Parrish, 1965) and Klug & Alexander (1974) describe details of the instrumentation and method.

2.3.1.1.1. *Geometrical instrument parameters*

The powder diffractometer is basically a single-axis goniometer with a large-diameter precision gear and worm drive. The detector and receiving-slit assembly are mounted on an arm attached to the gear in a radial position. The specimen is mounted in a holder carried by a shaft precisely positioned at the centre of the gear. 2/1 reduction gears drive the specimen post at one-half the speed of the detector. Some diffractometers have two large gears, making it possible to drive only the detector with the specimen fixed or *vice versa*, or to use 2/1 scanning. Synchronous motors have been used for continuous scanning for ratemeter recording and stepping motors for step-scanning with computer control.

The geometry of the method requires that the axis of rotation of the diffractometer be parallel to the X-ray tube focal line to obtain maximum intensity and resolution. The target is normal to the long axis of the tube; vertically mounted tubes require a diffractometer that scans in the vertical plane while a horizontal tube requires a horizontal diffractometer. The X-ray optics are the same for both. The incident angle θ and the reflection angle 2θ are defined with respect to the central ray that passes through the diffractometer axis of rotation *O*.

The axis of rotation of the specimen is the central axis of the main gear of the diffractometer, as shown in Fig. 2.3.1.3. The centre of the specimen is equidistant from the source *F* and receiving slit RS. The instrument radius $R_{DC} = F - O = O -$ RS. The radius of commercial instruments is in the range 150 to 250 mm, with 185 mm most common. Changing the radius affects the instrument parameters and a number of the aberrations. Larger radii have been used to obtain higher resolution and better profile shapes. For example, the asymmetric broadening caused by axial divergence is decreased because the chord of the diffraction cone intercepted by the receiving slit has less curvature. However, if the same entrance slit is used, moving the specimen further from the source proportionately increases the length of specimen irradiated and decreases the intensity.

The imaginary specimen focusing circle SFC passes through *F*, *O* and the middle of RS and its radius varies with θ:

$$R_{SFC} = R_{DC}/2\sin\theta. \quad (2.3.1.1)$$

The specimen holder is set parallel to the central ray at 0° and the gears drive the RS-detector arm at twice the speed of the specimen to maintain the θ–2θ relation at all angles. The source F is the line focus of the X-ray tube viewed at a take-off angle ψ. The actual width, F'_w, is foreshortened to

$$F_w = F'_w \sin\psi. \quad (2.3.1.2)$$

In a typical case, $F'_w = 0.4$ mm and, at $\psi = 5°$, $F_w = 0.03$ mm and the projected angular width is 0.025° for $R = 185$ mm. The angular aperture α_{ES} of the incident beam in the equatorial (focusing) plane is determined by the entrance slit width ES_w (also called the 'divergence slit' since it limits the divergence of the beam) and its distance D_1 from F:

$$ES_\alpha = 2\arctan[(ES_w + F_w)/2D_1]. \quad (2.3.1.3)$$

Because the beam is divergent, the length of specimen irradiated S_l in the direction of the incident beam normal to O varies with θ:

$$S_l = [\alpha(R - D')]/\sin\theta, \quad (2.3.1.4)$$

where α is in radians and D' is the distance from F to the crossover point before ES and is given by $F_w D_1/(F_w + ES)$. The approximate relation

$$S_l = \alpha R/\sin\theta \quad (2.3.1.5)$$

is close enough for practical purposes (Parrish, Mack & Taylor, 1966). The intensity is nearly proportional to ES_α but the maximum aperture that can be used is determined by S_l and the smallest angle to be scanned $2\theta_{min}$, as shown in Fig. 2.3.1.4. The entrance-slit width may be increased to obtain higher intensity at the upper angular range; for example, ES = 1° for the forward-reflection region and 4° for back-reflection.

Some slit designs are shown in Fig. 2.3.1.5. The base is machined with a pair of rectangular shoulders whose separation A is the sum of the diameters of the two rods (*a*) or bar widths (*b*) and the central spacers on both ends that determine the slit opening. The distance P between the centre of the slit opening and the edge of the slit frame is kept constant for all slits to avoid angular errors when changing slits. The rods may be molybdenum or other highly absorbing metal and are cemented in place. It may also be made in one piece (*c*) using machinable tungsten (Parrish & Vajda, 1966).

A variable ES whose width increases with 2θ so that the irradiated length is about the same at all angles has been described by Jenkins & Paolini (1974). It is called a θ-compensating slit in which a pair of semicircular cylinders with a fixed opening is rotated around the axis of the opening by a linkage attached to the specimen shaft of the diffractometer to vary the aperture continously with θ. The observed intensities must be corrected to obtain the relative intensities and the angular dependence of the aberrations is different from the fixed aperture slit.

Another way to irradiate constantly the entire specimen length is to use a self-centring slit which acts as an entrance and antiscatter slit (de Wolff, 1957). A 1 mm thick brass plate with rounded edge is mounted above the centre of the specimen and is moved in a plane normal to the specimen surface so that the aperture is proportional to sin θ. It can only be used for forward reflections.

Owing to the beam divergence, the geometric centre of the irradiated specimen length shifts a small amount during the scan (see also §2.3.5.1.5). It is generally advisable to centre the beam at the smallest 2θ to be scanned. Below about 20°, the irradiated length increases rapidly and it is essential to use small apertures and to align the entrance and antiscatter slits carefully. Failure to do this correctly could cause (*a*) errors in the relative intensities owing to the primary beam exceeding the specimen area, (*b*) cutoff by the walls of the specimen holder for low-absorbing thick specimens, and (*c*) increased background from scattering by the specimen holder or the primary beam entering the detector. The transmission specimen method (Subsection 2.3.1.2) has advantages in measuring large d's.

The beam converges after reflection on the receiving slit RS, whose width defines the reflection and profile width. Only those rays that are within the θ–2θ setting are in sharp convergence, *i.e.* 'in focus'. The reflections become broader with increasing distance from the RS, and, therefore, this method is not suited for position-sensitive detectors. The RS aperture

$$\alpha_{RS} = 2\arctan(RS_w/2R) \quad (2.3.1.6)$$

is the dominant factor in determining the intensity and resolution. For $RS_w = 0.1$ mm and $R = 185$ mm, $\alpha_{RS} = 0.031°$.

Antiscatter slits AS are slightly wider than the beam and are essential in this and other geometries to make certain the detector

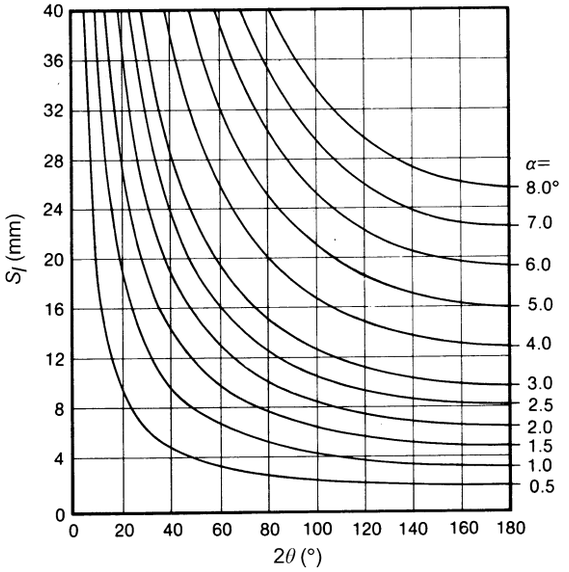

Fig. 2.3.1.4. Length of specimen irradiated, S_l, as a function of 2θ for various angular apertures. $S_l = \alpha R/\sin\theta$, $R = 185$ mm.

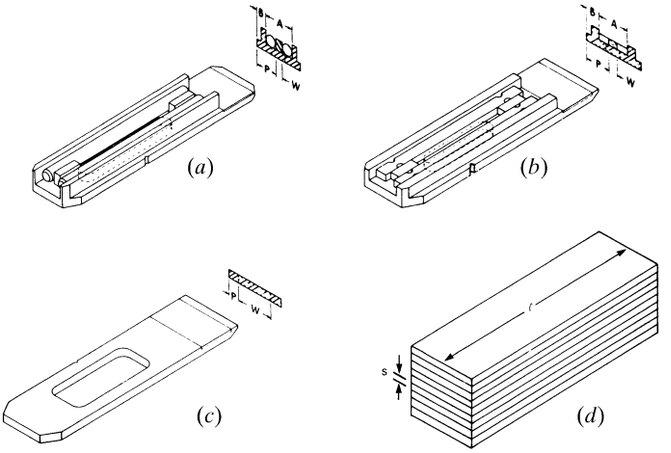

Fig. 2.3.1.5. Slit designs made with (*a*) rods, (*b*) bars, and (*c*) machined from single piece. (*d*) Parallel (Soller) slits made with spacers or slots cut into the two side pieces (not shown) to position the foils.

can receive X-rays only from the specimen area. They must be carefully aligned to avoid touching the beam.

The use of the long X-ray source makes it necessary to reduce the axial divergence, which would cause very large asymmetry. This is done with two sets of thin (25 to 50 μm) parallel metallic foils PS ('Soller slits'; Soller, 1924) placed before and after the specimen. If a monochromator is used, the set on the side of the monochromator is not essential because the crystal reduces the divergence. The angular aperture of a set of slits is

$$\delta = 2\arctan(\text{spacing/length}). \qquad (2.3.1.7)$$

The overall width of the set and δ determine the width of the specimen irradiated in the axial direction, which remains constant at all 2θ's. The construction is illustrated in Fig. 2.3.1.5(*d*). The aperture δ is usually 2 to 5°. Each set of parallel slits reduces the intensity; for example, with 12.5 mm long foils with 1 mm spacings, the intensity is about one-half of that without the parallel slits. The aperture can be selected with any combination of spacings and lengths but the greater the length, the fewer foils are needed, and the less is the intensity loss due to thickness of the metal foils (usually 0.025 mm). These slits can be made as interchangeable units of different apertures.

2.3.1.1.2. *Use of monochromators*

Many diffractometers are equipped with a curved highly-oriented pyrolytic graphite monochromator placed after the receiving slit as shown in Fig. 2.3.1.3. Although graphite has a large mosaic spread (~ 0.35 to 0.6°), the diffracted beam from the specimen is defined by the receiving slit, which determines the profile shape and width rather than the monochromator. The same results are obtained whether the monochromator is set in the parallel or antiparallel position with respect to the specimen. The most important advantage of graphite is its high reflectivity, which is about 25–50% for Cu $K\alpha$. This is much higher than LiF, Si or quartz monochromators that have been used for powder diffraction. The $K\beta$ filter and the parallel slits in the diffracted beam can be eliminated and, since each reduces the $K\alpha$ intensity by about a factor of two, the use of a graphite monochromator actually increases the available intensity. The diffracted-beam monochromator eliminates specimen fluorescence and the scattered background whose wavelengths are different from that of the monochromator setting. For example, a Cu tube can be used for specimens containing Co, Fe, or other elements with absorption edges at longer wavelengths than Cu $K\alpha$ to produce patterns with low background. Several monochromator geometries are described by Lang (1956).

A specimen in the reflection mode may be used with an incident-beam monochromator and θ–2θ scanning as shown in Fig. 2.3.1.1(*c*). One of the principal advantages is that it is possible to adjust the monochromator and slits to remove the $K\alpha_2$ component and produce patterns with only $K\alpha_1$ peaks. The profile symmetry, resolution and instrument function are thus greatly improved; see, for example, Warren (1969), Wölfel (1981), Göbel (1982) and Louër & Langford (1988). The high-quality crystal required causes a large loss of intensity and reduces specimen fluorescence but does not eliminate it. However, Soller slits in the incident beam and a β filter are no longer required and the net loss of intensity can be as low as 20%. Such monochromators can now be provided as standard by diffractometer manufacturers and their use is increasing, but they are not as widely used as the diffracted-beam monochromator.

2.3.1.1.3. *Alignment and angular calibration*

It is essential to align and calibrate the diffractometer properly. Failure to do so degrades the performance of the instrument, leading to a loss of intensity and resolution, increased background, incorrect profile shapes, and errors that cannot be readily diagnosed. Procedures and devices for this purpose are often provided by the manufacturer. The principles and mechanical devices to aid in making a proper alignment have been described by Parrish & Lowitzsch (1959) and the general procedure by Klug & Alexander (1974, p. 280).

The alignment requires setting the diffractometer axis of rotation to the selected X-ray tube take-off angle at a distance equal to the radius of the diffractometer. The long axes of the X-ray tube focal line, entrance, receiving, and antiscatter slits must be centred, be parallel to the axis of rotation, and lie in the same plane when the instrument is at 0°. The slits are made parallel to the axis of rotation in the manufacture of the diffractometer, and these steps require positioning of the instrument with respect to the line focus. The parallel-slit foils must also be normal to the rotation axis. A *flat* fluorescent screen made as a specimen to fit into the diffractometer specimen post is used to centre the primary beam by small movements of the ES and/or diffractometer. The diffracted beam can be centred on the curved monochromator with a narrow slit placed at the centre of the monochromator position (with the monochromator removed). The detector arm is then moved to the highest intensity. The procedure is repeated with the receiving slit in position. This is very close to the 0° position described below.

The angular calibration of the diffractometer is usually made by accurately measuring the 0° position to establish a fiducial point. It assumes that the gear system is accurate and that the receiving-slit arm moves exactly to the angle indicated on the scale at all 2θ positions. The determination of the angular precision of the gear train requires special equipment and methods; see, for example, Jenkins & Schreiner (1986). It is

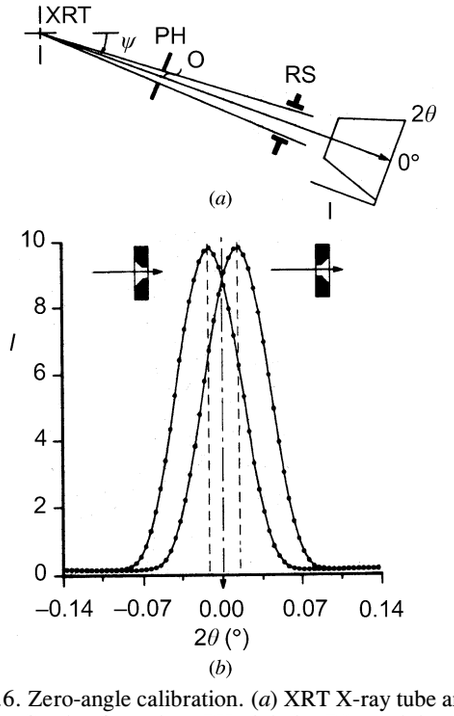

Fig. 2.3.1.6. Zero-angle calibration. (*a*) XRT X-ray tube anode, ψ take-off angle, *O* axis of rotation, PH pinhole, RS receiving slit. Intensity distribution at right. (*b*) 0° position is median of two curves recorded with 180° rotation of PH.

essential that the setting of the worm against the gear wheel be adjusted for smooth operation. In practice, this is a compromise between minimum backlash and jerky movement. The backlash can be avoided by scanning in the same direction and running the diffractometer beyond the starting angle before beginning the data collection. Incremental angle encoders have been used when very high precision is required.

The 0° position of the diffractometer scale, $2\theta_0$, can be determined with a pinhole placed in the specimen post as shown in Fig. 2.3.1.6(*a*) (Parrish & Lowitzsch, 1959). The receiving slit is step scanned in 0.01° or smaller increments and the midpoints of chords at various heights are used to determine the angle. To avoid mis-centring errors of the pin-hole, two measurements are made with the specimen post rotated 180° between measurements. The median angle of the two plots is the 0° position as shown in Fig. 2.3.1.6(*b*) and the diffractometer scale is then reset to this position. The shape of the curves is determined by the relative sizes of the pinhole and the receiving-slit width. With care, the position can be located to about 0.001°. The $2\theta_0$ position can be corrected by using it as a variable in the least-squares refinement of the lattice parameter of a standard specimen.

Another method measures the peak angles of a number of reflections on both sides of 0°, which is equivalent to measuring 4θ. This method may be mechanically impossible with some diffractometers.

The θ–2θ setting of the specimen post is made with the diffractometer locked in the predetermined 0° position and manually (or with a stepping motor) rotating the post to the maximum intensity. A flat plate can be used as illustrated in Fig. 2.3.1.7(*a*). The setting can be made to a small fraction of a degree. Fig. 2.3.1.7(*b*) shows the effect of incorrect θ–2θ setting, which combines with the flat-specimen aberration to cause a marked broadening and decrease of peak height but no apparent shift in peak position (Parrish, 1958). The effect increases with decreasing θ and could cause systematic errors in the peak intensities as well as incorrect profile broadening.

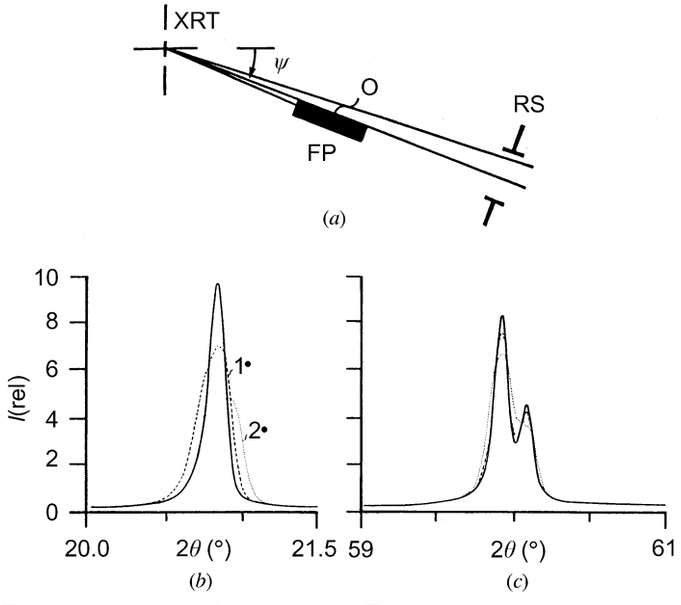

Fig. 2.3.1.7. (*a*) θ–2θ setting at 0°. Flat plate or long narrow slit is rotated to position of highest intensity. (*b*) and (*c*) Profiles obtained with correct θ–2θ setting (solid profile) and 1 and 2° mis-settings (dashed profiles) at (*b*) 21° and (*c*) 60° (2θ).

2.3.1.1.4. *Instrument broadening and aberrations*

The asymmetric form, broadening and angular shifts of the recorded profiles arise from the $K\alpha$ doublet and geometrical aberrations inherent in the imperfect focusing of the particular diffractometer method used. There are additional causes of distortions such as the time constant and scanning speed in rate-meter strip-chart recording, small crystallite size, strain, disorder stacking and similar properties of the specimen, and very small effects due to refractive index and related physical aberrations.

Perfect focusing in the sense of reflection from a mirror is never realized in powder diffractometry. The focusing is approximate (sometimes called 'parafocusing') and the practical selection of the instrument geometry and slit sizes is a compromise between intensity, resolution, and profile shape. Increasing the resolution causes a loss of intensity. When setting up a diffractometer, the effects of the various instrument and specimen factors should be taken into account as well as the required precision of the results so that they can be matched. There is no advantage in using high resolution, which increases the recording time (because of the lower intensity and smaller step increments), if the analysis does not require it. A set of runs to determine the best experimental conditions using the following descriptions as a guide should be helpful in obtaining the most useful results.

In the symmetrical geometries where the incident and reflected beams make the same angle with the specimen surface, the effect of absorption on the intensity is independent of the θ angle. This is an important advantage since the relative intensities can be compared directly without corrections. The actual intensities depend on the type of specimen. For a solid block of the material, or a compacted powder specimen, the intensity is proportional to μ^{-1}, where μ is the linear absorption coefficient of the material. The transparency aberration [equation (2.3.1.13)], however, depends on the effective absorption coefficient of the composite specimen.

The need to correct the experimental data for the various aberrations depends on the nature of the required analysis. For example, simple phase identifications can often be made using data in which the uncertainty of the lattice spacing $\Delta d/d$ is of the order of 1/1000, corresponding to about 0.025 to 0.05° precision in the useful identification range. This is readily attainable in routine practice if care is taken to minimize specimen displacement and the zero-angle calibration is properly carried out. The experimental data can then be used directly for peak search (Subsection 2.3.3.7) to determine the peak angles and intensities (Subsection 2.3.3.5) and the data entered in the search/match program for phase identification.

However, in many of the more advanced aspects of powder diffraction, as in crystal-structure determination and the characterization of materials for solid-state studies, much more detailed and more precise data are required, and this involves attention to the profile shapes. The following sections describe the origin of the instrumental factors that contribute to the shapes and shift the peaks from their correct positions. Many of these factors can be handled individually. With the use of computer programs, they can be determined collectively by using a standard sample without profile broadening and profile-fitting methods to determine the shapes (Subsection 2.3.3.6). The resulting instrument function can then be stored and used to determine the contribution of the specimen to the observed profiles.

A series of papers describing the geometrical and physical aberrations occurring in powder diffractometry has been

published by Wilson (1963, 1974). His work provides the mathematical foundation for understanding the origin and treatment of the various sources of errors. The major aberrations are described in the following and are illustrated with experimental profiles and plots of computed data for better visualization and interpretation of the effects. The information can be used to correct the experimental data, interpret the profile broadening and shifts, and evaluate the precision of the analysis. Chapter 5.2 contains tables listing the centroid displacements and variances of the various aberrations.

The magnitudes of the aberrations and their effects are illustrated in Figs. 2.3.1.8(*a*) and (*b*), which show the Cu $K\alpha_1, K\alpha_2$ spectrum inside the experimental profile. At high 2θ's, the shape of the experimental profile is largely determined by the spectral distribution, but at low 2θ's the aberrations are the principal contributors. The basic experimental high-resolution profile shapes from specimens without appreciable broadening effects (NIST silicon powder standard) are shown in Figs. 2.3.1.8(*c*)–(*f*). The solid-line profiles were obtained with a reflection specimen (Fig. 2.3.1.3), and the dashed-line profiles with transmission-specimen geometry (Fig. 2.3.1.12). The differences in the $K\alpha_1, K\alpha_2$ doublet separations are explained in Subsection 2.3.1.2. These profiles are the basic instrument functions which show the profile shapes contained in all reflections recorded with these methods. The shapes are modified by changing slit sizes.

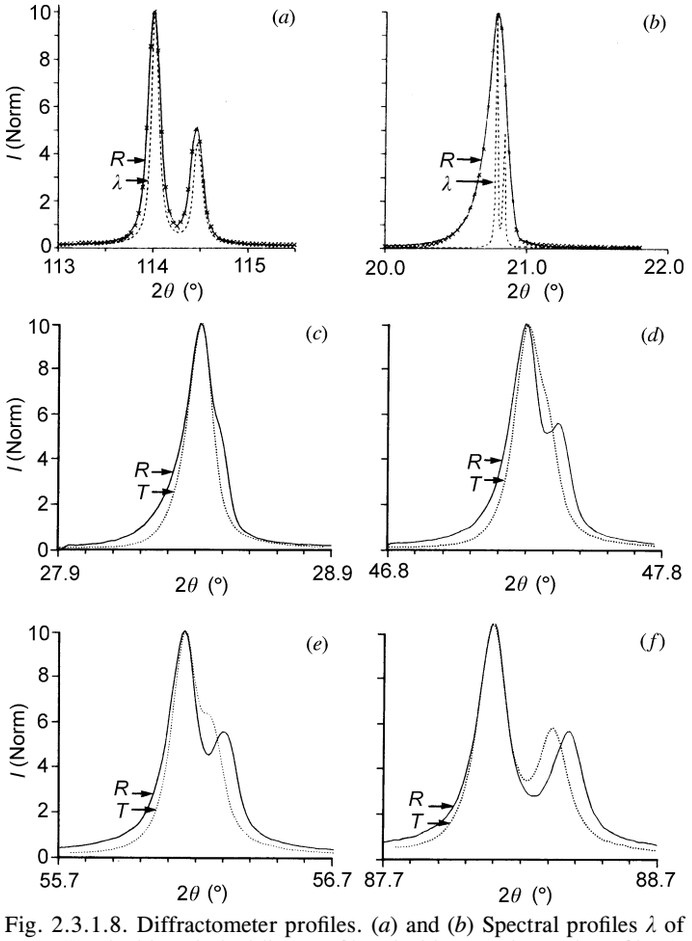

Fig. 2.3.1.8. Diffractometer profiles. (*a*) and (*b*) Spectral profiles λ of Cu $K\alpha$ doublet (dashed-line profiles) inside experimental profiles R (solid line). (*c*)–(*f*) Experimental profiles with reflection specimen (R) geometry (Fig. 2.3.1.3) with α_{ES} 1° and α_{RS} 0.046° (solid line profiles), and transmission specimen (T) (Fig. 2.3.1.12) with α_{ES} 2° and receiving axial divergence parallel slits (dotted profiles). Cu $K\alpha$ radiation. (*a*) Si(531), (*b*) quartz(100), (*c*) Si(111), (*d*) Si(220), (*e*) Si(311), and (*f*) Si(422).

2.3.1.1.5. *Focal line and receiving-slit widths*

The projected source width F_w and receiving-slit width RS_w each add a symmetrical broadening to the profiles that is constant for all angles. Both the profile width and the intensity increase with increasing take-off angle (Section 2.3.5). However, the contribution of F_w is small when the line focus is used, Fig. 2.3.1.9(*a*). The receiving slit can easily be changed and it is one of the most important elements in controlling the profile width, intensity, and peak-to-background ratio, as is shown in Figs. 2.3.1.9(*a*) and (*c*). Because of the contributions of other broadening factors, α_{RS} can be about twice α_F (line focus) without significant loss of resolution.

The projected width of the X-ray tube focus F_w is given in equation (2.3.1.2). The aperture is

$$\alpha_F = 2\arctan(F_w/2R). \qquad (2.3.1.8)$$

For a line focus with actual width $F'_w = 1\,\text{mm}$, $\psi = 5°$, and $R = 185\,\text{mm}$, $\alpha_F = 0.011°$. The receiving-slit aperture is

$$\alpha_{RS} = 2\arctan(RS_w/2R). \qquad (2.3.1.9)$$

For $RS_w = 0.2\,\text{mm}$ and $R = 185\,\text{mm}$. α_{RS} is 0.062°. The FWHM of the profiles is always greater than the receiving-slit aperture because of the other broadening factors.

2.3.1.1.6. *Aberrations related to the specimen*

The major displacement errors arising from the specimen are (1) displacement of the specimen surface from the axis of rotation, (2) use of a flat rather than a curved specimen, and (3) specimen transparency. These are illustrated schematically for the focusing plane in Fig. 2.3.1.10(*a*). The rays from a highly absorbing or very thin specimen with the same curvature as the focusing circle converge at A without broadening and at the correct 2θ. The rays from the flat surface cause an asymmetric profile shifted to B. Penetration of the beam below the surface combined with the flat specimen causes additional broadening and a shift to C.

The most frequent and usually the largest source of angular errors arises from displacement of the specimen surface from the diffractometer axis of rotation. It is not easy to avoid and may arise from several sources. It is advisable to check the reproducibility of inserting the specimen in the diffractometer by recording an isolated peak at low 2θ for each insertion. If only a radial displacement s occurs, the reflection is shifted

$$\Delta 2\theta(\text{rad}) = \pm 2s\cos\theta/R, \qquad (2.3.1.10)$$

where R is the diffractometer radius. A plot of equation (2.3.1.10) is shown in Fig. 2.3.1.10(*b*). The shift is to larger or smaller angles depending on the direction of the displacement and there is no broadening if the displacement is only radial and relatively small. Even a small displacement causes a relatively large shift; for example, if $s = +0.1\,\text{mm}$ and $R = 185\,\text{mm}$, $\Delta 2\theta = +0.06°$ at $20°2\theta$. This gives rise to a systematic error in the recorded reflection angles, which increases with decreasing 2θ. It could be handled with a $\cos\theta\cot\theta$ plot, providing it was the only source of error. There are other possible sources of displacement such as (*a*) if the bearing surface of the specimen post was not machined to lie exactly on the axis of rotation, (*b*) improper specimen preparation or insertion in which the surface was not exactly coincident with the bearing surface or (*c*) nonplanar specimen surface, irregularities, large particle sizes, and specimen transparency. Source (*a*) leads to a constant error

in all measurements, and errors due to (*b*) and (*c*) vary with each specimen.

Ideally, the specimen should be in the form of a focusing torus because of the beam divergence in the equatorial and axial planes. The curvatures would have to vary continuously and differently during the scan and it is impracticable to make specimens in such forms. An approximation is to make the specimen in a flexible cylindrical form with the radius of curvature increasing with decreasing 2θ (Ogilvie, 1963). This requires a very thin specimen (thus reducing the intensity) to avoid cracking and surface irregularities, and also introduces background from the substrate. A compromise uses rigid curved specimens, which match the SFC (Fig. 2.3.1.3) at the smallest 2θ angle to be scanned, and this eliminates most of the aberration (Parrish, 1968). A major disadvantage of the curvature is that it is not possible to spin the specimen.

In practice, a flat specimen is almost always used. The specimen surface departs from the focusing circle by an amount h at a distance $l/2$ from the specimen centre:

$$h = R_{\rm FC} - [R_{\rm FC}^2 - (l^2/2)]^{1/2}. \qquad (2.3.1.11)$$

This causes a broadening of the low-2θ side of the profile and shifts the centroid $\Delta 2\theta$ to lower 2θ:

$$\Delta 2\theta({\rm rad}) = -\alpha^2/(6\tan\theta). \qquad (2.3.1.12)$$

For $\alpha = 1^\circ$ and $2\theta = 20^\circ$, $\Delta 2\theta = -0.016^\circ$. The peak shift is about one-third as large as the centroid shift in the forward-reflection region. This aberration can be interpreted as a continuous series of specimen-surface displacements, which increase from 0 at the centre of the specimen to a maximum value at the ends. The effect increases with α and decreasing 2θ. The profile distortion is magnified in the small 2θ-angle region where the axial divergence also increases and causes similar effects. Typical flat-specimen profiles are shown in Fig. 2.3.1.10(*c*) and computed centroid shifts in Fig. 2.3.1.10(*d*).

The specimen-transparency aberration is caused by diffraction from below the surface of the specimen which asymmetrically broadens the profile (Langford & Wilson, 1962). The peak and centroid are shifted to smaller 2θ as shown in Fig. 2.3.1.10(*e*). For the case of a thick absorbing specimen, the centroid is shifted

$$\Delta 2\theta({\rm rad}) = \sin 2\theta/2\mu R \qquad (2.3.1.13)$$

and for a thin low-absorbing specimen

$$\Delta 2\theta({\rm rad}) = t\cos\theta/R, \qquad (2.3.1.14)$$

where μ is the effective linear absorption coefficient of the specimen used, t the thickness in cm, and R the diffractometer radius in cm. The intermediate absorption case is described by Wilson (1963). A plot of equation (2.3.1.13) for various values of μ is given in Fig. 2.3.1.10(*f*). The effect varies with $\sin 2\theta$ and is maximum at 90° and zero at 0° and 180°. For example, if $\mu = 50\,{\rm cm}^{-1}$, the centroid shift is -0.033° at 90° and falls to -0.012° at $20^\circ 2\theta$.

The observed intensity is reduced by absorption of the incident and diffracted beams in the specimen. The intensity loss is $\exp(-2\mu/x_s\,{\rm cosec}\,\theta)$, where μ is the linear absorption coefficient of the powder sample (it is almost always smaller than the solid material) and x_s is the distance below the surface, which may be equal to the thickness in the case of a thin film or low-absorbing material specimen. The thick (1 mm) specimen of LiF in Fig. 2.3.1.10(*e*) had twice the peak intensity of the thin (0.1 mm) specimen.

The aberration can be avoided by making the sample thin. However, the amount of incident-beam intensity contributing to the reflections could then vary with θ because different amounts are transmitted through the sample and this may require corrections of the experimental data. Because the effective reflecting volume of low-absorbing specimens lies below the surface, care must be taken to avoid blocking part of the diffracted beam with the antiscatter slits or the specimen holder, particularly at small 2θ.

There are additional problems related to the specimen such as preferred orientation, particle size, and other factors; these are discussed in Section 2.3.3.

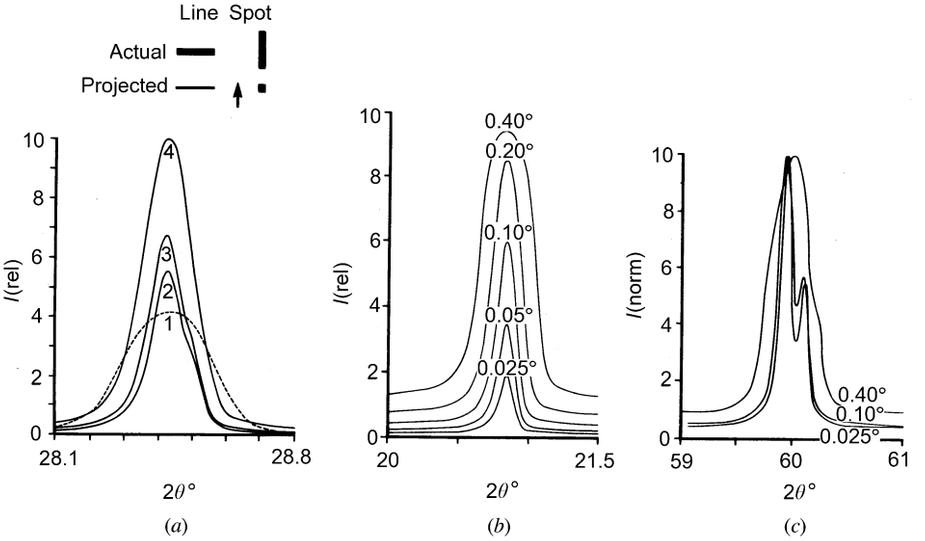

Fig. 2.3.1.9. (*a*) Effect of source size on profile shape, Cu $K\alpha$, $\alpha_{\rm ES}$ 1°, $\alpha_{\rm RS}$ 0.05°, Si(111).

No.	Projected size (mm)	FWHM (°2θ)
1	1.6 × 1.0 (spot)	0.31
2	0.32 × 10 (line)	0.11
3	0.16 × 10 (line)	0.13
4	0.32 × 12 (line)	0.17.

Effect of receiving-slit aperture $\alpha_{\rm RS}$ on profiles of quartz (*b*) (100) and (*c*) (121); peak intensities normalized, Cu $K\alpha$, $\alpha_{\rm ES}$ 1°.

2.3.1.1.7. *Axial divergence*

Divergence in the axial direction (formerly also called 'vertical divergence') causes asymmetric broadening and shifts the reflections. The aberration is illustrated in Fig. 2.3.1.11 for a low-2θ reflection in the transmission-specimen mode (Subsection 2.3.1.2). The narrow profile was obtained with $\delta = 4.4^\circ$ parallel slits placed between the monochromator and detector, and the broad profile with the slits removed. The slits caused a 33% reduction in peak intensity. This problem was recognized in the first design of the diffractometer using the X-ray tube line focus when parallel slits were used in the incident and diffracted beams to limit the effect (Parrish, 1949). Increasing the radius reduces the effect if the slit length is kept constant. The intensity is also reduced because the chord length intercepted is a smaller fraction of the longer radius diffraction cone. The construction of parallel (Soller) slits (Soller, 1924) is shown in Fig. 2.3.1.5(*d*).

The calculation of the aberration and the present status is summarized by Wilson (1963, pp. 40–45). The results depend on the aperture of the parallel slits, the length of the entrance and receiving slits, and 2θ. In the limit of small s, the shift of the centroid is

$$\Delta(2\theta, \text{rad}) = (s/l)^2 \cot 2\theta/6, \qquad (2.3.1.15)$$

where s is the spacing and l the length of the foils. The shift becomes very large at small 2θ's but not infinite as equation (2.3.1.15) implies. The shift is to smaller 2θ's in the forward-reflection region and to larger 2θ's in back-reflection. However, the mathematical formulation is difficult to quantify because in the forward-reflection region the axial divergence convolves with the flat-specimen aberration to increase the asymmetry. In the back-reflection region, the effect is not so obvious because the distortion is smaller and the Lorentz and dispersion factors also stretch the profiles to higher angles.

2.3.1.1.8. *Combined aberrations*

Additional aberrations are caused by inaccurate instrument set-up and alignment. For example, if the receiving-slit position is incorrect, the profiles are broadened. If, in addition, the incident beam is mis-centred or the θ–2θ is incorrect, a peak shift accompanies the broadening because the aberrations convolute, causing larger distortions and peak shifts than the individual aberrations, for example, flat-specimen, transparency, and axial divergence.

2.3.1.2. *Transmission specimen, θ–2θ scan*

Transmission-specimen methods are not as widely used as reflection methods but they provide important supplemental data and have advantages in a number of applications. Reflections occur from lattice planes oriented normal to the specimen surface rather than parallel. Reflection and transmission patterns can be compared to determine texture and preferred-orientation effects. The transmission method is better suited to the measurement of large d's. Smaller specimen volumes are required. The surface 'roughness' which may cause large intensity errors due to the microabsorption in reflection specimens is largely reduced.

The same basic diffractometer is used for both methods but the geometry is different because the diffracted beam continues to

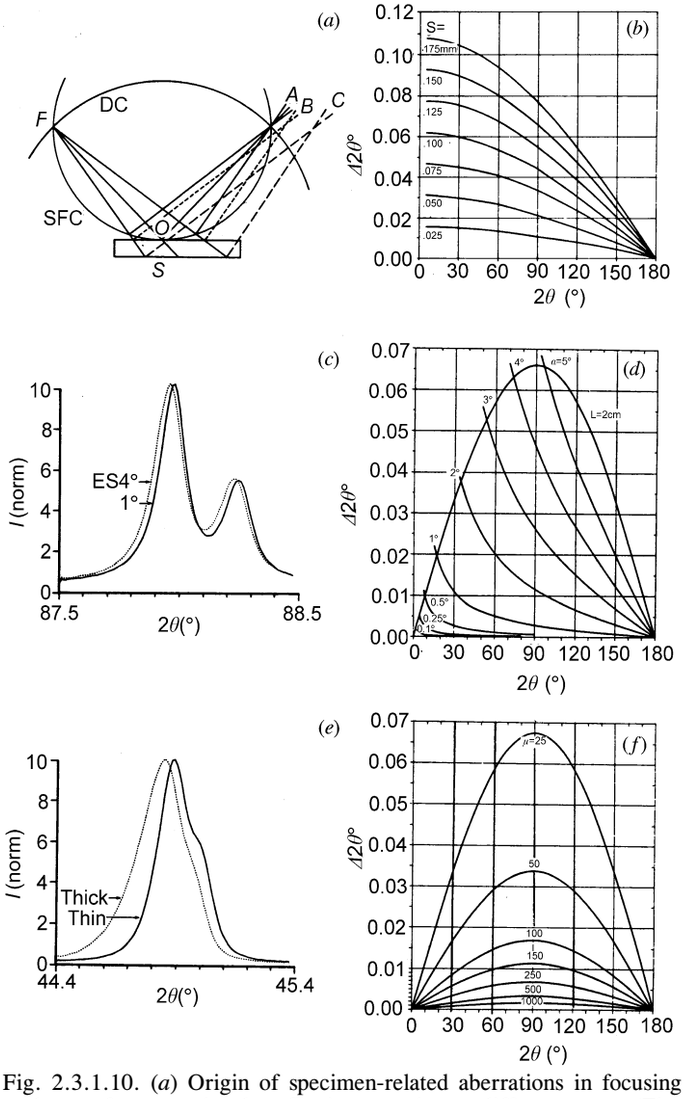

Fig. 2.3.1.10. (*a*) Origin of specimen-related aberrations in focusing plane of conventional reflection specimen diffractometer (Fig. 2.3.1.3). *A* no aberration from curved specimen; *B* flat specimen; *C* specimen displacement from 0. (*b*) Computed angular shifts caused by specimen displacement, $R = 185$ mm. (*c*) Flat-specimen asymmetric aberration, Si(422), Cu $K\alpha_1$, $K\alpha_2$ peak intensities normalized. (*d*) Computed flat-specimen centroid shifts for various apertures; parabola for constant irradiated 2 cm specimen length. (*e*) Transparency asymmetric aberration, LiF(200) powder reflection, Cu $K\alpha$, peak intensities normalized, thin specimen (solid-line profile) 0.1 mm thick; thick specimen (dotted-line profile) 1.0 mm, α_{ES} 1°, α_{RS} 0.046°. (*f*) Computed transparency centroid shifts for various values of linear absorption coefficient.

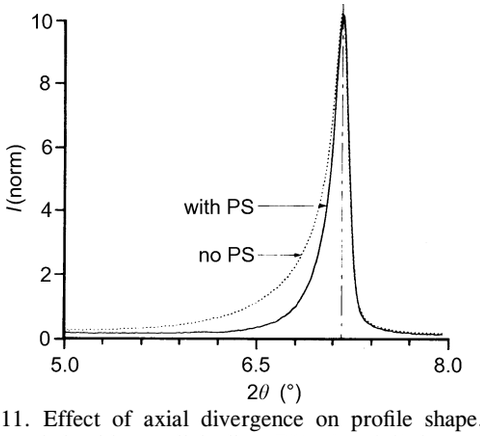

Fig. 2.3.1.11. Effect of axial divergence on profile shape. Narrow profile recorded with parallel slits (PS), $\delta = 4.4^\circ$ between monochromator and detector Fig. (2.3.1.12), and broad profile with these parallel slits removed. Faujasite, Cu $K\alpha$, α_{ES} 2°.

diverge after it passes through the specimen and the monochromator is required to refocus the beam, on the detector as shown in Fig. 2.3.1.12 (de Wolff, 1968*b*; Parrish, 1958). The monochromator can be placed before or after the specimen and the position has different effects on the pattern. Using the monochromator in the diffracted beam, the intensity and width of the profiles are determined by the X-ray focal line width and the quality of the bent monochromator rather than the receiving slit which serves as an antiscatter slit. This geometrical arrangement places the virtual image VI of the focal line at the intersection of the focusing circles. After reflection from the specimen, the divergent beam is again reflected by the focusing crystal M and converges on the detector. The pattern is recorded with θ–2θ scanning with the monochromator and detector both mounted on a rigid arm rotating around the diffractometer axis. A beam stop MS can be translated and moved in and out near the crossover point to prevent the primary beam from entering the detector at small 2θ's. To avoid long radii, the crystal surface is cut at an angle σ (about 3°) to the reflecting lattice plane. The distances are related by

$$\begin{aligned}(l_1 + l_2)/l_3 &= [\sin(\theta_M + \sigma)]/[\sin(\theta_M - \sigma)] \\ R_{\rm FC} &= [l_1 + l_2]/[2\sin(\theta_M + \sigma)] \\ &= l_3/[2\sin(\theta_M - \sigma)],\end{aligned} \tag{2.3.1.16}$$

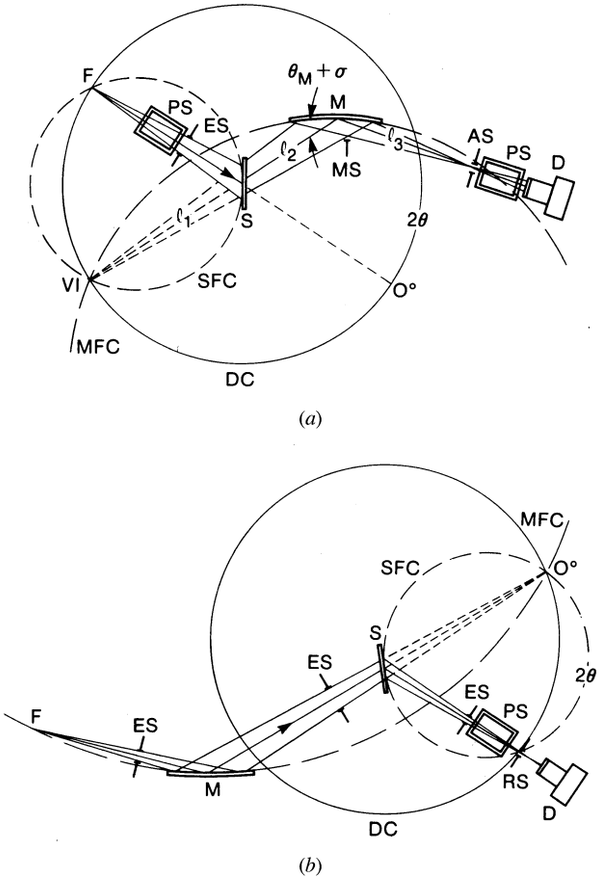

Fig. 2.3.1.12. X-ray optics of the transmission specimen with asymmetric focusing monochromator and θ–2θ scanning. (*a*) Monochromator in diffracted beam. θ_M Bragg angle of monochromator with surface cut at angle σ to reflecting plane, MS adjustable beam stop, I_1, I_2, and I_3 defined in text and other symbols listed in Fig. 2.3.1.3. (*b*) Monochromator in incident beam, equivalent to Guinier focusing camera.

where θ_M is the Bragg angle of the monochromator for the selected wavelength and the l's are shown in Fig. 2.3.2.12(*a*).

Because the profile shape and the intensity are determined by the monochromator, the crystal quality and the accuracy of the bending are crucial factors in determining the quality of the pattern. A flat thin quartz (101) wafer bent with a special device to approximate a section of a logarithmic spiral has been successfully used (de Wolff, 1968*b*). The curvature can be varied to obtain the sharpest focus. Thin silicon crystals that can be bent are now available, and Johann and Johannsen asymmetric crystals may be used. Pyrolytic graphite monochromators are not applicable; the radii would be longer because graphite is too soft to be cut at an angle, and a receiving slit would be necessary to define the diffracted beam because the monochromator produces a broad reflection.

A polarization factor is introduced by the monochromator,

$$p = (1 + k\cos^2 2\theta)/(1 + k), \tag{2.3.1.17}$$

where $k = \cos^2 2\theta_M$ for mosaic crystals and $k = \cos 2\theta_M$ for perfect crystals. The value of k is strongly dependent on the surface finish of the crystal and the crystal should be measured to determine the effect. A specimen with accurately known structure factors such as silicon can be used to calibrate the intensities.

The $K\alpha$-doublet separation is zero at the 2θ angle at which the dispersion of the specimen compensates that of the monochromator, *i.e.* the 2θ at which the monochromator is aligned and also depends on the distances. The $K\alpha_1$ and $K\alpha_2$ peaks are superposed and appear as a single peak over a small range of 2θ's. The $K\alpha_2$ peak gradually separates with increasing 2θ but the separation is less than calculated from the wavelengths and the intensity ratio may not be 2:1 until higher angles are reached as shown in Fig. 2.3.1.8.

A larger angular aperture α_T can be used for transmission than for reflection α_R because the specimen is more nearly normal to than parallel to the primary beam:

$$\alpha_T/\alpha_R = 2R_D/[1 + (R/l_2)L_s], \tag{2.3.1.18}$$

where the diffractometer radius $R_D = l_1$. For $R_D = 170$ mm, specimen length $L_S = 20$ mm and $l_2 = 65$ mm; α_T could be 4.7 times larger than α_R but the monochromator length usually limits it to about 3°. The smallest reflection angle that can be measured is

$$2\theta_{\rm min} = \alpha_T[(R_D + l_2)/l_2]. \tag{2.3.1.19}$$

Using $\alpha_T = 0.5°$, $2\theta_{\rm min} = 1.75°$ and $d = 50$ Å for Cu $K\alpha$ radiation.

Specimen preparation is not difficult and the preparation can be easily tested and changed. The specimen must be X-ray transparent and can be a free-standing film or foil, or a powder cemented to a thin substrate. The substrate selection is important because its pattern is included. If both transmission and reflection patterns are to be compared, the substrate should be selected to have a minimal contribution to both. For example, Mylar is a good substrate for transmission but has a strong reflection pattern, and although rolled Be foil has a few reflections it is often satisfactory for both.

The absorption factor is

$$A = (t/\cos\theta)\exp(-s/\cos\theta), \tag{2.3.1.20}$$

where t is the powder thickness and s is the sum of the products of the absorption coefficients and thicknesses of the powder and the substrate. The optimum specimen thickness to give the highest intensity is $\mu t = 1$, *i.e.* the specimen should transmit about 38% of the incident $K\alpha$ intensity. The transmission can be

easily measured with a standard specimen set to reflect the $K\alpha$ and the specimen to be measured inserted normal to the diffracted beam in front of the detector. It is not critical to achieve the exact value and a range of ±15–20% of the transmission can be tolerated. This minimizes the effect of the absorption change with 2θ, and corrections of the relative intensities are required only when accurate values are required.

The intensity of the incident beam can be measured at 0° in the same geometry and used to scale the relative intensities to 'absolute' values. The flat specimen, transparency, and specimen surface displacement aberrations are similar to those in reflection specimen geometry except that they vary as $\sin\theta$ rather than $\cos\theta$. This is an important factor in the measurement of large-d-spacing reflections. The flat-specimen effect is smaller because the irradiated specimen length is usually smaller. The transparency error is also usually smaller because thin specimens are used.

An important advantage of the method is that the specimen displacement can be directly determined by measuring the peak in the normal position and again after rotating the specimen holder 180°. The correct peak position is at one-half the angle between the two values. The axial divergence has the same effect as in reflection. The limitations are that only the forward-reflection region is accessible, and the intensity is about one-half of the reflection method (except at small angles) because smaller specimen volumes are used.

An alternative arrangement for the transmission specimen mode is to use an incident-beam monochromator as shown in Fig. 2.3.1.12(*b*). This is similar to the geometry used in the Guinier powder camera with the detector replacing the film. A high-quality focusing crystal is required. Wölfel (1981) used a symmetrical focusing monochromator with 260 mm focal length for quantitative analysis. Göbel (1982) used an asymmetric monochromator with a position-sensitive detector for high-speed scanning, see §2.3.5.4.1. By proper selection of the source size and distances, the $K\alpha_2$ can be eliminated and the pattern contains only the $K\alpha_1$ peaks (Guinier & Sébilleau, 1952). This geometry can have high resolution with the FWHM typically about 0.05 to 0.07°. The profile widths are narrower for the subtractive setting of the monochromator than for the additive setting.

The pattern is recorded with θ–2θ scanning. The 0° position can be determined by measuring 4θ, *i.e.* peaks above and below 0°, or calibration can be made with a standard specimen. A slit after the monochromator limits the size of the beam striking the specimen. The width and intensity of the powder reflections are limited by the receiving-slit width. A parallel slit is used between the specimen and detector to limit axial divergence.

The full spectrum from the X-ray tube strikes the monochromator and only the monochromatic beam reaches the specimen, so that it is preferred for radiation-sensitive materials. On the other hand, the radiation reaching the specimen may cause fluorescence (though considerably less than the full spectrum) which adds to the background.

2.3.1.3. *Seemann–Bohlin method*

The Seemann–Bohlin (*S–B*) diffractometer has the specimen mounted on a radial arm instead of the axis of rotation and a linkage or servomechanism moves the detector around the circumference of a fixed-radius focusing circle while keeping it pointed to the stationary specimen. All reflections occur simultaneously focused on the focusing circle as shown in Fig. 2.3.1.13(*a*). The method was originally developed for powder cameras by Seemann (1919) and Bohlin (1920) but was not widely used because of the limited angular range and the broad reflections caused by inclination of the rays to the film. The diffractometer eliminates the broadening and extends the angular range. Diffractometers designed for this geometry have been described by Wassermann & Wiewiorosky (1953), Segmüller (1957), Kunze (1964*a*,*b*), Parrish, Mack & Vajda (1967), King, Gillham & Huggins (1970), Feder & Berry (1970), and others.

The geometry is shown in Fig. 2.3.1.13(*b*) (Parrish & Mack, 1967). Reflections occur from lattice planes with varying inclinations β_H to the specimen surface. The reflecting position of a plane H is $\theta_H = \gamma + \beta_H$, where γ is the incidence angle and $4\theta_H$ the reflection angle. The maximum value of β_H is about 45°. It is essential to align the specimen tangent to FC. This is a critical adjustment because even a small misalignment causes profile broadening and loss of peak intensity.

The source may be the line focus of the X-ray tube [F in Fig. 2.3.1.13(*b*)] or at the focus of a monochromator [ES in Fig. 2.3.1.13(*a*)]; in the latter case, the entrance slit at F' limits the divergent beam reaching the specimen. The source, specimen centre O, and receiving slit RS lie on the specimen focusing circle SFC, which has a fixed radius r. The incidence angle γ is given by

$$\gamma = \arcsin(b/2r), \qquad (2.3.1.21)$$

where b is the distance from F or F' to O, or $2r\sin\gamma$. The γ angle determines the angular range that can be recorded with a given r, decreasing γ decreases $2\theta_{\min}$. The relationships of specimen position on the focusing circle and the recording range

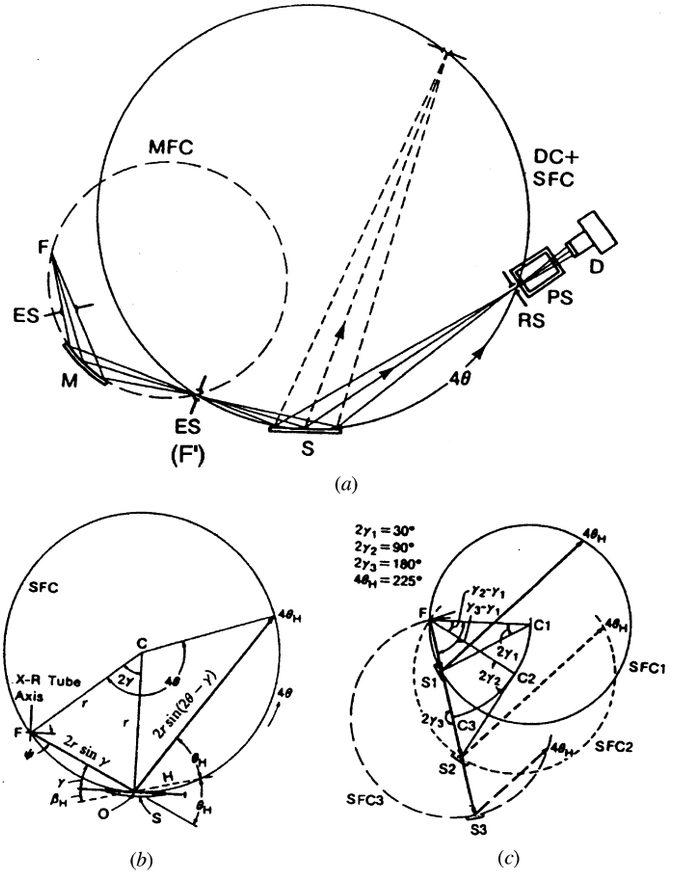

Fig. 2.3.1.13. Seemann–Bohlin method. (*a*) X-ray optics using incident-beam monochromator. (*b*) X-ray tube line-focus source showing geometrical relations: γ mean angle of incident beam, β_H inclination of reflecting plane H to specimen surface, θ_H Bragg angle of H plane, t tangent to focusing circle at O. (*c*) Diffractometer settings for various angular ranges.

are illustrated in Fig. 2.3.1.13(*c*). To change the range requires rotation of the X-ray tube axis or the diffractometer around *F*. The detector must also be repositioned. For forward-reflection measurements, γ is usually $\leq 10^\circ$. Extreme care must be used in the specimen preparation to avoid errors due to microabsorption (particle-shadowing) effects, which increase with decreasing γ. The 0° position cannot be measured directly and a standard is used for calibration. The range from 0° to about $15^\circ 2\theta$ is inaccessible because of mechanical dimensions. At $\gamma = 90^\circ$, only the back-reflection region can be scanned.

The aperture of the beam striking the specimen is

$$\alpha_{\rm SB} = 2\arctan({\rm ES}_w/2a), \qquad (2.3.1.22)$$

where $\rm ES_w$ is the entrance slit width and *a* the distance between *F* or *F'* and the slit. The irradiated specimen length *l* is constant at all angles, $l = 2\alpha r$. A large aperture can be used to increase intensity since the specimen is close to *F*. However, the selection of α is limited if γ is small, and also because of the large flat-specimen aberration.

The receiving-slit aperture varies with the distance of the slit to the specimen

$$\alpha_{\rm RS}(^\circ 4\theta) = 2\arctan {\rm RS}_w/[2r\sin(2\theta - \gamma)]. \qquad (2.3.1.23)$$

Consequently, the resolution and relative intensity gradually change across the pattern. The *S*–*B* has greater widths at the smaller 2θ's and nearly the same widths at the higher angles compared with the θ–2θ diffractometer. The aperture can be kept constant by using a special slit with offset sides (to avoid shadowing) and pointing the opening to *C* while the detector remains pointed to *O* (Parrish *et al.*, 1967). The slit opening is tangent to FC and inclined to the beam and rotates while scanning. The constant aperture slit has

$$\alpha_{\rm RS}(^\circ 4\theta) = 2\arctan({\rm RS}_w/2r). \qquad (2.3.1.24)$$

The axial divergence is limited by parallel slits as in conventional diffractometry and the effects are about the same. The equatorial aberrations are also similar but larger in magnitude. The specimen-aberration errors are listed in Table 5.2.7.1. The flat specimen causes asymmetric broadening; the shift is proportional to $\alpha_{\rm ES}^2$ and increases with decreasing θ. It can be eliminated by making the specimen with the same curvature as $r = {\rm FC}$. In this case, one curvature satisfies the entire angular range because the focusing circle has a fixed radius. However, the curvature precludes rotating the specimen. The specimen transparency also causes asymmetric broadening and a peak shift that increases with decreasing θ. For $\mu h \rightarrow 0$, the geometric term is the same as for specimen displacement (Mack & Parrish, 1967).

The diffracted intensity is proportional to $I_0 A(\mu h) TB$, where I_0 is the incident intensity determined by α, δ, and the axial length *L* of the incident-beam assembly, $A(\mu h)$ is the specimen absorption factor, *T* the transmission of the air path, and *B* the length $L_{\rm RS}$ of the diffracted ring intercepted by the slit. The X-rays reflected at a depth *x* below the specimen surface are attenuated by

$$\exp\{-[\mu x\,{\rm cosec}\,\delta + \mu x\,{\rm cosec}\,(2\theta - \delta)]\}, \qquad (2.3.1.25)$$

where μ is the linear absorption coefficient. The asymmetric geometry causes the absorption to vary with the reflection angle. The air absorption path varies with the distance *O* to RS and reaches a maximum at $180^\circ + 2\gamma$. The expression for air transmission includes the radius of the X-ray tube R_T, which is needed only for the case where the X-ray tube focal line is used as *F*. In a typical instrument with X-ray tube source *F* and $r = 174$ mm, the transmission of Cu $K\alpha$ decreases from 90% at $40^\circ 4\theta$ to 62% at 210°, and Cr $K\alpha$ from 73 to 23% at the same angles.

Some of the advantages of the method include the following: (*a*) the fixed specimen makes it possible to simplify the design of specimen environment devices; (*b*) a large aperture can be used and the intensities are higher than for conventional diffractometers; (*c*) the flat-specimen aberration can be eliminated by a single-curvature specimen; (*d*) a small γ angle can be used to increase the path length *l* in the specimen, and hence the intensity of low-absorbing thin-film samples ($l = t/\sin\gamma$ and for $\gamma = 5^\circ$, $l = 11.5t$); (*e*) the method is useful in thin-film and preferred-orientation studies because about a 45° range of lattice-plane orientations can be measured and compared with conventional patterns. The limitations include (*a*) the more complicated diffractometer and its alignment, (*b*) limited angular range of about 10 to $110^\circ 2\theta$ for the forward-reflection setting, (*c*) extreme care required in specimen preparation, and (*d*) larger aberration errors.

2.3.1.4. *Reflection specimen, θ–θ scan*

In this geometry, the specimen is fixed in the horizontal plane and the X-ray tube and detector are synchronously scanned in the vertical plane in opposite directions above the centre of the specimen as shown in Fig. 2.3.1.14. The distances source to *S* and *S* to RS are equal to that the angles of incidence and diffraction and a constant $\mathrm{d}\theta/\mathrm{d}t$ are maintained over the entire angular range. A focusing monochromator can be used in the incident or diffracted beam. High- and low-temperature chambers are simplified because the specimen does not move. The arms carrying the X-ray tube and detector must be counterbalanced because of the unequal weights. The method has advantages in certain applications such as the measurement of liquid scattering without a covering window, high-temperature molten samples, and other applications requiring a stationary horizontal sample (Kaplow & Averbach, 1963; Wagner, 1969).

2.3.1.5. *Microdiffractometry*

There are two types of microdiffraction: (*a*) only a very small amount of powder is available, and (*b*) information is required from very small areas of a conventional-size specimen. Small-volume samples have been analysed with a conventional diffractometer by concentrating the powder over a small spot centred on a single-crystal plate such as silicon (510) or an

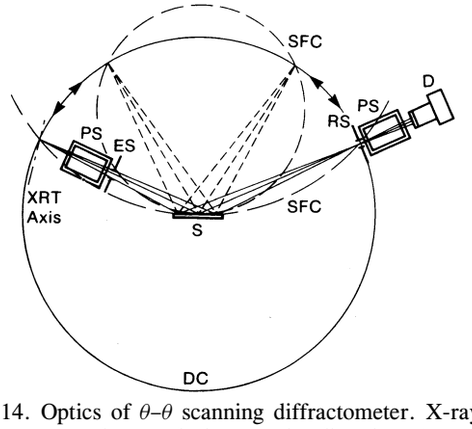

Fig. 2.3.1.14. Optics of θ–θ scanning diffractometer. X-ray tube and detector move synchronously in opposite directions (arrows) around fixed horizontal specimen. A focusing monochromator can be used after the receiving slit.

AT-cut quartz plate, or on Mylar for transmission. It is essential to rotate the specimen and increase the count time. A Gandolfi camera has also been used for very small specimens (see Section 2.3.4). A high-brilliance microfocus X-ray source has been used with a collimator made of 10 to 100 μm internal-diameter capillary tube. An *X*–*Y* stage is used with an optical microscope to locate selected areas of the specimen.

A microdiffractometer has been designed for microanalysis, Fig. 2.3.1.15 (Rigaku Corporation, 1990). It has been used to determine phases and stress in areas $< 10^4\ \mu m^2$ (Goldsmith & Walker, 1984). The key to the method is the use of an annular-ring receiving slit, which transmits the entire diffraction cone to the detector instead of a small chord as in conventional diffractometry, thereby utilizing all the available intensity. The pattern is scanned by translating the ring and detector along the direct-beam path so that

$$2\theta = \arctan(R_{RS}/L), \qquad (2.3.1.26)$$

where R_{RS} is the radius of the ring slit and L the distance from the fixed specimen. For $R_{RS} = 15$ mm, L varies from 171 to 9 mm in the transmission range 5 to 60°2θ; a 50 mm diameter scintillation counter is used. A doughnut-shaped proportional counter (3/4 of a full circle) is used for the 30 to 150° reflection specimen mode. The slit width is 0.2 mm and the aperture varies with 2θ. The intensities fall off at the higher 2θ's because of the small incidence angles to the slit. An alternative method uses a position-sensitive proportional counter. Steinmeyer (1986) has described applications of microdiffractometry.

By using synchrotron radiation (Section 2.3.2), single-crystal data for structure determination can now be obtained from a microcrystal about 5–10 μm in size; see Andrews *et al.* (1988), Bachmann, Kohler, Schultz & Weber (1985), Harding (1988), Newsam, King & Liang (1989), Cheetham, Harding, Mingos & Powell (1993), Harding & Kariuki (1994), and Harding, Kariuki, Cernik & Cressey (1994).

2.3.2. Parallel-beam geometries, synchrotron radiation

The radiation from the X-ray tube is divergent and various methods can be used to obtain a parallel beam as shown in Fig. 2.3.2.1. Symmetrical reflection from a flat crystal is the usual method. An asymmetric reflecting monochromator with small incidence angle and large exit angle expands the beam, or in reverse condenses it (§2.3.5.4.1). A channel monochromator has the advantage of not changing the beam direction. A receiving slit or preferably Soller slits can be used to define the diffracted beam. A graphite monochromator in the diffracted beam or a solid-state detector eliminates fluorescence. The incident-beam parallel slits limit vertical divergence. However, all the methods result in a large loss of intensity compared with conventional focusing. In contrast, the storage ring produces a virtually parallel beam with very small vertical divergence of about 0.1 mrad, and the monochromator is used only to select the wavelength. The rest of this section assumes a synchrotron-radiation source.

Storage-ring X-ray sources have a number of unique properties that are of great importance for powder diffraction. The advantages of synchrotron powder diffraction have been described by Hastings, Thomlinson & Cox (1984), Parrish & Hart (1987), Parrish (1988), and Finger (1989). Excellent patterns with high resolution and high peak-to-back ground ratio have been reported. These include the orders-of-magnitude higher intensity and nearly uniform spectral distribution compared with X-ray tubes, the wide continuous range of selectable wavelengths, and the single profile that avoids the problems caused by $K\alpha$ doublets and β filters. Owing to major differences in the diffractometer geometries, comparisons of intensities with X-ray tube focusing methods cannot be predicted simply from the number of source photons.

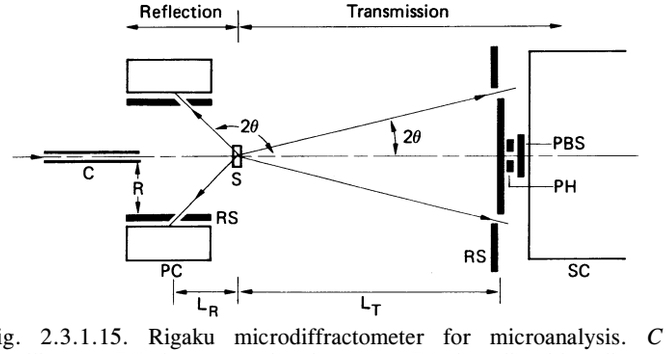

Fig. 2.3.1.15. Rigaku microdiffractometer for microanalysis. *C* collimator, PC ring proportional counter, RS ring slit with radius *r*, *S* specimen, SC scintillation counter, PBS primary beam stop, PH pinhole for alignment, *L* specimen-to-receiving-slit distance.

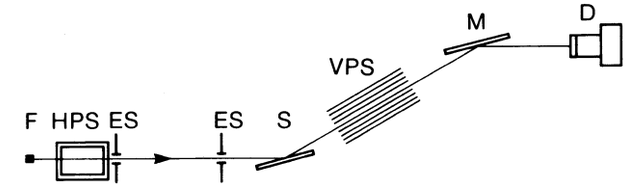

Fig. 2.3.2.1. Method to obtain parallel beam from X-ray tube for powder diffraction. HPS parallel slits to limit axial divergence, ES entrance slits (can be replaced by pair of flat parallel steel bars), *S* specimen, VPS parallel slits to define diffracted beam, *M* flat monochromator (can be omitted). *D* detector. See also Fig. 2.3.2.4(*a*).

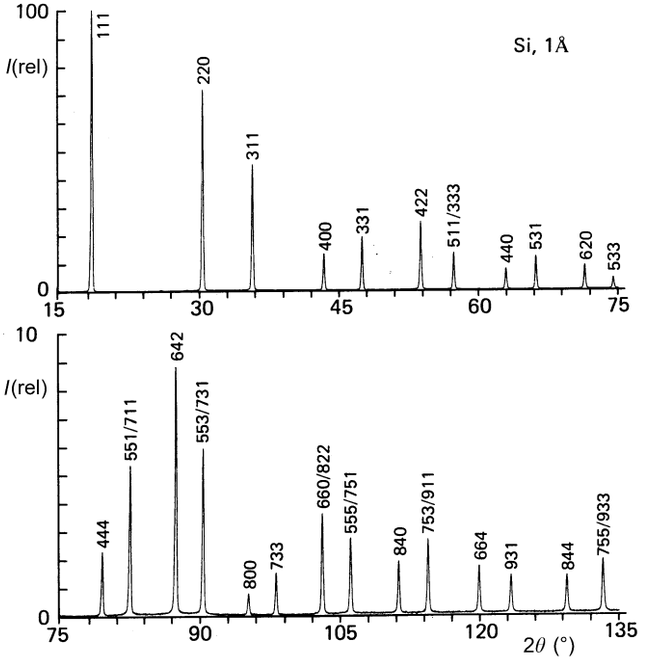

Fig. 2.3.2.2. Silicon powder pattern with 1 Å synchrotron radiation using method shown in Fig. 2.3.2.4(*a*). The 444 reflection is the limit for Cu $K\alpha$ radiation.

The easy wavelength selection makes it possible to avoid specimen fluorescence, to record data on both sides of an absorption edge for anomalous-scattering studies, to select optimum angles and wavelengths for lattice-parameter measurements, and to vary the dispersion. Short-wavelength radiation can be used for uncomplicated patterns without the background occurring in X-ray tube spectra. Fig. 2.3.2.2 shows a silicon pattern obtained with 1.0 Å X-rays in which there are twice as many reflections as can be recorded with Cu $K\alpha$, and the background remains very low out to the highest 2θ angles. The short wavelengths (~ 0.7 Å) are especially useful for samples mounted in cryostats, furnaces, and pressure cells.

Using an incident-beam tunable monochromator, no continuous radiation reaches the specimen and a wavelength can be selected that gives a high peak-to-background ratio and no specimen fluorescence. If the specimen contains different chemical phases, patterns can be recorded using wavelengths on both sides of the absorption edge to enhance one of the patterns as an aid in identification. This is illustrated in Fig. 2.3.2.3 for a mixture of Ni and ZnO powders. A pattern (*a*) with maximum peak-to-background ratio is obtained with a wavelength slightly longer than the Ni *K*-absorption edge but using a wavelength shorter than the edge (*b*) causes high Ni *K* fluorescence background. The relative intensities of the peaks in each compound are the same with both wavelengths. However, the large change in the Ni absorption across the edge caused a large difference in the ratio of Ni/ZnO intensities. The Ni(111) decreased by 85% and the intensity ratio Ni(111)/ZnO(102) dropped from 4.2 to 1.3.

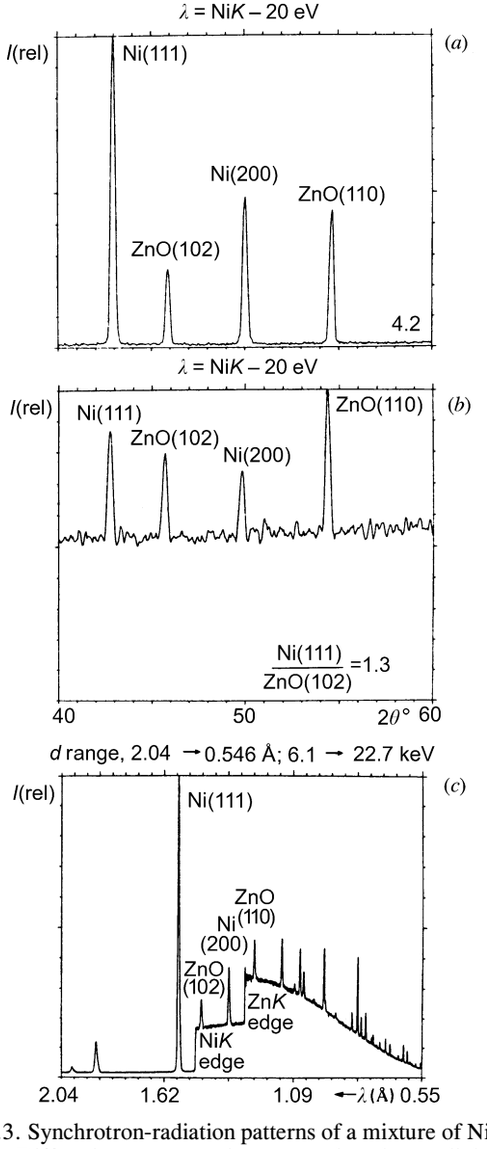

Fig. 2.3.2.3. Synchrotron-radiation patterns of a mixture of Ni and ZnO powders. Diffraction pattern using a wavelength (*a*) slightly longer than the Ni *K*-absorption edge and (*b*) slightly shorter. (*c*) High-resolution energy-dispersive diffraction (EDD) pattern.

Modified conventional vertical-scanning diffractometers are used to avoid intensity losses from the strong polarization in the horizontal plane. The six basic powder diffraction methods that have been used are:

(*a*) Monochromatic X-rays with θ–2θ scanning and flat specimen as in conventional X-ray tube methods but using parallel-beam X-ray optics. This is the most widely applicable method for polycrystalline materials.

(*b*) Monochromatic X-rays with fixed specimen and 2θ detector scan, used for analysing texture, preferred orientation, and grazing-incidence diffraction.

(*c*) Monochromatic X-rays with a capillary specimen and scanning receiving slit or position-sensitive detector.

(*d*) Energy-dispersive diffraction using a step-scanned channel monochromator, selectable fixed θ–2θ positions, and conventional scintillation counter and electronics. The instrumentation is the same as (*a*) and may be used in methods that require a stationary specimen.

(*e*) Energy-dispersive diffraction using the white beam, solid-state detector and multichannel analyser, and selected fixed θ–2θ. This is the method frequently used with synchrotron and X-ray tube sources but it has low pattern resolution (Giessen & Gordon, 1968).

(*f*) Angle-dispersive or energy-dispersive experiments with an imaging-plate detector, whereby complete Debye–Scherrer rings are recorded simultaneously, as in some film methods (Subsection 2.3.4.1) (*e.g.* Piltz *et al.*, 1992). This is a particularly useful technique for studies under non-ambient conditions, such as experiments at ultra-high pressure (*e.g.* McMahon & Nelmes, 1993).

2.3.2.1. *Monochromatic radiation, θ–2θ scan*

The X-ray optics of a plane-wave parallel-beam diffractometer is shown schematically in Fig. 2.3.2.4(*a*). The primary white beam is limited by slits at *C*1. A channel monochromator CM is used because it has the important property of maintaining the same direction and position for a wide range of wavelengths. It may be used in the dispersive setting with respect to the specimen or in the parallel setting [Fig. 2.3.2.4(*b*)]. The monochromatic beam is larger than the entrance slit ES and it is unnecessary to realign the powder diffractometer when changing wavelengths. The monochromator can be mounted on a stripped diffractometer for easy alignment and step scanning.

There are no characteristic spectral lines and the wavelength calibration of the monochromator is made by step scanning the monochromator across absorption edges of elements in a specimen or pure element foils placed in the beam. The wavelength accuracy is limited by the uncertainty as to what feature of the edge should be measured and which one was used for the wavelength tables. A standard powder sample such as NIST silicon 640b whose lattice parameter is known with moderately high precision can also be used. An alternative method is to measure the reflection angle of a single-crystal plate of float-zones oxygen-free silicon whose lattice parameter is known to 1 part in 10^{-7} and to determine the wavelength from

the Bragg equation (Hart, 1981). The accuracy is then limited by the angular accuracy of the diffractometer and the orientation setting.

It is necessary to monitor the monochromatic beam intensity I_0, which changes during the recording due to decreasing storage-ring current, orbital shifts or other factors. This can be done by inserting a low-absorbing ionization chamber in the beam or by using a scintillation counter to measure scattering from an inclined thin beryllium foil, kapton or other low-absorbing material. The data are recorded and used to correct the observed intensities. The monitored counts can also be used as a timer for step scanning if a sufficient number are recorded for good counting statistics.

The entrance slit ES determines the irradiated specimen length, which is equal to ES/sin θ_s. Vertical parallel slits VPS with $\delta \simeq 2^\circ$ are used to limit the axial divergence. The longer the distance between the specimen and detector, the smaller the asymmetry, and a vacuum path should be used to avoid air-absorption losses. The specimen may be used in either reflection or transmission simply by rotating it 90° around the diffractometer axis from its previous position.

The diffracted beam can be defined by a receiving slit (Parrish, Hart & Huang, 1986), horizontal parallel slits HPS [Fig. 2.3.2.4(*a*)] (Parrish & Hart, 1985) or a high-quality single-crystal plate which acts as a very narrow receiving slit [Fig. 2.3.2.4(*b*)] (Cox, Hastings, Thomlinson & Prewitt, 1983; Hastings *et al.*, 1984). If a receiving slit is used, the intensity, profile width and shape are determined by the widths of both ES and RS. If either one is much wider than the other, the profile has a flat top. Increasing the RS width and keeping ES constant causes symmetrical profile broadening and increases the intensity as in conventional focusing diffractometry. There are disadvantages in using a receiving slit because the intensities are low and it causes the same specimen-surface-displacement and transparency errors as the focusing geometries.

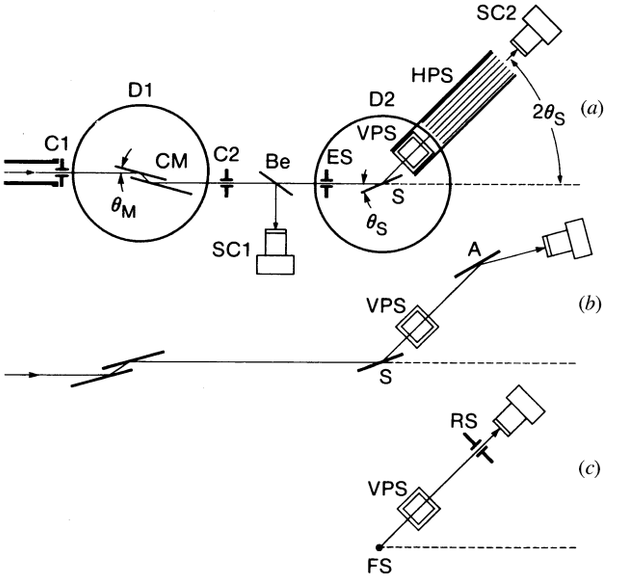

Fig. 2.3.2.4. (*a*) Optics of dispersive parallel-beam method for synchrotron X-rays. *C*1 primary-beam collimator, *D*1 diffractometer for channel monochromator CM, *C*2 antiscatter shield, Be beryllium foil for monitor, SC1 and SC2 scintillation counters, ES entrance slit on powder diffractometer *D*2, VPS vertical parallel slits to limit axial divergence, HPS horizontal parallel slits, which determine the resolution. (*b*) CM in nondispersive setting and crystal analyser *A* used as a narrow receiving slit. (*c*) Fibre specimen FS with receiving slit RS or with position-sensitive detector (not shown) with RS removed.

A set of horizontal parallel (Soller) slits is advantageous because of the much higher intensity and it eliminates the displacement errors. The profiles of specimens without broadening effects have the same FWHM as the aperture of the slits, equation (2.3.1.7). The FWHM increases as $\tan\theta$ due to wavelength dispersion. By increasing the length of the foils and keeping the same spacing, the aperture can be reduced to increase the resolution without large loss of intensity. A set of 365 mm long slits with 0.05° aperture has been used and even smaller apertures are feasible. Longer slits decrease the fluorescence intensity (if any) reaching the detector. They must be carefully made and aligned to avoid loss of intensity and should be evacuated or filled with He to avoid air-absorption losses.

The use of a crystal analyser eliminates fluorescence and gives the highest resolution powder profiles with FWHM = 0.02 to 0.05°2θ, depending on the quality of the crystal (Hastings *et al.*, 1984). The alignment of the crystal is critical and must be done with remote automated control every time the wavelength is changed. Displacement aberrations are eliminated but the intensity is much lower than the HPS because of the small rocking angle and low integrated reflectivity of the crystal.

The correct orientation of crystalline powder particles for reflection is far more restrictive for the parallel beam than the X-ray tube divergent beam. A much smaller number of particles will have the exact orientation for reflection, and thus the recorded intensity will be lower and relative intensities less accurate. If the specimen is stationary, the standard deviations of the intensities due to particle size are six to nine times higher than in focusing methods (Parrish, Hart & Huang, 1986). It also becomes more difficult to achieve the completely randomly oriented specimens required for structure determination and quantitative analysis and, as in X-ray tube data, a preferred-orientation term is included in the structure refinement. It is, therefore, essential to use small particles $< 10\,\mu$m and to rotate the specimen. Some investigators prefer to oscillate the specimen over a small angle but this is not as effective as rotation.

The profiles are virtually symmetrical except at small angles where axial divergence causes asymmetry. The profiles in Fig. 2.3.2.5 show the differences in the shape and resolution obtained with conventional focusing (*a*) and parallel-beam synchrotron methods (*b*). The effect of the higher resolution on a mixture of nearly equal volumes of quartz, orthoclase, and feldspar recorded with X-ray tube focusing methods is shown in Fig. 2.3.2.5(*c*) and with synchrotron radiation in Fig. 2.3.2.5(*d*). The symmetry and nearly constant simple instrument function make it easier to separate overlapping reflections and simplify the profile-fitting procedures and the interpretation of specimen-broadening effects.

The early crystal-structure studies using Rietveld refinement were not as successful with X-ray tube focusing methods as they were with neutron diffraction because the complicated instrument function made profile fitting difficult and inaccurate. The development of synchrotron powder methods with simple symmetrical instrument function, high resolution, and the use of longer wavelengths to increase the dispersion have made structural studies as successful as with neutrons, and have the advantage of orders-of-magnitude higher intensity. Some examples are described by Attfield, Cheetham, Cox & Sleight (1988), Lehmann, Christensen, Fjellvåg, Feidenhans'l & Nielsen (1987), and *ab initio* structure determinations by

McCusker (1988), Cernik *et al.* (1991), Morris, Harrison, Nicol, Wilkinson & Cheetham (1992), and others.

Structures have also been solved using a two-stage method in which the integrated intensities are determined by profile fitting the individual reflections and used in a powder least-squares refinement method (*POWLS*) (Will, Bellotto, Parrish & Hart, 1988). The method was tested with silicon, which gave R(Bragg) 0.7%, and quartz, which gave 1.6%, which is a good test of the high quality of the experimental data and the profile-fitting procedure. Fig. 2.3.2.6 shows Fourier maps of orthorhombic Mg_2GeO_4 calculated using Fourier coefficients taken directly from the profile-fitting intensities.

Other types of powder studies have been carried out successfully. For example, these have been used in anomalous-scattering studies (Will, Masciocchi, Hart & Parrish, 1987; Will, Masciocchi, Parrish & Hart, 1987), Warren–Averbach profile-broadening analysis (Huang, Hart, Parrish & Masciocchi, 1987), studies of texture in thin films (Hart, Parrish & Masciocchi, 1987), and precision lattice-parameter determination (Hart, Cernik, Parrish & Toraya, 1990).

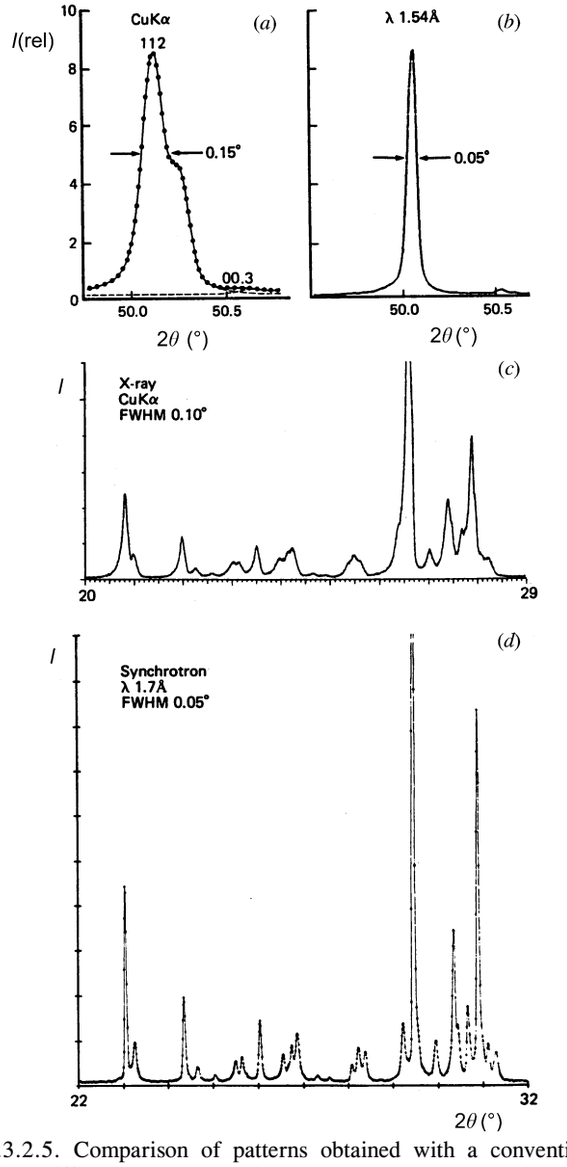

Fig. 2.3.2.5. Comparison of patterns obtained with a conventional focusing diffractometer (*a*) and (*c*), and synchrotron parallel-beam method (*b*) and (*d*). (*a*) and (*b*) quartz powder profiles; (*c*) and (*d*) mixture of equal amounts of quartz, orthoclase, and feldspar.

2.3.2.2. *Cylindrical specimen, 2θ scan*

The flat specimen can be replaced by a thin cylindrical [Fig. 2.3.2.4(*c*)] specimen as used in powder cameras. The powder can be coated on a thin fibre or reactive materials can be forced into a capillary to avoid contact with air. The intensity is lower than for flat specimens because of the smaller beam, and less powder is required. Thompson, Cox & Hastings (1987) used the method to determine the structure of Al_2O_3 by Rietveld refinement. They used a two-crystal incident-beam Si(111) monochromator; the first crystal was flat and the second a cylindrically bent triangular plate for sagittal focusing to form a 4×2 mm beam with spectral bandwidth $\Delta\lambda/\lambda \simeq 10^{-3}$.

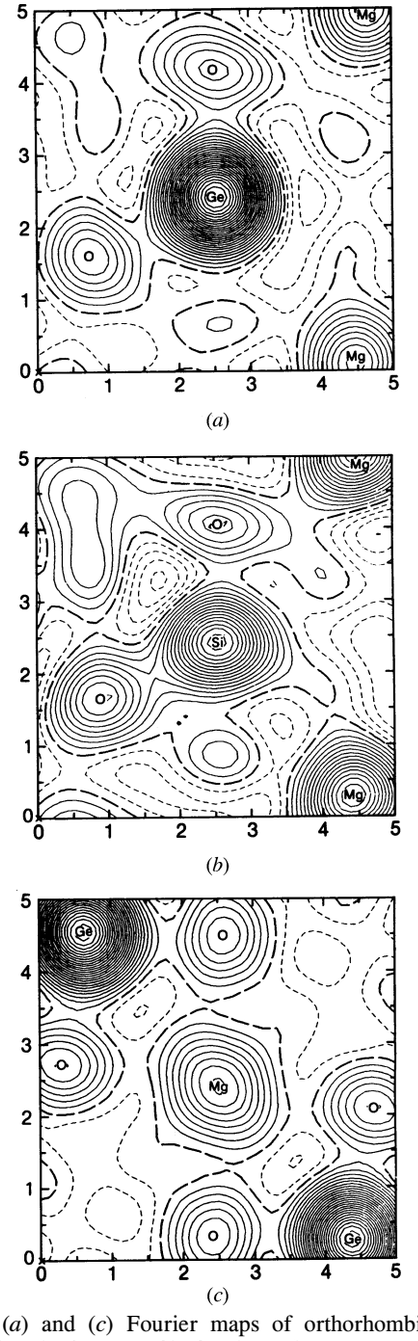

Fig. 2.3.2.6. (*a*) and (*c*) Fourier maps of orthorhombic Mg_2GeO_4 calculated directly from profile-fitted synchrotron powder data. (*b*) Fourier section of isostructural Mg_2SiO_4 calculated from single-crystal data for comparison with (*a*).

The method can also be used with a receiving slit or position-sensitive detectors (Lehmann *et al.*, 1987; Shishiguchi, Minato & Hashizume, 1986). The latter can be a short straight detector, which can be scanned to increase the data-collection speed (Göbel, 1982), or a longer curved detector.

2.3.2.3. *Grazing-incidence diffraction*

In conventional focusing geometry, the specimen and detector are coupled in θ–2θ relation at all 2θ's to avoid defocusing and profile broadening. In Seemann–Bohlin geometry, changing the specimen position necessitates realigning the diffractometer and very small incidence angles are inaccessible. In parallel-beam geometry, the specimen and detector positions can be uncoupled without loss of resolution. This freedom makes possible the use of different geometries for new applications. The specimen can be set at any angle from grazing incidence to slightly less than 2θ, and the detector scanned. Because the incident and exit angles are unequal, the relative intensities may differ by small amounts from those of the θ–2θ scan due to specimen absorption. The reflections occur from differently oriented crystallites whose planes are inclined (rather than parallel) to the specimen surface so that particle statistics becomes an important factor. The method is thus similar to Seemann–Bohlin but without focusing.

The method can be used for depth-profiling analysis of polycrystalline thin films using grazing-incidence diffraction (GID) (Lim, Parrish, Ortiz, Bellotto & Hart, 1987). If the angle of incidence θ_i is less than the critical angle of total reflection θ_c, diffraction occurs only from the top 35 to 60 Å of the film. Comparison of the GID pattern with a conventional θ–2θ pattern in which the penetration is much greater gives structural information for phase identification as a function of film depth. The intrinsic profile shapes are the same in the two patterns and broadening may indicate smaller particle sizes. However, if the film is epitaxic or highly oriented, it may not be possible to obtain a GID pattern.

For $\theta_i < \theta_c$, the penetration depth t' is (Vineyard, 1982)

$$t' \simeq \lambda/[2\pi(\theta_c^2 - \theta_i^2)^{1/2}] \qquad (2.3.2.1)$$

and, for $\theta_i > \theta_c$,

$$t' \simeq 2\theta_i/\mu, \qquad (2.3.2.2)$$

where μ is the linear absorption coefficient. The thinnest top layer of the film that can be sampled is determined by the film density, which may be less than the bulk value. As θ_i approaches θ_c, the penetration depth increases rapidly and fine control becomes more difficult. Fig. 2.3.2.7 shows this relation and the advantage of using longer wavelengths for a wider range of penetration control. For example, for a film with $\mu = 200\,\text{cm}^{-1}$, $\lambda = 1.75$ Å, and $\theta_i = 0.1°$, only the top 45 Å contribute, and increasing θ_i to 0.35° increases the depth to 130 Å. The patterns have much lower intensity than a θ–2θ scan because of the smaller diffracting volume.

Fig. 2.3.2.8 shows patterns of a 5000 Å polycrystalline film of iron oxide deposited on a glass substrate and recorded with (*a*) θ–2θ scanning and (*b*) 0.25° GID. The film has preferred orientation as shown by the numbers above the peaks in (*a*), which are the relative intensities of a random powder sample. The relative intensities are different because in (*a*) they come from planes oriented parallel to the surface and in (*b*) the planes are inclined. The glass scattering that is prominent in (*a*) is absent in (*b*) because the beam does not penetrate to the substrate.

2.3.2.4. *High-resolution energy-dispersive diffraction*

By step scanning the channel monochromator instead of the specimen, a different wavelength reaches the specimen at each step and the pattern is a plot of intensity *versus* wavelength or energy (Parrish & Hart, 1985, 1987). The X-ray optics can be the same as described in Subsection 2.3.2.1 and determines the resolution. A scintillation counter with conventional electronic circuits can be used. As in the conventional white-beam energy-

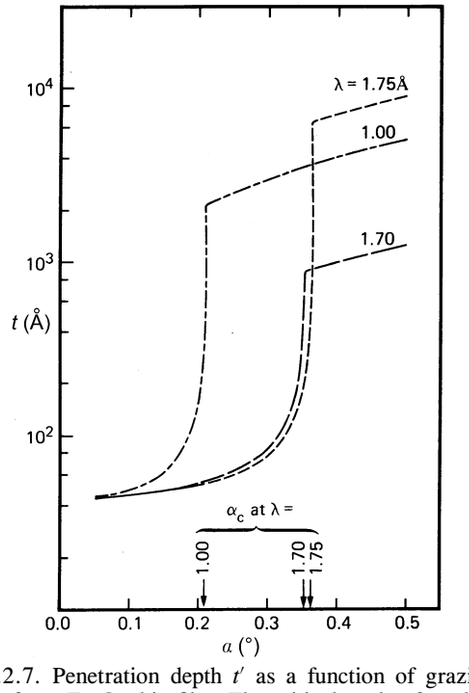

Fig. 2.3.2.7. Penetration depth t' as a function of grazing-incidence angle α for γ-Fe_2O_3 thin film. The critical angle of total reflection α_c is shown by the vertical arrows for different wavelengths.

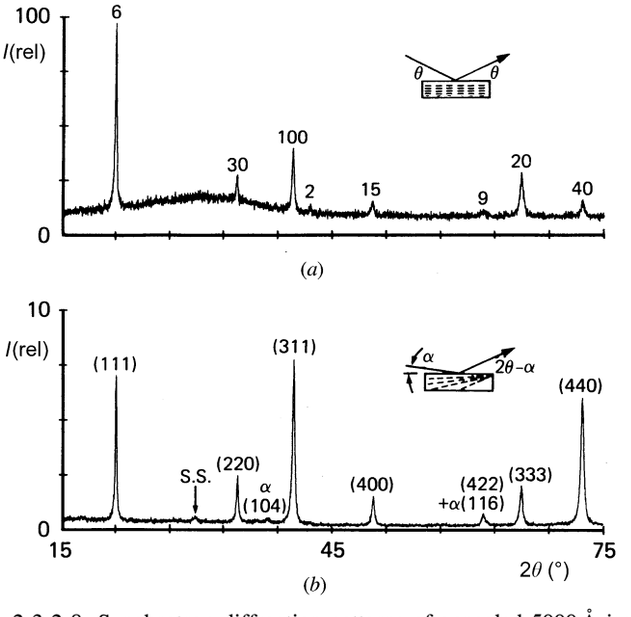

Fig. 2.3.2.8. Synchrotron diffraction patterns of annealed 5000 Å iron oxide film, $\lambda = 1.75$ Å, (*a*) θ–2θ scan; relative intensities of random powder sample shown above each reflection. (*b*) Grazing incidence pattern of same film with $\alpha = 0.25°$ showing only reflections from top 60 Å of film, superstructure peak S.S. and α-Fe_2O_3 peaks not seen in (*a*). Absolute intensity is an order of magnitude lower than (*a*).

dispersive diffraction (EDD) described in Section 2.5.1, the specimen and detector remain fixed at selected angles during the recording. This makes it possible to design special experiments that would not be possible with specimen-scanning methods. It also simplifies the design of specimen-environment chambers for high and low temperatures. The advantages of the method over conventional EDD are the order-of-magnitude higher resolution that can be controlled by the X-ray optics, the ability to handle high peak count rates with a high-speed scintillation counter and conventional circuits, and much lower count times for good statistical accuracy.

The accessible range of d's that can be recorded using a selected wavelength range is determined by the 2θ setting of the detector. Changing 2θ causes the separation of the peaks to expand or compress in a manner similar to a variation of λ in conventional diffractometry. This is illustrated in Figs. 2.3.2.9(*a*)–(*d*) for a quartz powder specimen using an Si(111) channel monochromator and $\theta_M = 19$ to 5° (2.04 to 0.55 Å, 6.1 to 22.7 keV) and four detector 2θ settings. At small 2θ settings, only the large d's are recorded and the peak separation is large. Increasing the 2θ setting decreases the d range and the separation of the peaks as shown in Fig. 2.3.2.9(*e*). These patterns were recorded with the pulse-height analyser set to discriminate only against scintillation counter noise.

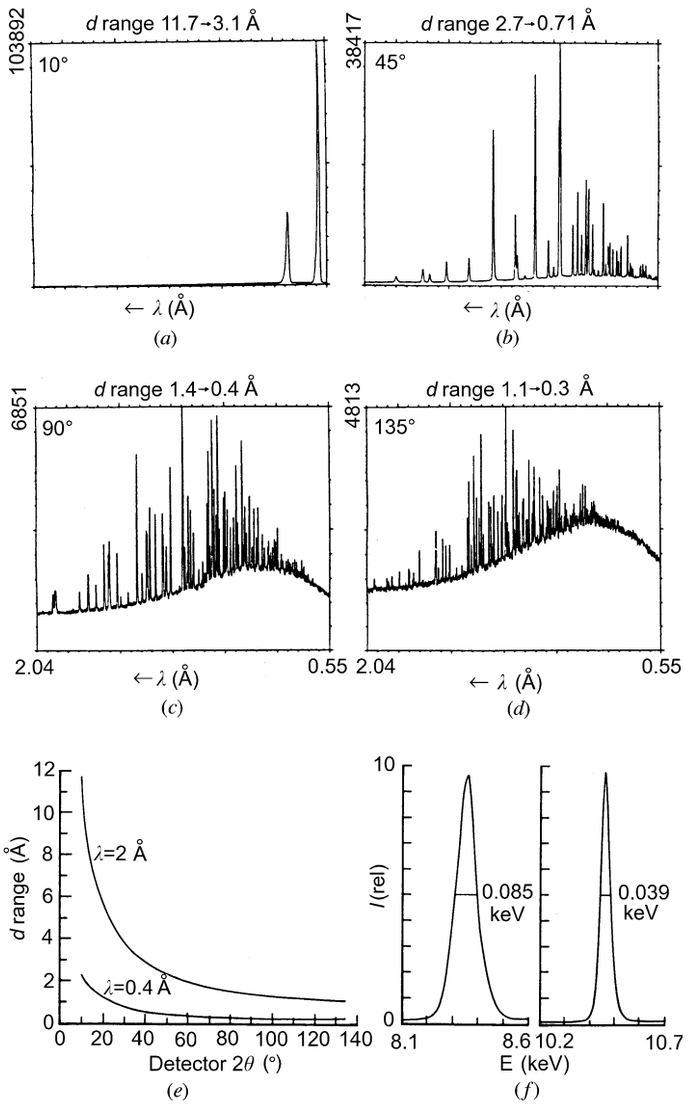

Fig. 2.3.2.9. (*a*)–(*d*) High-resolution energy-dispersive diffraction patterns of quartz powder sample obtained with 2θ settings shown in upper left corners. (*e*) d range as a function of detector 2θ setting for $\lambda = 0.4$ to 2 Å. (*f*) Effect of 2θ setting and E on profile widths of quartz. Right: 121 reflection, 20°2θ, E_p 10.45 keV; left: 100 reflection, 45°2θ, e_p 8.35; both reflections broadened by X-ray optics and peak intensity of 100 twice that of 121.

For given X-ray optics, the profiles symmetrically broaden with decreasing X-ray photon energy and with θ. This type of broadening remains symmetrical if E is increased and 2θ decreased, or *vice versa*, Fig. 2.3.2.9(*f*). The two profiles shown have been broadened by the X-ray optics but the intrinsic resolution is far better. The number of points recorded per profile thus decreases with decreasing profile width since $\Delta\theta_M$ is constant. At the higher energies, it may be desirable to use smaller $\Delta\theta_M$ steps to increase the number of points to define better the profile. Alternatively, increments in $\sin\theta$ steps rather than θ steps would eliminate this variation.

Many electronic solid-state devices use thin films that are purposely prepared to have single-crystal structure (*e.g.* epitaxic growth), or with a selected lattice plane oriented parallel or normal to the film surface to enhance certain properties. The properties vary with the degree of orientation and textural characterization is essential to make the correct film preparation. Preferred orientation can be detected by comparing the relative intensities of the thin-film pattern with those of a random powder. The pattern can be recorded with conventional θ–2θ scanning (λ fixed) or by EDD. However, this only gives information on the planes oriented parallel to the surface. To study inclined planes requires uncoupling the specimen surface and detector angles. This can be done with the EDD method described above without distorting the profiles (Hart *et al.*, 1987).

The principle of the method is illustrated in Fig. 2.3.2.10. The set of lattice planes (*hkl*) oriented parallel to the surface has its highest intensity in the symmetric θ–2θ position. Rotating the specimen by an angle θ_r while keeping 2θ fixed reduces the intensity of (*hkl*) and brings another set of planes (*pqr*), which are inclined to the surface, to its symmetrical reflecting position. The required rotation is determined by the interplanar angle between (*hkl*) and (*pqr*). The angular distribution of any plane can be measured with respect to the film surface by step scanning at small θ_r steps. The specimen is rotated clockwise with the limitation $\theta_s + \theta_r < 2\theta$. A computer automation program is desirable for large numbers of measurements.

Fig. 2.3.2.3(*c*) shows the appearance of a pattern of a specimen containing elements with absorption edges in the recording range and using electronic discrimination only against electronic noise. Starting at the incident high-energy side, the Zn and Ni K fluorescence increases as the energy approaches the edges (λ^3 law), decreases abruptly when the energy crosses each edge, and disappears beyond the Ni K edge. Long-wavelength fluorescence is absorbed in the windows and air path.

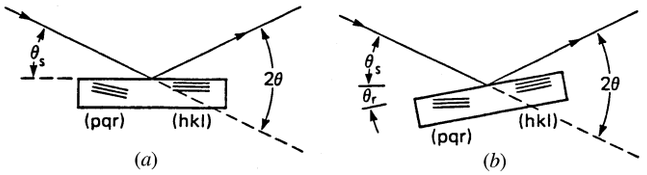

Fig. 2.3.2.10. Specimen orientation for symmetric reflection (*a*) from (*hkl*) planes and (*b*) specimen rotated θ_r for symmetric reflection from (*pqr*) planes.

The method is of doubtful use for structure determination or quantitative analysis. The wide range of wavelengths, continually varying absorption and profile widths, and other factors create a major difficulty in deriving accurate values of the relative intensities.

Conventional energy-dispersive diffraction methods using white X-rays and a solid-state detector are described in Chapter 2.5 and Section 5.2.7.

2.3.3. Specimen factors, angle, intensity, and profile-shape measurement

The basic experimental procedure in powder diffraction is the measurement of intensity as a function of scattering angle. The profile shapes and 2θ angles are derived from the observed intensities and hence the counting statistical accuracy has an important role. There is a wide range of precision requirements depending on the application and many factors are involved: instrument factors, counting statistics, profile shape, and particle-size statistics of the specimen. *The quality of the specimen preparation is often the most important factor in determining the precision of powder diffraction data.*

D. K. Smith and colleagues (see, for example, Borg & Smith, 1969; see also Yvon, Jeitschko & Parthé, 1977) developed a method for calculating theoretical powder patterns from well determined single-crystal structures and have made available a Fortran program (Smith, Nichols & Zolensky, 1983). This has important uses in powder diffraction studies because it provides reference data with correct I's and d's, free of sample defects, preferred orientation, statistical errors, and other factors. The data can be displayed as recorded patterns by using plot parameters corresponding to the experimental conditions (Subsection 2.3.3.9). Calculated patterns have been used in a large variety of studies such as identification standards, computing intermediate members of an isomorphous series, testing structure models, ordered and disordered structures, and others. Many experiments can be performed with simulated patterns to plan and guide research. The method must be used with some care because it is based on the small single crystal used in the crystal-structure determination and the large powder samples of minerals and ceramics, for example, may have a different composition. Errors in the structure analysis are magnified because the powder intensities are based on the squares of the structure factors.

The Lorentz and polarization factors for diffractometry geometry have been discussed by Ladell (1961) and Pike & Ladell (1961).

Smith & Snyder (1979) have developed a criterion for rating the quality of powder patterns; see also de Wolff (1968*a*).

2.3.3.1. *Specimen factors*

Ideally, the specimen should contain a large number of small equal-sized randomly oriented particles. The surface must be flat and smooth to avoid microabsorption effects, *i.e.* particle interferences which reduce the intensities of the incident and reflected beams and can lead to significant errors (Cline & Snyder, 1983). The specimen should be homogeneous, particularly if it is a mixture or if a standard has been added. Low packing density and specimen-surface displacement (§2.3.1.1.6) may cause significant errors. It is recommended that the powder and the prepared specimen be examined with a low-power binocular optical microscope. Smith & Barrett (1979), Jenkins, Fawcett, Smith, Visser, Morris & Frevel (1986), and Bish & Reynolds (1989) have surveyed methods of specimen preparation and they include bibliographies on special handling problems. Powder diffraction standards for angle and intensity calibration are described in Section 5.2.9.

2.3.3.1.1. *Preferred orientation*

Preferred orientation changes the relative intensities from those obtained with a randomly oriented powder sample. It occurs in materials that have good cleavage or a morphology that is platy, acicular or any special shape in which the particles tend to orient themselves in specimen preparation. The micas and clay minerals are examples of materials that exhibit very strong preferred orientation. When they are prepared as reflection specimens, the basal reflections dominate the pattern. It is common in prepared thin films where preferred orientation occurs frequently or may be purposely induced to enhance certain optical, electrical, or magnetic properties for electronic devices. By comparison of the relative intensities with the random powder pattern, the degree of preferred orientation can be observed.

Powder reflections take place from crystallites oriented in different ways in the instrument geometries as shown in Fig. 2.3.1.2. In reflection specimen geometry with θ–2θ scanning, reflections can occur only from lattice planes parallel to the surface and in the transmission mode they must be normal to the surface. In the Seemann–Bohlin and fixed specimen with 2θ scanning methods, the orientation varies from parallel to about 45° inclination to the surface. The effect of preferred orientation can be seen in diffraction patterns obtained by using the same specimen in the different geometries.

The effect is illustrated in Fig. 2.3.3.1 for *m*-chlorobenzoic acid, $C_7H_5ClO_2$, with reflection and transmission patterns and the pattern calculated from the crystal structure. The degree of preferred orientation is shown by comparing the peak intensities of four reflections in the three patterns:

(*hkl*)	(120)	(200)	(040)	(121)
Reflection	9.8	0.6	1.6	2.5
Transmission	5.2	0.5	0.7	9.3
Calculated	3.0	6.6	4.0	9.1.

Care is required to make certain the differences are not caused by a few fortuitously oriented large particles.

Various methods have been used to minimize preferred orientation in the specimen preparation (Calvert, Sirianni, Gainsford & Hubbard, 1983; Smith & Barrett, 1979; Jenkins *et al.*, 1986; Bish & Reynolds, 1989). These include using small particles, loading the powder from the back or side of the specimen holder, and cutting shallow grooves to roughen the surface. The powder has also been sifted directly on the surface of a microscope slide or single-crystal plate that has been wetted with the binder or petroleum jelly. Another method is to mix the powder with an inert amorphous powder such as Lindemann glass or rice starch, or add gum arabic, which after setting can be reground to obtain irregular particles. Any additive reduces the intensity and the peak-to-background ratio of the pattern. A promising method that requires a considerable amount of powder is to mix it with a binder and to use spray drying to encapsulate the particles into small spheres which are then used to prepare the specimen (Smith, Snyder & Brownell, 1979).

Preferred orientation would not cause a serious problem in routine identification providing the reference standard had a similar preferred orientation and both patterns were obtained with the same diffractometer geometry. However, when accurate values of the relative intensities are required, as in crystal-

structure refinement and quantitative analysis, it may be the major factor limiting the precision.

In practice, it is very difficult to prepare specimens that have a completely random orientation. Even materials that do not have good cleavage or special morphological forms, such as quartz and silicon, show small deviations from a completely random orientation. These show up as errors in the structure refinement and a correction factor is required.

An empirical correction factor determined by the acute angle φ between the preferred-orientation plane and the diffracting plane (hkl)

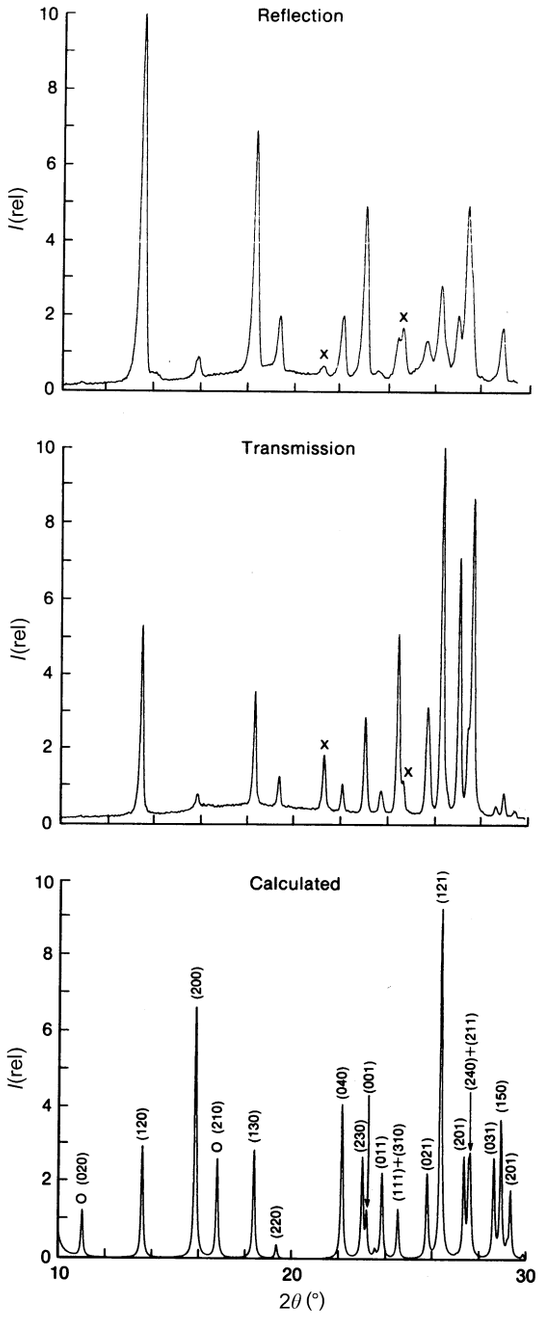

Fig. 2.3.3.1. Differences in relative intensities due to preferred orientation as seen in synchrotron X-ray patterns of *m*-chlorobenzoic acid obtained with a specimen in reflection and transmission compared with calculated pattern. Peaks marked × are impurities, *O* absent in experimental patterns.

Table 2.3.3.1. *Preferred-orientation data for silicon*

$h\ k\ l$	R(Bragg) (%)	GP
1 1 1	1.86	−0.11
2 2 0	2.02	−0.11
3 1 1	2.01	0.17
4 0 0*	0.86	−0.15
3 3 1	1.73	−0.19
4 2 2	2.43	0.04
5 1 1	1.36	0.19
5 3 1	2.44	−0.08
4 4 2	1.69	−0.19
6 2 0	1.25	0.29
5 3 3	2.40	−0.04

* Selected preferred orientation plane.

Table 2.3.3.2. *R(Bragg) values obtained with different preferred-orientation formulae*

	R(Bragg)		
	Si	SiO_2	Mg_2GeO_4
No corrections	3.50	2.57	12.5
Gaussian	1.65	1.60	5.71
Exponential	0.75	1.83	5.30
March/Dollase	0.75	1.64	4.87
Preferred-orientation plane	100	211	100

$$I(\text{corr.}) = I(hkl)P(hkl)\varphi \qquad (2.3.3.1)$$

can be used (Will *et al.*, 1988). Three functions have been used to represent $P(hkl)\varphi$ and the term GP is the variable refined:

$$P(hkl)\varphi = \exp(-\text{GP}\varphi^2) \qquad (2.3.3.2)$$

(Rietveld, 1969) for transmission specimens;

$$P(hkl)\varphi = \exp[\text{GP}(\pi/2 - \varphi^2)] \qquad (2.3.3.3)$$

for reflection specimens; and

$$P(hkl)\varphi = (\text{GP}^2 \cos^2\varphi + \sin^2\varphi/\text{GP})^{-3/2} \qquad (2.3.3.4)$$

(Dollase, 1986).

These functions are quite similar for small amounts of non-randomness. The preferred-orientation plane is selected by trial and error. For example, a modified fast routine of the powder least-squares refinement program with only seven cycles of refinement on each plane for the first dozen allowed Miller indices can be used to find the plane that gives the lowest R(Bragg) value as shown in Table 2.3.3.1. All three functions improve the R(Bragg) value as shown in Table 2.3.3.2 but the evidence is not conclusive as to which is the best. More research is required in this area. Several specimens made of the same material may show different preferred-orientation planes, and in some cases the preferred-orientation plane never occurred in the crystal morphology. A more complicated method examines the polar-axis density distribution using a cubic harmonic expansion to describe the crystallite orientation of a rotating sample (Järvinen, Merisalo, Pesonen & Inkinen, 1970; Ahtee, Nurmela, Suortti & Järvinen, 1989; Järvinen, 1993).

2.3.3.1.2. *Crystallite-size effects*

In addition to profile broadening, which begins to appear when the crystallite sizes are < 1–$2\,\mu m$, the sizes have a strong effect on the absolute and relative intensities (de Wolff, Taylor & Parrish, 1959; Parrish & Huang, 1983). The particle sizes have to be less than about $5\,\mu m$ to achieve 1% reproducible relative intensities from a stationary specimen in conventional diffractometer geometry (Klug & Alexander, 1974). The statistical errors arising from the number of particles irradiated can be greatly reduced by using smaller particles and rotating the specimen around the diffraction vector. This brings many more particles into reflecting orientations.

The particle-size effect is illustrated in Fig. 2.3.3.2 for specimens of NIST silicon standard powder 640 sifted to different size fractions. The powders were packed in a 1 mm deep cavity in a 25.4 mm diameter Al holder using 5% collodion/amyl acetate binder. They were rotated by a synchronous motor (a stepper motor can also be used) around the axis normal to the centre of the specimen surface with the detector arm fixed at the peak position and the intensity recorded with a strip-chart. Rapid rotation, $\sim 60\,r\,min^{-1}$, gives the average peak intensity for all azimuths of the specimen and the small variations result only from the counting statistics. Scaling the intensities to (111) = 100% for the 5–10 μm fraction, the 10–20 μm fraction is 94%, 20–30 μm 88% and > 30 μm 59%. The decrease is probably due to lower particle-packing density and increasing interparticle microabsorption. The > 5 μm fraction = 95% may be due to the larger ratio of oxide coating around the particles to the mass of the particles.

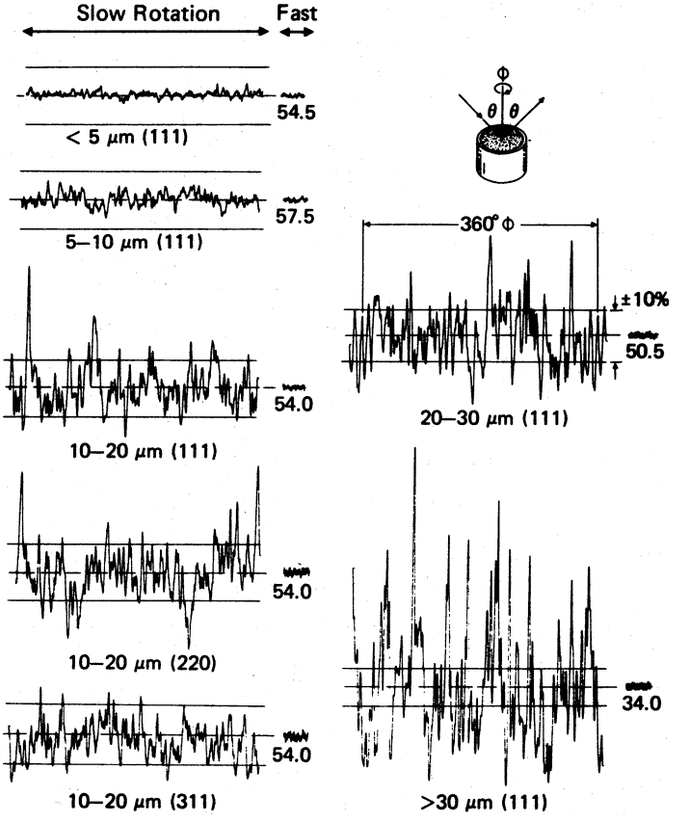

Fig. 2.3.3.2. Effect of specimen rotation and particle size on Si powder intensity using a conventional diffractometer (Fig. 2.3.1.3) and Cu $K\alpha$. Numbers below fast rotation are the average intensities.

Slow rotation, $\sim 1/7\,r\,min^{-1}$, shows the variation of the peak intensity with azimuth angle φ. The pattern repeats after 360° rotation and the magnitude of the fluctations increases with increasing particle sizes and resolution. There is no correlation between the fluctations of different reflections, as can be seen by comparing the 111, 220 and 311 reflections of the 10–20 μm specimen (lower left side) for which the incident-beam intensity was adjusted to give the same average amplitude. The horizontal lines are ±10% of the average. This shows the magnitude of errors that could occur using stationary specimens. Similar particle-size effects were found using the integrated intensities derived from profile fitting. The above discussion and Fig. 2.3.3.2 refer to a continuous scan. If the step-scan mode is used to collect data, it is clearly not necessary to rotate the specimen through more than one revolution at each step.

The rotating specimen also averages the in-plane preferred orientation but has virtually no effect on the planes oriented parallel to the specimen surface. The slow rotation method is useful in testing the grinding and sifting stages in specimen preparation. When calibrated with known size fractions, it can be used as a rough qualitative measure of the particle sizes.

2.3.3.2. *Problems arising from the Kα doublet*

A common source of error arises from the $K\alpha$ doublet which produces a pair of peaks for each reflection. The separation of the Cu $K\alpha_1$, $K\alpha_2$ peaks increases from 0.05° at 20°2θ to 1.08° at 150°2θ. The overlapping is also dependent on the instrument resolution and may cause errors in the peak angles and intensities when strip-chart recording or peak-search methods (described below) are used. The $K\alpha_1$ wavelength is generally used to calculate all the d's even when the low-angle peaks are unresolved. In the region where the doublet is only slightly resolved, the apparent $K\alpha_1$ peak angle is shifted to higher angles because of the overlapping $K\alpha_2$ tail and similarly the peak intensities will be in error. The relative peak intensities of a reflection with superposed doublet compared to a resolved doublet could have an error as large as 50%. Relative peak intensities are used in the ICDD standards file and cause no problem because the unknowns are measured in the same way. The integrated intensity avoids this difficulty but is impractical to use in routine identification.

Rachinger (1948) described a simple graphical procedure for removing $K\alpha_2$ peaks. The method causes errors because it makes the incorrect assumption that $K\alpha_2$ is the exact half-scale version of $K\alpha_1$. Ladell, Zagofsky & Pearlman (1975) developed an exact algorithm using the actual mathematical shapes observed with

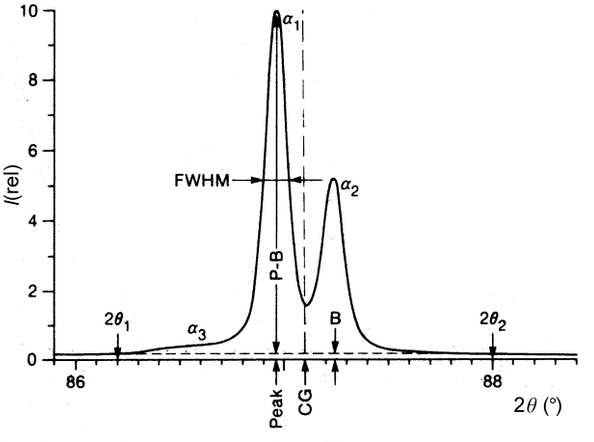

Fig. 2.3.3.3. Various measures of profile.

the user's diffractometer but, with line-profile-fitting programs now available, the $K\alpha_2$ component can be modelled precisely along with the $K\alpha_1$.

It is possible to isolate the $K\alpha_1$ line when using a high-quality incident-beam focusing monochromator as described in Subsection 2.3.1.2, Fig. 2.3.1.12(*b*), but there may be a loss of intensity. The source size must be narrow and the focal length long enough to separate the components.

2.3.3.3. *Use of peak or centroid for angle definition*

The most obvious and commonly used measure of the reflection angle of a profile is the position of maximum intensities (Fig. 2.3.3.3). The midpoints of chords at various heights have often been used but their values vary with the profile asymmetry. Another method is to connect the midpoints of chords near the top of the profile and extrapolate to the peak. The computer methods using derivatives are the most accurate and fastest as described in Subsection 2.3.3.7.

A more fundamental measure that uses the entire intensity distribution is the centre of gravity (or centroid) defined as

$$\langle 2\theta\rangle = \int 2\theta I(2\theta)\,\mathrm{d}(2\theta) \Big/ \int I(2\theta)\,\mathrm{d}(2\theta). \qquad (2.3.3.5)$$

The variance (mean-square deviation of the mean) is defined as

$$W_{2\theta} = \langle(2\theta - \langle 2\theta\rangle)^2\rangle = \int(2\theta - \langle 2\theta\rangle)^2 I(2\theta)\,\mathrm{d}(2\theta) \Big/ \int I(2\theta)\,\mathrm{d}(2\theta). \qquad (2.3.3.6)$$

The use of the centroid and variance has two important advantages: (1) most of the aberrations (§2.3.1.1.6) were derived in terms of the centroid and variance; and (2) they are additive, making it easy to determine the composite effect of a number of aberrations. Mathematically, the integration extends from $-\infty$ to $+\infty$ but the aberrations have a finite range. However, the practical use of these measures causes some difficulty. If the profile shapes are Lorentzian, the tails decay slowly. A very wide range would be required to reach points where the signal could no longer be separated from the background and the profiles must be truncated for the calculation. Truncation limits that have been used are 90% ordinate heights of $K\alpha_1$ (Ladell, Parrish & Taylor, 1959), and equal 2θ or λ limits from the centroid (Taylor, Mack & Parrish, 1964; Langford, 1982). The limits such as $2\theta_1$ and $2\theta_2$ in Fig. 2.3.3.3 must be carefully chosen to avoid errors and this involves the correct determination of the background level. It is not practical to use centroids for overlapping peak clusters unless the profile fitting can accurately resolve the individuals with their correct positions and intensities. Their use has, therefore, been confined to simple patterns with small unit cells in which the profiles were well separated.

The difference between the angle derived from the peak and the centroid depends on the asymmetry of the profile, which in turn varies with the $K\alpha$-doublet separation and the aberration broadening. Tournarie (1958) found that the centre of a horizontal chord at 60.6% of the $K\alpha_1$ peak height corresponds well to the centroid of that line in fairly well resolved doublets. The number, of course, depends on the profile shape. There is also the basic problem that most of the X-ray wavelengths were probably determined from the spectral peaks and, if the centroids are measured for the powder pattern, the Bragg equation becomes nonlinear in the sense that the 1:1 correspondence between λ and $\sin\theta$ is lost.

2.3.3.4. *Rate-meter/strip-chart recording*

Formerly, the most common method of obtaining diffractometer data was by using a rate-meter and strip-chart recorder with the paper moving synchronously with the constant angular velocity of the scan. This simple analogue method is still used and a large fraction of the JCPDS (ICDD) file prior to about 1982 was obtained in this way.

The method has several limitations: the data are not in the digital form required for computers, and are distorted; manual measurement of the chart takes a long time and has low accuracy. The output of the strip chart lags behind the input by an amount determined by the product of the scanning speed and the time constant of the rate-meter, including the speed of the recorder pen. The peak height is decreased and shifted in the direction of the scan causing asymmetric broadening with loss of resolution. The profile shape, $K\alpha$-doublet separation, and scan direction also contribute to distortion. When the product of the scan speed and time constant have the same value, the profile shapes are the same even though the total count is determined by the scan speed, Figs. 2.3.3.4(*a*) and (*b*). If the product is large, the distortion is severe (*c*), and very weak peaks may be lost.

2.3.3.5. *Computer-controlled automation*

Most diffractomers are now sold with computer automation. Older instruments can be easily upgraded by adding a stepping motor to the gear-drive shaft. A large variety of computers and programs is available, and it is not easy to make the best selection. Continuing improvements in computer technology have been made to handle expanded programs with increased speed and storage capabilities. The collected data are displayed on a VDU screen and/or computer printer and stored on hard disk or diskette for later use and analysis. Microprocessors are often used to select the X-ray-generator operating conditions, shutter control, specimen change, and similar tasks that were formerly performed manually. Aside from the elimination of much of the manual labour, automation provides far better control of the data-collection and data-reduction procedures. However, computers do not preclude the necessity of precise alignment and calibration. Smith (1989) has written a detailed description of computer analysis for phase identification and also includes related programs and their sources.

Personal computers are widely used for powder-diffraction automation and a typical arrangement is shown in Fig. 2.3.3.5(*a*). The automation may provide for step scanning,

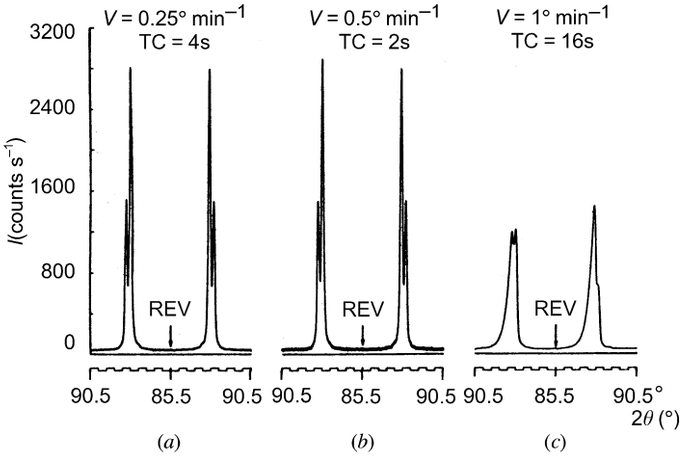

Fig. 2.3.3.4. Rate-meter strip-chart recordings. REV: scan direction reversed. Scan speed and time constant shown at top.

continuous scanning with read-out on the fly, or slewing to selected angles to read particular points. Step scanning is the method most frequently used. It is essential that absolute registration and step tracking be reliably maintained for all experimental conditions.

The step size or angular increment $\Delta 2\theta$ and count time t at each step, and the beginning and ending angles are selectable. For a given total time available for the experiment, it usually makes no difference in the counting statistical accuracy if a combination of small or large $\Delta 2\theta$ and t (within reasonable limits) is used. A minimal number of steps of the order of $\Delta 2\theta \simeq 0.1$ to 0.2 FWHM is required for profile fitting isolated peaks. It is clear that the greater the number of steps, the better the definition of the profile shape. The step size becomes important when using profile fitting to resolve patterns containing overlapped reflections and to detect closely spaced overlaps from the width and small changes in slopes of the profiles. A preliminary fast run to determine the nature of the pattern may be made to select the best run conditions for the final pattern. Will *et al.* (1988) recorded a quartz pattern with 1.28 Å synchrotron X-rays and 0.01° steps to test the step-size role. The profile fitting was done using all points and repeated with the omission of every second, third, and fourth point corresponding to $\Delta 2\theta = 0.02$, 0.03 and 0.04°. The R(Bragg) values were virtually the same (except for 0.04° where it increased), indicating the experimental time could have been reduced by a factor of three with little loss of precision; see also Hill & Madsen (1984). Patterns with more overlapping would require smaller steps. Ideally, the steps could be larger in the background but this also requires a prior knowledge of the pattern and special programming.

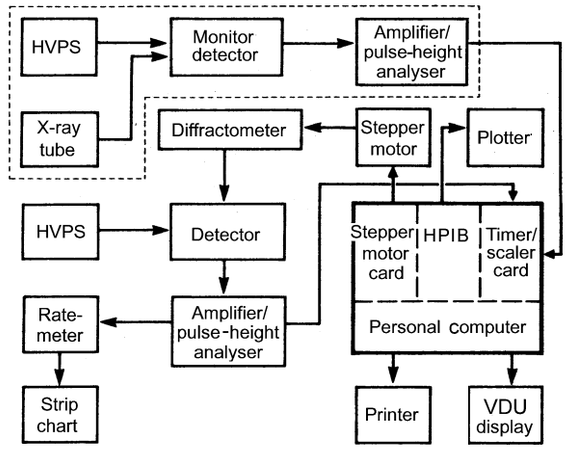

(*a*)

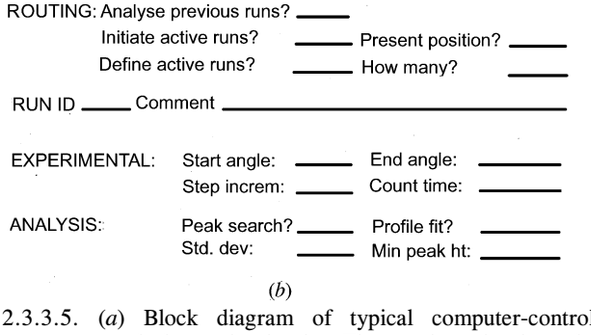

(*b*)

Fig. 2.3.3.5. (*a*) Block diagram of typical computer-controlled diffractometer and electronic circuits. The monitor circuit enclosed by the dashed line is optional. HPIB is the interface bus. (*b*) A full-screen menu with some typical entries.

A typical VDU screen menu for diffractometer-operation control is shown in Fig. 2.3.3.5(*b*). A number of runs can be defined with the same or different experimental parameters to run consecutively. The run log number, date, and time are usually automatically entered and together with the comment and parameters are carried forward and recorded on the print-outs and graphics to make certain the runs are completely identified. The menu is designed to prompt the operator to enter all the required information before a run can be started. Error messages appear if omissions or entry mistakes are made. There are, of course, many variations to the one shown.

2.3.3.6. *Counting statistics*

X-ray quanta arrive at the detector at random and varying rates and hence the rules of statistics govern the accuracy of the intensity measurements. The general problems in achieving maximum accuracy in minimum time and in assessing the accuracy are described in books on mathematical statistics. Chapter 7.5 reviews the pertinent theory; see also Wilson (1980). In this section, only the fixed-time method is described because the fixed-count method takes too long for most practical applications.

Let $\bar{N}$ be the average of N, the number of counts in a given time t, over a very large number of determinations. The spread is given by a Poisson probability distribution (if $\bar{N}$ is large) with standard deviation

$$\sigma = \bar{N}^{1/2}. \tag{2.3.3.7}$$

Any individual determination of N or the corresponding counting rate n $(= N/t)$ will be subject to a proportionate error ε which is also a function of the confidence level, *i.e.* the probability that the result deviates less than a certain percentage from the true value. If Q is the constant determined by the confidence level, then

$$\varepsilon = Q/N^{1/2}, \tag{2.3.3.8}$$

where $Q = 0.67$ for the probable relative error ε_{50} (50% confidence level) and $Q = 1.64$ and 2.58 for the 90 and 99% confidence levels (ε_{90}, ε_{99}), respectively. For a 1% error, $N = 4500$, 27 000, 67 000 for ε_{50}, ε_{90}, ε_{99}, respectively. Fig. 2.3.3.6 shows various percentage errors as a function of N for several confidence levels.

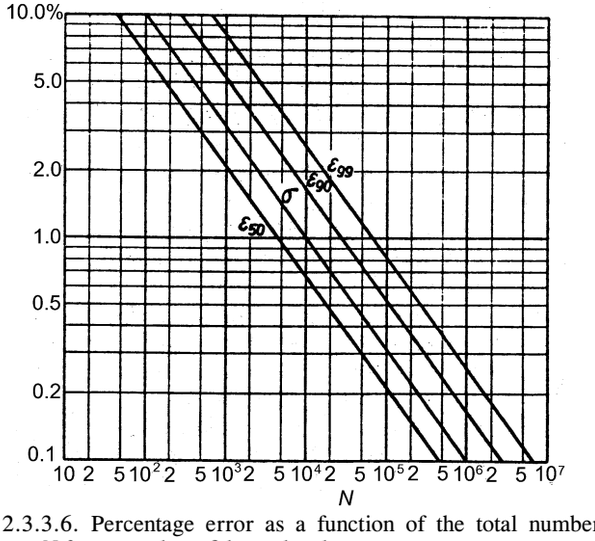

Fig. 2.3.3.6. Percentage error as a function of the total number of counts N for several confidence levels.

In practice, there is usually a background count N_B. The net peak count $N_{P+B} - N_B = N_{P-B}$ is dependent on the P/B radio as well as on N_{P+B} and N_B separately. The relative error ε_D of the net peak count is

$$\varepsilon_D = \frac{[(N_{P+B}\varepsilon_{P+B})^2 + (N_N\varepsilon_B)^2]^{1/2}}{N_{P-B}}, \qquad (2.3.3.9)$$

which shows that ε_D is similarly influenced by both absolute errors $N_{P+B}\varepsilon_{P+B}$ and $N_B\varepsilon_B$. The absolute standard deviation of the net peak height is

$$\sigma_{P-B} = (\sigma_{P+B}^2 + \sigma_B^2)^{1/2} \qquad (2.3.3.10)$$

and expressed as the per cent standard deviation is

$$\sigma_{P-B} = \frac{(N_{P+B} + N_B)^{1/2}}{N_{P-B}} \times 100. \qquad (2.3.3.11)$$

The accuracy of the net peak measurement decreases rapidly as the peak-to-background ratio falls below 1. For example, with $N_B = 50$, the dependence of σ_{P-B} on P/B is

P/B	σ_{P-B} (%)
0.1	205
1	24.5
10	4.9
100	1.43.

It is obviously desirable to minimize the background using the best possible experimental methods.

2.3.3.7. *Peak search*

The accurate location of the 2θ angle corresponding to the peak of the profile has been discussed in many papers (see, for example, Wilson, 1965). Computers are now widely used for data reduction, thereby greatly decreasing the labour, improving the accuracy, and making possible the use of specially designed algorithms. It is not possible to present a description of the large number of private and commercial programs. The peak-search and profile-fitting methods described below have been successfully used for a number of years and are representative of the results that can now be obtained. They have greatly improved the results in phase identification, integrated intensity measurement, and analyses requiring precise profile-shape determination. It is likely that even better programs and methods will be developed in this rapidly changing field.

There are two levels of the types of data reduction that may be done. The easiest and most frequently used method is usually called 'peak search'. It computes the 2θ angles and intensities of the peaks. The results have good precision for isolated peaks but give the values of the composite overlapping reflections as they appear, for example, on a strip-chart recording. The calculation is virtually instantaneous and is often all that is needed for phase identification, lattice-parameter determination, and similar analyses. The second, profile fitting, described below, is a more advanced procedure that can resolve overlapping peaks into individual reflections and determines the profile shape, width, peak and integrated intensities, and reflection angle of each resolved peak. This method requires a prior knowledge of the profile-fitting function. It is used to determine the integrated intensities for analyses requiring higher precision such as crystal-structure refinement and quantitative analysis, and profile-shape parameters for small crystallite size, microstrain and similar studies.

To measure weak peaks, the counting statistical accuracy must be sufficient to delineate the peak from the background. When the intensity and peak-to-background ratio are low, the computing time is much increased. Since powder patterns often contain a number of weak peaks that may not be required for the analysis, computer programs often permit the user to select a minimum peak height (MPH) and a standard deviation (SD) that the peak must exceed to be included in the data reduction. For example, MPH = 1 would reject peaks less than 1% of the highest peak in the recorded pattern, and SD = 4 requires the intensity to exceed the background adjacent to the peak by $4B^{1/2}$. The number of peaks rejected depends on the intensity and peak-to-background ratio as illustrated in Fig. 2.3.3.7, where the cut-off level was set at $\bar{B} + 4\bar{B}^{1/2}$ for two recordings of the same pattern with about a 40 times difference in intensities. All visible peaks are included in the high-intensity recording and several are rejected by the cut-off level selected in the lower-intensity pattern.

Before carrying out the computer calculations, it may be desirable to subtract unusual background such as is caused by a glass substrate in a thin-film pattern.

The following method was developed using computer-generated profiles having the same shapes as conventional diffractometer (Fig. 2.3.1.3) profiles and adding random counting statistical noise (Huang & Parrish, 1984; Huang, 1988). The best results were obtained using the first derivative ($dx/dy = 0$) of a least-squares-fitted cubic polynomial to locate the peaks, combined with the second derivative ($d^2y/dx^2 =$ minimum) of a quadratic/cubic polynomial to resolve overlapped reflections (Fig. 2.3.3.8). Overlaps with a separate ≥ 0.5 FWHM can be resolved and measured and the accuracy of the peak position is 0.001° for noise-free profiles. Real profiles with statistical noise have a precision of ±0.003 to 0.02° depending on the noise level. The Savitzky & Golay (1964) method (see also Ateiner, Termonia & Deltour, 1974; Edwards & Willson, 1974) was used for smoothing and differentiation of

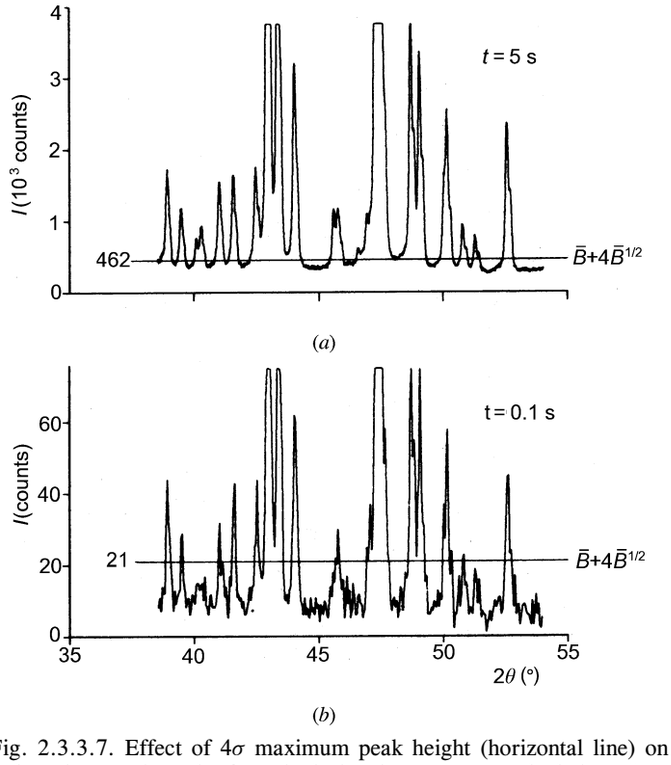

Fig. 2.3.3.7. Effect of 4σ maximum peak height (horizontal line) on dropping weak peaks from inclusion in computer calculation. Step scan with (*a*) $t = 5$ s and (*b*) $t = 0.1$ s. Five-compound mixture, Cu $K\alpha$.

the data by least squares in which the values of the derivatives can be calculated using a set of tabulated integers. The convolution range CR expressed as a multiple of the FWHM of the peak can be selected. A minimum of five points is required. For asymmetric peaks, such as occur at small 2θ's, a CR $\simeq 0.5$ FWHM gives the best precision. The larger the CR the larger the intrinsic error but the smaller the random error, and the smaller the number of peaks identified in overlapping patterns. The larger CR also avoids false peaks in patterns with poor counting statistics. Fig. 2.3.3.8(*c*) shows the dependence of the accuracy of the peak determination on P/σ. The computer results list the 2θ's, d's, absolute and relative intensities (scaled to 100) of the identified peaks. The calculation is made with a selected wavelength such as $K\alpha_1$ and the possible $K\alpha_2$ peaks are flagged.

2.3.3.8. *Profile fitting*

Profile fitting has greatly advanced powder diffractometry by making it possible to calculate the intensities, peak positions, widths, and shapes of the reflections with a far greater precision than had been possible with manual measurements or visual inspection of the experimental data. The method has better resolution than the original data and the entire scattering distribution is used instead of only a few features such as the peak and width. Individual profiles and clusters of reflections can be fitted, or the entire pattern as in the Rietveld method (Chapter 8.6).

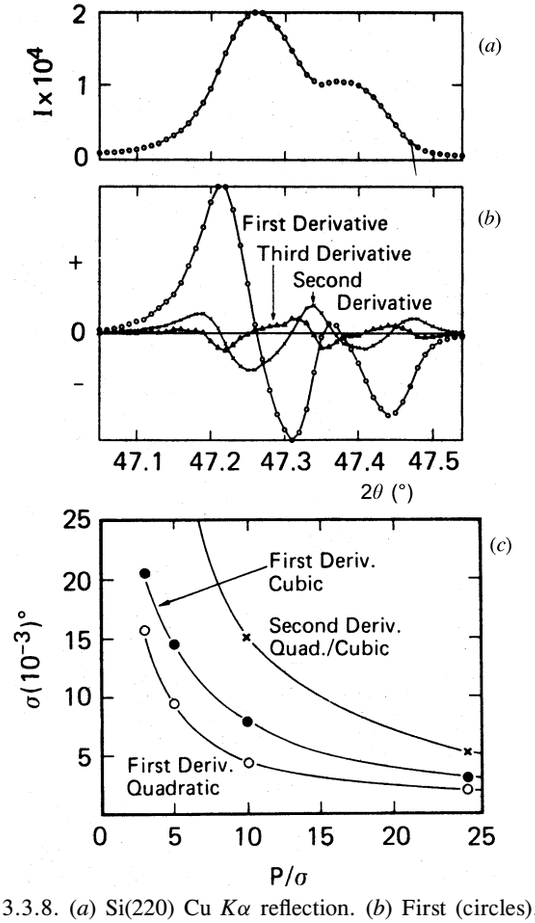

Fig. 2.3.3.8. (*a*) Si(220) Cu $K\alpha$ reflection. (*b*) First (circles), second (crosses), and third (triangles) derivatives of a seven-point polynomial of data in (*a*). (*c*) Average angular deviations as a function of P/σ for various derivatives.

The procedure is based on the least-squares fitting of theoretical profile intensities to the digitized powder pattern. The profile intensity at the ith step is calculated by

$$Y(x_i)_{\rm calc} = B(x_i) + \sum_j I_j P(x_i - T_j)_j, \qquad (2.3.3.12)$$

where $B(x_i)$ is the background intensity, I_j is the integrated intensity of the jth reflection, T_j is the peak-maximum position, $P(x_i)_j$ is the profile function to represent the profile shape, and $\sum_j$ is taken over j, in which the $P(x)_j$ has a finite value at x_i. Unlike the Rietveld method, a structure model is not used. In the least-squares fitting, I_j and T_j are refined together with background and profile shape parameters in $P(x)_j$. Smoothing the experimental data is not required because it underestimates the estimated standard deviations for the least-squares parameters, which are based on the counting statistics.

The experimental profiles are a convolution of the X-ray line spectrum λ and all the combined instrumental and geometrical

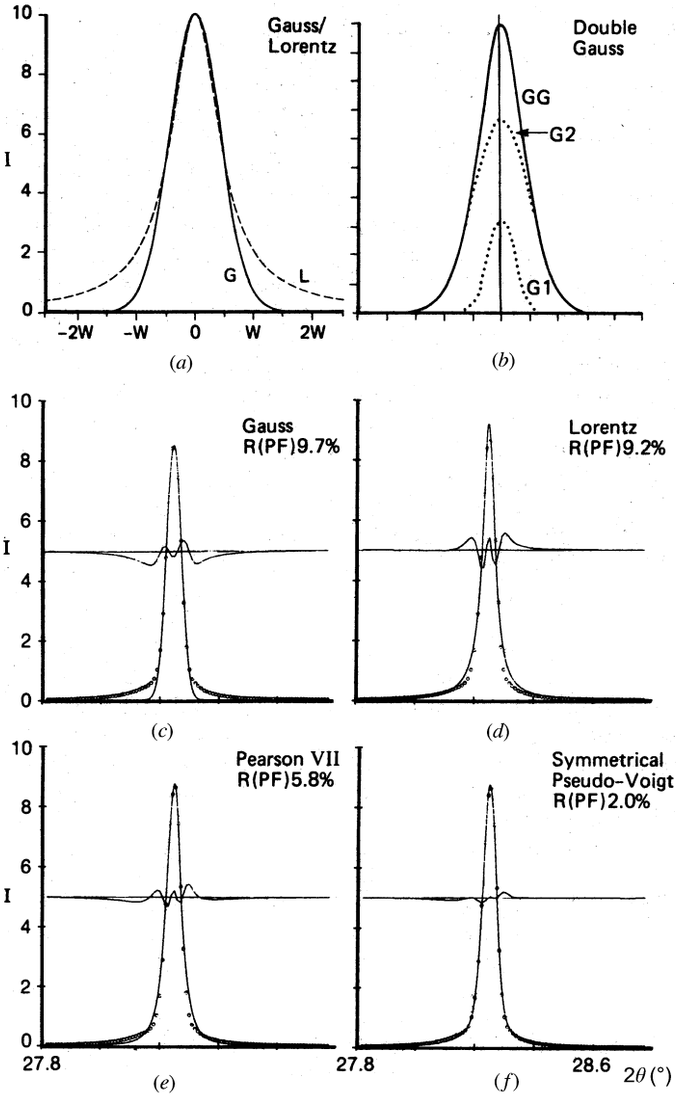

Fig. 2.3.3.9. (*a*) Computer-generated symmetrical Lorentzian profile L and Gaussian G with equal peak heights, 2θ and FWHM. (*b*) Double Gaussian GG shown as the sum of two Gaussians in which I and FWHM of $G1$ are twice those of $G2$ and 2θ is constant. (*c*)–(*f*) Profile fitting with different functions. Differences between experimental points and fitted profile shown at one-half height. Synchrotron radiation, Si(111).

aberrations G with the true diffraction effects of the specimen S (Parrish, Huang & Ayers, 1976), *i.e.*

$$\Omega(x) = (\lambda * G) * S + \text{background}. \qquad (2.3.3.13)$$

The profile shapes and resolution differ in the various diffractometer geometries and there is no universal profile-fitting function. In conventional X-ray tube focusing methods, the profiles are asymmetric and the shapes change continually across the scattering-angle range owing to the aberrations and the $K\alpha$ doublet. To avoid problems caused by the $K\alpha$ doublet, a few authors used the $K\beta$ line, but it has only about 1/7 the intensity. The profiles obtained with synchrotron radiation are symmetrical and narrower, and the widths increase with increasing 2θ. The different shapes and rates of decay of the tails make it necessary to find an analytical function that best fits the particular experimental profile. Langford (1987) and Young & Wiles (1982) have compiled and reviewed various profile-fitting functions and several are described below. Howard & Preston (1989) give details of the computations in their review of the method.

Early profile analyses used Gaussian or Lorentzian (Cauchy) curves. Fig. 2.3.3.9(*a*) shows that the most obvious difference is the rate of decay of the tails. X-ray synchrotron profiles lie between the two as shown in Figs. 2.3.3.9(*c*)–(*f*). The function must fit the tails as well as the main body and single-element functions are generally unsatisfactory. The Voigt function is a convolution of Lorenzian (L) and Gaussian (G) functions of different widths:

$$P(x)_V = \int L(x)G(x-u)\,\mathrm{d}u, \qquad (2.3.3.14)$$

where x corresponds to $2\theta - T_j$ (Langford, 1978). It has been used for profile fitting and also to determine certain physical properties such as crystallite size and strain broadening from the constituent L and G profiles (see, for example, Langford, 1978; Suortti, Ahtee & Unonius, 1979; de Keijser, Langford, Mittemeijer & Vogels, 1982; Langford, Delhez, de Keijser & Mittemeijer, 1988). Evaluation of a symmetrical Voigt function involves the real part of the complex error function and an algorithm for calculating this has been given by Langford (1992).

The two most frequently used functions are at present the pseudo-Voigt (Wertheim, Butler, West & Buchanan, 1974) and the Pearson VII (Hall, Veeraraghavan, Rubin & Winchell, 1977). They cannot be easily deconvoluted analytically and have no direct physical interpretation but the equivalent Voigt parameters can be derived. Both can be split into symmetric and asymmetric portions to adjust better to the profile asymmetries and tails. The shapes can also be varied systematically by changing the L/G ratio (de Keijser, Langford, Mittemeijer & Vogels, 1982).

The pseudo-Voigt function is similar to the Voigt except that an addition is used in place of the convolution. It is easier to use and Wertheim *et al.* (1974) found there was only a small difference in the intensities and widths obtained with this approximation. It is defined as

$$P(x)_{\mathrm{p-V}} = \eta L(x) + (1-\eta)G(x), \qquad (2.3.3.15)$$

where η is the ratio of Lorentz to Gauss and they have the same widths. The refined η and width of the full fitted profile can be related by a polynomial expansion (Hastings, Thomlinson & Cox, 1984; David, 1986; Cox, Toby & Eddy, 1988) to the widths of the L and G components of the original Voigt function. It is frequently used to fit synchrotron-radiation profiles. In the particular case shown in Figs. 2.3.3.9(*c*)–(*f*), the pseudo-Voigt has the best fit as shown by the difference curve at half-height and the lowest R_p[= R(PF)] value.

The Pearson VII function is defined as

$$P(x)_{\mathrm{PVII}} = a[1 + (x/b)^2]^{-m}, \qquad (2.3.3.16)$$

where m is a refinable parameter based on the G/L content (for $m = 1$, the curve is 100% Lorentzian and for $m = \infty$ it is 100% Gaussian), and $1/b = 2[2^{1/m} - 1]^{1/2}/W$, where W is the FWHM.

The peak asymmetry can be incorporated into the profile function in several ways. One is to multiply (or add) the symmetrical profile function with an asymmetric function (Rietveld, 1969). Another is to dispose two or three functions asymmetrically (Parrish, Huang & Ayers, 1976). A third is to use a split-type function, consisting of two profile functions, each of which defines one-half the total peak, *i.e.* the low- or high-angle sides of the peak and each has different profile widths and shapes but the same height (Toraya, Yoshimura & Somiya, 1983; Howard & Snyder, 1983).

Some other functions that have been used include the double Gaussian [Fig. 2.3.3.9(*b*)] for low-resolution synchrotron data (Will, Masciocchi, Parrish & Hart, 1987), a Gaussian with shifted Lorentzian component to account for the asymmetry on the low-2θ side of the tail (Will, Masciocchi, Parrish & Lutz, 1990), profile modelling of single isolated peaks with a rational function, *e.g.* the ratio of two polynomials (Pyrros & Hubbard, 1983). In contrast to these analytical-type functions, some empirical functions have been developed. They are the 'learned' (experimental) peak-shape function (Hepp & Baerlocher, 1988) and the direct fitting of experimental data represented by Fourier series (Mortier & Constenoble, 1973).

The sum of Lorentzians has been used for X-ray tube focusing profiles (Parrish & Huang, 1980; Taupin, 1973). The instrument function ($\lambda * G$) is determined (see below) by a sum of Lorentzian curves, three each for $K\alpha_1$ and $K\alpha_2$ and one for the weak $K\alpha_3$ satellite. Three Lorentzians were used to match the asymmetry although a greater or lesser number could be used depending on the profile symmetry. Each curve has three parameters (intensity, half-width at half-height, and peak position) and the 21 parameters are adjusted by the computer program to give the best fit to the experimental data, which may contain 150 to 300 points. This is done only once for each particular instrument set-up. After ($\lambda * G$) is determined, the profile fitting is easy and fast because only the specimen contribution S must be convoluted with ($\lambda * G$). If the specimen has no asymmetric broadening other than ($\lambda * G$), S can be approximated by a single symmetrical Lorentzian for each reflection; a split Lorentzian can be used if there is asymmetric broadening.

A function can be tested using isolated profiles of a standard specimen such as silicon, tungsten, quartz, and others which have $< 10\,\mu$m particles and no specimen broadening (Fawcett *et al.*, 1988). It is necessary to do this test carefully and whenever the instrument parameters are changed.

The instrument function can be measured using isolated profiles of standard specimens as stated above. The measurements should be made with small $\Delta 2\theta \simeq 0.01^\circ$ steps and count times long enough to accumulate about 25 000 to 50 000 counts on the $K\alpha_1$ peaks for good counting statistics. By measuring a number of profiles separated by no more than about 5 to 10°, the instrument function can be established for the angular range of interest. A linear interpolation of the profile-fitting parameter between adjacent profiles gives a continuous function for use at any 2θ in the range. The

intensities of the derived profile parameters are normalized and stored in the computer for later use. Note that any change in the X-ray spectrum or instrument geometry requires another set of measurements. The instrument function is also an important aid in computer graphics as described in Subsection 2.3.3.9.

The fitting of conventional diffractometer profiles was considerably improved by the use of a convolution function, in which the Pearson VII function is convoluted with the observed instrument function (Toraya *et al.*, 1983; Toraya, 1988). Enzo, Fagherrazzi, Benedetti & Polizzi (1988; Benedetti, Fagherazzi, Enzo & Battagliarin, 1988) used the convolution of a pseudo-Voigt function as the true data function and the convolution of exponential and pseudo-Voigt functions as the instrumental function for crystallite size and strain analysis. These functions have advantages in analysing the crystallite size and strain, although they require longer computation time for calculating the convolution.

Background intensity is usually included in the refinement. A first- or second-order polynomial is used to represent the background function $B(x)$ in equation (2.3.3.12) in a small 2θ range, and the polynomial coefficients are adjusted during the least-squares refinement. In some cases, the background is subtracted from the pattern before the refinement by using the lowest intensities between the reflections. The background in the vicinity of high-intensity peaks and peak clusters is usually higher and should be avoided.

In the least-squares refinement, the following quantity is minimized:

$$\Delta = \sum_{i=1}^{N} w_i [Y(x_i)_{\rm obs} - Y(x_i)_{\rm calc}]^2, \qquad (2.3.3.17)$$

where N is the number of observations, w_i is the weight assigned to the ith observation, and $Y(x_i)_{\rm obs}$ is the observed profile intensity. A statistical weighting factor such as $w_i = \sigma_i^2$, where $\sigma_i^2 = 1/Y(x_i)_{\rm obs}$, is frequently used. The quality of the fitting procedure is generally expressed by R factors such as R_{wp}, the weighted R factor for profile intensity, which includes the entire scattering range and the background. The definitions of these factors are summarized by Young, Prince & Sparks (1982). The R_p and R_{wp} factors are given as

$$R_p(\%) = 100 \sum_{i=1}^{N} |Y(x_i)_{\rm obs} - Y(x_i)_{\rm calc}| \Big/ \sum_{i=1}^{N} Y(x_i)_{\rm obs}, \qquad (2.3.3.18)$$

$$R_{wp}(\%) = 100 \left\{ \frac{\sum_{i=1}^{N} w_i \left[Y(x_i)_{\rm obs} - Y(x_i)_{\rm calc} \right]^2}{\sum_{i=1}^{N} w_i Y(x_i)_{\rm obs}^2} \right\}^{1/2}. \qquad (2.3.3.19)$$

If the selected function is inappropriate, it will show up on the difference curve (experimental – calculated; see Fig. 2.3.3.9), and high R_p and R_{wp} factors.

A whole-powder-pattern fitting technique without using the structural model was proposed for analysing neutron powder data (Pawley, 1981) and then extended to X-ray data (Toraya, 1986). The method executes the whole pattern decomposition (*i.e.* fitting all the profiles) in one step. In this technique, the peak position T_j in equation (2.3.3.12) is a function of unit-cell parameters, and the unit-cell parameters are refined instead of individual peak positions. Furthermore, the angular dependence of the profile width can be expressed approximately as

$$w(2\theta) = \sqrt{w_1 + w_2 \tan\theta + w_3 \tan^2\theta}, \qquad (2.3.3.20)$$

where w_1, w_2, and w_3 are adjustable parameters (Caglioti, Paoletti & Ricci, 1958); but see also Louër & Langford (1988). The profile-shape dependency on 2θ is ignored when fitting a small 2θ range, but it must be taken into account in the whole-powder-pattern fitting in both focusing and parallel-beam geometries. The least-squares ill conditioning is handled by imposing the constraints on the peak positions in the profile-fitting procedure.

Approximate unit-cell parameters are required to start the refinement. Advantages of this technique are: (1) the unit-cell parameters are refined to high precision; (2) the analysis is rapid and straightforward; (3) it is also powerful in analysing complex powder patterns. The output of indices and integrated intensities of all reflections can be used to calculate Patterson and Fourier diagrams, and thus used for *ab initio* structure determination (McCusker, 1988) and the structure refinement based on the integrated intensities such as used in the *POWLS* program (Will, 1979).

The convolution equation is used in place of $P(x)$ in equation (2.3.3.12), in which the true data function represented by a pseudo-Voigt or Pearson VII has adjustable parameters of crystallite size and strain (Toraya, 1989). The anisotropic crystallite size assuming cylindrical shape has been determined by whole-powder-pattern fitting for complex powder patterns.

The advantage of profile fitting is illustrated in Fig. 2.3.3.10 for the quartz cluster at 68° with Cu $K\alpha$ where the doublet separation is 0.19° and the FWHM is 0.14°. The relative intensities of the 122, 203, and 301 $K\alpha_1$ peaks are 81:97:100, which differ from the profile-fitted peaks, 90:100:67, due to the overlapping. The sum of the fitted curves is the solid line which passes through the experimental points. The peak-search (or strip-chart) intensities that are not corrected for overlaps are more likely to correspond to the ICDD powder file than the profile-fitted values. Profile fitting is capable of about $\pm 0.0004°2\theta$ and 0.2% intensity for good experimental data (Parrish & Huang, 1980). Even in data with poor counting

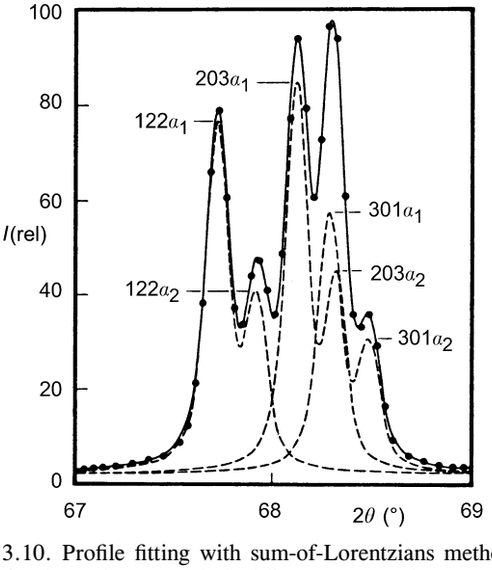

Fig. 2.3.3.10. Profile fitting with sum-of-Lorentzians method. Individual reflections shown as dashed-line curves and sum as solid line passing through experimental points. Quartz peak cluster, Cu $K\alpha_1$, $K\alpha_2$, conventional diffractomer.

statistical accuracy, it is possible to identify very weak peaks with low P/B as shown in Fig. 2.3.3.11.

2.3.3.9. *Computer graphics for powder patterns*

An interactive graphics display program is a very important asset for interpreting and analysing powder diffraction data. If a colour graphics station is used, the display can be enhanced by using various colours. The simplest form is the VDU display of experimental points connected with straight lines, which appears similar to a strip-chart recording but has no time-constant error and is printed on page-size paper. It avoids storing large numbers of charts because hundreds of patterns can be stored on a diskette and displayed and printed at any time.

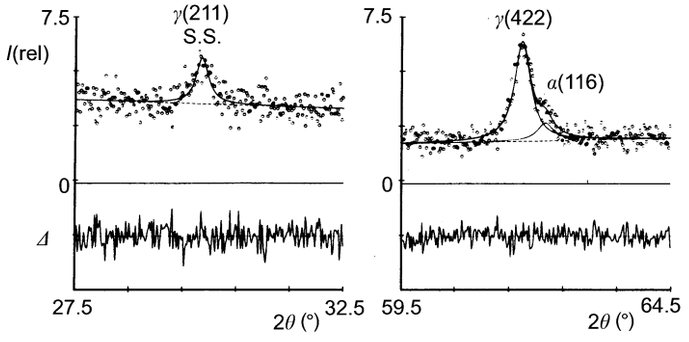

Fig. 2.3.3.11. Profile fitting of poor statistical data.

The basic parameters required in one of the published methods (Parrish, Huang & Ayers, 1984) are the d's and I's of the reflections, the wavelength and profile shapes ($\lambda * G$ instrument function). This makes it possible to produce a pattern exactly as it would appear on the user's diffractometer, aside from contributions arising from sample microstructure. The step size can be included if experimental patterns are to be reproduced or if patterns are to be subtracted. A section of the pattern can be enlarged to the full screen size by entering the desired angular range and highest peak intensity. A linear background can be added by entries at the low- and high-2θ points. Nonlinear background, *e.g.* from an amorphous substrate, can be transferred from a stored file. Counting statistical noise can be added to a simulated pattern by using a normally distributed random number with a standard deviation scaled to the calculated $I^{1/2}$. Noise in an experimental pattern can be smoothed. A profile broadening factor can be added to the $\lambda * G$ function. Quantitative synthesis of a mixture can be simulated by entering the relative weight percentage and reference intensity, the ratio of the intensities of the strongest lines of each pattern in a 50–50 mixture, or the ICDD values compared to α-Al_2O_3 (de Wolff & Visser, 1988; Davis & Smith, 1988). The program has access to the ICDD file stored on disk so that any card can be reproduced as a pattern using any wavelength. Some examples are shown in Fig. 2.3.3.12.

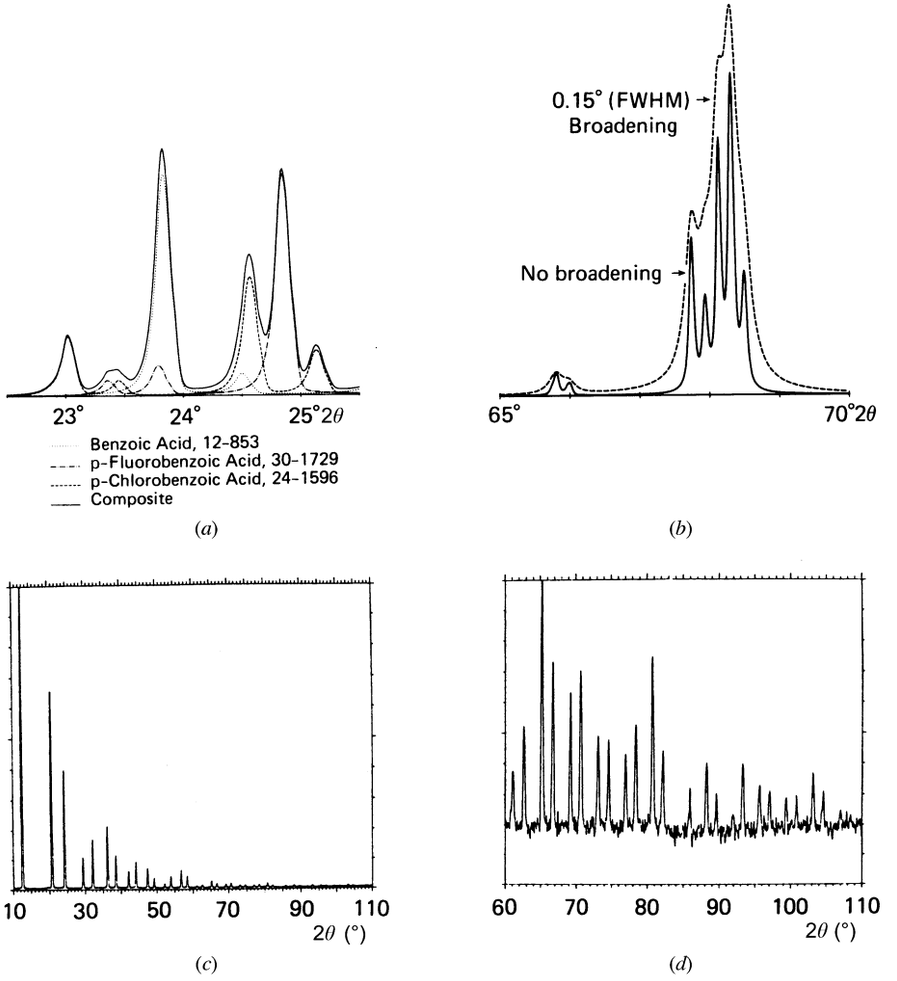

Fig. 2.3.3.12. Some examples of computer graphics of powder patterns. (*a*) Overlay of three patterns with ICDD card numbers. (*b*) Effect of adding 0.15° to FWHM. (*c*) Synchrotron 0.6888 Å radiation pattern of Si powder. (*d*) Low-intensity section enlarged and 11-point smoothing.

2.3.4. Powder cameras

The use of powder cameras has greatly diminished in recent years, having been largely replaced by diffractometers. Detailed descriptions of the many types of camera, their use, film measurement, and interpretation have been published in the books by Peiser, Rooksby & Wilson (1955), Azároff & Buerger (1958), Taylor (1961), Alexander (1969), Lipson & Steeple (1970), Klug & Alexander (1974), Cullity (1978), and Barrett & Massalski (1980). The following is an outline of the more important features.

The most commonly used cameras are:

(*a*) Cylindrical camera with narrow fibre-shaped specimen and Straumanis film mounting.

(*b*) Guinier focusing monochromator camera with flat transmission specimen and cylindrical film.

(*c*) Flat-film camera for Laue patterns and crystal orientation.

The best results are obtained using the X-ray tube spot focus for non-focusing methods as in (*a*) and (*c*), and the line focus for focusing cameras as in (*b*). A filter is used to eliminate the $K\beta$ lines in the methods that do not use a monochromator. Double-coated film is used for cameras in which the reflections are normal to the film. Single-coated film is used for focusing cameras; alternatively, double-coated film can be used if the second image is prevented from developing (Parrish, 1955).

In all film methods, it is necessary to account for film shrinkage in the development processing to obtain correct angle measurements. In the Straumanis film mounting, Fig. 2.3.4.1(*a*), the arcs can be measured around the incident and exit holes to obtain a linear measure of the effective camera diameter, *i.e.* $180^\circ 2\theta$. Other methods include exposing a transparent scale on the film prior to development, installing a pair of knife edges with accurately measured separation just above the film to cast sharp images on both ends of the film, or incorporating a standard material in the specimen. Exposure times vary from a few minutes to an hour or more depending on the specimen and the various camera parameters.

2.3.4.1. *Cylindrical cameras (Debye–Scherrer)*

The design of cylindrical powder cameras with Straumanis film mounting was described by Buerger (1945) and the collimators by Parrish & Cisney (1948). Straumanis developed the method to an art and used it to measure lattice parameters, thermal expansion, and other properties of many materials; see, for example, Straumanis (1959), which contains references to many of his papers. In the USA, the camera diameter was usually made 57.3 or 114.6 mm to simplify measuring the film with a millimetre scale, 1 mm = 1° or $2^\circ 2\theta$. One of the major advantages of the method is that the full reflection range is recorded simultaneously on the film. Other advantages are that the effects of preferred orientation are immediately apparent on a film, lines can have non-uniform intensity ('spottiness') owing to size effects or there can be broadening owing to structural imperfections. These visual effects, which are less evident with diffractometer data, can be valuable aids in identifying a mixture of substances.

The camera is basically a cylindrical light-tight metal body with removable cover, and the film is pressed around the inside circumference. The beam is defined by an entrance collimator and the undiffracted portion is conducted out by an exit tube; both are mounted on the central plane of the camera and extend inside nearly to the specimen. The specimen is centred and rotated continuously during the exposure; translation may be added to bring more particles into the beam. Evacuating the camera or filling it with helium removes the air scattering which darkens the film in the vicinity of the 0° hole.

If the specimen is too thick or has high absorption, the forward reflection lines split because the beam penetrates only the top and bottom of the rod. The diameter of the rod determines the widths of the lines. The line widths are about twice the diameter of the rod at small 2θ's and decrease with increasing 2θ. The absorption causes a systematic error in the positions of the lines, which can be handled with a $\cos^2\theta$ or Nelson–Riley plot (Section 5.2.8). The sample may be small – only about 0.1 mg is required. Axial divergence causes the well known 'umbrella' or 'broom' broadening illustrated in Fig. 2.3.4.1(*b*). It is essential to measure the film along the equator where the lines are narrowest and shifts the smallest. The specimens should be less than 0.5 mm diameter and may be coated on a fine wire or glass fibre (silica or Lindemann glass), or packed into a capillary (commercially available).

Read & Hensler (1972) modified a Debye–Scherrer camera to use flat specimens for thin-film analysis (Tao & Hewett, 1987).

2.3.4.2. *Focusing cameras (Guinier)*

The Guinier camera (Guinier, 1937, 1946; Guinier & Dexter, 1963) uses a high-quality asymmetric focusing monochromator and cylindrical camera with a thin transmission specimen, Fig. 2.3.4.1(*c*). The film must be placed at the focal point of the monochromator, which can be adjusted to reflect only the $K\alpha_1$ line. When the camera is in the position shown, the angular range is larger on one side of the film than the other (asymmetric

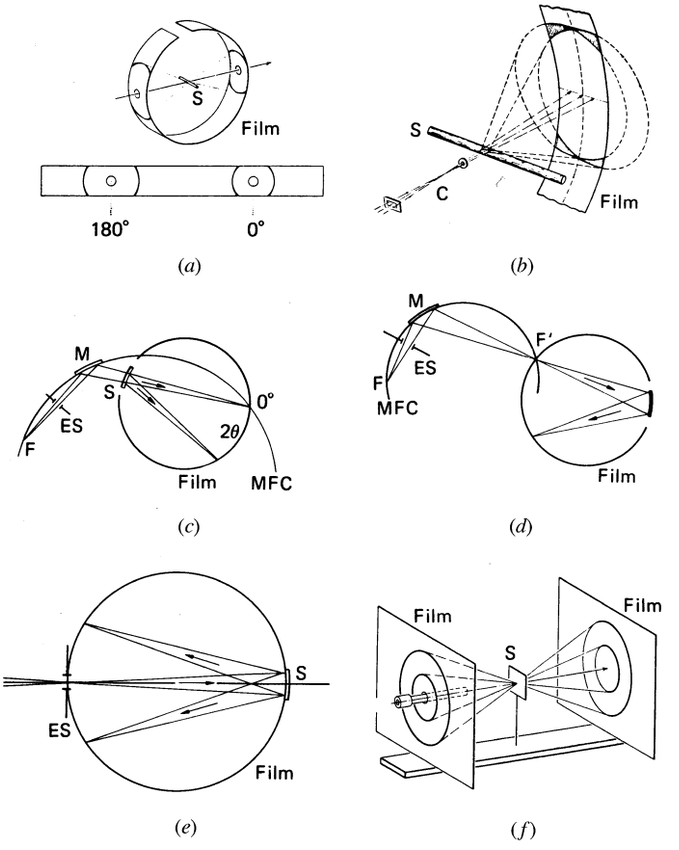

Fig. 2.3.4.1. Powder-camera geometries. (*a*) Straumanis film setting. (*b*) Origin of 'umbrella' effect (axial divergence). (*c*) Guinier camera with specimen in transmission and (*d*) in reflection. (*e*) Symmetrical back-reflection focusing camera. (*f*) Flat-film camera for forward- and back-reflection.

setting). If the camera is placed so that the rays from the monochromator are along the camera diameter, the angular range is the same on both sides of the 0° point (symmetric setting) and the usable range is about 60°2θ. The sharpest lines are obtained when the rays are nearly normal to the film. The lines are broadened by inclination of the rays to the film, axial divergence, and specimen thickness. The camera can also be used with the specimen in reflection so that it becomes a Seemann–Bohlin camera with only the back reflections accessible [Fig. 2.3.4.1(*d*)]. Hofmann & Jagodzinski (1955) designed a double camera in a single body that can record transmission and reflection patterns on separate films.

de Wolff (1948) described a novel Guinier-type camera that can simultaneously record up to four patterns of different specimens on one film with a single monochromator and long fine-focus X-ray tube. The patterns are separated by horizontal partitions. There are some differences in the line widths in the top and bottom patterns. Malmros & Werner (1973) developed an automated film-measuring densitometer to improve the precision in measuring the Guinier films; see also Sonneveld & Visser (1975).

2.3.4.3. *Miscellaneous camera types*

The symmetrical back-reflection camera, Fig. 2.3.4.1(*e*), is mainly used for lattice-parameter and solid-solution studies because the high reflection angles can be recorded. The specimen can be mounted on a curved holder matching the film curvature to obtain sharp lines and is oscillated during exposure.

The flat-plate camera, Fig. 2.3.4.1(*f*), can be used for forward- or back-reflection. The angular range is small and varies inversely with the specimen-to-film distance. Polaroid film is frequently used. The same method is used for Laue photographs, usually in back-reflection with a goniometer to orient the crystal. The method is often used for fibre and polymer specimens because the entire cone can be recorded (Alexander, 1969).

The Gandolfi (1967) camera produces a powder-like pattern from a tiny single crystal by simultaneous rotation of the crystal around two inclined axes. It is often made as a modification to the cylindrical camera. The crystal may be very small but the pattern is greatly improved by using several crystals. The smoothness of the lines depends on the chance orientation of the crystal with respect to the rotation axes, and the multiplicity of the reflection. The centring of the specimen and the rotation axes must be done precisely. Anderson, Zolensky, Smith, Freeborn & Scheetz (1981) obtained patterns routinely from 5 μm particles in 2–4 d exposure at 40 keV, 20 mA in an evacuated camera; see also Sussieck-Fornefeld & Schmetzer (1987) and Rendle (1983). A high-brilliance microfocus X-ray tube can greatly increase the intensity.

Another type of camera for the same purpose was developed by Parrish & Vajda (1971). The small crystal is mounted on a glass fibre at the end of a vertical shaft that rotates continuously and simultaneously scans about 90°. The film is mounted in a half-cylinder with about 20 mm radius. A microscope is used for precise alignment and centring.

A camera with a wide film cassette has been used for high-temperature diffraction patterns. The cassette can be translated synchronously with the change in temperature, or held in fixed positions during exposure at selected temperatures. The advantage is that all the patterns are recorded on a single film showing the phase changes and thermal expansion as a function of temperature. A Weissenberg camera can be adapted for this purpose.

2.3.5. Generation, modifications, and measurement of X-ray spectra

This section covers methods for using X-ray tubes and their operation. The methods of modifying the X-ray spectrum by crystal monochromators, filters, and the detector system apply to powder and single-crystal diffraction. Chapter 4.2 contains a more detailed description of the physics of X-ray sources.

2.3.5.1. *X-ray tubes*

Vacuum-sealed water-cooled X-ray tubes of the type shown in Fig. 2.3.5.1 are almost exclusively used for powder diffraction. They are installed in either a vertical or a horizontal shield (sometimes called a tower) mounted on the generator, or remotely operated with a long high-voltage cable. The shield is designed to seat the tube cap in the correct position, which allows tube replacement without realigning the instruments. Rotating-anode tubes are becoming more popular. They may be operated at higher currents and, although they require continual pumping, recent designs incorporating a ferromagnetic seal and turbomolecular pump make their use virtually as simple as sealed tubes. For additional background information see Phillips (1985) and Yoshimatsu & Kozaki (1977). End-window tubes with large focal spot have been used mainly for X-ray-fluorescence spectroscopy (Arai, Shoji & Omote, 1986), and fine-point-focus tubes for Kossel diagrams.

The maximum permissible power ratings for sealed water-cooled diffraction tubes are about 60 kV, 60 mA and 3 kW. The rating varies with the focal-spot size, anode element, and the particular manufacturer's specifications. Table 2.3.5.1 lists some typical maximum ratings of sealed and rotating-anode tubes. The brightness or specific loading, expressed as watts per square mm, increases with decreasing focal-spot size. There is a very large increase in brightness in the small microfocus sources that

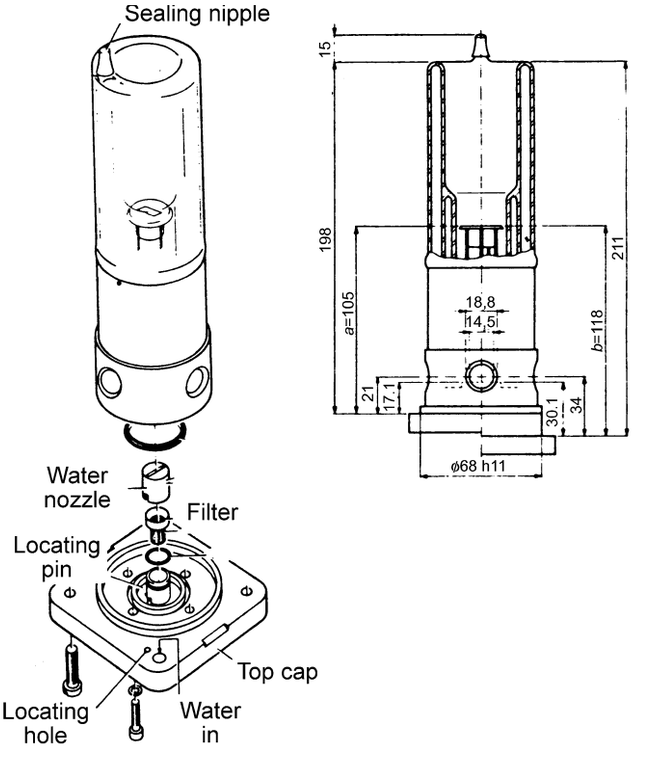

Fig. 2.3.5.1. Sealed X-ray diffraction tube (Philips), dimensions are given in mm. a = 'short' focus, b = 'long' focus.

Table 2.3.5.1. *X-ray tube maximum ratings*

Sealed-off (3 kW)*				Rotating anode (18 kW)†			
Anode	Focus (mm)	Power (kW)	Brightness ($W\,mm^{-2}$)	Anode	Focus (mm)	Power (kW)	Brightness ($W\,mm^{-2}$)
Mo	0.4 × 12	3.0	625	Mo, Cu	0.5 × 10	18.0	3600
	1 × 10	2.4	240		0.3 × 3	5.4	6000
	2 × 12	2.7	112		0.1 × 1	1.2	12000
Cu	0.4 × 12	2.2	460	Ag	0.5 × 10	12.0	2400
	1 × 10	2.0	200		0.3 × 3	5.4	6000
	2 × 12	2.7	112		0.1 × 1	1.2	12000
Cr	0.4 × 12	1.9	400	Cr	0.5 × 10	10.0	2000
	1 × 10	1.9	180		0.3 × 3	4.5	5000
	2 × 12	2.7	112		0.1 × 1	1.0	10000

* Philips. † Rigaku.

operate at lower total power. X-ray tubes normally have a life of several thousand hours. It varies with power, anode-cooling efficiency, on–off cycles, and similar factors.

Most X-ray generators are now designed for constant-potential operation using solid-state rectifiers and capacitors in the high-voltage transformer tank. They produce higher intensity at the same voltage than self-rectified or full-wave-rectified operation because the characteristic line spectrum is produced only in the portion of the cycle in which the voltage exceeds the critical excitation voltage of the target element. The gain thus increases with decreasing wavelength. The operation of modern X-ray generators is very simple and requires little attention. Safety interlocks provide electrical protection, and window-shutter interlocks aid in radiation safety. Large ray-proof plastic enclosures are available to surround the X-ray tube tower and diffraction instrumentation and are recommended for safety. Some legal requirements are outlined in Part 10.

Air-cooled tubes can operate at only a fraction of the power of water-cooled tubes and are used for special applications where low intensities can be tolerated. Small portable air-cooled X-ray tubes have recently become available in a variety of forms (see, for example, Kevex Corporation, 1990). The tube, high-voltage generator and control electronics are packaged in compact units with approximate dimensions 27 by 10 cm weighing about 3 kg. They have a single 0.13 mm Be window, a focal-spot size 0.25 to 0.50 mm, and are available with a number of target elements. They can be AC or battery operated. Some tubes are rated at 70 kV, 7W, and others at 30 kV, 200W, depending on the model.

2.3.5.1.1. *Stability*

Modern X-ray generators have a high degree of electrical stability, of the order of 0.1 to 0.005%, which is sufficient for most applications. The current is continually monitored in the generator and used in feedback circuits to regulate the output. The high voltage is also monitored in some generators. Maximum long-time stability is obtained if the generator and X-ray tube are run continuously over long periods of time so that they reach stable operating conditions. Experienced technicians often advise that the X-ray tube life is shortened by frequent on–off use because the filament receives maximum stress when turned on. The tube may be left operating at low power, 20 kV, 5–10 mA, when not being used. It is inadvisable to operate at voltages below about 20 kV for long periods of time because space charge builds up, causing excessive heating of the filament and shorter life. The stability can be determined by measuring the intensity of a diffraction peak or fluorescence as a function of time. This is not an easy experiment to perform because the stability of the detector system must first be determined with a radioactive source and a sufficient number of counts recorded for the required statistical accuracy.

Alternatively, a monitor method can be used to correct for drifts and instabilities. The monitor is another detector with a separate set of electronics. It can be used in several ways: (1) as a dosimeter to control the count time at each step; (2) to measure the counts at each step and use the data to make corrections, *i.e.* counts from specimen divided by monitor counts. (It is usually advisable to average the monitor counts over a number of steps to obtain better statistical accuracy.) A thin Be foil or Mylar film inclined to the beam is ideal because they have little absorption and strong scattering. The monitor detector can be mounted out of the beam path and must be able to handle very high count rates and have an extended linear range to avoid introducing errors. In synchrotron-radiation EXAFS experiments, the beam passes through an ionization chamber placed in the beam to monitor the incident intensity.

Spikes in the data may arise from transients in the electrical supply and filtering at the source is required, although modern diffractometer control systems have provision for removing aberrant data.

2.3.5.1.2. *Spectral purity*

Spectral contamination from metals inside the tube may occur and increase with tube use. This reduces the intensity by coating the anode and windows and may not be noticed when using an incident-beam or diffracted-beam monochromator. It can be measured by removing the monochromator or β filter, operating the tube at high kV, and recording the diffraction pattern of a simple powder (*e.g.* Si or W), a rolled metal foil, or a single-crystal plate (Ladell & Parrish, 1959). The contaminating elements can be identified from the extra peaks. It is advisable to check the spectral purity when the tube is new and periodically thereafter.

2.3.5.1.3. *Source intensity distribution and size*

The intensity distribution of the focal line is usually not uniform. This has no apparent effect on the shapes of powder reflections but may cause difficulties with single crystals (Parrish, Mack & Taylor, 1966). The distribution can be measured with a small pinhole placed between the X-ray tube focal line and a dental or Polaroid film. The ratio of the distances between line-to-pinhole and pinhole-to-film determines the magnification of the image. The pinhole diameter should be small for good resolution. About 0.1 mm diameter is satisfactory and can be made with a special microdrill, spark erosion or other methods. The thickness of the metal must be minimal to avoid having the aperture formed by the length and diameter of the pinhole limit the length of focus photographed. Avoid over-exposure which broadens the image. Also, the Polaroid film should be exposed outside the cassette to avoid broadening caused by the intensifying screen.

A more accurate method is to scan a slit and detector (mounted on the same arm) normal to the central ray from the focus as shown in Fig. 2.3.5.2(*b*) (Parrish, 1967). The slits are a pair of molybdenum rods (or other high-absorbing metal) with opening normal to the scan direction, and the slit width determines the resolution. This method gives a direct measurement of the intensity distribution from which the projected size can be determined.

The actual size of the focus F'_w is foreshortened to F_w by the small take-off angle ψ, $F_w = F'_w \sin\psi$. A typical 0.5×10 mm focus viewed at 6° appears to be a line 0.05×10 mm or a spot 0.05×1 mm [Fig. 2.3.1.9(*a*)]. The line focus is generally used for powder diffractometry and focusing cameras and the spot focus for powder cameras and single-crystal diffractometry.

X-rays emerge from three or four Be windows spaced 90° apart around the circumference. Their diameter and position with respect to the plane of the target determine the usable ψ-angle range. The length of line focus that can pass through the window can be seen with a flat fluorescent screen in the specimen holder using the largest entrance slit. The Be window thickness often used is 300 µm and the transmission as a function of wavelength is shown in Fig. 2.3.5.2(*a*).

2.3.5.1.4. *Air and window transmission*

The absorption of X-rays in air is also wavelength-dependent and increases rapidly with increasing wavelength, Fig. 2.3.5.2(*a*). The air absorption was calculated using a density

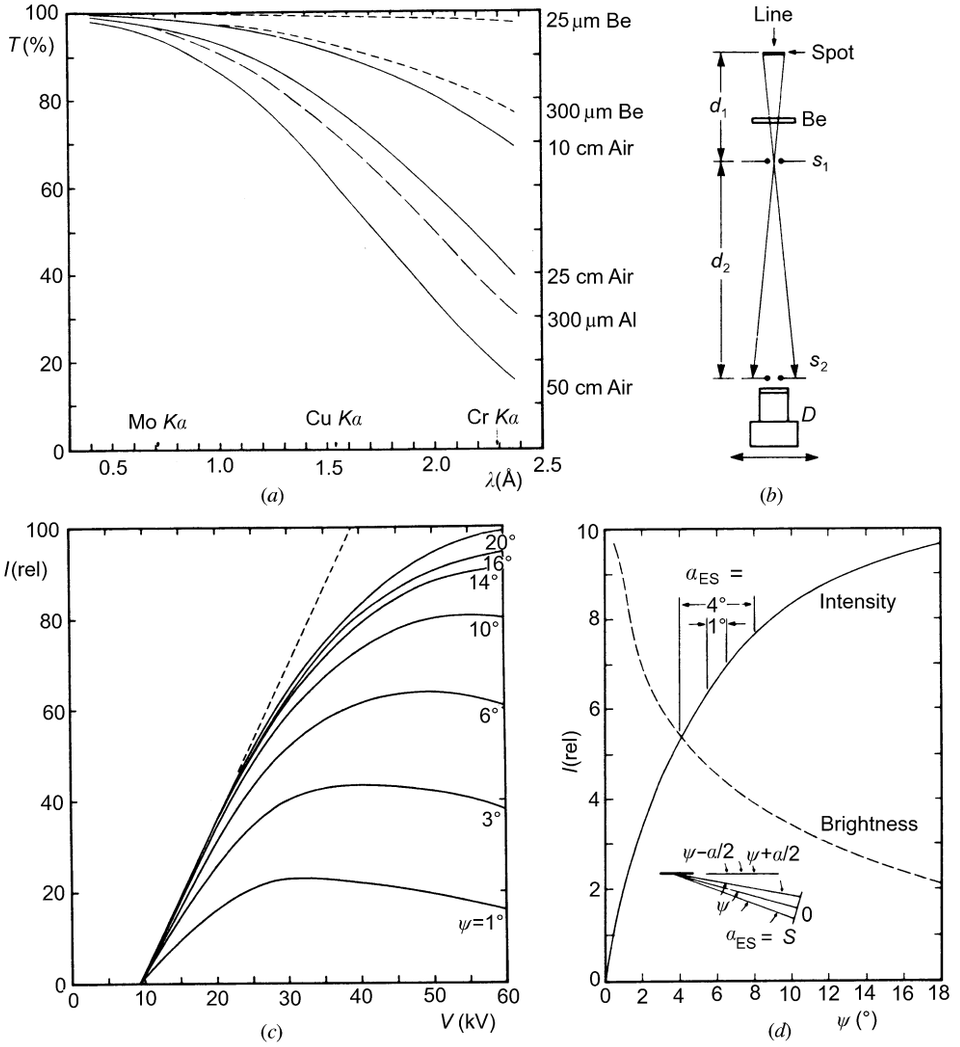

Fig. 2.3.5.2. (*a*) Transmission of Be, Al and air as a function of wavelegth. (*b*) Method for measuring X-ray tube focus by scanning slit S_2 and detector D. Slit S_1 is fixed and the radio of the distances d_2/d_1 gives the magnification. (*c*) Intensity of a copper target tube as a function of kV for various take-off angles. (*d*) Intensity and brightness as a function of take-off angle of a copper target tube operated at 50 kV. The intensity distributions for 1 and 4° entrance-slit apertures are shown at the top, and terms used to define ψ and α_{ES} are shown in the lower insert.

of $0.001\,205\,g\,cm^{-3}$ at 760 mm Hg pressure (1 mm Hg = 133 Pa), 293 K, and 0% humidity. Changes in the humidity and barometric pressure can cause small changes in the intensity. Baker, George, Bellamy & Causer (1968) measured the intensity of the Cu $K\alpha$ and barometric pressure over a 5 d period and found the counts increased 2.67% as the barometric pressure decreased 3.7%. However, they used an Xe proportional counter whose sensitivity is also pressure-dependent and a large amount of the change may have been due to changes in the detector efficiency.

Air scattering increases rapidly at small 2θ's, increasing the background. It is advisable to use a vacuum or helium path to avoid problems in this region.

2.3.5.1.5. *Intensity variation with take-off angle*

The intensity of the characteristic line spectrum emerging from the tube depends on the anode element, voltage, and take-off angle ψ. The depth of penetration of the electrons in the anode is approximately proportional to kV^2/ρ, where ρ is the density of the anode metal. The path length L of the X-rays to reach the surface depends on the depth D at which they are generated and the take-off angle, $L = D/\sin\psi$. Self-absorption in the anode causes a loss of intensity that increases with D and decreasing ψ. The intensity of Cu $K\alpha$ radiation at 50 kV as a function of take-off angle is shown in Fig. 2.3.5.2(*d*). This effect has been described in a number of publications: Green (1964), Brown & Ogilvie (1964), Birks, Seebold, Grant & Grosso (1965), Parrish (1968), and Phillips (1985). Because of the self-absorption, the wavelength distribution varies slightly with take-off angle (Wilson, 1963, pp. 61–63).

The optimum kV and mA operating conditions are not sharply defined and the range can be determined with a powder reflection or by using small apertures in the direct beam with balanced filters and pulse-amplitude discrimination. The intensity is measured at various voltages, keeping the current constant and converting the data to constant power. Typical experimental curves relating Cu $K\alpha$ intensity to kV for various ψ's are given in Fig. 2.3.5.2(*c*). At 50 kV, the intensity doubles by increasing ψ from 3 to 12° (although the projected width of the focal spot also increases). The effect is much larger for Cr $K\alpha$ and W $L\alpha$ because of their higher absorptions. The linear region of *I versus V* is relatively short and increases with ψ. At small ψ's, I is virtually independent of V and could decrease with increasing voltages; increasing the current would give a greater increase using the same power. For a tube with maximum power values of 60 kV, 55 mA and 2200 W, the relative intensites of Cu $K\alpha$ are about 100 for 40 kV/55 mA, 88 for 50 kV/44 mA and 74 for 60 kV/37 mA. However, the filament life decreases with increasing current and most manufacturers specify a maximum allowable current.

The intensity distribution reaching the specimen is not uniform over the entire illuminated area. In the direction normal to the specimen axis of rotation, one end of the specimen views the X-ray tube focus at an angle $\psi - (\alpha/2)$ and the other at $\psi + (\alpha/2)$, where α is the angular aperture of the entrance slit [Fig. 2.3.5.2(*d*)]. The intensity differences are determined by ψ and α_{ES} so that the centre of gravity does not coincide with the geometrical centre. The dependence of the diffracted-beam intensity on the aperture of the entrance slit α_{ES}, therefore, may also be nonlinear. For example, at $\psi = 6°$, the intensity difference at the ends of the specimen is 9% for $\alpha_{ES} = 1°$, and 44% for $\alpha_{ES} = 4°$; the corresponding numbers for $\psi = 12°$ are 2 and 10% respectively.

Although increasing ψ increases the intensity, it also increases the projected width and may increase the widths of the reflections (§2.3.1.1.5). The brightness expressed as $I(\text{rel})/\sin\psi$ also decreases rapidly. When one is working with small apertures, as in grazing incidence and the analysis of small samples, the brightness becomes a very important factor in obtaining the maximum number of counts. For example, the intensity at $\psi = 12°$ is twice that at 3° but the brightness is one half [Fig. 2.3.5.2(*d*)]. However, it should be noted that the smaller the take-off angle the greater the possibility of intensity losses due to target roughening.

2.3.5.2. *X-ray spectra*

The X-ray tube spectrum consists of sharp characteristic lines superposed on broad continuous radiation as shown in Fig. 2.3.5.3. The continuous spectrum begins at a wavelength determined by the voltage on the X-ray tube, $\lambda\,\text{min} \simeq 12.4/\text{kV}$. It reaches a maximum at about 1.5 to $2\lambda\,\text{min}$ and gradually falls off with increasing λ [Fig. 2.3.5.4(*a*)]. The intensity increases with voltage and current, and also with the atomic number of the target element. The integrated intensity is greater than that of the spectral lines. It is used for Laue patterns, fluorescence analysis, and energy-dispersive diffraction. It is troublesome in powder diffraction because it contributes to the background by scattering and by causing specimen fluorescence.

The wavelengths of the spectral lines decrease with increasing atomic number Z of the target element [Moseley's law, Fig. 2.3.5.4(*b*)]. All the lines in a series appear when the critical excitation voltage is exceeded. For a Cu target, this is 9 kV and the approximate relative intensities are Cu $K\alpha_2$ 50, $K\alpha_1$ 100 and $K\beta$ 20. The peak intensities of Cu $K\alpha_1$ and Cu $K\alpha_2$ in diffractometer patterns may not be exactly 2:1 but closer to 2.1:1 in resolved doublets because of the different profile widths. The profile widths of the spectral lines vary among the different elements used for X-ray tube targets (Compton & Allison, 1935), as does the $K\beta/K\alpha$ ratio (Smith, Reed & Ware, 1974). The observed ratio varies with the degree of overlap. The rate of increase with voltage and other factors is described above.

A broad weak group of satellite peaks, $K\alpha_3$, occurs near the bottom of the short-wavelength tail of the $K\alpha_1$ peak (see Fig. 2.3.3.3). The intensity varies with the target element and is about 0.5% for the Cu K spectrum. The satellites appear as a small, broad, ill defined peak in powder diffraction patterns (Parratt, 1936; Parrish, Mack & Taylor, 1963; Edwards & Langford, 1971).

The spectral lines have an approximately Lorentzian shape when measured with a two-crystal diffractometer. They usually have a small asymmetry and their widths vary among the elements and also in the same series of lines. Bearden (1964) defined the wavelength as the peak determined by extrapolation of the centres of chords near the top of the peak. The corresponding energy levels have been compiled by Bearden & Burr (1965). The centroid of the $K\alpha_1$, $K\alpha_2$ peaks of Cu and Fe has been calculated from the Bearden experimental two-crystal data (Mack, Parrish & Taylor, 1964). X-ray wavelengths are discussed in Chapter 4.2. The standard targets provide the K spectra of Ag, Mo, Cu, Co, Fe and Cr, and the W L spectrum. Other targets may be obtained on special order. The K spectra of the elements of high atomic number require a radiographic tube and power supply that can operate continuously at about 150 kV or higher. (**Caution:** The radiation-shielding problems multiply exponentially at high voltages.)

2.3.5.2.1. *Wavelength selection*

The selection of the X-ray tube anode is determined by several factors such as intensity, specimen fluorescence, and dispersion. The intensity of the characteristic line radiation varies among the target elements depending on the voltage and if a vacuum or He path is used. The recorded intensities also change abruptly at the absorption edges of the elements in the specimen. If a diffracted-beam monochromator or solid-state detector with narrow window centred on the characteristic line energy is used, the specimen fluorescence is elminated (except for the element that is the same as the anode), and one tube can be used for all compositions. If the pattern has severe overlapping, the separation of the peaks can be increased with longer wavelengths, which increase the dispersion

$$-\Delta\theta/\Delta d\theta = (180/\pi)(\sin\theta\tan\theta)/\lambda, \qquad (2.3.5.1)$$

expressed as $^\circ\theta\,\text{Å}^{-1}$ of d. Fig. 2.3.5.5 shows portions of diffractometer patterns of topaz in which the same d ranges were recorded with Cu $K\alpha$ (*a*) and Cr $K\alpha$ (*b*). The greater separation of the peaks is clearly advantageous in analysing the patterns.

Copper-anode tubes are most frequently used for powder work because of their high intensity and good dispersion. Chromium tubes are often used for specimens containing iron and other transition elements to avoid fluorescence, and for larger dispersion, but require a vacuum or helium path and the intensity is usually one-half or less than that of copper. Molybdenum tubes are often used for single-crystal analysis, but not often for powders because of the low dispersion.

2.3.5.3. *Other X-ray sources*

The remarkable properties of synchrotron-radiation sources, which produce very high intensity parallel beams of continuous 'white' radiation, are described in Subsection 4.2.1.5, and their use in powder diffraction in Section 2.3.2.

Fluorescent sources produced by primary X-ray tube excitation of a selected element have the advantage of a wide range of wavelengths but have too low brightness to be useful for powder diffraction. The intensity is 2–3 orders of magnitude lower than an X-ray tube source (Parrish, Lowitzsch & Spielberg, 1958).

Radionuclides that decay by *K*-electron capture and produce X-rays (*e.g.* Mn $K\alpha$ from ^{55}Fe) have too low brightness for use in powder diffraction. They are often used to calibrate detectors and to measure the stability of a counting system (Dyson, 1973).

2.3.5.4. *Methods for modifying the spectrum*

The powder method is based on approximately monochromatic radiation and requires the isolation of a spectral line and/or reduction of the white radiation, except of course for energy-

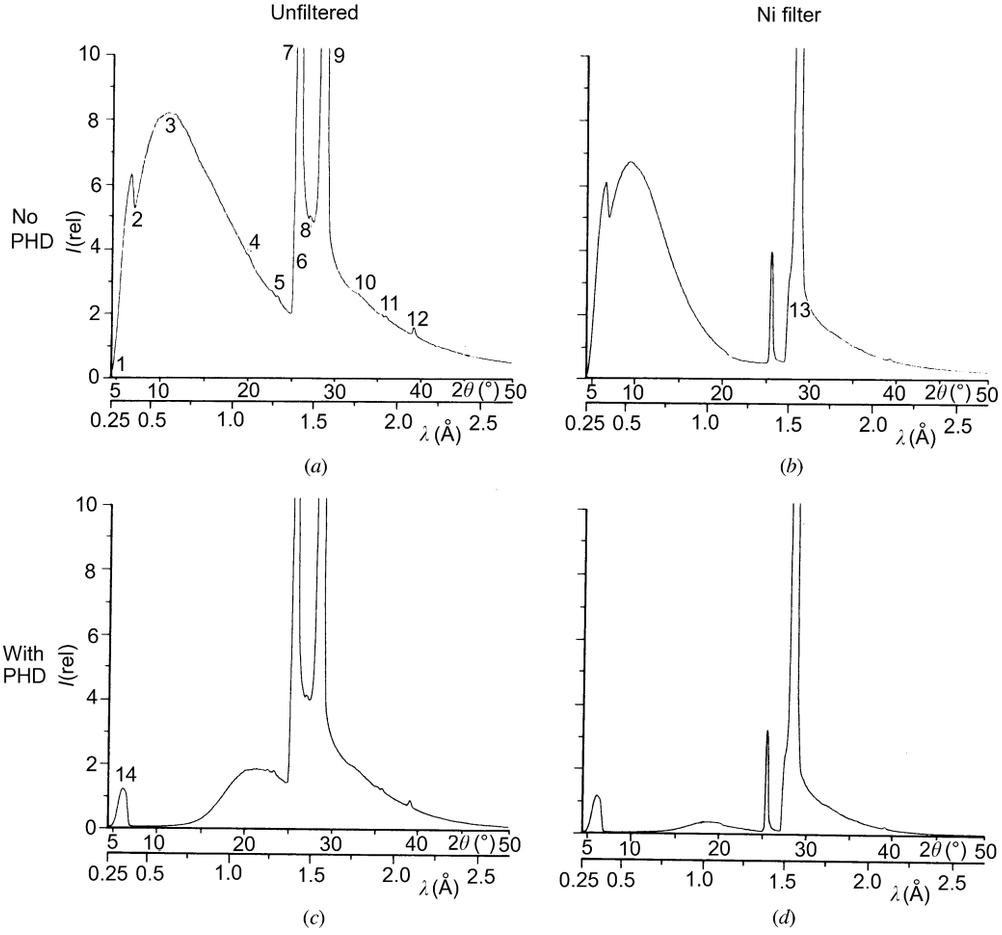

Fig. 2.3.5.3. X-ray spectrum of copper target tube with Be window, 50 kV constant potential, 12° take-off angle. (*a*) Unfiltered, (*b*) with Ni filter, (*c*) unfiltered with pulse-height discrimination (PHD), (*d*) Ni filter + PHD. (1) $\lambda\,\text{min} = 0.246$ Å (4.5°2θ), (2) I *K*-absorption edge (from NaI scintillation crystal), (3) peak of continuous radiation (about 19% of Cu $K\alpha$ peak), (4) W $L\gamma$ contaminant, (5) W $L\beta$, (6) Cu *K*-absorption edge, (7) Cu $K\beta$, (8) W $L\alpha$, (9) Cu $K\alpha_1 + K\alpha_2$, (10) Co $K\alpha$, (11) Fe $K\alpha$, (12) Mn $K\alpha$, (13) Ni *K*-absorption edge, (14) escape peak. Experimental conditions: Si(111) single-crystal analyser, vacuum path, Ni filter 0.18 mm, scintillation counter with 45% resolution for Cu $K\alpha$, lower-level discrimination only against circuit noise. ES 0.25 × 1.5 mm, AS 1.4 mm, no RS, $\Delta 2\theta$ 0.05°, FWHM 0.3°2θ.

dispersive diffraction. This is done with one or more of the following techniques:

–crystal monochromators;
–single or balanced filters; and the
–detector system.

Special methods such as total reflection from a highly polished surface are rarely used in powder diffraction.

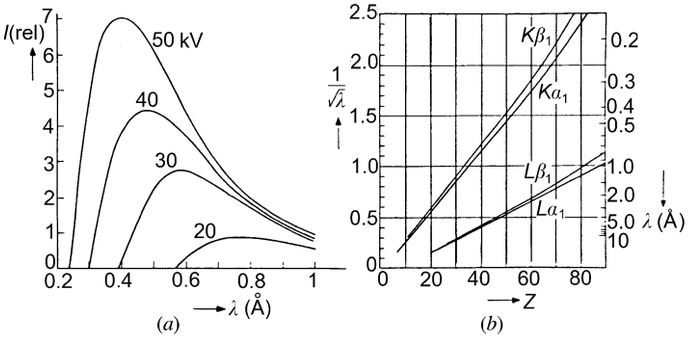

Fig. 2.3.5.4. (*a*) Continuous X-ray spectrum of tungsten target X-ray tube as a function of voltage and constant current. Full-wave rectification, silicon (111) crystal analyser, scintillation counter. (*b*) Plot of Moseley's law for four characteristic X-ray spectral lines.

2.3.5.4.1. *Crystal monochromators*

Reflection from a single-crystal plate is the most common way to obtain monochromatic X-rays. Although the reflected beam is not strictly monochromatic because of the natural width of the spectral line and the rocking angle of the crystal, it is sufficient for practical powder diffraction. The crystal reflects λ and may also reflect subharmonic wavelengths $\lambda/2$, $\lambda/3$, *etc.*, and higher-order *hkl*'s depending on its crystal structure. Crystals can be selected to avoid the subharmonics, for example, Si and Ge cut parallel to (111); they have a negligible 222 reflection and $\lambda/3$ can be easily rejected with pulse-amplitude discrimination. Crystals are selected with relatively small Bragg angles to minimize polarization effects. Virtually all monochromators are of the reflection type. Transmission monochromators such as thin mica have been used occasionally in X-ray spectroscopy but not in powder diffraction.

When a crystal monochromator is placed in the direct beam from an X-ray tube or synchrotron-radiation source, the crystal also reflects other wavelengths from the continuous radiation. It is necessary to take a photograph of the reflected beam to see if Laue spots may be close to the spectral line and might pass through. If Laue spots are a problem and a flat crystal is used, a small rotation will move the spots. The entrance and exit slits should be made as narrow as possible for the experiment and a

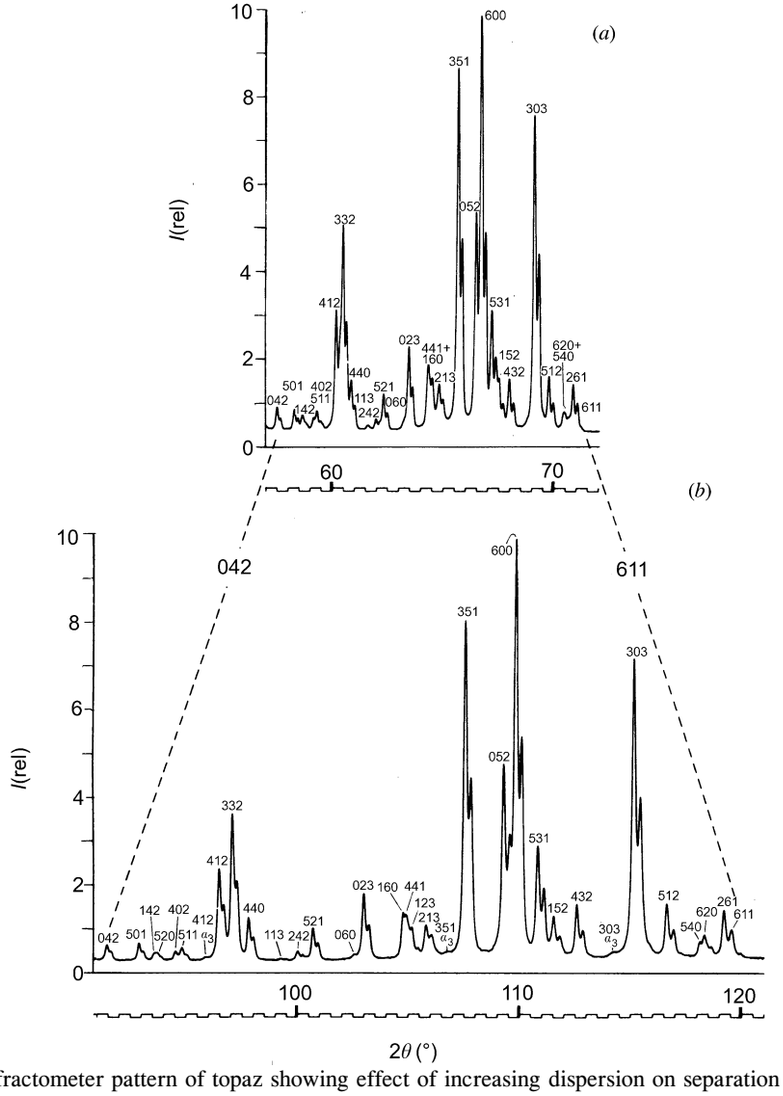

Fig. 2.3.5.5. Portion of diffractometer pattern of topaz showing effect of increasing dispersion on separation of peaks. (*a*) Cu $K\alpha$, (*b*) Cr $K\alpha$.

narrow pulse-height analyser window (see Section 7.1.2) may be helpful. In any case, a simple powder pattern will show if the unwanted wavelengths are reaching the specimen.

To achieve maximum performance in terms of intensity and resolution, it is essential to design the X-ray optics so that the properties of the monochromator match the characteristics of the source, specimen, and instrument geometry. A flat crystal is used for parallel beams and a curved crystal for focusing geometries. The curved crystal can accept a much larger divergent primary beam and has the property of converting the incident divergent beam to a convergent beam after reflection. The quality of the crystal and its surface preparation by fine lapping and etching are crucial.

The crystal materials most commonly used are silicon, germanium, and quartz, which have small rocking angles, and graphite and LiF which have large mosaic spreads. A large variety of crystals is available with large and small d spacings for use in X-ray fluorescence spectroscopy. The crystal must be chemically stable and not deteriorate with X-ray exposure. Synthetic multilayer microstructures have recently been developed for longer-wavelength X-rays. A lower atomic number element avoids fluorescence from the crystal.

The common types of monochromators are illustrated in Fig. 2.3.5.6. The beam reflected from a flat crystal (*a*) is nearly parallel. If the incident beam is divergent and the crystal is rotated, the reflection will broaden as the rays that make the correct Bragg angle 'walk' across the surface. If the crystal is cut at an angle γ to the reflecting plane, the beam is broadened as shown in (*b*) (or narrowed if reversed) (Fankuchen, 1937; Evans, Hirsch & Kellar, 1948).

A channel-cut monochromator [Fig. 2.3.5.6(*c*)] is cut from a single-crystal ingot and both plates, therefore, have exactly the same orientation (Bonse & Hart, 1965, 1966). They are usually made from a high-quality dislocation-free silicon ingot. They can also be designed to give more than two reflections per channel, and can be cut at an angle to the reflecting plane (Deutsch, 1980). Originally designed for small-angle scattering, they are now also used for parallel-beam diffractometry, interferometry, and spectroscopy. They have the important property that the position and direction of the monochromatic beam remain nearly the same for a wide range of wavelengths. This avoids realignment and recalibration of the diffractometer when changing wavelengths in synchrotron diffractometry. The reflections are narrow with minimal tails. The resolution is determined by the energy spread of the perfect-crystal bandpass [which is 1.33×10^{-4} for Si(111)] and the wavelength dispersion, which is small at small 2θ's and increases with $\tan\theta$ (Beaumont & Hart, 1974; Hart, Rodrigues & Siddons, 1984).

Thin crystals can be bent to form a section of a cylinder for focusing, Fig. 2.3.5.6(*d*) (Johann, 1931). The safe bending radius is of the order of 1000 to 2000 times the thickness of the crystal plate. The bending radius $2R$ forms a surface tangent to the focusing circle of radius R. The cylindrical form allows the line focus of the X-ray tube to be used. Because the lattice planes are not always tangent to the focusing circle, as would be required for perfect focusing, the aberrations broaden the focus, but this may not be a serious problem in powder diffraction. If the crystal is also ground so that its surface radius R matches the focusing circle, the aberrations are removed, Fig. 2.3.5.6(*e*) (DuMond & Kirkpatrick, 1930; Johannson, 1933). The crystal may be initially cut at an angle γ to the surface to change the focal length FL of the incident and reflected beams. Here, $\mathrm{FL}_1 = 2R\sin(\theta - \gamma)$ and $\mathrm{FL}_2 = 2R\sin(\theta + \gamma)$.

Another type of focusing monochromator requires a plane-parallel thin single-crystal plate bent into a section of a logarithmic spiral, Fig. 2.3.5.6(*f*) (Barraud, 1949). de Wolff (1968*b*) developed a method of applying unequal forces to the ends of the plate in adjusting the curvature to give a sharp focus (Subsection 2.3.1.2). It has the important advantage that the curvature can be changed while set on a reflection to obtain the best results in setting up the diffractometer.

The most widely used monochromator is highly oriented pyrolytic graphite in the form of a cylindrically curved plate. It is generally used in the diffracted beam after the receiving slit. The basal reflection $d(002) = 3.35$ Å. Because of its softness, it cannot be ground or cut at an angle to the plane. It is not a true single crystal and has a broad rocking angle of 0.3 to 0.6°, but this is not a problem when the receiving slit determines the profile. Its greatest advantage is the extraordinarily high reflectivity of about 50% for Cu $K\alpha$, which is far higher than any other crystal (Renninger, 1956). In practice, some graphite plates may have a reflectivity as low as about 25–30%.

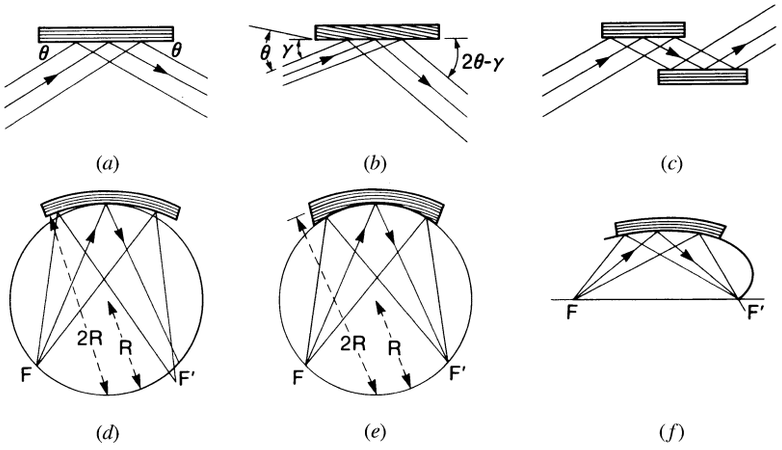

Fig. 2.3.5.6. Crystal monochromators most frequently used in powder diffraction. (*a*)-(*c*) Non-focusing parallel beam, (*d*)-(*f*) focusing bent crystals. All may be cut parallel to the reflecting lattice plane (symmetric cut) or inclined (asymmetric cut). The latter are used to expand or condense beam depending on the direction of inclination, and to change focal lengths. (*a*) Flat symmetric plate. (*b*) Flat asymmetric plate in orientation to expand beam and increase intensity (Fankuchen, 1937). (*c*) Channel monochromator cut from highly perfect ingot (Bonse & Hart, 1965). (*d*) Focusing crystal bent to radius $2R$ (Johann, 1931). (*e*) Crystal bent to $2R$ and surface ground to R (DuMond & Kirkpatrick, 1930; Johannson, 1933). (*f*) Crystal bent to section of logarithmic spiral (Barraud, 1949; de Wolff, 1968*b*).

Table 2.3.5.2. *β filters for common target elements*

Target element	β filter	$K\beta_1/K\alpha_1 = 1/100$ (mm)	g cm^{-2}	% loss $K\alpha_1$	$K\beta_1/K\alpha_1 = 1/500$ (mm)	g cm^{-2}	% loss $K\alpha_1$
Ag	Pd	0.62	0.074	60	0.092	0.110	74
	Rh	0.062	0.077	59	0.092	0.114	73
Mo	Zr	0.081	0.053	57	0.120	0.078	71
Cu	Ni	0.015	0.013	45	0.023	0.020	60
Ni	Co	0.013	0.011	42	0.020	0.017	57
Co	Fe	0.012	0.009	39	0.019	0.015	54
Fe	Mn	0.011	0.008	38	0.018	0.013	53
	Mn_2O_3	0.027	0.012	43	0.042	0.019	59
	MnO_2	0.026	0.013	45	0.042	0.021	61
Cr	V	0.011	0.007	37	0.017	0.010	51
	V_2O_5	0.036	0.012	48	0.056	0.019	64

The advantage of placing the monochromator in the diffracted beam is that it eliminates specimen fluorescence except for the wavelength to which it is tuned. In conventional focusing geometry, the receiving slit controls the resolution and intensity. The set of parallel slits that limits the axial divergence in the diffracted beam can be eliminated because the crystal has a smaller effective aperture. By eliminating the slits and the $K\beta$ filter, each of which reduces the intensity by about one half, there is about a twofold *gain* of intensity. The results are the same using the parallel or antiparallel position of the graphite with respect to the specimen. The dispersive setting makes it easier to use shielding for radioactive samples.

There is no advantage in using a perfect crystal such as Si after the receiving slit because it does not improve the resolution or profile shape, and the intensity is much lower. However, if the monochromator is to be used in the incident beam, it is advisable to use a high-quality crystal because the incident-beam aperture and profile shape are determined by the focusing properties of the monochromator. A narrow slit would be needed to reduce the reflected width of a graphite monochromator and would cause a large loss of intensity.

The use of a small solid-state detector in place of the monochromator should be considered if the count rates are not too high (see Subsection 7.1.5.1).

2.3.5.4.2. *Single and balanced filters*

Single filters to remove the $K\beta$ lines are also used, but better results are generally obtained with a crystal monochromator. The following description provides the basic information on the use of filters if monochromators are not used. A single thin filter made of, or containing, an element that has an absorption edge of wavelength just less than that of the $K\alpha_1$, $K\alpha_2$ doublet will absorb part of that doublet but much more of the $K\beta$ line and part of the white radiation, as shown in Fig. 2.3.5.3. The relative transmission throughout the spectrum depends on the filter element and its thickness.

A filter may be used to modify the X-ray spectral distribution by suppressing certain radiations for any of several reasons:

(1) *β lines*. β-line intensity need be reduced only enough to avoid overlaps and difficulties in identification in powder work. In single-crystal work, the large peak intensities may require a larger reduction of the β lines, which may be virtually eliminated if so desired. The $K\alpha$ intensity is also reduced by the filter. For example, a 0.015 mm thick Ni filter reduces Cu $K\beta$ by 99% but also reduces Cu $K\alpha_1$ by 60%.

(2) *Continuum*. The continuum is reduced by the filter but by no means eliminated (see Fig. 2.3.5.3). The greatest reduction occurs for those wavelengths just below the *K*-absorption edge of the filter. The reduction of the continuum appears greater for Mo than for Cu and lower atomic number targets because the Mo *K* lines occur near the peak of the continuum. Care must be taken in measuring integrated line intensities when using filters because the *K*-absorption edge of the filter may cause an abrupt change in the background level on the short-wavelength side of the line.

(3) *Contaminant lines*. Lines arising from an element other than the pure target element may be absorbed. For example, an Ni filter is an ideal absorber for the W *L* spectrum.

The filter thickness required to obtain a certain $K\beta_1$: $K\alpha_1$ peak or integrated-intensity ratio at the detector requires the unfiltered peak or integrated-intensity ratio under the same experimental conditions. Then,

$$t = \ln\left\{\left(\frac{K\beta_1}{K\alpha_1}\right)_{\text{unfilt}}\left(\frac{K\alpha_1}{K\beta_1}\right)_{\text{filt}}\right\}\Big/(\mu K\beta_1 - \mu K\alpha_1), \quad (2.3.5.2)$$

where the thickness t is in cm and μ is the linear absorption coefficient of the filter for the given wavelength. Table 2.3.5.2 lists the calculated thicknesses of β filters required to reduce the $K\beta_1$: $K\alpha_1$ integrated-intensity ratio to 1/100 and 1/500 for seven common targets. A brass filter has been used to isolate W $L\alpha$. The *L*-absorption edges of high atomic number elements have been used for filtering purposes, but the high absorption of these filters causes a large reduction of the $K\alpha$ intensity.

The object of filtering is to obtain an optimum effect at the measuring device (photographic film, counter, *etc*.), and the distribution of intensity before and after diffraction by the crystalline specimen has to be taken into account in deciding the best position of the filter. The continuum, line spectrum or both cause all specimens to fluoresce, that is, to produce *K*, *L*, and *M* line spectra characteristic of the elements in the specimen. The longer-wavelength fluorescence spectra ($\lambda > 2.5$ Å) are

usually absorbed in the air path or counter-tube window and, hence, are not observed. When using vacuum or helium-path instruments and low-absorbing detector windows, the longer-wavelength fluorescence spectra may appear.

When specimen fluorescence is present, the position of the β filter may have a marked effect on the background. If placed between the X-ray tube and specimen, the filter attenuates a portion of the primary spectrum just below the absorption edges of the elements in the specimen, thereby reducing the intensity of the fluorescence. When placed between the specimen and counter tube, the filter absorbes some of the fluorescence from the specimen. The choice of position will depend on the elements of the X-ray tube target and specimen. If the filter is placed after the specimen, it is advisable to place it close to the specimen to minimize the amount of fluorescence from the filter that reaches the detector. The fluorescence intensity decreases by the inverse-square law. Maximizing the distance between the specimen and detector also reduces the specimen fluorescence intensity detected for the same reason. If the filter is to be placed between the X-ray tube and specimen, the filter should be close to the tube to avoid fluorescence from the filter that might be recorded. It is sometimes useful to place the filter over only a portion of the film in powder cameras to facilitate the identification of the β lines.

If possible, the X-ray tube target element should be chosen so that its β filter also has a high absorption for the specimen X-ray fluorescence. For example, with a Cu target and Cu specimen, the continuum causes a large Cu K fluorescence that is transmitted by an Ni filter; if a Co target is used instead, the Cu K fluorescence is greatly decreased by an Fe $K\beta$ filter. A second filter may be useful in reducing the fluorescence background. For example, with a Ge specimen, the continuum from a Cu target causes strong Ge K fluorescence, which an Ni filter transmits. Addition of a thin Zn filter improves the peak/background ratio (P/B) of the Cu $K\alpha$ with only a small reduction of peak intensity (Ge $K\alpha$, $\lambda = 1.25$ Å; Zn K-absorption edge, $\lambda = 1.28$ Å).

X-ray background is also caused by scattering of the entire primary spectrum with varying efficiency by the specimen. The filter reduces the background by an amount dependent on its absorption characteristics. When using pulse-amplitude discrimination and specimens whose X-ray fluorescence is weak, the remaining observed background is largely due to characteristic line radiation. The β filter then usually reduces the background and the $K\alpha$ radiation by roughly the same amount and P/B is not changed markedly regardless of the position of the filter.

Table 2.3.5.3. *Calculated thickness of balanced filters for common target elements*

Target material	Filter pair (*A*)	Filter pair (*B*)	(*A*) Thickness mm	(*A*) Thickness g cm^{-3}	(*B*) Thickness mm	(*B*) Thickness g cm^{-2}
Ag	Pd	Mo	0.0275	0.033	0.039	0.040
Mo	Zr	Sr	0.0392	0.026	0.104	0.027
Mo	Zr	Y	0.0392	0.026	0.063	0.028
Cu	Ni	Co	0.0100	0.0089	0.0108	0.0095
Ni	Co	Fe	0.0094	0.0083	0.0113	0.0089
Co	Fe	Mn	0.0098	0.0077	0.0111	0.0083
Fe	Mn	Cr	0.0095	0.0071	0.0107	0.0077
Cr	V	Ti	0.0097	0.0059	0.0146	0.0066

The β filter is sometimes used instead of black paper or Al foil to screen out visible and ultraviolet light. Filters in the form of pure thin metal foils are available from a number of metal and chemical companies. They should be checked with a bright light source to make certain they are free of pinholes.

The balanced-filter technique uses two filters that have absorption edges just above and just below the $K\alpha_1$, $K\alpha_2$ wavelengths (Ross, 1928; Young, 1963). The difference between intensities of X-ray diffractometer or film recordings made with each filter arises from the band of wavelengths between the absorption edges, which is essential that of the $K\alpha_1$, $K\alpha_2$ wavelengths. The thicknesses of the two filters should be selected so that both have the same absorption for the $K\beta$ wavelength. Table 2.3.5.3 lists the calculated thicknesses of filter pairs for the common target elements. The (*A*) filter was chosen for a 67% transmission of the incident $K\alpha$ intensity, and only pure metal foils are used. Adjustment of the thickness is facilitated if the foil is mounted in a rotatable holder so that the ray-path thickness can be varied by changing the inclination of the foil to the beam.

Although the two filters can be experimentally adjusted to give the same $K\beta$ intensities, they are not exactly balanced at other wavelengths. The use of pulse-amplitude discrimination to remove most of the continuous radiation is desirable to reduce this effect. The limitations of the method are (*a*) the difficulties in adjusting the balance of the filters, (*b*) the band-pass is much wider that that of a crystal monochromator, and (*c*) it requires two sets of data, one of which has low intensity and consequently poor counting statistics.

2.4. Powder and related techniques: electron and neutron techniques

By J. M. Cowley and A. W. Hewat

2.4.1. Electron techniques (By J. M. Cowley)

2.4.1.1. *Powder-pattern geometry*

The electron wavelengths normally used to obtain powder patterns from thin films of polycrystalline materials lie in the range 8×10^{-2} to 2×10^{-2} Å (20 to 200 kV accelerating voltages). The maximum scattering angles ($2\theta_B$) observed are usually less than 10^{-1} rad.

Patterns are usually recorded on flat photographic plates or films and a small-angle approximation is applied. For a camera length L, the distance from the specimen to the photographic plate in the absence of any intervening electron lenses, the approximation is made that, for a diffraction ring of radius r,

$$\lambda/d = 2\sin\theta \simeq \tan 2\theta = r/L,$$

or the interplanar spacing, d, is given by

$$d = L\lambda/r. \qquad (2.4.1.1)$$

For a scattering angle of 10^{-1} rad, the error in this expression is 0.5%. A better approximation, valid to better than 0.1% at 10^{-1} rad, is

$$d = (L\lambda/r)(1 + 3r^2/8L^2). \qquad (2.4.1.2)$$

The 'camera constant' $L\lambda$ may be obtained by direct measurement of L and the accelerating voltage if there are no electron lenses following the specimen.

Direct electronic recording of intensities has great advantages over photographic recording (Tsypursky & Drits, 1977).

In recent years, electron diffraction patterns have been obtained most commonly in electron microscopes with three or more post-specimen lenses. The camera-constant values are then best obtained by calibration using samples of known structure.

With electron-optical instruments, it is possible to attain collimations of 10^{-6} rad so that for scattering angles of 10^{-1} rad an accuracy of 10^{-5} in d spacings should be possible in principle but is not normally achievable. In practice, accuracies of about 1% are expected. Some factors limiting the accuracy of measurement are mentioned in the following sections. The small-angle-scattering geometry precludes application of any of the special camera geometries used for high-accuracy measurements with X-rays (Chapter 2.3).

2.4.1.2. *Diffraction patterns in electron microscopes*

The specimens used in electron microscopes may be self-supporting thin films or fine powders supported on thin films, usually made of amorphous carbon. Specimen thicknesses must be less than about 10^3 Å in order to avoid perturbations of the diffraction patterns by strong multiple-scattering effects. The selected-area electron-diffraction (SAED) technique [see Section 2.5.1 in *IT* B (1993)] allows sharply focused diffraction patterns to be obtained from regions 10^3 to 10^5 Å in diameter. For the smaller ranges of selected-area regions, specimens may give single-crystal patterns or very spotty ring paterns, rather than continuous ring patterns, because the number of crystals present in the field of view is small unless the crystallite size is of the order of 100 Å or less. By use of the convergent-beam electron-diffraction (CBED) technique, diffraction patterns can be obtained from regions of diameter 100 Å [see Section 2.5.2 in *IT* B (1993)] or, in the case of some specialized instruments, regions less than 10 Å in diameter. For these reasons, the methods for phase identification from electron diffraction patterns and the corresponding databases (see Subsection 2.4.1.6) are increasingly concerned with single-crystal spot patterns in addition to powder patterns.

Instrument manufacturers usually provide values of camera lengths, L, or camera constants, $L\lambda$, for a wide range of designated lens-current settings. It is advisable to check these calibrations with samples of known structure and to determine calibrations for non-standard lens settings.

The effective camera length, L, is dependent on the specimen height within the objective-lens pole-piece. If a specimen-height adjustment (a z-lift) is provided, it should be adjusted to give a predetermined lens current, and hence focal length, of the objective lens.

In some microscopes, at particular lens settings the projector lenses may introduce a radial distortion of the diffraction pattern. This may be measured with a suitable standard specimen.

2.4.1.3. *Preferred orientations*

The techniques of specimen preparation may result in a strong preferred orientation of the crystallites, resulting in strong arcing of powder-pattern rings, the absence of some rings, and perturbations of relative intensities.

For example, small crystals of flaky habit deposited on a flat supporting film may be oriented with one reciprocal-lattice axis preferentially perpendicular to the plane of the support. A ring pattern obtained with the incident beam perpendicular to the support then shows only those rings for planes in the zone parallel to the preferred axis. Such orientation is detected by the appearance of arcing and additional reflections when the supporting film is tilted. Tilted specimens give the so-called oblique texture patterns which provide a rich source of three-dimensional diffraction information, used as a basis for crystal structure analysis.

A full discussion of the texture patterns resulting from preferred orientations is given in Section 2.5.3 of *IT* B (1993).

2.4.1.4. *Powder-pattern intensities*

In the kinematical approximation, the expression for intensities of electron diffraction follows that for X-ray diffraction with the exception that, because only small angles of diffraction are involved, no polarization factor is involved. Following Vainshtein (1964), the intensity per unit length of a powder line is

$$I(h) = J_0\lambda^2 \left| \frac{\Phi_h}{\Omega} \right|^2 V \frac{d_h^2 M}{4\pi L\lambda}, \qquad (2.4.1.3)$$

where J_0 is the incident-beam intensity, Φ_h is the structure factor, Ω is the unit-cell volume, V is the sample volume, and M is the multiplicity factor.

The kinematical approximation has limited validity. The deviations from this approximation are given to a first approximation by the two-beam approximation to the dynamical-scattering theory. Because an averaging over all orientations is involved, the many-beam dynamical-diffraction effects are less evident than for single-crystal patterns.

Copyright © 2006 International Union of Crystallography

By integrating the two-beam intensity expression over excitation error, Blackman (1939) obtained the expression for the ratio of dynamical to kinematical intensities:

$$I_{\rm dyn}/I_{\rm kin} = A_h^{-1} \int_0^{A_h} J_0(2x)\,{\rm d}x, \qquad (2.4.1.4)$$

where $J_o(x)$ is the zero-order Bessel function, $A_h = \sigma H \Phi_h$ with the interaction constant $\sigma = 2\pi me\lambda/h^2$, and H is the crystal thickness. Careful measurements on ring patterns from thin aluminium films by Horstmann & Meyer (1962) showed agreement with the 'Blackman curve' [from equation (2.4.1.4)] to within about 5% with some notable exceptions. Deviations of up to 40 to 50% from the Blackman curve occurred for several reflections, such as 222 and 400, which are second-order reflections from strong inner reflections. A practical algorithm for implementing Blackman corrections has been published by Dvoryankina & Pinsker (1958).

Such deviations result from plural-beam *systematic interactions*, the coherent multiple scattering between different orders of a strong inner reflection. When the Bragg condition is satisfied for one order, the excitation errors for the other orders are the same for all possible crystal orientations and these other orders contribute systematically to the ring-pattern intensities. A correction for the effects of systematic interactions may be made by use of the Bethe second approximation (Bethe, 1928) (see Chapter 8.8).

For non-systematic reflections, corresponding to reciprocal-lattice points not collinear with the origin and the reciprocal-lattice point of interest, the averaging over all crystal orientations ensures that the powder-pattern intensity calculated from the two-beam formula will not be appreciably affected. Appreciable effects from non-systematic interactions may, however, occur when the averaging is over a limited range of crystal orientations, as in the case of strong preferred orientations. It was shown theoretically by Turner & Cowley (1969) and experimentally by Imamov, Pannhorst, Avilov & Pinsker (1976) that appreciable modifications of intensities of oblique-texture patterns may result from non-systematic interactions for particular tilt angles, especially for heavy-atom materials [see also Avilov, Parmon, Semiletov & Sirota (1984)].

The techniques for the measurement of electron diffraction intensities are described in Chapter 7.2. Most commonly electron diffraction powder patterns are recorded by photographic methods and a microdensitometer is used for quantitative intensity measurement. The Grigson scanning method, using a scintillator and photomultiplier to record intensities as the pattern is scanned over a fine slit, has considerable advantages in terms of linearity and range of the intensity scale (Grigson, 1962). This method also has the advantage that it may readily be combined with an energy filter so that only elastically scattered electrons (or electrons inelastically scattered with a particular energy loss) may be recorded.

Small-angle electron diffraction may give useful information in some cases, but must be interpreted carefully because the features may result from multiple scattering or other artefacts. It may give additional details of periodicity (super-periods) and deviations of the real symmetry from the ideal symmetry suggested by other data. Care must be taken with the interpretation of additional reflections, as they may relate to the structure of small regions that are not typical of the bulk specimens such as are examined by X-ray diffraction.

The techniques for interpretation of electron diffraction powder-pattern intensities follow those for X-ray patterns when the kinematical approximation is valid. For very small crystals, giving very broad rings, it is possible to use the method, commonly applied for diffraction by gases, of performing a Fourier transform to obtain a radial distribution function (Goodman, 1963).

2.4.1.5. *Crystal-size analysis*

The methods used in X-ray diffraction for the determination of average crystal size or size distributions may be applied to electron diffraction powder patterns. Except in the case of very small crystal dimensions, several factors peculiar to electrons should be taken into consideration.

(*a*) Unless energy filtering is used to remove inelastically scattered electrons, a component is added to the rings broadened by the effects of inelastic scattering involving electronic excitations. Since the mean free paths for such processes are of the order of 10^3 Å and the angular spread of the scattered electrons is 10^{-3} to 10^{-4} rad, the ring broadening for thick samples may be equivalent to the broadening for a crystal size of the order of 100 Å.

(*b*) When a powder sample consists of separated crystallites having faces not predominantly parallel or perpendicular to the incident beam, the diffraction rings may be appreciably broadened by refraction effects. The refractive index for electrons is given, to a first approximation, by

$$n = 1 + \Phi_0/2E,$$

where Φ_0 is the mean inner potential of the crystal, typically 10 to 20 V, and E is the accelerating voltage of the incident electron beam. For the beam passing through the two faces of a 90° wedge, each at an angle $\alpha = 45^\circ$ to the beam, for example, the beam is deflected by an amount

$$\Delta = \Phi_0/E = 1.5 \times 10^{-4}\,{\rm rad}$$

for an inner potential of 15 V and $E = 100$ kV. The broadening of the ring by such deflections can correspond to the broadening due to a particle size of $\lambda/2\Delta \simeq 120$ Å.

For crystallites of regular habit, such as the small cubic crystals of MgO smoke, the ring broadening from this source is strongly dependent on the crystallographic planes involved (Sturkey & Frevel, 1945; Cowley & Rees, 1947; Honjo & Mihama, 1954). For more isometric crystal shapes, this dependence is less marked and the broadening has been estimated (Cowley & Rees, 1947) as equivalent to that due to a particle size of about 200 Å.

2.4.1.6. *Unknown-phase identification: databases*

To a limited extent, the compilations of data for X-ray diffraction, such as the ICDD Powder Diffraction File, may be used for the identification of phases from electron diffraction data. The nature of the electron diffraction data and the circumstances of its collection have prompted the compilation of databases specifically for use with electron diffraction. Factors taken into consideration include the following.

(*a*) Because of the increasing use of single-crystal patterns obtained in the SAED mode in an electron microscope, the use of single-crystal spot patterns, in addition to powder patterns, must be considered for purposes of identification. Methods for the analysis of single-crystal patterns are summarized in Section 5.4.1.

(*b*) The deviations from kinematical scattering conditions may be large, especially for single-crystal patterns, so that little reliance can be placed on relative intensities, and reflections kinematically forbidden may be present.

(*c*) Compositional information may be obtained by use of X-ray microanalysis (or electron-energy-loss spectroscopy) performed in the electron microscope and this provides an effective additional guide to identification.

(*d*) Electron diffraction data often extend to smaller d spacings than X-ray data because there is no wavelength limitation.

(*e*) The electron diffraction d-spacing information is rarely more precise than 1% and the uncertainty may be 5% for large d spacings.

With these points in mind, databases specially designed for use with electron diffraction have been developed. The NIST/Sandia/ICDD Electron Diffraction Database follows the design principles of Carr, Chambers, Melgaard, Himes, Stalick & Mighell (1987). The 1993 version contains crystallographic and chemical information on over 81 500 crystalline materials with, in most cases, calculated patterns to ensure that diagnostic high-d-spacing reflections can be matched. It is available on magnetic tape or floppy disks. The MAX-d index (Anderson & Johnson, 1979) has been expanded to 51 580 NSI-based entries (Mighell, Himes, Anderson & Carr, 1988) in book form for manual searching.

2.4.2. Neutron techniques (By A. W. Hewat)

Neutrons have advantages over X-rays for the refinement of crystal structures from powder data because systematic errors (Wilson, 1963) are smaller, and the absence of a form factor means that information is available at small d spacings. It is also easy to collect data at very low or high temperature; examining the structure as a function of temperature (or pressure) is much more useful than simply obtaining 'the' crystal structure at STP (standard temperature and pressure). In some cases, 'kinetics' measurements at intervals of only a few seconds are needed to follow chemical reactions.

A neutron powder diffractometer need not separate all of the Bragg peaks, since complex patterns can be analysed by Rietveld refinement (Rietveld, 1969), but high resolution will increase the information content of the profile, and permit the refinement of larger and more complex structures. Doubling the unit-cell volume doubles the number of Bragg peaks, requiring higher resolution, but also halves the average peak intensity. Resolution must not then be obtained at the expense of well defined line shape, essential for profile analysis, nor at the expense of intensity.

Two types of diffractometer are required in practice: a high-resolution machine with data-collection times of a few hours (or days) for Rietveld structure refinement, and a high-flux machine with data-collection times of a few seconds (or minutes) for kinetics measurements. In both cases, the data-collection rate depends on the product of the flux on the sample, the sample volume, and the solid angle of the detector (Hewat, 1975). The flux on the sample can be increased with a focusing monochromator, the sample volume by using large sample-detector distances or Soller collimators, and the detector solid angle by using a large multidetector.

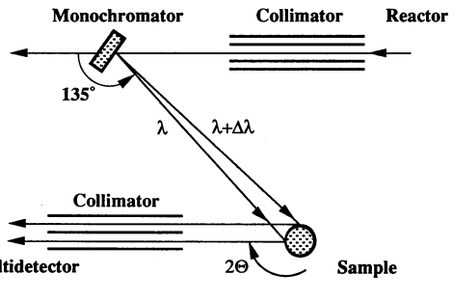

Fig. 2.4.2.1. Schematic drawing of the high-resolution neutron powder diffractometer D2B at ILL, Grenoble.

The focusing monochromator is usually made from horizontal strips of pyrolytic graphite or squashed germanium mounted on a vertically focusing plate 100 to 300 mm high. A large beam can thus be focused on a sample up to 50 mm high. Vertical divergence of 5° or more can be tolerated even for a high-resolution machine; the peak width is only increased (and made asymmetric) far from scattering angles of 90°, where most of the peaks occur. The effect is in any case purely geometrical, and can readily be included in the data analysis (Howard, 1982).

To increase the wavelength spread $\Delta\lambda/\lambda$, and hence intensity, monochromator mosaic can be large (20′) even for high resolution, since all wavelengths are focused back into the primary-beam direction at scattering angles equal to the monochromator take-off angle (Fig. 2.4.2.1).

Rather long wavelengths (1.5 to 3 Å) are favoured, to spread out the pattern, and to reduce the total number of reflections excited (increasing their average intensity). Data must then be collected at large scattering angles with good resolution to obtain sufficiently small d spacings, and this implies a large take-off angle. A graphite filter to remove $\lambda/2$ and higher-order contamination is a popular choice for a primary wavelength of 2.4 Å (Loopstra, 1966). Since germanium reflections such as *hhl* with h, $l = 2n + 1$ do not produce $\lambda/2$ contamination, a filter is not needed for primary wavelengths below about 1.6 Å with high-take-off-angle geometry, but is still necessary for longer wavelengths.

The multidetector can be an array of up to 64 individual detectors and Soller collimators for a high-resolution machine (Hewat & Bailey, 1976; Hewat, 1986*a*), or a position-sensitive detector (PSD) for a high-flux machine (Allemand *et al.*, 1975). Gas-filled (^{3}He or BF_3) detectors are usual, though scintillator and other types of solid-state detector are increasingly used; the PSD may be either a single horizontal wire with position-detection logic comparing the signals obtained at either end, or an array of vertical wire detectors within a common gas envelope. The vertical aperture of the single-wire detector seriously limits the efficiency of what is otherwise a very cheap solution, and of course large angular ranges cannot be covered by a single straight wire.

The vertical aperture should match the vertical divergence from the monochromator ($\sim 5°$). Composite detectors can be constructed by stacking elements both vertically to increase the aperture, and horizontally to increase the angular range. Construction of a wide-angle (160°) multiwire detector is difficult and expensive, but a solid angle of more than 0.1 sr may be obtained. The solid angle for a collimated multidetector, even if it covers 160°, may be less than 0.01 sr.

The sample volume limits the resolution of the PSD, since the detector resolution α_3 (typically 0.2°) is the mean of the element width and the sample diameter (typically 5 mm) divided by the sample-to-detector distance (typically 1500 mm). For a Soller collimator, α_3 can be as little as 5′, and does not depend on the sample volume, which can be large (20 mm diameter) even for high resolution. The PSD also requires special precautions to avoid background from the sample environment, while the collimated machine can handle difficult sample environments, especially for scattering near 90°.

The definition of the detector is the number of data points per degree. For profile analysis, unless the peak shape is well known *a priori*, about five points are needed per reflection half-width, which is more than usually available from a multiwire PSD.

However, a PSD may be scanned to increase the profile definition. The minimum scan angle is clearly the angle between elements, from 0.2° for a PSD to 2.5° or more for a multidetector in steps of from 0.025 to 0.1°. If larger scans are performed, it is most convenient to reduce the data to a single profile by averaging the counts from different detector elements at each point in the profile, after correcting for relative efficiencies and angular separations.

The resolution, of either machine, should be no better than really necessary for a particular sample: additional resolution merely reveals problems with sample perfection and line shape, making Rietveld refinement difficult, and of course reducing effective intensity. In any case, resolution is ultimately limited by the powder particle size and strain broadening (Hewat, 1975). As an order of magnitude, if $D = 1000$ Å is the effective size of the perfect crystallites that make up a much larger (1 to 10 μm) powder grain, then for lattice spacing $d = 1$ Å, the best resolution that one can hope to obtain is of the order $\Delta d/d = d/D = 10^{-3}$, corresponding to a line width of $\Delta(2\theta) \simeq 0.1°$. A few more perfect materials (usually those for which single crystals can be grown!) will produce higher-resolution patterns, but then primary extinction may not be negligible.

It is not even necessary to have the best possible resolution for all d spacings: ideally, the resolution should be proportional to the density of lines, and this increases with the surface area of the Ewald sphere of radius $1/d$. Then we want $\Delta d/d = d^2$ or $\Delta(2\theta) = \lambda^2/\sin 2\theta$. This has a minimum near $2\theta = 90°$. In fact, the full width at half-height is (Cagliotti, Paoletti & Ricci, 1958)

$$\Delta^2(2\theta) = U\tan^2\theta + V\tan\theta + W.$$

The parameters U, V, and W are functions of the monochromator mosaic spread and collimation, from which it follows that the minimum in $\Delta(2\theta)$ occurs for scattering angles $2\theta \simeq 2\theta_M$. The monochromator take-off angle should then be at least 90°; in practice, since $\Delta^2(2\theta)$ increases quadratically with $\tan\theta$ for angles larger than this focusing angle, the monochromator take-off should be even greater than 90°. A value of 120 to 135° is recommended.

For this focusing geometry, the different wavelengths $\lambda + \Delta\lambda$, reflected at different angles from the monochromator, are brought back parallel to the primary beam, and the line width becomes simply the convolution of the primary and detector collimations α_1 and α_3:

$$\Delta^2(2\theta) = \alpha_1^2 + \alpha_3^2.$$

The collimators α_1 and α_3 should then be equal and small. Such fine collimators are now made routinely from gadolinium oxide-coated stretched plastic foil (Carlile, Hey & Mack, 1977). The collimator α_2 should simply be large enough to pass all wavelengths reflected by the mosaic spread β of the monochromator, *i.e.* $\alpha_2 \simeq 2\beta$.

Neutron crystallographers have been reluctant to use large take-off angles because they seem to imply greatly reduced beam intensity. Indeed, large θ_M means small waveband $\Delta\lambda/\lambda$ since $\Delta\lambda/\lambda = \Delta d/d = \Delta(\theta_M)\cot\theta_M = \beta\cot\theta_M$. However, $\Delta\lambda/\lambda$ and therefore beam intensity can be recovered simply by increasing β. This has no effect on the resolution at focusing, but it does increase the line width at low angles where there are few lines. When large d spacings are needed, for example for magnetic structures, it is best for both resolution and intensity to retain the same high take-off geometry and increase the wavelength to bring these lines closer to the focusing angle. A large take-off angle also gives a large choice of high-index reflections and wavelengths up to 6 Å!

A fixed take-off angle greatly simplifies machine design: the multidetector collimation α_3 is also necessarily fixed, but the single primary collimator α_1 can readily be changed. It is useful to have a second choice, much larger than α_3, to boost intensity for poor samples or exploratory data collection. The resolution at low angles, largely determined by β (or α_2), is not much affected by increasing α_1.

Finally, the machine should be designed around the sample environment, since this is one of the strengths of neutron powder diffraction. There is no point in building a neutron machine with superb resolution and intensity (these can much more readily be obtained with X-rays) if it cannot produce precise results for the kind of experiments of most interest – those for which it is difficult to use any other technique (Hewat, 1986*b*).

International Tables for Crystallography (2006). Vol. C, Chapter 2.5, pp. 84–88.

2.5. Energy-dispersive techniques

BY B. BURAS, W. I. F. DAVID, L. GERWARD, J. D. JORGENSEN AND B. T. M. WILLIS

2.5.1. Techniques for X-rays (By B. Buras and L. Gerward)

X-ray energy-dispersive diffraction, XED, invented in the late sixties (Giessen & Gordon, 1968; Buras, Chwaszczewska, Szarras & Szmid 1968), utilizes a primary X-ray beam of polychromatic ('white') radiation. XED is the analogue of white-beam and time-of-flight neutron diffraction (*cf.* Section 2.5.2). In the case of powdered crystals, the photon energy (or wavelength) spectrum of the X-rays scattered through a fixed optimized angle is measured using a semiconductor detector connected to a multichannel pulse-height analyser. Single-crystal methods have also been developed.

2.5.1.1. *Recording of powder diffraction spectra*

In XED powder work, the incident- and scattered-beam directions are determined by slits (Fig. 2.5.1.1). A powder spectrum is shown in Fig. 2.5.1.2. The Bragg equation is

$$2d \sin\theta_0 = \lambda = hc/E, \qquad (2.5.1.1a)$$

where d is the lattice-plane spacing, θ_0 the Bragg angle, λ and E the wavelength and the photon energy, respectively, associated with the Bragg reflection, h is Planck's constant and c the velocity of light. In practical units, equation (2.5.1.1*a*) can be written

$$E(\text{keV})\, d(\text{Å}) \sin\theta_0 = 6.199. \qquad (2.5.1.1b)$$

The main features of the XED powder method where it differs from standard angle-dispersive methods can be summarized as follows:

(*a*) The incident beam is polychromatic.

(*b*) The scattering angle $2\theta_0$ is fixed during the measurement but can be optimized for each particular experiment. There is no mechanical movement during the recording.

(*c*) The whole energy spectrum of the diffracted photons is recorded simultaneously using an energy-dispersive detector.

The scattering angle is chosen to accommodate an appropriate number of Bragg reflections within the available photon-energy range and to avoid overlapping with fluorescence lines from the sample and, when using an X-ray tube, characteristic lines from the anode. Overlap can often be avoided because a change in the scattering angle shifts the diffraction lines to new energy positions, whereas the fluorescence lines always appear at the same energies. Severe overlap problems may be encountered when the sample contains several heavy elements.

The detector aperture usually collects only a small fraction of the Debye–Scherrer cone of diffracted X-rays. The collection of an entire cone of radiation greatly increases the intensities. Also, it makes it possible to overcome crystallite stratistics problems and preferred orientations in very small samples (Holzapfel & May, 1982; Häusermann, 1992).

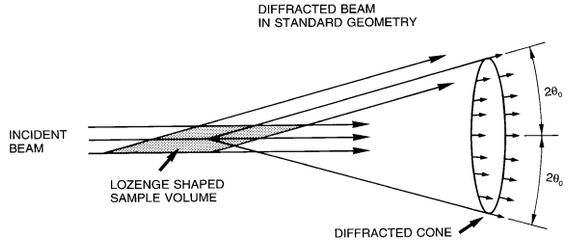

Fig. 2.5.1.1. Standard and conical diffraction geometries: $2\theta_0$ = fixed scattering angle. At low scattering angles, the lozenge-shaped sample volume is very long compared with the beam cross sections (after Häusermann, 1992).

2.5.1.2. *Incident X-ray beam*

(*a*) *Bremsstrahlung from an X-ray tube*

Bremsstrahlung from an X-ray diffraction tube provides a useful continuous spectrum for XED in the photon-energy range 2–60 keV. However, one has to avoid spectral regions close to the characteristic lines of the anode material. A tungsten anode is suitable because of its high output of white radiation having no characteristic lines in the 12–58 keV range.

A drawback of *Bremsstrahlung* is that its spectral distribution is difficult to measure or calculate with accuracy, which is necessary for a structure determination using integrated intensities [see equation (2.5.1.7)]. *Bremsstrahlung* is strongly polarized for photon energies near the high-energy limit, while the low-energy region has a weak polarization. The direction of polarization is parallel to the direction of the electron beam from the filament to the anode in the X-ray tube. Also, the polarization is difficult to measure or calculate.

(*b*) *Synchrotron radiation*

Synchrotron radiation emitted by electrons or positrons, when passing the bending magnets or insertion devices, such as wigglers, of a storage ring, provides an intense smooth spectrum for XED.

Both the spectral distribution and the polarization of the synchrotron radiation can be calculated from the parameters of the storage ring. Synchrotron radiation is almost fully polarized in the electron or positron orbit plane, *i.e.* the horizontal plane, and inherently collimated in the vertical plane. Full advantage of these features can be obtained using a vertical scattering plane. However, the mechanical construction of the diffractometer, the placing of furnaces, cryogenic equipment, *etc.* are easier to handle when the X-ray scattering is recorded in the horizontal plane. Recent XED facilities at synchrotron-radiation sources have been described by Besson & Weill (1992), Clark (1992), Häusermann (1992), Olsen (1992), and Otto (1997).

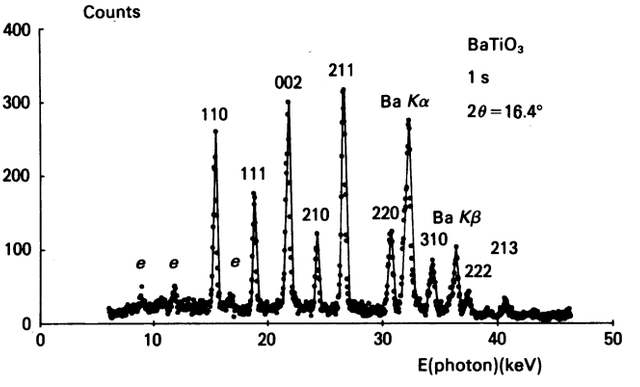

Fig. 2.5.1.2. XED powder spectrum of $BaTiO_3$ recorded with synchrotron radiation from the electron storage ring DORIS at DESY-HASYLAB in Hamburg, Germany. Counting time 1 s. Escape peaks due to the Ge detector are denoted by *e* (from Buras, Gerward, Glazer, Hidaka & Olsen, 1979).

Copyright © 2006 International Union of Crystallography

2.5.1.3. *Resolution*

The momentum resolution in energy-dispersive diffraction is limited by the angular divergence of the incident and diffracted X-ray beams and by the energy resolution of the detector system. The observed profile is a convolution of the profile due to the angular divergence and the profile due to the detector response. For resolution calculations, it is usually assumed that the profiles are Gaussian, although the real profiles might exhibit geometrical and physical aberrations (Subsection 2.5.1.5). The relative full width at half-maximum (FWHM) of a diffraction peak in terms of energy is then given by

$$\delta E/E = [(e_n/E)^2 + 5.546F\varepsilon/E + (\cot\theta_0\Delta\theta_0)^2]^{1/2}, \quad (2.5.1.2)$$

where e_n is the electronic noise contribution, F the Fano factor, ε the energy required for creating an electron–hole pair (*cf.* Subsection 7.1.5.1), and $\Delta\theta_0$ the overall angular divergence of the X-ray beam, resulting from a convolution of the incident- and the diffracted-beam profiles. For synchrotron radiation, $\Delta\theta_0$ can usually be replaced by the divergence of the diffracted beam because of the small divergence of the incident beam.

Fig. 2.5.1.3 shows $\delta E/E$ as a function of Bragg angle θ_0. The curves have been calculated from equations (2.5.1.1) and (2.5.1.2) for two values of the lattice-plane spacing and two values of $\Delta\theta_0$, typical for *Bremsstrahlung* and synchrotron radiation, respectively. It is seen that in all cases $\delta E/E$ decreases with decreasing angle (*i.e.* increasing energy) to a certain minimum and then increases rapidly. It is also seen that the minimum point of the $\delta E/E$ curve is lower for the small d value and shifts towards smaller θ_0 values for decreasing $\Delta\theta_0$. Calculations of this kind are valuable for optimizing the Bragg angle for a given sample and other experimental conditions (*cf.* Fukamachi, Hosoya & Terasaki, 1973; Buras, Niimura & Olsen, 1978).

The relative peak width at half-height is typically less than 1% for energies above 30 keV. When the observed peaks can be fitted with Gaussian functions, one can determine the centroids of the profiles by a factor of 10–100 better than the $\delta E/E$ value of equation (2.5.1.2) would indicate. Thus, it should be possible to achieve a relative resolution of about 10^{-4} for high energies. A resolution of this order is required for example in residual-stress measurements.

The detector broadening can be eliminated using a technique where the diffraction data are obtained by means of a scanning crystal monochromator and an energy-sensitive detector (Bourdillon, Glazer, Hidaka & Bordas, 1978; Parrish & Hart, 1987). A low-resolution detector is sufficient because its function (besides recording) is just to discriminate the monochromator harmonics. The Bragg reflections are not measured simultaneously as in standard XED. The monochromator-scan method can be useful when both a fixed scattering angle (*e.g.* for samples in special environments) and a high resolution are required.

2.5.1.4. *Integrated intensity for powder sample*

The kinematical theory of diffraction and a non-absorbing crystal with a 'frozen' lattice are assumed. Corrections for thermal vibrations, absorption, extinction, *etc.* are discussed in Subsection 2.5.1.5. The total diffracted power, $P_{\mathbf{h}}$, for a Bragg reflection of a powder sample can then be written (Buras & Gerward, 1975; Kalman, 1979)

$$P_{\mathbf{h}} = hcr_e^2 VN_c^2[i_0(E)jd^2|F|^2]_{\mathbf{h}} C_p(E,\theta_0)\cos\theta_0\Delta\theta_0, \quad (2.5.1.3)$$

where $\mathbf{h}$ is the diffraction vector, r_e the classical electron radius, $i_0(E)$ the intensity per unit energy range of the incident beam evaluated at the energy of the diffraction peak, V the irradiated sample volume, N_c the number of unit cells per unit volume, j the multiplicity factor, F the structure factor, and $C_p(E,\theta_0)$ the polarization factor. The latter is given by

$$C_p(E,\theta_0) = \tfrac{1}{2}[1 + \cos^2 2\theta_0 - P(E)\sin^2 2\theta_0], \quad (2.5.1.4)$$

where $P(E)$ is the degree of polarization of the incident beam. The definition of $P(E)$ is

$$P(E) = \frac{i_{0,p}(E) - i_{0,n}(E)}{i_0(E)}, \quad (2.5.1.5)$$

where $i_{0,p}(E)$ and $i_{0,n}(E)$ are the parallel and normal components of $i_0(E)$ with respect to the plane defined by the incident- and diffracted-beam directions.

Generally, $C_p(E,\theta_0)$ has to be calculated from equations (2.5.1.4) and (2.5.1.5). However, the following special cases are sometimes of interest:

$$P = 0: \quad C_p(\theta_0) = \tfrac{1}{2}(1 + \cos^2 2\theta_0) \quad (2.5.1.6a)$$

$$P = 1: \quad C_p(\theta_0) = \cos^2 2\theta_0 \quad (2.5.1.6b)$$

$$P = -1: \quad C_p = 1. \quad (2.5.1.6c)$$

Equation (2.5.1.6*a*) can often be used in connection with *Bremsstrahlung* from an X-ray tube. The primary X-ray beam can be treated as unpolarized for all photon energies when there is an angle of 45° between the plane defined by the primary and the diffraced beams and the plane defined by the primary beam and the electron beam of the X-ray tube. In standard configurations, the corresponding angle is 0° or 90° and equation (2.5.1.6*a*) is generally not correct. However, for $2\theta_0 < 20°$ it is correct to within 2.5% for all photon energies (Olsen, Buras, Jensen, Alstrup, Gerward & Selsmark, 1978).

Equations (2.5.1.6*b*) and (2.5.1.6*c*) are generally acceptable approximations for synchrotron radiation. Equation (2.5.1.6*b*) is used when the scattering plane is horizontal and (2.5.1.6*c*) when the scattering plane is vertical.

The diffraction directions appear as generatrices of a circular cone of semi-apex angle $2\theta_0$ about the direction of incidence. Equation (2.5.1.3) represents the total power associated with this

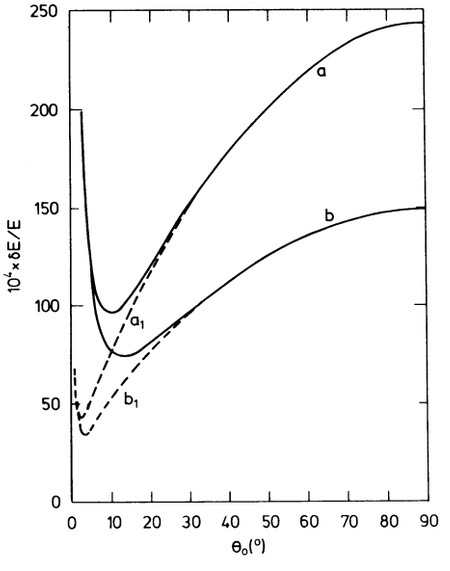

Fig. 2.5.1.3.Relative resolution, $\delta E/E$, as function of Bragg angle, θ_0, for two values of the lattice plane spacing: (*a*) 1 Å and (*b*) 0.5 Å. The full curves have been calculated for $\Delta\theta_0 = 10^{-3}$, the broken curves for $\Delta\theta_0 = 10^{-4}$.

cone. Generally, only a small fraction of this power is recorded by the detector. Thus, the useful quantity is the power per unit length of the diffraction circle on the receiving surface, $P'_{\mathbf{h}}$. At a distance r from the sample, the circumference of the diffraction circle is $2\pi r \sin 2\theta_0$ and one has (constants omitted)

$$P'_{\mathbf{h}} \propto r^{-1} V N_c^2 [i_0(E) j d^2 |F|^2]_{\mathbf{h}} \frac{C_p(E, \theta_0) \Delta\theta_0}{\sin \theta_0}. \qquad (2.5.1.7)$$

The peak areas in an XED powder spectrum are directly proportional to the $P'_{\mathbf{h}}$ of equation (2.5.1.7).

Quantitative structural analysis requires the knowledge of $i_0(E)$ and $P(E)$. As mentioned above, these quantities are not known with sufficient accuracy for *Bremsstrahlung*. For synchrotron radiation they can be calculated, but they will nevertheless contribute to the total uncertainty in the analysis. Accordingly, XED is used rather for identification of a known or assumed structure than for a full structure determination.

2.5.1.5. *Corrections*

(*a*) *Temperature effects*

The effect of thermal vibrations on the integrated intensities is expressed by the Debye–Waller factor in the same way as for standard angle-dispersive methods. Notice that $(\sin\theta)/\lambda = 1/2d$ irrespective of the method used. The contribution of the thermal diffuse scattering to the measured integrated intensities can be calculated if the elastic constants of the sample are known (Uno & Ishigaki 1975).

(*b*) *Absorption*

The transmission factor $A(E, \theta_0)$ for a small sample bathed in the incident beam and the factor $A_c(E, \theta_0)$ for a large sample intercepting the entire incident beam are the same as for monochromatic methods (Table 6.3.3.1). However, when they are applied to energy-dispersive techniques, one has to note that the absorption corrections are strongly varying with energy. In the special case of a symmetrical reflection where the incident and diffracted beams each make angles θ_0 with the face of a thick sample (powder or imperfect crystal), one has

$$A_c(E) = \frac{1}{2\mu(E)}, \qquad (2.5.1.8)$$

where $\mu(E)$ is the linear attentuation coefficient evaluated at the energy associated with the Bragg reflection.

(*c*) *Extinction and dispersion*

Extinction and dispersion corrections are applied in the same way as for angle-dispersive monochromatic methods. However, in XED, the energy dependence of the corrections has to be taken into account.

(*d*) *Geometrical aberrations*

These are distortions and displacements of the line profile by features of the geometry of the apparatus. Axial aberrations as well as equatorial divergence contribute to the angular range $\Delta\theta_0$ of the Bragg reflections. There is a predominance of positive contributions to $\Delta\theta_0$, so that the diffraction maxima are slightly displaced to the low-energy side, and show more tailing on the low-energy side than the high-energy side (Wilson, 1973).

(*e*) *Physical aberrations*

Displacements due to the energy-dependent absorption and reflectivity of the sample tend to cancel each other if the incident intensity, $i_0(E)$, can be assumed to be constant within the energy range of Bragg reflection. With synchrotron radiation, $i_0(E)$ varies rapidly with energy and its influence on the peak positions should be checked. Also, the detector response function will influence the line profile. Low-energy line shapes are particularly sensitive to the deadlayer absorption, which may cause tailing on the low-energy side of the peak. Integrated intensities, measured as peak areas in the diffraction spectrum, have to be corrected for detector efficiency and intensity losses due to escape peaks.

2.5.1.6. *The Rietveld method*

The Rietveld method (see Chapter 8.6) for refining structural variables has only recently been applied to energy-dispersive powder data. The ability to analyse diffraction patterns with overlapping Bragg peaks is particularly important for a low-resolution technique, such as XED (Glazer, Hidaka & Bordas, 1978; Buras, Gerward, Glazer, Hidaka & Olsen, 1979; Neuling & Holzapfel, 1992). In this section, it is assumed that the diffraction peaks are Gaussian in energy. It then follows from equation (2.5.1.7) that the measured profile y_i of the reflection k at energy E_i corresponding to the ith channel of the multichannel analyser can be written

$$y_i = \frac{c'}{H_k} i_0(E_i) A(E_i) j_k d_k^2 |F_k|^2 \exp\{-4 \ln 2[(E_k - E_i)^2 / H_k^2]\}, \qquad (2.5.1.9)$$

where c' is a constant, $i_0(E_i)$ is evaluated at the energy E_i, and H_k is the full width (in energy) at half-maximum of the diffraction peak. $A(E_i)$ is a factor that accounts for the absorption in the sample and elsewhere in the beam path. The number of overlapping peaks can be determined on the basis of their position and half-width. The full width at half-maximum can be expressed as a linear function of energy:

$$H_k = UE_k + V, \qquad (2.5.1.10)$$

where U and V are the half-width parameters.

2.5.1.7. *Single-crystal diffraction*

Energy-dispersive diffraction is mainly used for powdered crystals. However, it can also be applied to single-crystal diffraction.

A two-circle system for single-crystal diffraction in a diamond-anvil high-pressure cell with a polychromatic, synchrotron X-ray beam has been devised by Mao, Jephcoat, Hemley, Finger, Zha, Hazen & Cox (1988).

Formulae for single-crystal integrated intensities are well known from the classical Laue method. Adaptations to energy-dispersive work have been made by Buras, Olsen, Gerward, Selsmark & Lindegaard-Andersen (1975).

2.5.1.8. *Applications*

The unique features of energy-dispersive diffraction make it a complement to rather than a substitute for monochromatic angle-dispersive diffraction. Both techniques yield quantitative structural information, although XED is seldom used for a full structure determination. Because of the fixed geometry, energy-dispersive methods are particularly suited to *in situ* studies of samples in special environments, *e.g.* at high or low temperature and/or high pressure. The study of anomalous scattering and forbidden reflections is facilitated by the possibility of shifting the diffraction peaks on the energy scale by changing the scattering angle. Other applications are studies of Debye–Waller factors, determinative mineralogy, attenuation-coefficient measurements, on-stream measurements, particle-size and -strain

determination, and texture studies. These and other applications can be found in an annotated bibliography covering the period 1968–1978 (Laine & Lähteenmäki, 1980). The short counting time and the simultaneous recording of the diffraction spectrum permit the study of the kinetics of structural transformations in time frames of a few seconds or minutes.

Energy-dispersive powder diffraction has proved to be of great value for high-pressure structural studies in conjunction with synchrotron radiation. The brightness of the radiation source and the efficiency of the detector system permit the recording of a diffraction spectrum with satisfactory counting statistics in a reasonable time (100–1000 s) in spite of the extremely small sample volume (10^{-3}–10^{-5} mm^3). Reviews have been given by Buras & Gerward (1989) and Häusermann (1992). Recently, XED experiments have been performed at pressures above 400 GPa, and pressures near 1 TPa may be attainable in the near future (Ruoff, 1992). At this point, it should be mentioned that XED methods have limited resolution and generally give unreliable peak intensities. The situation has been transformed recently by the introduction of the image-plate area detector, which allows angle-dispersive, monochromatic methods to be used with greatly improved resolution and powder averaging (Nelmes & McMahon, 1994, and references therein).

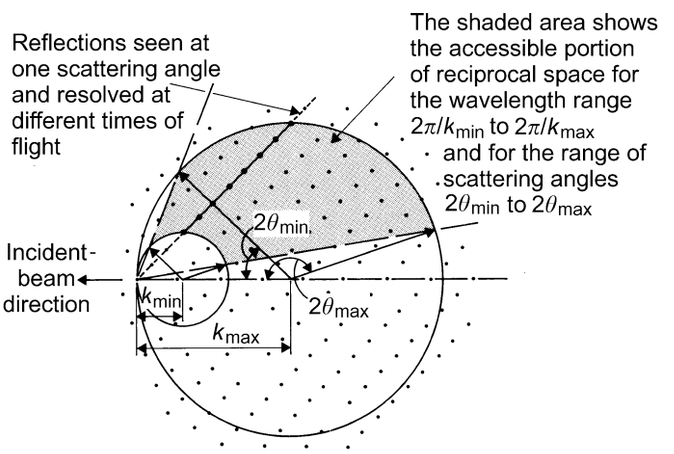

Fig. 2.5.2.1. Construction in reciprocal space to illustrate the use of multi-wavelength radiation in single-crystal diffraction. The circles with radii $k_{max} = 2\pi/\lambda_{min}$ and $k_{min} = 2\pi/\lambda_{max}$ are drawn through the origin. All reciprocal-lattice points within the shaded area may be sampled by a linear position-sensitive detector spanning the scattering angles from $2\theta_{min}$ to $2\theta_{max}$. With a position-sensitive area detector, a three-dimensional portion of reciprocal space may be examined (after Schultz, Srinivasan, Teller, Williams & Lukehart, 1984).

2.5.2. White-beam and time-of-flight neutron diffraction (By J. D. Jorgensen, W. I. F. David, and B. T. M. Willis)

2.5.2.1. *Neutron single-crystal Laue diffraction*

In traditional neutron-diffraction experiments, using a continuous source of neutrons from a nuclear reactor, a narrow wavelength band is selected from the wide spectrum of neutrons emerging from a moderator within the reactor. This monochromatization process is extremely inefficient in the utilization of the available neutron flux. If the requirement of discriminating between different orders of reflection is relaxed, then the entire white beam can be employed to contribute to the diffraction pattern and the count-rate may increase by several orders of magnitude. Further, by recording the scattered neutrons on photographic film or with a position-sensitive detector, it is possible to probe simultaneously many points in reciprocal space.

If the experiment is performed using a pulsed neutron beam, the different orders of a given reflection may be separated from one another by time-of-flight analysis. Consider a short polychromatic burst of neutrons produced within a moderator. The subsequent times-of-flight, t, of neutrons with differing wavelengths, λ, measured over a total flight path, L, may be discriminated one from another through the de Broglie relationship:

$$m_n(L/t) = h/\lambda, \qquad (2.5.2.1)$$

where m_n is the neutron mass and h is Planck's constant. Expressing t in microseconds, L in metres and λ in Å, equation (2.5.2.1) becomes

$$t = 252.7784\, L\lambda.$$

Inserting Bragg's law, $\lambda = 2(d/n)\sin\theta$, for the nth order of a fundamental reflection with spacing d in Å gives

$$t = (505.5568/n)Ld\sin\theta. \qquad (2.5.2.2)$$

Different orders may be measured simply by recording the time taken, following the release of the initial pulse from the moderator, for the neutron to travel to the sample and then to the detector.

The origins of pulsed neutron diffraction can be traced back to the work of Lowde (1956) and of Buras, Mikke, Lebech & Leciejewicz (1965). Later developments are described by Turberfield (1970) and Windsor (1981). Although a pulsed beam may be produced at a nuclear reactor using a chopper, the major developments in pulsed neutron diffraction have been associated with pulsed sources derived from particle accelerators. Spallation neutron sources, which are based on proton synchrotrons, allow optimal use of the Laue method because the pulse duration and pulse repetition rate can be matched to the experimental requirements. The neutron Laue method is particularly useful for examining crystals in special environments, where the incident and scattered radiations must penetrate heat shields or other window materials. [A good example is the study of the incommensurate structure of α-uranium at low temperature (Marmeggi & Delapalme, 1980).]

A typical time-of-flight single-crystal instrument has a large area detector. For a given setting of detector and sample, a three-dimensional region is viewed in reciprocal space, as shown in Fig. 2.5.2.1. Thus, many Bragg reflections can be measured at the same time. For an ideally imperfect crystal, with volume V_s and unit-cell volume v_c, the number of neutrons of wavelength λ reflected at Bragg angle θ by the planes with structure factor F is given by

$$N = i_0(\lambda)\lambda^4 V_s F^2/(2v_c^2\sin^2\theta), \qquad (2.5.2.3)$$

where $i_0(\lambda)$ is the number of incident neutrons per unit wavelength interval. In practice, the intensity in equation (2.5.2.3) must be corrected for wavelength-dependent factors, such as detector efficiency, sample absorption and extinction, and the contribution of thermal diffuse scattering. Jauch, Schultz & Schneider (1988) have shown that accurate structural data can be obtained using the single-crystal time-of-flight method despite the complexity of these wavelength-dependent corrections.

2.5.2.2. *Neutron time-of-flight powder diffraction*

This technique, first developed by Buras & Leciejewicz (1964), has made a unique impact in the study of powders in confined environments such as high-pressure cells (Jorgensen &

Worlton, 1985). As in single-crystal Laue diffraction, the time of flight is measured as the elapsed time from the emergence of the neutron pulse at the moderator through to its scattering by the sample and to its subsequent detection. This time is given by equation (2.5.2.2). Many Bragg peaks, each separated by time of flight, can be observed at a single fixed scattering angle, since there is a wide range of wavelengths available in the incident beam.

A good approximation to the resolution function of a time-of-flight powder diffractometer is given by the second-moment relationship

$$\Delta d/d = [(\Delta t/t)^2 + (\Delta\theta \cot\theta)^2 + (\Delta L/L)^2]^{1/2}, \qquad (2.5.2.4)$$

where Δd, Δt and $\Delta\theta$ are, respectively, the uncertainties in the d spacing, time of flight, and Bragg angle associated with a given reflection, and ΔL is the uncertainty in the total path length (Jorgensen & Rotella, 1982). Thus, the highest resolution is obtained in back scattering (large 2θ) where $\cot\theta$ is small. Time-of-flight instruments using this concept have been described by Steichele & Arnold (1975) and by Johnson & David (1985). With pulsed neutron sources a large source aperture can be viewed, as no chopper is required of the type used on reactor sources. Hence, long flight paths can be employed and this too [see equation (2.5.2.4)] leads to high resolution. For a well designed moderator the pulse width is approximately proportional to wavelength, so that the resolution is roughly constant across the whole of the diffraction pattern. For an ideal powder sample the number of neutrons diffracted into a complete Debye–Scherrer cone is proportional to

$$N' = i_0(\lambda)\lambda^4 V_s j F^2 \cos\theta \Delta\theta/(4v_c^2 \sin^2\theta) \qquad (2.5.2.5)$$

(Buras & Gerward, 1975). j is the multiplicity of the reflection and the remaining symbols in equation (2.5.2.5) are the same as those in equation (2.5.2.3).

International Tables for Crystallography (2006). Vol. C, Chapter 2.6, pp. 89–112.

2.6. Small-angle techniques

BY O. GLATTER AND R. MAY

2.6.1. X-ray techniques (By O. Glatter)

2.6.1.1. *Introduction*

The purpose of this section is to introduce small-angle scattering as a method for investigation of nonperiodic systems. It should create an understanding of the crucial points of this method, especially by showing the differences from wide-angle diffraction. The most important concepts will be explained. This article also contains a collection of the most important equations and methods for standard applications. For details and special applications, one must refer to the original literature or to textbooks; the reference list is extensive but, of course, not complete.

The physical principles of scattering are the same for wide-angle diffraction and small-angle X-ray scattering. The electric field of the incoming wave induces dipole oscillations in the atoms. The energy of X-rays is so high that all electrons are excited. The accelerated charges generate secondary waves that add at large distances (far-field approach) to give the overall scattering amplitude. All secondary waves have the same frequency but may have different phases caused by the different path lengths. Owing to the high frequency, it is only possible to detect the scattering intensity – the square of the scattering amplitude – and its dependence on the scattering angle.

The angle-dependent scattering amplitude is related to the electron-density distribution of the scatterer by a Fourier transformation. All this holds for both wide-angle diffraction and small-angle X-ray scattering. The main difference is that in the former we have a periodic arrangement of identical scattering centres (particles), *i.e.* the scattering medium is periodic in all three dimensions with a large number of repetitions, whereas in small-angle scattering these particles, for example proteins, are not ordered periodically. They are embedded with arbitrary orientation and with irregular distances in a matrix, such as water. The scattering centres are limited in size, non-oriented, and nonperiodic, but the number of particles is high and they can be assumed to be identical, as in crystallography.

The Fourier transform of a periodic structure in crystallography (crystal diffraction) corresponds to a Fourier series, *i.e.* a periodic structure is expanded in a periodic function system.

The Fourier transform of a non-periodic limited structure (small-angle scattering) corresponds to a Fourier integral. In mathematical terms, it is the expansion of a nonperiodic function by a periodic function system.

So the differences between crystallography and small-angle scattering are equivalent to the differences between a Fourier series and a Fourier integral. It may seem foolish to expand a non-periodic function with a periodic function system, but this is how scattering works and we do not have any other powerful physical process to study these structures.

The essential effect of these differences is that in small-angle scattering we measure a continuous angle-dependent scattering intensity at discrete points instead of sharp, point-like spots as in crystallography.

Another important point is that in small-angle scattering we have a linear increase of the signal (scattered intensity) with the number of particles in the measuring volume since intensities are adding. Amplitudes are adding in crystallography, so we have a quadratic relation between the signal and the number of particles.

In addition, there is a loss of information in small-angle scattering experiments caused by the averaging over all orientations in space. The three-dimensional structure is represented by a one-dimensional function – the dependence of the scattered intensity on the scattering angle. This is also true for powder diffraction. To recover the structure uniquely is therefore impossible.

The computation of the scattering function for a known structure is called the solution of the scattering problem. This problem can be solved exactly for many different structures. The inversion, *i.e.* the estimation of the structure of the scatterer from its scattering functions, is called the inverse scattering problem. This problem cannot be solved uniquely.

The description and solution of the scattering problem gives information to the experimenter concerning the scattering functions to be expected in a special situation. In addition, this knowledge is the starting point for the evaluation and interpretation of experimental data (solution of the inverse problem).

There are methods that give a rough first-order approximation to the solution of the inverse scattering problem using only a minimum amount of *a priori* information about the system to obtain an initial model. In order to improve this model, one has to solve the scattering problem. The resulting theoretical model functions are compared with the experimental data. If necessary, model modifications are deduced from the deviations. After some iterations, one obtains the final model.

It should be noticed that it is possible to find different models that fit the data within their statistical accuracy. In order to reduce this ambiguity, it is necessary to have additional independent information from other experiments. Incorrect models, however, can be rejected when their scattering functions differ significantly from the experimental data.

What type of investigations can be performed with small-angle scattering? It is possible to study monodisperse and polydisperse systems. In the case of monodisperse systems, it is possible to determine size, shape, and, under certain conditions, the internal structure. Monodispersity cannot be deduced from small-angle scattering data and must therefore be assumed or checked by independent methods.

For polydisperse systems, a size distribution can be evaluated under the assumption of a certain shape for the particles (*particle sizing*).

All these statements are strictly true for highly diluted systems where the interparticle distances are much larger than the particle dimensions. In the case of semi-dilute systems, the result of a small-angle scattering experiment is influenced by the structure of the particles and by their spatial arrangement. Then the scattering curve is the product of the particle scattering function and of the interparticle interference function. If the scattering function of one particle is known, it is possible to evaluate information about the radial distribution of these particles relative to each other. If the system is dense, *i.e.* if the volume fraction of the particles (scattering centres) is of the same order of magnitude as the volume fraction of the matrix, it is possible to determine these volume fractions and a characteristic length of the phases. The most important practical applications, however, pertain to dilute systems.

How are small-angle scattering experiments related to other scattering experiments? Small-angle scattering uses radiation with a wavelength in the range 10^{-1} to 10^{0} nm, depending on the

Copyright © 2006 International Union of Crystallography

problem and on the source used. This range is similar for X-rays and neutrons, but neutrons interact with the nuclei of the atoms whereas X-rays interact with the electrons. The scattering efficiency increases linearly with the atomic number for X-rays. The dependence is much more complicated for neutrons and does not show a systematic trend. The essential fact in neutron scattering is the pronounced difference in the scattering power between hydrogen and deuterium, which is important for varying the contrast between the particles and the matrix.

The wavelength and the scattering efficiency limit the range of small-angle scattering experiments to systems in the size range of a few nanometres up to about 100 nm. Special instruments permit the study of larger particles (Bonse & Hart, 1967; Koch, 1988). These instruments need a high intensity of the primary beam (synchrotron radiation) and are not very common.

Particles in the size range from 100 nm up to some micrometres can be investigated by static light-scattering techniques (Glatter, Hofer, Jorde & Eigner, 1985; Glatter & Hofer, 1988*a,b*; Hofer, Schurz & Glatter, 1989). Particles exceeding this limit can be seen in an optical microscope or can be studied with Fraunhofer diffraction (Bayvel & Jones, 1981).

Electron microscopy is in competition with all these scattering methods. It has the marked advantage of giving real pictures with rather high resolution but it has the inherent disadvantage that the preparation may introduce artefacts. Small-angle scattering, on the other hand, is a method to study macromolecules in solution, which is a very important advantage for biological samples and for polymers.

Crystallography gives more information about the particle (atomic structure) and can be applied to relatively large systems. It is possible to study particles as large as proteins and viruses if good crystals of these substances are available. The experiment needs synchrotron radiation for large molecules like proteins or viruses, *i.e.* access to a large research facility is necessary. Small-angle X-ray scattering with conventional generators is a typical next-door technique with the advantage of ready availability.

Small-angle scattering has developed into a standard measuring method during recent decades, being most powerful for the investigation of submicrometre particles.

2.6.1.2. *General principles*

In this subsection, we are concerned with X-rays only, but all equations may also be applied with slight modifications to neutron or electron diffraction. When a wave of X-rays strikes an object, every electron becomes the source of a scattered wave. All these waves have the same intensity given by the Thomson formula

$$I_e(\theta) = I_p T_f \frac{1}{a^2}\frac{1+\cos^2 2\theta}{2}, \qquad (2.6.1.1)$$

where I_p is the primary intensity and a the distance from the object to the detector. The factor T_f is the square of the classical electron radius ($e^2/mc^2 = 7.90 \times 10^{-26}$[cm^2]). The scattering angle 2θ is the angle between the primary beam and the scattered beam. The last term in (2.6.1.1) is the polarization factor and is practically equal to 1 for all problems dealt with in this subsection. I_e should appear in all following equations but will be omitted, *i.e.* the amplitude of the wave scattered by an electron will be taken to be of magnitude 1. I_e is only needed in cases where the absolute intensity is of interest.

The amplitudes differ only by their phases φ, which depend on the positions of the electrons in space. Incoherent (Compton) scattering can be neglected for small-angle X-ray scattering. The phase φ is $2\pi/\lambda$ times the difference between the optical path length of the wave and an arbitrary reference wave (with λ being the wavelength). The direction of the incident beam is defined by the unit vector $\mathbf{s}_0$ and of the scattered beam by $\mathbf{s}$. The angle between these two unit vectors (scattering angle) is 2θ. The path difference between the rays through a point P and an arbitrary origin O is $-\mathbf{r}(\mathbf{s}-\mathbf{s}_0)$. The phase is $\varphi = -\mathbf{h}\cdot\mathbf{r}$ if we define the scattering vector $\mathbf{h}$ as

$$\mathbf{h} = (2\pi/\lambda)(\mathbf{s}-\mathbf{s}_0). \qquad (2.6.1.2)$$

This vector bisects the angle between the scattered beam and the incident beam and has length $h = (4\pi/\lambda)\sin\theta$. We keep in mind that $\sin\theta$ may be replaced by θ in small-angle scattering. We now introduce the electron density $\rho(\mathbf{r})$. This is the number of electrons per unit volume at the position $\mathbf{r}$. A volume element $\mathrm{d}V$ at $\mathbf{r}$ contains $\rho(\mathbf{r})\,\mathrm{d}V$ electrons. The scattering amplitude of the whole irradiated volume V is given by

$$A(\mathbf{h}) = \iiint \rho(\mathbf{r})\exp(-i\mathbf{h}\cdot\mathbf{r})\,\mathrm{d}V. \qquad (2.6.1.3)$$

We see that the amplitude A is the Fourier transform of the electron-density distribution ρ. The intensity $I(\mathbf{h})$ of the complex amplitude $A(\mathbf{h})$ is the absolute square given by the product of the amplitude and its complex conjugate A^*,

$$I(\mathbf{h}) = A(\mathbf{h})A(\mathbf{h})^* = \iiint \widetilde{\rho}^2(\mathbf{r})\exp(-i\mathbf{h}\cdot\mathbf{r})\,\mathrm{d}V, \qquad (2.6.1.4)$$

where $\widetilde{\rho}^2(\mathbf{r})$ is the convolution square (Bracewell, 1986):

$$\widetilde{\rho}^2(\mathbf{r}) = \iiint \rho(\mathbf{r}_1)\rho(\mathbf{r}_1-\mathbf{r})\,\mathrm{d}V_1. \qquad (2.6.1.5)$$

The intensity distribution in $\mathbf{h}$ or reciprocal space is uniquely determined by the structure in real space.

Until now, we have discussed the scattering process of a particle in fixed orientation in vacuum. In most cases of small-angle scattering, the following situation is present:

–The scatterers (particles or inhomogeneities) are statistically isotropic and no long-range order exists, *i.e.* there is no correlation between points at great spatial distance.

–The scatterers are embedded in a matrix. The matrix is considered to be a homogeneous medium with the electron density ρ_0. This situation holds for particles in solution or for inhomogeneities in a solid. The electron density in equations (2.6.1.3)–(2.6.1.5) should be replaced by the difference in electron density $\Delta\rho = \rho - \rho_0$, which can take positive and negative values.

The average over all orientations $\langle\ \rangle$ leads to

$$\langle\exp(-i\mathbf{h}\cdot\mathbf{r})\rangle = \frac{\sin hr}{hr} \qquad (2.6.1.6)$$

(Debye, 1915) and (2.6.1.4) reduces to the form

$$I(h) = 4\pi\int_0^\infty r^2\Delta\widetilde{\rho}^2(r)\frac{\sin hr}{hr}\,\mathrm{d}r \qquad (2.6.1.7)$$

or, with

$$p(r) = r^2\Delta\widetilde{\rho}^2(r) = r^2 V\gamma(r), \qquad (2.6.1.8)$$

to

$$I(h) = 4\pi\int_0^\infty p(r)\frac{\sin hr}{hr}\,\mathrm{d}r; \qquad (2.6.1.9)$$

γ is the so-called correlation function (Debye & Bueche, 1949), or characteristic function (Porod, 1951). The function $p(r)$ is the so-called pair-distance distribution function PDDF (Guinier &

Fournet, 1955; Glatter, 1979). The inverse transform to (2.6.1.9) is given by

$$p(r) = \frac{1}{2\pi^2} \int_0^\infty I(h) hr \sin(hr)\, \mathrm{d}h \qquad (2.6.1.10)$$

or by

$$V\gamma(r) = \frac{1}{2\pi^2} \int_0^\infty I(h) h^2 \frac{\sin hr}{hr}\, \mathrm{d}h. \qquad (2.6.1.11)$$

The function $p(r)$ is directly connected with the measurable scattering intensity and is very important for the solution of the inverse scattering problem. Before working out details, we should first discuss equations (2.6.1.9) and (2.6.1.10).

The PDDF can be defined as follows: the function $p(r)$ gives the number of difference electron pairs with a mutual distance between r and $r + \mathrm{d}r$ within the particle. For homogeneous particles (constant electron density), this function has a simple and clear geometrical definition.

Let us subdivide the particle into a very large number of identical small volume elements. The function $p(r)$ is proportional to the number of lines with a length between r and $r + \mathrm{d}r$ which are found in the combination of any volume element i with any other volume element k of the particle (see Fig. 2.6.1.1). For $r = 0$, there is no other volume element, so $p(r)$ must be zero, increasing with r^2 as the number of possible neighbouring volume elements is proportional to the surface of a sphere with radius r. Starting from an arbitrary point in the particle, there is a certain probability that the surface will be reached within the distance r. This will cause the $p(r)$ function to drop below the r^2 parabola and finally the PDDF will be zero for all $r > D$, where D is the maximum dimension of the particle. So $p(r)$ is a distance histogram of the particle. There is no information about the orientation of these lines in $p(r)$, because of the spatial averaging.

In the case of inhomogeneous particles, we have to weight each line by the product of the difference in electron density $\Delta\rho$, and the differential volume element, $\mathrm{d}V$. This can lead to negative contributions to the PDDF.

We can see from equation (2.6.1.9) that every distance r gives a $\sin(hr)/(hr)$ contribution with the weight $p(r)$ to the total scattering intensity. $I(h)$ and $p(r)$ contain the same information, but in most cases it is easier to analyse in terms of distances than in terms of $\sin(x)/x$ contributions. The PDDF could be computed exactly with equation (2.6.1.10) if $I(h)$ were known for the whole reciprocal space.

For $h = 0$, we obtain from equation (2.6.1.9)

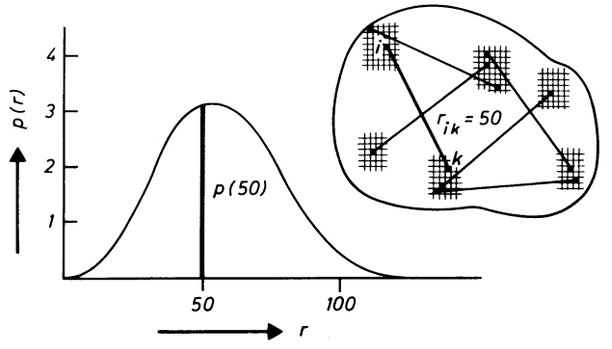

Fig. 2.6.1.1. The height of the $p(r)$ function for a certain value of r is proportional to the number of lines with a length between r and $r + \mathrm{d}r$ within the particle.

$$I(0) = I(\overline{\Delta\rho})^2 V^2 = 4\pi \int_0^\infty p(r)\, \mathrm{d}r, \qquad (2.6.1.12)$$

i.e. the scattering intensity at h equal to zero is proportional to the area under the PDDF. From equation (2.6.1.11), we find

$$V\gamma(0) = \frac{1}{2\pi^2} \int I(h) h^2\, \mathrm{d}h = V\overline{\Delta\rho^2} \qquad (2.6.1.13)$$

(Porod, 1982), *i.e.* the integral of the intensity times h^2 is related to the mean-square fluctuation of the electron density irrespective of the structure. We may modify the shape of a particle, the scattering function $I(h)$ might be altered considerably, but the integral (2.6.1.13) must remain invariant (Porod, 1951).

$$\text{Invariant } Q = \int_0^\infty I(h) h^2\, \mathrm{d}h. \qquad (2.6.1.14)$$

2.6.1.3. *Monodisperse systems*

In this subsection, we discuss scattering from monodisperse systems, *i.e.* all particles in the scattering volume have the same size, shape, and internal structure. These conditions are usually met by biological macromolecules in solution. Furthermore, we assume that these solutions are at infinite dilution, which is taken into account by measuring a series of scattering functions at different concentrations and by extrapolating these data to zero concentration. We continue with the notations defined in the previous subsection, which coincide to a large extent with the notations in the original papers and in the textbooks (Guinier & Fournet, 1955; Glatter & Kratky, 1982). There is a notation created by Luzzati (1960) that is quite different in many details. A comparison of the two notations is given in the Appendix of Pilz, Glatter & Kratky (1980).

The particles can be roughly described by some parameters that can be extracted from the scattering function. More information about the shape and structure of the particles can be found by detailed discussion of the scattering functions. At first, this discussion will be about homogeneous particles and will be followed by some aspects for inhomogeneous systems. Finally, we have to discuss the influence of finite concentrations on our results.

2.6.1.3.1. *Parameters of a particle*

Total scattering length. The scattering intensity at $h = 0$ must be equal to the square of the number of excess electrons, as follows from equations (2.6.1.7) and (2.6.1.12):

$$I(0) = (\Delta\rho)^2 V^2 = 4\pi \int_0^\infty p(r)\, \mathrm{d}r. \qquad (2.6.1.15)$$

This value is important for the determination of the molecular weight if we perform our experiments on an absolute scale (see below).

Radius of gyration. The electronic radius of gyration of the whole particle is defined in analogy to the radius of gyration in mechanics:

$$R_g^2 = \frac{\int_V \rho(r_i) r_i^2\, \mathrm{d}V_i}{\int_V \rho(r_i)\, \mathrm{d}V_i}. \qquad (2.6.1.16)$$

It can be obtained from the PDDF by

Table 2.6.1.1. *Formulae for the various parameters for h (left) and m (right) scales*

$R = K\sqrt{\tan\alpha}$ $\tan\alpha = \dfrac{\Delta \log I(h)}{\Delta h^2}$	$R = K\dfrac{\lambda a}{2\pi}\sqrt{\tan\alpha}$ $\tan\alpha = \dfrac{\Delta \log I(m)}{\Delta m^2}$
$K = \sqrt{\dfrac{3}{\log e}} = 2.628$	
$R_c = K_c\sqrt{\tan\alpha}$ $\tan\alpha = \dfrac{\Delta \log[I(h)h]}{\Delta h^2}$	$R_c = K_c\dfrac{\lambda a}{2\pi}\sqrt{\tan\alpha}$ $\tan\alpha = \dfrac{\Delta \log[I(m)m]}{\Delta m^2}$
$K_c = \sqrt{\dfrac{2}{\log e}} = 2.146$	
$R_t = K_t\sqrt{\tan\alpha}$ $\tan\alpha = \dfrac{\Delta \log[I(h)h^2]}{\Delta h^2}$	$R_t = K_t\dfrac{\lambda a}{2\pi}\sqrt{\tan\alpha}$ $\tan\alpha = \dfrac{\Delta \log[I(m)m^2]}{\Delta m^2}$
$K_t = \sqrt{\dfrac{1}{\log e}} = 1.517$	
$V = 2\pi^2\dfrac{I(0)}{Q}$ $Q = \int I(h)h^2\,\mathrm{d}h$	$V = \dfrac{\lambda^3 a^3}{4\pi}\dfrac{I(0)}{Q_m}$ $Q_m = \int I(m)m^2\,\mathrm{d}m$
$A = 2\pi\dfrac{[I(h)h]_0}{Q}$	$A = \dfrac{\lambda^2 a^2}{2\pi}\dfrac{[I(m)m]_0}{Q_m}$
$T = \pi\dfrac{[I(h)h^2]_0}{Q}$	$T = \dfrac{\lambda a}{2}\dfrac{[I(m)m^2]_0}{Q_m}$
$M = \dfrac{I(0)}{P}K\dfrac{a^2}{cd(\Delta z)^2}$	$K = \dfrac{1}{I_e N_L} = 21.0$
$M_c = \dfrac{[I(h)h]_0}{P}\dfrac{K}{\pi}\dfrac{a^2}{cd(\Delta z)^2}$	$M_c = \dfrac{[I(m)m]_0}{P}\dfrac{2K}{\lambda}\dfrac{a}{cd(\Delta z)^2}$
$M_t = \dfrac{[I(h)h^2]_0}{P}\dfrac{K}{2\pi}\dfrac{a^2}{cd(\Delta z)^2}$	$M_t = \dfrac{[I(m)m^2]_0}{P}\dfrac{2\pi K}{\lambda^2}\dfrac{1}{cd(\Delta z)^2}$
$\overline{(\Delta\rho)^2} = \dfrac{Q}{P}\dfrac{a^2}{2\pi^2 d}K$	$\overline{(\Delta\rho)^2} = \dfrac{Q_m}{P}\dfrac{4\pi}{\lambda^3 ad}K$
$K = 10^{24}/I_e$ $(10^{24} = [\mathrm{cm}/\text{Å}]^3)$	
$O_s = \pi\dfrac{K}{Q}$ $K = \lim\limits_{h\to\infty} I(h)h^4$	$O_s = \dfrac{2\pi^2}{\lambda a}\dfrac{K_m}{Q_m}$ $K = \lim\limits_{m\to\infty} I(m)m^4$

$$R_g^2 = \frac{\int_0^\infty p(r)r^2\,\mathrm{d}r}{2\int_0^\infty p(r)\,\mathrm{d}r} \qquad (2.6.1.17)$$

or from the innermost part of the scattering curve [Guinier approximation (Guinier, 1939)]:

$$I(h) = I(0)\exp(-h^2R_g^2/3). \qquad (2.6.1.18)$$

A plot of $\log[I(h)]$ *vs* h^2 (Guinier plot) shows at its innermost part a linear descent with a slope $\tan\alpha$, where

$$R_g = K\sqrt{\tan\alpha}$$

(see Table 2.6.1.1).

The radius of gyration is related to the geometrical parameters of simple homogeneous triaxial bodies as follows (Mittelbach, 1964):

sphere (radius R)	$R_g^2 = (3/5)R^2$
hollow sphere (radii R_1 and R_2)	$R_g^2 = (3/5)\dfrac{R_2^5 - R_1^5}{R_2^3 - R_1^3}$
ellipsoid (semi-axes a, b, c)	$R_g^2 = (1/5)(a^2 + b^2 + c^2)$
parallelepiped (edge lengths A, B, C)	$R_g^2 = (1/12)(A^2 + B^2 + C^2)$
elliptic cylinder (semi-axes a, b; height h)	$R_g^2 = \dfrac{a^2 + b^2}{4} + \dfrac{h^2}{12} = R_c^2 + \dfrac{h^2}{12}$
hollow cylinder (height h and radii r_1, r_2)	$R_g^2 = \dfrac{r_1^2 + r_2^2}{2} + \dfrac{h^2}{12}$.

Radius of gyration of the cross section. In the special case of rod-like particles, the two-dimensional analogue of R_g is called radius of gyration of the cross section R_c. It can be obtained from

$$R_c^2 = \frac{\int_0^\infty p_c(r)r^2\,\mathrm{d}r}{2\int_0^\infty p_c(r)\,\mathrm{d}r}, \qquad (2.6.1.19)$$

where $p_c(r)$ is the PDDF of the cross section or it can be calculated from the innermost part of the scattering intensity of the cross section $I_c(h)$:

$$I_c(h) = I_c(0)\exp(-h^2R_c^2/2), \qquad (2.6.1.20)$$

with $I_c(h) = I(h)h$ (see Table 2.6.1.1).

Radius of gyration of the thickness. A similar definition exists for lamellar particles. The one-dimensional radius of gyration of the thickness R_t can be calculated from

$$R_t^2 = \frac{\int_0^\infty p_t(r)r^2\,\mathrm{d}r}{2\int_0^\infty p_t(r)\,\mathrm{d}r}, \qquad (2.6.1.21)$$

or from the innermost part of the scattered intensity of thickness $I_t(h)$:

$$I_t(h) = I_t(0)\exp(-h^2R_t^2), \qquad (2.6.1.22)$$

with $I_t(h) = I(h)h^2$ (see Table 2.6.1.1 and §2.6.1.3.2.1).

Volume. The volume of a homogeneous particle is given by

$$V = 2\pi^2\frac{I(0)}{Q}. \qquad (2.6.1.23)$$

This equation follows from equations (2.6.1.12)–(2.6.1.14). Such volume determinations are subject to errors as they rely on the validity of an extrapolation to zero angle [to obtain $I(0)$] and to larger angles (h^{-4} extrapolation for Q). Scattering functions cannot be measured from h equal to zero to h equal to infinity.

Surface. The surface S of one particle is correlated with the scattering intensity $I_1(h)$ of this particle by

$$I_1(h)|_{h\to\infty} = (\Delta\rho)^2 \frac{2\pi}{h^4} S. \tag{2.6.1.24}$$

Determination of the absolute intensity can be avoided if we calculate the specific surface O_s (Mittelbach & Porod, 1965)

$$O_s = S/V = \pi \frac{\lim_{h\to\infty} [I(h)h^4]}{Q}. \tag{2.6.1.25}$$

Cross section, thickness, and correlation length. By similar equations, we can find the area A of the cross section of a rod-like particle

$$A = 2\pi \frac{[I(h)h]_{h\to 0}}{Q} \tag{2.6.1.26}$$

and the thickness T of lamellar particles by

$$T = \pi \frac{[I(h)h^2]_{h\to 0}}{Q} \tag{2.6.1.27}$$

but the experimental accuracy of the limiting values $[I(h)h]_{h\to 0}$ and $[I(h)h^2]_{h\to 0}$ is usually not very high.

The correlation length l_c is the mean width of the correlation function $\gamma(r)$ (Porod, 1982) and is given by

$$l_c = \frac{\pi}{Q} \int_0^\infty I(h)h \, \mathrm{d}h. \tag{2.6.1.28}$$

The *maximum dimension* D of a particle would be another important particle parameter, but it cannot be calculated directly from the scattering function and will be discussed later.

Persistence length a_p. An important model for polymers in solution is the so-called worm-like chain (Porod, 1949; Kratky & Porod, 1949). The degree of coiling can be characterized by the persistence length a_p (Kratky, 1982*b*). Under the assumption that the persistence length is much larger than the cross section of the polymer, it is possible to find a transition point h^+ in an $I(h)h^2$ *vs* h plot where the function starts to be proportional to h. There is an approximation

$$h^+ a_p \simeq 2.3, \tag{2.6.1.29}$$

depending on the length of the chain (Heine, Kratky & Roppert, 1962). For further details, see Kratky (1982*b*).

Molecular weight. Particles of arbitrary shape. The particle is measured at high dilution in a homogeneous solution and has an isopotential specific volume v_2' and z_2 mol. electrons per gram, *i.e.* the molecule contains $z_2 M$ electrons if M is the molecular weight. The number of effective mol. electrons per gram is given by

$$\Delta z_2 = (z_2 - v_2'\rho_0), \tag{2.6.1.30}$$

where ρ_0 is the mean electron density of the solvent. The molecular weight can be determined from the intensity at zero angle $I(0)$:

$$M = \frac{I(0)}{P} \frac{a^2}{\Delta z^2 dc I_e N_L} = \frac{I(0)}{P} \frac{21.0a^2}{\Delta z^2 dc} \tag{2.6.1.31}$$

(Kratky, Porod & Kahovec, 1951), where P is the total intensity per unit time irradiating the sample, a [cm] is the distance between the sample and the plane of registration, d [cm] is the thickness of the sample, c [g cm^{-3}] is the concentration, and N_L is Loschmidt's (Avogadro's) number.

Rod-like particles. The mass per unit length $M_c = M/L$, *i.e.* the mass related to the cross section of a rod-like particle with length L, is given by a similar equation (Kratky & Porod, 1953):

$$M_c = \frac{[I(h)h]_{h\to 0}}{P} \frac{a^2}{\pi \Delta z^2 dc I_e N_L} = \frac{[I(h)h]_{h\to 0}}{P} \frac{6.68a^2}{\Delta z^2 dc}. \tag{2.6.1.32}$$

Flat particles. A similar equation holds for the mass per unit area $M_t = M/A$:

$$M_t = \frac{[I(h)h^2]_{h\to 0}}{P} \frac{a^2}{2\pi \Delta z^2 dc I_e N_L} = \frac{[I(h)h^2]_{h\to 0}}{P} \frac{3.34a^2}{\Delta z^2 dc}. \tag{2.6.1.33}$$

Abscissa scaling. The various molecular parameters can be evaluated from scattered intensities with different abscissa scaling. The abscissa used in theoretical work is $h = (4\pi/\lambda)\sin\theta$. The most important experimental scale is m [cm], the distance of the detector from the centre of the primary beam with the distance a [cm] between the sample and the detector plane.

$$h[\mathrm{nm}^{-1}] = T_{hm}[\mathrm{cm}^{-1}\mathrm{nm}^{-1}]m[\mathrm{cm}], \tag{2.6.1.34}$$

with

$$T_{hm} = 2\pi/\lambda a. \tag{2.6.1.35}$$

The angular scale 2θ with

$$2\theta \simeq m/a = (\lambda/2\pi)h \tag{2.6.1.36}$$

was used in the early years of small-angle X-ray scattering experiments. The formulae for the various parameters for m and the h scale can be found in Table 2.6.1.1, the formulae for the 2θ scale can be found in Glatter & Kratky (1982, p. 158).

2.6.1.3.2. *Shape and structure of particles*

In this subsection, we have to discuss how shape, size, and structure of the scattering particle are reflected in the scattering function $I(h)$ and in the PDDF $p(r)$. In general, it is easier to discuss features of the PDDF, but some characteristics like symmetry give more pronounced effects in reciprocal space.

2.6.1.3.2.1. *Homogeneous particles*

Globular particles. Only a few scattering problems can be solved analytically. The most trivial shape is a sphere. Here we have analytical expressions for the scattering intensity

$$I(h) = \left(3\frac{\sin(hR) - hR\cos(hR)}{(hR)^3}\right)^2 \tag{2.6.1.37}$$

and for the PDDF (Porod, 1948)

$$p(r) = 12x^2(2 - 3x + x^3) \quad x = r/(2R) \le 1, \tag{2.6.1.38}$$

where R is the radius of the sphere. The graphical representation of scattering functions is usually made with a semi-log plot [$\log I(h)$ *vs* h] or with a log–log plot [$\log I(h)$ *vs* $\log h$]; the PDDF is shown in a linear plot. In order to compare functions from particles of different shape, it is preferable to keep the scattering intensity at zero angle (area under PDDF) and the radius of

gyration R_g [slope of the main maximum of $I(h)$ or the second moment of $p(r)$] constant.

The scattering function of a sphere with $R = 65$ is shown in Fig. 2.6.1.2 [dashed line, $\log I(0)$ normalized to 12]. We see distinct minima which are typical for particles of high symmetry. We can determine the size of the sphere directly from the position of the zeros h_{01} and h_{02} (Glatter, 1972).

$$R \simeq \frac{4.493}{h_{01}} \quad \text{or} \quad R \simeq \frac{7.725}{h_{02}} \tag{2.6.1.39}$$

or from the position of the first side maximum ($R_g \simeq 4.5/h_1$). The minima are considerably flattened in the case of cubes (full line in Fig. 2.6.1.2). The corresponding differences in real space are not so clear-cut (Fig. 2.6.1.3). The $p(r)$ function of the sphere has a maximum near $r = R = D/2$ ($x \simeq 0.525$) and drops to zero like every PDDF at $r = D$, where D is the maximum dimension of the particle – here the diameter. The $p(r)$ for the cube with the same R_g is zero at $r \simeq 175$. The function is very flat in this region. This fact demonstrates the problems of accuracy in this determination of D when we take into account experimental errors. In any case, this accuracy will be different for different shapes.

Any deviation from spherical symmetry will shift the maximum to smaller r values and the value for D will increase [$I(0)$ and R_g constant!]. A comparison of PDDF's for a sphere, an oblate ellipsoid of revolution (axial ratio 1:1:0.2), and a prolate ellipsoid of revolution (1:1:3) is shown in Fig. 2.6.1.4. The more we change from the compact, spherical structure to a two- and one-dimensionally elongated structure, the more the maximum shifts to smaller r values and at the same time we have an increase in D. We see that $p(r)$ is a very informative function. The interpretation of scattering functions in reciprocal space is hampered by the highly abstract nature of this domain. We can see this problem in Fig. 2.6.1.5, where the scattering functions of the sphere and the ellipsoids in Fig. 2.6.1.4 are plotted. A systematic discussion of the features of $p(r)$ can be found elsewhere (Glatter, 1979, 1982*b*).

Rod-like particles. The first example of a particle elongated in one direction (prolate ellipsoid) was given in Figs. 2.6.1.4 and 2.6.1.5. An important class is particles elongated in one

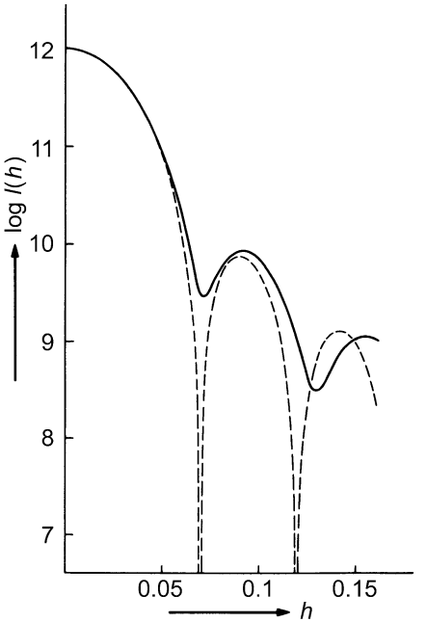

Fig. 2.6.1.2. Comparison of the scattering functions of a sphere (- - - -) and a cube (———) with same radius of gyration.

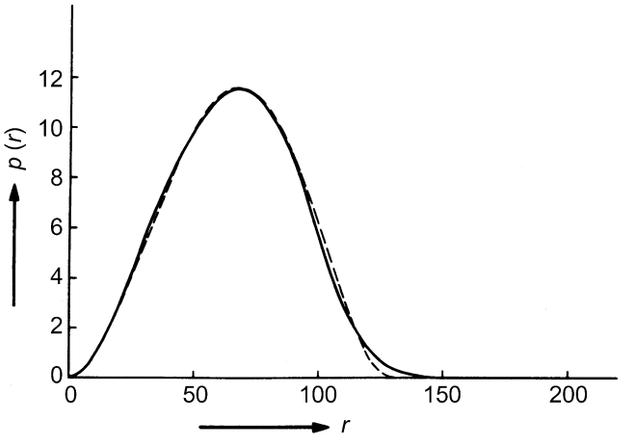

Fig. 2.6.1.3. Distance distribution function of a sphere (- - - -) and a cube (———) with the same radius of gyration and the same scattering intensity at zero angle.

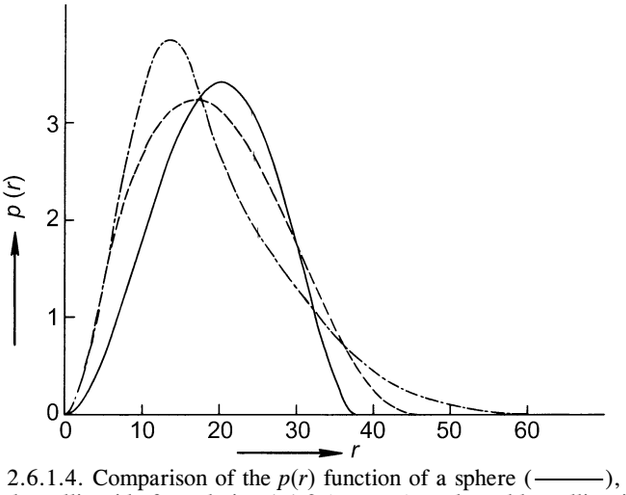

Fig. 2.6.1.4. Comparison of the $p(r)$ function of a sphere (———), a prolate ellipsoid of revolution 1:1:3 (—·—·—), and an oblate ellipsoid of revolution 1:1:0.2 (- - - -) with the same radius of gyration.

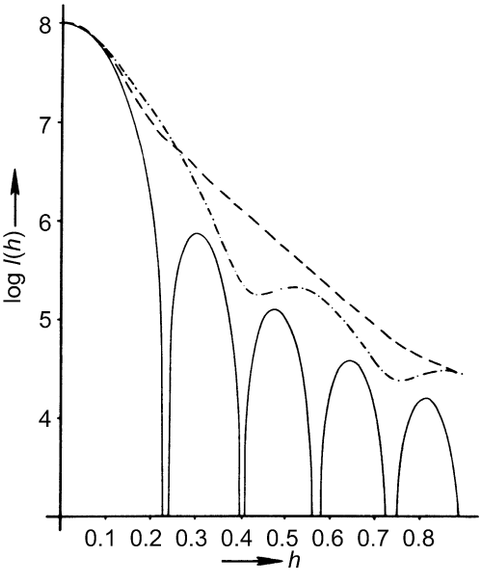

Fig. 2.6.1.5. Comparison of the $I(h)$ functions of a sphere, a prolate, and an oblate ellipsoid (see legend to Fig. 2.6.1.4).

direction with a constant cross section of arbitrary shape (long cylinders, parallelepipeds, *etc.*) The cross section A (with maximum dimension d) should be small in comparison to the length of the whole particle L:

$$d \ll L \quad L = (D^2 - d^2)^{1/2} \simeq D. \tag{2.6.1.40}$$

The scattering curve of such a particle can be written as

$$I(h) = L(\pi/h)I_c(h), \tag{2.6.1.41}$$

where the function $I_c(h)$ is related only to the cross section and the factor $1/h$ is characteristic for rod-like particles (Kratky & Porod, 1948; Porod, 1982). The cross-section function $I_c(h)$ is

$$I_c(h) = (L\pi)^{-1}I(h)h = \text{constant} \times I(h)h. \tag{2.6.1.42}$$

This function was used in the previous subsection for the determination of the cross-section parameters R_c, A, and M_c. In addition, we have

$$I_c(h) = 2\pi \int_0^\infty p_c(r)J_0(hr)\,\mathrm{d}r, \tag{2.6.1.43}$$

where $J_0(hr)$ is the zero-order Bessel function and

$$p_c(r) = \frac{1}{2\pi}\int_0^\infty I_c(h)(hr)J_0(hr)\,\mathrm{d}h \tag{2.6.1.44}$$

(Glatter, 1982*a*). The function $p_c(r)$ is the PDDF of the cross section with

$$p_c(r) = r\gamma_c(r) = \langle \Delta\rho(\mathbf{r}_c) * \Delta\rho(-\mathbf{r}_c)\rangle. \tag{2.6.1.45}$$

The symbol * stands for the mathematical operation called convolution and the symbol $\langle\ \rangle$ means averaging over all directions in the plane of the cross section. Rod-like particles with a constant cross section show a linear descent of $p(r)$ for $r \gg d$ if $D > 2.5d$. The slope of this linear part is proportional to the square of the area of the cross section,

$$\frac{\mathrm{d}p}{\mathrm{d}r} = -\frac{A^2\Delta\rho^2}{2}. \tag{2.6.1.46}$$

The PDDF's of parallelepipeds with the same cross section but different length L are shown in Fig. 2.6.1.6. The maximum corresponds to the cross section and the point of inflection r_i gives a rough indication for the size of the cross section. This is shown more clearly in Fig. 2.6.1.7, where three parallelepipeds with equal cross section area A but different cross-section dimensions are shown. If we find from the overall PDDF that the particle under investigation is a rod-like particle, we can use the PDDF of the cross section $p_c(r)$ to obtain more information on the cross section (Glatter, 1980*a*).

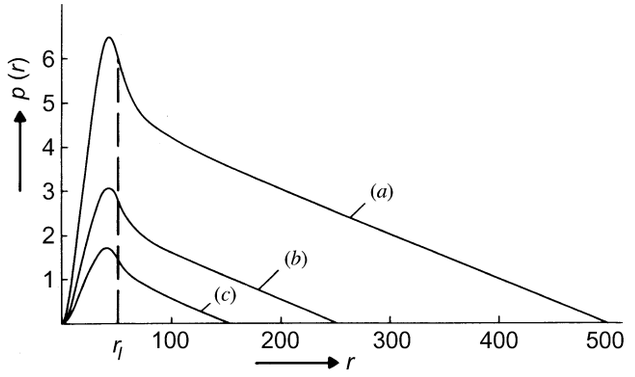

Fig. 2.6.1.6. Distance distributions from homogeneous parallelepipeds with edge lengths of: (*a*) 50 × 50 × 500 Å; (*b*) 50 × 50 × 250 Å; (*c*) 50 × 50 × 150 Å.

Flat particles. Flat particles, *i.e.* particles elongated in two dimensions (discs, flat parallelepipeds), with a constant thickness T much smaller than the overall dimensions D, can be treated in a similar way. The scattering function can be written as

$$I(h) = A\frac{2\pi}{h^2}I_t(h), \tag{2.6.1.47}$$

where $I_t(h)$ is the so-called thickness factor (Kratky & Porod, 1948) or

$$I_t(h) = (A2\pi)^{-1}I(h)h = \text{constant} \times I(h)h^2, \tag{2.6.1.48}$$

which can be used for the determination of R_t, T, and M_t. In addition, we have again:

$$I_t(h) = 2\int_0^\infty p_t(r)\cos(hr)\,\mathrm{d}r \tag{2.6.1.49}$$

and

$$p_t(r) = \gamma_t(r) - \frac{1}{\pi}\int_0^\infty I_t(h)\cos(hr)\,\mathrm{d}h$$
$$= \Delta\rho_t(r) * \Delta\rho_t(-r). \tag{2.6.1.50}$$

PDDF's from flat particles do not show clear features and therefore it is better to study $f(r) = p(r)/r$ (Glatter, 1979). The corresponding functions for lamellar particles with the same basal plane but different thickness are shown in Fig. 2.6.1.7(*b*). The marked transition points in Fig. 2.6.1.7(*b*) can be used to determine the thickness. The PDDF of the thickness $p_t(r)$ can give more information in such cases, especially for inhomogeneous particles (see below).

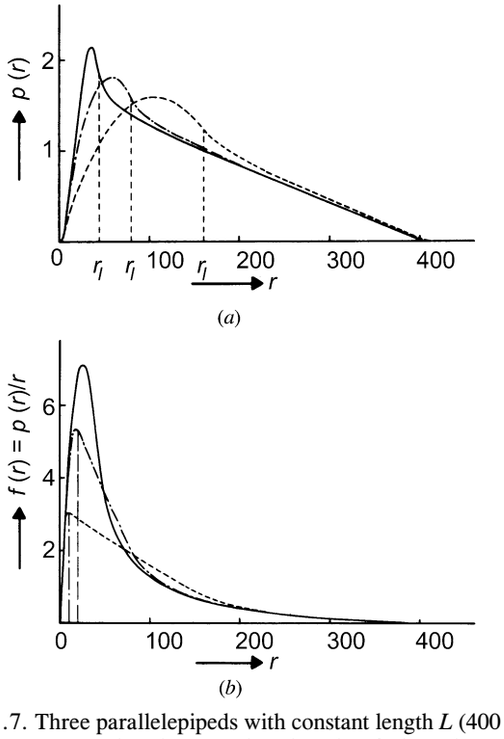

Fig. 2.6.1.7. Three parallelepipeds with constant length L (400 Å) and a constant cross section but varying length of the edges: ——— 40 × 40 Å; —·—·— 80 × 20 Å; - - - - 160 × 10 Å. (*a*) $p(r)$ function. (*b*) $f(r) = p(r)/r$.

Composite structures – aggregates, subunits. The formation of dimers can be analysed qualitatively with the $p(r)$ function (Glatter, 1979). For an approximate analysis, it is only necessary to know the PDDF of the monomer. Different types of aggregates will have distinct differences in their PDDF. Higher aggregates generally cannot be classified unambiguously. Additional information from other sources, such as the occurrence of symmetry, can simplify the problem.

Particles that consist of aggregates of a relatively large number of identical subunits show, at low resolution, the overall structure of the whole particle. At larger angles (higher resolution), the influence of the individual subunits can be seen. In the special case of globular subunits, it is possible to determine the size of the subunits from the position of the minima of the corresponding shape factors using equation (2.6.1.39) (Glatter, 1972; Pilz, Glatter, Kratky & Moring-Claesson, 1972).

2.6.1.3.2.2. *Hollow and inhomogeneous particles*

We have learned to classify homogeneous particles in the previous part of this section. It is possible to see from scattering data [$I(h)$ or $p(r)$] whether a particle is globular or elongated, flat or rod-like, *etc*., but it is impossible to determine uniquely a complicated shape with many parameters. If we allow internal inhomogeneities, we make things more complicated and it is clear that it is impossible to obtain a unique reconstruction of an inhomogeneous three-dimensional structure from its scattering function without additional *a priori* information. We restrict our considerations to special cases that are important in practical applications and that allow at least a solution in terms of a first-order approximation. In addition, we have to remember that the $p(r)$ function is weighted by the number of excess electrons that can be negative. Therefore, a minimum in the PDDF can be caused by a small number of distances, or by the addition of positive and negative contributions.

Spherically symmetric particles. In this case, it is possible to describe the particle by a one-dimensional radial excess density function $\Delta\rho(r)$. For convenience, we omit the Δ sign for excess in the following. As we do not have any angle-dependent terms, we have no loss of information from the averaging over angle. The scattering amplitude is simply the Fourier transform of the radial distribution:

$$A(h) = 4\pi \int_0^\infty r\rho(r)\frac{\sin(hr)}{h}\,\mathrm{d}r \qquad (2.6.1.51)$$

$[I(h) - A(h)^2]$ and

$$\rho(r) = \frac{1}{2\pi^2}\int_0^\infty hA(h)\frac{\sin(hr)}{r}\,\mathrm{d}h \qquad (2.6.1.52)$$

(Glatter, 1977*a*). These equations would allow direct analysis if $A(h)$ could be measured, but we can measure only $I(h)$. $\rho(r)$ can be calculated from $I(h)$ using equation (2.6.1.10) remembering that this function is the convolution square of $\rho(r)$ [equations (2.6.1.5) and (2.6.1.8)]. Using a *convolution square-root* technique, we can calculate $\rho(r)$ from $I(h)$ *via* the PDDF without having a 'phase problem' like that in crystallography; *i.e*. it is not necessary to calculate scattering amplitudes and phases (Glatter, 1981; Glatter & Hainisch, 1984; Glatter, 1988). This can be done because $p(r)$ differs from zero only in the limited range $0 < r < D$ (Hosemann & Bagchi, 1952, 1962). In mathematical terms, it is again the difference between a Fourier series and a Fourier integral.

Details of the technique cannot be discussed here, but it is a fact that we can calculate the radial distribution $\rho(r)$ from the scattering data assuming that the spherical scatterer is only of finite size. The hollow sphere can be treated either as a homogeneous particle with a special shape or as an inhomogeneous particle with spherical symmetry with a step function as radial distribution. The scattering function and the PDDF of a hollow sphere can be calculated analytically. The $p(r)$ of a hollow sphere has a triangular shape and the function $f(r) = p(r)/r$ shows a horizontal plateau (Glatter, 1982*b*).

Rod-like particles. Radial inhomogeneity. If we assume radial inhomogeneity of a circular cylinder, *i.e*. ρ is a function of the radius r but not of the angle φ or of the value of z in cylindrical coordinates, we can determine some structural details. We define $\bar{\rho}_c$ as the average excess electron density in the cross section. Then we obtain a PDDF with a linear part for $r > d$ and we have to replace $\Delta\rho$ in equation (2.6.1.46) by $\bar{\rho}_c$ with the maximum dimension of the cross section d. The $p(r)$ function differs from that of a homogeneous cylinder with the same $\bar{\rho}_c$ only in the range $0 < r \leq d$. A typical example is shown in Fig. 2.6.1.8. The functions for a homogeneous, a hollow, and an inhomogeneous cylinder with varying density $\rho_c(r)$ are shown.

Rod-like particles. Axial inhomogeneity. This is another special case for rod-like particles, *i.e*. the density is a function of the z coordinate. In Fig. 2.6.1.9, we compare two cylinders with the same size and diameter. One is a homogeneous cylinder with density $\bar{\rho}$, diameter $d = 48$ and length $L = 480$, and the other is an inhomogeneous cylinder of the same size and mean density $\bar{\rho}$, but this cylinder is made from slices with a thickness of 20 and alternating densities of $1.5\bar{\rho}$ and $0.5\bar{\rho}$, respectively. The PDDF of the inhomogeneous cylinder has ripples with the periodicity of 40 in the whole linear range. This periodicity leads to reflections in reciprocal space (first and third order in the h range of the figure).

Flat particles. Cross-sectional inhomogeneity. Lamellar particles with varying electron density perpendicular to the basal plane, where ρ is a function of the distance x from the central plane, show differences from a homogeneous lamella of the same size in the PDDF in the range $0 < r < T$, where T is the

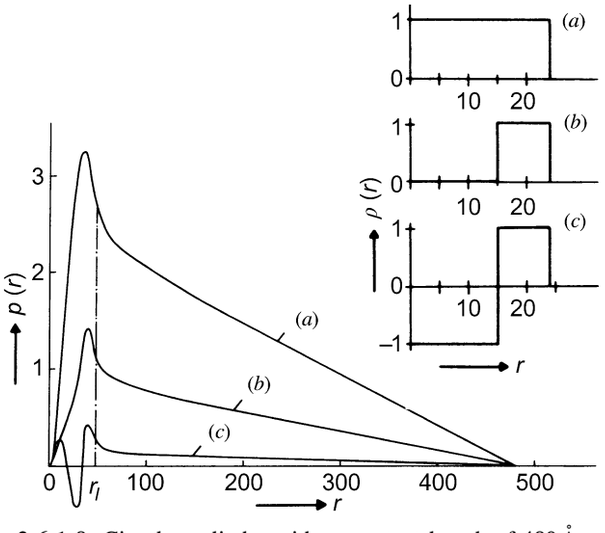

Fig. 2.6.1.8. Circular cylinder with a constant length of 480 Å and an outer diameter of 48 Å. (*a*) Homogeneous cylinder, (*b*) hollow cylinder, (*c*) inhomogeneous cylinder. The $p(r)$ functions are shown on the left, the corresponding electron-density distributions $\rho(r)$ on the right.

thickness of the lamella. An example is given in Fig. 2.6.1.10 where we compare a homogeneous lamellar particle (with $\rho = +\frac{1}{3}$) with an inhomogeneous one, $\rho_t(x)$ being a three-step function alternating between the values $+1$, -1, $+1$.

Flat particles. In-plane inhomogeneity. Lamellae with a homogeneous cross section but inhomogeneities along the basal plane have a PDDF that deviates from that of a homogeneous lamella in the whole range $0 < r < D$. These deviations are a measure of the in-plane inhomogeneites; a general evaluation method does not exist. Even more complicated is the situation that occurs in membranes: these have a pronounced cross-sectional structure with additional in-plane inhomogeneities caused by the membrane proteins (Laggner, 1982; Sadler & Worcester, 1982).

Contrast variation and labelling. An important method for studying inhomogeneous particles is the method of contrast variation (Stuhrmann, 1982). By changing the contrast of the solvent, we can obtain additional information about the inhomogeneities in the particles. This variation of the contrast is much easier for neutron scattering than for X-ray scattering because hydrogen and deuterium have significantly different scattering cross sections. This technique will therefore be discussed in the section on neutron small-angle scattering.

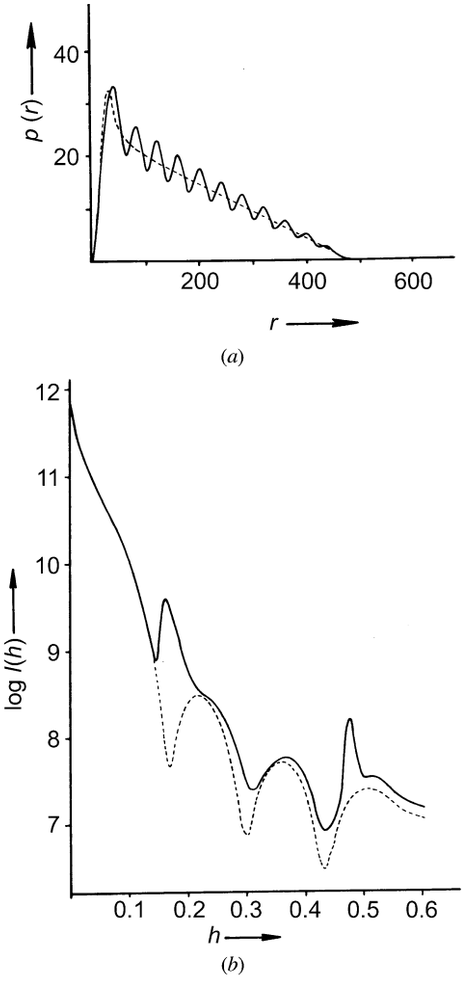

Fig. 2.6.1.9. Inhomogeneous circular cylinder with periodical changes of the electron density along the cylinder axis compared with a homogeneous cylinder with the same mean electron density. (*a*) $p(r)$ function; (*b*) scattering intensity; ——— inhomogeneous cylinder; - - - - homogeneous cylinder.

A method for distance determination with X-rays by heavy-atom labelling was developed by Kratky & Worthman (1947). These ideas are now used for the determination of distances between deuterated subunits of complex macromolecular structures with neutron scattering.

High-resolution experiments. A special type of study is the comparison of the structures of the same molecule in the crystal and in solution. This is done to investigate the influence of the crystal field on the polymer structure (Krigbaum & Kügler, 1970; Damaschun, Damaschun, Müller, Ruckpaul & Zinke, 1974; Heidorn & Trewhella, 1988) or to investigate structural changes (Ruckpaul, Damaschun, Damaschun, Dimitrov, Jänig, Müller, Pürschel & Behlke, 1973; Hubbard, Hodgson & Doniach, 1988). Sometimes such investigations are used to verify biopolymer structures predicted by methods of theoretical physics (Müller, Damaschun, Damaschun, Misselwitz, Zirwer & Nothnagel, 1984). In all cases, it is necessary to measure the small-angle scattering curves up to relatively high scattering angles ($h \simeq 30\,\mathrm{nm}^{-1}$, and more). Techniques for such experiments have been developed during recent years (Damaschun, Gernat, Damaschun, Bychkova & Ptitsyn, 1986; Gernat, Damaschun, Kröber, Bychkova & Ptitsyn, 1986; I'anson, Bacon, Lambert, Miles, Morris, Wright & Nave, 1987) and need special evaluation methods (Müller, Damaschun & Schrauber, 1990).

2.6.1.3.3. *Interparticle interference, concentration effects*

So far, only the scattering of single particles has been treated, though, of course, a great number of these are always present. It has been assumed that the intensities simply add to give the total diffraction pattern. This is true for a very dilute solution, but with increasing concentration interference effects will contribute. Biological samples often require higher concentrations for a sufficient signal strength. We can treat this problem in two different ways:

–We accept the interference terms as additional information about our system under investigation, thus observing the spatial arrangement of the particles.

–We treat the interference effect as a perturbation of our single-particle concept and discuss how to remove it.

The first point of view is the more general, but there are many open questions left. For many practical applications, the second point of view is important.

The radial distribution function. In order to find a general description, we have to restrict ourselves to an isotropic assembly of monodisperse spheres. This makes it possible to

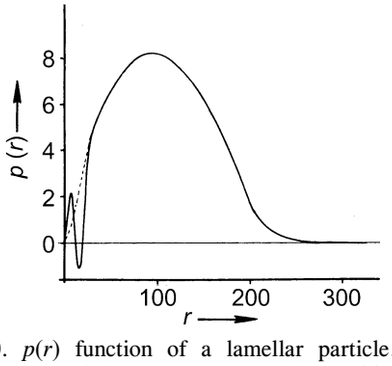

Fig. 2.6.1.10. $p(r)$ function of a lamellar particle. The full line corresponds to an inhomogeneous particle, $\rho_t(x)$ is a three-step function with the values $+1$, -1, $+1$. The broken line represents the homogeneous lamella with $\rho = +\frac{1}{3}$.

describe the situation by introducing a radial interparticle distribution function $P(r)$ (Zernicke & Prins, 1927; Debye & Menke, 1930). Each particle has the same surroundings. We consider one central particle and ask for the probability that another particle will be found in the volume element $\mathrm{d}V$ at a distance r apart. The mean value is $(N/v)\,\mathrm{d}V$; any deviation from this may be accounted for by a factor $P(r)$. In the range of impenetrability ($r < D$), we have $P(r) = 0$ and in the long range ($r \gg D$) $P(r) = 1$. So the corresponding equation takes the form

$$I(h) = NI_1(h)\left[1 + \frac{N}{V}\int_0^\infty 4\pi r^2[P(r) - 1]\frac{\sin(hr)}{hr}\,\mathrm{d}r\right]. \quad (2.6.1.53)$$

The second term contains all interparticle interferences. Its predominant part is the 'hole' of radius D, where $[P(r) - 1] = -1$. This leads to a decrease of the scattering intensity mainly in the central part, which results in a liquid-type pattern (Fig. 2.6.1.11). This can be explained by the reduction of the contrast caused by the high number of surrounding particles. Even if a size distribution for the spheres is assumed, the effect remains essentially the same (Porod, 1952). Up to now, no exact analytical expressions for $P(r)$ exist. The situation is even more complicated if one takes into account attractive or repulsive interactions or non-spherical particle shapes (orientation).

If we have a system of spheres with known size D, we can use equation (2.6.1.37) for $I_1(h)$ in equation (2.6.1.53), divide by this function, and calculate $P(r)$ from experimental data by Fourier inversion. The interference term can be used to study particle correlations of charged macromolecular solutions (Chen, Sheu, Kalus & Hoffmann, 1988).

If there are attractive forces, there will be a tendency for aggregation. This tendency may, for instance, be introduced by some steps in the procedure of preparation of biological samples. Such aggregation leads to an increase of the intensity in the central part (gas type). In this case, we will finally have a polydisperse system of monomers and oligomers. Again, there exist no methods to analyse such a system uniquely.

Elimination of concentration effects – liquid type. In most cases, the interference effect is a perturbation of our experiment where we are only interested in the particle scattering function. Any remaining concentration effect would lead to errors in the resulting parameters. As we have seen above, the effect is essential at low h values, thus influencing $I(0)$, R_g, and the PDDF at large r values.

The problem can be handled for the liquid-like type in the following way. We measure the scattering function $I(h)$ at different concentrations (typically from a few $\mathrm{mg\,ml^{-1}}$ up to about $50\,\mathrm{mg\,ml^{-1}}$). The influence of the concentration can be seen in a common plot of these scattering curves, divided by their concentrations. For large h values, these curves are identical. In the low-h range, the curves must be extrapolated to zero concentration. It depends on the problem as to whether a linear fit is sufficient or whether a second-degree polynomial has to be used. The extrapolation can be performed in a standard $I(h)/c$ *versus* h plot or in a Zimm plot $[I(h)/c]^{-1}$ *versus* h (Cleemann & Kratky, 1960; Kirste & Oberthür, 1982). The Zimm plot should be preferred when working with highly concentrated solutions (Pilz, 1982).

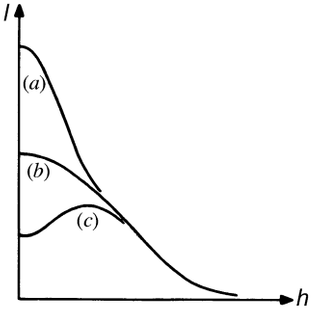

Fig. 2.6.1.11. Characteristic types of scattering functions: (*a*) gas type; (*b*) particle scattering; (*c*) liquid type.

As mentioned above, the innermost part of the scattering function is lowered and the apparent radius of gyration decreases with increasing concentration. The length of the linear range of the Guinier plot can be extended by the interference effect for non-spherical particles. Thus, an elongated linear Guinier plot is no guarantee of the completeness of the elimination of the concentration effect. Remaining interparticle interferences cannot be recognized in reciprocal space.

The PDDF is affected considerably by interparticle interference (Glatter, 1979). It is lowered with increasing distance r, goes through a negative minimum in the region of the maximum dimension D of the particle, and the oscillations vanish at larger r values. This is shown for the hard-sphere model in Fig. 2.6.1.12. The oscillations disappear when the concentration goes to zero.

The same behaviour can be found from experimental data even in the case of non-spherical data (Pilz, Goral, Hoylaerts, Witters & Lontie, 1980; Pilz, 1982).

In some cases, it may be impossible to carry out experiments with varying concentrations. This will be the case if the structure of the particles depends on concentration. Under certain circumstances, it is possible to find the particle parameters by neglecting the innermost part of the scattering function influenced by the concentration effect (Müller & Glatter, 1982).

Aggregates – gas type. When the particles show a tendency to aggregation with increasing concentration, we can follow the same procedures as discussed for the liquid type, *i.e.* perform a concentration series and extrapolate the $I(h)/c$ curves to zero concentration.

However, in most cases, the tendency to aggregation exists at any concentration, *i.e.* even at very high dilution we have a certain number of oligomers coexisting with monomers. There is no unique way to find the real particle parameters in these cases. It is not sufficient just to neglect the innermost part of the

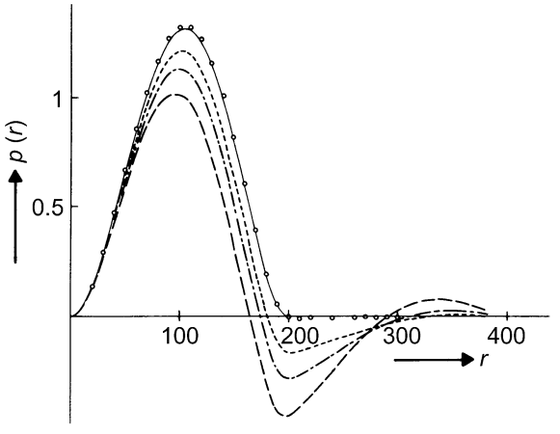

Fig. 2.6.1.12. Distance distribution – hard-sphere interference model. Theoretical $p(r)$ functions: ——— $\theta = 0$; - - - $\theta = 0.25$; —·—·— $\theta = 0.5$; — — — $\theta = 1.0$. Circles: results from indirect transformation: $\theta = 0.5$, $h_1R = 2.0$. 2% statistical noise, $D_{\max} = 300\,\text{Å}$, $\Delta R_g = 0.5\%$, $\Delta I_0 = 1.2\%$.

scattering function because that leads to an increasing loss of essential information about the particle (monomer) itself.

2.6.1.4. *Polydisperse systems*

In this subsection, we give a short survey of the problem of polydispersity. It is most important that there is no way to decide from small-angle scattering data whether the sample is mono- or polydisperse. Every data set can be evaluated in terms of monodisperse or polydisperse structures. Independent *a priori* information is necessary to make this decision. It has been shown analytically that a certain size distribution of spheres gives the same scattering function as a monodisperse ellipsoid with axes a, b and c (Mittelbach & Porod, 1962).

The scattering function of a polydisperse system is determined by the shape of the particles and by the size distribution. As mentioned above, we can assume a certain size distribution and can determine the shape, or, more frequently, we assume the shape and determine the size distribution. In order to do this we have to assume that the scattered intensity results from an ensemble of particles of the same shape whose size distribution can be described by $D_n(R)$, where R is a size parameter and $D_n(R)$ denotes the number of particles of size R. Let us further assume that there are no interparticle interferences or multiple scattering effects. Then the scattering function $I(h)$ is given by

$$I(h) = c_n \int_0^\infty D_n(R) R^6 i_0(hR)\, \mathrm{d}R, \qquad (2.6.1.54)$$

where c_n is a constant, the factor R^6 takes into account the fact that the particle volume is proportional to R^3, and $i_0(hR)$ is the normalized form factor of a particle size R. In many cases, one is interested in the mass distribution $D_m(R)$ [sometimes called volume distribution $D_c(R)$]. In this case, we have

$$I(h) = c_m \int_0^\infty D_m(R) R^3 i_0(hR)\, \mathrm{d}R. \qquad (2.6.1.55)$$

The solution of these integral equations, *i.e.* the computation of $D_n(R)$ or $D_m(R)$ from $I(h)$, needs rather sophisticated numerical or analytical methods and will be discussed later.

The problems of interparticle interference and multiple scattering in the case of polydisperse systems cannot be described analytically and have not been investigated in detail up to now. In general, interference effects start to influence data from small-angle scattering experiments much earlier, *i.e.* at lower concentration, than multiple scattering. Multiple scattering becomes more important with increasing size and contrast and is therefore dominant in light-scattering experiments in higher concentrations.

A concentration series and extrapolation to zero concentration as in monodisperse systems should be performed to eliminate these effects.

2.6.1.5. *Instrumentation*

X-ray sources are the same for small-angle scattering as for crystallographic experiments. One can use conventional generators with sealed tubes or rotating anodes for higher power. For the vast majority of applications, an X-ray tube with copper anode is used; the wavelength of its characteristic radiation (Cu $K\alpha$ line) is 0.154 nm. Different anode materials emit X-rays of different characteristic wavelengths.

X-rays from synchrotrons or storage rings have a continuous wavelength distribution and the actual wavelength for the experiment is selected by a monochromator. The intensity is much higher than for any type of conventional source but synchrotron radiation is available only at a few places in the world. Reviews on synchrotron radiation and its application have been published during recent years (Stuhrmann, 1978; Holmes, 1982; Koch, 1988). In these reviews, one can also find some remarks on the general principles of the systems including cameras and special detectors.

2.6.1.5.1. *Small-angle cameras*

General. In any small-angle scattering experiment, it is necessary to illuminate the sample with a well defined flux of X-rays. The ideal condition would be a parallel monochromatic beam of negligible dimension and very high intensity. These theoretical conditions can never be reached in practice (Pessen, Kumosinski & Timasheff, 1973). One of the main reasons is the fact that there are no lenses as in the visible range of electromagnetic radiation. The refractive index of all materials is equal to or very close to unity for X-rays. On the other hand, this fact has some important advantages. It is, for example, possible to use circular capillaries as sample holders without deflecting the beam. There are different ways of constructing a small-angle scattering system. Slit, pinhole, and block systems define a certain area where the X-rays can pass. Any slit or edge will give rise to secondary scattering (parasitic scattering). The special construction of the instrument has to provide at least a subspace in the detector plane (plane of registration) that is free from this parasitic scattering. The crucial point is of course to provide the conditions to measure at very small scattering angles.

The other possibility of building a small-angle scattering system is to use monochromator crystals and/or bent mirrors to select a narrow wavelength band from the radiation (important for synchrotron radiation) and to focus the X-ray beam to a narrow spot. These systems require slits in addition to eliminate stray radiation.

Block collimation – Kratky camera. The Kratky (1982*a*) collimation system consists of an entrance slit (edge) and two blocks – the *U*-shaped centre piece and a block called *bridge*. With this system, the problem of parasitic scattering can be largely removed for the upper half of the plane of registration and the smallest accessible scattering angle is defined by the size of the entrance slit (see Fig. 2.6.1.13). This system can be integrated in an evacuated housing (Kratky compact camera) and fixed on the top of the X-ray tube. It is widely used in many laboratories for different applications. In the Kratky system, the X-ray beam has a rectangular shape, the length being much larger than the width. Instrumental broadening can be corrected by special numerical routines. The advantage is a relatively high primary-beam intensity. The main disadvantage is that it cannot be used in special applications such as oriented systems where

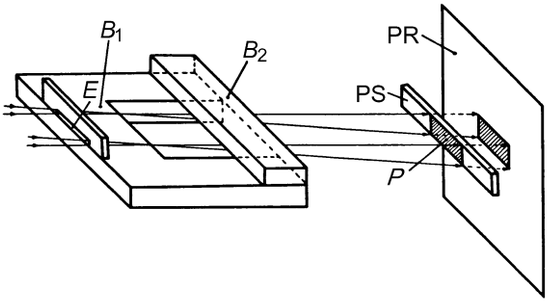

Fig. 2.6.1.13. Schematic drawing of the block collimation (Kratky camera): E edge; B_1 centre piece; B_2 bridge; P primary-beam profile; PS primary-beam stop; PR plane of registration.

the two-dimensional scattering pattern has to be recorded. For such applications, any type of point collimation can be used.

Slit and pinhole cameras. The simplest way to build a camera is to use two pairs of slits or pinholes at a certain distance apart (Kratky, 1982*a*; Holmes, 1982). The narrower the slits and the larger the distance between them, the smaller is the smallest attainable scattering angle (sometimes called the '*resolution*'). Parasitic scattering and difficult alignment are the main problems for all such systems (Guinier & Fournet, 1955). A slit camera that has been used very successfully is that of Beeman and co-workers (Ritland, Kaesberg & Beeman, 1950; Anderegg, Beeman, Shulman & Kaesberg, 1955). A rather unusual design is adopted in the slit camera of Stasiecki & Stuhrmann (1978), whose overall length is 50 m! A highly developed system is the ORNL 10 m camera at Oak Ridge (Hendricks, 1978).

Standard-size cameras for laboratory application are commercially available with different designs from various companies.

Bonse–Hart camera. The Bonse–Hart camera (Bonse & Hart, 1965, 1966, 1967) is based on multiple reflections of the primary beam from opposite sides of a groove in an ideal germanium crystal (collimator and monochromator). After penetrating the sample, the scattered beam runs through the groove of a second crystal (analyser). This selects the scattering angle. Rotation of the second crystal allows the measurement of the angle-dependent scattering function. The appealing feature of this design is that one can measure down to very small angles without a narrow entrance slit. The system is therefore favourable for the investigation of very large particles ($D > 350$ nm). For smaller particles, one obtains better results with block collimation (Kratky & Leopold, 1970).

Camera systems for synchrotron radiation. Small-angle scattering facilities at synchrotrons are built by the local staff and details of the construction are not important for the user in most cases. Descriptions of the instruments are available from the local contacts. These small-angle scattering systems are usually built with crystal monochromators and focusing mirrors (point collimation). All elements have to be operated under remote control for safety reasons. A review of the different instruments was published recently by Koch (1988).

2.6.1.5.2. *Detectors*

In this field, we are facing the same situation as we met for X-ray sources. The detectors for small-angle scattering experiments are the same as or slightly modified from the detectors used in crystallography. Therefore, it is sufficient to give a short summary of the detectors in the following; further details are given in Chapter 7.1. If we are not investigating the special cases of fully or partially oriented systems, we have to measure the dependence of the scattered intensity on the scattering angle, *i.e.* a one-dimensional function. This can be done with a standard gas-filled proportional counter that is operated in a sequential mode (Leopold, 1982), *i.e.* a positioning device moves the receiving slit and the detector to the desired angular position and the radiation detector senses the scattered intensity at that position. In order to obtain the whole scattering curve, a series of different angles must be positioned sequentially and the intensity readings at every position must be recorded. The system has a very high dynamic range, but – as the intensities at different angles are measured at different times – the stability of the primary beam is of great importance.

This drawback is eliminated in the parallel detection mode with the use of position-sensitive detectors. Such systems are in most cases proportional counters with sophisticated and expensive read-out electronics that can evaluate on-line the accurate position where the pulses have been created by the incoming radiation.

Two-dimensional position-sensitive detectors are necessary for oriented systems, but they also have advantages in the case of non-oriented samples when circular chambers are used or when integration techniques in square detectors lead to a higher signal at large scattering angles.

The simplest and cheapest two-dimensional detector is still film, but films are not used very frequently in small-angle scattering experiments because of limited linearity and dynamic range, and fog intensity.

Koch (1988) reviews the one- and two-dimensional detectors actually used in synchrotron small-angle scattering experiments. For a general review of detectors, see Hendrix (1985).

2.6.1.6. *Data evaluation and interpretation*

After having discussed the general principles and the basics of instrumentation in the previous subsections, we can now discuss how to handle measured data. This can only be a very short survey; a detailed description of data treatment and interpretation has been given previously (Glatter, 1982*a*,*b*).

Every physical investigation consists of three highly correlated parts: theory, experiment, and evaluation of data. The theory predicts a possible experiment, experimental data have to be collected in a way that the evaluation of the information wanted is possible, the experimental situation has to be described theoretically and has to be taken into account in the process of data evaluation *etc*. This correlation should be remembered at every stage of the investigation. Before we can start any discussion about interpretation, we have to describe the experimental situation carefully.

All the theoretical equations in the previous subsections correspond to ideal conditions as mentioned in the subsection on instrumentation. In real experiments, we do not measure with a point-like parallel and strictly monochromatic primary beam and our detector will have non-negligible dimensions. The finite size of the beam, its divergence, the size of the detector, and the wavelength distribution will lead to an instrumental broadening as in most physical investigations. The measured scattering curve is said to be *smeared* by these effects. So we find ourselves in the following situation.

The particle is represented by its PDDF $p(r)$. This function is not measured directly. In the scattering process it is Fourier-transformed into a scattering function $I(h)$ [equation (2.6.1.9)]. This function is smeared by the broadening effects and the final *smeared* scattering function $I_{\exp}(h)$ is measured with a certain experimental error $\sigma(h)$. In the case of polydisperse systems, the situation is very similar; we start from a size-distribution function $D(R)$ and have a different transformation [equations (2.6.1.54), (2.6.1.55)], but the smearing problem is the same.

2.6.1.6.1. *Primary data handling*

In order to obtain reliable results, we have to perform a series of experiments. We have to repeat the experiment for every sample, to be able to estimate a mean value and a standard deviation at every scattering angle. This experimentally determined standard deviation is often much higher than the standard deviation simply estimated from counting statistics. A blank experiment (cuvette filled with solvent only) is necessary to be able to subtract background scattering coming from the instrument and from the solvent (or *matrix* in the case of solid samples). Finally, we have to perform a series of such

experiments at different concentrations to extrapolate to zero concentration (elimination of interparticle interferences).

If the scattering efficiency of the sample is low (low contrast, small particles), it may be necessary to measure the outer part of the scattering function with a larger entrance slit and we will have to merge different parts of the scattering function. The intensity of the instrument (primary beam) should be checked before each measurement. This allows correction (normalization) for instabilities.

It is therefore necessary to have a so-called primary data-handling routine that performs all these preliminary steps like averaging, subtraction, normalization, overlapping, concentration extrapolation, and graphical representation on a graphics terminal or plotter. In addition, it is helpful to have the possibility of calculating the Guinier radius, Porod extrapolation [equations (2.6.1.24)], invariant, *etc*. from the raw data.

When all these preliminary steps have been performed, we have a smeared particle-scattering function $I_{\rm exp}(h)$ with a certain statistical accuracy. From this data set, we want to compute $I(h)$ and $p(r)$ [or $D(R)$] and all our particle parameters. In order to do this, we have to *smooth* and *desmear* our function $I_{\rm exp}(h)$. The smoothing operation is an absolute necessity because the desmearing process is comparable to a differentiation that is impossible for noisy data. Finally, we have to perform a Fourier transform (or other similar transformation) to invert equations (2.6.1.9) or (2.6.1.54), (2.6.1.55). Before we can discuss the desmearing process (collimation error correction) we have to describe the smearing process.

2.6.1.6.2. *Instrumental broadening – smearing*

These effects can be separated into three components: the two-dimensional geometrical effects and the wavelength effect. The geometrical effects can be separated into a slit-length (or slit-height) effect and a slit-width effect. The slit length is perpendicular to the direction of increasing scattering angle; the corresponding weighting function is usually called $P(t)$. The slit width is measured in the direction of increasing scattering angles and the weighting function is called $Q(x)$. If there is a wavelength distribution, we call the weighting function $W(\lambda')$ where $\lambda' = \lambda/\lambda_0$ and λ_0 is the reference wavelength used in equation (2.6.1.2). When a conventional X-ray source is used, it is sufficient in most cases to correct only for the $K\beta$ contribution. Instead of the weighting function $W(\lambda')$ one only needs the ratio between $K\beta$ and $K\alpha$ radiation, which has to be determined experimentally (Zipper, 1969). One or more smearing effects may be negligible, depending on the experimental situation.

Each effect can be described separately by an integral equation (Glatter, 1982*a*). The combined formula reads

$$\bar{I}_{\rm exp}(h) = 2 \int_{-\infty}^{\infty} \int_{0}^{\infty} \int_{0}^{\infty} Q(x)P(t)W(\lambda') \times I\left(\frac{[(m-x)^2 + t^2]^{1/2}}{\lambda'}\right) {\rm d}\lambda'\ {\rm d}t\ {\rm d}x. \quad (2.6.1.56)$$

This threefold integral equation cannot be solved analytically. Numerical methods must be used for its solution.

2.6.1.6.3. *Smoothing, desmearing, and Fourier transformation*

There are many methods published that offer a solution for this problem. Most are referenced and some are reviewed in the textbooks (Glatter, 1982*a*; Feigin & Svergun, 1987). The *indirect transformation method* in its original version (Glatter, 1977*a*,*b*, 1980*a*,*b*) or in modifications for special applications (Moore, 1980; Feigin & Svergun, 1987) is a well established method used in the majority of laboratories for different applications. This procedure solves the problems of smoothing, desmearing, and Fourier transformation [inversion of equations (2.6.1.9) or (2.6.1.54), (2.6.1.55)] in one step. A short description of this technique is given in the following.

Indirect transformation methods. The *indirect transformation method* combines the following demands: single-step procedure, optimized general-function system, weighted least-squares approximation, minimization of termination effect, error propagation, and consideration of the physical smoothing condition given by the maximum intraparticle distance. This smoothing condition requires an estimate $D_{\rm max}$ as an upper limit for the largest particle dimension:

$$D_{\rm max} \geq D. \quad (2.6.1.57)$$

For the following, it is not necessary for $D_{\rm max}$ to be a perfect estimate, but it must not be smaller than D.

As $p(r) = 0$ for $r \geq D_{\rm max}$, we can use a function system for the representation of $p(r)$ that is defined only in the subspace $0 \leq r \leq D_{\rm max}$. A linear combination

$$p_A(r) = \sum_{\nu=1}^{N} c_\nu \varphi_\nu(r) \quad (2.6.1.58)$$

is used as an approximation to the PDDF. Let N be the number of functions and c_ν be the unknowns. The functions $\varphi_\nu(r)$ are chosen as cubic B splines (Greville, 1969; Schelten & Hossfeld, 1971) as they represent smooth curves with a minimum second derivative.

Now we take advantage of two facts. The first is that we know precisely how to calculate a smeared scattering function $\bar{I}(h)$ from $I(h)$ [equation (2.6.1.56)] and how $p(r)$ or $D(R)$ is transformed into $I(h)$ [equations (2.6.1.9) or (2.6.1.54), (2.6.1.55)], but we do not know the inverse transformations. The second fact is that all these transformations are linear, *i.e*. they can be applied to all terms in a sum like that in equation (2.6.1.58) separately. So it is easy to start with our approximation in real space [equation (2.6.1.58)] taking into account the *a priori* information $D_{\rm max}$. The approximation $I_A(h)$ to the ideal (unsmeared) scattering function can be written as

$$I_A(h) = \sum_{\nu=1}^{N} c_\nu \Psi_\nu(h), \quad (2.6.1.59)$$

where the functions $\Psi_\nu(h)$ are calculated from $\varphi_\nu(r)$ by the transformations (2.6.1.9) or (2.6.1.54), (2.6.1.55), the coefficients c_ν remain unknown. The final fit in the smeared, experimental space is given by a similar series

$$\bar{I}_A(h) = \sum_{\nu=1}^{N} c_\nu \chi_\nu(h), \quad (2.6.1.60)$$

where the $\chi_\nu(h)$ are functions calculated from $\psi_\nu(h)$ by the transform (2.6.1.56). Equations (2.6.1.58), (2.6.1.59), and (2.6.1.60) are similar because of the linearity of the transforms. We see that the functions $\chi_\nu(h)$ are calculated from $\varphi_\nu(r)$ in the same way as the data $\bar{I}_{\rm exp}(h)$ were produced by the experiment from $p(r)$. Now we can minimize the expression

$$L = \sum_{k=1}^{M} [\bar{I}_{\rm exp}(h_k) - \bar{I}_A(h_k)]^2/\sigma^2(h_k), \quad (2.6.1.61)$$

where M is the number of experimental points. Such *least-squares problems* are in most cases *ill conditioned, i.e*. additional stabilization routines are necessary to find the best

solution. This problem is far from being trivial, but it can be solved with standard routines (Glatter, 1977*a*,*b*; Tikhonov & Arsenin, 1977).

The whole process of data evaluation is shown in Fig. 2.6.1.14. Similar routines cannot be used in crystallography (periodic structures) because there exists no estimate for D_{max} [equation (2.6.1.57)].

Maximum particle dimension. The sampling theorem of Fourier transformation (Shannon & Weaver, 1949; Bracewell, 1986) gives a clear answer to the question of how the size of the particle D is related to the smallest scattering angle h_1. If the scattering curve is observed at increments $\Delta h \leq h_1$ starting from a scattering angle h_1, the scattering data contain, at least theoretically, the full information for all particles with maximum dimension D

$$D \leq \pi/h_1. \tag{2.6.1.62}$$

The first application of this theorem to the problem of data evaluation was given by Damaschun & Pürschel (1971*a*,*b*). In practice, one should always try to stay below this limit, *i.e.*

$$h_1 < \pi/D \quad \text{and} \quad \Delta h \ll h_1, \tag{2.6.1.63}$$

taking into account the loss of information due to counting statistics and smearing effects. An optimum value for $\Delta h = \pi/(6D)$ is claimed by Walter, Kranold & Becherer (1974).

Information content. The number of *independent* parameters contained in a small-angle scattering curve is given by

$$N_{max} \leq h_2/h_1, \tag{2.6.1.64}$$

with h_1 and h_2 being the lower and upper limits of h. In practice, this limit certainly depends on the statistical accuracy of the data. It should be noted that the number of functions N in equations (2.6.1.58) to (2.6.1.60) may be larger than N_{max} because they are not independent. They are correlated by the stabilization routine. An example of this problem can be found in Glatter (1980*a*).

Resolution. There is no clear answer to the question concerning the smallest structural details, *i.e.* details in the $p(r)$ function that can be recognized from an experimental scattering function. The limiting factors are the maximum scattering angle h_2, the statistical error $\sigma(h)$, and the weighting functions $P(t)$, $Q(x)$, and $W(\lambda')$ (Glatter, 1982*a*). The resolution of standard experiments is not better than approximately 10% of the maximum dimension of the particle for a monodisperse system. In the case of polydisperse systems, resolution can be defined as the minimum relative peak distance that can be resolved in a bimodal distribution. We know from simulations that this value is of the order of 25%.

Special transforms. The PDDF $p(r)$ or the size distribution function $D(R)$ is related to $I(h)$ by equations (2.6.1.9) or (2.6.1.54), (2.6.1.55). In the special case of particles elongated in one direction (like cylinders), we can combine equations (2.6.1.41) and (2.6.1.43) and obtain

$$I(h) = 2\pi^2 L \int_0^\infty p_c(r) \frac{J_0(hr)}{h}\, \mathrm{d}r. \tag{2.6.1.65}$$

This Hankel transform can be used in the indirect transformation method for the calculation of $\psi_\nu(h)$ in (2.6.1.59). Doing this, we immediately obtain the PDDF of the cross section $p_c(r)$ from the smeared experimental data. It is not necessary to know the length L of the particle if the results are not needed on an absolute scale. For this application, we only need the information that the scatterers are elongated in one direction with a constant cross section. This information can be found from the overall PDDF of the particle or can be *a priori* information from other experiments, like electron microscopy. The estimate for the maximum dimension D_{max} (2.6.1.57) is related to the cross

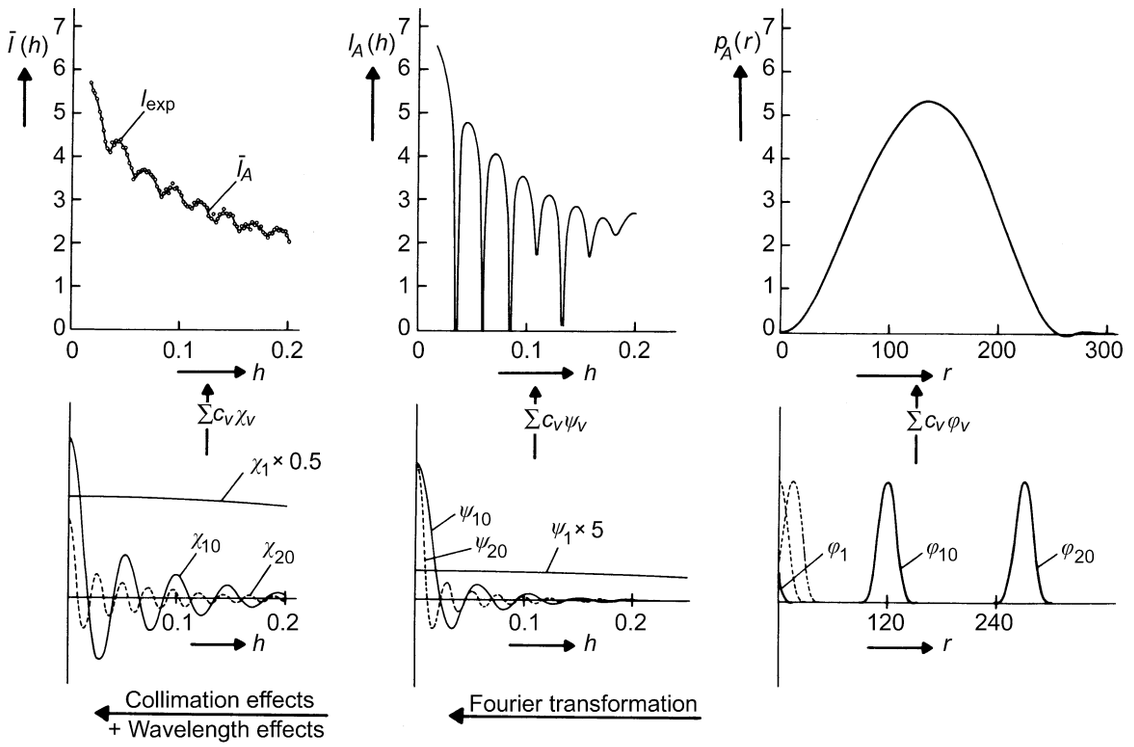

Fig. 2.6.1.14. Function systems $\varphi_\nu(r)$, $\Psi_\nu(h)$, and $\chi_\nu(h)$ used for the approximation of the scattering data in the indirect transformation method.

section in this application, *i.e.* the maximum dimension of the cross section must not be larger than $D_{\max}$.

The situation is quite similar for flat particles. If we combine (2.6.1.47) and (2.6.1.49), we obtain

$$I(h) = 4\pi A \int_0^\infty p_t(r) \frac{\cos(hr)}{h^2}\, \mathrm{d}r, \qquad (2.6.1.66)$$

$p_t(r)$ being the distance distribution function of the thickness. We have to check that the particles are flat with a constant thickness with maximum thickness $T \leq D_{\max}$. A is the area of the particles and would be needed only for experiments on an absolute scale.

2.6.1.6.4. *Direct structure analysis*

It is impossible to determine the three-dimensional structure $\rho(\mathbf{r})$ directly from the one-dimensional information $I(h)$ or $p(r)$. Any direct method needs additional *a priori information* – or assumptions – on the system under investigation. If this information tells us that the structure only depends on one variable, *i.e.* the structure is in a general sense *one dimensional*, we have a good chance of recovering the structure from our scattering data.

Examples for this case are particles with spherical symmetry, *i.e.* ρ depends only on the distance r from the centre, or particles with cylindrical or lamellar symmetry where ρ depends only on the distance from the cylinder axis or from the distance from the central plane in the lamella. We will restrict our discussion here to the spherical problem but we keep in mind that similar methods exist for the cylindrical and the lamellar case.

Spherical symmetry. This case is described by equations (2.6.1.51) and (2.6.1.52). As already mentioned in §2.6.1.3.2.2, we can solve the problem of the calculation of $\rho(r)$ from $I(h)$ in two different ways. We can calculate $\rho(r)$ *via* the distance distribution function $p(r)$ with a *convolution square-root* technique (Glatter, 1981; Glatter & Hainisch, 1984). The other way goes through the amplitude function $A(h)$ and its Fourier transform. In this case, one has to find the right phases (signs) in the square-root operation $\{A(h) = \pm[I(h)^{1/2}]\}$.The *box-function refinement* method by Svergun, Feigin & Schedrin (1984) is an iterative technique for the solution of the phase problem using the *a priori* information that $\rho(r)$ is equal to zero for $r \geq R_{\max}$ ($D_{\max}/2$). The same restriction is used in the convolution square-root technique. Under ideal conditions (perfect spherical symmetry), both methods give good results. In the case of deviations from spherical symmetry, one obtains better results with the convolution square-root technique (Glatter, 1988). With this method, the results are less distorted by non-spherical contributions.

Multipole expansions. A wide class of homogeneous particles can be represented by a boundary function that can be expanded into a series of spherical harmonics. The coefficients are related to the coefficients of a power series of the scattering function $I(h)$, which are connected with the moments of the PDDF (Stuhrmann, 1970*b*,*c*; Stuhrmann, Koch, Parfait, Haas, Ibel & Crichton, 1977). Of course, this expansion cannot be unique, *i.e.* for a certain scattering function $I(h)$ one can find a large variety of possible expansion coefficients and shapes. In any case, additional *a priori* information is necessary to reduce this number, which in turn influences the convergence of the expansion. Only compact, globular structures can be approximated with a small number of coefficients.

This concept is not restricted to the determination of the shape of the particles. Even inhomogeneous particles can be described using all possible radial terms in a general expansion (Stuhrmann, 1970*a*). The information content can be increased by contrast variation (Stuhrmann, 1982), but in any event one is left with the problem of how to find additional *a priori* information in order to reduce the possible structures. Any type of symmetry will lead to a considerable improvement. The case of axial symmetry is a good example. Svergun, Feigin & Schedrin (1982) have shown that the quality of the results can be further improved when upper and lower limits for $\rho(\mathbf{r})$ can be used. Such limits can come from a known chemical composition.

2.6.1.6.5. *Interpretation of results*

After having used all possible data-evaluation techniques, we end up with a desmeared scattering function $I(h)$, the PDDF $p(r)$ or the size-distribution function $D(R)$, and some special functions discussed in the previous subsections. Together with the particle parameters, we have a data set that can give us at least a rough classification of the substance under investigation.

The interpretation can be performed in reciprocal space (scattering function) or in real space (PDDF *etc*.). Any symmetry can be detected more easily in reciprocal space, but all other structural information can be found more easily in real space (Glatter, 1979, 1982*b*).

When a certain structure is estimated from the data and from *a priori* information, one has to test the corresponding model. That means one has to find the PDDF and $I(h)$ for the model and has to compare it with the experimental data. Every model that fits within the experimental errors can be true, all that do not fit have to be rejected. If the model does not fit, it has to be refined by trial and error. In most cases, this process is much easier in real space than in reciprocal space. Finally, we may end up with a set of possible structures that can be correct. Additional *a priori* information will be necessary to reduce this number.

2.6.1.7. *Simulations and model calculations*

2.6.1.7.1. *Simulations*

Simulations can help to find the limits of the method and to estimate the systematic errors introduced by the data-evaluation procedure. Simulations are performed with exactly known model systems (test functions). These systems should be similar to the structures of interest. The model data are transformed according to the special experimental situation (collimation profiles and wavelength distribution) starting from the theoretical PDDF (or scattering function). '*Experimental data points*' are generated by sampling in a limited h range and adding statistical noise from a random-number generator. If necessary, a certain amount of background scattering can also be added. This simulated data set is subjected to the data-evaluation procedure and the result is compared with the starting function. Such simulation can reveal the influence of each approximation applied in the various evaluation routines.

On the other hand, simulations can also be used for the optimization of the experimental design for a special application. The experiment situation is characterized by several contradictory effects: a large width for the functions $P(t)$, $Q(x)$, and $W(\lambda')$ leads to a high statistical accuracy but considerable smearing effects. The quality of the results of the desmearing procedure is increased by high statistical accuracy, but decreased by large smearing effects. Simulations can help to find the optimum for a special application.

2.6.1.7.2. *Model calculation*

In the section on data evaluation and interpretation, we have seen that we obtain a rough estimate for the structure of the particles under investigation directly from the experimental data. For further refinement, we have to compare our results with scattering functions or PDDF's from models

2.6.1.7.3. *Calculation of scattering intensities*

The scattering curves can be calculated semi-analytically for simple triaxial bodies and for models composed of some of these bodies. The scattering amplitude for regular bodies like ellipsoids, parallelepipeds, and cylinders can be calculated analytically for any orientation. The spatial averaging has to be performed numerically. Such calculations have been performed for a large number of different models by Porod (1948), Mittelbach & Porod (1961*a*,*b*, 1962), and by Mittelbach (1964). More complicated structures can be described by models composed of several such triaxial bodies, but the computing time necessary for such calculations can be hours on a mainframe computer.

Models composed only of spherical subunits can be evaluated with the Debye formula (Debye, 1915):

$$I(h) = i_{\rm el}(h) \sum_{i=1}^{N} \sum_{k=1}^{N} \rho_i V_i \rho_k V_k \Phi_i(h) \Phi_k(h) \frac{\sin(hd_{ik})}{hd_{ik}}, \quad (2.6.1.67)$$

where the spatial average is carried out analytically. Another possibility would be to use spherical harmonics as discussed in the previous section but the problem is how to find the expansion coefficients for a certain given geometrical structure.

2.6.1.7.4. *Method of finite elements*

Models of arbitrary shape can be approximated by a large number of very small homogeneous elements of variable electron density. These elements have to be smaller than the smallest structural detail of interest.

Sphere method. In this method, the elements consist of spheres of equal size. The diameter of these spheres must be chosen independently of the distance between nearest neighbours, in such a way that the total volume of the model is represented correctly by the sum of all volume elements (which corresponds to a slight formal overlap between adjacent spheres). The scattering intensity is calculated using the Debye formula (2.6.1.67), with $\Phi_i(h) = \Phi_k(h) = \Phi(h)$.

The computing time is mainly controlled by the number of mutual distances between the elements. The computing time can be lowered drastically by the use of approximate d_{ik} values in (2.6.1.67). Negligible errors in $I(h)$ result if d_{ik} values are quantized to $D_{\max}/10000$ (Glatter, 1980*c*). For the practical application (input operation), it is important that a certain number of elements can be combined to form so-called substructures that can be used in different positions with arbitrary weights and orientations to build the model.

The sphere method can also be used for the computation of scattering curves for macromolecules from a known crystal structure. The weights of the atoms are given by the effective number of electrons

$$Z_{\rm eff} = Z - \rho_0 V_{\rm eff}, \quad (2.6.1.68)$$

where $V_{\rm eff}$ is the apparent volume of the atom given by Langridge, Marvin, Seeds, Wilson, Cooper, Wilkins & Hamilton (1960).

Cube method. This method has been developed independently by Fedorov, Ptitsyn & Voronin (1972, 1974*a*,*b*) and by Ninio & Luzzati (1972) mainly for the computation of scattered intensities for macromolecules in solution whose crystal structure is known. In the cube method, the macromolecule is mentally placed in a parallelepiped, which is subdivided into small cubes (with edge lengths of 0.5–1.5 Å. Each cube is examined in order to decide whether it belongs to the molecule or to the solvent. Adjacent cubes in the z direction are joined to form parallelepipeds. The total scattering amplitude is the sum over the amplitudes from the parallelepipeds with different positions and lengths. The mathematical background is described by Fedorov, Ptitsyn & Voronin (1974*a*,*b*). The *modified cube method* of Fedorov & Denesyuk (1978) takes into account the possible penetration of the molecule by water molecules.

2.6.1.7.5. *Calculation of distance-distribution functions*

The PDDF can be calculated analytically only for a few simple models (Porod, 1948; Goodisman, 1980); in all other cases, we have to use a finite element method with spheres. It is possible to define an analogous equation to the Debye formula (2.6.1.67) in real space (Glatter, 1980*c*). The PDDF can be expressed as

$$p(r) = \sum_{i=1}^{N} \rho_i^2 p_0(r, R_i) + 2 \sum_{i=1}^{N-1} \sum_{k=i+1}^{N} \rho_i \rho_k p(r, d_{ik}, R_i, R_k). \quad (2.6.1.69)$$

$p_0(r, R_i)$ is the PDDF of a sphere with radius R_i and electron density equal to unity, $p(r, d_{ik}, R_i, R_k)$ is the cross-term distance distribution between the ith and kth spheres (radii R_i and R_k) with a mutal distance d_{ik}.

Equation (2.6.1.69) [and (2.6.1.67)] can be used in two different ways for the calculation of model functions. Sometimes, it is possible to approximate a macromolecule as an aggregate of some spheres of well defined size representing different globular subunits (Pilz, Glatter, Kratky & Moring-Claesson, 1972). The form factors of the subunits are in such cases real parameters of the model. However, in most cases we have no such possibility and we have to use the method of finite elements, *i.e.* we fit our model with a large number of sufficiently small spheres of equal size, and, if necessary, different weight. The form factor of the small spheres is now not a real model parameter and introduces a limit of resolution.

Fourier transformation [equation (2.6.1.10)] can be used for the computation of the PDDF of any arbitrary model if the scattering function of the model is known over a sufficiently large range of h values.

2.6.1.8. *Suggestions for further reading*

Only a few textbooks exist in the field of small-angle scattering. The classic monograph *Small-Angle Scattering of X-rays* by Gunier & Fournet (1955) was followed by the proceedings of the conference at Syracuse University, 1965, edited by Brumberger (1967) and by *Small-Angle X-ray Scattering* edited by Glatter & Kratky (1982). The several sections of this book are written by different authors being experts in the field and representing the state of the art at the beginning of the 1980's. The monograph *Structure Analysis by Small-Angle X-ray and Neutron Scattering* by Feigin & Svergun (1987) combines X-ray and neutron techniques.

2.6.2. Neutron techniques (By R. May)

Symbols used in the text

A	sample area
A_s	inner sample surface
b_i	coherent scattering length of atom i
B_i	spin-dependent scattering length of atom i
C	sample concentration in g l^{-1}
c	volume fraction occupied by matter
d	sample thickness
D	particle dimension
DCD	double-crystal diffractometer
d_0	Bragg spacing
$\mathbf{e}$, $\mathbf{e}_0$	unit vectors along the diffracted and incident beams
$\mathbf{I}$	nuclear spin
IFT	indirect Fourier transformation
N	number of particles in the sample
N_A	Avogadro's number
Q	momentum transfer [$= (4\pi/\lambda)\sin\theta$]
r	radius of a sphere
R_G	radius of gyration
$\mathbf{s}$	neutron spin
SANS	small-angle neutron scattering
SAXS	small-angle X-ray scattering
T	transmission
TOF	time of flight
v	partial specific volume
V_p	particle volume
V_s	sample volume
$\Delta\Omega$	solid angle subtended by a detection element
λ	wavelength
ρ	scattering-length density
2θ	full scattering angle
$\mathrm{d}\sigma(Q)/\mathrm{d}\Omega$	scattering cross section per particle and unit solid angle

2.6.2.1. *Relation of X-ray and neutron small-angle scattering*

X-ray and neutron small-angle scattering (SAXS and SANS, respectively) are dealing with the same family of problems, *i.e.* the investigation of 'inhomogeneities' in matter. These inhomogeneities have dimensions D of the order of 1 to 100 nm, which are larger than interatomic distances, *i.e.* 0.3 nm. The term inhomogeneities may mean clusters in metals, a small concentration of protonated chains in an otherwise identical deuterated polymer – or *vice versa* – but also particles as well defined as purified proteins in aqueous solution.

In most cases, the inhomogeneities are not ordered. This is where small-angle scattering is most useful: many systems are not crystalline, cannot be crystallized, or do not exhibit the same properties if they are. One field, if one may say so, of SANS where samples are ordered is low-resolution crystallography of biological macromolecules. It will not be treated further here. In the case of crystalline order, the scattering of the single particle is observed with an amplification factor of N^2 for N identical particles in the crystal, but only for those scattering vectors observing the Bragg condition $n\lambda = 2d_0\sin\theta$. For disordered, randomly oriented particles, the amplification is only N, and the scattering pattern is lacking all information on particle orientation. Moreover, the real-space information on the internal arrangement of atoms within the inhomogeneities is reduced to the 'distance distribution function', a sine Fourier transform of the scattering intensity.

The mathematical descriptions of SAXS and SANS are either identical or hold with equivalent terms. The reader is referred to Section 2.6.1 on X-ray small-angle scattering techniques for a general description of low-Q scattering. An abundant treatment of SAXS can be found in the book edited by Glatter & Kratky (1982), and in Guinier & Fournet (1955) and Guinier (1968). A general introduction to SANS is given, for example, by Kostorz (1979) and by Hayter (1985). This section deals mainly with the differences between the techniques.

Altogether, neutrons are used for low-Q scattering essentially for the same reasons as for other neutron experiments. These reasons are:

(1) neutrons are sensitive to the isotopic composition of the sample;

(2) neutrons possess a magnetic moment and, therefore, can be used as a magnetic probe of the sample; and

(3) because of their weak interaction with and consequent deep penetration into matter, neutrons allow us to investigate properties of the bulk;

(4) for similar reasons, strong transparent materials are available as sample-environment equipment.

The fact that the kinetic energies of thermal and cold neutrons are comparable to those of excitations in solids, which is a reason for the use of neutrons for inelastic scattering, is, with the exception of time-of-flight SANS (see §2.6.2.1.1), not of importance for SANS.

The information obtained from low-Q scattering is always an average over the irradiated sample volume and over time. This average may be purely static (in the case of solids) or also dynamic (liquids). The limited Q range used does not resolve interatomic scattering contributions. Thus, a 'scattering-length density' ρ can be introduced, $\rho = \sum b_i/V$, where b_i are the (coherent) scattering lengths of the atoms within a volume V with linear dimensions of at least λ/π. Inhomogeneities can then be understood as regions where the scattering-length density deviates from the prevailing average value.

2.6.2.1.1. *Wavelength*

In the case of SANS – as in that of X-rays from synchrotron sources – the wavelength dependence of the momentum transfer Q, $Q = (4\pi/\lambda)\sin\theta$, where θ is half the scattering angle and λ is the wavelength, has to be taken into account explicitly. Q corresponds to k, h, and $2\pi s$ used by other authors.

SANS offers an optimal choice of the wavelength: with sufficiently large wavelengths, for example, first-order Bragg scattering (and therefore the contribution of multiple Bragg scattering to small-angle scattering) can be suppressed: The Bragg condition written as $\lambda/d_{\max} = (2\sin\theta)/n < 2$ cannot hold for $\lambda \geq 2d_{\max}$, where $d_{\max}$ is the largest atomic distance in a crystalline sample. For the usually small scattering angles in SANS, even quite small λ will not produce first-order peaks.

The neutrons produced by the fuel element of a reactor or by a pulsed source are moderated by the (heavy) water surrounding the core. Normally, the neutrons leave the reactor with a thermal velocity distribution. Cold sources, small vessels filled with liquid deuterium in the reactor tank, permit the neutron velocity distribution to be slowed down ('cold' neutrons) and lead to neutron wavelengths (range 0.4 to 2 nm) which are more useful for SANS.

At reactors, a narrow wavelength band is usually selected for SANS either by an artificial-multilayer monochromator or – more frequently, owing to the slow speed of cold neutrons – by a velocity selector. This is a rotating drum with a large number (about 100) of helical slots at its circumference, situated at the entrance of the neutron guides used for collimation. Only neutrons of the suitable velocity are able to pass through this

drum. The wavelength resolution $\Delta\lambda/\lambda$ of velocity selectors is usually between 5 and 40% (full width at half-maximum, FWHM); 10 and 20% are frequently used values.

Alternatively, time-of-flight (TOF) SANS cameras have been developed on pulsed neutron sources (*e.g.* Hjelm, 1988). These use short bunches (about 100 μs long) of neutrons with a 'white' wavelength spectrum produced by a pulsed high-energy proton beam impinging on a target with a repetition rate of the order of 10 ms. The wavelength and, consequently, the Q value of a scattered neutron is determined by its flight time, if the scattering is assumed to be quasi-elastic. The dynamic Q range of TOF SANS instruments is rather large, especially in the high-Q limit, owing to the large number of rapid neutrons in the pulse. The low-Q limit is determined by the pulse-repetition rate of the source because of frame overlap with the following pulse. It can be decreased, if necessary with choppers turning in phase with the pulse production and selecting only every nth pulse. This disadvantage does not exist for reactor-based TOF SANS cameras, where the pulse-repetition rate can be optimally adapted to the chosen maximal and minimal wavelength. A principal problem for TOF SANS exists in the 'upscattering' of cold neutrons, *i.e.* their gain in energy, by ^{1}H-rich samples: The background scattering may not arrive simultaneously with the elastic signal, and may thus not be attributed to the correct Q value (Hjelm, 1988).

2.6.2.1.2. *Geometry*

With typical neutron wavelengths, low Q need not necessarily mean small angles: The interesting Q range for an inhomogeneity of dimension D can be estimated as $1/D < Q < 10/D$. The scattering angle corresponding to the upper Q limit for $D = 10$ nm is 1.4° for Cu $K\alpha$ radiation, but amounts to 9.1° for neutrons of 10 nm wavelength. Consequently, it is preferable to speak of low-Q rather than of small-angle neutron scattering.

'Pin-hole'-type cameras are the most frequently used SANS instruments; an example is the SANS camera D11 at the Institut Max von Laue–Paul Langevin in Grenoble, France (Ibel, 1976; Lindner, May & Timmins, 1992), from which some of the numbers below are quoted. Since the cross section of the primary beam is usually chosen to be rather large (*e.g.* 3×5 cm) for intensity reasons, pin-hole instruments tend to be large. The smallest Q value that can be measured at a given distance is just outside the image of the direct beam on the detector (which either has to be attenuated or is hidden behind a beamstop, a neutron-absorbing plate of several 10 cm^2, *e.g.* of cadmium). Very small Q values thus require long sample-to-detector distances. The area detector of D11, with a surface of 64×64 cm and resolution elements of 1 cm^2, moves within an evacuated tube of 1.6 m diameter and a length of 40 m. Thus, a Q range of 5×10^{-3} to 5 nm^{-1} is covered. The geometrical resolution is determined by the length of the free neutron flight path in front of the sample, moving sections of neutron guide into or out of the beam ('collimation'). In general, the collimation length is chosen roughly equal to the sample-to-detector distance. Thus, the geometrical and wavelength contributions to the Q resolution match at a certain distance of the scattered beam from the direct-beam position in the detector plane. In order to resolve scattering patterns with very detailed features, *e.g.* of particles with high symmetry, longer collimation lengths are sometimes required at the expense of intensity.

Much more compact double-crystal neutron diffractometers [described for X-rays by Bonse & Hart (1966)] are being used to reach the very small Q values of some 10^{-4} nm^{-1} typical of static light scattering. The sample is placed between two crystals. The first crystal defines the wavelength and the direction of the incoming beam. The other crystal scans the scattered intensity. The resolution of such an instrument is mainly determined by the Darwin widths of the ideal crystals. This fact is reflected in the low neutron yield. Slit geometry can be used, but not 2D detectors.

A recent development is the ellipsoidal-mirror SANS camera. The mirror, which needs to be of very high surface quality, focuses the divergent beam from a small (several mm^2) source through the sample onto a detector with a resolution of the order of 1×1 mm. Owing to the more compact beam image, all other dimensions of the SANS camera can be reduced drastically (Alefeld, Schwahn & Springer, 1989). Whether or not there is a gain in intensity as compared with pin-hole geometry is strongly determined by the maximal sample dimensions. Long mirror with cameras (*e.g.* 20 m) are always superior to double-crystal instruments in this respect (Alefeld, Schwahn & Springer, 1989), and can also reach the light-scattering Q domain ($Q_{\min}$ of some 10^{-4} nm^{-1}, corresponding to particles of several μm dimension).

2.6.2.1.3. *Correction of wavelength, slit, and detector-element effects*

Resolution errors affect SANS data in the same way as X-ray scattering data, for which one may find a detailed treatment in an article by Glatter (1982*b*); there is one exception to this; namely, gravity, which of course only concerns neutron scattering, and only in rare cases (Boothroyd, 1989). Since SANS cameras usually work with pin-hole geometry, the influences of the slit sizes, *i.e.* the effective source dimensions, on the scattering pattern are small; even less important is, in general, the pixel size of 2D detectors. The preponderant contribution to the resolution of the neutron-scattering pattern is the wavelength-distribution function after the monochromatizing device, especially at larger angles. The situation is more complicated for TOF SANS (Hjelm, 1988).

As has been shown in an analytical treatment of the resolution function by Pedersen, Posselt & Mortensen (1990), who also quote some relevant references, resolution effects have a small influence on the results of the data analysis for scattering patterns with a smooth intensity variation and without sharp features. Therefore, one may assume that a majority of SANS patterns are not subjected to desmearing procedures.

Resolution has to be considered for scattering patterns with distinct features, as from spherical latex particles (Wignall, Christen & Ramakrishnan, 1988) or from viruses (Cusack, 1984). Size-distribution and wavelength-smearing effects are similar; it is evident that wavelength effects have to be corrected for if the size distribution is to be obtained.

Since measured scattering curves contain errors and have to be smoothed before they can be desmeared, iterative indirect methods are, in general, superior: A guessed solution of the scattering curve is convoluted with known smearing parameters and iteratively fitted to the data by a least-squares procedure. The guessed solution can be a simply parameterized scattering curve, without knowledge of the sample (Schelten & Hossfeld, 1971), but it is of more interest to fit the smeared Fourier transform of the distance-distribution function (Glatter, 1979) or the radial density distribution (*e.g.* Cusack, Mellema, Krijgsman & Miller, 1981) of a real-space model to the data.

2.6.2.2. *Isotopic composition of the sample*

Unlike X-rays, which 'see' the electron clouds of atoms within a sample, neutrons interact with the point-like nuclei. Since their

form factor does not decay like the atomic form factor, an isotropic background from the nuclei is present in all SANS measurements.

While X-ray scattering amplitudes increase regularly with the atomic number, neutron coherent-scattering amplitudes that give rise to the interference scattering necessary for structural investigations vary irregularly (see Bacon, 1975). Isotopes of the same element often have considerably different amplitudes owing to their different resonant scattering. The most prominent example of this is the difference of the two stable isotopes of hydrogen, ^{1}H and ^{2}H (deuterium). The coherent-scattering length of ^{2}H is positive and of similar value to that of most other elements in organic matter, whereas that of ^{1}H is negative, *i.e.* for ^{1}H there is a 180° phase shift of the scattered neutrons with respect to other nuclei.

This latter difference has been exploited vastly in the fields of polymer science (*e.g.* Wignall, 1987) and structural molecular biology (*e.g.* Timmins & Zaccai, 1988), in mainly two complementary respects, contrast variation and specific isotopic labelling.

In the metallurgy field, other isotopes are being used frequently for similar purposes, for example the nickel isotope ^{62}Ni, which has a negative scattering length, and the silver isotopes ^{107}Ag and ^{109}Ag (see the review of Kostorz, 1988).

2.6.2.2.1. *Contrast variation*

The easiest way of using the scattering-amplitude difference between ^{1}H and ^{2}H is the so-called contrast variation. It was introduced into SANS by Ibel & Stuhrmann (1975) on the basis of X-ray crystallographic (Bragg & Perutz, 1952), SAXS (Stuhrmann & Kirste, 1965), and light-scattering (Benoit & Wippler, 1960) work. Most frequently, contrast variation is carried out with mixtures of light (^1H_2O) and heavy water (^2H_2O), but also with other solvents available in protonated and deuterated form (ethanol, cyclohexane, *etc.*). The scattering-length density of H_2O varies between -0.562×10^{10} cm^{-2} for normal water, which is nearly pure ^1H_2O, and 6.404×10^{10} cm^{-2} for pure heavy water.

The scattering-length densities of other molecules, in general, are different from each other and from pure protonated and deuterated solvents and can be matched by ^{1}H/^{2}H mixture ratios characteristic for their chemical compositions. This mixture ratio (or the corresponding absolute scattering-length density) is called the scattering-length-density match point, or, semantically incorrect, contrast match point. If a molecule contains non-covalently bound hydrogens, they can be exchanged for solvent hydrogens. This exchange is proportional to the ratio of all labile ^{1}H and ^{2}H present; in dilute aqueous solutions, it is dominated by the solvent hydrogens. A plot of the scattering-length density *versus* the ^{2}H/(^{2}H+^{1}H) ratio in the solvent shows a linear increase if there is exchange; the value of the match point also depends on solvent exchange. The fact that many particles have high contrast with respect to ^2H_2O makes neutrons superior to X-rays for studying small particles at low concentrations.

The scattered neutron intensity from N identical particles without long-range interactions in a (very) dilute solution with solvent scattering density ρ_s can be written as

$$I(Q) = [\mathrm{d}\sigma(Q)/\mathrm{d}\Omega]NTAI_0\Delta\Omega, \qquad (2.6.2.1)$$

with the scattering cross section per particle and unit solid angle

$$\mathrm{d}\sigma(Q)/\mathrm{d}\Omega = \left\langle \left| \int [\rho(\mathbf{r}) - \rho_s] \exp(i\mathbf{Q}\cdot\mathbf{r})\, \mathrm{d}\mathbf{r} \right|^2 \right\rangle. \qquad (2.6.2.1a)$$

The angle brackets indicate averaging over all particle orientations. With $\rho(r) = \sum b_i/V_p$ and $I(0) = \text{constant} \times \left\langle \left| \int [\rho(\mathbf{r}) - \rho_s]\, \mathrm{d}\mathbf{r} \right|^2 \right\rangle$, we find that the scattering intensity at zero angle is proportional to

$$\Delta\rho = \sum b_i/V_p - \rho_s, \qquad (2.6.2.2)$$

which is called the contrast. The exact meaning of V_p is discussed, for example, by Zaccai & Jacrot (1983), and for X-rays by Luzzati, Tardieu, Mateu & Stuhrmann (1976).

The scattering-length density $\rho(\mathbf{r})$ can be written as a sum

$$\rho(\mathbf{r}) = \rho_0 + \rho_F(\mathbf{r}), \qquad (2.6.2.3)$$

where ρ_0 is the average scattering-length density of the particle at zero contrast, $\Delta\rho = 0$, and $\rho_F(\mathbf{r})$ describes the fluctuations about this mean. $I(Q)$ can then be written

$$I(Q) = (\rho_0 - \rho_2)^2 I_c(Q) + (\rho_0 - \rho_s) I_{cs}(Q) + I_s(Q). \qquad (2.6.2.4)$$

I_s is the scattering intensity due to the fluctuations at zero contrast. The cross term $I_{cs}(Q)$ also has to take account of solvent-exchange phenomena in the widest sense (including solvent water molecules bound to the particle surface, which can have a density different from that of bulk water). This extension is mathematically correct, since one can assume that solvent exchange is proportional to $\Delta\rho$. The term I_c is due to the invariant volume inside which the scattering density is independent of the solvent (Luzzati, Tardieu, Mateu & Stuhrmann, 1976). This is usually not the scattering of a homogeneous particle at infinte contrast, if the exchange is not uniform over the whole particle volume, as is often the case, or if the particle can be imaged as a sponge (see Witz, 1983).

The method is still very valuable, since it allows calculation of the scattering at any given contrast on the basis of at least three measurements at well chosen ^{1}H/^{2}H ratios (including data near, but preferentially not exactly at, the lowest contrasts). It is sometimes limited by ^{2}H-dependent aggregation effects.

2.6.2.2.2. *Specific isotopic labelling*

Specific isotope labelling is a method that has created unique applications of SANS, especially in the polymer field. Again, it is mainly concerned with the exchange of ^{1}H by ^{2}H, this time in the particles to be studied themselves, at hydrogen positions that are not affected by exchange with solvent atoms, for example carbon-bound hydrogen sites.

With this technique, isolated polymer chains can be studied in the environment of other polymer chains which are identical except for the hydrogen atoms, which are either ^{1}H or ^{2}H. Even if some care has to be taken as far as slightly modified thermodynamics are concerned, there is no other method that could replace neutrons in this field.

Inverse contrast variation forms an intermediate between the two methods described above. The contrast with respect to the solvent of a whole particle or of well defined components of a particle, for example a macromolecular complex, is changed by varying its degree of deuteration. That of the solvent remains constant. Since solvent-exchange effects remain practically identical for all samples, the measurements can be more precise than in the classical contrast variation (Knoll, Schmidt & Ibel, 1985).

2.6.2.3. *Magnetic properties of the neutron*

Since the neutron possesses a magnetic moment, it is sensitive to the orientation of spins in the sample [see, for example, Abragam *et al.* (1982)]. Especially in the absence of any other (isotopic) contrast, an inhomogeneous distribution of spins in the

sample is detectable by neutron low-Q scattering. The neutron spins need not be oriented themselves, although important contributions can be expected from measuring the difference between the scattering of neutron beams with opposite spin orientation. At present, several low-Q instruments are being planned or even built including neutron polarization and polarization analysis.

Studies of magnetic SANS without (and rarely with) neutron polarization include dislocations in magnetic crystals and amorphous ferromagnets [see the review of Kostorz (1988)].

Janot & George (1985) have pointed out that it is important to apply contrast variation for suppressing surface-roughness scattering and/or volume scattering in order to isolate magnetic scattering contributions by matching the scattering-length density of the material with that of a mixture of heavy and light water or oil, *etc*.

2.6.2.3.1. *Spin-contrast variation*

For a long time, the magnetic properties of the neutron have been neglected as far as 'nonmagnetic' matter is concerned. Spin-contrast variation, proposed by Stuhrmann (Stuhrmann *et al.*, 1986; Knop *et al.*, 1986), takes advantage of the different scattering lengths of the hydrogen atoms in its spin-up and spin-down states. Normally, these two states are mixed, and the cross section of unpolarized neutrons with the undirected spins gives rise to the usual value of the scattering amplitude of hydrogen. If, however, one is able to orient the spins of a given atom, and especially hydrogen, then the interaction of *polarized* neutrons with the two different oriented states offers an important contribution to the scattering amplitude:

$$A = b + 2B\mathbf{I} \cdot \mathbf{s}, \qquad (2.6.2.5)$$

where b is the isotropic nuclear scattering amplitude, B is the spin-dependent scattering amplitude, $\mathbf{s}$ is the neutron spin, and $\mathbf{I}$ the nuclear spin. For hydrogen, $b = -0.374 \times 10^{-12}$ cm, $B = 2.9 \times 10^{-12}$ cm.

The sample protons are polarized at very low temperatures (order of mK) and high magnetic fields (several tesla) by dynamic nuclear polarization, *i.e.* by spin–spin coupling with the electron spins of a paramagnetic metallo-organic compound present in the sample, which are polarized by a resonant microwave frequency. It is clear that the principles mentioned above also apply to other than biological and chemical material.

2.6.2.4. *Long wavelengths*

An important aspect of neutron scattering is the ease of using long wavelengths: Long-wavelength X-rays are produced efficiently only by synchrotrons, and therefore their cost is similar to that of neutrons. Unlike neutrons, however, they suffer from their strong interaction with matter. This disadvantage, which is acceptable with the commonly used Cu $K\alpha$ radiation, is in most cases prohibitive for wavelengths of the order of 1 nm.

Very low Q values are more easily obtained with long wavelengths than with very small angles, as is necessary with X-rays, since the same Q value can be observed further away from the direct beam. Objects of linear dimensions of several 100 nm, *e.g.* opals, where spherical particles of amorphous silica form a close-packed lattice with cell dimensions of up to several hundreds of nm, can still be investigated easily with neutrons. X-ray double-crystal diffractometers (Bonse & Hart, 1966), which may also reach very low Q, are subject to transmission problems, and neutron DCD's again perform better.

2.6.2.5. *Sample environment*

Important new fields of low-Q scattering, such as dynamic studies of polymers in a shear gradient and time-resolved studies of samples under periodic stress or under high pressure, have become accessible by neutron scattering because the weak interaction of neutrons with (homogeneous) matter permits the use of relatively thick (several mm) sample container walls, for example of cryostats, Couette-type shearing apparatus (Lindner & Oberthür, 1985, 1988), and ovens. Air scattering is not prohibitive, and easy-to-handle standard quartz cells serve as sample containers rather than very thin ones with mica windows in the case of X-rays.

Unlike with X-rays, samples can be relatively thick, and nevertheless be studied to low Q values. This is particularly evident for metals, where X-rays are usually restricted to thin foils, but neutrons can easily accept samples 1–10 mm thick.

2.6.2.6. *Incoherent scattering*

Incoherent scattering is produced by the interaction of neutrons with nuclei that are not in a fixed phase relation with that of other nuclei. It arises, for example, when molecules do not all contain the same isotope of an element (isotopic incoherent scattering). The most important source of incoherent scattering in SANS, however, is the spin-incoherent scattering from protons. It results from the fact that only protons and neutrons with identical spin directions can form an intermediate compound nucleus. The statistical probabilities of the parallel and antiparallel spin orientations, the similarity in size of the scattering lengths for spin up and spin down and their opposite sign result in an extremely large incoherent scattering cross section for ^{1}H, together with a coherent cross section of normal magnitude (but negative sign). Incoherent scattering contributes a background that can be by orders of magnitude more important than the coherent signal, especially at larger Q. On the other hand, it can be used for the calibration of the incoming intensity and of the detector efficiency (see below).

2.6.2.6.1. *Absolute scaling*

Wignall & Bates (1987) compare many different methods of absolute calibration of SANS data. Since the scattering from a thin water sample is frequently already being used for correcting the detector response [see §2.6.2.6.2], there is an evident advantage for performing the absolute calibration by H_2O scattering.

For a purely isotropic scatterer, the intensity scattered into a detector element of surface ΔA spanning a solid angle $\delta\Omega = \Delta A/4\pi L^2$ can be expressed as

$$\Delta I = I_0(1 - T_i)\delta\Omega g/4\pi, \qquad (2.6.2.6)$$

with T_i the transmission of the isotropic scatterer, *i.e.* the relation of the number of neutrons in the primary beam measured within a time interval Δt after having passed through the sample, I_{Tr}, and the number of neutrons I_0 observed within Δt without the sample. In practice, T_i is measured with an attenuated beam; typical attenuation factors are about 100 to 1000. g is a geometrical factor taking into account the sample surface and the solid angle subtended by the apparent source, *i.e.* the cross section of the neutron guide exit.

Vanadium is an incoherent scatterer frequently used for absolute scaling. Its scattering cross section, however, is more than an order of magnitude lower than that of protons. Moreover, the surface of vanadium samples has to be handled with much care in order to avoid important contributions from

surface scattering by scratches. The vanadium sample has to be hermetically sealed to prevent hydrogen incorporation (Wignall & Bates, 1987).

The coherent cross sections of the two protons and one oxygen in light water add up to a nearly vanishing *coherent*-scattering-length density, whereas the incoherent scattering length of the water molecule remains very high. The (quasi)isotropic incoherent scattering from a thin, *i.e.* about 1 mm or less, sample of ^1H_2O, therefore, is an ideal means for determining the absolute intensity of the sample scattering (Jacrot, 1976; Stuhrmann *et al.*, 1976), on condition that the sample-to-detector distance L is not too large, *i.e.* up to about 10 m. A function $f(\sigma_t[H_2O], \lambda)$ that accounts for deviations from the isotropic behaviour due to inelastic incoherent-scattering contributions of ^1H_2O and for the influence of the wavelength dependence of the detector response has to be multiplied to the right-hand side of equation (2.6.2.6) (May, Ibel & Haas, 1982). f can be determined experimentally and takes values of around 1 for wavelengths around 1 nm.

Since the intensity scattered into a solid angle $\Delta\Omega$ is

$$I(Q) = P(Q)NT_sI_0g\left(\sum b_i - \rho_sV\right)^2, \qquad (2.6.2.7)$$

where $P(Q)$ is the form factor of the scattering of one particle, and the geometrical factor g can be chosen so that it is the same as that of equation (2.6.2.6) (same sample thickness and surface and identical collimation conditions), we obtain

$$I(Q) = 4\pi P(Q)NT_sf(\sigma_t[H_2O], \lambda)\left(\sum b_i - \rho_sV\right)^2/(1 - T[H_2O]). \qquad (2.6.2.8)$$

Note that the scattering intensities mentioned above are scattering intensities corrected for container scattering, electronic and neutron background noise, and, in the case of the sample, for the solvent scattering.

2.6.2.6.2. *Detector-response correction*

For geometrical reasons (*e.g.* sample absorption), and in the case of 2D detectors also for electronic reasons, the scattering curves cannot be measured with a sensitivity uniform over all the angular region. Therefore, the scattering curve has to be corrected by that of a sample with identical geometrical properties, but scattering the neutrons with the same probability into all angles (at least in the forward direction). As we have seen previously, such samples are vanadium and thin cells filled with light water. Again, water has the advantage of a much higher scattering cross section, and is less influenced by surface effects.

At large sample-to-detector distances (more than about 10 m), the scattering from water is not sufficiently strong to enable its use for correcting sample scattering curves obtained with the same settings. Experience shows that it is possible in this case to use a water scattering curve measured at a shorter sample-to-detector distance. This should be sufficiently large not to be influenced by the deviation of the (flat) detector surface from the spherical shape of the scattered waves and small enough so that the scattering intensity per detector element is still sufficient, for example about 3 m. It is necessary to know the intensity loss factor due to the different solid angles covered by the detector element and by the apparent source in both cases. This can be determined, for instance, by comparing the global scattering intensity of water on the whole detector for both conditions (after correction for the background scattering) or from the intensity shift of the same sample measured at both detector distances in a plot of the logarithm of the intensity *versus* Q.

2.6.2.6.3. *Estimation of the incoherent scattering level*

For an exact knowledge of the scattering curve, it is necessary to subtract the level of incoherent scattering from the scattering curve, which is initially a superposition of the (desired) coherent sample scattering, electronic and neutron background noise, and (sometimes dominant) incoherent scattering.

A frequently used technique is the subtraction of a reference sample that has the same level of incoherent scattering, but lacks the coherent scattering from the inhomogeneities under study. Although this seems simple in the case of solutions, in practice there are problems: Very often, the $^1H/^2H$ mixture is made by dialysis, and the last dialysis solution is taken as the reference. The dialysis has to be excessive to obtain really identical levels of ^1H, and in reality there is often a disagreement that is more important the lower the sample concentration is. If the concentration is high, then the incoherent scattering from the sample atoms (protons) themselves becomes important.

For dilute aqueous solutions, there is a procedure using the sample and reference transmissions for estimating the incoherent background level (May, Ibel & Haas, 1982): The incoherent scattering level from the sample, $I_{i,s}$, can be estimated as

$$I_{i,s} = I[H_2O]f_\lambda(1 - T_s)/(1 - T[H_2O]), \qquad (2.6.2.9)$$

where $I[H_2O]$ is the scattering from a water sample, $T[H_2O]$ is transmission, T_s that of the sample. f_λ is a factor depending on the wavelength, the detector sensibility, the solvent composition, and the sample thickness; it can be determined experimentally by plotting $I_{i,s}/I[H_2O]$ *versus* $(1 - T_s)/(1 - T[H_2O])$ for a number of partially deuterated solvent mixtures.

This procedure is justified because of the overwhelming contribution of the incoherent scattering of ^1H to the macroscopic scattering cross section of the solution, and therefore to its transmission. The procedure should also be valid for organic solvents. The precision of the estimation is limited by the precision of the transmission measurement, the relative error of which can hardly be much better than about 0.005 for reasonable measuring times and currently available equipment, and by the (usually small) contribution of the coherent cross section to the total cross section of the solution. A modified version of (2.6.2.9) can be used if a solvent with a transmission close to that of a sample has been measured, but the factor f_λ should not be omitted.

An equation similar to (2.6.2.9) holds for systems with a larger volume occupation c of particles in a (protonated) solvent with a scattering level $I_{\rm inc}$ in a cell with identical pathway (without the particles):

$$I_{i,s} = I_{\rm inc}(1 - T_{\rm inc}^{1-c})/(1 - T_{\rm inc}). \qquad (2.6.2.9a)$$

In this approximation, the particles' cross-section contribution is assumed to be zero, *i.e.* the particles are considered as bubbles.

In the case of dilute systems of monodisperse particles, the residual background (after initial corrections) can be quite well estimated from the zero-distance value of the distance-distribution function calculated by the indirect Fourier transformation of Glatter (1979).

2.6.2.6.4. *Inner surface area*

According to Porod (1951, 1982), small-angle scattering curves behave asymptotically like $I(Q) = \text{constant} \times A_sQ^{-4}$ for large Q, where A_s is the inner surface of the sample. Theoretically, fitting a straight line to $I(Q)Q^4$ *versus* Q^4 ('Porod plot') *at sufficiently large* Q therefore yields a zero intercept, which is proportional to the internal surface; a slope

can be interpreted as a residual constant background (including the self-term of the constant nuclear 'form factor'), which may be used for slightly correcting the estimated background and consequently improving the quality of the data. For monodispersed particles, a particle surface can be deduced from the overall surface. The value of the surface area so determined depends on the maximal Q to which the scattering curve can be obtained with good statistics. This depends also on the magnitude of the background. At least for weakly scattering particles in mixtures of ^1H_2O and ^2H_2O, and even more in pure ^1H_2O, the incoherent background level often cannot be determined precisely enough for interpreting the tail of the scattering curve in terms of the surface area.

2.6.2.7. *Single-particle scattering*

Single-particle scattering in this context means scattering from isolated structures (clusters in alloys, isolated polymer chains in a solvent, biological macromolecules, *etc*.) randomly distributed in space and sufficiently far away from each other so that interparticle contributions to the scattering (see Subsection 2.6.2.8) can be neglected. The tendency of polymerization of single particles, for example the monomer–dimer equilibrium of proteins or the formation of higher aggregates, and long-range (*e.g.* electrostatic) interactions between the particles disturb single-particle scattering. In the absence of such effects, samples with solute volume fractions below about 1% can be regarded as free of volume-exclusion interparticle effects for most purposes. For (monodispersed) protein samples, for example, this means that concentrations of about $5\,\mathrm{mg\,ml^{-1}}$ are often a good compromise between sufficient scattering intensity and concentration effects. In many cases, series of scattering measurements with increasing particle concentrations have been used for extrapolating the scattering to zero concentration. In the following, we assume that particle interactions are absent.

2.6.2.7.1. *Particle shape*

All X-ray and neutron small-angle scattering curves can be approximated by a parabolic fit in a narrow Q range near $Q = 0$ (Porod, 1951): $I(Q) \simeq I(0)\ (1 - a^2Q^2/3 + \ldots)$. In the case of single-particle scattering, a Gaussian approximation to the scattering curve is even more precise (Guinier & Fournet, 1955) in the zero-angle limit:

$$I(Q) \simeq I(0)\exp(-Q^2/3R_G^2), \qquad (2.6.2.10)$$

where R_G is the radius of gyration of the particle's excess scattering density.

The concept of R_G and the validity of the Guinier approximation is discussed in more detail in the SAXS section of this volume (§2.6.1). It might be mentioned here that the frequently used $QR_G < 1$ rule for the validity of the Guinier approximation is no more than an indication and should always be tested by a scattering calculation with the model obtained from the experiment: Spheres yield a deviation of 5% of the Gaussian approximation at $QR_G = 1.3$, rods at $QR_G = 0.6$; ellipsoids of revolution with an elongation factor of 2 can reach as far as $QR_G = 3$.

More detailed shape information requires a wider Q range. As indicated before, Fourier transforms may help to distinguish between conflicting models. In many instances (*e.g.* hollow bodies, cylinders), it is much easier to find the shape of the scattering particle from the distance distribution function than from the scattering curve [see §2.6.2.7.3].

2.6.2.7.2. *Particle mass*

With $N = CN_AV_s/M_r$, where N_A is Avogadro's number, C is the mass concentration of the solute in $\mathrm{g\,l^{-1}}$, and V_s is the sample volume in $\mathrm{cm^{-3}}$ (we assume N identical particles randomly distributed in dilute solution), we find that the relative molecular mass M_r of a particle can be determined from the intensity at zero angle, $I(0)$ in equation (2.6.2.10), using the relation (Jacrot & Zaccai, 1981), where the particle mass concentration C (in $\mathrm{mg\,ml^{-1}}$) is omitted:

$$I(0)/\{CI[\mathrm{H_2O}](0)\} = 4\pi f\, T_sM_rN_Ad_s\, 10^{-3}\left[\left(\sum b_i - \rho_sV\right)/M_r\right]^2/(1 - T[\mathrm{H_2O}]). \qquad (2.6.2.11)$$

d_s is the sample thickness. Note that $\sum b_i/M_r$ may depend on solvent exchange; in a given solvent, especially ^1H_2O, it is rather independent of the exact amino acid composition of proteins (Jacrot & Zaccai, 1981).

An alternative presentation of equation (2.6.2.11) is

$$I(0)/\{CI[\mathrm{H_2O}](0)\} = 4\pi f\, T_sM_rd_s\ 10^{-3}(v\Delta\rho)^2/N_A(1 - T[\mathrm{H_2O}]), \qquad (2.6.2.11a)$$

where $\Delta\rho = \rho_p(\rho_s) - \rho_s$ is the contrast; ρ_p is the particle scattering-length density (depending on the scattering-length density ρ_s of the solvent, in general) and v is the partial specific volume of the particle. Expression (2.6.2.11*a*) is of advantage when $(v\Delta\rho)$, which is a linear function of ρ_s, is known for a class of particles.

A thermodynamic approach to the particle-size problem, in view of the complementarity of different methods, has been given Zaccai, Wachtel & Eisenberg (1986) on the basis of the theory of Eisenberg (1981). It permits the determination of the molecular mass, of the hydration, and of the amount of bound salts.

2.6.2.7.3. *Real-space considerations*

The scattering from a large number of randomly oriented particles at infinite dilution, and as a first approximation that of particles at sufficiently high dilution (see above), is completely determined by a function $p(r)$ in real space, the distance-distribution function. It describes the probability p of finding a given distance r between any two volume elements within the particle, weighted with the product of the scattering-length densities of the two volume elements.

Theoretically, $p(r)$ can be obtained by an infinite sine Fourier transform of the isolated-particle scattering curve

$$I(Q) = \int_0^\infty [p(r)/Qr]\sin(Qr)\,\mathrm{d}r. \qquad (2.6.2.12)$$

In practice, the scattering curve can be measured neither to $Q = 0$ (but an extrapolation is possible to this limit), nor to $Q \to \infty$. In fact, neutrons allow us to measure more easily the sample scattering in the range near $Q = 0$; X-rays are superior for large Q values. Indirect iterative methods have been developed that fit the finite Fourier transform

$$I(Q) = \int_0^{D_{\max}} [p(r)/Qr]\sin(Qr)\,\mathrm{d}r \qquad (2.6.2.12a)$$

of a $p(r)$ function described by a limited number of parameters between $r = 0$ and a maximal chord length $D_{\max}$ within the particle to the experimental scattering curve. It differs from the $p(r)$ of Section 2.6.1 by a factor of 4π.

This procedure was termed the 'indirect Fourier transformation (IFT)' method by Glatter (1979), who uses equidistant B splines in real space that are correlated by a Lagrange parameter, thus reducing the number of independent parameters to be fitted. Errors in determining a residual flat background only affect the innermost spline at $r = 0$; the intensity at $Q = 0$ and the radius of gyration are not influenced by a (small) flat background.

Another IFT method was introduced by Moore (1980), who uses an orthogonal set of sine functions in real space. This procedure is more sensitive to the correct choice of $D_{\max}$ and to a residual background that might be present in the data.

A major advantage of IFT is the ease with which the deconvolution of the scattering intensities with respect to the wavelength distribution and to geometrical smearing due to the primary beam and sample sizes is calculated by smearing the theoretical scattering curve obtained from the real-space model. In fact, it is possible to convolute the scattering curves obtained from the single splines that are calculated only once at the beginning of the fit procedure. The convoluted constituent curves are then iteratively fitted to the experimental scattering curves.

With the exception of particle symmetry, which is better seen in the scattering curve, structural features are more easily recognized in the $p(r)$ function (Glatter, 1982*a*).

Once the $p(r)$ function is determined, the zero-angle intensity and the radius of gyration can be calculated from its integral and from its second moment, respectively.

2.6.2.7.4. *Particle-size distribution*

Indirect Fourier transformation also facilitates the evaluation of particle-size distributions on the assumption that all particles have the same shape and that the size distribution depends on only one parameter (Glatter, 1980).

2.6.2.7.5. *Model fitting*

As in small-angle X-ray scattering, the scattering curves can be compared with those of simple or more elaborate models. This is rather straightforward in the case of highly symmetric particles like icosahedral viruses that can be regarded as spherical at low resolution. The scattering curves of such viruses are easily adapted by spherical-shell models assigning different scattering-length densities to the different shells (*e.g.* Cusack, 1984). Neutron constrast variation helps decisively to distinguish between the shells.

Fitting complicated models to the scattering curves is more critical because of the averaging effect of small-angle scattering. While it is correct and easy to show that the scattering curve produced by a model body coincides with the measured curve, in general a unique model cannot be deduced from the scattering curve alone. Stuhrmann (1970) has presented a procedure using Lagrange polynomials to calculate low-resolution real-space models directly from the scattering information. It has been applied successfully to the scattering curves from ribosomes (Stuhrmann *et al.*, 1976).

2.6.2.7.6. *Label triangulation*

Triangulation is one of the techniques that make full use of the advantages of neutron scattering. It consists in specifically labelling single components of a multicomponent complex, measuring the scattering curves from (*a*) particles with two labelled components, (*b*) and (*c*) particles with either of the two components labelled, and (*d*) a (reference) particle that is not labelled at all. The comparison of the scattering from $(b) + (c)$ with that from $(a) + (d)$ yields information on the scattering originating exclusively from vectors combining volume elements in one component with volume elements in the other component.

From this scattering difference curve, the distances between the centres of mass of the components are obtained. A table of such distances yields the spatial arrangement of the components. If there are n components in the complex, at least $4n - 10$ for $n > 3$ distance values are needed to build this model: Three distances define a basic triangle, three more yield a basic tetrahedron, the handedness of which is arbitrary and has to be determined by independent means. At least four more distances are required to fix a further component in space. More than four distances are needed if the resulting tetrahedron is too flat.

Label triangulation is based on a technique developed by Kratky & Worthmann (1947) for determining heavy-metal distances in organometallic compounds by X-ray scattering, and was proposed originally by Hoppe (1972); Engelman & Moore (1972) first saw the advantage of neutrons. The need to mix preparations (*a*) plus (*d*) and (*b*) plus (*c*) for obtaining the desired scattering difference curve in the case of high concentrations and/or inhomogeneous complexes (consisting of different classes of matter) has been shown by Hoppe (1973). The complete map of all protein positions within the small subunit from *E. coli* ribosomes has been obtained with this method (Capel *et al.*, 1987). An alternative approach for obtaining the distance information contained in the scattering curves from pairs of proteins by fitting the Fourier transform of 'moving splines' to the scattering curves has been presented by May & Nowotny (1989) for data on the large ribosomal subunit.

The scattering curves should be measured at the scattering-length-density matching point of the reference particle for reducing undesired contributions. Naturally inhomogeneous particles can be rendered homogeneous by specific partial deuteration. This technique has been successfully applied for ribosomes (Nierhaus *et al.*, 1983).

2.6.2.7.7. *Triple isotropic replacement*

An elegant way of determining the structure of a component inside a molecular complex has been proposed by Pavlov & Serdyuk (1987). It is based on measuring the scattering curves from three preparations. Two contain the complex to be studied at two different levels of labelling, ρ_1 and ρ_2, and are mixed together to yield sample 1, the third contains the complex at an intermediate level of labelling, ρ_3 (sample 2). If the condition

$$\rho_3(\mathbf{r}) = (1 - \delta)\rho_1(\mathbf{r}) + \delta\rho_2(\mathbf{r}) \qquad (2.6.2.13)$$

is satisfied by δ, the relative concentration of particle 2 in sample 1, then the difference between the scattering from the two samples only contains contributions from the single component. Additionally, the contributions from contamination, aggregation, and interparticle effects are suppressed provided that they are the same in the three samples, *i.e.* independent of the partial-deuteration states.

In the case of small complexes, δ can be obtained by measuring the scattering curves $I_1(Q)$, $I_2(Q)$, and $I_3(Q)$ of the three particles as a function of contrast and by plotting the differences of the zero-angle scattering $I_1(0) - I_3(0)$ and $I_2(0) - I_3(0)$ *versus* δ. The two curves intercept at the correct ratio δ_0.

The method, which can be considered as a special case of a systematic inverse contrast variation of a selected component, holds if the concentrations, the complex occupations, and the aggregation behaviour of the three particles are identical. Mathematically, the difference curve is independent of the

contrast of the rest of the complex with respect to the solvent. In practice, it would be wise to follow the same considerations as with triangulation.

2.6.2.8. *Dense systems*

Especially in the case of polymers, but also in alloys, the scattering from the sample can often no longer be described, as in the previous section, as originating from a sum of isolated particles in different orientations. There may be two reasons for this: either the number concentration c of one of the components is higher than about 0.01, leading to excluded-volume effects, and/or there is an electrostatic interaction between components (for example, in solutions of polyelectrolytes, latex, or micelles). In these cases, it is usually the information about the *structure* of the sample caused by the interactions that is to be obtained rather than the shape of the inhomogeneities or particles in the sample, unless the interactions can be regarded as a weak disturbance.

An excellent introduction to the treatment of dense systems is found in the article of Hayter (1985). A detailed description of the theoretical interpretation of correlations in charged macromolecular and supramolecular solutions has been published by Chen, Sheu, Kalus & Hoffmann (1988).

The scattering from densely packed particles can be written as the product of the structure factor or structure function $S(Q)$, describing the arrangement of the inhomogeneities with respect to each other, in mathematical terms the interference effects of correlations between particle positions, in the sample,

$$S(Q) = \left\langle \sum \sum \exp[i\mathbf{Q}(\mathbf{r}_j - \mathbf{r}_k)] \right\rangle / N, \tag{2.6.2.14}$$

and of the form factor $P(Q)$ of the inhomogeneities (as before):

$$I(Q) = P(Q)S(Q). \tag{2.6.2.15}$$

Hayter & Penfold (1981) were the first to describe an analytic structure factor for macro-ion solutions.

If $P(Q)$ can be obtained from a measurement of a dilute solution of the particles under study, then the pure structure factor can be calculated by dividing the high-concentration intensity curve by the low-concentration curve. This procedure requires the form factor not to change with concentration, which is not necessarily the case for loosely arranged particles such as polymers. A technique that avoids this problem is contrast variation (see Subsection 2.6.2.2): introducing a fraction of a deuterated molecule into a bulk of identical protonated molecules (or *vice versa*, with the advantage of reduced incoherent background) yields the scattering of the 'isolated' labelled particle at high-concentration conditions.

Partial structure factors can be obtained from a contrast-variation series of a given system at different volume fractions of the particles. Similarly to equation (2.6.2.4), the structure factor can be decomposed into a quadratic function. In the ternary alloy Al–Ag–Zn, for example, the scattering has been decomposed into the contributions from the two minor species Ag and Zn, and their interference, *i.e.* the partial structure functions for Zn–Zn, Zn–Ag, and Ag–Ag, by using the scattering from three samples with different silver isotopes, and identical sample treatment (Salva-Ghilarducci, Simon, Guyot & Ansara, 1983).

International Tables for Crystallography (2006). Vol. C, Chapter 2.7, pp. 113–123.

2.7. Topography

BY A. R. LANG

2.7.1. Principles

The term diffraction topography covers techniques in which images of crystals are recorded by Bragg-diffracted rays issuing from them. It can be arranged at will for these rays to produce an image of a surface bounding the crystal, or of a thin slice cutting through the crystal, or of the projection of a selected volume of the crystal. The majority of present-day topographic techniques aim for as high a spatial resolution as possible in their point-by-point recording of intensity in the diffracted rays. In principle, any position-sensitive detector with adequate spatial resolution could be employed for recording the image. Photographic emulsions are most widely used in practice. In the following accounts of the various diffraction geometries developed for topographic experiments, the term 'film' will be used to stand for photographic emulsion coated on film or on glass plate, or for any other position-sensitive detector, either integrating or capable of real-time viewing, that could serve instead of photographic emulsion. (Position-sensitive detectors, TV cameras, and storage phosphors are described in Sections 7.1.6, 7.1.7, and 7.1.8.) All diffraction geometries described with reference to an X-ray source could in principle be used with neutron radiation of comparable wavelength (see Chapter 4.4).

Two factors, often largely independent and experimentally distinguishable, determine the intensity that reaches each point on the topograph image. The first is simply whether or not the corresponding point in the specimen is oriented so that some rays within the incident beam impinging upon it can satisfy the Bragg condition. The intensity of the Bragg-reflected rays will range between maximum and minimum values depending upon how well that condition is satisfied. The consequent intensity variation from point to point on the image is called *orientation contrast*, and it can be analysed to provide a map of lattice misorientations in the specimen. The sensitivity of misorientation measurement is controllable over a wide range by appropriate choice of diffraction geometry, as will be explained below. The second factor determining the diffracted intensity is the lattice perfection of the crystal. In this case, physical factors such as X-ray wavelength, specimen absorption, and structure factor of the active Bragg reflection fix the range within which the diffracted intensity can lie. One limit corresponds to the case of the *ideally perfect crystal*. This is a well defined entity, and its diffraction behaviour is well understood [see *IT* B (1996, Part 5)]. The other limit is that of the *ideally imperfect crystal*, a less precisely defined entity, but which, for practical purposes, may be taken as a crystal exhibiting negligible primary and secondary extinction. The magnitude, and sometimes also the sign, of the difference in intensity recorded from volume elements of ideally perfect as opposed to ideally imperfect crystals is to a large degree controllable by the choice of experimental parameters (in particular by choice of wavelength). Contrast on the topograph image arising from point-to-point differences in lattice perfection of the specimen crystal was called *extinction contrast* in earlier X-ray topographic work, but is now more usually called *diffraction contrast* to conform with terminology used in transmission electron microscopic observations of lattice defects, experiments which have many analogies with the X-ray case.

Figs. 2.7.1.1 and 2.7.1.2, respectively, show in plan view the simplest arrangements for taking a *reflection* topograph and a *transmission* topograph. The source of X-rays is shown as being point-like at S. If its wavelength spread is large then the Bragg condition may be satisfied over the whole length CD for Bragg planes oriented parallel to BB', and an image of CD will be formed on F by the Bragg-diffracted rays falling on it. The specimen is mounted on a rotatable axis (the ω axis) perpendicular to the plane of the drawing, which represents the median plane of incidence, in order that the angle of incidence on the planes BB' can be varied. The specimen is usually adjusted so that the diffraction vector, **h**, of the Bragg reflection of principal interest is perpendicular to the ω axis. Let the mean source-to-specimen and specimen-to-film distances be a and b, respectively. Suppose the source S is extended a distance s in the axial direction (*i.e.* perpendicular to the plane of incidence). Then diffracted rays from any point on CD will be spread on F over a distance $s(b/a)$ in the axial direction. This is the simple expression for the axial resolution of the topograph given by ray optics. Transmission topographs have the value of showing defects within the interior of specimens, which may be optically opaque, but are in practice limited to a specimen thickness, t, such that μt is less than a few units (μ being the normal linear absorption coefficient) unless the specimen structure and the perfection are such as to allow strong anomalous transmission [the Borrmann effect, see *IT* B (1996, Part 5)]. If a reflection topograph specimen is a nearly perfect crystal then the volume of crystal contributing to the image is restricted to a depth below the surface given approximately by the X-ray extinction distance, ξ_h, of the active Bragg reflection, which may be only a few micrometres, rather than the penetration distance, μ^{-1}, of the radiation used.

Besides the ratio b/a, other important experimental parameters are the degree of collimation of the incident beam and its wavelength spread. The manner in which X-ray topographs exhibit *orientation contrast* and *diffraction contrast* under different choices of these parameters is illustrated schematically in Fig. 2.7.1.3. There, (*a*) represents a hypothetical specimen consisting of a matrix of perfect crystal C in which are embedded two islands A and B whose lattices differ from C in the following respects. A has the same mean orientation as C but is a region of

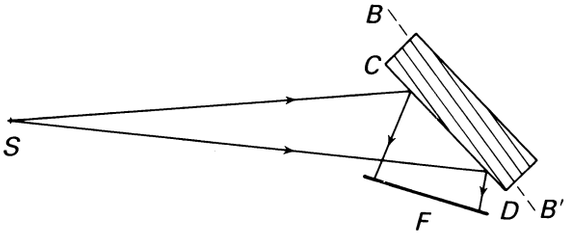

Fig. 2.7.1.1. Surface reflection topography with a point source of diverging continuous radiation.

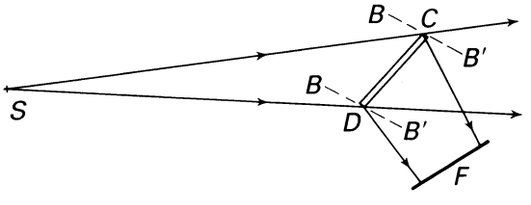

Fig. 2.7.1.2. Transmission topography with a point source of diverging continuous radiation.

Copyright © 2006 International Union of Crystallography

high imperfection. (In reflection topographs, imperfect regions will always produce stronger *integrated* reflections than perfect regions and will also do so in transmission topographs under low-absorption conditions.) The island B is assumed to be as perfect as C, but is slightly misoriented with respect to C. The topograph images sketched in (b)–(e) could represent either reflection topographs or transmission topographs from a specimen thin compared with the dimension CD in Fig. 2.7.1.2. [Possible distortion of the images relative to the shape of (a) is neglected: this matter is considered later.] First, suppose that continuous radiation is emitted from the source S. If the ratio b/a is quite small, the topograph image will resemble (b). The island A is detected by diffraction contrast whereas island B will not show any area contrast since by assumption the incident radiation contains wavelengths enabling B to satisfy the Bragg condition just as well as C. The low-angle B–C boundary may show up, however, since it contains dislocations that will produce diffraction contrast and might be individually resolvable with a high-resolution topographic technique. Orientation contrast of B becomes manifest when b is increased, and measurement of the misorientation is then possible from the displacement of the image of B [as shown in (c)] consequent upon the different direction of Bragg-reflected rays issuing from it compared with those from C.

Next, suppose that S emits a limited range of wavelengths, *e.g.* characteristic $K\alpha$ radiation, and let the incident beam be collimated to have an angular spread in the plane of incidence that is smaller than the component in that plane of the misorientation between B and C, but larger than the angular range of reflection of C or A. Then, if the specimen is rotated about the ω axis so that A and C satisfy the Bragg condition, B will not do so and the topograph will resemble (d). [Island A shows up in (d) by diffraction contrast, as in (b).]. Appropriate rotation of the specimen will bring B into the Bragg-reflecting orientation, but will eliminate reflection from A and C, as shown in (e). The images (d) and (e) will not undergo significant change with variation in the ratio b/a, except for loss of resolution as b/a increases. The sensitivity of misorientation measurement will increase as the angular and wavelength spread of the incident beam are reduced, but when the angular range of a monochromatic incident beam is lowered to a value comparable with the angular range of reflection of the perfect crystal (generally only a few seconds of arc), it will not be possible with one angular setting alone to obtain an image that will distinguish between diffraction contrast and orientation contrast in the clear way shown in (d). The distinction will require comparison of a series of topographs obtained during a step-wise sweep of the angular range of reflection by the specimen. This is the procedure adopted in double-crystal or multicrystal topography, as described in Sections 2.7.3 and Subsection 2.7.4.2.

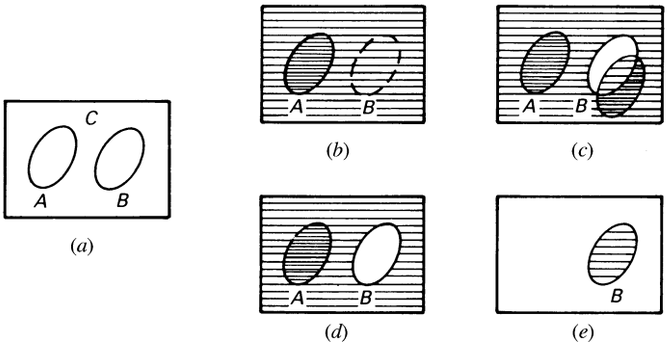

Fig. 2.7.1.3. Differentiation between orientation contrast and diffraction contrast in types of topograph images, (b)–(e), of a crystal surface (a).

Details concerning diverse variants in diffraction geometry used in X-ray topographic experiments, treatments of the diffraction contrast theory underlying X-ray topographic imaging of lattice defects, and listings of applications of X-ray topography can be found in reviews and monographs of which a selection follows. All aspects of X-ray topography are covered in the survey edited by Tanner & Bowen (1980). Armstrong & Wu (1973), Tanner (1976), and Lang (1978) describe experimental techniques and review their applications. The dynamical-diffraction theoretical basis of X-ray topography is emphasized by Authier (1970, 1977). Kato (1974) and Pinsker (1978) deal comprehensively with X-ray dynamical diffraction theory, which is also the topic of Part 5 of *IT* B (1996). Introductions to this theory have been presented by Batterman & Cole (1964), Hart (1971), and Hildebrandt (1982), the latter two being especially relevant to X-ray topography.

2.7.2. Single-crystal techniques

2.7.2.1. *Reflection topographs*

Combining the simple diffraction geometry of Fig. 2.7.1.1 with a laboratory microfocus source of continuous radiation offers a simple yet sensitive technique for mapping misorientation textures of large single crystals (Schulz, 1954). One laboratory X-ray source much used produces an apparent size of S 30 μm in the axial direction and 3 μm in the plane of incidence. Smaller source sizes can be achieved with X-ray tubes employing magnetic focusing of the electron beam. Then b/a ratios between $\frac{1}{2}$ and 1 can be adopted without serious loss of geometric resolution, and, with $a = 0.3$ m typically, misorientation angles of $10''$ can be measured on images of the type (c) in Fig. 2.7.1.3. The technique is most informative when the crystal is divided into well defined subgrains separated by low-angle boundaries, as is often the case with annealed melt-grown crystals. On the other hand, when continuous lattice curvature is present, as is usually the case in all but the simplest cases of plastic deformation, it is difficult to separate the relative contributions of orientation contrast and diffraction contrast on topographs taken by this method. In principle, the separation could be effected by recording a series of exposures with a wide range of values of b, and it becomes practicable to do so when exposures can be brief, as they can be with synchrotron-radiation sources (see Section 2.7.4.).

For easier separation of orientation contrast and diffraction contrast, and for quicker exposures with conventional X-ray sources, collimated characteristic radiation is used, as in the Berg–Barrett method. Barrett (1945) improved an arrangement earlier described by Berg (1931) by using fine-grain photographic emulsion and by minimizing the ratio b/a, and achieved high topographic resolution (~ 1 μm). The method was further developed by Newkirk (1958, 1959). A typical Berg–Barrett arrangement is sketched in Fig. 2.7.2.1. Usually, the source S is

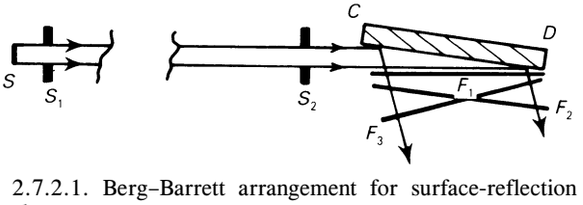

Fig. 2.7.2.1. Berg–Barrett arrangement for surface-reflection topographs.

the focal spot of a standard X-ray tube, giving an apparent source 1 mm square perpendicular to the incident beam. The openings of the slits S_1 and S_2 are also 1 mm in the plane of incidence, and the distance S_1–S_2 (which may be identified with the distance a) is typically 0.3 m. The specimen is oriented so as to Bragg reflect asymmetrically, as shown. Softer radiations, *e.g.* Cu $K\alpha$, Co $K\alpha$ or Cr $K\alpha$, are employed and higher-angle Bragg reflections are chosen ($2\theta_B \simeq 90^\circ$ is most convenient). Fig. 2.7.2.1 indicates three possible film orientations, F_1–F_3. (These possibilities apply in most X-ray topographic arrangements.) Choice of orientation is made from the following considerations. If minimum distance b is required over the whole length CD, then position F_1 is most appropriate. If a geometrically undistorted image of CD is needed, then position F_2, in which the film plane is parallel to the specimen surface, satisfies this condition. If a thick emulsion is used, it should receive X-rays at normal incidence, and be in orientation F_3. If high-resolution spectroscopic photographic plates are used, in which the emulsion thickness is $\sim 1\,\mu$m only, then considerable obliquity of incidence of the X-rays is tolerable. But these plates have low X-ray absorption efficiency. Nuclear emulsions (particularly Ilford type L4) are much used in X-ray topographic work. Ilford L4 is a high-density emulsion (halide weight fraction 83%) and hence has high X-ray stopping power. The usual minimum emulsion thickness is 25 μm. Such emulsions should be oriented not more than about 2° off perpendicularity to the X-ray beam if resolution loss due to oblique incidence is not to exceed 1 μm (with correspondingly closer limits on obliquity for thicker emulsions). With 1 mm openings of S_1 and S_2, and $a = 0.3$ m, most of the irradiated area of CD will receive an angular range of illumination sufficient to allow both components of the $K\alpha$ doublet to Bragg reflect. In these circumstances, the distance b must be everywhere less than 1–2 mm if image spreading due to superimposition of the α_1 and α_2 images is not to exceed a few micrometres. In order to eliminate this major cause of resolution loss (and, incidentally, gain sensitivity in misorientation measurements), the apertures S_1 and S_2 should be narrowed and/or a increased so that the angular range of incidence on the specimen is less than the difference in Bragg angle of the α_1 and α_2 components for the particular radiation and Bragg angle being used. (This condition applies equally in the transmission specimen techniques, described below.). With a narrower beam, the illuminated length of CD is reduced. This disadvantage may be overcome by mounting the specimen and film together on a linear traverse mechanism so that during the exposure all the length of CD of interest is scanned. In this way, surface-reflection X-ray topographs can be recorded for comparison with, say, etch patterns or cathodoluminescence patterns (Lang, 1974).

2.7.2.2. *Transmission topographs*

The term 'X-ray topograph' was introduced by Ramachandran (1944) who took transmission topographs of cleavage plates of diamond using essentially the arrangement shown in Fig. 2.7.1.2. (In this case, S was a 0.3 mm diameter pinhole placed in front of the window of a W-target X-ray tube so as to form a point source of diverging continuous radiation.) Ramachandran adopted a distance $a = 0.3$ m and ratio a/b of about 12, which produced images of about 25 μm geometrical resolution having the characteristics of Fig. 2.7.1.3(*b*), *i.e.* sensitive to diffraction contrast but not to orientation contrast. For each reflection under study, the film was inclined to the incident beam with that obliquity calculated to produce an undistorted image of the specimen plate. Guinier & Tennevin (1949) studied both diffraction contrast and orientation contrast in continuous-radiation transmission topograph images. Their minimum b/a ratio was set by the need to avoid overlap of Laue images of the crystal produced by different Bragg planes.

Collimated characteristic radiation is used in the methods of 'section topographs' (Lang, 1957) and 'projection topographs' (Lang, 1959*a*), the latter being sometimes called 'traverse topographs'. Fig. 2.7.2.2 explains both techniques. When taking a section topograph, the specimen CD, usually plate shaped, is stationary (disregard the double-headed arrow in the figure). The ribbon-shaped incident beam issuing from the slit P is Bragg reflected by planes normal, or not far from normal, to the major surfaces of the specimen. As drawn, the Bragg planes make an angle α with the normal to the X-ray entrance surface of the specimen, the positive sense of α being taken in the same sense as the deviation $2\theta_B$ of the Bragg-reflected rays. If the crystal is sufficiently perfect for multiple scattering to occur within it (with or without loss of coherence), then the multiply scattered rays associated with the Bragg reflection excited will fill the volume of the triangular prism whose base is ORT, the 'energy-flow triangle' or 'Borrmann triangle', contained between OT and OR whose directions are parallel to the incident wavevector, $\mathbf{K}_0$, and diffracted wavevector, $\mathbf{K}_h$, respectively. Both the $\mathbf{K}_0$ and $\mathbf{K}_h$ beams issuing from the X-ray exit surface of the crystal carry information about the lattice defects within the crystal. However, it is usual to record only the $\mathbf{K}_h$ beam. This falls on the film, F, in a strip extending normal to the plane of incidence, of height equal to the illuminated height of the specimen multiplied by the axial magnification factor $(a + b)/a$, and forms the section topograph image. The screen, Q, prevents the $\mathbf{K}_0$ beam from blackening the film but has a slot allowing the diffracted beam to fall on F. A diffraction-contrast-producing lattice defect cut by OT at I will generate supplementary rays parallel to $\mathbf{K}_h$ and will produce an identifiable image on F at I', the 'direct image' or 'kinematic image' of the defect. The depth of I within CD can be found *via* the measurement of $I'T'/R'T'$. From a series of section topographs taken with a known translation of the specimen between each topograph, a three-dimensional construction of the trajectory of defect I (*e.g.* a dislocation line) within the crystal can be built up. To obtain good definition of the spatial width of the ribbon incident beam cutting the crystal, the distance between P and the crystal is kept small. The minimum practicable opening of P is about 10 μm. If diffraction is occurring from planes perpendicular to the X-ray entrance surface of the specimen, *i.e. symmetrical Laue case* diffraction, the width $R'T'$ of the section topograph image is simply $2t \sin\theta_B$, t being the specimen thickness, and neglecting the contribution from the

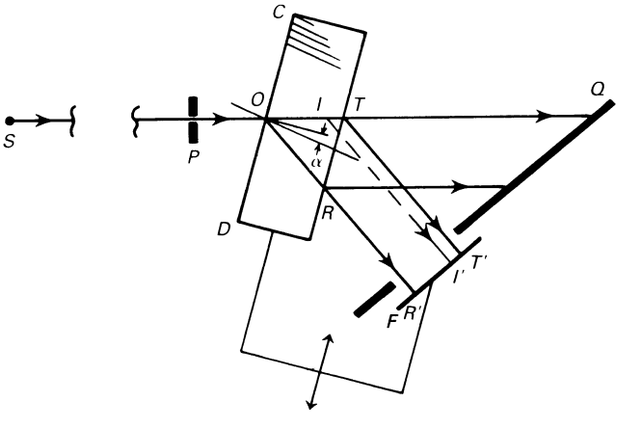

Fig. 2.7.2.2. Arrangements for section topographs and projection topographs.

width of the ribbon incident beam. With asymmetric transmission, as drawn in the figure, $R'T' = t\sec(\theta_B - \alpha)\sin 2\theta_B$. The distance b is made as small as is permitted by the specimen shape and the need to separate the emerging $\mathbf{K}_0$ and $\mathbf{K}_h$ beams. Suppose b is 10 mm. Then, with a source S having axial extension 100 μm, the distance $a = SP$ should be not less than 0.5 m in order to keep the geometrical resolution in the axial direction better than 2 μm, and should be correspondingly longer with larger source sizes.

To take a projection topograph, the specimen CD and the cassette holding the film F are together mounted on an accurate linear traversing mechanism that oscillates back and forth during the exposure so that the whole area of interest in the specimen is scanned by the ribbon beam from P. The screen Q is stationary. If the specimen is plate shaped, the best traverse direction to choose is that parallel to the plate, as indicated by the double-headed arrow, for then the diffracted beam will have minimum side-to-side oscillation during the traverse oscillation, the opening of Q can be held to a minimum, and thereby unwanted scattering reaching F kept low. The projection topograph image is an orthographic projection parallel to $\mathbf{K}_h$ of the crystal volume and its content of diffraction-contrast-producing lattice defects. If the specimen is plate-like, of length L in the plane of incidence, then, with F normal to $\mathbf{K}_h$, the magnification of the topograph image in the direction parallel to the plane of incidence is $L\cos(\theta_B + \alpha)$. There will generally be a small change of axial magnification $(a + b)/a$ along L. The loss of three-dimensional information occurring through projection can be recovered by taking stereopairs of projection topographs. The first method (Lang, 1959*a*,*b*) used hkl, $\bar{h}\bar{k}\bar{l}$ pairs of topographs as stereopairs. One disadvantage of this method is that the convergence angle is fixed at $2\theta_B$, which may be unsuitably large for thick specimens. The method of Haruta (1965) obtains two views of the specimen using the same hkl reflection, by making a small rotation of the specimen about the **h** vector between the two exposures, and has the advantage that this rotation, and hence the stereoscopic sensitivity, can be chosen at will. When taking projection topographs, the slit P can be wider than the narrow opening needed for high-resolution section topographs, but not so wide as to cause unwanted $K\alpha_2$ reflection to occur. Best use of the X-ray source is made when the width of P is the same as or somewhat greater than S.

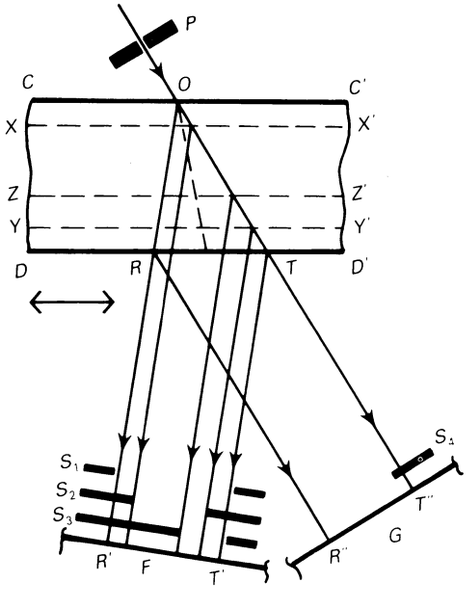

Fig. 2.7.2.3. Arrangements for limited projection topographs and direct-beam topographs.

In certain investigations, the methods of $\mathbf{K}_h$-beam 'limited projection topographs' (Lang, 1963) and of $\mathbf{K}_0$-beam section topographs and projection topographs are useful; Fig. 2.7.2.3 shows the arrangement of screens and diffracted-beam slits then adopted. The limited projection topograph technique can be employed with a plate-shaped specimen $CDD'C'$, as in the following examples. Suppose the surface of the plate contains abrasion damage that cannot be removed but that causes diffraction contrast obscuring the images of interior defects in the crystal. The diffracted-beam slit (equivalent to the opening in Q shown in Fig. 2.7.2.2), which is opened to the setting S_1 for a standard projection topograph, may now be closed down to setting S_2 so as to cut into the RR' and TT' edges of the $\mathbf{K}_h$ beam, and thereby prevent direct images of near-surface defects located between CC' and XX', and between YY' and DD', from reaching F. As another example, it may be desired to receive direct images from a specimen surface and a limited depth below it only (*e.g.* when correlating surface etch pits with dislocation outcrops). Then, setting S_3 of the diffracted-beam slit is adopted and only the direct images from defects lying between depth ZZ' and the surface DD' reach F.

To record the $\mathbf{K}_0$ beam image, either in a section topograph or a projection topograph, some interception of the $\mathbf{K}_0$ beam on the OTT'' side is needed to avoid intense blackening of the film G by radiation coming from the source, which will generally contain much energy in wavelengths other than those undergoing Bragg diffraction by the crystal. Screen S_4, critically adjusted, performs the required interception. Recording both $\mathbf{K}_0$-beam and $\mathbf{K}_h$-beam images is valuable in some studies of dynamical diffraction phenomena, such as the 'first-fringe contrast' in stacking-fault fringe patterns (Jiang & Lang, 1983). Such recording can be done simultaneously, on separate films, normal to $\mathbf{K}_0$ and $\mathbf{K}_h$, respectively, when $2\theta_B$ is sufficiently large.

When collimated characteristic radiation is used, recording projection topographs of reasonably uniform density becomes difficult when the specimen is bent. To keep the ω axis oriented at the peak of the Bragg reflection while the specimen is scanned, several devices for 'Bragg-angle control' have been designed, for example the servo system of Van Mellaert & Schwuttke (1972). The signal is taken from a detector registering the Bragg reflection through the film F, but this precludes use of glass-backed emulsions if X-ray wavelengths such as that of Cu K and softer are used. An alternative approach with thin, large-area transmission specimens is to revert to the geometry of Fig. 2.7.1.2 and deliberately elastically bend the crystal to such radius as will enable its whole length to Bragg diffract a single wavelength diverging from S, similar to a Cauchois focusing transmission monochromator (Wallace & Ward, 1975). No specimen traversing is then needed, but b cannot be made small if the wide $\mathbf{K}_0$ and $\mathbf{K}_h$ beams are to be spatially separated in the plane of F.

Quite simple experimental arrangements can be adopted for taking transmission topographs under high-absorption conditions, when only anomalously transmitted radiation can pass through the crystal. The technique has mainly been used in symmetrical transmission, as shown with the specimen $CC'D'D$ in Fig. 2.7.2.4. When the specimen perfection is sufficiently high for the Borrmann effect to be strongly manifested, and $\mu t > 10$, say, the energy flow transmitted within the Borrmann triangle is constricted to a narrow fan parallel to the Bragg planes, the fan opening angle being only a small fraction of $2\theta_B$ [see *IT* B (1996, Part 5)]. Radiation of a given wavelength coming from a small source at S and undergoing Bragg

diffraction in $CC'D'D$ will take the path shown by the heavy line in Fig. 2.7.2.4, simplifying the picture to the case of extreme confinement of energy flow to parallelism with the Bragg planes. At the X-ray exit surface DD', splitting into $\mathbf{K}_0$ and $\mathbf{K}_h$ beams occurs. A slit-less arrangement, as shown in the figure, may suffice. Then, when S is a point-like source of $K\alpha$ radiation, and distance a is sufficiently large, films F_1 and F_2 will each record a pair of narrow images formed by the α_1 and α_2 wavelengths, respectively. A wider area of specimen can be imaged if a line focus rather than a point focus is placed at S (Barth & Hosemann, 1958), but then the α_1 and α_2 images will overlap. Under conditions of high anomalous transmission, defects in the crystal cause a reduction in transmitted intensity, which appears similarly in the $\mathbf{K}_0$ and $\mathbf{K}_h$ images. Thus, it is possible to gain intensity and improve resolution by recording both images superimposed on a film F_3 placed in close proximity to the X-ray exit face DD' (Gerold & Meier, 1959).

2.7.3. Double-crystal topography

The foregoing description of single-crystal techniques will have indicated that in order to gain greater sensitivity in orientation contrast there are required incident beams with closer collimation, and limitation of dispersion due to wavelength spread of the characteristic X-ray lines used. It suggests turning to prior reflection of the incident beam by a perfect crystal as a means of meeting these needs. Moreover, the application of crystal-reflection-collimated radiation to probe angularly step by step as well as spatially point by point the intensity of Bragg reflection from the vicinity of an individual lattice defect such as a dislocation brings possibilities of new measurements beyond the scope provided by simply recording the local value of the integrated reflection. The X-ray optical principles of double-crystal X-ray topography are basically those of the double-crystal spectrometer (Compton & Allison, 1935). The properties of successive Bragg reflection by two or more crystals can be effectively displayed by a Du Mond diagram (Du Mond 1937), and such will now be applied to show how collimation and monochromatization result from successive reflection by two crystals, U and V, arranged as sketched in Fig. 2.7.3.1. They are in the dispersive, antiparallel, '$++$' setting, and are assumed to be identical perfect crystals set for the same symmetrical Bragg reflection. Only rays making the same glancing angle with both surfaces will be reflected by both U and V. For example, radiation of shorter wavelength reflected at a smaller glancing angle at U (the ray shown by the dashed line) will impinge at a larger glancing angle on V and not satisfy the Bragg condition. In this $++$ setting, with a given angle ω between the Bragg-reflecting planes of each crystal, $\theta_U + \theta_V = \omega$ and $\Delta\theta_U = -\Delta\theta_V$. The Du Mond diagram for the $++$ setting, Fig. 2.7.3.2, shows plots of Bragg's law for each crystal, the V curve being a reflection of the U curve in a vertical mirror line and differing by ω from the U curve in its coordinate of intersection with the axis of abscissa, in accord with the equations given above. The small angular range of reflection of a monochromatic ray by each perfect crystal is represented exaggeratedly by the band between the parallel curves. Where the band for crystal U superimposes on the band for V (the shaded area) defines semiquantitatively the divergence and wavelength spread in the rays successively reflected by U and V. (It is taken for granted that $\frac{1}{2}\omega$ lies between the maximum and minimum incident glancing angles on U, $\theta_{\max}$ and $\theta_{\min}$, afforded by the incident beam, assumed polychromatic.) The reflected beam from U alone contains wavelengths ranging from $\lambda_{\min}$ to $\lambda_{\max}$. Comparison of these θ and λ ranges with the extent of the shaded area illustrates the efficacy of the $++$ arrangement in providing a collimated and monochromatic beam, which can be employed to probe the reflecting properties of a third crystal (Nakayama, Hashizume, Miyoshi, Kikuta & Kohra, 1973). Techniques employing three or more successive Bragg reflections find considerable application when used with synchrotron X-ray sources, and will be considered below, in Section 2.7.4.

The most commonly used arrangement for double-crystal topography is shown in Fig. 2.7.3.3, in which U is the 'reference' crystal, assumed perfect, and V is the specimen crystal under examination. Crystals U and V are in the parallel, '$+-$' setting, which is non-dispersive when the Bragg planes of U and V have the same (or closely similar) spacings. Before considering the Du Mond diagram for this arrangement, note that Bragg reflection at the reference crystal U is asymmetric, from planes inclined at angle α to its surface. Asymmetric reflections have useful properties, discussed, for example, by Renninger (1961), Kohra (1972), Kuriyama & Boettinger (1976), and Boettinger, Burdette & Kuriyama (1979). The asymmetry factor, b, of magnitude $|\mathbf{K}_0 \cdot \mathbf{n}/\mathbf{K}_h \cdot \mathbf{n}|$, $\mathbf{n}$ being the

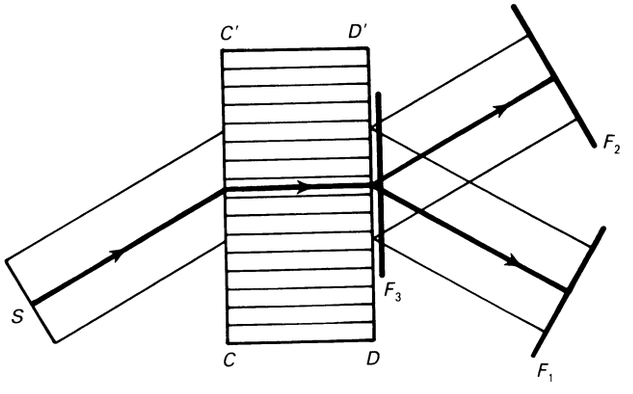

Fig. 2.7.2.4. Topographic techniques using anomalous transmission.

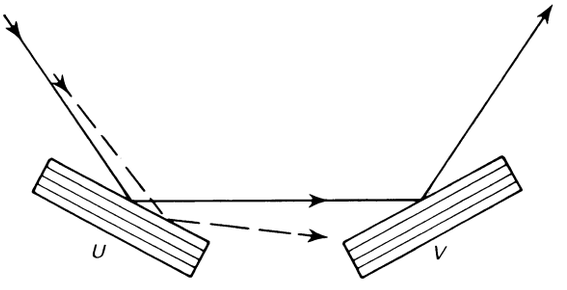

Fig. 2.7.3.1. Double-crystal $++$ setting.

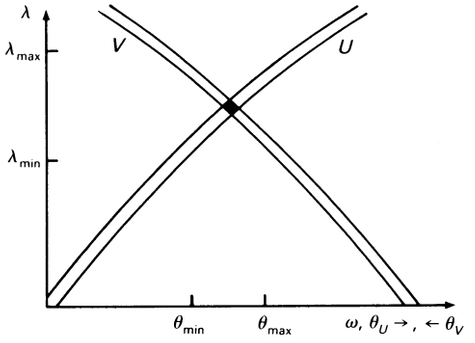

Fig. 2.7.3.2. Du Mond diagram for $++$ setting in Fig. 2.7.3.1.

crystal-surface normal, is also the ratio of spatial widths of the incoming to the outgoing beams, W_{in}/W_{out}. In the case of symmetric Bragg reflection, the perfect crystal U would totally reflect (in the zero-absorption case) over a small angular range, w_S. In the asymmetric case, the ranges of total reflection are w_{in} for the incoming rays and w_{out} for the outgoing. Dynamical-diffraction theory [*IT* B (1996, Part 5)] shows that $w_{out} = bw_{in} = b^{1/2} w_S$, so that $w_{in}W_{in} = w_{out}W_{out}$ (as would be expected from energy conservation). Thus, highly asymmetric reflection from the reference crystal U not only provides a spatially wide beam, able to cover a large area of V without recourse to any mechanical traversing motion of the components S, U or V, but also produces a desirably narrow angular probe for studying the angular breadth of reflection of V. In practice, values of b lower than 0.1 can be used.

Du Mond diagrams for the $+-$ arrangement are shown in Fig. 2.7.3.4(*a*) and (*b*). For simplicity, the curves (slope $d\lambda/d\theta = 2d\cos\theta$) are represented by straight lines. In the $+-$ setting, $\theta_V - \theta_U = \omega$ and $\Delta\theta_V = \Delta\theta_U$. In Fig. 2.7.3.4(*a*), the narrow band labelled U passing through the origin represents the beam of angular width w_{out} leaving U. It is assumed that all of the specimen crystal V has the same interplanar spacing as U but that it contains a slightly misoriented minor region V'(which may be located as shown in Fig. 2.7.3.3). When ω differs substantially from zero, the bands corresponding to crystal V and its minor part V' lie in positions V_1 and V_1', respectively, in Fig. 2.7.3.4(*a*). (Only the relevant part of the latter band is drawn, for simplicity.) The offset along the θ axis between V_1 and V_1' is the component $\Delta\varphi$ of the misorientation between V and V' that lies in the plane of incidence. If ω is reduced step-wise, a double-crystal topograph image being obtained at F at each angular setting, $\Delta\varphi$ can be found from film densitometry, which will show at what settings band U is most effectively overlapped by band V or by band V'. When ω is reduced to zero, the specimen crystal bands are at V_2 and V_2'. The drawing shows that V' has then passed right through the setting for its Bragg reflection, which occurred at a small positive value of ω. Since the U and V bands have identical slopes, their overlap occurs at all wavelengths when $\omega = 0$. In practice, only the shaded area is involved, corresponding to the wavelength range λ_{min} to λ_{max}, defined by the range of incidence angles, θ_{min} to θ_{max}, on the Bragg planes of crystal U. (The width of band U will generally be negligible compared with the range of θ allowed by source width and slit collimation system.) One component of $\Delta\varphi$ is found in the procedure just described. The second component needed to specify the difference between **h**-vector directions of the Bragg planes of V and V' is obtained by repeating the experiment after rotating V by 90° about **h**.

Next consider the more general case when V' differs from V in both orientation and interplanar spacing, and both V' and V have slightly different interplanar spacings from U. The difference in orientation between V' and V, $\Delta\varphi$, and their difference in interplanar spacing, $d(V') - d(V)$, can be distinguished by taking two series of double-crystal topographs, the orientation of the specimen in its own plane (its azimuthal angle, ψ) being changed by a 180° rotation about its **h** vector between taking the first and second series. As shown schematically in the Du Mond diagram, Fig. 2.7.3.4(*b*), the U, V, and V' bands now all have slightly different slopes. [Reference crystal U is reflecting the same small wavelength band as in Fig. 2.7.3.4(*a*).] The setting represented in the diagram is that putting V at the maximum of its Bragg reflection Let the V' band be then at position V_0', for the case when $\psi = 0°$. Assume that, when ψ is changed by 180°, the rotation of the specimen in its own plane can be made about the **h** vector of V precisely. (This assumption simplifies the diagram.) Then this 180° rotation will not cause any translation of the V band along the θ axis, but does transfer the V' band from V_0' to the position V_{180}'. With the sense of increasing ω taken as that translating the specimen bands to the right and $\Delta\omega$ taken as the difference in readings between peak reflection from V and that from V', the diagram shows that, with $\psi = 0°$, $\Delta\omega_0 = \theta(V') - \theta(V) + \Delta\varphi$, and, with $\psi = 180°$,

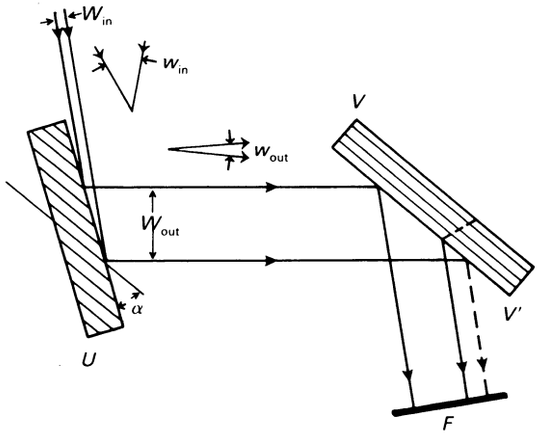

Fig. 2.7.3.3. Double-crystal topographic arrangement, $+-$ setting. Asymmetric reflection from reference crystal U. Specimen crystal divided into regions V and V'.

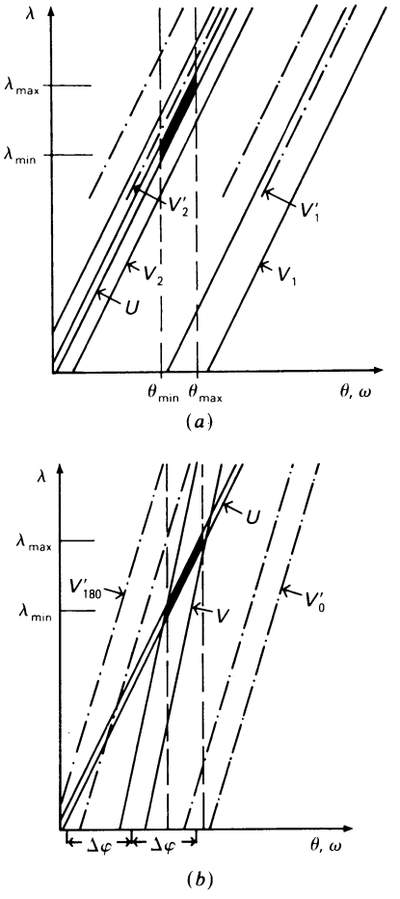

Fig. 2.7.3.4. Du Mond diagrams for $+-$ setting in Fig. 2.7.3.3. (*a*) Case when specimen region V' is misoriented with respect to V, but U, V, and V' all have the same interplanar spacing. (*b*) Case when V' differs from V in both orientation and interplanar spacing, and both differ from U in interplanar spacing.

$\Delta\omega_{180} = \theta(V') - \theta(V) - \Delta\varphi$, from which both $\Delta\varphi$ and the difference in Bragg angles can be found. The interplanar spacing difference is given by $d(V') - d(V) = [\theta(V) - \theta(V')]\bar{d}\cot\theta$, $\bar{d}$ being the mean interplanar spacing of V and V'. In practice, series of topographs are taken with azimuthal angles $\psi = 0$, 90, 180, and 270°, so that the two components needed to specify the misorientation vector between the Bragg-plane normals of V and V' can be determined. The Du Mond diagram shows that in this slightly dispersive experiment the range of overlap of the U band with any V band can be restricted by reducing the angular range or wavelength range of rays incident on U. Such reduction can be achieved by use of a small source S far distant from U, such as a synchrotron source. It can also be achieved by methods described in Subsection 2.7.4.2. As regards spatial resolution on double-crystal topographs, relations analogous to those for single-crystal topographs apply. If the reference crystal U unavoidably contains some defects, their images on F can deliberately be made diffuse compared with images of defects in V by making the UV distance relatively large. In a nearly dispersion-free arrangement, if the $K\alpha_1$ wavelength is being reflected, then so too will the $K\alpha_2$ if S is sufficiently widely extended in the incidence plane, as is usually necessary to image a usefully large area of V. If the distance VF cannot be made sufficiently small to reduce to a tolerable value the resolution loss due to simultaneous registration of the α_1 and α_2 images, then a source S of small apparent size, together with a collimating slit before U, will be needed. In order to obtain imaging of a large area of V, a linear scanning motion to and fro at an angle to SU in the plane of incidence must be performed by the source and collimator relative to the double-crystal camera. Whether it is the source and collimator or the camera that physically move depends upon their relative portability. When the source is a standard sealed-off X-ray tube, it is not difficult to arrange for it to execute the motion (Milne, 1971).

In some applications, it may occur that the specimen is so deformed that only a narrow strip of its surface will reflect at each ω setting. Then, a sequence of images can be superimposed on a single film, changing ω by a small step between each exposure. The 'zebra' patterns so obtained define contours of equal 'effective misorientation', the latter term describing the combined effect of variations in tilt $\Delta\varphi$ and of Bragg-angle changes due to variations in interplanar spacing (Renninger, 1965; Jacobs & Hart, 1977).

Double-crystal topography employing the parallel setting was developed independently by Bond & Andrus (1952) and by Bonse & Kappler (1958), and used by the former workers for studying reflections from surfaces of natural quartz crystals, and by the latter for detecting the strain fields surrounding outcrops of single dislocations at the surfaces of germanium crystals. Since then, the method has been much refined and widely applied. The detection of relative changes in interplanar spacing with a sensitivity of 10^{-8} is achievable using high-angle reflections and very perfect crystals. These developments have been reviewed by Hart (1968, 1981).

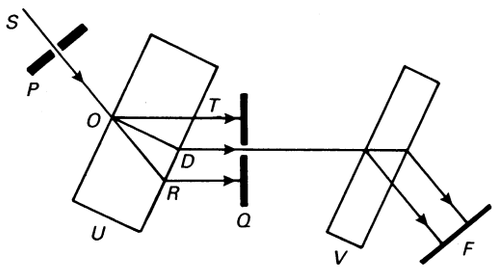

Fig. 2.7.3.5. Transmission double-crystal topography in + − setting with spatial limitation of beam leaving reference crystal.

Transmitted Bragg reflection (*i.e.* the Laue case) can be used for either or both crystals U and V, in both the + + and + − settings, if desired. When the reference crystal U is used in transmission, a technique due to Chikawa & Austerman (1968), shown in Fig. 2.7.3.5, can be employed if U is relatively thick and, preferably, not highly absorbing of the radiation used. This technique exploits a property of diffraction by ideally perfect crystals, that, for waves satisfying the Bragg condition exactly, the energy-flow vector (Poynting vector) within the energy-flow triangle (the triangle *ORT* in Figs. 2.7.2.2 and 2.7.2.3) is parallel to the Bragg planes. (In fact, the energy-flow vectors swing through the triangle *ORT* as the range of Bragg reflection is swept by the incident wave vector, $\mathbf{K}_0$.) Placing a slit Q as shown in Fig. 2.7.3.5 so as to transmit only those diffracted rays emerging from *RT* whose energy-flow direction in the crystal ran parallel, or nearly parallel, to the Bragg plane *OD* has the effect of selecting out from all diffracted rays only those that have zero or very small angular deviation from the exact Bragg condition. The slit Q thus provides an angularly narrower beam for studying the specimen crystal V than would be obtained if all diffracted rays from U were allowed to fall on V. The specimen is shown here in the + − setting, and also oriented to transmit its diffracted beam to the film F. This specimen arrangement is a likely embodiment of the technique but is incidental to the principle of employing *spatial* selection of transmitted diffraction rays to gain *angular* selection, a technique first used by Authier (1961). A practical limitation of this technique arises from angular spreading due to Fraunhofer diffraction by the slit Q: use of too fine an opening of Q will defeat the aim of securing an extremely angularly narrow beam for probing the specimen crystal.

2.7.4. Developments with synchrotron radiation

2.7.4.1. *White-radiation topography*

The generation and properties of synchrotron X-rays are discussed by Arndt in Subsection 4.2.1.5. For reference, his list of important attributes of synchrotron radiation is here repeated as follows: (1) high intensity, (2) continuous spectrum, (3) narrow angular collimation, (4) small source size, (5) polarization, (6) regularly pulsed time structure, and (7) computability of properties. All these items influence the design and scope of X-ray topographic experiments with synchrotron radiation, in some cases profoundly. The high intensity of continuous radiation delivered in comparison with the output of standard X-ray tubes, and hence the rapidity with which X-ray topographs could be produced, was the first attribute to attract attention, through the pioneer experiments of Tuomi, Naukkarinen & Rabe (1974), and of Hart (1975*a*). They used the simple diffraction geometry of the Ramachandran (Fig. 2.7.1.2) and Schulz (Fig.2.7.1.1) methods, respectively. [Since in the transmission-specimen case a multiplicity of Laue images can be recorded, it is usual to regard this work as a revival of the Guinier & Tennevin (1949) technique.] Subsequent developments in synchrotron X-ray topography have been reviewed by Tanner (1977) and by Kuriyama, Boettinger & Cohen (1982), and described in several chapters in Tanner & Bowen (1980). Some developments of methods and apparatus that have been stimulated by the advent of synchrotron-radiation sources will be described in this and in the following Subsection 2.7.4.2, the division illustrating two recognizable streams of development, the first exploiting the speed and relative instrumental simplicity

of white-radiation synchrotron X-ray topography, the second directed towards developing sophisticated 'beam conditioners' to extract highly collimated and monochromatic beams from the continuous-wavelength output of the synchrotron source. In both monochromatic and continuous-radiation experiments, the high intensity renders it more practicable than with conventional sources to apply electronic 'real-time' imaging systems (discussed in Sections 7.1.6 and 7.1.7, and Subsection 2.7.5.2).

At the experimental stations where synchrotron X-ray topography is performed, the distance a from the source (the tangent point on the electron orbit) is never less than some tens of metres, *e.g.* 40 m at the Deutsches Elektronen-Synchrotron, Hamburg (DESY), a maximum of 80 m at the Synchrotron Radiation Source, Daresbury (SRS), and 140 m at the European Synchrotron Radiation Facility (ESRF). The dimensions of the X-ray source (given by the cross section of the electron beam at the tangent point) vary widely between different installations (see Table 4.2.1.7), but the dimension in the plane of the electron orbit is usually several times that normal to it. If W_x and W_z are the corresponding full widths at half-maximum intensity of the source, then with the simple X-ray optics of a white-radiation topograph the geometrical resolution will be $W_x b/a$ and $W_z b/a$ in the orbit-plane (horizontal) and normal to the orbit-plane (vertical) directions, respectively, independent of the orientation of the plane of incidence of the Bragg reflection concerned. Representative dimensions might be $W_x = 2\,\text{mm}$, $W_z = 0.5\,\text{mm}$, and $a = 50\,\text{m}$. With $b = 100\,\text{mm}$, the horizontal and vertical resolutions of the topograph image would then be 4 and 1 μm, respectively, comparable with those on a conventional source, but with $b = 10\,\text{mm}$ only. Thus, even under synchrotron-source conditions, it is desirable that b should not exceed some centimetres in order to avoid geometrical factors causing a severer limitation of resolution (at least in one dimension) than other factors [such as photo-electron track lengths in the emulsion and point-by-point statistical fluctuations in absorbed photon dose (Lang, 1978)]. Since synchrotron X-rays are generated at all points along a curved electron trajectory, they spread out in a sheet parallel to the orbit plane. So there is in principle no limit to the specimen dimension in that plane that can be illuminated in a white-radiation topograph. However, increased background due to scattering from air and other sources imposes a practical limit of around 100 mm on the beam width. With electrons circulating in a planar orbit, the divergence of radiation normal to the orbit plane is strongly constricted, significant intensity being contained only within a fan of opening angle $\Omega \simeq mc^2/E$, *e.g.* $\Omega = 0.25\,\text{mrad}$ with electron energy $E = 2\,\text{GeV}$, equivalent to a vertical distance $\sim$12 mm with $a = 50\,\text{m}$. This does impose a significant restriction on the area of specimen that can be imaged in a transmission topograph unless recourse be had to beam expansion by an asymmetrically reflecting monochromator crystal.

For analysis of the three-dimensional configuration of defects within crystals, it is a useful feature of white-radiation transmission topography that different views of the specimen are presented simultaneously by the assemblage of Laue images, and that when studying reflection from a given Bragg plane there is freedom to vary the glancing angle upon it. When interpreting the diffraction contrast effects observed, the relative contributions of all the diffraction orders superimposed must be considered. However, after taking into account source spectral distribution, specimen structure factors, absorption losses and film efficiency, it is often found that a particular order of reflection is dominant in each Laue image (Tuomi, Naukkarinen & Rabe, 1974; Hart, 1975*a*). The variation of diffraction contrast with wavelength follows different trends for different types of defect (Lang, Makepeace, Moore & Machado, 1983), so the ability to vary the wavelength with which a given order of reflection is studied can help in identifying the type of defect.

If the orbiting electrons are confined to a plane, then the radiation emitted in that plane is completely linearly polarized with the **E** vector in that plane. It follows that diffraction with the plane of incidence normal to the orbit plane is in pure σ-polarization mode (polarization factor $P = 1$), and with plane of incidence parallel to the orbit plane in pure π-polarization mode ($P = |\cos 2\theta_B|$). The former, vertical plane of incidence is often chosen to avoid vanishing of reflections in the region of $2\theta_B = 90^\circ$. The ability to record patterns with either pure σ-mode or pure π-mode polarization is very helpful in the study of several dynamical diffraction phenomena. To facilitate switching of polarization mode, some diffractometers and cameras built for use with synchrotron sources are rotatable bodily about the incident-beam axis (Bonse & Fischer, 1981; Bowen, Clark, Davies, Nicholson, Roberts, Sherwood & Tanner, 1982; Bowen & Davies, 1983). From the diffraction-theoretical standpoint, it is the section topograph that provides the image of fundamental importance. High-resolution section-topograph patterns have been recorded with synchrotron radiation using a portable assembly combining crystal mount and narrow incident-beam slit. With the help of optical methods of alignment, this can be transferred between topograph cameras set up at a conventional source and at the synchrotron source (Lang, 1983).

The regularly pulsed time structure of synchrotron radiation can be exploited in stroboscopic X-ray topography. The wavefronts of travelling surface acoustic waves (SAW) on lithium niobate crystals have been imaged, and their perturbation by lattice defects disclosed (Whatmore, Goddard, Tanner & Clark, 1982; Cerva & Graeff, 1984, 1985). The latter workers made detailed studies of the relative contributions to the image made by orientation contrast and by 'wavefield deviation contrast' (*i.e.* contrast arising from deviation of the energy-flow vector in the elastically strained crystal).

2.7.4.2. *Incident-beam monochromatization*

In order to achieve extremely small beam divergences and wavelength pass bands ($\mathrm{d}\lambda/\lambda$), and, in particular, to suppress transmission of harmonic wavelengths, arrangements much more complicated than the double-crystal systems shown in Figs. 2.7.3.1 and 2.7.3.3 have been applied in synchrotron-radiation topography. The properties of monochromator crystals are discussed in Section 4.2.5. In synchrotron-radiation topographic applications, the majority of monochromators are constructed from perfect silicon, with occasional use of germanium. Damage-free surfaces of optical quality can be prepared in any orientation on silicon, and smooth-walled channels can be milled into silicon monoliths to produce multireflection devices. First, for simpler monochromatization systems, one possibility is to set up a monochromator crystal oriented for Bragg reflection with asymmetry $b \gg 1$ (*i.e.* giving $W_{\text{out}}/W_{\text{in}} \ll 1$) to produce a narrow monochromatic beam with which section topographs can be taken (Mai, Mardix & Lang, 1980). The standard $+-$ double-crystal topography arrangement is frequently used with synchrotron sources, the experimental procedure being as described in Section 2.7.3 and benefiting from the small divergence of the incident beam due to remoteness of the source. An example of a more refined angular probe is that obtainable by employing a pair of silicon crystals in $++$ setting to prepare the beam

Table 2.7.4.1. *Monolithic monochromator for plane-wave synchrotron-radiation topography*

Reflection 1	$\bar{3}33$
Reflection 2	$\bar{1}3\bar{1}$
Reflection 3	$1\bar{3}\bar{1}$
Output wavelength	0.12378 nm
Spectral pass band, $d\lambda/\lambda$	$\sim 7 \times 10^{-6}$
Angular divergence of exit beam	$\sim 1.4 \times 10^{-6}$
Size of exit beam	15×15 mm

incident on the specimen crystal, the three crystals together forming a $+ + -$ arrangement (Ishikawa, Kitano & Matsui, 1985). The first monochromator is oriented for asymmetric $11\bar{1}$ Bragg reflection, the second for highly asymmetric $55\bar{3}$ reflection ($W_{out}/W_{in} = 64$ at $\lambda = 0.12$ nm), resulting in a divergence of only 0.5×10^{-6} in the beam impinging on the specimen.

Multireflection systems, some of which were proposed by Du Mond (1937) but not at that time realizable, have become a practicality through the advent of perfect silicon and germanium. When multiple reflection occurs between the walls of a channel cut in a perfect crystal, the tails of the curve of angular dependence of reflection intensity can be greatly attenuated without much loss of reflectivity at the peak of the curve (Bonse & Hart, 1965*a*). Beaumont & Hart (1974) described combinations of such 'channel-cut' monochromators that were suitable for use with synchrotron sources. One combination, consisting of a pair of contra-rotating channel-cut crystals, with each channel acting as a pair of reflecting surfaces in symmetrical $+ -$ setting, has found much favour as a monochromatizing device producing neither angular deviation nor spatial displacement of the final beam, whatever the wavelength it is set to pass. The properties of monoliths with one or more channels and employing two or more asymmetric reflections in succession have been analysed by Kikuta & Kohra (1970), Kikuta (1971), and Matsushita, Kikuta & Kohra (1971).

Symmetric channel-cut monochromators in perfect undistorted crystals transmit harmonic reflections. Several approaches to the problem of harmonic elimination may be taken, such as one of the following procedures (or possibly more than one in combination).

(1) Using crystals of slightly different interplanar spacing (*e.g.* silicon and germanium) in the $+ -$ setting, which then becomes slightly dispersive (Bonse, Materlik & Schröder, 1976; Bauspiess, Bonse, Graeff & Rauch, 1977).

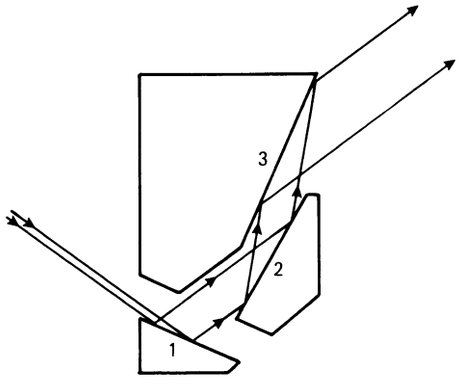

Fig. 2.7.4.1. Monolithic multiply reflecting monochromator for plane-wave topography.

(2) Laue case (transmission) followed by Bragg case (reflection), with deliberate slight misorientation between the diffracting elements (Materlik & Kostroun, 1980).

(3) Asymmetric reflection in non-parallel channel walls in a monolith (Hashizume, 1983).

(4) Misorientating a multiply reflecting channel, either one wall with respect to the opposite wall, or one length segment with respect to a following length segment (Hart & Rodrigues, 1978; Bonse, Olthoff-Münter & Rumpf, 1983; Hart, Rodrigues & Siddons, 1984).

For X-ray topographic applications, it is very desirable to have a spatially wide beam issuing from the multiply reflecting device. This is achieved, together with small angular divergence and spectral window, and without need of mechanical bending, in a monolith design by Hashizume, though it lacks wavelength tunability (Petroff, Sauvage, Riglet & Hashizume, 1980). The configuration of reflecting surfaces of this monolith is shown in Fig. 2.7.4.1. Reflection occurs in succession at surfaces 1, 2, and 3. The monochromator characteristics are listed in Table 2.7.4.1. The wavelength is very suitable in many topographic applications, and this design has proved to be an effective beam conditioner for use in synchrotron-radiation 'plane-wave' topography.

2.7.5. Some special techniques

2.7.5.1. *Moiré topography*

In X-ray optics, the same basic geometrical interpretation of moiré patterns applies as in light and electron optics. Suppose radiation passes successively through two periodic media, (1) and (2), whose reciprocal vectors are $\mathbf{h}_1$ and $\mathbf{h}_2$, so as to form a moiré pattern. Then, the reciprocal vector of the moiré fringes will be $\mathbf{H} = \mathbf{h}_1 - \mathbf{h}_2$. The magnitude, D, of the moiré fringe spacing is $|\mathbf{H}|^{-1}$ and may typically lie in the range 0.1 to 1 mm in the case of X-ray moiré patterns. Simple special cases are the 'rotation' moiré pattern in which $|\mathbf{h}_1| = |\mathbf{h}_2| = d^{-1}$, but $\mathbf{h}_1$ makes a small angle α with $\mathbf{h}_2$. Then, the spacing of the moiré fringes is d/α and the fringes run parallel to the bisector of the small angle α. The other special case is the 'compression' moiré pattern. Here, $\mathbf{h}_1$ and $\mathbf{h}_2$ are parallel but there is a small difference between their corresponding spacings, d_1 and d_2. The spacing D of compression moiré fringes is given by $D = d_1 d_2/(d_1 - d_2)$ and the fringes lie parallel to the grating rulings or Bragg planes in (1) and (2). X-ray moiré topographs achieve sensitivies of 10^{-7} to 10^{-8} in measuring orientation differences or relative differences in interplanar spacing. Moreover, if either periodic medium contains a lattice dislocation, Burgers vector $\mathbf{b}$, for which $\mathbf{b} \cdot \mathbf{h} \neq 0$, then a magnified image of the dislocation will appear in the moiré pattern, as one or more fringes terminating at the position of the dislocation, the number of terminating fringes being $\mathbf{b} \cdot \mathbf{h}$, which is necessarily integral (Hashimoto & Uyeda, 1957).

X-ray moiré topography has been performed with two quite different arrangements, the Bonse & Hart interferometer, and by superposition of separate crystals (Brádler & Lang, 1968). For accounts of the principles and applications of the interferometer, see, for example, Bonse & Hart (1965*b*, 1966), Hart (1968, 1975*b*), Bonse & Graeff (1977), Section 4.2.6 and §4.2.6.3.1. Fig. 2.7.5.1 shows the arrangement (Hart, 1968, 1972) for obtaining large-area moiré topographs by traversing the interferometer relative to a ribbon incident beam in similar fashion to taking a normal projection topograph (Fig. 2.7.2.2); P is the incident-beam slit, Q is a

stationary slit selecting the beam that it is desired to record, and film, *F*, and interferometer, *SMA*, together traverse to and fro as indicated by the double-headed arrow. In Fig. 2.7.5.1, *S*, *M*, and *A* are the three equally thick wafers of the interferometer that remain upstanding above the base of the monolithic interferometer after the gaps between *S* and *M*, and *M* and *A*, have been milled away. The elements *S*, *M* and *A* are called the splitter, mirror, and analyser, respectively. The moiré pattern is formed between the Bragg planes of *A* and the standing-wave pattern in the overlapping $\mathbf{K}_0$ and $\mathbf{K}_h$ beams entering it. Maximum fringe visibility occurs in the emerging beam that the slit *Q* is shown selecting. A dislocation will appear in the moiré pattern whether the lattice dislocation lies in *S*, *M*, or *A*, provided $\mathbf{b} \cdot \mathbf{h} \neq 0$. Moiré patterns formed in a number of Bragg reflections whose normals lie in, or not greatly inclined to, the plane of the wafers, can be recorded by appropriate orientation of the monolith. By this means, it is easily discovered in which wafer the dislocation lies, and its Burgers vector can be completely determined, including its sense, the latter being found by a deliberate slight elastic deformation of the interferometer (Hart, 1972). Satisfactory moiré topographs have been obtained with an interferometer in a synchrotron beam, despite thermal gradients due to the local intense irradiation (Hart, Sauvage & Siddons, 1980).

Fig. 2.7.5.2 shows crystal slices (1), *ABCD*, and (2), *EFGH*, superposed and simultaneously Bragg reflecting in the Brádler–Lang (1968) method of X-ray moiré topography. The slices could have been cut from separate crystals. In the case when the Bragg planes of (1) and (2) are in identical orientation but have a translational mismatch across *CD* and *EF* with a component parallel to **h**, strong scattering occurs towards *Z* as focus, producing extra intensity at T' in the $\mathbf{K}_0$ beam TT'' and at R' in the $\mathbf{K}_h$ beam RR''. It is usual to record the moiré pattern using the $\mathbf{K}_h$ beam. Projection moiré topographs are obtained by the standard procedure of traversing the crystal pair and film together with respect to the incident beam *SO*. The special procedure devised for mutually aligning the two crystals so that $\mathbf{h}_1$ and $\mathbf{h}_2$ coincide within their angular range of reflection is explained by Brádler & Lang (1968). This method has been applied to silicon and to natural (Lang, 1968) and synthetic quartz (Lang, 1978).

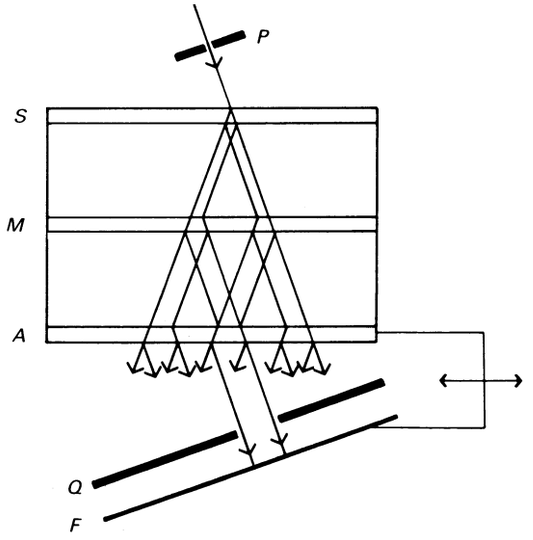

Fig. 2.7.5.1. Scanning arrangement for moiré topography with the Bonse–Hart interferometer.

2.7.5.2. *Real-time viewing of topograph images*

Position-sensitive detectors involving the production of electrons are described in Chapter 7.1, Sections 7.1.6 and 7.1.7, and Arndt (1986, 1990). Those descriptions cover all the image-forming devices that form the core of systems set up for 'live' X-ray topography. Here, discussion is limited to remarks on the historical development of techniques designed for making X-ray topographic images directly visible, and on the leading systems that are now sufficiently developed to be acceptable for routine use, in particular on topograph cameras set up at synchrotron X-ray sources. Two types of system became practicalities about the same time, that using direct conversion of X-rays to electronic signals by means of an X-ray-sensitive vidicon television camera tube (Chikawa & Fujimoto, 1968), and the indirect method using an external X-ray phosphor coupled to a multistage electronic image-intensifier tube (Reifsnider & Green, 1968; Lang & Reifsnider, 1969) or to a television-camera tube incorporating an image-intensifier stage (Meieran, Landre & O'Hara, 1969). These two approaches, the direct and the indirect, remain in competition. Developments up to the middle 1970's have been comprehensively reviewed by Hartman (1977). Since that time, Si-based, two-dimensional CCD (charge-coupled device) arrays have come into prominence as radiation detectors. They can be used for direct conversion of low-energy X-rays into electronic charges as well as for recording images of phosphor screens. As illustrated by Allinson (1994), four configurations employing CCD arrays for X-ray imaging can be considered: (i) direct detection by the 'naked' device; (ii) detection by phosphor coated directly on the CCD array; (iii) phosphor separate, and optically coupled to the CCD by lens or fibre-optics; and (iv) the addition to (iii) of an image intensifier

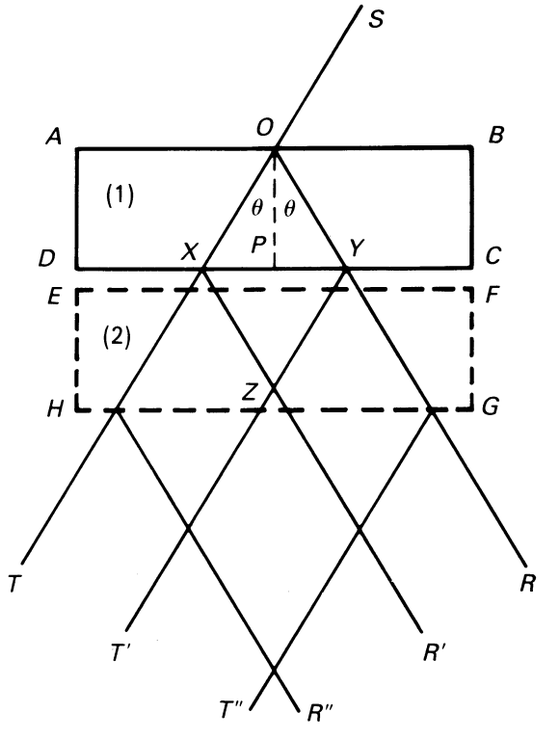

Fig. 2.7.5.2. Superposition of crystals (1) and (2) for production of moiré topographs. [Reproduced from *Diffraction and Imaging Techniques in Material Science*, Vol. II. *Imaging and Diffraction Techniques*, edited by S. Amelinckx, R. Gevers & J. Van Landuyt (1978), Fig. 21, p. 695. Amsterdam, New York, Oxford: North-Holland.]

or microchannel plate coupled to the phosphor screen. Consider first configuration (i). X-ray absorption efficiency in the active layer of silicon is near unity for radiations such as Cu $K\alpha$, and is not less than about 20% for Mo $K\alpha$ or Ag $K\alpha$. Since about one-third of the absorbed energy goes into electron–hole pair production, an absorbed 8 keV X-ray photon creates about 2000 pairs, a large number compared with a combined dark-current plus read-out noise level per photosite of a few tens of electrons r.m.s. Thus, single-photon counting is possible. Moreover, a cooled CCD can integrate the charge accumulated in each pixel for up to $\sim 10^3$ s. With pixel sizes in the range 10 to 30 μm square, and 1024×1024 (or 2048×2048) arrays in production, sensitive areas of 50 mm square, or greater, are available, sufficient for the majority of topographic applications.

For X-ray-sensitive TV-camera tubes, some major improvements in resolution and sensitivity have taken place since the first applications to X-ray topography of Be-windowed vidicons. Using the more sensitive 'Saticon' tube with incorporation of a 20 μm-thick Se–As target that provides good X-ray absorption efficiency, Chikawa, Sato & Fujimoto (1984) achieved a resolution as good as 6 μm at a modulation transfer function (MTF) of 5%. This betters that achieved with indirect systems or with standard-pixel-size CCD arrays used as direct detectors. The newer 'Harp' tube, which employs avalanche multiplication produced by a high field ($\sim 10^8$ V m^{-1}) applied across a 2 μm Se target to increase light sensitivity at least ten fold compared with the Saticon tube, has also been modified into a direct X-ray detector. Increasing the target thickness to 8 μm and adding an X-ray-transparent window provides satisfactory detector efficiency over a useful wavelength range (and the Se $K\alpha$-absorption edge at 0.098 nm causes absorption efficiencies for Cu $K\alpha$ and Mo $K\alpha$ to be similar, about 25%). The gain is sufficient for detection of single Cu $K\alpha$ photon-absorption events (at least for photons absorbed close to the target front, giving the maximum path for avalanche formation). A limiting resolution of about 25 μm (at MTF of ~33%) is exhibited (Sato, Maruyama, Goto, Fujimoto, Shidara, Kawamura, Hirai, Sakai & Chikawa, 1993), not yet as good as the 6 μm achieved with the Saticon tube. The rather small 6×9 mm sensitive areas of these camera tubes (when in standard '$\frac{2}{3}$ in' size) restricts their range of topographic applications as direct detectors compared with CCD arrays, but their amorphous Se targets are less likely to be degraded by X-radiation damage than crystalline-silicon CCD arrays. The latter do suffer degradation, but recover after treatment (Allinson, Allsopp, Quayle & Magorrian, 1991).

In the case of indirect systems, the lens or fibre-optic plate situated between phosphor and detector automatically protects the latter from radiation damage. Somewhat better resolution can be achieved by lens coupling than by fibre-optic coupling of phosphor to detector, but at the expense of loss of light-collection efficiency generally too great to be acceptable. In principle, magnification or de-magnification of the phosphor-screen image on the detector can be selected according to whether phosphor or detector has the better resolution, in order to maximize the system resolution as a whole. Phosphor resolution can be increased by diminishing its thickness below the value that would be chosen from consideration of X-ray absorption efficiency alone. Using a phosphor screen of Gd_2O_2S(Tb) only 5 μm thick, and lens-coupling it with tenfold magnification on to the target of a low-light-level television camera, Hartmann achieved a system resolution of about 10 μm (Queisser, Hartmann & Hagen, 1981), as good as any demonstrated so far with indirect systems.

The phosphors already used (or potentially usable) in real-time X-ray topography are inorganic compounds containing elements of medium or heavy atomic weight. They include ZnS(Ag), NaI(Tl), CsI(Tl), Y_2O_2S(Tb), Y_2O_2S(Eu), La_2O_2S(Eu) and Gd_2O_2S(Tb). Problems encountered are light loss by light trapping within single-crystal phosphor sheets, and resolution loss by light scattering from grain to grain in phosphor powders. Various ways of reducing lateral light-spreading within phosphor screens by imposing a columnar structure upon them have been tried. Most success has been achieved with CsI. Evaporated layers of this crystal have a natural tendency towards columnar cracking normal to the substrate. Then internal reflection within columns reduces 'cross talk' between columns (Stevels & Kühl, 1974). However, a columnar structure can be very effectively imposed on CsI films evaporated on to fibre-optic plates by etching away the cladding glass surrounding each fibre core to a depth of 10 μm, say. The evaporated CsI starts growing on the protruding cores, and continues as pillars physically separated and hence to a large degree optically separated from their neighbours (Ito, Yamaguchi & Oba, 1987; Allinson, 1994; Castelli, Allinson, Moon & Watson, 1994).

The drive to develop systems for 2D imaging of single-crystal or fibre diffraction patterns produced by synchrotron radiation that offer spatial resolution better than that within the grasp of position-sensitive multiwire gas proportional counters (say 100–200 μm) has produced several phosphor/fibre-optic/CCD combinations that with some modifications would be useful for real-time X-ray topography. Diffraction-pattern recording requires a sensitive area not less than about 50 mm in diameter, so most systems incorporate a fibre-optic taper to couple a larger phosphor screen with a small CCD array. Spatial resolution in the X-ray image cannot then be better than CCD pixel size multiplied by the taper ratio. In one system that has been fully described, this product is $20.5\ \mu m \times 2.6$, and a point-spread FWHM of 80 μm on a 51×51 mm input area was realised without benefit from a columnar-structure phosphor (Tate, Eikenberry, Barna, Wall, Lawrance & Gruner, 1995). More appropriate for X-ray topography would be unit-magnification optical coupling of phosphor with a CCD array of not less than 1024×1024 elements and not more than 20 μm square pixel size. With such a combination, a system resolution of ~25 μm should be achievable; and at a synchrotron X-ray topography station at least one device offering resolution no worse than this should be available. There is a scope for both high-resolution, small-sensitive-area and lower-resolution, large-sensitive-area imaging systems in real-time X-ray topography. It has been shown possible to incorporate both types in a single topography camera for use with synchrotron radiation (Suzuki, Ando, Hayakawa, Nittono, Hashizume, Kishino & Kohra, 1984).

International Tables for Crystallography (2006). Vol. C, Chapter 2.8, pp. 124–125.

2.8. Neutron diffraction topography

BY M. SCHLENKER AND J. BARUCHEL

2.8.1. Introduction

Some salient differences between neutron diffraction and X-ray diffraction are that

(*a*) neutron beams are not available in standard ('home') laboratories,

(*b*) the available neutron fluxes are small even at a high-flux reactor and even when compared with laboratory X-ray generators (Scherm & Fåk, 1993),

(*c*) absorption is negligible in most materials (see Section 4.4.6), and

(*d*) magnetic scattering is a strong component (see Section 4.4.5).

All these differences have effects on the use of neutrons for diffraction imaging (hereafter called, according to standard usage, neutron topography), while the obvious similarities in scattering amplitude and geometry make such topography possible. The effect of (*a*) is that the first attempts at neutron topography occurred late, with the work of Doi, Minakawa, Motohashi & Masaki (1971), Ando & Hosoya (1972), and Schlenker & Shull (1973), and that it is practised at very few places in the world, though one of them, at Institut Laue–Langevin (ILL), is open to external users.

2.8.2. Implementation

As a result of (*b*), the resolution of neutron topography is poor. It was estimated to be no better than 60 μm in non-polarized work on the instrument installed at ILL Grenoble, for exposure times of hours, as a result of roughly equal contributions from detector resolution, geometric blurring due to beam divergence, and shot noise, *i.e.* fluctuation in the number of diffracted neutrons reaching a pixel. The same reason leads to the technique being instrumentally simple because refinements that might lead, for example, to better resolution are discouraged by the increase in exposure time they would imply. Typically, a neutron beam with divergence of the order of 10′ is monochromated by a non-perfect crystal (mosaic spread a few minutes of arc), and the monochromatic beam illuminates the sample, which can be either a single crystal or a grain in a polycrystal. It is advantageous, but not mandatory, to use a white beam delivered by a curved neutron guide tube as the divergence is already limited and high-energy parts of the spectrum, which would contribute to unwanted background, as well as γ-rays, are eliminated. After the specimen is set for a chosen Bragg reflexion with the help of a detector and counter, a neutron-sensitive photographic detector (see §7.3.1.2.3) is placed across the diffracted beam, as near the sample as possible to minimize geometric blurring effects while avoiding the direct transmitted beam. Very crude but comparatively fast exposures can be made with Polaroid film and an isotopically enriched ^{6}LiF (ZnS) phosphor screen. Better topographs are obtained with X-ray film associated with a gadolinium foil (if possible isotopically enriched in ^{157}Gd) acting as an $n \rightarrow \beta$ converter, or with a track-etch plastic foil with an ^{6}LiF or $^{10}B_4C$ foil or layer ($n \rightarrow \alpha$ converter) (Malgrange, Petroff, Sauvage, Zarka & Englander, 1976). Alternatively, an electronic position-sensitive neutron detector can be used for both setting and imaging (Davidson & Case, 1976; Sillou *et al.*, 1989).

Polarized neutrons are extremely useful in the investigation of magnetic domains. The use of a polarizing monochromator and a crude attachment providing a guide field and the possibility to flip the polarization can provide this possibility as an option because the requirements are much less stringent than in quantitative structural polarized-neutron-diffraction work.

It is also possible to use the white beam from a curved guide tube directly (Boeuf, Lagomarsino, Rustichelli, Baruchel & Schlenker, 1975), in the same way as in synchrotron-radiation X-ray topography, that is to say making a Laue diagram, each spot of which is a topograph. The technique is then instrumentally extremely simple, but background is a problem. Because the beam divergence is so much larger than for synchrotron radiation, the resolution is much worse than in the latter case, but it is not expected to differ significantly from the monochromatic beam neutron version.

The ability of neutron beams to go through furnaces or cooling devices, one of the advantages in neutron diffraction work in general, is of course retained in topography. It is, however, desirable to retain a small ($\sim$<2 cm) specimen-to-film distance.

2.8.3. Application to investigations of heavy crystals

As indicated in (*c*) in Section 2.8.1, the absorption of neutrons by most materials is very small. As a result, it is possible to investigate the defect distribution in samples that are too large and/or contain elements too heavy to be suitable for X-ray topography. Another interesting potentiality is the investigation of crystals where X-rays induce a reaction, for example polymerization (Dudley, Baruchel & Sherwood, 1990). While there is no problem except for the resolution and exposure time with thin crystals of heavy materials (Baruchel, Schlenker, Zarka & Petroff, 1978), the observation of large crystals by the standard, wide-beam technique that corresponds to standard topography implies a superposition of the contributions of sizeable portions of the crystal. It is therefore convenient to restrict the observation to a virtual slice, exactly as in Lang's method of X-ray section topography in low-absorption cases (Schlenker, Baruchel, Perrier de la Bathie & Wilson, 1975; Davidson & Case, 1976). This method is useful in particular in the process of preparation of monochromator crystals (Hustache, 1979). It has been applied in metallographic investigations of large crystals of copper-based alloys (Tomimitsu, Doi & Kamada, 1983).

2.8.4. Investigation of magnetic domains and magnetic phase transitions

The strong contribution of electronic magnetic moments in materials to neutron diffraction [item (*d*) in Section 2.8.1] makes magnetic neutron scattering a unique tool in determining magnetic structures on the unit-cell level. When a single-crystal specimen contains regions with different magnetic structures, *i.e.* magnetic domains or coexisting phases with different magnetic structures, they will be imaged because of the local variations in structure amplitude, and hence in diffracted intensity, they entail. Ferromagnetic domains can be imaged by neutron topography (Schlenker & Shull, 1973). This is of restricted value because so many other and more efficient techniques are available, albeit not for observations in the bulk. But neutron topography is the only method available to visualize antiferromagnetic domains of various kinds. The pioneering work by Ando & Hosoya (1972, 1978) and Davidson, Werner &

Copyright © 2006 International Union of Crystallography

Arrott (1974) showed spin-density wave domains in antiferromagnetic chromium. Chirality domains (right/left-handed helix in helimagnets), as well as 180° antiferromagnetic domains, could also be observed for the first time using polarized neutron topography (Baruchel, Schlenker & Palmer, 1990). Neutron topography is also a valuable tool in the investigation of the coexistence of different magnetic phases, for example heli- and ferromagnetic, at a first-order phase transition, which can be driven either by temperature changes or by applying a magnetic field (Baruchel, 1989).

International Tables for Crystallography (2006). Vol. C, Chapter 2.9, pp. 126–146.

2.9. Neutron reflectometry

By G. S. Smith and C. F. Majkrzak

2.9.1. Introduction

The neutron reflectivity of a surface is defined as the ratio of the number of neutrons elastically and specularly reflected to the number of incident neutrons. When measured as a function of neutron wave-vector transfer, the reflectivity curve contains information regarding the profile of the in-plane average of the scattering-length density (or simply scattering density) normal to that surface. The concentration of a given atomic species at a particular depth can then be inferred. Although similar information can often be extracted from X-ray reflectivity data, an additional sensitivity is gained by using neutrons in those cases where elements with nearly the same number of electrons or different isotopes (especially hydrogen and deuterium) need to be distinguished. Furthermore, if the incident neutron beam is polarized and the resultant polarization of the reflected beam analysed, it is possible to determine, in both magnitude and direction, the in-plane magnetic moment depth profile. This latter capability is greatly facilitated by the simple correlation of the relative counts of neutron spin-flip and non-spin-flip scattering to magnetic moment orientation and by the relatively high instrumental polarization and spin-flipping efficiencies possible with neutrons. These properties make neutron reflectivity a powerful tool for the study of surface layers and interfaces.

2.9.2. Theory of elastic specular neutron reflection

Consider the glancing (small-angle) reflection of a neutron plane wave characterized by a wave vector $\mathbf{k}_i$ from a perfectly flat and smooth surface of infinite lateral extent, as depicted schematically in Fig. 2.9.2.1. Although the density of the material can, in general, vary as a function of depth [along the direction (z) of the surface normal], it is assumed that there are no in-plane variations of the density. If the scattering is also elastic, so that the neutron neither gains nor loses energy (*i.e.* $|\mathbf{k}_i| = |\mathbf{k}_f| = k = 2\pi/\lambda$, where the subscripts i and f signify initial and final values, respectively, and λ is the neutron wavelength), then the component of the neutron wave vector parallel to the surface must be conserved. In this case, the magnitude of the wave-vector transfer is $Q = |\mathbf{Q}| = |\mathbf{k}_f - \mathbf{k}_i| = 2k\sin(\theta) = 2k_z$, where the angles of incidence and reflection, θ, are equal, and the scattering is said to be *specular*. Since at low values of Q the neutrons are strongly scattered from the surface (*i.e.* the magnitude of the reflectivity approaches 1), the neutron wave function is significantly distorted from its free-space plane-wave form. The first Born approximation normally applied in the description of high-Q crystal diffraction is therefore not valid for the analysis of low-Q reflectivity measurements, and a more accurate, dynamical treatment is required.

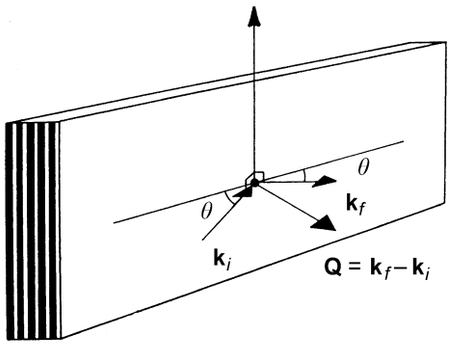

Fig. 2.9.2.1. Schematic diagram of reflection geometry.

Because the in-plane component of the neutron wave vector is a constant of the motion in the specular elastic reflection process described above, the appropriate equation of motion is the one-dimensional, time-independent, Schrödinger equation (see, for example, Merzbacher, 1970)

$$\psi''(z) + k_z^2\psi(z) = 0, \tag{2.9.2.1}$$

where ψ is the neutron wave function [which in free space is proportional to $\exp(ik_{0z}z)$, where k_{0z} is the magnitude of the z component of the neutron wave vector in vacuum]. If the infinite planar boundary from which the neutron wave reflects separates vacuum from a medium in which the neutron potential energy is V_1, conservation of the neutron's total energy requires that

$$k_{0z}^2 = k_{1z}^2 + \frac{2mV_1}{\hbar^2}, \tag{2.9.2.2}$$

where $\hbar$ is Planck's constant divided by 2π and m is the neutron mass. If $2\pi/Q$ has a magnitude much greater than interatomic distances in the medium, then the medium can be treated as if it were a continuum. In this limit, the potential energy V_1 can be expressed as (see, for example, Sears, 1989)

$$V_1 = \frac{2\pi\hbar^2\overline{Nb}}{m}, \tag{2.9.2.3}$$

where $\overline{Nb} = \sum N_i b_i$, i represents the ith atomic species in the material, N_i is the number density of that species and b_i is the coherent neutron scattering length for the ith atom (which is in general complex if absorption or an effective absorption such as isotopic incoherent scattering exists; magnetic contributions are not accounted for here but will be considered below). The quantity $\overline{Nb} \equiv \rho$ is the effective scattering density. Substituting the expression for V_1 given in equation (2.9.2.3) into (2.9.2.2) yields

$$k_{1z}^2 = k_{0z}^2 - 4\pi\rho(z). \tag{2.9.2.4}$$

In order to calculate the reflectivity, continuity of the wave function and its first derivative (with respect to z) are imposed. These boundary conditions are a consequence of restrictions on current densities required by particle and momentum conservation. In general, given a sample with layers of varying potentials where the boundaries of the jth layer are at z_{oj} and $z_{oj} + \delta_j$, and the potential, V_j, is constant over that layer, it can be shown that (see, for example, Yamada, Ebisawa, Achiwa, Akiyoshi & Okamoto, 1978)

$$\begin{aligned}\begin{pmatrix}\psi_j(z_{oj}+\delta_j)\\ \psi_j'(z_{oj}+\delta_j)\end{pmatrix} &= \mathbf{M}_j\begin{pmatrix}\psi_j(z_{oj})\\ \psi_j'(z_{oj})\end{pmatrix}\\ &= \begin{pmatrix}\psi_{j+1}(z_{oj}+\delta_j)\\ \psi_{j+1}'(z_{oj}+\delta_j)\end{pmatrix},\end{aligned} \tag{2.9.2.5}$$

where

$$\mathbf{M}_j = \begin{pmatrix}\cos(k_{jz}\delta_j) & (1/k_{jz})\sin(k_{jz}\delta_j)\\ -k_{jz}\sin(k_{jz}\delta_j) & \cos(k_{jz}\delta_j)\end{pmatrix}, \tag{2.9.2.6}$$

Copyright © 2006 International Union of Crystallography

and k_{jz} is the magnitude of the neutron wave vector in the jth layer [equation (2.9.2.4)].

The first equality in (2.9.2.5) relates the wave function at one boundary within the jth layer to the next boundary within the jth layer, whereas the second equality represents the continuity of the wave function and its derivative across the boundary between the jth and $(j+1)$th layers. When a neutron plane wave is incident on a multilayer sample, we can take the incident amplitude as unity, set up the coordinate system to have $z = 0$ at the air/sample interface, and write the wave function in air as the sum of the incident and reflected waves,

$$\psi_{\text{incident}}(z) = \exp(ik_{0z}z) + R\exp(-ik_{0z}z), \tag{2.9.2.7}$$

and the wave function in the substrate as a purely transmitted wave,

$$\psi_{\text{substrate}}(z) = T\exp(ik_{sz}z), \tag{2.9.2.8}$$

where k_{sz} is the magnitude of the z component of the neutron wave vector in the substrate. By combining equations (2.9.2.5) through (2.9.2.8), we obtain a working equation for calculating the reflectivity:

$$\begin{pmatrix} T \\ ik_{sz}T \end{pmatrix}\exp(ik_{sz}\Delta) = M_N M_{N-1}\ldots M_1\begin{pmatrix} (1+R) \\ ik_{0z}(1-R) \end{pmatrix}, \tag{2.9.2.9}$$

where $\Delta = \sum\delta \equiv$ total film thickness. The experimentally measured reflection and transmission coefficients $|R|^2$ and $|T|^2$ can be computed from (2.9.2.9). The procedure outlined above can be applied in piece-wise continuous fashion to arbitrary, smooth potentials, $\rho(z)$, which are approximated to any desired degree of accuracy by an appropriate number of consecutive rectangular slabs, each having its own uniform scattering density, ρ_j, and thickness, δ_j, as depicted in Fig. 2.9.2.2.

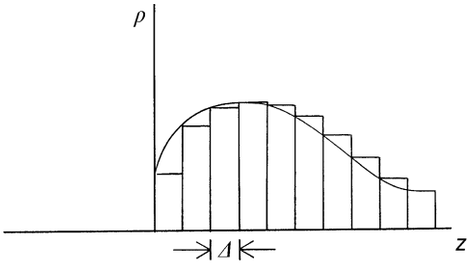

Fig. 2.9.2.2. Arbitrary scattering density profile represented by slabs of uniform potential.

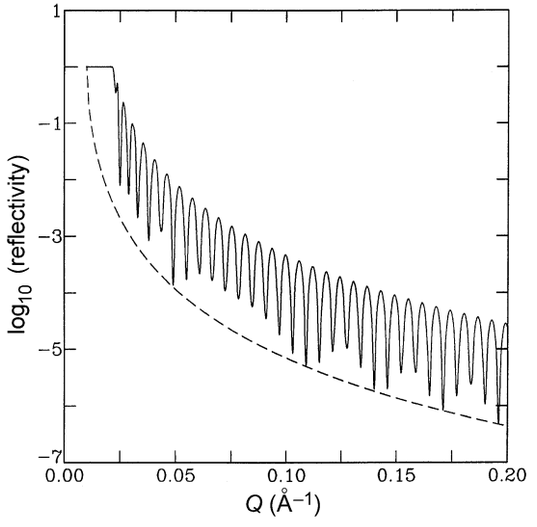

Fig. 2.9.2.3. Neutron reflectivities calculated for an infinite Si substrate (dashed line) and 1000 Å Ni film on an Si substrate (solid line).

If $k_{0z}^2 < 4\pi\rho_{\text{substrate}}$, then k_z becomes imaginary in the substrate, and total external reflection occurs. In addition, for a single layer deposited on the substrate, the reflectivity will oscillate with a periodicity characteristic of the layer thickness. Fig. 2.9.2.3 compares the ideal Fresnel reflectivity corresponding to an infinite silicon substrate and that of a 1000Å nickel film deposited on silicon. For a barrier of finite thickness, tunnelling phenomena can also be observed (see, for instance, Merzbacher, 1970; Buttiker, 1983; Nuñez, Majkrzak & Berk, 1993; Steinhauser, Steryl, Scheckenhofer & Malik, 1980).

With the matrix method described above, the reflectivity of any model scattering-density profile can be calculated with quantitative accuracy over many orders of magnitude. Unfortunately, the inverse computation of an unknown scattering density profile corresponding to a given reflectivity curve can be exceedingly difficult, in part due to the the lack of phase information on $R(Q)$, which forces one to use highly non-linear relations between $|R(Q)|^2$ and $\rho(z)$. Often, parameterized model scattering-density profiles are fit to the experimental data (Felcher & Russell, 1991). Recently, several authors have described model-independent methods for obtaining $\rho(z)$ from measured reflectivity curves (Zhou & Chen, 1993; Pedersen & Hamley, 1994; Berk & Majkrzak, 1995).

2.9.3. Polarized neutron reflectivity

Reflectivity measurements with polarized neutrons can reveal the in-plane magnetization-vector depth profile in magnetic thin films and multilayers. The interaction between the neutron and atomic magnetic moments is dependent upon their relative orientations. Two important yet simple selection rules apply in the case where the neutron polarization axis (defined by an applied magnetic field at the sample position) is perpendicular to **Q**. Any component of the in-plane magnetization parallel to this quantization axis gives rise to non-spin-flip (NSF) neutron scattering, which interferes with scattering due to the nuclear potential: any perpendicular magnetic component creates spin-flip (SF) scattering, which is purely magnetic. Consequently, the atomic magnetic moment's direction can be inferred by measuring the two NSF (++, −−) and two SF (+−, −+) reflectivities (where +− refers to a reflection measurement in which the incident neutron magnetic moment is parallel to the applied field and only neutrons with their magnetic moment antiparallel to the applied field are measured, *etc*.), in addition to its absolute magnitude (which is proportional to a magnetic scattering density $\rho_M = Np$, where p is a magnetic scattering length). The matrix formalism described earlier to obtain the reflectivity in the non-polarized-beam case can be extended to treat polarized beams as well. The resulting transfer matrix is, however, in the latter instance a 4×4 matrix relating two spin-dependent reflectivities and transmissions for each of two possible incident-neutron spin states. The matrix elements are given in Felcher, Hilleke, Crawford, Haumann, Kleb & Ostrowski (1987), and more detailed discussions of the method of polarized neutron reflectometry can be found in Majkrzak (1991) and Majkrzak, Ankner, Berk & Gibbs (1994).

2.9.4. Surface roughness

Up to this point, we have only considered reflection from smooth, flat surfaces. In reality, however, all surfaces have microscopic or mesoscopic imperfections such as steps, facets and rough hills and valleys. In this case, the potential must be represented by a three-dimensional function instead of the simple one-dimensional example discussed above. In addition, the roughness may not be confined to the outer surface or substrate, but the imperfections may propagate through several layers. This roughness at the interfaces modifies the specularly reflected beam and adds a diffuse component to the scattered beam (*i.e.* neutrons scattered at angles other than the incident angle). Theories based on the distorted-wave, Born approximation have been developed to describe this type of scattering (Nevot & Croce, 1980; Sinha, Sirota, Garroff & Stanley, 1988; Pynn, 1992; Sears, 1993; Holy, Kubena, Ohlidal, Lischka & Plotz, 1993; de Boer, 1994) for a microscopically rough surface. These theories give results consistent with the earlier work (Nevot & Croce, 1980) for the modification to the specular scattering due to a single rough surface. The reader is referred to Sinha, Sirota, Garroff & Stanley (1988) and Pynn (1992) for a more complete discussion of diffuse scattering.

In order to fit the specular scattering from a rough surface, two simple methods have been employed. First, using the matrix method discussed above, the rough interface can be modelled as a smoothly varying scattering density approximated as a series of steps. This has the advantage that complex interfaces that are combinations of rough surfaces and intermixed layers can be approximated. The other method is to extend the results of Nevot to each successive interface while iteratively calculating the reflection amplitude. This method works well for simple interfaces of Gaussian roughness and is faster, in general, than the matrix method, since fewer calculations are needed for each interface. However, this latter technique suffers from frequently yielding unphysical answers (*i.e.* surface widths greater than adjacent layer thicknesses). Both of these methods are inadequate, in that there is no way to separate the effects of graded interfaces from rough surfaces. This can only be done with a simultaneous examination of both the diffuse and specular scattering.

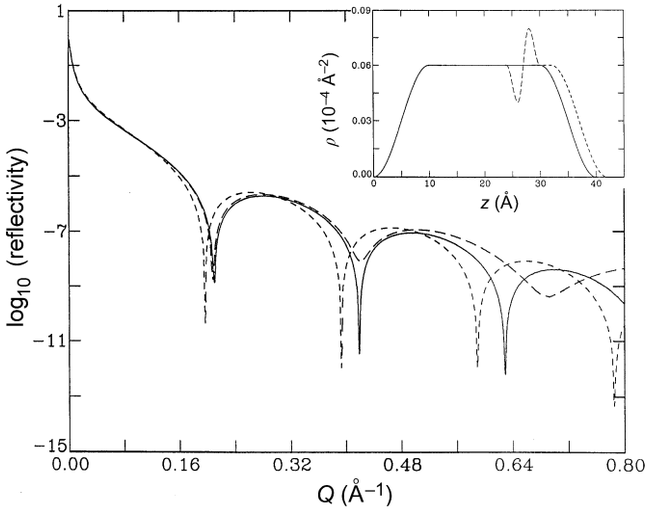

Fig. 2.9.6.1. Calculated neutron reflectivity curves corresponding to the three density profiles in the inset (*i.e.* solid line in density profile corresponds to solid line in reflectivity plot). Note that in the density plots the solid and long-dash curves coincide except at the oscillation on top of the plateau, whereas the solid and short-dashed curves coincide except at the trailing edge between 30 and 42 Å.

2.9.5. Experimental methodology

Neutron reflectivity measurements can be carried out in two principal ways: either (1) with a monochromatic incident beam of narrow angular divergence in the plane of reflection (defined by $\mathbf{k}_i$ and $\mathbf{k}_f$, where λ is constant, and Q is varied by changing the glancing angle of incidence, θ, relative to the sample surface; or (2) using a pulsed polychromatic incident beam, also of narrow angular divergence at fixed θ, and obtaining data over a range of Q values simultaneously by performing time-of-flight analysis on the reflected neutrons. For either method, the instrumental resolution is simply given as

$$\left(\frac{\Delta Q}{Q}\right)^2 = \left(\frac{\Delta\lambda}{\lambda}\right)^2 + \left(\frac{\Delta\theta}{\theta}\right)^2, \qquad (2.9.5.1)$$

where $\Delta\theta$ is the angular divergence of the reflected beam, and $\Delta\lambda$ is the wavelength spread. In the case of a steady-state source,

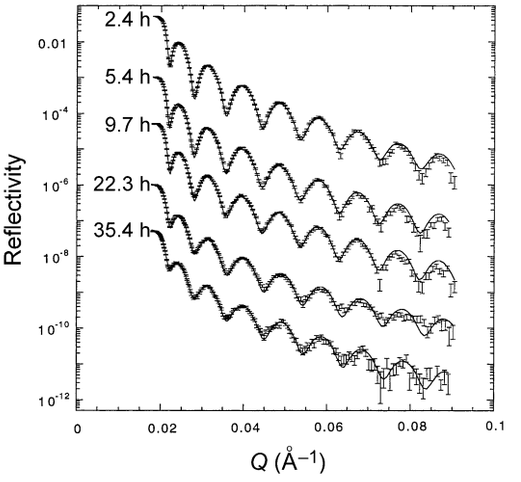

Fig. 2.9.7.1. Measured neutron reflectivities from boron bilayers [from Smith *et al.* (1992)].

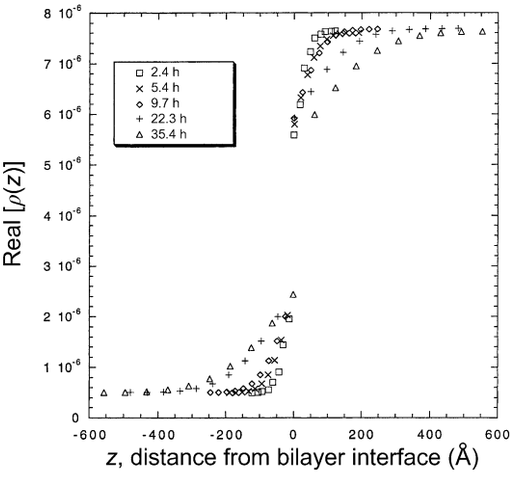

Fig. 2.9.7.2. The fitted real part of the scattering density profiles for the measured reflectivities of Fig. 2.9.7.1. Note the pinning of the concentration of ^{10}B at the interface [after Smith *et al.* (1992)].

the wavelength resolution is determined by the monochromator, whereas the timing and moderator characteristics determine the wavelength resolution on a time-of-flight instrument. Although the second term in equation (2.9.5.1) is standard in scattering, it has a unique characteristic, in that the angular divergence of the reflected beam determines the resolution. This is the case because the sample is a δ-function scatterer, so that the angle of the incident beam can be determined precisely by knowing the reflected angle (Hamilton, Hayter & Smith, 1994). For a more complete description of both types of neutron reflectometry instrumentation, see Russell (1990).

2.9.6. Resolution in real space

From Fig. 2.9.2.3, the period δQ of the reflectivity oscillation (in the region where the Born approximation becomes valid, sufficiently far away from the critical angle) is inversely proportional to the thickness t of the film. That is, $2\pi/(\delta Q) = t$. Consequently, in order to be able to resolve reflectivity oscillations for a film of thickness t, the instrumental Q resolution ΔQ [from equation (2.9.5.1)] must be approximately $2\pi/t$ or smaller. With sufficiently good instrumental resolution, even the thickness of a film with non-abrupt interfaces can be accurately determined, as demonstrated by the hypothetical case depicted in Fig. 2.9.6.1 (where the instrumental resolution is taken to be perfect): an overall film-thickness difference of 2 Å (between 42 and 40 Å films) is clearly resolved at a Q of about 0.2 Å^{-1}. In practice, differences even less than this can be distinguished. Note, however, that to 'see' more detailed features in the scattering-density profile (such as the oscillation on top of the plateau shown for the long-dash profile in the inset of Fig. 2.9.6.1), other than the overall film thickness, it can be necessary to make reflectivity measurements at values of Q corresponding to 2π/(characteristic dimension of the feature).

2.9.7. Applications of neutron reflectometry

2.9.7.1. *Self-diffusion*

One of the simplest, yet powerful, examples of the use of neutron reflectivity is in the study of self-diffusion. Most techniques to measure diffusion coefficients rely on chemical and mechanical methods to measure density profiles after a sample

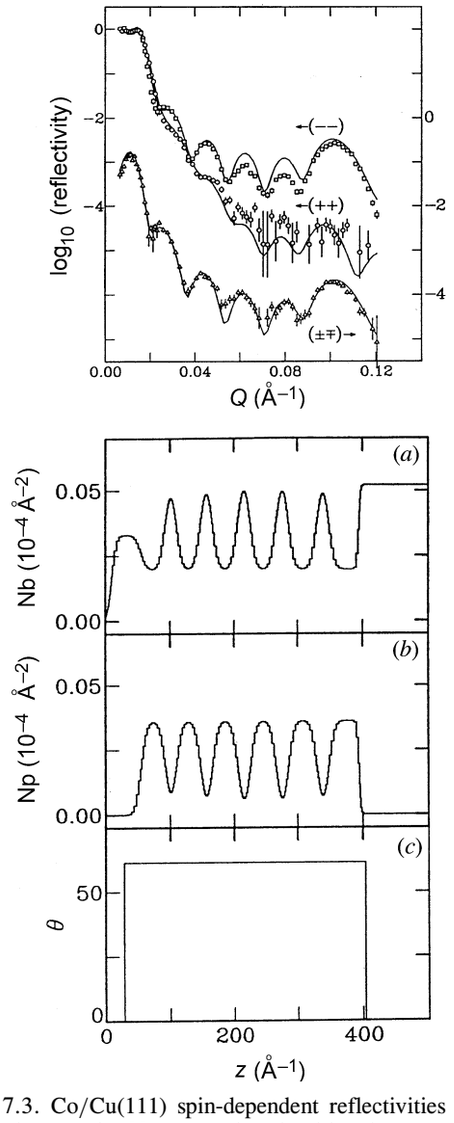

Fig. 2.9.7.3. Co/Cu(111) spin-dependent reflectivities (top). Nuclear (Nb) and magnetic (Np) scattering densities (bottom). Also shown is the (constant) moment direction [after Schreyer *et al.* (1993)].

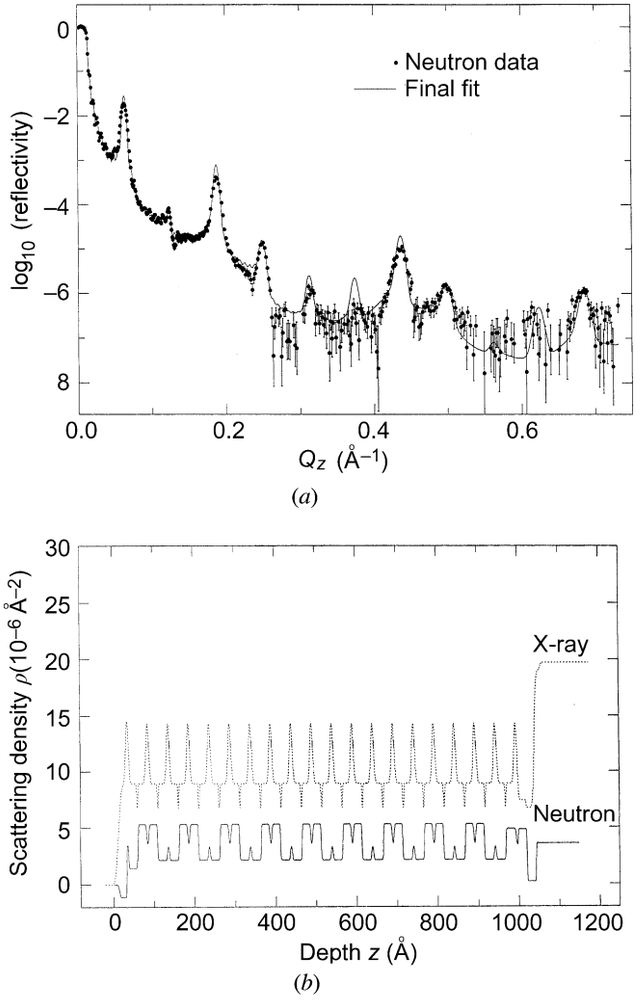

Fig. 2.9.7.4. (*a*) Measured neutron reflectivity for the Langmuir–Blodgett multilayer described in the text along with the fit. (*b*) Both corresponding neutron and X-ray scattering density profiles. The X-ray reflectivity is more sensitive to the high-Z barium in the head groups whereas the neutron reflectivity can distinguish mixing between adjacent hydrogenated and deuterated hydrocarbon tails [after Wiesler *et al.* (1995)].

has been annealed. Then a model for the diffusion is assumed, and the coefficients are calculated. Using standard techniques, researchers are unable to detect the movement of an atom through a sample of like atoms. However, using single bilayers of amorphous ^{10}B and ^{11}B, it was shown (Smith, Hamilton, Fitzsimmons, Baker, Hubbard, Nastasi, Hirvonen & Zocco, 1992) through neutron-reflectivity measurements that the diffusion of boron in boron could be measured by studying the density profile (see Figs. 2.9.7.1 and 2.9.7.2) of one isotope in the other as a function of annealing time. Also, because of the sensitivity of the technique to the interfacial density profile, it was found that standard Fickian diffusion models could not explain the measured density profiles.

2.9.7.2. *Magnetic multilayers*

In order to understand interlayer coupling mechanisms, it is necessary to know what the magnetic superstructure is for a given nonmagnetic spacer layer thickness and/or applied field strength. Fig. 2.9.7.3 shows the spin-dependent reflectivities for a Co/Cu (111) multilayer along with the nuclear (Nb) and magnetic (Np) scattering-density profiles deduced from the data of Schreyer, Zeidler, Morawe, Metoki, Zabel, Ankner & Majkrzak (1993). In this specific case, the in-plane ferromagnetic Co layers are themselves coupled ferromagnetically across the nonmagnetic Cu, all at a constant angle.

2.9.7.3. *Hydrogenous materials*

There are a substantial number of applications of neutron reflectometry in the study of hydrogenous films and multilayers, including diblock copolymer, surfactant, Langmuir–Blodgett, self-assembled monolayer, and lipid bilayer films. Reviews of the extensive research that has already been done have been written by Russell (1990) and Penfold & Thomas (1990). Only one specific example will be given here.

Fig. 2.9.7.4 shows neutron reflectivity data and the corresponding density profile for a Langmuir–Blodgett film composed of alternating bilayers of deuterated and hydrogenated stearic acid [after Wiesler, Feigin, Majkrzak, Ankner, Berzina & Troitsky (1995)]. Also shown in Fig. 2.9.7.4 is the scattering-density profile for the same sample as seen by X-rays. It is obvious that the X-rays are more sensitive to the high-Z barium in the head group, whereas the neutrons are especially good at distinguishing the degree of mixing between adjacent hydrogenated and deuterated hydrocarbon tails. This is a good example of the complementary nature of neutron and X-ray reflectivities.

References

2.1–2.2

Amorós, J. L., Buerger, M. J. & Amorós, M. C. (1975). *The Laue method*. New York: Academic Press.

Andrews, S. J., Hails, J. E., Harding, M. M. & Cruickshank, D. W. J. (1987). *Acta Cryst.* A**43**, 70–73.

Arndt, U. W. (1986). *X-ray position-sensitive detectors. J. Appl. Cryst.* **19**, 145–163.

Arndt, U. W. & Willis, B. T. M. (1966). *Single crystal diffractometry*. Cambridge University Press.

Arndt, U. W. & Wonacott, A. J. (1977). *The rotation method in crystallography*. Amsterdam: North-Holland.

Artymiuk, P. & Phillips, D. C. (1985). *On the design of diffractometers to measure a number of reflections simultaneously. Methods Enzymol.* **114**A, 397–415.

Bernal, J. D. (1927). *A universal X-ray photogoniometer. J. Sci. Instrum.* **4**, 273–284.

Bijvoet, J. M., Burgers, W. G. & Hägg, G. (1969). *Early papers on diffraction of X-rays by crystals*, Vol. I. Dordrecht: Kluwer Academic Publishers.

Bijvoet, J. M., Burgers, W. G. & Hägg, G. (1972). *Early papers on diffraction of X-rays by crystals*, Vol. II. Dordrecht: Kluwer Academic Publishers.

Blundell, T. L. & Johnson, L. N. (1976). *Protein crystallography*. New York: Academic Press.

Bonse, U., Materlik, G. & Schröder, W. (1976). *Perfect-crystal monochromators for synchrotron X-radiation. J. Appl. Cryst.* **9**, 223–230.

Bragg, W. H. (1928). *An introduction to crystal structure analysis*. London: Bell.

Bragg, W. L. (1949). *The crystalline state: a general survey*, pp. 30–33. London: Bell.

Brooks, I. & Moffat, K. (1991). *Laue diffraction from protein crystals using a sealed-tube X-ray source. J. Appl. Cryst.* **24**, 146–148.

Buerger, M. J. (1942). *X-ray crystallography*. New York: John Wiley.

Buerger, M. J. (1964). *The precession method*. New York: John Wiley.

Carr, P. D., Cruickshank, D. W. J. & Harding, M. M. (1992). *The determination of unit-cell parameters from Laue diffraction patterns using their gnomonic projections. J. Appl. Cryst.* **25**, 294–308.

Cassetta, A., Deacon, A., Emmerich, C., Habash, J., Helliwell, J. R., McSweeney, S., Snell, E., Thompson, A. W. & Weisgerber, S. (1993). *The emergence of the synchrotron Laue method for rapid data collection from protein crystals. Proc. R. Soc. London Ser. A*, **442**, 177–192.

Charpak, G., Demierre, C., Kahn, R., Santiard, J. C. & Sauli, F. (1977). *Some properties of spherical drift chambers. Nucl. Instrum. Methods*, **141**, 449.

Coppens, P. (1992). *Synchrotron radiation crystallography*. New York: Academic Press.

Cruickshank, D. W. J., Carr, P. D. & Harding, M. M. (1992). *Estimation of d_{min}, λ_{min} and λ_{max} from the gnomonic projections of Laue patterns. J. Appl. Cryst.* **25**, 285–293.

Cruickshank, D. W. J., Helliwell, J. R. & Moffat, K. (1987). *Multiplicity distribution of reflections in Laue diffraction. Acta Cryst.* A**43**, 656–674.

Cruickshank, D. W. J., Helliwell, J. R. & Moffat, K. (1991). *Angular distribution of reflections in Laue diffraction. Acta Cryst.* A**47**, 352–373.

Evans, H. T. & Lonsdale, K. (1959). *Diffraction geometry. International tables for X-ray crystallography*, Vol. II, p. 164. Birmingham: Kynoch Press.

Friedrich, W., Knipping, P. & von Laue, M. (1912). *Interferenz-Erscheinungen bei Röntgenstrahlen. Sitzungsber K. Bayer. Akad. Wiss. Muenchen*, pp. 303–322.

Glusker, J. P. & Trueblood, K. N. (1971). *Crystal structure analysis*, pp. 35–47. Oxford University Press.

Glusker, J. P. & Trueblood, K. N. (1985). *Crystal structure analysis*, 2nd ed., pp. 42–60. Oxford University Press.

2.1–2.2 (*cont.*)

Greenhough, T. J. & Helliwell, J. R. (1982). *Oscillation camera data processing: reflecting range and prediction of partiality. 2. Monochromatic synchrotron X-radiation from a singly bent triangular monochromator. J. Appl. Cryst.* **15**, 493–508.

Hamilton, W. C. (1974). *Angle settings for four-circle diffractometers. International tables for X-ray crystallography*, Vol. IV, pp. 273–284. Birmingham: Kynoch Press. (Present distributor Kluwer Academic Publishers, Dordrecht.)

Hamlin, R. (1985). *Multi-wire area X-ray diffractometers. Methods Enzymol.* **114**A, 416–451.

Hamlin, R., Cork, C., Howard, A., Nielsen, C., Vernon, W., Matthews, D., Xuong, Ng. H. & Perez-Mendez, V. (1981). *Characteristics of a flat multiwire area detector for protein crystallography. J. Appl. Cryst.* **14**, 85–93.

Harrison, S. C., Winkler, F. K., Schutt, C. E. & Durbin, R. (1985). *Oscillation method with large unit cells. Methods Enzymol.* **114**A, 211–236.

Hart, M. (1971). *Bragg reflection X-ray optics. Rep. Prog. Phys.* **34**, 435–490.

Hastings, J. B. (1977). *X-ray optics and monochromators for synchrotron radiation. J. Appl. Phys.* **48**, 1576–1584.

Hastings, J. B., Kincaid, B. M. & Eisenberger, P. (1978). *A separated function focussing monochromator system for synchrotron radiation. Nucl. Instrum. Methods*, **152**, 167–171.

Helliwell, J. R. (1984). *Synchrotron X-radiation protein crystallography: instrumentation, methods and applications. Rep. Prog. Phys.* **47**, 1403–1497.

Helliwell, J. R. (1985). *Protein crystallography with synchrotron radiation. J. Mol. Struct.* **130**, 63–91.

Helliwell, J. R. (1992). *Macromolecular crystallography with synchrotron radiation*. Cambridge University Press.

Helliwell, J. R. & Wilkinson, C. (1994). *X-ray and neutron Laue diffraction*. In *Neutron and synchrotron radiation for condensed matter studies: applications to soft condensed matter and biology*, Vol. III, edited by J. Baruchel, J. L. Hodeau, M. S. Lehmann, J. R. Regnard & C. Schlenker. Berlin: Springer Verlag.

Henry, N. F. M., Lipson, H. & Wooster, W. A. (1951). *The interpretation of X-ray diffraction photographs*. London: Macmillan.

Higashi, T. (1989). *The processing of diffraction data taken on a screenless Weissenberg camera for macromolecular crystallography. J. Appl. Cryst.* **22**, 9–18.

Howard, A., Nielsen, C. & Xuong, Ng. H. (1985). *Software for a diffractometer with multi-wire area detector. Methods Enzymol.* **114**A, 452–472.

International Tables for X-ray Crystallography (1959). Vol. II. Birmingham: Kynoch Press.

Jeffery, J. W. (1958). *An investigation of the blank areas on Laue photographs round: 1. The direct beam, and 2. Reflections with simple indices. Z. Kristallogr.* **110**, 321–328.

Kohra, K., Ando, M., Matsushita, T. & Hashizume, H. (1978). *Design of high-resolution X-ray optical system using dynamical diffraction for synchrotron radiation. Nucl. Instrum. Methods*, **152**, 161–166.

Lairson, B. M. & Bilderback, D. H. (1982). *Transmission X-ray mirror – a new optical element. Nucl. Instrum. Methods*, **195**, 79–83.

Lemonnier, M., Fourme, R., Rousseaux, F. & Kahn, R. (1978). *X-ray curved-crystal monochromator system at the storage ring DCI. Nucl. Instrum. Methods*, **152**, 173–177.

McKie, D. & McKie, C. (1986). *Essentials of crystallography*. Oxford: Blackwell Scientific Publications.

Moffat, K., Schildkamp, W., Bilderback, D. H. & Volz, K. (1986). *Laue diffraction from biological samples. Nucl. Instrum. Methods*, A**246**, 617–623.

Rabinovich, D. & Lourie, B. (1987). *Use of the polychromatic Laue method for short-exposure X-ray diffraction data acquisition. Acta Cryst.* A**43**, 774–780.

Rossmann, M. G. (1985). *Determining the intensity of Bragg reflections from oscillation photographs. Methods Enzymol.* **114**A, 237–280.

Sakabe, N. (1983). *A focusing Weissenberg camera with multilayer-line screens for macromolecular crystallography. J. Appl. Cryst.* **16**, 542–547.

Sakabe, N. (1991). *X-ray diffraction data collection systems for modern protein crystallography with a Weissenberg camera and an imaging plate using synchrotron radiation. Nucl. Instrum. Methods*, A**303**, 448–463.

Stout, G. H. & Jensen, L. H. (1968). *X-ray structure determination: a practical guide*, pp. 83–194. New York: Macmillan.

Vainshtein, B. K. (1981). *Modern crystallography*. I, pp. 297–300. Berlin: Springer.

Weisgerber, S. & Helliwell, J. R. (1993). *High-resolution crystallographic studies of native concanavalin A using rapid Laue data collection methods and the introduction of a monochromatic large-angle oscillation technique (LOT). J. Chem. Soc. Faraday Trans.* **89**, 2667–2675.

Weissenberg, K. (1924). *Ein neues Röntgengoniometer. Z. Phys.* **23**, 229–238.

Witz, J. (1969). *Focusing monochromators. Acta Cryst.* A**25**, 30–42.

Wlodawer, A. (1985). *Methods Enzymol.* **114**A, 551–564.

Woolfson, M. M. (1970). *Introduction to X-ray crystallography*. Cambridge University Press.

Woolfson, M. M. (1997). *Introduction to X-ray crystallography*, 2nd ed. Cambridge University Press.

Wyckoff, H. W. (1985). *Diffractometry. Methods Enzymol.* **114**A, 330–385.

Wyckoff, H. W., Hirs, C. H. W. & Timasheff, S. N. (1985). *Diffraction methods for biological macromolecules. Part A. Methods in Enzymol.* **114**A, 199–588.

Xuong, Ng. H., Nielsen, C., Hamlin, R. & Anderson, D. (1985). *Strategy for data collection from protein crystals using a multiwire counter area detector diffractometer. J. Appl. Cryst.* **18**, 342–350.

2.3

Ahtee, M., Nurmela, M., Suortti, P. & Järvinen, M. (1989). *Correction for preferred orientation in Rietveld refinement. J. Appl. Cryst.* **22**, 261–268.

Alexander, L. E. (1969). *X-ray diffraction methods in polymer science*. New York: John Wiley. [Reprint 1979; Huntington, New York: Krieger.]

Anderson, C. A. F., Zolensky, M. E., Smith, D. K., Freeborn, W. P. & Scheetz, B. E. (1981). *Applications of Gandolfi X-ray diffraction to the characterization of reaction products from the alteration of simulated nuclear wastes. Adv. X-ray Anal.* **24**, 265–269.

Andrews, S. J., Papiz, M. Z., McMeeking, R., Blake, A. J., Lowe, B. M., Franklin, K. R., Helliwell, J. R. & Harding, M. M. (1988). *Piperazine silicate (EU 19): the structure of a very small crystal determined with synchrotron radiation. Acta Cryst.* B**44**, 73–77.

2.3 (*cont.*)

Arai, T., Shoji, T. & Omote, K. (1986). *Measurement of the spectral distribution emitted from X-ray spectrographic tubes. Adv. X-ray Anal.* **29**, 413–422.

Ateiner, J., Termonia, Y. & Deltour, J. (1974). *Comments on smoothing and differentiation of data by simplified least squares procedures. Anal. Chem.* **44**, 1906–1909.

Attfield, J. P., Cheetham, A. K., Cox, D. E. & Sleight, A. W. (1988). *Synchrotron X-ray and neutron powder diffraction studies of the structure of α-$CrPO_4$. J. Appl. Cryst.* **21**, 452–457.

Australian Journal of Physics (1988). *X-ray powder diffractometry. Aust. J. Phys.* **41**(2), 101–335.

Azároff, L. V. & Buerger, M. J. (1958). *The powder method in X-ray crystallography*. New York: McGraw-Hill.

Bachmann, R., Kohler, H., Schultz, H. & Weber, H.-P. (1985). *Structure investigation of a 6 μm CaF_2 crystal with synchrotron radiation. Acta Cryst.* A**41**, 35–40.

Baker, T. W., George, J. D., Bellamy, B. A. & Causer, R. (1968). *Fully automated high-precision X-ray diffraction. Adv. X-ray Anal.* **11**, 359–375.

Barraud, J. (1949). *Monochromateur-focalisateur logarithmique: application à l'étude de la texture et des déformations des cristaux. C. R. Acad. Sci.* **229**, 378–380.

Barrett, C. S. & Massalski, T. B. (1980). *Structure of Metals*, 3rd revised ed. New York: McGraw-Hill.

Bearden, J. A. (1964). *X-ray wavelengths*. US Atomic Energy Commission, Div. Techn. Inf. Ext., Oak Ridge, TN, USA; (1967) *Rev. Mod. Phys.* **39**, 78–124; (1974) *International tables for X-ray crystallography*, Vol. IV, pp. 6–43.

Bearden, J. A. & Burr, A. F. (1965). *Atomic energy levels*. US Atomic Energy Commission, Div. Techn. Inf. Ext., Oak Ridge, TN, USA.

Beaumont, J. H. & Hart, M. (1974). *Multiple Bragg reflection monochromators for synchrotron radiation. J. Phys. E*, **7**, 823–829.

Benedetti, A., Fagherazzi, A., Enzo, S. & Battagliarin, M. (1988). *A profile-fitting procedure for analysis of broadened X-ray diffraction peaks. II. Application and discussion of the methodology. J. Appl. Cryst.* **21**, 543–549.

Birks, L. S., Seebold, R. E., Grant, B. K. & Grosso, J. S. (1965). *X-ray yield and line/background ratios for electron excitation. J. Appl. Phys.* **36**. 699–702.

Bish, D. L. & Post, J. E. (1989). Editors. *Modern powder diffraction. Reviews in Mineralogy*, Vol. 20. Washington: Mineralogical Society of America.

Bish, D. L. & Reynolds, R. C. (1989). *Sample preparation for X-ray diffraction. Modern powder diffraction*, edited by D. L. Bish & J. E. Post, Chap. 4. Washington: Mineralogical Society of America.

Bleeksma, J., Kloos, G. & DiGiovanni, H. J. (1948). *X-ray spectrometer with Geiger counter for measuring powder diffraction patterns. Philips Tech. Rev.* **10**, 1–12.

Block, S. & Hubbard, C. R. (1980). Editors. *Accuracy in powder diffraction. US Natl Bur. Stand. Spec. Publ.* No. 567.

Bohlin, H. (1920). *Eine neue Anordnung für röntgenkristallographische Untersuchungen von Kristallpulver. Ann. Phys. (Leipzig)*, **61**, 421–439.

Bojarski, Z. & Bołd, T. (1979). Editors. *Conference on applied crystallography*, 2 Vols. Silesian University, Katowice, Poland.

Bonse, U. & Hart, M. (1965). *An X-ray interferometer. Appl. Phys. Lett.* **6**, 155–156.

Bonse, U. & Hart, M. (1966). *Small angle X-ray scattering by spherical particles of polystyrene and polyvinyltoluene. Z. Phys.* **189**, 151–162.

Borg, I. Y. & Smith, D. K. (1969). *Calculated X-ray powder patterns for silicate minerals. Geol. Soc. Am. Mem.* **122**.

Bragg, W. H. (1921). *Application of the ionization chamber to the determination of the structure of minute crystals. Proc. Phys. Soc.* **33**, 222–224.

Brentano, J. C. M. (1946). *Parafocusing properties of microcrystalline powder layers in X-ray diffraction applied to the design of X-ray goniometers. J. Appl. Phys.* **17**, 420–434.

Brown, D. B. & Ogilvie, R. E. (1964). *Efficiency of production of characteristic X radiation from pure elements bombarded with electrons. J. Appl. Phys.* **35**, 309–314.

Buerger, M. J. (1945). *The design of X-ray powder cameras. J. Appl. Phys.* **16**, 501–510.

Caglioti, G., Paoletti, A. & Ricci, F. P. (1958). *Choice of collimators for a crystal spectrometer for neutron diffraction. Nucl. Instrum. Methods*, **3**, 223–226.

Calvert, L. D., Sirianni, A. F., Gainsford, G. J. & Hubbard, C. R. (1983). *A comparison of methods for reducing preferred orientation. Adv. X-ray Anal.* **26**, 105–110.

Cernik, R. J., Cheetham, A. K., Prout, C. K., Watkin, D. J., Wilkinson, A. P. & Willis, B. T. M. (1991). *The structure of cimetidine ($C_{10}H_{16}N_6S$) solved from synchrotron-radiation X-ray powder diffraction data. J. Appl. Cryst.* **24**, 222–226.

Cheetham, G. M. T., Harding, M. M., Mingos, D. M. P. & Powell, H. R. (1993). *Synthesis and microcrystal structure determination of $[Au_{10}(PPh_3)_7\{S_2C_2(CN)_2\}_2]$. J. Chem. Soc. Chem. Commun.* pp. 1000–1001.

Cline, J. P. & Snyder, R. L. (1983). *The dramatic effect of crystallite size on X-ray intensities. Adv. X-ray Anal.* **26**, 111–117.

Compton, A. H. & Allison, S. K. (1935). *X-rays in theory and experiment*. New York: D. van Nostrand Co.

Cox, D. E., Hastings, J. B., Thomlinson, W. & Prewitt, C. T. (1983). *Applications of synchrotron radiation to high resolution powder diffraction and Rietveld refinement. Nucl. Instrum. Methods*, **208**, 573–578.

Cox, D. E., Toby, B. H. & Eddy, M. M. (1988). *Acquisition of powder diffraction data with synchrotron radiation. Aust. J. Phys.* **41**, 117–131.

Cullity, B. D. (1978). *Elements of X-ray diffraction*, 2nd ed. Reading, Massachusetts: Addison-Wesley.

David, W. I. F. (1986). *Powder diffraction peak shapes. Parameterization of the pseudo-Voigt as a Voigt function. J. Appl. Cryst.* **19**, 63–64.

Davis, B. L. & Smith, D. K. (1988). *Tables of experimental reference intensity ratios. Powder Diffr.* **3**, 205–208.

Debye, P. & Scherrer, P. (1916). *Interferenzen an regellos orientierten Teilchen in Röntgenlicht. Phys. Z.* **17**, 277–283.

Deutsch, M. (1980). *The asymmetrically cut Bonse–Hart X-ray diffractometer. 1. Design principles and performance. J. Appl. Cryst.* **13**, 252–255.

Dollase, W. A. (1986). *Correction of intensities for preferred orientation in powder diffractometry: application of the March model. J. Appl. Cryst.* **19**, 267–272.

DuMond, J. W. M. & Kirkpatrick, H. (1930). *The multiple crystal X-ray spectrograph. Rev. Sci. Instrum.* **1**, 88–105.

Dyson, N. A. (1973). *X-rays in atomic and nuclear physics*. London: Longman.

Edwards, H. J. & Langford, J. I. (1971). *A comparison between the variances of the Cu Kα and Fe Kα spectral distributions. J. Appl. Cryst.* **4**, 43–50.

2.3 (*cont.*)

Edwards, T. H. & Willson, P. D. (1974). *Digital least squares smoothing of spectra*. *Appl. Spectrosc.* **28**, 541–545.

Enzo, S., Fagherazzi, G., Benedetti, A. & Polizzi, S. (1988). *A profile-fitting procedure for analysis of broadened X-ray diffraction peaks. I. Methodology*. *J. Appl. Cryst.* **21**, 536–542.

Evans, R. C., Hirsch, P. B. & Kellar, J. N. (1948). *A 'parallel-beam' concentrating monochromator for X-rays*. *Acta Cryst.* **1**, 124–129.

Fankuchen, I. (1937). *Condensing monochromator for X-rays*. *Nature (London)*, **139**, 193–194.

Fawcett, T. G., Crowder, C. E., Brownell, S. J., Zhang, Y., Hubbard, C., Schreiner, W., Hamill, G. P., Huang, T. C., Sabino, E., Langford, J. I., Hamilton, R. & Louër, D. (1988). *Establishing an instrument peak profile calibration standard for powder diffraction analyses: international round robin conducted by the JCPDS-ICDD and the US National Bureau of Standards*. *Powder Diffr.* **3**, 209–218.

Feder, R. & Berry, B. S. (1970). *Seeman–Bohlin X-ray diffractometer for thin films*. *J. Appl. Cryst.* **3**, 372–379.

Finger, L. W. (1989). *Synchrotron powder diffraction*. *Modern powder diffraction*, edited by D. L. Bish & J. E. Post, Chap. 10. Washington: Mineralogical Society of America.

Gandolfi, G. (1967). *Discussion upon methods to obtain X-ray 'powder patterns' from a single crystal*. *Mineral. Petrogr. Acta*, **13**, 67–74.

Giessen, B. C. & Gordon, G. E. (1968). *X-ray diffraction: a new high-speed technique based on X-ray spectrography*. *Science,* **159**, 973–975.

Göbel, H. E. (1982). *A Guinier diffractometer with a scanning position sensitive detector*. *Adv. X-ray Anal.* **25**, 315–324.

Goldsmith, C. C. & Walker, G. A. (1984). *Small area X-ray diffraction techniques; applications of the microdiffractometer to phase identification and strain determination*. *Adv. X-ray Anal.* **27**, 229–238.

Green, M. (1964). *The angular distribution of characteristic X radiation and its origin within a solid target*. *Proc. Phys. Soc.* **83**, 435–451.

Guinier, A. (1937). *Arrangement for obtaining intense diffraction diagrams of crystalline powders with monochromatic radiation*. *C. R. Acad. Sci.* **204**, 1115–1116.

Guinier, A. (1946). *Sur les monochromateurs à cristal courbé*. *C. R. Acad. Sci.* **223**, 31–32.

Guinier, A. (1956). *Théorie et technique de la radiocristallographie*. Paris: Dunod.

Guinier, A. (1963). *X-ray diffraction*. San Francisco: Freeman.

Guinier, A. & Dexter, D. L. (1963). *X-ray studies of materials*. New York: Interscience.

Guinier, A. & Sébilleau, F. (1952). *Montague achromatique pour la détermination du profile des raies des rayons X. C. R. Acad. Sci.* **235**, 888–890.

Hall, M. M. Jr., Veeraraghavan, V. G., Rubin, H. & Winchell, P. G. (1977). *The approximation of symmetric X-ray peaks by Pearson type VII distributions*. *J. Appl. Cryst.* **10**, 66–68.

Hanawalt, J. D. & Rinn, H. W. (1936). *Identification of crystalline materials. Classification and use of X-ray diffraction patterns*. *Ind. Eng. Chem. Anal. Ed.* **8**, 244–247.

Hanawalt, J. D., Rinn, H. W. & Frevel, L. K. (1938). *Chemical analysis by X-ray diffraction*. *Ind. Eng. Chem. Anal. Ed.* **10**, 457–512.

Harding, M. M. (1988). *The use of synchrotron radiation for Laue diffraction and for the study of very small crystals*. *Chemical crystallography with pulsed neutrons and synchrotron X-rays*, edited by M. A. Carrondo & G. A. Jeffrey, pp. 537–561. *NATO Advanced Study Institute Series C*, Vol. 221. Dordrecht: Kluwer Academic Publishers.

Harding, M. M. & Kariuki, B. M. (1994). *Microcrystal structure determination of $AlPO_4$-CHA using synchrotron radiation*. *Acta Cryst.* C**50**, 852–854.

Harding, M. M., Kariuki, B. M., Cernik, R. J. & Cressey, G. (1994). *The structure of aurichalcite, $(Cu,Zn)_5(OH)_6(CO_3)_2$, determined from a microcrystal*. *Acta Cryst.* B**50**, 673–676.

Hart, M. (1981). *Bragg angle measurement and mapping*. *J. Cryst. Growth*, **55**, 409–427.

Hart, M., Cernik, R. J., Parrish, W. & Toraya, H. (1990). *Lattice parameter determination for powders using synchrotron radiation*. *J. Appl. Cryst.* **23**, 286–291.

Hart, M., Parrish, W. & Masciocchi, N. (1987). *Studies of texture in thin films using synchrotron radiation and energy dispersive diffraction*. *Appl. Phys. Lett.* **50**, 897–899.

Hart, M., Rodrigues, A. R. D. & Siddons, D. P. (1984). *Adjustable resolution Bragg reflection systems*. *Acta Cryst.* A**40**, 502–507.

Hastings, J. B., Thomlinson, W. & Cox, D. E. (1984). *Synchrotron X-ray powder diffraction*. *J. Appl. Cryst.* **17**, 85–89.

Hepp, A. & Baerlocher, Ch. (1988). *Learned peak shape functions for powder diffraction data*. *Austr. J. Phys.* **41**, 229–236.

Hill, R. J. & Madsen, I. C. (1984). *The effect of profile step counting time on the determination of crystal structure parameters by X-ray Rietveld analysis*. *J. Appl. Cryst.* **17**, 297–306.

Hofmann, E. G. & Jagodzinski, H. (1955). *Eine neue, hochauflösende Röntgenfeinstruktur-Anlage mit verbessertem, fokussierendem Monochromator und Feinfokusröhe, Z. Metallkd.* **46**, 601–609.

Howard, S. A. & Preston, K. D. (1989). *Profile fitting of powder diffraction patterns*. *Modern powder diffraction*, edited by D. L. Bish & J. E. Post, Chap. 8. Washington: Mineralogical Society of America.

Howard, S. A. & Snyder, R. L. (1983). *An evaluation of some profile models and the optimization procedures used in profile fitting*. *Adv. X-ray Anal.* **26**, 73–80.

Huang, T. C. (1988). *Precision peak determination in X-ray powder diffraction*. *Aust. J. Phys.* **41**, 201–212.

Huang, T. C., Hart, M., Parrish, W. & Masciocchi, N. (1987). *Line-broadening analysis of synchrotron X-ray diffraction data*. *J. Appl. Phys.* **61**, 2813–2816.

Huang, T. C. & Parrish, W. (1984). *A combined derivative method for peak search analysis*. *Adv. X-ray Anal.* **27**, 45–52.

Hull, A. W. (1917). *A new method of X-ray crystal analysis*. *Phys. Rev.* **10**, 661–696.

Hull, A. W. (1919). *A new method of chemical analysis*. *J. Am. Chem. Soc.* **41**, 1168–1175.

Järvinen, M. (1993). *Application of symmetrized harmonics expansion to correction of the preferred orientation effect*. *J. Appl. Cryst.* **26**, 525–531.

Järvinen, M., Merisalo, M., Pesonen, A. & Inkinen, O. (1970). *Correction of integrated X-ray intensities for preferred orientation in cubic powders*. *J. Appl. Cryst.* **3**, 313–318.

Jenkins, R. (1989). *Instrumentation*. *Modern powder diffraction*, edited by D. L. Bish & J. E. Post, Chap. 2. Washington: Mineralogical Society of America. *Experimental procedures*. *ibid*, Chap. 3.

2.3 (*cont.*)

Jenkins, R., Fawcett, T. G., Smith, D. K., Visser, J. W., Morris, M. C. & Frevel, L. K. (1986). *International Centre for Diffraction Data. Sample preparation methods in X-ray powder diffraction. Powder Diffr.* **1**, 51–63.

Jenkins, R. & Paolini, F. R. (1974). *An automatic divergence slit for the powder diffractometer. Norelco Rep.* **21**, 9–14.

Jenkins, R. & Schreiner, W. N. (1986). *Considerations in the design of goniometers for use in X-ray powder diffractometers. Powder Diffr.* **1**, 305–319.

Jenkins, R. & Snyder, R. L. (1996). *Introduction to X-ray powder diffractometry*. New York: Wiley.

Johann, H. H. (1931). *Die Ergeugung lichstarker Röntgenspektren mit Hilfe von Konkavkristallen. Z. Phys.* **69**, 185–206.

Johansson, T. (1933). *Über ein neuartiges, genau fokussierendes Röntgenspektrometer. Z. Phys.* **82**, 507–528.

Kaplow, R. & Averbach, B. L. (1963). *X-ray diffractometer for the study of liquid structures. Rev. Sci. Instrum.* **34**, 579–581.

Keijser, Th. H. de, Langford, J. I., Mittemeijer, E. J. & Vogels, A. B. P. (1982). *Use of the Voigt function in a single-line method for the analysis of X-ray diffraction line broadening. J. Appl. Cryst.* **15**, 308–314.

Kevex Corporation (1990). Brochure describing equipment.

King, H. W., Gillham, C. J. & Huggins, F. G. (1970). *A versatile Bragg–Brentano/Seemann–Bohlin powder diffractometer. Adv. X-ray Anal.* **13**, 550–577.

Klug, H. P. & Alexander, L. E. (1974). *X-ray diffraction procedures for polycrystalline and amorphous materials*, 2nd ed. New York: John Wiley.

Kunze, G. (1964*a*). *Korrekturen höherer Ordnung für die mit Bragg–Brentano und Seemann–Bohlin Systemen gewonenen Messgrössen unter Berücksichtigung der Primärstrahldivergenz. Z. Angew. Phys.* **17**, 412–421.

Kunze, G. (1964*b*). *Intensitäts-, Absorptions- und Verschiebungsfaktoren von Interferenz-linien bei Bragg–Brentano und Seemann–Bohlin Diffraktometern. I. Z. Angew. Phys.* **17**, 522–534. *II. ibid*, **18**, 28–37.

Ladell, J. (1961). *Interpretation of diffractometer line profiles distortion due to the diffraction process. Acta Cryst.* **14**, 47–53.

Ladell, J. & Parrish, W. (1959). *Determination of spectral contamination of X-ray tubes. Philips Res. Rep.* **14**, 401–420.

Ladell, J., Parrish, W. & Taylor, J. (1959). *Interpretation of diffractometer line profiles. Acta Cryst.* **12**, 561–567.

Ladell, J., Zagofsky, A. & Pearlman, S. (1975). *Cu $K\alpha_2$ elimination algorithm. J. Appl. Cryst.* **8**, 499–506.

Lang, A. R. (1956). *Diffracted-beam monochromatization techniques in X-ray diffractometry. Rev. Sci. Instrum.* **27**, 17–25.

Langford, J. I. (1978). *A rapid method for analysing the breadths of diffraction and spectral lines using the Voigt function. J. Appl. Cryst.* **11**, 10–14.

Langford, J. I. (1982). *The variance as a measure of line broadening: corrections for truncation, curvature and instrument effects. J. Appl. Cryst.* **15**, 315–322.

Langford, J. I. (1987). *Some applications of pattern fitting to powder diffraction data. Prog. Cryst. Growth Charact.* **14**, 185–211.

Langford, J. I. (1992). *The use of the Voigt function in determining microstructural properties from diffraction data by means of pattern decomposition. Accuracy in Powder Diffraction II*, edited by E. Prince & J. K. Stalick, pp. 110–127. *NIST Spec. Publ.* No. 846. Gaithersburg, MA: US Department of Commerce.

Langford, J. I., Delhez, R., de Keijser, Th. H. & Mittemeijer, E. J. (1988). *Profile analysis for microcrystalline properties by the Fourier and other methods. Aust. J. Phys.* **41**, 173–187.

Langford, J. I. & Wilson, A. J. C. (1962). *Counter diffractometer: the effect of specimen transparency on the intensity, position and breadth of X-ray powder diffraction lines. J. Sci. Instrum.* **39**, 581–585.

LeGalley, D. P. (1935). *A type of Geiger–Müller counter suitable for the measurement of diffracted Mo K X-rays. Rev. Sci. Instrum.* **6**, 279–283.

Lehmann, M. S., Christensen, A. N., Fjellvåg, H., Feidenhans'l, R. & Nielsen, M. (1987). *Structure determination by use of pattern decomposition and the Rietveld method on synchrotron X-ray and neutron powder data; the structures of $Al_2Y_4O_9$ and I_2O_4. J. Appl. Cryst.* **20**, 123–129.

Lim, G., Parrish, W., Ortiz, C., Bellotto, M. & Hart, M. (1987). *Grazing incidence synchrotron X-ray diffraction method for analyzing thin films. J. Mater. Res.* **2**, 471–477.

Lindemann, R. & Trost, A. (1940). *Das Interferenz-Zählrohr als Hilfsmittel der Feinstrukturforschung mit Röntgenstrahlen. Z. Phys.* **115**, 456–468.

Lipson, H. & Steeple, H. (1970). *Interpretation of X-ray powder diffraction patterns*. London: Macmillan.

Louër, D. & Langford, J. I. (1988). *Peak shape and resolution in conventional diffractometry with monochromatic X-rays. J. Appl. Cryst.* **21**, 430–437.

McCusker, L. (1988). *The ab initio structure determination of Sigma-2 (a new clathrasil phase) from synchrotron powder diffraction data. J. Appl. Cryst.* **21**, 305–310.

Mack, M. & Parrish, W. (1967). *Seemann–Bohlin X-ray diffractometry. II. Comparison of aberrations and intensity with conventional diffractometer. Acta Cryst.* **23**, 693–700.

Mack, M., Parrish, W. & Taylor, J. (1964). *Methods of determining centroid X-ray wavelengths: Cu Kα and Fe Kα. J. Appl. Phys.* **35**, 118–127.

McMahon, M. I. & Nelmes, R. J. (1993). *New high-pressure phase of Si. Phys. Rev. B*, **47**, 8337–8340.

Malmros, G. & Werner, P. E. (1973). *Automatic densitometer measurement of powder diffraction photographs. Acta Chem. Scand.* **27**, 493–502.

Morris, R. E., Harrison, W. T. A., Nicol, J. M., Wilkinson, A. P. & Cheetham, A. K. (1992). *Determination of complex structures by combined neutron and synchrotron X-ray powder diffraction. Nature (London)*, **359**, 519–522.

Mortier, W. J. & Constenoble, M. L. (1973). *The separation of overlapping peaks in X-ray powder patterns with the use of an experimental profile. J. Appl. Cryst.* **6**, 488–490.

Newsam, J. M., King, H. E. Jr & Liang, K. S. (1989). *X-ray diffraction using synchrotron radiation – a catalysis perspective. Adv. X-ray Anal.* **32**, 9–20.

Ogilvie, R. E. (1963). *Parafocusing diffractometry. Rev. Sci. Instrum.* **34**, 1344–1347.

Parratt, L. G. (1936). *Kα satellite lines. Phys. Rev.* **50**, 1–15.

Parrish, W. (1949). *X-ray powder diffraction analysis: film and Geiger counter techniques. Science,* **110**, 368–371.

Parrish, W. (1955). *Elimination of the second image in double-coated film. Norelco Rep.* **2**, 67.

Parrish, W. (1958). *Advances in X-ray diffractometry of clay minerals. Seventh Natl Conf. Clays and Clay Minerals*, pp. 230–259. New York: Pergamon.

Parrish, W. (1965). *X-ray analysis papers*. Eindhoven: Centrex.

Parrish, W. (1967). *Improved method of measuring X-ray tube focus. Rev. Sci. Instrum.* **12**, 1779–1782.

2.3 (*cont.*)

Parrish, W. (1968). *X-ray diffractometry methods for complex powder patterns. X-ray and electron methods of analysis*, edited by H. van Alphen & W. Parrish, pp. 1–35. New York: Plenum.

Parrish, W. (1974). *Role of diffractometer geometry in the standardization of polycrystalline data. Adv. X-ray Anal.* **17**, 97–105.

Parrish, W. (1983). *History of the X-ray powder method in the USA. Crystallography in North America*, edited by D. M. McLachlan Jr & J. P. Glusker, pp. 201–214. American Crystallographic Association.

Parrish, W. (1988). *Advances in synchrotron X-ray polycrystalline diffraction. Aust. J. Phys.* **41**, 101–112.

Parrish, W. & Cisney, E. (1948). *An improved X-ray diffraction camera. Philips Tech. Rev.* **10**, 157–167.

Parrish, W., Hamacher, E. A. & Lowitzsch, K. (1954). *The 'Norelco' X-ray diffractometer. Philips Tech. Rev.* **16**, 123–133.

Parrish, W. & Hart, M. (1985). *Synchrotron experimental methods for powder structure refinement. Trans. Am. Crystallogr. Assoc.* **21**, 51–55.

Parrish, W. & Hart, M. (1987). *Advantages of synchrotron radiation for polycrystalline diffractometry. Z. Kristallogr.* **179**, 161–173.

Parrish, W., Hart, M. & Huang, T. C. (1986). *Synchrotron X-ray polycrystalline diffractometry. J. Appl. Cryst.* **19**, 92–100.

Parrish, W. & Huang, T. C. (1980). *Accuracy of the profile fitting method for X-ray polycrystalline diffractometry. US Natl Bur. Stand. Spec. Publ.* No. 457, pp. 95–110.

Parrish, W. & Huang, T. C. (1983). *Accuracy and precision in X-ray polycrystalline diffraction. Adv. X-ray Anal.* **26**, 35–44.

Parrish, W., Huang, T. C. & Ayers, G. L. (1976). *Profile fitting: a powerful method of computer X-ray instrumentation and analysis. Trans. Am. Crystallogr. Assoc.* **12**, 55–73.

Parrish, W., Huang, T. C. & Ayers, G. L. (1984). *Computer simulation of powder patterns. Adv. X-ray Anal.* **27**, 75–80.

Parrish, W. & Lowitzsch, K. (1959). *Geometry, alignment and angular calibration of X-ray diffractometers. Am. Mineral.* **44**, 564–583.

Parrish, W., Lowitzsch, K. & Spielberg, N. (1958). *Fluorescent sources for X-ray diffractometry. Acta Cryst.* **11**, 400–405.

Parrish, W. & Mack, M. (1967). *Seemann–Bohlin X-ray diffractometry. I. Instrumentation. Acta Cryst.* **23**, 687–692.

Parrish, W., Mack, M. & Taylor, J. (1963). *Kα satellite interference in X-ray diffractometer line profiles. J. Appl. Phys.* **34**, 2544–2548.

Parrish, W., Mack, M. & Taylor, J. (1966). *Determination of apertures in the focusing plane of X-ray powder diffractometers. J. Sci. Instrum.* **43**, 623–628.

Parrish, W., Mack, M. & Vajda, I. (1967). *Seemann–Bohlin linkage for Norelco diffractometer. Norelco Rep.* **14**, 56–59.

Parrish, W. & Vajda, I. (1966). *Ray-proof slit mount for X-ray powder diffractometers. Rev. Sci. Instrum.* **37**, 1607–1608.

Parrish, W. & Vajda, I. (1971). *X-ray camera having a semicylindrical film holder and means to simultaneously rotate a specimen about two mutually perpendicular axes.* US patent No. 3 626 185, 7 December 1971.

Pawley, G. S. (1981). *Unit-cell refinement from powder diffraction scans. J. Appl. Cryst.* **14**, 357–361.

Peiser, H. S., Rooksby, H. P. & Wilson, A. J. C. (1955). Editors. *X-ray diffraction by polycrystalline materials*. London: The Institute of Physics.

Phillips, W. C. (1985). *X-ray sources. Methods Enzymol.* **114**, 300–316.

Pike, E. R. & Ladell, J. (1961). *The Lorentz factor in powder diffraction. Acta Cryst.* **14**, 53–54.

Piltz, R. O., McMahon, M. I., Crain, J., Hatton, P. D., Nelmes, R. J., Cernik, R. J. & Bushnell-Wye, G. (1992). *An imaging plate system for high-pressure powder diffraction: the data processing side. Rev. Sci. Instrum.* **63**, 700–702.

Prince, E. & Stalick, J. K. (1992). *Accuracy in Powder Diffraction II, NIST Spec. Publ.* No. 846. Gaithersburg, MA: US Department of Commerce.

Pyrros, N. P. & Hubbard, C. R. (1983). *Rational functions as profile models in powder diffraction. J. Appl. Cryst.* **16**, 289–294.

Rachinger, W. A. (1948). *A correction for the $\alpha_1\alpha_2$ doublet in the measurement of widths of X-ray diffraction lines. J. Sci. Instrum.* **25**, 254–255.

Read, M. H. & Hensler, D. H. (1972). *X-ray analysis of sputtered films of beta-tantalum and body-centered cubic titanium. Thin Solid Films,* **10**, 123–135.

Rendle, D. F. (1983). *A simple Gandolfi attachment for a Debye–Scherrer camera and its use in a forensic science laboratory. J. Appl. Cryst.* **16**, 428–429.

Renninger, M. (1956). *Absolutvergleich der Stärksten Röntgenstrahl-Reflexe verschiedener Kristalle. Z. Kristallogr.* **107**, 464–470.

Reynolds, R. C. (1989). *Principles of powder diffraction. Modern powder diffraction*, edited by D. L. Bish & J. E. Post, Chap. 1. Washington: Mineralogical Society of America.

Rietveld, H. M. (1969). *A profile-refinement method for nuclear and magnetic structures. J. Appl. Cryst.* **2**, 65–71.

Rigaku Corporation (1990). Brochure describing equipment.

Ross, P. A. (1928). *A new method of spectroscopy for faint X-radiations. J. Opt. Soc. Am.* **16**, 433–438.

Savitzky, A. & Golay, M. J. E. (1964). *Smoothing and differentiation of data by simplified least squares procedures. Anal. Chem.* **36**, 1627–1639.

Schwartz, L. S. & Cohen, J. B. (1987). *Diffraction from materials,* 2nd ed. New York: Springer-Verlag.

Seemann, H. (1919). *Eine fokussierende röntgenspektroskopische Anordung für Kristallpulver. Ann. Phys. (Leipzig),* **55**, 455–464.

Segmüller, A. (1957). *Die Bestimmung von Glanzwinkeln, Linienbreiten und Intensitäten der Röntgen–interferenzen mit einem Geiger–Zählrohr-goniometer nach dem Seemann–Bohlin-prinzip. Z. Metallkd.* **48**, 448–454.

Shishiguchi, S., Minato, I. & Hashizume, H. (1986). *Rapid collection of X-ray powder data for pattern analysis by a cylindrical position-sensitive detector. J. Appl. Cryst.* **19**, 420–426.

Smith, D. G. W., Reed, S. J. B. & Ware, N. G. (1974). *$K\beta/K\alpha$ intensity ratios for elements of atomic number 20 to 30. X-ray Spectrosc.* **3**, 149–150.

Smith, D. K. (1989). *Computer analysis of diffraction data. Modern powder diffraction*, edited by D. L. Bish & J. E. Post, Chap. 7. Washington: Mineralogical Society of America.

Smith, D. K. & Barrett, C. S. (1979). *Special handling problems in X-ray diffractometry. Adv. X-ray Anal.* **22**, 1–12.

2.3 (*cont.*)

Smith, D. K., Nichols, M. C. & Zolensky, M. E. (1983). *POWD10 – a FORTRAN IV program for calculating X-ray powder diffraction patterns – version 10*. The Pennsylvania State University, University Park, PA, USA.

Smith, G. S. & Snyder, R. L. (1979). *F_N: a criterion for rating powder diffraction patterns and evaluating the reliability of powder-pattern indexing*. *J. Appl. Cryst.* **12**, 60–65.

Smith, S. T., Snyder, R. L. & Brownell, W. E. (1979). *Minimization of preferred orientation in powders by spray drying*. *Adv. X-ray Anal.* **22**, 77–88.

Soller, W. (1924). *A new precision X-ray spectrometer*. *Phys. Rev.* **24**, 158–167.

Sonneveld, E. J. & Visser, J. W. (1975). *Automatic collection of powder data from photographs*. *J. Appl. Cryst.* **8**, 1–7.

Steinmeyer, P. A. (1986). *Special applications of the Debye microdiffractometer*. *Adv. X-ray Anal.* **29**, 251–256.

Straumanis, M. E. (1959). *Absorption correction in precision determination of lattice parameters*. *J. Appl. Phys.* **30**, 1965–1969.

Suortti, P., Ahtee, M. & Unonius, L. (1979). *Voigt function fit of X-ray and neutron powder diffraction profiles*. *J. Appl. Cryst.* **12**, 365–369.

Sussieck-Fornefeld, C. & Schmetzer, K. (1987). *A modified Gandolfi camera with improved adjustment facilities*. *Powder Diffr.* **2**, 82–83.

Tao, K. & Hewett, C. A. (1987). *Thin film X-ray analysis using the Read camera: a refinement of the technique*. *Rev. Sci. Instrum.* **58**, 212–214.

Taupin, D. (1973). *Automatic peak determination in X-ray powder patterns*. *J. Appl. Cryst.* **6**, 266–273.

Taylor, A. (1961). *X-ray metallography*. New York: John Wiley.

Taylor, J., Mack, M. & Parrish, W. (1964). *Evaluation of truncation methods for accurate centroid lattice parameter determination*. *Acta Cryst.* **17**, 1229–1245.

Thompson, P., Cox, D. E. & Hastings, J. B. (1987). *Rietveld refinement of Debye–Scherrer synchrotron X-ray data from Al_2O_3*. *J. Appl. Cryst.* **20**, 79–83.

Toraya, H. (1986). *Whole-powder-pattern fitting without reference to a structural model: application to X-ray powder diffractometer data*. *J. Appl. Cryst.* **19**, 440–447.

Toraya, H. (1988). *The deconvolution of overlapping reflections by the procedure of direct fitting*. *J. Appl. Cryst.* **21**, 192–196.

Toraya, H. (1989). *The determination of direction-dependent crystallite size and strain by X-ray whole-powder-pattern fitting*. *Powder Diffr.* **4**, 130–136.

Toraya, H., Yoshimura, M. & Somiya, S. (1983). *A computer program for the deconvolution of X-ray diffraction profiles with the composite of Pearson type VII functions*. *J. Appl. Cryst.* **16**, 653–657.

Tournarie, M. (1958). *Méthode général de correction des effets instrumentaux appliquée à l'interprétation des diagrammes de rayons X*. *Bull. Soc. Fr. Minéral. Cristallogr.* **81**, 278–286.

Vineyard, G. H. (1982). *Grazing-incidence diffraction and the distorted-wave approximation for the study of surfaces*. *Phys. Rev. B*, **26**, 4146–4159.

Wagner, C. N. J. (1969). *Diffraction analysis of liquid and amorphous alloys*. *Adv. X-ray Anal.* **12**, 50–71.

Warren, B. E. (1969). *X-ray diffraction*. Reading, MA. Addison-Wesley.

Wassermann, G. & Wiewiorosky, J. (1953). *Uber ein Geiger-Zahlrohr-goniometer nach dem Seeman–Bohlin prinzip*. *Z. Metallkd.* **44**, 567–570.

Wertheim, G., Butler, M., West, K. & Buchanan, D. (1974). *Determination of the Gaussian and Lorentzian content of experimental line shapes*. *Rev. Sci. Instrum.* **45**, 1369–1371.

Will, G. (1979). *POWLS: a powder least-squares program*. *J. Appl. Cryst.* **12**, 483–485.

Will, G., Bellotto, M., Parrish, W. & Hart, M. (1988). *Crystal structures of quartz and magnesium germanate by profile analysis of synchrotron-radiation high-resolution powder data*. *J. Appl. Cryst.* **21**, 182–191.

Will, G., Masciocchi, N., Hart, M. & Parrish, W. (1987). *Ytterbium L_{III}-edge anomalous scattering measured with synchrotron radiation powder diffraction*. *Acta Cryst.* A**43**, 677–683.

Will, G., Masciocchi, N., Parrish, W. & Hart, M. (1987). *Refinement of simple crystal structures from synchrotron radiation powder diffraction data*. *J. Appl. Cryst.* **20**, 394–401.

Will, G., Masciocchi, N., Parrish, W. & Lutz, H. D. (1990). *Crystal structure and cation distribution of $MnCrInS_4$ from synchrotron powder diffraction data*. *Z. Kristallogr.* **190**. 277–285.

Wilson, A. J. C. (1963). *Mathematical theory of X-ray powder diffractometry*. Eindhoven: Philips Technical Library.

Wilson, A. J. C. (1965). *The location of peaks*. *Br. J. Appl. Phys.* **16**, 665–674.

Wilson, A. J. C. (1974). *Powder diffractometry*. *X-ray diffraction*, edited by L. V. Azároff, R. Kaplow, N. Kato, R. J. Weiss, A. J. C. Wilson & R. A. Young, Chap. 6. New York: McGraw-Hill.

Wilson, A. J. C. (1980). *Relationship between 'observed' and 'true' intensity: effect of various counting modes*. *Acta Cryst.* A**36**, 929–936.

Wölfel, E. R. (1981). *A new method for quantitative X-ray analysis of multiphase mixtures*. *J. Appl. Cryst.* **14**, 291–296.

Wolff, P. M. de (1948). *Multiple Guinier cameras*. *Acta Cryst.* **1**, 207–211.

Wolff, P. M. de (1957). *Self-centering combined aperture- and scatter-slit for powder diffractometry with constant effective specimen area*. *Appl. Sci. Res. B*, **6**, 296–300.

Wolff, P. M. de (1968*a*). *A simplified criterion for the reliability of a powder pattern indexing*. *J. Appl. Cryst.* **1**, 108–113.

Wolff, P. M. de (1968*b*). *Focusing monochromators and transmission techniques*. *Norelco Rep.* **15**, 44–49.

Wolff, P. M. de, Taylor, J. & Parrish, W. (1959). *Experimental study of effect of crystallite size statistics on X-ray diffractometer intensities*. *J. Appl. Phys.* **30**, 63–69.

Wolff, P. M. de & Visser, J. W. (1988). *Absolute intensities – outline of a recommended practice*. *Powder Diffr.* **3**, 202–204.

Yoshimatsu, M. & Kozaki, S. (1977). *High brilliance X-ray sources*. *Topics in applied physics*, Vol. 22, *X-ray optics*, edited by H.-J. Queisser, pp. 9–33. Berlin: Springer-Verlag.

Young, R. A. (1963). *Balanced filters for X-ray diffractometry*. *Z. Kristallogr.* **118**, 233–247.

Young, R. A., Prince, E. & Sparks, R. A. (1982). *Suggested guidelines for the publication of Rietveld analyses and pattern decomposition studies*. *J. Appl. Cryst.* **15**, 357–359.

Young, R. A. & Wiles, D. B. (1982). *Profile shape functions in Rietveld refinements*. *J. Appl. Cryst.* **15**, 430–438.

Yvon, K., Jeitschko, W. & Parthé, E. (1977). *LAZY PULVERIX, a computer program for calculating X-ray and neutron diffraction powder patterns*. *J. Appl. Cryst.* **10**, 73–74.

2.4.1

Anderson, R. & Johnson, G. G. Jr (1979). *The MAX-d alphabetical index to the JCPDS data base: a new tool for electron diffraction analysis. 37th Annu. Proc. Electron Microsc. Soc. Am.*, edited by G. W. Bailey, pp. 444–445. Baton Rouge: Claitors.

Avilov, A. S., Parmon, V. S., Semiletov, S. A. & Sirota, M. I. (1984). *Intensity calculations for many-wave diffraction of fast electrons in polycrystal specimens. Kristallografiya*, **29**, 11–15. [In Russian.]

Bethe, H. A. (1928). *Theorie der Beugung von Elektronen an Kristallen. Ann. Phys. (Leipzig)*, **87**, 55–129.

Blackman, M. (1939). *On the intensities of electron diffraction rings. Proc. R. Soc. London*, **173**, 68–82.

Carr, M. J., Chambers, W. F., Melgaard, D. K., Himes, V. L., Stalick, J. K. & Mighell, A. D. (1987). *NBS/Sandia/ICDD Electron Diffraction Data Base*. Report SAND87-1992-UC-13. Sandia National Laboratories, Albuquerque, NM 87185, USA.

Cowley, J. M & Rees, A. L. G. (1947). *Refraction effects in electron diffraction. Proc. Phys. Soc.* **59**, 287–302.

Dvoryankina, G. G. & Pinsker, Z. G. (1958). *The structural study of Fe_4N. Kristallografiya*, **3**, 438–445. [In Russian.]

Goodman, P. (1963). *Investigation of arsenic trisulphide by the electron diffraction radial distribution method. Acta Cryst.* **16**, A130.

Grigson, C. W. B. (1962). *On scanning electron diffraction. J. Electron. Control,* **12**, 209–232.

Honjo, G. & Mihama, K. (1954). *Fine structure due to refraction effect in electron diffraction pattern of powder sample. J. Phys. Soc. Jpn*, **9**, 184–198.

Horstmann, M. & Meyer, G. (1962). *Messung der Elastischen Electronenbeugungsintensitaten polykristalliner Aluminium-Schichten. Acta Cryst.* **15**, 271–281.

Imamov, R. M., Pannhorst, V., Avilov, A. S. & Pinsker, Z. G. (1976). *Experimental study of dynamic effects associated with electron diffraction in partly oriented films. Kristallografiya*, **21**, 364–369.

International Tables for Crystallography (1993). Vol. B. Dordrecht: Kluwer Academic Publishers.

Mighell, A. D., Himes, V. L., Anderson, R. & Carr, M. J. (1988). *d-spacing and formula index for compound identification using electron diffraction. 46th Annu. Proc. Electron Microsc. Soc. Am.*, edited by G. W. Bailey, pp. 912–913. San Francisco Press.

Sturkey, L. & Frevel, L. K. (1945). *Refraction effects in electron diffraction. Phys. Rev.* **68**, 56–57.

Tsypursky, S. I. & Drits, V. A. (1977). *The efficiency of the electronometric measurement of intensities in electron diffraction structural studies. Izv. Akad. Nauk SSSR Ser. Phys.* **41**, 2263–2271. [In Russian.]

Turner, P. S. & Cowley, J. M. (1969). *The effect of n-beam dynamical diffraction in electron diffraction intensities from polycrystalline materials. Acta Cryst.* A**25**, 475–481.

Vainshtein, B. K. (1964). *Structure analysis by electron diffraction*. Oxford: Pergamon Press. [Translated from the Russian: *Strukturnaya Electronografiya*.]

2.4.2

Allemand, R., Bordet, J., Roudaut, E., Convert, P., Ibel, K., Jacobe, J., Cotton, J. P. & Farnoux, B. (1975). *Position sensitive detectors for neutron diffraction. Nucl. Instrum. Methods*, **126**, 29–42.

Caglioti, G., Paoletti, A. & Ricci, F. P. (1958). *Choice of collimators for a crystal spectrometer for neutron diffraction. Nucl. Instrum. Methods*, **3**, 223–228.

Carlile, C. J., Hey, P. D. & Mack, B. (1977). *High efficiency Soller slit collimators for thermal neutrons. J. Phys. E*, **10**, 543–546.

Hewat, A. W. (1975). *Design for a conventional high resolution neutron powder diffractometer. Nucl. Instrum. Methods*, **127**, 361–370.

Hewat, A. W. (1986*a*). *D2B, a new high resolution neutron powder diffractometer at ILL Grenoble. Mater. Sci. Forum*, **9**, 69–79.

Hewat, A. W. (1986*b*). *High resolution neutron and synchrotron powder diffraction. Chem. Scr.* **26**A, 119–130.

Hewat, A. W. & Bailey, I. (1976). *D1A, a high resolution neutron powder diffractometer with a bank of Mylar collimators. Nucl. Instrum. Methods*, **137**, 463–471.

Howard, C. J. (1982). *The approximation of asymmetric neutron powder diffraction peaks by sums of Gaussians. J. Appl. Cryst.* **15**, 615–620.

Loopstra, B. O. (1966). *Neutron powder diffractometry using a wavelength of 2.6 Å. Nucl. Instrum. Methods*, **44**, 181–187.

Rietveld, H. M. (1969). *A profile refinement method for nuclear and magnetic structures. J. Appl. Cryst.* **2**, 65–71.

Wilson, A. J. C. (1963). *Mathematical theory of X-ray powder diffractometry*. Eindhoven: Centrex.

2.5.1

Besson, J. M. & Weill, G. (1992). *EDX station for high pressure at LURE (DCI). High Press. Res.* **8**, 715–716.

Bourdillon, A. J., Glazer, A. M., Hidaka, M. & Bordas, J. (1978). *High-resolution energy-dispersive diffraction using synchrotron radiation. J. Appl. Cryst.* **11**, 684–687.

Buras, B., Chwaszczewska, J., Szarras, S. & Szmid, Z. (1968). *Fixed angle scattering* (*FAS*) *method for X-ray crystal structure analysis*. Report No. 894/II/PS, 10 pp. Institute of Nuclear Research, Warsaw.

Buras, B. & Gerward, L. (1975). *Relations between integrated intensities in crystal diffraction methods for X-rays and neutrons. Acta Cryst.* A**31**, 372–374.

Buras, B. & Gerward, L. (1989). *Application of X-ray energy-dispersive diffraction for characterization of materials under high pressure. Prog. Cryst. Growth Charact.* **18**, 93–138.

Buras, B., Gerward, L., Glazer, A. M., Hidaka, M. & Olsen, J. S. (1979). *Quantitative structural studies by means of the energy-dispersive method with X-rays from a storage ring. J. Appl. Cryst.* **12**, 531–536.

Buras, B., Niimura, N. & Olsen, J. S. (1978). *Optimum resolution in X-ray energy-dispersive diffractometry. J. Appl. Cryst.* **11**, 137–140.

Buras, B., Olsen, J. S., Gerward, L., Selsmark, B. & Lindegaard-Andersen, A. (1975). *Energy-dispersive spectroscopic methods applied to X-ray diffraction in single crystals. Acta Cryst.* A**31**, 327–333.

Clark, S. M. (1992). *A new white beam single crystal and powder diffraction facility at the SRS. Rev. Sci. Instrum.* **63**, 1010–1012.

Fukamachi, T., Hosoya, S. & Terasaki, O. (1973). *The precision of interplanar distances measured by an energy-dispersive method. J. Appl. Cryst.* **6**, 117–122.

2.5.1 (*cont.*)

Giessen, B. C. & Gordon, G. E. (1968). *X-ray diffraction: new high-speed technique based on X-ray spectroscopy*. *Science*, **159**, 973–975.

Glazer, A. M., Hidaka, M. & Bordas, J. (1978). *Energy-dispersive powder profile refinement using synchrotron radiation*. *J. Appl. Cryst.* **11**, 165–172.

Häusermann, D. (1992). *New techniques for new sources: a fresh look at energy-dispersive diffraction for high-pressure studies*. *High Press. Res.* **8**, 647–654.

Holzapfel, W. B. & May, W. (1982). *Improvements in energy dispersive X-ray diffraction with conical slit and diamond cell*. *High-pressure research in geophysics*, edited by S. Akimoto & M. H. Manghnani, pp. 73–80, and references therein. Dordrecht: Reidel.

Kalman, Z. H. (1979). *On the derivation of integrated reflected energy formulae*. *Acta Cryst.* A**35**, 634–641.

Laine, E. & Lähteenmäki, I. (1980). *The energy-dispersive X-ray diffraction method*: *annotated bibliography 1968–78*. *J. Mater. Sci.* **15**, 269–278, and references therein.

Mao, H. K., Jephcoat, A. P., Hemley, R. J., Finger, L. W., Zha, C. S., Hazen, R. M. & Cox, D. E. (1988). *Synchrotron X-ray diffraction measurements of single crystal hydrogen to 26.5 GigaPascals*. *Science*, **239**, 1131–1134.

Nelmes, R. J. & McMahon, M. I. (1994). *High-pressure powder diffraction on synchrotron sources*. *J. Synchrotron Rad.* **1**, 69–73.

Neuling, H. W. & Holzapfel, W. B. (1992). *Rietveld analysis for energy dispersive X-ray diffraction under high pressure with synchrotron radiation*. *High Press. Res.* **8**, 665–660.

Olsen, J. S. (1992). *Instrumentation for high-pressure X-ray diffraction research at HASYLAB*. *Rev. Sci. Instrum.* **63**, 1058–1061.

Olsen, J. S., Buras, B., Jensen, T., Alstrup, O., Gerward, L. & Selsmark, B. (1978). *Influence of polarization of the incident beam on integrated intensities in X-ray energy-dispersive diffractometry*. *Acta Cryst.* A**34**, 84–87.

Otto, J. W. (1997). *A facility for high-pressure X-ray diffraction at HASYLAB*. *Nucl. Instrum. Methods*, A**384**, 552–557.

Parrish, W. & Hart, M. (1987). *Advantages of synchrotron radiation for polycrystalline diffractometry*. *Z. Kristallogr.* **179**, 161–173.

Ruoff, A. L. (1992). *EDXD studies above 400 GPa (and prospects for obtaining pressures near 1 TPa and doing EDXD studies at such pressures)*. *High Press. Res.* **8**, 639–645.

Uno, R. & Ishigaki, A. (1975). *The correction of experimental structure factors for thermal diffuse scattering in white X-ray diffraction*. *Jpn. J. Appl. Phys.* **14**, 291–292.

Wilson, A. J. C. (1973). *Note on the aberrations of a fixed-angle energy-dispersive powder diffractometer*. *J. Appl. Cryst.* **6**, 230–237.

2.5.2

Buras, B. & Gerward, L. (1975). *Relations between integrated intensities in crystal diffraction methods for X-rays and neutrons*. *Acta Cryst.* A**31**, 372–374.

Buras, B. & Leciejewicz, J. (1964). *A new method for neutron diffraction crystal structure investigations*. *Phys. Status Solidi*, **4**, 349–355.

Buras, B., Mikke, K., Lebech, B. & Leciejewicz, J. (1965). *The time-of-flight method for investigations of single-crystal structures*. *Phys. Status Solidi*, **11**, 567–573.

Jauch, W., Schultz, A. J. & Schneider, J. R. (1988). *Accuracy of single crystal time-of-flight neutron diffraction: a comparative study of MnF_2*. *J. Appl. Cryst.* **21**, 975–979.

Johnson, M. W. & David, W. I. F. (1985). *HPRD: the high resolution powder diffractometer at the spallation neutron source*. Report RAL-85-112. Rutherford Appleton Laboratory, Chilton, Didcot, Oxon, UK.

Jorgensen, J. D. & Rotella, F. J. (1982). *High-resolution time-of-flight powder diffractometer at the ZING-P′ pulsed neutron source*. *J. Appl. Cryst.* **15**, 27–34.

Jorgensen, J. D. & Worlton, T. G. (1985). *Disordered structure of D_2O ice VII from in situ neutron powder diffraction*. *J. Chem. Phys.* **83**, 329–333.

Lowde, R. D. (1956). *A new rationale of structure-factor measurement in neutron-diffraction analysis*. *Acta Cryst.* **9**, 151–155.

Marmeggi, J. C. & Delapalme, A. (1980). *Neutron Laue photographs of crystallographic satellite reflections in alpha-uranium*. *Physica (Utrecht)*, **102**B, 309–312.

Schultz, A. J., Srinivasan, K., Teller, R. G., Williams, J. M. & Lukehart, C. M. (1984). *Single-crystal time-of-flight neutron diffraction structure of hydrogen cis-diacetyltetracarbonylrhenate*. *J. Am. Chem. Soc.* **106**, 999–1003.

Steichele, E. & Arnold, P. (1975). *A high-resolution neutron time-of-flight diffractometer*. *Phys. Lett.* A**44**, 165–166.

Turberfield, K. C. (1970). *Time-of-flight neutron diffractometry*. *Thermal neutron diffraction*, edited by B. T. M. Willis, pp. 34–50. Oxford University Press.

Windsor, C. G. (1981). *Pulsed neutron diffraction*. London: Taylor & Francis.

2.6.1

Anderegg, J. W., Beeman, W. W., Shulman, S. & Kaesberg, P. J. (1955). *An investigation of the size, shape and hydration of serum albumin by small-angle X-ray scattering J. Am. Chem. Soc.* **77**, 2927–2937.

Bayvel, L. P. & Jones, A. R. (1981). *Electromagnetic scattering and its applications*. London: Applied Science Publishers.

Bonse, U. & Hart, M. (1965). *An X-ray interferometer*. *Appl. Phys. Lett.* **6**, 155–156.

Bonse, U. & Hart, M. (1966). *An X-ray interferometer*. *Z. Phys.* **189**, 151–156.

Bonse, U. & Hart, M. (1967). In *Small-angle X-ray scattering,* edited by H. Brumberger. New York: Gordon and Breach.

Bracewell, R. (1986). *Fourier transform and its applications*. New York: McGraw-Hill.

Brumberger, H. (1967). *Small-angle X-ray scattering*. New York: Gordon and Breach.

Chen, S. H., Sheu, E. Y., Kalus, J. & Hoffmann, H. (1988). *Small-angle neutron scattering investigation of correlations in charged macromolecular and supramolecular solutions*. *J. Appl. Cryst.* **21**, 751–769.

Cleemann, J. C. & Kratky, O. (1960). *Größe, Gestalt und Solvatation des Edestinmoleküls aus dem Studium der Röntgenkleinwinkelstreuung*. *Z. Naturforsch. Teil B*, **15**, 525–535.

Damaschun, G., Damaschun, H., Müller, J. J., Ruckpaul, K. & Zinke, M. (1974). *Vergleich der Struktur von Proteinen im Kristall und in Lösung; Theoretische und experimentelle Untersuchungen mittels der Röntgen-Klein-winkelstreuung am Hämoglobin*. *Stud. Biophys.* **47**, 27–39.

2.6.1 (*cont.*)

Damaschun, G., Gernat, C., Damaschun, H., Bychkova, V. E. & Ptitsyn, O. B. (1986). *Comparison of intramolecular packing of a protein in native and 'molten globule' states*. *Int. J. Biol. Macromol.* **8**, 226–230.

Damaschun, G. & Pürschel, H. V. (1971*a*). *Röntgen-Kleinwinkelstreuug von isotropen Proben ohne Fernordnung. I. Allgemeine Theorie*. *Acta Cryst.* A**27**, 193–197.

Damaschun, G. & Pürschel, H. V. (1971*b*). *Berechnung von Streumassenradien aus unverschmierten und spaltverschmierten Röntgen-Kleinwinkelstreukurven*. *Monatsh. Chem.* **102**, 1146–1155.

Debye, P. (1915). *Zerstreuung von Röntgenstrahlen*. *Ann. Phys. (Leipzig)*, **46**, 809–823.

Debye, P. & Bueche, A. M. (1949). *Scattering by an inhomogeneous solid*. *J. Appl. Phys.* **20**, 518–525.

Debye, P. & Menke, H. (1930). *Bestimmung der inneren Struktur von Flüssigkeiten mit Röntgenstrahlen*. *Phys. Z.* **31**, 797–798.

Fedorov, B. A. & Denesyuk, A. I. (1978). *Large-angle X-ray diffuse scattering, a new method for investigating changes in the conformation of globular proteins in solution*. *J. Appl. Cryst.* **11**, 473–477.

Fedorov, B. A., Ptitsyn, O. B. & Voronin, L. A. (1972). *X-ray diffuse scattering of globular protein solutions: consideration of the solvent influence*. *FEBS Lett.* **28**, 188–190.

Fedorov, B. A., Ptitsyn, O. B. & Voronin, L. A. (1974*a*). *Small-angle X-ray scattering of native hog thyroglobulin*. *J. Appl. Cryst.* **7**, 181.

Fedorov, B. A., Ptitsyn, O. B. & Voronin, L. A. (1974*b*). *X-ray diffuse scattering by polypeptides and proteins in solution. IV. Consideration of the solvent effect for globular protein solutions*. *Mol. Biol. (Moscow)*, **8**, 693–709.

Feigin, L. A. & Svergun, D. I. (1987). *Structure analysis by small-angle X-ray and neutron scattering*. New York: Plenum.

Gernat, C., Damaschun, G., Kröber, R., Bychkova, V. E. & Ptitsyn, O. B. (1986). *Large-angle diffuse X-ray scattering from a homopolypeptide and some proteins*. *Stud. Biophys.* **112**, 213–219.

Glatter, O. (1972). *X-ray small angle scattering of molecules composed of subunits*. *Acta Phys. Austriaca*, **36**, 307–315.

Glatter, O. (1977*a*). *Data evaluation in small-angle scattering: calculation of the radial electron density distribution by means of indirect Fourier transformation*. *Acta Phys. Austriaca,* **47**, 83–102.

Glatter, O. (1977*b*). *A new method for the evaluation of small-angle scattering data*. *J. Appl. Cryst.* **10**, 415–421.

Glatter, O. (1979). *The interpretation of real-space information from small-angle scattering experiments*. *J. Appl. Cryst.* **12**, 166–175.

Glatter, O. (1980*a*). *Evaluation of small-angle scattering data from lamellar and cylindrical particles by the indirect transformation method*. *J. Appl. Cryst.* **13**, 577–584.

Glatter, O. (1980*b*). *Determination of particle-size distribution functions from small-angle scattering data by means of the indirect transformation method*. *J. Appl. Cryst.* **13**, 7–11.

Glatter, O. (1980*c*). *Computation of distance distribution functions and scattering functions of models for small-angle scattering experiments*. *Acta Phys. Austriaca*, **52**, 243–256.

Glatter, O. (1981). *Convolution square root of band-limited symmetrical functions and its application to small-angle scattering data*. *J. Appl. Cryst.* **14**, 101–108.

Glatter, O. (1982*a*). In *Small angle X-ray scattering,* edited by O. Glatter & O. Kratky, Chap. 4. London: Academic Press.

Glatter, O. (1982*b*). In *Small angle X-ray scattering*, edited by O. Glatter & O. Kratky, Chap. 5. London: Academic Press.

Glatter, O. (1988). *Comparison of two different methods for direct structure analysis from small-angle scattering data*. *J. Appl. Cryst.* **21**, 886–890.

Glatter, O. & Hainisch, B. (1984). *Improvements in real-space deconvolution of small-angle scattering data*. *J. Appl. Cryst.* **17**, 435–441.

Glatter, O. & Hofer, M. (1988*a*). *Interpretation of elastic light-scattering data in real space. II. Nonspherical and inhomogeneous monodisperse systems*. *J. Colloid Interface Sci.* **112**, 484–495.

Glatter, O. & Hofer, M. (1988*b*). *Interpretation of elastic light-scattering data. III. Determination of size distributions of polydisperse systems*. *J. Colloid Interface Sci.* **122**, 496–506.

Glatter, O., Hofer, M., Jorde, C. & Eigner, W.-D. (1985). *Interpretation of elastic light-scattering data in real space*. *J. Colloid Interface Sci.* **105**, 577–586.

Glatter, O. & Kratky, O. (1982). *Small angle X-ray scattering*. London: Academic Press.

Goodisman, J. (1980). *The correlation function, intersect distribution and scattering from a cube*. *J. Appl. Cryst.* **13**, 132–134.

Greville, T. N. E. (1969). *Theory and applications of spline functions*. New York: Academic Press.

Guinier, A. (1939). *La diffraction des rayons X aux très petits angles: application à l'étude de phénomènes ultramicroscopiques*. *Ann. Phys. (Paris)*, **12**, 161–237.

Guinier, A. & Fournet, G. (1955). *Small angle scattering of X-rays*. New York: John Wiley.

Heidorn, D. B. & Trewhella, J. (1988). *Comparison of the crystal and solution structures of calmodulin and troponin C*. *Biochemistry*, **27**, 909–915.

Heine, S., Kratky, O. & Roppert, J. (1962). *Lichstreuung und Röntgenkleinwinkelstreuung von statistisch verknäuelter. Fadenmolekülen, berechnet nach der Monte Carlo Methode*. *Makromol. Chem.* **56**, 150–168.

Hendricks, R. W. (1978). *The ORNL 10-meter small-angle X-ray scattering camera*. *J. Appl. Cryst.* **11**, 15–30.

Hendrix, J. (1985). *Position-sensitive X-ray detectors*. *Adv. Polym. Sci.* **67**, 59–98.

Hofer, M., Schurz, J. & Glatter, O. (1989). *Oil–water emulsions: particle size distributions from elastic light-scattering data*. *J. Colloid Interface Sci.* **127**, 147–155.

Holmes, K. C. (1982). In *Small angle X-ray scattering,* edited by O. Glatter & O. Kratky, Chap. 3.II. London: Academic Press.

Hosemann, R. & Bagchi, S. N. (1952). *Existenzbeweis für eine eindeutige Röntgenstrukturanalyse durch Entfaltung. I. Entfaltung zentrosymmetrischer endlicher Massenverteilungen*. *Acta Cryst.* **5**, 749–762.

Hosemann, R. & Bagchi, S. N. (1962). *Direct analysis of diffraction by matter*. Amsterdam: North-Holland.

Hubbard, S. T., Hodgson, K. O. & Doniach, S. (1988). *Small-angle X-ray scattering investigation of the solution structure of troponin C*. *J. Biol Chem.* **263**, 4151–4158.

I'anson, K. J., Bacon, J. R., Lambert, N., Miles, M. J., Morris, V. J., Wright, D. J. & Nave, C. (1987). *Synchrotron radiation wide-angle X-ray scattering of glycinin solutions*. *Int. J. Biol. Macromol.* **9**, 368–370.

Kirste, R. G. & Oberthür, R. C. (1982). In *Small angle X-ray scattering*, edited by O. Glatter & O. Kratky, Chap. 12. London: Academic Press.

Koch, M. H. J. (1988). *Instruments and methods for small-angle scattering with synchrotron radiation*. *Macromol. Symp.* **15**, 79–90.

2.6.1 (*cont.*)

Kratky, O. (1982*a*). In *Small angle X-ray scattering*, edited by O. Glatter & O. Kratky, Chap. 3.I. London: Academic Press.

Kratky, O. (1982*b*). In *Small angle X-ray scattering,* edited by O. Glatter & O. Kratky, Chap. 11. London: Academic Press.

Kratky, O. & Leopold, H. (1970). *A comparison between Bonse–Hart and the block collimation system. Makromol. Chem.* **133**, 181–195.

Kratky, O. & Porod, G. (1948). *Die Abhängigkeit der Röntgen-Kleinwinkelstreuung von Form und Größe der kolloider Teilchen in verdünnten Systemen. III. Acta Phys. Austriaca*, **2**, 133–147.

Kratky, O. & Porod, G. (1949). *Röntgenuntersuchung gelöster Fadenmoleküle. Recl Trav. Chim. Pays-Bas*, **68**, 1106–1122.

Kratky, O. & Porod, G. (1953). In *Die Physik der Hochpolymere*, Vol. II, edited by H. A. Stuart. Berlin: Springer.

Kratky, O., Porod, G. & Kahovec, L. (1951). *Einige Neuerungen in der Technik und Auswertung von Röntgen-Kleinwinkelmessungen. Z. Elektrochem.* **55**, 53–59.

Kratky, O. & Worthmann, W. (1947). *Über die Bestimmbarkeit der Konfiguration gelöster organischer Moleküle durch interferometrische Vermessung mit Röntgenstrahlen. Monatsh. Chem.* **76**, 263–281.

Krigbaum, W. R. & Kügler, F. R. (1970). *Molecular conformation of egg-white lysozyme and bovine-lactalbumin in solution. Biochemistry*, **9**, 1216–1223.

Laggner, P. (1982). In *Small-angle X-ray scattering*, edited by O. Glatter & O. Kratky, Chap. 10. London: Academic Press.

Langridge, R., Marvin, D. A., Seeds, W. E., Wilson, H. R., Cooper, C. W., Wilkins, M. H. F. & Hamilton, L. D. (1960). *The molecular configuration of deoxyribonucleic acid. J. Mol. Biol.* **2**, 38–62.

Leopold, H. (1982). In *Small-angle X-ray scattering,* edited by O. Glatter & O. Kratky, Chap. 3.III. London: Academic Press.

Luzzati, V. (1960). *Interprétation des mesures absolues de diffusion centrale des rayons X en collimation ponctuelle ou linéaire: solutions de particules globulaires et de batonnets. Acta Cryst.* **13**, 939–945.

Mittelbach, P. (1964). *Zur Röntgenkleinwinkelstreuung verdünnter kolloider Systeme. VIII. Acta Phys. Austriaca*, **19**, 53–102.

Mittelbach, P. & Porod, G. (1961*a*). *Zur Röntgenkleinwinkelstreuung verdünnter kolloider Systeme. Die Berechnung der Streukurven von Parallelepipeden. Acta Phys. Austriaca*, **14**, 185–211.

Mittelbach, P. & Porod, G. (1961*b*). *Zur Röntgenkleinwinkelstreuung verdünnter kolloider Systeme. VI. Acta Phys. Austriaca*, **14**, 405.

Mittelbach, P. & Porod, G. (1962). *Zur Röntgenkleinwinkelstreuung verdünnter kolloider Systeme. VII. Die Berechnung der Streukurven von dreiachsigen Ellipsoiden. Acta Phys. Austriaca,* **15**, 122–147.

Mittelbach, P. & Porod, G. (1965). *Zur Röntgenkleinwinkelstreuung verdünnter kolloider Systeme. Kolloid Z. Z. Polym.* **202**, 40–49.

Moore, P. B. (1980). *Small-angle scattering. Information content and error analysis. J. Appl. Cryst.* **13**, 168–175.

Müller, J. J., Damaschun, G., Damaschun, H., Misselwitz, R., Zirwer, D. & Nothnagel, A. (1984). *X-ray scattering evidence that calf thymus DNA in solution is a double helix and not a warped zipper. Biomed. Biochim. Acta*, **43**, 929–936.

Müller, J. J., Damaschun, G. & Schrauber, H. (1990). *The highly resolved excess electron distance distribution of biopolymers in solution – calculation from intermediate-angle X-ray scattering and interpretation. J. Appl. Cryst.* **23**, 26–34.

Müller, K. & Glatter, O. (1982). *Practical aspects of the use of indirect Fourier transformation methods. Makromol. Chem.* **183**, 465–479.

Ninio, J. & Luzzati, V. (1972). *Comparative small-angle X-ray scattering studies on unacylated, acylated and cross-linked Escherichia coli transfer* RNA_1^{Val}. *J. Mol. Biol.* **71**, 217–229.

Pessen, H., Kumosinski, T. F. & Timasheff, S. N. (1973). *Small-angle X-ray scattering. Methods Enzymol.* **27**, 151–209.

Pilz, I. (1982). In *Small-angle X-ray scattering,* edited by O. Glatter & O. Kratky, Chap. 8. London: Academic Press.

Pilz, I., Glatter, O. & Kratky, O. (1980). *Small-angle X-ray scattering. Methods Enzymol.* **61**, 148–249.

Pilz, I., Glatter, O., Kratky, O. & Moring-Claesson, O. (1972). *Rötgenkleinwinkelstudien über die Substruktur von Helix pomatia Hämocyanin. Z. Naturforsch. Teil B*, **27**, 518.

Pilz, I., Goral, K., Hoylaerts, M., Witters, R. & Lontie, R. (1980). *Studies by small-angle X-ray scattering of the quaternary structure of the 24-S component of the haemocyanin of Astacus leptodactylus in solution. Eur. J. Biochem.* **105**, 539–543.

Porod, G. (1948). *Die Abhängigkeit der Röntgen-Kleinwinkelstreuung von Form und Größe der kolloiden Teilchen in verdünnten Systemen. IV. Acta Phys. Austriaca*, **2**, 255–292.

Porod, G. (1949). *Zusammenhang zwischen mittlerem Endpunktsabstand und Kettenlänge bei Fadenmolekülen. Monatsh. Chem.* **80**, 251–255.

Porod, G. (1951). *Die Röntgenkleinwinkelstreuung von dichtgepackten kolloiden Systemen. I. Kolloid Z.* **124**, 83–114.

Porod, G. (1952). *Die Röntgenkleinwinkelstreuung von dichtgepackten kolloiden Systemen. II. Kolloid Z.* **125**, 51–122.

Porod, G. (1982). In *Small-angle X-ray scattering*, edited by O. Glatter & O. Kratky, Chap. 2. London: Academic Press.

Ritland, H. N., Kaesberg, P. & Beeman, W. W. (1950). *Double crystal and slit methods in small angle X-ray scattering. J. Appl. Phys.* **21**, 838–841.

Ruckpaul, K., Damaschun, G., Damaschun, H., Dimitrov, D. P., Jänig, G. R., Müller, J. J., Pürschel, H.-V. & Behlke, J. (1973). *Der Einfluß verschiedener Pufferionen auf die Funktion und Struktur von adultem menschlichen Hämoglobin. Acta Biol. Med. Germ.* **31**, 679–690.

Sadler, D. M. & Worcester, D. L. (1982). *Neutron diffraction studies of oriented photosynthetic membranes. J. Mol. Biol.* **159**, 467–484.

Schelten, J. & Hossfeld, F. (1971). *Application of spline functions to the correction of resolution errors in small-angle scattering. J. Appl. Cryst.* **4**, 210–223.

Shannon, C. E. & Weaver, W. (1949). *The mathematical theory of communication*. Urbana: University of Illinois Press.

Stasiecki, P. & Stuhrmann, H. B. (1978). *Röntgenkleinstwinkelstreuung an Erythrocyten. J. Appl. Cryst.* **11**, 1–5.

Stuhrmann, H. B. (1970*a*). *Interpretation of small-angle scattering functions of dilute solutions and gases. A representation of the structures related to a one-particle-scattering function. Acta Cryst.* A**26**, 297–306.

Stuhrmann, H. B. (1970*b*). *Ein neus Verfahren zur Bestimmung der Oberflächenform und der inneren Struktur von gelösten globulären Proteinen aus Röntgenkleinwinkelmessungen. Z. Phys. Chem.* **72**, 177–184.

2.6.1 (*cont.*)

Stuhrmann, H. B. (1970*c*). *Die Bestimmung der Oberflächenform von gelöstem Myoglobin aus Röntgenkleinwinkelmessungen. Z. Phys. Chem.* **72**, 185–198.

Stuhrmann, H. B. (1978). *The use of X-ray synchrotron radiation for structural research in biology. Rev. Biophys.* **11**, 71–98.

Stuhrmann, H. B. (1982). In *Small-angle X-ray scattering,* edited by O. Glatter & O. Kratky, Chap. 6. London: Academic Press.

Stuhrmann, H. B., Koch, M. H. J., Parfait, J., Haas, J., Ibel, K. & Crichton, R. R. (1977). *Shape of the 50S subunit of Escherichia coli ribosomes. Proc. Natl Acad. Sci. USA*, **74**, 2316–2320.

Svergun, D. I., Feigin, L. A. & Schedrin, B. M. (1982). *Small-angle scattering: direct structure analysis. Acta Cryst.* A**38**, 827–835.

Svergun, D. I., Feigin, L. A. & Schedrin, B. M. (1984). *The solution of the one-dimensional sign problem for Fourier transforms. Acta Cryst.* A**40**, 137–142.

Tikhonov, A. N. & Arsenin, V. Ya. (1977). *Solution of ill-posed problems:* New York: John Wiley.

Walter, G., Kranold, R. & Becherer, G. (1974). *Zu Problemen der Ver- und Entschmierung von Röntgen-Kleinwinkel-Streukurven. Stud. Biophys.* **47**, 49–62.

Zernicke, F. & Prins, J. A. (1927). *Die Beugung von Röntgenstrahlen in Flüssigkeiten als Effekt der Molekülanordnung. Z. Phys.* **41**, 184–194.

Zipper, P. (1969). *Ein einfaches Verfahren zur Monochromatisierung von Streukurven. Acta Phys. Austriaca*, **30**, 143–151.

2.6.2

Abragam, A., Bacchella, C. L., Coustham, J., Glättli, H., Fourmond, M., Malinowski, A., Meriel, P., Pinot, M. & Roubeau, A. (1982). *The interest in spin dependent nuclear scattering amplitudes. J. Phys. (Paris)*, **43**(C7), 373–381.

Alefeld, B., Schwahn, D. & Springer, T. (1989). *New developments of small angle neutron scattering instruments with focusing. Nucl. Instrum. Methods*, A**274**, 210–216.

Bacon, G. E. (1975). *Neutron diffraction.* Oxford: Clarendon Press.

Benoit, H. & Wippler, C. (1960). *Répartition angulaire de la lumière diffusée par une solution de copolymères. J. Chim. Phys.* **57**, 524–527.

Bonse, M. & Hart, M. (1966). *Small-angle X-ray scattering by spherical particles of polystyrene and polyvinyltoluene. Z. Phys.* **189**, 151–162.

Boothroyd, A. T. (1989). *The effect of gravity on the resolution of small-angle neutron scattering. J. Appl. Cryst.* **22**, 252–255.

Bragg, W. L. & Perutz, M. F. (1952). *The external form of the haemoglobin molecule. I. Acta Cryst.* **5**, 277–283.

Capel, M. S., Engelman, D. M., Freeborn, B. R., Kjeldgaard, M., Langer, J. A., Ramakrishnan, V., Schindler, D. G., Schneider, D. K., Schoenborn, B. P., Sillers, I.-Y., Yabuki, S. & Moore, P. B. (1987). *A complete mapping of the proteins in the small ribosomal subunit of Escherichia coli. Science*, **238**, 1403–1406.

Chen, S. H., Sheu, E. Y., Kalus, J. & Hoffmann, H. (1988). *Small-angle neutron scattering investigation of correlations in charged macromolecular and supramolecular solutions. J. Appl. Cryst.* **21**, 751–769.

Cusack, S. (1984). *Neutron scattering studies of virus structure. Neutrons in biology; basic life sciences,* Vol. 27, edited by B. P. Schoenborn, pp. 173–188. New York: Plenum.

Cusack, S., Mellema, J. E., Krijgsman, P. C. J. & Miller, A. (1981). *An investigation of the structure of alfalfa mosaic virus by small-angle neutron scattering. J. Mol. Biol.* **145**, 525–543.

Eisenberg, H. (1981). *Forward scattering of light, X-rays and neutrons. Q. Rev. Biophys.* **14**, 141–172.

Engelman, D. M. & Moore, P. B. (1972). *A new method for the determination of biological quaternary structure by neutron scattering. Proc. Natl Acad. Sci. USA,* **69**, 1997–1999.

Glatter, O. (1979). *The interpretation of real-space information from small-angle scattering experiments. J. Appl. Cryst.* **12**, 166–175.

Glatter, O. (1980). *Determination of particle-size distribution functions from small-angle scattering data by means of the indirect transformation method. J. Appl. Cryst.* **13**, 7–11.

Glatter, O. (1982*a*). *Interpretation. Small-angle X-ray scattering*, edited by O. Glatter & O. Kratky, pp. 167–196. London: Academic Press.

Glatter, O. (1982*b*). *Data treatment. Small-angle X-ray scattering*, edited by O. Glatter & O. Kratky, pp. 119–165. London: Academic Press.

Glatter, O. & Kratky, O. (1982). Editors. *Small-angle X-ray scattering*. London: Academic Press.

Guinier, A. (1968). *Small-angle scattering. International Tables for X-ray crystallography*, Vol. III, 2nd ed., edited by C. H. Macgillavry & G. D. Rieck, pp. 324–329. Birmingham: Kynoch Press.

Guinier, A. & Fournet, G. (1955). Editors. *Small-angle scattering of X-rays*. New York: John Wiley.

Hayter, J. B. (1985). *Determination of the structure and dynamics of micellar solutions by neutron small-angle scattering. Physics of amphiphiles: micelles, vesicles and micro-emulsions,* edited by V. Degiorgio & M. Corti, pp. 59–93. Amsterdam: North-Holland.

Hayter, J. B. & Penfold, J. (1981). *An analytic structure factor for macro-ion solutions. Mol. Phys.* **42**, 109–118.

Hjelm, R. P. (1988). *The resolution of TOF low-Q diffractometers: instrumental, data acquisition and reduction factors. J. Appl. Cryst.* **21**, 618–628.

Hoppe, W. (1972). *A new X-ray method for the determination of the quaternary structure of protein complexes. Isr. J. Chem.* **10**, 321–333.

Hoppe, W. (1973). *The 'label triangulation' method and the 'mixed isomorphous replacement' principle. J. Mol. Biol.* **78**, 581–585.

Ibel, K. (1976). *The neutron small-angle camera D11 at the high-flux reactor, Grenoble. J. Appl. Cryst.* **9**, 296–309.

Ibel, K. & Stuhrmann, H. B. (1975). *Comparison of neutron and X-ray scattering of dilute myoglobin solutions. J. Mol. Biol.* **93**, 255–265.

Jacrot, B. (1976). *The study of biological structures by neutron scattering from solution. Rep. Prog. Phys.* **10**, 911–953.

Jacrot, B. & Zaccai, G. (1981). *Determination of molecular weight by neutron scattering. Biopolymers*, **20**, 2413–2426.

Janot, C. & George, B. (1985). *Surface states and magnetic heterogeneity in iron-based glasses. J. Phys. (Paris) Lett.* **46**, L85–L88.

Knoll, W., Schmidt, K. & Ibel, K. (1985). *The inverse contrast variation in small-angle neutron scattering: a sensitive technique for the evaluation of lipid phase diagrams. J. Appl. Cryst.* **18**, 65–70.

2.6.2 (*cont.*)

Knop, W., Nierhaus, K. H., Nowotny, V., Niinikoski, T. O., Krumpolc, M., Rieubland, J. M., Rijlart, A., Schärpf, O., Schink, H.-J., Stuhrmann, H. B. & Wagner, R. (1986). *Polarised neutron scattering from dynamic polarised targets of biological origin*. *Helv. Phys. Acta*, **59**, 741–746.

Kostorz, G. (1979). *Small-angle scattering and its applications to materials science*. *Treatise on materials science and technology,* Vol. 15, edited by G. Kostorz, pp. 227–289. New York: Academic Press.

Kostorz, G. (1988). *Small-angle neutron scattering – metallurgical applications*. *Materials science forum,* Vols. 27/28, edited by M. M. Elcombe & T. J. Hicks, pp. 325–344. Aedermannsdorf, Switzerland: Trans Tech Publications.

Kratky, O. & Worthmann, W. (1947). *Über die Bestimmbarkeit der Konfiguration gelöster organischer Moleküle durch interferometrische Vermessung mit Röntgenstrahlen*. *Monatsh. Chem.* **76**, 263–281.

Lindner, P., May, R. P. & Timmins, P. A. (1992). *Upgrading the SANS instrument D11 at the ILL*. *Physica (Utrecht)*, B**180–181**, 967–972.

Lindner, P. & Oberthür, R. C. (1985). *Shear induced deformation of polystyrene coils in dilute solution from small angle neutron scattering. 1. Shear gradient apparatus and first results*. *Colloid Polym. Sci.* **263**, 443–453.

Lindner, P. & Oberthür, R. C. (1988). *Shear-induced deformation of polystyrene coils in dilute solution from small angle neutron scattering. 2. Variation of shear gradient, molecular mass and solvent viscosity*. *Colloid Polym. Sci.,* **263**, 443–453.

Luzzati, V., Tardieu, A., Mateu, L. & Stuhrmann, H. B. (1976). *Structure of human serum lipoprotein in solution. I. Theory and techniques of an X-ray scattering approach using solvents of variable density*. *J. Mol. Biol.* **101**, 115–127.

May, R. P., Ibel, K. & Haas, J. (1982). *The forward scattering of cold neutrons by mixtures of light and heavy water*. *J. Appl. Cryst.* **15**, 15–19.

May, R. P. & Nowotny, V. (1989). *Distance information derived from neutron low-Q scattering*. *J. Appl. Cryst.* **22**, 231–237.

Moore, P. B. (1980). *Small-angle scattering. Information content and error analysis*. *J. Appl. Cryst.* **13**, 168–175.

Nierhaus, K. H., Lietzke, R., May, R. P., Nowotny, V., Schulze, H., Simpson, K., Wurmbach, P. & Stuhrmann, H. B. (1983). *Shape determination of ribosomal proteins in situ*. *Proc. Natl Acad. Sci. USA*, **80**, 2889–2893.

Pavlov, M. Yu. & Serdyuk, I. N. (1987). *Three-isotropic substitutions method in small-angle neutron scattering*. *J. Appl. Cryst.* **20**, 105–110.

Pedersen, J. S., Posselt, D. & Mortensen, K. (1990). *Analytical treatment of the resolution function for small-angle scattering*. *J. Appl. Cryst.* **23**, 321–333.

Porod, G. (1951). *Die Röntgenkleinwinkelstreuung von dichtgepackten kolloiden Systemen*. *Kolloid Z.* **124**, 83–114.

Porod, G. (1982). *General theory*. *Small-angle X-ray scattering,* edited by O. Glatter & O. Kratky, pp. 17–51. London: Academic Press.

Salva-Ghilarducci, A., Simon, J. P., Guyot, P. & Ansara, I. (1983). *Precipitation in ternary Al–Zn–Ag alloys studied by isotropic contrast in neutron small angle scattering*. *Acta Metall.* **31**, 1705–1713.

Schelten, J. & Hossfeld, F. (1971). *Application of spline functions to the correction of resolution errors in small-angle scattering*. *J. Appl. Cryst.* **4**, 210–223.

Stuhrmann, H. B. (1970). *Interpretation of small-angle scattering functions of dilute solutions and gases. A representation of the structures related to a one-particle-scattering function*. *Acta Cryst.* A**26**, 297–306.

Stuhrmann, H. B., Haas, J., Ibel, K., de Wolf, B., Koch, M. H. J., Parfait, R. & Crichton, R. R. (1976). *New low resolution model for 50S subunit of Escherichia coli ribosomes*. *Proc. Natl Acad. Sci. USA*, **73**, 2379–2383.

Stuhrmann, H. B. & Kirste, R. G. (1965). *Elimination der intrapartikulären Untergrundstreuung bei der Röntgenkleinwinkelstreuung an kompakten Teilchen (Proteinen)*. *Z. Phys. Chem. Neue Folge,* **46**, 247–250.

Stuhrmann, H. B., Schärpf, O., Krumpolc, M., Niinikoski, T. O., Rieubland, M. & Rijllart, A. (1986). *Dynamic nuclear polarisation of nuclear matter*. *Eur. Biophys. J.* **14**, 1–6.

Timmins, P. A. & Zaccai, G. (1988). *Low resolution structures of biological complexes studied by neutron scattering*. *Eur. Biophys. J.* **15**, 257–268.

Wignall, G. D. (1987). *Neutron scattering*. *Encyclopedia of polymer science and engineering,* Vol. 10, 2nd ed., edited by J. I. Kroschwitz, pp. 112–184. New York: John Wiley.

Wignall, G. D. & Bates, F. S. (1987). *Absolute calibration of small-angle neutron scattering data*. *J. Appl. Cryst.* **20**, 28–40.

Wignall, G. D., Christen, D. K. & Ramakrishnan, V. (1988). *Instrumental resolution effects in small-angle neutron scattering*. *J. Appl. Cryst.* **21**, 438–451.

Witz, J. (1983). *Contrast variation of the small-angle neutron scattering of globular particles: the influence of hydrogen exchange*. *Acta Cryst.* A**39**, 706–711.

Zaccai, G. & Jacrot, B. (1983). *Small angle neutron scattering*. *Annu. Rev. Biophys. Bioeng.* **12**, 139–157.

Zaccai, G., Wachtel, E. & Eisenberg, H. (1986). *Solution structure of halophilic malate dehydrogenase from small-angle neutron and X-ray scattering and ultracentrifugation*. *J. Mol. Biol.* **190**, 97–106.

2.7

Allinson, N. M. (1994). *Development of non-intensified charge-coupled device area X-ray detectors*. *J. Synchrotron Rad.* **1**, 54–62.

Allinson, N. M., Allsopp, D. W. E., Quayle, J. A. & Magorrian, B. G. (1991). *Effects of soft X-ray irradiation on solid-state imagers*. *Nucl. Instrum. Methods*, A**310**, 267–272.

Armstrong, R. W. & Wu, C. C. (1973) *X-ray diffraction microscopy*. *Tools and techniques for microstructural analysis*, edited by J. L. McCall & W. M. Mueller, pp. 169–219. New York: Plenum.

Arndt, U. W. (1986). *X-ray position-sensitive detectors*. *J. Appl. Cryst.* **19**, 145–163.

Arndt, U. W. (1990). *X-ray television area detectors*. *Synchrotron Radiat. News*, **3**, 17–22.

Authier, A. (1961). *Etude de la transmission anormale des rayons X dans des cristaux de silicium. I. Case des cristaux parfaits*. *Bull. Soc. Fr. Minéral. Cristallogr.* **84**, 51–89.

2.7 (*cont.*)

Authier, A. (1970). *Ewald waves in theory and experiment (dynamical theory of X-ray diffraction). Advances in structure research by diffraction methods*, Vol. 3, edited by R. Brill & R. Mason, pp. 1–51. Oxford: Pergamon Press.

Authier, A. (1977). *Section topography. X-ray optics. Applications to solids*, edited by H.-J. Queisser, Chap. 5, pp. 145–189. Berlin: Springer.

Barrett, C. S. (1945). *A new microscopy and its potentialities. Trans. Am. Inst. Min. Metall. Pet. Eng.* **161**, 15–64.

Barth, H. & Hosemann, R. (1958). *Anwendung der Parallelstrahlmethode in Durchstrahlungsfall zur Prüfung des Kristallinneren mit Röntgen-Strahlen. Z. Naturforsch. Teil A*, **13**, 792–794.

Batterman, B. W. & Cole, H. (1964). *Dynamical diffraction of X-rays by perfect crystals. Rev. Mod. Phys.* **36**, 681–717.

Bauspiess, W., Bonse, U., Graeff, W. & Rauch, H. (1977). *A bicrystal monochromator of moderate wavelength resolution for use with X-rays or thermal neutrons. J. Appl. Cryst.* **10**, 338–343.

Beaumont, J. H. & Hart, M. (1974). *Multiple Bragg reflection monochromators for synchrotron X radiation. J. Phys. E,* **7**, 823–829.

Berg, W. F. (1931). *Über ein röntgenographische Methode zur Untersuchung von Gitterstörungen an Kristallen. Naturwissenschaften*, **19**, 391–396.

Boettinger, W. J., Burdette, H. E. & Kuriyama, M. (1979). *X-ray magnifier. Rev. Sci. Instrum.* **50**, 26–30.

Bond, W. L. & Andrus, J. (1952). *Structural imperfections in quartz crystals. Am. Mineral.* **37**, 622–632.

Bonse, U. & Fischer, K. (1981). *The new multi-purpose two-axis diffractometer for synchrotron X-rays at DORIS. Nucl. Instrum. Methods*, **190**, 593–603.

Bonse, U. & Graeff, W. (1977). *X-ray and neutron interferometry. X-ray optics. Applications to solids*, edited by H.-J. Queisser, Chap. 4, pp. 93–143. Berlin: Springer.

Bonse, U. & Hart, M. (1965*a*). *Tailless X-ray single-crystal reflection curves obtained by multiple reflection. Appl. Phys. Lett.* **7**, 238–240.

Bonse, U. & Hart, M. (1965*b*). *An X-ray interferometer. Appl. Phys. Lett.* **6**, 155–158.

Bonse, U. & Hart, M. (1966). *Moiré patterns of atomic planes obtained by X-ray interferometry. Z. Phys.* **190**, 455–467.

Bonse, U. & Kappler, E. (1958). *Röntgenographische Abbildung des Verzerrungsfeldes einzelner Versetszungen in Germanium-Einkristallen. Z. Naturforsch. Teil A*, **13**, 348–349.

Bonse, U., Materlik, G. & Schröder, W. (1976). *Perfect-crystal monochromators for synchrotron X-radiation. J. Appl. Cryst.* **9**, 233–230.

Bonse, U., Olthoff-Münter, K. & Rumpf, A. (1983). *Monolithic double-grooved-crystal monochromators with tunable harmonic supression for neutrons and X-rays. J. Appl. Cryst.* **16**, 524–531.

Bowen, D. K., Clark, G. F., Davies, S. T., Nicholson, J. R. S., Roberts, K. J., Sherwood, J. N. & Tanner, B. K. (1982). *The X-ray topography station at Daresbury Laboratory. Nucl. Instrum. Methods*, **195**, 277–284.

Bowen, D. K. & Davies, S. T. (1983). *The double-crystal X-ray camera at Daresbury Laboratory. Nucl. Instrum. Methods*, **208**, 725–729.

Brádler, J. & Lang, A. R. (1968). *Use of the Ewald sphere in aligning crystal pairs to produce X-ray moiré fringes. Acta Cryst.* A**24**, 246–247.

Castelli, C. M., Allinson, N. M., Moon, K. J. & Watson, D. L. (1994). *High spatial resolution scintillation screens coupled to CCD detectors for X-ray imaging applications. Nucl. Instrum. Methods*, A**348**, 649–653.

Cerva, H. & Graeff, W. (1984). *Contrast investigation of surface acoustic waves by stroboscopic topography. I. Orientation contrast. Phys. Status Solidi A*, **82**, 34–45.

Cerva, H. & Graeff, W. (1985). *Contrast investigation of surface acoustic waves by stroboscopic topography. II. Wavefield deviation contrast. Phys. Status Solidi A*, **87**, 507–516.

Chikawa, J.-I. & Austerman, S. B. (1968). *X-ray double-crystal method of analyzing microstrains with BeO single crystals. Advances in X-ray analysis*, Vol. 11, edited by J. B. Newkirk & G. R. Mallett, pp. 393–400. New York: Plenum.

Chikawa, J.-I. & Fujimoto, I. (1968). *X-ray diffraction topography with a vidicon television image system. Appl. Phys. Lett.* **13**, 387–389.

Chikawa, J.-I., Sato, F. & Fujimoto, I. (1984). *High-resolution topography detector. Acta Cryst.* A**40**, C403.

Compton, A. H. & Allison, S. K. (1935). *X-rays in theory and experiment*. New York: Van Nostrand.

Du Mond, J. W. M. (1937). *Theory of the use of more than two successive X-ray crystal reflections to obtain increased resolving power. Phys. Rev.* **52**, 872–883.

Gerold, V. & Meier, F. (1959). *Der röntgenographische Nachweiss von Versetzungen in Germanium. Z. Phys.* **155**, 387–394.

Guinier, A. & Tennevin, J. (1949). *Sur deux variantes de la méthode de Laue et leurs applications. Acta Cryst.* **2**, 133–138.

Hart, M. (1968). *'Perfect crystals'. A study of their structural defects. Sci. Prog. Oxford*, **56**, 429–447.

Hart, M. (1971). *Bragg reflection X-ray optics. Rep. Prog. Phys.* **34**, 435–490.

Hart, M. (1972). *A complete determination of dislocation Burgers vectors by X-ray interferometry. Philos. Mag.* **26**, 821–831.

Hart, M. (1975*a*). *Synchrotron radiation – its application to high-speed, high-resolution X-ray diffraction topography. J. Appl. Cryst.* **8**, 436–444.

Hart, M. (1975*b*). *Ten years of X-ray interferometry. Proc. R. Soc. London Ser. A*, **346**, 1–22.

Hart, M. (1981). *Bragg angle measurement and mapping. J Cryst. Growth*, **55**, 409–427.

Hart, M. & Rodrigues, A. R. D. (1978). *Harmonic-free single-crystal monochromators for neutrons and X-rays. J. Appl. Cryst.* **11**, 248–253.

Hart, M., Rodrigues, A. R. D. & Siddons, D. P. (1984). *Adjustable resolution Bragg reflection systems. Acta Cryst.* A**40**, 502–507.

Hart, M., Sauvage, M. & Siddons, D. P. (1980). *'White beam' synchrotron X-ray interferometry. Acta Cryst.* A**36**, 947–951.

Hartmann, W. (1977). *Live topography. X-ray optics. Applications to solids*, edited by H.-J. Queisser, Chap. 6, pp. 191–219. Berlin: Springer.

Haruta, K. (1965). *A new method of obtaining stereoscopic pairs of X-ray diffraction topographs. J. Appl. Phys.* **36**, 1789–1790.

Hashimoto, H. & Uyeda, R. (1957). *Detection of dislocation by the moiré pattern in electron micrographs. Acta Cryst.* **10**, 143.

Hashizume, H. (1983). *Asymmetrically grooved monolithic crystal monochromators for suppression of harmonics in synchrotron X-radiation. J. Appl. Cryst.* **16**, 420–427; erratum: **16**, 648.

2.7 (*cont.*)

Hildebrandt, G. (1982). *X-ray wave fields in perfect and nearly perfect crystals – theoretical background and recent applications*. *J. Phys. E*, **15**, 1140–1155.

International Tables for Crystallography (1996). Vol. B. Dordrecht: Kluwer Academic Publishers.

Ishikawa, T., Kitano, T. & Matsui, J. (1985). *Synchrotron plane wave X-ray topography of GaAs with a separate (+, +) monochro-collimator*. *Jpn. J. Appl. Phys. Part 2*, **24**, L968–L971.

Ito, M., Yamaguchi, M. & Oba, K. (1987). *CsI(Na) scintillation plate with high spatial resolution*. *IEEE Trans. Nucl. Sci.* **34**, 401–405.

Jacobs, L. & Hart, M. (1977). *An X-ray topographic study of large crystals for a bent-crystal gamma diffractometer*. *Nucl. Instrum. Methods*, **143**, 319–325.

Jiang, S.-S. & Lang, A. R. (1983). *Stacking fault contrast in X-ray diffraction: a high resolution experimental study*. *Proc. R. Soc. London Ser. A*, **388**, 249–271.

Kato, N. (1974). *X-ray diffraction*, by L. V. Azaroff, R. Kaplow, N. Kato, R. J. Weiss, A. J. C. Wilson & R. A. Young, Chaps. 3–5, pp. 176–438. New York: McGraw–Hill.

Kikuta, S. (1971). *X-ray crystal collimators using successive asymmetric diffractions and their applications to measurements of diffraction curves. II. Type I collimator*. *J. Phys. Soc. Jpn*, **30**, 222–227.

Kikuta, S. & Kohra, K. (1970). *X-ray crystal collimators using successive asymmetric diffractions and their applications to measurements of diffraction curves. I. General considerations on collimators*. *J. Phys. Soc. Jpn*, **29**, 1322–1328.

Kohra, K. (1972). *Dynamical asymmetric diffraction and its applications to X-ray optical systems*. *Proceedings of the VIth International Conference on X-ray Optics and Microanalysis*, edited by G. Shinoda, K. Kohra & T. Ichinokawa, pp. 35–45. Tokyo: University of Tokyo Press.

Kuriyama, M. & Boettinger, W. J. (1976). *On the angular divergence of out-going beams in an asymmetric diffraction geometry*. *Acta Cryst.* A**32**, 511–512.

Kuriyama, M., Boettinger, W. J. & Cohen, G. G. (1982). *Synchrotron radiation topography*. *Annu. Rev. Mater. Sci.* **12**, 23–50.

Lang, A. R. (1957). *A method for the examination of crystal sections using penetrating charactistic radiation*. *Acta Metall.* **5**, 358–364.

Lang, A. R. (1959*a*). *The projection topograph: a new method in X-ray diffraction microradiography*. *Acta Cryst.* **12**, 249–250.

Lang, A. R. (1959*b*). *Studies of individual dislocations in crystals by X-ray diffraction microradiography*. *J. Appl. Phys.* **30**, 1748–1755.

Lang, A. R. (1963). *Applications of 'limited projection topographs' and 'direct beam topographs' in X-ray diffraction topography*. *Br. J. Appl. Phys.* **14**, 904–907.

Lang, A. R. (1968). *X-ray moiré topography of lattice defects in quartz*. *Nature (London)*, **220**, 652–657.

Lang, A. R. (1974). *On the growth-sectorial dependence of defects in natural diamonds*. *Proc. R. Soc. London Ser. A*, **340**, 233–248.

Lang, A. R. (1978). *Techniques and interpretation in X-ray topography*. *Diffraction and imaging techniques in material science*, 2nd, revised edition, edited by S. Amelinckx, R. Gevers & J. Van Landuyt, pp. 623–714. Amsterdam: North-Holland.

Lang, A. R. (1983). *Compact device for X-ray section topography with synchrotron sources*. *Rev. Sci. Instrum.* **54**, 897–899.

Lang, A. R., Makepeace, A. P. W., Moore, M. & Machado, W. G. (1983). *On the variation of X-ray diffraction contrast with wavelength: a study with synchrotron radiation*. *J. Appl. Cryst.* **16**, 113–125.

Lang, A. R. & Reifsnider, K. (1969). *Rapid X-ray diffraction topography using a high-gain image intensifier*. *Appl. Phys Lett.* **15**, 258–260.

Mai, Z.-H., Mardix, S. & Lang, A. R. (1980). *A high-resolution section topograph technique applicable to synchrotron radiation sources*. *J. Appl. Cryst.* **13**, 180–187.

Materlik, G. & Kostroun, V. O. (1980). *Monolithic crystal monochromators for synchrotron radiation with order sorting and polarising properties*. *Rev. Sci. Instrum.* **51**, 86–94.

Matsushita, T., Kikuta, S. & Kohra, K. (1971). *X-ray crystal collimators using successive asymmetric diffractions and their applications to measurements of diffraction curves. III. Type II collimator*. *J. Phys. Soc. Jpn*, **30**, 1136–1144.

Meieran, E. S., Landre, J. K. & O'Hara, S. (1969). *Direct video imaging of X-ray topographs*. *Appl. Phys. Lett.* **14**, 368–371.

Milne, A. D. (1971). *Scanning source X-ray topography*. *J. Appl. Cryst.* **4**, 251–252.

Nakayama, K., Hashizume, H., Miyoshi, A., Kikuta, S. & Kohra, K. (1973). *Use of asymmetrical dynamical diffraction of X-rays for multiple-crystal arrangements of the* $(n_1, +n_2)$ *setting*. *Z. Naturforsch. Teil. A*, **28**, 632–638.

Newkirk, J. B. (1958). *Method for the detection of dislocations in silicon by X-ray extinction contrast*. *Phys. Rev.* **110**, 1465–1466.

Newkirk, J. B. (1959). *The observation of dislocations and other imperfections by X-ray extinction contrast*. *Trans. TMS–AIME*, **215**, 483–497.

Petroff, J. F., Sauvage, M., Riglet, P. & Hashizume, H. (1980). *Synchrotron-radiation plane-wave topography. I. Application to misfit dislocation imaging in III–V heterojunctions*. *Philos. Mag.* A**42**, 319–338.

Pinsker, Z. G. (1978). *Dynamical scattering of X-rays in crystals*. Berlin: Springer.

Queisser, H.-J., Hartmann, W. & Hagen, W. (1981). *Real-time X-ray topography: defect dynamics and crystal growth*. *J. Cryst. Growth*. **52**, 897–906.

Ramachandran, G. N. (1944). *X-ray topographs of diamond*. *Proc. Indian Acad. Sci. Sect. A*, **19**, 280–292.

Reifsnider, K. & Green, R. E. Jr (1968). *Image intensifier system for dynamic X-ray diffraction studies*. *Rev. Sci. Instrum.* **39**, 1651–1655.

Renninger, M. (1961). *Asymmetrische Bragg-Reflexion am Idealkrystall zur Erhöhung des Doppelspekrometer-Auflösungsvermögens*. *Z. Naturforsch. Teil. A*, **16**, 1110–1111.

Renninger, M. (1965). *Beitrage zur doppeldiffraktometrischen Kristall-Topographic mit Röntgenstrahlen I. Methodik und Ergebnisse typischer Art*. *Z. Angew. Phys.* **19**, 20–33.

Sato, F., Maruyama, H., Goto, K., Fujimoto, I., Shidara, K., Kawamura, T., Hirai, T., Sakai, H. & Chikawa, J.-I. (1993). *Characteristics of a new high-sensitivity X-ray imaging tube for video topography*. *Jpn. J. Appl. Phys.* **32**, 2142–2146.

Schulz, L. G. (1954). *Method of using a fine-focus X-ray tube for examining the surface of single crystals*. *J. Met: Trans. AIME*, **200**, 1082–1083.

Stevels, A. L. N. & Kühl, W. (1974). *New phosphors for X-ray image intensifier tubes*. *Medicamundi*, **19**, 3–7.

2.7 (*cont.*)

Suzuki, S., Ando, M., Hayakawa, K., Nittono, O., Hashizume, H., Kishino, S. & Kohra, K. (1984). *A high-speed X-ray topography camera for use with synchrotron radiation at the photon factory*. *Nucl. Instrum. Methods*, **227**, 584–592.

Tanner, B. K. (1976). *X-ray diffraction topography*. Oxford: Pergamon Presss.

Tanner, B. K. (1977). *Crystal assessment by X-ray topography using synchrotron radiation*. *Prog. Cryst. Growth Charact.* **1**, 23–56.

Tanner, B. K. & Bowen, D. K. (1980). Editors. *Characterization of crystal growth defects by X-ray methods*. New York: Plenum.

Tate, M. W., Eikenberry, E. F., Barna, S. L., Wall, M. E., Lawrance, J. L. & Gruner, S. M. (1995). *A large-format high-resolution area X-ray detector based on a fiber-optically bonded charge-coupled device (CCD)*. *J. Appl. Cryst.* **28**, 196–205.

Tuomi, T., Naukkarinen, K. & Rabe, P. (1974). *Use of synchrotron radiation in X-ray diffraction topography*. *Phys. Status Solidi A*, **25**, 93–106.

Van Mellaert, L. & Schwuttke, G. H. (1972). *Feedback control system for scanning X-ray topography*. *J. Appl. Phys.* **43**, 687–692.

Wallace, C. A. & Ward, R. C. C. (1975). *A high-resolution X-ray topographical technique for thin flexible crystal plates*. *J. Appl. Cryst.* **8**, 281–286.

Whatmore, R. W., Goddard, P. A., Tanner, B. K. & Clark, G. F. (1982). *Direct imaging of travelling Rayleigh waves by stroboscopic X-ray topography*. *Nature (London)*, **299**, 44–46.

2.8

Ando, M. & Hosoya, S. (1972). *Q-switch and polarization domains in antiferromagnetic chromium observed with neutron diffraction topography*. *Phys. Rev. Lett.* **29**, 281–285.

Ando, M. & Hosoya, S. (1978). *Size and behavior of antiferromagnetic domains in Cr directly observed with X-ray and neutron topography*. *J. Appl. Phys.* **49**, 6045–6051.

Baruchel, J. (1989). *The contribution of neutron and synchrotron radiation topography to the investigation of first-order magnetic phase transitions*. *Phase Transit.* **14**, 21–29.

Baruchel, J., Schlenker, M. & Palmer, S. B. (1990). *Neutron diffraction topographic investigations of 'exotic' magnetic domains*. *Nondestr. Test. Eval.* **5**, 349–367

Baruchel, J., Schlenker, M., Zarka, A. & Petroff, J. F. (1978). *Neutron diffraction topographic investigation of growth defects in natural lead carbonate single crystals*. *J. Cryst. Growth*, **44**, 356–362.

Boeuf, A., Lagomarsino, S., Rustichelli, F., Baruchel, J. & Schlenker, M. (1975). *White beam neutron topography*. *Phys. Status Solidi A*, **31**, K91–K93.

Davidson, J. B. & Case, A. L. (1976). *Applications of the fly's eye neutron camera: diffraction tomography and phase transition studies*. Proc. Conf. on Neutron Scattering, ORNL, USERDA CONF 760601–P2, pp. 1124–1135.

Davidson, J. B., Werner, S. & Arrott, A. S. (1974). *Neutron microscopy of spin density wave domains in chromium*. *AIP Conf. Proc.*, edited by C. D. Graham & J. J. Rhyne, Vol. 18, pp. 396–400.

Doi, K., Minakawa, N., Motohashi, H. & Masaki, N. (1971). *A trial of neutron diffraction topography*. *J. Appl. Cryst.* **4**, 528–530.

Dudley, M., Baruchel, J. & Sherwood, J. N. (1990). *Neutron topography as a tool for studying reactive organic crystals: a feasibility study*. *J. Appl. Cryst.* **23**, 186–198.

Hustache, R. (1979). *Sélection de blocs monocristallins dans un cristal de beryllium par topographie neutronique*. *Nucl. Instrum. Methods*, **163**, 151–156.

Malgrange, C., Petroff, J. F., Sauvage, M., Zarka, A. & Englander, M. (1976). *Individual dislocation images and Pendellösung fringes in neutron topographs*. *Philos. Mag.* **33**, 743–751.

Scherm, R. & Fåk, B. (1993). *Neutrons*. In *Neutron and synchrotron radiation for condensed matter studies*, Vol. 1: *Theory, instruments and methods. HERCULES (Higher European Research Course for Users of Large Experimental Systems)*, *Grenoble*, edited by J. Baruchel, J. L. Hodeau, M. S. Lehmann, J. R. Regnard & C. Schlenker. Les Ulis: Les Editions de Physique; Berlin: Springer-Verlag.

Schlenker, M., Baruchel, J., Perrier de la Bathie, R. & Wilson, S. A. (1975). *Neutron diffraction section topography: observing crystal slices before cutting them*. *J. Appl. Phys.* **46**, 2845–2848.

Schlenker, M. & Shull, C. G. (1973). *Polarized neutron techniques for the observation of ferromagnetic domains*. *J. Appl. Phys.* **44**, 4181–4184.

Sillou, D., Baruchel, J., Kuroda, K., Michalowicz, A., Guigay, J. P. & Schlenker, M. (1989). *First experiments on flipping ratio mapping with the 'multi-PM' position-sensitive detector*. *Physica (Utrecht)*, B**156–157**, 581–583.

Tomimitsu, H., Doi, K. & Kamada, K. (1983). *Neutron diffraction topographic observations of substructures in Cu-based alloys*. *Physica (Utrecht)*, B**120**, 96–102.

2.9

Berk, N. F. & Majkrzak, C. F. (1995). *Using parametric B-splines to fit specular reflectivities*. *Phys. Rev. B*, **51**, 11296–11309.

Boer, D. K. G. de (1994). *Influence of the roughness profile on the specular reflectivity of X-rays and neutrons*. *Phys. Rev. B*, **49**, 5817–5820.

Buttiker, M. (1983). *Larmor precession and the traversal time for tunneling*. *Phys. Rev. B*, **27**, 6178–6188.

Felcher, G. P., Hilleke, R. O., Crawford, R. K., Haumann, J., Kleb, R. & Ostrowski, G. (1987). *Polarized neutron reflectometer: a new instrument to measure magnetic depth profiles*. *Rev. Sci. Instrum.* **58**, 609–619.

Felcher, G. P. & Russell, T. P. (1991). Editors. *Physica (Utrecht)*, B**173**, 1–210.

Hamilton, W. A., Hayter, J. B. & Smith, G. S. (1994). *Neutron reflectometry as optical imaging*. *J. Neutron Res.* **2**, 1–19.

Holy, V., Kubena, J., Ohlidal, I., Lischka, K. & Plotz, W. (1993). *X-ray reflection from rough layered systems*. *Phys. Rev. B*, **47**, 15896–15903.

Majkrzak, C. F. (1991). *Polarized neutron reflectometry*. *Physica (Utrecht)*, B**173**, 75–88.

Majkrzak, C. F., Ankner, J. F., Berk, N. F. & Gibbs, D. (1994) *Magnetic multilayers*, edited by L. H. Bennett & R. E. Watson, pp. 299–354. Singapore: World Scientific.

Merzbacher, E. (1970). *Quantum mechanics*, 2nd ed. New York: John Wiley.

2.9 (*cont.*)

Nevot, L. & Croce, P. (1980). *Caracterisation des surfaces par reflexion rasante de rayons X. Application a l'etude du polissage de quelques verres silicates*. *Rev. Phys. Appl.* **15**, 761–779.

Nuñez, V., Majkrzak, C. F. & Berk, N. F. (1993). *Dynamical scattering of polarized neutrons by thin magnetic films*. *MRS Symp. Proc.* **313**, 431–436.

Pedersen, J. S. & Hamley, I. W. (1994). *Analysis of neutron and X-ray reflectivity data by constrained least-squares methods*. *Physica (Utrecht)*, B**198**, 16–23.

Penfold, J. & Thomas, R. K. (1990). *The application of specular reflection of neutrons to the study of surfaces and interfaces*. *J. Phys. Condens. Matter*, **2**, 1369–1412.

Pynn, R. (1992). *Neutron scattering by rough surfaces at grazing incidence*. *Phys. Rev. B*, **45**, 602–612.

Russell, T. P. (1990). *X-ray and neutron reflectivity for the investigation of polymers*. *Mater. Sci. Rep.* **5**, 171–271.

Schreyer, A., Zeidler, T., Morawe, C., Metoki, N., Zabel, H., Ankner, J. F. & Majkrzak, C. F. (1993). *Spin polarized neutron reflectivity study of a Co/Cu superlattice*. *J. Appl. Phys.* **73**, 7616–7621.

Sears, V. F. (1989). *Neutron optics*. Oxford University Press.

Sears, V. F. (1993). *Generalized distorted-wave Born approximation for neutron reflection*. *Phys. Rev. B*, **48**, 17477–17485.

Sinha, S. K., Sirota, E. B., Garroff, S. & Stanley, H. B. (1988). *X-ray and neutron scattering from rough surfaces*. *Phys. Rev. B*, **38**, 2297–2311.

Smith, G. S., Hamilton, W., Fitzsimmons, M., Baker, S. M., Hubbard, K. M., Nastasi, M., Hirvonen, J.-P. & Zocco, T. G. (1992). *Neutron reflectivity study of thermally-induced boron diffusion in amorphous elemental boron*. *SPIE Proc. Ser.* **1738**, 246–253.

Steinhauser, K. A., Steryl, A., Scheckenhofer, H. & Malik, S. S. (1980). *Observation of quasibound states of the neutron in matter*. *Phys. Rev. Lett.* **44**, 1306–1309.

Wiesler, D. G., Feigin, L. A., Majkrzak, C. F., Ankner, J. F., Berzina, T. S. & Troitsky, V. I. (1995). *Neutron and X-ray reflectivity study of Ba salts of alternating bilayers of deuterated and hydrogenated stearic acid*. *Thin Solid Films*, **266**, 69–77.

Yamada, S., Ebisawa, T., Achiwa, N., Akiyoshi, T. & Okamoto, S. (1978). *Neutron-optical properties of a multilayer system*. *Annu. Rep. Res. React. Inst. Kyoto Univ.* **11**, 8–27.

Zhou, X.-L. & Chen, S.-H. (1993). *Model-independent method for reconstruction of scattering-length-density profiles using neutron or X-ray reflectivity data*. *Phys. Rev. E*, **47**, 3174–3190.

International Tables for Crystallography (2006). Vol. C, Chapter 3.1, pp. 148–155.

3.1. Preparation, selection, and investigation of specimens

By P. F. Lindley

3.1.1. Crystallization

3.1.1.1. *Introduction*

The preparation of single crystals probably constitutes the most important step in a crystal structure analysis, since without high-quality diffraction data many analyses will prove problematical, if not completely intractable; time and effort invested in crystallization procedures are rarely wasted. There is a wealth of literature available on the subject of growing crystals and this includes the *Journal of Crystal Growth* (Amsterdam: Elsevier). This section does not intend to be a comprehensive review of the subject, but rather to provide some key lines of approach with appropriate references. The field of crystallizing biological macromolecules is itself a growth area and, in consequence, has been given a special emphasis.

Useful general references for growing crystals for structure analysis include Bunn (1961), Stout & Jensen (1968), Blundell & Johnson (1976), McPherson (1976, 1982, 1990), Ducruix & Giegé (1992) and Helliwell (1992). Volume D50 (Part 4) of *Acta Crystallographica* (1994) reports the Proceedings of the Fifth International Conference on Crystallization of Biological Macromolecules (San Diego, California, 1993) and is essential reading for crystallization experiments in this area. A biological macromolecular database for crystallization conditions has also been initiated (Gilliland, Tung, Blakeslee & Ladner, 1994).

3.1.1.2. *Crystal growth*

Crystallization has long been used as a method of purification by chemists and biochemists, although lack of purity can severely hamper the growth of single crystals, particularly if the impurities have some structural resemblance to the molecule being crystallized (Giegé, Theobald-Dietrich & Lorber, 1993; Thatcher, 1993). The process of crystallization involves the ordering of ions, atoms, and molecules in the gas, liquid, or solution phases to take up regular positions in the solid state. The initial stage is nucleation, followed by deposition on the crystallite faces. The latter can be considered as a dynamic equilibrium between the fluid and the crystal, with growth occurring when the forward rate predominates. Factors that affect the equilibrium include the chemical nature of the crystal surface, the concentration of the material being crystallized, and the nature of the medium in and around the crystal. Relatively little research has been done concerning the process of nucleation, but crystal formation appears to be conditional on the appearance of nuclei of a critical size. Too small aggregates will have either a positive or an unfavourable free energy of formation, so that there is a tendency to dissolution, whilst above the critical size the intermolecular interactions will, on average, lead to an overall negative free energy of formation. The rate of nucleation will increase considerably with the degree of supersaturation, and, in order to limit the number of nuclei (and therefore number of crystals growing), the degree of supersaturation must be as low as possible. Supersaturation must be approached slowly, and, when a low degree has been achieved, it must be carefully controlled. Many factors can influence crystallization, but a conceptually simple explanation of crystal growth has been described in detail by Tipson (1956) and elaborated, for example, by Ries-Kautt & Ducruix (1992). These latter authors provide a useful schematic description of the two-dimensional solubility diagram relating the concentration of the molecule being crystallized to the concentration of the crystallizing agent. The presence of foreign bodies, such as dust particles, makes the nucleation process thermodynamically more favourable, and these should be removed by centrifugation and/or filtration. The addition of seed crystals can often be used to control the nucleation process (Thaller, Eichelle, Weaver, Wilson, Karlsson & Jansonius, 1985). In the case of the formation of crystals of macromolecules in solution, Ferré-D'Amaré & Burley (1994) have described the use of dynamic light scattering to screen crystallization conditions for monodispersity. Empirical observations suggest that macromolecules that have the same size under normal solvent conditions tend to form crystals, whereas those systems that are polydisperse, or where random aggregation occurs, rarely give rise to ordered crystals.

3.1.1.3. *Methods of growing crystals*

General strategies for crystallizing low-molecular-weight organic compounds have been reported by van der Sluis, Hezemans & Kroon (1989) and are listed in Table 3.1.1.1. Many of these strategies are also applicable to inorganic compounds. In the case of biological macromolecules, the main methods utilize one or more of the factors described in Subsection 3.1.1.5 and include batch crystallization, the hot-box technique, equilibrium dialysis, and vapour diffusion (see, for example, Blundell & Johnson, 1976; Helliwell, 1992). The growth of macromolecular crystals in silica hydrogels minimizes convection currents, turbidity, and any strain effects due to the presence of the crystallization vessel. Heterogeneous and secondary nucleation are also reduced (Robert, Provost & Lefaucheux, 1992; Cudney, Patel & McPherson, 1994; García-Ruiz & Moreno, 1994; Thiessen, 1994; Robert, Bernard & Lefaucheux, 1994; Bernard, Degoy, Lefaucheux & Robert, 1994; Sica *et al.*, 1994). Various apparata have been described for use with the vapour diffusion technique (see also Subsection 3.1.1.6) and include a simple capillary vapour diffusion device for preliminary screening of crystallization conditions (Luft & Cody, 1989), a double-cell device that decouples the crystal nucleation from the crystal growth, facilitating the control of nucleation and growth (Przybylska, 1989), microbridges for use with sitting drops in the 35–45 µl range (Harlos, 1992), and diffusion cells with varying depths, in order to control the time course of the equilibration between the macromolecule and the reservoir solution (Luft *et al.*, 1994).

3.1.1.4. *Factors affecting the solubility of biological macromolecules*

There are many factors that influence the crystallization of macromolecules (McPherson, 1985*a*; Giegé & Ducruix, 1992; Schick & Jurnak, 1994; Tissen, Fraaije, Drenth & Berendsen, 1994; Carter & Yin, 1994; Spangfort, Surin, Dixon & Svensson, 1994; Axelrod *et al.*, 1994; Konnert, D'Antonio & Ward, 1994; Forsythe, Ewing & Pusey, 1994; Diller, Shaw, Stura, Vacquier & Stout, 1994; Hennig & Schlesier, 1994), but the following are particularly important with respect to solubility (Blundell & Johnson, 1976).

Ionic strength. The solubility of macromolecules in aqueous solution depends on the ionic strength, since the presence of ions modifies the interactions of the macromolecule with the solvent. At low ion concentrations, the solubility of the macromolecule is

Copyright © 2006 International Union of Crystallography

Table 3.1.1.1. *Survey of crystallization techniques suitable for the crystallization of low-molecular-weight organic compounds for X-ray crystallography (adapted from van der Sluis, Hezemans & Kroon, 1989)*

Technique	Advantage(s)	Limitation(s)
Evaporation from a single solvent	Simple Inexpensive	Limitation to solvents with adequate vapour pressure Crust formation on tube walls Crystals that are dried are less suitable as seeds, may lose included solvent and become tightly adhered to the crystallization vessel Difficult to reproduce Limited number of solvents give concentration 5–200 mg ml^{-1} for a particular compound
Evaporation from a binary mixture of solvents (volatile solvent and non-volatile precipitant)	No crust formation on the tube walls Crystals are not dried	Stringent demands on solubility, miscibility and volatility of the two solvents Difficult to reproduce
Batch crystallization	No demands on the volatility of the solvent or precipitant Repeated seeding by thermal treatment is easy	Metastable zone with regard to supersaturation must be large High and almost uncontrollable crystallization rate Solvents must be miscible
Liquid–liquid diffusion	Favourable change in supersaturation at the interface during crystallization Repeated seeding by thermal treatment is easy	Density differences required for the two liquids (less stringent if capillaries are used) Viscosity of the liquids greater than water Solvents must be miscible High and almost uncontrollable crystallization rate
Sitting-drop vapour-phase diffusion	Crystallization rate can easily be controlled by changing the diffusion path, solvent, precipitant, or pH Repeated seeding easily implemented Highest number of independent variables to obtain wide variety of conditions	Solvents must be miscible Solvent preferably less volatile than precipitant
Hanging-drop vapour-phase diffusion	Crystallization rate can easily be controlled by changing solvent, precipitant, or pH Easy examination of crystallization outcome in array-like set-up	Only applicable in case of water-based solvents Diffusion rate is fast and difficult to control See previous method
Temperature change	Easily controllable parameter Repeated seeding extremely easily and accurately carried out With Dewar flask inexpensive and simple	Limited to thermally stable compounds and (pseudo)polymorphs
Gel crystallization	Suited for sparingly soluble or easily nucleating compounds	Limited variety of solvents possible Sampling of crystals difficult Laborious
Sublimation	No inclusion of solvent of crystallization	Limited to small hydrophobic molecules Laborious
Solidification	For liquids and gases the only applicable method	Limited to thermostable compounds High change of amorphicity Laborious

Table 3.1.1.2. *Commonly used ionic and organic precipitants, adapted from McPherson (1985a)*

(*a*) Ionic compounds	(*b*) Organic solvents*
Ammonium† or sodium sulfate	Ethanol
Sodium or ammonium citrate	Isopropanol
Sodium, potassium or ammonium chloride	2-Methyl-2,4-pentanediol (MPD)
Sodium or ammonium acetate	Dioxane
Magnesium sulfate	Acetone
Cetyltrimethylammonium salts	Butanol
Calcium chloride	Dimethyl sulfoxide
Ammonium nitrate	2,5-Hexanediol
Sodium formate	Methanol
Lithium chloride	1,3-Propanediol
	1,3-Butyrolactone
	Poly(ethylene glycol) 600–20000 (PEG)

* The volatility of solvents such as ethanol and acetone may cause handling problems. † Ammonium sulfate can cause problems when used as a precipitant, since pH changes occur owing to ammonium transfer following ammonium/ammonia equilibrium; this effect has been studied in detail by Mikol, Rodeau & Giegé (1989). Monaco (1994) has suggested that ammonium succinate is a useful substitute for ammonium sulfate.

increased, a phenomenon termed 'salting-in'. As the ionic strength is increased, the ions added compete with one another and the macromolecules for the surrounding water. The resulting removal of water molecules from the solute leads to a decrease in the solubility, a phenomenon termed 'salting-out'. Different ions will affect the solubility of the protein in different ways. Small highly charged ions will be more effective in the salting-out process than large low-charged ions. Commonly used ionic precipitants are listed in Table 3.1.1.2, column (*a*) (McPherson, 1985*a*).

pH and counterions. The net charge on a macromolecule in solution can be modified either by changing the pH (adding or removing protons) or by binding ions (counterions). In general terms, the protein solubility will increase with the overall net charge and will be least soluble when the net charge is zero (isoelectric point). In the latter case, the molecules can pack in the crystalline form without an overall, destabilizing accumulation of charge.

Temperature. Temperature has a marked affect on many of the factors that govern the solubility of a macromolecule. The dielectric constant decreases with increase in temperature, and the entropy terms in the free energy tend to dominate the enthalpy terms (Blundell & Johnson, 1976). The temperature coefficient of solubility varies with ionic strength and the presence of organic solvents. McPherson (1985*b*) gives a useful account of protein crystallization by variation of pH and temperature.

Organic solvents. Addition of organic solvents can produce a marked change in the solubility of a macromolecule in aqueous solution (care should be taken to avoid denaturation). This is partly due to a lowering of the dielectric constant, but may also involve specific solvation and displacement of water at the surface of the macromolecule. Generally, the solubility decreases with decrease of temperature when substantial amounts of organic solvent are present. Commonly used organic precipitants are listed in Table 3.1.1.2, column (*b*) (McPherson, 1985*a*).

3.1.1.5. *Screening procedures for the crystallization of biological macromolecules*

Optimal conditions for crystal growth are often very difficult to predict *a priori*, although many proteins crystallize close to their pI. In order to surmount the problem of testing a very large range of conditions, Carter & Carter (1979) devised the *incomplete factorial method*, in which a very coarse matrix of crystallization conditions is explored initially. Finer grids are then investigated around the most promising sets of coarse conditions. This technique has been further refined to yield the sparse-matrix sampling technique described by Jancarik & Kim (1991). Table 3.1.1.3 lists the crystallization parameters used by these authors. The 50 conditions constituting the sparse matrix are given in Table 3.1.1.4. A recent update of this matrix and a set of stock solutions in the form of a crystal screen kit can be obtained commercially from Hampton Research (1994). Further developments in screening methods are described in Volume D50 (Part 4) of *Acta Crystallographica* (1994).

3.1.1.6. *Automated protein crystallization*

Several liquid-handling systems have been described that can automatically set up, reproducibly, a range of crystallization conditions (different protein concentrations, ionic strengths, amounts of organic precipitant, *etc*.) for the hanging-drop, sitting-drop, and microbatch methods. A useful introduction describing a system for mixing both buffered protein solutions and the corresponding reservoirs is given by Cox & Weber (1987). Chayen, Shaw Stewart, Maeder & Blow (1990) describe an automatic dispenser involving a bank of Hamilton syringes driven by stepper motors under computer control that can be used to set up small samples (2 µl or less) for microbatch crystallization (or hanging drops). Further systems have been described by Oldfield, Ceska & Brady (1991), Eiselé (1993), Soriano & Fontecilla-Camps (1993), Sadaoui, Janin & Lewit-Bentley (1994), and Chayen, Shaw Stewart & Baldock (1994).

3.1.1.7. *Membrane proteins*

Integral membrane proteins can be considered as those whose polypeptide chains span the lipid bilayer at least once. The external membrane segments exposed to an aqueous environment are hydrophilic, but it is the tight interaction of the hydrophobic segments of the chain with the quasisolid lipid bilayer that constitutes the major problem in their crystallization. Crystallization trials require disruption of the membrane, isolation of the protein, and solubilization of the resultant hydrophobic region (McDermott, 1993). Organic solvents, chaotropic agents, and amphipathic detergents can be used to disrupt the membrane, but detergents such as β-octyl glucoside are most commonly

Table 3.1.1.3. *Crystallization matrix parameters for sparse-matrix sampling, adapted from Jancarik & Kim (1991)*

Precipitating agents			
Non-volatile	Salts	Volatile	Mixture
2-Methyl-2,4-pentanediol (MPD) Poly(ethylene glycol)(PEG) 400 PEG 4000 PEG 8000	Na, K tartrate NH_4 phosphate NH_4 sulfate Na acetate Li sulfate Na formate Na, K phosphate Na citrate Mg formate	2-Propanol	NH_4 sulfate + PEG 2-Propanol + PEG
Range of pH: 4.6, 5.6, 7.5, 8.5			
Salts, additives:	Ca chloride, Na citrate, Mg chloride, NH_4 acetate, NH_4 sulfate, Mg acetate, Zn acetate, Ca acetate		

used, since they minimize the loss of protein integrity. The several classes of detergent employed tend to be non-ionic or zwitterionic at the pH used, have a maximum hydrocarbon chain length of 12 carbon atoms, and possess a critical micelle concentration. The key to crystallizing membrane protein–detergent complexes appears to be the attainment of conditions in which the protein surfaces are moderately supersaturated and, in addition, the detergent micellar collar is at, or near, its solubility limit (Scarborough, 1994). Most successful integral membrane protein crystallizations are near the micellar aggregation point of the detergent (Garavito & Picot, 1990).

3.1.2. Selection of single crystals

3.1.2.1. *Introduction*

The final results of a structure analysis cannot be better than the imperfections of the crystal allow, and effort invested in producing crystals giving a clearly defined, high-resolution diffraction pattern is rarely wasted. The selection of twinned crystals, aggregates, or those with highly irregular shapes can lead to poor diffraction data and may prohibit a structure solution. There are many properties of crystals that can be examined prior, or in addition, to an X-ray or neutron diffraction study. These are summarized in Table 3.1.2.1. Many of these properties can yield useful information about the crystal packing and the overall molecular shape. For example, the shape and orientation of the optical indicatrix may be used to find the orientation of large atomic groups that possess shapes such as flat discs or rods and therefore also have strong anisotropic polarizability. A morphological examination can reveal information not only about the crystal quality but also in many cases about the crystal system, whilst identification of extinction directions can assist in crystal mounting. It is regrettable that many modern practitioners of the science of crystallography give little more than a cursory optical examination to their specimens before commencing data collection and a structure analysis.

3.1.2.2. *Size, shape, and quality*

A frequently occurring question involves the size and shape of single crystals required for successful diffraction studies. Among other factors, the intensity of diffraction is dependent on the volume of the crystal specimen bathed by the X-ray or neutron beam and is inversely proportional to the square of the unit-cell volume (see Chapter 6.4). Hence, small crystals with large unit cells will tend to give rise to weak diffraction patterns. This can be compensated for by increasing the incident intensity, *e.g.* using a synchrotron-radiation source in the case of X-rays. How large should a crystal be, and what is the smallest crystal size that can be accommodated? X-ray collimators, or slit systems, with diameters in the range 0.1 to 0.8 mm are commonly employed for single-crystal diffraction studies. For many diffractometers, the primary beam is arranged to have a plateau of uniform intensity with dimensions 0.5×0.5 mm. For most small inorganic and organic compounds, crystals with dimensions slightly smaller than this will suffice, depending on the strength of diffraction, although successful structure determinations have been reported on very small crystals (0.1 mm and less) with both conventional and synchrotron X-ray sources (Helliwell *et al.*, 1993). Microfocus beam lines at the third generation of synchrotron sources such as ESRF are designed to examine crystals routinely in the 10 μm range (Riekel, 1993). In the case of a biological macromolecule of molecular weight 50 kDa and using a conventional X-ray source (a rotating-anode generator), a crystal of 0.1 mm in all dimensions will probably give diffraction patterns from which the basic crystal system and unit-cell parameters can be deduced, but a crystal of 0.3 mm in each dimension, *i.e.* roughly 30 times the volume, would be required for the collection of high-resolution data (Blundell & Johnson, 1976). The higher intensity and smaller beam divergence inherent in a synchrotron X-ray source mean that high-resolution data of good quality could be obtained with the smaller crystal. Indeed, useful intensity data have been obtained with crystals with a maximum dimension of 50 μm (Subsection 3.4.1.5). At cryogenic temperatures, radiation damage is greatly reduced, and increased exposure times can be utilized (at the expense of increased background) to compensate for a small crystal volume. In the case of neutrons, the sample size is generally larger than for X-rays, owing to lower neutron flux and higher beam divergence. For a steady-state high-flux reactor such as that at the Institut Laue–Langevin (France), a crystal volume of 6 mm^3 or larger is recommended for biological samples. Unfortunately, crystals of this size are not readily obtainable in most cases.

The shape or habit of a single crystal is normally determined by the internal crystal structure and the growth

Table 3.1.1.4. *Reservoir solutions for sparse-matrix sampling (Jancarik & Kim 1991)*

No.	Salt	Buffer	Precipitant (% by mass)
1	0.02 *M* Ca chloride	0.1 *M* Acetate	30% MPD
2			0.4 *M* Na, K tartrate
3			0.4 *M* NH_4 phosphate
4		0.1 *M* Tris	2.0 *M* NH_4 sulfate
5	0.2 *M* Na citrate	0.1 *M* Hepes	40% MPD
6	0.2 *M* Mg chloride	0.1 *M* Tris	30% PEG 4000
7		0.1 *M* Cacodylate	1.4 *M* Na acetate
8	0.2 *M* Na citrate	0.1 *M* Cacodylate	30% 2-Propanol
9	0.2 *M* NH_4 acetate	0.1 *M* Citrate	30% PEG 4000
10	0.2 *M* NH_4 acetate	0.1 *M* Acetate	30% PEG 4000
11		0.1 *M* Citrate	1.0 *M* NH_4 phosphate
12	0.2 *M* Mg chloride	0.1 *M* Hepes	30% 2-Propanol
13	0.2 *M* Na citrate	0.1 *M* Tris	30% PEG 400
14	0.2 *M* Ca chloride	0.1 *M* Hepes	28% PEG 400
15	0.2 *M* NH_4 sulfate	0.1 *M* Cacodylate	30% PEG 8000
16		0.1 *M* Hepes	1.5 *M* Li sulfate
17	0.2 *M* Li sulfate	0.1 *M* Tris	30% PEG 4000
18	0.2 *M* Mg acetate	0.1 *M* Cacodylate	20% PEG 8000
19	0.2 *M* NH_4 acetate	0.1 *M* Tris	30% 2-Propanol
20	0.2 *M* NH_4 sulfate	0.1 *M* Acetate	25% PEG 4000
21	0.2 *M* Mg acetate	0.1 *M* Cacodylate	30% MPD
22	0.2 *M* Na acetate	0.1 *M* Tris	30% PEG 4000
23	0.2 *M* Mg chloride	0.1 *M* Hepes	30% PEG 400
24	0.2 *M* Ca chloride	0.1 *M* Acetate	20% 2-Propanol
25		0.1 *M* Imidazole	1.0 *M* Na acetate
26	0.2 *M* NH_4 acetate	0.1 *M* Citrate	30% MPD
27	0.2 *M* Na citrate	0.1 *M* Hepes	20% 2-Propanol
28	0.2 *M* Na acetate	0.1 *M* Cacodylate	30% PEG 8000
29		0.1 *M* Hepes	0.8 *M* Na, K tartrate
30	0.2 *M* NH_4 sulfate		30% PEG 8000
31	0.2 *M* NH_4 sulfate		30% PEG 4000
32			2.0 *M* NH_4 sulfate
33			4.0 *M* Na formate
34		0.1 *M* Acetate	2.0 *M* Na formate
35		0.1 *M* Hepes	1.6 *M* Na, K phosphate
36		0.1 *M* Tris	8% PEG 8000
37		0.1 *M* Acetate	8% PEG 4000
38		0.1 *M* Hepes	1.4 *M* Na citrate
39		0.1 *M* Hepes	2% PEG 400, 2.0 *M* Na sulfate
40		0.1 *M* Citrate	20% 2-Propanol + 20% PEG 4000
41		0.1 *M* Hepes	10% 2-Propanol + 20% PEG 4000
42	0.05 *M* K phosphate		20% PEG 8000
43			30% PEG 1500
44			0.2 *M* Mg formate
45	0.2 *M* Zn acetate	0.1 *M* Cacodylate	18% PEG 8000
46	0.2 *M* Ca acetate	0.1 *M* Cacodylate	18% PEG 8000
47		0.1 *M* Acetate	2.0 *M* NH_4 sulfate
48		0.1 *M* Tris	2.0 *M* NH_4 sulfate
49	1.0 *M* Li sulfate		2% PEG 8000
50	1.0 *M* Li sulfate		15% PEG 8000

Abbreviations: tris: 2-amino-2-(hydroxymethyl)-1,3-propanediol; hepes: 4-(2-hydroxyethyl)-1-piperazineethanesulfonic acid. Buffers: Na acetate buffer, pH = 4.6; Na citrate buffer, pH = 5.6; Na cacodylate buffer, pH = 6.5; Na hepes buffer, pH = 7.5; tris/HCl buffer, pH = 8.5.

conditions. For diffractometry purposes, it is customary to bathe the crystal in the X-ray beam, so that elongated crystals may require cutting with a razor blade in order to trim them to an appropriate size. Large crystals of hard materials can be ground into spheres or cylinders (Jeffery, 1977), so that corrections can be readily made to the observed intensities for systematic errors in absorption (see Chapter 6.3). Crystals that have elongated prismatic or needle shapes are often useful if data are collected using oscillation geometry, since the crystal can be translated in the X-ray beam at intervals during data collection to minimize radiation damage (Subsection 3.4.1.5). In general, all shapes can be accommodated, but those that are grossly asymmetric (*e.g.* very thin plates) may give elongated or distorted

Table 3.1.2.1. *Use of crystal properties for selection and preliminary study of crystals, adapted from MacGillavry & Henry (1962); morphological, optical, and mechanical properties*

Crystal property	Uses and comments	Relation with structure
Morphological properties		
Crystal habit	Setting crystal parallel to edge, or to symmetry axis, derived from goniometric measurement Habit can be influenced by solvent, crystallization conditions, trace impurities Well formed crystals can be accurately measured for analytical corrections for absorption	Morphological determination of crystal class may narrow down choice of space group Best-developed faces correspond to net planes with large density of lattice or pseudo-lattice nodes (Bravais' law, extended by Donnay & Harker) Prominent faces tend to be parallel to important bond systems Face development correlates inversely with surface free energy
Twinning	Twins may be hard to detect by morphological or diffraction methods. Investigate under the polarizing microscope: optical anomalies strongly indicate mimetic twinning, stacking faults, *etc*. Mechanical twinning may occur when a single crystal is cut or ground. In such cases, the crystal should be shaped by use of a solvent	May indicate hemimorphy or pseudo-hemimorphy of the cell or supercell; see Chapter 1.3 Pseudo-symmetrical stacking
Etch figures; epitaxy	See *IT* A (2002), Section 10.2.3 (pp. 805–806), and chemical properties below	
Optical properties		
Refractive index; birefringence (see IT *A*, Section 10.5.4, p. 790)	Checking quality of crystal: homogeneous extinction, interference figures Extinction direction is used for setting badly formed or ground crystals Magnitude of refractive index may be used for identification of crystal orientation	High refractive index may indicate close packing Shape and orientation of indicatrix may be useful for finding orientation of large atomic or ionic groups with strongly anisotropic polarizability (*e.g.* flat or rod-shaped groups)
Optical activity	Distinguishes between optical antipodes in studies of absolute configuration	Difficult to measure, or even detect, in optically biaxial crystals. No obvious relation with structure
Pleochroism	Identification of crystal orientation through dependence of colour on direction of light vibration	Extended conjugated-bond systems have strong absorption of light vibrating parallel to system; weak absorption perpendicular to system String-like arrangement of some atoms [*e.g.* iodine in poly(vinyl alcohol)] produces strong absorption parallel to string In inorganic compounds, absorption is greatest for light vibrating along directions in which ions are distorted
Reflection of light		Opaque substances contain loosely bound electrons
Raman effect		May give information on the orientation and symmetry of scattering groups
Mechanical properties		
Cleavage	Useful for obtaining good surfaces for crystal setting Useful for improving crystal shape	Correlates with bond-strength anisotropy
Hardness	Anisotropy of hardness may produce ellipsoids instead of spheres when an abrasion chamber is used	Hardness gives an indication of bond strength and bond density Hardness may be very sensitive to impurities, changes in texture through ageing or heat treatment, *etc*.
Plasticity	Single crystals: avoid cutting or grinding Polycrystalline material: plastic deformation is often strongly anisotropic, and may then be used to produce single or double orientation	Non-directive bonding between large strongly bonded units (long-chain paraffins, layer structures) Plastic flow may also be associated with mechanical twinning or lattice imperfections

Table 3.1.2.1. *Use of crystal properties for selection and preliminary study of crystals (cont.)*

Crystal property	Relation with structure
Magnetic properties	
Paramagnetism; diamagnetism	In an isomorphous series of paramagnetic salts, the values of the average susceptibility and of magnetic anisotropy are dependent on the nature of the paramagnetic ion. The shape of the coordination polyhedron may be found from the crystal anisotropies In aliphatic non-conjugated organic crystals, the numerically largest diamagnetic susceptibility is along the direction in which lie the largest molecular directions In crystals containing aromatic compounds or molecules with coplanar conjugated bonds, the numerically largest molecular diamagnetic susceptibility is normal to the plane of the molecular orbitals, and may thus indicate the molecular orientations
Ferromagnetism; antiferromagnetism; ferrimagnetism	Neutron diffraction by magnetic compounds may give information about the directions of the resultant spin and orbital moments. X-ray diffraction effects are usually unimportant In magnetic materials, the interatomic distances, and, in antiferromagnetic oxides, the valency angles at the oxygen ions are related to the diameter of the electron shell
Nuclear magnetic resonance	The line width in NMR spectra is related to the distances between the nuclei with magnetic moments
Electrical properties	
Ferroelectricity; pyroelectricity	See *IT* A (2002), Section 10.2.5, p. 807. Ferroelectricity indicates (i) a structure of polar symmetry, and (ii) the probability of another high-symmetry structure of nearly equal energy, derivable from the ferroelectric by a displacive transition. Often there are several related structures, some ferroelectric and some antiferroelectric Pyroelectricity indicates noncentrosymmetry. Second-harmonic generation is ordinarily a more sensitive test
Piezoelectricity	Piezoelectricity gives information on symmetry; it occurs only in ten crystal classes. See *IT* A, Section 10.2.6
Thermodynamic properties	
Heat capacity ('specific heat')	Anomalies indicate polymorphic transitions, disorder, approach to melting point, and temperature variation gives Einstein and/or Debye characteristic temperatures
Melting point	Atoms in crystals with a low melting point often have large thermal movements; diffraction experiments should preferably be carried out at low temperatures Anomalies in the variation of melting point in a series of homologues indicate a change in packing or bond type
Density	For measurement, see Chapter 3.2. Necessary for determination of number of formula weights per cell. May indicate liquid of crystallization, isomorphous replacement, degree of approach to close packing, first-order transitions with change of temperature or pressure
Thermal expansion	Thermal expansion is usually greatest in directions normal to layers or chains. Abrupt variation with change of temperature or pressure indicates a second-order transition
Chemical properties	
Chemical analysis	Gives kinds of atoms in the structure and (in conjunction with the density) the number of each kind in the unit cell
Attack of surface	May be used to shape crystals Etch figures are sensitive indicators of point-group symmetry (see *IT* A, Section 10.2.3). Change of orientation of etch figures on a face may reveal twinning. Rows of etch pits may reveal grain or sub-grain boundaries
Oriented growth on parent crystal	Epitaxy often reveals similarity of lattice parameters and even of atomic arrangement in the interface Grain boundaries and twinning orientations may be marked by epitaxic growth, or by oriented growth of crystals or reaction products on the mother crystal ('topotaxy')

reflections, leading to poor data quality in certain regions of the diffraction pattern.

The ultimate test of the quality of a crystal and its suitability for a structure analysis is the quality of the diffraction pattern. Ideally, the reflections should appear in the case of monochromatic radiation as single spots without satellites, tails, or streaks between the spots. The diffraction pattern should be indexable in terms of a single lattice.

3.1.2.3. *Optical examination [see IT A (2002), Section 10.2.4]*

Optical examination of a crystal under a polarizing microscope should be a prerequisite before mounting the specimen for a diffraction experiment. The presence of satellite crystals, inclusions, and other crystal imperfections will degrade the data quality, indicating the selection of a better specimen. The external morphology can often give a strong indication regarding

the nature of the crystal system. A preliminary examination under crossed polars will often show whether the crystal is isotropic, uniaxial or biaxial (see, for example, Hartshorne & Stuart, 1960; Bunn, 1961; Ladd & Palmer, 1985). Crystals that comprise two or more fragments will often be revealed by displaying both dark and light regions simultaneously. For uniaxial crystals, a birefringent orientation is always presented to the incident light beam if the unique axis is perpendicular to the microscope axis, and extinction will occur whenever the unique axis is parallel to the crosswires (assuming that the crosswires are parallel to the planes of polarization of the polarizer and analyser). If the unique axis is parallel to the microscope axis, a uniaxial crystal presents an isotropic cross section and will remain extinguished for all rotations of the crystal. Biaxial crystals have three principal refractive indices associated with light vibrating parallel to the three mutually perpendicular directions in the crystal. The two optic axes and their correspondingly isotropic cross sections that derive from this property are not directly related to the crystallographic axes. In the orthorhombic system, the three vibration directions are parallel to the crystallographic axes, often enabling identification of this crystal system. A monoclinic crystal lying with its unique axis parallel to the crosswires will always show straight extinction. If the crystal is oriented so that the unique axis lies along the microscope axis then, in general, the extinction directions will be oblique. In the triclinic case, the three mutually perpendicular vibration directions are arbitrarily related to the crystal axes. Even if it is not possible to discover the nature of the crystal system unequivocally, the extinction directions should at least enable the principal symmetry directions to be identified and therefore suggest how the crystals should be mounted for optimum data collection (see Chapter 3.4).

3.1.2.4. *Twinning (see Chapter 1.3)*

If at all possible, twinned crystals should *not* be used for structure analysis studies, but the recognition of twinning is critical, since unnoticed or misinterpreted twinning can prevent structure determination or lead to errors in the final structure solution. A distinction should be made between multiple crystal growth, whereby single crystals grow on or from the faces of a given single crystal, or from a common nucleation point, in non-specific orientations, and crystallographic twinning (see, for example, Phillips, 1971; Bishop, 1972). In the latter case, the relationship between the lattices of twinned crystals is normally that of rotation of 180° about a central lattice line, or reflection across a lattice plane. If the lattice is not geometrically symmetrical about the line or plane, two lattices with differing orientations will be produced, and the corresponding reciprocal lattices will be visible in the diffraction patterns. In ideal circumstances, the two patterns can be deconvoluted. If the lattice is geometrically symmetrical about the twin axis or plane, then the two reciprocal lattices will coincide and there may be no obvious signs of twinning in the diffraction pattern (merohedry). If the twins are present in almost equal amounts, the result will be an apparent mirror plane and perpendicular twofold axis in the Laue symmetry. It is therefore very important to examine carefully the Laue symmetry, preferably from a number of different crystals, if twinning is suspected. In some of these crystals, one twin component may be predominant, causing a breakdown in the pseudosymmetry.

Morphological evidence (a concave shape indicating an intersection between the two twin components) and optical examination under a polarizing microscope should also be employed to test for twinning. For lattices that are twinned in a geometrically nonsymmetrical manner, the different twin components will show extinction at different orientations. However, perfect optical extinction is not positive evidence of lack of twinning, since the geometrical symmetry plane (or axis) on which twinning takes place may be parallel to a symmetry plane (or axis) in the optical properties of the crystal.

Intensity statistics can also be used to detect twinning, particularly in the case of crystals twinned by merohedry (*e.g.* Britton, 1972; Fisher & Sweet, 1980). If crystallization conditions cannot be found that eliminate twinning, it is still possible, although difficult, to undertake structure analysis. Recent examples include Sr_3CuPtO_6 (Hodeau *et al.*, 1992), $RbLiCrO_4$ (Makarova, Verin & Aleksandrov, 1993), a serine protease from rat mast cells (Reynolds *et al.*, 1985) and plastocyanin from the green alga *Chlamydomonas reinhardtii* (Redinbo & Yeates, 1993).

International Tables for Crystallography (2006). Vol. C, Chapter 3.2, pp. 156–159.

3.2. Determination of the density of solids

By F. M. Richards and P. F. Lindley

3.2.1. Introduction (By P. F. Lindley)

The measurement of the density of a crystal has become a neglected art, and yet, in combination with an accurate knowledge of the unit-cell dimensions, it can provide vital information regarding the total molecular weight of the unit-cell contents. From this quantity, it is usually possible to determine the number of molecules in the unit cell and their individual molecular weights. The equation relating the crystal density (ρ), unit-cell volume (V), and the overall molecular weight is

$$\rho = Mm_a/V,$$

where m_a is the atomic mass unit (1.66057×10^{-24} g) and V is expressed in mm^3. Alternatively,

$$M = 0.602206V\rho,$$

where V is in units of Å^3. The mass per asymmetric unit can be determined by dividing M by the number of asymmetric units, Z (dependent on the space group), and this will normally correspond to the molecular weight. However, the quotient can either be a fraction of the molecular weight (normally 1/2) when the molecular symmetry permits the molecule to lie on a special position such as a centre of symmetry or a symmetry axis, or a multiple if the asymmetric unit contains more than one molecule. In either case, a special examination of the choice of unit cell and space group should be undertaken to ensure that the *correct* ones have been chosen. Normally, the measured and calculated densities should agree within at least 1.5%; discrepancies greater than this may indicate an incorrect molecular formula (not unknown in preparative chemistry) or the presence of solvent molecules or other additives. Incorrect choice of space group, inappropriate choice of unit cell, and incorrect asymmetric unit contents can all have profound effects on the success of a structure analysis and on the refinement of the resulting structure.

The classical techniques of density measurement are described by Tutton (1922) and by Reilly & Rae (1954). An excellent and detailed review of both the standard and the less common methods is given by Mason (1944), but, because this work can be difficult to obtain, some of the references compiled by this author are cited herein.

3.2.1.1. *General precautions*

Meticulous temperature control is essential for the highest precision. The allowable temperature fluctuation will depend on the thermal coefficient of expansion of the material and on the required accuracy of the measurement. The utmost care must be taken to avoid air bubbles and inclusions. In those techniques that require immersion of the solid in a liquid, it is assumed that no chemical or physical interaction occurs between the liquid and the solid, and that the volume of the liquid displaced represents the true volume of the solid. For most hard crystalline materials, liquids can easily be found for which these assumptions are valid. However, for amorphous powders, porous structures such as zeolites, crystalline proteins, and natural and synthetic fibres, the measured 'density' may depend markedly on the particular liquid chosen and on the details of the method applied. In these cases, *penetration* or *swelling* of the solid will depend on a variety of factors such as interfacial tension, the relation of pore size to molecular dimensions, adsorption, and electrostrictive forces. The structural unit to which the measured density applies may be very difficult to specify. Even with materials not subject to these difficulties, variability in the measured density is frequently found. Such variations may arise from differences in trace impurities or in the previous history of the sample (Johnston & Adams, 1912).

3.2.2. Description and discussion of techniques (By F. M. Richards)

The discussion here will be limited to six general methods, of which at least one may be adapted to the requirements of almost any problem. The method of choice will depend to a large extent on the nature of the material under study. The merits and disadvantages of each method will be discussed.

3.2.2.1. *Gradient tube*

This technique is simple, versatile, and capable of the greatest sensitivity. It is the method of choice except in those cases where immersion liquids with an appropriate density and chemical inertness cannot be found.

Originally devised by Linderstrom-Lang (Linderstrom-Lang, 1937; Linderstrom-Lang & Lanz, 1938) for the determination of the density of aqueous solutions, the procedure has been adapted for the measurement of crystal densities by Low & Richards (1952*a*). For the original solution measurements, a precision of 0.000001 g ml^{-1} was obtained, although no attempt has been made to attain that precision with solids. This technique was apparently developed and used quite independently in the sugar-cane industry [see, for example, Guo & White (1983) and earlier references contained therein].

3.2.2.1.1. *Technique*

When one liquid is layered over another of greater specific gravity, with which it is miscible, a linear gradient of density develops near the interface. Manipulation of a plunger-type stirrer in a vertical tube can extend the gradient over the greater part of the column. In the absence of convection, the process of diffusion in a column of this type is so slow that the gradient will be maintained virtually unchanged for many months.

A crystal introduced into the tube falls until it reaches a level corresponding to its own density, where it will remain stationary. The density gradient may be calibrated either by introducing immiscible liquid drops of known density, or by the use of a micro-Westphal balance designed for the purpose (Richards & Thompson, 1952).

With an adequate thermostat, measurements may be made at any temperature between the freezing and boiling points of the mixtures involved.

Powders and crystals with cavities or inclusions may be ground to a slurry with the lighter column liquid, subjected to reduced pressure to remove trapped air bubbles, and then introduced into the gradient tube. With hygroscopic materials, these operations are carried out in a dry atmosphere. Finely divided material settles rapidly if the tube is centrifuged. Although centrifugation does not markedly affect the gradient, the column should be calibrated after this step.

If such samples are homogeneous, they will form a thin layer after centrifuging. If, on the other hand, some air bubbles or

Copyright © 2006 International Union of Crystallography

Table 3.2.2.1. *Possible substances for use as gradient-column components*

Hydrophobic components			Hydrophilic components	
Liquid	Approximate density at 298 K (g ml^{-1})	α	Solute	Approximate maximum density of concentrated aqueous solution at 298 K (g ml^{-1})
Isooctane (2-methylheptane)	0.69	−0.8	Sodium chloride	1.20
Kerosene	0.79	−0.5 −0.8	Potassium chloride	1.40
m-Xylene	0.86	−0.85	Potassium iodide	1.63
Chlorobenzene	1.10	−1.1	Iron(III) sulfate	1.80
Bromobenzene	1.49	−1.3	Zinc bromide	2.00
Carbon tetrachloride	1.60	−1.9	Zinc iodide	2.39
Methyl iodide	2.28	−2.7	Thallium(I) formate	3.5
Bromoform	2.89	−0.9	Thallium(I) formate–malonate	4.3
s-Tetrabromoethane	2.96	−2.2		
Methylene iodide	3.32	−2.6	Ficoll* (60% *w*/*w* in water)	1.25

The density at temperature T K can be computed by substituting the values of the density at 298 K and α in the formula $d_T = d_{298} + 10^{-3}\alpha(T - 298)$. * Trade name for a synthetic high-molecular-weight polysaccharide derivative.

inclusions still remain, or if the sample is truly a mixture, a stable distribution of material will be observed. The density of the material of interest can then usually be obtained by measurement of the appropriate layer, generally the most dense, without further treatment of the sample. This is the only technique by which the homogeneity of the sample can be tested simply. All other methods provide an average density value. A satisfactory technique for removing crystalline powders from the gradient column has not been devised. If a precision of ±0.002 g ml^{-1} is adequate, it is simplest to prepare a new wide-range column for each determination in a 10 ml test tube.

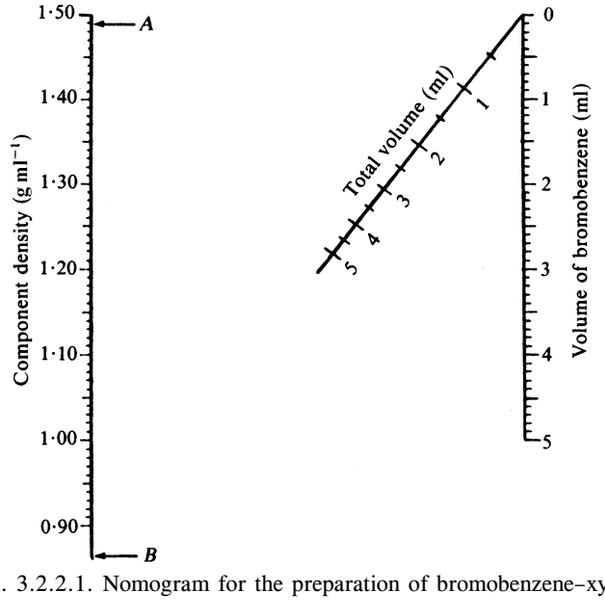

Fig. 3.2.2.1. Nomogram for the preparation of bromobenzene–xylene gradient column components at room temperature. From the desired component density and total volume, the required amount of bromobenzene is read from the chart, the volume difference being made up with xylene. To adapt this chart to any other pair of liquids, it is only necessary to change the component density scale. A uniform scale is drawn up such that the density of the heavy liquid lies at the point *A* while that of the light liquid is at *B*. The volume scales may be multiplied by any constant factor in order to change their range.

Detailed specifications for the preparation of large density-gradient columns are contained in the records of the British Standards Institution (1964). In the experience of the author, for ordinary laboratory use, the procedures described are unnecessarily complicated as is the large scale of the system. The large columns are not suitable for centrifuging and the settling times tend to be many hours. However, if extreme sensitivity (*i.e.* use of a shallow gradient) is required, the large column may be useful, as it was in the original studies of Linderstrom-Lang (Linderstrom-Lang, 1937; Linderstrom-Lang & Lanz, 1938).

In the specific application of this technique to protein crystals, where a gradient of organic liquids is used, it is necessary to have available crystals sufficiently large that they can individually be quickly wiped free of adhering mother liquor with dampened filter paper before insertion. The uncertainty of successful cleaning combined with rapid evaporation of liquid from the pores within the crystal always affect the estimated accuracy of the measurement. An important improvement in the technique has been made by Westbrook (1976, 1985) through the use of concentrated aqueous solutions of the water-soluble polymer Ficoll. This very high molecular weight polysaccharide can be dissolved in water to concentrations of at least 60% by weight. The solutions are very viscous but do provide satisfactory water-based gradient columns. The polymer is both too large to enter the solvent-filled pores of the protein crystals and too high in molecular weight to develop a significant osmotic pressure. An aqueous suspension of crystals can be added directly to the column. This procedure has been adapted for measurements of protein-crystal density under hydrostatic pressures from 1 to 2000 atm (1 atm ≡ 101 325 Pa) (Kundrot & Richards, 1988). The general principle of using high-polymer-based gradients can presumably be extended to other porous materials.

3.2.2.1.2. *Suitable substances for columns*

Some representative liquids are listed in Table 3.2.2.1; all are readily available. For further information, see Meyrowitz, Cuttitta & Hickling (1959), and for very heavy liquids Sullivan

(1927). Standardized solutions or mixtures from one list in Table 3.2.2.1 may be used as calibrating drops in gradients made from those of the other.

For rapid preparation of mixtures from stock solutions of the basic compounds, a nomogram is very useful, such as is given in Fig. 3.2.2.1 for the system bromobenzene–xylene at room temperature. In the construction of the nomogram, it has been assumed that the volumes of the liquids are additive. In general, this assumption is not valid, but it is a sufficiently good approximation for the purpose.

3.2.2.1.3. *Sensitivity*

The range of density covered by a column, and thus the accuracy of the determination, is controlled by the liquids or liquid mixtures chosen for the top and bottom components. A precision of about $\pm 0.002\ \mathrm{g\ ml^{-1}}$ can easily be obtained without any special precautions. If narrow-range columns are carefully protected from temperature changes and vibration, the accuracy of the measurement may be increased 10- to 100-fold.

3.2.2.2. *Flotation method*

Although historically used much earlier, this technique is essentially an approximation to the gradient-tube method. The specimen is immersed in a liquid, and a denser or less dense liquid miscible with the first is added until the sample neither rises nor sinks in the solution (Wulff & Heigl, 1931). The density of the immersion medium is then determined immediately by standard techniques such as pycnometry, by the Westphal balance, or by refractive index (Midgley, 1951). The method is reported as capable of a probable accuracy as great as 0.02%.

The compounds listed in Table 3.2.2.1 are also useful in this method. With slurries or with specimens smaller than $1\ \mathrm{mm^3}$, a centrifuge must be used to achieve a reasonable rate of settling. As little as 0.05 mg of material has been used with good results (Bernal & Crowfoot, 1934). A modification of this method has been described in which the density of the immersion medium is varied by altering the temperature (Reilly & Rae, 1954; Wunderlich, 1957).

3.2.2.3. *Pycnometry*

This is one of the most demanding of the available techniques. A previously calibrated pycnometer containing the sample is weighed. A liquid of known density is then introduced, air bubbles are removed by reducing the pressure, and the filled bottle is reweighed. The volume of the sample and its mass may thus be determined. With care, a probable accuracy of 0.02% may be achieved (Johnston & Adams, 1912). Contrary to many published statements, the accuracy of this technique is not dependent to any significant extent on the use of immersion media of high density.

Liquids with low surface tension will facilitate the removal of air bubbles. In some cases, it is advantageous to fill the bottle with the mother liquor from which the crystal grew. Powders or many small crystals may be used as well as large single specimens. There is no restriction on the density of the materials for which this technique is suitable.

A micropycnometer for use with samples of total volume as small as 0.01 ml has been described (Syromyatnikov, 1935). An accuracy of better than 1% has been achieved with this instrument.

3.2.2.4. *Method of Archimedes*

The specimen is weighed in air and again in a liquid of accurately known density. From the apparent loss of weight the volume is computed, and thence the density (Reilly & Rae, 1954). The technique requires little special equipment and is capable of great accuracy when used with large, well formed crystals. The accuracy is maximized by using immersion liquids of density as close to that of the crystals as possible. For precise work, correction must be made for the interfacial tension between the supporting wire and the upper surface of the suspending medium.

A torsion microbalance has been adapted to the determination of crystals as small as 25 mg (Berman, 1939). A probable accuracy of better than 1% may be achieved with this micromethod.

A densitometer based on Archimedes principle with control of the composition of the gas phase and a wide temperature range has been described by Graubner (1986). The method is not suitable for finely divided materials.

3.2.2.5. *Immersion microbalance*

Some crystals, such as those of globular proteins grown from alcohol–water mixtures, rapidly change their composition, and thus their density, when removed from the mother liquor in which they were grown. The density may then be computed from the weight of the crystal immersed in its mother liquor, the density of the latter, and the volume of the crystal (Low & Richards, 1952*b*, 1954; Richards, 1954).

A horizontal quartz fibre, free at one end, is mounted in a glass case that can be filled with liquid. After calibration, the deflection of the fibre gives the weight of an immersed crystal suspended on the free end. The volume is computed from the crystal dimensions as determined from two photomicrographs of the immersed crystal taken at right angles to each other. The density of the mother liquor is measured by one of the standard techniques for liquids.

The method is suitable for single, well formed crystals having a volume of about $0.1\ \mathrm{mm^3}$ or greater. The accuracy is related inversely to the difference in density between the crystal and its mother liquor.

3.2.2.6. *Volumenometry*

This is the only technique not requiring immersion of the sample in a liquid medium. The technique is therefore used in instances where the specimen would be attacked by the customary immersion media, or where one wishes to work over a temperature range where liquid media would be inappropriate.

The gas-pressure change caused by altering the volume of a calibrated vessel by a given amount is determined when the vessel is empty, and again after the weighed specimen has been introduced (Reilly & Rae, 1954).

Any gas inert to the crystal may be used. Powders and crystal fragments may be employed. A probable accuracy as great as 0.1% may be attained. Samples with an aggregate volume as low as 0.01 ml have been measured with a probable accuracy of 1% (Hauptmann & Schulze, 1934).

3.2.2.7. *Other procedures*

A novel procedure that may be useful in special circumstances is based on measuring the frequency of a vibrating string of the material in question. If the length of the string is fixed and the transverse deformation is small, the various harmonic frequen-

Table 3.2.3.1. *Typical calculations of the values of V_M and V_{solv} for proteins*

Protein	γB-Crystallin	γD-Crystallin	Ceruloplasmin
Space group	$P4_12_12$	$P2_12_12_1$	$P3_221$
Cell parameters (Å)	57.5×98.0	$57.8 \times 70.0 \times 117.3$	213.9×85.6
Molecular weight (kDa)	21	21	132
Z	8	4	6
V_M (Å^3 Da^{-1})	1.93	5.65*	4.95
$V_{\rm solv}$ (%)	36	78*	75
Resolution (Å)	1.5	2.0	3.1

* In the case of γD-crystallin, the values for V_M and $V_{\rm solv}$ are abnormally high. A recalculation assuming two molecules per asymmetric unit, $Z_a = 2$, gives more reasonable values of $V_M = 2.83$ Å^3 Da^{-1} and $V_{\rm solv} = 56\,\%$.

cies of vibration will be related inversely to the square root of the density for small oscillations. The potential accuracy of frequency measurements makes this useful for following density changes in the sample while altering the temperature or pressure; see Rabukhin (1982).

3.2.3. Biological macromolecules (By P. F. Lindley)

Biological macromolecules usually present particular difficulties with respect to density measurements and the determination of Z_a, the number of molecules per asymmetric unit, because of the presence in the crystals of variable amounts of solvent. However, it is often crucially important with respect to a structure determination, particularly using molecular-replacement techniques, to know Z_a. In many cases, $Z_a = 1$, although, as in the case of small molecules, crystals are also found with fractional values of Z_a when molecular symmetry axes coincide with crystal symmetry axes, or values greater than 1 if there are multiple copies of the molecule in the asymmetric unit. In practice, it is usually necessary only to know the solvent content of the crystals between rather coarse limits in order to distinguish possible values of Z_a, and this problem has been addressed for globular proteins by Matthews (1968). A rather more precise knowledge of the solvent may be essential for the use of density-modification techniques in phase refinement. Matthews defines a quantity, V_M, the crystal volume per unit of protein molecular weight (*i.e.* the ratio of the volume of the asymmetric unit determined from X-ray diffraction measurements to the molecular weight of the protein in the asymmetric unit) and shows that V_M bears a simple relationship to the fractional volume of solvent in the crystal. The range of observed values of V_M (1.68 to 3.53 Å^3 Da^{-1} for the 116 distinct crystal forms considered by Matthews with median and most common values of 2.61 and 2.15 Å^3 Da^{-1}, respectively) is essentially independent of the volume of the asymmetric unit. Matthews further defines the quantity $V_{\rm prot}$, the fraction of the crystal volume occupied by the protein:

$$V_{\rm prot} = 1.66\nu/V_M,$$

where ν is the partial specific volume of the protein in the crystal and for most proteins approximates to 0.74 ml g^{-1}. With this approximation,

$$V_{\rm prot} = 1.23/V_M$$

and, by difference, the fractional volume occupied by the solvent is therefore

$$V_{\rm solv} = 1 - 1.66\nu/V_M \approx 1 - 1.23/V_M.$$

On this basis, the range of V_M cited above converts to a solvent content ranging from 27 to 65%, with values near 43% occurring most frequently. For cases where the solvent content appears abnormally low or high in respect of the physical properties of the crystal and the resolution of the diffraction pattern, then some alteration to the value of Z_a may well be indicated. Some typical examples are given in Table 3.2.3.1. It should be noted that, although the method described above appears to obviate the need to measure the density of crystals, a precise experimental measurement of the crystal density, wherever practical, is always a useful investment.

In a recent development, Kwong, Pound & Hendrickson (1994) have devised an experimental method for the determination of Z_a using a volume-specific amino acid analysis. The crystal volume is determined from optical measurements of crystals mounted in glass capillaries, and the number of molecules in that volume is determined by amino acid analysis. From the unit-cell volume determined from X-ray measurements and the space-group symmetry, Z_a can be calculated from the number of molecules per crystal volume. The method requires extreme care to obtain precise measurements of the crystal volume and access to high-performance liquid chromatography and associated equipment for the amino acid analysis.

International Tables for Crystallography (2006). Vol. C, Chapter 3.3, pp. 160–161.

3.3. Measurement of refractive index*

BY E. S. LARSEN JR, R. MEYROWITZ AND A. J. C. WILSON

3.3.1. Introduction

The optical properties of crystals are complex, and it is planned to include a full account in Volume D. What follows is restricted to a brief description of immersion media for use in the measurement of indices of refraction. **WARNING. Many of the media, particularly those of high refractive index, are poisonous, or corrosive, or both.**

3.3.2. Media for general use

The immersion media listed in Table 3.3.2.1 are easily prepared, stable, and venerally satisfactory. They were selected because they require only a small number of liquids for their preparation. In general, each liquid is miscible in the liquids with higher and lower indices of refraction so that any intermediate mixture can be easily prepared.

The liquids up to $n = 1.770$ are measured on an Abbe refractometer; those with higher values for n are measured in a hollow glass prism prepared from selected object glasses and mounted on a goniometer or on a spectrometer (Butler, 1933; Larsen & Berman, 1934, pp. 18–20).

A set of immersion liquids with indices of refraction differing by one unit in the second decimal place (1.510, 1.520, 1.530, . . .) is used for routine work. The liquids are best kept in 15 ml dropping bottles with plastic caps and glass dropping rods. These bottles are more satisfactory than the more expensive dropping bottles with solid glass stoppers and ground-glass caps because there is less trouble with the stopper cementing to the bottle. The bottle should be about half full.

Some crystals dissolve rapidly in the liquids tested. A measurement can usually be made by performing the reading rapidly. If the crystal and the liquid have nearly the same indices of refraction, the index of the liquid is not much changed by the solution of the crystal.

* Editorial condensation of the entry by E. S. Larsen Jr and R. Meyrowitz in Volume III (*IT* III, 1962).

Table 3.3.4.1. *Aqueous solutions for use as immersion media for organic crystals*

Salt	$n_D^{20^\circ C}$ of saturated solution
Lithium iodide	1.490
Sodium iodide	1.496
Potassium iodide	1.456
Barium iodide	1.528
Tetrasodium dioxypentathiostannate	1.615

Table 3.3.4.2. *Organic immersion media for use with organic crystals of low solubility*

Compound	$n_D^{20^\circ C}$
Diethyl oxalate	1.41
Di-*n*-butyl carbonate	1.41
Triethyl citrate	1.44
Tri-*n*-butyl citrate	1.44
n-Butyl phthalate	1.49
α-Bromonaphthalene	1.66
α-Iodonaphthalene	1.70
Methylene iodide	1.74

3.3.3. High-index media

Refractive indices greater than 2.1 present special difficulties. Merwin & Larsen (1912) used melts of sulfur and selenium, satisfactory up to index 2.72. Mixtures of selenium and As_2Se_3 can be used up to index 3.17 (Larsen & Berman, 1934). Above about 2.2, the index must be determined at a wavelength for

Table 3.3.2.1. *Immersion media for general use in the measurement of index of refraction*

Note: Further lists are given by Hartshorne & Stuart (1960).

	$n_D^{20^\circ C}$	Temperature coefficient (dn/dT)	Dispersion
Water	1.333	1×10^{-4}	Slight
Glycerol	1.473	2.2×10^{-4}	Slight
n-Octane	1.400	4.8×10^{-4}	–
n-Hexadecane	1.434	3.8×10^{-4}	Slight
Kerosene (Paraffin)	1.448	3.5×10^{-4}	Slight
Petroleum oil (Nujol)	1.477	4×10^{-4}	Slight
α-Chloronaphthalene	1.626	4×10^{-4}	Moderate
Methylene iodide	1.740	6.4×10^{-4}	Rather strong
Methylene iodide saturated with sulfur	1.778	6×10^{-4}	Rather strong
$AsBr_3$ plus 10% sulfur (mix with methylene iodide or α-bromonapthalene for lower n)	1.814 (25° C)	7×10^{-4}	Rather strong
2S, $2AS_2S_2$, $6AsBr_3$ (mix with 10% sulfur in $AsBr_3$ for lower n)	2.003 (25° C)	6×10^{-4}	Rather strong
2Se, $2As_2S_2$, $6AsBr_3$ (mix with 10% sulfur in $AsBr_3$ for lower n)	2.11 (25° C)	6×10^{-4}	Rather strong

Copyright © 2006 International Union of Crystallography

which selenium is transparent; the red line of lithium is convenient.

3.3.4. Media for organic substances

Organic substances are usually soluble in organic liquids, but not usually in aqueous solutions. The saturated solutions listed in Table 3.3.4.1 (Jelley, 1934, p. 245) are generally satisfactory. For substances of low solubility, the organic liquids listed in Table 3.3.4.2 may be useful; the refractive index of diluted aqueous solutions changes with time because of evaporation.

If the index of refraction is greater than about 1.7, the media at the end of Table 3.3.2.1 have to be used. These usually dissolve organic crystals, so that the immersion liquid becomes saturated with the compound. The refractive index of the saturated medium is then measured with a microrefractometer (Jelley, 1934, pp. 236–240).

International Tables for Crystallography (2006). Vol. C, Chapter 3.4, pp. 162–170.

3.4. Mounting and setting of specimens for X-ray crystallographic studies

By P. F. Lindley

3.4.1. Mounting of specimens

3.4.1.1. *Introduction*

This section deals with the mounting of two categories of specimens:

(1) polycrystalline;

(2) single crystal.

Category 2 is further divided into single crystals of small organic and inorganic molecules, and those of biological macromolecules at both ambient and cryogenic temperatures. Commonly used methods of mounting specimens for both camera and diffractometer, and most other detector systems are described.

The bibliography is necessarily selective and wherever possible has been restricted to journals and textbooks that are readily accessible to a crystallographic laboratory. It should also be noted that there exist, worldwide, various centres specializing in synchrotron-radiation and neutron diffraction techniques. Within these centres lies a wealth of experience in sample handling and preparation. For specialist purposes, communication with local contacts at such centres may provide invaluable assistance.

3.4.1.2. *Polycrystalline specimens*

3.4.1.2.1. *General*

Informative accounts of the powder method of recording diffraction patterns have been given by Klug & Alexander (1954), D'Eye & Wait (1960) and Dent Glasser (1977). There are three principal methods of preparing polycrystalline specimens for mounting in powder cameras:

(1) encased;

(2) bonded;

(3) fibre supported.

The most common method of preparing samples of polycrystalline materials is to *encase* them in thin-walled capillary tubes, for Debye–Scherrer camera work, or into sample holders, for Guinier camera and diffractometer measurements. This technique has the advantage that the sample can be readily protected from attack by oxygen, carbon dioxide and water vapour, and, if necessary, the sample preparation can be undertaken in an inert atmosphere (Lange & Haendler, 1972; D'Eye & Wait, 1960). The precise details of sample preparation and mounting will be dependent on the type of camera or diffractometer used, but the particle size should be generally less than 10 μm for stationary samples and diffractometer work. A slightly larger particle size, 45 μm, can be used for Debye–Scherrer camera work if the specimen is rotated. Foit (1982) has described a simple method of filling thin-walled capillaries using an ultrasonic vibrator. A frequent problem affecting intensity measurements from powder specimens is caused by preferred orientation when powder samples are packed or pressed. McMurdie, Morris, Evans, Paretzkin & Wong-Ng (1986) have described a method of sample preparation suitable for a diffractometer that minimizes this problem.

Capillaries made from lithium beryllium borate (Lindemann glass), borosilicate (*e.g.* Pyrex glass), or fused silica are commercially available in a variety of internal diameters. For very high temperatures, thin-walled ceramic or metal capillaries can be used. The diffraction pattern of the metal can be used as an internal standard. Capillaries that are suitable for materials that react with glass can be made from various organic polymers. Table 3.4.1.1 lists details of capillaries and other containers suitable for encasing powder specimens.

In the *bonded* method, the polycrystalline material is mixed with an adhesive such as gum tragacanth or ethyl cellulose, and the mixture is wetted with water or aqueous alcohol to form a viscous paste. The paste is then rolled between two glass slides or extruded through a glass capillary, using a glass or metal piston, to form a cylindrical sample. This can be cut to length and either glued, fixed with plasticine, or cemented (for high-temperature work) to the camera mounting pin. Alternatively, the sample can be compressed and compacted in a die to form a solid rod, or, for diffractometers, into a disc. In the case of very small quantities of material, the powder can be smeared with silicone vacuum grease over the surface of a disc-shaped silica crystal. The silica can then be used as an internal standard.

In the *fibre-supported* method, a silica, Lindemann, or borosilicate glass fibre moistened with adhesive (Canada balsam diluted with xylene, collodion, gum tragacanth and water, dilute fish glue) is dipped into the powder. Experience has shown that powder adhesion to the fibre is often improved if non-drying glues or viscous oils are employed. Hairs of fine organic filaments have been used in place of glass fibres, and for high temperature above 1270° C metal wires are useful. Once again, the metal diffraction patterns can act as internal standards. For extruded metal wires, the wire itself acts as the specimen, and the diameter can be reduced by etching if it is too large, or a glancing-angle diffraction technique can be employed. Various specialized holders for diffraction studies of polycrystalline samples can be found in annual conference proceedings such as EPDIC (*European Powder Diffraction Conference*, Switzerland: Trans Tech Publications) and Advances in X-ray Analysis (*Proceedings of the Annual Conference on the Applications of X-ray Diffraction*, New York/London: Plenum). The journals *Reviews of Scientific Instruments* (American Institute of Physics) and *Nuclear Instruments and Methods* (Elsevier, North-Holland) also provide useful sources of information.

3.4.1.2.2. *Non-ambient conditions*

A number of devices have recently been described to study polycrystalline specimens under non-ambient conditions. Rink, Mathias & Schlenoff (1994) have designed a portable sample housing for work at room temperature with samples that are air or moisture sensitive. A review of designs and desirable features for high-temperature furnaces suitable for X-ray diffractometers has been given by McKinstry (1970). More recently, Puxley, Squire & Bates (1994) have described an *in situ* cell fitted to a Siemens D-500 powder diffractometer that allows samples in flowing or static reactive gas environments at atmospheric pressure and at temperatures up to 1273 K. These authors also review other developments in the field of high-temperature furnaces for polycrystalline X-ray diffraction published since the McKinstry article in 1970. Brown, Swapp, Bennett & Navrotsky (1993) have devised methods to minimize the uncertainties in temperature at the sample and in the position of the sample itself. Tarling, Barnes & Mackay (1984) have adapted a Guinier–Lenné high-temperature powder camera to include a gas rinsing system and a specially designed mini-environment cell in which conditions of industrial furnacing can be simulated. In the neutron area, Lorenz, Neder, Marxreiter, Frey & Schneider

Copyright © 2006 International Union of Crystallography

Table 3.4.1.1. *Single-crystal and powder mounting, capillary tubes and other containers*

Material	Temperature range (K)	Comments
(*A*) Capillary tubes		
Glass Lindemann glass Vitreous silica	< 773 < 773 < 1373	Lindemann glass scatters less, but is moisture sensitive Thinner walled tubes that are less sensitive to atmospheric influences can be obtained using other types of glass
Collodion Polyvinyl methylal resin (*e.g.* Formvar) Cellulose acetate	93 to 343 < 323 < 373	These capillaries can be made by coating a copper wire with a solution of the polymer in an appropriate organic solvent. When dry, the metal core may be removed by stretching, to reduce its diameter
Polyethylene	< 373	Tubes may be drawn from the molten polymer using a glass tube and a slow stream of air. The polymer gives a distinct diffraction pattern
(B) Other containers		
Gelatin capsules	< 303	Vessels with very thin, 20 μm, windows can be made
Methyl methacrylate resin (*e.g.* Perspex)	< 338	
Mica	< 1073	Mica windows useful in vessels for small-angle scattering, but the wall size is generally thicker, ~0.3 mm, and there are discrete lines at 10.00, 3.34 and 2.60 Å in the diffraction pattern
Regenerated cellulose film (*e.g.* cellophane)	Ambient	

For optimum results, tube diameters should be between 0.3 and 0.5 mm with wall thicknesses of 0.02 to 0.05 mm. The materials listed above, except where stated, give diffuse diffraction patterns. If necessary, control diffraction patterns, recorded only from the capillary or other container, should be taken.

(1993) have developed a mirror furnace working at up to 2300 K and suitable for polycrystalline or single-crystal samples.

A comprehensive account of cryogenic studies pertinent to both polycrystalline and single-crystal samples is given by Rudman (1976). Nieman, Evans, Heal & Powell (1984) have described a device for the preparation of low-temperature samples of noxious materials. The device is enclosed in a vanadium can and is therefore only suitable for neutron diffraction studies. Ihringer & Küster (1993) have described a cryostat for powder diffraction, temperature range 8–300 K, for use on a synchrotron-radiation beam line at HASYLAB, Germany (Arnold *et al.*, 1989).

3.4.1.3. *Single crystals (small molecules)*

3.4.1.3.1. *General*

Small single crystals of inorganic and organic materials, suitable for intensity data collection, are normally glued to the end of a glass or vitreous silica fibre, or capillary (Denne, 1971*b*; Stout & Jensen, 1968). A simple device that fits onto a conventional microscope stage to facilitate the procedure of cementing a single crystal to a glass fibre has been constructed by Bretherton & Kennard (1976). The support is in turn fixed to a metal pin that fits onto a goniometer head. For preliminary studies, plasticine or wax are useful fixatives, since it is then relatively easy to alter the orientation of the support, and hence the crystal, as required. For data-collection purposes, the support should be firmly fixed or glued to the goniometer head pin. The fibre should be sufficiently thin to minimize absorption effects but thick enough to form a rigid support. The length of the fibre is usually about 10 mm. Kennard (1994) has described a macroscope that allows specimens to be observed remotely during data collection and can also be used for measurement of crystal faces for absorption correction. Large specimens can be directly mounted onto a camera or onto a specially designed goniometer (Denne, 1971*a*; Shaham, 1982). A method using high-temperature diffusion to bond ductile single crystals to a metal backing, for strain-free mounting, has been described by Black, Burdette & Early (1986).

Prior to crystal mounting, it is always prudent to determine the nature of any spatial constraints that are applicable for the proposed experiment. Some diffractometers have relatively little translational flexibility, and the length of the fibre mount or capillary is critical. For some low-temperature devices where the cooling gas stream is coaxial with the specimen mount, the

Table 3.4.1.2. *Single-crystal mounting – adhesives*

Adhesive	Temperature range (K)	Comments
Durofix, Duco cement *etc.* (celluloid composition dissolved in organic solvent)	93 to 373	* Dries rapidly
Shellac dissolved in alcohol	<423	* Correct amount of solvent is critical
Fish glue (*e.g.* Seccotine)	<423	* Unsuitable for humid atmospheres
Dental cement	93 to 573	Adheres well to glass or asbestos, but not metals
Epoxy resin (epichlorohydrin, *e.g.* Araldite)	93 to 373	* Permanent fixing, fast (minutes) and slow (hours) available. 'Uncured' adhesive, *i.e.* minus hardener, useful for cryogenic mounting
Vacuum grease (*e.g.* Apiezon)	<473	Can protect crystal from moisture
Silicone high-vacuum grease	<373	Can protect crystal from moisture
Vaseline		Low temperatures down to liquid helium
Canada balsam	<333	† Dilute with xylene.
Mixture of wax and resin, ~1:1	93 to 303	†
Aluminium	<873	Large crystals set in molten metal, irradiate only protruding part of crystal
Aluminium cement	<1973	Irradiate only protruding part of crystal

* These glues tend to pull in setting and may require adjustment during the drying process. † Useful adhesives if the crystal requires grinding to shape after fixing.

orientation of the fibre (and crystal) on the goniometer head may also need careful alignment.

Many proprietary adhesives can be used (see Table 3.4.1.2), but it should be remembered that adhesives such as epoxy resins are often permanent, and attempts to dismount specimens lead to crystal damage. Some adhesives contain organic solvents that may react with the sample, and others may be X-ray sensitive and deteriorate with exposure. In low-temperature work, some adhesives shrink or become brittle. Ideally, the adhesive should have the same thermal characteristics as the crystal and its mount. An account of how strong stresses on adhesives, typically used to mount single crystals, induced by low and high temperatures is given by Argoud & Muller (1989*a*). The stresses appear to cause anisotropic modifications to secondary extinction, leading to discrepancies in the intensities of symmetry-related reflections. Beeswax and paraffin wax were found to be free from such stresses. Crystals that are sensitive to air can be mounted inside capillary tubes or other containers, as listed in Table 3.4.1.1. A useful summary of the methods available has been provided by Rao (1989). All adhesives and containers will give diffraction patterns, typically comprising diffuse bands, that contribute to the general background, and that may change with ageing. Minimal amounts of adhesive and thin-walled capillaries should be used. If the background diffraction is critical, it is highly recommended that diffraction patterns of the container and/or adhesive are recorded separately as controls.

The morphology of a given crystal will normally dictate the way that it is mounted, particularly for data-collection purposes. Thus, prismatic crystals and needle-shaped crystals are usually mounted with the longest dimension parallel to the fibre, in order to minimize systematic errors due to absorption. Jeffery (1971) and Wood, Tode & Welberry (1985) have described devices for shaping crystals into spheres and cylinders, respectively. A solvent lathe whereby a string moistened with solvent is used to shape the crystal is described by Stout & Jensen (1968).

3.4.1.3.2. *Non-ambient conditions*

As in the case of polycrystalline samples, a number of devices have been described to study single crystals at elevated pressures and at a range of temperatures. The mounting of the sample is very dependent on the device and radiation used. In recent years, the field of high-pressure crystallography has expanded significantly, and several sample holders based on the diamond-anvil cell have been reported for pressures up to 10 GPa. Recent papers include those by Alkire, Larson, Vergamini, Schirber & Morosin (1985) for neutron diffraction, and Malinowski (1987) and Leszczynski, Podlasin & Suski (1993) for X-ray diffraction.

Various types of furnace have been designed for high-temperature studies of single crystals. These are based either on radiative heat transfer mechanisms [*e.g.* Swanson & Prewitt (1986); temperatures up to 1400 K], electrically heated gas streams [*e.g.* Tsukimura, Sato-Sorensen & Ghose (1989); temperatures up to 1600 K], or flame heaters [*e.g.* Miyata, Ishizawa, Minato & Iwai (1979); temperatures up to 2600 K]. Furnaces specific to Weissenberg geometry (Adlhart, Tzafaras, Sueno, Jagodzinski & Huber, 1982) and Laue diffraction (Bhat, Clark, El Korashy & Roberts, 1990) have also been reported. There are many techniques available for mounting single crystals for high-temperature diffraction (Hazen & Finger, 1982), and a detailed account using an MgO-based ceramic cement is given by Swanson & Prewitt (1986). A recent paper by Peterson (1992) summarizes previous work in the design of high-temperature furnaces and describes a flame-heated gas-flow furnace operating in the range 373 to 1573 K. For this system, the crystals can be mounted either directly onto the thermocouple bead with a paste of fine platinum particles and oil, particularly useful if the crystal is to be exposed to a gas mixture that controls oxygen fugacity, or sealed under high vacuum in an ampoule made from 0.2 or 0.3 mm diameter silica capillary. In the latter case, the main support for the crystal is a 0.2 mm Pt wire threaded through a 0.3 mm diameter silica glass capillary. A 0.05 mm Pt/13Rh lead is welded to the end of this support to form the thermocouple bead. The wire is then wound around the outside of the capillary. A 0.05 mm Pt lead is welded to the other end of the 0.2 mm Pt wire and is threaded through a hole in the capillary near the base. The whole assembly can be mounted on a goniometer head that has only translational adjustments. For neutron diffraction, Lorenz, Neder, Marxreiter, Frey & Schneider (1993) have described a mirror furnace operating upto 2300 K. The sample support is normally a thin ceramic tube or rod of Al_2O_3 or ZrO_2 to which the sample may be glued with a ceramic cement. Neder, Frey & Schulz (1990) have described a versatile holder for high-temperature neutron studies. One part of the crystal is ground away to leave a stem, which is then fixed to an alumina rod with a ceramic glue based on zirconia. The ceramic glue is surrounded by a cylinder of BN to minimize spurious scattering.

A comprehensive account of low-temperature diffraction is given by Rudman (1976). Procedures for the selection and transfer of crystals to diffractometers have been described by Boese & Bläser (1989) and Kottke & Stalke (1993). These procedures are applicable down to temperatures of 213 and 193 K, respectively. The latter authors do not recommend the use of capillaries, but describe a device employing the oil-drop mounting technique pioneered by Hope (1987, 1988). Lippman & Rudman (1976) have used a mechanically refrigerated gas stream to achieve temperatures down to approximately 150 K, and the use of liquid nitrogen extends the range to 77 K. Devices such as the Oxford Cryostream can be readily fitted to diffractometers and other types of camera. Closed-cycle refrigerators, liquid-helium-based devices (*e.g.* Henriksen, Larsen & Rasmussen, 1986; Argoud & Muller, 1989*b*; Zobel & Luger, 1990; Graafsma, Sagerman & Coppens, 1991; Toyoshima, Hoya & Ohshima, 1991) further extend the low-temperature limit to 5 K, but often involve substantial blind regions and collision zones. For sample mounting in these devices, it is essential to have good heat conduction to the crystal. Zobel & Luger (1990) describe a taper-formed sample holder made of special copper screwed to the cold head. A steel injection needle with a Be wire inside (0.3 mm diameter and exactly 2 mm in length) is fitted into a 0.5 mm bore hole. The crystal is glued with Araldite to the Be needle, which has little X-ray absorption but good heat conduction. In addition to diffractometer-based devices, Moret & Dallé (1994) have described an adaptation of the closed-cycle refrigerator for a precession goniometer, and various authors have reported systems utilizing Weissenberg geometry for both X-rays and neutrons (*e.g.* Hohlwein & Wright, 1981; Aldhart & Huber, 1982; Allen *et al.*, 1982). Reference should be made to the individual papers for methods of mounting, including spatial and any other constraints.

3.4.1.4. *Single crystals of biological macromolecules at ambient temperatures*

Crystals of biological macromolecules are normally grown from an aqueous solution (see Subsection 3.1.1.2), and when growth is complete are in equilibrium with the mother liquor. Changes in this equilibrium may often result in crystal damage, so the most important aspect of crystal mounting in this case is to preserve the crystal in its state of hydration. This is most readily accomplished by sealing the crystal in a thin-walled quartz or glass capillary tube (King, 1954; Holmes & Blow, 1966). The crystal adheres to the inside of the tube by surface-tension effects through a small droplet of liquid, and a further pool of liquid at one end maintains the required degree of hydration. The general principles involved are well described by Rayment (1985). D'Aprile & Moretto (1975) have described two simple devices, a small electric heater for melting the wax used for sealing the capillary and a refrigerating microcell to prevent heat affecting the wet crystal, which are very useful for mounting wet single crystals in capillary tubes.

Alternatively, crystals can be grown directly within capillary tubes (Phillips, 1985) or microdialysis cells such as those described by Zeppezauer, Eklund & Zeppezauer (1968). A further mounting device particularly useful for enzymatic studies is the flow cell (Wyckoff *et al.*, 1967), in which the specimen is immobilized while mother liquor, or buffer with substrates or inhibitors, is allowed to flow over the crystal. A useful account of this device is given by Petsko (1985). More recently, Edwards (1993) has described a yokeless flow cell, which uses a plastic cone fixed to a brass mounting pin with a wire harness to support the quartz capillary. Although the device was originally designed for Laue studies, its simplicity and practicality should make it useful for a wide range of diffraction experiments. Pickford, Garman, Jones & Stuart (1993) have designed a mounting cell that allows the humidity around a protein crystal to be varied in a controlled manner. This may be particularly useful for crystals where the solvent content is high and the molecular packing, and hence the diffraction intensities, highly dependent on the precise amount of solvent present.

The relatively short crystal lifetimes and large volumes of intensity data often dictate that crystals of biological macromolecules be mounted so that data collection can be accomplished in the most efficient manner, for example, with a symmetry axis parallel to the rotation axis of the collection device. Samples crystallizing in the form of thin plates that have to be aligned perpendicular to the capillary axis can be wedged using cotton lint fibres (Narayana, Weininger, Huess & Argos, 1982), or mounted on a fibre plug (Przybylska, 1988).

One of the key problems in collecting diffraction data from wet crystals is movement of the specimen within the capillary, *i.e.* crystal slippage. Numerous ways have been suggested to surmount this problem, including flattening of the capillary surface, surrounding the crystal with a thin film of plastic (Rayment, Johnson & Suck, 1977) and supporting the crystal with fibre plugs in contact with the mother liquor.

Table 3.4.1.3. *Cryoprotectants commonly used for biological macromolecules*

Protectant	Concentration (% by volume)
Glycerol	13–25
Ethylene glycol	11–30
Poly(ethylene glycol) 400	25–35
Xylitol	22
(2*R*,3*R*)-Butane-2,3-diol	8
Erythritol	11
Glucose	25
2,4-Methylpentanediol	28–45

Pressure cells. Tilton (1988) has described an attachment that can be used on conventional diffractometers for collecting X-ray data from biomolecular crystals under gas pressures up to 300 atm (30 MPa). The crystals are coated with mineral oil to minimize dehydration (see Subsection 3.4.1.5) and mounted in a quartz glass capillary between two layers of cotton fibres. These fibres give mechanical support to the specimen and protect it from shock during gas pressurization. No plugs of mother liquor or oil are used so that the gas flow is unimpeded. Kundrot & Richards (1986) describe an adaptation of the flow cell for hydrostatic pressure studies up to 0.2 GPa. More recently, Kroeger & Kundrot (1994) have described a gas cell that allows data sets at several partial pressures to be collected from the same crystal.

3.4.1.5. *Cryogenic studies of biological macromolecules*

Useful recent reviews on protein crystallography at low temperatures have been written by Hope (1990) and Watenpaugh (1991).

3.4.1.5.1. *Radiation damage*

Crystals of biological macromolecules are very susceptible to radiation damage, and this can severely limit the amount and quality of diffraction data that can be collected per crystal. There have been relatively few systematic studies of this phenomenon (Young, Dewan, Nave & Tilton, 1993; Gonzalez & Nave, 1994; Nave 1995), but one of the first effects of radiation damage is the deterioration of the high-resolution regions of the pattern, followed by increasing loss of crystallinity. Improvement of crystal lifetime in X-ray beams has been obtained by the addition of free-radical scavengers (Zaloga & Sarma, 1974) and the replacement of the mother liquor with solutions containing 10–20% polyethylene glycol 4000 or 20000 (Cascio, Williams & McPherson, 1984). The use of synchrotron radiation has also led to improved data-per-crystal ratios (Lindley, 1988). The high intensity allows fast collection of data, and the high collimation permits different sections of the same crystal to be used for data collection. This is particularly useful for prismatic crystals, which can be mounted along their largest morphological axis. An alternative method of surmounting this problem, however, is to freeze the protein crystal. As the temperature is decreased, the rate of diffusion of free radicals is reduced, with a corresponding reduction in radiation damage. Appreciable reduction in diffusion rate is achieved even at 250 K, and at 100 K diffusion essentially ceases. Cryogenic measurements not only minimize radiation damage but often lead to improved resolution owing to decrease in thermal motion in the crystal. Increasing the crystal lifetime may be particularly important with respect to multiwavelength anomalous-dispersion measurements in order to derive phase information. Since crystals of biological macromolecules contain substantial amounts of solvent, typically between 35 and 80% by volume, the technical problem is to force the solvent to cool in an amorphous glass-like state, rather than as crystalline ice. The latter normally degrades the crystallinity by expansion and gives rise to powder rings, which complicate data measurement.

3.4.1.5.2. *Cryoprotectants*

Cryoprotectants are normally required to avoid ice formation, and the choice of cryoprotectant will depend on the nature of the mother liquor from which the crystals have been grown. Crystals grown from high salt will usually require high salt concentration in the cryobuffer to avoid dissolution, although the addition of organic solvents may be a useful alternative. Table 3.4.1.3 lists commonly used cryoprotectants and their typical concentrations (Gamblin & Rogers, 1993).

The introduction of the cryoprotectant can be achieved through: (*a*) crystal growth in the cryoprotectant; (*b*) direct transfer of crystal from mother liquor into cryoprotectant buffer either in a single step or in steps of increasing cryoprotectant concentration; (*c*) dialysis, either direct or stepwise; or (*d*) exchange of liquor using a flow cell and a gradient maker.

3.4.1.5.3. *Crystal mounting and cooling*

Experience indicates that small crystals are better for cryogenic purposes, presumably because the rate of diffusion of small molecules and the rate of heat loss during rapid freezing is significantly faster than for large crystals. In most cases, there is an increase in the mosaicity (typically by a factor of 2–3), and in large specimens the increase may render the crystals useless for data collection. Successful freezing is often indicated by the crystal remaining transparent. Opacity usually indicates considerable breakdown in the crystallinity. Three commonly used methods for mounting crystals of biological macromolecules for cryogenic measurements are detailed below.

(i) *Coating methods*. Useful accounts of this method are given by Dewan & Tilton (1987) and Hope (1988). The crystal is first transferred to a hydrocarbon environment, mounted on a glass fibre attached to a brass pin on a goniometer head, and then fast cooled by introduction into a nitrogen-gas stream. The crystal adheres to the fibre by surface-tension effects, and the hydrocarbon also prevents loss of solvent during transfer into the gas stream. Paratone-N (Exxon) mixed with mineral oil (25–50% mineral oil) has a suitable viscosity, and excess oil should be removed by draining. This method has been successfully used for a number of biological macromolecules including crambin (Teeter, Roe & Heo, 1993) and the bovine eye lens protein, γB-crystallin (Lindley *et al.*, 1993). In the case of γB-crystallin, it was found that large crystals, $0.5 \times 0.5 \times 1.0$ mm, often became opaque after freezing, indicating gross damage to the crystallinity, or showed appreciable mosaic spread in the subsequent diffraction patterns, rendering them useless for data collection. Smaller crystals, $0.2 \times 0.2 \times 0.8$ mm, gave good diffraction patterns with an increase in the mosaic spread of only a factor of

about two, compared with room-temperature measurements, presumably because of smaller angular and size distributions of the mosaic blocks. For γB-crystallin, the effective resolution was extended from 1.5 Å to at least 1.2 Å. A coating and flash-freezing method has been employed to obtain data from physically fragile and very radiation sensitive crystals of 50S ribosomal particles (Hope *et al.*, 1989). The crystals were transferred to an inert hydrocarbon environment, or to solutions similar to the crystallization medium but with higher viscosities, and flash frozen on a thin glass spatula by immersion in liquid propane. They were then transferred to a cold-nitrogen-gas stream for data measurement. The immersion in a slurry of propane near its melting point gives good wetting of the crystal surface and a heat transfer rate appreciably faster than direct introduction into a cold-gas stream. Transfer from the propane to the gas stream has to be achieved rapidly to avoid ice formation on the surface of the protein owing to condensation of moist air.

(ii) *Loop techniques*. Loops (Teng, 1990; Gamblin & Rogers, 1993), made from fine wire, glass, and a range of thin fibres, can provide very useful mounts for cryocrystallography. Typically, the loops are folded and the two ends glued inside a glass capillary mounted on a goniometer head. Rayon and hair fibres give relatively low backgrounds in diffraction patterns and can readily be made into loops with diameters from 200 to 800 μm. Larger-diameter loops tend to fold over, and glass fibres are more appropriate. Wire loops have a distinct disadvantage in that a plane of diffraction data in which the X-rays are blocked by the wire loop is inaccessible. The diameter is chosen so that the crystal just fits inside the loop and is held in place by surface tension with a thin film of the crystallization/cryoprotectant buffer. The loop with the crystal can then be flash frozen by immersing in liquid propane or fast frozen by direct introduction into a cold-gas stream. Hope (1990) describes a device that can rapidly transfer crystals mounted in loops from a liquid-propane bath to the cooled-gas stream. Indeed, once crystals have been frozen in loops they can be transferred to liquid-nitrogen containers and kept almost indefinitely. A typical application of the loop technique is provided by the crystal structure determination of an extracellular fragment of the rat CD4 receptor (Lange *et al.*, 1994).

(iii) *Liquid-helium cryostat: neutron diffraction*. Slow freezing using a liquid-helium cryostat (Archer & Lehmann, 1986), over a period of hours, has been successfully used with crystals of the coenzyme of vitamin B_{12} to 15 K (Bouquiere, Finney, Lehmann, Lindley & Savage, 1993), where the solvent content is relatively low, 16–17 water molecules per asymmetric unit. Whether biological macromolecular crystals can be annealed to low temperatures with progressive sets of cooling, heating and cooling stages is not well researched.

3.4.1.5.4. *Cooling devices*

Several airstream devices have been described to cool protein crystals to around 250 K [Marsh & Petsko (1973), temperature range 253 to 303 K; Rossi (1989), temperature range 242 to 335 K; Machin, Begg & Isaacs (1984), 258 to 293 K; Fischer, Moras & Thierry (1985), temperature range 263 to 293 K; Fraase Storm & Tuinstra (1986), 250 to 350 K; Arndt & Stubbings (1987), 248 to 353 K]. The devices of Machin, Begg & Isaacs, Fraase Storm & Tuinstra and Arndt & Stubbings involve thermoelectric modules utilizing the Peltier effect. The space available to accommodate the sample is usually very limited and care has to be taken with the length of the capillary and other aspects of crystal mounting. Hovmöller (1981) has designed an extension to the cooling delivery tube that minimizes air turbulence at the sample. Various devices have been described that operate down to near liquid-nitrogen temperature and that can be fitted to a variety of data-collection systems. These include the rotation camera (Bartunik & Schubert, 1982), and a universal cooling device for precession cameras, rotation cameras and diffractometers (Hajdu, McLaughlin, Helliwell, Sheldon & Thompson, 1985). One of the more versatile devices is the cryostream described by Cosier & Glazer (1986), which uses a pump to effectively separate the liquid-nitrogen supply from the gas outflow; this arrangement eliminates instabilities in the cooling-gas stream; the device works in the range 77.4 to 323.0 K and is commercially available (Oxford Cryosystems, England).

3.4.1.5.5. *General*

Cryocrystallography not only minimizes the effects of radiation damage but also often allows the collection of high-quality, high-resolution data from a single specimen. In the case of very labile systems such as ribosomal particles, it is sometimes the only means of obtaining useful diffraction data. Further, cryocrystallography permits the study of temperature effects on the structure and dynamics of biological macromolecules. In this latter regard, examples include multiple-temperature crystallographic studies on sperm whale myoglobin (Frauenfelder, Petsko & Tsernoglou, 1979; Hartmann *et al.*, 1982; Frauenfelder *et al.*, 1987) and, more recently, ribonuclease-A (Tilton, Dewan & Petsko, 1992; Rasmussen, Stock, Ringe & Petsko, 1992). The future will no doubt see the routine emergence of cryogenic techniques for data collection, using both conventional and synchrotron X-ray sources, from biological macromolecules, with consequent improvement in structure quality and detail.

3.4.2. Setting of single crystals by X-rays

3.4.2.1. *Introduction*

With regard to X-ray structure analysis, the use of automated data-collection devices in conjunction with sophisticated software packages has, in the most part, eliminated the need for accurate crystal-setting techniques, although it should be remembered that the determination of the precise crystal orientation with respect to the instrument axes is a prerequisite for data processing. Furthermore, in the case of samples that are highly radiation sensitive (*e.g.* viruses), the lifetime of the sample in the X-ray beam does not permit accurate setting. However, the exercise of setting a crystal so that a certain morphological feature and/or unit-cell edge is perpendicular or parallel to the X-ray beam at the start of the experiment is often very useful, not only in establishing the quality of the crystal diffraction pattern (spot dimensions, mosaicity, twinning, limit of resolution, susceptibility to radiation damage, *etc.*), but also in ensuring that intensity data are collected in the most efficient manner and that the data set is as complete as possible (see also Subsection 3.4.2.8). Mounting a crystal specimen in a random orientation can often lead to inefficient data collection (some reflections measured several times and volumes of reciprocal space not measured at all), and in extreme cases can lead to inappropriate or incorrect choice of cell and space group. Optical examination, crystal density measurement, and careful analysis of diffraction data should still be regarded as important components of crystal structure analysis, even though data collection may be fully automated.

In most cases, the problem of crystal setting by X-rays is composed of two parts (Jeffery, 1971):

(1) equatorial setting, whereby a particular reciprocal-lattice plane is aligned perpendicular to a given direction. This setting is equivalent to bringing a direct-lattice vector (perpendicular to the reciprocal-lattice plane) parallel to the given direction;

(2) azimuthal setting, whereby a reciprocal-lattice vector, in the equatorial plane, is positioned to make a given angle with the plane containing the given direction and the X-ray beam.

In the rotation or oscillation methods, the given direction is the camera rotation axis, but precession geometry requires a direct-lattice vector to be aligned along the X-ray beam. This section will briefly discuss:

(1) equatorial setting using a rotation camera;

(2) setting and orientation using stationary-crystal methods;

(3) rotation geometry setting for crystals with large unit cells;

(4) diffractometer setting considerations.

Specialized methods for orientating and cutting large single crystals are not covered, but two-axis goniometers have been designed by Denne (1971*a*) and Shaham (1982), and methods for cutting single crystals along any desired direction have been reported by Campos, Cardoso & Caticha-Ellis (1983) and Desai & Bhatt (1984).

3.4.2.2. *Preliminary considerations*

Prior to the commencement of the setting process, it is useful to align the crystal optically so that prominent morphological features bear fixed geometrical relationships with the component parts of the goniometer head. Thus, a prismatic crystal could be aligned with its longest axis parallel to the mount, but in addition with a face perpendicular to the rotation axis of one of the goniometer arcs. Many modern goniometer heads have a rotatable component to which the crystal mount can be fixed, and judicious use of this facility can considerably simplify the setting process. This may be particularly important for crystals that are very sensitive to X-radiation. It is also useful if the arc readings on the goniometer head are equal or close to zero. Large deviations away from the zero positions can lead to mechanical collision with other parts of the camera (*e.g.* the layer-line screens of a Weissenberg camera), or in extreme cases to interference with the primary or diffracted X-ray beams. If the crystal mount is fixed to the goniometer head with wax or plasticine, this can often be achieved by manual manipulation of the mount and the wax. The use of less-pliable adhesives requires careful monitoring during the hardening process. Although the detailed alignment will depend on the geometry of the recording device, care taken at the mounting stage will always result in increased efficiency in setting. Sensible orientation of the goniometer head on the camera may also lead to increased efficiency, and it is often useful to start with the axes of the goniometer arcs perpendicular and parallel to the X-ray beam.

3.4.2.3. *Equatorial setting using a rotation camera*

Methods for equatorial setting are well described by Jeffery (1971). The aim is to identify reciprocal-lattice layer lines from X-ray oscillation photographs and, by measuring the degree and directions of curvature of the zero-layer line, to adjust the crystal setting until the layer-line patterns are made perpendicular to the rotation axis, *i.e.* the crystal lattice vector perpendicular to these reciprocal-lattice layers lies parallel to the rotation axis. For crystals of well defined morphology, initial alignment of a crystal lattice vector with the rotation axis can be achieved optically, often to within a degree. For setting errors of less than 5°, reciprocal-lattice layer lines should be readily identifiable on X-ray oscillation diffraction patterns. The use of unfiltered X-radiation often assists in this regard (as well as reducing exposure times), and a device described by Kulpe (Kulpe, 1963; Kulpe & Dornberger-Schiff, 1965) may prove useful in the identification of the zero-layer equatorial pattern on photographic films.

For accurate final setting, a general 'double-oscillation' method such as that of Weisz & Cole as modified by Davies (Jeffery, 1971) is preferred, although Suh, Suh, Ko, Aoki & Yamazaki (1988) have provided a rationale for adjustment of both goniometer arcs simultaneously from a 'single-oscillation' photograph. With the 'double-oscillation' technique, two single oscillations, separated by a φ reading of 180°, are recorded on the same image, but with significantly different exposure times, so that the patterns are related by a mirror plane and are readily distinguishable. The goniometer arcs are placed at 45° to the X-ray beam. Measurements of the relative displacements of the two patterns at the $2\theta = 90°$ position on the image readily yield corrections to both goniometer-head arcs. No translational movement of the film cassette is required, but the crystal must diffract to at least a θ angle of 45°. Hanson (1981) has devised a technique suitable for a Weissenberg camera that is a combination of double oscillation with displacements and measurements at low-2θ angles. This method is particularly suitable for crystals with large unit cells.

In the case where layer lines are not readily locatable, but the crystal unit-cell dimensions are known, Jeffery (1971) also describes an equatorial setting technique that relies on the indexing of at least three low-angle Laue streaks.

Okasaki & Soejima (1986) have described two simple goniometer attachments that may prove useful for crystals that have been mounted so that the angular movements required to achieve setting exceed the range commonly available on goniometer heads.

3.4.2.4. *Precession geometry setting with moving-crystal methods*

Methods of setting crystals so that a crystal lattice vector lies along the X-ray beam have been fully described by Buerger (1964). Optical alignment precedes small-angle (typically 2–5°) precession photographs taken with unfiltered radiation. The use of a screen with a central hole may assist the identification of the outer ends of the white-radiation streaks on the zero-layer pattern by preventing the recording of the upper-layer patterns. The deviation of the zero-layer pattern from cylindrical symmetry about the direct beam leads to the measurement of simultaneous corrections for the spindle angle and goniometer-head arcs. These adjustments are particularly easy if the goniometer-head arcs are perpendicular and parallel to the X-ray beam, and both arcs read zero. Reider (1975) has proposed an approximate stereographic method of making appropriate corrections when these ideal conditions are not fulfilled. Where optical alignment is not possible, or recognition of a zero-layer pattern is difficult, reciprocal space can be systematically explored by taking a series of small-angle precession photographs at regular intervals (*e.g.* 15°) around the spindle axis until a suitable zero-layer pattern is found. In such cases, and particularly for non-orthogonal crystal systems, the use of the complementary rotation technique is recommended (see Subsection 3.4.2.3).

In the final alignment when the crystal lattice vector is parallel to the X-ray beam, it is also desirable to have a reciprocal axis parallel to the spindle axis. With this combined setting, it is possible to survey the whole of reciprocal space (to a θ limit equal to the maximum precession angle mechanically available) with one mounting of the crystal.

3.4.2.5. *Setting and orientation with stationary-crystal methods*

3.4.2.5.1. *Laue images – white radiation*

The azimuthal and back-reflection Laue methods for setting crystals with relatively small unit cells have been described by Jeffery (1971). The former is capable of achieving an accuracy of setting of $\pm 0.05^\circ$, whereas the latter is important in metallurgy, where the Laue method is often the only possibility because of the large size of the specimens. Schiller (1985) has emphasized the importance of the back-reflection Laue technique for setting specimens with a precision of 0.1° needed in semiconductor surface preparation.

In recent years, there has been a resurgence of the Laue technique, in conjunction with synchrotron radiation, to record intensity data from biological macromolecules in very short time scales. The overall experimental strategies involved are described by Helliwell *et al.* (1989) and Clifton, Elder & Hajdu (1991). Crystals are not usually set in a precise orientation for these types of experiment prior to data acquisition because of radiation damage. The post-determination of the precise crystal orientation with respect to the instrument axes from the recorded Laue pattern therefore forms an essential part of the data processing. Most methods are based on the indexing procedure of Riquet & Bonnet (1979), and an interactive computer program for the interpretation and simulation of Laue patterns has been written by Laugier & Filhol (1983). An orientation-matrix approach has been reported by Jacobson (1986), and the work of Helliwell *et al.* (1989) has led to a comprehensive set of Laue processing programs. In addition to enabling trial-and-error visual matching of images, this program suite includes an auto-indexing procedure based on a known unit cell, and refinement of the orientational parameters. More recently, Carr, Cruickshank & Harding (1992) have developed a method whereby a gnomonic projection of the Laue diffraction pattern can be used to determine the cell dimensions and orientation of a crystal. The axial ratios and interaxial angles can be determined precisely, but the absolute scaling of the cell is dependent on the accuracy with which the minimum wavelength used in the experiment is known.

3.4.2.5.2. *'Still' images – monochromatic radiation*

More recently, the azimuthal method has proved of great value in the rapid alignment of crystals with large unit cells prior to data collection on devices using rotation geometry. After optical alignment, a 'still' photograph taken with monochromatic radiation (or a very small angle rotation photograph, typically 0.05–0.20°), is used to locate a zero-layer reciprocal-lattice plane (Fig. 3.4.2.1). Such a plane will record on a flat detector placed at a distance D mm from the crystal, C, as an ellipsoidal trace of maximum dimension S mm from the direct-beam position, O'. In order to make the plane perpendicular to the X-ray beam (*i.e.* the real axis parallel to the X-ray beam), it must be rotated through an angle θ such that $\tan 2\theta = S/D$.

If the vector $O'P$ makes an angle α with the rotation axis, the angle θ can be resolved into a vertical component, $\theta \sin\alpha$, corresponding to a rotation of the spindle axis, and a horizontal component, $\theta \cos\alpha$, corresponding to a rotation of the goniometer arc whose axis is perpendicular to the X-ray beam (assuming a perpendicular and parallel setting of the goniometer head). Rotation of the reciprocal-lattice plane within its own plane can then be achieved with the goniometer arc whose axis is parallel to the beam. This technique is also applicable to preliminary setting on a precession camera.

However, with very radiation sensitive crystals, it is inadvisable to waste time accurately setting the crystal prior to data collection, since the crystal is subject to continuous radiation damage from the beginning of the first exposure (Rossmann & Erickson, 1983). In this case, two 'still' images are collected, preferably separated by a 90° rotation, after data collection but before the crystal is irretrievably damaged. In principle, the orientation can be determined from a single still, but the precise crystal orientation is better determined by identifying and measuring the orientations of two real axes relative to the camera axes, from the sets of ellipses on two stills. The orientation of the reciprocal axis, perpendicular to these two real axes, can then be calculated, and, provided that the unit-cell dimensions are known, the orientation of the third real axis readily determined. Given the directions of the three real axes, the direction cosines of the reciprocal axes can be computed and a matrix determined that specifies the crystal orientation with respect to the camera axes. This method obviates the need to index the 'partial' reflections on still images (Jones, Bartels & Schwager, 1977).

3.4.2.6. *Setting and orientation for crystals with large unit cells using oscillation geometry*

The use of the screenless rotation technique is now routine as a method for large-molecule data collection (Arndt & Wonacott, 1977; Usha *et al.*, 1984). In general, the setting of the crystal for data-collection purposes does not need to be precise, although efficient data collection may dictate that a particular direct axis is set along the rotation axis (Munshi & Murthy, 1986), and subsequent data processing may be simpler. An accurate knowledge of the crystal orientation relative to the axial system of the camera is, however, absolutely essential for the final data processing.

Historically, determination of the crystal setting was normally undertaken using 'still' photographs (see Subsection 3.4.2.5) and the final orientation then determined from two such photographs taken orthogonally (Jones, Bartels & Schwager, 1977; Rossmann

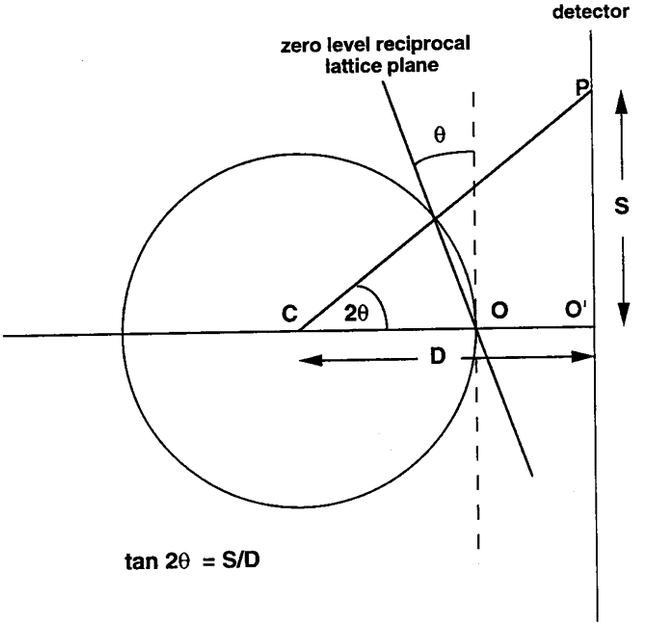

Fig. 3.4.2.1. A zero-layer reciprocal-lattice plane will record on a flat-plate detector placed at a distance D from the crystal C as an ellipsoid of maximum dimension S from the direct-beam position O'.

& Erickson, 1983). In order to minimize the problem of radiation damage, various graphical methods were then devised for determining the precise setting without the need to record 'still' images (Dumas & Ripp, 1986; Moews, Sakamaki & Knox, 1986; Sarma, McKeever, Gallo & Scuderi, 1986). Vriend, Rossmann, Arnold, Luo, Griffith & Moffat (1986) reported a 'post-refinement' technique in which the intensities of partially recorded reflections on oscillation images are compared with their full intensities observed elsewhere on the same or a different image. The degree of partiality is dependent on the crystal orientation so that this provides a very sensitive method of refining the setting parameters (cell parameters, crystal mosaicity and X-ray beam characteristics may also be refined). In a further development, Vriend & Rossmann (1987) described how to determine the orientation from a single oscillation photograph. The method was again devised for crystals that have short lifetimes in the X-ray beam and is based on correlating the unique set of calculated normals to reciprocal-lattice planes with the observed zone axes on the oscillation image.

Currently, auto-indexing procedures based on a single still/oscillation image or preferably several images well separated in reciprocal space are used to determine the precise crystal setting prior to data processing. Kim (1989) has devised an auto-indexing algorithm based on methods previously developed for four-circle diffractometers (*e.g.* Sparks, 1976). The algorithm includes *ab initio* cell-parameter and orientation-matrix determination, followed by reduced-cell calculation and transformation of the reduced cell to one of higher symmetry, where appropriate. Kim's method does require, however, that the diffraction image is large enough to display many lunes. Higashi (1990) has also developed an auto-indexing program for single and or multiple still/oscillation images. The very effective auto-indexing routine of Kabsch (1988*a*, 1993) has been incorporated into the *XDS* program suite (Kabsch, 1988*b*).

Several types of area-detector diffractometer have been developed for fast and accurate measurement of intensity data for macromolecular crystals. Crystal alignment and general strategies for typical devices are described by Xuong, Nielsen, Hamlin & Anderson (1985), Messerschmidt & Pflugrath, (1987), Higashi (1989), and Sato *et al.* (1992).

3.4.2.7. *Diffractometer-setting considerations*

General setting considerations for three- and four-circle diffractometers have been discussed by Busing & Levy (1967). In principle, crystals can be placed on a four-circle diffractometer in any general orientation, although it is often useful to have a setting such that the reciprocal-lattice axis lies parallel to the φ rotation axis. This setting is a prerequisite for effective use of the empirical absorption correction method of North, Phillips & Matthews (1968).

In the case where the crystal orientation is not precisely determined, setting is normally achieved using automatic procedures that involve finding a set of general reflections and generating a **UB** matrix from their angular positions. Generation of the **UB** matrix can be achieved by finding the shortest non-coplanar reciprocal-lattice vectors and assigning these as the reciprocal-cell axes (Hornstra & Vossers, 1974). The resulting unit cell is always primitive, and additional manipulations are required to determine the conventional cell and type of Bravais lattice. This reciprocal-space method is adopted by the Nonius CAD4 diffractometer software (CAD4 Manual, 1989). Alternatively, the 'auto-indexing' method originated by Sparks (1976, 1982) and Jacobson (1976) can be used whereby direct-lattice vectors are generated, again through an initial cell. Clegg (1984) has described an enhancement of the direct-lattice vector method so that the initial cell is used to produce direct-lattice vectors systematically. In order to confirm that a generated vector is a true direct vector, the condition is applied that the scalar multiplication of a true direct vector and any true reciprocal vector (*i.e.* the observed reflection vectors) results in an integer. If a great majority of the products of a putative direct vector and each of the measured observed reflection vectors are integers, the direct vector is accepted. The final cell can be obtained from the set of accepted direct vectors. Subsequently, Duisenberg (1992) developed a method of auto-indexing that is particularly applicable to difficult cases such as twin lattices, incommensurate structures, fragmented crystals, long axes, and even unreliable data. Finding the reciprocal lattice from a distribution of reciprocal-lattice points (*i.e.* observed reflections) is reduced to finding elementary periods in one-dimensional rows, obtained by projecting all observed points onto the normal to the plane formed by any three of these points. Row periodicity and offending reflections are readily recognized. Each row, by its direction and reciprocal spacing, defines one direct-axis vector, based upon all co-operating observations. A primitive cell can be obtained from the direct vectors and refined against the fitting reflections, resulting in one main lattice, or a main lattice and a set of alien reflections (see also Subsection 3.4.2.6).

3.4.2.8. *Crystal setting and data-collection efficiency*

Although it has become modern practice to determine the orientation of crystals after data collection using auto-indexing procedures, rather than to carry out accurate alignment prior to data collection, such a procedure, as indicated earlier in this section, can lead to inefficient data collection. In the case of anomalous-dispersion measurements, and particularly multiple-wavelength anomalous diffraction (MWAD) for phase determination (*e.g.* Kahn *et al.*, 1985), it is often very important to orientate the crystal so that Bijvoet pairs of reflections are recorded simultaneously. The use of synchrotron radiation, where access is usually very limited and crystals are highly radiation sensitive, often leads to insufficient care being taken in the data-collection procedure. An efficient data-collection strategy should aim to measure a set of data as complete as possible (preferably $> 90\%$) in the shortest possible time. Contiguous regions of reciprocal space, such as the 'cusp' region for oscillation geometry, and low-resolution shells should *not* be omitted. In addition, a reasonable number of reflections should be measured more than once to check for internal consistency in the data set. For biological macromolecules, in particular, the temptation to collect data beyond the practical resolution limit should be avoided. Two useful indicators from the outer resolution shell are (*a*) the proportion of significant data should not fall below 70%, and (*b*) the internal consistency index for data measured more than once should not rise above 20%. In general, rotation of crystals along the highest rotation symmetry axis (*i.e.* the fourfold axis for tetragonal systems) will require the least amount of data to be collected, and it is advisable to mount crystals so that this rotation axis is parallel to the fibre or capillary axis, provided that this is sensible in terms of the crystal morphology.

Munshi & Murthy (1986) have discussed strategies of data collection using the screenless oscillation method based on the Laue group and the nature of the crystal axis parallel to the rotation axis. More general strategies for area-detector systems have been reported by Xuong, Nielsen, Hamlin & Anderson (1985) and Zhang & Matthews (1993).

International Tables for Crystallography (2006). Vol. C, Chapter 3.5, pp. 171–176.

3.5. Preparation of specimens for electron diffraction and electron microscopy

By N. J. Tighe, J. R. Fryer, and H. M. Flower

3.5.1. Ceramics and rock minerals

Transmission-electron-microscopy studies of ceramics and rocks require electron-transparent specimens in the form of flakes, profiled thin-foil discs, and evaporated films. These specimens are made from bulk ceramics and minerals by techniques that retain the structure and composition of the original sample. All three specimen types may be required for some studies of a single material. Fragments are made easily and are used extensively for diffraction analysis and for high-resolution structure imaging. Evaporated films are made for composition standards as well as for material process samples. Profiled thin-foil discs are most useful where direct comparison is required between the disc and the bulk sample from which it is made.

The thin-foil disc-shaped specimen fits directly in the specimen holder of the electron microscope. There is a tapered thin region at the centre of electron transparency and a thick rim for rigidity and support. One surface can be flat or both surfaces can be tapered as needed. Profiled specimens retain the microstructure of a bulk sample and can be prepared from any material. This type of specimen can be made from cross sections of multilayer materials as well as from parallel sections of multilayer materials. They are handled easily with vacuum tweezers, cleaned when necessary, and examined in the microscope repeatedly. The profiling of a disc specimen is achieved during ion thinning or by mechanical grinding, trepanning with an ultrasonic tool, grit blasting, or chemical dissolution prior to ion thinning. Thinned, insulating specimens should be coated with carbon to reduce electron-beam charging in the electron microscope. Specialized preparation techniques for ceramics have been described by many authors (Amelinckx, 1964; Bach, 1970; Barber, 1970; Butler & Hale, 1981; Drum, 1965; Goodhew, 1972, 1993; Hobbs, 1970; Hirsch, Howie, Nicholson, Pashley & Whelan, 1965; Thomas, 1962; Tighe, 1976, 1983). The purpose of this section is to present brief descriptions of the techniques, to indicate where the techniques are used, and to describe artefacts that can result from specimen preparation. Considerable patience is required to develop an appreciation of the fragility of the specimens and the skill to handle them without expensive loss.

3.5.1.1. *Thin fragments, particles, and flakes*

Occasionally, processed powders and small flakes of many minerals are thin enough to be examined directly. For powders and chips that are not electron transparent, additional crushing in a mortar and pestle, or between glass or ceramic plates is required (Amelinckx, 1964; Goodhew, 1972). In some layer-structure minerals such as mica, graphite, and hematite, fracture occurs parallel to easy cleavage planes and produces fragments that are thin and parallel-sided over extensive areas. Most crushed flakes, however, are slightly wedge shaped and are electron transparent only near their edges.

The crushing stresses can introduce defects such as twins, micro cracks, and dislocations, which can be imaged and accounted for in diffraction analysis. During the crushing process, it is possible to introduce contamination such as wear debris, dust, and other foreign particles.

Thin flakes can be cut from a bulk specimen with a microtome that uses glass or diamond knives. This ultramicrotomy method is useful for producing flakes from cross sections of multilayer materials such as coated metals and multiphase ceramic devices. The bulk sample to be microtomed is encapsulated in epoxy or plastic; 20 to 80 nm slices are cut and then collected in a water bath. The cutting process produces surface striations and stress-induced damage that may interfere with the structure analysis, but should not affect the composition.

The particles and flakes are placed in an organic solvent, ultrasonically separated, and dispersed onto holey carbon films. Flakes can be stripped from a bulk sample with replicating tape (extraction replica) and redispersed onto a holey carbon film. The particles on the grid can be coated with an additional carbon film to provide an enveloping and conducting preparation. Instead of a holey carbon film, a supported collodion or other suitable organic film may be used (Zvyagin, 1967).

3.5.1.2. *Thin-section preparation*

Bulk samples are reduced in size by cutting slices with a slow-speed diamond-bladed saw or by grinding the sample flat with a diamond-impregnated grinding wheel. The surfaces are fine ground, polished or left in the as-received condition as required for the analysis. Typical petrographic sections are 100 to 200 μm thick. Disc-shaped specimens are cut from the petrographic thin sections with an ultrasonic drill or a diamond-core drill (Tighe, 1964).

Although discs and petrographic sections can be ground and polished as thin as 30 μm before ion thinning, experience has shown that such thin discs are extremely fragile and may not survive long enough for the complete analysis, which may require examination over long periods of time in different instruments. Extremely fragile materials and porous materials can be pressure impregnated with epoxy or bakelite before slicing and grinding. Cross-section specimens (Bach, 1970) can be stacked together and pressure mounted in epoxy or plastic before carrying out the slicing and cutting operations.

Before the element-analysis techniques were available, thin fragile specimens were cemented to copper single-hole grids. However, in X-ray microanalysis, spurious copper signals are obtained from the mounting grid and this practice is no longer recommended unless absolutely necessary. Beryllium grids are available and should be used when extra support is required.

The mechanical profiling of a disc specimen is carried out using a diamond-impregnated metal tool, a small wood dowel with diamond paste, a small metal disc or ball tool with diamond or alumina paste that is held in a variable-speed hand drill or in a semi-automated profiling machine. The specimen is cemented to a metal disc or glass slide and the processes are monitored carefully with a light microscope. When an ultrasonic tool is used it must be slightly rounded because a flat tool will produce a profile with a hump at the centre.

The mechanical profiling technique must be used with some care in order to minimize surface strain from grinding. The damage consists of cracks, embedded grinding debris, and pull-outs. It is possible for cracks to be introduced by grinding and then propagated by both the continuing contact pressure and the presence of the liquid abrasive carrier. In some cases, it may be necessary to maintain inert grinding conditions by selecting special lubricants or by chilling the sample. These mechanical profiling techniques require some practice to obtain reproducible sample conditions.

Profiling in the ion-beam thinner occurs when a well aligned beam that is smaller than the specimen diameter or less than

Copyright © 2006 International Union of Crystallography

2 mm in diameter is used or when the specimen edges are masked with the holder. The disc specimens can be profiled on both surfaces or one surface can be left flat. A flat surface is preferable for electron-diffraction analysis as well as for secondary electron imaging.

The mechanical preparation of specimens has been greatly simplified by the development of two instruments by Gatan Inc. (6678 Owens Drive, Pleasanton, CA 94566, USA) (Alani & Swann, 1990). The first is a holder for disc samples that is used on a polishing wheel to grind and polish discs to a specific thickness. This holder has a height adjustment for the specimen, which can be ground and polished to a thickness of 50 μm by the use of various grades of abrasive. With the second instrument, called a 'dimpler™', the polished disc is profiled or dimpled on one side. This dimple is ground and polished with a sensitivity of 1 μm. The dimpled disc is then ready to be thinned in an ion-bombardment instrument.

3.5.1.3. *Final thinning by argon-ion etching*

Argon-ion bombardment or sputter etching is the simplest method for the final thinning of electron-microscope specimens. The application of the technique to ceramics and minerals was demonstrated in the early and mid-1960's with an apparatus commercialized by Paulus & Reverchon (1961; Tighe & Hyman, 1968) or similar designs (Bach, 1964; Drum, 1965). Since that time, numerous commercial instruments have been developed and are available in most electron-microscope laboratories.

The schematics in Fig. 3.5.1.1 show two types of arrangement of the instruments. There are two ion sources for etching from both sides of a specimen, a specimen holder that can be rotated, a viewing port, and a vacuum system. In the instrument in Fig. 3.5.1.1(*b*), the ion sources tilt instead of the specimen holder and an airlock system is used for sample exchange and for monitoring the sample during thinning. The new instruments are relatively trouble free and simple to use compared with the first-generation instruments. The ion sources operate at 4 to 10 kV with variable current to control desired thinning rate and the amount of specimen damage. Thinning rates of 1 μm h^{-1} per ion source are average for normal specimens. The sputtering rates depend also on the angle of tilt (Fig 3.5.1.2) with respect to the ion beam. Faster rates cause more specimen heating and greater ion damage.

The Dual Ion Mill system has two chambers such as the one shown in Fig. 3.5.1.1(*b*) (Gatan Inc.). The chambers function independently, so that two specimens can be thinned simultaneously. The sample holder is raised through an airlock to the observation window at intervals in order to monitor the thinning process. A special beam detector can be used to stop the operation when the specimen perforates.

The specially designed Precision Ion Polishing System 'PIPS™' provides precise control over the specimen thinning area and is a dedicated low-angle instrument with a high thinning rate (Alani & Swann, 1992). The ion beams can be adjusted individually to specific angles, and can be switched on and off regularly during the thinning process. Additionally, the beams can be oriented with respect to specific line features of the sample to preserve edge detail, for example, in a stacked sample (Alani, Harper & Swann, 1992). Gases other than argon can be used for special etching conditions.

Ionic bombardment produces uniquely etched surfaces that are easily recognized in light and electron micrographs. With stationary specimens, closely spaced grooves and ridges are etched parallel to the direction of beam impingement. When the specimen is rotated slowly, these ridges are smoothed and an undulating orange-peel surface is produced. The severity of etching decreases when the angle of incidence to the ion beam is decreased to near grazing angles but uneven etching is never eliminated. The orange-peel texture is randomly located with

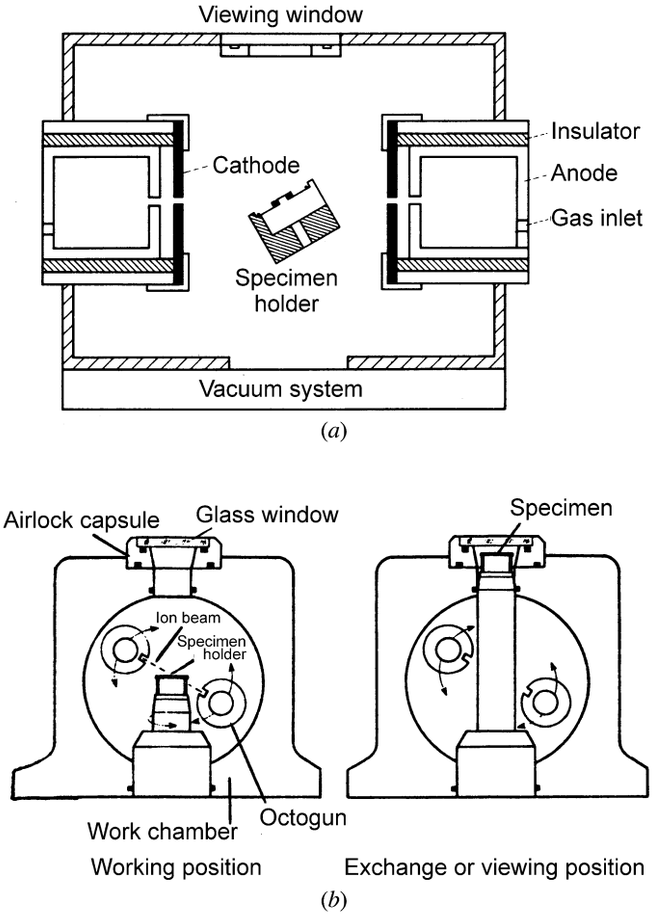

Fig. 3.5.1.1. The two types of arrangement for final thinning by argon-ion etching. (*a*) The system of Paulus & Reverchon (1961) with fixed ion sources, made by Alba. (*b*) The system of Swann with movable ion sources and an airlock for specimen viewing (drawing courtesy of Gatan, Inc.).

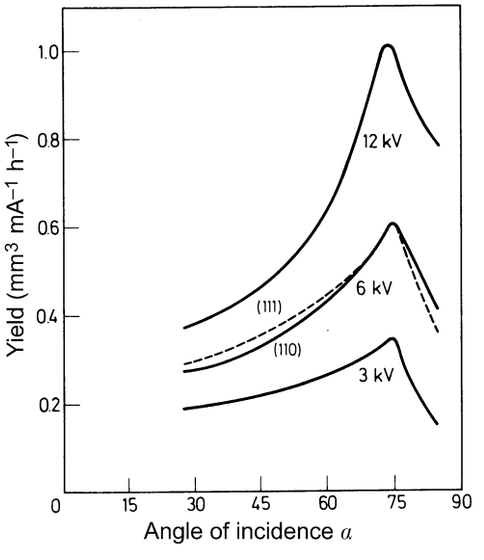

Fig. 3.5.1.2. Dependence of sputtering rate on the angle of tilt.

Table 3.5.1.1. *Chemical etchants used for preparing thin foils from single-crystal ceramic materials; symbols: I immersion method; SFJ separatory funnel jet; CJ convection jet; BJ boiling jet*

Material	Etchant		References
Al_2O_3	85% H_3PO_4, 723–733 K	*I*, BJ	Tighe (1964)
$BaTiO_3$	H_2SO_4	CJ	Kirkpatrick & Amelinckx (1962)
$CaCO_3$	$C_6H_8O_7$ (dilute)	*I*	Braillon *et al.* (1974)
CoO	85% H_3PO_4	CJ	Remaut *et al.* (1964)
$LiNbO_3$	KOH, 623–673 K	*I*	Wicks & Lewis (1968)
MgO	85% H_3PO_4, 373 K	*I*, SFJ	Washburn *et al.* (1960)
$MgAl_2O_4$	85% H_3PO_4, 523–723 K	*I*	Lewis (1966)
MnO	$HCl + NO_3$		Barber & Evans (1970)
SiO_2	$NH_4F{\cdot}HF$, 453–473 K	*I*	Tighe (unpublished)
	HF, 373 K	*I*	
TiO_2	NaOH, 823 K	*I*	Barber & Farabaugh (1965)
$ZrSiO_4$	$NH_4F{\cdot}HF$ + KF (1:1), 693–703 K	*I*	Tighe (unpublished)
$Y_3Al_5O_{12}$	85% H_3PO_4, 573 K	*I*	Keast (1967)

respect to grain boundaries, dislocations, and other types of interfaces found in the thin foils. The severity of the orange-peel texture increases with bombardment time.

Subsurface ion damage occurs and is imaged as spotty black-dot contrast that is typical of point-defect clusters. The presence of the ion damage affects experiments that involve heating of the thin foil but is otherwise accepted as an artefact of the process. In materials such as silicon, the ion damage is sufficient to cause vitrification of the specimen at or near the surface. The argon that is implanted in specimens can be detected with the element-analysis systems.

One troublesome artefact of the ion-thinning process is the surface contamination that is produced by sputtering from tantalum or molybdenum or stainless steel parts of the specimen holder and the cathode. Debris may interfere with the analysis. The sputter debris is frequently located along interfaces of cracks and pores and adds to the contrast effects. Additional contamination occurs during one-sided thinning. The sputter debris adheres to the non-thinning side and must be removed by light-ion etching at the end of the thinning process.

3.5.1.4. *Final thinning by chemical etching*

Chemical dissolution methods for preparing electron-transparent specimens were developed before ion thinning was perfected. These methods are not used extensively, but they have some advantages particularly where ion thinning may disturb the surface composition or structure of a particular material. It is advantageous to use chemical dissolution in some stages of specimen preparation, for example to relate etch pits to dislocations, to prepare a defect-free surface, and to remove the ion-damaged surface from thin disc specimens (Barber & Tighe, 1965). The thinning conditions must be chosen carefully to avoid artefacts such as preferential dissolution at grain boundaries, precipitates, and dislocations, or surface precipitates produced by a supersaturated solution.

Suitable solvents and dissolution conditions must be found for each new material. Some of the chemical etchants used for thin-section preparation are listed in Table 3.5.1.1.

Devices that squirt a jet of chemical solvent at the disc or slab specimen are used to obtain careful control over the final thinning to electron transparency (Kirkpatrick & Amelinckx, 1962; Tighe, 1964; Washburn, Groves, Kelly & Williamson, 1960).

Predictable dissolution rates are obtained by varying the concentration and temperature of the etchant. Solutions can be found that will produce a smooth surface polish or an etch-pitted surface. For example, corundum is etched in boiling phosphoric acid at a temperature approximately 50 K lower than the temperature used for polishing. Surfaces with different crystallographic orientations have different dissolution rates. Useful sources of information about possible etchants are mineralogical and chemical handbooks that discuss production of etch figures and crystallographic facets (Dana & Ford, 1922; Honess, 1927).

3.5.1.5. *Evaporated and sputtered thin films*

Thin nonmetallic films are prepared by electron-beam heating and by plasma sputtering for direct applications such as optical and dielectric films and for standard samples for calibration of the X-ray and electron-energy-loss element-analysis spectrometers on the electron microscopes. The thickness, crystallinity, and composition of the evaporated films are determined by the method of deposition. Co-evaporation from several electron-beam sources is used to produce films of different composition. Reproducible polycrystalline as well as amorphous microstructures are produced using heated and unheated substrates of glass, mica, metal, carbon. The crystalline electron-beam-evaporated films are used for diffraction standards and have been used to observe line broadening and lattice-spacing shifts that result from strain and compositional differences in the films.

Glasses with known compositions are used as sources for plasma sputtering to make thin-film composition standards. Such standards are required for quantitative analysis of ceramic transmission-electron-microscope specimens.

3.5.2. Metals

The aim of the specimen preparation is to obtain a sample (thin foil) of adequate electron transparency to permit the acquisition of images and diffraction patterns of the internal microstructure that is unaltered by the preparation method from that existing in the bulk material. When transmission electron microscopy is carried out at 100 to 200 keV, the sample thickness must lie in the range 0–1000 nm. The useable thickness decreases with increasing mean atomic number and with the requirement for ultra-high (atomic) resolution or for *in situ* chemical analysis by electron-energy-loss spectroscopy (Penneycook, 1981, 1982). In metallic systems, which can undergo plastic (permanent)

deformation as a consequence of the application of mechanical stress, it is most important that the stresses to which the samples are subjected during preparation are too small to result in deformation of the finished thin foil. It is also important that the chemical or electrochemical polishing employed in final thinning does not produce surface films that will either obscure the true microstructure or modify surface chemistry to the point where chemical analysis by X-ray energy-dispersive or electron-energy-loss techniques cannot be carried out. In a limited number of alloy systems, notably titanium alloys (Pennock, Flower & West, 1977), the absorption of hydrogen during preparation can also produce microstructural modifications and careful choice of electrochemical thinning conditions is required to minimize or eliminate the problem: in extreme cases, it may be necessary to resort to ion-beam thinning to reveal the true microstructure (Banerjee & Williams, 1983; see Subsection 3.5.1.3).

3.5.2.1. *Thin sections*

Samples are taken from the bulk material either by a mechanical cutting operation or by spark erosion. The former is the most common technique, but it necessarily produces a region of plastic deformation, and hence microstructural modification, in the material adjacent to the cut faces. The severity of the damage is greatest with cutting by a hacksaw or bandsaw and least with machine cutting using an oil- or water-cooled and lubricated abrasive wheel. The lubricant prevents heating of the sample, which can also lead to microstructural modification. Whatever method of mechanical cutting is adopted, it is necessary to remove a section of sufficient thickness that the slice will contain a central core of unmodified microstructure. The minimum thickness required is not only a function of the cutting method but also of the material cut since softer materials will be damaged to greater depths than hard ones. Typically, a hacksawn slice thickness will lie in the range 2–5 mm, whereas with abrasive cut-off the minimum useable slice thickness is reduced by an order of magnitude.

Subsequent thinning can be carried out by grinding using water-lubricated and -cooled silicon carbide abrasive discs to grind down from both faces of the sample to remove the regions of surface damage. As the section is reduced, successively finer grades of abrasive are required to reduce the depth of damage that they themselves introduce into the material. The depth of damage may be between 10 and 50× the depth of penetration of the abrasive particles depending on the hardness of the metal (*Metals Handbook*, 1985). Typically, grit sizes of 240 to 600 are employed to reduce the section thickness to 0.1 to 0.4 mm.

A spark-erosion method, which employs a high-voltage spark discharge between a tool and the work piece (immersed in paraffin or other insulating liquid with a high dielectric constant), can be used to perform the cutting. The metal is melted locally and eroded at the point of discharge. Both work piece and tool suffer erosion; for cutting slices, a continuously fed wire is used as the tool. With this method, cuts of the order of millimetres in depth may be made while retaining a constant tool profile. Damage at the sample surface is severe involving local melting and large thermally induced stresses. The depth of damage is typically less than 100 μm (Jansen & Zeedijk, 1972) and is readily removed from slices during subsequent thinning procedures.

From the slice, the thin foil may be prepared by either the disc or the window method. For the window technique, samples approximately 10 mm square are employed and electron-transparent sections are cut from them after the sample has been thinned chemically or electrochemically.

For the disc technique, samples of diameter to fit in the electron-microscope specimen holder (typically 3 mm) are cut from the thin sections. The discs may be cut from many materials mechanically using a suitable sample stamping machine. However, in cases where the material is either too hard to stamp successfully (*e.g.* tool steels) or so soft that unacceptable mechanical damage would result, the discs are cut out by spark machining. A tubular tool is employed and it is moved towards the sample in order to keep a constant spark gap. The edges of discs cut in this way, or by punching, require no treatment as only the central portion of the disc is subsequently thinned to electron transparency.

3.5.2.2. *Final thinning methods*

There are two main approaches to the final thinning methods: the window and disc methods (Goodhew, 1972, 1984). The window method is simple and relatively quick and produces small thin pieces of a sample that must be supported by a grid. The disc method produces a specimen where the thinned area is protected by the thick disc rim, which makes handling the foil easier. The disc method can be automated for routine specimen preparation.

In the window technique, a sample about 0.3 mm or less in thickness and ~10 mm square is held at the edge in a pair of metal tweezers. The tweezers and the sample edges are coated in protective lacquer to form a 'window frame' about 1 mm wide. The sample is immersed in an electrolyte contained in a stainless steel beaker as a cathode. The electrolyte is stirred magnetically using a PTFE(polytetrafluorethylene)-coated stirring bar. Temperature is controlled by immersing the beaker partially in a bath of alcohol cooled with solid carbon dioxide or liquid nitrogen. The polishing rate is seldom entirely uniform and best results can be obtained by setting the specimen faces parallel to the electrolyte flow at a distance of one-quarter to one-half of the beaker radius from the centre and turning the sample through 180° periodically. Polishing is carried out until a hole appears in the sample, typically along one window-frame edge. The sample is then repositioned to induce more rapid attack on the opposing edge (*e.g.* if the hole appears at the top edge the foil must be inverted in the tweezers) and thinning is continued until a second perforation forms and grows just into contact with the first. The sample is removed from the electrolyte as rapidly as possible (it may be necessary to switch off the power to avoid the risk of sparks igniting alcohol-based solutions) and washed thoroughly in alcohol. The protective lacquer is peeled off and the sample is further washed and then dried on fresh paper towelling.

Electron-transparent regions can then be cut from the sample using a sharp scalpel. The cutting is accomplished by a pressing action rather than by drawing the scalpel across the sample as the latter can induce substantial damage. The thin foils are then mounted in the microscope specimen holder sandwiched between copper-mesh grids. The technique is particularly appropriate where very large thin areas are required and for magnetic specimens since the total mass of material introduced into the pole-piece gap in the microscope and the consequent image distortion is kept to a minimum.

In the disc technique, the sample is about 0.3 mm in thickness but takes the form of a disc of diameter equal to that of the microscope specimen holder, generally 3 mm. The disc is held in an insulating, typically PTFE, holder, which leaves a large fraction of each face of the disc exposed. The disc is connected electrically to the polishing circuit *via* a platinum wire running

down the inside of the holder and connected to a ring of platinum foil in contact with the sample disc. The sample is immersed in the electrolyte, which contains two jets through which electrolyte is pumped onto the exposed disc faces. The electrolyte flow produces more rapid dissolution at the centre of the disc than at the edges and results in the formation of a central hole. The cross-sectional profile of the thinned section is affected strongly by the size of the jet orifices and electrolyte flow rate, which requires optimization for each electrolyte/metal combination. The hole may be detected by eye using a glass container rather than a stainless steel beaker for the electrolyte with a suitable cathode immersed in it. The greatest advantage of the method, however, lies in its ready automation.

The holder and jet assembly can be mounted inside a light-tight container with a light directed onto one disc face and a photosensor onto the opposite face. *Via* suitable circuitry, the sensitivity of the detector can be adjusted to detect a hole and to cut off the polishing power supply automatically. Several such automated thinners are available commercially and provide a good means of routinely preparing thin foils.

Thin foils should always be stored in a dry dust-free environment to minimize surface reaction with the atmosphere and contamination of the thin areas. Foils of reactive metals (*e.g.* Mg or Fe alloys) will have very limited storability whereas some metals can be stored for years with no loss in foil quality either as a result of their inactivity or as a consequence of the protective nature of the thin air-formed oxide film (*e.g.* Ti).

3.5.2.3. *Chemical and electrochemical thinning solutions*

The principal requirement of the thinning solution is that material is removed from the sample surfaces in as uniform a way as possible to produce flat, polished, and clean surfaces. Thinning is carried out until perforation of the foil occurs at which time the edges of the perforated region should be sufficiently thin for electron microscopy. In a limited number of cases such thinning can be obtained chemically using a suitable acid in an aqueous or organic solvent. Comprehensive lists of chemical and electrochemical thinning solutions appropriate to a wide range of metals and alloys are given in the general references (*Metals Handbook*, 1985; Edington, 1976; Hirsch *et al.*, 1965; Thomas, 1962; Goodhew, 1972, 1975). It must be stressed that in many cases mixtures of highly oxidizing acids are employed in organic solvents and the mixing of the solutions can be hazardous unless undertaken under carefully controlled conditions involving the slow addition of acid to solvent at low temperatures. The storage of such solutions can also produce a fire and explosion hazard and all safety aspects must be thoroughly considered before preparing and using these materials. In spite of continued reference to them in texts, *under no circumstances* should solutions containing acetic anhydride be employed since they can present extreme hazards and safer alternatives exist. The use of face shields and fume-cupboard facilities are mandatory for the preparation and use of all polishing solutions and protective gloves are required in cases where strong acid solutions are employed.

Where several alternative polishing solutions are available, selection should include consideration of safety and storage aspects (inorganic acids in organic solvents being generally the least hazardous), the speed and quality of the thinning/polishing action, and the nature of the surface film that the solution produces on the finished thin foil. The surface film is particularly important where microanalytical studies are undertaken since the chemistry of the surface film may differ markedly from that of the underlying metal (Morris, Davies & Treverton 1978).

Chemical polishing solutions are very simple to use since they require only immersion of the sample in the stirred solutions at an appropriate temperature for thinning and polishing to take place. They can be employed also to thin non-electrically conducting materials such as silicon. However, the thinning action can be stopped only by removal of the sample from the acid and thorough washing of the sample surfaces. Since this operation takes a finite time, it is difficult to stop thinning in a precise manner.

Electrochemical thinning involves the application of an anodic potential to the sample and a cathodic potential to a second electrode in contact with the solution. Electropolishing occurs over a limited range of voltage and temperature and attack can be greatly diminished or halted by switching off the power supply. Thus, more precise control can be obtained over the termination of thinning and automatic control circuitry can be devised. The typical anode current/voltage (i/V) relationship at a fixed temperature under potentiostatic conditions is shown schematically in Fig. 3.5.3.1.

In region I, etching of the sample occurs. In region II, a stable polishing condition is achieved and the current density is insensitive to voltage variations. It is associated with the presence of a viscous liquid layer on the sample surface. Protuberances on the surface extend further through this layer and polish faster hence resulting in their removal and the rapid establishment of a smooth polished surface. Variation in temperature can seriously alter viscosity and the thickness of this layer and increasing temperature reduces the voltage range of the polishing plateau. Region III, which occurs at high voltages, corresponds to breakdown of the solution and gas evolution. It is necessary to establish i/V curves experimentally for any combination of metal and electrolyte. True potential–current relationships can be obtained by potentiostatic techniques (West, 1970), but in practice determination of the applied-voltage range over which polishing occurs using an anode/cathode geometry appropriate to the thinning technique to be employed is generally adequate. Since local ohmic heating of the sample can raise the temperature substantially above that of the bulk solution (Cox & Mountfield, 1967), it is necessary in either case to stir the solution in a controlled manner and to note the effect of stirring-rate variations.

At the practical level, it is pertinent to note that electropolishing to produce thin foils is very much an art rather than an exact science because of the presence of many uncontrolled or unsuspected variables in the process. Firstly, a completely fresh solution often polishes poorly because it lacks an adequate

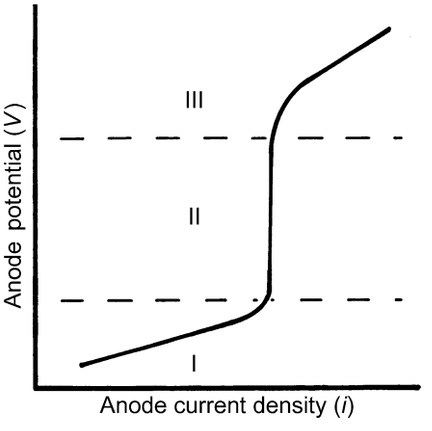

Fig. 3.5.3.1. Typical anode current/voltage relationship at fixed temperature under potentiostatic conditions.

concentration of the metal ions in solution; it is often worth adding a few drops of an exhausted solution to a fresh batch to remedy this. Secondly, solutions become exhausted, at least partially, as a result of selective evaporation, concentration of a metal-ion species, and contamination, particularly by water. Quite apart from the hazards of long-term storage, it is unwise to use solutions once these processes occur.

3.5.3. Polymers and organic specimens

The major difficulty with polymers and organic specimens is that they are rapidly degraded by the electron beam. The specimens become amorphous and sometimes volatilize (Fryer, 1987; Fryer, McConnell, Zemlin & Dorset, 1992). The rate of degradation can be reduced by encapsulating the specimen between two evaporated carbon films or by cooling the specimen to near liquid-nitrogen temperatures in the microscope (Fryer & Holland, 1984). When the specimen is encapsulated with carbon films, the structure can be preserved long enough to obtain electron-diffraction patterns. Therefore, a thin covering layer of carbon should be evaporated on top of the specimen.

Close contact of the specimen with the supporting carbon film is necessary to reduce electron-beam damage. Simple dusting of powdered specimens on carbon film is rarely satisfactory. A drop of the specimen in suspension often gives agglomerated specimens. Therefore, the powdered specimen should be dispersed in a solvent (2-propanol has proved satisfactory for aromatic compounds) with the aid of a low-power vibratory ultrasonic bath. The dispersion is then sprayed with a fine aerosol spray onto the carbon-covered grid.

For specimens where the original morphology is not important, a solution of the compound may be crystallized directly onto the carbon-covered grid. Low concentrations (1–2%) are necessary for good dispersions. Features of the crystal-growth morphology, *e.g.* spiral growth in paraffins, can be highlighted by heavy-metal shadowing. The morphology is often solvent dependent so that needles, platelets, monolayers or multilayers can be obtained as required.

3.5.3.1. *Cast films*

Thin films of polymeric compounds can be obtained by casting solutions of the polymer in a volatile, non-polar solvent onto a water surface and collecting a specimen by bringing a carbon-coated grid up though the film (Porat, Fryer, Huxham & Rubinstein, 1995). This technique is used for specimens of Langmuir–Blodgett monolayer films (Fryer, McConnell, Hann, Eyres & Gupta, 1990; Fryer *et al.*, 1991). The crystallinity of the film is often poor with this method of preparation; better crystals can be obtained by crystallizing the polymer from solution directly onto a carbon film. For many polymers, an ordered array is obtained when crystallization is performed on a cleaved alkali halide single-crystal surface. The monomer can be cast onto the crystalline substrate and polymerization performed thermally or by UV irradiation. After crystallization, the polymeric specimen is coated with carbon and floated off on a water surface. Specimens from bulk polymeric materials can be prepared also by microtome sectioning (see Subsection 3.5.1.1).

3.5.3.2. *Sublimed films*

Most organic compounds can be sublimed under vacuum to give an expitaxic layer on a suitable substrate. Specimens of compounds ranging from paraffins to polynuclear hydrocarbons (Fryer & Smith, 1982; Fryer & Ewins, 1992) and porphyrins (Fryer, 1994) have been prepared in this way. A small amount of material is placed in a molybdenum boat with a perforated cover and sublimed under high vacuum onto a heated substrate. Potassium chloride crystals cleaved in air (100) provide successful substrates. Crystal size and order increase with substrate temperature, however, and a high temperature leads to re-evaporation of the compound. Sometimes, the temperature difference between film deposition and re-evaporation is as small as 30 K. An empirical guide to the optimum substrate is one-third of the boiling-point temperature of the compound. Normally, the crystalline film produced is 10–15 nm thick and is discontinuous.

Following the compound sublimation, carbon is evaporated onto the compound and the film is floated off the KCl substrate onto a water surface. The carbon film can prevent disintegration of the organic compound. Specimens of the film are then picked up on grids.

Organic crystals easily undergo phase changes, so that the crystal modification of the evaporated epitaxic film may not be that of the bulk material. The structure may also vary between preparations on different substrates or between different temperatures on the same substrate.

3.5.3.3. *Oriented solidification*

Long-chain compounds, paraffins, phospholipids, *etc.*, can be prepared epitaxically from solution in molten naphthalene or benzoic acid (Fryer, McConnell, Dorset, Zemlin & Zeitler, 1997; Wittman & Lotz, 1990). For example, a dilute solution of a compound in naphthalene is alternatively solidified and liquified within a few degrees of the melting point to order the long-chain material relative to the naphthalene. When finally solidified, the compound is ordered along the (110) plane of the naphthalene. In practice, the final solidification is carried out on a carbon film and the naphthalene is removed under vacuum. The crystals are lath shaped and are aligned with the long-chain major axis on the carbon film across the lath and hence normal to the electron beam. Crystals of the same compounds prepared from normal organic solvents as described in Subsection 3.5.3.2 have the long-chain axis normal to the carbon-grid plane and thus parallel to the electron beam. The advantage of the normal orientation is that the large interplanar spacing along the chain axis is more accessible to direct imaging in the electron microscope.

3.6. Specimens for neutron diffraction

By B. T. M. Willis

Specimen preparation for neutron diffraction presents few of the problems encountered in electron diffraction and electron microscopy (Chapter 3.5). This is because – with the exception of a few isotopes – the atomic absorption cross section for slow neutrons is several orders of magnitude less than that for electrons. Whereas thin sections must be prepared from bulk samples for examination by electron microscopy, the bulk samples themselves are used in neutron diffraction.

For structural studies with single crystals, the size of crystal required depends on the magnitude of the incident neutron flux. The fluxes available worldwide from different sources are tabulated by Bacon (1987). If a flux of 10^{14} neutrons cm^{-2} s^{-1} is assumed, a crystal of linear dimension about 1 mm is necessary. Corrections for extinction, absorption, and multiple scattering are easier to apply if the crystal is in the form of a flat plate or sphere. Crystals containing hydrogen give rise to a uniform background from incoherent scattering. This background can be removed by deuteration, but for measuring Bragg intensities this is rarely essential. The sample can be examined *in vacuo* or in an inert atmosphere by sealing it inside a silica tube, which causes very little attenuation of the neutron beam for a wall thickness of 0.5 mm.

Structural studies on polycrystalline samples are often undertaken using a cylindrical volume of material, enclosed in a holder of aluminium or vanadium. Apart from its cost, vanadium is an ideal container because its atomic coherent scattering cross section (3.3×10^{-30} m^2) is negligible compared with its incoherent cross section (530×10^{-30} m^2); consequently, the container contributes significantly to the background, but gives no diffraction lines. Aluminium has negligible absorption and incoherent scattering, and weak coherent scattering. It therefore produces no background scattering, but it does give rise to diffraction peaks, which may be superimposed on those of the sample. Unlike in single-crystal work, it is usually necessary to replace hydrogen atoms by deuterium. By using a cylindrical sample, effects due to preferred orientation can be reduced by rotating the cylinder about its vertical axis.

Coherent inelastic scattering studies, used to investigate the lattice dynamics of crystalline solids [see Section 4.1.1 in *IT* B (1992)], require single crystals of high purity and crystalline perfection (mosaic spread less than 0.3°). Counting rates are, perhaps, one thousand times less than for structural studies, so that the crystal size is measured in centimetres rather than millimetres. Crystals up to 50 cm^3 in volume may be used. For such large crystals, there is an upper limit of about 10×10^{-30} m^2 to the atomic absorption cross section. This is considerably less than the effective absorption cross section of hydrogen (arising from incoherent scattering), so that hydrogenous compounds must be deuterated for neutron work in which coherent inelastic scattering is measured.

References

3.1

Axelrod, H. J., Feher, G., Allen, J. P., Chirino, A. J., Day, M. W., Hsu, B. T. & Rees, D. C. (1994). *Crystallization and X-ray structure determination of cytochrome c_2 from rhodobacter sphaeroides in three crystal forms*. *Acta Cryst*. D**50**, 596–602.

Bernard, Y., Degoy, S., Lefaucheux, F. & Robert, M. C. (1994). *A gel-mediatied feeding technique for protein crystal growth from hanging drops*. *Acta Cryst*. D**50**, 504–507.

Bishop, A. C. (1972). *An outline of crystal morphology*, 3rd ed., Chap. 11, pp. 254–282. London: Hutchinson Scientific and Technical.

Blundell, T. L. & Johnson, L. N. (1976). *Protein crystallography*, Chap. 3, pp. 59–82. New York: Academic Press.

Britton, D. (1972). *Estimation of twinning parameter for twins with exactly superposed reciprocal lattices*. *Acta Cryst*. A**28**, 296–297.

Bunn, C. W. (1961). *Chemical crystallography: an introduction to optical and X-ray methods*, 2nd ed., Chaps. 2, 3, 4, pp. 11–106. Oxford University Press.

Carter, C. W. Jr & Carter, C. W. (1979). *Protein crystallisation using incomplete factorial experiments*. *J. Biol. Chem*. **254**, 12219–12223.

Carter, C. W. Jr & Yin, Y. (1994). *Quantitative analysis in the characterization and optimization of protein crystal growth*. *Acta Cryst*. D**50**, 572–590.

Chayen, N. E., Shaw Stewart, P. D. & Baldock, P. (1994). *New developments of the IMPAX small-volume automated crystallization system*. *Acta Cryst*. D**50**, 456–458.

Chayen, N. E., Shaw Stewart, P. D., Maeder, D. L. & Blow, D. M. (1990). *An automated system for micro-batch protein crystallization and screening*. *J. Appl. Cryst*. **23**, 297–302.

Cox, M. J. & Weber, P. C. (1987). *Experiments with automated protein crystallization*. *J. Appl. Cryst*. **20**, 366–373.

Cudney, B., Patel, S. & McPherson, A. (1994). *Crystallization of macromolecules and silica gels*. *Acta Cryst*. D**50**, 479–483.

Diller, T. C., Shaw, A., Stura, E. A., Vacquier, V. D. & Stout, C. D. (1994). *Acid pH crystallization of the basic protein lysin from the spermatozoa of red abalone (Haliotis refescens)*. *Acta Cryst*. D**50**, 627–631.

Ducruix, A. & Giegé, R. (1992). Editors. *Crystallisation of nucleic acids and proteins: a practical approach*. Oxford University Press.

Eiselé, J.-L. (1993). *Preparation of protein crystallization buffers with a computer-controlled motorized pipette: PIPEX*. *J. Appl. Cryst*. **26**, 92–96.

Ferré-D'Amaré, A. R. & Burley, S. K. (1994). *Use of dynamic light scattering to assess crystallisability of macromolecules and macromolecular assemblies*. *Structure*, **2**(5), 357–359.

Fisher, R. G. & Sweet, R. M. (1980). *Treatment of diffraction data from protein crystals twinned by merohedry*. *Acta Cryst*. A**36**, 755–760.

Forsythe, E., Ewing, F. & Pusey, M. (1994). *Studies on tetragonal lysozyme crystal growth rates*. *Acta Cryst*. D**50**, 614–619.

Garavito, R. M. & Picot, D. (1990), *Methods: a companion to methods in enzymology*, Vol. 1, pp. 57–69. New York: Academic Press.

Copyright © 2006 International Union of Crystallography

3.1 (*cont.*)

García-Ruiz, J. M. & Moreno, A. (1994). *Investigations on protein crystal growth by the gel acupuncture method. Acta Cryst.* D**50**, 484–490.

Giegé, R. & Ducruix, A. (1992). *Crystallisation of nucleic acids and proteins: a practical approach*, edited by A. Ducruix & R. Giegé, pp. 1–15. Oxford University Press.

Giegé, R., Theobald-Dietrich, A. & Lorber, B. (1993). *Novel trends in protein and nucleic acid crystallisation: biochemical and physico-chemical aspects. Data collection and processing. Proceedings of the CCP4 Study Weekend*, edited by L. Sawyer, N. Isaacs & S. Bailey, pp. 12–19. SERC Daresbury Laboratory, Warrington WA4 4AD, England.

Gilliland, G. L., Tung, M., Blakeslee, D. M. & Ladner, J. E. (1994). *Biological macromolecule crystallization database, Version 3.0: new features, data and the NASA archive for protein crystal growth data. Acta Cryst.* D**50**, 408–413.

Hampton Research (1994). *Crystallisation research tools*, Vol.4, No. 2. Hampton Research, 5225 Canyon Crest Drive, Suite 71–336, Riverside, CA 92597, USA.

Harlos, K. (1992). *Micro-bridges for sitting-drop crystallizations. J. Appl. Cryst.* **25**, 536–538.

Hartshorne, N. H. & Stuart, A. (1960). *Crystals and the polarising microscope*, 3rd ed. London: Arnold.

Helliwell, J. R. (1992). *Macromolecular crystallography with synchrotron radiation*, Chap. 2, pp. 11–23. Cambridge University Press.

Helliwell, M., Kaucic, V., Cheetham, G. M. T., Harding, M. M., Kariuki, B. M. & Rizkallah, P. J. (1993). *Structure determination from small crystals of two aluminophosphates, CrAPO-14 and SAPO-43. Acta Cryst.* B**49**, 413–420.

Hennig, M. & Schlesier, B. (1994). *Crystallization of seed globulins from legumes. Acta Cryst.* D**50**, 627–631.

Hodeau, J. L., Tu, H. Y., Bordet, P., Fournier, T., Strobel, P., Marezio, M. & Chandrashekar, G. V. (1992). *Structure and twinning of Sr_3CuPtO_6. Acta Cryst.* B**48**, 1–11.

Jancarik, J. & Kim, S.-H. (1991). *Sparse matrix sampling: a screening method for crystallization of proteins. J. Appl. Cryst.* **24**, 409–411.

Jeffery, J. W. (1977). *Methods in X-ray crystallography*, pp. 441–443. London/New York: Academic Press.

Konnert, J. H., D'Antonio, P. & Ward, K. B. (1994). *Observation of growth steps, spiral dislocations and molecular packing on the surface of lysozyme crystals with the atomic force microscope. Acta Cryst.* D**50**, 603–613.

Ladd, M. F. C. & Palmer, R. A. (1985). *Structure determination by X-ray crystallography*, 2nd ed., Chap. 3, pp. 101–112. New York/London: Plenum.

Luft, J. & Cody, V. (1989). *A simple capillary vapor diffusion apparatus for surveying macromolecular crystallization conditions. J. Appl. Cryst.* **22**, 396.

Luft, J. R., Arakali, S. V., Kirisits, M. J., Kalenik, J., Waarzak, I., Cody, V., Pangborn, W. A. & DeTitta, G. T. (1994). *A macromolecular crystallization procedure employing diffusion cells of varying depths as reservoirs to tailor the time course of equilibration in hanging- and sitting-drop vapor-diffusion and microdialysis experiments. J. Appl. Cryst.* **27**, 443–452.

McDermott, G. (1993). *Crystallisation of membrane proteins. Data collection and processing. Proceedings of the CCP4 Study Weekend*, edited by L. Sawyer, N. Isaacs & S. Bailey, pp. 20–27. SERC Daresbury Laboratory, Warrington WA4 4AD, England.

MacGillavry, C. H. & Henry, N. F. M. (1962). *Preliminary investigation and selection of crystals for X-ray study. International tables for X-ray crystallography*, Vol. III, pp. 5–13. Birmingham: Kynoch Press.

McPherson, A. (1976). *The growth and preliminary investigation of protein and nucleic acid crystals for X-ray diffraction. Methods Biochem. Anal.*, **25**, 249–345.

McPherson, A. (1982). *The preparation and analysis of protein crystals*. New York: John Wiley.

McPherson, A. (1985*a*). *Crystallisation of macromolecules: general principles. Methods in enzymology*, Vol. 114, pp. 112–120. New York: Academic Press.

McPherson, A. (1985*b*). *Crystallisation of proteins by variation of pH and temperature. Methods in enzymology*, Vol. 114, pp. 125–127. New York: Academic Press.

McPherson, A. (1990). *Current approaches to macromolecular crystallisation. Eur. J. Biochem.* **189**, 1–23.

Makarova, I. P., Verin, I. A. & Aleksandrov, K. S. (1993). *Structure and twinning of $RbLiCrO_4$ crystals. Acta Cryst.* B**49**, 19–28.

Mikol, V., Rodeau, J.-L. & Giegé, R. (1989). *Changes of pH during biomacromolecule crystallization by vapour diffusion using ammonium sulfate as the precipitant. J. Appl. Cryst.* **22**, 155–161.

Monaco, H. L. (1994). *The use of ammonium succinate in protein crystallography. J. Appl. Cryst.* **27**, 1068.

Oldfield, T. J., Ceska, T. A. & Brady, R. L. (1991). *A flexible approach to automated protein crystallization. J. Appl. Cryst.* **24**, 255–260.

Phillips, F. C. (1971). *An introduction to crystallography*, 4th ed., Chap. 7, pp. 171–193. Edinburgh: Oliver & Boyd.

Przybylska, M. (1989). *A double cell for controlling nucleation and growth of protein crystals. J. Appl. Cryst.* **22**, 115–118.

Redinbo, M. R. & Yeates, T. O. (1993). *Structure determination of plastocyanin from a specimen with a hemihedral twinning fraction of one-half. Acta Cryst.*, D**49**, 375–380.

Reynolds, R. A., Remington, S. J., Weaver, L. H., Fisher, R. G., Anderson, W. F., Ammon, H. L. & Matthews, B. W. (1985). *Structure of a serine protease from rat mast cells determined from twinned crystals by isomorphous and molecular replacement. Acta Cryst.* B**41**, 139–147.

Riekel, C. (1993). *Beamline 1: microfocus beamline*. In Annual Report of the European Synchrotron Radiation Facility, Grenoble, France.

Ries-Kautt, M. & Ducruix, A. (1992). *Crystallisation of nucleic acids and proteins: a practical approach*, edited by A. Ducruix & R. Giegé, pp. 195–218. Oxford University Press.

Robert, M. C., Bernard, Y. & Lefaucheux, F. (1994). *Study of nucleation-related phenomena in lysozyme solutions. Application to gel growth. Acta Cryst.* D**50**, 496–503.

Robert, M. C., Provost, K. & Lefaucheux, F. (1992). *Crystallisation of nucleic acids and proteins: a practical approach*, edited by A. Ducruix & R. Giegé, pp. 127–143. Oxford University Press.

Sadaoui, N., Janin, J. & Lewit-Bentley, A. (1994). *TAOS: an automated system for protein crystallization. J. Appl. Cryst.* **27**, 622–626.

Scarborough, G. A. (1994). *Large single crystals of the nerospora crassa plasma membrane H^+-ATPase: an approach to the crystallization of integral membrane proteins. Acta Cryst.* D**50**, 643–649.

Schick, B. & Jurnak, F. (1994). *Extension of the diffraction resolution of crystals. Acta Cryst.* D**50**, 563–568.

3.1 (*cont.*)

Sica, F., Demasi, D., Mazzarella, L., Zagari, A., Capasso, S., Pearl, L. H., D'Auria, S., Raia, C. A. & Rossi, M. (1994). *Elimination of twinning in crystals of sulfolobus solfataricus alcohol dehydrogenase holo-enzyme by growth in agarose gels*. *Acta Cryst*. D**50**, 508–511.

Sluis, P. van der, Hezemans, A. M. F. & Kroon, J. (1989). *Crystallization of low-molecular-weight compounds for X-ray crystallography*. *J. Appl. Cryst*. **22**, 340–344.

Soriano, T. M. B. & Fontecilla-Camps, J. C. (1993). *ASTEC: an automated system for sitting-drop protein crystallization*. *J. Appl. Cryst*. **26**, 558–562.

Spangfort, M. D., Surin, B. P., Dixon, N. E. & Svensson, L. A. (1994). *Internal symmetry of the molecular chaperone cpn60 (GroEL) determined by X-ray crystallography*. *Acta Cryst*. D**50**, 591–595.

Stout, G. H. & Jensen, L. H. (1968). *X-ray structure determination: a practical guide*, Chap. 4, pp. 62–82. London: Macmillan.

Thaller, C., Eichelle, G., Weaver, L. H., Wilson, E., Karlsson, R. & Jansonius, J. N. (1985). *Seed enlargement and repeated seeding*. *Methods in enzymology*, Vol. 114, pp. 132–135. New York: Academic Press.

Thatcher, D. R. (1993). *Protein purification and analysis for crystallographic studies*. *Data collection and processing*. *Proceedings of the CCP4 Study Weekend*, edited by L. Sawyer, N. Isaacs & S. Bailey, pp. 2–11. SERC Daresbury Laboratory, Warrington WA4 4AD, England.

Thiessen, M. J. (1994). *The use of two novel methods to grow protein crystals by microdialysis and vapor diffusion in an agarose gel*. *Acta Cryst*. D**50**, 491–495.

Tipson, R. S. (1956). *Techniques of organic chemistry*, Vol. III, Part I, Chap. 3. New York: Interscience.

Tissen, J. T. W. M., Fraaije, J. G. E. M., Drenth, J. & Berendsen, H. J. C. (1994). *Mesoscopic theories for protein crystal growth*. *Acta Cryst*. D**50**, 569–571.

3.2

Berman, H. (1939). *A torsion microbalance for the determination of specific gravities of minerals*. *Am. Mineral*. **24**, 434–440.

Bernal, J. D. & Crowfoot, D. (1934). *Use of the centrifuge in determining the density of small crystals*. *Nature (London)*, **134**, 809–810.

British Standards Institution (1964). *Concentration gradient density columns*. British Standard 3715, pp. 1–17. British Standards Institution, London, England.

Graubner, H. (1986). *Densitometer for absolute measurements of the temperature dependence of density, partial volumes and thermal expansivity of solids and liquids*. *Rev. Sci. Instrum*. **57**, 2817–2826.

Guo, S. Y. & White, E. T. (1983). *Measurement on inclusions in sugar crystals using a density gradient column*. *Proc. Austr. Soc. Sugar Cane Technol*. pp. 219–224.

Hauptmann, H. & Schulze, G. E. R. (1934). *Über ein neues Microvolumenometer*. *Z. Phys. Chem. Abt. A*, **171**, 36–40.

Johnston, J. & Adams, L. H. (1912). *On the density of solid substances, with especial reference to permanent changes produced by high pressures*. *J. Am. Chem. Soc*. **34**, 563–584.

Kundrot, C. E. & Richards, F. M. (1988). *Effect of hydrostatic pressure on the solvent in crystals of hen egg-white lysozyme*. *J. Mol. Biol*. **200**, 401–410.

Kwong, P. D., Pound, A. & Hendrickson, W. A. (1994). *Volume-specific amino acid analysis: a method for Z_a determination*. *J. Appl. Cryst*. **27**, 504–509.

Linderstrom-Lang, K. (1937). *Dilatometric ultra-microestimation of peptidase activity*. *Nature (London)*, **139**, 713–714.

Linderstrom-Lang, K. & Lanz, H. Jr (1938). *Studies on enzymatic histochemistry*. *XXIX. Dilatometric micro-estimation of peptidase activity*. *C. R. Trav. Lab. Carlsberg Ser. Chim*. **21**, 315–338.

Low, B. W. & Richards, F. M. (1952*a*). *The use of the gradient tube for the determination of crystal densities*. *J. Am. Chem. Soc*. **74**, 1660–1666.

Low, B. W. & Richards, F. M. (1952*b*). *Determination of protein crystal densities*. *Nature (London)*, **170**, 412–415.

Low, B. W. & Richards, F. M. (1954). *Measurements of the density, composition and related unit cell dimensions of some protein crystals*. *J. Am. Chem. Soc*. **76**, 2511–2518.

Mason, B. (1944). *The determination of the density of solids*. *Geol. Foeren. Stockholm Foerh*. **66**, 27–51.

Matthews, B. W. (1968). *Solvent content of protein crystals*. *J. Mol. Biol*. **33**, 491–497.

Meyrowitz, R., Cuttitta, F. & Hickling, N. (1959). *A new diluent for bromoform in heavy liquid separation of minerals*. *Am. Mineral*. **44**, 884–885.

Midgley, H. G. (1951). *A quick method of determining the density of liquid mixtures*. *Acta Cryst*. **4**, 565.

Rabukhin, V. B. (1982). *String method of measuring the density of irradiated metallic crystals*. *At. Energ*. **52**, 131–132.

Reilly, J. & Rae, W. N. (1954). *Physico-chemical methods*, Vol. 1, 5th ed., pp. 577–608. New York: van Nostrand.

Richards, F. M. (1954). *A microbalance for the determination of protein crystal densities*. *Rev. Sci. Instrum*. **24**, 1029–1034.

Richards, F. M. & Thompson, T. E. (1952). *Application of Mohr–Westphal balance to rapid calibration of wide range density-gradient columns*. *Anal. Chem*. **24**, 1052–1053.

Sullivan, J. D. (1927). *Heavy liquids for mineralogical analyses*. *US Bur. Mines Tech. Pap*. No. 381.

Syromyatnikov, F. V. (1935). *The micropycnometric method for the determination of specific gravities of minerals*. *Am. Mineral*. **20**, 364–370.

Tutton, A. E. (1922). *Crystallography and practical crystal measurement*, Vol. 1, pp. 625–639. London: Macmillan.

Westbrook, E. M. (1976). *J. Mol. Biol*. **103**, 659–664.

Westbrook, E. M. (1985). *Methods Enzymol*. **114**, 187–196.

Wulff, P. & Heigl, A. (1931). *Methodisches zur Dichtebestimmung fester Stoffe, insbesondere anorganischer Salze*. *Z. Phys. Chem. Abt. A*, **153**, 187–209.

Wunderlich, J. A. (1957). *Un méthode rapide pour mésurer la densité d'un cristal*. *Acta Cryst*. **10**, 433–434.

3.3

Butler, R. D. (1933). *Immersion liquids of intermediate refraction*. *Am. Mineral*. **18**, 386–401.

Hartshorne, N. H. & Stuart, A. (1960). *Crystals and the polarising microscope*, 3rd ed. London: Arnold.

International Tables for X-ray Crystallography (1962). Vol. III. Birmingham: Kynoch Press.

Jelley, E. E. (1934). *A microfractometer and its use in chemical microscopy*. *J. R. Microsc. Soc*. **54**, 234–245.

Larsen, E. S. Jr & Berman, H. (1934). *The microscopic determination of nonopaque minerals*, 2nd ed. *US Geol. Survey Bull*. No. 848.

3.3 (*cont.*)

Merwin, H. E. & Larsen, E. S. Jr (1912). *Mixtures of amorphous sulphur and selenium as immersion media for the determination of high refractive indices with the microscope*. *Am. J. Sci.* **34**, 42–47.

3.4

Adlhart, W. & Huber, H. (1982). *A low-temperature X-ray Weissenberg goniometer with closed-cycle cooling to about 28 K*. *J. Appl. Cryst.* **15**, 241–244.

Adlhart, W., Tzafaras, N., Sueno, S., Jagodzinski, H. & Huber, H. (1982). *An X-ray camera for single-crystal studies at high temperatures under controlled atmosphere*. *J. Appl. Cryst.* **15**, 236–240.

Alkire, R. W., Larson, A. C., Vergamini, P. J., Schirber, J. E. & Morosin, B. (1985). *High-pressure single-crystal neutron diffraction (to 20 kbar) using a pulsed source: preliminary investigation of Tl_3PSe_4*. *J. Appl. Cryst.* **18**, 145–149.

Allen, S., Cosier, J., Glazer, A. M., Hastings, T. J., Smith, D. T. & Wood, I. G. (1982). *A microprocessor-controlled continuous-flow cryostat for single-crystal X-ray diffraction in the range 10–300 K*. *J. Appl. Cryst.* **15**, 382–387.

Archer, J. M. & Lehmann, M. S. (1986). *A simple adjustable mount for a two-stage cryorefrigerator on an Eulerian cradle*. *J. Appl. Cryst.* **19**, 456–458.

Argoud, R. & Muller, J. (1989*a*). *Effect of stress from the glue on single-crystal X-ray intensities at high or low temperatures*. *J. Appl. Cryst.* **22**, 378–380.

Argoud, R. & Muller, J. (1989*b*). *Magnetically coupled crystal holder and liquid-helium cryostat for X-ray four-circle diffractometer studies between 5 and 300 K*. *J. Appl. Cryst.* **22**, 584–591.

Arndt, U. W. & Stubbings, S. J. (1987). *A miniature Peltier-effect goniometer-head attachment*. *J. Appl. Cryst.* **20**, 445.

Arndt, U. W. & Wonacott, A. J. (1977). *The rotation method in crystallography*. Amsterdam/New York/Oxford: North-Holland.

Arnold, H., Bartl, H., Fuess, H., Ihringer, J., Kosten, K., Löchner, U., Pennartz, P. U., Prandl, W. & Wroblewski, T. (1989). *New powder diffractometer at HASYLAB/DESY*. *Rev. Sci. Instrum.* **60**, 2380–2381.

Bartunik, H. D. & Schubert, P. (1982). *Crystal cooling for protein crystallography with synchrotron radiation*. *J. Appl. Cryst.* **15**, 227–231.

Bhat, H. L., Clark, S. M., El Korashy, A. & Roberts, K. J. (1990). *A furnace for in situ synchrotron Laue diffraction and its application to studies of solid-state phase transformations*. *J. Appl. Cryst.* **23**, 545–549.

Black, D. R., Burdette, H. E. & Early, J. G. (1986). *Diffusion bonding of ductile single crystals for strain-free mounting*. *J. Appl. Cryst.* **19**, 279–280.

Boese, R. & Bläser, D. (1989). *A procedure for the selection and transferring of crystals at low temperatures to diffractometers*. *J. Appl. Cryst.* **22**, 394–395.

Bouquiere, J. P., Finney, J. L., Lehmann, M. S., Lindley, P. F. & Savage, H. F. J. (1993). *High-resolution neutron study of vitamin B_{12} coenzyme at 15 K: structure analysis and comparison with the structure at 279 K*. *Acta Cryst.* B**49**, 79–89.

Bretherton, L. & Kennard, C. H. L. (1976). *Crystal mounter*. *J. Appl. Cryst.* **9**, 416.

Brown, N. E., Swapp, S. M., Bennett, C. L. & Navrotsky, A. (1993). *High-temperature X-ray diffraction: solutions to uncertainties in temperature and sample position*. *J. Appl. Cryst.* **26**, 77–81.

Buerger, M. J. (1964). *The precession method in X-ray crystallography*. New York: John Wiley.

Busing, W. R. & Levy, H. A. (1967). *Angle calculations for 3- and 4-circle X-ray and neutron diffractometers*. *Acta Cryst.* **22**, 457–464.

CAD4 Manual (1989). Enraf–Nonius, Scientific Instruments Division, PB 483, NL-2600 AL, Delft, The Netherlands.

Campos, C., Cardoso, L. P. & Caticha-Ellis, S. (1983). *A simple method to cut a single crystal in any desired direction*. *J. Appl. Cryst.* **16**, 360.

Carr, P. D., Cruickshank, D. W. J. & Harding, M. M. (1992). *The determination of unit-cell parameters from Laue diffraction patterns using their gnomonic projections*. *J. Appl. Cryst.* **25**, 294–308.

Cascio, D., Williams, R. & McPherson, A. (1984). *The reduction of radiation damage in protein crystals by polyethylene glycol*. *J. Appl. Cryst.* **17**, 209–210.

Clegg, W. (1984). *Enhancements of the 'auto-indexing' method for cell determination in four-circle diffractometry*. *J. Appl. Cryst.* **17**, 334–336.

Clifton, I. J., Elder, M. & Hajdu, J. (1991). *Experimental strategies in Laue crystallography*. *J. Appl. Cryst.* **24**, 267–277.

Cosier, J. & Glazer, A. M. (1986). *A nitrogen-gas-stream cryostat for general X-ray diffraction studies*. *J. Appl. Cryst.* **19**, 105–107.

D'Aprile, F. & Moretto, R. (1975). *Two simple devices for sealing wet single crystals in capillary tubes*. *J. Appl. Cryst.* **8**, 696.

Denne, W. A. (1971*a*). *A new concept in goniometer head design*. *J. Appl. Cryst.* **4**, 60–66.

Denne, W. A. (1971*b*). *A technique for the rigid mounting of crystals in X-ray diffractometry*. *J. Appl. Cryst.* **4**, 400.

Dent Glasser, L. S. (1977). *Crystallography and its applications*, Chap. 6, pp. 125–155. New York/Cincinnati/Toronto/London/Melbourne: Van Nostrand Reinhold.

Desai, C. F. & Bhatt, V. P. (1984). *A sample holder for cutting single crystals along any desired X-ray orientated plane*. *J. Appl. Cryst.* **17**, 369–370.

Dewan, J. C. & Tilton, R. F. (1987). *Greatly reduced radiation damage in ribonuclease crystals mounted on glass fibres*. *J. Appl. Cryst.* **20**, 130–132.

D'Eye, R. W. M. & Wait, E. (1960). *X-ray powder photography*. London: Butterworth.

Duisenberg, A. J. M. (1992). *Indexing in single-crystal diffractometry with an obstinate list of reflections*. *J. Appl. Cryst.* **25**, 92–96.

Dumas, P. & Ripp, R. (1986). *A real-time interactive graphics program to determine crystal orientation for the analysis of oscillation diffraction photographs*. *J. Appl. Cryst.* **19**, 28–33.

Edwards, S. L. (1993). *Yokeless flow cell for Laue crystallography*. *J. Appl. Cryst.* **26**, 305–306.

Fischer, J., Moras, D. & Thierry, J. C. (1985). *Single-crystal diffractometry: strategy for rapidly decaying poorly diffracting crystals*. *J. Appl. Cryst.* **18**, 20–26.

Foit, F. F. Jr (1982). *A technique for loading glass capillaries used in X-ray powder diffraction*. *J. Appl. Cryst.* **15**, 357.

Fraase Storm, G. M. & Tuinstra, F. (1986). *A thermoelectric device for temperature-controlled single-crystal diffractometry*. *J. Appl. Cryst.* **19**, 372–373.

3.4 (*cont.*)

Frauenfelder, H., Hartmann, H., Karplus, M., Kuntz, I. D. Jr, Kuriyan, J., Parak, F., Petsko, G. A., Ringe, D., Tilton, R. F. Jr, Conolly, M. L. & Max, N. (1987). *Thermal expansion of a protein*. *Biochemistry*, **26**, 254–261.

Frauenfelder, H., Petsko, G. A. & Tsernoglou, D. (1979). *Temperature-dependent X-ray diffraction as a probe of protein structure dynamics*. *Nature (London)*, **280**, 558.

Gamblin, S. J. & Rogers, D. W. (1993). *Some practical details of data collection at 100 K*. In *Data collection and processing*. *Proceedings of the CCP4 Study Weekend*, edited by L. Sawyer, N. Isaacs & S. Bailey. Report DL/SCI/R34. SERC Daresbury Laboratory, Cheshire WA4 4AD, England.

Gonzalez, A. & Nave, C. (1994). *Radiation damage in protein crystals at low temperature*. *Acta Cryst*. D**50**, 874–877.

Graafsma, H., Sagerman, G. & Coppens, P. (1991). *Closed-cycle helium cryostat for the Huber 511.1 diffractometer circle*. *J. Appl. Cryst*. **24**, 961–962.

Hajdu, J., McLaughlin, P. J., Helliwell, J. R., Sheldon, J. & Thompson, A. W. (1985). *Universal cooling device for precession cameras, rotation cameras and diffractometers*. *J. Appl. Cryst*. **18**, 528–532.

Hanson, I. R. (1981). *A rapid and accurate method of aligning a crystal on a Weissenberg goniometer*. *J. Appl. Cryst*. **14**, 353.

Hartmann, H., Parak, F., Steigemann, W., Petsko, G. A., Ringe-Ponzi, D. & Frauenfelder, H. (1982). *Conformational substrates in a protein: structure and dynamics of metmyoglobin at 80 K*. *Proc. Natl Acad. Sci. USA*, **79**, 4967–4971.

Hazen, R. M. & Finger, L. W. (1982). *Comparative crystal chemistry*, pp. 5–16. New York: Wiley.

Helliwell, J. R., Habash, J., Cruickshank, D. W. J., Harding, M. M., Greenhough, T. J., Campbell, J. E., Clifton, I. J., Elder, M., Machin, P. A., Papiz, M. Z. & Zurek, S. (1989). *The recording and analysis of synchrotron X-radiation Laue diffraction photographs*. *J. Appl. Cryst*. **22**, 483–497.

Henriksen, K., Larsen, F. K. & Rasmussen, S. E. (1986). *Mounting a 10 K cooling device without rotating seals on a four-circle diffractometer*. *J. Appl. Cryst*. **19**, 390–394.

Higashi, T. (1989). *The processing of diffraction data taken on a screenless Weissenberg camera for macromolecular crystallography*. *J. Appl. Cryst*. **22**, 9–18.

Higashi, T. (1990). *Auto-indexing of oscillation images*. *J. Appl. Cryst*. **23**, 253–257.

Hohlwein, D. & Wright, A. F. (1981). *A low-temperature Weissenberg camera for neutrons*. *J. Appl. Cryst*. **14**, 82–84.

Holmes, K. C. & Blow, D. M. (1966). *The use of diffraction in the study of protein and nucleic acid structure*. New York: John Wiley.

Hope, H. (1987). *Experimental organometallic chemistry*. *Am. Chem. Soc. Symp. Ser.*, No. 357. Washington, DC: American Chemical Society.

Hope, H. (1988). *Cryocrystallography of biological macromolecules: a generally applicable method*. *Acta Cryst*. B**44**, 22–26.

Hope, H. (1990). *Crystallography of biological macromolecules at ultra-low temperatures*. *Ann. Rev. Biophys. Biophys. Chem*. **19**, 107–126.

Hope, H., Frolow, F., van Böhlen, K., Makowski, I., Kratky, C., Halfon, Y., Danz, H., Bartels, K. S., Wittmann, H. G. & Yonath, A. (1989). *Crystallography of ribosomal particles*. *Acta Cryst*. B**45**, 190–199.

Hornstra, J. & Vossers, H. (1974). *Philips Tech. Rundsch*. **33**, 65–78.

Hovmöller, S. (1981). *A device which improves the cooling of protein crystals during X-ray data collection*. *J. Appl. Cryst*. **14**, 75.

Ihringer, J. & Küster, A. (1993). *Cryostat for synchrotron powder diffraction with sample rotation and controlled gas atmosphere in the sample chamber*. *J. Appl. Cryst*. **26**, 135–137.

Jacobson, R. A. (1976). *A single-crystal automatic indexing procedure*. *J. Appl. Cryst*. **9**, 115–118.

Jacobson, R. A. (1986). *An orientation-matrix approach to Laue indexing*. *J. Appl. Cryst*. **19**, 283–286.

Jeffery, J. W. (1971). *Methods in X-ray crystallography*, pp. 149–169, 441–444. London/New York: Academic Press.

Jones, A., Bartels, K. & Schwager, P. (1977). *Refinement of crystal orientation parameters*. *The rotation method*, edited by U. W. Arndt & A. Wonacott, pp. 105–117. Amsterdam/New York/Oxford: North-Holland.

Kabsch, W. (1988*a*). *Automatic indexing of rotation diffraction patterns*. *J. Appl. Cryst*. **21**, 67–71.

Kabsch, W. (1988*b*). *Evaluation of single-crystal X-ray diffraction data from a position-sensitive detector*. *J. Appl. Cryst*. **21**, 916–924.

Kabsch, W. (1993). *Automatic processing of rotation diffraction data from crystals of initially unknown symmetry and cell constants*. *J. Appl. Cryst*. **26**, 795–800.

Kahn, R., Fourme, R., Bosshard, R., Chaimdi, M., Risler, J. L., Dideberg, O. & Wery, J. P. (1985). *Crystal structure study of Opsanus tau parvalbumin by multiwavelength anomalous diffraction*. *FEBS Lett*. **179**, 133–137.

Kennard, C. H. L. (1994). *Direct observation of a crystal during X-ray data collection using a macroscope*. *J. Appl. Cryst*. **27**, 668–669.

Kim, S. (1989). *Auto-indexing oscillation photographs*. *J. Appl. Cryst*. **22**, 53–60.

King, M. V. (1954). *An efficient method for mounting wet protein crystals for X-ray studies*. *Acta Cryst*. **7**, 601–602.

Klug, H. P. & Alexander, L. E. (1954). *X-ray diffractometer procedures for polycrystalline and amorphous materials*. New York: John Wiley.

Kottke, T. & Stalke, D. (1993). *Crystal handling at low temperatures*. *J. Appl. Cryst*. **26**, 616–619.

Kroeger, K. S. & Kundrot, C. E. (1994). *A gas cell for collecting X-ray diffraction data from proteins*. *J. Appl. Cryst*. **27**, 609–612.

Kulpe, S. (1963). *Instrument for setting single crystals from X-ray oscillation photographs*. *Acta Cryst*. **16**, 837–838.

Kulpe, S. & Dornberger-Schiff, K. (1965). *A special application of the crystal setter*. *Acta Cryst*. **18**, 812–813.

Kundrot, C. E. & Richards, F. M. (1986). *Collection and processing of X-ray diffraction data from protein crystals at high pressure*. *J. Appl. Cryst*. **19**, 208–213.

Lange, B. A. & Haendler, H. M. (1972). *A capillary support apparatus for use in glove bags and dry boxes*. *J. Appl. Cryst*. **5**, 310.

Lange, G., Lewis, S. J., Murshudov, G. N., Dodson, G. G., Moody, P. C. E., Turkenburg, J. P., Barclay, A. N. & Brady, R. L. (1994). *Crystal structure of an extracellular fragment of the rat CD4 receptor containing domains 3 and 4*. *Structure*, **2**, 469–481.

Laugier, J. & Filhol, A. (1983). *An interactive program for the interpretation and simulation of Laue patterns*. *J. Appl. Cryst*. **16**, 281–283.

Leszczynski, M., Podlasin, S. & Suski, T. (1993). *A 10^9 Pa high-pressure cell for X-ray and optical measurements*. *J. Appl. Cryst*. **26**, 1–4.

3.4 (*cont.*)

Lindley, P., Najmudin, S., Bateman, O., Slingsby, S., Myles, D., Kumaraswamy, S. & Glover, I. (1993). *Structure of bovine γB-crystallin at 150 K. J. Chem. Soc. Faraday Trans.* **89**, 2677–2682.

Lindley, P. F. (1988). *Crystallographic studies of biological macromolecules using synchrotron radiation. Chemical crystallography with pulsed neutrons and synchrotron X-rays*, edited by M. A. Carrondo & G. A. Jeffrey, pp. 509–536. Dordrecht: Reidel.

Lippman, R. & Rudman, R. (1976). *A mechanically refrigerated gas stream (to −120° C) and some useful accessories. J. Appl. Cryst.* **9**, 220–222.

Lorenz, G., Neder, R. B., Marxreiter, J., Frey, F. & Schneider, J. (1993). *A mirror furnace for neutron diffraction up to 2300 K. J. Appl. Cryst.* **26**, 632–635.

Machin, K. J., Begg, G. S. & Isaacs, N. W. (1984). *A low-temperature cooler for protein crystallography. J. Appl. Cryst.* **17**, 358–359.

McKinstry, H. A. (1970). *Low thermal gradient high-temperature furnace for X-ray diffraction. J. Appl. Phys.* **41**, 5074–5079.

McMurdie, H. F., Morris, M. C., Evans, E. H., Paretzkin, B. & Wong-Ng, W. (1986). *Methods of producing standard X-ray diffraction powder patterns. Powder Diffr.* **1**, 40–43.

Malinowski, M. (1987). *A diamond high-pressure cell for X-ray diffraction on a single crystal. J. Appl. Cryst.* **20**, 379–382.

Marsh, D. J. & Petsko, G. A. (1973). *A low-temperature device for protein crystallography. J. Appl. Cryst.* **6**, 76–80.

Messerschmidt, A. & Pflugrath, J. (1987). *Crystal orientation and X-ray pattern prediction routines for area-detector diffractometer systems in macromolecular crystallography. J. Appl. Cryst.* **20**, 306–315.

Miyata, T., Ishizawa, N., Minato, I. & Iwai, S. (1979). *Gas-flame heating equipment providing temperatures up to 2600 K for the four-circle diffractometer. J. Appl. Cryst.* **12**, 303–305.

Moews, P. C., Sakamaki, T. & Knox, J. R. (1986). *Interactive graphics for rapid indexing of oscillation films from large unit cells. J. Appl. Cryst.* **19**, 101–104.

Moret, R. & Dallé, D. (1994). *A novel X-ray precession goniometer for use with stationary single crystals in special environments. Adaptation of a closed-cycle refrigerator. J. Appl. Cryst.* **27**, 637–646.

Munshi, S. K. & Murthy, M. R. N. (1986). *Strategies for collecting screen-less oscillation data. J. Appl. Cryst.* **19**, 61–62.

Narayana, S. V. L., Weininger, M. S., Heuss, K. L. & Argos, P. (1982). *A method to increase protein-crystal lifetime during X-ray exposure. J. Appl. Cryst.* **15**, 571–573.

Nave, C. (1995). *Radiation damage in protein crystallography*. In *Radiation physics & chemistry*, edited by P. Barnes. Oxford: Pergamon.

Neder, R. B., Frey, F. & Schulz, H. (1990). *Defect structure of zirconia ($Zr_{0.85}Ca_{0.15}O_{1.85}$) at 290 and 1550 K. Acta Cryst.* A**46**, 799–809.

Nieman, H. F., Evans, J. C., Heal, K. M. & Powell, B. M. (1984). *A technique for the preparation of low-temperature powder samples of noxious materials. J. Appl. Cryst.* **17**, 372.

North, A. C. T., Phillips, D. C. & Mathews, F. S. (1968). *A semi-empirical method of absorption correction. Acta Cryst.* A**24**, 351–359.

Okazaki, A. & Soejima, Y. (1986). *Goniometer-head attachments for crystal characterization in Weissenberg or precession geometry. J. Appl. Cryst.* **19**, 412–413.

Peterson, R. C. (1992). *A flame-heated gas-flow furnace for single-crystal X-ray diffraction. J. Appl. Cryst.* **25**, 545–548.

Petsko, G. A. (1985). *Flow cell construction and use. Methods in enzymology*, Vol. 114, pp. 141–145. New York: Academic Press.

Phillips, G. N. Jr (1985). *Crystallisation in capillary tubes. Methods in enzymology*, Vol. 114, pp. 128–131. New York: Academic Press.

Pickford, M. G., Garman, E. F., Jones, E. Y. & Stuart, D. I. (1993). *A design of crystal mounting cell that allows the controlled variation of humidity at the protein crystal during X-ray diffraction. J. Appl. Cryst.* **26**, 465–466.

Przybylska, M. (1988) *A novel method of mounting a protein crystal on a surface perpendicular to the X-ray capillary. J. Appl. Cryst.* **21**, 272–273.

Puxley, D. C., Squire, G. D. & Bates, D. R. (1994). *A new cell for in situ X-ray diffraction studies of catalysts and other materials under reactive gas atmospheres. J. Appl. Cryst.* **27**, 585–594.

Rao, Ch. P. (1989). *Easy and economic ways of handling air-sensitive crystals for X-ray diffraction studies. J. Appl. Cryst.* **22**, 182–183.

Rasmussen, B. F., Stock, A. M., Ringe, D. & Petsko, G. A. (1992). *Crystalline ribonuclease A loses function below the dynamical transition at 220 K. Nature (London)*, **357**, 423–424.

Rayment, I. (1985). *Treatment and manipulation of crystals. Methods in enzymology*, Vol. 114, pp. 136–140. New York: Academic Press.

Rayment, I., Johnson, J. E. & Suck, D. (1977). *A method of preventing crystal slippage in macromolecular crystallography. J. Appl. Cryst.* **10**, 365.

Reider, M. (1975). *Precession photography: orientating crystals by means of the stereographic projection. J. Appl. Cryst.* **8**, 388–389.

Rink, W. J., Mathias, H. G. & Schlenoff, J. B. (1994). *Hermetic sample housing for X-ray diffraction studies. J. Appl. Cryst.* **27**, 666–668.

Riquet, J. P. & Bonnet, R. (1979). *Dépouillement par ordinator des clichés de diffraction obtenus par la méthode de Laue. J. Appl. Cryst.* **12**, 39–41.

Rossi, F. A. (1989). *Permanent cooling of protein crystals by a collinear air flow. J. Appl. Cryst.* **22**, 620–622.

Rossmann, M. G. & Erickson, J. W. (1983). *Oscillation photography of radiation-sensitive crystals using a synchrotron source. J. Appl. Cryst.* **16**, 629–636.

Rudman, R. (1976). *Low-temperature X-ray diffraction: apparatus and techniques*, Chap. 6, pp. 161–179. New York/London: Plenum.

Sarma, R., McKeever, B., Gallo, R. & Scuderi, J. (1986). *A new method for determination of the crystal setting matrix for interpreting oscillation photographs. J. Appl. Cryst.* **19**, 482–484.

Sato, M., Yamamoto, M., Imada, K., Katsube, Y., Tanaka, N. & Higashi, T. (1992). *A high-speed data-collection system for large-unit-cell crystals using an Imaging Plate as a detector. J. Appl. Cryst.* **25**, 348–357.

Schiller, C. (1985). *Precise orientation of semiconductor surfaces by the back-reflection Laue technique. J. Appl. Cryst.* **18**, 373.

Shaham, H. (1982). *A goniometer for large single crystals. J. Appl. Cryst.* **15**, 469.

Sparks, R. A. (1976). *Crystallographic computing techniques*, edited by F. R. Ahmed, K. Huml & B. Sedlcek, pp. 452–467. Copenhagen: Munksgaard.

3.4 (*cont.*)

Sparks, R. A. (1982). *Computational crystallography*, edited by D. Sayre, pp. 1–18. Oxford University Press.

Stout, G. H. & Jensen, L. H. (1968). *X-ray structure determination: a practical guide*, Chap. 4, pp. 71–79. London: Macmillan.

Suh, I.-H., Suh, J.-M., Ko, T.-S., Aoki, K. & Yamazaki, H. (1988). *Rationale of a quick adjustment method for crystal orientation in oscillation photography*. *J. Appl. Cryst.* **21**, 521–523.

Swanson, D. K. & Prewitt, C. T. (1986). *A new radiative single-crystal diffractometer microfurnace incorporating MgO as a high-temperature cement and internal temperature calibrant*. *J. Appl. Cryst.* **19**, 1–6.

Tarling, S. E., Barnes, P. & Mackay, A. L. (1984). *Simulation of industrial furnacing with powder X-ray diffraction*. *J. Appl. Cryst.* **17**, 96–99.

Teeter, M. M., Roe, S. M. & Heo, N. H. (1993). *Atomic resolution (0.83 Å) crystal structure of the hydrophobic protein crambin at 130 K*. *J. Mol. Biol.* **230**, 292–311.

Teng, T. Y. (1990). *Mounting of crystals for macromolecular crystallography in a free-standing thin film*. *J. Appl. Cryst.* **23**, 387–391.

Tilton, R. F. Jr (1988). *A fixture for X-ray crystallographic studies of biomolecules under high gas pressure*. *J. Appl. Cryst.* **21**, 4–9.

Tilton, R. F. Jr, Dewan, J. C. & Petsko, G. A. (1992). *Effects of temperature on protein structure and dynamics: X-ray crystallographic studies of the protein ribonuclease-A at nine different temperatures from 98 to 320 K*. *Biochemistry*, **31**, 2469–2481.

Toyoshima, N., Hoya, H. & Ohshima, K.-I. (1991). *A simple device for mounting a vacuum chamber on a four-circle diffractometer with central χ circle*. *J. Appl. Cryst.* **24**, 1074–1075.

Tsukimura, K., Sato-Sorensen, Y. & Ghose, S. (1989). *A gas-flow furnace for X-ray crystallography*. *J. Appl. Cryst.* **22**, 401–405.

Usha, R., Johnson, J. E., Moras, D., Thierry, J. C., Fourme, R. & Kahn, R. (1984). *Macromolecular crystallography with synchrotron radiation: collection and processing of data from crystals with a very large unit cell*. *J. Appl. Cryst.* **17**, 147–153.

Vriend, G. & Rossmann, M. G. (1987). *Determination of the orientation of a randomly placed crystal from a single oscillation photograph*. *J. Appl. Cryst.* **20**, 338–343.

Vriend, G., Rossmann, M. G., Arnold, E., Luo, M., Griffith, J. P. & Moffat, K. (1986). *Post-refinement of oscillation diffraction data collected at a synchrotron radiation source*. *J. Appl. Cryst.* **19**, 134–139.

Watenpaugh, K. D. (1991). *Macromolecular crystallography at cryogenic temperatures*. *Curr. Opin. Struct. Biol.* **1**, 1012–1015.

Wood, R. A., Tode, G. E. & Welberry, T. R. (1985). *A lathe-like crystal grinder for grinding pre-aligned crystals into cylindrical cross section*. *J. Appl. Cryst.* **18**, 371–372.

Wyckoff, H. W., Doscher, M. S., Tsernoglou, D., Inagami, T., Johnson, L. N., Hardman, K. D., Allewell, N. M., Kelley, D. M. & Richards, F. M. (1967). *Design of a diffractometer and flowcell system for X-ray analysis of crystalline proteins with applications to the crystal chemistry of ribonuclease-S*. *J. Mol. Biol.* **27**, 563–578.

Xuong, Ng. H., Nielsen, C., Hamlin, R. & Anderson, D. (1985). *Strategy for data collection from protein crystals using a multiwire counter area detector diffractometer*. *J. Appl. Cryst.* **18**, 342–350.

Young, A. C. M., Dewan, J. C., Nave, C. & Tilton, R. F. (1993). *Comparison of radiation-induced decay and structure refinement from X-ray data collected from lysozyme crystals at low and ambient temperatures*. *J. Appl. Cryst.* **26**, 309–319.

Zaloga, G. & Sarma, R. (1974). *New method for extending the diffraction patterns from protein crystals and preventing their radiation damage*. *Nature (London)*, **251**, 551–552.

Zeppezauer, M., Eklund, H. & Zeppezauer, E. S. (1968). *Micro diffusion cells for the growth of single protein crystals by means of equilibrium dialysis*. *Arch. Biochem. Biophys.* **126**, 564–573.

Zhang, X.-J. & Matthews, B. W. (1993). *STRAT: a program to optimize data collection on an area detector system*. *J. Appl. Cryst.* **26**, 457–462.

Zobel, D. & Luger, P. (1990). *A small 50 K device for a quarter-circle Eulerian cradle diffractometer*. *J. Appl. Cryst.* **23**, 175–179

3.5

Alani, R., Harper, R. G. & Swann, P. R. (1992). *Ion thinning of TEM cross sections under beam switching control*. *Proc. EMSA*, pp. 394–395. Baton Rouge: Claitor.

Alani, R. & Swann, P. R. (1990). *Workshop on specimen preparation for transmission electron microscopy of materials*. Materials Research Society, Vol. 199, p. 85.

Alani, R. & Swann, P. R. (1992). *Precision ion polishing system – a new instrument for TEM specimen preparation of materials*. *Mater. Res. Soc. Symp.* **254**, 43–63.

Amelinckx, S. (1964). *The direct observation of dislocations*. New York: Academic Press.

Bach, H. (1964). *Elektronenmikroskopische Durchstrahlungs-aufnahmen und Feinbereichselektronenbeugung an Al_2O_3 Keramik*. *BOSCH Techn. Ber.* **1**, 10–13.

Bach, H. (1970). *Application of ion sputtering in preparing glasses and their surface layers for electron microscope investigations*. *J. Non-Cryst. Solids*, **3**, 1–32.

Banerjee, D. & Williams, J. C. (1983). *The effect of foil preparation technique on interface phase formation in Ti alloys*. *Scr. Metall.* **17**, 1125.

Barber, D. J. (1970). *Thin foils of non-metals made for electron microscopy by sputter-etching*. *J. Mater. Sci.* **5**, 1–8.

Barber, D. J. & Evans, R. G. (1970). *Dislocations, ordering and antiferromagnetic domains in MnO*. *Proc. EMSA*, pp. 522–523. Baton Rouge: Claitor.

Barber, D. J. & Farabaugh, E. N. (1965). *Dislocations and stacking faults in rutile crystals grown by flame fusion methods*. *J. Appl. Phys.* **36**, 2803–2806.

Barber, D. J. & Tighe, N. J. (1965). *Electron microscopy and diffraction of synthetic corundum crystals. I. Pure aluminum oxide grown by the Verneuil process*. *Philos. Mag.* **11**, 495–512.

Braillon, P., Mughier, J. & Serughetti, J. (1974). *Transmission electron microscope observations of dislocations in calcite single crystals*. *Cryst. Lattice Defects*, **5**, 73–78.

Butler, E. P. & Hale, K. F. (1981). *Dynamic experiments in the electron microscope*. Amsterdam: North-Holland.

Cox, A. R. & Mountfield, M. J. (1967). *Specimen temperatures during electropolishing of thin films for electron microscopy*. *J. Instrum. Methods*, **95**, 347–349.

3.5 (*cont.*)

Dana, E. S. & Ford, W. E. (1922). *A textbook on mineralogy*. New York: John Wiley.

Drum, C. M. (1965). *Electron microscopy of dislocations and other defects in sapphire and in silicon carbide thinned by sputtering*. *Phys. Status Solidi*, **9**, 635–642.

Edington, J. W. (1976). *Practical electron microscopy in materials science*, Vols. 1–3. London: Macmillan.

Fryer, J. R. (1987). *The effect of dose rate on imaging aromatic organic crystals*. *Ultramicroscopy*, **23**, 321–328.

Fryer, J. R. (1994). *Electron microscopy of polymeric phthalocyanines*. *MSA Bull*. **24**, 521–526.

Fryer, J. R. & Ewins, C. (1992). *Epitaxial growth of thin films of perylene*. *Philos. Mag*. A**66**, 889–898.

Fryer, J. R. & Holland, F. M. (1984). *High resolution electron microscopy of molecular crystals. III. Radiation damage processes at room temperature*. *Proc. R. Soc. London Ser A*, **393**, 352–369.

Fryer, J. R., McConnell, C. H., Dorset, D. L., Zemlin, F. & Zeitler, E. (1997). *High resolution electron microscopy of molecular crystals. IV. Paraffins and their solid solutions*. *Proc. R. Soc. London*, A**453**, 1929–1946.

Fryer, J. R., McConnell, C. H., Grant, G. A., Hann, R. A., Eyres, B. L. & Gupta, S. K. (1991). *The structure of some Langmuir–Blodgett films. II. Aromatic polar molecules*. *Philos. Mag*. B**63**, 1193–1200.

Fryer, J. R., McConnell, C. H., Hann, R. A., Eyres, B. L. & Gupta, S. K. (1990). *The structure of some Langmuir–Blodgett films. I. Substituted phthalocyanines*. *Philos. Mag*. B**61**, 843–852.

Fryer, J. R., McConnell, C. H., Zemlin, F. & Dorset, D. L. (1992). *The effect of temperature on radiation damage to aromatic organic molecules*. *Ultramicroscopy*, **40**, 163–169.

Fryer, J. R. & Smith, D. J. (1982). *High resolution electron microscopy of molecular crystals. I. Quaterrylene*. *Proc. R. Soc London Ser. A*, **381**, 225–240.

Goodhew, P. J. (1972). *Specimen preparation in materials science*. *Practical methods in electron microscopy*, edited by A. M. Glauert, pp. 3–180. Amsterdam: North-Holland.

Goodhew, P. J. (1975). *Specimen preparation in materials science*. In *Electron microscopy and analysis*. Vol. 1, Part 1. London: Wykeham Publications; New York: Springer Verlag.

Goodhew, P. J. (1984). *Specimen preparation for transmission electron microscopy of materials*. *Royal Microscopy Society Handbook*. Oxford: Royal Microscopy Society.

Goodhew, P. J. (1993). *Preparation of plan view and cross-sectional specimens for TEM*. *Proc. EMSA*, edited by G. W. Bailey & C. L. Rieder. San Francisco Press.

Hirsch, P. B., Howie, A., Nicholson, R. B., Pashley, D. W. & Whelan, M. J. (1965). *Electron microscopy of thin crystals*. London: Butterworth.

Hobbs, L. W. (1970). *Preparation of thin films of moisture sensitive crystals for transmission electron microscopy*. *J. Phys. E*, **3**, 85–89.

Honess, A. P. (1927). *The nature, origin and interpretation of the etch figures on crystals*. New York: John Wiley.

Jansen, J. & Zeedijk, H. B. (1972). *Deformation layers in spark-machined and mechanically sectioned specimens of 0.2% mild steel*. *J. Phys. E*, **5**, 973–975.

Keast, D. J. (1967). *A chemical thinning technique for the simultaneous preparation of foils for transmission electron microscopy. Application to yttrium aluminum garnet (YAG)*. *J. Sci. Instrum.* **44**, 862–863.

Kirkpatrick, H. B. & Amelinckx, S. (1962). *Device for chemically thinning crystals for transmission electron microscopy*. *Rev. Sci. Instrum*. **33**, 488–489.

Lewis, M. H. (1966). *Defects in spinel crystals grown by the Verneuil process*. *Philos. Mag*. **14**, 1003–1008.

Metals Handbook (1985). Metals Park, Ohio. American Society for metals.

Morris, P. L., Davies, N. C. & Treverton, J. A. (1978). *Effects of a surface film upon thin foil microanalysis*. In *Developments in electron microscopy and analysis 1977*, edited by D. L. Misell. *Inst. Phys. Conf. Ser*. No. 36, pp. 377–380.

Paulus, M. & Reverchon, F. (1961). *Dispositif de bombardement inonique pour préparations micrographiques*. *J. Phys. Radium*, **22**, 103A–107A.

Penneycook, S. J. (1981). *Quantitative microanalysis with high spatial resolution*. Book 277. London: The Metals Society.

Penneycook, S. J. (1982). *High resolution electron microscopy and microanalysis*. *Contemp. Phys*. **23**, 371.

Pennock, G. M., Flower, H. M. & West, D. R. F. (1977). *The thinning transformation in Ti–Mo alloys*. *Metallography*, **10**, 43.

Porat, Z., Fryer, J. R., Huxham, M. & Rubinstein, I. (1995). *Electron microscope investigation of the microstructure of Nafion films*. *J. Phys. Chem*. **99**, 4667–71.

Remaut, G., Lagasse, A. & Amelinckx, S. (1964). *Electron microscope study of the domain structure in anti-ferromagnetic cobalteous oxide*. *Phys. Status Solidi*, **5**, 497–510.

Thomas, G. (1962). *Transmission electron microscopy of metals*. New York: John Wiley.

Tighe, N. J. (1964). *Jet thinning device for preparation of Al_2O_3 electron microscopy specimens*. *Rev. Sci. Instrum*. **35**, 520–521.

Tighe, N. J. (1976). *Experimental techniques*. *Electron microscopy in mineralogy*, pp. 144–174. New York: Springer Verlag.

Tighe, N. J. (1983). *Analysis of oxide and oxide/matrix interfaces in silicon nitride*. *Adv. Ceram*. **6**, 151–162.

Tighe, N. J. & Hyman, A. (1968). *Transmission electron microscopy of alumina ceramics*. In *Anisotropy in single crystal refractory compounds*, Vol. 2, edited by E. W. Vahldick & S. A. Mersol. New York: Plenum.

Washburn, J., Groves, G. W., Kelly, A. & Williamson, G. K. (1960). *Electron microscope observations of deformed magnesium oxide*. *Philos. Mag*. **5**, 991–999.

West, J. M. (1970). *Application of potentiostats in corrosion science*. *Br. Corros. J*. **5**, 65–71.

Wicks, B. J. & Lewis, M. H. (1968). *Direct observations of ferroelectric domains in lithium niobate*. *Phys. Status Solidi*, **26**, 571–576.

Wittmann, J. C. & Lotz, B. (1990). *Epitaxial crystal growth on organic and polymeric substrates*. *Electron Crystallography of Organic Molecules*, edited by J. R. Fryer & D. L. Dorset, pp. 241–254. Dordrecht: Kluwer Academic Publishers.

Zvyagin, B. B. (1967). *Electron diffraction analysis of clay mineral structures*. New York: Plenum.

3.6

Bacon, G. E. (1987). *Some statistics from the Neutron Diffraction Commission of the IUCr. Fifty years of neutron diffraction*, Chap. 6. London: Adam Hilger.

International Tables for Crystallography (1992). Vol. B. Dordrecht: Kluwer Academic Publishers.

4.1. Radiations used in crystallography

By V. Valvoda

4.1.1. Introduction

The radiations used in crystallography are either electromagnetic waves or beams of particles. The choice of radiation depends on the type of crystallographic information needed. The most general tool for obtaining any crystallographic information is diffraction but other types of scattering or reflection and absorption phenomena are also used in *general* crystallography (see Fig. 4.1.1.1).

4.1.2. Electromagnetic waves and particles

Both electromagnetic waves and particles can be described by the wavefunction $\psi(\mathbf{r})$, as a complex function of spatial coordinates, by the wavelength λ, the wavevector $\mathbf{k}$, which indicates the direction of propagation and is of magnitude $2\pi/\lambda$, the frequency ν or angular frequency ω in rad s^{-1}, and the phase velocity v (and the group velocity). Intensity in $\mathbf{r}$ is given by $|\psi(\mathbf{r})|^2$. These wavefunctions are solutions of the same type of differential equation [see, for example, Cowley (1975)]:

$$\nabla^2\psi + k^2\psi = 0. \tag{4.1.2.1}$$

For electromagnetic waves,

$$k^2 = \varepsilon\mu\omega^2 = \omega^2/v^2, \tag{4.1.2.2}$$

where k is the wavenumber, ε is the permittivity or dielectric constant and μ is the magnetic permeability of the medium; $\mu \approx 1$ for most cases. The velocity of the waves in free space is $c = 1/(\varepsilon_0\mu_0)^{1/2}$; otherwise $v = c/n$, where $n = (\varepsilon/\varepsilon_0)^{1/2}$ is the refraction index.

For particles of mass m and charge q with kinetic energy E_k in field-free space, the wave equation (4.1.2.1) is the time-independent Schrödinger equation and

$$k^2 = \frac{8\pi^2 m}{h^2}\{E_k + q\mathscr{S}(\mathbf{r})\}, \tag{4.1.2.3}$$

where $\mathscr{S}(\mathbf{r})$ is the electrostatic potential function and the bracket gives the sum of the kinetic and potential energies of the particles.

Important nontrivial solutions of (4.1.2.1) are (after adding the time dependence) the plane wavefunctions

$$\psi = \psi_0 \exp\{i(\omega t - \mathbf{k}\cdot\mathbf{r})\} \tag{4.1.2.4}$$

or the spherical wavefunctions

$$\psi = \psi_0 \frac{\exp\{i(\omega t - kr)\}}{r}. \tag{4.1.2.5}$$

Thus, relatively simple semi-classical wave mechanics, rather than full quantum mechanics, is needed for interactions with no appreciable loss of energy. The interaction of the waves with matter depends on the spatial variation of the refractive index given by the spatial variations of the electron density or the electrostatic potential functions.

Electromagnetic waves can also be described in terms of energy quanta, photons, with energy given by Planck's law

$$E = h\nu. \tag{4.1.2.6}$$

The values of E, ν, and λ of the electromagnetic waves used in general crystallography are scaled in Fig. 4.1.2.1. It should be noted that there are several types of electromagnetic waves in the most important wavelength range near 1 Å, which are called X-rays (when generated in X-ray tubes), γ-rays (when emitted by radioactive isotopes) or synchrotron radiation (emitted by electrons moving in a circular orbit).

On the other hand, the beam of particles of mass m, moving with velocity v, behaves like waves with wavelength given by de Broglie's law

$$\lambda = \frac{h}{mv} \tag{4.1.2.7}$$

or using $E_k = \frac{1}{2}mv^2$ for the kinetic energy of particles

$$\lambda = \frac{h}{(2mE_k)^{1/2}}. \tag{4.1.2.8}$$

When relativistic effects are taken into account,

$$\lambda = \lambda_0\left\{1 + \frac{E_k}{2m_0c^2}\right\}^{-1/2}, \tag{4.1.2.9}$$

where m_0 is the rest mass and λ_0 the non-relativistic wavelength. High-energy electrons ($E_k \approx 10^5$ eV, $\lambda \approx 10^{-2}$ Å) and neutrons ($E_k \approx 10^{-2}$ eV, $\lambda \approx 10^0$ Å) belong to the most prominent particles used in diffraction crystallography (see Table 4.1.3.1). However, low-energy electrons ($E_k \approx 10^2$ eV,

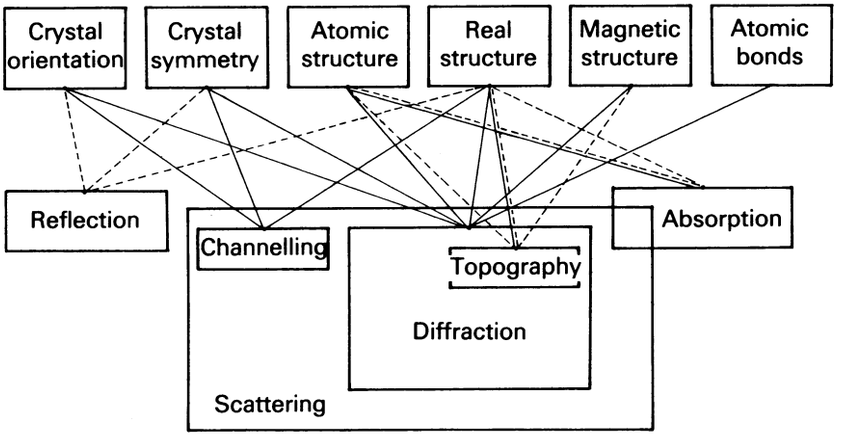

Fig. 4.1.1.1. Schematic diagram of the main types of radiation application in crystallography (dashed lines represent structure investigation on a larger than atomic scale).

Copyright © 2006 International Union of Crystallography

$\lambda \approx 10^0$ Å), protons or ions of elements with quite high atomic number and energy ($E_k \approx 10^3 - 10^6$ eV) are also used in scattering, channelling or shadowing experiments (see Section 4.1.5).

4.1.3. Most frequently used radiations

Average diffraction properties of X-rays, high-energy electrons, and neutrons are listed in Table 4.1.3.1. They can be varied with respect to the material analysed by changing the incident-beam operating conditions and they also greatly depend on the mutal interaction of radiation with the material. The values presented are typical rather than extreme ones and should be used as a guide for rough estimates and for general orientation in the subject. Details are given in the following sections. The properties of the radiations and the features of their interaction with crystals also impose limitations on the sample choice or preparation, on the recording of the diffraction data, and on the theoretical interpretation of these data. The different nature of the scattering of X-rays and electrons (interacting with the electron-density distribution or with the potential distribution) and neutrons (which are mainly scattered by nuclei) may be used in combined experiments to study details of thermal smearing of atomic positions and bonding characteristics of the electron-density distribution.

Table 4.1.3.1. *Average diffraction properties of X-rays, electrons, and neutrons*

	X-rays	Electrons	Neutrons
(1) Charge	0	-1 e	0
(2) Rest mass	0	9.11×10^{-31} kg	1.67×10^{-27} kg
(3) Energy	10 keV	100 keV	0.03 eV
(4) Wavelength	1.5 Å	0.04 Å	1.2 Å
(5) Bragg angles	Large	1°	Large
(6) Extinction length	10 μm	0.03 μm	100 μm
(7) Absorption length	100 μm	1 μm	5 cm
(8) Width of rocking curve	5"	0.6°	0.5"
(9) Refractive index	$n < 1$	$n > 1$	$n \lesssim 1$
$n = 1 + \delta$	$\delta \approx -1 \times 10^{-5}$	$\delta \approx +1 \times 10^{-4}$	$\delta \approx \mp 1 \times 10^{-6}$
(10) Atomic scattering amplitudes f	10^{-3} Å	10 Å	10^{-4} Å
(11) Dependence of f on the atomic number Z	$\sim Z$	$\sim Z^{2/3}$	Nonmonotonic
(12) Anomalous dispersion	Common	–	Rare
(13) Spectral breadth	1 eV $\Delta\lambda/\lambda \approx 10^{-4}$	3 eV $\Delta\lambda/\lambda \approx 10^{-5}$	500 eV $\Delta\lambda/\lambda \approx 2$

Notes to Table 4.1.3.1

(1) *Charge*. Charged electrons interact strongly with matter and must be used in vacuum whereas X-rays and neutrons can be used in air.

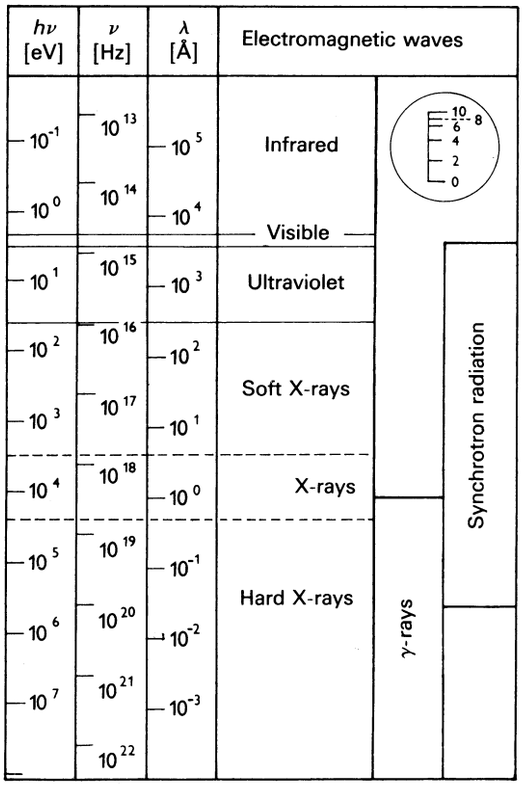

Fig. 4.1.2.1. Comparison of the energy, frequency, and wavelength of the electromagnetic waves used in crystallography (logarithmic scale).

(2) *Rest mass*. The wavelength of moving particles with the same energy is inversely proportional to the square root of their mass.

(3) *Energy*: Energies of X-rays generated in commonly used X-ray tubes range from 5 to 17 keV. High-energy electrons used in electron microscopes have energies from 40 to 300 keV, but energies of 1 MeV or more are achievable (for low-energy electrons, see Subsection 4.1.4.2). The extremely low energy of neutrons as compared with X-rays or electrons leads to their strong inelastic interaction with phonons (see Subsection 4.1.4.3).

(4) *Wavelength*. The radius of the Ewald sphere for electrons is much larger than that for X-rays or neutrons and thus part of the reciprocal-lattice plane image can be seen immediately if fixed-crystal electron diffraction is used. Wavelengths of electrons and neutrons are tunable by changing instrumental conditions (high voltage in the microscope and the temperature inside the reactor, respectively) whereas X-ray wavelengths are given by discrete lines of the characteristic spectra of the X-ray tube targets (for other X-ray sources, see Subsection 4.1.4.1).

(5) *Bragg angles*. The whole observable diffraction pattern obtained by electrons is contracted into small angles not exceeding 3–5° with the primary beam.

(6) *Extinction length*. The extinction length corresponds to the thickness of the crystal required for the whole incident beam to be scattered into the Bragg reflected beam and then to be scattered back into the direction of the incident beam. If the size of a nearly perfect crystal (or the size of the mosaic blocks) is comparable to or exceeds the extinction length for the given reflection then the dynamic diffraction theory (or the primary-extinction correction of applied kinematic theory in

the case of the mosaic crystal) must be used. The dynamical effects thus decrease when passing from electrons to X-rays and neutrons for a given crystal thickness.

(7) *Absorption length*. Absorption length is here estimated by the reciprocal values of the linear absorption coefficients. The value of the absorption length determines the size of the sample or the surface layer thickness accessible for diffraction analysis. The penetration of the electron beam into the crystal is severely limited by absorption or by diffraction when a strong reflection is excited and thus only 10–1000 Å surface layers contribute to the electron diffraction. Owing to the Borrmann effect, there occurs a substantial decrease of X-ray absorption for nearly perfect crystals in diffraction position. The relatively large crystals used for neutron diffraction in order to obtain useful diffraction intensities have been found to cause particularly important secondary-extinction effects due to disorientation of the mosaic blocks.

(8) *Width of rocking curve*. The range of angles between a crystal plane and the diffracted beam over which there is significant Bragg reflection is much larger for electrons than for X-rays or neutrons.

(9) *Refractive index*. The refractive index deviates slightly from unity for the radiations compared and the angle of refraction thus makes only a few angular minutes and increases with increasing wavelength. Negative values of δ for neutrons correspond to positive values of atomic scattering amplitudes and *vice versa*. The refraction effects will be considerable for the small angles of incidence of electrons needed in the Bragg case of diffraction (see *Bragg angles*) and the waves diffracted from planes parallel to the surface having spacings as small as 2 or 3 Å may suffer total internal reflection and be unable to leave the crystal.

(10) *Atomic scattering amplitudes*. The example given corresponds to the scattering of the atoms of lead at $(\sin\theta)/\lambda = 0.4\,\text{Å}^{-1}$. The absolute values of the atomic scattering amplitudes for electrons are considerably greater than for X-rays or neutrons; this is also reflected in the structure-amplitude values and in the corresponding intensities of the Bragg reflections. For the angular dependence of the atomic scattering amplitudes, see Fig. 4.1.3.1. The constant value of the atomic scattering amplitudes for neutrons (also often called the scattering length) makes neutron diffraction suitable for precise measurement of thermal parameters.

(11) *Dependence of atomic scattering amplitudes on the atomic number Z*. This kind of dependence is illustrated for neutral atoms in Fig. 4.1.3.2. Because of the relatively weaker dependence on the atomic number, the peaks of light atoms in the presence of heavy atoms are revealed more clearly in the Fourier synthesis of electron-density maps obtained by the electron-diffraction method than by X-ray diffraction. The same is generally true for neutron diffraction, which also enables atoms of elements with similar atomic numbers to be distinguished in certain cases (based on the irregular change of atomic scattering amplitudes with Z); different isotopes of the same element may also be distinguished.

(12) *Anomalous dispersion*. This effect is utilized for the solution of the phase problem in crystal structure analysis by X-ray diffraction. In the case of neutron diffraction, there are only a few stable isotopes convenient for this purpose (mainly ^{149}Sm, ^{157}Gd, and ^{113}Cd). The wavelength of the high-energy electrons is too short compared with the K-absorption edges of atoms and the resonance scattering of electrons is thus negligible.

(13) *Spectral breadth*. The value for X-rays corresponds to the characteristic lines of X-ray spectra. The spread of energies or wavelengths in the beam of neutrons obtained from a reactor is quite broad and for diffraction experiments a narrow range of wavelengths is usually selected by the use of a crystal monochromator or, especially for long wavelengths, by a time-of-flight chopper device that selects a range of neutron velocities.

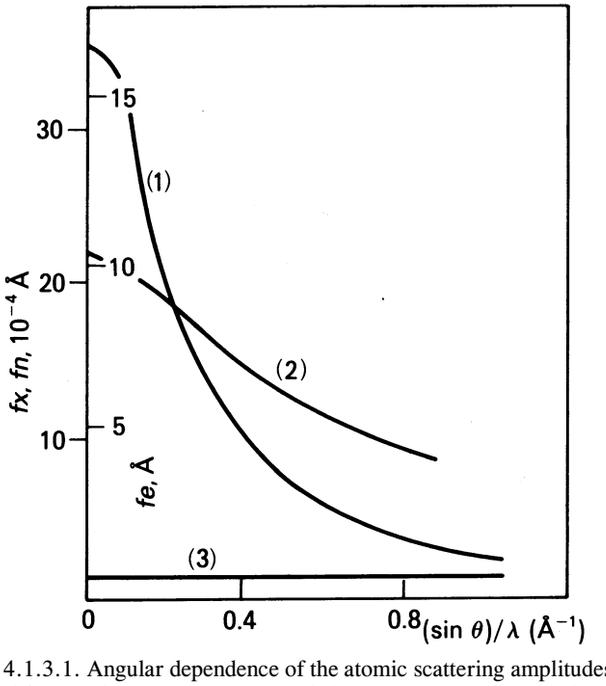

Fig. 4.1.3.1. Angular dependence of the atomic scattering amplitudes of lead for (1) electron, (2) X-ray, and (3) neutron scattering (in absolute values).

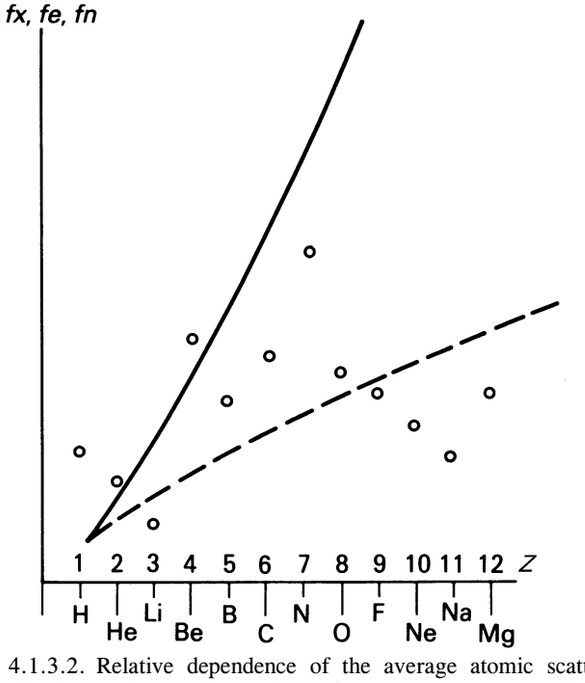

Fig. 4.1.3.2. Relative dependence of the average atomic scattering amplitudes on the atomic number Z for X-rays (———), electrons (— — —), and neutrons (○). The values plotted are averages over $(\sin\theta)/\lambda$.

4.1.4. Special applications of X-rays, electrons, and neutrons

Special sources and/or special properties of these radiations are used in general crystallography.

4.1.4.1. *X-rays, synchrotron radiation, and γ-rays*

X-ray beams from *rotating-anode tubes* are approximately one hundred times more intensive than those from normal X-ray tubes. *Laser plasma X-ray sources* yield intensive nanosecond pulses of the line spectrum of nearly electron-free ions in the X-ray region with a spectral breadth of $\Delta\lambda/\lambda \approx 10^{-3}$. Several such pulses may be repeated per hour (Frankel & Forsyth, 1979). *Synchrotron radiation* is characterized by a continuous spectrum of wavelengths, high spectral flux, high intensity, high brightness, extreme collimation, sharp time structure (pulses with 30–200 ps length emitted in ns intervals), and nearly 100% polarization in the orbital plane (Kuntz, 1979; Bonse, 1980). Some of these properties are utilized in ordinary structure analysis: for example, fine tuning of the wavelength of synchrotron radiation for the solution of the phase problem by resonant scattering on chosen atomic species constituting the material under study. But these radiations also offer new advantages in other fields of crystallography, as, for example, in X-ray topography (Tanner & Bowen, 1980), in time-resolving studies (Bordas, 1980), in X-ray microscopy (Parsons, 1980), in studies of local atomic arrangements by extended X-ray absorption fine structure (XAFS) investigations (Lee, Citrin, Eisenberger & Kincaid, 1981) or studies of surface structures by X-ray photoemission spectroscopy (XPS) (Plummer & Eberhardt, 1982), *etc*. *γ-rays* emitted by radioactive sources such as ^{198}Au ($t_{1/2} = 2.7$ d), ^{153}Sm ($t_{1/2} = 46.8$ h), ^{192}Ir ($t_{1/2} = 74.2$ d) or ^{137}Cs ($t_{1/2} = 29.9$ a) are characterized by short wavelengths (typically hundreds of Å), by narrow spectral breadth ($\Delta E \approx 10^{-8}$ eV, $\Delta\lambda/\lambda \approx 10^{-6}$) and by relatively low beam intensity ($\sim 10^8 - 10^9$ m^{-2} s^{-1}). They are mainly used for studies of the mosaic structure of single crystals (Schneider, 1983) or for the determination of charge density distribution (Hansen & Schneider, 1984). The typical absorption length of $\sim$ 1–4 cm and the increase of the extinction length by a factor of about 50 compared with ordinary X-rays are advantages utilized in these experiments. γ-rays also find applications in magnetic structure studies and in the determination of gradients of electric fields by Mössbauer diffraction and spectroscopy (Kuz'min, Kolpakov & Zhdanov, 1966).

For Compton scattering, see Sections 6.1.1 and 7.4.3.

4.1.4.2. *Electrons*

Low-energy electrons (10–200 eV) have wavelengths near 1 Å and a penetration of a few Å below the surface of a crystal. Low-energy electron diffraction (LEED) is thus used for the study of surface-layer structures (Ertl & Küppers, 1974). High-energy electrons are also currently used in electron microscopy in materials science. Under certain conditions, images of lattice planes with a resolution of 2 Å or better can be obtained. Transmission electron microscopy is also used for reconstruction of the three-dimensional structure of biological objects (such as viruses), alternatively in combination with X-ray diffraction (de Rossier & Klug, 1968).

4.1.4.3. *Neutrons*

The most important application of neutron diffraction is found in studies of magnetic structures (Marshall & Lovesey, 1971). The magnetic moment of neutrons is equal to $1.913\,\mu_N$, where μ_N is the nuclear magneton, and neutrons have spin $I = 1/2$. They can thus interact with the magnetic moments of nuclei or with the magnetic moments of the electron shells with uncompensated spins. Changes in wavelength from 1 to 30 Å enable one to study non-uniformities of different sizes and structures of polymers and biological objects by the small-angle method. Inelastic scattering of neutrons is used for determining phonon-dispersion curves. Neutron topography and neutron texture diffraction can be utilized for the relatively large samples used in technological applications. The *pulsed spallation neutron sources* are used for high-resolution time-of-flight powder diffraction (Windsor, 1981) or for time-resolved Laue diffraction.

4.1.5. Other radiations

4.1.5.1. *Atomic and molecular beams*

Fast charged particles like protons, deuterons or He^+ ions show preferential penetration through crystals when the direction of incidence is almost parallel to the prominent planes or axes of the lattice. The reverse effect of this *channelling* is *shadowing* when the centres of emission of the fast charged particles are the atoms of the crystal themselves. These methods are, for example, used in studies of surface structures, lattice defects, orientation, thermal vibrations, atomic displacements, and concentration profiles (Feldman, Mayer & Picraux, 1982). Ion beams are also applied in special analytical methods like Rutherford backscattering (RBS), inelastic scattering, proton-induced X-ray analysis (PIX), *etc*.

4.1.5.2. *Positrons and muons*

These elementary particles are used in crystallography mainly in studies of lattice defects (vacancies, interstitials, and impurity atoms) for the determination of their concentration, location, and diffusion by means of the techniques such as positron annihilation spectroscopy (PAS) and muon spin resonance (μSR) – see, for example, Siegel (1980) and Gyax, Kündig & Meier (1979). The positron implantation range in a solid is $\lesssim 100$ μm from the positron sources usually used (*e.g.* ^{22}Na, ^{64}Cu, ^{58}Co); these sources yield positrons with end-point energies of $\lesssim$1 MeV. The PAS techniques are based on lifetime, Doppler broadening or angular correlation measurements of γ-rays emitted by the decaying nucleus of the radioactive source and those resulting from the positron–electron annihilation process. Muon sources require intense primary medium-energy proton beams. The positive muon μ^+ has charge +e, spin 1/2, mass $105.659\,\mathrm{MeV}/c^2$ and a magnetic moment equal to 1.001 of the muon–magneton units. With a mean lifetime of 2.197 μs, the muon decays into a positron (e^+) and two neutrinos (ν_e and $\bar{\nu}_\mu$). The correlation between the direction of the emitted positron and the spin direction of the muon allows one to measure the spin precession frequency and/or the decay of the muon polarization of an ensemble of muons implanted in a solid.

4.1.5.3. *Infrared, visible, and ultraviolet light*

Visible light is one of the oldest tools used by crystallographers for macroscopic symmetry determination, for orientation of crystals, and in metallographic microscopes for phase analysis. Infrared and Raman spectroscopy are highly complementary methods in the infrared and visible range of wavelengths, respectively. The information content available with the two techniques is determined by molecular symmetry and polarity. This information is utilized for the identification of molecules or structural groups [symmetric

vibrations and nonpolar groups are most easily studied by Raman scattering, antisymmetric vibrations and polar groups by infrared scattering (Grasselli, Snavely & Bulkin, 1980)]. The valence states or the bonds of surface atoms and the local structure in the immediate neighbourhood of the chosen atoms can be studied by ultraviolet radiation in the energy range 10–50 eV by means of angle-resolved photoelectron emission (Plummer & Eberhardt, 1982).

4.1.5.4. *Radiofrequency and microwaves*

Electromagnetic waves of frequencies 10^6–10^{10} Hz are used in nuclear magnetic resonance (NMR) and electron paramagnetic resonance (EPR) experiments for studies of interatomic bonds, local atomic configurations, ordering, and relative population of atomic sites as well as for the determination of orientational features of magnetic structures (Kaufman & Shenoy, 1981).

International Tables for Crystallography (2006). Vol. C, Chapter 4.2, pp. 191–258.

4.2. X-rays

By U. W. Arndt, D. C. Creagh, R. D. Deslattes, J. H. Hubbell, P. Indelicato, E. G. Kessler Jr and E. Lindroth

4.2.1. Generation of X-rays (By U. W. Arndt)

X-rays are produced by the interaction of charged particles with an electromagnetic field. There are four sources of X-rays that are of interest to the crystallographer.

(1) The bombardment of a target by electrons produces a continuous ('white') X-ray spectrum, called *Bremsstrahlung*, which is accompanied by a number of discrete spectral lines characteristic of the target material. The high-vacuum, or Coolidge, X-ray tube is the most important X-ray source for crystallographic studies.

(2) The decay of natural or artificial radio isotopes is often accompanied by the emission of X-rays. Radioactive X-ray sources are often used for the calibration of X-ray detectors. Mössbauer sources have the narrowest known spectral bandwidth and are used in nuclear resonance scattering studies.

(3) Sources of synchrotron radiation produced by relativistic electrons in orbital motion are of growing importance.

(4) X-rays are also produced in plasmas generated by the bombardment of targets by high-energy laser beams, but to date the yield has been principally in the form of soft X-rays.

The classical text on the generation and properties of X-rays is that by Compton & Allison (1935), which still summarizes much of the information required by crystallographers. There is a more recent comprehensive book by Dyson (1973). X-ray physics has received a new impetus on the one hand through the development of X-ray microprobe analysis dealt with in a number of monographs (Reed, 1975; Scott & Love, 1983) and on the other hand through the increasing utilization of synchrotron-radiation sources (see Subsection 4.2.1.5).

4.2.1.1. *The characteristic line spectrum*

Characteristic X-ray emission originates from the radiative decay of electronically highly excited states of matter. We are concerned mostly with excitation by electron bombardment of a target that results in the emission of spectral lines characteristic of the target elements. The electronic states occurring as initial and final states of a process involving the absorption of emission of X-rays are called *X-ray levels*. Levels involving the removal of one electron from the configuration of the neutral ground state are called *normal X-ray levels* or *diagram levels*.

Table 4.2.1.1 shows the relation between diagram levels and electron configurations. The notation used here is the IUPAC notation (Jenkins, Manne, Robin & Senemaud, 1991), which uses arabic instead of the former roman subscripts for the levels. The IUPAC recommendations are to refer to X-ray lines by writing the initial and final levels separated by a hyphen, *e.g.* Cu K-L_3 and to abandon the Siegbahn (1925) notation, *e.g.* Cu $K\alpha_1$, which is based on the relative intensities of the lines. The correspondence between the two notations is shown in Table 4.2.1.2. Because this substitution has not yet become common practice, however, the Siegbahn notation is retained in Section 4.2.2, in which the wavelengths of the characteristic emission lines and absorption edges are discussed.

4.2.1.1.1. *The intensity of characteristic lines*

The efficiency of the production of characteristic radiation has been calculated by a number of authors (see, for example, Dyson, 1973, Chap. 3). For a particular line, it depends on the fluorescence yield, that is the probability that the decay of an excited state leads to the emission of a photon, on the statistical weights of the X-ray levels involved, on the effects of the penetration and slowing down of the bombarding electrons in the target, on the fraction of electrons back-scattered out of the target, and on the contribution caused by fluorescent X-rays produced indirectly by the continuous spectrum. The *emerging* X-ray intensity is further affected by the partial absorption of the generated X-rays in the target.

Dyson (1973) has also reviewed calculations and measurements made of the *relative* intensities of different lines in the K spectrum. The ratio of the $K\alpha_2$ to $K\alpha_3$ intensities is very close to

Table 4.2.1.1. *Correspondence between X-ray diagram levels and electron configurations; from Jenkins, Manne, Robin & Senemaud (1991), courtesy of IUPAC*

Level	Electron configuration	Level	Electron configuration	Level	Electron configuration
K	$1s^{-1}$	N_1	$4s^{-1}$	O_1	$5s^{-1}$
L_1	$2s^{-1}$	N_2	$4p_{1/2}^{-1}$	O_2	$5p_{1/2}^{-1}$
L_2	$2p_{1/2}^{-1}$	N_3	$4p_{3/2}^{-1}$	O_3	$5p_{3/2}^{-1}$
L_3	$2p_{3/2}^{-1}$	N_4	$4d_{3/2}^{-1}$	O_4	$5d_{3/2}^{-1}$
M_1	$3s^{-1}$	N_5	$4d_{5/2}^{-1}$	O_5	$5d_{5/2}^{-1}$
M_2	$3p_{1/2}^{-1}$	N_6	$4f_{5/2}^{-1}$	O_6	$5f_{5/2}^{-1}$
M_3	$3p_{3/2}^{-1}$	N_7	$4f_{7/2}^{-1}$	O_7	$5f_{7/2}^{-1}$
M_4	$3d_{3/2}^{-1}$				
M_5	$3d_{5/2}^{-1}$				

Table 4.2.1.2. *Correspondence between IUPAC and Siegbahn notations for X-ray diagram lines; from Jenkins, Manne, Robin & Senemaud (1991), courtesy of IUPAC*

Siegbahn	IUPAC	Siegbahn	IUPAC	Siegbahn	IUPAC
$K\alpha_1$	K-L_3	$L\alpha_1$	L_3-M_5	$L\gamma_1$	L_2-N_4
$K\alpha_2$	K-L_2	$L\alpha_2$	L_3-M_4	$L\gamma_2$	L_1-N_2
$K\beta_1^1$	K-M_3	$L\beta_1$	L_2-M_4	$L\gamma_3$	L_1-N_3
$K\beta_2^1$	K-N_3	$L\beta_2$	L_3-N_5	$L\gamma_4$	L_1-O_3
$K\beta_2^{11}$	K-N_2	$L\beta_3$	L_1-M_3	$L\gamma_4'$	L_1-O_2
$K\beta_3$	K-M_2	$L\beta_4$	L_1-M_2	$L\gamma_5$	L_2-N_1
$K\beta_4^1$	K-N_5	$L\beta_5$	L_3-$O_{4,5}$	$L\gamma_6$	L_2-O_4
$K\beta_4^{11}$	K-N_4	$L\beta_6$	L_3-N_1	$L\gamma_8$	L_2-O_1
$K\beta_{4x}$	K-N_4	$L\beta_7$	L_3-O_1	$L\gamma_8'$	L_2-$N_{6(7)}$
$K\beta_5^1$	K-M_5	$L\beta_7'$	L_3-$N_{6,7}$	L_η	L_2-M_1
$K\beta_5^{11}$	K-M_4	$L\beta_9$	L_1-M_5	Ll	L_3-M_1
		$L\beta_{10}$	L_1-M_4	Ls	L_3-M_3
		$L\beta_{15}$	L_3-N_4	Lt	L_3-M_2
		$L\beta_{17}$	L_2-M_3	Lu	L_3-$N_{6,7}$
				Lv	L_2-$N_{6(7)}$

Siegbahn	IUPAC
$M\alpha_1$	M_5-N_7
$M\alpha_2$	M_5-N_6
$M\beta$	M_4-N_6
$M\gamma$	M_3-N_5
$M\zeta$	$M_{4,5}$-$N_{2,3}$

In the case of unresolved lines, such as K-L_2 and K-L_3, the recommended IUPAC notation is K-$L_{2,3}$.

Copyright © 2006 International Union of Crystallography

0.5 for Z between 23 and 48. The ratio of $K\beta_3$ to $K\alpha_2$ rises fairly linearly with Z from 0.2 at $Z = 20$ to 0.4 at $Z = 80$ and that of $K\beta_1$ to $K\alpha_2$ is near zero at $Z = 29$ and rises linearly with Z to about 0.1 at $Z = 80$. Relative intensities of lines in the L spectrum are given by Goldberg (1961).

Green & Cosslett (1968) have made extensive measurements of the efficiency of the production of characteristic radiation for a number of targets and for a range of electron accelerating voltages. Their results can be expressed empirically in the form

$$N_K/4\pi = N_0/4\pi(E_0 - E_K - 1)^{1.63}, \qquad (4.2.1.1)$$

where $N_K/4\pi$ is the *generated* number of $K\alpha$ photons per steradian per incident electron, N_0 is a function of the atomic number of the target, E_0 is the electron energy in keV and E_K is the excitation potential in keV. It should be noted that $N_K/4\pi$ decreases with increasing Z.

For a copper target, this expression becomes

$$N_K/4\pi = 1.8 \times 10^{-6}\,(E_0 - 8.9)^{1.63} \qquad (4.2.1.2)$$

or

$$N'_K/4\pi = 1.1 \times 10^{10}\,(E_0 - 8.9)^{1.63}, \qquad (4.2.1.3)$$

where $N'_K/4\pi$ is the number of $K\alpha$ photons per steradian per second per milliampere of tube current.

These expressions are probably accurate to within a factor of 2 up to values of E_0/E_K of about 10. Guo & Wu (1985) found a linear relationship for the *emerging* number of photons with electron energy in the range $2 < E_0/E_K < 5$.

To obtain the number of photons that *emerge* from the target, the above expressions have to be corrected for absorption of the generated radiation in the target. The number of photons emerging at an angle φ to the surface, for normal electron incidence, is usually written

$$N_\varphi/4\pi = f(\chi)N/4\pi, \qquad (4.2.1.4)$$

where $\chi = (\mu/\rho)\,\mathrm{cosec}\,\varphi$ (Castaing & Descamps, 1955). Green (1963) gives experimental values of the correction factor $f(\chi)$ for a series of targets over a range of electron energies. His curves for a copper target are given in Fig. 4.2.1.1. It will be noticed that the correction factor increases with increasing electron energy since the effective depth of X-ray generation increases with voltage. As a result, curves of N_φ as a function of E_0 have a broad maximum that is displaced towards lower voltages as φ decreases, as shown in the experimental curves for copper K radiation due to Metchnik & Tomlin (1963) (Fig. 4.2.1.2). For very small take-off angles, therefore, X-ray tubes should be operated at lower than customary voltages. Note that the values in Fig. 4.2.1.2 agree to within $\sim 40\%$ with those of Green & Cosslett. $f(\chi)$ at constant E_0/E_K increases with increasing Z, thus partly compensating for the decrease in N_K, especially at small values of φ. A recent re-examination of the characteristic X-ray flux from Cr, Cu, Mo, Ag and W targets has been carried out by Honkimaki, Sleight & Suortti (1990).

4.2.1.2. *The continuous spectrum*

The shape of the continuous spectrum from a thick target is very simple: I_ν, the energy per unit frequency band in the spectrum, is given by the expression derived by Kramers (1923):

$$I_\nu = AZ(\nu_0 - \nu) + BZ^2, \qquad (4.2.1.5)$$

where Z is the atomic number of the target and A and B are constants independent of the applied voltage E_0. B/A is of the order of 0.0025 so that the term in Z^2 can usually be neglected (Fig. 4.2.1.3). ν_0 is the maximum frequency in the spectrum, *i.e.* the Duane–Hunt limit at which the entire energy of the bombarding electrons is converted into the quantum energy of the emitted photon, where

$$H\nu_0 = hc/\lambda_0 = E_0. \qquad (4.2.1.6)$$

Using the latest adjusted values of the fundamental constants (Cohen & Taylor, 1987):

$$hc = 1.23984244 \pm 0.00000037 \times 10^{-6}\ \text{eV m}$$
$$= 12.3984244 \pm 0.0000037\ \text{keV Å}.$$

Equation (4.2.1.5) can be rewritten in a number of forms. If $\mathrm{d}N_E$ is the number of photons of energy E per incident electron,

$$\mathrm{d}N_E = bZ(E_0/E - 1)\ \mathrm{d}E, \qquad (4.2.1.7)$$

where $b \sim 2 \times 10^{-9}$ photons eV^{-1} $\mathrm{electron}^{-1}$, and is known as Kramer's constant.

From (4.2.1.7), it follows that the total energy in the continuous spectrum per electron is

$$\int_0^{E_0} E\ \mathrm{d}N_E = bZE_0^2/2. \qquad (4.2.1.8)$$

Since the energy of the bombarding electron is E_0, the efficiency of production of the continuous radiation is

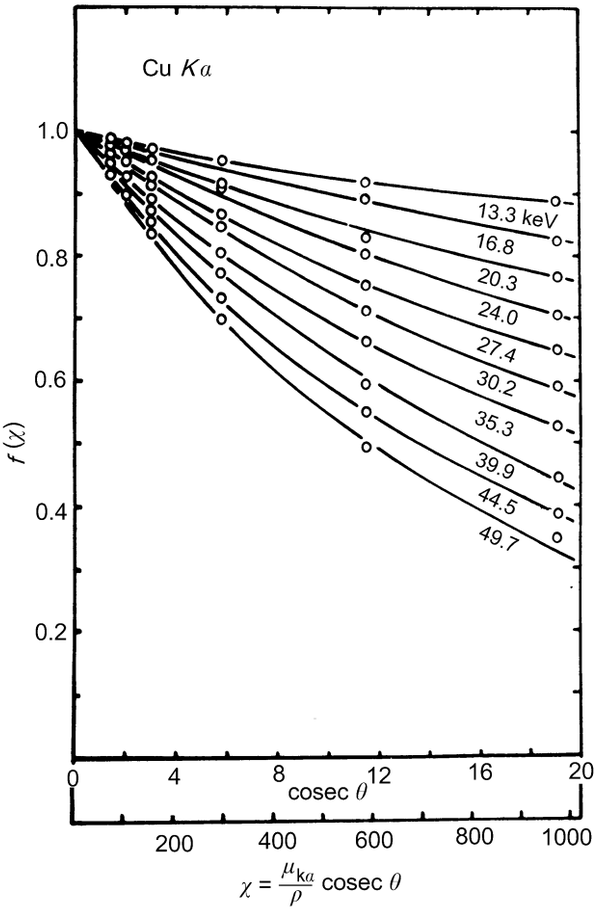

Fig. 4.2.1.1. $f(\chi)$ curves for Cu K-L_3 at a series of different accelerating voltages (in kV). From Green (1963).

$$\eta_c = bZE_0/2. \quad (4.2.1.9)$$

Crystallographers are more accustomed to thinking of the spectrum in terms of wavelength. Equation (4.2.1.7) can be transformed into

$$dN_\lambda = hcbZ(1/\lambda^2 - 1/\lambda\lambda_0)\, d\lambda, \quad (4.2.1.10)$$

which has a maximum at $\lambda = 2\lambda_0$. In practice, the *emerging* spectrum is modified by target absorption, which is greatest for the longer wavelengths and moves the maximum more nearly to $1.5\lambda_0$.

It is of interest to compare the X-ray flux in a narrow wavelength band selected by an appropriate monochromator with the flux in a characteristic spectral line, in order to examine the practicability of XAFS (X-ray absorption fine-structure spectroscopy) or optimized anomalous-dispersion diffractometry experiments. For these purposes, the maximum permissible wavelength band is about 10^{-3} Å. From equation (4.2.1.10), we see that, for a tungsten-target X-ray tube operated at 80 kV, dN_λ is about 1.1×10^{-5} photons with the $K\alpha$ energy electron^{-1} steradian^{-1} $(10^{-3}\,\delta\lambda/\lambda)^{-1}$ for an X-ray wavelength in the neighbourhood of 1.5 Å. By comparison, from equation (4.2.1.2), a copper-target tube operated at 40 kV produces about 5×10^{-4} $K\alpha$ photons electron^{-1} steradian^{-1}. In spite of this shortcoming by a factor of about 45, laboratory XAFS experiments are sufficiently common to have merited at least one specialized conference (Stern, 1980; see also Tohji, Udagawa, Kawasaki & Masuda, 1983; Sakurai, 1993; Sakurai & Sakurai, 1994).

The use of continuous radiation for diffraction experiments is complicated by the fact that the radiation is polarized. The degree of polarization may be defined as

$$p = (I_\parallel - I_\perp)/(I_\parallel + I_\perp), \quad (4.2.1.11)$$

where $I_\parallel$ and $I_\perp$ are the intensities of radiation with the electric vector parallel and perpendicular to the plane containing the incident electrons and the direction of the emitted photons. For an angle of $\pi/2$ between the electrons and the emitted beam, p varies smoothly through the spectrum; it is negative for the softest radiation, approximately zero at $\nu/\nu_0 \sim 0.1$ and reaches values between +0.7 and +0.9 near the Duane–Hunt limit (Kirkpatrick & Wiedmann, 1945). Since practical use of white radiation is likely to be in the vicinity of $\nu/\nu_0 \sim 0.1$, the effect is not a large one.

It should also be noted that the spatial distribution of the white spectrum, even after correction for absorption in the target, is not isotropic. The intensity has a maximum at about 50° to the electron beam and non-zero minima at 0 and 180° to that beam (Stephenson, 1957).

4.2.1.3. *X-ray tubes*

The commonest source of X-rays is the high-vacuum, or Coolidge, X-ray tube, which may be either demountable and pumped continuously when in operation or permanently sealed after evacuation. The vacuum tube contains an electron gun that incorporates a thermionic cathode, which produces a well defined electron beam that is accelerated towards the anode or target, formerly often called the anticathode. In most X-ray tubes intended for crystallographic purposes, the anode is massive, *i.e.* its thickness is large compared with the range of the electrons; it is usually water-cooled and its surface is normal to the incident electron beam. Usually, it is desirable for the X-ray source to be small (between 25 μm and 1 mm square) and for the X-ray intensity from the tube to be the maximum possible for the amount of power that can be dissipated in the target. These objectives are best achieved by

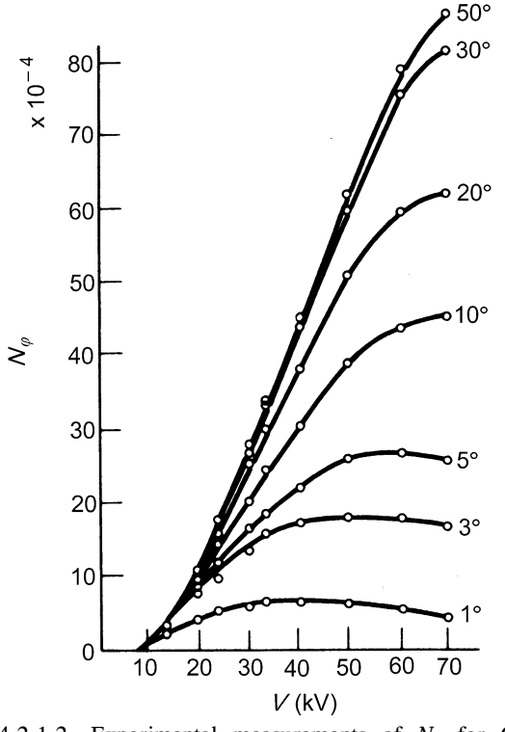

Fig. 4.2.1.2. Experimental measurements of N_φ for Cu K-L_3 as functions of the accelerating voltage for different take-off angles. From Metchnik & Tomlin (1963).

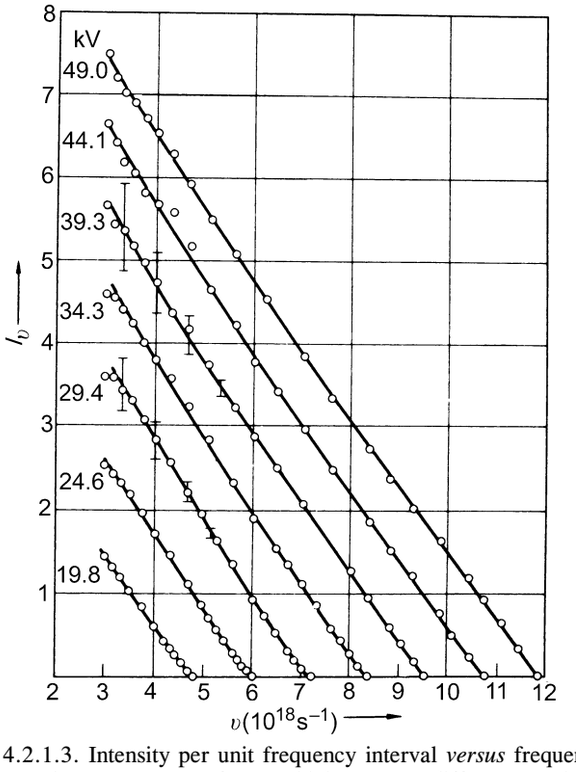

Fig. 4.2.1.3. Intensity per unit frequency interval *versus* frequency in the continuous spectrum from a thick target at different accelerating voltages. From Kuhlenkampff & Schmidt (1943).

Table 4.2.1.3. *Copper-target X-ray tubes and their loading*

X-ray tube	Anode diameter (mm)	Speed		$f_1 \times f_2$ (mm) (mm)	μ	Loading (kW)		Recommended specific loading (kW mm^{-2})
		r min^{-1}	mm s^{-1}			calc.	recommended	
Standard insert	–	–	–	8×0.15	0.295	1.0	0.8	0.67
	–	–	–	8×0.4	0.359	1.2	1.5	0.47
	–	–	–	10×1.0	0.425	1.8	2.0	0.20
	–	–	–	12×2.0	0.493	2.5	2.7	0.11
AEI-GX21	89	6000	28000	1×0.1	0.425	1.4	1.2	12.0
				2×0.2	0.425	3.95	3.2	8.0
				3×0.3	0.425	7.3	5.2	5.8
				5×0.5	0.425	15.6	15.0	6.0
AEI-GX13	457	4500	108000	1×0.1	0.425	2.7	2.7	27.0
Rigaku-RU200	99	6000	31000	1×0.1	0.425	1.5	1.2	12.0
				2×0.2	0.425	4.2	3.0	7.5
				3×0.3	0.425	7.6	5.4	6.0
Rigaku-RU500	400	1250	26200	10×0.5	0.359	26.8	30	6.0
Rigaku-RU1000	400	2500	52450	10×1	0.425	60	60	6.0
Rigaku-RU1500	250	10000	131000	10×1	0.425	96	90	9.0
KFA-Jülich	250	12000	157000	14×1.4	0.425	173	120	6.1

designing the electron gun to produce a line focus, that is the electron focus on the target face is approximately rectangular with the small dimension equal to the desired effective source size and the large dimension about 10 to 20 times larger. The focus is viewed at an angle between about 2 and 5° to the anode surface to produce an approximately square foreshortened effective source; and the X-ray windows are so positioned as to make these take-off angles possible. For some purposes, very fine line sources are required and windows may be provided to allow the focus to be viewed so as to foreshorten the line width. Higher power dissipation is possible in X-ray tubes in which the anode rotates: the line focus is now usually on the cylindrical surface of the anode with its long dimension parallel to the axis of rotation.

For focal-spot sizes down to about 100 μm, an electrostatic gun is adequate; this consists of a fine helical filament and a Wehnelt cathode, which produces a demagnified electron image of the filament on the anode. For most purposes, the Wehnelt cathode can be at the same potential as the filament but cleaner foci and adjustment of the focal spot size are possible when this electrode is negatively biased with respect to the filament. The filament is nearly always directly heated and made of tungsten. Lower filament temperatures, and smaller heating currents, could be achieved with activated heaters but the vacuum in high-power devices like X-ray tubes is rarely hard enough to permit their use since they are easily poisoned. However, Yao (1992) has reported successful operation of a hot-pressed polycrystalline lanthanum hexaboride cathode in an otherwise unmodified RU-1000 rotating-target X-ray generator.

Very fine focus tubes, with foci in the range between 25 and 1 μm, require magnetic lenses. At one time, the all-electrostatic X-ray tube of Ehrenberg & Spear (1951), which achieved foci between 20 and 80 μm, was very popular.

Sealed-off X-ray tubes for crystallographic use are nowadays made in the form of inserts containing a target of one of a range of standard metals to produce the desired characteristic radiation. A series of nominal focal-spot sizes, shown in Table 4.2.1.3, is commonly available. The insert is mounted inside a standard shield that is radiation- and shock-proof and that is fitted with X-ray shutters and filters and often also with a standardized track for mounting X-ray cameras. The water-cooled anode is normally at ground potential and the negative high voltage for the cathode, together with the filament supply, is brought in through a shielded shock-proof cable. The high voltage is nowadays generally of the constant-voltage type, that is, it is full-wave rectified and smoothed by means of solid-state rectifiers and capacitors housed in the high-voltage transformer tank, which also contains the filament transformer. The high tension and the tube current are frequently stabilized. Only the simplest X-ray generators now employ an alternating high tension that is rectified by the self-rectifying property of the X-ray tube itself.

A demountable continuously pumped form of construction is nowadays adopted mainly for rotating-anode and other specialized X-ray tubes. The pumping system must be capable of maintaining a vacuum of better than 10^{-5} Torr: filament life is critically dependent upon the quality of the vacuum.

Rotating-anode tubes have been reviewed by Yoshimatsu & Kozaki (1977). The first successful tube of this type that incorporated a vacuum shaft seal was described by Clay (1934). Modern tubes mostly contain vacuum-oil-lubricated shaft seals of the type due to Wilson (1941) and are based on, or are similar to, the rotating-anode tubes described by Taylor (1949, 1956). In some tubes, successful use has been made of ferro-fluidic vacuum seals (see Bailey, 1978). The main problems in the operation of rotating-anode tubes is the lifetime of the seals and of bearings that operate *in vacuo*. In successful tubes, *e.g.* those

manufactured by Enraf, Rigaku-Denki, and Siemens, these lifetimes are about the same as the lifetime of the filament under good vacuum conditions, that is, of the order of 1000 h.

Phillips (1985) has written a review article on stationary and rotating-anode X-ray tubes that contains many important practical details.

4.2.1.3.1. *Power dissipation in the anode*

The allowable power loading of X-ray tube targets is determined by the temperature of the target surface, which must remain below the melting point. Müller (1927, 1929, 1931) first calculated the maximum loading both for stationary and for rotating anodes. His calculations were refined by Oosterkamp (1948) who considered, in particular, targets of finite thickness, and who also treated pulsed operation of the tube. For normal conditions, Oosterkamp's conclusions and those of Ishimura, Shiraiwa & Sawada (1957) do not greatly differ from those of Müller, which are in adequate agreement with experimental observations.

For an elliptical focal spot with axes f_1 and f_2, Müller's formula for the maximum power dissipation on a stationary anode, assumed to be a water-cooled block of dimensions large compared with the focal-spot dimensions, can be written

$$W_{\rm stat} = 2.063(T_M - T_0)Kf_1\mu(f_1,f_2), \qquad (4.2.1.12)$$

where K is the specific thermal conductivity of the target material in $\mathrm{W\,mm^{-1}}$, T_M is the maximum temperature at the centre of the focal spot on the target, that is, a temperature well below the melting point of the target material, and T_0 is the temperature of the cold surface of the target, that is, of the cooling water. The function μ is shown in Fig. 4.2.1.4. For copper, K is $400\,\mathrm{W\,m^{-1}}$ and, with $T_M - T_0 = 500\,\mathrm{K}$,

$$W_{\rm stat} = 425\mu f_1. \qquad (4.2.1.13)$$

For $f_2/f_1 = 0.1$, and $\mu = 0.425$, this equation becomes

$$W_{\rm stat} = 180 f_1. \qquad (4.2.1.14)$$

In these last two equations, f_1 is in mm.

For a rotating target, Müller found that the permissible power dissipation was given by

$$W_{\rm rot} = 1.428\,K(T_M - T_0)f_1(f_2\rho Cv/2K)^{1/2}, \qquad (4.2.1.15)$$

where f_2 is the short dimension of the focus, assumed to be in the direction of motion of the target, v is the linear velocity, ρ is the density of the target material, and C is its specific heat.

For a copper target with f_1 and f_2 in mm and v in $\mathrm{mm\,s^{-1}}$,

$$W_{\rm rot} = 26.4 f_1(f_2 v)^{1/2}. \qquad (4.2.1.16)$$

Equation (4.2.1.16) shows that for very narrow focal spots rotating-anode tubes give useful improvements in permissible loading only if the surface speed is very high (see Table 4.2.1.3). The reason is that with large foci on stationary anodes the isothermal surfaces in the target are planar; with fine foci, these surfaces become cylindrical and this already makes for very efficient cooling without the need for rotation. Rotating anodes are thus most useful for medium-size foci (200 to 500 μm) since for the larger focal spots it becomes very expensive to construct power supplies capable of supplying the permissible amount of power.

Table 4.2.1.3 shows the recommended loading for a number of commercially available X-ray tubes with copper targets, which will be seen to be in qualitative agreement with the calculations. Some of the discrepancy is due to the fact that the value of $K(T_M - T_0)$ for the copper–chromium alloy targets used in actual X-ray tubes is appreciably lower than the value for pure copper used here. To a good approximation, the permissible loading for other targets can be derived by multiplying those in Table 4.2.1.3 by the factors shown in Table 4.2.1.4. It is worth noting that the recommended loading of commercial stationary-target X-ray tubes has increased steadily in recent years. This is largely due to improvements in the water cooling of the back surface of the target by increasing the turbulence of the water and the effective surface area of the cooled surface.

In considering Table 4.2.1.3, it should be noted that the linear velocities of the highest-power X-ray-tube anode have already reached a speed that Yoshimatsu & Kozaki (1977) consider the practical limit, which is set by the mechanical properties of engineering materials. It should also be noted that much higher specific loads can be achieved for true micro-focus tubes, *e.g.* $50\,\mathrm{kW\,mm^{-2}}$ for a 25 μm Ehrenberg & Spear tube and $1000\,\mathrm{kW\,mm^{-2}}$ for a tube with a 1 μm focus (Goldsztaub, 1947; Cosslett & Nixon, 1951, 1960).

Some tubes with focus spots of less than 10 μm utilize foil or needle targets. These targets and the heat dissipated in them have been discussed by Cosslett & Nixon (1960). The dissipation is less than that in a massive target by a factor of about 3 for a foil and 10 for a needle, but, in view of the low absolute power, target movement and even water-cooling can be dispensed with.

4.2.1.4. *Radioactive X-ray sources*

Radioactive sources of X-rays are mainly of interest to crystallographers for the calibration of X-ray detectors where they have the great advantage of being completely stable with time, or at least of having an accurately known decay rate. For some purposes, spectral purity of the radiation is important; radionuclides that decay wholly by electron capture are particularly useful as they produce little or no β or other radiation. In this type of decay, the atomic number of the daughter nucleus is one less than that of the decaying isotope, and the emitted X-rays are characteristic of the daughter nucleus. In some cases, the probability of electron capture taking place

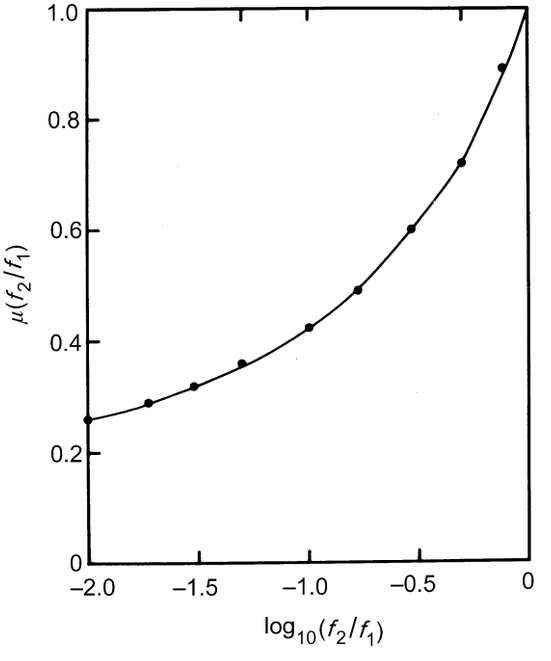

Fig. 4.2.1.4. The function μ in Müller's equation (equation 4.2.1.12) as a function of the ratio of width to length of the focal spot.

Table 4.2.1.4. *Relative permissible loading for different target materials*

Cu	Cr	Fe	Co	Mo	Ag	W
1.0	0.9	0.6	0.9	1.2	1.0	1.2

from some shell other than the K shell is very small and most of the photons emitted are K photons. The number of photons emitted into a solid angle of 4π, uncorrected for absorption, is given by the strength of the source in Curies (1 Curie = 3.7×10^{10} disintegrations s^{-1}), since each disintegration produces one photon. A list of these nuclei (after Dyson, 1973) is given in Table 4.2.1.5.

Useful radioactive sources are also made by mixing a pure β-emitter with a target material. These sources produce a continuous spectrum in addition to the characteristic line spectrum. The nuclide most commonly used for this purpose is tritium which emits β particles with an energy up to 18 keV and which has a half-life of 12.4 a.

Radioactive X-ray sources have been reviewed by Dyson (1973).

4.2.1.5. *Synchrotron-radiation sources*

The growing importance of synchrotron radiation is attested by a large number of monographs (Kunz, 1979; Winick, 1980; Stuhrmann, 1982; Koch, 1983) and review articles (Godwin, 1968; Kulipanov & Strinskii, 1977; Lea, 1978; Winick & Bienenstock, 1978; Helliwell, 1984; Buras, 1985). Project studies for storage rings such as the European Synchrotron Radiation Facility, the ESRF (Farge & Duke, 1979; Thompson & Poole, 1979; Buras & Marr, 1979; Buras & Tazzari, 1984) are still worth consulting for the reasoning that lay behind the design; the ESRF has, in fact, achieved or even exceeded the design parameters (Laclare, 1994).

A charged particle with energy E and mass m moving in a circular orbit of radius R at a constant speed v radiates a power P into a solid angle of 4π, where

$$P = 2e^2c(v/c)^4(E/mc^2)^4/3R^2. \qquad (4.2.1.17)$$

The orbit of the particle can be maintained only if the energy lost in the form of electromagnetic radiation is constantly replenished. In an electron synchrotron or in a storage ring, the circulating particles are electrons or positrons maintained in a closed orbit by a magnetic field; their energy is supplied or restored by means of an oscillating radio-frequency (RF) electric field at one or more places in the orbit. In a synchrotron, designed for nuclear-physics experiments, the circulating particles are injected from a linear accelerator, accelerated up to full energy by the RF field and then deflected into a target with a cycle frequency of about 50 Hz. The synchrotron radiation is thus produced in the form of pulses of this frequency. A storage ring, on the other hand, is filled with electrons or positrons and after acceleration the particle energy is maintained by the RF field; the current ideally circulates for many hours and decays only as a result of collisions with remaining gas molecules. At present, only storage rings are used as sources of synchrotron radiation and many of these are dedicated entirely to the production of radiation: they are not used at all, or are used only for limited periods, for nuclear-physics collision experiments.

In equation (4.2.1.17), we may substitute for the various constants and obtain for the radiated power

Table 4.2.1.5. *Radionuclides decaying wholly by electron capture, and yielding little or no γ-radiation*

Nuclide	Half-life	X-rays		Remarks
		Element	$K\alpha_1$ (keV)	
^{37}Ar	35 d	Cl	2.622	–
^{51}Cr	27.8 d	V	4.952	γ at 320 keV
^{55}Fe	2.6 a	Mn	5.898	–
^{71}Ge	11.4 d	Ga	9.251	–
^{103}Pd	17 d	Rh	20.214	Several γ's; all weak
^{109}Cd	453 d	Ag	22.16	γ at 88 keV
^{125}I	60 d	Te	27.47	γ at 35.4 keV
^{131}Cs	10 d	Xe	29.80	–
^{145}Pm	17.7a	Nd	37.36	γ's at 67 and 72 keV
^{145}Sm	340 d	Pm	38.65	γ's at 61 keV; weak γ at 485 keV
^{179}Ta	600 d	Hf	55.76	–
^{181}W	140 d	Ta	57.52	γ at 6.5 keV; weak γ's at 136, 153 keV
^{205}Pb	5×10^7a	Tl	L only (L_{α_1} = 10.27 keV)	–

$$P = 0.0885\,E^4I/R, \qquad (4.2.1.18)$$

where E is in GeV (10^9 eV), I is the circulating electron or positron current in milliamperes, and R is in metres. Thus, for example, at the Daresbury storage ring in England, $R = 5.5$ m and, for operation at 2 GeV and 200 mA, $P = 51.5$ kW. Storage rings with a total power of the order of 1 MW are planned.

For relativistic electrons, the electromagnetic radiation is compressed into a fan-shaped beam tangential to the orbit with a vertical opening angle $\psi \simeq mc^2/E$, *i.e.* ~ 0.25 mrad for $E = 2$ GeV (Fig. 4.2.1.5). This fan rotates with circulating electrons: if the ring is filled with n bunches of electrons, a stationary observer will see n flashes of radiation every $2\pi R/c$ s, the duration of each flash being less than 1 ns.

The spectral distribution of synchrotron radiation extends from the infrared to the X-ray region; Schwinger (1949) gives the instantaneous power radiated by a monoenergetic electron in a circular motion per unit wavelength interval as a function of wavelength (Winick, 1980). An important parameter specifying the distribution is the critical wavelength λ_c: half the total power radiated, but only $\sim 9\%$ of the total number of photons, is at $\lambda < \lambda_c$ (Fig. 4.2.1.6). λ_c is given by

$$\lambda_c = 4\pi R/3(E/mc^2)^3, \qquad (4.2.1.19)$$

from which it follows that λ_c in Å can be expressed as

$$\lambda_c = 18.64/(BE^2), \qquad (4.2.1.20)$$

where B (= 3.34 E/R) is the magnetic bending field in T, E is in GeV, and R is in metres.

Synchrotron radiation is highly polarized. In an ideal ring where all electrons are parallel to one another in a central orbit, the radiation in the orbital plane is linearly polarized with the electric vector lying in this plane. Outside the plane, the radiation is elliptically polarized.

In practice, the electron path in a storage ring is not a circle. The 'ring' consists of an alternation of straight sections and bending magnets and beam lines are installed at these magnets.

So-called *insertion devices* with a zero magnetic field integral, *i.e. wigglers* and *undulators*, may be inserted in the straight sections (Fig. 4.2.1.7). A wiggler consists of one or more dipole magnets with alternating magnetic field directions aligned transverse to the orbit. The critical wavelength can thus be shifted towards shorter values because the bending radius can be made small over a short section, especially when superconducting magnets are used. Such a device is called a *wavelength shifter*. If it has N dipoles, the radiation from the different poles is added to give an N-fold increase in intensity. Wigglers can be horizontal or vertical.

In a wiggler, the maximum divergence 2α of the electron beam is much larger than ψ, the vertical aperture of the radiation cone in the spectral region of interest (Fig. 4.2.1.5). If $2\alpha \ll \psi$ and if, in addition, the magnet poles of a multipole device have a short period λ_0, the device becomes an undulator: interference will take place between the radiation emitted at two points λ_0 apart on the electron trajectory (Fig. 4.2.1.8). The spectrum at an angle φ to the axis observed through a pin-hole will consist of a single spectral line and its harmonics of wavelengths

$$\lambda_i = i^{-1}\lambda_0[(E/mc^2)^{-2} + \alpha^2/2 + \theta^2]/2 \qquad (4.2.1.21)$$

(Hofmann, 1978). Typically, the bandwidth of the lines, $\delta\lambda/\lambda$, will be ~ 0.01 to 0.1 and the photon flux per unit band width from the undulator will be many orders of magnitude greater than that from a bending magnet. Existing undulators have been designed for photon energies below 2 keV; higher energies, because of the relatively weak magnetic fields necessitated by the need to keep λ_0 small [equation (4.2.1.21)], require a high electron energy: undulators with a fundamental wavelength in the neighbourhood of 0.86 Å are planned for the European storage ring (Buras & Tazzari, 1984).

The wavelength spectra for a bending magnet, a wiggler and an undulator for the ESRF, are shown in Fig. 4.2.1.9. A comparison of the spectra from an existing storage ring with the spectrum of a rotating-anode tube is shown in Fig. 4.2.1.10.

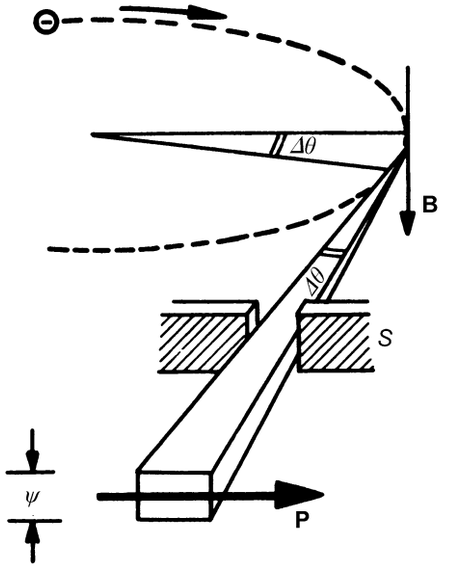

Fig. 4.2.1.5. Synchrotron radiation emitted by a relativistic electron travelling in a curved trajectory. B is the magnetic field perpendicular to the plane of the electron orbit; ψ is the natural opening angle in the vertical plane; P is the direction of polarization. The slit S defines the length of the arc of angle $\Delta\theta$ from which the radiation is taken. From Buras & Tazzari (1984); courtesy of ESRP.

The important properties of synchrotron-radiation sources are:
(1) high intensity;
(2) very broad continuous spectral range;
(3) narrow angular collimation;
(4) small source size;
(5) high degree of polarization;
(6) regularly pulsed time structure;
(7) computability of properties.

Table 4.2.1.6 (after Buras & Tazzari, 1984) compares the most important parameters of the European Synchrotron Radiation Facility (ESRF) with a number of other storage rings. In this table, BM and W signify bending-magnet and wiggler beam lines, respectively, σ_x and σ'_z is the source divergence; the flux is integrated in the vertical plane. The ESRF is seen to have a higher flux than other sources; even more impressive by virtue of the small dimensions of the source size and divergence are its improvements in spectral brightness (defined as the number of photons s^{-1} per unit solid angle per 0.1% bandwidth) and in spectral brilliance (defined as the number of photons s^{-1} per unit solid angle per unit area of the source per 0.1% bandwidth). In comparing different synchrotron-radiation sources with one another and with conventional sources (Fig. 4.2.1.10), the relative quantity for comparison may be flux, brightness or brilliance, depending on the type of diffraction experiment and the type of collimation adopted. Table 4.2.1.7 (due to Farge & Duke, 1979) attempts to compare intensity factors for a number of typical experiments. In general, a high brightness is important in experiments that do not embody focusing elements, such as mirrors or

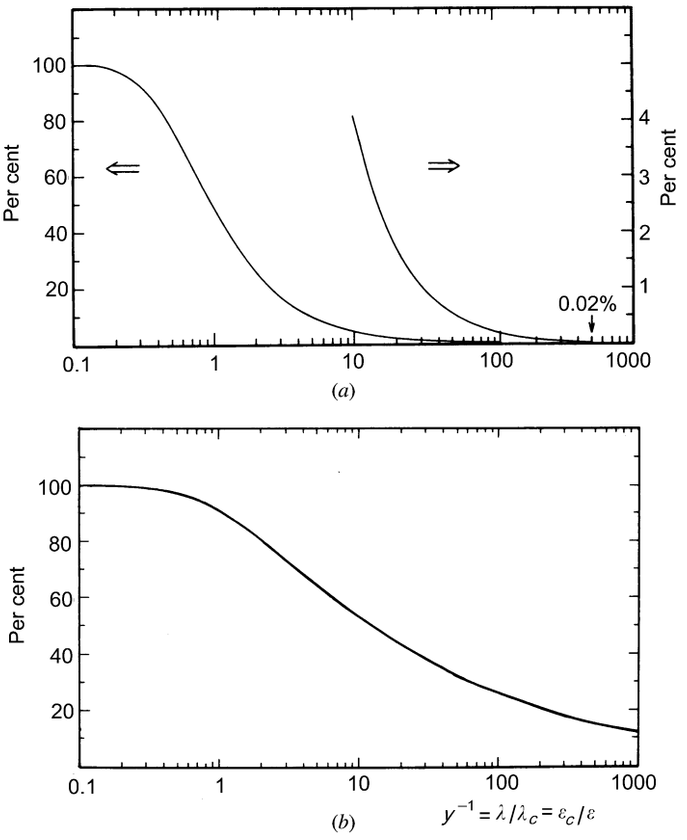

Fig. 4.2.1.6. Synchrotron-radiation spectrum: percentage per unit wavelength interval (*a*) of power of total power and (*b*) of number of photons of total number of photons at wavelengths greater than λ *versus* λ/λ_c. Note that half the power but only 9% of the photons are radiated at wavelengths less than λ_c; courtesy of H. Winick.

curved crystals, and a high brilliance in those experiments that do.

Many surveys of existing and planned synchrotron-radiation sources have been published since the compilation of Table 4.2.1.6. Figure 4.2.1.11, taken from a recent review (Suller, 1992), is a graphical illustration of the growth and the distribution of these sources. An earlier census is due to Huke & Kobayakawa (1989). Many detailed descriptions of beam lines for particular purposes, such as protein crystallography (*e.g* Fourme, 1992) or at individual storage rings (*e.g*. Kusev, Raiko & Skuratowski, 1992) have appeared: these are too numerous to list here and can be located by reference to *Synchrotron Radiation News*.

4.2.1.6. *Plasma X-ray sources*

Plasma sources of hard X-rays are being investigated in many laboratories. Most of the material in this section is derived from publications from the Laboratory for Laser Energetics, University of Rochester, USA. Plasma sources of very soft X-rays have been reviewed by Byer, Kuhn, Reed & Trail (1983).

The peak wavelength of emission from a black-body radiator falls into the ultraviolet at about 10^5 K and into the X-ray region between 10^6 and 10^7 K. At these temperatures, matter is in the form of a plasma that consists of highly ionized atoms and of electrons with energies of several keV. The only successful methods of heating plasmas to temperatures in excess of 10^6 K is by means of high-energy laser beams with intensities of 10^{12} W mm^{-2} or more. The duration of the laser pulse must be less than 1 ns so that the plasma cannot flow away from the pulse. When the plasmas are created from elements with $15 < Z < 25$, they consist mainly of ions stripped to the *K* shell, that is of hydrogen- and helium-like ions. The X-ray spectrum (Fig. 4.2.1.12) then contains a main group of lines with a bandwidth for the group of about 1%; the band is situated slightly below the *K*-absorption edge of the target material. The intensity of the band drops with increasing atomic number. For diffraction studies, Forsyth & Frankel (1980, 1984) and Frankel & Forsyth (1979, 1985) used a multi-stage Nd^{3+}:glass laser (Seka, Soures, Lewis, Bunkenburg, Brown, Jacobs, Mourou & Zimmermann, 1980), which was able to deliver up to 220 J per pulse of width 700 ps. They obtained 6×10^{14} photons pulse^{-1} for a Cl^{15+} plasma with a mean wavelength of about 4.45 Å and about 3×10^{13} photons pulse^{-1} for a Fe^{24+} plasma at about 1.87 Å (Yaakobi, Bourke, Conturie, Delettrez, Forsyth, Frankel, Goldman, McCrory, Seka, Soures, Burek & Deslattes, 1981). More recently, the laser was fitted

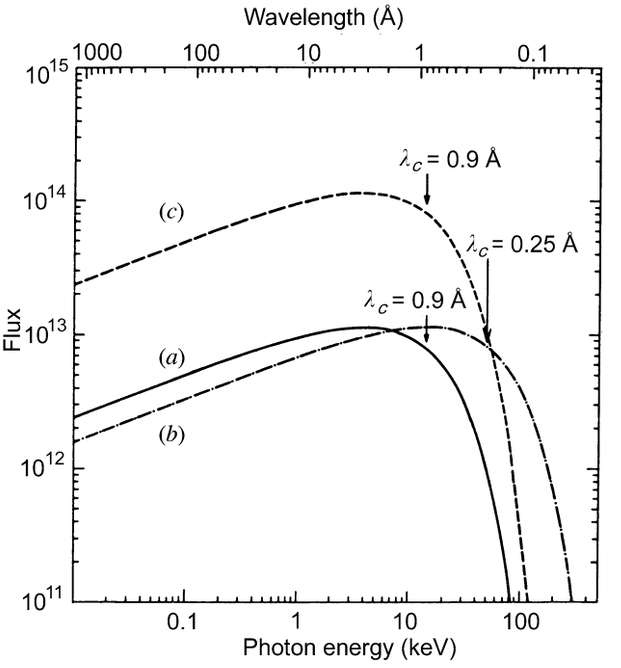

Fig. 4.2.1.9. Spectral distribution and critical wavelengths for (*a*) a dipole magnet, (*b*) a wavelength shifter, and (*c*) a multipole wiggler for the proposed ESRF. From Buras & Tazzari (1984); courtesy of ESRP.

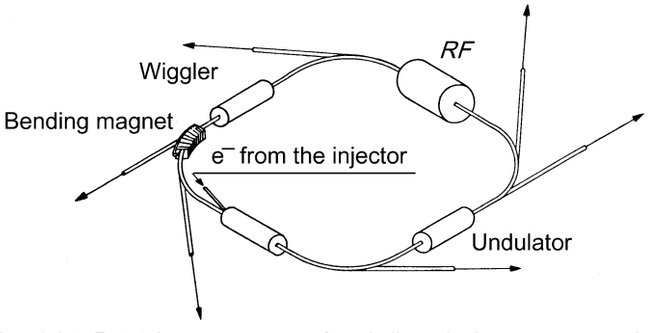

Fig. 4.2.1.7. Main components of a dedicated electron storage-ring synchrotron-radiation source. For clarity, only one bending magnet is shown. From Buras & Tazzari (1984); courtesy of ESRP.

Fig. 4.2.1.8. Electron trajectory within a multipole wiggler or undulator. λ_0 is the spatial period, α the maximum deflection angle, and θ the observation angle. From Buras & Tazzari (1984); courtesy of ESRP.

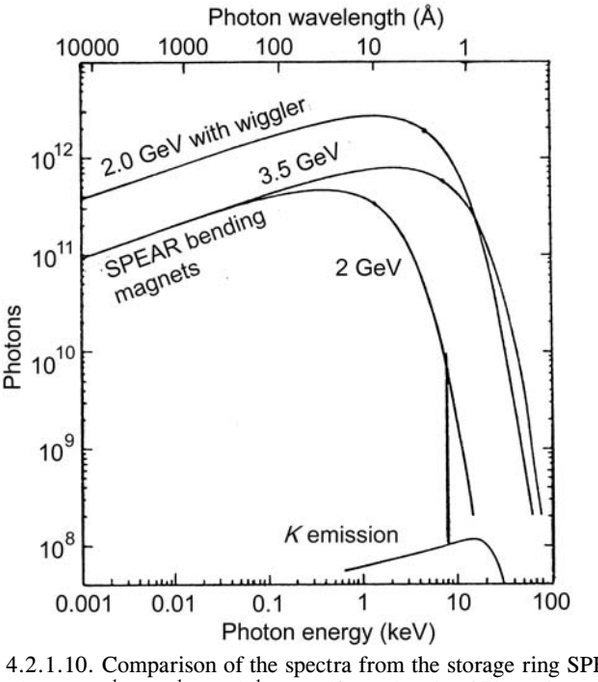

Fig. 4.2.1.10. Comparison of the spectra from the storage ring SPEAR in photons s^{-1} mA^{-1} mrad^{-1} per 1% passband (1978 performance) and a rotating-anode X-ray generator. From Nagel (1980); courtesy of K. O. Hodgson.

Table 4.2.1.6. *Comparison of storage-ring synchrotron-radiation sources; the parameters were correct in 1985 and, for some sources, may be substantially different from those at earlier or later periods; after Buras & Tazzari (1984), courtesy of ESRP*

Storage ring	Source type	No. of poles	I (mA)	E (GeV)	R (m)	σ_x (mm)*	σ_z (mm)*	σ'_z (mrad)*	λ_c (Å)	$E_{c(\mathrm{keV})}$	Flux $\left[\frac{\text{photons s}^{-1}}{\text{mrad} \times 0.1\%\ \text{BW}}\right]$ at λ^c	Flux at 1.54 Å
(1) ESRF	BM	–	100	5.0	20.0	0.092	0.100	0.008	0.9	14	8×10^{12}	1×10^{13}
(2) ESRF	W	30	100	5.0	11.56	0.062	0.040	0.016	0.5	24	2.4×10^{14}	3×10^{14}
(3) ADONE (Frascati)	BM	–	100	1.5	5.0	0.8	0.4	0.04	8.0	1.5	2.4×10^{12}	5×10^{10}
(4) ADONE (Frascati)	W	6	100	1.5	2.6	1.4	0.24	0.08	4.3	3	1.4×10^{13}	3.4×10^{12}
(5) SRS (Daresbury)	BM	–	300	2.0	5.56	2.7	0.23	0.05	4.0	3	1×10^{13}	3×10^{12}
(6) SRS (Daresbury)	W	1	300	2.0	1.33	5.3	0.17	0.05	0.9	13	1×10^{13}	1.2×10^{13}
(7) DCI (Orsay)	BM	–	250	1.8	3.82	2.72	1.06	0.06	3.6	3.4	7×10^{12}	2.4×10^{12}
(8) DORIS (Hamburg)	BM	–	100	3.7	12.22	1.0	0.3	0.05	1.3	9.2	6×10^{12}	6.4×10^{12}
(9) DORIS (Hamburg)	BM	–	40	5.0	12.22	1.3	0.65	0.065	0.55	23	3×10^{12}	4.4×10^{13}
(10) DORIS (Hamburg)	W	32	100	3.7	20.57	1.5	0.4	0.033	2.3	5.5	1.9×10^{14}	1.3×10^{14}
(11) CESR (Cornell)	BM	–	40	5.5	32.0	1.44	1.0	0.065	1.0	11.5	3.5×10^{12}	4×10^{12}
(12) CESR (Cornell)	W	6	40	5.5	13.2	1.9	1.2	0.05	0.4	28	2×10^{13}	3×10^{13}
(13) NSLS X-ray (Brookhaven)	BM	–	300	2.5	6.83	0.25	0.1	0.01	2.4	5	1×10^{13}	8×10^{12}
(14) SPEAR	BM	–	100	3.0	12.7	2.0	0.28	0.05	2.7	5	5×10^{12}	3×10^{12}
(15) SPEAR	W	8	100	3.0	5.57	3.2	0.15	0.03	1.0	10	3.8×10^{13}	4.5×10^{13}
(16) SPEAR	W	54	100	3.0	8.36	3.2	0.15	0.03	1.7	7	2.6×10^{14}	2.4×10^{14}
(17) Photon Factory (Tsukuba)	BM	–	150	2.5	8.66	2.2	0.6	0.14	3.0	4	6×10^{12}	3×10^{12}
(18) Photon Factory (Tsukuba)	W	3	150	2.5	1.85	1.9	0.7	0.18	0.7	19	1.8×10^{13}	2.5×10^{13}
(19) VEPP-3	BM	–	100	2.2	6.15	6.15	0.08	0.02	3.0	4	3.5×10^{12}	1.5×10^{12}

* One standard deviation of Gaussian distribution.

with a frequency conversion system that shifts the peak power of the laser light from the infrared (1.054 μm) to the ultraviolet (0.351 μm) (Seka, Soures, Lund & Craxton, 1981). This led to a more efficient X-ray production, which permitted a more than twofold increase in X-ray flux, even though the maximum pulse energies had to be reduced to ~ 50 J to prevent damage to the optical components (Yaakobi, Boehli, Bourke, Conturie, Craxton, Delettrez, Forsyth, Frankel, Goldman, McCrory, Richardson, Seka, Shvarts & Soures, 1981). Forsyth & Frankel (1984) used the plasma X-ray source for diffraction studies with 4.45 Å X-rays with a focusing collimation system that delivered up to 10^{10} photons pulse^{-1} to the specimen over an area approximately 150 μm in diameter. More recently, by special target design (Forsyth, 1986, unpublished), fluxes have been increased by factors of 2 to 3 without altering the laser output. Other plasma sources have been described by Collins, Davanloo & Bowen (1986) and by Rudakov, Baigarin, Kalimin, Korolev & Kumachov (1991).

The cost of plasma sources is about an order of magnitude greater than that of rotating-anode generators (Nagel, 1980). Their use is at present confined to flash-diffraction experiments, since the duty cycle is a maximum of one flash every 30 min. Attempts are being made to increase the laser repetition rate; a substantial improvement could lead to a source that would rival storage-ring sources.

4.2.1.7. *Other sources of X-rays*

Parametric X-ray generation can be described as the diffraction of virtual photons associated with the field of a relativistic charged particle passing through a crystal. These diffracted photons appear as real photons with an energy that satisfies Bragg's law for the reflecting crystal planes, so that the energy can be tuned between 5 and 45 keV by rotating the mosaic graphite crystal. Linear accelerators with an energy between 100 and 500 MeV produce the incident relativistic electron beam (Maruyama, Di Nova, Snyder, Piestrup, Li, Fiorito & Rule, 1993; Fiorito, Rule, Piestrup, Li, Ho & Maruyama, 1993).

Transition-radiation X-rays with peak energies between 10 and 30 keV are produced when electrons from 100 to 400 MeV strike a stack of thin foils (Piestrup, Moran, Boyers, Pincus, Kephart, Gearhart & Maruyama, 1991). Quasi-monochromatic X-rays result from a selection of target foils with appropriate *K*-, *L*- or *M*-edge frequencies (Piestrup, Boyers, Pincus, Harris, Maruyama, Bergstrom, Caplan, Silzer & Skopic, 1991).

Table 4.2.1.7. *Intensity gain with storage rings over conventional sources; from Farge & Duke (1979), courtesy of ESF*

	GX6 rotating-anode tube 2.4 kW (Cu $K\alpha$ emission)	DCI 1.72 GeV and 240 mA	ESRF 5 GeV and 565 mA
Brightness impact ▲	Small-angle scattering with a double monochromator	×500 to 1000	×15000 to 3000
	Protein crystallography with a single-focus monochromator 1 mm^3 samples Small samples	 ×50 to 160 ×30 to 60	 ×900 to 1800 ×650 to 1300
	Diffuse scattering (wide angles, low resolution and large samples) with a curved graphite monochromator	×20 to 40	×160 to 320
Non characteristic wavelength (continuous background) EXAFS experimental set-up with a 100 kW rotating anode		×10^4	×10^5

Channelling radiation, resulting from the incidence of electrons with an energy of only about 5 MeV on appropriately aligned diamond or silicon crystals hold out the hope of producing a bright tunable X-ray source.

One or more of these methods may, in the future, be developed as X-ray sources that can compete with synchrotron-radiation sources.

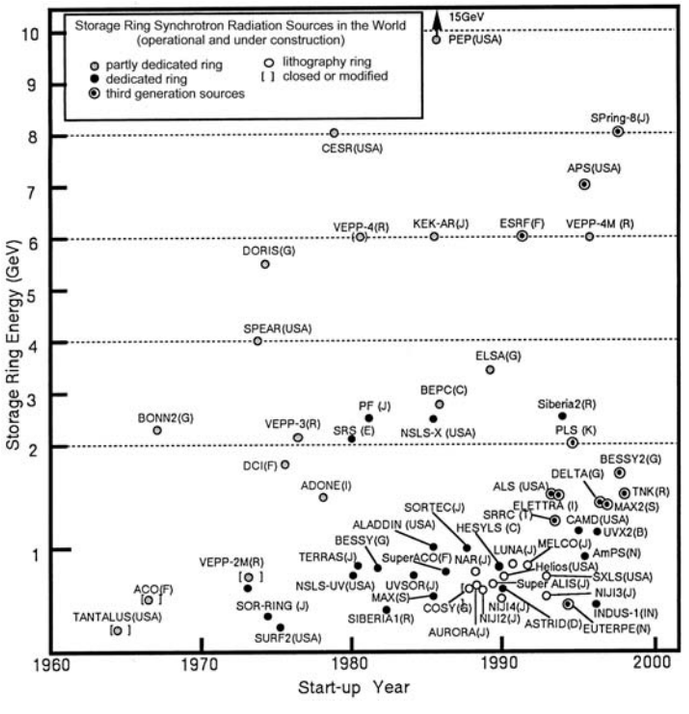

Fig. 4.2.1.11. The evolution of storage-ring synchrotron-radiation sources over the decades, as illustrated by their increasing number and range of machine energies (based on Suller, 1992).

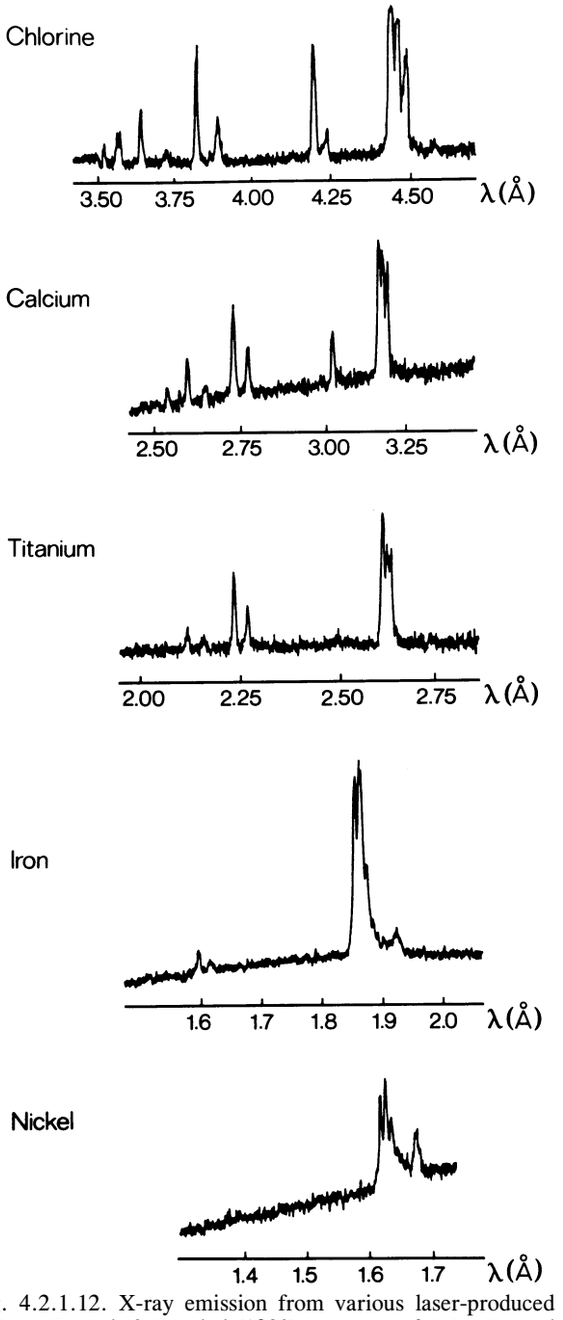

Fig. 4.2.1.12. X-ray emission from various laser-produced plasmas. From Forsyth & Frankel (1980); courtesy of J. M. Forsyth.

4.2.2. X-ray wavelengths (By R. D. Deslattes, E. G. Kessler Jr, P. Indelicato, and E. Lindroth)

4.2.2.1. *Historical introduction*

Wavelength tables in previous editions of this volume (Rieck, 1962; Arndt, 1992) were mainly obtained from the compilations prepared in Paris under the general direction of Professor Y. Cauchois (Cauchois & Hulubei, 1947; Cauchois & Senemaud, 1978). A separate effort by the late Professor J. A. Bearden and his collaborators (Bearden, 1967) has been widely used in other aggregations of tabular data and was made available for some time through the Standard Reference Data Program at the National Institute of Standards and Technology (NIST). For simplicity in the following discussion, we use the Bearden database as a frame of reference with respect to which our

current, and rather different, approach can be compared. Although a detailed comparison of the historical databases may be of some interest, the result would have only very small influence on the outcome presented here. To specify this framework, we begin with a brief description of the procedures used in establishing this reference database.

Bearden and his collaborators remeasured a group of five X-ray lines (Bearden, Henins, Marzolf, Sauder & Thomsen, 1964), with the remaining entries in the wavelength table coming from a critically reviewed, and re-scaled, subset of earlier measurements (Bearden, 1967). Line locations were given in Å* units, a scale defined by setting the wavelength of W $K\alpha_1 = 0.2090100$Å*. It was Bearden's intention that, for all but the most demanding applications, one could simply assign Å*/Å $= 1$, with an uncertainty arising from the fundamental physical constants, particularly N_A and hc/e, combined with uncertainties arising from the measurement technology (Bearden, 1965). Not long after the publication of the final compilation (Bearden, 1967), it became clear that the fundamental constants used in defining Å* needed significant revision (Cohen & Taylor, 1973), and that there were some inconsistencies in the metrology (Kessler, Deslattes & Henins, 1979).

4.2.2.2. *Known problems*

Aside from the particular issues noted above, all previous wavelength tables had certain limitations arising from the procedures used in their generation. In particular, except for a small group of five $K\alpha$ spectra (Bearden, Thomsen *et al.*, 1964), the Bearden tables relied entirely on data previously reported in the literature. Both of the other tabulations also proceeded using only reported experimental values (Cauchois & Hulubei, 1947; Cauchois & Senemaud, 1978). In the Bearden compilation process, available data for each emission line were weighted according to claimed uncertainties, modified in certain cases by Bearden's detailed knowledge of the measurement practices of the major sources of experimental wavelength values. The complete documentation of this remarkable undertaking is, unfortunately, not widely accessible. Our evident need to understand the origin of the 'recommended' values has been greatly aided by the availability of a copy of the full documentation (Bearden, Thomsen *et al.*, 1964).

The actual experimental data array from which the previous tables emerged is not complete, even for the prominent ('diagram') lines. In the cases where experimental data were not available [as can be seen only in the source documentation (Bearden, Thomsen *et al.*, 1964)], the gaps were filled by interpolated values based on measurements available from nearby elements, plotted on a modified Moseley diagram in which the Z^2 term dependence is taken into account (Burr, 1996). In the end, such a smooth scaling with respect to nuclear charge suppresses the effects of the atomic shell structure, a practice that must be avoided in order to obtain the significant improvement in the database that we hope to provide. Also obscured in smooth Z scaling are detectable contributions arising from the fact that nuclear sizes do not change smoothly as a function of the nuclear charge, Z.

4.2.2.3. *Alternative strategies*

There are several possible approaches to generating an improved, 'all-Z' table of X-ray wavelengths. These range from the option of conducting a massive measurement campaign to populate more fully the currently available tabular array to a large computational endeavor that might purport to carry out multiconfiguration, relativistic wavefunction calculations for the entire Periodic Table. It seems evident to us that there is little interest in, and even less support for, mounting the large effort needed to realize an improved tabulation of X-ray wavelengths by purely experimental means, while the possibility of proceeding in an entirely theoretical mode is not consistent with the evident need that at least some wavelengths be reported with uncertainties that approach the limit of what can be obtained from the naturally occurring X-ray lines. The actual location of any useful feature of a line is influenced not only by the physical and chemical environment of the emitting atom but also by inevitable multi-electron excitation processes that perturb the entire spectral profile. Calculation of such complexities currently lies beyond the limits of practicality, eliminating the option of proceeding without strong coupling to experimental profile locations, at least for crystallographically important X-ray lines. Similar considerations apply *a fortiori* to those lines needed as reference wavelengths for exotic atom measurements, such as those leading to masses of elementary particles and tests of basic theory [see *e.g.* Beyer, Indelicato, Finlayson, Liesen & Deslattes (1991)].

In constructing the accompanying tables, we have chosen a new procedure that differs from those described above, and accordingly requires some detailed commentary. We begin with the presently available network of well documented experimental measurements, originally established to provide a test bed for the theoretical methods developing at that time (Deslattes & Kessler, 1985). This modest network was the first compilation to make use of the, then newly available, connection between the X-ray region and the base unit of the International System of measurement (the SI) based on optical interferometric measurement of a lattice period as revealed by X-ray interferometry. Details of the generation of this network and its subsequent expansion will be given below. Using this network as a test set gave clearer suggestions as to specific limitations of the theoretical modelling than had been evident from using other, less selective, experimental reference compilations available at that time. Extensive theoretical developments before and, especially, after the appearance of this new experimental reference set have shown a steady convergence toward these critically evaluated data. Following this evolution further, our long-term plan is to use these new theoretical calculations to provide a more structured and accurate interpolation procedure for estimating the spectra of elements lying between those for which we have accurate measurements, or spectra well connected to a directly established reference wavelength. The present table provides experimental and theoretical values for some of the more prominent K and L series lines and is a subset of a larger effort for all K and L series lines connecting the $n = 1$ to $n = 4$ shells. The more complete table will be published elsewhere and be made available on the the NIST Physical Reference Data web site. In addition, experimental values for the K and L edges are provided. Although the reference data are inadequate in both low and high ranges of Z, the general consistency of theory and experiment through the region $20 < Z < 90$ for the strong K-series and L-series lines suggests that, in the absence of good reference measurements, the uncorrected theoretical values should be considered for applications not requiring the highest accuracy.

4.2.2.4. *The X-ray wavelength scales, old and new*

Historically, from the first realizations of refined spectroscopy in the X-ray region (*ca* 1915–1925) up to the period 1975–1985, the best measured X-ray wavelengths had to be expressed in some local unit, most often designated as the xu (x unit) or kxu

(kilo x unit). Uncertainty in the conversion factor between the X-ray and optical scales was the dominant contributor to the total uncertainties in the wavelength values of the sharper X-ray emission lines, such as those most frequently used in crystallography. (For a discussion of the present values in relation to previously assigned numerical values on the various scales, see Subsection 4.2.2.14.) This local unit was, for most of the time, 'officially' defined by assigning a specific numerical value to the lattice period of a particular reflection from 'the purest instance' of a particular crystal. Originally this was rocksalt; later it was calcite. In practice, most work used as *de facto* standards certain values for Cu $K\alpha_1$ and Mo $K\alpha_1$ whose inconsistency, though noted by some crystallographers earlier, was seriously addressed by Bearden and co-workers only in the 1960's (Bearden, Henins *et al.*, 1964). This early history was summarized in 1968 (Thomsen & Burr, 1968). Connection of the X-ray wavelength scale to the primary realizations of the length (wavelength) unit in the 'metric system' was primarily (at least after about 1930) through ruled grating measurements of longer-wavelength X-ray lines such as Al $K\alpha_{1,2}$.

The remainder of the X-ray wavelength database was derived from relative measurements using crystal diffraction spectroscopy. Unfortunately, even the most refined among the ruled grating measurements did not give accuracies comparable to the precision accessible by relative wavelength measurements (Henins, 1971). As noted above, in connection with establishing the previous wavelength table, Bearden introduced a new local unit, the Å*, based on an explicit value for the wavelength of W $K\alpha_1$, chosen to give a conversion factor near unity. This transitional period will not be treated further in the present documentation since, to a substantial extent, developments described in the following paragraphs have effectively eliminated the need for a local scale for X-ray wavelength metrology.

Following the demonstration of crystal lattice interferometry in the X-ray region (Bonse & Hart, 1965), efforts to combine such an X-ray interferometer with various optical interferometers were undertaken in several (mostly national standards) laboratories. Although the earliest of these, carried out at the National Bureau of Standards (NBS) (now the National Institute of Standards and Technology, NIST) (Deslattes & Henins, 1973) was, in the end, found to be burdened by a serious systematic error (1.8×10^{-6}) in later work at the Physikalisch Technishe Bundesanstalt (PTB) (Becker *et al.*, 1981; Becker, Seyfried & Siegert, 1982), it was clear that accuracy limitations associated with ruled grating measurements no longer dominated the metrology of X-ray wavelengths. The origin of the systematic error in the early NBS measurement was subsequently understood (Deslattes, Tanaka, Greene, Henins & Kessler, 1987), and, more recently, excellent results were obtained in Italy (Basile, Bergamin, Cavagnero, Mana, Vittone & Zosi, 1994, 1995) and Japan (Fujimoto, Fujii, Tanaka & Nakayama, 1997). In all cases, the goal was to obtain an optical measurement of a crystal lattice period (thus far, only Si 220) and to use the calibrated crystals in diffraction spectrometry to establish optically based X-ray wavelengths. Such exercises have been undertaken for several X-ray lines, but the most detailed and well documented results to date were obtained in Jena (Härtwig, Hölzer, Wolf & Förster, 1993; Hölzer, Fritsch, Deutsch, Härtwig & Förster, 1997), where the $K\alpha$ and $K\beta$ spectra of the elements Cr to Cu were evaluated using silicon crystals well connected with the crystal spacings measured at the PTB.

4.2.2.5. *K-series reference wavelengths*

In addition to the Jena measurements noted above, a number of characteristic X-ray lines were measured on the optically based scale at NBS/NIST. The set of directly measured reference wavelengths is given in Table 4.2.2.1 in bold type. Most of the originally published (NBS/NIST) values were burdened by the 1.8×10^{-6} error in the silicon lattice period, as noted above. These have been corrected in the numerical results summarized in the table. The directly measured elements and lines appearing in this table were often chosen to meet the need for specific reference values in locations near those of certain optical transitions in highly charged ion spectra or spectra from pionic atoms. In addition, early NBS measurements specifically addressed the lines most often used in crystallography and the W $K\alpha$ transition. In response to the needs of electron spectroscopy, Al and Mg K spectra were also determined (Schweppe, Deslattes, Mooney & Powell, 1994). In this case, the original lattice error had been previously recognized, so that no rescaling was required. The remaining directly measured entries were obtained as opportunities to do so emerged.

The optically based data set was expanded by noting that several groups of accurate (relative) measurements in the literature either contained one of the directly measured lines (bold type) in Table 4.2.2.1 or were explicitly connected to one of them. Most often this situation was realized in reports that indicated a specific reference value, *i.e.* where it was stated numerical values are based on a scale where, for example, the wavelength of Mo $K\alpha_1$ was taken as 707.831 xu. In such cases, and where other indicators of good measurement quality are presented, it is easy to re-scale the data reported so that it is consistent with the optically based data. This procedure was followed for important groups of measurements from earlier work by Bearden and co-workers, and from the X-ray laboratory at Uppsala. The rescaled numerical results are included in Table 4.2.2.1 in normal type along with the specific literature citations. The indicated uncertainties are standard uncertainties as defined by ISO (Taylor & Kuyatt, 1994; Schwarzenbach, Abrahams, Flack, Prince & Wilson, 1995).

4.2.2.6. *L-series reference wavelengths*

To date, only a very limited number of L-series emission lines have been directly measured on an optically based scale. Wavelengths for directly measured L-series lines are reported in Table 4.2.2.2 along with the literature citations. In the future, we hope to expand this limited data set by including other lines and elements that are well connected to these reference lines in the literature.

4.2.2.7. *Absorption-edge locations*

Only a small number of absorption-edge locations have been directly measured to high accuracy using the currently acceptable protocols. Some of the available data were obtained in order to provide wavelength determinations for spectra from highly charged and/or exotic atoms (Bearden, 1960; Lum *et al.*, 1981). This small group was, however, significantly expanded very recently by an important set of new measurements, extending to $Z = 51$, that are well coupled to the optical wavelength scale (Kraft, Stümpel, Becker & Kuetgens, 1996) The resulting experimental database is summarized in Table 4.2.2.3. The effort that would be needed to expand the experimental database in a systematic way is quite large. Thus, we make use of a procedure, not previously used for this purpose, that combines available electron binding energy data with emission-line locations from our expanded reference set of emission-line data and emission lines that have been rescaled to be consistent with the optically based scale. At the same time, calculation of the location of absorption thresholds within the

Table 4.2.2.1. *K-series reference wavelengths in Å; bold numbers indicate a directly measured line*

Numbers in parentheses are standard uncertainties in the least-significant figures.

Z	Symbol	A	$K\alpha_2$	$K\alpha_1$	$K\beta_3$	$K\beta_1$	References
12	Mg		**9.89153 (10)**	**9.889554 (88)**			(*a*)
13	Al		**8.341831 (58)**	**8.339514 (58)**			(*a*)
14	Si		**7.12801 (14)**	**7.125588 (78)**			(*b*)
16	S		**5.374960 (89)**	**5.372200 (78)**			(*b*)
17	Cl		**4.730693 (71)**	**4.727818 (71)**			(*b*)
18	Ar		**4.194939 (23)**	**4.191938 (23)**			(*c*)
19	K		**3.7443932 (68)**	**3.7412838 (56)**			(*d*)
24	Cr		**2.2936510 (30)**	**2.2897260 (30)**	**2.0848810 (40)**	**2.0848810 (40)**	(*e*)
25	Mn		**2.1058220 (30)**	**2.1018540 (30)**	**1.9102160 (40)**	**1.9102160 (40)**	(*e*)
26	Fe		**1.9399730 (30)**	**1.9360410 (30)**	**1.7566040 (40)**	**1.7566040 (40)**	(*e*)
27	Co		**1.7928350 (10)**	**1.7889960 (10)**	**1.6208260 (30)**	**1.6208260 (30)**	(*e*)
28	Ni		**1.6617560 (10)**	**1.6579300 (10)**	**1.5001520 (30)**	**1.5001520 (30)**	(*e*)
29	Cu		**1.54442740 (50)**	**1.54059290 (50)**	**1.3922340 (60)**	**1.3922340 (60)**	(*e*)
31	Ga		**1.3440260 (40)**	**1.3401270 (96)**	1.208390 (75)	1.207930 (34)	(*b*),(*f*)
33	As		**1.108830 (31)**	**1.104780 (12)**	0.992689 (79)	0.992189 (53)	(*b*),(*f*)
34	Se		1.043836 (30)	**1.039756 (30)**	0.933284 (74)	0.932804 (30)	(*b*),(*f*)
36	Kr		**0.9843590 (44)**	**0.9802670 (40)**	**0.8790110 (70)**	**0.8785220 (50)**	(*b*)
40	Zr		**0.7901790 (25)**	**0.7859579 (27)**	**0.7023554 (30)**	**0.7018008 (30)**	(*b*)
42	Mo		0.713607 (12)	**0.70931715 (41)**	0.632887 (13)	0.632303 (13)	(*d*),(*f*)
44	Ru		0.6474205 (61)	0.6430994 (61)	0.5730816 (42)	0.5724966 (42)	(*d*),(*f*)
45	Rh		0.6176458 (61)	0.6132937 (61)	0.5462139 (42)	0.5456189 (42)	(*d*),(*f*)
46	Pd		0.5898351 (60)	0.5854639 (46)	0.5211363 (41)	0.5205333 (41)	(*d*),(*f*)
47	Ag		**0.5638131 (26)**	**0.55942178 (76)**	0.4976977 (60)	0.4970817 (60)	(*d*),(*f*)
48	Cd		0.5394358 (46)	0.5350147 (46)	0.4757401 (71)	0.4751181 (71)	(*d*),(*f*)
49	In		0.5165572 (60)	0.5121251 (46)	0.4551966 (41)	0.4545616 (41)	(*d*),(*f*)
50	Sn		0.4950646 (46)	0.4906115 (46)	0.4358821 (51)	0.4352421 (51)	(*d*),(*f*)
51	Sb		0.4748391 (45)	0.4703700 (45)	0.4177477 (41)	0.4170966 (31)	(*d*),(*f*)
54	Xe		**0.42088103 (71)**	**0.4163508 (14)**	**0.3694051 (13)**	**0.3687346 (13)**	(*d*)
56	Ba		**0.38968378 (74)**	**0.38512464 (84)**	**0.3415228 (11)**	**0.34082708 (75)**	(*d*)
60	Nd		**0.3248079 (59)**	**0.3201648 (59)**	0.283634 (59)	0.282904 (44)	(*d*),(*f*)
62	Sm		**0.31369830 (79)**	**0.30904506 (46)**	0.273764 (30)	0.273014 (30)	(*d*),(*f*)
67	Ho		0.26549088 (84)	0.2607608 (42)	0.230834 (30)	0.230124 (30)	(*f*),(*g*)
68	Er		**0.2571133 (11)**	**0.25237359 (62)**	**0.2234766 (14)**	**0.22269866 (72)**	(*d*)
69	Tm		0.24910095 (61)	0.24434486 (44)	0.216366 (30)	0.21559182 (57)	(*f*),(*h*)
74	W		0.21383304 (50)	**0.20901314 (18)**	0.18518317 (70)	0.1843768 (30)	(*d*),(*f*)
79	Au		**0.18507664 (61)**	**0.18019780 (47)**	**0.1598249 (13)**	**0.15899527 (77)**	(*d*)
82	Pb		**0.17029527 (56)**	**0.16537816 (38)**	**0.1468129 (10)**	**0.14596836 (58)**	(*d*)
83	Bi		0.1657183 (20)	0.1607903 (46)	0.142780 (11)	0.1419492 (54)	(*f*),(*g*)
90	Th	230	**0.13782600 (31)**	**0.13282021 (36)**	**0.11828686 (78)**	**0.11740759 (59)**	(*d*)
91	Pa	231	0.1343516 (29)	0.1293302 (27)	0.1152427 (21)	0.1143583 (21)	(*i*)
92	U	238	**0.13099111 (78)**	**0.12595977 (36)**	**0.11228858 (66)**	**0.11140132 (65)**	(*d*)
93	Np	237	0.1277287 (39)	0.1226882 (36)	0.1094230 (39)	0.1085265 (28)	(*i*)
94	Pu	239	0.1245782 (15)	0.11952120 (69)			(*h*)
94	Pu	244	0.1245705 (25)	0.1195140 (23)	0.1066611 (18)	0.1057595 (18)	(*i*)
95	Am	243	0.1215158 (24)	0.1164463 (33)	0.1039794 (17)	0.1030803 (17)	(*i*)
96	Cm	248	0.1185427 (23)	0.1134635 (21)	0.1013753 (17)	0.1004708 (16)	(*i*)
97	Bk	249	0.1156630 (54)	0.1105745 (49)	0.0988598 (55)	0.0979514 (54)	(*i*)
98	Cf	250	0.1128799 (82)	0.1077793 (75)			(*i*)

References: (*a*) Schweppe *et al*. (1994); (*b*) Mooney (1996); (*c*) Schweppe (1995); (*d*) Deslattes & Kessler (1985); (*e*) Hölzer *et al*. (1997); (*f*) Bearden (1967); (*g*) Borchert, Hansen, Jonson, Ravn & Desclaux (1980); (*h*) Borchert (1976); (*i*) Barreau, Börner, Egidy & Hoff (1982).

theoretical framework (see below) has been undertaken and will be made available in the longer publication and on the web site.

The feature of absorption spectra customarily designated as 'the absorption edge' has been variously associated with: the first inflection point of the absorption spectrum; the energy needed to produce a single inner vacancy with the photo-electron 'at rest at infinity'; or the energy needed to remove an electron from an inner shell and place it in the lowest unoccupied energy level. A general discussion of this question has been given by Parratt (1959). If we choose the second alternative, then it is easy to see that, with some care for symmetry restrictions, one can estimate the absorption-edge energy by combining the binding energy for any accessible outer shell with the energy of an emission line for which the transition terminus lies in the same outer shell. Of course, this procedure does not focus on the details of absorption thresholds, the locations of which are important for a number of structural applications. On the other hand, our choice gives greater regularity with respect to nuclear charge and facilitates use of electron binding energies, since they are referenced to the Fermi energy or the vacuum.

Electron binding energies have been tabulated for the principal electron shells of all the elements considered in the present table (Fuggle, Burr, Watson, Fabian & Lang, 1974; Cardona & Ley, 1978; Nyholm, Berndtsson & Mårtensson,

Table 4.2.2.2. *Directly measured L-series reference wavelengths in Å*

Numbers in parentheses are standard uncertainties in the least-significant figures.

Z	Symbol	$L\alpha_2$	$L\alpha_1$	$L\beta_1$	References
36	Kr	7.82032(13)	7.82032(13)	7.574441(98)	(*a*)
40	Zr	6.07710(48)	6.070250(79)	5.836214(76)	(*a*)
54	Xe	3.025940(22)	3.016582(15)	2.806553(19)	(*b*)
60	Nd	2.38079(52)	2.370526(16)	2.167008(19)	(*a*)
62	Sm	2.210430(24)	2.199873(13)	1.998432(30)	(*a*)
67	Ho	1.856472(15)	1.845092(17)	1.647484(32)	(*a*)
68	Er	1.795701(45)	1.784481(20)	1.587466(86)	(*a*)
69	Tm	1.738003(19)	1.7267720(70)	1.5302410(70)	(*a*)

References: (*a*) Mooney (1996); (*b*) Mooney *et al*. (1992).

1980; Nyholm & Mårtensson, 1980; Lebugle, Axelsson, Nyholm & Mårtensson, 1981; Powell, 1995). The number of values available offers the possibility of consistency checking, since the K and L shells are connected by emission lines to several final hole states, each of which has (possibly) been evaluated by photoelectron spectroscopy. For each of the elements for which well qualified reference spectra are available, we evaluated edge location estimates using several alternative transition cycles and used the distribution of results to provide a measure of the uncertainty. Comparison of edge estimates obtained by this procedure with experimental data provides a quantitative test of the utility of the chosen approach to edge location estimation. In Table 4.2.2.3, the numerical results in the column labelled 'Emission + binding energies' were obtained by combining emission energies and electron binding energies using all possible redundancies. The estimated uncertainties indicated were obtained from the distribution of the redundant routes. As can be seen, the results are in general agreement with the available directly measured values. Accordingly, we have used this protocol to obtain the edge locations listed in the summary tables below.

4.2.2.8. *Outline of the theoretical procedures*

Only recently has it become possible to understand the relativistic many-body problem in atoms with sufficient detail to permit meaningful calculation of transition energies between hole states (Indelicato & Lindroth, 1992; Mooney, Lindroth, Indelicato, Kessler & Deslattes, 1992; Lindroth & Indelicato, 1993, 1994; Indelicato & Lindroth, 1996). To deal with those hole states for atomic numbers ranging from 10 to 100, one needs to consider five kinds of contributions, all of which must be calculated in a relativistic framework, and the relative influence of which can change strongly as a function of the atomic number:

(i) nuclear size;

(ii) relativistic effects (corrections to Coulomb energy, magnetic and retardation energy);

(iii) Coulomb and Breit correlation;

(iv) radiative (QED) corrections (one- and two-electron Lamb shift *etc*.);

(v) Auger shift.

Such an undertaking, although much more advanced than any other done in the past, still suffers from severe limitations that need to be understood fully to make the best use of the table. The main limitation is probably that most lines are emitted by atoms in an elemental solid or a compound, while the calculation at present deals only with atoms isolated in vacuum. (A purely experimental database would have a similar limitation.) The second limitation is that it is not possible at present to include the coupling between the hole and open outer shells. Coupling between a $j = \frac{1}{2}$, $j = \frac{3}{2}$ or $j = \frac{5}{2}$ hole and an external $3d$ or $4f$ shell can generate hundreds of levels, with splitting that can reach an eV. One then should calculate all radiative and Auger transition probabilities between hundreds of initial and final states. (The Auger final state would have one extra vacancy, leading eventually to thousands of final states.) Such an approach would give not only the mean line energy but also its shape and would thus be very desirable, but is impossible to do with present day theoretical tools and computers. We have thus limited ourselves to an approach in which one computes the weighted average energy for each hole state, and ignores possible distortion of the line profile due to the coupling between inner vacancies and outer shells.

Since we want to have good predictions for both light and heavy atoms, we have to include relativity non-perturbatively. To get a result approaching 1×10^{-6} for uranium $K\alpha$ by applying perturbation theory to the Schrödinger equation, for example, one would need to go to order 22 in powers of $Z\alpha = v/c$. The natural framework in this case is thus to do a calculation exact to all orders in $Z\alpha$ by using the Dirac equation. We thus have used many-body methods, based on the Dirac equation, in which the main contributions to the transition energy are evaluated using the Dirac–Fock method. We use the Breit operator for the electron–electron interaction, to include magnetic (spin–spin, spin–other orbit and orbit–orbit interactions in the lower orders in $Z\alpha$ and $(v/c)^2$ retardation effects. Higher-order retardation effects are also included.

Table 4.2.2.3. *Directly measured and emission + binding energies (see text) K-absorption edges in Å*

Numbers in parentheses are standard uncertainties in the least significant figures.

Z	Symbol	Directly measured	Emission + binding energies	References
23	V	2.269211(21)	2.26893(11)	(*a*)
24	Cr	2.070193(14)	2.07014(17)	(*a*)
25	Mn	1.8964592(58)	1.896457(42)	(*a*)
26	Fe	1.7436170(49)	1.743589(98)	(*a*)
27	Co	1.6083510(42)	1.60836(17)	(*a*)
28	Ni	1.4881401(36)	1.48823(25)	(*a*)
29	Cu	1.3805971(31)	1.38060(16)	(*a*)
30	Zn	1.2833798(40)	1.28338(15)	(*a*)
39	Y	0.7277514(21)	0.727750(23)	(*a*)
40	Zr	0.6889591(31)	0.688946(30)	(*a*)
41	Nb	0.6531341(14)	0.653112(29)	(*a*)
42	Mo	0.61991006(62)	0.619906(64)	(*a*)
45	Rh	0.5339086(69)	0.533951(10)	(*a*)
46	Pd	0.5091212(42)	0.509156(11)	(*a*)
47	Ag	0.4859155(57)	0.4859168(91)	(*a*)
48	Cd	0.4641293(35)	0.464135(12)	(*a*)
49	In	0.4437454(48)	0.443740(11)	(*a*)
50	Sn	0.4245978(29)	0.424590(13)	(*a*)
51	Sb	0.4066324(27)	0.406612(12)	(*a*)
68	Er	0.2156801(75)	0.2156762(50)	(*b*)
82	Pb	0.1408821(74)	0.1408836(11)	(*c*)

References: (*a*) Kraft *et al*. (1996); (*b*) Lum *et al*. (1981); (*c*) Bearden (1960).

Many-body effects are calculated by using relativistic many-body perturbation theory (RMBPT). Since inner vacancy levels are auto-ionizing, one must include shifts in their energy due to the coupling between the discrete levels and Auger decay continuua.

In the following subsections, we describe in more detail the calculation of the different contributions.

4.2.2.9. *Evaluation of the uncorrelated energy with the Dirac–Fock method*

The first step in the calculation, following Indelicato and collaborators (Indelicato & Desclaux, 1990; Indelicato & Lindroth, 1992; Mooney *et al.*, 1992; Lindroth & Indelicato, 1993; Indelicato & Lindroth, 1996) consists in evaluating the best possible energy with relativistic corrections, within the independent electron approximation, for each hole state (here $1s_{\frac{1}{2}}$, $2p_{\frac{1}{2}}$, $2p_{\frac{3}{2}}$, $3p_{\frac{1}{2}}$, $3p_{\frac{3}{2}}$ for K, $L_{\rm II}$, $L_{\rm III}$, $M_{\rm II}$, $M_{\rm III}$, respectively). Such a calculation must provide a suitable starting point for adding all many-body and QED contributions. We have thus chosen the Dirac–Fock method in the implementation of Desclaux (1975, 1993). This method, based on the Dirac equation, allows treatment of arbitrary atoms with arbitrary structure and has been widely used for this kind of calculation. We have used it with full exchange and relaxation (to account for inactive orbital rearrangment due to the hole presence). The electron–electron interaction used in this program contains all magnetic and retardation effects, which is very important to have good results at large Z. The magnetic interaction is treated on an equal footing with the Coulomb interaction, to account for higher-order effects in the wavefunction (which are also useful for evaluating radiative corrections to the electron–electron interaction). All these calculations must be done with proper nuclear charge models to account for finite-nuclear-size corrections to all contributions. For heavy nuclei, nuclear deformations must be accounted for (Blundell, Johnson & Sapirstein, 1990; Indelicato, 1990). For all elements for which experiments have been performed, we used experimental nuclear charge radii. For the others we used a formula from Johnson & Soff (1985), corrected for nuclear deformations for $Z > 90$. Contribution of deformation to the r.m.s. radius (the only parameter of importance to the atomic calculation) is roughly constant (0.11 fm) for $Z > 90$. There is an unknown region, between Bi and Th ($83 < Z < 90$), where deformation effects start to be important, but for which they are not known. When experiments are done for a particular isotope, we calculated separately the energies for each isotope.

As mentioned in the introduction, there are special difficulties involved when dealing with atoms with open outer shells (obviously this is the most common case). Computing all energies E_J for total angular momentum J would be both impossible and useless. The Dirac–Fock method circumvents this difficulty. One can evaluate directly an average energy that corresponds to the barycentre of all E_J with weight $(2J + 1)$. There are still a few cases for which the average calculation cannot converge (when the open shells have identical symmetry). In that case, the outer electrons have been rearranged in an identical fashion for all hole states of the atom, to minimize possible shifts due to this procedure.

4.2.2.10. *Correlation and Auger shifts*

Once the Dirac–Fock energy is obtained, many-body effects beyond Dirac–Fock relaxation must be taken into account. These include relaxation beyond the spherical average, correlation (due to both Coulomb and magnetic interaction), and corrections due to the autoionizing nature of hole states (Auger shift). Since the many-body generalization of the Dirac–Fock method, the so-called MCDF (multiconfiguration Dirac–Fock), is very inefficient for hole states, we turned to RMBPT to evaluate those quantities. These many-body effects contribute very significantly to the final value. Coulomb correlation is mostly constant along the Periodic Table (at the level of a few eV). Magnetic correlations are very strong at high Z. Auger shift is very important for p states. The interested reader will find more details of these complicated calculations in the original references (Indelicato & Lindroth, 1992; Mooney *et al.*, 1992; Lindroth & Indelicato, 1993; Indelicato & Lindroth, 1996). As these calculations are very time consuming, they are performed only for selected Z and interpolated. Since the Auger shifts do not always have a smooth Z dependence, care has been taken to evaluate them at as many different Z's as practical to ensure a good reproduction of irregularities.

4.2.2.11. *QED corrections*

The QED corrections originate in the quantum nature of both the electromagnetic and electron fields. They can be divided in two categories, radiative and non-radiative. The first one includes self-energy and vacuum polarization, which are the main contributions to the Lamb shift in one-electron atoms. These corrections scale as Z^4/n^3 (n being the principal quantum number) and are thus very important for inner shells and high Z. The second category is composed of corrections to the electron–electron interaction that cannot be accounted for by RMBPT or MCDF. These corrections start at the two-photon interaction and include three-body effects. The two-photon, non-radiative QED contribution has been calculated recently only for the ground

Table 4.2.2.4. *Wavelengths of K-emission lines and K-absorption edges in Å; see text for explanation of typefaces*

Numbers in parentheses are standard uncertainties in the least significant figures.

Z	Symbol	A	$K\alpha_2$	$K\alpha_1$	$K\beta_3$	$K\beta_1$	$K\beta_2^{II}$	$K\beta_2^{I}$	K abs. edge
10	Ne		*14.6020(93)*	*14.6006(93)*					*14.2391(26)*
			14.6102(44)	14.6102(44)	14.4522(74)	14.4522(74)			14.30201(15)
11	Na		*11.9013(59)*	*11.8994(59)*					*11.4784(16)*
			11.9103(13)	11.9103(13)	11.5752(30)	11.5752(30)			11.5692(15)
12	Mg		*9.8860(39)*	*9.8840(39)*					*9.4479(10)*
			9.89153(10)	**9.889554(88)**	9.5211(30)	9.5211(30)			9.51234(15)
13	Al		*8.3372(27)*	*8.3349(26)*	*7.9412(49)*				*7.89928(67)*
			8.341831(58)	**8.339514(58)**	7.9601(30)	7.9601(30)			7.948249(74)
14	Si		*7.1269(19)*	*7.1208(19)*	*6.7317(26)*				*6.70091(46)*
			7.12801(14)	**7.125588(78)**	6.7531(15)	6.7531(15)			6.7381(15)
15	P		*6.1587(14)*	*6.1539(14)*	*5.7834(16)*	*5.7914(27)*			*5.75537(33)*
			6.1601(15)	6.1571(15)	5.7961(30)	5.7961(30)			5.7841(15)
16	S		*5.3742(10)*	*5.3701(10)*	*5.0202(12)*	*5.0246(15)*			*4.99591(24)*
			5.374960(89)	**5.372200(78)**		5.03168(30)			5.01858(15)
17	Cl		*4.72993(80)*	*4.72560(77)*	*4.39810(99)*	*4.40038(77)*			*4.37679(18)*
			4.730693(71)	**4.727818(71)**	4.40347(44)	4.40347(44)			4.39717(15)
18	Ar		*4.19448(62)*	*4.19162(60)*	*3.88506(71)*	*3.88486(70)*			*3.86552(14)*
			4.194939(23)	**4.191938(23)**	3.88606(30)	3.88606(30)			3.870958(74)
19	K		*3.74352(50)*	*3.74055(48)*	*3.45189(69)*	*3.45216(58)*			*3.42856(11)*
			3.7443932(68)	**3.7412838(56)**	3.45395(30)	3.45395(30)			3.43655(15)
20	Ca		*3.36223(39)*	*3.35911(38)*	*3.08855(45)*	*3.08827(45)*			*3.061828(87)*
			3.361710(44)	3.358440(44)	3.08975(30)	3.08975(30)			3.07035(15)
21	Sc		*3.03479(33)*	*3.03129(31)*	*2.77919(50)*	*2.77809(49)*			*2.754176(71)*
			3.0344010(63)	3.030854(14)	2.77964(30)	2.77964(30)			2.7620(15)
22	Ti		*2.75272(27)*	*2.74886(26)*	*2.51445(43)*	*2.51262(45)*			*2.490681(59)*
			2.7521950(57)	2.7485471(57)	2.513960(30)	2.513960(30)			2.497377(74)
23	V		*2.50798(23)*	*2.50383(21)*	*2.28567(37)*	*2.28332(40)*			*2.263194(49)*
			2.507430(30)	2.503610(30)	2.284446(30)	2.284446(30)			**2.269211(21)**
24	Cr		*2.29428(19)*	*2.29012(18)*	*2.08702(32)*	*2.08478(35)*			*2.067898(41)*
			2.2936510(30)	**2.2897260(30)**	**2.0848810(40)**	**2.0848810(40)**			**2.070193(14)**
25	Mn		*2.10635(16)*	*2.10210(15)*	*1.91175(28)*	*1.90960(31)*			*1.892275(36)*
			2.1058220(30)	**2.1018540(30)**	**1.9102160(40)**	**1.9102160(40)**			**1.8964592(58)**
26	Fe		*1.94043(14)*	*1.93631(13)*	*1.75784(25)*	*1.75617(27)*			*1.739918(31)*
			1.9399730(30)	**1.9360410(30)**	**1.7566040(40)**	**1.7566040(40)**			**1.7436170(49)**
27	Co		*1.79321(12)*	*1.78919(11)*	*1.62166(22)*	*1.62039(24)*			*1.605127(27)*
			1.7928350(10)	**1.7889960(10)**	**1.6208260(30)**	**1.6208260(30)**			**1.6083510(42)**
28	Ni		*1.66199(10)*	*1.658049(96)*	*1.50059(19)*	*1.49964(21)*			*1.485300(24)*
			1.6617560(10)	**1.6579300(10)**	**1.5001520(30)**	**1.5001520(30)**			**1.4881401(36)**
29	Cu		*1.544324(93)*	*1.540538(85)*	*1.39246(17)*	*1.39201(18)*			*1.379448(23)*
			1.54442740(50)	**1.54059290(50)**	**1.3922340(60)**	**1.3922340(60)**			**1.3805971(31)**
30	Zn		*1.438963(84)*	*1.435151(74)*	*1.29544(17)*	*1.29506(16)*			*1.282346(20)*
			1.439029(12)	1.435184(12)	1.295276(30)	1.295276(30)	1.283739(30)	1.283739(30)	**1.2833798(40)**
31	Ga		*1.343987(72)*	*1.340095(65)*	*1.20821(13)*	*1.20774(14)*	*1.195547(25)*		*1.194711(18)*
			1.3440260(40)	**1.3401270(96)**	1.208390(75)	1.207930(34)	1.196018(30)	1.196018(30)	1.19582(15)
32	Ge		*1.257998(65)*	*1.254054(58)*	*1.12924(13)*	*1.12877(13)*	*1.116387(37)*		*1.115585(16)*
			1.258030(13)	1.254073(13)	1.12938(13)	1.128957(30)	1.116877(30)	1.116877(30)	1.116597(74)
33	As		*1.179921(57)*	*1.175932(52)*	*1.05774(11)*	*1.05724(11)*	*1.044699(56)*	*1.044836(20)*	*1.043925(16)*
			1.179959(17)	**1.17595600(90)**	1.057898(76)	1.057368(33)	1.045016(44)	1.045016(44)	1.04502(15)
34	Se		*1.108801(52)*	*1.104778(47)*	*0.992646(96)*	*0.992152(95)*	*0.979618(57)*	*0.979716(26)*	*0.978818(15)*
			1.108830(31)	**1.104780(12)**	0.992689(79)	0.992189(53)	0.979935(74)	0.979935(74)	0.979755(15)
35	Br		*1.043841(47)*	*1.039785(42)*	*0.933275(87)*	*0.932768(84)*	*0.920344(49)*	*0.920390(28)*	*0.919501(13)*
			1.043836(30)	1.039756(30)	0.933284(74)	0.932804(30)	0.920474(30)	0.920474(30)	0.92041(15)
36	Kr		*0.984347(42)*	*0.980267(38)*	*0.878967(81)*	*0.878495(75)*	*0.866209(36)*	*0.866169(35)*	*0.865324(12)*
			0.9843590(44)	**0.9802670(40)**	**0.8790110(70)**	**0.8785220(50)**	0.86611(15)	0.86611(15)	0.865533(15)
37	Rb		*0.929713(39)*	*0.925597(35)*	*0.829174(71)*	*0.828681(67)*	*0.816459(33)*	*0.816408(33)*	*0.815270(12)*
			0.929704(15)	0.925567(13)	0.829222(44)	0.828692(30)	0.816462(44)	0.816462(44)	0.815552(74)
38	Sr		*0.879444(36)*	*0.875298(32)*	*0.783413(63)*	*0.782911(58)*	*0.770774(33)*	*0.770718(20)*	*0.769359(11)*
			0.879443(15)	0.875273(15)	0.783462(44)	0.782932(30)	0.770822(44)	0.770822(44)	0.769742(74)
39	Y		*0.833059(32)*	*0.828875(29)*	*0.741232(58)*	*0.740716(53)*	*0.728801(27)*	*0.728663(21)*	*0.727270(10)*
			0.833063(15)	0.828852(15)	0.741271(44)	0.740731(30)	0.728651(59)	0.728651(59)	**0.7277514(21)**
40	Zr		*0.790181(30)*	*0.785960(27)*	*0.702296(53)*	*0.701766(48)*	*0.690079(28)*	*0.689895(21)*	*0.6884893(99)*
			0.7901790(25)	**0.7859579(27)**	**0.7023554(30)**	**0.7018008(30)**	0.689940(59)	0.689940(59)	**0.6889591(31)**
41	Nb		*0.750448(28)*	*0.746189(25)*	*0.666266(49)*	*0.665721(44)*	*0.654328(31)*	*0.654078(22)*	*0.6528690(93)*
			0.750451(15)	0.746211(15)	0.666350(44)	0.665770(30)	0.654170(59)	0.654170(59)	**0.6531341(14)**
42	Mo		*0.713612(25)*	*0.709328(22)*	*0.632900(44)*	*0.632345(38)*	*0.621162(35)*	*0.620941(21)*	*0.6196481(87)*
			0.713607(12)	**0.70931715(41)**	0.632887(13)	0.632303(13)	0.620999(30)	0.620999(30)	**0.61991006(62)**

Table 4.2.2.4. *Wavelengths of K-emission lines and K-absorption edges in Å (cont.)*

Z	Symbol	A	$K\alpha_2$	$K\alpha_1$	$K\beta_3$	$K\beta_1$	$K\beta_2^{II}$	$K\beta_2^{I}$	K abs. edge
43	Tc		*0.679318(24)*	*0.675017(21)*	*0.601881(40)*	*0.601318(35)*	*0.590423(40)*	*0.590231(22)*	*0.5889852(84)*
			0.679330(44)	0.675030(44)	0.601889(59)	0.601309(59)	0.590249(74)	0.590249(74)	0.589069(15)
44	Ru		*0.647415(22)*	*0.643088(20)*	*0.573053(37)*	*0.572478(32)*	*0.561748(44)*	*0.561587(22)*	*0.5603122(81)*
			0.6474205(61)	0.6430994(61)	0.5730816(42)	0.5724966(42)	0.561668(44)	0.561668(44)	0.560518(15)
45	Rh		*0.617652(21)*	*0.613305(18)*	*0.546191(34)*	*0.545606(29)*	*0.535110(48)*	*0.534977(22)*	*0.5337192(74)*
			0.6176458(61)	0.6132937(61)	0.5462139(42)	0.5456189(42)	0.535038(30)	0.535038(30)	**0.5339086(69)**
46	Pd		*0.589822(20)*	*0.585459(18)*	*0.521117(29)*	*0.520514(27)*	*0.510283(46)*	*0.510177(51)*	*0.5090158(75)*
			0.5898351(60)	0.5854639(46)	0.5211363(41)	0.5205333(41)	0.5102357(59)	0.5102357(59)	0.5091212(42)
47	Ag		*0.563804(18)*	*0.559420(17)*	*0.497673(29)*	*0.497069(25)*	*0.487060(55)*	*0.487019(38)*	*0.4857609(74)*
			0.5638131(26)	**0.55942178(76)**	0.4976977(60)	0.4970817(60)	0.4870393(59)	0.4870393(59)	**0.4859155(57)**
48	Cd		*0.539426(18)*	*0.535020(15)*	*0.475739(27)*	*0.475124(23)*	*0.465335(62)*	*0.465346(28)*	*0.4640026(71)*
			0.5394358(46)	0.5350147(46)	0.4757401(71)	0.4751181(71)	0.465335(10)	0.465335(10)	**0.4641293(35)**
49	In		*0.516551(17)*	*0.512124(15)*	*0.455178(25)*	*0.454552(22)*	*0.445014(58)*	*0.445011(27)*	*0.4435977(70)*
			0.5165572(60)	0.5121251(46)	0.4551966(41)	0.4545616(41)	0.445007(15)	0.445007(15)	**0.4437454(48)**
50	Sn		*0.495060(16)*	*0.490612(14)*	*0.435878(24)*	*0.435241(20)*	*0.426120(12)*	*0.425928(26)*	*0.4244611(68)*
			0.4950646(46)	0.4906115(46)	0.4358821(51)	0.4352421(51)	0.425921(12)	0.425921(12)	**0.4245978(29)**
51	Sb		*0.474840(15)*	*0.470373(13)*	*0.417736(22)*	*0.417089(19)*	*0.408017(57)*	*0.408004(25)*	*0.4064886(65)*
			0.4748391(45)	0.4703700(45)	0.4177477(41)	0.4170966(31)	0.4079791(74)	0.4079791(74)	**0.4066324(27)**
52	Te		*0.455795(14)*	*0.451310(13)*	*0.400664(21)*	*0.400008(18)*	*0.391161(56)*	*0.391135(27)*	*0.3895899(64)*
			0.4557908(44)	0.4513018(44)	0.4006650(59)	0.4000010(44)	0.3911079(89)	0.3911079(89)	0.389746(15)
53	I		*0.437834(13)*	*0.433330(12)*	*0.384576(20)*	*0.383910(17)*	*0.375286(54)*	*0.375234(29)*	*0.3736775(61)*
			0.437836(10)	0.4333245(74)	0.3845698(59)	0.3839108(59)	0.375236(30)	0.375236(30)	0.373816(15)
54	Xe		*0.420879(42)*	*0.416358(40)*	*0.369407(40)*	*0.368730(38)*	*0.360326(72)*	*0.36034(12)*	*0.358683(27)*
			0.42088103(71)	**0.4163508(14)**	**0.3694051(13)**	**0.3687346(13)**	0.360265(44)	0.360265(44)	0.35841(74)
55	Cs		*0.404848(13)*	*0.400310(11)*	*0.355067(17)*	*0.354385(16)*	*0.346197(49)*	*0.346102(37)*	*0.3444778(59)*
			0.4048411(59)	0.4002960(59)	0.3550553(59)	0.354369(10)	0.346115(30)	0.346115(30)	0.344515(15)
56	Ba		*0.389684(12)*	*0.385129(11)*	*0.341517(16)*	*0.340826(15)*	*0.33285(14)*	*0.332728(12)*	*0.3310639(56)*
			0.38968378(74)	**0.38512464(84)**	**0.3415228(11)**	**0.34082708(75)**	0.332775(15)	0.332775(15)	0.331045(15)
57	La		*0.375320(11)*	*0.370748(10)*	*0.328692(16)*	*0.327993(14)*	*0.32023(13)*	*0.320101(11)*	*0.3184025(55)*
			0.3753186(30)	0.3707426(30)	0.3286909(59)	0.3279879(44)	0.320122(10)	0.320122(10)	0.318445(74)
58	Ce		*0.361685(11)*	*0.3570964(97)*	*0.316507(15)*	*0.315795(14)*	*0.30827(12)*	*0.308131(10)*	*0.3065382(54)*
			0.3616884(30)	0.3570974(30)	0.3165248(59)	0.3158207(30)	0.308165(15)	0.308165(15)	0.306485(74)
59	Pr		*0.348755(10)*	*0.3441494(94)*	*0.304970(14)*	*0.304249(13)*	*0.29694(11)*	*0.2967952(99)*	*0.2952418(53)*
			0.3487542(30)	0.3441452(30)	0.3049796(74)	0.3042656(59)	0.296794(30)	0.296794(30)	0.295184(74)
60	Nd		*0.336473(10)*	*0.3318514(91)*	*0.294021(13)*	*0.293290(13)*	*0.28619(10)*	*0.2860408(94)*	*0.2845288(52)*
			0.33647921(73)	**0.33185689(62)**	0.2940366(40)	0.2933086(40)	0.28610(15)	0.28610(15)	0.284534(74)
61	Pm		*0.3247982(98)*	*0.3201607(88)*	*0.283620(13)*	*0.282880(12)*	*0.275992(98)*	*0.2758335(91)*	*0.2743634(53)*
			0.3248079(59)	0.3201648(59)	0.283634(59)	0.282904(44)	0.27590(15)	0.27590(15)	0.274314(74)
62	Sm		*0.3136913(94)*	*0.3090384(84)*	*0.273732(12)*	*0.272984(12)*	*0.266459(91)*	*0.2661277(87)*	*0.2647027(51)*
			0.31369830(79)	**0.30904506(46)**	0.273764(30)	0.273014(30)	0.26620(15)	0.26620(15)	0.264644(74)
63	Eu		*0.3031139(91)*	*0.2984457(81)*	*0.264322(12)*	*0.263567(11)*	*0.257069(85)*	*0.2569028(81)*	*0.2555123(51)*
			0.3031225(30)	0.2984505(30)	0.2643360(74)	0.2635810(74)	0.256927(12)	0.256927(12)	0.255534(15)
64	Gd		*0.2930400(89)*	*0.2883568(79)*	*0.255371(11)*	*0.254610(11)*	*0.248289(23)*	*0.2481186(76)*	*0.2467265(48)*
			0.2930424(30)	0.2883573(30)	0.255344(30)	0.254604(30)	0.248164(44)	0.248164(44)	0.246814(15)
65	Tb		*0.2834212(86)*	*0.2787234(76)*	*0.246818(11)*	*0.246054(11)*	*0.239916(21)*	*0.2397496(75)*	*0.2384335(49)*
			0.2834273(30)	0.2787242(30)	0.246834(30)	0.246084(30)	0.23970(30)	0.23970(30)	0.238414(15)
66	Dy		*0.2742462(84)*	*0.2695341(74)*	*0.238671(10)*	*0.237902(10)*	*0.231955(12)*	*0.2318190(53)*	*0.2304867(46)*
			0.2742511(30)	0.2695370(30)	0.238624(30)	0.237884(30)	0.23170(30)	0.23170(30)	0.230483(15)
67	Ho		*0.2654851(81)*	*0.2607589(72)*	*0.230896(10)*	*0.230122(10)*	*0.224320(18)*	*0.2241536(66)*	*0.2229099(45)*
			0.26549088(84)	0.2607608(42)	0.230834(30)	0.230124(30)	0.22410(30)	0.22410(30)	0.222913(15)
68	Er		*0.2571059(79)*	*0.2523659(71)*	*0.2234662(97)*	*0.2226875(98)*	*0.217046(16)*	*0.2168806(64)*	*0.2156719(45)*
			0.2571133(11)	**0.25237359(62)**	**0.2234766(14)**	**0.22269866(72)**	0.21670(30)	0.21670(30)	**0.2156801(75)**
69	Tm		*0.2490952(77)*	*0.2443415(68)*	*0.2163665(94)*	*0.2155833(95)*	*0.210099(15)*	*0.2099331(62)*	*0.2087587(44)*
			0.24910095(61)	0.24434486(44)	0.216366(30)	0.21559182(57)	0.20980(30)	0.20980(30)	0.208803(74)
70	Yb		*0.2414274(75)*	*0.2366603(67)*	*0.2095741(93)*	*0.2087863(95)*	*0.203456(14)*	*0.2032912(59)*	*0.2021481(43)*
			0.2414276(30)	0.2366586(30)	0.20960(15)	0.208843(30)	0.20330(30)	0.20330(30)	0.202243(74)
71	Lu		*0.2340857(73)*	*0.2293053(65)*	*0.2030802(88)*	*0.2022872(90)*	*0.197101(13)*	*0.1969329(58)*	*0.1957973(42)*
			0.2340845(30)	0.2293014(30)	0.203093(59)	0.202313(44)	0.19690(30)	0.19690(30)	0.195853(74)
72	Hf		*0.2270507(72)*	*0.2222572(64)*	*0.1968603(86)*	*0.1960622(88)*	*0.191017(13)*	*0.1908468(56)*	*0.1897176(42)*
			0.2270274(44)	0.2222303(44)	0.196863(59)	0.196073(44)	0.19080(30)	0.19080(30)	0.189823(74)
73	Ta		*0.2203039(70)*	*0.2154977(63)*	*0.1908986(83)*	*0.1900954(86)*	*0.185143(12)*	*0.1849702(54)*	*0.1838657(41)*
			0.2203083(59)	0.2155002(59)	0.1908929(30)	0.1900919(59)	0.185191(13)	0.185014(12)	0.183943(15)
74	W		*0.2138327(69)*	*0.2090134(61)*	*0.1851834(81)*	*0.1843751(83)*	*0.179595(12)*	*0.1794215(52)*	*0.1783098(41)*
			0.21383304(50)	**0.20901314(18)**	**0.18518317(70)**	**0.1843768(30)**	0.179603(15)	0.179424(10)	0.178373(15)
75	Re		*0.2076150(67)*	*0.2027835(60)*	*0.1796955(79)*	*0.1788824(81)*	*0.174234(11)*	*0.1740571(51)*	*0.1729509(40)*
			0.2076141(15)	0.2027840(30)	0.1796997(44)	0.1788827(44)	0.174253(15)	0.1740566(89)	0.173023(15)

Table 4.2.2.4. *Wavelengths of K-emission lines and K-absorption edges in Å (cont.)*

Z	Symbol	A	$K\alpha_2$	$K\alpha_1$	$K\beta_3$	$K\beta_1$	$K\beta_2^{II}$	$K\beta_2^{I}$	K abs. edge
76	Os		*0.2016443(66)*	*0.1968007(59)*	*0.1744279(77)*	*0.1736101(79)*	*0.169085(11)*	*0.1689066(50)*	*0.1678092(40)*
			0.2016420(30)	0.1967970(30)	0.1744336(44)	0.1736136(44)	0.169103(15)	0.1689085(89)	0.167873(15)
77	Ir		*0.1959045(65)*	*0.1910492(57)*	*0.1693667(75)*	*0.1685444(77)*	*0.164150(11)*	*0.1639697(51)*	*0.1628853(39)*
			0.1959069(30)	0.1910499(30)	0.1693695(30)	0.1685445(30)	0.164152(15)	0.163958(10)	0.162922(15)
78	Pt		*0.1903859(61)*	*0.1855187(55)*	*0.1645026(72)*	*0.1636756(74)*	*0.1593872(99)*	*0.1592048(46)*	*0.1581346(38)*
			0.1903839(59)	0.1855138(59)	0.1645035(44)	0.1636775(44)	0.159392(15)	0.159202(15)	0.158182(15)
79	Au		*0.1850702(64)*	*0.1801914(57)*	*0.1598202(73)*	*0.1589887(75)*	*0.1548206(99)*	*0.1546363(48)*	*0.1535699(40)*
			0.18507664(61)	**0.18019780(47)**	**0.1598249(13)**	**0.15899527(77)**	0.154832(30)	0.154620(13)	0.1535953(74)
80	Hg		*0.1799628(61)*	*0.1750720(54)*	*0.1553217(69)*	*0.1544857(72)*	*0.1504204(94)*	*0.1502334(46)*	*0.1491786(38)*
			0.1799607(44)	0.1750706(44)	0.1553233(44)	0.1544893(44)	0.150402(30)	0.150202(30)	0.149182(15)
81	Tl		*0.1750380(60)*	*0.1701355(53)*	*0.1509866(68)*	*0.1501462(70)*	*0.1461874(92)*	*0.1459989(77)*	*0.1449460(37)*
			0.1750386(30)	0.1701386(30)	0.1509823(89)	0.1501443(74)	0.146142(15)	0.145952(15)	0.144952(15)
82	Pb		*0.1702924(59)*	*0.1653781(53)*	*0.1468107(67)*	*0.1459663(68)*	*0.1421118(88)*	*0.1419201(75)*	*0.1408707(37)*
			0.17029527(56)	**0.16537816(38)**	**0.1468129(10)**	**0.14596836(58)**	0.142122(30)	0.141912(15)	0.1408821(74)
83	Bi	209	*0.1657170(58)*	*0.1607911(52)*	*0.1427865(65)*	*0.1419372(66)*	*0.1381841(87)*	*0.1379910(72)*	*0.1369439(37)*
			0.1657183(20)	0.1607903(46)	0.142780(11)	0.1419492(54)	0.138172(15)	0.137972(15)	0.136942(15)
84	Po	209	*0.1613031(58)*	*0.1563656(51)*	*0.1389056(63)*	*0.1380520(65)*	*0.1343966(85)*	*0.1342012(69)*	*0.1331589(36)*
			0.161302(15)	0.156362(15)	0.138922(30)	0.138072(30)	0.134382(30)	0.134182(30)	
85	At	210	*0.1570444(56)*	*0.1520953(50)*	*0.1351623(62)*	*0.1343044(63)*	*0.1307448(83)*	*0.1305470(67)*	*0.1295098(36)*
			0.157052(30)	0.152102(30)	0.135172(59)	0.134322(59)	0.130722(59)	0.130522(59)	
86	Rn	222	*0.1529334(56)*	*0.1479727(49)*	*0.1315499(61)*	*0.1306882(61)*	*0.1272218(79)*	*0.1270211(66)*	*0.1259898(35)*
			0.152942(44)	0.147982(44)	0.131552(74)	0.130692(74)	0.127192(74)	0.126982(74)	
87	Fr	223	*0.1489599(56)*	*0.1439878(50)*	*0.1280599(60)*	*0.1271937(61)*	*0.1238183(79)*	*0.1236157(63)*	*0.1225852(36)*
			0.148962(44)	0.143992(44)	0.128072(74)	0.127192(74)	0.123792(74)	0.123582(74)	
88	Ra	226	*0.1451209(54)*	*0.1401373(48)*	*0.1246890(58)*	*0.1238185(59)*	*0.1205312(77)*	*0.1203271(60)*	*0.1192985(35)*
			0.145119(20)	0.140132(19)	0.124689(15)	0.123815(15)	0.120535(14)	0.120320(14)	
89	Ac	227	*0.1414083(54)*	*0.1364131(47)*	*0.1214301(57)*	*0.1205554(58)*	*0.1173552(73)*	*0.1171477(59)*	*0.1161246(34)*
			0.141412(30)	0.136419(12)	0.121432(30)	0.120552(30)	0.117322(30)	0.117112(30)	
90	Th	232	*0.1378266(53)*	*0.1328194(47)*	*0.1182861(56)*	*0.1174071(56)*	*0.1142910(71)*	*0.1140810(57)*	*0.1130642(34)*
			0.13782600(31)	**0.13282021(36)**	**0.11828686(78)**	**0.11740759(59)**	0.114262(15)	0.114042(13)	0.113072(15)
91	Pa	231	*0.1343514(52)*	*0.1293324(46)*	*0.1152364(55)*	*0.1143530(55)*	*0.1113088(69)*	*0.1110964(56)*	*0.1101087(34)*
			0.1343516(29)	0.1293302(27)	0.1152427(21)	0.1143583(21)	0.111292(30)	0.111072(30)	
92	U	238	*0.1309879(52)*	*0.1259572(46)*	*0.1122860(53)*	*0.1113979(54)*	*0.1084449(67)*	*0.1082301(54)*	*0.1072452(33)*
			0.13099111(78)	**0.12595977(36)**	**0.11228858(66)**	**0.11140132(65)**	0.108372(15)	0.108182(15)	0.107232(15)
93	Np	237	*0.1277298(51)*	*0.1226871(45)*	*0.1094299(52)*	*0.1085378(53)*	*0.1056621(66)*	*0.1054450(53)*	*0.1044744(33)*
			0.1277287(39)	0.1226882(36)	0.1094230(39)	0.1085265(28)	0.105670(31)	0.105457(31)	0.1044605(62)
94	Pu	244	*0.1245763(50)*	*0.1195212(45)*	*0.1066627(51)*	*0.1057661(52)*	*0.1029688(64)*	*0.1027494(52)*	*0.1017982(33)*
			0.1245705(25)	0.1195140(23)	0.1066611(18)	0.1057595(18)	0.1029724(26)	0.1027429(26)	
95	Am	243	*0.1215172(50)*	*0.1164501(45)*	*0.1039811(51)*	*0.1030805(51)*	*0.1003579(63)*	*0.1001364(51)*	*0.0991999(33)*
			0.1215158(24)	0.1164463(33)	0.1039794(17)	0.1030803(17)	0.1003537(24)	0.1001357(24)	
96	Cm	248	*0.1185536(49)*	*0.1134742(44)*	*0.1013837(50)*	*0.1004790(50)*	*0.0978295(63)*	*0.0976059(50)*	*0.0966801(33)*
			0.1185427(23)	0.1134635(21)	0.1013753(17)	0.1004708(16)	0.0978355(23)	0.0975952(15)	
97	Bk	249	*0.1156777(49)*	*0.1105860(43)*	*0.0988636(48)*	*0.0979546(49)*	*0.0953724(61)*	*0.0951469(49)*	*0.0942405(32)*
			0.1156630(54)	0.1105745(49)	0.0988598(55)	0.0979514(54)		0.0942501(50)	
98	Cf	250	*0.1128873(48)*	*0.1077832(43)*	*0.0964130(47)*	*0.0955000(48)*	*0.0929867(61)*	*0.0927593(48)*	*0.0918695(32)*
			0.1128799(82)	0.1077793(75)	0.0963915(83)	0.0954860(90)	0.0929715(82)	0.0927508(84)	0.091862(10)
99	Es	251	*0.1101788(47)*	*0.1050620(43)*	*0.0940403(46)*	*0.0931231(47)*	*0.0906838(60)*	*0.0904543(47)*	*0.0895840(32)*
			0.1102072(98)	0.1050554(89)	0.094036(14)	0.093090(14)			0.0895878(97)
100	Fm	254	*0.1075497(47)*	*0.1024201(42)*	*0.0917379(45)*	*0.0908165(46)*	*0.0884443(59)*	*0.0882127(45)*	*0.0873575(32)*
			0.107514(14)	0.102386(13)	0.091715(10)	0.0907943(98)	0.0884212(100)	0.0881872(99)	0.0873356(80)

state of two-electron ions (Blundell, Mohr, Johnson & Sapirstein, 1993; Lindgren, Persson, Salomonson & Labzowsky, 1995) and cannot be evaluated in practice for atoms with more than two or three electrons.

The radiative corrections split up into two contributions. The first contribution is composed of one-electron radiative corrections (self-energy and vacuum polarization). For the self-energy and $Z > 10$, one must use all-order calculations (Mohr, 1974*a*,*b*, 1975, 1982, 1992; Mohr & Soff, 1993). Vacuum polarization can be evaluated at the Uehling (1935) and Wichmann & Kroll (1956) level. Higher-order effects are much smaller than for the self-energy (Soff & Mohr, 1988) and have been neglected. The second contribution is composed of radiative corrections to the electron–electron interaction, and scales as Z^3/n^3. *Ab initio* calculations have been performed only for few-electron ions (Indelicato & Mohr, 1990, 1991). Here we use the Welton approximation which has been shown to reproduce very closely *ab initio* results in all examples that have been calculated (Indelicato, Gorceix & Desclaux 1987; Indelicato & Desclaux 1990; Kim, Baik, Indelicato & Desclaux, 1991; Blundell, 1993*a*,*b*).

Table 4.2.2.5. *Wavelengths of L-emission lines and L-absorption edges in Å; see text for explanation of typefaces*

Numbers in parentheses are standard uncertainties in the least significant figures.

Z	Symbol	A	$L\alpha_2$	$L\alpha_1$	$L\beta_1$	$L\beta_2$	$L_{\rm I}$ abs. edge	$L_{\rm II}$ abs. edge	$L_{\rm III}$ abs. edge
20	Ca						*28.275(32)*	*35.384(40)*	*35.7704(68)*
			36.331(30)	36.331(30)	35.941(30)			35.131(15)	35.491(15)
21	Sc		*30.947(46)*		*30.587(47)*		*24.896(15)*	*30.718(17)*	*31.109(36)*
			31.350(44)	31.350(44)	31.020(30)				
22	Ti		*27.215(37)*		*26.843(37)*		*22.099(24)*	*26.953(14)*	*27.3105(36)*
			27.420(30)	27.420(30)	27.050(30)			27.290(15)	27.290(15)
23	V		*24.143(30)*		*23.764(30)*		*19.779(19)*	*23.8561(89)*	*24.206(10)*
			24.250(44)	24.250(44)	23.880(59)				
24	Cr		*21.640(24)*	*21.490(11)*	*21.276(24)*		*17.804(15)*	*21.246(18)*	*21.5867(49)*
			21.640(44)	21.640(44)	21.270(15)		16.70(15)	17.90(15)	20.70(15)
25	Mn		*19.390(20)*	*19.359(21)*	*19.036(20)*		*16.113(19)*	*19.0781(57)*	*19.4063(43)*
			19.450(15)	19.450(15)	19.110(30)				
26	Fe		*17.525(17)*	*17.503(17)*	*17.194(17)*		*14.611(34)*	*17.2248(92)*	*17.5402(35)*
			17.590(30)	17.590(30)	17.260(15)			17.2023(74)	17.5253(74)
27	Co		*15.922(14)*	*15.905(15)*	*15.610(14)*		*13.4000(86)*	*15.627(14)*	*15.9290(44)*
			15.9722(89)	15.9722(89)	15.666(12)			15.6182(74)	15.9152(74)
28	Ni		*14.532(12)*	*14.520(12)*	*14.236(12)*		*12.295(13)*	*14.251(23)*	*14.5396(57)*
			14.5612(44)	14.5612(44)	14.2712(89)			14.2422(74)	14.5252(74)
29	Cu		*13.341(10)*	*13.336(11)*	*13.063(10)*		*11.292(16)*	*13.016(14)*	*13.2934(64)*
			13.3362(44)	13.3362(44)	13.0532(44)			13.0142(15)	13.2882(15)
30	Zn		*12.2529(90)*	*12.2489(90)*	*11.9819(93)*		*10.361(12)*	*11.8652(66)*	*12.134(14)*
			12.2542(44)	12.2542(44)	11.9832(44)		13.060(15)	11.8622(15)	12.1312(15)
31	Ga		*11.2916(77)*	*11.2858(78)*	*11.0226(78)*		*9.518(11)*	*10.8414(29)*	*11.1040(29)*
			11.2922(15)	11.2922(15)	11.0232(30)		9.5171(74)	10.8282(74)	11.1002(15)
32	Ge		*10.4371(68)*	*10.4306(68)*	*10.1717(69)*		*8.775(12)*	*9.9340(27)*	*10.1849(46)*
			10.4363(12)	10.4363(12)	10.1752(15)		8.7731(15)	9.9241(15)	10.1872(15)
33	As		*9.6744(60)*	*9.6680(60)*	*9.4126(59)*		*8.092(13)*	*9.1182(17)*	*9.3649(29)*
			9.6710(12)	9.6710(12)	9.4142(12)		8.1071(15)	9.1251(15)	9.3671(15)
34	Se		*8.9914(52)*	*8.9852(52)*	*8.7335(52)*		*7.498(13)*	*8.4105(58)*	*8.64459(77)*
			8.99013(74)	8.99013(74)	8.73593(74)		7.5031(15)	8.4071(15)	8.6461(15)
35	Br		*8.3776(46)*	*8.3715(46)*	*8.1233(46)*		*6.958(14)*	*7.7669(35)*	*7.9991(30)*
			8.37473(74)	8.37473(74)	8.12522(74)		6.9591(74)	7.7531(74)	7.9841(74)
36	Kr		*7.8242(41)*	*7.8180(41)*	*7.5736(40)*		*6.4561(41)*	*7.1630(21)*	*7.3841(17)*
			7.82032(13)	**7.82032(13)**	**7.574441(98)**		6.470(15)	7.1681(15)	7.3921(15)
37	Rb		*7.3226(37)*	*7.3164(36)*	*7.0749(36)*		*6.0010(11)*	*6.6449(59)*	*6.8643(67)*
			7.32521(44)	7.31841(30)	7.07601(44)		6.0081(74)	6.6441(15)	6.8621(15)
38	Sr		*6.8674(33)*	*6.8610(32)*	*6.6224(33)*		*5.5945(16)*	*6.17624(70)*	*6.38937(84)*
			6.86980(44)	6.86290(30)	6.62400(44)		5.5921(74)	6.1731(15)	6.3871(15)
39	Y		*6.4539(30)*	*6.4466(29)*	*6.2110(29)*		*5.22968(53)*	*5.75742(82)*	*5.9658(15)*
			6.45590(44)	6.44890(30)	6.21209(44)		5.2171(74)	5.7561(15)	5.9621(15)
40	Zr		*6.0766(27)*	*6.0684(26)*	*5.8357(26)*		*4.89881(41)*	*5.3773(15)*	*5.5816(15)*
			6.0766(27)	**6.070250(79)**	**5.836214(76)**	5.58638(44)*	4.8791(74)	5.3781(15)	5.5791(15)
41	Nb		*5.7326(24)*	*5.7226(23)*	*5.4931(23)*		*4.59975(43)*	*5.03480(63)*	*5.23529(98)*
			5.73199(44)	5.72439(30)	5.49238(44)	5.23798(44)*	4.5751(74)	5.0311(15)	5.2301(15)
42	Mo		*5.4151(22)*	*5.4054(21)*	*5.1778(21)*	*4.91857(74)*	*4.32423(40)*	*4.72145(60)*	*4.9179(31)*
			5.41445(12)	5.40663(12)	5.17716(12)	4.92327(30)*	4.3041(74)	4.7191(15)	4.9131(15)
43	Tc		*5.1228(20)*	*5.1139(19)*	*4.8880(19)*	*4.6341(13)*		*4.4368(13)*	*4.62991(94)*
				5.11488(44)	4.8874(12)		4.0581(74)	4.4361(15)	4.6301(15)
44	Ru		*4.8541(18)*	*4.8449(17)*	*4.6210(17)*	*4.3681(13)*	*3.8443(16)*	*4.17814(78)*	*4.36776(32)*
			4.85388(10)	4.845823(74)	4.620649(44)	4.37187(30)*	3.8351(74)	4.1801(15)	4.3691(15)
45	Rh		*4.6055(16)*	*4.5966(16)*	*4.3744(16)*	*4.1277(12)*	*3.6334(17)*	*3.94053(55)*	*4.12730(50)*
			4.60552(13)	4.59750(13)	4.374206(59)	4.13106(30)*	3.6291(74)	3.94256(74)	4.12996(74)
46	Pd		*4.3753(15)*	*4.3672(15)*	*4.1461(14)*	*3.9088(10)*	*3.43948(61)*	*3.72251(52)*	*3.90655(62)*
			4.37595(10)	4.367736(74)	4.146282(74)	3.908929(59)*	3.4371(15)	3.72286(15)	3.90746(15)
47	Ag		*4.1623(14)*	*4.1541(13)*	*3.9347(13)*	*3.7034(10)*	*3.25639(29)*	*3.51704(26)*	*3.69817(53)*
			4.163002(74)	4.154492(44)	3.934789(44)	3.703406(44)*	3.25645(15)	3.51645(15)	3.69996(15)
48	Cd		*3.9644(13)*	*3.9560(12)*	*3.7382(12)*	*3.51355(97)*	*3.08443(17)*	*3.32528(29)*	*3.50348(45)*
			3.965020(89)	3.956409(59)	3.738286(59)	3.514133(59)*	3.08495(15)	3.32575(15)	3.50475(15)
49	In		*3.7802(12)*	*3.7716(11)*	*3.5553(11)*	*3.33796(83)*	*2.92533(19)*	*3.14784(47)*	*3.32322(42)*
			3.780787(89)	3.771977(59)	3.555363(59)	3.338430(44)*	2.92604(15)	3.14735(15)	3.32375(15)
50	Sn		*3.6084(11)*	*3.5997(10)*	*3.38472(100)*	*3.17475(77)*	*2.776792(71)*	*2.98309(56)*	*3.15521(70)*
			3.606964(59)	3.599994(44)	3.384921(44)	3.175098(44)*	2.77694(15)	2.98234(15)	3.15575(15)

* These values are for the unresolved $L\beta_2$ and $L\beta_{15}$ emission lines.

Table 4.2.2.5. *Wavelengths of L-emission lines and L-absorption edges in Å (cont.)*

Z	Symbol	A	$L\alpha_2$	$L\alpha_1$	$L\beta_1$	$L\beta_2$	$L_{\rm I}$ abs. edge	$L_{\rm II}$ abs. edge	$L_{\rm III}$ abs. edge
51	Sb		*3.44794(99)*	*3.43913(93)*	*3.22551(92)*	*3.02325(67)*	*2.638437(69)*	*2.82990(51)*	*2.99986(66)*
			3.448452(89)	3.439462(59)	3.225718(59)	3.023395(44)*	2.63884(15)	2.82944(74)	3.00035(15)
52	Te		*3.29788(92)*	*3.28894(86)*	*3.07663(85)*	*2.88209(61)*	*2.50998(50)*	*2.687685(87)*	*2.85523(35)*
			3.29851(13)	3.289249(89)	3.076816(89)	2.88221(12)*	2.50994(15)	2.68794(15)	2.85554(15)
53	I		*3.15734(85)*	*3.14828(81)*	*2.93720(78)*	*2.75031(54)*	*2.38965(37)*	*2.55532(31)*	*2.72067(32)*
			3.157957(89)	3.148647(89)	2.937484(89)	2.75057(12)*	2.38804(74)	2.55424(74)	2.71964(74)
54	Xe		*3.02568(78)*	*3.01640(76)*	*2.80659(69)*	*2.62740(47)*	*2.273869(70)*	*2.427862(95)*	*2.590303(89)*
			3.025940(22)	**3.016582(15)**	**2.806553(19)**		2.27373(15)	2.42924(15)	2.59264(15)
55	Cs		*2.90167(73)*	*2.89237(69)*	*2.68362(66)*	*2.51216(47)*	*2.1676(29)*	*2.3135(17)*	*2.47326(16)*
			2.90204(30)	2.89244(30)	2.68374(30)	2.51184(30)*	2.16733(74)	2.31393(15)	2.47404(15)
56	Ba		*2.78522(68)*	*2.77580(64)*	*2.56812(61)*	*2.40421(26)*	*2.0697(15)*	*2.20482(12)*	*2.363082(97)*
			2.785572(74)	2.775992(74)	2.568249(74)	2.404386(89)*	2.06783(74)	2.20483(15)	2.36294(15)
57	La		*2.67563(64)*	*2.66607(60)*	*2.45941(57)*	*2.30307(24)*	*1.97705(28)*	*2.10317(10)*	*2.25958(20)*
			2.675383(60)	2.665740(74)	2.458947(74)	2.303312(98)*	1.97803(74)	2.10533(74)	2.2610(15)
58	Ce		*2.57122(59)*	*2.56108(56)*	*2.35598(53)*	*2.20843(21)*	*1.89320(71)*	*2.01084(14)*	*2.16586(39)*
			2.57059(18)	2.56163(17)	2.35580(18)	2.20900(17)*	1.89343(74)	2.01243(74)	2.1660(15)
59	Pr		*2.47329(55)*	*2.46280(52)*	*2.25890(49)*	*2.11936(20)*	*1.81477(33)*	*1.92607(36)*	*2.07945(22)*
			2.47294(44)	2.46304(30)	2.25883(44)	2.11943(59)*	1.81413(74)	1.92553(74)	2.07913(74)
60	Nd		*2.38081(51)*	*2.36999(48)*	*2.16724(45)*	*2.03554(18)*	*1.73904(18)*	*1.84373(16)*	*1.99616(19)*
			2.38079(52)	**2.370526(16)**	**2.167008(19)**	2.035448(88)*	1.73903(15)	1.84403(15)	1.99673(15)
61	Pm		*2.29340(48)*	*2.28227(45)*	*2.08060(42)*	*1.95675(18)*			
			2.29263(59)	2.28223(44)	2.07973(59)	1.95593(89)*	1.66743(74)	1.76763(74)	1.91913(15)
62	Sm		*2.21054(48)*	*2.19926(42)*	*1.99850(42)*	*1.88225(17)*	*1.60201(12)*	*1.69495(13)*	*1.84534(42)*
			2.210430(24)	**2.199873(13)**	**1.998432(30)**	1.882206(41)*	1.60022(15)	1.69533(15)	1.84573(15)
63	Eu		*2.13214(42)*	*2.12081(40)*	*1.92080(37)*	*1.81237(16)*	*1.54065(17)*	*1.62830(21)*	*1.77767(16)*
			2.13156(17)	2.120673(95)	1.92053(17)	1.81215(17)*	1.53812(15)	1.62712(15)	1.77613(15)
64	Gd		*2.05817(40)*	*2.04670(37)*	*1.84744(34)*	*1.74582(14)*	*1.47922(25)*	*1.56264(23)*	*1.71092(21)*
			2.05783(30)	2.04683(30)	1.84683(30)	1.74553(30)*	1.47842(15)	1.56322(15)	1.71173(15)
65	Tb		*1.98699(37)*	*1.97586(35)*	*1.77701(32)*	*1.68377(14)*	*1.42285(98)*	*1.50195(80)*	*1.65023(44)*
			1.98753(30)	1.97653(30)	1.77683(44)	1.68303(30)*	1.42232(15)	1.50232(15)	1.64972(15)
66	Dy		*1.91986(35)*	*1.90883(33)*	*1.71052(30)*	*1.62497(12)*	*1.37058(41)*	*1.44500(20)*	*1.59241(33)*
			1.919939(44)	1.908839(44)	1.71065(10)	1.62371(10)*	1.36922(15)	1.44452(15)	1.59162(15)
67	Ho		*1.85606(33)*	*1.84511(31)*	*1.64732(28)*	*1.56818(11)*	*1.31957(28)*	*1.39091(27)*	*1.53614(34)*
			1.856472(15)	**1.845092(17)**	**1.647484(32)**	1.567168(50)*	1.31902(15)	1.39052(15)	1.53682(15)
68	Er		*1.79537(31)*	*1.78449(29)*	*1.58720(26)*	*1.51486(10)*	*1.27145(14)*	*1.33792(26)*	*1.48318(27)*
			1.795701(45)	**1.784481(20)**	**1.587466(86)**	1.51401(13)*	1.27062(15)	1.33862(15)	1.48352(15)
69	Tm		*1.73758(29)*	*1.72677(27)*	*1.52995(24)*	*1.464210(95)*	*1.22612(28)*	*1.28942(27)*	*1.43366(27)*
			1.738003(19)	**1.7267720(70)**	**1.5302410(70)**	1.46402(30)*	1.22502(15)	1.28922(15)	1.43342(15)
70	Yb		*1.68248(29)*	*1.67177(26)*	*1.47538(24)*	*1.416041(89)*	*1.18266(60)*	*1.243391(70)*	*1.3858(10)*
			1.682875(74)	1.671915(59)	1.475672(74)	1.415521(74)*	1.18182(15)	1.24282(15)	1.38622(15)
71	Lu		*1.63031(26)*	*1.61949(24)*	*1.42361(21)*	*1.370061(85)*	*1.14043(22)*	*1.197954(60)*	*1.341053(93)*
			1.630314(74)	1.619534(44)	1.423611(44)	1.370141(44)	1.14022(15)	1.19852(15)	1.34052(15)
72	Hf		*1.58049(25)*	*1.56959(23)*	*1.37419(20)*	*1.326241(78)*	*1.10009(24)*	*1.1550(10)*	*1.2972(14)*
			1.580484(74)	1.569604(74)	1.374121(74)	1.326410(74)	1.1002640(49)	1.1548587(22)	1.2971383(68)
73	Ta		*1.53290(23)*	*1.52194(22)*	*1.32697(19)*	*1.282314(74)*	*1.06152(30)*	*1.11368(14)*	*1.25506(34)*
			1.532953(30)	1.521993(30)	1.327000(44)	1.284559(30)	1.06132(15)	1.11372(15)	1.25532(15)
74	W		*1.48748(22)*	*1.47642(21)*	*1.28188(18)*	*1.244447(70)*	*0.91604(28)*	*1.07431(38)*	*1.21543(99)*
			1.487452(30)	1.4763112(95)	1.281812(13)	1.2443048(98)	1.024685(74)	1.07452(15)	1.21552(15)
75	Re		*1.44399(21)*	*1.43288(19)*	*1.23872(17)*	*1.206487(67)*	*0.98968(21)*	*1.03670(20)*	*1.17673(27)*
			1.443982(74)	1.432922(59)	1.238599(30)	1.206618(59)	0.98941(15)	1.03712(15)	1.17732(15)
76	Os		*1.40238(20)*	*1.39121(18)*	*1.19742(16)*	*1.170095(62)*	*0.95583(36)*	*1.000786(57)*	*1.14002(23)*
			1.402361(74)	1.391231(74)	1.197288(74)	1.16981(12)	0.95581(15)	1.00142(15)	1.14082(15)
77	Ir		*1.36252(19)*	*1.35130(19)*	*1.15786(15)*	*1.135812(72)*	*0.9240(12)*	*0.96675(18)*	*1.10535(22)*
			1.362520(74)	1.351300(44)	1.157827(44)	1.135337(44)	0.92361(15)	0.96711(15)	1.10582(15)
78	Pt		*1.32434(18)*	*1.31308(17)*	*1.11995(14)*	*1.102006(63)*	*0.8933(14)*	*0.93395(27)*	*1.07200(36)*
			1.324340(30)	1.313060(44)	1.119917(30)	1.102017(44)	0.893213(19)	0.9341861(21)	1.0722721(19)
79	Au		*1.28773(17)*	*1.27643(16)*	*1.08359(13)*	*1.070479(53)*	*0.86383(45)*	*0.90263(12)*	*1.04009(27)*
			1.287739(44)	1.276419(44)	1.083546(44)	1.070236(44)	0.863683(30)	0.9027409(46)	1.0401625(52)
80	Hg		*1.25261(16)*	*1.24126(15)*	*1.04869(13)*	*1.039584(51)*	*0.83546(43)*	*0.87238(26)*	*1.00919(30)*
			1.25266(10)	1.241219(74)	1.048696(74)	1.03977(10)	0.83531(15)	0.87221(15)	1.00912(15)
81	Tl		*1.21890(15)*	*1.20750(14)*	*1.01519(12)*	*1.01029(20)*	*0.80795(15)*	*0.843512(77)*	*0.97953(25)*
			1.218768(44)	1.207408(59)	1.015145(59)	1.010325(44)	0.80811(15)	0.84341(15)	0.97931(15)
82	Pb		*1.18651(15)*	*1.17507(14)*	*0.98298(11)*	*0.98221(19)*	*0.78172(24)*	*0.81575(18)*	*0.95113(22)*
			1.186498(74)	1.175028(30)	0.982925(44)	0.98222(10)	0.7818404(49)	0.8157395(16)	0.9511590(22)

* These values are for the unresolved $L\beta_2$ and $L\beta_{15}$ emission lines.

Table 4.2.2.5. *Wavelengths of L-emission lines and L-absorption edges in Å (cont.)*

Z	Symbol	A	$L\alpha_2$	$L\alpha_1$	$L\beta_1$	$L\beta_2$	$L_{\rm I}$ abs. edge	$L_{\rm II}$ abs. edge	$L_{\rm III}$ abs. edge
83	Bi	209	*1.15540(14)*	*1.14390(13)*	*0.95205(11)*	*0.95526(18)*	*0.75649(58)*	*0.789102(88)*	*0.92387(11)*
			1.155377(15)	1.143877(30)	0.951992(13)	0.955194(59)	0.75711(15)	0.78871(15)	0.92341(15)
84	Po	209	*1.12549(13)*	*1.11393(12)*	*0.92228(10)*	*0.92932(18)*	*0.7332(13)*	*0.76325(13)*	*0.897554(85)*
			1.125497(74)	1.113877(59)	0.92201(30)	0.929384(74)			
85	At	210	*1.09670(13)*	*1.08510(12)*	*0.893639(96)*	*0.90444(17)*		*0.73868(13)*	
			1.096726(74)	1.085016(74)	0.89350(13)				
86	Rn	222	*1.06900(12)*	*1.05735(11)*	*0.866054(91)*	*0.88055(15)*		*0.71511(13)*	
			1.069006(74)	1.057246(74)	0.86606(13)				
87	Fr	223	*1.04232(11)*	*1.03063(11)*	*0.839482(86)*	*0.85751(15)*		*0.69240(13)*	*0.8251(27)*
			1.042316(74)	1.030505(74)	0.83941(13)	0.8580(30)			
88	Ra	226	*1.01662(11)*	*1.00489(10)*	*0.813866(82)*	*0.83533(16)*	*0.64449(15)*	*0.67077(12)*	*0.802768(44)*
			1.016575(74)	1.004745(74)	0.813762(74)	0.835383(74)	0.64451(15)	0.67071(15)	0.80281(15)
89	Ac	227	*0.99185(11)*	*0.980070(98)*	*0.789163(78)*	*0.81406(14)*		*0.64970(13)*	
			0.991795(74)	0.979945(74)	0.78904(13)				
90	Th	232	*0.96798(10)*	*0.956154(94)*	*0.765343(75)*	*0.79354(13)*	*0.60569(11)*	*0.62966(11)*	*0.760637(99)*
			0.9679082(23)	0.9560826(15)	0.7652610(14)	0.7935516(15)	0.60591(15)	0.62991(15)	0.76071(15)
91	Pa	231	*0.944896(96)*	*0.933002(90)*	*0.742301(71)*	*0.77321(12)*	*0.58759(12)*	*0.610354(92)*	*0.740958(97)*
			0.944834(74)	0.932854(74)	0.742331(74)	0.77371(15)			
92	U	238	*0.922622(93)*	*0.910674(86)*	*0.720056(68)*	*0.75462(12)*	*0.569885(39)*	*0.591930(66)*	*0.722319(52)*
			0.922572(13)	0.910653(13)	0.719995(12)	0.754692(13)	0.56951(15)	0.59191(15)	0.72231(15)
93	Np	237	*0.901230(88)*	*0.889223(83)*	*0.698624(65)*	*0.73623(11)*			
			0.901059(13)	0.889141(13)	0.698488(13)	0.736241(13)	0.55239(34)	0.57368(37)	0.704136(20)
94	Pu	244	*0.880355(85)*	*0.868290(79)*	*0.677776(60)*	*0.71848(11)*			
							0.53651(15)	0.55721(15)	0.68671(15)
95	Am	243	*0.860288(84)*	*0.848190(81)*	*0.657686(59)*	*0.70134(10)*			
96	Cm	248	*0.840918(80)*	*0.828776(78)*	*0.638265(56)*	*0.684815(98)*			
97	Bk	249	*0.822159(76)*	*0.809987(69)*	*0.619449(53)*	*0.668638(94)*			
							0.49060(49)	0.50851(52)	0.63748(98)
98	Cf	250	*0.803608(73)*	*0.791421(66)*	*0.601005(50)*	*0.652873(89)*			
							0.476569(92)	0.493804(98)	0.62300(19)
99	Es	251	*0.786043(70)*	*0.773837(63)*	*0.583354(49)*	*0.638227(82)*			
100	Fm	254	*0.769077(67)*	*0.756843(60)*	*0.566272(47)*	*0.623826(82)*			
			0.76904(62)	0.75674(60)	0.56619(34)	0.62369(41)	0.44966(13)	0.46534(12)	0.59414(20)

* These values are for the unresolved $L\beta_2$ and $L\beta_{15}$ emission lines.

4.2.2.12. *Structure and format of the summary tables*

Table 4.2.2.4 summarizes the theoretical and experimental results for prominent *K*-series lines and the *K*-absorption edge. For the emission lines, the upper number (in italics) is the theoretical estimate for this line and the lower number is the experimentally measured value (1) from Table 4.2.2.1 or (2) from the Bearden database or a reference that appeared after the Bearden database corrected to the optically based scale. For the *K* absorption edge, the upper number (also in italics) was obtained by combining emission lines and photoelectron spectroscopy (see Subsection 4.2.2.7), and the lower number is the experimentally measured value (1) from Table 4.2.2.3 or (2) from the Bearden database or a reference that appeared after the Bearden database corrected to an optically based scale. For the experimental emission and absorption entries, bold type is used for wavelengths directly measured on an optically based scale. The numerical values for wavelengths in angstrom units (1 Å = 0.1 nm) are given to a number of significant figures commensurate with their estimated uncertainties, which appear in parentheses after each theoretical and experimental value.

Figure 4.2.2.1 shows plots of the relative deviation between theoretical and experimental values for the *K*-series lines and the *K*-absorption edge as a function of *Z*. The error bars shown in the figure are the experimental uncertainties. In general, these plots show good agreement between theory and experiment except in the low-*Z* and high-*Z* regions. At the low-*Z* end of the table, the particular calculational approach used is not optimum, and the experimental data are suprisingly weak. At the high end, experimental data have rather large uncertainties, and thus do not provide an accurate test of the theory.

Table 4.2.2.5 summarizes the theoretical and experimental results for prominent *L*-series lines and the *L*-absorption edges. The experimental database of high-accuracy emission data is much more limited than was the case for the *K* series, and there have been very few high-accuracy edge-location measurements. The format of this table is similar to that of Table 4.2.2.4. For the emission lines, the upper number (in italics) is the theoretical estimate for this line, and the lower number is the experimentally measured value. Numbers in bold type were directly measured on the optical scale (see Table 4.2.2.2), and numbers in normal type are from the Bearden database or a reference that appeared after the Bearden database corrected to an optically based scale. For the *L*-absorption edges, the upper number (also in italics) is obtained by combining emission lines and photoelectron spectroscopy (see Subsection 4.2.2.7) and the lower number is the experimentally measured value. The numbers in bold type

Table 4.2.2.6. *Wavelength conversion factors*

Numbers in parentheses are standard uncertainties in the least-significant figures.

	Cu $K\alpha_1$	Mo $K\alpha_1$	W $K\alpha_1$
λ (Å)	1.54059292(45)	0.70931713(41)	0.20901313(18)
λ (Å*)	1.540562(3)	0.709300(1)	0.2090100
1 kxu	1.537400	0.707831	
Å*/Å	1.0000201(20)	1.0000242(22)	1.00001498(86)
kxu/Å	1.00207683(29)	1.00209955(58)	

are recent measurements by Kraft, Stümpel, Becker & Kuetgens (1996), and the numbers in normal type are from the Bearden database or a reference that appeared after the Bearden database corrected to an optically based scale. Figure 4.2.2.2 shows relative deviations between the theoretical and experimental values for most of the tabulated data. The error bars shown in the figure are the experimental uncertainties.

4.2.2.13. *Availability of a more complete X-ray wavelength table*

This article and the accompanying X-ray wavelength tables are an up-dated version of the contribution to the *International Tables for Crystallography*, Volume C, 2nd edition that was published in 1999. This article has been subject to more critical review and analysis and the data are consistent with the most recent adjustment of the fundamental physical constants (Mohr & Taylor, 2000). We believe that these data represent a significant improvement in consistency, coverage and accuracy over previously available resources. The results presented here are a subset of a larger effort that includes all *K*- and *L*-series lines connecting the $n = 1$ to $n = 4$ shells. The more complete table has been submitted for archival publication and will be made avaialble on the NIST Physical Reference Data web site. Electronic publishing of this resource will provide a convenient data resource to the scientific community that can be more easily up-dated and expanded.

4.2.2.14. *Connection with scales used in previous literature*

In order to compare historical data for X-ray spectra with the results in the present tabulation, certain conversion factors are needed. As discussed in the introduction, the principal units found in the literature are the xu and the Å* unit. There is the additional complication that there were several different definitions in use at various times and at the same time in different laboratories. For the convenience of the reader, we summarize in Table 4.2.2.6 the main conversion factors needed. The numerical values for the wavelengths in Å can be converted to energies in electron volts by using the conversion factor 12 398.41857 (49) eV Å (Mohr & Taylor, 2000).

Our current efforts owe their inception to the encouragement of the late A. J. C. Wilson, who persistently communicated the need for an updated wavelength resource for the crystallographic community. The larger effort evolved at NIST with the support of the Standard Reference Data Program as established with the help of the late Jean Gallagher, and sustained by the program's current Director, John Rumble. Early phases of the preparation of this material benefited from the efforts of John Schweppe. Cedric Powell supplied valuable advice in the area of electron binding energies. We are particularly grateful to the Editor, E. Prince, for his help and patience in the development of these wavelength tables. Richard Deslattes died between the first publication of this article and this revision. This work would not have been possible without his dedication to this project over more than a decade. The earlier wavelength table of the late J. A. Bearden, under whom one of the present authors (RDD) studied, was a significant influence on this project.

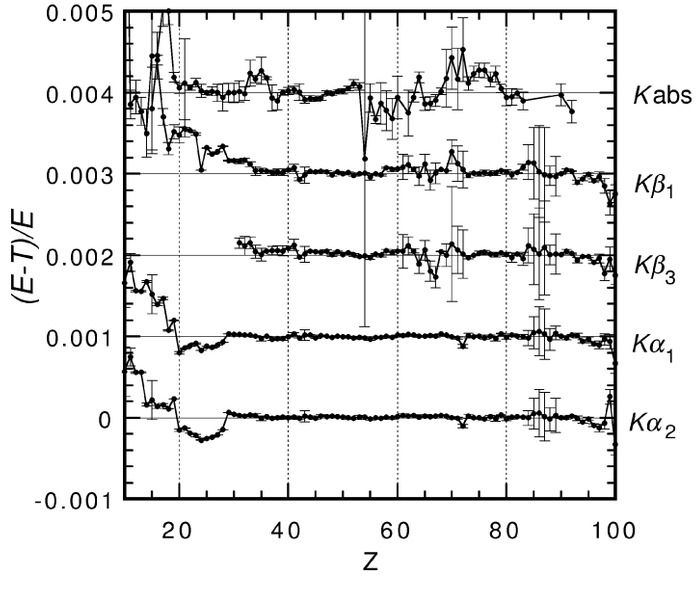

Fig. 4.2.2.1. Relative deviations between theoretical and experimental results for *K*-series spectra. The topmost data set concerns the *K*-edge location, while the other data sets, beginning at the bottom, refer to the $K\alpha_2$, $K\alpha_1$, $K\beta_3$ and $K\beta_1$, respectively. The ordinate scales have been displaced for clarity by the indicated multiples of 0.001.

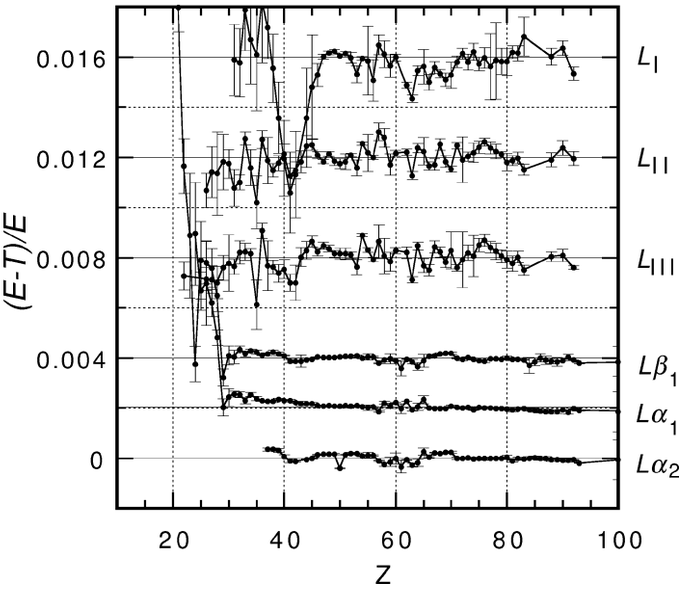

Fig. 4.2.2.2. Comparison of *L*-series data with experiment for the indicated range of *Z*. Indicated data, beginning at the bottom, refer to the $L\alpha_2$, $L\alpha_1$, and $L\beta_1$ emission lines and the L_{III}, L_{II}, and L_I absorption edges. For clarity, the plots have been displaced vertically by multiples of 0.002 for the emission lines and 0.004 for the absorption edges.

4.2.3. X-ray absorption spectra (by D. C. Creagh)

4.2.3.1. *Introduction*

4.2.3.1.1. *Definitions*

This section deals with the manner in which the photon scattering and absorption cross sections of an atom varies with the energy of the incident photon. Further information concerning these cross sections and tables of the X-ray attenuation coefficients are given in Section 4.2.4. Information concerning the anomalous-dispersion corrections is given in Section 4.2.6.

When a highly collimated beam of monoenergetic photons passes through a medium of thickness t, it suffers a decrease in intensity according to the relation

$$I = I_0 \exp(-\mu_l t), \tag{4.2.3.1}$$

where μ_l is the linear attenuation coefficient. Most tabulations express μ_l in c.g.s. units, μ_l having the units cm^{-1}.

An alternative, often more convenient, way of expressing the decrease in intensity involves the measurement of the mass per unit area m_A of the specimen rather than the specimen thickness, in which case equation (4.2.3.1) takes the form

$$I = I_0 \exp[-(\mu/\rho)m_A], \tag{4.2.3.2}$$

where ρ is the density of the material and (μ/ρ) is the mass absorption coefficient. The linear attenuation coefficient of a medium comprising atoms of different types is related to the mass absorption coefficients by

$$\mu_l = \rho \sum_i g_i(\mu/\rho)_i, \tag{4.2.3.3}$$

where g_i is the mass fraction of the atoms of the ith species for which the mass absorption coefficient is $(\mu/\rho)_i$. The summation extends over all the atoms comprising the medium. For a crystal having a unit-cell volume of V_c,

$$\mu_l = \frac{1}{V_c}\sum \sigma_i, \tag{4.2.3.4}$$

where σ_i is the photon scattering and absorption cross section. If σ_i is expressed in terms of barns/atom then V_c must be expressed in terms of Å^3 and μ_l is in cm^{-1}. (1 barn $= 10^{-28}$ m^2.)

The mass attenuation coefficient μ/ρ is related to the total photon–atom scattering cross section σ according to

$$\begin{aligned}\frac{\mu}{\rho}(\mathrm{cm}^2/\mathrm{g}) &= (N_\mathrm{A}/M)\sigma\,(\mathrm{cm}^2/\mathrm{atom}) \\ &= (N_\mathrm{A}/M) \times 10^{-24}\sigma\,(\mathrm{barns/atom}),\end{aligned} \tag{4.2.3.5}$$

where N_A = Avogadro's number $= 6.0221367\,(36) \times 10^{23}$ atoms/gram atom (Cohen & Taylor, 1987) and M = atomic weight relative to $M(^{12}\mathrm{C}) = 12.0000$.

4.2.3.1.2. *Variation of X-ray attenuation coefficients with photon energy*

When a photon interacts with an atom, a number of different absorption and scattering processes may occur. For an isolated atom at photon energies of less than 100 keV (the limit of most conventional X-ray generators), contributions to the total cross section come from the photo-effect, coherent (Rayleigh) scattering, and incoherent (Compton) scattering.

$$\sigma = \sigma_\mathrm{pe} + \sigma_R + \sigma_C. \tag{4.2.3.6}$$

The relation between the photo-effect absorption cross section σ_pe and the X-ray anomalous-dispersion corrections will be discussed in Section 4.2.6.

The magnitudes of these scattering cross sections depend on the type of atom involved in the interactions and on the energy of the photon with which it interacts. In Fig. 4.2.3.1, the theoretical cross sections for the interaction of photons with a carbon atom are given. Values of σ_pe are from calculations by Schofield (1973), and those for Rayleigh and Compton scattering are from tabulations by Hubbell & Øverbø (1979) and Hubbell (1969), respectively. Note the sharp discontinuities that occur in the otherwise smooth curves. These correspond to photon energies that correspond to the energies of the K and L_I L_II L_III shells of the carbon energies. Notice also that σ_pe is the dominant interaction cross section, and that the Rayleigh scattering cross section remains relatively constant for a broad range of photon energies, whilst the Compton scattering peaks at a particular photon energy (~ 100 keV). Other interaction mechanisms exist [*e.g.* Delbrück (Papatzacos & Mort, 1975; Alvarez, Crawford & Stevenson, 1958), pair production, nuclear Thompson], but these do not become significant interaction processes for photon energies less than 1 MeV. This section will not address the interaction of photons with atoms for which the photon energy exceeds 100 keV.

4.2.3.1.3. *Normal attenuation, XAFS, and XANES*

The curves shown in Fig. 4.2.3.1 are the result of theoretical calculations of the interactions of an isolated atom with a single photon. Experiments are not usually performed on isolated atoms, however. When experiments are performed on ensembles of atoms, a number of points of difference emerge between the experimental data and the theoretical calculations. These effects arise because the presence of atoms in proximity with one another can influence the scattering process. In short: the total attenuation coefficient of the system is *not* the sum of all the individual attenuation coefficients of the atoms that comprise the system.

Perhaps the most obvious manifestation of this occurs when the photon energy is close to an absorption edge of an atom. In Fig. 4.2.3.2, the mass attenuation of several germanium compounds is plotted as a function of photon energy. The

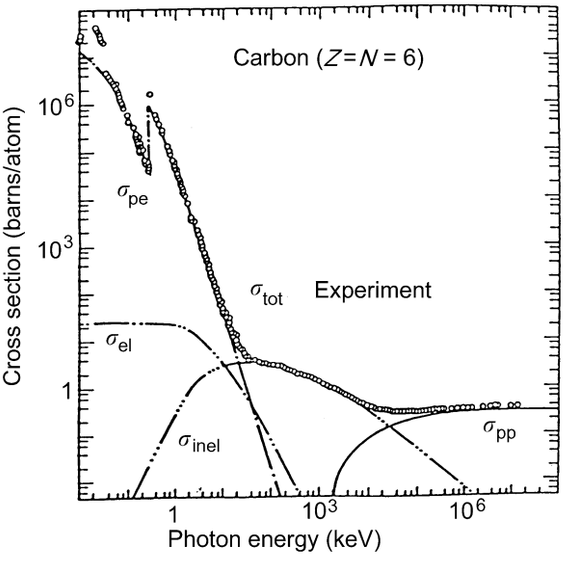

Fig. 4.2.3.1. Theoretical cross sections for photon interactions with carbon showing the contributions of photoelectric, elastic (Rayleigh), inelastic (Compton), and pair-production cross sections to the total cross sections. Also shown are the experimental data (open circles). From Gerstenberg & Hubbell (1982).

energy scale measures the distance from the *K*-shell edge energy of germanium (11.104 keV). These curves are taken from Hubbell, McMaster, Del Grande & Mallett (1974). Not only does the experimental curve depart significantly from the theoretically predicted curve, but there is a marked difference in the complexity of the curves between the various germanium compounds.

Far from the absorption edge, the theoretical calculations and the experimental data are in reasonable agreement with what one might expect using the sum rule for the various scattering cross sections and one could say that this region is one in which normal attenuation coefficients may be found.

Closer to the edge, the almost periodic variation of the mass attenuation coefficient is called the extended X-ray absorption fine structure (XAFS). Very close to the edge, more complicated fluctuations occur. These are referred to as X-ray absorption near edge fine structure (XANES). The boundary of the XAFS and XANES regions is somewhat arbitrary, and the physical basis for making the distinction between the two will be outlined in Subsection 4.2.3.4.

Even in the region where normal attenuation may be thought to occur, cooperative effects can exist, which can affect both the Rayleigh and the Compton scattering contributions to the total attenuation cross section. The effect of cooperative Rayleigh scattering has been discussed by Gerward, Thuesen, Stibius-Jensen & Alstrup (1979), Gerward (1981, 1982, 1983), Creagh & Hubbell (1987), and Creagh (1987*a*). That the Compton scattering contribution depends on the physical state of the scattering medium has been discussed by Cooper (1985).

Care must therefore be taken to consider the physical state of the system under investigation when estimates of the theoretical interaction cross sections are made.

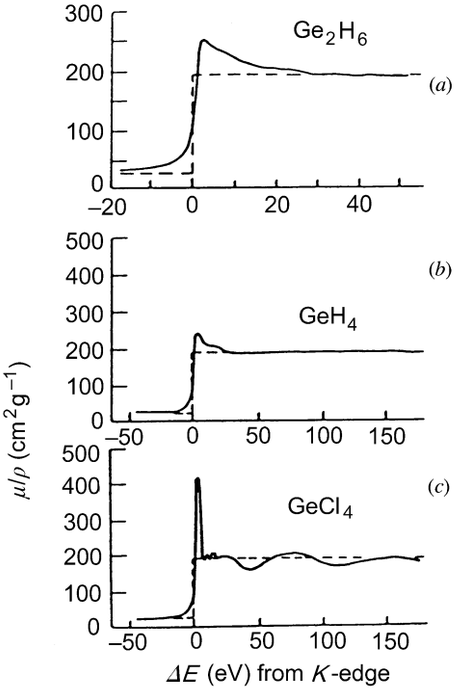

Fig. 4.2.3.2. The dependence of the X-ray attenuation coefficient on energy for a range of germanium compounds, taken in the neighbourhood of the germanium absorption edge (from *IT* IV, 1974).

4.2.3.2. *Techniques for the measurement of X-ray attenuation coefficients*

4.2.3.2.1. *Experimental configurations*

Experimental configurations that set out to determine the X-ray linear attenuation coefficient μ_l or the corresponding mass absorption coefficients (μ/ρ) must have characteristics that reflect the underlying assumptions from which equation (4.2.3.1) was derived, namely:

(i) the incident and transmitted beams are parallel and there is no divergence in the transmitted beam;

(ii) the photons in the incident and transmitted beams have the same energy;

(iii) the specimen is of sufficient thickness.

Because of the considerable discrepancies that often exist in X-ray attenuation measurements (see, for example, *IT* IV, 1974), the IUCr Commission on Crystallographic Apparatus set up a project to determine which, if any, of the many techniques for the measurement of X-ray attenuation coefficients is most likely to yield correct results. In the project, a number of different experimental configurations were used. These are shown in Fig. 4.2.3.3. The configurations used ranged in complexity from that

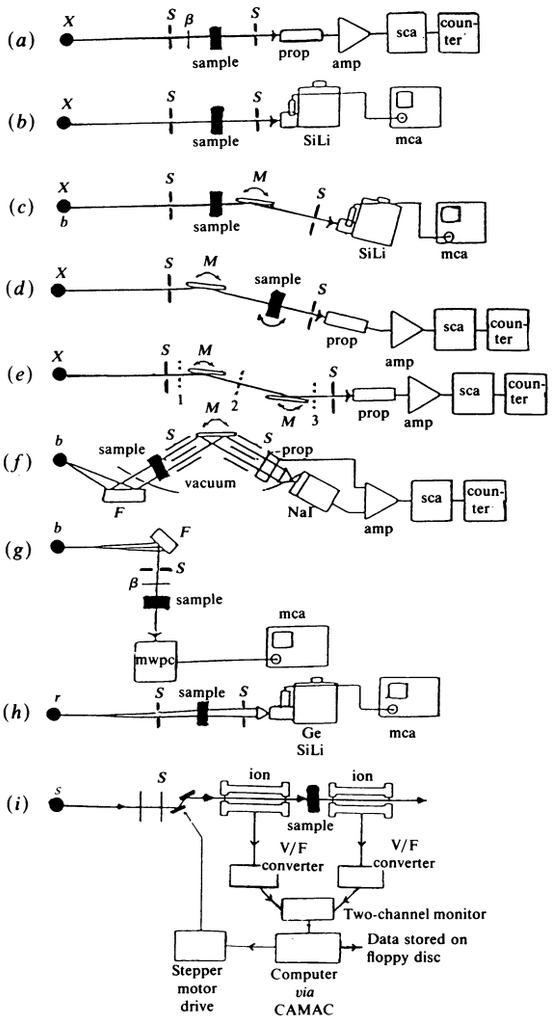

Fig. 4.2.3.3. Schematic representations of experimental apparatus used in the IUCr X-ray Attenuation Project (Creagh & Hubbell, 1987; Creagh, 1985). *X*: characteristic line from sealed X-ray tube; *b*: *Bremsstrahlung* from a sealed X-ray tube; *r*: radioactive source; *s*: synchrotron-radiation source; β: β-filter for characteristic X-rays; *S*: collimating slits; *M*: monochromator.

of Fig. 4.2.3.3(*a*), which uses a slit-collimated beam from a sealed tube and a β-filter to select its characteristic radiation, and a proportional counter and associated electronics to detect the transmitted-beam intensity, to that of Fig. 4.2.3.3(*f*), which uses a modification to a commercial X-ray-fluorescence analyser. Sources of X-rays included conventional sealed X-ray tubes, X-ray-fluorescence sources, radioisotope sources, and synchrotron-radiation sources. Detectors ranged from simple ionization chambers, which have no capacity for photon energy detection, to solid-state detectors, which provide a relatively high degree of energy discrimination. In a number of cases (Figs. 4.2.3.3*c*, *d*, *e*, and *f*), monochromatization of the beam was effected using single Bragg reflection from silicon single crystals. In Fig. 4.2.3.3(*i*), the incident-beam monochromator is using reflections from two Bragg reflectors tuned so as to eliminate harmonic radiation from the source.

The performance of these systems was evaluated for a range of materials that included:

(i) highly perfect silicon single crystals (Creagh & Hubbell, 1987);

(ii) polycrystalline copper foils that exhibited a high degree of preferred orientation; and

(iii) pyrolytic graphite that contained a high density of regular voids.

The results of this study are outlined in Section 4.2.3.2.3.

4.2.3.2.2. *Specimen selection*

Although the most important component in the experiment is the specimen itself, examination of the data files held at the US National Institute of Standards and Technology (Gerstenberg & Hubbell, 1982; Saloman & Hubbell, 1986; Hubbell, Gerstenberg & Saloman, 1986) has shown that, in general, insufficient care has been taken in the past to select an experimental device with characteristics that are appropriate to the specimen chosen. Nor has sufficient care been taken in the determination of the dimensions, homogeneity, and defect structure of the specimens. To achieve the best results, the following procedures should be followed.

(i) The *dimensions* of the specimen should be determined using at least two different techniques, and sample *thicknesses* should be chosen such that the Nordfors (1960) criterion, later confirmed by Sears (1983), that the condition

$$2 \leq \ln(I_0/I) \leq 4 \qquad (4.2.3.7)$$

be satisfied. This enables the best compromise between achieving good counting statistics and avoiding multiple photon scattering within the sample.

Wherever possible, different sample thicknesses should be chosen to enable a test of equation (4.2.3.1) to be made. If deviations from equation (4.2.3.1) exist, either the sample material or the experimental configuration, or both, are not appropriate for the measurement of μ_l. If the attenuation of the material under test falls outside the limits set by the Nordfors criterion and the material is in the form of a powder, the mixing of this powder with one with low attenuation and no absorption edge in the region of interest can be used to bring the total attenuation of the sample within the Nordfors range.

(ii) The sample should be examined by as many means as possible to ascertain its regularity, homogeneity, defect structure, and, especially for very thin specimens, freedom from pinholes and cracks. Where a diluent has been used to reduce the attenuation so that the Nordfors criterion is satisfied, care must be taken to ensure intimate mixing of the two materials and the absence of voids.

Since the theory upon which equation (4.2.3.1) is based envisages that each atom scatters as an individual, it is necessary to be aware of whether such cooperative effects as Laue–Bragg scattering (which may become significant in single-crystal specimens) and small-angle X-ray scattering (SAXS) (which may occur if a distribution of small voids or inclusions exists) occur in polycrystalline and amorphous specimens. Knowledge that cooperative scattering may occur influences the choice of collimation of the beam.

(iii) The sample should be mounted *normal* to the beam.

4.2.3.2.3. *Requirements for the absolute measurement of μ_l or (μ/ρ)*

The following prescription should be followed if accurate, absolute measurements of μ_l and (μ/ρ) are to be obtained.

(i) *X-ray source and X-ray monochromatization*. The *energy* of the incident photons should be measured directly using reflections from a single-crystal silicon monochromator, and the *energy spread* of the beam should be measured. Measurements should be made of the state of *polarization*, since X-ray-polarization effects are known to be significant in some measurements (Templeton & Templeton, 1982, 1985, 1986). The results of a survey on X-ray polarization were given by Jennings (1984). If a single-crystal monochromator is employed, it should be placed between the sample and the detector.

(ii) *Collimation*. It is of some advantage if both the incident-beam- and the transmitted-beam-defining slits can be varied in width.

Should it be necessary to combat the effects of Laue–Bragg scattering in a single-crystal specimen, an incident beam with a high degree of collimation is required (Gerward, 1981).

To counter the effects of small-angle X-ray scattering, it may be necessary to widen the detector aperture (Chipman, 1969). That these effects can be marked has been shown by Parratt, Porteus, Schnopper & Watanabe (1959), who investigated the influence collimator and monochromator configurations have on X-ray-attenuation measurements.

(iii) *Detection*. Detectors that give some degree of energy discrimination should be used. Compromise may be necessary between sensitivity and energy resolution, however, and these factors should be taken into account when a choice is being made between proportional and solid-state detectors.

Whichever detection system is chosen, it is essential that the system dead-time be determined experimentally. For descriptions of techniques for the determination of system dead-time, see, for example, Bertin (1975).

4.2.3.3. *Normal attenuation coefficients*

Fig. 4.2.3.1 shows that the X-ray attenuation coefficients are a smooth function of photon energy over a relatively large range of photon energies, and that discontinuities occur whenever the photon energy corresponds to a resonance in the electron cloud surrounding the nucleus. In Fig. 4.2.3.2, the effect of the interaction of the ejected photoelectron with the electron's neighbouring atoms is shown. Such edge effects (XAFS) can extend 1000 eV from the edge.

It is conventional, however, to extrapolate the smooth curve to the edge value, and a curve of *normal attenuation coefficients* results. These are taken to be the attenuation coefficients of the individual atoms. Tables of these *normal attenuation coefficients* are given in Section 4.2.4.

4.2.3.4. *Attenuation coefficients in the neighbourhood of an absorption edge*

4.2.3.4.1. *XAFS*

Although the existence of XAFS has been known for more than 60 years following experiments by Fricke (1920) and Hertz (1920), it is only in the last decade that a proper theoretical description has been developed. Kronig (1932*a*) suggested a long-range-order theory based on quantum-mechanical precepts, although later (Kronig, 1932*b*) he applied a short-range-order (SRO) theory to explain the existence of XAFS in molecular spectra. As time progressed, important suggestions were made by others, notably Kostarev (1941, 1949), who applied this SRO theory to condensed matter, Sawada, Tsutsumi, Shiraiwa, Ishimura & Obashi (1959), who accounted for the lifetime of the excited photoelectron and the core-hole state in terms of a mean free path, and Schmidt (1961*a*,*b*, 1963), who showed the influence atomic vibrations have on the phase of the back-scattered waves.

Nevertheless, neither the experimental data nor the theories were sufficiently good to enable Azaroff & Pease (1974) to decide which theory was the correct one to use. However, Sayers, Lytle & Stern (1970) produced a theoretical approach based on SRO theory, later extended by Lytle, Stern & Sayers (1975), and this is the foundation upon which all modern work has been built. Since 1970, a great deal of theoretical effort has been expended to improve the theory because of the need to interpret the wealth of data that became available through the increasing use of synchrotron-radiation sources in XAFS experiments.

A number of major reviews of XAFS theory and its use for the resolution of experimental data have been published. Contributions have been made by Stern, Sayers & Lytle (1975), Lee, Citrin, Eisenberger & Kincaid (1981), Lee (1981), and Teo (1981). The rapid growth of the use of synchrotron-radiation sources has led to the development of the use of XAFS in a wide variety of research fields. The XAFS community has met regularly at conferences, producing conference proceedings that demonstrate the maturation of the technique. The reader is directed to the proceedings edited by Mustre de Leon, Stern, Sayers, Ma & Rehr (1988), Hasnain (1990), and Kuroda, Ohta, Murata, Udagawa & Nomura (1992), and to the papers contained therein. In the following section, a brief, simplified, description will be given of the theory of XAFS and of the application of that theory to the interpretation of XAFS data.

4.2.3.4.1.1. *Theory*

The theory that will be outlined here has evolved through the efforts of many workers over the past decade. The oscillatory part of the X-ray attenuation relative to the 'background' absorption may be written as

$$\chi(E) = \frac{\mu_l(E) - \mu_{l0}(E)}{\mu_{l0}(E)}, \tag{4.2.3.8}$$

where $\mu_l(E)$ is the measured value of the linear attenuation coefficient at a photon energy E and $\mu_{l0}(E)$ is the 'background' linear attenuation coefficient. This is sometimes the extrapolation of the normal attenuation curve to the edge energy, although it is usually found necessary to modify this extrapolation somewhat to improve the matching of the higher-energy data with the XAFS data (Dreier, Rabe, Matzfeld & Niemann, 1984). In most computer programs, the normal attenuation curve is fitted to the data using cubic spline fitting routines.

The origin of XAFS lies in the interaction of the ejected photoelectron with electrons in its immediate vicinity. The wavelength of a photoelectron ejected when a photon is absorbed is given by $\lambda = 2\pi/k$, where

$$k = [(2m/\hbar^2)(E - E_0)]^{1/2}. \tag{4.2.3.9}$$

This outgoing spherical wave can be back-scattered by the electron clouds of neighbouring atoms. This back-scattered wave interferes with the outgoing wave, resulting in the oscillation of the absorption rate that is observed experimentally and called XAFS. Equation (4.2.3.8) was written with the assumption that the absorption rate was directly proportional to the linear absorption coefficient.

It is conventional to express $\chi(E)$ in terms of the momentum of the ejected electron, and the usual form of the theoretical expression for $\chi(\mathbf{k})$ is

$$\chi(\mathbf{k}) = \sum_i (N_i/kr_j^2)|f_i(k)| \exp(\sigma_i^2 k^2 - r_i/\rho) \sin[2kr_i + \varphi_i(k)]. \tag{4.2.3.10}$$

Here the summation extends over the shells of atoms that surround the absorbing atom, N_i representing the number of atoms in the ith shell, which is situated a distance r_i from the absorbing atom. The back-scattering amplitude from this shell is $f_i(k)$ for which the associated phase is $\varphi_i(k)$. Deviations due to thermal motions of the electrons are incorporated through a Debye–Waller factor, $\exp(-\sigma_i^2 k^2)$, and ρ is the mean free path of the electron.

The amplitude function $f_i(k)$ depends only on the type of back-scattering atom. The phase, however, contains contributions from both the absorber and the back-scatterer:

$$\varphi_i^l(k) = \varphi_j^l(k) + \varphi_i(k) - l\pi, \tag{4.2.3.11}$$

where $l = 1$ for K and $L_{\rm I}$ edges, and $l = 2$ or 0 for $L_{\rm II}$ and $L_{\rm III}$ edges. The phase is sensitive to variations in the energy threshold, the magnitude of the effect being larger for small electron energies than for electrons with considerable kinetic energy, *i.e.* the effect is more marked in the neighbourhood of the absorption edge. Since the position of the edge varies somewhat for different compounds (Azaroff & Pease, 1974), some impediment to the analysis of experimental data might occur, since the determination of the interatomic distance r_i depends upon the precise knowledge of the value of $\varphi_i(k)$.

In fitting the experimental data based on an empirical value of threshold energy using theoretically determined phase shifts, the difference between the theoretical and the experimental threshold energies ΔE_0 cannot produce a good fit at an arbitrarily chosen distance r_i, since the effect will be seen primarily at low k values ($\sim 0.3r\Delta E_0/k$), whereas changing r_i affects $\varphi_i(k)$ at high k values ($\sim 2k\Delta r$). This was first demonstrated by Lee & Beni (1977).

The significance of the Debye–Waller factor $\exp(-\sigma_i^2 k^2)$ should not be underestimated in this type of investigation. In XAFS studies, one is seeking to determine information regarding such properties of the system as nearest- and next-nearest-neighbour distances and the number of nearest and next-nearest neighbours. The theory is a short-range-order theory, hence deviations of atoms from their expected positions will influence the analysis significantly. Thus, it is often of value, experimentally, to work at liquid-nitrogen temperatures to reduce the effect of atomic vibrations.

Two distinct types of disorder are observed: vibrational, where the atom vibrates about a mean position in the structure, and static, where the atom occupies a position not expected theoretically. These terms can be separated from one

another if the variation of XAFS spectra with temperature is studied, because the two have different temperature dependences. A discussion of the effect of a thermally activated disorder that is large compared with the static order has been given by Sevillano, Meuth & Rehr (1978). For systems with large static disorders, *e.g.* liquids and amorphous solids, equation (4.2.3.10) has to be modified somewhat. The XAFS equation has to be averaged over the pair distribution function $g(r)$ for the system:

$$\chi(k) = \frac{F(k)}{k} \int_0^{\infty} g(r) \exp(-2r/\rho) \frac{\sin(2kr + \varphi_k)}{r^2} \, \mathrm{d}r. \quad (4.2.3.12)$$

Other factors that must be taken into account in XAFS analyses include: inelastic scattering (due to multiple scattering in the absorbing atom and excitations of the atoms surrounding the atom from which the photoelectron was ejected) and multiple scattering of the photoelectron. Should multiple scattering be significant, the simple model given in equation (4.2.3.10) is inappropriate, and more complex models such as those proposed by Pendry (1983), Durham (1983), Gurman (1988, 1995), Natoli (1990), and Rehr & Albers (1990) should be used. Several computer programs are now available commercially for use in personal computers (*EXCURVE*, *FEFF5*, *MSCALC*). Readers are referred to scientific journals to find how best to contact the suppliers of these programs.

4.2.3.4.1.2. *Techniques of data analysis*

Three assumptions must be made if XAFS data are to be used to provide accurate structural and chemical information:

(i) XAFS occurs through the interaction of waves *singly* scattered by neighbouring atoms;

(ii) the amplitude function of the atoms is insensitive to the type of chemical bond (the postulate of transferability), which implies that one can use the same amplitude function for a given atom in problems involving compounds of that atom, whatever the nature of its neighbours or the nature of the bond; and

(iii) the phase function can be transferred for each pair of absorber–back-scatterer atoms.

Of these three assumptions, (ii) is of the most questionable validity. See, for example, Stern, Bunker & Heald (1981).

It is usual, when analysing XAFS data, to search the literature for, or make sufficient measurements of, μ_{l0} remote from the absorption edge to produce a curve of $\mu_{l0}(E)$ *versus* E that can be extrapolated to the position of the edge. From equation (4.2.3.8), it is possible to produce a curve of $\chi(E)$ *versus* E from which the variation of $\chi(k)$ with k can be deduced using equation (4.2.3.9).

It is also customary to multiply $\chi(k)$ by some power of k to compensate for the damping of the XAFS amplitudes with increasing k. The power chosen is somewhat arbitrary but k^3 is a commonly used weighting function.

Two different techniques may be used to analyse the new data set, the *Fourier-transform technique* or the *curve-fitting technique*.

In the *Fourier-transform technique* (FF), the Fourier transform of the $k^n\chi(k)$ is determined for that region of momentum space from the smallest, k_1, to the largest, k_2, wavevectors of the photoelectron, yielding the radical distribution function $\rho_n(r')$ in coordinate (r') space.

$$\rho_n(r') = \frac{1}{(2\pi)^{1/2}} \int_{k_1}^{k_2} k^n \chi(k) \exp(i2kr') \, \mathrm{d}k. \quad (4.2.3.13)$$

The Fourier spectrum contains peaks indicating that the nearest-neighbour, next-nearest-neighbour, *etc.* distances will differ from the true spacings by between 0.2 to 0.5 Å depending on the elements involved. These position shifts are determined for model systems and then *transferred* to the unknown systems to predict interatomic spacings. Fig. 4.2.3.4 illustrates the various steps in the Fourier-transform analysis of XAFS data.

The technique works best for systems having well separated peaks. Its primary weakness as a technique lies in the fact that the phase functions are not linear functions of k, and the spacing shift will depend on E_0, the other factors including the weighting of data before the Fourier transforms are made, the range of k space transformed, and the Debye–Waller factors of the system.

In the *curve-fitting technique* (CF), least-squares refinement is used to fit the spectra in k space using some structural model for the system. Such techniques, however, can only indicate which of several possible choices is more likely to be correct, and *do not prove* that that structure is the correct structure.

It is possible to combine the FF and CF techniques to simplify the data analysis. Also, for data containing single-scatter peaks, the phase and amplitude components can be separated and analysed separately using either theory or model compounds (Stern, Sayers & Lytle, 1975).

Each XAFS data set depends on two sets of strongly correlated variables: $\{F(k), \sigma, \rho, N\}$ and $\{\varphi(k), E_0, r\}$. The elements of each set are not independent of one another. To determine N and σ,

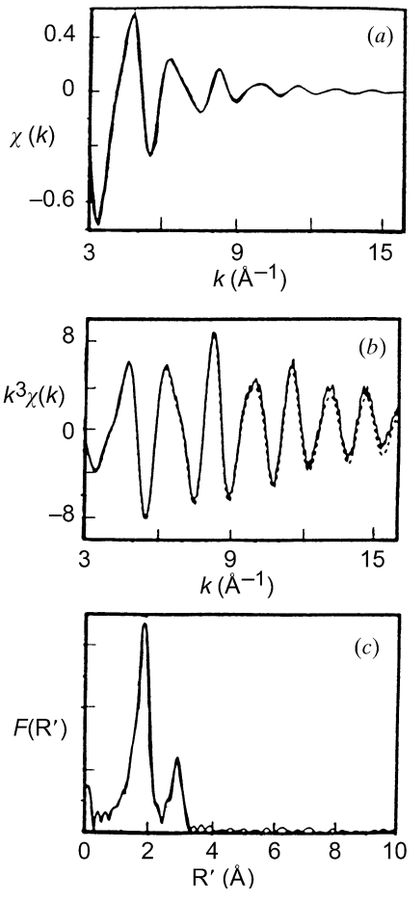

Fig. 4.2.3.4. Steps in the reduction of data from an XAFS experiment using the Fourier transform technique: (*a*) after the removal of background $\chi(k)$ *versus* k; (*b*) after multiplication by a weighting function (in this case k^3); (*c*) after Fourier transformation to determine r'.

one must know $F(k)$ well. To determine r, $\varphi(k)$ must be known accurately.

Attempts have been made by Teo & Lee (1979) to calculate $F(k)$ and $\varphi(k)$ from first principles using an electron–atom scattering model. Parametrized versions have been given by Teo, Lee, Simons, Eisenberger & Kincaid (1977) and Lee *et al.* (1981). Claimed accuracies for r, σ, and N in XAFS determinations are 0.5, 10, and 20%, respectively.

Acceptable methods for data analysis must conform to a number of basic criteria to have any validity. Amongst these are the following:

(i) the data analysis must not give rise to systematic error in the sense that it must provide unbiased estimates of parameters;

(ii) the assumed (hypothetical) model must be able to describe the data adequately;

(iii) the number of parameters used to describe the best fit of data must not exceed the number of independent data points;

(iv) where multiple solutions exist, supplementary information or assumptions used to resolve the ambiguity must conform to the philosophy of choice of the model structure.

The techniques for estimation of the parameters must always be given, including all known sources of uncertainty.

A complete list of criteria for the correct analysis and presentation of XAFS data is given in the reports of the International Workshops on Standards and Criteria in XAFS (Lytle, Sayers & Stern, 1989; Bunker, Hasnain & Sayers, 1990).

4.2.3.4.1.3. *XAFS experiments*

The variety and number of experiments in which XAFS experiments have been used is so large that it is not possible here to give a comprehensive list. By consulting the papers given in such texts as those edited by Winick & Doniach (1980), Teo & Joy (1981), Bianconi, Incoccia & Stipcich (1983), Mustre de Leon *et al.* (1988), Hasnain (1990), and Kuroda *et al.* (1992), the reader may find references to a wide variety of experiments in fields of research ranging from archaeology to zoology.

In *crystallography*, XAFS experiments have been used to assist in the solution of crystal structures; the large variations in the atomic scattering factors can be used to help solve the phase problem. Helliwell (1984) reviewed the use of these techniques in protein crystallography. A further discussion of the use of these anomalous-dispersion techniques in crystallography has been given by Creagh (1987*b*). The relation that exists between the attenuation (related to the imaginary part of the dispersion correction, f'') and intensity (related to the atomic form factor and the real part of the dispersion correction, f') is discussed by Creagh in Section 4.2.6. Specifically, modulations occur in the observed diffracted intensities from a specimen as the incident photon energy is scanned through the absorption edge of an atomic species present in the specimen. This technique, referred to as diffraction anomalous fine structure (DAFS) is complementary to XAFS. Because of the dependence of intensity on the geometrical structure factor, and the fact that the structure factor itself depends on the positional coordinates of the absorbing atom, it is possible to discriminate, in some favourable cases, between the anomalous scattering between atoms occupying different sites in the unit cell (Sorenson *et al.*, 1994).

In many systems of *biological* interest, the arrangement of radicals surrounding an active site must be found in order that the role of that site in biochemical processes may be assessed. A study of the XAFS spectrum of the active atom yields structural information that is specific to that site. Normal crystallographic techniques yield more general information concerning the crystal structure. An example of the use of XAFS in biological systems is the study of iron–sulfur proteins undertaken by Shulman, Weisenberger, Teo, Kincaid & Brown (1978). Other, more recent, studies of biological systems include the characterization of the Mn site in the photosynthetic oxygen evolving complexes including hydroxylamine and hydroquinone (Riggs, Mei, Yocum & Penner-Hahn, 1993) and an XAFS study with an *in situ* electrochemical cell on manganese Schiff-base complexes as a model of a photosystem (Yamaguchi *et al.*, 1993).

It must be stressed that the theoretical expression (equation 4.2.3.10) does not take into account the state of polarization of the incident photon. Templeton & Templeton (1986) have shown that polarization effects may be observed in some materials, *e.g.* sodium bromate. Given that most XAFS experiments are undertaken using the highly polarized radiation from synchrotron-radiation sources, it is of some importance to be aware of the possibility that dichroic effects may occur in some specimens.

Because XAFS is a short-range-order phenomenon, it is particularly useful for the structural study of such *disordered systems* as liquid metals and amorphous solids. The analysis of such disordered systems can be complicated, particularly in those cases where excluded-volume effects occur. Techniques for analysis for these cases have been suggested by Crozier & Seary (1980). Fuoss, Eisenberger, Warburton & Bienenstock (1981) suggested a technique for the investigation of amorphous solids, which they call the differential anomalous X-ray scattering (DAS) technique. This method has some advantages when compared with conventional XAFS methods because it makes more effective use of low-k information, and it does not depend on a knowledge of either the electron phase shifts or the mean free paths.

Both the conventional XAFS and DAS techniques may be used for studies of surface effects and catalytic processes such as those investigated by Sinfelt, Via & Lytle (1980), Hida *et al.* (1985), and Caballero, Villain, Dexpert, Le Peltier & Lynch (1993).

It must be stressed that in all the foregoing discussion it has been assumed that the detection of XAFS has been by measurement of the linear attenuation coefficient of the specimen. However, the process of photon absorption followed by the ejection of a photoelectron has as its consequence both *X-ray fluorescence* and *surface XAFS* (SEXAFS) and *Auger electron emission*. All of these techniques are extremely useful in the analysis of dilute systems.

SEXAFS techniques are extremely sensitive to surface conditions since the mean free path of electrons is only about 20 Å. Discussions of the use of SEXAFS techniques have been given by Citrin, Eisenberger & Hewitt (1978) and Stohr, Denley & Perfettii (1978). A major review of the topic is given in Lee *et al.* (1981). SEXAFS has the capacity of sensing thin films deposited on the surface of substrates, and has applications in experiments involving epitaxic growth and absorption by catalysts.

Fluorescence techniques are important in those systems for which the absorption of the specimen under investigation contributes only very slightly to the total attenuation coefficient since it detects the fluorescence of the absorbing atom directly. Experiments by Hastings, Eisenberger, Lengeler & Perlman (1975) and Marcus, Powers, Storm, Kincaid & Chance (1980) proved the importance of this technique in analysing dilute alloy and biological specimens. Materlik, Bedzyk & Frahm (1984) have demonstrated its use in determining the location of bromine atoms absorbed on single-crystal silicon substrates. Oyanagi, Matsushita, Tanoue, Ishiguro & Kohra (1985) and Oyanagi, Takeda, Matsushita, Ishiguro & Sasaki (1986) have also used fluorescence XAFS techniques for the characterization of very

Table 4.2.3.1. *Some synchrotron-radiation facilities providing XAFS databases and analysis utilities*

Country	Synchrotron source	Address
France	LURE	Université Paris-Sud, LURE, 91405 Orsay, France
Italy	Frascati	Laboratori Nationali di Frascati, CP 13, 00044 Frascati, Italy
Japan	Photon Factory	Photon Factory, National Laboratory for High Energy Physics, 1-1 Oho, Tsukuba-gun, Ibaraki 305, Japan
Germany	DESY	DESY, Notkestrasse 85, 2000 Hamburg 52, Germany
United Kingdom	SRC/ Daresbury	Daresbury Laboratory, Daresbury, Warrington WA4 4AD, England
USA	CHESS	CHESS, Cornell University, Ithaca, New York 14853, USA
	NSLS	NSLS, Brookhaven National Laboratory, Upton, New York 11973, USA
	SPEAR	SSRL, Stanford University, Bin 69, PO Box 4349, Stanford, California 94305, USA

thin films. More recently, Oyanagi *et al*. (1987) have applied the technique to the study of short-range order in high-temperature superconductors. Oyanagi, Martini, Saito & Haga (1995) have studied in detail the performance of a 19-element high-purity Ge solid-state detector array for fluorescence X-ray absorption fine structure studies.

A less-sensitive technique, but one that can be usefully employed for thin-film studies, is that in which XAFS modulations are detected in the beam reflected from a sample surface. This technique, *ReflEXAFS*, has been used by Martens & Rabe (1980) to investigate superficial regions of copper oxide films by means of reflection of the X-rays close to the critical angle for total reflection.

If a thin film is examined in a transmission electron microscope, the electron beam loses some of its kinetic energy in interactions between the electron beam and the electrons within the film. If the resultant energy loss is analysed using a magnetic analyser, XAFS-like modulations are observed in the electron energy spectrum. These modulations, electron-energy-loss fine structure (*EELS*), which were first observed in a conventional transmission electron microscope by Leapman & Cosslet (1976), are now used extensively for microanalyses of light elements incorporated into heavy-element matrices. Most major manufacturers of transmission electron microscopes supply electron-energy-loss spectrometers for their machines. There are more problems in analysing electron-energy-loss spectra than there are for XAFS spectra. Some of the difficulties encountered in producing reliable techniques for the routine analysis of EELS have been outlined by Joy & Maher (1985). This matter is discussed more fully in §4.3.4.4.2.

A more recent development has been the observation of *topographic XAFS* (Bowen, Stock, Davies, Pantos, Birnbaum & Chen, 1984). This fine structure is observed in white-beam topographs taken using synchrotron-radiation sources. The technique provides the means of simultaneously determining spatially resolved microstructural and spectroscopic information for the specimen under investigation.

In all the preceeding discussion, however, the electron was assumed to undergo only single-scattering processes. If multiple scattering occurs, then the theory has to be changed somewhat. §4.2.3.4.2 discusses the effect of multiple scattering.

4.2.3.4.2. *X-ray absorption near edge structure (XANES)*

In Fig. 4.2.3.2(*c*), there appears to be one cycle of strong oscillation in the neighbourhood of the absorption edge before the quasi-periodic variation of the XAFS commences. The electrons that cause this strong modulation of the photoelectric scattering cross section have low k values, and the electron is strongly scattered by neighbouring atoms. It was mentioned in §4.2.3.4.1 that conventional XAFS theory assumes a weak, single-scattering interaction between the ejected photoelectron and its environment. A schematic diagram illustrating the difference between single- and multiple-scattering processes is given in Fig. 4.2.3.5. Evidently, the multiple-scattering process is very complicated and a discussion of the theory of XANES is too complex to be given here. The reader is directed to papers by Pendry (1983), Lee (1981), and Durham (1983). A more recent review of the study of fine structure in ionization cross sections and their use in surface science has been given by Woodruff (1986).

The data from XANES experiments can be analysed to determine structural information such as coordination geometry, the symmetry of unoccupied valence electronic states, and the effective charge on the absorbing atom (Natoli, Misemer, Doniach & Kutzler, 1980; Kutzler, Natoli, Misemer, Doniach & Hodgson, 1981). XANES experiments have been performed to resolve many problems, *inter alia*: the origin of white lines (Lengeler, Materlik & Müller, 1983); absorption of gases on metal surfaces (Norman, Durham & Pendry, 1983); the effect of local symmetry in 3*d* elements (Petiau & Calas, 1983); and the determination of valence states in materials (Lereboures, Dürr, d'Huysser, Bonelle & Lenglet, 1980).

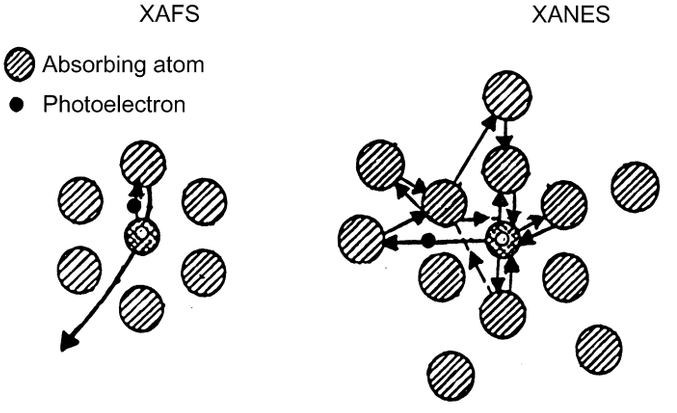

Fig. 4.2.3.5. Schematic representations of the scattering processes undergone by the ejected photoelectron in the single-scattering (XAFS) case and the full multiple-scattering regime (XANES).

4.2.3.5. *Comments*

For reliable experiments using XAFS and XANES to be undertaken, intense-radiation sources must be used. Synchrotron-radiation sources are such a source of highly intense X-rays. Their ready availability to experimenters and the comparative simplicity of the equipment required to perform the experiments have made experiments involving XAFS and XANES very much easier to perform than has hitherto been the case.

At some synchrotron-radiation sources, database and program libraries for the storage and analysis of XAFS and XANES data exist. These are usually part of the general computing facilities (Pantos, 1982).

Crystallographers seeking information concerning the nature and extent of these computer facilities can find such information by contacting the computer centre at one of the synchrotron-radiation establishments listed in Table 4.2.3.1.

4.2.4. X-ray absorption (or attenuation) coefficients (By D. C. Creagh and J. H. Hubbell)

4.2.4.1. *Introduction*

This data set is intended to supersede those data sets given in *International Tables for X-ray Crystallography*, Vols. III (Koch, MacGillavry & Milledge, 1962) and IV (Hubbell, McMaster, Del Grande & Mallett, 1974).

It is not intended here to give a detailed bibliography of experimental data that have been obtained in the past 90 years. This has been the subject of a number of publications, *e.g.* Saloman & Hubbell (1987), Hubbell, Gerstenberg & Saloman (1986), Saloman & Hubbell (1986), and Saloman, Hubbell & Scofield (1988). Further commentary on the validity and the quality of the experimental data in existing tabulations has been given by Creagh & Hubbell (1987) and Creagh (1987).

Existing tabulations of X-ray attenuation (or absorption) cross sections fall into three distinct categories: purely theoretical, purely experimental, and an evaluated mixture of theoretical and experimental data.

Compilations of the purely theoretically derived data exist for:

photo-effect absorption cross sections (Storm & Israel, 1970; Cromer & Liberman, 1970; Scofield, 1973; Hubbell, Veigele, Briggs, Brown, Cromer & Howerton, 1975; Band, Kharitonov & Trzhaskovskaya, 1979; Yeh & Lindau, 1985);

Compton scattering cross sections (Hubbell *et al.*, 1975);

Rayleigh scattering cross sections (Hubbell *et al.*, 1975; Hubbell & Øverbø, 1979; Schaupp, Schumacher, Smend, Rullhausen & Hubbell, 1983).

Many purely experimental compilations exist, and the cross-section data given in computer programs used in the analysis of results in X-ray-fluorescence spectroscopy, electron-probe microanalysis, and X-ray diffraction are usually (evaluated) compilations of several of the following compilations: Allen (1935, 1969), Victoreen (1949), Liebhafsky, Pfeiffer, Winslow & Zemany (1960), Koch *et al.* (1962), Heinrich (1966), Theisen & Vollath (1967), Veigele (1973), Leroux & Thinh (1977), Montenegro, Baptista & Duarte (1978), and Plechaty, Cullen & Howerton (1981). If a comparison is made between these data sets, significant discrepancies are found, and questions must be asked concerning the reliability of the data sets that are compared. Jackson & Hawkes (1981) and Gerward (1986) have produced sets of parametric tables to simplify the application of X-ray attenuation data for the solution of problems in computer-aided tomography and X-ray-fluorescence analysis.

Compilations by Henke, Lee, Tanaka, Shimambukuro & Fujikawa (1982) and the earlier tables of McMaster, Del Grande, Mallett & Hubbell (1969/1970) are examples of the judicious application of both theoretical and experimental data to produce a comprehensive data set of X-ray interaction cross sections.

Because of the discrepancies that appear to exist between experimental data sets, the IUCr Commission on Crystallographic Apparatus set up a project to establish which, if any, of the existing methods for measuring X-ray interaction cross sections (X-ray attenuation coefficients) and which theoretical calculations could be considered to be the most reliable. A discussion of some of the major results of this project is given in Section 4.2.3. A more detailed description of this project has been given by Creagh & Hubbell (1987, 1990).

In this section, tabulations of the total X-ray interaction cross sections σ and the mass absorption coefficient μ_m are given for a range of characteristic X-ray wavelengths [Ti $K\alpha$ 2.7440 Å (or 4.509 keV) to Ag $K\beta$ 0.4470 Å (or 24.942 keV)]. The interaction cross sections are expressed in units of barns/atom (1 barn $= 10^{-28}$ m^2) whilst the mass absorption coefficient is given in cm^2 g^{-1}. Table 4.2.4.1 sets out the wavelengths of the characteristic wavelengths used in Tables 4.2.4.2 and 4.2.4.3, which list values of σ and μ_m, respectively.

Users of these tables should be aware of three important facts.

(i) The values given in the tables are derived for the case of isolated atoms, and cooperative effects may become important in condensed phases (Section 4.2.3).

(ii) The values are based solely on theoretical calculations.

(iii) The limits to the reliability of the data when compared with experimental values are shown in Fig. 4.2.4.4.

The linear attenuation coefficient μ_l in units of cm^{-1} can be defined operationally as

$$\mu_l = \left(\ln \frac{I_o}{I}\right) \Big/ t \qquad (4.2.4.1)$$

from the exponential attenuation relationship

$$\frac{I}{I_0} = \exp(-\mu_l t) \qquad (4.2.4.2)$$

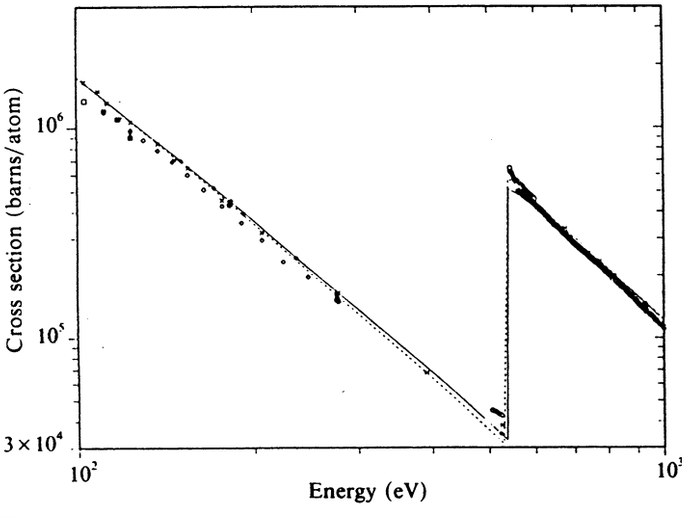

Fig. 4.2.4.1. Agreement between theory and experiment for oxygen ($Z = 8$) in the 'soft' X-ray region. The solid line is for the Scofield (1973) values without renormalization and the dotted line is for the semi-empirical data of Henke *et al.* (1982).

Table 4.2.4.1. *Table of wavelengths and energies for the characteristic radiations used in Tables 4.2.4.2 and 4.2.4.3*

Radiation	λ (Å)	E (keV)
Ag $K\bar{\alpha}$	0.5608	22.103
$K\beta_1$	0.4970	24.942
Pd $K\bar{\alpha}$	0.5869	21.125
$K\beta_1$	0.5205	23.819
Rh $K\bar{\alpha}$	0.6147	20.169
$K\beta_1$	0.5456	22.724
Mo $K\bar{\alpha}$	0.7107	17.444
$K\beta_1$	0.6323	19.608
Zn $K\bar{\alpha}$	1.4364	8.631
$K\beta_1$	1.2952	9.572
Cu $K\bar{\alpha}$	1.5418	8.041
$K\beta_1$	1.3922	8.905
Ni $K\bar{\alpha}$	1.6591	7.472
$K\beta_1$	1.5001	8.265
Co $K\bar{\alpha}$	1.7905	6.925
$K\beta_1$	1.6208	7.629
Fe $K\bar{\alpha}$	1.9373	6.400
$K\beta_1$	1.7565	7.038
Mn $K\bar{\alpha}$	2.1031	5.895
$K\beta_1$	1.9102	6.490
Cr $K\bar{\alpha}$	2.2909	5.412
$K\beta_1$	2.0848	5.947
Ti $K\bar{\alpha}$	2.7496	4.509
$K\beta_1$	2.5138	4.932

in which an idealized plane-parallel slab of material is interposed normally into a parallel beam of monoenergetic X-rays initially of intensity I_0, attenuated by the interposed slab to a reduced intensity I.

The linear attenuation coefficient μ_l for multi-element substances may be obtained in two ways. Through the mass absorption coefficients, we have

$$\mu_l = \rho \sum_i g_i(\mu_m)_i, \tag{4.2.4.3}$$

where g_i is the mass fraction of the element i for which the mass attenuation coefficient $(\mu_m)_i$ is in units of $\mathrm{cm^2\,g^{-1}}$, and ρ is the density of the material in units of $\mathrm{g\,cm^{-3}}$. The summation is over all the constituent elements. The mass attenuation coefficient μ_m is sometimes written as (μ_l/ρ).

For a crystal with unit-cell volume V_c,

$$\mu_l = \frac{1}{V_c}\sum_i \sigma_i, \tag{4.2.4.4}$$

where the summation is over all the atoms in the cell. If σ_i is in barns/atom and V_c is in $\mathrm{Å^3}$, then μ_l is in $\mathrm{cm^{-1}}$.

These tables list total interaction cross sections and mass attenuation coefficients for isolated atoms calculated for characteristic X-ray photon emissions ranging from Ti $K\alpha$ to Ag $K\beta$.

The total interaction cross section is defined by

$$\sigma = \sigma_{\mathrm{pe}} + \sigma_R + \sigma_C, \tag{4.2.4.5}$$

where σ_{pe} is the photo-effect cross section; σ_R is the Rayleigh (unmodified, elastic) cross section; σ_C is the Compton (modified, inelastic) cross section.

The reader's attention is drawn to the fact that in the neighbourhood of an absorption edge for aggregations of atoms significant deviations may be found because of cooperative effects (XAFS and XANES). A discussion of these effects is given in Section 4.2.3.

4.2.4.2. *Sources of information*

4.2.4.2.1. *Theoretical photo-effect data: σ_{pe}*

Of the many theoretical data sets in existence, those of Storm & Israel (1970), Cromer & Liberman (1970), and Scofield (1973) have often been used as bench marks against which both experimental and theoretical data have been compared. In particular, theoretical data produced using the **S**-matrix approach have been compared with these values. See, for example, Kissel, Roy & Pratt (1980). Some indication of the extent to which agreement exists between the different theoretical data sets is given in §4.2.6.2.4 (Tables 4.2.6.3 and 4.2.6.5). These tables show that the values of $f'(\omega, 0)$, which is proportional to σ, calculated using modern relativistic quantum mechanics, agree to better than 1%. It has also been demonstrated by Creagh & Hubbell (1987, 1990) in their analysis of the results of the IUCr X-ray Attenuation Project that there appears to be no rational basis for preferring one of these data sets over the other.

These tables do not list separately photo-effect cross sections. However, should these be required, the data can be found using Table 4.2.6.8. The cross section in barns/atom is related to $f'(\omega, 0)$ expressed in electrons/atom by $\sigma = 5636\lambda f'(\omega, 0)$, where λ is expressed in ångströms.

The values for σ_{pe} used in this compilation are derived from recent tabulations based on relativistic Hartree–Fock–Dirac–Slater calculations by Creagh. The extent to which this data set differs from other theoretical and experimental data sets has been discussed by Creagh (1990).

4.2.4.2.2. *Theoretical Rayleigh scattering data: σ_R*

If each of the atoms gives rise to scattering in which momentum but not energy changes occur, and if each of the atoms can be considered to scatter as if it were an isolated atom, the cross section may be written as

$$\sigma_R = \pi r_e^2 \int_{-1}^{1} (1 + \cos^2\varphi) f^2(q, Z)\, \mathrm{d}(\cos\varphi), \tag{4.2.4.6}$$

where

r_e is the classical radius of the electron;

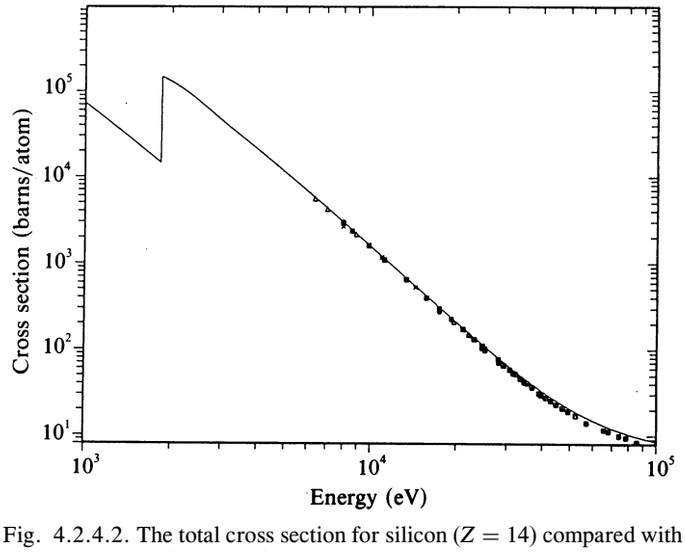

Fig. 4.2.4.2. The total cross section for silicon ($Z = 14$) compared with the unrenormalized Scofield values. The measured and theoretical attenuation coefficients show systematic differences of several percent for the photon energy range 10 to 100 keV.

φ is the angle of scattering ($= 2\theta$ if θ is the Bragg angle);

$2\pi\,\mathrm{d}(\cos\varphi)$ is the solid angle between cones with angles φ and $\varphi + \mathrm{d}\varphi$;

$f(q, Z)$ is the atomic scattering factor as defined by Cromer & Waber (1974);

q is $[\sin(\varphi/2)/\lambda]$, the momentum transfer parameter. Here λ is expressed in ångströms.

Reliable tables of $f(q, Z)$ exist and have been reviewed recently by Kane, Kissel, Pratt & Roy (1986). The most recent schematic tabulations of $f(q, Z)$ are those of Hubbell & Øverbø (1979) and Schaupp *et al.* (1983). The data used in these tables have been derived from the tabulation for $q = 0.02$ to 10^9 Å^{-1}, for all Z's from 1 to 100 by Hubbell & Øverbø (1979) based on the exact formula of Pirenne (1946) for H, and relativistic calculations by Doyle & Turner (1968), Cromer & Waber (1974), Øverbø (1977, 1978), and high-q extensions using the Bethe–Levinger expression in Levinger (1952).

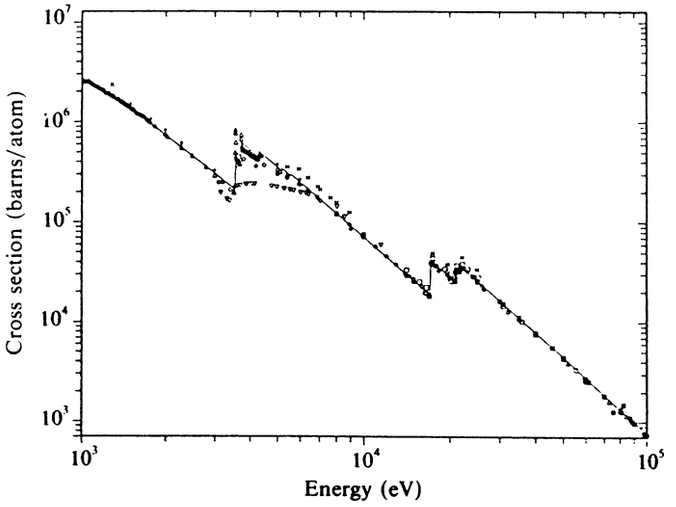

Fig. 4.2.4.3. The total cross section for uranium ($Z = 92$). The theoretical values (solid line) are partially obscured by the high density of available measurements. Deviations of the measured values from the theoretical predictions are mostly of the order of 5%, although a few data sets deviate by more than 30%.

As mentioned in Creagh & Hubbell (1987), the atoms in highly ordered single crystals do not scatter as though they are isolated atoms. Rather, cooperative effects become important. In this case, the Rayleigh scattering cross section must be replaced by two cross sections:

the Laue–Bragg cross section σ_{LB},

and the thermal diffuse scattering cross section σ_{TD}.

That is, σ_R is replaced by $\sigma_{\mathrm{LB}} + \sigma_{\mathrm{TD}}$.

These effects are discussed elsewhere (Subsection 4.2.3.2). Briefly,

$$\sigma_{\mathrm{LB}} = (r_e^2\lambda^2/2NV_c)\sum_H [C_p m d|F|^2 \exp(-2M)]_H. \qquad (4.2.4.7)$$

In equation (4.2.4.7), which is due to De Marco & Suortti (1971),

$C_p = \frac{1}{2}(1 + \cos^2\varphi)$;

d_H is the spacing of the (hkl) planes in the crystal;

m_H is the multiplicity of the hkl Bragg reflection;

F_H is the geometrical structure factor for the crystal structure that contains N atoms in a cell of volume V_c;

$\exp(-2M)_H$ is the Debye-Waller temperature factor.

It is assumed that the total thermal diffuse scattering is equal to the scattering lost from Laue–Bragg scattering because of thermal vibrations.

$$\sigma_{\mathrm{TD}} = (r_e^2\lambda^2/2NV_c)\sum_H \{C_p m d|F|^2[1 - \exp(-2M)]\}_H. \quad (4.2.4.8)$$

H[1] 20↑ 36↑																He[2] 16↑ 2↓
Li[3] 7↑ 12	Be[4] 13 17↓											B[5] 1 *	C[6] 5↓ 6	N[7] 6↑ 5	O[8] 9 6↓	F[9] 6 3	Ne[10] 3↓ 5
Na[11] 11 *	Mg[12] 4↓ 5											Al[13] 4 7	Si[14] 8↓ 2↓	P[15] 7↓ *	S[16] 4↓ 3	Cl[17] 5↑ 2	Ar[18] 5 14↑
K[19] 4 *	Ca[20] 7↓ 12↓	Sc[21] 6 8↑	Ti[22] 3 8↑	V[23] 4↓ 5	Cr[24] 4 14	Mn[25] 5↓ *	Fe[26] 3↓ 29↑	Co[27] 5↓ 5	Ni[28] 5 6	Cu[29] 5 27	Zn[30] 5↑ 6↑	Ga[31] 17↑ *	Ge[32] 3↓ 12	As[33] 9 *	Se[34] 7↑ 8↑	Br[35] 6↑ 4↓	Kr[36] 2 9↑
Rb[37] * *	Sr[38] 5 *	Y[39] 2↑ 3	Zr[40] 3↑ 3	Nb[41] 3 3	Mo[42] 5↑ 9↑	Tc[43] * *	Ru[44] * *	Rh[45] 4 25	Pd[46] 3↑ 6↑	Ag[47] 5↑ 10↑	Cd[48] 4↑ 13	In[49] 7↑ 22	Sn[50] 5↑ 7↑	Sb[51] 6↑ 42	Te[52] 9↑ 17↑	I[53] 5↑ 6↓	Xe[54] 3 10
Cs[55] * *	Ba[56] 4↓ 12↑	La[57] 7↓ 23↓	Hf[72] 3 10	Ta[73] 4 9↓	W[74] 5 8	Re[75] * 21↑	Os[76] * *	Ir[77] 3 *	Pt[78] 5↑ 14↓	Au[79] 4↓ 11↑	Hg[80] 9 2↑	Tl[81] 3 *	Pb[82] 4↑ 6↑	Bi[83] 7↑ 8↑	Po[84] * *	At[85] * *	Rn[86] * *
Fr[87] * *	Ra[88] * *	Ac[89] * *															

Ce[58] 4↑ 3↑	Pr[59] 2 5	Nd[60] 3 7↑	Pn[61] * *	Sm[62] 4↑ 5↑	Eu[63] * *	Gd[64] 3↑ 8↑	Tb[65] 2 *	Dy[66] 2 3	Ho[67] 3 10↑	Er[68] 3 3	Tm[69] 2 *	Yb[70] 3 24↑	Lu[71] * 80
Th[90] 4↓ 11↑	Pa[91] * *	U[92] 6 25↑	Np[93]	Pu[94]	Am[95]	Cm[96]	Bk[97]	Cf[98]	Es[99]	Fn[100]	Md[101]	No[102]	Lr[103]

Fig. 4.2.4.4. Comparison between this tabulation and experimental data contained in Saloman & Hubbell (1986). The upper set corresponds to the average percent deviation between the experimental data and this tabulation for the energy range 10 to 100 keV. The lower set corresponds to the energy range 1 to 10 keV. For explanation of symbols see text.

Table 4.2.4.2. *Total photon interaction cross section (barns/atom)*

Radiation	Energy (MeV)	1 Hydrogen	2 Helium	3 Lithium	4 Beryllium	5 Boron	6 Carbon	7 Nitrogen	8 Oxygen
Ag $K\beta_1$	2.494E−02	6.10E−01	1.26E+00	2.01E+00	2.97E+00	4.40E+00	6.59E+00	1.00E+01	1.52E+01
Pd $K\beta_1$	2.382E−02	6.10E−01	1.26E+00	2.01E+00	2.99E+00	4.44E+00	6.68E+00	1.02E+01	1.55E+01
Rh $K\beta_1$	2.272E−02	6.12E−01	1.27E+00	2.04E+00	3.06E+00	4.47E+00	6.78E+00	1.05E+01	1.62E+01
Ag $K\bar{\alpha}$	2.210E−02	6.14E−01	1.28E+00	2.06E+00	3.13E+00	4.79E+00	7.45E+00	1.17E+01	1.82E+01
Pd $K\bar{\alpha}$	2.112E−02	6.16E−01	1.29E+00	2.09E+00	3.23E+00	5.05E+00	8.02E+00	1.28E+01	2.02E+01
Rh $K\bar{\alpha}$	2.017E−02	6.18E−01	1.30E+00	2.13E+00	3.35E+00	5.35E+00	8.68E+00	1.41E+01	2.25E+01
Mo $K\beta_1$	1.961E−02	6.19E−01	1.31E+00	2.16E+00	3.42E+00	5.56E+00	9.14E+00	1.50E+01	2.41E+01
Mo $K\bar{\alpha}$	1.744E−02	6.24E−01	1.34E+00	2.28E+00	3.83E+00	6.61E+00	1.15E+01	1.96E+01	3.25E+01
Zn $K\beta_1$	9.572E−03	6.47E−01	1.69E+00	4.19E+00	1.07E+01	2.54E+01	5.37E+01	1.03E+02	1.80E+02
Cu $K\beta_1$	8.905E−03	6.50E−01	1.78E+00	4.74E+00	1.28E+01	3.10E+01	6.64E+01	1.27E+02	2.24E+02
Zn $K\bar{\alpha}$	8.631E−03	6.51E−01	1.82E+00	5.02E+00	1.38E+01	3.39E+01	7.28E+01	1.40E+02	2.46E+02
Ni $K\beta_1$	8.265E−03	6.53E−01	1.89E+00	5.46E+00	1.54E+01	3.83E+01	8.28E+01	1.59E+02	2.80E+02
Cu $K\bar{\alpha}$	8.041E−03	6.55E−01	1.94E+00	5.76E+00	1.66E+01	4.15E+01	8.99E+01	1.73E+02	3.04E+02
Co $K\beta_1$	7.649E−03	6.58E−01	2.04E+00	6.40E+00	1.90E+01	4.80E+01	1.04E+02	2.01E+02	3.54E+02
Ni $K\bar{\alpha}$	7.472E−03	6.59E−01	2.09E+00	6.73E+00	2.02E+01	5.14E+01	1.12E+02	2.16E+02	3.80E+02
Fe $K\beta_1$	7.058E−03	6.63E−01	2.23E+00	7.65E+00	2.37E+01	6.09E+01	1.33E+02	2.57E+02	4.51E+02
Co $K\bar{\alpha}$	6.925E−03	6.64E−01	2.28E+00	7.99E+00	2.50E+01	6.45E+01	1.41E+02	2.72E+02	4.78E+02
Mn $K\beta_1$	6.490E−03	6.69E−01	2.48E+00	9.34E+00	3.01E+01	7.84E+01	1.72E+02	3.31E+02	5.81E+02
Fe $K\bar{\alpha}$	6.400E−03	6.70E−01	2.53E+00	9.67E+00	3.13E+01	8.18E+01	1.79E+02	3.46E+02	6.06E+02
Cr $K\beta_1$	5.947E−03	6.77E−01	2.83E+00	1.16E+01	3.88E+01	1.02E+02	2.24E+02	4.32E+02	7.56E+02
Mn $K\bar{\alpha}$	5.895E−03	6.78E−01	2.87E+00	1.19E+01	3.99E+01	1.05E+02	2.30E+02	4.44E+02	7.76E+02
Cr $K\bar{\alpha}$	5.412E−03	6.89E−01	3.31E+00	1.50E+01	5.14E+01	1.36E+02	2.99E+02	5.75E+02	1.00E+03
Ti $K\beta_1$	4.932E−03	7.04E−01	3.94E+00	1.94E+01	6.82E+01	1.81E+02	3.98E+02	7.62E+02	1.33E+03
Ti $K\bar{\alpha}$	4.509E−03	7.24E−01	4.73E+00	2.51E+01	8.97E+01	2.39E+02	5.23E+02	1.00E+03	1.73E+03

		9 Fluorine	10 Neon	11 Sodium	12 Magnesium	13 Aluminium	14 Silicon	15 Phosphorus	16 Sulfur
Ag $K\beta_1$	2.494E−02	2.27E+01	3.33E+01	4.77E+01	6.68E+01	9.16E+01	1.23E+02	1.62E+02	2.10E+02
Pd $K\beta_1$	2.382E−02	2.32E+01	3.40E+01	4.88E+01	6.85E+01	9.40E+01	1.26E+02	1.67E+02	2.16E+02
Rh $K\beta_1$	2.272E−02	2.50E+01	3.62E+01	5.07E+01	8.26E+01	1.05E+02	1.40E+02	1.85E+02	2.02E+02
Ag $K\bar{\alpha}$	2.210E−02	2.77E+01	4.12E+01	5.96E+01	8.42E+01	1.16E+02	1.56E+02	2.06E+02	2.67E+02
Pd $K\bar{\alpha}$	2.112E−02	3.11E+01	4.65E+01	6.75E+01	9.55E+01	1.32E+02	1.78E+02	2.35E+02	3.05E+02
Rh $K\bar{\alpha}$	2.017E−02	3.50E+01	5.26E+01	7.67E+01	1.09E+02	1.51E+02	2.03E+02	2.69E+02	3.49E+02
Mo $K\beta_1$	1.961E−02	3.76E+01	5.68E+01	5.30E+01	1.18E+02	1.63E+02	2.20E+02	2.92E+02	3.78E+02
Mo $K\bar{\alpha}$	1.744E−02	5.15E+01	7.86E+01	1.16E+02	1.65E+02	2.29E+02	3.10E+02	4.10E+02	5.32E+02
Zn $K\beta_1$	9.572E−03	2.95E+02	4.57E+02	6.77E+02	9.67E+02	1.34E+03	1.79E+03	2.36E+03	3.03E+03
Cu $K\beta_1$	8.905E−03	3.66E+02	5.67E+02	8.39E+02	1.20E+03	1.65E+03	2.21E+03	2.90E+03	3.72E+03
Zn $K\bar{\alpha}$	8.631E−03	4.02E+02	6.22E+02	9.20E+02	1.31E+03	1.81E+03	2.42E+03	3.17E+03	4.06E+03
Ni $K\beta_1$	8.265E−03	4.58E+02	7.08E+02	1.05E+03	1.49E+03	2.05E+03	2.75E+03	3.59E+03	4.60E+03
Cu $K\bar{\alpha}$	8.041E−03	4.98E+02	7.68E+02	1.14E+03	1.61E+03	2.22E+03	2.97E+03	3.88E+03	4.97E+03
Co $K\beta_1$	7.649E−03	5.78E+02	8.92E+02	1.32E+03	1.87E+03	2.57E+03	3.43E+03	4.48E+03	5.72E+03
Ni $K\bar{\alpha}$	7.472E−03	6.20E+02	9.56E+02	1.41E+03	2.00E+03	2.75E+03	3.67E+03	4.78E+03	6.11E+03
Fe $K\beta_1$	7.058E−03	7.36E+02	1.13E+03	1.67E+03	2.36E+03	3.24E+03	4.32E+03	5.62E+03	7.17E+03
Co $K\bar{\alpha}$	6.925E−03	7.79E+02	1.20E+03	1.76E+03	2.50E+03	3.42E+03	4.56E+03	5.93E+03	7.56E+03
Mn $K\beta_1$	6.490E−03	9.46E+02	1.45E+03	2.13E+03	3.02E+03	4.13E+03	5.49E+03	7.12E+03	9.06E+03
Fe $K\bar{\alpha}$	6.400E−03	9.86E+02	1.51E+03	2.22E+03	3.14E+03	4.29E+03	5.71E+03	7.41E+03	9.42E+03
Cr $K\beta_1$	5.947E−03	1.23E+03	1.88E+03	2.75E+03	3.88E+03	5.30E+03	7.03E+03	9.10E+03	1.15E+04
Mn $K\bar{\alpha}$	5.895E−03	1.26E+03	1.93E+03	2.83E+03	3.98E+03	5.43E+03	7.20E+03	9.33E+03	1.18E+04
Cr $K\bar{\alpha}$	5.412E−03	1.62E+03	2.48E+03	3.62E+03	5.09E+03	6.93E+03	9.16E+03	1.18E+04	1.50E+04
Ti $K\beta_1$	4.932E−03	2.14E+03	3.26E+03	4.74E+03	6.64E+03	9.01E+03	1.19E+04	1.53E+04	1.93E+04
Ti $K\bar{\alpha}$	4.509E−03	2.79E+03	4.23E+03	6.13E+03	8.57E+03	1.16E+04	1.52E+04	1.95E+04	2.45E+04

Table 4.2.4.2. *Total photon interaction cross section (barns/atom) (cont.)*

Radiation	Energy (MeV)	17 Chlorine	18 Argon	19 Potassium	20 Calcium	21 Scandium	22 Titanium	23 Vanadium	24 Chromium
Ag $K\beta_1$	2.494E−02	2.68E+02	3.36E+02	4.17E+02	5.12E+02	6.20E+02	7.44E+02	8.85E+02	1.04E+03
Pd $K\beta_1$	2.382E−02	2.75E+02	3.45E+02	4.29E+02	5.26E+02	6.37E+02	7.64E+02	9.09E+02	1.07E+03
Rh $K\beta_1$	2.272E−02	3.15E+02	3.84E+02	4.84E+02	6.30E+02	7.25E+02	8.63E+02	9.98E+02	1.19E+03
Ag $K\bar{\alpha}$	2.210E−02	3.41E+02	4.29E+02	5.32E+02	6.52E+02	7.89E+02	9.47E+02	1.12E+03	1.33E+03
Pd $K\bar{\alpha}$	2.112E−02	3.89E+02	4.89E+02	6.06E+02	7.42E+02	8.99E+02	1.08E+03	1.28E+03	1.51E+03
Rh $K\bar{\alpha}$	2.017E−02	4.45E+02	5.59E+02	6.93E+02	8.48E+02	1.03E+03	1.23E+03	1.46E+03	1.72E+03
Mo $K\beta_1$	1.961E−02	4.83E+02	6.06E+02	7.52E+02	9.20E+02	1.11E+03	1.33E+03	1.58E+03	1.86E+03
Mo $K\bar{\alpha}$	1.744E−02	6.78E+02	8.51E+02	1.05E+03	1.29E+03	1.56E+03	1.86E+03	2.20E+03	2.58E+03
Zn $K\beta_1$	9.572E−03	3.82E+03	4.74E+03	5.80E+03	7.02E+03	8.38E+03	9.93E+03	1.16E+04	1.33E+04
Cu $K\beta_1$	8.905E−03	4.68E+03	5.80E+03	7.09E+03	8.57E+03	1.02E+04	1.21E+04	1.41E+04	1.60E+04
Zn $K\bar{\alpha}$	8.631E−03	5.11E+03	6.34E+03	7.73E+03	9.34E+03	1.11E+04	1.32E+04	1.53E+04	1.73E+04
Ni $K\beta_1$	8.265E−03	5.78E+03	7.15E+03	8.72E+03	1.05E+04	1.25E+04	1.48E+04	1.72E+04	1.96E+04
Cu $K\bar{\alpha}$	8.041E−03	6.24E+03	7.72E+03	9.40E+03	1.13E+04	1.35E+04	1.39E+04	1.85E+04	2.13E+04
Co $K\beta_1$	7.649E−03	7.17E+03	8.86E+03	1.08E+04	1.30E+04	1.54E+04	1.80E+04	2.11E+04	2.53E+04
Ni $K\bar{\alpha}$	7.472E−03	7.66E+03	9.46E+03	1.15E+04	1.38E+04	1.64E+04	1.91E+04	2.25E+04	2.74E+04
Fe $K\beta_1$	7.058E−03	8.97E+03	1.11E+04	1.34E+04	1.61E+04	1.91E+04	2.20E+04	2.62E+04	3.32E+04
Co $K\bar{\alpha}$	6.925E−03	9.46E+03	1.17E+04	1.41E+04	1.69E+04	2.01E+04	2.31E+04	2.75E+04	3.53E+04
Mn $K\beta_1$	6.490E−03	1.13E+04	1.39E+04	1.69E+04	2.01E+04	2.39E+04	2.74E+04	3.26E+04	4.15E+04
Fe $K\bar{\alpha}$	6.400E−03	1.18E+04	1.44E+04	1.75E+04	2.09E+04	2.47E+04	2.85E+04	3.37E+04	4.25E+04
Cr $K\beta_1$	5.947E−03	1.44E+04	1.76E+04	2.13E+04	2.54E+04	3.01E+04	3.53E+04	4.05E+04	5.79E+03
Mn $K\bar{\alpha}$	5.895E−03	1.47E+04	1.80E+04	2.18E+04	2.60E+04	3.08E+04	3.63E+04	4.14E+04	5.93E+03
Cr $K\bar{\alpha}$	5.412E−03	1.86E+04	2.27E+04	2.74E+04	3.26E+04	3.85E+04	4.69E+04	6.32E+03	7.50E+03
Ti $K\beta_1$	4.932E−03	2.38E+04	2.91E+04	3.49E+04	4.15E+04	4.87E+04	6.79E+03	8.16E+03	9.68E+03
Ti $K\bar{\alpha}$	4.509E−03	3.01E+04	3.69E+04	4.41E+04	5.20E+04	6.03E+04	8.68E+03	1.04E+04	1.24E+04

		25 Manganese	26 Iron	27 Cobalt	28 Nickel	29 Copper	30 Zinc	31 Gallium	32 Germanium
Ag $K\beta_1$	2.494E−02	1.22E+03	1.42E+03	1.64E+03	1.88E+03	2.14E+03	2.43E+03	2.74E+03	3.08E+03
Pd $K\beta_1$	2.382E−02	1.25E+03	1.46E+03	1.68E+03	1.93E+03	2.20E+03	2.49E+03	2.81E+03	3.16E+03
Rh $K\beta_1$	2.272E−02	1.37E+03	1.65E+03	1.89E+03	2.19E+03	2.49E+03	2.88E+03	3.21E+03	3.55E+03
Ag $K\bar{\alpha}$	2.210E−02	1.55E+03	1.80E+03	2.07E+03	2.38E+03	2.71E+03	3.07E+03	3.46E+03	3.87E+03
Pd $K\bar{\alpha}$	2.112E−02	1.76E+03	2.04E+03	2.35E+03	2.70E+03	3.07E+03	3.47E+03	3.91E+03	4.38E+03
Rh $K\bar{\alpha}$	2.017E−02	2.01E+03	2.33E+03	2.68E+03	3.07E+03	3.49E+03	3.95E+03	4.44E+03	4.97E+03
Mo $K\beta_1$	1.961E−02	2.17E+03	2.52E+03	2.90E+03	3.31E+03	3.77E+03	4.26E+03	4.80E+03	5.37E+03
Mo $K\bar{\alpha}$	1.744E−02	3.02E+03	3.49E+03	4.01E+03	4.57E+03	5.18E+03	5.86E+03	6.60E+03	7.38E+03
Zn $K\beta_1$	9.572E−03	1.55E+04	1.78E+04	2.02E+04	2.27E+04	2.53E+04	3.90E+03	4.46E+03	5.08E+03
Cu $K\beta_1$	8.905E−03	1.88E+04	2.15E+04	2.43E+04	2.72E+04	4.13E+03	4.75E+03	5.44E+03	6.19E+03
Zn $K\bar{\alpha}$	8.631E−03	2.05E+04	2.34E+04	2.63E+04	2.94E+04	4.50E+03	5.18E+03	5.92E+03	6.75E+03
Ni $K\beta_1$	8.265E−03	2.29E+04	2.61E+04	2.93E+04	4.41E+03	5.07E+03	5.83E+03	6.67E+03	7.60E+03
Cu $K\bar{\alpha}$	8.041E−03	2.46E+04	2.80E+04	3.14E+04	4.76E+03	5.47E+03	6.29E+03	7.19E+03	8.19E+03
Co $K\beta_1$	7.649E−03	2.80E+04	3.17E+04	4.71E+03	5.46E+03	6.27E+03	7.21E+03	8.24E+03	9.38E+03
Ni $K\bar{\alpha}$	7.472E−03	2.97E+04	3.35E+04	5.02E+03	5.82E+03	6.68E+03	7.68E+03	8.79E+03	1.00E+04
Fe $K\beta_1$	7.058E−03	3.42E+04	5.04E+03	5.87E+03	6.80E+03	7.81E+03	8.98E+03	1.03E+04	1.17E+04
Co $K\bar{\alpha}$	6.925E−03	3.58E+04	5.31E+03	6.18E+03	7.16E+03	8.23E+03	9.46E+03	1.08E+04	1.23E+04
Mn $K\beta_1$	6.490E−03	5.40E+03	6.34E+03	7.39E+03	8.56E+03	9.83E+03	1.13E+04	1.29E+04	1.47E+04
Fe $K\bar{\alpha}$	6.400E−03	5.62E+03	6.59E+03	7.68E+03	8.89E+03	1.02E+04	1.17E+04	1.34E+04	1.53E+04
Cr $K\beta_1$	5.947E−03	6.87E+03	8.06E+03	9.40E+03	1.09E+04	1.25E+04	1.43E+04	1.64E+04	1.86E+04
Mn $K\bar{\alpha}$	5.895E−03	7.04E+03	8.26E+03	9.62E+03	1.11E+04	1.28E+04	1.47E+04	1.68E+04	1,91E+04
Cr $K\bar{\alpha}$	5.412E−03	8.90E+03	1.04E+04	1.22E+04	1.41E+04	1.61E+04	1.85E+04	2.12E+04	2.41E+04
Ti $K\beta_1$	4.932E−03	1.15E+04	1.35E+04	1.57E+04	1.81E+04	2.08E+04	2.39E+04	2.72E+04	3.09E+04
Ti $K\bar{\alpha}$	4.509E−03	1.47E+04	1.72E+04	2.00E+04	2.31E+04	2.65E+04	3.04E+04	3.46E+04	3.93E+04

Table 4.2.4.2. *Total photon interaction cross section (barns/atom) (cont.)*

Radiation	Energy (MeV)	33 Arsenic	34 Selenium	35 Bromine	36 Krypton	37 Rubidium	38 Strontium	39 Yttrium	40 Zirconium
Ag $K\beta_1$	2.494E−02	3.44E+03	3.84E+03	4.26E+03	4.72E+03	5.21E+03	5.72E+03	6.25E+03	6.79E+03
Pd $K\beta_1$	2.382E−02	3.53E+03	3.94E+03	4.37E+03	4.84E+03	5.34E+03	5.86E+03	6.41E+03	6.96E+03
Rh $K\beta_1$	2.272E−02	4.04E+03	4.53E+03	5.00E+03	5.50E+03	5.98E+03	6.48E+03	7.27E+03	7.80E+03
Ag $K\bar{\alpha}$	2.210E−02	4.33E+03	4.82E+03	5.35E+03	5.92E+03	6.52E+03	7.15E+03	7.80E+03	8.47E+03
Pd $K\bar{\alpha}$	2.112E−02	4.89E+03	5.45E+03	6.04E+03	6.68E+03	7.35E+03	8.06E+03	8.79E+03	9.52E+03
Rh $K\bar{\alpha}$	2.017E−02	5.55E+03	6.18E+03	6.83E+03	7.55E+03	8.30E+03	9.09E+03	9.90E+03	1.07E+04
Mo $K\beta_1$	1.961E−02	5.99E+03	6.66E+03	7.36E+03	8.13E+03	8.94E+03	9.78E+03	1.06E+04	1.15E+04
Mo $K\bar{\alpha}$	1.744E−02	8.22E+03	9.11E+03	1.00E+04	1.10E+04	1.21E+04	1.32E+04	1.43E+04	2.47E+03
Zn $K\beta_1$	9.572E−03	5.77E+03	6.52E+03	7.34E+03	8.24E+03	9.21E+03	1.03E+04	1.14E+04	1.26E+04
Cu $K\beta_1$	8.905E−03	7.03E+03	7.94E+03	8.94E+03	1.00E+04	1.12E+04	1.25E+04	1.39E+04	1.54E+04
Zn $K\bar{\alpha}$	8.631E−03	7.65E+03	8.64E+03	9.73E+03	1.09E+04	1.22E+04	1.36E+04	1.51E+04	1.67E+04
Ni $K\beta_1$	8.265E−03	8.62E+03	9.73E+03	1.10E+04	1.23E+04	1.37E+04	1.53E+04	1.70E+04	1.88E+04
Cu $K\bar{\alpha}$	8.041E−03	9.29E+03	1.05E+04	1.18E+04	1.32E+04	1.48E+04	1.65E+04	1.83E+04	2.03E+04
Co $K\beta_1$	7.649E−03	1.06E+04	1.20E+04	1.35E+04	1.52E+04	1.69E+04	1.89E+04	2.09E+04	2.32E+04
Ni $K\bar{\alpha}$	7.472E−03	1.13E+04	1.28E+04	1.44E+04	1.61E+04	1.80E+04	2.01E+04	2.23E+04	2.47E+04
Fe $K\beta_1$	7.058E−03	1.32E+04	1.49E+04	1.68E+04	1.88E+04	2.10E+04	2.34E+04	2.60E+04	2.87E+04
Co $K\bar{\alpha}$	6.925E−03	1.39E+04	1.57E+04	1.77E+04	1.98E+04	2.22E+04	2.47E+04	2.73E+04	3.02E+04
Mn $K\beta_1$	6.490E−03	1.66E+04	1.88E+04	2.11E+04	2.36E+04	2.64E+04	2.94E+04	3.26E+04	3.60E+04
Fe $K\bar{\alpha}$	6.400E−03	1.73E+04	1.95E+04	2.19E+04	2.45E+04	2.74E+04	3.05E+04	3.38E+04	3.74E+04
Cr $K\beta_1$	5.947E−03	2.11E+04	2.38E+04	2.67E+04	2.99E+04	3.34E+04	3.72E+04	4.12E+04	4.55E+04
Mn $K\bar{\alpha}$	5.895E−03	2.16E+04	2.44E+04	2.74E+04	3.07E+04	3.42E+04	3.81E+04	4.22E+04	4.66E+04
Cr $K\bar{\alpha}$	5.412E−03	2.72E+04	3.07E+04	3.45E+04	3.85E+04	4.30E+04	4.78E+04	5.29E+04	5.84E+04
Ti $K\beta_1$	4.932E−03	3.50E+04	3.94E+04	4.42E+04	4.94E+04	5.51E+04	6.12E+04	6.77E+04	7.47E+04
Ti $K\bar{\alpha}$	4.509E−03	4.44E+04	5.00E+04	5.61E+04	6.27E+04	6.98E+04	7.75E+04	8.56E+04	9.43E+04
		41 Niobium	42 Molybdenum	43 Technetium	44 Ruthenium	45 Rhodium	46 Palladium	47 Silver	48 Cadmium
Ag $K\beta_1$	2.494E−02	7.41E+03	9.36E+03	8.65E+03	9.33E+03	1.00E+04	1.00E+04	2.00E+03	2.18E+03
Pd $K\beta_1$	2.382E−02	7.59E+03	9.61E+03	8.86E+03	9.56E+03	1.03E+04	1.88E+03	2.05E+03	2.23E+03
Rh $K\beta_1$	2.272E−02	8.57E+03	9.30E+03	9.95E+03	1.07E+04	1.18E+03	2.10E+03	2.29E+03	2.49E+03
Ag $K\bar{\alpha}$	2.210E−02	9.22E+03	1.15E+04	1.07E+04	1.92E+03	2.10E+03	2.30E+03	2.51E+03	2.73E+03
Pd $K\bar{\alpha}$	2.112E−02	1.04E+04	1.23E+04	1.20E+04	2.17E+03	2.38E+03	2.60E+03	2.84E+03	3.09E+03
Rh $K\bar{\alpha}$	2.017E−02	1.16E+04	1.27E+04	2.24E+03	2.46E+03	2.70E+03	2.94E+03	3.21E+03	3.50E+03
Mo $K\beta_1$	1.961E−02	1.25E+04	2.19E+03	2.42E+03	2.65E+03	2.91E+03	3.18E+03	3.47E+03	3.78E+03
Mo $K\bar{\alpha}$	1.744E−02	2.73E+03	3.00E+03	3.32E+03	3.64E+03	3.99E+03	4.36E+03	4.76E+03	5.18E+03
Zn $K\beta_1$	9.572E−03	1.40E+04	1.54E+04	1.69E+04	1.85E+04	2.02E+04	2.21E+04	2.40E+04	2.61E+04
Cu $K\beta_1$	8.905E−03	1.70E+04	1.87E+04	2.05E+04	2.25E+04	2.45E+04	2.67E+04	2.91E+04	3.16E+04
Zn $K\bar{\alpha}$	8.631E−03	1.85E+04	2.03E+04	2.23E+04	2.44E+04	2.67E+04	2.91E+04	3.16E+04	3.44E+04
Ni $K\beta_1$	8.265E−03	2.07E+04	2.28E+04	2.51E+04	2.74E+04	3.00E+04	3.27E+04	3.55E+04	3.86E+04
Cu $K\bar{\alpha}$	8.041E−03	2.23E+04	2.46E+04	2.70E+04	2.95E+04	3.23E+04	3.52E+04	3.82E+04	4.15E+04
Co $K\beta_1$	7.649E−03	2.55E+04	2.81E+04	3.08E+04	3.37E+04	3.68E+04	4.01E+04	4.36E+04	4.73E+04
Ni $K\bar{\alpha}$	7.472E−03	2.72E+04	2.99E+04	3.28E+04	3.59E+04	3.92E+04	4.27E+04	4.64E+04	5.03E+04
Fe $K\beta_1$	7.058E−03	3.17E+04	3.48E+04	3.82E+04	4.18E+04	4.56E+04	4.96E+04	5.39E+04	5.84E+04
Co $K\bar{\alpha}$	6.925E−03	3.33E+04	3.66E+04	4.02E+04	4.39E+04	4.79E+04	5.21E+04	5.66E+04	6.14E+04
Mn $K\beta_1$	6.490E−03	3.96E+04	4.36E+04	4.77E+04	5.22E+04	5.69E+04	6.19E+04	6.72E+04	7.28E+04
Fe $K\bar{\alpha}$	6.400E−03	4.12E+04	4.52E+04	4.95E+04	5.42E+04	5.91E+04	6.42E+04	6.97E+04	7.55E+04
Cr $K\beta_1$	5.947E−03	5.01E+04	5.50E+04	6.02E+04	6.58E+04	7.17E+04	7.79E+04	8.45E+04	9.15E+04
Mn $K\bar{\alpha}$	5.895E−03	5.13E+04	5.63E+04	6.16E+04	6.73E+04	7.34E+04	7.97E+04	8.64E+04	9.36E+04
Cr $K\bar{\alpha}$	5.412E−03	6.42E+04	7.05E+04	7.71E+04	8.41E+04	9.16E+04	9.94E+04	1.08E+05	1.17E+05
Ti $K\beta_1$	4.932E−03	8.21E+04	8.99E+04	9.83E+04	1.07E+05	1.17E+05	1.27E+05	1.37E+05	1.48E+05
Ti $K\bar{\alpha}$	4.509E−03	1.04E+05	1.13E+05	1.24E+05	1.35E+05	1.47E+05	1.59E+05	1.72E+05	1.86E+05

Table 4.2.4.2. *Total photon interaction cross section (barns/atom) (cont.)*

Radiation	Energy (MeV)	49 Indium	50 Tin	51 Antimony	52 Tellurium	53 Iodine	54 Xenon	55 Caesium	56 Barium
Ag $K\beta_1$	2.494E−02	2.37E+03	2.57E+03	2.79E+03	3.02E+03	3.26E+03	3.52E+03	3.79E+03	4.08E+03
Pd $K\beta_1$	2.382E−02	2.43E+03	2.64E+03	2.86E+03	3.09E+03	3.34E+03	3.61E+03	3.89E+03	4.18E+03
Rh $K\beta_1$	2.272E−02	2.64E+03	3.00E+03	3.20E+03	3.50E+03	3.71E+03	4.04E+03	4.04E+03	4.76E+03
Ag $K\bar{\alpha}$	2.210E−02	2.97E+03	3.23E+03	3.50E+03	3.78E+03	4.09E+03	4.41E+03	4.75E+03	5.11E+03
Pd $K\bar{\alpha}$	2.112E−02	3.36E+03	3.65E+03	3.95E+03	4.28E+03	4.62E+03	4.98E+03	5.37E+03	5.78E+03
Rh $K\bar{\alpha}$	2.017E−02	3.81E+03	4.13E+03	4.48E+03	4.85E+03	5.24E+03	5.65E+03	6.09E+03	6.55E+03
Mo $K\beta_1$	1.961E−02	4.11E+03	4.46E+03	4.84E+03	5.23E+03	5.65E+03	6.09E+03	6.57E+03	7.06E+03
Mo $K\bar{\alpha}$	1.744E−02	5.63E+03	6.11E+03	6.62E+03	7.16E+03	7.73E+03	8.34E+03	8.98E+03	9.65E+03
Zn $K\beta_1$	9.572E−03	2.83E+04	3.06E+04	3.31E+04	3.57E+04	3.84E+04	4.13E+04	4.44E+04	4.76E+04
Cu $K\beta_1$	8.905E−03	3.43E+04	3.71E+04	4.00E+04	4.32E+04	4.64E+04	4.99E+04	5.36E+04	5.74E+04
Zn $K\bar{\alpha}$	8.631E−03	3.72E+04	4.03E+04	4.35E+04	4.69E+04	5.04E+04	5.42E+04	5.81E+04	6.23E+04
Ni $K\beta_1$	8.265E−03	4.18E+04	4.52E+04	4.88E+04	5.25E+04	5.65E+04	6.07E+04	6.51E+04	6.98E+04
Cu $K\bar{\alpha}$	8.041E−03	4.50E+04	4.86E+04	5.25E+04	5.65E+04	6.07E+04	6.52E+04	7.00E+04	7.50E+04
Co $K\beta_1$	7.649E−03	5.12E+04	5.54E+04	5.98E+04	6.43E+04	6.92E+04	7.42E+04	7.96E+04	8.52E+04
Ni $K\bar{\alpha}$	7.472E−03	5.45E+04	5.89E+04	6.35E+04	6.84E+04	7.35E+04	7.88E+04	8.45E+04	9.04E+04
Fe $K\beta_1$	7.058E−03	6.32E+04	6.83E+04	7.37E+04	7.94E+04	8.52E+04	9.14E+04	9.77E+04	1.04E+05
Co $K\bar{\alpha}$	6.925E−03	6.64E+04	7.18E+04	7.74E+04	8.34E+04	8.96E+04	9.60E+04	1.03E+05	1.09E+05
Mn $K\beta_1$	6.490E−03	7.87E+04	8.50E+04	9.17E+04	9.88E+04	1.06E+05	1.13E+05	1.21E+05	1.29E+05
Fe $K\bar{\alpha}$	6.400E−03	8.17E+04	8.82E+04	9.51E+04	1.02E+05	1.10E+05	1.18E+05	1.26E+05	1.34E+05
Cr $K\beta_1$	5.947E−03	9.90E+04	1.07E+05	1.15E+05	1.24E+05	1.33E+05	1.42E+05	1.60E+05	1.47E+05
Mn $K\bar{\alpha}$	5.895E−03	1.01E+05	1.09E+05	1.18E+05	1.27E+05	1.36E+05	1.45E+05	1.63E+05	1.50E+05
Cr $K\bar{\alpha}$	5.412E−03	1.26E+05	1.36E+05	1.46E+05	1.57E+05	1.68E+05	1.57E+05	1.77E+05	1.34E+05
Ti $K\beta_1$	4.932E−03	1.60E+05	1.73E+05	1.85E+05	1.98E+05	2.11E+05	2.48E+05	5.70E+04	7.16E+04
Ti $K\bar{\alpha}$	4.509E−03	2.00E+05	2.15E+05	2.00E+05	1.60E+05	6.17E+04	5.78E+04	7.28E+04	7.62E+04

		57 Lanthanum	58 Cerium	59 Praseodymium	60 Neodymium	61 Promethium	62 Samarium	63 Europium	64 Gadolinium
Ag $K\beta_1$	2.494E−02	3.97E+03	4.26E+03	4.56E+03	4.89E+03	5.22E+03	5.57E+03	5.93E+03	6.32E+03
Pd $K\beta_1$	2.382E−02	4.05E+03	4.82E+03	5.15E+03	5.51E+03	5.90E+03	6.29E+03	6.71E+03	7.15E+03
Rh $K\beta_1$	2.272E−02	5.10E+03	5.47E+03	5.85E+03	6.25E+03	6.69E+03	7.14E+03	7.59E+03	8.09E+03
Ag $K\bar{\alpha}$	2.210E−02	5.49E+03	5.89E+03	6.29E+03	6.73E+03	7.20E+03	7.69E+03	8.17E+03	8.72E+03
Pd $K\bar{\alpha}$	2.112E−02	6.20E+03	6.63E+03	7.11E+03	7.62E+03	8.14E+03	8.69E+03	9.23E+03	9.84E+03
Rh $K\bar{\alpha}$	2.017E−02	7.03E+03	7.69E+03	8.07E+03	8.62E+03	9.22E+03	9.84E+03	1.05E+04	1.11E+04
Mo $K\beta_1$	1.961E−02	7.59E+03	8.12E+03	8.70E+03	9.29E+03	9.94E+03	1.06E+04	1.13E+04	1.20E+04
Mo $K\bar{\alpha}$	1.744E−02	1.04E+04	1.11E+04	1.19E+04	1.27E+04	1.36E+04	1.44E+04	1.54E+04	1.63E+04
Zn $K\beta_1$	9.572E−03	5.10E+04	5.42E+04	5.78E+04	6.15E+04	6.57E+04	6.97E+04	9.93E+04	7.83E+04
Cu $K\beta_1$	8.905E−03	6.14E+04	6.56E+04	7.00E+04	7.42E+04	7.90E+04	8.36E+04	8.88E+04	9.40E+04
Zn $K\bar{\alpha}$	8.631E−03	6.67E+04	7.12E+04	7.58E+04	8.04E+04	8.44E+04	9.06E+04	9.59E+04	1.02E+05
Ni $K\beta_1$	8.265E−03	7.47E+04	7.96E+04	8.49E+04	9.00E+04	9.56E+04	1.01E+05	1.07E+05	9.84E+04
Cu $K\bar{\alpha}$	8.041E−03	8.03E+04	8.56E+04	9.12E+04	9.68E+04	1.03E+05	1.08E+05	1.02E+05	1.05E+05
Co $K\beta_1$	7.649E−03	9.11E+04	9.70E+04	1.03E+05	1.09E+05	1.16E+05	1.07E+05	1.21E+05	8.75E+04
Ni $K\bar{\alpha}$	7.472E−03	9.68E+04	1.03E+05	1.09E+05	1.16E+05	1.23E+05	1.14E+05	8.70E+04	9.29E+04
Fe $K\beta_1$	7.058E−03	1.11E+05	1.19E+05	1.26E+05	1.18E+05	1.22E+05	9.56E+04	1.03E+05	3.99E+04
Co $K\bar{\alpha}$	6.925E−03	1.17E+05	1.24E+05	1.32E+05	1.21E+05	9.63E+04	9.89E+04	4.04E+04	4.20E+04
Mn $K\beta_1$	6.490E−03	1.38E+05	1.27E+05	1.39E+05	1.05E+05	1.13E+05	4.39E+04	4.67E+04	4.93E+04
Fe $K\bar{\alpha}$	6.400E−03	1.43E+05	1.31E+05	1.02E+05	1.09E+05	4.19E+04	4.59E+04	4.87E+04	5.09E+04
Cr $K\beta_1$	5.947E−03	1.48E+05	1.15E+05	1.22E+05	4.74E+04	5.01E+04	5.52E+04	5.65E+04	6.14E+04
Mn $K\bar{\alpha}$	5.895E−03	1.50E+05	1.19E+05	4.52E+04	4.86E+04	5.18E+04	5.64E+04	6.03E+04	6.29E+04
Cr $K\bar{\alpha}$	5.412E−03	5.19E+04	5.54E+04	5.57E+04	6.01E+04	6.43E+04	6.97E+04	7.54E+04	7.78E+04
Ti $K\beta_1$	4.932E−03	6.55E+04	6.98E+04	7.02E+04	7.52E+04	8.11E+04	8.74E+04	9.34E+04	9.76E+04
Ti $K\bar{\alpha}$	4.509E−03	8.19E+04	8.31E+04	8.77E+04	9.51E+04	1.02E+05	1.09E+05	1.16E+05	1.22E+05

Table 4.2.4.2. *Total photon interaction cross section (barns/atom) (cont.)*

Radiation	Energy (MeV)	65 Terbium	66 Dysprosium	67 Holmium	68 Erbium	69 Thulium	70 Ytterbium	71 Lutetium	72 Hafnium
Ag $K\beta_1$	2.494E−02	6.66E+03	7.15E+03	7.59E+03	8.05E+03	8.52E+03	9.02E+03	9.53E+03	1.01E+04
Pd $K\beta_1$	2.382E−02	7.52E+03	8.07E+03	8.57E+03	9.08E+03	9.62E+03	1.02E+04	1.08E+04	1.14E+04
Rh $K\beta_1$	2.272E−02	8.15E+03	9.15E+03	9.69E+03	1.03E+04	1.08E+04	1.15E+04	1.22E+04	1.29E+04
Ag $K\bar{\alpha}$	2.210E−02	9.16E+03	9.85E+03	1.01E+04	1.11E+04	1.17E+04	1.24E+04	1.31E+04	1.38E+04
Pd $K\bar{\alpha}$	2.112E−02	1.03E+04	1.11E+04	1.18E+04	1.25E+04	1.32E+04	1.40E+04	1.48E+04	1.56E+04
Rh $K\bar{\alpha}$	2.017E−02	1.17E+04	1.26E+04	1.33E+04	1.41E+04	1.50E+04	1.58E+04	1.67E+04	1.76E+04
Mo $K\beta_1$	1.961E−02	1.26E+04	1.35E+04	1.43E+04	1.52E+04	1.61E+04	1.70E+04	1.80E+04	1.90E+04
Mo $K\bar{\alpha}$	1.744E−02	1.72E+04	1.84E+04	1.95E+04	2.07E+04	2.19E+04	2.31E+04	2.44E+04	2.57E+04
Zn $K\beta_1$	9.572E−03	8.20E+04	8.74E+04	9.20E+04	8.53E+04	6.59E+04	6.90E+04	7.26E+04	7.70E+04
Cu $K\beta_1$	8.905E−03	9.87E+04	9.31E+04	7.17E+04	7.42E+04	8.27E+04	3.10E+04	3.52E+04	3.56E+04
Zn $K\bar{\alpha}$	8.631E−03	9.29E+04	1.02E+05	7.78E+04	7.97E+04	3.28E+04	3.36E+04	3.81E+04	3.85E+04
Ni $K\beta_1$	8.265E−03	1.08E+05	8.53E+04	8.60E+04	3.42E+04	3.67E+04	3.76E+04	4.24E+04	4.30E+04
Cu $K\bar{\alpha}$	8.041E−03	8.38E+04	9.23E+04	3.53E+04	3.67E+04	3.93E+04	4.08E+04	4.53E+04	4.59E+04
Co $K\beta_1$	7.649E−03	9.40E+04	3.72E+04	4.00E+04	4.14E+04	4.46E+04	4.57E+04	5.17E+04	5.21E+04
Ni $K\bar{\alpha}$	7.472E−03	3.89E+04	3.94E+04	4.24E+04	4.39E+04	4.47E+04	4.86E+04	5.49E+04	5.54E+04
Fe $K\beta_1$	7.058E−03	4.22E+04	4.53E+04	4.87E+04	5.05E+04	5.50E+04	5.63E+04	6.33E+04	6.40E+04
Co $K\bar{\alpha}$	6.925E−03	4.43E+04	4.75E+04	5.12E+04	5.30E+04	5.78E+04	5.92E+04	6.65E+04	6.73E+04
Mn $K\beta_1$	6.490E−03	5.22E+04	5.59E+04	6.02E+04	6.22E+04	6.82E+04	7.01E+04	7.84E+04	7.91E+04
Fe $K\bar{\alpha}$	6.400E−03	5.44E+04	5.77E+04	6.24E+04	6.44E+04	7.10E+04	7.21E+04	8.13E+04	8.21E+04
Cr $K\beta_1$	5.947E−03	6.46E+04	6.93E+04	7.45E+04	7.75E+04	8.55E+04	8.73E+04	9.85E+04	9.90E+04
Mn $K\bar{\alpha}$	5.895E−03	6.68E+04	7.07E+04	7.67E+04	7.92E+04	8.75E+04	8.94E+04	1.01E+05	1.01E+05
Cr $K\bar{\alpha}$	5.412E−03	8.29E+04	8.77E+04	9.51E+04	9.78E+04	1.08E+05	1.11E+05	1.25E+05	1.26E+05
Ti $K\beta_1$	4.932E−03	1.05E+05	1.11E+05	1.20E+05	1.23E+05	1.39E+05	1.41E+05	1.59E+05	1.60E+05
Ti $K\bar{\alpha}$	4.509E−03	1.31E+05	1.39E+05	1.50E+05	1.54E+05	1.73E+05	1.78E+05	2.00E+05	2.01E+05
		73 Tantalum	74 Tungsten	75 Rhenium	76 Osmium	77 Iridium	78 Platinum	79 Gold	80 Mercury
Ag $K\beta_1$	2.494E−02	1.17E+04	1.24E+04	1.30E+04	1.37E+04	1.44E+04	1.52E+04	1.60E+04	1.68E+04
Pd $K\beta_1$	2.382E−02	1.20E+04	1.27E+04	1.34E+04	1.41E+04	1.48E+04	1.56E+04	1.64E+04	1.72E+04
Rh $K\beta_1$	2.272E−02	1.35E+04	1.45E+04	1.52E+04	1.59E+04	1.69E+04	1.78E+04	1.77E+04	1.94E+04
Ag $K\bar{\alpha}$	2.210E−02	1.46E+04	1.54E+04	1.62E+04	1.71E+04	1.80E+04	1.89E+04	1.99E+04	2.09E+04
Pd $K\bar{\alpha}$	2.112E−02	1.65E+04	1.74E+04	1.83E+04	1.93E+04	2.02E+04	2.13E+04	2.24E+04	2.35E+04
Rh $K\bar{\alpha}$	2.017E−02	1.86E+04	1.96E+04	2.07E+04	2.17E+04	2.28E+04	2.40E+04	2.52E+04	2.65E+04
Mo $K\beta_1$	1.961E−02	2.00E+04	2.11E+04	2.22E+04	2.34E+04	2.46E+04	2.58E+04	2.71E+04	2.84E+04
Mo $K\bar{\alpha}$	1.744E−02	2.72E+04	2.86E+04	3.01E+04	3.16E+04	3.31E+04	3.48E+04	3.65E+04	3.82E+04
Zn $K\beta_1$	9.572E−03	3.30E+04	3.29E+04	3.67E+04	3.73E+04	4.01E+04	4.08E+04	4.24E+04	4.29E+04
Cu $K\beta_1$	8.905E−03	3.76E+04	3.97E+04	4.43E+04	4.48E+04	4.83E+04	4.89E+04	5.08E+04	5.18E+04
Zn $K\bar{\alpha}$	8.631E−03	4.05E+04	4.26E+04	4.78E+04	4.84E+04	5.20E+04	5.28E+04	5.58E+04	5.58E+04
Ni $K\beta_1$	8.265E−03	4.41E+04	4.80E+04	5.34E+04	5.41E+04	5.81E+04	5.66E+04	6.14E+04	6.20E+04
Cu $K\bar{\alpha}$	8.041E−03	4.85E+04	5.13E+04	5.72E+04	5.80E+04	6.24E+04	6.34E+04	6.69E+04	6.68E+04
Co $K\beta_1$	7.649E−03	5.39E+04	5.83E+04	6.50E+04	6.55E+04	7.09E+04	6.87E+04	7.49E+04	6.91E+04
Ni $K\bar{\alpha}$	7.472E−03	5.84E+04	6.19E+04	6.88E+04	6.97E+04	7.51E+04	7.62E+04	8.03E+04	8.02E+04
Fe $K\beta_1$	7.058E−03	6.60E+04	7.15E+04	7.95E+04	8.03E+04	8.68E+04	8.45E+04	9.17E+04	9.14E+04
Co $K\bar{\alpha}$	6.925E−03	6.92E+04	7.51E+04	8.33E+04	8.44E+04	9.11E+04	9.20E+04	9.71E+04	9.71E+04
Mn $K\beta_1$	6.490E−03	8.16E+04	8.82E+04	9.83E+04	9.94E+04	1.07E+05	1.04E+05	1.14E+05	1.09E+05
Fe $K\bar{\alpha}$	6.400E−03	8.46E+04	9.15E+04	1.02E+05	1.02E+05	1.11E+05	1.12E+05	1.18E+05	1.19E+05
Cr $K\beta_1$	5.947E−03	1.01E+05	1.10E+05	1.22E+05	1.23E+05	1.34E+05	1.31E+05	1.41E+05	1.36E+05
Mn $K\bar{\alpha}$	5.895E−03	1.06E+05	1.12E+05	1.25E+05	1.27E+05	1.37E+05	1.34E+05	1.45E+05	1.42E+05
Cr $K\bar{\alpha}$	5.412E−03	1.31E+05	1.40E+05	1.55E+05	1.57E+05	1.70E+05	1.66E+05	1.79E+05	1.80E+05
Ti $K\beta_1$	4.932E−03	1.64E+05	1.77E+05	1.96E+05	1.99E+05	2.15E+05	2.11E+05	2.23E+05	2.33E+05
Ti $K\bar{\alpha}$	4.509E−03	2.60E+05	2.18E+05	2.46E+05	2.49E+05	2.65E+05	2.66E+05	2.80E+05	2.98E+05

Table 4.2.4.2. *Total photon interaction cross section (barns/atom) (cont.)*

Radiation	Energy (MeV)	81 Thallium	82 Lead	83 Bismuth	84 Polonium	85 Astatine	86 Radon	87 Francium	88 Radium
Ag $K\beta_1$	2.494E−02	1.76E+04	1.84E+04	1.93E+04	2.02E+04	2.11E+04	2.20E+04	2.30E+04	2.41E+04
Pd $K\beta_1$	2.382E−02	1.80E+04	1.89E+04	1.98E+04	2.07E+04	2.16E+04	2.26E+04	2.36E+04	2.46E+04
Rh $K\beta_1$	2.272E−02	1.99E+04	2.05E+04	2.27E+04	2.37E+04	2.49E+04	2.55E+04	2.60E+04	2.68E+04
Ag $K\bar{\alpha}$	2.210E−02	2.19E+04	2.29E+04	2.40E+04	2.51E+04	2.62E+04	2.73E+04	2.85E+04	2.98E+04
Pd $K\bar{\alpha}$	2.112E−02	2.46E+04	2.58E+04	2.70E+04	2.82E+04	2.94E+04	3.07E+04	3.20E+04	3.34E+04
Rh $K\bar{\alpha}$	2.017E−02	2.78E+04	2.91E+04	3.04E+04	3.18E+04	3.31E+04	3.45E+04	3.60E+04	3.76E+04
Mo $K\beta_1$	1.961E−02	2.98E+04	3.12E+04	3.27E+04	3.41E+04	3.56E+04	3.71E+04	3.87E+04	4.03E+04
Mo $K\bar{\alpha}$	1.744E−02	4.01E+04	4.19E+04	4.38E+04	4.58E+04	4.07E+04	3.98E+04	3.22E+04	3.30E+04
Zn $K\beta_1$	9.572E−03	4.83E+04	5.11E+04	5.42E+04	5.66E+04	5.56E+04	6.22E+04	6.55E+04	6.56E+04
Cu $K\beta_1$	8.905E−03	5.81E+04	6.15E+04	6.51E+04	6.80E+04	6.68E+04	7.48E+04	7.87E+04	7.80E+04
Zn $K\bar{\alpha}$	8.631E−03	6.29E+04	6.66E+04	7.04E+04	7.35E+04	7.21E+04	8.11E+04	8.92E+04	8.55E+04
Ni $K\beta_1$	8.265E−03	7.03E+04	7.44E+04	7.86E+04	8.22E+04	8.04E+04	9.06E+04	9.94E+04	9.53E+04
Cu $K\bar{\alpha}$	8.041E−03	7.54E+04	7.98E+04	8.43E+04	8.81E+04	8.65E+04	9.72E+04	1.02E+05	1.02E+05
Co $K\beta_1$	7.649E−03	8.58E+04	9.01E+04	9.57E+04	1.00E+05	9.82E+04	1.11E+05	1.16E+05	1.16E+05
Ni $K\bar{\alpha}$	7.472E−03	9.11E+04	9.64E+04	1.02E+05	1.06E+05	1.04E+05	1.17E+05	1.23E+05	1.23E+05
Fe $K\beta_1$	7.058E−03	1.05E+05	1.12E+05	1.17E+05	1.22E+05	1.20E+05	1.36E+05	1.42E+05	1.43E+05
Co $K\bar{\alpha}$	6.925E−03	1.11E+05	1.17E+05	1.23E+05	1.29E+05	1.26E+05	1.43E+05	1.49E+05	1.49E+05
Mn $K\beta_1$	6.490E−03	1.31E+05	1.39E+05	1.46E+05	1.51E+05	1.49E+05	1.69E+05	1.77E+05	1.76E+05
Fe $K\bar{\alpha}$	6.400E−03	1.36E+05	1.48E+05	1.51E+05	1.57E+05	1.54E+05	1.75E+05	1.82E+05	1.83E+05
Cr $K\beta_1$	5.947E−03	1.64E+05	1.74E+05	1.82E+05	1.89E+05	1.86E+05	2.11E+05	2.21E+05	2.19E+05
Mn $K\bar{\alpha}$	5.895E−03	1.68E+05	1.78E+05	1.86E+05	1.93E+05	1.91E+05	2.16E+05	2.23E+05	2.25E+05
Cr $K\bar{\alpha}$	5.412E−03	2.22E+05	2.22E+05	2.32E+05	1.99E+05	2.37E+05	2.70E+05	2.82E+05	2.79E+05
Ti $K\beta_1$	4.932E−03	2.66E+05	2.82E+05	2.94E+05	2.88w+05	2.99E+05	3.43E+05	3.56E+05	3.53E+05
Ti $K\bar{\alpha}$	4.509E−03	3.36E+05	3.56E+05	3.67E+05	3.17E+05	3.78E+05	4.33E+05	4.49E+05	4.99E+05
		89 Actinium	90 Thorium	91 Protactinium	92 Uranium	93 Neptunium	94 Plutonium	95 Americium	96 Curium
Ag $K\beta_1$	2.494E−02	2.51E+04	2.62E+04	2.73E+04	2.84E+04	2.95E+04	3.07E+04	3.18E+04	2.89E+04
Pd $K\beta_1$	2.382E−02	2.57E+04	2.68E+04	2.79E+04	2.90E+04	3.02E+04	3.14E+04	3.26E+04	2.96E+04
Rh $K\beta_1$	2.272E−02	2.83E+04	3.09E+04	3.00E+04	3.54E+04	3.42E+04	3.03E+04	3.34E+04	2.36E+04
Ag $K\bar{\alpha}$	2.210E−02	3.11E+04	3.23E+04	3.42E+04	3.50E+04	2.99E+04	2.27E+04	2.50E+04	2.46E+04
Pd $K\bar{\alpha}$	2.112E−02	3.48E+04	3.62E+04	3.77E+04	3.40E+04	4.08E+04	4.24E+04	4.39E+04	4.05E+04
Rh $K\bar{\alpha}$	2.017E−02	3.92E+04	4.07E+04	4.24E+04	2.74E+04	4.58E+04	4.76E+04	4.93E+04	4.57E+04
Mo $K\beta_1$	1.961E−02	3.42E+04	3.80E+04	4.55E+04	2.96E+04	4.91E+04	5.10E+04	5.29E+04	4.92E+04
Mo $K\bar{\alpha}$	1.744E−02	5.40E+04	3.70E+04	3.87E+04	4.03E+04	2.57E+04	1.62E+04	1.89E+04	2.01E+04
Zn $K\beta_1$	9.572E−03	1.07E+05	6.57E+04	6.74E+04	7.11E+04	7.47E+04	7.29E+04	7.63E+04	7.95E+04
Cu $K\beta_1$	8.905E−03	1.14E+05	8.70E+04	8.11E+04	8.54E+04	8.92E+04	8.75E+04	9.27E+04	9.51E+04
Zn $K\bar{\alpha}$	8.631E−03	1.16E+05	9.84E+04	8.78E+04	9.23E+04	9.67E+04	9.48E+04	1.01E+05	1.03E+05
Ni $K\beta_1$	8.265E−03	1.19E+05	1.10E+05	9.82E+04	1.03E+05	1.08E+05	1.06E+05	1.14E+05	1.15E+05
Cu $K\bar{\alpha}$	8.041E−03	1.43E+05	1.18E+05	1.06E+05	1.12E+05	1.23E+05	1.13E+05	1.44E+05	1.38E+05
Co $K\beta_1$	7.649E−03	1.50E+05	1.34E+05	1.19E+05	1.26E+05	1.32E+05	1.28E+05	1.46E+05	1.41E+05
Ni $K\bar{\alpha}$	7.472E−03	1.67E+05	1.42E+05	1.27E+05	1.33E+05	1.40E+05	1.36E+05	1.48E+05	1.47E+05
Fe $K\beta_1$	7.058E−03	1.47E+05	1.54E+05	1.46E+05	1.54E+05	1.61E+05	1.57E+05	1.73E+05	1.73E+05
Co $K\bar{\alpha}$	6.925E−03	1.74E+05	1.72E+05	1.53E+05	1.61E+05	1.69E+05	1.65E+05	1.81E+05	1.79E+05
Mn $K\beta_1$	6.490E−03	1.96E+05	1.87E+05	1.81E+05	1.90E+05	1.98E+05	1.94E+05	2.15E+05	2.11E+05
Fe $K\bar{\alpha}$	6.400E−03	2.00E+05	1.96E+05	1.88E+05	1.97E+05	2.17E+05	2.02E+05	2.43E+05	2.42E+05
Cr $K\beta_1$	5.947E−03	2.32E+05	2.35E+05	2.27E+05	2.37E+05	2.48E+05	2.43E+05	2.72E+05	2.62E+05
Mn $K\bar{\alpha}$	5.895E−03	2.37E+05	2.40E+05	2.31E+05	2.43E+05	2.53E+05	2.48E+05	2.78E+05	2.68E+05
Cr $K\bar{\alpha}$	5.412E−03	2.79E+05	2.96E+05	2.88E+05	3.03E+05	3.14E+05	3.08E+05	3.49E+05	3.33E+05
Ti $K\beta_1$	4.932E−03	3.32E+05	3.77E+05	3.83E+05	3.82E+05	3.97E+05	3.90E+05	4.47E+05	4.22E+05
Ti $K\bar{\alpha}$	4.509E−03	3.95E+05	4.76E+05	4.84E+05	4.88E+05	3.79E+05	3.65E+05	4.26E+05	4.03E+05

Table 4.2.4.2. *Total photon interaction cross section (barns/atom) (cont.)*

Radiation	Energy (MeV)	97 Berkelium	98 Californium
Ag $K\beta_1$	2.494E−02	2.13E+04	3.06E+04
Pd $K\beta_1$	2.382E−02	2.18E+04	3.44E+04
Rh $K\beta_1$	2.272E−02	2.41E+04	3.86E+04
Ag $K\bar{\alpha}$	2.210E−02	2.50E+04	2.89E+04
Pd $K\bar{\alpha}$	2.112E−02	2.98E+04	4.62E+04
Rh $K\bar{\alpha}$	2.017E−02	3.37E+04	5.21E+04
Mo $K\beta_1$	1.961E−02	3.64E+04	5.59E+04
Mo $K\bar{\alpha}$	1.744E−02	2.01E+04	2.09E+04
Zn $K\beta_1$	9.572E−03	7.63E+04	8.67E+04
Cu $K\beta_1$	8.905E−03	9.27E+04	1.04E+04
Zn $K\bar{\alpha}$	8.631E−03	1.01E+05	1.13E+05
Ni $K\beta_1$	8.265E−03	1.13E+05	1.26E+05
Cu $K\bar{\alpha}$	8.041E−03	1.43E+05	1.50E+05
Co $K\beta_1$	7.649E−03	1.46E+05	1.52E+05
Ni $K\bar{\alpha}$	7.472E−03	1.48E+05	1.61E+05
Fe $K\beta_1$	7.058E−03	1.73E+05	1.87E+05
Co $K\bar{\alpha}$	6.925E−03	1.82E+05	1.96E+05
Mn $K\beta_1$	6.490E−03	2.16E+05	2.30E+05
Fe $K\bar{\alpha}$	6.400E−03	2.43E+05	2.53E+05
Cr $K\beta_1$	5.947E−03	2.72E+05	2.86E+05
Mn $K\bar{\alpha}$	5.895E−03	2.78E+05	2.93E+05
Cr $K\bar{\alpha}$	5.412E−03	3.49E+05	3.63E+05
Ti $K\beta_1$	4.932E−03	4.47E+05	4.59E+05
Ti $K\bar{\alpha}$	4.509E−03	4.26E+05	4.38E+05

This equation is not in a convenient form for computation and the alternative formalism presented by Sano, Ohtaka & Ohtsuki (1969) is often used in calculations. In this formalism,

$$\sigma_{\rm TD} = 2\pi r_e^2 \int_{-1}^{1} C_p f^2(q, Z)\{1 - \exp[-2M(q)]\}\, {\rm d}(\cos\varphi). \tag{4.2.4.9}$$

The values of $f(q, Z)$ are those of Cromer & Waber (1974).

Cross sections calculated using equation (4.2.4.8) tend to oscillate at low energy and this corresponds to the inclusion of Bragg peaks in the summation or integration. Eventually, these oscillations abate and $\sigma_{\rm TD}$ becomes a smoothly varying function of energy.

Creagh & Hubbell (1987) and Creagh (1987) have stressed that, before cross sections are calculated for a given ensemble of atoms, care should be taken to ascertain whether single-atom or single-crystal scattering is appropriate for that ensemble.

4.2.4.2.3. *Theoretical Compton scattering data: σ_C*

The bound-electron Compton scattering cross section is given by

$$\begin{aligned}\sigma_C = \pi r_e^2 \int_{-1}^{1} &[1 + k(1 - \cos\varphi)]^{-2} \\ &\times \{+\cos^2\varphi + k^2(1 - \cos\varphi)^2 \\ &\times [1 + k(1 - \cos\varphi)]^{-1}\} I(q, z)\, {\rm d}(\cos\varphi).\end{aligned} \tag{4.2.4.10}$$

Here $k = \hbar\omega/mc^2$ and $I(q, z)$ is the incoherent scattering intensity expressed in electron units. The other symbols have the meanings defined in §§4.2.4.2.1 and 4.2.4.2.2.

Values of σ_C incorporated into the tables of total cross section σ have been computed using the incoherent scattering intensities from the tabulation by Hubbell *et al.* (1975) based on the calculations by Cromer & Mann (1967) and Cromer (1969).

4.2.4.3. *Comparison between theoretical and experimental data sets*

Saloman & Hubbell (1986) and Saloman *et al.* (1988) have published an extensive comparison of the experimental database with the theoretical values of Scofield (1973, 1986) for photon energies between 0.1 and 100 keV. Some examples taken from Saloman & Hubbell (1986) are shown in Figs. 4.2.4.1, 4.2.4.2, and 4.2.4.3.

Comparisons between theory and experiment exist for about 80 elements and space does not permit reproduction of all the available information. This information has been summarized in Fig. 4.2.4.4. Superimposed on the Periodic Table of the elements are two sets of data. The upper set corresponds to the average percent deviation between experiment and theory for the photon energy range 10 to 100 keV. The lower set corresponds to the average percent deviation between experiment and theory for the photon energy range 1 to 10 keV. An upwards pointing arrow $\uparrow$ means that $(\sigma_{\rm exp} - \sigma_{\rm theor}) > 0$. No arrow implies that $(\sigma_{\rm exp} - \sigma_{\rm theor}) = 0$. A downwards pointing arrow $\downarrow$ means that $(\sigma_{\rm exp} - \sigma_{\rm theor}) < 0$. An asterisk means no experimental data set was available.

For example: for tin ($Z = 50$), the experimental data are on average 5% higher than the theoretical predictions for the range of photon energies from 10 to 100 keV. For the range 1 to 10 keV, the experimental data are on average 7% higher than the theoretical predictions.

Fig. 4.2.4.4 is given as a rapid means of comparing theory and experiment. For more detailed information, see Saloman & Hubbell (1986), Saloman *et al.* (1988), and Creagh (1990).

4.2.4.4. *Uncertainty in the data tables*

It is not possible to generalize on the accuracy of the experimental data sets. Creagh & Hubbell (1987) have shown that many experiments for which the precision quoted by the author is high differ from other accurate measurements by a considerable amount. It must be stressed that the experimental apparatus has to be chosen so that it is appropriate for the atomic system being investigated. Details concerning the proper choice of measuring system are given in Section 4.2.3. Within about 200 eV of an absorption edge, deviations of up to 200% may be observed between theory and experiment. This is the region in which XAFS and XANES oscillations occur.

With respect to the theoretical data: the detailed agreement between the several methods for calculating the photo-effect cross sections is quite remarkable and it is estimated that the reliability of these data is to within 2% for the energy range considered in this compilation. Some problems may exist, however, close to the absorption edges. Errors in the calculation of the Rayleigh and the Compton scattering cross sections are assessed to be of the order of 5%. Because the greater proportion of total attenuation is photoelectric, the accuracy of the total scattering cross section should be much better than 5% and usually close to 2%.

4.2.5. Filters and monochromators (By D. C. Creagh)

4.2.5.1. *Introduction*

All sources of X-rays, whether they be produced by conventional sealed tubes, rotating-anode systems, or synchrotron-radiation sources, emit over a broad spectral range. In many cases, this spectral diversity is of concern, and techniques have been developed to minimize the problem. These techniques

Table 4.2.4.3. *Mass attenuation coefficients ($cm^2\ g^{-1}$)*

Radiation	Energy (MeV)	1 Hydrogen	2 Helium	3 Lithium	4 Beryllium	5 Boron	6 Carbon	7 Nitrogen	8 Oxygen
Ag $K\beta_1$	2.494E−02	3.63E−01	1.89E−01	1.72E−01	1.95E−01	2.37E−01	3.15E−01	4.04E−01	3.29E−01
Pd $K\beta_1$	2.382E−02	3.65E−01	1.90E−01	1.74E−01	2.00E−01	2.47E−01	3.35E−01	4.37E−01	5.82E−01
Rh $K\beta_1$	2.272E−02	3.66E−01	1.92E−01	1.77E−01	2.05E−01	2.59E−01	3.58E−01	4.77E−01	6.44E−01
Ag $K\bar{\alpha}$	2.210E−02	3.67E−01	1.93E−01	1.79E−01	2.09E−01	2.67E−01	3.74E−01	5.03E−01	6.85E−01
Pd $K\bar{\alpha}$	2.112E−02	3.68E−01	1.94E−01	1.82E−01	2.16E−01	2.81E−01	4.02E−01	5.51E−01	7.60E−01
Rh $K\bar{\alpha}$	2.017E−02	3.69E−01	1.96E−01	1.85E−01	2.24E−01	2.98E−01	4.35E−01	6.07E−01	8.48E−01
Mo $K\beta_1$	1.961E−02	3.70E−01	1.97E−01	1.87E−01	2.29E−01	3.09E−01	4.58E−01	6.45E−01	9.08E−01
Mo $K\bar{\alpha}$	1.744E−02	3.73E−01	2.02E−01	1.98E−01	2.56E−01	3.68E−01	5.76E−01	8.45E−01	1.22E+00
Zn $K\beta_1$	9.572E−03	3.86E−01	2.55E−01	3.64E−01	7.16E−01	1.41E+00	2.69E+00	4.42E+00	6.78E+00
Cu $K\beta_1$	8.905E−03	3.88E−01	2.68E−01	4.12E−01	8.53E−01	1.73E+00	3.33E+00	5.48E+00	8.42E+00
Zn $K\bar{\alpha}$	8.631E−03	3.89E−01	2.74E−01	4.36E−01	9.23E−01	1.89E+00	3.65E+00	6.01E+00	9.25E+00
Ni $K\beta_1$	8.265E−03	3.90E−01	2.85E−01	4.73E−01	1.03E+00	2.14E+00	4.15E+00	6.85E+00	1.05E+01
Cu $K\bar{\alpha}$	8.041E−03	3.91E−01	2.92E−01	5.00E−01	1.11E+00	2.31E+00	4.51E+00	7.44E+00	1.15E+01
Co $K\beta_1$	7.649E−03	3.93E−01	3.07E−01	5.55E−01	1.27E+00	2.67E+00	5.24E+00	8.66E+00	1.33E+01
Ni $K\bar{\alpha}$	7.472E−03	3.94E−01	3.14E−01	5.84E−01	1.35E+00	2.87E+00	5.62E+00	9.29E+00	1.43E+01
Fe $K\beta_1$	7.058E−03	3.96E−01	3.35E−01	6.63E−01	1.58E+00	3.39E+00	6.68E+00	1.10E+01	1.70E+01
Co $K\bar{\alpha}$	6.925E−03	3.97E−01	3.43E−01	6.93E−01	1.67E+00	3.59E+00	7.07E+00	1.17E+01	1.80E+01
Mn $K\beta_1$	6.490E−03	4.00E−01	3.74E−01	8.10E−01	2.01E+00	4.37E+00	8.62E+00	1.42E+01	2.19E+01
Fe $K\bar{\alpha}$	6.400E−03	4.00E−01	3.81E−01	8.39E−01	2.09E+00	4.55E+00	8.99E+00	1.49E+01	2.28E+01
Cr $K\beta_1$	5.947E−03	4.05E−01	4.25E−01	1.01E+00	2.59E+00	5.69E+00	1.12E+01	1.86E+01	2.84E+01
Mn $K\bar{\alpha}$	5.895E−03	4.05E−01	4.31E−01	1.03E+00	2.66E+00	5.84E+00	1.16E+01	1.91E+01	2.92E+01
Cr $K\bar{\alpha}$	5.412E−03	4.12E−01	4.98E−01	1.30E+00	3.44E+00	7.59E+00	1.50E+01	2.47E+01	3.78E+01
Ti $K\beta_1$	4.932E−03	4.21E−01	5.92E−01	1.68E+00	4.56E+00	1.01E+01	1.99E+01	3.28E+01	4.99E+01
Ti $K\bar{\alpha}$	4.509E−03	4.33E−01	7.12E−01	2.18E+00	6.00E+00	1.33E+01	2.62E+01	4.30E+01	6.52E+01

		9 Fluorine	10 Neon	11 Sodium	12 Magnesium	13 Aluminium	14 Silicon	15 Phosphorus	16 Sulfur
Ag $K\beta_1$	2.494E−02	6.60E−01	9.06E−01	1.13E+00	1.50E+00	1.85E+00	2.38E+00	2.84E+00	3.55E+00
Pd $K\beta_1$	2.382E−02	7.35E−01	1.02E+00	1.28E+00	1.70E+00	2.10E+00	2.71E+00	3.24E+00	4.05E+00
Rh $K\beta_1$	2.272E−02	8.22E−01	1.15E+00	1.45E+00	1.93E+00	2.39E+00	3.09E+00	3.70E+00	4.64E+00
Ag $K\bar{\alpha}$	2.210E−02	8.79E−01	1.23E+00	1.56E+00	2.09E+00	2.59E+00	3.35E+00	4.01E+00	5.02E+00
Pd $K\bar{\alpha}$	2.112E−02	9.84E−01	1.39E+00	1.77E+00	2.37E+00	2.94E+00	3.81E+00	4.57E+00	5.72E+00
Rh $K\bar{\alpha}$	2.017E−02	1.11E+00	1.57E+00	2.01E+00	2.70E+00	3.36E+00	4.36E+00	5.23E+00	6.55E+00
Mo $K\beta_1$	1.961E−02	1.19E+00	1.69E+00	2.17E+00	2.92E+00	3.64E+00	4.73E+00	5.67E+00	7.11E+00
Mo $K\bar{\alpha}$	1.744E−02	1.63E+00	2.35E+00	3.03E+00	4.09E+00	5.11E+00	6.64E+00	7.97E+00	9.99E+00
Zn $K\beta_1$	9.572E−03	9.35E+00	1.36E+01	1.77E+01	2.40E+01	2.98E+01	3.85E+01	4.58E+01	5.68E+01
Cu $K\beta_1$	8.905E−03	1.16E+01	1.69E+01	2.20E+01	2.96E+01	3.68E+01	4.75E+01	5.64E+01	6.98E+01
Zn $K\bar{\alpha}$	8.631E−03	1.28E+01	1.86E+01	2.41E+01	3.25E+01	4.03E+01	5.20E+01	6.17E+01	7.63E+01
Ni $K\beta_1$	8.265E−03	1.45E+01	2.11E+01	2.74E+01	3.69E+01	4.58E+01	5.89E+01	6.98E+01	8.63E+01
Cu $K\bar{\alpha}$	8.041E−03	1.58E+01	2.29E+01	2.97E+01	4.00E+01	4.96E+01	6.37E+01	7.55E+01	9.33E+01
Co $K\beta_1$	7.649E−03	1.83E+01	2.66E+01	3.45E+01	4.63E+01	5.73E+01	7.36E+01	8.70E+01	1.07E+02
Ni $K\bar{\alpha}$	7.472E−03	1.97E+01	2.85E+01	3.69E+01	4.96E+01	6.13E+01	7.87E+01	9.30E+01	1.15E+02
Fe $K\beta_1$	7.058E−03	2.33E+01	3.38E+01	4.37E+01	5.85E+01	7.23E+01	9.27E+01	1.09E+02	1.35E+02
Co $K\bar{\alpha}$	6.925E−03	2.47E+01	3.58E+01	4.62E+01	6.19E+01	7.64E+01	9.78E+01	1.15E+02	1.42E+02
Mn $K\beta_1$	6.490E 03	3.00E+01	4.34E+01	5.59E+01	7.47E+01	9.21E+01	1.18E+02	1.39E+02	1.70E+02
Fe $K\bar{\alpha}$	6.400E−03	3.13E+01	4.52E+01	5.82E+01	7.78E+01	9.59E+01	1.22E+02	1.44E+02	1.77E+02
Cr $K\beta_1$	5.947E−03	3.89E+01	5.61E+01	7.21E+01	9.62E+01	1.18E+02	1.51E+02	1.77E+02	2.17E+02
Mn $K\bar{\alpha}$	5.895E−03	3.99E+01	5.76E+01	7.40E+01	9.87E+01	1.21E+02	1.54E+02	1.81E+02	2.22E+02
Cr $K\bar{\alpha}$	5.412E−03	5.15E+01	7.41E+01	9.49E+01	1.26E+02	1.55E+02	1.96E+02	2.30E+02	2.81E+02
Ti $K\beta_1$	4.932E−03	6.78E+01	9.72E+01	1.24E+02	1.65E+02	2.01E+02	2.55E+02	2.97E+02	3.62E+02
Ti $K\bar{\alpha}$	4.509E−03	8.84E+01	1.26E+02	1.61E+02	2.12E+02	2.59E+02	3.27E+02	3.79E+02	4.60E+02

Table 4.2.4.3. *Mass attenuation coefficients ($cm^2\ g^{-1}$) (cont.)*

Radiation	Energy (MeV)	17 Chlorine	18 Argon	19 Potassium	20 Calcium	21 Scandium	22 Titanium	23 Vanadium	24 Chromium
Ag $K\beta_1$	2.494E−02	4.09E+00	4.56E+00	5.78E+00	6.92E+00	7.47E+00	8.43E+00	9.42E+00	1.09E+01
Pd $K\beta_1$	2.382E−02	4.67E+00	5.21E+00	6.60E+00	7.90E+00	8.53E+00	9.61E+00	1.07E+01	1.24E+01
Rh $K\beta_1$	2.272E−02	5.35E+00	5.96E+00	7.56E+00	9.04E+00	9.76E+00	1.10E+01	1.23E+01	1.42E+01
Ag $K\bar{\alpha}$	2.210E−02	5.79E+00	6.46E+00	8.19E+00	9.79E+00	1.06E+01	1.19E+01	1.33E+01	1.54E+01
Pd $K\bar{\alpha}$	2.112E−02	6.61E+00	7.37E+00	9.33E+00	1.12E+01	1.20E+01	1.36E+01	1.51E+01	1.75E+01
Rh $K\bar{\alpha}$	2.017E−02	7.55E+00	8.42E+00	1.07E+01	1.27E+01	1.38E+01	1.55E+01	1.73E+01	1.99E+01
Mo $K\beta_1$	1.961E−02	8.20E+00	9.14E+00	1.16E+01	1.38E+01	1.49E+01	1.68E+01	1.87E+01	2.15E+01
Mo $K\bar{\alpha}$	1.744E−02	1.15E+01	1.28E+01	1.62E+01	1.93E+01	2.08E+01	2.34E+01	2.60E+01	2.99E+01
Zn $K\beta_1$	9.572E−03	6.48E+01	7.14E+01	8.94E+01	1.05E+02	1.12E+02	1.25E+02	1.37E+02	1.55E+02
Cu $K\beta_1$	8.905E−03	7.95E+01	8.75E+01	1.09E+02	1.29E+02	1.37E+02	1.52E+02	1.66E+02	1.85E+02
Zn $K\bar{\alpha}$	8.631E−03	8.69E+01	9.55E+01	1.19E+02	1.40E+02	1.49E+02	1.66E+02	1.81E+02	2.01E+02
Ni $K\beta_1$	8.265E−03	9.81E+01	1.08E+02	1.34E+02	1.58E+02	1.67E+02	1.86E+02	2.03E+02	2.27E+02
Cu $K\bar{\alpha}$	8.041E−03	1.06E+02	1.16E+02	1.45E+02	1.70E+02	1.80E+02	2.00E+02	2.19E+02	2.47E+02
Co $K\beta_1$	7.649E−03	1.22E+02	1.34E+02	1.66E+02	1.95E+02	2.06E+02	2.27E+02	2.50E+02	2.93E+02
Ni $K\bar{\alpha}$	7.472E−03	1.30E+02	1.43E+02	1.77E+02	2.08E+02	2.20E+02	2.40E+02	2.66E+02	3.18E+02
Fe $K\beta_1$	7.058E−03	1.52E+02	1.67E+02	2.07E+02	2.42E+02	2.56E+02	2.77E+02	3.09E+02	3.85E+02
Co $K\bar{\alpha}$	6.925E−03	1.61E+02	1.76E+02	2.18E+02	2.55E+02	2.69E+02	2.91E+02	3.25E+02	4.08E+02
Mn $K\beta_1$	6.490E−03	1.92E+02	2.10E+02	2.60E+02	3.03E+02	3.19E+02	3.45E+02	3.85E+02	4.80E+02
Fe $K\bar{\alpha}$	6.400E−03	2.00E+02	2.18E+02	2.70E+02	3.14E+02	3.32E+02	3.58E+02	3.99E+02	4.92E+02
Cr $K\beta_1$	5.947E−03	2.44E+02	2.66E+02	3.28E+02	3.82E+02	4.03E+02	4.44E+02	4.79E+02	6.70E+01
Mn $K\bar{\alpha}$	5.895E−03	2.50E+02	2.72E+02	3.36E+02	3.91E+02	4.12E+02	4.57E+02	4.89E+02	6.86E+01
Cr $K\bar{\alpha}$	5.412E−03	3.16E+02	3.42E+02	4.21E+02	4.90E+02	5.16E+02	5.90E+02	7.47E+01	8.68E+01
Ti $K\beta_1$	4.932E−03	4.04E+02	4.38E+02	5.38E+02	6.24E+02	6.52E+02	8.54E+01	9.65E+01	1.12E+02
Ti $K\bar{\alpha}$	4.509E−03	5.11E+02	5.56E+02	6.80E+02	7.81E+02	8.08E+02	1.09E+02	1.23E+02	1.43E+02

		25 Manganese	26 Iron	27 Cobalt	28 Nickel	29 Copper	30 Zinc	31 Gallium	32 Germanium
Ag $K\beta_1$	2.494E−02	1.21E+01	1.38E+01	1.51E+01	1.74E+01	1.83E+01	2.02E+01	2.14E+01	2.31E+01
Pd $K\beta_1$	2.382E−02	1.37E+01	1.57E+01	1.72E+01	1.98E+01	2.08E+01	2.30E+01	2.43E+01	2.62E+01
Rh $K\beta_1$	2.272E−02	1.57E+01	1.79E+01	1.96E+01	2.26E+01	2.38E+01	2.62E+01	2.77E+01	2.98E+01
Ag $K\bar{\alpha}$	2.210E−02	1.70E+01	1.94E+01	2.12E+01	2.44E+01	2.56E+01	2.82E+01	2.98E+01	3.21E+01
Pd $K\bar{\alpha}$	2.112E−02	1.93E+01	2.20E+01	2.41E+01	2.77E+01	2.91E+01	3.20E+01	3.38E+01	3.64E+01
Rh $K\bar{\alpha}$	2.017E−02	2.20E+01	2.51E+01	2.74E+01	3.15E+01	3.30E+01	3.63E+01	3.84E+01	4.13E+01
Mo $K\beta_1$	1.961E−02	2.38E+01	2.71E+01	2.96E+01	3.40E+01	3.57E+01	3.93E+01	4.15E+01	4.46E+01
Mo $K\bar{\alpha}$	1.744E−02	3.31E+01	3.76E+01	4.10E+01	4.69E+01	4.91E+01	5.40E+01	5.70E+01	6.12E+01
Zn $K\beta_1$	9.572E−03	1.70E+02	1.92E+02	2.06E+02	2.33E+02	2.40E+02	3.59E+01	3.85E+01	4.22E+01
Cu $K\beta_1$	8.905E−03	2.07E+02	2.32E+02	2.48E+02	2.79E+02	3.92E+01	4.38E+01	4.70E+01	5.14E+01
Zn $K\bar{\alpha}$	8.631E 03	2.24E+02	2.52E+02	2.69E+02	3.02E+02	4.27E+01	4.77E+01	5.12E+01	5.59E+01
Ni $K\beta_1$	8.265E−03	2.51E+02	2.81E+02	3.00E+02	4.53E+01	4.80E+01	5.37E+01	5.76E+01	6.30E+01
Cu $K\bar{\alpha}$	8.041E 03	2.70E+02	3.02E+02	3.21E+02	4.88E+01	5.18E+01	5.79E+01	6.21E+01	6.79E+01
Co $K\beta_1$	7.649E−03	3.06E+02	3.42E+02	4.81E+01	5.60E+01	5.94E+01	6.64E+01	7.12E+01	7.78E+01
Ni $K\bar{\alpha}$	7.472E−03	3.25E+02	3.62E+02	5.13E+01	5.97E+01	6.33E+01	7.08E+01	7.59E+01	8.29E+01
Fe $K\beta_1$	7.058E−03	3.75E+02	5.43E+01	6.00E+01	6.98E+01	7.40E+01	8.27E+01	8.86E+01	9.69E+01
Co $K\bar{\alpha}$	6.925E−03	3.93E+02	5.72E+01	6.32E+01	7.35E+01	7.80E+01	8.71E+01	9.34E+01	1.02E+02
Mn $K\beta_1$	6.490E−03	5.92E+01	6.84E+01	7.55E+01	8.78E+01	9.31E+01	1.04E+02	1.11E+02	1.22E+02
Fe $K\bar{\alpha}$	6.400E−03	6.16E+01	7.10E+01	7.85E+01	9.13E+01	9.68E+01	1.08E+02	1.16E+02	1.27E+02
Cr $K\beta_1$	5.947E−03	7.53E+01	8.69E+01	9.60E+01	1.12E+02	1.18E+02	1.32E+02	1.42E+02	1.55E+02
Mn $K\bar{\alpha}$	5.895E−03	7.72E+01	8.90E+01	9.83E+01	1.14E+02	1.21E+02	1.35E+02	1.45E+02	1.58E+02
Cr $K\bar{\alpha}$	5.412E−03	9.75E+01	1.13E+02	1.24E+02	1.44E+02	1.53E+02	1.71E+02	1.83E+02	1.99E+02
Ti $K\beta_1$	4.932E−03	1.26E+02	1.45E+02	1.60E+02	1.86E+02	1.97E+02	2.20E+02	2.35E+02	2.56E+02
Ti $K\bar{\alpha}$	4.509E−03	1.61E+02	1.85E+02	2.04E+02	2.37E+02	2.51E+02	2.80E+02	2.99E+02	3.26E+02

Table 4.2.4.3. *Mass attenuation coefficients ($cm^2\ g^{-1}$) (cont.)*

Radiation	Energy (MeV)	33 Arsenic	34 Selenium	35 Bromine	36 Krypton	37 Rubidium	38 Strontium	39 Yttrium	40 Zirconium
Ag $K\beta_1$	2.494E−02	2.50E+01	2.65E+01	2.91E+01	3.07E+01	3.32E+01	3.56E+01	3.84E+01	4.07E+01
Pd $K\beta_1$	2.382E−02	2.84E+01	3.00E+01	3.29E+01	3.48E+01	3.76E+01	4.03E+01	4.34E+01	4.60E+01
Rh $K\beta_1$	2.272E−02	3.23E+01	3.41E+01	3.74E+01	3.95E+01	4.27E+01	4.57E+01	4.91E+01	5.20E+01
Ag $K\bar{\alpha}$	2.210E−02	3.48E+01	3.68E+01	4.03E+01	4.25E+01	4.59E+01	4.91E+01	5.29E+01	5.59E+01
Pd $K\bar{\alpha}$	2.112E−02	3.93E+01	4.16E+01	4.55E+01	4.80E+01	5.18E+01	5.54E+01	5.95E+01	6.29E+01
Rh $K\bar{\alpha}$	2.017E−02	4.46E+01	4.71E+01	5.15E+01	5.43E+01	5.85E+01	6.25E+01	6.71E+01	6.25E+01
Mo $K\beta_1$	1.961E−02	4.82E+01	5.08E+01	5.55E+01	5.84E+01	6.30E+01	6.72E+01	7.21E+01	7.61E+01
Mo $K\bar{\alpha}$	1.744E−02	6.61E+01	6.95E+01	7.56E+01	7.93E+01	8.51E+01	9.06E+01	9.70E+01	1.63E+01
Zn $K\beta_1$	9.572E−03	4.64E+01	4.97E+01	5.53E+01	5.92E+01	6.49E+01	7.06E+01	7.73E+01	8.35E+01
Cu $K\beta_1$	8.905E−03	5.65E+01	6.05E+01	6.74E+01	7.21E+01	7.90E+01	8.59E+01	9.40E+01	1.01E+02
Zn $K\bar{\alpha}$	8.631E−03	6.15E+01	6.59E+01	7.33E+01	7.85E+01	8.60E+01	9.35E+01	1.02E+02	1.10E+02
Ni $K\beta_1$	8.265E−03	6.93E+01	7.42E+01	8.26E+01	8.83E+01	9.68E+01	1.05E+02	1.15E+02	1.24E+02
Cu $K\bar{\alpha}$	8.041E−03	7.47E+01	8.00E+01	8.90E+01	9.52E+01	1.04E+02	1.13E+02	1.24E+02	1.39E+02
Co $K\beta_1$	7.649E−03	8.55E+01	9.16E+01	1.02E+02	1.09E+02	1.19E+02	1.30E+02	1.42E+02	1.54E+02
Ni $K\bar{\alpha}$	7.472E−03	9.11E+01	9.76E+01	1.09E+02	1.16E+02	1.27E+02	1.38E+02	1.51E+02	1.63E+02
Fe $K\beta_1$	7.058E−03	1.06E+02	1.14E+02	1.27E+02	1.35E+02	1.48E+02	1.61E+02	1.76E+02	1.91E+02
Co $K\bar{\alpha}$	6.925E−03	1.12E+02	1.20E+02	1.33E+02	1.42E+02	1.56E+02	1.70E+02	1.85E+02	2.00E+02
Mn $K\beta_1$	6.490E−03	1.34E+02	1.43E+02	1.59E+02	1.70E+02	1.86E+02	2.02E+02	2.21E+02	2.38E+02
Fe $K\bar{\alpha}$	6.400E−03	1.39E+02	1.49E+02	1.65E+02	1.76E+02	1.93E+02	2.10E+02	2.29E+02	2.47E+02
Cr $K\beta_1$	5.947E−03	1.70E+02	1.82E+02	2.02E+02	2.15E+02	2.36E+02	2.56E+02	2.79E+02	3.00E+02
Mn $K\bar{\alpha}$	5.895E−03	1.74E+02	1.86E+02	2.06E+02	2.20E+02	2.41E+02	2.62E+02	2.86E+02	3.08E+02
Cr $K\bar{\alpha}$	5.412E−03	2.19E+02	2.34E+02	2.60E+02	2.77E+02	3.03E+02	3.28E+02	3.58E+02	3.86E+02
Ti $K\beta_1$	4.932E−03	2.81E+02	3.00E+02	3.33E+02	3.55E+02	3.88E+02	4.21E+02	4.59E+02	4.93E+02
Ti $K\bar{\alpha}$	4.509E−03	3.57E+02	3.81E+02	4.23E+02	4.50E+02	4.92E+02	5.32E+02	5.80E+02	6.22E+02
		41 Niobium	42 Molybdenum	43 Technetium	44 Ruthenium	45 Rhodium	46 Palladium	47 Silver	48 Cadmium
Ag $K\beta_1$	2.494E−02	4.36E+01	5.25E+01	4.84E+01	5.06E+01	5.35E+01	5.55E+01	1.01E+01	1.06E+01
Pd $K\beta_1$	2.382E−02	4.92E+01	6.03E+01	5.45E+01	5.69E+01	6.01E+01	1.06E+01	1.15E+01	1.20E+01
Rh $K\beta_1$	2.272E−02	5.56E+01	6.80E+01	6.15E+01	7.00E+01	1.14E+01	1.21E+01	1.30E+01	1.36E+01
Ag $K\bar{\alpha}$	2.210E−02	5.98E+01	7.20E+01	6.60E+01	1.14E+01	1.23E+01	1.30E+01	1.40E+01	1.46E+01
Pd $K\bar{\alpha}$	2.112E−02	6.71E+01	7.71E+01	7.41E+01	1.29E+01	1.39E+01	1.47E+01	1.58E+01	1.66E+01
Rh $K\bar{\alpha}$	2.017E−02	7.55E+01	7.95E+01	1.38E+01	1.47E+01	1.58E+01	1.67E+01	1.79E+01	1.88E+01
Mo $K\beta_1$	1.961E−02	8.10E+01	1.38E+01	1.49E+01	1.58E+01	1.70E+01	1.80E+01	1.94E+01	2.02E+01
Mo $K\bar{\alpha}$	1.744E−02	1.77E+01	1.88E+01	2.04E+01	2.17E+01	2.33E+01	2.47E+01	2.65E+01	2.78E+01
Zn $K\beta_1$	9.572E−03	9.04E+01	9.65E+01	1.04E+02	1.10E+02	1.18E+02	1.25E+02	1.34E+02	1.40E+02
Cu $K\beta_1$	8.905E−03	1.10E+02	1.17E+02	1.26E+02	1.34E+02	1.44E+02	1.51E+02	1.63E+02	1.69E+02
Zn $K\bar{\alpha}$	8.631E−03	1.20E+02	1.27E+02	1.37E+02	1.46E+02	1.56E+02	1.65E+02	1.77E+02	1.84E+02
Ni $K\beta_1$	8.265E−03	1.34E+02	1.43E+02	1.54E+02	1.63E+02	1.75E+02	1.85E+02	1.98E+02	2.07E+02
Cu $K\bar{\alpha}$	8.041E−03	1.45E+02	1.54E+02	1.66E+02	1.76E+02	1.89E+02	1.99E+02	2.13E+02	2.22E+02
Co $K\beta_1$	7.649E−03	1.66E+02	1.76E+02	1.90E+02	2.01E+02	2.16E+02	2.27E+02	2.43E+02	2.53E+02
Ni $K\bar{\alpha}$	7.472E−03	1.76E+02	1.88E+02	2.02E+02	2.14E+02	2.29E+02	2.41E+02	2.59E+02	2.69E+02
Fe $K\beta_1$	7.058E−03	2.05E+02	2.19E+02	2.35E+02	2.49E+02	2.67E+02	2.81E+02	3.01E+02	3.13E+02
Co $K\bar{\alpha}$	6.925E−03	2.16E+02	2.30E+02	2.47E+02	2.62E+02	2.80E+02	2.95E+02	3.16E+02	3.29E+02
Mn $K\beta_1$	6.490E−03	2.57E+02	2.73E+02	2.94E+02	3.11E+02	3.33E+02	3.50E+02	3.75E+02	3.90E+02
Fe $K\bar{\alpha}$	6.400E−03	2.67E+02	2.84E+02	3.05E+02	3.23E+02	3.46E+02	3.63E+02	3.89E+02	4.05E+02
Cr $K\beta_1$	5.947E−03	3.25E+02	3.45E+02	3.70E+02	3.92E+02	4.20E+02	4.41E+02	4.72E+02	4.90E+02
Mn $K\bar{\alpha}$	5.895E 03	3.32E+02	3.53E+02	3.79E+02	4.01E+02	4.29E+02	4.51E+02	4.83E+02	5.02E+02
Cr $K\bar{\alpha}$	5.412E−03	4.16E+02	4.42E+02	4.74E+02	5.01E+02	5.36E+02	5.63E+02	6.02E+02	6.26E+02
Ti $K\beta_1$	4.932E−03	5.32E+02	5.65E+02	6.04E+02	6.39E+02	6.83E+02	7.16E+02	7.65E+02	7.95E+02
Ti $K\bar{\alpha}$	4.509E−03	6.71E+02	7.12E+02	7.61E+02	8.04E+02	8.60E+02	9.01E+02	9.61E+02	9.95E+02

Table 4.2.4.3. *Mass attenuation coefficients ($cm^2\ g^{-1}$) (cont.)*

Radiation	Energy (MeV)	49 Indium	50 Tin	51 Antimony	52 Tellurium	53 Iodine	54 Xenon	55 Caesium	56 Barium
Ag $K\beta_1$	2.494E−02	1.13E+01	1.18E+01	1.25E+01	1.29E+01	1.40E+01	1.46E+01	1.56E+01	1.62E+01
Pd $K\beta_1$	2.382E−02	1.27E+01	1.34E+01	1.41E+01	1.46E+01	1.59E+01	1.65E+01	1.76E+01	1.83E+01
Rh $K\beta_1$	2.272E−02	1.45E+01	1.52E+01	1.60E+01	1.66E+01	1.80E+01	1.88E+01	2.00E+01	2.08E+01
Ag $K\bar{\alpha}$	2.210E−02	1.56E+01	1.64E+01	1.73E+01	1.79E+01	1.94E+01	2.02E+01	2.15E+01	2.24E+01
Pd $K\bar{\alpha}$	2.112E−02	1.76E+01	1.85E+01	1.96E+01	2.02E+01	2.19E+01	2.29E+01	2.43E+01	2.54E+01
Rh $K\bar{\alpha}$	2.017E−02	2.00E+01	2.10E+01	2.22E+01	2.29E+01	2.18E+01	2.27E+01	2.42E+01	2.52E+01
Mo $K\beta_1$	1.961E−02	2.16E+01	2.26E+01	2.39E+01	2.47E+01	2.68E+01	2.80E+01	2.98E+01	3.10E+01
Mo $K\bar{\alpha}$	1.744E−02	2.95E+01	3.10E+01	3.27E+01	3.38E+01	3.67E+01	3.82E+01	4.07E+01	4.23E+01
Zn $K\beta_1$	9.572E−03	1.48E+02	1.55E+02	1.64E+02	1.68E+02	1.82E+02	1.90E+02	2.01E+02	2.09E+02
Cu $K\beta_1$	8.905E−03	1.80E+02	1.88E+02	1.98E+02	2.04E+02	2.20E+02	2.29E+02	2.43E+02	2.52E+02
Zn $K\bar{\alpha}$	8.631E−03	1.95E+02	2.04E+02	2.15E+02	2.21E+02	2.39E+02	2.49E+02	2.63E+02	2.73E+02
Ni $K\beta_1$	8.265E−03	2.19E+02	2.29E+02	2.41E+02	2.48E+02	2.68E+02	2.78E+02	2.95E+02	3.06E+02
Cu $K\bar{\alpha}$	8.041E−03	2.36E+02	2.47E+02	2.59E+02	2.67E+02	2.88E+02	2.99E+02	3.17E+02	3.25E+02
Co $K\beta_1$	7.649E−03	2.69E+02	2.81E+02	2.96E+02	3.04E+02	3.30E+02	3.43E+02	3.63E+02	3.76E+02
Ni $K\bar{\alpha}$	7.472E−03	2.86E+02	2.99E+02	3.14E+02	3.23E+02	3.49E+02	3.62E+02	3.83E+02	3.96E+02
Fe $K\beta_1$	7.058E−03	3.32E+02	3.47E+02	3.65E+02	3.74E+02	4.08E+02	4.22E+02	4.46E+02	4.61E+02
Co $K\bar{\alpha}$	6.925E−03	3.49E+02	3.64E+02	3.83E+02	3.94E+02	4.25E+02	4.40E+02	4.65E+02	4.80E+02
Mn $K\beta_1$	6.490E−03	4.13E+02	4.31E+02	4.54E+02	4.66E+02	5.03E+02	5.20E+02	5.49E+02	5.66E+02
Fe $K\bar{\alpha}$	6.400E−03	4.28E+02	4.47E+02	4.71E+02	4.83E+02	5.22E+02	5.40E+02	5.69E+02	5.86E+02
Cr $K\beta_1$	5.947E−03	5.19E+02	5.42E+02	5.70E+02	5.85E+02	6.31E+02	6.52E+02	6.86E+02	6.45E+02
Mn $K\bar{\alpha}$	5.895E−03	5.31E+02	5.54E+02	5.82E+02	5.98E+02	6.45E+02	6.66E+02	7.00E+02	6.60E+02
Cr $K\bar{\alpha}$	5.412E−03	6.63E+02	6.91E+02	7.23E+02	7.40E+02	7.96E+02	7.21E+02	7.60E+02	5.70E+02
Ti $K\beta_1$	4.932E−03	8.41E+02	8.76E+02	9.15E+02	9.32E+02	1.00E+03	1.03E+03	2.60E+02	3.14E+02
Ti $K\bar{\alpha}$	4.509E−03	1.05E+03	1.09E+03	9.91E+02	7.51E+02	2.83E+02	2.65E+02	3.30E+02	3.34E+02
		57 Lanthanum	58 Cerium	59 Praseodymium	60 Neodymium	61 Promethium	62 Samarium	63 Europium	64 Gadolinium
Ag $K\beta_1$	2.494E−02	1.72E+01	1.83E+01	1.95E+01	2.04E+01	2.17E+01	2.23E+01	2.35E+01	2.42E+01
Pd $K\beta_1$	2.382E−02	1.95E+01	2.07E+01	2.20E+01	2.30E+01	2.45E+01	2.52E+01	2.66E+01	2.74E+01
Rh $K\beta_1$	2.272E−02	2.21E+01	2.35E+01	2.50E+01	2.61E+01	2.78E+01	2.86E+01	3.01E+01	3.10E+01
Ag $K\bar{\alpha}$	2.210E−02	2.38E+01	2.53E+01	2.69E+01	2.81E+01	2.99E+01	3.08E+01	3.24E+01	3.34E+01
Pd $K\bar{\alpha}$	2.112E−02	2.69E+01	2.86E+01	3.04E+01	3.18E+01	3.38E+01	3.48E+01	3.66E+01	3.77E+01
Rh $K\bar{\alpha}$	2.017E−02	3.05E+01	3.24E+01	3.45E+01	3.60E+01	3.83E+01	3.94E+01	4.15E+01	4.27E+01
Mo $K\beta_1$	1.961E−02	3.29E+01	3.49E+01	3.72E+01	3.88E+01	4.13E+01	4.24E+01	4.47E+01	4.60E+01
Mo $K\bar{\alpha}$	1.744E−02	4.49E+01	4.77E+01	5.07E+01	5.30E+01	5.63E+01	5.78E+01	6.09E+01	6.26E+01
Zn $K\beta_1$	9.572E−03	2.21E+02	2.33E+02	2.47E+02	2.57E+02	2.73E+02	2.79E+02	2.93E+02	3.00E+02
Cu $K\beta_1$	8.905E−03	2.66E+02	2.82E+02	2.99E+02	3.10E+02	3.28E+02	3.35E+02	3.52E+02	3.60E+02
Zn $K\bar{\alpha}$	8.631E−03	2.89E+02	3.06E+02	3.24E+02	3.36E+02	3.55E+02	3.63E+02	3.80E+02	3.89E+02
Ni $K\beta_1$	8.265E−03	3.24E+02	3.43E+02	3.63E+02	3.76E+02	3.97E+02	4.05E+02	4.24E+02	4.33E+02
Cu $K\bar{\alpha}$	8.041E−03	3.48E+02	3.68E+02	3.90E+02	4.04E+02	4.26E+02	4.34E+02	4.34E+02	4.03E+02
Co $K\beta_1$	7.649E−03	3.95E+02	4.17E+02	4.41E+02	4.57E+02	4.82E+02	3.54E+02	4.80E+02	3.35E+02
Ni $K\bar{\alpha}$	7.472E−03	4.19E+02	4.42E+02	4.68E+02	4.84E+02	5.11E+02	3.71E+02	3.75E+02	3.56E+02
Fe $K\beta_1$	7.058E−03	4.83E+02	5.10E+02	5.39E+02	4.92E+02	5.88E+02	1.63E+02	4.08E+02	1.53E+02
Co $K\bar{\alpha}$	6.925E−03	5.07E+02	5.35E+02	5.65E+02	5.05E+02	4.00E+02	1.76E+02	4.19E+02	1.61E+02
Mn $K\beta_1$	6.490E−03	5.97E+02	5.47E+02	6.16E+02	4.39E+02	4.68E+02	1.66E+02	1.95E+02	1.89E+02
Fe $K\bar{\alpha}$	6.400E−03	6.18E+02	5.61E+02	4.48E+02	4.55E+02	1.94E+02	2.04E+02	2.03E+02	1.95E+02
Cr $K\beta_1$	5.947E−03	7.44E+02	4.94E+02	1.88E+02	1.98E+02	2.32E+02	2.21E+02	2.44E+02	2.35E+02
Mn $K\bar{\alpha}$	5.895E−03	7.60E+02	5.12E+02	1.93E+02	2.03E+02	2.37E+02	2.25E+02	2.49E+02	2.41E+02
Cr $K\bar{\alpha}$	5.412E−03	2.25E+02	2.38E+02	2.38E+02	2.51E+02	2.94E+02	2.79E+02	3.09E+02	2.98E+02
Ti $K\beta_1$	4.932E−03	2.84E+02	3.00E+02	3.00E+02	3.14E+02	3.69E+02	3.50E+02	3.90E+02	3.74E+02
Ti $K\bar{\alpha}$	4.509E−03	3.55E+02	3.57E+02	3.75E+02	3.97E+02	4.62E+02	4.35E+02	4.88E+02	4.69E+02

Table 4.2.4.3. *Mass attenuation coefficients ($cm^2\ g^{-1}$) (cont.)*

Radiation	Energy (MeV)	65 Terbium	66 Dysprosium	67 Holmium	68 Erbium	69 Thulium	70 Ytterbium	71 Lutetium	72 Hafnium
Ag $K\beta_1$	2.494E−02	2.55E+01	2.65E+01	2.77E+01	2.90E+01	3.04E+01	3.14E+01	3.28E+01	3.40E+01
Pd $K\beta_1$	2.382E−02	2.88E+01	2.99E+01	3.13E+01	3.27E+01	3.43E+01	3.54E+01	3.71E+01	3.84E+01
Rh $K\beta_1$	2.272E−02	3.26E+01	3.39E+01	3.54E+01	3.71E+01	3.89E+01	4.01E+01	4.20E+01	4.35E+01
Ag $K\bar{\alpha}$	2.210E−02	3.51E+01	3.65E+01	3.81E+01	3.99E+01	4.18E+01	4.32E+01	4.51E+01	4.67E+01
Pd $K\bar{\alpha}$	2.112E−02	3.96E+01	4.12E+01	4.30E+01	4.50E+01	4.71E+01	4.87E+01	5.09E+01	5.27E+01
Rh $K\bar{\alpha}$	2.017E−02	4.49E+01	4.66E+01	4.87E+01	5.09E+01	5.33E+01	5.50E+01	5.75E+01	5.95E+01
Mo $K\beta_1$	1.961E−02	4.83E+01	5.02E+01	5.24E+01	5.48E+01	5.74E+01	5.93E+01	6.19E+01	6.41E+01
Mo $K\bar{\alpha}$	1.744E−02	6.58E+01	6.83E+01	7.13E+01	7.44E+01	7.79E+01	8.04E+01	8.40E+01	8.69E+01
Zn $K\beta_1$	9.572E−03	3.14E+02	3.24E+02	3.36E+02	3.49E+02	3.65E+02	3.75E+02	3.91E+02	1.00E+02
Cu $K\beta_1$	8.905E−03	3.76E+02	3.87E+02	4.02E+02	4.17E+02	1.08E+02	1.08E+02	1.21E+02	1.20E+02
Zn $K\bar{\alpha}$	8.631E−03	4.06E+02	4.19E+02	3.98E+02	2.87E+02	1.17E+02	1.17E+02	1.31E+02	1.30E+02
Ni $K\beta_1$	8.265E−03	4.52E+02	3.36E+02	4.44E+02	1.23E+02	1.31E+02	1.31E+02	1.46E+02	1.45E+02
Cu $K\bar{\alpha}$	8.041E−03	3.21E+02	3.62E+02	1.29E+02	1.32E+02	1.40E+02	1.42E+02	1.56E+02	1.55E+02
Co $K\beta_1$	7.649E−03	3.60E+02	1.38E+02	1.46E+02	1.49E+02	1.59E+02	1.59E+02	1.78E+02	1.76E+02
Ni $K\bar{\alpha}$	7.472E−03	1.49E+02	1.46E+02	1.55E+02	1.58E+02	1.69E+02	1.69E+02	1.89E+02	1.87E+02
Fe $K\beta_1$	7.058E−03	1.71E+02	1.68E+02	1.78E+02	1.82E+02	1.96E+02	1.96E+02	2.18E+02	2.16E+02
Co $K\bar{\alpha}$	6.925E−03	1.80E+02	1.76E+02	1.87E+02	1.91E+02	2.06E+02	2.06E+02	2.29E+02	2.27E+02
Mn $K\beta_1$	6.490E−03	2.11E+02	2.07E+02	2.20E+02	2.24E+02	2.43E+02	2.44E+02	2.70E+02	2.67E+02
Fe $K\bar{\alpha}$	6.400E−03	2.19E+02	2.14E+02	2.28E+02	2.32E+02	2.53E+02	2.51E+02	2.80E+02	2.77E+02
Cr $K\beta_1$	5.947E−03	2.63E+02	2.57E+02	2.72E+02	2.78E+02	3.05E+02	3.04E+02	3.39E+02	3.34E+02
Mn $K\bar{\alpha}$	5.895E−03	2.69E+02	2.62E+02	2.80E+02	2.85E+02	3.12E+02	3.11E+02	3.47E+02	3.41E+02
Cr $K\bar{\alpha}$	5.412E−03	3.32E+02	3.25E+02	3.47E+02	3.52E+02	3.86E+02	3.87E+02	4.31E+02	4.25E+02
Ti $K\beta_1$	4.932E−03	4.19E+02	4.10E+02	4.38E+02	4.43E+02	4.94E+02	4.92E+02	5.47E+02	5.39E+02
Ti $K\bar{\alpha}$	4.509E−03	5.24E+02	5.15E+02	5.47E+02	5.54E+02	6.21E+02	6.19E+02	6.88E+02	6.78E+02

		73 Tantalum	74 Tungsten	75 Rhenium	76 Osmium	77 Iridium	78 Platinum	79 Gold	80 Mercury
Ag $K\beta_1$	2.494E−02	3.54E+01	3.68E+01	3.83E+01	3.95E+01	4.11E+01	4.26E+01	4.44E+01	4.58E+01
Pd $K\beta_1$	2.382E−02	4.00E+01	4.15E+01	4.32E+01	4.45E+01	4.64E+01	4.80E+01	5.00E+01	5.16E+01
Rh $K\beta_1$	2.272E−02	4.53E+01	4.70E+01	4.89E+01	5.04E+01	5.24E+01	5.43E+01	5.65E+01	5.83E+01
Ag $K\bar{\alpha}$	2.210E−02	4.87E+01	5.05E+01	5.25E+01	5.41E+01	5.63E+01	5.83E+01	6.07E+01	6.26E+01
Pd $K\bar{\alpha}$	2.112E−02	5.48E+01	5.69E+01	5.92E+01	6.10E+01	6.34E+01	6.57E+01	6.83E+01	7.04E+01
Rh $K\bar{\alpha}$	2.017E−02	6.20E+01	6.43E+01	6.69E+01	6.89E+01	7.16E+01	7.41E+01	7.71E+01	7.95E+01
Mo $K\beta_1$	1.961E−02	6.67E+01	6.92E+01	7.19E+01	7.41E+01	7.70E+01	7.97E+01	8.29E+01	8.54E+01
Mo $K\bar{\alpha}$	1.744E−02	9.04E+01	9.38E+01	9.74E+01	1.00E+02	1.04E+02	1.07E+02	1.12E+02	1.15E+02
Zn $K\beta_1$	9.572E−03	1.02E+02	1.08E+02	1.19E+02	1.18E+02	1.23E+02	1.21E+02	1.30E+02	1.16E+02
Cu $K\beta_1$	8.905E−03	1.22E+02	1.30E+02	1.43E+02	1.42E+02	1.48E+02	1.45E+02	1.55E+02	1.41E+02
Zn $K\bar{\alpha}$	8.631E−03	1.32E+02	1.41E+02	1.55E+02	1.54E+02	1.60E+02	1.57E+02	1.68E+02	1.54E+02
Ni $K\beta_1$	8.265E−03	1.47E+02	1.57E+02	1.72E+02	1.71E+02	1.78E+02	1.75E+02	1.88E+02	1.74E+02
Cu $K\bar{\alpha}$	8.041E−03	1.58E+02	1.68E+02	1.87E+02	1.84E+02	1.91E+02	1.88E+02	2.01E+02	1.88E+02
Co $K\beta_1$	7.649E−03	1.79E+02	1.91E+02	2.09E+02	2.09E+02	2.16E+02	2.14E+02	2.29E+02	2.16E+02
Ni $K\bar{\alpha}$	7.472E−03	1.90E+02	2.03E+02	2.22E+02	2.21E+02	2.30E+02	2.27E+02	2.43E+02	2.30E+02
Fe $K\beta_1$	7.058E−03	2.20E+02	2.34E+02	2.57E+02	2.55E+02	2.65E+02	2.61E+02	2.79E+02	2.60E+02
Co $K\bar{\alpha}$	6.925E−03	2.31E+02	2.46E+02	2.68E+02	2.68E+02	2.78E+02	2.76E+02	2.95E+02	2.73E+02
Mn $K\beta_1$	6.490E−03	2.73E+02	2.88E+02	3.16E+02	3.14E+02	3.30E+02	3.25E+02	3.48E+02	3.27E+02
Fe $K\bar{\alpha}$	6.400E−03	2.83E+02	3.01E+02	3.27E+02	3.27E+02	3.40E+02	3.57E+02	3.61E+02	3.39E+02
Cr $K\beta_1$	5.947E−03	3.39E+02	3.61E+02	3.94E+02	3.92E+02	4.11E+02	4.23E+02	4.34E+02	4.16E+02
Mn $K\bar{\alpha}$	5.895E−03	3.46E+02	3.69E+02	4.05E+02	4.03E+02	4.18E+02	4.34E+02	4.45E+02	4.27E+02
Cr $K\bar{\alpha}$	5.412E−03	4.32E+02	4.57E+02	5.01E+02	4.99E+02	5.20E+02	5.41E+02	5.51E+02	5.41E+02
Ti $K\beta_1$	4.932E−03	5.46E+02	5.79E+02	6.33E+02	6.31E+02	6.59E+02	6.83E+02	6.99E+02	6.99E+02
Ti $K\bar{\alpha}$	4.509E−03	6.85E+02	7.25E+02	7.94E+02	7.92E+02	8.26E+02	8.19E+02	8.76E+02	8.97E+02

Table 4.2.4.3. *Mass attenuation coefficients ($cm^2\ g^{-1}$) (cont.)*

Radiation	Energy (MeV)	81 Thallium	82 Lead	83 Bismuth	84 Polonium	85 Astatine	86 Radon	87 Francium	88 Radium
Ag $K\beta_1$	2.494E−02	4.72E+01	4.88E+01	5.06E+01	5.30E+01	5.51E+01	5.45E+01	5.67E+01	5.84E+01
Pd $K\beta_1$	2.382E−02	5.31E+01	5.49E+01	5.70E+01	5.96E+01	6.20E+01	6.12E+01	6.37E+01	6.56E+01
Rh $K\beta_1$	2.272E−02	6.00E+01	6.20E+01	6.44E+01	6.73E+01	7.00E+01	6.90E+01	7.18E+01	7.40E+01
Ag $K\bar{\alpha}$	2.210E−02	6.45E+01	6.66E+01	6.91E+01	7.23E+01	7.51E+01	7.21E+01	7.70E+01	7.93E+01
Pd $K\bar{\alpha}$	2.112E−02	7.25E+01	7.49E+01	7.77E+01	8.12E+01	8.43E+01	8.32E+01	8.64E+01	8.90E+01
Rh $K\bar{\alpha}$	2.017E−02	8.18E+01	8.45E+01	8.76E+01	9.15E+01	9.50E+01	9.36E+01	9.72E+01	1.00E+02
Mo $K\beta_1$	1.961E−02	8.79E+01	9.08E+01	9.41E+01	9.83E+01	1.02E+02	1.01E+02	1.04E+02	1.08E+01
Mo $K\bar{\alpha}$	1.744E−02	1.18E+02	1.22E+02	1.26E+02	1.32E+02	1.17E+02	1.08E+02	8.70E+01	8.80E+01
Zn $K\beta_1$	9.572E−03	1.45E+02	1.51E+02	1.57E+02	1.63E+02	1.71E+02	1.71E+02	1.77E+02	1.75E+02
Cu $K\beta_1$	8.905E−03	1.75E+02	1.81E+02	1.88E+02	1.96E+02	1.86E+02	2.05E+02	2.13E+02	2.10E+02
Zn $K\bar{\alpha}$	8.631E−03	1.89E+02	1.96E+02	2.04E+02	2.12E+02	2.07E+02	2.23E+02	2.30E+02	2.28E+02
Ni $K\beta_1$	8.265E−03	2.11E+02	2.16E+02	2.28E+02	2.37E+02	2.31E+02	2.49E+02	2.57E+02	2.54E+02
Cu $K\bar{\alpha}$	8.041E−03	2.26E+02	2.35E+02	2.44E+02	2.54E+02	2.48E+02	2.67E+02	2.77E+02	2.73E+02
Co $K\beta_1$	7.649E−03	2.57E+02	2.67E+02	2.76E+02	2.88E+02	2.82E+02	3.04E+02	3.12E+02	3.10E+02
Ni $K\bar{\alpha}$	7.472E−03	2.71E+02	2.83E+02	2.95E+02	3.05E+02	2.99E+02	3.21E+02	3.32E+02	3.29E+02
Fe $K\beta_1$	7.058E−03	3.14E+02	3.27E+02	3.39E+02	3.54E+02	3.45E+02	3.73E+02	3.84E+02	3.80E+02
Co $K\bar{\alpha}$	6.925E−03	3.31E+02	3.43E+02	3.55E+02	3.70E+02	3.63E+02	3.92E+02	4.03E+02	3.98E+02
Mn $K\beta_1$	6.490E−03	3.90E+02	4.06E+02	4.21E+02	4.35E+02	4.26E+02	4.60E+02	4.77E+02	4.70E+02
Fe $K\bar{\alpha}$	6.400E−03	4.03E+02	4.20E+02	4.34E+02	4.52E+02	4.44E+02	4.77E+02	4.93E+02	4.87E+02
Cr $K\beta_1$	5.947E−03	4.87E+02	5.07E+02	5.24E+02	5.44E+02	5.33E+02	5.76E+02	5.97E+02	5.85E+02
Mn $K\bar{\alpha}$	5.895E−03	5.00E+02	5.18E+02	5.35E+02	5.58E+02	5.45E+02	5.89E+02	6.02E+02	5.99E+02
Cr $K\bar{\alpha}$	5.412E−03	5.97E+02	6.43E+02	6.66E+02	6.91E+02	6.80E+02	7.34E+02	7.58E+02	7.43E+02
Ti $K\beta_1$	4.932E−03	7.15E+02	8.15E+02	8.44E+02	8.30E+02	8.60E+02	9.32E+02	9.61E+02	9.41E+02
Ti $K\bar{\alpha}$	4.509E−03	9.89E+02	1.03E+03	1.06E+03	1.10E+03	1.08E+03	1.18E+03	1.21E+03	1.33E+03

		89 Actinium	90 Thorium	91 Protactinium	92 Uranium	93 Neptunium	94 Plutonium	95 Americium	96 Curium
Ag $K\beta_1$	2.494E−02	6.07E+01	6.19E+01	6.48E+01	6.55E+01	6.84E+01	7.05E+01	7.20E+01	7.35E+01
Pd $K\beta_1$	2.382E−02	6.82E+01	6.95E+01	7.27E+01	7.35E+01	7.67E+01	7.91E+01	8.08E+01	8.24E+01
Rh $K\beta_1$	2.272E−02	7.68E+01	7.82E+01	8.19E+01	8.27E+01	8.63E+01	8.89E+01	9.08E+01	6.00E+01
Ag $K\bar{\alpha}$	2.210E−02	8.24E+01	8.39E+01	8.78E+01	8.86E+01	9.25E+01	5.60E+01	5.95E+01	6.43E+01
Pd $K\bar{\alpha}$	2.112E−02	9.24E+01	9.41E+01	9.84E+01	9.93E+01	1.04E+02	1.07E+02	1.09E+02	1.11E+02
Rh $K\bar{\alpha}$	2.017E−02	1.04E+02	1.06E+02	1.11E+02	1.12E+02	1.16E+02	1.20E+02	1.22E+02	1.10E+02
Mo $K\beta_1$	1.961E−02	1.10E+02	9.87E+01	1.19E+02	7.49E+01	1.25E+02	1.29E+02	1.31E+02	1.34E+02
Mo $K\bar{\alpha}$	1.744E−02	9.08E+01	9.65E+01	1.01E+02	1.02E+02	4.22E+01	3.99E+01	4.81E+01	4.90E+01
Zn $K\beta_1$	9.572E−03	2.49E+02	1.70E+02	1.73E+02	1.85E+02	1.90E+02	1.80E+02	1.89E+02	1.94E+02
Cu $K\beta_1$	8.905E−03	2.85E+02	2.19E+02	2.08E+02	2.22E+02	2.27E+02	2.16E+02	2.27E+02	2.32E+02
Zn $K\bar{\alpha}$	8.631E−03	3.03E+02	2.55E+02	2.25E+02	2.40E+02	2.46E+02	2.34E+02	2.41E+02	2.51E+02
Ni $K\beta_1$	8.265E−03	3.09E+02	2.85E+02	2.52E+02	2.68E+02	2.75E+02	2.62E+02	2.73E+02	2.80E+02
Cu $K\bar{\alpha}$	8.041E−03	3.17E+02	3.06E+02	2.71E+02	2.88E+02	3.14E+02	2.80E+02	3.22E+02	3.38E+02
Co $K\beta_1$	7.649E−03	3.81E+02	3.48E+02	3.06E+02	3.26E+02	3.35E+02	3.17E+02	3.33E+02	3.43E+02
Ni $K\bar{\alpha}$	7.472E−03	3.99E+02	3.69E+02	3.25E+02	3.47E+02	3.55E+02	3.36E+02	3.52E+02	3.60E+02
Fe $K\beta_1$	7.058E−03	4.44E+02	3.89E+02	3.75E+02	4.00E+02	4.10E+02	3.89E+02	4.07E+02	4.21E+02
Co $K\bar{\alpha}$	6.925E−03	4.61E+02	4.06E+02	3.94E+02	4.20E+02	4.30E+02	4.08E+02	4.26E+02	4.37E+02
Mn $K\beta_1$	6.490E−03	5.21E+02	4.46E+02	4.65E+02	4.96E+02	5.05E+02	4.08E+02	5.03E+02	5.15E+02
Fe $K\bar{\alpha}$	6.400E−03	5.30E+02	4.85E+02	4.82E+02	5.28E+02	5.52E+02	4.98E+02	5.81E+02	5.90E+02
Cr $K\beta_1$	5.947E−03	6.18E+02	5.09E+02	5.82E+02	6.17E+02	6.30E+02	6.00E+02	6.27E+02	6.40E+02
Mn $K\bar{\alpha}$	5.895E−03	6.29E+02	6.23E+02	5.93E+02	6.32E+02	6.45E+02	6.12E+02	6.42E+02	6.55E+02
Cr $K\bar{\alpha}$	5.412E−03	7.39E+02	7.68E+02	7.38E+02	7.66E+02	8.00E+02	7.60E+02	7.95E+02	8.12E+02
Ti $K\beta_1$	4.932E−03	8.83E+02	9.78E+02	9.83E+02	9.66E+02	1.01E+03	9.62E+02	1.03E+03	1.03E+03
Ti $K\bar{\alpha}$	4.509E−03	1.05E+03	1.23E+03	1.24E+03	1.23E+03	9.65E+02	9.00E+02	9.55E+02	9.84E+02

Table 4.2.4.3. *Mass attenuation coefficients ($cm^2\ g^{-1}$) (cont.)*

Radiation	Energy (MeV)	97 Berkelium	98 Californium
Ag $K\beta_1$	2.494E−02	6.66E+01	7.35E+01
Pd $K\beta_1$	2.382E−02	7.52E+01	8.24E+01
Rh $K\beta_1$	2.272E−02	8.51E+01	9.26E+01
Ag $K\bar{\alpha}$	2.210E−02	6.10E+01	6.92E+01
Pd $K\bar{\alpha}$	2.112E−02	1.03E+02	1.11E+02
Rh $K\bar{\alpha}$	2.017E−02	1.02E+02	1.25E+02
Mo $K\beta_1$	1.961E−02	1.25E+02	1.34E+02
Mo $K\bar{\alpha}$	1.744E−02	4.90E+01	5.00E+01
Zn $K\beta_1$	9.572E−03	1.86E+02	2.08E+02
Cu $K\beta_1$	8.905E−03	2.26E+02	2.49E+02
Zn $K\bar{\alpha}$	8.631E−03	2.46E+02	2.70E+02
Ni $K\beta_1$	8.265E−03	2.77E+02	3.01E+02
Cu $K\bar{\alpha}$	8.041E−03	3.52E+02	3.60E+02
Co $K\beta_1$	7.649E−03	3.57E+02	3.66E+02
Ni $K\bar{\alpha}$	7.472E−03	3.62E+02	3.86E+02
Fe $K\beta_1$	7.058E−03	4.22E+02	4.48E+02
Co $K\bar{\alpha}$	6.925E−03	4.43E+02	4.69E+02
Mn $K\beta_1$	6.490E−03	5.26E+02	5.52E+02
Fe $K\bar{\alpha}$	6.400E−03	5.92E+02	6.07E+02
Cr $K\beta_1$	5.947E−03	6.64E+02	6.87E+02
Mn $K\bar{\alpha}$	5.895E−03	6.78E+02	7.03E+02
Cr $K\bar{\alpha}$	5.412E−03	8.52E+02	8.71E+02
Ti $K\beta_1$	4.932E−03	1.09E+03	1.10E+03
Ti $K\bar{\alpha}$	4.509E−03	1.04E+03	1.05E+03

involve the use of filters, mirrors, and Laue and Bragg crystal monochromators, chosen so as to provide the best compromise between flux and spectral purity in a particular experiment. In other chapters, authors have discussed the use of techniques to improve the spectral purity of X-ray sources. This section does not purport to be a comprehensive exposition on the topic of filters and monochromators. Rather, it seeks to point the reader towards the information given elsewhere in this volume, and to add complementary information where necessary. A search of the Subject Index will find references to filters and monochromators that are not explicitly mentioned in the text of this section.

The ability to select photon energies, or bands of energies, depends on the scattering power of the atoms from which the monochromator is made and the arrangement of the atoms within the monochromator. The scattering powers of the atoms and their dependence on the energy of the incident photons were discussed in Sections 4.2.3 and 4.2.4 and are discussed more fully in Section 4.2.6. In brief, the scattering power of the atom, or *atomic scattering factor*, is defined, for a given incident photon energy, as the ratio of the scattering power of the atom to that of a free Thomson electron. The scattering power is denoted by the symbol $f(\omega, \Delta)$ and is a complex quantity, the real part of which, $f'(\omega, \Delta)$, is related to the elastic scattering cross section, and the imaginary part of which, $f''(\omega, \Delta)$, is related directly to the photoelectric scattering cross section and therefore the linear attenuation coefficient μ_l.

At an interface between, say, air and the material from which the monochromator is made, reflection and refraction of the incident photons can occur, as dictated by Maxwell's equations. There is an associated refractive index n given by

$$n = (1 + \chi)^{1/2}, \qquad (4.2.5.1)$$

where

$$\chi = -(r_e\lambda^2/\pi)\sum_j N_j f_j(\omega, \Delta), \qquad (4.2.5.2)$$

r_e is the classical radius of the electron, and N_j is the number density of atoms of type j.

An angle of total external reflection α_c exists for the material, which is a function of the incident photon energy, since $f_j(\omega, \Delta)$ is a function of photon energy. Thus, a polychromatic beam incident at the critical angle of one of the photon energies (E) will reflect totally those components having energies less than E, and transmit those components with energies greater than E. Fig. 4.2.5.1 shows calculations by Fukumachi, Nakano & Kawamura (1986) for the reflectivity of single layers of aluminium, copper and platinum as a function of incident energy for a fixed angle of incidence (0.2°). For the aluminium specimen, the reflectivity curve shows the rapid decrease in reflectivity as the critical angle is exceeded. The reflectivity in this region varies as E^{-2}. The effect of increasing atomic number can be seen: the higher the atomic factor $f(\omega, \Delta)$, the greater the energy that can be reflected from the surface. Also visible are the effects of the dispersion corrections $f'(\omega, \Delta)$ and $f''(\omega, \Delta)$ on reflectivity. For copper, the K shell is excited, and for platinum the $L_{\rm I}$, $L_{\rm II}$ and $L_{\rm III}$ shells are excited by the polychromatic beam.

Interfaces can therefore be used to act as low-pass energy filters. The surface roughness and the existence of impurities and contaminants on the interface will, however, influence the characteristics of the reflecting surface, sometimes significantly.

4.2.5.2. *Mirrors and capillaries*

Whilst neither of these classes of X-ray optical device is strictly speaking a monochromator, they nevertheless form component parts of monochromator systems in the laboratory and at synchrotron-radiation sources.

4.2.5.2.1. *Mirrors*

In the laboratory, mirrors are used in conjunction with conventional sealed tubes and rotating-anode sources, the emission from which consists of *Bremsstrahlung* upon which is superimposed the characteristic spectrum of the anode material (Subsection 2.3.5.2). The shape of the *Bremsstrahlung* spectrum can be significantly modified by mirrors, and the intensity emitted at harmonics of the characteristic wavelength can be

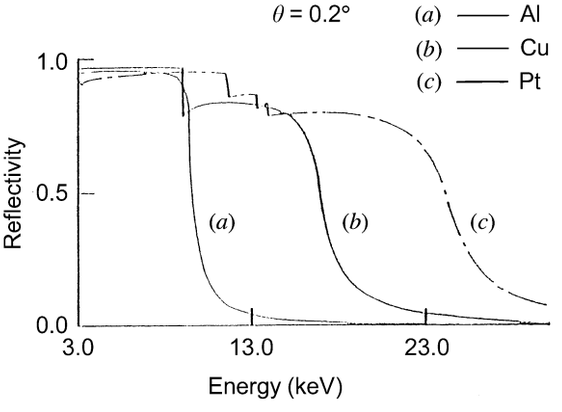

Fig. 4.2.5.1. The variation of specular reflectivity with incident photon energy is shown for materials of different atomic number and a constant angle of incidence of 0.2°. (*a*) Aluminium: note the rapid decrease of reflectivity with energy. (*b*) Copper: the sudden decrease of reflectivity is due to the modification of the scattering-length density owing to absorption at the K-absorption edge. (*c*) Platinum: the three discontinuities in the reflectivity curve are due to absorption at the $L_{\rm I}$-, $L_{\rm II}$-, and $L_{\rm III}$-absorption edges.

significantly reduced. More importantly, the mirrors can be fashioned into shapes that enable the emitted radiation to be brought to a focus. Ellipsoidal, logarithmic spiral, and toroidal mirrors have been manufactured commercially for use with laboratory X-ray sources. Since the X-rays are emitted isotropically from the anode surface, it is important to devise a mirror system that has a maximum angle of acceptance and a relatively long focal length.

At synchrotron-radiation sources, the high intensities that are generated over a very broad spectral range give rise to significant heat loading of subsequent monochromators and therefore degrade the performance of these elements. In many systems, mirrors are used as the first optical element in the monochromator, to reduce the heat load on the primary monochromator and to make it easier for the subsequent monochromators to reject harmonics of the chosen radiation. Shaped mirror geometries are often used to focus the beam in the horizontal plane (Subsection 2.2.7.3). A schematic diagram of the optical elements of a typical synchrotron-radiation beamline is shown in Fig. 4.2.5.2. In this, the primary mirror acts as a thermal shunt for the subsequent monochromator, minimizes the high-energy component that may give rise to possible harmonic content in the final beam, and acts as a vertical collimator. The radii of curvature of mirrors can be changed using a mechanical four-point bending system (Oshima, Harada & Sakabe, 1986). More recent advances in mirror technology enable the shape of the mirror to be changed through use of the piezoelectric effect (Sussini & Labergerie, 1995).

4.2.5.2.2. *Capillaries*

Capillaries, and bundles of capillaries, are finding increasing use in situations where a focused beam is required. The radiation is guided along the capillary by total external reflection, and the shape of the capillary determines the overall flux gain and the uniformity of the focused spot. Gains in flux of 100 and better have been reported. There is, however, a degradation in the angular divergence of the outgoing beam. For single capillaries, applications are laboratory-based protein crystallography, microtomography, X-ray microscopy, and micro-X-ray fluorescence spectroscopy. The design and construction of capillaries for use in the laboratory and at synchrotron-radiation sources has been discussed by Bilderback, Thiel, Pahl & Brister (1994), Balaic & Nugent (1995), Balaic, Nugent, Barnea, Garrett & Wilkins (1995), Balaic *et al.* (1996), and Engström, Rindby & Vincze (1996). They are usually used after other monochromators in these applications and their role as a low-pass energy filter is not of much significance.

Bundles of capillaries are currently being produced commercially to produce focused beams (ellipsoidally shaped bundles) and half-ellipsoidal bundles are used to form beams of large cross section from conventional laboratory sources (Peele *et al.*, 1996; Kumakov & Komarov, 1990).

4.2.5.2.3. *Quasi-Bragg reflectors*

For one interface, the reflectivity (R) and the transmissivity (T) of the surface are determined by the Fresnel equations, *viz*:

$$R = \left|(\theta_1 - \theta_2)/(\theta_1 + \theta_2)\right|^2, \tag{4.2.5.3}$$

and

$$T = \left|2\theta_1/(\theta_1 + \theta_2)\right|^2, \tag{4.2.5.4}$$

where θ_1 and θ_2 are the angles between the incident ray and the surface plane and the reflected ray and the surface plane, respectively.

If a succession of interfaces exists, the possibility of interference between successively reflected rays exists. Parameters that define the position of the interference maxima, the line breadths of those maxima, and the line intensity depend *inter alia* on the regularity in layer thickness, the interface surface roughness, and the existence of surface tilts between successive interfaces. Algorithms for solving this type of problem are incorporated in software currently available from a number of commercial sources (Bede Scientific, Siemens, and Philips). The reflectivity profile of a system having a periodic layer structure is shown in Fig. 4.2.5.3. This is the reflectivity profile for a multiple-quantum-well structure of alternating aluminium gallium arsenide and indium gallium arsenide layers (Holt, Brown, Creagh & Leon, 1997). Note the interference maxima that are superimposed on the Fresnel reflectivity curve. From the full width at half-maximum of these interference lines, it can be inferred that the energy discrimination of the system, $\Delta E/E$, is 2%. The energy range that can be reflected by such a multilayer system depends on the interlayer thickness: the higher the photon energy, the thinner the layer thickness.

Commercially available multilayer mirrors exist, and hitherto they have been used as monochromators in the soft X-ray region in X-ray fluorescence spectrometers. These monochromators are typically made of alternating layers of tungsten and carbon, to maximize the difference in scattering-

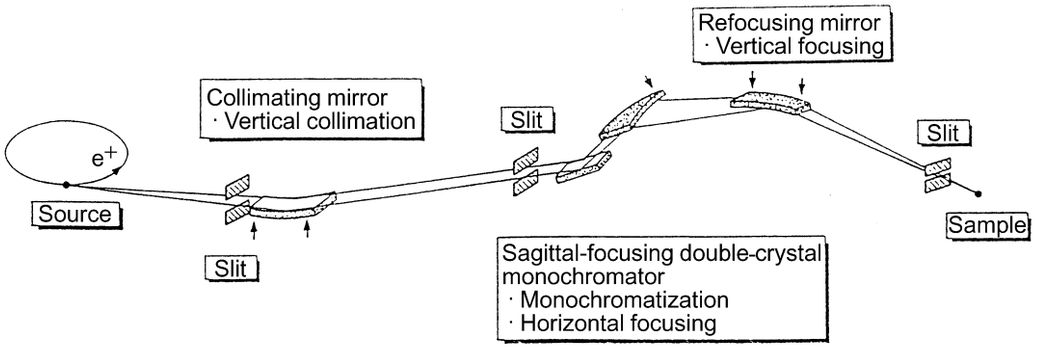

Fig. 4.2.5.2. The use of mirrors in a typical synchrotron-radiation beamline. The X-rays are emitted tangentially to the orbit of the stored positron beam. They pass through a beam-defining slit onto a mirror that serves three purposes, *viz* energy discrimination, heat absorption, and focusing, by means of a mechanical four-point bending system. The beam then passes into a double-crystal monochromator, which selects the desired photon energy. The second element of this monochromator is capable of being bent sagittally using a mechanical four-point bending system to focus the beam in the horizontal plane. The beam is then refocused and redirected by a second mirror.

length density at the interfaces. Whilst the energy resolution of such systems is not especially good, these monochromators have a good angle of acceptance for the incident beam, and reasonably high photon fluxes can be achieved using conventional laboratory sources.

A recent development of this, the Goebel mirror system, is supplied as an accessory to a commercially available diffractometer (Siemens, 1996*a*,*b*,*c*; OSMIC, 1996). This system combines the focusing capacity of a curved mirror with the energy selectivity of the multilayer system. The spacing between layers in this class of mirror multilayers can be laterally graded to enhance the incident acceptance angle. These multilayers can be fixed to mirrors of any figure to a precision of 0.3′ and can therefore can be used to form parallel beams (parabolic optical elements) as well as focused beams (elliptical optical elements) of high quality.

4.2.5.3. *Filters*

It is usual to consider only the cases where a quasimonochromatic beam is to be extracted from a polychromatic beam. Before discussing this class of usage, mention must be made of two simple forms of filtering of radiation.

In the first, *screening*, a thin layer of absorbing foil is used to reduce the effect of specimen fluorescence on photon counting, film and imaging-plate detectors. A typical example is the use of aluminium foil in front of a Polaroid camera used in a Laue camera to reduce the *K*-shell fluorescence radiation from a transition-metal crystal when using a conventional sealed molybdenum X-ray source. A 0.1 mm thick foil will reduce the fluorescent radiation from the crystal by a factor of about five, and this radiation is emitted isotropically from the specimen. In contrast, the wanted Laue-reflected beams are emitted as a nearly parallel beam, and the signal-to-noise ratio in the resulting photograph is much increased.

The second case is the ultimate limiting case of filtering, *shielding*. If it is necessary to shield an object completely from a polychromatic incident beam, a sufficient thickness of absorbing material, calculated using the data in Section 4.2.4, to reduce the beam intensity to the level of the ambient background is inserted in the beam. [The details of how shielding systems are designed are given in reference works such as the *Handbook of Radiation Measurement and Protection* (Brodsky, 1982).] In general, the use of an absorber of one atomic species will provide insufficient shielding. The use of composite absorbers is necessary to achieve a maximum of shielding for a minimum of weight. This is of utmost importance if one is designing, say, the shielding of an X-ray telescope to be carried in a rocket or a balloon (Grey, 1996). To produce shielding that satisfies the requirements of minimum weight, good mechanical rigidity, and ability to be constructed to good levels of mechanical tolerance, shielding must be constructed using a number of layers of different absorbers, chosen such that the highest-energy radiation is just stopped in the first layer, the *L*-shell fluorescent radiation created in the absorption process is stopped in the second, and the lower-energy *L* and *M* fluorescent radiation is stopped by the next layer, and so on until the desired radiation level is reached.

In the usual case involving filters, the problem is one of removing as much as possible of the *Bremsstrahlung* radiation and unwanted characteristic radiation from the spectrum of a laboratory sealed tube or rotating-anode source whilst retaining as much of the wanted radiation as is possible. To give an example, a thin characteristic radiation filter of nickel of appropriate thickness almost completely eliminates the *Bremsstrahlung* and $K\beta$ radiation from an X-ray source with a copper target, but reduces the intensity in the Cu $K\alpha$ doublet by only about a factor of two. For many applications, this is all that is necessary to provide the required degree of monochromatization. If there is a problem with the residual *Bremsstrahlung*, this problem may be averted by making a second set of measurements with a different filter, one having an absorption edge at an energy a little shorter than that of the desired emission line. The difference between the two sets of measurements corresponds to a comparatively small energy range spanning the emission line. This *balanced-filter* method is more cumbersome than the single-filter method, but no special equipment or difficult adjustments are required. In general, if the required emission is from an element of atomic number Z, the first foil is made from material having atomic number $Z-1$ and the second from atomic number $Z+1$. A better balance can be achieved using three foils (Young, 1963). The use of filters is discussed in more detail in §2.3.5.4.2. Data for filters for the radiations in common use are given in Tables 2.3.5.2 and 2.3.5.3. The information necessary for choosing filter materials and estimating their optimum thicknesses for other radiations is given in Sections 4.2.2, 4.2.3, and 4.2.4.

It should be remembered that filtration changes the wavelength of the emission line slightly, but this is only of significance for measurements of lattice parameters to high precision (Delf, 1961).

4.2.5.4. *Monochromators*

4.2.5.4.1. *Crystal monochromators*

Even multifoil balanced filters transmit a wide range of photon energies. Strictly monochromatic radiation is impossible, since all atomic energy levels have a finite width, and emission from these levels therefore is spread over a finite energy range. The corresponding radiative line width is important for the correct evaluation of the dispersion corrections in the neighbourhood of absorption edges (§4.2.6.3.3.2). Even Mössbauer lines, originating as they do from nuclear energy levels that are much narrower than atomic energy levels, have a finite line width. To achieve line widths comparable to these requires the use of monochromators using carefully selected single-crystal reflections.

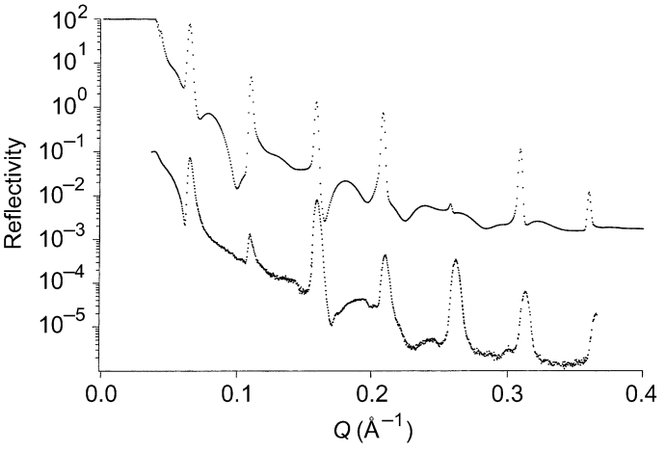

Fig. 4.2.5.3. The reflectivity of a multiple-quantum-well device is shown. This consists of 40 alternating layers of AlGaAs and InGaAs. Shown also, but shifted downwards on the vertical scale for the purpose of clarity, is the theoretical prediction based on standard electromagnetic theory.

Crystal monochromators make use of the periodicity of 'perfect' crystals to select the desired photon energy from a range of photon energies. This is described by Bragg's law,

$$2d_{hkl} \sin\theta = n\lambda, \qquad (4.2.5.5)$$

where d_{hkl} is the spacing between the planes having Miller indices hkl, θ is the angle of incidence, n is the order of a particular reflection ($n = 1, 2, 3, \ldots$), and λ is the wavelength.

If there are wavelength components with values near $\lambda/2$, $\lambda/3$, ..., these will be reflected as well as the wanted radiation, and harmonic contamination can result. This can be a difficulty in spectroscopic experiments, particularly XAFS, XANES and DAFS (Section 4.2.3).

Equation (4.2.5.5) neglects the effect of the refractive index of the material. This is usually omitted from Bragg's law, since it is of the order of 10^{-5} in magnitude. Because the refractive index is a strong function of wavelength, the angles at which the successive harmonics are reflected are slightly different from the Bragg angle of the fundamental. This fact can be used in multiple-reflection monochromators to minimize harmonic contamination.

As can be seen in Fig. 4.2.5.4, each Bragg reflection has a finite line width, the Darwin width, arising from the interaction of the radiation with the periodic electron charge distribution. [See, for example, Warren (1968) and Subsection 7.2.2.1.] Each Bragg reflection therefore contains a spread of photon energies. The higher the Miller indices, the narrower the Darwin width becomes. Thus, for experiments involving the Mössbauer effect, extreme back-reflection geometry is used at the expense of photon flux.

If the beam propagates through the specimen, the geometry is referred to as *transmission*, or *Laue*, geometry. If the beam is reflected from the surface, the geometry is referred to as *reflection*, or *Bragg*, geometry. Bragg geometry is the most commonly used in the construction of crystal monochromators. Laue geometry has been used in only a relatively few applications until recently. The need to handle high photon fluxes with their associated high power load has led to the use of diamond crystals in Laue configurations as one of the first components of X-ray optical systems (Freund, 1993). Phase plates can be created using the Laue geometry (Giles *et al.*, 1994). A schematic diagram of a system used at the European Synchrotron Radiation Facility is shown in Fig. 4.2.5.5. Radiation from an insertion device falls on a Laue-geometry pre-monochromator and then passes through a channel-cut (multiple-reflection) monochromator. The strong linear polarization from the source and the monochromators can be changed into circular polarization by the asymmetric Laue-geometry polarizer and analysed by a similar Laue-geometry analysing crystal.

More will be said about polarization in §4.2.5.4.4 and Section 6.2.2.

4.2.5.4.2. *Laboratory monochromator systems*

Many laboratories use powder diffractometers using the Bragg–Brentano configuration. For these, a sufficient degree of monochromatization is achieved through the use of a diffracted-beam monochromator consisting of a curved-graphite monochromator and a detector, both mounted on the 2θ arm of the diffractometer. Such a device rejects the unwanted $K\beta$ radiation and fluorescence from the sample with little change in the magnitude of the $K\alpha$ lines. Incident-beam monochromators are also used to produce closely monochromatic beams of the desired energy. Single-reflection monochromators used for the reduction of spectral energy spread are described in Subsections 2.2.7.2 and 2.3.5.4.

For most applications, this simple means of monochromatization is adequate. Increasingly, however, more versatility and accuracy are being demanded of laboratory diffractometer systems. Increased angular accuracy in both the θ and 2θ axes, excellent monochromatization, and parallel-beam geometry are all demands of a user community using improved techniques of data collection and data analysis. The necessity to study thin films has generated a need for accurately collimated beams of small cross section, and there is a need to have well collimated and monchromatic beams for the study of rough surfaces. This, coupled with the need to analyse data using the Rietveld method (Young, 1993), has caused a revolution in the design of commercial diffractometers, with the use of principles long since used in synchrotron-radiation research for the design of laboratory instruments. Monochromators of this type are briefly discussed in §4.2.5.4.3.

4.2.5.4.3. *Multiple-reflection monochromators for use with laboratory and synchrotron-radiation sources*

Single-reflection devices produce reflected beams with quite wide, quasi-Lorentzian, tails (Subsection 2.3.3.8), a situation

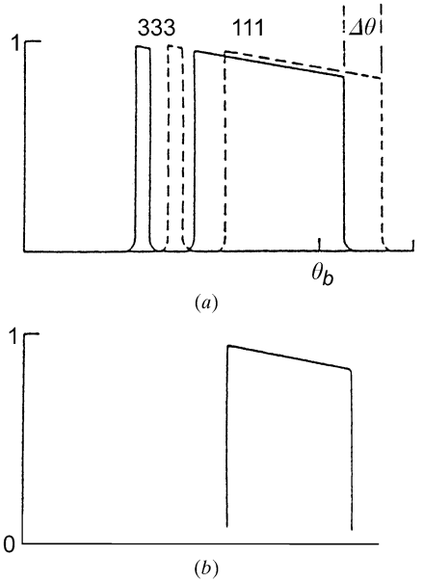

Fig. 4.2.5.4. In (*a*), the schematic rocking curve for a silicon crystal in the neighbourhood of the 111 Bragg peak is shown. The full curve is due to the crystal set to the true Bragg angle, and the dotted curve corresponds to a surface tilted at an angle of 2″ with respect to the beam prior to the acquisition of the rocking curve. Only the 111 and 333 reflections are shown for clarity. The 222 reflection is very weak because the geometrical structure factor is small. The separation of the 111 and 333 peaks occurs because the refractive index is different for these reflections. In a double-crystal monochromator, white radiation from the source will produce the scattered intensity given by the full curve. If that intensity distribution now falls on the second crystal, which is tilted with respect to the first, an angle of tilt can be found for which the Bragg condition is not fulfilled in the second crystal, and the 333 radiation cannot be reflected. The resultant reflected intensity is shown in (*b*). Note that this is an idealized case, and in practice the existence of tails in the reflectivity curve can allow the transmission of some harmonic radiation through the double-crystal monochromator.

that is not acceptable, for example, for the study of small-angle scattering (SAXS, Chapter 2.6). The effect of the tails can be reduced significantly through the use of multiple Bragg reflections.

The use of multiple Bragg reflections from a channel cut in a monolithic silicon crystal such that the channel lay parallel to the (111) planes of the crystal was shown by Bonse & Hart (1965) to remove the tails of reflections almost completely. This class of device, referred to as a (symmetrical) channel-cut crystal, is the most frequently used form of monochromator produced for modern X-ray laboratory diffractometers and beamlines at synchrotron-radiation sources (Figs. 4.2.5.2, 4.2.5.5).

The use of symmetrical and asymmetrical Bragg reflections for the production of highly collimated monochromatic beams has been discussed by Beaumont & Hart (1973). This paper contains descriptions of the configurations of channel-cut monochromators and combinations of channel-cut monochromators used in modern laboratory diffractometers produced by Philips, Siemens, and Bede Scientific. In another paper, Hart (1971) discussed the whole gamut of Bragg reflecting X-ray optical devices. Hart & Rodriguez (1978) extended this to include a class of device in which the second wafer of the channel-cut monochromator could be tilted with respect to the first (Fig. 4.2.5.6), thereby providing an offset of the crystal rocking curves with the consequent removal of most of the contaminant harmonic radiation (Fig. 4.2.5.4). The version of monochromator shown here is designed to provide thermal stability for high incident-photon fluxes. Berman & Hart (1991) have also devised a class of adaptive X-ray monochromators to be used at high thermal loads where thermal expansion can cause a significant degradation of the rocking curve, and therefore a significant loss of flux and spectral purity. The cooling of Bragg-geometry monochromators at high photon fluxes presents a difficult problem in design.

Kikuta & Kohra (1970), Matsushita, Kikuta & Kohra (1971) and Kikuta (1971) have discussed in some detail the performance of asymmetrical channel-cut monochromators. These find application under circumstances in which beam widths need to be condensed or expanded in X-ray tomography or for micro X-ray fluorescence spectroscopy. Hashizume (1983) has described the design of asymmetrical monolithic crystal monochromators for the elimination of harmonics from synchrotron-radiation beams.

Many installations use a system designed by the Kohzu Company as their primary monochromator. This is a separated element design in which the reference crystal is set on the axis of the monochromator and the first crystal is set so as to satisfy the Bragg condition in both elements. One element can be tilted slightly to reduce harmonic contamination. When the wavelength is changed (*i.e.* θ is changed), the position of the first wafer is changed either by mechanical linkages or by electronic positioning devices so as to maintain the position of the outgoing beam in the same place as it was initially. This design of a fixed-height, separated-element monochromator was due initially to Matsushita, Ishikawa & Oyanagi (1986). More recent designs incorporate liquid-nitrogen cooling of the first crystal for use with high-power insertion devices at synchrotron-radiation sources. In many installations, the second crystal can be bent into a cylindrical shape to focus the beam in the horizontal plane. The design of such a sagittally focusing monochromator is discussed by Stephens, Eng & Tse (1992). Creagh & Garrett (1965) have descibed the properties of a monochromator based on a primary monchromator (Berman & Hart, 1991) and a sagittally focusing second monochromator at the Australian National Beamline at the Photon Factory.

A recent innovation in X-ray optics has been made at the European Synchrotron Radiation Facility by the group led by Snigirev (1994). This combines Bragg reflection of X-rays from a silicon crystal with Fresnel reflection from a linear zone-plate structure lithographically etched on its surface. Hanfland *et al.* (1994) have reported the use of this class of reflecting optics for the focusing of 25 to 30 keV photon beams for high-pressure crystallography experiments (Fig. 4.2.5.7).

Further discussion on these monochromators is to be found in this volume in Subsection 2.2.7.2, §2.3.5.4.1, Chapter 2.7, and Section 7.4.2.

4.2.5.4.4. *Polarization*

All scattering of X-rays by atoms causes a probable change of polarization in the beam. Jennings (1981) has discussed the effects of monochromators on the polarization state for

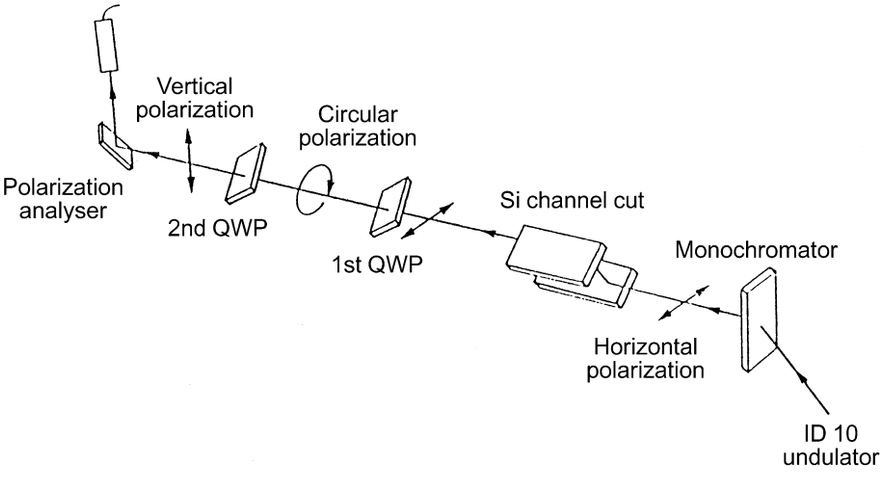

Fig. 4.2.5.5. A schematic diagram of a beamline designed to produce circularly polarized light from initially linearly polarized light using Laue-case reflections. Radiation from an insertion device is initially monochromated by a cooled diamond crystal, operating in Laue geometry. The outgoing radiation has linear polarization in the horizontal plane. It then passes through a silicon channel-cut monochromator and into a silicon crystal of a thickness chosen so as to produce equal amounts of radiation from the σ and π branches of the dispersion surface. These recombine to produce circularly polarized radiation at the exit surface of the crystal.

conventional diffractometers of that era. For accurate Rietveld modelling or accurate charge-density studies, the theoretical scattered intensity must be known. This is not a problem at synchrotron-radiation sources, where the incident beam is initially almost completely linearly polarized in the plane of the orbit, and is subsequently made more linearly polarized through Bragg reflection in the monochromator systems. Rather, it is a problem in the laboratory-based systems where the source is in general a source of elliptical polarization. It is essential to determine the polarization for the particular monochromator and the source combined to determine the correct form of the polarization factor to use in the formulae used to calculate scattered intensity (Chapter 6.2).

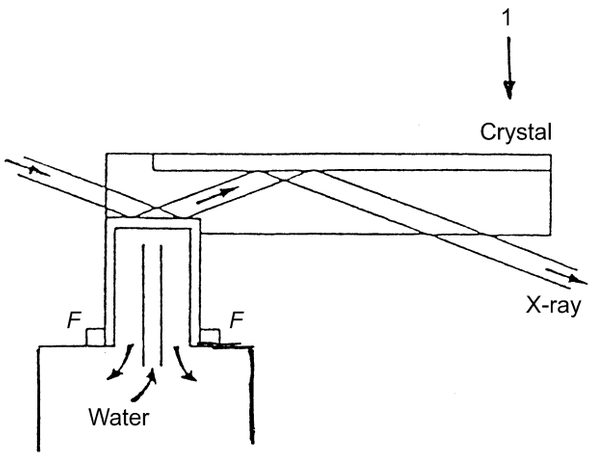

Fig. 4.2.5.6. A schematic diagram of a Hart-type tuneable channel-cut monochromator is shown. The monochromator is cut from a single piece of silicon. The reflecting surfaces lie parallel to the (111) planes. Cuts are made in the crystal block so as to form a lazy hinge, and the second wafer of the monochromator is able to be deflected by a force generated by a current in an electromagnet acting on an iron disc glued to the upper surface of the wafer. Cooling of the primary crystal of the monochromator is by a jet of water falling on the underside of the wafer. This type of system can tolerate incident-beam powers of 500 W mm^{-2} without significant change to the width of the reflectivity curve.

4.2.6. X-ray dispersion corrections (By D. C. Creagh)

The term 'anomalous dispersion' is often used in the literature. It has been dropped here because there is nothing 'anomalous' about these corrections. In fact, the scattering is totally predictable.

For many years after the theoretical prediction of the dispersion of X-rays by Waller (1928), and the application of this theory to the case of hydrogen-like atoms by Hönl (1933*a*,*b*), no real use was made by experimentalists of dispersion-correction effects in X-ray scattering experiments. The suggestion by Bijvoet, Peerdeman & Van Bommel (1951) that dispersion effects might be used to resolve the phase problem in the solution of crystal structures stimulated interest in the practical usefulness of this hitherto neglected aspect of the scattering of photons by atoms. In one of the first texts to discuss the problem, James (1955) collated experimental data and discussed both the classical and the non-relativistic theories of the anomalous scattering of X-rays. James's text remained the principal reference work until 1974, when an Inter-Congress Conference of the International Union of Crystallography dedicated to the discussion of the topic produced its proceedings (Ramaseshan & Abrahams, 1975).

At that conference, reference was made to a theoretical data set calculated by Cromer & Liberman (1970) using relativistic quantum mechanics. This data set was later used in *IT* IV (1974) and has been used extensively by crystallographers for more than a decade.

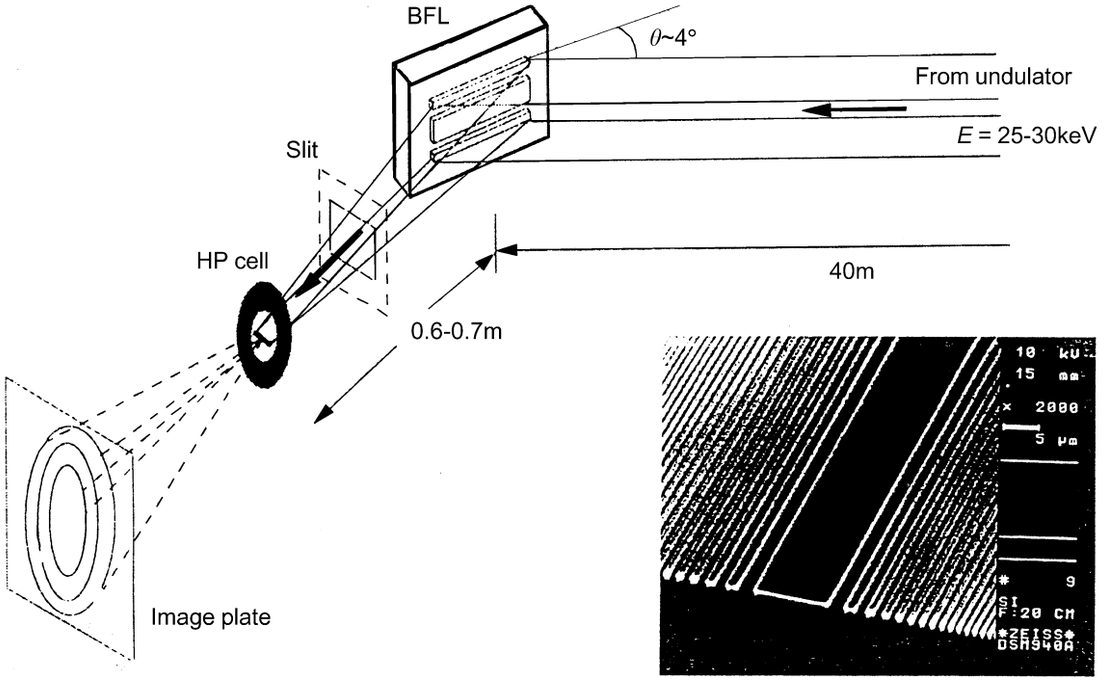

Fig. 4.2.5.7. A schematic diagram of the use of a Bragg–Fresnel lens to focus hard X-rays onto a high-pressure cell. The diameter of the sample in such a cell is typically 10 µm. The insert shows a scanning electron micrograph of the surface of the Bragg–Fresnel lens.

The rapid development in computing techniques, improvements in materials of construction and experimental equipment, and the use of synchrotron-radiation sources for X-ray scattering experiments have led to the production of a number of reviews of both the theoretical and the experimental aspects of the anomalous scattering of X-rays. Review articles by Gavrila (1981), Kissel, Pratt, Kane & Roy (1985), and Creagh (1985) discuss both the theoretical and the experimental techniques for the determination of the X-ray dispersion corrections. Creagh (1986) has discussed the use of X-ray anomalous scattering for the characterization of materials, and a review by Helliwell (1984) has described the anomalous scattering by atoms contained in proteins and its use for the solution of the structure of proteins. In a number of papers, Karle (1980, 1984*a*,*b*,*c*, 1985) has recently shown how powerful dispersion techniques can be in the solution of crystal structures. Indeed, the high intensity afforded by synchrotron-radiation sources, together with improvements in specimen-handling techniques, has led to the general use of dispersion techniques for the solution of the phase problem in crystal structures. In particular, the MAD (multiple-wavelength anomalous-dispersion) technique is used extensively for the solution of such macromolecular crystal structures as proteins and the like. The origin of the technique lies in the Bijvoet relations, but the implementation and the development of the technique is due to Hendrickson (1994).

In this section, a brief discussion of the physical principles underlying the theoretical tabulations of X-ray scattering will be given. This will be followed by a discussion of experimental techniques for the determination of the dispersion corrections. In the next section, theoretical and experimentally determined values for the dispersion corrections will be compared for a number of elements.

Currently, there is some discussion about the nature of the dispersion corrections: are they to be considered to exhibit tensor characteristics? It is clear that in all the theoretical calculations the atoms are considered to be isolated, and, therefore, if there is a tensor associated with the X-ray scattering, it must be associated with the reaction of the atoms with the polarization state of the incident radiation. Since the property of polarization of the X-ray beam is described by a first-rank tensor, it follows that the form factor must be described by a second-rank tensor (Templeton, 1994). Either the detection system of the experimental equipment must be capable of resolving the change in the polarization states of the incident and scattered radiation, or the incident radiation must be plane polarized for this property to be observable. Except for certain diffractometers at synchrotron-radiation sources, or for specially designed conventional laboratory equipment, it is not possible to determine the polarization states before and after scattering.

To a very good approximation, therefore, one can describe the form factor as being made up of a number of separate components, the largest of which is a zeroth-rank tensor that corresponds to the conventionally accepted description of the form factor. The magnitudes of any of the higher-order tensor components are small compared with this term. Whether or not they are observable depends on the characteristics of the diffraction system used in the experiment. The form-factor formalism in its zeroth-order mode has been used extremely successfully for the solution of crystal structures, the description of wavefields in crystals, the determination of the distribution of electron density in crystal structures, *etc*. as has been shown by Creagh (1993).

It must be stressed that all of the crystal structures solved so far have been solved using the conventionally accepted, zeroth-order, form-factor description of X-ray scattering. As well, all the data concerning the distribution of electron density within crystals have used this description.

Further discussion of this issue will be given in §4.2.6.3.3.4.

4.2.6.1. *Definitions*

4.2.6.1.1. *Rayleigh scattering*

When photons interact with atoms, a number of different scattering processes can occur. The dominant scattering mechanisms are: elastic scattering from the bound electrons (Rayleigh scattering); elastic scattering from the nucleus (nuclear Thomson scattering); virtual pair production in the field of the screened nucleus (Delbrück scattering); and inelastic scattering from the bound electrons (Compton scattering).

Of the elastic scattering processes, only Rayleigh scattering has a significant amplitude in the range of photon energies used by crystallographers (< 100 keV). Compton scattering will be discussed elsewhere (Section 4.2.4).

The essential feature of Rayleigh scattering is that the internal energy of the atom remains unchanged in the interaction. The momentum $\hbar\mathbf{k}_i$ and polarization $\boldsymbol{\varepsilon}_i$ of the incident photon may be modified during the process to $\hbar\mathbf{k}_f$ and $\boldsymbol{\varepsilon}_f$

$$(\hbar\mathbf{k}_i, \boldsymbol{\varepsilon}_i) + A \rightarrow A + (\hbar\mathbf{k}_f, \boldsymbol{\varepsilon}_f).$$

4.2.6.1.2. *Thomson scattering by a free electron*

From classical electromagnetic theory, it can be shown that the fraction of incident intensity scattered by a free electron is, at a position r, φ from the scattering electron,

$$I/I_0 = (r_e/r)^2 \tfrac{1}{2}(1 + \cos^2\varphi), \qquad (4.2.6.1)$$

where r_e is the classical radius of the electron ($= 2.817938 \times 10^{-15}$ m). The factor $\frac{1}{2}(1 + \cos^2\varphi)$ arises from the assumption that the electromagnetic wave is initially unpolarized. Should the wave be polarized, the factor is necessarily different from that given in equation (4.2.6.1).

Equation (4.2.6.1) is the basis on which the scattering power of ensembles of electrons is compared.

4.2.6.1.3. *Elastic scattering from electrons bound to atoms: the atomic scattering factor, the atomic form factor, and the dispersion corrections*

In considering the interaction of a photon with electrons bound in an atom, one assumes that each electron scatters independently of its fellows, and that the total scattering power of the atom is the sum of the contributions from all the electrons in the atom. Assuming that one can define an electron density $\rho(\mathbf{r})$ for an atom containing a single electron, one can show that the scattering power of that atom relative to the scattering power of a Thomson free electron is

$$f(\boldsymbol{\Delta}) = \int \rho(\mathbf{r}) \exp[i(\mathbf{k}_f - \mathbf{k}_i)\cdot\mathbf{r}]\,\mathrm{d}V, \qquad (4.2.6.2)$$

where

$$\boldsymbol{\Delta} = \mathbf{k}_f - \mathbf{k}_i \equiv \text{ change in photon momentum}$$
$$= 2|k|\sin(\theta/2),$$

θ being the total angle of scattering of the photon.

The scattering power for the atom relative to a free electron is referred to as the *atomic form factor* or the *atomic scattering factor* of the atom.

The result (4.2.6.2), which was derived using purely classical arguments, has been shown by Nelms & Oppenheimer (1955) to be identical to the result gained by quantum mechanics. If it is assumed that the atom has spherical symmetry,

$$f(\Delta) = 4\pi \int_0^\infty \rho(r) \frac{\sin \Delta r}{\Delta r} r^2 \, \mathrm{d}r. \tag{4.2.6.3}$$

For an atom containing Z electrons, the atomic form factor becomes

$$f(\Delta) = 4\pi \sum_{n=1}^{n=Z} \int_0^\infty \rho_n(r) \frac{\sin \Delta r}{\Delta r} r^2 \, \mathrm{d}r. \tag{4.2.6.4}$$

Exact solutions for the form factor are difficult to obtain, and therefore approximations have to be made to enable equation (4.2.6.4) to be evaluated. The two most commonly used approximations are the Thomas–Fermi (Thomas, 1927; Fermi, 1928) and the Hartree–Fock (Hartree, 1928; Fock, 1930) techniques.

In the Thomas–Fermi model, the atomic electrons are considered to be a degenerate gas obeying Fermi–Dirac statistics and the Pauli exclusion principle, the ground-state energy of the atom being equal to the zero-point energy of this gas. The average charge density can be written in terms of the radial potential function, $V(r)$, which may then be substituted into Poisson's equation, $\nabla^2 V(r) = \rho(r)/\varepsilon_0$, which can then be solved for $V(r)$ using the boundary conditions that $\lim_{r\to\infty} V(r) = 0$ and that $\lim_{r\to 0} rV(r) = Ze$.

The Thomas–Fermi charge distributions for different atoms are related to each other. If the form factor is known for a 'standard' atom for which the atomic number is Z_0 then, for an atom with atomic number Z,

$$f_Z(\mathbf{\Delta}) = (Z/Z_0) f_0(\mathbf{\Delta}'). \tag{4.2.6.5}$$

Here,

$$\Delta' = \Delta (Z/Z_0)^{1/3}.$$

The most accurate calculations of wavefunctions of many-electron atoms have been made using the self-consistent-field (Hartree–Fock) method. In this independent-particle model, each electron is assumed to move in the field of the nucleus and in an average field due to the other electrons. With this approach, the charge distribution can be written as

$$\rho(r) = \sum_{n=1}^{n=Z} \rho_n(r) = \sum_{n=1}^{n=Z} \Psi_n^*(r) \Psi_n(r), \tag{4.2.6.6}$$

where $\rho_n(r)$ is the charge-density distribution of the nth electron and $\Psi_n(r)$ is its wavefunction. The technique has been extended to include the effects of both exchange and correlation. Tables of relativistic Hartree–Fock values have been given by Cromer & Waber (1974). Their notation $F(x, Z)$ is related to the notation used earlier as follows:

$$f_Z(\Delta) \equiv F(x, Z),$$

where

$$x = \frac{|k|}{2\pi} \sin(\varphi/2) = \frac{\Delta}{4\pi}.$$

In the foregoing discussion, the fact that the electrons occupy definite energy levels within the atoms has been ignored: it has been assumed that the energy of the photon is very different from any of these energy levels. The theory for calculating the scattering power of an atom near a resonant energy level was supposed to be effectively the same as the well understood problem of the driven damped pendulum system. In this type of problem, the natural amplitude of the system was modified by a correction term (a real number) dependent on the proximity of the impressed frequency to the natural resonant frequency of the system and a loss term (an imaginary number) that was related to the damping factor for the resonant system. Thus the scattering power came to be written in the form

$$f = f_0 + \Delta f' + i\Delta f'', \tag{4.2.6.7}$$

where f_0 is the atomic scattering factor remote from the resonant energy levels, $\Delta f'$ is the real part of the anomalous-scattering factor, and $\Delta f''$ is the imaginary part of the anomalous-scattering factor. The nomenclature of (4.2.6.7) has been superseded, but one still encounters it occasionally in modern papers.

In what follows, a brief exposition of the various theories for the anomalous scattering of X-rays and descriptions of modern experimental techniques for their determination will be given. Comparisons will be made between the several theoretical and experimental results for a number of atomic species. From these comparisons, conclusions will be drawn as to the validity of the various theories and the relevance of certain experiments.

4.2.6.2. *Theoretical approaches for the calculation of the dispersion corrections*

All the theories that will be discussed here have the following assumptions in common: the elastic scattering is from an isolated neutral atom and that atom is spherically symmetrical. All but the most recent of the theoretical approaches neglect changes in polarization of the incident photon caused by the interaction of the photon with the atom. In the event, few experimental configurations are able to detect such changes in polarization, and the only observable for most experiments is the momentum change of the photon.

4.2.6.2.1. *The classical approach*

In the classical approach, electrons are thought of as occupying energy levels within the atom characterized by an angular frequency ω_n and a damping factor κ_n. The forced vibration of an electron gives rise to a dipolar radiation field, when the atomic scattering factor can be shown to be

$$f = \frac{\omega^2}{\omega^2 - \omega_n^2 - i\kappa_n \omega}. \tag{4.2.6.8}$$

If the probability that the electron is to be found in the nth orbit is g_n, the real part of the atomic scattering factor may be written as

$$\mathrm{Re}(f) = \sum_n g_n + \sum_n \frac{g_n \omega_n^2}{\omega^2 - \omega_n^2}. \tag{4.2.6.9}$$

The probability g_n is referred to as the oscillator strength corresponding to the virtual oscillator having natural frequency ω_n. Equation (4.2.6.9) may be written as

$$\mathrm{Re}(f) = f_0 + f', \tag{4.2.6.10}$$

where f_0 represents the sum of all the elements of the set of oscillator strengths and is unity for a single-electron atom. The second term may be written as

$$f' = \int_{\omega_{\kappa_i}}^\infty \frac{\omega'^2 (\mathrm{d}g_\kappa/\mathrm{d}\omega')}{\omega^2 - \omega'^2} \mathrm{d}\omega' \tag{4.2.6.11}$$

if the atom is assumed to have an infinite number of energy states. For an atom containing κ electrons, it is assumed that the overall value of f' is the coherent sum of the contribution of each individual electron, whence

$$f' = \sum_{\kappa} \int_{\omega_\kappa}^{\infty} \frac{\omega'^2 (\mathrm{d}g_\kappa/\mathrm{d}\omega')}{\omega^2 - \omega'^2} \mathrm{d}\omega' \qquad (4.2.6.12)$$

and the oscillator strength of the κth electron

$$g_\kappa = \int_{\omega_\kappa}^{\infty} \left[\frac{\mathrm{d}g}{\mathrm{d}\omega}\right]_\kappa \mathrm{d}\omega$$

is not unity, but the total oscillator strength for the atom must be equal to the total number of electrons in the atom.

The imaginary part of the dispersion correction f'' is associated with the damping of the incident wave by the bound electrons. It is therefore functionally related to the linear absorption coefficient, μ_l, which can be determined from experimental measurement of the decrease in intensity of the photon beam as it passes through a medium containing the atoms under investigation. It can be shown that the attenuation coefficient per atom μ_a is related to the density of the oscillator states by

$$\mu_a = \frac{2\pi^2 e^2}{\varepsilon_0 mc}\left[\frac{\mathrm{d}g}{\mathrm{d}\omega}\right], \qquad (4.2.6.13)$$

whence

$$f'' = \frac{\pi}{2}\omega\left[\frac{\mathrm{d}g_\kappa}{\mathrm{d}\omega}\right]. \qquad (4.2.6.14)$$

An expression linking the real and imaginary parts of the dispersion corrections can now be written:

$$f' = \frac{2}{\pi}\sum_{\kappa} P \int_{\omega_\kappa}^{\infty} \frac{\omega' f''(\omega', 0)}{\omega^2 - \omega'^2}\mathrm{d}\omega'. \qquad (4.2.6.15)$$

This is referred to as the Kramers–Kronig transform. Note that the term involving the restoring force has been omitted from this equation.

Equations (4.2.6.12), (4.2.6.14), and (4.2.6.15) are the fundamental equations of the classical theory of photon scattering, and it is to these equations that the predictions of other theories are compared.

4.2.6.2.2. *Non-relativistic theories*

The matrix element for Rayleigh scattering from an atom having a radially symmetric charge distribution may be written as

$$M = M_1(\boldsymbol{\varepsilon}_i \cdot \boldsymbol{\varepsilon}_f^*) + M_2(\boldsymbol{\varepsilon}_i \cdot \boldsymbol{\kappa}_f)(\boldsymbol{\varepsilon}_f^* \cdot \boldsymbol{\kappa}_i), \qquad (4.2.6.16)$$

where $\boldsymbol{\varepsilon}_i$ and $\boldsymbol{\varepsilon}_f$ represent the initial and final states of the photon. The matrix element M_1 represents scattering for polarizations $\boldsymbol{\varepsilon}_i$ and $\boldsymbol{\varepsilon}_f$ perpendicular to the plane of scattering and M_2 represents scattering for polarization states lying in the plane of scattering.

Averaged over polarization states, the differential scattering cross section takes the form

$$\frac{\mathrm{d}\sigma}{\mathrm{d}\Omega} = \frac{r_e^2}{2}(|M_1|^2 + |M_2|^2). \qquad (4.2.6.17)$$

Here σ is the photoelectric scattering cross section, which is related to the mass attenuation coefficient μ_m by

$$\sigma = (M/N_A)\mu_m \times 10^{-24}, \qquad (4.2.6.18)$$

where M is the molecular weight and N_A is Avogadro's number.

Using the vector potential of the wavefield $\mathbf{A}$, an expression for the perturbed Hamiltonian of a hydrogen-like atom coupled to the radiation field may be written as

$$\hat{\mathscr{H}} = \hat{\mathscr{H}}_0 - r_e c\mathbf{A}\cdot\mathbf{P} + \frac{r_e^2}{2}\mathbf{A}^2, \qquad (4.2.6.19)$$

where $\hat{\mathscr{H}}_0$ is the Hamiltonian for the unperturbed atom and $\mathbf{P} = i\hbar\nabla$.

After application of the second-order perturbation theory, the matrix element may be deduced to be

$$M = (\boldsymbol{\varepsilon}_i \cdot \boldsymbol{\varepsilon}_f^*) f_0(\Delta) + \frac{1}{m}\langle 1|T_1|1\rangle + \frac{1}{m}\langle 1|T_2|1\rangle. \qquad (4.2.6.20)$$

In this equation, the initial and final wavefunctions are designated as $\langle 1|$ and $|1\rangle$, respectively, and the terms T_1 and T_2 are given by

$$T_1 = \boldsymbol{\varepsilon}_f \cdot \mathbf{P}\exp(-i\mathbf{k}_f\cdot\mathbf{r})\frac{1}{E_1 - \mathscr{H}_0 + \hbar\omega + i\xi}\boldsymbol{\varepsilon}_i \cdot \mathbf{P}\exp(-i\mathbf{k}_i\cdot\mathbf{r})$$

and

$$T_2 = \boldsymbol{\varepsilon}_i \cdot \mathbf{P}\exp(-i\mathbf{k}_i\cdot\mathbf{r})\frac{1}{E_1 - \mathscr{H}_0 + \hbar\omega + i\xi}\boldsymbol{\varepsilon}_f \cdot \mathbf{P}\exp(-i\mathbf{k}_f\cdot\mathbf{r})$$

where ξ is an infinitesimal positive quantity.

The first term of equation (4.2.6.20) corresponds to the atomic scattering factor and is identical to the value given by classical theory. The terms involving T_1 and T_2 correspond to the dispersion corrections. Equation (4.2.6.20) contains no terms to account for radiation damping. More complete theories take the effect of the finite width of the radiating level into account.

It is necessary to realize that the atomic scattering factor depends on both the photon's frequency ω and the momentum vector $\boldsymbol{\Delta}$. To emphasize this dependence, equation (4.2.6.7) is rewritten as

$$f(\omega, \boldsymbol{\Delta}) = f_0(\boldsymbol{\Delta}) + f'(\omega, \boldsymbol{\Delta}) + if''(\omega, \boldsymbol{\Delta}). \qquad (4.2.6.21)$$

In the dipole approximation, it can be shown that

$$f'(\omega, 0) = \frac{2}{\pi}P\int_0^{\infty}\frac{\omega' f''(\omega', 0)}{\omega^2 - \omega'^2}\mathrm{d}\omega', \qquad (4.2.6.22)$$

which may be compared with equation (4.2.6.15) and

$$f''(\omega, 0) = \frac{\omega}{4\pi r_e c}\sigma(\omega), \qquad (4.2.6.23)$$

which may be compared with equation (4.2.6.14).

There is a direct correspondence between the predictions of the classical theory and the theory using second-order perturbation theory and non-relativistic quantum mechanics.

The extension of Hönl's (1933*a*,*b*) study of the scattering of X-rays by the K shell of atoms to other electron shells has been presented by Wagenfeld (1975).

In these calculations, the energy of the photon was assumed to be such that relativistic effects do not occur, nor do transitions within the discrete states of the atom occur. Transitions to continuum states do occur, and, using the analytical expressions for the wavefunctions of the hydrogen-like atom, analytical expressions may be developed for the photoelectric scattering cross sections. By expansion of the retardation factor $\exp(-i\mathbf{k}\cdot\mathbf{r})$ as the power series $1 - i\mathbf{k}\cdot\mathbf{r} - \frac{1}{2}(\mathbf{k}\cdot\mathbf{r})^2 + \ldots$, it is possible to determine dipolar, quadrupolar, and higher-order

terms in the analytical expression for the photoelectric scattering cross section.

The values of the cross section so obtained were used to calculate the values of $f'(\omega, \mathbf{\Delta})$ using the Kramers–Kronig transform [equation (4.2.6.22)] and $f''(\omega, \mathbf{\Delta})$ using equation (4.2.6.23). The work of Wagenfeld (1975) predicts that the values of $f'(\omega, \mathbf{\Delta})$ and $f''(\omega, \mathbf{\Delta})$ are functions of $\mathbf{\Delta}$. Whether or not this is a correct prediction will be discussed in Subsection 4.2.6.3.

Wang & Pratt (1983) have drawn attention to the importance of bound–bound transitions in the dispersion relation for the calculation of forward-scattering amplitudes. Their inclusion is especially important for elements with small atomic numbers. In a later paper, Wang (1986) has shown that, for silicon at the wavelengths of Mo $K\alpha$ and Ag $K\alpha_1$, values for $f'(\omega, 0)$ of 0.084 and 0.055, respectively, are obtained. These values should be compared with those listed in Table 4.2.6.4.

4.2.6.2.3. *Relativistic theories*

4.2.6.2.3.1. *Cromer and Liberman*: *relativistic dipole approach*

It is necessary to consider relativistic effects for atoms having all but the smallest atomic numbers. Cromer & Liberman (1970) produced a set of tables based on a relativistic approach to the scattering of photons by isolated atoms that was later reproduced in *IT* IV (1974). Subsequent experimental determinations drew attention to inaccuracies in these tables in the neighbourhood of absorption edges owing to the poor convergence of the Gaussian integration technique, which was used to evaluate the real part of the dispersion correction. In a later paper, Cromer & Liberman (1981) recalculated 34 instances for which the incident radiation lay close to the absorption edges of atoms using a modified integration procedure. Care should be exercised when using the Cromer & Liberman computer program, especially for calculations of $f'(\omega, 0)$ for high atomic weight elements at low photon energies. As Creagh (1990) and Chantler (1994) have shown, incorrect values of $f'(\omega, 0)$ can be calculated because an insufficient number of values of $f''(\omega, 0)$ are calculated prior to performing the Kramers–Kronig transform. In a new tabulation, Chantler (1995) presents the Cromer & Liberman data using a finer integrating grid. It should be noted that the relativistic correction is the same as that used in this tabulation.

These relativistic calculations are based on the scattering formula developed by Akhiezer & Berestetsky (1957) for the scattering amplitude for photons by a bound electron, *viz*:

$$S_{i\rightarrow f} = -2\pi i\delta(\varepsilon_1 + \hbar\omega_1 - \varepsilon_2 - \hbar\omega_2)\,\frac{4\pi(e\hbar c)^2}{2mc^2\hbar(\omega_1\omega_2)^{1/2}}\,f. \tag{4.2.6.24}$$

Here the angular frequencies of the incident and scattered photons are ω_1 and ω_2, respectively, and the initial and final energy states of the atom are ε_1 and ε_2, respectively. The scattering factor f is a complicated expression that includes the initial and final polarization states of the photon, the Dirac velocity operator, and the phase factors $\exp(i\mathbf{k}_1\cdot\mathbf{r})$ and $\exp(i\mathbf{k}_2\cdot\mathbf{r})$ for the incident and scattered waves, respectively. Summation is over all positive and negative intermediate states except those positive energy states occupied by other atomic electrons. The form of this expression is not easily related to the form-factor formalism that is most widely used by crystallographers, and a number of manipulations of the formula for the scattering factor are necessary to relate it more directly to the crystallographic formalism. In doing so, a number of assumptions and simplifications were made. Cromer & Liberman restricted their study to coherent, forward scatter in which changes in photon polarization did not occur. With these approximations, and using the electrical dipole approximation [$\exp(i\mathbf{k}\cdot\mathbf{r}) = 1$], they were able to show that

$$f(\omega, 0) = f(0) + f^+(\omega, 0) + \tfrac{5}{3}\frac{E_{\rm tot}}{mc^2} + if''(\omega, 0). \tag{4.2.6.25}$$

In equation (4.2.6.25), $f(0)$ is the atomic form factor for the case of forward scatter ($\mathbf{\Delta} = 0$), and the term $[+\frac{5}{3}(E_{\rm tot}/mc^2)]$ arises from the application of the dipole approximation to determine the contribution of bound electrons to the scattering process. The term $f''(\omega, 0)$ is related to the photoelectric scattering cross section expressed as a function of photon energy $\sigma(\hbar\omega)$ by

$$f''(\omega, 0) = \frac{mc}{4\pi\hbar e^2}\hbar\omega\,\sigma(\hbar\omega) \tag{4.2.6.26}$$

and

$$f^+(\omega, 0) = \left(\frac{1}{2\pi^2\hbar r_e c}\right)P\int_{mc^2}^{\infty}\frac{(\varepsilon^+ - \varepsilon_1)\sigma(\varepsilon + -\varepsilon_1)}{(\hbar\omega)^2 - (\varepsilon^+ - \varepsilon_1)^2}\,{\rm d}\varepsilon^+. \tag{4.2.6.27}$$

These equations may be compared with equations (4.2.6.23) and (4.2.6.22), respectively. But equation (4.2.6.25) differs from equation (4.2.6.21) by the term $\frac{5}{3}(E_{\rm tot}/mc^2)$, which is constant for each atomic species, and is related to the total Coulomb energy of the atom. Evidently, to keep the formalism the same, one must write

$$f'(\omega, 0) = f^+(\omega, 0) + \tfrac{5}{3}\frac{E_{\rm tot}}{mc^2}. \tag{4.2.6.28}$$

In Table 4.2.6.1, values of $E_{\rm tot}/mc^2$ are set out as a function of atomic number for elements ranging in atomic number from 3 to 98.

To develop their tables, Cromer & Liberman (1970) used the Brysk & Zerby (1968) computer code for the calculation of photoelectric cross sections, which was based on Dirac–Slater relativistic wavefunctions (Liberman, Waber & Cromer, 1965). They employed a value for the exchange potential of $0.667\rho(\mathbf{r})^{1/3}$ and experimental rather than computed values of the energy eigenvalues for the atoms.

The wide use of their tables by crystallographers inevitably meant that criticism of the accuracy of the tables was forthcoming on both theoretical and experimental grounds. Stibius-Jensen (1979) drew attention to the fact that the use of the dipole approximation too early in the argument caused an error of $-\frac{1}{2}Z(\hbar\omega/mc^2)^2$ in the tabulated values. More recently, Cromer & Liberman (1981) include this term in their calculations. Some experimental deficiencies of the tabulated values of $f'(\omega, 0)$ have been discussed by Cusatis & Hart (1977), Hart & Siddons (1981), Creagh (1980, 1984, 1985, 1986), Deutsch & Hart (1982), Dreier, Rabe, Malzfeldt & Niemann (1984), Bonse & Hartman-Lotsch (1984), and Bonse & Henning (1986).

In the latter two cases, the Kramers–Kronig transformation of photoelectric scattering results has been performed without taking into account the term that arises in the relativistic case for the total Coulomb energy of the atom. Although good agreement with the Cromer & Liberman tables is claimed, their failure to include this term is an implied criticism of the Cromer & Liberman tables. That this is unjustified can be seen by references to Fig. 4.2.6.2 taken from Bonse & Henning (1986), which shows that their interferometer results [which measure $f'(\omega, 0)$ directly] and the Kramers–Kronig results differ

from one another by $\sim E_{\rm tot}/mc^2$ in the neighbourhood of the *K*-absorption edge of niobium in the compound lithium niobate.

Further theoretical objections have been made by Creagh (1984) and Smith (1987), who has shown that the Stibius-Jensen correction is not valid, and that, when higher-order multipolar expansions and retardation are considered, the total self-energy correction becomes $E_{\rm tot}/mc^2$ rather than $\frac{5}{3}E_{\rm tot}/mc^2$. Fig. 4.2.6.1 shows the variation of the self-energy correction with atomic number for the modified form factor (Creagh, 1984; Smith, 1987; Cromer & Liberman, 1970).

For the imaginary part of the dispersion correction $f''(\omega, 0)$, which depends on the calculation of the photoelectric scattering cross section, better agreement is found between theoretical results and experimental data. Details of this comparison have been given elsewhere (Section 4.2.4). Suffice it to say that Creagh & Hubbell (1990), in reporting the results of the IUCr X-ray Attenuation Project, could find no rational basis for preferring the Scofield (1973) Hartree–Fock calculations to the Cromer & Liberman (1970, 1981) and Storm & Israel (1970) Dirac–Hartree–Fock–Slater calculations.

Computer programs based on the Cromer & Liberman program (Cromer & Liberman, 1983) are in use at all the major synchrotron-radiation laboratories. Many other laboratories have also acquired copies of their program. This program must be modified to remove the incorrect Stibius–Jensen correction term, and, as will be seen later, the energy term should be modified to be $E_{\rm tot}/mc^2$.

Table 4.2.6.1. *Values of E_{tot}/mc^2 listed as a function of atomic number Z*

Z	Symbol	$E_{\rm tot}/mc^2$
3	Li	−0.0004
4	Be	−0.0006
5	B	−0.0012
6	C	−0.0018
7	N	−0.0030
8	O	−0.0042
9	F	−0.0054
10	Ne	−0.0066
11	Na	−0.0084
12	Mg	−0.0110
13	Al	−0.0125
14	Si	−0.0158
15	P	−0.0180
16	S	−0.0210
17	Cl	−0.0250
18	Ar	−0.0285
19	K	−0.0320
20	Ca	−0.0362
21	Sc	−0.0410
22	Ti	−0.0460
23	V	−0.0510
24	Cr	−0.0560
25	Mn	−0.0616
26	Fe	−0.0680
27	Co	−0.0740
28	Ni	−0.0815
29	Cu	−0.0878
30	Zn	−0.0960
31	Ga	−0.104
32	Ge	−0.114
33	As	−0.120
34	Se	−0.132
35	Br	−0.141
36	Kr	−0.150
37	Rb	−0.159
38	Sr	−0.171
39	Y	−0.180
40	Zr	−0.192
41	Nb	−0.204
42	Mo	−0.216
43	Tc	−0.228
44	Ru	−0.246
45	Rh	−0.258
46	Pd	−0.270
47	Ag	−0.285
48	Cd	−0.300
49	In	−0.318
50	Sn	−0.330
51	Sb	−0.348
52	Te	−0.363
53	I	−0.384
54	Xe	−0.396
55	Cs	−0.414
56	Ba	−0.438
57	La	−0.456
58	Ce	−0.474
59	Pr	−0.492
60	Nd	−0.516
61	Pm	−0.534
62	Sm	−0.558
63	Eu	−0.582
64	Gd	−0.610
65	Tb	−0.624
66	Dy	−0.648
67	Ho	−0.672
68	Er	−0.696
69	Tm	−0.723
70	Yb	−0.750
71	Lu	−0.780
72	Hf	−0.804
73	Ta	−0.834
74	W	−0.864
75	Re	−0.900
76	Os	−0.919
77	Ir	−0.948
78	Pt	−0.984
79	Au	−1.014
80	Hg	−1.046
81	Tl	−1.080
82	Pb	−1.116
83	Bi	−1.149
84	Po	−1.189
85	At	−1.224
86	Rn	−1.260
87	Fr	−1.296
88	Ra	−1.332
89	Ac	−1.374
90	Th	−1.416
91	Pa	−1.458
92	U	−1.470
93	Np	−1.536
94	Pu	−1.584
95	Am	−1.626
96	Cm	−1.669
97	Bk	−1.716
98	Cf	−1.764

4.2.6.2.3.2. *The scattering matrix formalism*

Kissel, Pratt & Roy (1980) have developed a computer program based on the second-order *S*-matrix formalism suggested by Brown, Peierls & Woodward (1955). Their aim was to provide a prescription for the accurate ($\sim$1%) prediction of the total-atom Rayleigh scattering amplitudes.

Their model treats the elastic scattering as the sum of bound electron, nuclear, and Delbrück scattering cross sections, and treats the Rayleigh scattering by considering second-order, single-electron transitions from electrons bound in a relativistic, self-consistent, central potential. This potential was a Dirac–Hartree–Fock–Slater potential, and exchange was included by use of the Kohn & Sham (1965) exchange model. They omitted radiative corrections.

In principle, the observables in an elastic scattering process are momentum ($\hbar\mathbf{k}$) and polarization $\boldsymbol{\varepsilon}$. The complex polarization vectors $\boldsymbol{\varepsilon}$ satisfy the conditions

$$\boldsymbol{\varepsilon}^* \cdot \boldsymbol{\varepsilon} = 1'; \quad \boldsymbol{\varepsilon} \cdot \mathbf{k} = 0. \tag{4.2.6.29}$$

In quantum mechanics, elastic scattering is described in terms of a differential scattering amplitude, M, which is related to the elastic cross section by equation (4.2.6.16).

If polarization is not an observable, then the expression for the differential scattering cross section takes the form of equation (4.2.6.17). If polarization is taken into account, as may be the case when a polarizer is used on a beam scattered from a sample irradiated by the linearly polarized beam from a synchrotron-radiation source, the full equation, and not equation (4.2.6.17), must be used to compute the differential scattering cross section.

The principle of causality implies that the forward-scattering amplitude $M(\omega, 0)$ should be analytic in the upper half of the ω plane, and that the dispersion relation

$$\text{Re } M(\omega, 0) = \frac{2\omega^2}{\pi} \int_0^\infty \frac{\text{Im } M(\omega', 0)}{\omega'(\omega'^2 - \omega^2)} \text{d}\omega' \tag{4.2.6.30}$$

should hold, with the consequence that

$$\text{Re } M(\infty, 0) = -\frac{2}{\pi} \int_0^\infty \frac{\text{Im } M(\omega', 0)}{\omega'} \text{d}\omega'. \tag{4.2.6.31}$$

This may be rewritten as

$$M(\omega, 0) - M(\infty, 0) = f'(\omega, 0) + if''(\omega, 0), \qquad (4.2.6.32)$$

with the value of $f'(\omega, 0)$ defined by equation (4.2.6.15). Using the conservation of probability,

$$\text{Im } M(\omega, 0) = \frac{\omega}{4\pi r_e c}\sigma_{\text{tot}}, \qquad (4.2.6.33)$$

which is to be compared with equation (4.2.6.23).

Starting with Furry's extension of the formalism of quantum mechanics proposed by Feynman and Dyson, the total Rayleigh amplitude may be written as

$$M_n = \sum_p \left[\frac{\langle n|T_1^*|p\rangle\langle p|T_1|n\rangle}{E_n - E_p + \hbar\omega} + \frac{\langle n|T_2|p\rangle\langle n|T_2^*|p\rangle}{E_n - E_p + \hbar\omega} \right], \qquad (4.2.6.34)$$

where

$$T_1 = \boldsymbol{\alpha} \cdot \boldsymbol{\varepsilon}_i \cdot \exp(i\mathbf{k}_i \cdot \mathbf{r})$$

and

$$T_2 = \boldsymbol{\alpha} \cdot \boldsymbol{\varepsilon}_f^* \cdot \exp(-i\mathbf{k}_f \cdot \mathbf{r}).$$

The $|p\rangle$ are the complete set of bound and continuum states in the external field of the atomic potential. Singularities occur at all photon energies that correspond to transitions between bound $|n\rangle$ and bound state $|p\rangle$. These singularities are removed if the finite widths of these states are considered, and the energies E are replaced by $iE\Gamma/2$, where Γ is the total (radiative plus non-radiative) width of the state (Gavrila, 1981). By use of the formalism suggested by Brown *et al.* (1955), it is possible to reduce the numerical problems to one-dimensional radial integrals and differential equations. The required multipole expansions of T_1 and the specification of the radial perturbed orbitals that are characterized by angular-momentum quantum numbers have been discussed by Kissel (1977). Ultimately, all the angular dependence on the photon scattering angle is written in terms of the associated Legendre functions, and all the energy dependence is in terms of multipole amplitudes.

Solutions are not found for the inhomogeneous radial wave equations, and Kissel (1977) expressed the solution as the linear sum of two solutions of the homogeneous equation, one of which was regular at the origin and the other regular at infinity.

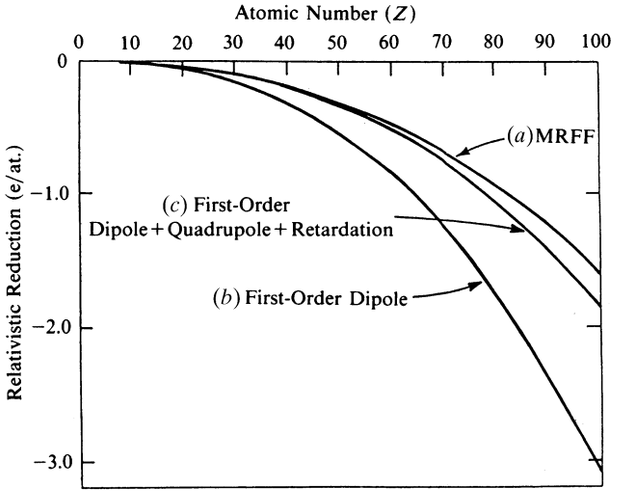

Fig. 4.2.6.1. The relativistic correction in electrons per atom for: (*a*) the modified form-factor approach; (*b*) the relativistic multipole approach; (*c*) the relativistic dipole approach.

Because excessive amounts of computer time are required to use these direct techniques for calculating the amplitudes from all the subshells, simpler methods are usually used for calculating outer-shell amplitudes. Kissel & Pratt (1985) used estimates for outer-shell amplitudes based on the predictions of the modified form-factor approach. A tabulation of the modified relativistic form factors has been given by Schaupp, Schumacher, Smend, Rullhusen & Hubbell (1983).

Because of the generality of their approach, the computer time required for the calculation of the scattering amplitudes for a particular energy is quite long, so that relatively few calculations have been made. Their approach, however, does not confine itself solely to the problem of forward scattering of photons as does the Cromer & Liberman (1970) approach. Using their model, Kissel *et al.* (1980) have been able to show that it is incorrect to assign a dependence of the dispersion corrections on the scattering vector $\boldsymbol{\Delta}$. This is at variance with some established crystallographic practices, in which the dispersion corrections are accorded the same dependence on $\boldsymbol{\Delta}$ as $f_0(\boldsymbol{\Delta})$, and also at

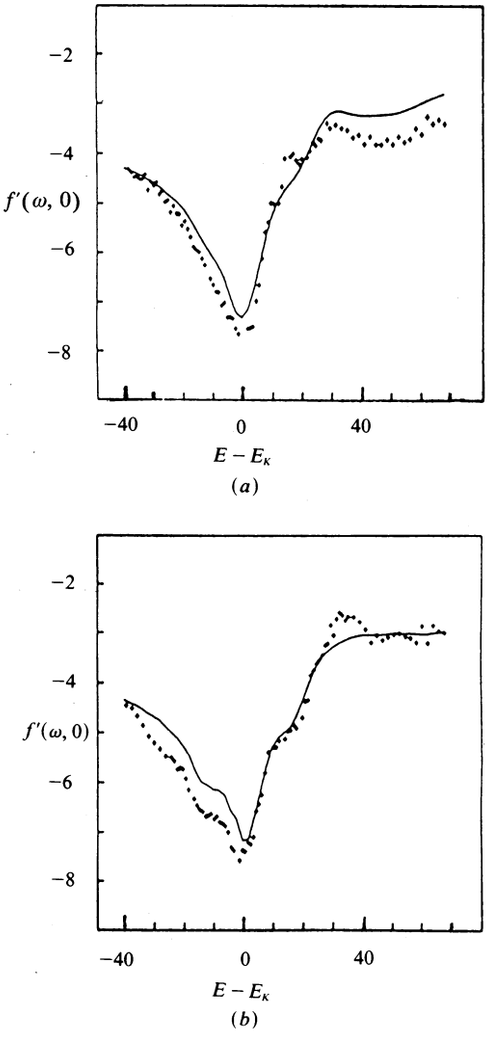

Fig. 4.2.6.2. Measured values of $f'(\omega, 0)$ at the *K*-edge of Nb in $LiNbO_3$ and the Kramers–Kronig transformation of $f''(\omega, 0)$. The curve is obtained by transformation and the points are measured by interferometry. For (*a*), the polarization of the incident radiation is parallel to the hexagonal *c* axis, and for (*b*) it is at right angles to the hexagonal *c* axis. After Bonse & Henning (1986). Note that the distortion of the dispersion curve is due to X-ray absorption near-edge structure (XANES) effects (Section 4.2.4).

variance with the predictions of Wagenfeld's (1975) non-relativistic model.

4.2.6.2.4. *Intercomparison of theories*

A discussion of the validity of the non-relativistic dipole approximation for the calculation of forward Rayleigh scattering amplitudes has been given by Roy & Pratt (1982). They compared their relativistic multipole calculations with the relativistic dipole approximation and with the non-relativistic dipole approximation for two elements, silver and lead. They concluded that a relativistic correction to the form factor of order $(Z\alpha)^2$ persists in the high-energy limit, and that this constant correction accounts for much of the deviation from the non-relativistic dipole approximation at all energies above threshold. In addition, their results illustrate that cancelling occurs amongst the relativistic, retardation, and higher multipole contributions to the scattering amplitude. This implies that care must be taken in assessing where to terminate the series that describes the multipolarity of the scattering process.

In a later paper, Roy, Kissel & Pratt (1983) discussed the elastic photon scattering for small momentum transfers and the validity of the form-factor theories. In this paper, which compares the relativistic modified form factor with experimental results for lead and a relativistic form factor and the tabulation by Hubbell, Veigele, Briggs, Brown, Cromer & Howerton (1975), it is shown that the modified relativistic form-factor approach gives better agreement with experiment for high momentum transfers ($<104\,\text{Å}^{-1}$) than the non-relativistic, form-factor theories.

Kissel *et al*. (1980) used the *S*-matrix technique to calculate the real part of the forward-scattering amplitude $f'(\omega, 0)$ for the inert gases at the wavelength of Mo $K\alpha_1$. These values are compared with the predictions of the relativistic dipole theory (RDP) and the relativistic multipole theory (RMP) in Table 4.2.6.2(*a*). In most cases, the agreement between the *S* matrix and the RMP theory is excellent, considering the differences in the methodology of the two sets of calculations. Table 4.2.6.2(*b*) shows comparisons of the real part of the forward-scattering amplitude $f''(\omega, 0)$ calculated for the atoms aluminium, silicon, zinc, germanium, silver, samarium, tantalum and lead using the approach of Kissel *et al*. (1980) with that of Cromer & Liberman (1970, 1981), with tabulations by Wagenfeld (1975), and with values taken from the tables in this section. Although reasonably satisfactory agreement exists between the relativistic values, large differences exist between the non-relativistic value (Wagenfeld, 1975) and the relativistic values. The major difference between the relativistic values occurs because of differences in estimation of the self-consistent-field term, which is proportional to E_{tot}/mc^2. The Cromer & Liberman (1970) relativistic dipole value is $+\frac{5}{3}(E_{\text{tot}}/mc^2)$, whereas the tabulation in this section uses the relativistic multipole value of $(+E_{\text{tot}}/mc^2)$. This causes a vertical shift of the curve, but does not alter its shape. Should better estimates of the self-energy term be found, the correction is simply that of adding a constant to each value of $f'(\omega, 0)$ for each atomic species. There is a significant discrepancy between the Kissel *et al*. (1980) result for ^{62}Sm and the other theoretical values. This is the only major point of difference, however, and the results are better in accord with the relativistic multipole approach than with the relativistic dipole approach. Note that the relativistic multipole approach does not include the Stibius-Jensen correction, which alters the shape of the curve.

In §4.2.6.3.3, some examples are given to illustrate the extent to which predictions of these theories agree with experimental data for $f'(\omega, 0)$.

That there is little to choose between the different theoretical approaches where the calculation of $f''(\omega, 0)$ is concerned is illustrated in Table 4.2.6.3. In most cases, the agreement between the scattering matrix, relativistic dipole, and relativistic multipole values is within 1%. In contrast, there are some significant differences between the relativistic and the non-relativistic values of $f''(\omega, 0)$. The extent of the discrepancies is greater the higher the atomic number, as one might expect from the assumptions made in the formulation of the non-relativistic model. Some detailed comparisons of theoretical and experimental data for linear attenuation coefficients [proportional to $f''(\omega, 0)$] have been given by Creagh & Hubbell (1987) for silicon, and for copper and carbon by Gerward (1982, 1983). These tend to confirm the assertion that, at the 1% level of accuracy, there is little to choose between the various relativistic models for computing scattering cross sections.

Further discussion of this is given in §4.2.6.3.3.

4.2.6.3. *Modern experimental techniques*

The atomic scattering factor enters directly into expressions for such macroscopic material properties as the *refractive index*, n, and the *linear attenuation coefficient*, μ_l. The refractive index depends on the dielectric susceptibility χ through

$$n = (1 + \chi)^{1/2}, \tag{4.2.6.35}$$

where

$$\chi = -\frac{r_e\lambda^2}{\pi}\sum_j N_j f_j(\omega, \mathbf{\Delta}) \tag{4.2.6.36}$$

and N_j is the number density of atoms of type j.

The imaginary part of the dispersion correction $f''(\omega, \mathbf{\Delta})$ for the case where $\mathbf{\Delta} = 0$ is related to the atomic scattering cross section through equation (4.2.6.23).

Experimental techniques that measure refractive indices or X-ray attenuation coefficients to determine the dispersion corrections involve measurements for which the scattering vector, $\mathbf{\Delta}$, is zero or close to it. Data from these experiments may be compared *directly* with data sets such as Cromer & Liberman (1970, 1981).

Other techniques measure the intensities of Bragg reflections from crystalline materials or the variation of intensities within one particular Laue reflection (*Pendellösung*). For these cases, $\mathbf{\Delta} = g_{hkl}$, the reciprocal-lattice vector for the reflection or reflections measured. These techniques can be compared only indirectly with existing relativistic tabulations, since these have been developed for the $\mathbf{\Delta} = 0$ case. Data are available for elements having atomic numbers less than 20 in the non-relativistic case (Wagenfeld, 1975).

The following sections will discuss some modern techniques for the measurement of dispersion corrections, and an intercomparison will be made between experimental data and theoretical calculations for a representative selection of atoms and at two extremes of photon energies: near to and remote from an absorption edge of those atoms.

4.2.6.3.1. *Determination of the real part of the dispersion correction*: $f'(\omega, 0)$

X-ray interferometer techniques are now used extensively for the measurement of the refractive index of materials and hence

Table 4.2.6.2(*a*). *Comparison between the S-matrix calculations of Kissel (K) (1977) and the form-factor calculations of Cromer & Liberman (C & L) (1970, 1981, 1983) and Creagh & McAuley (C & M) for the noble gases and several common metals; $f'(\omega, 0)$ values are given for two frequently used photon energies*

Energy (keV)	Element	RDP (C & L)	*S* matrix (*K*)	RMP (C & M)
17.479 (Mo $K\alpha_1$)	Ne	0.021	0.024	0.026
	Ar	0.155	0.170	0.174
	Kr	−0.652	−0.478	−0.557
	Xe	−0.684	−0.416	−0.428
22.613 (Ag $K\alpha_1$)	Al	0.032	0.039	0.041
	Zn	0.260	0.323	0.324
	Ta	−0.937	−0.375	−0.383
	Pb	−1.910	−1.034	−1.162

$f'(\omega, 0)$. All the interferometers are transmission-geometry LLL devices (Bonse & Hart, 1965, 1966*a*,*b*,*c*,*d*, 1970), and initially they were used to measure the X-ray refractive indices of such materials as the alkali halides, beryllium and silicon using the characteristic radiation emitted by sealed X-ray tubes. Measurements were made for such characteristic emissions as Ag $K\alpha_1$, Mo $K\alpha_1$, Cu $K\alpha_1$ and Cr $K\alpha_1$ by a variety of authors (Creagh & Hart, 1970; Creagh, 1970; Bonse & Hellkötter, 1969; Bonse & Materlik, 1972).

The ready availability of synchrotron-radiation sources led to the adaptation of the simple LLL interferometers to use this new radiation source. Bonse & Materlik (1975) reported measurements at DESY, Hamburg, made with a temporary adaptation of a diffraction-beam line. Recent advances in X-ray interferometry have led to the establishment of a permanent interferometer station at DESY (Bonse, Hartmann-Lotsch & Lotsch, 1983*b*). This, and many of the earlier interferometers invented by Bonse, makes its phase measurements by the rotation of a phase-shifting plate in the beams emanating from the first wafer of the interferometer.

In contrast, the LLL interferometer designed by Hart (1968) uses the movement of the position of lattice planes in the third wafer of the interferometer relative to the standing-wave field formed by the recombination of two of the diffracted beams within the interferometer. Measurements made with and without the specimen in position enabled both the refractive index and the linear attenuation coefficient to be determined. The use of energy-dispersive detection meant that these parameters could be determined for harmonics of the fundamental frequency to which the interferometer was tuned (Cusatis & Hart, 1975, 1977). Subsequently, measurements have been made by Siddons & Hart (1983) and Hart & Siddons (1981) for zirconium, niobium, nickel, and molybdenum. Hart (1985) planned to provide detailed dispersion curves for a large number of elements capable of being rolled into thin foils.

Both types of interferometers have yielded data of high quality, and accuracies better than 0.2 electrons have been claimed for measurements of $f'(\omega, 0)$ in the neighbourhood of the *K*- and *L*-absorption edges of a number of elements. The energy window has been claimed to be as low as 0.3 eV in width. However, on the basis of the measured values, it would seem that the width of the energy window is more likely to be about 2 eV for a primary wavelength of 5 keV.

Table 4.2.6.2(*b*). *A comparison of the real part of the forward-scattering amplitudes computed using different theoretical approaches: KPR (Kissel et al., 1980); C & L (Cromer & Liberman, 1970, 1981); W (Wagenfeld, 1975); and C & M (this data set)*

		$f'(\omega, 0)$				
			C & L			
Atom	Radiation	KPR	1970	1981	*W*	C & M
^{13}Al	Cr $K\alpha_1$	13.320	13.328	13.316	13.376	13.326
	Cu $K\alpha_1$	13.209	13.204	13.203	13.235	13.213
	Ag $K\alpha_1$	13.039	13.032	13.020	13.078	13.041
^{14}Si	Cr $K\alpha_1$		14.333	14.354	14.441	14.365
	Cu $K\alpha_1$		14.244	14.242	14.282	14.254
	Ag $K\alpha_1$		14.042	14.029	14.071	14.052
^{30}Zn	Cr $K\alpha_1$	29.161	29.316	29.314		29.383
	Cu $K\alpha_1$	28.369	28.388	28.383		28.451
	Ag $K\alpha_1$	30.323	30.260	30.232		30.324
^{32}Ge	Cr $K\alpha_1$		31.538	31.538	30.20	31.614
	Cu $K\alpha_1$		30.837	30.837	31.92	30.911
	Ag $K\alpha_1$		32.228	32.228	32.14	32.302
^{47}Ag	Cu $K\alpha_1$	47.075	46.940	46.936		47.131
^{62}Sm	Ag $K\alpha_1$	58.307	56.304	56.299		56.676
^{73}Ta	Ag $K\alpha_1$	72.625	72.063	71.994		72.617
^{82}Pb	Ag $K\alpha_1$	80.966	80.090	80.012		80.832

Apparently, the ångström-ruler design is the better of the two interferometer types, since the interferometer to be mounted at the EU storage ring is to be of this type (Buras & Tazzari, 1985).

Interferometers of this type have the advantage of enabling direct measurements of both refractive index and linear attenuation coefficients to be made. The determination of the energy scale and the assessment of the energy bandpass of such a system are two factors that may influence the accuracy of this type of interferometer.

One of the oldest techniques for determining refractive indices derives from measurement of the deviation produced when a prism of the material under investigation is placed in the photon beam. Recently, a number of groups have used this technique to determine the X-ray refractive index, and hence $f'(\omega, 0)$.

Deutsch & Hart (1984*a*,*b*) have designed a novel double-crystal transmission spectrometer for which they were able to detect to high accuracy the angular rotation of one element with respect to the other by reference to the *Pendellösung* maxima that are observed in the wave field of the primary wafer. In this second paper, data gained for beryllium and lithium fluoride wedges are discussed.

Several Japanese groups have used more conventional monochromator systems having Bragg-reflecting optics to determine the refractive indices of a number of materials. Hosoya, Kawamure, Hunter & Hakano (1978; cited by Bonse & Hartmann-Lotsch, 1984) made determinations of $f'(\omega, 0)$ in the region of the *K*-absorption edge for copper. More recently, Ishida & Katoh (1982) have described the use of a multiple-reflection diffractometer for the determination of X-ray refrac-

Table 4.2.6.3. *A comparison of the imaginary part of the forward-scattering amplitudes $f''(\omega, 0)$ computed using different theoretical approaches: KPR (Kissel et al., 1980); C & L (Cromer & Liberman, 1981); W (Wagenfeld, 1975); and C & M (this data set)*

Atom	Radiation	$f'(\omega, 0)$			
		KPR	C & L	*W*	C & M
^{13}Al	Cr $K\alpha_1$	0.514	0.522		0.512
	Cu $K\alpha_1$	0.243	0.246		0.246
	Ag $K\alpha_1$	0.031	0.031		0.031
^{14}Si	Cr $K\alpha_1$		0.694	0.70	0.692
	Cu $K\alpha_1$		0.330	0.33	0.330
	Ag $K\alpha_1$		0.043	0.047	0.043
^{30}Zn	Cr $K\alpha_1$	1.370	1.373		1.371
	Cu $K\alpha_1$	0.678	0.678		0.678
	Ag $K\alpha_1$	0.932	0.938		0.938
^{32}Ge	Cr $K\alpha_1$		1.786	1.84	1.784
	Cu $K\alpha_1$		0.886	0.87	0.886
	Ag $K\alpha_1$		1.190	1.23	1.190
^{47}Ag	Cu $K\alpha_1$	4.242	4.282		4.282
^{62}Sm	Cu $K\alpha_1$	12.16	12.218		12.218
^{73}Ta	Ag $K\alpha_1$	4.403	4.399		4.399
^{82}Pb	Ag $K\alpha_1$	6.937	6.929		6.929

tive indices. Later, Katoh *et al*. (1985*a*,*b*) described its use for the measurement of $f'(\omega, 0)$ for lithium fluoride and potassium chloride at a wavelength near that of Mo $K\alpha_1$ and for germanium in the neighbourhood of its *K*-absorption edge.

Measurements of the linear attenuation coefficient μ_l over an extended energy range can be used as a basis for the determination of the real part of the dispersion correction $f'(\omega, 0)$ because of the Kramers–Kronig relation, which links $f'(\omega, 0)$ and $f''(\omega, 0)$. However, as Creagh (1980) has pointed out, even if the integration can be performed accurately [implying the knowledge of $f''(\omega, 0)$ over several decades of photon energies and the exact energy at which the absorption edge occurs], there will still be some ambiguity in the result because there still has to be the inclusion of the appropriate relativistic correction term.

The experimental procedures that must be adopted to ensure that the linear attenuation coefficients are measured correctly have been given in Subsection 4.2.3.2. One other problem that must be addressed is the accuracy to which the photon energy can be measured. Accuracy in the energy scale becomes paramount in the neighbourhood of an absorption edge where large variations in $f'(\omega, 0)$ occur for very small changes in photon energy $\hbar\omega$.

Despite these difficulties, Creagh (1977, 1978, 1982) has used the technique to determine $f'(\omega, 0)$ and $f''(\omega, 0)$ for several alkali halides and Gerward, Thuesen, Stibius-Jensen & Alstrup (1979) used the technique to measure these dispersion corrections for germanium. More recently, the technique has been used by Dreier *et al*. (1984) to determine $f'(\omega, 0)$ and $f''(\omega, 0)$ for a number of transition metals and rare-earth atoms. The experimental configuration used by them was a conventional XAFS system. Similar techniques have been used by Fuoss & Bienenstock (1981) to study a variety of amorphous materials in the region of an absorption edge.

Henke *et al*. (1982) used the Kramers–Kronig relation to compute the real part of the dispersion correction for most of the atoms in the Periodic Table, given their measured scattering cross sections. This data set was computed specifically for the soft X-ray region ($\hbar\omega < 1.5$ keV).

Linear attenuation coefficient measurements yield $f'(\omega, 0)$ directly and $f''(\omega, 0)$ indirectly through use of the Kramers–Kronig integral. Data from these experiments do not have the reliability of those from refractive-index measurements because of the uncertainty in knowing the correct value for the relativistic correction term.

None of the previous techniques is useful for small photon energies. These photons would experience considerable attenuation in traversing both the specimen and the experimental apparatus. For small photon energies or large atomic numbers, reflection techniques are used, the most commonly used technique being that of total external reflection. As Henke *et al*. (1982) have shown, when reflection occurs at a smooth (vacuum–material) interface, the refractive index of the reflecting material can be written as a single complex constant, and measurement of the angle of total external reflection may be related directly to the refractive index and therefore to $f'(\omega, \mathbf{\Delta})$. Because the X-ray refractive indices of materials are only slightly less than unity, the scattering wavevector $\mathbf{\Delta}$ is small, and the scattering angle is only a few degrees in magnitude. Assuming that there is not a strong dependence of $f'(\omega, \mathbf{\Delta})$ with $\mathbf{\Delta}$, one may consider that this technique provides an estimate of $f'(\omega, 0)$ for a photon energy range that cannot be surveyed using more precise techniques. A recent review of the use of reflectometers to determine $f'(\omega, 0)$ has been given by Lengeler (1994).

4.2.6.3.2. *Determination of the real part of the dispersion correction*: $f'(\omega, \mathbf{\Delta})$

This classification includes those experiments in which measurements of the geometrical structure factors F_{hkl} for various Bragg reflections are undertaken. Into this category fall those techniques for which the period of standing-wave fields (*Pendellösung*) and reflectivity of perfect crystals in Laue or Bragg reflection are measured. Also included are those techniques from which the atomic scattering factors are inferred from measurements of Bijvoet- or Friedel-pair intensity ratios for noncentrosymmetric crystal structures.

4.2.6.3.2.1. *Measurements using the dynamical theory of X-ray diffraction*

The development of the dynamical theory of X-ray diffraction (see, for example, Section 5 in *IT* B, 1995) and recent advances in techniques for crystal growth have enabled experimentalists to determine the geometrical structure factor F_{hkl} for a variety of materials by measuring the spacing between minima in the internal standing wave fields within the crystal (*Pendellösung*).

Two classes of *Pendellösung* experiment exist: those for which the ratio $(\lambda/\cos\theta)$ is kept constant and the thickness of the samples varies; and those for which the specimen thickness remains constant and $(\lambda/\cos\theta)$ is allowed to vary.

Of the many experiments performed using the former technique, measurements by Aldred & Hart (1973*a*,*b*) for

silicon are thought to be the most accurate determinations of the atomic form factor $f(\omega, \mathbf{\Delta})$ for that material. From these data, Price, Maslen & Mair (1978) were able to refine values of $f'(\omega, \mathbf{\Delta})$ for a number of photon energies. Recently, Deutsch & Hart (1985) were able to extend the determination of the form factor to higher values of momentum transfer ($\hbar\mathbf{\Delta}$). This technique requires for its success the availability of large, strain-free crystals, which limits the range of materials that can be investigated.

A number of experimentalists have attempted to measure *Pendellösung* fringes for parallel-sided specimens illuminated by white radiation, usually from synchrotron-radiation sources. [See, for example, Hashimoto, Kozaki & Ohkawa (1965) and Aristov, Shmytko & Shulakov (1977).] A technique in which the *Pendellösung* fringes are detected using a solid-state detector has been reported by Takama, Kobayashi & Sato (1982). Using this technique, Takama and his co-workers have reported measurements for silicon (Takama, Iwasaki & Sato, 1980), germanium (Takama & Sato, 1984), copper (Takama & Sato, 1982), and aluminium (Takama, Kobayashi & Sato, 1982). A feature of this technique is that it can be used with small crystals, in contrast to the first technique in this section. However, it does not have the precision of that technique.

Another technique using the dynamical theory of X-ray diffraction determines the integrated reflectivity for a Bragg-case reflection that uses the expression for integrated reflectivity given by Zachariasen (1945). Using this approach, Freund (1975) determined the value of the atomic scattering factor $f(\omega, \mathbf{g}_{222})$ for copper. Measurements of intensity are difficult to make, and this method is not capable of yielding results having the precisions of the *Pendellösung* techniques.

4.2.6.3.2.2. *Friedel- and Bijvoet-pair techniques*

The Bijvoet-pair technique (Bijvoet *et al.*, 1951) is used extensively by crystallographers to assist in the resolution of the phase problem in the solution of crystal structures. Measurements of as many as several hundred values for the diffracted intensities I_{hkl} for a crystal may be made. When these are analysed, the Cole & Stemple (1962) observation that the ratio of the intensities scattered in the Bijvoet or Friedel pair is independent of the state of the crystal is assumed to hold. This is a necessary assumption since in a large number of structure analyses radiation damage occurs during the course of an experiment.

For simple crystal structures, Hosoya (1975) has outlined a number of ways in which values of $f'(\omega, \mathbf{g}_{hkl})$ and $f''(\omega, \mathbf{g}_{hkl})$ may be extracted from the Friedel-pair ratios. Measurements of these corrections for atoms such as gallium, indium, arsenic and selenium have been made.

In more complicated crystal structures for which the positional parameters are known, attempts have been made to determine the anomalous-scattering corrections by least-squares-refinement techniques. Measurements of these corrections for a number of atoms have been made, *inter alia*, by Engel & Sturm (1975), Templeton & Templeton (1978), Philips, Templeton, Templeton & Hodgson (1978), Templeton, Templeton, Philips & Hodgson (1980), Philips & Hodgson (1985), and Chapuis, Templeton & Templeton (1985). There are a number of problems with this approach, not the least of which are the requirement to measure intensities accurately for a large period of time and the assumption that specimen perfection does not affect the intensity ratio. Also, factors such as crystal shape and primary and secondary extinction may adversely affect the ability to measure intensity ratios correctly. One problem that has to be addressed in this type of determination is the fact that $f'(\omega, 0)$ and $f''(\omega, 0)$ are related to one another, and cannot be refined separately.

4.2.6.3.3. *Comparison of theory with experiment*

In this section, discussion will be focused on (i) the scattering of photons having energies considerably greater than that of the *K*-absorption edge of the atom from which they are scattered, and (ii) scattering of photons having energies in the neighbourhood of the *K*-absorption edge of the atom from which they are scattered.

4.2.6.3.3.1. *Measurements in the high-energy limit* $(\omega/\omega_\kappa \rightarrow 0)$

In this case, there is some possibility of testing the validity of the relativistic dipole and relativistic multipole theories since, in the high-energy limit, the value of $f'(\omega, 0)$ must approach a value related to the total self energy of the atom ($E_{\rm tot}/mc^2$). That there is an atomic number dependent systematic error in the relativistic dipole approach has been demonstrated by Creagh (1984). The question of whether the relativistic multipole approach yields a result in better accord with the experimental data is answered in Table 4.2.6.4, where a comparison of values of $f'(\omega, 0)$ is made for three theoretical data sets (this work; Cromer & Liberman, 1981; Wagenfeld, 1975) with a number of experimental results. These include the 'direct' measurements using X-ray interferometers (Cusatis & Hart, 1975; Creagh, 1984), the Kramers–Kronig integration of X-ray attenuation data (Gerward *et al.*, 1979), and the angle-of-the-prism data of Deutsch & Hart (1984*b*). Also included in the table are 'indirect' measurements: those of Price *et al.* (1978), based on *Pendellösung* measurements, and those of Grimvall & Persson (1969). These latter data estimate $f'(\omega, \mathbf{g}_{hkl})$ and not $f'(\omega, 0)$. Table 4.2.6.4 details values of the real part of the dispersion correction for LiF, Si, Al and Ge for the characteristic wavelengths Ag $K\alpha_1$, Mo $K\alpha_1$ and Cu $K\alpha_1$. Of the atomic species listed, the first three are approaching the high-energy limit at Ag $K\alpha_1$, whilst for germanium the *K*-shell absorption edge lies between Mo $K\alpha_1$ and Ag $K\alpha_1$.

The high-energy-limit case is considered first: both the relativistic dipole and relativistic multipole theories underestimate $f'(\omega, 0)$ for LiF whereas the non-relativistic theory overestimates $f'(\omega, 0)$ when compared with the experimental data. For silicon, however, the relativistic multipole yields values in good agreement with experiment. Further, the values derived from the work of Takama *et al.* (1982), who used a *Pendellösung* technique to measure the atomic form factor of aluminium are in reasonable agreement with the relativistic multipole approach. Also, some relatively imprecise measurements by Creagh (1985) are in better accordance with the relativistic multipole values than with the relativistic dipole values.

Further from the high-energy limit (smaller values of ω/ω_κ), the relativistic multipole approach appears to give better agreement with theory. It must be reported here that measurements by Katoh *et al.* (1985*a*) for lithium fluoride at a wavelength of 0.77366 Å yielded a value of 0.018 in good agreement with the relativistic multipole value 0.017.

At still smaller values of (ω/ω_κ), the non-relativistic theory yields values considerably at variance with the experimental data, except for the case of LiF using Cu $K\alpha_1$ radiation. The relativistic multipole approach seems, in general, to be a little better than the relativistic approach, although agreement between experiment and theory is not at all good for germanium. Neither

of the experiments cited here, however, has claims to high accuracy.

In Table 4.2.6.5, a comparison is made of measurements of $f''(\omega, 0)$ derived from the results of the IUCr X-ray Attenuation Project (Creagh & Hubbell, 1987, 1990) with a number of theoretical predictions. The measurements were made on carbon, silicon and copper specimens at the characteristic wavelengths Cu $K\alpha_1$, Mo $K\alpha_1$ and Ag $K\alpha_1$. The principal conclusion that can be drawn from perusal of Table 4.2.6.5 is that only minor, non-systematic differences exist between the predictions of the several relativistic approaches and the experimental results. In contrast, the non-relativistic theory fails for higher values of atomic number.

4.2.6.3.3.2. *Measurements in the vicinity of an absorption edge*

The advent of the synchrotron-radiation source as a routine experimental tool and the deep interest that many crystallographers have in both XAFS and the anomalous-scattering determinations of crystal structures have stimulated considerable interest in the determination of the dispersion corrections in the neighbourhood of absorption edges. In this region, the interaction of the ejected photoelectron with electrons belonging to neighbouring atoms causes the modulations that are referred to as XAFS. Both $f''(\omega, 0)$ (which is directly proportional to the X-ray scattering cross section) and $f'(\omega, 0)$ [which is linked to $f''(\omega, 0)$ through the Kramers–Kronig integral] exhibit these modulations. It is at this point that one must realize that the theoretical tabulations are for the interactions of photons with *isolated* atoms. At best, a comparison of theory and experiment can show that they follow the same trend.

Measurements have been made in the neighbourhood of the absorption edges of a variety of atoms using the 'direct' techniques interferometry, Kramers–Kronig, refraction of a prism and critical-angle techniques, and by the 'indirect' refinement techniques. In Table 4.2.6.6, a comparison is made of experimental values taken at or near the absorption edges of copper, nickel and niobium with theoretical predictions. These have not been adjusted for any energy window that might be thought to exist in any particular experimental configuration. The theoretical values for niobium have been calculated at the energy at which the experimentalists claimed the experiment was conducted.

Despite the considerable experimental difficulties and the wide variety of experimental apparatus, there appears to be close agreement between the experimental data for each type of atom. There appears to be, however, for both copper and nickel, a large discrepancy between the theoretical values and the experimental values. It must be remembered that the experimental values are averages of the value of $f'(\omega, 0)$, the average being taken over the range of photon energies that pass through the device when it is set to a particular energy value. Furthermore, the exact position of the wavelength chosen may be in doubt in absolute terms, especially when synchrotron-radiation sources are used. Therefore, to be able to make a more realistic comparison between theory and experiment, the theoretical data gained using the relativistic multipole approach (this work) were averaged over a rectangular energy window of 5 eV width in the region containing the absorption edge. The rectangular shape arises because of the shape of the reflectivity curve and 5 eV was chosen as a result of (i) analysis of the characteristics of the interferometers used by Bonse *et al*. and Hart *et al*., and (ii) a statement concerning the experimental bandpass of the interferometer used by Bonse & Henning (1986). It must also be borne in mind that mechanical vibrations and thermal fluctuations can broaden the energy window and that 5 eV is not an overestimate of the width of this window. Note that for elements with atomic numbers less than 40 the experimental width is greater than the line width.

For the Bonse & Henning (1986) data, two values are listed for each experiment. Their experiment demonstrates the effect the state of polarization of the incoming photon has on the value of $f'(\omega, 0)$. Similar X-ray dichroism has been shown for sodium bromate by Templeton & Templeton (1985) and Chapuis *et al*. (1985). The theoretical values are for averaged polarization in

Table 4.2.6.4. *Comparison of measurements of the real part of the dispersion correction for LiF, Si, Al and Ge for characteristic wavelengths Ag $K\alpha_1$, Mo $K\alpha_1$ and Cu $K\alpha_1$ with theoretical predictions; the experimental accuracy claimed for the experiments is shown thus: (10) = 10% error*

Sample	Reference	$f'(\omega, 0)$		
		Cu $K\alpha_1$	Mo $K\alpha_1$	Ag $K\alpha_1$
LiF	Theory			
	This work	0.075	0.017	0.010
	Cromer & Liberman (1981)	0.068	0.014	0.006
	Wagenfield (1975)	0.080	0.023	0.015
	Experiment			
	Creagh (1984)	0.085 (5)	0.020 (10)	0.014 (10)
	Deutsch & Hart (1984*b*)	–	0.0217 (1)	0.0133 (1)
Si	Theory			
	This work	0.254	0.817	0.052
	Cromer & Liberman (1981)	0.242	0.071	0.042
	Wagenfeld (1975)	0.282	0.101	0.071
	Experiment			
	Cusatis & Hart (1975)	–	0.0863 (2)	0.0568 (2)
	Price *et al*. (1978)	–	0.085 (7)	0.047 (7)
	Gerward *et al*. (1979)	0.244 (7)	0.099 (7)	0.070 (7)
	Creagh (1984)	0.236 (5)	0.091 (5)	0.060 (5)
	Deutsch & Hart (1984*b*)	–	0.0847 (1)	0.0537 (1)
Al	Theory			
	This work	0.213	0.0645	0.041
	Cromer & Liberman (1981)	0.203	0.0486	0.020
	Wagenfeld (1975)	0.235	0.076	0.553
	Experiment			
	Creagh (1985)	–	0.065 (20)	0.044 (20)
	Takama *et al*. (1982)	0.20 (5)	0.07 (5)	0.035 (10)
Ge	Theory			
	This work	−1.089	0.155	0.302
	Cromer & Liberman (1981)	−1.167	0.062	0.197
	Wagenfeld (1975)	−1.80	−0.08	0.14
	Experiment			
	Gerward *et al*. (1979)	−1.04	0.30	0.43
	Grimvall & Persson (1969)	−1.79	0.08	0.27

Table 4.2.6.5. *Comparison of measurements of $f'(\omega, 0)$ for C, Si and Cu for characteristic wavelengths Ag $K\alpha_1$, Mo $K\alpha_1$ and Cu $K\alpha_1$ with theoretical predictions; the measurements are from the IUCr X-ray Attenuation Project Report (Creagh & Hubbell, 1987, 1990), corrected for the effects of Compton, Laue–Bragg, and small-angle scattering*

Sample	Reference	$f'(\omega, 0)$		
		Cu $K\alpha_1$	Mo $K\alpha_1$	Ag $K\alpha_1$
^{6}C	Theory			
	This work	0.0091	0.0016	0.0009
	Cromer & Liberman (1981)	0.0091	0.0016	0.0009
	Wagenfeld (1975)	–	–	–
	Scofield (1973)	0.0093	0.0016	0.0009
	Storm & Israel (1970)	0.0090	0.0016	0.0009
	Experiment			
	IUCr Project	0.0093	0.0016	0.0009
^{14}Si	Theory			
	This work	0.330	0.070	0.043
	Cromer & Liberman (1981)	0.330	0.0704	0.0431
	Wagenfeld (1975)	0.330	0.071	0.044
	Scofield (1973)	0.332	0.0702	0.0431
	Storm & Israel (1970)	0.331	0.0698	0.0429
	Experiment			
	IUCr Project	0.332	0.0696	0.0429
^{29}Cu	Theory			
	This work	0.588	1.265	0.826
	Cromer & Liberman (1981)	0.589	1.265	0.826
	Scofield (1973)	0.586	1.256	0.826
	Experiment			
	IUCr Project	0.588	1.267	0.826

the incident photon beam. Another important feature is the difference of 0.16 electrons between the Kramers–Kronig and the interferometer values. Bonse & Henning (1986) did not add the relativistic correction term to their Kramers–Kronig values. Inclusion of this term would have reduced the quoted values by 0.20, bringing the two data sets into close agreement with one another.

Katoh *et al*. (1985*b*) have made measurements spanning the *K*-absorption edge of germanium using the deviation by a prism method, and these data have been shown to be in excellent agreement with the theory on which these tables are based (Creagh, 1993). In contrast, the theoretical approach of Pratt, Kissell & Bergstrom (1994) does not agree so well, especially near to, and at higher photon energies, than the *K*-edge energy. Also, Chapuis *et al*. (1985) have measured the dispersion corrections for holmium in $[HoNa(edta)]\cdot 8H_2O$ for the characteristic emission lines Cu $K\alpha_1$, Cu $K\alpha_2$, Cu $K\beta$, and Mo $K\alpha_1$ using a refinement technique. Their results are in reasonable agreement with the relativistic multipole theory, *e.g.* for $f'(\omega, \mathbf{\Delta})$ at the wavelength of Cu $K\alpha_1$ experiment gives $-(16.0 \pm 0.2)$ whereas the relative multipole approach yields -15.0. For Cu $K\alpha_2$, experiment yields $-(13.9 \pm 0.3)$ and theory gives -13.67. The discrepancy between theory and experiment may well be explained by the oxidation state of the holmium ion, which is in the form Ho^{3+}. The oxidation state of an atom affects both the position of the absorption edge and the magnitude of the relativistic correction. Both of these will have a large influence on the value of $f'(\omega, \mathbf{\Delta})$ in the neighbourhood of the absorption edge, Another problem that may be of some significance is the natural width of the absorption edge, about 60 eV. What is remarkable is the extent of the agreement between theory and experiment given the nature of the experiment. In these experiments, the intensities of many reflections (usually nearly 1000) are analysed and compared. Such a procedure can be followed only if there is no dependence of $f'(\omega, \mathbf{\Delta})$ on $\mathbf{\Delta}$.

It had often been thought that the dispersion corrections should exhibit some functional dependence on scattering angle. Indeed, some texts ascribe to these corrections the same functional dependence on angle of scattering as the form factor. A fundamental dependence was also predicted theoretically on the basis of non-relativistic quantum mechanics (Wagenfeld, 1975). This prediction is not supported by modern approaches using relativistic quantum mechanics [see, for example, Kissel *et al*. (1980)]. Reference to Tables 4.2.6.4 and 4.2.6.6 shows that the agreement between experimental values derived from diffraction experiments and those derived from 'direct' experiments is excellent. They are also in excellent agreement with the recent calculations, using relativistic quantum mechanics, so that it may be inferred that there is indeed no functional dependence of the dispersion corrections on scattering angle. Moreover, Suortti, Hastings & Cox (1985) have recently demonstrated that $f'(\omega, \mathbf{\Delta})$ was independent of $\mathbf{\Delta}$ in a powder-diffraction experiment using a nickel specimen.

4.2.6.3.3.3. *Accuracy in the tables of dispersion corrections*

Experimentalists must be aware of two potential sources of error in the values of $f'(\omega, 0)$ listed in Table 4.2.6.5. One is computational, arising from the error in calculating the relativistic correction. Stibius-Jensen (1980) has suggested that this error may be as large as $\pm 0.25(E_{\rm tot}/mc^2)$. This means, for example, that the real part of the dispersion correction $f'(\omega, 0)$ for lead at the wavelength of 0.55936 Å is $-(1.168 \pm 0.146)$. The effect of this error is to shift the dispersion curve vertically without distorting its shape. Note, however, that the direction of the shift is either up or down for all atoms: the effect of multipole cancellation and retardation will be in the same direction for all atoms.

The second possible source of error occurs because the position of the absorption edge varies somewhat depending on the oxidation state of the scattering atom. This has the effect of displacing the dispersion curve laterally. Large discrepancies may occur for those regions in which the dispersion corrections are varying rapidly with photon energy, *i.e.* near absorption edges.

It must also be borne in mind that in the neighbourhood of an absorption edge polarization effects may occur. The tables are valid only for average polarization.

4.2.6.3.3.4. *Towards a tensor formalism*

The question of how best to describe the interaction of X-rays with crystalline materials is quite difficult to answer. In the form factor formalism, the atoms are supposed to scatter as though they are isolated atoms situated at fixed positions in the unit cell. In the vast majority of cases, the polarization on scattering is not detected, and only the scattered intensities are measured. From the scattered intensities, the distribution of the electron density within the unit cell is calculated, and the difference between the form-factor model and that calculated from the intensities is taken as a measure of the nature and location of chemical bonds between atoms in the unit cell.

Table 4.2.6.6. *Comparison of $f'(\omega_A, 0)$ for copper, nickel, zirconium, and niobium for theoretical and experimental data sets; in this table: BR ≡ Bragg reflection; IN ≡ interferometer; KK ≡ Kramers–Kronig; CA = critical angle; and REF = reflectivity; measurements have been made for the K-absorption edges of copper and nickel and near the K-absorption edges of zirconium and niobium; claimed experimental errors are not worse than 5%*

Reference	Method	$f'(\omega_A, 0)$			
		Cu	Ni	Nb	Zr
Experiment					
Freund (1975)	BR	−8.2			
Begum, Hart, Lea & Siddons (1986)	IN	−7.84	−7.66		
Bonse & Materlik (1972)	IN		−8.1		
Bonse, Hartmann-Lotsch & Lotsch (1983*a*)	IN	−8.3			
Hart & Siddons (1981)	IN	−9.3	−9.2	−4.396	−6.670
Kawamura & Fukimachi (1978; cited in Bonse & Hartmann-Lotsch, 1984)	KK		−7.9		
Dreier *et al*. (1984)	KK	−8.2	−7.8		−7.83
	IN	−8.3	−8.1		
Bonse & Hartmann-Lotsch (1984)	KK	−8.3	−7.7		
Fukamachi *et al*. (1978; cited in Bonse & Hartmann-Lotsch, 1984)	KK	−8.8			
	CA	−10.0			
Bonse & Henning (1986)	IN			−7.37; −7.73	
	KK			−7.21; −7.62	
Stanglmeier, Lengeler, Weber, Gobel & Schuster (1992)	REF	−8.5	−8.1		
Creagh (1990, 1993)	REF	−8.2	−7.7		−6.8
Theory					
Cromer & Liberman (1981)		−13.50	−9.45	−4.20; −7.39	−6.207
This work		−9.5	−9.40	−4.04; −7.23	−6.056
Averaged values (5 eV) window)		−9.0	−7.53	−8.18	−6.04

This is the zeroth-order approximation to a solution, but it is in fact the only way crystal structures are solved *ab initio*.

The existence of chemical bonding imposes additional restrictions on the symmetry of lattices, and, if the associated influence this has on the complexity of energy levels is taken into account, significant changes in the scattering factors may occur in the neighbourhood of the absorption edges of the atoms comprising the crystal structure. The magnitudes of the dispersion corrections are sensitive to the chemical state, particularly oxidation state, and phenomena similar to those observed in the XAFS case (Section 4.2.4) are observed.

The XAFS interaction arising from the presence of neighbouring atoms is proportional to $f''(\omega, 0)$ and therefore is related to $f'(\omega, 0)$ through the Kramers–Kronig integral. It is not surprising that these modulations are observed in diffracted intensities in those X-ray diffraction experiments where the photon energy is scanned through the absorption edge of an atomic species in the crystal lattice. Studies of this type are referred to as diffraction absorption fine structure (DAFS) experiments. A recent review of work performed using counter techniques has been given by Sorenson (1994). Creagh & Cookson (1995) have described the use of imaging-plate techniques to study the structure and site symmetry using the DAFS technique. This technique has the ability to discriminate between different lattice sites in the unit cell occupied by an atomic species. XAFS cannot make this discrimination. The DAFS modulations are small perturbations to the diffracted intensities. They are, however, significantly larger than the tensor effects described in the following paragraphs.

In the case where the excited state lacks high symmetry and is oriented by crystal bonding, the scattering can no longer be described by a scalar scattering factor but must be described by a symmetric second-rank tensor. The consequences of this have been described by Templeton (1994). It follows therefore that material media can be optically active in the X-ray region. Hart (1994) has used his unique polarizing X-ray optical devices to study, for example, Faraday rotation in such materials as iron, in the region of the iron *K*-absorption edge, and cobalt(III) bromide monohydrate in the region of the cobalt *K*-absorption edge.

The theory of anisotropy in anomalous scattering has been treated extensively by Kirfel (1994), and Morgenroth, Kirfel

Table 4.2.6.7. *List of wavelengths, energies, and linewidths used in compiling the table of dispersion corrections (a) Agarwal (1979); (b) Deutsch & Hart (1982)*

Radiation	Wavelength (Å)	Energy (keV)	Linewidth (eV)
^{79}Au $K\alpha_1$	0.180195	68.803	46 (*a*)
^{74}W $K\alpha_1$	0.209010	59.318	43 (*a*)
^{73}Ta $K\alpha_1$	0.215947	57.412	42 (*a*)
^{47}Ag $K\alpha_1$	0.559360	22.165	7 (*a*)
^{42}Mo $K\alpha_1$	0.709260	17.480	4 (*a*)
^{29}Cu $K\alpha_1$	1.540520	8.04792	2.61 (*b*)
^{27}Co $K\alpha_1$	1.788965	6.9302	1.8
^{26}Fe $K\alpha_1$	1.93597	6.4040	1.6
^{24}Cr $K\alpha_1$	2.289620	5.4149	1.5
^{22}Ti $K\alpha_1$	2.748510	4.5108	1.4

Table 4.2.6.8. *Dispersion corrections for forward scattering*

Wavelength (Å)		2.748510	2.289620	1.935970	1.788965	1.540520	0.709260	0.559360	0.215947	0.209010	0.180195
Li	$f' =$	0.0035	0.0023	0.0015	0.0013	0.0008	−0.0003	−0.0004	−0.0006	−0.0006	−0.0006
	$f'' =$	0.0013	0.0008	0.0006	0.0005	0.0003	0.0001	0.0000	0.0000	0.0000	0.0000
Be	$f' =$	0.0117	0.0083	0.0060	0.0052	0.0038	0.0005	0.0001	−0.0005	−0.0005	−0.0005
	$f'' =$	0.0050	0.0033	0.0023	0.0019	0.0014	0.0002	0.0001	0.0000	0.0000	0.0000
B	$f' =$	0.0263	0.0190	0.0140	0.0121	0.0090	0.0013	0.0004	−0.0009	−0.0009	−0.0010
	$f'' =$	0.0139	0.0094	0.0065	0.0055	0.0039	0.0007	0.0004	0.0000	0.0000	0.0000
C	$f' =$	0.0490	0.0364	0.0273	0.0237	0.0181	0.0033	0.0015	−0.0012	−0.0013	−0.0014
	$f'' =$	0.0313	0.0213	0.0148	0.0125	0.0091	0.0016	0.0009	0.0001	0.0001	0.0001
N	$f' =$	0.0807	0.0606	0.0461	0.0403	0.0311	0.0061	0.0030	−0.0020	−0.0020	−0.0023
	$f'' =$	0.0606	0.0416	0.0293	0.0248	0.0180	0.0033	0.0019	0.0002	0.0002	0.0001
O	$f' =$	0.1213	0.0928	0.0716	0.0630	0.0492	0.0106	0.0056	−0.0025	−0.0026	−0.0030
	$f'' =$	0.1057	0.0731	0.0518	0.0440	0.0322	0.0060	0.0036	0.0004	0.0004	0.0003
F	$f' =$	0.1700	0.1324	0.1037	0.0920	0.0727	0.0171	0.0096	−0.0027	−0.0028	−0.0034
	$f'' =$	0.1710	0.1192	0.0851	0.0725	0.0534	0.0103	0.0061	0.0007	0.0007	0.0005
Ne	$f' =$	0.2257	0.1793	0.1426	0.1273	0.1019	0.0259	0.0152	−0.0025	−0.0028	−0.0037
	$f'' =$	0.2621	0.1837	0.1318	0.1126	0.0833	0.0164	0.0098	0.0012	0.0011	0.0008
Na	$f' =$	0.2801	0.2295	0.1857	0.1670	0.1353	0.0362	0.0218	−0.0028	−0.0031	−0.0044
	$f'' =$	0.3829	0.2699	0.1957	0.1667	0.1239	0.0249	0.0150	0.0019	0.0017	0.0012
Mg	$f' =$	0.3299	0.2778	0.2309	0.2094	0.1719	0.0486	0.0298	−0.0030	−0.0034	−0.0052
	$f'' =$	0.5365	0.3812	0.2765	0.2373	0.1771	0.0363	0.0220	0.0028	0.0026	0.0018
Al	$f' =$	0.3760	0.3260	0.2774	0.2551	0.2130	0.0645	0.0406	−0.0020	−0.0026	−0.0050
	$f'' =$	0.7287	0.5212	0.3807	0.3276	0.2455	0.0514	0.0313	0.0040	0.0037	0.0027
Si	$f' =$	0.3921	0.3647	0.3209	0.2979	0.2541	0.0817	0.0522	−0.0017	−0.0025	−0.0055
	$f'' =$	0.9619	0.6921	0.5081	0.4384	0.3302	0.0704	0.0431	0.0056	0.0052	0.0038
P	$f' =$	0.3821	0.3898	0.3592	0.3388	0.2955	0.1023	0.0667	−0.0002	−0.0012	−0.0050
	$f'' =$	1.2423	0.8984	0.6628	0.5731	0.4335	0.0942	0.0580	0.0077	0.0071	0.0052
S	$f' =$	0.3167	0.3899	0.3848	0.3706	0.3331	0.1246	0.0826	0.0015	0.0003	−0.0045
	$f'' =$	1.5665	1.1410	0.8457	0.7329	0.5567	0.1234	0.0763	0.0103	0.0096	0.0069
Cl	$f' =$	0.1832	0.3508	0.3920	0.3892	0.3639	0.1484	0.0998	0.0032	0.0017	−0.0042
	$f'' =$	1.9384	1.4222	1.0596	0.9202	0.7018	0.1585	0.0984	0.0134	0.0125	0.0091
Ar	$f' =$	−0.0656	0.2609	0.3696	0.3880	0.3843	0.1743	0.1191	0.0059	0.0041	−0.0030
	$f'' =$	2.3670	1.7458	1.3087	1.1388	0.8717	0.2003	0.1249	0.0174	0.0162	0.0118
K	$f' =$	−0.5083	0.0914	0.3068	0.3532	0.3868	0.2009	0.1399	0.0089	0.0067	−0.0017
	$f'' =$	2.8437	2.1089	1.5888	1.3865	1.0657	0.2494	0.1562	0.0219	0.0204	0.0149
Ca	$f' =$	−1.3666	−0.1987	0.1867	0.2782	0.3641	0.2262	0.1611	0.0122	0.0097	−0.0002
	$f'' =$	3.3694	2.5138	1.9032	0.6648	1.2855	0.3064	0.1926	0.0273	0.0255	0.0187
Sc	$f' =$	−5.4265	−0.6935	−0.0120	0.1474	0.3119	0.2519	0.1829	0.0159	0.0130	0.0015
	$f'' =$	4.0017	2.9646	2.2557	1.9774	1.5331	0.3716	0.2348	0.0338	0.0315	0.0231
Ti	$f' =$	−2.2250	−1.6394	−0.3318	−0.0617	0.2191	0.2776	0.2060	0.0212	0.0179	0.0047
	$f'' =$	0.5264	3.4538	2.6425	2.3213	1.8069	0.4457	0.2830	0.0414	0.0387	0.0284
V	$f' =$	−1.6269	−4.4818	−0.8645	−0.3871	0.0687	0.3005	0.2276	0.0259	0.0221	0.0070
	$f'' =$	0.6340	0.4575	3.0644	2.6994	2.1097	0.5294	0.3376	0.0500	0.0468	0.0344
Cr	$f' =$	−1.2999	−2.1308	−1.9210	−0.9524	−0.1635	0.3209	0.2496	0.0314	0.0272	0.0101
	$f'' =$	0.7569	0.5468	3.5251	3.1130	2.4439	0.6236	0.3992	0.0599	0.0561	0.0413
Mn	$f' =$	−1.0732	−1.5980	−3.5716	−2.0793	−0.5299	0.3368	0.2704	0.0377	0.0330	0.0139
	$f'' =$	0.8956	0.6479	0.4798	3.5546	2.8052	0.7283	0.4681	0.0712	0.0666	0.0492
Fe	$f' =$	−0.8901	−1.2935	−2.0554	−3.3307	−1.1336	0.3463	0.2886	0.0438	0.0386	0.0173
	$f'' =$	1.0521	0.7620	0.5649	0.4901	3.1974	0.8444	0.5448	0.0840	0.0787	0.0582
Co	$f' =$	−0.7307	−1.0738	−1.5743	−2.0230	−2.3653	0.3494	0.3050	0.0512	0.0454	0.0219
	$f'' =$	1.2272	0.8897	0.6602	0.5731	3.6143	0.9721	0.6296	0.0984	0.0921	0.0682
Ni	$f' =$	−0.5921	−0.9005	−1.2894	−1.5664	−3.0029	0.3393	0.3147	0.0563	0.0500	0.0244
	$f'' =$	1.4240	1.0331	0.7671	0.6662	0.5091	1.1124	0.7232	0.1146	0.1074	0.0796
Cu	$f' =$	−0.4430	−0.7338	−1.0699	−1.2789	−1.9646	0.3201	0.3240	0.0647	0.0579	0.0298
	$f'' =$	1.6427	1.1930	0.8864	0.7700	0.5888	1.2651	0.8257	0.1326	0.1242	0.0922
Zn	$f' =$	−0.3524	−0.6166	−0.9134	−1.0843	−1.5491	0.2839	0.3242	0.0722	0.0648	0.0344
	$f'' =$	1.8861	1.3712	1.0193	0.8857	0.6778	1.4301	0.9375	0.1526	0.1430	0.1063
Ga	$f' =$	−0.2524	−0.4989	−0.7701	−0.9200	−1.2846	0.2307	0.3179	0.0800	0.0721	0.0393
	$f'' =$	2.1518	1.5674	1.1663	1.0138	0.7763	1.6083	1.0589	0.1745	0.1636	0.1218
Ge	$f' =$	−0.1549	−0.3858	−0.6412	−0.7781	−1.0885	0.1547	0.3016	0.0880	0.0796	0.0445
	$f'' =$	2.4445	1.7841	1.3291	1.1557	0.8855	1.8001	1.1903	0.1987	0.1863	0.1389
As	$f' =$	−0.0687	−0.2871	−0.5260	−0.6523	−0.9300	0.0499	0.2758	0.0962	0.0873	0.0501
	$f'' =$	2.7627	2.0194	1.5069	1.3109	1.0051	2.0058	1.3314	0.2252	0.2112	0.1576
Se	$f' =$	0.0052	−0.1919	−0.4179	−0.5390	−0.7943	−0.0929	0.2367	0.1047	0.0954	0.0560
	$f'' =$	3.1131	2.2784	1.7027	1.4821	1.1372	2.2259	1.4831	0.2543	0.2386	0.1782
Br	$f' =$	0.0592	−0.1095	−0.3244	−0.4363	−0.6763	−0.2901	0.1811	0.1106	0.1026	0.0613
	$f'' =$	3.4901	2.5578	1.9140	1.6673	1.2805	2.4595	1.6452	0.2858	0.2682	0.2006
Kr	$f' =$	0.1009	−0.0316	−0.2303	−0.3390	−0.5657	−0.5574	0.1067	0.1180	0.1082	0.0668
	$f'' =$	3.9083	2.8669	2.1472	1.8713	1.4385	2.7079	1.8192	0.3197	0.3003	0.2251

Table 4.2.6.8. *Dispersion corrections for forward scattering (cont.)*

Wavelength (Å)		2.748510	2.289620	1.935970	1.788965	1.540520	0.709260	0.559360	0.215947	0.209010	0.180195
Rb	$f' =$	0.1056	0.0247	−0.1516	−0.2535	−0.4688	−0.9393	0.0068	0.1247	0.1146	0.0717
	$f'' =$	4.3505	3.1954	2.3960	2.0893	1.6079	2.9676	2.0025	0.3561	0.3346	0.2514
Sr	$f' =$	0.1220	0.1037	−0.0489	−0.1448	−0.3528	−1.5307	−0.1172	0.1321	0.1219	0.0769
	$f'' =$	4.8946	3.6029	2.7060	2.3614	1.8200	3.2498	2.2025	0.3964	0.3726	0.2805
Y	$f' =$	0.0654	0.1263	0.0138	−0.0720	−0.2670	−2.7962	−0.2879	0.1380	0.1278	0.0819
	$f'' =$	5.4198	3.9964	3.0054	2.6241	2.0244	3.5667	2.4099	0.4390	0.4128	0.3112
Zr	$f' =$	−0.0304	0.1338	0.0659	−0.0066	−0.1862	−2.9673	−0.5364	0.1431	0.1329	0.0863
	$f'' =$	5.9818	4.4226	3.3301	2.9086	2.2449	0.5597	2.6141	0.4852	0.4562	0.3443
Nb	$f' =$	−0.1659	0.1211	0.1072	0.0496	−0.1121	−2.0727	−0.8282	0.1471	0.1371	0.0905
	$f'' =$	6.5803	4.8761	3.6768	3.2133	2.4826	0.6215	2.8404	0.5342	0.5025	0.3797
Mo	$f' =$	−0.3487	0.0801	0.1301	0.0904	−0.0483	−1.6832	−1.2703	0.1487	0.1391	0.0934
	$f'' =$	7.2047	5.3484	4.0388	3.5326	2.7339	0.6857	3.0978	0.5862	0.5517	0.4177
Tc	$f' =$	−0.6073	−0.0025	0.1314	0.1164	0.0057	−1.4390	−2.0087	0.1496	0.1406	0.0960
	$f'' =$	7.8739	5.8597	4.4331	3.8799	3.0049	0.7593	3.3490	0.6424	0.6047	0.4582
Ru	$f' =$	−0.9294	−0.1091	0.1220	0.1331	0.0552	−1.2594	−5.3630	0.1491	0.1409	0.0981
	$f'' =$	8.5988	6.4069	4.8540	4.2509	3.2960	0.8363	3.6506	0.7016	0.6607	0.5014
Rh	$f' =$	−1.3551	−0.2630	0.0861	0.1305	0.0927	−1.1178	−2.5280	0.1445	0.1373	0.0970
	$f'' =$	9.3504	6.9820	5.2985	4.6432	3.6045	0.9187	0.5964	0.7639	0.7195	0.5469
Pd	$f' =$	−1.9086	−0.4640	0.0279	0.1128	0.1215	−0.9988	−1.9556	0.1387	0.1327	0.0959
	$f'' =$	10.1441	7.5938	5.7719	5.0613	3.9337	1.0072	0.6546	0.8302	0.7822	0.5955
Ag	$f' =$	−2.5003	−0.7387	−0.0700	0.0634	0.1306	−0.8971	−1.6473	0.1295	0.1251	0.0928
	$f'' =$	10.9916	8.2358	6.2709	5.5027	4.2820	1.1015	0.7167	0.9001	0.8484	0.6469
Cd	$f' =$	−3.5070	−1.1086	−0.2163	−0.0214	0.1185	−0.8075	−1.4396	0.1171	0.1147	0.0881
	$f'' =$	11.9019	8.9174	6.8017	5.9728	4.6533	1.2024	0.7832	0.9741	0.9185	0.7013
In	$f' =$	−5.1325	−1.5975	−0.4165	−0.1473	0.0822	−0.7276	−1.2843	0.1013	0.1012	0.0816
	$f'' =$	12.6310	9.6290	7.3594	6.4674	5.0449	1.3100	0.8542	1.0519	0.9922	0.7587
Sn	$f' =$	−7.5862	−2.2019	−0.6686	−0.3097	0.0259	−0.6537	−1.1587	0.0809	0.0839	0.0728
	$f'' =$	13.5168	10.3742	7.9473	6.9896	5.4591	1.4246	0.9299	1.1337	1.0697	0.8192
Sb	$f' =$	−9.2145	−3.0637	−0.9868	−0.5189	−0.0562	−0.5866	−1.0547	0.0559	0.0619	0.0613
	$f'' =$	12.7661	11.1026	8.5620	7.5367	5.8946	1.5461	1.0104	1.2196	1.1512	0.8830
Te	$f' =$	−11.6068	−4.2407	−1.4022	−0.7914	−0.1759	−0.5308	−0.9710	0.0216	0.0316	0.0435
	$f'' =$	−10.1013	11.8079	9.2067	8.1113	6.3531	1.6751	1.0960	1.3095	1.2366	0.9499
I	$f' =$	−13.9940	−5.6353	1.9032	1.1275	−0.3257	−0.4742	−0.8919	−0.0146	−0.0001	0.0259
	$f'' =$	3.4071	12.6156	9.8852	8.7159	6.8362	1.8119	1.1868	1.4037	1.3259	1.0201
Xe	$f' =$	−9.6593	−8.1899	−2.6313	−1.5532	−0.5179	−0.4205	−0.8200	−0.0565	−0.0367	0.0057
	$f'' =$	3.7063	11.7407	10.5776	9.3585	7.3500	1.9578	1.2838	1.5023	1.4195	1.0938
Cs	$f' =$	−8.1342	−10.3310	−3.5831	−2.1433	−0.7457	−0.3680	−0.7527	−0.1070	−0.0809	0.0194
	$f'' =$	4.0732	12.8551	11.2902	10.0454	7.9052	2.1192	1.3916	1.6058	1.5179	1.1714
Ba	$f' =$	−7.2079	−11.0454	−4.6472	−2.7946	−1.0456	−0.3244	−0.6940	−0.1670	−0.1335	−0.0494
	$f'' =$	4.4110	10.0919	12.0003	10.7091	8.4617	2.2819	1.5004	1.7127	1.6194	1.2517
La	$f' =$	−6.5722	−12.8190	−6.3557	−3.6566	−1.4094	−0.2871	−0.6411	−0.2363	−0.1940	−0.0835
	$f'' =$	4.7587	3.5648	12.8927	11.4336	9.0376	2.4523	1.6148	1.8238	1.7250	1.3353
Ce	$f' =$	−6.0641	−9.3304	−8.0962	−4.8792	−1.8482	−0.2486	−0.5890	−0.3159	−0.2633	−0.1222
	$f'' =$	5.1301	3.8433	11.8734	12.1350	9.6596	2.6331	1.7358	1.9398	1.8353	1.4227
Pr	$f' =$	−5.6727	−7.9841	−10.9279	−6.7923	−2.4164	−0.2180	−0.5424	−0.4096	−0.3443	−0.1666
	$f'' =$	5.5091	4.1304	9.2394	12.8653	10.2820	2.8214	1.8624	2.0599	1.9496	1.5136
Nd	$f' =$	−5.3510	−7.1451	−10.5249	−8.1618	−3.1807	−0.1943	−0.5012	−0.5194	−0.4389	−0.2183
	$f'' =$	5.9005	4.4278	9.9814	11.9121	10.9079	3.0179	1.9950	2.1843	2.0679	1.6077
Pm	$f' =$	−5.0783	−6.5334	−13.2062	−10.0720	−4.0598	−0.1753	−0.4626	−0.6447	−0.5499	−0.2776
	$f'' =$	6.3144	4.7422	3.6278	9.2324	11.5523	3.2249	2.1347	2.3143	2.1906	1.7056
Sm	$f' =$	−4.8443	−6.0570	−9.3497	−10.2609	−5.3236	−0.1638	−0.4287	−0.7989	−0.6734	−0.3455
	$f'' =$	6.7524	5.0744	3.8839	9.9412	12.2178	3.4418	2.2815	2.4510	2.3197	1.8069
Eu	$f' =$	−4.6288	−5.6630	−7.9854	−13.5405	−8.9294	−0.1578	−0.3977	−0.9903	−0.8137	−0.4235
	$f'' =$	7.2035	5.4178	4.1498	3.6550	11.1857	3.6682	2.4351	2.5896	2.4526	1.9120
Gd	$f' =$	−4.5094	−5.3778	−7.1681	−9.3863	−8.8380	−0.1653	−0.3741	−1.2279	−1.0234	−0.5140
	$f'' =$	7.6708	5.7756	4.4280	3.9016	11.9157	3.9035	2.5954	2.7304	2.5878	2.0202
Tb	$f' =$	−4.3489	−5.0951	−6.5583	−8.0413	−9.1472	−0.1723	−0.3496	−1.5334	−1.2583	−0.6165
	$f'' =$	8.1882	6.1667	4.7292	4.1674	9.1891	4.1537	2.7654	2.8797	2.7310	2.1330
Dy	$f' =$	−4.1616	−4.8149	−6.0597	−7.1503	−9.8046	−0.1892	−0.3302	−1.9594	−1.5632	−0.7322
	$f'' =$	8.6945	6.5527	5.0280	4.4320	9.8477	4.4098	2.9404	3.0274	2.8733	2.2494
Ho	$f' =$	−4.0280	−4.5887	−5.6628	−6.5338	−14.9734	−0.2175	−0.3168	−2.6705	−1.9886	−0.8709
	$f'' =$	9.2302	6.9619	5.3451	4.7129	3.7046	4.6783	3.1241	3.1799	3.0218	2.3711
Er	$f' =$	−3.9471	−4.4106	−5.3448	−6.0673	−9.4367	−0.2586	−0.3091	−5.5645	−2.6932	−1.0386
	$f'' =$	9.7921	7.3910	5.6776	5.0074	3.9380	4.9576	3.3158	0.6167	3.1695	2.4949
Tm	$f' =$	−3.9079	−4.2698	−5.0823	−5.6969	−8.0393	−0.3139	−0.3084	−2.8957	−5.6057	−1.2397
	$f'' =$	10.3763	7.8385	6.0249	5.3151	4.1821	5.2483	3.5155	0.6569	0.6192	2.6240
Yb	$f' =$	−3.8890	−4.1523	−4.8591	−5.3940	−7.2108	−0.3850	−0.3157	−2.4144	−2.9190	−1.4909
	$f'' =$	10.9742	8.2969	6.3813	5.6309	4.4329	5.5486	3.7229	0.6994	0.6592	2.7538

Table 4.2.6.8. *Dispersion corrections for forward scattering (cont.)*

Wavelength (Å)		2.748510	2.289620	1.935970	1.788965	1.540520	0.709260	0.559360	0.215947	0.209010	0.180195
Lu	$f' =$	−3.9056	−4.0630	−4.6707	−5.1360	−6.6179	−0.4720	−0.3299	−2.1535	−2.4402	−1.8184
	$f'' =$	11.5787	8.7649	6.7484	5.9574	4.6937	5.8584	3.9377	0.7436	0.7010	2.8890
Hf	$f' =$	−4.0452	−4.0564	−4.4593	−4.9466	−6.1794	−0.5830	−0.3548	−1.9785	−2.1778	−2.2909
	$f'' =$	12.2546	9.2832	7.1518	6.3150	4.9776	6.1852	4.1643	0.7905	0.7454	3.0246
Ta	$f' =$	−4.0905	−3.9860	−4.3912	−4.7389	5.7959	−0.7052	−0.3831	−1.8534	−2.0068	−3.1639
	$f'' =$	12.9479	9.8171	7.5686	6.6850	5.2718	6.5227	4.3992	0.8392	0.7915	3.1610
W	$f' =$	−4.1530	−3.9270	−4.2486	−4.5529	−5.4734	−0.8490	−0.4201	−1.7565	−1.8819	−3.8673
	$f'' =$	13.6643	10.3696	8.0005	7.0688	5.5774	6.8722	4.6430	0.8905	0.8388	0.6433
Re	$f' =$	−4.2681	−3.9052	−4.1390	−4.4020	−5.2083	−1.0185	−0.4693	−1.6799	−1.7868	−2.8429
	$f'' =$	14.3931	10.9346	8.4435	7.4631	5.8923	7.2310	4.8944	0.9441	0.8907	0.6827
Os	$f' =$	−4.4183	−3.9016	−4.0478	−4.2711	−4.9801	−1.2165	−0.5280	−1.6170	−1.7107	−2.4688
	$f'' =$	15.1553	11.5251	8.9067	7.8753	6.2216	7.6030	5.1558	1.0001	0.9437	0.7238
Ir	$f' =$	−4.5860	−3.9049	−3.9606	−4.1463	−4.7710	−1.4442	−0.5977	−1.5648	−1.6486	−2.2499
	$f'' =$	15.9558	12.1453	9.3923	8.3074	6.5667	7.9887	5.4269	1.0589	0.9993	0.7669
Pt	$f' =$	−4.8057	−3.9435	−3.8977	−4.0461	−4.5932	−1.7033	−0.6812	−1.5228	−1.5998	−2.1036
	$f'' =$	16.7870	12.7910	9.8985	8.7578	6.9264	8.3905	5.7081	1.1193	1.0565	0.8116
Au	$f' =$	−5.0625	−3.9908	−3.8356	−3.9461	−4.4197	−2.0133	−0.7638	−1.4693	−1.5404	−1.9775
	$f'' =$	17.6400	13.4551	10.4202	9.2222	7.2980	8.8022	5.9978	1.1833	1.1171	0.8589
Hg	$f' =$	−5.4327	−4.1029	−3.8228	−3.8921	−4.2923	−2.3894	−0.8801	−1.4389	−1.5055	−1.8958
	$f'' =$	18.5241	14.1473	10.9650	9.7076	7.6849	9.2266	6.2989	1.2483	1.1796	0.9080
TI	$f' =$	−5.8163	−4.2233	−3.8103	−3.8340	−4.1627	−2.8358	−1.0117	−1.4111	−1.4740	−1.8288
	$f'' =$	19.4378	14.8643	11.5300	10.2108	8.0900	9.6688	6.6090	1.3189	1.2456	0.9594
Pb	$f' =$	−6.4779	−4.4167	−3.8519	−3.8236	−4.0753	−3.3944	−1.1676	−1.3897	−1.4497	−1.7773
	$f'' =$	20.3336	15.5987	12.1106	10.7292	8.5060	10.1111	6.9287	1.3909	1.3137	1.0127
Bi	$f' =$	−7.0419	−4.6533	−3.9228	−3.8408	−4.0111	−4.1077	−1.3494	−1.3721	−1.4290	−1.7346
	$f'' =$	21.2196	16.3448	12.7017	11.2575	8.9310	10.2566	7.2566	1.4661	1.3851	1.0685
Po	$f' =$	−7.7195	−4.9604	−4.0267	−3.8855	−3.9670	−5.1210	−1.5613	−1.3584	−1.4133	−1.7005
	$f'' =$	22.1974	17.1410	13.3329	11.8209	9.3834	11.0496	7.5986	1.5443	1.4592	1.1266
At	$f' =$	−8.5994	−5.3399	−4.1781	−3.9706	−3.9588	−7.9122	−1.8039	−1.3540	−1.4066	−1.6784
	$f'' =$	23.2213	17.9390	13.9709	12.3915	9.8433	9.9777	7.9509	1.6260	1.5367	1.1876
Rn	$f' =$	−10.2749	−5.7275	−4.3331	−4.0549	−3.9487	−8.0659	−2.0847	−1.3475	−1.3982	−1.6571
	$f'' =$	24.2613	18.7720	14.6313	12.9815	10.3181	10.4580	8.3112	1.7103	1.6167	1.2504
Fr	$f' =$	−10.8938	−6.2180	−4.5387	−4.1818	−3.9689	−7.2224	−2.4129	−1.3404	−1.3892	−1.6367
	$f'' =$	24.3041	19.6009	15.3016	13.5825	10.8038	7.7847	8.6839	1.7986	1.7004	1.3162
Ra	$f' =$	−12.3462	−6.7502	−4.7764	−4.3309	−4.0088	−6.7704	−2.8081	−1.3462	−1.3931	−1.6299
	$f'' =$	25.5374	20.4389	15.9778	14.1902	11.2969	8.1435	9.0614	1.8891	1.7863	1.3840
Ac	$f' =$	−12.3496	−7.4161	−5.0617	−4.5270	−4.0794	−6.8494	−3.2784	−1.3473	−1.3922	−1.6190
	$f'' =$	25.1363	21.3053	16.6687	14.8096	11.7994	8.5178	9.4502	1.9845	1.8770	1.4553
Th	$f' =$	−13.6049	−8.2118	−5.3692	−4.7310	−4.1491	−7.2400	−3.8533	−1.3524	−1.3955	−1.6136
	$f'' =$	26.2511	22.2248	17.4018	15.4642	12.3296	8.8979	9.8403	2.0819	1.9695	1.5284
Pa	$f' =$	−14.4639	−9.4459	−5.7337	−4.9639	−4.2473	−8.0334	−4.6067	−1.3672	−1.4083	−1.6170
	$f'' =$	27.4475	23.1548	18.1406	16.1295	12.8681	9.2807	10.2413	2.1835	2.0661	1.6047
U	$f' =$	−12.3528	−9.9362	−6.1485	−5.2392	−4.3638	−9.6767	−5.7225	−1.3792	−1.4184	−1.6188
	$f'' =$	30.1725	23.1239	18.8728	16.7952	13.4090	9.6646	10.6428	2.2876	1.1650	1.6831
Np	$f' =$	−17.4143	−11.1080	−6.6136	−5.5633	−4.5053	−11.4937	−6.9995	−1.3941	−1.4312	−1.6231
	$f'' =$	31.7405	24.1168	19.6379	17.4837	13.9666	4.1493	9.5876	2.3958	2.2679	1.7648
Pu	$f' =$	−18.0862	−11.4073	−6.9721	−5.8130	−4.6563	−9.4100	−13.5905	−1.4180	−1.4527	−1.6351
	$f'' =$	33.8963	23.2960	20.1548	17.9579	14.3729	4.3056	6.9468	2.4979	2.3652	1.8430
Am	$f' =$	−19.7042	−11.7097	−7.7881	−6.2920	−4.8483	−7.8986	−6.7022	−1.4359	−1.4684	−1.6424
	$f'' =$	37.3716	24.5715	21.1738	18.8618	15.0877	4.5125	7.3108	2.6218	2.4829	1.9358
Cm	$f' =$	−24.9307	−10.4100	−8.6102	−6.7506	−5.0611	−7.3248	−6.2891	−1.4655	−1.4952	−1.6592
	$f'' =$	41.4852	25.8115	21.8880	19.5119	15.6355	4.6980	7.6044	2.7421	2.5974	2.0271
Bk	$f' =$	−32.8492	−9.2185	−9.3381	−7.4293	−5.3481	−6.8498	−6.3438	−1.4932	−1.5203	−1.6746
	$f'' =$	32.5421	29.3028	21.9514	20.3581	16.3190	4.9086	7.9477	2.8653	2.7147	2.1208
Cf	$f' =$	−23.6520	−23.5202	−9.7799	−7.8616	−5.5545	−6.6561	−6.4144	−1.5323	−1.5562	−1.6984
	$f'' =$	21.9334	31.2999	22.4858	20.8536	16.7428	5.0785	8.1930	2.9807	2.8250	2.2102

& Fischer (1994) have extended this to the description of kinematic diffraction intensities in lattices containing anisotropic anomalous scatterers. Their treatment was developed for space groups up to orthorhombic symmetry.

All the preceeding treatments apply to scattering in the neighbourhood of an absorption edge, and to a fairly restricted class of crystals for which the local site symmetry of the electron density of states in the excited state is very different from the apparent crystal symmetry.

These approaches seek to treat the scattering from the crystal as though the scattering from each atomic position can be described by a symmetric second-rank tensor whose properties are determined by the point-group symmetries of those sites. Clearly, this procedure cannot be followed unless the structure has been solved by the usual method. The tensor approach can then be used to explain apparent deficiencies in that model such as the existence of 'forbidden' reflections, birefringence, and circular dichroism.

Scattering of X-rays from the electron spins in antiferromagnetically ordered materials can also be described by imposing a tensor description on the form factor (Blume, 1994). The tensor in this case is a fourth-rank tensor, and the strength of the interaction, even for the favourable case of resonance scattering, is several orders of magnitude lower in intensity than the polarization effects. Nevertheless, studies have been made on holmium and uranium arsenide, and significant magnetic Bragg scattering has been observed.

All the cases cited above represent exciting, state-of-the-art, scientific studies. However, none of the work will assist in the solution of crystal structures directly. Researchers should avoid the temptation, in the first instance, to ascribe anything but a scalar value to the form factor.

4.2.6.3.3.5. *Summary*

For the imaginary part of the dispersion correction $f''(\omega, \mathbf{\Delta})$, the following observations can be made.

(i) Measurements of the linear absorption coefficient μ_l from which $f''(\omega, 0)$ is deduced should follow the recommendations set out in Subsection 4.2.3.2.

(ii) There is no rational basis for preferring one set of relativistic calculations of atomic scattering cross sections over another, as Creagh & Hubbell (1987, 1990) and Kissel *et al.* (1980) have shown.

(iii) The total scattering cross section for an ensemble of atoms is not simply the sum of the individual scattering cross sections in the neighbourhood of an absorption edge and therefore $f'(\omega, 0)$ will fluctuate as $\omega \rightarrow \omega_\kappa$.

(iv) There is no dependence of $f''(\omega, \mathbf{\Delta})$ and $\mathbf{\Delta}$.

For the real part of the dispersion correction $f'(\omega, \mathbf{\Delta})$, the following observations can be made.

(i) The relativistic multipole values listed here tend to accord better with experiment than the non-relativistic and relativistic dipole values.

(ii) There is no dependence of $f'(\omega, \mathbf{\Delta})$ on $\mathbf{\Delta}$.

(iii) The theoretical tables are calculated for averaged polarizations.

(iv) Experimentalists wishing to compare their data with theoretical predictions should take account of the energy bandpass of their system when determining the appropriate theoretical value. They should also be aware of the fact that the position of the absorption edge depends on the oxidation state of the scattering atom, and that there is an inaccuracy in the tables of $f'(\omega, 0)$ of either $+0.20(E_{\rm tot}/mc^2)$ or $-0.10(E_{\rm tot}/mc^2)$.

4.2.6.4. *Table of wavelengths, energies, and linewidths used in compiling the tables of the dispersion corrections*

Table 4.2.6.7 lists the characteristic emission wavelengths that are commonly used by crystallographers in their experiments. Also included are the emission energies (since many systems use energy rather than wavelength discrimination) and the line widths (full width at half-maximum) of these lines (Agarwal, 1979; Stearns, 1984; Deutsch & Hart, 1984*a*,*b*).

4.2.6.5. *Tables of the dispersion corrections for forward scattering, averaged polarization using the relativistic multipole approach*

See Subsection 4.2.6.3 for comments on the accuracy of these tables. Note also that in the neighbourhood of absorption edges the values for condensed matter may be significantly different from the values in the tables due to XAFS and XANES effects. The values in Table 4.2.6.8 are for scattering by isolated atoms.

International Tables for Crystallography (2006). Vol. C, Chapter 4.3, pp. 259–429.

4.3. Electron diffraction

By C. Colliex, J. M. Cowley, S. L. Dudarev, M. Fink, J. Gjønnes, R. Hilderbrandt, A. Howie, D. F. Lynch, L. M. Peng, G. Ren, A. W. Ross, V. H. Smith Jr, J. C. H. Spence, J. W. Steeds, J. Wang, M. J. Whelan and B. B. Zvyagin

4.3.1. Scattering factors for the diffraction of electrons by crystalline solids (By J. M. Cowley)

4.3.1.1. *Elastic scattering from a perfect crystal*

The most important interaction of electrons with crystalline matter is the interaction with the electrostatic potential field. The scattering into sharp, Bragg reflections is considered in terms of the interaction of an incident plane wave with a time-independent, averaged, periodic potential field which may be written

$$\varphi(\mathbf{r}) = \frac{1}{\Omega}\sum_{\mathbf{h}} V(\mathbf{h})\exp\{-2\pi i\mathbf{h}\cdot\mathbf{r}\}, \tag{4.3.1.1}$$

where Ω is the unit-cell volume and the Fourier coefficients, $V(\mathbf{h})$, may be referred to as the structure amplitudes corresponding to the reciprocal-lattice vectors $\mathbf{h}$. In conformity with the crystallographic sign convention used thoughout this volume [see also Volume B (*IT* B, 1992)], we choose a free-electron approximation for the incident electron beam of the form $\exp(-i\mathbf{k}\cdot\mathbf{r})$ and the interaction is represented by inserting the potential (4.3.1.1) in the Schrödinger wave equation

$$\nabla^2\psi(r) + 2k\sigma\{E + \varphi(r)\}\psi(r) = 0, \tag{4.3.1.2}$$

where eE is the kinetic energy of the incident beam, $k\,(= 2\pi/\lambda)$ is the magnitude of the wavevector for the incident electrons, and σ is an 'interaction constant' defined by

$$\sigma = 2\pi me\lambda/h^2, \tag{4.3.1.3}$$

where h is Planck's constant. Relativistic values of m and λ are assumed (see Subsection 4.3.1.4).

The solution of equation (4.3.1.2), subject to the boundary conditions imposed by the need to fit the waves in the crystal with the incoming and outgoing waves in vacuum at the crystal surfaces, then allows the directions and amplitudes of the diffracted beams to be obtained in terms of the crystal periodicities and the Fourier coefficients, $V(\mathbf{h})$, of $\varphi(\mathbf{r})$ by the eigenvalue or Bloch-wave method (Bethe, 1928).

Alternatively, the scattered amplitudes may be obtained from the integral form of (4.3.1.2),

$$\psi(\mathbf{r}) = \exp\{-i\mathbf{k}_0\cdot\mathbf{r}\} + K\int \frac{\exp\{-ik|\mathbf{r}-\mathbf{r}'|\}}{|\mathbf{r}-\mathbf{r}'|}\varphi(\mathbf{r}')\psi(\mathbf{r}')\,\mathrm{d}\tau_{\mathbf{r}'}, \tag{4.3.1.4}$$

where $\exp\{-i\mathbf{k}_0\cdot\mathbf{r}\}$ represents the incident beam, $K = \sigma/\lambda$, and the integral is taken over the space of the variable, $\mathbf{r}'$. An iterative solution of (4.3.1.4) leads to the Born series,

$$\psi = \psi_0 + \psi_1 + \psi_2 + \ldots,$$

where

$$\psi_0 = \exp\{-i\mathbf{k}_0\cdot\mathbf{r}\}$$

and

$$\psi_n(\mathbf{r}) = K\int \frac{\exp\{-ik|\mathbf{r}-\mathbf{r}'|\}}{|\mathbf{r}-\mathbf{r}'|}\varphi(\mathbf{r}')\psi_{n-1}(\mathbf{r}')\,\mathrm{d}\tau_{\mathbf{r}'}, \tag{4.3.1.5}$$

for $n \geq 1$. Terms of the series for $n = 1, 2, \ldots$ may be considered to represent the contributions from single, double and multiple scattering of the incident electron beam. This method has been applied to the diffraction from crystals by Fujiwara (1959).

A further formulation of the scattering problem in integral form is that due to Cowley & Moodie (1957) who considered the progressive modification of an incident plane wave as it passed through successive thin slices of a crystal. The effect of the nth slice on the incident electron wave is that of a phase-grating so that the wavefunction is modified by multiplication by a transmission function,

$$q_n(xy) = \exp\{-i\sigma\varphi_n(xy)\}, \tag{4.3.1.6}$$

where $\varphi_n(xy)$ is the projection of the potential distribution within the slice in the direction of the incident beam, taken to be the z axis;

$$\varphi_n(x, y) = \int_{z_n}^{z_n+\Delta z} \varphi(x, y, z)\,\mathrm{d}z. \tag{4.3.1.7}$$

Propagation of the wave between the centres of slices is represented by convolution with a propagation function, $p(xy)$, so that the wave entering the $(n+1)$th slice may be written

$$\psi_{n+1}(xy) = [\psi_n(xy)\cdot q_n(xy)] * p_n(xy). \tag{4.3.1.8}$$

In the small-angle approximation, the function $p_n(xy)$ is given by the usual Fresnel diffraction theory as

$$p(xy) = (i/\lambda\Delta z)\exp\{-ik(x^2+y^2)/2\Delta z\}. \tag{4.3.1.9}$$

In the limit that the slice thickness, Δz, tends to zero, the iteration of (4.3.1.8) gives an exact account of the diffraction by the crystal.

On the basis of the above-mentioned and other related formulations of the diffraction problem, several computing methods have been devised for calculation of the amplitudes and intensities of the many diffracted beams of appreciable intensity that may emerge simultaneously from a crystal (see Section 4.3.6). In this way, a degree of accuracy may be achieved in the calculation of the intensities of spots in diffraction patterns or of the contrast in electron-microscope images of crystals (Section 4.3.8).

4.3.1.2. *Atomic scattering factors*

All such calculations require a knowledge of the potential distribution, $\varphi(\mathbf{r})$, or its Fourier coefficients, $V(\mathbf{h})$. It is usually convenient to express the potential distribution in terms of the sum of contributions of individual atoms centred at the positions $\mathbf{r} = \mathbf{r}_i$. Thus:

$$\varphi(\mathbf{r}) = \sum_i \varphi_i(\mathbf{r} - \mathbf{r}_i) \tag{4.3.1.10}$$

or, in terms of the Fourier transforms, V_i, of the $\varphi_i(\mathbf{r})$

$$V(\mathbf{h}) = \sum_i V_i(\mathbf{h})\exp\{+2\pi i\mathbf{h}\cdot\mathbf{r}_i\}. \tag{4.3.1.11}$$

As a first approximation, the functions $\varphi_i(\mathbf{r})$ may be identified with the potential distributions for individual, isolated atoms or ions, with the usual spreading due to thermal motion. The interatomic binding and the interactions of ions that are thereby neglected may have important effects on diffraction intensities in some cases.

In this approximation, the Fourier transforms for individual atoms may be written

Copyright © 2006 International Union of Crystallography

$$V_i(s) = f_i^B(s)/K, \tag{4.3.1.12}$$

where $s = 4\pi\lambda^{-1}\sin\theta = |\mathbf{k} - \mathbf{k}_0|$ and the f^B are the Born electron scattering amplitudes, as conventionally defined, in units of Å. Here θ is half the scattering angle and, again, $K = \sigma/\lambda$. Some values of $f^B(s)$ listed in the accompanying Tables 4.3.1.1 and 4.3.1.2 are obtained from the atomic potentials $\varphi_0(\mathbf{r})$ for isolated, spherically symmetrical atoms or ions by the relation

$$f^B(s) = 4\pi K \int_0^\infty r^2\varphi(r)\frac{\sin sr}{sr}\,\mathrm{d}r. \tag{4.3.1.13}$$

By the use of Poisson's equation relating the potential and charge-density distributions, it is possible to derive the Mott–Bethe formula for $f^B(s)$ in terms of the atomic scattering factors for X-rays, $f_x(s)$:

$$f^B(s) = 2\pi\frac{me^2}{h^2\varepsilon_0}\{Z - f_x(s)\}/s^2, \tag{4.3.1.14}$$

where ε_0 is the permittivity of vacuum, or

$$f^B(s) = 0.023934\,\lambda^2\{Z - f_x(s)\}/\sin^2\theta \tag{4.3.1.15}$$

[for λ in Å, $f^B(s)$ in Å, and $f_x(s)$ in electron units]. This was used for the other listed $f^B(s)$ values.

4.3.1.3. *Approximations of restricted validity*

(*a*) *Kinematical approximation*. In the limiting case of a vanishingly weak interaction of the incident electrons with the scattering potential of the crystal, the Born series (4.3.1.5) may be terminated at the term ψ_1, corresponding to single scattering. Then the diffracted wave is given for a potential $\varphi(r)$ as $\psi(\mathbf{s})(\exp -ikR)/R$, with

$$\psi(\mathbf{s}) = K\int\varphi(\mathbf{r})\exp\{i[\mathbf{r}\cdot\mathbf{s}]\}\,\mathrm{d}\tau_\mathbf{r}, \tag{4.3.1.16}$$

where R is the distance to the point of observation. For a periodic potential, $\varphi(\mathbf{r})$, the scattering amplitude for the $\mathbf{h}$ beam is

$$\psi(\mathbf{h}) = NK\int\varphi(\mathbf{r})\exp\{2\pi i\mathbf{h}\cdot\mathbf{r}\}\,\mathrm{d}\tau_\mathbf{r}, \tag{4.3.1.17}$$

where the integral is taken over one unit cell and N is the number of unit cells. From (4.3.1.16), it then follows that the scattering amplitude $\psi(\mathbf{h})$ is proportional to the structure amplitude, $V(\mathbf{h})$;

$$\psi(\mathbf{h}) = NKV(h) \tag{4.3.1.18}$$

$$= NK\sum_i f_{\mathrm{el},i}(\mathbf{h})\exp\{2\pi i\,\mathbf{h}\cdot\mathbf{r}_i\}. \tag{4.3.1.19}$$

The intensity of the $\mathbf{h}$ diffracted beam is then proportional to $\psi(\mathbf{h})\psi^*(\mathbf{h})$, and so to $|V(\mathbf{h})|^2$.

Similarly, we may write the differential scattering cross section for the scattering from a single isolated atom as

$$|f^B(s)|^2 = K^2|V_i(s)|^2. \tag{4.3.1.20}$$

(*b*) *Two-beam approximation*. For some specific orientations of a crystal of relatively simple structure, the incident beam may be close to the Bragg angle for a strong, inner reflection but not for any other reflection. Then the approximation may be made that only those beams with indices $\mathbf{0}$ and $\mathbf{h}$ have appreciable intensity. The intensities of these beams for a parallel-sided, plate-shaped, centrosymmetric crystal are given in MacGillary's (1940) development of the theory of Bethe (1928) as

$$I(\mathbf{h}) = I_0\{\sigma V(\mathbf{h})\}^2\frac{\sin^2\{\pi t(\zeta_\mathbf{h}^2 + \xi_\mathbf{h}^{-2})^{1/2}\}}{\pi^2(\zeta_\mathbf{h}^2 + \xi_\mathbf{h}^{-2})} \tag{4.3.1.21}$$

and $I(\mathbf{0}) = I_0 - I(\mathbf{h})$, where I_0 is the incident-beam intensity, t is the crystal thickness, $\xi_\mathbf{h}$ is the extinction distance given by $\xi_\mathbf{h} = \pi/\sigma V(\mathbf{h})$, and $\zeta_\mathbf{h}$ is the excitation error which measures the distance of the reciprocal-lattice point $\mathbf{h}$ from the Ewald sphere.

A formula due to Blackman (1939), obtained by integrating (4.3.1.21) over $\xi_\mathbf{h}$, provides a useful first approximation for the intensities of ring or arc patterns given by polycrystalline material (see Section 2.5.2).

(*c*) *Phase-grating approximations*. For extremely thin crystals, the scattering can be approximated by that of a two-dimensional potential distribution given by projection of the three-dimensional distribution in the beam direction. Then, by analogy with (4.3.1.6), the emerging wave is

$$\psi(xy) = \exp\{-i\sigma\varphi(xy)\} \tag{4.3.1.22}$$

when

$$\varphi(xy) = \int_0^H \varphi(xyz)\,\mathrm{d}z \tag{4.3.1.23}$$

and the diffraction amplitudes are given by the Fourier transform of this expression.

For thicker crystals, this approximation applies in the limit of very high electron-accelerating voltage, with the value of σ appropriate for the Compton wavelength, $\lambda = 0.024262$ Å, *viz* $\sigma = 0.0005068$.

It may be noted that for the special case of a single layer of atoms the solution of the wave equations (4.3.1.2) or (4.3.1.4), with the real potential (4.3.1.1) inserted, leads to a form equivalent to the Moliere high-energy approximation for the scattering by single atoms, namely

$$KV(s) = -\frac{i}{\lambda}\int_{-\infty}^{\infty}\{\exp[-i\sigma\varphi(\boldsymbol{\rho})] - 1\}\exp\{i\,\boldsymbol{\rho}\cdot\mathbf{s}\}\,\mathrm{d}^2\boldsymbol{\rho}, \tag{4.3.1.24}$$

where $\boldsymbol{\rho}$ is a two-dimensional vector with components x, y, and

$$\varphi(\boldsymbol{\rho}) = \int_{-\infty}^{\infty}\varphi(\boldsymbol{\rho}, z)\,\mathrm{d}z, \tag{4.3.1.25}$$

and this, in the low-angle approximation, is the same as (4.3.1.23). Then the scattered amplitude can be considered as made up from contributions from individual atoms that are equal (apart from bonding effects) to the complex atomic scattering amplitudes tabulated in connection with the diffraction of electrons by gases.

4.3.1.4. *Relativistic effects*

It has been shown by Fujiwara (1961) that, at least for electron energies up to 1 MeV or so, the relativistic effects on diffraction amplitudes and geometry are adequately described by the use of relativisitically corrected values for the mass and wavelength of the electrons;

$$m = m_0(1 - \beta^2)^{-1/2} \tag{4.3.1.26}$$

$$\lambda = h\Big/\left[2em_0E\left(1 + \frac{eE}{2m_0c^2}\right)\right]^{1/2} = \lambda_c\frac{(1-\beta^2)^{1/2}}{\beta}$$
$$= 12.2639/(E + 0.97845\times10^{-6}E^2)^{1/2}, \tag{4.3.1.27}$$

where m_0 is the rest mass, λ_c is the Compton wavelength $\beta = \nu/c$, and λ is given in Å if E is in volts. Consequently, σ varies with the incident electron energy as $[1 + h^2/m_0^2c^2\lambda^2)]^{1/2}$, or

$$\sigma = 2\pi/\{\lambda E[1 + (1 - \beta^2)^{1/2}]\}.$$

Values of λ, λ^{-1}, m/m_0, $\beta = \nu/c$, and σ are listed for various values of the accelerating voltage, E, in Table 4.3.2.1 with λ in Å and E in volts.

4.3.1.5. *Absorption effects*

Any scattering process, whether elastic or inelastic, which removes energy from the set of diffracted beams being considered, may be said to constitute an absorption process. For example, for a measurement of the intensities of the elastically scattered, sharp Bragg reflections from a crystal, any process which gives diffuse background scattering or results in a detectable loss of energy gives rise to absorption.

The diffracted amplitudes in such cases may be calculated, at least as a first approximation, in terms of a complex potential, $\varphi_c(\mathbf{r})$, containing an imaginary part $\varphi_i(r)$ due to an 'absorption function' and a small added real part $\Delta\varphi(r)$. Then under the crystallographic sign convention, $\varphi_c(r) = \varphi(r) - i\varphi_i(r) + \Delta\varphi(r)$. Correspondingly, for a centrosymmetric crystal, the structure amplitude becomes complex and may be written

$$V(\mathbf{h}) = V_0(\mathbf{h}) - iV'(\mathbf{h}) + V''(\mathbf{h}). \qquad (4.3.1.28)$$

Under the appropriate conditions of observation, important contributions to the imaginary and real additions to the structure amplitudes may be given by the excitation of phonons, plasmons, or electron transitions, or by diffuse scattering due to crystal defects or disorder.

The additional terms $iV'(\mathbf{h})$ and $V''(\mathbf{h})$, however, are not invariant properties of the crystal structure but depend on the conditions of the diffraction experiment, such as the accelerating voltage and orientation of the incident beam, the aperture or resolution of the recording system, and the use of energy filtering or discrimination. In spite of this, it may often be convenient to treat them as being produced by phenomenological complex potentials, defined for a limited range of experimental conditions.

4.3.1.6. *Tables of atomic scattering amplitudes for electrons*

Tables 4.3.1.1 and 4.3.1.2 list values of $f^B(s)$ in Å for all neutral atoms and most chemically significant ions, respectively. The values have been given by Doyle & Turner (1968) for several cases, denoted by RHF using the relativistic Hartree–Fock atomic potentials of Coulthard (1967). For all other atoms and ions, $f^B(s)$ has been found using the Mott–Bethe formula [equation (4.3.1.15)] for $s \neq 0$, and the X-ray scattering factors of Table 2.2A of *IT* IV (1974). Thus all other neutral atoms except hydrogen are based on the relativistic Hartree–Fock wavefunctions of Mann (1968). These are designated by *RHF. For H and for ions below Rb, denoted by HF, $f^B(s)$ is ultimately based on the nonrelativistic Hartree–Fock wavefunctions of Mann (1968). For ions above Rb, denoted by *DS, modified relativistic Dirac–Slater wavefunctions calculated by Cromer & Waber (1974) are used.

For low values of s, the Mott formula becomes less accurate, since $[Z - f_x(s)]$ tends to zero with s for neutral atoms. Except for the RHF atoms, $f^B(s)$ for s from 0.01 to 0.03 are omitted in Table 4.3.1.1 and for s from 0.04 to 0.11, only two decimal places are given. $f^B(s)$ is then accurate to the figure quoted. For these atoms, $f^B(0)$ was found using the formula given by Ibers (1958):

$$f^B(0) = \frac{4\pi m e^2}{3h^2} Z\langle r^2\rangle, \qquad (4.3.1.29)$$

where $\langle r^2\rangle$ is the mean-square atomic radius.

For ionized atoms, $f_{\rm el}(0) = \pm\infty$. The values listed at $s = 0$ in Table 4.3.1.2 for RHF atoms were calculated by Doyle & Turner (1968) with $\varphi(r)$ in equation (4.3.1.13) replaced by $\varphi'(\mathbf{r})$, where

$$\varphi'(\mathbf{r}) = \varphi(\mathbf{r}) - e\Delta Z/r. \qquad (4.3.1.30)$$

Here, ΔZ is the ionic charge. This approach omits the Coulomb field due to the excess or deficiency of charge on the nucleus. With the use of these values, the structure factor for forward scattering by a neutral unit cell containing ions may be found in the conventional way. Similar values are not available for other ions because the atomic potential data are lacking.

For computer applications, numerical approximations to the $f(s)$ of these tables have been given by Doyle & Turner (1968) as sums of Gaussians for the range $s = 0$ to $2\,\text{Å}^{-1}$. An alternative is to make Gaussian fits to X-ray scattering factors, then use the Mott formula to derive electron scattering factors. As discussed by Peng & Cowley (1988), this practice may lead to problems for small values of s. An additional problem occurs in high-resolution electron-microscopy (HREM) image-simulation programs, where it is usually necessary to have electron scattering factors for the range 0 to $6\,\text{Å}^{-1}$. Fox, O'Keefe & Tabbernor (1989) point out that extrapolation of the Gaussian fits of Doyle & Turner (1968) to values past $2\,\text{Å}^{-1}$ can be highly inaccurate. For the range of s from 2 to $6\,\text{Å}^{-1}$, Fox *et al*. have used sums of polynomials to make accurate fits to the X-ray scattering factors of Doyle & Turner (1968) for many elements (Section 6.1.1), and electron scattering factors can be generated from these data by use of the Mott formula.

Recently, Rez, Rez & Grant (1994) have published new tables of X-ray scattering factors obtained using a multiconfiguration Dirac–Fock code and two parameterizations in terms of four Gaussians, one of higher accuracy over the range of about $2\,\text{Å}^{-1}$ and the other of lower accuracy over the extended range of about $6\,\text{Å}^{-1}$. These authors suggest that electron scattering factors may best be obtained from these X-ray scattering factors by using the Mott formula. They provide a table of values for the electron scattering factor values for zero scattering angle, $f_{\rm el}(0)$, for many elements and ions, which may be of value for the calculation of mean inner potentials.

4.3.1.7. *Use of Tables 4.3.1.1 and 4.3.1.2*

In order to calculate the Fourier coefficients $V(\mathbf{h})$ of the potential distribution $\varphi(\mathbf{r})$, for insertion in the formulae used to calculate intensities [such as (4.3.1.6), (4.3.1.20), (4.3.1.21)], or in the numerical methods for dynamical diffraction calculations, use

$$V(\mathbf{h})(\text{in volts}) = 47.87801\Phi(\mathbf{h})/\Omega, \qquad (4.3.1.31)$$

where

$$\Phi(\mathbf{h}) = \sum_i f_i \exp\{2\pi i\, \mathbf{h}\cdot\mathbf{r}_i\}. \qquad (4.3.1.32)$$

The f_i values are obtained from Tables 4.3.1.1 and 4.3.1.2, and Ω is the unit-cell volume in Å^3. The $V(\mathbf{h})$ and the f_i tabulated are properties of the crystal structure and the isolated atoms, respectively, and are independent of the particular scattering theory assumed.

Expressions for the calculation of intensities in the kinematical approximation are given for powder patterns and oblique texture patterns in Section 2.5.3, and for thin crystal plates in Section 2.5.1 of Volume B (*IT* B, 1992). Since the formulas for kinematical scattering, such as (4.3.1.19) and (4.3.1.20), include the parameter $K = \sigma/\lambda$, which varies with the energy of the electron beam through relativistic effects, it may be considered

that the electron scattering factors for kinematical calculations should be multiplied by relativistic factors.

For high-energy electrons, the relativistic variations of the electron mass, the electron wavelength and the interaction constant, σ, become significant. The relations are

$$m = m_0(1-\beta^2)^{-1/2},$$
$$\lambda = h\left[2em_0E\left(1+\frac{eE}{2m_0c^2}\right)\right]^{-1/2} = \lambda_c\frac{(1-\beta^2)^{1/2}}{\beta}, \quad (4.3.1.33)$$

where m_0 is the rest mass, λ_c is the Compton wavelength, h/m_0c, and $\beta = v/c$. Consequently, σ varies with the incident electron energy as

$$\sigma = 2\pi/\{\lambda E[1+(1-\beta^2)^{1/2}]\} = 2\pi e/hc\beta. \quad (4.3.1.34)$$

For the calculation of intensities in the kinematical approximation, the values of $f^B(s)$ listed in Tables 4.3.1.1 and 4.3.1.2, which were calculated using m_0, must be multiplied by $m/m_0 = (1-\beta^2)^{-1/2}$ for electrons of velocity v. Values of λ, $1/\lambda$, m/m_0, $\beta = v/c$, and σ are listed for various values of the accelerating voltage, E, in Table 4.3.2.1.

4.3.2. Parameterizations of electron atomic scattering factors (By J. M. Cowley, L. M. Peng, G. Ren, S. L. Dudarev, and M. J. Whelan)

For computer applications, numerical approximations to the $f(s)$ of Tables 4.3.1.1 or 4.3.1.2 are usually preferred and various approximations as sums of Gaussians have been proposed. The initial Gaussian fits were given by Doyle & Turner (1968) for the range $s = 0$ to $2\,\text{Å}^{-1}$. However, for some purposes, as in the image-simulation programs for high-resolution electron microscopy, atomic scattering factors are needed for higher s values, up to $6\,\text{Å}^{-1}$, and, as pointed out by Fox, O'Keefe & Tabbernor (1989), extrapolation of the Gaussian fits of Doyle & Turner to values above $2\,\text{Å}^{-1}$ can be highly inaccurate.

An alternative approach to obtaining numerical values for the electron scattering factors is to make use of the polynomial fits to X-ray scattering factors of Fox *et al*. or the more recent tables of X-ray scattering factors produced by Rez, Rez & Grant (1994), who used a multiconfiguration Dirac–Fock code and two parameterizations in terms of four Gaussians, one of higher accuracy over the range of about $2\,\text{Å}^{-1}$ and the other of lower accuracy over the extended range of about $6\,\text{Å}^{-1}$. The electron scattering factors may then be derived from the X-ray scattering factors by use of the Mott formula (4.3.1.14). For small angles of scattering, the determination of electron scattering factors in this way may give problems, since the X-ray scattering factor tends to the atomic number, and both the numerator and denominator of (4.3.1.14) tend to zero. However, the electron scattering factor may be determined for zero scattering angle using equation (4.3.1.29) and Rez, Rez & Grant (1994) listed values of $f_{\rm el}(0)$ for many elements and ions.

Recently, Peng, Ren, Dudarev & Whelan (1996) have developed a new algorithm, based on a combined modified simulated-annealing and least-squares method, to parameterize both the elastic and absorptive scattering factors as sums of five Gaussians of the form

$$f_{\rm el}(s) = \sum_{i=1}^{n} a_i \exp\left(-b_i s^2\right), \quad (4.3.2.1)$$

where a_i and b_i are fitting parameters. The values of their fitting parameters for the range of s values from 0 to 2.0 for elastic electron scattering factors for all neutral atoms with atomic numbers up to 98 are given in Table 4.3.2.2 and the values obtained separately for these atoms for the range of s from 0 to $6.0\,\text{Å}^{-1}$ are given in Table 4.3.2.3. For Table 4.3.2.2, the fitting was made to the values of f given in Table 4.3.1.1. For Table 4.3.2.3, the f values in the range of s from 2.0 to $6.0\,\text{Å}^{-1}$ were those obtained by using the Mott formula to convert the X-ray scattering factors derived from the Dirac–Fock calculations of Rez, Rez & Grant (1994). Similar tables for atomic scattering factors of ions can be found in Peng (1998).

As an indication of the accuracy with which the parameterized f values of (4.3.2.1) reproduce the numerical values of the reference f values, Peng *et al*. (1996) computed values of $\varepsilon = 100\,\sigma/f(0)$, where σ is the square root of the mean square deviation, σ^2, between the numerical and fitted scattering factors. The values of ε are typically in the range 0.02 to 0.05, and are consistently smaller (with a few exceptions) than the corresponding values given for the parameterizations of previous workers (Weickenmeier & Kohl, 1991; Bird & King, 1990; Doyle & Turner, 1968).

For the absorptive scattering factors, corresponding to the imaginary parts added to the real elastic scattering factors as a consequence of inelastic scattering processes, Peng *et al*. (1996) have tabulated values for particular elemental crystals and a selection of crystals of compounds having the zinc-blend structure. The main contribution to the absorptive scattering factors arises from the thermal vibrations of the atoms in the crystals so that the numerical values are not characteristic of the individual atom types but depend on the type of bonding of the atoms in the crystal, as indicated by the Debye–Waller factor, and must be calculated separately for each temperature. The authors offer copies of their computer programs, freely available *via* electronic mail, from which the parameterization of the absorptive scattering factors can be derived for other materials and temperatures, given the values of the atomic numbers of the elements, the Debye–Waller factor and the electron accelerating voltage.

4.3.3. Complex scattering factors for the diffraction of electrons by gases (By A. W. Ross, M. Fink, R. Hilderbrandt, J. Wang, and V. H. Smith Jr)

4.3.3.1. *Introduction*

This section includes tables of scattering factors of interest for gas-phase electron diffraction from atoms and molecules in the keV energy region. In addition to the tables and a description of their uses, a discussion of the theoretical uncertainties related to the material in the tables is also provided. The tables give scattering factors for elastic and inelastic scattering from free atoms. The theory of molecular scattering based on these atomic quantities is also discussed.

4.3.3.2. *Complex atomic scattering factors for electrons*

4.3.3.2.1. *Elastic scattering factors for atoms*

It has long been known that the first Born approximation provides an inadequate description at the 4% accuracy level for elastic and total differential cross sections in the 40 keV energy range for atoms heavier than Ne (Schomaker & Glauber, 1952; Glauber & Schomaker, 1953). Results of early experimental work have been confirmed for both atomic and molecular

(*continued on page* 388)

Table 4.3.1.1. *Atomic scattering amplitudes (Å) for electrons for neutral atoms*

Self-consistent field calculations: HF: non-relativistic Hartree–Fock; RHF, *RHF: relativistic Hartree–Fock.

$(\sin\theta)/\lambda$ (Å^{-1})	Element	H	He	Li	Be	B	C	N	O	F	Ne	Na
	Z	1	2	3	4	5	6	7	8	9	10	11
	Method	HF	RHF	RHF	RHF	RHF	RHF	RHF	RHF	RHF	RHF	RHF
0.00		0.529	0.418	3.286	3.052	2.794	2.509	2.211	1.983	1.801	1.652	4.778
0.01			0.418	3.265	3.042	2.788	2.505	2.209	1.982	1.800	1.651	4.749
0.02			0.417	3.200	3.011	2.768	2.492	2.201	1.976	1.796	1.648	4.663
0.03			0.415	3.097	2.961	2.736	2.471	2.187	1.966	1.789	1.642	4.527
0.04		0.51	0.413	2.961	2.892	2.693	2.442	2.168	1.953	1.779	1.635	4.348
0.05		0.51	0.410	2.800	2.807	2.638	2.406	2.144	1.937	1.767	1.626	4.138
0.06		0.50	0.407	2.622	2.710	2.574	2.363	2.116	1.917	1.752	1.615	3.908
0.07		0.49	0.404	2.435	2.601	2.502	2.313	2.083	1.893	1.735	1.602	3.667
0.08		0.48	0.399	2.245	2.484	2.423	2.259	2.047	1.867	1.716	1.587	3.425
0.09		0.47	0.395	2.058	2.362	2.339	2.200	2.007	1.839	1.694	1.570	3.190
0.10		0.45	0.390	1.879	2.237	2.250	2.138	1.963	1.808	1.671	1.552	2.967
0.11		0.44	0.384	1.710	2.111	2.159	2.072	1.918	1.774	1.646	1.533	2.759
0.12		0.425	0.378	1.554	1.987	2.067	2.005	1.870	1.739	1.619	1.512	2.569
0.13		0.411	0.372	1.411	1.865	1.974	1.936	1.821	1.702	1.591	1.490	2.395
0.14		0.396	0.366	1.282	1.748	1.882	1.866	1.770	1.664	1.562	1.467	2.239
0.15		0.382	0.359	1.166	1.635	1.791	1.796	1.718	1.625	1.532	1.443	2.099
0.16		0.366	0.352	1.063	1.528	1.702	1.727	1.666	1.585	1.501	1.418	1.974
0.17		0.353	0.345	0.971	1.427	1.616	1.658	1.614	1.545	1.469	1.393	1.863
0.18		0.338	0.338	0.889	1.332	1.533	1.591	1.561	1.504	1.436	1.367	1.763
0.19		0.324	0.330	0.817	1.243	1.453	1.524	1.510	1.463	1.404	1.340	1.674
0.20		0.311	0.323	0.753	1.161	1.377	1.460	1.458	1.422	1.371	1.313	1.594
0.22		0.285	0.308	0.646	1.013	1.235	1.337	1.358	1.341	1.304	1.259	1.458
0.24		0.261	0.293	0.562	0.887	1.107	1.222	1.262	1.261	1.238	1.204	1.344
0.25		0.249	0.286	0.526	0.832	1.048	1.168	1.216	1.222	1.206	1.176	1.295
0.26		0.238	0.278	0.494	0.781	0.993	1.117	1.171	1.184	1.173	1.149	1.249
0.28		0.218	0.264	0.440	0.690	0.892	1.020	1.085	1.110	1.110	1.095	1.167
0.30		0.199	0.250	0.396	0.614	0.803	0.932	1.006	1.040	1.049	1.043	1.095
0.32		0.182	0.236	0.359	0.549	0.725	0.853	0.932	0.974	0.991	0.991	1.031
0.34		0.167	0.224	0.328	0.494	0.657	0.781	0.863	0.911	0.935	0.942	0.973
0.35		0.160	0.217	0.314	0.469	0.625	0.748	0.831	0.881	0.908	0.918	0.946
0.36		0.153	0.211	0.301	0.446	0.596	0.717	0.800	0.853	0.882	0.894	0.921
0.38		0.141	0.200	0.279	0.406	0.543	0.658	0.742	0.798	0.831	0.849	0.872
0.40		0.130	0.189	0.259	0.371	0.497	0.606	0.689	0.747	0.784	0.805	0.827
0.42		0.120	0.178	0.241	0.341	0.455	0.559	0.641	0.700	0.739	0.764	0.785
0.44		0.111	0.169	0.226	0.314	0.419	0.517	0.596	0.656	0.697	0.725	0.746
0.45		0.107	0.164	0.219	0.302	0.402	0.497	0.575	0.635	0.677	0.706	0.727
0.46		0.103	0.159	0.212	0.291	0.387	0.479	0.555	0.615	0.658	0.687	0.709
0.48		0.096	0.151	0.200	0.271	0.358	0.444	0.518	0.577	0.621	0.652	0.675
0.50		0.089	0.143	0.188	0.253	0.333	0.413	0.484	0.542	0.586	0.619	0.642
0.55		0.075	0.125	0.164	0.215	0.280	0.348	0.411	0.466	0.510	0.544	0.569
0.60		0.064	0.110	0.145	0.186	0.239	0.297	0.353	0.403	0.445	0.479	0.505
0.65		0.055	0.097	0.128	0.164	0.207	0.256	0.305	0.350	0.390	0.424	0.450
0.70		0.048	0.086	0.115	0.145	0.182	0.223	0.266	0.307	0.344	0.376	0.403
0.80		0.037	0.068	0.093	0.117	0.144	0.175	0.208	0.241	0.272	0.300	0.325
0.90		0.029	0.055	0.077	0.096	0.118	0.141	0.167	0.193	0.219	0.244	0.266
1.00		0.024	0.046	0.064	0.081	0.098	0.117	0.137	0.159	0.180	0.201	0.221
1.10		0.020	0.038	0.054	0.069	0.083	0.099	0.115	0.133	0.150	0.168	0.185
1.20		0.017	0.032	0.046	0.059	0.072	0.085	0.098	0.113	0.128	0.143	0.158
1.30		0.014	0.028	0.040	0.051	0.062	0.073	0.085	0.097	0.110	0.123	0.135
1.40		0.012	0.024	0.035	0.045	0.055	0.064	0.074	0.085	0.095	0.106	0.117
1.50		0.011	0.021	0.031	0.040	0.048	0.057	0.065	0.074	0.084	0.093	0.103
1.60			0.019	0.028	0.035	0.043	0.051	0.058	0.066	0.074	0.083	0.092
1.70			0.016	0.024	0.031	0.038	0.045	0.052	0.059	0.066	0.074	0.081
1.80			0.015	0.022	0.028	0.035	0.041	0.047	0.053	0.060	0.066	0.073
1.90			0.013	0.019	0.026	0.031	0.037	0.043	0.048	0.054	0.060	0.065
2.00			0.012	0.017	0.023	0.028	0.034	0.039	0.044	0.049	0.054	0.059

Table 4.3.1.1. *Atomic scattering amplitudes (Å) for electrons for neutral atoms (cont.)*

$(\sin\theta)/\lambda$ (Å^{-1})	Element	Mg	Al	Si	P	S	Cl	Ar	K	Ca	Sc	Ti
	Z	12	13	14	15	16	17	18	19	20	21	22
	Method	RHF	RHF	RHF	RHF	RHF	RHF	RHF	RHF	RHF	RHF	RHF
0.00		5.207	5.889	5.828	5.488	5.161	4.857	4.580	8.984	9.913	9.307	8.776
0.01		5.187	5.867	5.810	5.476	5.152	4.851	4.576	8.921	9.860	9.264	8.740
0.02		5.124	5.800	5.759	5.439	5.124	4.830	4.559	8.731	9.699	9.134	8.631
0.03		5.022	5.692	5.675	5.378	5.079	4.795	4.531	8.434	9.442	8.926	8.455
0.04		4.884	5.547	5.561	5.296	5.016	4.746	4.493	8.054	9.104	8.649	8.220
0.05		4.717	5.371	5.421	5.192	4.938	4.685	4.444	7.619	8.703	8.318	7.937
0.06		4.527	5.170	5.258	5.071	4.845	4.613	4.386	7.157	8.258	7.946	7.618
0.07		4.320	4.949	5.077	4.935	4.740	4.529	4.320	6.691	7.789	7.548	7.274
0.08		4.102	4.717	4.882	4.785	4.623	4.436	4.245	6.239	7.312	7.139	6.917
0.09		3.879	4.478	4.677	4.625	4.496	4.335	4.163	5.815	6.841	6.729	6.556
0.10		3.656	4.237	4.467	4.457	4.362	4.227	4.074	5.426	6.388	6.328	6.199
0.11		3.437	3.999	4.255	4.285	4.222	4.113	3.980	5.073	5.959	5.944	5.853
0.12		3.226	3.767	4.043	4.109	4.078	3.994	3.881	4.756	5.560	5.580	5.522
0.13		3.025	3.544	3.835	3.933	3.931	3.871	3.779	4.474	5.192	5.239	5.209
0.14		2.835	3.330	3.632	3.758	3.783	3.746	3.674	4.222	4.855	4.924	4.916
0.15		2.657	3.128	3.437	3.586	3.635	3.620	3.566	3.997	4.550	4.633	4.643
0.16		2.492	2.938	3.249	3.417	3.487	3.493	3.458	3.795	4.273	4.366	4.390
0.17		2.340	2.760	3.070	3.253	3.342	3.367	3.348	3.612	4.023	4.122	4.157
0.18		2.199	2.595	2.900	3.094	3.200	3.242	3.239	3.446	3.797	3.899	3.943
0.19		2.071	2.441	2.740	2.942	3.061	3.118	3.130	3.295	3.593	3.695	3.745
0.20		1.953	2.299	2.589	2.796	2.927	2.997	3.022	3.154	3.408	3.509	3.564
0.22		1.748	2.046	2.315	2.525	2.671	2.763	2.811	2.902	3.086	3.183	3.242
0.24		1.577	1.832	2.076	2.281	2.436	2.543	2.609	2.680	2.815	2.906	2.967
0.25		1.502	1.737	1.969	2.169	2.326	2.438	2.512	2.578	2.695	2.783	2.844
0.26		1.434	1.650	1.869	2.064	2.221	2.337	2.417	2.481	2.584	2.669	2.730
0.28		1.313	1.495	1.689	1.872	2.026	2.148	2.238	2.299	2.383	2.462	2.523
0.30		1.211	1.363	1.534	1.702	1.851	1.974	2.070	2.134	2.206	2.281	2.341
0.32		1.123	1.251	1.400	1.553	1.694	1.816	1.915	1.982	2.048	2.119	2.178
0.34		1.047	1.154	1.284	1.422	1.554	1.672	1.772	1.842	1.905	1.974	2.032
0.35		1.013	1.111	1.231	1.362	1.490	1.606	1.705	1.776	1.838	1.906	1.964
0.36		0.980	1.070	1.182	1.306	1.429	1.542	1.641	1.714	1.775	1.842	1.899
0.38		0.921	0.997	1.094	1.205	1.318	1.425	1.522	1.595	1.657	1.722	1.778
0.40		0.868	0.932	1.017	1.115	1.218	1.319	1.412	1.487	1.548	1.612	1.668
0.42		0.821	0.875	0.949	1.036	1.130	1.224	1.313	1.387	1.449	1.511	1.566
0.44		0.777	0.825	0.888	0.965	1.051	1.138	1.223	1.295	1.357	1.418	1.472
0.45		0.757	0.801	0.861	0.933	1.014	1.098	1.181	1.252	1.314	1.374	1.428
0.46		0.738	0.779	0.834	0.903	0.980	1.061	1.141	1.211	1.272	1.332	1.385
0.48		0.701	0.737	0.786	0.847	0.917	0.991	1.066	1.134	1.194	1.252	1.305
0.50		0.667	0.700	0.743	0.797	0.860	0.928	0.998	1.064	1.123	1.179	1.230
0.55		0.592	0.618	0.651	0.692	0.741	0.796	0.854	0.912	0.966	1.018	1.067
0.60		0.528	0.551	0.578	0.610	0.648	0.692	0.740	0.790	0.838	0.885	0.930
0.65		0.473	0.494	0.517	0.543	0.573	0.609	0.648	0.690	0.733	0.775	0.816
0.70		0.425	0.445	0.465	0.487	0.513	0.541	0.574	0.609	0.647	0.684	0.721
0.80		0.347	0.366	0.383	0.401	0.419	0.440	0.462	0.488	0.515	0.544	0.573
0.90		0.286	0.304	0.320	0.335	0.350	0.366	0.383	0.402	0.422	0.444	0.467
1.00		0.239	0.255	0.270	0.284	0.298	0.311	0.324	0.339	0.354	0.371	0.389
1.10		0.202	0.217	0.231	0.243	0.255	0.267	0.278	0.290	0.303	0.316	0.330
1.20		0.172	0.185	0.198	0.210	0.221	0.232	0.242	0.252	0.262	0.273	0.285
1.30		0.148	0.160	0.172	0.183	0.193	0.202	0.212	0.220	0.230	0.239	0.249
1.40		0.129	0.139	0.150	0.160	0.169	0.178	0.187	0.194	0.202	0.211	0.219
1.50		0.113	0.123	0.132	0.141	0.150	0.158	0.166	0.174	0.181	0.188	0.195
1.60		0.100	0.109	0.117	0.125	0.133	0.141	0.148	0.156	0.162	0.169	0.175
1.70		0.089	0.096	0.104	0.111	0.119	0.126	0.132	0.138	0.144	0.151	0.157
1.80		0.080	0.087	0.093	0.100	0.107	0.113	0.119	0.127	0.132	0.137	0.143
1.90		0.072	0.078	0.084	0.090	0.096	0.102	0.108	0.112	0.118	0.124	0.129
2.00		0.065	0.070	0.076	0.082	0.087	0.093	0.098	0.101	0.107	0.112	0.117

Table 4.3.1.1. *Atomic scattering amplitudes (Å) for electrons for neutral atoms (cont.)*

$(\sin\theta)/\lambda$ (Å^{-1})	Element	V	Cr	Mn	Fe	Co	Ni	Cu	Zn	Ga	Ge	As
	Z	23	24	25	26	27	28	29	30	31	32	33
	Method	RHF	RHF	RHF	RHF	RHF	RHF	RHF	RHF	RHF	RHF	RHF
0.00		8.305	6.969	7.506	7.165	6.854	6.569	5.600	6.065	7.108	7.378	7.320
0.01		8.274	6.945	7.484	7.145	6.836	6.552	5.587	6.051	7.088	7.359	7.306
0.02		8.180	6.875	7.412	7.081	6.779	6.501	5.547	6.009	7.027	7.303	7.260
0.03		8.029	6.762	7.296	6.978	6.687	6.418	5.482	5.941	6.927	7.211	7.184
0.04		7.826	6.610	7.140	6.839	6.562	6.306	5.395	5.849	6.792	7.088	7.081
0.05		7.581	6.427	6.949	6.669	6.410	6.169	5.287	5.735	6.629	6.935	6.953
0.06		7.303	6.221	6.732	6.474	6.234	6.010	5.165	5.603	6.441	6.759	6.803
0.07		7.002	5.997	6.493	6.260	6.040	5.834	5.029	5.457	6.236	6.562	6.634
0.08		6.686	5.764	6.241	6.032	5.834	5.646	4.886	5.299	6.017	6.351	6.449
0.09		6.365	5.527	5.981	5.796	5.619	5.449	4.737	5.133	5.792	6.129	6.253
0.10		6.045	5.291	5.719	5.558	5.401	5.249	4.585	4.962	5.564	5.902	6.048
0.11		5.732	5.061	5.459	5.320	5.182	5.048	4.434	4.790	5.337	5.672	5.838
0.12		5.430	4.838	5.206	5.087	4.967	4.848	4.285	4.618	5.113	5.442	5.625
0.13		5.142	4.625	4.962	4.861	4.758	4.654	4.139	4.449	4.896	5.217	5.411
0.14		4.871	4.423	4.728	4.644	4.555	4.465	3.998	4.283	4.686	4.996	5.200
0.15		4.616	4.231	4.506	4.436	4.361	4.283	3.862	4.123	4.486	4.783	4.992
0.16		4.378	4.051	4.297	4.240	4.177	4.110	3.731	3.969	4.295	4.578	4.789
0.17		4.158	3.882	4.100	4.054	4.002	3.944	3.607	3.822	4.114	4.382	4.593
0.18		3.953	3.723	3.916	3.880	3.836	3.788	3.488	3.681	3.942	4.195	4.404
0.19		3.763	3.574	3.743	3.716	3.681	3.640	3.375	3.547	3.781	4.017	4.222
0.20		3.588	3.434	3.583	3.562	3.534	3.500	3.267	3.421	3.629	3.849	4.048
0.22		3.276	3.179	3.292	3.284	3.267	3.245	3.067	3.186	3.352	3.541	3.724
0.24		3.006	2.953	3.039	3.039	3.032	3.018	2.885	2.977	3.108	3.268	3.433
0.25		2.885	2.849	2.924	2.928	2.924	2.914	2.800	2.880	2.997	3.143	3.299
0.26		2.772	2.750	2.817	2.824	2.823	2.816	2.719	2.789	2.892	3.026	3.172
0.28		2.568	2.568	2.620	2.632	2.637	2.636	2.568	2.620	2.701	2.813	2.940
0.30		2.386	2.403	2.445	2.461	1.471	2.474	2.428	2.468	2.531	2.623	2.733
0.32		2.225	2.252	2.288	2.308	2.321	2.328	2.299	2.329	2.379	2.455	2.548
0.34		2.079	2.114	2.146	2.168	2.184	2.195	2.180	2.203	2.242	2.304	2.384
0.35		2.011	2.049	2.080	2.104	2.121	2.133	2.123	2.144	2.179	2.235	2.308
0.36		1.947	1.987	2.017	2.042	2.060	2.073	2.069	2.087	2.119	2.169	2.237
0.38		1.826	1.870	1.899	1.925	1.946	1.962	1.965	1.980	2.006	2.048	2.105
0.40		1.716	1.761	1.790	1.818	1.841	1.858	1.868	1.882	1.903	1.938	1.986
0.42		1.614	1.660	1.690	1.719	1.743	1.763	1.777	1.790	1.808	1.837	1.878
0.44		1.520	1.567	1.597	1.628	1.653	1.674	1.691	1.704	1.720	1.745	1.780
0.45		1.476	1.523	1.553	1.584	1.610	1.631	1.651	1.663	1.679	1.702	1.734
0.46		1.433	1.480	1.511	1.542	1.569	1.591	1.611	1.624	1.639	1.661	1.691
0.48		1.352	1.399	1.431	1.462	1.490	1.513	1.535	1.549	1.563	1.583	1.608
0.50		1.277	1.323	1.356	1.388	1.416	1.440	1.464	1.478	1.492	1.510	1.533
0.55		1.111	1.155	1.189	1.222	1.251	1.277	1.303	1.319	1.334	1.349	1.367
0.60		0.973	1.014	1.047	1.080	1.110	1.136	1.163	1.181	1.197	1.212	1.228
0.65		0.856	0.894	0.927	0.959	0.988	1.015	1.041	1.061	1.078	1.093	1.108
0.70		0.757	0.792	0.824	0.854	0.883	0.909	0.935	0.955	0.973	0.989	1.004
0.80		0.602	0.631	0.659	0.686	0.712	0.737	0.761	0.781	0.800	0.817	0.832
0.90		0.490	0.514	0.538	0.561	0.583	0.605	0.626	0.646	0.665	0.681	0.697
1.00		0.408	0.427	0.446	0.466	0.485	0.504	0.523	0.541	0.558	0.574	0.589
1.10		0.345	0.361	0.377	0.393	0.409	0.425	0.442	0.457	0.473	0.488	0.502
1.20		0.297	0.310	0.323	0.336	0.350	0.364	0.378	0.391	0.405	0.418	0.431
1.30		0.259	0.269	0.280	0.291	0.303	0.315	0.327	0.339	0.350	0.362	0.374
1.40		0.228	0.237	0.246	0.255	0.265	0.275	0.285	0.296	0.306	0.317	0.327
1.50		0.203	0.210	0.218	0.226	0.235	0.243	0.252	0.261	0.270	0.279	0.288
1.60		0.182	0.188	‘0.195	0.202	0.209	0.217	0.224	0.232	0.240	0.248	0.256
1.70		0.163	0.169	0.175	0.181	0.188	0.194	0.201	0.208	0.215	0.222	0.229
1.80		0.148	0.154	0.159	0.165	0.170	0.176	0.182	0.188	0.194	0.200	0.206
1.90		0.134	0.139	0.144	0.149	0.154	0.160	0.165	0.170	0.175	0.181	0.187
2.00		0.122	0.127	0.132	0.136	0.141	0.146	0.150	0.155	0.160	0.165	0.170

Table 4.3.1.1. *Atomic scattering amplitudes (Å) for electrons for neutral atoms (cont.)*

$(\sin\theta)/\lambda$ (Å^{-1})	Element	Se	Br	Kr	Rb	Sr	Y	Zr	Nb	Mo	Tc	Ru
	Z	34	35	36	37	38	39	40	41	42	43	44
	Method	RHF	RHF	RHF	RHF	RHF	*RHF	*RHF	*RHF	*RHF	*RHF	*RHF
0.00		7.205	7.060	6.897	11.778	13.109	12.674	12.166	10.679	10.260	10.856	9.558
0.01		7.192	7.049	6.889	11.699	13.035				10.230		
0.02		7.154	7.016	6.861	11.460	12.816				10.138		
0.03		7.090	6.962	6.814	11.088	12.468				9.989		
0.04		7.004	6.888	6.750	10.613	12.013	11.79	11.41	10.13	9.790	10.35	9.18
0.05		6.895	6.795	6.670	10.073	11.476	11.34	11.04	9.86	9.548	10.10	8.99
0.06		6.767	6.684	6.574	9.504	10.888	10.84	10.62	9.54	9.272	9.80	8.77
0.07		6.621	6.558	6.464	8.934	10.273	10.31	10.15	9.20	8.972	9.48	8.53
0.08		6.460	6.418	6.341	8.385	9.655	9.77	9.68	8.85	8.655	9.14	8.27
0.09		6.288	6.266	6.207	7.872	9.052	9.23	9.20	8.49	8.330	8.78	8.00
0.10		6.105	6.104	6.064	7.402	8.478	8.70	8.72	8.12	8.004	8.42	7.73
0.11		5.916	5.935	5.913	6.976	7.940	8.20	8.26	7.77	7.680	8.07	7.46
0.12		5.722	5.760	5.755	6.593	7.443	7.722	7.818	7.421	7.364	7.720	7.190
0.13		5.525	5.580	5.593	6.248	6.988	7.278	7.400	7.090	7.058	7.383	6.928
0.14		5.328	5.399	5.428	5.938	6.575	6.865	7.007	6.772	6.763	7.057	6.672
0.15		5.132	5.217	5.260	5.658	6.200	6.485	6.640	6.472	6.481	6.746	6.426
0.16		4.938	5.036	5.092	5.403	5.862	6.136	6.299	6.187	6.213	6.451	6.188
0.17		4.749	4.857	4.925	5.170	5.555	5.816	5.983	5.918	5.957	6.171	5.960
0.18		4.564	4.680	4.759	4.954	5.278	5.523	5.689	5.665	5.715	5.907	5.741
0.19		4.384	4.507	4.595	4.754	5.025	5.254	5.419	5.427	5.486	5.658	5.533
0.20		4.211	4.339	4.434	4.566	4.794	5.008	5.168	5.203	5.269	5.423	5.332
0.22		3.884	4.017	4.123	4.224	4.387	4.570	4.721	4.792	4.868	4.994	4.959
0.24		3.585	3.718	3.829	3.916	4.039	4.195	4.333	4.426	4.507	4.614	4.618
0.25		3.446	3.578	3.690	3.773	3.882	4.027	4.158	4.258	4.341	4.439	4.459
0.26		3.314	3.443	3.556	3.636	3.735	3.869	3.995	4.099	4.182	4.273	4.306
0.28		3.069	3.192	3.303	3.382	3.465	3.583	3.697	3.804	3.888	3.969	4.021
0.30		2.849	2.963	3.071	3.149	3.224	3.329	3.433	3.539	3.622	3.695	3.759
0.32		2.651	2.757	2.858	2.936	3.007	3.101	3.196	3.298	3.379	3.448	3.518
0.34		2.475	2.570	2.665	2.742	2.810	2.895	2.982	3.080	3.158	3.223	3.296
0.35		2.393	2.484	2.575	2.651	2.718	2.799	2.883	2.978	3.054	3.118	3.192
0.36		2.316	2.402	2.490	2.564	2.630	2.708	2.789	2.880	2.955	3.018	3.092
0.38		2.173	2.250	2.330	2.402	2.466	2.538	2.613	2.698	2.770	2.830	2.904
0.40		2.045	2.113	2.186	2.254	2.315	2.383	2.452	2.531	2.600	2.658	2.730
0.42		1.929	1.989	2.055	2.119	2.178	2.241	2.305	2.379	2.444	2.500	2.570
0.44		1.824	1.877	1.936	1.995	2.052	2.111	2.171	2.239	2.300	2.355	2.421
0.45		1.776	1.825	1.881	1.938	1.993	2.049	2.108	2.173	2.233	2.287	2.351
0.46		1.729	1.775	1.828	1.883	1.936	1.991	2.047	2.110	2.168	2.221	2.284
0.48		1.642	1.683	1.730	1.780	1.830	1.881	1.934	1.991	2.046	2.098	2.157
0.50		1.562	1.598	1.640	1.686	1.733	1.780	1.829	1.883	1.934	1.984	2.040
0.55		1.389	1.416	1.447	1.483	1.522	1.562	1.603	1.646	1.690	1.734	1.782
0.60		1.245	1.266	1.290	1.319	1.350	1.383	1.417	1.452	1.490	1.528	1.569
0.65		1.124	1.141	1.160	1.182	1.208	1.235	1.263	1.292	1.324	1.357	1.391
0.70		1.019	1.034	1.050	1.068	1.089	1.111	1.135	1.159	1.185	1.214	1.243
0.80		0.847	0.860	0.873	0.887	0.902	0.918	0.935	0.952	0.971	0.992	1.013
0.90		0.711	0.725	0.737	0.749	0.762	0.774	0.787	0.800	0.814	0.830	0.845
1.00		0.603	0.616	0.628	0.640	0.651	0.662	0.673	0.684	0.695	0.707	0.719
1.10		0.515	0.528	0.540	0.551	0.562	0.572	0.582	0.591	0.601	0.611	0.621
1.20		0.444	0.456	0.467	0.478	0.488	0.498	0.507	0.516	0.525	0.534	0.542
1.30		0.385	0.396	0.407	0.417	0.427	0.436	0.445	0.454	0.462	0.470	0.478
1.40		0.337	0.347	0.357	0.365	0.375	0.384	0.393	0.401	0.408	0.416	0.423
1.50		0.297	0.306	0.315	0.325	0.333	0.341	0.349	0.356	0.364	0.371	0.378
1.60		0.264	0.272	0.280	0.290	0.297	0.303	0.311	0.318	0.325	0.332	0.338
1.70		0.236	0.243	0.250	0.257	0.264	0.272	0.278	0.285	0.291	0.298	0.304
1.80		0.212	0.219	0.225	0.233	0.239	0.244	0.251	0.257	0.263	0.269	0.275
1.90		0.192	0.198	0.204	0.208	0.214	0.221	0.227	0.233	0.238	0.244	0.249
2.00		0.175	0.180	0.185	0.188	0.194	0.201	0.206	0.211	0.216	0.222	0.227

Table 4.3.1.1. *Atomic scattering amplitudes (Å) for electrons for neutral atoms (cont.)*

$(\sin\theta)/\lambda$ (Å^{-1})	Element	Rh	Pd	Ag	Cd	In	Sn	Sb	Te	I	Xe	Cs
	Z	45	46	47	48	49	50	51	52	53	54	55
	Method	*RHF	*RHF	RHF	RHF	RHF	RHF	RHF	*RHF	RHF	RHF	RHF
0.00		9.242	7.583	8.671	9.232	10.434	10.859	10.974	11.003	10.905	10.794	16.508
0.01				8.654	9.213	10.406	10.833	10.950		10.887	10.777	16.391
0.02				8.599	9.153	10.320	10.750	10.876		10.828	10.725	16.050
0.03				8.510	9.057	10.181	10.615	10.755		10.731	10.638	15.521
0.04		8.90	7.43	8.391	8.926	9.995	10.433	10.591	10.65	10.599	10.520	14.855
0.05		8.73	7.35	8.244	8.764	9.768	10.209	10.387	10.47	10.434	10.371	14.106
0.06		8.53	7.26	8.075	8.577	9.509	9.950	10.150	10.25	10.238	10.194	13.326
0.07		8.31	7.16	7.888	8.369	9.224	9.664	9.884	10.01	10.017	9.993	12.556
0.08		8.01	7.03	7.689	8.144	8.923	9.357	9.596	9.74	9.773	9.771	11.823
0.09		7.83	6.91	7.480	7.909	8.612	9.037	9.291	9.46	9.511	9.530	11.145
0.10		7.58	6.77	7.267	7.666	8.297	8.709	8.976	9.16	9.235	9.274	10.525
0.11		7.33	6.62	7.052	7.421	7.983	8.380	8.654	8.85	8.948	9.007	9.965
0.12		7.079	6.474	6.837	7.176	7.674	8.053	8.331	8.538	8.654	8.732	9.458
0.13		6.836	6.319	6.625	6.933	7.374	7.732	8.010	8.224	8.357	8.451	9.000
0.14		6.598	6.162	6.418	6.695	7.084	7.419	7.694	7.914	8.059	8.167	8.583
0.15		6.366	6.003	6.215	6.464	6.805	7.118	7.386	7.608	7.764	7.884	8.201
0.16		6.143	5.843	6.018	6.240	6.539	6.829	7.088	7.309	7.472	7.603	7.848
0.17		5.929	5.684	5.827	6.024	6.286	6.552	6.800	7.018	7.186	7.325	7.519
0.18		5.722	5.526	5.643	5.817	6.045	6.289	6.524	6.738	6.908	7.053	7.212
0.19		5.524	5.369	5.464	5.618	5.817	6.039	6.261	6.467	6.639	6.787	6.922
0.20		5.334	5.214	5.293	5.427	5.601	5.803	6.010	6.209	6.379	6.529	6.649
0.22		4.976	4.913	4.967	5.070	5.203	5.368	5.547	5.727	5.889	6.039	6.143
0.24		4.648	4.626	4.665	4.745	4.846	4.979	5.131	3.291	5.442	5.586	5.684
0.25		4.493	4.487	4.522	4.592	4.682	4.801	4.940	5.090	5.234	5.374	5.471
0.26		4.345	4.352	4.384	4.447	4.525	4.633	4.760	4.899	5.036	5.172	5.268
0.28		4.066	4.093	4.122	4.173	4.236	4.323	4.428	4.548	4.670	4.795	4.890
0.30		3.809	3.850	3.878	3.922	3.973	4.044	4.131	4.234	4.341	4.454	4.547
0.32		3.572	3.622	3.651	3.690	3.734	3.792	3.865	3.952	4.046	4.147	4.235
0.34		3.353	3.408	3.440	3.476	3.515	3.564	3.625	3.700	3.780	3.870	3.953
0.35		3.249	3.306	3.339	3.375	3.412	3.458	3.514	3.583	3.658	3.742	3.822
0.36		3.150	3.208	3.242	3.278	3.313	3.356	3.408	3.472	3.541	3.620	3.697
0.38		2.962	3.022	3.058	3.093	3.127	3.165	3.210	3.265	3.325	3.394	3.465
0.40		2.788	2.848	2.886	2.922	2.955	2.990	3.030	3.078	3.130	3.191	3.255
0.42		2.626	2.686	2.726	2.762	2.795	2.828	2.864	2.907	2.953	3.006	3.064
0.44		2.477	2.535	2.576	2.613	2.646	2.678	2.712	2.750	2.791	2.838	2.890
0.45		2.406	2.464	2.505	2.542	2.576	2.608	2.640	2.677	2.715	2.759	2.809
0.46		2.338	2.395	2.436	2.474	2.507	2.539	2.571	2.606	2.642	2.684	2.731
0.48		2.210	2.264	2.306	2.344	2.378	2.409	2.440	2.473	2.506	2.543	2.586
0.50		2.090	2.143	2.185	2.223	2.257	2.288	2.318	2.350	2.380	2.414	2.453
0.55		1.828	1.875	1.915	1.953	1.987	2.019	2.048	2.077	2.104	2.132	2.163
0.60		1.609	1.650	1.688	1.724	1.758	1.790	1.819	1.847	1.871	1.897	1.923
0.65		1.426	1.462	1.497	1.531	1.563	1.594	1.622	1.649	1.673	1.697	1.721
0.70		1.273	1.304	1.335	1.366	1.397	1.426	1.453	1.479	1.503	1.526	1.548
0.80		1.035	1.058	1.082	1.107	1.132	1.157	1.181	1.205	1.227	1.248	1.269
0.90		0.861	0.879	0.897	0.916	0.936	0.956	0.976	0.997	1.016	1.036	1.055
1.00		0.731	0.745	0.758	0.773	0.789	0.805	0.821	0.838	0.855	0.871	0.888
1.10		0.631	0.641	0.652	0.664	0.676	0.688	0.701	0.715	0.729	0.743	0.758
1.20		0.551	0.559	0.568	0.578	0.587	0.597	0.608	0.619	0.630	0.642	0.654
1.30		0.485	0.493	0.500	0.508	0.516	0.525	0.533	0.542	0.551	0.561	0.570
1.40		0.431	0.437	0.444	0.451	0.458	0.465	0.472	0.480	0.487	0.495	0.502
1.50		0.384	0.391	0.397	0.403	0.409	0.416	0.422	0.428	0.435	0.442	0.450
1.60		0.345	0.351	0.357	0.362	0.368	0.374	0.379	0.385	0.391	0.397	0.405
1.70		0.310	0.316	0.321	0.327	0.332	0.337	0.343	0.348	0.353	0.358	0.363
1.80		0.281	0.286	0.291	0.297	0.302	0.307	0.311	0.316	0.321	0.325	0.332
1.90		0.255	0.260	0.265	0.270	0.274	0.279	0.284	0.288	0.293	0.297	0.299
2.00		0.232	0.237	0.241	0.246	0.250	0.255	0.259	0.264	0.268	0.272	0.272

Table 4.3.1.1. *Atomic scattering amplitudes (Å) for electrons for neutral atoms (cont.)*

$(\sin\theta)/\lambda$ (Å^{-1})	Element	Ba	La	Ce	Pr	Nd	Pm	Sm	Eu	Gd	Tb	Dy
	Z	56	57	58	59	60	61	62	63	64	65	66
	Method	RHF	*RHF	*RHF	*RMF	*RHF	*RHF	*RHF	RHF	*RHF	*RHF	*RHF
0.00		18.267	17.805	17.378	16.987	16.606	16.243	15.897	15.563	15.266	14.974	14.641
0.01		18.157							15.486			
0.02		17.828							15.260			
0.03		17.309							14.898			
0.04		16.636	16.45	16.10	15.62	15.30	14.99	14.70	14.425	14.30	13.90	13.64
0.05		15.854	15.79	15.46	14.94	14.67	14.39	14.12	13.867	13.81	13.37	13.14
0.06		15.008	15.05	14.77	14.22	13.97	13.72	13.48	13.253	13.27	12.81	12.60
0.07		14.138	14.28	14.03	13.47	13.25	13.03	12.81	12.611	12.70	12.22	12.03
0.08		13.278	13.51	13.29	12.72	12.52	12.33	12.14	11.963	12.11	11.62	11.44
0.09		12.431	12.74	12.56	11.99	11.82	11.65	11.49	11.329	11.52	11.02	10.87
0.10		11.675	12.01	11.85	11.29	11.15	11.00	10.86	10.722	10.95	10.45	10.32
0.11		10.958	11.32	11.19	10.65	10.52	10.40	10.27	10.150	10.39	9.91	9.79
0.12		10.302	10.671	10.561	10.052	9.944	9.833	9.722	9.618	9.871	9.407	9.303
0.13		9.707	10.072	9.981	9.506	9.412	9.316	9.218	9.128	9.382	8.942	8.848
0.14		9.168	9.522	9.448	9.008	8.928	8.843	8.758	8.678	8.926	8.512	8.429
0.15		8.682	9.017	8.958	8.556	8.486	8.413	8.336	8.267	8.505	8.121	8.045
0.16		8.241	8.555	8.507	8.144	8.084	8.020	7.953	7.891	8.114	7.761	7.693
0.17		7.840	8.131	8.094	7.768	7.717	7.661	7.602	7.548	7.754	7.430	7.370
0.18		7.474	7.742	7.714	7.424	7.380	7.332	7.280	7.232	7.422	7.128	7.073
0.19		7.139	7.384	7.365	7.107	7.071	7.029	6.983	6.942	7.114	6.849	6.800
0.20		6.829	7.053	7.041	6.815	6.785	6.749	6.710	6.673	6.828	6.591	6.547
0.22		6.275	6.462	6.462	6.291	6.272	6.247	6.218	6.191	6.316	6.127	6.092
0.24		5.791	5.948	5.957	5.831	5.822	5.806	5.787	5.768	5.868	5.720	5.693
0.25		5.570	5.714	5.728	5.620	5.615	5.605	5.589	5.574	5.664	5.534	5.510
0.26		5.361	5.495	5.312	5.421	5.421	5.413	5.402	5.390	5.472	5.358	5.337
0.28		4.975	5.092	5.115	5.053	5.059	5.059	5.055	5.030	5.117	5.030	5.016
0.30		4.628	4.730	4.759	4.719	4.731	4.737	4.739	4.740	4.796	4.731	4.723
0.32		4.313	4.405	4.438	4.414	4.432	4.443	4.450	4.456	4.504	4.457	4.454
0.34		4.028	4.111	4.146	4.136	4.157	4.173	4.185	4.195	4.238	4.205	4.206
0.35		3.893	3.974	4.010	4.006	4.029	4.047	4.060	4.072	4.113	4.086	4.089
0.36		3.769	3.844	3.881	3.882	3.906	3.925	3.940	3.954	3.993	3.971	3.976
0.38		3.533	3.602	3.640	3.648	3.675	3.697	3.715	3.731	3.767	3.755	3.763
0.40		3.318	3.381	3.420	3.434	3.462	3.486	3.306	3.525	3.559	3.554	3.565
0.42		3.123	3.180	3.219	3.238	3.267	3.292	3.314	3.335	3.367	3.368	3.380
0.44		2.944	2.997	3.035	3.057	3.087	3.114	3.137	3.159	3.189	3.194	3.209
0.43		2.861	2.911	2.949	2.973	3.003	3.029	3.053	3.075	3.105	3.113	3.128
0.46		2.781	2.829	2.866	2.891	2.922	2.948	2.973	2.995	3.025	3.034	3.050
0.48		2.631	2.676	2.712	2.739	2.769	2.796	2.821	2.844	2.872	2.884	2.901
0.50		2.494	2.535	2.570	2.598	2.628	2.655	2.680	2.703	2.730	2.745	2.763
0.55		2.197	2.230	2.262	2.291	2.320	2.346	2.371	2.394	2.419	2.457	2.456
0.60		1.951	1.979	2.008	2.037	2.064	2.089	2.113	2.156	2.138	2.178	2.197
0.65		1.745	1.770	1.796	1.824	1.849	1.872	1.895	1.917	1.937	1.958	1.977
0.70		1.570	1.592	1.617	1.643	1.666	1.688	1.709	1.730	1.749	1.770	1.788
0.80		1.288	1.308	1.329	1.351	1.372	1.391	1.411	1.429	1.446	1.465	1.482
0.90		1.073	1.090	1.109	1.128	1.146	1.164	1.181	1.198	1.213	1.231	1.246
1.00		0.904	0.920	0.936	0.953	0.969	0.985	1.000	1.016	1.030	1.045	1.060
1.10		0.772	0.785	0.799	0.814	0.828	0.842	0.856	0.870	0.883	0.897	0.910
1.20		0.666	0.678	0.690	0.702	0.715	0.727	0.739	0.752	0.763	0.776	0.787
1.30		0.580	0.391	0.602	0.612	0.623	0.634	0.644	0.655	0.666	0.676	0.687
1.40		0.511	0.521	0.530	0.539	0.548	0.557	0.566	0.575	0.383	0.595	0.604
1.50		0.436	0.463	0.470	0.478	0.486	0.494	0.502	0.511	0.519	0.527	0.535
1.60		0.411	0.415	0.421	0.428	0.435	0.442	0.449	0.457	0.463	0.470	0.478
1.70		0.367	0.374	0.380	0.386	0.392	0.398	0.404	0.409	0.416	0.423	0.429
1.80		0.337	0.340	0.345	0.350	0.355	0.360	0.366	0.372	0.377	0.382	0.388
1.90		0.304	0.310	0.314	0.319	0.324	0.328	0.333	0.337	0.343	0.348	0.353
2.00		0.277	0.284	0.288	0.292	0.296	0.301	0.305	0.307	0.313	0.318	0.322

Table 4.3.1.1. *Atomic scattering amplitudes (Å) for electrons for neutral atoms (cont.)*

$(\sin\theta)/\lambda$ (Å^{-1})	Element	Ho	Er	Tm	Yb	Lu	Hf	Ta	W	Re	Os	Ir
	Z	67	68	69	70	71	72	73	74	75	76	77
	Method	*RHF	*RHF	*RHF	*RHF	*RHF	*RHF	*RHF	*RHF	*RHF	*RHF	*RHF
0.00		14.355	14.080	13.814	13.557	13.486	13.177	12.856	12.543	12.263	11.987	11.718
0.01												
0.02												
0.03												
0.04		13.57	13.16	12.92	12.70	12.74	12.55	12.31	12.06	11.83	11.59	11.37
0.05		13.14	12.70	12.48	12.28	12.38	12.23	12.01	11.80	11.60	11.39	11.18
0.06		12.66	12.19	12.00	11.81	11.95	11.85	11.69	11.51	11.34	11.15	10.96
0.07		12.15	11.66	11.48	11.31	11.50	11.45	11.33	11.18	11.04	10.88	10.72
0.08		11.61	11.11	10.96	10.80	11.03	11.02	10.95	10.83	10.73	10.59	10.45
0.09		11.08	10.58	10.44	10.29	10.55	10.59	10.55	10.47	10.40	10.29	10.17
0.10		10.55	10.06	9.93	9.80	10.08	10.16	10.15	10.10	10.05	9.98	9.88
0.11		10.05	9.56	9.45	9.33	9.62	9.73	9.75	9.74	9.71	9.65	9.58
0.12		9.562	9.095	8.994	8.892	9.180	9.308	9.363	9.369	9.366	9.334	9.281
0.13		9.108	8.662	8.571	8.480	8.762	8.907	8.982	9.011	9.028	9.016	8.982
0.14		8.681	8.262	8.180	8.098	8.370	8.525	8.616	8.663	8.697	8.702	8.686
0.15		8.284	7.895	7.821	7.746	8.001	8.163	8.266	8.327	8.376	8.396	8.395
0.16		7.917	7.557	7.490	7.421	7.660	7.822	7.933	8.006	8.067	8.099	8.111
0.17		7.577	7.247	7.185	7.123	7.343	7.502	7.617	7.699	7.769	7.813	7.836
0.18		7.262	6.962	6.905	6.849	7.047	7.202	7.321	7.408	7.485	7.537	7.570
0.19		6.971	6.698	6.646	6.595	6.774	6.922	7.040	7.132	7.213	7.272	7.313
0.20		6.700	6.454	6.407	6.360	6.520	6.660	6.776	6.870	6.954	7.019	7.067
0.22		6.213	6.017	5.978	5.938	6.063	6.185	6.295	6.388	6.475	6.547	6.604
0.24		5.788	5.632	5.601	5.568	5.664	5.768	5.867	5.957	6.043	6.117	6.180
0.25		5.595	5.457	5.428	5.398	5.483	5.578	5.672	5.759	5.843	5.917	5.982
0.26		5.412	5.290	5.265	5.238	5.312	5.399	5.487	5.571	5.653	5.727	5.792
0.28		5.075	4.981	4.961	4.940	4.996	5.069	5.147	5.224	5.301	5.372	5.437
0.30		4.771	4.699	4.685	4.669	4.712	4.772	4.840	4.910	4.981	5.049	5.113
0.32		4.494	4.440	4.430	4.419	4.453	4.503	4.563	4.626	4.691	4.755	4.816
0.34		4.240	4.200	4.195	4.188	4.215	4.258	4.310	4.366	4.425	4.485	4.543
0.35		4.121	4.087	4.084	4.078	4.103	4.143	4.191	4.245	4.301	4.359	4.415
0.36		4.007	3.978	3.976	3.973	3.996	4.033	4.078	4.129	4.182	4.237	4.293
0.38		3.790	3.771	3.773	3.773	3.793	3.825	3.865	3.910	3.959	4.010	4.061
0.40		3.591	3.579	3.583	3.586	3.604	3.632	3.668	3.709	3.753	3.800	3.848
0.42		3.405	3.399	3.406	3.411	3.429	3.454	3.486	3.523	3.563	3.606	3.651
0.44		3.233	3.232	3.241	3.248	3.265	3.288	3.317	3.350	3.387	3.427	3.468
0.45		3.151	3.153	3.162	3.170	3.187	3.209	3.237	3.269	3.304	3.342	3.382
0.46		3.073	3.076	3.086	3.095	3.111	3.133	3.159	3.190	3.224	3.260	3.299
0.48		2.924	2.930	2.942	2.952	2.968	2.988	3.013	3.041	3.072	3.105	3.141
0.50		2.785	2.793	2.806	2.818	2.834	2.853	2.876	2.902	2.930	2.961	2.994
0.55		2.477	2.490	2.505	2.518	2.534	2.551	2.571	2.592	2.616	2.641	2.669
0.60		2.216	2.232	2.248	2.263	2.278	2.294	2.311	2.330	2.349	2.371	2.394
0.65		1.995	2.012	2.028	2.043	2.058	2.073	2.089	2.105	2.122	2.140	2.160
0.70		1.085	1.823	1.839	1.854	1.868	1.882	1.896	1.911	1.926	1.942	1.959
0.80		1.497	1.515	1.530	1.545	1.558	1.571	1.583	1.596	1.608	1.621	1.634
0.90		1.260	1.276	1.291	1.305	1.317	1.329	1.341	1.352	1.363	1.374	1.385
1.00		1.073	1.088	1.101	1.114	1.126	1.138	1.148	1.159	1.169	1.179	1.189
1.10		0.922	0.935	0.948	0.960	0.971	0.982	0.993	1.003	1.012	1.022	1.031
1.20		0.799	0.811	0.822	0.833	0.844	0.854	0.864	0.874	0.883	0.892	0.901
1.30		0.698	0.708	0.719	0.729	0.739	0.748	0.758	0.767	0.776	0.784	0.793
1.40		0.614	0.623	0.632	0.642	0.651	0.660	0.668	0.677	0.685	0.694	0.702
1.50		0.544	0.552	0.560	0.569	0.577	0.585	0.593	0.601	0.609	0.617	0.624
1.60		0.485	0.492	0.500	0.507	0.515	0.522	0.530	0.537	0.544	0.551	0.558
1.70		0.436	0.442	0.449	0.455	0.462	0.469	0.475	0.482	0.489	0.495	0.502
1.80		0.394	0.399	0.405	0.411	0.417	0.423	0.429	0.435	0.441	0.447	0.453
1.90		0.358	0.363	0.368	0.373	0.379	0.384	0.389	0.395	0.400	0.406	0.411
2.00		0.327	0.331	0.336	0.341	0.345	0.350	0.355	0.360	0.365	0.370	0.374

Table 4.3.1.1. *Atomic scattering amplitudes (Å) for electrons for neutral atoms (cont.)*

$(\sin\theta)/\lambda$ (Å^{-1})	Element	Pt	Au	Hg	Tl	Pb	Bi	Po	At	Rn	Fr	Ra
	Z	78	79	80	81	82	83	84	85	86	87	88
	Method	*RHF	RHF	RHF	*RHF	RHF	RHF	*RHF	*RHF	RHF	*RHF	*RHF
0.00		10.813	10.573	10.964	12.109	12.597	13.096	13.368	13.473	13.492	18.715	20.561
0.01			10.559	10.948		12.573	13.070			13.470		
0.02			10.511	10.897		12.494	12.989			13.403		
0.03			10.434	10.813		12.366	12.857			13.292		
0.04		10.55	10.328	10.698	11.71	12.193	12.678	12.95	13.09	13.139	17.14	18.94
0.05		10.40	10.195	10.555	11.51	11.979	12.456	12.74	12.89	12.949	16.41	18.15
0.06		10.23	10.040	10.387	11.27	11.730	12.197	12.49	12.65	12.724	15.64	17.31
0.07		10.03	9.865	10.197	11.00	11.454	11.908	12.21	12.38	12.469	14.87	16.42
0.08		9.82	9.673	9.989	10.72	11.155	11.595	11.90	12.08	12.187	14.13	15.54
0.09		9.60	9.467	9.766	10.42	10.840	11.264	11.57	11.76	11.884	13.42	14.69
0.10		9.37	9.251	9.533	10.12	10.516	10.921	11.22	11.43	11.565	12.77	13.88
0.11		9.13	9.028	9.291	9.81	10.186	10.571	10.87	11.08	11.232	12.16	13.12
0.12		8.882	8.799	9.045	9.500	9.855	10.219	10.509	10.729	10.892	11.605	12.419
0.13		8.636	8.568	8.796	9.195	9.527	9.869	10.153	10.375	10.546	11.093	11.776
0.14		8.389	8.337	8.547	8.896	9.203	9.523	9.798	10.021	10.199	10.620	11.187
0.15		8.145	8.106	8.299	8.603	8.888	9.186	9.449	9.671	9.854	10.180	10.648
0.16		7.904	7.877	8.055	8.320	8.581	8.857	9.109	9.328	9.512	9.770	10.155
0.17		7.667	7.652	7.815	8.046	8.285	8.539	8.779	8.991	9.177	9.386	9.702
0.18		7.436	7.431	7.579	7.781	7.999	8.233	8.459	8.666	8.849	9.023	9.285
0.19		7.210	7.214	7.350	7.526	7.724	7.939	8.151	8.350	8.531	8.681	8.899
0.20		6.991	7.003	7.128	7.282	7.461	7.658	7.856	8.046	8.223	8.356	8.540
0.22		6.572	6.598	6.702	6.822	6.969	7.132	7.303	3.474	7.639	7.754	7.891
0.24		6.181	6.216	6.305	6.399	6.520	6.654	6.800	6.952	7.102	7.208	7.318
0.25		5.995	6.035	6.116	6.201	6.310	6.432	6.567	6.709	6.852	6.954	7.055
0.26		5.817	5.859	5.934	6.011	6.110	6.221	6.345	6.477	6.612	6.712	6.807
0.28		5.478	5.525	5.591	5.654	5.736	5.828	5.933	6.047	6.166	6.261	6.347
0.30		5.164	5.214	5.272	5.327	5.395	5.472	5.560	5.658	5.762	5.852	5.931
0.32		4.873	4.924	4.976	5.025	5.083	5.148	5.222	5.305	5.397	5.480	5.555
0.34		4.603	4.654	4.702	4.746	4.797	4.852	4.915	4.987	5.065	5.141	5.212
0.35		4.475	4.526	4.572	4.614	4.662	4.714	4.772	4.838	4.912	4.984	5.053
0.36		4.352	4.403	4.447	4.488	4.533	4.581	4.636	4.697	4.765	4.834	4.900
0.38		4.120	4.169	4.211	4.249	4.290	4.333	4.380	4.433	4.492	4.555	4.616
0.40		3.905	3.952	3.991	4.028	4.066	4.104	4.146	4.192	4.244	4.300	4.356
0.42		3.704	3.750	3.787	3.823	3.858	3.893	3.931	3.972	4.017	4.067	4.118
0.44		3.518	3.562	3.597	3.632	3.665	3.698	3.732	3.769	3.808	3.854	3.901
0.45		3.430	3.472	3.507	3.541	3.573	3.606	3.639	3.673	3.711	3.754	3.798
0.46		3.345	3.386	3.420	3.454	3.485	3.517	3.548	3.582	3.617	3.658	3.700
0.48		3.184	3.223	3.256	3.288	3.318	3.348	3.378	3.408	3.441	3.477	3.516
0.50		3.034	3.070	3.102	3.133	3.162	3.191	3.219	3.248	3.277	3.311	3.346
0.55		2.701	2.732	2.760	2.789	2.816	2.842	2.868	2.893	2.918	2.945	2.974
0.60		2.420	2.446	2.471	2.497	2.522	2.546	2.570	2.593	2.616	2.639	2.663
0.65		2.181	2.203	2.225	2.248	2.271	2.293	2.315	2.337	2.358	2.378	2.399
0.70		1.976	1.995	2.015	2.035	2.055	2.076	2.096	2.116	2.135	2.154	2.173
0.80		1.647	1.661	1.676	1.692	1.708	1.725	1.742	1.758	1.775	1.791	1.808
0.90		1.396	1.407	1.419	1.431	1.444	1.457	1.471	1.485	1.499	1.513	1.527
1.00		1.198	1.208	1.218	1.228	1.239	1.249	1.260	1.272	1.283	1.295	1.307
1.10		1.040	1.048	1.057	1.066	1.075	1.084	1.093	1.102	1.112	1.122	1.132
1.20		0.909	0.918	0.926	0.934	0.942	0.949	0.957	0.965	0.974	0.982	0.990
1.30		0.801	0.809	0.816	0.824	0.831	0.838	0.846	0.853	0.860	0.867	0.874
1.40		0.709	0.717	0.724	0.731	0.738	0.745	0.752	0.758	0.765	0.771	0.778
1.50		0.632	0.639	0.646	0.653	0.659	0.666	0.672	0.678	0.684	0.690	0.696
1.60		0.565	0.572	0.579	0.585	0.591	0.598	0.603	0.609	0.615	0.621	0.626
1.70		0.508	0.514	0.521	0.527	0.533	0.538	0.544	0.550	0.555	0.561	0.566
1.80		0.459	0.465	0.471	0.476	0.482	0.488	0.493	0.498	0.503	0.508	0.513
1.90		0.416	0.422	0.427	0.432	0.438	0.443	0.448	0.453	0.458	0.463	0.468
2.00		0.379	0.384	0.389	0.394	0.399	0.404	0.409	0.413	0.418	0.423	0.427

Table 4.3.1.1. *Atomic scattering amplitudes (Å) for electrons for neutral atoms (cont.)*

$(\sin\theta)/\lambda$ (Å^{-1})	Element	Ac	Th	Pa	U	Np	Pu	Am	Cm	Bk	Cf
	Z	89	90	91	92	93	94	95	96	97	98
	Method	*RHF	*RHF	*RHF	RHF	*RHF	*RHF	*RHF	*RHF	*RHF	*RHF
0.00		20.484	20.115	19.568	19.119	18.759	18.191	17.840	17.710	17.406	16.841
0.01					19.047						
0.02					18.825						
0.03					18.470						
0.04		19.10	18.92	18.37	17.999	17.70	17.10	16.80	16.80	16.53	16.28
0.05		18.41	18.33	17.77	17.436	17.16	16.55	16.28	16.33	16.08	15.85
0.06		17.64	17.66	17.11	16.805	16.55	15.95	15.70	15.80	15.58	15.37
0.07		16.84	16.93	16.39	16.131	15.91	15.31	15.09	15.24	15.04	14.84
0.08		16.01	16.19	15.66	15.436	15.25	14.65	14.47	14.66	14.48	14.30
0.09		15.19	15.43	14.92	14.738	14.58	14.00	13.84	14.06	13.91	13.75
0.10		14.40	14.68	14.20	14.052	13.92	13.37	13.24	13.47	13.33	13.20
0.11		13.64	13.95	13.51	13.389	13.28	12.76	12.65	12.90	12.78	12.66
0.12		12.923	13.255	12.850	12.756	12.665	12.191	12.095	12.344	12.241	12.135
0.13		12.253	12.594	12.228	12.157	12.085	11.653	11.572	11.817	11.729	11.637
0.14		11.632	11.972	11.646	11.595	11.540	11.149	11.083	11.319	11.243	11.164
0.15		11.058	11.388	11.102	11.069	11.029	10.679	10.626	10.848	10.784	10.716
0.16		10.528	10.845	10.597	10.579	10.551	10.243	10.200	10.407	10.353	10.294
0.17		10.038	10.339	10.128	10.122	10.104	9.836	9.803	9.993	9.948	9.898
0.18		9.586	9.868	9.691	9.696	9.688	9.457	9.433	9.605	9.568	9.527
0.19		9.168	9.430	9.285	9.299	9.300	9.102	9.086	9.241	9.212	9.178
0.20		8.780	9.022	8.906	8.928	8.936	8.770	8.760	8.900	8.878	8.850
0.22		8.083	8.287	8.221	8.254	8.275	8.163	8.164	8.277	8.266	8.249
0.24		7.474	7.645	7.617	7.659	7.689	7.619	7.631	7.721	7.720	7.713
0.25		7.196	7.353	7.341	7.387	7.420	7.368	7.384	7.465	7.468	7.466
0.26		6.935	7.079	7.081	7.129	7.165	7.129	7.148	7.222	7.229	7.231
0.28		6.455	6.578	6.600	6.652	6.694	6.683	6.708	6.770	6.784	6.793
0.30		6.025	6.129	6.167	6.221	6.266	6.274	6.304	6.358	6.378	6.393
0.32		5.637	5.727	5.775	5.830	5.878	5.899	5.933	5.981	6.006	6.026
0.34		5.285	5.364	5.418	5.473	5.523	5.553	5.591	5.635	5.664	5.687
0.35		5.122	5.196	5.252	5.307	5.357	5.391	5.429	5.472	5.502	5.528
0.36		4.966	5.036	5.093	5.148	5.197	5.235	5.274	5.316	5.347	5.374
0.38		4.675	4.738	4.796	4.850	4.899	4.940	4.981	5.021	5.055	5.084
0.40		4.410	4.466	4.524	4.576	4.625	4.669	4.710	4.749	4.784	4.815
0.42		4.168	4.218	4.275	4.325	4.372	4.417	4.459	4.497	4.532	4.565
0.44		3.946	3.992	4.046	4.094	4.140	4.185	4.226	4.263	4.299	4.333
0.45		3.842	3.885	3.938	3.985	4.030	4.076	4.116	4.152	4.189	4.222
0.46		3.742	3.784	3.835	3.881	3.925	3.970	4.010	4.046	4.082	4.116
0.48		3.554	3.592	3.641	3.685	3.727	3.771	3.810	3.844	3.880	3.914
0.50		3.381	3.416	3.462	3.503	3.543	3.586	3.624	3.657	3.693	3.726
0.55		3.003	3.032	3.071	3.106	3.141	3.179	3.213	3.244	3.277	3.309
0.60		2.687	2.712	2.744	2.775	2.805	2.839	2.869	2.897	2.927	2.957
0.65		2.421	2.442	2.470	2.495	2.522	2.551	2.578	2.603	2.630	2.657
0.70		2.193	2.212	2.235	2.257	2.280	2.306	2.330	2.352	2.376	2.400
0.80		1.824	1.840	1.857	1.875	1.893	1.912	1.930	1.949	1.968	1.987
0.90		1.541	1.554	1.568	1.582	1.597	1.611	1.626	1.641	1.657	1.673
1.00		1.318	1.330	1.342	1.353	1.365	1.377	1.389	1.402	1.415	1.427
1.10		1.142	1.152	1.161	1.171	1.181	1.191	1.201	1.212	1.222	1.233
1.20		0.999	1.007	1.016	1.024	1.033	1.041	1.049	1.058	1.067	1.076
1.30		0.882	0.889	0.896	0.904	0.911	0.918	0.926	0.933	0.941	0.948
1.40		0.784	0.791	0.797	0.803	0.810	0.816	0.823	0.830	0.836	0.843
1.50		0.702	0.708	0.714	0.720	0.725	0.731	0.737	0.743	0.748	0.754
1.60		0.632	0.637	0.643	0.649	0.653	0.659	0.664	0.669	0.674	0.679
1.70		0.571	0.576	0.581	0.585	0.591	0.596	0.601	0.606	0.611	0.165
1.80		0.518	0.523	0.528	0.534	0.537	0.542	0.547	0.551	0.555	0.560
1.90		0.472	0.477	0.481	0.485	0.490	0.495	0.499	0.503	0.507	0.511
2.00		0.432	0.436	0.440	0.443	0.449	0.453	0.457	0.461	0.465	0.469

Table 4.3.1.2. *Atomic scattering amplitudes (Å) for electrons for ionized atoms*

A discussion of the values quoted here for $s = 0$ is given in Subsection 4.3.1.6. Self-consistent field calculations: HF: non-relativistic Hartree–Fock; DS: modified Dirac–Slater; RHF, *RHF: relativistic Hartree–Fock.

$(\sin\theta)/\lambda$ (Å^{-1})	Element	H^{1-}	Li^{1+}	Be^{2+}	O^{1-}	F^{1-}	Na^{1+}	Mg^{2+}	Al^{3+}	Si^{4+}	Cl^{1-}	K^{1+}
	Z	1	3	4	8	9	11	12	13	14	17	19
	Method	HF	RHF	RHF	HF	HF	RHF	RHF	HF	HF	RHF	RHF
0.00			0.157	0.082			1.130	0.831			6.770	3.436
0.01			239.497	478.762			240.469	479.511			−232.585	242.773
0.02			59.992	119.752			60.963	120.500			−53.125	63.260
0.03			26.750	53.268			27.719	54.015			−19.957	30.004
0.04		−12.00	15.115	29.999	−11.74	−12.21	16.081	30.745	45.52	60.34	−8.423	18.349
0.05		−6.78	9.730	19.229	−6.41	−6.85	10.692	19.972	29.36	38.80	−3.162	12.939
0.06		−4.03	6.804	13.378	−3.55	−3.97	7.762	14.119	20.58	27.10	−0.381	9.983
0.07		−2.45	5.040	9.850	−1.86	−2.25	5.993	10.589	15.29	20.05	1.219	8.184
0.08		−1.48	3.894	7.560	−0.79	−1.16	4.841	8.296	11.85	15.46	2.187	6.999
0.09		−0.87	3.109	5.990	−0.09	−0.43	4.049	6.722	9.49	12.32	2.783	6.169
0.10		−0.47	2.546	4.867	0.39	0.08	3.480	5.595	7.81	10.08	3.147	5.559
0.11		−0.20	2.130	4.036	0.72	0.43	3.056	4.760	6.56	8.41	3.361	5.092
0.12		−0.023	1.813	3.404	0.949	0.688	2.731	4.123	5.610	7.147	3.472	4.720
0.13		0.095	1.567	2.912	1.107	0.870	2.475	3.626	4.868	6.162	3.513	4.416
0.14		0.173	1.370	2.522	1.215	1.000	2.269	3.230	4.280	5.379	3.504	4.160
0.15		0.224	1.212	2.207	1.285	1.092	2.100	2.909	3.804	4.747	3.461	3.939
0.16		0.257	1.082	1.949	1.329	1.157	1.960	2.645	3.413	4.230	3.393	3.745
0.17		0.276	0.974	1.735	1.352	1.200	1.841	2.425	3.089	3.800	3.308	3.571
0.18		0.286	0.883	1.556	1.359	1.226	1.738	2.239	2.817	3.440	3.211	3.414
0.19		0.288	0.806	1.404	1.355	1.239	1.650	2.081	2.585	3.135	3.108	3.269
0.20		0.287	0.740	1.274	1.343	1.242	1.571	1.944	2.387	2.873	3.000	3.135
0.22		0.276	0.634	1.066	1.300	1.228	1.440	1.720	2.066	2.451	2.779	2.893
0.24		0.259	0.552	0.907	1.243	1.194	1.332	1.546	1.819	2.129	2.563	2.676
0.25		0.250	0.518	0.841	1.212	1.173	1.284	1.472	1.716	1.995	2.458	2.575
0.26		0.240	0.487	0.783	1.179	1.150	1.240	1.406	1.624	1.876	2.357	2.479
0.28		0.221	0.435	0.685	1.112	1.099	1.161	1.290	1.466	1.674	2.165	2.300
0.30		0.203	0.393	0.605	1.046	1.046	1.092	1.193	1.336	1.509	1.988	2.135
0.32		0.186	0.357	0.539	0.981	0.992	1.029	1.110	1.228	1.372	1.827	1.983
0.34		0.170	0.327	0.485	0.918	0.939	0.972	1.038	1.136	1.257	1.680	1.843
0.35		0.163	0.314	0.461	0.889	0.912	0.946	1.005	1.094	1.206	1.613	1.778
0.36		0.156	0.301	0.439	0.860	0.887	0.920	0.974	1.056	1.159	1.548	1.715
0.38		0.143	0.279	0.400	0.804	0.837	0.872	0.917	0.987	1.075	1.429	1.596
0.40		0.132	0.259	0.366	0.753	0.789	0.827	0.866	0.925	1.001	1.322	1.488
0.42		0.122	0.242	0.337	0.704	0.744	0.785	0.820	0.871	0.937	1.226	1.388
0.44		0.112	0.227	0.312	0.660	0.702	0.746	0.777	0.822	0.880	1.139	1.296
0.45		0.108	0.220	0.300	0.639	0.682	0.727	0.757	0.799	0.853	1.099	1.253
0.46		0.104	0.213	0.290	0.618	0.662	0.709	0.738	0.778	0.829	1.061	1.212
0.48		0.096	0.200	0.270	0.580	0.625	0.675	0.701	0.737	0.783	0.991	1.135
0.50		0.090	0.189	0.252	0.544	0.590	0.642	0.668	0.701	0.741	0.928	1.064
0.55		0.075	0.165	0.216	0.467	0.512	0.569	0.593	0.620	0.652	0.796	0.912
0.60		0.064	0.145	0.188	0.403	0.446	0.506	0.529	0.553	0.580	0.691	0.789
0.65		0.055	0.129	0.165	0.351	0.391	0.451	0.474	0.496	0.519	0.608	0.690
0.70		0.048	0.115	0.146	0.307	0.345	0.403	0.426	0.447	0.468	0.541	0.609
0.80		0.037	0.093	0.118	0.241	0.272	0.325	0.347	0.367	0.385	0.439	0.488
0.90		0.029	0.077	0.097	0.193	0.219	0.266	0.286	0.305	0.321	0.366	0.402
1.00		0.024	0.064	0.081	0.159	0.180	0.221	0.239	0.256	0.271	0.311	0.338
1.10		0.020	0.054	0.069	0.133	0.150	0.185	0.201	0.217	0.231	0.267	0.290
1.20		0.017	0.046	0.059	0.113	0.128	0.157	0.172	0.186	0.198	0.232	0.252
1.30		0.014	0.040	0.052	0.097	0.110	0.135	0.148	0.160	0.172	0.202	0.221
1.40		0.012	0.035	0.045	0.085	0.095	0.118	0.129	0.140	0.150	0.178	0.195
1.50		0.011	0.031	0.040	0.075	0.084	0.103	0.113	0.123	0.132	0.158	0.173
1.60			0.027	0.035			0.091	0.100			0.141	0.155
1.70			0.024	0.032			0.081	0.089			0.126	0.139
1.80			0.022	0.028			0.073	0.080			0.113	0.125
1.90			0.020	0.026			0.066	0.072			0.102	0.114
2.00			0.018	0.023			0.060	0.065			0.093	0.103

Table 4.3.1.2. *Atomic scattering amplitudes (Å) for electrons for ionized atoms (cont.)*

$(\sin\theta)/\lambda$ (Å^{-1})	Element	Ca^{2+}	Sc^{3+}	Ti^{2+}	Ti^{3+}	Ti^{4+}	V^{2+}	V^{3+}	V^{5+}	Cr^{2+}	Cr^{3+}	Mn^{2+}
	Z	20	21	22	22	22	23	23	23	24	24	25
	Method	RHF	HF	HF	HF	HF	RHF	HF	HF	HF	HF	RHF
0.00		2.711					2.904					2.846
0.01		481.390					481.582					481.525
0.02		122.375					122.566					122.510
0.03		55.883					56.074					56.018
0.04		32.602	47.08	32.80	47.15	61.67	32.791	47.18	76.36	32.79	47.19	32.738
0.05		21.817	30.91	22.01	30.98	40.13	22.005	31.02	49.43	22.00	31.03	21.953
0.06		15.948	22.13	16.14	22.19	28.42	16.134	22.23	34.80	16.13	22.24	16.085
0.07		12.399	16.82	12.59	16.89	21.35	12.583	16.92	25.98	12.58	16.93	12.537
0.08		10.085	13.37	10.27	13.44	16.77	10.267	13.47	20.24	10.26	13.48	10.225
0.09		8.489	11.00	8.67	11.07	13.62	8.668	11.10	16.31	8.67	11.11	8.630
0.10		7.336	9.30	7.52	9.36	11.36	7.514	9.39	13.49	7.51	9.41	7.479
0.11		6.473	8.03	6.65	8.09	9.68	6.648	8.13	11.41	6.65	8.14	6.618
0.12		5.807	7.057	5.977	7.120	8.400	5.980	7.155	9.815	5.983	7.172	5.954
0.13		5.279	6.295	5.444	6.359	7.400	5.449	6.394	8.574	5.455	6.410	5.428
0.14		4.850	5.684	5.011	5.747	6.603	5.018	5.782	7.584	5.026	5.800	5.002
0.15		4.495	5.185	4.653	5.247	5.954	4.661	5.284	6.784	4.671	5.302	4.650
0.16		4.196	4.770	4.349	4.832	5.418	4.360	4.868	6.126	4.372	4.888	4.353
0.17		3.939	4.421	4.089	4.481	4.971	4.102	4.518	5.577	4.116	4.539	4.100
0.18		3.716	4.121	3.863	4.182	4.591	3.877	4.220	5.113	3.894	4.242	3.880
0.19		3.519	3.863	3.663	3.923	4.266	3.679	3.961	4.719	3.698	3.984	3.686
0.20		3.343	3.637	3.485	3.697	3.984	3.503	3.735	4.378	3.523	3.759	3.514
0.22		3.041	3.259	3.178	3.318	3.520	3.200	3.358	3.824	3.224	3.384	3.220
0.24		2.787	2.953	2.920	3.012	3.155	2.946	3.053	3.391	2.973	3.081	2.975
0.25		2.674	2.821	2.806	2.879	2.998	2.833	2.921	3.209	2.862	2.950	2.865
0.26		2.568	2.699	2.699	2.757	2.857	2.727	2.799	3.045	2.758	2.830	2.764
0.28		2.376	2.482	2.504	2.540	2.610	2.536	2.584	2.761	2.569	2.616	2.579
0.30		2.204	2.294	2.331	2.352	2.399	2.365	2.396	2.524	2.401	2.430	2.415
0.32		2.049	2.128	2.174	2.185	2.217	2.211	2.231	2.322	2.249	2.266	2.266
0.34		1.907	1.980	2.032	2.037	2.057	2.071	2.073	2.147	2.111	2.120	2.131
0.35		1.842	1.911	1.966	1.968	1.984	2.005	2.015	2.068	2.046	2.053	2.068
0.36		1.778	1.846	1.903	1.903	1.915	1.943	1.950	1.994	1.984	1.988	2.007
0.38		1.660	1.725	1.783	1.781	1.788	1.825	1.829	1.858	1.867	1.868	1.893
0.40		1.551	1.614	1.673	1.670	1.673	1.716	1.718	1.736	1.759	1.758	1.787
0.42		1.451	1.512	1.572	1.568	1.569	1.615	1.616	1.627	1.659	1.657	1.688
0.44		1.359	1.419	1.478	1.474	1.473	1.522	1.522	1.528	1.566	1.563	1.597
0.45		1.316	1.375	1.433	1.429	1.428	1.477	1.477	1.481	1.522	1.519	1.553
0.46		1.274	1.333	1.391	1.387	1.385	1.435	1.434	1.437	1.480	1.476	1.511
0.48		1.196	1.253	1.310	1.306	1.304	1.354	1.354	1.354	1.399	1.395	1.432
0.50		1.124	1.180	1.235	1.232	1.229	1.279	1.279	1.277	1.324	1.320	1.357
0.55		0.967	1.019	1.070	1.068	1.066	1.113	1.113	1.110	1.156	1.154	1.190
0.60		0.838	0.886	0.933	0.931	0.930	0.973	0.974	0.971	1.015	1.013	1.049
0.65		0.733	0.776	0.818	0.817	0.816	0.856	0.857	0.855	0.895	0.894	0.928
0.70		0.647	0.685	0.722	0.722	0.721	0.757	0.758	0.756	0.793	0.792	0.824
0.80		0.515	0.544	0.574	0.574	0.574	0.602	0.603	0.603	0.632	0.632	0.659
0.90		0.422	0.444	0.467	0.467	0.467	0.490	0.491	0.491	0.515	0.515	0.538
1.00		0.354	0.371	0.389	0.389	0.389	0.408	0.408	0.408	0.427	0.427	0.446
1.10		0.302	0.316	0.331	0.331	0.330	0.345	0.346	0.345	0.361	0.361	0.377
1.20		0.262	0.273	0.285	0.285	0.285	0.297	0.297	0.297	0.310	0.310	0.323
1.30		0.230	0.239	0.249	0.249	0.249	0.259	0.259	0.259	0.270	0.270	0.280
1.40		0.203	0.211	0.220	0.220	0.219	0.228	0.228	0.228	0.237	0.237	0.246
1.50		0.180	0.188	0.195	0.195	0.195	0.203	0.203	0.202	0.211	0.211	0.218
1.60		0.161					0.181					0.195
1.70		0.145					0.163					0.175
1.80		0.131					0.148					0.159
1.90		0.119					0.134					0.144
2.00		0.108					0.123					0.132

Table 4.3.1.2. *Atomic scattering amplitudes (Å) for electrons for ionized atoms (cont.)*

$(\sin\theta)/\lambda$ (Å^{-1})	Element	Mn^{3+}	Mn^{4+}	Fe^{2+}	Fe^{3+}	Co^{2+}	Co^{3+}	Ni^{2+}	Ni^{3+}	Cu^{1+}	Cu^{2+}	Zn^{2+}
	Z	25	25	26	26	27	27	28	28	29	29	30
	Method	HF	HF	RHF	RHF	RHF	HF	RHF	HF	RHF	HF	RHF
0.00				2.802	2.298	2.754		2.703		3.280		2.599
0.01				481.481	720.318	481.433		481.382		242.618		481.278
0.02				122.467	181.800	122.419		122.368		63.107		122.265
0.03				55.976	82.070	55.928		55.878		29.855		55.776
0.04		47.18	61.76	32.696	47.160	32.650	47.15	32.600	47.12	18.206	32.55	32.499
0.05		31.02	40.22	21.913	30.996	21.867	30.98	21.819	30.96	12.803	21.77	21.719
0.06		22.23	28.51	16.046	22.210	16.002	22.20	15.955	22.17	9.856	15.90	15.857
0.07		16.93	21.44	12.500	16.907	12.457	16.90	12.411	16.87	8.066	12.36	12.316
0.08		13.48	16.85	10.189	13.459	10.148	13.45	10.103	13.43	6.893	10.06	10.011
0.09		11.11	13.70	8.596	11.089	8.556	11.08	8.513	11.06	6.076	8.47	8.424
0.10		9.41	11.45	7.447	9.388	7.409	9.38	7.368	9.36	5.479	7.33	7.282
0.11		8.14	9.77	6.588	8.124	6.553	8.12	6.513	8.10	5.027	6.47	6.430
0.12		7.174	8.492	5.926	7.156	5.893	7.150	5.856	7.132	4.671	5.817	5.776
0.13		6.413	7.492	5.403	6.398	5.371	6.393	5.336	6.376	4.383	5.299	5.260
0.14		5.804	6.695	4.979	5.790	4.950	5.787	4.917	5.770	4.144	4.883	4.845
0.15		5.307	6.047	4.629	5.294	4.603	5.293	4.572	5.277	3.942	4.540	4.504
0.16		4.894	5.514	4.335	4.884	4.311	4.883	4.283	4.869	3.766	4.253	4.219
0.17		4.547	5.068	4.084	4.538	4.063	4.538	4.036	4.526	3.612	4.009	3.976
0.18		4.251	4.689	3.867	4.243	3.847	4.245	3.824	4.234	3.474	3.799	3.768
0.19		3.995	4.366	3.676	3.989	3.659	3.993	3.638	3.983	3.349	3.615	3.586
0.20		3.771	4.086	3.506	3.767	3.492	3.772	3.473	3.764	3.234	3.453	3.426
0.22		3.399	3.625	3.217	3.397	3.207	3.405	3.193	3.400	3.030	3.178	3.154
0.24		3.099	3.262	2.976	3.100	2.971	3.111	2.961	3.109	2.851	2.950	2.930
0.25		2.969	3.108	2.869	2.972	2.866	2.984	2.858	2.984	2.769	2.850	2.831
0.26		2.850	2.968	2.769	2.855	2.768	2.868	2.763	2.869	2.690	2.757	2.740
0.28		2.639	2.723	2.589	2.646	2.592	2.662	2.590	2.666	2.544	2.588	2.574
0.30		2.455	2.516	2.428	2.466	2.434	2.484	2.436	2.490	2.410	2.438	2.428
0.32		2.294	2.336	2.282	2.307	2.293	2.327	2.298	2.336	2.285	2.303	2.296
0.34		2.149	2.179	2.150	2.165	2.163	2.187	2.172	2.199	2.169	2.180	2.176
0.35		2.083	2.107	2.088	2.099	2.103	2.123	2.113	2.135	2.114	2.123	2.120
0.36		2.019	2.039	2.029	2.037	2.045	2.061	2.056	2.075	2.061	2.067	2.066
0.38		1.900	1.913	1.917	1.920	1.935	1.946	1.949	1.962	1.959	1.963	1.964
0.40		1.791	1.799	1.813	1.813	1.833	1.841	1.849	1.858	1.864	1.866	1.869
0.42		1.691	1.695	1.716	1.715	1.739	1.743	1.756	1.762	1.774	1.775	1.781
0.44		1.598	1.600	1.626	1.623	1.650	1.653	1.670	1.674	1.690	1.690	1.697
0.45		1.554	1.555	1.583	1.580	1.608	1.610	1.628	1.631	1.649	1.649	1.658
0.46		1.512	1.512	1.542	1.538	1.567	1.569	1.588	1.591	1.610	1.610	1.619
0.48		1.432	1.431	1.463	1.459	1.489	1.490	1.512	1.513	1.535	1.535	1.546
0.50		1.357	1.355	1.389	1.385	1.416	1.417	1.440	1.441	1.464	1.464	1.476
0.55		1.190	1.188	1.223	1.220	1.252	1.252	1.277	1.278	1.303	1.303	1.319
0.60		1.049	1.047	1.081	1.079	1.111	1.111	1.137	1.138	1.163	1.164	1.182
0.65		0.928	0.927	0.959	0.958	0.989	0.989	1.015	1.016	1.042	1.043	1.061
0.70		0.825	0.824	0.855	0.854	0.883	0.884	0.910	0.910	0.935	0.936	0.956
0.80		0.660	0.660	0.687	0.686	0.713	0.713	0.737	0.738	0.761	0.762	0.782
0.90		0.538	0.538	0.561	0.561	0.583	0.584	0.605	0.606	0.627	0.628	0.646
1.00		0.447	0.447	0.466	0.466	0.485	0.486	0.504	0.505	0.523	0.524	0.541
1.10		0.377	0.377	0.393	0.393	0.409	0.410	0.425	0.426	0.441	0.442	0.457
1.20		0.323	0.323	0.336	0.336	0.350	0.350	0.364	0.364	0.378	0.378	0.391
1.30		0.281	0.281	0.291	0.291	0.303	0.304	0.315	0.315	0.327	0.327	0.339
1.40		0.246	0.246	0.256	0.256	0.265	0.266	0.275	0.276	0.286	0.286	0.296
1.50		0.219	0.218	0.226	0.226	0.235	0.235	0.243	0.244	0.252	0.253	0.261
1.60				0.202	0.202	0.209		0.217		0.224		0.232
1.70				0.182	0.182	0.188		0.195		0.201		0.208
1.80				0.164	0.164	0.170		0.176		0.182		0.188
1.90				0.149	0.149	0.155		0.160		0.165		0.170
2.00				0.136	0.136	0.141		0.146		0.150		0.155

Table 4.3.1.2. *Atomic scattering amplitudes (Å) for electrons for ionized atoms (cont.)*

$(\sin\theta)/\lambda$ (Å^{-1})	Element	Ga^{3+}	Ge^{4+}	Br^{1}-	Rb^{1+}	Sr^{2+}	Y^{3+}	Zr^{4+}	Nb^{3+}	Nb^{5+}	Mo^{3+}	Mo^{5+}
	Z	31	32	35	37	38	39	40	41	41	42	42
	Method	HF	HF	RHF	RHF	RHF	*DS	*DS	*DS	*DS	*DS	*DS
0.00				9.357	5.545	4.642						
0.01				−230.004	244.880	483.320						
0.02				−50.565	65.359	124.299						
0.03				−17.431	32.090	57.798						
0.04		47.03	61.67	−5.942	20.419	34.505	48.84	63.31	49.33	77.86	49.44	78.04
0.05		30.87	40.13	−0.738	14.987	23.704	32.67	41.74	33.15	50.92	33.26	51.09
0.06		22.09	28.43	1.978	12.005	17.816	23.86	30.02	24.34	36.28	24.45	36.45
0.07		16.78	21.37	3.508	10.176	14.246	18.54	22.95	19.01	27.45	19.11	27.61
0.08		13.34	16.78	4.399	8.957	11.907	15.07	18.34	15.52	21.70	15.63	21.87
0.09		10.97	13.63	4.917	8.091	10.283	12.68	15.17	13.12	17.76	13.23	17.92
0.10		9.28	11.38	5.202	7.442	9.101	10.95	12.90	11.38	14.92	11.49	15.09
0.11		8.02	9.71	5.335	6.932	8.206	9.66	11.20	10.07	12.82	10.18	12.98
0.12		7.057	8.437	5.367	6.516	7.506	8.658	9.898	9.062	11.212	9.170	11.369
0.13		6.305	7.442	5.331	6.166	6.942	7.867	8.874	8.257	9.952	8.364	10.105
0.14		5.703	6.650	5.248	5.863	6.477	7.227	8.052	7.601	8.945	7.708	9.094
0.15		5.213	5.818	5.132	5.595	6.084	6.696	7.378	7.057	8.124	7.163	8.269
0.16		4.809	5.481	4.996	5.352	5.746	6.249	6.817	6.596	7.444	6.702	7.586
0.17		4.470	5.041	4.846	5.130	5.449	5.867	6.343	6.200	6.873	6.304	7.012
0.18		4.182	4.669	4.688	4.925	5.186	5.534	5.936	5.853	6.388	5.957	6.523
0.19		3.934	4.351	4.527	4.733	4.949	5.242	5.582	5.548	5.969	5.650	6.101
0.20		3.719	4.078	4.365	4.552	4.734	4.981	5.273	5.275	5.605	5.376	5.733
0.22		3.364	3.631	4.046	4.218	4.352	4.535	4.751	4.805	5.002	4.903	5.123
0.24		3.081	3.281	3.745	3.914	4.021	4.161	4.327	4.410	4.520	4.505	4.634
0.25		2.960	3.133	3.602	3.773	3.871	3.995	4.143	4.233	4.313	4.327	4.424
0.26		2.849	3.000	3.465	3.638	3.729	3.841	3.972	4.069	4.124	4.162	4.232
0.28		2.654	2.769	3.208	3.384	3.466	3.560	3.668	3.771	3.791	3.860	3.892
0.30		2.487	2.574	2.975	3.151	3.228	3.311	3.403	3.507	3.505	3.592	3.599
0.32		2.340	2.407	2.765	2.938	3.012	3.088	3.168	3.269	3.255	3.351	3.344
0.34		2.210	2.262	2.576	2.744	2.815	2.886	2.957	3.054	3.034	3.132	3.117
0.35		2.150	2.195	2.488	2.652	2.723	2.792	2.860	2.955	2.933	3.031	3.013
0.36		2.093	2.133	2.405	2.565	2.635	2.702	2.768	2.859	2.837	2.934	2.915
0.38		1.986	2.018	2.252	2.403	2.470	2.534	2.596	2.681	2.659	2.752	2.732
0.40		1.888	1.914	2.114	2.254	2.319	2.381	2.439	2.518	2.497	2.585	2.566
0.42		1.798	1.819	1.990	2.119	2.180	2.240	2.295	2.369	2.350	2.432	2.414
0.44		1.714	1.732	1.877	1.996	2.053	2.111	2.163	2.231	2.215	2.292	2.276
0.45		1.674	1.691	1.825	1.938	1.994	2.050	2.102	2.167	2.152	2.225	2.211
0.46		1.635	1.652	1.775	1.883	1.937	1.992	2.042	2.105	2.092	2.162	2.148
0.48		1.562	1.577	1.682	1.780	1.831	1.883	1.931	1.988	1.978	2.042	2.031
0.50		1.493	1.507	1.598	1.686	1.733	1.782	1.828	1.881	1.872	1.931	1.922
0.55		1.337	1.351	1.415	1.483	1.522	1.564	1.604	1.647	1.643	1.690	1.686
0.60		1.201	1.216	1.266	1.318	1.350	1.385	1.419	1.454	1.453	1.491	1.489
0.65		1.082	1.098	1.140	1.182	1.208	1.237	1.266	1.295	1.295	1.326	1.326
0.70		0.977	0.994	1.034	1.068	1.089	1.113	1.137	1.161	1.163	1.188	1.188
0.80		0.803	0.821	0.860	0.887	0.902	0.919	0.937	0.954	0.955	0.973	0.974
0.90		0.667	0.684	0.725	0.749	0.761	0.775	0.788	0.801	0.802	0.815	0.816
1.00		0.559	0.575	0.616	0.640	0.651	0.662	0.673	0.684	0.685	0.696	0.696
1.10		0.474	0.489	0.528	0.551	0.562	0.572	0.582	0.591	0.592	0.601	0.601
1.20		0.406	0.419	0.456	0.478	0.488	0.498	0.507	0.516	0.516	0.525	0.525
1.30		0.351	0.363	0.396	0.417	0.427	0.436	0.445	0.453	0.453	0.462	0.462
1.40		0.307	0.317	0.347	0.366	0.376	0.384	0.393	0.401	0.401	0.408	0.408
1.50		0.271	0.280	0.306	0.324	0.332	0.340	0.348	0.356	0.356	0.363	0.363
1.60				0.272	0.288	0.296	0.303	0.311	0.318	0.318	0.325	0.325
1.70				0.243	0.257	0.265	0.271	0.278	0.285	0.285	0.292	0.292
1.80				0.219	0.232	0.238	0.244	0.251	0.257	0.257	0.263	0.263
1.90				0.198	0.209	0.215	0.221	0.227	0.232	0.232	0.238	0.238
2.00				0.180	0.190	0.196	0.201	0.206	0.211	0.211	0.216	0.216

Table 4.3.1.2. *Atomic scattering amplitudes (Å) for electrons for ionized atoms (cont.)*

$(\sin\theta)/\lambda$ (Å^{-1})	Element	Mo^{3+}	Ru^{3+}	Ru^{4+}	Rh^{3+}	Rh^{4+}	Pd^{2+}	Pd^{4+}	Ag^{1+}	Ag^{2+}	Cd^{2+}	In^{3+}
	Z	42	44	44	45	45	46	46	47	47	48	49
	Method	*DS	*DS	*DS	*DS	*DS	*DS	*DS	*DS	*DS	*DS	*DS
0.00												
0.01												
0.02												
0.03												
0.04		92.49	49.53	63.83	49.53	63.87	35.30	63.89	21.21	35.23	35.15	49.41
0.05		60.17	33.34	42.27	33.35	42.31	24.50	42.32	15.77	24.43	24.36	33.23
0.06		42.61	24.54	30.54	24.55	30.58	18.61	30.61	12.79	18.54	18.47	24.43
0.07		32.01	19.21	23.46	19.22	23.50	15.03	23.52	10.96	14.97	14.90	19.11
0.08		25.13	15.73	18.85	15.74	18.89	12.69	18.92	9.73	12.63	12.56	15.65
0.09		20.40	13.33	15.68	13.34	15.72	11.06	15.75	8.87	11.00	10.94	13.26
0.10		17.02	11.59	13.39	11.61	13.44	9.87	13.46	8.22	9.82	9.76	11.53
0.11		14.50	10.29	11.69	10.31	11.74	8.97	11.76	7.70	8.92	8.87	10.24
0.12		12.585	9.281	10.381	9.301	10.430	8.259	10.458	7.287	8.217	8.169	9.249
0.13		11.086	8.480	9.351	8.502	9.399	7.687	9.431	6.935	7.652	7.608	8.463
0.14		9.891	7.827	8.521	7.853	8.571	7.214	8.603	6.631	7.184	7.146	7.826
0.15		8.919	7.286	7.840	7.313	7.891	6.813	7.924	6.361	6.789	6.756	7.299
0.16		8.118	6.827	7.271	6.858	7.322	6.467	7.357	6.117	6.448	6.419	6.856
0.17		7.449	6.432	6.788	6.465	6.841	6.163	6.877	5.894	6.149	6.126	6.476
0.18		6.881	6.088	6.372	6.124	6.426	5.892	6.464	5.687	5.883	5.865	6.147
0.19		6.395	5.784	6.011	5.822	6.065	5.647	6.105	5.494	5.643	5.629	5.858
0.20		5.975	5.511	5.692	5.553	5.747	5.423	5.788	5.312	5.424	5.416	5.600
0.22		5.283	5.042	5.153	5.087	5.211	5.026	5.255	4.975	5.036	5.036	5.158
0.24		4.739	4.646	4.712	4.695	4.771	4.679	4.818	4.667	4.697	4.705	4.786
0.25		4.508	4.469	4.519	4.520	4.578	4.521	4.626	4.522	4.541	4.553	4.621
0.26		4.297	4.304	4.340	4.356	4.400	4.370	4.449	4.383	4.394	4.410	4.466
0.28		3.931	4.003	4.020	4.057	4.080	4.090	4.130	4.120	4.121	4.142	4.184
0.30		3.620	3.733	3.738	3.789	3.799	3.836	3.850	3.876	3.871	3.898	3.930
0.32		3.352	3.490	3.488	3.547	3.548	3.601	3.601	3.649	3.640	3.672	3.701
0.34		3.118	3.269	3.263	3.327	3.323	3.385	3.376	3.437	3.427	3.463	3.490
0.35		3.011	3.166	3.158	3.224	3.218	3.284	3.271	3.336	3.327	3.363	3.390
0.36		2.910	3.067	3.058	3.125	3.118	3.185	3.171	3.239	3.230	3.268	3.295
0.38		2.725	2.882	2.872	2.939	2.931	3.000	2.984	3.055	3.046	3.086	3.115
0.40		2.557	2.711	2.702	2.768	2.759	2.828	2.812	2.883	2.875	2.917	2.947
0.42		2.406	2.553	2.545	2.609	2.601	2.668	2.653	2.723	2.716	2.759	2.790
0.44		2.267	2.408	2.400	2.462	2.454	2.520	2.505	2.573	2.567	2.611	2.643
0.45		2.202	2.339	2.332	2.393	2.385	2.450	2.436	2.502	2.497	2.541	2.574
0.46		2.140	2.273	2.266	2.326	2.319	2.382	2.369	2.434	2.429	2.473	2.506
0.48		2.024	2.148	2.143	2.199	2.193	2.253	2.242	2.304	2.300	2.343	2.378
0.50		1.916	2.033	2.028	2.082	2.077	2.133	2.124	2.182	2.179	2.222	2.258
0.55		1.682	1.779	1.776	1.823	1.820	1.869	1.863	1.913	1.912	1.953	1.989
0.60		1.487	1.568	1.567	1.607	1.606	1.647	1.644	1.687	1.686	1.725	1.760
0.65		1.325	1.392	1.392	1.426	1.426	1.461	1.460	1.496	1.496	1.531	1.564
0.70		1.189	1.244	1.244	1.274	1.274	1.304	1.304	1.335	1.335	1.367	1.397
0.80		0.975	1.014	1.015	1.036	1.037	1.059	1.060	1.083	1.083	1.107	1.132
0.90		0.817	0.846	0.846	0.863	0.863	0.880	0.880	0.898	0.898	0.917	0.936
1.00		0.696	0.719	0.720	0.732	0.732	0.745	0.746	0.759	0.759	0.774	0.789
1.10		0.602	0.621	0.621	0.631	0.631	0.642	0.642	0.653	0.653	0.664	0.676
1.20		0.525	0.542	0.542	0.551	0.551	0.560	0.560	0.569	0.569	0.578	0.588
1.30		0.462	0.477	0.477	0.485	0.485	0.493	0.493	0.501	0.501	0.508	0.516
1.40		0.409	0.423	0.423	0.430	0.430	0.437	0.437	0.444	0.444	0.451	0.458
1.50		0.363	0.377	0.377	0.384	0.384	0.391	0.391	0.397	0.397	0.403	0.409
1.60		0.325	0.338	0.338	0.344	0.344	0.350	0.350	0.356	0.356	0.362	0.368
1.70		0.292	0.304	0.304	0.310	0.310	0.316	0.316	0.322	0.322	0.327	0.332
1.80		0.263	0.275	0.275	0.280	0.280	0.286	0.286	0.291	0.291	0.296	0.301
1.90		0.238	0.249	0.249	0.254	0.254	0.260	0.260	0.265	0.265	0.270	0.274
2.00		0.216	0.227	0.227	0.232	0.232	0.237	0.237	0.241	0.241	0.246	0.251

Table 4.3.1.2. *Atomic scattering amplitudes (Å) for electrons for ionized atoms (cont.)*

$(\sin\theta)/\lambda$ (Å^{-1})	Element	Sn^{2+}	Sn^{4+}	Sb^{3+}	Sb^{5+}	I^{1-}	Cs^{1+}	Ba^{2+}	La^{3+}	Ce^{3+}	Ce^{4+}	Pr^{3+}
	Z	50	50	51	51	53	55	56	57	58	58	59
	Method	RHF	RHF	*DS	*DS	RHF	RHF	*DS	*DS	*DS	*DS	*DS
0.00		6.144	3.971			13.835	9.035					
0.01		484.819	961.330			−225.540	248.365					
0.02		125.792	243.305			−46.145	68.827					
0.03		59.280	110.331			−13.083	35.532					
0.04		35.972	63.782	50.16	78.38	−1.690	23.823	37.64	51.70	51.62	65.94	51.53
0.05		25.152	42.227	33.97	51.44	3.399	18.344	26.81	35.49	35.42	44.36	35.34
0.06		19.242	30.510	25.14	36.81	5.981	15.307	20.87	26.65	26.59	32.62	26.51
0.07		15.646	23.435	19.81	27.97	7.365	13.414	17.25	21.30	21.23	25.51	21.15
0.08		13.280	18.833	16.32	22.22	8.103	12.124	14.86	17.78	17.72	20.87	17.65
0.09		11.625	15.668	13.91	18.28	8.462	11.180	13.17	15.34	15.29	17.66	15.22
0.10		10.411	13.395	12.16	15.45	8.586	10.448	11.92	13.57	13.51	15.34	13.45
0.11		9.484	11.703	10.85	13.35	8.560	9.851	10.96	12.22	12.17	13.60	12.11
0.12		8.750	10.407	9.825	11.743	8.437	9.345	10.185	11.163	11.119	12.258	11.064
0.13		8.152	9.388	9.010	10.486	8.249	8.903	9.547	10.313	10.275	11.185	10.224
0.14		7.653	8.571	8.344	9.480	8.021	8.506	9.003	9.610	9.576	10.312	9.531
0.15		7.227	7.902	7.790	8.660	7.767	8.143	8.531	9.016	8.987	9.586	8.947
0.16		6.856	7.345	7.319	7.982	7.500	7.806	8.113	8.505	8.482	8.972	8.446
0.17		6.528	6.875	6.911	7.413	7.228	7.491	7.738	8.056	8.038	8.441	8.008
0.18		6.234	6.473	6.555	6.928	6.955	7.193	7.395	7.658	7.645	7.979	7.619
0.19		5.968	6.124	6.239	6.512	6.685	6.911	7.080	7.300	7.292	7.569	7.270
0.20		5.725	5.818	5.955	6.149	6.423	6.643	6.787	6.974	6.970	7.202	6.954
0.22		5.293	5.304	5.464	5.548	5.925	6.143	6.256	6.398	6.403	6.568	6.396
0.24		4.918	4.886	5.050	5.067	5.468	5.688	5.785	5.900	5.912	6.033	5.914
0.25		4.747	4.703	4.864	4.860	5.255	5.475	5.568	5.674	5.690	5.794	5.695
0.26		4.586	4.535	4.691	4.671	5.054	5.272	5.362	5.461	5.480	5.570	5.489
0.28		4.289	4.232	4.375	4.336	4.681	4.893	4.980	5.069	5.094	5.163	5.109
0.30		4.021	3.967	4.094	4.048	4.348	4.549	4.633	4.716	4.745	4.800	4.766
0.32		3.778	3.730	3.840	3.793	4.049	4.237	4.318	4.396	4.429	4.474	4.454
0.34		3.556	3.516	3.611	3.567	3.782	3.954	4.032	4.106	4.142	4.179	4.170
0.35		3.452	3.416	3.503	3.463	3.658	3.823	3.899	3.971	4.008	4.042	4.037
0.36		3.352	3.320	3.401	3.363	3.541	3.698	3.772	3.843	3.880	3.911	3.910
0.38		3.164	3.140	3.208	3.177	3.325	3.466	3.536	3.602	3.640	3.667	3.673
0.40		2.991	2.973	3.031	3.006	3.129	3.255	3.321	3.383	3.422	3.444	3.455
0.42		2.830	2.817	2.867	2.848	2.951	3.064	3.124	3.183	3.221	3.240	3.255
0.44		2.680	2.672	2.716	2.702	2.789	2.890	2.946	3.000	3.038	3.054	3.072
0.45		2.610	2.604	2.644	2.632	2.714	2.808	2.862	2.914	2.952	2.967	2.986
0.46		2.541	2.537	2.575	2.565	2.641	2.731	2.782	2.832	2.870	2.883	2.904
0.48		2.412	2.410	2.444	2.438	2.505	2.586	2.632	2.679	2.715	2.726	2.749
0.50		2.290	2.291	2.322	2.319	2.379	2.452	2.495	2.538	2.573	2.582	2.606
0.55		2.020	2.023	2.050	2.051	2.103	2.163	2.197	2.232	2.264	2.268	2.295
0.60		1.791	1.794	1.819	1.822	1.871	1.923	1.951	1.980	2.010	2.011	2.038
0.65		1.594	1.597	1.622	1.625	1.673	1.721	1.745	1.770	1.797	1.796	1.823
0.70		1.426	1.428	1.453	1.455	1.503	1.548	1.570	1.592	1.617	1.615	1.641
0.80		1.157	1.157	1.181	1.182	1.227	1.269	1.288	1.307	1.328	1.326	1.349
0.90		0.956	0.956	0.976	0.977	1.017	1.055	1.072	1.090	1.108	1.107	1.126
1.00		0.805	0.804	0.821	0.821	0.855	0.888	0.904	0.920	0.936	0.935	0.952
1.10		0.688	0.688	0.702	0.702	0.729	0.757	0.771	0.785	0.799	0.799	0.813
1.20		0.597	0.597	0.608	0.608	0.630	0.654	0.666	0.678	0.690	0.690	0.702
1.30		0.525	0.524	0.534	0.533	0.551	0.571	0.581	0.591	0.602	0.602	0.612
1.40		0.465	0.465	0.473	0.473	0.487	0.504	0.512	0.521	0.530	0.530	0.539
1.50		0.416	0.416	0.422	0.422	0.435	0.448	0.456	0.463	0.471	0.471	0.478
1.60		0.374	0.374	0.379	0.379	0.391	0.402	0.409	0.415	0.421	0.421	0.428
1.70		0.338	0.338	0.343	0.343	0.353	0.364	0.369	0.374	0.380	0.380	0.386
1.80		0.306	0.306	0.311	0.311	0.321	0.330	0.335	0.340	0.345	0.345	0.350
1.90		0.279	0.279	0.284	0.284	0.293	0.301	0.306	0.310	0.314	0.314	0.319
2.00		0.255	0.255	0.259	0.259	0.268	0.276	0.280	0.284	0.288	0.288	0.292

Table 4.3.1.2. *Atomic scattering amplitudes (Å) for electrons for ionized atoms (cont.)*

$(\sin\theta)/\lambda$ ($Å^{-1}$)	Element	Pr^{4+}	Nd^{3+}	Pm^{3+}	Sm^{3+}	Eu^{2+}	Eu^{3+}	Gd^{3+}	Tb^{3+}	Dy^{3+}	Ho^{3+}	Er^{3+}
	Z	59	60	61	62	63	63	64	65	66	67	68
	Method	*DS	*DS	*DS	*DS	*DS	*DS	*DS	*DS	*DS	*DS	*DS
0.00												
0.01												
0.02												
0.03												
0.04		65.86	51.44	51.35	51.26	36.99	51.17	51.08	51.04	50.92	50.83	50.74
0.05		44.30	35.25	35.15	35.07	26.17	34.97	34.90	34.85	34.72	34.64	34.55
0.06		32.55	26.42	26.33	26.25	20.26	26.15	26.08	26.02	25.92	25.83	25.74
0.07		25.44	21.07	20.98	20.90	16.67	20.81	20.74	20.68	20.58	20.50	20.41
0.08		20.81	17.57	17.49	17.41	14.30	17.32	17.25	17.19	17.09	17.01	16.93
0.09		17.60	15.14	15.06	14.98	12.65	14.90	14.83	14.77	14.68	14.60	14.53
0.10		15.29	13.38	13.30	13.23	11.44	13.15	13.08	13.02	12.94	12.86	12.79
0.11		13.55	12.04	11.97	11.90	10.51	11.83	11.76	11.71	11.62	11.55	11.48
0.12		12.210	11.003	10.937	10.870	9.770	10.802	10.739	10.681	10.604	10.538	10.469
0.13		11.141	10.167	10.106	10.044	9.167	9.979	9.919	9.863	9.792	9.728	9.664
0.14		10.272	9.480	9.422	9.366	8.663	9.305	9.248	9.194	9.128	9.068	9.007
0.15		9.550	8.901	8.849	8.796	8.229	8.740	8.686	8.634	8.574	8.517	8.460
0.16		8.939	8.405	8.357	8.310	7.850	8.257	8.207	8.158	8.102	8.049	7.995
0.17		8.413	7.972	7.930	7.886	7.511	7.838	7.791	7.746	7.694	7.645	7.594
0.18		7.955	7.589	7.551	7.512	7.206	7.468	7.425	7.383	7.335	7.290	7.242
0.19		7.549	7.245	7.212	7.177	6.927	7.138	7.099	7.059	7.016	6.974	6.930
0.20		7.187	6.932	6.904	6.874	6.669	6.839	6.804	6.768	6.729	6.690	6.650
0.22		6.561	6.384	6.364	6.342	6.204	6.316	6.289	6.258	6.227	6.196	6.162
0.24		6.033	5.910	5.899	5.884	5.792	5.865	5.845	5.822	5.798	5.773	5.745
0.25		5.797	5.695	5.687	5.677	5.601	5.661	5.645	5.625	5.604	5.582	5.557
0.26		5.577	5.492	5.488	5.481	5.419	5.469	5.456	5.439	5.421	5.402	5.380
0.28		5.176	5.118	5.121	5.120	5.080	5.115	5.107	5.096	5.085	5.071	5.055
0.30		4.818	4.780	4.789	4.793	4.768	4.794	4.792	4.787	4.780	4.772	4.760
0.32		4.496	4.473	4.486	4.496	4.482	4.501	4.504	4.504	4.502	4.498	4.492
0.34		4.205	4.193	4.210	4.224	4.218	4.233	4.240	4.244	4.247	4.247	4.244
0.35		4.069	4.061	4.081	4.096	4.093	4.107	4.116	4.122	4.126	4.128	4.128
0.36		3.939	3.936	3.956	3.973	3.973	3.987	3.997	4.005	4.011	4.014	4.016
0.38		3.697	3.700	3.724	3.743	3.748	3.759	3.773	3.784	3.793	3.799	3.804
0.40		3.476	3.484	3.509	3.531	3.540	3.550	3.566	3.579	3.590	3.600	3.607
0.42		3.273	3.285	3.312	3.335	3.347	3.356	3.374	3.389	3.403	3.414	3.423
0.44		3.087	3.103	3.130	3.155	3.168	3.176	3.196	3.213	3.228	3.241	3.253
0.45		3.000	3.017	3.045	3.069	3.084	3.092	3.112	3.130	3.146	3.160	3.172
0.46		2.916	2.934	2.962	2.988	3.003	3.010	3.031	3.049	3.066	3.081	3.094
0.48		2.759	2.779	2.807	2.833	2.850	2.856	2.878	2.897	2.915	2.931	2.945
0.50		2.614	2.636	2.664	2.690	2.709	2.714	2.736	2.756	2.775	2.791	2.807
0.55		2.299	2.324	2.351	2.376	2.397	2.400	2.423	2.444	2.463	2.481	2.498
0.60		2.040	2.065	2.091	2.115	2.137	2.138	2.160	2.181	2.201	2.220	2.237
0.65		1.823	1.848	1.872	1.895	1.917	1.917	1.939	1.959	1.978	1.997	2.014
0.70		1.639	1.664	1.686	1.708	1.730	1.729	1.749	1.769	1.788	1.806	1.823
0.80		1.347	1.369	1.389	1.408	1.428	1.427	1.445	1.463	1.480	1.497	1.513
0.90		1.125	1.144	1.162	1.179	1.197	1.196	1.212	1.228	1.244	1.260	1.274
1.00		0.951	0.968	0.984	0.999	1.015	1.014	1.029	1.044	1.058	1.072	1.086
1.10		0.813	0.827	0.841	0.855	0.869	0.869	0.882	0.895	0.908	0.921	0.934
1.20		0.702	0.714	0.727	0.739	0.751	0.751	0.763	0.775	0.787	0.798	0.810
1.30		0.612	0.623	0.634	0.644	0.655	0.655	0.666	0.676	0.687	0.697	0.708
1.40		0.539	0.548	0.557	0.567	0.576	0.576	0.585	0.595	0.604	0.613	0.623
1.50		0.478	0.486	0.494	0.502	0.510	0.510	0.519	0.527	0.535	0.544	0.552
1.60		0.428	0.435	0.442	0.449	0.456	0.456	0.463	0.470	0.478	0.485	0.492
1.70		0.386	0.392	0.398	0.404	0.410	0.410	0.416	0.423	0.429	0.436	0.442
1.80		0.350	0.355	0.360	0.366	0.371	0.371	0.377	0.382	0.388	0.394	0.399
1.90		0.319	0.324	0.328	0.333	0.338	0.338	0.343	0.348	0.353	0.358	0.363
2.00		0.292	0.296	0.301	0.305	0.309	0.309	0.313	0.318	0.322	0.327	0.331

Table 4.3.1.2. *Atomic scattering amplitudes (Å) for electrons for ionized atoms (cont.)*

$(\sin\theta)/\lambda$ (Å^{-1})	Element	Tm^{3+}	Yb^{2+}	Yb^{3+}	Lu^{3+}	Hf^{4+}	Ta^{5+}	W^{6+}	Os^{4+}	Ir^{3+}	Ir^{4+}	Pt^{2+}
	Z	69	70	70	71	72	73	74	76	77	77	78
	Method	*DS	*DS	*DS	*DS	*DS	*DS	*DS	*DS	*DS	*DS	*DS
0.00												
0.01												
0.02												
0.03												
0.04		50.67	36.30	50.58	50.50	64.91	79.42	94.00	65.56	51.44	65.65	37.41
0.05		34.47	25.49	34.40	34.32	43.35	52.47	61.68	44.00	35.25	44.09	26.60
0.06		25.67	19.61	25.59	25.52	31.63	37.84	44.11	32.26	26.43	32.36	20.68
0.07		20.34	16.03	20.27	20.19	24.54	28.99	33.51	25.17	21.09	25.26	17.09
0.08		16.86	13.68	16.79	16.72	19.93	23.24	26.62	20.55	17.60	20.64	14.72
0.09		14.46	12.05	14.39	14.32	16.76	19.29	21.89	17.36	15.18	17.45	13.06
0.10		12.72	10.86	12.65	12.59	14.47	16.45	18.50	15.06	13.42	15.15	11.84
0.11		11.42	9.95	11.35	11.29	12.77	14.34	15.98	13.34	12.10	13.43	10.91
0.12		10.406	9.243	10.343	10.282	11.463	12.727	14.051	12.019	11.071	12.108	10.170
0.13		9.603	8.669	9.542	9.484	10.432	11.460	12.545	10.971	10.248	11.061	9.567
0.14		8.950	8.191	8.891	8.835	9.600	10.443	11.341	10.122	9.571	10.211	9.058
0.15		8.405	7.788	8.349	8.296	8.918	9.613	10.361	9.421	9.006	9.510	8.623
0.16		7.943	7.436	7.890	7.839	8.348	8.924	9.550	8.833	8.523	8.919	8.241
0.17		7.545	7.128	7.495	7.447	7.863	8.343	8.870	8.330	8.104	8.415	7.902
0.18		7.196	6.852	7.150	7.104	7.445	7.847	8.292	7.895	7.734	7.978	7.595
0.19		6.888	6.601	6.843	6.801	7.081	7.418	7.795	7.512	7.404	7.594	7.314
0.20		6.610	6.372	6.569	6.529	6.760	7.042	7.364	7.172	7.107	7.253	7.055
0.22		6.128	5.962	6.093	6.058	6.214	6.415	6.650	6.591	6.585	6.668	6.587
0.24		5.717	5.601	5.688	5.659	5.765	5.907	6.080	6.107	6.138	6.181	6.173
0.25		5.532	5.434	5.505	5.479	5.566	5.687	5.836	5.893	5.936	5.965	5.981
0.26		5.358	5.276	5.334	5.310	5.382	5.485	5.613	5.693	5.745	5.764	5.799
0.28		5.038	4.980	5.019	5.000	5.049	5.124	5.220	5.331	5.395	5.398	5.458
0.30		4.748	4.708	4.734	4.720	4.754	4.809	4.882	5.009	5.078	5.072	5.145
0.32		4.484	4.456	4.474	4.464	4.489	4.530	4.586	4.719	4.789	4.779	4.857
0.34		4.240	4.221	4.234	4.228	4.247	4.279	4.323	4.456	4.524	4.512	4.590
0.35		4.126	4.110	4.122	4.117	4.134	4.162	4.201	4.333	4.400	4.387	4.464
0.36		4.015	4.003	4.013	4.010	4.025	4.051	4.086	4.215	4.280	4.267	4.343
0.38		3.806	3.800	3.807	3.807	3.821	3.843	3.872	3.994	4.055	4.042	4.114
0.40		3.612	3.609	3.616	3.618	3.632	3.650	3.675	3.789	3.845	3.834	3.900
0.42		3.431	3.432	3.437	3.442	3.455	3.473	3.495	3.599	3.651	3.641	3.702
0.44		3.262	3.266	3.271	3.277	3.291	3.307	3.327	3.423	3.471	3.462	3.518
0.45		3.182	3.187	3.191	3.199	3.213	3.229	3.248	3.340	3.385	3.377	3.430
0.46		3.105	3.110	3.115	3.123	3.137	3.153	3.172	3.259	3.303	3.295	3.346
0.48		2.958	2.965	2.969	2.979	2.993	3.009	3.027	3.106	3.146	3.140	3.186
0.50		2.820	2.829	2.833	2.844	2.859	2.875	2.892	2.963	3.000	2.995	3.036
0.55		2.514	2.526	2.528	2.541	2.557	2.573	2.590	2.646	2.675	2.672	2.704
0.60		2.253	2.267	2.269	2.283	2.299	2.315	2.331	2.375	2.399	2.398	2.423
0.65		2.031	2.046	2.047	2.061	2.077	2.092	2.108	2.144	2.164	2.164	2.184
0.70		1.839	1.855	1.855	1.870	1.885	1.900	1.914	1.945	1.962	1.962	1.979
0.80		1.529	1.544	1.544	1.558	1.572	1.585	1.598	1.623	1.636	1.636	1.649
0.90		1.289	1.304	1.303	1.317	1.329	1.341	1.353	1.375	1.386	1.386	1.397
1.00		1.099	1.113	1.112	1.125	1.137	1.148	1.159	1.179	1.189	1.189	1.199
1.10		0.946	0.959	0.958	0.970	0.981	0.992	1.002	1.021	1.031	1.031	1.040
1.20		0.821	0.833	0.832	0.843	0.854	0.864	0.873	0.892	0.901	0.901	0.909
1.30		0.718	0.728	0.728	0.738	0.748	0.757	0.766	0.784	0.792	0.792	0.800
1.40		0.632	0.641	0.641	0.650	0.659	0.668	0.677	0.693	0.701	0.701	0.709
1.50		0.560	0.569	0.569	0.577	0.585	0.593	0.601	0.616	0.624	0.624	0.631
1.60		0.500	0.507	0.507	0.515	0.522	0.529	0.537	0.551	0.558	0.558	0.565
1.70		0.449	0.455	0.455	0.462	0.469	0.475	0.482	0.495	0.502	0.502	0.508
1.80		0.405	0.411	0.411	0.417	0.423	0.429	0.435	0.447	0.453	0.453	0.459
1.90		0.368	0.373	0.373	0.379	0.384	0.389	0.395	0.405	0.411	0.411	0.416
2.00		0.336	0.341	0.341	0.345	0.350	0.355	0.360	0.370	0.374	0.374	0.379

Table 4.3.1.2. *Atomic scattering amplitudes (Å) for electrons for ionized atoms (cont.)*

$(\sin\theta)/\lambda$ ($Å^{-1}$)	Element	Pt^{4+}	Au^{1+}	Au^{3+}	Hg^{1+}	Hg^{2+}	Tl^{1+}	Tl^{3+}	Pb^{2+}	Pb^{4+}	Bi^{3+}	Bi^{5+}
	Z	78	79	79	80	80	81	81	82	82	83	83
	Method	*DS	*DS	*DS	*DS	*DS	*DS	*DS	*DS	*DS	*DS	*DS
0.00												
0.01												
0.02												
0.03												
0.04		65.73	23.52	51.50	23.84	37.35	24.11	51.46	37.98	65.83	52.12	80.28
0.05		44.16	18.07	35.32	18.38	26.53	18.65	35.29	27.15	44.27	35.91	53.34
0.06		32.42	15.05	26.49	15.36	20.63	15.62	26.48	21.23	32.54	27.09	38.69
0.07		25.33	13.19	21.15	13.49	17.04	13.74	21.15	17.62	25.45	21.74	29.85
0.08		20.71	11.94	17.67	12.23	14.67	12.47	17.67	15.24	20.83	18.23	24.09
0.09		17.52	11.04	15.25	11.31	13.03	11.54	15.26	13.57	17.65	15.81	20.13
0.10		15.22	10.35	13.50	10.60	11.82	10.83	13.51	12.34	15.35	14.04	17.29
0.11		13.50	9.80	12.18	10.04	10.89	10.26	12.20	11.40	13.64	12.70	15.17
0.12		12.178	9.341	11.153	9.565	10.165	9.775	11.178	10.642	12.316	11.663	13.539
0.13		11.130	8.946	10.331	9.156	9.569	9.356	10.362	10.024	11.272	10.827	12.262
0.14		10.281	8.599	9.660	8.795	9.072	8.983	9.696	9.500	10.427	10.138	11.234
0.15		9.579	8.285	9.097	8.466	8.644	8.645	9.139	9.049	9.730	9.559	10.392
0.16		8.988	7.997	8.617	8.166	8.271	8.335	8.664	8.653	9.144	9.061	9.690
0.17		8.484	7.731	8.201	7.887	7.940	8.045	8.253	8.297	8.644	8.629	9.097
0.18		8.047	7.480	7.834	7.624	7.640	7.773	7.890	7.975	8.211	8.245	8.587
0.19		7.662	7.243	7.506	7.376	7.367	7.516	7.567	7.679	7.830	7.901	8.144
0.20		7.320	7.018	7.211	7.141	7.114	7.272	7.275	7.406	7.492	7.589	7.755
0.22		6.735	6.598	6.693	6.703	6.658	6.817	6.765	6.912	6.913	7.040	7.100
0.24		6.246	6.210	6.247	6.301	6.253	6.400	6.326	6.472	6.429	6.566	6.564
0.25		6.029	6.028	6.046	6.112	6.065	6.205	6.127	6.268	6.214	6.351	6.329
0.26		5.827	5.852	5.855	5.930	5.886	6.017	5.939	6.075	6.014	6.148	6.111
0.28		5.459	5.519	5.505	5.587	5.550	5.664	5.591	5.714	5.647	5.773	5.721
0.30		5.131	5.209	5.186	5.270	5.240	5.337	5.275	5.383	5.320	5.433	5.377
0.32		4.385	4.921	4.895	4.975	4.953	5.035	4.985	5.078	5.023	5.123	5.069
0.34		4.565	4.652	4.627	4.702	4.686	4.756	4.718	4.797	4.751	4.838	4.790
0.35		4.439	4.525	4.501	4.573	4.560	4.624	4.591	4.664	4.623	4.704	4.660
0.36		4.318	4.402	4.379	4.448	4.437	4.497	4.469	4.536	4.501	4.576	4.535
0.38		4.090	4.170	4.149	4.212	4.206	4.257	4.238	4.295	4.269	4.333	4.300
0.40		3.880	3.953	3.936	3.993	3.990	4.034	4.022	4.072	4.053	4.108	4.083
0.42		3.684	3.752	3.737	3.789	3.788	3.827	3.821	3.864	3.851	3.899	3.881
0.44		3.502	3.564	3.552	3.599	3.600	3.635	3.633	3.671	3.663	3.705	3.692
0.45		3.416	3.475	3.464	3.509	3.511	3.544	3.544	3.579	3.574	3.613	3.603
0.46		3.333	3.389	3.379	3.422	3.424	3.456	3.457	3.491	3.488	3.524	3.516
0.48		3.176	3.225	3.218	3.258	3.260	3.290	3.293	3.323	3.323	3.355	3.351
0.50		3.028	3.073	3.068	3.104	3.107	3.134	3.139	3.166	3.168	3.197	3.197
0.55		2.700	2.735	2.733	2.762	2.765	2.790	2.795	2.819	2.823	2.847	2.850
0.60		2.422	2.449	2.448	2.474	2.476	2.498	2.502	2.524	2.528	2.549	2.554
0.96		2.184	2.206	2.206	2.227	2.229	2.249	2.252	2.272	2.276	2.295	2.300
0.70		1.980	1.998	1.998	2.017	2.017	2.036	2.038	2.057	2.059	2.077	2.080
0.80		1.650	1.663	1.663	1.678	1.678	1.693	1.694	1.709	1.710	1.726	1.727
0.90		1.397	1.408	1.408	1.420	1.420	1.432	1.432	1.445	1.445	1.458	1.458
1.00		1.199	1.208	1.209	1.218	1.218	1.229	1.228	1.239	1.239	1.250	1.249
1.10		1.040	1.048	1.048	1.057	1.057	1.066	1.066	1.075	1.075	1.084	1.084
1.20		0.909	0.917	0.917	0.926	0.925	0.934	0.933	0.942	0.941	0.950	0.949
1.30		0.800	0.808	0.808	0.816	0.816	0.824	0.824	0.831	0.831	0.838	0.838
1.40		0.709	0.717	0.716	0.724	0.724	0.731	0.731	0.738	0.738	0.745	0.745
1.50		0.631	0.638	0.638	0.645	0.645	0.652	0.652	0.659	0.659	0.665	0.665
1.60		0.565	0.572	0.572	0.578	0.578	0.585	0.585	0.591	0.591	0.597	0.597
1.70		0.508	0.514	0.514	0.520	0.520	0.526	0.527	0.532	0.533	0.538	0.538
1.80		0.459	0.465	0.465	0.470	0.470	0.476	0.476	0.482	0.482	0.487	0.487
1.90		0.416	0.422	0.422	0.427	0.427	0.432	0.432	0.438	0.438	0.443	0.443
2.00		0.379	0.384	0.384	0.389	0.389	0.394	0.394	0.399	0.399	0.404	0.404

Table 4.3.1.2. *Atomic scattering amplitudes (Å) for electrons for ionized atoms (cont.)*

$(\sin\theta)/\lambda$ (Å^{-1})	Element	Ra^{2+}	Ac^{3+}	U^{3+}	U^{4+}	U^{6+}
	Z	88	89	92	92	92
	Method	*DS	*DS	*DS	*DS	*DS
0.00						
0.01						
0.02						
0.03						
0.04		40.04	54.00	54.02	68.15	96.83
0.05		29.19	37.78	37.81	46.56	64.49
0.06		23.23	28.91	28.95	34.80	46.89
0.07		19.57	23.53	23.57	27.67	36.26
0.08		17.14	19.98	20.03	23.01	29.33
0.09		15.42	17.51	17.57	19.78	24.56
0.10		14.12	15.70	15.76	17.44	21.12
0.11		13.11	14.31	14.39	15.67	18.55
0.12		12.291	13.217	13.300	14.296	16.573
0.13		11.602	12.324	12.416	13.192	15.010
0.14		11.008	11.577	11.679	12.287	13.749
0.15		10.486	10.939	11.050	11.528	12.709
0.16		10.018	10.382	10.503	10.879	11.837
0.17		9.592	9.889	10.018	10.314	11.093
0.18		9.200	9.446	9.583	9.816	10.451
0.19		8.836	9.042	9.188	9.371	9.889
0.20		8.495	8.671	8.824	8.967	9.391
0.22		7.873	8.008	8.174	8.261	8.544
0.24		7.315	7.427	7.602	7.655	7.843
0.25		7.057	7.161	7.340	7.380	7.534
0.26		6.811	6.909	7.091	7.122	7.247
0.28		6.355	6.444	6.629	6.647	6.729
0.30		5.940	6.022	6.208	6.219	6.273
0.32		5.563	5.639	5.824	5.830	5.865
0.34		5.219	5.291	5.472	5.475	5.497
0.35		5.059	5.128	5.307	5.309	5.327
0.36		4.906	4.973	5.149	5.151	5.164
0.38		4.621	4.683	4.853	4.853	4.861
0.40		4.360	4.417	4.580	4.580	4.584
0.42		4.122	4.174	4.329	4.328	4.330
0.44		3.904	3.951	4.098	4.097	4.096
0.45		3.801	3.847	3.989	3.988	3.987
0.46		3.703	3.747	3.885	3.883	3.881
0.48		3.518	3.558	3.688	3.686	3.683
0.50		3.348	3.385	3.506	3.504	3.500
0.55		2.975	3.005	3.107	3.106	3.100
0.60		2.664	2.689	2.776	2.774	2.768
0.65		2.400	2.421	2.496	2.494	2.489
0.70		2.174	2.193	2.258	2.256	2.252
0.80		1.808	1.824	1.875	1.874	1.872
0.90		1.527	1.541	1.583	1.582	1.582
1.00		1.307	1.319	1.354	1.354	1.354
1.10		1.132	1.142	1.171	1.172	1.172
1.20		0.991	0.999	1.024	1.025	1.025
1.30		0.874	0.882	0.904	0.904	0.905
1.40		0.778	0.784	0.804	0.804	0.804
1.50		0.696	0.702	0.720	0.720	0.720
1.60		0.626	0.632	0.648	0.648	0.648
1.70		0.566	0.571	0.586	0.586	0.586
1.80		0.513	0.518	0.533	0.533	0.533
1.90		0.467	0.472	0.486	0.486	0.486
2.00		0.427	0.431	0.444	0.444	0.444

Table 4.3.2.1. *Parameters useful in electron diffraction as a function of accelerating voltage, E*

E (keV)	λ	$1/\lambda$	m/m_0	v/c	σ
1	0.387629	2.57979	1.00196	0.06247	0.0081126
2	0.273961	3.65016	1.00391	0.08821	0.0057448
3	0.223579	4.47270	1.00587	0.10788	0.0046975
4	0.193530	5.16715	1.00783	0.12439	0.0040741
5	0.173015	5.77986	1.00978	0.13887	0.0036493
6	0.157863	6.33460	1.01174	0.15191	0.0033361
7	0.146082	6.84548	1.01370	0.16384	0.0030931
8	0.136581	7.32168	1.01566	0.17490	0.0028975
9	0.128707	7.76958	1.01761	0.18524	0.0027358
10	0.122043	8.19383	1.01957	0.19498	0.0025991
15	0.099407	10.05963	1.02935	0.23711	0.0021374
20	0.085882	11.64383	1.03914	0.27186	0.0018641
25	0.076632	13.04940	1.04892	0.30184	0.0016790
30	0.069789	14.32899	1.05871	0.32837	0.0015433
35	0.064459	15.51381	1.06849	0.35227	0.0014386
40	0.060153	16.62414	1.07828	0.37406	0.0013548
45	0.056580	17.67403	1.08806	0.39410	0.0012859
50	0.053551	18.67366	1.09784	0.41268	0.0012280
55	0.050941	19.63072	1.10763	0.43000	0.0011786
60	0.048659	20.55115	1.11741	0.44622	0.0011357
65	0.046642	21.43968	1.12720	0.46147	0.0010982
70	0.044843	22.30012	1.13698	0.47586	0.0010650
75	0.043223	23.13560	1.14677	0.48948	0.0010354
80	0.041756	23.94874	1.15655	0.50239	0.0010087
85	0.040418	24.74173	1.16634	0.51467	0.0009847
90	0.039190	25.51646	1.17612	0.52637	0.0009628
95	0.038060	26.27454	1.18591	0.53754	0.0009428
100	0.037013	27.01738	1.19569	0.54822	0.0009244
120	0.033491	29.85866	1.23483	0.58667	0.0008638
140	0.030739	32.53222	1.27397	0.61956	0.0008180
160	0.028509	35.07642	1.31310	0.64810	0.0007820
180	0.026654	37.51759	1.35224	0.67314	0.0007529
200	0.025079	39.87466	1.39138	0.69531	0.0007289
250	0.021986	45.48412	1.48922	0.74101	0.0006839
300	0.019687	50.79517	1.58707	0.77652	0.0006526
350	0.017891	55.89295	1.68491	0.80483	0.0006297
400	0.016439	60.83109	1.78276	0.82786	0.0006122
450	0.015233	65.64563	1.88060	0.84691	0.0005984
500	0.014212	70.36195	1.97845	0.86286	0.0005873
550	0.013334	74.99858	2.07629	0.87638	0.0005783
600	0.012568	79.56945	2.17414	0.88794	0.0005707
650	0.011893	84.08529	2.27198	0.89793	0.0005644
700	0.011292	88.55452	2.36983	0.90661	0.0005590
750	0.010755	92.98385	2.46767	0.91421	0.0005543
800	0.010269	97.37874	2.56552	0.92091	0.0005503
850	0.009829	101.74364	2.66336	0.92684	0.0005468
900	0.009427	106.08226	2.76121	0.93212	0.0005437
950	0.009058	110.39769	2.85905	0.93684	0.0005410
1000	0.008719	114.69256	2.95690	0.94108	0.0005385
1100	0.008115	123.22919	3.15259	0.94836	0.0005344
1200	0.007593	131.70646	3.34828	0.95436	0.0005310
1300	0.007136	140.13516	3.54397	0.95936	0.0005282
1400	0.006733	148.52355	3.73966	0.96358	0.0005259
1500	0.006374	156.87810	3.93535	0.96718	0.0005240

Table 4.3.2.2. *Elastic atomic scattering factors of electrons for neutral atoms and s up to 2.0 $\AA^{-1}$*

Element	Z	a_1	a_2	a_3	a_4	a_5	b_1	b_2	b_3	b_4	b_5
H	1	0.0349	0.1201	0.1970	0.0573	0.1195	0.5347	3.5867	12.3471	18.9525	38.6269
He	2	0.0317	0.0838	0.1526	0.1334	0.0164	0.2507	1.4751	4.4938	12.6646	31.1653
Li	3	0.0750	0.2249	0.5548	1.4954	0.9354	0.3864	2.9383	15.3829	53.5545	138.7337
Be	4	0.0780	0.2210	0.6740	1.3867	0.6925	0.3131	2.2381	10.1517	30.9061	78.3273
B	5	0.0909	0.2551	0.7738	1.2136	0.4606	0.2995	2.1155	8.3816	24.1292	63.1314
C	6	0.0893	0.2563	0.7570	1.0487	0.3575	0.2465	1.7100	6.4094	18.6113	50.2523
N	7	0.1022	0.3219	0.7982	0.8197	0.1715	0.2451	1.7481	6.1925	17.3894	48.1431
O	8	0.0974	0.2921	0.6910	0.6990	0.2039	0.2067	1.3815	4.6943	12.7105	32.4726
F	9	0.1083	0.3175	0.6487	0.5846	0.1421	0.2057	1.3439	4.2788	11.3932	28.7881
Ne	10	0.1269	0.3535	0.5582	0.4674	0.1460	0.2200	1.3779	4.0203	9.4934	23.1278
Na	11	0.2142	0.6853	0.7692	1.6589	1.4482	0.3334	2.3446	10.0830	48.3037	138.2700
Mg	12	0.2314	0.6866	0.9677	2.1882	1.1339	0.3278	2.2720	10.9241	39.2898	101.9748
Al	13	0.2390	0.6573	1.2011	2.5586	1.2312	0.3138	2.1063	10.4163	34.4552	98.5344
Si	14	0.2519	0.6372	1.3795	2.5082	1.0500	0.3075	2.0174	9.6746	29.3744	80.4732
P	15	0.2548	0.6106	1.4541	2.3204	0.8477	0.2908	1.8740	8.5176	24.3434	63.2996
S	16	0.2497	0.5628	1.3899	2.1865	0.7715	0.2681	1.6711	7.0267	19.5377	50.3888
Cl	17	0.2443	0.5397	1.3919	2.0197	0.6621	0.2468	1.5242	6.1537	16.6687	42.3086
Ar	18	0.2385	0.5017	1.3428	1.8899	0.6079	0.2289	1.3694	5.2561	14.0928	35.5361
K	19	0.4115	1.4031	2.2784	2.6742	2.2162	0.3703	3.3874	13.1029	68.9592	194.4329
Ca	20	0.4054	1.3880	2.1602	3.7532	2.2063	0.3499	3.0991	11.9608	53.9353	142.3892
Sc	21	0.3787	1.2181	2.0594	3.2618	2.3870	0.3133	2.5856	9.5813	41.7688	116.7282
Ti	22	0.3825	1.2598	2.0008	3.0617	2.0694	0.3040	2.4863	9.2783	39.0751	109.4583
V	23	0.3876	1.2750	1.9109	2.8314	1.8979	0.2967	2.3780	8.7981	35.9528	101.7201
Cr	24	0.4046	1.3696	1.8941	2.0800	1.2196	0.2986	2.3958	9.1406	37.4701	113.7121
Mn	25	0.3796	1.2094	1.7815	2.5420	1.5937	0.2699	2.0455	7.4726	31.0604	91.5622
Fe	26	0.3946	1.2725	1.7031	2.3140	1.4795	0.2717	2.0443	7.6007	29.9714	86.2265
Co	27	0.4118	1.3161	1.6493	2.1930	1.2830	0.2742	2.0372	7.7205	29.9680	84.9383
Ni	28	0.3860	1.1765	1.5451	2.0730	1.3814	0.2478	1.7660	6.3107	25.2204	74.3146
Cu	29	0.4314	1.3208	1.5236	1.4671	0.8562	0.2694	1.9223	7.3474	28.9892	90.6246
Zn	30	0.4288	1.2646	1.4472	1.8294	1.0934	0.2593	1.7998	6.7500	25.5860	73.5284
Ga	31	0.4818	1.4032	1.6561	2.4605	1.1054	0.2825	1.9785	8.7546	32.5238	98.5523
Ge	32	0.4655	1.3014	1.6088	2.6998	1.3003	0.2647	1.7926	7.6071	26.5541	77.5238
As	33	0.4517	1.2229	1.5852	2.7958	1.2638	0.2493	1.6436	6.8154	22.3681	62.0390
Se	34	0.4477	1.1678	1.5843	2.8087	1.1956	0.2405	1.5442	6.3231	19.4610	52.0233
Br	35	0.4798	1.1948	1.8695	2.6953	0.8203	0.2504	1.5963	6.9653	19.8492	50.3233
Kr	36	0.4546	1.0993	1.7696	2.7068	0.8672	0.2309	1.4279	5.9449	16.6752	42.2243
Rb	37	1.0160	2.8528	3.5466	-7.7804	12.1148	0.4853	5.0925	25.7851	130.4515	138.6775
Sr	38	0.6703	1.4926	3.3368	4.4600	3.1501	0.3190	2.2287	10.3504	52.3291	151.2216
Y	39	0.6894	1.5474	3.2450	4.2126	2.9764	0.3189	2.2904	10.0062	44.0771	125.0120
Zr	40	0.6719	1.4684	3.1668	3.9557	2.8920	0.3036	2.1249	8.9236	36.8458	108.2049
Nb	41	0.6123	1.2677	3.0348	3.3841	2.3683	0.2709	1.7683	7.2489	27.9465	98.5624
Mo	42	0.6773	1.4798	3.1788	3.0824	1.8384	0.2920	2.0606	8.1129	30.5336	100.0658
Tc	43	0.7082	1.6392	3.1993	3.4327	1.8711	0.2976	2.2106	8.5246	33.1456	96.6377
Ru	44	0.6735	1.4934	3.0966	2.7254	1.5597	0.2773	1.9716	7.3249	26.6891	90.5581
Rh	45	0.6413	1.3690	2.9854	2.6952	1.5433	0.2580	1.7721	6.3854	23.2549	85.1517
Pd	46	0.5904	1.1775	2.6519	2.2875	0.8689	0.2324	1.5019	5.1591	15.5428	46.8213
Ag	47	0.6377	1.3790	2.8294	2.3631	1.4553	0.2466	1.6974	5.7656	20.0943	76.7372
Cd	48	0.6364	1.4247	2.7802	2.5973	1.7886	0.2407	1.6823	5.6588	20.7219	69.1109
In	49	0.6768	1.6589	2.7740	3.1835	2.1326	0.2522	1.8545	6.2936	25.1457	84.5448

Table 4.3.2.2. *Elastic atomic scattering factors of electrons for neutral atoms and s up to 2.0 Å^{-1} (cont.)*

Element	Z	a_1	a_2	a_3	a_4	a_5	b_1	b_2	b_3	b_4	b_5
Sn	50	0.7224	1.9610	2.7161	3.5603	1.8972	0.2651	2.0604	7.3011	27.5493	81.3349
Sb	51	0.7106	1.9247	2.6149	3.8322	1.8899	0.2562	1.9646	6.8852	24.7648	68.9168
Te	52	0.6947	1.8690	2.5356	4.0013	1.8955	0.2459	1.8542	6.4411	22.1730	59.2206
I	53	0.7047	1.9484	2.5940	4.1526	1.5057	0.2455	1.8638	6.7639	21.8007	56.4395
Xe	54	0.6737	1.7908	2.4129	4.2100	1.7058	0.2305	1.6890	5.8218	18.3928	47.2496
Cs	55	1.2704	3.8018	5.6618	0.9205	4.8105	0.4356	4.2058	23.4342	136.7783	171.7561
Ba	56	0.9049	2.6076	4.8498	5.1603	4.7388	0.3066	2.4363	12.1821	54.6135	161.9978
La	57	0.8405	2.3863	4.6139	5.1514	4.7949	0.2791	2.1410	10.3400	41.9148	132.0204
Ce	58	0.8551	2.3915	4.5772	5.0278	4.5118	0.2805	2.1200	10.1808	42.0633	130.9893
Pr	59	0.9096	2.5313	4.5266	4.6376	4.3690	0.2939	2.2471	10.8266	48.8842	147.6020
Nd	60	0.8807	2.4183	4.4448	4.6858	4.1725	0.2802	2.0836	10.0357	47.4506	146.9976
Pm	61	0.9471	2.5463	4.3523	4.4789	3.9080	0.2977	2.2276	10.5762	49.3619	145.3580
Sm	62	0.9699	2.5837	4.2778	4.4575	3.5985	0.3003	2.2447	10.6487	50.7994	146.4179
Eu	63	0.8694	2.2413	3.9196	3.9694	4.5498	0.2653	1.8590	8.3998	36.7397	125.7089
Gd	64	0.9673	2.4702	4.1148	4.4972	3.2099	0.2909	2.1014	9.7067	43.4270	125.9474
Tb	65	0.9325	2.3673	3.8791	3.9674	3.7996	0.2761	1.9511	8.9296	41.5937	131.0122
Dy	66	0.9505	2.3705	3.8218	4.0471	3.4451	0.2773	1.9469	8.8862	43.0938	133.1396
Ho	67	0.9248	2.2428	3.6182	3.7910	3.7912	0.2660	1.8183	7.9655	33.1129	101.8139
Er	68	1.0373	2.4824	3.6558	3.8925	3.0056	0.2944	2.0797	9.4156	45.8056	132.7720
Tm	69	1.0075	2.3787	3.5440	3.6932	3.1759	0.2816	1.9486	8.7162	41.8420	125.0320
Yb	70	1.0347	2.3911	3.4619	3.6556	3.0052	0.2855	1.9679	8.7619	42.3304	125.6499
Lu	71	0.9927	2.2436	3.3554	3.7813	3.0994	0.2701	1.8073	7.8112	34.4849	103.3526
Hf	72	1.0295	2.2911	3.4110	3.9497	2.4925	0.2761	1.8625	8.0961	34.2712	98.5295
Ta	73	1.0190	2.2291	3.4097	3.9252	2.2679	0.2694	1.7962	7.6944	31.0942	91.1089
W	74	0.9853	2.1167	3.3570	3.7981	2.2798	0.2569	1.6745	7.0098	26.9234	81.3910
Re	75	0.9914	2.0858	3.4531	3.8812	1.8526	0.2548	1.6518	6.8845	26.7234	81.7215
Os	76	0.9813	2.0322	3.3665	3.6235	1.9741	0.2487	1.5973	6.4737	23.2817	70.9254
Ir	77	1.0194	2.0645	3.4425	3.4914	1.6976	0.2554	1.6475	6.5966	23.2269	70.0272
Pt	78	0.9148	1.8096	3.2134	3.2953	1.5754	0.2263	1.3813	5.3243	17.5987	60.0171
Au	79	0.9674	1.8916	3.3993	3.0524	1.2607	0.2358	1.4712	5.6758	18.7119	61.5286
Hg	80	1.0033	1.9469	3.4396	3.1548	1.4180	0.2413	1.5298	5.8009	19.4520	60.5753
Tl	81	1.0689	2.1038	3.6039	3.4927	1.8283	0.2540	1.6715	6.3509	23.1531	78.7099
Pb	82	1.0891	2.1867	3.6160	3.8031	1.8994	0.2552	1.7174	6.5131	23.9170	74.7039
Bi	83	1.1007	2.2306	3.5689	4.1549	2.0382	0.2546	1.7351	6.4948	23.6464	70.3780
Po	84	1.1568	2.4353	3.6459	4.4064	1.7179	0.2648	1.8786	7.1749	25.1766	69.2821
At	85	1.0909	2.1976	3.3831	4.6700	2.1277	0.2466	1.6707	6.0197	20.7657	57.2663
Rn	86	1.0756	2.1630	3.3178	4.8852	2.0489	0.2402	1.6169	5.7644	19.4568	52.5009
Fr	87	1.4282	3.5081	5.6767	4.1964	3.8946	0.3183	2.6889	13.4816	54.3866	200.8321
Ra	88	1.3127	3.1243	5.2988	5.3891	5.4133	0.2887	2.2897	10.8276	43.5389	145.6109
Ac	89	1.3128	3.1021	5.3385	5.9611	4.7562	0.2861	2.2509	10.5287	41.7796	128.2973
Th	90	1.2553	2.9178	5.0862	6.1206	4.7122	0.2701	2.0636	9.3051	34.5977	107.9200
Pa	91	1.3218	3.1444	5.4371	5.6444	4.0107	0.2827	2.2250	10.2454	41.1162	124.4449
U	92	1.3382	3.2043	5.4558	5.4839	3.6342	0.2838	2.2452	10.2519	41.7251	124.9023
Np	93	1.5193	4.0053	6.5327	-.1402	6.7489	0.3213	2.8206	14.8878	68.9103	81.7257
Pu	94	1.3517	3.2937	5.3213	4.6466	3.5714	0.2813	2.2418	9.9952	42.7939	132.1739
Am	95	1.2135	2.7962	4.7545	4.5731	4.4786	0.2483	1.8437	7.5421	29.3841	112.4579
Cm	96	1.2937	3.1100	5.0393	4.7546	3.5031	0.2638	2.0341	8.7101	35.2992	109.4972
Bk	97	1.2915	3.1023	4.9309	4.6009	3.4661	0.2611	2.0023	8.4377	34.1559	105.8911
Cf	98	1.2089	2.7391	4.3482	4.0047	4.6497	0.2421	1.7487	6.7262	23.2153	80.3108

Table 4.3.2.3. *Elastic atomic scattering factors of electrons for neutral atoms and s up to 6.0 Å^{-1}*

Element	Z	a_1	a_2	a_3	a_4	a_5	b_1	b_2	b_3	b_4	b_5
H	1	0.0088	0.0449	0.1481	0.2356	0.0914	0.1152	1.0867	4.9755	16.5591	43.2743
He	2	0.0084	0.0443	0.1314	0.1671	0.0666	0.0596	0.5360	2.4274	7.7852	20.3126
Li	3	0.0478	0.2048	0.5253	1.5225	0.9853	0.2258	2.1032	12.9349	50.7501	136.6280
Be	4	0.0423	0.1874	0.6019	1.4311	0.7891	0.1445	1.4180	8.1165	27.9705	74.8684
B	5	0.0436	0.1898	0.6788	1.3273	0.5544	0.1207	1.1595	6.2474	21.0460	59.3619
C	6	0.0489	0.2091	0.7537	1.1420	0.3555	0.1140	1.0825	5.4281	17.8811	51.1341
N	7	0.0267	0.1328	0.5301	1.1020	0.4215	0.0541	0.5165	2.8207	10.6297	34.3764
O	8	0.0365	0.1729	0.5805	0.8814	0.3121	0.0652	0.6184	2.9449	9.6298	28.2194
F	9	0.0382	0.1822	0.5972	0.7707	0.2130	0.0613	0.5753	2.6858	8.8214	25.6668
Ne	10	0.0380	0.1785	0.5494	0.6942	0.1918	0.0554	0.5087	2.2639	7.3316	21.6912
Na	11	0.1260	0.6442	0.8893	1.8197	1.2988	0.1684	1.7150	8.8386	50.8265	147.2073
Mg	12	0.1130	0.5575	0.9046	2.1580	1.4735	0.1356	1.3579	6.9255	32.3165	92.1138
Al	13	0.1165	0.5504	1.0179	2.6295	1.5711	0.1295	1.2619	6.8242	28.4577	88.4750
Si	14	0.0567	0.3365	0.8104	2.4960	2.1186	0.0582	0.6155	3.2522	16.7929	57.6767
P	15	0.1005	0.4615	1.0663	2.5854	1.2725	0.0977	0.9084	4.9654	18.5471	54.3648
S	16	0.0915	0.4312	1.0847	2.4671	1.0852	0.0838	0.7788	4.3462	15.5846	44.6365
Cl	17	0.0799	0.3891	1.0037	2.3332	1.0507	0.0694	0.6443	3.5351	12.5058	35.8633
Ar	18	0.1044	0.4551	1.4232	2.1533	0.4459	0.0853	0.7701	4.4684	14.5864	41.2474
K	19	0.2149	0.8703	2.4999	2.3591	3.0318	0.1660	1.6906	8.7447	46.7825	165.6923
Ca	20	0.2355	0.9916	2.3959	3.7252	2.5647	0.1742	1.8329	8.8407	47.4583	134.9613
Sc	21	0.4636	2.0802	2.9003	1.4193	2.4323	0.3682	4.0312	22.6493	71.8200	103.3691
Ti	22	0.2123	0.8960	2.1765	3.0436	2.4439	0.1399	1.4568	6.7534	33.1168	101.8238
V	23	0.2369	1.0774	2.1894	3.0825	1.7190	0.1505	1.6392	7.5691	36.8741	107.8517
Cr	24	0.1970	0.8228	2.0200	2.1717	1.7516	0.1197	1.1985	5.4097	25.2361	94.4290
Mn	25	0.1943	0.8190	1.9296	2.4968	2.0625	0.1135	1.1313	5.0341	24.1798	80.5598
Fe	26	0.1929	0.8239	1.8689	2.3694	1.9060	0.1087	1.0806	4.7637	22.8500	76.7309
Co	27	0.2186	0.9861	1.8540	2.3258	1.4685	0.1182	1.2300	5.4177	25.7602	80.8542
Ni	28	0.2313	1.0657	1.8229	2.2609	1.1883	0.1210	1.2691	5.6870	27.0917	83.0285
Cu	29	0.3501	1.6558	1.9582	0.2134	1.4109	0.1867	1.9917	11.3396	53.2619	63.2520
Zn	30	0.1780	0.8096	1.6744	1.9499	1.4495	0.0876	0.8650	3.8612	18.8726	64.7016
Ga	31	0.2135	0.9768	1.6669	2.5662	1.6790	0.1020	1.0219	4.6275	22.8742	80.1535
Ge	32	0.2135	0.9761	1.6555	2.8938	1.6356	0.0989	0.9845	4.5527	21.5563	70.3903
As	33	0.2059	0.9518	1.6372	3.0490	1.4756	0.0926	0.9182	4.3291	19.2996	58.9329
Se	34	0.1574	0.7614	1.4834	3.0016	1.7978	0.0686	0.6808	3.1163	14.3458	44.0455
Br	35	0.1899	0.8983	1.6358	3.1845	1.1518	0.0810	0.7957	3.9054	15.7701	45.6124
Kr	36	0.1742	0.8447	1.5944	3.1507	1.1338	0.0723	0.7123	3.5192	13.7724	39.1148
Rb	37	0.3781	1.4904	3.5753	3.0031	3.3272	0.1557	1.5347	9.9947	51.4251	185.9828
Sr	38	0.3723	1.4598	3.5124	4.4612	3.3031	0.1480	1.4643	9.2320	49.8807	148.0937
Y	39	0.3234	1.2737	3.2115	4.0563	3.7962	0.1244	1.1948	7.2756	34.1430	111.2079
Zr	40	0.2997	1.1879	3.1075	3.9740	3.5769	0.1121	1.0638	6.3891	28.7081	97.4289
Nb	41	0.1680	0.9370	2.7300	3.8150	3.0053	0.0597	0.6524	4.4317	19.5540	85.5011
Mo	42	0.3069	1.1714	3.2293	3.4254	2.1224	0.1101	1.0222	5.9613	25.1965	93.5831
Tc	43	0.2928	1.1267	3.1675	3.6619	2.5942	0.1020	0.9481	5.4713	23.8153	82.8991
Ru	44	0.2604	1.0442	3.0761	3.2175	1.9448	0.0887	0.8240	4.8278	19.8977	80.4566
Rh	45	0.2713	1.0556	3.1416	3.0451	1.7179	0.0907	0.8324	4.7702	19.7862	80.2540
Pd	46	0.2003	0.8779	2.6135	2.8594	1.0258	0.0659	0.6111	3.5563	12.7638	44.4283
Ag	47	0.2739	1.0503	3.1564	2.7543	1.4328	0.0881	0.8028	4.4451	18.7011	79.2633
Cd	48	0.3072	1.1303	3.2046	2.9329	1.6560	0.0966	0.8856	4.6273	20.6789	73.4723
In	49	0.3564	1.3011	3.2424	3.4839	2.0459	0.1091	1.0452	5.0900	24.6578	88.0513

Table 4.3.2.3. *Elastic atomic scattering factors of electrons for neutral atoms and s up to 6.0 Å^{-1} (cont.)*

Element	Z	a_1	a_2	a_3	a_4	a_5	b_1	b_2	b_3	b_4	b_5
Sn	50	0.2966	1.1157	3.0973	3.8156	2.5281	0.0896	0.8268	4.2242	20.6900	71.3399
Sb	51	0.2725	1.0651	2.9940	4.0697	2.5682	0.0809	0.7488	3.8710	18.8800	60.6499
Te	52	0.2422	0.9692	2.8114	4.1509	2.8161	0.0708	0.6472	3.3609	16.0752	50.1724
I	53	0.2617	1.0325	2.8097	4.4809	2.3190	0.0749	0.6914	3.4634	16.3603	48.2522
Xe	54	0.2334	0.9496	2.6381	4.4680	2.5020	0.0655	0.6050	3.0389	14.0809	41.0005
Cs	55	0.5713	2.4866	4.9795	4.0198	4.4403	0.1626	1.8213	11.1049	49.0568	202.9987
Ba	56	0.5229	2.2874	4.7243	5.0807	5.6389	0.1434	1.6019	9.4511	42.7685	148.4969
La	57	0.5461	2.3856	5.0653	5.7601	4.0463	0.1479	1.6552	10.0059	47.3245	145.8464
Ce	58	0.2227	1.0760	2.9482	5.8496	7.1834	0.0571	0.5946	3.2022	16.4253	95.7030
Pr	59	0.5237	2.2913	4.6161	4.7233	4.8173	0.1360	1.5068	8.8213	41.9536	141.2424
Nd	60	0.5368	2.3301	4.6058	4.6621	4.4622	0.1378	1.5140	8.8719	43.5967	141.8065
Pm	61	0.5232	2.2627	4.4552	4.4787	4.5073	0.1317	1.4336	8.3087	40.6010	135.9196
Sm	62	0.5162	2.2302	4.3449	4.3598	4.4292	0.1279	1.3811	7.9629	39.1213	132.7846
Eu	63	0.5272	2.2844	4.3361	4.3178	4.0908	0.1285	1.3943	8.1081	40.9631	134.1233
Gd	64	0.9664	3.4052	5.0803	1.4991	4.2528	0.2641	2.6586	16.2213	80.2060	92.5359
Tb	65	0.5110	2.1570	4.0308	3.9936	4.2466	0.1210	1.2704	7.1368	35.0354	123.5062
Dy	66	0.4974	2.1097	3.8906	3.8100	4.3084	0.1157	1.2108	6.7377	32.4150	116.9225
Ho	67	0.4679	1.9693	3.7191	3.9632	4.2432	0.1069	1.0994	5.9769	27.1491	96.3119
Er	68	0.5034	2.1088	3.8232	3.7299	3.8963	0.1141	1.1769	6.6087	33.4332	116.4913
Tm	69	0.4839	2.0262	3.6851	3.5874	4.0037	0.1081	1.1012	6.1114	30.3728	110.5988
Yb	70	0.5221	2.1695	3.7567	3.6685	3.4274	0.1148	1.1860	6.7520	35.6807	118.0692
Lu	71	0.4680	1.9466	3.5428	3.8490	3.6594	0.1015	1.0195	5.6058	27.4899	95.2846
Hf	72	0.4048	1.7370	3.3399	3.9448	3.7293	0.0868	0.8585	4.6378	21.6900	80.2408
Ta	73	0.3835	1.6747	3.2986	4.0462	3.4303	0.0810	0.8020	4.3545	19.9644	73.6337
W	74	0.3661	1.6191	3.2455	4.0856	3.2064	0.0761	0.7543	4.0952	18.2886	68.0967
Re	75	0.3933	1.6973	3.4202	4.1274	2.6158	0.0806	0.7972	4.4237	19.5692	68.7477
Os	76	0.3854	1.6555	3.4129	4.1111	2.4106	0.0787	0.7638	4.2441	18.3700	65.1071
Ir	77	0.3510	1.5620	3.2946	4.0615	2.4382	0.0706	0.6904	3.8266	16.0812	58.7638
Pt	78	0.3083	1.4158	2.9662	3.9349	2.1709	0.0609	0.5993	3.1921	12.5285	49.7675
Au	79	0.3055	1.3945	2.9617	3.8990	2.0026	0.0596	0.5827	3.1035	11.9693	47.9106
Hg	80	0.3593	1.5736	3.5237	3.8109	1.6953	0.0694	0.6758	3.8457	15.6203	56.6614
Tl	81	0.3511	1.5489	3.5676	4.0900	2.5251	0.0672	0.6522	3.7420	15.9791	65.1354
Pb	82	0.3540	1.5453	3.5975	4.3152	2.7743	0.0668	0.6465	3.6968	16.2056	61.4909
Bi	83	0.3530	1.5258	3.5815	4.5532	3.0714	0.0661	0.6324	3.5906	15.9962	57.5760
Po	84	0.3673	1.5772	3.7079	4.8582	2.8440	0.0678	0.6527	3.7396	17.0668	55.9789
At	85	0.3547	1.5206	3.5621	5.0184	3.0075	0.0649	0.6188	3.4696	15.6090	49.4818
Rn	86	0.4586	1.7781	3.9877	5.7273	1.5460	0.0831	0.7840	4.3599	20.0128	62.1535
Fr	87	0.8282	2.9941	5.6597	4.9292	4.2889	0.1515	1.6163	9.7752	42.8480	190.7366
Ra	88	1.4129	4.4269	7.0460	-1.0573	8.6430	0.2921	3.1381	19.6767	102.0436	113.9798
Ac	89	0.7169	2.5710	5.1791	6.3484	5.6474	0.1263	1.2900	7.3686	32.4490	118.0558
Th	90	0.6958	2.4936	5.1269	6.6988	5.0799	0.1211	1.2247	6.9398	30.0991	105.1960
Pa	91	1.2502	4.2284	7.0489	1.1390	5.8222	0.2415	2.6442	16.3313	73.5757	91.9401
U	92	0.6410	2.2643	4.8713	5.9287	5.3935	0.1097	1.0644	5.7907	25.0261	101.3899
Np	93	0.6938	2.4652	5.1227	5.5965	4.8543	0.1171	1.1757	6.4053	27.5217	103.0482
Pu	94	0.6902	2.4509	5.1284	5.0339	4.8575	0.1153	1.1545	6.2291	27.0741	111.3150
Am	95	0.7577	2.7264	5.4184	4.8198	4.1013	0.1257	1.3044	7.1035	32.4649	118.8647
Cm	96	0.7567	2.7565	5.4364	5.1918	3.5643	0.1239	1.2979	7.0798	32.7871	110.1512
Bk	97	0.7492	2.7267	5.3521	5.0369	3.5321	0.1217	1.2651	6.8101	31.6088	106.4853
Cf	98	0.8100	3.0001	5.4635	4.1756	3.5066	0.1310	1.4038	7.6057	34.0186	90.5226

Table 4.3.3.1. *Partial wave elastic scattering factors for neutral atoms*
H; $Z = 1$

	10 keV		40 keV		60 keV		90 keV	
s	$\|f(s)\|$	$\eta(s)$	$\|f(s)\|$	$\eta(s)$	$\|f(s)\|$	$\eta(s)$	$\|f(s)\|$	$\eta(s)$
0	5.3956E−01	2.1835E−02	5.7106E−01	1.1403E−02	5.8501E−01	9.6111E−03	6.0222E−01	8.2636E−03
1	4.8779E−01	2.3657E−02	5.1682E−01	1.2341E−02	5.3150E−01	1.0363E−02	5.5125E−01	8.8468E−03
2	3.7546E−01	2.8959E−02	3.9784E−01	1.5102E−02	4.1121E−01	1.2624E−02	4.3188E−01	1.0653E−02
3	2.6709E−01	3.7159E−02	2.8276E−01	1.9391E−02	2.9248E−01	1.6207E−02	3.0790E−01	1.3658E−02
4	1.8733E−01	4.7280E−02	1.9824E−01	2.4676E−02	2.0522E−01	2.0617E−02	2.1554E−01	1.7432E−02
5	1.3383E−01	5.8258E−02	1.4159E−01	3.0404E−02	1.4658E−01	2.5411E−02	1.5436E−01	2.1443E−02
6	9.8468E−02	6.9249E−02	1.0417E−01	3.6134E−02	1.0784E−01	3.0211E−02	1.1349E−01	2.5524E−02
7	7.4696E−02	7.9743E−02	7.9010E−02	4.1605E−02	8.1814E−02	3.4784E−02	8.5989E−02	2.9437E−02
8	5.8260E−02	8.9502E−02	6.1621E−02	4.6690E−02	6.3786E−02	3.9055E−02	6.7184E−02	3.2990E−02
9	4.6554E−02	9.8462E−02	4.9235E−02	5.1360E−02	5.0981E−02	4.2952E−02	5.3638E−02	3.6328E−02
10	3.7970E−02	1.0665E−01	4.0156E−02	5.5626E−02	4.1569E−02	4.6535E−02	4.3702E−02	3.9395E−02
11	3.1489E−02	1.1414E−01	3.3300E−02	5.9528E−02	3.4468E−02	4.9806E−02	3.6249E−02	4.2156E−02
12	2.6551E−02	1.2100E−01	2.8077E−02	6.3104E−02	2.9065E−02	5.2796E−02	3.0577E−02	4.4678E−02
13	2.2685E−02	1.2732E−01	2.3987E−02	6.6395E−02	2.4832E−02	5.5549E−02	2.6126E−02	4.7004E−02
14	1.9591E−02	1.3316E−01	2.0715E−02	6.9437E−02	2.1445E−02	5.8097E−02	2.2568E−02	4.9149E−02
15	1.7086E−02	1.3858E−01	1.8065E−02	7.2263E−02	1.8702E−02	6.0463E−02	1.9680E−02	5.1163E−02
16	1.5030E−02	1.4364E−01	1.5891E−02	7.4898E−02	1.6451E−02	6.2669E−02	1.7307E−02	5.3039E−02
17	1.3322E−02	1.4838E−01	1.4085E−02	7.7366E−02	1.4581E−02	6.4736E−02	1.5344E−02	5.4773E−02
18	1.1889E−02	1.5283E−01	1.2569E−02	7.9685E−02	1.3012E−02	6.6678E−02	1.3692E−02	5.6427E−02
19	1.0674E−02	1.5703E−01	1.1285E−02	8.1873E−02	1.1682E−02	6.8509E−02	1.2290E−02	5.7987E−02
20	9.6365E−03	1.6100E−01	1.0188E−02	8.3943E−02	1.0546E−02	7.0243E−02	1.1097E−02	5.9439E−02
21	8.7427E−03	1.6477E−01	9.2423E−03	8.5908E−02	9.5673E−03	7.1887E−02	1.0067E−02	6.0840E−02
22	7.9675E−03	1.6836E−01	8.4226E−03	8.7776E−02	8.7186E−03	7.3452E−02	9.1718E−03	6.2174E−02
23	7.2908E−03	1.7178E−01	7.7070E−03	8.9558E−02	7.9778E−03	7.4943E−02	8.3943E−03	6.3421E−02
24	6.6968E−03	1.7505E−01	7.0789E−03	9.1261E−02	7.3275E−03	7.6369E−02	7.7096E−03	6.4635E−02
25	6.1724E−03	1.7818E−01	6.5244E−03	9.2892E−02	6.7534E−03	7.7734E−02	7.1041E−03	6.5801E−02
26	5.7072E−03	1.8118E−01	6.0325E−03	9.4456E−02	6.2442E−03	7.9043E−02	6.5697E−03	6.6894E−02
27	5.2927E−03	1.8407E−01	5.5942E−03	9.5959E−02	5.7904E−03	8.0301E−02	6.0920E−03	6.7965E−02
28	4.9217E−03	1.8685E−01	5.2019E−03	9.7406E−02	5.3842E−03	8.1512E−02	5.6635E−03	6.9001E−02
29	4.5884E−03	1.8952E−01	4.8494E−03	9.8800E−02	5.0193E−03	8.2679E−02	5.2805E−03	6.9974E−02
30	4.2878E−03	1.9211E−01	4.5316E−03	1.0014E−01	4.6903E−03	8.3805E−02	4.9342E−03	7.0931E−02
31	4.0157E−03	1.9460E−01	4.2440E−03	1.0145E−01	4.3925E−03	8.4893E−02	4.6200E−03	7.1865E−02
32	3.7688E−03	1.9702E−01	3.9829E−03	1.0270E−01	4.1222E−03	8.5946E−02	4.3363E−03	7.2741E−02
33	3.5440E−03	1.9936E−01	3.7451E−03	1.0392E−01	3.8760E−03	8.6966E−02	4.0773E−03	7.3607E−02
34	3.3387E−03	2.0162E−01	3.5280E−03	1.0510E−01	3.6513E−03	8.7954E−02	3.8401E−03	7.4456E−02
35	3.1507E−03	2.0382E−01	3.3293E−03	1.0625E−01	3.4455E−03	8.8913E−02	3.6241E−03	7.5254E−02
36	2.9781E−03	2.0596E−01	3.1468E−03	1.0736E−01	3.2566E−03	8.9845E−02	3.4254E−03	7.6044E−02
37	2.8194E−03	2.0804E−01	2.9790E−03	1.0844E−01	3.0828E−03	9.0751E−02	3.2419E−03	7.6823E−02
38	2.6730E−03	2.1006E−01	2.8242E−03	1.0949E−01	2.9226E−03	9.1631E−02	3.0738E−03	7.7555E−02
39	2.5377E−03	2.1202E−01	2.6812E−03	1.1052E−01	2.7745E−03	9.2489E−02	2.9180E−03	7.8282E−02
40	2.4124E−03	2.1394E−01	2.5487E−03	1.1152E−01	2.6374E−03	9.3324E−02	2.7732E−03	7.9002E−02
41	2.2962E−03	2.1581E−01	2.4258E−03	1.1249E−01	2.5101E−03	9.4138E−02	2.6397E−03	7.9679E−02
42	2.1882E−03	2.1763E−01	2.3116E−03	1.1344E−01	2.3919E−03	9.4934E−02	2.5153E−03	8.0351E−02
43	2.0876E−03	2.1941E−01	2.2053E−03	1.1437E−01	2.2818E−03	9.5709E−02	2.3991E−03	8.1021E−02
44	1.9939E−03	2.2115E−01	2.1061E−03	1.1527E−01	2.1791E−03	9.6466E−02	2.2913E−03	8.1649E−02
45	1.9062E−03	2.2284E−01	2.0134E−03	1.1616E−01	2.0832E−03	9.7207E−02	2.1905E−03	8.2275E−02
46	1.8243E−03	2.2451E−01	1.9268E−03	1.1702E−01	1.9935E−03	9.7931E−02	2.0957E−03	8.2901E−02
47	1.7475E−03	2.2613E−01	1.8456E−03	1.1787E−01	1.9095E−03	9.8638E−02	2.0075E−03	8.3489E−02
48	1.6755E−03	2.2771E−01	1.7694E−03	1.1870E−01	1.8306E−03	9.9331E−02	1.9246E−03	8.4073E−02
49	1.6078E−03	2.2927E−01	1.6979E−03	1.1951E−01	1.7565E−03	1.0001E−01	1.8463E−03	8.4662E−02
50	1.5441E−03	2.3080E−01	1.6306E−03	1.2030E−01	1.6868E−03	1.0068E−01	1.7732E−03	8.5214E−02
51	1.4842E−03	2.3229E−01	1.5672E−03	1.2108E−01	1.6212E−03	1.0133E−01	1.7042E−03	8.5761E−02
52	1.4277E−03	2.3376E−01	1.5074E−03	1.2184E−01	1.5593E−03	1.0197E−01	1.6388E−03	8.6315E−02
53	1.3743E−03	2.3519E−01	1.4510E−03	1.2259E−01	1.5009E−03	1.0259E−01	1.5775E−03	8.6837E−02
54	1.3239E−03	2.3660E−01	1.3977E−03	1.2333E−01	1.4457E−03	1.0321E−01	1.5195E−03	8.7353E−02
55	1.2762E−03	2.3798E−01	1.3473E−03	1.2405E−01	1.3935E−03	1.0381E−01	1.4644E−03	8.7876E−02
56	1.2311E−03	2.3934E−01	1.2995E−03	1.2476E−01	1.3441E−03	1.0440E−01	1.4125E−03	8.8368E−02
57	1.1882E−03	2.4068E−01	1.2543E−03	1.2545E−01	1.2972E−03	1.0499E−01	1.3633E−03	8.8858E−02
58	1.1476E−03	2.4199E−01	1.2113E−03	1.2614E−01	1.2528E−03	1.0556E−01	1.3162E−03	8.9357E−02
59	1.1091E−03	2.4327E−01	1.1706E−03	1.2681E−01	1.2105E−03	1.0612E−01	1.2719E−03	8.9826E−02
60	1.0724E−03	2.4454E−01	1.1319E−03	1.2746E−01	1.1705E−03	1.0667E−01	1.2301E−03	9.0263E−02

Table 4.3.3.1. *Partial wave elastic scattering factors for neutral atoms (cont.)*
He; $Z = 2$

	10 keV		40 keV		60 keV		90 keV	
s	$\|f(s)\|$	$\eta(s)$	$\|f(s)\|$	$\eta(s)$	$\|f(s)\|$	$\eta(s)$	$\|f(s)\|$	$\eta(s)$
0	4.2610E−01	4.1776E−02	4.4985E−01	2.1809E−02	4.6272E−01	1.8383E−02	4.7861E−01	1.5783E−02
1	4.0739E−01	4.3327E−02	4.3041E−01	2.2602E−02	4.4354E−01	1.9017E−02	4.6026E−01	1.6277E−02
2	3.5950E−01	4.7901E−02	3.8022E−01	2.4959E−02	3.9327E−01	2.0925E−02	4.1119E−01	1.7781E−02
3	2.9975E−01	5.5216E−02	3.1704E−01	2.8767E−02	3.2862E−01	2.4069E−02	3.4590E−01	2.0325E−02
4	2.4232E−01	6.4811E−02	2.5619E−01	3.3776E−02	2.6545E−01	2.8275E−02	2.7985E−01	2.3848E−02
5	1.9367E−01	7.6153E−02	2.0478E−01	3.9673E−02	2.1206E−01	3.3235E−02	2.2303E−01	2.8110E−02
6	1.5495E−01	8.8676E−02	1.6384E−01	4.6186E−02	1.6975E−01	3.8674E−02	1.7832E−01	3.2760E−02
7	1.2497E−01	1.0185E−01	1.3209E−01	5.3056E−02	1.3689E−01	4.4420E−02	1.4407E−01	3.7568E−02
8	1.0190E−01	1.1529E−01	1.0770E−01	6.0041E−02	1.1154E−01	5.0301E−02	1.1756E−01	4.2489E−02
9	8.4110E−02	1.2864E−01	8.8879E−02	6.6990E−02	9.2057E−02	5.6121E−02	9.6885E−02	4.7481E−02
10	7.0272E−02	1.4169E−01	7.4222E−02	7.3795E−02	7.6918E−02	6.1790E−02	8.0827E−02	5.2361E−02
11	5.9355E−02	1.5431E−01	6.2676E−02	8.0359E−02	6.4950E−02	6.7298E−02	6.8289E−02	5.6980E−02
12	5.0706E−02	1.6642E−01	5.3536E−02	8.6655E−02	5.5459E−02	7.2590E−02	5.8394E−02	6.1393E−02
13	4.3748E−02	1.7797E−01	4.6181E−02	9.2663E−02	4.7842E−02	7.7613E−02	5.0369E−02	6.5675E−02
14	3.8074E−02	1.8895E−01	4.0185E−02	9.8371E−02	4.1636E−02	8.2387E−02	4.3787E−02	6.9788E−02
15	3.3405E−02	1.9937E−01	3.5252E−02	1.0379E−01	3.6518E−02	8.6940E−02	3.8403E−02	7.3638E−02
16	2.9524E−02	2.0926E−01	3.1151E−02	1.0893E−01	3.2266E−02	9.1254E−02	3.3963E−02	7.7224E−02
17	2.6267E−02	2.1865E−01	2.7711E−02	1.1380E−01	2.8707E−02	9.5322E−02	3.0223E−02	8.0661E−02
18	2.3511E−02	2.2755E−01	2.4801E−02	1.1843E−01	2.5693E−02	9.9196E−02	2.7031E−02	8.4002E−02
19	2.1160E−02	2.3601E−01	2.2319E−02	1.2283E−01	2.3117E−02	1.0290E−01	2.4310E−02	8.7168E−02
20	1.9139E−02	2.4407E−01	2.0186E−02	1.2701E−01	2.0907E−02	1.0640E−01	2.1995E−02	9.0098E−02
21	1.7392E−02	2.5174E−01	1.8342E−02	1.3100E−01	1.8999E−02	1.0972E−01	1.9998E−02	9.2866E−02
22	1.5871E−02	2.5906E−01	1.6736E−02	1.3480E−01	1.7336E−02	1.1291E−01	1.8244E−02	9.5585E−02
23	1.4539E−02	2.6606E−01	1.5330E−02	1.3843E−01	1.5876E−02	1.1598E−01	1.6700E−02	9.8232E−02
24	1.3366E−02	2.7275E−01	1.4093E−02	1.4191E−01	1.4596E−02	1.1888E−01	1.5350E−02	1.0071E−01
25	1.2329E−02	2.7917E−01	1.2999E−02	1.4524E−01	1.3464E−02	1.2166E−01	1.4166E−02	1.0300E−01
26	1.1407E−02	2.8533E−01	1.2026E−02	1.4844E−01	1.2456E−02	1.2435E−01	1.3110E−02	1.0524E−01
27	1.0585E−02	2.9124E−01	1.1158E−02	1.5152E−01	1.1555E−02	1.2694E−01	1.2158E−02	1.0748E−01
28	9.8473E−03	2.9695E−01	1.0381E−02	1.5447E−01	1.0750E−02	1.2940E−01	1.1305E−02	1.0963E−01
29	9.1842E−03	3.0243E−01	9.6810E−03	1.5733E−01	1.0027E−02	1.3178E−01	1.0546E−02	1.1162E−01
30	8.5856E−03	3.0772E−01	9.0497E−03	1.6007E−01	9.3719E−03	1.3410E−01	9.8633E−03	1.1350E−01
31	8.0433E−03	3.1285E−01	8.4779E−03	1.6273E−01	8.7787E−03	1.3633E−01	9.2390E−03	1.1540E−01
32	7.5508E−03	3.1779E−01	7.9583E−03	1.6530E−01	8.2418E−03	1.3846E−01	8.6674E−03	1.1729E−01
33	7.1020E−03	3.2257E−01	7.4850E−03	1.6779E−01	7.7520E−03	1.4054E−01	8.1506E−03	1.1907E−01
34	6.6919E−03	3.2722E−01	7.0526E−03	1.7019E−01	7.3030E−03	1.4258E−01	7.6836E−03	1.2071E−01
35	6.3164E−03	3.3171E−01	6.6564E−03	1.7253E−01	6.8925E−03	1.4454E−01	7.2541E−03	1.2233E−01
36	5.9714E−03	3.3608E−01	6.2927E−03	1.7480E−01	6.5168E−03	1.4641E−01	6.8548E−03	1.2399E−01
37	5.6538E−03	3.4032E−01	5.9580E−03	1.7700E−01	6.1700E−03	1.4826E−01	6.4869E−03	1.2561E−01
38	5.3611E−03	3.4444E−01	5.6492E−03	1.7914E−01	5.8492E−03	1.5008E−01	6.1519E−03	1.2710E−01
39	5.0903E−03	3.4846E−01	5.3637E−03	1.8123E−01	5.5538E−03	1.5182E−01	5.8440E−03	1.2851E−01
40	4.8395E−03	3.5236E−01	5.0994E−03	1.8325E−01	5.2807E−03	1.5349E−01	5.5555E−03	1.2996E−01
41	4.6069E−03	3.5616E−01	4.8540E−03	1.8523E−01	5.0263E−03	1.5516E−01	5.2853E−03	1.3143E−01
42	4.3905E−03	3.5988E−01	4.6259E−03	1.8716E−01	4.7894E−03	1.5679E−01	5.0360E−03	1.3281E−01
43	4.1891E−03	3.6349E−01	4.4136E−03	1.8904E−01	4.5698E−03	1.5835E−01	4.8068E−03	1.3408E−01
44	4.0012E−03	3.6703E−01	4.2154E−03	1.9087E−01	4.3651E−03	1.5987E−01	4.5923E−03	1.3535E−01
45	3.8256E−03	3.7049E−01	4.0303E−03	1.9267E−01	4.1730E−03	1.6139E−01	4.3890E−03	1.3667E−01
46	3.6614E−03	3.7386E−01	3.8572E−03	1.9442E−01	3.9932E−03	1.6288E−01	4.1985E−03	1.3797E−01
47	3.5074E−03	3.7716E−01	3.6949E−03	1.9613E−01	3.8257E−03	1.6429E−01	4.0225E−03	1.3916E−01
48	3.3630E−03	3.8038E−01	3.5426E−03	1.9781E−01	3.6682E−03	1.6568E−01	3.8584E−03	1.4028E−01
49	3.2273E−03	3.8355E−01	3.3996E−03	1.9945E−01	3.5195E−03	1.6708E−01	3.7024E−03	1.4144E−01
50	3.0997E−03	3.8664E−01	3.2651E−03	2.0106E−01	3.3800E−03	1.6843E−01	3.5541E−03	1.4265E−01
51	2.9795E−03	3.8966E−01	3.1383E−03	2.0263E−01	3.2493E−03	1.6972E−01	3.4155E−03	1.4379E−01
52	2.8661E−03	3.9264E−01	3.0188E−03	2.0417E−01	3.1256E−03	1.7102E−01	3.2866E−03	1.4482E−01
53	2.7591E−03	3.9555E−01	2.9060E−03	2.0569E−01	3.0082E−03	1.7231E−01	3.1646E−03	1.4585E−01
54	2.6580E−03	3.9840E−01	2.7994E−03	2.0717E−01	2.8979E−03	1.7355E−01	3.0475E−03	1.4695E−01
55	2.5623E−03	4.0120E−01	2.6986E−03	2.0863E−01	2.7939E−03	1.7474E−01	2.9364E−03	1.4804E−01
56	2.4717E−03	4.0396E−01	2.6031E−03	2.1005E−01	2.6948E−03	1.7595E−01	2.8328E−03	1.4903E−01
57	2.3858E−03	4.0666E−01	2.5125E−03	2.1146E−01	2.6006E−03	1.7715E−01	2.7354E−03	1.4996E−01
58	2.3044E−03	4.0930E−01	2.4266E−03	2.1284E−01	2.5119E−03	1.7829E−01	2.6417E−03	1.5094E−01
59	2.2271E−03	4.1189E−01	2.3451E−03	2.1419E−01	2.4280E−03	1.7938E−01	2.5516E−03	1.5197E−01
60	2.1533E−03	4.1451E−01	2.2675E−03	2.1553E−01	2.3472E−03	1.8053E−01	2.4666E−03	1.5295E−01

Table 4.3.3.1. *Partial wave elastic scattering factors for neutral atoms (cont.)*
Li; $Z = 3$

	10 keV		40 keV		60 keV		90 keV	
s	$\|f(s)\|$	$\eta(s)$	$\|f(s)\|$	$\eta(s)$	$\|f(s)\|$	$\eta(s)$	$\|f(s)\|$	$\eta(s)$
0	3.3440E+00	3.4566E−02	3.5370E+00	1.8036E−02	3.6606E+00	1.5125E−02	3.8345E+00	1.2836E−02
1	2.2942E+00	4.6591E−02	2.4277E+00	2.4302E−02	2.5141E+00	2.0369E−02	2.6390E+00	1.7258E−02
2	1.0905E+00	8.0922E−02	1.1545E+00	4.2187E−02	1.1963E+00	3.5347E−02	1.2584E+00	2.9910E−02
3	5.7692E−01	1.2235E−01	6.1069E−01	6.3773E−02	6.3285E−01	5.3436E−02	6.6585E−01	4.5230E−02
4	3.6834E−01	1.5631E−01	3.8977E−01	8.1464E−02	4.0391E−01	6.8263E−02	4.2502E−01	5.7792E−02
5	2.6569E−01	1.8224E−01	2.8107E−01	9.4973E−02	2.9126E−01	7.9585E−02	3.0650E−01	6.7386E−02
6	2.0504E−01	2.0358E−01	2.1686E−01	1.0609E−01	2.2472E−01	8.8897E−02	2.3649E−01	7.5278E−02
7	1.6450E−01	2.2257E−01	1.7394E−01	1.1596E−01	1.8024E−01	9.7177E−02	1.8968E−01	8.2294E−02
8	1.3523E−01	2.4027E−01	1.4296E−01	1.2518E−01	1.4814E−01	1.0490E−01	1.5589E−01	8.8837E−02
9	1.1308E−01	2.5720E−01	1.1952E−01	1.3398E−01	1.2384E−01	1.1227E−01	1.3033E−01	9.5088E−02
10	9.5794E−02	2.7357E−01	1.0122E−01	1.4250E−01	1.0488E−01	1.1941E−01	1.1037E−01	1.0113E−01
11	8.2007E−02	2.8939E−01	8.6630E−02	1.5072E−01	8.9757E−02	1.2630E−01	9.4457E−02	1.0697E−01
12	7.0897E−02	3.0474E−01	7.4873E−02	1.5870E−01	7.7575E−02	1.3299E−01	8.1634E−02	1.1264E−01
13	6.1809E−02	3.1959E−01	6.5258E−02	1.6641E−01	6.7611E−02	1.3945E−01	7.1147E−02	1.1812E−01
14	5.4277E−02	3.3393E−01	5.7291E−02	1.7386E−01	5.9355E−02	1.4569E−01	6.2458E−02	1.2341E−01
15	4.7985E−02	3.4776E−01	5.0636E−02	1.8105E−01	5.2458E−02	1.5172E−01	5.5200E−02	1.2851E−01
16	4.2685E−02	3.6110E−01	4.5031E−02	1.8798E−01	4.6650E−02	1.5752E−01	4.9087E−02	1.3343E−01
17	3.8184E−02	3.7395E−01	4.0273E−02	1.9465E−01	4.1720E−02	1.6311E−01	4.3898E−02	1.3816E−01
18	3.4337E−02	3.8631E−01	3.6206E−02	2.0107E−01	3.7506E−02	1.6849E−01	3.9463E−02	1.4272E−01
19	3.1025E−02	3.9820E−01	3.2707E−02	2.0724E−01	3.3880E−02	1.7366E−01	3.5647E−02	1.4710E−01
20	2.8158E−02	4.0964E−01	2.9678E−02	2.1317E−01	3.0741E−02	1.7863E−01	3.2344E−02	1.5131E−01
21	2.5660E−02	4.2064E−01	2.7040E−02	2.1888E−01	2.8008E−02	1.8341E−01	2.9468E−02	1.5536E−01
22	2.3473E−02	4.3123E−01	2.4730E−02	2.2437E−01	2.5615E−02	1.8801E−01	2.6950E−02	1.5926E−01
23	2.1549E−02	4.4142E−01	2.2699E−02	2.2966E−01	2.3510E−02	1.9244E−01	2.4735E−02	1.6301E−01
24	1.9847E−02	4.5123E−01	2.0903E−02	2.3475E−01	2.1650E−02	1.9670E−01	2.2777E−02	1.6663E−01
25	1.8336E−02	4.6069E−01	1.9308E−02	2.3965E−01	1.9998E−02	2.0081E−01	2.1038E−02	1.7011E−01
26	1.6988E−02	4.6981E−01	1.7886E−02	2.4438E−01	1.8525E−02	2.0477E−01	1.9489E−02	1.7346E−01
27	1.5782E−02	4.7861E−01	1.6614E−02	2.4894E−01	1.7207E−02	2.0859E−01	1.8101E−02	1.7670E−01
28	1.4698E−02	4.8711E−01	1.5471E−02	2.5335E−01	1.6022E−02	2.1228E−01	1.6855E−02	1.7982E−01
29	1.3720E−02	4.9532E−01	1.4440E−02	2.5761E−01	1.4955E−02	2.1585E−01	1.5732E−02	1.8285E−01
30	1.2836E−02	5.0327E−01	1.3508E−02	2.6172E−01	1.3989E−02	2.1930E−01	1.4716E−02	1.8577E−01
31	1.2034E−02	5.1096E−01	1.2663E−02	2.6571E−01	1.3114E−02	2.2264E−01	1.3795E−02	1.8859E−01
32	1.1304E−02	5.1840E−01	1.1894E−02	2.6957E−01	1.2317E−02	2.2587E−01	1.2957E−02	1.9133E−01
33	1.0638E−02	5.2562E−01	1.1192E−02	2.7331E−01	1.1590E−02	2.2900E−01	1.2192E−02	1.9398E−01
34	1.0029E−02	5.3262E−01	1.0550E−02	2.7694E−01	1.0925E−02	2.3204E−01	1.1492E−02	1.9656E−01
35	9.4702E−03	5.3942E−01	9.9617E−03	2.8046E−01	1.0316E−02	2.3499E−01	1.0851E−02	1.9906E−01
36	8.9566E−03	5.4603E−01	9.4206E−03	2.8388E−01	9.7552E−03	2.3786E−01	1.0261E−02	2.0149E−01
37	8.4834E−03	5.5245E−01	8.9223E−03	2.8721E−01	9.2390E−03	2.4065E−01	9.7179E−03	2.0385E−01
38	8.0465E−03	5.5870E−01	8.4623E−03	2.9044E−01	8.7626E−03	2.4335E−01	9.2166E−03	2.0614E−01
39	7.6424E−03	5.6478E−01	8.0368E−03	2.9359E−01	8.3219E−03	2.4599E−01	8.7529E−03	2.0838E−01
40	7.2678E−03	5.7070E−01	7.6424E−03	2.9666E−01	7.9134E−03	2.4856E−01	8.3232E−03	2.1055E−01
41	6.9200E−03	5.7647E−01	7.2763E−03	2.9965E−01	7.5342E−03	2.5107E−01	7.9241E−03	2.1267E−01
42	6.5965E−03	5.8210E−01	6.9357E−03	3.0257E−01	7.1814E−03	2.5351E−01	7.5530E−03	2.1474E−01
43	6.2950E−03	5.8760E−01	6.6184E−03	3.0542E−01	6.8528E−03	2.5589E−01	7.2072E−03	2.1676E−01
44	6.0137E−03	5.9296E−01	6.3223E−03	3.0819E−01	6.5461E−03	2.5822E−01	6.8846E−03	2.1873E−01
45	5.7508E−03	5.9820E−01	6.0456E−03	3.1091E−01	6.2595E−03	2.6049E−01	6.5831E−03	2.2066E−01
46	5.5047E−03	6.0332E−01	5.7866E−03	3.1356E−01	5.9913E−03	2.6271E−01	6.3009E−03	2.2254E−01
47	5.2740E−03	6.0833E−01	5.5439E−03	3.1615E−01	5.7399E−03	2.6488E−01	6.0364E−03	2.2438E−01
48	5.0574E−03	6.1323E−01	5.3160E−03	3.1869E−01	5.5039E−03	2.6701E−01	5.7882E−03	2.2618E−01
49	4.8540E−03	6.1802E−01	5.1019E−03	3.2117E−01	5.2822E−03	2.6909E−01	5.5549E−03	2.2794E−01
50	4.6625E−03	6.2272E−01	4.9005E−03	3.2361E−01	5.0735E−03	2.7113E−01	5.3354E−03	2.2966E−01
51	4.4821E−03	6.2731E−01	4.7107E−03	3.2599E−01	4.8770E−03	2.7312E−01	5.1286E−03	2.3135E−01
52	4.3120E−03	6.3182E−01	4.5317E−03	3.2832E−01	4.6917E−03	2.7507E−01	4.9336E−03	2.3301E−01
53	4.1513E−03	6.3623E−01	4.3627E−03	3.3061E−01	4.5166E−03	2.7699E−01	4.7494E−03	2.3463E−01
54	3.9995E−03	6.4057E−01	4.2030E−03	3.3285E−01	4.3512E−03	2.7887E−01	4.5754E−03	2.3622E−01
55	3.8558E−03	6.4482E−01	4.0518E−03	3.3505E−01	4.1947E−03	2.8071E−01	4.4107E−03	2.3779E−01
56	3.7197E−03	6.4899E−01	3.9087E−03	3.3721E−01	4.0464E−03	2.8252E−01	4.2548E−03	2.3932E−01
57	3.5907E−03	6.5308E−01	3.7730E−03	3.3933E−01	3.9059E−03	2.8430E−01	4.1069E−03	2.4082E−01
58	3.4683E−03	6.5711E−01	3.6442E−03	3.4142E−01	3.7725E−03	2.8605E−01	3.9666E−03	2.4230E−01
59	3.3520E−03	6.6105E−01	3.5219E−03	3.4347E−01	3.6459E−03	2.8776E−01	3.8334E−03	2.4375E−01
60	3.2415E−03	6.6492E−01	3.4058E−03	3.4547E−01	3.5255E−03	2.8945E−01	3.7068E−03	2.4517E−01

Table 4.3.3.1. *Partial wave elastic scattering factors for neutral atoms (cont.)*
Be; $Z = 4$

	10 keV		40 keV		60 keV		90 keV	
s	$\|f(s)\|$	$\eta(s)$	$\|f(s)\|$	$\eta(s)$	$\|f(s)\|$	$\eta(s)$	$\|f(s)\|$	$\eta(s)$
0	3.1055E+00	5.8862E−02	3.2880E+00	3.0761E−02	3.4035E+00	2.5806E−02	3.5638E+00	2.1939E−02
1	2.5308E+00	6.9079E−02	2.6815E+00	3.6077E−02	2.7773E+00	3.0252E−02	2.9164E+00	2.5649E−02
2	1.5618E+00	9.9147E−02	1.6558E+00	5.1749E−02	1.7162E+00	4.3368E−02	1.8057E+00	3.6714E−02
3	9.0894E−01	1.4388E−01	9.6387E−01	7.5060E−02	9.9918E−01	6.2898E−02	1.0515E+00	5.3259E−02
4	5.6282E−01	1.9294E−01	5.9674E−01	1.0060E−01	6.1846E−01	8.4322E−02	6.5100E−01	7.1403E−02
5	3.8082E−01	2.3775E−01	4.0346E−01	1.2396E−01	4.1816E−01	1.0389E−01	4.4012E−01	8.7995E−02
6	2.7803E−01	2.7538E−01	2.9434E−01	1.4359E−01	3.0510E−01	1.2032E−01	3.2108E−01	1.0193E−01
7	2.1472E−01	3.0659E−01	2.2727E−01	1.5979E−01	2.3550E−01	1.3394E−01	2.4788E−01	1.1345E−01
8	1.7255E−01	3.3310E−01	1.8254E−01	1.7362E−01	1.8915E−01	1.4552E−01	1.9908E−01	1.2327E−01
9	1.4259E−01	3.5654E−01	1.5076E−01	1.8585E−01	1.5625E−01	1.5573E−01	1.6443E−01	1.3194E−01
10	1.2020E−01	3.7796E−01	1.2712E−01	1.9689E−01	1.3170E−01	1.6504E−01	1.3862E−01	1.3980E−01
11	1.0282E−01	3.9793E−01	1.0872E−01	2.0725E−01	1.1263E−01	1.7373E−01	1.1855E−01	1.4716E−01
12	8.9120E−02	4.1676E−01	9.4178E−02	2.1709E−01	9.7574E−02	1.8195E−01	1.0269E−01	1.5414E−01
13	7.8000E−02	4.3478E−01	8.2389E−02	2.2648E−01	8.5364E−02	1.8980E−01	8.9832E−02	1.6080E−01
14	6.8793E−02	4.5213E−01	7.2641E−02	2.3549E−01	7.5262E−02	1.9735E−01	7.9199E−02	1.6720E−01
15	6.1093E−02	4.6886E−01	6.4491E−02	2.4417E−01	6.6814E−02	2.0463E−01	7.0308E−02	1.7336E−01
16	5.4587E−02	4.8503E−01	5.7604E−02	2.5256E−01	5.9677E−02	2.1166E−01	6.2796E−02	1.7932E−01
17	4.9039E−02	5.0066E−01	5.1732E−02	2.6068E−01	5.3593E−02	2.1846E−01	5.6392E−02	1.8508E−01
18	4.4271E−02	5.1580E−01	4.6688E−02	2.6853E−01	4.8365E−02	2.2503E−01	5.0890E−02	1.9065E−01
19	4.0146E−02	5.3045E−01	4.2324E−02	2.7612E−01	4.3843E−02	2.3140E−01	4.6130E−02	1.9604E−01
20	3.6555E−02	5.4463E−01	3.8526E−02	2.8348E−01	3.9907E−02	2.3756E−01	4.1988E−02	2.0126E−01
21	3.3411E−02	5.5836E−01	3.5202E−02	2.9059E−01	3.6463E−02	2.4352E−01	3.8364E−02	2.0631E−01
22	3.0645E−02	5.7166E−01	3.2279E−02	2.9748E−01	3.3433E−02	2.4929E−01	3.5175E−02	2.1120E−01
23	2.8200E−02	5.8454E−01	2.9695E−02	3.0416E−01	3.0756E−02	2.5488E−01	3.2357E−02	2.1594E−01
24	2.6029E−02	5.9701E−01	2.7401E−02	3.1062E−01	2.8379E−02	2.6029E−01	2.9856E−02	2.2052E−01
25	2.4093E−02	6.0910E−01	2.5357E−02	3.1688E−01	2.6261E−02	2.6554E−01	2.7627E−02	2.2497E−01
26	2.2361E−02	6.2081E−01	2.3528E−02	3.2295E−01	2.4366E−02	2.7062E−01	2.5633E−02	2.2927E−01
27	2.0805E−02	6.3217E−01	2.1886E−02	3.2883E−01	2.2665E−02	2.7554E−01	2.3843E−02	2.3344E−01
28	1.9403E−02	6.4318E−01	2.0406E−02	3.3453E−01	2.1132E−02	2.8032E−01	2.2230E−02	2.3749E−01
29	1.8135E−02	6.5387E−01	1.9069E−02	3.4006E−01	1.9747E−02	2.8495E−01	2.0772E−02	2.4141E−01
30	1.6986E−02	6.6424E−01	1.7857E−02	3.4542E−01	1.8491E−02	2.8944E−01	1.9451E−02	2.4521E−01
31	1.5941E−02	6.7431E−01	1.6755E−02	3.5064E−01	1.7349E−02	2.9381E−01	1.8249E−02	2.4891E−01
32	1.4988E−02	6.8410E−01	1.5750E−02	3.5570E−01	1.6308E−02	2.9805E−01	1.7154E−02	2.5250E−01
33	1.4116E−02	6.9361E−01	1.4832E−02	3.6061E−01	1.5357E−02	3.0217E−01	1.6153E−02	2.5599E−01
34	1.3318E−02	7.0286E−01	1.3990E−02	3.6540E−01	1.4486E−02	3.0617E−01	1.5236E−02	2.5938E−01
35	1.2584E−02	7.1186E−01	1.3218E−02	3.7005E−01	1.3686E−02	3.1007E−01	1.4395E−02	2.6268E−01
36	1.1909E−02	7.2061E−01	1.2507E−02	3.7458E−01	1.2949E−02	3.1386E−01	1.3620E−02	2.6589E−01
37	1.1286E−02	7.2914E−01	1.1851E−02	3.7899E−01	1.2270E−02	3.1755E−01	1.2905E−02	2.6902E−01
38	1.0711E−02	7.3745E−01	1.1245E−02	3.8328E−01	1.1642E−02	3.2115E−01	1.2245E−02	2.7207E−01
39	1.0177E−02	7.4555E−01	1.0684E−02	3.8747E−01	1.1061E−02	3.2465E−01	1.1633E−02	2.7504E−01
40	9.6828E−03	7.5345E−01	1.0164E−02	3.9155E−01	1.0522E−02	3.2807E−01	1.1066E−02	2.7793E−01
41	9.2231E−03	7.6116E−01	9.6798E−03	3.9554E−01	1.0021E−02	3.3140E−01	1.0539E−02	2.8076E−01
42	8.7950E−03	7.6869E−01	9.2296E−03	3.9942E−01	9.5549E−03	3.3466E−01	1.0049E−02	2.8351E−01
43	8.3959E−03	7.7603E−01	8.8098E−03	4.0322E−01	9.1202E−03	3.3784E−01	9.5912E−03	2.8621E−01
44	8.0231E−03	7.8321E−01	8.4179E−03	4.0693E−01	8.7143E−03	3.4095E−01	9.1642E−03	2.8884E−01
45	7.6745E−03	7.9023E−01	8.0514E−03	4.1055E−01	8.3348E−03	3.4398E−01	8.7648E−03	2.9141E−01
46	7.3479E−03	7.9710E−01	7.7081E−03	4.1410E−01	7.9793E−03	3.4695E−01	8.3909E−03	2.9392E−01
47	7.0417E−03	8.0381E−01	7.3862E−03	4.1757E−01	7.6460E−03	3.4985E−01	8.0403E−03	2.9638E−01
48	6.7541E−03	8.1038E−01	7.0840E−03	4.2096E−01	7.3330E−03	3.5270E−01	7.7110E−03	2.9879E−01
49	6.4837E−03	8.1682E−01	6.7998E−03	4.2429E−01	7.0388E−03	3.5548E−01	7.4015E−03	3.0114E−01
50	6.2291E−03	8.2312E−01	6.5324E−03	4.2754E−01	6.7618E−03	3.5820E−01	7.1102E−03	3.0345E−01
51	5.9892E−03	8.2930E−01	6.2803E−03	4.3073E−01	6.5008E−03	3.6087E−01	6.8356E−03	3.0571E−01
52	5.7627E−03	8.3535E−01	6.0425E−03	4.3386E−01	6.2545E−03	3.6349E−01	6.5765E−03	3.0793E−01
53	5.5489E−03	8.4129E−01	5.8179E−03	4.3692E−01	6.0220E−03	3.6606E−01	6.3319E−03	3.1010E−01
54	5.3467E−03	8.4711E−01	5.6056E−03	4.3993E−01	5.8021E−03	3.6858E−01	6.1006E−03	3.1224E−01
55	5.1553E−03	8.5282E−01	5.4046E−03	4.4288E−01	5.5940E−03	3.7105E−01	5.8817E−03	3.1433E−01
56	4.9740E−03	8.5843E−01	5.2141E−03	4.4578E−01	5.3968E−03	3.7347E−01	5.6743E−03	3.1638E−01
57	4.8020E−03	8.6394E−01	5.0336E−03	4.4862E−01	5.2099E−03	3.7585E−01	5.4776E−03	3.1840E−01
58	4.6388E−03	8.6934E−01	4.8622E−03	4.5142E−01	5.0325E−03	3.7819E−01	5.2911E−03	3.2037E−01
59	4.4837E−03	8.7465E−01	4.6995E−03	4.5416E−01	4.8640E−03	3.8049E−01	5.1137E−03	3.2233E−01
60	4.3361E−03	8.7993E−01	4.5450E−03	4.5683E−01	4.7036E−03	3.8276E−01	4.9449E−03	3.2425E−01

Table 4.3.3.1. *Partial wave elastic scattering factors for neutral atoms (cont.)*
B; $Z = 5$

	10 keV		40 keV		60 keV		90 keV	
s	$\|f(s)\|$	$\eta(s)$	$\|f(s)\|$	$\eta(s)$	$\|f(s)\|$	$\eta(s)$	$\|f(s)\|$	$\eta(s)$
0	2.8358E+00	8.0833E−02	3.0075E+00	4.2321E−02	3.1129E+00	3.5528E−02	3.2589E+00	3.0233E−02
1	2.4610E+00	9.0430E−02	2.6117E+00	4.7318E−02	2.7056E+00	3.9689E−02	2.8411E+00	3.3677E−02
2	1.7329E+00	1.1818E−01	1.8407E+00	6.1786E−02	1.9083E+00	5.1793E−02	2.0083E+00	4.3863E−02
3	1.1285E+00	1.6052E−01	1.1995E+00	8.3854E−02	1.2437E+00	7.0287E−02	1.3092E+00	5.9526E−02
4	7.4063E−01	2.1145E−01	7.8730E−01	1.1039E−01	8.1629E−01	9.2525E−02	8.5934E−01	7.8374E−02
5	5.0784E−01	2.6434E−01	5.3954E−01	1.3794E−01	5.5940E−01	1.1562E−01	5.8894E−01	9.7936E−02
6	3.6682E−01	3.1415E−01	3.8937E−01	1.6389E−01	4.0365E−01	1.3737E−01	4.2492E−01	1.1638E−01
7	2.7788E−01	3.5851E−01	2.9466E−01	1.8701E−01	3.0544E−01	1.5675E−01	3.2151E−01	1.3281E−01
8	2.1893E−01	3.9718E−01	2.3195E−01	2.0716E−01	2.4041E−01	1.7363E−01	2.5306E−01	1.4710E−01
9	1.7797E−01	4.3078E−01	1.8843E−01	2.2464E−01	1.9528E−01	1.8830E−01	2.0553E−01	1.5955E−01
10	1.4819E−01	4.6047E−01	1.5680E−01	2.4010E−01	1.6250E−01	2.0124E−01	1.7104E−01	1.7050E−01
11	1.2565E−01	4.8713E−01	1.3288E−01	2.5397E−01	1.3771E−01	2.1286E−01	1.4494E−01	1.8035E−01
12	1.0830E−01	5.1149E−01	1.1450E−01	2.6662E−01	1.1865E−01	2.2346E−01	1.2487E−01	1.8934E−01
13	9.4491E−02	5.3411E−01	9.9864E−02	2.7837E−01	1.0348E−01	2.3331E−01	1.0890E−01	1.9769E−01
14	8.3219E−02	5.5541E−01	8.7920E−02	2.8942E−01	9.1096E−02	2.4257E−01	9.5866E−02	2.0553E−01
15	7.3891E−02	5.7562E−01	7.8037E−02	2.9991E−01	8.0853E−02	2.5136E−01	8.5084E−02	2.1298E−01
16	6.6065E−02	5.9496E−01	6.9747E−02	3.0994E−01	7.2261E−02	2.5977E−01	7.6040E−02	2.2010E−01
17	5.9424E−02	6.1353E−01	6.2712E−02	3.1957E−01	6.4970E−02	2.6783E−01	6.8366E−02	2.2694E−01
18	5.3731E−02	6.3143E−01	5.6683E−02	3.2886E−01	5.8722E−02	2.7561E−01	6.1789E−02	2.3353E−01
19	4.8811E−02	6.4873E−01	5.1474E−02	3.3782E−01	5.3323E−02	2.8312E−01	5.6106E−02	2.3989E−01
20	4.4527E−02	6.6548E−01	4.6940E−02	3.4650E−01	4.8623E−02	2.9039E−01	5.1160E−02	2.4605E−01
21	4.0775E−02	6.8171E−01	4.2968E−02	3.5491E−01	4.4507E−02	2.9743E−01	4.6828E−02	2.5201E−01
22	3.7469E−02	6.9746E−01	3.9469E−02	3.6306E−01	4.0882E−02	3.0426E−01	4.3012E−02	2.5780E−01
23	3.4541E−02	7.1274E−01	3.6372E−02	3.7098E−01	3.7672E−02	3.1089E−01	3.9634E−02	2.6341E−01
24	3.1936E−02	7.2760E−01	3.3617E−02	3.7866E−01	3.4817E−02	3.1732E−01	3.6629E−02	2.6887E−01
25	2.9609E−02	7.4202E−01	3.1157E−02	3.8612E−01	3.2268E−02	3.2358E−01	3.3946E−02	2.7416E−01
26	2.7522E−02	7.5605E−01	2.8951E−02	3.9338E−01	2.9982E−02	3.2965E−01	3.1540E−02	2.7931E−01
27	2.5643E−02	7.6970E−01	2.6966E−02	4.0044E−01	2.7925E−02	3.3556E−01	2.9376E−02	2.8431E−01
28	2.3947E−02	7.8296E−01	2.5174E−02	4.0730E−01	2.6068E−02	3.4130E−01	2.7422E−02	2.8918E−01
29	2.2410E−02	7.9588E−01	2.3551E−02	4.1397E−01	2.4387E−02	3.4690E−01	2.5652E−02	2.9392E−01
30	2.1014E−02	8.0845E−01	2.2077E−02	4.2046E−01	2.2860E−02	3.5233E−01	2.4045E−02	2.9852E−01
31	1.9741E−02	8.2069E−01	2.0734E−02	4.2679E−01	2.1469E−02	3.5763E−01	2.2581E−02	3.0301E−01
32	1.8579E−02	8.3261E−01	1.9508E−02	4.3295E−01	2.0198E−02	3.6279E−01	2.1245E−02	3.0738E−01
33	1.7515E−02	8.4423E−01	1.8386E−02	4.3895E−01	1.9036E−02	3.6781E−01	2.0021E−02	3.1163E−01
34	1.6538E−02	8.5555E−01	1.7356E−02	4.4480E−01	1.7969E−02	3.7271E−01	1.8899E−02	3.1578E−01
35	1.5639E−02	8.6660E−01	1.6409E−02	4.5049E−01	1.6988E−02	3.7748E−01	1.7866E−02	3.1982E−01
36	1.4811E−02	8.7737E−01	1.5536E−02	4.5605E−01	1.6084E−02	3.8213E−01	1.6915E−02	3.2376E−01
37	1.4046E−02	8.8788E−01	1.4730E−02	4.6148E−01	1.5249E−02	3.8667E−01	1.6037E−02	3.2760E−01
38	1.3338E−02	8.9813E−01	1.3984E−02	4.6677E−01	1.4476E−02	3.9110E−01	1.5224E−02	3.3135E−01
39	1.2681E−02	9.0815E−01	1.3293E−02	4.7193E−01	1.3760E−02	3.9543E−01	1.4471E−02	3.3502E−01
40	1.2071E−02	9.1794E−01	1.2651E−02	4.7698E−01	1.3096E−02	3.9965E−01	1.3771E−02	3.3860E−01
41	1.1503E−02	9.2750E−01	1.2054E−02	4.8191E−01	1.2477E−02	4.0378E−01	1.3121E−02	3.4209E−01
42	1.0975E−02	9.3684E−01	1.1498E−02	4.8673E−01	1.1901E−02	4.0781E−01	1.2515E−02	3.4550E−01
43	1.0481E−02	9.4598E−01	1.0979E−02	4.9144E−01	1.1364E−02	4.1175E−01	1.1949E−02	3.4885E−01
44	1.0020E−02	9.5492E−01	1.0494E−02	4.9605E−01	1.0861E−02	4.1561E−01	1.1421E−02	3.5211E−01
45	9.5878E−03	9.6366E−01	1.0040E−02	5.0055E−01	1.0391E−02	4.1938E−01	1.0927E−02	3.5530E−01
46	9.1830E−03	9.7223E−01	9.6145E−03	5.0496E−01	9.9510E−03	4.2308E−01	1.0463E−02	3.5843E−01
47	8.8031E−03	9.8062E−01	9.2153E−03	5.0929E−01	9.5377E−03	4.2670E−01	1.0029E−02	3.6150E−01
48	8.4461E−03	9.8882E−01	8.8405E−03	5.1351E−01	9.1495E−03	4.3024E−01	9.6201E−03	3.6449E−01
49	8.1102E−03	9.9687E−01	8.4878E−03	5.1766E−01	8.7844E−03	4.3370E−01	9.2360E−03	3.6743E−01
50	7.7938E−03	1.0048E+00	8.1556E−03	5.2173E−01	8.4404E−03	4.3711E−01	8.8742E−03	3.7031E−01
51	7.4955E−03	1.0125E+00	7.8425E−03	5.2571E−01	8.1161E−03	4.4044E−01	8.5332E−03	3.7313E−01
52	7.2138E−03	1.0201E+00	7.5469E−03	5.2961E−01	7.8102E−03	4.4371E−01	8.2113E−03	3.7590E−01
53	6.9476E−03	1.0275E+00	7.2676E−03	5.3345E−01	7.5209E−03	4.4692E−01	7.9071E−03	3.7862E−01
54	6.6958E−03	1.0348E+00	7.0034E−03	5.3721E−01	7.2474E−03	4.5007E−01	7.6194E−03	3.8128E−01
55	6.4574E−03	1.0420E+00	6.7533E−03	5.4090E−01	6.9885E−03	4.5316E−01	7.3471E−03	3.8390E−01
56	6.2314E−03	1.0490E+00	6.5164E−03	5.4452E−01	6.7432E−03	4.5619E−01	7.0891E−03	3.8647E−01
57	6.0169E−03	1.0560E+00	6.2915E−03	5.4808E−01	6.5104E−03	4.5917E−01	6.8442E−03	3.8899E−01
58	5.8134E−03	1.0627E+00	6.0781E−03	5.5159E−01	6.2894E−03	4.6210E−01	6.6118E−03	3.9147E−01
59	5.6199E−03	1.0694E+00	5.8752E−03	5.5503E−01	6.0795E−03	4.6498E−01	6.3910E−03	3.9391E−01
60	5.4357E−03	1.0760E+00	5.6826E−03	5.5838E−01	5.8801E−03	4.6779E−01	6.1810E−03	3.9631E−01

Table 4.3.3.1. *Partial wave elastic scattering factors for neutral atoms (cont.)*
C; $Z = 6$

	10 keV		40 keV		60 keV		90 keV	
s	$\|f(s)\|$	$\eta(s)$	$\|f(s)\|$	$\eta(s)$	$\|f(s)\|$	$\eta(s)$	$\|f(s)\|$	$\eta(s)$
0	2.5385E+00	1.0201E−01	2.6187E+00	5.4129E−02	2.7926E+00	4.4969E−02	2.9237E+00	3.8293E−02
1	2.2870E+00	1.1089E−01	2.3744E+00	5.8509E−02	2.5202E+00	4.8805E−02	2.6459E+00	4.1447E−02
2	1.7503E+00	1.3649E−01	1.8390E+00	7.1297E−02	1.9324E+00	5.9971E−02	2.0345E+00	5.0798E−02
3	1.2403E+00	1.7586E−01	1.3145E+00	9.1277E−02	1.3709E+00	7.7184E−02	1.4432E+00	6.5396E−02
4	8.6647E−01	2.2496E−01	9.2238E−01	1.1646E−01	9.5829E−01	9.8626E−02	1.0093E+00	8.3540E−02
5	6.1651E−01	2.7910E−01	6.5717E−01	1.4446E−01	6.8179E−01	1.2225E−01	7.1786E−01	1.0359E−01
6	4.5256E−01	3.3405E−01	4.8230E−01	1.7300E−01	5.0003E−01	1.4625E−01	5.2662E−01	1.2390E−01
7	3.4376E−01	3.8662E−01	3.6595E−01	2.0039E−01	3.7936E−01	1.6919E−01	3.9938E−01	1.4338E−01
8	2.6960E−01	4.3505E−01	2.8663E−01	2.2565E−01	2.9704E−01	1.9037E−01	3.1277E−01	1.6129E−01
9	2.1743E−01	4.7877E−01	2.3089E−01	2.4845E−01	2.3927E−01	2.0944E−01	2.5186E−01	1.7749E−01
10	1.7954E−01	5.1788E−01	1.9042E−01	2.6886E−01	1.9728E−01	2.2656E−01	2.0769E−01	1.9197E−01
11	1.5103E−01	5.5297E−01	1.6004E−01	2.8716E−01	1.6578E−01	2.4188E−01	1.7452E−01	2.0494E−01
12	1.2931E−01	5.8472E−01	1.3692E−01	3.0367E−01	1.4183E−01	2.5569E−01	1.4929E−01	2.1667E−01
13	1.1222E−01	6.1369E−01	1.1876E−01	3.1873E−01	1.2302E−01	2.6830E−01	1.2947E−01	2.2736E−01
14	9.8441E−02	6.4040E−01	1.0412E−01	3.3262E−01	1.0784E−01	2.7992E−01	1.1350E−01	2.3721E−01
15	8.7158E−02	6.6532E−01	9.2143E−02	3.4556E−01	9.5434E−02	2.9076E−01	1.0043E−01	2.4639E−01
16	7.7780E−02	6.8876E−01	8.2192E−02	3.5772E−01	8.5123E−02	3.0094E−01	8.9579E−02	2.5502E−01
17	6.9881E−02	7.1099E−01	7.3814E−02	3.6925E−01	7.6443E−02	3.1060E−01	8.0441E−02	2.6320E−01
18	6.3155E−02	7.3218E−01	6.6680E−02	3.8025E−01	6.9052E−02	3.1980E−01	7.2661E−02	2.7099E−01
19	5.7368E−02	7.5251E−01	6.0545E−02	3.9078E−01	6.2697E−02	3.2862E−01	6.5971E−02	2.7847E−01
20	5.2350E−02	7.7206E−01	5.5226E−02	4.0091E−01	5.7186E−02	3.3710E−01	6.0171E−02	2.8565E−01
21	4.7965E−02	7.9094E−01	5.0578E−02	4.1069E−01	5.2371E−02	3.4528E−01	5.5103E−02	2.9258E−01
22	4.4109E−02	8.0920E−01	4.6492E−02	4.2014E−01	4.8138E−02	3.5319E−01	5.0647E−02	2.9929E−01
23	4.0697E−02	8.2690E−01	4.2878E−02	4.2930E−01	4.4395E−02	3.6086E−01	4.6707E−02	3.0578E−01
24	3.7664E−02	8.4408E−01	3.9665E−02	4.3819E−01	4.1066E−02	3.6830E−01	4.3204E−02	3.1208E−01
25	3.4954E−02	8.6077E−01	3.6795E−02	4.4683E−01	3.8094E−02	3.7553E−01	4.0076E−02	3.1820E−01
26	3.2523E−02	8.7701E−01	3.4222E−02	4.5522E−01	3.5429E−02	3.8255E−01	3.7270E−02	3.2415E−01
27	3.0334E−02	8.9280E−01	3.1905E−02	4.6339E−01	3.3029E−02	3.8939E−01	3.4744E−02	3.2994E−01
28	2.8355E−02	9.0820E−01	2.9812E−02	4.7134E−01	3.0861E−02	3.9604E−01	3.2462E−02	3.3558E−01
29	2.6561E−02	9.2319E−01	2.7915E−02	4.7909E−01	2.8895E−02	4.0253E−01	3.0394E−02	3.4107E−01
30	2.4929E−02	9.3782E−01	2.6190E−02	4.8664E−01	2.7109E−02	4.0884E−01	2.8514E−02	3.4642E−01
31	2.3441E−02	9.5207E−01	2.4617E−02	4.9400E−01	2.5480E−02	4.1501E−01	2.6800E−02	3.5164E−01
32	2.2080E−02	9.6599E−01	2.3179E−02	5.0118E−01	2.3991E−02	4.2101E−01	2.5233E−02	3.5673E−01
33	2.0832E−02	9.7957E−01	2.1861E−02	5.0819E−01	2.2626E−02	4.2688E−01	2.3797E−02	3.6170E−01
34	1.9686E−02	9.9283E−01	2.0651E−02	5.1503E−01	2.1373E−02	4.3260E−01	2.2478E−02	3.6654E−01
35	1.8630E−02	1.0058E+00	1.9537E−02	5.2171E−01	2.0219E−02	4.3819E−01	2.1263E−02	3.7128E−01
36	1.7656E−02	1.0184E+00	1.8509E−02	5.2823E−01	1.9154E−02	4.4365E−01	2.0143E−02	3.7590E−01
37	1.6754E−02	1.0308E+00	1.7558E−02	5.3461E−01	1.8170E−02	4.4898E−01	1.9108E−02	3.8042E−01
38	1.5920E−02	1.0429E+00	1.6678E−02	5.4083E−01	1.7259E−02	4.5420E−01	1.8149E−02	3.8483E−01
39	1.5145E−02	1.0547E+00	1.5862E−02	5.4693E−01	1.6413E−02	4.5929E−01	1.7260E−02	3.8914E−01
40	1.4424E−02	1.0663E+00	1.5103E−02	5.5288E−01	1.5628E−02	4.6428E−01	1.6433E−02	3.9337E−01
41	1.3754E−02	1.0776E+00	1.4397E−02	5.5871E−01	1.4896E−02	4.6915E−01	1.5663E−02	3.9750E−01
42	1.3128E−02	1.0887E+00	1.3738E−02	5.6441E−01	1.4214E−02	4.7393E−01	1.4946E−02	4.0153E−01
43	1.2543E−02	1.0995E+00	1.3123E−02	5.6999E−01	1.3578E−02	4.7860E−01	1.4276E−02	4.0549E−01
44	1.1997E−02	1.1102E+00	1.2548E−02	5.7546E−01	1.2982E−02	4.8317E−01	1.3649E−02	4.0936E−01
45	1.1484E−02	1.1206E+00	1.2009E−02	5.8081E−01	1.2424E−02	4.8765E−01	1.3063E−02	4.1315E−01
46	1.1004E−02	1.1308E+00	1.1504E−02	5.8606E−01	1.1901E−02	4.9204E−01	1.2513E−02	4.1687E−01
47	1.0553E−02	1.1408E+00	1.1030E−02	5.9120E−01	1.1411E−02	4.9634E−01	1.1996E−02	4.2051E−01
48	1.0128E−02	1.1506E+00	1.0584E−02	5.9624E−01	1.0949E−02	5.0055E−01	1.1511E−02	4.2408E−01
49	9.7287E−03	1.1602E+00	1.0164E−02	6.0118E−01	1.0515E−02	5.0469E−01	1.1054E−02	4.2758E−01
50	9.3522E−03	1.1696E+00	9.7690E−03	6.0602E−01	1.0106E−02	5.0875E−01	1.0624E−02	4.3102E−01
51	8.9969E−03	1.1789E+00	9.3961E−03	6.1078E−01	9.7196E−03	5.1272E−01	1.0218E−02	4.3438E−01
52	8.6613E−03	1.1880E+00	9.0439E−03	6.1545E−01	9.3550E−03	5.1662E−01	9.8344E−03	4.3768E−01
53	8.3439E−03	1.1969E+00	8.7110E−03	6.2003E−01	9.0104E−03	5.2046E−01	9.4719E−03	4.4093E−01
54	8.0435E−03	1.2056E+00	8.3959E−03	6.2453E−01	8.6843E−03	5.2422E−01	9.1289E−03	4.4412E−01
55	7.7589E−03	1.2142E+00	8.0975E−03	6.2894E−01	8.3757E−03	5.2791E−01	8.8042E−03	4.4724E−01
56	7.4891E−03	1.2227E+00	7.8147E−03	6.3328E−01	8.0829E−03	5.3154E−01	8.4964E−03	4.5031E−01
57	7.2329E−03	1.2310E+00	7.5463E−03	6.3755E−01	7.8051E−03	5.3511E−01	8.2042E−03	4.5334E−01
58	6.9897E−03	1.2392E+00	7.2914E−03	6.4174E−01	7.5413E−03	5.3862E−01	7.9268E−03	4.5631E−01
59	6.7584E−03	1.2472E+00	7.0491E−03	6.4586E−01	7.2908E−03	5.4205E−01	7.6632E−03	4.5922E−01
60	6.5381E−03	1.2551E+00	6.8186E−03	6.4992E−01	7.0517E−03	5.4549E−01	7.4122E−03	4.6210E−01

Table 4.3.3.1. *Partial wave elastic scattering factors for neutral atoms (cont.)*
N; $Z = 7$

	10 keV		40 keV		60 keV		90 keV	
s	$\|f(s)\|$	$\eta(s)$	$\|f(s)\|$	$\eta(s)$	$\|f(s)\|$	$\eta(s)$	$\|f(s)\|$	$\eta(s)$
0	2.2348E+00	1.2336E−01	2.3809E+00	6.4945E−02	2.4654E+00	5.4566E−02	2.5816E+00	4.6486E−02
1	2.0680E+00	1.3129E−01	2.2051E+00	6.9067E−02	2.2852E+00	5.7987E−02	2.3986E+00	4.9287E−02
2	1.6835E+00	1.5435E−01	1.7974E+00	8.1099E−02	1.8645E+00	6.8024E−02	1.9632E+00	5.7642E−02
3	1.2750E+00	1.9031E−01	1.3628E+00	9.9882E−02	1.4138E+00	8.3773E−02	1.4889E+00	7.0988E−02
4	9.4122E−01	2.3626E−01	1.0071E+00	1.2383E−01	1.0450E+00	1.0384E−01	1.1006E+00	8.8003E−02
5	6.9683E−01	2.8880E−01	7.4580E−01	1.5122E−01	7.7392E−01	1.2679E−01	8.1539E−01	1.0742E−01
6	5.2467E−01	3.4462E−01	5.6149E−01	1.8025E−01	5.8258E−01	1.5114E−01	6.1355E−01	1.2810E−01
7	4.0419E−01	4.0074E−01	4.3205E−01	2.0952E−01	4.4829E−01	1.7565E−01	4.7225E−01	1.4883E−01
8	3.1894E−01	4.5502E−01	3.4051E−01	2.3775E−01	3.5321E−01	1.9933E−01	3.7199E−01	1.6893E−01
9	2.5750E−01	5.0604E−01	2.7443E−01	2.6438E−01	2.8464E−01	2.2164E−01	2.9972E−01	1.8784E−01
10	2.1220E−01	5.5319E−01	2.2579E−01	2.8896E−01	2.3414E−01	2.4224E−01	2.4658E−01	2.0526E−01
11	1.7790E−01	5.9639E−01	1.8903E−01	3.1144E−01	1.9598E−01	2.6110E−01	2.0636E−01	2.2125E−01
12	1.5171E−01	6.3586E−01	1.6098E−01	3.3201E−01	1.6687E−01	2.7834E−01	1.7568E−01	2.3587E−01
13	1.3114E−01	6.7197E−01	1.3899E−01	3.5081E−01	1.4406E−01	2.9409E−01	1.5164E−01	2.4924E−01
14	1.1461E−01	7.0515E−01	1.2136E−01	3.6806E−01	1.2577E−01	3.0855E−01	1.3238E−01	2.6149E−01
15	1.0116E−01	7.3584E−01	1.0702E−01	3.8401E−01	1.1091E−01	3.2191E−01	1.1673E−01	2.7281E−01
16	9.0036E−02	7.6443E−01	9.5191E−02	3.9884E−01	9.8637E−02	3.3434E−01	1.0381E−01	2.8335E−01
17	8.0725E−02	7.9124E−01	8.5294E−02	4.1274E−01	8.8376E−02	3.4598E−01	9.3003E−02	2.9321E−01
18	7.2838E−02	8.1654E−01	7.6917E−02	4.2586E−01	7.9692E−02	3.5697E−01	8.3861E−02	3.0252E−01
19	6.6089E−02	8.4056E−01	6.9753E−02	4.3830E−01	7.2265E−02	3.6739E−01	7.6042E−02	3.1135E−01
20	6.0261E−02	8.6348E−01	6.3570E−02	4.5016E−01	6.5856E−02	3.7732E−01	6.9295E−02	3.1976E−01
21	5.5188E−02	8.8544E−01	5.8191E−02	4.6152E−01	6.0279E−02	3.8684E−01	6.3425E−02	3.2782E−01
22	5.0741E−02	9.0656E−01	5.3476E−02	4.7244E−01	5.5392E−02	3.9598E−01	5.8280E−02	3.3557E−01
23	4.6817E−02	9.2693E−01	4.9317E−02	4.8297E−01	5.1082E−02	4.0480E−01	5.3743E−02	3.4304E−01
24	4.3335E−02	9.4663E−01	4.5628E−02	4.9315E−01	4.7258E−02	4.1333E−01	4.9718E−02	3.5026E−01
25	4.0230E−02	9.6572E−01	4.2339E−02	5.0301E−01	4.3849E−02	4.2158E−01	4.6130E−02	3.5725E−01
26	3.7447E−02	9.8425E−01	3.9392E−02	5.1257E−01	4.0795E−02	4.2959E−01	4.2916E−02	3.6404E−01
27	3.4944E−02	1.0022E+00	3.6741E−02	5.2187E−01	3.8048E−02	4.3737E−01	4.0024E−02	3.7063E−01
28	3.2682E−02	1.0198E+00	3.4348E−02	5.3091E−01	3.5567E−02	4.4494E−01	3.7413E−02	3.7704E−01
29	3.0632E−02	1.0368E+00	3.2179E−02	5.3972E−01	3.3319E−02	4.5231E−01	3.5048E−02	3.8328E−01
30	2.8768E−02	1.0535E+00	3.0206E−02	5.4830E−01	3.1276E−02	4.5950E−01	3.2896E−02	3.8937E−01
31	2.7067E−02	1.0697E+00	2.8408E−02	5.5666E−01	2.9412E−02	4.6650E−01	3.0936E−02	3.9529E−01
32	2.5512E−02	1.0856E+00	2.6764E−02	5.6483E−01	2.7709E−02	4.7333E−01	2.9142E−02	4.0108E−01
33	2.4085E−02	1.1011E+00	2.5256E−02	5.7280E−01	2.6147E−02	4.8001E−01	2.7498E−02	4.0674E−01
34	2.2774E−02	1.1162E+00	2.3871E−02	5.8059E−01	2.4711E−02	4.8653E−01	2.5988E−02	4.1225E−01
35	2.1565E−02	1.1310E+00	2.2595E−02	5.8820E−01	2.3389E−02	4.9290E−01	2.4597E−02	4.1765E−01
36	2.0450E−02	1.1454E+00	2.1417E−02	5.9564E−01	2.2169E−02	4.9912E−01	2.3312E−02	4.2292E−01
37	1.9417E−02	1.1596E+00	2.0327E−02	6.0292E−01	2.1040E−02	5.0521E−01	2.2125E−02	4.2808E−01
38	1.8460E−02	1.1734E+00	1.9318E−02	6.1003E−01	1.9994E−02	5.1117E−01	2.1024E−02	4.3313E−01
39	1.7571E−02	1.1870E+00	1.8380E−02	6.1700E−01	1.9023E−02	5.1701E−01	2.0003E−02	4.3806E−01
40	1.6744E−02	1.2003E+00	1.7509E−02	6.2382E−01	1.8120E−02	5.2271E−01	1.9052E−02	4.4289E−01
41	1.5973E−02	1.2132E+00	1.6697E−02	6.3050E−01	1.7279E−02	5.2830E−01	1.8167E−02	4.4763E−01
42	1.5254E−02	1.2260E+00	1.5939E−02	6.3705E−01	1.6494E−02	5.3378E−01	1.7342E−02	4.5226E−01
43	1.4581E−02	1.2385E+00	1.5231E−02	6.4346E−01	1.5761E−02	5.3914E−01	1.6570E−02	4.5681E−01
44	1.3952E−02	1.2507E+00	1.4569E−02	6.4974E−01	1.5075E−02	5.4440E−01	1.5849E−02	4.6125E−01
45	1.3362E−02	1.2627E+00	1.3948E−02	6.5590E−01	1.4432E−02	5.4956E−01	1.5173E−02	4.6562E−01
46	1.2808E−02	1.2745E+00	1.3366E−02	6.6195E−01	1.3829E−02	5.5461E−01	1.4538E−02	4.6990E−01
47	1.2288E−02	1.2860E+00	1.2819E−02	6.6786E−01	1.3263E−02	5.5957E−01	1.3942E−02	4.7409E−01
48	1.1798E−02	1.2974E+00	1.2304E−02	6.7368E−01	1.2730E−02	5.6443E−01	1.3382E−02	4.7821E−01
49	1.1336E−02	1.3085E+00	1.1819E−02	6.7939E−01	1.2228E−02	5.6921E−01	1.2854E−02	4.8226E−01
50	1.0901E−02	1.3194E+00	1.1363E−02	6.8499E−01	1.1755E−02	5.7389E−01	1.2357E−02	4.8622E−01
51	1.0491E−02	1.3302E+00	1.0932E−02	6.9048E−01	1.1309E−02	5.7849E−01	1.1887E−02	4.9011E−01
52	1.0102E−02	1.3407E+00	1.0524E−02	6.9588E−01	1.0887E−02	5.8301E−01	1.1444E−02	4.9394E−01
53	9.7352E−03	1.3511E+00	1.0139E−02	7.0119E−01	1.0488E−02	5.8745E−01	1.1024E−02	4.9769E−01
54	9.3874E−03	1.3612E+00	9.7746E−03	7.0640E−01	1.0111E−02	5.9180E−01	1.0627E−02	5.0138E−01
55	9.0578E−03	1.3712E+00	9.4292E−03	7.1152E−01	9.7534E−03	5.9608E−01	1.0251E−02	5.0500E−01
56	8.7450E−03	1.3811E+00	9.1015E−03	7.1655E−01	9.4142E−03	6.0030E−01	9.8944E−03	5.0857E−01
57	8.4481E−03	1.3908E+00	8.7904E−03	7.2151E−01	9.0922E−03	6.0444E−01	9.5557E−03	5.1208E−01
58	8.1659E−03	1.4003E+00	8.4949E−03	7.2638E−01	8.7864E−03	6.0851E−01	9.2342E−03	5.1552E−01
59	7.8974E−03	1.4096E+00	8.2141E−03	7.3115E−01	8.4957E−03	6.1251E−01	8.9284E−03	5.1891E−01
60	7.6418E−03	1.4189E+00	7.9471E−03	7.3582E−01	8.2189E−03	6.1645E−01	8.6373E−03	5.2226E−01

Table 4.3.3.1. *Partial wave elastic scattering factors for neutral atoms (cont.)*
O; $Z = 8$

	10 keV		40 keV		60 keV		90 keV	
s	$\|f(s)\|$	$\eta(s)$	$\|f(s)\|$	$\eta(s)$	$\|f(s)\|$	$\eta(s)$	$\|f(s)\|$	$\eta(s)$
0	1.9959E+00	1.4403E−01	2.1119E+00	7.6444E−02	2.2088E+00	6.3972E−02	2.3140E+00	5.4509E−02
1	1.8787E+00	1.5125E−01	1.9924E+00	8.0108E−02	2.0827E+00	6.7068E−02	2.1859E+00	5.7045E−02
2	1.5943E+00	1.7229E−01	1.6986E+00	9.0879E−02	1.7721E+00	7.6214E−02	1.8657E+00	6.4628E−02
3	1.2675E+00	2.0544E−01	1.3557E+00	1.0800E−01	1.4107E+00	9.0760E−02	1.4866E+00	7.6903E−02
4	9.7811E−01	2.4839E−01	1.0491E+00	1.3025E−01	1.0904E+00	1.0954E−01	1.1484E+00	9.2878E−02
5	7.5031E−01	2.9858E−01	8.0606E−01	1.5631E−01	8.3734E−01	1.3145E−01	8.8238E−01	1.1141E−01
6	5.8005E−01	3.5335E−01	6.2353E−01	1.8477E−01	6.4731E−01	1.5539E−01	6.8227E−01	1.3167E−01
7	4.5495E−01	4.1030E−01	4.8897E−01	2.1435E−01	5.0759E−01	1.8018E−01	5.3468E−01	1.5276E−01
8	3.6316E−01	4.6723E−01	3.8989E−01	2.4398E−01	4.0460E−01	2.0505E−01	4.2634E−01	1.7377E−01
9	2.9510E−01	5.2266E−01	3.1636E−01	2.7283E−01	3.2814E−01	2.2928E−01	3.4578E−01	1.9428E−01
10	2.4394E−01	5.7543E−01	2.6102E−01	3.0035E−01	2.7077E−01	2.5227E−01	2.8511E−01	2.1389E−01
11	2.0472E−01	6.2496E−01	2.1862E−01	3.2620E−01	2.2675E−01	2.7392E−01	2.3871E−01	2.3224E−01
12	1.7445E−01	6.7117E−01	1.8593E−01	3.5031E−01	1.9278E−01	2.9414E−01	2.0299E−01	2.4933E−01
13	1.5055E−01	7.1403E−01	1.6018E−01	3.7266E−01	1.6604E−01	3.1287E−01	1.7482E−01	2.6520E−01
14	1.3133E−01	7.5371E−01	1.3951E−01	3.9335E−01	1.4459E−01	3.3021E−01	1.5222E−01	2.7986E−01
15	1.1567E−01	7.9052E−01	1.2272E−01	4.1252E−01	1.2716E−01	3.4626E−01	1.3387E−01	2.9347E−01
16	1.0276E−01	8.2479E−01	1.0888E−01	4.3033E−01	1.1282E−01	3.6117E−01	1.1874E−01	3.0614E−01
17	9.1961E−02	8.5681E−01	9.7346E−02	4.4697E−01	1.0085E−01	3.7512E−01	1.0614E−01	3.1792E−01
18	8.2843E−02	8.8688E−01	8.7616E−02	4.6256E−01	9.0759E−02	3.8817E−01	9.5520E−02	3.2899E−01
19	7.5063E−02	9.1524E−01	7.9326E−02	4.7726E−01	8.2168E−02	4.0047E−01	8.6462E−02	3.3945E−01
20	6.8366E−02	9.4213E−01	7.2198E−02	4.9119E−01	7.4773E−02	4.1216E−01	7.8684E−02	3.4931E−01
21	6.2554E−02	9.6773E−01	6.6017E−02	5.0443E−01	6.8368E−02	4.2323E−01	7.1941E−02	3.5869E−01
22	5.7473E−02	9.9219E−01	6.0618E−02	5.1708E−01	6.2775E−02	4.3381E−01	6.6045E−02	3.6769E−01
23	5.3002E−02	1.0157E+00	5.5870E−02	5.2921E−01	5.7849E−02	4.4400E−01	6.0866E−02	3.7627E−01
24	4.9044E−02	1.0382E+00	5.1668E−02	5.4087E−01	5.3498E−02	4.5373E−01	5.6286E−02	3.8452E−01
25	4.5521E−02	1.0600E+00	4.7931E−02	5.5211E−01	4.9627E−02	4.6314E−01	5.2206E−02	3.9252E−01
26	4.2370E−02	1.0811E+00	4.4589E−02	5.6298E−01	4.6161E−02	4.7227E−01	4.8561E−02	4.0022E−01
27	3.9539E−02	1.1015E+00	4.1588E−02	5.7351E−01	4.3054E−02	4.8104E−01	4.5292E−02	4.0765E−01
28	3.6986E−02	1.1213E+00	3.8881E−02	5.8372E−01	4.0250E−02	4.8959E−01	4.2337E−02	4.1492E−01
29	3.4673E−02	1.1405E+00	3.6431E−02	5.9365E−01	3.7709E−02	4.9793E−01	3.9665E−02	4.2196E−01
30	3.2572E−02	1.1593E+00	3.4205E−02	6.0331E−01	3.5406E−02	5.0597E−01	3.7241E−02	4.2877E−01
31	3.0656E−02	1.1775E+00	3.2177E−02	6.1271E−01	3.3305E−02	5.1385E−01	3.5028E−02	4.3546E−01
32	2.8905E−02	1.1954E+00	3.0323E−02	6.2189E−01	3.1382E−02	5.2156E−01	3.3006E−02	4.4197E−01
33	2.7299E−02	1.2127E+00	2.8624E−02	6.3084E−01	2.9625E−02	5.2900E−01	3.1156E−02	4.4827E−01
34	2.5823E−02	1.2298E+00	2.7063E−02	6.3958E−01	2.8007E−02	5.3633E−01	2.9453E−02	4.5448E−01
35	2.4463E−02	1.2464E+00	2.5625E−02	6.4812E−01	2.6516E−02	5.4350E−01	2.7884E−02	4.6055E−01
36	2.3207E−02	1.2626E+00	2.4297E−02	6.5647E−01	2.5143E−02	5.5044E−01	2.6439E−02	4.6643E−01
37	2.2045E−02	1.2785E+00	2.3070E−02	6.6464E−01	2.3871E−02	5.5730E−01	2.5101E−02	4.7222E−01
38	2.0967E−02	1.2941E+00	2.1931E−02	6.7263E−01	2.2691E−02	5.6400E−01	2.3859E−02	4.7792E−01
39	1.9966E−02	1.3093E+00	2.0875E−02	6.8046E−01	2.1598E−02	5.7050E−01	2.2709E−02	4.8342E−01
40	1.9035E−02	1.3242E+00	1.9891E−02	6.8813E−01	2.0579E−02	5.7695E−01	2.1638E−02	4.8885E−01
41	1.8166E−02	1.3389E+00	1.8975E−02	6.9564E−01	1.9630E−02	5.8324E−01	2.0638E−02	4.9421E−01
42	1.7355E−02	1.3532E+00	1.8120E−02	7.0300E−01	1.8746E−02	5.8935E−01	1.9707E−02	4.9939E−01
43	1.6597E−02	1.3673E+00	1.7321E−02	7.1021E−01	1.7917E−02	5.9544E−01	1.8837E−02	5.0448E−01
44	1.5887E−02	1.3811E+00	1.6573E−02	7.1729E−01	1.7142E−02	6.0135E−01	1.8021E−02	5.0954E−01
45	1.5221E−02	1.3947E+00	1.5871E−02	7.2424E−01	1.6417E−02	6.0711E−01	1.7257E−02	5.1443E−01
46	1.4596E−02	1.4080E+00	1.5213E−02	7.3105E−01	1.5735E−02	6.1287E−01	1.6541E−02	5.1923E−01
47	1.4008E−02	1.4210E+00	1.4595E−02	7.3774E−01	1.5095E−02	6.1844E−01	1.5866E−02	5.2401E−01
48	1.3454E−02	1.4339E+00	1.4013E−02	7.4430E−01	1.4493E−02	6.2389E−01	1.5233E−02	5.2864E−01
49	1.2933E−02	1.4465E+00	1.3464E−02	7.5075E−01	1.3924E−02	6.2935E−01	1.4636E−02	5.3317E−01
50	1.2441E−02	1.4588E+00	1.2947E−02	7.5708E−01	1.3389E−02	6.3460E−01	1.4073E−02	5.3769E−01
51	1.1976E−02	1.4710E+00	1.2459E−02	7.6330E−01	1.2884E−02	6.3978E−01	1.3541E−02	5.4209E−01
52	1.1536E−02	1.4830E+00	1.1997E−02	7.6942E−01	1.2406E−02	6.4496E−01	1.3039E−02	5.4638E−01
53	1.1120E−02	1.4947E+00	1.1561E−02	7.7543E−01	1.1954E−02	6.4993E−01	1.2563E−02	5.5067E−01
54	1.0726E−02	1.5063E+00	1.1147E−02	7.8133E−01	1.1527E−02	6.5486E−01	1.2113E−02	5.5486E−01
55	1.0352E−02	1.5177E+00	1.0755E−02	7.8714E−01	1.1120E−02	6.5978E−01	1.1688E−02	5.5892E−01
56	9.9977E−03	1.5288E+00	1.0384E−02	7.9286E−01	1.0736E−02	6.6450E−01	1.1282E−02	5.6299E−01
57	9.6607E−03	1.5398E+00	1.0031E−02	7.9847E−01	1.0371E−02	6.6921E−01	1.0898E−02	5.6700E−01
58	9.3404E−03	1.5507E+00	9.6952E−03	8.0400E−01	1.0023E−02	6.7387E−01	1.0534E−02	5.7085E−01
59	9.0356E−03	1.5613E+00	9.3762E−03	8.0944E−01	9.6947E−03	6.7829E−01	1.0187E−02	5.7468E−01
60	8.7453E−03	1.5719E+00	9.0724E−03	8.1480E−01	9.3803E−03	6.8278E−01	9.8539E−03	5.7861E−01

Table 4.3.3.1. *Partial wave elastic scattering factors for neutral atoms (cont.)*
F; $Z = 9$

	10 keV		40 keV		60 keV		90 keV	
s	$\|f(s)\|$	$\eta(s)$	$\|f(s)\|$	$\eta(s)$	$\|f(s)\|$	$\eta(s)$	$\|f(s)\|$	$\eta(s)$
0	1.8023E+00	1.6411E−01	1.9323E+00	8.7053E−02	2.0022E+00	7.3216E−02	2.0984E+00	6.2406E−02
1	1.7164E+00	1.7076E−01	1.8420E+00	9.0491E−02	1.9098E+00	7.6062E−02	2.0047E+00	6.4733E−02
2	1.5003E+00	1.9016E−01	1.6125E+00	1.0064E−01	1.6740E+00	8.4489E−02	1.7623E+00	7.1697E−02
3	1.2370E+00	2.2094E−01	1.3316E+00	1.1676E−01	1.3827E+00	9.8003E−02	1.4577E+00	8.3057E−02
4	9.8895E−01	2.6122E−01	1.0663E+00	1.3781E−01	1.1072E+00	1.1567E−01	1.1668E+00	9.8079E−02
5	7.8208E−01	3.0892E−01	8.4435E−01	1.6269E−01	8.7712E−01	1.3649E−01	9.2429E−01	1.1575E−01
6	6.1949E−01	3.6194E−01	6.6931E−01	1.9031E−01	6.9525E−01	1.5966E−01	7.3312E−01	1.3531E−01
7	4.9500E−01	4.1823E−01	5.3482E−01	2.1960E−01	5.5551E−01	1.8422E−01	5.8563E−01	1.5616E−01
8	4.0042E−01	4.7594E−01	4.3234E−01	2.4963E−01	4.4912E−01	2.0935E−01	4.7327E−01	1.7752E−01
9	3.2842E−01	5.3352E−01	3.5412E−01	2.7960E−01	3.6776E−01	2.3449E−01	3.8768E−01	1.9874E−01
10	2.7314E−01	5.8974E−01	2.9397E−01	3.0888E−01	3.0520E−01	2.5907E−01	3.2172E−01	2.1954E−01
11	2.3010E−01	6.4374E−01	2.4713E−01	3.3703E−01	2.5652E−01	2.8266E−01	2.7032E−01	2.3956E−01
12	1.9645E−01	6.9511E−01	2.1051E−01	3.6382E−01	2.1846E−01	3.0510E−01	2.3017E−01	2.5859E−01
13	1.6965E−01	7.4354E−01	1.8139E−01	3.8908E−01	1.8820E−01	3.2627E−01	1.9825E−01	2.7654E−01
14	1.4799E−01	7.8898E−01	1.5790E−01	4.1278E−01	1.6379E−01	3.4611E−01	1.7249E−01	2.9341E−01
15	1.3029E−01	8.3153E−01	1.3873E−01	4.3496E−01	1.4388E−01	3.6472E−01	1.5149E−01	3.0917E−01
16	1.1564E−01	8.7138E−01	1.2292E−01	4.5571E−01	1.2744E−01	3.8213E−01	1.3419E−01	3.2388E−01
17	1.0340E−01	9.0873E−01	1.0973E−01	4.7514E−01	1.1376E−01	3.9838E−01	1.1975E−01	3.3769E−01
18	9.3051E−02	9.4383E−01	9.8614E−02	4.9337E−01	1.0222E−01	4.1366E−01	1.0758E−01	3.5067E−01
19	8.4230E−02	9.7690E−01	8.9156E−02	5.1054E−01	9.2392E−02	4.2808E−01	9.7247E−02	3.6283E−01
20	7.6644E−02	1.0082E+00	8.1038E−02	5.2675E−01	8.3973E−02	4.4162E−01	8.8378E−02	3.7432E−01
21	7.0069E−02	1.0378E+00	7.4014E−02	5.4210E−01	7.6690E−02	4.5447E−01	8.0697E−02	3.8525E−01
22	6.4330E−02	1.0661E+00	6.7893E−02	5.5671E−01	7.0335E−02	4.6675E−01	7.4009E−02	3.9561E−01
23	5.9289E−02	1.0930E+00	6.2522E−02	5.7064E−01	6.4766E−02	4.7840E−01	6.8149E−02	4.0546E−01
24	5.4833E−02	1.1189E+00	5.7780E−02	5.8398E−01	5.9853E−02	4.8953E−01	6.2970E−02	4.1494E−01
25	5.0874E−02	1.1437E+00	5.3571E−02	5.9679E−01	5.5484E−02	5.0030E−01	5.8371E−02	4.2404E−01
26	4.7338E−02	1.1676E+00	4.9814E−02	6.0911E−01	5.1589E−02	5.1062E−01	5.4275E−02	4.3275E−01
27	4.4166E−02	1.1907E+00	4.6447E−02	6.2101E−01	4.8103E−02	5.2053E−01	5.0601E−02	4.4118E−01
28	4.1308E−02	1.2130E+00	4.3414E−02	6.3251E−01	4.4957E−02	5.3020E−01	4.7289E−02	4.4936E−01
29	3.8723E−02	1.2347E+00	4.0673E−02	6.4366E−01	4.2113E−02	5.3955E−01	4.4298E−02	4.5726E−01
30	3.6377E−02	1.2557E+00	3.8186E−02	6.5447E−01	3.9539E−02	5.4854E−01	4.1587E−02	4.6489E−01
31	3.4240E−02	1.2761E+00	3.5922E−02	6.6499E−01	3.7192E−02	5.5737E−01	3.9116E−02	4.7236E−01
32	3.2288E−02	1.2960E+00	3.3854E−02	6.7522E−01	3.5046E−02	5.6597E−01	3.6859E−02	4.7964E−01
33	3.0499E−02	1.3154E+00	3.1961E−02	6.8519E−01	3.3087E−02	5.7426E−01	3.4795E−02	4.8667E−01
34	2.8856E−02	1.3344E+00	3.0222E−02	6.9491E−01	3.1285E−02	5.8240E−01	3.2899E−02	4.9355E−01
35	2.7343E−02	1.3529E+00	2.8621E−02	7.0441E−01	2.9623E−02	5.9040E−01	3.1151E−02	5.0031E−01
36	2.5946E−02	1.3709E+00	2.7144E−02	7.1368E−01	2.8094E−02	5.9811E−01	2.9541E−02	5.0687E−01
37	2.4653E−02	1.3886E+00	2.5777E−02	7.2275E−01	2.6679E−02	6.0567E−01	2.8052E−02	5.1327E−01
38	2.3455E−02	1.4059E+00	2.4511E−02	7.3162E−01	2.5365E−02	6.1317E−01	2.6671E−02	5.1957E−01
39	2.2342E−02	1.4229E+00	2.3336E−02	7.4030E−01	2.4148E−02	6.2040E−01	2.5388E−02	5.2573E−01
40	2.1307E−02	1.4395E+00	2.2242E−02	7.4880E−01	2.3017E−02	6.2746E−01	2.4197E−02	5.3173E−01
41	2.0341E−02	1.4557E+00	2.1223E−02	7.5714E−01	2.1959E−02	6.3451E−01	2.3087E−02	5.3763E−01
42	1.9439E−02	1.4717E+00	2.0272E−02	7.6530E−01	2.0973E−02	6.4133E−01	2.2048E−02	5.4344E−01
43	1.8596E−02	1.4873E+00	1.9382E−02	7.7331E−01	2.0054E−02	6.4796E−01	2.1080E−02	5.4910E−01
44	1.7806E−02	1.5027E+00	1.8550E−02	7.8117E−01	1.9190E−02	6.5459E−01	2.0173E−02	5.5463E−01
45	1.7066E−02	1.5178E+00	1.7769E−02	7.8888E−01	1.8381E−02	6.6106E−01	1.9322E−02	5.6011E−01
46	1.6370E−02	1.5326E+00	1.7036E−02	7.9644E−01	1.7624E−02	6.6731E−01	1.8523E−02	5.6548E−01
47	1.5716E−02	1.5471E+00	1.6348E−02	8.0387E−01	1.6910E−02	6.7357E−01	1.7773E−02	5.7071E−01
48	1.5100E−02	1.5614E+00	1.5699E−02	8.1117E−01	1.6237E−02	6.7972E−01	1.7067E−02	5.7588E−01
49	1.4519E−02	1.5755E+00	1.5089E−02	8.1834E−01	1.5606E−02	6.8563E−01	1.6401E−02	5.8098E−01
50	1.3971E−02	1.5893E+00	1.4512E−02	8.2538E−01	1.5009E−02	6.9154E−01	1.5774E−02	5.8595E−01
51	1.3453E−02	1.6028E+00	1.3968E−02	8.3231E−01	1.4445E−02	6.9740E−01	1.5181E−02	5.9083E−01
52	1.2963E−02	1.6162E+00	1.3454E−02	8.3912E−01	1.3913E−02	7.0301E−01	1.4620E−02	5.9567E−01
53	1.2499E−02	1.6293E+00	1.2967E−02	8.4580E−01	1.3409E−02	7.0860E−01	1.4090E−02	6.0041E−01
54	1.2059E−02	1.6422E+00	1.2506E−02	8.5238E−01	1.2931E−02	7.1419E−01	1.3589E−02	6.0504E−01
55	1.1643E−02	1.6549E+00	1.2068E−02	8.5886E−01	1.2479E−02	7.1954E−01	1.3112E−02	6.0963E−01
56	1.1247E−02	1.6675E+00	1.1653E−02	8.6524E−01	1.2050E−02	7.2483E−01	1.2660E−02	6.1416E−01
57	1.0870E−02	1.6798E+00	1.1259E−02	8.7150E−01	1.1640E−02	7.3017E−01	1.2231E−02	6.1858E−01
58	1.0513E−02	1.6919E+00	1.0885E−02	8.7767E−01	1.1253E−02	7.3528E−01	1.1824E−02	6.2292E−01
59	1.0172E−02	1.7038E+00	1.0528E−02	8.8375E−01	1.0886E−02	7.4020E−01	1.1435E−02	6.2726E−01
60	9.8480E−03	1.7156E+00	1.0189E−02	8.8974E−01	1.0532E−02	7.4543E−01	1.1066E−02	6.3151E−01

Table 4.3.3.1. *Partial wave elastic scattering factors for neutral atoms (cont.)*
Ne; $Z = 10$

	10 keV		40 keV		60 keV		90 keV	
s	$\|f(s)\|$	$\eta(s)$	$\|f(s)\|$	$\eta(s)$	$\|f(s)\|$	$\eta(s)$	$\|f(s)\|$	$\eta(s)$
0	1.6416E+00	1.8367E−01	1.7500E+00	9.8299E−02	1.8315E+00	8.2346E−02	1.9202E+00	7.0210E−02
1	1.5766E+00	1.8982E−01	1.6841E+00	1.0140E−01	1.7616E+00	8.4983E−02	1.8494E+00	7.2364E−02
2	1.4086E+00	2.0785E−01	1.5114E+00	1.1057E−01	1.5783E+00	9.2804E−02	1.6616E+00	7.8813E−02
3	1.1946E+00	2.3660E−01	1.2873E+00	1.2537E−01	1.3414E+00	1.0543E−01	1.4147E+00	8.9387E−02
4	9.8264E−01	2.7450E−01	1.0625E+00	1.4501E−01	1.1054E+00	1.2210E−01	1.1656E+00	1.0354E−01
5	7.9732E−01	3.1983E−01	8.6405E−01	1.6857E−01	8.9880E−01	1.4193E−01	9.4736E−01	1.2041E−01
6	6.4543E−01	3.7084E−01	7.0032E−01	1.9512E−01	7.2862E−01	1.6420E−01	7.6840E−01	1.3924E−01
7	5.2482E−01	4.2582E−01	5.6975E−01	2.2373E−01	5.9271E−01	1.8823E−01	6.2533E−01	1.5954E−01
8	4.3037E−01	4.8318E−01	4.6714E−01	2.5354E−01	4.8598E−01	2.1322E−01	5.1245E−01	1.8081E−01
9	3.5663E−01	5.4148E−01	3.8675E−01	2.8383E−01	4.0238E−01	2.3859E−01	4.2418E−01	2.0235E−01
10	2.9884E−01	5.9953E−01	3.2361E−01	3.1400E−01	3.3655E−01	2.6394E−01	3.5494E−01	2.2373E−01
11	2.5314E−01	6.5635E−01	2.7359E−01	3.4355E−01	2.8444E−01	2.8874E−01	2.9994E−01	2.4477E−01
12	2.1690E−01	7.1135E−01	2.3388E−01	3.7219E−01	2.4311E−01	3.1274E−01	2.5622E−01	2.6520E−01
13	1.8777E−01	7.6404E−01	2.0195E−01	3.9964E−01	2.0985E−01	3.3580E−01	2.2113E−01	2.8470E−01
14	1.6404E−01	8.1416E−01	1.7597E−01	4.2578E−01	1.8279E−01	3.5776E−01	1.9263E−01	3.0323E−01
15	1.4453E−01	8.6164E−01	1.5466E−01	4.5054E−01	1.6061E−01	3.7850E−01	1.6922E−01	3.2086E−01
16	1.2833E−01	9.0650E−01	1.3700E−01	4.7393E−01	1.4225E−01	3.9808E−01	1.4980E−01	3.3755E−01
17	1.1475E−01	9.4884E−01	1.2222E−01	4.9600E−01	1.2687E−01	4.1663E−01	1.3360E−01	3.5319E−01
18	1.0325E−01	9.8881E−01	1.0975E−01	5.1680E−01	1.1390E−01	4.3409E−01	1.1995E−01	3.6791E−01
19	9.3428E−02	1.0266E+00	9.9136E−02	5.3644E−01	1.0287E−01	4.5049E−01	1.0830E−01	3.8191E−01
20	8.4979E−02	1.0623E+00	9.0026E−02	5.5499E−01	9.3402E−02	4.6606E−01	9.8298E−02	3.9517E−01
21	7.7655E−02	1.0963E+00	8.2148E−02	5.7257E−01	8.5204E−02	4.8086E−01	8.9682E−02	4.0760E−01
22	7.1262E−02	1.1285E+00	7.5289E−02	5.8926E−01	7.8080E−02	4.9482E−01	8.2187E−02	4.1939E−01
23	6.5648E−02	1.1593E+00	6.9278E−02	6.0515E−01	7.1844E−02	5.0809E−01	7.5597E−02	4.3074E−01
24	6.0690E−02	1.1887E+00	6.3979E−02	6.2032E−01	6.6334E−02	5.2087E−01	6.9788E−02	4.4159E−01
25	5.6287E−02	1.2168E+00	5.9281E−02	6.3484E−01	6.1451E−02	5.3308E−01	6.4659E−02	4.5182E−01
26	5.2358E−02	1.2439E+00	5.5095E−02	6.4877E−01	5.7112E−02	5.4468E−01	6.0092E−02	4.6164E−01
27	4.8837E−02	1.2699E+00	5.1347E−02	6.6218E−01	5.3223E−02	5.5590E−01	5.5986E−02	4.7124E−01
28	4.5667E−02	1.2951E+00	4.7977E−02	6.7509E−01	4.9718E−02	5.6682E−01	5.2295E−02	4.8048E−01
29	4.2802E−02	1.3193E+00	4.4934E−02	6.8758E−01	4.6561E−02	5.7725E−01	4.8979E−02	4.8924E−01
30	4.0205E−02	1.3429E+00	4.2176E−02	6.9966E−01	4.3706E−02	5.8729E−01	4.5974E−02	4.9774E−01
31	3.7840E−02	1.3657E+00	3.9669E−02	7.1137E−01	4.1101E−02	5.9717E−01	4.3227E−02	5.0615E−01
32	3.5682E−02	1.3879E+00	3.7381E−02	7.2275E−01	3.8724E−02	6.0675E−01	4.0723E−02	5.1428E−01
33	3.3706E−02	1.4094E+00	3.5288E−02	7.3381E−01	3.6557E−02	6.1592E−01	3.8445E−02	5.2202E−01
34	3.1892E−02	1.4304E+00	3.3367E−02	7.4458E−01	3.4567E−02	6.2492E−01	3.6353E−02	5.2958E−01
35	3.0222E−02	1.4509E+00	3.1600E−02	7.5508E−01	3.2729E−02	6.3381E−01	3.4417E−02	5.3714E−01
36	2.8682E−02	1.4709E+00	2.9970E−02	7.6532E−01	3.1039E−02	6.4237E−01	3.2634E−02	5.4447E−01
37	2.7257E−02	1.4905E+00	2.8464E−02	7.7532E−01	2.9481E−02	6.5064E−01	3.0996E−02	5.5143E−01
38	2.5937E−02	1.5096E+00	2.7068E−02	7.8510E−01	2.8032E−02	6.5888E−01	2.9477E−02	5.5829E−01
39	2.4711E−02	1.5283E+00	2.5773E−02	7.9466E−01	2.6686E−02	6.6697E−01	2.8057E−02	5.6520E−01
40	2.3570E−02	1.5466E+00	2.4568E−02	8.0402E−01	2.5440E−02	6.7471E−01	2.6740E−02	5.7189E−01
41	2.2507E−02	1.5645E+00	2.3446E−02	8.1319E−01	2.4278E−02	6.8233E−01	2.5521E−02	5.7824E−01
42	2.1514E−02	1.5821E+00	2.2399E−02	8.2217E−01	2.3189E−02	6.8997E−01	2.4381E−02	5.8455E−01
43	2.0586E−02	1.5994E+00	2.1419E−02	8.3097E−01	2.2174E−02	6.9733E−01	2.3308E−02	5.9092E−01
44	1.9717E−02	1.6163E+00	2.0503E−02	8.3961E−01	2.1227E−02	7.0443E−01	2.2306E−02	5.9710E−01
45	1.8902E−02	1.6329E+00	1.9644E−02	8.4808E−01	2.0335E−02	7.1158E−01	2.1374E−02	6.0295E−01
46	1.8136E−02	1.6492E+00	1.8837E−02	8.5639E−01	1.9496E−02	7.1864E−01	2.0496E−02	6.0878E−01
47	1.7415E−02	1.6652E+00	1.8079E−02	8.6456E−01	1.8712E−02	7.2537E−01	1.9664E−02	6.1472E−01
48	1.6737E−02	1.6810E+00	1.7365E−02	8.7258E−01	1.7974E−02	7.3202E−01	1.8885E−02	6.2045E−01
49	1.6098E−02	1.6965E+00	1.6692E−02	8.8046E−01	1.7274E−02	7.3874E−01	1.8156E−02	6.2586E−01
50	1.5494E−02	1.7117E+00	1.6058E−02	8.8820E−01	1.6616E−02	7.4523E−01	1.7465E−02	6.3130E−01
51	1.4924E−02	1.7266E+00	1.5458E−02	8.9582E−01	1.5998E−02	7.5146E−01	1.6808E−02	6.3686E−01
52	1.4384E−02	1.7414E+00	1.4891E−02	9.0330E−01	1.5410E−02	7.5778E−01	1.6189E−02	6.4220E−01
53	1.3873E−02	1.7558E+00	1.4355E−02	9.1067E−01	1.4852E−02	7.6406E−01	1.5608E−02	6.4723E−01
54	1.3389E−02	1.7701E+00	1.3847E−02	9.1791E−01	1.4327E−02	7.7001E−01	1.5055E−02	6.5232E−01
55	1.2929E−02	1.7841E+00	1.3365E−02	9.2504E−01	1.3829E−02	7.7589E−01	1.4526E−02	6.5756E−01
56	1.2493E−02	1.7980E+00	1.2908E−02	9.3206E−01	1.3353E−02	7.8191E−01	1.4028E−02	6.6254E−01
57	1.2078E−02	1.8116E+00	1.2473E−02	9.3897E−01	1.2903E−02	7.8770E−01	1.3557E−02	6.6723E−01
58	1.1683E−02	1.8250E+00	1.2060E−02	9.4577E−01	1.2477E−02	7.9322E−01	1.3108E−02	6.7203E−01
59	1.1308E−02	1.8382E+00	1.1667E−02	9.5247E−01	1.2069E−02	7.9882E−01	1.2676E−02	6.7700E−01
60	1.0950E−02	1.8512E+00	1.1292E−02	9.5906E−01	1.1678E−02	8.0465E−01	1.2267E−02	6.8173E−01

Table 4.3.3.1. *Partial wave elastic scattering factors for neutral atoms (cont.)*
Na; $Z = 11$

	10 keV		40 keV		60 keV		90 keV	
s	$\|f(s)\|$	$\eta(s)$	$\|f(s)\|$	$\eta(s)$	$\|f(s)\|$	$\eta(s)$	$\|f(s)\|$	$\eta(s)$
0	4.7823E+00	9.9384E−02	5.1198E+00	5.3502E−02	5.3083E+00	4.5039E−02	5.5741E+00	3.8348E−02
1	3.4260E+00	1.3450E−01	3.6809E+00	7.2184E−02	3.8196E+00	6.0722E−02	4.0180E+00	5.1618E−02
2	1.9625E+00	2.1863E−01	2.1215E+00	1.1663E−01	2.2038E+00	9.8007E−02	2.3226E+00	8.3181E−02
3	1.3298E+00	2.9721E−01	1.4427E+00	1.5792E−01	1.4994E+00	1.3265E−01	1.5810E+00	1.1255E−01
4	1.0167E+00	3.5796E−01	1.1057E+00	1.8976E−01	1.1495E+00	1.5935E−01	1.2123E+00	1.3519E−01
5	8.1364E−01	4.1211E−01	8.8654E−01	2.1809E−01	9.2185E−01	1.8310E−01	9.7242E−01	1.5532E−01
6	6.6281E−01	4.6596E−01	7.2329E−01	2.4619E−01	7.5222E−01	2.0666E−01	7.9358E−01	1.7529E−01
7	5.4547E−01	5.2136E−01	5.9581E−01	2.7505E−01	6.1971E−01	2.3085E−01	6.5384E−01	1.9579E−01
8	4.5282E−01	5.7840E−01	4.9477E−01	3.0474E−01	5.1463E−01	2.5573E−01	5.4299E−01	2.1687E−01
9	3.7923E−01	6.3655E−01	4.1421E−01	3.3498E−01	4.3082E−01	2.8108E−01	4.5455E−01	2.3835E−01
10	3.2049E−01	6.9509E−01	3.4969E−01	3.6543E−01	3.6367E−01	3.0659E−01	3.8366E−01	2.5998E−01
11	2.7332E−01	7.5314E−01	2.9774E−01	3.9564E−01	3.0958E−01	3.3191E−01	3.2656E−01	2.8143E−01
12	2.3532E−01	8.1020E−01	2.5580E−01	4.2535E−01	2.6591E−01	3.5681E−01	2.8045E−01	3.0254E−01
13	2.0442E−01	8.6564E−01	2.2166E−01	4.5425E−01	2.3036E−01	3.8104E−01	2.4290E−01	3.2307E−01
14	1.7904E−01	9.1910E−01	1.9362E−01	4.8214E−01	2.0116E−01	4.0442E−01	2.1207E−01	3.4289E−01
15	1.5803E−01	9.7036E−01	1.7043E−01	5.0890E−01	1.7701E−01	4.2685E−01	1.8657E−01	3.6191E−01
16	1.4049E−01	1.0193E+00	1.5109E−01	5.3445E−01	1.5688E−01	4.4828E−01	1.6532E−01	3.8007E−01
17	1.2572E−01	1.0659E+00	1.3484E−01	5.5879E−01	1.3996E−01	4.6868E−01	1.4746E−01	3.9737E−01
18	1.1317E−01	1.1102E+00	1.2108E−01	5.8191E−01	1.2564E−01	4.8806E−01	1.3235E−01	4.1380E−01
19	1.0244E−01	1.1523E+00	1.0934E−01	6.0386E−01	1.1342E−01	5.0646E−01	1.1945E−01	4.2940E−01
20	9.3180E−02	1.1924E+00	9.9242E−02	6.2470E−01	1.0293E−01	5.2393E−01	1.0838E−01	4.4420E−01
21	8.5147E−02	1.2304E+00	9.0507E−02	6.4449E−01	9.3844E−02	5.4052E−01	9.8803E−02	4.5826E−01
22	7.8130E−02	1.2667E+00	8.2899E−02	6.6332E−01	8.5938E−02	5.5629E−01	9.0466E−02	4.7163E−01
23	7.1965E−02	1.3012E+00	7.6232E−02	6.8125E−01	7.9012E−02	5.7131E−01	8.3164E−02	4.8436E−01
24	6.6517E−02	1.3343E+00	7.0357E−02	6.9836E−01	7.2911E−02	5.8565E−01	7.6733E−02	4.9650E−01
25	6.1680E−02	1.3659E+00	6.5153E−02	7.1472E−01	6.7507E−02	5.9935E−01	7.1039E−02	5.0811E−01
26	5.7364E−02	1.3962E+00	6.0519E−02	7.3038E−01	6.2698E−02	6.1247E−01	6.5971E−02	5.1922E−01
27	5.3496E−02	1.4254E+00	5.6375E−02	7.4543E−01	5.8396E−02	6.2506E−01	6.1440E−02	5.2989E−01
28	5.0015E−02	1.4535E+00	5.2652E−02	7.5990E−01	5.4534E−02	6.3717E−01	5.7371E−02	5.4015E−01
29	4.6871E−02	1.4806E+00	4.9294E−02	7.7384E−01	5.1050E−02	6.4885E−01	5.3702E−02	5.5003E−01
30	4.4021E−02	1.5067E+00	4.6254E−02	7.8731E−01	4.7897E−02	6.6012E−01	5.0382E−02	5.5958E−01
31	4.1428E−02	1.5321E+00	4.3492E−02	8.0033E−01	4.5033E−02	6.7102E−01	4.7366E−02	5.6880E−01
32	3.9063E−02	1.5567E+00	4.0975E−02	8.1295E−01	4.2423E−02	6.8158E−01	4.4618E−02	5.7774E−01
33	3.6898E−02	1.5806E+00	3.8674E−02	8.2520E−01	4.0037E−02	6.9182E−01	4.2106E−02	5.8642E−01
34	3.4912E−02	1.6038E+00	3.6564E−02	8.3710E−01	3.7850E−02	7.0178E−01	3.9803E−02	5.9485E−01
35	3.3084E−02	1.6264E+00	3.4624E−02	8.4867E−01	3.5839E−02	7.1146E−01	3.7687E−02	6.0304E−01
36	3.1399E−02	1.6484E+00	3.2837E−02	8.5995E−01	3.3986E−02	7.2090E−01	3.5736E−02	6.1103E−01
37	2.9841E−02	1.6699E+00	3.1185E−02	8.7095E−01	3.2274E−02	7.3010E−01	3.3935E−02	6.1882E−01
38	2.8398E−02	1.6909E+00	2.9657E−02	8.8168E−01	3.0690E−02	7.3907E−01	3.2267E−02	6.2642E−01
39	2.7059E−02	1.7114E+00	2.8238E−02	8.9217E−01	2.9220E−02	7.4785E−01	3.0720E−02	6.3384E−01
40	2.5813E−02	1.7315E+00	2.6920E−02	9.0242E−01	2.7853E−02	7.5642E−01	2.9282E−02	6.4110E−01
41	2.4652E−02	1.7511E+00	2.5691E−02	9.1245E−01	2.6581E−02	7.6481E−01	2.7943E−02	6.4820E−01
42	2.3568E−02	1.7703E+00	2.4546E−02	9.2228E−01	2.5394E−02	7.7303E−01	2.6693E−02	6.5515E−01
43	2.2555E−02	1.7892E+00	2.3475E−02	9.3190E−01	2.4285E−02	7.8108E−01	2.5526E−02	6.6196E−01
44	2.1607E−02	1.8077E+00	2.2473E−02	9.4134E−01	2.3246E−02	7.8896E−01	2.4434E−02	6.6864E−01
45	2.0717E−02	1.8259E+00	2.1534E−02	9.5059E−01	2.2273E−02	7.9670E−01	2.3410E−02	6.7518E−01
46	1.9882E−02	1.8437E+00	2.0652E−02	9.5967E−01	2.1360E−02	8.0429E−01	2.2449E−02	6.8160E−01
47	1.9096E−02	1.8612E+00	1.9823E−02	9.6858E−01	2.0501E−02	8.1174E−01	2.1546E−02	6.8791E−01
48	1.8356E−02	1.8784E+00	1.9043E−02	9.7734E−01	1.9693E−02	8.1906E−01	2.0696E−02	6.9410E−01
49	1.7659E−02	1.8953E+00	1.8308E−02	9.8594E−01	1.8932E−02	8.2625E−01	1.9895E−02	7.0019E−01
50	1.7000E−02	1.9119E+00	1.7615E−02	9.9439E−01	1.8214E−02	8.3332E−01	1.9139E−02	7.0616E−01
51	1.6378E−02	1.9283E+00	1.6960E−02	1.0027E+00	1.7536E−02	8.4026E−01	1.8425E−02	7.1204E−01
52	1.5790E−02	1.9444E+00	1.6340E−02	1.0109E+00	1.6894E−02	8.4709E−01	1.7751E−02	7.1781E−01
53	1.5232E−02	1.9602E+00	1.5754E−02	1.0189E+00	1.6287E−02	8.5380E−01	1.7112E−02	7.2350E−01
54	1.4704E−02	1.9757E+00	1.5199E−02	1.0268E+00	1.5712E−02	8.6041E−01	1.6507E−02	7.2909E−01
55	1.4202E−02	1.9911E+00	1.4672E−02	1.0346E+00	1.5166E−02	8.6692E−01	1.5933E−02	7.3459E−01
56	1.3726E−02	2.0062E+00	1.4172E−02	1.0423E+00	1.4649E−02	8.7332E−01	1.5389E−02	7.4000E−01
57	1.3274E−02	2.0211E+00	1.3697E−02	1.0498E+00	1.4157E−02	8.7962E−01	1.4872E−02	7.4533E−01
58	1.2843E−02	2.0357E+00	1.3245E−02	1.0572E+00	1.3689E−02	8.8583E−01	1.4380E−02	7.5059E−01
59	1.2433E−02	2.0502E+00	1.2815E−02	1.0646E+00	1.3244E−02	8.9194E−01	1.3912E−02	7.5576E−01
60	1.2042E−02	2.0644E+00	1.2406E−02	1.0718E+00	1.2820E−02	8.9796E−01	1.3466E−02	7.6084E−01

Table 4.3.3.1. *Partial wave elastic scattering factors for neutral atoms (cont.)*
Mg; $Z = 12$

	10 keV		40 keV		60 keV		90 keV	
s	$\|f(s)\|$	$\eta(s)$	$\|f(s)\|$	$\eta(s)$	$\|f(s)\|$	$\eta(s)$	$\|f(s)\|$	$\eta(s)$
0	5.1990E+00	1.1836E−01	5.5799E+00	6.3908E−02	5.7880E+00	5.3816E−02	6.0792E+00	4.5838E−02
1	4.0878E+00	1.4577E−01	4.4006E+00	7.8538E−02	4.5679E+00	6.6096E−02	4.8079E+00	5.6191E−02
2	2.4698E+00	2.2243E−01	2.6760E+00	1.1921E−01	2.7807E+00	1.0024E−01	2.9317E+00	8.5105E−02
3	1.5529E+00	3.1959E−01	1.6913E+00	1.7043E−01	1.7586E+00	1.4322E−01	1.8547E+00	1.2157E−01
4	1.1017E+00	4.0638E−01	1.2033E+00	2.1601E−01	1.2516E+00	1.8145E−01	1.3205E+00	1.5398E−01
5	8.4946E−01	4.7758E−01	9.2971E−01	2.5331E−01	9.6728E−01	2.1274E−01	1.0209E+00	1.8047E−01
6	6.8426E−01	5.3991E−01	7.5017E−01	2.8589E−01	7.8060E−01	2.4007E−01	8.2385E−01	2.0367E−01
7	5.6388E−01	5.9897E−01	6.1899E−01	3.1671E−01	6.4419E−01	2.6590E−01	6.7986E−01	2.2559E−01
8	4.7110E−01	6.5741E−01	5.1751E−01	3.4716E−01	5.3866E−01	2.9140E−01	5.6862E−01	2.4716E−01
9	3.9760E−01	7.1608E−01	4.3683E−01	3.7768E−01	4.5469E−01	3.1697E−01	4.7999E−01	2.6883E−01
10	3.3855E−01	7.7492E−01	3.7178E−01	4.0826E−01	3.8691E−01	3.4264E−01	4.0833E−01	2.9065E−01
11	2.9058E−01	8.3370E−01	3.1874E−01	4.3882E−01	3.3166E−01	3.6825E−01	3.4996E−01	3.1237E−01
12	2.5152E−01	8.9187E−01	2.7540E−01	4.6911E−01	2.8653E−01	3.9362E−01	3.0236E−01	3.3382E−01
13	2.1941E−01	9.4903E−01	2.3971E−01	4.9889E−01	2.4934E−01	4.1857E−01	2.6309E−01	3.5495E−01
14	1.9279E−01	1.0048E+00	2.1009E−01	5.2795E−01	2.1847E−01	4.4293E−01	2.3047E−01	3.7560E−01
15	1.7060E−01	1.0588E+00	1.8538E−01	5.5615E−01	1.9271E−01	4.6657E−01	2.0325E−01	3.9564E−01
16	1.5194E−01	1.1110E+00	1.6463E−01	5.8337E−01	1.7108E−01	4.8939E−01	1.8040E−01	4.1499E−01
17	1.3616E−01	1.1611E+00	1.4709E−01	6.0953E−01	1.5280E−01	5.1133E−01	1.6108E−01	4.3359E−01
18	1.2270E−01	1.2091E+00	1.3217E−01	6.3461E−01	1.3725E−01	5.3235E−01	1.4466E−01	4.5141E−01
19	1.1115E−01	1.2550E+00	1.1938E−01	6.5858E−01	1.2394E−01	5.5246E−01	1.3059E−01	4.6845E−01
20	1.0116E−01	1.2988E+00	1.0837E−01	6.8148E−01	1.1247E−01	5.7165E−01	1.1848E−01	4.8473E−01
21	9.2480E−02	1.3407E+00	9.8818E−02	7.0333E−01	1.0253E−01	5.8997E−01	1.0799E−01	5.0025E−01
22	8.4883E−02	1.3808E+00	9.0489E−02	7.2418E−01	9.3860E−02	6.0745E−01	9.8842E−02	5.1507E−01
23	7.8199E−02	1.4190E+00	8.3184E−02	7.4409E−01	8.6262E−02	6.2413E−01	9.0826E−02	5.2921E−01
24	7.2288E−02	1.4557E+00	7.6745E−02	7.6312E−01	7.9566E−02	6.4008E−01	8.3762E−02	5.4272E−01
25	6.7035E−02	1.4908E+00	7.1039E−02	7.8132E−01	7.3635E−02	6.5533E−01	7.7508E−02	5.5564E−01
26	6.2345E−02	1.5245E+00	6.5960E−02	7.9876E−01	6.8358E−02	6.6993E−01	7.1943E−02	5.6802E−01
27	5.8141E−02	1.5568E+00	6.1419E−02	8.1549E−01	6.3640E−02	6.8395E−01	6.6970E−02	5.7989E−01
28	5.4357E−02	1.5880E+00	5.7341E−02	8.3157E−01	5.9406E−02	6.9741E−01	6.2507E−02	5.9130E−01
29	5.0938E−02	1.6180E+00	5.3665E−02	8.4705E−01	5.5590E−02	7.1037E−01	5.8486E−02	6.0227E−01
30	4.7838E−02	1.6470E+00	5.0340E−02	8.6197E−01	5.2138E−02	7.2286E−01	5.4849E−02	6.1285E−01
31	4.5019E−02	1.6750E+00	4.7320E−02	8.7638E−01	4.9005E−02	7.3492E−01	5.1549E−02	6.2306E−01
32	4.2447E−02	1.7021E+00	4.4570E−02	8.9031E−01	4.6151E−02	7.4658E−01	4.8544E−02	6.3294E−01
33	4.0094E−02	1.7284E+00	4.2058E−02	9.0382E−01	4.3545E−02	7.5788E−01	4.5799E−02	6.4250E−01
34	3.7935E−02	1.7540E+00	3.9756E−02	9.1691E−01	4.1157E−02	7.6884E−01	4.3284E−02	6.5178E−01
35	3.5950E−02	1.7788E+00	3.7641E−02	9.2963E−01	3.8964E−02	7.7948E−01	4.0975E−02	6.6079E−01
36	3.4119E−02	1.8030E+00	3.5693E−02	9.4200E−01	3.6945E−02	7.8983E−01	3.8849E−02	6.6955E−01
37	3.2427E−02	1.8265E+00	3.3895E−02	9.5405E−01	3.5080E−02	7.9991E−01	3.6886E−02	6.7808E−01
38	3.0860E−02	1.8495E+00	3.2231E−02	9.6579E−01	3.3355E−02	8.0972E−01	3.5070E−02	6.8638E−01
39	2.9406E−02	1.8719E+00	3.0688E−02	9.7724E−01	3.1756E−02	8.1931E−01	3.3386E−02	6.9449E−01
40	2.8054E−02	1.8938E+00	2.9254E−02	9.8843E−01	3.0270E−02	8.2866E−01	3.1822E−02	7.0241E−01
41	2.6795E−02	1.9153E+00	2.7920E−02	9.9937E−01	2.8886E−02	8.3780E−01	3.0366E−02	7.1015E−01
42	2.5619E−02	1.9363E+00	2.6675E−02	1.0101E+00	2.7596E−02	8.4675E−01	2.9009E−02	7.1771E−01
43	2.4521E−02	1.9568E+00	2.5512E−02	1.0205E+00	2.6392E−02	8.5550E−01	2.7741E−02	7.2512E−01
44	2.3492E−02	1.9770E+00	2.4424E−02	1.0308E+00	2.5264E−02	8.6407E−01	2.6554E−02	7.3238E−01
45	2.2528E−02	1.9967E+00	2.3405E−02	1.0408E+00	2.4208E−02	8.7248E−01	2.5443E−02	7.3949E−01
46	2.1623E−02	2.0161E+00	2.2448E−02	1.0507E+00	2.3217E−02	8.8072E−01	2.4400E−02	7.4646E−01
47	2.0771E−02	2.0351E+00	2.1549E−02	1.0604E+00	2.2285E−02	8.8880E−01	2.3419E−02	7.5330E−01
48	1.9970E−02	2.0538E+00	2.0703E−02	1.0699E+00	2.1409E−02	8.9674E−01	2.2497E−02	7.6001E−01
49	1.9214E−02	2.0721E+00	1.9906E−02	1.0792E+00	2.0583E−02	9.0453E−01	2.1628E−02	7.6660E−01
50	1.8501E−02	2.0902E+00	1.9153E−02	1.0884E+00	1.9804E−02	9.1219E−01	2.0808E−02	7.7308E−01
51	1.7827E−02	2.1079E+00	1.8443E−02	1.0974E+00	1.9068E−02	9.1971E−01	2.0034E−02	7.7945E−01
52	1.7190E−02	2.1253E+00	1.7771E−02	1.1062E+00	1.8372E−02	9.2711E−01	1.9303E−02	7.8570E−01
53	1.6586E−02	2.1425E+00	1.7136E−02	1.1149E+00	1.7714E−02	9.3439E−01	1.8610E−02	7.9186E−01
54	1.6014E−02	2.1594E+00	1.6533E−02	1.1235E+00	1.7090E−02	9.4155E−01	1.7954E−02	7.9791E−01
55	1.5471E−02	2.1761E+00	1.5962E−02	1.1319E+00	1.6499E−02	9.4859E−01	1.7332E−02	8.0387E−01
56	1.4955E−02	2.1925E+00	1.5420E−02	1.1402E+00	1.5937E−02	9.5552E−01	1.6741E−02	8.0974E−01
57	1.4465E−02	2.2086E+00	1.4905E−02	1.1484E+00	1.5404E−02	9.6235E−01	1.6180E−02	8.1551E−01
58	1.3999E−02	2.2245E+00	1.4415E−02	1.1564E+00	1.4897E−02	9.6907E−01	1.5647E−02	8.2119E−01
59	1.3554E−02	2.2402E+00	1.3949E−02	1.1644E+00	1.4414E−02	9.7569E−01	1.5139E−02	8.2679E−01
60	1.3131E−02	2.2557E+00	1.3505E−02	1.1722E+00	1.3954E−02	9.8222E−01	1.4655E−02	8.3235E−01

Table 4.3.3.1. *Partial wave elastic scattering factors for neutral atoms (cont.)*
Al; $Z = 13$

	10 keV		40 keV		60 keV		90 keV	
s	$\|f(s)\|$	$\eta(s)$	$\|f(s)\|$	$\eta(s)$	$\|f(s)\|$	$\eta(s)$	$\|f(s)\|$	$\eta(s)$
0	5.8588E+00	1.3210E−01	6.3025E+00	7.1601E−02	6.5403E+00	6.0318E−02	6.8747E+00	5.1372E−02
1	4.6839E+00	1.5975E−01	5.0545E+00	8.6406E−02	5.2486E+00	7.2754E−02	5.5260E+00	6.1871E−02
2	2.8993E+00	2.3638E−01	3.1505E+00	1.2722E−01	3.2750E+00	1.0703E−01	3.4536E+00	9.0908E−02
3	1.7944E+00	3.4084E−01	1.9621E+00	1.8246E−01	2.0413E+00	1.5340E−01	2.1539E+00	1.3024E−01
4	1.2198E+00	4.4565E−01	1.3385E+00	2.3762E−01	1.3932E+00	1.9968E−01	1.4705E+00	1.6949E−01
5	9.0675E−01	5.3577E−01	9.9701E−01	2.8493E−01	1.0379E+00	2.3937E−01	1.0957E+00	2.0316E−01
6	7.1549E−01	6.1144E−01	7.8795E−01	3.2457E−01	8.2038E−01	2.7264E−01	8.6618E−01	2.3136E−01
7	5.8495E−01	6.7819E−01	6.4509E−01	3.5947E−01	6.7174E−01	3.0191E−01	7.0934E−01	2.5616E−01
8	4.8851E−01	7.4063E−01	5.3930E−01	3.9204E−01	5.6169E−01	3.2918E−01	5.9317E−01	2.7929E−01
9	4.1370E−01	8.0125E−01	4.5698E−01	4.2360E−01	4.7600E−01	3.5562E−01	5.0268E−01	3.0170E−01
10	3.5399E−01	8.6110E−01	3.9104E−01	4.5470E−01	4.0727E−01	3.8173E−01	4.3007E−01	3.2384E−01
11	3.0538E−01	9.2064E−01	3.3713E−01	4.8566E−01	3.5110E−01	4.0766E−01	3.7073E−01	3.4583E−01
12	2.6561E−01	9.7964E−01	2.9285E−01	5.1638E−01	3.0494E−01	4.3339E−01	3.2198E−01	3.6761E−01
13	2.3268E−01	1.0380E+00	2.5607E−01	5.4673E−01	2.6659E−01	4.5882E−01	2.8146E−01	3.8916E−01
14	2.0517E−01	1.0953E+00	2.2528E−01	5.7658E−01	2.3448E−01	4.8384E−01	2.4751E−01	4.1037E−01
15	1.8206E−01	1.1513E+00	1.9939E−01	6.0579E−01	2.0747E−01	5.0833E−01	2.1895E−01	4.3112E−01
16	1.6253E−01	1.2058E+00	1.7749E−01	6.3423E−01	1.8462E−01	5.3217E−01	1.9479E−01	4.5133E−01
17	1.4592E−01	1.2586E+00	1.5886E−01	6.6180E−01	1.6518E−01	5.5528E−01	1.7424E−01	4.7093E−01
18	1.3169E−01	1.3096E+00	1.4292E−01	6.8843E−01	1.4856E−01	5.7762E−01	1.5667E−01	4.8986E−01
19	1.1943E−01	1.3586E+00	1.2922E−01	7.1409E−01	1.3426E−01	5.9913E−01	1.4156E−01	5.0810E−01
20	1.0881E−01	1.4058E+00	1.1736E−01	7.3875E−01	1.2190E−01	6.1981E−01	1.2849E−01	5.2563E−01
21	9.9546E−02	1.4511E+00	1.0705E−01	7.6242E−01	1.1116E−01	6.3965E−01	1.1714E−01	5.4246E−01
22	9.1426E−02	1.4946E+00	9.8045E−02	7.8511E−01	1.0177E−01	6.5868E−01	1.0723E−01	5.5859E−01
23	8.4269E−02	1.5363E+00	9.0132E−02	8.0686E−01	9.3529E−02	6.7692E−01	9.8521E−02	5.7405E−01
24	7.7931E−02	1.5763E+00	8.3147E−02	8.2772E−01	8.6256E−02	6.9440E−01	9.0842E−02	5.8886E−01
25	7.2292E−02	1.6148E+00	7.6953E−02	8.4771E−01	7.9809E−02	7.1115E−01	8.4037E−02	6.0307E−01
26	6.7252E−02	1.6517E+00	7.1436E−02	8.6689E−01	7.4069E−02	7.2723E−01	7.7980E−02	6.1669E−01
27	6.2730E−02	1.6873E+00	6.6501E−02	8.8531E−01	6.8937E−02	7.4266E−01	7.2565E−02	6.2977E−01
28	5.8656E−02	1.7215E+00	6.2070E−02	9.0302E−01	6.4330E−02	7.5750E−01	6.7706E−02	6.4234E−01
29	5.4974E−02	1.7544E+00	5.8076E−02	9.2007E−01	6.0179E−02	7.7178E−01	6.3329E−02	6.5443E−01
30	5.1634E−02	1.7863E+00	5.4463E−02	9.3650E−01	5.6425E−02	7.8553E−01	5.9371E−02	6.6608E−01
31	4.8595E−02	1.8170E+00	5.1183E−02	9.5235E−01	5.3019E−02	7.9880E−01	5.5781E−02	6.7732E−01
32	4.5822E−02	1.8468E+00	4.8198E−02	9.6767E−01	4.9918E−02	8.1163E−01	5.2514E−02	6.8818E−01
33	4.3284E−02	1.8757E+00	4.5471E−02	9.8249E−01	4.7088E−02	8.2403E−01	4.9531E−02	6.9869E−01
34	4.0955E−02	1.9037E+00	4.2973E−02	9.9685E−01	4.4496E−02	8.3605E−01	4.6800E−02	7.0886E−01
35	3.8813E−02	1.9308E+00	4.0680E−02	1.0108E+00	4.2116E−02	8.4770E−01	4.4294E−02	7.1873E−01
36	3.6838E−02	1.9573E+00	3.8569E−02	1.0243E+00	3.9926E−02	8.5902E−01	4.1987E−02	7.2831E−01
37	3.5013E−02	1.9830E+00	3.6621E−02	1.0375E+00	3.7906E−02	8.7003E−01	3.9859E−02	7.3762E−01
38	3.3322E−02	2.0080E+00	3.4819E−02	1.0503E+00	3.6037E−02	8.8074E−01	3.7891E−02	7.4669E−01
39	3.1754E−02	2.0325E+00	3.3149E−02	1.0628E+00	3.4305E−02	8.9118E−01	3.6068E−02	7.5552E−01
40	3.0296E−02	2.0563E+00	3.1599E−02	1.0749E+00	3.2697E−02	9.0135E−01	3.4375E−02	7.6414E−01
41	2.8937E−02	2.0796E+00	3.0155E−02	1.0868E+00	3.1201E−02	9.1129E−01	3.2800E−02	7.7255E−01
42	2.7670E−02	2.1024E+00	2.8810E−02	1.0984E+00	2.9806E−02	9.2100E−01	3.1332E−02	7.8076E−01
43	2.6486E−02	2.1247E+00	2.7554E−02	1.1098E+00	2.8504E−02	9.3050E−01	2.9961E−02	7.8879E−01
44	2.5377E−02	2.1466E+00	2.6378E−02	1.1209E+00	2.7286E−02	9.3979E−01	2.8679E−02	7.9666E−01
45	2.4338E−02	2.1680E+00	2.5278E−02	1.1318E+00	2.6145E−02	9.4888E−01	2.7478E−02	8.0435E−01
46	2.3362E−02	2.1890E+00	2.4244E−02	1.1424E+00	2.5074E−02	9.5780E−01	2.6352E−02	8.1189E−01
47	2.2445E−02	2.2096E+00	2.3274E−02	1.1529E+00	2.4069E−02	9.6654E−01	2.5293E−02	8.1929E−01
48	2.1582E−02	2.2298E+00	2.2361E−02	1.1632E+00	2.3123E−02	9.7511E−01	2.4298E−02	8.2654E−01
49	2.0768E−02	2.2496E+00	2.1501E−02	1.1732E+00	2.2232E−02	9.8353E−01	2.3360E−02	8.3366E−01
50	2.0000E−02	2.2691E+00	2.0690E−02	1.1831E+00	2.1391E−02	9.9179E−01	2.2476E−02	8.4065E−01
51	1.9274E−02	2.2883E+00	1.9924E−02	1.1928E+00	2.0598E−02	9.9991E−01	2.1641E−02	8.4751E−01
52	1.8587E−02	2.3071E+00	1.9200E−02	1.2024E+00	1.9848E−02	1.0079E+00	2.0852E−02	8.5426E−01
53	1.7937E−02	2.3257E+00	1.8514E−02	1.2118E+00	1.9138E−02	1.0157E+00	2.0105E−02	8.6090E−01
54	1.7321E−02	2.3439E+00	1.7865E−02	1.2210E+00	1.8465E−02	1.0235E+00	1.9398E−02	8.6742E−01
55	1.6737E−02	2.3619E+00	1.7249E−02	1.2301E+00	1.7828E−02	1.0310E+00	1.8727E−02	8.7384E−01
56	1.6182E−02	2.3796E+00	1.6665E−02	1.2390E+00	1.7222E−02	1.0385E+00	1.8090E−02	8.8016E−01
57	1.5654E−02	2.3970E+00	1.6109E−02	1.2478E+00	1.6647E−02	1.0459E+00	1.7485E−02	8.8638E−01
58	1.5152E−02	2.4142E+00	1.5581E−02	1.2565E+00	1.6100E−02	1.0531E+00	1.6910E−02	8.9250E−01
59	1.4673E−02	2.4311E+00	1.5079E−02	1.2651E+00	1.5580E−02	1.0602E+00	1.6363E−02	8.9853E−01
60	1.4218E−02	2.4478E+00	1.4600E−02	1.2734E+00	1.5085E−02	1.0673E+00	1.5842E−02	9.0448E−01

Table 4.3.3.1. *Partial wave elastic scattering factors for neutral atoms (cont.)*
Si; $Z = 14$

	10 keV		40 keV		60 keV		90 keV	
s	$\|f(s)\|$	$\eta(s)$	$\|f(s)\|$	$\eta(s)$	$\|f(s)\|$	$\eta(s)$	$\|f(s)\|$	$\eta(s)$
0	5.7670E+00	1.5342E−01	6.2279E+00	8.3536E−02	6.4654E+00	7.0425E−02	6.7983E+00	6.0010E−02
1	4.8204E+00	1.7816E−01	5.2205E+00	9.6834E−02	5.4236E+00	8.1585E−02	5.7124E+00	6.9415E−02
2	3.1875E+00	2.4867E−01	3.4760E+00	1.3453E−01	3.6152E+00	1.1325E−01	3.8137E+00	9.6236E−02
3	2.0207E+00	3.5156E−01	2.2195E+00	1.8911E−01	2.3103E+00	1.5910E−01	2.4388E+00	1.3513E−01
4	1.3552E+00	4.6543E−01	1.4952E+00	2.4918E−01	1.5573E+00	2.0952E−01	1.6445E+00	1.7791E−01
5	9.8182E−01	5.7164E−01	1.0853E+00	3.0509E−01	1.1307E+00	2.5643E−01	1.1942E+00	2.1770E−01
6	7.5804E−01	6.6307E−01	8.3889E−01	3.5311E−01	8.7403E−01	2.9671E−01	9.2322E−01	2.5186E−01
7	6.1157E−01	7.4140E−01	6.7753E−01	3.9414E−01	7.0598E−01	3.3113E−01	7.4578E−01	2.8105E−01
8	5.0775E−01	8.1102E−01	5.6308E−01	4.3055E−01	5.8679E−01	3.6166E−01	6.1992E−01	3.0693E−01
9	4.2953E−01	8.7578E−01	4.7675E−01	4.6432E−01	4.9689E−01	3.8996E−01	5.2497E−01	3.3092E−01
10	3.6811E−01	9.3811E−01	4.0879E−01	4.9671E−01	4.2608E−01	4.1710E−01	4.5017E−01	3.5392E−01
11	3.1849E−01	9.9907E−01	3.5366E−01	5.2841E−01	3.6861E−01	4.4366E−01	3.8945E−01	3.7643E−01
12	2.7802E−01	1.0590E+00	3.0848E−01	5.5962E−01	3.2149E−01	4.6983E−01	3.3964E−01	3.9860E−01
13	2.4442E−01	1.1183E+00	2.7084E−01	5.9046E−01	2.8221E−01	4.9567E−01	2.9812E−01	4.2050E−01
14	2.1623E−01	1.1768E+00	2.3915E−01	6.2089E−01	2.4915E−01	5.2117E−01	2.6315E−01	4.4212E−01
15	1.9242E−01	1.2343E+00	2.1234E−01	6.5082E−01	2.2115E−01	5.4626E−01	2.3354E−01	4.6338E−01
16	1.7220E−01	1.2905E+00	1.8952E−01	6.8015E−01	1.9733E−01	5.7084E−01	2.0834E−01	4.8421E−01
17	1.5492E−01	1.3454E+00	1.7000E−01	7.0877E−01	1.7694E−01	5.9484E−01	1.8677E−01	5.0456E−01
18	1.4006E−01	1.3987E+00	1.5321E−01	7.3662E−01	1.5941E−01	6.1819E−01	1.6822E−01	5.2435E−01
19	1.2721E−01	1.4504E+00	1.3870E−01	7.6363E−01	1.4426E−01	6.4083E−01	1.5220E−01	5.4355E−01
20	1.1604E−01	1.5003E+00	1.2610E−01	7.8975E−01	1.3111E−01	6.6274E−01	1.3828E−01	5.6213E−01
21	1.0627E−01	1.5485E+00	1.1511E−01	8.1497E−01	1.1964E−01	6.8389E−01	1.2615E−01	5.8006E−01
22	9.7686E−02	1.5950E+00	1.0548E−01	8.3928E−01	1.0959E−01	7.0428E−01	1.1553E−01	5.9734E−01
23	9.0108E−02	1.6398E+00	9.7002E−02	8.6268E−01	1.0074E−01	7.2390E−01	1.0617E−01	6.1398E−01
24	8.3384E−02	1.6830E+00	8.9502E−02	8.8521E−01	9.2919E−02	7.4278E−01	9.7910E−02	6.2999E−01
25	7.7393E−02	1.7245E+00	8.2842E−02	9.0687E−01	8.5977E−02	7.6095E−01	9.0575E−02	6.4539E−01
26	7.2032E−02	1.7645E+00	7.6904E−02	9.2771E−01	7.9790E−02	7.7842E−01	8.4039E−02	6.6020E−01
27	6.7216E−02	1.8031E+00	7.1587E−02	9.4777E−01	7.4253E−02	7.9523E−01	7.8192E−02	6.7444E−01
28	6.2873E−02	1.8403E+00	6.6811E−02	9.6707E−01	6.9280E−02	8.1141E−01	7.2942E−02	6.8815E−01
29	5.8944E−02	1.8762E+00	6.2503E−02	9.8568E−01	6.4797E−02	8.2699E−01	6.8211E−02	7.0136E−01
30	5.5377E−02	1.9108E+00	5.8606E−02	1.0036E+00	6.0743E−02	8.4202E−01	6.3933E−02	7.1409E−01
31	5.2130E−02	1.9444E+00	5.5068E−02	1.0209E+00	5.7064E−02	8.5652E−01	6.0052E−02	7.2638E−01
32	4.9165E−02	1.9768E+00	5.1847E−02	1.0377E+00	5.3716E−02	8.7053E−01	5.6521E−02	7.3824E−01
33	4.6449E−02	2.0082E+00	4.8906E−02	1.0538E+00	5.0660E−02	8.8408E−01	5.3299E−02	7.4972E−01
34	4.3957E−02	2.0387E+00	4.6212E−02	1.0695E+00	4.7862E−02	8.9719E−01	5.0349E−02	7.6082E−01
35	4.1663E−02	2.0683E+00	4.3740E−02	1.0847E+00	4.5294E−02	9.0990E−01	4.7642E−02	7.7159E−01
36	3.9547E−02	2.0970E+00	4.1464E−02	1.0994E+00	4.2931E−02	9.2224E−01	4.5153E−02	7.8203E−01
37	3.7592E−02	2.1250E+00	3.9364E−02	1.1138E+00	4.0752E−02	9.3422E−01	4.2856E−02	7.9217E−01
38	3.5780E−02	2.1522E+00	3.7423E−02	1.1277E+00	3.8737E−02	9.4587E−01	4.0734E−02	8.0203E−01
39	3.4099E−02	2.1788E+00	3.5624E−02	1.1412E+00	3.6871E−02	9.5720E−01	3.8768E−02	8.1163E−01
40	3.2536E−02	2.2046E+00	3.3955E−02	1.1545E+00	3.5138E−02	9.6825E−01	3.6944E−02	8.2097E−01
41	3.1080E−02	2.2299E+00	3.2401E−02	1.1673E+00	3.3527E−02	9.7902E−01	3.5247E−02	8.3009E−01
42	2.9722E−02	2.2546E+00	3.0954E−02	1.1799E+00	3.2026E−02	9.8954E−01	3.3666E−02	8.3899E−01
43	2.8452E−02	2.2788E+00	2.9602E−02	1.1922E+00	3.0625E−02	9.9980E−01	3.2191E−02	8.4768E−01
44	2.7263E−02	2.3024E+00	2.8339E−02	1.2042E+00	2.9314E−02	1.0099E+00	3.0812E−02	8.5617E−01
45	2.6149E−02	2.3255E+00	2.7155E−02	1.2160E+00	2.8088E−02	1.0197E+00	2.9520E−02	8.6448E−01
46	2.5103E−02	2.3482E+00	2.6045E−02	1.2275E+00	2.6937E−02	1.0293E+00	2.8309E−02	8.7262E−01
47	2.4120E−02	2.3704E+00	2.5002E−02	1.2387E+00	2.5856E−02	1.0387E+00	2.7172E−02	8.8059E−01
48	2.3194E−02	2.3922E+00	2.4022E−02	1.2498E+00	2.4840E−02	1.0480E+00	2.6102E−02	8.8841E−01
49	2.2322E−02	2.4136E+00	2.3098E−02	1.2606E+00	2.3883E−02	1.0570E+00	2.5095E−02	8.9607E−01
50	2.1499E−02	2.4346E+00	2.2227E−02	1.2713E+00	2.2980E−02	1.0659E+00	2.4145E−02	9.0359E−01
51	2.0721E−02	2.4553E+00	2.1405E−02	1.2817E+00	2.2128E−02	1.0746E+00	2.3248E−02	9.1097E−01
52	1.9986E−02	2.4755E+00	2.0627E−02	1.2920E+00	2.1323E−02	1.0832E+00	2.2401E−02	9.1822E−01
53	1.9289E−02	2.4955E+00	1.9892E−02	1.3021E+00	2.0561E−02	1.0916E+00	2.1600E−02	9.2535E−01
54	1.8629E−02	2.5151E+00	1.9195E−02	1.3120E+00	1.9839E−02	1.0999E+00	2.0840E−02	9.3236E−01
55	1.8003E−02	2.5345E+00	1.8535E−02	1.3218E+00	1.9155E−02	1.1081E+00	2.0120E−02	9.3925E−01
56	1.7408E−02	2.5535E+00	1.7908E−02	1.3314E+00	1.8506E−02	1.1161E+00	1.9437E−02	9.4603E−01
57	1.6843E−02	2.5722E+00	1.7312E−02	1.3408E+00	1.7889E−02	1.1240E+00	1.8788E−02	9.5270E−01
58	1.6305E−02	2.5907E+00	1.6746E−02	1.3501E+00	1.7303E−02	1.1317E+00	1.8172E−02	9.5926E−01
59	1.5793E−02	2.6088E+00	1.6207E−02	1.3593E+00	1.6744E−02	1.1394E+00	1.7585E−02	9.6573E−01
60	1.5305E−02	2.6268E+00	1.5693E−02	1.3683E+00	1.6213E−02	1.1470E+00	1.7025E−02	9.7211E−01

Table 4.3.3.1. *Partial wave elastic scattering factors for neutral atoms (cont.)*
P; $Z = 15$

	10 keV		40 keV		60 keV		90 keV	
s	$\|f(s)\|$	$\eta(s)$	$\|f(s)\|$	$\eta(s)$	$\|f(s)\|$	$\eta(s)$	$\|f(s)\|$	$\eta(s)$
0	5.4043E+00	1.7700E−01	5.8630E+00	9.6904E−02	6.0901E+00	8.1757E−02	6.4054E+00	6.9716E−02
1	4.6991E+00	1.9853E−01	5.1119E+00	1.0850E−01	5.3138E+00	9.1488E−02	5.5987E+00	7.7888E−02
2	3.3312E+00	2.6134E−01	3.6481E+00	1.4221E−01	3.7964E+00	1.1981E−01	4.0063E+00	1.0187E−01
3	2.2044E+00	3.5783E−01	2.4327E+00	1.9360E−01	2.5340E+00	1.6299E−01	2.6761E+00	1.3851E−01
4	1.4906E+00	4.7310E−01	1.6542E+00	2.5457E−01	1.7242E+00	2.1419E−01	1.8217E+00	1.8196E−01
5	1.0670E+00	5.8970E−01	1.1870E+00	3.1606E−01	1.2376E+00	2.6579E−01	1.3080E+00	2.2573E−01
6	8.1013E−01	6.9558E−01	9.0182E−01	3.7181E−01	9.4031E−01	3.1258E−01	9.9378E−01	2.6542E−01
7	6.4462E−01	7.8740E−01	7.1774E−01	4.2010E−01	7.4839E−01	3.5310E−01	7.9094E−01	2.9979E−01
8	5.3036E−01	8.6737E−01	5.9083E−01	4.6203E−01	6.1611E−01	3.8827E−01	6.5119E−01	3.2960E−01
9	4.4664E−01	9.3899E−01	4.9795E−01	4.9945E−01	5.1930E−01	4.1964E−01	5.4887E−01	3.5621E−01
10	3.8226E−01	1.0056E+00	4.2643E−01	5.3419E−01	4.4475E−01	4.4875E−01	4.7010E−01	3.8088E−01
11	3.3092E−01	1.0692E+00	3.6927E−01	5.6730E−01	3.8514E−01	4.7650E−01	4.0710E−01	4.0440E−01
12	2.8940E−01	1.1310E+00	3.2289E−01	5.9937E−01	3.3675E−01	5.0338E−01	3.5595E−01	4.2717E−01
13	2.5504E−01	1.1915E+00	2.8435E−01	6.3082E−01	2.9653E−01	5.2974E−01	3.1342E−01	4.4951E−01
14	2.2620E−01	1.2511E+00	2.5185E−01	6.6181E−01	2.6260E−01	5.5570E−01	2.7752E−01	4.7151E−01
15	2.0180E−01	1.3097E+00	2.2427E−01	6.9233E−01	2.3379E−01	5.8128E−01	2.4704E−01	4.9319E−01
16	1.8100E−01	1.3673E+00	2.0070E−01	7.2233E−01	2.0916E−01	6.0642E−01	2.2098E−01	5.1450E−01
17	1.6317E−01	1.4238E+00	1.8044E−01	7.5176E−01	1.8799E−01	6.3109E−01	1.9857E−01	5.3541E−01
18	1.4779E−01	1.4790E+00	1.6294E−01	7.8054E−01	1.6970E−01	6.5522E−01	1.7921E−01	5.5587E−01
19	1.3444E−01	1.5327E+00	1.4775E−01	8.0861E−01	1.5382E−01	6.7875E−01	1.6240E−01	5.7582E−01
20	1.2280E−01	1.5849E+00	1.3451E−01	8.3592E−01	1.3999E−01	7.0165E−01	1.4775E−01	5.9523E−01
21	1.1260E−01	1.6356E+00	1.2292E−01	8.6242E−01	1.2787E−01	7.2388E−01	1.3493E−01	6.1408E−01
22	1.0361E−01	1.6847E+00	1.1272E−01	8.8810E−01	1.1722E−01	7.4541E−01	1.2366E−01	6.3234E−01
23	9.5662E−02	1.7322E+00	1.0373E−01	9.1294E−01	1.0782E−01	7.6625E−01	1.1371E−01	6.5000E−01
24	8.8597E−02	1.7781E+00	9.5753E−02	9.3695E−01	9.9495E−02	7.8638E−01	1.0490E−01	6.6707E−01
25	8.2290E−02	1.8225E+00	8.8657E−02	9.6012E−01	9.2088E−02	8.0581E−01	9.7067E−02	6.8355E−01
26	7.6640E−02	1.8653E+00	8.2320E−02	9.8249E−01	8.5476E−02	8.2457E−01	9.0075E−02	6.9945E−01
27	7.1557E−02	1.9067E+00	7.6641E−02	1.0041E+00	7.9552E−02	8.4267E−01	8.3812E−02	7.1479E−01
28	6.6968E−02	1.9467E+00	7.1532E−02	1.0249E+00	7.4225E−02	8.6013E−01	7.8184E−02	7.2959E−01
29	6.2812E−02	1.9854E+00	6.6921E−02	1.0450E+00	6.9420E−02	8.7698E−01	7.3108E−02	7.4387E−01
30	5.9036E−02	2.0228E+00	6.2747E−02	1.0644E+00	6.5072E−02	8.9324E−01	6.8515E−02	7.5766E−01
31	5.5594E−02	2.0590E+00	5.8956E−02	1.0832E+00	6.1125E−02	9.0896E−01	6.4348E−02	7.7097E−01
32	5.2449E−02	2.0940E+00	5.5504E−02	1.1013E+00	5.7532E−02	9.2415E−01	6.0554E−02	7.8384E−01
33	4.9567E−02	2.1280E+00	5.2350E−02	1.1188E+00	5.4251E−02	9.3884E−01	5.7092E−02	7.9629E−01
34	4.6920E−02	2.1610E+00	4.9463E−02	1.1358E+00	5.1247E−02	9.5307E−01	5.3924E−02	8.0834E−01
35	4.4482E−02	2.1930E+00	4.6811E−02	1.1523E+00	4.8491E−02	9.6686E−01	5.1016E−02	8.2002E−01
36	4.2232E−02	2.2241E+00	4.4371E−02	1.1683E+00	4.5954E−02	9.8023E−01	4.8342E−02	8.3134E−01
37	4.0151E−02	2.2543E+00	4.2120E−02	1.1838E+00	4.3616E−02	9.9322E−01	4.5876E−02	8.4234E−01
38	3.8223E−02	2.2838E+00	4.0039E−02	1.1989E+00	4.1454E−02	1.0058E+00	4.3598E−02	8.5302E−01
39	3.6433E−02	2.3125E+00	3.8111E−02	1.2136E+00	3.9452E−02	1.0181E+00	4.1488E−02	8.6341E−01
40	3.4768E−02	2.3405E+00	3.6322E−02	1.2278E+00	3.7595E−02	1.0301E+00	3.9530E−02	8.7353E−01
41	3.3217E−02	2.3678E+00	3.4657E−02	1.2418E+00	3.5867E−02	1.0417E+00	3.7710E−02	8.8338E−01
42	3.1769E−02	2.3944E+00	3.3107E−02	1.2553E+00	3.4258E−02	1.0531E+00	3.6015E−02	8.9299E−01
43	3.0415E−02	2.4205E+00	3.1659E−02	1.2686E+00	3.2756E−02	1.0641E+00	3.4434E−02	9.0237E−01
44	2.9148E−02	2.4459E+00	3.0306E−02	1.2816E+00	3.1353E−02	1.0750E+00	3.2956E−02	9.1152E−01
45	2.7960E−02	2.4709E+00	2.9040E−02	1.2942E+00	3.0039E−02	1.0855E+00	3.1572E−02	9.2048E−01
46	2.6844E−02	2.4953E+00	2.7852E−02	1.3066E+00	2.8807E−02	1.0959E+00	3.0275E−02	9.2924E−01
47	2.5795E−02	2.5192E+00	2.6736E−02	1.3187E+00	2.7650E−02	1.1060E+00	2.9057E−02	9.3781E−01
48	2.4808E−02	2.5426E+00	2.5687E−02	1.3306E+00	2.6562E−02	1.1160E+00	2.7912E−02	9.4621E−01
49	2.3878E−02	2.5656E+00	2.4699E−02	1.3423E+00	2.5538E−02	1.1257E+00	2.6834E−02	9.5444E−01
50	2.3000E−02	2.5882E+00	2.3767E−02	1.3537E+00	2.4573E−02	1.1352E+00	2.5818E−02	9.6251E−01
51	2.2170E−02	2.6104E+00	2.2888E−02	1.3649E+00	2.3662E−02	1.1446E+00	2.4859E−02	9.7043E−01
52	2.1385E−02	2.6322E+00	2.2057E−02	1.3759E+00	2.2801E−02	1.1538E+00	2.3953E−02	9.7821E−01
53	2.0643E−02	2.6536E+00	2.1271E−02	1.3867E+00	2.1986E−02	1.1628E+00	2.3096E−02	9.8584E−01
54	1.9939E−02	2.6746E+00	2.0527E−02	1.3973E+00	2.1215E−02	1.1717E+00	2.2285E−02	9.9334E−01
55	1.9271E−02	2.6954E+00	1.9821E−02	1.4078E+00	2.0484E−02	1.1804E+00	2.1515E−02	1.0007E+00
56	1.8636E−02	2.7157E+00	1.9151E−02	1.4181E+00	1.9790E−02	1.1890E+00	2.0785E−02	1.0080E+00
57	1.8033E−02	2.7358E+00	1.8515E−02	1.4282E+00	1.9131E−02	1.1974E+00	2.0092E−02	1.0151E+00
58	1.7460E−02	2.7556E+00	1.7910E−02	1.4381E+00	1.8504E−02	1.2057E+00	1.9433E−02	1.0221E+00
59	1.6914E−02	2.7750E+00	1.7334E−02	1.4479E+00	1.7908E−02	1.2139E+00	1.8806E−02	1.0290E+00
60	1.6394E−02	2.7943E+00	1.6786E−02	1.4575E+00	1.7340E−02	1.2220E+00	1.8208E−02	1.0359E+00

Table 4.3.3.1. *Partial wave elastic scattering factors for neutral atoms (cont.)*
S; $Z = 16$

	10 keV		40 keV		60 keV		90 keV	
s	$\|f(s)\|$	$\eta(s)$	$\|f(s)\|$	$\eta(s)$	$\|f(s)\|$	$\eta(s)$	$\|f(s)\|$	$\eta(s)$
0	5.0445E+00	1.9983E−01	5.5003E+00	1.1006E−01	5.7166E+00	9.2940E−02	6.0148E+00	7.9309E−02
1	4.5062E+00	2.1901E−01	4.9261E+00	1.2043E−01	5.1240E+00	1.0162E−01	5.4007E+00	8.6578E−02
2	3.3751E+00	2.7550E−01	3.7136E+00	1.5086E−01	3.8669E+00	1.2720E−01	4.0828E+00	1.0821E−01
3	2.3354E+00	3.6478E−01	2.5903E+00	1.9859E−01	2.6999E+00	1.6733E−01	2.8526E+00	1.4229E−01
4	1.6115E+00	4.7690E−01	1.7993E+00	2.5809E−01	1.8770E+00	2.1731E−01	1.9843E+00	1.8470E−01
5	1.1541E+00	5.9775E−01	1.2931E+00	3.2194E−01	1.3494E+00	2.7091E−01	1.4270E+00	2.3017E−01
6	8.6808E−01	7.1423E−01	9.7316E−01	3.8340E−01	1.0157E+00	3.2250E−01	1.0741E+00	2.7395E−01
7	6.8299E−01	8.1899E−01	7.6521E−01	4.3867E−01	7.9856E−01	3.6889E−01	8.4450E−01	3.1330E−01
8	5.5679E−01	9.1077E−01	6.2350E−01	4.8699E−01	6.5066E−01	4.0943E−01	6.8801E−01	3.4771E−01
9	4.6595E−01	9.9171E−01	5.2180E−01	5.2946E−01	5.4451E−01	4.4508E−01	5.7581E−01	3.7790E−01
10	3.9738E−01	1.0649E+00	4.4520E−01	5.6770E−01	4.6461E−01	4.7711E−01	4.9129E−01	4.0510E−01
11	3.4348E−01	1.1330E+00	3.8498E−01	6.0318E−01	4.0179E−01	5.0685E−01	4.2485E−01	4.3031E−01
12	3.0042E−01	1.1976E+00	3.3678E−01	6.3679E−01	3.5148E−01	5.3503E−01	3.7169E−01	4.5417E−01
13	2.6504E−01	1.2601E+00	2.9705E−01	6.6926E−01	3.1001E−01	5.6223E−01	3.2783E−01	4.7722E−01
14	2.3542E−01	1.3212E+00	2.6366E−01	7.0098E−01	2.7513E−01	5.8881E−01	2.9093E−01	4.9973E−01
15	2.1040E−01	1.3811E+00	2.3533E−01	7.3211E−01	2.4553E−01	6.1489E−01	2.5960E−01	5.2184E−01
16	1.8907E−01	1.4399E+00	2.1108E−01	7.6271E−01	2.2019E−01	6.4054E−01	2.3277E−01	5.4358E−01
17	1.7075E−01	1.4977E+00	1.9019E−01	7.9279E−01	1.9834E−01	6.6575E−01	2.0963E−01	5.6494E−01
18	1.5490E−01	1.5543E+00	1.7208E−01	8.2231E−01	1.7940E−01	6.9049E−01	1.8958E−01	5.8591E−01
19	1.4113E−01	1.6097E+00	1.5631E−01	8.5122E−01	1.6290E−01	7.1473E−01	1.7210E−01	6.0646E−01
20	1.2909E−01	1.6638E+00	1.4252E−01	8.7947E−01	1.4847E−01	7.3842E−01	1.5682E−01	6.2654E−01
21	1.1851E−01	1.7165E+00	1.3040E−01	9.0702E−01	1.3579E−01	7.6152E−01	1.4339E−01	6.4613E−01
22	1.0918E−01	1.7678E+00	1.1971E−01	9.3384E−01	1.2461E−01	7.8401E−01	1.3154E−01	6.6520E−01
23	1.0090E−01	1.8176E+00	1.1025E−01	9.5990E−01	1.1472E−01	8.0587E−01	1.2106E−01	6.8373E−01
24	9.3536E−02	1.8660E+00	1.0185E−01	9.8519E−01	1.0593E−01	8.2708E−01	1.1176E−01	7.0171E−01
25	8.6951E−02	1.9128E+00	9.4349E−02	1.0097E+00	9.8093E−02	8.4763E−01	1.0346E−01	7.1915E−01
26	8.1041E−02	1.9582E+00	8.7643E−02	1.0334E+00	9.1084E−02	8.6754E−01	9.6043E−02	7.3603E−01
27	7.5719E−02	2.0022E+00	8.1623E−02	1.0564E+00	8.4795E−02	8.8681E−01	8.9388E−02	7.5237E−01
28	7.0908E−02	2.0448E+00	7.6200E−02	1.0786E+00	7.9133E−02	9.0546E−01	8.3398E−02	7.6817E−01
29	6.6546E−02	2.0861E+00	7.1301E−02	1.1001E+00	7.4019E−02	9.2349E−01	7.7990E−02	7.8346E−01
30	6.2579E−02	2.1261E+00	6.6862E−02	1.1210E+00	6.9388E−02	9.4093E−01	7.3093E−02	7.9825E−01
31	5.8960E−02	2.1648E+00	6.2827E−02	1.1411E+00	6.5180E−02	9.5782E−01	6.8646E−02	8.1256E−01
32	5.5649E−02	2.2024E+00	5.9150E−02	1.1606E+00	6.1347E−02	9.7415E−01	6.4596E−02	8.2640E−01
33	5.2613E−02	2.2389E+00	5.5790E−02	1.1795E+00	5.7846E−02	9.8998E−01	6.0898E−02	8.3981E−01
34	4.9821E−02	2.2743E+00	5.2712E−02	1.1978E+00	5.4640E−02	1.0053E+00	5.7513E−02	8.5280E−01
35	4.7249E−02	2.3087E+00	4.9885E−02	1.2155E+00	5.1697E−02	1.0202E+00	5.4406E−02	8.6539E−01
36	4.4873E−02	2.3422E+00	4.7282E−02	1.2328E+00	4.8989E−02	1.0346E+00	5.1548E−02	8.7761E−01
37	4.2675E−02	2.3747E+00	4.4882E−02	1.2495E+00	4.6492E−02	1.0486E+00	4.8913E−02	8.8946E−01
38	4.0636E−02	2.4064E+00	4.2662E−02	1.2657E+00	4.4184E−02	1.0622E+00	4.6478E−02	9.0098E−01
39	3.8743E−02	2.4372E+00	4.0605E−02	1.2816E+00	4.2046E−02	1.0754E+00	4.4224E−02	9.1219E−01
40	3.6980E−02	2.4673E+00	3.8696E−02	1.2969E+00	4.0062E−02	1.0883E+00	4.2133E−02	9.2308E−01
41	3.5337E−02	2.4967E+00	3.6921E−02	1.3119E+00	3.8218E−02	1.1008E+00	4.0188E−02	9.3370E−01
42	3.3803E−02	2.5253E+00	3.5267E−02	1.3266E+00	3.6500E−02	1.1131E+00	3.8378E−02	9.4404E−01
43	3.2368E−02	2.5533E+00	3.3724E−02	1.3408E+00	3.4898E−02	1.1250E+00	3.6689E−02	9.5414E−01
44	3.1025E−02	2.5807E+00	3.2281E−02	1.3547E+00	3.3400E−02	1.1366E+00	3.5111E−02	9.6398E−01
45	2.9765E−02	2.6075E+00	3.0930E−02	1.3683E+00	3.1999E−02	1.1480E+00	3.3634E−02	9.7361E−01
46	2.8581E−02	2.6337E+00	2.9664E−02	1.3816E+00	3.0684E−02	1.1591E+00	3.2250E−02	9.8301E−01
47	2.7468E−02	2.6594E+00	2.8475E−02	1.3946E+00	2.9451E−02	1.1700E+00	3.0951E−02	9.9221E−01
48	2.6421E−02	2.6845E+00	2.7357E−02	1.4074E+00	2.8291E−02	1.1806E+00	2.9730E−02	1.0012E+00
49	2.5433E−02	2.7092E+00	2.6304E−02	1.4199E+00	2.7199E−02	1.1911E+00	2.8580E−02	1.0100E+00
50	2.4501E−02	2.7334E+00	2.5312E−02	1.4321E+00	2.6171E−02	1.2013E+00	2.7497E−02	1.0187E+00
51	2.3620E−02	2.7571E+00	2.4375E−02	1.4441E+00	2.5200E−02	1.2113E+00	2.6475E−02	1.0272E+00
52	2.2787E−02	2.7805E+00	2.3491E−02	1.4559E+00	2.4282E−02	1.2211E+00	2.5510E−02	1.0355E+00
53	2.1998E−02	2.8034E+00	2.2653E−02	1.4674E+00	2.3415E−02	1.2308E+00	2.4597E−02	1.0436E+00
54	2.1250E−02	2.8259E+00	2.1861E−02	1.4788E+00	2.2593E−02	1.2403E+00	2.3732E−02	1.0516E+00
55	2.0541E−02	2.8481E+00	2.1109E−02	1.4899E+00	2.1815E−02	1.2496E+00	2.2912E−02	1.0595E+00
56	1.9867E−02	2.8698E+00	2.0396E−02	1.5009E+00	2.1076E−02	1.2587E+00	2.2135E−02	1.0673E+00
57	1.9227E−02	2.8913E+00	1.9719E−02	1.5117E+00	2.0374E−02	1.2678E+00	2.1397E−02	1.0749E+00
58	1.8617E−02	2.9124E+00	1.9076E−02	1.5223E+00	1.9707E−02	1.2766E+00	2.0695E−02	1.0824E+00
59	1.8038E−02	2.9332E+00	1.8463E−02	1.5328E+00	1.9073E−02	1.2853E+00	2.0028E−02	1.0898E+00
60	1.7485E−02	2.9537E+00	1.7880E−02	1.5430E+00	1.8469E−02	1.2939E+00	1.9393E−02	1.0970E+00

Table 4.3.3.1. *Partial wave elastic scattering factors for neutral atoms (cont.)*
Cl; $Z = 17$

	10 keV		40 keV		60 keV		90 keV	
s	$\|f(s)\|$	$\eta(s)$	$\|f(s)\|$	$\eta(s)$	$\|f(s)\|$	$\eta(s)$	$\|f(s)\|$	$\eta(s)$
0	4.7069E+00	2.2194E−01	5.1598E+00	1.2301E−01	5.3666E+00	1.0397E−01	5.6495E+00	8.8780E−02
1	4.2877E+00	2.3926E−01	4.7120E+00	1.3241E−01	4.9046E+00	1.1184E−01	5.1712E+00	9.5354E−02
2	3.3531E+00	2.9056E−01	3.7081E+00	1.6015E−01	3.8640E+00	1.3516E−01	4.0819E+00	1.1505E−01
3	2.4173E+00	3.7298E−01	2.6954E+00	2.0440E−01	2.8115E+00	1.7238E−01	2.9718E+00	1.4669E−01
4	1.7110E+00	4.7986E−01	1.9222E+00	2.6133E−01	2.0068E+00	2.2022E−01	2.1230E+00	1.8727E−01
5	1.2362E+00	6.0057E−01	1.3953E+00	3.2524E−01	1.4575E+00	2.7389E−01	1.5423E+00	2.3284E−01
6	9.2764E−01	7.2310E−01	1.0483E+00	3.9001E−01	1.0952E+00	3.2826E−01	1.1591E+00	2.7895E−01
7	7.2468E−01	8.3821E−01	8.1807E−01	4.5087E−01	8.5463E−01	3.7935E−01	9.0437E−01	3.2233E−01
8	5.8626E−01	9.4156E−01	6.6076E−01	5.0550E−01	6.9014E−01	4.2523E−01	7.3026E−01	3.6123E−01
9	4.8753E−01	1.0330E+00	5.4885E−01	5.5374E−01	5.7320E−01	4.6570E−01	6.0644E−01	3.9558E−01
10	4.1394E−01	1.1146E+00	4.6582E−01	5.9658E−01	4.8643E−01	5.0167E−01	5.1462E−01	4.2608E−01
11	3.5679E−01	1.1890E+00	4.0153E−01	6.3545E−01	4.1929E−01	5.3427E−01	4.4359E−01	4.5371E−01
12	3.1166E−01	1.2581E+00	3.5082E−01	6.7145E−01	3.6636E−01	5.6442E−01	3.8759E−01	4.7927E−01
13	2.7490E−01	1.3237E+00	3.0947E−01	7.0556E−01	3.2318E−01	5.9299E−01	3.4191E−01	5.0349E−01
14	2.4430E−01	1.3870E+00	2.7494E−01	7.3840E−01	2.8711E−01	6.2051E−01	3.0374E−01	5.2680E−01
15	2.1853E−01	1.4486E+00	2.4576E−01	7.7036E−01	2.5661E−01	6.4729E−01	2.7146E−01	5.4949E−01
16	1.9661E−01	1.5088E+00	2.2082E−01	8.0164E−01	2.3054E−01	6.7350E−01	2.4385E−01	5.7170E−01
17	1.7779E−01	1.5679E+00	1.9933E−01	8.3235E−01	2.0806E−01	6.9923E−01	2.2004E−01	5.9350E−01
18	1.6151E−01	1.6258E+00	1.8067E−01	8.6250E−01	1.8853E−01	7.2450E−01	1.9936E−01	6.1492E−01
19	1.4734E−01	1.6827E+00	1.6439E−01	8.9210E−01	1.7149E−01	7.4931E−01	1.8130E−01	6.3595E−01
20	1.3494E−01	1.7383E+00	1.5011E−01	9.2112E−01	1.5654E−01	7.7364E−01	1.6545E−01	6.5657E−01
21	1.2403E−01	1.7927E+00	1.3753E−01	9.4953E−01	1.4337E−01	7.9746E−01	1.5149E−01	6.7676E−01
22	1.1438E−01	1.8458E+00	1.2640E−01	9.7728E−01	1.3172E−01	8.2073E−01	1.3914E−01	6.9649E−01
23	1.0582E−01	1.8976E+00	1.1653E−01	1.0044E+00	1.2138E−01	8.4344E−01	1.2819E−01	7.1575E−01
24	9.8189E−02	1.9481E+00	1.0774E−01	1.0307E+00	1.1217E−01	8.6556E−01	1.1843E−01	7.3451E−01
25	9.1356E−02	1.9971E+00	9.9880E−02	1.0564E+00	1.0395E−01	8.8709E−01	1.0971E−01	7.5276E−01
26	8.5216E−02	2.0448E+00	9.2835E−02	1.0813E+00	9.6575E−02	9.0801E−01	1.0190E−01	7.7050E−01
27	7.9680E−02	2.0911E+00	8.6500E−02	1.1056E+00	8.9947E−02	9.2833E−01	9.4880E−02	7.8773E−01
28	7.4671E−02	2.1361E+00	8.0785E−02	1.1291E+00	8.3970E−02	9.4804E−01	8.8551E−02	8.0444E−01
29	7.0124E−02	2.1797E+00	7.5615E−02	1.1519E+00	7.8565E−02	9.6716E−01	8.2829E−02	8.2066E−01
30	6.5984E−02	2.2221E+00	7.0925E−02	1.1740E+00	7.3664E−02	9.8570E−01	7.7641E−02	8.3638E−01
31	6.2204E−02	2.2633E+00	6.6658E−02	1.1954E+00	6.9207E−02	1.0037E+00	7.2926E−02	8.5162E−01
32	5.8742E−02	2.3033E+00	6.2766E−02	1.2162E+00	6.5144E−02	1.0211E+00	6.8628E−02	8.6640E−01
33	5.5565E−02	2.3421E+00	5.9207E−02	1.2364E+00	6.1430E−02	1.0380E+00	6.4700E−02	8.8073E−01
34	5.2642E−02	2.3799E+00	5.5944E−02	1.2560E+00	5.8027E−02	1.0544E+00	6.1103E−02	8.9463E−01
35	4.9945E−02	2.4166E+00	5.2946E−02	1.2750E+00	5.4902E−02	1.0703E+00	5.7801E−02	9.0811E−01
36	4.7453E−02	2.4523E+00	5.0186E−02	1.2934E+00	5.2025E−02	1.0858E+00	5.4762E−02	9.2120E−01
37	4.5146E−02	2.4871E+00	4.7638E−02	1.3113E+00	4.9371E−02	1.1008E+00	5.1959E−02	9.3392E−01
38	4.3004E−02	2.5210E+00	4.5282E−02	1.3288E+00	4.6918E−02	1.1154E+00	4.9369E−02	9.4628E−01
39	4.1013E−02	2.5540E+00	4.3099E−02	1.3457E+00	4.4646E−02	1.1296E+00	4.6971E−02	9.5830E−01
40	3.9159E−02	2.5862E+00	4.1072E−02	1.3622E+00	4.2537E−02	1.1434E+00	4.4746E−02	9.6999E−01
41	3.7430E−02	2.6176E+00	3.9187E−02	1.3783E+00	4.0577E−02	1.1568E+00	4.2677E−02	9.8138E−01
42	3.5814E−02	2.6483E+00	3.7431E−02	1.3940E+00	3.8751E−02	1.1700E+00	4.0752E−02	9.9248E−01
43	3.4302E−02	2.6783E+00	3.5792E−02	1.4093E+00	3.7047E−02	1.1827E+00	3.8955E−02	1.0033E+00
44	3.2886E−02	2.7076E+00	3.4260E−02	1.4242E+00	3.5455E−02	1.1952E+00	3.7277E−02	1.0138E+00
45	3.1557E−02	2.7362E+00	3.2826E−02	1.4387E+00	3.3966E−02	1.2074E+00	3.5707E−02	1.0242E+00
46	3.0308E−02	2.7642E+00	3.1481E−02	1.4530E+00	3.2569E−02	1.2193E+00	3.4235E−02	1.0342E+00
47	2.9134E−02	2.7917E+00	3.0218E−02	1.4669E+00	3.1258E−02	1.2309E+00	3.2854E−02	1.0441E+00
48	2.8027E−02	2.8186E+00	2.9031E−02	1.4805E+00	3.0026E−02	1.2423E+00	3.1556E−02	1.0537E+00
49	2.6984E−02	2.8450E+00	2.7914E−02	1.4939E+00	2.8867E−02	1.2535E+00	3.0334E−02	1.0631E+00
50	2.5999E−02	2.8708E+00	2.6860E−02	1.5069E+00	2.7774E−02	1.2644E+00	2.9183E−02	1.0724E+00
51	2.5068E−02	2.8962E+00	2.5866E−02	1.5197E+00	2.6742E−02	1.2751E+00	2.8097E−02	1.0814E+00
52	2.4187E−02	2.9211E+00	2.4927E−02	1.5323E+00	2.5768E−02	1.2856E+00	2.7071E−02	1.0903E+00
53	2.3353E−02	2.9456E+00	2.4039E−02	1.5446E+00	2.4847E−02	1.2959E+00	2.6102E−02	1.0990E+00
54	2.2562E−02	2.9696E+00	2.3198E−02	1.5568E+00	2.3975E−02	1.3060E+00	2.5184E−02	1.1076E+00
55	2.1812E−02	2.9933E+00	2.2401E−02	1.5687E+00	2.3149E−02	1.3159E+00	2.4314E−02	1.1160E+00
56	2.1099E−02	3.0165E+00	2.1644E−02	1.5803E+00	2.2365E−02	1.3257E+00	2.3489E−02	1.1242E+00
57	2.0422E−02	3.0394E+00	2.0926E−02	1.5918E+00	2.1621E−02	1.3353E+00	2.2705E−02	1.1323E+00
58	1.9777E−02	3.0619E+00	2.0243E−02	1.6031E+00	2.0913E−02	1.3447E+00	2.1961E−02	1.1403E+00
59	1.9164E−02	3.0840E+00	1.9593E−02	1.6142E+00	2.0240E−02	1.3540E+00	2.1252E−02	1.1481E+00
60	1.8579E−02	3.1059E+00	1.8975E−02	1.6251E+00	1.9599E−02	1.3631E+00	2.0578E−02	1.1558E+00

Table 4.3.3.1. *Partial wave elastic scattering factors for neutral atoms (cont.)*
Ar; $Z = 18$

	10 keV		40 keV		60 keV		90 keV	
s	$\|f(s)\|$	$\eta(s)$	$\|f(s)\|$	$\eta(s)$	$\|f(s)\|$	$\eta(s)$	$\|f(s)\|$	$\eta(s)$
0	4.3973E+00	2.4333E−01	4.8477E+00	1.3577E−01	5.0459E+00	1.1486E−01	5.3150E+00	9.8141E−02
1	4.0647E+00	2.5913E−01	4.4918E+00	1.4437E−01	4.6788E+00	1.2206E−01	4.9352E+00	1.0416E−01
2	3.2894E+00	3.0611E−01	3.6573E+00	1.6988E−01	3.8140E+00	1.4350E−01	4.0312E+00	1.2223E−01
3	2.4585E+00	3.8233E−01	2.7563E+00	2.1099E−01	2.8772E+00	1.7811E−01	3.0431E+00	1.5165E−01
4	1.7868E+00	4.8330E−01	2.0198E+00	2.6497E−01	2.1106E+00	2.2348E−01	2.2340E+00	1.9017E−01
5	1.3088E+00	6.0117E−01	1.4882E+00	3.2755E−01	1.5561E+00	2.7606E−01	1.6479E+00	2.3480E−01
6	9.8520E−01	7.2591E−01	1.1228E+00	3.9359E−01	1.1744E+00	3.3150E−01	1.2438E+00	2.8188E−01
7	7.6737E−01	8.4801E−01	8.7381E−01	4.5824E−01	9.1391E−01	3.8581E−01	9.6800E−01	3.2791E−01
8	6.1755E−01	9.6119E−01	7.0153E−01	5.1825E−01	7.3356E−01	4.3619E−01	7.7672E−01	3.7073E−01
9	5.1086E−01	1.0631E+00	5.7893E−01	5.7223E−01	6.0516E−01	4.8154E−01	6.4071E−01	4.0917E−01
10	4.3187E−01	1.1540E+00	4.8858E−01	6.2030E−01	5.1062E−01	5.2188E−01	5.4053E−01	4.4341E−01
11	3.7106E−01	1.2361E+00	4.1940E−01	6.6343E−01	4.3828E−01	5.5806E−01	4.6390E−01	4.7411E−01
12	3.2346E−01	1.3112E+00	3.6552E−01	7.0271E−01	3.8196E−01	5.9101E−01	4.0427E−01	5.0203E−01
13	2.8499E−01	1.3813E+00	3.2206E−01	7.3920E−01	3.3653E−01	6.2160E−01	3.5619E−01	5.2796E−01
14	2.5315E−01	1.4478E+00	2.8607E−01	7.7376E−01	2.9892E−01	6.5055E−01	3.1638E−01	5.5248E−01
15	2.2648E−01	1.5118E+00	2.5584E−01	8.0694E−01	2.6733E−01	6.7834E−01	2.8294E−01	5.7604E−01
16	2.0386E−01	1.5739E+00	2.3012E−01	8.3913E−01	2.4043E−01	7.0531E−01	2.5445E−01	5.9889E−01
17	1.8448E−01	1.6345E+00	2.0799E−01	8.7058E−01	2.1727E−01	7.3165E−01	2.2992E−01	6.2120E−01
18	1.6773E−01	1.6939E+00	1.8879E−01	9.0139E−01	1.9718E−01	7.5747E−01	2.0862E−01	6.4308E−01
19	1.5317E−01	1.7521E+00	1.7202E−01	9.3163E−01	1.7962E−01	7.8281E−01	1.9001E−01	6.6455E−01
20	1.4042E−01	1.8091E+00	1.5729E−01	9.6132E−01	1.6419E−01	8.0769E−01	1.7366E−01	6.8564E−01
21	1.2919E−01	1.8650E+00	1.4430E−01	9.9044E−01	1.5058E−01	8.3210E−01	1.5922E−01	7.0633E−01
22	1.1926E−01	1.9197E+00	1.3279E−01	1.0190E+00	1.3851E−01	8.5603E−01	1.4642E−01	7.2661E−01
23	1.1044E−01	1.9732E+00	1.2254E−01	1.0469E+00	1.2778E−01	8.7945E−01	1.3504E−01	7.4647E−01
24	1.0256E−01	2.0254E+00	1.1341E−01	1.0742E+00	1.1820E−01	9.0234E−01	1.2488E−01	7.6588E−01
25	9.5506E−02	2.0764E+00	1.0522E−01	1.1008E+00	1.0962E−01	9.2469E−01	1.1578E−01	7.8483E−01
26	8.9160E−02	2.1260E+00	9.7868E−02	1.1268E+00	1.0192E−01	9.4649E−01	1.0761E−01	8.0331E−01
27	8.3432E−02	2.1744E+00	9.1245E−02	1.1522E+00	9.4977E−02	9.6772E−01	1.0026E−01	8.2132E−01
28	7.8244E−02	2.2215E+00	8.5260E−02	1.1768E+00	8.8709E−02	9.8839E−01	9.3612E−02	8.3885E−01
29	7.3530E−02	2.2674E+00	7.9839E−02	1.2007E+00	8.3033E−02	1.0085E+00	8.7596E−02	8.5589E−01
30	6.9235E−02	2.3120E+00	7.4913E−02	1.2241E+00	7.7878E−02	1.0280E+00	8.2134E−02	8.7246E−01
31	6.5309E−02	2.3554E+00	7.0428E−02	1.2467E+00	7.3185E−02	1.0470E+00	7.7164E−02	8.8856E−01
32	6.1712E−02	2.3976E+00	6.6332E−02	1.2687E+00	6.8903E−02	1.0655E+00	7.2629E−02	9.0421E−01
33	5.8407E−02	2.4387E+00	6.2583E−02	1.2901E+00	6.4985E−02	1.0834E+00	6.8481E−02	9.1941E−01
34	5.5364E−02	2.4787E+00	5.9145E−02	1.3109E+00	6.1392E−02	1.1008E+00	6.4679E−02	9.3417E−01
35	5.2555E−02	2.5176E+00	5.5983E−02	1.3311E+00	5.8090E−02	1.1178E+00	6.1186E−02	9.4852E−01
36	4.9956E−02	2.5555E+00	5.3070E−02	1.3507E+00	5.5050E−02	1.1342E+00	5.7971E−02	9.6246E−01
37	4.7548E−02	2.5925E+00	5.0380E−02	1.3698E+00	5.2244E−02	1.1502E+00	5.5004E−02	9.7602E−01
38	4.5312E−02	2.6285E+00	4.7891E−02	1.3884E+00	4.9649E−02	1.1658E+00	5.2262E−02	9.8920E−01
39	4.3231E−02	2.6636E+00	4.5585E−02	1.4064E+00	4.7244E−02	1.1809E+00	4.9721E−02	1.0020E+00
40	4.1293E−02	2.6979E+00	4.3442E−02	1.4240E+00	4.5013E−02	1.1956E+00	4.7364E−02	1.0145E+00
41	3.9483E−02	2.7313E+00	4.1450E−02	1.4412E+00	4.2937E−02	1.2100E+00	4.5173E−02	1.0267E+00
42	3.7791E−02	2.7640E+00	3.9593E−02	1.4579E+00	4.1004E−02	1.2240E+00	4.3132E−02	1.0385E+00
43	3.6207E−02	2.7959E+00	3.7859E−02	1.4742E+00	3.9200E−02	1.2377E+00	4.1229E−02	1.0501E+00
44	3.4722E−02	2.8272E+00	3.6239E−02	1.4902E+00	3.7515E−02	1.2510E+00	3.9450E−02	1.0614E+00
45	3.3328E−02	2.8577E+00	3.4722E−02	1.5057E+00	3.5937E−02	1.2640E+00	3.7786E−02	1.0724E+00
46	3.2017E−02	2.8876E+00	3.3299E−02	1.5209E+00	3.4459E−02	1.2767E+00	3.6227E−02	1.0831E+00
47	3.0784E−02	2.9169E+00	3.1964E−02	1.5358E+00	3.3071E−02	1.2891E+00	3.4763E−02	1.0936E+00
48	2.9621E−02	2.9455E+00	3.0708E−02	1.5503E+00	3.1766E−02	1.3012E+00	3.3388E−02	1.1039E+00
49	2.8524E−02	2.9736E+00	2.9526E−02	1.5645E+00	3.0538E−02	1.3131E+00	3.2094E−02	1.1140E+00
50	2.7489E−02	3.0012E+00	2.8411E−02	1.5785E+00	2.9382E−02	1.3248E+00	3.0875E−02	1.1238E+00
51	2.6510E−02	3.0282E+00	2.7360E−02	1.5921E+00	2.8290E−02	1.3362E+00	2.9725E−02	1.1335E+00
52	2.5583E−02	3.0547E+00	2.6367E−02	1.6055E+00	2.7259E−02	1.3474E+00	2.8639E−02	1.1429E+00
53	2.4705E−02	3.0808E+00	2.5427E−02	1.6186E+00	2.6284E−02	1.3583E+00	2.7612E−02	1.1522E+00
54	2.3872E−02	3.1064E+00	2.4537E−02	1.6315E+00	2.5361E−02	1.3691E+00	2.6640E−02	1.1613E+00
55	2.3082E−02	3.1316E+00	2.3694E−02	1.6442E+00	2.4487E−02	1.3796E+00	2.5720E−02	1.1702E+00
56	2.2331E−02	3.1563E+00	2.2894E−02	1.6566E+00	2.3657E−02	1.3900E+00	2.4846E−02	1.1790E+00
57	2.1618E−02	3.1806E+00	2.2135E−02	1.6688E+00	2.2870E−02	1.4002E+00	2.4017E−02	1.1876E+00
58	2.0939E−02	3.2046E+00	2.1413E−02	1.6808E+00	2.2121E−02	1.4102E+00	2.3229E−02	1.1960E+00
59	2.0292E−02	3.2281E+00	2.0726E−02	1.6926E+00	2.1409E−02	1.4201E+00	2.2480E−02	1.2044E+00
60	1.9675E−02	3.2513E+00	2.0072E−02	1.7042E+00	2.0731E−02	1.4297E+00	2.1767E−02	1.2125E+00

Table 4.3.3.1. *Partial wave elastic scattering factors for neutral atoms (cont.)*
K; $Z = 19$

	10 keV		40 keV		60 keV		90 keV	
s	$\|f(s)\|$	$\eta(s)$	$\|f(s)\|$	$\eta(s)$	$\|f(s)\|$	$\eta(s)$	$\|f(s)\|$	$\eta(s)$
0	8.7237E+00	1.6059E−01	9.5161E+00	9.0866E−02	9.8965E+00	7.6992E−02	1.0427E+01	6.5797E−02
1	6.0203E+00	2.2522E−01	6.6280E+00	1.2640E−01	6.9024E+00	1.0697E−01	7.2836E+00	9.1288E−02
2	3.5970E+00	3.4923E−01	4.0137E+00	1.9370E−01	4.1878E+00	1.6365E−01	4.4276E+00	1.3942E−01
3	2.5066E+00	4.5491E−01	2.8249E+00	2.5068E−01	2.9511E+00	2.1160E−01	3.1230E+00	1.8017E−01
4	1.8328E+00	5.5955E−01	2.0834E+00	3.0678E−01	2.1789E+00	2.5879E−01	2.3076E+00	2.2025E−01
5	1.3635E+00	6.7457E−01	1.5603E+00	3.6805E−01	1.6331E+00	3.1028E−01	1.7305E+00	2.6397E−01
6	1.0361E+00	7.9761E−01	1.1898E+00	4.3333E−01	1.2458E+00	3.6511E−01	1.3205E+00	3.1051E−01
7	8.0891E−01	9.2197E−01	9.2903E−01	4.9927E−01	9.7286E−01	4.2049E−01	1.0312E+00	3.5752E−01
8	6.4976E−01	1.0412E+00	7.4457E−01	5.6262E−01	7.7950E−01	4.7371E−01	8.2613E−01	4.0268E−01
9	5.3560E−01	1.1516E+00	6.1180E−01	6.2129E−01	6.4027E−01	5.2299E−01	6.7839E−01	4.4452E−01
10	4.5112E−01	1.2518E+00	5.1374E−01	6.7455E−01	5.3745E−01	5.6774E−01	5.6931E−01	4.8250E−01
11	3.8644E−01	1.3421E+00	4.3916E−01	7.2231E−01	4.5931E−01	6.0784E−01	4.8644E−01	5.1654E−01
12	3.3605E−01	1.4245E+00	3.8140E−01	7.6572E−01	3.9883E−01	6.4427E−01	4.2234E−01	5.4744E−01
13	2.9559E−01	1.5004E+00	3.3528E−01	8.0543E−01	3.5057E−01	6.7758E−01	3.7122E−01	5.7568E−01
14	2.6230E−01	1.5713E+00	2.9746E−01	8.4239E−01	3.1102E−01	7.0855E−01	3.2933E−01	6.0192E−01
15	2.3454E−01	1.6387E+00	2.6593E−01	8.7735E−01	2.7805E−01	7.3784E−01	2.9441E−01	6.2674E−01
16	2.1108E−01	1.7034E+00	2.3924E−01	9.1087E−01	2.5013E−01	7.6592E−01	2.6484E−01	6.5053E−01
17	1.9104E−01	1.7660E+00	2.1637E−01	9.4332E−01	2.2620E−01	7.9309E−01	2.3949E−01	6.7355E−01
18	1.7377E−01	1.8271E+00	1.9658E−01	9.7493E−01	2.0548E−01	8.1958E−01	2.1753E−01	6.9599E−01
19	1.5876E−01	1.8868E+00	1.7931E−01	1.0059E+00	1.8739E−01	8.4549E−01	1.9835E−01	7.1794E−01
20	1.4563E−01	1.9452E+00	1.6415E−01	1.0362E+00	1.7150E−01	8.7090E−01	1.8150E−01	7.3947E−01
21	1.3408E−01	2.0025E+00	1.5076E−01	1.0660E+00	1.5747E−01	8.9585E−01	1.6662E−01	7.6062E−01
22	1.2387E−01	2.0586E+00	1.3888E−01	1.0952E+00	1.4501E−01	9.2034E−01	1.5340E−01	7.8137E−01
23	1.1479E−01	2.1136E+00	1.2830E−01	1.1238E+00	1.3392E−01	9.4437E−01	1.4163E−01	8.0174E−01
24	1.0668E−01	2.1674E+00	1.1884E−01	1.1519E+00	1.2400E−01	9.6791E−01	1.3110E−01	8.2170E−01
25	9.9416E−02	2.2200E+00	1.1036E−01	1.1794E+00	1.1510E−01	9.9096E−01	1.2166E−01	8.4125E−01
26	9.2877E−02	2.2714E+00	1.0273E−01	1.2063E+00	1.0709E−01	1.0135E+00	1.1316E−01	8.6036E−01
27	8.6971E−02	2.3216E+00	9.5839E−02	1.2326E+00	9.9866E−02	1.0355E+00	1.0549E−01	8.7904E−01
28	8.1619E−02	2.3706E+00	8.9606E−02	1.2582E+00	9.3329E−02	1.0570E+00	9.8559E−02	8.9727E−01
29	7.6754E−02	2.4184E+00	8.3951E−02	1.2832E+00	8.7400E−02	1.0780E+00	9.2270E−02	9.1506E−01
30	7.2317E−02	2.4650E+00	7.8807E−02	1.3076E+00	8.2009E−02	1.0984E+00	8.6551E−02	9.3239E−01
31	6.8259E−02	2.5104E+00	7.4117E−02	1.3313E+00	7.7094E−02	1.1184E+00	8.1340E−02	9.4928E−01
32	6.4538E−02	2.5547E+00	6.9830E−02	1.3544E+00	7.2604E−02	1.1377E+00	7.6580E−02	9.6572E−01
33	6.1117E−02	2.5979E+00	6.5902E−02	1.3769E+00	6.8492E−02	1.1566E+00	7.2223E−02	9.8172E−01
34	5.7965E−02	2.6399E+00	6.2296E−02	1.3988E+00	6.4719E−02	1.1750E+00	6.8225E−02	9.9730E−01
35	5.5053E−02	2.6810E+00	5.8978E−02	1.4202E+00	6.1248E−02	1.1929E+00	6.4549E−02	1.0125E+00
36	5.2359E−02	2.7210E+00	5.5918E−02	1.4409E+00	5.8049E−02	1.2103E+00	6.1162E−02	1.0272E+00
37	4.9859E−02	2.7600E+00	5.3092E−02	1.4611E+00	5.5096E−02	1.2272E+00	5.8036E−02	1.0416E+00
38	4.7536E−02	2.7980E+00	5.0475E−02	1.4808E+00	5.2363E−02	1.2437E+00	5.5145E−02	1.0556E+00
39	4.5374E−02	2.8352E+00	4.8049E−02	1.5000E+00	4.9830E−02	1.2598E+00	5.2466E−02	1.0692E+00
40	4.3357E−02	2.8714E+00	4.5795E−02	1.5187E+00	4.7478E−02	1.2754E+00	4.9979E−02	1.0824E+00
41	4.1474E−02	2.9069E+00	4.3697E−02	1.5369E+00	4.5290E−02	1.2907E+00	4.7666E−02	1.0954E+00
42	3.9712E−02	2.9415E+00	4.1742E−02	1.5547E+00	4.3252E−02	1.3056E+00	4.5512E−02	1.1080E+00
43	3.8061E−02	2.9753E+00	3.9916E−02	1.5720E+00	4.1350E−02	1.3201E+00	4.3503E−02	1.1202E+00
44	3.6513E−02	3.0085E+00	3.8209E−02	1.5889E+00	3.9572E−02	1.3343E+00	4.1625E−02	1.1322E+00
45	3.5058E−02	3.0408E+00	3.6611E−02	1.6055E+00	3.7907E−02	1.3481E+00	3.9868E−02	1.1439E+00
46	3.3689E−02	3.0726E+00	3.5112E−02	1.6216E+00	3.6347E−02	1.3616E+00	3.8222E−02	1.1554E+00
47	3.2401E−02	3.1036E+00	3.3704E−02	1.6374E+00	3.4883E−02	1.3748E+00	3.6676E−02	1.1666E+00
48	3.1186E−02	3.1340E+00	3.2380E−02	1.6529E+00	3.3506E−02	1.3877E+00	3.5224E−02	1.1775E+00
49	3.0039E−02	3.1639E+00	3.1134E−02	1.6680E+00	3.2211E−02	1.4003E+00	3.3858E−02	1.1882E+00
50	2.8955E−02	3.1931E+00	2.9960E−02	1.6828E+00	3.0990E−02	1.4127E+00	3.2571E−02	1.1987E+00
51	2.7930E−02	3.2218E+00	2.8851E−02	1.6973E+00	2.9838E−02	1.4248E+00	3.1356E−02	1.2089E+00
52	2.6959E−02	3.2500E+00	2.7804E−02	1.7115E+00	2.8751E−02	1.4367E+00	3.0210E−02	1.2189E+00
53	2.6040E−02	3.2776E+00	2.6813E−02	1.7254E+00	2.7722E−02	1.4483E+00	2.9126E−02	1.2288E+00
54	2.5167E−02	3.3048E+00	2.5876E−02	1.7391E+00	2.6748E−02	1.4598E+00	2.8100E−02	1.2384E+00
55	2.4339E−02	3.3315E+00	2.4987E−02	1.7525E+00	2.5826E−02	1.4710E+00	2.7128E−02	1.2479E+00
56	2.3551E−02	3.3577E+00	2.4144E−02	1.7657E+00	2.4951E−02	1.4820E+00	2.6206E−02	1.2572E+00
57	2.2803E−02	3.3835E+00	2.3343E−02	1.7786E+00	2.4120E−02	1.4928E+00	2.5332E−02	1.2663E+00
58	2.2090E−02	3.4089E+00	2.2582E−02	1.7914E+00	2.3330E−02	1.5034E+00	2.4500E−02	1.2753E+00
59	2.1411E−02	3.4339E+00	2.1858E−02	1.8039E+00	2.2580E−02	1.5138E+00	2.3709E−02	1.2841E+00
60	2.0763E−02	3.4585E+00	2.1168E−02	1.8161E+00	2.1865E−02	1.5240E+00	2.2957E−02	1.2928E+00

Table 4.3.3.1. *Partial wave elastic scattering factors for neutral atoms (cont.)*
Ca; $Z = 20$

	10 keV		40 keV		60 keV		90 keV	
s	$\|f(s)\|$	$\eta(s)$	$\|f(s)\|$	$\eta(s)$	$\|f(s)\|$	$\eta(s)$	$\|f(s)\|$	$\eta(s)$
0	9.6204E+00	1.7308E−01	1.0517E+01	9.8165E−02	1.0941E+01	8.3216E−02	1.1532E+01	7.1133E−02
1	7.0378E+00	2.2767E−01	7.7570E+00	1.2836E−01	8.0803E+00	1.0870E−01	8.5292E+00	9.2808E−02
2	4.0325E+00	3.6260E−01	4.5139E+00	2.0193E−01	4.7122E+00	1.7071E−01	4.9839E+00	1.4551E−01
3	2.6145E+00	5.0011E−01	2.9605E+00	2.7615E−01	3.0951E+00	2.3319E−01	3.2771E+00	1.9861E−01
4	1.8783E+00	6.1900E−01	2.1461E+00	3.4001E−01	2.2462E+00	2.8692E−01	2.3802E+00	2.4426E−01
5	1.4068E+00	7.3535E−01	1.6192E+00	4.0218E−01	1.6963E+00	3.3919E−01	1.7987E+00	2.8865E−01
6	1.0791E+00	8.5643E−01	1.2478E+00	4.6659E−01	1.3080E+00	3.9331E−01	1.3874E+00	3.3460E−01
7	8.4690E−01	9.8059E−01	9.8064E−01	5.3253E−01	1.0281E+00	4.4871E−01	1.0907E+00	3.8162E−01
8	6.8091E−01	1.1031E+00	7.8721E−01	5.9768E−01	8.2520E−01	5.0344E−01	8.7535E−01	4.2808E−01
9	5.6044E−01	1.2196E+00	6.4574E−01	6.5975E−01	6.7664E−01	5.5560E−01	7.1756E−01	4.7238E−01
10	4.7093E−01	1.3274E+00	5.4049E−01	7.1731E−01	5.6609E−01	6.0398E−01	6.0013E−01	5.1345E−01
11	4.0241E−01	1.4258E+00	4.6030E−01	7.6970E−01	4.8189E−01	6.4800E−01	5.1073E−01	5.5083E−01
12	3.4924E−01	1.5157E+00	3.9845E−01	8.1739E−01	4.1701E−01	6.8805E−01	4.4186E−01	5.8483E−01
13	3.0669E−01	1.5982E+00	3.4934E−01	8.6084E−01	3.6554E−01	7.2453E−01	3.8727E−01	6.1577E−01
14	2.7182E−01	1.6745E+00	3.0936E−01	9.0086E−01	3.2367E−01	7.5809E−01	3.4288E−01	6.4423E−01
15	2.4285E−01	1.7462E+00	2.7626E−01	9.3822E−01	2.8902E−01	7.8940E−01	3.0616E−01	6.7076E−01
16	2.1844E−01	1.8144E+00	2.4842E−01	9.7357E−01	2.5988E−01	8.1902E−01	2.7528E−01	6.9586E−01
17	1.9765E−01	1.8798E+00	2.2467E−01	1.0074E+00	2.3503E−01	8.4736E−01	2.4894E−01	7.1987E−01
18	1.7977E−01	1.9430E+00	2.0419E−01	1.0401E+00	2.1359E−01	8.7475E−01	2.2622E−01	7.4306E−01
19	1.6426E−01	2.0045E+00	1.8638E−01	1.0719E+00	1.9492E−01	9.0139E−01	2.0643E−01	7.6563E−01
20	1.5072E−01	2.0645E+00	1.7075E−01	1.1030E+00	1.7855E−01	9.2742E−01	1.8907E−01	7.8768E−01
21	1.3881E−01	2.1233E+00	1.5696E−01	1.1335E+00	1.6409E−01	9.5292E−01	1.7373E−01	8.0929E−01
22	1.2830E−01	2.1808E+00	1.4472E−01	1.1633E+00	1.5126E−01	9.7795E−01	1.6011E−01	8.3050E−01
23	1.1895E−01	2.2372E+00	1.3382E−01	1.1926E+00	1.3982E−01	1.0025E+00	1.4797E−01	8.5132E−01
24	1.1061E−01	2.2925E+00	1.2406E−01	1.2214E+00	1.2958E−01	1.0266E+00	1.3710E−01	8.7176E−01
25	1.0314E−01	2.3466E+00	1.1530E−01	1.2496E+00	1.2038E−01	1.0503E+00	1.2733E−01	8.9182E−01
26	9.6410E−02	2.3996E+00	1.0741E−01	1.2773E+00	1.1209E−01	1.0735E+00	1.1853E−01	9.1148E−01
27	9.0334E−02	2.4514E+00	1.0028E−01	1.3044E+00	1.0460E−01	1.0962E+00	1.1058E−01	9.3074E−01
28	8.4827E−02	2.5021E+00	9.3815E−02	1.3309E+00	9.7819E−02	1.1184E+00	1.0338E−01	9.4959E−01
29	7.9818E−02	2.5517E+00	8.7945E−02	1.3568E+00	9.1656E−02	1.1402E+00	9.6834E−02	9.6802E−01
30	7.5249E−02	2.6001E+00	8.2598E−02	1.3821E+00	8.6045E−02	1.1614E+00	9.0877E−02	9.8603E−01
31	7.1069E−02	2.6474E+00	7.7717E−02	1.4068E+00	8.0923E−02	1.1821E+00	8.5441E−02	1.0036E+00
32	6.7234E−02	2.6936E+00	7.3250E−02	1.4309E+00	7.6238E−02	1.2024E+00	8.0469E−02	1.0208E+00
33	6.3707E−02	2.7386E+00	6.9154E−02	1.4545E+00	7.1943E−02	1.2221E+00	7.5912E−02	1.0375E+00
34	6.0455E−02	2.7826E+00	6.5390E−02	1.4774E+00	6.7997E−02	1.2414E+00	7.1728E−02	1.0539E+00
35	5.7450E−02	2.8256E+00	6.1923E−02	1.4998E+00	6.4366E−02	1.2601E+00	6.7877E−02	1.0698E+00
36	5.4666E−02	2.8676E+00	5.8725E−02	1.5216E+00	6.1016E−02	1.2785E+00	6.4327E−02	1.0853E+00
37	5.2083E−02	2.9085E+00	5.5768E−02	1.5429E+00	5.7921E−02	1.2963E+00	6.1047E−02	1.1004E+00
38	4.9682E−02	2.9485E+00	5.3029E−02	1.5637E+00	5.5055E−02	1.3137E+00	5.8011E−02	1.1152E+00
39	4.7444E−02	2.9876E+00	5.0487E−02	1.5839E+00	5.2398E−02	1.3306E+00	5.5198E−02	1.1295E+00
40	4.5357E−02	3.0258E+00	4.8125E−02	1.6036E+00	4.9929E−02	1.3472E+00	5.2584E−02	1.1435E+00
41	4.3405E−02	3.0632E+00	4.5926E−02	1.6229E+00	4.7632E−02	1.3633E+00	5.0153E−02	1.1572E+00
42	4.1579E−02	3.0997E+00	4.3875E−02	1.6417E+00	4.5491E−02	1.3791E+00	4.7888E−02	1.1705E+00
43	3.9867E−02	3.1354E+00	4.1960E−02	1.6600E+00	4.3492E−02	1.3944E+00	4.5775E−02	1.1836E+00
44	3.8260E−02	3.1703E+00	4.0169E−02	1.6779E+00	4.1623E−02	1.4094E+00	4.3799E−02	1.1963E+00
45	3.6749E−02	3.2046E+00	3.8491E−02	1.6954E+00	3.9874E−02	1.4241E+00	4.1950E−02	1.2087E+00
46	3.5327E−02	3.2381E+00	3.6917E−02	1.7125E+00	3.8233E−02	1.4384E+00	4.0217E−02	1.2208E+00
47	3.3987E−02	3.2709E+00	3.5439E−02	1.7293E+00	3.6693E−02	1.4524E+00	3.8591E−02	1.2326E+00
48	3.2723E−02	3.3031E+00	3.4048E−02	1.7456E+00	3.5246E−02	1.4661E+00	3.7062E−02	1.2442E+00
49	3.1529E−02	3.3346E+00	3.2739E−02	1.7616E+00	3.3883E−02	1.4794E+00	3.5624E−02	1.2556E+00
50	3.0400E−02	3.3656E+00	3.1505E−02	1.7773E+00	3.2599E−02	1.4926E+00	3.4269E−02	1.2666E+00
51	2.9332E−02	3.3959E+00	3.0341E−02	1.7927E+00	3.1388E−02	1.5054E+00	3.2991E−02	1.2775E+00
52	2.8320E−02	3.4257E+00	2.9240E−02	1.8077E+00	3.0243E−02	1.5180E+00	3.1784E−02	1.2881E+00
53	2.7361E−02	3.4550E+00	2.8199E−02	1.8225E+00	2.9161E−02	1.5303E+00	3.0643E−02	1.2986E+00
54	2.6451E−02	3.4837E+00	2.7213E−02	1.8370E+00	2.8137E−02	1.5424E+00	2.9563E−02	1.3088E+00
55	2.5586E−02	3.5120E+00	2.6279E−02	1.8512E+00	2.7166E−02	1.5542E+00	2.8540E−02	1.3188E+00
56	2.4763E−02	3.5397E+00	2.5393E−02	1.8651E+00	2.6246E−02	1.5659E+00	2.7570E−02	1.3287E+00
57	2.3981E−02	3.5670E+00	2.4551E−02	1.8788E+00	2.5372E−02	1.5773E+00	2.6649E−02	1.3383E+00
58	2.3236E−02	3.5938E+00	2.3751E−02	1.8922E+00	2.4541E−02	1.5885E+00	2.5774E−02	1.3478E+00
59	2.2526E−02	3.6203E+00	2.2990E−02	1.9055E+00	2.3752E−02	1.5996E+00	2.4942E−02	1.3572E+00
60	2.1849E−02	3.6463E+00	2.2265E−02	1.9185E+00	2.3000E−02	1.6104E+00	2.4150E−02	1.3663E+00

Table 4.3.3.1. *Partial wave elastic scattering factors for neutral atoms (cont.)*
Sc; $Z = 21$

	10 keV		40 keV		60 keV		90 keV	
s	$\|f(s)\|$	$\eta(s)$	$\|f(s)\|$	$\eta(s)$	$\|f(s)\|$	$\eta(s)$	$\|f(s)\|$	$\eta(s)$
0	8.9757E+00	1.8778E−01	9.8570E+00	1.0735E−01	1.0261E+01	9.1119E−02	1.0820E+01	7.7965E−02
1	6.8266E+00	2.3883E−01	7.5574E+00	1.3573E−01	7.8775E+00	1.1508E−01	8.3189E+00	9.8340E−02
2	4.0920E+00	3.6725E−01	4.6023E+00	2.0609E−01	4.8079E+00	1.7442E−01	5.0878E+00	1.4879E−01
3	2.6762E+00	5.0666E−01	3.0475E+00	2.8159E−01	3.1889E+00	2.3802E−01	3.3785E+00	2.0286E−01
4	1.9252E+00	6.3055E−01	2.2134E+00	3.4834E−01	2.3189E+00	2.9419E−01	2.4589E+00	2.5060E−01
5	1.4489E+00	7.4933E−01	1.6789E+00	4.1199E−01	1.7607E+00	3.4773E−01	1.8683E+00	2.9609E−01
6	1.1179E+00	8.7097E−01	1.3025E+00	4.7687E−01	1.3669E+00	4.0227E−01	1.4511E+00	3.4240E−01
7	8.8117E−01	9.9590E−01	1.0290E+00	5.4336E−01	1.0802E+00	4.5814E−01	1.1470E+00	3.8983E−01
8	7.0984E−01	1.1208E+00	8.2826E−01	6.0988E−01	8.6941E−01	5.1404E−01	9.2312E−01	4.3729E−01
9	5.8427E−01	1.2418E+00	6.7955E−01	6.7445E−01	7.1306E−01	5.6831E−01	7.5692E−01	4.8338E−01
10	4.9047E−01	1.3558E+00	5.6796E−01	7.3544E−01	5.9566E−01	6.1958E−01	6.3208E−01	5.2692E−01
11	4.1856E−01	1.4611E+00	4.8258E−01	7.9180E−01	5.0584E−01	6.6697E−01	5.3657E−01	5.6717E−01
12	3.6276E−01	1.5581E+00	4.1665E−01	8.4357E−01	4.3652E−01	7.1049E−01	4.6288E−01	6.0413E−01
13	3.1817E−01	1.6472E+00	3.6442E−01	8.9089E−01	3.8166E−01	7.5024E−01	4.0460E−01	6.3787E−01
14	2.8172E−01	1.7295E+00	3.2207E−01	9.3432E−01	3.3723E−01	7.8670E−01	3.5744E−01	6.6881E−01
15	2.5150E−01	1.8063E+00	2.8719E−01	9.7457E−01	3.0066E−01	8.2046E−01	3.1865E−01	6.9743E−01
16	2.2608E−01	1.8787E+00	2.5799E−01	1.0123E+00	2.7007E−01	8.5208E−01	2.8621E−01	7.2423E−01
17	2.0447E−01	1.9476E+00	2.3321E−01	1.0481E+00	2.4411E−01	8.8203E−01	2.5868E−01	7.4961E−01
18	1.8592E−01	2.0137E+00	2.1192E−01	1.0823E+00	2.2181E−01	9.1070E−01	2.3504E−01	7.7389E−01
19	1.6986E−01	2.0777E+00	1.9345E−01	1.1153E+00	2.0246E−01	9.3837E−01	2.1452E−01	7.9733E−01
20	1.5585E−01	2.1398E+00	1.7730E−01	1.1474E+00	1.8553E−01	9.6525E−01	1.9656E−01	8.2009E−01
21	1.4355E−01	2.2004E+00	1.6306E−01	1.1788E+00	1.7060E−01	9.9149E−01	1.8072E−01	8.4232E−01
22	1.3269E−01	2.2597E+00	1.5044E−01	1.2094E+00	1.5736E−01	1.0172E+00	1.6668E−01	8.6407E−01
23	1.2306E−01	2.3177E+00	1.3920E−01	1.2395E+00	1.4557E−01	1.0423E+00	1.5415E−01	8.8540E−01
24	1.1447E−01	2.3745E+00	1.2914E−01	1.2689E+00	1.3500E−01	1.0670E+00	1.4293E−01	9.0633E−01
25	1.0677E−01	2.4301E+00	1.2010E−01	1.2979E+00	1.2551E−01	1.0913E+00	1.3285E−01	9.2689E−01
26	9.9847E−02	2.4846E+00	1.1196E−01	1.3263E+00	1.1695E−01	1.1151E+00	1.2376E−01	9.4706E−01
27	9.3595E−02	2.5381E+00	1.0459E−01	1.3541E+00	1.0921E−01	1.1384E+00	1.1554E−01	9.6686E−01
28	8.7930E−02	2.5904E+00	9.7907E−02	1.3814E+00	1.0219E−01	1.1613E+00	1.0808E−01	9.8626E−01
29	8.2779E−02	2.6416E+00	9.1831E−02	1.4082E+00	9.5807E−02	1.1838E+00	1.0129E−01	1.0053E+00
30	7.8080E−02	2.6917E+00	8.6293E−02	1.4343E+00	8.9987E−02	1.2057E+00	9.5109E−02	1.0239E+00
31	7.3780E−02	2.7407E+00	8.1231E−02	1.4599E+00	8.4669E−02	1.2272E+00	8.9460E−02	1.0421E+00
32	6.9836E−02	2.7886E+00	7.6595E−02	1.4850E+00	7.9800E−02	1.2482E+00	8.4289E−02	1.0599E+00
33	6.6206E−02	2.8355E+00	7.2340E−02	1.5095E+00	7.5332E−02	1.2687E+00	7.9543E−02	1.0774E+00
34	6.2859E−02	2.8813E+00	6.8426E−02	1.5334E+00	7.1223E−02	1.2888E+00	7.5181E−02	1.0944E+00
35	5.9766E−02	2.9261E+00	6.4818E−02	1.5567E+00	6.7438E−02	1.3084E+00	7.1164E−02	1.1110E+00
36	5.6899E−02	2.9699E+00	6.1487E−02	1.5796E+00	6.3944E−02	1.3275E+00	6.7456E−02	1.1272E+00
37	5.4238E−02	3.0127E+00	5.8406E−02	1.6018E+00	6.0714E−02	1.3462E+00	6.4029E−02	1.1430E+00
38	5.1762E−02	3.0546E+00	5.5549E−02	1.6236E+00	5.7720E−02	1.3644E+00	6.0855E−02	1.1585E+00
39	4.9455E−02	3.0955E+00	5.2898E−02	1.6448E+00	5.4943E−02	1.3822E+00	5.7911E−02	1.1736E+00
40	4.7302E−02	3.1356E+00	5.0432E−02	1.6655E+00	5.2362E−02	1.3996E+00	5.5175E−02	1.1883E+00
41	4.5287E−02	3.1748E+00	4.8135E−02	1.6858E+00	4.9958E−02	1.4166E+00	5.2629E−02	1.2027E+00
42	4.3401E−02	3.2131E+00	4.5992E−02	1.7055E+00	4.7717E−02	1.4332E+00	5.0256E−02	1.2168E+00
43	4.1632E−02	3.2506E+00	4.3990E−02	1.7249E+00	4.5624E−02	1.4493E+00	4.8040E−02	1.2305E+00
44	3.9970E−02	3.2874E+00	4.2116E−02	1.7437E+00	4.3667E−02	1.4652E+00	4.5969E−02	1.2439E+00
45	3.8407E−02	3.3234E+00	4.0361E−02	1.7622E+00	4.1834E−02	1.4806E+00	4.4030E−02	1.2570E+00
46	3.6935E−02	3.3587E+00	3.8714E−02	1.7802E+00	4.0115E−02	1.4957E+00	4.2212E−02	1.2697E+00
47	3.5547E−02	3.3932E+00	3.7167E−02	1.7979E+00	3.8501E−02	1.5105E+00	4.0505E−02	1.2823E+00
48	3.4237E−02	3.4271E+00	3.5711E−02	1.8152E+00	3.6983E−02	1.5249E+00	3.8901E−02	1.2945E+00
49	3.3000E−02	3.4604E+00	3.4340E−02	1.8321E+00	3.5554E−02	1.5391E+00	3.7392E−02	1.3065E+00
50	3.1829E−02	3.4930E+00	3.3048E−02	1.8486E+00	3.4208E−02	1.5529E+00	3.5969E−02	1.3182E+00
51	3.0720E−02	3.5250E+00	3.1828E−02	1.8648E+00	3.2937E−02	1.5665E+00	3.4628E−02	1.3297E+00
52	2.9669E−02	3.5564E+00	3.0675E−02	1.8807E+00	3.1737E−02	1.5798E+00	3.3361E−02	1.3409E+00
53	2.8672E−02	3.5873E+00	2.9584E−02	1.8963E+00	3.0602E−02	1.5928E+00	3.2163E−02	1.3519E+00
54	2.7726E−02	3.6176E+00	2.8551E−02	1.9116E+00	2.9527E−02	1.6056E+00	3.1029E−02	1.3627E+00
55	2.6826E−02	3.6474E+00	2.7572E−02	1.9266E+00	2.8509E−02	1.6181E+00	2.9955E−02	1.3733E+00
56	2.5971E−02	3.6767E+00	2.6643E−02	1.9413E+00	2.7543E−02	1.6304E+00	2.8936E−02	1.3837E+00
57	2.5156E−02	3.7055E+00	2.5761E−02	1.9558E+00	2.6626E−02	1.6424E+00	2.7970E−02	1.3939E+00
58	2.4381E−02	3.7339E+00	2.4922E−02	1.9700E+00	2.5755E−02	1.6543E+00	2.7051E−02	1.4039E+00
59	2.3641E−02	3.7617E+00	2.4124E−02	1.9839E+00	2.4926E−02	1.6659E+00	2.6178E−02	1.4138E+00
60	2.2935E−02	3.7892E+00	2.3364E−02	1.9976E+00	2.4138E−02	1.6774E+00	2.5347E−02	1.4234E+00

Table 4.3.3.1. *Partial wave elastic scattering factors for neutral atoms (cont.)*
Ti; $Z = 22$

	10 keV		40 keV		60 keV		90 keV	
s	$\|f(s)\|$	$\eta(s)$	$\|f(s)\|$	$\eta(s)$	$\|f(s)\|$	$\eta(s)$	$\|f(s)\|$	$\eta(s)$
0	8.4030E+00	2.0031E−01	9.2695E+00	1.1551E−01	9.6563E+00	9.8169E−02	1.0186E+01	8.4087E−02
1	6.5652E+00	2.4904E−01	7.3006E+00	1.4273E−01	7.6151E+00	1.2118E−01	8.0455E+00	1.0365E−01
2	4.0822E+00	3.7245E−01	4.6135E+00	2.1068E−01	4.8233E+00	1.7852E−01	5.1069E+00	1.5242E−01
3	2.7075E+00	5.1119E−01	3.1010E+00	2.8612E−01	3.2477E+00	2.4210E−01	3.4430E+00	2.0650E−01
4	1.9587E+00	6.3742E−01	2.2663E+00	3.5434E−01	2.3767E+00	2.9955E−01	2.5220E+00	2.5533E−01
5	1.4827E+00	7.5771E−01	1.7300E+00	4.1900E−01	1.8162E+00	3.5396E−01	1.9287E+00	3.0157E−01
6	1.1508E+00	8.7970E−01	1.3512E+00	4.8425E−01	1.4196E+00	4.0883E−01	1.5084E+00	3.4818E−01
7	9.1135E−01	1.0050E+00	1.0735E+00	5.5106E−01	1.1284E+00	4.6498E−01	1.1992E+00	3.9586E−01
8	7.3617E−01	1.1314E+00	8.6714E−01	6.1846E−01	9.1151E−01	5.2163E−01	9.6879E−01	4.4396E−01
9	6.0657E−01	1.2555E+00	7.1252E−01	6.8481E−01	7.4875E−01	5.7740E−01	7.9564E−01	4.9133E−01
10	5.0917E−01	1.3743E+00	5.9541E−01	7.4847E−01	6.2536E−01	6.3094E−01	6.6428E−01	5.3680E−01
11	4.3428E−01	1.4855E+00	5.0528E−01	8.0821E−01	5.3037E−01	6.8119E−01	5.6314E−01	5.7949E−01
12	3.7608E−01	1.5889E+00	4.3544E−01	8.6371E−01	4.5678E−01	7.2787E−01	4.8480E−01	6.1915E−01
13	3.2962E−01	1.6844E+00	3.8009E−01	9.1479E−01	3.9851E−01	7.7082E−01	4.2280E−01	6.5563E−01
14	2.9167E−01	1.7727E+00	3.3531E−01	9.6176E−01	3.5142E−01	8.1029E−01	3.7273E−01	6.8914E−01
15	2.6023E−01	1.8549E+00	2.9854E−01	1.0052E+00	3.1280E−01	8.4674E−01	3.3170E−01	7.2008E−01
16	2.3383E−01	1.9320E+00	2.6788E−01	1.0456E+00	2.8062E−01	8.8068E−01	2.9754E−01	7.4885E−01
17	2.1140E−01	2.0050E+00	2.4195E−01	1.0837E+00	2.5342E−01	9.1257E−01	2.6868E−01	7.7589E−01
18	1.9216E−01	2.0747E+00	2.1976E−01	1.1198E+00	2.3016E−01	9.4284E−01	2.4400E−01	8.0153E−01
19	1.7551E−01	2.1416E+00	2.0057E−01	1.1544E+00	2.1004E−01	9.7183E−01	2.2266E−01	8.2608E−01
20	1.6101E−01	2.2063E+00	1.8382E−01	1.1878E+00	1.9248E−01	9.9980E−01	2.0403E−01	8.4977E−01
21	1.4829E−01	2.2692E+00	1.6909E−01	1.2203E+00	1.7704E−01	1.0269E+00	1.8764E−01	8.7276E−01
22	1.3707E−01	2.3304E+00	1.5606E−01	1.2519E+00	1.6337E−01	1.0534E+00	1.7313E−01	8.9516E−01
23	1.2712E−01	2.3902E+00	1.4446E−01	1.2828E+00	1.5119E−01	1.0793E+00	1.6020E−01	9.1708E−01
24	1.1826E−01	2.4486E+00	1.3409E−01	1.3130E+00	1.4030E−01	1.1046E+00	1.4863E−01	9.3855E−01
25	1.1033E−01	2.5059E+00	1.2478E−01	1.3427E+00	1.3051E−01	1.1295E+00	1.3823E−01	9.5962E−01
26	1.0320E−01	2.5620E+00	1.1638E−01	1.3718E+00	1.2168E−01	1.1539E+00	1.2885E−01	9.8030E−01
27	9.6764E−02	2.6170E+00	1.0878E−01	1.4004E+00	1.1370E−01	1.1778E+00	1.2036E−01	1.0006E+00
28	9.0936E−02	2.6708E+00	1.0188E−01	1.4284E+00	1.0645E−01	1.2013E+00	1.1266E−01	1.0205E+00
29	8.5639E−02	2.7236E+00	9.5611E−02	1.4559E+00	9.9850E−02	1.2244E+00	1.0564E−01	1.0401E+00
30	8.0809E−02	2.7753E+00	8.9888E−02	1.4829E+00	9.3832E−02	1.2470E+00	9.9245E−02	1.0593E+00
31	7.6391E−02	2.8260E+00	8.4655E−02	1.5093E+00	8.8328E−02	1.2692E+00	9.3393E−02	1.0781E+00
32	7.2338E−02	2.8756E+00	7.9857E−02	1.5352E+00	8.3284E−02	1.2909E+00	8.8032E−02	1.0965E+00
33	6.8610E−02	2.9241E+00	7.5451E−02	1.5605E+00	7.8651E−02	1.3122E+00	8.3108E−02	1.1145E+00
34	6.5172E−02	2.9716E+00	7.1395E−02	1.5854E+00	7.4388E−02	1.3330E+00	7.8577E−02	1.1321E+00
35	6.1993E−02	3.0182E+00	6.7653E−02	1.6096E+00	7.0457E−02	1.3533E+00	7.4400E−02	1.1494E+00
36	5.9048E−02	3.0637E+00	6.4196E−02	1.6333E+00	6.6825E−02	1.3732E+00	7.0543E−02	1.1663E+00
37	5.6313E−02	3.1083E+00	6.0996E−02	1.6565E+00	6.3465E−02	1.3927E+00	6.6975E−02	1.1828E+00
38	5.3768E−02	3.1519E+00	5.8028E−02	1.6792E+00	6.0350E−02	1.4117E+00	6.3668E−02	1.1989E+00
39	5.1396E−02	3.1946E+00	5.5271E−02	1.7014E+00	5.7458E−02	1.4303E+00	6.0598E−02	1.2147E+00
40	4.9180E−02	3.2364E+00	5.2705E−02	1.7231E+00	5.4767E−02	1.4485E+00	5.7744E−02	1.2301E+00
41	4.7108E−02	3.2774E+00	5.0314E−02	1.7443E+00	5.2262E−02	1.4662E+00	5.5086E−02	1.2452E+00
42	4.5166E−02	3.3175E+00	4.8083E−02	1.7650E+00	4.9924E−02	1.4836E+00	5.2608E−02	1.2599E+00
43	4.3344E−02	3.3568E+00	4.5997E−02	1.7852E+00	4.7740E−02	1.5006E+00	5.0293E−02	1.2743E+00
44	4.1632E−02	3.3953E+00	4.4044E−02	1.8051E+00	4.5697E−02	1.5172E+00	4.8129E−02	1.2883E+00
45	4.0021E−02	3.4330E+00	4.2214E−02	1.8244E+00	4.3783E−02	1.5334E+00	4.6101E−02	1.3021E+00
46	3.8503E−02	3.4700E+00	4.0496E−02	1.8434E+00	4.1987E−02	1.5493E+00	4.4200E−02	1.3155E+00
47	3.7071E−02	3.5063E+00	3.8882E−02	1.8619E+00	4.0300E−02	1.5648E+00	4.2415E−02	1.3287E+00
48	3.5718E−02	3.5419E+00	3.7363E−02	1.8801E+00	3.8714E−02	1.5800E+00	4.0737E−02	1.3416E+00
49	3.4440E−02	3.5768E+00	3.5932E−02	1.8979E+00	3.7220E−02	1.5949E+00	3.9157E−02	1.3542E+00
50	3.3230E−02	3.6110E+00	3.4582E−02	1.9153E+00	3.5812E−02	1.6095E+00	3.7668E−02	1.3665E+00
51	3.2083E−02	3.6447E+00	3.3308E−02	1.9324E+00	3.4483E−02	1.6238E+00	3.6264E−02	1.3786E+00
52	3.0996E−02	3.6777E+00	3.2104E−02	1.9491E+00	3.3228E−02	1.6378E+00	3.4937E−02	1.3904E+00
53	2.9964E−02	3.7102E+00	3.0964E−02	1.9655E+00	3.2040E−02	1.6515E+00	3.3683E−02	1.4021E+00
54	2.8984E−02	3.7421E+00	2.9885E−02	1.9816E+00	3.0916E−02	1.6649E+00	3.2496E−02	1.4134E+00
55	2.8052E−02	3.7734E+00	2.8861E−02	1.9974E+00	2.9851E−02	1.6781E+00	3.1371E−02	1.4246E+00
56	2.7165E−02	3.8043E+00	2.7890E−02	2.0129E+00	2.8840E−02	1.6911E+00	3.0305E−02	1.4355E+00
57	2.6321E−02	3.8346E+00	2.6968E−02	2.0281E+00	2.7881E−02	1.7038E+00	2.9292E−02	1.4463E+00
58	2.5516E−02	3.8644E+00	2.6091E−02	2.0431E+00	2.6969E−02	1.7163E+00	2.8330E−02	1.4568E+00
59	2.4748E−02	3.8938E+00	2.5257E−02	2.0577E+00	2.6102E−02	1.7285E+00	2.7415E−02	1.4672E+00
60	2.4016E−02	3.9227E+00	2.4462E−02	2.0722E+00	2.5276E−02	1.7406E+00	2.6545E−02	1.4774E+00

Table 4.3.3.1. *Partial wave elastic scattering factors for neutral atoms (cont.)*
V; $Z = 23$

	10 keV		40 keV		60 keV		90 keV	
s	$\|f(s)\|$	$\eta(s)$	$\|f(s)\|$	$\eta(s)$	$\|f(s)\|$	$\eta(s)$	$\|f(s)\|$	$\eta(s)$
0	7.8964E+00	2.1149E−01	8.7493E+00	1.2304E−01	9.1204E+00	1.0472E−01	9.6240E+00	8.9803E−02
1	6.2982E+00	2.5844E−01	7.0348E+00	1.4941E−01	7.3431E+00	1.2702E−01	7.7618E+00	1.0876E−01
2	4.0368E+00	3.7776E−01	4.5843E+00	2.1546E−01	4.7966E+00	1.8281E−01	5.0815E+00	1.5622E−01
3	2.7172E+00	5.1504E−01	3.1298E+00	2.9041E−01	3.2809E+00	2.4601E−01	3.4805E+00	2.1000E−01
4	1.9800E+00	6.4225E−01	2.3056E+00	3.5939E−01	2.4204E+00	3.0412E−01	2.5702E+00	2.5942E−01
5	1.5083E+00	7.6333E−01	1.7722E+00	4.2469E−01	1.8626E+00	3.5909E−01	1.9795E+00	3.0615E−01
6	1.1778E+00	8.8534E−01	1.3935E+00	4.9014E−01	1.4659E+00	4.1416E−01	1.5589E+00	3.5293E−01
7	9.3731E−01	1.0106E+00	1.1136E+00	5.5707E−01	1.1720E+00	4.7043E−01	1.2469E+00	4.0073E−01
8	7.5963E−01	1.1377E+00	9.0330E−01	6.2497E−01	9.5091E−01	5.2751E−01	1.0117E+00	4.4920E−01
9	6.2699E−01	1.2639E+00	7.4402E−01	6.9250E−01	7.8307E−01	5.8429E−01	8.3302E−01	4.9743E−01
10	5.2664E−01	1.3863E+00	6.2226E−01	7.5818E−01	6.5460E−01	6.3953E−01	6.9612E−01	5.4436E−01
11	4.4921E−01	1.5023E+00	5.2792E−01	8.2068E−01	5.5500E−01	6.9212E−01	5.8993E−01	5.8905E−01
12	3.8892E−01	1.6113E+00	4.5445E−01	8.7942E−01	4.7741E−01	7.4155E−01	5.0721E−01	6.3106E−01
13	3.4075E−01	1.7127E+00	3.9610E−01	9.3399E−01	4.1584E−01	7.8747E−01	4.4159E−01	6.7008E−01
14	3.0144E−01	1.8068E+00	3.4891E−01	9.8443E−01	3.6609E−01	8.2990E−01	3.8861E−01	7.0612E−01
15	2.6889E−01	1.8945E+00	3.1022E−01	1.0311E+00	3.2536E−01	8.6914E−01	3.4527E−01	7.3944E−01
16	2.4156E−01	1.9766E+00	2.7803E−01	1.0745E+00	2.9151E−01	9.0559E−01	3.0927E−01	7.7037E−01
17	2.1834E−01	2.0540E+00	2.5089E−01	1.1152E+00	2.6299E−01	9.3968E−01	2.7898E−01	7.9928E−01
18	1.9842E−01	2.1276E+00	2.2773E−01	1.1535E+00	2.3867E−01	9.7182E−01	2.5315E−01	8.2653E−01
19	1.8120E−01	2.1979E+00	2.0775E−01	1.1900E+00	2.1771E−01	1.0024E+00	2.3090E−01	8.5243E−01
20	1.6619E−01	2.2655E+00	1.9037E−01	1.2250E+00	1.9947E−01	1.0317E+00	2.1153E−01	8.7724E−01
21	1.5304E−01	2.3310E+00	1.7511E−01	1.2587E+00	1.8346E−01	1.0599E+00	1.9454E−01	9.0117E−01
22	1.4145E−01	2.3945E+00	1.6164E−01	1.2915E+00	1.6932E−01	1.0874E+00	1.7952E−01	9.2438E−01
23	1.3117E−01	2.4563E+00	1.4966E−01	1.3234E+00	1.5674E−01	1.1141E+00	1.6617E−01	9.4699E−01
24	1.2203E−01	2.5167E+00	1.3896E−01	1.3545E+00	1.4550E−01	1.1401E+00	1.5423E−01	9.6908E−01
25	1.1385E−01	2.5757E+00	1.2935E−01	1.3850E+00	1.3541E−01	1.1657E+00	1.4350E−01	9.9072E−01
26	1.0650E−01	2.6335E+00	1.2070E−01	1.4149E+00	1.2631E−01	1.1907E+00	1.3383E−01	1.0119E+00
27	9.9870E−02	2.6901E+00	1.1286E−01	1.4442E+00	1.1808E−01	1.2153E+00	1.2508E−01	1.0328E+00
28	9.3872E−02	2.7456E+00	1.0576E−01	1.4730E+00	1.1060E−01	1.2394E+00	1.1713E−01	1.0532E+00
29	8.8424E−02	2.7999E+00	9.9293E−02	1.5013E+00	1.0380E−01	1.2631E+00	1.0989E−01	1.0733E+00
30	8.3459E−02	2.8532E+00	9.3391E−02	1.5290E+00	9.7585E−02	1.2863E+00	1.0329E−01	1.0929E+00
31	7.8920E−02	2.9054E+00	8.7992E−02	1.5562E+00	9.1902E−02	1.3091E+00	9.7241E−02	1.1123E+00
32	7.4758E−02	2.9566E+00	8.3040E−02	1.5828E+00	8.6690E−02	1.3315E+00	9.1697E−02	1.1313E+00
33	7.0930E−02	3.0068E+00	7.8488E−02	1.6090E+00	8.1900E−02	1.3534E+00	8.6602E−02	1.1498E+00
34	6.7401E−02	3.0559E+00	7.4295E−02	1.6346E+00	7.7488E−02	1.3749E+00	8.1910E−02	1.1681E+00
35	6.4140E−02	3.1041E+00	7.0427E−02	1.6597E+00	7.3418E−02	1.3959E+00	7.7582E−02	1.1859E+00
36	6.1118E−02	3.1513E+00	6.6849E−02	1.6843E+00	6.9655E−02	1.4166E+00	7.3581E−02	1.2034E+00
37	5.8312E−02	3.1975E+00	6.3535E−02	1.7083E+00	6.6171E−02	1.4368E+00	6.9877E−02	1.2205E+00
38	5.5701E−02	3.2428E+00	6.0460E−02	1.7319E+00	6.2939E−02	1.4565E+00	6.6443E−02	1.2373E+00
39	5.3267E−02	3.2872E+00	5.7602E−02	1.7550E+00	5.9936E−02	1.4759E+00	6.3253E−02	1.2537E+00
40	5.0993E−02	3.3307E+00	5.4941E−02	1.7775E+00	5.7142E−02	1.4948E+00	6.0285E−02	1.2697E+00
41	4.8866E−02	3.3734E+00	5.2460E−02	1.7996E+00	5.4538E−02	1.5133E+00	5.7520E−02	1.2854E+00
42	4.6873E−02	3.4152E+00	5.0144E−02	1.8212E+00	5.2107E−02	1.5314E+00	5.4940E−02	1.3008E+00
43	4.5001E−02	3.4561E+00	4.7977E−02	1.8424E+00	4.9835E−02	1.5492E+00	5.2529E−02	1.3159E+00
44	4.3242E−02	3.4963E+00	4.5948E−02	1.8631E+00	4.7708E−02	1.5665E+00	5.0274E−02	1.3306E+00
45	4.1587E−02	3.5357E+00	4.4046E−02	1.8834E+00	4.5715E−02	1.5835E+00	4.8161E−02	1.3450E+00
46	4.0026E−02	3.5744E+00	4.2260E−02	1.9032E+00	4.3845E−02	1.6001E+00	4.6178E−02	1.3591E+00
47	3.8553E−02	3.6123E+00	4.0581E−02	1.9226E+00	4.2088E−02	1.6164E+00	4.4316E−02	1.3728E+00
48	3.7162E−02	3.6496E+00	3.9000E−02	1.9417E+00	4.0435E−02	1.6324E+00	4.2565E−02	1.3863E+00
49	3.5845E−02	3.6861E+00	3.7511E−02	1.9603E+00	3.8878E−02	1.6480E+00	4.0917E−02	1.3996E+00
50	3.4599E−02	3.7220E+00	3.6105E−02	1.9786E+00	3.7409E−02	1.6633E+00	3.9363E−02	1.4125E+00
51	3.3418E−02	3.7573E+00	3.4779E−02	1.9965E+00	3.6024E−02	1.6782E+00	3.7897E−02	1.4252E+00
52	3.2297E−02	3.7919E+00	3.3524E−02	2.0141E+00	3.4714E−02	1.6929E+00	3.6511E−02	1.4376E+00
53	3.1233E−02	3.8259E+00	3.2337E−02	2.0313E+00	3.3475E−02	1.7073E+00	3.5202E−02	1.4498E+00
54	3.0222E−02	3.8594E+00	3.1212E−02	2.0482E+00	3.2302E−02	1.7215E+00	3.3962E−02	1.4618E+00
55	2.9259E−02	3.8923E+00	3.0145E−02	2.0648E+00	3.1190E−02	1.7353E+00	3.2787E−02	1.4735E+00
56	2.8343E−02	3.9246E+00	2.9133E−02	2.0810E+00	3.0135E−02	1.7489E+00	3.1673E−02	1.4850E+00
57	2.7471E−02	3.9565E+00	2.8171E−02	2.0970E+00	2.9134E−02	1.7623E+00	3.0615E−02	1.4963E+00
58	2.6639E−02	3.9878E+00	2.7257E−02	2.1127E+00	2.8182E−02	1.7754E+00	2.9610E−02	1.5074E+00
59	2.5844E−02	4.0186E+00	2.6387E−02	2.1281E+00	2.7276E−02	1.7883E+00	2.8654E−02	1.5183E+00
60	2.5086E−02	4.0490E+00	2.5558E−02	2.1433E+00	2.6414E−02	1.8009E+00	2.7744E−02	1.5290E+00

Table 4.3.3.1. *Partial wave elastic scattering factors for neutral atoms (cont.)*
Cr; $Z = 24$

	10 keV		40 keV		60 keV		90 keV	
s	$\|f(s)\|$	$\eta(s)$	$\|f(s)\|$	$\eta(s)$	$\|f(s)\|$	$\eta(s)$	$\|f(s)\|$	$\eta(s)$
0	6.5487E+00	2.3087E−01	7.3124E+00	1.3592E−01	7.6308E+00	1.1590E−01	8.0559E+00	9.9555E−02
1	5.3648E+00	2.7679E−01	6.0387E+00	1.6179E−01	6.3105E+00	1.3779E−01	6.6750E+00	1.1813E−01
2	3.6934E+00	3.8330E−01	4.2223E+00	2.2100E−01	4.4225E+00	1.8781E−01	4.6887E+00	1.6068E−01
3	2.6401E+00	5.0123E−01	3.0602E+00	2.8576E−01	3.2112E+00	2.4247E−01	3.4091E+00	2.0721E−01
4	1.9810E+00	6.1693E−01	2.3230E+00	3.4881E−01	2.4413E+00	2.9563E−01	2.5945E+00	2.5245E−01
5	1.5285E+00	7.3384E−01	1.8101E+00	4.1210E−01	1.9048E+00	3.4893E−01	2.0261E+00	2.9778E−01
6	1.2016E+00	8.5497E−01	1.4339E+00	4.7727E−01	1.5104E+00	4.0378E−01	1.6078E+00	3.4439E−01
7	9.6026E−01	9.8061E−01	1.1516E+00	5.4458E−01	1.2138E+00	4.6039E−01	1.2926E+00	3.9248E−01
8	7.8043E−01	1.1090E+00	9.3749E−01	6.1326E−01	9.8843E−01	5.1814E−01	1.0528E+00	4.4153E−01
9	6.4530E−01	1.2374E+00	7.7399E−01	6.8203E−01	8.1595E−01	5.7597E−01	8.6901E−01	4.9066E−01
10	5.4255E−01	1.3629E+00	6.4812E−01	7.4950E−01	6.8294E−01	6.3273E−01	7.2713E−01	5.3888E−01
11	4.6303E−01	1.4831E+00	5.5005E−01	8.1435E−01	5.7922E−01	6.8730E−01	6.1642E−01	5.8526E−01
12	4.0097E−01	1.5969E+00	4.7331E−01	8.7589E−01	4.9802E−01	7.3912E−01	5.2971E−01	6.2931E−01
13	3.5135E−01	1.7035E+00	4.1220E−01	9.3355E−01	4.3338E−01	7.8766E−01	4.6070E−01	6.7058E−01
14	3.1085E−01	1.8029E+00	3.6273E−01	9.8720E−01	3.8109E−01	8.3283E−01	4.0492E−01	7.0897E−01
15	2.7731E−01	1.8958E+00	3.2217E−01	1.0371E+00	3.3828E−01	8.7476E−01	3.5928E−01	7.4460E−01
16	2.4914E−01	1.9828E+00	2.8845E−01	1.0834E+00	3.0274E−01	9.1375E−01	3.2143E−01	7.7771E−01
17	2.2521E−01	2.0648E+00	2.6007E−01	1.1268E+00	2.7286E−01	9.5016E−01	2.8963E−01	8.0861E−01
18	2.0467E−01	2.1425E+00	2.3590E−01	1.1676E+00	2.4743E−01	9.8438E−01	2.6260E−01	8.3763E−01
19	1.8690E−01	2.2165E+00	2.1509E−01	1.2062E+00	2.2557E−01	1.0167E+00	2.3936E−01	8.6507E−01
20	1.7141E−01	2.2875E+00	1.9702E−01	1.2430E+00	2.0659E−01	1.0476E+00	2.1919E−01	8.9121E−01
21	1.5783E−01	2.3559E+00	1.8120E−01	1.2784E+00	1.8997E−01	1.0772E+00	2.0154E−01	9.1629E−01
22	1.4586E−01	2.4221E+00	1.6724E−01	1.3125E+00	1.7531E−01	1.1058E+00	1.8597E−01	9.4048E−01
23	1.3526E−01	2.4863E+00	1.5486E−01	1.3456E+00	1.6230E−01	1.1335E+00	1.7215E−01	9.6395E−01
24	1.2582E−01	2.5489E+00	1.4380E−01	1.3778E+00	1.5069E−01	1.1605E+00	1.5981E−01	9.8679E−01
25	1.1737E−01	2.6099E+00	1.3389E−01	1.4093E+00	1.4027E−01	1.1868E+00	1.4873E−01	1.0091E+00
26	1.0980E−01	2.6696E+00	1.2497E−01	1.4401E+00	1.3088E−01	1.2126E+00	1.3875E−01	1.0309E+00
27	1.0297E−01	2.7280E+00	1.1689E−01	1.4702E+00	1.2239E−01	1.2378E+00	1.2973E−01	1.0523E+00
28	9.6791E−02	2.7851E+00	1.0957E−01	1.4998E+00	1.1469E−01	1.2626E+00	1.2153E−01	1.0733E+00
29	9.1183E−02	2.8411E+00	1.0291E−01	1.5288E+00	1.0767E−01	1.2869E+00	1.1407E−01	1.0939E+00
30	8.6076E−02	2.8960E+00	9.6828E−02	1.5573E+00	1.0127E−01	1.3108E+00	1.0726E−01	1.1141E+00
31	8.1410E−02	2.9499E+00	9.1263E−02	1.5852E+00	9.5408E−02	1.3342E+00	1.0102E−01	1.1340E+00
32	7.7134E−02	3.0026E+00	8.6158E−02	1.6126E+00	9.0031E−02	1.3572E+00	9.5296E−02	1.1535E+00
33	7.3204E−02	3.0544E+00	8.1464E−02	1.6395E+00	8.5087E−02	1.3798E+00	9.0035E−02	1.1726E+00
34	6.9582E−02	3.1051E+00	7.7139E−02	1.6659E+00	8.0532E−02	1.4019E+00	8.5186E−02	1.1914E+00
35	6.6236E−02	3.1549E+00	7.3145E−02	1.6918E+00	7.6326E−02	1.4236E+00	8.0711E−02	1.2098E+00
36	6.3137E−02	3.2037E+00	6.9452E−02	1.7172E+00	7.2436E−02	1.4449E+00	7.6572E−02	1.2278E+00
37	6.0260E−02	3.2516E+00	6.6028E−02	1.7421E+00	6.8833E−02	1.4658E+00	7.2738E−02	1.2455E+00
38	5.7583E−02	3.2985E+00	6.2850E−02	1.7665E+00	6.5488E−02	1.4862E+00	6.9180E−02	1.2629E+00
39	5.5088E−02	3.3445E+00	5.9895E−02	1.7904E+00	6.2379E−02	1.5063E+00	6.5874E−02	1.2799E+00
40	5.2758E−02	3.3897E+00	5.7142E−02	1.8138E+00	5.9484E−02	1.5259E+00	6.2796E−02	1.2966E+00
41	5.0578E−02	3.4339E+00	5.4574E−02	1.8367E+00	5.6785E−02	1.5452E+00	5.9927E−02	1.3129E+00
42	4.8535E−02	3.4774E+00	5.2175E−02	1.8592E+00	5.4264E−02	1.5640E+00	5.7249E−02	1.3288E+00
43	4.6616E−02	3.5200E+00	4.9931E−02	1.8812E+00	5.1907E−02	1.5825E+00	5.4745E−02	1.3445E+00
44	4.4813E−02	3.5618E+00	4.7829E−02	1.9028E+00	4.9700E−02	1.6005E+00	5.2401E−02	1.3598E+00
45	4.3115E−02	3.6028E+00	4.5857E−02	1.9239E+00	4.7631E−02	1.6182E+00	5.0205E−02	1.3748E+00
46	4.1514E−02	3.6431E+00	4.4004E−02	1.9446E+00	4.5688E−02	1.6356E+00	4.8144E−02	1.3895E+00
47	4.0003E−02	3.6827E+00	4.2262E−02	1.9649E+00	4.3862E−02	1.6526E+00	4.6207E−02	1.4039E+00
48	3.8574E−02	3.7215E+00	4.0622E−02	1.9848E+00	4.2144E−02	1.6692E+00	4.4385E−02	1.4180E+00
49	3.7223E−02	3.7597E+00	3.9076E−02	2.0043E+00	4.0525E−02	1.6855E+00	4.2669E−02	1.4318E+00
50	3.5943E−02	3.7972E+00	3.7617E−02	2.0234E+00	3.8998E−02	1.7015E+00	4.1051E−02	1.4454E+00
51	3.4729E−02	3.8340E+00	3.6239E−02	2.0421E+00	3.7556E−02	1.7172E+00	3.9525E−02	1.4587E+00
52	3.3577E−02	3.8702E+00	3.4935E−02	2.0605E+00	3.6194E−02	1.7326E+00	3.8082E−02	1.4717E+00
53	3.2483E−02	3.9058E+00	3.3701E−02	2.0785E+00	3.4904E−02	1.7477E+00	3.6717E−02	1.4845E+00
54	3.1442E−02	3.9408E+00	3.2532E−02	2.0962E+00	3.3683E−02	1.7625E+00	3.5425E−02	1.4970E+00
55	3.0452E−02	3.9752E+00	3.1423E−02	2.1135E+00	3.2526E−02	1.7770E+00	3.4201E−02	1.5093E+00
56	2.9508E−02	4.0091E+00	3.0371E−02	2.1306E+00	3.1427E−02	1.7912E+00	3.3040E−02	1.5213E+00
57	2.8609E−02	4.0424E+00	2.9371E−02	2.1474E+00	3.0384E−02	1.8052E+00	3.1937E−02	1.5332E+00
58	2.7752E−02	4.0753E+00	2.8419E−02	2.1638E+00	2.9393E−02	1.8190E+00	3.0889E−02	1.5448E+00
59	2.6933E−02	4.1076E+00	2.7514E−02	2.1799E+00	2.8450E−02	1.8325E+00	2.9893E−02	1.5562E+00
60	2.6151E−02	4.1394E+00	2.6652E−02	2.1958E+00	2.7552E−02	1.8457E+00	2.8944E−02	1.5674E+00

Table 4.3.3.1. *Partial wave elastic scattering factors for neutral atoms (cont.)*
Mn; $Z = 25$

	10 keV		40 keV		60 keV		90 keV	
s	$\|f(s)\|$	$\eta(s)$	$\|f(s)\|$	$\eta(s)$	$\|f(s)\|$	$\eta(s)$	$\|f(s)\|$	$\eta(s)$
0	7.0380E+00	2.3139E−01	7.8661E+00	1.3708E−01	8.2111E+00	1.1703E−01	8.6717E+00	1.0059E−01
1	5.7919E+00	2.7543E−01	6.5264E+00	1.6210E−01	6.8223E+00	1.3822E−01	7.2186E+00	1.1860E−01
2	3.8974E+00	3.8806E−01	4.4682E+00	2.2511E−01	4.6827E+00	1.9151E−01	4.9667E+00	1.6398E−01
3	2.6962E+00	5.2180E−01	3.1400E+00	2.9878E−01	3.2977E+00	2.5373E−01	3.5031E+00	2.1697E−01
4	1.9947E+00	6.4920E−01	2.3517E+00	3.6836E−01	2.4739E+00	3.1241E−01	2.6311E+00	2.6692E−01
5	1.5387E+00	7.7067E−01	1.8327E+00	4.3431E−01	1.9306E+00	3.6799E−01	2.0551E+00	3.1419E−01
6	1.2156E+00	8.9207E−01	1.4600E+00	4.9985E−01	1.5396E+00	4.2317E−01	1.6402E+00	3.6111E−01
7	9.7702E−01	1.0163E+00	1.1803E+00	5.6662E−01	1.2457E+00	4.7935E−01	1.3278E+00	4.0885E−01
8	7.9768E−01	1.1434E+00	9.6638E−01	6.3473E−01	1.0203E+00	5.3664E−01	1.0879E+00	4.5752E−01
9	6.6153E−01	1.2715E+00	8.0116E−01	7.0343E−01	8.4591E−01	5.9442E−01	9.0193E−01	5.0660E−01
10	5.5715E−01	1.3982E+00	6.7259E−01	7.7156E−01	7.0992E−01	6.5174E−01	7.5676E−01	5.5531E−01
11	4.7592E−01	1.5210E+00	5.7156E−01	8.3790E−01	6.0292E−01	7.0758E−01	6.4243E−01	6.0277E−01
12	4.1228E−01	1.6386E+00	4.9192E−01	9.0162E−01	5.1849E−01	7.6123E−01	5.5217E−01	6.4838E−01
13	3.6135E−01	1.7497E+00	4.2821E−01	9.6197E−01	4.5096E−01	8.1207E−01	4.7996E−01	6.9162E−01
14	3.1976E−01	1.8541E+00	3.7653E−01	1.0186E+00	3.9619E−01	8.5979E−01	4.2143E−01	7.3220E−01
15	2.8534E−01	1.9520E+00	3.3412E−01	1.0716E+00	3.5131E−01	9.0438E−01	3.7349E−01	7.7011E−01
16	2.5642E−01	2.0439E+00	2.9888E−01	1.1210E+00	3.1406E−01	9.4597E−01	3.3374E−01	8.0545E−01
17	2.3184E−01	2.1305E+00	2.6925E−01	1.1672E+00	2.8278E−01	9.8482E−01	3.0039E−01	8.3845E−01
18	2.1074E−01	2.2124E+00	2.4405E−01	1.2106E+00	2.5622E−01	1.0213E+00	2.7210E−01	8.6938E−01
19	1.9246E−01	2.2903E+00	2.2240E−01	1.2515E+00	2.3342E−01	1.0556E+00	2.4783E−01	8.9852E−01
20	1.7653E−01	2.3647E+00	2.0363E−01	1.2904E+00	2.1367E−01	1.0882E+00	2.2683E−01	9.2614E−01
21	1.6254E−01	2.4362E+00	1.8722E−01	1.3275E+00	1.9641E−01	1.1193E+00	2.0848E−01	9.5250E−01
22	1.5021E−01	2.5052E+00	1.7277E−01	1.3631E+00	1.8123E−01	1.1492E+00	1.9234E−01	9.7779E−01
23	1.3928E−01	2.5720E+00	1.5997E−01	1.3976E+00	1.6777E−01	1.1780E+00	1.7804E−01	1.0022E+00
24	1.2954E−01	2.6369E+00	1.4855E−01	1.4310E+00	1.5577E−01	1.2059E+00	1.6529E−01	1.0259E+00
25	1.2084E−01	2.7000E+00	1.3833E−01	1.4634E+00	1.4502E−01	1.2331E+00	1.5386E−01	1.0489E+00
26	1.1303E−01	2.7616E+00	1.2913E−01	1.4951E+00	1.3535E−01	1.2596E+00	1.4357E−01	1.0713E+00
27	1.0599E−01	2.8218E+00	1.2082E−01	1.5261E+00	1.2660E−01	1.2856E+00	1.3427E−01	1.0933E+00
28	9.9633E−02	2.8807E+00	1.1328E−01	1.5565E+00	1.1867E−01	1.3110E+00	1.2583E−01	1.1149E+00
29	9.3861E−02	2.9384E+00	1.0643E−01	1.5863E+00	1.1145E−01	1.3360E+00	1.1815E−01	1.1360E+00
30	8.8608E−02	2.9950E+00	1.0017E−01	1.6155E+00	1.0486E−01	1.3604E+00	1.1113E−01	1.1567E+00
31	8.3812E−02	3.0504E+00	9.4442E−02	1.6442E+00	9.8823E−02	1.3844E+00	1.0471E−01	1.1771E+00
32	7.9419E−02	3.1047E+00	8.9188E−02	1.6723E+00	9.3286E−02	1.4080E+00	9.8811E−02	1.1971E+00
33	7.5385E−02	3.1580E+00	8.4356E−02	1.6999E+00	8.8194E−02	1.4312E+00	9.3388E−02	1.2167E+00
34	7.1669E−02	3.2103E+00	7.9903E−02	1.7271E+00	8.3501E−02	1.4540E+00	8.8390E−02	1.2360E+00
35	6.8238E−02	3.2616E+00	7.5791E−02	1.7537E+00	7.9166E−02	1.4763E+00	8.3774E−02	1.2549E+00
36	6.5062E−02	3.3119E+00	7.1985E−02	1.7798E+00	7.5155E−02	1.4982E+00	7.9503E−02	1.2735E+00
37	6.2116E−02	3.3613E+00	6.8457E−02	1.8055E+00	7.1436E−02	1.5197E+00	7.5544E−02	1.2917E+00
38	5.9376E−02	3.4098E+00	6.5180E−02	1.8306E+00	6.7984E−02	1.5408E+00	7.1868E−02	1.3096E+00
39	5.6822E−02	3.4573E+00	6.2132E−02	1.8553E+00	6.4773E−02	1.5615E+00	6.8450E−02	1.3272E+00
40	5.4438E−02	3.5040E+00	5.9292E−02	1.8795E+00	6.1782E−02	1.5818E+00	6.5267E−02	1.3444E+00
41	5.2207E−02	3.5499E+00	5.6641E−02	1.9033E+00	5.8991E−02	1.6017E+00	6.2298E−02	1.3613E+00
42	5.0117E−02	3.5949E+00	5.4164E−02	1.9266E+00	5.6384E−02	1.6213E+00	5.9526E−02	1.3779E+00
43	4.8155E−02	3.6390E+00	5.1845E−02	1.9494E+00	5.3946E−02	1.6404E+00	5.6932E−02	1.3941E+00
44	4.6310E−02	3.6824E+00	4.9672E−02	1.9718E+00	5.1661E−02	1.6592E+00	5.4504E−02	1.4100E+00
45	4.4573E−02	3.7250E+00	4.7633E−02	1.9937E+00	4.9518E−02	1.6776E+00	5.2227E−02	1.4256E+00
46	4.2935E−02	3.7669E+00	4.5718E−02	2.0152E+00	4.7506E−02	1.6956E+00	5.0089E−02	1.4409E+00
47	4.1389E−02	3.8080E+00	4.3915E−02	2.0364E+00	4.5614E−02	1.7133E+00	4.8080E−02	1.4559E+00
48	3.9927E−02	3.8484E+00	4.2218E−02	2.0570E+00	4.3833E−02	1.7306E+00	4.6189E−02	1.4706E+00
49	3.8544E−02	3.8881E+00	4.0617E−02	2.0773E+00	4.2154E−02	1.7476E+00	4.4407E−02	1.4850E+00
50	3.7233E−02	3.9271E+00	3.9106E−02	2.0973E+00	4.0570E−02	1.7643E+00	4.2727E−02	1.4991E+00
51	3.5990E−02	3.9655E+00	3.7678E−02	2.1168E+00	3.9074E−02	1.7807E+00	4.1141E−02	1.5130E+00
52	3.4809E−02	4.0032E+00	3.6328E−02	2.1360E+00	3.7660E−02	1.7967E+00	3.9642E−02	1.5266E+00
53	3.3688E−02	4.0403E+00	3.5049E−02	2.1548E+00	3.6322E−02	1.8125E+00	3.8224E−02	1.5399E+00
54	3.2621E−02	4.0768E+00	3.3837E−02	2.1732E+00	3.5054E−02	1.8279E+00	3.6881E−02	1.5530E+00
55	3.1605E−02	4.1127E+00	3.2687E−02	2.1914E+00	3.3852E−02	1.8431E+00	3.5608E−02	1.5658E+00
56	3.0637E−02	4.1481E+00	3.1595E−02	2.2092E+00	3.2711E−02	1.8580E+00	3.4401E−02	1.5784E+00
57	2.9714E−02	4.1829E+00	3.0558E−02	2.2267E+00	3.1627E−02	1.8726E+00	3.3254E−02	1.5908E+00
58	2.8833E−02	4.2172E+00	2.9571E−02	2.2439E+00	3.0597E−02	1.8870E+00	3.2164E−02	1.6030E+00
59	2.7992E−02	4.2509E+00	2.8632E−02	2.2608E+00	2.9617E−02	1.9011E+00	3.1128E−02	1.6149E+00
60	2.7188E−02	4.2841E+00	2.7737E−02	2.2774E+00	2.8683E−02	1.9150E+00	3.0141E−02	1.6266E+00

Table 4.3.3.1. *Partial wave elastic scattering factors for neutral atoms (cont.)*
Fe; $Z = 26$

	10 keV		40 keV		60 keV		90 keV	
s	$\|f(s)\|$	$\eta(s)$	$\|f(s)\|$	$\eta(s)$	$\|f(s)\|$	$\eta(s)$	$\|f(s)\|$	$\eta(s)$
0	6.6697E+00	2.4041E−01	7.4861E+00	1.4374E−01	7.8200E+00	1.2290E−01	8.2623E+00	1.0577E−01
1	5.5574E+00	2.8320E−01	6.2891E+00	1.6818E−01	6.5791E+00	1.4362E−01	6.9649E+00	1.2338E−01
2	3.8154E+00	3.9291E−01	4.3944E+00	2.2990E−01	4.6092E+00	1.9587E−01	4.8917E+00	1.6789E−01
3	2.6722E+00	5.2480E−01	3.1286E+00	3.0289E−01	3.2889E+00	2.5755E−01	3.4961E+00	2.2045E−01
4	1.9914E+00	6.5182E−01	2.3619E+00	3.7253E−01	2.4873E+00	3.1632E−01	2.6473E+00	2.7049E−01
5	1.5453E+00	7.7314E−01	1.8527E+00	4.3863E−01	1.9539E+00	3.7206E−01	2.0817E+00	3.1792E−01
6	1.2275E+00	8.9404E−01	1.4850E+00	5.0411E−01	1.5680E+00	4.2722E−01	1.6719E+00	3.6484E−01
7	9.9133E−01	1.0176E+00	1.2073E+00	5.7068E−01	1.2759E+00	4.8326E−01	1.3613E+00	4.1247E−01
8	8.1244E−01	1.1442E+00	9.9315E−01	6.3867E−01	1.0502E+00	5.4046E−01	1.1209E+00	4.6107E−01
9	6.7562E−01	1.2724E+00	8.2638E−01	7.0753E−01	8.7396E−01	5.9839E−01	9.3292E−01	5.1030E−01
10	5.7003E−01	1.4002E+00	6.9555E−01	7.7631E−01	7.3543E−01	6.5626E−01	7.8492E−01	5.5947E−01
11	4.8748E−01	1.5251E+00	5.9202E−01	8.4388E−01	6.2562E−01	7.1314E−01	6.6748E−01	6.0782E−01
12	4.2259E−01	1.6458E+00	5.0989E−01	9.0936E−01	5.3841E−01	7.6830E−01	5.7412E−01	6.5472E−01
13	3.7056E−01	1.7608E+00	4.4390E−01	9.7197E−01	4.6830E−01	8.2105E−01	4.9905E−01	6.9959E−01
14	3.2807E−01	1.8695E+00	3.9021E−01	1.0312E+00	4.1128E−01	8.7100E−01	4.3800E−01	7.4208E−01
15	2.9289E−01	1.9719E+00	3.4609E−01	1.0870E+00	3.6445E−01	9.1798E−01	3.8789E−01	7.8205E−01
16	2.6334E−01	2.0683E+00	3.0940E−01	1.1392E+00	3.2556E−01	9.6200E−01	3.4631E−01	8.1949E−01
17	2.3821E−01	2.1593E+00	2.7855E−01	1.1882E+00	2.9290E−01	1.0032E+00	3.1142E−01	8.5454E−01
18	2.1662E−01	2.2453E+00	2.5233E−01	1.2342E+00	2.6519E−01	1.0419E+00	2.8185E−01	8.8741E−01
19	1.9790E−01	2.3271E+00	2.2982E−01	1.2776E+00	2.4144E−01	1.0783E+00	2.5653E−01	9.1833E−01
20	1.8156E−01	2.4052E+00	2.1034E−01	1.3186E+00	2.2089E−01	1.1128E+00	2.3465E−01	9.4757E−01
21	1.6721E−01	2.4800E+00	1.9332E−01	1.3577E+00	2.0297E−01	1.1456E+00	2.1557E−01	9.7536E−01
22	1.5454E−01	2.5521E+00	1.7836E−01	1.3951E+00	1.8723E−01	1.1769E+00	1.9882E−01	1.0019E+00
23	1.4330E−01	2.6216E+00	1.6512E−01	1.4311E+00	1.7329E−01	1.2070E+00	1.8399E−01	1.0274E+00
24	1.3328E−01	2.6890E+00	1.5333E−01	1.4658E+00	1.6089E−01	1.2361E+00	1.7080E−01	1.0521E+00
25	1.2432E−01	2.7546E+00	1.4278E−01	1.4995E+00	1.4979E−01	1.2643E+00	1.5900E−01	1.0759E+00
26	1.1628E−01	2.8184E+00	1.3329E−01	1.5323E+00	1.3981E−01	1.2918E+00	1.4838E−01	1.0992E+00
27	1.0904E−01	2.8806E+00	1.2473E−01	1.5643E+00	1.3079E−01	1.3185E+00	1.3879E−01	1.1218E+00
28	1.0249E−01	2.9415E+00	1.1697E−01	1.5956E+00	1.2262E−01	1.3447E+00	1.3009E−01	1.1440E+00
29	9.6545E−02	3.0010E+00	1.0991E−01	1.6262E+00	1.1519E−01	1.3704E+00	1.2218E−01	1.1657E+00
30	9.1140E−02	3.0592E+00	1.0347E−01	1.6562E+00	1.0840E−01	1.3955E+00	1.1495E−01	1.1870E+00
31	8.6208E−02	3.1163E+00	9.7577E−02	1.6856E+00	1.0219E−01	1.4201E+00	1.0834E−01	1.2078E+00
32	8.1694E−02	3.1723E+00	9.2172E−02	1.7145E+00	9.6494E−02	1.4443E+00	1.0227E−01	1.2284E+00
33	7.7550E−02	3.2272E+00	8.7202E−02	1.7429E+00	9.1253E−02	1.4681E+00	9.6691E−02	1.2485E+00
34	7.3736E−02	3.2810E+00	8.2621E−02	1.7708E+00	8.6421E−02	1.4914E+00	9.1544E−02	1.2683E+00
35	7.0216E−02	3.3339E+00	7.8390E−02	1.7981E+00	8.1958E−02	1.5144E+00	8.6789E−02	1.2877E+00
36	6.6960E−02	3.3858E+00	7.4474E−02	1.8250E+00	7.7827E−02	1.5369E+00	8.2387E−02	1.3068E+00
37	6.3941E−02	3.4367E+00	7.0842E−02	1.8514E+00	7.3997E−02	1.5590E+00	7.8307E−02	1.3256E+00
38	6.1135E−02	3.4867E+00	6.7469E−02	1.8773E+00	7.0439E−02	1.5808E+00	7.4516E−02	1.3440E+00
39	5.8521E−02	3.5358E+00	6.4330E−02	1.9027E+00	6.7129E−02	1.6021E+00	7.0990E−02	1.3621E+00
40	5.6081E−02	3.5840E+00	6.1404E−02	1.9277E+00	6.4044E−02	1.6230E+00	6.7704E−02	1.3799E+00
41	5.3800E−02	3.6314E+00	5.8673E−02	1.9522E+00	6.1165E−02	1.6436E+00	6.4639E−02	1.3973E+00
42	5.1663E−02	3.6779E+00	5.6120E−02	1.9762E+00	5.8475E−02	1.6638E+00	6.1774E−02	1.4144E+00
43	4.9657E−02	3.7236E+00	5.3729E−02	1.9998E+00	5.5957E−02	1.6836E+00	5.9094E−02	1.4312E+00
44	4.7771E−02	3.7685E+00	5.1488E−02	2.0230E+00	5.3597E−02	1.7030E+00	5.6583E−02	1.4476E+00
45	4.5996E−02	3.8126E+00	4.9384E−02	2.0457E+00	5.1383E−02	1.7220E+00	5.4228E−02	1.4638E+00
46	4.4323E−02	3.8560E+00	4.7407E−02	2.0680E+00	4.9303E−02	1.7407E+00	5.2016E−02	1.4797E+00
47	4.2743E−02	3.8987E+00	4.5547E−02	2.0899E+00	4.7347E−02	1.7591E+00	4.9936E−02	1.4952E+00
48	4.1249E−02	3.9406E+00	4.3794E−02	2.1114E+00	4.5504E−02	1.7771E+00	4.7978E−02	1.5105E+00
49	3.9835E−02	3.9818E+00	4.2140E−02	2.1325E+00	4.3768E−02	1.7947E+00	4.6133E−02	1.5254E+00
50	3.8495E−02	4.0223E+00	4.0579E−02	2.1532E+00	4.2129E−02	1.8121E+00	4.4392E−02	1.5401E+00
51	3.7224E−02	4.0622E+00	3.9103E−02	2.1735E+00	4.0580E−02	1.8291E+00	4.2748E−02	1.5545E+00
52	3.6017E−02	4.1014E+00	3.7707E−02	2.1934E+00	3.9116E−02	1.8458E+00	4.1194E−02	1.5687E+00
53	3.4870E−02	4.1400E+00	3.6385E−02	2.2130E+00	3.7729E−02	1.8622E+00	3.9724E−02	1.5826E+00
54	3.3778E−02	4.1780E+00	3.5131E−02	2.2323E+00	3.6416E−02	1.8783E+00	3.8331E−02	1.5962E+00
55	3.2738E−02	4.2154E+00	3.3941E−02	2.2512E+00	3.5170E−02	1.8941E+00	3.7010E−02	1.6096E+00
56	3.1747E−02	4.2522E+00	3.2811E−02	2.2697E+00	3.3988E−02	1.9096E+00	3.5757E−02	1.6227E+00
57	3.0802E−02	4.2885E+00	3.1737E−02	2.2880E+00	3.2864E−02	1.9249E+00	3.4567E−02	1.6357E+00
58	2.9900E−02	4.3242E+00	3.0715E−02	2.3059E+00	3.1796E−02	1.9399E+00	3.3436E−02	1.6483E+00
59	2.9038E−02	4.3594E+00	2.9743E−02	2.3235E+00	3.0779E−02	1.9546E+00	3.2360E−02	1.6608E+00
60	2.8214E−02	4.3940E+00	2.8816E−02	2.3408E+00	2.9811E−02	1.9691E+00	3.1336E−02	1.6730E+00

Table 4.3.3.1. *Partial wave elastic scattering factors for neutral atoms (cont.)*
Co; $Z = 27$

	10 keV		40 keV		60 keV		90 keV	
s	$\|f(s)\|$	$\eta(s)$	$\|f(s)\|$	$\eta(s)$	$\|f(s)\|$	$\eta(s)$	$\|f(s)\|$	$\eta(s)$
0	6.3345E+00	2.4885E−01	7.1396E+00	1.5015E−01	7.4634E+00	1.2860E−01	7.8891E+00	1.1082E−01
1	5.3351E+00	2.9049E−01	6.0630E+00	1.7408E−01	6.3475E+00	1.4890E−01	6.7232E+00	1.2806E−01
2	3.7285E+00	3.9756E−01	4.3138E+00	2.3464E−01	4.5284E+00	2.0021E−01	4.8089E+00	1.7179E−01
3	2.6415E+00	5.2758E−01	3.1086E+00	3.0694E−01	3.2710E+00	2.6136E−01	3.4795E+00	2.2392E−01
4	1.9824E+00	6.5400E−01	2.3650E+00	3.7653E−01	2.4932E+00	3.2012E−01	2.6556E+00	2.7398E−01
5	1.5471E+00	7.7496E−01	1.8668E+00	4.4268E−01	1.9711E+00	3.7592E−01	2.1018E+00	3.2149E−01
6	1.2354E+00	8.9524E−01	1.5051E+00	5.0805E−01	1.5912E+00	4.3102E−01	1.6982E+00	3.6837E−01
7	1.0023E+00	1.0180E+00	1.2302E+00	5.7437E−01	1.3019E+00	4.8688E−01	1.3905E+00	4.1586E−01
8	8.2457E−01	1.1438E+00	1.0168E+00	6.4212E−01	1.0768E+00	5.4390E−01	1.1505E+00	4.6433E−01
9	6.8764E−01	1.2718E+00	8.4926E−01	7.1097E−01	8.9961E−01	6.0184E−01	9.6144E−01	5.1357E−01
10	5.8130E−01	1.4001E+00	7.1684E−01	7.8012E−01	7.5926E−01	6.6003E−01	8.1138E−01	5.6302E−01
11	4.9779E−01	1.5266E+00	6.1133E−01	8.4855E−01	6.4721E−01	7.1764E−01	6.9143E−01	6.1200E−01
12	4.3188E−01	1.6497E+00	5.2710E−01	9.1542E−01	5.5763E−01	7.7396E−01	5.9543E−01	6.5989E−01
13	3.7895E−01	1.7679E+00	4.5911E−01	9.7988E−01	4.8525E−01	8.2829E−01	5.1782E−01	7.0611E−01
14	3.3570E−01	1.8803E+00	4.0361E−01	1.0414E+00	4.2617E−01	8.8015E−01	4.5445E−01	7.5024E−01
15	2.9989E−01	1.9867E+00	3.5789E−01	1.0996E+00	3.7752E−01	9.2927E−01	4.0230E−01	7.9204E−01
16	2.6980E−01	2.0873E+00	3.1984E−01	1.1545E+00	3.3707E−01	9.7557E−01	3.5896E−01	8.3144E−01
17	2.4420E−01	2.1825E+00	2.8782E−01	1.2062E+00	3.0308E−01	1.0191E+00	3.2258E−01	8.6846E−01
18	2.2220E−01	2.2726E+00	2.6061E−01	1.2548E+00	2.7424E−01	1.0600E+00	2.9174E−01	9.0325E−01
19	2.0311E−01	2.3582E+00	2.3727E−01	1.3006E+00	2.4954E−01	1.0985E+00	2.6535E−01	9.3600E−01
20	1.8642E−01	2.4399E+00	2.1707E−01	1.3439E+00	2.2819E−01	1.1350E+00	2.4257E−01	9.6692E−01
21	1.7175E−01	2.5181E+00	1.9945E−01	1.3851E+00	2.0959E−01	1.1695E+00	2.2274E−01	9.9625E−01
22	1.5878E−01	2.5933E+00	1.8397E−01	1.4244E+00	1.9327E−01	1.2025E+00	2.0535E−01	1.0242E+00
23	1.4725E−01	2.6658E+00	1.7028E−01	1.4620E+00	1.7884E−01	1.2340E+00	1.8999E−01	1.0509E+00
24	1.3698E−01	2.7359E+00	1.5810E−01	1.4983E+00	1.6601E−01	1.2644E+00	1.7634E−01	1.0767E+00
25	1.2778E−01	2.8039E+00	1.4722E−01	1.5333E+00	1.5455E−01	1.2938E+00	1.6413E−01	1.1015E+00
26	1.1951E−01	2.8701E+00	1.3744E−01	1.5674E+00	1.4425E−01	1.3222E+00	1.5317E−01	1.1256E+00
27	1.1206E−01	2.9345E+00	1.2861E−01	1.6004E+00	1.3496E−01	1.3499E+00	1.4328E−01	1.1490E+00
28	1.0532E−01	2.9974E+00	1.2062E−01	1.6327E+00	1.2654E−01	1.3769E+00	1.3432E−01	1.1719E+00
29	9.9215E−02	3.0588E+00	1.1335E−01	1.6642E+00	1.1888E−01	1.4033E+00	1.2617E−01	1.1942E+00
30	9.3657E−02	3.1190E+00	1.0673E−01	1.6951E+00	1.1190E−01	1.4291E+00	1.1874E−01	1.2161E+00
31	8.8586E−02	3.1778E+00	1.0067E−01	1.7254E+00	1.0551E−01	1.4544E+00	1.1193E−01	1.2375E+00
32	8.3946E−02	3.2355E+00	9.5111E−02	1.7550E+00	9.9652E−02	1.4793E+00	1.0569E−01	1.2586E+00
33	7.9689E−02	3.2921E+00	9.0001E−02	1.7842E+00	9.4262E−02	1.5037E+00	9.9943E−02	1.2793E+00
34	7.5773E−02	3.3475E+00	8.5292E−02	1.8127E+00	8.9294E−02	1.5276E+00	9.4648E−02	1.2995E+00
35	7.2162E−02	3.4020E+00	8.0942E−02	1.8408E+00	8.4703E−02	1.5512E+00	8.9755E−02	1.3195E+00
36	6.8823E−02	3.4554E+00	7.6917E−02	1.8684E+00	8.0454E−02	1.5743E+00	8.5226E−02	1.3391E+00
37	6.5729E−02	3.5079E+00	7.3183E−02	1.8955E+00	7.6514E−02	1.5970E+00	8.1025E−02	1.3583E+00
38	6.2854E−02	3.5594E+00	6.9715E−02	1.9222E+00	7.2852E−02	1.6193E+00	7.7122E−02	1.3773E+00
39	6.0178E−02	3.6100E+00	6.6487E−02	1.9483E+00	6.9445E−02	1.6413E+00	7.3490E−02	1.3959E+00
40	5.7682E−02	3.6598E+00	6.3477E−02	1.9740E+00	6.6269E−02	1.6628E+00	7.0105E−02	1.4141E+00
41	5.5350E−02	3.7087E+00	6.0667E−02	1.9993E+00	6.3304E−02	1.6840E+00	6.6945E−02	1.4321E+00
42	5.3165E−02	3.7567E+00	5.8040E−02	2.0240E+00	6.0532E−02	1.7048E+00	6.3992E−02	1.4497E+00
43	5.1116E−02	3.8039E+00	5.5580E−02	2.0484E+00	5.7938E−02	1.7252E+00	6.1227E−02	1.4670E+00
44	4.9190E−02	3.8503E+00	5.3272E−02	2.0723E+00	5.5505E−02	1.7452E+00	5.8636E−02	1.4840E+00
45	4.7377E−02	3.8959E+00	5.1106E−02	2.0958E+00	5.3222E−02	1.7649E+00	5.6205E−02	1.5007E+00
46	4.5668E−02	3.9408E+00	4.9069E−02	2.1188E+00	5.1076E−02	1.7843E+00	5.3921E−02	1.5171E+00
47	4.4056E−02	3.9849E+00	4.7152E−02	2.1415E+00	4.9057E−02	1.8032E+00	5.1772E−02	1.5332E+00
48	4.2531E−02	4.0283E+00	4.5345E−02	2.1637E+00	4.7156E−02	1.8219E+00	4.9749E−02	1.5490E+00
49	4.1088E−02	4.0710E+00	4.3641E−02	2.1856E+00	4.5362E−02	1.8402E+00	4.7842E−02	1.5645E+00
50	3.9720E−02	4.1130E+00	4.2031E−02	2.2070E+00	4.3670E−02	1.8582E+00	4.6042E−02	1.5797E+00
51	3.8423E−02	4.1543E+00	4.0509E−02	2.2281E+00	4.2070E−02	1.8758E+00	4.4342E−02	1.5947E+00
52	3.7191E−02	4.1950E+00	3.9068E−02	2.2488E+00	4.0557E−02	1.8931E+00	4.2734E−02	1.6094E+00
53	3.6020E−02	4.2351E+00	3.7703E−02	2.2691E+00	3.9124E−02	1.9102E+00	4.1212E−02	1.6238E+00
54	3.4905E−02	4.2745E+00	3.6409E−02	2.2891E+00	3.7766E−02	1.9269E+00	3.9771E−02	1.6380E+00
55	3.3844E−02	4.3134E+00	3.5181E−02	2.3087E+00	3.6478E−02	1.9433E+00	3.8404E−02	1.6519E+00
56	3.2832E−02	4.3516E+00	3.4014E−02	2.3280E+00	3.5254E−02	1.9595E+00	3.7106E−02	1.6655E+00
57	3.1866E−02	4.3893E+00	3.2905E−02	2.3470E+00	3.4092E−02	1.9753E+00	3.5874E−02	1.6790E+00
58	3.0944E−02	4.4265E+00	3.1849E−02	2.3656E+00	3.2987E−02	1.9909E+00	3.4702E−02	1.6922E+00
59	3.0063E−02	4.4631E+00	3.0844E−02	2.3840E+00	3.1935E−02	2.0062E+00	3.3587E−02	1.7052E+00
60	2.9220E−02	4.4991E+00	2.9886E−02	2.4020E+00	3.0933E−02	2.0213E+00	3.2526E−02	1.7179E+00

Table 4.3.3.1. *Partial wave elastic scattering factors for neutral atoms (cont.)*
Ni; $Z = 28$

	10 keV		40 keV		60 keV		90 keV	
s	$\|f(s)\|$	$\eta(s)$	$\|f(s)\|$	$\eta(s)$	$\|f(s)\|$	$\eta(s)$	$\|f(s)\|$	$\eta(s)$
0	6.0281E+00	2.5677E−01	6.8220E+00	1.5635E−01	7.1366E+00	1.3413E−01	7.5470E+00	1.1574E−01
1	5.1251E+00	2.9736E−01	5.8484E+00	1.7981E−01	6.1275E+00	1.5405E−01	6.4937E+00	1.3265E−01
2	3.6392E+00	4.0197E−01	4.2290E+00	2.3932E−01	4.4432E+00	2.0451E−01	4.7213E+00	1.7568E−01
3	2.6058E+00	5.3016E−01	3.0820E+00	3.1095E−01	3.2460E+00	2.6513E−01	3.4555E+00	2.2740E−01
4	1.9688E+00	6.5582E−01	2.3620E+00	3.8040E−01	2.4927E+00	3.2383E−01	2.6572E+00	2.7742E−01
5	1.5449E+00	7.7628E−01	1.8757E+00	4.4652E−01	1.9828E+00	3.7964E−01	2.1161E+00	3.2496E−01
6	1.2398E+00	8.9586E−01	1.5207E+00	5.1173E−01	1.6097E+00	4.3464E−01	1.7196E+00	3.7176E−01
7	1.0103E+00	1.0177E+00	1.2494E+00	5.7776E−01	1.3241E+00	4.9028E−01	1.4155E+00	4.1909E−01
8	8.3425E−01	1.1426E+00	1.0374E+00	6.4522E−01	1.1002E+00	5.4708E−01	1.1769E+00	4.6738E−01
9	6.9771E−01	1.2701E+00	8.6981E−01	7.1392E−01	9.2287E−01	6.0491E−01	9.8746E−01	5.1653E−01
10	5.9103E−01	1.3986E+00	7.3638E−01	7.8322E−01	7.8131E−01	6.6323E−01	8.3601E−01	5.6611E−01
11	5.0685E−01	1.5261E+00	6.2937E−01	8.5224E−01	6.6755E−01	7.2135E−01	7.1412E−01	6.1552E−01
12	4.4017E−01	1.6510E+00	5.4343E−01	9.2013E−01	5.7601E−01	7.7854E−01	6.1592E−01	6.6415E−01
13	3.8650E−01	1.7717E+00	4.7371E−01	9.8608E−01	5.0167E−01	8.3413E−01	5.3609E−01	7.1145E−01
14	3.4263E−01	1.8873E+00	4.1661E−01	1.0495E+00	4.4074E−01	8.8761E−01	4.7065E−01	7.5696E−01
15	3.0628E−01	1.9973E+00	3.6944E−01	1.1099E+00	3.9043E−01	9.3861E−01	4.1661E−01	8.0038E−01
16	2.7575E−01	2.1017E+00	3.3011E−01	1.1672E+00	3.4850E−01	9.8696E−01	3.7160E−01	8.4155E−01
17	2.4977E−01	2.2007E+00	2.9700E−01	1.2214E+00	3.1324E−01	1.0326E+00	3.3378E−01	8.8043E−01
18	2.2743E−01	2.2946E+00	2.6884E−01	1.2725E+00	2.8330E−01	1.0757E+00	3.0170E−01	9.1708E−01
19	2.0803E−01	2.3840E+00	2.4469E−01	1.3207E+00	2.5767E−01	1.1163E+00	2.7426E−01	9.5164E−01
20	1.9106E−01	2.4692E+00	2.2379E−01	1.3664E+00	2.3552E−01	1.1547E+00	2.5058E−01	9.8428E−01
21	1.7611E−01	2.5508E+00	2.0557E−01	1.4097E+00	2.1624E−01	1.1912E+00	2.2999E−01	1.0152E+00
22	1.6288E−01	2.6291E+00	1.8958E−01	1.4510E+00	1.9933E−01	1.2258E+00	2.1195E−01	1.0446E+00
23	1.5111E−01	2.7046E+00	1.7544E−01	1.4904E+00	1.8441E−01	1.2589E+00	1.9603E−01	1.0727E+00
24	1.4060E−01	2.7775E+00	1.6287E−01	1.5283E+00	1.7115E−01	1.2907E+00	1.8190E−01	1.0996E+00
25	1.3117E−01	2.8482E+00	1.5164E−01	1.5648E+00	1.5931E−01	1.3213E+00	1.6929E−01	1.1255E+00
26	1.2270E−01	2.9168E+00	1.4156E−01	1.6002E+00	1.4869E−01	1.3509E+00	1.5797E−01	1.1506E+00
27	1.1506E−01	2.9835E+00	1.3247E−01	1.6345E+00	1.3911E−01	1.3796E+00	1.4776E−01	1.1749E+00
28	1.0814E−01	3.0486E+00	1.2424E−01	1.6679E+00	1.3043E−01	1.4075E+00	1.3853E−01	1.1985E+00
29	1.0187E−01	3.1121E+00	1.1677E−01	1.7004E+00	1.2255E−01	1.4347E+00	1.3013E−01	1.2215E+00
30	9.6158E−02	3.1742E+00	1.0995E−01	1.7322E+00	1.1537E−01	1.4613E+00	1.2248E−01	1.2441E+00
31	9.0948E−02	3.2349E+00	1.0372E−01	1.7633E+00	1.0880E−01	1.4874E+00	1.1548E−01	1.2661E+00
32	8.6182E−02	3.2944E+00	9.8012E−02	1.7938E+00	1.0277E−01	1.5129E+00	1.0906E−01	1.2877E+00
33	8.1810E−02	3.3527E+00	9.2761E−02	1.8237E+00	9.7232E−02	1.5380E+00	1.0315E−01	1.3089E+00
34	7.7790E−02	3.4098E+00	8.7923E−02	1.8531E+00	9.2125E−02	1.5625E+00	9.7710E−02	1.3298E+00
35	7.4084E−02	3.4659E+00	8.3454E−02	1.8819E+00	8.7407E−02	1.5867E+00	9.2679E−02	1.3502E+00
36	7.0660E−02	3.5210E+00	7.9319E−02	1.9102E+00	8.3040E−02	1.6104E+00	8.8023E−02	1.3703E+00
37	6.7488E−02	3.5750E+00	7.5484E−02	1.9381E+00	7.8990E−02	1.6337E+00	8.3703E−02	1.3901E+00
38	6.4543E−02	3.6281E+00	7.1921E−02	1.9654E+00	7.5226E−02	1.6566E+00	7.9689E−02	1.4095E+00
39	6.1804E−02	3.6802E+00	6.8605E−02	1.9923E+00	7.1723E−02	1.6791E+00	7.5953E−02	1.4286E+00
40	5.9249E−02	3.7315E+00	6.5513E−02	2.0187E+00	6.8458E−02	1.7013E+00	7.2470E−02	1.4473E+00
41	5.6864E−02	3.7818E+00	6.2626E−02	2.0446E+00	6.5409E−02	1.7230E+00	6.9218E−02	1.4658E+00
42	5.4630E−02	3.8314E+00	5.9926E−02	2.0701E+00	6.2557E−02	1.7444E+00	6.6178E−02	1.4839E+00
43	5.2537E−02	3.8800E+00	5.7397E−02	2.0952E+00	5.9887E−02	1.7654E+00	6.3331E−02	1.5017E+00
44	5.0570E−02	3.9279E+00	5.5025E−02	2.1198E+00	5.7384E−02	1.7861E+00	6.0662E−02	1.5192E+00
45	4.8720E−02	3.9750E+00	5.2798E−02	2.1440E+00	5.5034E−02	1.8064E+00	5.8157E−02	1.5364E+00
46	4.6976E−02	4.0213E+00	5.0703E−02	2.1678E+00	5.2824E−02	1.8263E+00	5.5802E−02	1.5533E+00
47	4.5331E−02	4.0669E+00	4.8731E−02	2.1912E+00	5.0745E−02	1.8459E+00	5.3587E−02	1.5699E+00
48	4.3776E−02	4.1118E+00	4.6872E−02	2.2142E+00	4.8785E−02	1.8651E+00	5.1501E−02	1.5863E+00
49	4.2305E−02	4.1559E+00	4.5118E−02	2.2367E+00	4.6937E−02	1.8841E+00	4.9533E−02	1.6023E+00
50	4.0911E−02	4.1994E+00	4.3461E−02	2.2589E+00	4.5192E−02	1.9026E+00	4.7675E−02	1.6181E+00
51	3.9589E−02	4.2422E+00	4.1894E−02	2.2807E+00	4.3542E−02	1.9209E+00	4.5921E−02	1.6335E+00
52	3.8333E−02	4.2843E+00	4.0410E−02	2.3021E+00	4.1982E−02	1.9389E+00	4.4261E−02	1.6487E+00
53	3.7139E−02	4.3258E+00	3.9005E−02	2.3232E+00	4.0504E−02	1.9565E+00	4.2689E−02	1.6637E+00
54	3.6003E−02	4.3667E+00	3.7671E−02	2.3439E+00	3.9102E−02	1.9738E+00	4.1200E−02	1.6784E+00
55	3.4921E−02	4.4069E+00	3.6406E−02	2.3642E+00	3.7773E−02	1.9909E+00	3.9787E−02	1.6928E+00
56	3.3889E−02	4.4466E+00	3.5203E−02	2.3843E+00	3.6510E−02	2.0076E+00	3.8446E−02	1.7070E+00
57	3.2904E−02	4.4857E+00	3.4059E−02	2.4039E+00	3.5310E−02	2.0241E+00	3.7172E−02	1.7209E+00
58	3.1964E−02	4.5243E+00	3.2971E−02	2.4233E+00	3.4169E−02	2.0403E+00	3.5961E−02	1.7346E+00
59	3.1065E−02	4.5623E+00	3.1934E−02	2.4423E+00	3.3082E−02	2.0562E+00	3.4808E−02	1.7481E+00
60	3.0205E−02	4.5997E+00	3.0946E−02	2.4611E+00	3.2046E−02	2.0719E+00	3.3710E−02	1.7614E+00

Table 4.3.3.1. *Partial wave elastic scattering factors for neutral atoms (cont.)*
Cu; $Z = 29$

	10 keV		40 keV		60 keV		90 keV	
s	$\|f(s)\|$	$\eta(s)$	$\|f(s)\|$	$\eta(s)$	$\|f(s)\|$	$\eta(s)$	$\|f(s)\|$	$\eta(s)$
0	5.0642E+00	2.7713E−01	5.7822E+00	1.7072E−01	6.0572E+00	1.4676E−01	6.4098E+00	1.2687E−01
1	4.3690E+00	3.1776E−01	5.0303E+00	1.9423E−01	5.2779E+00	1.6671E−01	5.5985E+00	1.4378E−01
2	3.2591E+00	4.1339E−01	3.8162E+00	2.4878E−01	4.0147E+00	2.1298E−01	4.2702E+00	1.8320E−01
3	2.4617E+00	5.2313E−01	2.9296E+00	3.1045E−01	3.0891E+00	2.6522E−01	3.2913E+00	2.2779E−01
4	1.9223E+00	6.3324E−01	2.3205E+00	3.7172E−01	2.4517E+00	3.1705E−01	2.6158E+00	2.7199E−01
5	1.5337E+00	7.4484E−01	1.8750E+00	4.3330E−01	1.9844E+00	3.6908E−01	2.1198E+00	3.1633E−01
6	1.2413E+00	8.6014E−01	1.5344E+00	4.9643E−01	1.6264E+00	4.2236E−01	1.7392E+00	3.6170E−01
7	1.0166E+00	9.8006E−01	1.2680E+00	5.6165E−01	1.3457E+00	4.7734E−01	1.4403E+00	4.0848E−01
8	8.4223E−01	1.1043E+00	1.0572E+00	6.2890E−01	1.1230E+00	5.3399E−01	1.2027E+00	4.5666E−01
9	7.0608E−01	1.2319E+00	8.8921E−01	6.9773E−01	9.4508E−01	5.9194E−01	1.0125E+00	5.0593E−01
10	5.9918E−01	1.3609E+00	7.5470E−01	7.6744E−01	8.0223E−01	6.5063E−01	8.5955E−01	5.5581E−01
11	5.1455E−01	1.4896E+00	6.4631E−01	8.3716E−01	6.8684E−01	7.0934E−01	7.3579E−01	6.0574E−01
12	4.4731E−01	1.6163E+00	5.5884E−01	9.0608E−01	5.9352E−01	7.6741E−01	6.3556E−01	6.5512E−01
13	3.9310E−01	1.7394E+00	4.8760E−01	9.7340E−01	5.1742E−01	8.2416E−01	5.5374E−01	7.0341E−01
14	3.4875E−01	1.8578E+00	4.2908E−01	1.0385E+00	4.5484E−01	8.7907E−01	4.8642E−01	7.5015E−01
15	3.1200E−01	1.9710E+00	3.8062E−01	1.1009E+00	4.0302E−01	9.3174E−01	4.3066E−01	7.9500E−01
16	2.8112E−01	2.0788E+00	3.4014E−01	1.1603E+00	3.5975E−01	9.8194E−01	3.8412E−01	8.3775E−01
17	2.5485E−01	2.1813E+00	3.0601E−01	1.2168E+00	3.2330E−01	1.0296E+00	3.4494E−01	8.7832E−01
18	2.3224E−01	2.2788E+00	2.7697E−01	1.2702E+00	2.9234E−01	1.0747E+00	3.1169E−01	9.1671E−01
19	2.1261E−01	2.3717E+00	2.5205E−01	1.3207E+00	2.6580E−01	1.1173E+00	2.8322E−01	9.5299E−01
20	1.9541E−01	2.4603E+00	2.3048E−01	1.3686E+00	2.4288E−01	1.1576E+00	2.5866E−01	9.8731E−01
21	1.8024E−01	2.5452E+00	2.1169E−01	1.4141E+00	2.2294E−01	1.1959E+00	2.3731E−01	1.0198E+00
22	1.6679E−01	2.6267E+00	1.9518E−01	1.4574E+00	2.0545E−01	1.2323E+00	2.1862E−01	1.0507E+00
23	1.5482E−01	2.7051E+00	1.8060E−01	1.4987E+00	1.9002E−01	1.2670E+00	2.0214E−01	1.0802E+00
24	1.4411E−01	2.7809E+00	1.6765E−01	1.5384E+00	1.7633E−01	1.3003E+00	1.8752E−01	1.1084E+00
25	1.3449E−01	2.8542E+00	1.5608E−01	1.5765E+00	1.6411E−01	1.3322E+00	1.7449E−01	1.1355E+00
26	1.2583E−01	2.9254E+00	1.4570E−01	1.6133E+00	1.5315E−01	1.3630E+00	1.6280E−01	1.1616E+00
27	1.1802E−01	2.9946E+00	1.3634E−01	1.6489E+00	1.4327E−01	1.3929E+00	1.5227E−01	1.1869E+00
28	1.1093E−01	3.0619E+00	1.2787E−01	1.6835E+00	1.3433E−01	1.4218E+00	1.4275E−01	1.2114E+00
29	1.0451E−01	3.1276E+00	1.2018E−01	1.7172E+00	1.2622E−01	1.4500E+00	1.3410E−01	1.2352E+00
30	9.8651E−02	3.1918E+00	1.1317E−01	1.7500E+00	1.1883E−01	1.4775E+00	1.2622E−01	1.2585E+00
31	9.3307E−02	3.2545E+00	1.0677E−01	1.7821E+00	1.1207E−01	1.5043E+00	1.1902E−01	1.2812E+00
32	8.8417E−02	3.3159E+00	1.0090E−01	1.8135E+00	1.0588E−01	1.5306E+00	1.1242E−01	1.3035E+00
33	8.3931E−02	3.3760E+00	9.5503E−02	1.8443E+00	1.0018E−01	1.5564E+00	1.0634E−01	1.3253E+00
34	7.9807E−02	3.4350E+00	9.0533E−02	1.8745E+00	9.4933E−02	1.5816E+00	1.0075E−01	1.3466E+00
35	7.6006E−02	3.4928E+00	8.5944E−02	1.9041E+00	9.0086E−02	1.6064E+00	9.5577E−02	1.3676E+00
36	7.2494E−02	3.5495E+00	8.1697E−02	1.9332E+00	8.5600E−02	1.6307E+00	9.0792E−02	1.3882E+00
37	6.9242E−02	3.6052E+00	7.7760E−02	1.9617E+00	8.1439E−02	1.6547E+00	8.6353E−02	1.4085E+00
38	6.6225E−02	3.6599E+00	7.4102E−02	1.9898E+00	7.7573E−02	1.6782E+00	8.2228E−02	1.4284E+00
39	6.3420E−02	3.7136E+00	7.0697E−02	2.0174E+00	7.3975E−02	1.7013E+00	7.8388E−02	1.4480E+00
40	6.0805E−02	3.7664E+00	6.7523E−02	2.0445E+00	7.0620E−02	1.7240E+00	7.4808E−02	1.4673E+00
41	5.8365E−02	3.8183E+00	6.4559E−02	2.0712E+00	6.7487E−02	1.7464E+00	7.1464E−02	1.4862E+00
42	5.6081E−02	3.8693E+00	6.1786E−02	2.0974E+00	6.4557E−02	1.7683E+00	6.8338E−02	1.5048E+00
43	5.3942E−02	3.9195E+00	5.9190E−02	2.1232E+00	6.1813E−02	1.7899E+00	6.5410E−02	1.5231E+00
44	5.1933E−02	3.9689E+00	5.6754E−02	2.1485E+00	5.9239E−02	1.8112E+00	6.2664E−02	1.5411E+00
45	5.0044E−02	4.0175E+00	5.4466E−02	2.1734E+00	5.6823E−02	1.8320E+00	6.0086E−02	1.5588E+00
46	4.8265E−02	4.0653E+00	5.2315E−02	2.1979E+00	5.4550E−02	1.8526E+00	5.7663E−02	1.5762E+00
47	4.6586E−02	4.1123E+00	5.0289E−02	2.2220E+00	5.2411E−02	1.8728E+00	5.5383E−02	1.5934E+00
48	4.5001E−02	4.1586E+00	4.8379E−02	2.2456E+00	5.0396E−02	1.8926E+00	5.3234E−02	1.6102E+00
49	4.3501E−02	4.2042E+00	4.6576E−02	2.2689E+00	4.8494E−02	1.9121E+00	5.1207E−02	1.6267E+00
50	4.2081E−02	4.2491E+00	4.4873E−02	2.2918E+00	4.6698E−02	1.9313E+00	4.9294E−02	1.6430E+00
51	4.0734E−02	4.2934E+00	4.3262E−02	2.3143E+00	4.5000E−02	1.9501E+00	4.7485E−02	1.6589E+00
52	3.9454E−02	4.3369E+00	4.1736E−02	2.3365E+00	4.3393E−02	1.9687E+00	4.5774E−02	1.6747E+00
53	3.8239E−02	4.3799E+00	4.0291E−02	2.3582E+00	4.1870E−02	1.9869E+00	4.4153E−02	1.6901E+00
54	3.7082E−02	4.4222E+00	3.8919E−02	2.3796E+00	4.0427E−02	2.0048E+00	4.2618E−02	1.7053E+00
55	3.5979E−02	4.4639E+00	3.7617E−02	2.4007E+00	3.9057E−02	2.0225E+00	4.1161E−02	1.7202E+00
56	3.4929E−02	4.5049E+00	3.6379E−02	2.4214E+00	3.7755E−02	2.0398E+00	3.9777E−02	1.7349E+00
57	3.3926E−02	4.5455E+00	3.5202E−02	2.4418E+00	3.6518E−02	2.0568E+00	3.8462E−02	1.7494E+00
58	3.2969E−02	4.5854E+00	3.4082E−02	2.4618E+00	3.5341E−02	2.0736E+00	3.7212E−02	1.7636E+00
59	3.2053E−02	4.6248E+00	3.3014E−02	2.4815E+00	3.4221E−02	2.0901E+00	3.6022E−02	1.7775E+00
60	3.1178E−02	4.6636E+00	3.1996E−02	2.5010E+00	3.3153E−02	2.1064E+00	3.4888E−02	1.7913E+00

Table 4.3.3.1. *Partial wave elastic scattering factors for neutral atoms (cont.)*
Zn; $Z = 30$

	10 keV		40 keV		60 keV		90 keV	
s	$\|f(s)\|$	$\eta(s)$	$\|f(s)\|$	$\eta(s)$	$\|f(s)\|$	$\eta(s)$	$\|f(s)\|$	$\eta(s)$
0	5.4874E+00	2.7128E−01	6.2593E+00	1.6820E−01	6.5575E+00	1.4480E−01	6.9412E+00	1.2528E−01
1	4.7400E+00	3.0996E−01	5.4522E+00	1.9082E−01	5.7212E+00	1.6402E−01	6.0698E+00	1.4161E−01
2	3.4593E+00	4.1012E−01	4.0540E+00	2.4844E−01	4.2664E+00	2.1298E−01	4.5393E+00	1.8338E−01
3	2.5248E+00	5.3472E−01	3.0146E+00	3.1876E−01	3.1811E+00	2.7259E−01	3.3912E+00	2.3430E−01
4	1.9313E+00	6.5860E−01	2.3419E+00	3.8781E−01	2.4767E+00	3.3103E−01	2.6444E+00	2.8416E−01
5	1.5308E+00	7.7778E−01	1.8807E+00	4.5373E−01	1.9925E+00	3.8675E−01	2.1302E+00	3.3166E−01
6	1.2397E+00	8.9576E−01	1.5405E+00	5.1854E−01	1.6347E+00	4.4147E−01	1.7496E+00	3.7827E−01
7	1.0187E+00	1.0156E+00	1.2779E+00	5.8393E−01	1.3579E+00	4.9663E−01	1.4546E+00	4.2522E−01
8	8.4717E−01	1.1385E+00	1.0703E+00	6.5067E−01	1.1385E+00	5.5288E−01	1.2205E+00	4.7308E−01
9	7.1254E−01	1.2644E+00	9.0415E−01	7.1882E−01	9.6237E−01	6.1028E−01	1.0322E+00	5.2189E−01
10	6.0616E−01	1.3923E+00	7.7017E−01	7.8798E−01	8.2000E−01	6.6852E−01	8.7964E−01	5.7141E−01
11	5.2145E−01	1.5206E+00	6.6144E−01	8.5750E−01	7.0417E−01	7.2708E−01	7.5534E−01	6.2120E−01
12	4.5381E−01	1.6476E+00	5.7310E−01	9.2664E−01	6.0983E−01	7.8534E−01	6.5395E−01	6.7075E−01
13	3.9913E−01	1.7719E+00	5.0075E−01	9.9466E−01	5.3243E−01	8.4269E−01	5.7064E−01	7.1955E−01
14	3.5433E−01	1.8924E+00	4.4103E−01	1.0609E+00	4.6848E−01	8.9858E−01	5.0175E−01	7.6713E−01
15	3.1720E−01	2.0082E+00	3.9142E−01	1.1249E+00	4.1531E−01	9.5258E−01	4.4446E−01	8.1313E−01
16	2.8601E−01	2.1189E+00	3.4988E−01	1.1862E+00	3.7079E−01	1.0044E+00	3.9648E−01	8.5726E−01
17	2.5948E−01	2.2247E+00	3.1479E−01	1.2447E+00	3.3321E−01	1.0538E+00	3.5601E−01	8.9938E−01
18	2.3666E−01	2.3255E+00	2.8491E−01	1.3003E+00	3.0125E−01	1.1008E+00	3.2161E−01	9.3941E−01
19	2.1683E−01	2.4217E+00	2.5925E−01	1.3532E+00	2.7384E−01	1.1454E+00	2.9214E−01	9.7739E−01
20	1.9945E−01	2.5136E+00	2.3705E−01	1.4033E+00	2.5016E−01	1.1877E+00	2.6671E−01	1.0134E+00
21	1.8411E−01	2.6016E+00	2.1769E−01	1.4509E+00	2.2955E−01	1.2278E+00	2.4460E−01	1.0475E+00
22	1.7049E−01	2.6862E+00	2.0069E−01	1.4963E+00	2.1150E−01	1.2660E+00	2.2525E−01	1.0800E+00
23	1.5834E−01	2.7675E+00	1.8568E−01	1.5395E+00	1.9557E−01	1.3024E+00	2.0821E−01	1.1109E+00
24	1.4746E−01	2.8461E+00	1.7235E−01	1.5810E+00	1.8144E−01	1.3372E+00	1.9310E−01	1.1405E+00
25	1.3768E−01	2.9221E+00	1.6045E−01	1.6208E+00	1.6884E−01	1.3706E+00	1.7964E−01	1.1688E+00
26	1.2886E−01	2.9958E+00	1.4977E−01	1.6591E+00	1.5755E−01	1.4027E+00	1.6758E−01	1.1960E+00
27	1.2088E−01	3.0673E+00	1.4014E−01	1.6961E+00	1.4738E−01	1.4337E+00	1.5673E−01	1.2223E+00
28	1.1365E−01	3.1370E+00	1.3144E−01	1.7320E+00	1.3818E−01	1.4638E+00	1.4692E−01	1.2477E+00
29	1.0707E−01	3.2049E+00	1.2353E−01	1.7668E+00	1.2984E−01	1.4929E+00	1.3802E−01	1.2724E+00
30	1.0108E−01	3.2711E+00	1.1633E−01	1.8008E+00	1.2224E−01	1.5213E+00	1.2991E−01	1.2964E+00
31	9.5606E−02	3.3358E+00	1.0976E−01	1.8339E+00	1.1529E−01	1.5490E+00	1.2251E−01	1.3199E+00
32	9.0596E−02	3.3991E+00	1.0373E−01	1.8662E+00	1.0893E−01	1.5761E+00	1.1572E−01	1.3428E+00
33	8.5998E−02	3.4611E+00	9.8190E−02	1.8978E+00	1.0308E−01	1.6025E+00	1.0948E−01	1.3652E+00
34	8.1770E−02	3.5219E+00	9.3090E−02	1.9288E+00	9.7689E−02	1.6285E+00	1.0373E−01	1.3871E+00
35	7.7874E−02	3.5814E+00	8.8381E−02	1.9592E+00	9.2714E−02	1.6539E+00	9.8425E−02	1.4087E+00
36	7.4275E−02	3.6398E+00	8.4024E−02	1.9891E+00	8.8110E−02	1.6789E+00	9.3512E−02	1.4298E+00
37	7.0943E−02	3.6971E+00	7.9985E−02	2.0184E+00	8.3840E−02	1.7034E+00	8.8955E−02	1.4506E+00
38	6.7853E−02	3.7534E+00	7.6233E−02	2.0472E+00	7.9873E−02	1.7275E+00	8.4720E−02	1.4710E+00
39	6.4980E−02	3.8087E+00	7.2741E−02	2.0755E+00	7.6181E−02	1.7512E+00	8.0779E−02	1.4911E+00
40	6.2305E−02	3.8631E+00	6.9486E−02	2.1033E+00	7.2738E−02	1.7745E+00	7.7103E−02	1.5108E+00
41	5.9809E−02	3.9165E+00	6.6446E−02	2.1306E+00	6.9523E−02	1.7974E+00	7.3671E−02	1.5302E+00
42	5.7475E−02	3.9690E+00	6.3603E−02	2.1575E+00	6.6516E−02	1.8199E+00	7.0460E−02	1.5493E+00
43	5.5289E−02	4.0207E+00	6.0940E−02	2.1840E+00	6.3700E−02	1.8421E+00	6.7453E−02	1.5681E+00
44	5.3238E−02	4.0715E+00	5.8442E−02	2.2100E+00	6.1058E−02	1.8639E+00	6.4633E−02	1.5865E+00
45	5.1311E−02	4.1215E+00	5.6096E−02	2.2356E+00	5.8577E−02	1.8853E+00	6.1985E−02	1.6047E+00
46	4.9496E−02	4.1708E+00	5.3889E−02	2.2608E+00	5.6244E−02	1.9064E+00	5.9495E−02	1.6226E+00
47	4.7785E−02	4.2192E+00	5.1811E−02	2.2855E+00	5.4047E−02	1.9272E+00	5.7151E−02	1.6402E+00
48	4.6170E−02	4.2670E+00	4.9851E−02	2.3099E+00	5.1977E−02	1.9476E+00	5.4942E−02	1.6575E+00
49	4.4642E−02	4.3140E+00	4.8002E−02	2.3338E+00	5.0023E−02	1.9677E+00	5.2857E−02	1.6745E+00
50	4.3196E−02	4.3603E+00	4.6254E−02	2.3574E+00	4.8177E−02	1.9874E+00	5.0889E−02	1.6913E+00
51	4.1825E−02	4.4059E+00	4.4600E−02	2.3806E+00	4.6432E−02	2.0069E+00	4.9028E−02	1.7077E+00
52	4.0524E−02	4.4509E+00	4.3034E−02	2.4034E+00	4.4780E−02	2.0260E+00	4.7268E−02	1.7239E+00
53	3.9287E−02	4.4952E+00	4.1550E−02	2.4258E+00	4.3215E−02	2.0448E+00	4.5600E−02	1.7399E+00
54	3.8111E−02	4.5388E+00	4.0142E−02	2.4479E+00	4.1730E−02	2.0633E+00	4.4019E−02	1.7555E+00
55	3.6990E−02	4.5819E+00	3.8805E−02	2.4697E+00	4.0321E−02	2.0815E+00	4.2518E−02	1.7709E+00
56	3.5922E−02	4.6244E+00	3.7533E−02	2.4911E+00	3.8982E−02	2.0994E+00	4.1093E−02	1.7861E+00
57	3.4903E−02	4.6662E+00	3.6324E−02	2.5121E+00	3.7710E−02	2.1170E+00	3.9739E−02	1.8010E+00
58	3.3930E−02	4.7075E+00	3.5173E−02	2.5329E+00	3.6498E−02	2.1343E+00	3.8451E−02	1.8157E+00
59	3.2999E−02	4.7483E+00	3.4076E−02	2.5533E+00	3.5345E−02	2.1514E+00	3.7224E−02	1.8302E+00
60	3.2109E−02	4.7885E+00	3.3029E−02	2.5733E+00	3.4245E−02	2.1682E+00	3.6056E−02	1.8444E+00

Table 4.3.3.1. *Partial wave elastic scattering factors for neutral atoms (cont.)*
Ga; $Z = 31$

	10 keV		40 keV		60 keV		90 keV	
s	$\|f(s)\|$	$\eta(s)$	$\|f(s)\|$	$\eta(s)$	$\|f(s)\|$	$\eta(s)$	$\|f(s)\|$	$\eta(s)$
0	6.4743E+00	2.5242E−01	7.3483E+00	1.5747E−01	7.6949E+00	1.3573E−01	8.1454E+00	1.1752E−01
1	5.4069E+00	2.9717E−01	6.1985E+00	1.8391E−01	6.5025E+00	1.5827E−01	6.8986E+00	1.3676E−01
2	3.7407E+00	4.1105E−01	4.3829E+00	2.4991E−01	4.6136E+00	2.1445E−01	4.9098E+00	1.8479E−01
3	2.6231E+00	5.5253E−01	3.1399E+00	3.3009E−01	3.3155E+00	2.8248E−01	3.5363E+00	2.4294E−01
4	1.9583E+00	6.9214E−01	2.3839E+00	4.0807E−01	2.5233E+00	3.4851E−01	2.6960E+00	2.9929E−01
5	1.5352E+00	8.2193E−01	1.8942E+00	4.8000E−01	2.0089E+00	4.0933E−01	2.1493E+00	3.5116E−01
6	1.2401E+00	9.4514E−01	1.5478E+00	5.4787E−01	1.6443E+00	4.6667E−01	1.7613E+00	4.0002E−01
7	1.0205E+00	1.0665E+00	1.2863E+00	6.1432E−01	1.3684E+00	5.2275E−01	1.4671E+00	4.4778E−01
8	8.5101E−01	1.1889E+00	1.0811E+00	6.8101E−01	1.1514E+00	5.7899E−01	1.2355E+00	4.9565E−01
9	7.1785E−01	1.3136E+00	9.1680E−01	7.4864E−01	9.7717E−01	6.3598E−01	1.0491E+00	5.4413E−01
10	6.1215E−01	1.4401E+00	7.8370E−01	8.1721E−01	8.3568E−01	6.9375E−01	8.9749E−01	5.9326E−01
11	5.2753E−01	1.5675E+00	6.7504E−01	8.8635E−01	7.1986E−01	7.5200E−01	7.7314E−01	6.4279E−01
12	4.5965E−01	1.6944E+00	5.8621E−01	9.5544E−01	6.2492E−01	8.1022E−01	6.7104E−01	6.9231E−01
13	4.0459E−01	1.8194E+00	5.1304E−01	1.0238E+00	5.4657E−01	8.6788E−01	5.8664E−01	7.4138E−01
14	3.5941E−01	1.9412E+00	4.5237E−01	1.0909E+00	4.8149E−01	9.2445E−01	5.1647E−01	7.8954E−01
15	3.2193E−01	2.0591E+00	4.0177E−01	1.1560E+00	4.2717E−01	9.7948E−01	4.5785E−01	8.3642E−01
16	2.9046E−01	2.1724E+00	3.5928E−01	1.2189E+00	3.8153E−01	1.0326E+00	4.0859E−01	8.8169E−01
17	2.6371E−01	2.2809E+00	3.2333E−01	1.2793E+00	3.4293E−01	1.0836E+00	3.6693E−01	9.2515E−01
18	2.4070E−01	2.3847E+00	2.9267E−01	1.3369E+00	3.1003E−01	1.1323E+00	3.3145E−01	9.6667E−01
19	2.2071E−01	2.4839E+00	2.6632E−01	1.3918E+00	2.8179E−01	1.1787E+00	3.0102E−01	1.0062E+00
20	2.0319E−01	2.5789E+00	2.4350E−01	1.4440E+00	2.5738E−01	1.2228E+00	2.7474E−01	1.0438E+00
21	1.8772E−01	2.6700E+00	2.2360E−01	1.4938E+00	2.3614E−01	1.2648E+00	2.5189E−01	1.0796E+00
22	1.7396E−01	2.7575E+00	2.0614E−01	1.5412E+00	2.1752E−01	1.3048E+00	2.3190E−01	1.1136E+00
23	1.6168E−01	2.8417E+00	1.9071E−01	1.5864E+00	2.0110E−01	1.3429E+00	2.1429E−01	1.1459E+00
24	1.5066E−01	2.9230E+00	1.7701E−01	1.6296E+00	1.8655E−01	1.3793E+00	1.9870E−01	1.1769E+00
25	1.4074E−01	3.0016E+00	1.6477E−01	1.6711E+00	1.7357E−01	1.4141E+00	1.8480E−01	1.2065E+00
26	1.3178E−01	3.0777E+00	1.5380E−01	1.7111E+00	1.6194E−01	1.4476E+00	1.7237E−01	1.2349E+00
27	1.2366E−01	3.1517E+00	1.4392E−01	1.7496E+00	1.5147E−01	1.4799E+00	1.6119E−01	1.2623E+00
28	1.1629E−01	3.2237E+00	1.3498E−01	1.7868E+00	1.4201E−01	1.5111E+00	1.5108E−01	1.2887E+00
29	1.0958E−01	3.2938E+00	1.2686E−01	1.8229E+00	1.3343E−01	1.5413E+00	1.4192E−01	1.3143E+00
30	1.0346E−01	3.3621E+00	1.1947E−01	1.8580E+00	1.2562E−01	1.5707E+00	1.3359E−01	1.3392E+00
31	9.7870E−02	3.4289E+00	1.1272E−01	1.8922E+00	1.1849E−01	1.5993E+00	1.2597E−01	1.3634E+00
32	9.2745E−02	3.4942E+00	1.0653E−01	1.9255E+00	1.1195E−01	1.6272E+00	1.1900E−01	1.3870E+00
33	8.8040E−02	3.5581E+00	1.0085E−01	1.9581E+00	1.0595E−01	1.6544E+00	1.1259E−01	1.4100E+00
34	8.3711E−02	3.6206E+00	9.5619E−02	1.9899E+00	1.0042E−01	1.6811E+00	1.0669E−01	1.4326E+00
35	7.9721E−02	3.6820E+00	9.0789E−02	2.0212E+00	9.5312E−02	1.7072E+00	1.0124E−01	1.4547E+00
36	7.6035E−02	3.7421E+00	8.6322E−02	2.0518E+00	9.0589E−02	1.7328E+00	9.6200E−02	1.4764E+00
37	7.2623E−02	3.8011E+00	8.2180E−02	2.0819E+00	8.6209E−02	1.7580E+00	9.1525E−02	1.4977E+00
38	6.9459E−02	3.8590E+00	7.8334E−02	2.1114E+00	8.2141E−02	1.7827E+00	8.7181E−02	1.5186E+00
39	6.6519E−02	3.9159E+00	7.4755E−02	2.1404E+00	7.8355E−02	1.8070E+00	8.3137E−02	1.5391E+00
40	6.3782E−02	3.9718E+00	7.1418E−02	2.1689E+00	7.4825E−02	1.8308E+00	7.9367E−02	1.5594E+00
41	6.1229E−02	4.0268E+00	6.8303E−02	2.1970E+00	7.1528E−02	1.8543E+00	7.5846E−02	1.5792E+00
42	5.8843E−02	4.0808E+00	6.5390E−02	2.2245E+00	6.8445E−02	1.8774E+00	7.2553E−02	1.5988E+00
43	5.6609E−02	4.1340E+00	6.2661E−02	2.2517E+00	6.5557E−02	1.9001E+00	6.9468E−02	1.6180E+00
44	5.4515E−02	4.1863E+00	6.0101E−02	2.2784E+00	6.2848E−02	1.9225E+00	6.6574E−02	1.6370E+00
45	5.2547E−02	4.2377E+00	5.7697E−02	2.3046E+00	6.0304E−02	1.9445E+00	6.3856E−02	1.6556E+00
46	5.0696E−02	4.2884E+00	5.5435E−02	2.3304E+00	5.7911E−02	1.9661E+00	6.1300E−02	1.6740E+00
47	4.8952E−02	4.3383E+00	5.3305E−02	2.3559E+00	5.5658E−02	1.9874E+00	5.8894E−02	1.6920E+00
48	4.7306E−02	4.3874E+00	5.1297E−02	2.3809E+00	5.3533E−02	2.0084E+00	5.6626E−02	1.7098E+00
49	4.5751E−02	4.4358E+00	4.9402E−02	2.4055E+00	5.1529E−02	2.0290E+00	5.4486E−02	1.7273E+00
50	4.4278E−02	4.4835E+00	4.7610E−02	2.4297E+00	4.9635E−02	2.0493E+00	5.2464E−02	1.7445E+00
51	4.2884E−02	4.5305E+00	4.5915E−02	2.4536E+00	4.7843E−02	2.0693E+00	5.0552E−02	1.7614E+00
52	4.1560E−02	4.5768E+00	4.4310E−02	2.4771E+00	4.6148E−02	2.0889E+00	4.8743E−02	1.7781E+00
53	4.0303E−02	4.6225E+00	4.2788E−02	2.5002E+00	4.4541E−02	2.1083E+00	4.7029E−02	1.7945E+00
54	3.9107E−02	4.6676E+00	4.1344E−02	2.5229E+00	4.3016E−02	2.1274E+00	4.5404E−02	1.8106E+00
55	3.7969E−02	4.7120E+00	3.9972E−02	2.5453E+00	4.1569E−02	2.1461E+00	4.3861E−02	1.8265E+00
56	3.6884E−02	4.7558E+00	3.8669E−02	2.5674E+00	4.0194E−02	2.1646E+00	4.2396E−02	1.8422E+00
57	3.5849E−02	4.7990E+00	3.7428E−02	2.5891E+00	3.8886E−02	2.1828E+00	4.1003E−02	1.8576E+00
58	3.4861E−02	4.8416E+00	3.6247E−02	2.6105E+00	3.7641E−02	2.2006E+00	3.9677E−02	1.8727E+00
59	3.3916E−02	4.8837E+00	3.5121E−02	2.6315E+00	3.6456E−02	2.2183E+00	3.8415E−02	1.8876E+00
60	3.3013E−02	4.9252E+00	3.4047E−02	2.6523E+00	3.5325E−02	2.2356E+00	3.7213E−02	1.9023E+00

Table 4.3.3.1. *Partial wave elastic scattering factors for neutral atoms (cont.)*
Ge; $Z = 32$

	10 keV		40 keV		60 keV		90 keV	
s	$\|f(s)\|$	$\eta(s)$	$\|f(s)\|$	$\eta(s)$	$\|f(s)\|$	$\eta(s)$	$\|f(s)\|$	$\eta(s)$
0	6.6981E+00	2.6067E−01	7.6145E+00	1.6293E−01	7.9769E+00	1.4055E−01	8.4472E+00	1.2177E−01
1	5.6931E+00	3.0111E−01	6.5316E+00	1.8695E−01	6.8541E+00	1.6105E−01	7.2738E+00	1.3926E−01
2	3.9785E+00	4.1065E−01	4.6644E+00	2.5086E−01	4.9115E+00	2.1551E−01	5.2283E+00	1.8587E−01
3	2.7452E+00	5.5806E−01	3.2934E+00	3.3485E−01	3.4796E+00	2.8685E−01	3.7132E+00	2.4690E−01
4	2.0062E+00	7.1109E−01	2.4511E+00	4.2056E−01	2.5966E+00	3.5947E−01	2.7762E+00	3.0891E−01
5	1.5507E+00	8.5381E−01	1.9211E+00	4.9980E−01	2.0394E+00	4.2650E−01	2.1836E+00	3.6609E−01
6	1.2449E+00	9.8548E−01	1.5601E+00	5.7250E−01	1.6590E+00	4.8795E−01	1.7784E+00	4.1847E−01
7	1.0233E+00	1.1109E+00	1.2952E+00	6.4139E−01	1.3793E+00	5.4613E−01	1.4801E+00	4.6803E−01
8	8.5457E−01	1.2344E+00	1.0906E+00	7.0889E−01	1.1628E+00	6.0307E−01	1.2489E+00	5.1652E−01
9	7.2243E−01	1.3585E+00	9.2759E−01	7.7641E−01	9.8991E−01	6.6001E−01	1.0639E+00	5.6497E−01
10	6.1735E−01	1.4839E+00	7.9544E−01	8.4452E−01	8.4938E−01	7.1741E−01	9.1319E−01	6.1380E−01
11	5.3292E−01	1.6103E+00	6.8711E−01	9.1320E−01	7.3387E−01	7.7528E−01	7.8913E−01	6.6302E−01
12	4.6491E−01	1.7366E+00	5.9811E−01	9.8202E−01	6.3871E−01	8.3328E−01	6.8674E−01	7.1236E−01
13	4.0956E−01	1.8617E+00	5.2442E−01	1.0505E+00	5.5974E−01	8.9100E−01	6.0162E−01	7.6148E−01
14	3.6404E−01	1.9844E+00	4.6302E−01	1.1180E+00	4.9380E−01	9.4798E−01	5.3046E−01	8.0999E−01
15	3.2625E−01	2.1037E+00	4.1162E−01	1.1840E+00	4.3853E−01	1.0037E+00	4.7074E−01	8.5749E−01
16	2.9452E−01	2.2190E+00	3.6831E−01	1.2481E+00	3.9192E−01	1.0579E+00	4.2036E−01	9.0366E−01
17	2.6756E−01	2.3300E+00	3.3158E−01	1.3100E+00	3.5239E−01	1.1102E+00	3.7762E−01	9.4824E−01
18	2.4439E−01	2.4364E+00	3.0020E−01	1.3694E+00	3.1863E−01	1.1604E+00	3.4115E−01	9.9107E−01
19	2.2427E−01	2.5384E+00	2.7320E−01	1.4262E+00	2.8962E−01	1.2085E+00	3.0981E−01	1.0320E+00
20	2.0664E−01	2.6363E+00	2.4981E−01	1.4804E+00	2.6452E−01	1.2543E+00	2.8272E−01	1.0711E+00
21	1.9106E−01	2.7302E+00	2.2941E−01	1.5322E+00	2.4266E−01	1.2981E+00	2.5916E−01	1.1084E+00
22	1.7720E−01	2.8204E+00	2.1149E−01	1.5815E+00	2.2350E−01	1.3398E+00	2.3853E−01	1.1439E+00
23	1.6482E−01	2.9074E+00	1.9566E−01	1.6287E+00	2.0660E−01	1.3795E+00	2.2037E−01	1.1778E+00
24	1.5369E−01	2.9913E+00	1.8161E−01	1.6738E+00	1.9162E−01	1.4175E+00	2.0429E−01	1.2101E+00
25	1.4365E−01	3.0725E+00	1.6905E−01	1.7170E+00	1.7827E−01	1.4539E+00	1.8997E−01	1.2410E+00
26	1.3458E−01	3.1511E+00	1.5780E−01	1.7586E+00	1.6631E−01	1.4888E+00	1.7716E−01	1.2707E+00
27	1.2634E−01	3.2275E+00	1.4765E−01	1.7986E+00	1.5555E−01	1.5224E+00	1.6564E−01	1.2992E+00
28	1.1885E−01	3.3017E+00	1.3848E−01	1.8373E+00	1.4583E−01	1.5549E+00	1.5524E−01	1.3267E+00
29	1.1203E−01	3.3741E+00	1.3016E−01	1.8747E+00	1.3701E−01	1.5862E+00	1.4582E−01	1.3533E+00
30	1.0580E−01	3.4446E+00	1.2258E−01	1.9110E+00	1.2899E−01	1.6166E+00	1.3725E−01	1.3790E+00
31	1.0009E−01	3.5134E+00	1.1565E−01	1.9463E+00	1.2166E−01	1.6462E+00	1.2942E−01	1.4040E+00
32	9.4861E−02	3.5807E+00	1.0931E−01	1.9807E+00	1.1495E−01	1.6750E+00	1.2226E−01	1.4284E+00
33	9.0054E−02	3.6465E+00	1.0349E−01	2.0143E+00	1.0879E−01	1.7030E+00	1.1568E−01	1.4522E+00
34	8.5629E−02	3.7109E+00	9.8122E−02	2.0471E+00	1.0312E−01	1.7305E+00	1.0962E−01	1.4754E+00
35	8.1548E−02	3.7741E+00	9.3172E−02	2.0792E+00	9.7884E−02	1.7573E+00	1.0403E−01	1.4981E+00
36	7.7777E−02	3.8360E+00	8.8593E−02	2.1107E+00	9.3041E−02	1.7837E+00	9.8861E−02	1.5204E+00
37	7.4286E−02	3.8967E+00	8.4350E−02	2.1416E+00	8.8552E−02	1.8095E+00	9.4067E−02	1.5422E+00
38	7.1049E−02	3.9563E+00	8.0408E−02	2.1718E+00	8.4382E−02	1.8348E+00	8.9613E−02	1.5636E+00
39	6.8041E−02	4.0148E+00	7.6742E−02	2.2016E+00	8.0501E−02	1.8597E+00	8.5468E−02	1.5847E+00
40	6.5241E−02	4.0723E+00	7.3324E−02	2.2308E+00	7.6884E−02	1.8841E+00	8.1603E−02	1.6054E+00
41	6.2630E−02	4.1288E+00	7.0133E−02	2.2595E+00	7.3506E−02	1.9082E+00	7.7993E−02	1.6258E+00
42	6.0191E−02	4.1844E+00	6.7149E−02	2.2878E+00	7.0347E−02	1.9318E+00	7.4617E−02	1.6458E+00
43	5.7909E−02	4.2391E+00	6.4355E−02	2.3156E+00	6.7388E−02	1.9551E+00	7.1455E−02	1.6655E+00
44	5.5769E−02	4.2929E+00	6.1733E−02	2.3429E+00	6.4612E−02	1.9780E+00	6.8488E−02	1.6849E+00
45	5.3761E−02	4.3458E+00	5.9271E−02	2.3698E+00	6.2005E−02	2.0005E+00	6.5702E−02	1.7040E+00
46	5.1873E−02	4.3979E+00	5.6956E−02	2.3963E+00	5.9552E−02	2.0227E+00	6.3082E−02	1.7228E+00
47	5.0094E−02	4.4492E+00	5.4775E−02	2.4224E+00	5.7243E−02	2.0445E+00	6.0614E−02	1.7413E+00
48	4.8417E−02	4.4998E+00	5.2719E−02	2.4481E+00	5.5067E−02	2.0660E+00	5.8288E−02	1.7595E+00
49	4.6832E−02	4.5496E+00	5.0778E−02	2.4733E+00	5.3012E−02	2.0872E+00	5.6093E−02	1.7774E+00
50	4.5334E−02	4.5987E+00	4.8943E−02	2.4982E+00	5.1070E−02	2.1080E+00	5.4019E−02	1.7951E+00
51	4.3914E−02	4.6470E+00	4.7207E−02	2.5227E+00	4.9234E−02	2.1286E+00	5.2057E−02	1.8125E+00
52	4.2568E−02	4.6947E+00	4.5563E−02	2.5468E+00	4.7495E−02	2.1488E+00	5.0201E−02	1.8296E+00
53	4.1290E−02	4.7418E+00	4.4005E−02	2.5706E+00	4.5847E−02	2.1687E+00	4.8441E−02	1.8464E+00
54	4.0076E−02	4.7881E+00	4.2526E−02	2.5940E+00	4.4284E−02	2.1883E+00	4.6773E−02	1.8630E+00
55	3.8920E−02	4.8339E+00	4.1121E−02	2.6170E+00	4.2799E−02	2.2076E+00	4.5189E−02	1.8794E+00
56	3.7818E−02	4.8790E+00	3.9785E−02	2.6397E+00	4.1389E−02	2.2266E+00	4.3684E−02	1.8955E+00
57	3.6768E−02	4.9236E+00	3.8514E−02	2.6621E+00	4.0047E−02	2.2453E+00	4.2253E−02	1.9114E+00
58	3.5766E−02	4.9675E+00	3.7304E−02	2.6841E+00	3.8770E−02	2.2637E+00	4.0891E−02	1.9270E+00
59	3.4808E−02	5.0109E+00	3.6150E−02	2.7058E+00	3.7553E−02	2.2818E+00	3.9595E−02	1.9423E+00
60	3.3892E−02	5.0538E+00	3.5049E−02	2.7272E+00	3.6392E−02	2.2997E+00	3.8359E−02	1.9575E+00

Table 4.3.3.1. *Partial wave elastic scattering factors for neutral atoms (cont.)*
As; $Z = 33$

	10 keV		40 keV		60 keV		90 keV	
s	$\|f(s)\|$	$\eta(s)$	$\|f(s)\|$	$\eta(s)$	$\|f(s)\|$	$\eta(s)$	$\|f(s)\|$	$\eta(s)$
0	6.6112E+00	2.7657E−01	7.5499E+00	1.7312E−01	7.9099E+00	1.4950E−01	8.3809E+00	1.2961E−01
1	5.7554E+00	3.1195E−01	6.6239E+00	1.9427E−01	6.9531E+00	1.6751E−01	7.3824E+00	1.4496E−01
2	4.1475E+00	4.1229E−01	4.8706E+00	2.5321E−01	5.1306E+00	2.1774E−01	5.4636E+00	1.8797E−01
3	2.8694E+00	5.5772E−01	3.4504E+00	3.3657E−01	3.6475E+00	2.8861E−01	3.8942E+00	2.4865E−01
4	2.0681E+00	7.1917E−01	2.5359E+00	4.2733E−01	2.6887E+00	3.6555E−01	2.8765E+00	3.1438E−01
5	1.5764E+00	8.7454E−01	1.9610E+00	5.1379E−01	2.0836E+00	4.3872E−01	2.2327E+00	3.7682E−01
6	1.2551E+00	1.0169E+00	1.5790E+00	5.9259E−01	1.6806E+00	5.0533E−01	1.8030E+00	4.3363E−01
7	1.0284E+00	1.1488E+00	1.3065E+00	6.6531E−01	1.3925E+00	5.6676E−01	1.4955E+00	4.8598E−01
8	8.5870E−01	1.2753E+00	1.1001E+00	7.3466E−01	1.1740E+00	6.2530E−01	1.2619E+00	5.3584E−01
9	7.2682E−01	1.4000E+00	9.3737E−01	8.0274E−01	1.0013E+00	6.8272E−01	1.0771E+00	5.8472E−01
10	6.2211E−01	1.5248E+00	8.0594E−01	8.7069E−01	8.6148E−01	7.4002E−01	9.2713E−01	6.3348E−01
11	5.3781E−01	1.6503E+00	6.9823E−01	9.3894E−01	7.4636E−01	7.9758E−01	8.0346E−01	6.8245E−01
12	4.6971E−01	1.7758E+00	6.0919E−01	1.0074E+00	6.5123E−01	8.5527E−01	7.0106E−01	7.3154E−01
13	4.1412E−01	1.9007E+00	5.3512E−01	1.0757E+00	5.7191E−01	9.1288E−01	6.1552E−01	7.8056E−01
14	3.6830E−01	2.0237E+00	4.7319E−01	1.1435E+00	5.0536E−01	9.7002E−01	5.4365E−01	8.2921E−01
15	3.3022E−01	2.1441E+00	4.2113E−01	1.2100E+00	4.4932E−01	1.0263E+00	4.8305E−01	8.7712E−01
16	2.9824E−01	2.2609E+00	3.7713E−01	1.2751E+00	4.0190E−01	1.0812E+00	4.3173E−01	9.2396E−01
17	2.7108E−01	2.3738E+00	3.3971E−01	1.3381E+00	3.6155E−01	1.1346E+00	3.8804E−01	9.6945E−01
18	2.4776E−01	2.4826E+00	3.0769E−01	1.3989E+00	3.2702E−01	1.1861E+00	3.5065E−01	1.0134E+00
19	2.2752E−01	2.5871E+00	2.8010E−01	1.4574E+00	2.9729E−01	1.2356E+00	3.1848E−01	1.0556E+00
20	2.0980E−01	2.6875E+00	2.5617E−01	1.5134E+00	2.7153E−01	1.2830E+00	2.9063E−01	1.0961E+00
21	1.9414E−01	2.7841E+00	2.3528E−01	1.5670E+00	2.4909E−01	1.3284E+00	2.6638E−01	1.1348E+00
22	1.8021E−01	2.8770E+00	2.1693E−01	1.6182E+00	2.2940E−01	1.3717E+00	2.4514E−01	1.1717E+00
23	1.6774E−01	2.9665E+00	2.0072E−01	1.6672E+00	2.1205E−01	1.4131E+00	2.2643E−01	1.2070E+00
24	1.5653E−01	3.0530E+00	1.8632E−01	1.7140E+00	1.9666E−01	1.4527E+00	2.0987E−01	1.2407E+00
25	1.4641E−01	3.1367E+00	1.7346E−01	1.7590E+00	1.8294E−01	1.4907E+00	1.9512E−01	1.2730E+00
26	1.3724E−01	3.2177E+00	1.6193E−01	1.8021E+00	1.7065E−01	1.5270E+00	1.8194E−01	1.3039E+00
27	1.2891E−01	3.2964E+00	1.5153E−01	1.8436E+00	1.5960E−01	1.5620E+00	1.7008E−01	1.3336E+00
28	1.2133E−01	3.3729E+00	1.4213E−01	1.8837E+00	1.4962E−01	1.5957E+00	1.5939E−01	1.3622E+00
29	1.1440E−01	3.4474E+00	1.3360E−01	1.9224E+00	1.4057E−01	1.6283E+00	1.4970E−01	1.3898E+00
30	1.0807E−01	3.5201E+00	1.2583E−01	1.9599E+00	1.3233E−01	1.6598E+00	1.4089E−01	1.4166E+00
31	1.0226E−01	3.5910E+00	1.1873E−01	1.9964E+00	1.2482E−01	1.6904E+00	1.3286E−01	1.4425E+00
32	9.6935E−02	3.6603E+00	1.1223E−01	2.0318E+00	1.1794E−01	1.7201E+00	1.2550E−01	1.4676E+00
33	9.2034E−02	3.7281E+00	1.0626E−01	2.0663E+00	1.1162E−01	1.7491E+00	1.1875E−01	1.4921E+00
34	8.7519E−02	3.7944E+00	1.0076E−01	2.1000E+00	1.0580E−01	1.7773E+00	1.1254E−01	1.5160E+00
35	8.3352E−02	3.8594E+00	9.5683E−02	2.1329E+00	1.0044E−01	1.8049E+00	1.0680E−01	1.5394E+00
36	7.9499E−02	3.9231E+00	9.0988E−02	2.1651E+00	9.5472E−02	1.8320E+00	1.0150E−01	1.5623E+00
37	7.5932E−02	3.9855E+00	8.6637E−02	2.1967E+00	9.0871E−02	1.8585E+00	9.6586E−02	1.5847E+00
38	7.2622E−02	4.0469E+00	8.2598E−02	2.2276E+00	8.6599E−02	1.8845E+00	9.2021E−02	1.6067E+00
39	6.9547E−02	4.1071E+00	7.8839E−02	2.2580E+00	8.2624E−02	1.9100E+00	8.7773E−02	1.6283E+00
40	6.6684E−02	4.1662E+00	7.5335E−02	2.2878E+00	7.8919E−02	1.9350E+00	8.3813E−02	1.6495E+00
41	6.4015E−02	4.2243E+00	7.2064E−02	2.3172E+00	7.5459E−02	1.9597E+00	8.0115E−02	1.6703E+00
42	6.1522E−02	4.2815E+00	6.9005E−02	2.3460E+00	7.2224E−02	1.9839E+00	7.6657E−02	1.6908E+00
43	5.9191E−02	4.3377E+00	6.6141E−02	2.3743E+00	6.9194E−02	2.0077E+00	7.3417E−02	1.7110E+00
44	5.7006E−02	4.3930E+00	6.3453E−02	2.4022E+00	6.6351E−02	2.0311E+00	7.0378E−02	1.7308E+00
45	5.4956E−02	4.4474E+00	6.0929E−02	2.4296E+00	6.3682E−02	2.0542E+00	6.7524E−02	1.7504E+00
46	5.3029E−02	4.5009E+00	5.8555E−02	2.4566E+00	6.1171E−02	2.0769E+00	6.4839E−02	1.7696E+00
47	5.1215E−02	4.5537E+00	5.6319E−02	2.4831E+00	5.8807E−02	2.0993E+00	6.2311E−02	1.7886E+00
48	4.9505E−02	4.6057E+00	5.4211E−02	2.5093E+00	5.6577E−02	2.1213E+00	5.9928E−02	1.8072E+00
49	4.7891E−02	4.6569E+00	5.2221E−02	2.5350E+00	5.4473E−02	2.1430E+00	5.7678E−02	1.8256E+00
50	4.6365E−02	4.7074E+00	5.0339E−02	2.5603E+00	5.2485E−02	2.1644E+00	5.5553E−02	1.8437E+00
51	4.4921E−02	4.7571E+00	4.8558E−02	2.5853E+00	5.0604E−02	2.1854E+00	5.3543E−02	1.8615E+00
52	4.3552E−02	4.8062E+00	4.6872E−02	2.6099E+00	4.8823E−02	2.2061E+00	5.1639E−02	1.8791E+00
53	4.2253E−02	4.8546E+00	4.5273E−02	2.6341E+00	4.7135E−02	2.2266E+00	4.9836E−02	1.8964E+00
54	4.1019E−02	4.9023E+00	4.3756E−02	2.6579E+00	4.5534E−02	2.2467E+00	4.8125E−02	1.9134E+00
55	3.9845E−02	4.9494E+00	4.2313E−02	2.6814E+00	4.4013E−02	2.2665E+00	4.6500E−02	1.9302E+00
56	3.8727E−02	4.9959E+00	4.0942E−02	2.7046E+00	4.2567E−02	2.2860E+00	4.4957E−02	1.9468E+00
57	3.7662E−02	5.0417E+00	3.9637E−02	2.7274E+00	4.1192E−02	2.3052E+00	4.3489E−02	1.9631E+00
58	3.6645E−02	5.0870E+00	3.8394E−02	2.7498E+00	3.9883E−02	2.3242E+00	4.2092E−02	1.9791E+00
59	3.5674E−02	5.1317E+00	3.7209E−02	2.7720E+00	3.8635E−02	2.3429E+00	4.0761E−02	1.9949E+00
60	3.4746E−02	5.1758E+00	3.6078E−02	2.7938E+00	3.7446E−02	2.3613E+00	3.9493E−02	2.0105E+00

Table 4.3.3.1. *Partial wave elastic scattering factors for neutral atoms (cont.)*
Se; $Z = 34$

	10 keV		40 keV		60 keV		90 keV	
s	$\|f(s)\|$	$\eta(s)$	$\|f(s)\|$	$\eta(s)$	$\|f(s)\|$	$\eta(s)$	$\|f(s)\|$	$\eta(s)$
0	6.4543E+00	2.9336E−01	7.3989E+00	1.8414E−01	7.7633E+00	1.5910E−01	8.2306E+00	1.3803E−01
1	5.7250E+00	3.2496E−01	6.6111E+00	2.0304E−01	6.9468E+00	1.7524E−01	7.3799E+00	1.5176E−01
2	4.2546E+00	4.1681E−01	5.0079E+00	2.5721E−01	5.2786E+00	2.2149E−01	5.6238E+00	1.9139E−01
3	2.9808E+00	5.5661E−01	3.5930E+00	3.3778E−01	3.8008E+00	2.9008E−01	4.0599E+00	2.5016E−01
4	2.1362E+00	7.2123E−01	2.6289E+00	4.3070E−01	2.7897E+00	3.6893E−01	2.9866E+00	3.1758E−01
5	1.6101E+00	8.8679E−01	2.0113E+00	5.2302E−01	2.1393E+00	4.4711E−01	2.2941E+00	3.8432E−01
6	1.2707E+00	1.0404E+00	1.6048E+00	6.0824E−01	1.7099E+00	5.1921E−01	1.8360E+00	4.4582E−01
7	1.0364E+00	1.1809E+00	1.3208E+00	6.8591E−01	1.4094E+00	5.8487E−01	1.5148E+00	5.0180E−01
8	8.6408E−01	1.3124E+00	1.1102E+00	7.5824E−01	1.1861E+00	6.4597E−01	1.2760E+00	5.5386E−01
9	7.3156E−01	1.4392E+00	9.4644E−01	8.2769E−01	1.0122E+00	7.0459E−01	1.0898E+00	6.0379E−01
10	6.2678E−01	1.5643E+00	8.1505E−01	8.9601E−01	8.7245E−01	7.6222E−01	9.3981E−01	6.5284E−01
11	5.4243E−01	1.6893E+00	7.0736E−01	9.6414E−01	7.5757E−01	8.1966E−01	8.1636E−01	7.0173E−01
12	4.7421E−01	1.8141E+00	6.1854E−01	1.0322E+00	6.6256E−01	8.7708E−01	7.1407E−01	7.5059E−01
13	4.1839E−01	1.9384E+00	5.4444E−01	1.1003E+00	5.8308E−01	9.3447E−01	6.2834E−01	7.9944E−01
14	3.7228E−01	2.0615E+00	4.8217E−01	1.1680E+00	5.1612E−01	9.9160E−01	5.5599E−01	8.4807E−01
15	3.3391E−01	2.1824E+00	4.2963E−01	1.2349E+00	4.5950E−01	1.0481E+00	4.9472E−01	8.9619E−01
16	3.0168E−01	2.3004E+00	3.8506E−01	1.3005E+00	4.1141E−01	1.1036E+00	4.4262E−01	9.4349E−01
17	2.7432E−01	2.4149E+00	3.4706E−01	1.3645E+00	3.7036E−01	1.1577E+00	3.9812E−01	9.8967E−01
18	2.5085E−01	2.5255E+00	3.1447E−01	1.4266E+00	3.3514E−01	1.2103E+00	3.5993E−01	1.0345E+00
19	2.3050E−01	2.6323E+00	2.8635E−01	1.4866E+00	3.0476E−01	1.2610E+00	3.2698E−01	1.0778E+00
20	2.1269E−01	2.7350E+00	2.6194E−01	1.5443E+00	2.7840E−01	1.3099E+00	2.9842E−01	1.1195E+00
21	1.9696E−01	2.8340E+00	2.4061E−01	1.5996E+00	2.5541E−01	1.3568E+00	2.7352E−01	1.1595E+00
22	1.8297E−01	2.9294E+00	2.2186E−01	1.6527E+00	2.3523E−01	1.4017E+00	2.5169E−01	1.1978E+00
23	1.7045E−01	3.0214E+00	2.0529E−01	1.7035E+00	2.1743E−01	1.4447E+00	2.3246E−01	1.2345E+00
24	1.5918E−01	3.1103E+00	1.9057E−01	1.7522E+00	2.0164E−01	1.4858E+00	2.1543E−01	1.2696E+00
25	1.4900E−01	3.1963E+00	1.7742E−01	1.7989E+00	1.8756E−01	1.5253E+00	2.0026E−01	1.3032E+00
26	1.3976E−01	3.2797E+00	1.6563E−01	1.8438E+00	1.7496E−01	1.5631E+00	1.8670E−01	1.3354E+00
27	1.3136E−01	3.3607E+00	1.5500E−01	1.8870E+00	1.6362E−01	1.5995E+00	1.7452E−01	1.3663E+00
28	1.2369E−01	3.4394E+00	1.4539E−01	1.9287E+00	1.5338E−01	1.6345E+00	1.6353E−01	1.3961E+00
29	1.1668E−01	3.5161E+00	1.3666E−01	1.9689E+00	1.4410E−01	1.6683E+00	1.5358E−01	1.4247E+00
30	1.1026E−01	3.5908E+00	1.2871E−01	2.0078E+00	1.3566E−01	1.7010E+00	1.4453E−01	1.4525E+00
31	1.0437E−01	3.6638E+00	1.2145E−01	2.0456E+00	1.2795E−01	1.7326E+00	1.3628E−01	1.4793E+00
32	9.8957E−02	3.7351E+00	1.1480E−01	2.0823E+00	1.2090E−01	1.7633E+00	1.2873E−01	1.5053E+00
33	9.3972E−02	3.8048E+00	1.0869E−01	2.1180E+00	1.1443E−01	1.7932E+00	1.2181E−01	1.5306E+00
34	8.9374E−02	3.8730E+00	1.0306E−01	2.1529E+00	1.0847E−01	1.8224E+00	1.1543E−01	1.5553E+00
35	8.5126E−02	3.9399E+00	9.7872E−02	2.1869E+00	1.0297E−01	1.8508E+00	1.0956E−01	1.5794E+00
36	8.1197E−02	4.0054E+00	9.3072E−02	2.2201E+00	9.7882E−02	1.8786E+00	1.0412E−01	1.6029E+00
37	7.7556E−02	4.0696E+00	8.8623E−02	2.2527E+00	9.3171E−02	1.9059E+00	9.9085E−02	1.6259E+00
38	7.4177E−02	4.1327E+00	8.4492E−02	2.2846E+00	8.8796E−02	1.9325E+00	9.4408E−02	1.6485E+00
39	7.1036E−02	4.1946E+00	8.0649E−02	2.3159E+00	8.4726E−02	1.9587E+00	9.0057E−02	1.6706E+00
40	6.8112E−02	4.2554E+00	7.7068E−02	2.3466E+00	8.0932E−02	1.9844E+00	8.6002E−02	1.6923E+00
41	6.5386E−02	4.3151E+00	7.3725E−02	2.3768E+00	7.7391E−02	2.0096E+00	8.2215E−02	1.7137E+00
42	6.2840E−02	4.3739E+00	7.0600E−02	2.4065E+00	7.4079E−02	2.0344E+00	7.8674E−02	1.7347E+00
43	6.0458E−02	4.4316E+00	6.7674E−02	2.4356E+00	7.0978E−02	2.0588E+00	7.5357E−02	1.7553E+00
44	5.8227E−02	4.4885E+00	6.4929E−02	2.4643E+00	6.8069E−02	2.0828E+00	7.2246E−02	1.7756E+00
45	5.6135E−02	4.5444E+00	6.2352E−02	2.4925E+00	6.5337E−02	2.1064E+00	6.9324E−02	1.7956E+00
46	5.4168E−02	4.5995E+00	5.9928E−02	2.5203E+00	6.2768E−02	2.1297E+00	6.6575E−02	1.8153E+00
47	5.2318E−02	4.6537E+00	5.7646E−02	2.5477E+00	6.0348E−02	2.1525E+00	6.3987E−02	1.8347E+00
48	5.0575E−02	4.7071E+00	5.5495E−02	2.5747E+00	5.8067E−02	2.1751E+00	6.1547E−02	1.8538E+00
49	4.8931E−02	4.7597E+00	5.3464E−02	2.6012E+00	5.5914E−02	2.1973E+00	5.9244E−02	1.8726E+00
50	4.7377E−02	4.8116E+00	5.1544E−02	2.6273E+00	5.3880E−02	2.2192E+00	5.7068E−02	1.8911E+00
51	4.5907E−02	4.8628E+00	4.9729E−02	2.6531E+00	5.1955E−02	2.2407E+00	5.5009E−02	1.9094E+00
52	4.4514E−02	4.9132E+00	4.8009E−02	2.6785E+00	5.0132E−02	2.2620E+00	5.3060E−02	1.9274E+00
53	4.3194E−02	4.9630E+00	4.6378E−02	2.7034E+00	4.8405E−02	2.2829E+00	5.1213E−02	1.9451E+00
54	4.1940E−02	5.0120E+00	4.4831E−02	2.7281E+00	4.6765E−02	2.3035E+00	4.9460E−02	1.9626E+00
55	4.0748E−02	5.0605E+00	4.3361E−02	2.7524E+00	4.5209E−02	2.3239E+00	4.7796E−02	1.9798E+00
56	3.9613E−02	5.1083E+00	4.1964E−02	2.7763E+00	4.3729E−02	2.3439E+00	4.6215E−02	1.9967E+00
57	3.8532E−02	5.1554E+00	4.0633E−02	2.7999E+00	4.2321E−02	2.3636E+00	4.4711E−02	2.0135E+00
58	3.7502E−02	5.2020E+00	3.9367E−02	2.8231E+00	4.0981E−02	2.3831E+00	4.3279E−02	2.0299E+00
59	3.6518E−02	5.2480E+00	3.8159E−02	2.8461E+00	3.9704E−02	2.4023E+00	4.1915E−02	2.0462E+00
60	3.5577E−02	5.2935E+00	3.7007E−02	2.8687E+00	3.8486E−02	2.4212E+00	4.0615E−02	2.0622E+00

Table 4.3.3.1. *Partial wave elastic scattering factors for neutral atoms (cont.)*
Br; $Z = 35$

	10 keV		40 keV		60 keV		90 keV	
s	$\|f(s)\|$	$\eta(s)$	$\|f(s)\|$	$\eta(s)$	$\|f(s)\|$	$\eta(s)$	$\|f(s)\|$	$\eta(s)$
0	6.2644E+00	3.1037E−01	7.2156E+00	1.9538E−01	7.5777E+00	1.6896E−01	8.0394E+00	1.4670E−01
1	5.6398E+00	3.3900E−01	6.5399E+00	2.1255E−01	6.8776E+00	1.8362E−01	7.3109E+00	1.5916E−01
2	4.3108E+00	4.2341E−01	5.0893E+00	2.6255E−01	5.3679E+00	2.2636E−01	5.7221E+00	1.9578E−01
3	3.0732E+00	5.5614E−01	3.7143E+00	3.3948E−01	3.9317E+00	2.9193E−01	4.2021E+00	2.5201E−01
4	2.2045E+00	7.1996E−01	2.7230E+00	4.3236E−01	2.8919E+00	3.7082E−01	3.0981E+00	3.1951E−01
5	1.6488E+00	8.9233E−01	2.0690E+00	5.2874E−01	2.2029E+00	4.5248E−01	2.3643E+00	3.8925E−01
6	1.2908E+00	1.0564E+00	1.6372E+00	6.1998E−01	1.7463E+00	5.2970E−01	1.8766E+00	4.5516E−01
7	1.0473E+00	1.2066E+00	1.3393E+00	7.0323E−01	1.4305E+00	6.0013E−01	1.5388E+00	5.1522E−01
8	8.7105E−01	1.3448E+00	1.1222E+00	7.7958E−01	1.2001E+00	6.6465E−01	1.2921E+00	5.7022E−01
9	7.3704E−01	1.4754E+00	9.5597E−01	8.5135E−01	1.0234E+00	7.2527E−01	1.1027E+00	6.2189E−01
10	6.3172E−01	1.6020E+00	8.2389E−01	9.2070E−01	8.8282E−01	7.8380E−01	9.5182E−01	6.7171E−01
11	5.4706E−01	1.7272E+00	7.1609E−01	9.8908E−01	7.6781E−01	8.4148E−01	8.2819E−01	7.2081E−01
12	4.7860E−01	1.8515E+00	6.2734E−01	1.0570E+00	6.7286E−01	8.9876E−01	7.2594E−01	7.6957E−01
13	4.2250E−01	1.9753E+00	5.5318E−01	1.1248E+00	5.9332E−01	9.5593E−01	6.4013E−01	8.1824E−01
14	3.7608E−01	2.0982E+00	4.9067E−01	1.1923E+00	5.2609E−01	1.0129E+00	5.6746E−01	8.6677E−01
15	3.3741E−01	2.2193E+00	4.3776E−01	1.2593E+00	4.6905E−01	1.0695E+00	5.0570E−01	9.1495E−01
16	3.0491E−01	2.3380E+00	3.9275E−01	1.3253E+00	4.2042E−01	1.1253E+00	4.5299E−01	9.6251E−01
17	2.7734E−01	2.4537E+00	3.5425E−01	1.3900E+00	3.7879E−01	1.1800E+00	4.0780E−01	1.0092E+00
18	2.5370E−01	2.5659E+00	3.2117E−01	1.4531E+00	3.4297E−01	1.2334E+00	3.6891E−01	1.0547E+00
19	2.3324E−01	2.6745E+00	2.9257E−01	1.5142E+00	3.1201E−01	1.2852E+00	3.3528E−01	1.0990E+00
20	2.1534E−01	2.7793E+00	2.6770E−01	1.5733E+00	2.8510E−01	1.3353E+00	3.0606E−01	1.1417E+00
21	1.9955E−01	2.8805E+00	2.4596E−01	1.6302E+00	2.6159E−01	1.3835E+00	2.8055E−01	1.1829E+00
22	1.8552E−01	2.9781E+00	2.2684E−01	1.6849E+00	2.4095E−01	1.4298E+00	2.5817E−01	1.2225E+00
23	1.7295E−01	3.0724E+00	2.0994E−01	1.7374E+00	2.2272E−01	1.4743E+00	2.3843E−01	1.2604E+00
24	1.6164E−01	3.1636E+00	1.9491E−01	1.7879E+00	2.0655E−01	1.5170E+00	2.2095E−01	1.2968E+00
25	1.5141E−01	3.2519E+00	1.8149E−01	1.8363E+00	1.9214E−01	1.5579E+00	2.0538E−01	1.3317E+00
26	1.4212E−01	3.3375E+00	1.6944E−01	1.8828E+00	1.7922E−01	1.5972E+00	1.9145E−01	1.3652E+00
27	1.3366E−01	3.4207E+00	1.5858E−01	1.9276E+00	1.6761E−01	1.6350E+00	1.7894E−01	1.3973E+00
28	1.2594E−01	3.5016E+00	1.4876E−01	1.9708E+00	1.5712E−01	1.6713E+00	1.6766E−01	1.4283E+00
29	1.1886E−01	3.5804E+00	1.3984E−01	2.0124E+00	1.4761E−01	1.7064E+00	1.5744E−01	1.4581E+00
30	1.1237E−01	3.6572E+00	1.3172E−01	2.0528E+00	1.3896E−01	1.7403E+00	1.4816E−01	1.4868E+00
31	1.0641E−01	3.7322E+00	1.2430E−01	2.0918E+00	1.3107E−01	1.7730E+00	1.3969E−01	1.5146E+00
32	1.0092E−01	3.8054E+00	1.1750E−01	2.1298E+00	1.2385E−01	1.8048E+00	1.3195E−01	1.5416E+00
33	9.5858E−02	3.8771E+00	1.1125E−01	2.1666E+00	1.1721E−01	1.8357E+00	1.2485E−01	1.5677E+00
34	9.1185E−02	3.9472E+00	1.0550E−01	2.2025E+00	1.1111E−01	1.8658E+00	1.1832E−01	1.5932E+00
35	8.6865E−02	4.0159E+00	1.0019E−01	2.2376E+00	1.0548E−01	1.8951E+00	1.1229E−01	1.6180E+00
36	8.2865E−02	4.0833E+00	9.5281E−02	2.2718E+00	1.0028E−01	1.9237E+00	1.0673E−01	1.6422E+00
37	7.9155E−02	4.1493E+00	9.0731E−02	2.3053E+00	9.5452E−02	1.9517E+00	1.0157E−01	1.6659E+00
38	7.5710E−02	4.2141E+00	8.6505E−02	2.3381E+00	9.0975E−02	1.9791E+00	9.6778E−02	1.6890E+00
39	7.2507E−02	4.2777E+00	8.2575E−02	2.3702E+00	8.6809E−02	2.0059E+00	9.2323E−02	1.7118E+00
40	6.9523E−02	4.3402E+00	7.8912E−02	2.4017E+00	8.2927E−02	2.0323E+00	8.8171E−02	1.7340E+00
41	6.6741E−02	4.4016E+00	7.5493E−02	2.4326E+00	7.9304E−02	2.0581E+00	8.4295E−02	1.7559E+00
42	6.4142E−02	4.4620E+00	7.2297E−02	2.4630E+00	7.5915E−02	2.0835E+00	8.0671E−02	1.7774E+00
43	6.1711E−02	4.5213E+00	6.9304E−02	2.4929E+00	7.2743E−02	2.1085E+00	7.7277E−02	1.7985E+00
44	5.9435E−02	4.5797E+00	6.6498E−02	2.5223E+00	6.9767E−02	2.1331E+00	7.4094E−02	1.8193E+00
45	5.7299E−02	4.6372E+00	6.3863E−02	2.5512E+00	6.6973E−02	2.1572E+00	7.1104E−02	1.8397E+00
46	5.5293E−02	4.6938E+00	6.1385E−02	2.5796E+00	6.4345E−02	2.1810E+00	6.8292E−02	1.8599E+00
47	5.3407E−02	4.7495E+00	5.9052E−02	2.6077E+00	6.1871E−02	2.2044E+00	6.5644E−02	1.8797E+00
48	5.1630E−02	4.8044E+00	5.6853E−02	2.6352E+00	5.9538E−02	2.2275E+00	6.3147E−02	1.8992E+00
49	4.9954E−02	4.8585E+00	5.4777E−02	2.6624E+00	5.7336E−02	2.2502E+00	6.0791E−02	1.9184E+00
50	4.8371E−02	4.9118E+00	5.2816E−02	2.6892E+00	5.5255E−02	2.2726E+00	5.8564E−02	1.9374E+00
51	4.6875E−02	4.9643E+00	5.0960E−02	2.7155E+00	5.3287E−02	2.2947E+00	5.6458E−02	1.9561E+00
52	4.5458E−02	5.0161E+00	4.9203E−02	2.7415E+00	5.1423E−02	2.3164E+00	5.4463E−02	1.9745E+00
53	4.4115E−02	5.0673E+00	4.7537E−02	2.7671E+00	4.9657E−02	2.3379E+00	5.2573E−02	1.9927E+00
54	4.2840E−02	5.1177E+00	4.5956E−02	2.7924E+00	4.7980E−02	2.3590E+00	5.0779E−02	2.0105E+00
55	4.1630E−02	5.1675E+00	4.4454E−02	2.8173E+00	4.6388E−02	2.3798E+00	4.9076E−02	2.0282E+00
56	4.0478E−02	5.2166E+00	4.3026E−02	2.8418E+00	4.4875E−02	2.4003E+00	4.7457E−02	2.0456E+00
57	3.9382E−02	5.2651E+00	4.1667E−02	2.8660E+00	4.3435E−02	2.4206E+00	4.5918E−02	2.0627E+00
58	3.8337E−02	5.3130E+00	4.0373E−02	2.8898E+00	4.2064E−02	2.4405E+00	4.4452E−02	2.0796E+00
59	3.7340E−02	5.3603E+00	3.9139E−02	2.9134E+00	4.0757E−02	2.4602E+00	4.3055E−02	2.0963E+00
60	3.6387E−02	5.4071E+00	3.7962E−02	2.9365E+00	3.9511E−02	2.4796E+00	4.1724E−02	2.1127E+00

Table 4.3.3.1. *Partial wave elastic scattering factors for neutral atoms (cont.)*
Kr; $Z = 36$

	10 keV		40 keV		60 keV		90 keV	
s	$\|f(s)\|$	$\eta(s)$	$\|f(s)\|$	$\eta(s)$	$\|f(s)\|$	$\eta(s)$	$\|f(s)\|$	$\eta(s)$
0	6.0600E+00	3.2728E−01	7.0151E+00	2.0669E−01	7.3740E+00	1.7892E−01	7.8299E+00	1.5545E−01
1	5.5219E+00	3.5349E−01	6.4320E+00	2.2246E−01	6.7701E+00	1.9238E−01	7.2009E+00	1.6691E−01
2	4.3272E+00	4.3146E−01	5.1262E+00	2.6884E−01	5.4109E+00	2.3205E−01	5.7716E+00	2.0088E−01
3	3.1447E+00	5.5680E−01	3.8119E+00	3.4187E−01	4.0378E+00	2.9437E−01	4.3178E+00	2.5439E−01
4	2.2687E+00	7.1718E−01	2.8126E+00	4.3323E−01	2.9897E+00	3.7205E−01	3.2052E+00	3.2087E−01
5	1.6900E+00	8.9301E−01	2.1308E+00	5.3184E−01	2.2710E+00	4.5566E−01	2.4393E+00	3.9236E−01
6	1.3142E+00	1.0658E+00	1.6748E+00	6.2809E−01	1.7884E+00	5.3716E−01	1.9236E+00	4.6191E−01
7	1.0607E+00	1.2257E+00	1.3617E+00	7.1702E−01	1.4560E+00	6.1242E−01	1.5675E+00	5.2615E−01
8	8.7963E−01	1.3719E+00	1.1364E+00	7.9811E−01	1.2165E+00	6.8100E−01	1.3108E+00	5.8462E−01
9	7.4347E−01	1.5077E+00	9.6636E−01	8.7311E−01	1.0355E+00	7.4439E−01	1.1166E+00	6.3867E−01
10	6.3715E−01	1.6372E+00	8.3272E−01	9.4426E−01	8.9312E−01	8.0448E−01	9.6369E−01	6.8985E−01
11	5.5191E−01	1.7635E+00	7.2435E−01	1.0134E+00	7.7746E−01	8.6284E−01	8.3933E−01	7.3954E−01
12	4.8305E−01	1.8879E+00	6.3546E−01	1.0815E+00	6.8237E−01	9.2026E−01	7.3692E−01	7.8843E−01
13	4.2659E−01	2.0114E+00	5.6122E−01	1.1491E+00	6.0274E−01	9.7731E−01	6.5100E−01	8.3700E−01
14	3.7980E−01	2.1340E+00	4.9853E−01	1.2164E+00	5.3532E−01	1.0342E+00	5.7811E−01	8.8540E−01
15	3.4079E−01	2.2551E+00	4.4533E−01	1.2834E+00	4.7796E−01	1.0907E+00	5.1599E−01	9.3354E−01
16	3.0800E−01	2.3742E+00	3.9996E−01	1.3496E+00	4.2892E−01	1.1466E+00	4.6279E−01	9.8122E−01
17	2.8018E−01	2.4907E+00	3.6106E−01	1.4147E+00	3.8680E−01	1.2017E+00	4.1705E−01	1.0282E+00
18	2.5637E−01	2.6042E+00	3.2754E−01	1.4785E+00	3.5048E−01	1.2557E+00	3.7756E−01	1.0743E+00
19	2.3577E−01	2.7143E+00	2.9852E−01	1.5406E+00	3.1900E−01	1.3083E+00	3.4332E−01	1.1192E+00
20	2.1778E−01	2.8210E+00	2.7325E−01	1.6009E+00	2.9159E−01	1.3594E+00	3.1351E−01	1.1629E+00
21	2.0193E−01	2.9241E+00	2.5114E−01	1.6591E+00	2.6761E−01	1.4088E+00	2.8745E−01	1.2051E+00
22	1.8785E−01	3.0238E+00	2.3167E−01	1.7153E+00	2.4654E−01	1.4565E+00	2.6454E−01	1.2458E+00
23	1.7526E−01	3.1202E+00	2.1445E−01	1.7694E+00	2.2792E−01	1.5023E+00	2.4433E−01	1.2849E+00
24	1.6391E−01	3.2135E+00	1.9914E−01	1.8214E+00	2.1138E−01	1.5464E+00	2.2641E−01	1.3226E+00
25	1.5365E−01	3.3040E+00	1.8545E−01	1.8715E+00	1.9664E−01	1.5888E+00	2.1045E−01	1.3587E+00
26	1.4433E−01	3.3917E+00	1.7317E−01	1.9196E+00	1.8343E−01	1.6295E+00	1.9617E−01	1.3935E+00
27	1.3583E−01	3.4770E+00	1.6210E−01	1.9660E+00	1.7155E−01	1.6686E+00	1.8334E−01	1.4268E+00
28	1.2806E−01	3.5599E+00	1.5208E−01	2.0107E+00	1.6082E−01	1.7063E+00	1.7176E−01	1.4589E+00
29	1.2093E−01	3.6407E+00	1.4298E−01	2.0538E+00	1.5109E−01	1.7427E+00	1.6129E−01	1.4898E+00
30	1.1438E−01	3.7195E+00	1.3469E−01	2.0955E+00	1.4224E−01	1.7778E+00	1.5177E−01	1.5197E+00
31	1.0836E−01	3.7965E+00	1.2711E−01	2.1359E+00	1.3416E−01	1.8117E+00	1.4309E−01	1.5485E+00
32	1.0281E−01	3.8717E+00	1.2017E−01	2.1751E+00	1.2677E−01	1.8446E+00	1.3516E−01	1.5764E+00
33	9.7684E−02	3.9453E+00	1.1379E−01	2.2132E+00	1.1998E−01	1.8765E+00	1.2788E−01	1.6034E+00
34	9.2946E−02	4.0173E+00	1.0791E−01	2.2502E+00	1.1374E−01	1.9075E+00	1.2119E−01	1.6297E+00
35	8.8561E−02	4.0878E+00	1.0249E−01	2.2863E+00	1.0798E−01	1.9378E+00	1.1502E−01	1.6553E+00
36	8.4496E−02	4.1570E+00	9.7470E−02	2.3215E+00	1.0265E−01	1.9672E+00	1.0932E−01	1.6803E+00
37	8.0723E−02	4.2248E+00	9.2819E−02	2.3560E+00	9.7717E−02	1.9960E+00	1.0403E−01	1.7046E+00
38	7.7217E−02	4.2913E+00	8.8500E−02	2.3897E+00	9.3137E−02	2.0242E+00	9.9132E−02	1.7284E+00
39	7.3955E−02	4.3567E+00	8.4483E−02	2.4226E+00	8.8876E−02	2.0517E+00	9.4573E−02	1.7517E+00
40	7.0915E−02	4.4209E+00	8.0739E−02	2.4550E+00	8.4906E−02	2.0788E+00	9.0324E−02	1.7746E+00
41	6.8079E−02	4.4840E+00	7.7244E−02	2.4867E+00	8.1199E−02	2.1053E+00	8.6359E−02	1.7970E+00
42	6.5429E−02	4.5460E+00	7.3977E−02	2.5179E+00	7.7735E−02	2.1313E+00	8.2651E−02	1.8190E+00
43	6.2950E−02	4.6069E+00	7.0919E−02	2.5485E+00	7.4491E−02	2.1569E+00	7.9179E−02	1.8406E+00
44	6.0628E−02	4.6669E+00	6.8051E−02	2.5786E+00	7.1448E−02	2.1820E+00	7.5923E−02	1.8619E+00
45	5.8450E−02	4.7260E+00	6.5358E−02	2.6082E+00	6.8591E−02	2.2067E+00	7.2865E−02	1.8828E+00
46	5.6404E−02	4.7841E+00	6.2826E−02	2.6373E+00	6.5905E−02	2.2311E+00	6.9990E−02	1.9034E+00
47	5.4481E−02	4.8413E+00	6.0442E−02	2.6660E+00	6.3376E−02	2.2550E+00	6.7282E−02	1.9237E+00
48	5.2670E−02	4.8977E+00	5.8195E−02	2.6942E+00	6.0991E−02	2.2786E+00	6.4729E−02	1.9436E+00
49	5.0962E−02	4.9532E+00	5.6074E−02	2.7220E+00	5.8741E−02	2.3019E+00	6.2320E−02	1.9633E+00
50	4.9350E−02	5.0080E+00	5.4070E−02	2.7494E+00	5.6614E−02	2.3248E+00	6.0043E−02	1.9827E+00
51	4.7827E−02	5.0620E+00	5.2175E−02	2.7764E+00	5.4602E−02	2.3473E+00	5.7889E−02	2.0018E+00
52	4.6385E−02	5.1152E+00	5.0380E−02	2.8029E+00	5.2697E−02	2.3696E+00	5.5849E−02	2.0206E+00
53	4.5019E−02	5.1677E+00	4.8679E−02	2.8292E+00	5.0892E−02	2.3915E+00	5.3916E−02	2.0392E+00
54	4.3724E−02	5.2196E+00	4.7064E−02	2.8550E+00	4.9178E−02	2.4131E+00	5.2082E−02	2.0575E+00
55	4.2494E−02	5.2707E+00	4.5531E−02	2.8805E+00	4.7551E−02	2.4345E+00	5.0340E−02	2.0755E+00
56	4.1325E−02	5.3212E+00	4.4073E−02	2.9056E+00	4.6005E−02	2.4555E+00	4.8685E−02	2.0933E+00
57	4.0212E−02	5.3710E+00	4.2685E−02	2.9304E+00	4.4533E−02	2.4762E+00	4.7110E−02	2.1109E+00
58	3.9152E−02	5.4202E+00	4.1364E−02	2.9548E+00	4.3132E−02	2.4966E+00	4.5610E−02	2.1282E+00
59	3.8142E−02	5.4689E+00	4.0104E−02	2.9789E+00	4.1797E−02	2.5168E+00	4.4182E−02	2.1453E+00
60	3.7177E−02	5.5169E+00	3.8902E−02	3.0027E+00	4.0523E−02	2.5367E+00	4.2820E−02	2.1621E+00

Table 4.3.3.1. *Partial wave elastic scattering factors for neutral atoms (cont.)*
Rb; $Z = 37$

	10 keV		40 keV		60 keV		90 keV	
s	$\|f(s)\|$	$\eta(s)$	$\|f(s)\|$	$\eta(s)$	$\|f(s)\|$	$\eta(s)$	$\|f(s)\|$	$\eta(s)$
0	1.0749E+01	2.2111E−01	1.2119E+01	1.4172E−01	1.2690E+01	1.2303E−01	1.3445E+01	1.0707E−01
1	7.4644E+00	3.0977E−01	8.5844E+00	1.9532E−01	9.0189E+00	1.6907E−01	9.5832E+00	1.4675E−01
2	4.5885E+00	4.7190E−01	5.4384E+00	2.9089E−01	5.7421E+00	2.5080E−01	6.1261E+00	2.1698E−01
3	3.1976E+00	6.2097E−01	3.8864E+00	3.7750E−01	4.1196E+00	3.2470E−01	4.4079E+00	2.8041E−01
4	2.3153E+00	7.8149E−01	2.8786E+00	4.6924E−01	3.0621E+00	4.0276E−01	3.2848E+00	3.4729E−01
5	1.7283E+00	9.5641E−01	2.1871E+00	5.6771E−01	2.3332E+00	4.8632E−01	2.5080E+00	4.1874E−01
6	1.3398E+00	1.1332E+00	1.7149E+00	6.6649E−01	1.8331E+00	5.7002E−01	1.9733E+00	4.9022E−01
7	1.0768E+00	1.3008E+00	1.3879E+00	7.5987E−01	1.4856E+00	6.4908E−01	1.6009E+00	5.5771E−01
8	8.9022E−01	1.4548E+00	1.1536E+00	8.4563E−01	1.2362E+00	7.2167E−01	1.3331E+00	6.1965E−01
9	7.5122E−01	1.5969E+00	9.7851E−01	9.2448E−01	1.0495E+00	7.8835E−01	1.1326E+00	6.7652E−01
10	6.4345E−01	1.7307E+00	8.4223E−01	9.9838E−01	9.0412E−01	8.5080E−01	9.7631E−01	7.2976E−01
11	5.5732E−01	1.8592E+00	7.3272E−01	1.0689E+00	7.8717E−01	9.1038E−01	8.5050E−01	7.8052E−01
12	4.8789E−01	1.9847E+00	6.4327E−01	1.1378E+00	6.9145E−01	9.6847E−01	7.4737E−01	8.2999E−01
13	4.3092E−01	2.1084E+00	5.6877E−01	1.2055E+00	6.1155E−01	1.0257E+00	6.6115E−01	8.7870E−01
14	3.8367E−01	2.2308E+00	5.0587E−01	1.2728E+00	5.4391E−01	1.0825E+00	5.8803E−01	9.2704E−01
15	3.4425E−01	2.3519E+00	4.5242E−01	1.3396E+00	4.8629E−01	1.1389E+00	5.2562E−01	9.7510E−01
16	3.1110E−01	2.4713E+00	4.0674E−01	1.4058E+00	4.3692E−01	1.1948E+00	4.7204E−01	1.0228E+00
17	2.8300E−01	2.5883E+00	3.6749E−01	1.4712E+00	3.9440E−01	1.2501E+00	4.2585E−01	1.0700E+00
18	2.5896E−01	2.7027E+00	3.3361E−01	1.5355E+00	3.5764E−01	1.3046E+00	3.8586E−01	1.1164E+00
19	2.3819E−01	2.8141E+00	3.0422E−01	1.5984E+00	3.2572E−01	1.3578E+00	3.5109E−01	1.1618E+00
20	2.2009E−01	2.9222E+00	2.7859E−01	1.6596E+00	2.9787E−01	1.4097E+00	3.2076E−01	1.2062E+00
21	2.0416E−01	3.0270E+00	2.5613E−01	1.7190E+00	2.7347E−01	1.4601E+00	2.9419E−01	1.2493E+00
22	1.9002E−01	3.1286E+00	2.3634E−01	1.7765E+00	2.5199E−01	1.5089E+00	2.7081E−01	1.2909E+00
23	1.7739E−01	3.2269E+00	2.1883E−01	1.8320E+00	2.3300E−01	1.5560E+00	2.5014E−01	1.3312E+00
24	1.6602E−01	3.3222E+00	2.0325E−01	1.8855E+00	2.1613E−01	1.6014E+00	2.3181E−01	1.3700E+00
25	1.5574E−01	3.4146E+00	1.8932E−01	1.9370E+00	2.0107E−01	1.6451E+00	2.1547E−01	1.4073E+00
26	1.4639E−01	3.5043E+00	1.7681E−01	1.9867E+00	1.8758E−01	1.6872E+00	2.0084E−01	1.4433E+00
27	1.3786E−01	3.5916E+00	1.6554E−01	2.0346E+00	1.7544E−01	1.7277E+00	1.8770E−01	1.4778E+00
28	1.3005E−01	3.6765E+00	1.5533E−01	2.0808E+00	1.6447E−01	1.7667E+00	1.7585E−01	1.5111E+00
29	1.2289E−01	3.7592E+00	1.4606E−01	2.1254E+00	1.5453E−01	1.8043E+00	1.6512E−01	1.5431E+00
30	1.1630E−01	3.8399E+00	1.3761E−01	2.1685E+00	1.4548E−01	1.8406E+00	1.5537E−01	1.5740E+00
31	1.1022E−01	3.9188E+00	1.2988E−01	2.2102E+00	1.3722E−01	1.8757E+00	1.4648E−01	1.6039E+00
32	1.0462E−01	3.9958E+00	1.2280E−01	2.2506E+00	1.2967E−01	1.9097E+00	1.3835E−01	1.6327E+00
33	9.9441E−02	4.0712E+00	1.1629E−01	2.2899E+00	1.2273E−01	1.9427E+00	1.3090E−01	1.6607E+00
34	9.4648E−02	4.1451E+00	1.1029E−01	2.3281E+00	1.1635E−01	1.9747E+00	1.2405E−01	1.6879E+00
35	9.0205E−02	4.2174E+00	1.0476E−01	2.3653E+00	1.1046E−01	2.0059E+00	1.1773E−01	1.7143E+00
36	8.6083E−02	4.2883E+00	9.9637E−02	2.4016E+00	1.0501E−01	2.0363E+00	1.1190E−01	1.7400E+00
37	8.2254E−02	4.3579E+00	9.4889E−02	2.4370E+00	9.9967E−02	2.0659E+00	1.0649E−01	1.7651E+00
38	7.8692E−02	4.4262E+00	9.0478E−02	2.4716E+00	9.5284E−02	2.0949E+00	1.0148E−01	1.7896E+00
39	7.5374E−02	4.4932E+00	8.6375E−02	2.5055E+00	9.0928E−02	2.1232E+00	9.6810E−02	1.8135E+00
40	7.2281E−02	4.5591E+00	8.2550E−02	2.5387E+00	8.6869E−02	2.1509E+00	9.2464E−02	1.8370E+00
41	6.9394E−02	4.6238E+00	7.8981E−02	2.5713E+00	8.3081E−02	2.1781E+00	8.8409E−02	1.8600E+00
42	6.6695E−02	4.6875E+00	7.5644E−02	2.6032E+00	7.9540E−02	2.2048E+00	8.4617E−02	1.8825E+00
43	6.4170E−02	4.7500E+00	7.2519E−02	2.6346E+00	7.6224E−02	2.2310E+00	8.1067E−02	1.9047E+00
44	6.1804E−02	4.8116E+00	6.9589E−02	2.6654E+00	7.3115E−02	2.2567E+00	7.7738E−02	1.9264E+00
45	5.9584E−02	4.8722E+00	6.6838E−02	2.6957E+00	7.0195E−02	2.2820E+00	7.4612E−02	1.9478E+00
46	5.7500E−02	4.9319E+00	6.4251E−02	2.7255E+00	6.7450E−02	2.3069E+00	7.1672E−02	1.9689E+00
47	5.5540E−02	4.9906E+00	6.1816E−02	2.7548E+00	6.4865E−02	2.3314E+00	6.8904E−02	1.9896E+00
48	5.3694E−02	5.0485E+00	5.9522E−02	2.7837E+00	6.2429E−02	2.3556E+00	6.6295E−02	2.0100E+00
49	5.1954E−02	5.1055E+00	5.7356E−02	2.8122E+00	6.0129E−02	2.3793E+00	6.3833E−02	2.0301E+00
50	5.0313E−02	5.1617E+00	5.5310E−02	2.8402E+00	5.7957E−02	2.4027E+00	6.1506E−02	2.0499E+00
51	4.8762E−02	5.2171E+00	5.3374E−02	2.8678E+00	5.5902E−02	2.4258E+00	5.9304E−02	2.0694E+00
52	4.7295E−02	5.2718E+00	5.1542E−02	2.8950E+00	5.3956E−02	2.4485E+00	5.7220E−02	2.0887E+00
53	4.5905E−02	5.3257E+00	4.9805E−02	2.9218E+00	5.2111E−02	2.4710E+00	5.5244E−02	2.1077E+00
54	4.4588E−02	5.3789E+00	4.8157E−02	2.9482E+00	5.0361E−02	2.4931E+00	5.3370E−02	2.1264E+00
55	4.3338E−02	5.4314E+00	4.6592E−02	2.9743E+00	4.8699E−02	2.5149E+00	5.1590E−02	2.1448E+00
56	4.2151E−02	5.4832E+00	4.5104E−02	3.0000E+00	4.7120E−02	2.5364E+00	4.9898E−02	2.1630E+00
57	4.1021E−02	5.5344E+00	4.3687E−02	3.0254E+00	4.5616E−02	2.5576E+00	4.8288E−02	2.1810E+00
58	3.9946E−02	5.5849E+00	4.2339E−02	3.0504E+00	4.4185E−02	2.5785E+00	4.6755E−02	2.1987E+00
59	3.8922E−02	5.6348E+00	4.1053E−02	3.0751E+00	4.2821E−02	2.5991E+00	4.5295E−02	2.2162E+00
60	3.7945E−02	5.6842E+00	3.9826E−02	3.0994E+00	4.1520E−02	2.6195E+00	4.3902E−02	2.2334E+00

Table 4.3.3.1. *Partial wave elastic scattering factors for neutral atoms (cont.)*
Sr; $Z = 38$

	10 keV		40 keV		60 keV		90 keV	
s	$\|f(s)\|$	$\eta(s)$	$\|f(s)\|$	$\eta(s)$	$\|f(s)\|$	$\eta(s)$	$\|f(s)\|$	$\eta(s)$
0	1.2019E+01	2.2526E−01	1.3533E+01	1.4349E−01	1.4169E+01	1.2451E−01	1.5012E+01	1.0832E−01
1	8.6382E+00	3.0252E−01	9.8978E+00	1.9041E−01	1.0394E+01	1.6486E−01	1.1042E+01	1.4313E−01
2	4.9783E+00	4.8384E−01	5.8977E+00	2.9752E−01	6.2275E+00	2.5654E−01	6.6448E+00	2.2199E−01
3	3.2826E+00	6.6408E−01	3.9973E+00	4.0195E−01	4.2396E+00	3.4563E−01	4.5385E+00	2.9847E−01
4	2.3569E+00	8.3296E−01	2.9372E+00	4.9862E−01	3.1267E+00	4.2793E−01	3.3560E+00	3.6900E−01
5	1.7627E+00	1.0073E+00	2.2376E+00	5.9710E−01	2.3891E+00	5.1157E−01	2.5700E+00	4.4057E−01
6	1.3655E+00	1.1853E+00	1.7550E+00	6.9681E−01	1.8778E+00	5.9611E−01	2.0232E+00	5.1281E−01
7	1.0942E+00	1.3580E+00	1.4164E+00	7.9333E−01	1.5177E+00	6.7788E−01	1.6370E+00	5.8264E−01
8	9.0209E−01	1.5193E+00	1.1730E+00	8.8345E−01	1.2582E+00	7.5420E−01	1.3581E+00	6.4779E−01
9	7.5997E−01	1.6683E+00	9.9209E−01	9.6652E−01	1.0651E+00	8.2451E−01	1.1503E+00	7.0779E−01
10	6.5046E−01	1.8072E+00	8.5254E−01	1.0436E+00	9.1597E−01	8.8973E−01	9.8987E−01	7.6342E−01
11	5.6327E−01	1.9391E+00	7.4120E−01	1.1164E+00	7.9694E−01	9.5123E−01	8.6170E−01	8.1584E−01
12	4.9310E−01	2.0663E+00	6.5094E−01	1.1864E+00	7.0031E−01	1.0103E+00	7.5755E−01	8.6619E−01
13	4.3555E−01	2.1908E+00	5.7601E−01	1.2547E+00	6.1995E−01	1.0680E+00	6.7081E−01	9.1531E−01
14	3.8776E−01	2.3135E+00	5.1280E−01	1.3221E+00	5.5200E−01	1.1249E+00	5.9736E−01	9.6377E−01
15	3.4785E−01	2.4347E+00	4.5908E−01	1.3889E+00	4.9411E−01	1.1813E+00	5.3465E−01	1.0118E+00
16	3.1429E−01	2.5542E+00	4.1312E−01	1.4551E+00	4.4444E−01	1.2373E+00	4.8076E−01	1.0595E+00
17	2.8584E−01	2.6716E+00	3.7357E−01	1.5206E+00	4.0159E−01	1.2926E+00	4.3418E−01	1.1067E+00
18	2.6152E−01	2.7867E+00	3.3937E−01	1.5852E+00	3.6446E−01	1.3473E+00	3.9377E−01	1.1534E+00
19	2.4055E−01	2.8990E+00	3.0964E−01	1.6486E+00	3.3215E−01	1.4010E+00	3.5856E−01	1.1992E+00
20	2.2229E−01	3.0084E+00	2.8369E−01	1.7105E+00	3.0391E−01	1.4535E+00	3.2777E−01	1.2441E+00
21	2.0626E−01	3.1147E+00	2.6092E−01	1.7709E+00	2.7912E−01	1.5048E+00	3.0074E−01	1.2879E+00
22	1.9206E−01	3.2178E+00	2.4084E−01	1.8295E+00	2.5728E−01	1.5545E+00	2.7691E−01	1.3304E+00
23	1.7938E−01	3.3179E+00	2.2306E−01	1.8862E+00	2.3795E−01	1.6027E+00	2.5584E−01	1.3716E+00
24	1.6798E−01	3.4150E+00	2.0722E−01	1.9411E+00	2.2075E−01	1.6493E+00	2.3712E−01	1.4115E+00
25	1.5767E−01	3.5092E+00	1.9307E−01	1.9941E+00	2.0540E−01	1.6942E+00	2.2042E−01	1.4499E+00
26	1.4830E−01	3.6008E+00	1.8035E−01	2.0452E+00	1.9164E−01	1.7376E+00	2.0546E−01	1.4869E+00
27	1.3974E−01	3.6899E+00	1.6888E−01	2.0945E+00	1.7926E−01	1.7794E+00	1.9202E−01	1.5226E+00
28	1.3191E−01	3.7767E+00	1.5850E−01	2.1422E+00	1.6806E−01	1.8197E+00	1.7990E−01	1.5570E+00
29	1.2472E−01	3.8613E+00	1.4906E−01	2.1882E+00	1.5791E−01	1.8586E+00	1.6892E−01	1.5902E+00
30	1.1810E−01	3.9438E+00	1.4046E−01	2.2327E+00	1.4868E−01	1.8961E+00	1.5894E−01	1.6222E+00
31	1.1199E−01	4.0245E+00	1.3260E−01	2.2757E+00	1.4025E−01	1.9324E+00	1.4984E−01	1.6531E+00
32	1.0634E−01	4.1034E+00	1.2538E−01	2.3175E+00	1.3253E−01	1.9676E+00	1.4153E−01	1.6830E+00
33	1.0112E−01	4.1806E+00	1.1875E−01	2.3580E+00	1.2545E−01	2.0016E+00	1.3390E−01	1.7119E+00
34	9.6275E−02	4.2561E+00	1.1264E−01	2.3974E+00	1.1893E−01	2.0347E+00	1.2689E−01	1.7399E+00
35	9.1783E−02	4.3302E+00	1.0700E−01	2.4357E+00	1.1291E−01	2.0668E+00	1.2043E−01	1.7672E+00
36	8.7611E−02	4.4029E+00	1.0177E−01	2.4730E+00	1.0735E−01	2.0981E+00	1.1446E−01	1.7937E+00
37	8.3730E−02	4.4742E+00	9.6931E−02	2.5095E+00	1.0220E−01	2.1286E+00	1.0893E−01	1.8196E+00
38	8.0118E−02	4.5442E+00	9.2431E−02	2.5451E+00	9.7412E−02	2.1584E+00	1.0380E−01	1.8448E+00
39	7.6751E−02	4.6129E+00	8.8244E−02	2.5799E+00	9.2962E−02	2.1876E+00	9.9033E−02	1.8694E+00
40	7.3609E−02	4.6805E+00	8.4341E−02	2.6140E+00	8.8816E−02	2.2160E+00	9.4590E−02	1.8935E+00
41	7.0674E−02	4.7469E+00	8.0697E−02	2.6474E+00	8.4946E−02	2.2439E+00	9.0444E−02	1.9171E+00
42	6.7930E−02	4.8122E+00	7.7291E−02	2.6801E+00	8.1328E−02	2.2713E+00	8.6568E−02	1.9402E+00
43	6.5360E−02	4.8764E+00	7.4101E−02	2.7123E+00	7.7941E−02	2.2982E+00	8.2940E−02	1.9629E+00
44	6.2952E−02	4.9396E+00	7.1109E−02	2.7439E+00	7.4764E−02	2.3245E+00	7.9538E−02	1.9852E+00
45	6.0693E−02	5.0017E+00	6.8300E−02	2.7749E+00	7.1782E−02	2.3504E+00	7.6343E−02	2.0071E+00
46	5.8570E−02	5.0630E+00	6.5660E−02	2.8054E+00	6.8978E−02	2.3759E+00	7.3340E−02	2.0286E+00
47	5.6575E−02	5.1233E+00	6.3174E−02	2.8354E+00	6.6338E−02	2.4010E+00	7.0512E−02	2.0498E+00
48	5.4696E−02	5.1827E+00	6.0831E−02	2.8650E+00	6.3850E−02	2.4256E+00	6.7846E−02	2.0707E+00
49	5.2925E−02	5.2412E+00	5.8621E−02	2.8941E+00	6.1502E−02	2.4499E+00	6.5330E−02	2.0912E+00
50	5.1254E−02	5.2989E+00	5.6532E−02	2.9227E+00	5.9284E−02	2.4739E+00	6.2953E−02	2.1115E+00
51	4.9676E−02	5.3558E+00	5.4557E−02	2.9510E+00	5.7185E−02	2.4975E+00	6.0704E−02	2.1314E+00
52	4.8183E−02	5.4119E+00	5.2687E−02	2.9788E+00	5.5198E−02	2.5207E+00	5.8575E−02	2.1511E+00
53	4.6770E−02	5.4672E+00	5.0915E−02	3.0062E+00	5.3315E−02	2.5436E+00	5.6557E−02	2.1705E+00
54	4.5432E−02	5.5218E+00	4.9233E−02	3.0333E+00	5.1529E−02	2.5662E+00	5.4643E−02	2.1896E+00
55	4.4162E−02	5.5757E+00	4.7636E−02	3.0599E+00	4.9832E−02	2.5885E+00	5.2825E−02	2.2085E+00
56	4.2956E−02	5.6289E+00	4.6118E−02	3.0863E+00	4.8219E−02	2.6105E+00	5.1096E−02	2.2271E+00
57	4.1810E−02	5.6814E+00	4.4674E−02	3.1122E+00	4.6685E−02	2.6322E+00	4.9452E−02	2.2454E+00
58	4.0720E−02	5.7333E+00	4.3298E−02	3.1378E+00	4.5224E−02	2.6536E+00	4.7887E−02	2.2635E+00
59	3.9682E−02	5.7846E+00	4.1987E−02	3.1630E+00	4.3832E−02	2.6747E+00	4.6395E−02	2.2814E+00
60	3.8692E−02	5.8352E+00	4.0736E−02	3.1880E+00	4.2504E−02	2.6955E+00	4.4973E−02	2.2990E+00

Table 4.3.3.1. *Partial wave elastic scattering factors for neutral atoms (cont.)*
Y; $Z = 39$

	10 keV		40 keV		60 keV		90 keV	
s	$\|f(s)\|$	$\eta(s)$	$\|f(s)\|$	$\eta(s)$	$\|f(s)\|$	$\eta(s)$	$\|f(s)\|$	$\eta(s)$
0	1.1519E+01	2.4347E−01	1.3035E+01	1.5527E−01	1.3660E+01	1.3481E−01	1.4482E+01	1.1736E−01
1	8.6824E+00	3.1259E−01	9.9798E+00	1.9728E−01	1.0486E+01	1.7095E−01	1.1145E+01	1.4854E−01
2	5.1872E+00	4.8364E−01	6.1563E+00	2.9865E−01	6.5034E+00	2.5779E−01	6.9418E+00	2.2327E−01
3	3.3892E+00	6.7070E−01	4.1376E+00	4.0719E−01	4.3911E+00	3.5045E−01	4.7031E+00	3.0285E−01
4	2.4133E+00	8.4790E−01	3.0161E+00	5.0877E−01	3.2130E+00	4.3697E−01	3.4509E+00	3.7704E−01
5	1.7998E+00	1.0263E+00	2.2923E+00	6.0983E−01	2.4495E+00	5.2285E−01	2.6368E+00	4.5056E−01
6	1.3913E+00	1.2077E+00	1.7950E+00	7.1169E−01	1.9225E+00	6.0927E−01	2.0730E+00	5.2444E−01
7	1.1119E+00	1.3854E+00	1.4451E+00	8.1123E−01	1.5501E+00	6.9364E−01	1.6733E+00	5.9653E−01
8	9.1454E−01	1.5531E+00	1.1932E+00	9.0521E−01	1.2812E+00	7.7327E−01	1.3841E+00	6.6453E−01
9	7.6927E−01	1.7084E+00	1.0066E+00	9.9222E−01	1.0816E+00	8.4698E−01	1.1691E+00	7.2746E−01
10	6.5792E−01	1.8527E+00	8.6348E−01	1.0727E+00	9.2851E−01	9.1510E−01	1.0042E+00	7.8560E−01
11	5.6956E−01	1.9884E+00	7.5004E−01	1.1480E+00	8.0708E−01	9.7876E−01	8.7329E−01	8.3990E−01
12	4.9858E−01	2.1181E+00	6.5865E−01	1.2196E+00	7.0918E−01	1.0393E+00	7.6771E−01	8.9147E−01
13	4.4037E−01	2.2440E+00	5.8307E−01	1.2888E+00	6.2811E−01	1.0977E+00	6.8019E−01	9.4129E−01
14	3.9199E−01	2.3674E+00	5.1945E−01	1.3566E+00	5.5973E−01	1.1550E+00	6.0626E−01	9.9008E−01
15	3.5157E−01	2.4889E+00	4.6542E−01	1.4236E+00	5.0151E−01	1.2115E+00	5.4321E−01	1.0382E+00
16	3.1755E−01	2.6086E+00	4.1917E−01	1.4898E+00	4.5155E−01	1.2675E+00	4.8899E−01	1.0859E+00
17	2.8871E−01	2.7264E+00	3.7933E−01	1.5554E+00	4.0839E−01	1.3230E+00	4.4209E−01	1.1332E+00
18	2.6408E−01	2.8421E+00	3.4483E−01	1.6202E+00	3.7094E−01	1.3778E+00	4.0131E−01	1.1800E+00
19	2.4287E−01	2.9552E+00	3.1481E−01	1.6839E+00	3.3828E−01	1.4318E+00	3.6571E−01	1.2261E+00
20	2.2443E−01	3.0656E+00	2.8856E−01	1.7465E+00	3.0970E−01	1.4849E+00	3.3451E−01	1.2714E+00
21	2.0827E−01	3.1732E+00	2.6551E−01	1.8076E+00	2.8457E−01	1.5367E+00	3.0707E−01	1.3157E+00
22	1.9398E−01	3.2777E+00	2.4516E−01	1.8671E+00	2.6240E−01	1.5873E+00	2.8286E−01	1.3590E+00
23	1.8124E−01	3.3793E+00	2.2713E−01	1.9250E+00	2.4275E−01	1.6364E+00	2.6140E−01	1.4010E+00
24	1.6980E−01	3.4781E+00	2.1107E−01	1.9810E+00	2.2526E−01	1.6840E+00	2.4232E−01	1.4418E+00
25	1.5947E−01	3.5740E+00	1.9670E−01	2.0353E+00	2.0964E−01	1.7301E+00	2.2528E−01	1.4812E+00
26	1.5008E−01	3.6674E+00	1.8379E−01	2.0877E+00	1.9563E−01	1.7747E+00	2.1002E−01	1.5193E+00
27	1.4151E−01	3.7582E+00	1.7214E−01	2.1385E+00	1.8301E−01	1.8177E+00	1.9629E−01	1.5561E+00
28	1.3366E−01	3.8467E+00	1.6159E−01	2.1875E+00	1.7160E−01	1.8592E+00	1.8390E−01	1.5915E+00
29	1.2644E−01	3.9331E+00	1.5200E−01	2.2348E+00	1.6125E−01	1.8993E+00	1.7268E−01	1.6258E+00
30	1.1980E−01	4.0174E+00	1.4326E−01	2.2807E+00	1.5183E−01	1.9381E+00	1.6248E−01	1.6588E+00
31	1.1366E−01	4.0998E+00	1.3526E−01	2.3251E+00	1.4324E−01	1.9756E+00	1.5319E−01	1.6908E+00
32	1.0798E−01	4.1804E+00	1.2792E−01	2.3681E+00	1.3536E−01	2.0118E+00	1.4469E−01	1.7217E+00
33	1.0272E−01	4.2593E+00	1.2118E−01	2.4099E+00	1.2814E−01	2.0470E+00	1.3689E−01	1.7515E+00
34	9.7840E−02	4.3366E+00	1.1495E−01	2.4504E+00	1.2149E−01	2.0811E+00	1.2973E−01	1.7805E+00
35	9.3308E−02	4.4124E+00	1.0921E−01	2.4899E+00	1.1535E−01	2.1143E+00	1.2312E−01	1.8087E+00
36	8.9092E−02	4.4868E+00	1.0389E−01	2.5283E+00	1.0967E−01	2.1465E+00	1.1702E−01	1.8360E+00
37	8.5168E−02	4.5597E+00	9.8954E−02	2.5658E+00	1.0441E−01	2.1779E+00	1.1137E−01	1.8627E+00
38	8.1511E−02	4.6314E+00	9.4368E−02	2.6024E+00	9.9529E−02	2.2086E+00	1.0612E−01	1.8886E+00
39	7.8099E−02	4.7018E+00	9.0099E−02	2.6382E+00	9.4986E−02	2.2385E+00	1.0125E−01	1.9139E+00
40	7.4914E−02	4.7710E+00	8.6120E−02	2.6732E+00	9.0753E−02	2.2678E+00	9.6709E−02	1.9387E+00
41	7.1935E−02	4.8391E+00	8.2403E−02	2.7075E+00	8.6802E−02	2.2964E+00	9.2472E−02	1.9629E+00
42	6.9149E−02	4.9060E+00	7.8928E−02	2.7411E+00	8.3108E−02	2.3245E+00	8.8512E−02	1.9867E+00
43	6.6538E−02	4.9718E+00	7.5674E−02	2.7741E+00	7.9649E−02	2.3520E+00	8.4805E−02	2.0099E+00
44	6.4090E−02	5.0366E+00	7.2622E−02	2.8064E+00	7.6406E−02	2.3791E+00	8.1329E−02	2.0328E+00
45	6.1793E−02	5.1004E+00	6.9756E−02	2.8382E+00	7.3361E−02	2.4056E+00	7.8066E−02	2.0552E+00
46	5.9634E−02	5.1632E+00	6.7061E−02	2.8695E+00	7.0498E−02	2.4317E+00	7.4998E−02	2.0773E+00
47	5.7604E−02	5.2250E+00	6.4525E−02	2.9002E+00	6.7803E−02	2.4573E+00	7.2109E−02	2.0989E+00
48	5.5692E−02	5.2860E+00	6.2134E−02	2.9305E+00	6.5263E−02	2.4826E+00	6.9387E−02	2.1203E+00
49	5.3891E−02	5.3460E+00	5.9878E−02	2.9602E+00	6.2866E−02	2.5074E+00	6.6818E−02	2.1413E+00
50	5.2191E−02	5.4052E+00	5.7747E−02	2.9895E+00	6.0601E−02	2.5319E+00	6.4390E−02	2.1620E+00
51	5.0585E−02	5.4636E+00	5.5732E−02	3.0184E+00	5.8459E−02	2.5560E+00	6.2094E−02	2.1823E+00
52	4.9067E−02	5.5212E+00	5.3824E−02	3.0469E+00	5.6431E−02	2.5798E+00	5.9920E−02	2.2024E+00
53	4.7631E−02	5.5780E+00	5.2016E−02	3.0749E+00	5.4509E−02	2.6032E+00	5.7860E−02	2.2222E+00
54	4.6270E−02	5.6340E+00	5.0300E−02	3.1026E+00	5.2686E−02	2.6263E+00	5.5905E−02	2.2418E+00
55	4.4980E−02	5.6893E+00	4.8671E−02	3.1298E+00	5.0955E−02	2.6491E+00	5.4049E−02	2.2610E+00
56	4.3756E−02	5.7439E+00	4.7123E−02	3.1567E+00	4.9309E−02	2.6715E+00	5.2284E−02	2.2800E+00
57	4.2593E−02	5.7979E+00	4.5650E−02	3.1833E+00	4.7743E−02	2.6937E+00	5.0606E−02	2.2988E+00
58	4.1486E−02	5.8511E+00	4.4248E−02	3.2094E+00	4.6252E−02	2.7156E+00	4.9008E−02	2.3173E+00
59	4.0434E−02	5.9037E+00	4.2911E−02	3.2353E+00	4.4832E−02	2.7371E+00	4.7485E−02	2.3355E+00
60	3.9431E−02	5.9557E+00	4.1636E−02	3.2608E+00	4.3477E−02	2.7584E+00	4.6033E−02	2.3536E+00

Table 4.3.3.1. *Partial wave elastic scattering factors for neutral atoms (cont.)*
Zr; $Z = 40$

	10 keV		40 keV		60 keV		90 keV	
s	$\|f(s)\|$	$\eta(s)$	$\|f(s)\|$	$\eta(s)$	$\|f(s)\|$	$\eta(s)$	$\|f(s)\|$	$\eta(s)$
0	1.0956E+01	2.5995E−01	1.2463E+01	1.6634E−01	1.3073E+01	1.4456E−01	1.3869E+01	1.2595E−01
1	8.5337E+00	3.2396E−01	9.8489E+00	2.0528E−01	1.0357E+01	1.7807E−01	1.1014E+01	1.5486E−01
2	5.2935E+00	4.8516E−01	6.2997E+00	3.0108E−01	6.6589E+00	2.6020E−01	7.1114E+00	2.2558E−01
3	3.4785E+00	6.7142E−01	4.2594E+00	4.0944E−01	4.5235E+00	3.5277E−01	4.8476E+00	3.0513E−01
4	2.4695E+00	8.5310E−01	3.0966E+00	5.1379E−01	3.3015E+00	4.4170E−01	3.5482E+00	3.8142E−01
5	1.8376E+00	1.0354E+00	2.3489E+00	6.1732E−01	2.5123E+00	5.2974E−01	2.7064E+00	4.5682E−01
6	1.4175E+00	1.2205E+00	1.8362E+00	7.2149E−01	1.9687E+00	6.1817E−01	2.1246E+00	5.3247E−01
7	1.1302E+00	1.4030E+00	1.4749E+00	8.2396E−01	1.5838E+00	7.0508E−01	1.7112E+00	6.0675E−01
8	9.2756E−01	1.5767E+00	1.2146E+00	9.2158E−01	1.3055E+00	7.8784E−01	1.4116E+00	6.7747E−01
9	7.7909E−01	1.7383E+00	1.0221E+00	1.0125E+00	1.0993E+00	8.6489E−01	1.1892E+00	7.4329E−01
10	6.6583E−01	1.8880E+00	8.7514E−01	1.0965E+00	9.4184E−01	9.3607E−01	1.0194E+00	8.0407E−01
11	5.7622E−01	2.0281E+00	7.5930E−01	1.1746E+00	8.1767E−01	1.0022E+00	8.8538E−01	8.6048E−01
12	5.0439E−01	2.1609E+00	6.6650E−01	1.2482E+00	7.1817E−01	1.0645E+00	7.7799E−01	9.1360E−01
13	4.4547E−01	2.2888E+00	5.9008E−01	1.3188E+00	6.3616E−01	1.1241E+00	6.8941E−01	9.6441E−01
14	3.9646E−01	2.4133E+00	5.2592E−01	1.3873E+00	5.6719E−01	1.1820E+00	6.1484E−01	1.0137E+00
15	3.5547E−01	2.5355E+00	4.7150E−01	1.4546E+00	5.0858E−01	1.2388E+00	5.5136E−01	1.0622E+00
16	3.2095E−01	2.6557E+00	4.2494E−01	1.5210E+00	4.5830E−01	1.2949E+00	4.9681E−01	1.1100E+00
17	2.9169E−01	2.7740E+00	3.8481E−01	1.5867E+00	4.1485E−01	1.3504E+00	4.4958E−01	1.1573E+00
18	2.6670E−01	2.8901E+00	3.5003E−01	1.6516E+00	3.7709E−01	1.4054E+00	4.0847E−01	1.2042E+00
19	2.4520E−01	3.0040E+00	3.1973E−01	1.7156E+00	3.4414E−01	1.4596E+00	3.7253E−01	1.2505E+00
20	2.2655E−01	3.1153E+00	2.9321E−01	1.7786E+00	3.1524E−01	1.5130E+00	3.4098E−01	1.2961E+00
21	2.1023E−01	3.2239E+00	2.6990E−01	1.8403E+00	2.8981E−01	1.5654E+00	3.1319E−01	1.3408E+00
22	1.9582E−01	3.3297E+00	2.4931E−01	1.9006E+00	2.6734E−01	1.6166E+00	2.8861E−01	1.3846E+00
23	1.8300E−01	3.4327E+00	2.3105E−01	1.9594E+00	2.4740E−01	1.6665E+00	2.6681E−01	1.4274E+00
24	1.7151E−01	3.5329E+00	2.1477E−01	2.0165E+00	2.2964E−01	1.7151E+00	2.4739E−01	1.4689E+00
25	1.6115E−01	3.6304E+00	2.0020E−01	2.0719E+00	2.1376E−01	1.7622E+00	2.3005E−01	1.5092E+00
26	1.5173E−01	3.7253E+00	1.8711E−01	2.1256E+00	1.9951E−01	1.8078E+00	2.1449E−01	1.5483E+00
27	1.4315E−01	3.8178E+00	1.7529E−01	2.1776E+00	1.8667E−01	1.8519E+00	2.0050E−01	1.5861E+00
28	1.3528E−01	3.9079E+00	1.6459E−01	2.2279E+00	1.7506E−01	1.8946E+00	1.8785E−01	1.6226E+00
29	1.2805E−01	3.9959E+00	1.5486E−01	2.2766E+00	1.6453E−01	1.9359E+00	1.7640E−01	1.6579E+00
30	1.2139E−01	4.0819E+00	1.4598E−01	2.3237E+00	1.5494E−01	1.9758E+00	1.6599E−01	1.6919E+00
31	1.1523E−01	4.1659E+00	1.3786E−01	2.3694E+00	1.4618E−01	2.0145E+00	1.5650E−01	1.7249E+00
32	1.0953E−01	4.2482E+00	1.3040E−01	2.4137E+00	1.3816E−01	2.0519E+00	1.4782E−01	1.7568E+00
33	1.0424E−01	4.3288E+00	1.2355E−01	2.4567E+00	1.3079E−01	2.0881E+00	1.3986E−01	1.7876E+00
34	9.9331E−02	4.4077E+00	1.1723E−01	2.4985E+00	1.2401E−01	2.1233E+00	1.3254E−01	1.8176E+00
35	9.4765E−02	4.4852E+00	1.1138E−01	2.5391E+00	1.1776E−01	2.1575E+00	1.2579E−01	1.8466E+00
36	9.0514E−02	4.5612E+00	1.0597E−01	2.5786E+00	1.1197E−01	2.1907E+00	1.1956E−01	1.8748E+00
37	8.6553E−02	4.6358E+00	1.0095E−01	2.6172E+00	1.0661E−01	2.2231E+00	1.1379E−01	1.9023E+00
38	8.2857E−02	4.7091E+00	9.6279E−02	2.6548E+00	1.0163E−01	2.2546E+00	1.0843E−01	1.9290E+00
39	7.9406E−02	4.7812E+00	9.1932E−02	2.6916E+00	9.6993E−02	2.2854E+00	1.0345E−01	1.9551E+00
40	7.6181E−02	4.8520E+00	8.7879E−02	2.7275E+00	9.2675E−02	2.3155E+00	9.8816E−02	1.9805E+00
41	7.3164E−02	4.9217E+00	8.4092E−02	2.7627E+00	8.8643E−02	2.3449E+00	9.4489E−02	2.0054E+00
42	7.0339E−02	4.9902E+00	8.0550E−02	2.7972E+00	8.4875E−02	2.3737E+00	9.0445E−02	2.0298E+00
43	6.7690E−02	5.0576E+00	7.7233E−02	2.8310E+00	8.1346E−02	2.4019E+00	8.6659E−02	2.0537E+00
44	6.5206E−02	5.1240E+00	7.4121E−02	2.8642E+00	7.8036E−02	2.4296E+00	8.3110E−02	2.0771E+00
45	6.2873E−02	5.1894E+00	7.1199E−02	2.8968E+00	7.4929E−02	2.4568E+00	7.9778E−02	2.1000E+00
46	6.0680E−02	5.2537E+00	6.8451E−02	2.9288E+00	7.2008E−02	2.4835E+00	7.6646E−02	2.1226E+00
47	5.8617E−02	5.3172E+00	6.5864E−02	2.9602E+00	6.9257E−02	2.5098E+00	7.3697E−02	2.1448E+00
48	5.6674E−02	5.3797E+00	6.3426E−02	2.9912E+00	6.6665E−02	2.5356E+00	7.0918E−02	2.1666E+00
49	5.4842E−02	5.4412E+00	6.1125E−02	3.0216E+00	6.4219E−02	2.5610E+00	6.8295E−02	2.1881E+00
50	5.3114E−02	5.5020E+00	5.8952E−02	3.0516E+00	6.1908E−02	2.5861E+00	6.5817E−02	2.2092E+00
51	5.1482E−02	5.5619E+00	5.6896E−02	3.0812E+00	5.9723E−02	2.6107E+00	6.3473E−02	2.2301E+00
52	4.9939E−02	5.6209E+00	5.4950E−02	3.1102E+00	5.7654E−02	2.6350E+00	6.1254E−02	2.2506E+00
53	4.8480E−02	5.6792E+00	5.3107E−02	3.1389E+00	5.5693E−02	2.6589E+00	5.9151E−02	2.2708E+00
54	4.7097E−02	5.7367E+00	5.1357E−02	3.1672E+00	5.3833E−02	2.6825E+00	5.7156E−02	2.2908E+00
55	4.5787E−02	5.7934E+00	4.9697E−02	3.1951E+00	5.2066E−02	2.7058E+00	5.5262E−02	2.3104E+00
56	4.4543E−02	5.8495E+00	4.8118E−02	3.2226E+00	5.0388E−02	2.7287E+00	5.3461E−02	2.3298E+00
57	4.3363E−02	5.9048E+00	4.6616E−02	3.2497E+00	4.8791E−02	2.7514E+00	5.1748E−02	2.3490E+00
58	4.2241E−02	5.9595E+00	4.5187E−02	3.2764E+00	4.7270E−02	2.7737E+00	5.0117E−02	2.3679E+00
59	4.1173E−02	6.0135E+00	4.3825E−02	3.3029E+00	4.5821E−02	2.7958E+00	4.8563E−02	2.3865E+00
60	4.0157E−02	6.0668E+00	4.2525E−02	3.3289E+00	4.4440E−02	2.8175E+00	4.7081E−02	2.4049E+00

Table 4.3.3.1. *Partial wave elastic scattering factors for neutral atoms (cont.)*
Nb; $Z = 41$

	10 keV		40 keV		60 keV		90 keV	
s	$\|f(s)\|$	$\eta(s)$	$\|f(s)\|$	$\eta(s)$	$\|f(s)\|$	$\eta(s)$	$\|f(s)\|$	$\eta(s)$
0	9.4533E+00	2.8664E−01	1.0859E+01	1.8480E−01	1.1409E+01	1.6086E−01	1.2118E+01	1.4036E−01
1	7.6822E+00	3.4475E−01	8.9406E+00	2.2013E−01	9.4162E+00	1.9125E−01	1.0025E+01	1.6655E−01
2	5.1468E+00	4.8463E−01	6.1561E+00	3.0354E−01	6.5136E+00	2.6282E−01	6.9617E+00	2.2818E−01
3	3.5240E+00	6.5147E−01	4.3323E+00	4.0115E−01	4.6046E+00	3.4630E−01	4.9378E+00	2.9999E−01
4	2.5263E+00	8.2739E−01	3.1820E+00	5.0257E−01	3.3955E+00	4.3281E−01	3.6520E+00	3.7425E−01
5	1.8783E+00	1.0119E+00	2.4129E+00	6.0756E−01	2.5834E+00	5.2214E−01	2.7854E+00	4.5081E−01
6	1.4447E+00	1.2020E+00	1.8811E+00	7.1480E−01	2.0190E+00	6.1323E−01	2.1809E+00	5.2876E−01
7	1.1487E+00	1.3907E+00	1.5062E+00	8.2099E−01	1.6193E+00	7.0334E−01	1.7512E+00	6.0581E−01
8	9.4076E−01	1.5711E+00	1.2367E+00	9.2265E−01	1.3307E+00	7.8958E−01	1.4402E+00	6.7953E−01
9	7.8916E−01	1.7391E+00	1.0381E+00	1.0176E+00	1.1176E+00	8.7009E−01	1.2101E+00	7.4834E−01
10	6.7400E−01	1.8945E+00	8.8722E−01	1.1052E+00	9.5563E−01	9.4440E−01	1.0351E+00	8.1184E−01
11	5.8313E−01	2.0391E+00	7.6884E−01	1.1863E+00	8.2855E−01	1.0131E+00	8.9780E−01	8.7049E−01
12	5.1041E−01	2.1753E+00	6.7448E−01	1.2622E+00	7.2726E−01	1.0773E+00	7.8837E−01	9.2532E−01
13	4.5075E−01	2.3056E+00	5.9707E−01	1.3343E+00	6.4415E−01	1.1383E+00	6.9855E−01	9.7732E−01
14	4.0110E−01	2.4317E+00	5.3226E−01	1.4038E+00	5.7448E−01	1.1971E+00	6.2320E−01	1.0274E+00
15	3.5951E−01	2.5549E+00	4.7740E−01	1.4716E+00	5.1539E−01	1.2544E+00	5.5921E−01	1.0762E+00
16	3.2447E−01	2.6757E+00	4.3048E−01	1.5383E+00	4.6475E−01	1.3107E+00	5.0427E−01	1.1243E+00
17	2.9475E−01	2.7945E+00	3.9005E−01	1.6042E+00	4.2099E−01	1.3664E+00	4.5672E−01	1.1717E+00
18	2.6938E−01	2.9112E+00	3.5499E−01	1.6693E+00	3.8295E−01	1.4215E+00	4.1530E−01	1.2187E+00
19	2.4757E−01	3.0257E+00	3.2442E−01	1.7335E+00	3.4971E−01	1.4759E+00	3.7904E−01	1.2651E+00
20	2.2867E−01	3.1379E+00	2.9765E−01	1.7968E+00	3.2054E−01	1.5295E+00	3.4718E−01	1.3109E+00
21	2.1216E−01	3.2474E+00	2.7410E−01	1.8590E+00	2.9483E−01	1.5823E+00	3.1906E−01	1.3561E+00
22	1.9761E−01	3.3543E+00	2.5328E−01	1.9200E+00	2.7208E−01	1.6341E+00	2.9416E−01	1.4003E+00
23	1.8470E−01	3.4585E+00	2.3480E−01	1.9795E+00	2.5188E−01	1.6847E+00	2.7205E−01	1.4436E+00
24	1.7314E−01	3.5601E+00	2.1833E−01	2.0375E+00	2.3387E−01	1.7340E+00	2.5233E−01	1.4858E+00
25	1.6273E−01	3.6590E+00	2.0357E−01	2.0939E+00	2.1776E−01	1.7820E+00	2.3470E−01	1.5269E+00
26	1.5329E−01	3.7554E+00	1.9031E−01	2.1487E+00	2.0329E−01	1.8286E+00	2.1887E−01	1.5668E+00
27	1.4468E−01	3.8494E+00	1.7834E−01	2.2019E+00	1.9024E−01	1.8738E+00	2.0462E−01	1.6055E+00
28	1.3680E−01	3.9411E+00	1.6749E−01	2.2534E+00	1.7844E−01	1.9175E+00	1.9174E−01	1.6430E+00
29	1.2956E−01	4.0307E+00	1.5763E−01	2.3033E+00	1.6773E−01	1.9599E+00	1.8007E−01	1.6793E+00
30	1.2288E−01	4.1182E+00	1.4863E−01	2.3517E+00	1.5798E−01	2.0010E+00	1.6945E−01	1.7143E+00
31	1.1671E−01	4.2038E+00	1.4039E−01	2.3986E+00	1.4907E−01	2.0407E+00	1.5977E−01	1.7483E+00
32	1.1099E−01	4.2876E+00	1.3283E−01	2.4441E+00	1.4090E−01	2.0792E+00	1.5092E−01	1.7811E+00
33	1.0568E−01	4.3698E+00	1.2587E−01	2.4883E+00	1.3341E−01	2.1165E+00	1.4280E−01	1.8130E+00
34	1.0074E−01	4.4503E+00	1.1945E−01	2.5313E+00	1.2651E−01	2.1528E+00	1.3533E−01	1.8438E+00
35	9.6151E−02	4.5294E+00	1.1351E−01	2.5731E+00	1.2013E−01	2.1880E+00	1.2844E−01	1.8737E+00
36	9.1871E−02	4.6070E+00	1.0801E−01	2.6137E+00	1.1424E−01	2.2222E+00	1.2208E−01	1.9028E+00
37	8.7879E−02	4.6832E+00	1.0291E−01	2.6534E+00	1.0878E−01	2.2555E+00	1.1619E−01	1.9311E+00
38	8.4151E−02	4.7581E+00	9.8162E−02	2.6920E+00	1.0370E−01	2.2879E+00	1.1073E−01	1.9586E+00
39	8.0667E−02	4.8317E+00	9.3741E−02	2.7298E+00	9.8981E−02	2.3196E+00	1.0565E−01	1.9855E+00
40	7.7408E−02	4.9042E+00	8.9616E−02	2.7667E+00	9.4580E−02	2.3505E+00	1.0091E−01	2.0117E+00
41	7.4356E−02	4.9754E+00	8.5762E−02	2.8028E+00	9.0471E−02	2.3807E+00	9.6497E−02	2.0372E+00
42	7.1497E−02	5.0455E+00	8.2156E−02	2.8382E+00	8.6628E−02	2.4103E+00	9.2369E−02	2.0623E+00
43	6.8814E−02	5.1146E+00	7.8777E−02	2.8729E+00	8.3030E−02	2.4393E+00	8.8506E−02	2.0868E+00
44	6.6296E−02	5.1825E+00	7.5608E−02	2.9069E+00	7.9656E−02	2.4677E+00	8.4883E−02	2.1108E+00
45	6.3931E−02	5.2495E+00	7.2630E−02	2.9403E+00	7.6487E−02	2.4955E+00	8.1483E−02	2.1343E+00
46	6.1706E−02	5.3154E+00	6.9830E−02	2.9731E+00	7.3508E−02	2.5229E+00	7.8286E−02	2.1574E+00
47	5.9612E−02	5.3804E+00	6.7194E−02	3.0053E+00	7.0703E−02	2.5498E+00	7.5276E−02	2.1802E+00
48	5.7640E−02	5.4444E+00	6.4709E−02	3.0370E+00	6.8059E−02	2.5762E+00	7.2440E−02	2.2025E+00
49	5.5780E−02	5.5076E+00	6.2364E−02	3.0681E+00	6.5564E−02	2.6022E+00	6.9763E−02	2.2245E+00
50	5.4025E−02	5.5698E+00	6.0148E−02	3.0988E+00	6.3207E−02	2.6278E+00	6.7235E−02	2.2461E+00
51	5.2368E−02	5.6312E+00	5.8053E−02	3.1290E+00	6.0978E−02	2.6530E+00	6.4843E−02	2.2674E+00
52	5.0801E−02	5.6918E+00	5.6069E−02	3.1588E+00	5.8868E−02	2.6779E+00	6.2580E−02	2.2883E+00
53	4.9318E−02	5.7516E+00	5.4190E−02	3.1881E+00	5.6868E−02	2.7023E+00	6.0434E−02	2.3090E+00
54	4.7915E−02	5.8106E+00	5.2407E−02	3.2170E+00	5.4971E−02	2.7264E+00	5.8399E−02	2.3294E+00
55	4.6584E−02	5.8688E+00	5.0714E−02	3.2455E+00	5.3170E−02	2.7502E+00	5.6466E−02	2.3495E+00
56	4.5322E−02	5.9263E+00	4.9105E−02	3.2736E+00	5.1458E−02	2.7736E+00	5.4629E−02	2.3693E+00
57	4.4124E−02	5.9831E+00	4.7575E−02	3.3013E+00	4.9829E−02	2.7968E+00	5.2882E−02	2.3888E+00
58	4.2986E−02	6.0392E+00	4.6118E−02	3.3287E+00	4.8279E−02	2.8196E+00	5.1218E−02	2.4081E+00
59	4.1904E−02	6.0946E+00	4.4730E−02	3.3557E+00	4.6802E−02	2.8421E+00	4.9633E−02	2.4272E+00
60	4.0874E−02	6.1493E+00	4.3406E−02	3.3823E+00	4.5393E−02	2.8644E+00	4.8122E−02	2.4460E+00

Table 4.3.3.1. *Partial wave elastic scattering factors for neutral atoms (cont.)*
Mo; $Z = 42$

	10 keV		40 keV		60 keV		90 keV	
s	$\|f(s)\|$	$\eta(s)$	$\|f(s)\|$	$\eta(s)$	$\|f(s)\|$	$\eta(s)$	$\|f(s)\|$	$\eta(s)$
0	9.0059E+00	3.0131E−01	1.0400E+01	1.9512E−01	1.0938E+01	1.7004E−01	1.1626E+01	1.4852E−01
1	7.4550E+00	3.5648E−01	8.7167E+00	2.2870E−01	9.1886E+00	1.9894E−01	9.7897E+00	1.7341E−01
2	5.1330E+00	4.8964E−01	6.1622E+00	3.0831E−01	6.5251E+00	2.6728E−01	6.9784E+00	2.3230E−01
3	3.5642E+00	6.5168E−01	4.3971E+00	4.0341E−01	4.6770E+00	3.4869E−01	5.0187E+00	3.0236E−01
4	2.5684E+00	8.2601E−01	3.2475E+00	5.0418E−01	3.4683E+00	4.3470E−01	3.7329E+00	3.7626E−01
5	1.9124E+00	1.0109E+00	2.4674E+00	6.0963E−01	2.6443E+00	5.2450E−01	2.8532E+00	4.5325E−01
6	1.4701E+00	1.2030E+00	1.9236E+00	7.1821E−01	2.0668E+00	6.1677E−01	2.2345E+00	5.3225E−01
7	1.1670E+00	1.3955E+00	1.5381E+00	8.2673E−01	1.6554E+00	7.0890E−01	1.7920E+00	6.1105E−01
8	9.5419E−01	1.5811E+00	1.2603E+00	9.3162E−01	1.3576E+00	7.9793E−01	1.4707E+00	6.8719E−01
9	7.9948E−01	1.7552E+00	1.0554E+00	1.0303E+00	1.1375E+00	8.8170E−01	1.2328E+00	7.5882E−01
10	6.8243E−01	1.9164E+00	9.0033E−01	1.1217E+00	9.7064E−01	9.5929E−01	1.0522E+00	8.2516E−01
11	5.9034E−01	2.0661E+00	7.7908E−01	1.2062E+00	8.4024E−01	1.0309E+00	9.1113E−01	8.8635E−01
12	5.1676E−01	2.2063E+00	6.8287E−01	1.2848E+00	7.3680E−01	1.0975E+00	7.9924E−01	9.4325E−01
13	4.5639E−01	2.3396E+00	6.0427E−01	1.3589E+00	6.5231E−01	1.1603E+00	7.0785E−01	9.9679E−01
14	4.0608E−01	2.4678E+00	5.3866E−01	1.4298E+00	5.8175E−01	1.2202E+00	6.3150E−01	1.0479E+00
15	3.6388E−01	2.5924E+00	4.8323E−01	1.4985E+00	5.2207E−01	1.2783E+00	5.6686E−01	1.0974E+00
16	3.2828E−01	2.7142E+00	4.3590E−01	1.5657E+00	4.7100E−01	1.3350E+00	5.1147E−01	1.1458E+00
17	2.9806E−01	2.8337E+00	3.9513E−01	1.6318E+00	4.2691E−01	1.3909E+00	4.6356E−01	1.1934E+00
18	2.7225E−01	2.9511E+00	3.5977E−01	1.6971E+00	3.8857E−01	1.4461E+00	4.2183E−01	1.2405E+00
19	2.5007E−01	3.0663E+00	3.2894E−01	1.7615E+00	3.5505E−01	1.5007E+00	3.8528E−01	1.2871E+00
20	2.3088E−01	3.1791E+00	3.0192E−01	1.8251E+00	3.2561E−01	1.5546E+00	3.5312E−01	1.3331E+00
21	2.1413E−01	3.2896E+00	2.7813E−01	1.8877E+00	2.9964E−01	1.6076E+00	3.2471E−01	1.3784E+00
22	1.9941E−01	3.3975E+00	2.5710E−01	1.9491E+00	2.7664E−01	1.6598E+00	2.9952E−01	1.4230E+00
23	1.8637E−01	3.5028E+00	2.3841E−01	2.0092E+00	2.5620E−01	1.7109E+00	2.7712E−01	1.4668E+00
24	1.7472E−01	3.6055E+00	2.2175E−01	2.0680E+00	2.3796E−01	1.7609E+00	2.5712E−01	1.5096E+00
25	1.6424E−01	3.7058E+00	2.0682E−01	2.1253E+00	2.2163E−01	1.8097E+00	2.3922E−01	1.5514E+00
26	1.5476E−01	3.8035E+00	1.9340E−01	2.1811E+00	2.0695E−01	1.8571E+00	2.2314E−01	1.5920E+00
27	1.4613E−01	3.8989E+00	1.8128E−01	2.2353E+00	1.9371E−01	1.9033E+00	2.0865E−01	1.6315E+00
28	1.3823E−01	3.9920E+00	1.7029E−01	2.2880E+00	1.8173E−01	1.9481E+00	1.9555E−01	1.6699E+00
29	1.3097E−01	4.0830E+00	1.6030E−01	2.3391E+00	1.7085E−01	1.9915E+00	1.8366E−01	1.7070E+00
30	1.2428E−01	4.1720E+00	1.5119E−01	2.3886E+00	1.6094E−01	2.0336E+00	1.7286E−01	1.7431E+00
31	1.1809E−01	4.2591E+00	1.4284E−01	2.4367E+00	1.5189E−01	2.0744E+00	1.6299E−01	1.7780E+00
32	1.1236E−01	4.3444E+00	1.3518E−01	2.4834E+00	1.4359E−01	2.1140E+00	1.5397E−01	1.8118E+00
33	1.0704E−01	4.4281E+00	1.2812E−01	2.5288E+00	1.3597E−01	2.1523E+00	1.4570E−01	1.8445E+00
34	1.0208E−01	4.5101E+00	1.2161E−01	2.5729E+00	1.2895E−01	2.1896E+00	1.3808E−01	1.8763E+00
35	9.7467E−02	4.5907E+00	1.1559E−01	2.6158E+00	1.2247E−01	2.2258E+00	1.3107E−01	1.9071E+00
36	9.3164E−02	4.6698E+00	1.1001E−01	2.6576E+00	1.1648E−01	2.2610E+00	1.2458E−01	1.9371E+00
37	8.9145E−02	4.7475E+00	1.0483E−01	2.6983E+00	1.1092E−01	2.2952E+00	1.1858E−01	1.9662E+00
38	8.5390E−02	4.8240E+00	1.0001E−01	2.7380E+00	1.0575E−01	2.3286E+00	1.1300E−01	1.9945E+00
39	8.1877E−02	4.8991E+00	9.5517E−02	2.7768E+00	1.0095E−01	2.3612E+00	1.0782E−01	2.0222E+00
40	7.8588E−02	4.9731E+00	9.1324E−02	2.8147E+00	9.6463E−02	2.3929E+00	1.0299E−01	2.0491E+00
41	7.5506E−02	5.0459E+00	8.7406E−02	2.8517E+00	9.2278E−02	2.4240E+00	9.8488E−02	2.0754E+00
42	7.2615E−02	5.1176E+00	8.3738E−02	2.8880E+00	8.8364E−02	2.4543E+00	9.4278E−02	2.1011E+00
43	6.9902E−02	5.1881E+00	8.0301E−02	2.9236E+00	8.4698E−02	2.4841E+00	9.0337E−02	2.1263E+00
44	6.7354E−02	5.2577E+00	7.7075E−02	2.9584E+00	8.1259E−02	2.5132E+00	8.6643E−02	2.1509E+00
45	6.4958E−02	5.3261E+00	7.4044E−02	2.9926E+00	7.8030E−02	2.5418E+00	8.3174E−02	2.1750E+00
46	6.2704E−02	5.3937E+00	7.1193E−02	3.0262E+00	7.4993E−02	2.5698E+00	7.9913E−02	2.1987E+00
47	6.0581E−02	5.4602E+00	6.8509E−02	3.0592E+00	7.2134E−02	2.5973E+00	7.6843E−02	2.2220E+00
48	5.8581E−02	5.5258E+00	6.5978E−02	3.0917E+00	6.9439E−02	2.6244E+00	7.3950E−02	2.2448E+00
49	5.6695E−02	5.5904E+00	6.3589E−02	3.1235E+00	6.6896E−02	2.6510E+00	7.1221E−02	2.2673E+00
50	5.4914E−02	5.6542E+00	6.1332E−02	3.1549E+00	6.4494E−02	2.6772E+00	6.8642E−02	2.2894E+00
51	5.3232E−02	5.7172E+00	5.9197E−02	3.1858E+00	6.2221E−02	2.7029E+00	6.6203E−02	2.3112E+00
52	5.1642E−02	5.7793E+00	5.7176E−02	3.2163E+00	6.0070E−02	2.7283E+00	6.3894E−02	2.3326E+00
53	5.0138E−02	5.8405E+00	5.5261E−02	3.2462E+00	5.8032E−02	2.7533E+00	6.1706E−02	2.3537E+00
54	4.8713E−02	5.9010E+00	5.3444E−02	3.2758E+00	5.6098E−02	2.7779E+00	5.9630E−02	2.3745E+00
55	4.7363E−02	5.9607E+00	5.1720E−02	3.3049E+00	5.4262E−02	2.8022E+00	5.7659E−02	2.3951E+00
56	4.6083E−02	6.0197E+00	5.0081E−02	3.3336E+00	5.2517E−02	2.8262E+00	5.5786E−02	2.4153E+00
57	4.4868E−02	6.0779E+00	4.8521E−02	3.3620E+00	5.0857E−02	2.8498E+00	5.4004E−02	2.4352E+00
58	4.3715E−02	6.1354E+00	4.7037E−02	3.3899E+00	4.9277E−02	2.8731E+00	5.2308E−02	2.4549E+00
59	4.2618E−02	6.1922E+00	4.5623E−02	3.4175E+00	4.7772E−02	2.8961E+00	5.0692E−02	2.4744E+00
60	4.1575E−02	6.2484E+00	4.4275E−02	3.4447E+00	4.6336E−02	2.9188E+00	4.9151E−02	2.4936E+00

Table 4.3.3.1. *Partial wave elastic scattering factors for neutral atoms (cont.)*
Tc; $Z = 43$

	10 keV		40 keV		60 keV		90 keV	
s	$\|f(s)\|$	$\eta(s)$	$\|f(s)\|$	$\eta(s)$	$\|f(s)\|$	$\eta(s)$	$\|f(s)\|$	$\eta(s)$
0	9.5099E+00	3.0091E−01	1.0981E+01	1.9529E−01	1.1551E+01	1.7032E−01	1.2279E+01	1.4887E−01
1	7.8509E+00	3.5633E−01	9.1816E+00	2.2917E−01	9.6802E+00	1.9951E−01	1.0315E+01	1.7404E−01
2	5.3042E+00	4.9705E−01	6.3791E+00	3.1346E−01	6.7578E+00	2.7193E−01	7.2300E+00	2.3648E−01
3	3.6232E+00	6.7061E−01	4.4829E+00	4.1530E−01	4.7716E+00	3.5912E−01	5.1231E+00	3.1156E−01
4	2.6008E+00	8.5112E−01	3.2985E+00	5.1973E−01	3.5256E+00	4.4830E−01	3.7970E+00	3.8820E−01
5	1.9393E+00	1.0372E+00	2.5104E+00	6.2610E−01	2.6927E+00	5.3894E−01	2.9075E+00	4.6595E−01
6	1.4928E+00	1.2291E+00	1.9611E+00	7.3483E−01	2.1092E+00	6.3140E−01	2.2822E+00	5.4515E−01
7	1.1848E+00	1.4226E+00	1.5690E+00	8.4416E−01	1.6906E+00	7.2427E−01	1.8318E+00	6.2463E−01
8	9.6761E−01	1.6115E+00	1.2844E+00	9.5107E−01	1.3853E+00	8.1506E−01	1.5022E+00	7.0230E−01
9	8.0986E−01	1.7905E+00	1.0739E+00	1.0529E+00	1.1587E+00	9.0149E−01	1.2570E+00	7.7625E−01
10	6.9093E−01	1.9574E+00	9.1441E−01	1.1479E+00	9.8684E−01	9.8220E−01	1.0708E+00	8.4529E−01
11	5.9766E−01	2.1122E+00	7.9008E−01	1.2358E+00	8.5283E−01	1.0569E+00	9.2554E−01	9.0916E−01
12	5.2329E−01	2.2570E+00	6.9178E−01	1.3176E+00	7.4693E−01	1.1263E+00	8.1079E−01	9.6845E−01
13	4.6229E−01	2.3939E+00	6.1177E−01	1.3942E+00	6.6079E−01	1.1912E+00	7.1750E−01	1.0239E+00
14	4.1137E−01	2.5247E+00	5.4520E−01	1.4670E+00	5.8914E−01	1.2527E+00	6.3991E−01	1.0764E+00
15	3.6858E−01	2.6512E+00	4.8911E−01	1.5368E+00	5.2873E−01	1.3118E+00	5.7445E−01	1.1268E+00
16	3.3241E−01	2.7744E+00	4.4128E−01	1.6048E+00	4.7714E−01	1.3693E+00	5.1849E−01	1.1758E+00
17	3.0165E−01	2.8949E+00	4.0012E−01	1.6714E+00	4.3266E−01	1.4255E+00	4.7017E−01	1.2237E+00
18	2.7537E−01	3.0131E+00	3.6445E−01	1.7369E+00	3.9400E−01	1.4810E+00	4.2811E−01	1.2710E+00
19	2.5278E−01	3.1290E+00	3.3333E−01	1.8016E+00	3.6020E−01	1.5357E+00	3.9126E−01	1.3177E+00
20	2.3324E−01	3.2426E+00	3.0606E−01	1.8653E+00	3.3050E−01	1.5897E+00	3.5882E−01	1.3638E+00
21	2.1622E−01	3.3539E+00	2.8203E−01	1.9282E+00	3.0428E−01	1.6430E+00	3.3014E−01	1.4093E+00
22	2.0128E−01	3.4627E+00	2.6078E−01	1.9900E+00	2.8104E−01	1.6955E+00	3.0468E−01	1.4542E+00
23	1.8807E−01	3.5691E+00	2.4189E−01	2.0507E+00	2.6037E−01	1.7471E+00	2.8202E−01	1.4983E+00
24	1.7630E−01	3.6729E+00	2.2504E−01	2.1101E+00	2.4191E−01	1.7976E+00	2.6177E−01	1.5416E+00
25	1.6574E−01	3.7743E+00	2.0995E−01	2.1682E+00	2.2537E−01	1.8470E+00	2.4362E−01	1.5839E+00
26	1.5619E−01	3.8733E+00	1.9637E−01	2.2248E+00	2.1050E−01	1.8952E+00	2.2730E−01	1.6252E+00
27	1.4751E−01	3.9700E+00	1.8411E−01	2.2800E+00	1.9708E−01	1.9422E+00	2.1258E−01	1.6655E+00
28	1.3959E−01	4.0644E+00	1.7300E−01	2.3336E+00	1.8493E−01	1.9878E+00	1.9927E−01	1.7046E+00
29	1.3231E−01	4.1568E+00	1.6289E−01	2.3858E+00	1.7389E−01	2.0322E+00	1.8719E−01	1.7427E+00
30	1.2560E−01	4.2472E+00	1.5366E−01	2.4365E+00	1.6384E−01	2.0753E+00	1.7620E−01	1.7796E+00
31	1.1940E−01	4.3357E+00	1.4521E−01	2.4857E+00	1.5465E−01	2.1172E+00	1.6616E−01	1.8154E+00
32	1.1366E−01	4.4224E+00	1.3746E−01	2.5336E+00	1.4622E−01	2.1577E+00	1.5698E−01	1.8501E+00
33	1.0832E−01	4.5074E+00	1.3031E−01	2.5801E+00	1.3849E−01	2.1972E+00	1.4855E−01	1.8838E+00
34	1.0335E−01	4.5909E+00	1.2372E−01	2.6253E+00	1.3135E−01	2.2354E+00	1.4080E−01	1.9165E+00
35	9.8716E−02	4.6729E+00	1.1762E−01	2.6693E+00	1.2477E−01	2.2726E+00	1.3365E−01	1.9482E+00
36	9.4392E−02	4.7534E+00	1.1196E−01	2.7122E+00	1.1867E−01	2.3088E+00	1.2705E−01	1.9790E+00
37	9.0352E−02	4.8326E+00	1.0671E−01	2.7539E+00	1.1302E−01	2.3440E+00	1.2093E−01	2.0089E+00
38	8.6573E−02	4.9105E+00	1.0182E−01	2.7947E+00	1.0777E−01	2.3783E+00	1.1525E−01	2.0381E+00
39	8.3035E−02	4.9871E+00	9.7257E−02	2.8345E+00	1.0288E−01	2.4117E+00	1.0997E−01	2.0665E+00
40	7.9720E−02	5.0626E+00	9.3001E−02	2.8733E+00	9.8320E−02	2.4444E+00	1.0505E−01	2.0942E+00
41	7.6610E−02	5.1368E+00	8.9021E−02	2.9114E+00	9.4061E−02	2.4762E+00	1.0046E−01	2.1212E+00
42	7.3692E−02	5.2100E+00	8.5295E−02	2.9485E+00	9.0078E−02	2.5074E+00	9.6171E−02	2.1476E+00
43	7.0951E−02	5.2821E+00	8.1801E−02	2.9850E+00	8.6346E−02	2.5379E+00	9.2154E−02	2.1734E+00
44	6.8375E−02	5.3531E+00	7.8521E−02	3.0207E+00	8.2845E−02	2.5678E+00	8.8388E−02	2.1987E+00
45	6.5951E−02	5.4231E+00	7.5439E−02	3.0557E+00	7.9557E−02	2.5970E+00	8.4852E−02	2.2235E+00
46	6.3670E−02	5.4921E+00	7.2539E−02	3.0901E+00	7.6464E−02	2.6258E+00	8.1528E−02	2.2478E+00
47	6.1521E−02	5.5602E+00	6.9807E−02	3.1239E+00	7.3552E−02	2.6540E+00	7.8398E−02	2.2716E+00
48	5.9495E−02	5.6273E+00	6.7231E−02	3.1571E+00	7.0807E−02	2.6817E+00	7.5449E−02	2.2950E+00
49	5.7583E−02	5.6935E+00	6.4800E−02	3.1897E+00	6.8216E−02	2.7089E+00	7.2666E−02	2.3180E+00
50	5.5779E−02	5.7588E+00	6.2502E−02	3.2219E+00	6.5768E−02	2.7357E+00	7.0037E−02	2.3406E+00
51	5.4074E−02	5.8232E+00	6.0328E−02	3.2535E+00	6.3453E−02	2.7620E+00	6.7551E−02	2.3628E+00
52	5.2461E−02	5.8868E+00	5.8271E−02	3.2846E+00	6.1261E−02	2.7879E+00	6.5197E−02	2.3847E+00
53	5.0936E−02	5.9495E+00	5.6320E−02	3.3152E+00	5.9184E−02	2.8135E+00	6.2966E−02	2.4063E+00
54	4.9491E−02	6.0115E+00	5.4470E−02	3.3454E+00	5.7213E−02	2.8387E+00	6.0850E−02	2.4276E+00
55	4.8123E−02	6.0727E+00	5.2714E−02	3.3752E+00	5.5343E−02	2.8635E+00	5.8841E−02	2.4485E+00
56	4.6825E−02	6.1331E+00	5.1045E−02	3.4045E+00	5.3565E−02	2.8879E+00	5.6932E−02	2.4692E+00
57	4.5593E−02	6.1928E+00	4.9457E−02	3.4335E+00	5.1874E−02	2.9121E+00	5.5116E−02	2.4895E+00
58	4.4424E−02	6.2518E+00	4.7946E−02	3.4620E+00	5.0264E−02	2.9359E+00	5.3387E−02	2.5096E+00
59	4.3313E−02	6.3101E+00	4.6506E−02	3.4902E+00	4.8731E−02	2.9594E+00	5.1740E−02	2.5295E+00
60	4.2257E−02	6.3676E+00	4.5134E−02	3.5180E+00	4.7268E−02	2.9825E+00	5.0170E−02	2.5491E+00

Table 4.3.3.1. *Partial wave elastic scattering factors for neutral atoms (cont.)*
Ru; $Z = 44$

	10 keV		40 keV		60 keV		90 keV	
s	$\|f(s)\|$	$\eta(s)$	$\|f(s)\|$	$\eta(s)$	$\|f(s)\|$	$\eta(s)$	$\|f(s)\|$	$\eta(s)$
0	8.2183E+00	3.2751E−01	9.5878E+00	2.1419E−01	1.0104E+01	1.8712E−01	1.0755E+01	1.6380E−01
1	6.9854E+00	3.7863E−01	8.2449E+00	2.4539E−01	8.7075E+00	2.1399E−01	9.2906E+00	1.8693E−01
2	5.0257E+00	5.0145E−01	6.0814E+00	3.1917E−01	6.4503E+00	2.7740E−01	6.9077E+00	2.4161E−01
3	3.5929E+00	6.5343E−01	4.4653E+00	4.0890E−01	4.7572E+00	3.5433E−01	5.1116E+00	3.0791E−01
4	2.6283E+00	8.2136E−01	3.3493E+00	5.0655E−01	3.5832E+00	4.3781E−01	3.8621E+00	3.7971E−01
5	1.9698E+00	1.0034E+00	2.5644E+00	6.1095E−01	2.7536E+00	5.2683E−01	2.9759E+00	4.5612E−01
6	1.5164E+00	1.1964E+00	2.0047E+00	7.2046E−01	2.1587E+00	6.2001E−01	2.3380E+00	5.3598E−01
7	1.2018E+00	1.3937E+00	1.6019E+00	8.3205E−01	1.7283E+00	7.1485E−01	1.8746E+00	6.1717E−01
8	9.8019E−01	1.5878E+00	1.3089E+00	9.4213E−01	1.4135E+00	8.0837E−01	1.5344E+00	6.9721E−01
9	8.1970E−01	1.7727E+00	1.0922E+00	1.0475E+00	1.1799E+00	8.9794E−01	1.2813E+00	7.7388E−01
10	6.9914E−01	1.9452E+00	9.2838E−01	1.1463E+00	1.0030E+00	9.8190E−01	1.0892E+00	8.4575E−01
11	6.0483E−01	2.1052E+00	8.0105E−01	1.2378E+00	8.6543E−01	1.0596E+00	9.3992E−01	9.1227E−01
12	5.2976E−01	2.2545E+00	7.0069E−01	1.3226E+00	7.5708E−01	1.1317E+00	8.2237E−01	9.7391E−01
13	4.6815E−01	2.3949E+00	6.1928E−01	1.4018E+00	6.6929E−01	1.1988E+00	7.2717E−01	1.0313E+00
14	4.1665E−01	2.5285E+00	5.5173E−01	1.4764E+00	5.9651E−01	1.2620E+00	6.4828E−01	1.0852E+00
15	3.7330E−01	2.6572E+00	4.9493E−01	1.5477E+00	5.3531E−01	1.3223E+00	5.8194E−01	1.1367E+00
16	3.3657E−01	2.7819E+00	4.4658E−01	1.6165E+00	4.8316E−01	1.3806E+00	5.2537E−01	1.1864E+00
17	3.0530E−01	2.9037E+00	4.0500E−01	1.6837E+00	4.3825E−01	1.4374E+00	4.7659E−01	1.2348E+00
18	2.7855E−01	3.0228E+00	3.6898E−01	1.7497E+00	3.9925E−01	1.4931E+00	4.3417E−01	1.2823E+00
19	2.5554E−01	3.1396E+00	3.3758E−01	1.8146E+00	3.6516E−01	1.5481E+00	3.9701E−01	1.3292E+00
20	2.3565E−01	3.2541E+00	3.1004E−01	1.8786E+00	3.3519E−01	1.6023E+00	3.6430E−01	1.3755E+00
21	2.1834E−01	3.3662E+00	2.8578E−01	1.9418E+00	3.0873E−01	1.6558E+00	3.3536E−01	1.4212E+00
22	2.0317E−01	3.4759E+00	2.6432E−01	2.0039E+00	2.8527E−01	1.7086E+00	3.0965E−01	1.4663E+00
23	1.8977E−01	3.5833E+00	2.4524E−01	2.0650E+00	2.6438E−01	1.7605E+00	2.8674E−01	1.5107E+00
24	1.7786E−01	3.6882E+00	2.2822E−01	2.1250E+00	2.4572E−01	1.8115E+00	2.6625E−01	1.5544E+00
25	1.6719E−01	3.7907E+00	2.1296E−01	2.1837E+00	2.2898E−01	1.8615E+00	2.4787E−01	1.5972E+00
26	1.5757E−01	3.8909E+00	1.9924E−01	2.2411E+00	2.1393E−01	1.9103E+00	2.3134E−01	1.6391E+00
27	1.4884E−01	3.9887E+00	1.8684E−01	2.2971E+00	2.0034E−01	1.9580E+00	2.1641E−01	1.6800E+00
28	1.4088E−01	4.0844E+00	1.7560E−01	2.3517E+00	1.8803E−01	2.0045E+00	2.0290E−01	1.7198E+00
29	1.3357E−01	4.1781E+00	1.6538E−01	2.4048E+00	1.7685E−01	2.0498E+00	1.9063E−01	1.7586E+00
30	1.2685E−01	4.2698E+00	1.5605E−01	2.4565E+00	1.6665E−01	2.0938E+00	1.7947E−01	1.7963E+00
31	1.2063E−01	4.3596E+00	1.4751E−01	2.5068E+00	1.5733E−01	2.1366E+00	1.6927E−01	1.8330E+00
32	1.1487E−01	4.4476E+00	1.3966E−01	2.5558E+00	1.4879E−01	2.1781E+00	1.5993E−01	1.8685E+00
33	1.0952E−01	4.5340E+00	1.3244E−01	2.6033E+00	1.4094E−01	2.2185E+00	1.5137E−01	1.9031E+00
34	1.0454E−01	4.6188E+00	1.2576E−01	2.6497E+00	1.3370E−01	2.2578E+00	1.4348E−01	1.9367E+00
35	9.9895E−02	4.7022E+00	1.1959E−01	2.6948E+00	1.2702E−01	2.2959E+00	1.3621E−01	1.9692E+00
36	9.5556E−02	4.7841E+00	1.1386E−01	2.7387E+00	1.2083E−01	2.3331E+00	1.2949E−01	2.0009E+00
37	9.1498E−02	4.8647E+00	1.0854E−01	2.7815E+00	1.1509E−01	2.3692E+00	1.2326E−01	2.0317E+00
38	8.7700E−02	4.9440E+00	1.0358E−01	2.8233E+00	1.0976E−01	2.4044E+00	1.1748E−01	2.0617E+00
39	8.4141E−02	5.0220E+00	9.8962E−02	2.8640E+00	1.0479E−01	2.4387E+00	1.1211E−01	2.0909E+00
40	8.0804E−02	5.0989E+00	9.4646E−02	2.9039E+00	1.0015E−01	2.4722E+00	1.0710E−01	2.1193E+00
41	7.7672E−02	5.1746E+00	9.0608E−02	2.9429E+00	9.5824E−02	2.5050E+00	1.0242E−01	2.1471E+00
42	7.4730E−02	5.2492E+00	8.6827E−02	2.9810E+00	9.1773E−02	2.5369E+00	9.8051E−02	2.1742E+00
43	7.1965E−02	5.3228E+00	8.3280E−02	3.0183E+00	8.7978E−02	2.5682E+00	9.3959E−02	2.2007E+00
44	6.9365E−02	5.3953E+00	7.9949E−02	3.0549E+00	8.4417E−02	2.5988E+00	9.0123E−02	2.2266E+00
45	6.6917E−02	5.4668E+00	7.6818E−02	3.0908E+00	8.1071E−02	2.6288E+00	8.6521E−02	2.2520E+00
46	6.4611E−02	5.5373E+00	7.3871E−02	3.1260E+00	7.7924E−02	2.6583E+00	8.3134E−02	2.2769E+00
47	6.2438E−02	5.6068E+00	7.1094E−02	3.1606E+00	7.4960E−02	2.6872E+00	7.9946E−02	2.3013E+00
48	6.0389E−02	5.6754E+00	6.8474E−02	3.1946E+00	7.2165E−02	2.7155E+00	7.6941E−02	2.3253E+00
49	5.8454E−02	5.7431E+00	6.6001E−02	3.2280E+00	6.9528E−02	2.7434E+00	7.4105E−02	2.3488E+00
50	5.6627E−02	5.8099E+00	6.3664E−02	3.2608E+00	6.7035E−02	2.7708E+00	7.1426E−02	2.3720E+00
51	5.4901E−02	5.8759E+00	6.1452E−02	3.2932E+00	6.4678E−02	2.7977E+00	6.8893E−02	2.3947E+00
52	5.3268E−02	5.9410E+00	5.9359E−02	3.3250E+00	6.2446E−02	2.8242E+00	6.6494E−02	2.4171E+00
53	5.1723E−02	6.0052E+00	5.7374E−02	3.3563E+00	6.0330E−02	2.8503E+00	6.4221E−02	2.4392E+00
54	5.0259E−02	6.0687E+00	5.5491E−02	3.3872E+00	5.8323E−02	2.8761E+00	6.2065E−02	2.4609E+00
55	4.8873E−02	6.1314E+00	5.3703E−02	3.4176E+00	5.6418E−02	2.9014E+00	6.0018E−02	2.4823E+00
56	4.7558E−02	6.1933E+00	5.2004E−02	3.4476E+00	5.4608E−02	2.9264E+00	5.8073E−02	2.5034E+00
57	4.6311E−02	6.2545E+00	5.0388E−02	3.4772E+00	5.2885E−02	2.9511E+00	5.6222E−02	2.5242E+00
58	4.5127E−02	6.3150E+00	4.8850E−02	3.5063E+00	5.1246E−02	2.9754E+00	5.4461E−02	2.5447E+00
59	4.4002E−02	6.3747E+00	4.7385E−02	3.5351E+00	4.9684E−02	2.9993E+00	5.2783E−02	2.5649E+00
60	4.2933E−02	6.4338E+00	4.5987E−02	3.5635E+00	4.8195E−02	3.0230E+00	5.1183E−02	2.5849E+00

Table 4.3.3.1. *Partial wave elastic scattering factors for neutral atoms (cont.)*
Rh; $Z = 45$

	10 keV		40 keV		60 keV		90 keV	
s	$\|f(s)\|$	$\eta(s)$	$\|f(s)\|$	$\eta(s)$	$\|f(s)\|$	$\eta(s)$	$\|f(s)\|$	$\eta(s)$
0	7.8710E+00	3.3930E−01	9.2282E+00	2.2307E−01	9.7341E+00	1.9512E−01	1.0369E+01	1.7100E−01
1	6.7562E+00	3.8897E−01	8.0117E+00	2.5343E−01	8.4692E+00	2.2128E−01	9.0430E+00	1.9351E−01
2	4.9472E+00	5.0781E−01	6.0112E+00	3.2498E−01	6.3814E+00	2.8281E−01	6.8387E+00	2.4658E−01
3	3.5861E+00	6.5507E−01	4.4738E+00	4.1217E−01	4.7703E+00	3.5762E−01	5.1291E+00	3.1110E−01
4	2.6461E+00	8.1902E−01	3.3853E+00	5.0780E−01	3.6249E+00	4.3944E−01	3.9098E+00	3.8152E−01
5	1.9924E+00	9.9845E−01	2.6055E+00	6.1096E−01	2.8004E+00	5.2746E−01	3.0289E+00	4.5712E−01
6	1.5365E+00	1.1904E+00	2.0421E+00	7.2014E−01	2.2014E+00	6.2042E−01	2.3865E+00	5.3683E−01
7	1.2177E+00	1.3888E+00	1.6329E+00	8.3249E−01	1.7638E+00	7.1594E−01	1.9151E+00	6.1865E−01
8	9.9234E−01	1.5860E+00	1.3333E+00	9.4443E−01	1.4418E+00	8.1108E−01	1.5668E+00	7.0010E−01
9	8.2924E−01	1.7754E+00	1.1111E+00	1.0526E+00	1.2019E+00	9.0309E−01	1.3066E+00	7.7888E−01
10	7.0709E−01	1.9531E+00	9.4309E−01	1.1548E+00	1.0200E+00	9.8998E−01	1.1089E+00	8.5330E−01
11	6.1184E−01	2.1182E+00	8.1266E−01	1.2498E+00	8.7883E−01	1.0708E+00	9.5534E−01	9.2249E−01
12	5.3616E−01	2.2722E+00	7.1010E−01	1.3379E+00	7.6784E−01	1.1457E+00	8.3469E−01	9.8667E−01
13	4.7407E−01	2.4166E+00	6.2714E−01	1.4199E+00	6.7819E−01	1.2154E+00	7.3731E−01	1.0462E+00
14	4.2210E−01	2.5534E+00	5.5849E−01	1.4968E+00	6.0411E−01	1.2806E+00	6.5691E−01	1.1020E+00
15	3.7824E−01	2.6845E+00	5.0089E−01	1.5698E+00	5.4200E−01	1.3424E+00	5.8952E−01	1.1548E+00
16	3.4100E−01	2.8112E+00	4.5194E−01	1.6400E+00	4.8918E−01	1.4018E+00	5.3222E−01	1.2054E+00
17	3.0922E−01	2.9345E+00	4.0990E−01	1.7080E+00	4.4378E−01	1.4593E+00	4.8291E−01	1.2544E+00
18	2.8199E−01	3.0549E+00	3.7350E−01	1.7745E+00	4.0440E−01	1.5155E+00	4.4008E−01	1.3024E+00
19	2.5854E−01	3.1727E+00	3.4177E−01	1.8398E+00	3.6999E−01	1.5708E+00	4.0259E−01	1.3495E+00
20	2.3826E−01	3.2881E+00	3.1396E−01	1.9041E+00	3.3975E−01	1.6252E+00	3.6959E−01	1.3959E+00
21	2.2062E−01	3.4011E+00	2.8945E−01	1.9676E+00	3.1305E−01	1.6789E+00	3.4039E−01	1.4418E+00
22	2.0518E−01	3.5118E+00	2.6777E−01	2.0300E+00	2.8935E−01	1.7320E+00	3.1444E−01	1.4871E+00
23	1.9157E−01	3.6201E+00	2.4849E−01	2.0915E+00	2.6825E−01	1.7842E+00	2.9130E−01	1.5318E+00
24	1.7948E−01	3.7260E+00	2.3129E−01	2.1519E+00	2.4940E−01	1.8355E+00	2.7059E−01	1.5758E+00
25	1.6868E−01	3.8296E+00	2.1587E−01	2.2112E+00	2.3248E−01	1.8860E+00	2.5200E−01	1.6190E+00
26	1.5896E−01	3.9308E+00	2.0200E−01	2.2692E+00	2.1725E−01	1.9354E+00	2.3526E−01	1.6613E+00
27	1.5016E−01	4.0299E+00	1.8947E−01	2.3260E+00	2.0350E−01	1.9837E+00	2.2013E−01	1.7028E+00
28	1.4214E−01	4.1267E+00	1.7812E−01	2.3814E+00	1.9104E−01	2.0309E+00	2.0644E−01	1.7433E+00
29	1.3480E−01	4.2216E+00	1.6779E−01	2.4354E+00	1.7971E−01	2.0770E+00	1.9400E−01	1.7828E+00
30	1.2805E−01	4.3145E+00	1.5836E−01	2.4880E+00	1.6939E−01	2.1218E+00	1.8266E−01	1.8212E+00
31	1.2181E−01	4.4055E+00	1.4973E−01	2.5393E+00	1.5995E−01	2.1655E+00	1.7231E−01	1.8586E+00
32	1.1603E−01	4.4948E+00	1.4179E−01	2.5893E+00	1.5129E−01	2.2080E+00	1.6283E−01	1.8950E+00
33	1.1067E−01	4.5825E+00	1.3449E−01	2.6379E+00	1.4333E−01	2.2493E+00	1.5412E−01	1.9304E+00
34	1.0567E−01	4.6686E+00	1.2774E−01	2.6852E+00	1.3599E−01	2.2895E+00	1.4611E−01	1.9648E+00
35	1.0101E−01	4.7532E+00	1.2150E−01	2.7313E+00	1.2922E−01	2.3286E+00	1.3872E−01	1.9982E+00
36	9.6661E−02	4.8364E+00	1.1570E−01	2.7763E+00	1.2294E−01	2.3666E+00	1.3189E−01	2.0307E+00
37	9.2588E−02	4.9183E+00	1.1032E−01	2.8201E+00	1.1712E−01	2.4037E+00	1.2556E−01	2.0624E+00
38	8.8773E−02	4.9989E+00	1.0530E−01	2.8629E+00	1.1170E−01	2.4398E+00	1.1968E−01	2.0931E+00
39	8.5196E−02	5.0783E+00	1.0062E−01	2.9047E+00	1.0666E−01	2.4750E+00	1.1421E−01	2.1231E+00
40	8.1840E−02	5.1565E+00	9.6252E−02	2.9455E+00	1.0195E−01	2.5094E+00	1.0911E−01	2.1523E+00
41	7.8687E−02	5.2337E+00	9.2161E−02	2.9854E+00	9.7558E−02	2.5429E+00	1.0436E−01	2.1808E+00
42	7.5724E−02	5.3097E+00	8.8327E−02	3.0245E+00	9.3443E−02	2.5757E+00	9.9910E−02	2.2087E+00
43	7.2938E−02	5.3846E+00	8.4730E−02	3.0627E+00	8.9586E−02	2.6078E+00	9.5746E−02	2.2359E+00
44	7.0315E−02	5.4585E+00	8.1351E−02	3.1002E+00	8.5967E−02	2.6392E+00	9.1841E−02	2.2625E+00
45	6.7845E−02	5.5314E+00	7.8173E−02	3.1369E+00	8.2565E−02	2.6700E+00	8.8174E−02	2.2885E+00
46	6.5517E−02	5.6034E+00	7.5181E−02	3.1730E+00	7.9365E−02	2.7001E+00	8.4726E−02	2.3140E+00
47	6.3322E−02	5.6744E+00	7.2360E−02	3.2084E+00	7.6351E−02	2.7297E+00	8.1479E−02	2.3391E+00
48	6.1251E−02	5.7445E+00	6.9699E−02	3.2431E+00	7.3508E−02	2.7587E+00	7.8419E−02	2.3636E+00
49	5.9295E−02	5.8137E+00	6.7186E−02	3.2773E+00	7.0825E−02	2.7872E+00	7.5532E−02	2.3877E+00
50	5.7447E−02	5.8819E+00	6.4810E−02	3.3109E+00	6.8289E−02	2.8152E+00	7.2803E−02	2.4114E+00
51	5.5700E−02	5.9494E+00	6.2562E−02	3.3440E+00	6.5890E−02	2.8428E+00	7.0223E−02	2.4346E+00
52	5.4048E−02	6.0160E+00	6.0433E−02	3.3765E+00	6.3618E−02	2.8699E+00	6.7781E−02	2.4575E+00
53	5.2484E−02	6.0817E+00	5.8414E−02	3.4085E+00	6.1465E−02	2.8966E+00	6.5466E−02	2.4801E+00
54	5.1003E−02	6.1467E+00	5.6499E−02	3.4401E+00	5.9422E−02	2.9229E+00	6.3270E−02	2.5022E+00
55	4.9600E−02	6.2109E+00	5.4681E−02	3.4712E+00	5.7483E−02	2.9488E+00	6.1185E−02	2.5241E+00
56	4.8269E−02	6.2743E+00	5.2952E−02	3.5018E+00	5.5640E−02	2.9743E+00	5.9204E−02	2.5456E+00
57	4.7007E−02	6.3370E+00	5.1308E−02	3.5320E+00	5.3886E−02	2.9995E+00	5.7319E−02	2.5669E+00
58	4.5808E−02	6.3989E+00	4.9743E−02	3.5618E+00	5.2217E−02	3.0243E+00	5.5525E−02	2.5878E+00
59	4.4670E−02	6.4601E+00	4.8252E−02	3.5912E+00	5.0628E−02	3.0488E+00	5.3816E−02	2.6085E+00
60	4.3589E−02	6.5206E+00	4.6831E−02	3.6202E+00	4.9112E−02	3.0729E+00	5.2186E−02	2.6289E+00

Table 4.3.3.1. *Partial wave elastic scattering factors for neutral atoms (cont.)*
Pd; $Z = 46$

	10 keV		40 keV		60 keV		90 keV	
s	$\|f(s)\|$	$\eta(s)$	$\|f(s)\|$	$\eta(s)$	$\|f(s)\|$	$\eta(s)$	$\|f(s)\|$	$\eta(s)$
0	6.2666E+00	3.9922E−01	7.4746E+00	2.6234E−01	7.9081E+00	2.2956E−01	8.4411E+00	2.0131E−01
1	5.7508E+00	4.2928E−01	6.9084E+00	2.8076E−01	7.3202E+00	2.4538E−01	7.8297E+00	2.1480E−01
2	4.6398E+00	5.1221E−01	5.6764E+00	3.3110E−01	6.0342E+00	2.8872E−01	6.4738E+00	2.5215E−01
3	3.5349E+00	6.3449E−01	4.4296E+00	4.0416E−01	4.7276E+00	3.5151E−01	5.0873E+00	3.0636E−01
4	2.6576E+00	7.8602E−01	3.4153E+00	4.9305E−01	3.6604E+00	4.2766E−01	3.9512E+00	3.7196E−01
5	2.0138E+00	9.6024E−01	2.6475E+00	5.9355E−01	2.8486E+00	5.1348E−01	3.0837E+00	4.4573E−01
6	1.5554E+00	1.1510E+00	2.0803E+00	7.0224E−01	2.2453E+00	6.0608E−01	2.4364E+00	5.2517E−01
7	1.2323E+00	1.3509E+00	1.6640E+00	8.1549E−01	1.7999E+00	7.0242E−01	1.9564E+00	6.0771E−01
8	1.0034E+00	1.5514E+00	1.3577E+00	9.2943E−01	1.4703E+00	7.9929E−01	1.5996E+00	6.9069E−01
9	8.3800E−01	1.7453E+00	1.1301E+00	1.0405E+00	1.2241E+00	8.9374E−01	1.3321E+00	7.7158E−01
10	7.1450E−01	1.9281E+00	9.5785E−01	1.1459E+00	1.0373E+00	9.8351E−01	1.1288E+00	8.4851E−01
11	6.1846E−01	2.0983E+00	8.2437E−01	1.2444E+00	8.9241E−01	1.0673E+00	9.7102E−01	9.2033E−01
12	5.4232E−01	2.2569E+00	7.1963E−01	1.3358E+00	7.7880E−01	1.1452E+00	8.4727E−01	9.8705E−01
13	4.7985E−01	2.4053E+00	6.3512E−01	1.4208E+00	6.8726E−01	1.2174E+00	7.4766E−01	1.0489E+00
14	4.2748E−01	2.5455E+00	5.6534E−01	1.5001E+00	6.1183E−01	1.2848E+00	6.6568E−01	1.1065E+00
15	3.8320E−01	2.6793E+00	5.0691E−01	1.5751E+00	5.4874E−01	1.3483E+00	5.9716E−01	1.1608E+00
16	3.4550E−01	2.8082E+00	4.5732E−01	1.6466E+00	4.9521E−01	1.4089E+00	5.3905E−01	1.2125E+00
17	3.1325E−01	2.9332E+00	4.1478E−01	1.7157E+00	4.4927E−01	1.4674E+00	4.8915E−01	1.2624E+00
18	2.8555E−01	3.0550E+00	3.7797E−01	1.7830E+00	4.0947E−01	1.5242E+00	4.4587E−01	1.3109E+00
19	2.6168E−01	3.1740E+00	3.4591E−01	1.8488E+00	3.7472E−01	1.5799E+00	4.0803E−01	1.3583E+00
20	2.4100E−01	3.2905E+00	3.1780E−01	1.9135E+00	3.4419E−01	1.6346E+00	3.7473E−01	1.4050E+00
21	2.2302E−01	3.4045E+00	2.9304E−01	1.9772E+00	3.1723E−01	1.6886E+00	3.4527E−01	1.4511E+00
22	2.0728E−01	3.5162E+00	2.7113E−01	2.0400E+00	2.9331E−01	1.7419E+00	3.1908E−01	1.4966E+00
23	1.9343E−01	3.6255E+00	2.5165E−01	2.1018E+00	2.7201E−01	1.7944E+00	2.9571E−01	1.5415E+00
24	1.8115E−01	3.7324E+00	2.3427E−01	2.1626E+00	2.5295E−01	1.8461E+00	2.7479E−01	1.5857E+00
25	1.7020E−01	3.8370E+00	2.1869E−01	2.2224E+00	2.3586E−01	1.8969E+00	2.5599E−01	1.6293E+00
26	1.6036E−01	3.9394E+00	2.0467E−01	2.2810E+00	2.2046E−01	1.9468E+00	2.3905E−01	1.6720E+00
27	1.5147E−01	4.0395E+00	1.9202E−01	2.3384E+00	2.0656E−01	1.9957E+00	2.2375E−01	1.7140E+00
28	1.4338E−01	4.1375E+00	1.8054E−01	2.3945E+00	1.9395E−01	2.0435E+00	2.0988E−01	1.7550E+00
29	1.3599E−01	4.2335E+00	1.7011E−01	2.4493E+00	1.8249E−01	2.0903E+00	1.9727E−01	1.7951E+00
30	1.2920E−01	4.3275E+00	1.6059E−01	2.5028E+00	1.7204E−01	2.1358E+00	1.8578E−01	1.8342E+00
31	1.2294E−01	4.4197E+00	1.5186E−01	2.5550E+00	1.6249E−01	2.1803E+00	1.7528E−01	1.8724E+00
32	1.1714E−01	4.5102E+00	1.4385E−01	2.6059E+00	1.5372E−01	2.2236E+00	1.6566E−01	1.9095E+00
33	1.1176E−01	4.5991E+00	1.3647E−01	2.6555E+00	1.4566E−01	2.2658E+00	1.5683E−01	1.9457E+00
34	1.0675E−01	4.6864E+00	1.2966E−01	2.7038E+00	1.3823E−01	2.3069E+00	1.4870E−01	1.9808E+00
35	1.0208E−01	4.7722E+00	1.2335E−01	2.7509E+00	1.3136E−01	2.3469E+00	1.4119E−01	2.0151E+00
36	9.7712E−02	4.8567E+00	1.1749E−01	2.7969E+00	1.2500E−01	2.3859E+00	1.3425E−01	2.0484E+00
37	9.3625E−02	4.9398E+00	1.1205E−01	2.8417E+00	1.1910E−01	2.4238E+00	1.2782E−01	2.0808E+00
38	8.9795E−02	5.0217E+00	1.0698E−01	2.8855E+00	1.1361E−01	2.4608E+00	1.2184E−01	2.1124E+00
39	8.6203E−02	5.1024E+00	1.0224E−01	2.9282E+00	1.0850E−01	2.4969E+00	1.1629E−01	2.1432E+00
40	8.2829E−02	5.1820E+00	9.7819E−02	2.9700E+00	1.0372E−01	2.5321E+00	1.1111E−01	2.1731E+00
41	7.9660E−02	5.2604E+00	9.3678E−02	3.0108E+00	9.9262E−02	2.5665E+00	1.0627E−01	2.2024E+00
42	7.6678E−02	5.3377E+00	8.9796E−02	3.0508E+00	9.5086E−02	2.6001E+00	1.0175E−01	2.2310E+00
43	7.3873E−02	5.4141E+00	8.6151E−02	3.0899E+00	9.1171E−02	2.6330E+00	9.7514E−02	2.2589E+00
44	7.1230E−02	5.4893E+00	8.2727E−02	3.1283E+00	8.7495E−02	2.6652E+00	9.3542E−02	2.2861E+00
45	6.8740E−02	5.5637E+00	7.9504E−02	3.1659E+00	8.4041E−02	2.6967E+00	8.9812E−02	2.3128E+00
46	6.6392E−02	5.6370E+00	7.6470E−02	3.2028E+00	8.0789E−02	2.7276E+00	8.6304E−02	2.3390E+00
47	6.4177E−02	5.7094E+00	7.3608E−02	3.2390E+00	7.7726E−02	2.7578E+00	8.3001E−02	2.3646E+00
48	6.2086E−02	5.7810E+00	7.0907E−02	3.2745E+00	7.4837E−02	2.7875E+00	7.9887E−02	2.3898E+00
49	6.0111E−02	5.8516E+00	6.8356E−02	3.3095E+00	7.2109E−02	2.8167E+00	7.6948E−02	2.4144E+00
50	5.8244E−02	5.9213E+00	6.5943E−02	3.3438E+00	6.9531E−02	2.8454E+00	7.4171E−02	2.4386E+00
51	5.6479E−02	5.9902E+00	6.3659E−02	3.3777E+00	6.7091E−02	2.8736E+00	7.1545E−02	2.4625E+00
52	5.4808E−02	6.0583E+00	6.1496E−02	3.4109E+00	6.4781E−02	2.9013E+00	6.9059E−02	2.4859E+00
53	5.3227E−02	6.1255E+00	5.9445E−02	3.4436E+00	6.2591E−02	2.9286E+00	6.6702E−02	2.5089E+00
54	5.1729E−02	6.1920E+00	5.7498E−02	3.4759E+00	6.0512E−02	2.9555E+00	6.4467E−02	2.5316E+00
55	5.0310E−02	6.2577E+00	5.5649E−02	3.5076E+00	5.8540E−02	2.9819E+00	6.2344E−02	2.5539E+00
56	4.8964E−02	6.3226E+00	5.3892E−02	3.5390E+00	5.6664E−02	3.0080E+00	6.0327E−02	2.5759E+00
57	4.7687E−02	6.3868E+00	5.2221E−02	3.5698E+00	5.4880E−02	3.0337E+00	5.8408E−02	2.5976E+00
58	4.6476E−02	6.4502E+00	5.0629E−02	3.6003E+00	5.3182E−02	3.0591E+00	5.6582E−02	2.6190E+00
59	4.5325E−02	6.5129E+00	4.9113E−02	3.6303E+00	5.1564E−02	3.0840E+00	5.4842E−02	2.6401E+00
60	4.4232E−02	6.5749E+00	4.7667E−02	3.6599E+00	5.0022E−02	3.1087E+00	5.3183E−02	2.6609E+00

Table 4.3.3.1. *Partial wave elastic scattering factors for neutral atoms (cont.)*
Ag; $Z = 47$

	10 keV		40 keV		60 keV		90 keV	
s	$\|f(s)\|$	$\eta(s)$	$\|f(s)\|$	$\eta(s)$	$\|f(s)\|$	$\eta(s)$	$\|f(s)\|$	$\eta(s)$
0	7.2512E+00	3.6073E−01	8.5834E+00	2.3973E−01	9.0713E+00	2.1025E−01	9.6770E+00	1.8469E−01
1	6.3204E+00	4.0822E−01	7.5642E+00	2.6885E−01	8.0112E+00	2.3535E−01	8.5668E+00	2.0627E−01
2	4.7638E+00	5.2076E−01	5.8368E+00	3.3689E−01	6.2073E+00	2.9393E−01	6.6619E+00	2.5684E−01
3	3.5410E+00	6.5960E−01	4.4518E+00	4.1956E−01	4.7550E+00	3.6496E−01	5.1200E+00	3.1817E−01
4	2.6597E+00	8.1524E−01	3.4295E+00	5.1091E−01	3.6787E+00	4.4324E−01	3.9737E+00	3.8562E−01
5	2.0247E+00	9.8793E−01	2.6712E+00	6.1076E−01	2.8766E+00	5.2857E−01	3.1163E+00	4.5901E−01
6	1.5697E+00	1.1759E+00	2.1083E+00	7.1810E−01	2.2778E+00	6.2008E−01	2.4737E+00	5.3756E−01
7	1.2456E+00	1.3739E+00	1.6910E+00	8.3052E−01	1.8312E+00	7.1576E−01	1.9923E+00	6.1959E−01
8	1.0142E+00	1.5747E+00	1.3811E+00	9.4472E−01	1.4975E+00	8.1290E−01	1.6309E+00	7.0281E−01
9	8.4656E−01	1.7712E+00	1.1492E+00	1.0573E+00	1.2465E+00	9.0865E−01	1.3581E+00	7.8485E−01
10	7.2158E−01	1.9580E+00	9.7315E−01	1.1652E+00	1.0553E+00	1.0006E+00	1.1497E+00	8.6368E−01
11	6.2474E−01	2.1328E+00	8.3665E−01	1.2668E+00	9.0683E−01	1.0871E+00	9.8775E−01	9.3789E−01
12	5.4819E−01	2.2959E+00	7.2964E−01	1.3616E+00	7.9042E−01	1.1680E+00	8.6069E−01	1.0072E+00
13	4.8548E−01	2.4486E+00	6.4346E−01	1.4497E+00	6.9681E−01	1.2430E+00	7.5862E−01	1.0715E+00
14	4.3286E−01	2.5924E+00	5.7247E−01	1.5318E+00	6.1988E−01	1.3128E+00	6.7485E−01	1.1313E+00
15	3.8827E−01	2.7292E+00	5.1313E−01	1.6091E+00	5.5570E−01	1.3784E+00	6.0504E−01	1.1874E+00
16	3.5020E−01	2.8606E+00	4.6285E−01	1.6825E+00	5.0137E−01	1.4406E+00	5.4600E−01	1.2405E+00
17	3.1752E−01	2.9876E+00	4.1977E−01	1.7529E+00	4.5482E−01	1.5002E+00	4.9542E−01	1.2914E+00
18	2.8938E−01	3.1111E+00	3.8252E−01	1.8211E+00	4.1455E−01	1.5579E+00	4.5162E−01	1.3405E+00
19	2.6507E−01	3.2315E+00	3.5008E−01	1.8876E+00	3.7942E−01	1.6141E+00	4.1339E−01	1.3885E+00
20	2.4399E−01	3.3492E+00	3.2165E−01	1.9527E+00	3.4858E−01	1.6693E+00	3.7976E−01	1.4356E+00
21	2.2564E−01	3.4644E+00	2.9661E−01	2.0168E+00	3.2134E−01	1.7235E+00	3.5002E−01	1.4819E+00
22	2.0958E−01	3.5771E+00	2.7446E−01	2.0799E+00	2.9719E−01	1.7770E+00	3.2358E−01	1.5275E+00
23	1.9545E−01	3.6875E+00	2.5476E−01	2.1421E+00	2.7566E−01	1.8297E+00	2.9999E−01	1.5726E+00
24	1.8295E−01	3.7954E+00	2.3719E−01	2.2033E+00	2.5642E−01	1.8817E+00	2.7886E−01	1.6171E+00
25	1.7181E−01	3.9011E+00	2.2144E−01	2.2634E+00	2.3914E−01	1.9329E+00	2.5986E−01	1.6609E+00
26	1.6183E−01	4.0045E+00	2.0728E−01	2.3225E+00	2.2358E−01	1.9832E+00	2.4274E−01	1.7040E+00
27	1.5282E−01	4.1057E+00	1.9449E−01	2.3805E+00	2.0952E−01	2.0325E+00	2.2726E−01	1.7463E+00
28	1.4465E−01	4.2048E+00	1.8290E−01	2.4372E+00	1.9678E−01	2.0809E+00	2.1322E−01	1.7878E+00
29	1.3719E−01	4.3018E+00	1.7235E−01	2.4927E+00	1.8519E−01	2.1283E+00	2.0046E−01	1.8285E+00
30	1.3035E−01	4.3969E+00	1.6273E−01	2.5470E+00	1.7462E−01	2.1746E+00	1.8882E−01	1.8682E+00
31	1.2405E−01	4.4903E+00	1.5393E−01	2.6000E+00	1.6495E−01	2.2198E+00	1.7818E−01	1.9070E+00
32	1.1822E−01	4.5819E+00	1.4584E−01	2.6518E+00	1.5608E−01	2.2639E+00	1.6843E−01	1.9448E+00
33	1.1282E−01	4.6718E+00	1.3839E−01	2.7023E+00	1.4792E−01	2.3069E+00	1.5947E−01	1.9817E+00
34	1.0779E−01	4.7603E+00	1.3151E−01	2.7515E+00	1.4040E−01	2.3488E+00	1.5122E−01	2.0176E+00
35	1.0310E−01	4.8473E+00	1.2514E−01	2.7996E+00	1.3345E−01	2.3897E+00	1.4361E−01	2.0526E+00
36	9.8715E−02	4.9329E+00	1.1922E−01	2.8465E+00	1.2701E−01	2.4295E+00	1.3656E−01	2.0867E+00
37	9.4614E−02	5.0172E+00	1.1372E−01	2.8923E+00	1.2103E−01	2.4683E+00	1.3003E−01	2.1199E+00
38	9.0769E−02	5.1003E+00	1.0860E−01	2.9370E+00	1.1547E−01	2.5062E+00	1.2397E−01	2.1523E+00
39	8.7161E−02	5.1822E+00	1.0381E−01	2.9807E+00	1.1029E−01	2.5431E+00	1.1833E−01	2.1838E+00
40	8.3772E−02	5.2630E+00	9.9342E−02	3.0234E+00	1.0545E−01	2.5792E+00	1.1307E−01	2.2146E+00
41	8.0586E−02	5.3426E+00	9.5154E−02	3.0652E+00	1.0093E−01	2.6144E+00	1.0816E−01	2.2445E+00
42	7.7587E−02	5.4212E+00	9.1226E−02	3.1060E+00	9.6696E−02	2.6488E+00	1.0356E−01	2.2738E+00
43	7.4764E−02	5.4988E+00	8.7538E−02	3.1460E+00	9.2725E−02	2.6825E+00	9.9258E−02	2.3024E+00
44	7.2103E−02	5.5754E+00	8.4070E−02	3.1853E+00	8.8996E−02	2.7154E+00	9.5221E−02	2.3304E+00
45	6.9595E−02	5.6511E+00	8.0807E−02	3.2237E+00	8.5491E−02	2.7477E+00	9.1429E−02	2.3578E+00
46	6.7228E−02	5.7258E+00	7.7731E−02	3.2614E+00	8.2191E−02	2.7793E+00	8.7863E−02	2.3846E+00
47	6.4994E−02	5.7996E+00	7.4831E−02	3.2985E+00	7.9081E−02	2.8103E+00	8.4504E−02	2.4108E+00
48	6.2885E−02	5.8724E+00	7.2092E−02	3.3348E+00	7.6146E−02	2.8407E+00	8.1338E−02	2.4365E+00
49	6.0891E−02	5.9444E+00	6.9504E−02	3.3705E+00	7.3375E−02	2.8705E+00	7.8349E−02	2.4618E+00
50	5.9006E−02	6.0156E+00	6.7056E−02	3.4057E+00	7.0755E−02	2.8998E+00	7.5525E−02	2.4866E+00
51	5.7223E−02	6.0859E+00	6.4738E−02	3.4402E+00	6.8276E−02	2.9287E+00	7.2853E−02	2.5109E+00
52	5.5536E−02	6.1554E+00	6.2541E−02	3.4742E+00	6.5928E−02	2.9570E+00	7.0323E−02	2.5349E+00
53	5.3938E−02	6.2241E+00	6.0459E−02	3.5076E+00	6.3702E−02	2.9849E+00	6.7926E−02	2.5584E+00
54	5.2424E−02	6.2920E+00	5.8481E−02	3.5406E+00	6.1589E−02	3.0124E+00	6.5651E−02	2.5816E+00
55	5.0990E−02	6.3591E+00	5.6604E−02	3.5730E+00	5.9583E−02	3.0394E+00	6.3492E−02	2.6044E+00
56	4.9629E−02	6.4255E+00	5.4818E−02	3.6050E+00	5.7676E−02	3.0660E+00	6.1439E−02	2.6269E+00
57	4.8339E−02	6.4911E+00	5.3120E−02	3.6365E+00	5.5862E−02	3.0923E+00	5.9487E−02	2.6490E+00
58	4.7115E−02	6.5560E+00	5.1502E−02	3.6676E+00	5.4135E−02	3.1181E+00	5.7628E−02	2.6708E+00
59	4.5952E−02	6.6202E+00	4.9961E−02	3.6983E+00	5.2490E−02	3.1436E+00	5.5858E−02	2.6923E+00
60	4.4848E−02	6.6837E+00	4.8492E−02	3.7285E+00	5.0921E−02	3.1688E+00	5.4169E−02	2.7136E+00

Table 4.3.3.1. *Partial wave elastic scattering factors for neutral atoms (cont.)*
Cd; $Z = 48$

	10 keV		40 keV		60 keV		90 keV	
s	$\|f(s)\|$	$\eta(s)$	$\|f(s)\|$	$\eta(s)$	$\|f(s)\|$	$\eta(s)$	$\|f(s)\|$	$\eta(s)$
0	7.7381E+00	3.5275E−01	9.1431E+00	2.3538E−01	9.6614E+00	2.0666E−01	1.0307E+01	1.8169E−01
1	6.7020E+00	4.0107E−01	8.0107E+00	2.6521E−01	8.4836E+00	2.3241E−01	9.0722E+00	2.0389E−01
2	4.9257E+00	5.2316E−01	6.0413E+00	3.3924E−01	6.4268E+00	2.9621E−01	6.8996E+00	2.5902E−01
3	3.5790E+00	6.7652E−01	4.5124E+00	4.3044E−01	4.8230E+00	3.7458E−01	5.1962E+00	3.2669E−01
4	2.6683E+00	8.4097E−01	3.4516E+00	5.2688E−01	3.7053E+00	4.5723E−01	4.0051E+00	3.9794E−01
5	2.0338E+00	1.0157E+00	2.6916E+00	6.2807E−01	2.9009E+00	5.4374E−01	3.1449E+00	4.7237E−01
6	1.5817E+00	1.2022E+00	2.1319E+00	7.3481E−01	2.3053E+00	6.3480E−01	2.5056E+00	5.5058E−01
7	1.2576E+00	1.3981E+00	1.7150E+00	8.4628E−01	1.8591E+00	7.2973E−01	2.0245E+00	6.3200E−01
8	1.0244E+00	1.5982E+00	1.4029E+00	9.6015E−01	1.5230E+00	8.2663E−01	1.6605E+00	7.1506E−01
9	8.5473E−01	1.7959E+00	1.1677E+00	1.0734E+00	1.2683E+00	9.2306E−01	1.3835E+00	7.9771E−01
10	7.2829E−01	1.9857E+00	9.8841E−01	1.1833E+00	1.0733E+00	1.0166E+00	1.1707E+00	8.7795E−01
11	6.3062E−01	2.1645E+00	8.4911E−01	1.2875E+00	9.2150E−01	1.1055E+00	1.0049E+00	9.5420E−01
12	5.5368E−01	2.3320E+00	7.3986E−01	1.3854E+00	8.0237E−01	1.1890E+00	8.7457E−01	1.0259E+00
13	4.9079E−01	2.4888E+00	6.5199E−01	1.4766E+00	7.0666E−01	1.2668E+00	7.6999E−01	1.0926E+00
14	4.3803E−01	2.6364E+00	5.7976E−01	1.5617E+00	6.2818E−01	1.3392E+00	6.8434E−01	1.1547E+00
15	3.9325E−01	2.7764E+00	5.1949E−01	1.6414E+00	5.6284E−01	1.4070E+00	6.1315E−01	1.2127E+00
16	3.5490E−01	2.9104E+00	4.6849E−01	1.7168E+00	5.0765E−01	1.4710E+00	5.5309E−01	1.2674E+00
17	3.2188E−01	3.0396E+00	4.2484E−01	1.7888E+00	4.6044E−01	1.5321E+00	5.0174E−01	1.3196E+00
18	2.9335E−01	3.1649E+00	3.8712E−01	1.8582E+00	4.1965E−01	1.5908E+00	4.5738E−01	1.3697E+00
19	2.6864E−01	3.2870E+00	3.5428E−01	1.9256E+00	3.8411E−01	1.6478E+00	4.1870E−01	1.4183E+00
20	2.4716E−01	3.4061E+00	3.2552E−01	1.9914E+00	3.5293E−01	1.7035E+00	3.8471E−01	1.4658E+00
21	2.2843E−01	3.5225E+00	3.0019E−01	2.0560E+00	3.2541E−01	1.7581E+00	3.5467E−01	1.5124E+00
22	2.1204E−01	3.6364E+00	2.7777E−01	2.1195E+00	3.0099E−01	1.8119E+00	3.2798E−01	1.5583E+00
23	1.9762E−01	3.7479E+00	2.5785E−01	2.1820E+00	2.7925E−01	1.8649E+00	3.0416E−01	1.6036E+00
24	1.8487E−01	3.8569E+00	2.4007E−01	2.2435E+00	2.5980E−01	1.9171E+00	2.8282E−01	1.6483E+00
25	1.7352E−01	3.9637E+00	2.2415E−01	2.3040E+00	2.4234E−01	1.9686E+00	2.6363E−01	1.6923E+00
26	1.6337E−01	4.0681E+00	2.0983E−01	2.3635E+00	2.2662E−01	2.0192E+00	2.4633E−01	1.7357E+00
27	1.5423E−01	4.1704E+00	1.9690E−01	2.4220E+00	2.1241E−01	2.0690E+00	2.3068E−01	1.7783E+00
28	1.4595E−01	4.2705E+00	1.8519E−01	2.4793E+00	1.9952E−01	2.1178E+00	2.1648E−01	1.8203E+00
29	1.3840E−01	4.3686E+00	1.7454E−01	2.5355E+00	1.8781E−01	2.1657E+00	2.0356E−01	1.8614E+00
30	1.3150E−01	4.4648E+00	1.6482E−01	2.5904E+00	1.7712E−01	2.2126E+00	1.9178E−01	1.9016E+00
31	1.2515E−01	4.5592E+00	1.5593E−01	2.6442E+00	1.6734E−01	2.2585E+00	1.8101E−01	1.9410E+00
32	1.1928E−01	4.6519E+00	1.4776E−01	2.6967E+00	1.5837E−01	2.3033E+00	1.7113E−01	1.9795E+00
33	1.1385E−01	4.7429E+00	1.4024E−01	2.7480E+00	1.5012E−01	2.3471E+00	1.6205E−01	2.0170E+00
34	1.0879E−01	4.8325E+00	1.3329E−01	2.7982E+00	1.4251E−01	2.3898E+00	1.5369E−01	2.0537E+00
35	1.0408E−01	4.9205E+00	1.2686E−01	2.8471E+00	1.3548E−01	2.4314E+00	1.4597E−01	2.0894E+00
36	9.9683E−02	5.0073E+00	1.2090E−01	2.8949E+00	1.2897E−01	2.4721E+00	1.3883E−01	2.1242E+00
37	9.5565E−02	5.0927E+00	1.1534E−01	2.9416E+00	1.2292E−01	2.5117E+00	1.3221E−01	2.1582E+00
38	9.1705E−02	5.1769E+00	1.1017E−01	2.9873E+00	1.1729E−01	2.5504E+00	1.2606E−01	2.1913E+00
39	8.8082E−02	5.2600E+00	1.0534E−01	3.0319E+00	1.1204E−01	2.5882E+00	1.2033E−01	2.2236E+00
40	8.4677E−02	5.3419E+00	1.0082E−01	3.0755E+00	1.0714E−01	2.6251E+00	1.1500E−01	2.2550E+00
41	8.1475E−02	5.4227E+00	9.6590E−02	3.1181E+00	1.0257E−01	2.6611E+00	1.1001E−01	2.2858E+00
42	7.8460E−02	5.5025E+00	9.2619E−02	3.1599E+00	9.8275E−02	2.6963E+00	1.0535E−01	2.3158E+00
43	7.5620E−02	5.5813E+00	8.8890E−02	3.2008E+00	9.4251E−02	2.7308E+00	1.0098E−01	2.3451E+00
44	7.2942E−02	5.6592E+00	8.5383E−02	3.2409E+00	9.0471E−02	2.7645E+00	9.6878E−02	2.3737E+00
45	7.0417E−02	5.7361E+00	8.2080E−02	3.2802E+00	8.6916E−02	2.7975E+00	9.3026E−02	2.4018E+00
46	6.8033E−02	5.8121E+00	7.8967E−02	3.3187E+00	8.3569E−02	2.8298E+00	8.9404E−02	2.4292E+00
47	6.5781E−02	5.8872E+00	7.6030E−02	3.3566E+00	8.0414E−02	2.8616E+00	8.5991E−02	2.4561E+00
48	6.3654E−02	5.9614E+00	7.3255E−02	3.3937E+00	7.7437E−02	2.8927E+00	8.2773E−02	2.4824E+00
49	6.1643E−02	6.0347E+00	7.0632E−02	3.4302E+00	7.4624E−02	2.9232E+00	7.9736E−02	2.5082E+00
50	5.9741E−02	6.1072E+00	6.8150E−02	3.4661E+00	7.1965E−02	2.9532E+00	7.6865E−02	2.5336E+00
51	5.7942E−02	6.1789E+00	6.5800E−02	3.5014E+00	6.9447E−02	2.9826E+00	7.4149E−02	2.5585E+00
52	5.6238E−02	6.2498E+00	6.3572E−02	3.5361E+00	6.7062E−02	3.0116E+00	7.1577E−02	2.5830E+00
53	5.4625E−02	6.3199E+00	6.1458E−02	3.5703E+00	6.4801E−02	3.0401E+00	6.9139E−02	2.6071E+00
54	5.3096E−02	6.3893E+00	5.9452E−02	3.6039E+00	6.2654E−02	3.0682E+00	6.6826E−02	2.6307E+00
55	5.1647E−02	6.4578E+00	5.7545E−02	3.6371E+00	6.0616E−02	3.0958E+00	6.4630E−02	2.6540E+00
56	5.0273E−02	6.5256E+00	5.5733E−02	3.6697E+00	5.8678E−02	3.1230E+00	6.2542E−02	2.6770E+00
57	4.8970E−02	6.5927E+00	5.4008E−02	3.7019E+00	5.6834E−02	3.1497E+00	6.0557E−02	2.6996E+00
58	4.7733E−02	6.6591E+00	5.2365E−02	3.7336E+00	5.5079E−02	3.1762E+00	5.8666E−02	2.7219E+00
59	4.6559E−02	6.7247E+00	5.0800E−02	3.7649E+00	5.3406E−02	3.2022E+00	5.6865E−02	2.7438E+00
60	4.5444E−02	6.7896E+00	4.9307E−02	3.7958E+00	5.1811E−02	3.2279E+00	5.5148E−02	2.7655E+00

Table 4.3.3.1. *Partial wave elastic scattering factors for neutral atoms (cont.)*
In; $Z = 49$

	10 keV		40 keV		60 keV		90 keV	
s	$\|f(s)\|$	$\eta(s)$	$\|f(s)\|$	$\eta(s)$	$\|f(s)\|$	$\eta(s)$	$\|f(s)\|$	$\eta(s)$
0	8.8299E+00	3.2999E−01	1.0367E+01	2.2127E−01	1.0945E+01	1.9451E−01	1.1670E+01	1.7117E−01
1	7.3855E+00	3.8743E−01	8.7935E+00	2.5697E−01	9.3076E+00	2.2539E−01	9.9503E+00	1.9789E−01
2	5.1550E+00	5.2904E−01	6.3239E+00	3.4300E−01	6.7286E+00	2.9960E−01	7.2249E+00	2.6209E−01
3	3.6353E+00	7.0107E−01	4.5945E+00	4.4515E−01	4.9136E+00	3.8737E−01	5.2966E+00	3.3790E−01
4	2.6811E+00	8.7715E−01	3.4778E+00	5.4827E−01	3.7362E+00	4.7576E−01	4.0411E+00	4.1410E−01
5	2.0422E+00	1.0560E+00	2.7099E+00	6.5193E−01	2.9228E+00	5.6441E−01	3.1708E+00	4.9040E−01
6	1.5921E+00	1.2419E+00	2.1522E+00	7.5861E−01	2.3293E+00	6.5547E−01	2.5335E+00	5.6865E−01
7	1.2685E+00	1.4358E+00	1.7366E+00	8.6913E−01	1.8844E+00	7.4966E−01	2.0537E+00	6.4948E−01
8	1.0341E+00	1.6345E+00	1.4234E+00	9.8234E−01	1.5471E+00	8.4605E−01	1.6883E+00	7.3213E−01
9	8.6262E−01	1.8326E+00	1.1857E+00	1.0959E+00	1.2895E+00	9.4271E−01	1.4081E+00	8.1501E−01
10	7.3473E−01	2.0246E+00	1.0035E+00	1.2070E+00	1.0912E+00	1.0374E+00	1.1916E+00	8.9626E−01
11	6.3621E−01	2.2067E+00	8.6159E−01	1.3135E+00	9.3632E−01	1.1283E+00	1.0222E+00	9.7420E−01
12	5.5886E−01	2.3782E+00	7.5019E−01	1.4141E+00	8.1454E−01	1.2142E+00	8.8877E−01	1.0480E+00
13	4.9582E−01	2.5390E+00	6.6066E−01	1.5084E+00	7.1675E−01	1.2947E+00	7.8168E−01	1.1171E+00
14	4.4298E−01	2.6902E+00	5.8718E−01	1.5963E+00	6.3668E−01	1.3697E+00	6.9412E−01	1.1815E+00
15	3.9809E−01	2.8335E+00	5.2597E−01	1.6787E+00	5.7015E−01	1.4398E+00	6.2148E−01	1.2416E+00
16	3.5955E−01	2.9703E+00	4.7424E−01	1.7563E+00	5.1405E−01	1.5058E+00	5.6032E−01	1.2981E+00
17	3.2626E−01	3.1019E+00	4.2999E−01	1.8302E+00	4.6614E−01	1.5684E+00	5.0816E−01	1.3516E+00
18	2.9740E−01	3.2292E+00	3.9179E−01	1.9010E+00	4.2480E−01	1.6284E+00	4.6317E−01	1.4029E+00
19	2.7232E−01	3.3530E+00	3.5854E−01	1.9694E+00	3.8882E−01	1.6864E+00	4.2400E−01	1.4523E+00
20	2.5047E−01	3.4736E+00	3.2942E−01	2.0360E+00	3.5727E−01	1.7427E+00	3.8963E−01	1.5004E+00
21	2.3139E−01	3.5914E+00	3.0378E−01	2.1012E+00	3.2944E−01	1.7979E+00	3.5927E−01	1.5474E+00
22	2.1466E−01	3.7066E+00	2.8109E−01	2.1651E+00	3.0476E−01	1.8520E+00	3.3230E−01	1.5936E+00
23	1.9994E−01	3.8193E+00	2.6093E−01	2.2280E+00	2.8278E−01	1.9053E+00	3.0824E−01	1.6391E+00
24	1.8692E−01	3.9295E+00	2.4294E−01	2.2899E+00	2.6313E−01	1.9578E+00	2.8668E−01	1.6840E+00
25	1.7535E−01	4.0374E+00	2.2683E−01	2.3508E+00	2.4548E−01	2.0095E+00	2.6730E−01	1.7282E+00
26	1.6501E−01	4.1429E+00	2.1234E−01	2.4107E+00	2.2959E−01	2.0605E+00	2.4982E−01	1.7719E+00
27	1.5571E−01	4.2463E+00	1.9927E−01	2.4696E+00	2.1522E−01	2.1106E+00	2.3400E−01	1.8148E+00
28	1.4730E−01	4.3475E+00	1.8743E−01	2.5274E+00	2.0220E−01	2.1599E+00	2.1964E−01	1.8571E+00
29	1.3966E−01	4.4467E+00	1.7666E−01	2.5841E+00	1.9036E−01	2.2083E+00	2.0658E−01	1.8986E+00
30	1.3267E−01	4.5439E+00	1.6685E−01	2.6397E+00	1.7955E−01	2.2557E+00	1.9466E−01	1.9393E+00
31	1.2626E−01	4.6394E+00	1.5787E−01	2.6942E+00	1.6967E−01	2.3021E+00	1.8376E−01	1.9792E+00
32	1.2034E−01	4.7331E+00	1.4962E−01	2.7475E+00	1.6060E−01	2.3476E+00	1.7376E−01	2.0183E+00
33	1.1487E−01	4.8252E+00	1.4203E−01	2.7995E+00	1.5226E−01	2.3920E+00	1.6457E−01	2.0564E+00
34	1.0978E−01	4.9157E+00	1.3502E−01	2.8505E+00	1.4457E−01	2.4355E+00	1.5611E−01	2.0937E+00
35	1.0505E−01	5.0048E+00	1.2854E−01	2.9003E+00	1.3746E−01	2.4779E+00	1.4829E−01	2.1301E+00
36	1.0063E−01	5.0926E+00	1.2251E−01	2.9489E+00	1.3087E−01	2.5193E+00	1.4105E−01	2.1656E+00
37	9.6487E−02	5.1791E+00	1.1691E−01	2.9965E+00	1.2475E−01	2.5598E+00	1.3434E−01	2.2003E+00
38	9.2609E−02	5.2644E+00	1.1169E−01	3.0430E+00	1.1906E−01	2.5993E+00	1.2811E−01	2.2341E+00
39	8.8969E−02	5.3485E+00	1.0682E−01	3.0885E+00	1.1375E−01	2.6378E+00	1.2230E−01	2.2671E+00
40	8.5548E−02	5.4315E+00	1.0226E−01	3.1330E+00	1.0880E−01	2.6755E+00	1.1689E−01	2.2993E+00
41	8.2329E−02	5.5135E+00	9.7984E−02	3.1765E+00	1.0416E−01	2.7123E+00	1.1184E−01	2.3308E+00
42	7.9298E−02	5.5944E+00	9.3974E−02	3.2191E+00	9.9820E−02	2.7483E+00	1.0710E−01	2.3615E+00
43	7.6442E−02	5.6744E+00	9.0207E−02	3.2609E+00	9.5745E−02	2.7836E+00	1.0267E−01	2.3915E+00
44	7.3748E−02	5.7534E+00	8.6662E−02	3.3018E+00	9.1917E−02	2.8180E+00	9.8511E−02	2.4208E+00
45	7.1206E−02	5.8315E+00	8.3323E−02	3.3419E+00	8.8316E−02	2.8518E+00	9.4602E−02	2.4495E+00
46	6.8805E−02	5.9087E+00	8.0174E−02	3.3813E+00	8.4924E−02	2.8849E+00	9.0924E−02	2.4776E+00
47	6.6537E−02	5.9850E+00	7.7203E−02	3.4199E+00	8.1726E−02	2.9173E+00	8.7460E−02	2.5051E+00
48	6.4393E−02	6.0605E+00	7.4394E−02	3.4579E+00	7.8707E−02	2.9491E+00	8.4192E−02	2.5321E+00
49	6.2366E−02	6.1352E+00	7.1739E−02	3.4952E+00	7.5855E−02	2.9803E+00	8.1107E−02	2.5585E+00
50	6.0448E−02	6.2090E+00	6.9225E−02	3.5318E+00	7.3157E−02	3.0110E+00	7.8191E−02	2.5845E+00
51	5.8633E−02	6.2820E+00	6.6843E−02	3.5679E+00	7.0602E−02	3.0411E+00	7.5431E−02	2.6099E+00
52	5.6913E−02	6.3543E+00	6.4585E−02	3.6033E+00	6.8182E−02	3.0707E+00	7.2818E−02	2.6349E+00
53	5.5285E−02	6.4257E+00	6.2442E−02	3.6382E+00	6.5886E−02	3.0998E+00	7.0341E−02	2.6595E+00
54	5.3742E−02	6.4965E+00	6.0408E−02	3.6725E+00	6.3707E−02	3.1284E+00	6.7990E−02	2.6837E+00
55	5.2279E−02	6.5664E+00	5.8474E−02	3.7064E+00	6.1637E−02	3.1566E+00	6.5758E−02	2.7076E+00
56	5.0892E−02	6.6356E+00	5.6635E−02	3.7397E+00	5.9669E−02	3.1844E+00	6.3636E−02	2.7310E+00
57	4.9576E−02	6.7042E+00	5.4884E−02	3.7726E+00	5.7796E−02	3.2118E+00	6.1617E−02	2.7541E+00
58	4.8328E−02	6.7719E+00	5.3217E−02	3.8050E+00	5.6012E−02	3.2387E+00	5.9695E−02	2.7768E+00
59	4.7143E−02	6.8390E+00	5.1628E−02	3.8369E+00	5.4313E−02	3.2653E+00	5.7864E−02	2.7992E+00
60	4.6018E−02	6.9054E+00	5.0113E−02	3.8684E+00	5.2692E−02	3.2915E+00	5.6118E−02	2.8213E+00

Table 4.3.3.1. *Partial wave elastic scattering factors for neutral atoms (cont.)*
Sn; $Z = 50$

	10 keV		40 keV		60 keV		90 keV	
s	$\|f(s)\|$	$\eta(s)$	$\|f(s)\|$	$\eta(s)$	$\|f(s)\|$	$\eta(s)$	$\|f(s)\|$	$\eta(s)$
0	9.1786E+00	3.3340E−01	1.0780E+01	2.2360E−01	1.1382E+01	1.9664E−01	1.2139E+01	1.7311E−01
1	7.7393E+00	3.8759E−01	9.2128E+00	2.5743E−01	9.7520E+00	2.2594E−01	1.0427E+01	1.9848E−01
2	5.3724E+00	5.2997E−01	6.5939E+00	3.4428E−01	7.0175E+00	3.0092E−01	7.5367E+00	2.6341E−01
3	3.7159E+00	7.1361E−01	4.7069E+00	4.5338E−01	5.0366E+00	3.9471E−01	5.4318E+00	3.4446E−01
4	2.7051E+00	9.0281E−01	3.5185E+00	5.6406E−01	3.7826E+00	4.8957E−01	4.0938E+00	4.2625E−01
5	2.0528E+00	1.0891E+00	2.7304E+00	6.7207E−01	2.9471E+00	5.8197E−01	3.1993E+00	5.0580E−01
6	1.6019E+00	1.2768E+00	2.1705E+00	7.7998E−01	2.3508E+00	6.7413E−01	2.5587E+00	5.8503E−01
7	1.2786E+00	1.4695E+00	1.7557E+00	8.9007E−01	1.9067E+00	7.6799E−01	2.0796E+00	6.6562E−01
8	1.0433E+00	1.6666E+00	1.4421E+00	1.0025E+00	1.5690E+00	8.6377E−01	1.7138E+00	7.4778E−01
9	8.7022E−01	1.8643E+00	1.2027E+00	1.1158E+00	1.3096E+00	9.6027E−01	1.4316E+00	8.3055E−01
10	7.4090E−01	2.0575E+00	1.0181E+00	1.2277E+00	1.1086E+00	1.0556E+00	1.2120E+00	9.1237E−01
11	6.4147E−01	2.2422E+00	8.7398E−01	1.3358E+00	9.5107E−01	1.1479E+00	1.0395E+00	9.9159E−01
12	5.6366E−01	2.4172E+00	7.6054E−01	1.4388E+00	8.2683E−01	1.2359E+00	9.0317E−01	1.0672E+00
13	5.0046E−01	2.5817E+00	6.6939E−01	1.5358E+00	7.2701E−01	1.3188E+00	7.9365E−01	1.1385E+00
14	4.4761E−01	2.7365E+00	5.9468E−01	1.6266E+00	6.4536E−01	1.3964E+00	7.0416E−01	1.2051E+00
15	4.0268E−01	2.8830E+00	5.3252E−01	1.7117E+00	5.7761E−01	1.4689E+00	6.3002E−01	1.2673E+00
16	3.6405E−01	3.0227E+00	4.8006E−01	1.7917E+00	5.2057E−01	1.5371E+00	5.6772E−01	1.3257E+00
17	3.3058E−01	3.1567E+00	4.3522E−01	1.8675E+00	4.7194E−01	1.6015E+00	5.1469E−01	1.3809E+00
18	3.0147E−01	3.2862E+00	3.9653E−01	1.9399E+00	4.3002E−01	1.6629E+00	4.6903E−01	1.4334E+00
19	2.7609E−01	3.4118E+00	3.6286E−01	2.0096E+00	3.9357E−01	1.7220E+00	4.2933E−01	1.4838E+00
20	2.5390E−01	3.5341E+00	3.3338E−01	2.0772E+00	3.6163E−01	1.7792E+00	3.9453E−01	1.5326E+00
21	2.3448E−01	3.6534E+00	3.0742E−01	2.1431E+00	3.3348E−01	1.8349E+00	3.6383E−01	1.5802E+00
22	2.1743E−01	3.7700E+00	2.8444E−01	2.2076E+00	3.0852E−01	1.8896E+00	3.3657E−01	1.6268E+00
23	2.0240E−01	3.8840E+00	2.6403E−01	2.2710E+00	2.8629E−01	1.9432E+00	3.1226E−01	1.6726E+00
24	1.8911E−01	3.9955E+00	2.4581E−01	2.3333E+00	2.6641E−01	1.9960E+00	2.9048E−01	1.7177E+00
25	1.7730E−01	4.1045E+00	2.2950E−01	2.3946E+00	2.4857E−01	2.0480E+00	2.7090E−01	1.7622E+00
26	1.6676E−01	4.2113E+00	2.1484E−01	2.4548E+00	2.3250E−01	2.0993E+00	2.5323E−01	1.8060E+00
27	1.5728E−01	4.3157E+00	2.0161E−01	2.5142E+00	2.1798E−01	2.1497E+00	2.3725E−01	1.8493E+00
28	1.4873E−01	4.4181E+00	1.8963E−01	2.5724E+00	2.0482E−01	2.1994E+00	2.2273E−01	1.8918E+00
29	1.4097E−01	4.5183E+00	1.7875E−01	2.6297E+00	1.9284E−01	2.2482E+00	2.0953E−01	1.9337E+00
30	1.3389E−01	4.6167E+00	1.6883E−01	2.6858E+00	1.8192E−01	2.2961E+00	1.9748E−01	1.9748E+00
31	1.2740E−01	4.7131E+00	1.5976E−01	2.7409E+00	1.7193E−01	2.3431E+00	1.8645E−01	2.0152E+00
32	1.2142E−01	4.8078E+00	1.5144E−01	2.7948E+00	1.6277E−01	2.3891E+00	1.7633E−01	2.0547E+00
33	1.1590E−01	4.9009E+00	1.4377E−01	2.8476E+00	1.5434E−01	2.4342E+00	1.6703E−01	2.0934E+00
34	1.1077E−01	4.9925E+00	1.3670E−01	2.8993E+00	1.4657E−01	2.4783E+00	1.5847E−01	2.1313E+00
35	1.0600E−01	5.0826E+00	1.3015E−01	2.9499E+00	1.3938E−01	2.5214E+00	1.5055E−01	2.1683E+00
36	1.0155E−01	5.1714E+00	1.2408E−01	2.9993E+00	1.3272E−01	2.5635E+00	1.4322E−01	2.2045E+00
37	9.7390E−02	5.2589E+00	1.1843E−01	3.0477E+00	1.2654E−01	2.6047E+00	1.3643E−01	2.2399E+00
38	9.3491E−02	5.3452E+00	1.1317E−01	3.0951E+00	1.2078E−01	2.6450E+00	1.3011E−01	2.2744E+00
39	8.9832E−02	5.4303E+00	1.0825E−01	3.1414E+00	1.1542E−01	2.6843E+00	1.2423E−01	2.3080E+00
40	8.6393E−02	5.5144E+00	1.0365E−01	3.1867E+00	1.1041E−01	2.7228E+00	1.1875E−01	2.3410E+00
41	8.3157E−02	5.5974E+00	9.9337E−02	3.2311E+00	1.0572E−01	2.7604E+00	1.1363E−01	2.3731E+00
42	8.0110E−02	5.6795E+00	9.5291E−02	3.2745E+00	1.0133E−01	2.7972E+00	1.0883E−01	2.4045E+00
43	7.7237E−02	5.7605E+00	9.1487E−02	3.3171E+00	9.7207E−02	2.8331E+00	1.0434E−01	2.4352E+00
44	7.4526E−02	5.8407E+00	8.7908E−02	3.3589E+00	9.3333E−02	2.8684E+00	1.0012E−01	2.4652E+00
45	7.1967E−02	5.9199E+00	8.4535E−02	3.3998E+00	8.9688E−02	2.9029E+00	9.6154E−02	2.4945E+00
46	6.9551E−02	5.9983E+00	8.1353E−02	3.4400E+00	8.6253E−02	2.9367E+00	9.2424E−02	2.5233E+00
47	6.7267E−02	6.0758E+00	7.8349E−02	3.4794E+00	8.3014E−02	2.9698E+00	8.8909E−02	2.5514E+00
48	6.5107E−02	6.1525E+00	7.5509E−02	3.5182E+00	7.9956E−02	3.0023E+00	8.5593E−02	2.5790E+00
49	6.3063E−02	6.2284E+00	7.2823E−02	3.5562E+00	7.7065E−02	3.0342E+00	8.2461E−02	2.6061E+00
50	6.1130E−02	6.3035E+00	7.0279E−02	3.5936E+00	7.4330E−02	3.0655E+00	7.9501E−02	2.6326E+00
51	5.9299E−02	6.3778E+00	6.7868E−02	3.6304E+00	7.1741E−02	3.0963E+00	7.6700E−02	2.6586E+00
52	5.7565E−02	6.4514E+00	6.5581E−02	3.6666E+00	6.9286E−02	3.1265E+00	7.4046E−02	2.6842E+00
53	5.5922E−02	6.5242E+00	6.3410E−02	3.7022E+00	6.6957E−02	3.1562E+00	7.1530E−02	2.7094E+00
54	5.4365E−02	6.5962E+00	6.1348E−02	3.7373E+00	6.4746E−02	3.1855E+00	6.9143E−02	2.7341E+00
55	5.2889E−02	6.6676E+00	5.9388E−02	3.7718E+00	6.2646E−02	3.2143E+00	6.6875E−02	2.7584E+00
56	5.1489E−02	6.7382E+00	5.7524E−02	3.8058E+00	6.0648E−02	3.2426E+00	6.4719E−02	2.7823E+00
57	5.0162E−02	6.8081E+00	5.5749E−02	3.8394E+00	5.8747E−02	3.2706E+00	6.2668E−02	2.8059E+00
58	4.8902E−02	6.8773E+00	5.4058E−02	3.8724E+00	5.6936E−02	3.2981E+00	6.0715E−02	2.8291E+00
59	4.7706E−02	6.9458E+00	5.2446E−02	3.9050E+00	5.5211E−02	3.3252E+00	5.8855E−02	2.8519E+00
60	4.6571E−02	7.0136E+00	5.0908E−02	3.9372E+00	5.3565E−02	3.3519E+00	5.7080E−02	2.8745E+00

Table 4.3.3.1. *Partial wave elastic scattering factors for neutral atoms (cont.)*
Sb; $Z = 51$

	10 keV		40 keV		60 keV		90 keV	
s	$\|f(s)\|$	$\eta(s)$	$\|f(s)\|$	$\eta(s)$	$\|f(s)\|$	$\eta(s)$	$\|f(s)\|$	$\eta(s)$
0	9.2392E+00	3.4422E−01	1.0879E+01	2.3076E−01	1.1493E+01	2.0299E−01	1.2263E+01	1.7877E−01
1	7.9140E+00	3.9358E−01	9.4351E+00	2.6168E−01	9.9910E+00	2.2979E−01	1.0686E+01	2.0197E−01
2	5.5606E+00	5.3038E−01	6.8317E+00	3.4546E−01	7.2727E+00	3.0219E−01	7.8130E+00	2.6472E−01
3	3.8093E+00	7.1939E−01	4.8361E+00	4.5798E−01	5.1775E+00	3.9897E−01	5.5863E+00	3.4839E−01
4	2.7389E+00	9.2084E−01	3.5723E+00	5.7575E−01	3.8431E+00	4.9992E−01	4.1618E+00	4.3545E−01
5	2.0668E+00	1.1169E+00	2.7552E+00	6.8939E−01	2.9759E+00	5.9716E−01	3.2326E+00	5.1918E−01
6	1.6121E+00	1.3087E+00	2.1883E+00	7.9986E−01	2.3717E+00	6.9153E−01	2.5831E+00	6.0035E−01
7	1.2883E+00	1.5015E+00	1.7729E+00	9.1023E−01	1.9269E+00	7.8570E−01	2.1031E+00	6.8123E−01
8	1.0521E+00	1.6972E+00	1.4592E+00	1.0220E+00	1.5890E+00	8.8098E−01	1.7371E+00	7.6301E−01
9	8.7762E−01	1.8939E+00	1.2186E+00	1.1348E+00	1.3284E+00	9.7709E−01	1.4536E+00	8.4547E−01
10	7.4689E−01	2.0876E+00	1.0323E+00	1.2469E+00	1.1254E+00	1.0726E+00	1.2318E+00	9.2750E−01
11	6.4648E−01	2.2743E+00	8.8612E−01	1.3562E+00	9.6556E−01	1.1659E+00	1.0566E+00	1.0076E+00
12	5.6814E−01	2.4521E+00	7.7083E−01	1.4612E+00	8.3910E−01	1.2557E+00	9.1763E−01	1.0847E+00
13	5.0474E−01	2.6200E+00	6.7813E−01	1.5606E+00	7.3737E−01	1.3407E+00	8.0580E−01	1.1579E+00
14	4.5189E−01	2.7782E+00	6.0222E−01	1.6541E+00	6.5416E−01	1.4207E+00	7.1440E−01	1.2266E+00
15	4.0700E−01	2.9279E+00	5.3913E−01	1.7418E+00	5.8519E−01	1.4956E+00	6.3876E−01	1.2910E+00
16	3.6835E−01	3.0704E+00	4.8593E−01	1.8242E+00	5.2720E−01	1.5660E+00	5.7529E−01	1.3514E+00
17	3.3479E−01	3.2070E+00	4.4051E−01	1.9022E+00	4.7782E−01	1.6323E+00	5.2134E−01	1.4082E+00
18	3.0550E−01	3.3387E+00	4.0132E−01	1.9764E+00	4.3531E−01	1.6954E+00	4.7496E−01	1.4622E+00
19	2.7987E−01	3.4663E+00	3.6724E−01	2.0476E+00	3.9837E−01	1.7557E+00	4.3470E−01	1.5138E+00
20	2.5740E−01	3.5903E+00	3.3739E−01	2.1163E+00	3.6603E−01	1.8139E+00	3.9945E−01	1.5635E+00
21	2.3767E−01	3.7112E+00	3.1109E−01	2.1831E+00	3.3753E−01	1.8705E+00	3.6837E−01	1.6117E+00
22	2.2031E−01	3.8293E+00	2.8783E−01	2.2483E+00	3.1227E−01	1.9257E+00	3.4081E−01	1.6588E+00
23	2.0499E−01	3.9447E+00	2.6715E−01	2.3122E+00	2.8978E−01	1.9798E+00	3.1623E−01	1.7050E+00
24	1.9143E−01	4.0575E+00	2.4870E−01	2.3750E+00	2.6968E−01	2.0329E+00	2.9422E−01	1.7504E+00
25	1.7937E−01	4.1678E+00	2.3218E−01	2.4367E+00	2.5164E−01	2.0853E+00	2.7443E−01	1.7951E+00
26	1.6861E−01	4.2758E+00	2.1733E−01	2.4974E+00	2.3539E−01	2.1368E+00	2.5658E−01	1.8392E+00
27	1.5895E−01	4.3815E+00	2.0394E−01	2.5571E+00	2.2070E−01	2.1876E+00	2.4042E−01	1.8827E+00
28	1.5025E−01	4.4849E+00	1.9182E−01	2.6158E+00	2.0739E−01	2.2376E+00	2.2576E−01	1.9255E+00
29	1.4235E−01	4.5863E+00	1.8081E−01	2.6735E+00	1.9528E−01	2.2868E+00	2.1241E−01	1.9677E+00
30	1.3516E−01	4.6857E+00	1.7079E−01	2.7302E+00	1.8424E−01	2.3351E+00	2.0022E−01	2.0092E+00
31	1.2858E−01	4.7832E+00	1.6162E−01	2.7858E+00	1.7415E−01	2.3826E+00	1.8907E−01	2.0499E+00
32	1.2253E−01	4.8790E+00	1.5321E−01	2.8404E+00	1.6488E−01	2.4291E+00	1.7884E−01	2.0899E+00
33	1.1695E−01	4.9731E+00	1.4547E−01	2.8938E+00	1.5637E−01	2.4748E+00	1.6944E−01	2.1291E+00
34	1.1177E−01	5.0657E+00	1.3833E−01	2.9462E+00	1.4851E−01	2.5195E+00	1.6077E−01	2.1676E+00
35	1.0696E−01	5.1568E+00	1.3173E−01	2.9975E+00	1.4125E−01	2.5632E+00	1.5276E−01	2.2052E+00
36	1.0247E−01	5.2465E+00	1.2560E−01	3.0477E+00	1.3452E−01	2.6061E+00	1.4535E−01	2.2420E+00
37	9.8285E−02	5.3350E+00	1.1990E−01	3.0968E+00	1.2828E−01	2.6479E+00	1.3847E−01	2.2779E+00
38	9.4360E−02	5.4223E+00	1.1460E−01	3.1450E+00	1.2246E−01	2.6889E+00	1.3208E−01	2.3131E+00
39	9.0678E−02	5.5084E+00	1.0964E−01	3.1921E+00	1.1704E−01	2.7290E+00	1.2612E−01	2.3474E+00
40	8.7219E−02	5.5935E+00	1.0500E−01	3.2382E+00	1.1198E−01	2.7682E+00	1.2057E−01	2.3810E+00
41	8.3964E−02	5.6775E+00	1.0065E−01	3.2834E+00	1.0724E−01	2.8065E+00	1.1538E−01	2.4138E+00
42	8.0898E−02	5.7605E+00	9.6569E−02	3.3277E+00	1.0280E−01	2.8440E+00	1.1053E−01	2.4459E+00
43	7.8008E−02	5.8426E+00	9.2732E−02	3.3711E+00	9.8635E−02	2.8808E+00	1.0597E−01	2.4772E+00
44	7.5281E−02	5.9239E+00	8.9119E−02	3.4137E+00	9.4718E−02	2.9167E+00	1.0170E−01	2.5079E+00
45	7.2705E−02	6.0042E+00	8.5715E−02	3.4554E+00	9.1031E−02	2.9519E+00	9.7682E−02	2.5379E+00
46	7.0272E−02	6.0837E+00	8.2502E−02	3.4964E+00	8.7556E−02	2.9864E+00	9.3900E−02	2.5673E+00
47	6.7971E−02	6.1623E+00	7.9468E−02	3.5366E+00	8.4278E−02	3.0203E+00	9.0336E−02	2.5961E+00
48	6.5796E−02	6.2402E+00	7.6598E−02	3.5761E+00	8.1182E−02	3.0535E+00	8.6974E−02	2.6243E+00
49	6.3737E−02	6.3173E+00	7.3883E−02	3.6149E+00	7.8255E−02	3.0861E+00	8.3798E−02	2.6519E+00
50	6.1788E−02	6.3936E+00	7.1310E−02	3.6531E+00	7.5485E−02	3.1180E+00	8.0795E−02	2.6790E+00
51	5.9942E−02	6.4692E+00	6.8872E−02	3.6906E+00	7.2861E−02	3.1495E+00	7.7953E−02	2.7057E+00
52	5.8193E−02	6.5440E+00	6.6558E−02	3.7275E+00	7.0374E−02	3.1803E+00	7.5260E−02	2.7318E+00
53	5.6536E−02	6.6181E+00	6.4361E−02	3.7638E+00	6.8013E−02	3.2107E+00	7.2707E−02	2.7575E+00
54	5.4966E−02	6.6914E+00	6.2273E−02	3.7996E+00	6.5772E−02	3.2406E+00	7.0283E−02	2.7827E+00
55	5.3477E−02	6.7641E+00	6.0288E−02	3.8349E+00	6.3641E−02	3.2700E+00	6.7981E−02	2.8076E+00
56	5.2064E−02	6.8361E+00	5.8399E−02	3.8695E+00	6.1615E−02	3.2989E+00	6.5792E−02	2.8320E+00
57	5.0725E−02	6.9073E+00	5.6600E−02	3.9038E+00	5.9686E−02	3.3274E+00	6.3709E−02	2.8561E+00
58	4.9454E−02	6.9779E+00	5.4886E−02	3.9375E+00	5.7849E−02	3.3555E+00	6.1726E−02	2.8797E+00
59	4.8248E−02	7.0479E+00	5.3252E−02	3.9707E+00	5.6098E−02	3.3831E+00	5.9836E−02	2.9031E+00
60	4.7103E−02	7.1171E+00	5.1693E−02	4.0035E+00	5.4428E−02	3.4104E+00	5.8033E−02	2.9261E+00

Table 4.3.3.1. *Partial wave elastic scattering factors for neutral atoms (cont.)*
Te; $Z = 52$

	10 keV		40 keV		60 keV		90 keV	
s	$\|f(s)\|$	$\eta(s)$	$\|f(s)\|$	$\eta(s)$	$\|f(s)\|$	$\eta(s)$	$\|f(s)\|$	$\eta(s)$
0	9.1728E+00	3.5733E−01	1.0839E+01	2.3954E−01	1.1459E+01	2.1079E−01	1.2233E+01	1.8571E−01
1	7.9735E+00	4.0253E−01	9.5306E+00	2.6793E−01	1.0098E+01	2.3540E−01	1.0805E+01	2.0702E−01
2	5.7059E+00	5.3203E−01	7.0211E+00	3.4755E−01	7.4772E+00	3.0427E−01	8.0354E+00	2.6674E−01
3	3.9052E+00	7.2120E−01	4.9692E+00	4.6048E−01	5.3228E+00	4.0147E−01	5.7457E+00	3.5083E−01
4	2.7806E+00	9.3204E−01	3.6376E+00	5.8376E−01	3.9160E+00	5.0718E−01	4.2433E+00	4.4202E−01
5	2.0847E+00	1.1388E+00	2.7858E+00	7.0358E−01	3.0111E+00	6.0971E−01	3.2729E+00	5.3032E−01
6	1.6234E+00	1.3370E+00	2.2071E+00	8.1787E−01	2.3937E+00	7.0738E−01	2.6086E+00	6.1435E−01
7	1.2981E+00	1.5316E+00	1.7891E+00	9.2953E−01	1.9458E+00	8.0269E−01	2.1252E+00	6.9626E−01
8	1.0609E+00	1.7266E+00	1.4749E+00	1.0411E+00	1.6074E+00	8.9786E−01	1.7585E+00	7.7798E−01
9	8.8498E−01	1.9223E+00	1.2335E+00	1.1534E+00	1.3460E+00	9.9353E−01	1.4741E+00	8.6009E−01
10	7.5280E−01	2.1158E+00	1.0457E+00	1.2653E+00	1.1415E+00	1.0890E+00	1.2506E+00	9.4206E−01
11	6.5134E−01	2.3037E+00	8.9789E−01	1.3753E+00	9.7970E−01	1.1829E+00	1.0732E+00	1.0227E+00
12	5.7234E−01	2.4839E+00	7.8094E−01	1.4817E+00	8.5125E−01	1.2739E+00	9.3198E−01	1.1009E+00
13	5.0869E−01	2.6546E+00	6.8681E−01	1.5832E+00	7.4772E−01	1.3608E+00	8.1801E−01	1.1757E+00
14	4.5581E−01	2.8160E+00	6.0973E−01	1.6791E+00	6.6303E−01	1.4429E+00	7.2479E−01	1.2464E+00
15	4.1099E−01	2.9687E+00	5.4573E−01	1.7694E+00	5.9285E−01	1.5201E+00	6.4765E−01	1.3128E+00
16	3.7239E−01	3.1141E+00	4.9182E−01	1.8543E+00	5.3391E−01	1.5927E+00	5.8298E−01	1.3752E+00
17	3.3881E−01	3.2532E+00	4.4582E−01	1.9345E+00	4.8377E−01	1.6611E+00	5.2810E−01	1.4339E+00
18	3.0942E−01	3.3872E+00	4.0616E−01	2.0106E+00	4.4065E−01	1.7259E+00	4.8098E−01	1.4894E+00
19	2.8361E−01	3.5168E+00	3.7166E−01	2.0834E+00	4.0322E−01	1.7877E+00	4.4012E−01	1.5423E+00
20	2.6092E−01	3.6427E+00	3.4144E−01	2.1535E+00	3.7046E−01	1.8471E+00	4.0440E−01	1.5930E+00
21	2.4092E−01	3.7653E+00	3.1482E−01	2.2213E+00	3.4160E−01	1.9046E+00	3.7293E−01	1.6421E+00
22	2.2328E−01	3.8849E+00	2.9126E−01	2.2874E+00	3.1604E−01	1.9605E+00	3.4504E−01	1.6898E+00
23	2.0768E−01	4.0018E+00	2.7031E−01	2.3520E+00	2.9328E−01	2.0151E+00	3.2018E−01	1.7364E+00
24	1.9385E−01	4.1160E+00	2.5162E−01	2.4153E+00	2.7294E−01	2.0687E+00	2.9792E−01	1.7822E+00
25	1.8156E−01	4.2277E+00	2.3488E−01	2.4774E+00	2.5469E−01	2.1214E+00	2.7792E−01	1.8272E+00
26	1.7057E−01	4.3369E+00	2.1984E−01	2.5386E+00	2.3824E−01	2.1733E+00	2.5988E−01	1.8715E+00
27	1.6072E−01	4.4439E+00	2.0628E−01	2.5987E+00	2.2339E−01	2.2244E+00	2.4355E−01	1.9153E+00
28	1.5185E−01	4.5486E+00	1.9400E−01	2.6579E+00	2.0993E−01	2.2747E+00	2.2872E−01	1.9583E+00
29	1.4381E−01	4.6511E+00	1.8286E−01	2.7160E+00	1.9769E−01	2.3242E+00	2.1523E−01	2.0008E+00
30	1.3650E−01	4.7516E+00	1.7272E−01	2.7732E+00	1.8652E−01	2.3730E+00	2.0291E−01	2.0426E+00
31	1.2982E−01	4.8502E+00	1.6345E−01	2.8293E+00	1.7631E−01	2.4209E+00	1.9164E−01	2.0837E+00
32	1.2368E−01	4.9471E+00	1.5495E−01	2.8844E+00	1.6695E−01	2.4679E+00	1.8130E−01	2.1241E+00
33	1.1802E−01	5.0422E+00	1.4713E−01	2.9385E+00	1.5835E−01	2.5141E+00	1.7178E−01	2.1638E+00
34	1.1279E−01	5.1357E+00	1.3993E−01	2.9915E+00	1.5041E−01	2.5593E+00	1.6302E−01	2.2027E+00
35	1.0793E−01	5.2278E+00	1.3326E−01	3.0434E+00	1.4308E−01	2.6037E+00	1.5492E−01	2.2408E+00
36	1.0340E−01	5.3185E+00	1.2708E−01	3.0943E+00	1.3628E−01	2.6471E+00	1.4742E−01	2.2782E+00
37	9.9179E−02	5.4079E+00	1.2134E−01	3.1442E+00	1.2997E−01	2.6897E+00	1.4047E−01	2.3147E+00
38	9.5224E−02	5.4962E+00	1.1598E−01	3.1931E+00	1.2410E−01	2.7313E+00	1.3400E−01	2.3505E+00
39	9.1516E−02	5.5832E+00	1.1098E−01	3.2410E+00	1.1863E−01	2.7721E+00	1.2797E−01	2.3854E+00
40	8.8033E−02	5.6692E+00	1.0631E−01	3.2878E+00	1.1351E−01	2.8120E+00	1.2236E−01	2.4197E+00
41	8.4756E−02	5.7542E+00	1.0192E−01	3.3338E+00	1.0873E−01	2.8510E+00	1.1710E−01	2.4531E+00
42	8.1670E−02	5.8383E+00	9.7809E−02	3.3789E+00	1.0424E−01	2.8893E+00	1.1219E−01	2.4858E+00
43	7.8761E−02	5.9214E+00	9.3940E−02	3.4231E+00	1.0003E−01	2.9267E+00	1.0758E−01	2.5178E+00
44	7.6016E−02	6.0036E+00	9.0297E−02	3.4664E+00	9.6070E−02	2.9634E+00	1.0325E−01	2.5492E+00
45	7.3423E−02	6.0850E+00	8.6862E−02	3.5089E+00	9.2343E−02	2.9993E+00	9.9183E−02	2.5798E+00
46	7.0972E−02	6.1655E+00	8.3621E−02	3.5507E+00	8.8831E−02	3.0345E+00	9.5352E−02	2.6098E+00
47	6.8655E−02	6.2453E+00	8.0558E−02	3.5917E+00	8.5515E−02	3.0691E+00	9.1742E−02	2.6392E+00
48	6.6463E−02	6.3242E+00	7.7661E−02	3.6319E+00	8.2384E−02	3.1029E+00	8.8335E−02	2.6681E+00
49	6.4388E−02	6.4024E+00	7.4918E−02	3.6715E+00	7.9422E−02	3.1362E+00	8.5116E−02	2.6963E+00
50	6.2424E−02	6.4799E+00	7.2319E−02	3.7104E+00	7.6619E−02	3.1688E+00	8.2072E−02	2.7240E+00
51	6.0563E−02	6.5567E+00	6.9854E−02	3.7487E+00	7.3963E−02	3.2009E+00	7.9190E−02	2.7512E+00
52	5.8800E−02	6.6327E+00	6.7515E−02	3.7863E+00	7.1444E−02	3.2324E+00	7.6459E−02	2.7779E+00
53	5.7129E−02	6.7080E+00	6.5293E−02	3.8233E+00	6.9053E−02	3.2634E+00	7.3869E−02	2.8041E+00
54	5.5545E−02	6.7827E+00	6.3181E−02	3.8598E+00	6.6782E−02	3.2939E+00	7.1410E−02	2.8299E+00
55	5.4042E−02	6.8566E+00	6.1172E−02	3.8958E+00	6.4623E−02	3.3239E+00	6.9074E−02	2.8553E+00
56	5.2618E−02	6.9299E+00	5.9260E−02	3.9311E+00	6.2569E−02	3.3534E+00	6.6853E−02	2.8802E+00
57	5.1266E−02	7.0025E+00	5.7438E−02	3.9660E+00	6.0614E−02	3.3825E+00	6.4740E−02	2.9048E+00
58	4.9984E−02	7.0745E+00	5.5702E−02	4.0004E+00	5.8751E−02	3.4111E+00	6.2726E−02	2.9290E+00
59	4.8768E−02	7.1458E+00	5.4046E−02	4.0343E+00	5.6975E−02	3.4393E+00	6.0808E−02	2.9528E+00
60	4.7614E−02	7.2165E+00	5.2466E−02	4.0677E+00	5.5280E−02	3.4672E+00	5.8978E−02	2.9762E+00

Table 4.3.3.1. *Partial wave elastic scattering factors for neutral atoms (cont.)*
I; $Z = 53$

	10 keV		40 keV		60 keV		90 keV	
s	$\|f(s)\|$	$\eta(s)$	$\|f(s)\|$	$\eta(s)$	$\|f(s)\|$	$\eta(s)$	$\|f(s)\|$	$\eta(s)$
0	9.0369E+00	3.7139E−01	1.0721E+01	2.4909E−01	1.1343E+01	2.1928E−01	1.2118E+01	1.9328E−01
1	7.9578E+00	4.1306E−01	9.5424E+00	2.7532E−01	1.0117E+01	2.4203E−01	1.0832E+01	2.1296E−01
2	5.8096E+00	5.3506E−01	7.1635E+00	3.5060E−01	7.6325E+00	3.0719E−01	8.2057E+00	2.6950E−01
3	3.9965E+00	7.2104E−01	5.0976E+00	4.6199E−01	5.4633E+00	4.0314E−01	5.9001E+00	3.5257E−01
4	2.8274E+00	9.3788E−01	3.7108E+00	5.8889E−01	3.9976E+00	5.1199E−01	4.3344E+00	4.4651E−01
5	2.1062E+00	1.1550E+00	2.8223E+00	7.1468E−01	3.0529E+00	6.1965E−01	3.3205E+00	5.3924E−01
6	1.6360E+00	1.3612E+00	2.2280E+00	8.3374E−01	2.4179E+00	7.2142E−01	2.6367E+00	6.2682E−01
7	1.3083E+00	1.5594E+00	1.8051E+00	9.4775E−01	1.9644E+00	8.1879E−01	2.1468E+00	7.1053E−01
8	1.0698E+00	1.7548E+00	1.4895E+00	1.0598E+00	1.6245E+00	9.1439E−01	1.7784E+00	7.9267E−01
9	8.9245E−01	1.9497E+00	1.2474E+00	1.1717E+00	1.3623E+00	1.0098E+00	1.4931E+00	8.7456E−01
10	7.5879E−01	2.1428E+00	1.0585E+00	1.2833E+00	1.1566E+00	1.1050E+00	1.2684E+00	9.5633E−01
11	6.5614E−01	2.3314E+00	9.0926E−01	1.3935E+00	9.9331E−01	1.1991E+00	1.0893E+00	1.0372E+00
12	5.7636E−01	2.5132E+00	7.9084E−01	1.5009E+00	8.6315E−01	1.2910E+00	9.4609E−01	1.1162E+00
13	5.1234E−01	2.6864E+00	6.9537E−01	1.6041E+00	7.5801E−01	1.3793E+00	8.3019E−01	1.1922E+00
14	4.5940E−01	2.8506E+00	6.1719E−01	1.7021E+00	6.7190E−01	1.4634E+00	7.3525E−01	1.2646E+00
15	4.1465E−01	3.0062E+00	5.5231E−01	1.7948E+00	6.0056E−01	1.5428E+00	6.5666E−01	1.3329E+00
16	3.7615E−01	3.1544E+00	4.9770E−01	1.8821E+00	5.4067E−01	1.6175E+00	5.9080E−01	1.3973E+00
17	3.4261E−01	3.2960E+00	4.5114E−01	1.9646E+00	4.8978E−01	1.6880E+00	5.3496E−01	1.4578E+00
18	3.1319E−01	3.4323E+00	4.1101E−01	2.0427E+00	4.4605E−01	1.7546E+00	4.8707E−01	1.5150E+00
19	2.8727E−01	3.5640E+00	3.7611E−01	2.1173E+00	4.0811E−01	1.8180E+00	4.4561E−01	1.5693E+00
20	2.6440E−01	3.6917E+00	3.4554E−01	2.1888E+00	3.7493E−01	1.8787E+00	4.0939E−01	1.6213E+00
21	2.4419E−01	3.8161E+00	3.1859E−01	2.2579E+00	3.4571E−01	1.9373E+00	3.7751E−01	1.6713E+00
22	2.2630E−01	3.9373E+00	2.9474E−01	2.3249E+00	3.1983E−01	1.9940E+00	3.4927E−01	1.7197E+00
23	2.1045E−01	4.0557E+00	2.7352E−01	2.3903E+00	2.9680E−01	2.0494E+00	3.2412E−01	1.7670E+00
24	1.9638E−01	4.1714E+00	2.5458E−01	2.4542E+00	2.7621E−01	2.1035E+00	3.0161E−01	1.8132E+00
25	1.8384E−01	4.2845E+00	2.3762E−01	2.5169E+00	2.5773E−01	2.1567E+00	2.8138E−01	1.8585E+00
26	1.7264E−01	4.3951E+00	2.2237E−01	2.5786E+00	2.4110E−01	2.2089E+00	2.6314E−01	1.9032E+00
27	1.6259E−01	4.5033E+00	2.0863E−01	2.6391E+00	2.2606E−01	2.2603E+00	2.4663E−01	1.9471E+00
28	1.5354E−01	4.6093E+00	1.9619E−01	2.6987E+00	2.1244E−01	2.3110E+00	2.3164E−01	1.9905E+00
29	1.4535E−01	4.7130E+00	1.8491E−01	2.7573E+00	2.0006E−01	2.3608E+00	2.1800E−01	2.0332E+00
30	1.3791E−01	4.8147E+00	1.7464E−01	2.8149E+00	1.8877E−01	2.4099E+00	2.0555E−01	2.0753E+00
31	1.3111E−01	4.9145E+00	1.6526E−01	2.8716E+00	1.7845E−01	2.4582E+00	1.9415E−01	2.1167E+00
32	1.2488E−01	5.0124E+00	1.5667E−01	2.9272E+00	1.6899E−01	2.5057E+00	1.8370E−01	2.1575E+00
33	1.1915E−01	5.1085E+00	1.4877E−01	2.9818E+00	1.6029E−01	2.5523E+00	1.7408E−01	2.1976E+00
34	1.1384E−01	5.2031E+00	1.4149E−01	3.0354E+00	1.5227E−01	2.5981E+00	1.6522E−01	2.2369E+00
35	1.0893E−01	5.2962E+00	1.3476E−01	3.0880E+00	1.4486E−01	2.6430E+00	1.5703E−01	2.2755E+00
36	1.0435E−01	5.3878E+00	1.2852E−01	3.1395E+00	1.3800E−01	2.6870E+00	1.4945E−01	2.3134E+00
37	1.0008E−01	5.4782E+00	1.2273E−01	3.1901E+00	1.3162E−01	2.7301E+00	1.4241E−01	2.3505E+00
38	9.6094E−02	5.5673E+00	1.1733E−01	3.2396E+00	1.2569E−01	2.7724E+00	1.3588E−01	2.3868E+00
39	9.2354E−02	5.6553E+00	1.1229E−01	3.2882E+00	1.2017E−01	2.8138E+00	1.2979E−01	2.4223E+00
40	8.8843E−02	5.7423E+00	1.0758E−01	3.3359E+00	1.1500E−01	2.8544E+00	1.2410E−01	2.4572E+00
41	8.5541E−02	5.8282E+00	1.0316E−01	3.3826E+00	1.1017E−01	2.8941E+00	1.1879E−01	2.4912E+00
42	8.2432E−02	5.9131E+00	9.9012E−02	3.4284E+00	1.0564E−01	2.9330E+00	1.1382E−01	2.5246E+00
43	7.9502E−02	5.9972E+00	9.5113E−02	3.4733E+00	1.0139E−01	2.9712E+00	1.0915E−01	2.5572E+00
44	7.6736E−02	6.0804E+00	9.1440E−02	3.5174E+00	9.7390E−02	3.0085E+00	1.0477E−01	2.5892E+00
45	7.4124E−02	6.1627E+00	8.7978E−02	3.5607E+00	9.3626E−02	3.0452E+00	1.0066E−01	2.6205E+00
46	7.1656E−02	6.2443E+00	8.4709E−02	3.6032E+00	9.0076E−02	3.0811E+00	9.6779E−02	2.6511E+00
47	6.9321E−02	6.3251E+00	8.1619E−02	3.6449E+00	8.6726E−02	3.1163E+00	9.3123E−02	2.6811E+00
48	6.7112E−02	6.4051E+00	7.8696E−02	3.6859E+00	8.3560E−02	3.1508E+00	8.9673E−02	2.7105E+00
49	6.5021E−02	6.4844E+00	7.5928E−02	3.7262E+00	8.0566E−02	3.1848E+00	8.6413E−02	2.7394E+00
50	6.3041E−02	6.5630E+00	7.3304E−02	3.7659E+00	7.7731E−02	3.2181E+00	8.3329E−02	2.7677E+00
51	6.1164E−02	6.6409E+00	7.0815E−02	3.8049E+00	7.5044E−02	3.2508E+00	8.0409E−02	2.7954E+00
52	5.9386E−02	6.7181E+00	6.8452E−02	3.8432E+00	7.2495E−02	3.2829E+00	7.7642E−02	2.8227E+00
53	5.7701E−02	6.7946E+00	6.6206E−02	3.8810E+00	7.0075E−02	3.3145E+00	7.5016E−02	2.8495E+00
54	5.6103E−02	6.8705E+00	6.4071E−02	3.9181E+00	6.7776E−02	3.3456E+00	7.2524E−02	2.8758E+00
55	5.4587E−02	6.9457E+00	6.2039E−02	3.9548E+00	6.5590E−02	3.3762E+00	7.0155E−02	2.9017E+00
56	5.3150E−02	7.0202E+00	6.0105E−02	3.9908E+00	6.3510E−02	3.4063E+00	6.7903E−02	2.9272E+00
57	5.1787E−02	7.0942E+00	5.8262E−02	4.0264E+00	6.1528E−02	3.4360E+00	6.5759E−02	2.9522E+00
58	5.0494E−02	7.1674E+00	5.6504E−02	4.0614E+00	5.9641E−02	3.4652E+00	6.3716E−02	2.9769E+00
59	4.9267E−02	7.2401E+00	5.4828E−02	4.0960E+00	5.7840E−02	3.4940E+00	6.1770E−02	3.0012E+00
60	4.8104E−02	7.3122E+00	5.3228E−02	4.1301E+00	5.6123E−02	3.5224E+00	5.9913E−02	3.0251E+00

Table 4.3.3.1. *Partial wave elastic scattering factors for neutral atoms (cont.)*
Xe; $Z = 54$

	10 keV		40 keV		60 keV		90 keV	
s	$\|f(s)\|$	$\eta(s)$	$\|f(s)\|$	$\eta(s)$	$\|f(s)\|$	$\eta(s)$	$\|f(s)\|$	$\eta(s)$
0	8.8612E+00	3.8581E−01	1.0559E+01	2.5901E−01	1.1181E+01	2.2811E−01	1.1952E+01	2.0116E−01
1	7.8913E+00	4.2448E−01	9.4973E+00	2.8340E−01	1.0077E+01	2.4927E−01	1.0795E+01	2.1946E−01
2	5.8763E+00	5.3932E−01	7.2637E+00	3.5450E−01	7.7435E+00	3.1086E−01	8.3291E+00	2.7293E−01
3	4.0788E+00	7.2011E−01	5.2157E+00	4.6316E−01	5.5931E+00	4.0455E−01	6.0431E+00	3.5410E−01
4	2.8766E+00	9.3973E−01	3.7883E+00	5.9189E−01	4.0841E+00	5.1501E−01	4.4309E+00	4.4947E−01
5	2.1306E+00	1.1658E+00	2.8642E+00	7.2290E−01	3.1006E+00	6.2716E−01	3.3746E+00	5.4609E−01
6	1.6501E+00	1.3809E+00	2.2515E+00	8.4724E−01	2.4451E+00	7.3347E−01	2.6680E+00	6.3760E−01
7	1.3190E+00	1.5843E+00	1.8215E+00	9.6456E−01	1.9834E+00	8.3371E−01	2.1688E+00	7.2381E−01
8	1.0790E+00	1.7815E+00	1.5036E+00	1.0779E+00	1.6409E+00	9.3043E−01	1.7974E+00	8.0695E−01
9	9.0018E−01	1.9761E+00	1.2605E+00	1.1897E+00	1.3776E+00	1.0259E+00	1.5110E+00	8.8891E−01
10	7.6498E−01	2.1688E+00	1.0706E+00	1.3010E+00	1.1710E+00	1.1208E+00	1.2852E+00	9.7046E−01
11	6.6103E−01	2.3576E+00	9.2015E−01	1.4112E+00	1.0063E+00	1.2150E+00	1.1047E+00	1.0514E+00
12	5.8032E−01	2.5406E+00	8.0044E−01	1.5192E+00	8.7473E−01	1.3073E+00	9.5984E−01	1.1308E+00
13	5.1580E−01	2.7158E+00	7.0376E−01	1.6236E+00	7.6814E−01	1.3967E+00	8.4223E−01	1.2078E+00
14	4.6270E−01	2.8825E+00	6.2454E−01	1.7235E+00	6.8072E−01	1.4824E+00	7.4570E−01	1.2816E+00
15	4.1799E−01	3.0409E+00	5.5882E−01	1.8183E+00	6.0826E−01	1.5637E+00	6.6571E−01	1.3517E+00
16	3.7959E−01	3.1916E+00	5.0353E−01	1.9079E+00	5.4746E−01	1.6406E+00	5.9869E−01	1.4179E+00
17	3.4614E−01	3.3358E+00	4.5644E−01	1.9926E+00	4.9582E−01	1.7131E+00	5.4190E−01	1.4803E+00
18	3.1675E−01	3.4743E+00	4.1586E−01	2.0728E+00	4.5148E−01	1.7816E+00	4.9325E−01	1.5392E+00
19	2.9079E−01	3.6080E+00	3.8057E−01	2.1492E+00	4.1304E−01	1.8467E+00	4.5115E−01	1.5950E+00
20	2.6781E−01	3.7376E+00	3.4966E−01	2.2224E+00	3.7943E−01	1.9089E+00	4.1442E−01	1.6483E+00
21	2.4743E−01	3.8637E+00	3.2240E−01	2.2928E+00	3.4985E−01	1.9686E+00	3.8211E−01	1.6994E+00
22	2.2934E−01	3.9866E+00	2.9825E−01	2.3609E+00	3.2365E−01	2.0264E+00	3.5352E−01	1.7487E+00
23	2.1327E−01	4.1066E+00	2.7677E−01	2.4272E+00	3.0033E−01	2.0825E+00	3.2806E−01	1.7966E+00
24	1.9896E−01	4.2238E+00	2.5758E−01	2.4919E+00	2.7949E−01	2.1373E+00	3.0528E−01	1.8434E+00
25	1.8620E−01	4.3383E+00	2.4039E−01	2.5552E+00	2.6079E−01	2.1909E+00	2.8482E−01	1.8892E+00
26	1.7479E−01	4.4504E+00	2.2494E−01	2.6174E+00	2.4395E−01	2.2436E+00	2.6637E−01	1.9341E+00
27	1.6455E−01	4.5600E+00	2.1100E−01	2.6785E+00	2.2873E−01	2.2954E+00	2.4968E−01	1.9784E+00
28	1.5532E−01	4.6672E+00	1.9840E−01	2.7385E+00	2.1495E−01	2.3464E+00	2.3453E−01	2.0220E+00
29	1.4697E−01	4.7723E+00	1.8697E−01	2.7975E+00	2.0242E−01	2.3966E+00	2.2074E−01	2.0650E+00
30	1.3939E−01	4.8752E+00	1.7657E−01	2.8556E+00	1.9100E−01	2.4460E+00	2.0814E−01	2.1074E+00
31	1.3248E−01	4.9761E+00	1.6707E−01	2.9127E+00	1.8056E−01	2.4947E+00	1.9662E−01	2.1491E+00
32	1.2614E−01	5.0752E+00	1.5838E−01	2.9688E+00	1.7099E−01	2.5425E+00	1.8606E−01	2.1902E+00
33	1.2032E−01	5.1724E+00	1.5039E−01	3.0240E+00	1.6219E−01	2.5896E+00	1.7633E−01	2.2306E+00
34	1.1494E−01	5.2680E+00	1.4303E−01	3.0781E+00	1.5409E−01	2.6358E+00	1.6737E−01	2.2703E+00
35	1.0996E−01	5.3621E+00	1.3623E−01	3.1313E+00	1.4660E−01	2.6812E+00	1.5910E−01	2.3094E+00
36	1.0532E−01	5.4547E+00	1.2994E−01	3.1834E+00	1.3967E−01	2.7258E+00	1.5143E−01	2.3477E+00
37	1.0101E−01	5.5460E+00	1.2409E−01	3.2346E+00	1.3323E−01	2.7695E+00	1.4432E−01	2.3853E+00
38	9.6976E−02	5.6361E+00	1.1864E−01	3.2848E+00	1.2725E−01	2.8124E+00	1.3771E−01	2.4221E+00
39	9.3200E−02	5.7250E+00	1.1356E−01	3.3341E+00	1.2167E−01	2.8544E+00	1.3156E−01	2.4583E+00
40	8.9656E−02	5.8128E+00	1.0881E−01	3.3824E+00	1.1646E−01	2.8956E+00	1.2581E−01	2.4936E+00
41	8.6326E−02	5.8996E+00	1.0436E−01	3.4299E+00	1.1158E−01	2.9360E+00	1.2044E−01	2.5283E+00
42	8.3191E−02	5.9855E+00	1.0018E−01	3.4764E+00	1.0701E−01	2.9756E+00	1.1541E−01	2.5622E+00
43	8.0236E−02	6.0704E+00	9.6251E−02	3.5220E+00	1.0272E−01	3.0143E+00	1.1069E−01	2.5955E+00
44	7.7448E−02	6.1546E+00	9.2551E−02	3.5669E+00	9.8678E−02	3.0524E+00	1.0627E−01	2.6280E+00
45	7.4816E−02	6.2378E+00	8.9061E−02	3.6109E+00	9.4877E−02	3.0897E+00	1.0210E−01	2.6599E+00
46	7.2327E−02	6.3204E+00	8.5767E−02	3.6541E+00	9.1293E−02	3.1262E+00	9.8178E−02	2.6912E+00
47	6.9974E−02	6.4021E+00	8.2652E−02	3.6966E+00	8.7909E−02	3.1621E+00	9.4480E−02	2.7218E+00
48	6.7747E−02	6.4831E+00	7.9704E−02	3.7383E+00	8.4711E−02	3.1973E+00	9.0988E−02	2.7518E+00
49	6.5638E−02	6.5635E+00	7.6912E−02	3.7793E+00	8.1686E−02	3.2319E+00	8.7688E−02	2.7813E+00
50	6.3641E−02	6.6431E+00	7.4265E−02	3.8197E+00	7.8820E−02	3.2659E+00	8.4566E−02	2.8101E+00
51	6.1749E−02	6.7221E+00	7.1753E−02	3.8594E+00	7.6104E−02	3.2992E+00	8.1610E−02	2.8385E+00
52	5.9955E−02	6.8004E+00	6.9367E−02	3.8984E+00	7.3527E−02	3.3320E+00	7.8807E−02	2.8663E+00
53	5.8255E−02	6.8781E+00	6.7099E−02	3.9369E+00	7.1079E−02	3.3642E+00	7.6148E−02	2.8937E+00
54	5.6643E−02	6.9551E+00	6.4942E−02	3.9747E+00	6.8753E−02	3.3959E+00	7.3622E−02	2.9205E+00
55	5.5114E−02	7.0315E+00	6.2889E−02	4.0120E+00	6.6541E−02	3.4271E+00	7.1222E−02	2.9469E+00
56	5.3663E−02	7.1073E+00	6.0934E−02	4.0488E+00	6.4435E−02	3.4578E+00	6.8939E−02	2.9729E+00
57	5.2288E−02	7.1825E+00	5.9070E−02	4.0850E+00	6.2429E−02	3.4881E+00	6.6766E−02	2.9985E+00
58	5.0984E−02	7.2571E+00	5.7293E−02	4.1207E+00	6.0517E−02	3.5179E+00	6.4695E−02	3.0236E+00
59	4.9746E−02	7.3311E+00	5.5597E−02	4.1559E+00	5.8694E−02	3.5472E+00	6.2721E−02	3.0484E+00
60	4.8573E−02	7.4045E+00	5.3977E−02	4.1907E+00	5.6954E−02	3.5761E+00	6.0838E−02	3.0728E+00

Table 4.3.3.1. *Partial wave elastic scattering factors for neutral atoms (cont.)*
Cs; $Z = 55$

	10 keV		40 keV		60 keV		90 keV	
s	$\|f(s)\|$	$\eta(s)$	$\|f(s)\|$	$\eta(s)$	$\|f(s)\|$	$\eta(s)$	$\|f(s)\|$	$\eta(s)$
0	1.4193E+01	2.7595E−01	1.6416E+01	1.8841E−01	1.7294E+01	1.6648E−01	1.8423E+01	1.4715E−01
1	9.7690E+00	3.8976E−01	1.1616E+01	2.6003E−01	1.2299E+01	2.2878E−01	1.3156E+01	2.0146E−01
2	6.0528E+00	5.8607E−01	7.4903E+00	3.7997E−01	7.9876E+00	3.3251E−01	8.5940E+00	2.9152E−01
3	4.1291E+00	7.8092E−01	5.2915E+00	4.9684E−01	5.6776E+00	4.3325E−01	6.1375E+00	3.7880E−01
4	2.9194E+00	9.9977E−01	3.8546E+00	6.2538E−01	4.1582E+00	5.4362E−01	4.5138E+00	4.7413E−01
5	2.1575E+00	1.2297E+00	2.9089E+00	7.5881E−01	3.1512E+00	6.5788E−01	3.4320E+00	5.7261E−01
6	1.6666E+00	1.4523E+00	2.2786E+00	8.8763E−01	2.4762E+00	7.6806E−01	2.7036E+00	6.6747E−01
7	1.3311E+00	1.6619E+00	1.8397E+00	1.0088E+00	2.0043E+00	8.7162E−01	2.1929E+00	7.5659E−01
8	1.0890E+00	1.8620E+00	1.5182E+00	1.1241E+00	1.6576E+00	9.7013E−01	1.8168E+00	8.4129E−01
9	9.0852E−01	2.0574E+00	1.2734E+00	1.2365E+00	1.3926E+00	1.0661E+00	1.5284E+00	9.2375E−01
10	7.7178E−01	2.2501E+00	1.0823E+00	1.3479E+00	1.1847E+00	1.1611E+00	1.3012E+00	1.0054E+00
11	6.6628E−01	2.4389E+00	9.3080E−01	1.4579E+00	1.0190E+00	1.2551E+00	1.1196E+00	1.0862E+00
12	5.8456E−01	2.6229E+00	8.0986E−01	1.5663E+00	8.8602E−01	1.3478E+00	9.7320E−01	1.1660E+00
13	5.1937E−01	2.7998E+00	7.1203E−01	1.6717E+00	7.7810E−01	1.4381E+00	8.5407E−01	1.2437E+00
14	4.6594E−01	2.9686E+00	6.3182E−01	1.7730E+00	6.8947E−01	1.5250E+00	7.5609E−01	1.3186E+00
15	4.2116E−01	3.1293E+00	5.6527E−01	1.8696E+00	6.1594E−01	1.6080E+00	6.7480E−01	1.3901E+00
16	3.8282E−01	3.2826E+00	5.0933E−01	1.9613E+00	5.5425E−01	1.6867E+00	6.0665E−01	1.4580E+00
17	3.4946E−01	3.4290E+00	4.6170E−01	2.0482E+00	5.0188E−01	1.7612E+00	5.4892E−01	1.5222E+00
18	3.2013E−01	3.5698E+00	4.2069E−01	2.1305E+00	4.5694E−01	1.8316E+00	4.9949E−01	1.5828E+00
19	2.9417E−01	3.7055E+00	3.8504E−01	2.2088E+00	4.1800E−01	1.8985E+00	4.5676E−01	1.6403E+00
20	2.7112E−01	3.8370E+00	3.5379E−01	2.2836E+00	3.8397E−01	1.9622E+00	4.1950E−01	1.6949E+00
21	2.5062E−01	3.9649E+00	3.2624E−01	2.3554E+00	3.5402E−01	2.0233E+00	3.8676E−01	1.7472E+00
22	2.3237E−01	4.0894E+00	3.0181E−01	2.4248E+00	3.2750E−01	2.0821E+00	3.5779E−01	1.7975E+00
23	2.1611E−01	4.2109E+00	2.8006E−01	2.4921E+00	3.0390E−01	2.1392E+00	3.3202E−01	1.8463E+00
24	2.0160E−01	4.3297E+00	2.6063E−01	2.5577E+00	2.8280E−01	2.1947E+00	3.0897E−01	1.8936E+00
25	1.8863E−01	4.4457E+00	2.4321E−01	2.6217E+00	2.6387E−01	2.2489E+00	2.8826E−01	1.9399E+00
26	1.7702E−01	4.5592E+00	2.2754E−01	2.6845E+00	2.4682E−01	2.3021E+00	2.6960E−01	1.9853E+00
27	1.6658E−01	4.6702E+00	2.1342E−01	2.7461E+00	2.3141E−01	2.3543E+00	2.5271E−01	2.0299E+00
28	1.5718E−01	4.7788E+00	2.0064E−01	2.8066E+00	2.1746E−01	2.4057E+00	2.3739E−01	2.0738E+00
29	1.4868E−01	4.8852E+00	1.8905E−01	2.8662E+00	2.0477E−01	2.4562E+00	2.2344E−01	2.1171E+00
30	1.4095E−01	4.9894E+00	1.7851E−01	2.9247E+00	1.9321E−01	2.5060E+00	2.1071E−01	2.1598E+00
31	1.3391E−01	5.0915E+00	1.6889E−01	2.9823E+00	1.8265E−01	2.5550E+00	1.9906E−01	2.2018E+00
32	1.2746E−01	5.1917E+00	1.6008E−01	3.0389E+00	1.7297E−01	2.6033E+00	1.8837E−01	2.2432E+00
33	1.2154E−01	5.2901E+00	1.5200E−01	3.0945E+00	1.6407E−01	2.6507E+00	1.7855E−01	2.2839E+00
34	1.1608E−01	5.3868E+00	1.4456E−01	3.1492E+00	1.5588E−01	2.6974E+00	1.6949E−01	2.3240E+00
35	1.1102E−01	5.4818E+00	1.3769E−01	3.2029E+00	1.4832E−01	2.7433E+00	1.6112E−01	2.3635E+00
36	1.0633E−01	5.5754E+00	1.3133E−01	3.2556E+00	1.4131E−01	2.7883E+00	1.5338E−01	2.4022E+00
37	1.0196E−01	5.6677E+00	1.2542E−01	3.3074E+00	1.3481E−01	2.8326E+00	1.4619E−01	2.4402E+00
38	9.7878E−02	5.7587E+00	1.1993E−01	3.3582E+00	1.2877E−01	2.8760E+00	1.3951E−01	2.4776E+00
39	9.4060E−02	5.8485E+00	1.1481E−01	3.4081E+00	1.2313E−01	2.9186E+00	1.3329E−01	2.5142E+00
40	9.0479E−02	5.9372E+00	1.1001E−01	3.4571E+00	1.1787E−01	2.9604E+00	1.2748E−01	2.5501E+00
41	8.7115E−02	6.0249E+00	1.0553E−01	3.5052E+00	1.1295E−01	3.0014E+00	1.2205E−01	2.5853E+00
42	8.3949E−02	6.1116E+00	1.0132E−01	3.5524E+00	1.0834E−01	3.0415E+00	1.1697E−01	2.6198E+00
43	8.0967E−02	6.1974E+00	9.7357E−02	3.5987E+00	1.0401E−01	3.0810E+00	1.1220E−01	2.6536E+00
44	7.8154E−02	6.2824E+00	9.3629E−02	3.6442E+00	9.9933E−02	3.1196E+00	1.0773E−01	2.6868E+00
45	7.5498E−02	6.3666E+00	9.0113E−02	3.6890E+00	9.6096E−02	3.1576E+00	1.0352E−01	2.7192E+00
46	7.2988E−02	6.4500E+00	8.6793E−02	3.7329E+00	9.2479E−02	3.1948E+00	9.9550E−02	2.7511E+00
47	7.0614E−02	6.5327E+00	8.3654E−02	3.7761E+00	8.9063E−02	3.2313E+00	9.5809E−02	2.7823E+00
48	6.8367E−02	6.6147E+00	8.0684E−02	3.8185E+00	8.5835E−02	3.2672E+00	9.2278E−02	2.8129E+00
49	6.6239E−02	6.6960E+00	7.7869E−02	3.8602E+00	8.2780E−02	3.3024E+00	8.8941E−02	2.8429E+00
50	6.4224E−02	6.7766E+00	7.5200E−02	3.9013E+00	7.9886E−02	3.3370E+00	8.5782E−02	2.8724E+00
51	6.2315E−02	6.8566E+00	7.2666E−02	3.9416E+00	7.7141E−02	3.3710E+00	8.2790E−02	2.9013E+00
52	6.0505E−02	6.9360E+00	7.0258E−02	3.9814E+00	7.4537E−02	3.4044E+00	7.9953E−02	2.9297E+00
53	5.8789E−02	7.0148E+00	6.7970E−02	4.0205E+00	7.2063E−02	3.4372E+00	7.7261E−02	2.9576E+00
54	5.7162E−02	7.0929E+00	6.5792E−02	4.0591E+00	6.9711E−02	3.4695E+00	7.4704E−02	2.9850E+00
55	5.5618E−02	7.1705E+00	6.3719E−02	4.0971E+00	6.7474E−02	3.5013E+00	7.2274E−02	3.0119E+00
56	5.4155E−02	7.2475E+00	6.1744E−02	4.1345E+00	6.5344E−02	3.5326E+00	6.9962E−02	3.0384E+00
57	5.2767E−02	7.3239E+00	5.9861E−02	4.1714E+00	6.3314E−02	3.5634E+00	6.7759E−02	3.0645E+00
58	5.1450E−02	7.3997E+00	5.8064E−02	4.2077E+00	6.1380E−02	3.5938E+00	6.5662E−02	3.0902E+00
59	5.0202E−02	7.4749E+00	5.6350E−02	4.2436E+00	5.9534E−02	3.6237E+00	6.3661E−02	3.1154E+00
60	4.9019E−02	7.5496E+00	5.4712E−02	4.2790E+00	5.7771E−02	3.6532E+00	6.1751E−02	3.1403E+00

Table 4.3.3.1. *Partial wave elastic scattering factors for neutral atoms (cont.)*
Ba; $Z = 56$

	10 keV		40 keV		60 keV		90 keV	
s	$\|f(s)\|$	$\eta(s)$	$\|f(s)\|$	$\eta(s)$	$\|f(s)\|$	$\eta(s)$	$\|f(s)\|$	$\eta(s)$
0	1.5858E+01	2.7398E−01	1.8280E+01	1.8580E−01	1.9247E+01	1.6404E−01	2.0496E+01	1.4490E−01
1	1.1064E+01	3.7833E−01	1.3088E+01	2.5185E−01	1.3845E+01	2.2156E−01	1.4802E+01	1.9511E−01
2	6.3513E+00	6.0578E−01	7.8595E+00	3.9070E−01	8.3821E+00	3.4167E−01	9.0196E+00	2.9944E−01
3	4.1858E+00	8.2674E−01	5.3728E+00	5.2269E−01	5.7677E+00	4.5539E−01	6.2377E+00	3.9794E−01
4	2.9561E+00	1.0484E+00	3.9108E+00	6.5308E−01	4.2213E+00	5.6739E−01	4.5847E+00	4.9472E−01
5	2.1843E+00	1.2793E+00	2.9529E+00	7.8723E−01	3.2012E+00	6.8232E−01	3.4886E+00	5.9382E−01
6	1.6841E+00	1.5068E+00	2.3084E+00	9.1908E−01	2.5104E+00	7.9513E−01	2.7428E+00	6.9097E−01
7	1.3437E+00	1.7226E+00	1.8597E+00	1.0441E+00	2.0274E+00	9.0205E−01	2.2195E+00	7.8301E−01
8	1.0994E+00	1.9272E+00	1.5331E+00	1.1624E+00	1.6748E+00	1.0032E+00	1.8366E+00	8.7000E−01
9	9.1745E−01	2.1246E+00	1.2860E+00	1.2764E+00	1.4071E+00	1.1005E+00	1.5451E+00	9.5366E−01
10	7.7912E−01	2.3179E+00	1.0937E+00	1.3881E+00	1.1978E+00	1.1959E+00	1.3165E+00	1.0357E+00
11	6.7215E−01	2.5071E+00	9.4098E−01	1.4982E+00	1.0309E+00	1.2899E+00	1.1335E+00	1.1165E+00
12	5.8911E−01	2.6915E+00	8.1899E−01	1.6066E+00	8.9688E−01	1.3827E+00	9.8601E−01	1.1963E+00
13	5.2303E−01	2.8695E+00	7.2013E−01	1.7124E+00	7.8783E−01	1.4733E+00	8.6562E−01	1.2744E+00
14	4.6913E−01	3.0401E+00	6.3898E−01	1.8148E+00	6.9808E−01	1.5612E+00	7.6634E−01	1.3501E+00
15	4.2417E−01	3.2030E+00	5.7163E−01	1.9130E+00	6.2356E−01	1.6456E+00	6.8383E−01	1.4229E+00
16	3.8583E−01	3.3585E+00	5.1505E−01	2.0066E+00	5.6101E−01	1.7260E+00	6.1462E−01	1.4923E+00
17	3.5254E−01	3.5072E+00	4.6691E−01	2.0955E+00	5.0793E−01	1.8023E+00	5.5597E−01	1.5582E+00
18	3.2329E−01	3.6501E+00	4.2548E−01	2.1798E+00	4.6240E−01	1.8746E+00	5.0578E−01	1.6205E+00
19	2.9737E−01	3.7878E+00	3.8947E−01	2.2600E+00	4.2297E−01	1.9432E+00	4.6242E−01	1.6795E+00
20	2.7430E−01	3.9212E+00	3.5792E−01	2.3365E+00	3.8853E−01	2.0086E+00	4.2463E−01	1.7357E+00
21	2.5373E−01	4.0508E+00	3.3008E−01	2.4099E+00	3.5822E−01	2.0710E+00	3.9144E−01	1.7892E+00
22	2.3536E−01	4.1770E+00	3.0538E−01	2.4806E+00	3.3138E−01	2.1311E+00	3.6209E−01	1.8407E+00
23	2.1894E−01	4.3001E+00	2.8339E−01	2.5490E+00	3.0749E−01	2.1892E+00	3.3599E−01	1.8903E+00
24	2.0426E−01	4.4203E+00	2.6372E−01	2.6156E+00	2.8614E−01	2.2455E+00	3.1266E−01	1.9384E+00
25	1.9110E−01	4.5379E+00	2.4607E−01	2.6804E+00	2.6697E−01	2.3005E+00	2.9171E−01	1.9853E+00
26	1.7930E−01	4.6528E+00	2.3020E−01	2.7439E+00	2.4971E−01	2.3542E+00	2.7282E−01	2.0312E+00
27	1.6869E−01	4.7653E+00	2.1587E−01	2.8061E+00	2.3411E−01	2.4069E+00	2.5574E−01	2.0762E+00
28	1.5912E−01	4.8753E+00	2.0292E−01	2.8672E+00	2.1997E−01	2.4587E+00	2.4024E−01	2.1205E+00
29	1.5045E−01	4.9830E+00	1.9117E−01	2.9272E+00	2.0713E−01	2.5097E+00	2.2613E−01	2.1640E+00
30	1.4258E−01	5.0885E+00	1.8048E−01	2.9862E+00	1.9543E−01	2.5598E+00	2.1325E−01	2.2069E+00
31	1.3541E−01	5.1919E+00	1.7072E−01	3.0443E+00	1.8474E−01	2.6092E+00	2.0147E−01	2.2492E+00
32	1.2885E−01	5.2933E+00	1.6180E−01	3.1014E+00	1.7494E−01	2.6578E+00	1.9067E−01	2.2909E+00
33	1.2283E−01	5.3928E+00	1.5362E−01	3.1575E+00	1.6594E−01	2.7056E+00	1.8073E−01	2.3320E+00
34	1.1727E−01	5.4906E+00	1.4609E−01	3.2127E+00	1.5766E−01	2.7527E+00	1.7157E−01	2.3724E+00
35	1.1214E−01	5.5868E+00	1.3914E−01	3.2669E+00	1.5001E−01	2.7990E+00	1.6312E−01	2.4122E+00
36	1.0738E−01	5.6814E+00	1.3271E−01	3.3202E+00	1.4293E−01	2.8445E+00	1.5529E−01	2.4513E+00
37	1.0294E−01	5.7746E+00	1.2674E−01	3.3725E+00	1.3636E−01	2.8893E+00	1.4802E−01	2.4898E+00
38	9.8810E−02	5.8665E+00	1.2120E−01	3.4239E+00	1.3026E−01	2.9332E+00	1.4127E−01	2.5276E+00
39	9.4944E−02	5.9572E+00	1.1602E−01	3.4744E+00	1.2457E−01	2.9763E+00	1.3498E−01	2.5647E+00
40	9.1321E−02	6.0468E+00	1.1119E−01	3.5240E+00	1.1926E−01	3.0187E+00	1.2912E−01	2.6011E+00
41	8.7919E−02	6.1354E+00	1.0667E−01	3.5728E+00	1.1429E−01	3.0602E+00	1.2363E−01	2.6368E+00
42	8.4720E−02	6.2230E+00	1.0243E−01	3.6206E+00	1.0964E−01	3.1010E+00	1.1850E−01	2.6718E+00
43	8.1706E−02	6.3096E+00	9.8435E−02	3.6676E+00	1.0527E−01	3.1410E+00	1.1368E−01	2.7062E+00
44	7.8865E−02	6.3955E+00	9.4678E−02	3.7138E+00	1.0116E−01	3.1803E+00	1.0916E−01	2.7399E+00
45	7.6182E−02	6.4805E+00	9.1136E−02	3.7592E+00	9.7286E−02	3.2188E+00	1.0490E−01	2.7729E+00
46	7.3648E−02	6.5648E+00	8.7792E−02	3.8038E+00	9.3637E−02	3.2567E+00	1.0089E−01	2.8053E+00
47	7.1251E−02	6.6484E+00	8.4630E−02	3.8476E+00	9.0190E−02	3.2938E+00	9.7114E−02	2.8371E+00
48	6.8982E−02	6.7312E+00	8.1637E−02	3.8907E+00	8.6932E−02	3.3303E+00	9.3544E−02	2.8683E+00
49	6.6834E−02	6.8135E+00	7.8801E−02	3.9331E+00	8.3849E−02	3.3661E+00	9.0170E−02	2.8989E+00
50	6.4800E−02	6.8951E+00	7.6110E−02	3.9748E+00	8.0927E−02	3.4014E+00	8.6976E−02	2.9289E+00
51	6.2872E−02	6.9760E+00	7.3556E−02	4.0159E+00	7.8156E−02	3.4360E+00	8.3950E−02	2.9584E+00
52	6.1044E−02	7.0564E+00	7.1128E−02	4.0563E+00	7.5526E−02	3.4700E+00	8.1081E−02	2.9873E+00
53	5.9311E−02	7.1362E+00	6.8820E−02	4.0961E+00	7.3027E−02	3.5034E+00	7.8357E−02	3.0157E+00
54	5.7668E−02	7.2154E+00	6.6623E−02	4.1354E+00	7.0651E−02	3.5363E+00	7.5770E−02	3.0437E+00
55	5.6109E−02	7.2941E+00	6.4531E−02	4.1740E+00	6.8390E−02	3.5687E+00	7.3310E−02	3.0712E+00
56	5.4631E−02	7.3722E+00	6.2537E−02	4.2121E+00	6.6237E−02	3.6006E+00	7.0969E−02	3.0982E+00
57	5.3230E−02	7.4498E+00	6.0635E−02	4.2496E+00	6.4185E−02	3.6320E+00	6.8740E−02	3.1248E+00
58	5.1901E−02	7.5268E+00	5.8821E−02	4.2866E+00	6.2228E−02	3.6629E+00	6.6615E−02	3.1509E+00
59	5.0641E−02	7.6033E+00	5.7089E−02	4.3231E+00	6.0361E−02	3.6934E+00	6.4589E−02	3.1767E+00
60	4.9446E−02	7.6792E+00	5.5433E−02	4.3591E+00	5.8577E−02	3.7234E+00	6.2655E−02	3.2021E+00

Table 4.3.3.1. *Partial wave elastic scattering factors for neutral atoms (cont.)*
La; $Z = 57$

	10 keV		40 keV		60 keV		90 keV	
s	$\|f(s)\|$	$\eta(s)$	$\|f(s)\|$	$\eta(s)$	$\|f(s)\|$	$\eta(s)$	$\|f(s)\|$	$\eta(s)$
0	1.5321E+01	2.9216E−01	1.7751E+01	1.9782E−01	1.8708E+01	1.7466E−01	1.9937E+01	1.5431E−01
1	1.1194E+01	3.8584E−01	1.3274E+01	2.5709E−01	1.4049E+01	2.2628E−01	1.5026E+01	1.9938E−01
2	6.5722E+00	6.0440E−01	8.1428E+00	3.9079E−01	8.6868E+00	3.4202E−01	9.3500E+00	2.9995E−01
3	4.2776E+00	8.3544E−01	5.5016E+00	5.2875E−01	5.9089E+00	4.6091E−01	6.3933E+00	4.0296E−01
4	3.0013E+00	1.0653E+00	3.9788E+00	6.6396E−01	4.2974E+00	5.7709E−01	4.6699E+00	5.0339E−01
5	2.2117E+00	1.3012E+00	2.9961E+00	8.0123E−01	3.2503E+00	6.9474E−01	3.5443E+00	6.0486E−01
6	1.7023E+00	1.5342E+00	2.3368E+00	9.3642E−01	2.5431E+00	8.1045E−01	2.7803E+00	7.0456E−01
7	1.3573E+00	1.7554E+00	1.8791E+00	1.0650E+00	2.0499E+00	9.2042E−01	2.2455E+00	7.9926E−01
8	1.1107E+00	1.9639E+00	1.5478E+00	1.1861E+00	1.6918E+00	1.0240E+00	1.8563E+00	8.8841E−01
9	9.2702E−01	2.1634E+00	1.2982E+00	1.3017E+00	1.4212E+00	1.1228E+00	1.5616E+00	9.7338E−01
10	7.8706E−01	2.3572E+00	1.1045E+00	1.4139E+00	1.2105E+00	1.2187E+00	1.3313E+00	1.0559E+00
11	6.7891E−01	2.5466E+00	9.5105E−01	1.5242E+00	1.0428E+00	1.3130E+00	1.1475E+00	1.1369E+00
12	5.9430E−01	2.7314E+00	8.2784E−01	1.6328E+00	9.0753E−01	1.4059E+00	9.9868E−01	1.2168E+00
13	5.2700E−01	2.9103E+00	7.2781E−01	1.7392E+00	7.9721E−01	1.4970E+00	8.7690E−01	1.2953E+00
14	4.7236E−01	3.0823E+00	6.4573E−01	1.8425E+00	7.0641E−01	1.5857E+00	7.7640E−01	1.3718E+00
15	4.2697E−01	3.2470E+00	5.7760E−01	1.9421E+00	6.3095E−01	1.6712E+00	6.9276E−01	1.4456E+00
16	3.8842E−01	3.4045E+00	5.2039E−01	2.0374E+00	5.6758E−01	1.7532E+00	6.2253E−01	1.5164E+00
17	3.5508E−01	3.5553E+00	4.7176E−01	2.1282E+00	5.1382E−01	1.8313E+00	5.6300E−01	1.5838E+00
18	3.2581E−01	3.7002E+00	4.2995E−01	2.2146E+00	4.6774E−01	1.9055E+00	5.1207E−01	1.6478E+00
19	2.9986E−01	3.8400E+00	3.9362E−01	2.2968E+00	4.2784E−01	1.9759E+00	4.6809E−01	1.7085E+00
20	2.7673E−01	3.9753E+00	3.6178E−01	2.3752E+00	3.9300E−01	2.0429E+00	4.2978E−01	1.7662E+00
21	2.5606E−01	4.1068E+00	3.3369E−01	2.4502E+00	3.6234E−01	2.1070E+00	3.9615E−01	1.8211E+00
22	2.3756E−01	4.2349E+00	3.0876E−01	2.5225E+00	3.3520E−01	2.1684E+00	3.6643E−01	1.8737E+00
23	2.2099E−01	4.3599E+00	2.8655E−01	2.5923E+00	3.1105E−01	2.2276E+00	3.4002E−01	1.9244E+00
24	2.0615E−01	4.4820E+00	2.6668E−01	2.6600E+00	2.8947E−01	2.2851E+00	3.1641E−01	1.9735E+00
25	1.9282E−01	4.6015E+00	2.4885E−01	2.7259E+00	2.7009E−01	2.3409E+00	2.9522E−01	2.0212E+00
26	1.8086E−01	4.7184E+00	2.3279E−01	2.7903E+00	2.5262E−01	2.3954E+00	2.7612E−01	2.0677E+00
27	1.7009E−01	4.8329E+00	2.1828E−01	2.8533E+00	2.3684E−01	2.4487E+00	2.5884E−01	2.1131E+00
28	1.6037E−01	4.9449E+00	2.0516E−01	2.9151E+00	2.2254E−01	2.5010E+00	2.4316E−01	2.1578E+00
29	1.5159E−01	5.0546E+00	1.9327E−01	2.9758E+00	2.0955E−01	2.5525E+00	2.2889E−01	2.2018E+00
30	1.4362E−01	5.1621E+00	1.8246E−01	3.0355E+00	1.9772E−01	2.6031E+00	2.1588E−01	2.2451E+00
31	1.3636E−01	5.2674E+00	1.7260E−01	3.0941E+00	1.8691E−01	2.6529E+00	2.0398E−01	2.2877E+00
32	1.2973E−01	5.3707E+00	1.6357E−01	3.1518E+00	1.7701E−01	2.7020E+00	1.9306E−01	2.3297E+00
33	1.2366E−01	5.4721E+00	1.5530E−01	3.2085E+00	1.6791E−01	2.7503E+00	1.8302E−01	2.3711E+00
34	1.1808E−01	5.5717E+00	1.4769E−01	3.2643E+00	1.5954E−01	2.7978E+00	1.7376E−01	2.4119E+00
35	1.1292E−01	5.6695E+00	1.4067E−01	3.3191E+00	1.5182E−01	2.8445E+00	1.6522E−01	2.4520E+00
36	1.0815E−01	5.7657E+00	1.3419E−01	3.3730E+00	1.4468E−01	2.8905E+00	1.5732E−01	2.4915E+00
37	1.0371E−01	5.8604E+00	1.2819E−01	3.4259E+00	1.3806E−01	2.9357E+00	1.4999E−01	2.5304E+00
38	9.9585E−02	5.9538E+00	1.2261E−01	3.4780E+00	1.3191E−01	2.9802E+00	1.4317E−01	2.5686E+00
39	9.5737E−02	6.0459E+00	1.1740E−01	3.5291E+00	1.2617E−01	3.0238E+00	1.3682E−01	2.6062E+00
40	9.2139E−02	6.1368E+00	1.1254E−01	3.5794E+00	1.2082E−01	3.0667E+00	1.3090E−01	2.6430E+00
41	8.8765E−02	6.2265E+00	1.0799E−01	3.6287E+00	1.1581E−01	3.1088E+00	1.2537E−01	2.6792E+00
42	8.5593E−02	3.2019E−02	1.0373E−01	3.6772E+00	1.1112E−01	3.1502E+00	1.2018E−01	2.7148E+00
43	8.2607E−02	1.1973E−01	9.9723E−02	3.7248E+00	1.0673E−01	3.1907E+00	1.1533E−01	2.7497E+00
44	7.9795E−02	2.0651E−01	9.5953E−02	3.7716E+00	1.0259E−01	3.2306E+00	1.1077E−01	2.7839E+00
45	7.7145E−02	2.9241E−01	9.2398E−02	3.8176E+00	9.8693E−02	3.2697E+00	1.0647E−01	2.8174E+00
46	7.4643E−02	3.7747E−01	8.9039E−02	3.8629E+00	9.5016E−02	3.3081E+00	1.0243E−01	2.8503E+00
47	7.2278E−02	4.6173E−01	8.5864E−02	3.9073E+00	9.1544E−02	3.3458E+00	9.8608E−02	2.8826E+00
48	7.0037E−02	5.4525E−01	8.2860E−02	3.9511E+00	8.8264E−02	3.3829E+00	9.5005E−02	2.9143E+00
49	6.7912E−02	6.2806E−01	8.0015E−02	3.9940E+00	8.5162E−02	3.4193E+00	9.1601E−02	2.9454E+00
50	6.5899E−02	7.1017E−01	7.7315E−02	4.0363E+00	8.2221E−02	3.4550E+00	8.8379E−02	2.9760E+00
51	6.3991E−02	7.9159E−01	7.4749E−02	4.0780E+00	7.9430E−02	3.4901E+00	8.5324E−02	3.0059E+00
52	6.2180E−02	8.7234E−01	7.2310E−02	4.1189E+00	7.6778E−02	3.5247E+00	8.2424E−02	3.0354E+00
53	6.0461E−02	9.5245E−01	6.9989E−02	4.1593E+00	7.4258E−02	3.5587E+00	7.9671E−02	3.0643E+00
54	5.8828E−02	1.0319E+00	6.7780E−02	4.1991E+00	7.1861E−02	3.5921E+00	7.7055E−02	3.0927E+00
55	5.7274E−02	1.1109E+00	6.5677E−02	4.2382E+00	6.9582E−02	3.6250E+00	7.4570E−02	3.1207E+00
56	5.5797E−02	1.1892E+00	6.3671E−02	4.2768E+00	6.7412E−02	3.6573E+00	7.2207E−02	3.1481E+00
57	5.4393E−02	1.2670E+00	6.1757E−02	4.3148E+00	6.5342E−02	3.6892E+00	6.9953E−02	3.1751E+00
58	5.3059E−02	1.3441E+00	5.9929E−02	4.3522E+00	6.3365E−02	3.7205E+00	6.7803E−02	3.2017E+00
59	5.1789E−02	1.4207E+00	5.8183E−02	4.3892E+00	6.1478E−02	3.7515E+00	6.5751E−02	3.2279E+00
60	5.0582E−02	1.4968E+00	5.6514E−02	4.4257E+00	5.9676E−02	3.7819E+00	6.3794E−02	3.2537E+00

Table 4.3.3.1. *Partial wave elastic scattering factors for neutral atoms (cont.)*
Ce; $Z = 58$

	10 keV		40 keV		60 keV		90 keV	
s	$\|f(s)\|$	$\eta(s)$	$\|f(s)\|$	$\eta(s)$	$\|f(s)\|$	$\eta(s)$	$\|f(s)\|$	$\eta(s)$
0	1.4874E+01	2.9574E−01	1.7273E+01	2.0146E−01	1.8215E+01	1.7813E−01	1.9420E+01	1.5758E−01
1	1.0952E+01	3.8819E−01	1.3017E+01	2.6018E−01	1.3785E+01	2.2932E−01	1.4750E+01	2.0229E−01
2	6.4941E+00	6.0425E−01	8.0664E+00	3.9278E−01	8.6108E+00	3.4419E−01	9.2733E+00	3.0218E−01
3	4.2539E+00	8.3296E−01	5.4869E+00	5.2972E−01	5.8972E+00	4.6227E−01	6.3846E+00	4.0455E−01
4	2.9989E+00	1.0601E+00	3.9892E+00	6.6363E−01	4.3121E+00	5.7740E−01	4.6891E+00	5.0412E−01
5	2.2156E+00	1.2941E+00	3.0143E+00	7.9999E−01	3.2730E+00	6.9433E−01	3.5719E+00	6.0502E−01
6	1.7069E+00	1.5271E+00	2.3549E+00	9.3532E−01	2.5654E+00	8.1020E−01	2.8071E+00	7.0490E−01
7	1.3618E+00	1.7499E+00	1.8949E+00	1.0649E+00	2.0692E+00	9.2114E−01	2.2688E+00	8.0045E−01
8	1.1152E+00	1.9606E+00	1.5613E+00	1.1875E+00	1.7083E+00	1.0260E+00	1.8761E+00	8.9073E−01
9	9.3151E−01	2.1618E+00	1.3101E+00	1.3044E+00	1.4357E+00	1.1259E+00	1.5788E+00	9.7674E−01
10	7.9124E−01	2.3569E+00	1.1151E+00	1.4176E+00	1.2233E+00	1.2227E+00	1.3467E+00	1.0600E+00
11	6.8260E−01	2.5474E+00	9.6054E−01	1.5287E+00	1.0543E+00	1.3177E+00	1.1613E+00	1.1417E+00
12	5.9746E−01	2.7333E+00	8.3631E−01	1.6380E+00	9.1786E−01	1.4112E+00	1.0111E+00	1.2222E+00
13	5.2973E−01	2.9137E+00	7.3536E−01	1.7452E+00	8.0645E−01	1.5030E+00	8.8800E−01	1.3013E+00
14	4.7483E−01	3.0874E+00	6.5245E−01	1.8496E+00	7.1464E−01	1.5927E+00	7.8631E−01	1.3786E+00
15	4.2933E−01	3.2540E+00	5.8363E−01	1.9505E+00	6.3828E−01	1.6794E+00	7.0158E−01	1.4535E+00
16	3.9080E−01	3.4136E+00	5.2584E−01	2.0473E+00	5.7415E−01	1.7628E+00	6.3038E−01	1.5255E+00
17	3.5754E−01	3.5664E+00	4.7674E−01	2.1399E+00	5.1975E−01	1.8424E+00	5.7002E−01	1.5943E+00
18	3.2837E−01	3.7133E+00	4.3454E−01	2.2280E+00	4.7312E−01	1.9183E+00	5.1837E−01	1.6599E+00
19	3.0251E−01	3.8549E+00	3.9790E−01	2.3120E+00	4.3276E−01	1.9904E+00	4.7379E−01	1.7220E+00
20	2.7943E−01	3.9920E+00	3.6579E−01	2.3921E+00	3.9753E−01	2.0590E+00	4.3497E−01	1.7811E+00
21	2.5876E−01	4.1252E+00	3.3744E−01	2.4687E+00	3.6653E−01	2.1244E+00	4.0090E−01	1.8374E+00
22	2.4022E−01	4.2549E+00	3.1228E−01	2.5424E+00	3.3909E−01	2.1872E+00	3.7080E−01	1.8913E+00
23	2.2358E−01	4.3815E+00	2.8985E−01	2.6135E+00	3.1467E−01	2.2477E+00	3.4406E−01	1.9431E+00
24	2.0863E−01	4.5051E+00	2.6977E−01	2.6823E+00	2.9283E−01	2.3061E+00	3.2016E−01	1.9930E+00
25	1.9518E−01	4.6260E+00	2.5173E−01	2.7493E+00	2.7322E−01	2.3629E+00	2.9871E−01	2.0415E+00
26	1.8308E−01	4.7444E+00	2.3548E−01	2.8146E+00	2.5555E−01	2.4181E+00	2.7938E−01	2.0887E+00
27	1.7217E−01	4.8604E+00	2.2079E−01	2.8784E+00	2.3958E−01	2.4722E+00	2.6189E−01	2.1348E+00
28	1.6232E−01	4.9739E+00	2.0750E−01	2.9409E+00	2.2510E−01	2.5251E+00	2.4602E−01	2.1800E+00
29	1.5339E−01	5.0850E+00	1.9544E−01	3.0023E+00	2.1194E−01	2.5771E+00	2.3159E−01	2.2243E+00
30	1.4529E−01	5.1939E+00	1.8447E−01	3.0626E+00	1.9996E−01	2.6282E+00	2.1842E−01	2.2680E+00
31	1.3791E−01	5.3006E+00	1.7448E−01	3.1218E+00	1.8902E−01	2.6785E+00	2.0638E−01	2.3110E+00
32	1.3117E−01	5.4052E+00	1.6533E−01	3.1800E+00	1.7899E−01	2.7279E+00	1.9533E−01	2.3534E+00
33	1.2500E−01	5.5079E+00	1.5694E−01	3.2373E+00	1.6978E−01	2.7766E+00	1.8518E−01	2.3951E+00
34	1.1932E−01	5.6088E+00	1.4923E−01	3.2936E+00	1.6131E−01	2.8246E+00	1.7581E−01	2.4362E+00
35	1.1408E−01	5.7079E+00	1.4213E−01	3.3489E+00	1.5349E−01	2.8718E+00	1.6717E−01	2.4767E+00
36	1.0923E−01	5.8053E+00	1.3557E−01	3.4034E+00	1.4627E−01	2.9182E+00	1.5918E−01	2.5166E+00
37	1.0473E−01	5.9012E+00	1.2950E−01	3.4569E+00	1.3958E−01	2.9639E+00	1.5177E−01	2.5559E+00
38	1.0054E−01	5.9956E+00	1.2385E−01	3.5095E+00	1.3336E−01	3.0088E+00	1.4489E−01	2.5945E+00
39	9.6640E−02	6.0887E+00	1.1859E−01	3.5612E+00	1.2757E−01	3.0530E+00	1.3847E−01	2.6325E+00
40	9.2993E−02	6.1807E+00	1.1368E−01	3.6121E+00	1.2216E−01	3.0963E+00	1.3249E−01	2.6698E+00
41	8.9575E−02	6.2714E+00	1.0909E−01	3.6620E+00	1.1710E−01	3.1390E+00	1.2689E−01	2.7064E+00
42	8.6364E−02	7.7888E−02	1.0479E−01	3.7111E+00	1.1237E−01	3.1809E+00	1.2166E−01	2.7425E+00
43	8.3343E−02	1.6656E−01	1.0076E−01	3.7594E+00	1.0794E−01	3.2220E+00	1.1675E−01	2.7778E+00
44	8.0499E−02	2.5429E−01	9.6957E−02	3.8068E+00	1.0376E−01	3.2624E+00	1.1215E−01	2.8126E+00
45	7.7819E−02	3.4114E−01	9.3374E−02	3.8535E+00	9.9834E−02	3.3021E+00	1.0781E−01	2.8466E+00
46	7.5291E−02	4.2713E−01	8.9991E−02	3.8993E+00	9.6126E−02	3.3411E+00	1.0372E−01	2.8801E+00
47	7.2901E−02	5.1234E−01	8.6793E−02	3.9445E+00	9.2624E−02	3.3794E+00	9.9866E−02	2.9129E+00
48	7.0638E−02	5.9680E−01	8.3767E−02	3.9889E+00	8.9316E−02	3.4171E+00	9.6227E−02	2.9451E+00
49	6.8493E−02	6.8057E−01	8.0901E−02	4.0325E+00	8.6187E−02	3.4541E+00	9.2789E−02	2.9768E+00
50	6.6460E−02	7.6366E−01	7.8181E−02	4.0754E+00	8.3221E−02	3.4904E+00	8.9534E−02	3.0079E+00
51	6.4534E−02	8.4607E−01	7.5598E−02	4.1177E+00	8.0405E−02	3.5261E+00	8.6447E−02	3.0384E+00
52	6.2706E−02	9.2783E−01	7.3141E−02	4.1594E+00	7.7730E−02	3.5613E+00	8.3517E−02	3.0684E+00
53	6.0972E−02	1.0090E+00	7.0803E−02	4.2004E+00	7.5187E−02	3.5958E+00	8.0735E−02	3.0978E+00
54	5.9324E−02	1.0895E+00	6.8577E−02	4.2408E+00	7.2769E−02	3.6299E+00	7.8091E−02	3.1267E+00
55	5.7756E−02	1.1695E+00	6.6456E−02	4.2806E+00	7.0468E−02	3.6633E+00	7.5580E−02	3.1552E+00
56	5.6267E−02	1.2490E+00	6.4435E−02	4.3198E+00	6.8277E−02	3.6962E+00	7.3189E−02	3.1832E+00
57	5.4851E−02	1.3278E+00	6.2505E−02	4.3584E+00	6.6187E−02	3.7287E+00	7.0910E−02	3.2107E+00
58	5.3505E−02	1.4062E+00	6.0661E−02	4.3966E+00	6.4190E−02	3.7606E+00	6.8736E−02	3.2378E+00
59	5.2226E−02	1.4840E+00	5.8900E−02	4.4342E+00	6.2284E−02	3.7921E+00	6.6661E−02	3.2645E+00
60	5.1009E−02	1.5612E+00	5.7216E−02	4.4713E+00	6.0464E−02	3.8231E+00	6.4681E−02	3.2908E+00

Table 4.3.3.1. *Partial wave elastic scattering factors for neutral atoms (cont.)*
Pr; $Z = 59$

	10 keV		40 keV		60 keV		90 keV	
s	$\|f(s)\|$	$\eta(s)$	$\|f(s)\|$	$\eta(s)$	$\|f(s)\|$	$\eta(s)$	$\|f(s)\|$	$\eta(s)$
0	1.4512E+01	2.8608E−01	1.6848E+01	1.9741E−01	1.7769E+01	1.7504E−01	1.8948E+01	1.5520E−01
1	1.0419E+01	3.8583E−01	1.2410E+01	2.6125E−01	1.3151E+01	2.3077E−01	1.4080E+01	2.0395E−01
2	6.1589E+00	6.0624E−01	7.6787E+00	3.9703E−01	8.2049E+00	3.4850E−01	8.8434E+00	3.0641E−01
3	4.1269E+00	8.2224E−01	5.3415E+00	5.2700E−01	5.7461E+00	4.6069E−01	6.2256E+00	4.0375E−01
4	2.9543E+00	1.0364E+00	3.9465E+00	6.5387E−01	4.2698E+00	5.6988E−01	4.6468E+00	4.9826E−01
5	2.1988E+00	1.2621E+00	3.0085E+00	7.8570E−01	3.2703E+00	6.8300E−01	3.5721E+00	5.9594E−01
6	1.6997E+00	1.4905E+00	2.3617E+00	9.1849E−01	2.5761E+00	7.9675E−01	2.8218E+00	6.9402E−01
7	1.3584E+00	1.7116E+00	1.9055E+00	1.0471E+00	2.0838E+00	9.0681E−01	2.2874E+00	7.8886E−01
8	1.1138E+00	1.9222E+00	1.5725E+00	1.1696E+00	1.7231E+00	1.0117E+00	1.8947E+00	8.7921E−01
9	9.3138E−01	2.1243E+00	1.3207E+00	1.2872E+00	1.4495E+00	1.1123E+00	1.5960E+00	9.6578E−01
10	7.9190E−01	2.3206E+00	1.1248E+00	1.4015E+00	1.2359E+00	1.2100E+00	1.3621E+00	1.0498E+00
11	6.8371E−01	2.5126E+00	9.6933E−01	1.5136E+00	1.0656E+00	1.3059E+00	1.1751E+00	1.1324E+00
12	5.9879E−01	2.7001E+00	8.4423E−01	1.6241E+00	9.2788E−01	1.4005E+00	1.0234E+00	1.2138E+00
13	5.3117E−01	2.8822E+00	7.4246E−01	1.7325E+00	8.1538E−01	1.4934E+00	8.9893E−01	1.2939E+00
14	4.7635E−01	3.0578E+00	6.5883E−01	1.8382E+00	7.2262E−01	1.5842E+00	7.9603E−01	1.3722E+00
15	4.3096E−01	3.2264E+00	5.8939E−01	1.9405E+00	6.4543E−01	1.6722E+00	7.1025E−01	1.4483E+00
16	3.9258E−01	3.3880E+00	5.3109E−01	2.0389E+00	5.8058E−01	1.7569E+00	6.3813E−01	1.5215E+00
17	3.5949E−01	3.5428E+00	4.8156E−01	2.1331E+00	5.2557E−01	1.8381E+00	5.7698E−01	1.5917E+00
18	3.3047E−01	3.6916E+00	4.3902E−01	2.2229E+00	4.7843E−01	1.9155E+00	5.2465E−01	1.6586E+00
19	3.0474E−01	3.8350E+00	4.0208E−01	2.3086E+00	4.3763E−01	1.9891E+00	4.7949E−01	1.7222E+00
20	2.8175E−01	3.9739E+00	3.6971E−01	2.3903E+00	4.0203E−01	2.0593E+00	4.4017E−01	1.7827E+00
21	2.6113E−01	4.1087E+00	3.4113E−01	2.4685E+00	3.7070E−01	2.1262E+00	4.0567E−01	1.8403E+00
22	2.4260E−01	4.2401E+00	3.1576E−01	2.5436E+00	3.4297E−01	2.1903E+00	3.7520E−01	1.8954E+00
23	2.2594E−01	4.3681E+00	2.9312E−01	2.6160E+00	3.1829E−01	2.2519E+00	3.4813E−01	1.9483E+00
24	2.1093E−01	4.4933E+00	2.7285E−01	2.6861E+00	2.9621E−01	2.3115E+00	3.2395E−01	1.9993E+00
25	1.9740E−01	4.6157E+00	2.5462E−01	2.7541E+00	2.7639E−01	2.3693E+00	3.0224E−01	2.0486E+00
26	1.8520E−01	4.7356E+00	2.3818E−01	2.8204E+00	2.5851E−01	2.4254E+00	2.8268E−01	2.0966E+00
27	1.7418E−01	4.8530E+00	2.2332E−01	2.8851E+00	2.4234E−01	2.4802E+00	2.6498E−01	2.1433E+00
28	1.6421E−01	4.9680E+00	2.0986E−01	2.9484E+00	2.2768E−01	2.5338E+00	2.4892E−01	2.1891E+00
29	1.5518E−01	5.0806E+00	1.9764E−01	3.0105E+00	2.1436E−01	2.5864E+00	2.3431E−01	2.2340E+00
30	1.4697E−01	5.1909E+00	1.8653E−01	3.0715E+00	2.0223E−01	2.6381E+00	2.2099E−01	2.2782E+00
31	1.3948E−01	5.2990E+00	1.7640E−01	3.1313E+00	1.9115E−01	2.6889E+00	2.0880E−01	2.3216E+00
32	1.3264E−01	5.4050E+00	1.6713E−01	3.1902E+00	1.8100E−01	2.7388E+00	1.9762E−01	2.3644E+00
33	1.2637E−01	5.5091E+00	1.5863E−01	3.2480E+00	1.7168E−01	2.7880E+00	1.8734E−01	2.4065E+00
34	1.2061E−01	5.6113E+00	1.5081E−01	3.3049E+00	1.6310E−01	2.8364E+00	1.7787E−01	2.4480E+00
35	1.1529E−01	5.7116E+00	1.4362E−01	3.3609E+00	1.5519E−01	2.8841E+00	1.6913E−01	2.4888E+00
36	1.1037E−01	5.8103E+00	1.3698E−01	3.4159E+00	1.4788E−01	2.9310E+00	1.6105E−01	2.5291E+00
37	1.0580E−01	5.9074E+00	1.3083E−01	3.4700E+00	1.4111E−01	2.9771E+00	1.5356E−01	2.5688E+00
38	1.0155E−01	6.0030E+00	1.2512E−01	3.5232E+00	1.3483E−01	3.0225E+00	1.4660E−01	2.6078E+00
39	9.7589E−02	6.0973E+00	1.1981E−01	3.5755E+00	1.2897E−01	3.0672E+00	1.4011E−01	2.6462E+00
40	9.3893E−02	6.1903E+00	1.1484E−01	3.6269E+00	1.2350E−01	3.1111E+00	1.3406E−01	2.6839E+00
41	9.0430E−02	6.2821E+00	1.1021E−01	3.6775E+00	1.1840E−01	3.1542E+00	1.2841E−01	2.7210E+00
42	8.7177E−02	8.9579E−02	1.0587E−01	3.7272E+00	1.1362E−01	3.1966E+00	1.2312E−01	2.7575E+00
43	8.4116E−02	1.7926E−01	1.0179E−01	3.7761E+00	1.0914E−01	3.2383E+00	1.1817E−01	2.7934E+00
44	8.1236E−02	2.6799E−01	9.7961E−02	3.8241E+00	1.0493E−01	3.2793E+00	1.1351E−01	2.8286E+00
45	7.8525E−02	3.5581E−01	9.4348E−02	3.8714E+00	1.0097E−01	3.3195E+00	1.0913E−01	2.8631E+00
46	7.5968E−02	4.4278E−01	9.0937E−02	3.9179E+00	9.7224E−02	3.3591E+00	1.0500E−01	2.8971E+00
47	7.3551E−02	5.2894E−01	8.7714E−02	3.9637E+00	9.3691E−02	3.3980E+00	1.0111E−01	2.9304E+00
48	7.1263E−02	6.1437E−01	8.4665E−02	4.0087E+00	9.0354E−02	3.4362E+00	9.7433E−02	2.9632E+00
49	6.9094E−02	6.9912E−01	8.1778E−02	4.0530E+00	8.7198E−02	3.4738E+00	9.3961E−02	2.9954E+00
50	6.7039E−02	7.8320E−01	7.9039E−02	4.0965E+00	8.4207E−02	3.5107E+00	9.0674E−02	3.0270E+00
51	6.5092E−02	8.6661E−01	7.6436E−02	4.1395E+00	8.1368E−02	3.5470E+00	8.7556E−02	3.0580E+00
52	6.3246E−02	9.4937E−01	7.3960E−02	4.1818E+00	7.8669E−02	3.5827E+00	8.4596E−02	3.0885E+00
53	6.1494E−02	1.0315E+00	7.1604E−02	4.2235E+00	7.6102E−02	3.6179E+00	8.1784E−02	3.1185E+00
54	5.9829E−02	1.1131E+00	6.9361E−02	4.2645E+00	7.3662E−02	3.6525E+00	7.9113E−02	3.1479E+00
55	5.8246E−02	1.1942E+00	6.7225E−02	4.3050E+00	7.1341E−02	3.6865E+00	7.6575E−02	3.1769E+00
56	5.6741E−02	1.2748E+00	6.5187E−02	4.3448E+00	6.9130E−02	3.7200E+00	7.4160E−02	3.2054E+00
57	5.5312E−02	1.3548E+00	6.3242E−02	4.3840E+00	6.7020E−02	3.7530E+00	7.1856E−02	3.2334E+00
58	5.3954E−02	1.4342E+00	6.1383E−02	4.4228E+00	6.5005E−02	3.7855E+00	6.9658E−02	3.2610E+00
59	5.2662E−02	1.5132E+00	5.9607E−02	4.4611E+00	6.3079E−02	3.8175E+00	6.7559E−02	3.2882E+00
60	5.1435E−02	1.5917E+00	5.7908E−02	4.4988E+00	6.1241E−02	3.8491E+00	6.5556E−02	3.3150E+00

Table 4.3.3.1. *Partial wave elastic scattering factors for neutral atoms (cont.)*
Nd; $Z = 60$

	10 keV		40 keV		60 keV		90 keV	
s	$\|f(s)\|$	$\eta(s)$	$\|f(s)\|$	$\eta(s)$	$\|f(s)\|$	$\eta(s)$	$\|f(s)\|$	$\eta(s)$
0	1.4119E+01	2.8873E−01	1.6423E+01	2.0045E−01	1.7330E+01	1.7798E−01	1.8487E+01	1.5802E−01
1	1.0206E+01	3.8730E−01	1.2180E+01	2.6378E−01	1.2914E+01	2.3333E−01	1.3832E+01	2.0647E−01
2	6.0770E+00	6.0589E−01	7.5938E+00	3.9891E−01	8.1191E+00	3.5059E−01	8.7556E+00	3.0858E−01
3	4.0922E+00	8.2028E−01	5.3104E+00	5.2825E−01	5.7165E+00	4.6231E−01	6.1973E+00	4.0556E−01
4	2.9430E+00	1.0317E+00	3.9433E+00	6.5384E−01	4.2696E+00	5.7046E−01	4.6496E+00	4.9923E−01
5	2.1968E+00	1.2549E+00	3.0173E+00	7.8447E−01	3.2827E+00	6.8261E−01	3.5884E+00	5.9612E−01
6	1.7004E+00	1.4824E+00	2.3737E+00	9.1683E−01	2.5919E+00	7.9603E−01	2.8414E+00	6.9396E−01
7	1.3600E+00	1.7040E+00	1.9174E+00	1.0458E+00	2.0991E+00	9.0649E−01	2.3062E+00	7.8917E−01
8	1.1160E+00	1.9158E+00	1.5834E+00	1.1693E+00	1.7370E+00	1.0122E+00	1.9117E+00	8.8024E−01
9	9.3389E−01	2.1191E+00	1.3307E+00	1.2878E+00	1.4620E+00	1.1136E+00	1.6113E+00	9.6756E−01
10	7.9448E−01	2.3165E+00	1.1340E+00	1.4028E+00	1.2473E+00	1.2120E+00	1.3761E+00	1.0523E+00
11	6.8613E−01	2.5094E+00	9.7772E−01	1.5156E+00	1.0760E+00	1.3085E+00	1.1878E+00	1.1354E+00
12	6.0093E−01	2.6978E+00	8.5185E−01	1.6267E+00	9.3737E−01	1.4036E+00	1.0349E+00	1.2173E+00
13	5.3305E−01	2.8810E+00	7.4934E−01	1.7358E+00	8.2397E−01	1.4972E+00	9.0940E−01	1.2979E+00
14	4.7806E−01	3.0581E+00	6.6503E−01	1.8424E+00	7.3036E−01	1.5887E+00	8.0546E−01	1.3769E+00
15	4.3262E−01	3.2284E+00	5.9499E−01	1.9458E+00	6.5239E−01	1.6777E+00	7.1872E−01	1.4538E+00
16	3.9429E−01	3.3918E+00	5.3618E−01	2.0456E+00	5.8686E−01	1.7637E+00	6.4574E−01	1.5282E+00
17	3.6131E−01	3.5485E+00	4.8624E−01	2.1413E+00	5.3126E−01	1.8462E+00	5.8382E−01	1.5996E+00
18	3.3244E−01	3.6990E+00	4.4336E−01	2.2327E+00	4.8362E−01	1.9251E+00	5.3083E−01	1.6679E+00
19	3.0684E−01	3.8442E+00	4.0614E−01	2.3200E+00	4.4241E−01	2.0003E+00	4.8510E−01	1.7329E+00
20	2.8396E−01	3.9848E+00	3.7353E−01	2.4034E+00	4.0644E−01	2.0719E+00	4.4530E−01	1.7948E+00
21	2.6342E−01	4.1212E+00	3.4475E−01	2.4831E+00	3.7480E−01	2.1403E+00	4.1038E−01	1.8537E+00
22	2.4492E−01	4.2540E+00	3.1918E−01	2.5597E+00	3.4679E−01	2.2058E+00	3.7955E−01	1.9100E+00
23	2.2824E−01	4.3836E+00	2.9636E−01	2.6334E+00	3.2186E−01	2.2687E+00	3.5216E−01	1.9641E+00
24	2.1319E−01	4.5101E+00	2.7590E−01	2.7047E+00	2.9956E−01	2.3294E+00	3.2769E−01	2.0161E+00
25	1.9959E−01	4.6340E+00	2.5749E−01	2.7739E+00	2.7952E−01	2.3882E+00	3.0573E−01	2.0664E+00
26	1.8731E−01	4.7553E+00	2.4088E−01	2.8412E+00	2.6144E−01	2.4452E+00	2.8594E−01	2.1152E+00
27	1.7619E−01	4.8741E+00	2.2584E−01	2.9068E+00	2.4508E−01	2.5008E+00	2.6803E−01	2.1627E+00
28	1.6612E−01	4.9906E+00	2.1222E−01	2.9709E+00	2.3025E−01	2.5551E+00	2.5178E−01	2.2090E+00
29	1.5697E−01	5.1046E+00	1.9985E−01	3.0338E+00	2.1677E−01	2.6084E+00	2.3700E−01	2.2545E+00
30	1.4865E−01	5.2163E+00	1.8859E−01	3.0954E+00	2.0449E−01	2.6606E+00	2.2352E−01	2.2991E+00
31	1.4106E−01	5.3258E+00	1.7832E−01	3.1559E+00	1.9327E−01	2.7119E+00	2.1119E−01	2.3430E+00
32	1.3412E−01	5.4332E+00	1.6892E−01	3.2154E+00	1.8299E−01	2.7624E+00	1.9988E−01	2.3861E+00
33	1.2776E−01	5.5387E+00	1.6031E−01	3.2738E+00	1.7355E−01	2.8120E+00	1.8948E−01	2.4286E+00
34	1.2191E−01	5.6421E+00	1.5239E−01	3.3313E+00	1.6486E−01	2.8609E+00	1.7990E−01	2.4704E+00
35	1.1651E−01	5.7438E+00	1.4510E−01	3.3878E+00	1.5686E−01	2.9090E+00	1.7106E−01	2.5117E+00
36	1.1151E−01	5.8437E+00	1.3837E−01	3.4434E+00	1.4946E−01	2.9563E+00	1.6288E−01	2.5523E+00
37	1.0687E−01	5.9420E+00	1.3215E−01	3.4980E+00	1.4262E−01	3.0029E+00	1.5531E−01	2.5924E+00
38	1.0256E−01	6.0387E+00	1.2637E−01	3.5517E+00	1.3626E−01	3.0488E+00	1.4827E−01	2.6318E+00
39	9.8547E−02	6.1341E+00	1.2099E−01	3.6046E+00	1.3034E−01	3.0939E+00	1.4172E−01	2.6705E+00
40	9.4797E−02	6.2282E+00	1.1598E−01	3.6566E+00	1.2481E−01	3.1383E+00	1.3560E−01	2.7087E+00
41	9.1286E−02	3.7860E−02	1.1129E−01	3.7078E+00	1.1966E−01	3.1819E+00	1.2989E−01	2.7462E+00
42	8.7989E−02	1.2957E−01	1.0691E−01	3.7581E+00	1.1483E−01	3.2248E+00	1.2455E−01	2.7831E+00
43	8.4888E−02	2.2024E−01	1.0280E−01	3.8075E+00	1.1031E−01	3.2670E+00	1.1954E−01	2.8194E+00
44	8.1972E−02	3.0993E−01	9.8933E−02	3.8562E+00	1.0606E−01	3.3085E+00	1.1484E−01	2.8551E+00
45	7.9227E−02	3.9870E−01	9.5290E−02	3.9041E+00	1.0206E−01	3.3493E+00	1.1042E−01	2.8902E+00
46	7.6637E−02	4.8660E−01	9.1852E−02	3.9512E+00	9.8288E−02	3.3894E+00	1.0625E−01	2.9246E+00
47	7.4192E−02	5.7369E−01	8.8603E−02	3.9976E+00	9.4726E−02	3.4289E+00	1.0232E−01	2.9584E+00
48	7.1876E−02	6.6005E−01	8.5532E−02	4.0432E+00	9.1361E−02	3.4676E+00	9.8609E−02	2.9917E+00
49	6.9682E−02	7.4573E−01	8.2624E−02	4.0881E+00	8.8179E−02	3.5057E+00	9.5104E−02	3.0243E+00
50	6.7604E−02	8.3073E−01	7.9865E−02	4.1323E+00	8.5163E−02	3.5432E+00	9.1785E−02	3.0564E+00
51	6.5635E−02	9.1508E−01	7.7243E−02	4.1758E+00	8.2299E−02	3.5801E+00	8.8637E−02	3.0880E+00
52	6.3769E−02	9.9881E−01	7.4750E−02	4.2188E+00	7.9579E−02	3.6164E+00	8.5648E−02	3.1190E+00
53	6.1997E−02	1.0819E+00	7.2378E−02	4.2611E+00	7.6991E−02	3.6521E+00	8.2809E−02	3.1495E+00
54	6.0314E−02	1.1645E+00	7.0119E−02	4.3028E+00	7.4530E−02	3.6873E+00	8.0112E−02	3.1795E+00
55	5.8714E−02	1.2466E+00	6.7967E−02	4.3438E+00	7.2190E−02	3.7219E+00	7.7548E−02	3.2090E+00
56	5.7194E−02	1.3282E+00	6.5914E−02	4.3843E+00	6.9959E−02	3.7559E+00	7.5108E−02	3.2380E+00
57	5.5751E−02	1.4093E+00	6.3954E−02	4.4242E+00	6.7830E−02	3.7895E+00	7.2781E−02	3.2665E+00
58	5.4378E−02	1.4899E+00	6.2081E−02	4.4636E+00	6.5797E−02	3.8225E+00	7.0560E−02	3.2946E+00
59	5.3074E−02	1.5700E+00	6.0291E−02	4.5024E+00	6.3854E−02	3.8551E+00	6.8439E−02	3.3222E+00
60	5.1835E−02	1.6496E+00	5.8579E−02	4.5408E+00	6.1998E−02	3.8872E+00	6.6415E−02	3.3495E+00

Table 4.3.3.1. *Partial wave elastic scattering factors for neutral atoms (cont.)*
Pm; $Z = 61$

	10 keV		40 keV		60 keV		90 keV	
s	$\|f(s)\|$	$\eta(s)$	$\|f(s)\|$	$\eta(s)$	$\|f(s)\|$	$\eta(s)$	$\|f(s)\|$	$\eta(s)$
0	1.3747E+01	2.9104E−01	1.6020E+01	2.0326E−01	1.6912E+01	1.8074E−01	1.8049E+01	1.6067E−01
1	9.9991E+00	3.8845E−01	1.1955E+01	2.6611E−01	1.2682E+01	2.3572E−01	1.3590E+01	2.0884E−01
2	5.9933E+00	6.0533E−01	7.5052E+00	4.0065E−01	8.0292E+00	3.5255E−01	8.6632E+00	3.1065E−01
3	4.0542E+00	8.1824E−01	5.2740E+00	5.2945E−01	5.6811E+00	4.6388E−01	6.1626E+00	4.0735E−01
4	2.9286E+00	1.0271E+00	3.9353E+00	6.5381E−01	4.2640E+00	5.7105E−01	4.6465E+00	5.0021E−01
5	2.1926E+00	1.2476E+00	3.0226E+00	7.8317E−01	3.2912E+00	6.8216E−01	3.6002E+00	5.9626E−01
6	1.6997E+00	1.4737E+00	2.3834E+00	9.1492E−01	2.6049E+00	7.9511E−01	2.8580E+00	6.9372E−01
7	1.3605E+00	1.6955E+00	1.9276E+00	1.0441E+00	2.1125E+00	9.0576E−01	2.3231E+00	7.8913E−01
8	1.1172E+00	1.9083E+00	1.5932E+00	1.1682E+00	1.7496E+00	1.0121E+00	1.9274E+00	8.8076E−01
9	9.3559E−01	2.1126E+00	1.3398E+00	1.2875E+00	1.4737E+00	1.1142E+00	1.6257E+00	9.6874E−01
10	7.9641E−01	2.3109E+00	1.1425E+00	1.4033E+00	1.2580E+00	1.2133E+00	1.3893E+00	1.0541E+00
11	6.8802E−01	2.5045E+00	9.8556E−01	1.5167E+00	1.0859E+00	1.3103E+00	1.1999E+00	1.1377E+00
12	6.0264E−01	2.6938E+00	8.5904E−01	1.6283E+00	9.4643E−01	1.4059E+00	1.0460E+00	1.2200E+00
13	5.3456E−01	2.8781E+00	7.5588E−01	1.7380E+00	8.3222E−01	1.5000E+00	9.1951E−01	1.3011E+00
14	4.7944E−01	3.0565E+00	6.7095E−01	1.8454E+00	7.3782E−01	1.5923E+00	8.1463E−01	1.3808E+00
15	4.3397E−01	3.2283E+00	6.0036E−01	1.9499E+00	6.5913E−01	1.6822E+00	7.2699E−01	1.4585E+00
16	3.9570E−01	3.3934E+00	5.4107E−01	2.0509E+00	5.9296E−01	1.7693E+00	6.5319E−01	1.5338E+00
17	3.6283E−01	3.5519E+00	4.9075E−01	2.1479E+00	5.3681E−01	1.8531E+00	5.9055E−01	1.6064E+00
18	3.3412E−01	3.7042E+00	4.4755E−01	2.2409E+00	4.8870E−01	1.9333E+00	5.3693E−01	1.6759E+00
19	3.0867E−01	3.8511E+00	4.1007E−01	2.3298E+00	4.4708E−01	2.0100E+00	4.9065E−01	1.7423E+00
20	2.8593E−01	3.9932E+00	3.7725E−01	2.4147E+00	4.1077E−01	2.0831E+00	4.5037E−01	1.8055E+00
21	2.6548E−01	4.1312E+00	3.4827E−01	2.4960E+00	3.7884E−01	2.1529E+00	4.1505E−01	1.8658E+00
22	2.4704E−01	4.2655E+00	3.2253E−01	2.5740E+00	3.5057E−01	2.2198E+00	3.8387E−01	1.9234E+00
23	2.3039E−01	4.3964E+00	2.9954E−01	2.6492E+00	3.2540E−01	2.2840E+00	3.5616E−01	1.9786E+00
24	2.1532E−01	4.5244E+00	2.7891E−01	2.7217E+00	3.0288E−01	2.3459E+00	3.3142E−01	2.0317E+00
25	2.0168E−01	4.6497E+00	2.6034E−01	2.7920E+00	2.8263E−01	2.4057E+00	3.0921E−01	2.0830E+00
26	1.8933E−01	4.7723E+00	2.4356E−01	2.8603E+00	2.6436E−01	2.4637E+00	2.8919E−01	2.1326E+00
27	1.7814E−01	4.8926E+00	2.2837E−01	2.9269E+00	2.4783E−01	2.5201E+00	2.7108E−01	2.1809E+00
28	1.6798E−01	5.0104E+00	2.1459E−01	2.9919E+00	2.3282E−01	2.5752E+00	2.5464E−01	2.2279E+00
29	1.5874E−01	5.1258E+00	2.0207E−01	3.0555E+00	2.1918E−01	2.6291E+00	2.3969E−01	2.2739E+00
30	1.5033E−01	5.2389E+00	1.9067E−01	3.1179E+00	2.0675E−01	2.6819E+00	2.2605E−01	2.3191E+00
31	1.4264E−01	5.3498E+00	1.8026E−01	3.1790E+00	1.9539E−01	2.7338E+00	2.1358E−01	2.3634E+00
32	1.3561E−01	5.4586E+00	1.7074E−01	3.2392E+00	1.8499E−01	2.7848E+00	2.0213E−01	2.4070E+00
33	1.2916E−01	5.5654E+00	1.6200E−01	3.2982E+00	1.7543E−01	2.8349E+00	1.9161E−01	2.4499E+00
34	1.2323E−01	5.6702E+00	1.5398E−01	3.3563E+00	1.6663E−01	2.8842E+00	1.8192E−01	2.4921E+00
35	1.1775E−01	5.7731E+00	1.4659E−01	3.4134E+00	1.5853E−01	2.9328E+00	1.7297E−01	2.5337E+00
36	1.1268E−01	5.8743E+00	1.3977E−01	3.4695E+00	1.5105E−01	2.9806E+00	1.6471E−01	2.5747E+00
37	1.0798E−01	5.9738E+00	1.3347E−01	3.5247E+00	1.4412E−01	3.0276E+00	1.5705E−01	2.6151E+00
38	1.0360E−01	6.0718E+00	1.2762E−01	3.5790E+00	1.3769E−01	3.0740E+00	1.4993E−01	2.6548E+00
39	9.9530E−02	6.1683E+00	1.2218E−01	3.6324E+00	1.3170E−01	3.1195E+00	1.4330E−01	2.6940E+00
40	9.5728E−02	6.2635E+00	1.1711E−01	3.6850E+00	1.2612E−01	3.1644E+00	1.3712E−01	2.7325E+00
41	9.2167E−02	7.4180E−02	1.1237E−01	3.7367E+00	1.2091E−01	3.2085E+00	1.3135E−01	2.7705E+00
42	8.8824E−02	1.6693E−01	1.0795E−01	3.7876E+00	1.1603E−01	3.2519E+00	1.2595E−01	2.8078E+00
43	8.5682E−02	2.5860E−01	1.0380E−01	3.8376E+00	1.1147E−01	3.2946E+00	1.2090E−01	2.8445E+00
44	8.2727E−02	3.4927E−01	9.9893E−02	3.8869E+00	1.0718E−01	3.3366E+00	1.1615E−01	2.8807E+00
45	7.9945E−02	4.3899E−01	9.6218E−02	3.9353E+00	1.0314E−01	3.3779E+00	1.1169E−01	2.9162E+00
46	7.7323E−02	5.2783E−01	9.2752E−02	3.9830E+00	9.9334E−02	3.4186E+00	1.0748E−01	2.9511E+00
47	7.4845E−02	6.1585E−01	8.9478E−02	4.0300E+00	9.5740E−02	3.4585E+00	1.0351E−01	2.9854E+00
48	7.2500E−02	7.0313E−01	8.6383E−02	4.0762E+00	9.2347E−02	3.4978E+00	9.9763E−02	3.0191E+00
49	7.0279E−02	7.8972E−01	8.3452E−02	4.1217E+00	8.9139E−02	3.5365E+00	9.6224E−02	3.0523E+00
50	6.8176E−02	8.7564E−01	8.0673E−02	4.1666E+00	8.6098E−02	3.5745E+00	9.2874E−02	3.0849E+00
51	6.6184E−02	9.6091E−01	7.8033E−02	4.2107E+00	8.3211E−02	3.6119E+00	8.9696E−02	3.1169E+00
52	6.4295E−02	1.0456E+00	7.5522E−02	4.2543E+00	8.0468E−02	3.6488E+00	8.6680E−02	3.1484E+00
53	6.2502E−02	1.1296E+00	7.3133E−02	4.2972E+00	7.7860E−02	3.6851E+00	8.3815E−02	3.1794E+00
54	6.0799E−02	1.2132E+00	7.0858E−02	4.3395E+00	7.5380E−02	3.7208E+00	8.1091E−02	3.2099E+00
55	5.9181E−02	1.2963E+00	6.8691E−02	4.3811E+00	7.3019E−02	3.7559E+00	7.8503E−02	3.2399E+00
56	5.7644E−02	1.3789E+00	6.6624E−02	4.4222E+00	7.0770E−02	3.7905E+00	7.6040E−02	3.2694E+00
57	5.6184E−02	1.4610E+00	6.4649E−02	4.4627E+00	6.8623E−02	3.8246E+00	7.3689E−02	3.2984E+00
58	5.4796E−02	1.5426E+00	6.2762E−02	4.5027E+00	6.6572E−02	3.8582E+00	7.1446E−02	3.3270E+00
59	5.3478E−02	1.6238E+00	6.0959E−02	4.5422E+00	6.4613E−02	3.8914E+00	6.9304E−02	3.3551E+00
60	5.2225E−02	1.7046E+00	5.9234E−02	4.5811E+00	6.2740E−02	3.9240E+00	6.7259E−02	3.3828E+00

Table 4.3.3.1. *Partial wave elastic scattering factors for neutral atoms (cont.)*
Sm; $Z = 62$

	10 keV		40 keV		60 keV		90 keV	
s	$\|f(s)\|$	$\eta(s)$	$\|f(s)\|$	$\eta(s)$	$\|f(s)\|$	$\eta(s)$	$\|f(s)\|$	$\eta(s)$
0	1.3395E+01	2.9309E−01	1.5635E+01	2.0589E−01	1.6514E+01	1.8334E−01	1.7631E+01	1.6319E−01
1	9.7992E+00	3.8936E−01	1.1735E+01	2.6827E−01	1.2455E+01	2.3797E−01	1.3352E+01	2.1109E−01
2	5.9092E+00	6.0457E−01	7.4147E+00	4.0225E−01	7.9369E+00	3.5441E−01	8.5680E+00	3.1262E−01
3	4.0140E+00	8.1613E−01	5.2337E+00	5.3059E−01	5.6414E+00	4.6541E−01	6.1230E+00	4.0909E−01
4	2.9118E+00	1.0224E+00	3.9232E+00	6.5380E−01	4.2540E+00	5.7164E−01	4.6385E+00	5.0120E−01
5	2.1866E+00	1.2402E+00	3.0246E+00	7.8186E−01	3.2961E+00	6.8171E−01	3.6082E+00	5.9639E−01
6	1.6976E+00	1.4648E+00	2.3907E+00	9.1286E−01	2.6154E+00	7.9406E−01	2.8719E+00	6.9338E−01
7	1.3600E+00	1.6864E+00	1.9363E+00	1.0420E+00	2.1243E+00	9.0473E−01	2.3381E+00	7.8883E−01
8	1.1175E+00	1.8998E+00	1.6019E+00	1.1667E+00	1.7611E+00	1.0115E+00	1.9418E+00	8.8088E−01
9	9.3658E−01	2.1051E+00	1.3481E+00	1.2866E+00	1.4844E+00	1.1142E+00	1.6392E+00	9.6943E−01
10	7.9774E−01	2.3041E+00	1.1503E+00	1.4030E+00	1.2681E+00	1.2139E+00	1.4017E+00	1.0553E+00
11	6.8943E−01	2.4984E+00	9.9286E−01	1.5170E+00	1.0952E+00	1.3115E+00	1.2115E+00	1.1394E+00
12	6.0396E−01	2.6884E+00	8.6579E−01	1.6291E+00	9.5504E−01	1.4075E+00	1.0566E+00	1.2221E+00
13	5.3574E−01	2.8737E+00	7.6206E−01	1.7394E+00	8.4010E−01	1.5022E+00	9.2925E−01	1.3037E+00
14	4.8052E−01	3.0533E+00	6.7658E−01	1.8475E+00	7.4500E−01	1.5950E+00	8.2350E−01	1.3839E+00
15	4.3502E−01	3.2265E+00	6.0549E−01	1.9529E+00	6.6565E−01	1.6858E+00	7.3503E−01	1.4624E+00
16	3.9681E−01	3.3932E+00	5.4576E−01	2.0550E+00	5.9889E−01	1.7738E+00	6.6047E−01	1.5386E+00
17	3.6407E−01	3.5533E+00	4.9508E−01	2.1534E+00	5.4221E−01	1.8588E+00	5.9714E−01	1.6122E+00
18	3.3551E−01	3.7073E+00	4.5158E−01	2.2478E+00	4.9365E−01	1.9404E+00	5.4292E−01	1.6829E+00
19	3.1024E−01	3.8558E+00	4.1387E−01	2.3382E+00	4.5165E−01	2.0184E+00	4.9612E−01	1.7506E+00
20	2.8764E−01	3.9995E+00	3.8085E−01	2.4246E+00	4.1502E−01	2.0930E+00	4.5539E−01	1.8151E+00
21	2.6732E−01	4.1389E+00	3.5169E−01	2.5074E+00	3.8281E−01	2.1642E+00	4.1968E−01	1.8767E+00
22	2.4897E−01	4.2746E+00	3.2579E−01	2.5868E+00	3.5429E−01	2.2324E+00	3.8815E−01	1.9356E+00
23	2.3236E−01	4.4070E+00	3.0265E−01	2.6633E+00	3.2890E−01	2.2979E+00	3.6014E−01	1.9920E+00
24	2.1731E−01	4.5363E+00	2.8188E−01	2.7371E+00	3.0617E−01	2.3610E+00	3.3513E−01	2.0462E+00
25	2.0365E−01	4.6629E+00	2.6316E−01	2.8086E+00	2.8573E−01	2.4219E+00	3.1268E−01	2.0984E+00
26	1.9126E−01	4.7870E+00	2.4623E−01	2.8779E+00	2.6727E−01	2.4808E+00	2.9244E−01	2.1490E+00
27	1.8001E−01	4.9085E+00	2.3089E−01	2.9455E+00	2.5057E−01	2.5382E+00	2.7413E−01	2.1980E+00
28	1.6978E−01	5.0277E+00	2.1696E−01	3.0114E+00	2.3540E−01	2.5940E+00	2.5750E−01	2.2457E+00
29	1.6047E−01	5.1445E+00	2.0430E−01	3.0758E+00	2.2161E−01	2.6487E+00	2.4238E−01	2.2924E+00
30	1.5197E−01	5.2590E+00	1.9276E−01	3.1390E+00	2.0903E−01	2.7022E+00	2.2858E−01	2.3381E+00
31	1.4421E−01	5.3712E+00	1.8222E−01	3.2009E+00	1.9753E−01	2.7547E+00	2.1596E−01	2.3830E+00
32	1.3709E−01	5.4814E+00	1.7257E−01	3.2616E+00	1.8699E−01	2.8062E+00	2.0438E−01	2.4270E+00
33	1.3057E−01	5.5895E+00	1.6372E−01	3.3213E+00	1.7732E−01	2.8568E+00	1.9374E−01	2.4703E+00
34	1.2456E−01	5.6957E+00	1.5558E−01	3.3800E+00	1.6841E−01	2.9066E+00	1.8393E−01	2.5129E+00
35	1.1901E−01	5.7999E+00	1.4810E−01	3.4377E+00	1.6021E−01	2.9556E+00	1.7488E−01	2.5549E+00
36	1.1387E−01	5.9023E+00	1.4119E−01	3.4944E+00	1.5263E−01	3.0039E+00	1.6652E−01	2.5962E+00
37	1.0910E−01	6.0031E+00	1.3480E−01	3.5501E+00	1.4562E−01	3.0514E+00	1.5877E−01	2.6370E+00
38	1.0467E−01	6.1023E+00	1.2888E−01	3.6050E+00	1.3911E−01	3.0982E+00	1.5157E−01	2.6772E+00
39	1.0054E−01	6.1999E+00	1.2337E−01	3.6590E+00	1.3305E−01	3.1442E+00	1.4487E−01	2.7167E+00
40	9.6681E−02	1.3042E−02	1.1824E−01	3.7122E+00	1.2741E−01	3.1895E+00	1.3863E−01	2.7556E+00
41	9.3071E−02	1.0804E−01	1.1345E−01	3.7644E+00	1.2214E−01	3.2341E+00	1.3280E−01	2.7939E+00
42	8.9682E−02	2.0184E−01	1.0898E−01	3.8159E+00	1.1722E−01	3.2780E+00	1.2734E−01	2.8317E+00
43	8.6498E−02	2.9453E−01	1.0479E−01	3.8665E+00	1.1261E−01	3.3212E+00	1.2224E−01	2.8688E+00
44	8.3503E−02	3.8619E−01	1.0085E−01	3.9163E+00	1.0828E−01	3.3637E+00	1.1744E−01	2.9054E+00
45	8.0683E−02	4.7688E−01	9.7137E−02	3.9653E+00	1.0420E−01	3.4055E+00	1.1293E−01	2.9413E+00
46	7.8025E−02	5.6666E−01	9.3640E−02	4.0136E+00	1.0036E−01	3.4466E+00	1.0868E−01	2.9767E+00
47	7.5515E−02	6.5561E−01	9.0339E−02	4.0612E+00	9.6738E−02	3.4871E+00	1.0468E−01	3.0114E+00
48	7.3139E−02	7.4381E−01	8.7219E−02	4.1080E+00	9.3315E−02	3.5269E+00	1.0089E−01	3.0456E+00
49	7.0889E−02	8.3131E−01	8.4266E−02	4.1540E+00	9.0080E−02	3.5661E+00	9.7324E−02	3.0793E+00
50	6.8759E−02	9.1814E−01	8.1465E−02	4.1995E+00	8.7014E−02	3.6047E+00	9.3942E−02	3.1123E+00
51	6.6741E−02	1.0043E+00	7.8805E−02	4.2442E+00	8.4104E−02	3.6426E+00	9.0736E−02	3.1449E+00
52	6.4827E−02	1.0899E+00	7.6277E−02	4.2883E+00	8.1339E−02	3.6800E+00	8.7692E−02	3.1769E+00
53	6.3011E−02	1.1749E+00	7.3871E−02	4.3319E+00	7.8710E−02	3.7168E+00	8.4800E−02	3.2083E+00
54	6.1287E−02	1.2594E+00	7.1581E−02	4.3747E+00	7.6210E−02	3.7531E+00	8.2052E−02	3.2393E+00
55	5.9648E−02	1.3434E+00	6.9398E−02	4.4170E+00	7.3831E−02	3.7887E+00	7.9440E−02	3.2698E+00
56	5.8092E−02	1.4270E+00	6.7316E−02	4.4587E+00	7.1563E−02	3.8239E+00	7.6953E−02	3.2997E+00
57	5.6614E−02	1.5101E+00	6.5328E−02	4.4998E+00	6.9399E−02	3.8585E+00	7.4580E−02	3.3292E+00
58	5.5209E−02	1.5928E+00	6.3428E−02	4.5404E+00	6.7331E−02	3.8927E+00	7.2316E−02	3.3583E+00
59	5.3875E−02	1.6751E+00	6.1611E−02	4.5805E+00	6.5355E−02	3.9263E+00	7.0153E−02	3.3869E+00
60	5.2607E−02	1.7569E+00	5.9873E−02	4.6200E+00	6.3467E−02	3.9595E+00	6.8088E−02	3.4151E+00

Table 4.3.3.1. *Partial wave elastic scattering factors for neutral atoms (cont.)*
Eu; $Z = 63$

	10 keV		40 keV		60 keV		90 keV	
s	$\|f(s)\|$	$\eta(s)$	$\|f(s)\|$	$\eta(s)$	$\|f(s)\|$	$\eta(s)$	$\|f(s)\|$	$\eta(s)$
0	1.3056E+01	2.9531E−01	1.5264E+01	2.0862E−01	1.6130E+01	1.8604E−01	1.7227E+01	1.6580E−01
1	9.6092E+00	3.9035E−01	1.1526E+01	2.7045E−01	1.2239E+01	2.4023E−01	1.3126E+01	2.1335E−01
2	5.8309E+00	6.0373E−01	7.3302E+00	4.0376E−01	7.8508E+00	3.5618E−01	8.4793E+00	3.1453E−01
3	3.9757E+00	8.1406E−01	5.1952E+00	5.3170E−01	5.6035E+00	4.6691E−01	6.0853E+00	4.1082E−01
4	2.8951E+00	1.0181E+00	3.9107E+00	6.5391E−01	4.2434E+00	5.7234E−01	4.6298E+00	5.0228E−01
5	2.1802E+00	1.2334E+00	3.0255E+00	7.8079E−01	3.2998E+00	6.8145E−01	3.6147E+00	5.9669E−01
6	1.6952E+00	1.4565E+00	2.3970E+00	9.1106E−01	2.6247E+00	7.9323E−01	2.8844E+00	6.9323E−01
7	1.3591E+00	1.6778E+00	1.9441E+00	1.0402E+00	2.1350E+00	9.0389E−01	2.3519E+00	7.8871E−01
8	1.1175E+00	1.8918E+00	1.6097E+00	1.1653E+00	1.7716E+00	1.0111E+00	1.9552E+00	8.8114E−01
9	9.3720E−01	2.0978E+00	1.3557E+00	1.2859E+00	1.4945E+00	1.1144E+00	1.6518E+00	9.7023E−01
10	7.9876E−01	2.2976E+00	1.1575E+00	1.4029E+00	1.2775E+00	1.2146E+00	1.4135E+00	1.0566E+00
11	6.9058E−01	2.4925E+00	9.9970E−01	1.5174E+00	1.1040E+00	1.3127E+00	1.2224E+00	1.1411E+00
12	6.0506E−01	2.6832E+00	8.7216E−01	1.6300E+00	9.6323E−01	1.4092E+00	1.0668E+00	1.2243E+00
13	5.3672E−01	2.8693E+00	7.6794E−01	1.7408E+00	8.4765E−01	1.5043E+00	9.3862E−01	1.3063E+00
14	4.8140E−01	3.0500E+00	6.8196E−01	1.8495E+00	7.5191E−01	1.5977E+00	8.3208E−01	1.3870E+00
15	4.3588E−01	3.2246E+00	6.1040E−01	1.9557E+00	6.7195E−01	1.6892E+00	7.4285E−01	1.4661E+00
16	3.9771E−01	3.3927E+00	5.5028E−01	2.0588E+00	6.0463E−01	1.7781E+00	6.6758E−01	1.5431E+00
17	3.6509E−01	3.5544E+00	4.9924E−01	2.1584E+00	5.4746E−01	1.8642E+00	6.0360E−01	1.6177E+00
18	3.3668E−01	3.7099E+00	4.5547E−01	2.2541E+00	4.9847E−01	1.9469E+00	5.4881E−01	1.6895E+00
19	3.1157E−01	3.8600E+00	4.1753E−01	2.3459E+00	4.5612E−01	2.0263E+00	5.0150E−01	1.7583E+00
20	2.8914E−01	4.0052E+00	3.8432E−01	2.4338E+00	4.1918E−01	2.1022E+00	4.6034E−01	1.8241E+00
21	2.6895E−01	4.1461E+00	3.5502E−01	2.5181E+00	3.8670E−01	2.1748E+00	4.2424E−01	1.8870E+00
22	2.5070E−01	4.2832E+00	3.2897E−01	2.5989E+00	3.5794E−01	2.2444E+00	3.9239E−01	1.9471E+00
23	2.3417E−01	4.4169E+00	3.0569E−01	2.6767E+00	3.3234E−01	2.3112E+00	3.6409E−01	2.0047E+00
24	2.1915E−01	4.5475E+00	2.8479E−01	2.7518E+00	3.0942E−01	2.3754E+00	3.3881E−01	2.0600E+00
25	2.0550E−01	4.6754E+00	2.6593E−01	2.8244E+00	2.8879E−01	2.4374E+00	3.1613E−01	2.1133E+00
26	1.9309E−01	4.8007E+00	2.4887E−01	2.8949E+00	2.7017E−01	2.4974E+00	2.9567E−01	2.1648E+00
27	1.8181E−01	4.9236E+00	2.3339E−01	2.9634E+00	2.5329E−01	2.5556E+00	2.7716E−01	2.2146E+00
28	1.7153E−01	5.0441E+00	2.1933E−01	3.0303E+00	2.3797E−01	2.6124E+00	2.6036E−01	2.2631E+00
29	1.6215E−01	5.1622E+00	2.0653E−01	3.0956E+00	2.2402E−01	2.6677E+00	2.4507E−01	2.3105E+00
30	1.5359E−01	5.2780E+00	1.9485E−01	3.1595E+00	2.1130E−01	2.7219E+00	2.3111E−01	2.3568E+00
31	1.4575E−01	5.3916E+00	1.8419E−01	3.2221E+00	1.9967E−01	2.7750E+00	2.1834E−01	2.4021E+00
32	1.3857E−01	5.5031E+00	1.7442E−01	3.2836E+00	1.8901E−01	2.8271E+00	2.0663E−01	2.4467E+00
33	1.3197E−01	5.6126E+00	1.6545E−01	3.3439E+00	1.7921E−01	2.8783E+00	1.9586E−01	2.4904E+00
34	1.2589E−01	5.7201E+00	1.5721E−01	3.4032E+00	1.7020E−01	2.9286E+00	1.8594E−01	2.5334E+00
35	1.2027E−01	5.8256E+00	1.4962E−01	3.4615E+00	1.6189E−01	2.9781E+00	1.7679E−01	2.5758E+00
36	1.1507E−01	5.9293E+00	1.4262E−01	3.5188E+00	1.5422E−01	3.0268E+00	1.6833E−01	2.6176E+00
37	1.1024E−01	6.0313E+00	1.3615E−01	3.5752E+00	1.4712E−01	3.0748E+00	1.6049E−01	2.6587E+00
38	1.0575E−01	6.1317E+00	1.3015E−01	3.6306E+00	1.4053E−01	3.1220E+00	1.5321E−01	2.6992E+00
39	1.0156E−01	6.2306E+00	1.2457E−01	3.6851E+00	1.3441E−01	3.1685E+00	1.4643E−01	2.7391E+00
40	9.7655E−02	4.4808E−02	1.1938E−01	3.7388E+00	1.2870E−01	3.2143E+00	1.4012E−01	2.7784E+00
41	9.3996E−02	1.4091E−01	1.1454E−01	3.7917E+00	1.2338E−01	3.2593E+00	1.3422E−01	2.8172E+00
42	9.0562E−02	2.3577E−01	1.1001E−01	3.8437E+00	1.1840E−01	3.3037E+00	1.2872E−01	2.8553E+00
43	8.7334E−02	3.2950E−01	1.0577E−01	3.8948E+00	1.1374E−01	3.3473E+00	1.2356E−01	2.8928E+00
44	8.4299E−02	4.2216E−01	1.0179E−01	3.9452E+00	1.0937E−01	3.3903E+00	1.1871E−01	2.9298E+00
45	8.1441E−02	5.1383E−01	9.8049E−02	3.9948E+00	1.0525E−01	3.4326E+00	1.1416E−01	2.9661E+00
46	7.8746E−02	6.0456E−01	9.4520E−02	4.0437E+00	1.0137E−01	3.4742E+00	1.0987E−01	3.0019E+00
47	7.6201E−02	6.9445E−01	9.1189E−02	4.0918E+00	9.7719E−02	3.5152E+00	1.0582E−01	3.0371E+00
48	7.3793E−02	7.8356E−01	8.8043E−02	4.1392E+00	9.4267E−02	3.5556E+00	1.0201E−01	3.0718E+00
49	7.1513E−02	8.7197E−01	8.5066E−02	4.1858E+00	9.1003E−02	3.5952E+00	9.8404E−02	3.1059E+00
50	6.9354E−02	9.5970E−01	8.2243E−02	4.2318E+00	8.7912E−02	3.6343E+00	9.4991E−02	3.1394E+00
51	6.7308E−02	1.0468E+00	7.9563E−02	4.2771E+00	8.4978E−02	3.6728E+00	9.1756E−02	3.1724E+00
52	6.5369E−02	1.1333E+00	7.7017E−02	4.3218E+00	8.2192E−02	3.7107E+00	8.8685E−02	3.2048E+00
53	6.3528E−02	1.2192E+00	7.4594E−02	4.3659E+00	7.9542E−02	3.7480E+00	8.5767E−02	3.2368E+00
54	6.1780E−02	1.3046E+00	7.2287E−02	4.4094E+00	7.7022E−02	3.7848E+00	8.2994E−02	3.2682E+00
55	6.0120E−02	1.3896E+00	7.0089E−02	4.4522E+00	7.4624E−02	3.8210E+00	8.0358E−02	3.2992E+00
56	5.8542E−02	1.4741E+00	6.7992E−02	4.4945E+00	7.2339E−02	3.8567E+00	7.7849E−02	3.3296E+00
57	5.7044E−02	1.5582E+00	6.5990E−02	4.5362E+00	7.0157E−02	3.8918E+00	7.5455E−02	3.3596E+00
58	5.5620E−02	1.6419E+00	6.4077E−02	4.5774E+00	6.8073E−02	3.9265E+00	7.3169E−02	3.3891E+00
59	5.4268E−02	1.7251E+00	6.2247E−02	4.6180E+00	6.6081E−02	3.9607E+00	7.0987E−02	3.4182E+00
60	5.2984E−02	1.8081E+00	6.0497E−02	4.6582E+00	6.4178E−02	3.9944E+00	6.8902E−02	3.4469E+00

Table 4.3.3.1. *Partial wave elastic scattering factors for neutral atoms (cont.)*
Gd; $Z = 64$

	10 keV		40 keV		60 keV		90 keV	
s	$\|f(s)\|$	$\eta(s)$	$\|f(s)\|$	$\eta(s)$	$\|f(s)\|$	$\eta(s)$	$\|f(s)\|$	$\eta(s)$
0	1.2712E+01	3.0927E−01	1.4919E+01	2.1809E−01	1.5776E+01	1.9448E−01	1.6860E+01	1.7334E−01
1	9.6906E+00	3.9480E−01	1.1638E+01	2.7378E−01	1.2361E+01	2.4330E−01	1.3261E+01	2.1618E−01
2	5.9880E+00	5.9894E−01	7.5269E+00	4.0180E−01	8.0624E+00	3.5475E−01	8.7090E+00	3.1350E−01
3	4.0295E+00	8.1801E−01	5.2714E+00	5.3518E−01	5.6878E+00	4.7022E−01	6.1791E+00	4.1395E−01
4	2.9114E+00	1.0307E+00	3.9386E+00	6.6254E−01	4.2760E+00	5.8011E−01	4.6676E+00	5.0930E−01
5	2.1882E+00	1.2497E+00	3.0418E+00	7.9175E−01	3.3195E+00	6.9127E−01	3.6383E+00	6.0551E−01
6	1.7007E+00	1.4745E+00	2.4096E+00	9.2329E−01	2.6402E+00	8.0417E−01	2.9032E+00	7.0305E−01
7	1.3633E+00	1.6977E+00	1.9543E+00	1.0537E+00	2.1477E+00	9.1595E−01	2.3674E+00	7.9953E−01
8	1.1212E+00	1.9136E+00	1.6183E+00	1.1801E+00	1.7823E+00	1.0243E+00	1.9684E+00	8.9303E−01
9	9.4073E−01	2.1212E+00	1.3633E+00	1.3019E+00	1.5039E+00	1.1287E+00	1.6633E+00	9.8305E−01
10	8.0207E−01	2.3219E+00	1.1646E+00	1.4197E+00	1.2862E+00	1.2296E+00	1.4241E+00	1.0701E+00
11	6.9349E−01	2.5173E+00	1.0064E+00	1.5346E+00	1.1122E+00	1.3281E+00	1.2324E+00	1.1549E+00
12	6.0745E−01	2.7083E+00	8.7838E−01	1.6473E+00	9.7095E−01	1.4247E+00	1.0762E+00	1.2383E+00
13	5.3859E−01	2.8948E+00	7.7369E−01	1.7582E+00	8.5486E−01	1.5199E+00	9.4746E−01	1.3204E+00
14	4.8285E−01	3.0761E+00	6.8723E−01	1.8672E+00	7.5857E−01	1.6136E+00	8.4029E−01	1.4013E+00
15	4.3705E−01	3.2517E+00	6.1520E−01	1.9739E+00	6.7806E−01	1.7054E+00	7.5041E−01	1.4807E+00
16	3.9876E−01	3.4211E+00	5.5466E−01	2.0777E+00	6.1021E−01	1.7950E+00	6.7449E−01	1.5583E+00
17	3.6612E−01	3.5842E+00	5.0327E−01	2.1782E+00	5.5256E−01	1.8819E+00	6.0991E−01	1.6336E+00
18	3.3779E−01	3.7413E+00	4.5922E−01	2.2751E+00	5.0316E−01	1.9657E+00	5.5457E−01	1.7064E+00
19	3.1281E−01	3.8928E+00	4.2105E−01	2.3682E+00	4.6045E−01	2.0463E+00	5.0677E−01	1.7763E+00
20	2.9053E−01	4.0394E+00	3.8767E−01	2.4575E+00	4.2322E−01	2.1235E+00	4.6519E−01	1.8433E+00
21	2.7048E−01	4.1816E+00	3.5823E−01	2.5432E+00	3.9049E−01	2.1975E+00	4.2873E−01	1.9074E+00
22	2.5235E−01	4.3200E+00	3.3206E−01	2.6254E+00	3.6152E−01	2.2684E+00	3.9655E−01	1.9688E+00
23	2.3589E−01	4.4549E+00	3.0866E−01	2.7046E+00	3.3572E−01	2.3364E+00	3.6797E−01	2.0276E+00
24	2.2092E−01	4.5868E+00	2.8764E−01	2.7809E+00	3.1261E−01	2.4019E+00	3.4245E−01	2.0841E+00
25	2.0729E−01	4.7159E+00	2.6866E−01	2.8547E+00	2.9182E−01	2.4650E+00	3.1953E−01	2.1384E+00
26	1.9488E−01	4.8425E+00	2.5148E−01	2.9263E+00	2.7303E−01	2.5261E+00	2.9887E−01	2.1908E+00
27	1.8356E−01	4.9665E+00	2.3588E−01	2.9959E+00	2.5600E−01	2.5853E+00	2.8017E−01	2.2416E+00
28	1.7324E−01	5.0883E+00	2.2169E−01	3.0636E+00	2.4053E−01	2.6428E+00	2.6319E−01	2.2909E+00
29	1.6381E−01	5.2076E+00	2.0876E−01	3.1298E+00	2.2644E−01	2.6990E+00	2.4774E−01	2.3389E+00
30	1.5518E−01	5.3248E+00	1.9696E−01	3.1945E+00	2.1358E−01	2.7539E+00	2.3363E−01	2.3858E+00
31	1.4728E−01	5.4397E+00	1.8616E−01	3.2579E+00	2.0181E−01	2.8076E+00	2.2071E−01	2.4318E+00
32	1.4003E−01	5.5525E+00	1.7627E−01	3.3200E+00	1.9102E−01	2.8603E+00	2.0886E−01	2.4768E+00
33	1.3336E−01	5.6633E+00	1.6719E−01	3.3810E+00	1.8110E−01	2.9120E+00	1.9797E−01	2.5210E+00
34	1.2722E−01	5.7721E+00	1.5884E−01	3.4409E+00	1.7198E−01	2.9629E+00	1.8794E−01	2.5644E+00
35	1.2154E−01	5.8789E+00	1.5115E−01	3.4998E+00	1.6357E−01	3.0128E+00	1.7868E−01	2.6072E+00
36	1.1627E−01	5.9839E+00	1.4406E−01	3.5577E+00	1.5580E−01	3.0620E+00	1.7012E−01	2.6493E+00
37	1.1138E−01	6.0871E+00	1.3750E−01	3.6147E+00	1.4861E−01	3.1105E+00	1.6219E−01	2.6908E+00
38	1.0684E−01	6.1887E+00	1.3142E−01	3.6707E+00	1.4195E−01	3.1581E+00	1.5482E−01	2.7317E+00
39	1.0260E−01	5.5211E−03	1.2577E−01	3.7258E+00	1.3575E−01	3.2050E+00	1.4797E−01	2.7720E+00
40	9.8639E−02	1.0408E−01	1.2051E−01	3.7800E+00	1.2998E−01	3.2512E+00	1.4159E−01	2.8116E+00
41	9.4930E−02	2.0128E−01	1.1561E−01	3.8334E+00	1.2459E−01	3.2967E+00	1.3563E−01	2.8507E+00
42	9.1450E−02	2.9720E−01	1.1103E−01	3.8859E+00	1.1956E−01	3.3415E+00	1.3006E−01	2.8892E+00
43	8.8180E−02	3.9195E−01	1.0675E−01	3.9376E+00	1.1485E−01	3.3856E+00	1.2485E−01	2.9271E+00
44	8.5104E−02	4.8560E−01	1.0272E−01	3.9885E+00	1.1043E−01	3.4291E+00	1.1996E−01	2.9645E+00
45	8.2207E−02	5.7823E−01	9.8942E−02	4.0387E+00	1.0628E−01	3.4718E+00	1.1536E−01	3.0012E+00
46	7.9474E−02	6.6990E−01	9.5380E−02	4.0881E+00	1.0237E−01	3.5139E+00	1.1103E−01	3.0374E+00
47	7.6892E−02	7.6071E−01	9.2020E−02	4.1367E+00	9.8676E−02	3.5554E+00	1.0695E−01	3.0731E+00
48	7.4451E−02	8.5072E−01	8.8846E−02	4.1847E+00	9.5194E−02	3.5962E+00	1.0310E−01	3.1081E+00
49	7.2139E−02	9.3999E−01	8.5844E−02	4.2319E+00	9.1902E−02	3.6364E+00	9.9457E−02	3.1426E+00
50	6.9950E−02	1.0286E+00	8.2998E−02	4.2784E+00	8.8784E−02	3.6760E+00	9.6013E−02	3.1766E+00
51	6.7876E−02	1.1165E+00	8.0298E−02	4.3243E+00	8.5827E−02	3.7150E+00	9.2748E−02	3.2101E+00
52	6.5908E−02	1.2039E+00	7.7733E−02	4.3696E+00	8.3019E−02	3.7534E+00	8.9651E−02	3.2430E+00
53	6.4041E−02	1.2907E+00	7.5293E−02	4.4142E+00	8.0350E−02	3.7912E+00	8.6710E−02	3.2754E+00
54	6.2268E−02	1.3770E+00	7.2970E−02	4.4583E+00	7.7811E−02	3.8285E+00	8.3913E−02	3.3073E+00
55	6.0584E−02	1.4628E+00	7.0757E−02	4.5017E+00	7.5394E−02	3.8652E+00	8.1254E−02	3.3387E+00
56	5.8984E−02	1.5482E+00	6.8646E−02	4.5445E+00	7.3091E−02	3.9014E+00	7.8721E−02	3.3696E+00
57	5.7464E−02	1.6332E+00	6.6630E−02	4.5868E+00	7.0892E−02	3.9371E+00	7.6306E−02	3.4000E+00
58	5.6020E−02	1.7178E+00	6.4704E−02	4.6285E+00	6.8793E−02	3.9722E+00	7.4001E−02	3.4300E+00
59	5.4649E−02	1.8021E+00	6.2862E−02	4.6697E+00	6.6786E−02	4.0069E+00	7.1800E−02	3.4596E+00
60	5.3347E−02	1.8860E+00	6.1100E−02	4.7104E+00	6.4868E−02	4.0412E+00	6.9698E−02	3.4887E+00

Table 4.3.3.1. *Partial wave elastic scattering factors for neutral atoms (cont.)*
Tb; $Z = 65$

	10 keV		40 keV		60 keV		90 keV	
s	$\|f(s)\|$	$\eta(s)$	$\|f(s)\|$	$\eta(s)$	$\|f(s)\|$	$\eta(s)$	$\|f(s)\|$	$\eta(s)$
0	1.2423E+01	2.9911E−01	1.4568E+01	2.1364E−01	1.5408E+01	1.9105E−01	1.6468E+01	1.7068E−01
1	9.2443E+00	3.9180E−01	1.1121E+01	2.7443E−01	1.1819E+01	2.4443E−01	1.2687E+01	2.1759E−01
2	5.6735E+00	6.0164E−01	7.1565E+00	4.0647E−01	7.6731E+00	3.5946E−01	8.2954E+00	3.1811E−01
3	3.8950E+00	8.0964E−01	5.1101E+00	5.3371E−01	5.5185E+00	4.6972E−01	5.9996E+00	4.1410E−01
4	2.8568E+00	1.0095E+00	3.8769E+00	6.5403E−01	4.2124E+00	5.7366E−01	4.6015E+00	5.0437E−01
5	2.1635E+00	1.2197E+00	3.0200E+00	7.7852E−01	3.2988E+00	6.8084E−01	3.6184E+00	5.9721E−01
6	1.6874E+00	1.4391E+00	2.4041E+00	9.0710E−01	2.6371E+00	7.9125E−01	2.9024E+00	6.9265E−01
7	1.3549E+00	1.6591E+00	1.9556E+00	1.0357E+00	2.1520E+00	9.0155E−01	2.3746E+00	7.8787E−01
8	1.1155E+00	1.8736E+00	1.6225E+00	1.1613E+00	1.7895E+00	1.0092E+00	1.9785E+00	8.8078E−01
9	9.3672E−01	2.0808E+00	1.3686E+00	1.2829E+00	1.5120E+00	1.1135E+00	1.6743E+00	9.7069E−01
10	7.9930E−01	2.2818E+00	1.1701E+00	1.4010E+00	1.2943E+00	1.2146E+00	1.4349E+00	1.0580E+00
11	6.9163E−01	2.4778E+00	1.0118E+00	1.5164E+00	1.1200E+00	1.3136E+00	1.2426E+00	1.1433E+00
12	6.0623E−01	2.6696E+00	8.8363E−01	1.6298E+00	9.7826E−01	1.4108E+00	1.0857E+00	1.2272E+00
13	5.3781E−01	2.8571E+00	7.7864E−01	1.7415E+00	8.6164E−01	1.5067E+00	9.5619E−01	1.3099E+00
14	4.8238E−01	3.0396E+00	6.9186E−01	1.8513E+00	7.6483E−01	1.6011E+00	8.4830E−01	1.3915E+00
15	4.3683E−01	3.2164E+00	6.1951E−01	1.9589E+00	6.8382E−01	1.6938E+00	7.5774E−01	1.4716E+00
16	3.9877E−01	3.3872E+00	5.5867E−01	2.0637E+00	6.1551E−01	1.7843E+00	6.8119E−01	1.5500E+00
17	3.6637E−01	3.5518E+00	5.0703E−01	2.1654E+00	5.5745E−01	1.8722E+00	6.1604E−01	1.6263E+00
18	3.3827E−01	3.7103E+00	4.6275E−01	2.2635E+00	5.0769E−01	1.9571E+00	5.6019E−01	1.7000E+00
19	3.1351E−01	3.8633E+00	4.2441E−01	2.3579E+00	4.6467E−01	2.0389E+00	5.1195E−01	1.7710E+00
20	2.9142E−01	4.0113E+00	3.9088E−01	2.4485E+00	4.2716E−01	2.1173E+00	4.6997E−01	1.8392E+00
21	2.7155E−01	4.1549E+00	3.6130E−01	2.5354E+00	3.9420E−01	2.1925E+00	4.3317E−01	1.9045E+00
22	2.5357E−01	4.2946E+00	3.3502E−01	2.6190E+00	3.6502E−01	2.2647E+00	4.0068E−01	1.9670E+00
23	2.3723E−01	4.4308E+00	3.1152E−01	2.6994E+00	3.3903E−01	2.3339E+00	3.7183E−01	2.0269E+00
24	2.2234E−01	4.5640E+00	2.9039E−01	2.7770E+00	3.1575E−01	2.4006E+00	3.4607E−01	2.0845E+00
25	2.0877E−01	4.6943E+00	2.7131E−01	2.8520E+00	2.9480E−01	2.4648E+00	3.2294E−01	2.1398E+00
26	1.9639E−01	4.8221E+00	2.5403E−01	2.9246E+00	2.7586E−01	2.5269E+00	3.0207E−01	2.1932E+00
27	1.8508E−01	4.9474E+00	2.3831E−01	2.9952E+00	2.5869E−01	2.5870E+00	2.8319E−01	2.2449E+00
28	1.7475E−01	5.0704E+00	2.2401E−01	3.0640E+00	2.4307E−01	2.6455E+00	2.6604E−01	2.2950E+00
29	1.6530E−01	5.1910E+00	2.1097E−01	3.1310E+00	2.2885E−01	2.7025E+00	2.5042E−01	2.3438E+00
30	1.5665E−01	5.3094E+00	1.9905E−01	3.1966E+00	2.1585E−01	2.7582E+00	2.3616E−01	2.3914E+00
31	1.4871E−01	5.4256E+00	1.8814E−01	3.2608E+00	2.0396E−01	2.8126E+00	2.2311E−01	2.4379E+00
32	1.4141E−01	5.5398E+00	1.7814E−01	3.3237E+00	1.9305E−01	2.8659E+00	2.1113E−01	2.4835E+00
33	1.3470E−01	5.6518E+00	1.6895E−01	3.3854E+00	1.8302E−01	2.9183E+00	2.0011E−01	2.5282E+00
34	1.2851E−01	5.7619E+00	1.6050E−01	3.4460E+00	1.7379E−01	2.9697E+00	1.8996E−01	2.5722E+00
35	1.2278E−01	5.8700E+00	1.5272E−01	3.5055E+00	1.6528E−01	3.0202E+00	1.8059E−01	2.6154E+00
36	1.1747E−01	5.9763E+00	1.4553E−01	3.5641E+00	1.5742E−01	3.0699E+00	1.7193E−01	2.6580E+00
37	1.1253E−01	6.0808E+00	1.3889E−01	3.6216E+00	1.5014E−01	3.1188E+00	1.6391E−01	2.6999E+00
38	1.0794E−01	6.1836E+00	1.3273E−01	3.6782E+00	1.4340E−01	3.1670E+00	1.5646E−01	2.7411E+00
39	1.0365E−01	1.6799E−03	1.2701E−01	3.7339E+00	1.3712E−01	3.2144E+00	1.4954E−01	2.7818E+00
40	9.9648E−02	1.0143E−01	1.2169E−01	3.7887E+00	1.3128E−01	3.2611E+00	1.4308E−01	2.8219E+00
41	9.5898E−02	1.9978E−01	1.1672E−01	3.8427E+00	1.2584E−01	3.3070E+00	1.3706E−01	2.8613E+00
42	9.2376E−02	2.9682E−01	1.1209E−01	3.8958E+00	1.2075E−01	3.3523E+00	1.3143E−01	2.9002E+00
43	8.9065E−02	3.9266E−01	1.0775E−01	3.9481E+00	1.1599E−01	3.3969E+00	1.2616E−01	2.9385E+00
44	8.5950E−02	4.8737E−01	1.0369E−01	3.9995E+00	1.1152E−01	3.4408E+00	1.2121E−01	2.9763E+00
45	8.3015E−02	5.8103E−01	9.9865E−02	4.0503E+00	1.0732E−01	3.4840E+00	1.1657E−01	3.0134E+00
46	8.0247E−02	6.7370E−01	9.6265E−02	4.1002E+00	1.0337E−01	3.5266E+00	1.1219E−01	3.0500E+00
47	7.7631E−02	7.6548E−01	9.2872E−02	4.1494E+00	9.9645E−02	3.5685E+00	1.0807E−01	3.0861E+00
48	7.5156E−02	8.5644E−01	8.9668E−02	4.1979E+00	9.6130E−02	3.6098E+00	1.0418E−01	3.1216E+00
49	7.2812E−02	9.4666E−01	8.6638E−02	4.2457E+00	9.2809E−02	3.6505E+00	1.0051E−01	3.1565E+00
50	7.0592E−02	1.0362E+00	8.3768E−02	4.2928E+00	8.9664E−02	3.6906E+00	9.7036E−02	3.1909E+00
51	6.8487E−02	1.1250E+00	8.1046E−02	4.3393E+00	8.6681E−02	3.7301E+00	9.3742E−02	3.2248E+00
52	6.6491E−02	1.2133E+00	7.8459E−02	4.3851E+00	8.3850E−02	3.7690E+00	9.0617E−02	3.2582E+00
53	6.4596E−02	1.3010E+00	7.6000E−02	4.4303E+00	8.1158E−02	3.8073E+00	8.7648E−02	3.2910E+00
54	6.2796E−02	1.3882E+00	7.3659E−02	4.4749E+00	7.8598E−02	3.8451E+00	8.4826E−02	3.3234E+00
55	6.1086E−02	1.4750E+00	7.1429E−02	4.5188E+00	7.6163E−02	3.8823E+00	8.2144E−02	3.3552E+00
56	5.9461E−02	1.5613E+00	6.9302E−02	4.5622E+00	7.3841E−02	3.9190E+00	7.9590E−02	3.3866E+00
57	5.7918E−02	1.6473E+00	6.7272E−02	4.6051E+00	7.1626E−02	3.9552E+00	7.7153E−02	3.4175E+00
58	5.6451E−02	1.7329E+00	6.5332E−02	4.6474E+00	6.9509E−02	3.9908E+00	7.4827E−02	3.4479E+00
59	5.5058E−02	1.8181E+00	6.3477E−02	4.6892E+00	6.7487E−02	4.0261E+00	7.2607E−02	3.4779E+00
60	5.3734E−02	1.9031E+00	6.1702E−02	4.7304E+00	6.5554E−02	4.0608E+00	7.0485E−02	3.5075E+00

Table 4.3.3.1. *Partial wave elastic scattering factors for neutral atoms (cont.)*
Dy; $Z = 66$

	10 keV		40 keV		60 keV		90 keV	
s	$\|f(s)\|$	$\eta(s)$	$\|f(s)\|$	$\eta(s)$	$\|f(s)\|$	$\eta(s)$	$\|f(s)\|$	$\eta(s)$
0	1.2127E+01	3.0077E−01	1.4241E+01	2.1597E−01	1.5068E+01	1.9340E−01	1.6111E+01	1.7300E−01
1	9.0699E+00	3.9231E−01	1.0926E+01	2.7626E−01	1.1617E+01	2.4639E−01	1.2474E+01	2.1960E−01
2	5.5957E+00	6.0041E−01	7.0691E+00	4.0768E−01	7.5833E+00	3.6098E−01	8.2021E+00	3.1980E−01
3	3.8535E+00	8.0732E−01	5.0649E+00	5.3461E−01	5.4728E+00	4.7104E−01	5.9531E+00	4.1567E−01
4	2.8359E+00	1.0051E+00	3.8565E+00	6.5406E−01	4.1931E+00	5.7429E−01	4.5830E+00	5.0539E−01
5	2.1536E+00	1.2128E+00	3.0141E+00	7.7738E−01	3.2947E+00	6.8052E−01	3.6163E+00	5.9745E−01
6	1.6823E+00	1.4303E+00	2.4052E+00	9.0502E−01	2.6406E+00	7.9018E−01	2.9083E+00	6.9228E−01
7	1.3520E+00	1.6494E+00	1.9596E+00	1.0332E+00	2.1584E+00	9.0016E−01	2.3837E+00	7.8727E−01
8	1.1137E+00	1.8638E+00	1.6275E+00	1.1589E+00	1.7969E+00	1.0079E+00	1.9885E+00	8.8027E−01
9	9.3574E−01	2.0714E+00	1.3739E+00	1.2808E+00	1.5196E+00	1.1125E+00	1.6842E+00	9.7049E−01
10	7.9892E−01	2.2728E+00	1.1755E+00	1.3993E+00	1.3017E+00	1.2141E+00	1.4445E+00	1.0581E+00
11	6.9160E−01	2.4693E+00	1.0171E+00	1.5151E+00	1.1272E+00	1.3134E+00	1.2518E+00	1.1438E+00
12	6.0635E−01	2.6615E+00	8.8873E−01	1.6289E+00	9.8510E−01	1.4110E+00	1.0944E+00	1.2280E+00
13	5.3796E−01	2.8496E+00	7.8347E−01	1.7410E+00	8.6809E−01	1.5072E+00	9.6439E−01	1.3111E+00
14	4.8252E−01	3.0328E+00	6.9636E−01	1.8513E+00	7.7084E−01	1.6020E+00	8.5593E−01	1.3930E+00
15	4.3697E−01	3.2107E+00	6.2369E−01	1.9595E+00	6.8938E−01	1.6952E+00	7.6479E−01	1.4736E+00
16	3.9897E−01	3.3826E+00	5.6255E−01	2.0650E+00	6.2064E−01	1.7864E+00	6.8769E−01	1.5526E+00
17	3.6667E−01	3.5484E+00	5.1064E−01	2.1676E+00	5.6218E−01	1.8751E+00	6.2200E−01	1.6296E+00
18	3.3872E−01	3.7083E+00	4.6614E−01	2.2667E+00	5.1207E−01	1.9609E+00	5.6567E−01	1.7042E+00
19	3.1413E−01	3.8627E+00	4.2762E−01	2.3623E+00	4.6875E−01	2.0438E+00	5.1700E−01	1.7762E+00
20	2.9223E−01	4.0121E+00	3.9395E−01	2.4541E+00	4.3098E−01	2.1234E+00	4.7464E−01	1.8454E+00
21	2.7253E−01	4.1570E+00	3.6425E−01	2.5424E+00	3.9779E−01	2.1998E+00	4.3750E−01	1.9118E+00
22	2.5469E−01	4.2979E+00	3.3787E−01	2.6272E+00	3.6842E−01	2.2731E+00	4.0473E−01	1.9755E+00
23	2.3848E−01	4.4353E+00	3.1428E−01	2.7089E+00	3.4226E−01	2.3436E+00	3.7562E−01	2.0365E+00
24	2.2369E−01	4.5696E+00	2.9307E−01	2.7877E+00	3.1883E−01	2.4114E+00	3.4962E−01	2.0952E+00
25	2.1018E−01	4.7011E+00	2.7390E−01	2.8639E+00	2.9773E−01	2.4768E+00	3.2628E−01	2.1516E+00
26	1.9784E−01	4.8300E+00	2.5652E−01	2.9376E+00	2.7865E−01	2.5399E+00	3.0523E−01	2.2060E+00
27	1.8655E−01	4.9565E+00	2.4071E−01	3.0092E+00	2.6134E−01	2.6011E+00	2.8617E−01	2.2585E+00
28	1.7622E−01	5.0807E+00	2.2631E−01	3.0789E+00	2.4560E−01	2.6605E+00	2.6885E−01	2.3095E+00
29	1.6676E−01	5.2025E+00	2.1316E−01	3.1469E+00	2.3124E−01	2.7183E+00	2.5308E−01	2.3591E+00
30	1.5808E−01	5.3222E+00	2.0114E−01	3.2133E+00	2.1812E−01	2.7747E+00	2.3867E−01	2.4074E+00
31	1.5010E−01	5.4396E+00	1.9012E−01	3.2783E+00	2.0610E−01	2.8299E+00	2.2548E−01	2.4546E+00
32	1.4277E−01	5.5550E+00	1.8001E−01	3.3419E+00	1.9508E−01	2.8839E+00	2.1337E−01	2.5007E+00
33	1.3602E−01	5.6684E+00	1.7072E−01	3.4044E+00	1.8494E−01	2.9368E+00	2.0223E−01	2.5460E+00
34	1.2978E−01	5.7797E+00	1.6217E−01	3.4657E+00	1.7560E−01	2.9888E+00	1.9197E−01	2.5904E+00
35	1.2401E−01	5.8891E+00	1.5428E−01	3.5259E+00	1.6699E−01	3.0399E+00	1.8250E−01	2.6341E+00
36	1.1865E−01	5.9966E+00	1.4701E−01	3.5850E+00	1.5903E−01	3.0901E+00	1.7374E−01	2.6771E+00
37	1.1367E−01	6.1023E+00	1.4028E−01	3.6432E+00	1.5167E−01	3.1395E+00	1.6562E−01	2.7194E+00
38	1.0903E−01	6.2064E+00	1.3404E−01	3.7004E+00	1.4484E−01	3.1881E+00	1.5809E−01	2.7610E+00
39	1.0470E−01	2.5636E−02	1.2825E−01	3.7567E+00	1.3849E−01	3.2360E+00	1.5108E−01	2.8021E+00
40	1.0066E−01	1.2655E−01	1.2285E−01	3.8121E+00	1.3258E−01	3.2832E+00	1.4455E−01	2.8425E+00
41	9.6865E−02	2.2604E−01	1.1783E−01	3.8666E+00	1.2707E−01	3.3296E+00	1.3846E−01	2.8824E+00
42	9.3303E−02	3.2419E−01	1.1314E−01	3.9202E+00	1.2192E−01	3.3753E+00	1.3277E−01	2.9216E+00
43	8.9953E−02	4.2111E−01	1.0875E−01	3.9731E+00	1.1710E−01	3.4203E+00	1.2745E−01	2.9603E+00
44	8.6800E−02	5.1686E−01	1.0464E−01	4.0251E+00	1.1259E−01	3.4647E+00	1.2245E−01	2.9985E+00
45	8.3829E−02	6.1152E−01	1.0077E−01	4.0764E+00	1.0835E−01	3.5084E+00	1.1776E−01	3.0360E+00
46	8.1024E−02	7.0518E−01	9.7137E−02	4.1269E+00	1.0436E−01	3.5514E+00	1.1334E−01	3.0730E+00
47	7.8374E−02	7.9791E−01	9.3709E−02	4.1766E+00	1.0059E−01	3.5938E+00	1.0917E−01	3.1095E+00
48	7.5865E−02	8.8981E−01	9.0474E−02	4.2257E+00	9.7047E−02	3.6356E+00	1.0525E−01	3.1453E+00
49	7.3489E−02	9.8094E−01	8.7416E−02	4.2740E+00	9.3695E−02	3.6768E+00	1.0154E−01	3.1807E+00
50	7.1237E−02	1.0713E+00	8.4520E−02	4.3216E+00	9.0522E−02	3.7173E+00	9.8035E−02	3.2155E+00
51	6.9101E−02	1.1611E+00	8.1774E−02	4.3686E+00	8.7514E−02	3.7573E+00	9.4712E−02	3.2498E+00
52	6.7075E−02	1.2502E+00	7.9166E−02	4.4150E+00	8.4658E−02	3.7966E+00	9.1558E−02	3.2836E+00
53	6.5151E−02	1.3388E+00	7.6687E−02	4.4607E+00	8.1945E−02	3.8354E+00	8.8564E−02	3.3169E+00
54	6.3323E−02	1.4269E+00	7.4329E−02	4.5059E+00	7.9365E−02	3.8737E+00	8.5718E−02	3.3497E+00
55	6.1586E−02	1.5145E+00	7.2082E−02	4.5504E+00	7.6910E−02	3.9114E+00	8.3012E−02	3.3820E+00
56	5.9936E−02	1.6018E+00	6.9939E−02	4.5943E+00	7.4570E−02	3.9486E+00	8.0436E−02	3.4138E+00
57	5.8367E−02	1.6887E+00	6.7894E−02	4.6377E+00	7.2338E−02	3.9853E+00	7.7979E−02	3.4451E+00
58	5.6876E−02	1.7751E+00	6.5940E−02	4.6806E+00	7.0206E−02	4.0215E+00	7.5633E−02	3.4760E+00
59	5.5459E−02	1.8613E+00	6.4073E−02	4.7229E+00	6.8168E−02	4.0571E+00	7.3394E−02	3.5064E+00
60	5.4114E−02	1.9473E+00	6.2286E−02	4.7647E+00	6.6220E−02	4.0924E+00	7.1254E−02	3.5365E+00

Table 4.3.3.1. *Partial wave elastic scattering factors for neutral atoms (cont.)*
Ho; $Z = 67$

	10 keV		40 keV		60 keV		90 keV	
s	$\|f(s)\|$	$\eta(s)$	$\|f(s)\|$	$\eta(s)$	$\|f(s)\|$	$\eta(s)$	$\|f(s)\|$	$\eta(s)$
0	1.1843E+01	3.0231E−01	1.3925E+01	2.1822E−01	1.4740E+01	1.9568E−01	1.5766E+01	1.7525E−01
1	8.9007E+00	3.9271E−01	1.0735E+01	2.7799E−01	1.1419E+01	2.4826E−01	1.2266E+01	2.2153E−01
2	5.5189E+00	5.9908E−01	6.9821E+00	4.0879E−01	7.4936E+00	3.6241E−01	8.1088E+00	3.2141E−01
3	3.8117E+00	8.0493E−01	5.0185E+00	5.3543E−01	5.4258E+00	4.7229E−01	5.9051E+00	4.1718E−01
4	2.8141E+00	1.0009E+00	3.8344E+00	6.5407E−01	4.1716E+00	5.7490E−01	4.5622E+00	5.0639E−01
5	2.1428E+00	1.2061E+00	3.0064E+00	7.7624E−01	3.2887E+00	6.8020E−01	3.6120E+00	5.9770E−01
6	1.6766E+00	1.4215E+00	2.4048E+00	9.0291E−01	2.6423E+00	7.8908E−01	2.9124E+00	6.9190E−01
7	1.3485E+00	1.6395E+00	1.9625E+00	1.0306E+00	2.1636E+00	8.9867E−01	2.3913E+00	7.8658E−01
8	1.1114E+00	1.8537E+00	1.6317E+00	1.1562E+00	1.8033E+00	1.0064E+00	1.9974E+00	8.7961E−01
9	9.3435E−01	2.0615E+00	1.3786E+00	1.2784E+00	1.5264E+00	1.1112E+00	1.6933E+00	9.7007E−01
10	7.9816E−01	2.2633E+00	1.1803E+00	1.3973E+00	1.3086E+00	1.2132E+00	1.4534E+00	1.0580E+00
11	6.9125E−01	2.4601E+00	1.0219E+00	1.5135E+00	1.1338E+00	1.3128E+00	1.2604E+00	1.1440E+00
12	6.0619E−01	2.6527E+00	8.9342E−01	1.6276E+00	9.9150E−01	1.4107E+00	1.1027E+00	1.2285E+00
13	5.3787E−01	2.8412E+00	7.8795E−01	1.7400E+00	8.7416E−01	1.5073E+00	9.7218E−01	1.3119E+00
14	4.8244E−01	3.0252E+00	7.0058E−01	1.8507E+00	7.7654E−01	1.6025E+00	8.6323E−01	1.3942E+00
15	4.3691E−01	3.2039E+00	6.2763E−01	1.9594E+00	6.9468E−01	1.6961E+00	7.7157E−01	1.4752E+00
16	3.9896E−01	3.3770E+00	5.6621E−01	2.0657E+00	6.2555E−01	1.7878E+00	6.9395E−01	1.5547E+00
17	3.6676E−01	3.5440E+00	5.1406E−01	2.1690E+00	5.6673E−01	1.8773E+00	6.2778E−01	1.6323E+00
18	3.3896E−01	3.7052E+00	4.6936E−01	2.2692E+00	5.1629E−01	1.9640E+00	5.7100E−01	1.7077E+00
19	3.1455E−01	3.8609E+00	4.3067E−01	2.3658E+00	4.7268E−01	2.0478E+00	5.2192E−01	1.7806E+00
20	2.9283E−01	4.0115E+00	3.9687E−01	2.4588E+00	4.3467E−01	2.1286E+00	4.7920E−01	1.8508E+00
21	2.7330E−01	4.1576E+00	3.6708E−01	2.5483E+00	4.0128E−01	2.2061E+00	4.4174E−01	1.9183E+00
22	2.5562E−01	4.2998E+00	3.4061E−01	2.6344E+00	3.7173E−01	2.2807E+00	4.0869E−01	1.9830E+00
23	2.3954E−01	4.4384E+00	3.1694E−01	2.7173E+00	3.4541E−01	2.3523E+00	3.7934E−01	2.0452E+00
24	2.2486E−01	4.5738E+00	2.9566E−01	2.7973E+00	3.2183E−01	2.4213E+00	3.5312E−01	2.1050E+00
25	2.1144E−01	4.7064E+00	2.7641E−01	2.8746E+00	3.0059E−01	2.4877E+00	3.2958E−01	2.1624E+00
26	1.9915E−01	4.8365E+00	2.5896E−01	2.9494E+00	2.8139E−01	2.5519E+00	3.0835E−01	2.2178E+00
27	1.8789E−01	4.9640E+00	2.4306E−01	3.0220E+00	2.6395E−01	2.6141E+00	2.8912E−01	2.2713E+00
28	1.7758E−01	5.0893E+00	2.2857E−01	3.0927E+00	2.4809E−01	2.6744E+00	2.7164E−01	2.3231E+00
29	1.6812E−01	5.2123E+00	2.1532E−01	3.1616E+00	2.3361E−01	2.7331E+00	2.5572E−01	2.3735E+00
30	1.5942E−01	5.3331E+00	2.0320E−01	3.2289E+00	2.2037E−01	2.7903E+00	2.4117E−01	2.4225E+00
31	1.5143E−01	5.4518E+00	1.9209E−01	3.2947E+00	2.0824E−01	2.8462E+00	2.2785E−01	2.4703E+00
32	1.4407E−01	5.5684E+00	1.8188E−01	3.3591E+00	1.9710E−01	2.9008E+00	2.1561E−01	2.5171E+00
33	1.3728E−01	5.6830E+00	1.7249E−01	3.4223E+00	1.8685E−01	2.9544E+00	2.0435E−01	2.5629E+00
34	1.3101E−01	5.7955E+00	1.6384E−01	3.4842E+00	1.7741E−01	3.0070E+00	1.9398E−01	2.6079E+00
35	1.2520E−01	5.9062E+00	1.5586E−01	3.5451E+00	1.6870E−01	3.0587E+00	1.8440E−01	2.6520E+00
36	1.1981E−01	6.0149E+00	1.4850E−01	3.6049E+00	1.6065E−01	3.1094E+00	1.7554E−01	2.6955E+00
37	1.1479E−01	6.1219E+00	1.4168E−01	3.6637E+00	1.5319E−01	3.1593E+00	1.6733E−01	2.7382E+00
38	1.1012E−01	6.2272E+00	1.3536E−01	3.7215E+00	1.4628E−01	3.2085E+00	1.5971E−01	2.7803E+00
39	1.0575E−01	4.7612E−02	1.2950E−01	3.7784E+00	1.3986E−01	3.2568E+00	1.5263E−01	2.8217E+00
40	1.0167E−01	1.4970E−01	1.2404E−01	3.8344E+00	1.3388E−01	3.3044E+00	1.4602E−01	2.8625E+00
41	9.7836E−02	2.5032E−01	1.1895E−01	3.8894E+00	1.2830E−01	3.3513E+00	1.3986E−01	2.9027E+00
42	9.4238E−02	3.4959E−01	1.1420E−01	3.9437E+00	1.2309E−01	3.3975E+00	1.3411E−01	2.9424E+00
43	9.0852E−02	4.4758E−01	1.0976E−01	3.9970E+00	1.1823E−01	3.4430E+00	1.2873E−01	2.9815E+00
44	8.7663E−02	5.4438E−01	1.0560E−01	4.0496E+00	1.1366E−01	3.4878E+00	1.2368E−01	3.0200E+00
45	8.4657E−02	6.4007E−01	1.0169E−01	4.1014E+00	1.0937E−01	3.5319E+00	1.1893E−01	3.0579E+00
46	8.1818E−02	7.3471E−01	9.8011E−02	4.1525E+00	1.0534E−01	3.5754E+00	1.1447E−01	3.0953E+00
47	7.9134E−02	8.2841E−01	9.4547E−02	4.2028E+00	1.0154E−01	3.6183E+00	1.1027E−01	3.1321E+00
48	7.6592E−02	9.2125E−01	9.1279E−02	4.2524E+00	9.7957E−02	3.6605E+00	1.0630E−01	3.1684E+00
49	7.4183E−02	1.0133E+00	8.8191E−02	4.3012E+00	9.4573E−02	3.7021E+00	1.0256E−01	3.2042E+00
50	7.1900E−02	1.1046E+00	8.5268E−02	4.3494E+00	9.1371E−02	3.7431E+00	9.9022E−02	3.2394E+00
51	6.9733E−02	1.1952E+00	8.2497E−02	4.3969E+00	8.8336E−02	3.7836E+00	9.5667E−02	3.2741E+00
52	6.7677E−02	1.2852E+00	7.9867E−02	4.4438E+00	8.5456E−02	3.8234E+00	9.2486E−02	3.3083E+00
53	6.5723E−02	1.3747E+00	7.7368E−02	4.4901E+00	8.2720E−02	3.8627E+00	8.9465E−02	3.3420E+00
54	6.3867E−02	1.4636E+00	7.4990E−02	4.5358E+00	8.0120E−02	3.9014E+00	8.6595E−02	3.3752E+00
55	6.2101E−02	1.5521E+00	7.2725E−02	4.5808E+00	7.7645E−02	3.9396E+00	8.3866E−02	3.4079E+00
56	6.0424E−02	1.6402E+00	7.0567E−02	4.6253E+00	7.5287E−02	3.9773E+00	8.1267E−02	3.4402E+00
57	5.8828E−02	1.7280E+00	6.8506E−02	4.6692E+00	7.3037E−02	4.0144E+00	7.8789E−02	3.4719E+00
58	5.7312E−02	1.8154E+00	6.6538E−02	4.7126E+00	7.0888E−02	4.0511E+00	7.6424E−02	3.5032E+00
59	5.5870E−02	1.9025E+00	6.4657E−02	4.7555E+00	6.8836E−02	4.0873E+00	7.4166E−02	3.5341E+00
60	5.4501E−02	1.9894E+00	6.2857E−02	4.7978E+00	6.6873E−02	4.1230E+00	7.2008E−02	3.5646E+00

Table 4.3.3.1. *Partial wave elastic scattering factors for neutral atoms (cont.)*
Er; $Z = 68$

	10 keV		40 keV		60 keV		90 keV	
s	$\|f(s)\|$	$\eta(s)$	$\|f(s)\|$	$\eta(s)$	$\|f(s)\|$	$\eta(s)$	$\|f(s)\|$	$\eta(s)$
0	1.1570E+01	3.0375E−01	1.3621E+01	2.2038E−01	1.4424E+01	1.9788E−01	1.5433E+01	1.7744E−01
1	8.7366E+00	3.9302E−01	1.0549E+01	2.7965E−01	1.1226E+01	2.5007E−01	1.2063E+01	2.2341E−01
2	5.4435E+00	5.9766E−01	6.8956E+00	4.0981E−01	7.4044E+00	3.6376E−01	8.0159E+00	3.2296E−01
3	3.7698E+00	8.0248E−01	4.9713E+00	5.3618E−01	5.3778E+00	4.7348E−01	5.8558E+00	4.1865E−01
4	2.7917E+00	9.9659E−01	3.8108E+00	6.5405E−01	4.1485E+00	5.7549E−01	4.5394E+00	5.0738E−01
5	2.1312E+00	1.1994E+00	2.9971E+00	7.7510E−01	3.2809E+00	6.7989E−01	3.6056E+00	5.9795E−01
6	1.6703E+00	1.4127E+00	2.4031E+00	9.0078E−01	2.6426E+00	7.8797E−01	2.9147E+00	6.9150E−01
7	1.3445E+00	1.6294E+00	1.9642E+00	1.0279E+00	2.1676E+00	8.9711E−01	2.3976E+00	7.8583E−01
8	1.1088E+00	1.8433E+00	1.6350E+00	1.1534E+00	1.8089E+00	1.0048E+00	2.0052E+00	8.7882E−01
9	9.3259E−01	2.0512E+00	1.3825E+00	1.2758E+00	1.5324E+00	1.1098E+00	1.7016E+00	9.6945E−01
10	7.9707E−01	2.2533E+00	1.1846E+00	1.3950E+00	1.3147E+00	1.2120E+00	1.4617E+00	1.0577E+00
11	6.9059E−01	2.4504E+00	1.0263E+00	1.5115E+00	1.1400E+00	1.3119E+00	1.2685E+00	1.1440E+00
12	6.0578E−01	2.6433E+00	8.9771E−01	1.6259E+00	9.9747E−01	1.4102E+00	1.1105E+00	1.2288E+00
13	5.3756E−01	2.8323E+00	7.9209E−01	1.7387E+00	8.7987E−01	1.5070E+00	9.7958E−01	1.3124E+00
14	4.8216E−01	3.0168E+00	7.0452E−01	1.8497E+00	7.8193E−01	1.6025E+00	8.7020E−01	1.3950E+00
15	4.3666E−01	3.1964E+00	6.3132E−01	1.9589E+00	6.9973E−01	1.6966E+00	7.7808E−01	1.4763E+00
16	3.9876E−01	3.3703E+00	5.6967E−01	2.0657E+00	6.3025E−01	1.7888E+00	7.0000E−01	1.5563E+00
17	3.6667E−01	3.5385E+00	5.1729E−01	2.1699E+00	5.7109E−01	1.8789E+00	6.3338E−01	1.6345E+00
18	3.3900E−01	3.7009E+00	4.7241E−01	2.2709E+00	5.2035E−01	1.9665E+00	5.7617E−01	1.7106E+00
19	3.1476E−01	3.8578E+00	4.3357E−01	2.3685E+00	4.7648E−01	2.0512E+00	5.2670E−01	1.7844E+00
20	2.9322E−01	4.0097E+00	3.9965E−01	2.4626E+00	4.3824E−01	2.1329E+00	4.8364E−01	1.8555E+00
21	2.7387E−01	4.1571E+00	3.6977E−01	2.5533E+00	4.0465E−01	2.2116E+00	4.4589E−01	1.9240E+00
22	2.5636E−01	4.3004E+00	3.4323E−01	2.6405E+00	3.7493E−01	2.2873E+00	4.1257E−01	1.9898E+00
23	2.4042E−01	4.4401E+00	3.1949E−01	2.7246E+00	3.4846E−01	2.3601E+00	3.8299E−01	2.0531E+00
24	2.2586E−01	4.5766E+00	2.9815E−01	2.8058E+00	3.2475E−01	2.4302E+00	3.5656E−01	2.1139E+00
25	2.1253E−01	4.7103E+00	2.7884E−01	2.8842E+00	3.0340E−01	2.4977E+00	3.3283E−01	2.1724E+00
26	2.0031E−01	4.8414E+00	2.6132E−01	2.9601E+00	2.8407E−01	2.5629E+00	3.1142E−01	2.2287E+00
27	1.8911E−01	4.9701E+00	2.4535E−01	3.0338E+00	2.6652E−01	2.6260E+00	2.9203E−01	2.2832E+00
28	1.7882E−01	5.0964E+00	2.3078E−01	3.1054E+00	2.5054E−01	2.6873E+00	2.7441E−01	2.3359E+00
29	1.6937E−01	5.2205E+00	2.1745E−01	3.1752E+00	2.3595E−01	2.7468E+00	2.5834E−01	2.3870E+00
30	1.6068E−01	5.3425E+00	2.0524E−01	3.2433E+00	2.2261E−01	2.8049E+00	2.4366E−01	2.4368E+00
31	1.5268E−01	5.4623E+00	1.9404E−01	3.3099E+00	2.1036E−01	2.8615E+00	2.3020E−01	2.4853E+00
32	1.4531E−01	5.5801E+00	1.8374E−01	3.3751E+00	1.9912E−01	2.9169E+00	2.1785E−01	2.5327E+00
33	1.3850E−01	5.6958E+00	1.7425E−01	3.4390E+00	1.8876E−01	2.9711E+00	2.0647E−01	2.5791E+00
34	1.3220E−01	5.8096E+00	1.6551E−01	3.5017E+00	1.7922E−01	3.0243E+00	1.9599E−01	2.6246E+00
35	1.2636E−01	5.9215E+00	1.5744E−01	3.5633E+00	1.7041E−01	3.0765E+00	1.8630E−01	2.6693E+00
36	1.2094E−01	6.0314E+00	1.4999E−01	3.6237E+00	1.6227E−01	3.1279E+00	1.7734E−01	2.7132E+00
37	1.1589E−01	6.1396E+00	1.4310E−01	3.6832E+00	1.5473E−01	3.1783E+00	1.6904E−01	2.7563E+00
38	1.1118E−01	6.2461E+00	1.3670E−01	3.7416E+00	1.4774E−01	3.2279E+00	1.6134E−01	2.7988E+00
39	1.0678E−01	6.7708E−02	1.3076E−01	3.7991E+00	1.4123E−01	3.2768E+00	1.5417E−01	2.8407E+00
40	1.0267E−01	1.7095E−01	1.2523E−01	3.8556E+00	1.3518E−01	3.3249E+00	1.4749E−01	2.8819E+00
41	9.8806E−02	2.7272E−01	1.2008E−01	3.9113E+00	1.2954E−01	3.3722E+00	1.4127E−01	2.9225E+00
42	9.5175E−02	3.7310E−01	1.1527E−01	3.9661E+00	1.2427E−01	3.4189E+00	1.3545E−01	2.9625E+00
43	9.1757E−02	4.7217E−01	1.1078E−01	4.0200E+00	1.1935E−01	3.4648E+00	1.3000E−01	3.0019E+00
44	8.8536E−02	5.7003E−01	1.0656E−01	4.0731E+00	1.1473E−01	3.5101E+00	1.2490E−01	3.0408E+00
45	8.5496E−02	6.6673E−01	1.0261E−01	4.1255E+00	1.1040E−01	3.5547E+00	1.2011E−01	3.0791E+00
46	8.2625E−02	7.6238E−01	9.8890E−02	4.1771E+00	1.0632E−01	3.5986E+00	1.1560E−01	3.1169E+00
47	7.9909E−02	8.5704E−01	9.5388E−02	4.2279E+00	1.0248E−01	3.6419E+00	1.1135E−01	3.1541E+00
48	7.7335E−02	9.5082E−01	9.2086E−02	4.2780E+00	9.8862E−02	3.6846E+00	1.0735E−01	3.1908E+00
49	7.4895E−02	1.0438E+00	8.8966E−02	4.3274E+00	9.5445E−02	3.7267E+00	1.0357E−01	3.2269E+00
50	7.2580E−02	1.1360E+00	8.6014E−02	4.3761E+00	9.2213E−02	3.7681E+00	9.9996E−02	3.2626E+00
51	7.0383E−02	1.2275E+00	8.3218E−02	4.4242E+00	8.9150E−02	3.8090E+00	9.6611E−02	3.2977E+00
52	6.8296E−02	1.3184E+00	8.0563E−02	4.4716E+00	8.6245E−02	3.8493E+00	9.3401E−02	3.3323E+00
53	6.6313E−02	1.4087E+00	7.8042E−02	4.5184E+00	8.3486E−02	3.8891E+00	9.0354E−02	3.3664E+00
54	6.4427E−02	1.4985E+00	7.5645E−02	4.5646E+00	8.0863E−02	3.9283E+00	8.7458E−02	3.4000E+00
55	6.2633E−02	1.5878E+00	7.3362E−02	4.6102E+00	7.8368E−02	3.9669E+00	8.4706E−02	3.4331E+00
56	6.0927E−02	1.6768E+00	7.1186E−02	4.6552E+00	7.5991E−02	4.0051E+00	8.2085E−02	3.4658E+00
57	5.9304E−02	1.7654E+00	6.9109E−02	4.6996E+00	7.3724E−02	4.0427E+00	7.9586E−02	3.4980E+00
58	5.7760E−02	1.8537E+00	6.7127E−02	4.7436E+00	7.1559E−02	4.0798E+00	7.7202E−02	3.5297E+00
59	5.6292E−02	1.9417E+00	6.5232E−02	4.7870E+00	6.9491E−02	4.1164E+00	7.4925E−02	3.5610E+00
60	5.4896E−02	2.0294E+00	6.3419E−02	4.8298E+00	6.7513E−02	4.1526E+00	7.2749E−02	3.5919E+00

Table 4.3.3.1. *Partial wave elastic scattering factors for neutral atoms (cont.)*
Tm; $Z = 69$

	10 keV		40 keV		60 keV		90 keV	
s	$\|f(s)\|$	$\eta(s)$	$\|f(s)\|$	$\eta(s)$	$\|f(s)\|$	$\eta(s)$	$\|f(s)\|$	$\eta(s)$
0	1.1308E+01	3.0510E−01	1.3328E+01	2.2247E−01	1.4119E+01	2.0003E−01	1.5112E+01	1.7958E−01
1	8.5773E+00	3.9326E−01	1.0368E+01	2.8123E−01	1.1037E+01	2.5182E−01	1.1865E+01	2.2523E−01
2	5.3695E+00	5.9615E−01	6.8101E+00	4.1075E−01	7.3160E+00	3.6504E−01	7.9236E+00	3.2444E−01
3	3.7281E+00	7.9997E−01	4.9235E+00	5.3686E−01	5.3290E+00	4.7461E−01	5.8056E+00	4.2005E−01
4	2.7687E+00	9.9236E−01	3.7859E+00	6.5402E−01	4.1238E+00	5.7606E−01	4.5149E+00	5.0835E−01
5	2.1192E+00	1.1928E+00	2.9865E+00	7.7397E−01	3.2714E+00	6.7958E−01	3.5974E+00	5.9821E−01
6	1.6635E+00	1.4039E+00	2.4002E+00	8.9865E−01	2.6415E+00	7.8685E−01	2.9155E+00	6.9110E−01
7	1.3402E+00	1.6193E+00	1.9651E+00	1.0252E+00	2.1704E+00	8.9550E−01	2.4026E+00	7.8503E−01
8	1.1058E+00	1.8326E+00	1.6375E+00	1.1504E+00	1.8135E+00	1.0030E+00	2.0120E+00	8.7792E−01
9	9.3051E−01	2.0406E+00	1.3859E+00	1.2729E+00	1.5378E+00	1.1081E+00	1.7091E+00	9.6868E−01
10	7.9567E−01	2.2429E+00	1.1883E+00	1.3924E+00	1.3204E+00	1.2106E+00	1.4693E+00	1.0572E+00
11	6.8966E−01	2.4402E+00	1.0302E+00	1.5092E+00	1.1456E+00	1.3108E+00	1.2760E+00	1.1437E+00
12	6.0513E−01	2.6334E+00	9.0161E−01	1.6239E+00	1.0030E+00	1.4093E+00	1.1178E+00	1.2287E+00
13	5.3704E−01	2.8227E+00	7.9590E−01	1.7369E+00	8.8522E−01	1.5064E+00	9.8658E−01	1.3126E+00
14	4.8170E−01	3.0078E+00	7.0817E−01	1.8483E+00	7.8702E−01	1.6022E+00	8.7683E−01	1.3954E+00
15	4.3624E−01	3.1880E+00	6.3477E−01	1.9579E+00	7.0452E−01	1.6966E+00	7.8432E−01	1.4771E+00
16	3.9840E−01	3.3629E+00	5.7291E−01	2.0653E+00	6.3473E−01	1.7893E+00	7.0581E−01	1.5575E+00
17	3.6640E−01	3.5321E+00	5.2034E−01	2.1701E+00	5.7527E−01	1.8800E+00	6.3877E−01	1.6363E+00
18	3.3887E−01	3.6957E+00	4.7529E−01	2.2719E+00	5.2425E−01	1.9683E+00	5.8117E−01	1.7131E+00
19	3.1479E−01	3.8538E+00	4.3631E−01	2.3705E+00	4.8013E−01	2.0539E+00	5.3135E−01	1.7875E+00
20	2.9343E−01	4.0068E+00	4.0229E−01	2.4656E+00	4.4167E−01	2.1366E+00	4.8797E−01	1.8596E+00
21	2.7426E−01	4.1553E+00	3.7232E−01	2.5574E+00	4.0790E−01	2.2163E+00	4.4993E−01	1.9290E+00
22	2.5691E−01	4.2998E+00	3.4572E−01	2.6458E+00	3.7803E−01	2.2931E+00	4.1636E−01	1.9958E+00
23	2.4113E−01	4.4406E+00	3.2193E−01	2.7310E+00	3.5143E−01	2.3669E+00	3.8655E−01	2.0601E+00
24	2.2670E−01	4.5782E+00	3.0053E−01	2.8133E+00	3.2759E−01	2.4381E+00	3.5993E−01	2.1220E+00
25	2.1347E−01	4.7129E+00	2.8118E−01	2.8928E+00	3.0612E−01	2.5067E+00	3.3602E−01	2.1815E+00
26	2.0134E−01	4.8450E+00	2.6360E−01	2.9697E+00	2.8669E−01	2.5730E+00	3.1445E−01	2.2388E+00
27	1.9019E−01	4.9747E+00	2.4758E−01	3.0444E+00	2.6904E−01	2.6371E+00	2.9491E−01	2.2942E+00
28	1.7995E−01	5.1021E+00	2.3294E−01	3.1170E+00	2.5296E−01	2.6992E+00	2.7714E−01	2.3477E+00
29	1.7052E−01	5.2273E+00	2.1954E−01	3.1877E+00	2.3827E−01	2.7597E+00	2.6094E−01	2.3997E+00
30	1.6185E−01	5.3503E+00	2.0725E−01	3.2567E+00	2.2481E−01	2.8185E+00	2.4613E−01	2.4502E+00
31	1.5385E−01	5.4712E+00	1.9597E−01	3.3242E+00	2.1247E−01	2.8759E+00	2.3255E−01	2.4995E+00
32	1.4647E−01	5.5901E+00	1.8558E−01	3.3902E+00	2.0112E−01	2.9320E+00	2.2007E−01	2.5475E+00
33	1.3965E−01	5.7070E+00	1.7601E−01	3.4548E+00	1.9067E−01	2.9869E+00	2.0858E−01	2.5945E+00
34	1.3334E−01	5.8220E+00	1.6718E−01	3.5182E+00	1.8103E−01	3.0408E+00	1.9799E−01	2.6406E+00
35	1.2748E−01	5.9350E+00	1.5903E−01	3.5804E+00	1.7213E−01	3.0936E+00	1.8820E−01	2.6858E+00
36	1.2203E−01	6.0462E+00	1.5149E−01	3.6416E+00	1.6390E−01	3.1454E+00	1.7915E−01	2.7301E+00
37	1.1696E−01	6.1556E+00	1.4452E−01	3.7016E+00	1.5627E−01	3.1964E+00	1.7076E−01	2.7738E+00
38	1.1223E−01	6.2632E+00	1.3804E−01	3.7607E+00	1.4920E−01	3.2466E+00	1.6296E−01	2.8167E+00
39	1.0780E−01	8.6016E−02	1.3203E−01	3.8187E+00	1.4262E−01	3.2959E+00	1.5572E−01	2.8589E+00
40	1.0366E−01	1.9042E−01	1.2643E−01	3.8759E+00	1.3649E−01	3.3445E+00	1.4897E−01	2.9006E+00
41	9.9769E−02	2.9331E−01	1.2122E−01	3.9321E+00	1.3079E−01	3.3923E+00	1.4267E−01	2.9416E+00
42	9.6110E−02	3.9480E−01	1.1635E−01	3.9875E+00	1.2546E−01	3.4394E+00	1.3678E−01	2.9820E+00
43	9.2663E−02	4.9496E−01	1.1180E−01	4.0420E+00	1.2047E−01	3.4858E+00	1.3128E−01	3.0218E+00
44	8.9412E−02	5.9386E−01	1.0754E−01	4.0957E+00	1.1581E−01	3.5315E+00	1.2612E−01	3.0610E+00
45	8.6344E−02	6.9160E−01	1.0353E−01	4.1486E+00	1.1142E−01	3.5766E+00	1.2127E−01	3.0997E+00
46	8.3443E−02	7.8825E−01	9.9774E−02	4.2007E+00	1.0730E−01	3.6210E+00	1.1672E−01	3.1379E+00
47	8.0696E−02	8.8388E−01	9.6233E−02	4.2521E+00	1.0342E−01	3.6648E+00	1.1243E−01	3.1755E+00
48	7.8093E−02	9.7861E−01	9.2895E−02	4.3027E+00	9.9765E−02	3.7079E+00	1.0839E−01	3.2125E+00
49	7.5623E−02	1.0725E+00	8.9743E−02	4.3527E+00	9.6314E−02	3.7504E+00	1.0457E−01	3.2490E+00
50	7.3278E−02	1.1656E+00	8.6761E−02	4.4019E+00	9.3050E−02	3.7923E+00	1.0096E−01	3.2850E+00
51	7.1051E−02	1.2580E+00	8.3937E−02	4.4505E+00	8.9958E−02	3.8336E+00	9.7545E−02	3.3205E+00
52	6.8934E−02	1.3497E+00	8.1258E−02	4.4984E+00	8.7027E−02	3.8744E+00	9.4305E−02	3.3556E+00
53	6.6921E−02	1.4409E+00	7.8713E−02	4.5458E+00	8.4243E−02	3.9146E+00	9.1231E−02	3.3900E+00
54	6.5005E−02	1.5315E+00	7.6295E−02	4.5925E+00	8.1598E−02	3.9543E+00	8.8310E−02	3.4241E+00
55	6.3182E−02	1.6217E+00	7.3992E−02	4.6385E+00	7.9082E−02	3.9934E+00	8.5533E−02	3.4576E+00
56	6.1447E−02	1.7115E+00	7.1798E−02	4.6841E+00	7.6686E−02	4.0319E+00	8.2890E−02	3.4907E+00
57	5.9795E−02	1.8009E+00	6.9706E−02	4.7290E+00	7.4401E−02	4.0700E+00	8.0370E−02	3.5233E+00
58	5.8223E−02	1.8901E+00	6.7707E−02	4.7735E+00	7.2219E−02	4.1076E+00	7.7966E−02	3.5554E+00
59	5.6727E−02	1.9790E+00	6.5798E−02	4.8174E+00	7.0134E−02	4.1447E+00	7.5670E−02	3.5871E+00
60	5.5304E−02	2.0676E+00	6.3972E−02	4.8608E+00	6.8142E−02	4.1814E+00	7.3477E−02	3.6184E+00

Table 4.3.3.1. *Partial wave elastic scattering factors for neutral atoms (cont.)*
Yb; $Z = 70$

	10 keV		40 keV		60 keV		90 keV	
s	$\|f(s)\|$	$\eta(s)$	$\|f(s)\|$	$\eta(s)$	$\|f(s)\|$	$\eta(s)$	$\|f(s)\|$	$\eta(s)$
0	1.1055E+01	3.0638E−01	1.3045E+01	2.2449E−01	1.3824E+01	2.0212E−01	1.4801E+01	1.8168E−01
1	8.4228E+00	3.9343E−01	1.0191E+01	2.8274E−01	1.0853E+01	2.5350E−01	1.1671E+01	2.2700E−01
2	5.2969E+00	5.9457E−01	6.7255E+00	4.1161E−01	7.2284E+00	3.6625E−01	7.8321E+00	3.2586E−01
3	3.6866E+00	7.9742E−01	4.8754E+00	5.3748E−01	5.2797E+00	4.7568E−01	5.7547E+00	4.2141E−01
4	2.7454E+00	9.8816E−01	3.7599E+00	6.5395E−01	4.0980E+00	5.7660E−01	4.4890E+00	5.0930E−01
5	2.1066E+00	1.1863E+00	2.9746E+00	7.7286E−01	3.2606E+00	6.7927E−01	3.5876E+00	5.9847E−01
6	1.6563E+00	1.3952E+00	2.3962E+00	8.9653E−01	2.6391E+00	7.8573E−01	2.9147E+00	6.9069E−01
7	1.3356E+00	1.6092E+00	1.9650E+00	1.0224E+00	2.1723E+00	8.9384E−01	2.4064E+00	7.8420E−01
8	1.1025E+00	1.8219E+00	1.6393E+00	1.1474E+00	1.8172E+00	1.0012E+00	2.0179E+00	8.7694E−01
9	9.2815E−01	2.0297E+00	1.3886E+00	1.2699E+00	1.5424E+00	1.1063E+00	1.7157E+00	9.6777E−01
10	7.9400E−01	2.2321E+00	1.1915E+00	1.3895E+00	1.3254E+00	1.2090E+00	1.4763E+00	1.0564E+00
11	6.8849E−01	2.4297E+00	1.0336E+00	1.5066E+00	1.1508E+00	1.3095E+00	1.2830E+00	1.1432E+00
12	6.0426E−01	2.6231E+00	9.0512E−01	1.6216E+00	1.0081E+00	1.4082E+00	1.1246E+00	1.2285E+00
13	5.3634E−01	2.8126E+00	7.9938E−01	1.7349E+00	8.9021E−01	1.5055E+00	9.9320E−01	1.3126E+00
14	4.8108E−01	2.9981E+00	7.1154E−01	1.8465E+00	7.9181E−01	1.6016E+00	8.8314E−01	1.3956E+00
15	4.3567E−01	3.1790E+00	6.3798E−01	1.9565E+00	7.0905E−01	1.6963E+00	7.9027E−01	1.4776E+00
16	3.9789E−01	3.3547E+00	5.7594E−01	2.0643E+00	6.3898E−01	1.7895E+00	7.1139E−01	1.5584E+00
17	3.6597E−01	3.5249E+00	5.2320E−01	2.1697E+00	5.7926E−01	1.8807E+00	6.4398E−01	1.6376E+00
18	3.3857E−01	3.6895E+00	4.7800E−01	2.2723E+00	5.2798E−01	1.9696E+00	5.8602E−01	1.7150E+00
19	3.1464E−01	3.8487E+00	4.3890E−01	2.3718E+00	4.8363E−01	2.0560E+00	5.3586E−01	1.7902E+00
20	2.9346E−01	4.0029E+00	4.0478E−01	2.4679E+00	4.4498E−01	2.1396E+00	4.9217E−01	1.8630E+00
21	2.7446E−01	4.1526E+00	3.7474E−01	2.5607E+00	4.1104E−01	2.2203E+00	4.5386E−01	1.9334E+00
22	2.5729E−01	4.2981E+00	3.4808E−01	2.6502E+00	3.8102E−01	2.2980E+00	4.2006E−01	2.0012E+00
23	2.4166E−01	4.4399E+00	3.2425E−01	2.7365E+00	3.5429E−01	2.3730E+00	3.9004E−01	2.0664E+00
24	2.2737E−01	4.5785E+00	3.0282E−01	2.8198E+00	3.3035E−01	2.4452E+00	3.6323E−01	2.1293E+00
25	2.1426E−01	4.7143E+00	2.8343E−01	2.9004E+00	3.0877E−01	2.5148E+00	3.3915E−01	2.1897E+00
26	2.0222E−01	4.8474E+00	2.6581E−01	2.9784E+00	2.8925E−01	2.5821E+00	3.1742E−01	2.2480E+00
27	1.9114E−01	4.9780E+00	2.4973E−01	3.0541E+00	2.7150E−01	2.6472E+00	2.9773E−01	2.3043E+00
28	1.8095E−01	5.1064E+00	2.3504E−01	3.1276E+00	2.5533E−01	2.7103E+00	2.7983E−01	2.3588E+00
29	1.7156E−01	5.2326E+00	2.2158E−01	3.1992E+00	2.4054E−01	2.7716E+00	2.6350E−01	2.4116E+00
30	1.6291E−01	5.3567E+00	2.0923E−01	3.2691E+00	2.2700E−01	2.8312E+00	2.4857E−01	2.4629E+00
31	1.5493E−01	5.4787E+00	1.9787E−01	3.3374E+00	2.1456E−01	2.8894E+00	2.3487E−01	2.5129E+00
32	1.4755E−01	5.5987E+00	1.8740E−01	3.4041E+00	2.0311E−01	2.9462E+00	2.2228E−01	2.5616E+00
33	1.4073E−01	5.7167E+00	1.7775E−01	3.4695E+00	1.9257E−01	3.0018E+00	2.1068E−01	2.6092E+00
34	1.3441E−01	5.8328E+00	1.6885E−01	3.5337E+00	1.8284E−01	3.0563E+00	1.9999E−01	2.6558E+00
35	1.2854E−01	5.9470E+00	1.6062E−01	3.5966E+00	1.7385E−01	3.1097E+00	1.9010E−01	2.7016E+00
36	1.2308E−01	6.0593E+00	1.5300E−01	3.6584E+00	1.6553E−01	3.1622E+00	1.8095E−01	2.7464E+00
37	1.1799E−01	6.1699E+00	1.4595E−01	3.7191E+00	1.5782E−01	3.2137E+00	1.7247E−01	2.7905E+00
38	1.1324E−01	6.2787E+00	1.3940E−01	3.7787E+00	1.5066E−01	3.2644E+00	1.6459E−01	2.8339E+00
39	1.0880E−01	1.0263E−01	1.3331E−01	3.8374E+00	1.4401E−01	3.3143E+00	1.5726E−01	2.8766E+00
40	1.0463E−01	2.0817E−01	1.2765E−01	3.8952E+00	1.3781E−01	3.3633E+00	1.5044E−01	2.9186E+00
41	1.0072E−01	3.1219E−01	1.2237E−01	3.9520E+00	1.3204E−01	3.4116E+00	1.4407E−01	2.9600E+00
42	9.7036E−02	4.1477E−01	1.1744E−01	4.0080E+00	1.2665E−01	3.4592E+00	1.3812E−01	3.0008E+00
43	9.3565E−02	5.1601E−01	1.1284E−01	4.0630E+00	1.2161E−01	3.5061E+00	1.3255E−01	3.0410E+00
44	9.0290E−02	6.1597E−01	1.0852E−01	4.1173E+00	1.1688E−01	3.5522E+00	1.2734E−01	3.0806E+00
45	8.7195E−02	7.1474E−01	1.0447E−01	4.1707E+00	1.1245E−01	3.5977E+00	1.2244E−01	3.1197E+00
46	8.4267E−02	8.1238E−01	1.0067E−01	4.2234E+00	1.0828E−01	3.6426E+00	1.1784E−01	3.1582E+00
47	8.1493E−02	9.0899E−01	9.7085E−02	4.2753E+00	1.0436E−01	3.6868E+00	1.1350E−01	3.1962E+00
48	7.8862E−02	1.0047E+00	9.3709E−02	4.3265E+00	1.0067E−01	3.7304E+00	1.0942E−01	3.2336E+00
49	7.6364E−02	1.0995E+00	9.0523E−02	4.3769E+00	9.7180E−02	3.7733E+00	1.0556E−01	3.2705E+00
50	7.3991E−02	1.1935E+00	8.7510E−02	4.4267E+00	9.3884E−02	3.8157E+00	1.0192E−01	3.3069E+00
51	7.1735E−02	1.2867E+00	8.4657E−02	4.4758E+00	9.0762E−02	3.8575E+00	9.8470E−02	3.3428E+00
52	6.9589E−02	1.3793E+00	8.1951E−02	4.5243E+00	8.7803E−02	3.8987E+00	9.5200E−02	3.3781E+00
53	6.7547E−02	1.4713E+00	7.9383E−02	4.5721E+00	8.4995E−02	3.9393E+00	9.2098E−02	3.4130E+00
54	6.5602E−02	1.5628E+00	7.6942E−02	4.6193E+00	8.2326E−02	3.9794E+00	8.9151E−02	3.4474E+00
55	6.3749E−02	1.6538E+00	7.4620E−02	4.6659E+00	7.9789E−02	4.0190E+00	8.6350E−02	3.4814E+00
56	6.1985E−02	1.7444E+00	7.2407E−02	4.7119E+00	7.7372E−02	4.0580E+00	8.3684E−02	3.5148E+00
57	6.0304E−02	1.8347E+00	7.0296E−02	4.7574E+00	7.5068E−02	4.0965E+00	8.1143E−02	3.5478E+00
58	5.8702E−02	1.9247E+00	6.8282E−02	4.8024E+00	7.2869E−02	4.1346E+00	7.8718E−02	3.5804E+00
59	5.7178E−02	2.0144E+00	6.6358E−02	4.8468E+00	7.0768E−02	4.1721E+00	7.6404E−02	3.6125E+00
60	5.5727E−02	2.1039E+00	6.4517E−02	4.8907E+00	6.8761E−02	4.2092E+00	7.4193E−02	3.6442E+00

Table 4.3.3.1. *Partial wave elastic scattering factors for neutral atoms (cont.)*
Lu; $Z = 71$

	10 keV		40 keV		60 keV		90 keV	
s	$\|f(s)\|$	$\eta(s)$	$\|f(s)\|$	$\eta(s)$	$\|f(s)\|$	$\eta(s)$	$\|f(s)\|$	$\eta(s)$
0	1.0943E+01	3.1759E−01	1.2941E+01	2.3177E−01	1.3721E+01	2.0859E−01	1.4697E+01	1.8747E−01
1	8.5956E+00	3.9524E−01	1.0394E+01	2.8379E−01	1.1070E+01	2.5451E−01	1.1905E+01	2.2797E−01
2	5.4783E+00	5.8749E−01	6.9420E+00	4.0753E−01	7.4594E+00	3.6289E−01	8.0814E+00	3.2310E−01
3	3.7447E+00	8.0077E−01	4.9509E+00	5.4004E−01	5.3623E+00	4.7814E−01	5.8458E+00	4.2377E−01
4	2.7567E+00	1.0028E+00	3.7768E+00	6.6330E−01	4.1179E+00	5.8494E−01	4.5126E+00	5.1678E−01
5	2.1084E+00	1.2058E+00	2.9786E+00	7.8527E−01	3.2664E+00	6.9028E−01	3.5956E+00	6.0829E−01
6	1.6571E+00	1.4161E+00	2.3990E+00	9.0994E−01	2.6436E+00	7.9764E−01	2.9212E+00	7.0133E−01
7	1.3362E+00	1.6305E+00	1.9682E+00	1.0362E+00	2.1771E+00	9.0619E−01	2.4132E+00	7.9524E−01
8	1.1031E+00	1.8436E+00	1.6427E+00	1.1618E+00	1.8222E+00	1.0140E+00	2.0246E+00	8.8843E−01
9	9.2889E−01	2.0521E+00	1.3920E+00	1.2849E+00	1.5473E+00	1.1197E+00	1.7223E+00	9.7976E−01
10	7.9486E−01	2.2551E+00	1.1950E+00	1.4051E+00	1.3303E+00	1.2228E+00	1.4828E+00	1.0689E+00
11	6.8939E−01	2.4530E+00	1.0372E+00	1.5225E+00	1.1557E+00	1.3237E+00	1.2894E+00	1.1560E+00
12	6.0507E−01	2.6465E+00	9.0872E−01	1.6377E+00	1.0130E+00	1.4226E+00	1.1309E+00	1.2414E+00
13	5.3695E−01	2.8361E+00	8.0292E−01	1.7510E+00	8.9498E−01	1.5200E+00	9.9934E−01	1.3256E+00
14	4.8145E−01	3.0218E+00	7.1494E−01	1.8628E+00	7.9641E−01	1.6161E+00	8.8908E−01	1.4087E+00
15	4.3582E−01	3.2030E+00	6.4120E−01	1.9728E+00	7.1344E−01	1.7109E+00	7.9595E−01	1.4908E+00
16	3.9788E−01	3.3794E+00	5.7895E−01	2.0809E+00	6.4312E−01	1.8043E+00	7.1675E−01	1.5717E+00
17	3.6588E−01	3.5504E+00	5.2601E−01	2.1867E+00	5.8312E−01	1.8958E+00	6.4901E−01	1.6512E+00
18	3.3846E−01	3.7160E+00	4.8062E−01	2.2898E+00	5.3159E−01	1.9852E+00	5.9071E−01	1.7290E+00
19	3.1460E−01	3.8763E+00	4.4138E−01	2.3900E+00	4.8701E−01	2.0722E+00	5.4023E−01	1.8048E+00
20	2.9353E−01	4.0315E+00	4.0715E−01	2.4869E+00	4.4817E−01	2.1566E+00	4.9625E−01	1.8783E+00
21	2.7467E−01	4.1822E+00	3.7704E−01	2.5807E+00	4.1406E−01	2.2381E+00	4.5769E−01	1.9495E+00
22	2.5764E−01	4.3287E+00	3.5033E−01	2.6712E+00	3.8390E−01	2.3169E+00	4.2365E−01	2.0182E+00
23	2.4215E−01	4.4716E+00	3.2647E−01	2.7585E+00	3.5706E−01	2.3928E+00	3.9343E−01	2.0844E+00
24	2.2799E−01	4.6112E+00	3.0500E−01	2.8429E+00	3.3301E−01	2.4660E+00	3.6644E−01	2.1482E+00
25	2.1499E−01	4.7478E+00	2.8558E−01	2.9245E+00	3.1135E−01	2.5367E+00	3.4220E−01	2.2096E+00
26	2.0304E−01	4.8818E+00	2.6793E−01	3.0035E+00	2.9173E−01	2.6050E+00	3.2033E−01	2.2689E+00
27	1.9204E−01	5.0134E+00	2.5183E−01	3.0802E+00	2.7391E−01	2.6710E+00	3.0051E−01	2.3261E+00
28	1.8190E−01	5.1427E+00	2.3710E−01	3.1547E+00	2.5765E−01	2.7350E+00	2.8248E−01	2.3815E+00
29	1.7255E−01	5.2699E+00	2.2358E−01	3.2272E+00	2.4278E−01	2.7972E+00	2.6603E−01	2.4351E+00
30	1.6393E−01	5.3949E+00	2.1117E−01	3.2979E+00	2.2915E−01	2.8577E+00	2.5098E−01	2.4872E+00
31	1.5596E−01	5.5179E+00	1.9974E−01	3.3670E+00	2.1662E−01	2.9167E+00	2.3717E−01	2.5379E+00
32	1.4859E−01	5.6390E+00	1.8921E−01	3.4345E+00	2.0509E−01	2.9742E+00	2.2447E−01	2.5873E+00
33	1.4177E−01	5.7581E+00	1.7949E−01	3.5007E+00	1.9446E−01	3.0305E+00	2.1277E−01	2.6356E+00
34	1.3545E−01	5.8752E+00	1.7051E−01	3.5655E+00	1.8464E−01	3.0856E+00	2.0197E−01	2.6828E+00
35	1.2957E−01	5.9905E+00	1.6220E−01	3.6291E+00	1.7556E−01	3.1397E+00	1.9199E−01	2.7290E+00
36	1.2410E−01	6.1040E+00	1.5451E−01	3.6916E+00	1.6716E−01	3.1927E+00	1.8275E−01	2.7744E+00
37	1.1900E−01	6.2156E+00	1.4738E−01	3.7529E+00	1.5936E−01	3.2448E+00	1.7417E−01	2.8190E+00
38	1.1423E−01	4.2364E−02	1.4075E−01	3.8132E+00	1.5213E−01	3.2960E+00	1.6621E−01	2.8628E+00
39	1.0977E−01	1.5062E−01	1.3460E−01	3.8725E+00	1.4540E−01	3.3464E+00	1.5880E−01	2.9059E+00
40	1.0559E−01	2.5726E−01	1.2887E−01	3.9309E+00	1.3913E−01	3.3959E+00	1.5190E−01	2.9483E+00
41	1.0165E−01	3.6238E−01	1.2352E−01	3.9883E+00	1.3329E−01	3.4447E+00	1.4546E−01	2.9901E+00
42	9.7950E−02	4.6604E−01	1.1854E−01	4.0448E+00	1.2784E−01	3.4927E+00	1.3945E−01	3.0313E+00
43	9.4458E−02	5.6833E−01	1.1387E−01	4.1004E+00	1.2273E−01	3.5401E+00	1.3382E−01	3.0719E+00
44	9.1160E−02	6.6932E−01	1.0950E−01	4.1552E+00	1.1796E−01	3.5867E+00	1.2855E−01	3.1119E+00
45	8.8042E−02	7.6908E−01	1.0541E−01	4.2092E+00	1.1347E−01	3.6326E+00	1.2360E−01	3.1513E+00
46	8.5089E−02	8.6771E−01	1.0156E−01	4.2624E+00	1.0926E−01	3.6779E+00	1.1894E−01	3.1902E+00
47	8.2290E−02	9.6528E−01	9.7934E−02	4.3148E+00	1.0530E−01	3.7225E+00	1.1456E−01	3.2285E+00
48	7.9633E−02	1.0619E+00	9.4520E−02	4.3665E+00	1.0156E−01	3.7666E+00	1.1044E−01	3.2663E+00
49	7.7109E−02	1.1576E+00	9.1298E−02	4.4175E+00	9.8038E−02	3.8100E+00	1.0654E−01	3.3036E+00
50	7.4709E−02	1.2524E+00	8.8253E−02	4.4678E+00	9.4707E−02	3.8527E+00	1.0286E−01	3.3403E+00
51	7.2425E−02	1.3465E+00	8.5370E−02	4.5174E+00	9.1555E−02	3.8949E+00	9.9380E−02	3.3766E+00
52	7.0251E−02	1.4400E+00	8.2637E−02	4.5664E+00	8.8568E−02	3.9366E+00	9.6080E−02	3.4123E+00
53	6.8180E−02	1.5328E+00	8.0044E−02	4.6147E+00	8.5733E−02	3.9777E+00	9.2949E−02	3.4476E+00
54	6.6206E−02	1.6251E+00	7.7580E−02	4.6624E+00	8.3041E−02	4.0182E+00	8.9976E−02	3.4824E+00
55	6.4324E−02	1.7169E+00	7.5236E−02	4.7095E+00	8.0481E−02	4.0582E+00	8.7150E−02	3.5167E+00
56	6.2530E−02	1.8083E+00	7.3004E−02	4.7561E+00	7.8044E−02	4.0977E+00	8.4461E−02	3.5506E+00
57	6.0819E−02	1.8993E+00	7.0876E−02	4.8020E+00	7.5721E−02	4.1366E+00	8.1898E−02	3.5840E+00
58	5.9188E−02	1.9901E+00	6.8845E−02	4.8475E+00	7.3504E−02	4.1751E+00	7.9454E−02	3.6169E+00
59	5.7634E−02	2.0806E+00	6.6905E−02	4.8924E+00	7.1387E−02	4.2131E+00	7.7121E−02	3.6494E+00
60	5.6154E−02	2.1709E+00	6.5050E−02	4.9368E+00	6.9364E−02	4.2506E+00	7.4892E−02	3.6815E+00

Table 4.3.3.1. *Partial wave elastic scattering factors for neutral atoms (cont.)*
Hf; $Z = 72$

	10 keV		40 keV		60 keV		90 keV	
s	$\|f(s)\|$	$\eta(s)$	$\|f(s)\|$	$\eta(s)$	$\|f(s)\|$	$\eta(s)$	$\|f(s)\|$	$\eta(s)$
0	1.0603E+01	3.3167E−01	1.2587E+01	2.4153E−01	1.3356E+01	2.1737E−01	1.4316E+01	1.9538E−01
1	8.5530E+00	4.0215E−01	1.0359E+01	2.8874E−01	1.1037E+01	2.5904E−01	1.1875E+01	2.3212E−01
2	5.5915E+00	5.8256E−01	7.0794E+00	4.0530E−01	7.6076E+00	3.6123E−01	8.2428E+00	3.2187E−01
3	3.8068E+00	7.9686E−01	5.0313E+00	5.3889E−01	5.4508E+00	4.7751E−01	5.9438E+00	4.2350E−01
4	2.7788E+00	1.0066E+00	3.8079E+00	6.6705E−01	4.1536E+00	5.8857E−01	4.5536E+00	5.2024E−01
5	2.1162E+00	1.2155E+00	2.9904E+00	7.9273E−01	3.2813E+00	6.9714E−01	3.6138E+00	6.1455E−01
6	1.6607E+00	1.4288E+00	2.4050E+00	9.1954E−01	2.6519E+00	8.0637E−01	2.9320E+00	7.0922E−01
7	1.3384E+00	1.6447E+00	1.9724E+00	1.0472E+00	2.1833E+00	9.1609E−01	2.4215E+00	8.0416E−01
8	1.1046E+00	1.8590E+00	1.6463E+00	1.1738E+00	1.8276E+00	1.0248E+00	2.0319E+00	8.9816E−01
9	9.3006E−01	2.0684E+00	1.3954E+00	1.2978E+00	1.5524E+00	1.1313E+00	1.7291E+00	9.9019E−01
10	7.9575E−01	2.2721E+00	1.1983E+00	1.4188E+00	1.3351E+00	1.2351E+00	1.4891E+00	1.0799E+00
11	6.8963E−01	2.4704E+00	1.0400E+00	1.5367E+00	1.1599E+00	1.3364E+00	1.2950E+00	1.1674E+00
12	6.0517E−01	2.6642E+00	9.1187E−01	1.6522E+00	1.0175E+00	1.4356E+00	1.1367E+00	1.2531E+00
13	5.3685E−01	2.8540E+00	8.0629E−01	1.7658E+00	8.9967E−01	1.5331E+00	1.0053E+00	1.3374E+00
14	4.8099E−01	3.0401E+00	7.1829E−01	1.8776E+00	8.0104E−01	1.6293E+00	8.9498E−01	1.4205E+00
15	4.3504E−01	3.2220E+00	6.4446E−01	1.9877E+00	7.1793E−01	1.7241E+00	8.0166E−01	1.5026E+00
16	3.9687E−01	3.3992E+00	5.8208E−01	2.0959E+00	6.4742E−01	1.8175E+00	7.2222E−01	1.5836E+00
17	3.6475E−01	3.5715E+00	5.2899E−01	2.2020E+00	5.8721E−01	1.9093E+00	6.5419E−01	1.6632E+00
18	3.3734E−01	3.7386E+00	4.8348E−01	2.3056E+00	5.3547E−01	1.9990E+00	5.9559E−01	1.7413E+00
19	3.1358E−01	3.9004E+00	4.4413E−01	2.4063E+00	4.9069E−01	2.0865E+00	5.4482E−01	1.8175E+00
20	2.9268E−01	4.0574E+00	4.0984E−01	2.5041E+00	4.5166E−01	2.1715E+00	5.0057E−01	1.8916E+00
21	2.7406E−01	4.2097E+00	3.7969E−01	2.5986E+00	4.1741E−01	2.2538E+00	4.6176E−01	1.9634E+00
22	2.5729E−01	4.3578E+00	3.5296E−01	2.6900E+00	3.8713E−01	2.3333E+00	4.2750E−01	2.0329E+00
23	2.4207E−01	4.5021E+00	3.2908E−01	2.7783E+00	3.6018E−01	2.4102E+00	3.9708E−01	2.0999E+00
24	2.2817E−01	4.6431E+00	3.0761E−01	2.8636E+00	3.3603E−01	2.4843E+00	3.6992E−01	2.1645E+00
25	2.1543E−01	4.7811E+00	2.8818E−01	2.9461E+00	3.1428E−01	2.5558E+00	3.4552E−01	2.2269E+00
26	2.0372E−01	4.9164E+00	2.7052E−01	3.0259E+00	2.9459E−01	2.6249E+00	3.2351E−01	2.2870E+00
27	1.9294E−01	5.0491E+00	2.5440E−01	3.1034E+00	2.7668E−01	2.6918E+00	3.0355E−01	2.3450E+00
28	1.8300E−01	5.1794E+00	2.3964E−01	3.1787E+00	2.6035E−01	2.7566E+00	2.8540E−01	2.4011E+00
29	1.7383E−01	5.3075E+00	2.2609E−01	3.2519E+00	2.4539E−01	2.8195E+00	2.6882E−01	2.4555E+00
30	1.6536E−01	5.4335E+00	2.1362E−01	3.3233E+00	2.3167E−01	2.8807E+00	2.5365E−01	2.5083E+00
31	1.5753E−01	5.5573E+00	2.0213E−01	3.3929E+00	2.1905E−01	2.9403E+00	2.3972E−01	2.5596E+00
32	1.5028E−01	5.6790E+00	1.9152E−01	3.4610E+00	2.0743E−01	2.9984E+00	2.2691E−01	2.6096E+00
33	1.4355E−01	5.7987E+00	1.8173E−01	3.5277E+00	1.9670E−01	3.0552E+00	2.1509E−01	2.6584E+00
34	1.3731E−01	5.9164E+00	1.7266E−01	3.5930E+00	1.8678E−01	3.1108E+00	2.0418E−01	2.7061E+00
35	1.3149E−01	6.0321E+00	1.6427E−01	3.6570E+00	1.7761E−01	3.1653E+00	1.9410E−01	2.7528E+00
36	1.2606E−01	6.1459E+00	1.5649E−01	3.7198E+00	1.6910E−01	3.2187E+00	1.8475E−01	2.7985E+00
37	1.2099E−01	6.2579E+00	1.4926E−01	3.7815E+00	1.6121E−01	3.2712E+00	1.7607E−01	2.8435E+00
38	1.1623E−01	6.3680E+00	1.4255E−01	3.8422E+00	1.5388E−01	3.3227E+00	1.6801E−01	2.8876E+00
39	1.1176E−01	6.4764E+00	1.3630E−01	3.9018E+00	1.4706E−01	3.3734E+00	1.6051E−01	2.9310E+00
40	1.0756E−01	6.5831E+00	1.3048E−01	3.9604E+00	1.4070E−01	3.4232E+00	1.5352E−01	2.9737E+00
41	1.0359E−01	6.6882E+00	1.2505E−01	4.0181E+00	1.3477E−01	3.4723E+00	1.4699E−01	3.0158E+00
42	9.9844E−02	6.7918E+00	1.1998E−01	4.0749E+00	1.2924E−01	3.5206E+00	1.4090E−01	3.0572E+00
43	9.6296E−02	6.8939E+00	1.1523E−01	4.1308E+00	1.2405E−01	3.5682E+00	1.3519E−01	3.0980E+00
44	9.2931E−02	6.9948E+00	1.1079E−01	4.1858E+00	1.1920E−01	3.6150E+00	1.2984E−01	3.1383E+00
45	8.9736E−02	7.0944E+00	1.0661E−01	4.2400E+00	1.1464E−01	3.6612E+00	1.2483E−01	3.1779E+00
46	8.6697E−02	7.1929E+00	1.0269E−01	4.2935E+00	1.1037E−01	3.7067E+00	1.2011E−01	3.2170E+00
47	8.3804E−02	7.2903E+00	9.8996E−02	4.3461E+00	1.0634E−01	3.7516E+00	1.1567E−01	3.2556E+00
48	8.1047E−02	7.3867E+00	9.5515E−02	4.3981E+00	1.0254E−01	3.7959E+00	1.1148E−01	3.2936E+00
49	7.8417E−02	7.4823E+00	9.2229E−02	4.4493E+00	9.8959E−02	3.8395E+00	1.0754E−01	3.3311E+00
50	7.5906E−02	7.5771E+00	8.9122E−02	4.4998E+00	9.5574E−02	3.8826E+00	1.0380E−01	3.3681E+00
51	7.3508E−02	7.6712E+00	8.6181E−02	4.5497E+00	9.2370E−02	3.9250E+00	1.0027E−01	3.4046E+00
52	7.1216E−02	7.7646E+00	8.3393E−02	4.5989E+00	8.9335E−02	3.9669E+00	9.6929E−02	3.4406E+00
53	6.9025E−02	7.8576E+00	8.0747E−02	4.6475E+00	8.6455E−02	4.0083E+00	9.3756E−02	3.4761E+00
54	6.6931E−02	7.9501E+00	7.8232E−02	4.6954E+00	8.3719E−02	4.0490E+00	9.0743E−02	3.5112E+00
55	6.4928E−02	8.0422E+00	7.5840E−02	4.7428E+00	8.1117E−02	4.0893E+00	8.7879E−02	3.5457E+00
56	6.3014E−02	8.1340E+00	7.3561E−02	4.7897E+00	7.8640E−02	4.1291E+00	8.5153E−02	3.5799E+00
57	6.1185E−02	8.2257E+00	7.1388E−02	4.8360E+00	7.6280E−02	4.1684E+00	8.2556E−02	3.6135E+00
58	5.9437E−02	8.3172E+00	6.9314E−02	4.8817E+00	7.4028E−02	4.2071E+00	8.0080E−02	3.6468E+00
59	5.7770E−02	8.4086E+00	6.7333E−02	4.9270E+00	7.1877E−02	4.2455E+00	7.7716E−02	3.6796E+00
60	5.6180E−02	8.5000E+00	6.5440E−02	4.9717E+00	6.9822E−02	4.2833E+00	7.5458E−02	3.7119E+00

Table 4.3.3.1. *Partial wave elastic scattering factors for neutral atoms (cont.)*
Ta; $Z = 73$

	10 keV		40 keV		60 keV		90 keV	
s	$\|f(s)\|$	$\eta(s)$	$\|f(s)\|$	$\eta(s)$	$\|f(s)\|$	$\eta(s)$	$\|f(s)\|$	$\eta(s)$
0	1.0252E+01	3.4524E−01	1.2220E+01	2.5112E−01	1.2978E+01	2.2603E−01	1.3921E+01	2.0321E−01
1	8.4411E+00	4.1045E−01	1.0249E+01	2.9477E−01	1.0927E+01	2.6456E−01	1.1761E+01	2.3716E−01
2	5.6583E+00	5.8029E−01	7.1658E+00	4.0479E−01	7.7018E+00	3.6107E−01	8.3465E+00	3.2197E−01
3	3.8629E+00	7.9165E−01	5.1069E+00	5.3696E−01	5.5339E+00	4.7621E−01	6.0357E+00	4.2267E−01
4	2.8046E+00	1.0060E+00	3.8463E+00	6.6807E−01	4.1971E+00	5.8988E−01	4.6029E+00	5.2172E−01
5	2.1272E+00	1.2204E+00	3.0086E+00	7.9718E−01	3.3027E+00	7.0144E−01	3.6390E+00	6.1865E−01
6	1.6661E+00	1.4377E+00	2.4145E+00	9.2656E−01	2.6637E+00	8.1291E−01	2.9466E+00	7.1529E−01
7	1.3417E+00	1.6565E+00	1.9784E+00	1.0560E+00	2.1911E+00	9.2425E−01	2.4315E+00	8.1166E−01
8	1.1071E+00	1.8728E+00	1.6507E+00	1.1841E+00	1.8335E+00	1.0343E+00	2.0396E+00	9.0679E−01
9	9.3225E−01	2.0837E+00	1.3991E+00	1.3093E+00	1.5574E+00	1.1418E+00	1.7356E+00	9.9974E−01
10	7.9782E−01	2.2883E+00	1.2018E+00	1.4311E+00	1.3397E+00	1.2464E+00	1.4951E+00	1.0901E+00
11	6.9154E−01	2.4871E+00	1.0434E+00	1.5497E+00	1.1644E+00	1.3482E+00	1.3008E+00	1.1781E+00
12	6.0684E−01	2.6812E+00	9.1521E−01	1.6656E+00	1.0219E+00	1.4477E+00	1.1424E+00	1.2641E+00
13	5.3819E−01	2.8711E+00	8.0957E−01	1.7792E+00	9.0400E−01	1.5454E+00	1.0109E+00	1.3486E+00
14	4.8195E−01	3.0572E+00	7.2144E−01	1.8911E+00	8.0525E−01	1.6416E+00	9.0037E−01	1.4318E+00
15	4.3563E−01	3.2393E+00	6.4743E−01	2.0012E+00	7.2197E−01	1.7364E+00	8.0686E−01	1.5138E+00
16	3.9714E−01	3.4170E+00	5.8486E−01	2.1095E+00	6.5124E−01	1.8299E+00	7.2718E−01	1.5948E+00
17	3.6480E−01	3.5900E+00	5.3158E−01	2.2159E+00	5.9081E−01	1.9218E+00	6.5888E−01	1.6746E+00
18	3.3726E−01	3.7579E+00	4.8588E−01	2.3198E+00	5.3883E−01	2.0119E+00	6.0000E−01	1.7529E+00
19	3.1346E−01	3.9207E+00	4.4640E−01	2.4211E+00	4.9384E−01	2.0998E+00	5.4895E−01	1.8295E+00
20	2.9258E−01	4.0786E+00	4.1199E−01	2.5195E+00	4.5464E−01	2.1854E+00	5.0444E−01	1.9042E+00
21	2.7403E−01	4.2320E+00	3.8176E−01	2.6148E+00	4.2023E−01	2.2684E+00	4.6539E−01	1.9767E+00
22	2.5736E−01	4.3811E+00	3.5498E−01	2.7071E+00	3.8982E−01	2.3488E+00	4.3093E−01	2.0469E+00
23	2.4225E−01	4.5265E+00	3.3108E−01	2.7963E+00	3.6276E−01	2.4265E+00	4.0033E−01	2.1147E+00
24	2.2846E−01	4.6685E+00	3.0959E−01	2.8826E+00	3.3853E−01	2.5015E+00	3.7300E−01	2.1803E+00
25	2.1583E−01	4.8074E+00	2.9015E−01	2.9661E+00	3.1671E−01	2.5740E+00	3.4846E−01	2.2435E+00
26	2.0422E−01	4.9436E+00	2.7248E−01	3.0469E+00	2.9695E−01	2.6441E+00	3.2632E−01	2.3045E+00
27	1.9352E−01	5.0772E+00	2.5635E−01	3.1253E+00	2.7898E−01	2.7119E+00	3.0624E−01	2.3635E+00
28	1.8365E−01	5.2085E+00	2.4157E−01	3.2015E+00	2.6258E−01	2.7777E+00	2.8798E−01	2.4205E+00
29	1.7455E−01	5.3376E+00	2.2799E−01	3.2756E+00	2.4757E−01	2.8414E+00	2.7130E−01	2.4757E+00
30	1.6612E−01	5.4645E+00	2.1549E−01	3.3478E+00	2.3378E−01	2.9034E+00	2.5603E−01	2.5293E+00
31	1.5833E−01	5.5893E+00	2.0396E−01	3.4183E+00	2.2109E−01	2.9638E+00	2.4200E−01	2.5814E+00
32	1.5111E−01	5.7121E+00	1.9331E−01	3.4871E+00	2.0939E−01	3.0227E+00	2.2909E−01	2.6320E+00
33	1.4441E−01	5.8328E+00	1.8346E−01	3.5545E+00	1.9859E−01	3.0802E+00	2.1718E−01	2.6815E+00
34	1.3818E−01	5.9516E+00	1.7433E−01	3.6205E+00	1.8860E−01	3.1364E+00	2.0619E−01	2.7298E+00
35	1.3238E−01	6.0684E+00	1.6588E−01	3.6853E+00	1.7934E−01	3.1915E+00	1.9600E−01	2.7771E+00
36	1.2697E−01	6.1833E+00	1.5803E−01	3.7488E+00	1.7076E−01	3.2455E+00	1.8657E−01	2.8234E+00
37	1.2190E−01	6.2964E+00	1.5074E−01	3.8111E+00	1.6280E−01	3.2985E+00	1.7781E−01	2.8688E+00
38	1.1716E−01	6.4076E+00	1.4396E−01	3.8724E+00	1.5539E−01	3.3506E+00	1.6967E−01	2.9134E+00
39	1.1269E−01	6.5171E+00	1.3765E−01	3.9326E+00	1.4850E−01	3.4018E+00	1.6209E−01	2.9573E+00
40	1.0849E−01	6.6248E+00	1.3176E−01	3.9918E+00	1.4208E−01	3.4522E+00	1.5502E−01	3.0004E+00
41	1.0452E−01	6.7310E+00	1.2627E−01	4.0501E+00	1.3608E−01	3.5017E+00	1.4843E−01	3.0428E+00
42	1.0077E−01	6.8357E+00	1.2114E−01	4.1074E+00	1.3048E−01	3.5505E+00	1.4226E−01	3.0847E+00
43	9.7222E−02	6.9388E+00	1.1634E−01	4.1638E+00	1.2524E−01	3.5985E+00	1.3649E−01	3.1258E+00
44	9.3850E−02	7.0407E+00	1.1184E−01	4.2194E+00	1.2033E−01	3.6458E+00	1.3109E−01	3.1664E+00
45	9.0645E−02	7.1413E+00	1.0762E−01	4.2742E+00	1.1572E−01	3.6924E+00	1.2601E−01	3.2064E+00
46	8.7595E−02	7.2406E+00	1.0365E−01	4.3281E+00	1.1139E−01	3.7384E+00	1.2125E−01	3.2459E+00
47	8.4688E−02	7.3389E+00	9.9911E−02	4.3813E+00	1.0732E−01	3.7837E+00	1.1676E−01	3.2848E+00
48	8.1914E−02	7.4362E+00	9.6389E−02	4.4337E+00	1.0348E−01	3.8283E+00	1.1253E−01	3.3232E+00
49	7.9265E−02	7.5326E+00	9.3066E−02	4.4854E+00	9.9858E−02	3.8724E+00	1.0854E−01	3.3610E+00
50	7.6734E−02	7.6281E+00	8.9924E−02	4.5364E+00	9.6436E−02	3.9158E+00	1.0477E−01	3.3984E+00
51	7.4313E−02	7.7230E+00	8.6950E−02	4.5868E+00	9.3199E−02	3.9587E+00	1.0120E−01	3.4352E+00
52	7.1996E−02	7.8172E+00	8.4132E−02	4.6364E+00	9.0132E−02	4.0010E+00	9.7825E−02	3.4715E+00
53	6.9779E−02	7.9108E+00	8.1458E−02	4.6855E+00	8.7224E−02	4.0427E+00	9.4622E−02	3.5074E+00
54	6.7656E−02	8.0040E+00	7.8917E−02	4.7339E+00	8.4461E−02	4.0839E+00	9.1581E−02	3.5428E+00
55	6.5623E−02	8.0967E+00	7.6500E−02	4.7818E+00	8.1835E−02	4.1246E+00	8.8690E−02	3.5777E+00
56	6.3678E−02	8.1892E+00	7.4199E−02	4.8291E+00	7.9335E−02	4.1648E+00	8.5939E−02	3.6122E+00
57	6.1816E−02	8.2815E+00	7.2005E−02	4.8758E+00	7.6953E−02	4.2044E+00	8.3319E−02	3.6462E+00
58	6.0035E−02	8.3736E+00	6.9912E−02	4.9220E+00	7.4681E−02	4.2436E+00	8.0821E−02	3.6798E+00
59	5.8333E−02	8.4656E+00	6.7913E−02	4.9677E+00	7.2512E−02	4.2823E+00	7.8437E−02	3.7130E+00
60	5.6707E−02	8.5576E+00	6.6002E−02	5.0129E+00	7.0439E−02	4.3206E+00	7.6160E−02	3.7457E+00

Table 4.3.3.1. *Partial wave elastic scattering factors for neutral atoms (cont.)*
W; $Z = 74$

	10 keV		40 keV		60 keV		90 keV	
s	$\|f(s)\|$	$\eta(s)$	$\|f(s)\|$	$\eta(s)$	$\|f(s)\|$	$\eta(s)$	$\|f(s)\|$	$\eta(s)$
0	9.9115E+00	3.5816E−01	1.1863E+01	2.6042E−01	1.2610E+01	2.3446E−01	1.3535E+01	2.1086E−01
1	8.2957E+00	4.1927E−01	1.0102E+01	3.0129E−01	1.0776E+01	2.7053E−01	1.1606E+01	2.4263E−01
2	5.6909E+00	5.7992E−01	7.2132E+00	4.0557E−01	7.7550E+00	3.6206E−01	8.4066E+00	3.2309E−01
3	3.9107E+00	7.8642E−01	5.1727E+00	5.3510E−01	5.6066E+00	4.7499E−01	6.1167E+00	4.2192E−01
4	2.8318E+00	1.0027E+00	3.8873E+00	6.6760E−01	4.2435E+00	5.8992E−01	4.6555E+00	5.2211E−01
5	2.1405E+00	1.2214E+00	3.0308E+00	7.9949E−01	3.3287E+00	7.0391E−01	3.6694E+00	6.2119E−01
6	1.6729E+00	1.4430E+00	2.4268E+00	9.3153E−01	2.6788E+00	8.1770E−01	2.9648E+00	7.1987E−01
7	1.3458E+00	1.6651E+00	1.9859E+00	1.0632E+00	2.2006E+00	9.3099E−01	2.4433E+00	8.1795E−01
8	1.1102E+00	1.8840E+00	1.6559E+00	1.1931E+00	1.8403E+00	1.0426E+00	2.0482E+00	9.1448E−01
9	9.3494E−01	2.0969E+00	1.4032E+00	1.3198E+00	1.5628E+00	1.1514E+00	1.7426E+00	1.0086E+00
10	8.0033E−01	2.3029E+00	1.2054E+00	1.4428E+00	1.3444E+00	1.2571E+00	1.5012E+00	1.0999E+00
11	6.9387E−01	2.5025E+00	1.0468E+00	1.5621E+00	1.1688E+00	1.3596E+00	1.3064E+00	1.1885E+00
12	6.0890E−01	2.6969E+00	9.1852E−01	1.6784E+00	1.0262E+00	1.4596E+00	1.1478E+00	1.2750E+00
13	5.3988E−01	2.8870E+00	8.1279E−01	1.7923E+00	9.0818E−01	1.5574E+00	1.0162E+00	1.3596E+00
14	4.8322E−01	3.0732E+00	7.2452E−01	1.9042E+00	8.0931E−01	1.6537E+00	9.0554E−01	1.4428E+00
15	4.3648E−01	3.2555E+00	6.5034E−01	2.0144E+00	7.2586E−01	1.7485E+00	8.1185E−01	1.5249E+00
16	3.9763E−01	3.4336E+00	5.8757E−01	2.1228E+00	6.5494E−01	1.8420E+00	7.3195E−01	1.6059E+00
17	3.6501E−01	3.6072E+00	5.3409E−01	2.2292E+00	5.9428E−01	1.9340E+00	6.6340E−01	1.6858E+00
18	3.3729E−01	3.7758E+00	4.8821E−01	2.3335E+00	5.4209E−01	2.0243E+00	6.0426E−01	1.7643E+00
19	3.1339E−01	3.9396E+00	4.4857E−01	2.4352E+00	4.9690E−01	2.1126E+00	5.5296E−01	1.8412E+00
20	2.9249E−01	4.0985E+00	4.1405E−01	2.5342E+00	4.5751E−01	2.1987E+00	5.0820E−01	1.9163E+00
21	2.7398E−01	4.2528E+00	3.8374E−01	2.6303E+00	4.2295E−01	2.2824E+00	4.6892E−01	1.9893E+00
22	2.5738E−01	4.4030E+00	3.5691E−01	2.7234E+00	3.9242E−01	2.3635E+00	4.3426E−01	2.0602E+00
23	2.4236E−01	4.5493E+00	3.3297E−01	2.8135E+00	3.6526E−01	2.4420E+00	4.0348E−01	2.1289E+00
24	2.2868E−01	4.6923E+00	3.1147E−01	2.9007E+00	3.4095E−01	2.5180E+00	3.7600E−01	2.1952E+00
25	2.1614E−01	4.8321E+00	2.9203E−01	2.9851E+00	3.1905E−01	2.5914E+00	3.5133E−01	2.2594E+00
26	2.0462E−01	4.9692E+00	2.7436E−01	3.0669E+00	2.9924E−01	2.6624E+00	3.2906E−01	2.3213E+00
27	1.9401E−01	5.1038E+00	2.5822E−01	3.1462E+00	2.8121E−01	2.7311E+00	3.0888E−01	2.3811E+00
28	1.8422E−01	5.2360E+00	2.4343E−01	3.2232E+00	2.6476E−01	2.7977E+00	2.9051E−01	2.4390E+00
29	1.7517E−01	5.3660E+00	2.2984E−01	3.2982E+00	2.4969E−01	2.8623E+00	2.7374E−01	2.4950E+00
30	1.6680E−01	5.4938E+00	2.1731E−01	3.3712E+00	2.3584E−01	2.9251E+00	2.5837E−01	2.5494E+00
31	1.5905E−01	5.6196E+00	2.0575E−01	3.4425E+00	2.2309E−01	2.9863E+00	2.4425E−01	2.6022E+00
32	1.5186E−01	5.7434E+00	1.9505E−01	3.5122E+00	2.1133E−01	3.0459E+00	2.3125E−01	2.6536E+00
33	1.4519E−01	5.8651E+00	1.8515E−01	3.5803E+00	2.0046E−01	3.1041E+00	2.1926E−01	2.7037E+00
34	1.3899E−01	5.9850E+00	1.7598E−01	3.6470E+00	1.9040E−01	3.1610E+00	2.0817E−01	2.7526E+00
35	1.3321E−01	6.1029E+00	1.6747E−01	3.7124E+00	1.8108E−01	3.2168E+00	1.9791E−01	2.8005E+00
36	1.2782E−01	6.2189E+00	1.5956E−01	3.7766E+00	1.7242E−01	3.2714E+00	1.8838E−01	2.8473E+00
37	1.2277E−01	6.3330E+00	1.5221E−01	3.8396E+00	1.6439E−01	3.3250E+00	1.7954E−01	2.8933E+00
38	1.1803E−01	6.4453E+00	1.4537E−01	3.9014E+00	1.5691E−01	3.3776E+00	1.7132E−01	2.9384E+00
39	1.1358E−01	6.5558E+00	1.3900E−01	3.9623E+00	1.4995E−01	3.4293E+00	1.6367E−01	2.9827E+00
40	1.0938E−01	6.6647E+00	1.3305E−01	4.0221E+00	1.4346E−01	3.4801E+00	1.5653E−01	3.0262E+00
41	1.0542E−01	6.7719E+00	1.2750E−01	4.0809E+00	1.3740E−01	3.5302E+00	1.4986E−01	3.0691E+00
42	1.0168E−01	6.8776E+00	1.2232E−01	4.1388E+00	1.3173E−01	3.5794E+00	1.4363E−01	3.1113E+00
43	9.8125E−02	6.9818E+00	1.1746E−01	4.1958E+00	1.2643E−01	3.6279E+00	1.3780E−01	3.1529E+00
44	9.4751E−02	7.0846E+00	1.1291E−01	4.2519E+00	1.2146E−01	3.6756E+00	1.3234E−01	3.1938E+00
45	9.1542E−02	7.1861E+00	1.0863E−01	4.3072E+00	1.1681E−01	3.7227E+00	1.2721E−01	3.2342E+00
46	8.8484E−02	7.2864E+00	1.0462E−01	4.3616E+00	1.1243E−01	3.7691E+00	1.2239E−01	3.2740E+00
47	8.5567E−02	7.3856E+00	1.0084E−01	4.4153E+00	1.0831E−01	3.8148E+00	1.1785E−01	3.3133E+00
48	8.2781E−02	7.4837E+00	9.7274E−02	4.4683E+00	1.0443E−01	3.8599E+00	1.1358E−01	3.3520E+00
49	8.0118E−02	7.5809E+00	9.3912E−02	4.5205E+00	1.0076E−01	3.9043E+00	1.0954E−01	3.3902E+00
50	7.7569E−02	7.6773E+00	9.0734E−02	4.5719E+00	9.7304E−02	3.9482E+00	1.0573E−01	3.4279E+00
51	7.5129E−02	7.7728E+00	8.7727E−02	4.6227E+00	9.4032E−02	3.9914E+00	1.0213E−01	3.4650E+00
52	7.2790E−02	7.8678E+00	8.4878E−02	4.6729E+00	9.0933E−02	4.0341E+00	9.8720E−02	3.5017E+00
53	7.0549E−02	7.9621E+00	8.2175E−02	4.7224E+00	8.7995E−02	4.0763E+00	9.5485E−02	3.5379E+00
54	6.8400E−02	8.0559E+00	7.9607E−02	4.7713E+00	8.5205E−02	4.1179E+00	9.2414E−02	3.5736E+00
55	6.6340E−02	8.1493E+00	7.7165E−02	4.8196E+00	8.2553E−02	4.1589E+00	8.9496E−02	3.6089E+00
56	6.4365E−02	8.2424E+00	7.4840E−02	4.8673E+00	8.0029E−02	4.1995E+00	8.6720E−02	3.6437E+00
57	6.2471E−02	8.3352E+00	7.2625E−02	4.9145E+00	7.7625E−02	4.2396E+00	8.4076E−02	3.6781E+00
58	6.0657E−02	8.4279E+00	7.0511E−02	4.9612E+00	7.5332E−02	4.2791E+00	8.1556E−02	3.7120E+00
59	5.8921E−02	8.5206E+00	6.8493E−02	5.0073E+00	7.3144E−02	4.3182E+00	7.9151E−02	3.7455E+00
60	5.7260E−02	8.6132E+00	6.6564E−02	5.0529E+00	7.1053E−02	4.3568E+00	7.6855E−02	3.7786E+00

Table 4.3.3.1. *Partial wave elastic scattering factors for neutral atoms (cont.)*
Re; $Z = 75$

	10 keV		40 keV		60 keV		90 keV	
s	$\|f(s)\|$	$\eta(s)$	$\|f(s)\|$	$\eta(s)$	$\|f(s)\|$	$\eta(s)$	$\|f(s)\|$	$\eta(s)$
0	9.6041E+00	3.7069E−01	1.1541E+01	2.6947E−01	1.2279E+01	2.4267E−01	1.3189E+01	2.1831E−01
1	8.1535E+00	4.2816E−01	9.9578E+00	3.0788E−01	1.0630E+01	2.7656E−01	1.1454E+01	2.4815E−01
2	5.7116E+00	5.8065E−01	7.2475E+00	4.0704E−01	7.7945E+00	3.6365E−01	8.4521E+00	3.2473E−01
3	3.9544E+00	7.8203E−01	5.2339E+00	5.3372E−01	5.6745E+00	4.7418E−01	6.1925E+00	4.2153E−01
4	2.8597E+00	9.9894E−01	3.9297E+00	6.6687E−01	4.2914E+00	5.8974E−01	4.7098E+00	5.2232E−01
5	2.1553E+00	1.2213E+00	3.0555E+00	8.0109E−01	3.3575E+00	7.0578E−01	3.7028E+00	6.2321E−01
6	1.6809E+00	1.4469E+00	2.4412E+00	9.3572E−01	2.6960E+00	8.2184E−01	2.9854E+00	7.2387E−01
7	1.3507E+00	1.6727E+00	1.9947E+00	1.0698E+00	2.2116E+00	9.3719E−01	2.4568E+00	8.2377E−01
8	1.1138E+00	1.8946E+00	1.6618E+00	1.2017E+00	1.8479E+00	1.0506E+00	2.0578E+00	9.2188E−01
9	9.3805E−01	2.1098E+00	1.4077E+00	1.3301E+00	1.5686E+00	1.1609E+00	1.7499E+00	1.0173E+00
10	8.0323E−01	2.3174E+00	1.2092E+00	1.4544E+00	1.3493E+00	1.2678E+00	1.5074E+00	1.1097E+00
11	6.9655E−01	2.5181E+00	1.0503E+00	1.5747E+00	1.1732E+00	1.3712E+00	1.3120E+00	1.1991E+00
12	6.1130E−01	2.7131E+00	9.2184E−01	1.6917E+00	1.0304E+00	1.4717E+00	1.1531E+00	1.2860E+00
13	5.4191E−01	2.9034E+00	8.1598E−01	1.8059E+00	9.1226E−01	1.5699E+00	1.0213E+00	1.3709E+00
14	4.8479E−01	3.0898E+00	7.2757E−01	1.9179E+00	8.1325E−01	1.6662E+00	9.1051E−01	1.4543E+00
15	4.3760E−01	3.2723E+00	6.5321E−01	2.0281E+00	7.2964E−01	1.7611E+00	8.1666E−01	1.5364E+00
16	3.9835E−01	3.4508E+00	5.9024E−01	2.1365E+00	6.5852E−01	1.8546E+00	7.3656E−01	1.6174E+00
17	3.6541E−01	3.6248E+00	5.3655E−01	2.2431E+00	5.9766E−01	1.9466E+00	6.6778E−01	1.6973E+00
18	3.3745E−01	3.7942E+00	4.9049E−01	2.3475E+00	5.4525E−01	2.0371E+00	6.0840E−01	1.7759E+00
19	3.1341E−01	3.9588E+00	4.5068E−01	2.4496E+00	4.9986E−01	2.1257E+00	5.5684E−01	1.8531E+00
20	2.9245E−01	4.1187E+00	4.1603E−01	2.5491E+00	4.6030E−01	2.2122E+00	5.1185E−01	1.9286E+00
21	2.7393E−01	4.2740E+00	3.8563E−01	2.6459E+00	4.2558E−01	2.2965E+00	4.7236E−01	2.0021E+00
22	2.5738E−01	4.4252E+00	3.5874E−01	2.7397E+00	3.9493E−01	2.3783E+00	4.3750E−01	2.0736E+00
23	2.4243E−01	4.5725E+00	3.3477E−01	2.8307E+00	3.6767E−01	2.4576E+00	4.0655E−01	2.1430E+00
24	2.2883E−01	4.7163E+00	3.1326E−01	2.9187E+00	3.4328E−01	2.5343E+00	3.7892E−01	2.2101E+00
25	2.1639E−01	4.8571E+00	2.9381E−01	3.0040E+00	3.2132E−01	2.6086E+00	3.5412E−01	2.2750E+00
26	2.0495E−01	4.9951E+00	2.7614E−01	3.0867E+00	3.0145E−01	2.6805E+00	3.3174E−01	2.3378E+00
27	1.9441E−01	5.1305E+00	2.6001E−01	3.1669E+00	2.8338E−01	2.7501E+00	3.1146E−01	2.3985E+00
28	1.8469E−01	5.2636E+00	2.4521E−01	3.2449E+00	2.6687E−01	2.8175E+00	2.9299E−01	2.4572E+00
29	1.7570E−01	5.3945E+00	2.3161E−01	3.3207E+00	2.5175E−01	2.8830E+00	2.7613E−01	2.5141E+00
30	1.6739E−01	5.5232E+00	2.1907E−01	3.3946E+00	2.3786E−01	2.9467E+00	2.6068E−01	2.5692E+00
31	1.5968E−01	5.6500E+00	2.0748E−01	3.4666E+00	2.2505E−01	3.0086E+00	2.4647E−01	2.6228E+00
32	1.5254E−01	5.7747E+00	1.9676E−01	3.5370E+00	2.1324E−01	3.0689E+00	2.3339E−01	2.6749E+00
33	1.4590E−01	5.8975E+00	1.8682E−01	3.6059E+00	2.0231E−01	3.1279E+00	2.2131E−01	2.7257E+00
34	1.3973E−01	6.0183E+00	1.7760E−01	3.6733E+00	1.9218E−01	3.1855E+00	2.1014E−01	2.7753E+00
35	1.3397E−01	6.1372E+00	1.6904E−01	3.7394E+00	1.8279E−01	3.2418E+00	1.9980E−01	2.8237E+00
36	1.2860E−01	6.2543E+00	1.6108E−01	3.8042E+00	1.7408E−01	3.2970E+00	1.9020E−01	2.8711E+00
37	1.2357E−01	6.3695E+00	1.5367E−01	3.8678E+00	1.6597E−01	3.3512E+00	1.8128E−01	2.9176E+00
38	1.1885E−01	6.4829E+00	1.4678E−01	3.9303E+00	1.5843E−01	3.4044E+00	1.7298E−01	2.9632E+00
39	1.1442E−01	6.5945E+00	1.4035E−01	3.9917E+00	1.5140E−01	3.4566E+00	1.6525E−01	3.0080E+00
40	1.1023E−01	6.7044E+00	1.3435E−01	4.0521E+00	1.4484E−01	3.5080E+00	1.5804E−01	3.0520E+00
41	1.0628E−01	6.8127E+00	1.2874E−01	4.1115E+00	1.3872E−01	3.5585E+00	1.5131E−01	3.0952E+00
42	1.0255E−01	6.9194E+00	1.2350E−01	4.1700E+00	1.3299E−01	3.6082E+00	1.4501E−01	3.1379E+00
43	9.9000E−02	7.0246E+00	1.1859E−01	4.2275E+00	1.2763E−01	3.6572E+00	1.3912E−01	3.1798E+00
44	9.5629E−02	7.1284E+00	1.1398E−01	4.2842E+00	1.2261E−01	3.7053E+00	1.3359E−01	3.2211E+00
45	9.2420E−02	7.2309E+00	1.0966E−01	4.3400E+00	1.1790E−01	3.7528E+00	1.2840E−01	3.2619E+00
46	8.9360E−02	7.3321E+00	1.0560E−01	4.3950E+00	1.1347E−01	3.7996E+00	1.2353E−01	3.3020E+00
47	8.6439E−02	7.4321E+00	1.0177E−01	4.4492E+00	1.0930E−01	3.8458E+00	1.1895E−01	3.3416E+00
48	8.3645E−02	7.5311E+00	9.8170E−02	4.5026E+00	1.0538E−01	3.8913E+00	1.1463E−01	3.3807E+00
49	8.0971E−02	7.6291E+00	9.4769E−02	4.5553E+00	1.0167E−01	3.9361E+00	1.1055E−01	3.4192E+00
50	7.8409E−02	7.7262E+00	9.1555E−02	4.6073E+00	9.8178E−02	3.9804E+00	1.0670E−01	3.4573E+00
51	7.5953E−02	7.8225E+00	8.8513E−02	4.6586E+00	9.4870E−02	4.0241E+00	1.0306E−01	3.4948E+00
52	7.3596E−02	7.9182E+00	8.5632E−02	4.7092E+00	9.1739E−02	4.0671E+00	9.9614E−02	3.5318E+00
53	7.1334E−02	8.0132E+00	8.2899E−02	4.7592E+00	8.8769E−02	4.1097E+00	9.6347E−02	3.5683E+00
54	6.9162E−02	8.1076E+00	8.0304E−02	4.8085E+00	8.5951E−02	4.1516E+00	9.3246E−02	3.6044E+00
55	6.7076E−02	8.2017E+00	7.7836E−02	4.8573E+00	8.3272E−02	4.1931E+00	9.0300E−02	3.6400E+00
56	6.5073E−02	8.2954E+00	7.5487E−02	4.9054E+00	8.0724E−02	4.2340E+00	8.7498E−02	3.6751E+00
57	6.3150E−02	8.3888E+00	7.3249E−02	4.9530E+00	7.8297E−02	4.2745E+00	8.4830E−02	3.7098E+00
58	6.1304E−02	8.4821E+00	7.1115E−02	5.0001E+00	7.5983E−02	4.3144E+00	8.2287E−02	3.7441E+00
59	5.9535E−02	8.5753E+00	6.9077E−02	5.0467E+00	7.3774E−02	4.3539E+00	7.9861E−02	3.7780E+00
60	5.7839E−02	8.6685E+00	6.7129E−02	5.0927E+00	7.1665E−02	4.3929E+00	7.7544E−02	3.8114E+00

Table 4.3.3.1. *Partial wave elastic scattering factors for neutral atoms (cont.)*
Os; $Z = 76$

	10 keV		40 keV		60 keV		90 keV	
s	$\|f(s)\|$	$\eta(s)$	$\|f(s)\|$	$\eta(s)$	$\|f(s)\|$	$\eta(s)$	$\|f(s)\|$	$\eta(s)$
0	9.3019E+00	3.8287E−01	1.1224E+01	2.7839E−01	1.1952E+01	2.5078E−01	1.2847E+01	2.2570E−01
1	7.9932E+00	4.3726E−01	9.7929E+00	3.1472E−01	1.0461E+01	2.8284E−01	1.1279E+01	2.5391E−01
2	5.7088E+00	5.8245E−01	7.2547E+00	4.0927E−01	7.8055E+00	3.6592E−01	8.4672E+00	3.2699E−01
3	3.9885E+00	7.7808E−01	5.2837E+00	5.3268E−01	5.7303E+00	4.7367E−01	6.2553E+00	4.2141E−01
4	2.8862E+00	9.9394E−01	3.9707E+00	6.6547E−01	4.3379E+00	5.8900E−01	4.7626E+00	5.2205E−01
5	2.1708E+00	1.2186E+00	3.0821E+00	8.0126E−01	3.3883E+00	7.0644E−01	3.7385E+00	6.2420E−01
6	1.6897E+00	1.4478E+00	2.4574E+00	9.3820E−01	2.7155E+00	8.2453E−01	3.0085E+00	7.2664E−01
7	1.3561E+00	1.6773E+00	2.0048E+00	1.0747E+00	2.2241E+00	9.4199E−01	2.4721E+00	8.2838E−01
8	1.1178E+00	1.9026E+00	1.6685E+00	1.2089E+00	1.8564E+00	1.0574E+00	2.0684E+00	9.2823E−01
9	9.4147E−01	2.1205E+00	1.4127E+00	1.3392E+00	1.5749E+00	1.1694E+00	1.7579E+00	1.0252E+00
10	8.0643E−01	2.3301E+00	1.2132E+00	1.4651E+00	1.3544E+00	1.2777E+00	1.5138E+00	1.1188E+00
11	6.9955E−01	2.5321E+00	1.0539E+00	1.5866E+00	1.1777E+00	1.3821E+00	1.3176E+00	1.2092E+00
12	6.1403E−01	2.7278E+00	9.2519E−01	1.7043E+00	1.0346E+00	1.4834E+00	1.1583E+00	1.2967E+00
13	5.4426E−01	2.9186E+00	8.1918E−01	1.8190E+00	9.1627E−01	1.5820E+00	1.0263E+00	1.3820E+00
14	4.8668E−01	3.1052E+00	7.3060E−01	1.9312E+00	8.1710E−01	1.6785E+00	9.1533E−01	1.4656E+00
15	4.3902E−01	3.2879E+00	6.5606E−01	2.0415E+00	7.3332E−01	1.7734E+00	8.2130E−01	1.5477E+00
16	3.9932E−01	3.4667E+00	5.9287E−01	2.1499E+00	6.6201E−01	1.8669E+00	7.4101E−01	1.6287E+00
17	3.6600E−01	3.6413E+00	5.3898E−01	2.2565E+00	6.0094E−01	1.9590E+00	6.7202E−01	1.7086E+00
18	3.3776E−01	3.8114E+00	4.9271E−01	2.3612E+00	5.4833E−01	2.0496E+00	6.1240E−01	1.7874E+00
19	3.1353E−01	3.9768E+00	4.5274E−01	2.4636E+00	5.0274E−01	2.1384E+00	5.6062E−01	1.8647E+00
20	2.9246E−01	4.1376E+00	4.1795E−01	2.5636E+00	4.6300E−01	2.2253E+00	5.1540E−01	1.9404E+00
21	2.7391E−01	4.2939E+00	3.8745E−01	2.6609E+00	4.2814E−01	2.3100E+00	4.7570E−01	2.0145E+00
22	2.5737E−01	4.4460E+00	3.6049E−01	2.7554E+00	3.9735E−01	2.3924E+00	4.4065E−01	2.0865E+00
23	2.4247E−01	4.5942E+00	3.3649E−01	2.8471E+00	3.6999E−01	2.4724E+00	4.0954E−01	2.1565E+00
24	2.2893E−01	4.7390E+00	3.1495E−01	2.9360E+00	3.4552E−01	2.5499E+00	3.8177E−01	2.2243E+00
25	2.1656E−01	4.8807E+00	2.9550E−01	3.0221E+00	3.2350E−01	2.6250E+00	3.5684E−01	2.2901E+00
26	2.0520E−01	5.0195E+00	2.7784E−01	3.1057E+00	3.0358E−01	2.6978E+00	3.3435E−01	2.3536E+00
27	1.9474E−01	5.1558E+00	2.6171E−01	3.1868E+00	2.8546E−01	2.7682E+00	3.1397E−01	2.4151E+00
28	1.8509E−01	5.2898E+00	2.4692E−01	3.2655E+00	2.6892E−01	2.8365E+00	2.9542E−01	2.4747E+00
29	1.7616E−01	5.4215E+00	2.3332E−01	3.3422E+00	2.5376E−01	2.9028E+00	2.7847E−01	2.5323E+00
30	1.6790E−01	5.5512E+00	2.2077E−01	3.4169E+00	2.3982E−01	2.9673E+00	2.6294E−01	2.5883E+00
31	1.6024E−01	5.6788E+00	2.0916E−01	3.4897E+00	2.2697E−01	3.0300E+00	2.4866E−01	2.6426E+00
32	1.5314E−01	5.8045E+00	1.9842E−01	3.5608E+00	2.1511E−01	3.0911E+00	2.3550E−01	2.6954E+00
33	1.4654E−01	5.9282E+00	1.8845E−01	3.6304E+00	2.0412E−01	3.1507E+00	2.2334E−01	2.7469E+00
34	1.4039E−01	6.0500E+00	1.7919E−01	3.6985E+00	1.9394E−01	3.2090E+00	2.1210E−01	2.7971E+00
35	1.3467E−01	6.1700E+00	1.7059E−01	3.7653E+00	1.8449E−01	3.2660E+00	2.0167E−01	2.8461E+00
36	1.2932E−01	6.2881E+00	1.6258E−01	3.8308E+00	1.7571E−01	3.3218E+00	1.9200E−01	2.8941E+00
37	1.2432E−01	6.4043E+00	1.5513E−01	3.8950E+00	1.6755E−01	3.3765E+00	1.8300E−01	2.9411E+00
38	1.1962E−01	6.5187E+00	1.4818E−01	3.9581E+00	1.5994E−01	3.4303E+00	1.7463E−01	2.9872E+00
39	1.1520E−01	6.6314E+00	1.4169E−01	4.0202E+00	1.5285E−01	3.4831E+00	1.6683E−01	3.0325E+00
40	1.1104E−01	6.7424E+00	1.3564E−01	4.0812E+00	1.4623E−01	3.5349E+00	1.5955E−01	3.0769E+00
41	1.0711E−01	6.8517E+00	1.2998E−01	4.1411E+00	1.4004E−01	3.5859E+00	1.5275E−01	3.1207E+00
42	1.0338E−01	6.9594E+00	1.2468E−01	4.2002E+00	1.3426E−01	3.6361E+00	1.4639E−01	3.1637E+00
43	9.9843E−02	7.0656E+00	1.1972E−01	4.2583E+00	1.2885E−01	3.6855E+00	1.4043E−01	3.2060E+00
44	9.6481E−02	7.1704E+00	1.1507E−01	4.3155E+00	1.2377E−01	3.7342E+00	1.3485E−01	3.2477E+00
45	9.3277E−02	7.2738E+00	1.1070E−01	4.3718E+00	1.1900E−01	3.7821E+00	1.2961E−01	3.2888E+00
46	9.0220E−02	7.3759E+00	1.0659E−01	4.4273E+00	1.1452E−01	3.8293E+00	1.2468E−01	3.3294E+00
47	8.7298E−02	7.4769E+00	1.0272E−01	4.4820E+00	1.1031E−01	3.8759E+00	1.2005E−01	3.3693E+00
48	8.4501E−02	7.5767E+00	9.9077E−02	4.5360E+00	1.0634E−01	3.9218E+00	1.1568E−01	3.4087E+00
49	8.1821E−02	7.6755E+00	9.5637E−02	4.5891E+00	1.0260E−01	3.9671E+00	1.1156E−01	3.4476E+00
50	7.9250E−02	7.7734E+00	9.2386E−02	4.6416E+00	9.9059E−02	4.0117E+00	1.0767E−01	3.4859E+00
51	7.6782E−02	7.8705E+00	8.9310E−02	4.6933E+00	9.5716E−02	4.0558E+00	1.0399E−01	3.5238E+00
52	7.4410E−02	7.9668E+00	8.6397E−02	4.7444E+00	9.2550E−02	4.0993E+00	1.0051E−01	3.5611E+00
53	7.2131E−02	8.0625E+00	8.3633E−02	4.7948E+00	8.9549E−02	4.1422E+00	9.7209E−02	3.5980E+00
54	6.9938E−02	8.1576E+00	8.1009E−02	4.8447E+00	8.6701E−02	4.1846E+00	9.4078E−02	3.6344E+00
55	6.7830E−02	8.2523E+00	7.8515E−02	4.8938E+00	8.3995E−02	4.2264E+00	9.1103E−02	3.6703E+00
56	6.5802E−02	8.3466E+00	7.6141E−02	4.9425E+00	8.1421E−02	4.2677E+00	8.8274E−02	3.7058E+00
57	6.3851E−02	8.4406E+00	7.3880E−02	4.9905E+00	7.8970E−02	4.3085E+00	8.5581E−02	3.7408E+00
58	6.1976E−02	8.5344E+00	7.1723E−02	5.0380E+00	7.6634E−02	4.3489E+00	8.3014E−02	3.7754E+00
59	6.0174E−02	8.6282E+00	6.9665E−02	5.0850E+00	7.4405E−02	4.3887E+00	8.0567E−02	3.8096E+00
60	5.8444E−02	8.7219E+00	6.7698E−02	5.1315E+00	7.2276E−02	4.4281E+00	7.8230E−02	3.8434E+00

Table 4.3.3.1. *Partial wave elastic scattering factors for neutral atoms (cont.)*
Ir; $Z = 77$

	10 keV		40 keV		60 keV		90 keV	
s	$\|f(s)\|$	$\eta(s)$	$\|f(s)\|$	$\eta(s)$	$\|f(s)\|$	$\eta(s)$	$\|f(s)\|$	$\eta(s)$
0	9.0094E+00	3.9465E−01	1.0915E+01	2.8713E−01	1.1634E+01	2.5876E−01	1.2514E+01	2.3298E−01
1	7.8231E+00	4.4641E−01	9.6163E+00	3.2167E−01	1.0280E+01	2.8924E−01	1.1091E+01	2.5978E−01
2	5.6873E+00	5.8508E−01	7.2404E+00	4.1210E−01	7.7938E+00	3.6873E−01	8.4580E+00	3.2972E−01
3	4.0132E+00	7.7474E−01	5.3222E+00	5.3206E−01	5.7741E+00	4.7355E−01	6.3052E+00	4.2163E−01
4	2.9103E+00	9.8831E−01	4.0090E+00	6.6376E−01	4.3815E+00	5.8800E−01	4.8124E+00	5.2156E−01
5	2.1863E+00	1.2141E+00	3.1093E+00	8.0039E−01	3.4200E+00	7.0623E−01	3.7752E+00	6.2443E−01
6	1.6988E+00	1.4462E+00	2.4750E+00	9.3923E−01	2.7366E+00	8.2599E−01	3.0335E+00	7.2837E−01
7	1.3618E+00	1.6793E+00	2.0161E+00	1.0780E+00	2.2380E+00	9.4548E−01	2.4889E+00	8.3189E−01
8	1.1219E+00	1.9080E+00	1.6760E+00	1.2146E+00	1.8658E+00	1.0629E+00	2.0800E+00	9.3354E−01
9	9.4506E−01	2.1289E+00	1.4181E+00	1.3471E+00	1.5817E+00	1.1769E+00	1.7664E+00	1.0322E+00
10	8.0983E−01	2.3409E+00	1.2175E+00	1.4748E+00	1.3598E+00	1.2867E+00	1.5205E+00	1.1272E+00
11	7.0279E−01	2.5444E+00	1.0576E+00	1.5977E+00	1.1823E+00	1.3924E+00	1.3233E+00	1.2187E+00
12	6.1704E−01	2.7411E+00	9.2861E−01	1.7163E+00	1.0388E+00	1.4945E+00	1.1635E+00	1.3070E+00
13	5.4690E−01	2.9325E+00	8.2241E−01	1.8316E+00	9.2024E−01	1.5937E+00	1.0312E+00	1.3928E+00
14	4.8887E−01	3.1194E+00	7.3365E−01	1.9441E+00	8.2089E−01	1.6905E+00	9.2001E−01	1.4766E+00
15	4.4071E−01	3.3024E+00	6.5890E−01	2.0545E+00	7.3693E−01	1.7855E+00	8.2581E−01	1.5589E+00
16	4.0054E−01	3.4816E+00	5.9550E−01	2.1630E+00	6.6543E−01	1.8791E+00	7.4533E−01	1.6399E+00
17	3.6681E−01	3.6566E+00	5.4139E−01	2.2697E+00	6.0415E−01	1.9712E+00	6.7613E−01	1.7198E+00
18	3.3824E−01	3.8274E+00	4.9492E−01	2.3745E+00	5.5133E−01	2.0618E+00	6.1629E−01	1.7986E+00
19	3.1378E−01	3.9936E+00	4.5476E−01	2.4772E+00	5.0555E−01	2.1508E+00	5.6429E−01	1.8760E+00
20	2.9256E−01	4.1553E+00	4.1982E−01	2.5775E+00	4.6563E−01	2.2380E+00	5.1885E−01	1.9520E+00
21	2.7393E−01	4.3125E+00	3.8921E−01	2.6753E+00	4.3061E−01	2.3231E+00	4.7895E−01	2.0264E+00
22	2.5737E−01	4.4655E+00	3.6217E−01	2.7704E+00	3.9970E−01	2.4061E+00	4.4372E−01	2.0989E+00
23	2.4249E−01	4.6147E+00	3.3812E−01	2.8628E+00	3.7224E−01	2.4867E+00	4.1245E−01	2.1695E+00
24	2.2900E−01	4.7604E+00	3.1656E−01	2.9525E+00	3.4769E−01	2.5649E+00	3.8453E−01	2.2380E+00
25	2.1669E−01	4.9030E+00	2.9711E−01	3.0394E+00	3.2561E−01	2.6408E+00	3.5949E−01	2.3044E+00
26	2.0540E−01	5.0427E+00	2.7945E−01	3.1238E+00	3.0563E−01	2.7143E+00	3.3689E−01	2.3688E+00
27	1.9500E−01	5.1799E+00	2.6333E−01	3.2057E+00	2.8748E−01	2.7856E+00	3.1642E−01	2.4311E+00
28	1.8541E−01	5.3146E+00	2.4855E−01	3.2854E+00	2.7090E−01	2.8547E+00	2.9778E−01	2.4914E+00
29	1.7654E−01	5.4472E+00	2.3495E−01	3.3628E+00	2.5570E−01	2.9218E+00	2.8076E−01	2.5498E+00
30	1.6833E−01	5.5778E+00	2.2240E−01	3.4383E+00	2.4173E−01	2.9871E+00	2.6515E−01	2.6065E+00
31	1.6072E−01	5.7063E+00	2.1079E−01	3.5119E+00	2.2884E−01	3.0505E+00	2.5080E−01	2.6616E+00
32	1.5366E−01	5.8328E+00	2.0002E−01	3.5838E+00	2.1693E−01	3.1123E+00	2.3757E−01	2.7152E+00
33	1.4710E−01	5.9575E+00	1.9003E−01	3.6540E+00	2.0591E−01	3.1727E+00	2.2534E−01	2.7673E+00
34	1.4099E−01	6.0803E+00	1.8075E−01	3.7229E+00	1.9568E−01	3.2316E+00	2.1403E−01	2.8182E+00
35	1.3530E−01	6.2013E+00	1.7211E−01	3.7903E+00	1.8618E−01	3.2892E+00	2.0353E−01	2.8678E+00
36	1.2998E−01	6.3203E+00	1.6407E−01	3.8564E+00	1.7734E−01	3.3457E+00	1.9379E−01	2.9164E+00
37	1.2500E−01	6.4376E+00	1.5656E−01	3.9213E+00	1.6912E−01	3.4010E+00	1.8472E−01	2.9639E+00
38	1.2033E−01	6.5531E+00	1.4957E−01	3.9850E+00	1.6145E−01	3.4553E+00	1.7628E−01	3.0105E+00
39	1.1593E−01	6.6668E+00	1.4304E−01	4.0477E+00	1.5430E−01	3.5087E+00	1.6841E−01	3.0563E+00
40	1.1179E−01	6.7788E+00	1.3693E−01	4.1092E+00	1.4762E−01	3.5610E+00	1.6106E−01	3.1012E+00
41	1.0788E−01	6.8891E+00	1.3122E−01	4.1698E+00	1.4138E−01	3.6125E+00	1.5420E−01	3.1453E+00
42	1.0417E−01	6.9979E+00	1.2587E−01	4.2294E+00	1.3554E−01	3.6632E+00	1.4777E−01	3.1888E+00
43	1.0065E−01	7.1051E+00	1.2086E−01	4.2880E+00	1.3006E−01	3.7131E+00	1.4176E−01	3.2315E+00
44	9.7301E−02	7.2108E+00	1.1616E−01	4.3458E+00	1.2493E−01	3.7622E+00	1.3612E−01	3.2736E+00
45	9.4107E−02	7.3152E+00	1.1174E−01	4.4026E+00	1.2011E−01	3.8106E+00	1.3082E−01	3.3151E+00
46	9.1058E−02	7.4182E+00	1.0759E−01	4.4587E+00	1.1559E−01	3.8582E+00	1.2584E−01	3.3560E+00
47	8.8140E−02	7.5200E+00	1.0368E−01	4.5139E+00	1.1133E−01	3.9052E+00	1.2115E−01	3.3963E+00
48	8.5345E−02	7.6207E+00	9.9995E−02	4.5683E+00	1.0731E−01	3.9516E+00	1.1674E−01	3.4361E+00
49	8.2663E−02	7.7204E+00	9.6516E−02	4.6220E+00	1.0352E−01	3.9972E+00	1.1258E−01	3.4753E+00
50	8.0088E−02	7.8190E+00	9.3228E−02	4.6749E+00	9.9950E−02	4.0423E+00	1.0864E−01	3.5140E+00
51	7.7612E−02	7.9169E+00	9.0117E−02	4.7272E+00	9.6569E−02	4.0868E+00	1.0493E−01	3.5521E+00
52	7.5230E−02	8.0139E+00	8.7171E−02	4.7787E+00	9.3368E−02	4.1306E+00	1.0141E−01	3.5898E+00
53	7.2937E−02	8.1102E+00	8.4377E−02	4.8296E+00	9.0335E−02	4.1739E+00	9.8074E−02	3.6270E+00
54	7.0728E−02	8.2060E+00	8.1724E−02	4.8799E+00	8.7457E−02	4.2167E+00	9.4911E−02	3.6637E+00
55	6.8600E−02	8.3013E+00	7.9202E−02	4.9295E+00	8.4722E−02	4.2589E+00	9.1906E−02	3.7000E+00
56	6.6549E−02	8.3961E+00	7.6803E−02	4.9785E+00	8.2122E−02	4.3006E+00	8.9050E−02	3.7358E+00
57	6.4573E−02	8.4907E+00	7.4517E−02	5.0270E+00	7.9647E−02	4.3418E+00	8.6331E−02	3.7712E+00
58	6.2670E−02	8.5851E+00	7.2338E−02	5.0750E+00	7.7288E−02	4.3825E+00	8.3740E−02	3.8061E+00
59	6.0838E−02	8.6793E+00	7.0258E−02	5.1224E+00	7.5038E−02	4.4227E+00	8.1270E−02	3.8406E+00
60	5.9076E−02	8.7736E+00	6.8272E−02	5.1693E+00	7.2889E−02	4.4625E+00	7.8912E−02	3.8747E+00

Table 4.3.3.1. *Partial wave elastic scattering factors for neutral atoms (cont.)*
Pt; $Z = 78$

	10 keV		40 keV		60 keV		90 keV	
s	$\|f(s)\|$	$\eta(s)$	$\|f(s)\|$	$\eta(s)$	$\|f(s)\|$	$\eta(s)$	$\|f(s)\|$	$\eta(s)$
0	8.1369E+00	4.2159E−01	9.9585E+00	3.0728E−01	1.0636E+01	2.7707E−01	1.1459E+01	2.4960E−01
1	7.2202E+00	4.6777E−01	8.9504E+00	3.3800E−01	9.5853E+00	3.0414E−01	1.0357E+01	2.7335E−01
2	5.4793E+00	5.9022E−01	7.0083E+00	4.1799E−01	7.5519E+00	3.7447E−01	8.2030E+00	3.3522E−01
3	3.9884E+00	7.6099E−01	5.3007E+00	5.2663E−01	5.7540E+00	4.6951E−01	6.2864E+00	4.1864E−01
4	2.9278E+00	9.6231E−01	4.0413E+00	6.5143E−01	4.4191E+00	5.7811E−01	4.8557E+00	5.1354E−01
5	2.2025E+00	1.1843E+00	3.1415E+00	7.8616E−01	3.4577E+00	6.9477E−01	3.8190E+00	6.1512E−01
6	1.7081E+00	1.4186E+00	2.4970E+00	9.2638E−01	2.7630E+00	8.1577E−01	3.0648E+00	7.2015E−01
7	1.3670E+00	1.6564E+00	2.0296E+00	1.0681E+00	2.2548E+00	9.3779E−01	2.5093E+00	8.2589E−01
8	1.1256E+00	1.8902E+00	1.6845E+00	1.2079E+00	1.8764E+00	1.0581E+00	2.0932E+00	9.3000E−01
9	9.4859E−01	2.1152E+00	1.4238E+00	1.3433E+00	1.5889E+00	1.1746E+00	1.7754E+00	1.0309E+00
10	8.1345E−01	2.3300E+00	1.2219E+00	1.4733E+00	1.3653E+00	1.2865E+00	1.5273E+00	1.1277E+00
11	7.0637E−01	2.5355E+00	1.0613E+00	1.5978E+00	1.1869E+00	1.3936E+00	1.3289E+00	1.2205E+00
12	6.2040E−01	2.7333E+00	9.3205E−01	1.7176E+00	1.0429E+00	1.4967E+00	1.1685E+00	1.3098E+00
13	5.4985E−01	2.9253E+00	8.2563E−01	1.8335E+00	9.2412E−01	1.5965E+00	1.0359E+00	1.3961E+00
14	4.9130E−01	3.1126E+00	7.3666E−01	1.9463E+00	8.2457E−01	1.6936E+00	9.2453E−01	1.4801E+00
15	4.4260E−01	3.2959E+00	6.6170E−01	2.0568E+00	7.4043E−01	1.7887E+00	8.3015E−01	1.5625E+00
16	4.0190E−01	3.4754E+00	5.9807E−01	2.1653E+00	6.6874E−01	1.8822E+00	7.4949E−01	1.6435E+00
17	3.6773E−01	3.6509E+00	5.4372E−01	2.2721E+00	6.0726E−01	1.9742E+00	6.8010E−01	1.7233E+00
18	3.3880E−01	3.8223E+00	4.9704E−01	2.3769E+00	5.5423E−01	2.0649E+00	6.2005E−01	1.8021E+00
19	3.1407E−01	3.9893E+00	4.5670E−01	2.4798E+00	5.0825E−01	2.1541E+00	5.6783E−01	1.8796E+00
20	2.9269E−01	4.1518E+00	4.2161E−01	2.5805E+00	4.6816E−01	2.2415E+00	5.2219E−01	1.9558E+00
21	2.7396E−01	4.3099E+00	3.9088E−01	2.6787E+00	4.3299E−01	2.3270E+00	4.8210E−01	2.0305E+00
22	2.5735E−01	4.4639E+00	3.6377E−01	2.7744E+00	4.0195E−01	2.4104E+00	4.4669E−01	2.1035E+00
23	2.4248E−01	4.6140E+00	3.3967E−01	2.8675E+00	3.7439E−01	2.4916E+00	4.1527E−01	2.1745E+00
24	2.2902E−01	4.7606E+00	3.1809E−01	2.9579E+00	3.4977E−01	2.5705E+00	3.8722E−01	2.2437E+00
25	2.1676E−01	4.9040E+00	2.9863E−01	3.0456E+00	3.2763E−01	2.6471E+00	3.6206E−01	2.3108E+00
26	2.0552E−01	5.0446E+00	2.8097E−01	3.1308E+00	3.0761E−01	2.7214E+00	3.3936E−01	2.3758E+00
27	1.9519E−01	5.1826E+00	2.6486E−01	3.2135E+00	2.8942E−01	2.7935E+00	3.1880E−01	2.4389E+00
28	1.8565E−01	5.3182E+00	2.5010E−01	3.2939E+00	2.7281E−01	2.8634E+00	3.0009E−01	2.5000E+00
29	1.7684E−01	5.4516E+00	2.3651E−01	3.3721E+00	2.5759E−01	2.9313E+00	2.8299E−01	2.5592E+00
30	1.6868E−01	5.5830E+00	2.2396E−01	3.4484E+00	2.4358E−01	2.9973E+00	2.6732E−01	2.6167E+00
31	1.6112E−01	5.7124E+00	2.1235E−01	3.5227E+00	2.3066E−01	3.0615E+00	2.5290E−01	2.6725E+00
32	1.5410E−01	5.8398E+00	2.0158E−01	3.5953E+00	2.1872E−01	3.1240E+00	2.3960E−01	2.7267E+00
33	1.4758E−01	5.9654E+00	1.9158E−01	3.6663E+00	2.0765E−01	3.1851E+00	2.2732E−01	2.7796E+00
34	1.4151E−01	6.0892E+00	1.8227E−01	3.7358E+00	1.9738E−01	3.2447E+00	2.1593E−01	2.8311E+00
35	1.3585E−01	6.2111E+00	1.7360E−01	3.8039E+00	1.8783E−01	3.3030E+00	2.0538E−01	2.8813E+00
36	1.3056E−01	6.3312E+00	1.6552E−01	3.8707E+00	1.7895E−01	3.3600E+00	1.9556E−01	2.9305E+00
37	1.2562E−01	6.4495E+00	1.5798E−01	3.9362E+00	1.7067E−01	3.4160E+00	1.8643E−01	2.9786E+00
38	1.2097E−01	6.5659E+00	1.5095E−01	4.0005E+00	1.6295E−01	3.4708E+00	1.7792E−01	3.0257E+00
39	1.1661E−01	6.6807E+00	1.4437E−01	4.0638E+00	1.5574E−01	3.5247E+00	1.6999E−01	3.0719E+00
40	1.1249E−01	6.7937E+00	1.3822E−01	4.1259E+00	1.4901E−01	3.5776E+00	1.6258E−01	3.1173E+00
41	1.0860E−01	6.9051E+00	1.3246E−01	4.1871E+00	1.4271E−01	3.6296E+00	1.5565E−01	3.1619E+00
42	1.0492E−01	7.0149E+00	1.2707E−01	4.2472E+00	1.3681E−01	3.6807E+00	1.4916E−01	3.2058E+00
43	1.0142E−01	7.1231E+00	1.2201E−01	4.3064E+00	1.3129E−01	3.7311E+00	1.4309E−01	3.2490E+00
44	9.8086E−02	7.2298E+00	1.1726E−01	4.3647E+00	1.2610E−01	3.7807E+00	1.3738E−01	3.2914E+00
45	9.4908E−02	7.3351E+00	1.1280E−01	4.4221E+00	1.2123E−01	3.8295E+00	1.3203E−01	3.3333E+00
46	9.1871E−02	7.4390E+00	1.0860E−01	4.4787E+00	1.1666E−01	3.8776E+00	1.2700E−01	3.3746E+00
47	8.8963E−02	7.5417E+00	1.0465E−01	4.5344E+00	1.1235E−01	3.9250E+00	1.2227E−01	3.4152E+00
48	8.6175E−02	7.6433E+00	1.0092E−01	4.5893E+00	1.0829E−01	3.9718E+00	1.1780E−01	3.4553E+00
49	8.3497E−02	7.7438E+00	9.7405E−02	4.6435E+00	1.0446E−01	4.0178E+00	1.1360E−01	3.4949E+00
50	8.0922E−02	7.8432E+00	9.4081E−02	4.6969E+00	1.0085E−01	4.0633E+00	1.0962E−01	3.5339E+00
51	7.8443E−02	7.9418E+00	9.0935E−02	4.7496E+00	9.7430E−02	4.1082E+00	1.0587E−01	3.5724E+00
52	7.6055E−02	8.0395E+00	8.7956E−02	4.8016E+00	9.4194E−02	4.1524E+00	1.0231E−01	3.6104E+00
53	7.3752E−02	8.1366E+00	8.5131E−02	4.8530E+00	9.1128E−02	4.1961E+00	9.8942E−02	3.6479E+00
54	7.1530E−02	8.2330E+00	8.2448E−02	4.9037E+00	8.8219E−02	4.2392E+00	9.5746E−02	3.6850E+00
55	6.9386E−02	8.3288E+00	7.9899E−02	4.9538E+00	8.5456E−02	4.2818E+00	9.2711E−02	3.7215E+00
56	6.7316E−02	8.4243E+00	7.7473E−02	5.0033E+00	8.2829E−02	4.3239E+00	8.9827E−02	3.7577E+00
57	6.5319E−02	8.5194E+00	7.5163E−02	5.0522E+00	8.0328E−02	4.3655E+00	8.7081E−02	3.7933E+00
58	6.3390E−02	8.6143E+00	7.2961E−02	5.1005E+00	7.7945E−02	4.4065E+00	8.4466E−02	3.8286E+00
59	6.1531E−02	8.7091E+00	7.0859E−02	5.1483E+00	7.5673E−02	4.4471E+00	8.1973E−02	3.8634E+00
60	5.9738E−02	8.8039E+00	6.8852E−02	5.1957E+00	7.3503E−02	4.4872E+00	7.9593E−02	3.8978E+00

Table 4.3.3.1. *Partial wave elastic scattering factors for neutral atoms (cont.)*
Au; $Z = 79$

	10 keV		40 keV		60 keV		90 keV	
s	$\|f(s)\|$	$\eta(s)$	$\|f(s)\|$	$\eta(s)$	$\|f(s)\|$	$\eta(s)$	$\|f(s)\|$	$\eta(s)$
0	7.8823E+00	4.3323E−01	9.6874E+00	3.1605E−01	1.0356E+01	2.8511E−01	1.1165E+01	2.5697E−01
1	7.0483E+00	4.7730E−01	8.7687E+00	3.4536E−01	9.3982E+00	3.1093E−01	1.0161E+01	2.7960E−01
2	5.4262E+00	5.9447E−01	6.9567E+00	4.2198E−01	7.5006E+00	3.7832E−01	8.1514E+00	3.3890E−01
3	3.9916E+00	7.5941E−01	5.3128E+00	5.2717E−01	5.7696E+00	4.7042E−01	6.3060E+00	4.1978E−01
4	2.9439E+00	9.5661E−01	4.0694E+00	6.4976E−01	4.4517E+00	5.7716E−01	4.8936E+00	5.1312E−01
5	2.2163E+00	1.1771E+00	3.1672E+00	7.8383E−01	3.4877E+00	6.9333E−01	3.8540E+00	6.1432E−01
6	1.7171E+00	1.4124E+00	2.5160E+00	9.2480E−01	2.7858E+00	8.1501E−01	3.0918E+00	7.1998E−01
7	1.3726E+00	1.6528E+00	2.0426E+00	1.0682E+00	2.2708E+00	9.3857E−01	2.5287E+00	8.2707E−01
8	1.1296E+00	1.8901E+00	1.6933E+00	1.2103E+00	1.8876E+00	1.0608E+00	2.1070E+00	9.3293E−01
9	9.5204E−01	2.1185E+00	1.4301E+00	1.3482E+00	1.5969E+00	1.1795E+00	1.7853E+00	1.0357E+00
10	8.1688E−01	2.3362E+00	1.2267E+00	1.4804E+00	1.3713E+00	1.2933E+00	1.5349E+00	1.1343E+00
11	7.0983E−01	2.5438E+00	1.0654E+00	1.6067E+00	1.1918E+00	1.4021E+00	1.3350E+00	1.2285E+00
12	6.2379E−01	2.7431E+00	9.3566E−01	1.7279E+00	1.0472E+00	1.5065E+00	1.1738E+00	1.3189E+00
13	5.5299E−01	2.9359E+00	8.2898E−01	1.8447E+00	9.2810E−01	1.6071E+00	1.0407E+00	1.4060E+00
14	4.9404E−01	3.1238E+00	7.3978E−01	1.9581E+00	8.2831E−01	1.7047E+00	9.2905E−01	1.4905E+00
15	4.4484E−01	3.3075E+00	6.6459E−01	2.0689E+00	7.4396E−01	1.8001E+00	8.3445E−01	1.5731E+00
16	4.0365E−01	3.4874E+00	6.0072E−01	2.1776E+00	6.7206E−01	1.8937E+00	7.5359E−01	1.6542E+00
17	3.6900E−01	3.6635E+00	5.4614E−01	2.2844E+00	6.1036E−01	1.9858E+00	6.8400E−01	1.7340E+00
18	3.3967E−01	3.8355E+00	4.9922E−01	2.3893E+00	5.5713E−01	2.0765E+00	6.2374E−01	1.8128E+00
19	3.1463E−01	4.0032E+00	4.5867E−01	2.4924E+00	5.1094E−01	2.1657E+00	5.7131E−01	1.8904E+00
20	2.9301E−01	4.1666E+00	4.2341E−01	2.5933E+00	4.7066E−01	2.2533E+00	5.2547E−01	1.9667E+00
21	2.7413E−01	4.3256E+00	3.9255E−01	2.6920E+00	4.3533E−01	2.3391E+00	4.8518E−01	2.0416E+00
22	2.5744E−01	4.4805E+00	3.6533E−01	2.7881E+00	4.0416E−01	2.4230E+00	4.4960E−01	2.1149E+00
23	2.4253E−01	4.6316E+00	3.4117E−01	2.8818E+00	3.7649E−01	2.5047E+00	4.1802E−01	2.1865E+00
24	2.2907E−01	4.7791E+00	3.1955E−01	2.9728E+00	3.5178E−01	2.5842E+00	3.8984E−01	2.2561E+00
25	2.1683E−01	4.9234E+00	3.0007E−01	3.0613E+00	3.2958E−01	2.6614E+00	3.6456E−01	2.3238E+00
26	2.0563E−01	5.0648E+00	2.8242E−01	3.1472E+00	3.0952E−01	2.7364E+00	3.4177E−01	2.3895E+00
27	1.9535E−01	5.2036E+00	2.6632E−01	3.2307E+00	2.9129E−01	2.8092E+00	3.2112E−01	2.4533E+00
28	1.8586E−01	5.3401E+00	2.5157E−01	3.3118E+00	2.7465E−01	2.8799E+00	3.0234E−01	2.5151E+00
29	1.7709E−01	5.4743E+00	2.3799E−01	3.3908E+00	2.5940E−01	2.9485E+00	2.8517E−01	2.5751E+00
30	1.6898E−01	5.6065E+00	2.2546E−01	3.4678E+00	2.4538E−01	3.0153E+00	2.6943E−01	2.6333E+00
31	1.6146E−01	5.7367E+00	2.1385E−01	3.5429E+00	2.3243E−01	3.0802E+00	2.5496E−01	2.6898E+00
32	1.5448E−01	5.8650E+00	2.0308E−01	3.6162E+00	2.2046E−01	3.1435E+00	2.4160E−01	2.7448E+00
33	1.4800E−01	5.9915E+00	1.9307E−01	3.6879E+00	2.0936E−01	3.2052E+00	2.2925E−01	2.7983E+00
34	1.4196E−01	6.1162E+00	1.8374E−01	3.7581E+00	1.9905E−01	3.2655E+00	2.1781E−01	2.8505E+00
35	1.3634E−01	6.2390E+00	1.7506E−01	3.8268E+00	1.8946E−01	3.3244E+00	2.0719E−01	2.9014E+00
36	1.3108E−01	6.3601E+00	1.6695E−01	3.8942E+00	1.8053E−01	3.3821E+00	1.9732E−01	2.9511E+00
37	1.2617E−01	6.4793E+00	1.5938E−01	3.9604E+00	1.7221E−01	3.4386E+00	1.8813E−01	2.9997E+00
38	1.2156E−01	6.5968E+00	1.5231E−01	4.0253E+00	1.6444E−01	3.4940E+00	1.7956E−01	3.0474E+00
39	1.1722E−01	6.7126E+00	1.4569E−01	4.0891E+00	1.5718E−01	3.5484E+00	1.7156E−01	3.0941E+00
40	1.1314E−01	6.8266E+00	1.3950E−01	4.1519E+00	1.5040E−01	3.6019E+00	1.6409E−01	3.1400E+00
41	1.0927E−01	6.9390E+00	1.3370E−01	4.2136E+00	1.4404E−01	3.6544E+00	1.5710E−01	3.1851E+00
42	1.0561E−01	7.0498E+00	1.2826E−01	4.2743E+00	1.3809E−01	3.7060E+00	1.5055E−01	3.2294E+00
43	1.0214E−01	7.1589E+00	1.2316E−01	4.3340E+00	1.3252E−01	3.7569E+00	1.4442E−01	3.2729E+00
44	9.8830E−02	7.2666E+00	1.1837E−01	4.3929E+00	1.2728E−01	3.8069E+00	1.3866E−01	3.3158E+00
45	9.5672E−02	7.3729E+00	1.1386E−01	4.4508E+00	1.2236E−01	3.8562E+00	1.3326E−01	3.3581E+00
46	9.2652E−02	7.4778E+00	1.0962E−01	4.5079E+00	1.1774E−01	3.9047E+00	1.2817E−01	3.3997E+00
47	8.9759E−02	7.5814E+00	1.0563E−01	4.5641E+00	1.1338E−01	3.9525E+00	1.2339E−01	3.4407E+00
48	8.6982E−02	7.6838E+00	1.0186E−01	4.6196E+00	1.0928E−01	3.9997E+00	1.1888E−01	3.4812E+00
49	8.4312E−02	7.7850E+00	9.8306E−02	4.6742E+00	1.0541E−01	4.0462E+00	1.1463E−01	3.5211E+00
50	8.1742E−02	7.8853E+00	9.4945E−02	4.7281E+00	1.0176E−01	4.0921E+00	1.1061E−01	3.5604E+00
51	7.9265E−02	7.9846E+00	9.1764E−02	4.7813E+00	9.8301E−02	4.1373E+00	1.0681E−01	3.5993E+00
52	7.6875E−02	8.0830E+00	8.8752E−02	4.8338E+00	9.5030E−02	4.1820E+00	1.0322E−01	3.6376E+00
53	7.4566E−02	8.1807E+00	8.5895E−02	4.8856E+00	9.1930E−02	4.2260E+00	9.9815E−02	3.6755E+00
54	7.2336E−02	8.2778E+00	8.3183E−02	4.9368E+00	8.8989E−02	4.2696E+00	9.6586E−02	3.7128E+00
55	7.0180E−02	8.3743E+00	8.0605E−02	4.9873E+00	8.6197E−02	4.3125E+00	9.3520E−02	3.7497E+00
56	6.8094E−02	8.4703E+00	7.8153E−02	5.0372E+00	8.3542E−02	4.3550E+00	9.0606E−02	3.7861E+00
57	6.6078E−02	8.5660E+00	7.5818E−02	5.0866E+00	8.1015E−02	4.3969E+00	8.7834E−02	3.8221E+00
58	6.4127E−02	8.6614E+00	7.3592E−02	5.1353E+00	7.8608E−02	4.4383E+00	8.5193E−02	3.8577E+00
59	6.2242E−02	8.7566E+00	7.1468E−02	5.1836E+00	7.6313E−02	4.4793E+00	8.2676E−02	3.8928E+00
60	6.0421E−02	8.8518E+00	6.9439E−02	5.2313E+00	7.4122E−02	4.5198E+00	8.0274E−02	3.9275E+00

Table 4.3.3.1. *Partial wave elastic scattering factors for neutral atoms (cont.)*
Hg; $Z = 80$

	10 keV		40 keV		60 keV		90 keV	
s	$\|f(s)\|$	$\eta(s)$	$\|f(s)\|$	$\eta(s)$	$\|f(s)\|$	$\eta(s)$	$\|f(s)\|$	$\eta(s)$
0	8.1999E+00	4.2779E−01	1.0057E+01	3.1227E−01	1.0747E+01	2.8183E−01	1.1585E+01	2.5414E−01
1	7.2950E+00	4.7334E−01	9.0609E+00	3.4264E−01	9.7088E+00	3.0862E−01	1.0495E+01	2.7765E−01
2	5.5456E+00	5.9611E−01	7.1072E+00	4.2293E−01	7.6629E+00	3.7927E−01	8.3282E+00	3.3985E−01
3	4.0362E+00	7.6853E−01	5.3757E+00	5.3276E−01	5.8394E+00	4.7544E−01	6.3839E+00	4.2432E−01
4	2.9635E+00	9.7105E−01	4.0999E+00	6.5858E−01	4.4866E+00	5.8500E−01	4.9337E+00	5.2014E−01
5	2.2288E+00	1.1940E+00	3.1874E+00	7.9423E−01	3.5113E+00	7.0258E−01	3.8817E+00	6.2259E−01
6	1.7262E+00	1.4301E+00	2.5315E+00	9.3598E−01	2.8042E+00	8.2500E−01	3.1137E+00	7.2894E−01
7	1.3791E+00	1.6717E+00	2.0545E+00	1.0803E+00	2.2853E+00	9.4930E−01	2.5462E+00	8.3671E−01
8	1.1342E+00	1.9106E+00	1.7022E+00	1.2235E+00	1.8987E+00	1.0727E+00	2.1206E+00	9.4356E−01
9	9.5569E−01	2.1414E+00	1.4367E+00	1.3631E+00	1.6053E+00	1.1928E+00	1.7958E+00	1.0476E+00
10	8.2022E−01	2.3616E+00	1.2319E+00	1.4972E+00	1.3779E+00	1.3083E+00	1.5430E+00	1.1477E+00
11	7.1313E−01	2.5713E+00	1.0696E+00	1.6253E+00	1.1971E+00	1.4188E+00	1.3417E+00	1.2434E+00
12	6.2710E−01	2.7723E+00	9.3942E−01	1.7481E+00	1.0518E+00	1.5245E+00	1.1794E+00	1.3350E+00
13	5.5620E−01	2.9664E+00	8.3243E−01	1.8662E+00	9.3223E−01	1.6262E+00	1.0457E+00	1.4231E+00
14	4.9698E−01	3.1550E+00	7.4299E−01	1.9804E+00	8.3213E−01	1.7246E+00	9.3365E−01	1.5083E+00
15	4.4739E−01	3.3393E+00	6.6758E−01	2.0917E+00	7.4753E−01	1.8205E+00	8.3877E−01	1.5914E+00
16	4.0573E−01	3.5197E+00	6.0348E−01	2.2007E+00	6.7541E−01	1.9144E+00	7.5768E−01	1.6727E+00
17	3.7062E−01	3.6963E+00	5.4865E−01	2.3077E+00	6.1350E−01	2.0066E+00	6.8786E−01	1.7527E+00
18	3.4087E−01	3.8689E+00	5.0150E−01	2.4128E+00	5.6005E−01	2.0974E+00	6.2740E−01	1.8315E+00
19	3.1547E−01	4.0374E+00	4.6073E−01	2.5160E+00	5.1365E−01	2.1867E+00	5.7476E−01	1.9091E+00
20	2.9358E−01	4.2016E+00	4.2527E−01	2.6171E+00	4.7317E−01	2.2744E+00	5.2870E−01	1.9855E+00
21	2.7449E−01	4.3616E+00	3.9424E−01	2.7161E+00	4.3766E−01	2.3605E+00	4.8822E−01	2.0606E+00
22	2.5767E−01	4.5175E+00	3.6690E−01	2.8127E+00	4.0634E−01	2.4446E+00	4.5246E−01	2.1342E+00
23	2.4268E−01	4.6695E+00	3.4264E−01	2.9069E+00	3.7856E−01	2.5268E+00	4.2072E−01	2.2060E+00
24	2.2919E−01	4.8179E+00	3.2097E−01	2.9985E+00	3.5375E−01	2.6068E+00	3.9240E−01	2.2762E+00
25	2.1694E−01	4.9631E+00	3.0147E−01	3.0876E+00	3.3148E−01	2.6846E+00	3.6700E−01	2.3444E+00
26	2.0576E−01	5.1054E+00	2.8380E−01	3.1742E+00	3.1136E−01	2.7603E+00	3.4411E−01	2.4108E+00
27	1.9550E−01	5.2450E+00	2.6771E−01	3.2584E+00	2.9310E−01	2.8338E+00	3.2338E−01	2.4752E+00
28	1.8605E−01	5.3823E+00	2.5296E−01	3.3403E+00	2.7643E−01	2.9052E+00	3.0452E−01	2.5377E+00
29	1.7732E−01	5.5173E+00	2.3940E−01	3.4201E+00	2.6116E−01	2.9745E+00	2.8729E−01	2.5984E+00
30	1.6925E−01	5.6503E+00	2.2688E−01	3.4978E+00	2.4711E−01	3.0420E+00	2.7150E−01	2.6573E+00
31	1.6176E−01	5.7813E+00	2.1529E−01	3.5736E+00	2.3414E−01	3.1077E+00	2.5697E−01	2.7145E+00
32	1.5482E−01	5.9105E+00	2.0452E−01	3.6476E+00	2.2215E−01	3.1716E+00	2.4356E−01	2.7702E+00
33	1.4837E−01	6.0378E+00	1.9450E−01	3.7199E+00	2.1102E−01	3.2340E+00	2.3116E−01	2.8244E+00
34	1.4236E−01	6.1634E+00	1.8517E−01	3.7908E+00	2.0068E−01	3.2950E+00	2.1966E−01	2.8772E+00
35	1.3677E−01	6.2871E+00	1.7647E−01	3.8602E+00	1.9106E−01	3.3545E+00	2.0899E−01	2.9287E+00
36	1.3155E−01	6.4091E+00	1.6834E−01	3.9282E+00	1.8210E−01	3.4128E+00	1.9906E−01	2.9790E+00
37	1.2667E−01	6.5293E+00	1.6075E−01	3.9950E+00	1.7373E−01	3.4699E+00	1.8981E−01	3.0282E+00
38	1.2209E−01	6.6478E+00	1.5365E−01	4.0605E+00	1.6592E−01	3.5259E+00	1.8119E−01	3.0764E+00
39	1.1778E−01	6.7646E+00	1.4700E−01	4.1249E+00	1.5861E−01	3.5808E+00	1.7313E−01	3.1237E+00
40	1.1373E−01	6.8796E+00	1.4077E−01	4.1882E+00	1.5178E−01	3.6348E+00	1.6560E−01	3.1700E+00
41	1.0989E−01	6.9930E+00	1.3493E−01	4.2505E+00	1.4538E−01	3.6878E+00	1.5855E−01	3.2155E+00
42	1.0626E−01	7.1047E+00	1.2945E−01	4.3117E+00	1.3938E−01	3.7400E+00	1.5195E−01	3.2603E+00
43	1.0281E−01	7.2149E+00	1.2431E−01	4.3720E+00	1.3375E−01	3.7913E+00	1.4576E−01	3.3043E+00
44	9.9531E−02	7.3235E+00	1.1947E−01	4.4314E+00	1.2847E−01	3.8418E+00	1.3995E−01	3.3476E+00
45	9.6396E−02	7.4307E+00	1.1493E−01	4.4899E+00	1.2350E−01	3.8915E+00	1.3449E−01	3.3902E+00
46	9.3398E−02	7.5365E+00	1.1065E−01	4.5475E+00	1.1883E−01	3.9405E+00	1.2935E−01	3.4322E+00
47	9.0523E−02	7.6410E+00	1.0661E−01	4.6042E+00	1.1443E−01	3.9888E+00	1.2452E−01	3.4736E+00
48	8.7761E−02	7.7442E+00	1.0281E−01	4.6602E+00	1.1028E−01	4.0363E+00	1.1996E−01	3.5144E+00
49	8.5104E−02	7.8463E+00	9.9216E−02	4.7153E+00	1.0637E−01	4.0833E+00	1.1566E−01	3.5547E+00
50	8.2543E−02	7.9473E+00	9.5819E−02	4.7697E+00	1.0268E−01	4.1295E+00	1.1160E−01	3.5944E+00
51	8.0072E−02	8.0474E+00	9.2604E−02	4.8234E+00	9.9183E−02	4.1752E+00	1.0777E−01	3.6335E+00
52	7.7685E−02	8.1465E+00	8.9558E−02	4.8763E+00	9.5875E−02	4.2202E+00	1.0414E−01	3.6722E+00
53	7.5375E−02	8.2449E+00	8.6670E−02	4.9286E+00	9.2741E−02	4.2647E+00	1.0069E−01	3.7104E+00
54	7.3140E−02	8.3426E+00	8.3928E−02	4.9802E+00	8.9769E−02	4.3086E+00	9.7431E−02	3.7480E+00
55	7.0976E−02	8.4396E+00	8.1322E−02	5.0312E+00	8.6946E−02	4.3519E+00	9.4334E−02	3.7852E+00
56	6.8879E−02	8.5362E+00	7.8843E−02	5.0815E+00	8.4262E−02	4.3947E+00	9.1390E−02	3.8220E+00
57	6.6847E−02	8.6324E+00	7.6482E−02	5.1313E+00	8.1709E−02	4.4370E+00	8.8590E−02	3.8583E+00
58	6.4878E−02	8.7283E+00	7.4232E−02	5.1805E+00	7.9277E−02	4.4788E+00	8.5923E−02	3.8942E+00
59	6.2970E−02	8.8240E+00	7.2085E−02	5.2291E+00	7.6958E−02	4.5201E+00	8.3381E−02	3.9296E+00
60	6.1124E−02	8.9197E+00	7.0035E−02	5.2772E+00	7.4745E−02	4.5609E+00	8.0956E−02	3.9646E+00

Table 4.3.3.1. *Partial wave elastic scattering factors for neutral atoms (cont.)*
Tl; $Z = 81$

	10 keV		40 keV		60 keV		90 keV	
s	$\|f(s)\|$	$\eta(s)$	$\|f(s)\|$	$\eta(s)$	$\|f(s)\|$	$\eta(s)$	$\|f(s)\|$	$\eta(s)$
0	9.2105E+00	3.9940E−01	1.1194E+01	2.9255E−01	1.1941E+01	2.6432E−01	1.2856E+01	2.3856E−01
1	7.9146E+00	4.5692E−01	9.7722E+00	3.3091E−01	1.0459E+01	2.9821E−01	1.1297E+01	2.6842E−01
2	5.7389E+00	6.0136E−01	7.3448E+00	4.2509E−01	7.9173E+00	3.8108E−01	8.6035E+00	3.4143E−01
3	4.0865E+00	7.8942E−01	5.4453E+00	5.4443E−01	5.9161E+00	4.8553E−01	6.4693E+00	4.3315E−01
4	2.9819E+00	9.9963E−01	4.1276E+00	6.7481E−01	4.5183E+00	5.9907E−01	4.9702E+00	5.3246E−01
5	2.2410E+00	1.2250E+00	3.2058E+00	8.1208E−01	3.5328E+00	7.1809E−01	3.9069E+00	6.3618E−01
6	1.7357E+00	1.4615E+00	2.5465E+00	9.5428E−01	2.8220E+00	8.4095E−01	3.1349E+00	7.4296E−01
7	1.3860E+00	1.7034E+00	2.0666E+00	1.0990E+00	2.2999E+00	9.6569E−01	2.5638E+00	8.5114E−01
8	1.1392E+00	1.9437E+00	1.7115E+00	1.2433E+00	1.9102E+00	1.0899E+00	2.1347E+00	9.5878E−01
9	9.5953E−01	2.1767E+00	1.4438E+00	1.3843E+00	1.6142E+00	1.2114E+00	1.8068E+00	1.0640E+00
10	8.2365E−01	2.3993E+00	1.2374E+00	1.5203E+00	1.3848E+00	1.3286E+00	1.5516E+00	1.1656E+00
11	7.1651E−01	2.6113E+00	1.0741E+00	1.6503E+00	1.2027E+00	1.4407E+00	1.3485E+00	1.2627E+00
12	6.3053E−01	2.8141E+00	9.4333E−01	1.7748E+00	1.0565E+00	1.5480E+00	1.1852E+00	1.3558E+00
13	5.5957E−01	3.0095E+00	8.3598E−01	1.8942E+00	9.3644E−01	1.6510E+00	1.0508E+00	1.4450E+00
14	5.0013E−01	3.1991E+00	7.4629E−01	2.0095E+00	8.3600E−01	1.7503E+00	9.3827E−01	1.5310E+00
15	4.5017E−01	3.3840E+00	6.7064E−01	2.1214E+00	7.5114E−01	1.8468E+00	8.4307E−01	1.6146E+00
16	4.0808E−01	3.5650E+00	6.0630E−01	2.2308E+00	6.7878E−01	1.9410E+00	7.6173E−01	1.6963E+00
17	3.7250E−01	3.7421E+00	5.5123E−01	2.3380E+00	6.1664E−01	2.0334E+00	6.9169E−01	1.7764E+00
18	3.4231E−01	3.9154E+00	5.0382E−01	2.4433E+00	5.6296E−01	2.1243E+00	6.3100E−01	1.8553E+00
19	3.1653E−01	4.0846E+00	4.6281E−01	2.5466E+00	5.1635E−01	2.2137E+00	5.7815E−01	1.9330E+00
20	2.9432E−01	4.2497E+00	4.2714E−01	2.6480E+00	4.7566E−01	2.3015E+00	5.3188E−01	2.0095E+00
21	2.7501E−01	4.4106E+00	3.9594E−01	2.7473E+00	4.3997E−01	2.3878E+00	4.9121E−01	2.0847E+00
22	2.5802E−01	4.5675E+00	3.6846E−01	2.8443E+00	4.0850E−01	2.4722E+00	4.5527E−01	2.1584E+00
23	2.4292E−01	4.7204E+00	3.4410E−01	2.9389E+00	3.8058E−01	2.5547E+00	4.2337E−01	2.2306E+00
24	2.2937E−01	4.8698E+00	3.2236E−01	3.0311E+00	3.5567E−01	2.6352E+00	3.9491E−01	2.3012E+00
25	2.1709E−01	5.0159E+00	3.0281E−01	3.1208E+00	3.3332E−01	2.7136E+00	3.6939E−01	2.3699E+00
26	2.0591E−01	5.1590E+00	2.8513E−01	3.2081E+00	3.1315E−01	2.7898E+00	3.4640E−01	2.4368E+00
27	1.9566E−01	5.2995E+00	2.6903E−01	3.2930E+00	2.9484E−01	2.8640E+00	3.2559E−01	2.5018E+00
28	1.8623E−01	5.4376E+00	2.5430E−01	3.3756E+00	2.7815E−01	2.9360E+00	3.0665E−01	2.5650E+00
29	1.7752E−01	5.5734E+00	2.4075E−01	3.4560E+00	2.6285E−01	3.0061E+00	2.8936E−01	2.6263E+00
30	1.6948E−01	5.7071E+00	2.2824E−01	3.5344E+00	2.4879E−01	3.0743E+00	2.7351E−01	2.6859E+00
31	1.6202E−01	5.8390E+00	2.1666E−01	3.6109E+00	2.3581E−01	3.1406E+00	2.5893E−01	2.7438E+00
32	1.5511E−01	5.9690E+00	2.0590E−01	3.6856E+00	2.2379E−01	3.2053E+00	2.4547E−01	2.8002E+00
33	1.4869E−01	6.0971E+00	1.9589E−01	3.7586E+00	2.1264E−01	3.2683E+00	2.3302E−01	2.8550E+00
34	1.4272E−01	6.2235E+00	1.8656E−01	3.8301E+00	2.0228E−01	3.3299E+00	2.2148E−01	2.9084E+00
35	1.3715E−01	6.3482E+00	1.7785E−01	3.9001E+00	1.9263E−01	3.3901E+00	2.1076E−01	2.9606E+00
36	1.3196E−01	6.4711E+00	1.6971E−01	3.9688E+00	1.8363E−01	3.4490E+00	2.0078E−01	3.0115E+00
37	1.2711E−01	6.5923E+00	1.6209E−01	4.0361E+00	1.7523E−01	3.5067E+00	1.9148E−01	3.0613E+00
38	1.2256E−01	6.7117E+00	1.5496E−01	4.1023E+00	1.6738E−01	3.5633E+00	1.8280E−01	3.1100E+00
39	1.1829E−01	6.8294E+00	1.4828E−01	4.1673E+00	1.6003E−01	3.6187E+00	1.7469E−01	3.1578E+00
40	1.1426E−01	6.9454E+00	1.4202E−01	4.2311E+00	1.5315E−01	3.6732E+00	1.6710E−01	3.2046E+00
41	1.1046E−01	7.0598E+00	1.3615E−01	4.2940E+00	1.4671E−01	3.7268E+00	1.6000E−01	3.2506E+00
42	1.0686E−01	7.1725E+00	1.3063E−01	4.3558E+00	1.4066E−01	3.7794E+00	1.5334E−01	3.2958E+00
43	1.0344E−01	7.2836E+00	1.2545E−01	4.4166E+00	1.3499E−01	3.8312E+00	1.4709E−01	3.3402E+00
44	1.0019E−01	7.3932E+00	1.2058E−01	4.4765E+00	1.2966E−01	3.8821E+00	1.4123E−01	3.3839E+00
45	9.7080E−02	7.5013E+00	1.1600E−01	4.5355E+00	1.2464E−01	3.9323E+00	1.3572E−01	3.4270E+00
46	9.4106E−02	7.6080E+00	1.1168E−01	4.5936E+00	1.1993E−01	3.9818E+00	1.3053E−01	3.4694E+00
47	9.1253E−02	7.7134E+00	1.0761E−01	4.6508E+00	1.1548E−01	4.0305E+00	1.2565E−01	3.5111E+00
48	8.8512E−02	7.8175E+00	1.0376E−01	4.7073E+00	1.1129E−01	4.0785E+00	1.2105E−01	3.5523E+00
49	8.5872E−02	7.9204E+00	1.0013E−01	4.7629E+00	1.0734E−01	4.1258E+00	1.1671E−01	3.5929E+00
50	8.3324E−02	8.0222E+00	9.6702E−02	4.8178E+00	1.0361E−01	4.1725E+00	1.1260E−01	3.6329E+00
51	8.0864E−02	8.1230E+00	9.3453E−02	4.8720E+00	1.0007E−01	4.2185E+00	1.0873E−01	3.6725E+00
52	7.8483E−02	8.2228E+00	9.0375E−02	4.9254E+00	9.6730E−02	4.2640E+00	1.0506E−01	3.7114E+00
53	7.6177E−02	8.3218E+00	8.7456E−02	4.9781E+00	9.3562E−02	4.3088E+00	1.0158E−01	3.7499E+00
54	7.3942E−02	8.4201E+00	8.4684E−02	5.0302E+00	9.0557E−02	4.3531E+00	9.8283E−02	3.7879E+00
55	7.1773E−02	8.5178E+00	8.2049E−02	5.0816E+00	8.7704E−02	4.3968E+00	9.5154E−02	3.8255E+00
56	6.9669E−02	8.6149E+00	7.9543E−02	5.1324E+00	8.4992E−02	4.4400E+00	9.2179E−02	3.8625E+00
57	6.7625E−02	8.7116E+00	7.7157E−02	5.1826E+00	8.2411E−02	4.4826E+00	8.9350E−02	3.8991E+00
58	6.5641E−02	8.8080E+00	7.4882E−02	5.2322E+00	7.9953E−02	4.5248E+00	8.6657E−02	3.9353E+00
59	6.3714E−02	8.9042E+00	7.2712E−02	5.2812E+00	7.7610E−02	4.5664E+00	8.4090E−02	3.9711E+00
60	6.1845E−02	9.0003E+00	7.0639E−02	5.3298E+00	7.5374E−02	4.6076E+00	8.1641E−02	4.0064E+00

Table 4.3.3.1. *Partial wave elastic scattering factors for neutral atoms (cont.)*
Pb; $Z = 82$

	10 keV		40 keV		60 keV		90 keV	
s	$\|f(s)\|$	$\eta(s)$	$\|f(s)\|$	$\eta(s)$	$\|f(s)\|$	$\eta(s)$	$\|f(s)\|$	$\eta(s)$
0	9.6136E+00	3.9757E−01	1.1662E+01	2.9059E−01	1.2436E+01	2.6253E−01	1.3386E+01	2.3696E−01
1	8.2645E+00	4.5390E−01	1.0184E+01	3.2827E−01	1.0895E+01	2.9585E−01	1.1765E+01	2.6634E−01
2	5.9257E+00	6.0212E−01	7.5761E+00	4.2504E−01	8.1652E+00	3.8106E−01	8.8720E+00	3.4146E−01
3	4.1547E+00	8.0058E−01	5.5382E+00	5.5077E−01	6.0180E+00	4.9111E−01	6.5818E+00	4.3812E−01
4	3.0066E+00	1.0203E+00	4.1641E+00	6.8679E−01	4.5595E+00	6.0954E−01	5.0171E+00	5.4170E−01
5	2.2543E+00	1.2507E+00	3.2252E+00	8.2711E−01	3.5553E+00	7.3123E−01	3.9331E+00	6.4777E−01
6	1.7456E+00	1.4887E+00	2.5609E+00	9.7046E−01	2.8389E+00	8.5513E−01	3.1548E+00	7.5548E−01
7	1.3935E+00	1.7310E+00	2.0783E+00	1.1157E+00	2.3139E+00	9.8034E−01	2.5806E+00	8.6411E−01
8	1.1445E+00	1.9721E+00	1.7208E+00	1.2606E+00	1.9216E+00	1.1052E+00	2.1485E+00	9.7231E−01
9	9.6355E−01	2.2067E+00	1.4510E+00	1.4028E+00	1.6232E+00	1.2277E+00	1.8179E+00	1.0785E+00
10	8.2709E−01	2.4314E+00	1.2430E+00	1.5404E+00	1.3918E+00	1.3463E+00	1.5604E+00	1.1813E+00
11	7.1981E−01	2.6456E+00	1.0787E+00	1.6722E+00	1.2085E+00	1.4600E+00	1.3557E+00	1.2799E+00
12	6.3387E−01	2.8503E+00	9.4731E−01	1.7984E+00	1.0614E+00	1.5689E+00	1.1911E+00	1.3743E+00
13	5.6292E−01	3.0471E+00	8.3957E−01	1.9193E+00	9.4072E−01	1.6732E+00	1.0560E+00	1.4647E+00
14	5.0333E−01	3.2378E+00	7.4962E−01	2.0357E+00	8.3990E−01	1.7736E+00	9.4293E−01	1.5517E+00
15	4.5309E−01	3.4234E+00	6.7374E−01	2.1485E+00	7.5476E−01	1.8708E+00	8.4738E−01	1.6360E+00
16	4.1061E−01	3.6050E+00	6.0917E−01	2.2584E+00	6.8217E−01	1.9655E+00	7.6576E−01	1.7181E+00
17	3.7460E−01	3.7827E+00	5.5386E−01	2.3659E+00	6.1980E−01	2.0582E+00	6.9549E−01	1.7985E+00
18	3.4397E−01	3.9566E+00	5.0621E−01	2.4714E+00	5.6589E−01	2.1493E+00	6.3458E−01	1.8775E+00
19	3.1780E−01	4.1266E+00	4.6495E−01	2.5750E+00	5.1905E−01	2.2388E+00	5.8150E−01	1.9552E+00
20	2.9526E−01	4.2926E+00	4.2906E−01	2.6765E+00	4.7816E−01	2.3267E+00	5.3503E−01	2.0318E+00
21	2.7568E−01	4.4544E+00	3.9766E−01	2.7761E+00	4.4228E−01	2.4131E+00	4.9415E−01	2.1071E+00
22	2.5850E−01	4.6122E+00	3.7002E−01	2.8734E+00	4.1064E−01	2.4978E+00	4.5803E−01	2.1810E+00
23	2.4326E−01	4.7661E+00	3.4555E−01	2.9685E+00	3.8258E−01	2.5806E+00	4.2597E−01	2.2535E+00
24	2.2961E−01	4.9165E+00	3.2372E−01	3.0611E+00	3.5756E−01	2.6615E+00	3.9737E−01	2.3244E+00
25	2.1729E−01	5.0635E+00	3.0412E−01	3.1514E+00	3.3512E−01	2.7404E+00	3.7173E−01	2.3935E+00
26	2.0608E−01	5.2076E+00	2.8640E−01	3.2393E+00	3.1489E−01	2.8172E+00	3.4863E−01	2.4609E+00
27	1.9582E−01	5.3489E+00	2.7030E−01	3.3249E+00	2.9653E−01	2.8920E+00	3.2773E−01	2.5265E+00
28	1.8640E−01	5.4877E+00	2.5557E−01	3.4081E+00	2.7981E−01	2.9647E+00	3.0873E−01	2.5903E+00
29	1.7771E−01	5.6244E+00	2.4203E−01	3.4893E+00	2.6449E−01	3.0354E+00	2.9138E−01	2.6523E+00
30	1.6968E−01	5.7589E+00	2.2954E−01	3.5684E+00	2.5041E−01	3.1042E+00	2.7548E−01	2.7125E+00
31	1.6225E−01	5.8916E+00	2.1797E−01	3.6455E+00	2.3741E−01	3.1713E+00	2.6084E−01	2.7711E+00
32	1.5536E−01	6.0223E+00	2.0722E−01	3.7209E+00	2.2538E−01	3.2366E+00	2.4734E−01	2.8281E+00
33	1.4897E−01	6.1513E+00	1.9722E−01	3.7946E+00	2.1421E−01	3.3003E+00	2.3485E−01	2.8836E+00
34	1.4302E−01	6.2786E+00	1.8789E−01	3.8667E+00	2.0383E−01	3.3625E+00	2.2326E−01	2.9377E+00
35	1.3748E−01	6.4041E+00	1.7918E−01	3.9373E+00	1.9416E−01	3.4233E+00	2.1249E−01	2.9904E+00
36	1.3232E−01	6.5279E+00	1.7103E−01	4.0065E+00	1.8513E−01	3.4828E+00	2.0247E−01	3.0419E+00
37	1.2750E−01	6.6500E+00	1.6340E−01	4.0745E+00	1.7670E−01	3.5411E+00	1.9312E−01	3.0923E+00
38	1.2298E−01	6.7704E+00	1.5625E−01	4.1412E+00	1.6882E−01	3.5982E+00	1.8439E−01	3.1415E+00
39	1.1874E−01	6.8891E+00	1.4955E−01	4.2068E+00	1.6143E−01	3.6542E+00	1.7623E−01	3.1898E+00
40	1.1474E−01	7.0061E+00	1.4326E−01	4.2712E+00	1.5451E−01	3.7092E+00	1.6860E−01	3.2372E+00
41	1.1098E−01	7.1214E+00	1.3735E−01	4.3346E+00	1.4803E−01	3.7633E+00	1.6144E−01	3.2836E+00
42	1.0741E−01	7.2351E+00	1.3181E−01	4.3969E+00	1.4194E−01	3.8164E+00	1.5473E−01	3.3293E+00
43	1.0402E−01	7.3471E+00	1.2659E−01	4.4583E+00	1.3622E−01	3.8687E+00	1.4844E−01	3.3741E+00
44	1.0080E−01	7.4577E+00	1.2169E−01	4.5187E+00	1.3084E−01	3.9201E+00	1.4252E−01	3.4183E+00
45	9.7720E−02	7.5667E+00	1.1707E−01	4.5782E+00	1.2579E−01	3.9707E+00	1.3696E−01	3.4617E+00
46	9.4775E−02	7.6743E+00	1.1271E−01	4.6368E+00	1.2103E−01	4.0206E+00	1.3173E−01	3.5045E+00
47	9.1949E−02	7.7806E+00	1.0860E−01	4.6946E+00	1.1654E−01	4.0697E+00	1.2679E−01	3.5466E+00
48	8.9231E−02	7.8855E+00	1.0472E−01	4.7516E+00	1.1231E−01	4.1182E+00	1.2215E−01	3.5882E+00
49	8.6612E−02	7.9892E+00	1.0106E−01	4.8077E+00	1.0832E−01	4.1659E+00	1.1776E−01	3.6291E+00
50	8.4083E−02	8.0918E+00	9.7593E−02	4.8631E+00	1.0454E−01	4.2130E+00	1.1362E−01	3.6695E+00
51	8.1637E−02	8.1933E+00	9.4312E−02	4.9177E+00	1.0098E−01	4.2595E+00	1.0970E−01	3.7093E+00
52	7.9268E−02	8.2939E+00	9.1202E−02	4.9716E+00	9.7596E−02	4.3053E+00	1.0599E−01	3.7487E+00
53	7.6970E−02	8.3936E+00	8.8252E−02	5.0248E+00	9.4394E−02	4.3505E+00	1.0247E−01	3.7875E+00
54	7.4739E−02	8.4925E+00	8.5450E−02	5.0773E+00	9.1356E−02	4.3952E+00	9.9143E−02	3.8258E+00
55	7.2571E−02	8.5907E+00	8.2787E−02	5.1291E+00	8.8471E−02	4.4393E+00	9.5980E−02	3.8636E+00
56	7.0463E−02	8.6884E+00	8.0254E−02	5.1803E+00	8.5730E−02	4.4828E+00	9.2975E−02	3.9010E+00
57	6.8412E−02	8.7856E+00	7.7842E−02	5.2310E+00	8.3122E−02	4.5258E+00	9.0117E−02	3.9379E+00
58	6.6416E−02	8.8825E+00	7.5542E−02	5.2810E+00	8.0638E−02	4.5683E+00	8.7396E−02	3.9744E+00
59	6.4474E−02	8.9791E+00	7.3349E−02	5.3305E+00	7.8270E−02	4.6103E+00	8.4803E−02	4.0104E+00
60	6.2586E−02	9.0756E+00	7.1254E−02	5.3794E+00	7.6011E−02	4.6519E+00	8.2330E−02	4.0461E+00

Table 4.3.3.1. *Partial wave elastic scattering factors for neutral atoms (cont.)*
Bi; $Z = 83$

	10 keV		40 keV		60 keV		90 keV	
s	$\|f(s)\|$	$\eta(s)$	$\|f(s)\|$	$\eta(s)$	$\|f(s)\|$	$\eta(s)$	$\|f(s)\|$	$\eta(s)$
0	1.0041E+01	3.9630E−01	1.2160E+01	2.8892E−01	1.2962E+01	2.6098E−01	1.3950E+01	2.3554E−01
1	8.6225E+00	4.5221E−01	1.0606E+01	3.2640E−01	1.1343E+01	2.9415E−01	1.2246E+01	2.6483E−01
2	6.1233E+00	6.0352E−01	7.8215E+00	4.2529E−01	8.4282E+00	3.8127E−01	9.1568E+00	3.4168E−01
3	4.2324E+00	8.1143E−01	5.6435E+00	5.5684E−01	6.1331E+00	4.9643E−01	6.7088E+00	4.4284E−01
4	3.0352E+00	1.0414E+00	4.2057E+00	6.9896E−01	4.6063E+00	6.2016E−01	5.0701E+00	5.5106E−01
5	2.2688E+00	1.2781E+00	3.2456E+00	8.4310E−01	3.5788E+00	7.4517E−01	3.9604E+00	6.6004E−01
6	1.7560E+00	1.5186E+00	2.5750E+00	9.8806E−01	2.8554E+00	8.7051E−01	3.1743E+00	7.6903E−01
7	1.4014E+00	1.7613E+00	2.0898E+00	1.1338E+00	2.3275E+00	9.9623E−01	2.5968E+00	8.7814E−01
8	1.1503E+00	2.0028E+00	1.7301E+00	1.2791E+00	1.9329E+00	1.1215E+00	2.1622E+00	9.8675E−01
9	9.6782E−01	2.2386E+00	1.4583E+00	1.4223E+00	1.6323E+00	1.2449E+00	1.8292E+00	1.0936E+00
10	8.3059E−01	2.4653E+00	1.2488E+00	1.5612E+00	1.3991E+00	1.3647E+00	1.5695E+00	1.1975E+00
11	7.2309E−01	2.6815E+00	1.0835E+00	1.6947E+00	1.2144E+00	1.4799E+00	1.3631E+00	1.2975E+00
12	6.3718E−01	2.8881E+00	9.5137E−01	1.8226E+00	1.0664E+00	1.5903E+00	1.1973E+00	1.3933E+00
13	5.6627E−01	3.0865E+00	8.4322E−01	1.9451E+00	9.4508E−01	1.6961E+00	1.0612E+00	1.4850E+00
14	5.0660E−01	3.2783E+00	7.5299E−01	2.0628E+00	8.4386E−01	1.7976E+00	9.4765E−01	1.5731E+00
15	4.5614E−01	3.4648E+00	6.7689E−01	2.1765E+00	7.5842E−01	1.8957E+00	8.5170E−01	1.6581E+00
16	4.1331E−01	3.6470E+00	6.1210E−01	2.2871E+00	6.8558E−01	1.9910E+00	7.6979E−01	1.7408E+00
17	3.7689E−01	3.8254E+00	5.5654E−01	2.3951E+00	6.2297E−01	2.0841E+00	6.9927E−01	1.8215E+00
18	3.4584E−01	3.9999E+00	5.0864E−01	2.5008E+00	5.6884E−01	2.1754E+00	6.3813E−01	1.9007E+00
19	3.1926E−01	4.1707E+00	4.6714E−01	2.6046E+00	5.2177E−01	2.2650E+00	5.8483E−01	1.9786E+00
20	2.9638E−01	4.3374E+00	4.3102E−01	2.7064E+00	4.8066E−01	2.3531E+00	5.3815E−01	2.0552E+00
21	2.7651E−01	4.5002E+00	3.9941E−01	2.8062E+00	4.4458E−01	2.4397E+00	4.9707E−01	2.1306E+00
22	2.5910E−01	4.6590E+00	3.7161E−01	2.9039E+00	4.1276E−01	2.5246E+00	4.6077E−01	2.2047E+00
23	2.4370E−01	4.8139E+00	3.4699E−01	2.9993E+00	3.8456E−01	2.6077E+00	4.2853E−01	2.2774E+00
24	2.2994E−01	4.9653E+00	3.2506E−01	3.0925E+00	3.5942E−01	2.6890E+00	3.9979E−01	2.3485E+00
25	2.1755E−01	5.1132E+00	3.0540E−01	3.1833E+00	3.3689E−01	2.7683E+00	3.7402E−01	2.4181E+00
26	2.0629E−01	5.2582E+00	2.8764E−01	3.2718E+00	3.1658E−01	2.8456E+00	3.5082E−01	2.4859E+00
27	1.9601E−01	5.4004E+00	2.7152E−01	3.3579E+00	2.9818E−01	2.9209E+00	3.2983E−01	2.5520E+00
28	1.8658E−01	5.5401E+00	2.5678E−01	3.4419E+00	2.8141E−01	2.9942E+00	3.1076E−01	2.6164E+00
29	1.7789E−01	5.6775E+00	2.4325E−01	3.5236E+00	2.6607E−01	3.0656E+00	2.9334E−01	2.6790E+00
30	1.6987E−01	5.8128E+00	2.3077E−01	3.6034E+00	2.5197E−01	3.1351E+00	2.7739E−01	2.7398E+00
31	1.6246E−01	5.9462E+00	2.1922E−01	3.6812E+00	2.3896E−01	3.2027E+00	2.6271E−01	2.7991E+00
32	1.5558E−01	6.0778E+00	2.0849E−01	3.7572E+00	2.2692E−01	3.2687E+00	2.4917E−01	2.8567E+00
33	1.4921E−01	6.2077E+00	1.9850E−01	3.8315E+00	2.1574E−01	3.3330E+00	2.3664E−01	2.9128E+00
34	1.4328E−01	6.3357E+00	1.8917E−01	3.9042E+00	2.0534E−01	3.3959E+00	2.2501E−01	2.9675E+00
35	1.3777E−01	6.4621E+00	1.8046E−01	3.9755E+00	1.9565E−01	3.4573E+00	2.1420E−01	3.0208E+00
36	1.3263E−01	6.5868E+00	1.7231E−01	4.0453E+00	1.8660E−01	3.5174E+00	2.0413E−01	3.0729E+00
37	1.2784E−01	6.7098E+00	1.6467E−01	4.1139E+00	1.7815E−01	3.5762E+00	1.9474E−01	3.1238E+00
38	1.2335E−01	6.8311E+00	1.5751E−01	4.1811E+00	1.7023E−01	3.6339E+00	1.8597E−01	3.1737E+00
39	1.1913E−01	6.9507E+00	1.5079E−01	4.2473E+00	1.6281E−01	3.6904E+00	1.7776E−01	3.2225E+00
40	1.1517E−01	7.0687E+00	1.4447E−01	4.3122E+00	1.5586E−01	3.7460E+00	1.7008E−01	3.2703E+00
41	1.1144E−01	7.1850E+00	1.3855E−01	4.3762E+00	1.4934E−01	3.8005E+00	1.6288E−01	3.3172E+00
42	1.0791E−01	7.2996E+00	1.3297E−01	4.4390E+00	1.4321E−01	3.8542E+00	1.5612E−01	3.3633E+00
43	1.0455E−01	7.4127E+00	1.2772E−01	4.5009E+00	1.3745E−01	3.9069E+00	1.4978E−01	3.4086E+00
44	1.0136E−01	7.5242E+00	1.2278E−01	4.5619E+00	1.3204E−01	3.9588E+00	1.4381E−01	3.4532E+00
45	9.8317E−02	7.6341E+00	1.1813E−01	4.6219E+00	1.2694E−01	4.0099E+00	1.3820E−01	3.4970E+00
46	9.5402E−02	7.7426E+00	1.1374E−01	4.6810E+00	1.2214E−01	4.0602E+00	1.3292E−01	3.5402E+00
47	9.2606E−02	7.8498E+00	1.0960E−01	4.7393E+00	1.1761E−01	4.1098E+00	1.2794E−01	3.5827E+00
48	8.9916E−02	7.9555E+00	1.0569E−01	4.7968E+00	1.1334E−01	4.1586E+00	1.2325E−01	3.6246E+00
49	8.7322E−02	8.0601E+00	1.0199E−01	4.8534E+00	1.0930E−01	4.2068E+00	1.1882E−01	3.6659E+00
50	8.4816E−02	8.1634E+00	9.8492E−02	4.9092E+00	1.0549E−01	4.2543E+00	1.1463E−01	3.7067E+00
51	8.2389E−02	8.2657E+00	9.5178E−02	4.9643E+00	1.0189E−01	4.3011E+00	1.1067E−01	3.7469E+00
52	8.0036E−02	8.3670E+00	9.2037E−02	5.0187E+00	9.8471E−02	4.3474E+00	1.0693E−01	3.7865E+00
53	7.7751E−02	8.4673E+00	8.9057E−02	5.0723E+00	9.5235E−02	4.3930E+00	1.0338E−01	3.8256E+00
54	7.5528E−02	8.5669E+00	8.6226E−02	5.1253E+00	9.2164E−02	4.4380E+00	1.0001E−01	3.8643E+00
55	7.3365E−02	8.6657E+00	8.3536E−02	5.1776E+00	8.9249E−02	4.4825E+00	9.6814E−02	3.9025E+00
56	7.1258E−02	8.7639E+00	8.0976E−02	5.2292E+00	8.6478E−02	4.5264E+00	9.3778E−02	3.9401E+00
57	6.9203E−02	8.8616E+00	7.8537E−02	5.2803E+00	8.3842E−02	4.5698E+00	9.0890E−02	3.9774E+00
58	6.7200E−02	8.9589E+00	7.6213E−02	5.3307E+00	8.1331E−02	4.6126E+00	8.8141E−02	4.0141E+00
59	6.5247E−02	9.0560E+00	7.3996E−02	5.3806E+00	7.8938E−02	4.6550E+00	8.5522E−02	4.0505E+00
60	6.3343E−02	9.1529E+00	7.1878E−02	5.4299E+00	7.6655E−02	4.6969E+00	8.3024E−02	4.0864E+00

Table 4.3.3.1. *Partial wave elastic scattering factors for neutral atoms (cont.)*
Po; $Z = 84$

	10 keV		40 keV		60 keV		90 keV	
s	$\|f(s)\|$	$\eta(s)$	$\|f(s)\|$	$\eta(s)$	$\|f(s)\|$	$\eta(s)$	$\|f(s)\|$	$\eta(s)$
0	1.0207E+01	4.0280E−01	1.2373E+01	2.9270E−01	1.3191E+01	2.6430E−01	1.4198E+01	2.3850E−01
1	8.8298E+00	4.5584E−01	1.0863E+01	3.2830E−01	1.1618E+01	2.9582E−01	1.2543E+01	2.6633E−01
2	6.2962E+00	6.0432E−01	8.0395E+00	4.2550E−01	8.6624E+00	3.8151E−01	9.4112E+00	3.4197E−01
3	4.3175E+00	8.1693E−01	5.7595E+00	5.6004E−01	6.2598E+00	4.9932E−01	6.8483E+00	4.4549E−01
4	3.0694E+00	1.0565E+00	4.2558E+00	7.0787E−01	4.6624E+00	6.2802E−01	5.1332E+00	5.5805E−01
5	2.2853E+00	1.3011E+00	3.2688E+00	8.5672E−01	3.6053E+00	7.5712E−01	3.9910E+00	6.7060E−01
6	1.7672E+00	1.5453E+00	2.5894E+00	1.0041E+00	2.8721E+00	8.8462E−01	3.1938E+00	7.8150E−01
7	1.4100E+00	1.7891E+00	2.1010E+00	1.1507E+00	2.3407E+00	1.0112E+00	2.6125E+00	8.9136E−01
8	1.1566E+00	2.0309E+00	1.7393E+00	1.2965E+00	1.9439E+00	1.1368E+00	2.1755E+00	1.0003E+00
9	9.7242E−01	2.2676E+00	1.4657E+00	1.4403E+00	1.6414E+00	1.2608E+00	1.8403E+00	1.1078E+00
10	8.3420E−01	2.4959E+00	1.2547E+00	1.5803E+00	1.4065E+00	1.3816E+00	1.5787E+00	1.2125E+00
11	7.2632E−01	2.7139E+00	1.0883E+00	1.7153E+00	1.2204E+00	1.4982E+00	1.3706E+00	1.3137E+00
12	6.4039E−01	2.9225E+00	9.5548E−01	1.8449E+00	1.0714E+00	1.6101E+00	1.2035E+00	1.4108E+00
13	5.6954E−01	3.1224E+00	8.4690E−01	1.9689E+00	9.4950E−01	1.7172E+00	1.0666E+00	1.5039E+00
14	5.0985E−01	3.3154E+00	7.5639E−01	2.0880E+00	8.4785E−01	1.8200E+00	9.5243E−01	1.5931E+00
15	4.5923E−01	3.5028E+00	6.8006E−01	2.2028E+00	7.6210E−01	1.9191E+00	8.5606E−01	1.6790E+00
16	4.1612E−01	3.6858E+00	6.1506E−01	2.3141E+00	6.8900E−01	2.0152E+00	7.7383E−01	1.7623E+00
17	3.7933E−01	3.8647E+00	5.5928E−01	2.4227E+00	6.2617E−01	2.1088E+00	7.0304E−01	1.8435E+00
18	3.4788E−01	4.0400E+00	5.1114E−01	2.5288E+00	5.7180E−01	2.2004E+00	6.4166E−01	1.9230E+00
19	3.2092E−01	4.2114E+00	4.6939E−01	2.6329E+00	5.2451E−01	2.2902E+00	5.8815E−01	2.0010E+00
20	2.9767E−01	4.3791E+00	4.3303E−01	2.7349E+00	4.8318E−01	2.3785E+00	5.4125E−01	2.0777E+00
21	2.7751E−01	4.5427E+00	4.0121E−01	2.8350E+00	4.4690E−01	2.4652E+00	4.9997E−01	2.1532E+00
22	2.5986E−01	4.7025E+00	3.7321E−01	2.9329E+00	4.1489E−01	2.5503E+00	4.6347E−01	2.2274E+00
23	2.4427E−01	4.8585E+00	3.4845E−01	3.0288E+00	3.8653E−01	2.6336E+00	4.3107E−01	2.3003E+00
24	2.3037E−01	5.0108E+00	3.2641E−01	3.1224E+00	3.6126E−01	2.7152E+00	4.0217E−01	2.3717E+00
25	2.1787E−01	5.1597E+00	3.0666E−01	3.2137E+00	3.3862E−01	2.7949E+00	3.7628E−01	2.4416E+00
26	2.0655E−01	5.3056E+00	2.8885E−01	3.3027E+00	3.1824E−01	2.8727E+00	3.5297E−01	2.5099E+00
27	1.9623E−01	5.4487E+00	2.7270E−01	3.3895E+00	2.9978E−01	2.9485E+00	3.3189E−01	2.5764E+00
28	1.8677E−01	5.5892E+00	2.5795E−01	3.4740E+00	2.8297E−01	3.0224E+00	3.1274E−01	2.6413E+00
29	1.7808E−01	5.7275E+00	2.4442E−01	3.5564E+00	2.6760E−01	3.0944E+00	2.9526E−01	2.7044E+00
30	1.7006E−01	5.8636E+00	2.3195E−01	3.6368E+00	2.5348E−01	3.1645E+00	2.7925E−01	2.7659E+00
31	1.6264E−01	5.9978E+00	2.2041E−01	3.7152E+00	2.4046E−01	3.2328E+00	2.6453E−01	2.8257E+00
32	1.5578E−01	6.1302E+00	2.0970E−01	3.7919E+00	2.2841E−01	3.2993E+00	2.5095E−01	2.8840E+00
33	1.4942E−01	6.2608E+00	1.9972E−01	3.8668E+00	2.1722E−01	3.3643E+00	2.3838E−01	2.9407E+00
34	1.4351E−01	6.3898E+00	1.9040E−01	3.9401E+00	2.0681E−01	3.4278E+00	2.2672E−01	2.9960E+00
35	1.3802E−01	6.5170E+00	1.8170E−01	4.0120E+00	1.9710E−01	3.4898E+00	2.1587E−01	3.0499E+00
36	1.3290E−01	6.6426E+00	1.7354E−01	4.0824E+00	1.8804E−01	3.5504E+00	2.0577E−01	3.1026E+00
37	1.2813E−01	6.7665E+00	1.6590E−01	4.1515E+00	1.7956E−01	3.6098E+00	1.9634E−01	3.1541E+00
38	1.2366E−01	6.8887E+00	1.5873E−01	4.2193E+00	1.7162E−01	3.6681E+00	1.8753E−01	3.2044E+00
39	1.1948E−01	7.0093E+00	1.5200E−01	4.2860E+00	1.6418E−01	3.7252E+00	1.7928E−01	3.2538E+00
40	1.1555E−01	7.1282E+00	1.4567E−01	4.3515E+00	1.5719E−01	3.7812E+00	1.7155E−01	3.3021E+00
41	1.1185E−01	7.2454E+00	1.3972E−01	4.4160E+00	1.5064E−01	3.8363E+00	1.6431E−01	3.3495E+00
42	1.0835E−01	7.3610E+00	1.3412E−01	4.4794E+00	1.4447E−01	3.8904E+00	1.5750E−01	3.3961E+00
43	1.0503E−01	7.4750E+00	1.2884E−01	4.5418E+00	1.3868E−01	3.9436E+00	1.5111E−01	3.4418E+00
44	1.0188E−01	7.5874E+00	1.2388E−01	4.6033E+00	1.3322E−01	3.9960E+00	1.4510E−01	3.4868E+00
45	9.8866E−02	7.6983E+00	1.1919E−01	4.6638E+00	1.2809E−01	4.0475E+00	1.3945E−01	3.5311E+00
46	9.5986E−02	7.8078E+00	1.1477E−01	4.7234E+00	1.2325E−01	4.0983E+00	1.3412E−01	3.5746E+00
47	9.3223E−02	7.9158E+00	1.1060E−01	4.7822E+00	1.1868E−01	4.1483E+00	1.2910E−01	3.6175E+00
48	9.0564E−02	8.0224E+00	1.0666E−01	4.8401E+00	1.1437E−01	4.1975E+00	1.2436E−01	3.6598E+00
49	8.7999E−02	8.1278E+00	1.0293E−01	4.8973E+00	1.1030E−01	4.2461E+00	1.1988E−01	3.7015E+00
50	8.5519E−02	8.2319E+00	9.9396E−02	4.9536E+00	1.0645E−01	4.2940E+00	1.1566E−01	3.7425E+00
51	8.3116E−02	8.3350E+00	9.6052E−02	5.0091E+00	1.0281E−01	4.3413E+00	1.1166E−01	3.7831E+00
52	8.0783E−02	8.4369E+00	9.2880E−02	5.0640E+00	9.9356E−02	4.3879E+00	1.0787E−01	3.8231E+00
53	7.8515E−02	8.5380E+00	8.9871E−02	5.1181E+00	9.6086E−02	4.4339E+00	1.0429E−01	3.8625E+00
54	7.6306E−02	8.6381E+00	8.7012E−02	5.1715E+00	9.2983E−02	4.4793E+00	1.0088E−01	3.9015E+00
55	7.4152E−02	8.7375E+00	8.4294E−02	5.2242E+00	9.0037E−02	4.5242E+00	9.7656E−02	3.9400E+00
56	7.2050E−02	8.8363E+00	8.1707E−02	5.2763E+00	8.7236E−02	4.5684E+00	9.4588E−02	3.9780E+00
57	6.9997E−02	8.9345E+00	7.9243E−02	5.3278E+00	8.4572E−02	4.6122E+00	9.1670E−02	4.0155E+00
58	6.7991E−02	9.0323E+00	7.6895E−02	5.3787E+00	8.2034E−02	4.6554E+00	8.8893E−02	4.0526E+00
59	6.6030E−02	9.1297E+00	7.4654E−02	5.4289E+00	7.9616E−02	4.6981E+00	8.6247E−02	4.0892E+00
60	6.4114E−02	9.2270E+00	7.2514E−02	5.4787E+00	7.7309E−02	4.7403E+00	8.3724E−02	4.1254E+00

Table 4.3.3.1. *Partial wave elastic scattering factors for neutral atoms (cont.)*
At; $Z = 85$

	10 keV		40 keV		60 keV		90 keV	
s	$\|f(s)\|$	$\eta(s)$	$\|f(s)\|$	$\eta(s)$	$\|f(s)\|$	$\eta(s)$	$\|f(s)\|$	$\eta(s)$
0	1.0239E+01	4.1248E−01	1.2437E+01	2.9883E−01	1.3265E+01	2.6974E−01	1.4283E+01	2.4336E−01
1	8.9380E+00	4.6234E−01	1.1010E+01	3.3233E−01	1.1777E+01	2.9940E−01	1.2718E+01	2.6955E−01
2	6.4388E+00	6.0566E−01	8.2238E+00	4.2631E−01	8.8612E+00	3.8231E−01	9.6278E+00	3.4277E−01
3	4.4043E+00	8.1918E−01	5.8788E+00	5.6154E−01	6.3903E+00	5.0078E−01	6.9920E+00	4.4692E−01
4	3.1079E+00	1.0666E+00	4.3131E+00	7.1406E−01	4.7264E+00	6.3357E−01	5.2052E+00	5.6307E−01
5	2.3038E+00	1.3199E+00	3.2955E+00	8.6805E−01	3.6357E+00	7.6713E−01	4.0258E+00	6.7952E−01
6	1.7794E+00	1.5693E+00	2.6047E+00	1.0187E+00	2.8896E+00	8.9751E−01	3.2143E+00	7.9294E−01
7	1.4192E+00	1.8149E+00	2.1122E+00	1.1668E+00	2.3537E+00	1.0253E+00	2.6278E+00	9.0395E−01
8	1.1636E+00	2.0573E+00	1.7484E+00	1.3130E+00	1.9547E+00	1.1515E+00	2.1885E+00	1.0134E+00
9	9.7745E−01	2.2946E+00	1.4731E+00	1.4572E+00	1.6504E+00	1.2759E+00	1.8513E+00	1.1212E+00
10	8.3802E−01	2.5240E+00	1.2607E+00	1.5982E+00	1.4139E+00	1.3974E+00	1.5879E+00	1.2267E+00
11	7.2958E−01	2.7438E+00	1.0932E+00	1.7345E+00	1.2265E+00	1.5151E+00	1.3782E+00	1.3288E+00
12	6.4352E−01	2.9541E+00	9.5963E−01	1.8656E+00	1.0766E+00	1.6285E+00	1.2099E+00	1.4272E+00
13	5.7271E−01	3.1556E+00	8.5058E−01	1.9912E+00	9.5397E−01	1.7371E+00	1.0721E+00	1.5215E+00
14	5.1304E−01	3.3499E+00	7.5978E−01	2.1116E+00	8.5186E−01	1.8412E+00	9.5726E−01	1.6119E+00
15	4.6233E−01	3.5383E+00	6.8324E−01	2.2276E+00	7.6580E−01	1.9413E+00	8.6044E−01	1.6989E+00
16	4.1900E−01	3.7220E+00	6.1804E−01	2.3398E+00	6.9244E−01	2.0382E+00	7.7787E−01	1.7830E+00
17	3.8190E−01	3.9016E+00	5.6205E−01	2.4490E+00	6.2938E−01	2.1324E+00	7.0681E−01	1.8647E+00
18	3.5008E−01	4.0775E+00	5.1368E−01	2.5556E+00	5.7478E−01	2.2244E+00	6.4520E−01	1.9445E+00
19	3.2273E−01	4.2497E+00	4.7169E−01	2.6600E+00	5.2727E−01	2.3145E+00	5.9145E−01	2.0227E+00
20	2.9914E−01	4.4181E+00	4.3510E−01	2.7624E+00	4.8572E−01	2.4030E+00	5.4434E−01	2.0996E+00
21	2.7866E−01	4.5827E+00	4.0305E−01	2.8627E+00	4.4923E−01	2.4899E+00	5.0285E−01	2.1752E+00
22	2.6074E−01	4.7435E+00	3.7486E−01	2.9610E+00	4.1703E−01	2.5751E+00	4.6616E−01	2.2496E+00
23	2.4495E−01	4.9005E+00	3.4993E−01	3.0572E+00	3.8850E−01	2.6588E+00	4.3358E−01	2.3226E+00
24	2.3089E−01	5.0538E+00	3.2776E−01	3.1512E+00	3.6309E−01	2.7407E+00	4.0453E−01	2.3943E+00
25	2.1828E−01	5.2037E+00	3.0791E−01	3.2430E+00	3.4034E−01	2.8207E+00	3.7850E−01	2.4644E+00
26	2.0687E−01	5.3506E+00	2.9004E−01	3.3325E+00	3.1986E−01	2.8989E+00	3.5508E−01	2.5330E+00
27	1.9649E−01	5.4946E+00	2.7384E−01	3.4199E+00	3.0134E−01	2.9753E+00	3.3390E−01	2.6000E+00
28	1.8700E−01	5.6360E+00	2.5908E−01	3.5050E+00	2.8449E−01	3.0496E+00	3.1467E−01	2.6654E+00
29	1.7828E−01	5.7751E+00	2.4555E−01	3.5880E+00	2.6908E−01	3.1222E+00	2.9713E−01	2.7290E+00
30	1.7025E−01	5.9120E+00	2.3308E−01	3.6690E+00	2.5494E−01	3.1928E+00	2.8107E−01	2.7910E+00
31	1.6283E−01	6.0470E+00	2.2155E−01	3.7480E+00	2.4191E−01	3.2617E+00	2.6631E−01	2.8514E+00
32	1.5596E−01	6.1802E+00	2.1085E−01	3.8253E+00	2.2984E−01	3.3289E+00	2.5269E−01	2.9103E+00
33	1.4961E−01	6.3117E+00	2.0089E−01	3.9008E+00	2.1865E−01	3.3945E+00	2.4008E−01	2.9676E+00
34	1.4371E−01	6.4414E+00	1.9158E−01	3.9747E+00	2.0823E−01	3.4585E+00	2.2839E−01	3.0235E+00
35	1.3823E−01	6.5695E+00	1.8289E−01	4.0472E+00	1.9851E−01	3.5211E+00	2.1751E−01	3.0780E+00
36	1.3313E−01	6.6959E+00	1.7474E−01	4.1182E+00	1.8944E−01	3.5823E+00	2.0737E−01	3.1312E+00
37	1.2838E−01	6.8207E+00	1.6709E−01	4.1878E+00	1.8094E−01	3.6423E+00	1.9791E−01	3.1833E+00
38	1.2394E−01	6.9438E+00	1.5992E−01	4.2562E+00	1.7298E−01	3.7011E+00	1.8906E−01	3.2342E+00
39	1.1978E−01	7.0653E+00	1.5317E−01	4.3234E+00	1.6552E−01	3.7587E+00	1.8077E−01	3.2840E+00
40	1.1588E−01	7.1852E+00	1.4683E−01	4.3895E+00	1.5851E−01	3.8152E+00	1.7301E−01	3.3328E+00
41	1.1221E−01	7.3034E+00	1.4086E−01	4.4544E+00	1.5192E−01	3.8708E+00	1.6572E−01	3.3807E+00
42	1.0874E−01	7.4200E+00	1.3524E−01	4.5184E+00	1.4572E−01	3.9254E+00	1.5888E−01	3.4278E+00
43	1.0546E−01	7.5349E+00	1.2995E−01	4.5813E+00	1.3990E−01	3.9791E+00	1.5244E−01	3.4740E+00
44	1.0234E−01	7.6483E+00	1.2496E−01	4.6433E+00	1.3441E−01	4.0319E+00	1.4639E−01	3.5194E+00
45	9.9368E−02	7.7601E+00	1.2025E−01	4.7043E+00	1.2923E−01	4.0839E+00	1.4069E−01	3.5640E+00
46	9.6525E−02	7.8705E+00	1.1580E−01	4.7644E+00	1.2435E−01	4.1351E+00	1.3532E−01	3.6080E+00
47	9.3797E−02	7.9794E+00	1.1159E−01	4.8237E+00	1.1975E−01	4.1856E+00	1.3025E−01	3.6513E+00
48	9.1172E−02	8.0869E+00	1.0762E−01	4.8821E+00	1.1540E−01	4.2353E+00	1.2547E−01	3.6939E+00
49	8.8640E−02	8.1931E+00	1.0386E−01	4.9397E+00	1.1130E−01	4.2843E+00	1.2096E−01	3.7360E+00
50	8.6190E−02	8.2980E+00	1.0030E−01	4.9965E+00	1.0741E−01	4.3326E+00	1.1669E−01	3.7774E+00
51	8.3815E−02	8.4018E+00	9.6930E−02	5.0525E+00	1.0373E−01	4.3802E+00	1.1265E−01	3.8183E+00
52	8.1507E−02	8.5045E+00	9.3730E−02	5.1078E+00	1.0025E−01	4.4273E+00	1.0883E−01	3.8586E+00
53	7.9260E−02	8.6062E+00	9.0692E−02	5.1624E+00	9.6946E−02	4.4736E+00	1.0521E−01	3.8984E+00
54	7.7068E−02	8.7070E+00	8.7806E−02	5.2162E+00	9.3811E−02	4.5194E+00	1.0177E−01	3.9377E+00
55	7.4928E−02	8.8070E+00	8.5061E−02	5.2694E+00	9.0834E−02	4.5647E+00	9.8507E−02	3.9765E+00
56	7.2836E−02	8.9063E+00	8.2448E−02	5.3220E+00	8.8004E−02	4.6093E+00	9.5407E−02	4.0148E+00
57	7.0789E−02	9.0050E+00	7.9959E−02	5.3739E+00	8.5311E−02	4.6534E+00	9.2459E−02	4.0526E+00
58	6.8784E−02	9.1032E+00	7.7586E−02	5.4251E+00	8.2747E−02	4.6970E+00	8.9653E−02	4.0900E+00
59	6.6821E−02	9.2011E+00	7.5322E−02	5.4759E+00	8.0303E−02	4.7400E+00	8.6980E−02	4.1269E+00
60	6.4897E−02	9.2987E+00	7.3159E−02	5.5260E+00	7.7972E−02	4.7826E+00	8.4431E−02	4.1635E+00

Table 4.3.3.1. *Partial wave elastic scattering factors for neutral atoms (cont.)*
Rn; $Z = 86$

	10 keV		40 keV		60 keV		90 keV	
s	$\|f(s)\|$	$\eta(s)$	$\|f(s)\|$	$\eta(s)$	$\|f(s)\|$	$\eta(s)$	$\|f(s)\|$	$\eta(s)$
0	1.0192E+01	4.2365E−01	1.2415E+01	3.0614E−01	1.3248E+01	2.7626E−01	1.4271E+01	2.4921E−01
1	8.9775E+00	4.7052E−01	1.1080E+01	3.3764E−01	1.1857E+01	3.0415E−01	1.2808E+01	2.7383E−01
2	6.5512E+00	6.0787E−01	8.3738E+00	4.2787E−01	9.0241E+00	3.8379E−01	9.8062E+00	3.4420E−01
3	4.4885E+00	8.1955E−01	5.9962E+00	5.6211E−01	6.5188E+00	5.0146E−01	7.1338E+00	4.4769E−01
4	3.1495E+00	1.0726E+00	4.3761E+00	7.1803E−01	4.7967E+00	6.3723E−01	5.2840E+00	5.6648E−01
5	2.3241E+00	1.3345E+00	3.3258E+00	8.7715E−01	3.6702E+00	7.7525E−01	4.0653E+00	6.8681E−01
6	1.7923E+00	1.5903E+00	2.6213E+00	1.0318E+00	2.9086E+00	9.0910E−01	3.2363E+00	8.0328E−01
7	1.4292E+00	1.8388E+00	2.1237E+00	1.1819E+00	2.3668E+00	1.0387E+00	2.6432E+00	9.1590E−01
8	1.1712E+00	2.0821E+00	1.7575E+00	1.3289E+00	1.9653E+00	1.1656E+00	2.2011E+00	1.0260E+00
9	9.8302E−01	2.3199E+00	1.4805E+00	1.4735E+00	1.6593E+00	1.2904E+00	1.8621E+00	1.1342E+00
10	8.4213E−01	2.5503E+00	1.2667E+00	1.6151E+00	1.4214E+00	1.4125E+00	1.5970E+00	1.2402E+00
11	7.3293E−01	2.7715E+00	1.0981E+00	1.7524E+00	1.2327E+00	1.5312E+00	1.3859E+00	1.3432E+00
12	6.4661E−01	2.9835E+00	9.6379E−01	1.8849E+00	1.0818E+00	1.6457E+00	1.2164E+00	1.4426E+00
13	5.7577E−01	3.1866E+00	8.5425E−01	2.0120E+00	9.5847E−01	1.7557E+00	1.0776E+00	1.5382E+00
14	5.1614E−01	3.3821E+00	7.6315E−01	2.1339E+00	8.5589E−01	1.8611E+00	9.6214E−01	1.6298E+00
15	4.6539E−01	3.5715E+00	6.8641E−01	2.2511E+00	7.6950E−01	1.9624E+00	8.6484E−01	1.7178E+00
16	4.2191E−01	3.7560E+00	6.2103E−01	2.3643E+00	6.9589E−01	2.0603E+00	7.8193E−01	1.8027E+00
17	3.8454E−01	3.9363E+00	5.6485E−01	2.4743E+00	6.3260E−01	2.1552E+00	7.1058E−01	1.8851E+00
18	3.5240E−01	4.1129E+00	5.1626E−01	2.5815E+00	5.7779E−01	2.2477E+00	6.4872E−01	1.9654E+00
19	3.2470E−01	4.2858E+00	4.7405E−01	2.6863E+00	5.3005E−01	2.3382E+00	5.9475E−01	2.0439E+00
20	3.0075E−01	4.4551E+00	4.3722E−01	2.7890E+00	4.8828E−01	2.4269E+00	5.4742E−01	2.1210E+00
21	2.7996E−01	4.6206E+00	4.0495E−01	2.8896E+00	4.5158E−01	2.5139E+00	5.0573E−01	2.1968E+00
22	2.6177E−01	4.7823E+00	3.7655E−01	2.9882E+00	4.1919E−01	2.5994E+00	4.6884E−01	2.2712E+00
23	2.4575E−01	4.9403E+00	3.5145E−01	3.0847E+00	3.9048E−01	2.6833E+00	4.3608E−01	2.3444E+00
24	2.3152E−01	5.0946E+00	3.2913E−01	3.1792E+00	3.6492E−01	2.7654E+00	4.0687E−01	2.4163E+00
25	2.1877E−01	5.2456E+00	3.0917E−01	3.2714E+00	3.4205E−01	2.8458E+00	3.8070E−01	2.4867E+00
26	2.0726E−01	5.3934E+00	2.9122E−01	3.3614E+00	3.2147E−01	2.9244E+00	3.5715E−01	2.5556E+00
27	1.9681E−01	5.5383E+00	2.7497E−01	3.4493E+00	3.0287E−01	3.0012E+00	3.3588E−01	2.6230E+00
28	1.8727E−01	5.6807E+00	2.6017E−01	3.5350E+00	2.8597E−01	3.0761E+00	3.1657E−01	2.6888E+00
29	1.7851E−01	5.8206E+00	2.4663E−01	3.6186E+00	2.7053E−01	3.1491E+00	2.9896E−01	2.7529E+00
30	1.7045E−01	5.9584E+00	2.3416E−01	3.7002E+00	2.5636E−01	3.2203E+00	2.8285E−01	2.8154E+00
31	1.6301E−01	6.0942E+00	2.2264E−01	3.7798E+00	2.4331E−01	3.2898E+00	2.6804E−01	2.8764E+00
32	1.5614E−01	6.2282E+00	2.1195E−01	3.8577E+00	2.3123E−01	3.3576E+00	2.5438E−01	2.9358E+00
33	1.4978E−01	6.3605E+00	2.0200E−01	3.9338E+00	2.2003E−01	3.4237E+00	2.4174E−01	2.9937E+00
34	1.4388E−01	6.4910E+00	1.9271E−01	4.0083E+00	2.0961E−01	3.4883E+00	2.3001E−01	3.0501E+00
35	1.3841E−01	6.6199E+00	1.8402E−01	4.0813E+00	1.9988E−01	3.5515E+00	2.1911E−01	3.1052E+00
36	1.3332E−01	6.7472E+00	1.7588E−01	4.1528E+00	1.9080E−01	3.6133E+00	2.0894E−01	3.1590E+00
37	1.2859E−01	6.8729E+00	1.6825E−01	4.2230E+00	1.8229E−01	3.6738E+00	1.9945E−01	3.2116E+00
38	1.2417E−01	6.9970E+00	1.6107E−01	4.2920E+00	1.7431E−01	3.7331E+00	1.9057E−01	3.2630E+00
39	1.2004E−01	7.1194E+00	1.5432E−01	4.3597E+00	1.6683E−01	3.7912E+00	1.8225E−01	3.3134E+00
40	1.1616E−01	7.2402E+00	1.4797E−01	4.4263E+00	1.5979E−01	3.8483E+00	1.7445E−01	3.3627E+00
41	1.1252E−01	7.3593E+00	1.4199E−01	4.4918E+00	1.5318E−01	3.9044E+00	1.6712E−01	3.4111E+00
42	1.0909E−01	7.4769E+00	1.3635E−01	4.5562E+00	1.4696E−01	3.9594E+00	1.6024E−01	3.4586E+00
43	1.0584E−01	7.5928E+00	1.3104E−01	4.6196E+00	1.4110E−01	4.0136E+00	1.5377E−01	3.5052E+00
44	1.0276E−01	7.7071E+00	1.2602E−01	4.6821E+00	1.3558E−01	4.0669E+00	1.4767E−01	3.5510E+00
45	9.9822E−02	7.8199E+00	1.2129E−01	4.7436E+00	1.3037E−01	4.1193E+00	1.4193E−01	3.5961E+00
46	9.7016E−02	7.9312E+00	1.1681E−01	4.8043E+00	1.2546E−01	4.1710E+00	1.3652E−01	3.6405E+00
47	9.4326E−02	8.0409E+00	1.1259E−01	4.8640E+00	1.2082E−01	4.2219E+00	1.3141E−01	3.6842E+00
48	9.1738E−02	8.1493E+00	1.0859E−01	4.9229E+00	1.1644E−01	4.2720E+00	1.2659E−01	3.7272E+00
49	8.9241E−02	8.2564E+00	1.0480E−01	4.9810E+00	1.1230E−01	4.3214E+00	1.2204E−01	3.7696E+00
50	8.6825E−02	8.3621E+00	1.0121E−01	5.0383E+00	1.0838E−01	4.3701E+00	1.1773E−01	3.8114E+00
51	8.4481E−02	8.4667E+00	9.7812E−02	5.0948E+00	1.0467E−01	4.4182E+00	1.1365E−01	3.8526E+00
52	8.2202E−02	8.5701E+00	9.4584E−02	5.1505E+00	1.0115E−01	4.4656E+00	1.0979E−01	3.8933E+00
53	7.9981E−02	8.6725E+00	9.1519E−02	5.2055E+00	9.7815E−02	4.5124E+00	1.0613E−01	3.9334E+00
54	7.7812E−02	8.7739E+00	8.8607E−02	5.2598E+00	9.4649E−02	4.5585E+00	1.0266E−01	3.9730E+00
55	7.5690E−02	8.8745E+00	8.5836E−02	5.3135E+00	9.1641E−02	4.6041E+00	9.9366E−02	4.0121E+00
56	7.3613E−02	8.9744E+00	8.3198E−02	5.3664E+00	8.8782E−02	4.6491E+00	9.6235E−02	4.0507E+00
57	7.1576E−02	9.0736E+00	8.0684E−02	5.4187E+00	8.6061E−02	4.6936E+00	9.3256E−02	4.0889E+00
58	6.9578E−02	9.1723E+00	7.8287E−02	5.4704E+00	8.3470E−02	4.7375E+00	9.0421E−02	4.1266E+00
59	6.7616E−02	9.2705E+00	7.6000E−02	5.5216E+00	8.1000E−02	4.7809E+00	8.7720E−02	4.1638E+00
60	6.5689E−02	9.3685E+00	7.3815E−02	5.5721E+00	7.8644E−02	4.8238E+00	8.5145E−02	4.2006E+00

Table 4.3.3.1. *Partial wave elastic scattering factors for neutral atoms (cont.)*
Fr; $Z = 87$

	10 keV		40 keV		60 keV		90 keV	
s	$\|f(s)\|$	$\eta(s)$	$\|f(s)\|$	$\eta(s)$	$\|f(s)\|$	$\eta(s)$	$\|f(s)\|$	$\eta(s)$
0	1.4986E+01	3.2129E−01	1.7704E+01	2.3520E−01	1.8776E+01	2.1286E−01	2.0130E+01	1.9247E−01
1	1.0705E+01	4.3797E−01	1.3040E+01	3.1288E−01	1.3917E+01	2.8171E−01	1.5001E+01	2.5356E−01
2	6.7315E+00	6.4961E−01	8.6029E+00	4.4955E−01	9.2706E+00	4.0203E−01	1.0074E+01	3.5974E−01
3	4.5441E+00	8.7458E−01	6.0739E+00	5.9164E−01	6.6045E+00	5.2651E−01	7.2291E+00	4.6919E−01
4	3.1886E+00	1.1283E+00	4.4328E+00	7.4805E−01	4.8599E+00	6.6277E−01	5.3550E+00	5.8845E−01
5	2.3471E+00	1.3946E+00	3.3598E+00	9.0990E−01	3.7086E+00	8.0318E−01	4.1091E+00	7.1090E−01
6	1.8070E+00	1.6564E+00	2.6408E+00	1.0683E+00	2.9307E+00	9.4031E−01	3.2618E+00	8.3024E−01
7	1.4404E+00	1.9089E+00	2.1365E+00	1.2211E+00	2.3813E+00	1.0724E+00	2.6600E+00	9.4499E−01
8	1.1799E+00	2.1539E+00	1.7672E+00	1.3695E+00	1.9764E+00	1.2004E+00	2.2141E+00	1.0562E+00
9	9.8953E−01	2.3926E+00	1.4883E+00	1.5147E+00	1.6684E+00	1.3258E+00	1.8730E+00	1.1649E+00
10	8.4708E−01	2.6240E+00	1.2730E+00	1.6570E+00	1.4289E+00	1.4486E+00	1.6062E+00	1.2715E+00
11	7.3670E−01	2.8464E+00	1.1033E+00	1.7951E+00	1.2390E+00	1.5679E+00	1.3937E+00	1.3751E+00
12	6.4997E−01	3.0600E+00	9.6811E−01	1.9288E+00	1.0871E+00	1.6836E+00	1.2230E+00	1.4756E+00
13	5.7898E−01	3.2646E+00	8.5801E−01	2.0572E+00	9.6304E−01	1.7948E+00	1.0833E+00	1.5722E+00
14	5.1929E−01	3.4614E+00	7.6656E−01	2.1804E+00	8.5997E−01	1.9014E+00	9.6709E−01	1.6649E+00
15	4.6848E−01	3.6519E+00	6.8959E−01	2.2989E+00	7.7322E−01	2.0040E+00	8.6929E−01	1.7540E+00
16	4.2487E−01	3.8372E+00	6.2403E−01	2.4132E+00	6.9935E−01	2.1028E+00	7.8601E−01	1.8399E+00
17	3.8729E−01	4.0182E+00	5.6766E−01	2.5240E+00	6.3583E−01	2.1985E+00	7.1437E−01	1.9230E+00
18	3.5485E−01	4.1954E+00	5.1889E−01	2.6319E+00	5.8081E−01	2.2916E+00	6.5226E−01	2.0038E+00
19	3.2682E−01	4.3690E+00	4.7646E−01	2.7372E+00	5.3286E−01	2.3825E+00	5.9806E−01	2.0827E+00
20	3.0254E−01	4.5391E+00	4.3940E−01	2.8403E+00	4.9088E−01	2.4715E+00	5.5052E−01	2.1601E+00
21	2.8143E−01	4.7054E+00	4.0691E−01	2.9413E+00	4.5397E−01	2.5588E+00	5.0861E−01	2.2360E+00
22	2.6297E−01	4.8681E+00	3.7831E−01	3.0402E+00	4.2138E−01	2.6445E+00	4.7153E−01	2.3106E+00
23	2.4671E−01	5.0271E+00	3.5302E−01	3.1371E+00	3.9249E−01	2.7286E+00	4.3859E−01	2.3840E+00
24	2.3229E−01	5.1825E+00	3.3054E−01	3.2319E+00	3.6677E−01	2.8111E+00	4.0921E−01	2.4560E+00
25	2.1939E−01	5.3345E+00	3.1046E−01	3.3246E+00	3.4376E−01	2.8918E+00	3.8289E−01	2.5266E+00
26	2.0776E−01	5.4833E+00	2.9241E−01	3.4151E+00	3.2308E−01	2.9708E+00	3.5922E−01	2.5959E+00
27	1.9722E−01	5.6292E+00	2.7609E−01	3.5035E+00	3.0439E−01	3.0479E+00	3.3784E−01	2.6636E+00
28	1.8760E−01	5.7724E+00	2.6125E−01	3.5897E+00	2.8743E−01	3.1233E+00	3.1844E−01	2.7297E+00
29	1.7879E−01	5.9132E+00	2.4768E−01	3.6739E+00	2.7194E−01	3.1968E+00	3.0076E−01	2.7943E+00
30	1.7069E−01	6.0519E+00	2.3521E−01	3.7561E+00	2.5774E−01	3.2685E+00	2.8458E−01	2.8574E+00
31	1.6323E−01	6.1885E+00	2.2369E−01	3.8363E+00	2.4467E−01	3.3385E+00	2.6973E−01	2.9188E+00
32	1.5634E−01	6.3233E+00	2.1301E−01	3.9147E+00	2.3258E−01	3.4069E+00	2.5603E−01	2.9787E+00
33	1.4996E−01	6.4564E+00	2.0307E−01	3.9914E+00	2.2137E−01	3.4736E+00	2.4336E−01	3.0372E+00
34	1.4406E−01	6.5878E+00	1.9379E−01	4.0665E+00	2.1094E−01	3.5387E+00	2.3160E−01	3.0942E+00
35	1.3859E−01	6.7175E+00	1.8512E−01	4.1400E+00	2.0121E−01	3.6024E+00	2.2067E−01	3.1498E+00
36	1.3350E−01	6.8457E+00	1.7699E−01	4.2121E+00	1.9211E−01	3.6648E+00	2.1048E−01	3.2042E+00
37	1.2878E−01	6.9722E+00	1.6935E−01	4.2828E+00	1.8360E−01	3.7258E+00	2.0096E−01	3.2573E+00
38	1.2437E−01	7.0972E+00	1.6218E−01	4.3523E+00	1.7561E−01	3.7856E+00	1.9205E−01	3.3092E+00
39	1.2026E−01	7.2205E+00	1.5543E−01	4.4205E+00	1.6811E−01	3.8443E+00	1.8370E−01	3.3601E+00
40	1.1641E−01	7.3422E+00	1.4907E−01	4.4876E+00	1.6106E−01	3.9019E+00	1.7586E−01	3.4099E+00
41	1.1279E−01	7.4623E+00	1.4308E−01	4.5536E+00	1.5443E−01	3.9584E+00	1.6851E−01	3.4588E+00
42	1.0939E−01	7.5808E+00	1.3743E−01	4.6186E+00	1.4818E−01	4.0140E+00	1.6159E−01	3.5067E+00
43	1.0618E−01	7.6977E+00	1.3210E−01	4.6825E+00	1.4229E−01	4.0686E+00	1.5508E−01	3.5538E+00
44	1.0313E−01	7.8130E+00	1.2707E−01	4.7455E+00	1.3674E−01	4.1224E+00	1.4895E−01	3.6001E+00
45	1.0023E−01	7.9267E+00	1.2232E−01	4.8075E+00	1.3151E−01	4.1753E+00	1.4317E−01	3.6456E+00
46	9.7461E−02	8.0389E+00	1.1782E−01	4.8686E+00	1.2656E−01	4.2273E+00	1.3772E−01	3.6903E+00
47	9.4809E−02	8.1496E+00	1.1357E−01	4.9288E+00	1.2190E−01	4.2786E+00	1.3257E−01	3.7344E+00
48	9.2260E−02	8.2588E+00	1.0955E−01	4.9882E+00	1.1748E−01	4.3292E+00	1.2771E−01	3.7778E+00
49	8.9800E−02	8.3667E+00	1.0573E−01	5.0467E+00	1.1330E−01	4.3790E+00	1.2312E−01	3.8206E+00
50	8.7420E−02	8.4732E+00	1.0212E−01	5.1045E+00	1.0935E−01	4.4281E+00	1.1877E−01	3.8627E+00
51	8.5111E−02	8.5786E+00	9.8693E−02	5.1614E+00	1.0561E−01	4.4766E+00	1.1466E−01	3.9043E+00
52	8.2863E−02	8.6827E+00	9.5441E−02	5.2176E+00	1.0206E−01	4.5244E+00	1.1076E−01	3.9453E+00
53	8.0671E−02	8.7858E+00	9.2350E−02	5.2731E+00	9.8691E−02	4.5716E+00	1.0707E−01	3.9858E+00
54	7.8528E−02	8.8878E+00	8.9412E−02	5.3278E+00	9.5494E−02	4.6181E+00	1.0356E−01	4.0257E+00
55	7.6429E−02	8.9890E+00	8.6616E−02	5.3819E+00	9.2457E−02	4.6641E+00	1.0023E−01	4.0651E+00
56	7.4370E−02	9.0894E+00	8.3953E−02	5.4353E+00	8.9569E−02	4.7094E+00	9.7071E−02	4.1041E+00
57	7.2348E−02	9.1891E+00	8.1416E−02	5.4880E+00	8.6820E−02	4.7543E+00	9.4062E−02	4.1425E+00
58	7.0360E−02	9.2883E+00	7.8996E−02	5.5402E+00	8.4202E−02	4.7986E+00	9.1198E−02	4.1805E+00
59	6.8404E−02	9.3869E+00	7.6686E−02	5.5917E+00	8.1707E−02	4.8423E+00	8.8469E−02	4.2180E+00
60	6.6477E−02	9.4853E+00	7.4480E−02	5.6426E+00	7.9326E−02	4.8856E+00	8.5867E−02	4.2551E+00

Table 4.3.3.1. *Partial wave elastic scattering factors for neutral atoms (cont.)*
Ra; $Z = 88$

	10 keV		40 keV		60 keV		90 keV	
s	$\|f(s)\|$	$\eta(s)$	$\|f(s)\|$	$\eta(s)$	$\|f(s)\|$	$\eta(s)$	$\|f(s)\|$	$\eta(s)$
0	1.6691E+01	3.1495E−01	1.9618E+01	2.2844E−01	2.0782E+01	2.0642E−01	2.2262E+01	1.8643E−01
1	1.1932E+01	4.2553E−01	1.4444E+01	3.0237E−01	1.5393E+01	2.7202E−01	1.6574E+01	2.4470E−01
2	7.0122E+00	6.6802E−01	8.9517E+00	4.5834E−01	9.6437E+00	4.0928E−01	1.0477E+01	3.6584E−01
3	4.6033E+00	9.1683E−01	6.1543E+00	6.1453E−01	6.6928E+00	5.4600E−01	7.3270E+00	4.8598E−01
4	3.2239E+00	1.1739E+00	4.4825E+00	7.7296E−01	4.9152E+00	6.8404E−01	5.4172E+00	6.0682E−01
5	2.3704E+00	1.4419E+00	3.3942E+00	9.3596E−01	3.7474E+00	8.2550E−01	4.1533E+00	7.3023E−01
6	1.8223E+00	1.7079E+00	2.6623E+00	1.0971E+00	2.9553E+00	9.6506E−01	3.2901E+00	8.5171E−01
7	1.4518E+00	1.9649E+00	2.1504E+00	1.2529E+00	2.3972E+00	1.0997E+00	2.6785E+00	9.6875E−01
8	1.1891E+00	2.2127E+00	1.7773E+00	1.4033E+00	1.9878E+00	1.2297E+00	2.2274E+00	1.0816E+00
9	9.9688E−01	2.4528E+00	1.4963E+00	1.5497E+00	1.6775E+00	1.3560E+00	1.8837E+00	1.1913E+00
10	8.5269E−01	2.6853E+00	1.2794E+00	1.6926E+00	1.4364E+00	1.4794E+00	1.6152E+00	1.2984E+00
11	7.4116E−01	2.9089E+00	1.1085E+00	1.8315E+00	1.2453E+00	1.5995E+00	1.4014E+00	1.4026E+00
12	6.5362E−01	3.1238E+00	9.7251E−01	1.9661E+00	1.0924E+00	1.7160E+00	1.2295E+00	1.5038E+00
13	5.8225E−01	3.3298E+00	8.6181E−01	2.0957E+00	9.6765E−01	1.8282E+00	1.0890E+00	1.6014E+00
14	5.2244E−01	3.5279E+00	7.6997E−01	2.2202E+00	8.6405E−01	1.9361E+00	9.7207E−01	1.6952E+00
15	4.7155E−01	3.7194E+00	6.9275E−01	2.3399E+00	7.7694E−01	2.0397E+00	8.7376E−01	1.7854E+00
16	4.2783E−01	3.9056E+00	6.2701E−01	2.4553E+00	7.0280E−01	2.1396E+00	7.9009E−01	1.8722E+00
17	3.9006E−01	4.0874E+00	5.7048E−01	2.5670E+00	6.3907E−01	2.2361E+00	7.1816E−01	1.9561E+00
18	3.5737E−01	4.2652E+00	5.2152E−01	2.6756E+00	5.8384E−01	2.3299E+00	6.5580E−01	2.0375E+00
19	3.2905E−01	4.4395E+00	4.7889E−01	2.7815E+00	5.3569E−01	2.4214E+00	6.0138E−01	2.1169E+00
20	3.0445E−01	4.6103E+00	4.4163E−01	2.8851E+00	4.9350E−01	2.5108E+00	5.5361E−01	2.1946E+00
21	2.8304E−01	4.7775E+00	4.0892E−01	2.9864E+00	4.5638E−01	2.5984E+00	5.1150E−01	2.2708E+00
22	2.6430E−01	4.9411E+00	3.8011E−01	3.0858E+00	4.2360E−01	2.6844E+00	4.7422E−01	2.3456E+00
23	2.4780E−01	5.1010E+00	3.5463E−01	3.1830E+00	3.9453E−01	2.7687E+00	4.4110E−01	2.4191E+00
24	2.3317E−01	5.2574E+00	3.3199E−01	3.2782E+00	3.6864E−01	2.8514E+00	4.1154E−01	2.4913E+00
25	2.2010E−01	5.4104E+00	3.1177E−01	3.3713E+00	3.4549E−01	2.9324E+00	3.8507E−01	2.5622E+00
26	2.0834E−01	5.5603E+00	2.9361E−01	3.4623E+00	3.2469E−01	3.0117E+00	3.6127E−01	2.6316E+00
27	1.9769E−01	5.7072E+00	2.7721E−01	3.5512E+00	3.0591E−01	3.0893E+00	3.3977E−01	2.6997E+00
28	1.8799E−01	5.8513E+00	2.6232E−01	3.6380E+00	2.8886E−01	3.1650E+00	3.2028E−01	2.7662E+00
29	1.7912E−01	5.9931E+00	2.4871E−01	3.7227E+00	2.7333E−01	3.2390E+00	3.0253E−01	2.8312E+00
30	1.7097E−01	6.1326E+00	2.3622E−01	3.8054E+00	2.5909E−01	3.3113E+00	2.8629E−01	2.8946E+00
31	1.6347E−01	6.2701E+00	2.2470E−01	3.8862E+00	2.4599E−01	3.3818E+00	2.7138E−01	2.9566E+00
32	1.5655E−01	6.4057E+00	2.1402E−01	3.9652E+00	2.3389E−01	3.4507E+00	2.5764E−01	3.0170E+00
33	1.5015E−01	6.5396E+00	2.0409E−01	4.0425E+00	2.2266E−01	3.5179E+00	2.4494E−01	3.0760E+00
34	1.4424E−01	6.6718E+00	1.9482E−01	4.1181E+00	2.1223E−01	3.5836E+00	2.3315E−01	3.1335E+00
35	1.3875E−01	6.8024E+00	1.8616E−01	4.1922E+00	2.0249E−01	3.6479E+00	2.2220E−01	3.1897E+00
36	1.3367E−01	6.9314E+00	1.7804E−01	4.2648E+00	1.9339E−01	3.7107E+00	2.1198E−01	3.2445E+00
37	1.2894E−01	7.0589E+00	1.7042E−01	4.3360E+00	1.8487E−01	3.7723E+00	2.0243E−01	3.2982E+00
38	1.2455E−01	7.1847E+00	1.6325E−01	4.4060E+00	1.7687E−01	3.8326E+00	1.9350E−01	3.3507E+00
39	1.2045E−01	7.3090E+00	1.5650E−01	4.4748E+00	1.6936E−01	3.8918E+00	1.8512E−01	3.4020E+00
40	1.1662E−01	7.4316E+00	1.5014E−01	4.5424E+00	1.6229E−01	3.9499E+00	1.7726E−01	3.4523E+00
41	1.1303E−01	7.5527E+00	1.4415E−01	4.6089E+00	1.5564E−01	4.0069E+00	1.6987E−01	3.5017E+00
42	1.0965E−01	7.6721E+00	1.3849E−01	4.6743E+00	1.4938E−01	4.0629E+00	1.6292E−01	3.5501E+00
43	1.0647E−01	7.7899E+00	1.3315E−01	4.7387E+00	1.4347E−01	4.1180E+00	1.5638E−01	3.5976E+00
44	1.0345E−01	7.9062E+00	1.2810E−01	4.8021E+00	1.3790E−01	4.1722E+00	1.5022E−01	3.6443E+00
45	1.0059E−01	8.0208E+00	1.2333E−01	4.8646E+00	1.3263E−01	4.2255E+00	1.4440E−01	3.6902E+00
46	9.7861E−02	8.1339E+00	1.1881E−01	4.9262E+00	1.2766E−01	4.2780E+00	1.3891E−01	3.7354E+00
47	9.5248E−02	8.2455E+00	1.1454E−01	4.9869E+00	1.2296E−01	4.3298E+00	1.3373E−01	3.7799E+00
48	9.2738E−02	8.3557E+00	1.1050E−01	5.0468E+00	1.1852E−01	4.3808E+00	1.2883E−01	3.8236E+00
49	9.0318E−02	8.4644E+00	1.0666E−01	5.1058E+00	1.1431E−01	4.4310E+00	1.2421E−01	3.8668E+00
50	8.7977E−02	8.5718E+00	1.0303E−01	5.1640E+00	1.1033E−01	4.4805E+00	1.1982E−01	3.9093E+00
51	8.5704E−02	8.6778E+00	9.9575E−02	5.2214E+00	1.0655E−01	4.5294E+00	1.1567E−01	3.9512E+00
52	8.3492E−02	8.7827E+00	9.6298E−02	5.2781E+00	1.0297E−01	4.5776E+00	1.1174E−01	3.9926E+00
53	8.1333E−02	8.8865E+00	9.3183E−02	5.3340E+00	9.9573E−02	4.6251E+00	1.0801E−01	4.0333E+00
54	7.9219E−02	8.9893E+00	9.0221E−02	5.3892E+00	9.6347E−02	4.6720E+00	1.0447E−01	4.0736E+00
55	7.7147E−02	9.0910E+00	8.7402E−02	5.4437E+00	9.3281E−02	4.7184E+00	1.0111E−01	4.1133E+00
56	7.5112E−02	9.1920E+00	8.4716E−02	5.4975E+00	9.0364E−02	4.7641E+00	9.7915E−02	4.1526E+00
57	7.3109E−02	9.2922E+00	8.2156E−02	5.5507E+00	8.7588E−02	4.8093E+00	9.4876E−02	4.1914E+00
58	7.1135E−02	9.3918E+00	7.9713E−02	5.6032E+00	8.4944E−02	4.8540E+00	9.1983E−02	4.2297E+00
59	6.9190E−02	9.4909E+00	7.7381E−02	5.6551E+00	8.2423E−02	4.8980E+00	8.9226E−02	4.2675E+00
60	6.7270E−02	9.5896E+00	7.5153E−02	5.7064E+00	8.0018E−02	4.9416E+00	8.6598E−02	4.3049E+00

Table 4.3.3.1. *Partial wave elastic scattering factors for neutral atoms (cont.)*
Ac; $Z = 89$

	10 keV		40 keV		60 keV		90 keV	
s	$\|f(s)\|$	$\eta(s)$	$\|f(s)\|$	$\eta(s)$	$\|f(s)\|$	$\eta(s)$	$\|f(s)\|$	$\eta(s)$
0	1.6519E+01	3.3109E−01	1.9489E+01	2.3865E−01	2.0660E+01	2.1539E−01	2.2143E+01	1.9437E−01
1	1.2277E+01	4.2997E−01	1.4870E+01	3.0467E−01	1.5848E+01	2.7397E−01	1.7065E+01	2.4639E−01
2	7.2733E+00	6.6761E−01	9.2827E+00	4.5758E−01	9.9986E+00	4.0858E−01	1.0862E+01	3.6523E−01
3	4.6917E+00	9.3102E−01	6.2761E+00	6.2243E−01	6.8259E+00	5.5281E−01	7.4737E+00	4.9195E−01
4	3.2633E+00	1.1975E+00	4.5384E+00	7.8641E−01	4.9773E+00	6.9568E−01	5.4867E+00	6.1702E−01
5	2.3938E+00	1.4703E+00	3.4272E+00	9.5233E−01	3.7845E+00	8.3972E−01	4.1955E+00	7.4270E−01
6	1.8379E+00	1.7405E+00	2.6832E+00	1.1162E+00	2.9789E+00	9.8161E−01	3.3173E+00	8.6624E−01
7	1.4635E+00	2.0010E+00	2.1645E+00	1.2744E+00	2.4132E+00	1.1184E+00	2.6969E+00	9.8522E−01
8	1.1985E+00	2.2513E+00	1.7877E+00	1.4266E+00	1.9996E+00	1.2500E+00	2.2411E+00	1.0995E+00
9	1.0043E+00	2.4929E+00	1.5044E+00	1.5741E+00	1.6868E+00	1.3774E+00	1.8946E+00	1.2101E+00
10	8.5840E−01	2.7265E+00	1.2860E+00	1.7178E+00	1.4441E+00	1.5015E+00	1.6244E+00	1.3179E+00
11	7.4568E−01	2.9514E+00	1.1139E+00	1.8575E+00	1.2517E+00	1.6223E+00	1.4091E+00	1.4228E+00
12	6.5733E−01	3.1676E+00	9.7696E−01	1.9930E+00	1.0978E+00	1.7396E+00	1.2361E+00	1.5247E+00
13	5.8556E−01	3.3750E+00	8.6564E−01	2.1237E+00	9.7230E−01	1.8529E+00	1.0947E+00	1.6232E+00
14	5.2559E−01	3.5744E+00	7.7340E−01	2.2495E+00	8.6816E−01	1.9619E+00	9.7708E−01	1.7180E+00
15	4.7463E−01	3.7670E+00	6.9592E−01	2.3704E+00	7.8067E−01	2.0667E+00	8.7825E−01	1.8092E+00
16	4.3081E−01	3.9541E+00	6.2998E−01	2.4869E+00	7.0625E−01	2.1676E+00	7.9419E−01	1.8970E+00
17	3.9288E−01	4.1366E+00	5.7329E−01	2.5996E+00	6.4229E−01	2.2650E+00	7.2195E−01	1.9818E+00
18	3.5996E−01	4.3151E+00	5.2417E−01	2.7090E+00	5.8687E−01	2.3596E+00	6.5934E−01	2.0639E+00
19	3.3136E−01	4.4901E+00	4.8135E−01	2.8155E+00	5.3852E−01	2.4516E+00	6.0468E−01	2.1438E+00
20	3.0647E−01	4.6616E+00	4.4388E−01	2.9195E+00	4.9613E−01	2.5414E+00	5.5670E−01	2.2218E+00
21	2.8475E−01	4.8295E+00	4.1097E−01	3.0214E+00	4.5881E−01	2.6294E+00	5.1439E−01	2.2983E+00
22	2.6574E−01	4.9940E+00	3.8195E−01	3.1211E+00	4.2583E−01	2.7157E+00	4.7691E−01	2.3733E+00
23	2.4899E−01	5.1549E+00	3.5628E−01	3.2187E+00	3.9658E−01	2.8002E+00	4.4360E−01	2.4470E+00
24	2.3415E−01	5.3124E+00	3.3347E−01	3.3143E+00	3.7052E−01	2.8832E+00	4.1387E−01	2.5194E+00
25	2.2090E−01	5.4664E+00	3.1310E−01	3.4079E+00	3.4722E−01	2.9645E+00	3.8725E−01	2.5905E+00
26	2.0900E−01	5.6173E+00	2.9482E−01	3.4993E+00	3.2629E−01	3.0442E+00	3.6331E−01	2.6602E+00
27	1.9823E−01	5.7652E+00	2.7833E−01	3.5887E+00	3.0741E−01	3.1221E+00	3.4170E−01	2.7285E+00
28	1.8844E−01	5.9103E+00	2.6338E−01	3.6760E+00	2.9029E−01	3.1983E+00	3.2210E−01	2.7954E+00
29	1.7949E−01	6.0530E+00	2.4973E−01	3.7613E+00	2.7469E−01	3.2727E+00	3.0427E−01	2.8608E+00
30	1.7128E−01	6.1934E+00	2.3721E−01	3.8445E+00	2.6041E−01	3.3454E+00	2.8796E−01	2.9247E+00
31	1.6373E−01	6.3318E+00	2.2567E−01	3.9259E+00	2.4728E−01	3.4165E+00	2.7300E−01	2.9870E+00
32	1.5677E−01	6.4682E+00	2.1499E−01	4.0054E+00	2.3516E−01	3.4858E+00	2.5922E−01	3.0480E+00
33	1.5035E−01	6.6030E+00	2.0507E−01	4.0832E+00	2.2392E−01	3.5536E+00	2.4648E−01	3.1074E+00
34	1.4441E−01	6.7360E+00	1.9581E−01	4.1594E+00	2.1348E−01	3.6198E+00	2.3467E−01	3.1655E+00
35	1.3891E−01	6.8674E+00	1.8716E−01	4.2340E+00	2.0373E−01	3.6846E+00	2.2368E−01	3.2221E+00
36	1.3382E−01	6.9973E+00	1.7905E−01	4.3071E+00	1.9463E−01	3.7480E+00	2.1344E−01	3.2775E+00
37	1.2909E−01	7.1256E+00	1.7144E−01	4.3789E+00	1.8610E−01	3.8101E+00	2.0387E−01	3.3317E+00
38	1.2470E−01	7.2524E+00	1.6428E−01	4.4494E+00	1.7810E−01	3.8709E+00	1.9492E−01	3.3846E+00
39	1.2061E−01	7.3776E+00	1.5754E−01	4.5187E+00	1.7058E−01	3.9305E+00	1.8652E−01	3.4365E+00
40	1.1679E−01	7.5012E+00	1.5118E−01	4.5868E+00	1.6350E−01	3.9891E+00	1.7863E−01	3.4873E+00
41	1.1322E−01	7.6232E+00	1.4518E−01	4.6537E+00	1.5684E−01	4.0466E+00	1.7122E−01	3.5371E+00
42	1.0987E−01	7.7436E+00	1.3952E−01	4.7196E+00	1.5056E−01	4.1031E+00	1.6424E−01	3.5859E+00
43	1.0671E−01	7.8624E+00	1.3417E−01	4.7845E+00	1.4463E−01	4.1586E+00	1.5767E−01	3.6339E+00
44	1.0373E−01	7.9796E+00	1.2911E−01	4.8484E+00	1.3903E−01	4.2133E+00	1.5147E−01	3.6810E+00
45	1.0091E−01	8.0952E+00	1.2432E−01	4.9114E+00	1.3375E−01	4.2670E+00	1.4562E−01	3.7274E+00
46	9.8214E−02	8.2092E+00	1.1979E−01	4.9735E+00	1.2875E−01	4.3200E+00	1.4010E−01	3.7729E+00
47	9.5641E−02	8.3217E+00	1.1550E−01	5.0346E+00	1.2402E−01	4.3721E+00	1.3489E−01	3.8178E+00
48	9.3172E−02	8.4328E+00	1.1144E−01	5.0949E+00	1.1955E−01	4.4235E+00	1.2996E−01	3.8620E+00
49	9.0794E−02	8.5424E+00	1.0758E−01	5.1544E+00	1.1531E−01	4.4742E+00	1.2529E−01	3.9055E+00
50	8.8493E−02	8.6506E+00	1.0393E−01	5.2131E+00	1.1130E−01	4.5241E+00	1.2087E−01	3.9484E+00
51	8.6261E−02	8.7575E+00	1.0045E−01	5.2709E+00	1.0750E−01	4.5734E+00	1.1669E−01	3.9906E+00
52	8.4087E−02	8.8631E+00	9.7155E−02	5.3280E+00	1.0389E−01	4.6220E+00	1.1272E−01	4.0323E+00
53	8.1964E−02	8.9676E+00	9.4018E−02	5.3844E+00	1.0046E−01	4.6699E+00	1.0896E−01	4.0735E+00
54	7.9885E−02	9.0710E+00	9.1034E−02	5.4400E+00	9.7207E−02	4.7172E+00	1.0539E−01	4.1140E+00
55	7.7844E−02	9.1734E+00	8.8192E−02	5.4950E+00	9.4112E−02	4.7639E+00	1.0199E−01	4.1541E+00
56	7.5836E−02	9.2749E+00	8.5484E−02	5.5492E+00	9.1168E−02	4.8100E+00	9.8768E−02	4.1937E+00
57	7.3856E−02	9.3757E+00	8.2902E−02	5.6028E+00	8.8365E−02	4.8556E+00	9.5699E−02	4.2327E+00
58	7.1903E−02	9.4757E+00	8.0437E−02	5.6557E+00	8.5695E−02	4.9005E+00	9.2777E−02	4.2713E+00
59	6.9972E−02	9.5752E+00	7.8084E−02	5.7081E+00	8.3148E−02	4.9450E+00	8.9993E−02	4.3095E+00
60	6.8063E−02	9.6743E+00	7.5835E−02	5.7598E+00	8.0719E−02	4.9889E+00	8.7338E−02	4.3471E+00

Table 4.3.3.1. *Partial wave elastic scattering factors for neutral atoms (cont.)*
Th; $Z = 90$

	10 keV		40 keV		60 keV		90 keV	
s	$\|f(s)\|$	$\eta(s)$	$\|f(s)\|$	$\eta(s)$	$\|f(s)\|$	$\eta(s)$	$\|f(s)\|$	$\eta(s)$
0	1.6064E+01	3.4887E−01	1.9046E+01	2.5047E−01	2.0209E+01	2.2590E−01	2.1675E+01	2.0375E−01
1	1.2347E+01	4.3840E−01	1.4991E+01	3.1016E−01	1.5984E+01	2.7884E−01	1.7217E+01	2.5075E−01
2	7.4837E+00	6.6515E−01	9.5564E+00	4.5620E−01	1.0294E+01	4.0745E−01	1.1182E+01	3.6433E−01
3	4.7871E+00	9.3543E−01	6.4103E+00	6.2512E−01	6.9729E+00	5.5525E−01	7.6358E+00	4.9420E−01
4	3.3061E+00	1.2117E+00	4.6007E+00	7.9490E−01	5.0467E+00	7.0314E−01	5.5644E+00	6.2365E−01
5	2.4180E+00	1.4911E+00	3.4615E+00	9.6477E−01	3.8231E+00	8.5062E−01	4.2393E+00	7.5236E−01
6	1.8542E+00	1.7660E+00	2.7045E+00	1.1316E+00	3.0029E+00	9.9517E−01	3.3448E+00	8.7824E−01
7	1.4758E+00	2.0301E+00	2.1789E+00	1.2923E+00	2.4294E+00	1.1342E+00	2.7156E+00	9.9916E−01
8	1.2083E+00	2.2829E+00	1.7983E+00	1.4463E+00	2.0115E+00	1.2674E+00	2.2549E+00	1.1149E+00
9	1.0120E+00	2.5260E+00	1.5128E+00	1.5950E+00	1.6962E+00	1.3959E+00	1.9057E+00	1.2265E+00
10	8.6437E−01	2.7608E+00	1.2927E+00	1.7394E+00	1.4519E+00	1.5207E+00	1.6336E+00	1.3349E+00
11	7.5037E−01	2.9869E+00	1.1194E+00	1.8800E+00	1.2581E+00	1.6422E+00	1.4168E+00	1.4404E+00
12	6.6114E−01	3.2045E+00	9.8150E−01	2.0163E+00	1.1032E+00	1.7602E+00	1.2428E+00	1.5430E+00
13	5.8891E−01	3.4132E+00	8.6951E−01	2.1480E+00	9.7696E−01	1.8744E+00	1.1004E+00	1.6423E+00
14	5.2873E−01	3.6140E+00	7.7683E−01	2.2750E+00	8.7227E−01	1.9845E+00	9.8210E−01	1.7382E+00
15	4.7768E−01	3.8077E+00	6.9907E−01	2.3971E+00	7.8439E−01	2.0904E+00	8.8274E−01	1.8304E+00
16	4.3376E−01	3.9957E+00	6.3294E−01	2.5148E+00	7.0969E−01	2.1924E+00	7.9828E−01	1.9192E+00
17	3.9570E−01	4.1789E+00	5.7609E−01	2.6284E+00	6.4551E−01	2.2908E+00	7.2573E−01	2.0048E+00
18	3.6259E−01	4.3582E+00	5.2681E−01	2.7387E+00	5.8989E−01	2.3861E+00	6.6286E−01	2.0877E+00
19	3.3374E−01	4.5337E+00	4.8383E−01	2.8459E+00	5.4135E−01	2.4788E+00	6.0798E−01	2.1681E+00
20	3.0857E−01	4.7059E+00	4.4617E−01	2.9505E+00	4.9878E−01	2.5691E+00	5.5979E−01	2.2466E+00
21	2.8657E−01	4.8747E+00	4.1305E−01	3.0528E+00	4.6126E−01	2.6575E+00	5.1728E−01	2.3234E+00
22	2.6728E−01	5.0400E+00	3.8384E−01	3.1529E+00	4.2809E−01	2.7441E+00	4.7961E−01	2.3987E+00
23	2.5029E−01	5.2019E+00	3.5797E−01	3.2510E+00	3.9865E−01	2.8290E+00	4.4611E−01	2.4726E+00
24	2.3523E−01	5.3603E+00	3.3498E−01	3.3470E+00	3.7242E−01	2.9122E+00	4.1621E−01	2.5452E+00
25	2.2180E−01	5.5153E+00	3.1446E−01	3.4410E+00	3.4897E−01	2.9938E+00	3.8942E−01	2.6165E+00
26	2.0974E−01	5.6672E+00	2.9605E−01	3.5329E+00	3.2791E−01	3.0738E+00	3.6534E−01	2.6865E+00
27	1.9885E−01	5.8161E+00	2.7946E−01	3.6227E+00	3.0891E−01	3.1521E+00	3.4360E−01	2.7550E+00
28	1.8895E−01	5.9623E+00	2.6443E−01	3.7105E+00	2.9170E−01	3.2287E+00	3.2391E−01	2.8222E+00
29	1.7992E−01	6.1059E+00	2.5073E−01	3.7963E+00	2.7603E−01	3.3035E+00	3.0598E−01	2.8879E+00
30	1.7164E−01	6.2472E+00	2.3818E−01	3.8801E+00	2.6170E−01	3.3767E+00	2.8961E−01	2.9522E+00
31	1.6403E−01	6.3864E+00	2.2662E−01	3.9620E+00	2.4854E−01	3.4482E+00	2.7459E−01	3.0150E+00
32	1.5702E−01	6.5238E+00	2.1593E−01	4.0421E+00	2.3639E−01	3.5181E+00	2.6076E−01	3.0764E+00
33	1.5056E−01	6.6594E+00	2.0601E−01	4.1205E+00	2.2514E−01	3.5863E+00	2.4799E−01	3.1363E+00
34	1.4459E−01	6.7933E+00	1.9677E−01	4.1972E+00	2.1468E−01	3.6531E+00	2.3615E−01	3.1948E+00
35	1.3907E−01	6.9256E+00	1.8812E−01	4.2723E+00	2.0494E−01	3.7183E+00	2.2514E−01	3.2520E+00
36	1.3396E−01	7.0563E+00	1.8002E−01	4.3460E+00	1.9583E−01	3.7822E+00	2.1487E−01	3.3079E+00
37	1.2922E−01	7.1855E+00	1.7242E−01	4.4183E+00	1.8730E−01	3.8448E+00	2.0528E−01	3.3625E+00
38	1.2482E−01	7.3132E+00	1.6527E−01	4.4893E+00	1.7929E−01	3.9061E+00	1.9631E−01	3.4160E+00
39	1.2074E−01	7.4393E+00	1.5853E−01	4.5590E+00	1.7176E−01	3.9663E+00	1.8789E−01	3.4683E+00
40	1.1693E−01	7.5638E+00	1.5218E−01	4.6276E+00	1.6468E−01	4.0253E+00	1.7998E−01	3.5196E+00
41	1.1337E−01	7.6868E+00	1.4618E−01	4.6950E+00	1.5800E−01	4.0833E+00	1.7254E−01	3.5699E+00
42	1.1005E−01	7.8082E+00	1.4052E−01	4.7614E+00	1.5171E−01	4.1402E+00	1.6554E−01	3.6192E+00
43	1.0692E−01	7.9279E+00	1.3516E−01	4.8268E+00	1.4577E−01	4.1962E+00	1.5894E−01	3.6676E+00
44	1.0397E−01	8.0461E+00	1.3009E−01	4.8911E+00	1.4015E−01	4.2513E+00	1.5271E−01	3.7152E+00
45	1.0117E−01	8.1627E+00	1.2530E−01	4.9546E+00	1.3484E−01	4.3055E+00	1.4684E−01	3.7619E+00
46	9.8520E−02	8.2777E+00	1.2076E−01	5.0171E+00	1.2982E−01	4.3589E+00	1.4129E−01	3.8079E+00
47	9.5988E−02	8.3912E+00	1.1645E−01	5.0787E+00	1.2507E−01	4.4114E+00	1.3604E−01	3.8531E+00
48	9.3560E−02	8.5031E+00	1.1237E−01	5.1395E+00	1.2058E−01	4.4633E+00	1.3108E−01	3.8977E+00
49	9.1224E−02	8.6136E+00	1.0850E−01	5.1994E+00	1.1632E−01	4.5143E+00	1.2638E−01	3.9416E+00
50	8.8967E−02	8.7227E+00	1.0482E−01	5.2585E+00	1.1228E−01	4.5646E+00	1.2193E−01	3.9848E+00
51	8.6777E−02	8.8304E+00	1.0133E−01	5.3168E+00	1.0844E−01	4.6143E+00	1.1771E−01	4.0274E+00
52	8.4644E−02	8.9368E+00	9.8010E−02	5.3744E+00	1.0481E−01	4.6632E+00	1.1371E−01	4.0695E+00
53	8.2561E−02	9.0420E+00	9.4852E−02	5.4312E+00	1.0135E−01	4.7116E+00	1.0991E−01	4.1109E+00
54	8.0520E−02	9.1461E+00	9.1847E−02	5.4872E+00	9.8071E−02	4.7593E+00	1.0631E−01	4.1519E+00
55	7.8514E−02	9.2492E+00	8.8984E−02	5.5426E+00	9.4949E−02	4.8063E+00	1.0288E−01	4.1922E+00
56	7.6537E−02	9.3513E+00	8.6255E−02	5.5973E+00	9.1979E−02	4.8528E+00	9.9629E−02	4.2321E+00
57	7.4586E−02	9.4525E+00	8.3652E−02	5.6513E+00	8.9150E−02	4.8987E+00	9.6530E−02	4.2715E+00
58	7.2657E−02	9.5531E+00	8.1167E−02	5.7046E+00	8.6454E−02	4.9440E+00	9.3579E−02	4.3104E+00
59	7.0746E−02	9.6530E+00	7.8794E−02	5.7574E+00	8.3883E−02	4.9889E+00	9.0768E−02	4.3488E+00
60	6.8853E−02	9.7524E+00	7.6525E−02	5.8095E+00	8.1430E−02	5.0331E+00	8.8086E−02	4.3868E+00

Table 4.3.3.1. *Partial wave elastic scattering factors for neutral atoms (cont.)*
Pa; $Z = 91$

	10 keV		40 keV		60 keV		90 keV	
s	$\|f(s)\|$	$\eta(s)$	$\|f(s)\|$	$\eta(s)$	$\|f(s)\|$	$\eta(s)$	$\|f(s)\|$	$\eta(s)$
0	1.5526E+01	3.4745E−01	1.8450E+01	2.5180E−01	1.9588E+01	2.2756E−01	2.1020E+01	2.0560E−01
1	1.1835E+01	4.4153E−01	1.4422E+01	3.1463E−01	1.5390E+01	2.8330E−01	1.6590E+01	2.5511E−01
2	7.2413E+00	6.6824E−01	9.2829E+00	4.6070E−01	1.0008E+01	4.1196E−01	1.0880E+01	3.6876E−01
3	4.7331E+00	9.2483E−01	6.3574E+00	6.2151E−01	6.9197E+00	5.5276E−01	7.5818E+00	4.9254E−01
4	3.3065E+00	1.1884E+00	4.6188E+00	7.8388E−01	5.0696E+00	6.9432E−01	5.5927E+00	6.1655E−01
5	2.4253E+00	1.4621E+00	3.4894E+00	9.5045E−01	3.8568E+00	8.3902E−01	4.2794E+00	7.4289E−01
6	1.8596E+00	1.7373E+00	2.7269E+00	1.1174E+00	3.0304E+00	9.8370E−01	3.3778E+00	8.6892E−01
7	1.4799E+00	2.0048E+00	2.1948E+00	1.2801E+00	2.4490E+00	1.1245E+00	2.7395E+00	9.9145E−01
8	1.2123E+00	2.2614E+00	1.8096E+00	1.4369E+00	2.0255E+00	1.2601E+00	2.2720E+00	1.1093E+00
9	1.0163E+00	2.5080E+00	1.5212E+00	1.5882E+00	1.7065E+00	1.3909E+00	1.9182E+00	1.2230E+00
10	8.6865E−01	2.7455E+00	1.2994E+00	1.7348E+00	1.4598E+00	1.5178E+00	1.6432E+00	1.3331E+00
11	7.5447E−01	2.9739E+00	1.1247E+00	1.8771E+00	1.2645E+00	1.6409E+00	1.4245E+00	1.4401E+00
12	6.6496E−01	3.1932E+00	9.8603E−01	2.0150E+00	1.1085E+00	1.7603E+00	1.2492E+00	1.5440E+00
13	5.9246E−01	3.4036E+00	8.7343E−01	2.1480E+00	9.8151E−01	1.8757E+00	1.1058E+00	1.6444E+00
14	5.3205E−01	3.6057E+00	7.8029E−01	2.2761E+00	8.7627E−01	1.9868E+00	9.8689E−01	1.7411E+00
15	4.8080E−01	3.8007E+00	7.0220E−01	2.3993E+00	7.8799E−01	2.0937E+00	8.8702E−01	1.8342E+00
16	4.3670E−01	3.9897E+00	6.3582E−01	2.5179E+00	7.1298E−01	2.1966E+00	8.0217E−01	1.9238E+00
17	3.9842E−01	4.1737E+00	5.7875E−01	2.6324E+00	6.4856E−01	2.2958E+00	7.2932E−01	2.0101E+00
18	3.6508E−01	4.3537E+00	5.2928E−01	2.7433E+00	5.9273E−01	2.3918E+00	6.6620E−01	2.0936E+00
19	3.3597E−01	4.5300E+00	4.8611E−01	2.8512E+00	5.4400E−01	2.4850E+00	6.1111E−01	2.1746E+00
20	3.1054E−01	4.7028E+00	4.4827E−01	2.9563E+00	5.0124E−01	2.5758E+00	5.6272E−01	2.2535E+00
21	2.8828E−01	4.8723E+00	4.1497E−01	3.0591E+00	4.6355E−01	2.6645E+00	5.2002E−01	2.3306E+00
22	2.6874E−01	5.0384E+00	3.8557E−01	3.1596E+00	4.3020E−01	2.7514E+00	4.8217E−01	2.4062E+00
23	2.5151E−01	5.2011E+00	3.5953E−01	3.2581E+00	4.0059E−01	2.8366E+00	4.4850E−01	2.4803E+00
24	2.3625E−01	5.3604E+00	3.3638E−01	3.3545E+00	3.7421E−01	2.9202E+00	4.1844E−01	2.5531E+00
25	2.2264E−01	5.5164E+00	3.1572E−01	3.4490E+00	3.5062E−01	3.0021E+00	3.9151E−01	2.6247E+00
26	2.1043E−01	5.6693E+00	2.9721E−01	3.5413E+00	3.2945E−01	3.0824E+00	3.6730E−01	2.6948E+00
27	1.9941E−01	5.8191E+00	2.8052E−01	3.6317E+00	3.1035E−01	3.1610E+00	3.4545E−01	2.7637E+00
28	1.8940E−01	5.9662E+00	2.6542E−01	3.7200E+00	2.9306E−01	3.2380E+00	3.2566E−01	2.8312E+00
29	1.8028E−01	6.1107E+00	2.5167E−01	3.8063E+00	2.7732E−01	3.3133E+00	3.0765E−01	2.8972E+00
30	1.7193E−01	6.2529E+00	2.3908E−01	3.8906E+00	2.6294E−01	3.3869E+00	2.9121E−01	2.9619E+00
31	1.6427E−01	6.3931E+00	2.2751E−01	3.9731E+00	2.4974E−01	3.4588E+00	2.7613E−01	3.0251E+00
32	1.5721E−01	6.5313E+00	2.1681E−01	4.0537E+00	2.3757E−01	3.5292E+00	2.6226E−01	3.0869E+00
33	1.5070E−01	6.6677E+00	2.0689E−01	4.1326E+00	2.2630E−01	3.5979E+00	2.4945E−01	3.1473E+00
34	1.4470E−01	6.8024E+00	1.9765E−01	4.2098E+00	2.1584E−01	3.6652E+00	2.3758E−01	3.2063E+00
35	1.3916E−01	6.9356E+00	1.8902E−01	4.2855E+00	2.0609E−01	3.7309E+00	2.2654E−01	3.2639E+00
36	1.3403E−01	7.0672E+00	1.8093E−01	4.3597E+00	1.9698E−01	3.7953E+00	2.1626E−01	3.3203E+00
37	1.2928E−01	7.1974E+00	1.7334E−01	4.4325E+00	1.8844E−01	3.8584E+00	2.0665E−01	3.3754E+00
38	1.2488E−01	7.3259E+00	1.6620E−01	4.5039E+00	1.8044E−01	3.9202E+00	1.9765E−01	3.4293E+00
39	1.2079E−01	7.4530E+00	1.5947E−01	4.5742E+00	1.7290E−01	3.9808E+00	1.8922E−01	3.4821E+00
40	1.1699E−01	7.5785E+00	1.5313E−01	4.6432E+00	1.6582E−01	4.0403E+00	1.8129E−01	3.5339E+00
41	1.1345E−01	7.7025E+00	1.4713E−01	4.7111E+00	1.5913E−01	4.0987E+00	1.7383E−01	3.5846E+00
42	1.1014E−01	7.8249E+00	1.4147E−01	4.7780E+00	1.5283E−01	4.1561E+00	1.6681E−01	3.6344E+00
43	1.0704E−01	7.9457E+00	1.3611E−01	4.8438E+00	1.4687E−01	4.2126E+00	1.6019E−01	3.6832E+00
44	1.0412E−01	8.0649E+00	1.3104E−01	4.9087E+00	1.4124E−01	4.2681E+00	1.5394E−01	3.7312E+00
45	1.0137E−01	8.1825E+00	1.2624E−01	4.9725E+00	1.3592E−01	4.3227E+00	1.4803E−01	3.7784E+00
46	9.8752E−02	8.2985E+00	1.2169E−01	5.0355E+00	1.3088E−01	4.3765E+00	1.4245E−01	3.8247E+00
47	9.6262E−02	8.4129E+00	1.1737E−01	5.0976E+00	1.2611E−01	4.4295E+00	1.3718E−01	3.8704E+00
48	9.3879E−02	8.5258E+00	1.1328E−01	5.1588E+00	1.2159E−01	4.4817E+00	1.3219E−01	3.9153E+00
49	9.1589E−02	8.6372E+00	1.0939E−01	5.2192E+00	1.1731E−01	4.5332E+00	1.2746E−01	3.9596E+00
50	8.9379E−02	8.7472E+00	1.0570E−01	5.2787E+00	1.1324E−01	4.5839E+00	1.2298E−01	4.0032E+00
51	8.7236E−02	8.8558E+00	1.0219E−01	5.3375E+00	1.0939E−01	4.6340E+00	1.1873E−01	4.0462E+00
52	8.5151E−02	8.9630E+00	9.8857E−02	5.3955E+00	1.0573E−01	4.6833E+00	1.1470E−01	4.0886E+00
53	8.3113E−02	9.0690E+00	9.5682E−02	5.4527E+00	1.0225E−01	4.7320E+00	1.1087E−01	4.1304E+00
54	8.1115E−02	9.1738E+00	9.2658E−02	5.5092E+00	9.8939E−02	4.7801E+00	1.0724E−01	4.1716E+00
55	7.9150E−02	9.2775E+00	8.9776E−02	5.5650E+00	9.5792E−02	4.8275E+00	1.0378E−01	4.2123E+00
56	7.7212E−02	9.3802E+00	8.7029E−02	5.6201E+00	9.2796E−02	4.8744E+00	1.0050E−01	4.2525E+00
57	7.5296E−02	9.4821E+00	8.4407E−02	5.6745E+00	8.9943E−02	4.9206E+00	9.7371E−02	4.2922E+00
58	7.3398E−02	9.5831E+00	8.1904E−02	5.7283E+00	8.7223E−02	4.9663E+00	9.4392E−02	4.3314E+00
59	7.1514E−02	9.6834E+00	7.9511E−02	5.7814E+00	8.4628E−02	5.0115E+00	9.1554E−02	4.3701E+00
60	6.9643E−02	9.7833E+00	7.7224E−02	5.8340E+00	8.2152E−02	5.0561E+00	8.8847E−02	4.4084E+00

Table 4.3.3.1. *Partial wave elastic scattering factors for neutral atoms (cont.)*
U; $Z = 92$

	10 keV		40 keV		60 keV		90 keV	
s	$\|f(s)\|$	$\eta(s)$	$\|f(s)\|$	$\eta(s)$	$\|f(s)\|$	$\eta(s)$	$\|f(s)\|$	$\eta(s)$
0	1.5083E+01	3.5370E−01	1.7980E+01	2.5724E−01	1.9103E+01	2.3266E−01	2.0511E+01	2.1038E−01
1	1.1598E+01	4.4626E−01	1.4175E+01	3.1909E−01	1.5136E+01	2.8755E−01	1.6325E+01	2.5913E−01
2	7.1875E+00	6.6900E−01	9.2358E+00	4.6273E−01	9.9621E+00	4.1411E−01	1.0835E+01	3.7094E−01
3	4.7328E+00	9.2179E−01	6.3709E+00	6.2130E−01	6.9374E+00	5.5299E−01	7.6043E+00	4.9309E−01
4	3.3185E+00	1.1823E+00	4.6467E+00	7.8195E−01	5.1024E+00	6.9312E−01	5.6313E+00	6.1589E−01
5	2.4367E+00	1.4547E+00	3.5159E+00	9.4777E−01	3.8880E+00	8.3721E−01	4.3160E+00	7.4175E−01
6	1.8679E+00	1.7309E+00	2.7474E+00	1.1153E+00	3.0548E+00	9.8244E−01	3.4068E+00	8.6830E−01
7	1.4862E+00	2.0009E+00	2.2097E+00	1.2797E+00	2.4670E+00	1.1247E+00	2.7610E+00	9.9213E−01
8	1.2177E+00	2.2604E+00	1.8206E+00	1.4385E+00	2.0387E+00	1.2622E+00	2.2879E+00	1.1116E+00
9	1.0212E+00	2.5096E+00	1.5296E+00	1.5917E+00	1.7165E+00	1.3947E+00	1.9303E+00	1.2269E+00
10	8.7314E−01	2.7492E+00	1.3060E+00	1.7400E+00	1.4677E+00	1.5231E+00	1.6528E+00	1.3384E+00
11	7.5850E−01	2.9795E+00	1.1302E+00	1.8838E+00	1.2709E+00	1.6475E+00	1.4323E+00	1.4466E+00
12	6.6860E−01	3.2005E+00	9.9061E−01	2.0229E+00	1.1140E+00	1.7681E+00	1.2557E+00	1.5515E+00
13	5.9581E−01	3.4124E+00	8.7737E−01	2.1572E+00	9.8616E−01	1.8846E+00	1.1115E+00	1.6529E+00
14	5.3522E−01	3.6160E+00	7.8378E−01	2.2864E+00	8.8035E−01	1.9968E+00	9.9181E−01	1.7506E+00
15	4.8384E−01	3.8121E+00	7.0535E−01	2.4108E+00	7.9165E−01	2.1048E+00	8.9140E−01	1.8447E+00
16	4.3961E−01	4.0022E+00	6.3873E−01	2.5305E+00	7.1634E−01	2.2087E+00	8.0615E−01	1.9352E+00
17	4.0120E−01	4.1871E+00	5.8148E−01	2.6459E+00	6.5167E−01	2.3087E+00	7.3298E−01	2.0223E+00
18	3.6767E−01	4.3678E+00	5.3183E−01	2.7576E+00	5.9564E−01	2.4055E+00	6.6961E−01	2.1065E+00
19	3.3835E−01	4.5447E+00	4.8849E−01	2.8662E+00	5.4672E−01	2.4994E+00	6.1429E−01	2.1881E+00
20	3.1267E−01	4.7182E+00	4.5047E−01	2.9719E+00	5.0378E−01	2.5907E+00	5.6570E−01	2.2675E+00
21	2.9015E−01	4.8885E+00	4.1698E−01	3.0752E+00	4.6591E−01	2.6799E+00	5.2280E−01	2.3450E+00
22	2.7036E−01	5.0553E+00	3.8740E−01	3.1762E+00	4.3238E−01	2.7672E+00	4.8477E−01	2.4209E+00
23	2.5290E−01	5.2189E+00	3.6118E−01	3.2752E+00	4.0260E−01	2.8527E+00	4.5093E−01	2.4953E+00
24	2.3742E−01	5.3791E+00	3.3786E−01	3.3721E+00	3.7606E−01	2.9366E+00	4.2070E−01	2.5683E+00
25	2.2363E−01	5.5360E+00	3.1706E−01	3.4669E+00	3.5232E−01	3.0188E+00	3.9362E−01	2.6400E+00
26	2.1125E−01	5.6898E+00	2.9841E−01	3.5597E+00	3.3101E−01	3.0994E+00	3.6927E−01	2.7104E+00
27	2.0009E−01	5.8406E+00	2.8162E−01	3.6505E+00	3.1181E−01	3.1784E+00	3.4730E−01	2.7796E+00
28	1.8997E−01	5.9886E+00	2.6643E−01	3.7394E+00	2.9442E−01	3.2557E+00	3.2740E−01	2.8473E+00
29	1.8075E−01	6.1341E+00	2.5261E−01	3.8262E+00	2.7861E−01	3.3314E+00	3.0931E−01	2.9137E+00
30	1.7232E−01	6.2773E+00	2.3998E−01	3.9110E+00	2.6417E−01	3.4055E+00	2.9279E−01	2.9787E+00
31	1.6458E−01	6.4183E+00	2.2838E−01	3.9940E+00	2.5093E−01	3.4778E+00	2.7765E−01	3.0423E+00
32	1.5746E−01	6.5574E+00	2.1767E−01	4.0752E+00	2.3873E−01	3.5486E+00	2.6373E−01	3.1045E+00
33	1.5091E−01	6.6947E+00	2.0774E−01	4.1546E+00	2.2744E−01	3.6179E+00	2.5088E−01	3.1653E+00
34	1.4486E−01	6.8303E+00	1.9851E−01	4.2323E+00	2.1696E−01	3.6856E+00	2.3898E−01	3.2247E+00
35	1.3928E−01	6.9643E+00	1.8988E−01	4.3085E+00	2.0721E−01	3.7518E+00	2.2792E−01	3.2828E+00
36	1.3412E−01	7.0968E+00	1.8181E−01	4.3832E+00	1.9809E−01	3.8167E+00	2.1761E−01	3.3397E+00
37	1.2935E−01	7.2278E+00	1.7422E−01	4.4565E+00	1.8956E−01	3.8802E+00	2.0798E−01	3.3952E+00
38	1.2494E−01	7.3574E+00	1.6710E−01	4.5285E+00	1.8155E−01	3.9425E+00	1.9897E−01	3.4496E+00
39	1.2085E−01	7.4854E+00	1.6038E−01	4.5992E+00	1.7401E−01	4.0036E+00	1.9052E−01	3.5029E+00
40	1.1705E−01	7.6119E+00	1.5404E−01	4.6687E+00	1.6692E−01	4.0635E+00	1.8257E−01	3.5551E+00
41	1.1352E−01	7.7368E+00	1.4805E−01	4.7371E+00	1.6023E−01	4.1224E+00	1.7510E−01	3.6063E+00
42	1.1022E−01	7.8602E+00	1.4239E−01	4.8044E+00	1.5392E−01	4.1803E+00	1.6806E−01	3.6565E+00
43	1.0714E−01	7.9820E+00	1.3704E−01	4.8707E+00	1.4795E−01	4.2372E+00	1.6141E−01	3.7057E+00
44	1.0425E−01	8.1023E+00	1.3196E−01	4.9360E+00	1.4231E−01	4.2931E+00	1.5514E−01	3.7542E+00
45	1.0152E−01	8.2209E+00	1.2716E−01	5.0003E+00	1.3698E−01	4.3482E+00	1.4921E−01	3.8017E+00
46	9.8945E−02	8.3379E+00	1.2260E−01	5.0637E+00	1.3192E−01	4.4024E+00	1.4361E−01	3.8485E+00
47	9.6495E−02	8.4534E+00	1.1828E−01	5.1263E+00	1.2713E−01	4.4558E+00	1.3831E−01	3.8946E+00
48	9.4155E−02	8.5672E+00	1.1417E−01	5.1879E+00	1.2260E−01	4.5084E+00	1.3329E−01	3.9399E+00
49	9.1910E−02	8.6796E+00	1.1028E−01	5.2487E+00	1.1829E−01	4.5602E+00	1.2853E−01	3.9845E+00
50	8.9747E−02	8.7905E+00	1.0657E−01	5.3087E+00	1.1421E−01	4.6114E+00	1.2402E−01	4.0285E+00
51	8.7652E−02	8.8999E+00	1.0305E−01	5.3679E+00	1.1033E−01	4.6618E+00	1.1975E−01	4.0718E+00
52	8.5614E−02	9.0080E+00	9.9696E−02	5.4264E+00	1.0664E−01	4.7115E+00	1.1569E−01	4.1145E+00
53	8.3623E−02	9.1147E+00	9.6504E−02	5.4840E+00	1.0314E−01	4.7606E+00	1.1183E−01	4.1567E+00
54	8.1671E−02	9.2203E+00	9.3464E−02	5.5409E+00	9.9807E−02	4.8091E+00	1.0817E−01	4.1983E+00
55	7.9750E−02	9.3247E+00	9.0565E−02	5.5972E+00	9.6636E−02	4.8569E+00	1.0468E−01	4.2393E+00
56	7.7854E−02	9.4280E+00	8.7800E−02	5.6527E+00	9.3616E−02	4.9041E+00	1.0137E−01	4.2798E+00
57	7.5976E−02	9.5304E+00	8.5161E−02	5.7075E+00	9.0739E−02	4.9507E+00	9.8216E−02	4.3198E+00
58	7.4113E−02	9.6320E+00	8.2640E−02	5.7617E+00	8.7996E−02	4.9968E+00	9.5211E−02	4.3593E+00
59	7.2260E−02	9.7328E+00	8.0230E−02	5.8152E+00	8.5378E−02	5.0423E+00	9.2346E−02	4.3984E+00
60	7.0415E−02	9.8330E+00	7.7924E−02	5.8682E+00	8.2879E−02	5.0872E+00	8.9613E−02	4.4369E+00

Table 4.3.3.2. *Inelastic scattering factors*

Element *Z* *s*	H 1	He 2	Li 3	Be 4	B 5	C 6	N 7	O 8	F 9
0	0.00000	0.00000	0.00000	0.00000	0.00000	0.00000	0.00000	0.00000	0.00000
1	0.23712	0.20585	0.88290	1.11410	0.97969	0.82589	0.70270	0.64471	0.58625
2	0.62750	0.67665	1.29649	2.05741	2.35860	2.30155	2.12384	2.05154	1.93281
3	0.85836	1.15502	1.58907	2.33547	3.03124	3.35857	3.37855	3.44994	3.38314
4	0.95050	1.50584	1.89856	2.54347	3.31571	3.92722	4.23128	4.52527	4.60924
5	0.98252	1.72314	2.17978	2.76339	3.50570	4.23471	4.76279	5.26209	5.53803
6	0.99349	1.84691	2.41052	2.97864	3.68270	4.43840	5.09842	5.74264	6.19823
7	0.99740	1.91496	2.58662	3.17603	3.85613	4.60589	5.32971	6.05888	6.65331
8	0.99889	1.95208	2.71445	3.34823	4.02198	4.75972	5.50893	6.28032	6.96851
9	0.99949	1.97248	2.80427	3.49247	4.17553	4.90533	5.66203	6.45035	7.19556
10	0.99976	1.98385	2.86613	3.60942	4.31351	5.04263	5.80060	6.59304	7.36980
11	0.99988	1.99032	2.90828	3.70189	4.43432	5.17019	5.92915	6.72061	7.51316
12	0.99993	1.99407	2.93687	3.77366	4.53780	5.28663	6.04900	6.83868	7.63830
13	0.99996	1.99629	2.95627	3.82863	4.62485	5.39115	6.16020	6.94951	7.75211
14	0.99998	1.99763	2.96947	3.87036	4.69701	5.48356	6.26247	7.05375	7.85802
15	0.99999	1.99846	2.97851	3.90185	4.75615	5.56419	6.35555	7.15137	7.95762
16	0.99999	1.99898	2.98474	3.92555	4.80418	5.63375	6.43942	7.24214	8.05146
17	1.00000	1.99931	2.98907	3.94336	4.84294	5.69320	6.51429	7.32588	8.13968
18	1.00000	1.99953	2.99209	3.95676	4.87406	5.74363	6.58055	7.40250	8.22220
19	1.00000	1.99968	2.99423	3.96686	4.89897	5.78614	6.63878	7.47210	8.29896
20	1.00000	1.99977	2.99576	3.97448	4.91886	5.82179	6.68961	7.53488	8.36993
21	1.00000	1.99984	2.99685	3.98027	4.93474	5.85157	6.73375	7.59117	8.43516
22	1.00000	1.99988	2.99764	3.98466	4.94741	5.87639	6.77191	7.64136	8.49480
23	1.00000	1.99991	2.99822	3.98802	4.95752	5.89702	6.80478	7.68590	8.54904
24	1.00000	1.99994	2.99865	3.99060	4.96560	5.91415	6.83300	7.72528	8.59816
25	1.00000	1.99995	2.99897	3.99259	4.97207	5.92836	6.85718	7.75997	8.64246
26	1.00000	1.99996	2.99920	3.99413	4.97726	5.94015	6.87785	7.79043	8.68227
27	1.00000	1.99997	2.99938	3.99532	4.98143	5.94992	6.89550	7.81712	8.71793
28	1.00000	1.99998	2.99952	3.99626	4.98479	5.95804	6.91055	7.84046	8.74980
29	1.00000	1.99998	2.99962	3.99699	4.98750	5.96477	6.92339	7.86084	8.77820
30	1.00000	1.99999	2.99970	3.99757	4.98970	5.97038	6.93433	7.87860	8.80347
31	1.00000	1.99999	2.99976	3.99803	4.99149	5.97504	6.94365	7.89407	8.82591
32	1.00000	1.99999	2.99981	3.99840	4.99294	5.97893	6.95160	7.90753	8.84581
33	1.00000	1.99999	2.99985	3.99869	4.99413	5.98217	6.95838	7.91925	8.86344
34	1.00000	2.00000	2.99988	3.99892	4.99510	5.98489	6.96416	7.92943	8.87904
35	1.00000	2.00000	2.99990	3.99911	4.99590	5.98716	6.96910	7.93829	8.89284
36	1.00000	2.00000	2.99992	3.99927	4.99656	5.98907	6.97332	7.94600	8.90503
37	1.00000	2.00000	2.99993	3.99939	4.99711	5.99068	6.97693	7.95270	8.91581
38	1.00000	2.00000	2.99994	3.99949	4.99756	5.99203	6.98003	7.95854	8.92532
39	1.00000	2.00000	2.99995	3.99958	4.99794	5.99318	6.98268	7.96362	8.93373
40	1.00000	2.00000	2.99996	3.99964	4.99825	5.99414	6.98496	7.96804	8.94116
41	1.00000	2.00000	2.99997	3.99970	4.99851	5.99496	6.98692	7.97190	8.94772
42	1.00000	2.00000	2.99997	3.99975	4.99873	5.99566	6.98860	7.97526	8.95352
43	1.00000	2.00000	2.99998	3.99979	4.99891	5.99625	6.99006	7.97820	8.95864
44	1.00000	2.00000	2.99998	3.99982	4.99907	5.99675	6.99131	7.98077	8.96317
45	1.00000	2.00000	2.99998	3.99984	4.99920	5.99719	6.99240	7.98301	8.96718
46	1.00000	2.00000	2.99999	3.99987	4.99931	5.99755	6.99334	7.98498	8.97073
47	1.00000	2.00000	2.99999	3.99989	4.99940	5.99787	6.99415	7.98670	8.97387
48	1.00000	2.00000	2.99999	3.99990	4.99948	5.99814	6.99486	7.98822	8.97666
49	1.00000	2.00000	2.99999	3.99992	4.99955	5.99838	6.99547	7.98954	8.97913
50	1.00000	2.00000	2.99999	3.99993	4.99961	5.99858	6.99601	7.99071	8.98132
51	1.00000	2.00000	2.99999	3.99994	4.99966	5.99876	6.99647	7.99174	8.98327
52	1.00000	2.00000	2.99999	3.99995	4.99970	5.99891	6.99688	7.99264	8.98500
53	1.00000	2.00000	3.00000	3.99995	4.99974	5.99904	6.99724	7.99344	8.98654
54	1.00000	2.00000	3.00000	3.99996	4.99977	5.99915	6.99755	7.99415	8.98791
55	1.00000	2.00000	3.00000	3.99996	4.99980	5.99925	6.99783	7.99477	8.98913
56	1.00000	2.00000	3.00000	3.99997	4.99983	5.99934	6.99807	7.99532	8.99021
57	1.00000	2.00000	3.00000	3.99997	4.99985	5.99941	6.99828	7.99581	8.99119
58	1.00000	2.00000	3.00000	3.99998	4.99986	5.99948	6.99846	7.99624	8.99205
59	1.00000	2.00000	3.00000	3.99998	4.99988	5.99954	6.99863	7.99663	8.99283
60	1.00000	2.00000	3.00000	3.99998	4.99989	5.99959	6.99877	7.99697	8.99352

Table 4.3.3.2. *Inelastic scattering factors (cont.)*

Element	Ne	Na	Mg	Al	Si	P	S	Cl	Ar
Z	10	11	12	13	14	15	16	17	18
s									
0	0.00000	0.00000	0.00000	0.00000	0.00000	0.00000	0.00000	0.00000	0.00000
1	0.53234	1.20747	1.61544	1.72194	1.65386	1.53700	1.49816	1.42156	1.33265
2	1.80053	2.28779	2.94235	3.50721	3.78096	3.80549	3.95432	3.94695	3.84282
3	3.24475	3.49193	3.94530	4.52834	5.07436	5.40954	5.80343	6.00685	6.03450
4	4.54966	4.70014	5.01729	5.47022	6.01322	6.52767	7.06849	7.48589	7.72422
5	5.61925	5.77806	6.03833	6.41063	6.88008	7.40945	7.98702	8.53330	8.96990
6	6.44652	6.68058	6.94760	7.29048	7.71078	8.20204	8.75585	9.33634	9.88639
7	7.06089	7.40330	7.72396	8.07744	8.48211	8.94372	9.46405	10.03048	10.61498
8	7.50742	7.96372	8.36460	8.75902	9.17588	9.62983	10.12957	10.67346	11.25279
9	7.83224	8.39028	8.87926	9.33363	9.78380	10.25033	10.74677	11.27732	11.84272
10	8.07400	8.71388	9.28563	9.80759	10.30489	10.79947	11.30797	11.83831	12.39562
11	8.26134	8.96233	9.60450	10.19272	10.74365	11.27657	11.80888	12.35087	12.90995
12	8.41386	9.15796	9.85601	10.50348	11.10840	11.68496	12.24905	12.81180	13.38195
13	8.54414	9.31737	10.05748	10.75458	11.40955	12.03077	12.63101	13.22075	13.80922
14	8.65993	9.45219	10.22270	10.95937	11.65803	12.32173	12.95942	13.57972	14.19149
15	8.76576	9.57025	10.36206	11.12908	11.86416	12.56614	13.24013	13.89228	14.53031
16	8.86416	9.67661	10.48302	11.27266	12.03702	12.77207	13.47958	14.16303	14.82851
17	8.95646	9.77440	10.59078	11.39691	12.18418	12.94685	13.68412	14.39702	15.08974
18	9.04331	9.86554	10.68886	11.50688	12.31167	13.09681	13.85970	14.59936	15.31806
19	9.12498	9.95113	10.77955	11.60616	12.42419	13.22723	14.01162	14.77489	15.51761
20	9.20160	10.03176	10.86431	11.69727	12.52524	13.34234	14.14443	14.92805	15.69240
21	9.27319	10.10777	10.94406	11.78195	12.61744	13.44547	14.26190	15.06274	15.84616
22	9.33982	10.17933	11.01935	11.86133	12.70264	13.53918	14.36711	15.18230	15.98223
23	9.40157	10.24653	11.09051	11.93618	12.78217	13.62538	14.46250	15.28952	16.10354
24	9.45854	10.30944	11.15772	12.00698	12.85695	13.70552	14.54998	15.38669	16.21260
25	9.51090	10.36817	11.22111	12.07405	12.92761	13.78062	14.63102	15.47564	16.31151
26	9.55885	10.42279	11.28077	12.13758	12.99459	13.85143	14.70673	15.55783	16.40201
27	9.60262	10.47344	11.33679	12.19771	13.05816	13.91849	14.77793	15.63441	16.48552
28	9.64244	10.52026	11.38925	12.25454	13.11853	13.98216	14.84524	15.70626	16.56318
29	9.67857	10.56342	11.43824	12.30814	13.17583	14.04271	14.90911	15.77405	16.63589
30	9.71128	10.60310	11.48389	12.35861	13.23017	14.10034	14.96988	15.83830	16.70436
31	9.74083	10.63950	11.52631	12.40603	13.28163	14.15517	15.02777	15.89938	16.76915
32	9.76748	10.67281	11.56565	12.45048	13.33028	14.20732	15.08297	15.95759	16.83069
33	9.79146	10.70323	11.60205	12.49206	13.37621	14.25686	15.13561	16.01315	16.88931
34	9.81302	10.73097	11.63566	12.53089	13.41949	14.30387	15.18580	16.06621	16.94527
35	9.83238	10.75622	11.66665	12.56708	13.46020	14.34842	15.23360	16.11691	16.99876
36	9.84974	10.77917	11.69517	12.60075	13.49843	14.39057	15.27911	16.16535	17.04993
37	9.86530	10.80002	11.72137	12.63202	13.53427	14.43041	15.32237	16.21159	17.09890
38	9.87924	10.81893	11.74542	12.66102	13.56783	14.46799	15.36345	16.25573	17.14577
39	9.89171	10.83606	11.76747	12.68789	13.59919	14.50341	15.40243	16.29780	17.19062
40	9.90287	10.85158	11.78765	12.71273	13.62846	14.53673	15.43935	16.33789	17.23350
41	9.91286	10.86562	11.80612	12.73569	13.65576	14.56805	15.47428	16.37603	17.27449
42	9.92179	10.87832	11.82300	12.75688	13.68117	14.59744	15.50730	16.41229	17.31364
43	9.92977	10.88980	11.83842	12.77642	13.70481	14.62500	15.53847	16.44672	17.35099
44	9.93691	10.90018	11.85250	12.79442	13.72678	14.65080	15.56786	16.47938	17.38661
45	9.94330	10.90956	11.86534	12.81100	13.74718	14.67494	15.59554	16.51033	17.42053
46	9.94901	10.91803	11.87705	12.82625	13.76610	14.69750	15.62159	16.53964	17.45281
47	9.95412	10.92569	11.88773	12.84028	13.78364	14.71857	15.64608	16.56736	17.48351
48	9.95870	10.93260	11.89747	12.85317	13.79988	14.73823	15.66909	16.59355	17.51267
49	9.96279	10.93885	11.90634	12.86501	13.81492	14.75656	15.69068	16.61828	17.54035
50	9.96646	10.94449	11.91442	12.87589	13.82884	14.77364	15.71093	16.64161	17.56660
51	9.96974	10.94959	11.92178	12.88588	13.84172	14.78955	15.72991	16.66360	17.59148
52	9.97269	10.95420	11.92849	12.89505	13.85362	14.80435	15.74768	16.68431	17.61504
53	9.97533	10.95837	11.93460	12.90346	13.86462	14.81813	15.76432	16.70381	17.63733
54	9.97770	10.96214	11.94017	12.91118	13.87478	14.83093	15.77989	16.72216	17.65841
55	9.97983	10.96555	11.94525	12.91827	13.88417	14.84284	15.79444	16.73941	17.67833
56	9.98174	10.96863	11.94987	12.92477	13.89284	14.85390	15.80804	16.75562	17.69714
57	9.98346	10.97143	11.95409	12.93074	13.90085	14.86418	15.82075	16.77085	17.71490
58	9.98500	10.97396	11.95793	12.93621	13.90824	14.87373	15.83262	16.78514	17.73166
59	9.98639	10.97625	11.96143	12.94124	13.91507	14.88259	15.84370	16.79856	17.74746
60	9.98765	10.97832	11.96463	12.94585	13.92137	14.89082	15.85405	16.81114	17.76235

Table 4.3.3.2. *Inelastic scattering factors (cont.)*

Element *Z* *s*	K 19	Ca 20	Sc 21	Ti 22	V 23	Cr 24	Mn 25	Fe 26	Co 27
0	0.00000	0.00000	0.00000	0.00000	0.00000	0.00000	0.00000	0.00000	0.00000
1	1.95409	2.48962	2.47505	2.41147	2.34470	1.87338	2.20760	2.15605	2.09981
2	4.16743	4.63722	4.74095	4.73155	4.71014	4.31232	4.61890	4.62675	4.60110
3	6.28656	6.63788	6.79142	6.81860	6.82580	6.58097	6.75751	6.80527	6.79526
4	8.01589	8.34650	8.56715	8.67221	8.74208	8.59326	8.76139	8.86447	8.88855
5	9.37354	9.75686	10.05075	10.24289	10.38420	10.33687	10.51832	10.68060	10.75511
6	10.40504	10.88531	11.27230	11.56360	11.78746	11.84876	12.05425	12.27171	12.40221
7	11.20105	11.76628	12.24977	12.64663	12.96597	13.14017	13.39278	13.66798	13.86069
8	11.85904	12.47072	13.02927	13.51955	13.93468	14.22015	14.54015	14.87959	15.14206
9	12.44416	13.06908	13.67229	14.23079	14.72718	15.11304	15.50762	15.91441	16.25102
10	12.98647	13.60753	14.23080	14.83118	15.38717	15.85527	16.31906	16.78966	17.19864
11	13.49465	14.10800	14.73745	15.35997	15.95492	16.48500	17.00553	17.53092	18.00479
12	13.96833	14.57744	15.20828	15.84156	16.46015	17.03426	17.59751	18.16629	18.69422
13	14.40504	15.01608	15.64906	16.28847	16.92150	17.52612	18.12000	18.72120	19.29164
14	14.80303	15.42228	16.06067	16.70589	17.34908	17.97537	18.59107	19.21579	19.81842
15	15.16201	15.79475	16.44246	17.09532	17.74762	18.39057	19.02256	19.66452	20.29119
16	15.48312	16.13321	16.79376	17.45682	18.11901	18.77626	19.42164	20.07700	20.72194
17	15.76851	16.43845	17.11456	17.79031	18.46388	19.13474	19.79241	20.45925	21.11878
18	16.02103	16.71212	17.40559	18.09602	18.78257	19.46719	20.13716	20.81484	21.48693
19	16.24393	16.95643	17.66824	18.37470	19.07558	19.77444	20.45724	21.14592	21.82968
20	16.44057	17.17399	17.90434	18.62758	19.34372	20.05728	20.75361	21.45382	22.14909
21	16.61428	17.36753	18.11606	18.85623	19.58811	20.31668	21.02715	21.73952	22.44651
22	16.76819	17.53980	18.30570	19.06249	19.81018	20.55380	21.27883	22.00392	22.72298
23	16.90520	17.69348	18.47561	19.24834	20.01151	20.77001	21.50974	22.24793	22.97940
24	17.02787	17.83103	18.62806	19.41579	20.19384	20.96677	21.72111	22.47258	23.21667
25	17.13845	17.95471	18.76522	19.56682	20.35893	21.14567	21.91428	22.67895	23.43574
26	17.23887	18.06655	18.88908	19.70334	20.50852	21.30828	22.09062	22.86824	23.63764
27	17.33077	18.16830	19.00144	19.82710	20.64429	21.45620	22.25155	23.04170	23.82343
28	17.41550	18.26148	19.10390	19.93973	20.76783	21.59092	22.39849	23.20059	23.99424
29	17.49419	18.34738	19.19786	20.04268	20.88059	21.71390	22.53279	23.34616	24.15122
30	17.56774	18.42708	19.28454	20.13724	20.98391	21.82646	22.65576	23.47965	24.29549
31	17.63689	18.50150	19.36496	20.22456	21.07897	21.92983	22.76860	23.60223	24.42819
32	17.70222	18.57136	19.44000	20.30560	21.16684	22.02511	22.87245	23.71501	24.55037
33	17.76420	18.63728	19.51040	20.38121	21.24845	22.11329	22.96833	23.81902	24.66306
34	17.82320	18.69974	19.57676	20.45211	21.32459	22.19525	23.05717	23.91523	24.76720
35	17.87951	18.75913	19.63959	20.51889	21.39596	22.27176	23.13979	24.00449	24.86369
36	17.93334	18.81578	19.69928	20.58206	21.46316	22.34348	23.21694	24.08758	24.95334
37	17.98488	18.86994	19.75618	20.64204	21.52669	22.41099	23.28926	24.16522	25.03688
38	18.03427	18.92181	19.81056	20.69918	21.58697	22.47478	23.35731	24.23800	25.11498
39	18.08161	18.97154	19.86264	20.75377	21.64436	22.53529	23.42158	24.30650	25.18823
40	18.12700	19.01926	19.91259	20.80603	21.69915	22.59286	23.48250	24.37117	25.25716
41	18.17051	19.06508	19.96056	20.85616	21.75159	22.64781	23.54043	24.43245	25.32224
42	18.21221	19.10909	20.00667	20.90432	21.80189	22.70038	23.59568	24.49069	25.38389
43	18.25215	19.15135	20.05100	20.95063	21.85021	22.75079	23.64851	24.54620	25.44246
44	18.29039	19.19192	20.09364	20.99521	21.89670	22.79921	23.69914	24.59926	25.49826
45	18.32697	19.23087	20.13466	21.03813	21.94146	22.84580	23.74777	24.65009	25.55156
46	18.36193	19.26822	20.17411	21.07948	21.98460	22.89069	23.79455	24.69889	25.60260
47	18.39533	19.30404	20.21204	21.11931	22.02620	22.93396	23.83961	24.74583	25.65158
48	18.42720	19.33836	20.24849	21.15767	22.06632	22.97572	23.88308	24.79104	25.69868
49	18.45760	19.37122	20.28352	21.19462	22.10502	23.01604	23.92503	24.83464	25.74404
50	18.48657	19.40267	20.31714	21.23020	22.14236	23.05497	23.96556	24.87675	25.78778
51	18.51415	19.43274	20.34941	21.26443	22.17837	23.09258	24.00473	24.91744	25.83002
52	18.54040	19.46147	20.38036	21.29737	22.21309	23.12890	24.04261	24.95678	25.87085
53	18.56535	19.48890	20.41003	21.32904	22.24656	23.16398	24.07923	24.99485	25.91035
54	18.58906	19.51509	20.43845	21.35948	22.27882	23.19785	24.11464	25.03170	25.94858
55	18.61157	19.54005	20.46565	21.38871	22.30989	23.23056	24.14889	25.06736	25.98561
56	18.63294	19.56385	20.49168	21.41677	22.33980	23.26212	24.18200	25.10189	26.02148
57	18.65319	19.58651	20.51656	21.44370	22.36859	23.29257	24.21401	25.13532	26.05624
58	18.67240	19.60808	20.54034	21.46952	22.39628	23.32193	24.24495	25.16768	26.08992
59	18.69058	19.62860	20.56305	21.49427	22.42290	23.35024	24.27484	25.19900	26.12257
60	18.70781	19.64811	20.58472	21.51797	22.44848	23.37752	24.30371	25.22931	26.15420

Table 4.3.3.2. *Inelastic scattering factors (cont.)*

Element	Ni	Cu	Zn	Ga	Ge	As	Se	Br	Kr
Z	28	29	30	31	32	33	34	35	36
s									
0	0.00000	0.00000	0.00000	0.00000	0.00000	0.00000	0.00000	0.00000	0.00000
1	2.04471	1.69573	1.93762	2.05186	2.02388	1.94862	1.96187	1.92529	1.86388
2	4.57025	4.20291	4.48366	4.79699	4.96356	4.96762	5.16391	5.22242	5.17677
3	6.78094	6.60632	6.71087	6.99727	7.31756	7.53254	7.87187	8.08782	8.15809
4	8.90504	8.78952	8.87296	9.07164	9.37130	9.69780	10.09282	10.44730	10.70005
5	10.81621	10.72987	10.85168	11.03258	11.28885	11.60839	11.98915	12.39473	12.77835
6	12.51132	12.47751	12.62492	12.81781	13.06230	13.35790	13.70612	14.09835	14.51642
7	14.02217	14.05989	14.22287	14.42883	14.67729	14.96447	15.29281	15.66034	16.06428
8	15.36345	15.48041	15.66617	15.88673	16.14378	16.43328	16.75585	17.10934	17.49432
9	16.53914	16.73670	16.96032	17.20429	17.47556	17.77364	18.09916	18.44981	18.82545
10	17.55583	17.83189	18.10676	18.38602	18.68056	18.99403	19.32906	19.68468	20.06045
11	18.42792	18.77754	19.11098	19.43536	19.76289	20.09987	20.45124	20.81812	21.20099
12	19.17588	19.59174	19.98462	20.35933	20.72723	21.09536	21.47006	21.85427	22.24990
13	19.82231	20.29556	20.74392	21.16939	21.58126	21.98591	22.38987	22.79705	23.21055
14	20.38840	20.90979	21.40691	21.87992	22.33572	22.77927	23.21633	23.65097	24.08679
15	20.89193	21.45278	21.99101	22.50626	23.00321	23.48524	23.95687	24.42167	24.88315
16	21.34665	21.93949	22.51151	23.06295	23.59669	24.11476	24.62031	25.11610	25.60513
17	21.76253	22.38138	22.98092	23.56269	24.12833	24.67882	25.21613	25.74214	26.25912
18	22.14646	22.78682	23.40889	24.01592	24.60873	25.18761	25.75365	26.30797	26.85209
19	22.50302	23.16168	23.80261	24.43082	25.04664	25.65004	26.24150	26.82157	27.39114
20	22.83520	23.51000	24.16724	24.81353	25.44900	26.07350	26.68718	27.29024	27.88309
21	23.14497	23.83452	24.50642	25.16859	25.82113	26.46391	27.09700	27.72039	28.33419
22	23.43371	24.13716	24.82271	25.49929	26.16701	26.82591	27.47606	28.11740	28.74992
23	23.70247	24.41932	25.11795	25.80799	26.48960	27.16300	27.82837	28.48569	29.13493
24	23.95219	24.68209	25.39353	26.09645	26.79109	27.47786	28.15706	28.82879	29.49305
25	24.18376	24.92646	25.65055	26.36601	27.07314	27.77250	28.46453	29.14946	29.82740
26	24.39808	25.15335	25.88998	26.61776	27.33704	28.04847	28.75264	29.44989	30.14045
27	24.59612	25.36367	26.11272	26.85266	27.58385	28.30702	29.02284	29.73179	30.43417
28	24.77888	25.55837	26.31965	27.07158	27.81449	28.54916	29.27632	29.99650	30.71014
29	24.94740	25.73841	26.51166	27.27537	28.02983	28.77579	29.51404	30.24515	30.96963
30	25.10270	25.90478	26.68965	27.46487	28.23066	28.98774	29.73688	30.47868	31.21369
31	25.24584	26.05845	26.85452	27.64092	28.41779	29.18578	29.94561	30.69790	31.44321
32	25.37784	26.20040	27.00720	27.80439	28.59202	29.37066	30.14099	30.90357	31.65898
33	25.49968	26.33158	27.14857	27.95609	28.75413	29.54314	30.32373	31.09639	31.86171
34	25.61229	26.45293	27.27951	28.09689	28.90492	29.70396	30.49453	31.27706	32.05209
35	25.71658	26.56530	27.40089	28.22758	29.04515	29.85384	30.65409	31.44623	32.23076
36	25.81336	26.66955	27.51352	28.34897	29.17560	29.99353	30.80309	31.60456	32.39834
37	25.90339	26.76643	27.61817	28.46182	29.29699	30.12372	30.94223	31.75270	32.55546
38	25.98737	26.85668	27.71557	28.56685	29.41005	30.24510	31.07215	31.89127	32.70272
39	26.06594	26.94095	27.80641	28.66476	29.51546	30.35836	31.19351	32.02090	32.84072
40	26.13966	27.01985	27.89131	28.75617	29.61385	30.46411	31.30692	32.14220	32.97004
41	26.20905	27.09393	27.97085	28.84170	29.70584	30.56298	31.41300	32.25575	33.09125
42	26.27456	27.16367	28.04555	28.92188	29.79200	30.65553	31.51232	32.36212	33.20489
43	26.33659	27.22952	28.11590	28.99724	29.87284	30.74230	31.60540	32.46184	33.31151
44	26.39551	27.29187	28.18232	29.06822	29.94886	30.82380	31.69278	32.55544	33.41161
45	26.45162	27.35108	28.24521	29.13525	30.02050	30.90049	31.77492	32.64339	33.50568
46	26.50519	27.40746	28.30490	29.19870	30.08816	30.97279	31.85227	32.72615	33.59417
47	26.55647	27.46126	28.36171	29.25892	30.15222	31.04111	31.92524	32.80415	33.67753
48	26.60565	27.51275	28.41590	29.31621	30.21302	31.10580	31.99422	32.87778	33.75616
49	26.65293	27.56211	28.46773	29.37085	30.27084	31.16719	32.05955	32.94742	33.83044
50	26.69844	27.60954	28.51740	29.42307	30.32596	31.22558	32.12156	33.01340	33.90072
51	26.74233	27.65519	28.56509	29.47310	30.37863	31.28122	32.18052	33.07602	33.96734
52	26.78471	27.69920	28.61097	29.52111	30.42906	31.33437	32.23672	33.13559	34.03060
53	26.82567	27.74169	28.65519	29.56728	30.47743	31.38524	32.29038	33.19235	34.09077
54	26.86530	27.78276	28.69787	29.61175	30.52393	31.43403	32.34172	33.24654	34.14811
55	26.90368	27.82249	28.73910	29.65465	30.56870	31.48089	32.39094	33.29838	34.20285
56	26.94086	27.86098	28.77900	29.69610	30.61187	31.52600	32.43820	33.34806	34.25521
57	26.97690	27.89827	28.81764	29.73619	30.65357	31.56948	32.48367	33.39576	34.30537
58	27.01185	27.93444	28.85509	29.77501	30.69389	31.61145	32.52749	33.44162	34.35352
59	27.04575	27.96953	28.89142	29.81264	30.73292	31.65203	32.56977	33.48580	34.39980
60	27.07863	28.00358	28.92667	29.84914	30.77075	31.69130	32.61063	33.52842	34.44437

Table 4.3.3.2. *Inelastic scattering factors (cont.)*

Element *Z* *s*	Rb 37	Sr 38	Y 39	Zr 40	Nb 41	Mo 42	Tc 43	Ru 44	Rh 45
0	0.00000	0.00000	0.00000	0.00000	0.00000	0.00000	0.00000	0.00000	0.00000
1	2.47108	3.04685	3.14857	3.13536	2.71132	2.62807	2.98330	2.57466	2.52855
2	5.52799	5.98984	6.23152	6.31697	6.07762	6.02878	6.36677	6.13781	6.12994
3	8.42971	8.78804	9.05817	9.20196	9.10320	9.08596	9.36034	9.30184	9.34697
4	10.98758	11.30230	11.58543	11.79126	11.80981	11.84206	12.07333	12.11783	12.19330
5	13.15459	13.52254	13.85142	14.12392	14.25176	14.35492	14.55835	14.70247	14.80976
6	14.95100	15.38843	15.79296	16.15287	16.39784	16.60221	16.83500	17.06754	17.22869
7	16.50508	16.96971	17.42770	17.86266	18.21807	18.53376	18.84164	19.15747	19.39679
8	17.91915	18.37743	18.85174	19.32606	19.75964	20.16607	20.55607	20.94877	21.27607
9	19.23525	19.67796	20.14726	20.63128	21.10549	21.56834	22.02040	22.47422	22.88053
10	20.46323	20.89436	21.35427	21.83462	22.32362	22.81354	23.30155	23.79566	24.26063
11	21.60452	22.03122	22.48536	22.96037	23.45249	23.95215	24.45652	24.97275	25.47475
12	22.66058	23.08945	23.54310	24.01599	24.50867	25.01107	25.52134	26.04805	26.57052
13	23.63390	24.07058	24.52855	25.00342	25.49806	26.00220	26.51474	27.04651	27.57948
14	24.52760	24.97699	25.44341	25.92401	26.42303	26.93042	27.44542	27.98082	28.51972
15	25.34529	25.81159	26.29007	26.77965	27.28544	27.79829	28.31748	28.85706	29.40064
16	26.09128	26.57772	27.07138	27.57279	28.08753	28.60801	29.13355	29.67848	30.22717
17	26.77063	27.27935	27.79065	28.30631	28.83193	29.36203	29.89596	30.44747	31.00229
18	27.38906	27.92103	28.45165	28.98346	29.52168	30.06306	30.60716	31.16636	31.72846
19	27.95268	28.50783	29.05861	29.60784	30.16004	30.71409	31.26982	31.83769	32.40810
20	28.46765	29.04513	29.61611	30.18338	30.75055	31.31829	31.88675	32.46417	33.04374
21	28.93986	29.53825	30.12888	30.71422	31.29692	31.87899	32.46091	33.04863	33.63805
22	29.37468	29.99232	30.60160	31.20455	31.80291	32.39960	32.99536	33.59396	34.19377
23	29.77685	30.41201	31.03868	31.65846	32.27225	32.88351	33.49318	34.10309	34.71364
24	30.15044	30.80144	31.44418	32.07980	32.70854	33.33406	33.95743	34.57888	35.20037
25	30.49879	31.16418	31.82168	32.47208	33.11511	33.75438	34.39106	35.02411	35.65660
26	30.82469	31.50320	32.17429	32.83842	33.49499	34.14739	34.79684	35.44141	36.08482
27	31.13035	31.82098	32.50463	33.18153	33.85088	34.51575	35.17737	35.83324	36.48738
28	31.41757	32.11952	32.81489	33.50371	34.18512	34.86180	35.53497	36.20184	36.86647
29	31.68781	32.40048	33.10687	33.80689	34.49971	35.18758	35.87171	36.54925	37.22407
30	31.94225	32.66518	33.38206	34.09271	34.79636	35.49488	36.18941	36.87726	37.56196
31	32.18187	32.91474	33.64170	34.36249	35.07650	35.78518	36.48965	37.18746	37.88172
32	32.40754	33.15010	33.88680	34.61738	35.34134	36.05979	36.77377	37.48122	38.18473
33	32.61999	33.37204	34.11825	34.85831	35.59190	36.31977	37.04294	37.75971	38.47222
34	32.81991	33.58129	34.33679	35.08610	35.82904	36.56607	37.29814	38.02398	38.74524
35	33.00795	33.77849	34.54311	35.30147	36.05353	36.79949	37.54022	38.27490	39.00470
36	33.18470	33.96426	34.73782	35.50504	36.26602	37.02072	37.76993	38.51325	39.25140
37	33.35077	34.13916	34.92149	35.69741	36.46712	37.23038	37.98791	38.73969	39.48604
38	33.50674	34.30375	35.09466	35.87911	36.65738	37.42904	38.19475	38.95482	39.70923
39	33.65317	34.45859	35.25788	36.05068	36.83731	37.61721	38.39097	39.15918	39.92152
40	33.79063	34.60420	35.41165	36.21259	37.00740	37.79540	38.57707	39.35328	40.12342
41	33.91965	34.74111	35.55648	36.36536	37.16815	37.96406	38.75351	39.53756	40.31539
42	34.04078	34.86983	35.69286	36.50944	37.31999	38.12364	38.92072	39.71247	40.49786
43	34.15452	34.99086	35.82127	36.64531	37.46339	38.27458	39.07914	39.87842	40.67125
44	34.26139	35.10468	35.94218	36.77342	37.59879	38.41732	39.22917	40.03581	40.83593
45	34.36186	35.21178	36.05605	36.89421	37.72663	38.55226	39.37123	40.18504	40.99231
46	34.45640	35.31260	36.16334	37.00813	37.84731	38.67981	39.50570	40.32650	41.14075
47	34.54543	35.40758	36.26446	37.11559	37.96126	38.80039	39.63297	40.46055	41.28160
48	34.62938	35.49713	36.35984	37.21700	38.06888	38.91438	39.75343	40.58757	41.41524
49	34.70863	35.58165	36.44986	37.31275	38.17056	39.02216	39.86744	40.70792	41.54201
50	34.78356	35.66151	36.53491	37.40322	38.26666	39.12409	39.97536	40.82195	41.66225
51	34.85449	35.73706	36.61534	37.48878	38.35755	39.22055	40.07755	40.93001	41.77630
52	34.92175	35.80863	36.69148	37.56975	38.44358	39.31186	40.17434	41.03243	41.88449
53	34.98564	35.87653	36.76366	37.64647	38.52507	39.39836	40.26607	41.12953	41.98714
54	35.04642	35.94105	36.83217	37.71924	38.60233	39.48037	40.35304	41.22163	42.08455
55	35.10435	36.00244	36.89729	37.78834	38.67566	39.55818	40.43556	41.30903	42.17703
56	35.15964	36.06095	36.95927	37.85405	38.74534	39.63208	40.51392	41.39202	42.26486
57	35.21253	36.11682	37.01836	37.91662	38.81162	39.70233	40.58838	41.47088	42.34833
58	35.26319	36.17023	37.07477	37.97628	38.87475	39.76919	40.65921	41.54587	42.42770
59	35.31180	36.22140	37.12872	38.03324	38.93497	39.83290	40.72666	41.61725	42.50322
60	35.35851	36.27048	37.18038	38.08771	38.99247	39.89368	40.79095	41.68524	42.57515

Table 4.3.3.2. *Inelastic scattering factors (cont.)*

Element	Pd	Ag	Cd	In	Sn	Sb	Te	I	Xe
Z	46	47	48	49	50	51	52	53	54
s									
0	0.00000	0.00000	0.00000	0.00000	0.00000	0.00000	0.00000	0.00000	0.00000
1	2.13081	2.42343	2.70975	2.83441	2.81535	2.73816	2.77296	2.74654	2.68555
2	5.95961	6.03591	6.30459	6.63451	6.84114	6.87653	7.11536	7.21010	7.17883
3	9.23632	9.33858	9.51999	9.81909	10.16026	10.44583	10.81525	11.09773	11.24839
4	12.07598	12.23784	12.46054	12.72978	13.05475	13.41599	13.82032	14.22622	14.58946
5	14.75560	14.90041	15.11768	15.37682	15.67918	16.02031	16.40069	16.81256	17.24286
6	17.27178	17.40539	17.59096	17.82417	18.10185	18.41562	18.76463	19.14401	19.55212
7	19.54545	19.71426	19.90073	20.11901	20.37444	20.66395	20.98609	21.33615	21.71173
8	21.52940	21.77057	22.00282	22.24093	22.49751	22.77720	23.08280	23.41315	23.76633
9	23.22845	23.55443	23.85882	24.14878	24.43757	24.73296	25.04189	25.36736	25.71067
10	24.68459	25.08751	25.46742	25.82409	26.16687	26.50212	26.83738	27.17764	27.52690
11	25.95299	26.41494	26.85884	27.28022	27.68354	28.07182	28.45037	28.82353	29.19578
12	27.08363	27.58563	28.07659	28.55092	29.00920	29.45143	29.87984	30.29667	30.70506
13	28.11340	28.64026	29.16253	29.67532	30.17704	30.66588	31.14154	31.60411	32.05470
14	29.06590	29.60758	30.14943	30.68802	31.22095	31.74576	32.26075	32.76453	33.25645
15	29.95479	30.50579	31.05985	31.61513	32.16920	32.71973	33.26464	33.80183	34.32964
16	30.78766	31.34559	31.90798	32.47438	33.04260	33.61083	34.17721	34.73959	35.29596
17	31.56892	32.13323	32.70240	33.27702	33.85522	34.43575	35.01722	35.59782	36.17566
18	32.30163	32.87265	33.44836	34.03004	34.61612	35.20579	35.79817	36.39189	36.98544
19	32.98838	33.56677	34.14941	34.73796	35.33110	35.92835	36.52924	37.13281	37.73796
20	33.63173	34.21817	34.80832	35.40399	36.00409	36.60835	37.21658	37.82815	38.44232
21	34.23429	34.82936	35.42759	36.03077	36.63803	37.24925	37.86439	38.48306	39.10481
22	34.79871	35.40286	36.00964	36.62069	37.23540	37.85373	38.47574	39.10122	39.72986
23	35.32765	35.94119	36.55686	37.17607	37.79848	38.42413	39.05314	39.68537	40.32066
24	35.82374	36.44685	37.07161	37.69917	38.32947	38.96261	39.59874	40.23781	40.87972
25	36.28950	36.92226	37.55620	38.19222	38.83052	39.47124	40.11461	40.76059	41.40916
26	36.72736	37.36974	38.01286	38.65737	39.30370	39.95205	40.60268	41.25563	41.91088
27	37.13958	37.79149	38.44370	39.09668	39.75100	40.40697	41.06486	41.72476	42.38669
28	37.52826	38.18955	38.85072	39.51207	40.17433	40.83784	41.50293	42.16973	42.83831
29	37.89533	38.56581	39.23576	39.90537	40.57546	41.24642	41.91862	42.59223	43.26737
30	38.24253	38.92198	39.60052	40.27825	40.95605	41.63434	42.31353	42.99385	43.67544
31	38.57142	39.25963	39.94654	40.63222	41.31759	42.00309	42.68916	43.37606	44.06399
32	38.88338	39.58012	40.27521	40.96869	41.66149	42.35407	43.04689	43.74024	44.43437
33	39.17963	39.88470	40.58776	41.28889	41.98898	42.68851	43.38796	44.08765	44.78786
34	39.46123	40.17445	40.88531	41.59393	42.30118	43.00755	43.71351	44.41943	45.12561
35	39.72910	40.45030	41.16881	41.88479	42.59909	43.31218	44.02456	44.73661	45.44865
36	39.98406	40.71310	41.43912	42.16236	42.88359	43.60332	44.32203	45.04011	45.75792
37	40.22683	40.96359	41.69700	42.42739	43.15548	43.88176	44.60672	45.33077	46.05429
38	40.45802	41.20239	41.94311	42.68057	43.41544	44.14821	44.87936	45.60932	46.33848
39	40.67820	41.43009	42.17803	42.92249	43.66408	44.40329	45.14059	45.87642	46.61118
40	40.88788	41.64720	42.40230	43.15369	43.90195	44.64756	45.39097	46.13264	46.87297
41	41.08751	41.85418	42.61638	43.37466	44.12954	44.88151	45.63102	46.37851	47.12440
42	41.27753	42.05147	42.82071	43.58582	44.34730	45.10560	45.86118	46.61449	47.36592
43	41.45833	42.23947	43.01568	43.78758	44.55561	45.32023	46.08187	46.84098	47.59796
44	41.63032	42.41855	43.20167	43.98031	44.75486	45.52577	46.29346	47.05837	47.82090
45	41.79386	42.58909	43.37904	44.16435	44.94538	45.72255	46.49628	47.26699	48.03509
46	41.94930	42.75142	43.54813	44.34004	45.12751	45.91091	46.69066	47.46717	48.24083
47	42.09701	42.90589	43.70925	44.50771	45.30155	46.09115	46.87690	47.65920	48.43843
48	42.23733	43.05284	43.86275	44.66765	45.46779	46.26354	47.05527	47.84334	48.62815
49	42.37059	43.19258	44.00892	44.82017	45.62655	46.42839	47.22605	48.01988	48.81026
50	42.49714	43.32545	44.14808	44.96556	45.77809	46.58596	47.38950	48.18906	48.98499
51	42.61729	43.45175	44.28053	45.10413	45.92270	46.73651	47.54589	48.35114	49.15259
52	42.73137	43.57180	44.40658	45.23615	46.06065	46.88032	47.69546	48.50634	49.31330
53	42.83969	43.68589	44.52650	45.36191	46.19222	47.01765	47.83846	48.65492	49.46733
54	42.94256	43.79434	44.64060	45.48169	46.31767	47.14874	47.97514	48.79711	49.61492
55	43.04027	43.89743	44.74916	45.59576	46.43727	47.27386	48.10575	48.93314	49.75629
56	43.13311	43.99544	44.85245	45.70439	46.55128	47.39326	48.23052	49.06324	49.89165
57	43.22136	44.08864	44.95074	45.80784	46.65995	47.50718	48.34969	49.18764	50.02123
58	43.30529	44.17732	45.04430	45.90638	46.76355	47.61588	48.46350	49.30657	50.14524
59	43.38515	44.26171	45.13338	46.00026	46.86231	47.71958	48.57219	49.42024	50.26389
60	43.46119	44.34207	45.21823	46.08971	46.95647	47.81853	48.67597	49.52889	50.37741

Table 4.3.3.2. *Inelastic scattering factors (cont.)*

Element *Z* *s*	Cs 55	Ba 56	La 57	Ce 58	Pr 59	Nd 60	Pm 61	Sm 62	Eu 63
0	0.00000	0.00000	0.00000	0.00000	0.00000	0.00000	0.00000	0.00000	0.00000
1	3.26056	3.86513	3.98173	3.82992	3.79780	3.76602	3.73391	3.70093	3.66574
2	7.51043	7.93796	8.16628	7.95853	7.92593	7.89361	7.86055	7.81853	7.76614
3	11.50727	11.82172	12.07836	11.89091	11.86936	11.85347	11.84146	11.81226	11.76155
4	14.94313	15.29163	15.59334	15.41466	15.40728	15.40977	15.42104	15.40725	15.35978
5	17.68653	18.13325	18.54373	18.38275	18.42223	18.46877	18.52393	18.54486	18.51896
6	19.99684	20.46851	20.94271	20.84073	20.93672	21.03547	21.14100	21.20679	21.21677
7	22.12327	22.56799	23.03816	23.01484	23.15493	23.29454	23.43911	23.54344	23.58933
8	24.14779	24.55922	25.00033	25.04584	25.21725	25.38565	25.55681	25.69054	25.76819
9	26.07414	26.46226	26.87743	26.97495	27.17051	27.36050	27.55050	27.70729	27.81321
10	27.88767	28.26625	28.66647	28.80594	29.02323	29.23184	29.43711	29.61325	29.74482
11	29.57070	29.95527	30.35349	30.53305	30.77376	31.00189	31.22252	31.41694	31.57265
12	31.10881	31.51424	31.92398	32.14682	32.41595	32.66791	32.90744	33.12205	33.30236
13	32.49628	32.93352	33.36671	33.63749	33.94154	34.22365	34.48807	34.72733	34.93493
14	33.73826	34.21247	34.67707	34.99934	35.34403	35.66263	35.95863	36.22826	36.46740
15	34.84870	35.35955	35.85864	36.23339	36.62203	36.98171	37.31495	37.62034	37.89555
16	35.84631	36.38969	36.92200	37.34741	37.78028	38.18301	38.55691	38.90190	39.21679
17	36.75052	37.32054	37.88201	38.35393	38.82863	39.27368	39.68908	40.07535	40.43188
18	37.57867	38.16937	38.75472	39.26759	39.77988	40.26438	40.71987	41.14694	41.54518
19	38.34476	38.95105	39.55512	40.10283	40.64762	41.16740	41.65990	42.12558	42.56396
20	39.05936	39.67740	40.29583	40.87249	41.44464	41.99498	42.52055	43.02149	43.49721
21	39.73002	40.35724	40.98674	41.58717	42.18196	42.75827	43.31265	43.84501	44.35455
22	40.36211	40.99692	41.63525	42.25515	42.86863	43.46675	44.04590	44.60572	45.14531
23	40.95944	41.60099	42.24674	42.88273	43.51172	44.12817	44.72844	45.31205	45.87800
24	41.52485	42.17275	42.82512	43.47463	44.11671	44.74866	45.36699	45.97111	46.56001
25	42.06062	42.71475	43.37330	44.03444	44.68778	45.33303	45.96689	46.58874	47.19760
26	42.56873	43.22905	43.89358	44.56494	45.22821	45.88506	46.53242	47.16970	47.79597
27	43.05095	43.71747	44.38788	45.06842	45.74062	46.40777	47.06702	47.71785	48.35940
28	43.50897	44.18169	44.85790	45.54682	46.22720	46.90364	47.57351	48.23636	48.89142
29	43.94439	44.62325	45.30520	46.00186	46.68983	47.37476	48.05422	48.72785	49.39496
30	44.35873	45.04367	45.73127	46.43513	47.13020	47.82296	48.51119	49.19458	49.87253
31	44.75343	45.44433	46.13749	46.84809	47.54986	48.24990	48.94618	49.63849	50.32626
32	45.12986	45.82660	46.52519	47.24213	47.95022	48.65706	49.36081	50.06129	50.75804
33	45.48926	46.19170	46.89561	47.61852	48.33261	49.04583	49.75652	50.46456	51.16953
34	45.83279	46.54079	47.24991	47.97846	48.69825	49.41747	50.13464	50.84968	51.56224
35	46.16150	46.87495	47.58915	48.32305	49.04827	49.77315	50.49640	51.21796	51.93753
36	46.47636	47.19512	47.91432	48.65331	49.38372	50.11396	50.84292	51.57057	52.29665
37	46.77820	47.50220	48.22631	48.97016	49.70555	50.44089	51.17523	51.90859	52.64073
38	47.06781	47.79696	48.52592	49.27443	50.01462	50.75482	51.49427	52.23300	52.97081
39	47.34587	48.08010	48.81386	49.56689	50.31171	51.05658	51.80089	52.54470	53.28783
40	47.61299	48.35226	49.09079	49.84820	50.59753	51.34690	52.09586	52.84449	53.59264
41	47.86970	48.61399	49.35727	50.11898	50.87271	51.62645	52.37989	53.13312	53.88602
42	48.11650	48.86579	49.61382	50.37975	51.13781	51.89581	52.65358	53.41122	54.16865
43	48.35382	49.10810	49.86090	50.63099	51.39333	52.15551	52.91750	53.67940	54.44116
44	48.58204	49.34133	50.09891	50.87315	51.63972	52.40602	53.17213	53.93818	54.70412
45	48.80151	49.56583	50.32821	51.10658	51.87737	52.64775	53.41794	54.18803	54.95801
46	49.01255	49.78191	50.54913	51.33164	52.10664	52.88109	53.65529	54.42936	55.20329
47	49.21545	49.98988	50.76197	51.54863	52.32785	53.10636	53.88456	54.66254	55.44034
48	49.41048	50.19001	50.96700	51.75783	52.54128	53.32387	54.10604	54.88791	55.66953
49	49.59791	50.38254	51.16446	51.95950	52.74720	53.53388	54.32003	55.10577	55.89117
50	49.77796	50.56773	51.35460	52.15386	52.94584	53.73663	54.52677	55.31637	56.10553
51	49.95088	50.74578	51.53763	52.34116	53.13743	53.93236	54.72650	55.51997	56.31287
52	50.11688	50.91692	51.71377	52.52158	53.32217	54.12127	54.91942	55.71677	56.51342
53	50.27620	51.08137	51.88321	52.69532	53.50027	54.30355	55.10575	55.90699	56.70740
54	50.42903	51.23932	52.04615	52.86259	53.67190	54.47940	55.28566	56.09081	56.89499
55	50.57560	51.39097	52.20279	53.02357	53.83725	54.64898	55.45932	56.26840	57.07636
56	50.71611	51.53654	52.35332	53.17843	53.99650	54.81247	55.62691	56.43994	57.25170
57	50.85077	51.67621	52.49792	53.32736	54.14981	54.97004	55.78858	56.60557	57.42115
58	50.97979	51.81018	52.63677	53.47053	54.29736	55.12184	55.94450	56.76546	57.58487
59	51.10338	51.93866	52.77008	53.60813	54.43931	55.26804	56.09482	56.91976	57.74301
60	51.22173	52.06182	52.89802	53.74033	54.57584	55.40880	56.23968	57.06860	57.89571

Table 4.3.3.2. *Inelastic scattering factors (cont.)*

Element	Gd	Tb	Dy	Ho	Er	Tm	Yb	Lu	Hf
Z	64	65	66	67	68	69	70	71	72
s									
0	0.00000	0.00000	0.00000	0.00000	0.00000	0.00000	0.00000	0.00000	0.00000
1	3.71361	3.61003	3.58129	3.55174	3.52320	3.49352	3.46493	3.55150	3.53769
2	7.85846	7.71283	7.67561	7.63634	7.60049	7.56010	7.51513	7.64243	7.65165
3	11.87023	11.75719	11.73154	11.70630	11.68736	11.65817	11.61547	11.69634	11.69972
4	15.51039	15.40658	15.39347	15.38593	15.38890	15.37564	15.33913	15.42634	15.47770
5	18.74647	18.64177	18.65196	18.67051	18.70234	18.71081	18.68517	18.82076	18.94311
6	21.51468	21.43284	21.47837	21.53281	21.60137	21.64017	21.63498	21.83614	22.03782
7	23.91627	23.88725	23.96877	24.05874	24.16249	24.23254	24.25196	24.49728	24.75775
8	26.09535	26.12906	26.24261	26.36312	26.49629	26.59446	26.63899	26.90009	27.18736
9	28.13360	28.22255	28.36456	28.51140	28.66909	28.79252	28.86244	29.12578	29.41882
10	30.06041	30.19256	30.35998	30.52974	30.70818	30.85451	30.94989	31.21431	31.50686
11	31.88606	32.05250	32.24256	32.43217	32.62811	32.79487	32.91479	33.18232	33.47536
12	33.61615	33.81265	34.02361	34.23101	34.44208	34.62698	34.76985	35.04127	35.33636
13	35.25308	35.47907	35.71101	35.93593	36.16142	36.36324	36.52769	36.80277	37.10023
14	36.79567	37.05282	37.30767	37.55182	37.79297	38.01213	38.19791	38.47694	38.77678
15	38.24058	38.53150	38.81250	39.07905	39.33878	39.57731	39.78550	40.07028	40.37345
16	39.58478	39.91198	40.22273	40.51552	40.79768	41.05867	41.29145	41.58529	41.89416
17	40.82754	41.19272	41.53630	41.85898	42.16747	42.45440	42.71447	43.02162	43.33975
18	41.97127	42.37492	42.75330	43.10864	43.44678	43.76280	44.05283	44.37769	44.70926
19	43.02132	43.46263	43.87646	44.26601	44.63605	44.98352	45.30566	45.65219	46.00131
20	43.98512	44.46218	44.91082	45.33481	45.73781	46.11808	46.47366	46.84497	47.21519
21	44.87117	45.38131	45.86307	46.32062	46.75648	47.16983	47.55927	47.95743	48.35143
22	45.68820	46.22827	46.74079	47.23010	47.69780	48.14358	48.56642	48.99245	49.41196
23	46.44445	47.01119	47.55172	48.07047	48.56826	49.04508	49.50015	49.95417	50.39996
24	47.14738	47.73763	48.30329	48.84887	49.37460	49.88057	50.36614	50.84752	51.31957
25	47.80343	48.41429	49.00232	49.57206	50.12337	50.65631	51.17032	51.67789	52.17554
26	48.41809	49.04700	49.65483	50.24620	50.82069	51.37830	51.91852	52.45076	52.97288
27	48.99594	49.64070	50.26607	50.87671	51.47209	52.05210	52.61627	53.17146	53.71663
28	49.54081	50.19957	50.84048	51.46830	52.08245	52.68272	53.26864	53.84498	54.41164
29	50.05590	50.72711	51.38187	52.02503	52.65604	53.27458	53.88020	54.47593	55.06245
30	50.54390	51.22628	51.89346	52.55037	53.19655	53.83157	54.45500	55.06843	55.67321
31	51.00714	51.69962	52.37799	53.04730	53.70715	54.35706	54.99660	55.62616	56.24769
32	51.44764	52.14932	52.83784	53.51836	54.19060	54.85399	55.50813	56.15239	56.78923
33	51.86716	52.57728	53.27506	53.96579	54.64928	55.32491	55.99230	56.64997	57.30083
34	52.26731	52.98520	53.69148	54.39154	55.08529	55.77207	56.45152	57.12145	57.78512
35	52.64951	53.37461	54.08870	54.79733	55.50047	56.19744	56.88790	57.56904	58.24446
36	53.01508	53.74685	54.46818	55.18470	55.89647	56.60278	57.30331	57.99473	58.68094
37	53.36518	54.10319	54.83122	55.55503	56.27474	56.98964	57.69941	58.40029	59.09641
38	53.70092	54.44473	55.17900	55.90957	56.63663	57.35943	58.07770	58.78729	59.49253
39	54.02325	54.77251	55.51260	56.24946	56.98331	57.71342	58.43952	59.15715	59.87082
40	54.33309	55.08747	55.83299	56.57572	57.31587	58.05275	58.78608	59.51116	60.23260
41	54.63124	55.39043	56.14107	56.88928	57.63530	58.37845	59.11849	59.85047	60.57912
42	54.91843	55.68217	56.43763	57.19099	57.94249	58.69148	59.43774	60.17613	60.91146
43	55.19531	55.96338	56.72340	57.48161	58.23823	58.99268	59.74472	60.48910	61.23063
44	55.46248	56.23467	56.99903	57.76182	58.52327	59.28282	60.04027	60.79022	61.53755
45	55.72046	56.49660	57.26511	58.03226	58.79826	59.56261	60.32511	61.08030	61.83303
46	55.96972	56.74968	57.52217	58.29348	59.06380	59.83267	60.59992	61.36002	62.11783
47	56.21069	56.99434	57.77068	58.54598	59.32041	60.09357	60.86531	61.63005	62.39262
48	56.44373	57.23098	58.01106	58.79021	59.56858	60.34582	61.12181	61.89094	62.65802
49	56.66918	57.45995	58.24368	59.02657	59.80874	60.58989	61.36992	62.14323	62.91457
50	56.88734	57.68157	58.46890	59.25542	60.04126	60.82617	61.61007	62.38738	63.16278
51	57.09846	57.89613	58.68699	59.47708	60.26650	61.05505	61.84266	62.62381	63.40309
52	57.30280	58.10387	58.89824	59.69184	60.48475	61.27683	62.06804	62.85289	63.63591
53	57.50057	58.30503	59.10288	59.89994	60.69629	61.49183	62.28653	63.07498	63.86160
54	57.69196	58.49981	59.30113	60.10163	60.90137	61.70030	62.49842	63.29036	64.08049
55	57.87716	58.68840	59.49319	60.29711	61.10021	61.90249	62.70394	63.49931	64.29285
56	58.05634	58.87098	59.67924	60.48657	61.29301	62.09859	62.90334	63.70208	64.49897
57	58.22965	59.04771	59.85944	60.67018	61.47995	62.28882	63.09682	63.89888	64.69906
58	58.39725	59.21873	60.03396	60.84811	61.66120	62.47333	63.28456	64.08991	64.89334
59	58.55928	59.38420	60.20294	61.02050	61.83691	62.65230	63.46674	64.27535	65.08201
60	58.71589	59.54426	60.36651	61.18749	62.00723	62.82588	63.64352	64.45537	65.26522

Table 4.3.3.2. *Inelastic scattering factors (cont.)*

Element *Z* *s*	Ta 73	W 74	Re 75	Os 76	Ir 77	Pt 78	Au 79	Hg 80	Tl 81
0	0.00000	0.00000	0.00000	0.00000	0.00000	0.00000	0.00000	0.00000	0.00000
1	3.51110	3.47440	3.42084	3.39710	3.35665	2.62718	2.92007	3.21624	3.35316
2	7.66380	7.67506	7.62562	7.69565	7.70093	7.28299	7.38597	7.64856	7.98942
3	11.69611	11.69835	11.62131	11.73418	11.75575	11.40374	11.54618	11.74935	12.05736
4	15.50242	15.51176	15.45172	15.58139	15.62856	15.28380	15.43449	15.65381	15.91600
5	19.03205	19.08462	19.08376	19.22645	19.31307	19.11956	19.21786	19.38841	19.60547
6	22.21447	22.35035	22.44359	22.62667	22.77449	22.75224	22.84500	22.97772	23.15315
7	25.01132	25.23775	25.43378	25.68056	25.90537	26.02263	26.17202	26.32856	26.50417
8	27.48515	27.77632	28.05343	28.36068	28.65719	28.88260	29.11511	29.33911	29.56069
9	29.73240	30.05529	30.37962	30.72615	31.07261	31.37642	31.68425	31.98262	32.27085
10	31.82262	32.15546	32.49975	32.86379	33.23607	33.58901	33.94846	34.30452	34.65371
11	33.79048	34.12464	34.47451	34.84275	35.22395	35.60220	35.98954	36.38055	36.77187
12	35.65180	35.98581	36.33640	36.70384	37.08589	37.47454	37.87334	38.28093	38.69506
13	37.41684	37.75117	38.10173	38.46783	38.84850	39.24070	39.64231	40.05533	40.47858
14	39.09480	39.42981	39.78048	40.14591	40.52538	40.91911	41.32016	41.73338	42.15838
15	40.69343	41.02943	41.38044	41.74578	42.12467	42.51974	42.91950	43.33120	43.75506
16	42.21771	42.55571	42.90766	43.27348	43.65234	44.04884	44.44763	44.85771	45.27989
17	43.66969	44.01175	44.36609	44.73342	45.11300	45.51094	45.90946	46.31852	46.73945
18	45.04926	45.39840	45.75753	46.12814	46.50976	46.90936	47.30865	47.71764	48.13811
19	46.35531	46.71511	47.08215	47.45859	47.84426	48.24630	48.64781	49.05803	49.47908
20	47.58687	47.96098	48.33936	48.72466	49.11697	49.52295	49.92857	50.34169	50.76463
21	48.74383	49.13553	49.52858	49.92586	50.32771	50.73978	51.15174	51.56978	51.99627
22	49.82728	50.23921	50.64979	51.06198	51.47623	51.89694	52.31766	52.74286	53.17482
23	50.83952	51.27353	51.70388	52.13342	52.56264	52.99462	53.42649	53.86116	54.30069
24	51.78390	52.24104	52.69265	53.14138	53.58768	54.03338	54.47860	54.92490	55.37411
25	52.66446	53.14507	53.61877	54.08786	54.55277	55.01429	55.47468	55.93453	56.39540
26	53.48571	53.98955	54.48551	54.97556	55.46004	55.93896	56.41593	56.89088	57.36512
27	54.25230	54.77868	55.29660	55.80766	56.31214	56.80952	57.30402	57.79523	58.28421
28	54.96886	55.51676	56.05594	56.58766	57.11212	57.62853	58.14109	58.64929	59.15401
29	55.63980	56.20800	56.76750	57.31920	57.86326	58.39880	58.92956	59.45512	59.97622
30	56.26923	56.85643	57.43512	58.00591	58.56891	59.12335	59.67213	60.21510	60.75286
31	56.86093	57.46579	58.06247	58.65132	59.23243	59.80523	60.37161	60.93174	61.48617
32	57.41832	58.03952	58.65296	59.25877	59.85704	60.44746	61.03082	61.60768	62.17854
33	57.94447	58.58075	59.20973	59.83140	60.44580	61.05295	61.65256	62.24557	62.83242
34	58.44213	59.09230	59.73566	60.37207	61.00158	61.62451	62.23954	62.84799	63.45027
35	58.91374	59.57669	60.23333	60.88343	61.52702	62.16472	62.79433	63.41746	64.03451
36	59.36149	60.03620	60.70509	61.36788	62.02456	62.67603	63.31935	63.95636	64.58745
37	59.78733	60.47288	61.15307	61.82759	62.49642	63.16068	63.81684	64.46693	65.11132
38	60.19301	60.88854	61.57916	62.26453	62.94463	63.62073	64.28890	64.95127	65.60820
39	60.58011	61.28485	61.98508	62.68050	63.37103	64.05808	64.73746	65.41133	66.08005
40	60.95004	61.66329	62.37241	63.07711	63.77731	64.47447	65.16428	65.84891	66.52868
41	61.30409	62.02520	62.74254	63.45584	64.16499	64.87147	65.57101	66.26568	66.95579
42	61.64342	62.37182	63.09676	63.81802	64.53547	65.25055	65.95912	66.66316	67.36294
43	61.96908	62.70424	63.43623	64.16487	64.89001	65.61303	66.33000	67.04278	67.75158
44	62.28204	63.02348	63.76202	64.49750	65.22977	65.96012	66.68491	67.40582	68.12304
45	62.58316	63.33045	64.07507	64.81692	65.55582	66.29295	67.02499	67.75348	68.47856
46	62.87323	63.62598	64.37627	65.12405	65.86912	66.61251	67.35131	68.08686	68.81925
47	63.15296	63.91083	64.66642	65.41973	66.17054	66.91974	67.66483	68.40696	69.14617
48	63.42301	64.18568	64.94624	65.70471	66.46088	67.21549	67.96644	68.71470	69.46027
49	63.68397	64.45116	65.21638	65.97970	66.74089	67.50053	68.25694	69.01093	69.76243
50	63.93635	64.70783	65.47745	66.24532	67.01122	67.77557	68.53709	69.29641	70.05346
51	64.18064	64.95619	65.72997	66.50215	67.27247	68.04124	68.80754	69.57187	70.33409
52	64.41727	65.19670	65.97444	66.75069	67.52519	68.29812	69.06891	69.83793	70.60500
53	64.64663	65.42978	66.21130	66.99142	67.76989	68.54675	69.32177	70.09520	70.86682
54	64.86905	65.65578	66.44094	67.22475	68.00700	68.78759	69.56661	70.34419	71.12009
55	65.08486	65.87506	66.66371	67.45107	68.23692	69.02108	69.80389	70.58540	71.36534
56	65.29432	66.08789	66.87993	67.67072	68.46003	69.24762	70.03403	70.81927	71.60303
57	65.49770	66.29456	67.08989	67.88399	68.67665	69.46754	70.25740	71.04618	71.83358
58	65.69521	66.49531	67.29386	68.09118	68.88708	69.68116	70.47434	71.26651	72.05737
59	65.88707	66.69034	67.49205	68.29252	69.09158	69.88876	70.68515	71.48058	72.27474
60	66.07345	66.87986	67.68468	68.48825	69.29039	70.09061	70.89009	71.68866	72.48602

Table 4.3.3.2. *Inelastic scattering factors (cont.)*

Element	Pb	Bi	Po	At	Rn	Fr	Ra	Ac	Th
Z	82	83	84	85	86	87	88	89	90
s									
0	0.00000	0.00000	0.00000	0.00000	0.00000	0.00000	0.00000	0.00000	0.00000
1	3.34621	3.27806	3.33281	3.32115	3.26930	3.83241	4.44464	4.60565	4.53225
2	8.22217	8.29008	8.55914	8.68626	8.67890	9.01288	9.43761	9.70196	9.73030
3	12.41125	12.73684	13.12943	13.45896	13.67755	13.96293	14.28181	14.56415	14.68382
4	16.22970	16.58625	16.98331	17.39841	17.80231	18.20342	18.59738	18.95415	19.10180
5	19.86837	20.17179	20.51378	20.88858	21.29218	21.72790	22.18172	22.62985	22.83294
6	23.37158	23.62798	23.91920	24.23940	24.58760	24.97453	25.39443	25.83912	26.08504
7	26.70653	26.93777	27.19750	27.48284	27.79204	28.13066	28.49894	28.89569	29.15467
8	29.78902	30.02992	30.28696	30.56176	30.85496	31.16853	31.50434	31.86395	32.12548
9	32.55386	32.83610	33.12152	33.41324	33.71411	34.02674	34.35324	34.69753	34.96690
10	34.99597	35.33272	35.66572	35.99589	36.32636	36.66045	36.99990	37.34880	37.63823
11	37.16069	37.54632	37.92853	38.30468	38.67709	39.04766	39.41742	39.78790	40.11077
12	39.11241	39.53176	39.95218	40.36861	40.78241	41.19310	41.60084	42.00369	42.36942
13	40.90935	41.34687	41.79059	42.23479	42.68028	43.12499	43.56818	44.00554	44.41624
14	42.59319	43.03767	43.49207	43.95125	44.41593	44.88381	45.35352	45.82004	46.27058
15	44.18948	44.63479	45.09182	45.55657	46.02985	46.51011	46.99576	47.48239	47.96308
16	45.71259	46.15634	46.61211	47.07707	47.55215	48.03675	48.52946	49.02718	49.52726
17	47.17058	47.61243	48.06580	48.52881	49.00237	49.48660	49.98052	50.48246	50.99268
18	48.56838	49.00889	49.46012	49.92093	50.39203	50.87389	51.36601	51.86803	52.38179
19	49.90941	50.34947	50.79941	51.25863	51.72758	52.20682	52.69615	53.19634	53.70975
20	51.19617	51.63680	52.08653	52.54511	53.01275	53.49000	53.97677	54.47467	54.98596
21	52.43042	52.87284	53.32354	53.78256	54.24992	54.72616	55.21118	55.70716	56.21594
22	53.61325	54.05891	54.51192	54.97254	55.44075	55.91711	56.40144	56.89625	57.40291
23	54.74527	55.19583	55.65265	56.11619	56.58647	57.06414	57.54895	58.04351	58.54882
24	55.82679	56.28406	56.74634	57.21425	57.68794	58.16821	58.65471	59.15007	59.65498
25	56.85810	57.32388	57.79336	58.26721	58.74575	59.22997	59.71947	60.21675	60.72234
26	57.83958	58.31562	58.79400	59.27537	59.76029	60.24988	60.74374	61.24415	61.75155
27	58.77191	59.25976	59.74862	60.23906	60.73186	61.22825	61.72786	62.23269	62.74312
28	59.65612	60.15705	60.65779	61.15870	61.66081	62.16539	62.67210	63.18267	63.69739
29	60.49357	61.00858	61.52233	62.03492	62.54761	63.06165	63.57676	64.09436	64.61464
30	61.28596	61.81573	62.34333	62.86859	63.39292	63.91754	64.44222	64.96805	65.49516
31	62.03522	62.58016	63.12218	63.66083	64.19764	64.73377	65.26900	65.80418	66.33929
32	62.74351	63.30374	63.86049	64.41300	64.96290	65.51124	66.05784	66.60329	67.14746
33	63.41306	63.98851	64.56004	65.12666	65.69003	66.25108	66.80966	67.36615	67.92027
34	64.04617	64.63658	65.22276	65.80353	66.38054	66.95460	67.52556	68.09365	68.65848
35	64.64514	65.25011	65.85064	66.44543	67.03606	67.62324	68.20682	68.78691	69.36298
36	65.21220	65.83123	66.44569	67.05424	67.65832	68.25858	68.85483	69.44713	70.03482
37	65.74952	66.38202	67.00992	67.63183	68.24908	68.86224	69.47109	70.07566	70.67518
38	66.25915	66.90451	67.54527	68.18009	68.81013	69.43589	70.05715	70.67391	71.28532
39	66.74304	67.40061	68.05362	68.70083	69.34321	69.98121	70.61459	71.24336	71.86659
40	67.20301	67.87214	68.53677	69.19582	69.85004	70.49985	71.14499	71.78549	72.42036
41	67.64078	68.32080	68.99643	69.66673	70.33226	70.99341	71.64990	72.30179	72.94803
42	68.05791	68.74819	69.43420	70.11516	70.79145	71.46344	72.13082	72.79371	73.45099
43	68.45590	69.15581	69.85158	70.54262	71.22912	71.91143	72.58923	73.26267	73.93061
44	68.83610	69.54503	70.24999	70.95052	71.64668	72.33878	73.02652	73.71006	74.38824
45	69.19977	69.91716	70.63072	71.34019	72.04547	72.74685	73.44402	74.13719	74.82516
46	69.54808	70.27337	70.99501	71.71287	72.42674	73.13689	73.84301	74.54533	75.24264
47	69.88210	70.61478	71.34398	72.06972	72.79167	73.51008	74.22466	74.93566	75.64185
48	70.20283	70.94241	71.67868	72.41180	73.14134	73.86754	74.59011	75.30931	76.02393
49	70.51118	71.25721	72.00009	72.74012	73.47678	74.21030	74.94041	75.66736	76.38996
50	70.80798	71.56003	72.30911	73.05561	73.79895	74.53935	75.27655	76.01079	76.74094
51	71.09401	71.85169	72.60656	73.35912	74.10871	74.85557	75.59945	76.34056	77.07783
52	71.36997	72.13291	72.89322	73.65144	74.40690	75.15982	75.90996	76.65754	77.40152
53	71.63652	72.40439	73.16978	73.93331	74.69426	75.45287	76.20890	76.96255	77.71286
54	71.89424	72.66672	73.43689	74.20539	74.97149	75.73544	76.49700	77.25636	78.01262
55	72.14367	72.92050	73.69514	74.46831	75.23925	76.00821	76.77496	77.53968	78.30154
56	72.38531	73.16622	73.94509	74.72264	75.49811	76.27179	77.04342	77.81316	78.58030
57	72.61959	73.40436	74.18721	74.96890	75.74864	76.52674	77.30296	78.07743	78.84953
58	72.84694	73.63536	74.42198	75.20756	75.99132	76.77359	77.55413	78.33304	79.10982
59	73.06770	73.85959	74.64979	75.43905	76.22661	77.01282	77.79743	78.58052	79.36171
60	73.28222	74.07742	74.87103	75.66378	76.45494	77.24487	78.03332	78.82035	79.60571

Table 4.3.3.2. *Inelastic scattering factors (cont.)*

Element Z s	Pa 91	U 92
0	0.00000	0.00000
1	4.48605	4.46901
2	9.64760	9.65990
3	14.50305	14.53454
4	18.88630	18.93052
5	22.67010	22.75975
6	26.01979	26.15376
7	29.17627	29.33734
8	32.20889	32.38794
9	35.09984	35.29714
10	37.82179	38.04410
11	40.35125	40.60907
12	42.67134	42.97470
13	44.77871	45.13292
14	46.68677	47.09059
15	48.42205	48.86853
16	50.01657	50.49569
17	51.50089	52.00222
18	52.89990	53.41447
19	54.23161	54.75278
20	55.50792	56.03139
21	56.73622	57.25961
22	57.92097	58.44323
23	59.06486	59.58582
24	60.16964	60.68962
25	61.23646	61.75612
26	62.26615	62.78632
27	63.25930	63.78093
28	64.21633	64.74047
29	65.13757	65.66531
30	66.02329	66.55575
31	66.87380	67.41207
32	67.68946	68.23461
33	68.47077	69.02374
34	69.21834	69.77999
35	69.93291	70.50398
36	70.61540	71.19646
37	71.26680	71.85830
38	71.88825	72.49049
39	72.48094	73.09410
40	73.04613	73.67027
41	73.58512	74.22018
42	74.09919	74.74506
43	74.58967	75.24613
44	75.05784	75.72462
45	75.50493	76.18173
46	75.93219	76.61863
47	76.34076	77.03649
48	76.73178	77.43640
49	77.10631	77.81941
50	77.46537	78.18654
51	77.80991	78.53875
52	78.14084	78.87696
53	78.45901	79.20201
54	78.76522	79.51472
55	79.06021	79.81586
56	79.34470	80.10614
57	79.61932	80.38622
58	79.88468	80.65672
59	80.14135	80.91823
60	80.38984	81.17129

scattering (Kimura, Schomaker, Smith & Weinstock, 1968; Bartell & Brockway, 1953; Hanson, 1962; Fink & Kessler, 1966; Geiger, 1964; Kessler, 1959; Seip, 1965; Schäfer & Seip, 1967; Kohl & Bonham, 1967; Bonham & Cox, 1967; Seip & Stølevik, 1966; Seip & Seip, 1966; Arnesen & Seip, 1966; McClelland & Fink, 1985; Coffman, Fink & Wellenstein, 1985). New partial wave scattering factors based on relativistic Hartree–Fock fields (Biggs, Mendelsohn & Mann, 1975) are presented here at a number of energies (Table 4.3.3.1). Because of the availability of these partial wave results, first Born approximation results are no longer needed for gas-phase work in this energy range.

The scattering of keV electrons from atoms is calculated in the central-field approximation in which the potential of the target is averaged over the angular coordinates and the resulting spherically symmetric potential $V(r)$ is used in the computation. In order to take the relativistic effects properly into account, the Dirac equation has been used. In addition to the straightforward correction for the electron mass, spin-polarization effects are also included in these calculations. The scattering wavefunctions are four-component spinors that can be reduced to two components as shown by Mott & Massey (1965). This reduction leads to two decoupled second-order differential equations in Schrödinger form:

$$\frac{\mathrm{d}^2 g_l(r)}{\mathrm{d}r^2} + \left[k^2 - \frac{l(l+1)}{r^2} - U_l(r)\right] g_l(r) = 0,$$

where

$$-U_l(r) = -2\gamma V(r) + \alpha^2 V^2(r) + \frac{n}{r}\frac{\beta'}{\beta} - \tfrac{3}{4}\left(\frac{\beta'}{\beta}\right)^2 + \tfrac{1}{2}\frac{\beta''}{\beta},$$

and

$$\alpha = \frac{e^2}{\hbar c},$$

$$\gamma = \left(1 - \frac{v^2}{c^2}\right)^{-1/2}$$

$$\beta = \left[\frac{\gamma+1}{\alpha} - \alpha V(r)\right],$$

$$n = \begin{cases} -l-1 & \text{for } j = l + \tfrac{1}{2} \\ l & \text{for } j = l - \tfrac{1}{2}, \end{cases}$$

where j is the total angular momentum for the lth partial wave including the two spin directions. Asymptotic solutions are available when $U_l(r)$ is small relative to the centrifugal term, $l(l+1)/r^2$. If this term is taken into account, but $U_l(r)$ is neglected, $g_l(r)$ approaches

$$g_l(r) \sim j_l(kr)\cos(\eta_l) + n_l(kr)\sin(\eta_l)$$

with a similar limit holding for the $-l-1$ solution. These limits lead directly to the scattering factors

$$f(\theta) = \frac{1}{2ki}\sum \big((l+1)[\exp(2i\eta_l) - 1] + l\{\exp[2i\eta_{(-l-1)}] - 1\}\big) P_l(\cos\theta)$$

$$g(\theta) = \frac{1}{2ki}\sum \{-\exp(2i\eta_l) + \exp[2i\eta_{(-l-1)}]\} P_l^1(\cos\theta)$$

and the elastic differential scattering cross section

$$\frac{\mathrm{d}\sigma}{\mathrm{d}\Omega} = |f|^2 + |g|^2 + (fg^* - f^*g) \times \left\{\frac{-AB^* \exp(i\varphi) + A^*B \exp(-i\varphi)}{|A|^2 + |B|^2}\right\},$$

where A, B and φ describe the direction and degree of spin polarization of the incoming electrons. The latter term is equal to 0 when unpolarized electrons ($A = B = 1$) are used in the scattering experiment.

The results printed in the tables were obtained in three steps. First, atomic wavefunctions were calculated and transformed into centrosymmetric potentials *via* Poisson's equation. Second, a sufficient number of phases, η_l and $\eta_{(-l-1)}$, were computed in order to calculate the scattering factors f and g by performing the partial wave sums. Finally, the results were smoothed, because small oscillations were seen between nearest neighbours in the second difference function. These oscillations were only of the order of 0.1% of the data, so smoothing only had an effect in the third or fourth significant figure.

For the scattering potentials, we used relativistic Hartree–Fock wavefunctions calculated by Biggs, Mendelsohn & Mann (1975). The wavefunctions were used to calculate the potentials and their derivatives since they are needed for $U_l(r)$ to solve the appropriate Dirac equation.

In order to solve the second-order differential equation, one must take advantage of the known asymptotic solutions. Following the procedure developed by Numerov (Numerov, 1924; Melkanov, Sawada & Raynal, 1966), an auxiliary function, $\xi_l(r)$ is introduced:

$$\xi_l(r_i) = \left[1 - \frac{\Delta r^2}{12} B_l(r_i)\right] g_l(r_i),$$

where

$$B_l(r_i) = -k^2 + \frac{l(l+1)}{r^2} + U_l(r_i)$$

and

$$r_i = i\Delta r, \quad i = 0, 1, 2, \ldots.$$

Now $\xi_l(r)$ is computed. Starting with $\xi_l(r_0) = \xi_l(0) = 0$ and $\xi_l(r_1) = \xi_l(\Delta r) = 0.2(\Delta r)^{l+1}$, the integration of ξ following the Numerov procedure is given by

$$\xi_l(r_{i+1}) = [2 + \Delta r^2 B_l(r_i) + \Delta r^4 B_l^2(r_i)/12]\xi_l(r_i) - \xi_l(r_{i-1}).$$

This recurrence relation is carried through for $a/\Delta r$ steps, where a is the asymptotic limit. At the asymptotic limit $g_l(r)$ is

$$\lim g_l(r) \sim B_l(r) j_l(kr) \cos(\eta_l) - B_l(r) n_l(kr) \sin(\eta_l).$$

The proportionality factor is eliminated by matching the logarithmic derivative of $\xi_l(r)$ [$= \xi'(r)/\xi(r)$] to the same derivative of $g_l(r)$ at $r = a$. From this equality, the partial wave phase shifts are calculated as follows:

$$\frac{1}{\xi_l(a)} \frac{\mathrm{d}\xi_l}{\mathrm{d}r}(a) = \{[B_l'(a) j_l(ka) + kB_l(a) j_l'(ka)] \cos(\eta_1) - [B_l'(a) n_l(ka) + kB_l(a) n_l'(ka)] \sin(\eta_l)\} \times [B_l(a) j_l(ka) \cos(\eta_l) - B_l(a) n_l(ka) \sin(\eta_l)]^{-1}.$$

Solving for η_l leads to

$$\tan(\eta_l) = [B_l'(a) j_l(ka) + kB_l(a) j_l'(ka) - \omega B_l(a) j_l(ka)] \times [B_l'(a) n_l(ka) + kB_l(a) n_l'(ka) - \omega B_l(a) n_l(ka)]^{-1},$$

where

$$\omega = \frac{1}{\xi_l(a)} \frac{\mathrm{d}\xi_l}{\mathrm{d}r}(a),$$

$$B_l(a) = -k^2 + \frac{l(l+1)}{a^2}$$

and

$$B_l'(a) = -\frac{2l(l+1)}{a^3}.$$

It is straightforward to calculate the scattering amplitudes by partial wave summation since stable numerical methods are readily available for the spherical Bessel functions, $j_l(kr)$, the Neumann functions, $n_l(kr)$, and the Legendre polynomials, $P_l(\cos\theta)$ (Yates, 1971).

Particular attention was given to the choices of the integration step size, Δr, and the matching radius, a. Both were varied to ensure the stability of the scattering factors to 0.1% for light atoms and to 0.3% for heavier atoms and higher incident energies. The results of the sensitivity calculations are summarized elsewhere (Ross & Fink, 1986).

Smoothing was carried out by the following procedure: Sixteen data points, quarter s units apart, were least-squares fit to a cubic polynomial and the eighth point was changed to lie on this analytical curve. This procedure was repeated in running point average mode for $s > 10\,\text{Å}^{-1}$. The points for $s < 10\text{Å}^{-1}$ were left unchanged since no oscillations were seen. Smoothed and unsmoothed data in quarter s units for f and g are available on tape at cost from the authors.

4.3.3.2.2. *Total inelastic scattering factors*

Total inelastic scattering in the first Born approximation (Bonham & Fink, 1974) is obtained by including all possible excitation processes:

$$S(s)_{\text{inel}} = \mathbf{S} \frac{k_n}{k} |\langle\psi_n| \sum_{i=1}^{N} \exp(is_{0n} \cdot r_i)|\psi_0\rangle|^2,$$

where r_i is the nuclear electron vector, $k_n = k^2 - \Delta E_{0n}$, $s_{0n} = [k^2 + k_n^2 - 2kk_n \cos(2\theta)]^{1/2}$, ΔE_{0n} is the energy loss of the incident electron upon excitation of the scatterer to the nth state, θ is the Bragg angle, $\mathbf{S}$ signifies a sum over all bound states and an integration over the continuum, and N is equal to the number of electrons in the atom. The sum is carried out over all states ψ_n for which ΔE_{0n} is less than the incident electron energy. The Morse approximation is obtained by making three assumptions: (1) that the incident energy is so high that $N \sim \infty$, *i.e.* that all states are accessible; (2) that the ratio k_n/k is unity for all inelastic processes of any importance; and (3) that s_{0n} may be replaced by its elastic value s. With these approximations, closure may be used to obtain (Morse, 1932; Heisenberg, 1931; Bethe, 1930):

$$S(s) = Z - F_x^2(s) + \sum_i^N \sum_{j \neq i}^N \langle\psi_0| \exp(is \cdot r_{ij})|\psi_0\rangle.$$

The function $S(s)$ is the X-ray incoherent scattering factor (Wang, Sagar, Schmider & Smith, 1993) and is related to the inelastic electron scattering cross section by

$$\sigma_{\text{inel}}(s) = 4S(s)/a^2s^4.$$

Inelastic scattering factors for X-rays and electrons are given in Table 4.3.3.2 in the Morse (1932) approximation for elements $Z = 1$ to $Z = 92$ with HF wave functions (Bunge, Barrientos & Bunge, 1993; McLean & McLean, 1981).

There are two kinds of relativistic correction that can be made on inelastic scattering factors. The first is for relativistic effects on the atomic field and has been neglected. This should not be too serious since HF wavefunctions are used and the corrections are only large for the heavier atoms where the contribution to the total scattering for $s > 3 - 4\,\text{Å}^{-1}$ tends to be negligible. The other correction is for effects in the scattering process, which can be significant above 40 keV, but again these corrections tend to be localized to the small-angle region ($s < 3\,\text{Å}^{-1}$) (Yates, 1970). Hence the tables of inelastic scattering factors given here are based on HF atomic fields since these appear to be the most accurate results presently available.

The inelastic scattering equations must be modified in order to compare theory with experiment. First, the Morse theory is corrected to ensure that both energy and momentum are conserved in the scattering process. In the description of the elastic scattering process, no transformation is required from the centre-of-mass system (CMS), where the scattering factors are calculated, to the laboratory system (LS), where data are taken, since the nuclei are heavy compared with the incident electrons. In the inelastic channels, a similar argument holds for scattering involving the bound states. However, for ionizing processes, the interaction can be assumed to take place between the incident electron and the ejected electron, so that the CMS is entirely different from the LS. Considering the atomic electrons as free particles and considering only the ionization process, the transformation between the CMS and the LS is possible and leads to the Bethe modification (Tavard & Bonham, 1969) for inelastic scattering. The inelastic cross section can now be given by

$$\sigma_{\text{inel}} = \frac{4\cos(2\theta)S(s\cos\theta)}{a^2s^4\cos^4\theta}$$

for $\theta < \pi/4$ and by $\sigma_{\text{inel}} = 0$ for $\theta > \pi/4$.

Another modification is necessary because the average energy of inelastically scattered electrons varies with energy and is given from approximate conservation of energy and momentum for a fast incident particle by $k^2\cos^2(2\theta)$. This means that for $s > 30\text{Å}^{-1}$ at 40 keV the average energy of inelastically scattered electrons may be around 30 keV and the fact that the response of the detector may be different for the 40keV inelastically scattered electrons and the elastic ones may have to be considered (Fink, Bonham, Lee & Ng, 1969).

In addition to the values given in Table 4.3.3.2, a few calculations of $S(s)$ have been carried out with very exact wavefunctions that include more than 85% of the correlation energy (Kohl & Bonham, 1967; Bartell & Gavin, 1964; Peixoto, Bunge & Bonham, 1969; Thakkar & Smith, 1978; Wang, Esquivel, Smith & Bunge, 1995).

4.3.3.2.3. *Corrections for defects in the theory of atomic scattering*

Errors in the inelastic scattering factors from the three approximations made in the Morse theory have been investigated (Tavard & Bonham, 1969; Bonham, 1965*b*). The Morse theory breaks down at very large scattering angles ($\theta > 30^\circ$), and is incorrect at small angles. Investigations carried out so far indicate that the small-angle failure is not serious outside $s = 1\,\text{Å}^{-1}$. It must be stressed that these uncertainties do not introduce important errors into the analysis of molecular structure using theoretical atomic scattering amplitudes. This is mainly because such deviations are smooth compared with molecular features and thus do not interfere with the analysis of molecular structure.

4.3.3.3. *Molecular scattering factors for electrons*

The simplest theory of molecular scattering assumes that a molecule consists of spherical atoms and that each electron is scattered by only one atom in the molecule. If only single scattering is allowed within each atom, the molecular intensity can be written as

$$\begin{aligned} I(s) &= I_a(s) + I_m(s) \\ &= \left[\frac{4I_0}{a^2s^4R^2}\right]\left[\sum_{i=1}^{M}\{[Z_i - F_i(s)]^2 + S_i(s)\}\right. \\ &\quad + \sum_{i}^{M}\sum_{j\neq i}^{M}[Z_i - F_i(s)][Z_j - F_j(s)] \\ &\quad \left.\times \int_0^\infty \mathrm{d}r\, P_{ij}(r,T)(\sin sr)/sr\right], \end{aligned} \tag{4.3.3.1}$$

where M is the number of constituent atoms in the molecule, $F_i(s)$ and $S_i(s)$ are the coherent and incoherent X-ray scattering factors, and $P_{ij}(r,T)$ is the probability of finding atom i at a distance r from atom j at the temperature T (Bonham & Su, 1966; Kelley & Fink, 1982*b*; Mawhorter, Fink & Archer, 1983; Mawhorter & Fink, 1983; Miller & Fink, 1985; Hilderbrandt & Kohl, 1981; Kohl & Hilderbrandt, 1981). The constant I_0 is proportional to the product of the intensities of the electron and molecular beams and R is the distance from the point of scattering to the detector. The single sum is the atomic intensity $I_a(s)$ and the double sum is the molecular intensity $I_m(s)$. This expression, referred to here as the independent atom model (IAM), may be improved by replacing the atomic elastic electron scattering factors by their partial wave counterparts. This modification is necessary to explain the failure of the Born approximation observed in molecules containing light and heavy atoms in proximity (Schomaker & Glauber, 1952; Seip, 1965), and may be written as

$$\begin{aligned} I(s) &= I_a(s) + I_m(s) \\ &= \frac{I_0}{R^2}\left\{\sum_{i=1}^{M}[|f_i|^2 + 4S_i(s)/(a^2s^4)]\right. \\ &\quad + \sum_{i}^{M}\sum_{j\neq i}^{M}|f_i|\,|f_j|\cos(\eta_i - \eta_j) \\ &\quad \left.\times \int_0^\infty \mathrm{d}r\, P_{ij}(r,T)(\sin sr)/sr\right\}. \end{aligned} \tag{4.3.3.2}$$

This is the most commonly used expression for the interpretation of molecular gas electron-diffraction patterns in the keV energy range. If it is necessary to consider relativistic effects in the scattering intensity, equation (4.3.3.2) becomes (Yates & Bonham, 1969)

$$I(s) = I_a(s) + I_m(s)$$
$$= \frac{I_0}{R^2}\left\{\sum_{i=1}^{M}[|f_i|^2 + |g_i|^2 + 4S_i(s)/(a^2s^4)] + \sum_{i}^{M}\sum_{j\neq i}^{M}[|f_i|\,|f_j|\cos(\eta_i^f - \eta_j^f) + |g_i|\,|g_j|\cos(\eta_i^g - \eta_j^g)] \times \int_0^\infty \mathrm{d}r\, P_{ij}(r,T)(\sin sr)/sr\right\}, \quad (4.3.3.3)$$

where $|g_i|$ and η_i^g refer to the scattering-factor magnitude and phase for electrons that have changed their electron spin state during the scattering process and $|f_i|$ and η_i^f refer to retention of spin orientation. The incident electron beam is assumed to be unpolarized and no attempt has been made to consider relativistic effects on the inelastic scattering cross section, which is usually negligible in the structural s range.

If it is necessary to consider binding effects, the first Born approximation may usually be used in describing molecular scattering, since binding effects are largest for molecules containing small atoms where the Born approximation is most valid.

The exact expression for $I(s)$ in the first Born approximation can be written as (Bonham & Fink, 1974; Tavard & Roux, 1965; Tavard, Rouault & Roux, 1965; Iijima, Bonham & Ando, 1963; Bonham, 1967)

$$I(s) = \frac{4I_0}{a^2s^4R^2}\left\{\sum_{i=1}^{M}(Z_i^2 + Z_i) + \sum_{i}^{M}\sum_{j\neq i}^{M} Z_iZ_j\int_0^\infty \mathrm{d}r\, P_{ij}(r,T)(\sin sr)/sr - 2\sum_{i=1}^{M} Z_i\left\langle\int \mathrm{d}r\,\rho(r+r_i)(\sin sr)/sr\right\rangle_{\mathrm{vib}} + \left\langle\int \mathrm{d}r\,\rho_c(r)(\sin sr)/sr\right\rangle_{\mathrm{vib}}\right\},$$

where

$$\rho(r) = \sum_{i=1}^{N}\int \mathrm{d}r_1 \ldots \int \mathrm{d}r_N\,|\psi(r_1,\ldots,r_N)|^2\delta(r - r_i)$$

and

$$\rho_c(r) = \sum_{i}^{N}\sum_{j\neq i}^{N}\int \mathrm{d}r_1 \ldots \int \mathrm{d}r_N\,|\psi(r_1,\ldots,r_N)|^2\delta(r - r_i + r_j).$$

The brackets $\langle\,\rangle_{\mathrm{vib}}$ denote averaging over the vibrational motion, $\delta(r)$ is the Dirac delta function, and $\psi(r_i,\ldots,r_n)$ is the molecular wavefunction. Binding effects appear to be proportional to the ratio of the number of electrons involved in binding to the total number of electrons in the system (Kohl & Bonham, 1967; Bonham & Iijima, 1965) so that binding effects in molecules containing mainly heavy atoms should be quite small.

The intensities, $I(s)$, for many small molecules have been calculated based on molecular Hartree–Fock wavefunctions. In most cases, a distinctive minimum has been found at about $s = 3 - 4\,\text{Å}^{-1}$ and a much small maximum at $s = 8 - 10\,\text{Å}^{-1}$ in the cross-sectional difference curve between the IAM and the molecular HF results (Pulay, Mawhorter, Kohl & Fink, 1983; Kohl & Bartell, 1969; Liu & Smith, 1977; Epstein & Stewart, 1977; Sasaki, Konaka, Iijima & Kimura, 1982; Shibata, Hirota, Kakuta & Muramatsu, 1980; Horota, Kakuta & Shibata, 1981; Xie, Fink & Kohl, 1984). Further studies using correlated wavefunctions (accounting for up to 60% of the correlation energy) showed that in the elastic channel the binding effects are only weakly modified; only the maximum at $s = 8 - 10\,\text{Å}^{-1}$ is further reduced. However, strong effects are seen in the inelastic channel, deepening the minimum at $s = 3 - 4\,\text{Å}^{-1}$ significantly (Breitenstein, Endesfelder, Meyer, Schweig & Zittlau, 1983; Breitenstein, Endesfelder, Meyer & Schweig, 1984; Breitenstein, Mawhorter, Meyer & Schweig, 1984; Wang, Tripathi & Smith, 1994). Detailed calculations on CO_2 and H_2O averaging over many internuclear distances and applying the pair distribution functions $P_{ij}(r)$ showed that vibrational effects do not alter the binding effects (Breitenstein, Mawhorter, Meyer & Schweig, 1986). For CO_2, the calculations have been confirmed in essence by an experimental set of data (McClelland & Fink, 1985). However, more molecules and more detailed analysis will be available in the future. The binding effects make it desirable to avoid the small-angle-scattering range when structural information is the main goal of a diffraction analysis.

The problem of intramolecular multiple scattering may necessitate corrections to the molecular intensity when three or more closely spaced heavy atoms are present. This correction (Karle & Karle, 1950; Hoerni, 1956; Bunyan, 1963; Gjønnes, 1964; Bonham, 1965*a*, 1966) appears to be more serious for three atoms in a right triangular configuration than for a collinear arrangement of three atoms. A case study by Kohl & Arvedson (1980) on SF_6 showed the importance of multiple scattering. However, their approach is too cumbersome to be used in routine structure work. A very good approximate technique is available utilizing the Glauber approximation (Bartell & Miller, 1980; Bartell & Wong, 1972; Wong & Bartell, 1973; Bartell, 1975); Kohl's results are reproduced quite well using the atomic scattering factors only. Several applications of the multiple scattering routines showed that the internuclear distances are rather insensitive to this perturbation, but the mean amplitudes of vibration can easily change by 10% (Miller & Fink, 1981; Kelley & Fink, 1982*a*; Ketkar & Fink, 1985).

Acknowledgements

The authors acknowledge with gratitude the contributions of Kenneth and Lise Hedberg, who made many helpful suggestions regarding the manuscript and carefully checked the numerical results for smoothness and consistency.

4.3.4. Electron energy-loss spectroscopy on solids (By C. Colliex)

4.3.4.1. *Definitions*

4.3.4.1.1. *Use of electron beams*

Among the different spectroscopies available for investigating the electronic excitation spectrum of solids, inelastic electron scattering experiments are very useful because the range of accessible energy and momentum transfer is very large, as illustrated in Fig. 4.3.4.1 taken from Schnatterly (1979). Absorption measurements with photon beams follow the photon dispersion curve, because it is impossible to vary independently the energy and the momentum of a photon. In a scattering experiment, a quasi-parallel beam of monochromatic particles is incident on the specimen and one measures the changes in energy and momentum that can be attributed to the creation of a given excitation in the target. Inelastic neutron scattering is the most

powerful technique for the low-energy range ($\lesssim 0.1$ eV). On the other hand, inelastic X-ray scattering is well suited for the study of high momentum and large energy transfers because the energy resolution is limited to ~ 1 eV and the cross section increases with momentum transfer. In the intermediate range, inelastic electron scattering [or electron energy-loss spectroscopy (EELS)] is the most useful technique. For recent reviews on different aspects of the subject, the reader may consult the texts by Schnatterly (1979), Raether (1980), Colliex (1984), Egerton (1986), and Spence (1988).

4.3.4.1.2. *Parameters involved in the description of a single inelastic scattering event*

The importance of inelastic scattering as a function of energy and momentum transfer is governed by a double differential cross section:

$$\frac{\mathrm{d}^2\sigma}{\mathrm{d}\Omega\,\mathrm{d}(\Delta E)}, \tag{4.3.4.1}$$

where $\mathrm{d}\Omega$ corresponds to the solid angle of acceptance of the detector and $\mathrm{d}(\Delta E)$ to the energy window transmitted by the spectrometer. The experimental conditions must therefore be defined before any interpretation of the data is possible. Integrations of the cross section over the relevant angular and energy-loss domains correspond to partial or total cross sections, depending on the feature measured. For instance, the total inelastic cross section (σ_i) corresponds to the probability of suffering any energy loss while being scattered into all solid angles. The discrimination between elastic and inelastic signal is generally defined by the energy resolution of the spectrometer, that is the minimum energy loss that can be unambiguously distinguished from the zero-loss peak; it is therefore very dependent on the instrumentation used.

The kinematics of a single inelastic event can be described as shown in Fig. 4.3.4.2. In contrast to the elastic case, there is no simple relation between the scattering angle θ and the transfer of momentum $\hbar\mathbf{q}$. One has also to take into account the energy loss ΔE. Combining both equations of conservation of momentum and energy,

$$\frac{\hbar^2 k'^2}{2m_0} + \Delta E = \frac{\hbar^2 k^2}{2m_0}, \tag{4.3.4.2}$$

and

$$q^2 = k^2 + k'^2 - 2kk'\cos\theta, \tag{4.3.4.3}$$

one obtains

$$(qa_0)^2 = \frac{2E_0}{R}\left[1 - \left(1 - \frac{\Delta E}{E_0}\right)^{1/2}\cos\theta\right] - \frac{\Delta E}{R}, \tag{4.3.4.4}$$

where the fundamental units $a_0 = \hbar^2/m_0e^2 =$ Bohr radius and $R = m_0e^4/2\hbar^2 =$ Rydberg energy are used to introduce dimensionless quantities. In this kinematical description, one deals only with factors concerning the primary or the scattered particle, without considering specifically the information on the ejected electron. For a core-electron excitation of an atom, one distinguishes $\mathbf{q}$ (the momentum exchanged by the incident particle) and $\boldsymbol{\chi}$ (the momentum gained by the excited electron), the difference being absorbed by the recoil of the target nucleus (Maslen & Rossouw, 1983).

4.3.4.1.3. *Problems associated with multiple scattering*

The strong coupling potential between the primary electron and the solid target is responsible for the occurrence of multiple inelastic events (and of mixed inelastic–elastic events) for thick specimens. To describe the interaction of a primary particle with an assembly of randomly distributed scattering centres (with a density N per unit volume), a useful concept is the mean free path defined as

$$\Lambda = 1/N\sigma \tag{4.3.4.5}$$

for the cross section σ. The ratio t/Λ measures the probability of occurrence of the event associated with the cross section σ when the incident particle travels a given length t through the material. This is true in the single scattering case, that is when $t/\Lambda \ll 1$.

For increased thicknesses, one must take into account all multiple scattering events and this contribution begins to be non-negligible for $t \gtrsim$ a few tens of nanometres. Multiple scattering is responsible for a broadening of the angular distribution of the

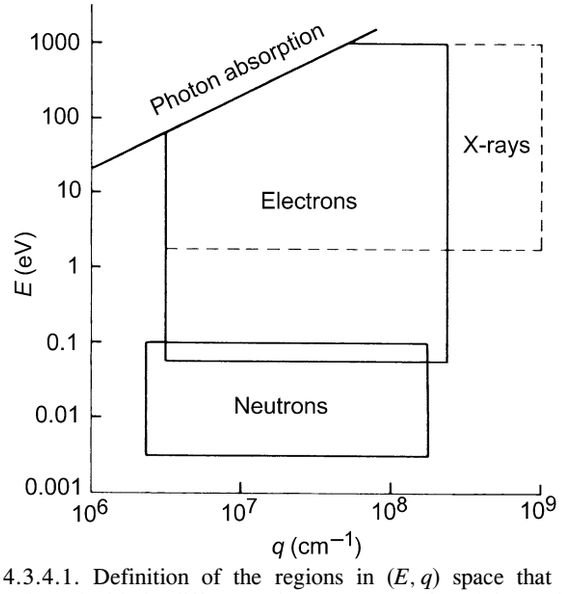

Fig. 4.3.4.1. Definition of the regions in (E, q) space that can be investigated with the different primary sources of particles available at present [courtesy of Schnatterly (1979)].

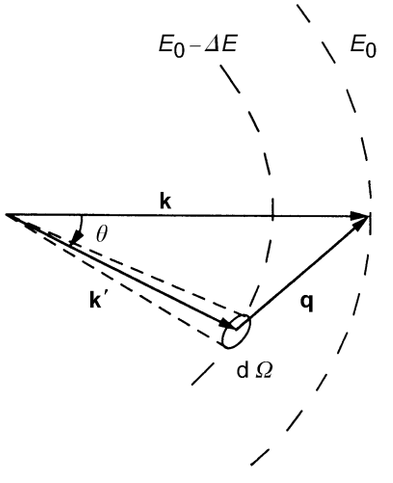

Fig. 4.3.4.2. A primary electron of energy E_0 and wavevector $\mathbf{k}$ is inelastically scattered into a state of energy $E_0 - \Delta E$ and wavevector $\mathbf{k}'$. The energy loss is ΔE and the momentum change is $\hbar\mathbf{q}$. The scattering angle is θ and the scattered electron is collected within an aperture of solid angle $\mathrm{d}\Omega$.

scattering electrons – mostly due to single or multiple elastic events – and of an important fraction of inelastic electrons suffering more than one energy loss. The probability of having n inelastic processes of mean free path Λ is governed by the Poisson distribution:

$$P_n(t) = \frac{1}{n!}\left(\frac{t}{\Lambda}\right)^{-n} \exp\left(-\frac{t}{\Lambda}\right). \qquad (4.3.4.6)$$

Multiple losses introduce additional peaks in the energy-loss spectrum; they are also responsible for an increased background that complicates the detection of single characteristic core-loss signals. Consequently, when the specimen thickness is not very small (*i.e.* for $t \gtrsim 50$ nm for 100 keV primary electrons), it is necessary to retrieve the single scattering profile that is truly representative of the electronic and chemical properties of the specimen.

Deconvolution techniques have therefore been developed to remove the effects of plural scattering from the low-loss spectrum (up to 100 eV) or from ionization edges but very few treatments deal with both angle and energy-loss distributions. Batson & Silcox (1983) have made a detailed study of the inelastic scattering properties of incident 75 keV electrons through a ~100 nm thick polycrystalline aluminium film, over the full range of transferred wavevectors ($0 \rightarrow 3$ Å^{-1}) and energy losses ($0 \rightarrow 100$ eV). Schattschneider (1983) has proposed a matrix approach that is sufficiently elaborate to handle angle-resolved energy-loss data. Simpler deconvolution schemes have been proposed and used for processing multiple losses without specific consideration of angular truncation effects. They are valid when the data have been recorded over sufficiently large angles of collection so that all appreciable inelastic scattering is included. They are generally based on Fourier transform techniques, except for the iterative approach of Daniels, Festenberg, Raether & Zeppenfeld (1970), which has been used for energy losses up to about 60 eV (Colliex, Gasgnier & Trebbia, 1976). The most accurate current methods are the Fourier-log method of Johnson & Spence (1974) and Spence (1979), and the Fourier-ratio method of Swyt & Leapman (1982), which only applies to the core-loss region. The first is far more complete and accurate and applies to any spectral range when one has recorded a full spectrum in unsaturated conditions.

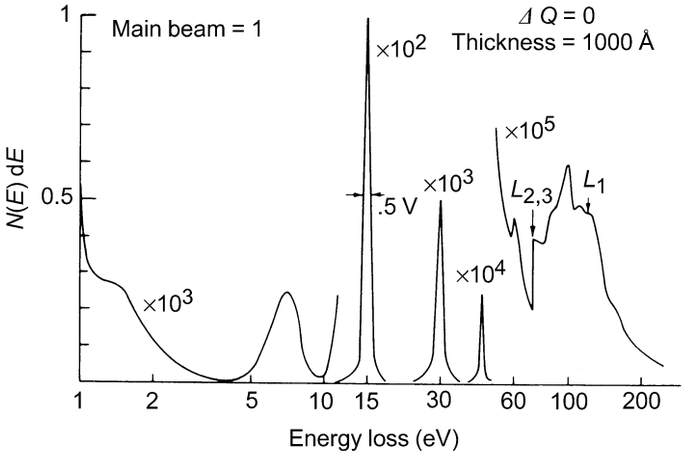

Fig. 4.3.4.3. Excitation spectrum of aluminium from 1 to 250 eV, investigated by EELS on 300 keV primary electrons [courtesy of Schnatterly (1979)].

4.3.4.1.4. *Classification of the different types of excitations contained in an electron energy-loss spectrum*

Figs. 4.3.4.3 and 4.3.4.4 display examples of electron energy-loss spectra over large energy domains, typically from 1 to about 2000 eV. With one instrument, all elementary excitations from the near infrared to the X-ray domain can be investigated. Apart from the main beam or zero-loss peak, two major families of electronic transitions can be distinguished in such spectra:

(*a*) The excitations in the low or moderate energy-loss region ($1 < \Delta E < 50$ eV) concern the quasifree (valence and conduction) electron gas. In a pure metal, such as Al, the dominant feature is the intense narrow peak at 15 eV with its multiple satellites at about 30, 45, and 60 eV. One also detects an interband transition at 1.5 eV and a surface plasmon peak at ~ 7 eV. For the more complex mineral specimen, rhodizite, this contribution lies in the intense and broad, but not very specific, peak around 25 eV. All these features are discussed in detail in Subsection 4.3.4.3.

(*b*) The excitations in the high-energy-loss domain ($50 < \Delta E < 2000$ eV) concern excitation and ionization processes from core atomic orbitals: in Al, the $L_{2,3}$ edge is associated with the creation of holes on the $2p$ level, L_1 is due to the excitation of $2s$, and K of $1s$ electrons. These contributions appear as edges superposed on a regularly decreasing background. In the complex specimen, the succession of these

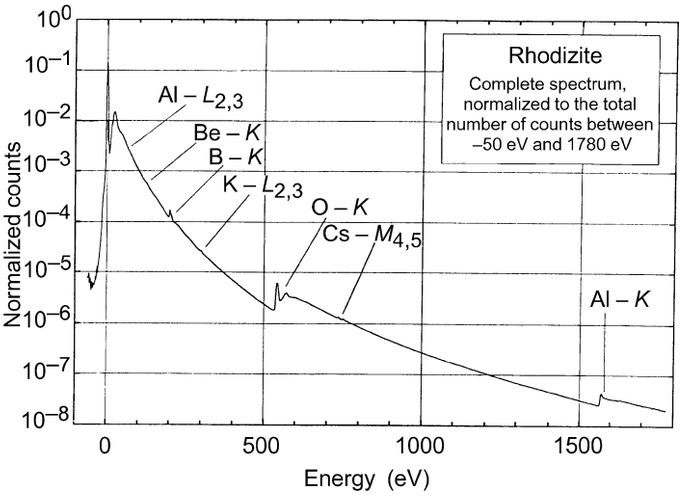

Fig. 4.3.4.4. Complete electron energy-loss spectrum of a thin rhodizite crystal (thickness ~60 nm). Separate spectra from eight significantly overlapping energy ranges were measured and matched. Primary energy 60 keV. Semi-angle of collection 5 mrad. Recording time 300 s (parallel acquisition). Scanned area 30×40 nm. Analysed mass 2×10^{-15} g [courtesy of Engel, Sauer, Zeitler, Brydson, Williams & Thomas (1988)].

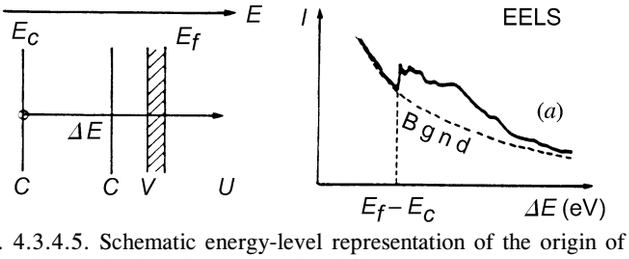

Fig. 4.3.4.5. Schematic energy-level representation of the origin of a core-loss excitation (from a core level C at energy E_c to an unoccupied state U above the Fermi level E_f) and its general shape in EELS, as superimposed on a continuously decreasing background.

different edges on top of the monotonously decaying background is a signature of the elemental composition, the intensity of the signals being roughly proportional to the relative concentration in the associated element. Core-level EELS spectroscopy therefore investigates transitions from one well defined atomic orbital to a vacant state above the Fermi level: it is a probe of the energy distribution of vacant states in a solid, see Fig. 4.3.4.5. As the excited electron is promoted on a given atomic site, the information involved has two specific characters: it provides the local atomic point of view and it reflects the existence of the hole created, which can be more or less screened by the surrounding population of electrons in the solid. The properties of this family of excitations are the subject of Subsection 4.3.4.4.

The non-characteristic background is due to the superposition of several contributions: the high-energy tail of valence-electron scattering, the tails of core losses with lower binding energy, *Bremsstrahlung* energy losses, plural scattering, *etc*. It is therefore rather difficult to model its behaviour, although some efforts have been made along this direction using Monte Carlo simulation of multiple scattering (Jouffrey, Sevely, Zanchi & Kihn, 1985).

When one monochromatizes the natural energy width of the primary beam to much smaller values (about a few meV) than its natural width, one has access to the infrared part of the electromagnetic spectrum. An example is provided in Fig. 4.3.4.6 for a specimen of germanium in the energy-loss range 0 up to 500 meV. In this case, one can investigate phonon modes, or the bonding states of impurities on surfaces. This field has been much less extensively studied than the higher-energy-loss range [for references see Ibach & Mills (1982)].

Generally, EELS techniques can be applied to a large variety of specimens. However, for the following review to remain of limited size, it is restricted to electron energy-loss spectroscopy on solids and surfaces in transmission and reflection. It omits some important aspects such as electron energy-loss spectroscopy in gases with its associated information on atomic and molecular states. In this domain, a bibliography of inner-shell excitation studies of atoms and molecules by electrons, photons or theory is available from Hitchcock (1982).

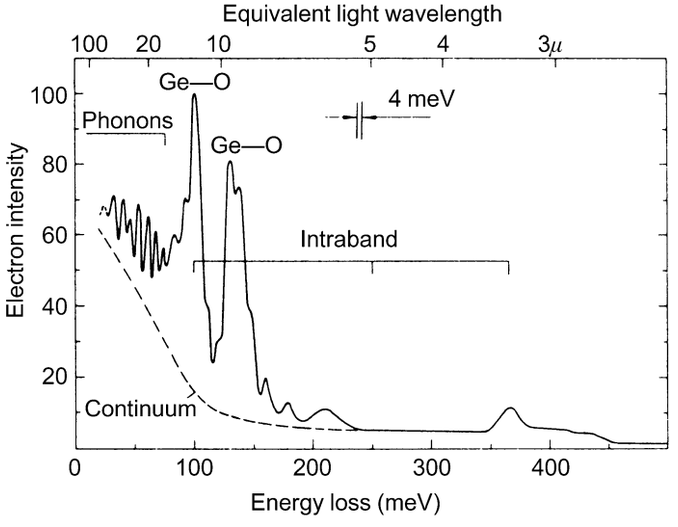

Fig. 4.3.4.6. Energy-loss spectrum, in the meV region, of an evaporated germanium film (thickness $\simeq 25$ nm). Primary electron energy 25 keV. Scattering angle $< 10^{-4}$. One detects the contributions of the phonon excitation, of the Ge—O bonding, and of intraband transitions [courtesy of Schröder & Geiger (1972)].

Table 4.3.4.1. *Different possibilities for using EELS information as a function of the different accessible parameters* ($\mathbf{r}$, θ, ΔE)

	Integration parameter	Selection parameter	Results	Working mode of the spectrometer
1	$\boldsymbol{\theta}$	$\mathbf{r}$	Spectrum $I_{\mathbf{r}}$ (ΔE)	Analyser
2	$\mathbf{r}$	$\boldsymbol{\theta}$	Spectrum $I_{\boldsymbol{\theta}}$ (ΔE)	Analyser
3	$\boldsymbol{\theta}$	ΔE	Energy-filtered image $I_{\Delta E}(\mathbf{r})$	Filter
4	$\mathbf{r}$	ΔE	Energy-filtered diffraction pattern $I_{\Delta E}(\boldsymbol{\theta})$	Filter

4.3.4.2. *Instrumentation*

4.3.4.2.1. *General instrumental considerations*

In a dedicated instrument for electron inelastic scattering studies, one aims at the best momentum and energy resolution with a well collimated and monochromatized primary beam. This is achieved at the cost of poor spatial localization of the incident electrons and one assumes the specimens to be homogeneous over the whole irradiated volume. In a sophisticated instrument such as that built by Fink & Kisker (1980), the energy resolution can be varied from 0.08 to 0.7 eV, and the momentum transfer resolution between 0.03 and 0.2 Å^{-1}, but typical values for the electron-beam diameter are about 0.2 to 1 mm. Nowadays, many energy-analysing devices are coupled with an electron microscope: consequently, an inelastic scattering study involves recording for a primary intensity I_0, the current $I(\mathbf{r}, \boldsymbol{\theta}, \Delta E)$ scattered or transmitted at the position $\mathbf{r}$ on the specimen, in the direction $\boldsymbol{\theta}$ with respect to the primary beam, and with an energy loss ΔE. Spatial resolution is achieved either with a focused probe or by a selected area method, angular acceptance is defined by an aperture, and energy width is controlled by a detector function after the spectrometer. It is not possible from signal-to-noise considerations to reduce simultaneously all instrumental widths to very small values. One of the parameters ($\mathbf{r}$, $\boldsymbol{\theta}$ or ΔE) is chosen for signal integration, another for selection, and the last is the variable. Table 4.3.4.1. classifies these different possibilities for inelastic scattering studies.

Because of the great variety of possible EELS experiments, it is impossible to build an optimum spectrometer for all applications. For instance, the design of a spectrometer for low-energy incident electrons and surface studies is different from that for high-energy incident electrons and transmission work. In the latter category, instruments built for dedicated EELS studies (Killat, 1974; Gibbons, Ritsko & Schnatterly, 1975; Fink & Kisker, 1980; *etc*.) are different from those inserted within an electron-microscope environment, in which case it is possible to investigate the excitation spectrum from a specimen area well characterized in image and diffraction [see the reviews by Colliex (1984) and Egerton (1986)].

The literature on dispersive electron–optical systems (equivalent to optical prisms) is very large. For example, the theory of uniform field magnets, which constitute an important family of analysing devices, has been extensively developed for the components in high-energy particle accelerators (Enge, 1967; Livingood, 1969). As for EELS spectrometers, they can be classified as:

(*a*) *Monochromators*, which filter the incident beam to obtain the smallest primary energy width. The natural width for a heated W filament is about 1 eV, possibly rising to about a few eV as a consequence of stochastic interactions [Boersch (1954) effect, analysed for instance by Rose & Spehr (1980)]. For a low-temperature field-emission source, this energy spread is only ~0.3 eV. This constitutes a clear gain but remains insufficient for meV studies. In this case, one has to introduce a filter lens such as the three-electrode design developed by Hartl (1966) or a cylindrical electrostatic deflector before the accelerator [Kuyatt & Simpson (1967) or Gibbons *et al.* (1975)]. In both cases, an energy resolution of 50 meV has been achieved for electron beams of 50–300 keV at the specimen.

(*b*) *Analysers*, which measure the energy distribution of the beam scattered from the specimen. They can be used either strictly as analysers displaying the energy loss from a given specimen volume, or as filters (or selecting devices) that provide 2D images or diffraction patterns with a given energy loss.

4.3.4.2.2. *Spectrometers*

Fig. 4.3.4.7 defines the basic parameters of a 'general' energy-loss spectrometer: a region of electrostatic **E** and/or magnetic **B** fields transforms a distribution of electrons I_0 $(x_0, y_0, t_0, u_0, \rho)$ in the object plane of coordinate z_0 along the principal trajectory, into a distribution of electrons I_1 $(x_1, y_1, t_1, u_1, \rho)$ in the object plane of coordinate z_1, coincident with the detector plane (or optically conjugate to it). The transverse coordinates are labelled as (x, y), the angular ones as (t, u), and $\rho = \Delta p/p = \Delta E/2E$ is the relative change in absolute momentum value associated with the energy loss.

Common properties of such systems are:

(*a*) first-order imaging properties or stigmatism, *i.e.* all electrons leaving (x_0, y_0) are focused at the same (x_1, y_1) point, independently of their inclination on the optical axis;

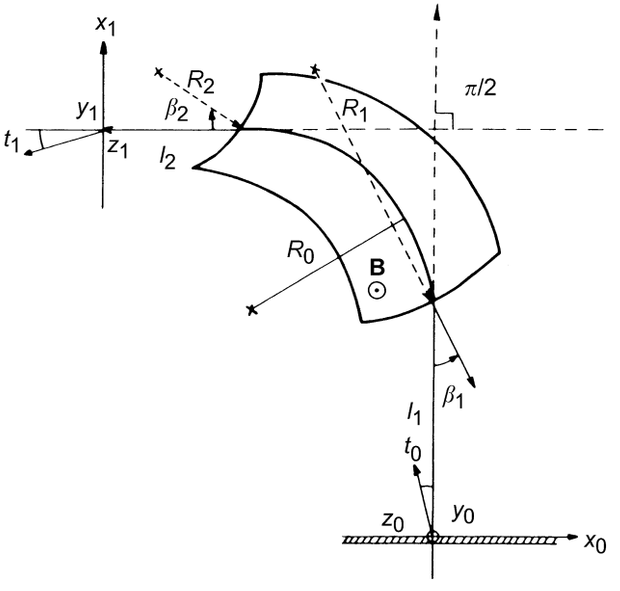

Fig. 4.3.4.7. Schematic drawing of a uniform magnetic sector spectrometer with induction **B** normal to the plane of the figure. Definition of the coordinates used in the text (the object plane at coordinate z_0 along the mean trajectory coincides with the specimen, and the image plane at z_1 coincides with the dispersion plane and the detector level).

(*b*) strong chromatic aberration in order to realize an efficient discrimination between electrons of different ρ.

The spectrometer performance can be evaluated with the following parameters:

$D = dispersion =$ beam displacement in the spectrometer image plane for a given momentum change ρ; it is generally expressed in cm/eV. The higher the dispersion, the easier it is to resolve small energy losses. For a straight-edge 90° magnetic sector, $D \propto 2R/E_0$, where R is the curvature radius of the mean trajectory and E_0 is the primary energy.

$\delta E_{\min} = energy\ resolution$. This corresponds to the minimum-energy variation that can be resolved by the instrument. It takes into account the width of the image $\Delta x_{\text{image}} = Mr$, where M is the spectrometer magnification and r the radius of the spectrometer source, as well as the second- and higher-order angular aberrations. These are responsible for the imperfect focusing of the electrons that enter the spectrometer within a cone of angular acceptance β_0 and contribute through a term $\Delta x_{\text{aber}} = C\beta_0^2$. Moreover, one must convolute these terms with the natural width δE_0 of the primary beam, including AC fields, and with the detection slit width Δx_{slit}. Combining all these effects, as shown schematically in Fig. 4.3.4.8, one obtains approximately:

$$\Delta x_{\text{tot}} = [(\Delta x_{\text{slit}})^2 + (\Delta x_{\text{image}})^2 + (\Delta x_{\text{aber}})^2 + D\delta E_0^2]^{1/2} \quad (4.3.4.7)$$

and the corresponding energy resolution is defined as $\delta E_{\min} = (\Delta x_{\text{tot}})_{\min}/D$. In many situations, the dominant factor is the second-order aberration term $C\beta_0^2$ so that the figure of merit F, defined as $F = \pi\beta_0 E_0/\delta E_{\min}$, is of the order of unity for an uncorrected magnetic spectrometer.

From this simplified discussion, one deduces that there is generally competition between large angular acceptance for the inelastic signal, which is very important for obtaining a high signal-to-noise ratio (SNR) for core-level excitations, and good energy resolution. Two solutions have been used to remedy this limitation. The first is to improve spectrometer design, for example by correcting second-order aberrations in a homogeneous magnetic prism (Crewe, 1977*a*; Parker, Utlaut & Isaacson, 1978; Egerton, 1980*b*; Krivanek & Swann, 1981; *etc*). This can enhance the figure of merit by at least a factor of 100. The second possibility is to transform the distribution of electrons to be analysed at the exit surface of the specimen into a more convenient distribution at the spectrometer entrance. This can be done by introducing versatile transfer optics (see Crewe, 1977*b*; Egerton, 1980*a*; Johnson, 1980; Craven & Buggy, 1981; *etc*.). As a final remark on the energy resolution of a spectrometer, it is meaningless to define it without reference to the size and the angular aperture of the analysed beam.

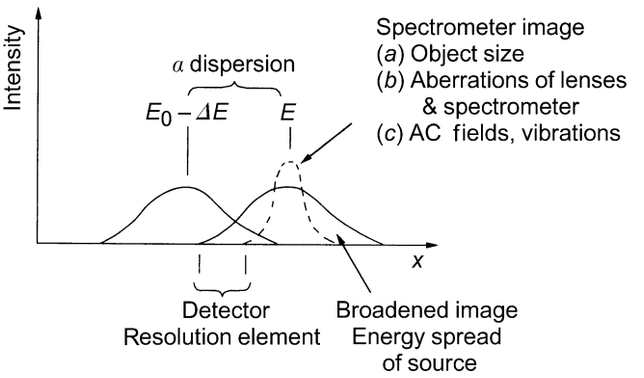

Fig. 4.3.4.8. Different factors contributing to the energy resolution in the dispersion plane [courtesy of Johnson (1979)].

Historically, many types of spectrometer have been used since the first suggestion by Wien (1897) that an energy analyser could be designed by employing crossed electric and magnetic fields. Reviews have been published by Klemperer (1965), Metherell (1971), Pearce-Percy (1978), and Egerton (1986). Nowadays, two configurations are mostly used and have become commercially available on modern electron microscopes: these are spectrometers on TEM/STEM instruments and filters on CTEM ones. In the first case, *homogeneous magnetic sectors* are the simplest and most widely used devices. Recent instrumental developments by Shuman (1980), Krivanek & Swann (1981), and Scheinfein & Isaacson (1984) have given birth to a generation of spectrometers with the following major characteristics: double focusing, correction for second-order aberrations, dispersion plane perpendicular to the trajectory. This has been made possible by a suitable choice of several parameters, such as the tilt angles and the radius of curvature for the entrance and exit faces and the correct choice of the object source position. As an example, for a 100 keV STEM equipped with a field emission gun, the coupling illustrated in Fig. 4.3.4.9 leads to an energy resolution of 0.35 eV for $\beta_0 = 7.5$ mrad on the specimen as visible on the elastic peak, and 0.6 eV for $\alpha_0 = 25$ mrad as checked on the fine structures on core losses. Krivanek, Manoubi & Colliex (1985) demonstrated a sub-eV energy resolution over the whole range of energy losses up to 1 or 2 keV.

A very competitive solution is the *Wien filter*, which consists of uniform electric and magnetic fields crossed perpendicularly, see Fig. 4.3.4.10. An electron travelling along the axis with a velocity $\mathbf{v}_0$ such that $|\mathbf{v}_0| = E/B$ is not deflected, the net force on it being null. All electrons with different velocities, or at some angle with respect to the optical axis, are deflected. The dispersion of the system is greatly enhanced by decelerating the electrons to about 100 eV within the filter, in which case $D \simeq$ a few 100 μm/eV. A presently achievable energy resolution of 150 meV at a spectrometer collection half-angle of 12.5 mrad has been demonstrated by Batson (1986, 1989). It allows the study of the detailed shape of the energy distribution of the electrons emitted from a field emission source and the taking of it into account in the investigation of band-gap states in semiconductors (Batson, 1987).

Filtering devices have been designed to form an energy-filtered image or diffraction pattern in a CTEM. The first

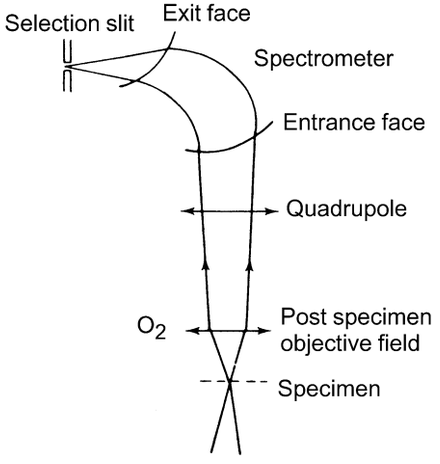

Fig. 4.3.4.9. Optical coupling of a magnetic sector spectrometer on a STEM column.

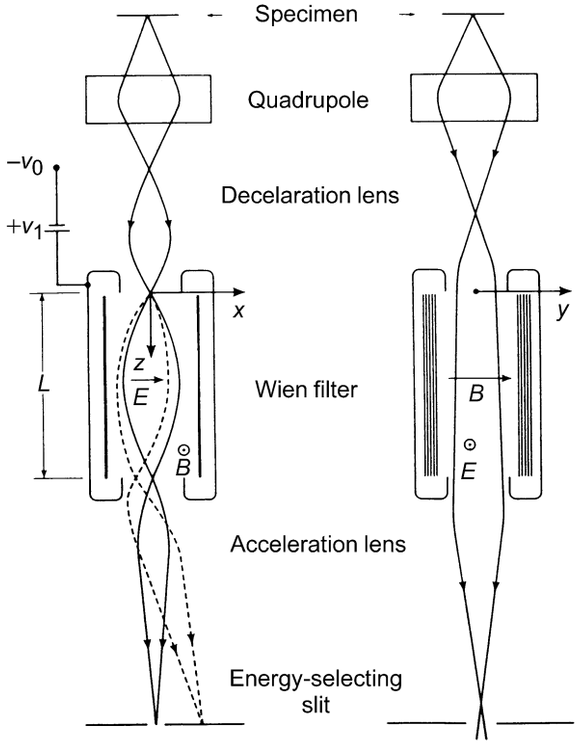

Fig. 4.3.4.10. Principle of the Wien filter used as an EELS spectrometer: the trajectories are shown in the two principal (dispersive and focusing) sections.

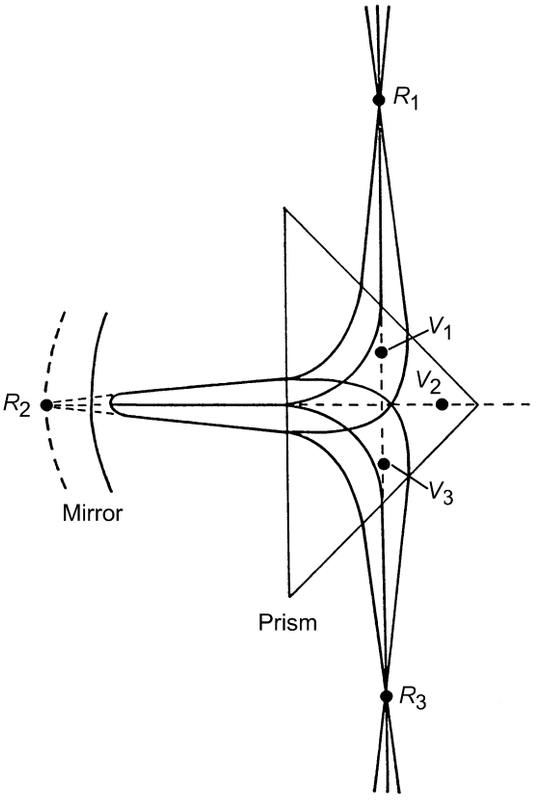

Fig. 4.3.4.11. Principle of the Castaing & Henry filter made from a magnetic prism and an electrostatic mirror. (R_1, R_2, and R_3 are the real conjugate stigmatic points, and V_1, V_2, and V_3 the virtual ones: the dispersion plane coincides with the R_3 level and achromatic one with the V_3 level.)

Table 4.3.4.2. *Plasmon energies measured (and calculated) for a few simple metals; most data have been extracted from Raether (1980)*

Monovalent			Divalent			Trivalent			Tetravalent		
$\hbar\omega_p$ (eV)			$\hbar\omega_p$ (eV)			$\hbar\omega_p$ (eV)			$\hbar\omega_p$ (eV)		
	Meas.	Calc.		Meas.	Calc.		Meas.	Calc.		Meas.	Calc.
Li	7.1	(8.0)	Be	18.7	(18.4)	B	22.7	(?)	C	34.0	(31)
Na	5.7	(5.9)	Mg	10.4	(10.9)	Al	14.95	(15.8)	Si	16.5	(16.6)
K	3.7	(4.3)	Ca	8.8	(8.0)	Ga	13.8	(14.5)	Ge	16.0	(15.6)
Rb	3.4	(3.9)	Sr	8.0	(7.0)	In	11.4	(12.5)	Sn	13.7	(14.3)
Cs	2.9	(3.4)	Ba	7.2	(6.7)	Sc	14.0	(12.9)	Pb	(13)	(13.5)

solution, reproduced in Fig. 4.3.4.11, is due to Castaing & Henry (1962). It consists of a double magnetic prism and a concave electrostatic mirror biased at the potential of the microscope cathode. The system possesses two pairs of stigmatic points that may coincide with a diffraction plane and an image plane of the electron-microscope column. One of these sets of points is achromatic and can be used for image filtering. The other is strongly chromatic and is used for spectrum analysis. Zanchi, Sevely & Jouffrey (1977) and Rose & Plies (1974) have proposed replacing this system, which requires an extra source of high voltage for the mirror, by a purely magnetic equivalent device. Several solutions, known as the α and ω filters, with three or four magnets, have thus been built, both on very high voltage microscopes (Zanchi, Perez & Sevely, 1975) and on more conventional ones (Krahl & Herrmann, 1980), the latest version now being available from one EM manufacturer (Zeiss EM S12).

4.3.4.2.3. *Detection systems*

The final important component in EELS is the detector that measures the electron flux in the dispersion plane of the spectrometer and transfers it through a suitable interface to the data storage device for further computer processing. Until about 1990, all systems were operated in a sequential acquisition mode. The dispersed beam was scanned in front of a narrow slit located in the spectrometer dispersion plane. Electrons were then generally recorded by a combination of scintillator and photomultiplier capable of single electron counting.

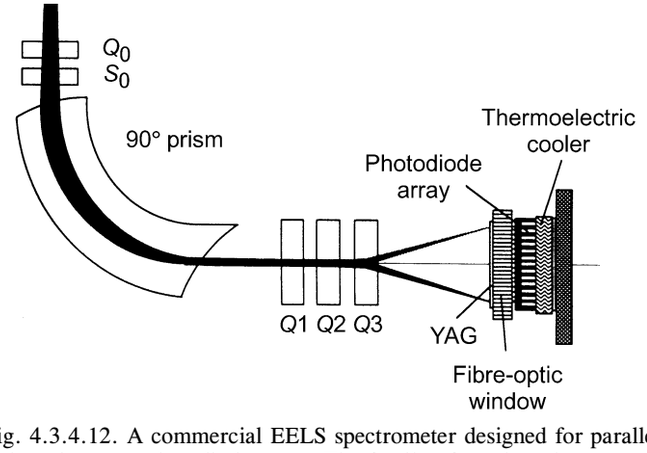

Fig. 4.3.4.12. A commercial EELS spectrometer designed for parallel detection on a photodiode array. The family of quadrupoles controls the dispersion on the detector level [courtesy of Krivanek *et al.* (1987))].

This process is, however, highly inefficient: while the counts are measured in one channel, all information concerning the other channels is lost. These requirements for improved detection efficiency have led to the consideration of possible solutions for parallel detection of the EELS spectrum. They use a multiarray of detectors, the position, the size and the number of which have to be adapted to the spectral distribution delivered by the spectrometer. In most cases with magnetic type devices, auxiliary electron optics has to be introduced between the spectrometer and the detector so that the dispersion matches the size of the individual detection cells. Different systems have been proposed and tested for recording media, the most widely used solutions at present being the photodiode and the charge-coupled diode arrays described by Shuman & Kruit (1985), Krivanek, Ahn & Keeney (1987), Strauss, Naday, Sherman & Zaluzec (1987), Egerton & Crozier (1987), Berger & McMullan (1989), *etc.* Fig. 4.3.4.12 shows a device, now commercially available from Gatan, that is made of a convenient combination of these different components. This progress in detection has led to significant improvements in many areas of EELS: enhanced detection limits, reduced beam damage in sensitive materials, data of improved quality in terms of both SNR and resolution, and access to time-resolved spectroscopy at the ms time scale (chronospectra). Several of these important consequences are illustrated in the following sections.

4.3.4.3. *Excitation spectrum of valence electrons*

Most inelastic interaction of fast incident electrons is with outer atomic shells in atoms, or in solids with valence electrons (referred to as conduction electrons in metals). These involve excitations in the 0–50 eV range, but, in a few cases, interband transitions from low-binding-energy shells may also contribute.

4.3.4.3.1. *Volume plasmons*

The basic concept introduced by the many-body theory in the interacting free electron gas is the volume plasmon. In a condensed material, the assembly of loosely bound electrons behaves as a plasma in which collective oscillations can be induced by a fast external charged particle. These eigenmodes, known as *volume plasmons*, are longitudinal charge-density fluctuations around the average bulk density in the plasma $n \simeq 10^{28}$ e^-/m^3). Their eigen frequency is given, in the free electron gas, as

$$\omega_p = \left(\frac{n e^2}{m\varepsilon_0}\right)^{1/2}. \qquad (4.3.4.8)$$

The corresponding $\hbar\omega_p$ energy, measured in an energy-loss spectrum (see the famous example of the plasmon in aluminium

Table 4.3.4.3. *Experimental and theoretical values for the coefficient α in the plasmon dispersion curve together with estimates of the cut-off wavevector (from Raether, 1980)*

	Measured α	Calculated α	q_c (Å^{-1})
Li	0.24	0.35	0.9
Na	0.24	0.32	0.8
K	0.14	0.29	0.8
Mg	0.35	0.39	1.0
Al	0.2 (<0.5 Å^{-1})		
	0.45 (>0.5 Å^{-1})	0.43	1.3
In	0.40 (<0.5 Å^{-1})		
	0.66 (>0.5 Å^{-1})		
Si	0.41		
	0.3	0.45	1.1

Table 4.3.4.4. *Comparison of measured and calculated values for the halfwidth $\Delta E_{1/2}(0)$ of the plasmon line (from Raether, 1980)*

	Experimental (eV)	Theory (eV)
Li	2.2	2.55
Na	0.3	0.12
K	0.25	0.15
Rb	0.6	0.64
Cs	1.2	0.96
Al	0.53	0.43
Mg	0.7	0.7
Si	3.2	5.4
Ge	3.1	3.9

in Fig. 4.3.4.3), is the *plasmon energy*, for which typical values in a selection of pure solid elements are gathered in Table 4.3.4.2. The accuracies of the measured values depend on several instrumental parameters. Moreover, they are sensitive to the specimen crystalline state and to its degree of purity. Consequently, there exist slight discrepancies between published values. Numbers listed in Table 4.3.4.2 must therefore be accepted with a 0.1 eV confidence. Some specific cases require comments: amorphous boron, when prepared by vacuum evaporation, is not a well defined specimen. Carbon exists in several allotropic varieties. The selection of the diamond type in the table is made for direct comparison with the other tetravalent specimens (Si, Ge, Sn). The results for lead (Pb) are still subject to confirmation. The volumic mass density is an important factor (through n) in governing the value of the plasmon energy. It varies with temperature and may be different in the crystal, in the amorphous, and in the liquid phases. In simple metals, the amorphous state is generally less dense than the crystalline one, so that its plasmon energy shifts to lower energies.

The above description applies only to very small scattering vectors $\mathbf{q}$. In fact, the plasmon energy increases with scattering angle (and with momentum transfer $\hbar\mathbf{q}$). This dependence is known as the dispersion relation, in which two distinct behaviours can be described:

(a) For small momentum transfers ($q \lesssim q_c$), the dispersion curve is parabolic:

$$\hbar\omega_p(q) = \hbar\omega_p(0) + \frac{\alpha\hbar^2}{m_0} q^2. \qquad (4.3.4.9)$$

The coefficient α has been measured in a number of substances and calculated for the free-electron case in the random phase approximation (Lindhard, 1954); see Table 4.3.4.3 for some data. A simple expression for α is

$$\alpha = \tfrac{3}{5}\frac{E_F}{\hbar\omega_p(0)}, \qquad (4.3.4.10)$$

where E_F is the Fermi energy of the electron gas. More detailed observations indicated that it is not possible to describe the dispersion curve over a large momentum range with a single q^2 law. In fact, one has to fit the experiment data with different linear or quadratic slopes as a function of q [see values indicated for Al and In in Table 4.3.4.3, and Hohberger, Otto & Petri (1975)]. Moreover, anisotropy has been found along different $\mathbf{q}$ directions in monocrystals (Manzke, 1980). In parallel, refinements have been brought into the calculations by including band-structure effects to deal with the anisotropy of the dispersion relation and with the bending of the experimental curves. Electron–electron correlations have also been considered, which has slightly improved the agreement between calculated and measured values of α (Bross, 1978*a*, *b*).

(b) For large momentum transfers, there exists a critical wavevector q_c, which corresponds to a strong decay of the plasmon mode into single electron–hole pair excitations. This can be calculated using conservation rules in energy and momentum, giving

$$\hbar\omega_p(0) + \alpha\frac{\hbar^2}{m_0} q_c^2 = \frac{\hbar^2}{2m_0}(q_c^2 + 2q_c q_F), \qquad (4.3.4.11)$$

where q_F is the Fermi wavevector. A simple approximation is $q_c \simeq \omega_p/v_F$, v_F being the Fermi velocity. Single pair excitations can be created by fast incoming electrons in the domain of scattering conditions contained between the two curves:

$$\left.\begin{aligned} \Delta E_{\max} &= \frac{\hbar^2}{2m_0}(q^2 + 2qq_F) \\ \Delta E_{\min} &= \frac{\hbar^2}{2m_0}(q^2 - 2qq_F) \end{aligned}\right\} \qquad (4.3.4.12)$$

shown in Fig. 4.3.4.13. They bracket the curve $\Delta E = \hbar^2 q^2/2m_0$ corresponding to the transfer of energy and momentum to an isolated free electron. For momentum transfers such as $q > q_c$, the plasmon mode is heavily damped and it is difficult to distinguish its own specific behaviour from the electron–hole continuum. A few studies, *e.g.* Batson & Silcox (1983), indicate that the plasmon dispersion curve flattens as it enters the

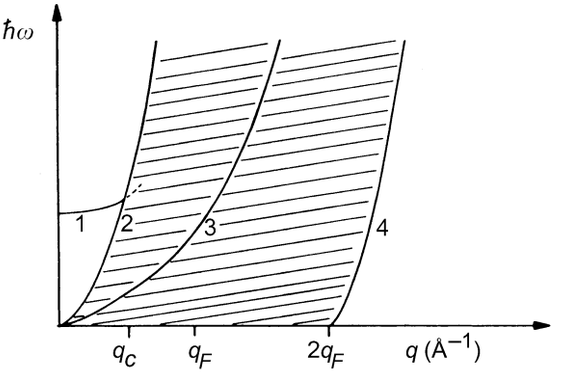

Fig. 4.3.4.13. The dispersion curve for the excitation of a plasmon (curve 1) merges into the continuum of individual electron–hole excitations (between curves 2 and 4) for a critical wavevector q_c. The intermediate curve (3) corresponds to Compton scattering on a free electron.

quasiparticle domain and approaches the centre of the continuum close to the free-electron curve. However, not only is the scatter between measurements fairly high, but a satisfactory theory is not yet available [see Schattschneider (1989) for a compilation of data on the subject].

Plasmon lifetime is inversely proportional to the energy width of the plasmon peak $\Delta E_{1/2}$. Even for Al, with one of the smallest plasmon energy widths ($\simeq 0.5$ eV), the lifetime is very short: after about five oscillations, their amplitude is reduced to $1/e$. Such a damping demonstrates the strength of the coupling of the collective modes with other processes. Several mechanisms compete for plasmon decay:

(*a*) For small momentum transfer, it is generally attributed to vertical interband transitions. Table 4.3.4.4, extracted from Raether (1980), compares a few measured values of $\Delta E_{1/2}(0)$, with values calculated using band-structure descriptions.

(*b*) For moderate momentum transfer q, a variation law such as

$$\Delta E_{1/2}(q) = \Delta E_{1/2}(0) + Bq^2 + O(q^4) \qquad (4.3.4.13)$$

has been measured. The q dependence of $\Delta E_{1/2}$ is mainly accounted for by non-vertical transitions compatible with the band structure, the number of these transitions increasing with q (Sturm, 1982). Other mechanisms have also been suggested, such as phonons, *umklapp* processes, scattering on surfaces, *etc*.

(*c*) For large momentum transfer (*i.e.* of the order of the critical wavevector q_c), the collective modes decay into the strong electron–hole-pair channels already described giving rise to a clear increase of the damping for values of $q > q_c$.

Within this free-electron-gas description, the differential cross section for the excitation of bulk plasmons by incident electrons of velocity v is given by

$$\frac{\mathrm{d}\sigma_p}{\mathrm{d}\Omega}(\theta) = \frac{\Delta E_p}{2\pi N a_0 m_0 v^2} \frac{1}{\theta^2 + \theta_E^2}, \qquad (4.3.4.14)$$

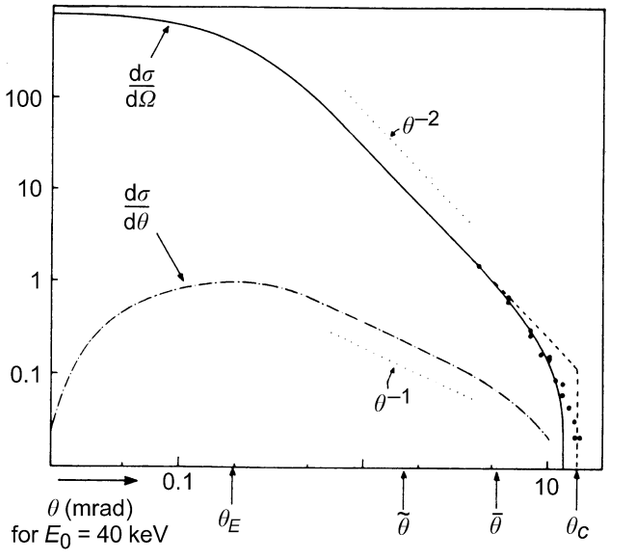

Fig. 4.3.4.14. Measured angular dependence of the differential cross section $\mathrm{d}\sigma/\mathrm{d}\Omega$ for the 15 eV plasmon loss in Al (dots) compared with a calculated curve by Ferrell (solid curve) and with a sharp cut-off approximation at θ_c (dashed curved). Also shown along the scattering angle axis, θ_E = characteristic inelastic angle defined as $\Delta E/2E_0$, $\tilde{\theta}$ = median inelastic angle defined by $\int_0^{\tilde{\theta}} (\mathrm{d}\sigma/\mathrm{d}\Omega)\,\mathrm{d}\Omega = 1/2 \int_0^{\theta_c} (\mathrm{d}\sigma/\mathrm{d}\Omega)\,\mathrm{d}\Omega$, and $\bar{\theta}$ = average inelastic angle defined by $\bar{\theta} = \int \theta(\mathrm{d}\sigma/\mathrm{d}\Omega)\,\mathrm{d}\Omega / \int (\mathrm{d}\sigma/\mathrm{d}\Omega)\,\mathrm{d}\Omega$ [courtesy of Egerton (1986)].

where N is the density of atoms per volume unit and θ_E is the characteristic inelastic angle defined as $\Delta E_p/2E_0$ in the non-relativistic description and as $\Delta E_p/\gamma m_0 v^2$ {with $\gamma = [1 - (v^2/c^2)]^{-1/2}$} in the relativistic case. The angular dependence of the differential cross section for plasmon scattering is shown in Fig. 4.3.4.14. The integral cross section up to an angle β_0 is

$$\sigma_p(\beta_0) = \int_0^{\beta_0} \left(\frac{\mathrm{d}\sigma_p}{\mathrm{d}\Omega}\right) \mathrm{d}\Omega = \frac{\Delta E_p \log(\beta_0/\theta_E)}{N a_0 m_0 v^2}. \qquad (4.3.4.15)$$

The total plasmon cross section is calculated for $\beta_0 = \theta_c = q_c/k_0$. Converted into mean free path, this becomes

$$\Lambda_p = \frac{1}{N\sigma_p} = \frac{a_0}{\theta_E} \left(\log \frac{\theta_c}{\theta_E}\right)^{-1} \quad \text{(non-relativistic formula);} \qquad (4.3.4.16)$$

and

$$\Lambda_p = \frac{a_0 \gamma m_0 v^2}{\Delta E_p} \left(\log \frac{\hbar q_c v}{1.132 \hbar \omega_p}\right)^{-1} \quad \text{(relativistic formula).} \qquad (4.3.4.17)$$

The behaviour of Λ_p as a function of the primary electron energy is shown in Fig. 4.3.4.15.

4.3.4.3.2. *Dielectric description*

The description of the bulk plasmon in the free-electron gas can be extended to any type of condensed material by introducing the dielectric response function $\varepsilon(\mathbf{q}, \omega)$, which describes the frequency and wavevector-dependent polarizability of the medium; *cf*. Daniels *et al* (1970). One associates, respectively, the ε_T and ε_L functions with the propagation of transverse and longitudinal EM modes through matter. In the small-$\mathbf{q}$ limit, these tend towards the same value:

$$\lim_{q\to 0} \varepsilon_T(\mathbf{q}, \omega) = \lim_{q\to 0} \varepsilon_L(\mathbf{q}, \omega) = \varepsilon(0, \omega).$$

As transverse dielectric functions are only used for wavevectors close to zero, the T and L indices can be omitted so that:

$$\varepsilon_L(\mathbf{q}, \omega) = \varepsilon(\mathbf{q}, \omega) \quad \text{and} \quad \varepsilon_T(\mathbf{q}, \omega) = \varepsilon(0, \omega).$$

The transverse solution corresponds to the normal propagation of EM waves in a medium of dielectric coefficient $\varepsilon(0, \omega)$, *i.e.* to

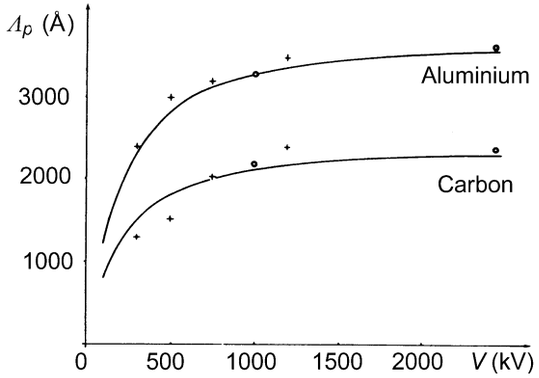

Fig. 4.3.4.15. Variation of plasmon excitation mean free path Λ_p as a function of accelerating voltage V in the case of carbon and aluminium [courtesy of Sevely (1985)].

$$\frac{q^2c^2}{\omega^2} - \varepsilon(0,\omega) = 0. \qquad (4.3.4.18)$$

For longitudinal fields, the only solution is $\varepsilon(\mathbf{q},\omega) = 0$, which is basically the dispersion relation for the bulk plasmon.

In the framework of the Maxwell description of wave propagation in matter, it has been shown by several authors [see, for instance, Ritchie (1957)] that the transfer of energy between the beam electron and the electrons in the solid is governed by the magnitude of the energy-loss function $-\mathrm{Im}[1/\varepsilon(\mathbf{q},\omega)]$, so that

$$\frac{\mathrm{d}^2\sigma}{\mathrm{d}(\Delta E)\,\mathrm{d}\Omega} = \frac{1}{N(e\pi a_0)^2}\,\frac{1}{q^2}\,\mathrm{Im}\left(-\frac{1}{\varepsilon(\mathbf{q},\omega)}\right). \qquad (4.3.4.19)$$

One can deduce (4.3.4.14) by introducing a δ function at energy loss ω_p for the energy-loss function:

$$\mathrm{Im}\left(-\frac{1}{\varepsilon(\mathbf{q},\omega)}\right) = \frac{\pi}{2}\,\omega_p\delta(\omega-\omega_p). \qquad (4.3.4.20)$$

As a consequence of the causality principle, a knowledge of the energy-loss function $-\mathrm{Im}[1/\varepsilon(\omega)]$ over the complete frequency (or energy-loss) range enables one to calculate $\mathrm{Re}[1/\varepsilon(\omega)]$ by Kramers–Kronig analysis:

$$\mathrm{Re}\frac{1}{\varepsilon(\omega)} = 1 - \frac{2}{\pi}\mathrm{PP}\int_0^\infty \mathrm{Im}\left(-\frac{1}{\varepsilon(\omega')}\right)\frac{\omega'}{\omega'^2-\omega^2}\,\mathrm{d}\omega', \qquad (4.3.4.21)$$

where PP denotes the principal part of the integral. For details of efficient practical evaluation of the above equation, see Johnson (1975).

The dielectric functions can be easily calculated for simple descriptions of the electron gas. In the Drude model, *i.e.* for a free-electron plasma with a relaxation time τ, the dielectric function at long wavelengths ($q \to 0$) is

$$\varepsilon(\omega) = \varepsilon_1(\omega) + i\varepsilon_2(\omega) = 1 - \frac{\omega_p^2}{\omega^2}\,\frac{1}{(1-1/i\omega\tau),} \qquad (4.3.4.22)$$

with $\omega_p^2 = ne^2/m\varepsilon_0$, as above. The behaviour of the different functions, the real and imaginary terms in ε, and the energy-loss function are shown in Fig. 4.3.4.16. The energy-loss term exhibits a sharp Lorentzian profile centred at $\omega = \omega_p$ and of width $1/\tau$. The narrower and more intense this plasmon peak, the more the involved valence electrons behave like free electrons.

In the Lorentz model, *i.e.* for a gas of bound electrons with one or several excitation eigenfrequencies ω_i, the dielectric function is

$$\varepsilon(\omega) = 1 + \sum_i \frac{n_i e^2}{m\varepsilon_0}\,\frac{1}{\omega_i^2 - \omega^2 + i\omega/\tau_i}, \qquad (4.3.4.23)$$

where n_i denotes the density of electrons oscillating with the frequency ω_i and τ_i is the associated relaxation time. The characteristic ε_1, ε_2, and $-\mathrm{Im}(1/\varepsilon)$ behaviours are displayed in Fig. 4.3.4.17: a typical 'interband' transition (in solid-state terminology) can be revealed as a maximum in the ε_2 function, simultaneous with a 'plasmon' mode associated with a maximum in the energy-loss function and slightly shifted to higher energies with respect to the annulation conditions of the ε_1 function.

In most practical situations, there coexist a family of n_f free electrons (with plasma frequency $\omega_p^2 = n_f e^2/m\varepsilon_0$) and one or several families of n_i bound electrons (with eigenfrequencies ω_i). The influence of bound electrons is to shift the plasma frequency towards lower values if $\omega_i > \omega_p$ and to higher values if $\omega_i < \omega_p$. As a special case, in an insulator, $n_f = 0$ and all the electrons ($n_i = n$) have a binding energy at least equal to the band gap $E_g \simeq \hbar\omega_i$, giving $\omega_p^2 = (E_g/\hbar)^2 + ne^2/m\varepsilon_0$.

This description constitutes a satisfactory first step into the world of real solids with a complex system of valence and conduction bands between which there is a strong transition rate of individual electrons under the influence of photon or electron beams. In optical spectroscopy, for instance, this transition rate, which governs the absorption coefficient, can be deduced from the calculation of the factor ε_2 as

$$\varepsilon_2(\omega) = \frac{A}{\omega^2}|M_{jj'}|^2 J_{jj'}(\omega), \qquad (4.3.4.24)$$

where $M_{jj'}$ is the matrix element for the transition from the occupied level j in the valence band to the unoccupied level j' in the conduction band, both with the same $\mathbf{k}$ value (which means for a vertical transition). $J_{jj'}(\omega)$ is the joint density of states (JDOS) with the energy difference $\hbar\omega$. This formula is also valid

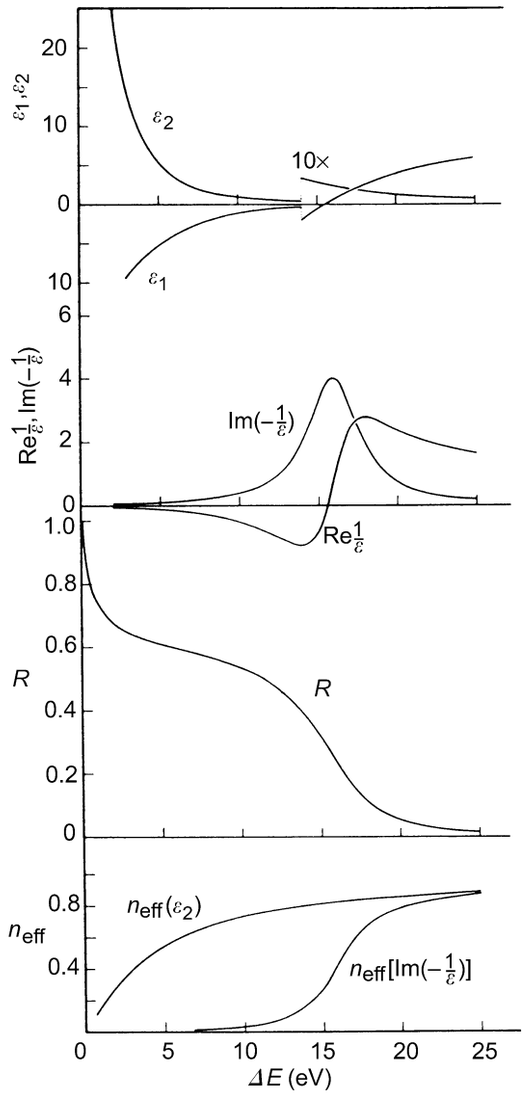

Fig. 4.3.4.16. Dielectric and optical functions calculated in the Drude model of a free-electron gas with $\hbar\omega_p = 16\,\mathrm{eV}$ and $\tau = 1.64 \times 10^{-16}\,\mathrm{s}$. R is the optical reflection coefficient in normal incidence, *i.e.* $R = [(n-1)^2 + k^2]/[(n+1)^2 + k^2]$ with n and k the real and imaginary parts of $\sqrt{\varepsilon}$. The effective numbers $n_{\mathrm{eff}}(\varepsilon_2)$ and $n_{\mathrm{eff}}[\mathrm{Im}(-1/\varepsilon)]$ are defined in Subsection 4.3.4.5 [courtesy of Daniels *et al.* (1970)].

for small-angle-scattering electron inelastic processes. When parabolic bands are used to represent, respectively, the upper part of the valence band and the lower part of the conduction band in a semiconductor, the dominant JDOS term close to the onset of the interband transitions takes the form

$$\text{JDOS} \propto (E - E_g)^{1/2}, \tag{4.3.4.25}$$

where E_g is the band-gap energy. This concept has been successfully used by Batson (1987) for the detection of gap energy variations between the bulk and the vicinity of a single misfit dislocation in a GaAs specimen. The case of non-vertical transitions involving integration over **k**-space has also been considered (Fink *et al.*, 1984; Fink & Leising, 1986).

4.3.4.3.3. *Real solids*

The dielectric constants of many solids have been deduced from a number of methods involving either primary photon or electron beams. In optical measurements, one obtains the values of ε_1 and ε_2 from a Krakers–Kronig analysis of the optical absorption and reflection curves, while in electron energy-loss measurements they are deduced from Kramers–Kronig analysis of energy-loss functions.

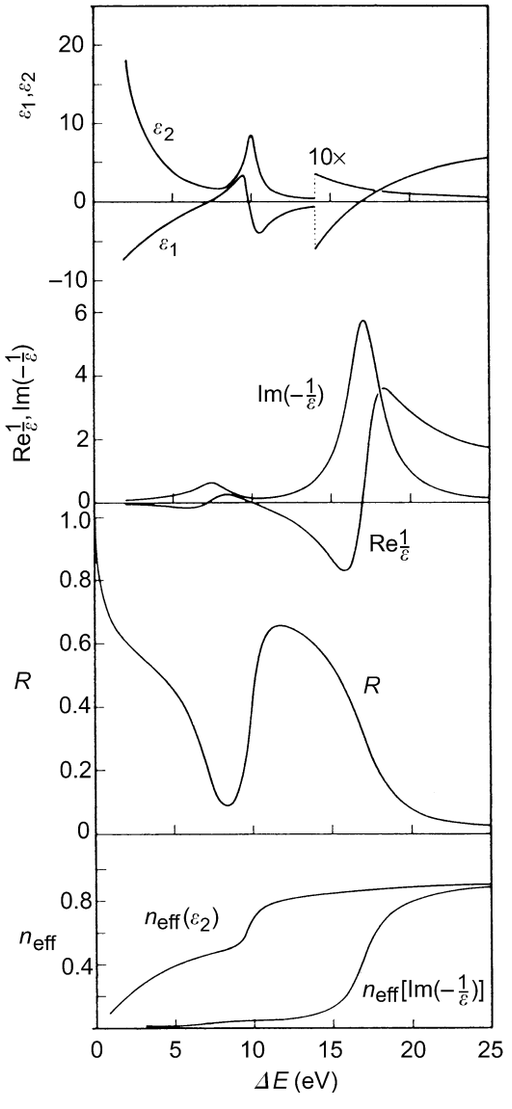

Fig. 4.3.4.17. Same as previous figure, but for a Lorentz model with an oscillator of eigenfrequency $\hbar\omega_0 = 10\,\text{eV}$ and relaxation time $\tau_0 = 6.6 \times 10^{-16}\,\text{s}$ superposed on the free-electron term [courtesy of Daniels *et al.* (1970)].

Fig. 4.3.4.18 shows typical behaviours of the dielectric and energy-loss functions.

(*a*) For a free-electron metal (Al), the Drude model is a satisfactory description with a well defined narrow and intense maximum of $\text{Im}(-1/\varepsilon)$ corresponding to the collective plasmon excitation together with typical conditions $\varepsilon_1 \simeq \varepsilon_2 \simeq 0$ for this energy $\hbar\omega_p$. One also notices a weak interband transition below 2 eV.

(*b*) For transition and noble metals (such as Au), the results strongly deviate from the free-electron gas function as a consequence of intense interband transitions originating mostly from the partially or fully filled *d* band lying in the vicinity of, or just below, the Fermi level. There is no clear condition for satisfying the criterion of plasma excitation ($\varepsilon = 0$) so that the collective modes are strongly damped. However, the higher-lying peak is more generally of a collective nature because it coincides with the exhaustion of all oscillator strengths for interband transitions.

(*c*) Similar arguments can be developed for a semiconductor (InSb) or an insulator (Xe solid). In the first case, one detects a few interband transitions at small energies that do not prevent the occurrence of a pronounced volume plasmon peak rather similar to the free-electron case. The difference between the gap and the plasma energy is so great that the valence electrons behave collectively as an assembly of free particles. In contrast, for wide gap insulators (alkali halides, oxides, solid rare gases), a number of peaks are seen, owing to different interband transitions and exciton peaks. Excitons are quasi-particles consisting of a conduction-band electron and a valence-band hole bound to each other by Coloumb interaction. One observes the existence of a band gap [no excitation either in ε_2 or in $\text{Im}(-1/\varepsilon)$ below a given critical value E_g] and again the higher-lying peak is generally of a rather collective nature.

Čerenkov radiation is emitted when the velocity v of an electron travelling through a medium exceeds the speed of light for a particular frequency in this medium. The criterion for Čerenkov emission is

$$\varepsilon_1(\omega) > \frac{c^2}{v^2} = \beta^{-2}. \tag{4.3.4.26}$$

In an insulator, ε_1 is positive at low energies and can considerably exceed unity, so that a 'radiation peak' can be detected in the corresponding energy-loss range (between 2 and 4 eV in Si, Ge, III–V compounds, diamond, ...); see Von Festenberg (1968), Kröger (1970), and Chen & Silcox (1971). The associated scattering angle, $\theta \simeq \lambda_{\text{el}}/\lambda_{\text{ph}} \simeq 10^{-5}\,\text{rad}$ for high-energy electrons, is very small and this contribution can only be detected using a limited forward-scattering angular acceptance.

In an *anisotropic* crystal, the dielectric function has the character of a tensor, so that the energy-loss function is expressed as

$$\text{Im}\left(-\frac{1}{\sum_i \sum_j \varepsilon_{ij}\, q_i\, q_j}\right). \tag{4.3.4.27}$$

If it is transformed to its orthogonal principal axes $(\varepsilon_{11}, \varepsilon_{22}, \varepsilon_{33})$, and if the **q** components in this system are q_1, q_2, q_3, the above expression simplifies to

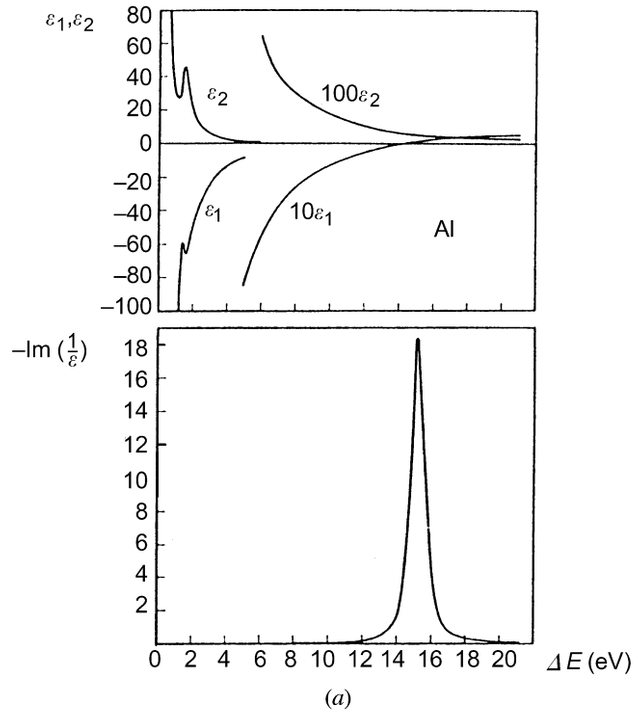

(a)

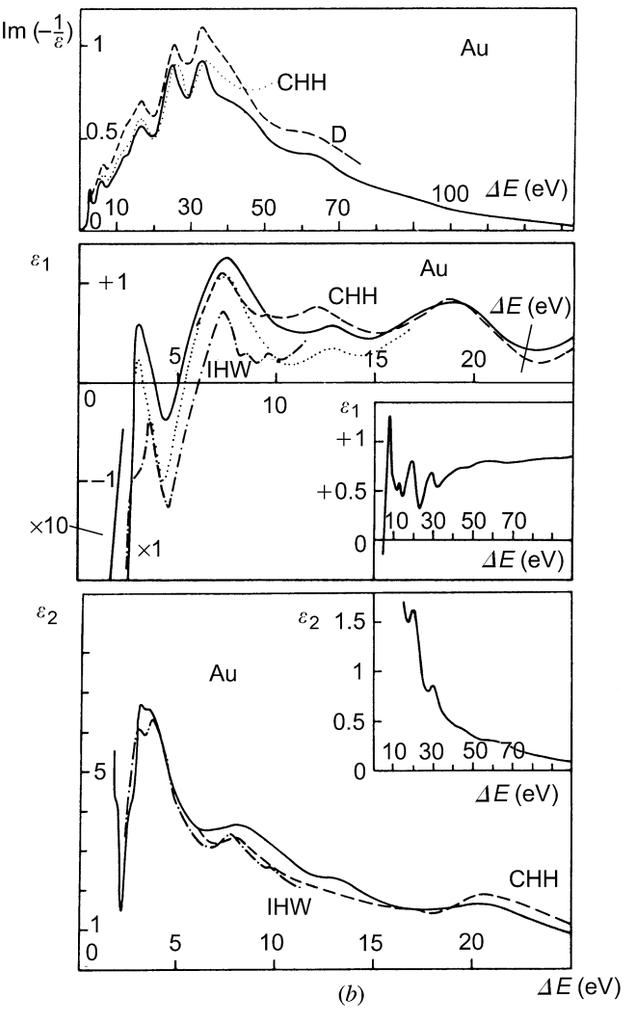

(b)

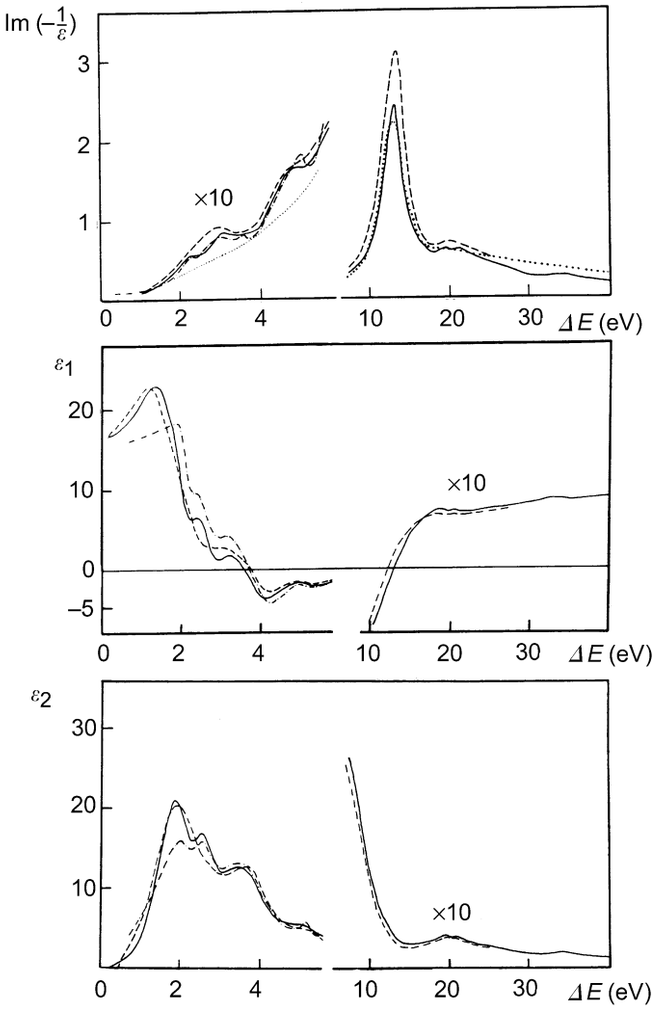

(c)

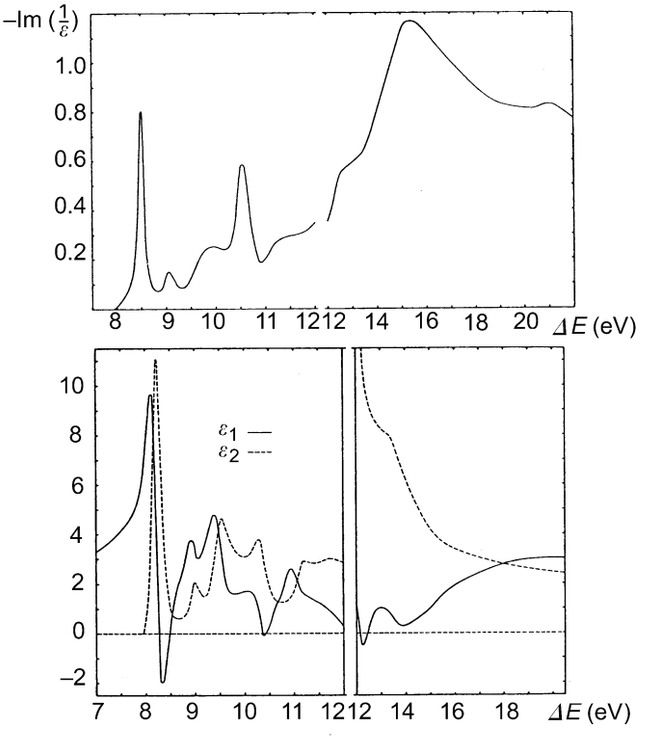

(d)

Fig. 4.3.4.18. Dielectric coefficients ε_1, ε_2 and $\mathrm{Im}(-1/\varepsilon)$ from a collection of typical real solids: (*a*) aluminium [courtesy of Raether (1965)]; (*b*) gold [courtesy of Wehenkel (1975)]; (*c*) InSb [courtesy of Zimmermann (1976)]; (*d*) solid xenon at *ca* 5 K [courtesy of Keil (1968)].

$$\mathrm{Im}\left(-\frac{1}{\sum_i \varepsilon_{ii} q_i^2}\right). \qquad (4.3.4.28)$$

In a uniaxial crystal, such as a graphite, $\varepsilon_{11} = \varepsilon_{22} = \varepsilon_\perp$ and $\varepsilon_{33} = \varepsilon_\parallel$ (*i.e.* parallel to the c axis):

$$\varepsilon(\mathbf{q}, \omega) = \varepsilon_\perp \sin^2\theta + \varepsilon_\parallel \cos^2\theta, \qquad (4.3.4.29)$$

where θ is the angle between $\mathbf{q}$ and the c axis. The spectrum depends on the direction of $\mathbf{q}$, either parallel or perpendicular to the c axis, as shown in Fig. 4.3.4.19 from Venghaus (1975). These experimental conditions may be achieved by tilting the graphite layer at 45° with respect to the incident axis, and recording spectra in two directions at $\pm\theta_E$ with respect to it (see Fig. 4.3.4.20).

4.3.4.3.4. *Surface plasmons*

Volume plasmons are longitudinal waves of charge density propagating through the bulk of the solid. Similarly, three exist longitudinal waves of charge density travelling along the surface between two media A and B (one may be a vacuum): these are the surface plasmons (Kliewer & Fuchs, 1974). Boundary conditions imply that

$$\varepsilon_A(\omega) + \varepsilon_B(\omega) = 0. \qquad (4.3.4.30)$$

The corresponding charge-density fluctuation is contained within the (**x**) boundary plane, z being normal to the surface:

$$\rho(\mathbf{x}, z) \simeq \cos(\mathbf{q}\cdot\mathbf{x} - \omega t)\delta(z), \qquad (4.3.4.31)$$

and the associated electrostatic potential oscillates in space and time as

$$\varphi(\mathbf{x}, z)\, \alpha \cos(\mathbf{q}\cdot\mathbf{x} - \omega t)\exp(-q|z|). \qquad (4.3.4.32)$$

The characteristic energy ω_s of this surface mode is estimated in the free electron case as:

In the planar interface case:

$$\left.\begin{aligned} &\omega_s = \frac{\omega_p}{\sqrt{2}} \\ &\quad \text{(interface metal–vacuum);} \\ &\omega_s = \frac{\omega_p}{(1+\varepsilon_d)^{1/2}} \\ &\quad \text{(interface metal–dielectric of constant } \varepsilon_d\text{);} \\ &\omega_s = \left(\frac{\omega_{p_A}^2 + \omega_{p_B}^2}{2}\right)^{1/2} \\ &\quad \text{(interface metal } A\text{–metal } B\text{).} \end{aligned}\right\} \qquad (4.3.4.33)$$

In the spherical interface case:

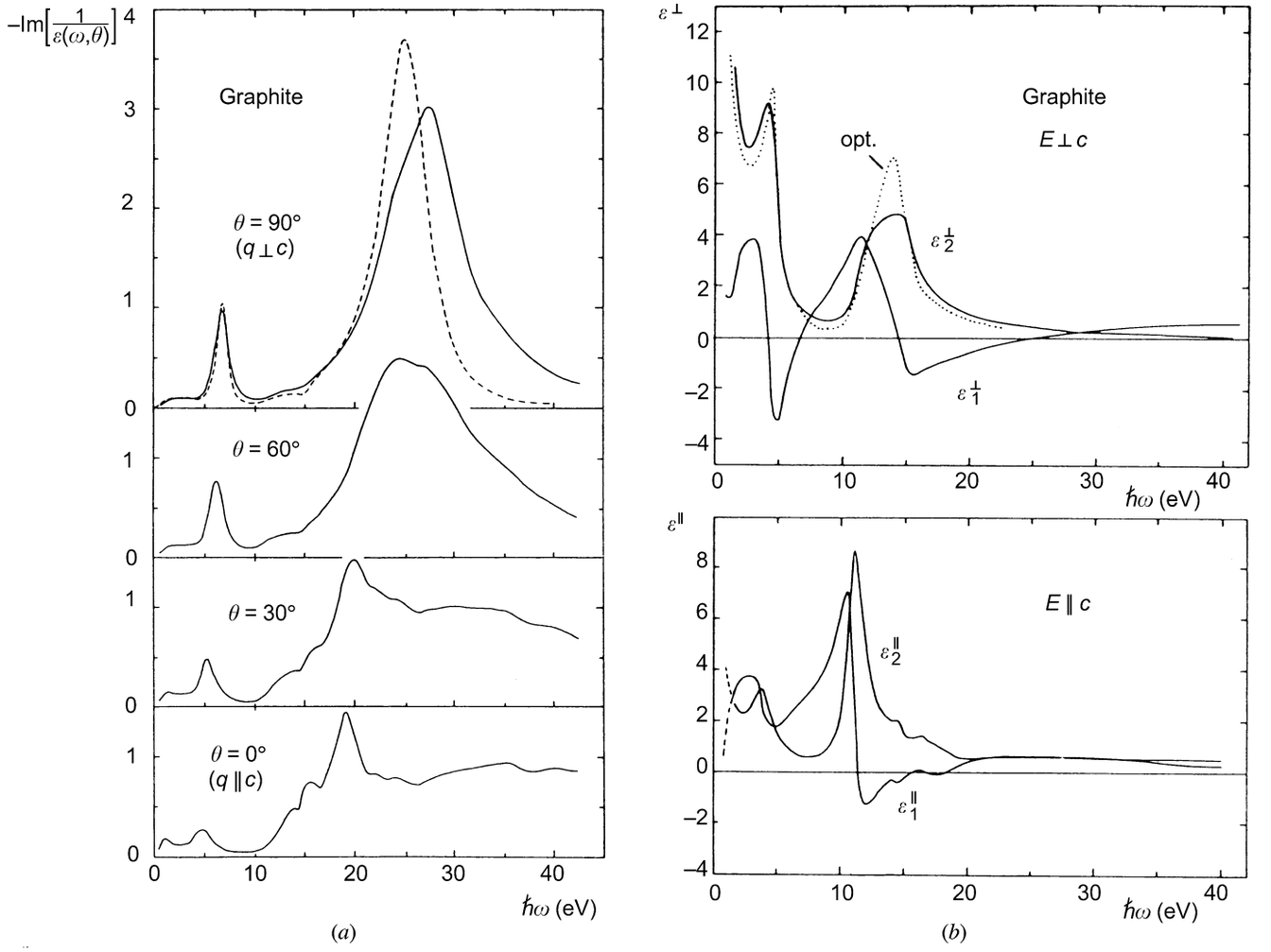

Fig. 4.3.4.19. Dielectic functions in graphite derived from energy losses for $E \perp c$ (*i.e.* the electric field vector being in the layer plane) and for $E \parallel c$ [from Daniels *et al.* (1970)]. The dashed line represents data extracted from optical reflectivity measurements [from Taft & Philipp (1965)].

$$(\omega_s)_l = \frac{\omega_p}{[(2l+1)/l]^{1/2}} \qquad (4.3.4.34a)$$

(metal sphere in vacuum – the modes are now quantified following the l quantum number in spherical geometry);

$$(\omega_s)_l = \frac{\omega_p}{[(2l+1)/(l+1)]^{1/2}} \qquad (4.3.4.34b)$$

(spherical void within metal).

Thin-film geometry:

$$(\omega_s)^{\pm} = \omega_p \left[\frac{1 \pm \exp(-qt)}{1+\varepsilon_d}\right]^{1/2} \qquad (4.3.4.35)$$

(metal layer of thickness t embedded in dielectric films of constant ε_d). The two solutions result from the coupling of the oscillations on the two surfaces, the electric field being symmetric for the $(\omega_s)^-$ mode and antisymmetric for the $(\omega_s)^+$.

In a real solid, the surface plasmon modes are determined by the roots of the equation $\varepsilon(\omega_s) = -1$ for vacuum coating [or $\varepsilon(\omega_s) = -\varepsilon_d$ for dielectric coating].

The probability of surface-loss excitation P_s is mostly governed by the $\mathrm{Im}\{-1/[1+\varepsilon(\omega)]\}$ energy-loss function, which is analogous for surface modes to the bulk $\mathrm{Im}\{-1/[\varepsilon(\omega)]\}$ energy-loss function. In normal incidence, the differential scattering cross section $\mathrm{d}P_s/\mathrm{d}\Omega$ is zero in the forward direction, reaches a maximum for $\theta = \pm\theta_E/3^{1/2}$, and decreases as θ^{-3} at large angles. In non-normal incidence, the angular distribution is asymmetrical, goes through a zero value for momentum transfer $\hbar\mathbf{q}$ in a direction perpendicular to the interface, and the total probability increases as

$$P_s(\varphi) = \frac{P_s(O)}{\cos\varphi}, \qquad (4.3.4.36)$$

where φ is the incidence angle between the primary beam and the normal to the surface. As a consequence, the probability of producing one (and several) surface losses increases rapidly for grazing incidences.

4.3.4.4. *Excitation spectrum of core electrons*

4.3.4.4.1. *Definition and classification of core edges*

As for any core-electron spectroscopy, EELS spectroscopy at higher energy losses mostly deals with the excitation of well defined atomic electrons. When considering solid specimens, both initial and final states in the transition are actually eigenstates in the solid state. However, the initial wavefunction can be considered as purely atomic for core excitations. As a first consequence, one can classify these transitions as a function of the parameters of atomic physics: Z is the atomic number of the element; n, l, and $j = l + s$ are the quantum numbers describing the subshells from which the electron has been excited. The spectroscopy notation used is shown in Fig. 4.3.4.21. The list of major transitions is displayed as a function of Z and E_c in Fig. 4.3.4.22.

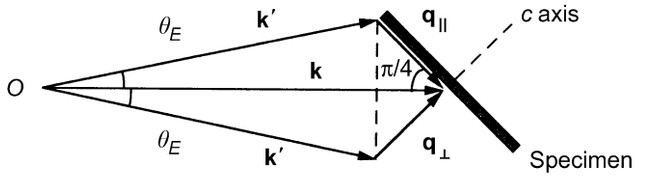

Fig. 4.3.4.20. Geometric conditions for investigating the anisotropic energy-loss function.

Core excitations appear as edges superimposed, from the threshold energy E_c upwards, above a regularly decreasing background. As explained below, the basic matrix element governing the probability of transition is similar for optical absorption spectroscopy and for small-angle-scattering EELS spectroscopy. Consequently, selection rules for dipole transitions define the dominant transitions to be observed, *i.e.*

$$l' - l = \Delta l = \pm 1 \quad \text{and} \quad j' - j = \Delta j = 0, \pm 1. \qquad (4.3.4.37)$$

This major rule has important consequences for the edge shapes to be observed: approximate behaviours are also shown in Fig. 4.3.4.22. A very useful library of core edges can be found in the EELS atlas (Ahn & Krivanek, 1982), from which we have selected the family of edges gathered in Fig. 4.3.4.23. They display the following typical profiles:

(i) *K edges for low-Z elements* ($3 \leq Z \leq 14$). The carbon K edge occurring at 284 eV is a nice example with a clear hydrogenic or saw-tooth profile and fine structures on threshold depending on the local environment (amorphous, graphite, diamond, organic molecules, ...); see Isaacson (1972*a*,*b*).

(ii) *$L_{2,3}$ edges for medium-Z elements* ($11 \lesssim Z \lesssim 45$). The $L_{2,3}$ edges exhibit different shapes when the outer occupied shell changes in nature: a delayed profile is observed as long as the first vacant d states are located, along the energy scale, rather above the Fermi level (sulfur case). When these d states coincide with the first accessible levels, sharp peaks, generally known as 'white lines', appear at threshold (this is the case for transition elements with the Fermi level inside the d band). These lines are generally split by the spin-orbit term on the initial level into $2p^{3/2}$ and $2p^{1/2}$ (or L_3 and L_2) terms. For higher-Z elements, the bound d levels are fully occupied, and

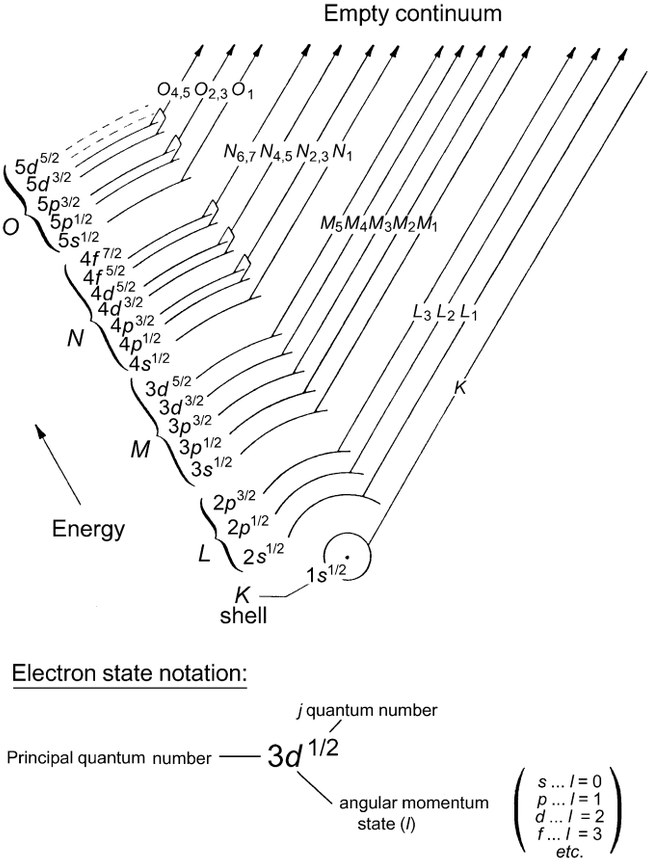

Fig. 4.3.4.21. Definition of electron shells and transitions involved in core-loss spectroscopy [from Ahn & Krivanek (1982)].

no longer contribute as host orbitals for the excited $2p$ electrons. One finds again a more traditional hydrogenic profile (such as for the germanium case).

(iii) *$M_{4,5}$ edges for heavier-Z elements* ($37 \lesssim Z \lesssim 83$). A sequence of $M_{4,5}$ edge profiles, rather similar to $L_{2,3}$ edges, is observed, the difference being that one then investigates the density of the final *f* states. White lines can also be detected when the *f* levels lie in the neighbourhood of the Fermi level, *e.g.* for rare-earth elements.

The deeper accessible signals, for incident electrons in the range of 100–400 kV primary voltage, lie between 2500 and 3000 eV, which corresponds roughly to the middle of the second row of transition elements (Mo–Ru) for the $L_{2,3}$ edge and to the very heavy metals (Pb–Bi) for the $M_{4,5}$ edge.

(iv) A final example in Fig. 4.3.4.23 concerns one of these resonant peaks associated with the excitation of levels just below the conduction band. These are features with high intensity of the same order or even superior to that of plasmons of conduction

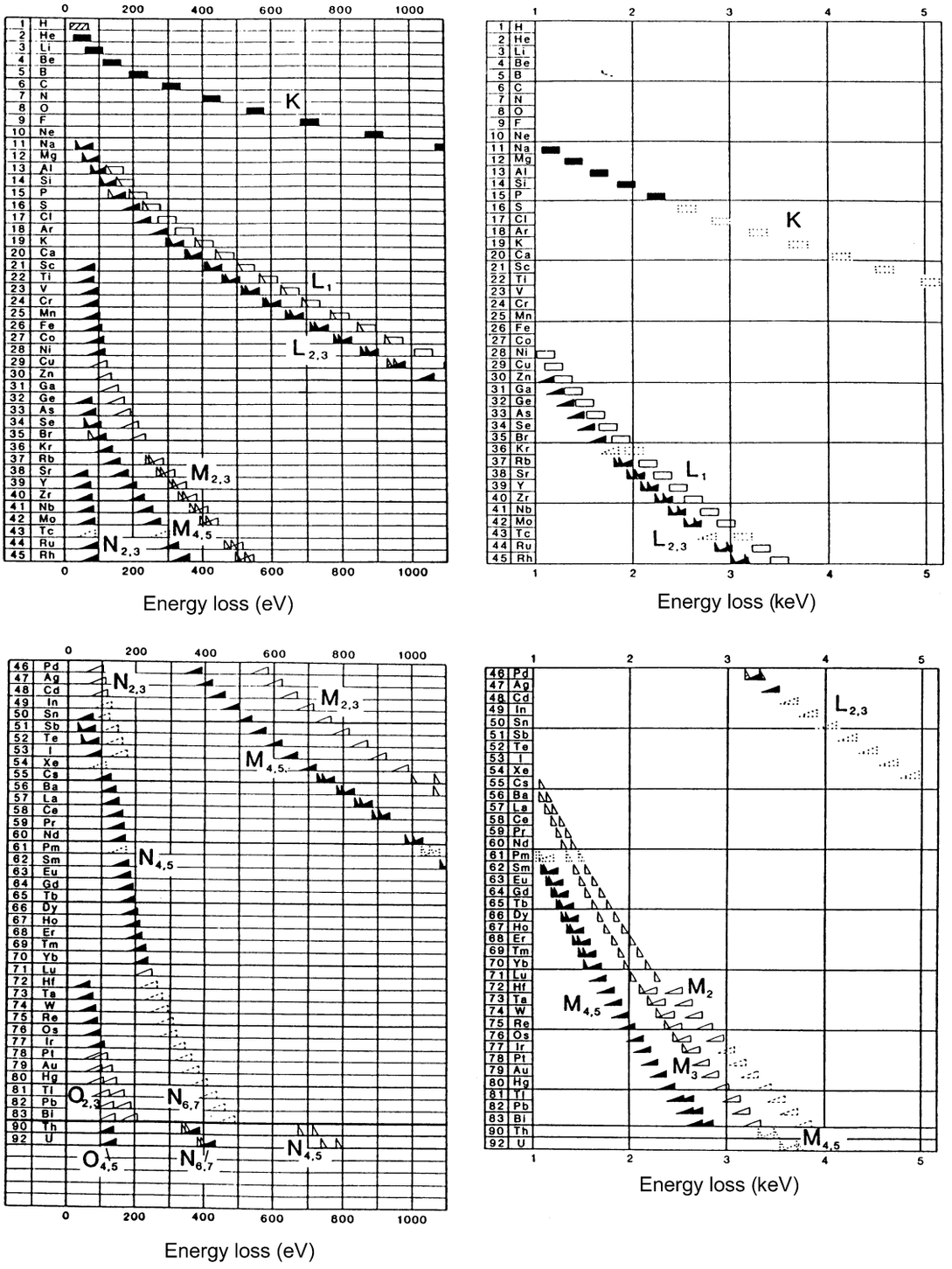

Fig. 4.3.4.22. Chart of edges encountered in the 50 eV up to 3 keV energy-loss range with symbols identifying the types of shapes [see Ahn & Krivanek (1982) for further comments].

band electrons previously described in Subsection 4.3.4.3. It occurs with the $M_{2,3}$ level for the first transition series, with the $N_{2,3}$ level for the second series (for example, strontium in Fig. 4.3.4.23) or with the $O_{2,3}$ level for the third series, including the rare-earth elements. The shape varies gradually from a plasmon-like peak with a short lifetime to an asymmetric Fano-type profile, a consequence of the coupling between discrete and continuum final states of the same energy (Fano, 1961).

4.3.4.4.2. *Bethe theory for inelastic scattering by an isolated atom (Bethe, 1930; Inokuti, 1971, 1979)*

As a consequence of the atomic nature of the excited wavefunction in core-loss spectroscopy, the first step involves deriving a useful theoretical expression for inelastic scattering by an isolated atom. The differential cross section for an electron of wavevector $\mathbf{k}$ to be scattered into a final plane wave of vector $\mathbf{k}'$, while promoting one atomic electron from ψ_0 to ψ_n, is given in a one-electron excitation description by

$$\frac{\mathrm{d}\sigma_n}{\mathrm{d}\Omega\,\mathrm{d}(\Delta E)} = \left(\frac{m_0}{2\pi\hbar^2}\right)^2 \frac{k'}{k} |\langle \psi_n \mathbf{k}' | V(\mathbf{r}) | \psi_0 \mathbf{k} \rangle|^2; \qquad (4.3.4.38)$$

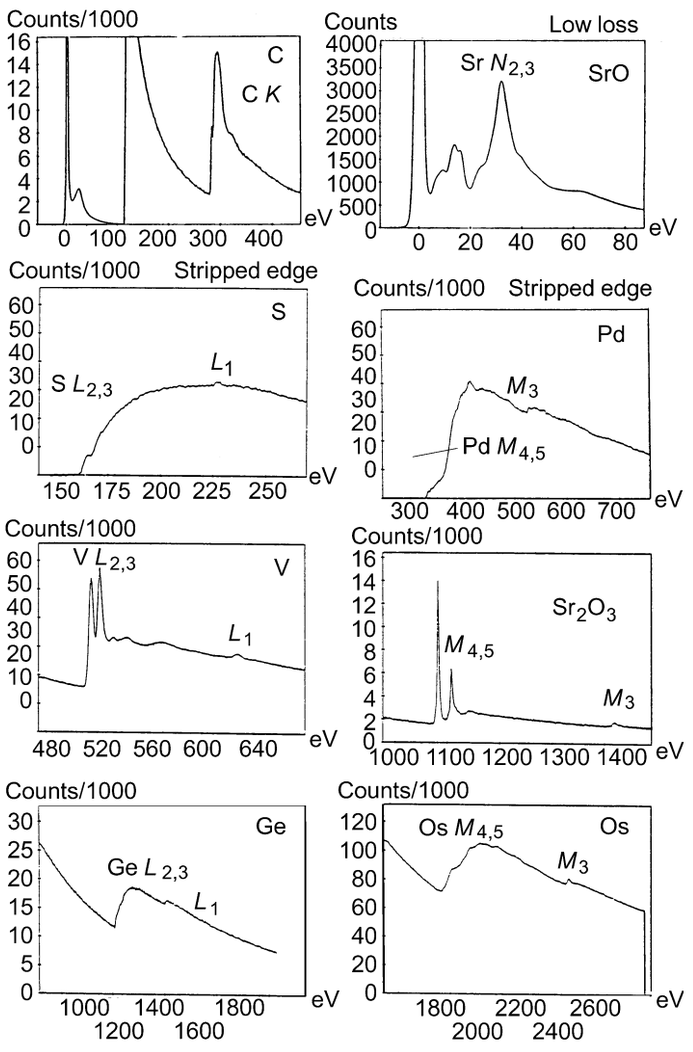

Fig. 4.3.4.23. A selection of typical profiles ($K, L_{2,3}, M_{4,5}$, and $N_{2,3}$) illustrating the most important behaviours encountered on major edges through the Periodic Table. A few edges are displayed prior to and others after background stripping. [Data extracted from Ahn & Krivanek (1982).]

see, for instance, Landau & Lifchitz (1966) and Mott & Massey (1952). The potential $V(\mathbf{r})$ corresponds to the Coulomb interaction with all charges (both in the nucleus and in the electron cloud) of the atom. The momentum change in the scattering event is $\hbar\mathbf{q} = \hbar(\mathbf{k} - \mathbf{k}')$. The final-state wavefunction is normalized per unit energy range. The orthogonality between initial- and final-state wavefunctions restricts the inelastic scattering to the only interactions with atomic electrons:

$$\frac{\mathrm{d}\sigma_n}{\mathrm{d}\Omega\,\mathrm{d}(\Delta E)} = \frac{4\gamma^2}{a_0^2 q^4} \frac{k'}{k} |\mathscr{E}_n(\mathbf{q}, \Delta E)|^2. \qquad (4.3.4.39)$$

The first part of the above expression has the form of Rutherford scattering. γ is introduced to deal, to a first approximation, with relativistic effects. The ratio k'/k is generally assumed to be equal to unity. This kinematic scattering factor is modified by the second term, or matrix element, which describes the response of the atomic electrons:

$$\mathscr{E}_n(\mathbf{q}, \Delta E) = \left\langle \psi_n \left| \sum_j \exp(i\mathbf{q}\cdot\mathbf{r}_j) \right| \psi_0 \right\rangle, \qquad (4.3.4.40)$$

where the sum extends over all atomic electrons at positions $\mathbf{r}_j$. The dimensionless quantity is known as the *inelastic form factor*.

For a more direct comparison with photoabsorption measurements, one introduces the generalized oscillator strength (GOS) as

$$\frac{\mathrm{d}f(\mathbf{q}, \Delta E)}{\mathrm{d}(\Delta E)} = \frac{\Delta E}{R} \frac{|\mathscr{E}_n(\mathbf{q}, \Delta E)|^2}{(qa_0)^2} \qquad (4.3.4.41)$$

for transitions towards final states ψ_ε in the continuum [ΔE is then the energy difference between the core level and the final state of kinetic energy ε above the Fermi level, scaled in energy to the Rydberg energy (R)]. Also,

$$f_n(\mathbf{q}) = \frac{E_n}{R} \frac{|\mathscr{E}_n(\mathbf{q})|^2}{(qa_0)^2} \qquad (4.3.4.42)$$

for transition towards bound states. In this case, E_n is the energy difference between the two states involved.

The generalized oscillator strength is a function of both the energy ΔE and the momentum $\hbar\mathbf{q}$ transferred to the atom. It is displayed as a three-dimensional surface known as the Bethe surface (Fig. 4.3.4.24), which embodies all information concerning the inelastic scattering of charged particles by atoms. The angular dependence of the cross section is proportional to

$$\frac{1}{q^2} \frac{\mathrm{d}f(\mathbf{q}, \Delta E)}{\mathrm{d}(\Delta E)}$$

at a given energy loss ΔE.

In the small-angle limit ($qr_c \ll 1$, where r_c is the average radius of the initial orbital), the GOS reduces to the optical oscillator strength

$$\frac{\mathrm{d}f(\mathbf{q}, \Delta E)}{\mathrm{d}(\Delta E)} \rightarrow \frac{\mathrm{d}f(0, \Delta E)}{\mathrm{d}(\Delta E)}$$

and

$$\mathscr{E}_n(\mathbf{q}, \Delta E) \rightarrow \mathscr{E}_n(0, \Delta E) = q^2 \left| \left\langle \psi_n \left| \sum_j \mathbf{u}\cdot\mathbf{r}_j \right| \psi_0 \right\rangle \right|^2, \qquad (4.3.4.43)$$

where $\mathbf{u}$ is the unit vector in the $\mathbf{q}$ direction. When one is concerned with a given orbital excitation, the sum over $\mathbf{r}_j$ reduces to a single term $\mathbf{r}$ for this electron. With some elementary calculations, the resulting cross section is

$$\frac{\mathrm{d}^2\sigma}{\mathrm{d}\Omega\,\mathrm{d}(\Delta E)} = \frac{4\gamma^2 R}{\Delta E\, k^2}\,\frac{1}{\theta^2+\theta_E^2}\,\frac{\mathrm{d}f(0,\Delta E)}{\mathrm{d}(\Delta E)}. \qquad (4.3.4.44)$$

The major angular dependence is contained, as in the low-loss domain, in the Lorentzian factor $(\theta^2+\theta_E^2)^{-1}$, with the characteristic inelastic angle θ_E being again equal to $\Delta E/\gamma m_0 v^2$. Over this reduced scattering-angle domain, known as the dipole region, the GOS is approximately constant and the inner-shell EELS spectrum is directly proportional to the photoabsorption cross section $\sigma_{\rm opt}$, whose data can be used to test the results of single-atom calculations. For larger scattering angles, Fig. 4.3.4.24 exhibits two distinct behaviours for energy losses just above the edge ($\mathrm{d}f/\mathrm{d}\Delta E$ drops regularly to zero), and for energy losses much greater than the core-edge threshold. In the latter case, the oscillator strength is mostly concentrated in the Bethe ridge, the maximum of which occurs for:

$$\left.\begin{aligned}(qa_0)^2 &= \frac{\Delta E}{R} \quad \text{(non-relativistic formula)},\\ (qa_0)^2 &= \frac{\Delta E}{R}\frac{(\Delta E)^2}{2m_0c^2R} \quad \text{(relativistic formula)}.\end{aligned}\right\} \qquad (4.3.4.45)$$

This contribution at large scattering angles is equivalent to direct knock-on collisions of free electrons, *i.e.* to the curve $\Delta E = \hbar^2 q^2/2m_0$ lying in the middle of the valence-electron–hole excitations continuum (see Fig. 4.3.4.13). The non-zero width of the Bethe ridge can be used as an electron Compton profile to analyse the momentum distribution of the atomic electrons [see also §4.3.4.4.4(*c*)].

The energy dependence of the cross section, responsible for the various edge shapes discussed in §4.3.4.4.1, is governed by

$$\frac{1}{\Delta E}\,\frac{\mathrm{d}f(\mathbf{q},\Delta E)}{\mathrm{d}(\Delta E)},$$

i.e. it corresponds to sections through the Bethe surface at constant $\mathbf{q}$. Within the general theory described above, various models have been developed for practical calculations of energy differential cross sections.

The hydrogenic model due to Egerton (1979) is an extension of the quantum-mechanical calculations for a hydrogen atom to inner-shell electron excitations in an atom Z by introduction of some useful parametrization (effective nuclear charge, effective threshold energy). It is applied in practice for K and $L_{2,3}$ shells.

In the Hartree–Slater (or Dirac–Slater) description, one calculates the final continuum-state wavefunction in a self-consistent central field atomic potential (Leapman, Rez & Mayers, 1980; Rez, 1989). The radial dependence of these wavefunctions is given by the solution of a Schrödinger equation with an effective potential:

$$V_{\rm eff}(r) = V(r) + \frac{l'(l'+1)\hbar^2}{2m_0r^2}, \qquad (4.3.4.46)$$

where $[l'(l'+1)\hbar^2]/2m_0r^2$ is the centrifugal potential, which is important for explaining the occurrence of delayed maxima in spectra involving final states of higher l'. This approach is now useful for any major K, $L_{2,3}$, $M_{4,5}$, ... edge, as illustrated by Ahn & Rez (1985) and more specifically in rare-earth elements by Manoubi, Rez & Colliex (1989).

These differential cross sections can be integrated over the relevant angular and energy domains to provide data comparable with experimental measurements. In practice, one records the energy spectral distribution of electrons scattered into all angles up to the acceptance value β of the collection aperture. The integration has therefore to be made from $q_{\rm min} \simeq k\theta_E$ for the zero scattering-angle limit, up to $q_{\rm max} \simeq k\beta$. Fig. 4.3.4.25 shows how such calculated profiles can be used for fitting experimental data.

Setting $\beta = \pi$ [or equal to an effective upper limit $\theta_{\rm max} \simeq (\Delta E/E_0)^{1/2}$ corresponding to the criterion $q_{\rm max} r \simeq 1$], the integral cross section is the total cross section for the excitation of a given core level. These ionization cross sections are required for quantification in all analytical techniques using core-level excitations and de-excitations, such as EELS, Auger electron spectroscopy, and X-ray microanalysis (see Powell, 1976, 1984). A convenient way of comparing total cross sections is to rewrite the Bethe asymptotic cross section as

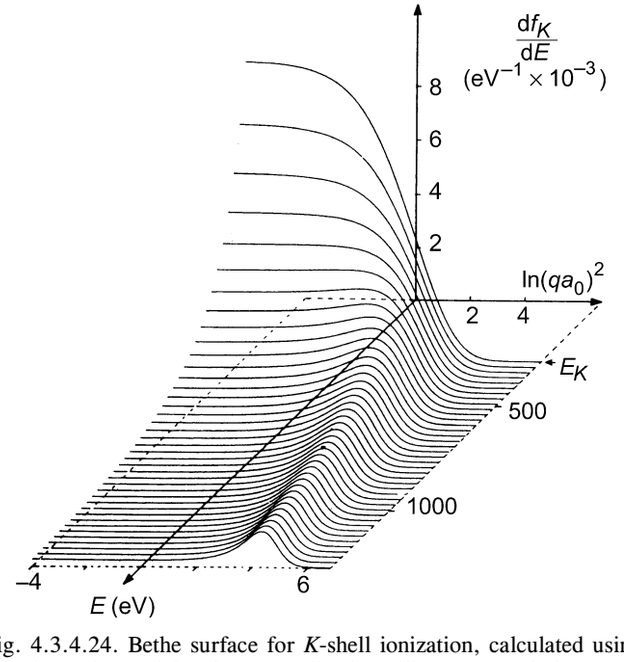

Fig. 4.3.4.24. Bethe surface for K-shell ionization, calculated using a hydrogenic model. The generalized oscillator strength is zero for energy loss E below the threshold E_K. The horizontal coordinate is related to scattering angle through q [from Egerton (1979)].

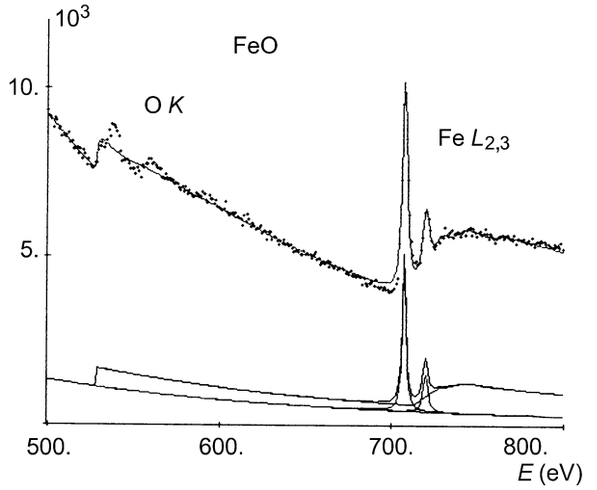

Fig. 4.3.4.25. A novel technique for simulating an energy-loss spectrum with two distinct edges as a superposition of theoretical contributions (hydrogenic saw-tooth for O K, Lorentzian white lines and delayed continuum for Fe $L_{2,3}$ calculated with the Hartree–Slater description). The best fit between the experimental and the simulated spectra is shown; it can be used to evaluate the relative concentration of the two elements [see Manoubi *et al.* (1990)].

$$\sigma_{nl}E_{nl}^2 = 6.51 \times 10^{-14} Z_{nl} b_{nl} \frac{\log(C_{nl}U_{nl})}{U_{nl}}, \qquad (4.3.4.47)$$

when the result is given in cm^2, σ_{nl} is the total cross section per atom or molecule or ionization of the *nl* subshell with edge energy E_{nl}, Z_{nl} is the number of electrons on the *nl* level, and U_{nl} is the overvoltage defined as E_0/E_{nl}. b_{nl} and c_{nl} are two parameters representing phenomenologically the average number of electrons involved in the excitation and their average energy loss (one finds for the major K and $L_{2,3}$ edges $b_{nl} \simeq 0.6$–0.9 and $c_{nl} \simeq 0.5$–0.7). These values are in practice estimated from plots of curves $\sigma_{nl}E_{nl}^2U_{nl}$ as a function of $\log U_{nl}$, known as Fano plots. From least-squares fits to linear regions, one can evaluate the values of b_{nl} (slope of the curves) and of $\log c_{nl}$ (coordinate at the origin) for various elements and shells. However, it has been shown more recently (Powell, 1989) that the interpretation of Fano plots is not always simple, since they typically display two linear regions. It is only in the linear region for the higher incident energies that the plots show the asymptotic Bethe dependence with the slope directly related to the optical data. At lower incident energies, another linear region is found with a slope typically 10–20% greater. Despite great progress over the last two decades, more cross-section data, either theoretical or experimental, are still required to improve to the 1% level the accuracy in all techniques using these signals.

4.3.4.4.3. *Solid-state effects*

The characteristic core edges recorded from solid specimens display complex structures different from those described in atomic terms. Moreover, their detailed spectral distributions depend on the type of compound in which the element is present (Leapman, Grunes & Fejes, 1982; Grunes, Leapman, Wilker, Hoffmann & Kunz, 1982; Colliex, Manoubi, Gasgnier & Brown, 1985). Modifications induced by the local solid-state environment concern (see Fig. 4.3.4.26) the following:

(*a*) *The threshold* (or edge itself), which may vary in position, slope, and associated fine structures. From photoelectron spectroscopies (UPS, XPS), an edge displacement along the energy scale is known as a 'chemical shift': it is due to a shift in the energy of the initial level as a consequence of the atomic potential modifications induced by valence-electron charge transfer (*e.g.* from metal to oxide). EELS is actually a two-level spectroscopy and the observed changes at edge onset concern both initial and final states. Consequently, measured shifts are due to a combination of core-level energy shift with bandgap and exciton creation. Some important shifts have been measured in EELS such as:

– carbon K: 284 to 288 eV from graphite to diamond;

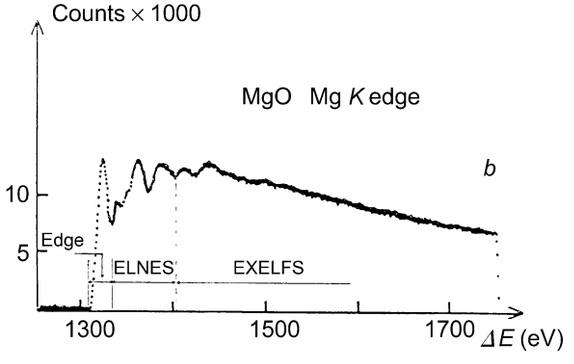

Fig. 4.3.4.26. Definition of the different fine structures visible on a core-loss edge.

– aluminium $L_{2,3}$: 73 to 77 eV from metal to Al_2O_3;

– silicon $L_{2,3}$: 99.5 to 106 eV from Si to SiO_2.

However, 'chemical shift' constitutes a simplified description of the more complex changes that may occur at a given threshold in various compounds. It assumes a rigid translation of the edge, but in most cases the onset changes in shape and there are no simple features to correlate through the different spectra. This remark is more relevant with the increased energy resolution that is now available. With a sub-eV value, extra peaks or splittings can frequently be detected on edges that exhibit simple shapes when recorded at lower resolution. Among others, the L_{32} white lines in transition metals show different behaviours when involved in various environments:

– crystal-field-induced splitting for each line in the oxides Sc_2O_3, TiO_2 when compared with the metal (see Fig. 4.3.4.27).

– relative change in L_3/L_2 intensity ratio between different ionic species [most important when the occupancy degree n for the d band is of the order of 5, *i.e.* around the middle of the transition series, *e.g.* Mn and Fe oxides; see for instance, Rask, Miner & Buseck (1987) and Rao, Thomas, Williams & Sparrow (1984)].

– presence of a narrow white line instead of a hydrogenic profile when the electron transfer from the metal to its ligand induces the existence of vacant d states at the Fermi level (CuO compared with Cu, see Fig. 4.3.4.28).

(*b*) *The near-edge fine structures* (ELNES), which extend over the first 20 or 30 eV above threshold (Taftø & Zhu, 1982; Colliex *et al.*, 1985). These are very similar to XANES structures in X-ray photoabsorption spectroscopy: they mostly reflect the spectral distribution of vacant accessible levels and are consequently very sensitive to site symmetry and charge transfer. Several approaches have been proposed to interpret them. A molecular-orbital description [*e.g.* Fischer (1970) or Tossell, Vaughan & Johnson (1974)] classifies the energy levels, both occupied and unoccupied, for clusters comprising the central excited ion and its first shell of neighbours. Its major success lies in the interpretation of level splitting on edges.

A one-electron band calculation constitutes a second step with noticeable successes in the case of metals (Müller, Jepsen &

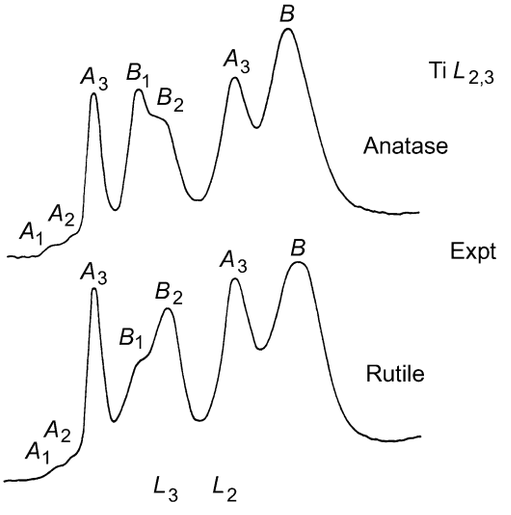

Fig. 4.3.4.27. High-energy resolution spectra on the $L_{2,3}$ titanium edge from two phases (rutile and anatase) of TiO_2. Each atomic line L_3 and L_2 is split into two components A and B by crystal-field effects. The new level of splitting B_1B_2 that distinguishes the two spectra is not yet understood. In Ti metal, the L_3 and L_2 lines are not split by structural effects [courtesy of Brydson *et al.* (1989)].

Wilkins, 1982). Core-loss spectroscopy, however, imposes specific conditions on the accessible final state: the overlap with the initial core wavefunction involves a projection in space on the site of the core hole, and the dominant dipole selection rules are responsible for angular symmetry selection. When extending the band-structure calculations to energy states rather high above the Fermi level, more elaborate methods, combining the conceptual advantage of the tight-binding method with the accuracy of *ab initio* pseudopotential calculations, have been developed (Janssen & Sankey, 1987). This self-consistent pseudo-atomic orbital band calculation has been used to describe ELNES structures on different covalent solids (Weng, Rez & Ma, 1989; Weng, Rez & Sankey, 1989).

The most promising description at present is the multiple scattering method developed for X-ray absorption spectra by Durham, Pendry & Hodges (1981) and Vvedensky, Saldin & Pendry (1985). It interprets the spectral modulations, in the energy range 10 to 30 eV above the edge, as due to interference effects, on the excited site, between all waves back-scattered by the neighbouring atoms (see Fig. 4.3.4.29). This multiple scattering description in real space should in principle converge towards the local point of view in the solid-state band model, calculated in reciprocal space (Heine, 1980). As an example investigated by EELS, the oxygen and magnesium K edges in MgO have been calculated by Lindner, Sauer, Engel & Kambe (1986) and by Weng & Rez (1989) for increased numbers of coordination shells and different potential models (representing variable ionicities). Fig. 4.3.4.30 shows the comparison of an experimental spectrum with such a calculation. Another useful idea emerging from this model is the simple relation, expressed by Bianconi, Fritsch, Calas & Petiau (1985):

$$(E_r - E_b)\, d^2 = C, \qquad (4.3.4.48)$$

where E_r is the energy position of a given resonance peak attributed to multiple scattering from a given shell of neighbours (d is the distance to this shell), and E_b is a reference energy close to the threshold energy. This simple law, advertised as the way of measuring 'bond lengths with a ruler' (Stohr, Sette & Jonson, 1984), seems to be quite useful when comparing similar structures (Lytle, Greegor & Panson, 1988).

Other effects, generally described as multi-electron contributions, cannot be systematically omitted. They all deal with the presence of a core hole on the excited atom and with its influence on the distribution of accessible electron states. Of particular importance are the intra-atomic configuration interactions for white lines, as explained by Zaanen, Sawatsky, Fink, Speier & Fuggle (1985) for L_3 and L_2 lines in transition metals and by Thole, van der Laan, Fuggle, Swatsky, Karnatak & Esteva (1985) for $M_{4,5}$ lines in rare-earth elements.

(*c*) *The extended fine structures* (EXELFS) are equivalent to the well known EXAFS oscillations in X-ray absorption spectroscopy (Sayers, Stern & Lytle, 1971; Teo & Joy, 1981). Within the previously described multiscattering theory, it corresponds to the first step, the single scattering regime (see Fig. 4.3.4.29*a*). These extended oscillations are due to the interference on the excited atom between the outgoing excited

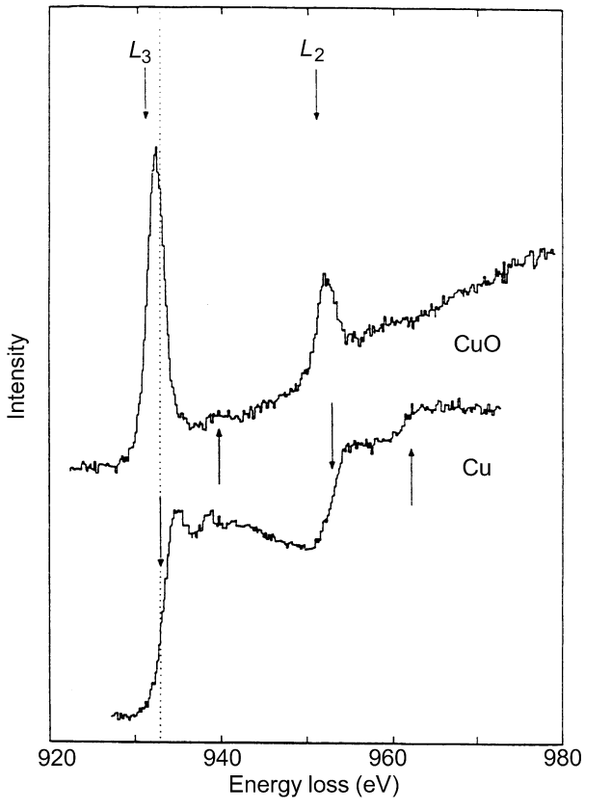

Fig. 4.3.4.28. The dramatic change in near-edge fine structures on the L_3 and L_2 lines of Cu, from Cu metal to CuO. The appearance of the intense narrow white lines is due to the existence of vacant d states close to the Fermi level [courtesy of Leapman *et al.* (1982)].

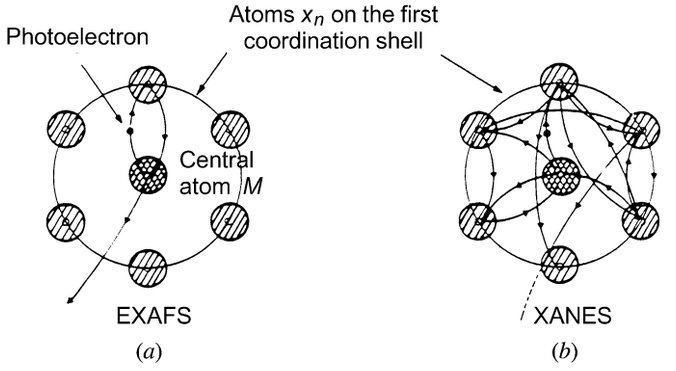

Fig. 4.3.4.29. Illustration of the single and multiple scattering effects used to describe the final wavefunction on the excited site. This theory is very fruitful for understanding and interpreting EXELFS and ELNES features, respectively equivalent to EXAFS and XANES encountered in X-ray absorption spectra.

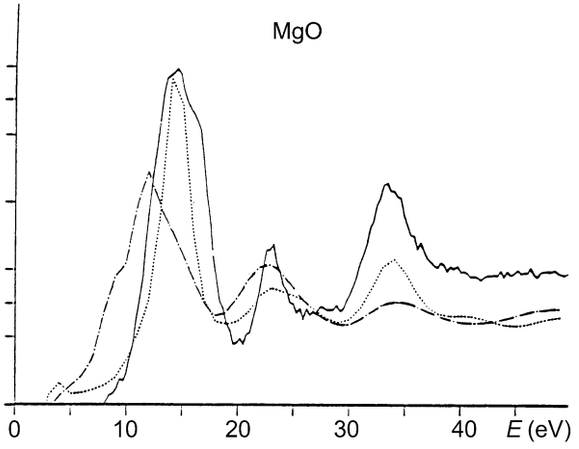

Fig. 4.3.4.30. Comparison of the experimental O K edge (solid line) with calculated profiles in the multiple scattering approach [courtesy of Weng & Rez (1989)].

electron wavefunction and its components reflected on the nearest-neighbour atoms. This interference is destructive or constructive depending on the ratio between the return path length $2r_i$ (where r_i is the radial distance with the ith shell of backscattering atoms) and the wavelength of the excited electron. Fourier analysis of EXELFS structures, from 50 eV above the ionization threshold, gives the radial distribution function around this specific site. This is mostly a technique for measuring the local short-range order. Its accuracy has been established to be better than 0.1 Å on nearest-neighbour distances with test specimens, but such performance requires correction procedures for phase shifts. The method therefore seems more promising for measuring changes in interatomic distances in specimens of the same chemical composition. The major advantage of EXELFS is its applicability for small specimen volumes that can moreover be characterized by other high-resolution electron-microscopy modes. It is also possible to investigate bond lengths in different directions by selecting the scattering angle of the transmitted electron and the specimen orientation (Disko, Krivanek & Rez, 1982). On the other hand, the major limitations of EXELFS are due to the dose requirements for sufficient SNR and to the fact that the accessible excitation range is limited to edges below ~2–3 keV and to oscillation domains ~200 or 300 eV at the maximum.

4.3.4.4.4. *Applications for core-loss spectroscopy*

(*a*) *Quantitative microanalysis*

The main field of application of core-loss EELS spectroscopy has been its use for local chemical analysis (Maher, 1979; Colliex, 1984; Egerton, 1986). The occurrence of an edge superimposed on the regularly decreasing background of an EELS spectrum is an indication of the presence of the associated element within the analysed volume.

Methods have been developed to extract quantitative composition information from these spectra. The basic idea lies in the linear relationship between the measured signal (S) and the number (N) of atoms responsible for it (this is valid in the single core-loss domain for specimen thickness, *i.e.* up to several micrometres):

$$S = I_0 N \sigma, \tag{4.3.4.49}$$

where I_0 is the incident-beam intensity and σ the relevant excitation cross section in the experimental conditions used, and N is the number of atoms per unit area of specimen. As a satisfactory approximation for taking into account multiple scattering events (either elastic or inelastic in the low-loss region), Egerton (1978) has proposed that equation (4.3.4.49) be rewritten:

$$S(\beta, \Delta) = I_0(\beta, \Delta) N \sigma(\beta, \Delta), \tag{4.3.4.50}$$

where all quantities correspond to a limited angle of collection β and to a limited integration window Δ (eV) above threshold for signal measurement.

A major problem is the evaluation of the signal itself after background subtraction. The method generally used, demonstrated in Fig. 4.3.4.31, involves extrapolating a modelized background profile below the core loss of interest. Following Egerton (1978), the choice of a power law $B(\Delta E) = A \Delta E^{-R}$ is satisfactory in many cases, and the signal is then defined as

$$S(\Delta) = \int_{E_c}^{E_c+\Delta} [I(\Delta E) - B(\Delta E)] \, \mathrm{d}(\Delta E). \tag{4.3.4.51}$$

Numerical methods have been developed to perform this process with a well controlled analysis of statistical errors (Trebbia, 1988).

In many cases, one is interested in elemental ratios; consequently, the useful formula becomes

$$\frac{N_A}{N_B} = \frac{S_A(\beta, \Delta)}{S_B(\beta, \Delta)} \frac{\sigma_B(\beta, \Delta)}{\sigma_A(\beta, \Delta)}. \tag{4.3.4.52}$$

This can be used to determine the N_A/N_B ratio without standards, if the cross-section ratio σ_B/σ_A (also called the k_{AB} factor) is previously known: accuracy at present is limited to ±5% for most edges. But it is also possible to extract from this formula the cross-section (or k factor) experimental values for comparison with the calculated ones, if the local stoichiometry of the specimen is satisfactorily known [Hofer, Golob & Brunegger (1988) and Manoubi *et al.* (1989) for the $M_{4,5}$ edges].

Improvements have recently been made in order to reduce the different sources of errors. For medium-thickness specimens (*i.e.* for $t \simeq \lambda_p$ where λ_P is the mean free path for plasmon excitation), deconvolution techniques are introduced for a safer determination of the signal. When the background extrapolation method cannot be used, *i.e.* when edges overlap noticeably, new approaches (such as illustrated in Fig. 4.3.4.25) try to determine the best simulated profile over the whole energy-loss range of interest. It requires several contributions, either deduced from previous measurements on standard (Shuman & Somlyo, 1987; Leapman & Swyt, 1988), or from reasonable mathematical models with different contributions for dealing with transitions towards bound states or continuum states (Manoubi, Tence, Walls & Colliex, 1990).

(*b*) *Detection limits*

This method has been shown to be the most successful of all EM techniques in terms of ultimate mass sensitivity and associated spatial resolution. This is due to the strong probability of excitation for the signals of interest (primary ionization event) and to the good localization of the characteristic even within the irradiated volume of material. Variations in composition have been recorded at a subnanometre level (Scheinfein & Isaacson, 1986; Colliex, 1985; Colliex, Maurice & Ugarte, 1989). In terms of ultimate sensitivity (minimum number of identified atoms), the range of a few tens of atoms (~10^{-21} g) has been reached as early as about 15 years ago in the pioneering work of

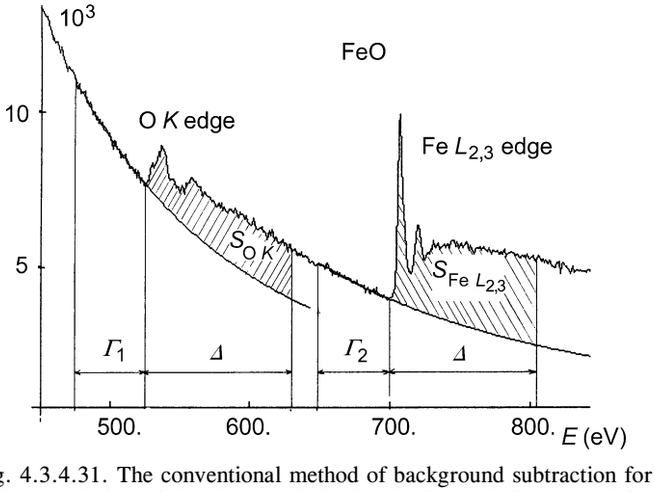

Fig. 4.3.4.31. The conventional method of background subtraction for the evalulation of the characteristic signals S_{OK} and $S_{Fe L_{2,3}}$ used for quantitative elemental analysis (to be compared with the approach described in Fig. 4.3.4.25).

Isaacson & Johnson (1975). Very recently, a level close to the single-atom identification has been demonstrated (Mory & Colliex, 1989). A major obstacle is then often radiation damage, and consequent specimen modification induced by the very intense primary dose required for obtaining sufficient SNR values.

On the other hand, the EELS technique has long been less fruitful for investigating low concentrations of impurities within a matrix. This is a consequence of the very high intrinsic background under the edges of interest: in most applications, the atomic concentration detection limit was in the range 10^{-3} to 10^{-2}. The introduction of satisfactory methods for processing the systematic sources of noise in spectra acquired with parallel detection devices (Shuman & Kruit, 1985) has greatly modified this situation. One can now take full benefit from the very high number of counts thus recorded within a reasonable time (10^6 to 10^7 counts per channel) and detection of calcium of the order of 10^{-5} atomic concentration in an organic matrix has been demonstrated by Shuman & Somlyo (1987).

(*c*) *Crystallographic information in EELS*

Although not particularly suited to solving crystal-structure problems, EELS carries structural information at different levels:

In a crystalline specimen, one detects orientation effects on the intensity of core-loss edges. This is a consequence of the channelling of the Bloch standing waves as a function of the crystal orientation This observation requires well collimated angular conditions and inelastic localization better than the lattice spacing responsible for elastic diffraction. When these criteria apply, the changes in core-loss excitations with crystallographic orientation can be used to determine the crystallographic site of specific atoms (Tafto & Krivanek, 1982). An equivalent method, known as ALCHEMI (atom location by channelling enhanced microanalysis), which involves measuring the change of X-ray production as a function of crystal orientation, has been applied to the determination of the preferential site for substitutional impurities in many crystals (Spence & Tafto, 1983).

Energy-filtered electron-diffraction patterns of core-loss edges could reveal the symmetry of the local coordination of selected atomic species rather than the symmetry of the crystal as a whole. This type of information should be compared with ELNES data (Spence, 1981).

At large scattering angles, and for energy losses far beyond the excitation threshold, the Bethe ridge [or electron Compton profile (see §§4.3.4.3.3 and 4.3.4.4.2)] constitutes a major feature easily observable in energy-filtered diffraction patterns (Reimer & Rennekamp, 1989). The width of this feature is associated with the momentum distribution of the excited electrons (Williams & Bourdillon, 1982). Quantitative analysis of the data is similar to the Fourier method for EXELFS oscillations. After subtracting the background contribution, the spectrum is converted into momentum space and Fourier transformed to obtain the reciprocal form factor $B(r)$: it is the autocorrelation of the ground-state wavefunction in a direction specified by the scattering vector $\mathbf{q}$. This technique of data analysis to study electron momentum densities is directly developed from high-energy photon-scattering experiments (Williams, Sparrow & Egerton, 1984).

4.3.4.5. *Conclusions*

Since the early work of Hillier & Baker (1944), EELS spectroscopy has established itself as a prominent technique for investigating various aspects of the electronic structure of solids, As a fundamental application, it is now possible to construct a self-consistent set of data for a substance by combination of optical or energy-loss functions over a wide spectral range (Altarelli & Smith, 1974; Shiles, Sazaki, Inokuti & Smith, 1980: Hagemann, Gudat & Kunz, 1975). Sum-rule tests provide useful guidance in selecting the best values from the available measurements. The Thomas–Reiche–Kuhn *f*-sum rule can be expressed in a number of equivalent forms, which all require the knowledge of a function $[\varepsilon_2, \kappa, \mathrm{Im}(-1/\varepsilon)]$ describing dissipative processes over all frequencies:

$$\left.\begin{aligned} \int_0^\infty \omega\varepsilon_2(\omega)\,\mathrm{d}\omega &= \frac{\pi}{2}\omega_p^2, \\ \int_0^\infty \omega\kappa(\omega)\,\mathrm{d}\omega &= \frac{\pi}{4}\omega_p^2, \\ \int_0^\infty \omega\left(-\frac{1}{\varepsilon(\omega)}\right)\mathrm{d}\omega &= \frac{\pi}{2}\omega_p^2. \end{aligned}\right\} \tag{4.3.4.53}$$

One defines the effective number density n_{eff} of electrons contributing to these various absorption processes at an energy $\hbar\omega$ by the partial *f* sums:

$$\left.\begin{aligned} n_{\mathrm{eff}}(\omega)|_{\varepsilon_2} &= \frac{m_0}{2\pi^2 e^2}\int_0^\omega \omega'\varepsilon_2(\omega')\,\mathrm{d}\omega', \\ n_{\mathrm{eff}}(\omega)|_{\kappa} &= \frac{m_0}{\pi^2 e^2}\int_0^\omega \omega'\kappa(\omega')\,\mathrm{d}\omega', \\ n_{\mathrm{eff}}(\omega)|_{-1/\varepsilon} &= \frac{m_0}{2\pi^2 e^2}\int_0^\omega \omega'\left[-\frac{1}{\varepsilon(\omega')}\right]\mathrm{d}\omega'. \end{aligned}\right\} \tag{4.3.4.54}$$

As an example, the values of $n_{\mathrm{eff}}(\omega)$ from the infrared to beyond the *K*-shell excitation energy for metallic aluminium are shown in Fig. 4.3.4.32. In this case, the conduction and core-electron contributions are well separated. One sees that the excitation of conduction electrons is virtually completed above the plasmon resonance only, but the different behaviour of the integrands below this value is a consequence of the fact that they describe different properties of matter: $\varepsilon_2(\omega)$ is a measure of the rate of energy dissipation from an electromagnetic wave, $\kappa(\omega)$ describes

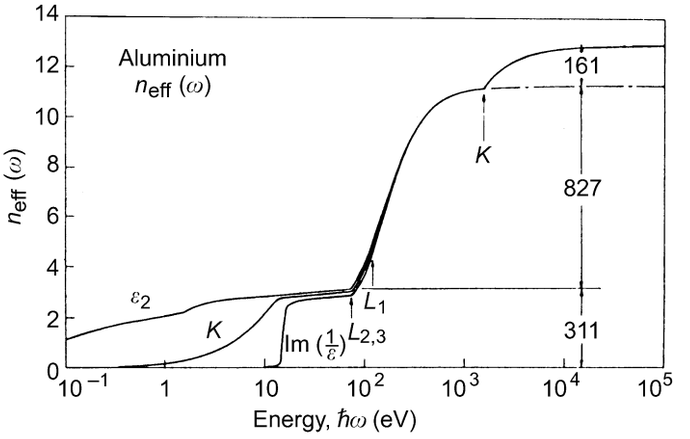

Fig. 4.3.4.32. Values of n_{eff} for metallic aluminium based on composite optical data [courtesy of Shiles *et al.* (1980)].

the decrease in amplitude of the wave, and $\mathrm{Im}[-\varepsilon^{-1}(\omega)]$ is related to the energy loss of a fast electron. The above curve shows some exchange of oscillator strength from core to valence electrons, arising from the Pauli principle, which forbids transitions to occupied states for the deeper electrons.

More practically, in the microanalytical domain, the combination of high performance attained by using EELS with parallel detection (*i.e.* energy resolution below 1 eV, spatial resolution below 1 nm, minimum concentration below 10^{-3} atom, time resolution below 10 ms) makes it a unique tool for studying local electronic properties in solid specimens.

4.3.5. Oriented texture patterns (By B. B. Zvyagin)

4.3.5.1. *Texture patterns*

The formation of textures in specimens for diffraction experiments is a natural consequence of the tendency for crystals of a highly anisotropic shape to deposit with a preferred orientation. The corresponding diffraction patterns may present some special advantages for the solution of problems of phase and structure analysis. Lamellar textures composed of crystals with the most fully developed face parallel to a plane but randomly rotated about its normal are specially important. The ease of interpretation of patterns of such textures when oriented obliquely to the primary beam (*OT* patterns) is a valuable property of the electron-diffraction method (Pinsker, 1953; Vainshtein, 1964; Zvyagin, 1967; Zvyagin, Vrublevskaya, Zhukhlistov, Sidorenko, Soboleva & Fedotov, 1979). Texture patterns (*T* patterns) are also useful in X-ray diffraction (Krinary, 1975; Mamy & Gaultier, 1976; Plançon, Rousseaux, Tchoubar, Tchoubar, Krinari & Drits, 1982).

4.3.5.2. *Lattice plane oriented perpendicular to a direction (lamellar texture)*

If in the plane of orientation (the texture basis) the crystal has a two-dimensional cell a, b, γ, the c^* axis of the reciprocal cell will be the texture axis. Reciprocal-lattice rods parallel to c^* intersect the plane normal to them (the ab plane of the direct lattice) in the positions hk of a two-dimensional net that has periods $1/a\sin\gamma$ and $1/b\sin\gamma$ with an angle $\gamma' = \pi - \gamma$ between them, whatever the direction of the c axis in the direct lattice.

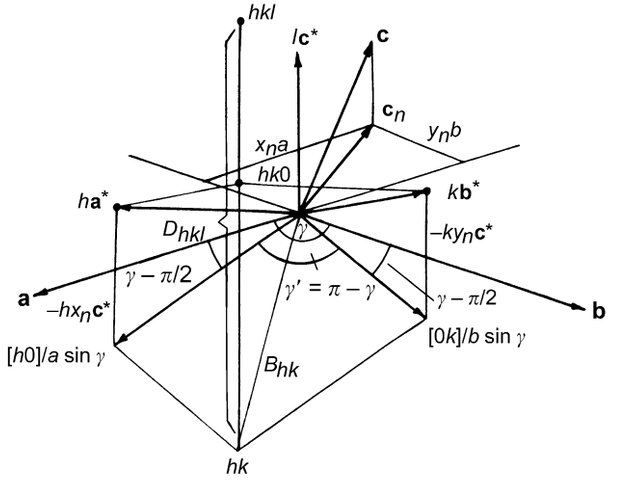

Fig. 4.3.5.1. The relative orientations of the direct and the reciprocal axes and their projections on the plane ab, with indication of the distances B_{hk} and D_{hkl} that define the positions of reflections in lamellar texture patterns.

The latter is defined by the absolute value c and the normal projection c_n on the ab plane, with components x_n, y_n along the axes a, b. In the triclinic case,

$$x_n = (c/a)(\cos\beta - \cos\alpha\cos\gamma)/\sin^2\gamma \qquad (4.3.5.1)$$

$$y_n = (c/b)(\cos\alpha - \cos\beta\cos\gamma)/\sin^2\gamma \qquad (4.3.5.2)$$

(Zvyagin *et al.*, 1979). The lattice points of each rod with constant hk and integer l are at intervals of $c^* = 1/d_{001}$, but their real positions, described by their distances D_{hkl} from the plane ab, depend on the projections of the axes a^* and b^* on c^* (see Fig. 4.3.5.1), the equations

$$x_n = -a^*\cos\beta^*/c^* \qquad (4.3.5.3)$$

$$y_n = -b^*\cos\alpha^*/c^* \qquad (4.3.5.4)$$

being satisfied.

The reciprocal-space representation of a lamellar texture is formed by the rotation of the reciprocal lattice of a single crystal about the c^* axis. The rods hk become cylinders and the lattice points become circles lying on the cylinders. In the case of high-energy electron diffraction (HEED), the wavelength of the electrons is very short, and the Ewald sphere, of radius $1/\lambda$, is so great that it may be approximated by a plane passing through the origin of reciprocal space and normal to the incident beam. The patterns differ in their geometry, depending on the angle φ through which the specimen is tilted from perpendicularity to the primary beam. At $\varphi = 0$, the pattern consists of hk rings. When $\varphi \neq 0$ it contains a two-dimensional set of reflections hkl falling on hk ellipses formed by oblique sections of the hk cylinders. In the limiting case of $\varphi = \pi/2$, the ellipses degenerate into pairs of parallel straight lines theoretically containing the maximum numbers of reflections. The reflection positions are defined by two kinds of distances: (1) between the straight lines hk (length of the short axes of the ellipses hk):

$$B_{hk} = (1/\sin\gamma)(h^2/a^2 + k^2/b^2 - 2hk\cos\gamma/ab)^{1/2} \qquad (4.3.5.5)$$

and (2) from the reflection hkl to the line of the short axes:

$$D_{hkl} = (ha^*\cos\beta^*/c^* + kb^*\cos\alpha^*/c^* + l)c^* \qquad (4.3.5.6)$$

$$= (-hx_n - ky_n + l)/d_{001}. \qquad (4.3.5.7)$$

In patterns obtained under real conditions ($0 < \varphi < \pi/2$, accelerating voltage V proportional to λ^{-2}, distance L between the specimen and the screen), these values are presented in the scale of $L\lambda$, D_{hkl} also being proportional to $1/\sin\varphi$ with maximum value $D_{\max} = B_{hk}\tan\varphi$ for the registrable reflections. The values of B_{hk} and D_{hkl}, determined by the unit cells and the indices hkl, are the objects of the geometrical analysis of the *OT* patterns. When the symmetry is higher than triclinic, the expression for B_{hk} and D_{hkl} are much simpler.

Such *OT* patterns are very informative, because the regular two-dimensional distribution of the hkl reflections permits definite indexing, cell determination, and intensity measurements. For low-symmetry and fine-grained substances, they present unique advantages for phase identification, polytypism studies, and structure analysis.

In the X-ray study of textures, it is impossible to neglect the curvature of the Ewald sphere and the number of reflections recorded is restricted to larger d values. However, there are advantages in that thicker specimens can be used and reflections with small values of B_{hk}, especially the $00l$ reflections, can be recorded. Such patterns are obtained in usual powder cameras with the incident beam parallel to the platelets of the oriented aggregate and are recorded on photographic film in the form of hkl reflection sequences along hk lines, as was demonstrated by

Mamy & Gaultier (1976). The *hk* lines are no longer straight, but have the shapes described by Bernal (1926) for rotation photographs. It is difficult, however, to prepare good specimens. Other arrangements have been developed recently with advantages for precise intensity measurements. The reflections are recorded consecutively by means of a powder diffractometer fitted with a goniometer head. The relation between the angle of tilt φ and the angle of diffraction (twice the Bragg angle) 2θ depends on the reciprocal-lattice point to be recorded. If the latter is defined by a vector of length $H = (2\sin\theta)/\lambda$ and by the angle ω between the vector and the plane of orientation (texture basis), the relation $\varphi = \theta - \omega$ permits scanning of reciprocal space along any trajectory by proper choice of consecutive values of ω or θ. In particular, if ω is constant, the trajectory is a straight line passing through the origin at an angle ω to the plane of orientation (Krinary, 1975). Using additional conditions [$\omega = \arctan(D/B)$, $H = (B^2 + D^2)^{1/2}$], Plançon *et al.* (1982) realized the recording and the measurement of intensities along the cylinder-generating *hk* rods for different shapes of the misorientation function $N(\alpha)$.

In the course of development of electron diffractometry, a deflecting system has been developed that permits scanning the electron diffraction pattern across the fixed detector along any direction over any interval (Fig. 4.3.5.2). The intensities are measured point by point in steps of variable length. This system is applicable to any kind of two-dimensional intensity pattern, and in particular to texture patterns (Zvyagin, Zhukhlistov & Plotnikev, 1996). Electron diffractometry provides very precise intensity measurements and very reliable structural data (Zhukhlistov *et al.*, 1997).

If the effective thickness of the lamellae is very small, of the order of the lattice parameter c, the diffraction pattern generates into a combination of broad but recognizably distinct $00l$ reflections and broad asymmetrical *hk* bands (Warren, 1941). The classical treatments of the shape of the bands were given by Méring (1949) and Wilson (1949) [for an elementary introduction see Wilson (1962)].

(*a*)

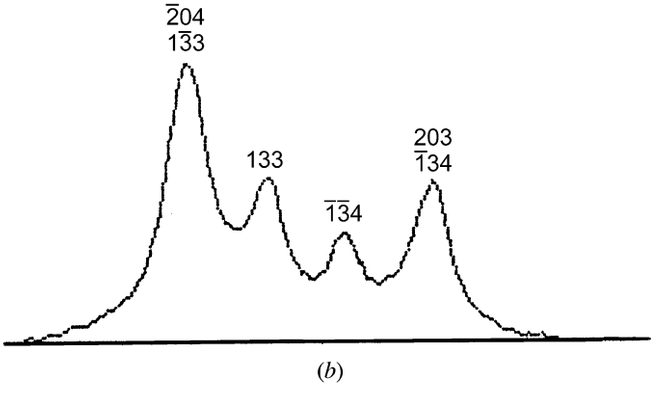

(*b*)

Fig. 4.3.5.2. (*a*) Part of the OTED pattern of the clay mineral kaolinite and (*b*) the intensity profile of a characteristic quadruplet of reflections recorded with the electron diffractometry system. The scanning direction is indicated in (*a*).

4.3.5.3. *Lattice direction oriented parallel to a direction (fibre texture)*

A fibre texture occurs when the crystals forming the specimen have a single direction in common. Each point of the reciprocal lattice describes a circle lying in a plane normal to the texture axis. The pattern, considered as plane sections of the reciprocal-lattice representation, resembles rotation diagrams of single crystals and approximates to the patterns given by cylindrical lattices (characteristic, for example, of tubular crystals).

If the *a* axis is the texture axis, the *hk* rods are at distances

$$B_{hk} = (-h\cos\gamma/a + k/b)/\sin\gamma \qquad (4.3.5.8)$$

from the texture axis and

$$D_{hk} = h/a \qquad (4.3.5.9)$$

from the plane normal to the texture axis (the zero plane b^*c^*). On rotation, they intersect the plane normal to the incident beam and pass through the texture axis in layer lines at distances D_{hk} from the zero line, while the reflection positions along these lines are defined by their distances from the textures axis (see Fig. 4.3.5.3):

$$B_{hkl} = [B_{hk}^2 + (-hx_n - ky_n + l)^2/d_{001}^2]^{1/2}. \qquad (4.3.5.10)$$

If the texture axis forms an angle ε with the *a* axis and $\delta = \varepsilon - \gamma + \pi/2$ with the projection of a^* on the plane *ab*, then

$$B_{hk} = \{-h(\sin\delta)/a + k[\sin(\gamma' - \delta)]/b\}/\sin\gamma \qquad (4.3.5.11)$$

$$= \{-h[\cos(\gamma - \varepsilon)]/a + k\cos\varepsilon/b\}/\sin\gamma \qquad (4.3.5.12)$$

$$D_{hk} = \{h(\cos\delta)/a + k[\cos(\gamma' - \delta)]/b\}/\sin\gamma \qquad (4.3.5.13)$$

$$= \{h[\sin(\gamma - \varepsilon)]/a + k\sin\varepsilon/b\}/\sin\gamma. \qquad (4.3.5.14)$$

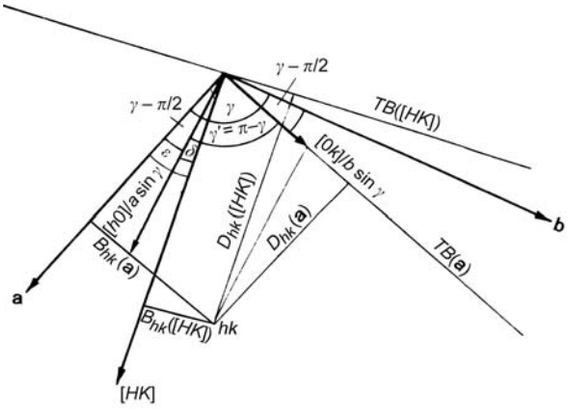

Fig. 4.3.5.3. The projections of the reciprocal axes on the plane *ab* of the direct lattice, with indications of the distances *B* and *D* of the *hk* rows from the fibre-texture axes *a* or [*hk*].

The relation between the angles δ, ε, and the direction $[hk]$ of the texture axis is given by the expression

$$\begin{aligned}\cos\delta &= \sin(\gamma-\varepsilon)\\ &= [h/a - k(\cos\gamma)/b]\\ &\quad\times[h^2a^{-2}+k^2b^{-2}-2hk(\cos\gamma)/ab]^{-1/2}.\end{aligned}\qquad(4.3.5.15)$$

The layer lines with constant h that coincide when $\varepsilon = 0$ are split when $\varepsilon \neq 0$ according to the sign of k, since then $D_{hk} \neq D_{h\bar{k}}$ and B_{hk} and B_{hkl} defining the reflection positions along the layer line take other values. Such peculiarities have been observed by means of selected-area electron diffraction for tabular particles and linear crystal aggregates of some phyllosilicates in the simple case of $\gamma = \pi/2$ (Gritsaenko, Zvyagin, Boyarskaya, Gorshkov, Samotoin & Frolova, 1969).

When fibres or linear aggregates are deposited on a film (for example, in specimens for high-resolution electron diffraction) with one direction parallel to a plane, they form a texture that is intermediate between lamellar and fibre. The points of the reciprocal lattice are subject to two rotations: around the fibre axis and around the normal to the plane. The first rotation results in circles, the second in spherical bands of different widths, depending on the position of the initial point relative to the texture axis and the zero plane normal to it. The diffraction patterns correspond to oblique plane sections of reciprocal space, and consist of arcs having intensity maxima near their ends; in some cases, the arcs close to form complete circles. In particular, when the particle elongation is in the a direction, the angular range of the arcs decreases with h and increases with k (Zvyagin, 1967).

4.3.5.4. *Applications to metals and organic materials*

The above treatment, though general, had layer silicates primarily in view. Texture studies are particularly important for metal specimens that have been subjected to cold work or other treatments; the phenomena and their interpretation occupy several chapters of the book by Barrett & Massalski (1980). Similarly, Kakudo & Kasai (1972) devote much space to texture in polymer specimens, and Guinier (1956) gives a good treatment of the whole subject. The mathematical methods for describing and analysing textures of all types have been described by Bunge (1982; the German edition of 1969 was revised in many places and a few errors were corrected for the English translation).

4.3.6. Computation of dynamical wave amplitudes

4.3.6.1. *The multislice method (By D. F. Lynch)*

The calculation of very large numbers of diffracted orders, *i.e.* more than 100 and often several thousand, requires the multislice procedure. This occurs because, for N diffracted orders, the multislice procedure involves the manipulation of arrays of size N, whereas the scattering matrix or the eigenvalue procedures involve manipulation of arrays of size N by N.

The simplest form of the multislice procedure presumes that the specimen is a parallel-sided plate. The surface normal is usually taken to be the z axis and the crystal structure axes are often chosen or transformed such that the c axis is parallel to z and the a and b axes are in the xy plane. This can often lead to rather unconventional choices for the unit-cell parameters. The maximum tilt of the incident beam from the surface normal is restricted to be of the order of 0.1 rad. For the calculation of wave amplitudes for larger tilts, the structure must be reprojected down an axis close to the incident-beam direction. For simple calculations, other crystal shapes are generally treated by the column approximation, that is the crystal is presumed to consist of columns parallel to the z axis, each column of different height and tilt in order to approximate the desired shape and variation of orientation.

The numerical procedure involves calculation of the transmission function through a thin slice, calculation of the vacuum propagation between centres of neighbouring slices, followed by evaluation in a computer of the iterated equation

$$u_n(h,k) = p_n\{p_{n-1}\ldots p_3[p_2(p_1q_1 * q_2) * q_3] * \ldots * q_n\} \quad (4.3.6.1)$$

in order to obtain the scattered wavefunction, $u_n(h,k)$, emitted from slice n, *i.e.* for crystal thickness $H = \Delta z_1 + \Delta z_2 + \ldots + \Delta z_n$; the symbol $*$ indicates the operation 'convolution' defined by

$$f_1(x) * f_2(x) = \int_{-\infty}^{\infty} f_1(w) f_2(x-w)\,\mathrm{d}w,$$

and

$$p_n = \exp\left(-i2\pi\Delta z_n(\lambda/2)\{[h(h-h'')/a^2] + [k(k-k'')/b^2]\}\right)$$

is the propagation function in the small-angle approximation between slice $n-1$ and slice n over the slice spacing Δz_n. For simplicity, the equation is given for orthogonal axes and h'', k'' are the usually non-integral intercepts of the Laue circle on the reciprocal-space axes in units of $(1/a)$, $(1/b)$. The excitation errors, $\zeta(h,k)$, can be evaluated using

$$\zeta(h,k) = -(\lambda/2)\{[h(h-h'')/a^2] + [k(k-k'')/b^2]\}. \quad (4.3.6.2)$$

The transmission function for slice n is

$$q_n(h,k) = F\{\exp[i\sigma\varphi_n(x,y)\Delta z_n]\}, \quad (4.3.6.3)$$

where F denotes Fourier transformation from real to reciprocal space, and

$$\varphi_n(x,y)\Delta z_n = {}^p\varphi(x,y) = \int_{z_{n-1}}^{z_{n-1}+\Delta z_n} \varphi(x,y,z)\,\mathrm{d}z$$

and

$$\sigma = \frac{\pi}{W\lambda}\,\frac{2}{1+(1-\beta^2)^{1/2}}$$

and

$$\beta = \frac{v}{c},$$

where W is the beam voltage, v is the relativistic velocity of the electron, c is the velocity of light, and λ is the relativistic wavelength of the electron.

The operation $*$ in (4.3.6.1) is most effectively carried out for large N by the use of the convolution theorem of Fourier transformations. This efficiency presumes that there is available an efficient fast-Fourier-transform subroutine that is suitable for crystallographic computing, that is, that contains the usual crystallographic normalization factors and that can deal with a range of values for h, k that go from negative to positive. Then,

$$u_n(h,k) = F\{F^{-1}[u_{n-1}(h,k)]F^{-1}[q_n(h,k)]\}, \quad (4.3.6.4)$$

where F denotes

$$u(h,k) = \frac{1}{n_x n_y}\sum_{x=1}^{n_x}\sum_{y=1}^{n_y} U(x,y)\exp\left\{2\pi i\left[\frac{hx}{n_x},\frac{ky}{n_y}\right]\right\}$$

and F^{-1} denotes

$$U(x,y) = \sum_{h=-n_h}^{n_h} \sum_{k=-n_k}^{n_k} u(h,k) \exp\left\{2\pi i \left[\frac{hx}{n_x}, \frac{ky}{n_y}\right]\right\},$$

where $n_h = (n_x/2) - 1$, $n_k = (n_y/2) - 1$, and n_x, n_y are the sampling intervals in the unit cell. The array sizes used in the calculations of the Fourier transforms are commonly powers of 2 as is required by many fast Fourier subroutines. The array for $u_n(h,k)$ is usually defined over the central portion of the reserved computer array space in order to avoid oscillation in the Fourier transforms (Gibbs instability). It is usual to carry out a 64×64 beam calculation in an array of 128×128, hence the critical timing interval in a multislice calculation is that interval taken by a fast Fourier transform for $4N$ coefficients. If the number of beams, N, is such that there is still appreciable intensity being scattered outside the calculation aperture, then it is usually necessary to impose a circular aperture on the calculation in order to prevent the symmetry of the calculation aperture imposing itself on the calculated wavefunction. This is most conveniently achieved by setting all $p(h,k)$ coefficients outside the desired circular aperture to zero.

It is clear that the iterative procedure of (4.3.6.1) means that care must be taken to avoid accumulation of error due to the precision of representation of numbers in the computer that is to be used. Practical experience indicates that a precision of nine significant figures (decimal) is more than adequate for most calculations. A precision of six to seven (decimal) figures (a common 32-bit floating-point representation) is only barely satisfactory. A computer that uses one of the common 64-bit representations (12 to 16 significant figures) is satisfactory even for the largest calculations currently contemplated.

The choice of slice thickness depends upon the maximum value of the projected potential within a slice and upon the validity of separation of the calculation into transmission function and propagation function. The second criterion is not severe and in practice sets an upper limit to slice thickness of about 10 Å. The first criterion depends upon the atomic number of atoms in the trial structure. In practice, the slice thickness will be too large if two atoms of medium to heavy atomic weight ($Z \geq 30$) are projected onto one another. It is not necessary to take slices less than one atomic diameter for calculations for fast electron (acceleration voltages greater than 50 keV) diffraction or microscopy. If the trial structure is such that the symmetry of the diffraction pattern is not strongly dependent upon the structure of the crystal parallel to the slice normal, then the slices may be all identical and there is no requirement to have a slice thickness related to the periodicity of the structure parallel to the surface normal. This is called the 'no upper-layer-line' approximation. If the upper-layer lines are important, then the slice thickness will need to be a discrete fraction of the c axis, and the contents of each slice will need to reflect the actual atomic contents of each slice. Hence, if there were four slices per unit cell, then there would need to be four distinct $q(h,k)$, each taken in the appropriate order as the multislice operation proceeds in thickness.

The multislice procedure has two checks that can be readily performed during a calculation. The first is applied to the transmission function, $q(h,k)$, and involves the evaluation of a unitarity test by calculation of

$$\sum_{h'} \sum_{k'} q(h',k') q^*(h+h', k+k') = \delta(h,k) \qquad (4.3.6.5)$$

for all h, k, where q^* denotes the complex conjugate of q, and $\delta(h,k)$ is the Kronecker delta function. The second test can be applied to any calculation for which no phenomenological absorption potential has been used in the evaluation of the $q(h,k)$. In that case, the sum of intensities of all beams at the final thickness should be no less than 0.9, the incident intensity being taken as 1.0. A value of this sum that is less than 0.9 indicates that the number of beams, N, has been insufficient. In some rare cases, the sum can be greater than 1.0; this is usually an indication that the number of beams has been allowed to come very close to the array size used in the convolution procedure. This last result does not occur if the convolution is carried out directly rather than by use of fast-Fourier-transform methods.

A more complete discussion of the multislice procedure can be obtained from Cowley (1975) and Goodman & Moodie (1974). These references are not exhaustive, but rather an indication of particularly useful articles for the novice in this subject.

4.3.6.2. *The Bloch-wave method (By A. Howie)*

Bloch waves, familiar in solid-state valence-band theory, arise as the basic wave solutions for a periodic structure. They are thus always implicit and often explicit in dynamical diffraction calculations, whether applied in perfect crystals, in almost perfect crystals with slowly varying defect strain fields or in more general structures that (see Subsection 4.3.6.1) can always, for computations, be treated by periodic continuation.

The Schrödinger wave equation in a periodic structure,

$$\nabla^2 \psi + 4\pi^2 \left[\chi^2 + \sum_{\mathbf{g}} U_{\mathbf{g}} \exp(2\pi i \mathbf{g} \cdot \mathbf{r})\right] \psi = 0, \qquad (4.3.6.6)$$

can be applied to high-energy, relativistic electron diffraction, taking $\chi = \lambda^{-1}$ as the relativistically corrected electron wave number (see Subsection 4.3.1.4). The Fourier coefficients in the expression for the periodic potential are defined at reciprocal-lattice points $\mathbf{g}$ by the expression

$$U_{\mathbf{g}} = U^*_{-\mathbf{g}} = \frac{m}{m_0} \frac{\exp(-M_{\mathbf{g}})}{\pi \Omega} \sum_j f_j[\sin(\theta_{\mathbf{g}})/\lambda] \exp(-2\pi i \mathbf{g} \cdot \mathbf{r}_j), \qquad (4.3.6.7)$$

where f_j is the Born scattering amplitude (see Subsection 4.3.1.2) of the jth atom at position $\mathbf{r}_j$ in the unit cell of volume Ω and $M_{\mathbf{g}}$ is the Debye–Waller factor.

The simplest solution to (4.3.6.6) is a single Bloch wave, consisting of a linear combination of plane-wave beams coupled by Bragg reflection.

$$\psi(\mathbf{r}) = b(\mathbf{k}, \mathbf{r}) = \sum_h C_{\mathbf{h}} \exp[2\pi i(\mathbf{k} + \mathbf{h}) \cdot \mathbf{r}]. \qquad (4.3.6.8)$$

In practice, only a limited number of terms N, corresponding to the most strongly excited Bragg beams, is included in (4.3.6.8). Substitution in (4.3.6.6) then yields N simultaneous equations for the wave amplitudes $C_{\mathbf{g}}$.

$$[\chi^2 + U_0 - (\mathbf{k} + \mathbf{g})^2] C_{\mathbf{g}} + \sum_{\mathbf{g}' \neq 0} U_{\mathbf{g}'} C_{\mathbf{g}-\mathbf{g}'} = 0. \qquad (4.3.6.9)$$

Usually, χ and the two tangential components k_x and k_y are fixed by matching to the incident wave at the crystal entrance surface. k_z then emerges as a root of the determinant of coefficients appearing in (4.3.6.9).

Numerical solution of (4.3.6.9) is considerably simplified (Hirsch, Howie, Nicholson, Pashley & Whelan, 1977) in cases of transmission high-energy electron diffraction where all the important reciprocal-lattice points lie in the zero-order Laue zone $g_z = 0$ and $\chi^2 \gg |U_{\mathbf{g}}|$. The equations then reduce to a

standard matrix eigenvalue problem (for which efficient subroutines are widely available):

$$\sum_{\mathbf{h}} M_{\mathbf{gh}} C_{\mathbf{h}} = \gamma C_{\mathbf{g}}, \tag{4.3.6.10}$$

where $M_{\mathbf{gh}} = U_{\mathbf{g}-\mathbf{h}}/2\chi + s_{\mathbf{g}}\delta_{\mathbf{gh}}$ and $s_{\mathbf{g}} = [k^2 - (\mathbf{k}+\mathbf{g})^2]/2\chi$ is the distance, measured in the z direction, of the reciprocal-lattice point $\mathbf{g}$ from the Ewald sphere.

There will in general be N distinct eigenvalues $\gamma = k_z - \chi_z$ corresponding to N possible values $k_z^{(j)}$, $j = 1, 2, \cdots N$, each with its eigenfunction defined by N wave amplitudes $C_0^{(j)}, C_{\mathbf{g}}^{(j)}, \ldots, C_{\mathbf{h}}^{(j)}$. The waves are normalized and orthogonal so that

$$\sum_{\mathbf{g}} C_{\mathbf{g}}^{(j)*} C_{\mathbf{g}}^{(l)} = \delta_{jl}; \quad \sum_{j} C_{\mathbf{g}}^{(j)*} C_{\mathbf{h}}^{(l)} = \delta_{\mathbf{gh}}. \tag{4.3.6.11}$$

In simple transmission geometry, the complete solution for the total coherent wavefunction $\psi(\mathbf{r})$ is

$$\psi(\mathbf{r}) = \sum_{j} \psi^{(j)} \exp[-2\pi q^{(j)} z] \sum_{\mathbf{g}} C_{\mathbf{g}}^{(j)} \exp[2\pi i(\chi + \mathbf{g}) \cdot \mathbf{r}]. \tag{4.3.6.12}$$

Inelastic and thermal-diffuse-scattering processes cause anomalous absorption effects whereby the amplitude of each component Bloch wave decays with depth z in the crystal from its initial value $\psi^{(j)} = C_0^{(j)*}$. The decay constant is computed using an imaginary optical potential $iU'(\mathbf{r})$ with Fourier coefficients $iU'_{\mathbf{g}} = iU'^{*}_{-\mathbf{g}}$ (for further details of these see Humphreys & Hirsch, 1968, and Subsection 4.3.1.5 and Section 4.3.2).

$$q^{(j)} = \frac{m}{h^2 \chi_z} \sum_{\mathbf{g},\mathbf{h}} C_{\mathbf{g}}^{(j)*} U'_{\mathbf{h}} C_{\mathbf{g}-\mathbf{h}}^{(j)}. \tag{4.3.6.13}$$

The Bloch-wave, matrix-diagonalization method has been extended to include reciprocal-lattice points in higher-order Laue zones (Jones, Rackham & Steeds, 1977) and, using pseudopotential scattering amplitudes, to the case of low-energy electrons (Pendry, 1974).

The Bloch-wave picture may be compared with other variants of dynamical diffraction theory, which, like the multislice method (Subsection 4.3.6.1), for example, employ plane waves whose amplitudes vary with position in real space and are determined by numerical integration of first-order coupled differential equations. For cases with $N < 50$ beams in perfect crystals or in crystals containing localized defects such as stacking faults or small point-defect clusters, the Bloch-wave method offers many advantages, particularly in thicker crystals with $t > 1000$ Å. For high-resolution image calculations in thin crystals where the periodic continuation process may lead to several hundred diffracted beams, the multislice method is more efficient. For cases of defects with extended strain fields or crystals illuminated at oblique incidence, coupled plane-wave integrations along columns in real space (Howie & Basinski, 1968) can be the most efficient method.

The general advantage of the Bloch-wave method, however, is the picture it affords of wave propagation and scattering in both perfect and imperfect crystals. For this purpose, solutions of equations (4.3.6.9) allow dispersion surfaces to be plotted in k space, covering with several sheets j all the wave points $\mathbf{k}^{(j)}$ for a given energy E. Thickness fringes and other interference effects then arise because of interference between waves excited at different points $\mathbf{k}^{(j)}$. The average current flow at each point is normal to the dispersion surface and anomalous-absorption effects can be understood in terms of the distribution of Bloch-wave current within the unit cell. Detailed study of these effects, and the behaviour of dispersion surfaces as a function of energy, yields accurate data on scattering amplitudes *via* the critical-voltage effect (see Section 4.3.7). Static crystal defects induce elastic scattering transitions $\mathbf{k}^{(j)} \rightarrow \mathbf{k}^{(l)}$ on sheets of the same dispersion surface. Transitions between points on dispersion surfaces of different energies occur because of thermal diffuse scattering, generation of electronic excitations or the emission of radiation by the fast electron. The Bloch-wave picture and the dispersion surface are central to any description of these phenomena. For further information and references, the reader may find it helpful to consult Section 5.2.10 of Volume B (*IT* B, 1996).

4.3.7. Measurement of structure factors and determination of crystal thickness by electron diffraction (by J. Gjønnes and J. W. Steeds)

Current advances in quantitative electron diffraction are connected with improved experimental facilities, notably the combination of convergent-beam electron diffraction (CBED) with new detection systems. This is reflected in extended applications of electron diffraction intensities to problems in crystallography, ranging from valence-electron distributions in crystals with small unit cells to structure determination of biological molecules in membranes. The experimental procedures can be seen in relation to the two main principles for measurement of diffracted intensities from crystals:

– *rocking curves*, *i.e.* intensity profiles measured as function of deviation, s_g, from the Bragg condition, and

– *integrated intensities*, which form the well known basis for X-ray and neutron diffraction determination of crystal structure.

Integrated intensities are not easily defined in the most common type of electron-diffraction pattern, *viz* the selected-area (SAD) spot pattern. This is due to the combination of dynamical scattering and the orientation and thickness variations usually present within the typically micrometre-size illuminated area. This combination leads to spot pattern intensities that are poorly defined averages over complicated scattering functions of many structure factors. Convergent-beam electron diffraction is a better alternative for intensity measurements, especially for inorganic structures with small-to-moderate unit cells. In CBED, a fine beam is focused within an area of a few hundred ångströms, with a divergence of the order of a tenth of a degree. The diffraction pattern then appears in the form of discs, which are essentially two-dimensional rocking curves from a small illuminated area, within which thickness and orientation can be regarded as constant. These intensity distributions are obtained under well defined conditions and are well suited for comparison with theoretical calculations. The intensity can be recorded either photographically, or with other parallel recording systems, *viz* YAG screen/CCD camera (Krivanek, Mooney, Fan, Leber & Meyer, 1991) or image plates (Mori, Oikawa & Harada, 1990) – or sequentially by a scanning system. The inelastic background can be removed by an energy filter (Krahl, Pätzold & Swoboda,1990; Krivanek, Gubbens, Dellby & Meyer, 1991). Detailed intensity profiles in one or two dimensions can then be measured with high precision for low-order reflections from simple structures. But there are limitations also with the CBED technique: the crystal should be fairly perfect within the illuminated area and the unit cell relatively small, so that overlap between discs can be avoided. The current development of electron diffraction is therefore characterized by a wide range of techniques, which extend from the traditional spot pattern to two-dimensional, filtered rocking curves, adapted to the

structure problems under study and the specimens that are available.

Spot-pattern intensities are best for thin samples of crystals with light atoms, especially organic and biological materials. Dorset and co-workers (Dorset, Jap, Ho & Glaeser, 1979; Dorset, 1991) have shown how conventional crystallographic techniques ('direct phasing') can be applied in *ab initio* structure determination of thin organic crystals from spot intensities in projections. Two main complications were treated by them: bending of the crystal and dynamical scattering. Thin crystals will frequently be bent; this will give some integration of the reflection, but may also produce a slight distortion of the structure, as pointed out by Cowley (1961), who proposed a correction formula. The thickness range for which a kinematical approach to intensities is valid was estimated theoretically by Dorset *et al*. (1979). For organic crystals, they quoted a few hundred ångströms as a limit for kinematical scattering in dense projections at 100 kV.

Radiation damage is a problem, but with low-dose and cryo-techniques, electron-microscopy methods can be applied to many organic crystals, as shown by several recent investigations. Voigt-Martin, Yan, Gilmore, Shankland & Bricogne (1994) collected electron-diffraction intensities from a beam-sensitive dione and constructed a 1.4 Å Fourier map by a direct method based on maximum entropy. Large numbers of electron-diffraction intensities have been collected from biological molecules crystallized in membranes. The structure amplitudes can be combined with phases extracted from high-resolution micrographs, following Unwin & Henderson's (1975) early work. Kühlbrandt, Wang & Fujiyoshi (1994) collected about 18 000 amplitudes and 15 000 phases for a protein complex in an electron cryomicroscope operating at 4.2 K (Fujiyoshi *et al.*, 1991). Using these data, they determined the structure from a three-dimensional Fourier map calculated to 3.4 Å resolution. The assumption of kinematical scattering in such studies has been investigated by Spargo (1994), who found the amplitudes to be kinematic within 4% but with somewhat larger deviations for phases.

For inorganic structures, spot-pattern intensities are less useful because of the stronger dynamical interactions, especially in dense zones. Nevertheless, it may be possible to derive a structure and refine parameters from spot-pattern intensities. Andersson (1975) used experimental intensities from selected projections for comparison with dynamical calculations, including an empirical correction factor for orientation spread, in a structure determination of $V_{14}O_8$. Recently, Zou, Sukharev & Hovmöller (1993) combined spot-pattern intensities read from film by the program *ELD* with image processing of high-resolution micrographs for structure determination of a complex perovskite.

A considerable improvement over the spot pattern has been obtained by the elegant double-precession technique devised by Vincent & Midgley (1994). They programmed scanning coils above and below the specimen in the electron microscope so as to achieve simultaneous precession of the focused incident beam and the diffraction pattern around the optical axis. The net effect is equivalent to a precession of the specimen with a stationary incident beam. Integrated intensities can be obtained from reflections out to a Bragg angle θ equal to the precession angle φ for the zeroth Laue zone. In addition, reflections in the first and second Laue zones appear as broad concentric rings. Dynamical effects are reduced appreciably by this procedure, especially in the non-zero Laue zones. The experimental integrated intensities, I_g, must be multiplied with a geometrical factor analogous to the Lorentz factor in X-ray diffraction, *viz*

$$I_g = I_G^{\rm exp} \sin\varepsilon; \quad \cos\varepsilon = \frac{(g^2 - 2nkh)}{2k\phi g}, \tag{4.3.7.1}$$

where nh is the reciprocal spacing between the zeroth and nth layers. The intensities can be used for structure determination by procedures taken over from X-ray crystallography, *e.g.* the conditional Patterson projections that are used by the Bristol group (Vincent, Bird & Steeds, 1984). The precession method may be seen as intermediate between the spot pattern and the CBED technique. Another intermediate approach was proposed by Goodman (1976) and used later by Olsen, Goodman & Whitfield (1985) in the structure determination of a series of selenides. CBED patterns from thin crystals were taken in dense zones; intensities were measured at corresponding points in the discs, *e.g.* at the zone-axis position. Structure parameters were determined by fitting the observed intensities to dynamical calculations.

Higher precision and more direct comparisons with dynamical scattering calculations are achieved by measurements of intensity distributions within the CBED discs, *i.e.* one- or two-dimensional rocking curves. An up-to-date review of these techniques is found in the recent book by Spence & Zuo (1992), where all aspects of the CBED technique, theory and applications are covered, including determination of lattice constants and strains, crystal symmetry, and fault vectors of defects. Refinement of structure factors in crystals with small unit cells are treated in detail. For determination of bond charges, the structure factors (Fourier potentials) should be determined to an accuracy of a few tenths of a percent; calculations must then be based on many-beam dynamical scattering theory, see Chapter 8.8. Removal of the inelastic background by an energy filter will improve the data considerably; analytical expressions for the inelastic background including multiple-scattering contributions may be an alternative (Marthinsen, Holmestad & Høier, 1994).

Early CBED applications to the determination of structure factors were based on features that can be related to dynamical effects in the two-beam case. Although insufficient for most accurate analyses, the two-beam expression for the intensity profile may be a useful guide. In its standard form,

$$I_g(s) = \frac{(U_g/k)^2}{s_g^2 + (U_g/k)^2} \sin^2\left[\pi t\sqrt{s_g^2 + (U_g/k)^2}\right], \tag{4.3.7.2}$$

where U_g and s_g are Fourier potential and excitation error for the reflection g, k wave number and t thickness. The expression can be rewritten in terms of the eigenvalues $\gamma^{(i,j)}$ that correspond to the two Bloch-wave branches, i, j:

$$I_g^{i,j}(s_g) = \frac{(U_g/k)^2}{(\gamma^{(i)} - \gamma^{(j)})^2} \sin^2[\pi t(\gamma^{(i)} - \gamma^{(j)})], \tag{4.3.7.3}$$

where

$$\gamma^{i,j} = \tfrac{1}{2}\left[s_g^2 \pm \sqrt{s_g^2 + (U_g/k)^2}\,\right].$$

Note that the minimum separation between the branches i,j or the gap at *the dispersion surface* is

$$(\gamma^{(j)} - \gamma^{(i)})_{\rm min} = U_g/k = 1/\xi_g, \tag{4.3.7.4}$$

where $\xi_{\rm g}$ is an extinction distance. The two-beam form is often found to be a good approximation to an intensity profile $I_g(s_g)$ even when other beams are excited, provided an *effective potential* $U_g^{\rm eff}$, which corresponds to the gap at the dispersion surface, is substituted for U_g. This is suggested by many features in CBED and Kikuchi patterns and borne out by detailed calculations, see *e.g.* Høier (1972). Approximate expressions for

$U_g^{\rm eff}$ have been developed along different lines; the best known is the Bethe potential

$$U_g^{\rm eff} = U_g - \sum_h \frac{U_{g-h}U_h}{2ks_h}. \qquad (4.3.7.5)$$

Other perturbation approaches are based on scattering between Bloch waves, in analogy with the 'interband scattering' introduced by Howie (1963) for diffuse scattering; the term 'Bloch-wave hybridization' was introduced by Buxton (1976). Exact treatment of symmetrical few-beam cases is possible (see Fukuhara, 1966; Kogiso & Takahashi, 1977). The three-beam case (Kambe, 1957; Gjønnes & Høier 1971) is described in detail in the book by Spence & Zuo (1992).

Many intensity features can be related to the structure of the dispersion surface, as represented by the function $\gamma(k_x,k_y)$. The gap [equation (4.3.7.4)] is an important parameter, as in the four-beam symmetrical case in Fig. 4.3.7.1. Intensity measurements along one dimension can then be referred to three groups, according to the width of the gap, *viz*:

small gap – integrated intensity;

large gap – rocking curve, thickness fringes;

zero gap – critical effects.

A small gap at the dispersion surface implies that the two-beam-like rocking curve above approaches a kinematical form and can be represented by an integrated intensity. Within a certain thickness range, this intensity may be proportional to $|U_g^{\rm eff}|^2$, with an angular width inversely proportional to gt. Several schemes have been proposed for measurement of relative integrated intensities for reflections in the outer, high-angle region, where the lines are narrow and can be easily separated from the background. Steeds (1984) proposed use of the HOLZ (high-order Laue-zone) lines, which appear in CBED patterns taken with the central disc at the zone-axis position. Along a ring that defines the first-order Laue zone (FOLZ), reflections appear as segments that can be associated with scattering from strongly excited Bloch waves in the central ZOLZ part into the FOLZ reflections. Vincent, Bird & Steeds (1984) proposed an intensity expression

$$I_g^{(j)} \propto |\varepsilon^{(j)}\beta_g^{(j)}|^2 \exp(-2\mu t)\frac{1-\exp[-2(\mu^{(j)}-\mu)t]}{2(\mu^{(j)}-\mu)} \qquad (4.3.7.6)$$

for integrated intensity for a line segment associated with scattering from (or into) the ZOLZ Bloch wave j. $\varepsilon^{(j)}$ is here the excitation coefficient and $\beta^{(j)}$ the matrix element for scattering between the Bloch wave j and the plane wave g. $\mu^{(j)}$ and μ are absorption coefficients for the Bloch wave and plane wave, respectively; t is the thickness. From measurements of a number of such FOLZ (or SOLZ) reflections, they were able to carry out *ab initio* structure determinations using so-called conditional Patterson projections and coordinate refinement. Tanaka & Tsuda (1990) have refined atomic positions from zone-axis HOLZ intensities. Ratios between HOLZ intensities have been used for determination of the Debye–Waller factor (Holmestad, Weickenmeier, Zuo, Spence & Horita, 1993).

Another CBED approach to integrated intensities is due to Taftø & Metzger (1985). They measured a set of high-order reflections along a systematic row with a wide-aperture CBED tilted off symmetrical incidence. A number of high-order reflections are then simultaneously excited in a range where the reflections are narrow and do not overlap. Gjønnes & Bøe (1994) and Ma, Rømming, Lebech & Gjønnes (1992) applied the technique to the refinement of coordinates and thermal parameters in high-T_c superconductors and intermetallic compounds. The validity and limitation of the kinematical approximation and dynamic potentials in this case has been discussed by Gjønnes & Bøe (1994).

Zero gap at the dispersion surface corresponds to zero effective Fourier potential or, to be more exact, an accidental degeneracy, $\gamma^{(i)} = \gamma^{(j)}$, in the Bloch-wave solution. This is the basis for the critical-voltage method first shown by Watanabe, Uyeda & Fukuhara (1969). From vanishing contrast of the Kikuchi line corresponding to a second-order reflection $2g$, they determined a relation between the structure factors U_g and U_{2g}. Gjønnes & Høier (1971) derived the condition for the accidental degeneracy in the general centrosymmetrical three-beam case $0,g,h$, expressed in terms of the excitation errors $s_{g,h}$ and Fourier potentials $U_{g,h,g-h}$, *viz*

$$2ks_g = \frac{U_g(U_h^2 - U_{g-h}^2)m}{U_hU_{g-h}m_0}; \quad 2ks_h = \frac{U_h(U_g^2 - U_{g-h}^2)m}{U_gU_{g-h}m_0}; \qquad (4.3.7.7)$$

where m and m_0 are the relativistic and rest mass of the incident electron. Experimentally, this condition is obtained at a particular voltage and diffraction condition as vanishing line contrast of a Kikuchi or Kossel line – or as a reversal of a contrast feature. The second-order critical-voltage effect is then obtained as a special case, *e.g.* by the mass ratio:

$$(m/m_0)_{\rm crit} = \frac{U_{2h}h^2}{U_h^2 - U_{2h}^2}. \qquad (4.3.7.8)$$

Measurements have been carried out for a number of elements and alloy phases; see the review by Fox & Fisher (1988) and later work on alloys by Fox & Tabbernor (1991). Zone-axis critical voltages have been used by Matsuhata & Steeds (1987). For analytical expressions and experimental determination of non-systematic critical voltages, see Matsuhata & Gjønnes (1994).

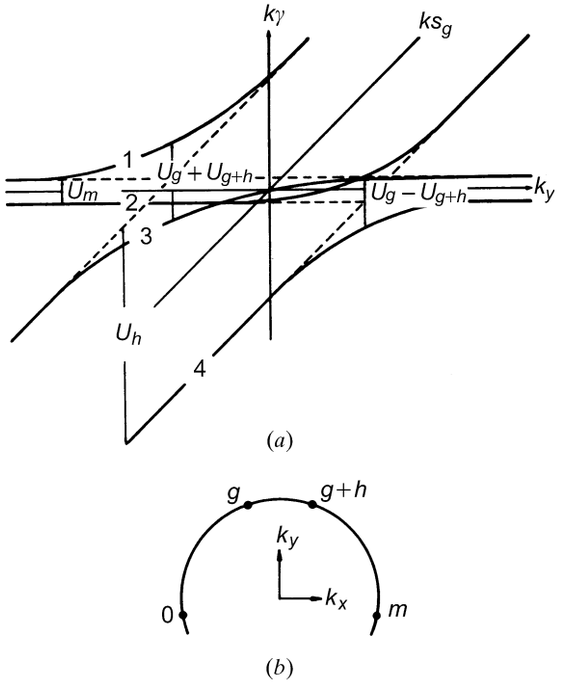

Fig. 4.3.7.1. (*a*) Dispersion-surface section for the symmetric four-beam case (0, *g*, *g*+*h*, *m*), γk is a function of k_x, referred to (*b*), where $k_x = k_y = 0$ corresponds to the exact Bragg condition for all three reflections. The two gaps appear at $s_g = \pm(U_h - U_m)/k$ with widths $(U_g \pm U_{g+h})/k$.

Large gaps at the dispersion surface are associated with strong inner reflections – and a strong dynamical effect of two-beam-like character. The absolute magnitude of the gap – or its inverse, the extinction distance – can be obtained in different ways. Early measurements were based on the split of diffraction spots from a wedge, see Lehmpfuhl (1974), or the corresponding fringe periods measured in bright- and dark-field micrographs (Ando, Ichimiya & Uyeda, 1974). The most precise and applicable large-gap methods are based on the refinement of the fringe pattern in CBED discs from strong reflections, as developed by Goodman & Lehmpfuhl (1967) and Voss, Lehmpfuhl & Smith (1980). In recent years, this technique has been developed to high perfection by means of filtered CBED patterns, see Spence & Zuo (1992) and papers referred to therein. See also Chapter 8.8.

The gap at the dispersion surface can also be obtained directly from the split observed at the crossing of a weak Kikuchi line with a strong band. Gjønnes & Høier (1971) showed how this can be used to determine strong low-order reflections. High voltage may improve the accuracy (Terasaki, Watanabe & Gjønnes, 1979). The sensitivity of the intersecting Kikuchi-line (IKL) method was further increased by the use of CBED instead of Kikuchi patterns (Matsuhata, Tomokiyo, Watanabe & Eguchi, 1984; Taftø & Gjønnes, 1985). In a recent development, Høier, Bakken, Marthinsen & Holmestad (1993) have measured the intensity distribution in the CBED discs around such intersections and have refined the main structure factors involved.

Two-dimensional rocking curves collected by CBED patterns around the axis of a dense zone are complicated by extensive many-beam dynamical interactions. The Bristol–Bath group (Saunders, Bird, Midgley & Vincent, 1994) claim that the strong dynamic effects can be exploited to yield high sensitivity in refinement of low-order structure factors. They have also developed procedures for *ab initio* structure determination based on zone-axis patterns (Bird & Saunders, 1992), see Chapter 8.8.

Determination of phase invariants. It has been known for some time (*e.g* Kambe, 1957) that the dynamical three-beam case contains information about phase. As in the X-ray case, measurement of dynamical effects can be used to determine the value of triplets (Zuo, Høier & Spence, 1989) and to determine phase angles to better than one tenth of a degree (Zuo, Spence, Downs & Mayer, 1993) which is far better than any X-ray method. Bird (1990) has pointed out that the phase of the absorption potential may differ from the phase of the real potential.

Thickness is an important parameter in electron-diffraction experiments. In structure-factor determination based on CBED patterns, thickness is often included in the refinement. Thickness can also be determined directly from profiles connected with large gaps at the dispersion surface (Goodman & Lehmpfuhl, 1967; Blake, Jostsons, Kelly & Napier, 1978; Glazer, Ramesh, Hilton & Sarikaya, 1985). The method is based on the outer part of the fringe profile, which is not so sensitive to the structure factor. The intensity minimum of the *i*th fringe in the diffracted disc occurs at a position corresponding to the excitation error s_i and expressed as

$$(s_i^2 + 1/\varepsilon_g^2)t^2 = n_i^2, \qquad (4.3.7.9)$$

where n_i is a small integer describing the order of the minimum. This equation can be arranged in two ways for graphic determination of thickness. The commonest method appears to be to plot $(s_i/n_i)^2$ against $1/{n_i}^2$ and then determine the thickness from the intersection with the ordinate axis (Kelly, Jostsons, Blake & Napier, 1975). Glazer *et al*. (1985) claim that the method originally proposed by Ackermann (1948), where s_i^2 is plotted against n_i and the thickness is taken from the slope, is more accurate. In both cases, the outer part of the rocking curve is emphasized; exact knowledge of the gap is not necessary for a good determination of thickness, provided the assumption of a two-beam-like rocking curve is valid.

4.3.8. Crystal structure determination by high-resolution electron microscopy
(By J. C. H. Spence and J. M. Cowley)

4.3.8.1. *Introduction*

For the crystallographic study of real materials, high-resolution electron microscopy (HREM) can provide a great deal of information that is complementary to that obtainable by X-ray and neutron diffraction methods. In contrast to the statistically averaged information that these other methods provide, the great power of HREM lies in its ability to elucidate the detailed atomic arrangements of individual defects and the microcrystalline structure in real crystals. The defects and inhomogeneities of real crystals frequently exert a controlling influence on phase-transition mechanisms and more generally on all the electrical, mechanical, and thermal properties of solids. The real-space images that HREM provides (such as that shown in Fig. 4.3.8.1) can give an immediate and dramatic impression of chemical crystallography processes, unobtainable by other methods. Their atomic structure is of the utmost importance for

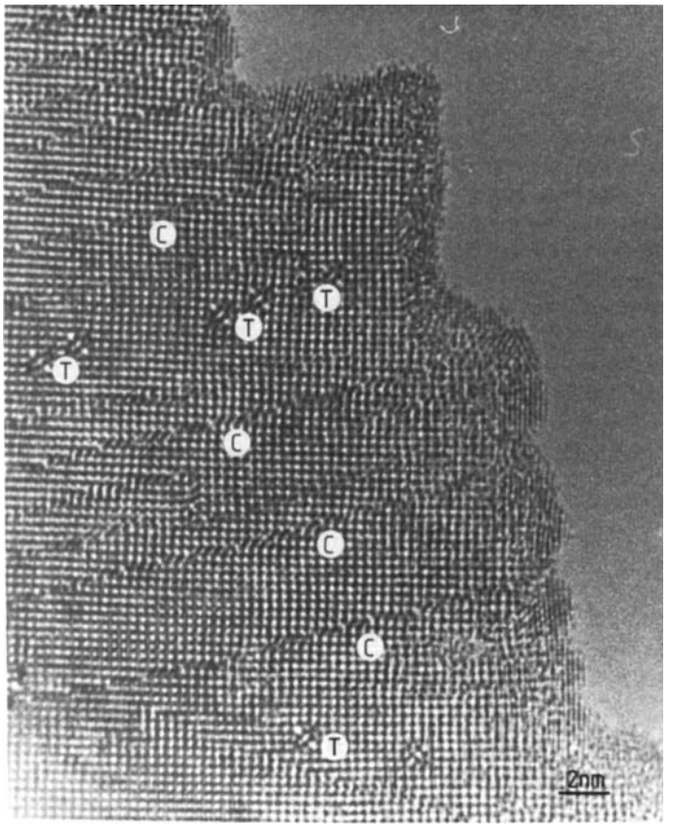

Fig. 4.3.8.1. Atomic resolution image of a tantalum-doped tungsten trioxide crystal (pseudo-cubic structure) showing extended crystallographic shear-plane defects (C), pentagonal-column hexagonal-tunnel (PCHT) defects (T), and metallization of the surface due to oxygen desorption (JEOL 4000EX, crystal thickness less than 200 Å, 400 kV, $C_s = 1$ mm). Atomic columns are black. [Smith, Bursill & Wood (1985).]

an understanding of the properties of real materials. The HREM method has proven powerful for the determination of the structure of such defects and of the submicrometre-sized microcrystals that constitute many polyphase materials.

In summary, HREM should be considered the technique of choice where a knowledge of microcrystal size, shape or morphology is required. In addition, it can be used to reveal the presence of line and planar defects, inclusions, grain boundaries and phase boundaries, and, in favourable cases, to determine atomic structure. Surface atomic structure and reconstruction have also been studied by HREM. However, meaningful results in this field require accurately controlled ultra-high-vacuum conditions. The determination of the atomic structure of point defects by HREM so far has proven extremely difficult, but this situation is likely to change in the near future.

The following sections are not intended to review the applications of HREM, but rather to provide a summary of the main theoretical results of proven usefulness in the field, a selected bibliography, and recommendations for good experimental practice. At the time of writing (1997), the point resolution of HREM machines lies between 1 and 2 Å.

The function of the objective lens in an electron microscope is to perform a Fourier synthesis of the Bragg-diffracted electron beams scattered (in transmission) by a thin crystal, in order to produce a real-space electron image in the plane r. This electron image intensity can be written

$$|\psi(\mathbf{r})|^2 = \left| \int \Psi(\mathbf{u}) \exp\{2\pi i \mathbf{u}\cdot\mathbf{r}\} P(\mathbf{u}) \exp\{i\chi(\mathbf{u})\}\, \mathrm{d}\mathbf{u} \right|^2, \quad (4.3.8.1)$$

where $\Psi(\mathbf{u})$ represents the complex amplitude of the diffracted wave after diffraction in the crystal as a function of the reciprocal-lattice vector $\mathbf{u}$ [magnitude $(2\sin\theta)/\lambda$] in the plane perpendicular to the beam, so that the wavevector of an incident plane wave is written $\mathbf{K}_0 = \mathbf{k}_z + 2\pi\mathbf{u}$. Following the convention of Section 2.5.1 in *IT* B (1992), we write $|\mathbf{K}_0| = 2\pi\lambda^{-1}$. The function $\chi(\mathbf{u})$ is the phase factor for the objective-lens transfer function and $P(\mathbf{u})$ describes the effect of the objective aperture:

$$P(\mathbf{u}) = \begin{cases} 1 & \text{for } |\mathbf{u}| < u_0 \\ 0 & \text{for } |\mathbf{u}| \geq u_0. \end{cases}$$

For a periodic object, the image wavefunction is given by summing the contributions from the set of reciprocal-lattice points, $\mathbf{g}$, so that

$$|\psi(\mathbf{r})|^2 = \left| \sum_{\mathbf{g}} \Psi_{\mathbf{g}} \exp\{2\pi i \mathbf{g}\cdot\mathbf{r}\} P(\mathbf{g}) \exp\{i\chi(\mathbf{g})\} \right|^2. \quad (4.3.8.2)$$

For atomic resolution, with $u_0 \approx 1\text{Å}^{-1}$, it is apparent that, for all but the simplest structures and smallest unit cells, this synthesis will involve many hundreds of Bragg beams. A scattering calculation must involve an even larger number of beams than those that contribute resolvable detail to the image, since, as described in Section 2.5.1 in *IT* B (1992), all beams interact strongly through multiple coherent scattering. The theoretical basis for HREM image interpretation is therefore the dynamical theory of electron diffraction in the transmission (or Laue) geometry [see Chapter 5.2 in *IT* B (1992)]. The resolution of HREM images is limited by the aberrations of the objective electron lens (notably spherical aberration) and by electronic instabilities. An intuitive understanding of the complicated effect of these factors on image formation from multiply scattered Bragg beams is generally not possible. To provide a basis for understanding, therefore, the following section treats the simplified case of few-beam 'lattice-fringe' images, in order to expose the relationship between the crystal potential, its structure factors, electron-lens aberrations, and the electron image.

Image formation in the transmission electron microscope is conventionally treated by analogy with the Abbe theory of coherent optical imaging. The overall process is subdivided as follows. (*a*) The problem of beam–specimen interaction for a collimated kilovolt electron beam traversing a thin parallel-sided slab of crystal in a given orientation. The solution to this problem gives the elastically scattered dynamical electron wavefunction $\psi(\mathbf{r})$, where $\mathbf{r}$ is a two-dimensional vector lying in the downstream surface of the slab. Computer algorithms for dynamical scattering are described in Section 4.3.6. (*b*) The effects of the objective lens are incorporated by multiplying the Fourier transform of $\psi(\mathbf{r})$ by a function $T(\mathbf{u})$, which describes both the wavefront aberration of the lens and the diffraction-limiting effects of any apertures. The dominant aberrations are spherical aberration, astigmatism, and defect of focus. The image intensity is then formed from the modulus squared of the Fourier transform of this product. (*c*) All partial coherence effects may be incorporated by repeating this procedure for each of the component energies and directions that make up the illumination from an extended electron source, and summing the resulting intensities. Because this procedure requires a separate dynamical calculation for each component direction of the incident beam, a number of useful approximations of restricted validity have been developed; these are described in Subsection 4.3.8.4. This treatment of partial coherence assumes that a perfectly incoherent effective source can be identified. For field-emission HREM instruments, a coherent sum (over directions) of complex image wavefunctions may be required.

General treatments of the subject of HREM can be found in the texts by Cowley (1981) and Spence (1988). The sign

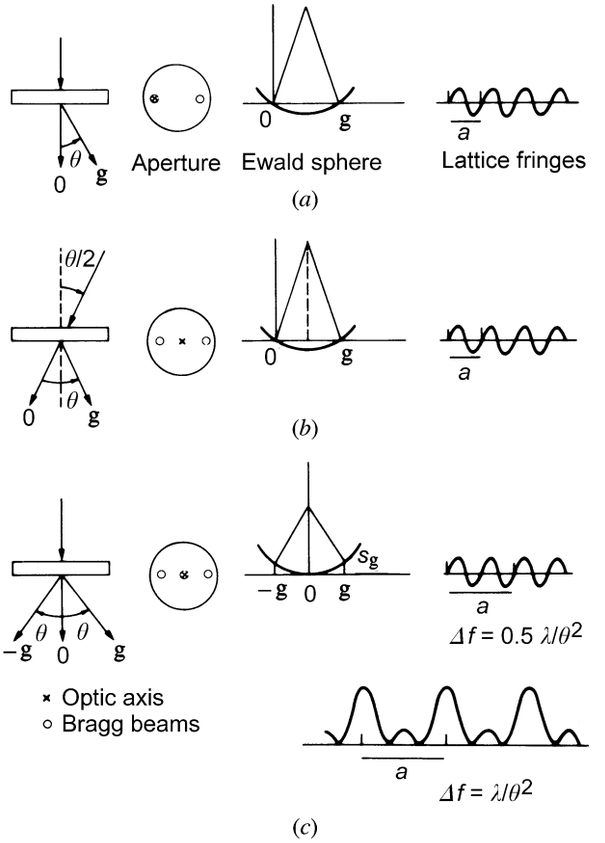

Fig. 4.3.8.2. Imaging conditions for few-beam lattice images. For three-beam axial imaging shown in (*c*), the formation of half-period fringes is also shown.

conventions used throughout the following are consistent with the standard crystallographic convention of Section 2.5.1 of *IT* B (1992), which assumes a plane wave of form $\exp\{-i(\mathbf{k}\cdot\mathbf{r}-\omega t)\}$ and so is consistent with X-ray usage.

4.3.8.2. *Lattice-fringe images*

We consider few-beam lattice images, in order to understand the effects of instrumental factors on electron images, and to expose the conditions under which they faithfully represent the scattering object. The case of two-beam lattice images is instructive and contains, in simplified form, most of the features seen in more complicated many-beam images. These fringes were first observed by Menter (1956) and further studied in the pioneering work of Komoda (1964) and others [see Spence (1988) for references to early work]. The electron-microscope optic-axis orientation, the electron beam, and the crystal setting are indicated in Fig. 4.3.8.2. If an objective aperture is used that excludes all but the two beams shown from contributing to the image, equation (4.3.8.2) gives the image intensity along direction **g** for a centrosymmetric crystal of thickness t as

$$I(x,t) = |\Psi_0(t)|^2 + |\Psi_\mathbf{g}(t)|^2 + 2|\Psi_0||\Psi_\mathbf{g}|\cos\{2\pi x/d_\mathbf{g} + \chi(u_\mathbf{g})\eta_\mathbf{g}(t) - \eta_0(t)\}. \quad (4.3.8.3)$$

The Bragg-diffracted beams have complex amplitudes $\Psi_\mathbf{g}(t) = |\Psi_\mathbf{g}(t)|\exp\{i\eta_\mathbf{g}(t)\}$. The lattice-plane period is $d_\mathbf{g}$ in direction **g** [Miller indices (hkl)]. The lens-aberration phase function, including only the effects of defocus Δf and spherical aberration (coefficient C_s), is given by

$$\chi(u_\mathbf{g}) = (2\pi/\lambda)\{(\Delta f\lambda^2 u_\mathbf{g}^2/2) + C_s\lambda^4 u_\mathbf{g}^4/4\}. \quad (4.3.8.4)$$

The effects of astigmatism and higher-order aberrations have been ignored. The defocus, Δf, is negative for the objective lens weakened (*i.e.* the focal length increased, giving a bright first Fresnel-edge fringe). The magnitude of the reciprocal-lattice vector $u_g = d_g^{-1} = (2\sin\theta_B)/\lambda$, where θ_B is the Bragg angle. If these two Bragg beams were the only beams excited in the crystal (a poor approximation for quantitative work), their amplitudes would be given by the 'two-beam' dynamical theory of electron diffraction as

$$\begin{aligned}\Psi_0(t) &= \{\cos[\pi t(1+w^2)^{1/2}/\xi_\mathbf{g}] + iw(1+w^2)^{-1/2} \\ &\quad\times \sin[\pi t(1+w^2)^{1/2}/\xi_\mathbf{g}]\}\exp(-i\pi s_\mathbf{g} t) \\ \Psi_\mathbf{g}(t) &= i(1+w^2)^{-1/2}\sin[\pi t(1+w^2)^{1/2}/\xi_\mathbf{g}] \\ &\quad\times \exp(-\pi i s_\mathbf{g} t), \end{aligned} \quad (4.3.8.5)$$

where $\xi_\mathbf{g}$ is the two-beam extinction distance, $V_\mathbf{g} = \pi/(\sigma\xi_\mathbf{g})$ is a Fourier coefficient of crystal potential, $s_\mathbf{g}$ is the excitation error (see Fig. 4.3.8.2), $w = s_\mathbf{g}\xi_\mathbf{g}$, and the interaction parameter σ is defined in Section 2.5.1 of *IT* B (1992).

The two-beam image intensity given by equation (4.3.8.3) therefore depends on the parameters of crystal thickness (t), orientation ($s_\mathbf{g}$), structure factor ($V_\mathbf{g}$), objective-lens defocus Δf, and spherical-aberration constant C_s. We consider first the variation of lattice fringes with crystal thickness in the two-beam approximation (Cowley, 1959; Hashimoto, Mannami & Naiki, 1961). At the exact Bragg condition ($s_\mathbf{g} = 0$), equations (4.3.8.5) and (4.3.8.3) give

$$I(x,t) = 1 - \sin(2\pi t/\xi_\mathbf{g})\sin[2\pi x/d + \chi(u_\mathbf{g})]. \quad (4.3.8.6)$$

If we consider a wedge-shaped crystal with the electron beam approximately normal to the wedge surface and edge, and take x and **g** parallel to the edge, this equation shows that sinusoidal lattice fringes are expected whose contrast falls to zero (and reverses sign) at thicknesses of $t_n = n\xi_\mathbf{g}/2$. This apparent abrupt translation of fringes (by $d/2$ in the direction x) at particular thicknesses is also seen in some experimental many-beam images. The effect of changes in focus (due perhaps to variations in lens current) is seen to result in a translation of the fringes (in direction x), while time-dependent variations in the accelerating voltage have a similar effect. Hence, time-dependent variations of the lens focal length or the accelerating voltage result in reduced image contrast (see below). If the illumination makes a small angle $\alpha = \lambda u'$ with the optic axis, the intensity becomes

$$I(x,\alpha) = |\Psi_0|^2 + |\Psi_\mathbf{g}|^2 + 2|\Psi_\mathbf{g}||\Psi_0| \times \cos[\chi(-u_\mathbf{g} - u') - \chi(u') + 2\pi x/d + \eta_\mathbf{g}(t) - \eta_0(t)].$$

For a uniformly intense line source subtending a semiangle θ_c, the total lattice-fringe intensity is

$$I(x) = (1/\theta_c)\int I(x,\alpha)\,\mathrm{d}\alpha.$$

The resulting fringe visibility $C = (I_{\max} - I_{\min})/(I_{\max} + I_{\min})$ is proportional to $C = (\sin\beta)/\beta$, where $\beta = 2\pi\Delta f\theta_c/d$. The contrast falls to zero for $\beta = \pi$, so that the range of focus over which fringes are expected is $\Delta z = d/\theta_c$. This is the approximate depth of field for lattice images due to the effects of the finite source size alone.

The case of three-beam fringes in the axial orientation is of more practical importance [see Fig. 4.3.8.2(*b*)]. The image intensity for $\Psi_\mathbf{g} = \Psi_{-\mathbf{g}}$ and $s_\mathbf{g} = s_{-\mathbf{g}}$ is

$$\begin{aligned} I(x,t) &= |\Psi_0|^2 + 2|\Psi_\mathbf{g}|^2 + 2|\Psi_\mathbf{g}|^2\cos(4\pi x/d) \\ &\quad + 4|\Psi_0||\Psi_\mathbf{g}|\cos(2\pi x/d) \\ &\quad\times \cos[\chi(u_\mathbf{g}) + \eta_\mathbf{g}(t) - \eta_0(t)]. \end{aligned} \quad (4.3.8.7)$$

The lattice image is seen to consist of a constant background plus cosine fringes with the lattice spacing, together with cosine fringes of half this spacing. The contribution of the half-spacing fringes is independent of instrumental parameters (and therefore of electronic instabilities if $\theta_c = 0$). These fringes constitute an important HREM image artifact. For kinematic scattering, $\eta_\mathbf{g}(t) - \eta_0(t) = -\pi/2$ and only the half-period fringes will then be seen if $\chi(u_\mathbf{g}) = n\pi$, or for focus settings

$$\Delta f = n\lambda^{-1}u_\mathbf{g}^{-2} - C_s\lambda^2 u_\mathbf{g}^2/2. \quad (4.3.8.8)$$

Fig. 4.3.8.2(*c*) indicates the form of the fringes expected for two focus settings with differing half-period contributions. As in the case of two-beam fringes, dynamical scattering may cause Ψ_0 to be severely attenuated at certain thicknesses, resulting also in a strong half-period contribution to the image.

Changes of 2π in $\chi(u_\mathbf{g})$ in equation (4.3.8.7) leave $I(x,t)$ unchanged. Thus, changes of defocus by amounts

$$\Delta f_f = 2n/(\lambda u_\mathbf{g}^2) \quad (4.3.8.9)$$

or changes in C_s by

$$\Delta C_s = 4n/(\lambda^3 u_\mathbf{g}^4) \quad (4.3.8.10)$$

yield identical images. The images are thus periodic in both Δf and C_s. This is a restricted example of the more general phenomenon of n-beam Fourier imaging discussed in Subsection 4.3.8.3.

We note that only a single Fourier period will be seen if Δf_f is less than the depth of field Δz. This leads to the approximate condition $\Theta_c > \lambda/d$, which, when combined with the Bragg law, indicates that a single period only of images will be seen when adjacent diffraction discs just overlap.

The axial three-beam fringes will coincide with the lattice planes, and show atom positions as dark if $\chi(u_{\mathbf{g}}) = (2n - 1/2)\pi$ and $\eta_0(t) - \eta_{\mathbf{g}}(t) = -\pi/2$. This total phase shift of $-\pi$ between Ψ_0 and the scattered beams is the desirable imaging condition for phase contrast, giving rise to dark atom positions on a bright background. This requires

$$C_s = (4n - 1)/(\lambda^3 u_{\mathbf{g}}^4) - 2\Delta f/(\lambda^2 u_{\mathbf{g}}^2)$$

as a condition for identical axial three-beam lattice images for $n = 0, 1, 2, \ldots$. This family of lines has been plotted in Fig. 4.3.8.3 for the (111) planes of silicon. Dashed lines denote the locus of 'white-atom' images (reversed contrast fringes), while the dotted lines indicate half-period images. In practice, the depth of field is limited by the finite illumination aperture θ_c, and few-beam lattice-image contrast will be a maximum at the stationary-phase focus setting, given by

$$\Delta f_0 = -C_s \lambda^2 u_{\mathbf{g}}^2. \qquad (4.3.8.11)$$

This choice of focus ensures $\nabla\chi(u) = 0$ for $u = u_{\mathbf{g}}$, and thus ensures the most favourable trade-off between increasing θ_c and loss of fringe contrast for lattice planes $\mathbf{g}$. Note that Δf_0 is not equal to the Scherzer focus Δf_s (see below). This focus setting is also indicated on Fig. 4.3.8.3, and indicates the instrumental conditions which produce the most intense (111) three- (or five-) beam axial fringes in silicon. For three-beam axial fringes of spacing d, it can be shown that the depth of field Δz is approximately

$$\Delta z = (\ln 2)^{1/2} d/\theta_c \pi. \qquad (4.3.8.12)$$

This depth of field, within which strong fringes will be seen, is indicated as a boundary on Fig. 4.3.8.3. Thus, the finer the image detail, the smaller is the focal range over which it may be observed, for a given illumination aperture θ_c.

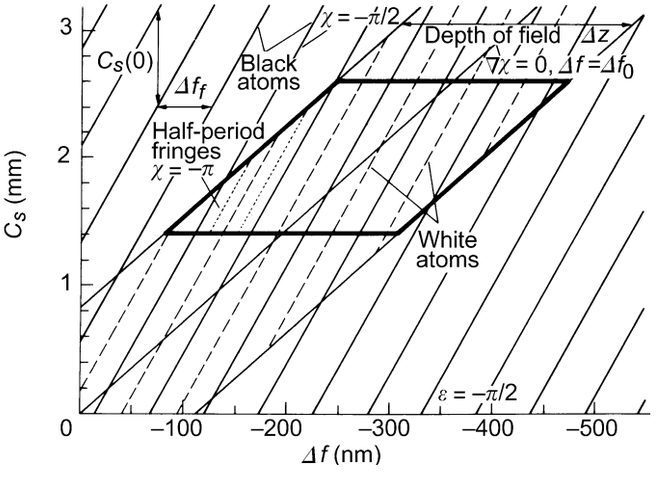

Fig. 4.3.8.3. A summary of three- (or five-) beam axial imaging conditions. Here, Δf_f is the Fourier image period, Δf_0 the stationary-phase focus, $C_s(0)$ the image period in C_s, and a scattering phase of $-\pi/2$ is assumed. The lines are drawn for the (111) planes of silicon at 100 kV with $\theta_c = 1.4$ mrad.

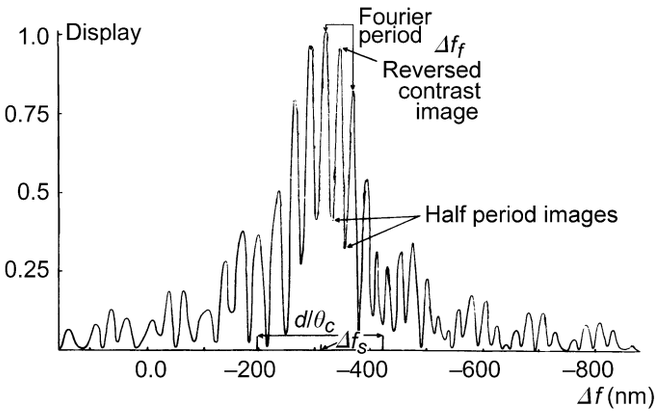

Fig. 4.3.8.4. The contrast of few-beam lattice images as a function of focus in the neighbourhood of the stationary-phase focus [see Olsen & Spence (1981)].

Fig. 4.3.8.4 shows an exact dynamical calculation for the contrast of three-beam axial fringes as a function of Δf in the neighbourhood of Δf_0. Both reversed contrast and half-period fringes are noted. The effects of electronic instabilities on lattice images are discussed in Subsection 4.3.8.3. It is assumed above that θ_c is sufficiently small to allow the neglect of any changes in diffraction conditions (Ewald-sphere orientation) within Θ_c. Under a similar approximation but without the approximations of transfer theory, Desseaux, Renault & Bourret (1977) have analysed the effect of beam divergence on two-dimensional five-beam axial lattice fringes.

When two-dimensional patterns of fringes are considered, the Fourier imaging conditions become more complex (see Subsection 4.3.8.3), but half-period fringe systems and reversed-contrast images are still seen. For example, in a cubic projection, a focus change of $\Delta f_f/2$ results in an image shifted by half a unit cell along the cell diagonal. It is readily shown that

$$\exp[i\chi(\Delta f)] = \exp[i\chi(\Delta f + \Delta f_f)]$$

if $\Delta f_f = 2na^2/\lambda + 2mb^2/\lambda$ when n, m are integers and a and b are the two dimensions of any orthogonal unit cell that can be chosen for $\Psi_p(x, y)$. Thus, changes in focus by $\Delta f_f(n, m)$ produce identical images in crystals for which such a cell can be chosen, regardless of the number of beams contributing (Cowley & Moodie, 1960).

For closed-form expressions for the few-beam (up to 10 beams) two-dimensional dynamical Bragg-beam amplitudes $\Psi_{\mathbf{g}}$ in orientations of high symmetry, the reader is referred to the work of Fukuhara (1966).

4.3.8.3. *Crystal structure images*

We define a crystal structure image as a high-resolution electron micrograph that faithfully represents a projection of a crystal structure to some limited resolution, and which was obtained using instrumental conditions that are independent of the structure, and so require no *a priori* knowledge of the structure. The resolution of these images is discussed in Subsection 4.3.8.6, and their variation with instrumental parameters in Subsection 4.3.8.4.

Equation (4.3.8.2) must now be modified to take account of the finite electron source size used and of the effects of the range of energies present in the electron beam. For a perfect crystal we may write, as in equation (2.5.1.36) in *IT* B (1992),

$$I_T(\mathbf{r}) = \iint |\psi(\mathbf{u}', \Delta f, \mathbf{r})|^2 \, G(\mathbf{u}') \, B(\Delta f, \mathbf{u}') \, \mathrm{d}\mathbf{u}' \, \mathrm{d}\Delta f \qquad (4.3.8.13a)$$

for the total image intensity due to an electron source whose normalized distribution of wavevectors is $G(\mathbf{u}')$, where $\mathbf{u}'$ has components u_1, v_1, and which extends over a range of energies corresponding to the distribution of focus $B(\Delta f, \mathbf{u})$. If χ is also assumed to vary linearly across θ_c and changes in the diffraction conditions over this range are assumed to make only negligible changes in the diffracted-beam amplitude $\Psi_{\mathbf{g}}$, the expression for a Fourier coefficient of the total image intensity $I_T(\mathbf{r})$ becomes

$$I_{\mathbf{g}} = \sum_{\mathbf{h}} \Psi_{\mathbf{h}} \exp\{-i\chi(\mathbf{h})\}\gamma\{\nabla\chi(\mathbf{h}) - \nabla\chi(\mathbf{h}-\mathbf{g})\} \times \psi^*_{\mathbf{h}-\mathbf{g}} \exp\{i\chi(\mathbf{h}-\mathbf{g})\}\beta\{\tfrac{1}{2}(\mathbf{h}^2 - |\mathbf{h}-\mathbf{g}|^2)^2\}, \quad (4.3.8.13b)$$

where $\gamma(\mathbf{h})$ and $\beta(\mathbf{g})$ are the Fourier transforms of $G(\mathbf{u}')$ and $B(\Delta f, \mathbf{u}')$, respectively.

For the imaging of very thin crystals, and particularly for the case of defects in crystals, which are frequently the objects of particular interest, we give here some useful approximations for HREM structure images in terms of the continuous projected crystal potential

$$\varphi(x, y) = (1/t)\int_0^t \varphi(x, y, z)\,\mathrm{d}z,$$

where the projection is taken in the electron-beam direction. A brief summary of the use of these approximations is included in Section 2.5.1 of *IT* B (1992) and computing methods are discussed in Subsection 4.3.8.5 and Section 4.3.4.

The projected-charge-density (PCD) approximation (Cowley & Moodie, 1960) gives the HREM image intensity (for the simplified case where $C_s = 0$) as

$$I(x, y) = 1 + (\Delta f\lambda\sigma/2\pi\varepsilon_0\varepsilon)\rho_p(x, y), \quad (4.3.8.13c)$$

where $\rho_p(x, y)$ is the projected charge density for the specimen (including the nuclear contribution) and is related to $\varphi_p(x, y)$ through Poisson's equation. Here, $\varepsilon_0\varepsilon$ is the specimen dielectric constant. This approximation, unlike the weak-phase-object approximation (WPO), includes multiple scattering to all orders of the Born series, within the approximation that the component of the scattering vector is zero in the beam direction (a 'flat' Ewald sphere). Contrast is found to be proportional to defocus and to $\rho_p(x, y)$. The failure conditions of this approximation are discussed by Lynch, Moodie & O'Keefe (1975); briefly, it fails for $\chi(u_0) > \pi/2$ (and hence if C_s, Δf or u_0 becomes large) or for large thicknesses t ($t < 7$ nm is suggested for specimens of medium atomic weight and $\lambda = 0.037$ Å). The PCD result becomes increasingly accurate with increasing accelerating voltage for small C_s.

The WPO approximation has been used extensively in combination with the Scherzer-focus condition (Scherzer, 1949) for the interpretation of structure images (Cowley & Iijima, 1972). This approximation neglects multiple scattering of the beam electron and thereby allows the application of the methods of linear transfer theory from optics. The image intensity is then given, for plane-wave illumination, by

$$I(x, y) = 1 + 2\sigma\varphi_p(x, y) * \mathcal{F}\{\sin\chi(u, v)P(u, v)\} = 1 + 2\sigma\varphi_p(x, y) * S(x, y), \quad (4.3.8.14)$$

where $\mathcal{F}$ denotes Fourier transform, $*$ denotes convolution, and u and v are orthogonal components of the two-dimensional scattering vector $\mathbf{u}$. The function $S(x, y)$ is sharply peaked and negative at the 'Scherzer focus'

$$\Delta f = \Delta f_s = 1.2(C_s\lambda)^{1/2} \quad (4.3.8.15a)$$

and the optimum objective aperture size

$$\theta_0 = 1.5(\lambda/C_s)^{1/4}. \quad (4.3.8.15b)$$

It forms the impulse response of an electron microscope for phase contrast. Contrast is found to be proportional to φ_p and to the interaction parameter σ, which increases very slowly with accelerating voltage above about 500 keV. The point resolution [see Subsection 2.5.1.9 of *IT* B (1992) and Subsection 4.3.8.6] is conventionally defined from equation (4.3.8.15*b*) as λ/θ_0, or

$$d_p = 0.66\,C_s^{1/4}\lambda^{3/4}. \quad (4.3.8.16)$$

The occurrence of appreciable multiple scattering, and therefore of the failure of the WPO approximation, depends on specimen thickness, orientation, and accelerating voltage. Detailed comparisons between accurate multiple-scattering calculations, the PCD approximation, and the WPO approximation can be found in Lynch, Moodie & O'Keefe (1975) and Jap & Glaeser (1978). As a very rough guide, equation (4.3.8.14) can be expected to fail for light elements at 100 keV and thicknesses greater than about 5.0 nm. Multiple-scattering effects have been predicted within single atoms of gold at 100 keV.

The WPO approximation may be extended to include the effects of an extended source (partial spatial coherence) and a range of incident electron-beam energies (temporal coherence). General methods for incorporating these effects in the presence of multiple scattering are described in Subsection 4.3.8.5. Under the approximations of linear imaging outlined below, it can be shown (Wade & Frank, 1977; Fejes, 1977) that $\sin\chi(u, v)P(u, v)$ in equation (4.3.8.14) may be replaced by

$$A'(\mathbf{u}) = P(\mathbf{u})\exp[i\chi(\mathbf{u})]\exp(-\pi^2\Delta^2\lambda^2\mathbf{u}^4/2)\gamma(\nabla\chi/2\pi) = P(\mathbf{u})\exp[i\chi(\mathbf{u})]\exp(i\pi^2\Delta^2\lambda^2\mathbf{u}^4/2)\exp(-\pi^2u_0^2q) \quad (4.3.8.17)$$

if astigmatism is absent. Here, $\mathbf{u} = u\mathbf{i} + v\mathbf{j}$ and $|\mathbf{u}| = 2\theta/\lambda = (u^2 + v^2)^{1/2}$. In addition, $\gamma(\mathbf{u}')$ is the Fourier transform of the source intensity distribution (assumed Gaussian), so that $\gamma(\nabla\chi/2\pi)$ is small in regions where the slope of $\chi(\mathbf{u}')$ is large, resulting in severe attenuation of these spatial frequencies. If the illuminating beam divergence Θ_c is chosen as the angular half width for which the distribution of source intensity falls to half its maximum value, then

$$\theta_c = \lambda u_0(\ln 2)^{1/2}. \quad (4.3.8.18)$$

The quantity q is defined by

$$q = (C_s\lambda^3\mathbf{u}^3 + \Delta f\lambda\mathbf{u})^2 + T2,$$

where $T2$ expresses a coupling between the effects of partial spatial coherence and temporal coherence. This term can frequently be neglected under HREM conditions [see Wade & Frank (1977) for details]. The damping envelope due to chromatic effects is described by the parameter

$$\Delta = C_cQ = C_c\{[\sigma^2(V_0)]/V_0^2 + [4\sigma^2(I_0)]/I_0^2 + [\sigma^2(E_0)]/E_0^2\}^{1/2}, \quad (4.3.8.19)$$

where $\sigma^2(V_0)$ and $\sigma^2(I_0)$ are the variances in the statistically independent fluctuations of accelerating voltage V_0 and objective-lens current I_0. The r.m.s. value of the high voltage fluctuation is equal to the standard deviation $\sigma(V_0) = [\sigma^2(V_0)]^{1/2}$. The full width at half-maximum height of the energy distribution of electrons leaving the filament is

$$\Delta E = 2(2\ln 2)^{1/2}\sigma(E_0) = 2.355[\sigma^2(E_0)]^{1/2}. \quad (4.3.8.20)$$

Here, C_c is the chromatic aberration constant of the objective lens.

Equations (4.3.8.14) and (4.3.8.17) indicate that under linear imaging conditions the transfer function for HREM contains a chromatic damping envelope more severely attenuating than a Gaussian of width

$$U_0(\Delta) = [2/\pi\lambda\Delta]^{1/2},$$

which is present in the absence of any objective aperture $P(\mathbf{u})$. The resulting resolution limit

$$d_i = [\pi\lambda\Delta/2]^{1/2} \qquad (4.3.8.21)$$

is known as the information resolution limit (see Subsection 4.3.8.6) and depends on electronic instabilities and the thermal-energy spread of electrons leaving the filament. The reduction in the contribution of particular diffracted beams to the image due to limited spatial coherence is minimized over those extended regions for which $\nabla\chi(\mathbf{u})$ is small, called passbands, which occur when

$$\Delta f_n = [C_s\lambda(8n+3)/2]^{1/2}. \qquad (4.3.8.22)$$

The Scherzer focus Δf_s corresponds to $n = 0$. These passbands become narrower and move to higher $\mathbf{u}$ values with increasing n, but are subject also to chromatic damping effects. The passbands occur between spatial frequencies U_1 and U_2, where

$$U_{1,2} = C_s^{-1/4}\lambda^{-3/4}\{[(8n+2)/2]^{1/2} \pm 1\}^{1/2}. \qquad (4.3.8.23)$$

Their use for extracting information beyond the point resolution of an electron microscope is further discussed in Subsection 4.3.8.6.

Fig. 4.3.8.5 shows transfer functions for a modern instrument for $n = 0$ and 1. Equations (4.3.8.14) and (4.3.8.17) provide a simple, useful, and popular approach to the interpretation of HREM images and valuable insights into resolution-limiting factors. However, it must be emphasized that these results apply only (amongst other conditions) for $\Phi_0 \gg \Phi_{\mathbf{g}}$ (in crystals) and therefore do not apply to the usual case of strong multiple electron scattering. Equation (4.3.8.13*b*) does not make this approximation. In real space, for crystals, the alignment of columns of atoms in the beam direction rapidly leads to phase changes in the electron wavefunction that exceed $\pi/2$, leading to the failure of equation (4.3.8.14). Accurate quantitative comparisons of experimental and simulated HREM images must be based on equation (4.3.8.13*a*), or possibly (4.3.8.13*b*), with $\psi(\mathbf{u}', \Delta f, \mathbf{r})$ obtained from many-beam dynamical calculations of the type described in Subsection 4.3.8.5.

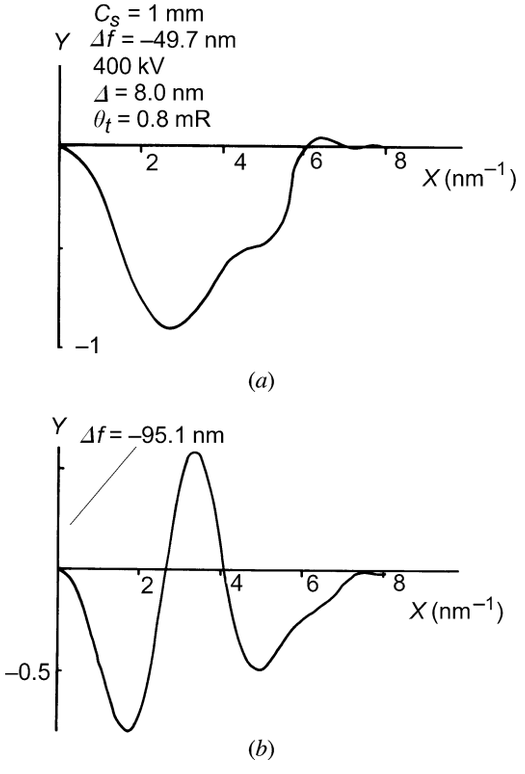

Fig. 4.3.8.5. (*a*) The transfer function for a 400 kV electron microscope with a point resolution of 1.7 Å at the Scherzer focus; the curve is based on equation (4.3.8.17). In (*b*) is shown a transfer function for similar conditions at the first 'passband' focus [$n = 1$ in equation (4.3.8.22)].

For the structure imaging of specific types of defects and materials, the following references are relevant. (i) For line defects viewed parallel to the line, d'Anterroches & Bourret (1984); viewed normal to the line, Alexander, Spence, Shindo, Gottschalk & Long (1986). (ii) For problems of variable lattice spacing (*e.g.* spinodal decomposition), Cockayne & Gronsky (1981). (iii) For point defects and their ordering, in tunnel structures, Yagi & Cowley (1978); in semiconductors, Zakharov, Pasemann & Rozhanski (1982); in metals, Fields & Cowley (1978). (iv) For interfaces, see the proceedings reported in *Ultramicroscopy* (1992), Vol. 40, No. 3. (v) For metals, Lovey, Coene, Van Dyck, Van Tendeloo, Van Landuyt & Amelinckx (1984). (vi) For organic crystals, Kobayashi, Fujiyoshi & Uyeda (1982). (vii) For a general review of applications in solid-state chemistry, see the collection of papers reported in *Ultramicroscopy* (1985), Vol. 18, Nos. 1–4. (viii) Radiation-damage effects are observed at atomic resolution by Horiuchi (1982).

4.3.8.4. *Parameters affecting HREM images*

The *instrumental parameters* that affect HREM images include accelerating voltage, astigmatism, optic-axis alignment, focus setting Δf, spherical-aberration constant C_s, beam divergence θ_c, and chromatic aberration constant C_c. Crystal parameters influencing HREM images include thickness, absorption, ionicity, and the alignment of the crystal zone axis with the beam, in addition to the structure factors and atom positions of the sample. The accurate measurement of electron wavelength or accelerating voltage has been discussed by many workers, including Uyeda, Hoier and others [see Fitzgerald & Johnson (1984) for references]. The measurement of Kikuchi-line spacings from crystals of known structure appears to be the most accurate and convenient method for HREM work, and allows an overall accuracy of better than 0.2% in accelerating voltage. Fluctuations in accelerating voltage contribute to the chromatic damping term Δ in equation (4.3.8.19) through the variance $\sigma^2(V_0)$. With the trend toward the use of higher accelerating voltages for HREM work, this term has become especially significant for the consideration of the information resolution limit [equation (4.3.8.21)].

Techniques for the accurate measurement of astigmatism and chromatic aberration are described by Spence (1988). The displacement of images of small crystals with beam tilt may be used to measure C_s; alternatively, the curvature of higher-order Laue-zone lines in CBED patterns has been used. The method of Budinger & Glaeser (1976) uses a similar dark-field image-displacement method to provide values for both Δf and C_s, and appears to be the most convenient and accurate for HREM work. The analysis of optical diffractograms initiated by Thon and co-workers from HREM images of thin amorphous films provides an invaluable diagnostic aid for HREM work; however, the determination of C_s by this method is prone to large errors, especially at small defocus. Diffractograms provide a rapid method for the determination of focus setting (see Krivanek, 1976) and in addition provide a sensitive indicator of specimen movement, astigmatism, and the damping-envelope constants Δ and Θ_c.

Misalignment of the electron beam, optic axis, and crystal axis in bright-field HREM work becomes increasingly important with increasing resolution and specimen thickness. The first-order effects of optical misalignment are an artifactual translation of spatial frequencies in the direction of misalignment by an amount proportional to the misalignment and to the square of spatial frequency. The corresponding phase shift is not observable in diffractograms. The effects of astigmatism on transfer functions for inclined illumination are discussed in Saxton (1978).

The effects of misalignment of the beam with respect to the optic axis are discussed in detail by Smith, Saxton, O'Keefe, Wood & Stobbs (1983), where it is found that all symmetry elements (except a mirror plane along the tilt direction) may be destroyed by misalignment. The maximum allowable misalignment for a given resolution δ in a specimen of thickness t is proportional to

$$\alpha = \delta/8t. \qquad (4.3.8.24)$$

Misalignment of a crystalline specimen with respect to the beam may be distinguished from misalignment of the optic axis with respect to the beam by the fact that, in very thin crystals, the former does not destroy centres of symmetry in the image.

The use of known defect point-group symmetry (for example in stacking faults) to identify a point in a HREM image with a point in the structure and so to resolve the black or white atomic contrast ambiguity has been described (Olsen & Spence, 1981). Structures containing screw or glide elements normal to the beam are particularly sensitive to misalignment, and errors as small as 0.2 mrad may substantially alter the image appearance.

A rapid comparison of images of amorphous material with the beam electronically tilted into several directions appears to be the best current method of aligning the beam with the optic axis, while switching to convergent-beam mode appears to be the most effective method of aligning the beam with the crystal axis. However, there is evidence that the angle of incidence of the incident beam is altered by this switching procedure.

The effects of misalignment and choice of beam divergence Θ_c on HREM images of crystals containing dynamically forbidden reflections are reviewed by Nagakura, Nakamura & Suzuki (1982) and Smith, Bursill & Wood (1985). Here the dramatic example of rutile in the [001] orientation is used to demonstrate how a misalignment of less than 0.2 mrad of the electron beam with respect to the crystal axis can bring up a coarse set of fringes (4.6 Å), which produce an image of incorrect symmetry, since these correspond to structure factors that are forbidden both dynamically and kinematically.

Crystal thickness is most accurately determined from images of planar faults in known orientations, or from crystal morphology for small particles. It must otherwise be treated as a refinement parameter. Since small crystals (such as MgO smoke particles, which form as perfect cubes) provide such an independent method of thickness determination, they provide the most convincing test of dynamical imaging theory. *The ability to match the contrast reversals and other detailed changes in HREM images as a function of either thickness or focus (or both) where these parameters have been measured by an independent method gives the greatest confidence in image interpretation.* This approach, which has been applied in rather few cases [see, for example, O'Keefe, Spence, Hutchinson & Waddington (1985)] is strongly recommended. The tendency for n-beam dynamical HREM images to repeat with increasing thickness in cases where the wavefunction is dominated by just two Bloch waves has been analysed by several workers (Kambe, 1982).

Since electron scattering factors are proportional to the difference between atomic number and X-ray scattering factors, and inversely proportional to the square of the scattering angle (see Section 4.3.1), it has been known for many years that the low-order reflections that contribute to HREM images are extremely sensitive to the distribution of bonding electrons and so to the degree of ionicity of the species imaged. This observation has formed the basis of several charge-density-map determinations by convergent-beam electron diffraction [see, for example, Zuo, Spence & O'Keefe (1988)]. Studies of ionicity effects on HREM imaging can be found in Anstis, Lynch, Moodie & O'Keefe (1973) and Fujiyoshi, Ishizuka, Tsuji, Kobayashi & Uyeda (1983).

The depletion of the elastic portion of the dynamical electron wavefunction by inelastic crystal excitations (chiefly phonons, single-electron excitations, and plasmons) may have dramatic effects on the HREM images of thicker crystals (Pirouz, 1974). For image formation by the elastic component, these effects may be described through the use of a complex 'optical' potential and the appropriate Debye–Waller factor (see Section 2.5.1). However, existing calculations for the absorption coefficients derived from the imaginary part of this potential are frequently not applicable to lattice images because of the large objective apertures used in HREM work. It has been suggested that HREM images formed from electrons that suffer small energy losses (and so remain 'in focus') but large-angle scattering events (within the objective aperture) due to phonon excitation may contribute high-resolution detail to images (Cowley, 1988). For measurements of the imaginary part of the optical potential by electron diffraction, the reader is referred to the work of Voss, Lehmpfuhl & Smith (1980), and references therein. All evidence suggests, however, that for the crystal thicknesses generally used for HREM work ($t < 200$ Å) the effects of 'absorption' are small.

In summary, the general approach to the matching of computed and experimental HREM images proceeds as follows (Wilson, Spargo & Smith, 1982). (i) Values of Δ, Θ_c, and C_s are determined by careful measurements under well defined conditions (electron-gun bias setting, illumination aperture size, specimen height as measured by focusing-lens currents, electron-source size, *etc*). These parameters are then taken as constants for all subsequent work under these instrumental conditions (assuming also continuous monitoring of electronic instabilities). (ii) For a particular structure refinement, the parameters of thickness and focus are then varied, together with the choice of atomic model, in dynamical computer simulations until agreement is obtained. Every effort should be made to match images as a function of thickness and focus. (iii) If agreement cannot be obtained, the effects of small misalignments must be investigated (Smith *et al.*, 1985). Crystals most sensitive to these include those containing reflections that are absent due to the presence of screw or glide elements normal to the beam.

4.3.8.5. *Computing methods*

The general formulations for the dynamical theory of electron diffraction in crystals have been described in Section 5.2 of *IT* B (1992). In Section 4.3.6, the computing methods used for calculating diffraction-beam amplitudes have been outlined.

Given the diffracted-beam amplitudes, Ψ_g, the image is calculated by use of equations (4.3.8.2), including, when appropriate, the modifications of (4.3.8.13*b*).

The numerical methods that can be employed in relation to crystal-structure imaging make use of algorithms based on (i) matrix diagonalization, (ii) fast Fourier transforms, (iii) real-space convolution (Van Dyck, 1980), (iv) Runge-Kutta (or similar) methods, or (v) power-series evaluation. Two other solutions, the Cowley–Moodie polynomial solution and the

Feynman path-integral solution, have not been used extensively for numerical work. Methods (i) and (ii) have proven the most popular, with (ii) (the multislice method) being used most extensively for HREM image simulations. The availability of inexpensive array processors has made this technique highly efficient. A comparison of these two N-beam methods is given by Self, O'Keefe, Buseck & Spargo (1983), who find the multislice method to be faster (time proportional to $N \log_2 N$) than the diagonalization method (time proportional to N^2) for $N > 16$. Computing space increases roughly as N^2 for the diagonalization method, and as N for the multislice. The problem of steeply inclined boundary conditions for multislice computations has been discussed by Ishizuka (1982).

In the Bloch-wave formulation, the lattice image is given by

$$I(\mathbf{r}) = \sum_{i,j} \sum_{\mathbf{h},\mathbf{g}} C_0^{(i)} C_0^{(j)} C_{\mathbf{g}}^{(i)} C_{\mathbf{h}}^{(j)} \exp\{i[2\pi(\gamma^{(i)} - \gamma^{(j)})t + 2\pi(\mathbf{g} - \mathbf{h}) \cdot \mathbf{r} - \chi(\Delta f, C_s, \mathbf{g}) + \chi(\Delta f, C_s, \mathbf{h})]\}, \quad (4.3.8.25)$$

where $C_{\mathbf{g}}^{(i)}$ and $\gamma^{(i)}$ are the eigenvector elements and eigenvalues of the structure matrix [see Hirsch, Howie, Nicholson, Pashley & Whelan (1977) and Section 4.3.4].

Using modern personal computers or workstations, it is now possible to build efficient single-user systems that allow interactive dynamical structure-image calculations. Either an image intensifier or a cooled scientific grade charge-coupled device and single-crystal scintillator screen may be used to record the images, which are then transferred into a computer (Daberkow, Herrman, Liu & Rau, 1991). This then allows for the possibility of automated alignment, stigmation and focusing to the level of accuracy needed at 0.1 nm point resolution (Krivanek & Mooney, 1993). An image-matching search through trial structures, thickness and focus parameters can then be completed rapidly. Where large numbers of pixels, large dynamic range and high sensitivity are required, the Image Plate has definite advantages and so should find application in electron holography and biology (Shindo, Hiraga, Oikawa & Mori, 1990).

For the calculation of images of defects, the method of periodic continuation has been used extensively (Grinton & Cowley, 1971). Since, for kilovolt electrons traversing thin crystals, the transverse spreading of the dynamical wavefunction is limited (Cowley, 1981), the complex image amplitude at a particular point on the specimen exit face depends only on the crystal potential within a cylinder a few ångströms in diameter, erected about that point (Spence, O'Keefe & Iijima, 1978). The width of this cylinder depends on accelerating voltage, specimen thickness, and focus setting (see above references). Thus, small overlapping 'patches' of exit-face wavefunction may be calculated in successive computations, and the results combined to form a larger area of image. The size of the 'artificial superlattice' used should be increased until no change is found in the wavefunction over the central region of interest. For most defects, the positions of only a few atoms are important and, since the electron wavefunction is locally determined (for thin specimens at Scherzer focus), it appears that very large calculations are rarely needed for HREM work. The simulation of profile images of crystal surfaces at large defocus settings will, however, frequently be found to require large amounts of storage.

A new program should be tested to ensure that (*a*) under approximate two-beam conditions the calculated extinction distances for small-unit-cell crystals agree roughly with tabulated values (Hirsch *et al.*, 1977), (*b*) the simulated dynamical images have the correct symmetry, (*c*) for small thickness, the Scherzer-focus images agree with the projected potential, and (*d*) images and beam intensities agree with those of a program known to be correct. The damping envelope (product representation) [equation (4.3.8.17)] should only be used in a thin crystal with $\Phi_0 > \Phi_{\mathbf{g}}$; in general, the effects of partial spatial and temporal coherence must be incorporated using equation (4.3.8.13*a*) or (4.3.8.13*b*), depending on whether variations in diffraction conditions over θ_c are important. Thus, a separate multislice dynamical-image calculation for each component plane wave in the incident cone of illumination may be required, followed by an incoherent sum of all resulting images.

The outlook for obtaining higher resolution at the time of writing (1997) is broadly as follows. (1) The highest point resolution currently obtainable is close to 0.1 nm, and this has been obtained by taking advantage of the reduction in electron wavelength that occurs at high voltage [equation (4.3.8.16)]. A summary of results from these machines can be found in *Ultramicroscopy* (1994), Vol. 56, Nos. 1–3, where applications to fullerenes, glasses, quasicrystals, interfaces, ceramics, semiconductors, metals and oxides and other systems may be found. Fig. 4.2.8.6 shows a typical result. High cost, and the effects of radiation damage (particularly at larger thickness where defects with higher free energies are likely to be found), may limit these machines to a few specialized laboratories in the future. The attainment of higher resolution through this approach depends on advances in high-voltage engineering. (2) Aberration coefficients may be reduced if higher magnetic fields can be produced in the pole piece, beyond the saturation flux of the specialized iron alloys currently used. Research into superconducting lenses has therefore continued for many years in a few laboratories. Fluctuations in lens current are also eliminated by this method. (3) Electron holography was originally developed for the purpose of improving electron-microscope resolution, and this approach is reviewed in the following section. (4) Electron–optical correction of aberrations has been under study for many years in work by Scherzer, Crewe, Beck, Krivanek, Lanio, Rose and others – results of recent experimental tests are described in Haider & Zach (1995) and Krivanek, Dellby, Spence, Camps & Brown (1997). The attainment of 0.1 nm point resolution is considered feasible. Aberration correctors will also provide benefits other than increased resolution, including greater space in the pole piece for increased sample tilt and access to X-ray detectors, *etc*.

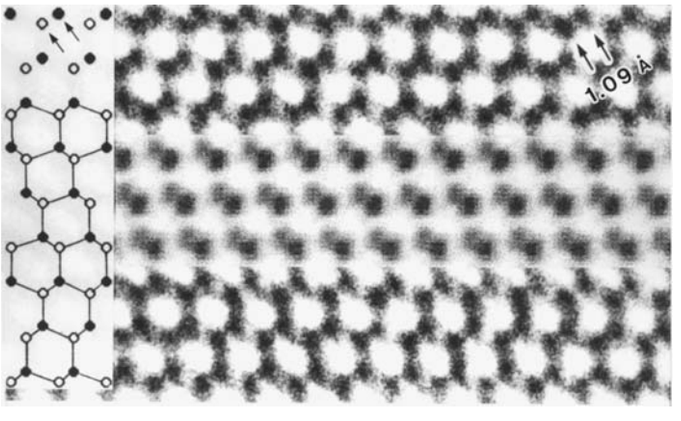

Fig. 4.3.8.6. Structure image of a thin lamella of the 6*H* polytype of SiC projected along [110] and recorded at 1.2 MeV. Every atomic column (darker dots) is separately resolved at 0.109 nm spacing. The central horizontal strip contains a computer-simulated image; the structure is sketched at the left. [Courtesy of H. Ichinose (1994).]

The need for resolution improvement beyond 0.1 nm has been questioned – the structural information retrievable by a single HREM image is always limited by the fact that a projection is obtained. (This problem is particularly acute for glasses.) Methods for combining different projected images (particularly of defects) from the same region (Downing, Meisheng, Wenk & O'Keefe, 1990) may now be as important as the search for higher resolution.

4.3.8.6. *Resolution and hyper-resolution*

Since the resolution of an instrument is a property of the instrument alone, whereas the ability to distinguish HREM image features due to adjacent atoms depends on the scattering properties of the atoms, the resolution of an electron microscope cannot easily be defined [see Subsection 2.5.1.9 in *IT* B (1992)]. The Rayleigh criterion was developed for the incoherent imaging of point sources and cannot be applied to coherent phase contrast. Only for very thin specimens of light elements for which it can be assumed that the scattering phase is $-\pi/2$ can the straightforward definition of point resolution d_p [equation (4.3.8.16)] be applied. In general, the dynamical wavefunction across the exit face of a crystalline sample bears no simple relationship to the crystal structure, other than to preserve its symmetry and to be determined by the 'local' crystal potential. The use of a dynamical '*R* factor' between computed and experimental images of a known structure has been suggested by several workers as the basis for a more general resolution definition.

For weakly scattering specimens, the most satisfactory method of measuring either the point resolution d_p or the information limit d_i [see equation (4.3.8.21)] appears to be that of Frank (1975). Here two successive micrographs of a thin amorphous film are recorded (under identical conditions) and the superimposed pair used to obtain a coherent optical diffractogram crossed by fringes. The fringes, which result from small displacements of the micrographs, extend only to the band limit d_i^{-1} of information common to both micrographs, and cannot be extended by photographic processing, noise, or increased exposure. By plotting this band limit against defocus, it is possible to determine both Δ and θ_c. As an alternative, for thin crystalline samples of large-unit-cell materials, the parameters Δ, θ_c, and C_s can be determined by matching computed and experimental images of crystals of known structure. It is the specification of these parameters (for a given electron intensity and wavelength) that is important in describing the performance of high-resolution electron microscopes. We note that certain conditions of focus or thickness may give a spurious impression of ultra-high resolution [see equations (4.3.8.7) and (4.3.8.8)].

Within the domain of linear imaging, implying, for the most part, the validity of the WPO approximation, many forms of image processing have been employed. These have been of particular importance for crystalline and non-crystalline biological materials and include image reconstruction [see Section 2.5.4 in *IT* B (1992)] and the derivation of three-dimensional structures from two-dimensional projections [see Section 2.5.5 in *IT* B (1992)]. For reviews, see also Saxton (1980*a*), Frank (1980), and Schiske (1975). Several software packages now exist that are designed for image manipulation, Fourier analysis, and cross correlation; for details of these, see Saxton (1980*a*) and Frank (1980). The theoretical basis for the WPO approximation closely parallels that of axial holography in coherent optics, thus much of that literature can be applied to HREM image processing. Gabor's original proposal for holography was intended for electron microscopy [see Cowley (1981) for a review].

The aim of image-processing schemes is the restoration of the exit-face wavefunction, given in equation (4.3.8.13*a*). The reconstruction of the crystal potential $\varphi_p(\mathbf{r})$ from this is a separate problem, since these are only simply related under the approximation of Subsection 4.3.8.3. For a non-linear method that allows the reconstruction of the dynamical image wavefunction, based on equation (4.3.8.13*b*), which thus includes the effects of multiple scattering, see Saxton (1980*b*).

The concept of holographic reconstruction was introduced by Gabor (1948, 1949) as a means of enhancing the resolution of electron microscopes. Gabor proposed that, if the information on relative phases of the image wave could be recorded by observing interference with a known reference wave, the phase modification due to the objective-lens aberrations could be removed. Of the many possible forms of electron holography (Cowley, 1994), two show particular promise of useful improvements of resolution. In what may be called in-line TEM holography, a through-focus series of bright-field images is obtained with near-coherent illumination. With reference to the relatively strong transmitted beam, the relative phase and amplitude changes due to the specimen are derived from the variations of image intensity (see Van Dyck, Op de Beeck & Coene, 1994). The tilt-series reconstruction method also shows considerable promise (Kirkland, Saxton, Chau, Tsuno & Kawasaki, 1995).

In the alternative off-axis approach, the reference wave is that which passes by the specimen area in vacuum, and which is made to interfere with the wave transmitted through the specimen by use of an electrostatic biprism (Möllenstedt & Düker, 1956). The hologram consists of a modulated pattern of interference fringes. The image wavefunction amplitude and phase are deduced from the contrast and lateral displacements of the fringes (Lichte, 1991; Tonomura, 1992). The process of reconstruction from the hologram to give the image wavefunction may be performed by optical-analogue or digital methods and can include the correction of the phase function to remove the effects of lens aberrations and the attendant limitation of resolution. The point resolution of electron microscopes has recently been exceeded by this method (Orchowski, Rau & Lichte, 1995).

The aim of the holographic reconstructions is the restoration of the wavefunction at the exit face of the specimen as given by equation (4.3.8.13*a*). The reconstruction of the crystal potential $\varphi(\mathbf{r})$ from this is a separate problem, since the exit-face wavefunction and $\varphi(\mathbf{r})$ are simply related only under the WPO approximations of Subsection 4.3.8.3. The possibility of deriving reconstructions from wavefunctions strongly affected by dynamical diffraction has been considered by a number of authors (for example, Van Dyck *et al.*, 1994). The problem does not appear to be solvable in general, but for special cases, such as perfect thin single crystals in exact axial orientations, considerable progress may be possible.

Since a single atom, or a column of atoms, acts as a lens with negative spherical aberration, methods for obtaining super-resolution using atoms as lenses have recently been proposed (Cowley, Spence & Smirnov, 1997).

4.3.8.7. *Alternative methods*

A number of non-conventional imaging modes have been found useful in electron microscopy for particular applications. In scanning transmission electron microscopy (STEM), powerful electron lenses are used to focus the beam from a very small bright source, formed by a field-emission gun, to form a small probe that is scanned across the specimen. Some selected part of the transmitted electron beam (part of the coherent convergent-

beam electron diffraction pattern produced) is detected to provide the image signal that is displayed or recorded in synchronism with the incident-beam scan. The principle of reciprocity suggests that, for equivalent lenses, apertures and column geometry, the resolution and contrast of STEM and TEM images will be identical (Cowley, 1969). Practical considerations of instrumental convenience distinguish particularly useful STEM modes.

Crewe & Wall (1970) showed that, if an annular detector is used to detect all electrons scattered outside the incident-beam cone, dark-field images could be obtained with high efficiency and with a resolution better than that of the bright-field mode by a factor of about 1.4. If the inner radius of the annular detector is made large (of the order of 10^{-1} rad for 100 kV electrons), the strong diffracted beams occurring for lower angles do not contribute to the resulting high-angle annular dark-field (HAADF) image (Howie, 1979), which is produced mainly by thermal diffuse scattering. The HAADF mode has important advantages for particular purposes because the contrast is strongly dependent on the atomic number, Z, of the atoms present but is not strongly affected by dynamical diffraction effects and so shows near-linear variation with Z and with the atom-number density in the sample. Applications have been made to the imaging of small high-Z particles in low-Z supports, such as in supported metal catalysts (Treacy & Rice, 1989) and to the high-resolution imaging of individual atomic rows in semiconductor crystals, showing the variations of composition across planar interfaces (Pennycook & Jesson, 1991).

The STEM imaging modes may be readily correlated with microchemical analysis of selected specimen areas having lateral dimensions in the nanometre range, by application of the techniques of electron energy-loss spectroscopy or X-ray energy-dispersive analysis (Williams & Carter, 1996; Section 4.3.4). Also, diffraction patterns (coherent convergent-beam electron diffraction patterns) may be obtained from any chosen region having dimensions equal to those of the incident-beam diameter and as small as about 0.2 nm (Cowley, 1992). The coherent interference between diffracted beams within such a pattern may provide information on the symmetries, and, ultimately, the atomic arrangement, within the illuminated area, which may be smaller than the projection of the crystal unit cell in the beam direction. This geometry has been used to extend resolution for crystalline samples beyond even the information resolution limit, d_i (Nellist, McCallum & Rodenburg, 1995), and is the basis for an exact, non-perturbative inversion scheme for dynamical electron diffraction (Spence, 1998).

The detection of secondary radiations (light, X-rays, low-energy 'secondary' electrons, *etc.*) in STEM or the detection of energy losses of the incident electrons, resulting from particular elementary excitations of the atoms in a crystal, in TEM or STEM, may be used to form images showing the distributions in a crystal structure of particular atomic species. In principle, this may be extended to the chemical identification of individual atom types in the projection of crystal structures, but only limited success has been achieved in this direction because of the relatively low level of the signals available. The formation of atomic resolution images using inner-shell excitations, for example, is complicated by the Bragg scattering of these inelastically scattered electrons (Endoh, Hashimoto & Makita, 1994; Spence & Lynch, 1982).

Reflection electron microscopy (REM) has been shown to be a powerful technique for the study of the structures and defects of crystal surfaces with moderately high spatial resolution (Larsen & Dobson, 1988), especially when performed in a specially built electron microscope having an ultra-high-vacuum specimen environment (Yagi, 1993). Images are formed by detecting strong diffracted beams in the RHEED patterns produced when kilovolt electron beams are incident on flat crystal surfaces at grazing incidence angles of a few degrees. The images suffer from severe foreshortening in the beam direction, but, in directions at right angles to the beam, resolutions approaching 0.3 nm have been achieved (Koike, Kobayashi, Ozawa & Yagi, 1989). Single-atom-high surface steps are imaged with high contrast, surface reconstructions involving only one or two monolayers are readily seen and phase transitions of surface superstructures may be followed.

The study of surface structure by use of high-resolution transmission electron microscopes has also been productive in particular cases. Images showing the structures of surface layers with near-atomic resolution have been obtained by the use of 'forbidden' or 'termination' reflections (Cherns, 1974; Takayanagi, 1984) and by phase-contrast imaging (Moodie & Warble, 1967; Iijima, 1977). The imaging of the profiles of the edges of thin or small crystals with clear resolution of the surface atomic layers has also been effective (Marks, 1986). The introduction of the scanning tunnelling microscope (Binnig, Rohrer, Gerber & Weibel, 1983) and other scanning probe microscopies has broadened the field of high-resolution surface structure imaging considerably.

4.3.8.8. *Combined use of HREM and electron diffraction*

For many materials of organic or biological origin, it is possible to obtain very thin crystals, only one or a few molecules thick, extending laterally over micrometre-size areas. These may give selected-area electron-diffraction patterns in electron microscopes with diffraction spots extending out to angles corresponding to d spacings as low as 0.1 nm. Because the materials are highly sensitive to electron irradiation, conventional bright-field images cannot be obtained with resolutions better than several nanometres. However, if images are obtained with very low electron doses and then a process of averaging over the content of a very large number of unit cells of the image is carried out, images showing detail down to the scale of 1 nm or less may be derived for the periodically repeated unit. From such images, it is possible to derive both the magnitudes and phases of the Fourier coefficients, the structure factors, out to some limit of d spacings, say d_m. From the diffraction patterns, the magnitudes of the structure factors may be deduced, with greater accuracy, out to a much smaller limit, d_d. By combination of the information from these two sources, it may be possible to obtain a greatly improved resolution for an enhanced image of the structure. This concept was first introduced by Unwin & Henderson (1975), who derived images of the purple membrane from *Halobacterium halobium*, with greatly improved resolution, revealing its essential molecular configuration.

Recently, several methods of phase extension have been developed whereby the knowledge of the relative phases may be extended from the region of the diffraction pattern covered by the electron-microscope image transform to the outer parts. These include methods based on the use of the tangent formula or Sayre's equation (Dorset, 1994; Dorset, McCourt, Fryer, Tivol & Turner, 1994) and on the use of maximum-entropy concepts (Fryer & Gilmore, 1992). Such methods have also been applied, with considerable success, to the case of some thin inorganic crystals (Fu *et al.*, 1994). In this case, the limitation on the resolution set by the electron-microscope images may be that due to the transfer function of the microscope, since radiation-damage effects are not so limiting. Then, the resolution achieved

by the combined application of the electron diffraction data may represent an advance beyond that of normal HREM imaging. Difficulties may well arise, however, because the theoretical basis for the phase-extension methods is currently limited to the WPO approximation. A summary of the present situation is given in the book by Dorset (1995).

International Tables for Crystallography (2006). Vol. C, Chapter 4.4, pp. 430–487.

4.4. Neutron techniques

By I. S. Anderson, P. J. Brown, J. M. Carpenter, G. Lander, R. Pynn, J. M. Rowe, O. Schärpf, V. F. Sears and B. T. M. Willis

4.4.1. Production of neutrons (By J. M. Carpenter and G. Lander)

The production of neutrons of sufficient intensity for scattering experiments is a 'big-machine' operation; there is no analogue to the small laboratory X-ray unit. The most common sources of neutrons, and those responsible for the great bulk of today's successful neutron scattering programs, are the nuclear reactors. These are based on the continuous, self-sustaining fission reaction. Research-reactor design emphasizes power density, that is the highest power within a small 'leaky' volume, whereas power reactors generate large amounts of power over a large core volume. In research reactors, fuel rods are of highly enriched ^{235}U. Neutrons produced are distributed in a fission spectrum centred about 1 MeV: Most of the neutrons within the reactor are moderated (*i.e.* slowed down) by collisions in the cooling liquid, normally D_2O or H_2O, and are absorbed in fuel to propagate the reaction. As large a fraction as possible is allowed to leak out as fast neutrons into the surrounding moderator (D_2O and Be are best) and to slow down to equilibrium with this moderator. The neutron spectrum is Maxwellian with a mean energy of ~300 K (= 25 meV), which for neutrons corresponds to 1.8 Å since

$$E_n\,(\mathrm{meV}) = 81.8/\lambda^2\ (\text{Å}^2).$$

Neutrons are extracted in beams through holes that penetrate the moderator.

There are two points to remember: (*a*) neutrons are neutral so that we cannot *focus* the beams and (*b*) the spectrum is broad and continuous; there is no analogy to the characteristic wavelength found with X-ray tubes, or to the high directionality of synchrotron-radiation sources.

Neutron production and versatility in reactors reached a new level with the construction of the High-Flux Reactor at the French-German-English Institut Laue-Langevin (ILL) in Grenoble, France. An overview of the reactor and beam-tube assembly is shown in Fig. 4.4.1.1. To shift the spectrum in energy, both a cold source (25 l of liquid deuterium at 25 K) and a hot source (graphite at 2400 K) have been inserted into the D_2O moderator. Special beam tubes view these sources allowing a range of wavelengths from ~ 0.3 to ~17 Å to be used. Over 30 instruments are in operation at the ILL, which started in 1972.

The second method of producing neutrons, which historically predates the discovery of fission, is with charged particles (α particles, protons, *etc.*) striking a target nuclei. The most powerful source of neutrons of this type uses proton beams. These are accelerated in short bursts (< 1 μs) to 500–1000 MeV, and after striking the target produce an instantaneous supply of high-energy 'evaporation' neutrons. These extend up in energy close to that of the incident proton beam. Shielding for spallation sources tends to be even more massive than that for reactors. The targets, usually tungsten or uranium and typically much smaller than a reactor core, are surrounded by hydrogenous moderators such as polyethylene (often at different temperatures) to produce the 'slow' neutrons (E_n < 10 eV) used in scattering experiments. The moderators are very different from those of reactors; they are designed to slow down neutrons rapidly and to let them leak out, rather than to store them for a long time. If the accelerated

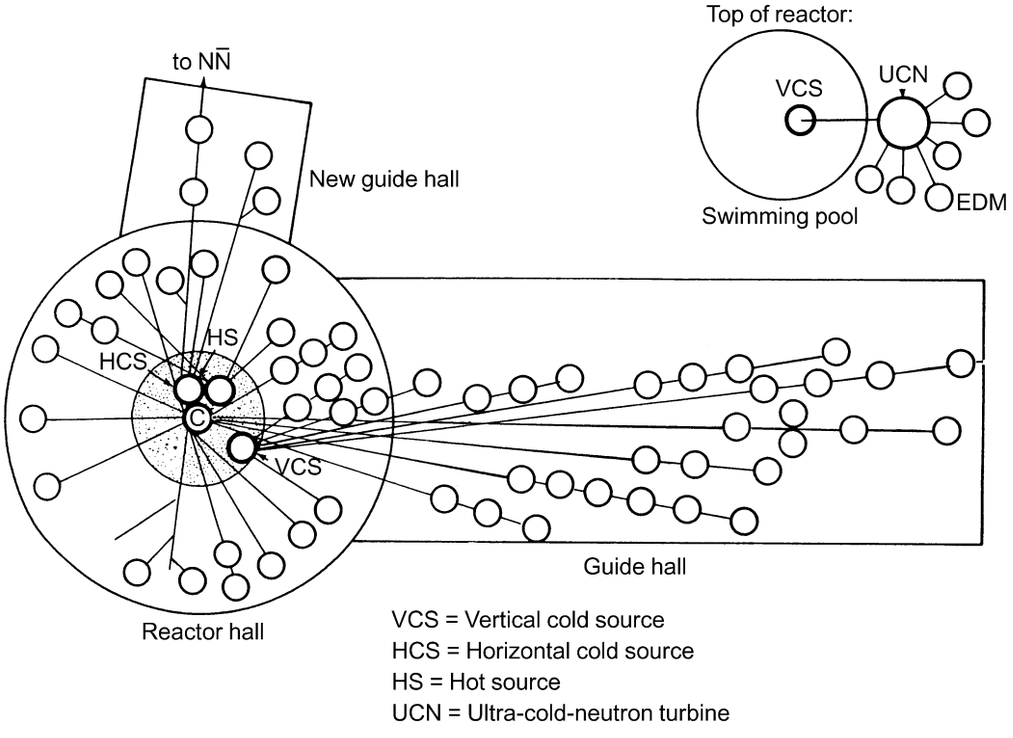

Fig. 4.4.1.1. A plane view of the installation at the Institut Laue–Langevin, Grenoble. Note especially the guide tubes exiting from the reactor that transport the neutron beams to a variety of instruments; these guide tubes are made of nickel-coated glass from which the neutrons are totally internally reflected.

Copyright © 2006 International Union of Crystallography

particle pulse is short enough, the duration of the moderated neutron pulses is roughly inversely proportional to the neutron speed.

These accelerator-driven pulsed sources are pulsed at frequencies of between 10 and 100 Hz.

There are two fundamental differences between a reactor and a pulsed source.

(1) *All* experiments at a pulsed source must be performed with time-of-flight techniques. The pulsed source produces neutrons in bursts of 1 to 50 μs duration, depending on the energy, spaced about 10 to 100 ms apart, so that the duty cycle is low but there is very high neutron intensity within each pulse. The time-of-flight technique makes it possible to exploit that high intensity. With the de Broglie relationship, for neutrons

$$\lambda\,(\text{Å}) = 0.3966\,t\,(\mu s)/L\,(\text{cm}),$$

where t is the flight time in μs and L is the total flight path in cm.

(2) The spectral characteristics of pulsed sources are somewhat different from reactors in that they have a much larger component of higher-energy (above 100 meV) neutrons than the thermal spectrum at reactors. The exploitation of this new energy regime accompanied by the short pulse duration is one of the great opportunities presented by spallation sources.

Fig. 4.4.1.2 illustrates the essential difference between experiments at a steady-state source (left panel) and a pulsed source (right panel). We confine the discussion here to diffraction. If the time over which useful information is gathered is equivalent to the full period of the source Δt (the case suggested by the lower-right figure), the *peak flux* of the pulsed source is the effective parameter to compare with the flux of the steady-state source. Often this is not the case, so one makes a comparison in terms of *time-averaged flux* (centre panel). For the pulsed source, this is lowered from the peak flux by the duty cycle, but with the time-of-flight method one uses a large interval of the spectrum (shaded area). For the steady-state source, the time-averaged flux is high, but only a small wavelength slice (stippled area) is used in the experiment. It is the *integrals* of the two areas which must be compared; for the pulsed sources now being designed, the integral is generally favourable compared with present-day reactors. Finally, one can see from the central panel that high-energy neutrons (100–1000 meV) are especially plentiful at the pulsed sources. These various features can be exploited in the design of different kinds of experiments at pulsed sources.

4.4.2. Beam-definition devices (By I. S. Anderson and O. Schärpf)

4.4.2.1. *Introduction*

Neutron scattering, when compared with X-ray scattering techniques developed on modern synchrotron sources, is flux limited, but the method remains unique in the resolution and range of energy and momentum space that can be covered. Furthermore, the neutron magnetic moment allows details of microscopic magnetism to be examined, and polarized neutrons can be exploited through their interaction with both nuclear and electron spins.

Owing to the low primary flux of neutrons, the beam definition devices that play the role of defining the beam conditions (direction, divergence, energy, polarization, *etc.*) have to be highly efficient. Progress in the development of such devices not only results in higher-intensity beams but also allows new techniques to be implemented.

The following sections give a (non-exhaustive) review of commonly used beam-definition devices. The reader should keep in mind the fact that neutron scattering experiments are typically carried out with large beams (1 to 50 cm^2) and divergences between 5 and 30 mrad.

4.4.2.2. *Collimators*

A collimator is perhaps the simplest neutron optical device and is used to define the direction and divergence of a neutron beam. The most rudimentary collimator consists of two slits or pinholes

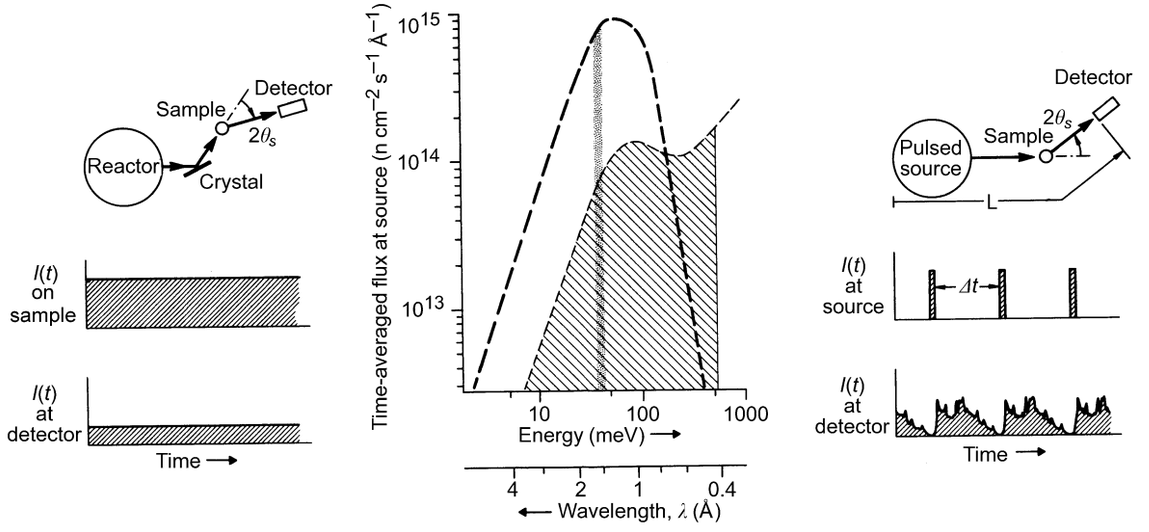

Fig. 4.4.1.2. Schematic diagram for performing diffraction experiments at steady-state and pulsed neutron sources. On the left we see the familiar monochromator crystal allowing a constant (in time) beam to fall on the sample (centre left), which then diffracts the beam through an angle $2\theta_s$ into the detector. The signal in the latter is also constant in time (lower left). On the right, the pulsed source allows a wide spectrum of neutrons to fall on the sample in sharp pulses separated by Δt (centre right). The neutrons are then diffracted by the sample through $2\theta_s$ and their time of arrival in the detector is analysed (lower right). The centre figure shows the time-averaged flux at the source. At a reactor, we make use of a narrow band of neutrons (heavy shading), here chosen with $\lambda = 1.5$ Å. At a pulsed source, we use a wide spectral band, here chosen from 0.4 to 3 Å and each one is identified by its time-of-flight. For the experimentalist, an important parameter is the integrated area of the two-shaded areas. Here they have been made identical.

cut into an absorbing material and placed one at the beginning and one at the end of a collimating distance L. The maximum beam divergence that is transmitted with this configuration is

$$\alpha_{\max} = (a_1 + a_2)/L, \qquad (4.4.2.1)$$

where a_1 and a_2 are the widths of the slits or pinholes.

Such a device is normally used for small-angle scattering and reflectometry. In order to avoid parasitic scattering by reflection from slit edges, very thin sheets of a highly absorbing material, *e.g.* gadolinium foils, are used as the slit material. Sometimes wedge-formed cadmium plates are sufficient. In cases where a very precise edge is required, cleaved single-crystalline absorbers such as gallium gadolinium garnet (GGG) can be employed.

To avoid high intensity losses when the distances are large, sections of neutron guide can be introduced between the collimators, as in, for example, small-angle scattering instruments with variable collimation. In this case, for maximum intensity at a given resolution (divergence), the collimator length should be equal to the camera length, *i.e.* the sample–detector distance (Schmatz, Springer, Schelten & Ibel, 1974).

As can be seen from (4.4.2.1), the beam divergence from a simple slit or pinhole collimator depends on the aperture size. In order to collimate (in one dimension) a beam of large cross section within a reasonable distance L, Soller collimators, composed of a number of equidistant neutron absorbing blades, are used. To avoid losses, the blades must be as thin and as flat as possible. If their surfaces do not reflect neutrons, which can be achieved by using blades with rough surfaces or materials with a negative scattering length, such as foils of hydrogen-containing polymers (Mylar is commonly used) or paper coated with neutron-absorbing paint containing boron or gadolinium (Meister & Weckerman, 1973; Carlile, Hey & Mack, 1977), the angular dependence of the transmission function is close to the ideal triangular form, and transmissions of 96% of the theoretical value can be obtained with 10′ collimation. If the blades of the Soller collimator are coated with a material whose critical angle of reflection is equal to $\alpha_{\max}/2$ (for one particular wavelength), then a square angular transmission function is obtained instead of the normal triangular function, thus doubling the theoretical transmission (Meardon & Wroe, 1977).

Soller collimators are often used in combination with single-crystal monochromators to define the wavelength resolution of an instrument but the Soller geometry is only useful for one-dimensional collimation. For small-angle scattering applications, where two-dimensional collimation is required, a converging 'pepper pot' collimator can be used (Nunes, 1974; Glinka, Rowe & LaRock, 1986).

Cylindrical collimators with radial blades are sometimes used to reduce background scattering from the sample environment. This type of collimator is particularly useful with position-sensitive detectors and may be oscillated about the cylinder axis to reduce the shadowing effect of the blades (Wright, Berneron & Heathman, 1981).

4.4.2.3. *Crystal monochromators*

Bragg reflection from crystals is the most widely used method for selecting a well defined wavelength band from a white neutron beam. In order to obtain reasonable reflected intensities and to match the typical neutron beam divergences, crystals that reflect over an angular range of 0.2 to 0.5° are typically employed. Traditionally, mosaic crystals have been used in preference to perfect crystals, although reflection from a mosaic crystal gives rise to an increase in beam divergence with a concomitant broadening of the selected wavelength band. Thus, collimators are often used together with mosaic monochromators to define the initial and final divergences and therefore the wavelength spread.

Because of the beam broadening produced by mosaic crystals, it was soon recognised that elastically deformed perfect crystals and crystals with gradients in lattice spacings would be more suitable candidates for focusing applications since the deformation can be modified to optimize focusing for different experimental conditions (Maier-Leibnitz, 1969).

Perfect crystals are used commonly in high-energy-resolution backscattering instruments, interferometry and Bonse–Hart cameras for ultra-small-angle scattering (Bonse & Hart, 1965).

An ideal mosaic crystal is assumed to comprise an agglomerate of independently scattering domains or mosaic blocks that are more or less perfect, but small enough that primary extinction does not come into play, and the intensity reflected by each block may be calculated using the kinematic theory (Zachariasen, 1945; Sears, 1997). The orientation of the mosaic blocks is distributed inside a finite angle, called the mosaic spread, following a distribution that is normally assumed to be Gaussian. The ideal neutron mosaic monochromator is not an ideal mosaic crystal but rather a mosaic crystal that is sufficiently thick to obtain a high reflectivity. As the crystal thickness increases, however, secondary extinction becomes important and must be accounted for in the calculation of the reflectivity. The model normally used is that developed by Bacon & Lowde (1948), which takes into account strong secondary extinction and a correction factor for primary extinction (Freund, 1985). In this case, the mosaic spread (usually defined by neutron scatterers as the full width at half maximum of the reflectivity curve) is not an intrinsic crystal property, but increases with wavelength and crystal thickness and can become quite appreciable at longer wavelengths.

Ideal monochromator materials should have a large scattering-length density, low absorption, incoherent and inelastic cross sections, and should be available as large single crystals with a suitable defect concentration. Relevant parameters for some typical neutron monochromator crystals are given in Table 4.4.2.1.

In principle, higher reflectivities can be obtained in neutron monochromators that are designed to operate in reflection geometry, but, because reflection crystals must be very large when takeoff angles are small, transmission geometry may be used. In that case, the optimization of crystal thickness can only be achieved for a small wavelength range.

Nickel has the highest scattering-length density, but, since natural nickel comprises several isotopes, the incoherent cross section is quite high. Thus, isotopic ^{58}Ni crystals have been grown as neutron monochromators despite their expense. Beryllium, owing to its large scattering-length density and low incoherent and absorption cross sections, is also an excellent candidate for neutron monochromators, but the mosaic structure of beryllium is difficult to modify, and the availability of good-quality single crystals is limited (Mücklich & Petzow, 1993). These limitations may be overcome in the near future, however, by building composite monochromators from thin beryllium blades that have been plastically deformed (May, Klimanek & Magerl, 1995).

Pyrolytic graphite is a highly efficient neutron monochromator if only a medium resolution is required (the minimum mosaic spread is of the order of 0.4°), owing to high reflectivities, which may exceed 90% (Shapiro & Chesser, 1972), but its use is limited to wavelengths above 1.5Å, owing to the rather large d spacing of the 002 reflection. Whenever better resolution at

Table 4.4.2.1. *Some important properties of materials used for neutron monochromator crystals (in order of increasing unit-cell volume)*

Material	Structure	Lattice constant(s) at 300 K a, c (Å)	Unit-cell volume $V_0(10^{-24}$ cm$^3)$	Coherent scattering length b (10^{-12} cm)	Square of scattering-length density 10^{-21} cm^{-4}	Ratio of incoherent to total scattering cross section $\sigma_{\rm inc}/\sigma_s$	Absorption cross section $\sigma_{\rm abs}$ (barns)* (at $\lambda = 1.8$ Å)	Atomic mass A	Debye temperature θ_D (K)	$A\theta_D^2$ (10^6 K^2)
Beryllium	h.c.p	a : 2.2856 c : 3.5832	16.2	0.779 (1)	9.25	6.5×10^{-4}	0.0076 (8)	9.013	1188	12.7
Iron	b.c.c.	a : 2.8664	23.5	0.954 (6)	6.59	0.033	2.56 (3)	55.85	411	9.4
Zinc	h.c.p.	a : 2.6649 c : 4.9468	30.4	0.5680 (5)	1.50	0.019	1.11 (2)	65.38	253	4.2
Pyrolytic graphite	layer hexag.	a : 2.461 c : 6.708	35.2	0.66484 (13)	5.71	$< 2 \times 10^{-4}$	0.00350 (7)	12.01	800	7.7
Niobum	b.c.c.	3.3006	35.9	0.7054 (3)	1.54	4×10^{-4}	1.15 (5)	92.91	284	7.5
Nickel (^{58}Ni)	f.c.c.	3.5241	43.8	1.44 (1)	17.3	0	4.6 (3)	58.71	417	9.9
Copper	f.c.c.	3.6147	47.2	0.7718 (4)	4.28	0.065	3.78 (2)	63.54	307	6.0
Aluminium	f.c.c.	4.0495	66.4	0.3449 (5)	0.43	5.6×10^{-3}	0.231 (3)	26.98	402	4.4
Lead	f.c.c.	4.9502	121	0.94003 (14)	0.97	2.7×10^{-4}	0.171 (2)	207.21	87	1.6
Silicon	diamond	5.4309	160	0.41491 (10)	0.43	6.9×10^{-3}	0.171 (3)	28.09	543	8.3
Germanium	diamond	5.6575	181	0.81929 (7)	1.31	0.020	2.3 (2)	72.60	290	6.1

* 1 barn= 10^{-28} m^2.

shorter wavelengths is required, copper (220 and 200) or germanium (311 and 511) monochromators are frequently used. The advantage of copper is that the mosaic structure can be easily modified by plastic deformation at high temperature. As with most face-centred cubic crystals, it is the (111) slip planes that are functional in generating the dislocation density needed for the desired mosaic spread, and, depending on the required orientation, either isotropic or anisotropic mosaics can be produced (Freund, 1976). The latter is interesting for vertical focusing applications, where a narrow vertical mosaic is required regardless of the resolution conditions.

Although both germanium and silicon are attractive as monochromators, owing to the absence of second-order neutrons for odd-index reflections, it is difficult to produce a controlled uniform mosaic spread in bulk samples by plastic deformation at high temperature because of the difficulty in introducing a spatially homogenous microstructure in large single crystals (Freund, 1975). Recently this difficulty has been overcome by building up composite monochromators from a stack of thin wafers, as originally proposed by Maier-Leibnitz (1967; Frey, 1974).

In practice, an artificial mosaic monochromator can be built up in two ways. In the first approach, illustrated in Fig. 4.4.2.1(*a*), the monochromator comprises a stack of crystalline wafers, each of which has a mosaic spread close to the global value required for the entire stack. Each wafer in the stack must be plastically deformed (usually by alternated bending) to produce the correct mosaic spread. For certain crystal orientations, the plastic deformation may result in an anisotropic mosaic spread. This method has been developed in several laboratories to construct germanium monochromators (Vogt, Passell, Cheung & Axe, 1994; Schefer *et al.*, 1996).

In the second approach, shown in Fig. 4.4.2.1(*b*), the global reflectivity distribution is obtained from the contributions of several stacked thin crystalline wafers, each with a rather narrow mosaic spread compared with the composite value but slightly misoriented with respect to the other wafers in the stack. If the misorientation of each wafer can be correctly controlled, this technique has the major advantage of producing monochromators with a highly anisotropic mosaic structure. The shape of the reflectivity curve can be chosen at will (Gaussian, Lorentzian, rectangular), if required. Moreover, because the initial mosaicity required is small, it is not necessary to use mosaic wafers and therefore for each wafer to undergo a long and tedious plastic deformation process. Recently, this method has been applied successfully to construct copper monochromators (Hamelin, Anderson, Berneron, Escoffier, Foltyn & Hehn, 1997), in which individual copper wafers were cut in a cylindrical form and then slid across one another to produce the required mosaic spread in the scattering plane. This technique looks very promising for the production of anisotropic mosaic monochromators.

The reflection from a mosaic crystal is visualized in Fig. 4.4.2.2(*b*). An incident beam with small divergence is transformed into a broad exit beam. The range of **k** vectors, Δk, selected in this process depends on the mosaic spread, η, and the incoming and outgoing beam divergences, α_1 and α_2.

$$\Delta k/k = \Delta\tau/\tau + \alpha \cot\theta, \tag{4.4.2.2}$$

where τ is the magnitude of the crystal reciprocal-lattice vector ($\tau = 2\pi/d$) and α is given by

$$\alpha = \sqrt{\frac{\alpha_1^2\alpha_2^2 + \alpha_1^2\eta^2 + \alpha_2^2\eta^2}{\alpha_1^2 + \alpha_2^2 + 4\eta^2.}} \tag{4.4.2.3}$$

The resolution can therefore be defined by collimators, and the highest resolution is obtained in backscattering, where the wavevector spread depends only on the intrinsic $\Delta d/d$ of the crystal.

In some applications, the beam broadening produced by mosaic crystals can be detrimental to the instrument performance. An interesting alternative is a gradient crystal, *i.e.* a single crystal with a smooth variation of the interplanar lattice spacing along a defined crystallographic direction. As shown in Fig. 4.4.2.2(*c*), the diffracted phase-space element has a different shape from that obtained from a mosaic crystal. Gradients in d spacing can be produced in various ways,

including thermal gradients (Alefeld, 1972), vibrating crystals by piezoelectric excitation (Hock, Vogt, Kulda, Mursic, Fuess & Magerl, 1993), and mixed crystals with concentration gradients, *e.g.* Cu–Ge (Freund, Guinet, Maréschal, Rustichelli & Vanoni, 1972) and Si–Ge (Maier-Leibnitz & Rustichelli, 1968; Magerl, Liss, Doll, Madar & Steichele, 1994).

Both vertically and horizontally focusing assemblies of mosaic crystals are employed to make better use of the neutron flux when making measurements on small samples. Vertical focusing can lead to intensity gain factors of between two and five without affecting resolution (real-space focusing) (Riste, 1970; Currat, 1973). Horizontal focusing changes the k-space volume that is selected by the monochromator through the variation in Bragg angle across the monochromator surface (k-space focusing) (Scherm, Dolling, Ritter, Schedler, Teuchert & Wagner, 1977). The orientation of the diffracted k-space volume can be modified by variation of the horizontal curvature, so that the resolution of the monochromator may be optimized with respect to a particular sample or experiment without loss of illumination. Monochromatic focusing can be achieved. Furthermore, asymmetrically cut crystals may be used, allowing focusing effects in real space and k space to be decoupled (Scherm & Kruger, 1994).

Traditionally, focusing monochromators consist of rectangular crystal plates mounted on an assembly that allows the orientation of each crystal to be varied in a correlated manner (Bührer, 1994). More recently, elastically deformed perfect crystals (in particular silicon) have been exploited as focusing elements for monochromators and analysers (Magerl & Wagner, 1994).

Since thermal neutrons have velocities that are of the order of km s^{-1}, their wavelengths can be Doppler shifted by diffraction from moving crystals. The k-space representation of the diffraction from a crystal moving perpendicular to its lattice planes is shown in Fig. 4.4.2.3(*a*). This effect is most commonly used in backscattering instruments on steady-state sources to vary the energy of the incident beam. Crystal velocities of 9–10 m s^{-1} are practically achievable, corresponding to energy variations of the order of $\pm$ 60 μeV.

The Doppler shift is also important in determining the resolution of the rotating-crystal time-of-flight (TOF) spectrom-

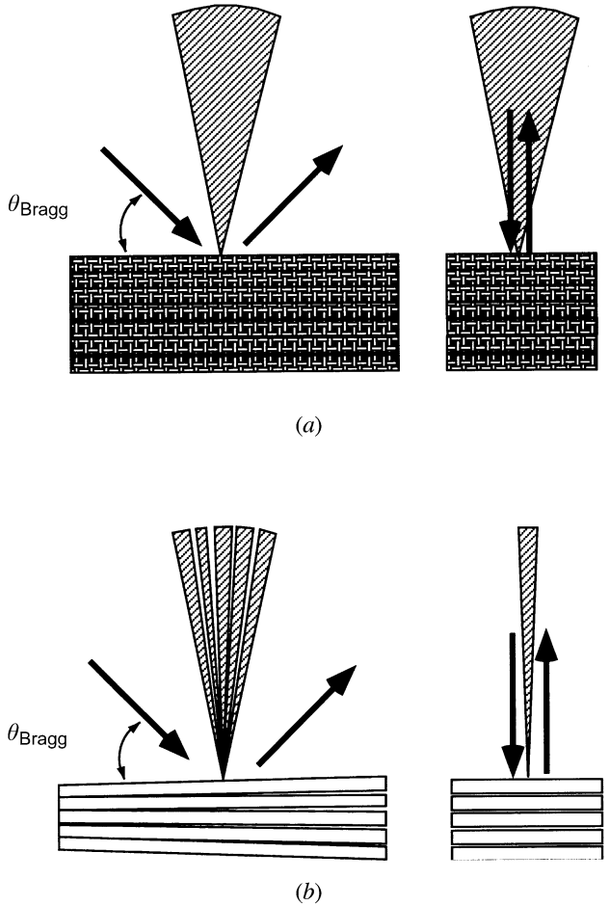

Fig. 4.4.2.1. Two methods by which artificial mosaic monochromators can be constructed: (*a*) out of a stack of crystalline wafers, each with a mosaicity close to the global value. The increase in divergence due to the mosaicity is the same in the horizontal (left picture) and the vertical (right picture) directions; (*b*) out of several stacked thin crystalline wafers each with a rather narrow mosaic but slightly misoriented in a perfectly controlled way. This allows the shape of the reflectivity curve to be rectangular, Gaussian, Lorentzian, *etc.*, and highly anisotropic, *i.e.* vertically narrow (right picture) and horizontally broad (left figure).

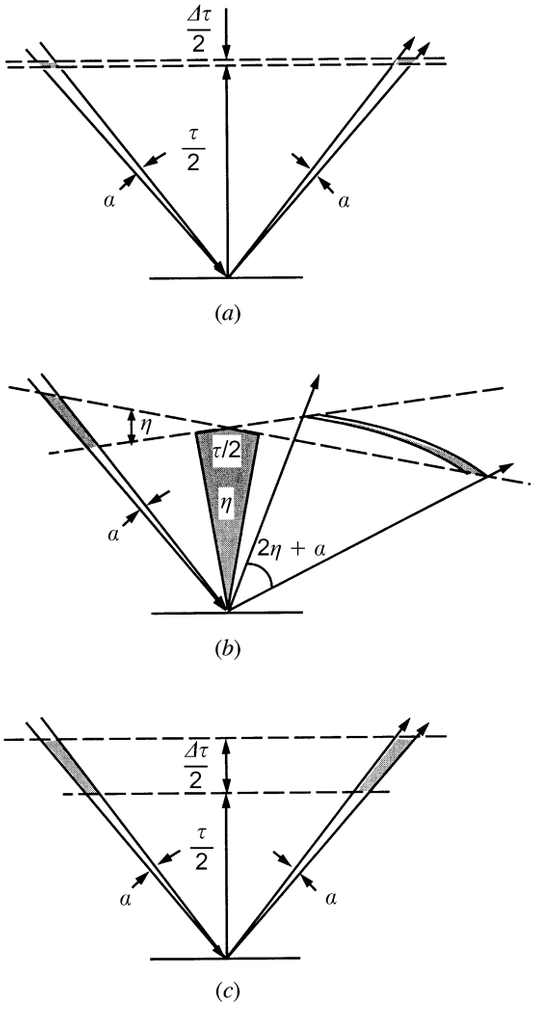

Fig. 4.4.2.2. Reciprocal-lattice representation of the effect of a monochromator with reciprocal-lattice vector τ on the reciprocal-space element of a beam with divergence α. (*a*) For an ideal crystal with a lattice constant width $\Delta\tau$; (*b*) for a mosaic crystal with mosaicity η, showing that a beam with small divergence, α, is transformed into a broad exit beam with divergence $2\eta + \alpha$; (*c*) for a gradient crystal with interplanar lattice spacing changing over $\Delta\tau$, showing that the divergence is not changed in this case.

eter, first conceived by Brockhouse (1958). A pulse of monochromatic neutrons is obtained when the reciprocal-lattice vector of a rotating crystal bisects the angle between two collimators. Effectively, the neutron **k** vector is changed in both direction and magnitude, depending on whether the crystal is moving towards or away from the neutron. For the rotating crystal, both of these situations occur simultaneously for different halves of the crystal, so that the net effect over the beam cross section is that a wider energy band is reflected than from the crystal at rest, and that, depending on the sense of rotation, the beam is either focused or defocused in time (Meister & Weckerman, 1972).

The Bragg reflection of neutrons from a crystal moving parallel to its lattice planes is illustrated in Fig. 4.4.2.3(*b*). It can be seen that the moving crystal selects a larger Δk than the crystal at rest, so that the reflected intensity is higher. Furthermore, it is possible under certain conditions to orientate the diffracted phase-space volume orthogonal to the diffraction vector. In this way, a monochromatic divergent beam can be obtained from a collimated beam with a larger energy spread. This provides an elegant means of producing a divergent beam with a sufficiently wide momentum spread to be scanned by the Doppler crystal of a backscattering instrument (Schelten & Alefeld, 1984).

Finally, an alternative method of scanning the energy of a monochromator in backscattering is to apply a steady but uniform temperature variation. The monochromator crystal must have a reasonable thermal expansion coefficient, and care has to be taken to ensure a uniform temperature across the crystal.

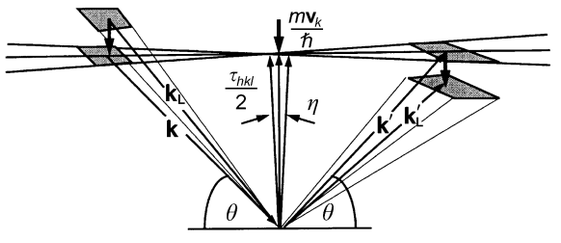

(*a*)

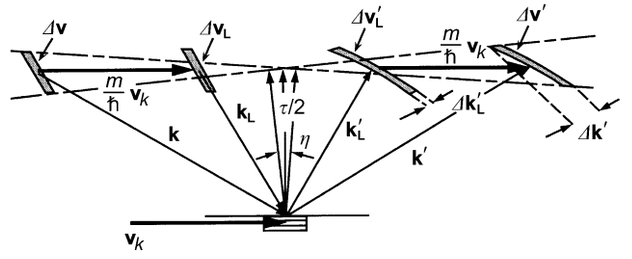

(*b*)

Fig. 4.4.2.3. Momentum-space representation of Bragg scattering from a crystal moving (*a*) perpendicular and (*b*) parallel to the diffracting planes with a velocity $\mathbf{v}_k$. The vectors $\mathbf{k}_L$ and $\mathbf{k}'_L$ refer to the incident and reflected wavevectors in the laboratory frame of reference. In (*a*), depending on the direction of $\mathbf{v}_k$, the reflected wavevector is larger or smaller than the incident wavevector, $\mathbf{k}_L$. In (*b*), a larger incident reciprocal-space volume, $\Delta\mathbf{v}_L$, is selected by the moving crystal than would have been selected by the crystal at rest. The reflected reciprocal-space element, $\Delta\mathbf{v}'_L$, has a large divergence, but can be arranged to be normal to $\mathbf{k}'_L$, hence improving the resolution $\Delta\mathbf{k}'_L$.

Table 4.4.2.2. *Neutron scattering-length densities, Nb_{coh}, for some commonly used materials*

Material	Nb (10^{-6} Å^{-2})
^{58}Ni	13.31
Diamond	11.71
Nickel	9.40
Quartz	3.64
Germanium	3.62
Silver	3.50
Aluminium	2.08
Silicon	2.08
Vanadium	−0.27
Titanium	−1.95
Manganese	−2.95

4.4.2.4. *Mirror reflection devices*

The refractive index, n, for neutrons of wavelength λ propagating in a nonmagnetic material of atomic density N is given by the expression

$$n^2 = 1 - \frac{\lambda^2 Nb_{\rm coh}}{\pi,} \qquad (4.4.2.4)$$

where $b_{\rm coh}$ is the mean coherent scattering length. Values of the scattering-length density $Nb_{\rm coh}$ for some common materials are listed in Table 4.4.2.2, from which it can be seen that the refractive index for most materials is slightly less than unity, so that total external reflection can take place. Thus, neutrons can be reflected from a smooth surface, but the critical angle of reflection, γ_c, given by

$$\gamma_c = \lambda \sqrt{\frac{Nb_{\rm coh}}{\pi}}, \qquad (4.4.2.5)$$

is small, so that reflection can only take place at grazing incidence. The critical angle for nickel, for example, is 0.1° Å^{-1}.

Because of the shallowness of the critical angle, reflective optics are traditionally bulky, and focusing devices tend to have long focal lengths. In some cases, however, depending on the beam divergence, a long mirror can be replaced by an equivalent stack of shorter mirrors.

4.4.2.4.1. *Neutron guides*

The principle of mirror reflection is the basis of neutron guides, which are used to transmit neutron beams to instruments that may be situated up to 100 m away from the source (Christ & Springer, 1962; Maier-Leibnitz & Springer, 1963). A standard neutron guide is constructed from boron glass plates assembled to form a rectangular tube, the dimensions of which may be up to 200 mm high by 50 mm wide. The inner surface of the guide is coated with approximately 1200 Å of either nickel, ^{58}Ni ($\gamma_c = 0.12^\circ$ Å^{-1}), or a 'supermirror' (described below). The guide is usually evacuated to reduce losses due to absorption and scattering of neutrons in air.

Theoretically, a neutron guide that is fully illuminated by the source will transmit a beam with a square divergence of full width $2\gamma_c$ in both the horizontal and vertical directions, so that the transmitted solid angle is proportional to λ^2. In practice, owing to imperfections in the assembly of the guide system, the divergence profile is closer to Gaussian than square at the end of a long guide. Since the neutrons may undergo a large number of reflections in the guide, it is important to achieve a high reflectivity. The specular reflectivity is determined by the surface roughness, and typically values in the range 98.5 to 99% are

achieved. Further transmission losses occur due to imperfections in the alignment of the sections that make up the guide.

The great advantage of neutron guides, in addition to the transport of neutrons to areas of low background, is that they can be multiplexed, *i.e.* one guide can serve many instruments. This is achieved either by deflecting only a part of the total cross section to a given instrument or by selecting a small wavelength range from the guide spectrum. In the latter case, the selection device (usually a crystal monochromator) must have a high transmission at other wavelengths.

If the neutron guide is curved, the transmission becomes wavelength dependent, as illustrated in Fig. 4.4.2.4. In this case, one can define a characteristic wavelength, λ^*, given by the relation $\theta^* = \sqrt{2a/\rho}$, so that

$$\lambda^* = \sqrt{\frac{\pi}{Nb_{\rm coh}}}\sqrt{\frac{2a}{\rho}} \qquad (4.4.2.6)$$

(where a is the guide width and ρ the radius of curvature), for which the theoretical transmission drops to 67%. For wavelengths less than λ^*, neutrons can only be transmitted by 'garland' reflections along the concave wall of the curved guide. Thus, the guide acts as a low-pass energy filter as long as its length is longer than the direct line-of-sight length $L_1 = \sqrt{8a\rho}$. For example, a 3 cm wide nickel-coated guide whose characteristic wavelength is 4 Å (radius of curvature 1300 m) must be at least 18 m long to act as a filter. The line-of-sight length can be reduced by subdividing the guide into a number of narrower channels, each of which acts as a miniguide. The resulting device, often referred to as a neutron bender, since deviation of the beam is achieved more rapidly, is used in beam deviators (Alefeld *et al.*, 1988) or polarizers (Hayter, Penfold & Williams, 1978). A microbender was devised by Marx (1971) in which the channels were made by evaporating alternate layers of aluminium (transmission layer) and nickel (mirror layer) onto a flexible smooth substrate.

Tapered guides can be used to reduce the beam size in one or two dimensions (Rossbach *et al.*, 1988), although, since mirror reflection obeys Liouville's theorem, focusing in real space is achieved at the expense of an increase in divergence. This fact can be used to calculate analytically the expected gain in neutron flux at the end of a tapered guide (Anderson, 1988). Alternatively, focusing can be achieved in one dimension using a bender in which the individual channel lengths are adjusted to create a focus (Freund & Forsyth, 1979).

4.4.2.4.2. *Focusing mirrors*

Optical imaging of neutrons can be achieved using ellipsoidal or torroidal mirrors, but, owing to the small critical angle of reflection, the dimensions of the mirrors themselves and the radii of curvature must be large. For example, a 4 m long toroidal mirror has been installed at the IN15 neutron spin echo spectrometer at the Institut Laue–Langevin, Grenoble (Hayes *et al.*, 1996), to focus neutrons with wavelengths greater than 15Å. The mirror has an in-plane radius of curvature of 408.75 m, and the sagittal radius is 280 mm. A coating of ^{65}Cu is used to obtain a high critical angle of reflection while maintaining a low surface roughness. Slope errors of less than 2.5×10^{-5} rad (r.m.s.) combined with a surface roughness of less than 3Å allow a minimum resolvable scattering vector of about 5×10^{-4} Å^{-1} to be reached.

For best results, the slope errors and the surface roughness must be low, in particular in small-angle scattering applications, since diffuse scattering from surface roughness gives rise to a halo around the image point. Owing to its low thermal expansion coefficient, highly polished Zerodur is often chosen as substrate.

4.4.2.4.3. *Multilayers*

Schoenborn, Caspar & Kammerer (1974) first pointed out that multibilayers, comprising alternating thin films of different scattering-length densities ($Nb_{\rm coh}$) act like two-dimensional crystals with a d spacing given by the bilayer period. With modern deposition techniques (usually sputtering), uniform films of thickness ranging from about twenty to a few hundred ångströms can be deposited over large surface areas of the order of 1 m^2. Owing to the rather large d spacings involved, the Bragg reflection from multilayers is generally at grazing incidence, so that long devices are required to cover a typical beam width, or a stacked device must be used. However, with judicious choice of the scattering-length contrast, the surface and interface roughness, and the number of layers, reflectivities close to 100% can be reached.

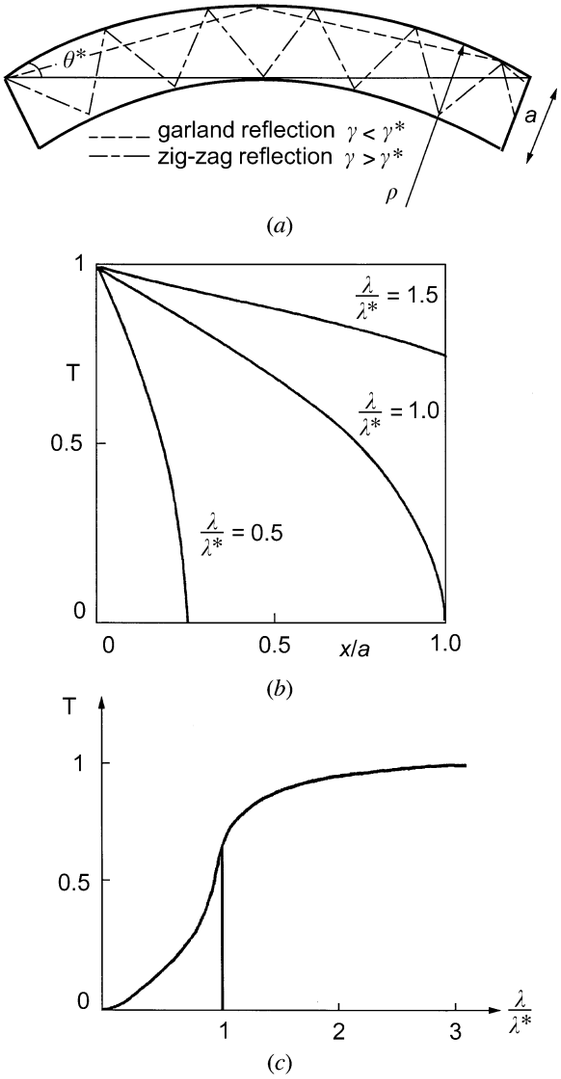

Fig. 4.4.2.4. In a curved neutron guide, the transmission becomes λ dependent: (*a*) the possible types of reflection (garland and zig-zag), the direct line-of-sight length, the critical angle θ^*, which is related to the characteristic wavelength $\lambda^* = \theta^*\sqrt{\pi/Nb_{\rm coh}}$; (*b*) transmission across the exit of the guide for different wavelengths, normalized to unity at the outside edge; (*c*) total transmission of the guide as a function of λ.

Fig. 4.4.2.5 illustrates how variation in the bilayer period can be used to produce a monochromator (the minimum $\Delta\lambda/\lambda$ that can be achieved is of the order of 0.5%), a broad-band device, or a 'supermirror', so called because it is composed of a particular sequence of bilayer thicknesses that in effect extends the region of total mirror reflection beyond the ordinary critical angle (Turchin, 1967; Mezei, 1976; Hayter & Mook, 1989). Supermirrors have been produced that extend the critical angle of nickel by a factor, m, of between three and four with reflectivities better than 90%. Such high reflectivities enable supermirror neutron guides to be constructed with flux gains, compared with nickel guides, close to the theoretical value of m^2.

The choice of the layer pairs depends on the application. For non-polarizing supermirrors and broad-band devices (Høghøj, Anderson, Ebisawa & Takeda, 1996), the Ni/Ti pair is commonly used, either pure or with some additions to relieve strain and stabilize interfaces (Elsenhans *et al.*, 1994) or alter the magnetism (Anderson & Høghøj, 1996), owing to the high contrast in scattering density, while for narrow-band monochromators a low contrast pair such as W/Si is more suitable.

4.4.2.4.4. *Capillary optics*

Capillary neutron optics, in which hollow glass capillaries act as waveguides, are also based on the concept of total external reflection of neutrons from a smooth surface. The advantage of capillaries, compared with neutron guides, is that the channel sizes are of the order of a few tens of micrometres, so that the radius of curvature can be significantly decreased for a given characteristic wavelength [see equation (4.4.2.6)]. Thus, neutrons can be efficiently deflected through large angles, and the device can be more compact.

Two basic types of capillary optics exist, and the choice depends on the beam characteristics required. Polycapillary fibres are manufactured from hollow glass tubes several centimetres in diameter, which are heated, fused and drawn multiple times until bundles of thousands of micrometre-sized channels are formed having an open area of up to 70% of the cross section. Fibre outer diameters range from 300 to 600 μm and contain hundreds or thousands of individual channels with inner diameters between 3 and 50 μm. The channel cross section is usually hexagonal, though square channels have been produced, and the inner channel wall surface roughness is typically less than 10 Å r.m.s., giving rise to very high reflectivities. The principal limitations on transmission efficiency are the open area, the acceptable divergence (note that the critical angle for glass is 1 mrad Å^{-1}) and reflection losses due to absorption and scattering. A typical optical device will comprise hundreds or thousands of fibres threaded through thin screens to produce the required shape.

Fig. 4.4.2.6 shows typical applications of polycapillary devices. In Fig. 4.4.2.6(*a*), a polycapillary lens is used to refocus neutrons collected from a divergent source. The half lens depicted in Fig. 4.4.2.6(*b*) can be used either to produce a nearly parallel (divergence $= 2\gamma_c$) beam from a divergent source or (in the reverse sense) to focus a nearly parallel beam, *e.g.* from a neutron guide. The size of the focal point depends on the channel size, the beam divergence, and the focal length of the lens. For example, a polycapillary lens used in a prompt γ-activation analysis instrument at the National Institute of Standards and Technology to focus a cold neutron beam from a neutron guide results in a current density gain of 80 averaged over the focused beam size of 0.53 mm (Chen *et al.*, 1995).

Fig. 4.4.2.6(*c*) shows another simple application of polycapillaries as a compact beam bender. In this case, such a bender may be more compact than an equivalent multichannel guide bender, although the accepted divergence will be less. Furthermore, as with curved neutron guides, owing to the wavelength dependence of the critical angle the capillary curvature can be used to filter out thermal or high-energy neutrons.

It should be emphasized that the applications depicted in Fig. 4.4.2.6 obey Liouville's theorem, in that the density of neutrons in phase space is not changed, but the shape of the phase-space volume is altered to meet the requirements of the experiment,

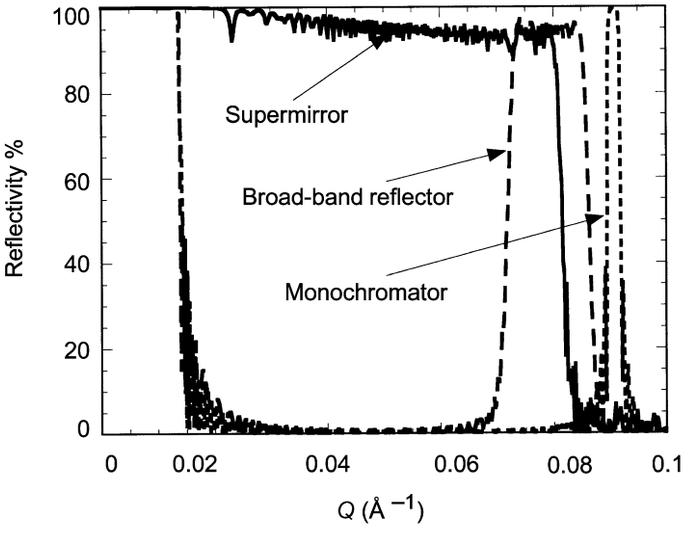

Fig. 4.4.2.5. Illustration of how a variation in the bilayer period can be used to produce a monochromator, a broad-band device, or a supermirror.

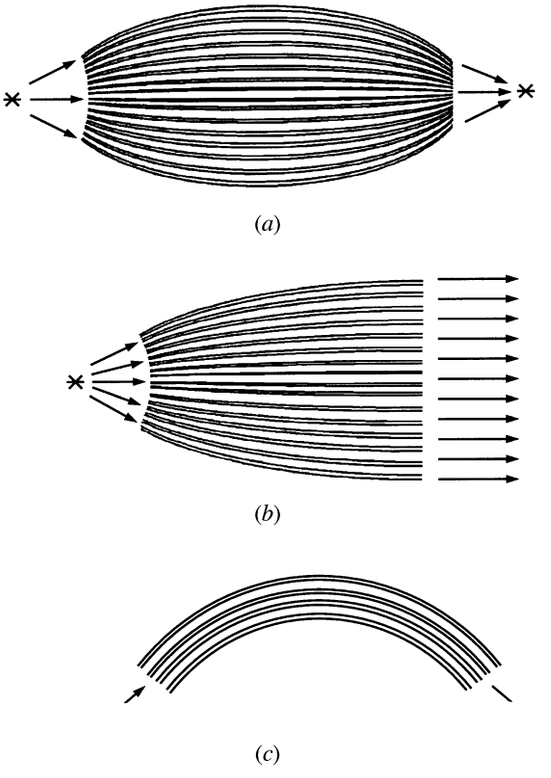

Fig. 4.4.2.6. Typical applications of polycapillary devices: (*a*) lens used to refocus a divergent beam; (*b*) half-lens to produce a nearly parallel beam or to focus a nearly parallel beam; (*c*) a compact bender.

i.e. there is a simple trade off between beam dimension and divergence.

The second type of capillary optic is a monolithic configuration. The individual capillaries in monolithic optics are tapered and fused together, so that no external frame assembly is necessary (Chen-Mayer *et al.*, 1996). Unlike the multifibre devices, the inner diameters of the channels that make up the monolithic optics vary along the length of the component, resulting in a smaller more compact design.

Further applications of capillary optics include small-angle scattering (Mildner, 1994) and lenses for high-spatial-resolution area detection.

4.4.2.5. *Filters*

Neutron filters are used to remove unwanted radiation from the beam while maintaining as high a transmission as possible for the neutrons of the required energy. Two major applications can be identified: removal of fast neutrons and γ-rays from the primary beam and reduction of higher-order contributions (λ/n) in the secondary beam reflected from crystal monochromators. In this section, we deal with non-polarizing filters, *i.e.* those whose transmission and removal cross sections are independent of the neutron spin. Polarizing filters are discussed in the section concerning polarizers.

Filters rely on a strong variation of the neutron cross section with energy, usually either the wavelength-dependent scattering cross section of polycrystals or a resonant absorption cross section. Following Freund (1983), the total cross section determining the attenuation of neutrons by a crystalline solid can be written as a sum of three terms,

$$\sigma = \sigma_{\rm abs} + \sigma_{\rm tds} + \sigma_{\rm Bragg}. \qquad (4.4.2.7)$$

Here, $\sigma_{\rm abs}$ is the true absorption cross section, which, at low energy, away from resonances, is proportional to $E^{-1/2}$. The temperature-dependent thermal diffuse cross section, $\sigma_{\rm tds}$, describing the attenuation due to inelastic processes, can be split into two parts depending on the neutron energy. At low energy, $E \ll k_b\Theta_D$, where k_b is Boltzmann's constant and Θ_D is the characteristic Debye temperature, single-phonon processes dominate, giving rise to a cross section, $\sigma_{\rm sph}$, which is also proportional to $E^{-1/2}$. The single-phonon cross section is proportional to $T^{7/2}$ at low temperatures and to T at higher temperatures. At higher energies, $E \geq k_b\Theta_D$, multiphonon and multiple-scattering processes come into play, leading to a cross section, $\sigma_{\rm mph}$, that increases with energy and temperature. The third contribution, $\sigma_{\rm Bragg}$, arises due to Bragg scattering in single- or polycrystalline material. At low energies, below the Bragg cut-off ($\lambda > 2d_{\rm max}$), $\sigma_{\rm Bragg}$ is zero. In polycrystalline materials, the cross section rises steeply above the Bragg cut-off and oscillates with increasing energy as more reflections come into play. At still higher energies, $\sigma_{\rm Bragg}$ decreases to zero.

In single-crystalline material above the Bragg cut-off, $\sigma_{\rm Bragg}$ is characterized by a discrete spectrum of peaks whose heights and widths depend on the beam collimation, energy resolution, and the perfection and orientation of the crystal. Hence a monocrystalline filter has to be tuned by careful orientation.

The resulting attenuation cross section for beryllium is shown in Fig. 4.4.2.7. Cooled polycrystalline beryllium is frequently used as a filter for neutrons with energies less than 5 meV, since there is an increase of nearly two orders of magnitude in the attenuation cross section for higher energies. BeO, with a Bragg cut-off at approximately 4 meV, is also commonly used.

Pyrolytic graphite, being a layered material with good crystalline properties along the *c* direction but random orientation perpendicular to it, lies somewhere between a polycrystal and a single crystal as far as its attenuation cross section is concerned. The energy-dependent cross section for a neutron beam incident along the *c* axis of a pyrolytic graphite filter is shown in Fig. 4.4.2.8, where the attenuation peaks due to the 00ξ reflections can be seen. Pyrolytic graphite serves as an efficient second- or third-order filter (Shapiro & Chesser, 1972) and can be 'tuned' by slight misorientation away from the *c* axis.

Further examples of typical filter materials (*e.g.* silicon, lead, bismuth, sapphire) can be found in the paper by Freund (1983).

Resonant absorption filters show a large increase in their attenuation cross sections at the resonant energy and are therefore used as selective filters for that energy. A list of typical filter materials and their resonance energies is given in Table 4.4.2.3.

4.4.2.6. *Polarizers*

Methods used to polarize a neutron beam are many and varied, and the choice of the best technique depends on the instrument and the experiment to be performed. The main parameter that has to be considered when describing the effectiveness of a given polarizer is the polarizing efficiency, defined as

$$P = (N_+ - N_-)/(N_+ + N_-), \qquad (4.4.2.8)$$

where N_+ and N_- are the numbers of neutrons with spin parallel (+) or antiparallel (−) to the guide field in the outgoing beam. The second important factor, the transmission of the wanted spin state, depends on various factors, such as acceptance angles, reflection, and absorption.

4.4.2.6.1. *Single-crystal polarizers*

The principle by which ferromagnetic single crystals are used to polarize and monochromate a neutron beam simultaneously is shown in Fig. 4.4.2.9. A field **B**, applied perpendicular to the scattering vector $\boldsymbol{\kappa}$, saturates the atomic moments $\mathbf{M}_\nu$ along the field direction. The cross section for Bragg reflection in this geometry is

$$(\mathrm{d}\sigma/\mathrm{d}\Omega) = F_N(\boldsymbol{\kappa})^2 + 2F_N(\boldsymbol{\kappa})F_M(\boldsymbol{\kappa})(\mathbf{P}\cdot\boldsymbol{\mu}) + F_M(\boldsymbol{\kappa})^2, \quad (4.4.2.9)$$

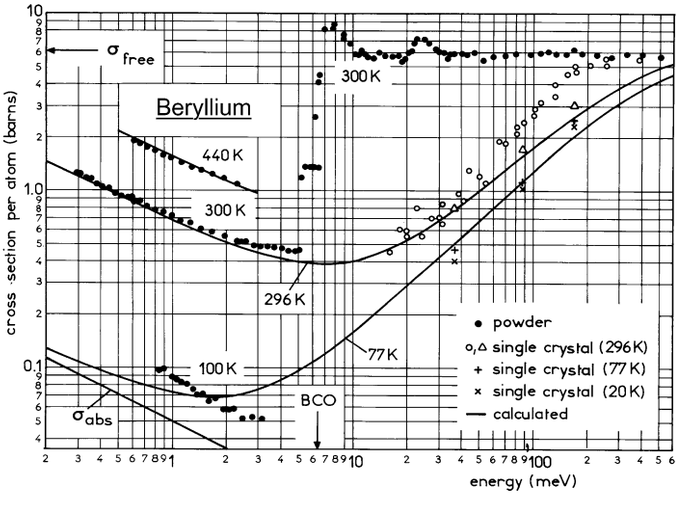

Fig. 4.4.2.7. Total cross section for beryllium in the energy range where it can be used as a filter for neutrons with energy below 5 meV (Freund, 1983).

Table 4.4.2.3. *Characteristics of some typical elements and isotopes used as neutron filters*

Element or isotope	Resonance (eV)	σ_s (resonance) (barns)	λ (Å)	$\sigma_s(\lambda)$ (barns)	$\frac{\sigma_s(\lambda/2)}{\sigma_s(\lambda)}$
In	1.45	30000	0.48	94	319
Rh	1.27	4500	0.51	76	59.2
Hf	1.10	5000	0.55	58	86.2
^{240}Pu	1.06	115000	9.55	145	793
Ir	0.66	4950	0.70	183	27.0
^{229}Th	0.61	6200	0.73	<100	>62.0
Er	0.58	1500	0.75	127	11.8
Er	0.46	2300	0.84	125	18.4
Eu	0.46	10100	0.84	1050	9.6
^{231}Pa	0.39	4900	0.92	116	42.2
^{239}Pu	0.29	5200	1.06	700	7.4

1 barn $= 10^{-28}$ m^2.

where $F_N(\boldsymbol{\kappa})$ is the nuclear structure factor and $F_M(\boldsymbol{\kappa}) = [(\gamma/2)r_0] \sum_\nu M_\nu f(hkl) \exp[2\pi(hx + ky + lz)]$ is the magnetic structure factor, with $f(hkl)$ the magnetic form factor of the magnetic atom at the position (x, y, z) in the unit cell. The vector $\mathbf{P}$ describes the polarization of the incoming neutron with respect to $\mathbf{B}$; $\mathbf{P} = 1$ for $+$ spins and $\mathbf{P} = -1$ for $-$ spins and $\boldsymbol{\mu}$ is a unit vector in the direction of the atomic magnetic moments. Hence, for neutrons polarized parallel to $\mathbf{B}$ $(\mathbf{P} \cdot \boldsymbol{\mu} = 1)$, the diffracted intensity is proportional to $[F_N(\boldsymbol{\kappa}) + F_M(\boldsymbol{\kappa})]^2$, while, for neutrons polarized antiparallel to $\mathbf{B}$ $(\mathbf{P} \cdot \boldsymbol{\mu} = -1)$, the diffracted intensity is proportional to $[F_N(\boldsymbol{\kappa}) - F_M(\boldsymbol{\kappa})]^2$. The polarizing efficiency of the diffracted beam is then

$$P = \pm 2F_N(\boldsymbol{\kappa})F_M(\boldsymbol{\kappa})/[F_N(\boldsymbol{\kappa})^2 + F_M(\boldsymbol{\kappa})^2], \qquad (4.4.2.10)$$

which can be either positive or negative and has a maximum value for $|F_N(\boldsymbol{\kappa})| = |F_M(\boldsymbol{\kappa})|$. Thus, a good single-crystal polarizer, in addition to possessing a crystallographic structure in which F_N and F_M are matched, must be ferromagnetic at room temperature and should contain atoms with large magnetic moments. Furthermore, large single crystals with 'controllable' mosaic should be available. Finally, the structure factor for the required reflection should be high, while those for higher-order reflections should be low.

None of the three naturally occurring ferromagnetic elements (iron, cobalt, nickel) makes efficient single-crystal polarizers. Cobalt is strongly absorbing and the nuclear scattering lengths of iron and nickel are too large to be balanced by their weak magnetic moments. An exception is ^{57}Fe, which has a rather low nuclear scattering length, and structure-factor matching can be achieved by mixing ^{57}Fe with Fe and 3% Si (Reed, Bolling & Harmon, 1973).

In general, in order to facilitate structure-factor matching, alloys rather than elements are used. The characteristics of some alloys used as polarizing monochromators are presented in Table 4.4.2.4. At short wavelengths, the 200 reflection of $Co_{0.92}Fe_{0.08}$ is used to give a positively polarized beam [$F_N(\boldsymbol{\kappa})$ and $F_M(\boldsymbol{\kappa})$ both positive], but the absorption due to cobalt is high. At longer wavelengths, the 111 reflection of the Heusler alloy Cu_2MnAl (Delapalme, Schweizer, Couderchon & Perrier de la Bathie, 1971; Freund, Pynn, Stirling & Zeyen, 1983) is commonly used, since it has a higher reflectivity and a larger d spacing than $Co_{0.92}Fe_{0.08}$. Since for the 111 reflection $F_N \approx -F_M$, the diffracted beam is negatively polarized. Unfortunately, the structure factor of the 222 reflection is higher than that of the 111 reflection, leading to significant higher-order contamination of the beam.

Other alloys that have been proposed as neutron polarizers are $Fe_{3-x}Mn_xSi$, $^7Li_{0.5}Fe_{2.5}O_4$ (Bednarski, Dobrzynski & Steinsvoll, 1980), Fe_3Si (Hines *et al.*, 1976), Fe_3Al (Pickart & Nathans, 1961), and $HoFe_2$ (Freund & Forsyth, 1979).

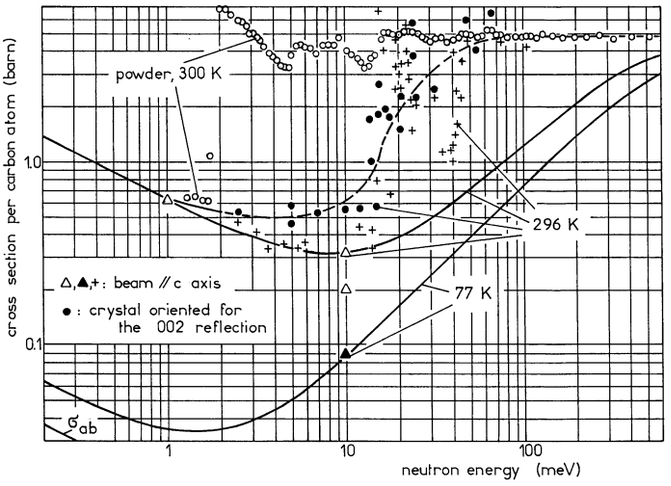

Fig. 4.4.2.8. Energy-dependent cross section for a neutron beam incident along the c axis of a pyrolytic graphite filter. The attenuation peaks due to the 00ξ reflections can be seen.

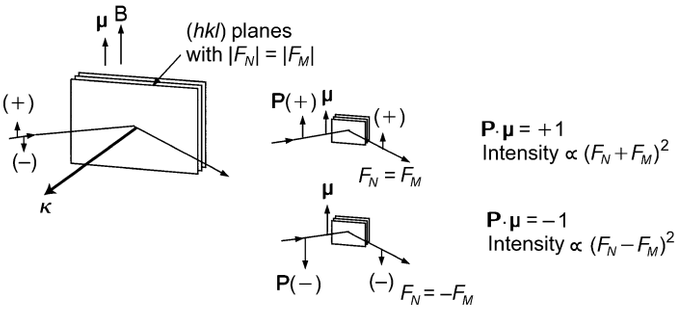

Fig. 4.4.2.9. Geometry of a polarizing monochromator showing the lattice planes (hkl) with $|F_N| = |F_M|$, the direction of $\mathbf{P}$ and $\boldsymbol{\mu}$, the expected spin direction and intensity.

Table 4.4.2.4. *Properties of polarizing crystal monochromators (Williams, 1988)*

	$Co_{0.92}Fe_{0.08}$	Cu_2MnAl	Fe_3Si	^{57}Fe:Fe	$HoFe_2$
Matched reflection $\|F_N\| \sim \|F_M\|$	200	111	111	110	620
d spacing (Å)	1.76	3.43	3.27	2.03	1.16
Take-off angle $2\theta_B$ at 1Å (°)	33.1	16.7	17.6	28.6	50.9
Cut-off wavelength, λ_{max} (Å)	3.5	6.9	6.5	4.1	2.3

4.4.2.6.2. *Polarizing mirrors*

For a ferromagnetic material, the neutron refractive index is given by

$$n_{\pm}^2 = 1 - \lambda^2 N(b_{coh} \pm p)/\pi, \qquad (4.4.2.11)$$

where the magnetic scattering length, p, is defined by

$$p = 2\mu(B - H)m\pi/h^2N. \qquad (4.4.2.12)$$

Here, m and μ are the neutron mass and magnetic moment, B is the magnetic induction in an applied field H, and h is Planck's constant.

The $-$ and $+$ signs refer, respectively, to neutrons whose moments are aligned parallel and antiparallel to B. The refractive index depends on the orientation of the neutron spin with respect to the film magnetization, thus giving rise to two critical angles of total reflection, γ_- and γ_+. Thus, reflection in an angular range between these two critical angles gives rise to polarized beams in reflection and in transmission. The polarization efficiency, P, is defined in terms of the reflectivity r_+ and r_- of the two spin states,

$$P = (r_+ - r_-)/(r_+ + r_-). \qquad (4.4.2.13)$$

The first polarizers using this principle were simple cobalt mirrors (Hughes & Burgy, 1950), while Schaerpf (1975) used FeCo sheets to build a polarizing guide. It is more common these days to use thin films of ferromagnetic material deposited onto a substrate of low surface roughness (*e.g.* float glass or polished silicon). In this case, the reflection from the substrate can be eliminated by including an antireflecting layer made from, for example, Gd–Ti alloys (Drabkin *et al.*, 1976). The major limitation of these polarizers is that grazing-incidence angles must be used and the angular range of polarization is small. This limitation can be partially overcome by using multilayers, as described above, in which one of the layer materials is ferromagnetic. In this case, the refractive index of the ferromagnetic material is matched for one spin state to that of the non-magnetic material, so that reflection does not occur. A polarizing supermirror made in this way has an extended angular range of polarization, as indicated in Fig. 4.4.2.10. It should be noted that modern deposition techniques allow the refractive index to be adjusted readily, so that matching is easily achieved. The scattering-length densities of some commonly used layer pairs are given in Table 4.4.2.5

Polarizing multilayers are also used in monochromators and broad-band devices. Depending on the application, various layer pairs have been used: Co/Ti, Fe/Ag, Fe/Si, Fe/Ge, Fe/W, FeCoV/TiN, FeCoV/TiZr, $^{63}Ni_{0.66}{}^{54}Fe_{0.34}$/V and the range of fields used to achieve saturation varies from about 100 to 500 Gs.

Polarizing mirrors can be used in reflection or transmission with polarization efficiencies reaching 97%, although, owing to the low incidence angles, their use is generally restricted to wavelengths above 2 Å.

Various devices have been constructed that use mirror polarizers, including simple reflecting mirrors, V-shaped transmission polarizers (Majkrzak, Nunez, Copley, Ankner & Greene, 1992), cavity polarizers (Mezei, 1988), and benders (Hayter, Penfold & Williams, 1978; Schaerpf, 1989). Perhaps the best known device is the polarizing bender developed by Schärpf. The device consists of 0.2 mm thick glass blades coated on both sides with a Co/Ti supermirror on top of an antireflecting Gd/Ti coating designed to reduce the scattering of the unwanted spin state from the substrate to a very low Q value. The device is quite compact (typically 30 cm long for a beam cross section up to 6×5 cm) and transmits over 40% of an unpolarized beam with the collimation from a nickel-coated guide for wavelengths above 4.5 Å. Polarization efficiencies of over 96% can be achieved with these benders.

4.4.2.6.3. *Polarizing filters*

Polarizing filters operate by selectively removing one of the neutron spin states from an incident beam, allowing the other spin state to be transmitted with only moderate attenuation. The spin selection is obtained by preferential absorption or scattering, so the polarizing efficiency usually increases with the thickness of the filter, whereas the transmission decreases. A compromise must therefore be made between polarization, P, and transmission, T. The 'quality factor' often used is $P\sqrt{T}$ (Tasset & Resouche, 1995).

The total cross sections for a generalized filter may be written as

$$\sigma_{\pm} = \sigma_0 \pm \sigma_p, \qquad (4.4.2.14)$$

where σ_0 is a spin-independent cross section and $\sigma_p = (\sigma_+ + \sigma_-)/2$ is the polarization cross section. It can be

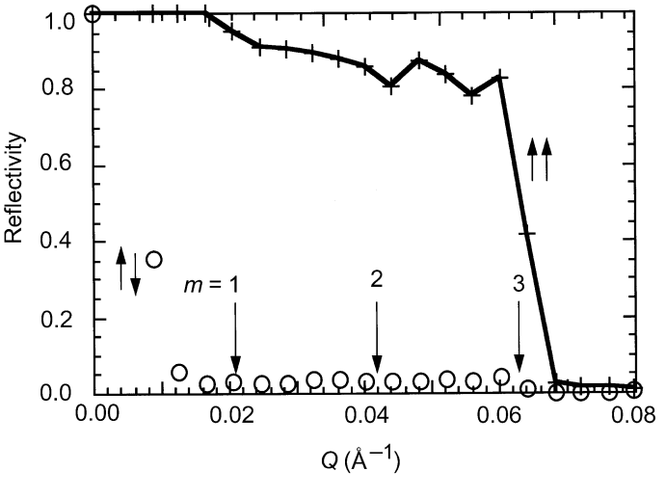

Fig. 4.4.2.10. Measured reflectivity curve of an FeCoV/TiZr polarizing supermirror with an extended angular range of polarization of three times that of γ_c(Ni) for neutrons without spin flip, ↑↑, and with spin flip, ↑↓.

Table 4.4.2.5. *Scattering-length densities for some typical materials used for polarizing multilayers*

Magnetic layer	$N(b+p)$ (10^{-6} Å^{-2})	$N(b-p)$ (10^{-6} Å^{-2})	Nb (10^{-6} Å^{-2})	Nonmagnetic layer
Fe	13.04	3.08	3.64	Ge
			3.50	Ag
			3.02	W
			2.08	Si
			2.08	Al
Fe:Co (50:50)	10.98	−0.52	−0.27	V
			−1.95	Ti
Ni	10.86	7.94		
Fe:Co:V (49:49:2)	10.75	−0.63	−0.27	V
			−1.95	Ti
Fe:Co:V (50:48:2)	10.66	−0.64	−0.27	V
			−1.95	Ti
Fe:Ni (50:50)	10.53	6.65		
Co	6.65	−2.00	−1.95	Ti
Fe:Co:V (52:38:10)	6.27	2.12	2.08	Si
			2.08	Al

For the non-magnetic layer we have only listed the simple elements that give a close match to the $N(b-p)$ value of the corresponding magnetic layer. In practice excellent matching can be achieved by using alloys (*e.g.* Ti_xZr_y alloys allow Nb values between −1.95 and 3.03×10^{-6}Å^{-2} to be selected) or reactive sputtering (*e.g.*TiN_x).

shown (Williams, 1988) that the ratio σ_p/σ_0 must be ≥ 0.65 to achieve $|P| > 0.95$ and $T > 0.2$.

Magnetized iron was the first polarizing filter to be used (Alvarez & Bloch, 1940). The method relies on the spin-dependent Bragg scattering from a magnetized polycrystalline block, for which σ_p approaches 10 barns near the Fe cut-off at 4 Å (Steinberger & Wick, 1949). Thus, for wavelengths in the range 3.6 to 4 Å, the ratio $\sigma_p/\sigma_0 \simeq 0.59$, resulting in a theoretical polarizing efficiency of 0.8 for a transmittance of ~ 0.3. In practice, however, since iron cannot be fully saturated, depolarization occurs, and values of $P \simeq 0.5$ with $T \sim 0.25$ are more typical.

Resonance absorption polarization filters rely on the spin dependence of the absorption cross section of polarized nuclei at their nuclear resonance energy and can produce efficient polarization over a wide energy range. The nuclear polarization is normally achieved by cooling in a magnetic field, and filters based on ^{149}Sm ($E_r = 0.097$ eV) (Freeman & Williams, 1978) and ^{151}Eu ($E_r = 0.32$ and 0.46 eV) have been successfully tested. The ^{149}Sm filter has a polarizing efficiency close to 1 within a small wavelength range (0.85 to 1.1 Å), while the transmittance is about 0.15. Furthermore, since the filter must be operated at temperatures of the order of 15 mK, it is very sensitive to heating by γ-rays.

Broad-band polarizing filters, based on spin-dependent scattering or absorption, provide an interesting alternative to polarizing mirrors or monochromators, owing to the wider range of energy and scattering angle that can be accepted. The most promising such filter is polarized ^{3}He, which operates through the huge spin-dependent neutron capture cross section that is totally dominated by the resonance capture of neutrons with antiparallel spin. The polarization efficiency of an ^{3}He neutron spin filter of length l can be written as

$$P_n(\lambda) = \tanh[\mathcal{O}(\lambda)P_{\rm He}], \qquad (4.4.2.15)$$

where $P_{\rm He}$ is the ^{3}He polarization, and $\mathcal{O}(\lambda) = [^3\mathrm{He}]l\sigma_0(\lambda)$ is the dimensionless effective absorption coefficient, also called the opacity (Surkau *et al.*, 1997). For gaseous ^{3}He, the opacity can be written in more convenient units as

$$\mathcal{O}' = p[\mathrm{bar}] \times l[\mathrm{cm}] \times \lambda[\text{Å}], \qquad (4.4.2.16)$$

where p is the ^{3}He pressure (1 bar = 10^5 Pa) and $\mathcal{O} = 7.33 \times 10^{-2}\mathcal{O}'$. Similarly, the residual transmission of the spin filter is given by

$$T_n(\lambda) = \exp[-\mathcal{O}(\lambda)]\cosh[\mathcal{O}(\lambda)P_{\rm He}]. \qquad (4.4.2.17)$$

It can be seen that, even at low ^{3}He polarization, full neutron polarization can be achieved in the limit of large absorption at the cost of the transmission.

^{3}He can be polarized either by spin exchange with optically pumped rubidium (Bouchiat, Carver & Varnum, 1960; Chupp, Coulter, Hwang, Smith & Welsh, 1996; Wagshul & Chupp, 1994) or by pumping of metastable ^{3}He* atoms followed by metastable exchange collisions (Colegrove, Schearer & Walters, 1963). In the former method, the ^{3}He gas is polarized at the required high pressure, whereas ^{3}He* pumping takes place at a pressure of about 1 mbar, followed by a polarization conserving compression by a factor of nearly 10 000. Although the polarization time constant for Rb pumping is of the order of several hours compared with fractions of a second for ^{3}He* pumping, the latter requires several 'fills' of the filter cell to achieve the required pressure.

An alternative broad-band spin filter is the polarized proton filter, which utilizes the spin dependence of nuclear scattering. The spin-dependent cross section can be written as (Lushchikov, Taran & Shapiro, 1969)

$$\sigma_\pm = \sigma_1 + \sigma_2 P_{\rm H}^2 \mp \sigma_3 P_{\rm H}, \qquad (4.4.2.18)$$

where σ_1, σ_2, and σ_3 are empirical constants. The viability of the method relies on achieving a high nuclear polarization $P_{\rm H}$. A polarization $P_{\rm H} = 0.7$ gives $\sigma_p/\sigma_0 \approx 0.56$ in the cold-neutron region. Proton polarizations of the order of 0.8 are required for a useful filter (Schaerpf & Stuesser, 1989). Polarized proton filters can polarize very high energy neutrons even in the eV range.

4.4.2.6.4. *Zeeman polarizer*

The reflection width of perfect silicon crystals for thermal neutrons and the Zeeman splitting ($\Delta E = 2\mu B$) of a field of about 10 kGs are comparable and therefore can be used to polarize a neutron beam. For a monochromatic beam (energy E_0) in a strong magnetic field region, the result of the Zeeman splitting will be a separation into two polarized subbeams, one polarized along **B** with energy $E_0 + \mu B$, and the other polarized antiparallel to **B** with energy $E_0 - \mu B$. The two polarized beams can be selected by rocking a perfect crystal in the field region B (Forte & Zeyen, 1989).

4.4.2.7. *Spin-orientation devices*

Polarization is the state of spin orientation of an assembly of particles in a target or beam. The beam polarization vector **P** is defined as the vector average of this spin state and is often described by the density matrix $\rho = \frac{1}{2}(1 + \sigma\mathbf{P})$. The polarization is then defined as $\mathbf{P} = \mathrm{Tr}(\rho\sigma)$. If the polarization vector is inclined to the field direction in a homogenous magnetic field, **B**, the polarization vector will precess with the classical Larmor frequency $\omega_L = |\gamma|B$. This results in a precessing spin polarization. For most experiments, it is sufficient to consider the linear polarization vector in the direction of an applied magnetic field. If, however, the magnetic field direction changes along the path of the neutron, it is also possible that the direction of **P** will change. If the frequency, Ω, with which the magnetic field changes is such that

$$\Omega = \mathrm{d}(\mathbf{B}/|\mathbf{B}|)/\,\mathrm{d}t \ll \omega_L, \qquad (4.4.2.19)$$

then the polarization vector follows the field rotation adiabatically. Alternatively, when $\Omega \gg \omega_L$, the magnetic field changes so rapidly that **P** cannot follow, and the condition is known as non-adiabatic fast passage. All spin-orientation devices are based on these concepts.

4.4.2.7.1. *Maintaining the direction of polarization*

A polarized beam will tend to become depolarized during passage through a region of zero field, since the field direction is ill defined over the beam cross section. Thus, in order to keep the polarization direction aligned along a defined quantization axis, special precautions must be taken.

The simplest way of maintaining the polarization of neutrons is to use a guide field to produce a well defined field **B** over the whole flight path of the beam. If the field changes direction, it has to fulfil the adiabatic condition $\Omega \ll \omega_L$, *i.e.* the field changes must take place over a time interval that is long compared with the Larmor period. In this case, the polarization follows the field direction adiabatically with an angle of deviation $\Delta\theta \leq 2\arctan(\Omega/\omega_L)$ (Schärpf, 1980).

Alternatively, some instruments (*e.g.* zero-field spin-echo spectrometers and polarimeters) use polarized neutron beams in regions of zero field. The spin orientation remains constant in a zero-field region, but the passage of the neutron beam into and out of the zero-field region must be well controlled. In order to provide a well defined region of transition from a guide-field region to a zero-field region, a non-adiabatic fast passage through the windings of a rectangular input solenoid can be used, either with a toroidal closure of the outside field or with a μ-metal closure frame. The latter serves as a mirror for the coil ends, with the effect of producing the field homogeneity of a long coil but avoiding the field divergence at the end of the coil.

4.4.2.7.2. *Rotation of the polarization direction*

The polarization direction can be changed by the adiabatic change of the guide-field direction so that the direction of the polarization follows it. Such a rotation is performed by a spin turner or spin rotator (Schärpf & Capellmann, 1993; Williams, 1988).

Alternatively, the direction of polarization can be rotated relative to the guide field by using the property of precession described above. If a polarized beam enters a region where the field is inclined to the polarization axis, then the polarization vector **P** will precess about the new field direction. The precession angle will depend on the magnitude of the field and the time spent in the field region. By adjustment of these two parameters together with the field direction, a defined, though wavelength-dependent, rotation of **P** can be achieved. A simple device uses the non-adiabatic fast passage through the windings of two rectangular solenoids, wound orthogonally one on top of the other. In this way, the direction of the precession field axis is determined by the ratio of the currents in the two coils, and the sizes of the fields determine the angle φ of the precession. The orientation of the polarization vector can therefore be defined in any direction.

In order to produce a continuous rotation of the polarization, *i.e.* a well defined precession, as required in neutron spin-echo (NSE) applications, precession coils are used. In the simplest case, these are long solenoids where the change of the field integral over the cross section can be corrected by Fresnel coils (Mezei, 1972). More recently, Zeyen & Rem (1996) have developed and implemented optimal field-shape (OFS) coils. The field in these coils follows a cosine squared shape that results from the optimization of the line integral homogeneity. The OFS coils can be wound over a very small diameter, thereby reducing stray fields drastically.

4.4.2.7.3. *Flipping of the polarization direction*

The term 'flipping' was originally applied to the situation where the beam polarization direction is reversed with respect to a guide field, *i.e.* it describes a transition of the polarization direction from parallel to antiparallel to the guide field and *vice versa*. A device that produces this 180° rotation is called a π flipper. A $\pi/2$ flipper, as the name suggests, produces a 90° rotation and is normally used to initiate precession by turning the polarization at 90° to the guide field.

The most direct wavelength-independent way of producing such a transition is again a non-adiabatic fast passage from the region of one field direction to the region of the other field direction. This can be realized by a current sheet like the Dabbs foil (Dabbs, Roberts & Bernstein, 1955), a Kjeller eight (Abrahams, Steinsvoll, Bongaarts & De Lange, 1962) or a cryoflipper (Forsyth, 1979).

Alternatively, a spin flip can be produced using a precession coil, as described above, in which the polarization direction makes a precession of just π about a direction orthogonal to the guide field direction (Mezei, 1972). Normally, two orthogonally wound coils are used, where the second, correction, coil serves to compensate the guide field in the interior of the precession coil. Such a flipper is wavelength dependent and can be easily tuned by varying the currents in the coils.

Another group of flippers uses the non-adiabatic transition through a well defined region of zero field. Examples of this type of flipper are the two-coil flipper of Drabkin, Zabidarov, Kasman & Okorokov (1969) and the line-shape flipper of Korneev & Kudriashov (1981).

Historically, the first flippers used were radio-frequency coils set in a homogeneous magnetic field. These devices are wavelength dependent, but may be rendered wavelength independent by replacing the homogeneous magnetic field with a gradient field (Egorov, Lobashov, Nazarento, Porsev & Serebrov, 1974).

In some devices, the flipping action can be combined with another selection function. The wavelength-dependent magnetic wiggler flipper proposed by Agamalyan, Drabkin & Sbitnev (1988) in combination with a polarizer can be used as a polarizing monochromator (Majkrzak & Shirane, 1982). Badurek & Rauch (1978) have used flippers as choppers to pulse a polarized beam.

In neutron resonance spin echo (NRSE) (Gähler & Golub, 1987), the precession coil of the conventional spin-echo configuration is replaced by two resonance spin flippers separated by a large zero-field region. The radio-frequency field of amplitude B_1 is arranged orthogonal to the DC field, B_0, with a frequency $\omega = \omega_L$, and an amplitude defined by the relation $\omega_1 \tau = \pi$, where τ is the flight time in the flipper coil and $\omega_1 = \gamma B_1$. In this configuration, the neutron spin precesses through an angle π about the resonance field in each coil and leaves the coil with a phase angle φ. The total phase angle after passing through both coils, $\varphi = 2\omega L/v$, depends on the velocity v of the neutron and the separation L between the two coils. Thus, compared with conventional NSE, where the phase angle comes from the precession of the neutron spin in a strong magnetic field compared with a static flipper field, in NRSE the neutron spin does not precess, but the flipper field rotates. Effectively, the NRSE phase angle φ is a factor of two larger than the NSE phase angle for the same DC field B_0. Furthermore, the resolution is determined by the precision of the RF frequencies and the zero-field flight path L rather than the homogeneity of the line integral of the field in the NSE precession coil.

4.4.2.8. *Mechanical choppers and selectors*

Thermal neutrons have relatively low velocities (a 4 Å neutron has a reciprocal velocity of approximately $1000\,\mu s\,m^{-1}$), so that mechanical selection devices and simple flight-time measurements can be used to make accurate neutron energy determinations.

Disc choppers rotating at speeds up to 20 000 revolutions per minute about an axis that is parallel to the neutron beam are used to produce a well defined pulse of neutrons. The discs are made from absorbing material (at least where the beam passes) and comprise one or more neutron-transparent apertures or slits. For polarized neutrons, these transparent slits should not be metallic, as the eddy currents in the metal moving in even a weak guide field will strongly depolarize the beam. The pulse frequency is determined by the number of apertures and the rotation frequency, while the duty cycle is given by the ratio of open time to closed time in one rotation. Two such choppers rotating in phase can be used to monochromate and pulse a beam simultaneously (Egelstaff, Cocking & Alexander, 1961). In practice, more than two choppers are generally used to avoid frame overlap of the incident and scattered beams. The time resolution of disc choppers (and hence the energy resolution of the instrument) is determined by the beam size, the aperture size and the rotation speed. For a realistic beam size, the rotation speed limits the resolution. Therefore, in modern instruments, it is normal to replace a single chopper with two counter-rotating choppers (Hautecler *et al.*, 1985; Copley, 1991). The low duty cycle of a simple disc chopper can be improved by replacing the single slit with a series of slits either in a regular sequence (Fourier chopper) (Colwell, Miller & Whittemore, 1968; Hiismäki, 1997) or a pseudostatistical sequence (pseudostatistical chopper) (Hossfeld, Amadori & Scherm, 1970), with duty cycles of 50 and 30%, respectively.

The Fermi chopper is an alternative form of neutron chopper that simultaneously pulses and monochromates the incoming beam. It consists of a slit package, essentially a collimator, rotating about an axis that is perpendicular to the beam direction (Turchin, 1965). For optimum transmission at the required wavelength, the slits are usually curved to provide a straight collimator in the neutron frame of reference. The curvature also eliminates the 'reverse burst', *i.e.* a pulse of neutrons that passes when the chopper has rotated by 180°.

A Fermi chopper with straight slits in combination with a monochromator assembly of wide horizontal divergence can be used to time focus a polychromatic beam, thus maintaining the energy resolution while improving the intensity (Blanc, 1983).

Velocity selectors are used when a continuous beam is required with coarse energy resolution. They exist in either multiple disc configurations or helical channels rotating about an axis parallel to the beam direction (Dash & Sommers, 1953). Modern helical channel selectors are made up of lightweight absorbing blades slotted into helical grooves on the rotation axis (Wagner, Friedrich & Wille, 1992). At higher energies where no suitable absorbing material is available, highly scattering polymers [poly(methyl methacrylate)] can be used for the blades, although in this case adequate shielding must be provided. The neutron wavelength is determined by the rotation speed, and resolutions, $\Delta\lambda/\lambda$, ranging from 5% to practically 100% ($\lambda/2$ filter) can be achieved. The resolution is fixed by the geometry of the device, but can be slightly improved by tilting the rotation axis or relaxed by rotating in the reverse direction for shorter wavelengths. Transmissions of up to 94% are typical.

4.4.3. Resolution functions (By R. Pynn and J. M. Rowe)

In a *Gedanken* neutron scattering experiment, neutrons of wavevector $\mathbf{k}_I$ impinge on a sample and the wavevector, $\mathbf{k}_F$, of the scattered neutrons is determined. A number of different types of spectrometer are used to achieve this goal (*cf.* Pynn, 1984). In each case, finite instrumental resolution is a result of uncertainties in the definition of $\mathbf{k}_I$ and $\mathbf{k}_F$. Propagation directions for neutrons are generally defined by Soller collimators for which the transmission as a function of divergence angle generally has a triangular shape. Neutron monochromatization may be achieved either by Bragg reflection from a (usually) mosaic crystal or by a time-of-flight method. In the former case, the mosaic leads to a spread of $|k_I|$ while, in the latter, pulse length and uncertainty in the lengths of flight paths (including sample size and detector thickness) produce a similar effect. Calculations of instrumental resolution are generally lengthy and lack of space prohibits their detailed presentation here. In the following paragraphs, the concepts involved are indicated and references to original articles are provided.

In resolution calculations for neutron spectrometers, it is usually assumed that the uncertainty of the neutron wavevector does not vary spatially across the neutron beam, although this reasoning may not apply to the case of small samples and compact spectrometers. To calculate the resolution of the spectrometer in the large-beam approximation, one writes the measured intensity I as

$$I \propto \int \mathrm{d}^3k_i \int \mathrm{d}^3k_f P_i(\mathbf{k}_i) S(\mathbf{k}_i \rightarrow \mathbf{k}_f) P_f(\mathbf{k}_f), \qquad (4.4.3.1)$$

where $P_i(\mathbf{k}_i)$ is the probability that a neutron of wavevector $\mathbf{k}_i$ is incident on the sample, $P_f(\mathbf{k}_f)$ is the probability that a neutron of wavevector $\mathbf{k}_f$ is transmitted by the analyser system and $S(\mathbf{k}_i \rightarrow \mathbf{k}_f)$ is the probability that the sample scatters a neutron from $\mathbf{k}_i$ to $\mathbf{k}_f$. The fluctuation spectrum of the sample, $S(\mathbf{k}_i \rightarrow \mathbf{k}_f)$, does not depend separately on $\mathbf{k}_i$ and $\mathbf{k}_f$ but rather on the scattering vector $\mathbf{Q}$ and energy transfer $\hbar\omega$ defined by the conservation equations

$$\mathbf{Q} = \mathbf{k}_i - \mathbf{k}_f; \quad \hbar\omega = \frac{\hbar^2}{2m}(k_i^2 - k_f^2), \qquad (4.4.3.2)$$

where m is the neutron mass.

A number of methods of calculating the distribution functions $P_i(\mathbf{k}_i)$ and $P_f(\mathbf{k}_f)$ have been proposed. The method of independent distributions was used implicitly by Stedman (1968) and in more detail by Bjerrum Møller & Nielson (MN) (Nielsen & Bjerrum Møller, 1969; Bjerrum Møller & Nielsen, 1970) for three-axis spectrometers. Subsequently, the method has been extended to perfect-crystal monochromators (Pynn, Fujii & Shirane, 1983) and to time-of-flight spectrometers (Steinsvoll, 1973; Robinson, Pynn & Eckert, 1985). The method involves separating P_i and P_f into a product of independent distribution functions each of which can be convolved separately with the fluctuation spectrum $S(\mathbf{Q}, \omega)$ [*cf.* equation (4.4.3.1)]. Extremely simple results are obtained for the widths of scans through a phonon dispersion surface for spectrometers where the energy of scattered neutrons is analysed (Nielson & Bjerrum Møller, 1969). For diffractometers, the width of a scan through a Bragg peak may also be obtained (Pynn *et al.*, 1983), yielding a result equivalent to that given by Caglioti, Paoletti & Ricci (1960). In this case, however, the singular nature of the Bragg scattering process introduces a correlation between the distribution functions that contribute to P_i and P_f and the calculation is less transparent than it is for phonons.

A somewhat different approach, which does not explicitly separate the various contributions to the resolution, was proposed by Cooper & Nathans (CN) (Cooper & Nathans, 1967, 1968; Cooper, 1968). Minor errors were corrected by several authors (Werner & Pynn, 1971; Chesser & Axe, 1973). The CN method calculates the instrumental resolution function $R(\mathbf{Q} - \mathbf{Q}_0, \omega - \omega_0)$ as

$$R(\Delta\mathbf{Q}, \Delta\omega) = R_0 \exp -\tfrac{1}{2} \sum_{\alpha,\beta} M_{\alpha\beta} X_\alpha X_\beta, \qquad (4.4.3.3)$$

where X_1, X_2, and X_3 are the three components of $\Delta\mathbf{Q}$, $X_4 = \Delta\omega$, and $\mathbf{Q}_0$ and ω_0 are obtained from (4.4.3.2) by replacing $\mathbf{k}_i$ and $\mathbf{k}_f$ by $\mathbf{k}_I$ and $\mathbf{k}_F$, respectively. The matrix $\boldsymbol{M}$ is given in explicit form by several authors (Cooper & Nathans, 1967, 1968; Cooper, 1968; Werner & Pynn, 1971; Chesser & Axe, 1973) and the normalization R_0 has been discussed in detail by Dorner (1972). [A refutation (Tindle, 1984) of Dorner's work is incorrect.] Equation (4.4.3.3) implies that contours of constant transmission for the spectrometer [$R(\Delta\mathbf{Q}, \Delta\omega) = \text{constant}$] are ellipsoids in the four-dimensional $\mathbf{Q}$–ω space. Optimum resolution (focusing) is achieved by a scan that causes the resolution function to intersect the feature of interest in $S(\mathbf{Q}, \omega)$ (*e.g.* Bragg peak or phonon dispersion surface) for the minimum scan interval. The optimization of scans for a diffractometer has been considered by Werner (1971).

The MN and CN methods are equivalent. Using the MN formalism, it can be shown that

$$\boldsymbol{M} = (\boldsymbol{A})^{-1} \quad \text{with} \quad A_{\alpha\beta} = \sum_j \chi_{j\alpha}\chi_{j\beta}, \qquad (4.4.3.4)$$

where the $\chi_{j\alpha}$ are the components of the standard deviations of independent distributions (labelled by index j) defined by Bjerrum Møller & Nielsen (1970). In the limit $Q \rightarrow 0$, the matrices $\boldsymbol{M}$ and $\boldsymbol{A}$ are of rank three and other methods must be used to calculate the resolution ellipsoid (Mitchell, Cowley & Higgins, 1984). Nevertheless, the MN method may be used even in this case to calculate widths of scans.

To obtain the resolution function of a diffractometer (in which there is no analysis of scattered neutron energy) from the CN form for $\boldsymbol{M}$, it is sufficient to set to zero those contributions that arise from the mosaic of the analyser crystal. For elastic Bragg scattering, the problem is further simplified because X_4 [*cf.* equation (4.4.3.3)] is zero. The spectrometer resolution function is then an ellipsoid in $\mathbf{Q}$ space.

For the measurement of integrated intensities (of Bragg peaks for example), the normalization R_0 in (4.4.3.3) is required in order to obtain the Lorentz factor. The latter has been calculated for an arbitrary scan of a three-axis spectrometer (Pynn, 1975) and the results may be modified for a diffractometer as described in the preceding paragraph.

4.4.4. Scattering lengths for neutrons (By V. F. Sears)

The use of neutron diffraction for crystal-structure determinations requires a knowledge of the scattering lengths and the corresponding scattering and absorption cross sections of the elements and, in some cases, of individual isotopes. This information is needed to calculate unit-cell structure factors and to correct for effects such as absorption, self-shielding, extinction, thermal diffuse scattering, and detector efficiency (Bacon, 1975; Sears, 1989). Table 4.4.4.1 lists the best values of the neutron scattering lengths and cross sections that are available at the time of writing (January 1995). We begin by summarizing the basic relationships between the scattering lengths and cross sections of the elements and their isotopes that have been used in the compilation of this table. More background information can be found in, for example, the book by Sears (1989).

4.4.4.1. *Scattering lengths*

The scattering of a neutron by a single bound nucleus is described within the Born approximation by the Fermi pseudopotential,

$$V(\mathbf{r}) = \left(\frac{2\pi\hbar^2}{m}\right) b\delta(\mathbf{r}), \qquad (4.4.4.1)$$

in which $\mathbf{r}$ is the position of the neutron relative to the nucleus, m the neutrons mass, and b the bound scattering length. The neutron has spin $\mathbf{s}$ and the nucleus spin $\mathbf{I}$ so that, if $I \neq 0$, the Fermi pseudopotential and, hence, the bound scattering length will be spin dependent. Since $s = 1/2$, the most general rotationally invariant expression for b is

$$b = b_c + \frac{2b_i}{\sqrt{I(I+1)}}\,\mathbf{s}\cdot\mathbf{I}, \qquad (4.4.4.2)$$

in which the coefficients b_c and b_i are called the bound coherent and incoherent scattering lengths. If $I = 0$, then $b_i = 0$ by convention.

Table 4.4.4.1. *Bound scattering lengths, b, in fm and cross sections, σ, in barns (1 barn = 100 fm²) of the elements and their isotopes*

Z: atomic number; A: mass number; $I(\pi)$: spin (parity) of the nuclear ground state; c: % natural abundance (for radioisotopes, the half-life is given instead in annums); b_c: bound coherent scattering length; b_i: bound incoherent scattering length; σ_c: bound coherent scattering cross section; σ_i: bound incoherent scattering cross section; σ_s: total bound scattering cross section; σ_a: absorption cross section for 2200 m s^{-1} neutrons (E = 25.30 meV, k = 3.494 Å^{-1}, λ = 1.798 Å); $i = \sqrt{-1}$.

Element	Z	A	$I(\pi)$	c	b_c	b_i	σ_c	σ_i	σ_s	σ_a
H	1				−3.7390(11)		1.7568(10)	80.26(6)	82.02(6)	0.3326(7)
		1	1/2(+)	99.985	−3.7406(11)	25.274(9)	1.7583(10)	80.27(6)	82.03(6)	0.3326(7)
		2	1(+)	0.015	6.671(4)	4.04(3)	5.592(7)	2.05(3)	7.64(3)	0.000519(7)
		3	1/2(+)	(12.32a)	4.792(27)	−1.04(17)	2.89(3)	0.14(4)	3.03(5)	0
He	2				3.26(3)		1.34(2)	0.00	1.34(2)	0.00747(1)
		3	1/2(+)	0.00014	5.74(7)	−2.5(6)	4.42(10)	1.6(4)	6.0(4)	5333.(7.)
					−1.483(2)i	+2.568(3)i				
		4	0(+)	99.99986	3.26(3)	0	1.34(2)	0	1.34(2)	0
Li	3				−1.90(2)		0.454(14)	0.92(3)	1.37(3)	70.5(3)
		6	1(+)	7.5	2.00(11)	−1.89(5)	0.51(5)	0.46(2)	0.97(7)	940.(4.)
					−0.261(1)i	0.257(11)i				
		7	3/2(−)	92.5	−2.22(2)	−2.49(5)	0.619(11)	0.78(3)	1.40(3)	0.0454(3)
Be	4	9	3/2(−)	100	7.79(1)	0.12(3)	7.63(2)	0.0018(9)	7.63(2)	0.0076(8)
B	5				5.30(4)		3.54(5)	1.70(12)	5.24(11)	767.(8.)
					0.213(2)i					
		10	3(+)	20.0	−0.1(3)	−4.7(3)	0.144(8)	3.0(4)	3.1(4)	3835.(9.)
					1.066(3)i	1.231(3)i				
		11	3/2(−)	80.0	6.65(4)	−1.3(2)	5.56(7)	0.22(6)	5.78(9)	0.0055(33)
C	6				6.6460(12)		5.550(2)	0.001(4)	5.551(3)	0.00350(7)
		12	0(+)	98.90	6.6511(16)	0	5.559(3)	0	5.559(3)	0.00353(7)
		13	1/2(−)	1.10	6.19(9)	−0.52(9)	4.81(14)	0.034(12)	4.84(14)	0.00137(4)
N	7				9.36(2)		11.01(5)	0.50(12)	11.51(11)	1.90(3)
		14	1(+)	99.63	9.37(2)	2.0(2)	11.03(5)	0.5(1)	11.53(11)	1.91(3)
		15	1/2(−)	0.37	6.44(3)	−0.02(2)	5.21(5)	0.00005(10)	5.21(5)	0.000024(8)
O	8				5.803(4)		4.232(6)	0.000(8)	4.232(6)	0.00019(2)
		16	0(+)	99.762	5.803(4)	0	4.232(6)	0	4.232(6)	0.00010(2)
		17	5/2(+)	0.038	5.78(12)	0.18(6)	4.20(22)	0.004(3)	4.20(22)	0.236(10)
		18	0(+)	0.200	5.84(7)	0	4.29(10)	0	4.29(10)	0.00016(1)
F	9	19	1/2(+)	100	5.654(10)	−0.082(9)	4.017(17)	0.0008(2)	4.018(14)	0.0096(5)
Ne	10				4.566(6)		2.620(7)	0.008(9)	2.628(6)	0.039(4)
		20	0(+)	90.51	4.631(6)	0	2.695(7)	0	2.695(7)	0.036(4)
		21	3/2(+)	0.27	6.66(19)	±0.6(1)	5.6(3)	0.05(2)	5.7(3)	0.67(11)
		22	0(+)	9.22	3.87(1)	0	1.88(1)	0	1.88(1)	0.046(6)
Na	11	23	3/2(+)	100	3.63(2)	3.59(3)	1.66(2)	1.62(3)	3.28(4)	0.530(5)
Mg	12				5.375(4)		3.631(5)	0.08(6)	3.71(4)	0.063(3)
		24	0(+)	78.99	5.66(3)	0	4.03(4)	0	4.03(4)	0.050(5)
		25	5/2(+)	10.00	3.62(14)	1.48(10)	1.65(13)	0.28(4)	1.93(14)	0.19(3)
		26	0(+)	11.01	4.89(15)	0	3.00(18)	0	3.00(18)	0.0382(8)
Al	13	27	5/2(+)	100	3.449(5)	0.256(10)	1.495(4)	0.0082(7)	1.503(4)	0.231(3)
Si	14				4.1491(10)		2.1633(10)	0.004(8)	2.167(8)	0.171(3)
		28	0(+)	92.23	4.107(6)	0	2.120(6)	0	2.120(6)	0.177(3)
		29	1/2(+)	4.67	4.70(10)	0.09(9)	2.78(12)	0.001(2)	2.78(12)	0.101(14)
		30	0(+)	3.10	4.58(8)	0	2.64(9)	0	2.64(9)	0.107(2)
P	15	31	1/2(+)	100	5.13(1)	0.2(2)	3.307(13)	0.005(10)	3.312(16)	0.172(6)
S	16				2.847(1)		1.0186(7)	0.007(5)	1.026(5)	0.53(1)
		32	0(+)	95.02	2.804(2)	0	0.9880(14)	0	0.9880(14)	0.54(4)
		33	3/2(+)	0.75	4.74(19)	1.5(1.5)	2.8(2)	0.3(6)	3.1(6)	0.54(4)
		34	0(+)	4.21	3.48(3)	0	1.52(3)	0	1.52(3)	0.227(5)
		36	0(+)	0.02	3.(1.) E	0	1.1(8)	0	1.1(8)	0.15(3)

Table 4.4.4.1. *Bound scattering lengths (cont.)*

Element	Z	A	$I(\pi)$	c	b_c	b_i	σ_c	σ_i	σ_s	σ_a
Cl	17				9.5770(8)		11.526(2)	5.3(5)	16.8(5)	33.5(3)
		35	3/2(+)	75.77	11.65(2)	6.1(4)	17.06(6)	4.7(6)	21.8(6)	44.1(4)
		37	3/2(+)	24.23	3.08(6)	0.1(1)	1.19(5)	0.001(3)	1.19(5)	0.433(6)
Ar	18				1.909(6)		0.458(3)	0.22(2)	0.683(4)	0.675(9)
		36	0(+)	0.337	24.90(7)	0	77.9(4)	0	77.9(4)	5.2(5)
		38	0(+)	0.063	3.5(3.5)	0	1.5(3.1)	0	1.5(3.1)	0.8(2)
		40	0(+)	99.600	1.830(6)	0	0.421(3)	0	0.421(3)	0.660(9)
K	19				3.67(2)		1.69(2)	0.27(11)	1.96(11)	2.1(1)
		39	3/2(+)	93.258	3.74(2)	1.4(3)	1.76(2)	0.25(11)	2.01(11)	2.1(1)
		40	4(−)	0.012	3.(1.) *E*		1.1(8)	0.5(5)	1.6(9)	35.(8.)
		41	3/2(+)	6.730	2.69(8)	1.5(1.5)	0.91(5)	0.3(6)	1.2(6)	1.46(3)
Ca	20				4.70(2)		2.78(2)	0.05(3)	2.83(2)	0.43(2)
		40	0(+)	96.941	4.80(2)	0	2.90(2)	0	2.90(2)	0.41(2)
		42	0(+)	0.647	3.36(10)	0	1.42(8)	0	1.42(8)	0.68(7)
		43	7/2(−)	0.135	−1.56(9)	0.31(4)	0.5(5) *E*		0.8(5)	6.2(6)
		44	0(+)	2.086	1.42(6)	0	0.25(2)	0	0.25(2)	0.88(5)
		46	0(+)	0.004	3.6(2)	0	1.6(2)	0	1.6(2)	0.74(7)
		48	0(+)	0.187	0.39(9)	0	0.019(9)	0	0.019(9)	1.09(14)
Sc	21	45	7/2(−)	100	12.29(11)	−6.0(3)	19.0(3)	4.5(5)	23.5(6)	27.5(2)
Ti	22				−3.370(13)		1.427(11)	2.63(3)	4.06(3)	6.43(6)
		46	0(+)	8.2	4.725(5)	0	2.80(6)	0	2.80(6)	0.59(18)
		47	5/2(−)	7.4	3.53(7)	−3.5(2)	1.57(6)	1.5(2)	3.1(2)	1.7(2)
		48	0(+)	73.8	−5.86(2)	0	4.32(3)	0	4.32(3)	8.30(9)
		49	7/2(−)	5.4	0.98(5)	5.1(2)	0.12(1)	3.3(3)	3.4(3)	2.2(3)
		50	0(+)	5.2	5.88(10)	0	4.34(15)	0	4.34(15)	0.179(3)
V	23				−0.3824(12)		0.01838(12)	5.08(6)	5.10(6)	5.08(2)
		50	6(+)	0.250	7.6(6)		7.3(1.1)	0.5(5) *E*	7.8(1.0)	60.(40.)
		51	7/2(−)	99.750	−0.402(2)	6.435(4)	0.0203(2)	5.07(6)	5.09(6)	4.9(1)
Cr	24				3.635(7)		1.660(6)	1.83(2)	3.49(2)	3.05(8)
		50	0(+)	4.35	−4.50(5)	0	2.54(6)	0	2.54(6)	15.8(2)
		52	0(+)	83.79	4.920(10)	0	3.042(12)	0	3.042(12)	0.76(6)
		53	3/2(−)	9.50	−4.20(3)	6.87(10)	2.22(3)	5.93(17)	8.15(17)	18.1(1.5)
		54	0(+)	2.36	4.55(10)	0	2.60(11)	0	2.60(11)	0.36(4)
Mn	25	55	5/2(−)	100	−3.750(18)	1.79(4)	1.77(2)	0.40(2)	2.17(3)	13.3(2)
Fe	26				9.45(2)		11.22(5)	0.40(11)	11.62(10)	2.56(3)
		54	0(+)	5.8	4.2(1)	0	2.2(1)	0	2.2(1)	2.25(18)
		56	0(+)	91.7	9.94(3)	0	12.42(7)	0	12.42(7)	2.59(14)
		57	1/2(−)	2.2	2.3(1)	0.66(6)		0.3(3) *E*	1.0(3)	2.48(30)
		58	0(+)	0.3	15.(7.)	0	28.(26.)	0	28.(26.)	1.28(5)
Co	27	59	7/2(−)	100	2.49(2)	−6.2(2)	0.779(13)	4.8(3)	5.6(3)	37.18(6)
Ni	28				10.3(1)		13.3(3)	5.2(4)	18.5(3)	4.49(16)
		58	0(+)	68.27	14.4(1)	0	26.1(4)	0	26.1(4)	4.6(3)
		60	0(+)	26.10	2.8(1)	0	0.99(7)	0	0.99(7)	2.9(2)
		61	3/2(−)	1.13	7.60(6)	±3.9(3)	7.26(11)	1.9(3)	9.2(3)	2.5(8)
		62	0(+)	3.59	−8.7(2)	0	9.5(4)	0	9.5(4)	14.5(3)
		64	0(+)	0.91	−0.37(7)	0	0.017(7)	0	0.017(7)	1.52(3)
Cu	29				7.718(4)		7.485(8)	0.55(3)	8.03(3)	3.78(2)
		63	3/2(−)	69.17	6.43(15)	0.22(2)	5.2(2)	0.006(1)	5.2(2)	4.50(2)
		65	3/2(−)	30.83	10.61(19)	1.79(10)	14.1(5)	0.40(4)	14.5(5)	2.17(3)
Zn	30				5.60(5)		4.054(7)	0.077(7)	4.131(10)	1.11(2)
		64	0(+)	48.6	5.22(4)	0	3.42(5)	0	3.42(5)	0.93(9)
		66	0(+)	27.9	5.97(5)	0	4.48(8)	0	4.48(8)	0.62(6)
		67	5/2(−)	4.1	7.56(8)	−1.50(7)	7.18(15)	0.28(3)	7.46(15)	6.8(8)
		68	0(+)	18.8	6.03(3)	0	4.57(5)	0	4.57(5)	1.1(1)
		70	0(+)	0.6	6.(1.) *E*	0	4.5(1.5)	0	4.5(1.5)	0.092(5)

Table 4.4.4.1. *Bound scattering lengths (cont.)*

Element	Z	A	$I(\pi)$	c	b_c	b_i	σ_c	σ_i	σ_s	σ_a
Ga	31				7.288(2)		6.675(4)	0.16(3)	6.83(3)	2.75(3)
		69	3/2(−)	60.1	7.88(2)	−0.85(5)	7.80(4)	0.091(11)	7.89(4)	2.18(5)
		71	3/2(−)	39.9	6.40(3)	−0.82(4)	5.15(5)	0.084(8)	5.23(5)	3.61(10)
Ge	32				8.185(20)		8.42(4)	0.18(7)	8.60(6)	2.20(4)
		70	0(+)	20.5	10.0(1)	0	12.6(3)	0	12.6(3)	3.0(2)
		72	0(+)	27.4	8.51(10)	0	9.1(2)	0	9.1(2)	0.8(2)
		73	9/2(+)	7.8	5.02(4)	3.4(3)	3.17(5)	1.5(3)	4.7(3)	15.1(4)
		74	0(+)	36.5	7.58(10)	0	7.2(2)	0	7.2(2)	0.4(2)
		76	0(+)	7.8	8.21(1.5)	0	8.(3.)	0	8.(3.)	0.16(2)
As	33	75	3/2(−)	100	6.58(1)	−0.69(5)	5.44(2)	0.060(10)	5.50(2)	4.5(1)
Se	34				7.970(9)		7.98(2)	0.33(6)	8.30(6)	11.7(2)
		74	0(+)	0.9	0.8(3.0)	0	0.1(6)	0	0.1(6)	51.8(1.2)
		76	0(+)	9.0	12.2(1)	0	18.7(3)	0	18.7(3)	85.(7.)
		77	1/2(−)	7.6	8.25(8)	±0.6(1.6)	8.6(2)	0.05(26)	8.65(16)	42.(4.)
		78	0(+)	23.5	8.24(9)	0	8.5(2)	0	8.5(2)	0.43(2)
		80	0(+)	49.6	7.48(3)	0	7.03(6)	0	7.03(6)	0.61(5)
		82	0(+)	9.4	6.34(8)	0	5.05(13)	0	5.05(13)	0.044(3)
Br	35				6.795(15)		5.80(3)	0.10(9)	5.90(9)	6.9(2)
		79	3/2(−)	50.69	6.80(7)	−1.1(2)	5.81(12)	0.15(6)	5.96(13)	11.0(7)
		81	3/2(−)	49.31	6.79(7)	0.6(1)	5.79(12)	0.05(2)	5.84(12)	2.7(2)
Kr	36				7.81(2)		7.67(4)	0.01(14)	7.68(13)	25.(1.)
		78	0(+)	0.35		0		0		6.4(9)
		80	0(+)	2.25		0		0		11.8(5)
		82	0(+)	11.6		0		0		29.(20.)
		83	9/2(+)	11.5		185(30.)				
		84	0(+)	57.0		0		0		0.113(15)
		86	0(+)	17.3	8.1(2)	0	8.2(4)	0	8.2(4)	0.003(2)
Rb	37				7.09(2)		6.32(4)	0.5(4)	6.8(4)	0.38(4)
		85	5/2(−)	72.17	7.03(10)	6.2(2)	0.5(5)	*E*	6.7(5)	0.48(1)
		87	3/2(−)	27.83	7.23(12)	6.6(2)	0.5(5)	*E*	7.1(5)	0.12(3)
Sr	38				7.02(2)		6.19(4)	0.06(11)	6.25(10)	1.28(6)
		84	0(+)	0.56	7.(1.) *E*	0	6.(2.)	0	6.(2.)	0.87(7)
		86	0(+)	9.86	5.67(5)	0	4.04(7)	0	4.04(7)	1.04(7)
		87	9/2(+)	7.00	7.40(7)	6.88(13)	0.5(5)	*E*	7.4(5)	16.(3.)
		88	0(+)	82.58	7.15(6)	0	6.42(11)	0	6.42(11)	0.058(4)
Y	39	89	1/2(−)	100	7.75(2)	1.1(3)	7.55(4)	0.15(8)	7.70(9)	1.28(2)
Zr	40				7.16(3)		6.44(5)	0.02(15)	6.46(14)	0.185(3)
		90	0(+)	51.45	6.4(1)	0	5.1(2)	0	5.1(2)	0.011(5)
		91	5/2(+)	11.32	8.7(1)	−1.08(15)	9.5(2)	0.15(4)	9.7(2)	1.17(10)
		92	0(+)	17.19	7.4(2)	0	6.9(4)	0	6.9(4)	0.22(6)
		94	0(+)	17.28	8.2(2)	0	8.4(4)	0	8.4(4)	0.0499(24)
		96	0(+)	2.76	5.5(1)	0	3.8(1)	0	3.8(1)	0.0229(10)
Nb	41	93	9/2(+)	100	7.054(3)	−0.139(10)	6.253(5)	0.0024(3)	6.255(5)	1.15(5)
Mo	42				6.715(2)		5.67(3)	0.04(5)	5.71(4)	2.48(4)
		92	0(+)	14.84	6.91(8)	0	6.00(14)	0	6.00(14)	0.019(2)
		94	0(+)	9.25	6.80(7)	0	5.81(12)	0	5.81(12)	0.015(2)
		95	5/2(+)	15.92	6.91(6)	6.00(10)	0.5(5)	*E*	6.5(5)	13.1(3)
		96	0(+)	16.68	6.20(6)	0	4.83(9)	0	4.83(9)	0.5(2)
		97	5/2(+)	9.55	7.24(8)	6.59(15)	0.5(5)	*E*	7.1(5)	2.5(2)
		98	0(+)	24.13	6.58(7)	0	5.44(12)	0	5.44(12)	0.127(6)
		100	0(+)	9.63	6.73(7)	0	5.69(12)	0	5.69(12)	0.4(2)
Tc	43									
		99	9/2(+)	$(2.13\times10^5$a)	6.8(3)	5.8(5)	0.5(5)	*E*	6.3(7)	20.(1.)

Table 4.4.4.1. *Bound scattering lengths (cont.)*

Element	Z	A	$I(\pi)$	c	b_c	b_i	σ_c	σ_i	σ_s	σ_a
Ru	44				7.03(3)		6.21(5)	0.4(1)	6.6(1)	2.56(13)
		96	0(+)	5.5	0	0	0.28(2)			
		98	0(+)	1.9	0	0	<8.0			
		99	5/2(+)	12.7	6.9(1.0)					
		100	0(+)	12.6	0	0	4.8(6)			
		101	5/2(+)	17.0	3.3(9)					
		102	0(+)	31.6	0	0	1.17(7)			
		104	0(+)	18.7	0	0	0.31(2)			
Rh	45	103	1/2(−)	100	5.88(4)	4.34(6)	0.3(3)	*E*	4.6(3)	144.8(7)
Pd	46				5.91(6)		4.39(9)	0.093(9)	4.48(9)	6.9(4)
		102	0(+)	1.02	7.7(7) *E*	0	7.5(1.4)	0	7.5(1.4)	3.4(3)
		104	0(+)	11.14	7.7(7) *E*	0	7.5(1.4)	0	7.5(1.4)	0.6(3)
		105	5/2(+)	22.33	5.5(3)	−2.6(1.6)	3.8(4)	0.8(1.0)	4.6(1.1)	20.(3.)
		106	0(+)	27.33	6.4(4)	0	5.1(6)	0	5.1(6)	0.304(29)
		108	0(+)	26.46	4.1(3)	0	2.1(3)	0	2.1(3)	8.5(5)
		110	0(+)	11.72	7.7(7)*E*	0	7.5(1.4)	0	7.5(1.4)	0.226(31)
Ag	47				5.922(7)		4.407(10)	0.58(3)	4.99(3)	63.3(4)
		107	1/2(−)	51.839	7.555(11)	1.00(13)	7.17(2)	0.13(3)	7.30(4)	37.6(1.2)
		109	1/2(−)	48.161	4.165(11)	−1.60(13)	2.18(1)	0.32(5)	2.50(5)	91.0(1.0)
Cd	48				4.87(5)		3.04(6)	3.46(13)	6.50(12)	2520.(50.)
					−0.70(1)*i*					
		106	0(+)	1.25	5.(2.) *E*	0	3.1(2.5)	0	3.1(2.5)	1.
		108	0(+)	0.89	5.4(1)	0	3.7(1)	0	3.7(1)	1.1(3)
		110	0(+)	12.51	5.9(1)	0	4.4(1)	0	4.4(1)	11.(1.)
		111	1/2(+)	12.81	6.5(1)	5.3(2)	0.3(3)	*E*	5.6(4)	24(3.)
		112	0(+)	24.13	6.4(1)	0	5.1(2)	0	5.1(2)	2.2(5)
		*113	1/2(+)	12.22	−8.0(2)	12.1(4)	0.3(3) *E*	12.4(5)		20600(400.)
					−5.73(11)*i*					
		114	0(+)	28.72	7.5(1)	0	7.1(2)	0	7.1(2)	0.34(2)
		116	0(+)	7.47	6.3(1)	0	5.0(2)	0	5.0(2)	0.075(13)
In	49			4.065(20)	2.08(2)	0.54(11)	2.62(11)	193.8(1.5)		
					−0.0539(4)*i*					
		113	9/2(+)	43	5.39(6)	±0.017(1)	3.65(8)	0.000037(5)	3.65(8)	12.0(1.1)
		115	9/2(+)	957	4.01(2)	−2.1(2)	2.02(2)	0.55(11)	2.57(11)	202(2.)
					−0.0562(6)*i*					
Sn	50				6.225(2)		4.870(3)	0.022(5)	4.892(6)	0.626(9)
		112	0(+)	1.0	6.1(1.) *E*	0	4.5(1.5)	0	4.5(1.5)	1.01(11)
		114	0(+)	0.7	6.2(3)	0	4.8(5)	0	4.8(5)	0.114(30)
		115	1/2(+)	0.4	6.(1.) *E*	4.5(1.5)	0.3(3) *E*	4.8(1.5)	30(7.)	
		116	0(+)	14.7	5.93(5)	0	4.42(7)	0	4.42(7)	0.14(3)
		117	1/2(+)	7.7	6.48(5)	5.28(8)	0.3(3) *E*	5.6(3)	2.3(5)	
		118	0(+)	24.3	6.07(5)	0	4.63(8)	0	4.63(8)	0.22(5)
		119	1/2(+)	8.6	6.12(5)	4.71(8)	0.3(3) *E*	5.0(3)	2.2(5)	
		120	0(+)	32.4	6.49(5)	0	5.29(8)	0	5.29(8)	0.14(3)
		122	0(+)	4.6	5.74(5)	0	4.14(7)	0	4.14(7)	0.18(2)
		124	0(+)	5.6	5.97(5)	0	4.48(8)	0	4.48(8)	0.133(5)
Sb	51				5.57(3)		3.90(4)	0.00(7)	3.90(6)	4.91(5)
		121	7/2(+)	57.3	5.71(6)	−0.05(15)	4.10(9)	0.0003(19)	4.10(9)	5.75(12)
		123	5/2(+)	42.7	5.38(7)	−0.10(15)	3.64(9)	0.001(4)	3.64(9)	3.8(2)
Te	52				5.80(3)		4.23(4)	0.09(1)	4.32(4)	4.05(5)
		120	0(+)	0.096	5.3(5)	0	3.5(7)	0	3.4(7)	2.3(3)
		122	0(+)	2.60	3.8(2)	0	1.8(2)	0	1.8(2)	3.4(5)
		123	1/2(+)	0.908	−0.05(25)	−2.04(9)	0.002(3)	0.52(5)	0.52(5)	418(30.)
					−0.116(8)*i*					
		124	0(+)	4.816	7.96(10)	0	8.0(2)	0	8.0(2)	6.8(1.3)
		125	1/2(+)	7.14	5.02(8)	−0.26(13)	3.17(10)	0.008(8)	3.18(10)	1.55(16)
		126	0(+)	18.95	5.56(7)	0	3.88(10)	0	3.88(10)	1.04(15)
		128	0(+)	31.69	5.89(7)	0	4.36(10)	0	4.36(10)	0.215(8)
		130	0(+)	33.80	6.02(7)	0	4.55(11)	0	4.55(11)	0.29(6)

Table 4.4.4.1. *Bound scattering lengths (cont.)*

Element	Z	A	$I(\pi)$	c	b_c	b_i	σ_c	σ_i	σ_s	σ_a
I	53	127	5/2(+)	100	5.28(2)	1.58(15)	3.50(3)	0.31(6)	3.81(7)	6.15(6)
Xe	54				4.92(3)		3.04(4)			23.9(1.2)
		124	0(+)	0.10		0		0		165.(20.)
		126	0(+)	0.09		0		0		3.5(8)
		128	0(+)	1.91		0		0		< 8.
		129	1/2(+)	26.4						21.(5.)
		130	0(+)	4.1		0		0		< 26.
		131	3/2(+)	21.2						85.(10.)
		132	0(+)	26.9		0		0		0.45(6)
		134	0(+)	10.4		0		0		0.265(20)
		136	0(+)	8.9		0		0		0.26(2)
Cs	55	133	7/2(+)	100	5.42(2)	1.29(15)	3.69(3)	0.21(5)	3.90(6)	29.0(1.5)
Ba	56				5.07(3)		3.23(4)	0.15(11)	3.38(10)	1.1(1)
		130	0(+)	0.11	−3.6(6)	0	1.6(5)	0	1.6(5)	30(5.)
		132	0(+)	0.10	7.8(3)	0	7.6(6)	0	7.6(6)	7.0(8)
		134	0(+)	2.42	5.7(1)	0	4.08(14)	0	4.08(14)	2.0(1.6)
		135	3/2(+)	6.59	4.67(10)		2.74(12)	0.5(5) *E*	3.2(5)	5.8(9)
		136	0(+)	7.85	4.91(8)	0	3.03(10)	0	3.03(10)	0.68(17)
		137	3/2(+)	11.23	6.83(10)		5.86(17)	0.5(5) *E*	6.4(5)	3.6(2)
		138	0(+)	71.70	4.84(8)	0	2.94(10)	0	2.94(10)	0.27(14)
La	57				8.24(4)		8.53(8)	1.13(19)	9.66(17)	8.97(5)
		138	5(+)	0.09	8.(2.) *E*	8.(4.)	0.5(5) *E*	8.5(4.0)	57.(6.)	
		139	7/2(+)	99.91	8.24(4)	3.0(2)	8.53(8)	1.13(15)	9.66(17)	8.93(4)
Ce	58				4.84(2)		2.94(2)	0.00(10)	2.94(10)	0.63(4)
		136	0(+)	0.19	5.80(9)	0	4.23(13)	0	4.23(13)	7.3(1.5)
		138	0(+)	0.25	6.70(9)	0	5.64(15)	0	5.64(15)	1.1(3)
		140	0(+)	88.48	4.84(9)	0	2.94(11)	0	2.94(11)	0.57(4)
		142	0(+)	11.08	4.75(9)	0	2.84(11)	0	2.84(11)	0.95(5)
Pr	59	141	5/2(+)	100	4.58(5)	−0.35(3)	2.64(6)	0.015(3)	2.66(6)	11.5(3)
Nd	60				7.69(5)		7.43(10)	9.2(8)	16.6(8)	50.5(1.2)
		142	0(+)	27.16	7.7(3)	0	7.5(6)	0	7.5(6)	18.7(7)
		143	7/2(−)	12.18	14.2(5) *E*	±21.1(6)	25.(7.)	55.(7.)	80.(2.)	334.(10.)
		144	0(+)	23.80	2.8(3)	0	1.0(2)	0	1.0(2)	3.6(3)
		145	7/2(−)	8.29	14.2(5)	*E*	25.(7.)	5.(5.) *E*	30.(9.)	42.(2.)
		146	0(+)	17.19	8.7(2)	0	9.5(4)	0	9.5(4)	1.4(1)
		148	0(+)	5.75	5.7(3)	0	4.1(4)	0	4.1(4)	2.5(2)
		150	0(+)	5.63	5.3(2)	0	3.5(3)	0	3.5(3)	1.2(2)
Pm	61									
		147	7/2(+)	(2.62a)	12.6(4)	±3.2(2.5)	20.0(1.3)	1.3(2.0)	21.3(1.5)	168.4(3.5)
Sm	62				0.80(2)		0.422(9)	39.(3.)	39.(3.)	5922.(56.)
					−1.65(2)*i*					
		144	0(+)	3.1	−3.(4.) *E*	0	1.(3.)	0	1.(3.)	0.7(3)
		147	7/2(−)	15.1	14(3.)	±11.(7.)	25.(11.)	14.(19.)	39(16.)	57(3.)
		148	0(+)	11.3	−3.(4.) *E*	0	1.(3.)	0	1.(3.)	2.4(6)
		*149	7/2(−)	13.9	−19.2(1)	±31.4(6)	63.5(6)	137.(5.)	200.(5.)	42080.(400.)
					−11.7(1)*i*	−10.3(1)*i*				
		150	0(+)	7.4	14(3.)	0	25(11.)	0	25(11.)	104(4.)
		152	0(+)	26.6	−5.0(6)	0	3.1(8)	0	3.1(8)	206.(6.)
		154	0(+)	22.6	9.3(1.0)	0	11.(2.)	0	11.(2.)	8.4(5)
Eu	63				7.22(2)		6.75(4)	2.5(4)	9.2(4)	4530.(40.)
					−1.26(1)*i*					
		*151	5/2(+)	47.8	6.13(14)	±4.5(4)	5.5(2)	3.1(4)	8.4(4)	9100(100.)
					−2.53(3)*i*	−2.14(2)*i*				
		153	5/2(+)	52.2	8.22(12)	±3.2(9)	8.5(2)	1.3(7)	9.8(7)	312.(7.)

Table 4.4.4.1.*Bound scattering lengths (cont.)*

Element	Z	A	$I(\pi)$	c	b_c	b_i	σ_c	σ_i	σ_s	σ_a
Gd	64				6.5(5) −13.82(3)*i*		29.3(8)	151.(2.)	180.(2.)	49700.(125.)
		152	0(+)	0.2	10.(3.) *E*	0	13.(8.)	0	13.(8.)	735.(20.)
		154	0(+)	2.1	10.(3.) *E*	0	13.(8.)	0	13.(8.)	85.(12.)
		*155	3/2(−)	14.8	6.0(1) −17.0(1)*i*	±5.(5.) *E* −13.16(9)*i*	40.8(4.)	25.(6.)	66.(6.)	61100.(400.)
		156	0(+)	20.6	6.3(4)	0	5.0(6)	0	5.0(6)	1.5(1.2)
		*157	3/2(−)	15.7	−1.14(2) −71.9(2)*i*	±5.(5.) *E* −55.8(2)*i*	650(4.)	394.(7.)	1044.(8.)	259000.(700.)
		158	0(+)	24.8	9.(2.)	0	10.(5.)	0	10.(5.)	2.2(2)
		160	0(+)	21.8	9.15(5)	0	10.52(11)	0	10.52(11)	0.77(2)
Tb	65	159	3/2(+)	100	7.38(3)	−0.17(7)	6.84(6)	0.004(3)	6.84(6)	23.4(4)
Dy	66				16.9(2) −0.276(4)*i*		35.9(8)	54.4(1.2)	90.3(9)	994.(13.)
		156	0(+)	0.06	6.1(5)	0	4.7(8)	0	4.7(8)	33.(3.)
		158	0(+)	0.10	6.(4.) *E*	0	5.(6.)	0	5.(6.)	43.(6.)
		160	0(+)	2.34	6.7(4)	0	5.6(7)	0	5.6(7)	56.(5.)
		161	5/2(+)	19.0	10.3(4)	±4.9(8)	13.3(1.0)	3.(1.)	16.(1.)	600.(25.)
		162	0(+)	25.5	−1.4(5)	0	0.25(18)	0	0.25(18)	194.(10.)
		163	5/2(−)	24.9	5.0(4)	1.3(3)	3.1(5)	0.21(10)	3.3(5)	124.(7.)
		164	0(+)	28.1	49.4(5) −0.79(1)*i*	0	307.(3.)	0	307.(3.)	2840.(40.)
Ho	67	165	7/2(−)	100	8.01(8)	−1.70(8)	8.06(16)	0.36(3)	8.42(16)	64.7(1.2)
Er	68				7.79(2)		7.63(4)	1.1(3)	8.7(3)	159.(4.)
		162	0(+)	0.14	8.8(2)	0	9.7(4)	0	9.7(4)	19.(2.)
		164	0(+)	1.56	8.2(2)	0	8.4(4)	0	8.4(4)	13.(2.)
		166	0(+)	33.4	10.6(2)	0	14.1(5)	0	14.1(5)	19.6(1.5)
		167	7/2(+)	22.9	3.0(3)	1.0(3)	1.1(2)	0.13(8)	1.2(2)	659.(16.)
		168	0(+)	27.1	7.4(4)	0	6.8(7)	0	6.9(7)	2.74(8)
		170	0(+)	14.9	9.6(5)	0	11.6(1.2)	0	11.6(1.2)	5.8(3)
Tm	69	169	1/2(+)	100	7.07(3)	0.9(3)	6.28(5)	0.10(7)	6.38(9)	100.(2.)
Yb	70				12.43(3)		19.42(9)	4.0(2)	23.05(18)	34.8(8)
		168	0(+)	0.14	−4.07(2) −0.62(1)*i*	0	2.13(2)	0	2.13(2)	2230.(40.)
		170	0(+)	3.06	6.77(10)	0	5.8(2)	0	5.8(2)	11.4(1.0)
		171	1/2(−)	143	9.66(10)	−5.59(17)	11.7(2)	3.9(2)	15.6(3)	48.6(2.5)
		172	0(+)	21.9	9.43(10)	0	11.2(2)	0	11.2(2)	0.8(4)
		173	5/2(−)	16.1	9.56(7)	−5.3(2)	11.5(2)	3.5(3)	15.0(4)	17.1(1.3)
		174	0(+)	31.8	19.3(1)	0	46.8(5)	0	46.8(5)	69.4(5.0)
		176	0(+)	12.7	8.72(10)	0	9.6(2)	0	9.6(2)	2.85(5)
Lu	71				7.21(3)		6.53(5)	0.7(4)	7.2(4)	74.(2.)
		175	7/2(+)	97.39	7.24(3)	±2.2(7)	6.59(5)	0.6(4)	7.2(4)	21.(3.)
		*176	7(−)	2.61	6.1(1) −0.57(1)*i*	±3.0(4) +0.61(1)*i*	4.7(2)	1.2(3)	5.9(4)	2065.(35.)
Hf	72				7.77(14)		7.6(3)	2.6(5)	10.2(4)	104.1(0.5)
		174	0(+)	0.2	10.9(1.1)	0	15.(3.)	0	15.(3.)	561.(35.)
		176	0(+)	5.2	6.61(18)	0	5.5(3)	0	5.5(3)	23.5(3.1)
		177	7/2(−)	18.6	0.8(1.0) *E*	±0.9(1.3)	0.1(2)	0.1(3)	0.2(2)	373.(10.)
		178	0(+)	27.1	5.9(2)	0	4.4(3)	0	4.4(3)	84.(4.)
		179	9/2(+)	13.7	7.46(16)	±1.06(8)	7.0(3)	0.14(2)	7.1(3)	41.(3.)
		180	0(+)	35.2	13.2(3)	0	21.9(1.0)	0	21.9(1.0)	13.04(7)
Ta	73				6.91(7)		6.00(12)	0.01(17)	6.01(12)	20.6(5)
		*180	9(−)	0.012	7.(2.) *E*	6.2(3.5)	0.5(5)	*E*	7.(4.)	563.(60.)
		181	7/2(+)	99.988	6.91(7)	−0.29(3)	6.00(12)	0.011(2)	6.01(12)	20.5(5)

Table 4.4.4.1. *Bound scattering lengths (cont.)*

Element	Z	A	$I(\pi)$	c	b_c	b_i	σ_c	σ_i	σ_s	σ_a
W	74				4.86(2)		2.97(2)	1.63(6)	4.60(6)	18.3(2)
		180	0(+)	0.1	5.(3.) *E*	0	3.(4.)	0	3.(4.)	30.(20.)
		182	0(+)	26.3	6.97(14)	0	6.10(7)	0	6.10(7)	20.7(5)
		183	1/2(−)	14.3	6.53(4)		5.36(7)	0.3(3) *E*	5.7(3)	10.1(3)
		184	0(+)	30.7	7.48(6)	0	7.03(11)	0	7.03(11)	1.7(1)
		186	0(+)	28.6	−0.72(4)	0	0.065(7)	0	0.065(7)	37.9(0.6)
Re	75				9.2(2)		10.6(5)	0.9(6)	11.5(3)	89.7(1.0)
		185	5/2(+)	37.40	9.0(3)	±2.0(1.8)	10.2(7)	0.5(9)	10.7(6)	112.(2.)
		187	5/2(+)	62.60	9.3(3)	±2.8(1.1)	10.9(7)	1.0(8)	11.9(4)	76.4(1.0)
Os	76				10.7(2)		14.4(5)	0.3(8)	14.7(6)	16.0(4)
		184	0(+)	0.02	10.(2.) *E*	0	13.(5.)	0	13.(5.)	3000.(150.)
		186	0(+)	1.58	11.6(1.7)	0	17.(5.)	0	17.(5.)	80.(13.)
		187	1/2(−)	1.6	10.(2.) *E*	13.(5.)	0.3(3)	*E*	13.(5.)	320(10.)
		188	0(+)	13.3	7.6(3)	0	7.3(6)	0	7.3(6)	4.7(5)
		189	3/2(−)	16.1	10.7(3)		14.4(8)	0.5(5) *E*	14.9(9)	25(4.)
		190	0(+)	26.4	11.0(3)	0	15.2(9)	0	15.2(8)	13.1(3)
		192	0(+)	41.0	11.5(4)	0	16.6(1.2)	0	16.6(1.2)	2.0(1)
Ir	77				10.6(3)		14.1(8)	0.(3.)	14.(3.)	425.3(2.4)
		191	3/2(+)	37.3						954.(10.)
		193	3/2(+)	62.7						111.(5.)
Pt	78				9.60(1)		11.58(2)	0.13(11)	11.71(11)	10.3(3)
		190	0(+)	0.01	9.0(1.0)	0	10.(2.)	0	10.(2.)	152.(4.)
		192	0(+)	0.79	9.9(5)	0	12.3(1.2)	0	12.3(1.2)	10.0(2.5)
		194	0(+)	32.9	10.55(8)	0	14.0(2)	0	14.0(2)	1.44(19)
		195	1/2(−)	33.8	8.83(9)	−1.00(17)	9.8(2)	0.13(4)	9.9(2)	27.5(1.2)
		196	0(+)	25.3	9.89(8)	0	12.3(2)	0	12.3(2)	0.72(4)
		198	0(+)	7.2	7.8(1)	0	7.7(2)	0	7.6(2)	3.66(19)
Au	79	197	3/2(+)	100	7.63(6)	−1.84(10)	7.32(12)	0.43(5)	7.75(13)	98.65(9)
Hg	80				12.692(15)		20.24(5)	6.6(1)	26.8(1)	372.3(4.0)
		196	0(+)	0.2	30.3(1.0)	0	115(8.)	0	115(8.)	3080(180.)
		198	0(+)	10.1		0		0		2.0(3)
		199	1/2(−)	17.0	16.9(4)	±15.5(8)	36.(2.)	30.(3.)	66.(2.)	2150.(48.)
		200	0(+)	23.1		0		0		<60.
		201	3/2(−)	13.2			7.8(2.0)			
		202	0(+)	29.6		0		0		4.89(5)
		204	0(+)	6.8		0		0		0.43(10)
Tl	81				8.776(5)		9.678(11)	0.21(15)	9.89(15)	3.43(6)
		203	1/2(+)	29.524	6.99(16)	1.06(14)	6.14(28)	0.14(4)	6.28(28)	11.4(2)
		205	1/2(+)	70.476	9.52(7)	−0.242(17)	11.39(17)	0.007(1)	11.40(17)	0.104(17)
Pb	82				9.405(3)		11.115(7)	0.0030(7)	11.118(7)	0.171(2)
		204	0(+)	1.4	9.90(10)	0	12.3(2)	0	12.3(2)	0.65(7)
		206	0(+)	24.1	9.22(5)	0	10.68(12)	0	10.68(12)	0.0300(8)
		207	1/2(−)	22.1	9.28(4)	0.14(6)	10.82(9)	0.002(2)	10.82(9)	0.699(10)
		208	0(+)	52.4	9.50(2)	0	11.34(5)	0	11.34(5)	0.00048(3)
Bi	83	209	9/2(−)	100	8.532(2)	0.259(15)	9.148(4)	0.0084(10)	9.156(4)	0.0338(7)
Po	84									
At	85									
Rn	86									
Fr	87									
Ra	88									
		226	0(+)	$(1.60\times10^3$a)	10.0(1.0)	0	13.(3.)	0	13.(3.)	12.8(1.5)

Table 4.4.4.1. *Bound scattering lengths (cont.)*

Element	Z	A	$I(\pi)$	c	b_c	b_i	σ_c	σ_i	σ_s	σ_a
Ac	89									
Th	90	232	0(+)	100	10.31(3)	0	13.36(8)	0	13.36(8)	7.37(6)
Pa	91									
		231	3/2(−)	(3.28×10^4a)	9.1(3)	1	0.4(7)	0.1(3.3)	10.5(3.2)	200.6(2.3)
U	92				8.417(5)		8.903(11)	0.005(16)	8.908(11)	7.57(2)
		233	5/2(+)	(1.59×10^5a)	10.1(2)	±1.(3.)	12.8(5)	0.1(6)	12.9(3)	574.7(1.0)
		234	0(+)	0.005	12.4(3)	0	19.3(9)	0	19.3(9)	100.1(1.3)
		235	7/2(−)	0.720	10.47(3)	±1.3(6)	13.78(11)	0.2(2)	14.0(2)	680.9(1.1)
		238	0(+)	99.275	8.402(5)	0	8.871(11)	0	8.871(11)	2.68(2)
Np	93									
		237	5/2(+)	(2.14×10^6a)	10.55(10)		14.0(3)	0.5(5)*E*	14.5(6)	175.9(2.9)
Pu	94									
		238	0(+)	(87.74a)	14.1(5)	0	25.0(1.8)	0	25.0(1.8)	558.(7.)
		239	1/2(+)	(2.41×10^4a)	7.7(1)	±1.3(1.9)	7.5(2)	0.2(6)	7.7(6)	1017.3(2.1)
		240	0(+)	(6.56×10^3a)	3.5(1)	0	1.54(9)	0	1.54(9)	289.6(1.4)
		242	0(+)	(3.76×10^5a)	8.1(1)	0	8.2(2)	0	8.2(2)	18.5(5)
Am	95									
		243	5/2(−)	(7.37×10^3a)	8.3(2)	±2.(7.)	8.7(4)	0.3(2.6)	9.0(2.6)	75.3(1.8)
Cm	96									
		244	0(+)	(18.10a)	9.5(3)	0	11.3(7)	0	11.3(7)	16.2(1.2)
		246	0(+)	(4.7×10^3a)	9.3(2)	0	10.9(5)	0	10.9(5)	1.36(17)
		248	0(+)	(3.5×10^5a)	7.7(2)	0	7.5(4)	0	7.5(4)	3.00(26)

4.4.4.2. *Scattering and absorption cross sections*

When a thermal neutron collides with a nucleus, it may be either scattered or absorbed. By absorption, we mean reactions such as (n,γ), (n,p), or (n,α), in which there is no neutron in the final state. The effect of absorption can be included by allowing the bound scattering length to be complex,

$$b = b' - ib''. \tag{4.4.4.3}$$

The total bound scattering cross section is then given by

$$\sigma_s = 4\pi\langle|b|^2\rangle, \tag{4.4.4.4}$$

in which $\langle\,\rangle$ denotes a statistical average over the neutron and nuclear spins and the absorption cross section is given by

$$\sigma_a = \frac{4\pi}{k}\langle b''\rangle, \tag{4.4.4.5}$$

where $k = 2\pi/\lambda$ is the wavevector of the incident neutron and λ is the wavelength.

If the neutron and/or the nucleus is unpolarized, then the total bound scattering cross section is of the form

$$\sigma_s = \sigma_c + \sigma_i, \tag{4.4.4.6}$$

in which σ_c and σ_i are called the bound coherent and incoherent scattering cross sections and are given by

$$\sigma_c = 4\pi|b_c|^2, \quad \sigma_i = 4\pi|b_i|^2. \tag{4.4.4.7}$$

Also,

$$b_c = \langle b\rangle, \tag{4.4.4.8}$$

so that the absorption cross section is given by

$$\sigma_a = \frac{4\pi}{k}\, b_c''. \tag{4.4.4.9}$$

The absorption cross section is therefore uniquely determined by the imaginary part of the bound coherent scattering length. It is only when the neutron and the nucleus are both polarized that the imaginary part of the bound incoherent scattering length contributes to the value of σ_a.

For most nuclides, the scattering lengths and, hence, the scattering cross sections are constant in the thermal-neutron region, and the absorption cross sections are inversely proportional to k. Since k is proportional to the neutron velocity v, the absorption is said to obey a $1/v$ law. By convention, absorption cross sections are tabulated for a velocity $v = 2200\ \mathrm{m\,s^{-1}}$, which corresponds to a wavevector $k = 3.494\ \mathrm{\AA^{-1}}$, a wavelength $\lambda = 1.798$ Å, or an energy $E = 25.30$ meV.

The only major deviations from the $1/v$ law are for a few heavy nuclides (specifically, ^{113}Cd, ^{149}Sm, ^{151}Eu, ^{155}Gd, ^{157}Gd, ^{176}Lu, and ^{180}Ta), which have an (n,γ) resonance at thermal-neutron energies. For these nuclides (which are indicated by the symbol * in Table 4.4.4.1), the scattering lengths and cross sections are strongly energy dependent. The scattering lengths of the resonant rare-earth nuclides have been tabulated as a function of energy by Lynn & Seeger (1990).

4.4.4.3. *Isotope effects*

The coefficients b_c and b_i in (4.4.4.2) for the bound scattering length depend on the particular isotope under consideration, and this provides an additional source of incoherence in the scattering of neutrons by a mixture of isotopes. If $\langle\,\rangle$ is now taken to denote an average over both the spin and isotope distributions, then the expressions (4.4.4.8) for b_c, (4.4.4.4) for σ_s, and (4.4.4.5) for

σ_a also apply to a mixture of isotopes. Hence, if c_l denotes the mole fraction of isotopes of type l, so that

$$\sum_l c_l = 1, \tag{4.4.4.10}$$

then, for an isotopic mixture,

$$b_c = \sum_l c_l b_{cl}, \tag{4.4.4.11}$$

$$\sigma_s = \sum_l c_l \sigma_{sl}, \tag{4.4.4.12}$$

and

$$\sigma_a = \sum_l c_l \sigma_{al}. \tag{4.4.4.13}$$

The bound coherent scattering cross section of the mixture is given, as before, by

$$\sigma_c = 4\pi|b_c|^2, \tag{4.4.4.14}$$

while the bound incoherent scattering cross section is defined as

$$\sigma_i = \sigma_s - \sigma_c. \tag{4.4.4.15}$$

Hence, it follows that

$$\sigma_i \equiv 4\pi|b_i|^2 = \sigma_i(\text{spin}) + \sigma_i(\text{isotope}), \tag{4.4.4.16}$$

in which the contribution from spin incoherence is given by

$$\sigma_i(\text{spin}) = \sum_l c_l \sigma_{il} = 4\pi \sum_l c_l |b_{il}|^2, \tag{4.4.4.17}$$

and that from isotope incoherence is given by

$$\sigma_i(\text{isotope}) = 4\pi \sum_{l<l'} c_l c_{l'} |b_{cl} - b_{cl'}|^2. \tag{4.4.4.18}$$

Note that for a mixture of isotopes only the magnitude of b_i is defined by (4.4.4.16), and its sign is arbitrary. However, for the individual isotopes, both the magnitude and sign (or complex phase) of b_i are defined in (4.4.4.2).

4.4.4.4. *Correction for electromagnetic interactions*

The effective bound coherent scattering length that describes the interaction of a neutron with an atom includes additional contributions from electromagnetic interactions (Bacon, 1975; Sears, 1986*a*, 1996). For a neutral atom with atomic number Z, this quantity is of the form

$$b_c(q) = b_c(0) - b_e[Z - f(q)], \tag{4.4.4.19}$$

where q is the wavevector transfer in the collision, $b_c(0)$ and b_e are constants, and $f(q)$ is the atomic scattering factor (Section 6.1.1). The latter quantity is the Fourier transform of the electron number density and is normalized such that $f(0) = Z$.

The main contribution to $b_c(0)$ is from the nuclear interaction between the neutron and the nucleus but there is also a small electrostatic contribution ($\leq$0.5%) arising from the neutron electric polarizability. The coefficient b_e is called the neutron–electron scattering length and has the value $-1.32\ (4) \times 10^{-3}$ fm (Koester, Waschkowksi & Meier, 1988). This quantity is due mainly to the Foldy interaction with a small additional contribution (~10%) from the intrinsic charge distribution of the neutron.

The correction of the bound coherent scattering length for electromagnetic interactions requires a knowledge of the atomic scattering factor $f(q)$. Tables 6.1.1.1 and 6.1.1.3 provide accurate values of $f(q)$ obtained from relativistic Hartree–Fock calculations for all the atoms and chemically important ions in the Periodic Table. Alternatively, since the correction is small (~1%), one can often use the approximate analytical expression (Sears, 1986*a*, 1996)

$$f(q) = \frac{Z}{\sqrt{1 + 3(q/q_0)^2}} \tag{4.4.4.20}$$

with $q_0 = \gamma Z^{1/3}$. The value $\gamma = 1.90 \pm 0.07$ Å^{-1} provides a good fit to the Hartree–Fock results in Table 6.1.1.1 for $Z \geq 20$.

4.4.4.5. *Measurement of scattering lengths*

The development of modern neutron-optical techniques during the past 25 years has produced a dramatic increase in the accuracy with which scattering lengths can be measured (Koester, 1977; Klein & Werner, 1983; Werner & Klein, 1986; Sears, 1989; Koester, Rauch & Seymann, 1991). The measurements employ a number of effects – mirror reflection, prism refraction, gravity refractometry, Christiansen filter, and interferometry – all of which are based on the fact that the neutron index of refraction, n, is uniquely determined by $b_c(0)$ through the relation

$$n^2 = 1 - \frac{4\pi}{k^2}\rho b_c(0), \tag{4.4.4.21}$$

in which ρ is the number of atoms per unit volume. Apart from a small ($\leq$0.01%) local-field correction (Sears, 1985, 1989), this expression is exact.

In methods based on diffraction, such as Bragg reflection by powders or dynamical diffraction by perfect crystals, the measured quantity is the unit-cell structure factor $|F_{hkl}|$. This quantity depends on $b_c(q)$ in which q is equal to the magnitude of the reciprocal-lattice vector corresponding to the relevant Bragg planes, *i.e.*

$$q = 2k \sin\theta_{hkl}, \tag{4.4.4.22}$$

where θ_{hkl} is the Bragg angle. In dynamical diffraction measurements, it is usual for the authors to correct their results for electromagnetic interactions so that the published quantity is again $b_c(0)$. In the past, this correction has not usually been made for the scattering lengths obtained from Bragg reflection by powders. However, these latter measurements are accurate only to ±2 or 3% so that the correction is then relatively unimportant.

The essential point is that all the bound coherent scattering lengths in Table 4.4.4.1 with the experimental uncertainties less than 1% represent $b_c(0)$ and should therefore be corrected for electromagnetic interactions before being used in the interpretation of neutron diffraction experiments. Failure to make this correction will introduce systematic errors of 0.5 to 2% in the unit-cell structure factors at large q, and corresponding errors of 1 to 4% in the calculated intensities.

Expression (4.4.4.21) assumed that the neutrons and/or the nuclei are unpolarized. If the neutrons and the nuclei are both polarized then $b_c(0)$ is replaced by $\langle b(0)\rangle$, which depends on both the coherent and incoherent scattering lengths. If the coherent scattering length is known, neutron-optical experiments with polarized neutrons and nuclei can then be used to determine the incoherent scattering length (Glättli & Goldman, 1987).

4.4.4.6. *Compilation of scattering lengths and cross sections*

The bound scattering lengths and cross sections of almost all the elements in the Periodic Table, as well as those of the individual isotopes, are listed in Table 4.4.4.1. As in earlier versions of this table (Sears, 1984, 1986*b*, 1992*a,b*), our primary aim, has been to take the best current values of the bound coherent and incoherent neutron scattering lengths and to

Table 4.4.5.1. $\langle j_0 \rangle$ *form factors for 3d transition elements and their ions*

Atom or ion	*A*	*a*	*B*	*b*	*C*	*c*	*D*	*e*
Sc	0.2512	90.030	0.3290	39.402	0.4235	14.322	−0.0043	0.2029
Sc^{+}	0.4889	51.160	0.5203	14.076	−0.0286	0.179	0.0185	0.1217
Sc^{2+}	0.5048	31.403	0.5186	10.990	−0.0241	1.183	0.0000	0.0578
Ti	0.4657	33.590	0.5490	9.879	−0.0291	0.323	0.0123	0.1088
Ti^{+}	0.5093	36.703	0.5032	10.371	−0.0263	0.311	0.0116	0.1125
Ti^{2+}	0.5091	24.976	0.5162	8.757	−0.0281	0.916	0.0015	0.0589
Ti^{3+}	0.3571	22.841	0.6688	8.931	−0.0354	0.483	0.0099	0.0575
V	0.4086	28.811	0.6077	8.544	−0.0295	0.277	0.0123	0.0970
V^{+}	0.4444	32.648	0.5683	9.097	−0.2285	0.022	0.2150	0.1111
V^{2+}	0.4085	23.853	0.6091	8.246	−0.1676	0.041	0.1496	0.0593
V^{3+}	0.3598	19.336	0.6632	7.617	−0.3064	0.030	0.2835	0.0515
V^{4+}	0.3106	16.816	0.7198	7.049	−0.0521	0.302	0.0221	0.0433
Cr	0.1135	45.199	0.3481	19.493	0.5477	7.354	−0.0092	0.1975
Cr^{+}	−0.0977	0.047	0.4544	26.005	0.5579	7.489	0.0831	0.1114
Cr^{2+}	1.2024	−0.005	0.4158	20.548	0.6032	6.956	−1.2218	0.0572
Cr^{3+}	−0.3094	0.027	0.3680	17.035	0.6559	6.524	0.2856	0.0436
Cr^{4+}	−0.2320	0.043	0.3101	14.952	0.7182	6.173	0.2042	0.0419
Mn	0.2438	24.963	0.1472	15.673	0.6189	6.540	−0.0105	0.1748
Mn^{+}	−0.0138	0.421	0.4231	24.668	0.5905	6.655	−0.0010	0.1242
Mn^{2+}	0.4220	17.684	0.5948	6.0050	0.0043	−0.609	−0.0219	0.0589
Mn^{3+}	0.4198	14.283	0.6054	5.469	0.9241	−0.009	−0.9498	0.0392
Mn^{4+}	0.3760	12.566	0.6602	5.133	−0.0372	0.563	0.0011	0.0393
Fe	0.0706	35.008	0.3589	15.358	0.5819	5.561	−0.0114	0.1398
Fe^{+}	0.1251	34.963	0.3629	15.514	0.5223	5.591	−0.0105	0.1301
Fe^{2+}	0.0263	34.960	0.3668	15.943	0.6188	5.594	−0.0119	0.1437
Fe^{3+}	0.3972	13.244	0.6295	4.903	−0.0314	0.350	0.0044	0.0441
Fe^{4+}	0.3782	11.380	0.6556	4.592	−0.0346	0.483	0.0005	0.0362
Co	0.4139	16.162	0.6013	4.780	−0.1518	0.021	0.1345	0.1033
Co^{+}	0.0990	33.125	0.3645	15.177	0.5470	5.008	−0.0109	0.0983
Co^{2+}	0.4332	14.355	0.5857	4.608	−0.0382	0.134	0.0179	0.0711
Co^{3+}	0.3902	12.508	0.6324	4.457	−0.1500	0.034	0.1272	0.0515
Co^{4+}	0.3515	10.778	0.6778	4.234	−0.0389	0.241	0.0098	0.0390
Ni	−0.0172	35.739	0.3174	14.269	0.7136	4.566	−0.0143	0.1072
Ni^{+}	0.0705	35.856	0.3984	13.804	0.5427	4.397	−0.0118	0.0738
Ni^{2+}	0.0163	35.883	0.3916	13.223	0.6052	4.339	−0.0133	0.0817
Ni^{3+}	0.0012	35.000	0.3468	11.987	0.6667	4.252	−0.0148	0.0883
Ni^{4+}	−0.0090	35.861	0.2776	11.790	0.7474	4.201	−0.0163	0.0966
Cu	0.0909	34.984	0.4088	11.443	0.5128	3.825	−0.0124	0.0513
Cu^{+}	0.0749	34.966	0.4147	11.764	0.5238	3.850	−0.0127	0.0591
Cu^{2+}	0.0232	34.969	0.4023	11.564	0.5882	3.843	−0.0137	0.0532
Cu^{3+}	0.0031	34.907	0.3582	10.914	0.6531	3.828	−0.0147	0.0665
Cu^{4+}	−0.0132	30.682	0.2801	11.163	0.7490	3.817	−0.0165	0.0767

compute from them a consistent set of bound scattering cross sections. In the present version, we have used the values of the coherent and incoherent scattering lengths recommended by Koester, Rauch & Seymann (1991), supplemented with a few more recently measured values, and have computed from them the corresponding scattering cross sections. The trailing digits in parentheses give the standard errors calculated from the errors in the input data using the statistical theory of error propagation (Young, 1962). The imaginary parts of the scattering lengths, which are appreciable only for strongly absorbing nuclides, were calculated from the measured absorption cross sections (Mughabghab, Divadeenam & Holden, 1981; Mughabghab, 1984) and are listed beneath the real parts of Table 4.4.4.1.

In a few cases, where the scattering lengths have not yet been measured directly, the available scattering cross-section data (Mughabghab, Divadeenam & Holden, 1981; Mughabghab, 1984) were used to obtain the scattering lengths. Equations (4.4.4.11), (4.4.4.12), and (4.4.4.13) were used, where necessary, to fill gaps in Table 4.4.4.1. For some elements, these relations indicated inconsistencies in the data. In such cases, appropriate adjustments in the values of some of the quantities were made. In almost all cases, such adjustments were comparable with the stated errors. Finally, for some elements, it was necessary to estimate arbitrarily the scattering lengths of one or two isotopes in order to be able to complete the table. Such estimates are indicated by the letter '*E*' and were usually made only for isotopes of low natural abundance where the estimated values have only a marginal effect on the final results. Apart from the inclusion of new data for Ti and Mn, the values listed in Table 4.4.4.1 are the same as in Sears (1992*b*).

4.4.5. Magnetic form factors (By P. J. Brown)

The form factors used in the calculations of the cross sections for magnetic scattering of neutrons are defined in Subsection 6.1.2.3 as

$$\langle j_l(k) \rangle = \int_0^\infty U^2(r) j_l(kr) 4\pi r^2 \, \mathrm{d}r, \qquad (4.4.5.1)$$

Table 4.4.5.2. $\langle j_0 \rangle$ *form factors for 4d atoms and their ions*

Atom or ion	*A*	*a*	*B*	*b*	*C*	*c*	*D*	*e*
Y	0.5915	67.608	1.5123	17.900	−1.1130	14.136	0.0080	0.3272
Zr	0.4106	59.996	1.0543	18.648	−0.4751	10.540	0.0106	0.3667
Zr^{+}	0.4532	59.595	0.7834	21.436	−0.2451	9.036	0.0098	0.3639
Nb	0.3946	49.230	1.3197	14.822	−0.7269	9.616	0.0129	0.3659
Nb^{+}	0.4572	49.918	1.0274	15.726	−0.4962	9.157	0.0118	0.3403
Mo	0.1806	49.057	1.2306	14.786	−0.4268	6.987	0.0171	0.4135
Mo^{+}	0.3500	48.035	1.0305	15.060	−0.3929	7.479	0.0139	0.3510
Tc	0.1298	49.661	1.1656	14.131	−0.3134	5.513	0.0195	0.3869
Tc^{+}	0.2674	48.957	0.9569	15.141	−0.2387	5.458	0.0160	0.3412
Ru	0.1069	49.424	1.1912	12.742	−0.3176	4.912	0.0213	0.3597
Ru^{+}	0.4410	33.309	1.4775	9.553	−0.9361	6.722	0.0176	0.2608
Rh	0.0976	49.882	1.1601	11.831	−0.2789	4.127	0.0234	0.3263
Rh^{+}	0.3342	29.756	1.2209	9.438	−0.5755	5.332	0.0210	0.2574
Pd	0.2003	29.363	1.1446	9.599	−0.3689	4.042	0.0251	0.2453
Pd^{+}	0.5033	24.504	1.9982	6.908	−1.5240	5.513	0.0213	0.1909

Table 4.4.5.3. $\langle j_0 \rangle$ *form factors for rare-earth ions*

Ion	*A*	*a*	*B*	*b*	*C*	*c*	*D*	*e*
Ce^{2+}	0.2953	17.685	0.2923	6.733	0.4313	5.383	−0.0194	0.0845
Nd^{2+}	0.1645	25.045	0.2522	11.978	0.6012	4.946	−0.0180	0.0668
Nd^{3+}	0.0540	25.029	0.3101	12.102	0.6575	4.722	−0.0216	0.0478
Sm^{2+}	0.0909	25.203	0.3037	11.856	0.6250	4.237	−0.0200	0.0408
Sm^{3+}	0.0288	25.207	0.2973	11.831	0.6954	4.212	−0.0213	0.0510
Eu^{2+}	0.0755	25.296	0.3001	11.599	0.6438	4.025	−0.0196	0.0488
Eu^{3+}	0.0204	25.308	0.3010	11.474	0.7005	3.942	−0.0220	0.0356
Gd^{2+}	0.0636	25.382	0.3033	11.212	0.6528	3.788	−0.0199	0.0486
Gd^{3+}	0.0186	25.387	0.2895	11.142	0.7135	3.752	−0.0217	0.0489
Tb^{2+}	0.0547	25.509	0.3171	10.591	0.6490	3.517	−0.0212	0.0342
Tb^{3+}	0.0177	25.510	0.2921	10.577	0.7133	3.512	−0.0231	0.0512
Dy^{2+}	0.1308	18.316	0.3118	7.665	0.5795	3.147	−0.0226	0.0315
Dy^{3+}	0.1157	15.073	0.3270	6.799	0.5821	3.020	−0.0249	0.0146
Ho^{2+}	0.0995	18.176	0.3305	7.856	0.5921	2.980	−0.0230	0.1240
Ho^{3+}	0.0566	18.318	0.3365	7.688	0.6317	2.943	−0.0248	0.0068
Er^{2+}	0.1122	18.122	0.3462	6.911	0.5649	2.761	−0.0235	0.0207
Er^{3+}	0.0586	17.980	0.3540	7.096	0.6126	2.748	−0.0251	0.0171
Tm^{2+}	0.0983	18.324	0.3380	6.918	0.5875	2.662	−0.0241	0.0404
Tm^{3+}	0.0581	15.092	0.2787	7.801	0.6854	2.793	−0.0224	0.0351
Yb^{2+}	0.0855	18.512	0.2943	7.373	0.6412	2.678	−0.0213	0.0421
Yb^{3+}	0.0416	16.095	0.2849	7.834	0.6961	2.672	−0.0229	0.0344

Table 4.4.5.4 $\langle j_0 \rangle$ *form factors for actinide ions*

Ion	*A*	*a*	*B*	*b*	*C*	*c*	*D*	*e*
U^{3+}	0.5058	23.288	1.3464	7.003	−0.8724	4.868	0.0192	0.1507
U^{4+}	0.3291	23.548	1.0836	8.454	−0.4340	4.120	0.0214	0.1757
U^{5+}	0.3650	19.804	3.2199	6.282	−2.6077	5.301	0.0233	0.1750
Np^{3+}	0.5157	20.865	2.2784	5.893	−1.8163	4.846	0.0211	0.1378
Np^{4+}	0.4206	19.805	2.8004	5.978	−2.2436	4.985	0.0228	0.1408
Np^{5+}	0.3692	18.190	3.1510	5.850	−2.5446	4.916	0.0248	0.1515
Np^{6+}	0.2929	17.561	3.4866	5.785	−2.8066	4.871	0.0267	0.1698
Pu^{3+}	0.3840	16.679	3.1049	5.421	−2.5148	4.551	0.0263	0.1280
Pu^{4+}	0.4934	16.836	1.6394	5.638	−1.1581	4.140	0.0248	0.1242
Pu^{5+}	0.3888	16.559	2.0362	5.657	−1.4515	4.255	0.0267	0.1287
Pu^{6+}	0.3172	16.051	3.4654	5.351	−2.8102	4.513	0.0281	0.1382
Am^{2+}	0.4743	21.776	1.5800	5.690	−1.0779	4.145	0.0218	0.1253
Am^{3+}	0.4239	19.574	1.4573	5.872	−0.9052	3.968	0.0238	0.1054
Am^{4+}	0.3737	17.862	1.3521	6.043	−0.7514	3.720	0.0258	0.1113
Am^{5+}	0.2956	17.372	1.4525	6.073	−0.7755	3.662	0.0277	0.1202
Am^{6+}	0.2302	16.953	1.4864	6.116	−0.7457	3.543	0.0294	0.1323
Am^{7+}	0.3601	12.730	1.9640	5.120	−1.3560	3.714	0.0316	0.1232

Table 4.4.5.5. $\langle j_2 \rangle$ *form factors for 3d transition elements and their ions*

Atom or ion	*A*	*a*	*B*	*b*	*C*	*c*	*D*	*e*
Sc	10.8172	54.327	4.7353	14.847	0.6071	4.218	0.0011	0.1212
Sc^{+}	8.5021	34.285	3.2116	10.994	0.4244	3.605	0.0009	0.1037
Sc^{2+}	4.3683	28.654	3.7231	10.823	0.6074	3.668	0.0014	0.0681
Ti	4.3583	36.056	3.8230	11.133	0.6855	3.469	0.0020	0.0967
Ti^{+}	6.1567	27.275	2.6833	8.983	0.4070	3.052	0.0011	0.0902
Ti^{2+}	4.3107	18.348	2.0960	6.797	0.2984	2.548	0.0007	0.0640
Ti^{3+}	3.3717	14.444	1.8258	5.713	0.2470	2.265	0.0005	0.0491
V	3.7600	21.831	2.4026	7.546	0.4464	2.663	0.0017	0.0556
V^{+}	4.7474	23.323	2.3609	7.808	0.4105	2.706	0.0014	0.0800
V^{2+}	3.4386	16.530	1.9638	6.141	0.2997	2.267	0.0009	0.0565
V^{3+}	2.3005	14.682	2.0364	6.130	0.4099	2.382	0.0014	0.0252
V^{4+}	1.8377	12.267	1.8247	5.458	0.3979	2.248	0.0012	0.0399
Cr	3.4085	20.127	2.1006	6.802	0.4266	2.394	0.0019	0.0662
Cr^{+}	3.7768	20.346	2.1028	6.893	0.4010	2.411	0.0017	0.0686
Cr^{2+}	2.6422	16.060	1.9198	6.253	0.4446	2.372	0.0020	0.0480
Cr^{3+}	1.6262	15.066	2.0618	6.284	0.5281	2.368	0.0023	0.0263
Cr^{4+}	1.0293	13.950	1.9933	6.059	0.5974	2.346	0.0027	0.0366
Mn	2.6681	16.060	1.7561	5.640	0.3675	2.049	0.0017	0.0595
Mn^{+}	3.2953	18.695	1.8792	6.240	0.3927	2.201	0.0022	0.0659
Mn^{2+}	2.0515	15.556	1.8841	6.063	0.4787	2.232	0.0027	0.0306
Mn^{3+}	1.2427	14.997	1.9567	6.118	0.5732	2.258	0.0031	0.0336
Mn^{4+}	0.7879	13.886	1.8717	5.743	0.5981	2.182	0.0034	0.0434
Fe	1.9405	18.473	1.9566	6.323	0.5166	2.161	0.0036	0.0394
Fe^{+}	2.6290	18.660	1.8704	6.331	0.4690	2.163	0.0031	0.0491
Fe^{2+}	1.6490	16.559	1.9064	6.133	0.5206	2.137	0.0035	0.0335
Fe^{3+}	1.3602	11.998	1.5188	5.003	0.4705	1.991	0.0038	0.0374
Fe^{4+}	1.5582	8.275	1.1863	3.279	0.1366	1.107	−0.0022	0.0327
Co	1.9678	14.170	1.4911	4.948	0.3844	1.797	0.0027	0.0452
Co^{+}	2.4097	16.161	1.5780	5.460	0.4095	1.914	0.0031	0.0581
Co^{2+}	1.9049	11.644	1.3159	4.357	0.3146	1.645	0.0017	0.0459
Co^{3+}	1.7058	8.859	1.1409	3.309	0.1474	1.090	−0.0025	0.0462
Co^{4+}	1.3110	8.025	1.1551	3.179	0.1608	1.130	−0.0011	0.0374
Ni	1.0302	12.252	1.4669	4.745	0.4521	1.744	0.0036	0.0338
Ni^{+}	2.1040	14.866	1.4302	5.071	0.4031	1.778	0.0034	0.0561
Ni^{2+}	1.7080	11.016	1.2147	4.103	0.3150	1.533	0.0018	0.0446
Ni^{3+}	1.4683	8.671	0.1794	1.106	1.1068	3.257	−0.0023	0.0373
Ni^{4+}	1.1612	7.700	1.0027	3.263	0.2719	1.378	0.0025	0.0326
Cu	1.9182	14.490	1.3329	4.730	0.3842	1.639	0.0035	0.0617
Cu^{+}	1.8814	13.433	1.2809	4.545	0.3646	1.602	0.0033	0.0590
Cu^{2+}	1.5189	10.478	1.1512	3.813	0.2918	1.398	0.0017	0.0429
Cu^{3+}	1.2797	8.450	1.0315	3.280	0.2401	1.250	0.0015	0.0389
Cu^{4+}	0.9568	7.448	0.9099	3.396	0.3729	1.494	0.0049	0.0330

Table 4.4.5.6. $\langle j_2 \rangle$ *form factors for 4d atoms and their ions*

Atom or ion	*A*	*a*	*B*	*b*	*C*	*c*	*D*	*e*
Y	14.4084	44.658	5.1045	14.904	−0.0535	3.319	0.0028	0.1093
Zr	10.1378	35.337	4.7734	12.545	−0.0489	2.672	0.0036	0.0912
Zr^{+}	11.8722	34.920	4.0502	12.127	−0.0632	2.828	0.0034	0.0737
Nb	7.4796	33.179	5.0884	11.571	−0.0281	1.564	0.0047	0.0944
Nb^{+}	8.7735	33.285	4.6556	11.605	−0.0268	1.539	0.0044	0.0855
Mo	5.1180	23.422	4.1809	9.208	−0.0505	1.743	0.0053	0.0655
Mo^{+}	7.2367	28.128	4.0705	9.923	−0.0317	1.455	0.0049	0.0798
Tc	4.2441	21.397	3.9439	8.375	−0.0371	1.187	0.0066	0.0645
Tc^{+}	6.4056	24.824	3.5400	8.611	−0.0366	1.485	0.0044	0.0806
Ru	3.7445	18.613	3.4749	7.420	−0.0363	1.007	0.0073	0.0533
Ru^{+}	5.2826	23.683	3.5813	8.152	−0.0257	0.426	0.0131	0.0830
Rh	3.3651	17.344	3.2121	6.804	−0.0350	0.503	0.0146	0.0545
Rh^{+}	4.0260	18.950	3.1663	7.000	−0.0296	0.486	0.0127	0.0629
Pd	3.3105	14.726	2.6332	5.862	−0.0437	1.130	0.0053	0.0492
Pd^{+}	4.2749	17.900	2.7021	6.354	−0.0258	0.700	0.0071	0.0768

Table 4.4.5.7. $\langle j_2 \rangle$ *form factors for rare-earth ions*

Ion	*A*	*a*	*B*	*b*	*C*	*c*	*D*	*e*
Ce^{2+}	0.9809	18.063	1.8413	7.769	0.9905	2.845	0.0120	0.0448
Nd^{2+}	1.4530	18.340	1.6196	7.285	0.8752	2.622	0.0126	0.0461
Nd^{3+}	0.6751	18.342	1.6272	7.260	0.9644	2.602	0.0150	0.0450
Sm^{2+}	1.0360	18.425	1.4769	7.032	0.8810	2.437	0.0152	0.0345
Sm^{3+}	0.4707	18.430	1.4261	7.034	0.9574	2.439	0.0182	0.0510
Eu^{2+}	0.8970	18.443	1.3769	7.005	0.9060	2.421	0.0190	0.0511
Eu^{3+}	0.3985	18.451	1.3307	6.956	0.9603	2.378	0.0197	0.0447
Gd^{2+}	0.7756	18.469	1.3124	6.899	0.8956	2.338	0.0199	0.0441
Gd^{3+}	0.3347	18.476	1.2465	6.877	0.9537	2.318	0.0217	0.0484
Tb^{2+}	0.6688	18.491	1.2487	6.822	0.8888	2.275	0.0215	0.0439
Tb^{3+}	0.2892	18.497	1.1678	6.797	0.9437	2.257	0.0232	0.0458
Dy^{2+}	0.5917	18.511	1.1828	6.747	0.8801	2.214	0.0229	0.0439
Dy^{3+}	0.2523	18.517	1.0914	6.736	0.9345	2.208	0.0250	0.0476
Ho^{2+}	0.5094	18.515	1.1234	6.706	0.8727	2.159	0.0242	0.0560
Ho^{3+}	0.2188	18.516	1.0240	6.707	0.9251	2.161	0.0268	0.0503
Er^{2+}	0.4693	18.528	1.0545	6.649	0.8679	2.120	0.0261	0.0413
Er^{3+}	0.1710	18.534	0.9879	6.625	0.9044	2.100	0.0278	0.0489
Tm^{2+}	0.4198	18.542	0.9959	6.600	0.8593	2.082	0.0284	0.0457
Tm^{3+}	0.1760	18.542	0.9105	6.579	0.8970	2.062	0.0294	0.0468
Yb^{2+}	0.3852	18.550	0.9415	6.551	0.8492	2.043	0.0301	0.0478
Yb^{3+}	0.1570	18.555	0.8484	6.540	0.8880	2.037	0.0318	0.0498

Table 4.4.5.8. $\langle j_2 \rangle$ *form factors for actinide ions*

Ion	*A*	*a*	*B*	*b*	*C*	*c*	*D*	*e*
U^{3+}	4.1582	16.534	2.4675	5.952	−0.0252	0.765	0.0057	0.0822
U^{4+}	3.7449	13.894	2.6453	4.863	−0.5218	3.192	0.0009	0.0928
U^{5+}	3.0724	12.546	2.3076	5.231	−0.0644	1.474	0.0035	0.0477
Np^{3+}	3.7170	15.133	2.3216	5.503	−0.0275	0.800	0.0052	0.0948
Np^{4+}	2.9203	14.646	2.5979	5.559	−0.0301	0.367	0.0141	0.0532
Np^{5+}	2.3308	13.654	2.7219	5.494	−0.1357	0.049	0.1224	0.0553
Np^{6+}	1.8245	13.180	2.8508	5.407	−0.1579	0.044	0.1438	0.0585
Pu^{3+}	2.0885	12.871	2.5961	5.190	−0.1465	0.039	0.1343	0.0866
Pu^{4+}	2.7244	12.926	2.3387	5.163	−0.1300	0.046	0.1177	0.0490
Pu^{5+}	2.1409	12.832	2.5664	5.152	−0.1338	0.046	0.1210	0.0491
Pu^{6+}	1.7262	12.324	2.6652	5.066	−0.1695	0.041	0.1550	0.0502
Am^{2+}	3.5237	15.955	2.2855	5.195	−0.0142	0.585	0.0033	0.1120
Am^{3+}	2.8622	14.733	2.4099	5.144	−0.1326	0.031	0.1233	0.0727
Am^{4+}	2.4141	12.948	2.3687	4.945	−0.2490	0.022	0.2371	0.0502
Am^{5+}	2.0109	12.053	2.4155	4.836	−0.2264	0.027	0.2128	0.0414
Am^{6+}	1.6778	11.337	2.4531	4.725	−0.2043	0.034	0.1892	0.0387
Am^{7+}	1.8845	9.161	2.0746	4.042	−0.1318	1.723	0.0020	0.0379

Table 4.4.5.9. $\langle j_4 \rangle$ *form factors for 3d atoms and their ions*

Atom or ion	*A*	*a*	*B*	*b*	*C*	*c*	*D*	*e*
Sc	1.3420	10.200	0.3837	3.079	0.0468	0.118	−0.0328	0.1343
Sc^{+}	7.1167	15.487	−6.6671	18.269	0.4900	2.992	0.0047	0.1624
Sc^{2+}	−1.6684	15.648	1.7742	9.062	0.4075	2.412	0.0042	0.1105
Ti	−2.1515	11.271	2.5149	8.859	0.3555	2.149	0.0045	0.1244
Ti^{+}	−1.0383	16.190	1.4699	8.924	0.3631	2.283	0.0044	0.1270
Ti^{2+}	−1.3242	15.310	1.2042	7.899	0.3976	2.156	0.0051	0.0820
Ti^{3+}	−1.1117	14.635	0.7689	6.927	0.4385	2.089	0.0060	0.0572
V	−0.9633	15.273	0.9274	7.732	0.3891	2.053	0.0063	0.0840
V^{+}	−0.9606	15.545	1.1278	8.118	0.3653	2.097	0.0056	0.1027
V^{2+}	−1.1729	14.973	0.9092	7.613	0.4105	2.039	0.0067	0.0719
V^{3+}	−0.9417	14.205	0.5284	6.607	0.4411	1.967	0.0076	0.0569
V^{4+}	−0.7654	13.097	0.3071	5.674	0.4476	1.871	0.0081	0.0518
Cr	−0.6670	19.613	0.5342	6.478	0.3641	1.905	0.0073	0.0628
Cr^{+}	−0.8309	18.043	0.7252	7.531	0.3828	2.003	0.0073	0.0781
Cr^{2+}	−0.8930	15.664	0.5590	7.033	0.4093	1.924	0.0081	0.0631
Cr^{3+}	−0.7327	14.073	0.3268	5.674	0.4114	1.810	0.0085	0.0505
Cr^{4+}	−0.6748	12.946	0.1805	6.753	0.4526	1.800	0.0098	0.0644
Mn	−0.5452	15.471	0.4406	4.902	0.2884	1.543	0.0059	0.0488
Mn^{+}	−0.7947	17.867	0.6078	7.704	0.3798	1.905	0.0087	0.0737
Mn^{2+}	−0.7416	15.255	0.3831	6.469	0.3935	1.800	0.0093	0.0577
Mn^{3+}	−0.6603	13.607	0.2322	6.218	0.4104	1.740	0.0101	0.0579
Mn^{4+}	−0.5127	13.461	0.0313	7.763	0.4282	1.701	0.0113	0.0693
Fe	−0.5029	19.677	0.2999	3.776	0.2576	1.424	0.0071	0.0292
Fe^{+}	−0.5109	19.250	0.3896	4.891	0.2810	1.526	0.0069	0.0375
Fe^{2+}	−0.5401	17.227	0.2865	3.742	0.2658	1.424	0.0076	0.0278
Fe^{3+}	−0.5507	11.493	0.2153	4.906	0.3468	1.523	0.0095	0.0314
Fe^{4+}	−0.5352	9.507	0.1783	5.175	0.3584	1.469	0.0097	0.0360
Co	−0.4221	14.195	0.2900	3.979	0.2469	1.286	0.0063	0.0400
Co^{+}	−0.4115	14.561	0.3580	4.717	0.2644	1.418	0.0074	0.0541
Co^{2+}	0.4759	14.046	0.2747	3.731	0.2458	1.250	0.0057	0.0282
Co^{3+}	−0.4466	13.391	0.1419	3.011	0.2773	1.335	0.0093	0.0341
Co^{4+}	−0.4091	13.194	−0.0194	3.417	0.3534	1.421	0.0112	0.0622
Ni	−0.4428	14.485	0.0870	3.234	0.2932	1.331	0.0096	0.0554
Ni^{+}	−0.3836	13.425	0.3116	4.462	0.2471	1.309	0.0079	0.0515
Ni^{2+}	−0.3803	10.403	0.2838	3.378	0.2108	1.104	0.0050	0.0474
Ni^{3+}	−0.4014	9.046	0.2314	3.075	0.2192	1.084	0.0060	0.0323
Ni^{4+}	−0.3509	8.157	0.2220	2.106	0.1567	0.925	0.0065	0.0352
Cu	−0.3204	15.132	0.2335	4.021	0.2312	1.196	0.0068	0.0457
Cu^{+}	−0.3572	15.125	0.2336	3.966	0.2315	1.197	0.0070	0.0397
Cu^{2+}	−0.3914	14.740	0.1275	3.384	0.2548	1.255	0.0103	0.0394
Cu^{3+}	−0.3671	14.082	−0.0078	3.315	0.3154	1.377	0.0132	0.0534
Cu^{4+}	−0.2915	14.124	−0.1065	4.201	0.3247	1.352	0.0148	0.0579

Table 4.4.5.10. $\langle j_4 \rangle$ *form factors for 4d atoms and their ions*

Atom or ion	*A*	*a*	*B*	*b*	*C*	*c*	*D*	*e*
Y	−8.0767	32.201	7.9197	25.156	1.4067	6.827	−0.0001	0.1031
Zr	−5.2697	32.868	4.1930	24.183	1.5202	6.048	−0.0002	0.0855
Zr^{+}	−5.6384	33.607	4.6729	22.338	1.3258	5.924	−0.0003	0.0674
Nb	−3.1377	25.595	2.3411	16.569	1.2304	4.990	−0.0005	0.0615
Nb^{+}	−3.3598	25.820	2.8297	16.427	1.1203	4.982	−0.0005	0.0724
Mo	−2.8860	20.572	1.8130	14.628	1.1899	4.264	−0.0008	0.0410
Mo^{+}	−3.2618	25.486	2.3596	16.462	1.1164	4.491	−0.0007	0.0592
Tc	−2.7975	20.159	1.6520	16.261	1.1726	3.943	−0.0008	0.0657
Tc^{+}	−2.0470	19.683	1.6306	11.592	0.8698	3.769	−0.0010	0.0723
Ru	−1.5042	17.949	0.6027	9.961	0.9700	3.393	−0.0010	0.0338
Ru^{+}	1.6278	18.506	1.1828	10.189	0.8138	3.418	−0.0009	0.0673
Rh	−1.3492	17.577	0.4527	10.507	0.9285	3.155	−0.0009	0.0483
Rh^{+}	−1.4673	17.957	0.7381	9.944	0.8485	3.126	−0.0012	0.0487
Pd	−1.1955	17.628	0.3183	11.309	0.8696	2.909	−0.0006	0.0555
Pd^{+}	−1.4098	17.765	0.7927	9.999	0.7710	2.930	−0.0006	0.0530

Table 4.4.5.11. $\langle j_4 \rangle$ *form factors for rare-earth ions*

Ion	*A*	*a*	*B*	*b*	*C*	*c*	*D*	*e*
Ce^{2+}	−0.6468	10.533	0.4052	5.624	0.3412	1.535	0.0080	0.0522
Nd^{2+}	−0.5416	12.204	0.3571	6.169	0.3154	1.485	0.0098	0.0519
Nd^{3+}	−0.4053	14.014	0.0329	7.005	0.3759	1.707	0.0209	0.0372
Sm^{2+}	−0.4150	14.057	0.1368	7.032	0.3272	1.582	0.0192	0.0319
Sm^{3+}	−0.4288	10.052	0.1782	5.019	0.2833	1.236	0.0088	0.0328
Eu^{2+}	−0.4145	10.193	0.2447	5.164	0.2661	1.205	0.0065	0.0516
Eu^{3+}	−0.4095	10.211	0.1485	5.175	0.2720	1.237	0.0131	0.0494
Gd^{2+}	−0.3824	10.344	0.1955	5.306	0.2622	1.203	0.0097	0.0363
Gd^{3+}	−0.3621	10.353	0.1016	5.310	0.2649	1.219	0.0147	0.0494
Tb^{2+}	−0.3443	10.469	0.1481	5.416	0.2575	1.182	0.0104	0.0280
Tb^{3+}	−0.3228	10.476	0.0638	5.419	0.2566	1.196	0.0159	0.0439
Dy^{2+}	−0.3206	12.071	0.0904	8.026	0.2616	1.230	0.0143	0.0767
Dy^{3+}	−0.2829	9.525	0.0565	4.429	0.2437	1.066	0.0092	0.0181
Ho^{2+}	−0.2976	9.719	0.1224	4.635	0.2279	1.005	0.0063	0.0452
Ho^{3+}	−0.2717	9.731	0.0474	4.638	0.2292	1.047	0.0124	0.0310
Er^{2+}	−0.2975	9.829	0.1189	4.741	0.2116	1.004	0.0117	0.0524
Er^{3+}	−0.2568	9.834	0.0356	4.741	0.2172	1.028	0.0148	0.0434
Tm^{2+}	−0.2677	9.888	0.0925	4.784	0.2056	0.990	0.0124	0.0396
Tm^{3+}	−0.2292	9.895	0.0124	4.785	0.2108	1.007	0.0151	0.0334
Yb^{2+}	−0.2393	9.947	0.0663	4.823	0.2009	0.965	0.0122	0.0311
Yb^{3+}	−0.2121	8.197	0.0325	3.153	0.1975	0.884	0.0093	0.0435

Table 4.4.5.12. $\langle j_4 \rangle$ *form factors for actinide ions*

Ion	*A*	*a*	*B*	*b*	*C*	*c*	*D*	*e*
U^{3+}	−0.9859	16.601	0.6116	6.515	0.6020	2.597	−0.0010	0.0599
U^{4+}	−1.0540	16.605	0.4339	6.512	0.6746	2.599	−0.0011	0.0471
U^{5+}	−0.9588	16.485	0.1576	6.440	0.7785	2.640	−0.0010	0.0493
Np^{3+}	0.9029	16.586	0.4006	6.470	0.6545	2.563	−0.0004	0.0470
Np^{4+}	−0.9887	12.441	0.5918	5.294	0.5306	2.263	−0.0021	0.0583
Np^{5+}	−0.8146	16.581	−0.0055	6.475	0.7956	2.562	−0.0004	0.0600
Np^{6+}	0.6738	16.553	−0.2297	6.505	0.8513	2.553	−0.0003	0.0623
Pu^{3+}	−0.7014	16.369	−0.1162	6.697	0.7778	2.450	0.0000	0.0546
Pu^{4+}	−0.9160	12.203	0.4891	5.127	0.5290	2.149	−0.0022	0.0520
Pu^{5+}	−0.7035	16.360	−0.0979	6.706	0.7726	2.447	0.0000	0.0610
Pu^{6+}	−0.5560	16.322	−0.3046	6.768	0.8146	2.426	0.0001	0.0596
Am^{2+}	−0.7433	16.416	0.3481	6.788	0.6014	2.346	0.0000	0.0566
Am^{3+}	0.8092	12.854	0.4161	5.459	0.5476	2.172	−0.0011	0.0530
Am^{4+}	−0.8548	12.226	0.3037	5.909	0.6173	2.188	−0.0016	0.0456
Am^{5+}	−0.6538	15.462	−0.0948	5.997	0.7295	2.297	0.0000	0.0594
Am^{6+}	−0.5390	15.449	−0.2689	6.017	0.7711	2.297	0.0002	0.0729
Am^{7+}	−0.4688	12.019	−0.2692	7.042	0.7297	2.164	−0.0011	0.0262

Table 4.4.5.13. $\langle j_6 \rangle$ *form factors for rare-earth ions*

Ion	*A*	*a*	*B*	*b*	*C*	*c*	*D*	*e*
Ce^{2+}	−0.1212	7.994	−0.0639	4.024	0.1519	1.096	0.0078	0.0388
Nd^{2+}	−0.1600	8.009	0.0272	4.028	0.1104	1.068	0.0139	0.0363
Nd^{3+}	0.0416	8.014	−0.1261	4.040	0.1400	1.087	0.0102	0.0367
Sm^{2+}	0.1428	6.041	0.0723	2.033	0.0550	0.513	0.0081	0.0450
Sm^{3+}	−0.0944	6.030	−0.0498	2.074	0.1372	0.645	−0.0132	0.0387
Eu^{2+}	−0.1252	6.049	0.0507	2.085	0.0572	0.646	0.0132	0.0403
Eu^{3+}	−0.0817	6.039	−0.0596	2.120	0.1243	0.764	−0.0001	0.0206
Gd^{2+}	−0.1351	5.030	0.0828	2.025	0.0315	0.503	0.0187	0.0453
Gd^{3+}	−0.0662	6.031	−0.0850	2.154	0.1323	0.891	0.0048	0.0371
Th^{2+}	−0.0758	6.032	−0.0540	2.158	0.1199	0.890	0.0051	0.0488
Tb^{3+}	−0.0559	6.031	−0.1020	2.237	0.1264	1.107	0.0167	0.0170
Dy^{2+}	−0.0568	6.032	−0.1003	2.240	0.1401	1.106	0.0109	0.0463
Dy^{3+}	−0.0423	6.038	−0.1248	2.244	0.1359	1.200	0.0188	0.0350
Ho^{2+}	−0.0725	6.045	−0.0318	2.243	0.0738	1.202	0.0252	0.0634
Ho^{3+}	−0.0289	6.050	−0.1545	2.230	0.1550	1.260	0.0177	0.0351
Er^{2+}	0.0648	6.056	−0.0515	2.230	0.0825	1.264	0.0250	0.0409
Er^{3+}	−0.0110	6.061	−0.1954	2.224	0.1818	1.296	0.0149	0.0455
Tm^{2+}	0.0842	4.070	0.0807	0.849	−0.2087	0.039	0.2095	0.0360
Tm^{3+}	0.0727	4.073	0.0243	0.689	3.9459	0.002	−3.9076	0.0502
Yb^{2+}	−0.0739	5.031	0.0140	2.030	0.0351	0.508	0.0174	0.0434
Yb^{3+}	−0.0345	5.007	−0.0677	2.020	0.0985	0.549	−0.0076	0.0359

Table 4.4.5.14. $\langle j_6 \rangle$ *form factors for actinide ions*

Ion	*A*	*a*	*B*	*b*	*C*	*c*	*D*	*e*
U^{3+}	−0.3797	9.953	0.0459	5.038	0.2748	1.607	0.0016	0.0345
U^{4+}	−0.1793	11.896	−0.2269	5.428	0.3291	1.701	0.0030	0.0472
U^{5+}	−0.0399	11.891	−0.3458	5.580	0.3340	1.645	0.0029	0.0444
Np^{3+}	−0.2427	11.844	−0.1129	5.377	0.2848	1.568	0.0022	0.0368
Np^{4+}	−0.2436	9.599	−0.1317	4.101	0.3029	1.545	0.0019	0.0500
Np^{5+}	−0.1157	9.565	−0.2654	4.260	0.3298	1.549	0.0025	0.0495
Np^{6+}	−0.0128	9.569	−0.3611	4.304	0.3419	1.541	0.0032	0.0520
Pu^{3+}	−0.0364	9.572	−0.3181	4.342	0.3210	1.523	0.0041	0.0496
Pu^{4+}	−0.2394	7.837	−0.0785	4.024	0.2643	1.378	0.0012	0.0414
Pu^{5+}	−0.1090	7.819	−0.2243	4.100	0.2947	1.404	0.0015	0.0477
Pu^{6+}	−0.0001	7.820	−0.3354	4.144	0.3097	1.403	0.0020	0.0513
Am^{2+}	−0.3176	7.864	0.0771	4.161	0.2194	1.339	0.0018	0.0374
Am^{3+}	−0.3159	6.982	0.0682	3.995	0.2141	1.188	−0.0015	0.0281
Am^{4+}	−0.1787	7.880	−0.1274	4.090	0.2565	1.315	0.0017	0.0419
Am^{5+}	−0.0927	6.073	−0.2227	3.784	0.2916	1.372	0.0026	0.0485
Am^{6+}	0.0152	6.079	−0.3549	3.861	0.3125	1.403	0.0036	0.0732
Am^{7+}	0.1292	6.082	−0.4689	3.879	0.3234	1.393	0.0042	0.0475

in which $U(r)$ is the radial wavefunction for the unpaired electrons in the atom, k is the length of the scattering vector, and $j_l(kr)$ is the lth-order spherical Bessel function.

Tables 4.4.5.1–4.4.5.8 give the coefficients in an analytical approximation to the $\langle j_0 \rangle$ magnetic form factors for the 3*d* and 4*d* transition series, the 4*f* electrons of rare-earth ions, and the 5*f* electrons of some actinide ions. The approximation has the form used by Forsyth & Wells (1959) but allowing three instead of two exponential terms:

$$\langle j_0(s) \rangle = A \exp(-as^2) + B \exp(-bs^2) + C \exp(-cs^2) + D, \quad (4.4.5.2)$$

where s is the value of $(\sin\theta)/\lambda$ in Å^{-1}.

Tables 4.4.5.9–4.4.5.14 give coefficients in the approximation used by Lisher & Forsyth (1971) to the $\langle j_2 \rangle$, $\langle j_4 \rangle$, and $\langle j_6 \rangle$ form factors for the same series of atoms and ions, again using three rather than two exponential terms, *viz* for $l \neq 0$:

$$\langle j_l(s) \rangle = As^2 \exp(-as^2) + Bs^2 \exp(-bs^2) + Cs^2 \exp(-cs^2) + Ds^2. \quad (4.4.5.3)$$

For the transition-metal series, the coefficients of the approximation have been obtained by fitting to form factors calculated from the Hartree–Fock wavefunctions given by Clementi & Roetti (1974) in terms of Slater-type functions in the form

$$U(r) = \sum_{nj} N_{nl}\, r^2 A_{nlj} \exp(-a_{nlj}\, r) \quad (4.4.5.4)$$

by using the identity:

$$\int_0^\infty j_l(kr) r^n \exp(-pr) 4\pi r^2 \, dr = \frac{\pi^{3/2}\Gamma(n+l+3)k^l}{2^{l-1}\Gamma(l+3/2)(k^2+p^2)^{(n+l+3)/2}} \times {}_2F_1\left(\frac{n+l+3}{2}; \frac{l-n+3}{2}; l+\frac{3}{2}; \frac{k^2}{k^2+p^2}\right). \quad (4.4.5.5)$$

The form factors have been calculated from these relationships in the range $(\sin\theta)/\lambda = 0$ to $1.5\,\text{Å}^{-1}$ at intervals of $0.05\,\text{Å}^{-1}$, and the coefficients of the exponential expansion fitted by a least-squares procedure at the calculated points.

For the atoms of the rare-earth and actinide series, the wavefunctions and form factors have been calculated by Freeman & Desclaux (1979) and Desclaux & Freeman (1978) using Dirac–Fock theory. The constants given in Tables 4.4.5.3, 4.4.5.4, 4.4.5.7, 4.4.5.8, and 4.4.5.11–4.4.5.14 have been fitted to the results of these calculations. For the rare-earth ions, the form factors are given in the range $(\sin\theta)/\lambda = 0$ to $0.5\,\text{Å}^{-1}$ at intervals of $0.5\,\text{Å}^{-1}$ and in the range 0.5 to $1.2\,\text{Å}^{-1}$ at intervals of $0.1\,\text{Å}^{-1}$. For the actinide ions, the calculations extend to $1.5\,\text{Å}^{-1}$. All the values given in the publications cited were included in the fitting procedure. The accuracy with which the exponential expansions fit the theoretical form factors can be judged from the value of the parameter e given in the tables, and defined by:

$$e = 100\left(\frac{\sum_i \delta_i^2}{N}\right)^{1/2}, \quad (4.4.5.6)$$

where δ_i is the difference between the ith fitted point and its theoretical value. The sum is over the N points included in the fitting procedure.

4.4.6. Absorption coefficients for neutrons (By B. T. M. Willis)

The cross sections σ discussed in Section 4.4.4 represent the area of each nucleus as seen by the neutron. To calculate the beam attenuation arising from absorption it is more convenient to use the macroscopic cross section Σ, which is the cross section per unit volume in units of cm^{-1}. Σ is derived by multiplying σ for the element by the number of atoms per unit volume. Thus, for element j, with density ρ_j and atomic weight A_j,

$$\Sigma_j = N_A \rho_j \sigma_j / A_j,$$

where N_A is Avogadro's number.

Table 4.4.6.1 gives the macroscopic absorption cross sections Σ_a of the elements. They are tabulated for a neutron velocity $v = 2200\ \text{m s}^{-1}$, corresponding to a wavelength of 1.80 Å. The cross sections are larger at longer wavelengths (Section 4.4.4). Apart from a few exceptions, such as boron and cadmium, the absorption cross section is vastly smaller than for X-rays. The $1/e$ penetration depth (l) is listed separately – most metals, for example, have a penetration depth of several cm. The data in Table 4.4.6.1 have been derived from the review article by Hutchings & Windsor (1987).

Table 4.4.6.1. *Absorption of the elements for neutrons ($\lambda = 1.80$ Å)*

Atom	Σ_a (cm^{-1})	l (cm)	Atom	Σ_a (cm^{-1})	l (cm)
H	0.0141	0.288	Rh	10.544	0.092
D	0.0000	6.17	Pd	0.4687	1.29
He	0.0001	20.22	Ag	3.7120	0.249
Li	3.2698	0.300	Cd	116.80	0.008
Be	0.0009	1.059	In	7.4135	0.133
B	105.41	0.009	Sn	0.0231	4.87
C	0.0004	1.58	Sb	0.1689	3.20
N	0.0662	2.14	Te	0.1386	4.01
O	0.0001	5.52	I	0.1458	4.36
F	0.0003	6.82	Xe	0.3904	2.27
Ne	0.0017	8.71	Cs	0.2458	3.57
Na	0.0135	10.22	Ba	0.0189	13.39
Mg	0.0027	6.11	La	0.2402	2.00
Al	0.0139	9.48	Ce	0.0182	9.60
Si	0.0085	8.45	Pr	0.3333	2.46
P	0.0061	8.04	Nd	1.4763	0.496
S	0.0208	16.14	Sm	171.23	0.005
Cl	0.9109	0.731	Eu	95.715	0.010
Ar	0.0143	2.03	Gd	1474.1	0.000
K	0.0279	18.12	Tb	0.7334	1.05
Ca	0.0099	12.35	Dy	29.731	0.030
Sc	1.0906	0.491	Ho	2.0791	0.424
Ti	0.3453	1.74	Er	5.1861	0.182
V	0.3658	1.35	Tm	3.4919	0.269
Cr	0.2558	1.82	Yb	0.8513	0.717
Mn	1.0900	0.789	Lu	2.5889	0.354
Fe	0.2174	0.82	Hf	4.6648	0.195
Co	3.3440	0.260	Ta	1.1434	0.676
Ni	0.4104	0.475	W	1.1609	0.681
Cu	0.3202	1.00	Re	6.1692	0.143
Zn	0.0730	2.89	Os	1.1444	0.442
Ga	0.1480	2.04	Ir	30.064	0.032
Ge	0.1016	2.07	Pt	0.6843	0.682
As	0.2091	2.15	Au	5.8181	0.159
Se	0.4292	1.36	Hg	15.146	0.061
Br	0.1623	3.31	Tl	0.1200	2.15
Kr	0.3882	1.97	Pb	0.0056	2.68
Rb	0.0041	13.09	Bi	0.0009	3.84
Sr	0.0227	7.44	Ra	0.1706	2.95
Y	0.0388	3.66	Th	0.2244	1.68
Zr	0.0079	3.42	Pa	8.0405	0.118
Nb	0.0640	2.42	U	0.3650	1.26
Mo	0.1637	1.75	Np	9.0534	0.10
Tc	1.4281	0.542	Pu	14.481	0.069
Ru	0.1886	1.48	Am	2.5522	0.351

References

4.1

Bonse, U. (1980). *X-ray sources. Characterization of crystal growth defects by X-ray methods*, edited by B. K. Tanner & D. K. Bowen, Chap. 11, pp. 298–319. New York: Plenum. [NATO Advanced Study Institute Series B63.]

Bordas, J. (1980). *A synchrotron radiation camera and data acquisition system for time resolved X-ray scattering studies. J. Phys. E*, **13**, 938–944.

Cowley, J. M. (1975). *Diffraction physics*, Chap. 1. Amsterdam: North-Holland.

Ertl, G. & Küppers, J. (1974). *Monographs in modern chemistry*, Vol. 4. *Energy electrons and surface chemistry*, edited by H. F. Ebel, Chap. 9, pp. 129–192. Weinheim: Verlag Chemie.

Feldman, C., Mayer, J. W. & Picraux, S. T. (1982). *Materials analysis by ion channeling*. London: Academic Press.

Frankel, R. D. & Forsyth, J. M. (1979). *Nanosecond X-ray diffraction from biological samples with a laser-produced plasma source. Science*, **204**, 622–624.

Grasselli, J. G., Snavely, M. K. & Bulkin, B. J. (1980). *Applications of Raman spectroscopy. Physics reports* 65, No. 4, pp. 231–344. Amsterdam: North-Holland.

Gyax, F. N., Kündig, W. & Meier, P. F. (1979). Editors. *Muon spin rotation*. Amsterdam: North-Holland.

Hansen, N. K. & Schneider, J. R. (1984). *Charge-density distribution of Be metal studied by γ-ray diffractometry. Phys. Rev. B*, **29**, 917–926.

Kaufmann, E. N. & Shenoy, G. K. (1981). Editors. *MRS symposia proceedings*, Vol. 3. *Nuclear and electron resonance spectroscopies applied to materials science*. New York: North-Holland.

Kunz, C. (1979). Editor. *Topics in current physics*, Vol. 10. *Synchrotron radiation, techniques and applications*. Berlin: Springer Verlag.

Kuz'min, R. N., Kolpakov, A. V. & Zhdanov, G. S. (1966). *Rassejanie messbauerovskovo izlutschenija kristallami. Kristallografiya*, **11**, 511–519. [English translation: *Sov. Phys. Crystallogr.* (1967), **11**, 457–465.]

Lee, P. A., Citrin, P. H., Eisenberger, P. & Kincaid, B. M. (1981). *Extended X-ray absorption fine structure – its strengths and limitations as a structural tool. Rev. Mod. Phys.* **53**, 769–806.

Marshall, W. & Lovesey, S. W. (1971). *Theory of thermal neutron scattering*. Oxford: Clarendon Press.

Parsons, D. F. (1980). Editor. *Ultrasoft X-ray microscopy: its application to biological and physical sciences*. New York: New York Academy of Sciences.

Plummer, E. W. & Eberhardt, W. (1982). *Advances in chemical physics*, Vol. XLIX. *Angle-resolved photoemission as a tool for the study of surfaces*, edited by I. Prigogine & S. I. Rice. New York: John Wiley.

Rosier, D. J. de & Klug, A. (1968). *Reconstruction of three dimensional structures from electron micrographs. Nature (London)*, **217**, 130–134.

Schneider, J. R. (1983). *Characterization of crystals by γ-ray and neutron diffraction methods. J. Cryst. Growth*, **65**, 660–671.

Siegel, R. W. (1980). *Positron annihilation spectroscopy. Annu. Rev. Mater. Sci.* **10**, 393–425.

Tanner, B. K. & Bowen, D. K. (1980). Editors. *Characterization of crystal growth defects by X-ray methods*. NATO Advanced Study Institute Series B63. New York: Plenum.

Windsor, C. G. (1981). *Pulsed neutron scattering*. London: Taylor and Francis.

4.2.1

Bailey, R. L. (1978). *The design and operation of magnetic liquid shaft seals*. In *Thermomechanics of magnetic fluids*, edited by B. Berkovsky. London: Hemisphere.

Buras, B. (1985). *The European Synchrotron Radiation Project. Nucl. Sci. Appl.* **2**, 127–143.

Buras, B. & Marr, G. V. (1979). Editors. *European Synchrotron Radiation Facility*. Suppl. III: *Instrumentation*. Strasbourg: ESF.

Buras, B. & Tazzari, S. (1984). Editors. *European Synchrotron Radiation Facility*. Geneva: ESRP c/o CERN.

Byer, R. L., Kuhn, K., Reed, M. & Trail, J. (1983). *Progress in high peak and average power lasers for soft X-ray production. Proc. SPIE*, **448**, 2–7.

Castaing, R. & Descamps, J. (1955). *Sur les bases physiques de l'analyse ponctuelle par spectrographie X. J. Phys. Radium*, **16**, 304–317.

Clay, R. E. (1934). *A 5 kW X-ray generator with a spinning target. Proc. Phys. Soc. London*, **46**, 703–712.

Cohen, E. R. & Taylor, B. N. (1987). *The 1986 adjustment of the fundamental physical constants. Rev. Mod. Phys.* **89**, 1121–1148.

Collins, C. B., Davanloo, F. & Bowen, T. S. (1986). *Flash X-ray source of intense nanosecond pulses produced at high repetition rates. Rev. Sci. Instrum.* **57**, 863–865.

Compton, A. H. & Allison, S. K. (1935). *X-rays in theory and experiment*. New York: Van Nostrand.

Cosslett, V. E. & Nixon, W. C. (1951). *X-ray shadow microscope. Nature (London)*, **168**, 24–25.

Cosslett, V. E. & Nixon, W. C. (1960). *X-ray microscopy*, pp. 217–222. Cambridge University Press.

Dyson, N. A. (1973). *X-rays in atomic and nuclear physics*. London: Longman.

Ehrenberg, W. & Spear, W. E. (1951). *An electrostatic focusing system and its application to a fine focus X-ray tube. Proc. Phys. Soc. London Sect. B*, **64**, 67–75.

Farge, Y. & Duke, P. J. (1979). Editors. *European Synchrotron Radiation Facility*. Suppl. 1: *The scientific case*. Strasbourg: ESF.

Fiorito, R. B., Rule, D. W., Piestrup, M. A., Li, Q., Ho, A. H. & Maruyama, X. K. (1993). *Parametric X-ray generation from moderate-energy electron beams. Nucl. Instrum. Methods*, B**79**, 758–761.

Forsyth, J. M. & Frankel, R. D. (1980). *Flash X-ray diffraction from biological specimens using a laser-produced plasma source*. Report No. 106. Laboratory for Laser Energetics, University of Rochester, USA.

Forsyth, J. M. & Frankel, R. D. (1984). *Experimental facility for nanosecond time-resolved low-angle X-ray diffraction experiments using a laser-produced plasma source. Rev. Sci. Instrum.* **55**, 1235–1242.

Fourme, R. (1992). *Sources X intenses et cristallographie biologique. Ann. Phys. (Leipzig)*, **17**, 247–255.

Frankel, R. D. & Forsyth, J. M. (1979). *Nanosecond exposure X-ray diffraction patterns from biological specimens using a laser plasma source. Science*, **204**, 622–624.

4.2.1 (*cont.*)

Frankel, R. D. & Forsyth, J. M. (1985). *Time-resolved X-ray diffraction study of photo stimulated purple membrane*. *Biophys. J.* **47**, 387–393.

Godwin, R. P. (1968). *Synchrotron radiation light source*. *Springer Tracts Mod. Phys.* **51**, 1–69.

Goldberg, M. (1961). *Intensités relatives des raies X du spectre L excité par bombardement électronique des éléments lourds*. *J. Phys. Radium*, **22**, 743–748.

Goldsztaub, S. (1947). *Tube à rayons X de grande brilliance à foyer ponctuel*. *CR Acad. Sci.* **224**, 458–459.

Green, M. (1963). *The target absorption correction in X-ray microanalysis*. *X-ray optics and X-ray microanalysis*, edited by H. Pattee, V. E. Cosslett & A. Engstrom, pp. 361–377. London: Academic Press.

Green, M. & Cosslett, V. E. (1968). *Measurement of K, L and M shell X-ray production efficiencies*. *Br. J. Appl. Phys. Ser.* 2, **1**, 425–436.

Guo, C.-L. & Wu, Y.-Q. (1985). *Empirical relationship between the characteristic X-ray intensity and the incident electron energy*. *Kexue Tongbao*, **30**, 1621–1627.

Helliwell, J. R. (1984). *Synchrotron X-radiation protein crystallography*. *Rep. Progr. Phys.* **47**, 1403–1497.

Hofmann, A. (1978). *Quasi-monochromatic synchrotron radiation from undulators*. *Nucl. Instrum. Methods*, **152**, 17–21.

Honkimaki, V., Sleight, J. & Suortti, P. (1990). *Characteristic X-ray flux from sealed Cr, Cu, Mo, Ag and W tubes*. *J. Appl. Cryst.* **23**, 412–417.

Huke, K. & Kobayakawa, M. (1989). *World-wide census of SR facilities*. *Rev. Sci. Instrum.* **60**, 2548–2561.

Ishimura, T., Shiraiwa, Y. & Sawada, M. (1957). *The input power limit of the cylindrical rotating anode of an X-ray tube*. *J. Phys. Soc. Jpn*, **12**, 1064–1070.

Jenkins, R., Manne, R., Robin, J. & Senemaud, C. (1991). *Nomenclature, symbols, units and their usuage in spectrochemical analysis*. *VIII Nomenclature system for X-ray spectroscopy*. *Pure Appl. Chem.* **63**, 735–746.

Kirkpatrick, P. & Wiedmann, L. (1945). *Theoretical continuous X-ray energy and polarization*. *Phys. Rev.* **67**, 321–339.

Koch, E. E. (1983). Editor. *Handbook on synchrotron radiation*. Amsterdam: North-Holland.

Kramers, H. A. (1923). *On the theory of X-ray absorption and of the continuous X-ray spectrum*. *Philos. Mag.* **46**, 836–871.

Kulenkampff, H. & Schmidt, L. (1943). *Die Energieverteilung im Spektrum der Röntgen Bremsstrahlung*. *Ann. Phys. (Leipzig)*, **43**, 494–512.

Kulipanov, G. N. & Strinskii, A. N. (1977). *Utilization of synchrotron radiation: current status and propsects*. *Usp. Fiz. Nauk,* **122**, 369–418. English translation: *Sov. Phys. Usp.* **20**, 559–586.

Kunz, C. (1979). Editor. *Synchrotron radiation*. Berlin: Springer.

Kusev, S. V., Raiko, V. I. & Skuratowski, I., Ya. (1992). *The status of beam lines for macromolecular crystallography at the Siberia-2 storage ring*. *Rev. Sci. Instrum.* **63**, 1055–1057.

Laclare, J. L. (1994). *Target specifications and performance of the ESRF source*. *J. Synchrotron Rad.* **1**, 12–18.

Lea, K. (1978). *Highlights of synchrotron radiation*. *Phys. Rep.* **43**, 337–375.

Maruyama, X. K., Di Nova, K., Snyder, D., Piestrup, M. A., Li, Q., Fiorito, R. B. & Rule, D. W. (1993). *A compact tunable X-ray source based on parametric X-ray generation by moderate-energy linacs*. *Proc. 1993 Particle Accelerator Conference*. *IEEE*, **2**, 1620–1622.

Metchnik, V. & Tomlin, S. G. (1963). *On the absolute intensity of emission of characteristic X radiation*. *Proc. Phys. Soc. London*, **81**, 956–964.

Müller, A. (1927). *Input limits of X-ray generators*. *Proc. R. Soc. London Ser. A*, **117**, 30–42.

Müller, A. (1929). *A spinning-target X-ray generator and its input limit*. *Proc. R. Soc. London Ser. A*, **125**, 507–516.

Müller, A. (1931). *Further estimates of the input limits of X-ray generators*. *Proc. R. Soc. London Ser. A*, **132**, 646–649.

Nagel, D. J. (1980). *Comparison of X-ray sources for exposure of photo resists*. *Ann. NY Acad. Sci*, **342**, 235–247.

Oosterkamp, W. J. (1948). *The heat dissipation in the anode of an X-ray tube*. *Philips Res.* **3**, 49–59, 161–173, 303–317.

Phillips, W. C. (1985). *X-ray sources*. *Methods Enzymol.* **114**, 300–316.

Piestrup, M. A., Boyers, D. G., Pincus, C. I., Harris, J. L., Maruyama, X. K., Bergstrom, J. C., Caplan, H. S., Silzer, R. M. & Skopik, D. M. (1991). *Quasimonochromatic X-ray source using photo-absorption edge transition radiation*. *Phys. Rev. A*, **43**, 3653–3661.

Piestrup, M. A., Moran, M. J., Boyers, D. G., Pincus, C. I., Kephart, J. O., Gearhart, R. A. & Maruyama, X. K. (1991). *Generation of hard X-rays from transition radiation using high-density foils and moderate-energy electrons*. *Phys. Rev. A*, **43**, 2387–2396.

Reed, S. J. B. (1975). *Electron microprobe analysis*. Cambridge University Press.

Rudakov, L. I., Baigarin, K. A., Kalinin, Y. G., Korolev, V. D. & Kumachov, M. A. (1991). *Pulsed-plasma-based X-ray source and new X-ray optics*. *Phys. Fluids B (Plasma Phys.)*, **3**, 2414–2419.

Sakurai, K. (1993). *High-intensity X-ray line-focal spot for laboratory EXAFS measurements*. *Rev. Sci. Instrum.* **64**, 267–268.

Sakurai, K. & Sakurai, H. (1994). *Comment on High intensity low tube-voltage X-ray source for laboratory EXAFS measurements*. *Rev. Sci. Instrum.* **65**, 2417–2418.

Schwinger, J. (1949). *On the classical radiation of accelerated electrons*. *Phys. Rev.* **75**, 1912–1925.

Scott, V. D. & Love, G. (1983). *Quantitative electron microprobe analysis*. Cambridge University Press.

Seka, W., Soures, J. M., Lewis, O., Bunkenburg, J., Brown, D., Jacobs, S., Mourou, X. & Zimmermann, J. (1980). *High-power phosphate-glass laser system: design and performance characteristics*. *Appl. Opt.* **19**, 409–419.

Seka, W., Soures, J. M., Lund, L. & Craxton, R. S. (1981). *GDL: a high-power 0.35 μm laser irradiation facility*. *IEEE J. Quantum Electron. QE*-**17**, 1689–1693.

Siegbahn, M. (1925). *The spectroscopy of X-rays*. Oxford University Press.

Stephenson, S. T. (1957). *The continuous X-ray spectrum*. *Handbuch der Physik*. XXX: *X-rays*, edited by S. Flügge, pp. 337–370. Berlin: Springer.

Stern, E. A. (1980). Editor. *Laboratory EXAFS facilities 1980*. *AIP Conf. Proc.* No. 64.

Stuhrmann, H. (1982). Editor. *Uses of synchrotron radiation in biology*. Esp. *Properties of synchrotron radiation*, Chap. 1, by G. Materlik. London: Academic Press.

Suller, V. P. (1992). *Review of the status of synchrotron radiation storage rings*. *Third European Particle Accelerator Conference*. *Editions Frontières*, **1**, 77–81.

Taylor, A. (1949). *A 5 kW crystallographic X-ray tube with a rotating anode*. *J. Sci. Instrum.* **26**, 225–229.

Taylor, A. (1956). *Improved demountable crystallographic rotating anode X-ray tube*. *Rev. Sci. Instrum.* **27**, 757–759.

4.2.1 (*cont.*)

Thompson, D. J. & Poole, M. W. (1979). Editors. *European Synchrotron Radiation Facility*. Suppl. II: *The machine*. Strasbourg: ESF.

Tohji, K., Udagawa, Y., Kawasaki, T. & Masuda, K. (1983). *Laboratory EXAFS spectrometer with a bent-crystal, a solid-state detector, and a fast detection system. Rev. Sci. Instrum.* **54**, 1482–1487.

Wilson, R. R. (1941). *A vacuum-tight sliding seal. Rev. Sci. Instrum.* **12**, 91–93.

Winick, H. (1980). *Properties of synchrotron radiation*. In *Synchrotron radiation research*, edited by H. Winick & S. Doniach. New York: Plenum.

Winick, H. & Bienenstock, A. (1978). *Synchrotron radiation research. Ann. Rev. Nucl. Sci.* **28**, 33–113.

Yaakobi, B., Boehli, T., Bourke, P., Conturie, Y., Craxton, R. S., Delettrez, J., Forsyth, J. M., Frankel, R. D., Goldman, L. M., McCrory, L. R., Richardson, M. C., Seka, W., Shvarts, D. & Soures, J. M. (1981). *Characteristics of target interaction with high-power UV laser radiation. Opt. Commun.* **39**, 175–179.

Yaakobi, B., Bourke, P., Conturie, Y., Delettrez, J., Forsyth, J. M., Frankel, R. D., Goldman, L. M., McCrory, L. R., Seka, W., Soures, J. M., Burek, A. J. & Deslattes, R. D. (1981). *High X-ray conversion efficiency with target irradiation by a frequency-tripled Nd:glass laser. Opt. Commun.* **38**, 196–200.

Yao, T. (1992). *Lanthanum hexaboride filament in an X-ray generator of a laboratory EXAFS facility. Rev. Sci. Instrum.* **63**, 2103–2104.

Yoshimatsu, M. & Kozaki, S. (1977). *High-brilliance X-ray sources. X-ray optics*, edited by H.-J. Queisser, Chap. 2. Berlin: Springer.

4.2.2

Arndt, U. W. (1992). *X-ray wavelengths. International Tables for Crystallography*, Vol. C, edited by A. J. C. Wilson, pp. 176–182. Dordrecht: Kluwer Academic Publishers.

Barreau, G. H., Börner, H. G., Egidy, T. V. & Hoff, R. W. (1982). *Precision measurement of X-ray energies, natural widths and intensities in the actinide region. Z. Phys.* A**308**, 209–213.

Basile, G., Bergamin, A., Cavagnero, G., Mana, G., Vittone, E. & Zosi, G. (1994). *Measurement of the silicon (220) lattice spacing. Phys. Rev. Lett.* **72**, 3133–3136.

Basile, G., Bergamin, A., Cavagnero, G., Mana, G., Vittone, E. & Zosi, G. (1995). *The (220) lattice spacing of silicon. IEEE Trans. Instrum. Meas.* **44**, 526–529.

Bearden, J. A. (1960). *Lead K absorption edge for μ-meson mass determination. Phys. Rev. Lett.* **4**, 240–241.

Bearden, J. A. (1965). *Selection of W $K\alpha_1$ as the X-ray wavelength standard. Phys. Rev. B,* **137**, 455–461.

Bearden, J. A. (1967). *X-ray wavelengths. Rev. Mod. Phys.* **39**, 78–100.

Bearden, J. A., Henins, A., Marzolf, J. G., Sauder, W. C. & Thomsen, J. S. (1964). *Precision redetermination of standard reference wavelengths for X-ray spectroscopy. Phys. Rev. A,* **135**, 899–910.

Bearden, J. A., Thomsen, J. S., Burr, A. F., Yap, F. Y., Huffman, F. N., Henins, A. & Matthews, G. D. (1964). *Remeasurement of selected X-ray lines and reevaluation of all published wavelengths on a consistent and absolute scale.* Baltimore, Maryland: The Johns Hopkins University.

Becker, P., Dorenwendt, K., Ebeling, G., Lauer, R., Lucas, W., Probst, R., Rademacher, H.-J., Reim, G., Seyfried, P. & Siegert, H. (1981). *Absolute measurement of the (220) lattice plane spacing in a silicon crystal. Phys. Rev. Lett.* **46**, 1540–1543.

Becker, P., Seyfried, P. & Siegert, H. (1982). *The lattice parameter of highly pure silicon single crystals. Z. Phys.* B**48**, 17–21.

Beyer, H., Indelicato, P., Finlayson, H., Liesen, D. & Deslattes, R. D. (1991). *Measurement of the 1s Lamb-shift in hydrogenlike nickel. Phys. Rev. A,* **43**, 223–227.

Blundell, S. A. (1993*a*). *Ab initio calculations of QED effects of Li-like, Na-like and Cu-like ions. Phys. Scr.* T**46**, 144–149.

Blundell, S. A. (1993*b*). *Calculations of the screened self-energy and vacuum polarization in Li-like, Na-like and Cu-like ions. Phys. Rev. A*, **47**, 1790–1803.

Blundell, S. A., Johnson, W. R. & Sapirstein, J. (1990). *Improved many-body perturbation theory calculations of the $n=2$ states of lithiumlike uranium. Phys. Rev. A*, **41**, 1698–1700.

Blundell, S. A., Mohr, P. J., Johnson, W. R. & Sapirstein, J. (1993). *Evaluation of two-photon exchange graphs for highly charged heliumlike ions. Phys. Rev. A*, **48**, 2615–2626.

Bonse, U. & Hart, M. (1965). *An X-ray interferometer. Appl. Phys. Lett.* **6**, 155–156.

Borchert, G. L. (1976). *Precise energies of K-Röntgen-lines of Tm, Th, U and Pu. Z. Naturforsh. Teil A*, **31**, 102–104.

Borchert, G. L., Hansen, P. G., Jonson, B., Ravn, H. L. & Desclaux, J. P. (1980). *Comparison of the K X-ray energy ratios of high Z and low Z elements with relativistic SCF DF calculations. Atomic massses and fundamental constants*, edited by J. E. Nolen & W. Benenson, Vol. 6, pp. 189–201. New York: Plenum Press.

Burr, A. F. (1996). Personal communication.

Cardona, M. & Ley, L. (1978). *Photemission in Solids I. Top. Appl. Phys.* **26**, 265–276.

Cauchois, Y. & Hulubei, H. (1947). *Tables de constantes et données numeriques. I. Longueurs d'onde des emissions X et des discontinuites d'absorption X.* Paris: Herman.

Cauchois, Y. & Senemaud, C. (1978). *Tables internationales de constantes selectionnées. 18. Longeurs d'onde des emissions X et des discontinuités d'absorption X.* London: Pergamon Press.

Cohen, E. R. & Taylor, B. N. (1973). *The 1973 least-squares adjustment of the fundamental constants. J. Phys. Chem. Ref. Data*, **2**, 663–734.

Desclaux, J. P. (1975). *A multiconfiguration relativistic Dirac–Fock program. Comput. Phys. Commun.* **9**, 31–45.

Desclaux, J. P. (1993). *Relativistic multiconfiguration Dirac–Fock package. Methods and techniques in computational chemistry – 94*, Vol. A, edited by E. Clementi. Cagliary: STEF.

Deslattes, R. D. & Henins, A. (1973). *X-ray to visible wavelength ratios. Phys. Rev. Lett.* **31**, 972–975.

Deslattes, R. D. & Kessler, E. G. Jr (1985). *Experimental evaluation of inner-vacancy level energies for comparison with theory. Atomic inner-shell physics,* edited by B. Crasemann, pp. 181–235. New York: Plenum.

Deslattes, R. D., Tanaka, M., Greene, G. L., Henins, A. & Kessler, E. G. (1987). *Remeasurement of a silicon lattice period. IEEE Trans. Instrum. Meas.* IM-**36**, 166.

Fuggle, J. C., Burr, A. F., Watson, L. M., Fabian, D. J. & Lang, W. (1974). *X-ray photoelectron studies of thorium and uranium. J. Phys. F*, **4**, 335–342.

4.2.2 (*cont.*)

Fujimoto, Z., Fujii, K., Tanaka, M. & Nakayama, K. (1997). *Lattice measurement in silicon. IEEE Trans. Instrum. Meas.* **50**, 123–124.

Härtwig, J., Hölzer, G., Förster, E., Goetz, K., Wokulska, K. & Wolf, J. (1994). *Remeasurement of characteristic X-ray emission lines and their application to line profile analysis and lattice parameter determination. Phys. Status Solidi. A,* **143**, 23–34.

Härtwig, J., Hölzer, G., Wolf, J. & Förster, E. (1993). *Remeasurement of the profile of the characteristic Cu Kα emission line with high precision and accuracy. J. Appl. Cryst.* **26**, 539–548.

Henins, A. (1971). *Ruled grating measurements of the Al $K\alpha_{1,2}$ wavelength. Precision measurements and fundamental constants*, edited by D. N. Langenberg & B. N. Taylor, pp. 255–258. *Natl Bur. Stand. (US) Spec. Publ.* No. 343. Gaithersburg, Maryland: National Bureau of Standards.

Hölzer, G., Fritsch, M., Deutsch, M., Härtwig, J. & Förster, E. (1997). *$K\alpha_{1,2}$ and $K\beta_{1,3}$ X-ray emission lines of the 3d transition metals. Phys. Rev. A*, **56**, 4554–4568.

Indelicato, P. (1990). *Kα transitions in few-electron ions and in atoms. X-ray and inner-shell processes*, edited by T. A. Carlson, M. O. Krause & S. T. Manson, pp. 591–601. New York: American Institute of Physics.

Indelicato, P. & Desclaux, J. P. (1990). *Multiconfiguration Dirac–Fock calculations of transition energies with QED corrections in three-electron ions. Phys. Rev. A*, **42**, 5139–5149.

Indelicato, P., Gorceix, O. & Desclaux, J. P. (1987). *MCDF studies of two electron ions II: radiative corrections and comparison with experiment. J. Phys. B*, **20**, 651.

Indelicato, P. & Lindroth, E. (1992). *Relativistic effects, correlation, and QED corrections on Kα transitions in medium to very heavy atoms. Phys. Rev. A*, **46**, 2426–2436.

Indelicato, P. & Lindroth, E. (1996). *Current status of the relativistic theory of inner hole states in heavy atoms. Comments At. Mol. Phys.* **32**, 197–208.

Indelicato, P. & Mohr, P. J. (1990). *Electron screening correction to the self energy in high-Z atoms.* 12th International Conference on Atomic Physics, Ann Arbor, Michigan, USA.

Indelicato, P. & Mohr, P. J. (1991). *Quantum electrodynamic effects in atomic structure. Theor. Chim. Acta*, **80**, 207–214.

Johnson, W. R. & Soff, G. (1985). *The Lamb shift in hydrogenlike atoms, $1 \leq Z \leq 110$. At. Data Nucl. Data Tables*, **33**, 405.

Kessler, E. G. Jr, Deslattes, R. D. & Henins, A. (1979). *Wavelength of the W $K\alpha_1$ X-ray line. Phys. Rev. A*, **19**, 215–218.

Kim, Y. K., Baik, D. H., Indelicato, P. & Desclaux, J. P. (1991). *Resonance transition energies of Li-, Na-, and Cu-like ions. Phys. Rev. A*, **44**, 148–166.

Kraft, S., Stümpel, J., Becker, P. & Kuetgens, U. (1996). *High resolution X-ray absorption spectroscopy with absolute energy calibration for the determination of absorption edge energies. Rev. Sci. Instrum.* **67**, 681–687.

Lebugle, A., Axelsson, U., Nyholm, R. & Mårtensson, N. (1981). *Experimental L and M core level binding energies for the metals 22Ti to 30Zn. Phys Scr.* **23**, 825–827.

Lindgren, I., Persson, H., Salomonson, S. & Labzowsky, L. (1995). *Full QED calculations of two-photon exchange for heliumlike systems: analysis in the Coulomb and Feynman gauge. Phys. Rev. A*, **51**, 1167–1195.

Lindroth, E. & Indelicato, P. (1993). *Inner shell transitions in heavy atoms. Phys. Scr.* T**46**, 139–143.

Lindroth, E. & Indelicato, P. (1994). *High precision calculations of inner shell transitions in heavy elements. Nucl. Instrum. Methods*, B**87**, 222–226.

Lum, G. K., Wiegand, C. E., Kessler, E. G. Jr, Deslattes, R. D., Jacobs, L., Schwitz, W. & Seki, R. (1981). *Kaonic mass by critical absorption of kaonic-atom X-rays. Phys. Rev. D,* **23**, 2522–2532.

Mohr, P. J. (1974*a*). *Numerical evaluation of the 1S1/2 state radiative level shift. Ann. Phys. (Leipzig)*, **88**, 52–87.

Mohr, P. J. (1974*b*). *Self-energy radiative corrections in hydrogen-like systems. Ann. Phys. (Leipzig)*, **88**, 26–51.

Mohr, P. J. (1975). *Lamb shift in a strong Coulomb potential. Phys. Rev. Lett.* **34**, 1050–1052.

Mohr, P. J. (1982). *Self-energy of the $n = 2$ states in a strong Coulomb field. Phys. Rev. A*, **26**, 2338–2354.

Mohr, P. J. (1992). *Self-energy correction to one-electron energy levels in a strong Coulomb field. Phys. Rev. A*, **46**, 4421–4424.

Mohr, P. J. & Soff, G. (1993). *Nuclear size correction to the electron self-energy. Phys. Rev. Lett.* **70**, 158–161.

Mohr, P. J. & Taylor, B. N. (2000). *CODATA recommended values of the fundamental physical constants: 1998. Rev. Mod. Phys.* **72**, 351–495.

Mooney, T., Lindroth, E., Indelicato, P., Kessler, E. & Deslattes, R. D. (1992). *Precision measurements of K and L transitions in xenon: experiment and theory for the K, L and M levels. Phys. Rev. A*, **45**, 1531–1543.

Mooney, T. M. (1996). Personal communication.

Nyholm, R., Berndtsson, A. & Mårtensson, N. (1980). *Core level binding energies for the elements Hf to Bi ($Z = 72$–83). J. Phys. C*, **13**, L1091–l1096.

Nyholm, R. & Mårtensson, N. (1980). *Core level binding energies for the elements Zr–Te ($Z = 40$–52). J. Phys. C,* **13**, L279–L284.

Parratt, L. G. (1959). *Electronic band structure of solids by X-ray spectroscopy. Rev. Mod. Phys.* **31**, 616–645.

Powell, C. J. (1995). *Elemental binding energies for X-ray photelectron spectroscopy. Appl. Surf. Sci.* **89**, 141–149.

Rieck, C. D. (1962). *Tables relating to the production, wavelengths, and intensities of X-rays. International tables for X-ray crystallography*, Vol. III, edited by C. H. MacGillavry & G. D. Rieck, pp. 59–72. Birmingham: Kynoch Press.

Schwarzenbach, D., Abrahams, S. C., Flack, H. D., Prince, E. & Wilson, A. J. C. (1995). *Statistical descriptors in crystallography. II. Report of a Working Group on Expression of Uncertainty in Measurement. Acta Cryst.* A**51**, 565–569.

Schweppe, J., Deslattes, R. D., Mooney, T. & Powell, C. J. (1994). *Accurate measurement of Mg and Al $K\alpha_{1,2}$ X-ray energy profiles. J. Electron Spectrosc. Relat. Phenom.* **67**, 463–478.

Schweppe, J. E. (1995). Personal communication.

Soff, G. & Mohr, P. J. (1988). *Vacuum polarization in a strong external field. Phys. Rev. A*, **38**, 5066–5075.

Taylor, B. N. & Kuyatt, C. E. (1994). *Guidelines for evaluating and expressing the uncertainty of NIST measurement results. NIST Technical Note* No. 1297. Gaithersburg, MD: National Institute of Standards and Technology.

Thomsen, J. S. & Burr, A. F. (1968). *Biography of the x-unit – the X-ray wavelength scale. Am. J. Phys.* **36**, 803–810.

Uehling, E. A. (1935). *Polarization effects in the positron theory. Phys. Rev.* **48**, 55–63.

4.2.2 (*cont.*)

Wichmann, E. H. & Kroll, N. M. (1956). *Vacuum polarization in a strong Coulomb field. Phys. Rev.* **101**, 843–859.

4.2.3

Alvarez, L. W., Crawford, F. S. & Stevenson, M. L. (1958). *Elastic scattering of 1.6 MeV gamma rays from H, Li, C and Al nuclei. Phys. Rev.* **112**, 1267–1273.

Azaroff, L. V. & Pease, D. M. (1974). *X-ray absorption spectra. X-ray spectroscopy*, edited by L. V. Azaroff, Chap. 6, pp. 284–337. New York: McGraw-Hill.

Bertin, E. P. (1975). *Principles and practice of X-ray spectrometric analysis*. New York: Plenum.

Bianconi, A., Incoccia, L. & Stipcich, S. (1983). Editors. *EXAFS and near edge structure*. Berlin: Springer.

Bowen, D. K., Stock, S. R., Davies, S. T., Pantos, E., Birnbaum, H. R. & Chen, H. (1984). *Topographic EXAFS. Nature (London)*, **309**, 336–338.

Bunker, G., Hasnain, S. S. & Sayers, D. E. (1990). *Report of the International Workshops on Standards and Criteria in XAFS*. In *X-ray absorption spectroscopy*, edited by S. S. Hasnain. London: Ellis Horwood.

Caballero, A., Villain, F., Dexpert, H., Le Peltier, F. & Lynch, J. (1993). *Characterization by in situ EXAFS spectroscopy of Pt/Al_2O_3 and $PtRe/Al_2O_3$ catalysts under reaction conditions. Jpn. J. Appl. Phys.* **32**, Suppl. 32–2, 439–441.

Chipman, D. R. (1969). *Conversion of relative intensities to an absolute scale. Acta Cryst.* A**25**, 209–214.

Citrin, P. H., Eisenberger, P. & Hewitt, R. (1978). *Extended X-ray absorption fine structure of surface atoms on single crystal substrates: iodine absorbed on Ag(111). Phys. Rev. Lett.* **41**, 309–312.

Cohen, E. R. & Taylor, B. N. (1987). *The 1986 adjustment of the fundamental physical constants. Rev. Mod. Phys.* **89**, 1121–1148.

Cooper, M. J. (1985). *Compton scattering and electron momentum determination. Rep. Prog. Phys.* **48**, 415–481.

Creagh, D. C. (1985). *Theoretical and experimental techniques for the determination of X-ray dispersion corrections. Aust. J. Phys.* **38**, 371–404.

Creagh, D. C. (1987*a*). *The resolution of discrepancies in tables of photon attenuation coefficients. Nucl. Instrum. Methods*, A**255**, 1–16.

Creagh, D. C. (1987*b*). *The X-ray anomalous dispersion corrections and their use for the characterization of materials*. In *Progress in crystal growth and characterization*, Vol. 14, edited by P. Krishna, Chap. 7, pp. 1–46. Oxford: Pergamon Press.

Creagh, D. C. & Hubbell, J. H. (1987). *Problems associated with the measurement of X-ray attenuation coefficients. I. Silicon. Acta Cryst.* A**43**, 102–112.

Crozier, E. D. & Seary, A. J. (1980). *Asymmetric effects in the extended X-ray absorption fine structure. Analysis of solid and liquid zinc. Can. J. Phys.* **58**, 1388–1399.

Dreier, P., Rabe, P., Matzfeld, W. & Niemann, W. (1984). *Anomalous X-ray scattering factors calculated from experimental absorption factor. J. Phys. C*, **17**, 3123–3136.

Durham, P. J. (1983). *Multiple scattering calculations of XANES. EXAFS and near edge structure*, edited by A. Bianconi, L. Incoccia & S. Stipcich, pp. 37–43. Berlin: Springer.

Fricke, H. (1920). *The K-characteristic absorption frequencies for the chemical elements magnesium to chromium. Phys. Rev.* **16**, 202–212.

Fuoss, P. H., Eisenberger, P., Warburton, W. K. & Bienenstock, A. (1981). *Application of differential anomalous X-ray scattering to structural studies of amorphous materials. Phys. Rev. Lett.* **46**, 1537–1540.

Gerstenberg, H. & Hubbell, J. H. (1982). *Comparison of experimental with theoretical photon attenuation cross sections between 10 eV and 100 GeV. Nuclear data for science and technology*, edited by K. H. Bockhoff, pp. 1007–1009. Amsterdam: North-Holland.

Gerward, L. (1981). *X-ray attenuation coefficients and atomic photoelectric absorption cross sections of silicon. J. Phys. B*, **14**, 3389–3395.

Gerward, L. (1982). *X-ray attenuation coefficients of copper in the energy range 5 to 50 keV. Z. Naturforsch. Teil A*, **37**, 451–459.

Gerward, L. (1983). *X-ray attenuation coefficients of carbon in the energy range 5 to 50 keV. Acta Cryst.* A**39**, 322–325.

Gerward. L., Thuesen, G., Stibius-Jensen, M. & Alstrup, I. (1979). *X-ray anomalous scattering factors for silicon and germanium. Acta Cryst.* A**35**, 852–857.

Gurman, S. J. (1988). *The small atom approximation in EXAFS and surface EXAFS. J. Phys. C*, **21**, 3699–3717.

Gurman, S. J. (1995). *Interpretation of EXAFS data. J. Synchrotron Rad.* **2**, 56–63.

Hasnain, S. S. (1990). *X-ray absorption fine structure*. London: Ellis Horwood.

Hastings, J. B., Eisenberger, P., Lengeler, B. & Perlman, M. L. (1975). *Local structure determination at high dilution: internal oxidation at 75 ppm Fe in Cu. Phys. Rev. Lett.* **43**, 1807–1810.

Helliwell, J. R. (1984). *Synchrotron X-radiation protein crystallography. Rep. Prog. Phys.* A**7**, 1403–1497.

Hertz, G. (1920). *Über die Absorptionsgrenzen in den L-Serie. Z. Phys.* **3**, 19–27.

Hida, M., Wada, N., Maeda, H., Hikaru, T., Tsu, Y. & Kamino, N. (1985). *An EXAFS investigation on the lattice relaxation of Ni fine particles prepared by gas evaporation. Jpn. J. Appl. Phys.* **24**, L3–L5.

Hubbell, J. H. (1969). *Phonon cross sections, attenuation coefficients, and energy absorption coefficients from 10 keV to 100 GeV*. Report NRDS-NBS29. National Institute of Standards and Technology, Gaithersburg, MD, USA.

Hubbell, J. H., Gerstenberg, H. M. & Saloman, E. B. (1986). *Bibliography of photon total cross section (attenuation coefficient) measurements 10 eV to 13.5 GeV*. Report NBSIR 86-3461. US Department of Commerce, Gaithersburg, MD, USA.

Hubbell, J. H., McMaster, W. H., Del Grande, N. K. & Mallett, J. H. (1974). *X-ray cross sections and attenuation coefficients. International tables for X-ray crystallography,* Vol. IV, edited by J. A. Ibers & W. C. Hamilton, pp. 47–70. Birmingham: Kynoch Press. (Present distributor Kluwer Academic Publishers, Dordrecht.)

Hubbell, J. H. & Øverbø, I. (1979). *Relativistic atomic form factors and photon coherent scattering cross sections. J. Phys. Chem. Ref. Data*, **8**, 69–105.

International Tables for X-ray Crystallography (1974). Vol. IV. Birmingham: Kynoch Press. (Present distributor Kluwer Academic Publishers, Dordrecht.)

Jennings, L. D. (1984). *The polarization ratio of crystal monochromators. Acta Cryst.* A**40**, 12–16.

4.2.3 (*cont.*)

Joy, D. C. & Maher, D. (1985). *Quantitative electron energy loss spectroscopy: an introduction to the power of Kevex Elstar software*. *Kevex Analyst*, **10**, 6–9.

Kostarev, A. L. (1941). *Theory of the fine structure of X-ray absorption spectra in solids*. *Zh. Eksper Teor. Fiz.* **11**, 60–73.

Kostarev, A. L. (1949). *Elucidation of the super-fine structure of X-ray absorption spectra in solids*. *Zh. Eksper. Teor. Fiz.* **19**, 413–420.

Kronig, R. de L. (1932*a*). *Zur Theorie der Feinstruktur in den Röntgenabsorptionspecktren II. Z. Phys.* **75**, 191–210.

Kronig, R. de L. (1932*b*). *Zur Theorie der Feinstruktur in den Röntgenabsorptionspecktren III. Z. Phys.* **75**, 468–475.

Kuroda, H., Ohta, T., Murata, T., Udagawa, Y. & Nomura, M. (1992). *XAFS VII: Proceedings of the Seventh Conference on X-ray Absorption Fine Structure*. *Jpn. J. Appl. Phys.* **32**, Suppl. 32–2.

Kutzler, F. W., Natoli, C. R., Misemer, D. K., Doniach, S. & Hodgson, K. O. (1981). *Use of one electron theory for the interpretation of near edge structure in K-shell X-ray absorption spectra of transition metal complexes*. *J. Chem. Phys.* **73**, 3274–3288.

Leapman, R. D. & Cosslet, V. E. (1976). *Extended fine structure above the X-ray edge in electron energy loss spectra*. *J. Phys. D*, **9**, L29–L31.

Lee, P. A. (1981). *Theory of extended X-ray absorption fine structure*. *EXAFS spectroscopy: techniques and applications*, edited by B. K. Teo & D. C. Joy, Chap. 2, pp. 5–13. New York: Plenum.

Lee, P. A. & Beni, G. (1977). *New method for the calculation of atomic phase shifts: application to extended X-ray absorption fine structure (EXAFS) in molecules and crystals*. *Phys. Rev. B*, **15**, 2862–2883.

Lee, P. A., Citrin, P. H., Eisenberger, P. & Kincaid, B. M. (1981). *Extended X-ray absorption fine structure – its strengths and limitations as a structural tool*. *Rev. Mod. Phys.* **53**, 769–787.

Lengeler, B., Materlik, G. & Müller, J. E. (1983). *Near edge structure in cerium and cerium compounds*. *EXAFS and near edge structure*, edited by A. Bianconi, L. Incoccia & S. Stipcich, pp. 150–153. Berlin: Springer.

Lereboures, B., Dürr, J., d'Huysser, A., Bonelle, J. P. & Lenglet, M. (1980). *Phys. Status Solidi*, **62**, K175.

Lytle, F. W., Sayers, D. E. & Stern, E. A. (1989). *Report of the International Workshops on Standards and Criteria in XAFS*. In *X-ray absorption spectroscopy*. *Physica (Utrecht)*, **B158**, 701–722.

Lytle, F. W., Stern, E. A. & Sayers, D. E. (1975). *Extended X-ray-absorption fine-structure technique II. Experimental practice and selected results*. *Phys. Rev. B*, **11**, 4825–4835.

Marcus, M., Powers, L. S., Storm, A. R., Kincaid, B. M. & Chance, B. (1980). *Curved-crystal (LiF) X-ray focusing array for fluorescence EXAFS in dilute samples*. *Rev. Sci. Instrum.* **51**, 1023–1029.

Martens, G. & Rabe, P. (1980). *EXAFS studies on superficial regions by means of total reflection*. *Phys. Status Solidi A*, **58**, 415–425.

Materlik, G., Bedzyk, M. J. & Frahm, A. (1984). Report SR-84-07. DESY, Hamburg, Germany.

Mustre de Leon, J., Stern, E. A., Sayers, D. E., Ma, Y. & Rehr, J. J. (1988). *XAFS V: Proceedings of the Fifth International Conference on X-ray Absorption Fine Structure*. Amsterdam: North-Holland.

Natoli, C. R. (1990). *Multichannel multiple scattering theory with general potentials*. *Phys. Rev. B*, **42**, 1944–1968.

Natoli, C. R., Misemer, D. K., Doniach, S. & Kutzler, F. W. (1980). *First principles calculation of X-ray absorption edge structure in molecular clusters*. *Phys. Rev. A*, **22**, 1104–1108.

Nordfors, B. (1960). *The statistical error in X-ray absorption measurements*. *Ark. Fys.* **18**, 37–47.

Norman, D., Durham, P. J. & Pendry, J. B. (1983). *The absorption of oxygen on nickel (001) studied by XANES*. *EXAFS and near edge structure*, edited by A. Bianconi, L. Incoccia & S. Stipcich, pp. 144–146. Berlin: Springer.

Oyanagi, H., Ihara, H., Matsushita, T., Hirabayashi, M., Terada, N., Tokumoto, M., Senzaki, K., Kimura, T. & Yao, T. (1987). *Short range order in high T_c superconductors $Ba_xY_{1-x}CuO_{3-y}$ and $Sr_xLa_{2-x}CuO_{4-7}$*. *Jpn. J. Appl. Phys.* **26**, L828–L831.

Oyanagi, H., Martini, M., Saito, M. & Haga, K. (1995). *Nineteen element high purity Ge solid state detector array for fluorescence X-ray absorption fine structure studies*. Submitted to *Rev. Sci. Instrum.*

Oyanagi, H., Matsushita, T., Tanoue, H., Ishiguro, T. & Kohra, K. (1985). *Fluorescence-detected X-ray absorption spectroscopy applied to structural characterization of very thin films: ion-beam-induced modification of thin Ni layers on Si (100)*. *Jpn. J. Appl. Phys.* **24**, 610–619.

Oyanagi, H., Takeda, T., Matsushita, T., Ishiguro, T. & Sasaki, A. (1986). *Local structure in InGaAsP I quaternary alloys*. *J. Phys. (Paris)*, **28**, Suppl. 12, C8, 423–426.

Pantos, E. (1982). *The SRS program library documentation*. Daresbury: SRC.

Papatzacos, P. & Mort, K. (1975). *Delbrück scattering calculations*. *Phys. Rev. D*, **12**, 206–221.

Parratt, L. G., Porteus, I. O., Schnopper, H. W. & Watanabe, T. (1959). *X-ray absorption coefficients and geometrical collimation of the beam*. *Rev. Sci. Instrum.* **30**, 344–347.

Pendry, J. B. (1983). *The transition region between XANES and EXAFS*. *EXAFS and near edge structure*, edited by A. Bianconi, L. Incoccia & S. Stipcich, pp. 4–10. Berlin: Springer.

Petiau, J. & Calas, G. (1983). *EXAFS for inorganic systems*, pp. 127–129. Daresbury: SRC.

Rehr, J. J. & Albers, R. C. (1990). *Phys. Rev. B*, **41**, 8139–8144.

Riggs, P. J., Mei, R., Yocum, C. F. & Penner-Hahn, J. E. (1993). *The characterization of the Mn site in the photosynthetic oxygen evolving complexes: the effect of hydroxylamine and hydroquinone on the XAFS*. *Jpn. J. Appl. Phys.* **32**, Suppl. 32–2, 527–529.

Saloman, E. B. & Hubbell, J. H. (1986). *X-ray attenuation coefficients (total cross sections): comparison of the data base with the experimental values of Henke and the theoretical values of Schofield for energies between 0.1–100 keV*. Report NBSIR 86–3431. US Department of Commerce, Gaithersburg, MD, USA.

Sawada, M., Tsutsumi, K., Shiraiwa, T., Ishimura, T. & Obashi, M. (1959). *Some contributions to the X-ray spectroscopy of solid state*. *Annu. Rep. Sci. Works Osaka Univ.* **7**, R–87.

Sayers, D. E., Lytle, F. W. & Stern, E. A. (1970). *Point scattering theory of X-ray K absorption fine structure*. *Adv. X-ray Anal.* **13**, 248–256.

Schmidt, V. V. (1961*a*). *Contribution to the theory of the temperature dependence of the fine structure of X-ray absorption spectra*. *Bull. Acad. Sci. USSR Phys. Ser.* **25**, 988–993.

4.2.3 (*cont.*)

Schmidt, V. V. (1961*b*). *On the effect of the temperature dependence of the fine structure of X-ray absorption spectra*. *J. Exp. Theor. Phys.* **12**, 886–890.

Schmidt, V. V. (1963). *Contributions to the theory of the dependence of the fine structure of X-ray absorption spectra II. Case of high temperatures*. *Bull. Acad. Sci. USSR Phys. Ser.* **27**, 392–397.

Scofield, J. H. (1973). *Theoretical photoionization cross sections from 1 to 1500 keV*. Report UCRL-51326. Lawrence Livermore Laboratory, Livermore, CA, USA.

Sears, V. F. (1983). *Optimum sample thickness for total cross section measurements*. *Nucl. Instrum. Methods*, **213**, 561–562.

Sevillano, E., Meuth, H. & Rehr, J. J. (1978). *Extended X-ray absorption fine structure Debye Waller factors. I. Monatomic crystals*. *Phys. Rev. B*, **20**, 4908–4911.

Shulman, R. G., Weisenberger, P., Teo, B. K., Kincaid, B. M. & Brown, G. S. (1978). *Fluorescence X-ray absorption studies of rubendoxin and its compounds*. *J. Mol. Biol.* **124**, 305–315.

Sinfelt, J. H., Via, G. H. & Lytle, F. W. (1980). *Structures of biometallic clusters. Extended X-ray absorption fine structure (EXAFS) studies of Ru–Cu clusters*. *J. Chem. Phys.* **72**, 4832–4843.

Sorenson, L. B., Cross, J. O., Newville, M., Ravel, B., Rehr, J. J., Stragier, H., Bouldin, C. E. & Woicik, J. C. (1994). *Diffraction anomalous fine structure: unifying X-ray diffraction and X-ray absorption with DAFS. Diffraction anomalous fine structure*, edited by G. Materlik, C. J. Sparks & K. Fischer, pp. 389–420. Amsterdam: North Holland.

Stern, E. A., Bunker, B. & Heald, A. (1981). *Understanding the causes of non-transferability of EXAFS amplitude. EXAFS spectroscopy: techniques and applications*, edited by B. K. Teo & D. C. Joy, pp. 59–79. New York: Plenum.

Stern, E. A., Sayers, D. E. & Lytle, F. W. (1975). *Extended X-ray absorption fine structure technique. III. Determination of physical parameters*. *Phys. Rev. B*, **11**, 4836–4846.

Stohr, J., Denley, D. & Perfettii, P. (1978). *Surface extended X-ray absorption fine structure in the soft X-ray region: study of an oxidized Al surface*. *Phys. Rev. B*, **18**, 4132–4135.

Templeton, D. H. & Templeton, L. K. (1982). *X-ray dichroism and polarized anomalous scattering of the uranyl ion*. *Acta Cryst.* A**38**, 62–67.

Templeton, D. H. & Templeton, L. K. (1985). *X-ray dichroism and anomalous scattering of potassium tetrachloroplatinate*. *Acta Cryst.* A**41**, 133–142.

Templeton, D. H. & Templeton, L. K. (1986). *X-ray birefringence and forbidden reflections in sodium bromate*. *Acta Cryst.* A**42**, 478–481.

Teo, B. K. (1981). *EXAFS spectroscopy: techniques and applications*, edited by B. K. Teo & D. C. Joy, Chap. 3, pp. 13–59. New York: Plenum.

Teo, B. K. & Joy, D. C. (1981). Editors. *EXAFS spectroscopy: techniques and applications*. New York: Plenum.

Teo, B. K. & Lee, P. A. (1979). *Ab initio calculations of amplitude and phase functions for extended X-ray absorption fine structure spectroscopy*. *J. Am. Chem. Soc.* **101**, 2815–2832.

Teo, B. K., Lee, P. A., Simons, A. L., Eisenberger, P. & Kincaid, B. M. (1977). *EXAFS. Approximation, parameterization and chemical transferability of amplitude function*. *J. Am. Chem. Soc.* **99**, 3854–3856.

Winick, H. & Doniach, S. (1980). Editors. *Synchrotron radiation research*. New York: Plenum.

Woodruff, D. P. (1986). *Fine structure in ionization cross sections and applications to surface science*. *Rep. Prog. Phys.* **49**, 683–723.

Yamaguchi, T., Mitsunaga, T., Yoshida, N., Wakita, H., Fujiwara, M., Matsushita, T., Ikeda, S. & Nomura, M. (1993). *XAFS study with an in situ electrochemical cell on manganese Schiff base complexes as a model of a photosystem*. *Jpn. J. Appl. Phys.* **32**, Suppl. 32-2, 533–535.

4.2.4

Allen, S. J. M. (1935). *X-rays in theory and experiment*, edited by A. H. Compton & S. K. Allison, pp. 799–806. New York: Van Nostrand.

Allen, S. J. M. (1969). *Handbook of chemistry and physics*, edited by R. C. Weast, pp. E143–E144. Cleveland: The Chemical Rubber Co.

Band, I. M., Kharitonov, Yu. I. & Trzhaskovskaya, M. B. (1979). *Photoionization cross sections and photoelectron angular distributions for X-ray line energies in the range 0.132–4.509 keV*. *At. Data Nucl. Data Tables*, **23**, 443–505.

Creagh, D. C. (1987). *Resolution of discrepancies in tables of photon attenuation cross sections*. *Nucl. Instrum. Methods*, A**255**, 38–42.

Creagh, D. C. (1990). *An evaluation of tabulations of X-ray attenuation coefficients: the new versus the old*. *Nucl. Instrum. Methods*, A**295**, 417–439.

Creagh, D. C. & Hubbell, J. H. (1987). *Problems associated with the measurement of X-ray attenuation coefficients. I. Silicon*. *Acta Cryst.* A**43**, 102–112.

Creagh, D. C. & Hubbell, J. H. (1990). *Problems associated with the measurement of X-ray attenuation coefficients. II. Carbon*. *Acta Cryst.* A**46**, 402–408.

Cromer, D. T. (1969). *Anomalous dispersion corrections computed from self consistent field relativistic Dirac–Slater wavefunctions*. *J. Chem. Phys.* **50**, 4857–4859.

Cromer, D. T. & Liberman, D. (1970). *Relativistic calculation of anomalous scattering for X-rays*. *J. Chem. Phys.* **53**, 1891–1898.

Cromer, D. T. & Mann, J. B. (1967). *Compton scattering factors for spherically symmetric free atoms*. *J. Chem. Phys.* **47**, 1892–1893.

Cromer, D. T. & Waber, J. T. (1974). *Atomic scattering factors for X-rays*. Section 2.2. *International tables for X-ray crystallography*, Vol. IV, edited by J. A. Ibers & W. C. Hamilton, pp. 71–147. Birmingham: Kynoch Press. (Present distributor Kluwer Academic Publishers, Dordrecht.)

De Marco, J. J. & Suortti, P. (1971). *Effect of scattering on the attenuation of X-rays*. *Phys. Rev. B*, **4**, 1028–1033.

Doyle, P. A. & Turner, P. S. (1968). *Relativistic Hartree–Fock X-ray and electron scattering factors*. *Acta Cryst.* A**24**, 390–397.

Gerward, L. (1986). *Empirical absorption equations for use in X-ray spectrometric analysis*. *X-ray Spectrom.* **15**, 29–33.

Heinrich, K. F. J. (1966). *X-ray absorption uncertainty*. *The electron microprobe*, edited by T. D. McKinley, K. F. J. Heinrich & D. B. Wittrey, pp. 296–377. New York: John Wiley.

Henke, B. L., Lee, P., Tanaka, T. J., Shimambukuro, R. L. & Fujikawa, B. K. (1982). *Low-energy X-ray interaction coefficients: photoabsorption, scattering and reflection*. *At. Data Nucl. Data Tables*, **27**, 1–144.

4.2.4 (*cont.*)

Hubbell, J. H., Gerstenberg, H. M. & Saloman, E. B. (1986). *Bibliography of photon total cross section (attenuation coefficient) measurements 10 eV to 13.5 GeV*. Report NBSIR 86–3461. National Institute of Standards and Technology, Gaithersburg, MD, USA.

Hubbell, J. H., McMaster, W. H., Del Grande, N. K. & Mallett, J. H. (1974). *X-ray cross sections and attenuation coefficients. International tables for X-ray crystallography*, Vol. IV, pp. 47–70. Birmingham: Kynoch Press. (Present distributor Kluwer Academic Publishers, Dordrecht.)

Hubbell, J. H. & Øverbø, I. (1979). *Relativistic atomic form factors and photon coherent scattering cross sections. J. Phys. Chem. Ref. Data*, **8**, 69–105.

Hubbell, J. H., Veigele, W. J., Briggs, E. A., Brown, R. T., Cromer, D. T. & Howerton, R. J. (1975). *Atomic form factors, incoherent scattering functions and photon scattering cross sections. J. Phys. Chem. Ref. Data*, **4**, 471–538.

Jackson, D. F. & Hawkes, D. J. (1981). *X-ray attenuation coefficients of elements and mixtures. Phys. Rep.* **70**, 169–233.

Kane, P. P., Kissel, L., Pratt, R. H. & Roy, S. C. (1986). *Elastic scattering of γ-rays and X-rays by atoms. Phys. Rep.* **150**, 75–159.

Kissel, L., Roy, S. C. & Pratt, R. H. (1980). *Rayleigh scattering by neutral atoms 100 eV to 10 MeV. Phys. Rev. A*, **22**, 1970–2004.

Koch, B., MacGillavry, C. H. & Milledge, H. J. (1962). *Absorption. International tables for X-ray crystallography*, Vol. III, Section 2.2, pp. 157–192. Birmingham: Kynoch Press.

Leroux, J. & Thinh, T. P. (1977). *Revised tables of X-ray mass attenuation coefficients*. Quebec: Corporation Scientifique Claisse, Inc.

Levinger, J. S. (1952). *Small angle coherent scattering of gammas by bound electrons. Phys. Rev.* **87**, 656–662.

Liebhafsky, H. A., Pfeiffer, H. G., Winslow, E. H. & Zemany, P. D. (1960). *X-ray absorption and emission analytical chemistry*, pp. 313–317. New York: John Wiley.

McMaster, W. H., Del Grande, N. K., Mallett, J. H. & Hubbell, J. H. (1969/1970). *Compilation of X-ray cross sections*. Report UCRL-50174. (Section I, 1970; Section II, 1969; Section III, 1969; Section IV 1969.) Lawrence Livermore National Laboratory, Livermore, CA, USA.

Montenegro, E. C., Baptista, G. B. & Duarte, P. W. E. P. (1978). *K and L X-rays mass attenuation coefficients for low-Z materials. At. Data Nucl. Data Tables*, **22**, 131–177.

Øverbø, I. (1977). *The Coulomb correction to electron pair production by intermediate-energy photons. Phys. Lett. B*, **71**, 412–414.

Øverbø, I. (1978). *Large-q form factors for light atoms. Phys. Scr.* **17**, 547–549.

Pirenne, M. H. (1946). *The diffraction of X-rays and electrons by free molecules*. Cambridge University Press.

Plechaty, E. F., Cullen, E. E. & Howerton, R. J. (1981). *Tables and graphs of photon-interaction cross sections from 0.1 keV to 100 MeV*. Derived from the LLL Evaluated-Nuclear-Data Library. Report UCRL-50400, Vol. 6, Rev. 3. Lawrence Livermore National Laboratory, Livermore, CA, USA.

Saloman, E. B. & Hubbell, J. H. (1986). *X-ray attenuation coefficients (total cross sections): comparison of the experimental data base with the recommended values of Henke and the theoretical values of Scofield for energies between 0.1–100 keV*. Report NBSIR 86–3431. National Institute of Standards and Technology, Gaithersburg, MD, USA.

Saloman, E. B. & Hubbell, J. H. (1987). *Critical analysis of soft X-ray cross section data. Nucl. Instrum. Methods*, A**255**, 38–42.

Saloman, E. B., Hubbell, J. H. & Scofield, J. H. (1988). *At. Data Nucl. Data Tables*, **38**, 1–197.

Sano, H., Ohtaka, K. & Ohtsuki, Y. H. (1969). *Normal and abnormal absorption coefficients of X-rays. J. Phys. Soc. Jpn*, **27**, 1254–1261.

Schaupp, D., Schumacher, M., Smend, F., Rullhausen, P. & Hubbell, J. H. (1983). *Small-angle Rayleigh scattering of photons at high energies: tabulations of relativistic HFS modified atomic form factors. J. Phys. Chem. Ref. Data*, **12**, 467–512.

Scofield, J. H. (1973). *Theoretical photoionization cross sections from 1 to 1500 keV*. UCRL-51326. Lawrence Livermore National Laboratory, Livermore, CA, USA.

Scofield, J. H. (1986). Personal communication to E. B. Saloman and J. H. Hubbell. *Calculated photoeffect values 0.1 to 1.0 keV*. [Presented in Saloman & Hubbell (1986) and Saloman *et al.* (1988).]

Storm, E. & Israel, H. I. (1970). *Photon cross sections from 0.001 to 100 MeV for elements 1 through 100. Nucl. Data Tables*, A**7**, 565–681.

Theisen, R. & Vollath, D. (1967). *Tables of X-ray mass attenuation coefficients*. Düsseldorf: Verlag Stahleisen.

Veigele, W. J. (1973). *Photon cross sections from 0.1 keV to 1 MeV for elements $Z = 1$ to $Z = 94$. At. Data*, **5**, 51–111.

Victoreen, J. A. (1949). *The calculation of X-ray mass absorption coefficients. J. Appl. Phys.* **20**, 1141–1147.

Yeh, J. J. & Lindau, I. (1985). *Atomic subshell photoionization cross sections and asymmetry parameters: $1 \leq Z \leq 103$. At. Data Nucl. Data Tables*, **32**, 1–156.

4.2.5

Balaic, D. X., Barnea, Z., Nugent, K. A., Garrett, R. F., Varghese, J. N. & Wilkins, S. W. (1996). *Protein crystal diffraction patterns using a capillary-focused synchrotron X-ray beam. J. Synchrotron Rad.* **3**, 289–295.

Balaic, D. X. & Nugent, K. A. (1995). *The X-ray optics of tapered capillaries. Appl. Opt.* **34**, 7263–7272.

Balaic, D. X., Nugent, K. A., Barnea, Z., Garrett, R. & Wilkins, S. W. (1995). *Focusing of X-rays by total external reflection from a paraboloidally tapered glass capillary. J. Synchrotron Rad.* **2**, 296–299.

Beaumont, J. H. & Hart, M. (1973). *Multiple-Bragg reflection monochromators for synchrotron radiation. J. Phys. E,* **7**, 823–829.

Berman, L. E. & Hart, M. (1991). *Adaptive crystal optics for high power synchrotron sources. Nucl. Instrum. Methods,* A**302**, 558–562.

Bilderback, D. H., Thiel, D. J., Pahl, R. & Brister, K. E. (1994). *X-ray applications with glass-capillary optics. J. Synchrotron Rad.* **1**, 37–42.

Bonse, U. & Hart, M. (1965). *Tailless X-ray single-crystal reflection curves obtained by multiple reflection. Appl. Phys. Lett.* **7**, 238–240.

Brodsky, A. (1982). Editor. *Handbook of radiation measurement and protection*, Vols. 1 and 2. Florida: CRC Press.

4.2.5 (*cont.*)

Creagh, D. C. & Garrett, R. F. (1995). *Testing of a sagittal focusing monochromator at BL 20B at the Photon Factory*. *Access to major facilities program*, edited by J. W. Boldeman, pp. 251–252. Sydney: ANSTO.

Delf, B. W. (1961). *The effect of absorption in the β-filter on the mean wavelength of X-ray emission lines*. *Proc. Phys. Soc. London*, **78**, 305–306.

Engström, P., Rindby, A. & Vincze, L. (1996). *Capillary optics*. *ESRF Newsletter,* **26**, 30–31.

Freund, A. K. (1993). *Thin is beautiful*. *ESRF Newsletter,* **19**, 11–13.

Fukumachi, T., Nakano, Y. & Kawamura, T. (1986). *Energy dependence of X-ray reflectivity from multi-layer mirrors*. *X-ray instrumentation for the Photon Factory: dynamic analyses of micro-structures in matter*, edited by S. Hosoya, Y. Iitaka & H. Hashizume, pp. 25–34. Japan: Photon Factory.

Giles, C., Vettier, C., de Bergevin, F., Grubel, G., Goulon, J. & Grossi, F. (1994). *X-ray polarimetry with phase plates*. *ESRF Newsletter,* **21**, 16–17.

Grey, D. (1996). *Instrumentation developments and observations in hard X-ray astronomy*. PhD thesis. The University of New South Wales, Australia.

Hanfland, M., Häusermann, D., Snigirev, A., Snigireva, I., Ahahama, Y. & McMahon, M. (1994). *Bragg–Fresnel lens for high pressure studies*. *ESRF Newsletter,* **22**, 8–9.

Hart, M. (1971). *Bragg reflection X-ray optics*. *Rep. Prog. Phys.* **34**, 435–490.

Hart, M. & Rodrigues, A. R. D. (1978). *Harmonic-free single-crystal monochromators for neutrons and X-rays*. *J. Appl. Cryst.* **11**, 248–253.

Hashizume, H. (1983). *Asymmetrically grooved monolithic crystal monochromators for suppression of harmonics in synchrotron X-radiation*. *J. Appl. Cryst.* **16**, 420–427.

Holt, S. A., Brown, A. S., Creagh, D. C. & Leon, R. (1997). *The application of grazing incidence X-ray diffraction and specular reflectivity to the structural investigation of multiple quantum well and quantum dot semiconductor devices*. *J. Synchrotron Rad.* **4**, 169–174.

Jennings, L. D. (1981). *Extinction, polarization and crystal monochromators*. *Acta Cryst.* A**37**, 584–593.

Kikuta, S. (1971). *X-ray crystal monochromators using successive asymmetric diffractions and their applications to measurements of diffraction curves. II. Type I collimator*. *J. Phys. Soc. Jpn,* **30**, 222–227.

Kikuta, S. & Kohra, K. (1970). *X-ray crystal collimators using successive asymmetric diffractions and their applications to measurements of diffraction curves. I. General considerations on collimators*. *J. Phys. Soc. Jpn,* **29**, 1322–1328.

Kumakov, M. A. & Komarov, F. F. (1990). *Multiple reflection from surface X-ray optics*. *Phys. Rep.* **191**(5), 284–350.

Matsushita, T., Ishikawa, T. & Oyanagi, H. (1986). *Sagitally focusing double-crystal monochromator with constant exit height at the Photon Factory*. *Nucl. Instrum. Methods*, A**246**, 377–379.

Matsushita, T., Kikuta, S. & Kohra, K. (1971). *X-ray crystal monochromators using successive asymmetric diffractions and their applications to measurements of diffraction curves. III. Type II collimators*. *J. Phys. Soc. Jpn*, **30**, 1136–1144.

Oshima, K., Harada, J. & Sakabe, N. (1986). *Curved crystal monochromator. X-ray instrumentation for the Photon Factory: dynamic analyses of micro-structures in matter*, edited by S. Hosoya, Y. Iitaka & H.Hashizume, pp. 35–41. Japan: Photon Factory.

OSMIC (1996). Catalogue. *A new family of collimating and focusing optics for X-ray analysis*. OSMIC, Michigan, USA.

Peele, A. G., Nugent, K. A., Rode, A. V., Gabel, K., Richardson, M. C. M., Strack, R. & Siegmund, W. (1996). *X-ray focusing with lobster-eye optics: a comparison of theory with experiment*. *Appl. Opt.* **35**, 4420–4425.

Siemens (1996*a*). *Parallel beam optics for measurements of samples with irregularly shaped surfaces*. Laboratory Report X-ray Analysis, DXRD, 13. Karlsruhe: Siemens.

Siemens (1996*b*). *Goebel mirrors for X-ray reflectometry investigations*. Laboratory Report X-ray Analysis, DXRD, 14. Karlsruhe: Siemens.

Siemens (1996*c*) *Grazing incidence diffraction with Goebel mirrors*. Laboratory Report X-ray Analysis, DXRD, 15. Karlsruhe: Siemens.

Snigirev, A. (1994). *Bragg–Fresnel optics: new fields of applications*. *ESRF Newsletter,* **22**, 20–21.

Stephens, P. W., Eng, P. J. & Tse, T. (1992). *Construction and performance of a bent crystal X-ray monochromator*. *Rev. Sci. Instrum.* **64**, 374–378.

Sussini, J. & Labergerie, D. (1995). *Bi-morph piezo-electric mirror: a novel active mirror*. *Synchrotron Rad. News,* **8**, 21–26.

Warren, B. E. (1968). *X-ray diffraction*. New York: Addison-Wesley.

Young, R. A. (1963). *Balanced filters for X-ray diffractometry*. *Z. Kristallogr.* **118**, 233–247.

Young, R. A. (1993). *The Rietveld method*. Oxford University Press.

4.2.6

Agarwal, B. K. (1979). *X-ray spectroscopy*, p. 215. Berlin: Springer-Verlag.

Akhiezer, A. I. & Berestetsky, V. B. (1957). *Quantum electrodynamics*. TESE, Oak Ridge, Tennessee, USA.

Aldred, P. J. E. & Hart, M. (1973*a*). *The electron distribution in silicon. I. Experiment*. *Proc. R. Soc. London Ser. A*, **332**, 233–238.

Aldred, P. J. E. & Hart, M. (1973*b*). *The electron distribution in silicon. II. Theoretical interpretation*. *Proc. R. Soc. London Ser. A*, **332**, 239–254.

Aristov, V. V., Shmytko, I. M. & Shulakov, E. V. (1977). *Dynamical contrast of the topographic image of a crystal with continuous X-radiation*. *Acta Cryst.* A**33**, 412–418.

Begum, R., Hart, M., Lea, K. R. & Siddons, D. P. (1986). *Direct measurements of the complex X-ray atomic scattering factors for elements by X-ray interferometry at the Daresbury synchrotron radiation source*. *Acta Cryst.* A**42**, 456–463.

Bijvoet, J. M., Peerdeman, A. F. & Van Bommel, A. J. (1951). *Determination of the absolute configuration of optically active compounds by means of X-rays*. *Nature (London)*, **168**, 271.

Blume, M. (1994). *Magnetic effects in anomalous dispersion*. *Resonant anomalous X-ray scattering*, edited by G. Materlik, C. J. Sparks & K. Fischer, pp. 495–512. Amsterdam: North Holland.

Bonse, U. & Hart, M. (1965). *Tailless X-ray single crystal reflection curves obtained by multiple reflection*. *Appl. Phys. Lett.* **1**, 238–242.

Bonse, U. & Hart, M. (1966*a*). *A Laue-case X-ray interferometer*. *Z. Phys.* **188**, 154–162.

Bonse, U. & Hart, M. (1966*b*). *An X-ray interferometer with Bragg-case beam splitting*. *Z. Phys.* **194**, 1–17.

4.2.6 (*cont.*)

Bonse, U. & Hart, M. (1966*c*). *Moire patterns of atomic planes obtained by X-ray interferometry*. *Z. Phys.* **190**, 455–467.

Bonse, U. & Hart, M. (1966*d*). *Small single X-ray scattering by spherical particles*. *Z. Phys.* **189**, 151–165.

Bonse, U. & Hart, M. (1970). *Interferometry with X-rays*. *Phys. Today*, **23**(8), 26–31.

Bonse, U. & Hartmann-Lotsch, I. (1984). *Kramers–Kronig correlation of measured f′(E) and f″(E) values*. *Nucl. Instrum. Methods*, **222**, 185–188.

Bonse, U., Hartmann-Lotsch, I. & Lotsch, H. (1983*a*). *Interferometric measurement of absorption $\mu(E)$ and dispersion $f'(E)$ at the K edge of copper*. *EXAFS and near edge structure*, edited by A. Bianconi, I. Incoccia & A. S. Stipcich, pp. 376–377. Berlin: Springer.

Bonse, U., Hartmann-Lotsch, I. & Lotsch, H. (1983*b*). *The X-ray interferometer for high resolution measurement of anomalous dispersion at HASYLAB*. *Nucl. Instrum. Methods*, **208**, 603–604.

Bonse, U. & Hellkötter, H. (1969). *Interferometrische Messung des Brechungsindex für Röntgenstrahlen*. *Z. Phys.* **223**, 345–352.

Bonse, U. & Henning, A. (1986). *Measurement of polarization isotropy of the anomalous forward scattering amplitude at the niobium K-edge in $LiNbO_3$*. *Nucl. Instrum. Methods*, A**246**, 814–816.

Bonse, U. & Materlik, G. (1972). *Dispersionskorrektur für Nickel nahe der K-Absorptionskante*. *Z. Phys.* **253**, 232–239.

Bonse, U. & Materlik, G. (1975). *Dispersion correction measurements by X-ray interferometry*. *Anomalous scattering*, edited by S. Ramaseshan & S. C. Abrahams, pp. 107–109. Copenhagen: Munksgaard.

Brown, G. E., Peierls, R. E. & Woodward, J. B. (1955). *The coherent scattering of γ-rays by K electrons in heavy atoms: method*. *Proc. R. Soc. London Ser. A*, **227**, 51–63.

Brysk, H. & Zerby, C. D. (1968). *Photoelectric cross sections in the keV range*. *Phys. Rev.* **171**, 292–298.

Buras, B. & Tazzari, S. (1985). *The European Synchrotron Radiation Facility*. *Report of the ESRP*, pp. 6–32. European Synchrotron Radiation Project, CERN, LEP Division, Geneva, Switzerland.

Chantler, C. T. (1994). *Towards improved form factor tables*. *Resonant anomalous X-ray scattering*, edited by G. Materlik, C. J. Sparks & K. Fischer, pp. 61–79. Amsterdam: North Holland.

Chantler, C. T. (1995). *Theoretical form factor, attenuation and scattering tabulation for $Z = 1$–92 from 1–$10\,eV$ to $E = 0.4$–$1.0\,MeV$*. *J. Phys. Chem. Ref. Data*, **24**, 71–643.

Chapuis, G., Templeton, D. H. & Templeton, L. K. (1985). *Solving crystal structures using several wavelengths from conventional sources*. *Anomalous scattering by holmium*. *Acta Cryst.* A**41**, 274–278.

Cole, H. & Stemple, N. R. (1962). *Effect of crystal perfection and polarity on absorption edges seen in Bragg diffraction*. *J. Appl. Phys.* **33**, 2227–2233.

Creagh, D. C. (1970). *On the measurement of X-ray dispersion corrections using X-ray interferometers*. *Aust. J. Phys.* **23**, 99–103.

Creagh, D. C. (1977). *Determination of the mass attenuation coefficients and the anomalous dispersion corrections for calcium at X-ray wavelengths from I $K\alpha_1$ to Cu $K\alpha_1$*. *Phys. Status Solidi A*, **39**, 705–715.

Creagh, D. C. (1978). *A new device for the precise measurement of X-ray attenuation coefficients and dispersion corrections*. *Advances in X-ray analysis*, Vol. 21, edited by C. S. Barrett & D. E. Leyden, pp. 149–153. New York: Plenum.

Creagh, D. C. (1980). *X-ray interferometer measurements of the anomalous dispersion correction $f'(\omega,0)$ for some low Z elements*. *Phys. Lett. A*, **77**, 129–132.

Creagh, D. C. (1982). *On the use of photoelectric attenuation coefficients for the determination of the anomalous dispersion coefficient f′ for X-rays*. *Phys. Lett. A*, **103**, 52–56.

Creagh, D. C. (1984). *The real part of the forward scattering factor for aluminium*. Unpublished.

Creagh, D. C. (1985). *Theoretical and experimental techniques for the determination of X-ray anomalous dispersion corrections*. *Aust. J. Phys.* **38**, 371–404.

Creagh, D. C. (1986). *The X-ray anomalous dispersion of materials*. In *Recent advances in X-ray characterization of materials*, edited by P. Krishna, Chap. 7. Oxford: Pergamon Press.

Creagh, D. C. (1990). *Tables of X-ray dispersion corrections and attenuation coefficients: the new versus the old*. *Nucl. Instrum. Methods*, A**295**, 417–434.

Creagh, D. C. (1993). *f′: its present and its future*. *Ind. J. Phys.* **67**B, 511–525.

Creagh, D. C. & Cookson, D. J. (1995). *Diffraction anomalous fine structure study of basic zinc sulphate and basic zinc sulphonate*. In *Photon Factory Activity Report 1994*, edited by K. Nasu. National Laboratory for High Energy Physics, Tsukuba 93-0305, Japan.

Creagh, D. C. & Hart, M. (1970). *X-ray interferometric measurements of the forward scattering amplitude of lithium fluoride*. *Phys. Status Solidi*, **37**, 753–758.

Creagh, D. C. & Hubbell, J. H. (1987). *Problems associated with the measurement of X-ray attenuation coefficients. I. Silicon*. *Acta Cryst.* A**43**, 102–112.

Creagh, D. C. & Hubbell, J. H. (1990). *Problems associated with the measurement of X-ray attenuation coefficients. II. Carbon*. *Acta Cryst.* A**46**, 402–408.

Cromer, D. T. & Liberman, D. A. (1970). *Relativistic calculation of anomalous scattering factors for X-rays*. *J. Chem. Phys.* **53**, 1891–1898.

Cromer, D. T. & Liberman, D. A. (1981). *Anomalous dispersion calculations near to and on the long-wavelength side of an absorption edge*. *Acta Cryst.* A**37**, 267–268.

Cromer, D. T. & Liberman, D. A. (1983). *Calculation of anomalous scattering factors at arbitrary wavelengths*. *J. Appl. Cryst.* **16**, 437.

Cromer, D. T. & Waber, J. T. (1974). *Atomic scattering factors for X-rays*. *International tables for X-ray crystallography*, Vol. IV, edited by J. A. Ibers & W. C. Hamilton, Chap. 2.2, pp. 71–147. Birmingham: Kynoch Press. (Present distributor Kluwer Academic Publishers, Dordrecht.)

Cusatis, C. & Hart, M. (1975). *Dispersion correction measurements by X-ray interferometry*. *Anomalous scattering*, edited by S. Ramaseshan & S. C. Abrahams, pp. 57–68. Copenhagen: Munksgaard.

Cusatis, C. & Hart, M. (1977). *The anomalous dispersion corrections for zirconium*. *Proc. R. Soc. London Ser. A*, **354**, 291–302.

Deutsch, M. & Hart, M. (1982). *Wavelength energy shape and structure of the Cu $K\alpha_1$ X-ray emission line*. *Phys. Rev. B*, **26**, 5550–5567.

Deutsch, M. & Hart, M. (1984*a*). *Noninterferometric measurement of the X-ray refractive index of beryllium*. *Phys. Rev. B*, **30**, 643–646.

4.2.6 (*cont.*)

Deutsch, M. & Hart, M. (1984*b*). *X-ray refractive-index measurement in silicon and lithium fluoride*. *Phys. Rev. B*, **30**, 640–642.

Deutsch, M. & Hart, M. (1985). *A new approach to the measurement of X-ray structure amplitudes determined by the Pendellösung method*. *Acta Cryst.* A**41**, 48–55.

Dreier, P., Rabe, P., Malzfeldt, W. & Niemann, W. (1984). *Anomalous X-ray scattering factors calculated from experimental absorption factor*. *J. Phys. C*, **7**, 3123–3136.

Engel, D. H. & Sturm, M. (1975). *Experimental determination of f″ for heavy atoms*. *Anomalous scattering*, edited by S. Ramaseshan & S. C. Abrahams, pp. 93–100. Copenhagen: Munksgaard.

Fermi, E. (1928). *Eine statistiche Methode zur Bestimmung einiger geschaften des Atoms und ihre Anwendung auf die Theorie des periodische Systems der Elemente*. *Z. Phys.* **48**, 73–79.

Fock, V. (1930). *Näherungsmethode zur Lösung des quantenmechanischen Mehrkörperproblems*. *Z. Phys.* **61**, 126–148.

Freund, A. (1975). *Anomalous scattering of X-rays in copper*. *Anomalous scattering,* edited by S. Ramaseshan & S. C. Abrahams, pp. 69–86. Copenhagen: Munksgaard.

Fuoss, P. H. & Bienenstock, A. (1981). *X-ray anomalous scattering factors – measurements and applications*. *Inner-shell and X-ray physics of atoms and solids*, edited by D. J. Fabian, A. Kleinpoppen & L. M. Watson, pp. 875–884. New York: Plenum.

Gavrila, M. (1981). *Photon atom elastic scattering in inner-shell and X-ray physics of atoms and solids*, edited by B. Craseman. New York: Plenum.

Gerward, L. (1982). *X-ray attenuation coefficients of copper in the energy range 5 to 50 keV*. *Z. Naturforsch. Teil A*, **37**, 451–459.

Gerward, L. (1983). *X-ray attenuation coefficients of carbon in the energy range 5 to 20 keV*. *Acta Cryst.* A**39**, 322–325.

Gerward, L., Thuesen, G., Stibius-Jensen, M. & Alstrup, I. (1979). *X-ray anomalous scattering factors for silicon and germanium*. *Acta Cryst.* A**35**, 852–857.

Grimvall, G. & Persson, E. (1969). *Absorption of X-rays in germanium*. *Acta Cryst.* A**25**, 417–422.

Hart, M. (1968). *An ångström ruler*. *J. Phys. D*, **1**, 1405–1408.

Hart, M. (1985). *Private communication*.

Hart, M. (1994). *Polarizing X-ray optics and anomalous dispersion in chiral systems*. *Resonant anomalous X-ray scattering*, edited by G. Materlik, C. J. Sparks & K. Fischer, pp. 103–118. Amsterdam: North Holland.

Hart, M. & Siddons, D. P. (1981). *Measurements of anomalous dispersion corrections made from X-ray interferometers*. *Proc. R. Soc. London Ser. A*, **376**, 465–482.

Hartree, D. R. (1928). *The wavemechanics of an atom with a non-Coulomb central field*. *Proc. Cambridge Philos. Soc.* **24**, 89–132.

Hashimoto, H., Kozaki, S. & Ohkawa, T. (1965). *Observations of Pendellösung fringes and images of dislocations by X-ray shadow micrographs of silicon crystals*. *Appl. Phys. Lett.* **6**, 16–17.

Helliwell, J. R. (1984). *Synchrotron X-radiation protein crystallography*. *Rep. Prog. Phys.* **47**, 1403–1497.

Hendrickson, W. A. (1994). *MAD phasing for macromolecular structures*. *Resonant anomalous X-ray scattering*, edited by G. Materlik, C. J. Sparks & K. Fischer, pp. 159–173. Amsterdam: North Holland.

Henke, B. L., Lee, P., Tanaka, T. J., Shimambukuro, R. L. & Fujikawa, B. K. (1982). *Low-energy interaction coefficients: photoabsorption, scattering, and reflection*. *At. Data Nucl. Data Tables*, **27**, 1–144.

Hönl, H. (1933*a*). *Zur Dispersions theorie der Röntgenstrahlen*. *Z. Phys.* **84**, 1–16.

Hönl, H. (1933*b*). *Atomfactor für Röntgenstrahlen als Problem der Dispersionstheorie (K-Schale)*. *Ann. Phys. (Leipzig)*, **18**, 625–657.

Hosoya, S. (1975). *Anomalous scattering measurements and amplitude and phase determinations with continuous X-rays*. *Anomalous scattering*, edited by S. Ramaseshan & S. C. Abrahams, pp. 275–287. Copenhagen: Munksgaard.

Hubbell, J. H., Veigele, W. J., Briggs, E. A., Brown, R. T., Cromer, D. T. & Howerton, R. J. (1975). *Atomic form factors, incoherent scattering functions and photon scattering cross section*. *J. Chem. Phys. Ref. Data*, **4**, 471–538.

International Tables for Crystallography (1995). Vol. B. Dordrecht: Kluwer Academic Publishers.

International Tables for X-ray Crystallography (1974). Vol. IV. Birmingham: Kynoch Press. (Present distributor Kluwer Academic Publishers, Dordrecht.)

Ishida, K. & Katoh, H. (1982). *Use of multiple reflection diffraction to measure X-ray refractive index*. *Jpn. J. Appl. Phys.* **21**, 1109.

James, R. W. (1955). *The optical principles of the diffraction of X-rays*. Ithaca: Cornell University Press.

Karle, J. (1980). *Anomalous dispersion and the use of triplet phase invariants*. *Int. J. Quantum. Chem.* **7**, 357–367.

Karle, J. (1984*a*). *Rules for evaluating triplet phase invariants by use of anomalous dispersion data*. *Acta Cryst.* A**40**, 366–379.

Karle, J. (1984*b*). *The relative scaling of multiple wavelength anomalous dispersion data*. *Acta Cryst.* A**40**, 1–4.

Karle, J. (1984*c*). *Triplet phase invariants from and exact algebraic analysis of anomalous dispersion*. *Acta Cryst.* A**40**, 526–532.

Karle, J. (1985). *Many algebraic formulas for the evaluation of triplet phase invariants from isomorphous replacement and anomalous dispersion data*. *Acta Cryst.* A**41**, 182–189.

Katoh, H., Shimakura, H., Ogawa, T., Hattori, S., Kobayashi, Y., Umezawa, K., Ishikawa, T. & Ishida, K. (1985*a*). *Measurement of X-ray refractive index by multiple reflection diffractometer*. Activity Report, KEK, Tsukuba, Japan.

Katoh, H., Shimakura, H., Ogawa, T., Hattori, S., Kobayashi, Y., Umezawa, K., Ishikawa, T. & Ishida, K. (1985*b*). *Measurement of the X-ray anomalous scattering of the germanium K-edge with synchrotron radiation*. *J. Phys. Soc. Jpn*, **54**, 881–884.

Kirfel, A. (1994). *Anisotropy of anomalous scattering in single crystals*. *Resonant anomalous X-ray scattering*, edited by G. Materlik, C. J. Sparks & K. Fischer, pp. 231–256. Amsterdam: North Holland.

Kissel, L. (1977). *Rayleigh scattering: elastic scattering by bound electrons*. PhD thesis, University of Pittsburgh, PA, USA.

Kissel, L. & Pratt, R. H. (1985). *Rayleigh scattering: elastic photon scattering by bound electrons*. In *Atomic inner-shell physics*, edited by B. Craseman. New York: Plenum.

Kissel, L., Pratt, R. H., Kane, P. P. & Roy, S. C. (1985). *Elastic scattering of X-rays and γ-rays by atoms*. Sandia Report SANDE5-0501J. Sandia, Albuquerque, NM, USA.

Kissel, L., Pratt, R. H. & Roy, S. C. (1980). *Rayleigh scattering by neutral atoms, 100 eV to 10 MeV*. *Phys. Rev. A*, **22**, 1970–2004.

4.2.6 (*cont.*)

Kohn, W. & Sham, L. S. (1965). *Self consistent equations including exchange and correlation effects. Phys. Rev. A*, **140**, 1133–1138.

Lengeler, B. (1994). *Experimental determination of the dispersion correction f′(E) to the atomic scattering factor. Resonant anomalous X-ray scattering*, edited by G. Materlik, C. J. Sparks & K. Fischer, pp. 35–69. Amsterdam: North Holland.

Liberman, D., Waber, J. T. & Cromer, D. T. (1965). *Self-consistent field Dirac–Slater wavefunctions for atoms and ions. I. Comparison with previous calculations. Phys. Rev. A*, **137**, 27–34.

Morgenroth, W., Kirfel, A. & Fischer, K. (1994). *Computing kinematic diffraction intensities with anomalous scatterers – 'forbidden' axial reflections in space groups up to orthorhombic symmetry. Resonant anomalous X-ray scattering*, edited by G. Materlik, C. J. Sparks & K. Fischer, pp. 257–264. Amsterdam: North Holland.

Nelms, A. T. & Oppenheimer, I. (1955). *J. Res. Natl Bur. Stand.* **55**, 53–62.

Philips, J. C. & Hodgson, K. O. (1985). *Single-crystal X-ray diffraction and anomalous scattering using synchrotron radiation. Synchrotron radiation research*, edited by H. Winick & S. Doniach, pp. 565–604. New York: Plenum.

Philips, J. C., Templeton, D. H., Templeton, L. K. & Hodgson, K. O. (1978). *L-III edge anomalous X-ray scattering by cesium measured with synchrotron radiation. Science*, **201**, 257–259.

Pratt, R. H., Kissel, L. & Bergstrom, P. M. Jr (1994). *New relativistic S-matrix results for scattering – beyond the anomalous factors/beyond impulse approximation. Resonant anomalous X-ray scattering*, edited by G. Materlik, C. J. Sparks & K. Fischer, pp. 9–34. Amsterdam: North Holland.

Price, P. F., Maslen, E. N. & Mair, S. L. (1978). *Electron-density studies. III. A re-evaluation of the electron distribution in crystalline silicon. Acta Cryst.* A**34**, 183–193.

Ramaseshan, S. & Abrahams, S. C. (1975). *Anomalous scattering*. Copenhagen: Munksgaard.

Roy, S. C., Kissel, L. & Pratt, R. H. (1983). *Elastic photon scattering at small momentum transfer and validity of form-factor theories. Phys. Rev. A*, **27**, 285–290.

Roy, S. C. & Pratt, R. H. (1982). *Validity of non relativistic dipole approximation for forward Rayleigh scattering. Phys. Rev. A*, **26**, 651–653.

Schaupp, D., Schumacher, M., Smend, F., Rullhausen, P. & Hubbell, J. H. (1983). *Small-angle Rayleigh scattering of photons at high energies: tabulations of relativistic HFS modified atomic form factors. J. Phys. Chem. Ref. Data*, **12**, 467–511.

Scofield, J. (1973). *Theoretical photoionization cross sections from 1 to 1500 keV*. Report UCRL-51326. Lawrence Livermore National Laboratory, Livermore, USA.

Siddons, P. & Hart, M. (1983). *Simultaneous measurements of the real and imaginary parts of the X-ray anomalous dispersion using X-ray interferometers. EXAFS and near edge structure*, edited by A. Branconi, L. Incoccia & S. Stipcich, pp. 373–375. Berlin: Springer.

Smith, D. Y. (1987). *Anomalous X-ray scattering: relativistic effects in X-ray dispersion analysis. Phys. Rev. A*, **35**, 3381–3387.

Sorenson, L. O. (1994). *Diffraction anomalous fine structure*, edited by G. Materlik, C. J. Sparks & K. Fischer, pp. 389–420. Amsterdam: North Holland.

Stanglmeier, F., Lengeler, B., Weber, W., Gobel, H. & Schuster, M. (1992). *Determination of the dispersive correction f′(E) to the atomic form factor from X-ray reflection. Acta Cryst.* A**48**, 626–639.

Stearns, D. G. (1984). *Broadening of extended X-ray absorption fine structure ensuing from the finite lifetime of the K hole. Philos. Mag.* **49**, 541–558.

Stibius-Jensen, M. (1979). *Some remarks on the anomalous scattering factors for X-rays. Phys. Lett. A*, **74**, 41–44.

Stibius-Jensen, M. (1980). *Atomic X-ray scattering factors for forward scattering beyond the dipole approximation*. Personal communication.

Storm, E. & Israel, H. (1970). *Photon cross sections from 0.001 to 100 MeV for elements 1 through 100. Nucl. Data Tables*, A**7**, 565–681.

Suortti, P., Hastings, J. B. & Cox, D. E. (1985). *Powder diffraction with synchrotron radiation. II. Dispersion factors of Ni. Acta Cryst.* A**41**, 417–420.

Takama, T., Iwasaki, N. & Sato, S. (1980). *Measurement of X-ray Pendellösung intensity beats in diffracted white radiation from silicon wafers. Acta Cryst.* A**36**, 1025–1030.

Takama, T., Kobayashi, K., Hyogah, H., Wittono, G. & Sato, S. (1984). *Atomic scattering factors of Zn determined from measurement of Pendellösung intensity beats using white radiation. Jpn. J. Appl. Phys.* **23**, 11–14.

Takama, T., Kobayashi, K. & Sato, S. (1982). *Determination of the atomic scattering factor of aluminium by the Pendellösung-beat measurement using white radiation. Trans. Jpn. Inst. Met.* **23**, 153–160.

Takama, T. & Sato, S. (1982). *Atomic scattering factors of copper determined by Pendellösung beat measurements using white radiation. Philos. Mag.* **45**, 615–626.

Takama, T. & Sato, S. (1984). *Determination of the atomic scattering factors of germanium by means of the Pendellösung beat measurement using white radiation. Jpn. J. Appl. Phys.* **20**, 1183–1190.

Templeton, D. H. (1994). *X-ray resonance, then and now. Resonant anomalous X-ray scattering*, edited by G. Materlik, C. J. Sparks & K. Fischer, pp. 1–7. Amsterdam: North Holland.

Templeton, D. H. & Templeton, L. K. (1978). *Cesium hydrogen tartrate and anomalous dispersion of cesium. Acta Cryst.* A**34**, 368–373.

Templeton, D. H. & Templeton, L. K. (1985). *Tensor X-ray optical properties of the bromate ion. Acta Cryst.* A**41**, 133–142.

Templeton, D. H., Templeton, L. K., Philips, J. C. & Hodgson, K. O. (1980). *Anomalous scattering of X-rays by cesium and cobalt measured with synchrotron radiation. Acta Cryst.* A**36**, 436–442.

Thomas, L. H. (1927). *The calculation of atomic fields. Proc. Cambridge Philos. Soc.* **23**, 542–548.

Wagenfeld, H. (1975). *Theoretical computations of X-ray dispersion corrections. Anomalous scattering*, edited by S. Ramaseshan & S. C. Abrahams, pp. 12–23. Copenhagen: Munksgaard.

Waller, I. (1928). *Über eine verallgemeinerte Streuringsformel. Z. Phys.* **51**, 213–231.

Wang, M. S. (1986). *Relativistic dispersion relation for X-ray anomalous scattering factor. Phys. Ref. A*, **34**, 636–637.

Wang, M. S. & Pratt, R. H. (1983). *Importance of bound–bound transitions in the dispersion relation for calculation of soft-X-ray forward Rayleigh scattering from light elements. Phys. Rev. A*, **28**, 3115–3116.

4.2.6 (*cont.*)

Zachariasen, W. H. (1945). *Theory of X-ray diffraction in crystals*. New York: Dover.

4.3.1

Bethe, H. A. (1928). *Theorie der Beugung von Elektronen an Kristallen*. *Ann. Phys (Leipzig)*, **87**, 55–129.

Blackman, M. (1939). *On the intensities of electron diffraction rings*. *Proc. R. Soc. London Ser A*, **173**, 68–82.

Coulthard, M. A. (1967). *A relativistic Hartree–Fock atomic field calculation*. *Proc. Phys. Soc.* **91**, 44–49.

Cowley, J. M. & Moodie, A. F. (1957). *The scattering of electrons by atoms and crystals. I. A new theoretical approach*. *Acta Cryst.* **10**, 609–619.

Cromer, D. T. & Waber, J. T. (1974). *Atomic scattering factors for X-rays*. *International tables for X-ray crystallography*, Vol. IV, Section 2.2. Birmingham: Kynoch Press. (Present distributor Kluwer Academic Publishers, Dordrecht.)

Doyle, P. A. & Turner, P. S. (1968). *Relativistic Hartree–Fock X-ray and electron scattering factors*. *Acta Cryst.* A**24**, 390–397.

Fox, A. G., O'Keefe, M. A. & Tabbernor, M. A. (1989). *Relativistic Hartree–Fock X-ray and electron atomic scattering factors at high angles*. *Acta Cryst.* A**45**, 786–793.

Fujiwara, K. (1959). *Application of higher-order Born approximation to multiple elastic scattering of electrons in crystals*. *J. Phys. Soc. Jpn*, **14**, 1513–1524.

Fujiwara, K. (1961). *Relativistic dynamical theory of electron diffraction*. *J. Phys. Soc. Jpn*, **16**, 2226–2238.

Ibers, J. A. (1958). *Atomic scattering amplitudes for electrons*. *Acta Cryst.* **11**, 178–183.

International Tables for Crystallography (1992). Vol. B. Dordrecht: Kluwer Academic Publishers.

International Tables for X-ray Crystallography (1974). Vol. IV. Birmingham: Kynoch Press. (Present distributor Kluwer Academic Publishers, Dordrecht.)

MacGillavry, C. H. (1940). *Zur Prufung der Dynamischen Theorie der Elektronenbeugung an Kristallgitter*. *Physica (Utrecht)*, **7**, 329–343.

Mann, J. B. (1968). Los Alamos Scientific Laboratory Report LA3691, p. 168.

Peng, L. M. & Cowley, J. M. (1988). *Errors arising from numerical use of the Mott formula in electron image simulation*. *Acta Cryst.* A**44**, 1–5.

Rez, D., Rez, P. & Grant, I. (1994). *Dirac–Fock calculations of X-ray scattering factors and contributions to the mean inner potential for electron scattering*. *Acta Cryst.* A**50**, 481–497.

4.3.2

Bird, D. M. & King, Q. A. (1990). *Absorptive form factors for high-energy electron diffraction*. *Acta Cryst.* A**46**, 202–208.

Doyle, P. A. & Turner, P. S. (1968). *Relativistic Hartree–Fock X-ray and electron scattering factors*. *Acta Cryst.* A**24**, 390–397.

Fox, A. G., O'Keefe, M. A. & Tabbernor, M. A. (1989). *Relativistic Hartree–Fock X-ray and electron atomic scattering factors at high angles*. *Acta Cryst.* A**45**, 786–793.

Peng, L.-M. (1998). *Electron scattering factors of ions and their parameterization*. *Acta Cryst.* A**54**, 481–485.

Peng, L. M., Ren, G., Dudarev, S. L. & Whelan, M. J. (1996). *Robust parameterization of elastic and absorptive electron atomic scattering factors*. *Acta Cryst.* A**52**, 257–276.

Rez, D., Rez, P. & Grant, I. (1994). *Dirac–Fock calculations of X-ray scattering factors and contributions to the mean inner potential for electron scattering*. *Acta Cryst.* A**50**, 481–497.

Weickenmeier, A. & Kohl, H. (1991). *Computation of absorptive form factors for high-energy electron diffraction*. *Acta Cryst.* A**47**, 590–597.

4.3.3

Arnesen, S. P. & Seip, H. M. (1966). *Studies on the failure of the first Born approximation in electron diffraction. V. Molybdenum- and tungsten hexacarbonyl*. *Acta Chem. Scand.* **20**, 2711–2727.

Bartell, L. S. (1975). *Modification of Glauber theory for dynamic scattering of electrons by polyatomic molecules*. *J. Chem. Phys.* **63**, 3750–3755.

Bartell, L. S. & Brockway, L. O. (1953). *The investigation of electron distribution in atoms by electron diffraction*. *Phys Rev.* **90**, 833–838.

Bartell, L. S. & Gavin, R. M. Jr (1964). *Effects of electron correlation in X-ray and electron diffraction*. *J. Am. Chem. Soc.* **86**, 3493–3498.

Bartell, L. S. & Miller, B. (1980). *Extension of Glauber theory to account for intratarget diffraction in multicenter scattering*. *J. Chem. Phys.* **72**, 800–807.

Bartell, L. S. & Wong, T. C. (1972). *Three-atom scattering in gas-phase electron diffraction: a tractable limiting case*. *J. Chem. Phys.* **56**, 2364–2367.

Bethe, H. A. (1930). *Zur Theorie des Durchgangs Schneller Korpuskularstrahlen durch Materie*. *Ann. Phys. (Leipzig)*, **5**, 325–400.

Biggs, F., Mendelsohn, L. B. & Mann, J. B. (1975). *Hartree–Fock Compton profiles for the elements*. *At. Data Nucl. Data Tables*, **16**, 210–309.

Bonham, R. A. (1965*a*). *Multiple elastic intramolecular scattering in gas electron diffraction*. *J. Chem. Phys.* **43**, 1103–1109.

Bonham, R. A. (1965*b*). *Corrections to the incoherent scattering factor for electrons and X-rays*. *J. Chem. Phys.* **43**, 1460–1464.

Bonham, R. A. (1966). *Dynamic effects in gas electron diffraction*. *Trans. Am. Crystallogr. Assoc.* **2**, 165–172.

Bonham, R. A. (1967). *Some new relations connecting molecular properties and electron and X-ray diffraction intensities*. *J. Phys. Chem.* **71**, 856–862.

Bonham, R. A. & Cox, H. L. Jr (1967). *40-kV elecron scattering fom Ne, Ar, Kr, and Xe measured by the sector-microphotometer electron-diffraction method*. *J. Chem. Phys.* **47**, 3508–3517.

Bonham, R. A. & Fink, M. (1974). *High energy electron scattering*, Chaps. 5 and 6. New York: Van Nostrand Reinhold.

Bonham, R. A. & Iijima, T. (1965). *Preliminary electron-diffraction study of H_2 at small scattering angles*. *J. Chem. Phys.* **42**, 2612–2614.

Bonham, R. A. & Su, L. S. (1966). *Use of Hellman–Feynman and hyperviral theorems to obtain anharmonic vibration–rotation expectation values and their application to gas diffraction*. *J. Chem. Phys.* **45**, 2827–2831.

4.3.3 (*cont.*)

Breitenstein, M., Endesfelder, A., Meyer, H. & Schweig, A. (1984). *CI calculations of electron-scattering cross sections for some linear molecules. Chem. Phys. Lett.* **108**, 430–434.

Breitenstein, M., Endesfelder, A., Meyer, H., Schweig, A. & Zittlau, W. (1983). *Electron correlation effects in electron scattering cross-section calculations of N_2. Chem. Phys. Lett.* **97**, 403–409.

Breitenstein, M., Mawhorter, R. J., Meyer, H. & Schweig, A. (1984). *Theoretical study of potential-energy differences from high-energy electron scattering cross sections of CO_2. Phys. Rev. Lett.* **53**, 2398–2401.

Breitenstein, M., Mawhorter, R. J., Meyer, H. & Schweig, A. (1986). *Vibrational effects on electron–molecule scattering for polyatomics in the first Born approximation: H_2O. Mol. Phys.* **57**, 81–88.

Bunge, C. F., Barrientos, J. & Bunge, A. V. (1993). *Roothaan–Hartree–Fock ground-state atomic wave functions: Slater-type orbital expansions and expectation values. At. Data Nucl. Data Tables*, **53**, 113–162.

Bunyan, P. J. (1963). *The effect of multiple elastic scattering in gas electron diffraction. Proc. Phys. Soc.* **82**, 1051–1057.

Coffman, D., Fink, M. & Wellenstein, H. (1985). *Elastic small-angle electron scattering by He, Ne, and Ar at 35 keV. Phys. Rev. Lett.* **55**, 1392–1394.

Epstein, J. & Stewart, R. F. (1977). *X-ray and electron scattering from diatomic molecules in the first Born approximation. J. Chem. Phys.* **66**, 4057–4064.

Fink, M., Bonham, R. A., Lee, J. S. & Ng, E. W. (1969). *Large angle scattering from N_2 with 40 keV electrons. Chem. Phys. Lett.* **4**, 347–351.

Fink, M. & Kessler, J. (1966). *Absolute Wirkungsquerschnitte für Elektronenstreuung um Kleine Winkel. Experimente sum Gültigkeitsbereich der Ersten Bornschen Näherung. Z. Phys.* **196**, 1–15.

Geiger, J. (1964). *Streuung von 25 keV-Elektronen an Gasen. II. Streuung an Neon, Argon, Krypton und Xenon. Z. Phys.* **177**, 138–145.

Gjønnes, J. (1964). *A dynamic effect in electron diffraction by molecules. Acta Cryst.* **17**, 1075–1076.

Glauber, R. & Schomacher, V. (1953). *The theory of electron diffraction. Phys. Rev.* **89**, 667–671.

Hanson, H. P. (1962). *Experimental f values and electron diffraction amplitudes for bromine. J. Chem. Phys.* **36**, 1043–1049.

Heisenberg, W. (1931). *Über die Inkohärente Streuung von Röntgenstrahlen. Phys. Z.* **32**, 737–740.

Hilderbrandt, R. L. & Kohl, D. A. (1981). *A variational treatment of the effects of vibrational anharmonicity on gas-phase electron diffraction intensities. Part I. Molecular scattering function. J. Mol. Struct. Theochem.* **85**, 25–36.

Hoerni, J. A. (1956). *Multiple elastic scattering in electron diffraction by molecules. Phys. Rev.* **102**, 1530–1533.

Horota, F., Kakuta, N. & Shibata, S. (1981). *High energy electron scattering by diborane. J. Phys. B*, **14**, 3299–3304.

Iijima, T., Bonham, R. A. & Ando, T. (1963). *The theory of electron scattering from molecules. I. Theoretical development. J. Phys. Chem.* **67**, 1472–1474.

Karle, I. L. & Karle, J. (1950). *Internal motion and molecular structure studies by electron diffraction. III. Structure of CH_2CF_2 and CF_2CF_2. J. Chem. Phys.* **18**, 963–971.

Kelley, M. H. & Fink, M. (1982*a*). *The molecular structure of dimolybdenum tetraacetate. J. Chem. Phys.* **76**, 1407–1416.

Kelley, M. H. & Fink, M. (1982*b*). *The temperture dependence of the molecular structure parameters in SF_6. J. Chem. Phys.* **77**, 1813–1817.

Kessler, J. (1959). *Einzelstreuung Mittelschneller Elektronen an Schweren Atomkernen. Z. Phys.* **155**, 350–367.

Ketkar, S. N. & Fink, M. (1985). *Structure of dichromium tetraacetate by gas-phase electron diffraction. J. Am. Chem. Soc.* **107**, 338–340.

Kimura, M., Schomaker, V., Smith, D. & Weinstock, B. (1968). *Electron-diffraction investigation of the hexafluorides of tungsten, osmium, iridium, uranium, neptunium, and plutonium. J. Chem. Phys.* **48**, 4001–4012.

Kohl, D. A. & Arvedson, M. (1980). *Elastic electron scattering from molecular potentials. J. Chem. Phys.* **73**, 3818–3822.

Kohl, D. A. & Bartell, L. S. (1969). *Electron densities from gas-phase electron diffraction intensities. II. Molecular Hartree–Fock cross sections. J. Chem. Phys.* **51**, 2896–2904.

Kohl, D. A. & Bonham, R. A. (1967). *Effect of bond formation on electron scattering cross sections for molecules. J. Chem. Phys.* **47**, 1634–1646.

Kohl, D. A. & Hilderbrandt, R. L. (1981). *A variational treatment of the effects of vibrational anharmonicity on gas-phase electron diffraction intensities. Part II. Temperature dependence. J. Mol. Struct. Theochem.* **85**, 325–335.

Liu, J. W. & Smith, V. H. (1977). *A critical study of high energy electron scattering from H_2. Chem. Phys. Lett.* **45**, 59–63.

McClelland, J. J. & Fink, M. (1985). *Electron correlation and binding effects in measured electron-scattering cross sections of CO_2. Phys. Rev. Lett.* **54**, 2218–2221.

McLean, A. D. & McLean, R. S. (1981). *Roothaan–Hartree–Fock atomic wave functions: Slater basis-set expansions for $Z = 55$–92. At. Data Nucl. Data Tables*, **26**, 197–381.

Mawhorter, R. J. & Fink, M. (1983). *The vibrationally averaged, temperture-dependent structure of polyatomic molecules. II. SO_2. J. Chem. Phys.* **79**, 3292–3296.

Mawhorter, R. J., Fink, M. & Archer, B. T. (1983). *The vibrationally averaged, temperature-dependent strucure of polyatomic molecules. I. CO_2. J. Chem. Phys.* **79**, 170–174.

Melkanov, M. A., Sawada, T. & Raynal, J. (1966). *Nuclear optical model calculations. Meth. Comput. Phys.* **6**, 1–80.

Miller, B. R. & Fink, M. (1981). *Mean amplitudes of vibration of SF_6 and intramolecular multiple scattering. J. Chem. Phys.* **75**, 5326–5328.

Miller, B. R. & Fink, M. (1985). *The vibrationally averaged, temperature-dependent structure of polyatomic molecules. III. NO_2. J. Chem. Phys.* **83**, 939–944.

Morse, P. M. (1932). *Unelastische Streuung von Kathodenstrahlen. Phys. Z.* **33**, 443–445.

Mott, N. I. & Massey, H. S. W. (1965). *The theory of atomic collisions*, 3rd ed., Chap. IX, Section 4, equations (22) and (23). Oxford University Press.

Numerov, B. V. (1924). *A method of extrapolation of perturbations. Mon. Not. R. Astron. Soc.* **84**, 592–601.

Peixoto, E. M. A., Bunge, C. F. & Bonham, R. A. (1969). *Elastic and inelastic electron scattering by He and Ne atoms in their ground states. Phys. Rev.* **181**, 322–328.

Pulay, P., Mawhorter, R. J., Kohl, D. A. & Fink, M. (1983). *Ab initio Hartree–Fock calculation of the elastic electron scattering cross section of sulphur hexafluoride. J. Chem. Phys.* **79**, 185–191.

Ross, A. W. & Fink, M. (1986). *Atomic scattering factor and spin polarization calculations. Phys. Rev.* **85**, 6810–6811.

Sasaki, H., Konaka, S., Iijima, T. & Kimura, M. (1982). *Small-angle electron scattering and electron density in carbon dioxide. Int. J. Quantum Chem.* **21**, 475–485.

4.3.3 (*cont.*)

Schäfer, L. & Seip, H. M. (1967). *Studies on the failure of the first Born approximation in electron diffraction. VI. Ruthenium tetraoxide. Acta Chem. Scand.* **21**, 737–744.

Schomaker, V. & Glauber, R. (1952). *The Born approximation in electron diffraction. Nature (London)*, **170**, 290–291.

Seip, H. M. (1965). *Studies on the failiure of the first Born approximation in electron diffraction. I. Uranium hexafluoride. Acta Chem. Scand.* **19**, 1955–1968.

Seip, H. M. & Seip, R. (1966). *Studies on the failure of the first Born approximation in electron diffraction. IV. Molybdenum- and tungsten hexafluoride. Acta Chem. Scand.* **20**, 2698–2711.

Seip, H. M. & Stølevik, V. (1966). *Studies on the failure of the first Born approximation in electron diffraction. II. Osmium tetraoxide. III. Tellurium hexafluoride. Acta Chem. Scand.* **20**, 385–394, 1535–1545.

Shibata, S., Hirota, F., Kakuta, N. & Muramatsu, T. (1980). *Electron distribution in water by high-energy electron scattering. Int. J. Quantum Chem.* **18**, 281–285.

Tavard, C. & Bonham, R. A. (1969). *Quantum-mechanical formulas for the inelastic scattering of fast electrons and their Compton line shape. Nonrelativistic approximation. J. Chem. Phys.* **50**, 1736–1747.

Tavard, C., Rouault, M. & Roux, M. (1965). *Diffraction des rayons X et des électrons par les molécules. III. Une méthode de detémination des densités électroniques moléculaires. J. Chim. Phys.* **62**, 1410–1417.

Tavard, C. & Roux, M. (1965). *Calcul des intensités de diffraction de rayons X et de électrons par les molécules. C. R. Acad. Sci.* **260**, 4933–4936.

Thakkar, A. J. & Smith, V. H. Jr (1978). *Form factors and total scattering intensities for the helium-like ions from explicitly correlated wavefunctions. J. Phys. B*, **11**, 3803–3820.

Wang, J., Esquivel, R. O., Smith, V. H. Jr & Bunge, C. (1995). *Accurate elastic and inelastic scattering factors from He to Ne using correlated wavefunctions. Phys. Rev. A*, **51**, 3812–3818.

Wang, J., Sagar, R. P., Schmider, H. & Smith, V. H. Jr (1993). *X-ray elastic and inelastic scattering factors for neutral atoms $Z = 2 - 92$. At. Data Nucl. Data Tables*, **53**, 233–269.

Wang, J., Tripathi, A. N. & Smith, V. H. Jr (1994). *Chemical binding and electron correlation effects in X-ray and high energy electron scattering. J. Chem. Phys.* **101**, 4842–4854.

Wong, T. C. & Bartell, L. S. (1973). *Three atom scattering in gas-phase electron diffraction. II. A general treatment. J. Chem. Phys.* **58**, 5654–5660.

Xie, S.-D., Fink, M. & Kohl, D. A. (1984). *Basis set dependence of ab initio SCF elastic, Born, electron scattering cross sections for C_2H_4. J. Chem. Phys.* **81**, 1940–1942.

Yates, A. C. (1970). *Relativistic effects in high-energy inelastic electron–atom collisions. Chem. Phys. Lett.* **6**, 49–53.

Yates, A. C. (1971). *A program for calculating relativistic elastic electron–atom collision data. Comput. Phys. Commun.* **2**, 175–179.

Yates, A. C. & Bonham, R. A. (1969). *Use of relativistic electron scattering factors in electron diffraction analysis. J. Chem. Phys.* **50**, 1056–1058.

4.3.4

Ahn, C. C. & Krivanek, O. L. (1982). *An EELS atlas*. Available from Center for Solid State Science, Arizona State University, Tempe, AZ 85287, USA.

Ahn, C. C. & Rez, P. (1985). *Inner shell edge profiles in electron energy loss spectroscopy. Ultramicroscopy*, **17**, 105–116.

Altarelli, M. & Smith, S. Y. (1974). *Superconvergence and sum rules for the optical constants: physical meaning, comparison with experiment and generalization. Phys Rev. B*, **9**, 1290–1298.

Batson, P. E. (1986). *High energy resolution electron spectrometer for a 1 nm spatial analysis. Rev. Sci. Instrum* **57**, 43–48.

Batson, P. E. (1987). *Spatially resolved interband spectroscopy. Physical aspects of microscopic characterization of materials*, edited by J. Kirschner, K. Murata & J. A. Venables, pp. 189–195. *Scanning Microscopy*, Suppl. I.

Batson, P. E. (1989). *High resolution energy-loss spectroscopy. Ultramicroscopy*, **28**, 32–39.

Batson, P. E. & Silcox, J. (1983). *Experimental energy loss function, $Im[-1/\varepsilon(q,\omega)]$, for aluminium. Phys. Rev. B*, **27**, 5224–5239.

Berger, S. D. & McMullan, D. (1989). *Parallel recording for an electron spectrometer on a scanning transmission electron microscope. Ultramicroscopy*, **28**, 122–125.

Bethe, H. A. (1930). *Zur Theorie des Durchgangs schneller Korpuskularstrahlen durch Materie. Ann. Phys. (Leipzig)*, **5**, 325–400.

Bianconi, A., Fritsch, E., Calas, G. & Petiau, J. (1985). *X-ray absorption near edge structure of 3d transition elements in tetrahedral coordination: the effect of bond length variation. Phys. Rev. B*, **32**, 4292–4295.

Boersch, H. (1954). *Experimentelle Bestimmung der Energieverteilung in thermisch ausgelosten Elektronenstrahlen. Z. Phys.* **139**, 115–146.

Bross, H. (1978*a*). *Anisotropy of plasmon dispersion in Al. Phys. Lett. A*, **64**, 418–420.

Bross, H. (1978*b*). *Pseudopotential theory of the dielectric function of Al – the volume plasmon dispersion. J. Phys. F*, **8**, 2631–2649.

Brydson, R., Sauer, H., Engel, W., Thomas, J. M., Zeitler, E., Kosugi, N. & Kuroda, H. (1989). *Electron energy loss and X-ray absorption spectroscopy of rutile and anatase: a test of structural sensitivity. J. Phys. Condens. Matter,* **1**, 797–812.

Castaing, R. & Henry, L. (1962). *Filtrage magnétique des vitesses en microscopie électronique. C. R. Acad. Sci. Sér. B*, **255**, 76–78.

Chen, C. H. & Silcox, J. (1971). *Detection of optical surface guided modes in thin graphite films by high energy electron scattering. Phys. Rev. Lett.* **35**, 390–393.

Colliex, C. (1984). *Electron energy loss spectroscopy in the electron microscope. Advances in optical and electron microscopy,* Vol. 9, edited by V. E. Cosslett & R. Barer, pp. 65–177. London: Academic Press.

Colliex, C. (1985). *An illustrated review on various factors governing the high spatial resolution capabilities in EELS microanalysis. Ultramicroscopy*, **18**, 131–150.

Colliex, C., Gasgnier, M. & Trebbia, P. (1976). *Analysis of the electron excitation spectra in heavy rare earth metals, hydrides and oxides. J. Phys. (Paris)*, **27**, 397–406.

Colliex, C., Manoubi, T., Gasgnier, M. & Brown, L. M. (1985). *Near edge structures on EELS core-loss edges. Scanning Electron Microsc.* **2**, 489–512.

Colliex, C., Maurice, J. L. & Ugarte, D. (1989). *Frontiers of analytical electron microscopy with special reference to cluster and interface problems. Ultramicroscopy*, **29**, 31–43.

Craven, A. J. & Buggy, T. W. (1981). *Design considerations and performance of an analytical STEM. Ultramicroscopy*, **7**, 27–37.

4.3.4 (*cont.*)

Crewe, A. V. (1977*a*). *Post specimen optics in the STEM. I. General information. Optik (Stuttgart)*, **47**, 299-312.

Crewe, A. V. (1977*b*). *Post specimen optics in the STEM. II. Optik (Stuttgart)*, **47**, 371–380.

Daniels, J., Festenberg, C. V., Raether, H. & Zeppenfeld, K. (1970). *Optical constants of solids by electron spectroscopy. Springer tracts in modern physics*, Vol. 54, pp. 78–135. New York: Springer-Verlag.

Disko, M. M., Krivanek, O. L. & Rez, P. (1982). *Orientation dependent extended fine structure in EELS. Phys. Rev. B*, **25**, 4252–4255.

Durham, J. P., Pendry, J. B. & Hodges, C. H. (1981). *XANES: determination of bond angles and multi-atom correlations in ordered and disordered systems. Solid State Commun.* **8**, 159–162.

Egerton, R. F. (1978). *Formulae for light element analysis by electron energy loss spectrometry. Ultramicroscopy*, **3**, 243–351.

Egerton, R. F. (1979). *K-shell ionization cross sections for use in microanalysis. Ultramicroscopy*, **4**, 169–179.

Egerton, R. F. (1980*a*). *The use of electron lenses between a TEM specimen and an electron spectrometer. Optik (Stuttgart)*, **56**, 363–376.

Egerton, R. F. (1980*b*). *Design of an aberration-corrected electron spectrometer for the TEM. Optik (Stuttgart)*, **57**, 229–242.

Egerton, R. F. (1986). *Electron energy loss spectroscopy in the electron microscope*. New York/London: Plenum.

Egerton, R. F. & Crozier, P. A. (1987). *A compact parallel recording. J. Microsc.* **148**, 157.

Enge, H. A. (1967). *Deflecting magnets. Focusing of charged particles*, Vol. 2, edited by A. Septier, pp. 203–264. New York: Academic Press.

Engel, W., Sauer, H., Zeitler, E., Brydson, R., Williams, B. G. & Thomas, J. M. (1988). *Electron energy loss spectroscopy and the crystal chemistry of rhodizite. J. Chem. Soc. Faraday Trans. 1*, **84**, 617–629.

Fano, U. (1961). *Effects of configuration interaction on intensities and phase shifts. Phys. Rev.* **124**, 1966–1978.

Fink, J. & Kisker, E. (1980). *A method for rapid calculation of electron trajectories in multielement electrostatic cylinder lenses. Rev. Sci. Instrum.* **51**, 918–920.

Fink, J. & Leising, G. (1986). *Momentum dependent dielectric functions of oriented trans-polyacetylen. Phys. Rev. B*, **34**, 5320–5328.

Fink, J., Müller-Heinzerling, T., Pflüger, J., Scheerer, B., Dischler, B., Koidl, P., Bubenzer, A. & Sah, R. E. (1984). *Investigation of hydrocarbon-plasma-generated carbon films by EELS. Phys. Rev. B*, **30**, 4713–4718.

Fischer, D. W. (1970). *Molecular orbital interpretation of the soft X-ray L_{23} emission and absorption spectra from some titanium and vanadium compounds. J. Appl. Phys.* **41**, 3561–3569.

Gibbons, P. C., Ritsko, J. J. & Schnatterly, S. E. (1975). *Inelastic electron scattering spectrometer. Rev. Sci. Instrum.* **46**, 1546–1554.

Grunes, L. A., Leapman, R. D., Wilker, C. N., Hoffmann, R. & Kunz, A. B. (1982). *Oxygen K near-edge fine structure: an electron energy-loss investigation with comparisons to new theory for selected 3d transition-metal oxides. Phys. Rev. B*, **25**, 7157–7173.

Hagemann, H. J., Gudat, W. & Kunz, C. (1975). *Optical constants from the far infrared to the X-ray region: Mg, Al, Cu, Ag, Au, Bi, C, and Al_2O_3. J. Opt. Soc. Am.* **65**, 742–748.

Hartl, W. A. M. (1966). *Die Filterlinse als Monochromator für schnelle Elektronen. Z. Phys.* **191**, 487–502.

Heine, V. (1980). *Electronic structure from the point of view of the local atomic environment. Solid State Phys.* **35**, 1–127.

Hillier, J. & Baker, R. F. (1944). *Microanalysis by means of electrons. J. Appl. Phys.* **15**, 663–675.

Hitchcock, A. P. (1982). *Bibliography of atomic and molecular inner-shell excitation studies. J. Electron Spectrosc. Relat. Phenom.* **25**, 245–275. [Updated copies of this bibliography are available from the author on request.]

Hofer, F., Golob, P. & Brunegger, A. (1988). *EELS quantification of the elements Sr to W by means of M_{45} edges. Ultramicroscopy*, **25**, 81–84.

Hohberger, H. I., Otto, A. & Petri, E. (1975). *Plasmon resonance in Al, devations from quadratic dispersion observed. Solid State Commun.* **16**, 175–179.

Ibach, H. & Mills, D. L. (1982). *Electron energy-loss spectroscopy and surface vibrations*. New York: Academic Press.

Inokuti, M. (1971). *Inelastic collisions of fast charged particles with atoms and molecules. The Bethe theory revisited. Rev. Mod. Phys.* **43**, 297–344; *Addenda: Rev. Mod. Phys.* **50**, 23–26.

Inokuti, M. (1979). *Electron scattering cross sections pertinent to electron microscopy. Ultramicroscopy*, **3**, 423–427.

Isaacson, M. (1972*a*). *Interaction of 24 keV electrons with the nucleic acid bases, adenine, thymine and uracil. I. Outer shell excitation. J. Chem. Phys.* **56**, 1803–1812.

Isaacson, M. (1972*b*). *Interaction of 25 keV electsons with the nucleic acid bases, adenine, thymine and uracil. II. Inner shell excitation and inelastic scattering cross section. J. Chem. Phys.* **56**, 1813–1818.

Isaacson, M. & Johnson, D. (1975). *The microanalysis of light elements using transmitted energy-loss electrons. Ultramicroscopy*, **1**, 33–52.

Janssen, R. W. & Sankey, O. F. (1987). *Ab inito linear combination of pseudo-atomic orbital scheme for the electronic properties of semiconductors. Results for ten materials. Phys. Rev. B*, **36**, 6520–6531.

Johnson, D. E. (1979). *Basic aspects of energy-loss spectrometer systems. Ultramicroscopy*, **3**, 361–365.

Johnson, D. E. (1980). *Post specimen optics for energy loss spectrometry. Scanning Electron. Microsc.* **1**, 33–40.

Johnson, D. W. (1975). *A Fourier method for numerical Kramers–Kronig analysis. J. Phys. A*, **8**, 490–495.

Johnson, D. W. & Spence, J. C. H. (1974). *Determination of the single scattering probability distribution from plural scattering data. J. Phys. D*, **7**, 771–780.

Jouffrey, B., Sevely, J., Zanchi, G. & Kihn, Y. (1985). *Characteristic energy losses with high energy electrons up to 2.5 MeV. Scanning Electron Microsc.* **3**, 1063–1070.

Keil, P. (1968). *Elektronen-Energieverlustmessungen und Berechnung optischer Konstanten. I. Festes Xenon. Z. Phys.* **214**, 251–265.

Killat, U. (1974). *Optical properties of C_6H_{12}, C_6H_{10}, C_6H_8, C_6H_6, C_7H_8, C_6H_5Cl and C_5H_5N in the solid and gaseous state derived from electron energy losses. J. Phys. C*, **7**, 2396–2408.

Klemperer, O. (1965). *Electron beam spectroscopy. Rev. Prog. Phys.* **28**, 77–111.

Kliewer, K. & Fuchs, R. (1974). *Theory of dynamical properties of dielectric surfaces. Adv. Chem. Phys.* **27**, 355–541.

4.3.4 (*cont.*)

Krahl, D. & Herrmann, K. H. (1980). *Experiments with an imaging energy filter in the CTEM*. *Micron*, **11**, 287–289.

Krivanek, O. L., Ahn, C. C. & Keeney, R. B. (1987). *Parallel detection electron spectrometer using quadrupole lens*. *Ultramicroscopy*, **22**, 103–115.

Krivanek, O. L., Manoubi, T. & Colliex, C. (1985). *Sub 1 eV resolution EELS at energy losses greater than 1 keV*. *Ultramicroscopy*, **18**, 155–158.

Krivanek, O. L. & Swann, P. R. (1981). *An advanced electron energy loss spectrometer*. *Quantitative microanalysis with high spatial resolution*, pp. 136–140. London: The Metals Society.

Kröger, E. Z. (1970). *Transition radiation, Čerenkov radiation and energy losses of relativistic charged particles traversing thin foils at oblique incidence*. *Z. Phys.* **235**, 403–421.

Kuyatt, C. E. & Simpson, J. A. (1967). *Electron monochromator design*. *Rev. Sci. Instrum.* **38**, 103–111.

Landau, L. & Lifchitz, E. (1966). *Mécanique quantique. Théorie non relativiste*, pp. 632–690. Moscow: Editions Mir.

Leapman, R. D., Grunes, L. A. & Fejes, P. L. (1982). *Study of the L_{23} edges in the 3d transition metals and their oxides by electron energy loss spectroscopy with comparisons to theory*. *Phys. Rev. B*, **26**, 614–635.

Leapman, R. D., Rez, P. & Mayers, D. F. (1980). *K, L and M shell generalized oscillator strengths and ionization cross sections for fast electron collisions*. *J. Chem. Phys.* **72**, 1232–1243.

Leapman, R. D. & Swyt, C. R. (1988). *Separation of overlapping core edges in EELS spectra by mutiple least-squares fitting*. *Ultramicroscopy*, **26**, 393–404.

Lindhard, J. (1954). *On the properties of a gas of charged particles*. *Dan. Vidensk. Selsk. Mat. Fys. Medd.* **28**, 1–57.

Lindner, T., Sauer, H., Engel, W. & Kambe, K. (1986). *Near-edge structure in electron energy loss spectra of MgO*. *Phys. Rev. B*, **33**, 22–24.

Livingood, J. J. (1969). *The optics of dipole magnets*. New York: Academic Press.

Lytle, F. W., Greegor, R. B. & Panson, A. Y. (1988). *Discussion of X-ray asorption near edge structure: application to Cu in the high T_c superconductors $La_{1.8}Sr_{0.2}Cu_4$ and $YBa_2Cu_3O_7$*. *Phys. Rev. B*, **37**, 1550–1562.

Maher, D. M. (1979). *Elemental analysis using inner-shell excitations: a microanalytical technique for materials characterization*. *Introduction to analytical electron microscopy*, edited by J. J. Hren, J. I. Goldstein & D. C. Joy, pp. 259–294. New York: Plenum.

Manoubi, T., Rez, P. & Colliex, C. (1989). *Quantitative electron energy loss spectroscopy on M_{45} edges in rare earth oxides*. *J. Electron Spectrosc. Relat. Phenom.* **50**, 1–18.

Manoubi, T., Tence, M., Walls, M. G. & Colliex, C. (1990). *Curve fitting methods for quantitative analysis in EELS*. *Microsc. Microanal. Microstruct.* **1**, 23–39.

Manzke, R. (1980). *Wavevector dependence of the volume plasmon of GaAs and InSb*. *J. Phys. C*, **13**, 911–917.

Maslen, V. M. & Rossouw, C. J. (1983). *The inelastic scattering matrix element and its application to electron energy loss spectroscopy*. *Philos. Mag.* A**47**, 119–130.

Metherell, A. J. F. (1971). *Energy analysing and energy selecting electron microscopes*. *Adv. Opt. Electron Microsc.* **4**, 263–361.

Mory, C. & Colliex, C. (1989). *Elemental analysis near the single-atom detection level by processing sequences of energy-filtered images*. *Ultramicroscopy*, **28**, 339–346.

Mott, N. F. & Massey, H. S. W. (1952). *The theory of atomic collisions*, pp. 224–248. Oxford: Clarendon Press.

Müller, J. E., Jepsen, O. & Wilkins, J. W. (1982). *X-ray absorption spectra: K edges of 3d transition metals, L edges of 3d and 4d metals and M edges of palladium*. *Solid State Commun.* **42**, 365–368.

Parker, N. W., Utlaut, M. & Isaacson, M. S. (1978). *Design of magnetic spectrometers with second order aberrations corrected*. *Optik (Stuttgart)*, **51**, 333–351.

Pearce-Percy, H. T. (1978). *The design of spectrometers for energy loss spectroscopy*. *Scanning Electron Microsc.* **1**, 41–51.

Powell, C. J. (1976). *Cross sections for ionization of inner-shell electrons by electrons*. *Rev. Mod. Phys.* **48**, 33–47.

Powell, C. J. (1984). *Inelastic scattering of electrons in solids*. *Electron beam interactions with solids for microscopy, microanalysis and micro-lithography*, edited by D. F. Kyser, H. Niedrig, D. E. Newbury & R. Shimizu, pp. 19–31. Chicago: SEM, Inc,.

Powell, C. J. (1989). *Cross sections for inelastic electron scattering in solids*. *Ultramicroscopy*, **28**, 24–31.

Raether, H. (1965). *Electron energy loss spectroscopy*. *Springer Tracts Mod. Phys.* Vol. 38, pp. 85–170. Berlin: Springer.

Raether, H. (1980). *Excitation of plasmons and interband transitions by electrons*. *Springer Tracts in Modern Physics*, Vol. 88. Berlin: Springer.

Rao, C. N., Thomas, J. M., Williams, B. G. & Sparrow, T. G. (1984). *Determination of the number of d-electron states in transition metal compounds*. *J. Phys. Chem.* **88**, 5769–5770.

Rask, J. H., Miner, B. A. & Buseck, P. (1987). *Determination of manganese oxidation states in solids by EELS*. *Ultramicroscopy*, **21**, 321–326.

Reimer, L. & Rennekamp. R. (1989). *Imaging and recording of multiple scattering effects by angular resolved electron energy loss spectroscopy*. *Ultramicroscopy*, **28**, 258–265.

Rez, P. (1989). *Inner shell spectroscopy: an atomic view*. *Ultramicroscopy*, **28**, 16–23.

Ritchie, R. H. (1957). *Plasmon losses by fast electrons in thin films*. *Phys. Rev.* **106**, 874–881.

Rose, H. & Plies, E. (1974). *Entwurf eines fehlerarmen magnetischen Energie Analysators*. *Optik (Stuttgart)*, **40**, 336–341.

Rose, H. & Spehr, R. (1980). *On the theory of the Boersch effect*. *Optik (Stuttgart)*, **57**, 339–364.

Sayers, D. E., Stern, E. A. & Lytle, F. W. (1971). *New technique for investigating noncrystalline structures: Fourier analysis of the extended X-ray absorption fine structure*. *Phys. Rev. Lett.* **27**, 1204–1207.

Schattschneider, P. (1983). *A performance test of the recovery of single energy loss profiles via matrix analysis*. *Ultramicroscopy*, **11**, 321–322.

Schattschneider, P. (1989). *The dielectric description of inelastic electron scattering*. *Ultramicroscopy*, **28**, 1–15.

Scheinfein, M. & Isaacson, M. S. (1984). *Design and performance of second order aberration corrected spectrometers for use with the scanning transmission electron microscope*. *Scanning Electron Microsc.* **4**, 1681–1696.

Scheinfein, M. & Isaacson, M. S. (1986). *Electronic and chemical analysis of fluoride interface structures at subnanometer spatial resolution*. *J. Vac. Sci. Technol.* B**4**, 326–332.

Schnatterly, S. E. (1979). *Inelastic electron scattering spectroscopy*. *Solid State Phys.* **14**, 275–358.

Schröder, B. & Geiger, J. (1972). *Electron spectrometric study of amorphous germanium and silicon in the two phonon region*. *Phys. Rev. Lett.* **28**, 301–303.

4.3.4 (*cont.*)

Sevely, J. (1985). *Voltage dependence in electron energy loss spectroscopy*. *Inst. Phys. Conf. Ser.* **78**, 155–160.

Shiles, E., Sazaki, T., Inokuti, M. & Smith, D. Y. (1980). *Self consistency and sum-rule tests in the Kramers Kronig analysis of optical data: applications to aluminium*. *Phys. Rev. B*, **22**, 1612–1628.

Shuman, H. (1980). *Correction of the second order aberrations of uniform field magnetic sections*. *Ultramicroscopy*, **5**, 45–53.

Shuman, H. & Kruit, P. (1985). *Quantitative data processing of parallel recorded electron energy-loss spectra with low signal to background*. *Rev. Sci. Instrum.* **56**, 231–239.

Shuman, H. & Somlyo, A. P. (1987). *Electron energy loss analysis of near-trace-element concentrations of calcium*. *Ultramicroscopy*, **21**, 23–32.

Spence, J. C. H. (1979). *Uniqueness and the inversion problem of incoherent multiple scattering*. *Ultramicroscopy*, **4**, 9–12.

Spence, J. C. H. (1981). *The crystallographic information in localized characteristic-loss electron images and diffraction patterns*. *Ultramicroscopy*, **7**, 59–64.

Spence, J. C. H. (1988). *Inelastic electron scattering: Parts I and II*. *High resolution transmission electron microscopy and associated techniques*, edited by P. R. Buseck, J. M. Cowley & L. Eyring, pp. 129–189. Oxford University Press.

Spence, J. C. H. & Tafto, J. (1983). *ALCHEMI: a new technique for locating atioms in small crystals*. *J. Microsc.* **130**, 147–154.

Stohr, J., Sette, F. & Johnson, A. L. (1984). *Near edge X-ray absorption fine structure studies of chemisorbed hydrocarbons: bond lengths with a ruler*. *Phys. Rev. Lett.* **53**, 1684–1687.

Strauss, M. G., Naday, Y., Sherman, I. S. & Zaluzec, N. J. (1987). *CCD base parallel detection system for EELS spectroscopy and imaging*. *Ultramicroscopy*, **22**, 117–124.

Sturm, K. (1982). *Electron energy loss in simple metals and semiconductors*. *Adv. Phys.* **31**, 1–64.

Swyt, C. R. & Leapman, R. D. (1982). *Plural scattering in electron energy loss analysis*. *Scanning Electron Microsc.* **1**, 73–82.

Taft, E. A. & Philipp, H. R. (1965). *Optical properties of graphite*. *Phys. Rev. A*, **138**, 197–202.

Tafto, J. & Krivanek, O. L. (1982). *Site specific valence determination by EELS*. *Phys. Rev. Lett.* **48**, 560–563.

Tafto, J. & Zhu, J. (1982). *Electron energy-loss near edge structure (ELNES), A potential technique in the studies of local atomic arrangements*. *Ultramicroscopy*, **9**, 349–354.

Teo, B. K. & Joy, D. C. (1981). *EXAFS spectroscopy techniques and applications*. New York: Plenum.

Thole, B. T., van der Laan, G., Fuggle, J. C., Sawatsky, G. A., Karnatak, R. C. & Esteva, J. M. (1985). *3d X-ray absorption lines and the $3d^9 4f^{n+1}$ multiplets of the lanthanides*. *Phys. Rev. B*, **32**, 5107–5118.

Tossel, J. A., Vaughan, D. J. & Johnson, K. H. (1974). *The electronic structure of rutile, wustite and hematite from molecular orbital calculations*. *Am. Mineral.* **59**, 319–334.

Trebbia, P. (1988). *Unbiased method for signal estimation in EELS. Concentration measurements and detection limits in quantitative analysis: methods and programs*. *Ultramicroscopy*, **24**, 399–408.

Venghaus, H. (1975). *Redetermination of the dielectric function of graphite*. *Phys. Status Solidi B*, **71**, 609–614.

Von Festenberg, C. (1968). *Retardierungseffekte im Energieverlustspektrum von GaP*. *Z. Phys.* **214**, 464.

Vvedensky, D. D., Saldin, D. K. & Pendry, J. B. (1985). *Azimuthal and polar angle dependence in XANES of low symmetry adsorption sites*. *Surf. Sci.* **162**, 909–912.

Wehenkel, C. (1975). *Mise au point d'une nouvelle méthode d'analyse quantitative des spectres de pertes d'énergie d'électrons rapides diffusés dans la direction du faisceau incident: application à l'étude des métaux nobles*. *J. Phys. (Paris)*, **36**, 199–207.

Weng, X. D. & Rez, P. (1989). *Multiple scattering approach to oxygen K near edge structures in EELS spectroscopy of alkaline earths*. *Phys. Rev. B*, **39**, 7405–7412.

Weng, X. D., Rez, P. & Ma, H. (1989). *Carbon K-shell near-edge structure: multiple scattering and band theory calculations*. *Phys. Rev. B*, **40**, 4175–4178.

Weng, X. D., Rez, P. & Sankey, O. F. (1989). *Pseudo-atomic orbital band theory applied to EELS near edge structures*. *Phys. Rev. B*, **40**, 5694–5704.

Wien, W. (1897). *Vert. Deutschen Phys. Res.* **16**, 165.

Williams, B. G. & Bourdillon, A. J. (1982). *Localised Compton scattering using EELS*. *J. Phys. C*, **15**, 6881–6890.

Williams, B. G., Sparrow, T. G. & Egerton, R. F. (1984). *Electron Compton scattering from solids*. *Proc. R. Soc. London Ser. A*, **393**, 409–422.

Zaanen, J., Sawatsky, G. A., Fink, J., Speier, W. & Fuggle, J. C. (1985). *L_{23} absorption spectra of the lighter 3d transition metals*. *Phys. Rev. B*, **32**, 4905–4913.

Zanchi, G., Perez, J. P. & Sevely, J. (1975). *Adaptation of magnetic filtering device on a one megavolt electron microscope*. *Optik (Stuttgart)*, **43**, 495–501.

Zanchi, G., Sevely, J. & Jouffrey, B. (1977). *Second order image aberration of a one megavolt magnetic filter*. *Optik (Stuttgart)*, **48**, 173–192.

Zimmermann, S. (1976). *The dielectric function of InSb determined by electron energy losses*. *J. Phys. C*, **9**, 2643–2649.

4.3.5

Barrett, C. S. & Massalski, T. B. (1980). *Structure of metals*, 3rd revised ed. Oxford: Pergamon Press.

Bernal, J. D. (1926). *On the interpretation of X-ray single-crystal rotation photographs*. *Proc. R. Soc. London Ser. A*, **113**, 117–160.

Bunge, H.-J. (1982). *Texture analysis in materials science*. London: Butterworth.

Gritsaenko, G. S., Zvyagin, B. B., Boyarskaya, R. V., Gorshkov, A. I., Samotoin, N. D. & Frolova, K. E. (1969). *Methods of electron microscopy of minerals*. Moscow: Nauka.

Guinier, A. (1956). *Théorie et technique de la radiocristallographie,* 2nd ed. Paris: Dunod.

Kakudo, M. & Kasai, N. (1972). *X-ray diffraction by polymers*. Tokyo: Kodanska; Amsterdam: Elsevier.

Krinary, G. A. (1975). *On the possibilities to use oriented specimens for recording of non-basal X-ray reflexions of fine-grained layer silicates*. *Crystal chemistry of minerals and geological problems*, pp. 132–138. Moscow: Nauka.

Mamy, J. & Gaultier, J.-P. (1976). *Evolution structurale de la montmorillonite associée au phénomène de fixation irréversible du potassium*. *An. Agron.* **27**(1), 1–16.

Méring, J. (1949). *L'interférence des rayons X dans les systèmes à stratification désordonnée*. *Acta Cryst.* **2**, 371–377.

Pinsker, Z. G. (1953). *Electron diffraction*. London: Butterworth.

4.3.5 (*cont.*)

Plançon, A., Rousseaux, F., Tchoubar, D., Tchoubar, C., Krinari, G. & Drits, V. A. (1982). *Recording and calculation of hk rod intensities in case of diffraction by highly oriented powders of lamellar samples. J. Appl. Cryst.* **15**, 509–512.

Vainshtein, B. K. (1964). *Structure analysis by electron diffraction*. Oxford: Pergamon Press.

Warren, B. E. (1941). *X-ray diffraction in random layer lattices. Phys. Rev.* **59**, 693–698.

Wilson, A. J. C. (1949). *Diffraction by random layers: ideal line profiles and determination of structure amplitudes from observed line profiles. Acta Cryst.* **2**, 245–251.

Wilson, A. J. C. (1962). *X-ray optics,* 2nd ed. London: Methuen.

Zhukhlistov, A. P., Avilov, A. S., Ferraris, G., Zvyagin, B. B. & Plotnikov, V. P. (1997). *Statistical distribution of hydrogen over three positions in brucite $Mg(OH)_2$ structure from electron diffractometry data. Crystallogr. Rep.* **42**, 774–777.

Zvyagin, B. B. (1967). *Electron diffraction analysis of clay mineral structures*. New York: Plenum.

Zvyagin, B. B., Vrublevskaya, Z. V., Zhukhlistov, A. P., Sidorenko, O. V., Soboleva, S. V. & Fedotov, A. F. (1979). *High-voltage electron diffraction in the study of layered minerals*. Moscow: Nauka.

Zvyagin, B. B., Zhukhlistov, A. P. & Plotnikov, V. P. (1996). *The development of electron diffractometry of minerals. Structural studies of crystals (For the 75th birthday of B. K. Vainshtein)*, pp. 225–234. Moscow: Nauka Physmathgis.

4.3.6.1

Cowley, J. M. (1975). *Diffraction physics*. New York: North-Holland.

Goodman, P. & Moodie, A. F. (1974). *Numerical evaluation of N-beam wave functions in electron scattering by the multislice method. Acta Cryst.* A**30**, 280–290.

4.3.6.2

International Tables for Crystallography (1996). Vol. B. Dordrecht: Kluwer Academic Publishers.

Hirsch, P. B., Howie, A., Nicholson, R. B., Pashley, D. W. & Whelan, M. J. (1977). *Electron microscopy of thin crystals*. New York: Krieger.

Howie, A. & Basinski, Z. S. (1968). *Approximations of the dynamical theory of diffraction contrast. Philos. Mag.* **17**, 1039–1063.

Humphreys, C. J. & Hirsch, P. B. (1968). *Absorption parameters in electron diffraction theory. Philos. Mag.* **18**, 115–122.

Jones, P. M., Rackham, G. M. & Steeds, J. W. (1977). *High-order Laue zone electron diffraction. Proc. R. Soc. London Ser. A*, **354**, 192–222.

Pendry, J. B. (1974). *Low energy electron diffraction*. New York: Academic Press.

4.3.7

Ackermann, I. (1948). *Observations on the dynamical interference phenomena in convergent electron beams. II. Ann. Phys. (Leipzig)*, **2**, 41–54.

Andersson, B. (1975). *Structure analysis of the γ-phase in the vanadium oxide system by electron diffraction studies. Acta Cryst.* A**31**, 63–70.

Ando, Y., Ichimiya, A. & Uyeda, R. (1974). *A determination of values and signs of the 111 and 222 structure factors of silicon. Acta Cryst.* A**30**, 600–601.

Bird, D. M. (1990). *Absorption in high-energy electron diffraction from non-centrosymmetrical crystals. Acta Cryst.* A**46**, 208–214.

Bird, D. M. & Saunders, M. (1992). *Inversion of convergent-beam electron diffraction patterns. Acta Cryst.* A**48**, 555–562.

Blake, R. G., Jostsons, A., Kelly, P. M. & Napier, J. G. (1978). *The determination of extinction distances and anomalous absorption coefficients by scanning electron microscopy. Philos. Mag.* A**37**, 1–16.

Buxton, B. F. (1976). *Bloch waves in high order Laue zone effects in high energy electron diffraction. Proc. R. Soc. London Ser. A*, **300**, 335–361.

Cowley, J. M. (1961). *Diffraction intensities from bent crystals. Acta Cryst.* **14**, 920–926.

Dorset, D. L. (1991). *Is electron crystallography possible? The direct determination of organic crystal structures. Ultramicroscopy*, **38**, 23–40.

Dorset, D. L., Jap, B. K., Ho, M. M. & Glaeser, R. M. (1979). *Direct phasing of electron diffraction data from organic crystals: the effect of n-beam dynamical scattering. Acta Cryst.* A**35**, 1001–1009.

Fox, A. G. & Fisher, R. M. (1988). *A summary of low-angle X-ray atomic scattering factors measured by the critical voltage effect in high energy electron diffraction. Aust. J. Phys.* **41**, 461–468.

Fox, A. G. & Tabbernor, M. A. (1991). *The bonding charge density of β′NiAl″. Acta Metall.* **39**, 669–678.

Fujiyoshi, Y., Mizusaki, T., Morikawa, K., Yamagishi, H., Aoki, Y., Kihara, H. & Harada, Y. (1991). *Development of a superfluid helium stage for high-resolution electron microscopy. Ultramicroscopy*, **38**, 241–251.

Fukuhara, A. (1966). *Many-ray approximation in the dynamical theory of electron diffraction. J. Phys. Soc. Jpn*, **21**, 2645–2662.

Gjønnes, J. & Høier, R. (1971). *The application of non-systematic many-beam dynamic effects to structure-factor determination. Acta Cryst.* A**27**, 313–316.

Gjønnes, K. & Bøe, N. (1994). *Refinement of temperature factors and charge distributions in $YBa_2Cu_3O_7$ and $YBa_2(Cu,Co)_3O_7$ from CBED intensities. Micron Microsc. Acta*, **25**, 29–44.

Glazer, J., Ramesh, R., Hilton, M. R. & Sarikaya, M. (1985). *Comparison of convergent beam electron diffraction methods for determination of foil thickness. Philos. Mag.* A**52**, 59–63.

Goodman, P. (1976). *Examination of the graphite structure using convergent-beam electron diffraction. Acta Cryst.* A**32**, 793–798.

Goodman, P. & Lehmpfuhl, G. (1967). *Electron diffraction study of MgO h00 systematic interactions. Acta Cryst.* **22**, 14–24.

Høier, R. (1972). *Displaced lines in Kikuchi patterns. Phys. Status Solidi A*, **11**, 597–610.

Høier, R., Bakken, L. N., Marthinsen, K. & Holmestad, R. (1993). *Structure factor determination in non-centrosymmetrical crystals by a two-dimensional CBED-based multi-parameter refinement method. Ultramicroscopy,* **49**, 159–170.

Holmestad, R., Weickenmeier, A. L., Zuo, J. M., Spence, J. C. H. & Horita, Z. (1993). *Debye–Waller factor measurement in TiAl from HOLZ reflections. Electron microscopy and analysis 1993,* pp. 141–144. Bristol: IOP Publishing.

4.3.7 (*cont.*)

Howie, A. (1963). *Inelastic scattering of electrons by crystals. I. The theory of small angle inelastic scattering*. *Proc. R. Soc. London Ser. A*, **271**, 268–287.

Kambe, K. (1957). *Study of simultaneous reflections in electron diffraction by crystals*. *J. Phys. Soc. Jpn*, **12**, 13–36.

Kelly, P. M., Jostsons, A., Blake, R. G. & Napier, J. G. (1975). *The determination of foil thickness by scanning transmission electron microscopy*. *Phys. Status Solidi A*, **31**, 771–780.

Kogiso, M. & Takahashi, H. (1977). *Group-theoretical method in the many-beam theory in electron diffraction*. *J. Phys Soc. Jpn*, **42**, 223–229.

Krahl, D., Pätzold, H. & Swoboda, M. (1990). *An aberration-minimized imaging energy filter of simple design*. Proceedings of 12th International Conference on Electron Microscopy 1990, Vol. 2, pp. 60–61.

Krivanek, O. L., Gubbens, A. J., Dellby, N. & Meyer, C. E. (1991). *Design and first applications of a post-column imaging filter*. *Microsc. Microanal. Microstruct. (France)*, **3**, 187–199.

Krivanek, O. L., Mooney, P. E., Fan, G. Y., Leber, M. L. & Meyer, C. E. (1991). *Slow-scan CCD cameras for transmission electron microscopy*. *Electron microscopy and analysis 1991*, pp. 523–526. Bristol: IOP Publishing.

Kühlbrandt, W., Wang, D. N. & Fujiyoshi, Y. (1994). *Atomic model of plan light-harvesting complex by electron crystallography*. *Nature (London)*, **367**, 614–621.

Lehmpfuhl, G. (1974). *Dynamical interaction of electron waves in a perfect single crystal*. *Z. Naturforsch. Teil A*, **27**, 424–433.

Ma, Y., Rømming, C., Lebech, B. & Gjønnes, J. (1992). *Structure refinement of Al_3Zr using single-crystal X-ray diffraction, powder neutron diffraction and CBED*. *Acta Cryst.* B**48**, 11–16.

Marthinsen, K., Holmestad, R. & Høier, R. (1994). *Analytical filtering of low-angle inelastic scattering contributions to CBED contrast*. *Ultramicroscopy*, **55**, 268–275.

Matsuhata, H. & Gjønnes, J. (1994). *Bloch-wave degeneracies and non-systematic critical voltage: a method for structure-factor determination*. *Acta Cryst.* A**50**, 107–115.

Matsuhata, H. & Steeds, J. W. (1987). *Observation of accidental Bloch-wave degeneracies of zone-axis critical voltge*. *Philos. Mag.* B**55**, 39–54.

Matsuhata, H., Tomokiyo, Y., Watanabe, H. & Eguchi, T. (1984). *Determination of the structure factors of Cu and Cu_3Au by the intersecting Kikuchi-line method*. *Acta Cryst.* B**40**, 544–549.

Mori, N., Oikawa, T. & Harada, Y. (1990). *Development of the imaging plate for the transmission electron microscope and its characteristics*. *J. Electron Microsc. (Japan)*, **39**, 433–436.

Olsen, A., Goodman, P. & Whitfield, H. (1985). *Tl_3SbS_3, Tl_3SbSe_3, $Tl_3Sb_{3-x}Se_x$ and $Tl_3Sb_yAs_{1-y}Se_3$*. *J. Solid State Chem.* **60**, 305–315.

Saunders, M., Bird, D. M., Midgley, P. A. & Vincent, R. (1994). *Structure factor refinement by zone-axis CBED pattern matching*. Proceedings of 13th International Congress on Electron Microscopy, Paris, France, 17–22 July 1994, Vol. 1, pp. 847–848.

Spargo, A. E. C. (1994). *Electron crystallography and crystal structure*. Proceedings of 13th International Congress on Electron Microscopy, Paris, France, 17–22 July 1994, Vol. 1, pp. 959–960.

Spence, J. C. H. & Zuo, J. M. (1992). *Electron microdiffraction*. New York: Plenum.

Steeds, J. W. (1984). *Further development in the analysis of convergent beam electron diffraction (CBED) data. EMAG 1983. Inst. Phys. Conf. Ser.* No. 69, pp. 31–36.

Taftø, J. & Gjønnes, J. (1985). *The intersecting Kikuchi line technique: critical voltage at any voltage*. *Ultramicroscopy,* **17**, 329–334.

Taftø, J. & Metzger, T. H. (1985). *Large-angle convergent-beam electron diffraction; a simple technique for the study of modulated structures with application to V_2D*. *J. Appl. Cryst.* **18**, 110–113.

Tanaka, M. & Tsuda, K. (1990). *Determination of positional parameters by convergent-beam electron diffraction*. Proceedings of 12th International Congress on Electron Microscopy 1990, Vol. 2, pp. 518–519.

Terasaki, O., Watanabe, D. & Gjønnes, J. (1979). *Determination of crystal structure factor of Si by the intersecting-Kikuchi-line method*. *Acta Cryst.* A**35**, 895–900.

Unwin, P. N. T. & Henderson, R. J. (1975). *Three-dimensional model of purple membrane obtained by electron microscopy*. *Mol. Biol.* **94**, 425–430.

Vincent, R., Bird, D. M. & Steeds, J. W. (1984). *Structure of AuGeAs determined by convergent beam electron diffraction. II. Refinement of structural parameters*. *Philos. Mag.* A**50**, 765–786.

Vincent, R. & Midgley, P. A. (1994). *Double conical beam-rocking system for measurement of integrated electron diffraction intensities*. *Ultramicroscopy*, **53**, 271–284.

Voigt-Martin, I. G., Yan, D. H., Gilmore, C. J., Shankland, K. & Bricogne, G. (1994). *The use of maximum entropy and likelihood ranking to determine the crystal structure of 4-[4′-(N-dimethylamino)benzylidene]pyrazolidine-3,5-dione at 1.4 Å resolution from electron diffraction and high-resolution electron microscopy image data*. *Ultramicroscopy*, **56**, 271–288.

Voss, R., Lehmpfuhl, G. & Smith, D. J. (1980). *Influence of doping on the crystal potential of silicon investigated by the convergent beam electron diffraction technique*. *Z. Naturforsch. Teil A*, **35**, 973–984.

Watanabe, D., Uyeda, R. & Fukuhara, A. (1969). *Determination of the atomic form factor by high–voltage electron diffraction*. *Acta Cryst.* A**25**, 138–140.

Zou, X. D., Sukharev, Y. & Hovmöller, S. (1993). *ELD – a computer program for extracting intensities from electron diffraction patterns*. *Ultramicroscopy,* **49**, 147–158.

Zuo, J. M., Høier, R. & Spence, J. C. H. (1989). *Three-beam and many-beam theory in electron diffraction and its use for structure-factor phase determination in non-centrosymmetrical crystal structures*. *Acta Cryst.* A**45**, 839–851.

Zuo, J. M., Spence, J. C. H., Downs, J. & Mayer, J. (1993). *Measurement of individual structure-factor phases with tenth-degree accuracy: the 00.2 reflection in BeO studied with electron and X-ray diffraction*. *Acta Cryst.* A**49**, 422–429.

4.3.8

Alexander, H., Spence, J. C. H., Shindo, D., Gottschalk, H. & Long, N. (1986). *Forbidden reflection lattice imaging for the determination of kink densities on partial dislocations*. *Philos. Mag.* A**53**, 627–643.

Anstis, G. R., Lynch, D. F., Moodie, A. F. & O'Keefe, M. A. (1973). *n-Beam lattice imges. III. Upper limits of ionicity in $W_4Nb_{26}P_{77}$*. *Acta Cryst.* A**29**, 138–147.

d'Anterroches, C. & Bourret, A. (1984). *Atomic structure of [011] and [001] near-coincident tilt boundaries in germanium and silicon*. *Philos. Mag.* A**49**, 783–807.

4.3.8 (*cont.*)

Binnig, G., Rohrer, H., Gerber, C. & Weibel, E. (1983). *Direct imaging of semiconductor surfaces. Phys. Rev. Lett.* **50**, 120–123.

Budinger, T. F. & Glaeser, R. M. (1976). *Measurement of focus and spherical aberration of an electron microscope objective lens. Ultramicroscopy*, **2**, 31–41.

Cherns, D. (1974). *Direct resolution of surface steps by transmission electron microscopy. Philos. Mag.* **30**, 549–557.

Cockayne, D. J. H. & Gronsky, R. (1981). *Lattice fringe imaging of modulated structures. Philos. Mag.* A**44**, 159–175.

Cowley, J. M. (1959). *The electron-optical imaging of crystal lattices. Acta Cryst.* **12**, 367–375.

Cowley, J. M. (1969). *Image contrast in transmission scanning electron microscope. Appl. Phys. Lett.* **15**, 58–59.

Cowley, J. M. (1981). *Diffraction physics*, 2nd ed. New York: North-Holland.

Cowley, J. M. (1988). *Electron microscopy of crystals with time-dependent perturbations. Acta Cryst.* A**44**, 847–853.

Cowley, J. M. (1992). *Coherent convergent beam diffraction. Electron diffraction techniques*, Vol. 1, edited by J. M. Cowley, pp. 439–464. Oxford University Press.

Cowley, J. M. (1994). *Applications of electron holography*. In *Handbook of advanced materials testing*, edited by N. P. Cheremisinoff & P. N. Cheremisinoff. New York: Marcel Dekker, Inc.

Cowley, J. M. & Iijima, S. (1972). *Electron microscope image contrast for thin crystals. Z. Naturforsch. Teil A,* **27**, 445–451.

Cowley, J. M. & Moodie, A. F. (1960). *Fourier images IV: the phase grating. Proc. Phys. Soc. (London)*, **76**, 378–384.

Cowley, J. M., Spence, J. C. & Smirnov, V. V. (1997). *The enhancement of electron microscope resolution by the use of atomic focusers. Ultramicroscopy*, **68**, 135–148.

Crewe, A. V. & Wall, J. (1970). *A scanning microscope with 5 Å resolution. J. Mol. Biol.* **48**, 375–393.

Daberkow, I., Herrman, K., Liu, L. & Rau, W. (1991). *Performance of electron image converters with YAG and CCD. Ultramicroscopy*, **38**, 215–224.

Desseaux, J., Renault, A. & Bourret, A. (1977). *Multibeam lattice images from germanium oriented in (001). Philos Mag.* **35**, 357–363.

Dorset, D. L. (1994). *Electron crystallography of organic molecules. Adv. Electron. Electron Phys.* **88**, 111–197.

Dorset, D. L. (1995). Editor. *Structural electron crystallography*. New York/London: Plenum Press.

Dorset, D. L., McCourt, M. P., Fryer, J. R., Tivol, W. F. & Turner, J. N. (1994). *The tangent formula in electron crystallography. Phase determination of copper perchlorophthalocyanine. Microsc. Soc. Am. Bull.* **24**, 398–404.

Downing, K. H., Meisheng, H., Wenk, H. R. & O'Keefe, M. A. (1990). *Resolution of oxygen atoms in staurolife by three dimensional transmission electron microscopy. Nature (London)*, **348**, 525.

Endoh, H., Hashimoto, H. & Makita, Y. (1994). *Theoretical and observed images of impurity atoms formed by L-shell ionization. Ultramicroscopy*, **56**, 108–120.

Fejes, P. L. (1977). *Approximations for the calculation of high-resolution electron-microscope images of thin films. Acta Cryst.* A**33**, 109–113.

Fields, P. M. & Cowley, J. M. (1978). *Computed electron microscope images of atomic defects in f.c.c. metals. Acta Cryst.* A**34**, 103–112.

Fitzgerald, J. D. & Johnson, A. W. S. (1984). *A simplified method of electron microscope voltage measurement. Ultramicroscopy*, **12**, 231–236.

Frank, J. (1975). *A practical resolution criterion in optics and electron microscopy. Optik (Stuttgart)*, **43**, 25–34.

Frank, J. (1980). *The role of correlation techniques in computer image processing. Computer processing of electron microscope images. Topics in current physics*, Vol. 13, edited by P. W. Hawkes, p. 187. Berlin/Heidelberg/New York: Springer Verlag.

Fryer, J. R. & Gilmore, C. J. (1992). *Structure determination by electron crystallography. Trans. Am. Crystallogr. Assoc.* **28**, 57–75.

Fu, Z. Q., Huang, D. X., Li, F. H., Li, J. Q., Zhao, Z. X., Cheng, T. Z. & Fan, H. F. (1994). *Incommensurate modulation in minute crystals revealed by combining high-resolution electron microscopy and electron diffraction. Ultramicroscopy*, **54**, 229–236.

Fujiyoshi, Y., Ishizuka, K., Tsuji, M., Kobayashi, T. & Uyeda, N. (1983). *Charge density distribution from high resolution molecular images*. Proceedings of the 17th International Conference on High Voltage Electron Microscopy, p. 21.

Fukuhara, A. (1966). *Many-ray approximation in the dynamical theory of electron diffraction. J. Phys. Soc. Jpn*, **21**, 2645–2662.

Gabor, D. (1948). *A new microscope principle. Nature (London)*, **161**, 777–778.

Gabor, D. (1949). *Microscopy of reconstructed wavefronts. Proc. R. Soc. London Ser. A*, **197**, 454–487.

Grinton, G. R. & Cowley, J. M. (1971). *Phase and amplitude contrast in electron micrographs of biological materials. Optik (Stuttgart)*, **34**, 221–233.

Haider, M. & Zach, J. (1995). *Multipole correctors. Proceedings of Microscopy and Microanalysis*, edited by G. Bailey, pp. 596–567. New York: Jones and Bigell.

Hashimoto, H., Mannami, M. & Naiki, T. (1961). *Theory of lattice images. Philos. Trans. R. Soc. London*, **253**, 459–489.

Hirsch, P. B., Howie, A., Nicholson, R. B., Pashley, D. W. & Whelan, M. J. (1977). *Electron microscopy of thin crystals*, p. 190. London: Butterworth.

Horiuchi, S. (1982). *Reduction in a niobium tungsten bronze. J. Appl. Cryst.* **15**, 323–329.

Howie, A. (1979). *Image contrast and localized signal selection techniques. J. Micros. (Oxford)*, **117**, 11–23.

Iijima, S. (1977). *High resolution electron microscopy of phase objects: observation of small holes and steps on graphite crystals. Optik (Stuttgart)*, **47**, 437–452.

International Tables for Crystallography (1992). Vol. B. Dordrecht: Kluwer Academic Publishers.

Ishizuka, K. (1982). *Multislice formula for inclined illumination. Acta Cryst.* A**38**, 773–779.

Jap, B. K. & Glaeser, R. M. (1978). *The scattering of high energy electrons. Acta Cryst.* A**34**, 94–102.

Kambe, K. (1982). *Visualization of Bloch waves of high energy electrons in high resolution electron microscopy. Ultramicroscopy*, **10**, 223–228.

Kirkland, A., Saxton, W., Chau, K., Tsuno, K. & Kawasaki, M. (1995). *Super-resolution by aperture synthesis. Ultramicroscopy*, **57**, 355–374.

Kobayashi, T., Fujiyoshi, Y. & Uyeda, N. (1982). *The observation of molecular orientations in crystal defects and the growth mechanism of thin phthalocyanine films. Acta Cryst.* A**38**, 356–362.

4.3.8 (*cont.*)

Koike, H., Kobayashi, K., Ozawa, S. & Yagi, K. (1989). *High resolution reflection electron microscopy of Si(111) 7 × 7 surfaces using a high voltage electron microscope*. *Jpn. J. Appl. Phys.* **28**, 861–865.

Komoda, T. (1964). *On the resolution of the lattice image in the electron microscope*. *Optik (Stuttgart)*, **21**, 94–110.

Krivanek, O. L. (1976). *A method for determining the coefficient of spherical aberration from a single electron micrograph*. *Optik (Stuttgart)*, **45**, 97–101.

Krivanek, O. L., Dellby, N., Spence, A. J., Camps, R. A. & Brown, L. M. (1997). *Aberration correction in the STEM*. *Proc EMAG 1997*, edited by S. McVitie. London: Institute of Physics.

Krivanek, O. L. & Mooney, P. E. (1993). *Applications of slow-scan CCD cameras in HREM*. *Ultramicroscopy*, **49**, 95–108.

Larsen, P. K. & Dobson, P. J. (1988). Editors. *Reflection high energy electron diffraction and reflection electron imaging of surfaces*. *NATO ASI Series*. New York/London: Plenum Press.

Lichte, H. (1991). *Electron image plane off-axis holography of atomic structures*. *Adv. Opt. Electron Microsc.* **12**, 25–91.

Lovey, F. C., Coene, W., Van Dyck, D., Van Tendeloo, G., Van Landuyt, J. & Amelinckx, S. (1984). *HREM imaging conditions for stacking sequences in 18R martensite of Cu–Al alloys*. *Ultramicroscopy*, **15**, 345–356.

Lynch, D. F., Moodie, A. F. & O'Keefe, M. A. (1975). *n-Beam lattice images. V. The use of the charge-density approximation in the interpretation of lattice images*. *Acta Cryst.* A**31**, 300–307.

Marks, L. (1986). *High resolution electron microscopy of surfaces*. In *Topics in current physics*, Vol. 41. *Structure and dynamics of surfaces. I*, edited by W. Schommers & P. Von Blackenhagen. Berlin/Heidelberg: Springer Verlag.

Menter, J. W. (1956). *The resolution of crystal lattices*. *Proc. R. Soc. London Ser. A*, **236**, 119.

Möllenstedt, G. & Düker, H. (1956). *Beobachtungen und Messungen an Biprisma-Interferenzen mit Elektronenwellen*. *Z. Phys.* **145**, 377–397.

Moodie, A. F. & Warble, C. E. (1967). *The observation of primary step growth in magnesium oxide by direct transmission electron microscopy*. *Philos. Mag.* **16**, 891–904.

Nagakura, S., Nakamura, Y. & Suzuki, T. (1982). *Forbidden reflection intensity in electron diffraction and its influence on the crystal structure image*. *Jpn. J. Appl. Phys.* **21**, L449–L451.

Nellist, P., McCallum, B. & Rodenburg, J. (1995). *Resolution beyond the information limit in STEM*. *Nature (London)*, **374**, 630–632.

O'Keefe, M. A., Spence, J. C. H., Hutchinson, J. L. & Waddington, W. G. (1985). *Proc. 43rd EMSA Meeting*, p. 64. San Francisco: San Francisco Press. [See also H. Hashimoto in *Ultramicroscopy* (1985), **18**, 19–32.]

Olsen, A. & Spence, J. C. H. (1981). *Distinguishing dissociated glide and shuffle set dislocations by high resolution electron microscopy*. *Philos. Mag.* A**43**, 945–965.

Orchowski, A., Rau, W. D. & Lichte, H. (1995). *Electron holography surmounts resolution limit of electron microscopy*. *Phys. Rev. Lett.* **74**, 399.

Pennycook, S. J. & Jesson, D. E. (1991). *High-resolution Z-contrast imaging of crystals*. *Ultramicroscopy*, **37**, 14–38.

Pirouz, P. (1974). *Effects of absorption on lattice images*. *Optik (Stuttgart)*, **54**, 69–74.

Saxton, W. O. (1978). *Computer techniques for image processing in electron microscopy*, pp. 9–19. New York: Academic Press.

Saxton, W. O. (1980*a*). *Recovery of specimen information for strongly scattering objects*. In *Computer processing of electron microscopy images*. *Topics in current physics*, Vol. 13, edited by P. W. Hawkes, p. 35. Berlin/Heidelberg/New York: Springer Verlag.

Saxton, W. O. (1980*b*). *Correction of artifacts in linear and nonlinear high resolution electron micrographs*. *J. Microsc. Spectrosc. Electron*, **5**, 665–674.

Scherzer, O. (1949). *The theoretical resolution limit of the electron microscope*. *J. Appl. Phys.* **20**, 20–29.

Schiske, P. (1975). *Phase determination from a focal series and the corresponding diffraction pattern in electron microscopy for strongly scattering objects*. *J. Phys. D*, **8**, 1372–1386.

Self, P. G., O'Keefe, M. A., Buseck, P. R. & Spargo, A. E. C. (1983). *Practical computation of amplitudes and phases in electron diffraction*. *Ultramicroscopy*, **11**, 35–52.

Shindo, D., Hiraga, K., Oikawa, T. & Mori, N. (1990). *Quantification of electron diffraction with imaging plate*. *J. Electron Microsc.* **39**, 449–453.

Smith, D. J., Bursill, L. A. & Wood, G. J. (1985). *Non-anomalous high-resolution imaging of crystalline materials*. *Ultramicroscopy*, **16**, 19–32.

Smith, D. J., Saxton, W. O., O'Keefe, M. A., Wood, G. J. & Stobbs, W. M. (1983). *The importance of beam alignment and crystal tilt in high resolution electron microscopy*. *Ultramicroscopy*, **11**, 263–282.

Spence, J. C. H. (1988). *High resolution electron microscopy*, 2nd ed. New York: Oxford University Press.

Spence, J. C. H. (1998). *Direct inversion of dynamical electron difffraction patterns to structure factors*. *Acta Cryst.* A**54**, 7–18.

Spence, J. C. H. & Lynch, J. (1982). *STEM microanalysis and inelastic imaging in crystals*. *Ultramicroscopy*, **9**, 267–278.

Spence, J. C. H., O'Keefe, M. A. & Iijima, S. (1978). *On the thickness periodicity of atomic-resolution images of dislocation cores*. *Philos. Mag.* A**38**, 463–482.

Takayanagi, K. (1984). *Surface structure imaging by electron microscopy*. *J. Microsc.*, **136**, 287–298.

Tonomura, A. (1992). *Electron-holographic interference microscopy*. *Adv. Phys.* **41**, 59–103.

Treacy, M. M. J. & Rice, S. B. (1989).*Catalyst particle sizes from Rutherford scattered intensities*. *J. Microsc.* **156**, 211–234.

Unwin, P. N. T. & Henderson, R. (1975). *Molecular structure determination by electron microscopy of unstained crystalline specimens*. *J. Mol. Biol.* **94**, 425–440.

Van Dyck, D. (1980). *Fast computational procedures for the simulation of structure images in complex or disordered crystals*. *J. Microsc.* **119**, 141.

Van Dyck, D., Op de Beeck, M. & Coene, W. M. J. (1994). *Information in electron microscopy*. *Microsc. Soc. Am. Bull.* **24**, 427–437.

Voss, R., Lehmpfuhl, G. & Smith, D. J. (1980). *Influence of doping on the crystal potential of silicon*. *Z. Naturforsch. Teil A*, **35**, 973–984.

Wade, R. H. & Frank, J. (1977). *Electron microscope transfer functions for partially coherent axial illumination*. *Optik (Stuttgart)*, **49**, 81–92.

Williams, D. B. & Carter, C. B. (1996). *Transmission electron microscopy*. New York: Plenum Press.

Wilson, A. R., Spargo, A. E. C. & Smith, D. J. (1982). *The characterisation of instrumental parameters in the high resolution electron microscope. Optik (Stuttgart)*, **61**, 63–78.
Yagi, K. (1993). *RHEED and REM*. In *Electron diffraction techniques*, Vol. 2, edited by J. M. Cowley. IUCr/Oxford University Press.
Yagi, K. & Cowley, J. M. (1978). *Electron microscopy study of ordering of potassium ions in cubic $KSbO_3$. Acta Cryst.* A**34**, 625–634.
Zakharov, N. D., Pasemann, M. & Rozhanski, V. N. (1982). *Observations of point defects in silicon by means of dark-field lattice plane imaging. Phys. Status Solidi A*, **71**, 275–281.
Zuo, J. M., Spence, J. C. H. & O'Keefe, M. A. (1988). *Bonding in GaAs. Phys. Rev. Lett.* **61**, 353–356.

4.4.2

Abrahams, K., Steinsvoll, O., Bongaarts, P. J. M. & De Lange, P. W. (1962). *Reversal of the spin of polarized thermal neutrons without depolarization. Rev. Sci. Instrum.* **33**, 524–529.
Agamalyan, M. M., Drabkin, G. M. & Sbitnev, V. I. (1988). *Spatial spin resonances of polarized neutrons. A tunable slow neutron filter. Phys. Rep.* **168**, 265–303.
Alefeld, B. (1972). *Neutronen-Rückstreuspektrometer. Kerntechnik,* **14**, 15–17.
Alefeld, B., Duppich, J., Schärpf, O., Schirmer, A., Springer, T. & Werner, K. (1988). *The new neutron guide laboratory at the FRJ-2 reactor in the KFA Jülich and its special beam forming devices. Thin film neutron optical devices: mirrors, supermirrors, multilayer monochromators, polarizers, and beam guides*, edited by C. F. Majkrzak, pp. 75–83. *SPIE Proc.* No. 983. Bellingham, WA: SPIE.
Alvarez, L. W. & Bloch, F. (1940). *A quantitative determination of the neutron moment in absolute nuclear magnetons. Phys. Rev.* **57**, 111–122.
Anderson, I. S. (1988). *Neutron beam focusing using supermirrors. Thin film neutron optical devices: mirrors, supermirrors, multilayer monochromators, polarizers, and beam guides*, edited by C. F. Majkrzak, pp. 84–92. *SPIE Proc.* No. 983. Bellingham, WA: SPIE.
Anderson, I. S. & Høghøj, P. (1996). *New developments in Ni/Ti multilayers.* ILL 1996 Annual Report, pp. 84–85. Institut Laue–Langevin, Grenoble, France
Bacon, G. E. & Lowde, R. D. (1948). *Secondary extinction and neutron crystallography. Acta Cryst.* **1**, 303–314.
Badurek, G. & Rauch, H. (1978). *Experimental capability study of non-conventional methods in neutron time-of-flight analysis. Neutron Inelastic Scattering Proceedings*, Vol. I, pp. 211–227. Vienna: IAEA.
Bednarski, S., Dobrzynski, L. & Steinsvoll, O. (1980). *Experimental test on $Fe_3Si(Mn)$ and $Li_{.5}Fe_{2.5}O_4$ crystals as polarizers for slow neutrons. Phys. Scr.* **21**, 217–219.
Blanc, Y. (1983). *Le spectrometre à temps de vol IN6: characteristiques techniques et performances.* ILL Internal Report No. 83BL21G. Institut Laue–Langevin, Grenoble, France.
Bonse, U. & Hart, M. (1965). *Tailless X-ray single crystal reflection curves obtained by multiple reflection. Appl. Phys. Lett.* **7**, 238–240.
Bouchiat, M. A., Carver, T. R. & Varnum, C. M. (1960). *Nuclear polarization in ^{3}He gas induced by optical pumping and dipolar exchange. Phys. Rev. Lett.* **5**, 373–375.
Brockhouse, B. N. (1958). *Bull. Am. Phys. Soc.* **3**, 233.
Bührer, W. (1994). *Triple axis instrument with doubly focusing ('zoom') monochromator and horizontally focusing analyser: seven years experience. Nucl. Instrum. Methods*, A**338**, 44–52.
Carlile, C. J., Hey, P. D. & Mack, B. J. (1977). *High-efficiency Soller slit collimators for thermal neutrons. J. Phys. E,* **10**, 543–546.
Chen, H., Sharov, V. A., Mildner, D. F. R., Downing, R. G., Paul, R. L., Lindstrom, R. M., Zeissler, C. J. & Xiao, Q. F. (1995). *Prompt gamma activation analysis enhanced by a neutron focusing capillary lens. Nucl. Instrum. Methods*, B**95**, 107–114.
Chen-Mayer, H. H., Mildner, D. F. R., Sharov, V. A., Ullrich, J. B., Ponomarev, I. Yu. & Downing, R. G. (1996). *Monolithic polycapillary neutron focusing lenses: experimental characterizations. J. Phys. Soc. Jpn,* **65**, Suppl. A, 319–321.
Christ, J. & Springer, T. (1962). *Über die Entwicklung eines Neutronenleiters am FRM-Reaktor. Nukleonik,* **4**, 23–25.
Chupp, T. E., Coulter, K. P., Hwang, S. R., Smith, T. B. & Welsh, R. C. J. (1996). *Progress toward a spin exchange pumped ^{3}He neutron spin filter. J. Neutron Res.* **5**, 11–24.
Colegrove, F. D., Schearer, L. D. & Walters, K. (1963). *Polarization of ^{3}He gas by optical pumping. Phys. Rev.* **132**, 2561–2572.
Colwell, J. F., Miller, P. H. & Whittemore, W. L. (1968). *A new high-efficiency time-of-flight system. Neutron inelastic scattering*, Vol. II, IAEA Conference Proceedings, pp. 429–437. Vienna: IAEA.
Copley, J. R. D. (1991). *Transmission properties of a counter-rotationg pair of disk choppers. Nucl. Instrum. Methods*, A**303**, 332–341.
Currat, R. (1973). *The efficiency of vertically bent neutron monochromators. Nucl. Instrum. Methods*, **107**, 21–28.
Dabbs, J. W. T., Roberts, L. D. & Bernstein, S. (1955). *Direct polarization of ^{115}In nuclei; J value for 1.456 eV resonance.* Report ORNL-CF-55-5-126. Oak Ridge National Laboratory, TN, USA.
Dash, J. G. & Sommers, H. S. (1953). *A high transmission slow neutron velocity selector. Rev. Sci. Instrum.* **24**, 91–96.
Delapalme, A., Schweizer, J., Couderchon, G. & Perrier de la Bathie, R. (1971). *Étude de l'alliage Heusler (Cu_2MnAl) comme monochromateur de neutrons polarizés. Nucl. Instrum. Methods*, **95**, 589–594.
Drabkin, G. M., Okorokov, A. I., Schebetov, A. F., Borovilova, N. V., Kugasov, A. G., Kudriashov, V. A., Runov, V. V. & Korneev, D. A. (1976). *Multilayer Fe–Co mirror polarizing neutron guide. Nucl. Instrum. Methods*, **133**, 453–456.
Drabkin, G. M., Zabidarov, E. I., Kasman, Ya. A. & Okorokov, A. I. (1969). *Investigation of a phase transition in nickel with polarized neutrons. Sov. Phys. JETP*, **29**, 261–266.
Egelstaff, P. A., Cocking, S. J. & Alexander, T. K. (1961). *A four-rotor thermal-neutron analyser. Inelastic scattering of neutrons in solids and liquids*, pp. 165–177. Vienna: IAEA.
Egorov, A. I., Lobashov, V. M., Nazarenko, V. A., Porsev, G. D. & Serebrov, A. P. (1974). *Production, storage, and polarization of ultracold neutrons. Sov. J. Nucl. Phys.* **19**, 147–152.
Elsenhans, O., Böni, P., Friedli, H. P., Grimmer, H., Buffat, P., Leifer, K., Söchtig, J. & Anderson, I. S. (1994). *Development of Ni/Ti multilayer supermirrors for neutron optics. Thin Solid Films*, **246**, 110–119.

4.4.2 (*cont.*)

Forsyth, J. B. (1979). *Magnetic neutron scattering and the chemical bond*. *At. Energy Rev*. **17**, 345–412.

Forte, M. & Zeyen, C. M. E. (1989). *Neutron optical spin-orbit rotation in dynamical diffraction*. *Nucl. Instrum. Methods*, A**284**, 147–150.

Freeman, F. F. & Williams W. G. (1978). *A ^{149}Sm polarizing filter for thermal neutrons*. *J. Phys. E*, **11**, 459–467.

Freund, A. K. (1975). *A neutron monochromator system consisting of deformed crystals with anisotropic mosaic structure*. *Nucl. Instrum. Methods*, **124**, 93–99.

Freund, A. K. (1976). *Progress in neutron monochromator development at the Institut Laue–Langevin*. *Conference on Neutron Scattering*. Report CONF-760601-p2, pp. 1143–1150. Oak Ridge National Laboratory, TN, USA.

Freund, A. K. (1983). *Cross sections of materials used as neutron monochromators and filters*. *Nucl. Instrum. Methods*, **213**, 495–501.

Freund, A. K. (1985). *On the wavelength dependence of neutron monochromator reflectivities*. *Nucl. Instrum. Methods*, A**238**, 570–571.

Freund, A. K. & Forsyth, J. B. (1979). *Materials problems in neutron devices*. *Neutron scattering*, edited by G. Kostorz, pp. 462–507. New York: Academic Press.

Freund, A. K., Guinet, P., Maréschal, J., Rustichelli, F. & Vanoni, F. (1972). *Cristaux á gradient de maille*. *J. Cryst. Growth*, **13/14**, 726.

Freund, A. K., Pynn, R., Stirling, W. G. & Zeyen, C. M. E. (1983). *Vertically focusing Heusler alloy monochromators for polarized neutrons*. *Physica (Utrecht) B*, **120**, 86–90.

Frey, F. (1974). *A packet of ideal-crystalline lamellae as neutron monochromator*. *Nucl. Instrum. Methods*, **115**, 277–284.

Gähler, R. & Golub, R. (1987). *A high resolution neutron spectrometer for quasielastic scattering on the basis of spin-echo and magnetic resonance*. *Z. Phys. B*, **65**, 269–273.

Glinka, C. J., Rowe, J. M. & LaRock, J. G. (1986). *The small-angle neutron scattering spectrometer at the National Bureau of Standards*. *J. Appl. Cryst*. **19**, 427–439.

Hamelin, B., Anderson, I., Berneron, M., Escoffier, A., Foltyn, T. & Hehn, R. (1997). *Nucl. Instrum. Methods*. Submitted.

Hautecler, S., Legrand, E., Vansteelandt, L., d'Hooghe, P., Rooms, G., Seeger, A., Schalt, W. & Gobert, G. (1985). *Mibemol: a six chopper TOF spectrometer installed on a neutron guide at the Orphée reactor*. Proceedings of the Conference on Neutron Scattering in the Nineties, Jülich, pp. 211–215. Vienna: IAEA.

Hayes, C., Lartigue, C., Copley, J. R. D., Alefeld, B., Mezei, F., Richter, D. & Springer, T. (1996). *The focusing mirror at the ILL spin-echo spectrometer IN15; experimental results*. *J. Phys. Soc. Jpn*, **65**, Suppl. A, 312–315.

Hayter, J. B. & Mook, H. A. (1989). *Discrete thin-film multilayer design for X-ray and neutron supermirrors*. *J. Appl. Cryst*. **22**, 35–41.

Hayter, J. B., Penfold, J. & Williams, W. G. (1978). *Compact polarizing Soller guides for cold neutrons*. *J. Phys. E*, **11**, 454–458.

Hiismäki, P. (1997). *Modulation spectroscopy of neutrons with diffractometry applications*. Singapore: World Science Publishing.

Hines, W. A., Menotti, A. H., Budnick, J. L., Burch, T. J., Litrenta, T., Niculescu, V. & Raj, K. (1976). *Magnetization studies of binary and ternary alloys based on Fe_3Si*. *Phys. Rev. B*, **13**, 4060–4068.

Hock, R., Vogt, T., Kulda, J., Mursic, Z., Fuess, H. & Magerl, A. (1993). *Neutron backscattering on vibrating silicon crystals – experimental results on the neutron backscattering spectrometer IN10*. *Z. Phys. B*, **90**, 143–153.

Høghøj, P., Anderson, I. S., Ebisawa, T. & Takeda, T. (1996). *Fabrication and performance of a large wavelength band multilayer monochromator*. *J. Phys. Soc. Jpn*, **65**, Suppl. A, 296–298.

Hossfeld, F., Amadori, R. & Scherm, R. (1970). Proceedings of Instrumentation for Neutron Inelastic Scattering, IAEA, Vienna, Austria, p. 117.

Hughes, D. J. & Burgy, M. T. (1951). *Reflection of neutrons from magnetized mirrors*. *Phys. Rev*. **81**, 498–506.

Korneev, D. A. & Kudriashov, V. A. (1981). *Experimental determination of the characteristics of a spin-flipper with a prolonged working area*. *Nucl. Instrum. Methods*, **179**, 509–513.

Lushchikov, V. I., Taran, Yu. V. & Shapiro, F. L. (1969). *Polarized proton target as neutron polarizer*. *Sov. J. Nucl. Phys*. **10**, 669–677.

Magerl, A., Liss, K.-D., Doll, C., Madar, R. & Steichele, E. (1994). *Will gradient crystals become available for neutron diffraction? Nucl. Instrum. Methods*, A**338**, 83–89.

Magerl, A. & Wagner, V. (1994). Editors. *Focusing neutron optics*. *Nucl. Instrum. Methods*, A**338**, 1–150.

Maier-Leibnitz, H. (1967). *Einige Vorschläge für die Verwendung von zusammengesetzten Monochromatorkristallen fur Neutronenbeugungs- und Streumessungen*. *Ann. Acad. Sci. Fenn. Ser. A*, **267**, 3–17.

Maier-Leibnitz, H. (1969). Summer School on Neutron Physics, Alushta. Dubna: Joint Institute of Nuclear Physics.

Maier-Leibnitz, H. & Rustichelli, F. (1968). German Patent No. 1816542.

Maier-Leibnitz, H. & Springer, T. (1963). *The use of neutron optical devices on beam-hole experiments*. *J. Nucl. Energy A/B*, **17**, 217–225.

Majkrzak, C. F., Nunez, V., Copley, J. R. D., Ankner, J. F. & Greene, G. C. (1992). *Supermirror transmission polarizers for neutrons*. *Neutron optical devices and applications*, edited by C. F. Majkrzak & J. L. Wood, pp. 90–106. *SPIE Proc*. No. 1738. Bellingham, WA: SPIE.

Majkrzak, C. F. & Shirane, G. (1982). *Polarized neutron spectrometer developments and experiments at Brookhaven*. *J. Phys. (Paris)*, **43**, C7, 215–220.

Marx, D. (1971). *Microguides for neutrons*. *Nucl. Instrum. Methods*, **94**, 533–536.

May, C., Klimanek, P. & Magerl, A. (1995). *Plastic bending of thin beryllium blades for neutron monochromators*. *Nucl. Instrum. Methods*, A**357**, 511–518.

Meardon, B. H. & Wroe, H. (1977). Report RL-77-059/A. Rutherford Laboratory, Oxon, England.

Meister, H. & Weckerman, B. (1972). *A high resolution time focusing spectrometer for quasi-elastic neutron scattering*. Proceedings of the Symposium on Inelastic Neutron Scattering of Neutrons in Solids and Liquids. Vienna: IAEA.

Meister, H. & Weckerman, B. (1973). *Neutron collimators with plates of self-contracting foils*. *Nucl. Instrum. Methods*, **108**, 107–111.

Mezei, F. (1972). *Neutron spin-echo: a new concept in polarized thermal neutron techniques*. *Z. Phys*. **255**, 146–160.

Mezei, F. (1976). *Novel polarized neutron devices: supermirror and spin component amplifier*. *Commun. Phys*. **1**, 81–85.

4.4.2 (*cont.*)

Mezei, F. (1988). *Very high reflectivity supermirrors and their applications. Thin film neutron optical devices: mirrors, supermirrors, multilayer monochromators, polarizers, and beam guides*, edited by C. F. Majkrzak, pp. 10–17. *SPIE Proc.* No. 983. Bellingham, WA: SPIE.

Mildner, D. F. R. (1994). *Neutron focusing optics for low-resolution small-angle scattering. J. Appl. Cryst.* **27**, 521–526.

Mücklich, F. & Petzow, G. (1993). *Development of beryllium single crystal material for monochromator applications. Mineral processing & extractive metallurgy review, beryllium – issue*. New York: Gordon and Breach.

Nunes, A. C. (1974). *A focusing low-angle neutron diffractometer. Nucl. Instrum. Methods*, **119**, 291–293.

Pickart, S. J. & Nathans, R. (1961). *Unpaired spin density in ordered Fe_3Al. Phys. Rev.* **123**, 1163–1171.

Reed, R. E., Bolling, E. D. & Harmon, H. E. (1973). Solid State Division Report, pp. 129–131. Oak Ridge National Laboratory, TN, USA.

Riste, T. (1970). *Singly bent graphite monochromators for neutrons. Nucl. Instrum. Methods*, **86**, 1–4.

Rossbach, M., Schärpf, O., Kaiser, W., Graf, W., Schirmer, A., Faber, W., Duppich, J. & Zeisler, R. (1988). *The use of focusing supermirror neutron guides to enhance cold neutron fluence rates. Nucl. Instrum. Methods*, B**35**, 181–190.

Schaerpf, O. (1975). *Magnetic neutron guide tube for polarization of thermal neutrons with $P = 97\%$ irrespective of wavelength. J. Phys. E*, **8**, 268–269.

Schaerpf, O. (1989). *Properties of beam bender type neutron polarizers using supermirrors. Physica (Utrecht) B*, **156&157**, 639–646.

Schaerpf, O. & Stuesser, N. (1989). *Recent progress in neutron polarizers. Nucl. Instrum. Methods*, A**284**, 208–211.

Schärpf, O. (1980). *Neutron spin echo. Lecture notes in physics*, Vol. 128, edited by F. Mezei, pp. 27–52. Heidelberg: Springer-Verlag.

Schärpf, O. & Capellmann, H. (1993). *The xyz-difference method with polarized neutrons and the separation of coherent, spin-incoherent, and magnetic scattering cross sections in a multidetector. Phys. Status Solidi A*, **135**, 359–379.

Schefer, J., Medarde, M., Fischer, S., Thut, R., Koch, M., Fischer, P., Staub, U., Horisberger, M., Böttger, G. & Dönni, A. (1996). *Sputtering method for improving neutron composite germanium monochromators. Nucl. Instrum. Methods*, A**372**, 229–232.

Schelten, J. & Alefeld, B. (1984). *Backscattering spectrometer with adapted Q-resolution at the pulsed neutron source*. Report No. 1954, pp. 378–389. KFA Jülich, Germany.

Scherm, R., Dolling, G., Ritter, R., Schedler, E., Teuchert, W. & Wagner, V. (1977). *A variable-curvature analyser crystal for three axis spectrometers. Nucl. Instrum. Methods*, **143**, 77–85.

Scherm, R. H. & Kruger, E. (1994). *Bragg optics – focusing in real and k space. Nucl. Instrum. Methods*, A**338**, 1–8.

Schmatz, W., Springer, T., Schelten, J. & Ibel, K. (1974). *Neutron small-angle scattering: experimental techniques and applications. J. Appl. Cryst.* **7**, 96–116.

Schoenborn, B. P., Caspar, D. L. D. & Kammerer, O. F. (1974). *A novel neutron monochromator. J. Appl. Cryst.* **7**, 508–510.

Sears, V. F. (1997). *Bragg reflection in mosaic crystals. Acta Cryst.* A**53**, 35–54.

Shapiro, S. M. & Chesser, N. J. (1972). *Characteristics of pyrolytic graphite as an analyser and higher order filter in neutron scattering experiments. Nucl. Instrum. Methods*, **101**, 183–186.

Steinberger, J. & Wick, G. C. (1949). *On the polarization of slow neutrons. Phys. Rev.* **76**, 994–995.

Surkau, R., Becker, J., Ebert, M., Grossman, T., Heil, W., Hofmann, D., Humblot, H., Leduc, M., Otten, E. W., Rohe, D., Siemensmeyer, K., Steiner, M., Tasset, F. & Trautmann, N. (1997). *Realization of a broad band neutron spin filter with compressed, polarized ^3He gas. Nucl. Instrum. Methods*, A**384**, 444–450.

Tasset, F. & Resouche, E. (1995). *Optimum transmission for a ^3He neutron polarizer. Nucl. Instrum. Methods*, A**359**, 537–541.

Turchin, V. F. (1965). *Slow neutrons*. Jerusalem: Israel Program for Scientific Translations.

Turchin, V. F. (1967). Deposited Paper, Atomic Energy 22.

Vogt, T., Passell, L., Cheung, S. & Axe, J. D. (1994). *Using wafer stacks as neutron monochromators. Nucl. Instrum. Methods*, A**338**, 71–77.

Wagner, V., Friedrich, H. & Wille, P. (1992). *Performance of a high-tech neutron velocity selector. Physica (Utrecht), B* **180&181**, 938–940.

Wagshul, M. E. & Chupp, T. E. (1994). *Laser optical pumping of high-density Rb in polarized ^3He targets. Phys. Rev. A*, **49**, 3854–3869.

Williams, W. G. (1988). *Polarised neutrons. Oxford Series on Neutron Scattering in Condensed Matter*, Vol. 1. Oxford: Clarendon Press.

Wright, A. F., Berneron, M. & Heathman, S. P. (1981). *Radial collimator system for reducing background noise during neutron diffraction with area detectors. Nucl. Instrum. Methods*, **180**, 655–658.

Zachariasen, W. H. (1945). *Theory of X-ray diffraction in crystals*. New York: Wiley.

Zeyen, C. M. E. & Rem, P. C. (1996). *Optimal Larmor precession magnetic field shapes: application to neutron spin echo three-axis spectrometry. Meas. Sci. Tech.* **7**, 782–791.

4.4.3

Bjerrum Møller, H. & Nielson, M. (1970). *Proceedings of IAEA panel meeting on instrumentation for neutron inelastic scattering research*. Vienna: IAEA.

Caglioti, G., Paoletti, A. & Ricci, F. P. (1960). *On resolution and luminosity of a neutron diffraction spectrometer for single crystal analysis. Nucl. Insrum. Methods*, **9**, 195–198.

Chesser, N. J. & Axe, J. D. (1973). *Derivation and experimental verifiation of the normalised resolution function for inelastic neutron scattering. Acta Cryst.* A**29**, 160–169.

Cooper, M. J. (1968). *The resolution function in neutron diffractometry. IV. Application of the resolution function to the measurement of Bragg peaks. Acta Cryst.* A**24**, 624–627.

Cooper, M. J. & Nathans, R. (1967). *The resolution function in neutron diffractometry. I. The resolution function of a neutron diffractometer and its application to phonon measurements. Acta Cryst.* **23**, 357–367.

Cooper, M. J. & Nathans, R. (1968). *The resolution function in neutron diffractometry. II. Experimental determination and properties of the 'elastic two-crystal' resolution function. Acta Cryst.* A**24**, 619–624.

4.4.3 (*cont.*)

Dorner, B. (1972). *The normalization of the resolution function for inelastic neutron scattering and its applications*. *Acta Cryst*. A**28**, 319–327.

Mitchell, P. W., Cowley, R. A. & Higgins, S. A. (1984). *The resolution fuction of triple-axis neutron spectrometers in the limit of small scattering angles*. *Acta Cryst*. A**40**, 152–160.

Nielsen, M. & Bjerrum Møller, H. (1969). *Resolution of a triple-axis spectrometer*. *Acta Cryst*. A**25**, 547–550.

Pynn, R. (1975). *Lorentz factor for triple-axis spectrometers*. *Acta Cryst*. B**31**, 2555–2556.

Pynn, R. (1984). *Reactor based neutron scattering instrumentation*. *Rev. Sci. Instrum*. **55**, 837–848.

Pynn, R., Fujii, Y. & Shirane, G. (1983). *The resolution function of a perfect-crystal three-axis X-ray spectrometer*. *Acta Cryst*. A**39**, 38–46. [There is an omission in equation (*A*3) of this reference; the relation $X_3 = k/\alpha_A$ should be added.]

Robinson, R. A., Pynn, R. & Eckert, J. (1985). *An improved constant-Q spectrometer for pulsed neutron sources*. *Nucl. Instrum. Methods*, A**241**, 312–324.

Stedman, R. (1968). *Energy resolution and focusing in inelastic scattering experiments*. *Rev. Sci. Instrum*. **39**, 878–883.

Steinsvoll, O. (1973). *The resolution function of a hybrid neutron spectrometer*. *Nucl. Instrum. Methods*, **106**, 453–459.

Tindle, G. L. (1984). *A new instrumental factor in triple-axis spectrometry and Bragg reflectivity measurements*. *Acta Cryst*. A**40**, 103–107.

Werner, S. A. (1971). *Choice of scans in neutron diffraction*. *Acta Cryst*. A**27**, 665–669.

Werner, S. A. & Pynn, R. (1971). *Resolution effects in the measurement of phonons in sodium metal*. *J. Appl. Phys*. **42**, 4736–4749.

4.4.4

Bacon, G. E. (1975). *Neutron diffraction*, 3rd ed. Oxford: Clarendon Press.

Glättli, H. & Goldman, M. (1987). *Nuclear magnetism. Methods of experimental physics*, Vol. 23, *Neutron scattering* Part C, edited by K. Sköld & D. L. Price, pp. 241–286. New York: Academic Press.

Klein, A. G. & Werner, S. A. (1983). *Neutron optics*. *Rep. Prog. Phys*. **46**, 259–335.

Koester, L. (1977). *Neutron scattering lengths and fundamental neutron interactions. Springer Tracts in Modern Physics*, Vol. 80, pp. 1–55. Berlin: Springer Verlag.

Koester, L., Rauch, H. & Seymann, E. (1991). *Neutron scattering lengths: a survey of experimental data and methods*. *At. Data Nucl. Data Tables*, **49**, 65–120.

Koester, L., Waschkowski, W. & Meier, J. (1988). *Experimental study on the electric polarizability of the neutron*. *Z. Phys*. A**329**, 229–234.

Lynn, J. E. & Seegar, P. A. (1990). *Resonance effects in neutron scattering lengths of rare-earth nuclides*. *At. Data Nucl. Data Tables*, **44**, 191–207.

Mughabghab, S. F. (1984). *Neutron cross sections*, Vol. 1, Part *B: Z = 61–100*. New York: Academic Press.

Mughabghab, S. F., Divadeenam, M. & Holden, N. E. (1981). *Neutron cross sections*, Vol. 1, Part *A: Z = 1–60*. New York: Academic Press.

Sears, V. F. (1984). *Thermal-neutron scattering lengths and cross sections for condensed-matter research*. Report AECL-8490. Atomic Energy of Canada Limited, Chalk River, Ontario, Canada.

Sears, V. F. (1985). *Local-field refinement of neutron scattering lengths*. *Z. Phys*. A**321**, 443–449.

Sears, V. F. (1986*a*). *Electromagnetic neutron–atom interactions*. *Phys. Rep*. **141**, 281–317.

Sears, V. F. (1986*b*). *Neutron scattering lengths and cross sections*. *Methods of experimental physics*, Vol. 23, *Neutron scattering*, Part *A*, edited by K. Sköld & D. L. Price, pp. 521–550. New York: Academic Press.

Sears, V. F. (1989). *Neutron optics*. Oxford University Press.

Sears, V. F. (1992*a*). *Scattering lengths for neutrons*. *International tables for crystallography*, Vol. C, edited by A. J. C. Wilson, pp. 383–391. Dordrecht: Kluwer Academic Publishers.

Sears, V. F. (1992*b*). *Neutron scattering lengths and cross sections*. *Neutron News*, **3**, 26–37.

Sears, V. F. (1996). *Correction of neutron scattering lengths for electromagnetic interactions*. *J. Neutron Res*. **3**, 53–62.

Werner, S. A. & Klein, A. G. (1986). *Neutron optics. Methods of experimental physics*, Vol. 23, *Neutron scattering*, Part *A*, edited by K. Sköld & D. L. Price, pp. 259–337. New York: Academic Press.

Young, H. D. (1962). *Statistical treatment of experimental data*. New York: McGraw–Hill.

4.4.5

Clementi, E. & Roetti, C. (1974). *Roothan–Hartree–Fock atomic wavefunctions*. *At. Data Nucl. Data Tables*, **14**, 177–478.

Desclaux, J. P. & Freeman, A. J. (1978). *Dirac–Fock studies of some electronic properties of actinide ions*. *J. Magn. Magn. Mater*. **8**, 119–129.

Forsyth, J. B. & Wells, M. (1959). *On an analytic approximation to the atomic scattering factor*. *Acta Cryst*. **12**, 412–414.

Freeman, A. J. & Desclaux, J. P. (1979). *Dirac–Fock studies of some electronic properties of rare-earth ions*. *J. Magn. Magn. Mater*. **12**, 11–21.

Lisher, E. J. & Forsyth, J. B. (1971). *Analytic approximations to form factors*. *Acta Cryst*. A**27**, 545–549.

4.4.6

Hutchings, M. T. & Windsor, C. G. (1987). *Industrial applications of neutron scattering*. In *Methods of experimental physics*, Vol. 23, Part C, edited by K. Sköld & D. L Price. New York: Academic Press.

5.1. Introduction

BY A. J. C. WILSON

Precise and accurate lattice parameters can be obtained by X-ray methods, both polycrystalline and single crystal. The literature on X-ray lattice-parameter determination is voluminous, involving hundreds of publications. For powder-camera methods most of it is fairly old; summaries with sufficient detail for most purposes will be found in Klug & Alexander (1974) and Peiser, Rooksby & Wilson (1960). The proceedings of the symposium on *Accuracy in Powder Diffraction* held in Gaithersburg in 1979 (Block & Hubbard, 1980) are particularly valuable as a source of information on developments of all aspects of powder diffraction up to 1979; the publication includes a review of accuracy in lattice-parameter measurements (Wilson, 1980), which contains about twice as many references as Chapter 5.2. A more recent symposium was held in Fremantle in 1987 (CSIRO, 1988); it contains several papers relevant to accuracy in lattice-parameter determination, as well as papers on other applications of powder diffractometry. References to papers published in these symposia are included in Chapter 5.2 where appropriate. A second Gaithersburg conference with the same title (Prince & Stalick, 1992) covered many aspects of powder diffraction, but not lattice-parameter determination. Unfortunately there seem to be no comparable reviews of single-crystal methods, so that Chapter 5.3 is somewhat more detailed than Chapter 5.2.

Electron- and neutron-diffraction methods are less used and are (in general) less precise than X-ray methods. They are, however, applicable to some problems for which X-ray methods are inappropriate, and are described in Chapters 5.4 and 5.5.

Whatever the radiation, perhaps the most important factor in obtaining accurate and precise lattice parameters is careful experimental technique; lack of care can produce larger errors than lack of the latest equipment. Measurements should be repeated to check the precision (reproducibility) of the determination; periodical check measurements of a standard specimen (for example, high-purity silicon) should be undertaken to check the accuracy (absence of, or satisfactory correction for, systematic errors).

The lattice parameter of silicon is discussed in Section 4.2.1. There is said to be a difference between the lattice parameters of high-quality single-crystal silicon plates and silicon powder samples. The lattice parameter of the powder is reported as 1.5×10^{-5} nm lower at room temperature (Okada & Tokumaru, 1984; see also Hubbard, 1983).

Copyright © 2006 International Union of Crystallography

International Tables for Crystallography (2006). Vol. C, Chapter 5.2, pp. 491–504.

5.2. X-ray diffraction methods: polycrystalline

By W. Parrish, A. J. C. Wilson and J. I. Langford

5.2.1. Introduction

5.2.1.1. *The techniques available*

X-ray powder methods for the accurate determination of lattice parameters can be divided broadly into four groups, depending on the type of dispersion, type of source, and the type of detector. They are:

(1) angle-dispersive: diffractometer methods, conventional tube source (Section 2.3.2);

(2) angle-dispersive: diffractometer methods, synchrotron sources (Subsections 2.3.3.1, 2.3.3.2);

(3) energy-dispersive: diffractometer methods (Subsection 2.3.3.3, Chapter 2.5);

(4) angle-dispersive: camera methods (Section 2.3.4).

The geometry, advantages, and some practical details of the methods are given in the sections whose numbers are given in parentheses. The techniques will be discussed in the above order in Sections 5.2.4–5.2.8. More details of systematic errors in diffractometry are given in Wilson (1963, 1965*c*, 1974). Some general points on checking precision and accuracy were made in Chapter 5.1. Many of them are treated in greater detail in Section 2.3.5, and are recapitulated in Section 5.2.13.

The technique of choice will depend on the accuracy required and on the nature and quantity of the material available. At present, the technique most frequently used for the purposes of this chapter is angle-dispersive diffractometry with a conventional tube source (1). Angle-dispersive diffractometry with synchrotron radiation (2) is capable of greater precision and accuracy, but access to the synchrotron sources is cumbersome and may involve long waiting periods. Energy-dispersive methods (3) would ordinarily be adopted only if the required environmental conditions (high or low temperatures, high pressures, ...) can be achieved most readily by means of a fixed-angle diffractometer. Camera methods (4) are adaptable to small quantities of material, but microdiffractometers (Subsection 2.3.1.5) can be used with similar or even smaller quantities.

5.2.1.2. *Errors and aberrations: general discussion*

The relation between the lattice spacing d, the angle of incidence (Bragg angle) θ, and the wavelength λ is Bragg's law:

$$\lambda = 2d \sin\theta. \qquad (5.2.1.1)$$

The lattice spacing d is related to the lattice parameters a, b, c, α, β, γ and the indices of reflection h, k, l. In the simple case of cubic crystals, the relation is

$$d^{-2} = a^{-2}(h^2 + k^2 + l^2), \qquad (5.2.1.2)$$

where a is the single lattice parameter. The general relation is

$$d^{-2} = G^{-1}(abc)^{-2}[A(hbc)^2 + B(kca)^2 + C(lab)^2 + 2abc(Dkla + Elhb + Fhkc)], \qquad (5.2.1.3)$$

where a, b, c are the edges of the unit cell, and $A, \ldots, G$ are the functions of the angles of the unit cell given in Table 5.2.1.1.

Differentiation of (5.2.1.1) shows that the errors in the measurement of d are related to the errors in the measurement of λ and θ by the equation

$$(\Delta d)/d = (\Delta\lambda)/\lambda - \cot\theta(\Delta\theta). \qquad (5.2.1.4)$$

Wavelength and related problems are discussed in Section 5.2.2 and geometrical and other aberration problems in Section 5.2.3.

5.2.1.3. *Errors of the Bragg angle*

The error in the Bragg angle, $\Delta\theta$, will ordinarily consist of both random and systematic components. The random components (as the name implies) have an expected value zero, but the systematic errors will affect all measurements consistently to a greater or lesser extent. The systematic errors may be, and usually are, functions of θ and/or λ. Such errors would ordinarily reveal themselves in checks of internal consistency: the values of the apparent lattice parameter, plotted as a function of θ, would show a systematic drift, not a random scatter. The success or otherwise of attempts to eliminate or account for them would be subject to statistical tests (Section 5.2.9 and Chapter 8.5). There is an exception to the 'ordinarily'; if the variation of $\Delta\theta$ with θ happens to be of the form $K\tan\theta$, where K does not depend on θ either explicitly or through λ, the resultant fractional error $(\Delta d)/d$ is a constant, and would not be revealed either by systematic drift of the apparent lattice parameter with θ or by statistical tests.

5.2.1.4. *Bragg angle: operational definitions*

The Bragg angles are determined from the observations by a series of operations that are often quite complex.

For film cameras of diameter 57.3 or 114.6 mm, a simple measurement with a millimetre scale gives θ in degrees (1 mm = 1 or 0.5°). This determination is crude, and ordinarily the lines on the film would be measured with a low-power travelling microscope or a densitometer. The effective camera diameter is found from measurements of fiducial marks imprinted on the film, or by use of the Straumanis film mounting. References to detailed descriptions are given in Section 2.3.4.

For Bragg–Brentano (Parrish) and Seemann–Bohlin diffractometers, rate-meter measurements with strip-chart recordings have time-constant errors, and precision measurements require step-scanning (Subsection 2.3.3.5). The data may be analysed to give one or more of the following measures of position:

(*a*) The centroid of the reflection (Subsection 2.3.3.3).

(*b*) The peak of the reflection (Subsection 2.3.3.3). The extrapolated mid-point of chords is a kind of modified peak determination, but the best method of locating peaks so far in operation is that called 'peak search' (Subsection 2.3.3.7).

(*c*) Profile fitting (Subsection 2.3.3.8). In principle, profile fitting could give the Bragg angle corresponding to any desired feature of the diffraction maximum (centroid peak, median, ...), but it has been used in practice mainly for locating the Bragg angle corresponding to the peak.

As usual, it is necessary to distinguish between the precision (reproducibility) of a measurement and its accuracy (extent to which it is affected by systematic errors). In principle, it does not matter if the Bragg angle obtained by any of the above operations is affected by systematic errors, as these can be calculated and allowed for, as described in the following paragraphs. The most precise methods are the peak-search and individual profile-fitting computer procedures. They are routinely capable of a precision of about 0.001°(2θ) for reasonably sharp reflections, and are free from the subjective effects that may influence, for example, film measurements or the graphical extrapolation of the mid-points of chords. As well as a measure of the peak position, the peak-search procedure gives a measure of the peak intensity, and the

Copyright © 2006 International Union of Crystallography

Table 5.2.1.1. *Functions of the cell angles in equation (5.2.1.3) for the possible unit cells*

Function	Cell				
	Cubic tetragonal orthorhombic	Hexagonal	Monoclinic (c unique)	Rhombohedral	Triclinic
A	1	1	1	$\sin^2\alpha$	$\sin^2\alpha$
B	1	1	1	$\sin^2\alpha$	$\sin^2\beta$
C	1	$\frac{3}{4}$	$\sin^2\gamma$	$\sin^2\alpha$	$\sin^2\gamma$
D	0	0	0	$\cos^2\alpha-\cos\alpha$	$\cos\beta\cos\gamma-\cos\alpha$
E	0	0	0	$\cos^2\alpha-\cos\alpha$	$\cos\gamma\cos\alpha-\cos\beta$
F	0	$\frac{1}{2}$	$-\cos\gamma$	$\cos^2\alpha-\cos\alpha$	$\cos\alpha\cos\beta-\cos\gamma$
G	1	$\frac{3}{4}$	$\sin^2\gamma$	$1+2\cos^3\alpha-3\cos^2\alpha$	$1+2\cos\alpha\cos\beta\cos\gamma$ $-\cos^2\alpha-\cos^2\beta-\cos^2\gamma$

profile-fitting procedure gives a measure of the peak intensity and (if desired) a measure of the integrated intensity.

5.2.2. Wavelength and related problems

5.2.2.1. *Errors and uncertainties in wavelength*

In diffractometry, the errors in wavelength, $\Delta\lambda$, are usually entirely systematic; the crystallographer accepts whatever wavelength the spectroscopist provides, so that an error that was random in the spectroscopy becomes systematic in the diffractometry. One or two exceptions to this rule are noted below, as they are encountered in the discussion of the various techniques. Equation (5.2.1.4) shows that such a systematic error in wavelength, arising either from uncertainty in the wavelength scale (affecting all wavelengths) or from a systematic error in one wavelength (possibly arising from a random error in its determination) produces a constant fractional error in the spacing, an error that is not detectable by any of the usual tests for systematic error.

Ordinarily, the wavelength to be inserted in (5.2.1.1) is not known with high accuracy. The emission wavelengths given by spectroscopists – the exact feature to which they refer is usually not known, but is probably nearer to the peak of the wavelength distribution than to its centroid – are subject to uncertainties of one part in 50 000 [see, for example, Sandström (1957, especially p. 157)], though this uncertainty is reduced by a factor of ten for some more recent measurements known to refer to the peak defined by, say, the extrapolated mid-points of chords (Thomsen, 1974). Energy-dispersive and synchrotron devices are usually calibrated by reference to such X-ray wavelengths, and thus their scales are uncertain to at least the same extent. Use of a standard silicon sample (Sections 5.2.5 and 5.2.10) will ordinary give greater accuracy. There are a few wavelengths determined by interferometric comparison with optical standards where the uncertainty may be less than one part in a million (Deslattes, Henins & Kessler, 1980); see Section 4.2.2.

The wavelength distributions in the emission spectra of the elements ordinarily used in crystallography are not noticeably affected by the methods used in preparing targets. There is a slight dependence, at about the limit of detectability, on operating voltage, take-off angle, and degree of filtration (Wilson, 1963, pp. 60–63), and even the fundamental emission profile is affected somewhat by the excitation conditions (Chevallier, Travennier & Briand, 1978). Effective monochromators, capable of separating the $K\alpha_1$ and $K\alpha_2$ components (Barth, 1960), produce large variations. However, (5.2.1.1) depends only on the ratio of d to λ, so that *relative* spacings can be determined without regard to the accuracy of λ, provided that nothing is done that alters the wavelength distribution between measurements, and that the same identifiable feature of the distribution (peak, centroid, mid-point of chord, ...) is used throughout.

5.2.2.2. *Refraction*

X-rays, unless incident normally, are refracted away from the normal on entering matter, and while inside matter they have a longer wavelength than *in vacuo*. Both effects are small, but the former leads to a measurable error for solid specimens (that is, specimens without voids or binder) with flat surfaces (single crystals or polished metal blocks). This effect becomes prominent at grazing incidence, and may lead to total external reflection. For the usual powder compacts (Section 2.3.4), refraction leads to a broadening rather than a displacement (Wilson, 1940, 1962; Wilkens, 1960; Hart, Parrish, Bellotto & Lim, 1988; Greenberg, 1989). The greater wavelength within the powder grain leads to a pseudo-aberration; the actual wavelength ought to be used in (5.2.1.1), and if the *in vacuo* wavelength is used instead the lattice spacing obtained will be too small by a fraction equal to the amount by which the refractive index differs from unity. The difference is typically in the fourth decimal place in the lattice parameter expressed in Å. The need for any refraction correction for very fine powders has been questioned.

5.2.2.3. *Statistical fluctuations*

Statistical fluctuations in the number of counts recorded are not aberrations, but random errors. They influence the precision with which the angles of diffraction, and hence the lattice parameters, can be determined. The fluctuations arise from at least two sources: emission of X-ray quanta from the source is random, and the number of crystallites in an orientation to reflect varies with position within the specimen and with the relative orientations of the specimen and the incident beam. The theory of fluctuations in recording counts is discussed in Chapter 7.5; their effect can be reduced as much as is desired by increases in the counting times. Fluctuations in particle orientation are more difficult to control; use of smaller particles, larger illuminated volumes, and rotation of the specimen are helpful, but may conflict with other requirements of the experiment. The section on specimen preparation in Chapter 2.3 should be consulted.

Among the many papers relevant to the problem are Mack & Spielberg (1958), Pike & Wilson (1959), Thomsen & Yap (1968*a,b*), Wilson (1965*a,b,c*, 1967, 1971), Wilson, Thomsen & Yap (1965), and Zevin, Umanskij, Khejker & Pančenko (1961). The formulae are complicated, and depend on the measure of location that is adopted for the diffraction profile. In general, however, the variance of the angle is inversely proportional to the number of counts accumulated.

5.2.3. Geometrical and physical aberrations

5.2.3.1. *Aberrations*

The systematic errors are generally called aberrations; they differ from random errors in that in principle they can be calculated for any particular experimental arrangement and the observations corrected for them, leaving only the random error. In practice, of course, the calculation may be difficult. Aberrations can be divided broadly into two classes: (i) geometrical and (ii) physical. The geometrical aberrations are those that depend on the dimensions of the source, specimen, and detector (or of the slits that limit their effective dimensions). In angle-dispersive techniques, the physical aberrations depend on the intensity distribution in the range of wavelengths used, and in both angle- and energy-dispersive techniques they depend on the response characteristics of the detector and associated circuits.

The aberrations shift and distort the diffraction maxima. The study of their effects can be divided into four stages, corresponding to four levels of mathematical difficulty, and the stage to which it is necessary to carry the calculation depends on the purpose in view and the identifiable feature (Subsection 5.2.2.1) of the wavelength distribution that it is intended to adopt as a measure of the position of the line profile. The three usual features are:

(i) the centroid (centre of gravity, mean, average) of the wavelength distribution;

(ii) the peak (mode, maximum); and

(iii) the best overall fit between the observed and the synthesized line profile.

The first of these, the centroid, requires only the first stage of the calculation for the geometrical aberrations and the first and second for the physical; the second, the peak, logically requires all four stages, but approximations can be obtained at the second stage; and the third, the best overall fit, requires all four stages.

The first stage of the calculation is the determination of the effect of the aberration on the centroid of the diffraction maximum, and ordinarily this gives rise to no insurmountable difficulty (Spencer, 1931, 1935, 1937, 1939, 1941, 1949; Wilson, 1950; Ladell, Parrish & Taylor, 1959; Pike & Wilson, 1959). It is all that is required for the correction of centroid positions for geometrical aberrations, which should be strictly additive. There is some limitation for physical aberrations (Edwards & Toman, 1970; Wilson, 1970*b*).

The second stage is the calculation of the mean-square broadening (variance). This can be used to obtain a reasonable approximation to the correction of peak positions over a wide range of Bragg angle (Wilson, 1961; Gale, 1963, 1968). To this approximation, the position of the observed peak is given by

$$(2\theta)_{\rm obs} = (2\theta)_{\rm true} + \langle \Delta(2\theta) \rangle + WI'''/2I'', \qquad (5.2.3.1)$$

where $\langle \Delta(2\theta) \rangle$ is the centroid and W the variance of the geometrical aberrations and I'' and I''' are second and third derivatives of the observed line profile evaluated at its maximum. The physical aberrations of the centroid depend on the variance of the part of the wavelength distribution used in determining the centroid (Wilson, 1958, 1963; Wilson & Delf, 1961). Those of the peak depend on the ratio of the peak intensity I to its second derivative I'' (Wilson, 1961, 1963, 1965*c*).

Often an aberration can be expressed in the form

$$\Delta(2\theta) = KF(2\theta), \qquad (5.2.3.2)$$

where the function F gives the angular variation of the aberration and K depends only on dimensions *etc*. that are fixed for a particular experiment but whose actual measurement is too difficult or tedious. The constant K can then be treated along with the lattice parameters as an adjustable parameter in least-squares refinement (analytical extrapolation; see Subsection 5.2.3.2).

The third stage is the calculation of the line profile corresponding to each geometrical aberration. These aberration profiles can be combined by convolution (folding), either directly or by Fourier methods, and, in the fourth stage, the combined aberration profile can be convoluted with the emission profile of the X-ray source (or the emission profile as trimmed by a monochromator, pulse-height analyser, filter *etc*.) and with the diffraction profile corresponding to the state of strain, crystallite size, *etc*. of the specimen. This calculation of the composite line profile would be a necessary preliminary to an exact use of peak positions or of overall-profile fitting in lattice-parameter determination.

Such calculations were proposed many years ago (for example, by Alexander, 1948, 1950, 1953, 1954), and have been used by Beu and co-workers (see Section 5.2.9), and also by Boom and Smits (Boom & Smits, 1965; Boom, 1966). With the development of more powerful computer methods, such calculations can now be carried out routinely (*e.g.* Cheary & Coelho, 1992, 1994; Kogan & Kupriyanov, 1992; Timmers, Delhez, Tuinstra & Peerdeman, 1992). However, not all the relevant instrumental parameters can in general be determined with sufficient accuracy and overall instrumental line profiles are normally obtained by means of a suitable standard material, for which sample broadening is negligible (Section 5.2.12). There is, however, a related common approach, empirical rather than fundamental, based on the proposal of Rietveld (1967, 1969). Its use in structure determination is treated in detail in Chapter 8.6, and its use in lattice-parameter determination in Section 5.2.6. There seems to be no detailed published study of the accuracy attainable for lattice parameters, but the estimated standard deviations quoted (see, for example, Young, 1988) are comparable with those obtained for simpler structures giving resolved reflections.

5.2.3.2. *Extrapolation, graphical and analytical*

Equation (5.2.1.4) indicates that for a given error in θ the fractional error in the spacing d approaches zero as θ approaches 90°. The errors in θ – expressed as $\Delta(2\theta) = KF(2\theta)$ in (5.2.3.2) – arising from any specified aberration may increase as θ increases, but ordinarily this increase is insufficient to outweigh the effect of the $\cot\theta$ factor. In the simple cubic case, one can write

$$a_{\rm true} = [(h^2 + k^2 + l^2)^{1/2}\lambda/2\sin\theta] + KF(\theta), \qquad (5.2.3.3)$$

where K is a proportionality factor and $F(\theta)$ represents the angular variation of the systematic errors in the lattice parameter. The functions F in (5.2.3.2) and (5.2.3.3) are not exactly the same; they are transformed into one another by the use of (5.2.1.4). Functions suitable for different experimental arrangements are quoted in the following sections; see, for example, equation (5.2.8.1) for the Debye–Scherrer camera and Tables 5.2.4.1 and 5.2.7.1 for diffractometers. Simple graphical

Table 5.2.4.1. *Centroid displacement* $\langle \Delta\theta/\theta \rangle$ *and variance* W *of certain aberrations of an angle-dispersive diffractometer; for references see Wilson (1963, 1965c, 1974) and Gillham (1971)*

For the Seemann–Bohlin arrangement, S and R are given by equations (5.2.4.1) and (5.2.4.2); for the symmetrical arrangement, they are equal to R_0. Other notation is explained at the end of the table.

Aberration	$\langle \Delta(2\theta) \rangle$	W
Zero-angle calibration	Constant	0
Specimen displacement	$-s\{R^{-1}\cos(2\theta-\varphi)+S^{-1}\cos\varphi\}$	0
Specimen transparency Thick specimen	$-\sin 2\varphi/\mu(R+S)$	$\sin^2 2\varphi/\mu^2(R+S)^2$
Thin specimen	See Wilson (1974, p. 547)	
2:1 mis-setting	Zero if centroid of illuminated area is centred	$\beta^2A^2[R^{-1}\cos(2\theta-\varphi)+S^{-1}\cos\varphi]^2/3$
Inclination of plane of specimen to axis of rotation	Zero if centroid of illuminated area on equator of specimen	$\gamma^2h^2[R^{-1}\cos(2\theta-\varphi)+S^{-1}\cos\varphi]^2/3$ for uniform illumination
Flat specimen	$-A^2\sin 2\theta/3RS$	$4A^4\sin^2 2\theta/45R^2S^2$
Focal-line width	Small	$\sim f_1^2/12S^2$
Receiving-slit width	Small	$\sim r_1^2/12R^2$
Interaction terms	Small if adjustment reasonably good	See Wilson (1963, 1974)
Axial divergence No Soller slits, source, specimen and receiver equal	$-h^2[(S^{-2}+R^{-2})\cot 2\theta+(RS)^{-1}\operatorname{cosec}2\theta]/3$	$h^4[\{7S^{-4}+2(RS)^{-2}+7R^{-4}\}\cot^2 2\theta$ $+14(RS)^{-1}(S^{-2}+R^{-2})\cot 2\theta\operatorname{cosec}2\theta$ $+19(RS)^{-2}\operatorname{cosec}^2 2\theta]/45$
Narrow Soller slits One set in incident beam	$-[\Delta^2/12+h^2/3R^2]\cot 2\theta$	$7[\Delta^4/720+h^4/45R^2]\cot^2 2\theta$ $+h^2\operatorname{cosec}^2 2\theta/9R^2$
One set in diffracted beam	Replace R by S in the above	
Two sets	$-(\Delta^2\cot 2\theta)/6$	$\Delta^4(10+17\cot^2 2\theta)/360$
Wide Soller slits	Complex. See Pike (1957), Langford & Wilson (1962), Wilson (1963, 1974), and Gillham (1971)	
Refraction	$\sim -2\delta\tan\theta$	$\sim \delta^2[-6\ln(\Delta/2)+25]/4\mu p$
Physical aberrations	See Wilson (1963, 1965*c*, 1970*a*, 1974) and Gillham & King (1972)	

Notation: $2A$ = illuminated length of specimen; β = angle of equatorial mis-setting of specimen; γ = angle of inclination of plane of specimen to axis of rotation; Δ = angular aperture of Soller slits; μ = linear absorption coefficient of specimen; r_1 = width of receiving slit (varies with θ in some designs of diffractometer); s = specimen-surface displacement; f_1 = projected width of focal line; h = half height of focal line, specimen, and receiving slit, taken as equal; $1-\delta$ = index of refraction; p = effective particle size.

extrapolation is quick and easy for cubic substances, and by the use of successive approximations it can be applied to hexagonal (Wilson & Lipson, 1941), tetragonal, and even orthorhombic materials. It is, however, very cumbersome for non-cubic substances, and impracticable if the symmetry is less than orthorhombic.

Analytic extrapolation seems to have been first used by Cohen (1936*a*,*b*). It is now usual even in the cubic case: programs are often included in the software accompanying powder diffractometers, and many others are available separately. Some programs that are frequently referred to are described by Appleman & Evans (1973), Mighell, Hubbard & Stalick (1981), and Ferguson, Rogerson, Wolstenholme, Hughes & Huyton (1987); for a comparison, see Kelly (1988). If the precision warrants it, the single function $KF(\theta)$ may be replaced by a sum of functions $K_iF_i(\theta)$, one for each of the larger aberrations listed in Tables 5.2.4.1, 5.2.7.1, and 5.2.8.1. Two – the zero error and a function corresponding to specimen-surface displacement and transparency – must be used routinely; one or two more may be added if the precision warrants it.

5.2.4. Angle-dispersive diffractometer methods: conventional sources

The symmetrical Bragg–Brentano (Parrish) and the Seemann–Bohlin angle-dispersive diffractometers are fully described in Chapter 2.3. The centroid and peak displacements and the variances of the aberrations of the symmetrical diffractometer have been collected by Wilson (1961, 1963, 1965*c*, 1970*a*, 1974). For the Seemann–Bohlin type, they are collected in Table 5.2.4.1, mainly from Wilson (1974). They are expressed in inverse powers of the source–specimen distance S and the specimen–detector distance R, and tend to be larger for the Seemann–Bohlin arrangement than for the symmetrical arrangement. For the latter, S and R are constant and equal to the radius, say R_0, of the diffractometer, whereas, for the former,

$$S = 2R_0 \sin\varphi \qquad (5.2.4.1)$$

and

$$R = 2R_0 \sin(2\theta - \varphi), \qquad (5.2.4.2)$$

where φ is the constant angle that the incident X-rays make with the specimen surface. In the Seemann–Bohlin case, S will be constant at a value depending on the choice of angle φ, but usually less than R_0, and R will vary with 2θ, approaching zero as θ approaches $\varphi/2$. There will thus be a range of 2θ for which the Seeman–Bohlin aberrations containing R become very large. Mack & Parrish (1967) have confirmed experimentally the expected differences in favour of the symmetrical arrangement for general use, even though the effective equatorial divergence ('flat-specimen error') can be greatly reduced by curving the specimen appropriately in the Seemann–Bohlin arrangement. The aberrations for the symmetrical arrangement are found by putting $R = S = R_0$, $\varphi = \theta$ in the expression in Table 5.2.4.1; they are given explicitly by Wilson (1963, 1965*c*, 1970*a*).

5.2.5. Angle-dispersive diffractometer methods: synchrotron sources

Lattice-parameter determination with synchrotron radiation has a number of advantages over focusing methods (Parrish, Hart, Huang, & Bellotto, 1987; Parrish, 1988; Huang, 1988). The $K\alpha$-doublet problem does not arise; the symmetrical single profiles greatly simplify the accurate angular measurement of peaks. The higher intensity and low uniform background out to the highest θ values give a higher statistical counting precision, an important factor in accurate measurements. Short wavelengths (0.65 to 1.4 Å) can be used to increase greatly the number of reflections without compromising the accuracy of the peak measurements. If desired, the patterns can be recorded with two or more wavelengths of about the same intensity, instead of being confined to the $K\alpha$ and $K\beta$ lines (Popović, 1973). The large specimen-surface-displacement and flat-specimen errors associated with most other methods do not occur, so that systematic errors are small or absent. The wavelength can be selected to obtain the desired dispersion, to avoid fluorescence, and to reduce specimen transparency.

The reflections are virtually symmetrical narrow peaks (Subsection 2.3.2.1), with widths of the order of 0.02–0.04°(2θ) when an analysing crystal is used instead of a receiving slit, and of the order of 0.05° when a long Soller slit is used as a collimator. These increase with increasing 2θ because of wavelength dispersion and small particle size. The angular positions of the peaks can be determined with high precision by the use of profile-fitting or peak-search measurements, and the only significant geometrical aberration is axial divergence.

There are no lines in the synchrotron-radiation spectrum, and this creates the problem of determining the wavelength selected by the monochromator. If a highly accurate diffractometer were used for the monochromator and the monochromator d spacing were known accurately, the wavelength could be determined directly from θ_M. The angular accuracy of the diffractometer would have to be 0.0002° to achieve an accuracy of one part in 10^6 in the wavelength at $\lambda = 1.54$ Å.

In practice, the wavelengths can often be determined by scanning the absorption edges of elements in the specimen or a metal foil placed in the beam. There is no feature of the absorption edge that is accurately measurable, and the wavelengths are usually listed to one or two decimal places fewer than those for the emission lines.

The wavelength problem could be avoided by using the ratio of the lattice parameter of the specimen to that of an accurately known standard measured with the same experimental conditions (Parrish *et al.*, 1987). The standard may be mixed with the specimen or measured separately, as there is no specimen-surface displacement shift. Mixing reduces the intensity of both patterns and worsens the peak-to-background ratio. The limitation is the accuracy of the lattice parameter of the standard. The only widely available one is the National Institute of Standards and Technology [NIST, formerly National Bureau of Standards (NBS)] silicon powder 640b (see Section 5.2.10). This accuracy may not be sufficient for measuring doping levels, stoichiometry, and similar analyses now possible with synchrotron-radiation methods and the wavelength is normally determined directly from data for a standard whose lattice parameter is known with a high degree of precision, such as NIST SRM silicon 640b.

The most promising method is to use a high-quality single-crystal plate of float-zoned oxygen-free silicon, now widely available. Its lattice parameter is known to about one part in 10^7 (Hart, 1981), which is much higher accuracy than that of the published lists of X-ray wavelengths. Several orders of reflection (for example 111, 333, 444) should be used to improve the accuracy of the measurement.

Data are usually collected by step-scanning with selected constant angular increments and count times. To avoid interruptions due to refilling of the synchrotron ring, it is better to make a number of short runs rather than one long one. The data can then be added together and treated as a single data set. A shift in the orbit may cause a change in the wavelength reflected by the monochromator, and it is important to be aware of this in accurate lattice-parameter determination. The peaks are narrow, and the angle increments should be small enough to produce at least a dozen points in each peak. In practice, the scans may be made to cover a range of one to two half-widths (full widths at half height) on both sides of the peak, with increments of about 0.1 to 0.2 of the half-width, in order to record a sufficient number of data points for accurate profile fitting. The count time, which depends on the intensity, should be checked by determining the goodness-of-fit of the calculated profiles and the experimental points (Subsection 2.3.3.8 and Chapters 8.4 and 8.6).

The lower-angle peaks generally have higher intensities and are therefore preferred to the higher-angle peaks because of the better counting statistics. If the diffractometer can scan to negative angles, the number of strong peaks can be doubled by measuring the reflections on both sides of the zero position. The specimen can be used in either reflection or transmission, but reflection generally gives higher intensity. The lattice parameters are determined by a least-squares analysis of the peak angles determined by profile fitting, and it is therefore necessary to measure a sufficient number of reflections to give a statistically

valid result. The zero-angle position should be included as a variable parameter in the least-squares calculation.

A precision of a few parts per million in the lattice parameter of NIST silicon has been reached with the high-precision diffractometer in the Daresbury Laboratory (Hart, Cernik, Parrish & Toraya, 1990). This instrument has an accurate gear and an incremental encoder driven by a DC servomotor with a feedback servoloop capable of positioning the detector arm within $0.36''$. A large number of repeated measurements showed a statistical accuracy of $0.0001^\circ(2\theta)$, corresponding to 1 in the fifth decimal place of d for $\lambda = 1\,\text{Å}$ and $2\theta = 20^\circ$.

5.2.6. Whole-pattern methods

The recent large increase in the use of powder samples for crystal-structure refinement and analysis has also stimulated interest in lattice-parameter determinations, which are derived during the course of the calculation. The most frequently used method is that of Rietveld (1967, 1969) described in Chapter 8.6. In outline, a profile-fitting function containing adjustable parameters to vary the width and shape with 2θ is selected. The parameters corresponding to the atomic positions, multiplicity, lattice parameters, *etc*. of the selected structure model are varied until the best least-squares fit between the whole observed diffraction pattern and the whole calculated pattern of the model is obtained. There is no detailed published study of the accuracy of the lattice parameters that is attained but the estimated standard deviations quoted in a number of papers (see, for example, Young, 1988) appear to be comparable with those published for simple structures having no overlapped reflections. In this type of calculation, the accuracy of the lattice parameters is tied to the accuracy of the refined structure because it includes the model errors in the least-squares residuals.

An alternative to the Rietveld method is the pattern-decomposition method in which the integrated intensities are derived from profile fitting and the data used in a powder least-squares-refinement program. The reflections may be fitted individually or in small clusters (Parrish & Huang, 1980) or the whole pattern can be fitted (Pawley, 1981; Langford, Louër, Sonneveld & Visser, 1986; Toraya, 1986, 1988); unlike the Rietveld method, no crystal-structure model is required and only the first stage is used for lattice parameters. The Pawley method was developed for neutron-diffraction data and uses slack constraints to handle the problem of least-squares ill-conditioning due to overlapping reflections, and the positions of the reflections are constrained by the lattice parameters. The refinement also determines the zero-angle calibration correction.

Toraya extended the Pawley method to X-ray powder diffractometry. He first determined the profile shapes and peak positions of several standard samples by individual profile fittings to generate a curve relating the peak shifts to 2θ. A pair of split Pearson VII profiles was used for conventional patterns to handle the $K\alpha$ doublets and the profile asymmetries, and a pseudo-Voight function for the nearly symmetrical synchrotron-radiation profiles. The program is set up so that the parameters of the fitting function are varied with 2θ to account for the increasing widths and the peak shifts and the whole pattern is automatically fitted. The positions of the individual reflections are a function of the calculated lattice parameters, which are refined together with the integrated intensities as independent variables. This method also permits simultaneous refinement of several phases present in the pattern. Unit cells calculated from whole-pattern profile fitting and incorporating the peak-shift corrections had estimated standard deviations an order of magnitude smaller than those not using the systematic error correction. It is also possible to use an internal standard and to make the corrections by refining the cell parameters of the sample and holding constant the parameters of the standard.

Good results can also be obtained using selected peaks rather than the whole pattern (Parrish & Huang, 1980). Peak search or profile fitting is used to determine the observed peak positions. The least-squares refinement is used to minimize $\Delta(2\theta)$ (observed − calculated). It also determines the average and the standard deviation of all the d's and 2θ's. In principle, all the aberrations causing shifts can be incorporated in the refinement. There are, however, large correlations between aberrations with similar angular dependencies. In practice, the zero-angle calibration correction is always determined, and the specimen-surface displacement shift is usually included.

The lattice-parameter determination requires an indexed pattern in which the peak angles have been determined by peak search or profile fitting. Reflections known to have poor precision because of very low intensity or close overlapping should be omitted. The estimated standard deviation is dependent on the number of reflections used and it is better to use all the well measured peaks. There is the question of using a weighting scheme in which the high-angle reflections are given greater weight because of their higher accuracy for a given 2θ error. As noted in Subsection 5.2.13, higher-order reflections usually have low intensities and much overlapping. Some judgement and critical tests are often required.

5.2.7. Energy-dispersive techniques

There are now two basic energy-dispersive techniques available. In both, the specimen and detector are fixed in a selectable θ–2θ setting. The method (Giessen & Gordon, 1968) first described and most widely used requires a solid-state detector and a multichannel pulse-height analyser (Section 2.3.2 and Chapter 2.5). The resolution of the pattern is determined by the energy resolution of the detector and is considerably poorer than that of conventional angle-dispersive techniques, thereby greatly limiting its applications. The second method uses an incident-beam monochromator, a conventional scintillation counter, and a single-channel pulse-height analyser. The monochromator is step-scanned to select a gradually increasing (or decreasing) single wavelength (Parrish & Hart, 1987). This method permits much higher count rates, thereby reducing the time required for the experiment. Since the resolution is determined by the X-ray optics, the resolution is the same as in angle-dispersive diffractometry (Subsection 2.3.2.4). The method has, however, the disadvantage that the widths of the profiles vary with energy, and unless care is taken with the step size there may be too few points per reflection to define the profile adequately. The method is particularly applicable to synchrotron radiation, but there have been no publications to date on its use for lattice-parameter determination.

Energy-dispersive techniques (Section 2.2.3 and Chapter 2.5) are not ordinarily the method of choice for lattice-parameter determination. Relative to angle-dispersive techniques, they suffer from the following disadvantages:

(1) lower resolution;

(2) need for absolute energy calibration of the multichannel pulse-height analyser;

(3) need to know the energy distribution in the incident beam;

(4) specimen transparency varies with energy; even tungsten becomes transparent for 35 keV radiation.

Nevertheless, the advantage of stationary specimen and detector may outweigh these disadvantages for special applications.

Table 5.2.7.1. *Centroid displacement $\langle \Delta E/E \rangle$ and variance W of certain aberrations of an energy-dispersive diffractometer [mainly from Wilson (1973), where more detailed results are given for the aberrations marked with an asterisk]*

The Soller slits are taken to be in the original orientation (Soller, 1924). For the notation, see the footnote.

Aberration	$\langle \Delta E/E \rangle$	W
Specimen displacement	~ 0	Included in equatorial divergence
Specimen transparency*	~ 0	?
Equatorial divergence*	~ 0	$\cot^2\theta(A^2+B^2)/24$ for narrow Soller slits
Axial divergence	$-R^{-2}\,\mathrm{cosec}^2\,\theta[X^2\cos 2\theta + 4Y^2\cos^2\theta + Z^2\cos 2\theta]/24$	$R^{-4}\,\mathrm{cosec}^4\,\theta[X^4\cos^2 2\theta + 4Y^4(1+\cos 2\theta)^2 + Z^4\cos^2 2\theta + 5X^2Z^2 + 5Y^2(X^2+Z^2) \times (1+\cos 2\theta)^2]/720$
Refraction*	Probably negligible at the present stage of technique	
Response variations Centroid	$[Vf' + f''(\mu_3/2 - V^2f'/f)]/Ef$	?
Peak	$-f'I/EfI''$	?
Interaction of Lorentz *etc.* factors and geometrical aberrations	$\langle(\Delta\theta)^2\rangle/2 - \cot\theta[\langle\Delta\theta\rangle + (g'/g)\langle(\Delta\theta)^2\rangle] + \cot^2\theta(EI'/I)\langle(\Delta\theta)^2\rangle$	$-\cot\theta[\langle(\Delta\theta)^3\rangle - \langle\Delta\theta\rangle\langle(\Delta\theta)^2\rangle] + \cot^2\theta\{\langle(\Delta\theta)^2\rangle - \langle\Delta\theta\rangle^2 + (2g'/g)[\langle(\Delta\theta)^3\rangle - \langle\Delta\theta\rangle\langle(\Delta\theta)^2\rangle]\}$

Notation: A and B are the angular apertures (possibly equal) of the two sets of Soller slits; E is the energy of the detected photon; $f(E)$ is the variation of a response (energy of the continuous radiation, absorption in the specimen *etc.*) with E; $g(\theta)$ is an angle-dependent response (Lorentz factor *etc.*); $I(E-E_1)\,\mathrm{d}E$ is the counting rate recorded at E when the energy of the incident photons is actually E_1; R is the diffractometer radius; V is the variance and μ_3 is the third central moment of the energy-resoluton function I; $2X, 2Y, 2Z$ are the effective dimensions (possibly equal) of the source, specimen, and detector; the primes indicate differentiation; the averages $\langle(\Delta\theta)^2\rangle$ *etc.* are over the range of Bragg angles permitted by the slits *etc.*

A diffractometer can be converted from angle-dispersive to energy-dispersive by (i) replacing the usual counter by a solid-state detector, (ii) replacing the usual electronic circuits by a multichannel pulse-height analyser, and (iii) keeping the specimen and detector stationary while the counts are accumulated. When so used, the geometrical aberrations are essentially the same as those of an angle-dispersive diffractometer, though the greater penetrating power of the higher-energy X-rays means that greater attention must be paid to the irradiated volume and the specimen transparency (Langford & Wilson, 1962; Mantler & Parrish, 1977). As Sparks & Gedcke (1972)* emphasize, spacing measurements made with such an arrangement are subject to large specimen-surface displacement and transparency aberrations, and the corrections required to allow for them are difficult to make. Fukamachi, Hosoya & Terasaki (1973) and Nakajima, Fukamachi, Terasaki & Hosoya (1976) showed that this difficulty can be avoided if the Soller slits are rotated about the beam directions by 90°, so that they limit the equatorial divergence instead of the axial; this was, of course, the orientation used by Soller (1924) himself. Any effect of specimen-surface displacement and transparency is then negligible if ordinary care in adjustment is used, and the specimen may be placed in the reflection, or the symmetrical transmission, or the unsymmetrical transmission position (Wilson, 1973). The geometrical aberrations are collected in Table 5.2.7.1, and apply to the original orientation of the Soller slits; in the Sparks & Gedcke (1972) orientation, the usual ones apply. In general, the physical aberrations are the same for both orientations. The most difficult correction is that for the energy distribution in the incident X-ray beam; aspects of this have been discussed by Bourdillon, Glazer, Hidaka & Bordas (1978), Glazer, Hidaka & Bordas (1978), Buras, Olsen, Gerward, Will & Hinze (1977), Fukamachi, Hosoya & Terasaki (1973), Laguitton & Parrish (1977) and Wilson (1973). Only the last of these is directly relevant to the lattice-spacing problem. The best results reported so far seem to be those of Fukamachi, Hosoya & Terasaki (1973) (0.01% in the lattice parameter).

Okazaki & Kawaminami (1973) have suggested the use of a stationary specimen followed by analysis of the diffracted X-rays with a single-crystal spectrometer. This would give some of the advantages of energy-dispersive diffractometry (easy control of temperature *etc.*, because only small windows would be needed), but there would be no reduction in the time required for recording a pattern.

5.2.8. Camera methods

The types of powder camera frequently used in the determination of lattice parameters are described in Section 2.3.4. The main geometrical aberrations affecting measurements made with them are summarized in Table 5.2.8.1. At high angles, most of them vary *approximately* as $(\pi - 2\theta)^2$, and one would thus expect to obtain an approximately straight-line extrapolation if the apparent values of the lattice parameter were plotted against a function something like $(\pi - 2\theta)^2$. A function that has been

* There seems to be an error in their equation (5), which carries over into the equations they derive from it.

Table 5.2.8.1. *Some geometrical aberrations in the Debye–Scherrer method [increase in $\theta = +$, decrease $= -$]*

Source of aberration	Effect on θ	Angle variation of Δd	Remarks
Specimen displacement towards exit towards entrance sideways	 $-$ $+$ ~ 0*	 $\cos^2\theta$ $\cos^2\theta$ $\sim\theta$*	 Minimized by accurate construction and centring Extrapolates to zero
Beam divergence perpendicular to axis parallel to axis	 $+$ $+$ or $-$	 $\cos\theta\cot\theta$ or $\cos^2\theta/2\theta$ Complex	 Minimized by reducing collimator dimensions See Langford, Pike & Beau (1964)
Film shrinkage	$+$	$(\pi - 2\theta)\cot\theta$	Affects only van Arkel arrangement
Knife-edge calibration	$+$ or $-$	$\theta\cot\theta$	Affects only Bradley–Jay arrangement. Partly eliminated by usual extrapolation
Specimen absorption	$+$	$\cos\theta\cot\theta$ or $\cos^2\theta/2\theta$	Minimized by reducing specimen diameter or dilution. Extrapolates to zero

* For van Arkel and Bradley–Jay arrangements. For Straumanis–Ievins', $+$ or $-$ and $(\pi - 2\theta)\cot\theta$, respectively.

found very satisfactory in practice was suggested by Nelson & Riley (1945) [see also Taylor & Sinclair (1945*a*,*b*)]:

$$\cos^2\theta(\mathrm{cosec}\,\theta + \theta^{-1})/2. \qquad (5.2.8.1)$$

This function gives linear plots down to quite small values of θ.

5.2.9. Testing for remanent systematic error

Since about 1930, it has been claimed that the lattice parameters of cubic substances could be measured within one part in 50 000. Precision (that is, reproducibility of measurements by one technique within one laboratory) of this order is achieved, but accuracy (agreement between determinations by different techniques or by the same technique in different laboratories) is lower. The IUCr lattice-parameter project (Parrish, 1960) showed a standard deviation of 1 in 30 000 in inter-laboratory comparisons, with some outlying values differing from the mean by one or two parts in 10 000. At that time, therefore, precision was considerably better than accuracy (absence of significant remanent systematic error). Testing for remanent systematic error is thus valuable as an occasional test of methodology, though not undertaken as routine. The principle is outlined here, and more details are given in Chapters 8.4 and 8.5.

When refinement of parameters is performed by least squares, weighted in accordance with the reciprocal of the estimated variance, the expected value of the weighted sum of squares is

$$\langle S\rangle = n - p, \qquad (5.2.9.1)$$

where n is the number of terms summed and p is the number of parameters determined. The standard deviation of the sum S is expected to be

$$\sigma_S = [2(n-p)]^{1/2} \qquad (5.2.9.2)$$

approximately (Wilson, 1980), so that if the actual value of S exceeds

$$\begin{aligned}\langle S\rangle + k\sigma_S &= n - p + k\sigma_S \\ &= n - p + k[2(n-p)]^{1/2} \qquad (5.2.9.3)\end{aligned}$$

(where $k = 2$ or 3), one can reasonably conclude that there are defects in the model (remanent systematic errors). If S is less than this value, one can reasonably conclude that any defects in the model (systematic errors) are at worst of the same order of magnitude as the statistical fluctuations; the sensitivity of the test increases rather slowly with $n - p$. The method was advocated by Beu and his collaborators (Beu, Musil & Whitney, 1962, 1963; Beu, 1964; Beu & Whitney, 1967; Langford, Pike & Beu, 1964; see also Mitra, Ahmed & Das Gupta, 1985) because tests of the hypothesis 'no remaining systematic error' based on likelihood were available; they assumed a normal distribution of errors, possibly without realizing, and certainly without emphasizing, that the method was then equivalent to least squares. Their application of the method to testing for remanent systematic error in lattice-parameter determination was successful: the aberrations of the counter diffractometer were found to be adequately accounted for: additional aberrations were found for the Bond method (see Chapter 5.3); Boom (1966) used it in testing the accuracy of the Debye–Scherrer method.

In statistical literature, the weighted sum of squares S is often called the *scaled deviance*, and

$$E = [S - (n-p)]/[2(n-p)]^{1/2} \qquad (5.2.9.4)$$

is called the *excess*. The test for the absence of significant systematic error is then that the excess should be less than three.

5.2.10. Powder-diffraction standards

The use of properly characterized materials is an important step in determining the performance characteristics of instruments and methods. The best documented and most widely used standards for powder diffraction are those from the [US] National Institute of Standards and Technology* (Dragoo, 1986).

Such standards are used as specimens in diffractometers and cameras for angular calibration to determine systematic errors in the observed 2θ's for profile shapes and in intensities for quantitative analysis and for determining instrumental line profiles. The standard may be used separately as an independent specimen ('external standard'), or mixed with the powder to be investigated ('internal standard'). Some examples of the use of

* http://srmcatalog.nist.gov.

Table 5.2.10.1. *NIST values for silicon standards ($\lambda = 1.5405929$ Å, $T = 298$ K for 640, 640a and 640b, $T = 295.6$ K for 640c, $a_0 \pm 0.000035$ Å, no refraction correction)*

Standard	Year issued	a_0 (Å)	Cu $K\alpha_1$	
			111 (°2θ)	444 (°2θ)
640	1974*	5.43086	28.4427	158.6382
640a	1982†	5.430806	28.4430	158.6443
640b	1987	5.430922	28.4424	158.6315
640c	2000	5.4311946	28.4410	158.6031

* Hubbard, Swanson & Mauer (1975). † Hubbard (1983).

standards are given by Hubbard (1983) and Wong-Ng & Hubbard (1987).

The current silicon-powder standard for 2θ calibration is Standard Reference Material (hereinafter abbreviated SRM) 640c; SRM 640, SRM 640a and SRM 640b are no longer available, but data for all four are listed in Table 5.2.10.1 for the use of workers who may still have stocks of the earlier standards. The median particle size (mass-weighted distribution) is about 5 μm, and 95% of the particles are < 10 μm. There is a wide range of particle sizes in SRM 640, and sieving is necessary to remove the larger particles. The agreement between SRM's 640 and 640a and between 640 and 640b is one part in 10^{-5}, and between 640a and 640b is two parts in 10^{-5}. The accuracy is given as 3.5×10^{-5} for each. All were calculated by the use of the Deslattes & Henins (1973) Cu $K\alpha_1$ wavelength of 1.5405981 Å, without refraction correction, and corrected to 298 K. Because this wavelength was later found to have a systematic error (see Section 4.2.2), and a more accurate value, 1.5405929(5) Å (see Table 4.2.2.1), is now available, this wavelength was used for SRM 640c, with the temperature adjusted to 295.6 K. The data for the earlier SRMs have also been adjusted to reflect this more accurate wavelength.

Table 5.2.10.2 lists the reflection angles for silicon 640c, silver and tungsten calculated from the adjusted NIST lattice parameters and the Table 4.2.2.1 value for the Cu $K\alpha_1$ wavelength. Table 5.2.10.3 lists the reflection angles of silicon 640c calculated from the Table 4.2.2.1 wavelengths for Mo $K\alpha_1$, Cr $K\alpha_1$ and other wavelengths selected for synchrotron radiation users. The high-angle reflections of silicon for Mo $K\alpha_1$ are listed in Table 5.2.10.4. NIST does not provide a tungsten standard, but reflection angles calculated from $a = 3.16523(4)$ Å at 298 K for Cu $K\alpha_1 = 1.5405929$ Å are given in Table 5.2.10.2 and in Table 5.2.10.5 for a number of other wavelengths.

For calibration at small diffraction angles, NIST provides fluorophlogopite, a synthetic mica, as SRM 675. The (001) lattice spacing, adjusted for the revised wavelength of Cu $K\alpha_1$, is 9.98101(7) Å at 298 K. Table 5.2.10.6 lists the diffraction angles for Cu $K\alpha_1$. NIST advises mixing it with silicon because the higher-angle reflections may be in error because of specimen transparency. SRM 675 was purposely prepared as large particles (up to 75 μm) to encourage preferred orientation of the mica flakes; only the 00l reflections are then observed. The first reflection with Cu $K\alpha_1$ radiation for SRM 675 occurs at 8.853°(2θ) (Table 5.2.10.6) and a material that extends the coverage of NIST SRMs down to very low angles is silver behenate (Huang, Toraya, Blanton & Wu, 1993). The long spacing for this material, obtained with synchrotron radiation and by using SRM 640a as an internal standard, is $d_{001} = 58.380$ (3) Å and, for Cu $K\alpha_1$ radiation, there are 13 well defined and evenly spaced 00l reflections in the range 1.5 to 20°(2θ) (Table 5.2.10.7). This material is suitable for use as an external or an internal low-angle calibration standard for the analysis of materials with large unit-cell dimensions and modulated multilayers with large layer periodicity.

Table 5.2.10.2. *Reflection angles (°) for tungsten, silver, and silicon ($\lambda = 1.5405929$ Å, $T = 298$ K for tungsten and silver, $T = 295.6$ K for silicon)*

hkl	Tungsten $a_0 =$ 3.16523 (4) Å	Silver $a_0 =$ 4.08650 (2) Å	Silicon $a_0 =$ 5.431195 (9) Å (SRM 640c)
110	40.262		
111		38.112	28.441
200	58.251	44.295	
211	73.184		
220	86.996	64.437	47.300
310	100.632		
311		77.390	56.120
222	114.923	81.533	
321	131.171		
400	153.535	97.875	69.126
331		110.499	76.372
420		114.914	
422		134.871	88.025
511/333		156.737	94.947
440			106.701
531			114.084
620			127.534
533			136.880
444			158.603

Although the reflection angles are given to three decimal places in the tables in this section, the accuracy is lower by an amount that is not known with certainty. The lower accuracy arises from three factors: uncertainties in the lattice parameters of the W and Ag internal standards, the experimental precision, and the methods used. The wavelength given in Table 4.2.2.1 is far more accurate than these factors. The tables can probably be used to two places of decimals, the 2θ errors increasing with increasing 2θ.

In using an external standard for calibrating an instrument (without a wide receiving slit), it is essential to minimize specimen-surface displacement, which shifts the measured position of the reflection (Subsection 5.2.3.1). The amount of the shift and even its direction may vary when the specimen is remounted, and it is advisable to make several measurements after removal and replacement, in order to determine the degree of reproducibility. Specimen transparency is equivalent to a variable specimen-surface displacement, since the effective depth of penetration varies with the angle of incidence of the beam. The maximum shift occurs at 2θ equal to 90°, and it vanishes at 0 and 180°. For example, for silicon, the linear absorption coefficient is 133 cm^{-1} for $\lambda = 1.54$ Å and 15 cm^{-1} for 0.7 Å, shifting the 422 reflection by −0.01° at 88° and −0.05° at 37°, respectively. It should be noted that SRM silicon 640b, as supplied by NIST, exhibits measurable sample broadening (van Berkum, Sprong, de Keijser, Delhez & Sonneveld, 1995) and is thus not suitable for determining instrumental line profiles.

Table 5.2.10.3. *Silicon standard reflection angles (°) (NIST SRM 640c, $a_0 = 5.431195$ Å, $T = 295.6$ K)*

h k l	d (Å)	I	Mo $K\alpha_1$ 0.709317 Å	1.000000 Å	1.250000 Å	1.500000 Å	1.750000 Å	Cr $K\alpha_1$ 2.289746 Å
1 1 1	3.13570	100.0	12.988	18.350	22.994	27.676	32.406	42.829
2 2 0	1.92022	71.1	21.287	30.186	37.990	45.981	54.217	73.202
3 1 1	1.63757	43.5	25.016	35.556	44.873	54.516	64.597	88.714
4 0 0	1.35780	11.8	30.283	43.215	54.813	67.059	80.245	114.955
3 3 1	1.24600	17.4	33.074	47.317	60.213	74.016	89.215	133.514
4 2 2	1.10864	22.3	37.314	53.616	68.635	85.142	104.232	
5 1 1	1.04523	8.7	39.670	57.157	73.447	91.704	113.678	
3 3 3	1.04523	2.9	39.670	57.157	73.447	91.704	113.678	
4 4 0	0.96011	6.0	43.356	62.768	81.229	102.734	131.386	
5 3 1	0.91804	9.8	45.452	66.000	85.812	109.563	144.772	
6 2 0	0.85871	7.1	48.789	71.221	93.411	121.713		
5 3 3	0.82825	2.9	50.707	74.268	97.981	129.788		
4 4 4	0.78393	1.5	53.797	79.258	105.739	146.162		
7 1 1	0.76052	1.9	55.594	82.211	110.532	160.918		
5 5 1	0.76052	1.9	55.594	82.211	110.532	160.918		
6 4 2	0.72577	5.7	58.506	87.090	118.893			
7 3 1	0.70708	2.4	60.209	90.004	124.237			
5 5 3	0.70708	1.2	60.209	90.004	124.237			
8 0 0	0.67890	0.5	62.987	94.866	134.030			
7 3 3	0.66353	0.8	64.620	97.797	140.757			
6 6 0	0.64007	0.7	67.297	102.735	155.085			
8 2 2	0.64007	1.3	67.297	102.735	155.085			
7 5 1	0.62714	1.7	68.876	105.740	170.531			
5 5 5	0.62714	0.2	68.876	105.740	170.531			
8 4 0	0.60723	0.9	71.473	110.855				
9 1 1	0.59615	0.4	73.013	114.009				
7 5 3	0.59615	0.8	73.013	114.009				
6 6 4	0.57897	0.7	75.551	119.447				
9 3 1	0.56934	0.6	77.061	122.854				
8 4 4	0.55432	0.5	79.555	128.846				
9 3 3	0.54586	0.2	81.042	132.692				
7 7 1	0.54586	0.2	81.042	132.692				
7 5 5	0.54586	0.2	81.042	132.692				
10 2 0	0.53257	0.4	83.509	139.717				
8 6 2	0.53257	0.8	83.509	139.717				
9 5 1	0.52505	0.4	84.982	144.460				
7 7 3	0.52505	0.2	84.982	144.460				
9 5 3	0.50646	0.3	88.897	161.678				
10 4 2	0.49580	0.5	91.340					
11 1 1	0.48971	0.1	92.808					
7 7 5	0.48971	0.1	92.808					
8 8 0	0.48005	0.1	95.258					
11 3 1	0.47453	0.2	96.729					
9 7 1	0.47453	0.2	96.729					
9 5 5	0.47453	0.1	96.729					

5.2.11. Intensity standards

The measurement of intensity falls within the scope of Parts 6 and 7. However, powder methods are much used in quantitative analysis, and the National Institute of Standards and Technology provides five standards for use as internal standards for this purpose and for checking the accuracy of diffractometer and camera intensity measurements. The five materials, certified as SRM 674, are α-Al_2O_3 (corundum), ZnO, TiO_2 (rutile), Cr_2O_3, and CeO_2. Table 5.2.11.1, taken from the NIST certificate, is a partial list of pertinent data. The lattice parameters have an uncertainty of 3 parts in 10^5, which must be increased by a factor of 2 or 3 because of uncertainty in internal standards and thermal expansion. The five materials have a wide range of absorption coefficient and the crystallite size (about 2 μm) causes a small profile broadening. The table gives the intensities of the second- and third-strongest lines relative to the strongest = 100, and the final column gives the ratio of the strongest peak to the strongest peak of Al_2O_3.

Table 5.2.10.4. *Silicon standard high reflection angles (°) (NIST SRM 640c, $a_0 = 5.431195$ Å, $T = 295.6$ K, $\lambda = 0.709317$ Å)*

h	k	l	d (Å)	2θ	h	k	l	d (Å)	2θ
10	6	0	0.46572	99.198	9	9	5	0.39717	126.497
8	6	6	0.46572	99.198	8	8	8	0.39196	129.600
11	3	3	0.46067	100.686	13	5	1	0.38894	131.530
9	7	3	0.46067	100.686	11	7	5	0.38894	131.530
12	0	0	0.45260	103.183	10	10	0	0.38404	134.882
8	8	4	0.45260	103.183	10	8	6	0.38404	134.882
11	5	1	0.44796	104.694	14	2	0	0.38404	134.882
7	7	7	0.44796	104.694	13	5	3	0.38120	136.990
12	2	2	0.44053	107.235	11	9	1	0.38120	136.990
10	6	4	0.44053	107.235	12	8	0	0.37659	140.703
11	5	3	0.43624	108.777	11	9	3	0.37390	143.079
9	7	5	0.43624	108.777	9	9	7	0.37390	143.079
12	4	0	0.42937	111.378	12	6	6	0.36955	147.363
9	9	1	0.42540	112.961	10	10	4	0.36955	147.363
10	8	2	0.41903	115.642	14	4	2	0.36955	147.363
9	9	3	0.41533	117.279	13	7	1	0.36701	150.191
11	7	1	0.41533	117.279	11	7	7	0.36701	150.191
11	5	5	0.41533	117.279	13	5	5	0.36701	150.191
13	1	1	0.41533	117.279	12	8	4	0.36289	155.551
12	4	4	0.40939	120.064	11	9	5	0.36048	159.376
11	7	3	0.40595	121.773	15	1	1	0.36048	159.376
13	3	1	0.40595	121.773	13	7	3	0.36048	159.376
9	7	7	0.40595	121.773	14	6	0	0.35658	168.113
12	6	2	0.40039	124.694					
13	3	3	0.39717	126.497					

5.2.12. Instrumental line-profile-shape standards

The need for standard reference materials to determine instrumental line profiles arose from the increased use in recent years of whole-pattern methods (Section 5.2.6) in several applications of powder diffraction. Instrumental line-profile standards are required to determine resolution, as a check that alignment has been optimized, or to compare the performance of different diffractometers, and to obtain sample contributions from observed data in line-profile analysis. Different standards may therefore be required if samples of interest do not have a high absorption coefficient for the radiation used.

In addition to the usual requirements for SRMs, suitable substances for instrument characterization clearly should not exhibit any measurable sample broadening, even when used with high-resolution diffractometers. Various materials were considered by the Technical Committee of the JCPDS–ICDD, in association with NIST, and lanthanum hexaboride [LaB_6: $a_0 = 4.15695(6)$ Å at $T = 299$ K] was selected for use as an instrumental standard (Fawcett *et al.*, 1988). This was subsequently marketed by NIST as SRM 660 and it also serves as a line position standard. Other materials used as instrumental standards include BaF_2 (Louër & Langford, 1988) and KCl (Scardi, Lutterotti & Maistrelli, 1994). Both are low-cost materials, are available in large quantities, and can readily be annealed to minimize sample broadening. Although KCl introduces a measurable contribution to line breadth owing to sample transparency, it can be used to advantage for correcting data from materials having a similar absorption coefficient, such as many ceramics. van Berkum, Sprong, de Keijser, Delhez & Sonneveld (1995) selected a 5–10 μm size fraction from silicon SRM 640b, deposited about 1.5 Mg m^{-2} uniformly on a (510)-oriented single-crystal silicon wafer and annealed the whole assemblage to produce an instrument line-profile standard. The resulting line-profile widths were found to be slightly less than for LaB_6 at angles below about 100°(2θ) with Cu $K\alpha$ radiation.

5.2.13. Factors determining accuracy

Many factors influencing accuracy in lattice-parameter determination have been mentioned in passing or discussed at length in this and previous chapters. This section attempts to summarize them and put them into perspective. Accuracy in the range of 1 to 0.1% can now be achieved routinely with average care. Increasing the accuracy to 0.01% requires considerable care in specimen preparation, data collection, instrument alignment, and calibration. The range 0.001 to 0.0001% is rarely reached and each determination is virtually a research project. The more important factors are:

(1) Differentiation of the Bragg equation, as in (5.2.1.4), shows the advantage of using the highest-angle reflections; because of the $\cot\theta$ term, the error in Δd is smaller for a given angular accuracy $\Delta\theta$. The gain is not as great as one might expect at first, as the experimental accuracy of the back reflections is lowered because of (i) their lower intensity, (ii) their lower peak-to-background ratio, (iii) their broadening by wavelength dispersion and crystallite imperfection, and (iv) problems of overlapping.

(2) The lower-angle reflections show the converse effects of (i) higher intensity, (ii) higher peak-to-background ratio, (iii) less broadening, and (iv) fewer problems of overlapping. In any particular case, a balance of advantage must be sought.

Table 5.2.10.5. *Tungsten reflection angles (°) ($a_0 = 3.16523$ Å, $T = 298$ K)*

h k l	d (Å)	I	Mo $K\alpha_1$ 0.709317 Å	1.000000 Å	1.250000 Å	1.500000 Å	1.750000 Å	Cr $K\alpha_1$ 2.289746 Å
1 1 0	2.23816	100.0	18.235	25.817	32.431	39.157	46.027	61.531
2 0 0	1.58262	18.1	25.899	36.834	46.521	56.575	67.130	92.672
2 1 1	1.29220	37.0	31.860	45.528	57.851	70.958	85.241	124.747
2 2 0	1.11908	11.1	36.953	53.076	67.903	84.164	102.868	
3 1 0	1.00093	14.4	41.505	59.938	77.279	97.059	121.896	
2 2 2	0.91372	3.3	45.679	66.352	86.316	110.333	146.518	
3 2 1	0.84594	14.2	49.574	72.464	95.262	124.894		
4 0 0	0.79131	1.3	53.255	78.376	104.339	142.810		
3 3 0	0.74605	2.0	56.768	84.164	113.805			
4 1 1	0.74605	4.0	56.768	84.164	113.805			
4 2 0	0.70777	3.1	60.145	89.893	124.027			
3 3 2	0.67483	2.5	63.411	95.621	135.687			
4 2 2	0.64610	2.0	66.586	101.406	150.632			
5 1 0	0.62075	1.6	69.687	107.312				
4 3 1	0.62075	3.2	69.687	107.312				
5 2 1	0.57789	2.2	75.717	119.815				
4 4 0	0.55954	0.5	78.668	126.656				
5 3 0	0.54283	0.8	81.589	134.172				
4 3 3	0.54283	0.8	81.589	134.172				
6 0 0	0.52754	0.2	84.488	142.810				
4 4 2	0.52754	0.7	84.488	142.810				
6 1 1	0.51347	0.6	87.373	153.695				
5 3 2	0.51347	1.2	87.373	153.695				
6 2 0	0.50047	0.5	90.251	175.042				
5 4 1	0.48841	1.0	93.129					
6 2 2	0.47718	0.4	96.016					
6 3 1	0.46669	0.8	98.919					
4 4 4	0.45686	0.1	101.845					
5 5 0	0.44763	0.2	104.802					
7 1 0	0.44763	0.3	104.802					
5 4 3	0.44763	0.7	104.802					
6 4 0	0.43894	0.3	107.800					
5 5 2	0.43073	0.3	110.851					
6 3 3	0.43073	0.3	110.851					
7 2 1	0.43073	0.6	110.851					
6 4 2	0.42297	0.6	113.963					
7 3 0	0.41562	0.3	117.150					
7 3 2	0.40198	0.5	123.837					
6 5 1	0.40198	0.5	123.837					
8 0 0	0.39565	0.1	127.376					
7 4 1	0.38961	0.5	131.091					
8 1 1	0.38961	0.3	131.091					
5 5 4	0.38961	0.3	131.091					
8 2 0	0.38384	0.3	135.029					
6 4 4	0.38384	0.3	135.029					
6 5 3	0.37832	0.6	139.257					
8 2 2	0.37303	0.3	143.877					
6 6 0	0.37303	0.1	143.877					
7 4 3	0.36795	0.6	149.106					
7 5 0	0.36795	0.3	149.106					
8 3 1	0.36795	0.6	149.106					
6 6 2	0.36308	0.4	155.271					
7 5 2	0.35839	1.1	163.450					

Table 5.2.10.6. *Fluorophlogopite 00l standard reflection angles [NIST SRM 675, $d(001) = 9.98104\,(7)$ Å, $T = 298$ K, $\lambda = 1.5405929$ Å]*

l	2θ (°)
1	8.853
2	17.759
3	26.774
4	35.962
5	45.397
6	55.169
7	65.399
8	76.255
10	101.025
11	116.193
12	135.674

Table 5.2.10.7. *Silver behenate 00l standard reflection angles [$d(001) = 58.380\,(3)$ Å, $\lambda = 1.5405929$ Å (Huang, Toraya, Blanton & Wu, 1993)]*

l	2θ (°)
1	1.512
2	3.024
3	4.537
4	6.051
5	7.565
6	9.081
7	10.599
8	12.118
9	13.640
10	15.164
11	16.691
12	18.221
13	19.754

The forward reflections have been used in parallel-beam synchrotron-radiation lattice-parameter studies (Parrish *et al.*, 1987).

(3) The profile shape has a strong influence on the accuracy of the angle measurement. The geometrical aberrations produce asymmetries that reduce the accuracy; the effects can be minimized by a proper selection of slit sizes. In most cases, it is inadvisable to use $K\beta$ radiation to avoid $K\alpha$-doublet splitting, as the intensity is reduced by a factor of seven. Symmetrical profiles are obtained with parallel-beam optics, but it is usually necessary to use synchrotron radiation to achieve sufficient intensity.

(4) The largest and commonest source of systematic error in focusing geometry is the specimen-surface displacement. Several remountings of the specimen in the diffractometer and measurement of some low-angle reflections may be helpful in determining and minimizing the error. This aberration does not occur in parallel-beam geometry unless a receiving slit is used.

(5) The precision of the diffractometer gears (or the equivalent) may be the limiting factor in high-precision measurements. The use of an electromagnetic encoder mounted on the 2θ-output shaft can increase the precision considerably. It is not normally included in commercial diffractometers because of its cost, but it is essential for adequate accuracy when the 2θ angles must be determined to better than 0.001°. The various types of mechanical error have been described by Jenkins & Schreiner (1986).

The diffractometer must be carefully adjusted to avoid mechanical problems. The effect of backlash can be minimized by slewing beyond and then returning to the starting angle, and by always scanning in the same direction. It is essential to avoid over-tight worm-and-gear meshing, as it causes jerky rather than smooth movement.

(6) The beam must be precisely centred, the slits and monochromator (if used) must be parallel to the line focus of the X-ray tube, and the scanning plane must be perpendicular to the line focus.

(7) The use of standard specimens with accurately known lattice parameters (Section 5.2.10) and ideally free of line broadening is strongly recommended as a test of the overall precision of the instrumentation and method.

(8) For a given total time available for an experiment, it is necessary to strike a balance between numerous short steps with short counting times and fewer longer steps with longer counting times. The former alternative may give a better definition of the line shape; the latter may give lower calculated standard uncertainties (formerly called estimated standard deviations) in any derived parameters. Obviously, the step length must be considerably shorter than the width of any feature of the profile that is considered to be of importance.

(9) Least-squares refinement is discussed in Subsection 5.2.3.2. The programs and the methods of handling the data should be carefully checked, as various programs have been found to give slightly different values from the same experimental data (see, for example, JCPDS – International Centre for Diffraction Data, 1986; Kelly, 1988).

(10) Specimen preparation is very important; the particle size should preferably be less than 10 μm, and a flat smooth surface normal to the diffraction vector is essential. The linearity of the detector and the temperature of the

Table 5.2.11.1. *NIST intensity standards, SRM 674*

Standard	Crystal system	a_0 (Å)	c_0 (Å)	I_{rel} *hkl*		$I_1/I_c(113)$
				2	3	
Al_2O_3 (corundum)	Trigonal	4.75893 (10)	12.9917 (7)	92.5 (26) 116	87.4 (19) 104	—
ZnO	Hexagonal	3.24981 (12)	5.20653 (13)	57.6 (11) 100	40.2 (14) 002	5.17 (13) 101
TiO_2 (rutile)	Tetragonal	4.59365 (10)	2.95874 (8)	56.9 (28) 211	44.0 (17) 101	3.39 (12) 110
Cr_2O_3	Trigonal	4.95916 (12)	13.5972 (6)	94.5 (22) 116	87.1 (23) 110	2.10 (5) 104
CeO_2	Cubic	5.41129 (8)	—	53.5 (20) 220	43.4 (23) 311	7.5 (2) 111

specimen must be properly controlled during the collection of the experimental data.

(11) The accuracy of the 2θ measurements is directly dependent on the individual step-scanned points. The counting statistical accuracy is determined by the intensity and the background level, and is a major factor in lattice-parameter precision. Preliminary tests on typical profiles ensure that fullest advantage can be taken of the experimental conditions.

(12) At present (2003), the best approach to precision lattice-parameter determination is to follow the suggestions listed above, and to use peak search or profile fitting to calculate the observed 2θ positions. All the well determined peaks are used in the least-squares refinement against 2θ to obtain the zero-angle calibration correction, and in the case of focusing methods the specimen-surface displacement is added. The use of standards is recommended.

International Tables for Crystallography (2006). Vol. C, Chapter 5.3, pp. 505–536.

5.3. X-ray diffraction methods: single crystal

By E. Gałdecka

5.3.1. Introduction

5.3.1.1. *General remarks*

The starting point for lattice-parameter measurements by X-ray diffraction methods and evaluation of their accuracy and precision is the Bragg law, combining diffraction conditions (the Bragg angle θ and the wavelength λ) with the parameters of the lattice to be determined:

$$2d\sin\theta = n\lambda, \tag{5.3.1.1}$$

in which d is the interplanar spacing, being a function of direct-lattice parameters a, b, c, α, β, γ, and n is the order of interference. Before calculating the lattice parameters, corrections for *refraction* should be introduced to d values determined from (5.3.1.1) [James (1967); Isherwood & Wallace (1971); Lisoivan (1974); Hart (1981); Hart, Parrish, Bellotto & Lim (1988); *cf.* §5.3.3.4.3.2, paragraph (2) below].

Since only d values result directly from (5.3.1.1) and the non-linear dependence of direct-lattice parameters on d is, in a general case, rather complicated (see, for example, Buerger, 1942, p. 103), it is convenient to introduce reciprocal-cell parameters (a^*, b^*, c^*, α^*, β^*, γ^*) and to write the Bragg law in the form:

$$\begin{aligned}4\sin^2\theta/\lambda^2 &= n^2/d^2 \\ &= h^2a^{*2} + k^2b^{*2} + l^2c^{*2} + 2hka^*b^*\cos\gamma^* \\ &\quad + 2hla^*c^*\cos\beta^* + 2klb^*c^*\cos\alpha^*,\end{aligned} \tag{5.3.1.2}$$

where h, k and l are the indices of reflection, and then those of the direct cell are calculated from suitable equations given elsewhere (Buerger, 1942, p. 361, Table 2). The minimum number of equations, and therefore number of measurements, necessary to obtain all the lattice parameters is equal to the number of parameters, but many more measurements are usually made, to make possible least-squares refinement to diminish the statistical error of the estimates. In some methods, extrapolation of the results is used to remove the θ-dependent systematic errors (Wilson, 1980, Section 5, and references therein) and requires several measurements for various θ.

Measurements of lattice dimensions can be divided into *absolute*, in which lattice dimensions are determined under defined environmental conditions, and *relative*, in which, compared to a reference crystal, small changes of lattice parameters (resulting from changes of temperature, pressure, electric field, mechanical stress *etc.*) or differences in the cell dimensions of a given specimen (influenced by point defects, deviation from exact stoichiometry, irradiation damage or other factors) are examined.

In the particular case when the lattice parameter of the reference crystal has been very accurately determined, precise determination of the ratio of two lattice parameters enables one to obtain an accurate value of the specimen parameter (Baker & Hart, 1975; Windisch & Becker, 1990; Bowen & Tanner, 1995).

Absolute methods can be characterized by the *accuracy* δd, defined as the difference between measured and real (unknown) interplanar spacings or, more frequently, by using the relative accuracy $\delta d/d$, defined by the formula obtained as a result of differentiation of the Bragg law [equation (5.3.1.1)]:

$$\delta d/d = \delta\lambda/\lambda - \cot\theta\,\delta\theta, \tag{5.3.1.3}$$

where $\delta\lambda/\lambda$ is the relative accuracy of the wavelength determination in relation to the commonly accepted wavelength standard, and $\delta\theta$ is the error in the Bragg angle determined.

The analogous criterion used for characterization of relative methods may be the *precision*, defined by the variance $\sigma^2(d)$ [or its square root – the standard deviation, $\sigma(d)$] of the measured interplanar spacing d as the measure of repeatability of experimental results.

The relative precision of lattice-spacing determination can be presented in the form:

$$\sigma(d)/d = \cot\theta\,\sigma(\theta), \tag{5.3.1.4}$$

where $\sigma(\theta)$ is the standard deviation of the measured Bragg angle θ.

Another mathematical criterion proposed especially for relative methods is the *sensitivity*, defined (Okazaki & Ohama, 1979) as the ratio $\delta\theta/\delta d$, *i.e.* the change in the θ value owing to the unit change in d.

The main task in unit-cell determination is the *measurement of the Bragg angle*. For a given θ angle, the accuracy $\delta\theta$ and precision $\sigma(\theta)$ affect those of the lattice parameter [equations (5.3.1.3) and (5.3.1.4)]. To achieve the desired value of $\delta d/d$, the accuracy $\delta\theta$ must be no worse than resulting from the Bragg law (Bond, 1960):

$$|\delta\theta| = (|\delta d|/d)\tan\theta. \tag{5.3.1.5}$$

An analogous equation can be obtained for $\sigma(\theta)$ as a function of $\sigma(d)/d$. The values $\delta\theta$ and $\sigma(\theta)$ depend not only on the measurement *technique* (X-ray source, device, geometry) and the *crystal* (its structure, perfection, shape, physical properties), but also on the *processing of the experimental data*.

The first two factors affect the measured profile [which will be denoted here – apart from the means of recording – by $h(\theta)$], being a convolution of several distributions (Alexander, 1948, 1950, 1954; Alexander & Smith, 1962; Härtwig & Grosswig, 1989; Härtwig, Hölzer, Forster, Goetz, Wokulska & Wolf, 1994) and the third permits calculations of the Bragg angle and the lattice parameters with an accuracy and a precision as high as possible in given conditions, *i.e.* for a given profile $h(\theta)$.

In the general case, $h(\theta)$ can be described as a convolution:

$$h(\theta) = h_\lambda(\theta) * h_A(\theta) * h_C(\theta), \tag{5.3.1.6}$$

where $h_\lambda(\theta)$ is an original profile due to wavelength distribution; $h_A(\theta)$ is a distribution depending on various apparatus factors, such as tube-focus emissivity, collimator parameters, detector aperture; and $h_C(\theta)$ is a function (the crystal profile) depending on the crystal, its perfection, mosaic structure, shape (flatness), and absorption coefficient.

The functions $h_A(\theta)$ and $h_C(\theta)$ are again convolutions of appropriate factors.

Each of the functions $h_\lambda(\theta)$, $h_A(\theta)$, and $h_C(\theta)$ has its own shape and a finite width, which affect the shape and the width ω_h of the resulting profile $h(\theta)$.

Since $h_A(\theta)$ and $h_C(\theta)$ are ordinarily asymmetric, the profile $h(\theta)$ is also asymmetric and may be considerably shifted in relation to the original one, $h_\lambda(\theta)$, leading to systematic errors in lattice-parameter determination.

The finite precision $\sigma(d)/d$, on the other hand, results from the fact that the two measured variables – the intensity h and the angle θ – are random variables.

Copyright © 2006 International Union of Crystallography

The half-width ω_λ of $h_\lambda(\theta)$ defines the minimum half-width of $h(\theta)$ that it is possible to achieve with a given X-ray source:

$$\omega_h \gtrsim \omega_\lambda. \quad (5.3.1.7)$$

It can be assumed from the Bragg law that:

$$\omega_\lambda = (w_\lambda/\lambda)\tan\theta, \quad (5.3.1.8)$$

where w_λ is the half-width of the wavelength distribution. In commonly used X-ray sources, $w_\lambda/\lambda \approx 300 \times 10^{-6}$.

Combination of (5.3.1.5) and (5.3.1.8), and with (5.3.1.7) taken into consideration, gives an estimate of the ratio of the admissible error $\delta\theta$ to the half-width of the measured profile:

$$\frac{|\delta\theta|}{\omega_h} \leq \frac{|\delta d|/d}{w_\lambda/\lambda}. \quad (5.3.1.9)$$

To obtain the highest possible accuracy and precision for a given experiment (given diffraction profile), mathematical methods of data analysis and processing and programming of the experiment are used (Bačkovský, 1965; Wilson, 1965, 1967; Barns, 1972; Thomsen & Yap, 1968; Segmüller, 1970; Thomsen, 1974; Urbanowicz, 1981*a*; Grosswig, Jäckel & Kittner, 1986; Gałdecka, 1993*a*,*b*; Mendelssohn & Milledge, 1999).

Measurements of lattice parameters can be realized both with *powder samples* and with *single crystals*. At the first stage of the development of X-ray diffraction methods, the highest precision was obtained with powder samples, which were easier to obtain and set, rather than with single crystals. The latter were considered to be more suitable in the case of lower-symmetry systems only. In the last 35 years, many single-crystal methods have been developed that allow the achievement of very high precision and accuracy and, at the same time, allow the investigation of different specific features characterizing single crystals only (defects and strains of a single-crystal sample, epitaxic layers).

Some elements are common to both powder and single-crystal methods: the application of the basic equations (5.3.1.1) and (5.3.1.2); the use of the same formulae defining the precision and the accuracy [equations (5.3.1.4) and (5.3.1.3)] and – as a consequence – the tendency to use θ values as large as possible; the means of evaluation of some systematic errors due to photographic cameras or to counter diffractometers (Parrish & Wilson, 1959; Beu, 1967; Wilson, 1980); the methods of estimating statistical errors based on the analysis of the diffraction profile and some methods of increasing the accuracy (Straumanis & Ieviņš, 1940). In other aspects, powder and single-crystal methods have developed separately, though some present-day high-resolution methods are not restricted to a particular crystalline form (Fewster & Andrew, 1995). In special cases, the combination of X-ray powder diffraction and single-crystal Laue photography, reported by Davis & Johnson (1984), can be useful for the determination of the unit-cell parameters.

Small but remarkable differences in lattice parameters determined by powder and single-crystal methods have been observed (Straumanis, Borgeaud & James, 1961; Hubbard, Swanson & Mauer, 1975; Wilson 1980, Sections 6 and 7), which may result from imperfections introduced in the process of powdering or from uncorrected systematic errors (due to refractive-index correction, for example; *cf.* Hart, Parrish, Bellotto & Lim, 1988). The first case was studied by Gamarnik (1990) – both theoretically and experimentally. As shown by the author, the relative increase of lattice parameters in ultradispersed crystals of diamond in comparison with massive crystals was as high as $\Delta d/d = 2.05 \times 10^{-3} \pm 10^{-4}$. Analysis of results of lattice-parameter measurements of silicon single crystals and powders, performed by different authors (Fewster & Andrew, 1995, p. 455, Table 1), may lead to the opposite conclusion: The weighted-mean lattice parameter of silicon powder proved to be about 0.0002 Å smaller ($\Delta d/d \simeq -4 \times 10^{-5}$) than that of the bulk silicon.

5.3.1.2. *Introduction to single-crystal methods*

The essential feature of single-crystal methods is the necessity for the very *accurate setting* of the diffracting planes of the crystal in relation to the axes or planes of the instrument; this may be achieved manually or automatically. The fully automated four-circle diffractometer permits measurements to be made with an arbitrarily oriented single crystal, since its original position in relation to the axes of the device can be determined by means of a computer (calculation of the orientation matrix); the crystal can then be automatically displaced into each required diffracting position. Misalignment of the crystal and/or of element(s) of the device (the collimator, for example) may be a source of serious error (Burke & Tomkeieff, 1968, 1969; Halliwell, 1970; Walder & Burke, 1971; Filscher & Unangst, 1980; Larson, 1974). On the other hand, a well defined single-crystal setting allows the unequivocal indexing of recorded reflections (moving-film methods, counter diffractometer) and the accurate determination of Bragg angles. In the particular case of large, specially cut and set, single crystals and a suitable measurement geometry, it is possible to avoid some sources of systematic error (Bond, 1960).

Single-crystal methods are realized by a great variety of techniques.

(i) Usually, a *single diffraction* phenomenon, which occurs when only one set of planes is in position to diffract the incident X-ray beam at a given moment, is applied in lattice-parameter measurements. A separate group of so-called *multiple-diffraction* methods is formed by methods in which two or more sets of planes simultaneously fulfil the diffraction condition [equations (5.3.1.1) and (5.3.1.2)]. Some photographic divergent-beam methods (Lonsdale, 1947; Heise, 1962; Morris, 1968; Isherwood & Wallace, 1971; Lang & Pang, 1995) and methods with counter recording in which a collimated beam is used (Renninger, 1937; Post, 1975) belong to this group.

(ii) In *traditional methods*, the unit-cell dimensions are determined in relation to the wavelength of a given X-radiation. Their accuracy and precision [equations (5.3.1.3) and (5.3.1.4)] are limited to those determined by the accuracy and precision of the wavelength determination and the width w_λ of the wavelength distribution [see equations (5.3.1.7) and (5.3.1.9)], so that the accuracy cannot exceed the limit of about 1 part in 10^6. To surmount these difficulties, new methods have been introduced. Combined X-ray and optical interferometry (applied simultaneously) permits the determination both of the lattice parameter and of the X-ray wavelength in terms of the visible wavelength standard so that interplanar distances can be 'non-dispersively' (independently of the optical and X-ray wavelength values and their dispersions) measured in metric units with an accuracy of 1 part in 10^7. These methods (Deslattes, 1969; Deslattes & Henins, 1973; Becker *et al.*, 1981; see also Section 4.4.2) are so-called *non-dispersive* methods. Various *pseudo-non-dispersive* methods, in which the width of the diffraction profile has been reduced owing to the use of two- or three-crystal spectrometers (Godwod, Kowalczyk & Szmid, 1974; Hart & Lloyd, 1975; Buschert, 1965) and/or multiple-beam techniques (Hart, 1969; Larson, 1974; Kishino, 1973; Ando, Bailey & Hart, 1978; Buschert, Pace, Inzaghi & Merlini, 1980; Buschert, Meyer, Stuckey Kauffman & Gotwals, 1983; Häusermann & Hart, 1990), are a very suitable tool for high-precision (up to 1 part in 10^9) differential measurements. In multiple-diffraction methods, an interesting

type of '*n*-crystal spectrometer' is generated within the specimen (Post, 1975), so that the resulting diffraction profiles are also narrow.

(iii) In traditional methods, usually only *one single crystal* (the specimen) is used to determine a given lattice parameter, while, in the non-dispersive and pseudo-non-dispersive methods, *two, three or more single crystals* are required, which play the role of the monochromator and/or the reference crystal.

(iv) In the majority of methods, a *single X-ray beam* is used, which is usually well *collimated*. In some methods, however, in which the sample remains stationary, a *highly divergent beam* is applied to satisfy the Bragg law for various sets of planes. These are the Kossel (1936) method and the divergent-beam techniques developed by Lonsdale (1947). The original conception of *multiple-beam* measurement was introduced by Hart (1969). The beams may come from two sources (as in the original paper) or may be separated from only one source (Kishino, 1973).

(v) Most frequently, only *one wavelength* of characteristic X-radiation is used. Sometimes, a monochromator is applied – in particular, in two- or three-crystal spectrometers [see, for example, Fewster (1989) and Obaidur (2002)]. *White* X-radiation may also be used in the Laue method, recently introduced for absolute measurements of the unit-cell dimensions (Carr, Cruickshank & Harding, 1992), or in connection with the two-crystal spectrometer (Okazaki & Kawaminami, 1973*a*,*b*; Okazaki & Ohama, 1979; Ohama, Sakashita & Okazaki, 1979; Okazaki & Soejima, 2001), to allow measurements at extremely large θ angles, or in *energy-dispersive* diffractometers (Buras, Olsen, Gerward, Will & Hinze, 1977), which make short exposures possible.

In the second case, the measurement is based on a principle different from that of traditional methods: a continuous incident X-ray spectrum and a fixed Bragg angle $2\theta_0$ are used. The relation between the interplanar spacing d_H and the energy E_H of the scattered photons is given by

$$E_H\, d_H \sin\theta = \tfrac{1}{2}hc = 6.199 \text{ (keV Å)}, \qquad (5.3.1.10)$$

where H denotes *hkl*.

The *resolved* $K\alpha_{1,2}$ *doublet* is often used in various methods (photographic moving-crystal methods as well as divergent-beam diffractometers) to base the measurements on two independent constant values (Main & Woolfson, 1963; Polcarová & Zůra, 1977; Schwartzenberger, 1959; Mackay, 1966; Isherwood & Wallace, 1971; Spooner & Wilson, 1973; Heise, 1962) or to obtain two independent X-ray beams from a single X-ray source (the multiple-beam method proposed by Kishino, 1973). Sometimes, the $K\beta$ line is also applied (Popović, 1971; Kishino, 1973).

(vi) More and more frequently, new sources of radiation are introduced instead of traditional laboratory *Bremsstrahlung* sources. In the case of methods using a divergent beam, the excitation of the characteristic X-rays may be performed both by primary *X-rays* (Lonsdale, 1947) and by *electron* bombardment (Kossel, 1936; Gielen, Yakowitz, Ganow & Ogilvie, 1965; Ullrich & Schulze, 1972), or by *proton* irradiation (Geist & Ascheron, 1984). Also, a *Mössbauer* source (because of its short wavelength) (Bearden, Marzolf & Thomsen, 1968) and *synchrotron radiation* (Buras *et al.*, 1977; Ando, Hagashi, Usuda, Yasuami & Kawata, 1989) may be used (see also §5.3.3.9 below). The latter is considered to be an ideal X-ray source because of the short exposure required.

When making a choice of the method, the aim of the measurement, the required accuracy and/or precision as well as the laboratory equipment available should be taken into account.

(i) In the case when unit-cell parameters of a *standard crystal* are to be determined, the highest accuracy is needed. This special task is sometimes realized by unique, sophisticated and time-consuming methods (Baker, George, Bellamy & Causer, 1968; Deslattes & Henins, 1973; Becker, Seyfried & Siegert, 1982; Härtwig & Grosswig, 1989): the sample has to be of high quality (pure, defect-free, suitably prepared) and should have a small thermal-expansion coefficient. A detailed error analysis is required. Such measurement is often reduced to only one parameter, since high-symmetry crystals are generally used as standard.

(ii) The second special problem is to determine *all the lattice parameters* of a lower-symmetry system with high, though not necessarily the highest, accuracy.

The most suitable tool for this task is the automated four-circle diffractometer, which permits a proper setting of the crystal for each possible *hkl* reflection. *One crystal mounting* is then sufficient to determine the unit cell with rather high (10 parts in 10^6) accuracy. The measurements can also be performed using a two-circle diffractometer (Clegg & Sheldrick, 1984); these are, however, more troublesome since, in this case, only two rotations are motor-driven while the two remaining angles must be set by hand.

When the diffractometer is to be used, preliminary measurements with photographic methods are advisable. A single rotation photograph allows one to determine one lattice parameter only, a single moving-film photograph makes it possible to obtain a two-dimensional picture of the reciprocal cell, and a suitable combination of two photographic techniques can be the basis for the determination of all the lattice parameters from a single mounting of the crystal (Buerger, 1942; Hulme, 1966; Hebert, 1978; Wölfel, 1971) with moderate accuracy (not better than 1 part in 10^4).

The above counter and photographic methods are suitable for small, preferable spherical, crystals. In the case of one-crystal spectrometers, which give better accuracy (from 10 to 1 parts in 10^6), in particular when the Bond (1960) arrangement is used and when all necessary corrections are taken into account, the preferable form of the sample is a large, flat slab, the surface of which is parallel to the planes of interest. Usually, several samples from one single crystal are needed in order to determine the unit cell of a lower-symmetry system (Cooper, 1962). It is possible, however, to determine coplanar lattice parameters using a single sample, in one crystal mounting, when reflections from different crystal planes are taken into consideration (Luger, 1980, Section 4.2.2; Grosswig, Jäckel, Kittner, Dietrich & Schellenberger, 1985), and a special combination of reflection and transmission geometries enables one to determine all the lattice parameters from a single sample (Lisoivan, 1974, 1981, 1982).

Multiple-diffraction methods, both photographic and with counter recording, can provide a large number of reflections from one crystal mounting. In spite of this, these methods are as yet applied to mainly cubic lattices and exceptionally to other (orthogonal) lattices, because the interpretation of multiple-diffraction patterns is rather complicated (Chang, 1984; and references therein).

High-precision multiple-crystal spectrometers are suitable for comparison measurements in which differences in interplanar spacings rather than absolute values of the spacings are determined.

(iii) When the *lattice-parameter changes* caused by changes of environmental conditions are to be determined, high precision and sensitivity are more important than high accuracy.

In the case of temperature dependence, an additional low- and/or high-temperature attachment is necessary for the precise

establishment and control of the temperature (Baker, George, Bellamy & Causer, 1968; Łukaszewicz, Kucharczyk, Malinowski & Pietraszko, 1978; Okazaki & Ohama, 1979; Okada, 1982; Soejima, Tomonaga, Onitsuka & Okazaki, 1991), so that the basic instrument should be relatively simple (Glazer, 1972; Berger, 1984; Clegg & Sheldrick, 1984). Since measurements at many temperatures are then performed, the problem is to obtain the desired precision in as short a time as possible by using automatic control (Baker, George, Bellamy & Causer, 1968), special strategy of measurement (Barns, 1972; Urbanowicz, 1981*a*), and special sources of radiation [synchrotron radiation used by Buras *et al*. (1977) and Ando, Hagashi, Usuda, Yasuami & Kawata (1989)]. Analogous problems appear when the effects of other factors such as pressure (Mauer, Hubbard, Piermarini & Block, 1975; d'Amour, Denner, Schulz & Cardona, 1982; Leszczyński, Podlasin & Suski, 1993), or electric field (Kobayashi, Yamada & Nakamura, 1963) are examined.

(iv) To detect *small differences of lattice parameter* between the sample and the standard or between two points of the same specimen, the highest precision is required. To improve resolution in traditional methods, a finely collimated X-ray beam (Kobayashi, Yamada & Nakamura, 1963) and cameras with large radius (Kobayashi, Yamada & Azumi, 1968) are required. Really high precision, which reaches 1 part in 10^9, can be obtained with multiple-crystal (pseudo-non-dispersive) techniques (Hart, 1969; Buschert, Meyer, Stuckey Kauffman & Gotwals, 1983).

In the present review, all the methods are classified with respect to the measurement technique, in particular into photographic and counter-diffractometer techniques. Moreover, the methods will be described in approximately chronological sequence,* *i.e.* from the earliest and simplest rotating-crystal method to the latest more-complex non-dispersive techniques, and at the same time from those of poor accuracy and precision to those attaining the highest precision and/or accuracy. In each of the methods realizing a given technique, first the absolute and then the relative methods will be described.

5.3.2. Photographic methods

5.3.2.1. *Introduction*

Photographic single-crystal techniques used for unit-cell determination can be divided into three main groups:

(1) the Laue method with a well collimated beam of polychromatic X-radiation with a stationary crystal;

(2) methods with a well collimated beam of characteristic radiation and a moving crystal;

(3) methods with a highly divergent X-ray beam of monochromatic radiation (usually combined with white radiation).

In the past, only techniques belonging to groups (2) and (3) were used in absolute lattice-parameter measurements. As recently shown by Carr, Cruickshank & Harding (1992), a single synchrotron-radiation Laue photograph can provide all necessary information for the determination of unit-cell dimensions on an absolute scale (though with low accuracy for the present).

The methods of the second group are popular moving-crystal methods or their modifications especially adapted for lattice-parameter determination. Cameras and other equipment for performing these measurements – with the exception of special designs – are available in every typical X-ray diffraction laboratory. At present, these methods of poor (1 part in 10^2) or moderate (up to 1 part in 10^4) accuracy are suitable only for preliminary measurements.

Less popular and more specific divergent-beam methods (third group) give satisfactory accuracy (1 part in 10^4 or 1 part in 10^5), comparable with that obtained by counter-diffractometer methods, by means of very simple equipment.

In spite of the common use of counter diffractometers, and of the increasing use of imaging plates (and synchrotron radiation), traditional photographic methods of the second and the third groups are still popular and new designs are reported.

5.3.2.2. *The Laue method*

As based on polychromatic radiation, the Laue method is, in principle, useless for accurate lattice-parameter determination. It is true that, from a single Laue diffraction pattern (in transmission), one can determine precisely the axial ratios and interaxial angles (a method based on the gnomonic projection is described by Amorós, Buerger & Amorós, 1975), but the unit cell determined will differ from the true cell by a simple scale factor.

The problem of absolute scaling of the cell is important nowadays, when synchrotron-radiation Laue diffraction patterns are currently being used for collecting X-ray data (from single-crystal systems including proteins, for example). As shown by Cruickshank, Carr & Harding (1992), it is possible to estimate the scale factor using the minimum wavelength present in the incident X-ray beam. A method proposed by the authors (Carr, Cruickshank & Harding, 1992) allows one to determine the unit cell and orientation of an unknown crystal (in a general orientation) from a single Laue pattern. The accuracy of the absolute lattice-parameter determination depends on the accuracy with which the minimum wavelength is known for the experiment and is, at present, about 5% in favourable cases (while the error in axial ratio determination after refinement is typically 0.25%). To increase the accuracy, the authors propose either to record the Laue patterns with an attenuator in the incident beam that has a suitable absorption edge ($\lambda_{\min}$ can become a sharp and accurately known limit) or to locate the bromine-absorption edge, if the X-ray detector contains bromine, as in photographic films and image plates.

5.3.2.3. *Moving-crystal methods*

Moving-crystal methods of lattice-parameter determination apply basic photographic techniques, such as:

(1) the rotating- or oscillating-crystal method;

(2) the Weissenberg method;

(3) the technique of de Jong–Bouman; or

(4) the Buerger precession method.

In the first of these methods, the film remains stationary, while in the others it is moved during the exposure. The principles and detailed descriptions of these techniques have been presented elsewhere (Buerger, 1942; Henry, Lipson & Wooster, 1960; Evans & Lonsdale, 1959; Stout & Jensen, 1968, Chapter 5; Sections 2.2.3, 2.2.4, and 2.2.5 of this volume) and only their use in lattice-parameter measurements will be considered here.

5.3.2.3.1. *Rotating-crystal method*

The rotating-crystal method – the simplest of the moving-crystal methods – determines the identity period I along the axis of rotation (or oscillation), $\mathbf{r} = u\mathbf{a} + v\mathbf{b} + w\mathbf{c}$, from the formula

$$I(uvw) = n\lambda/\sin\nu, \qquad (5.3.2.1)$$

* With some exceptions; for example, multiple-diffraction methods introduced by Renninger (1937) are placed after the Bond (1960) method.

in which n is the number of the layer line and ν is the angle between the directions of the primary and diffracted beams.

The angle ν is determined from the measurement of the distance l_n between two lines corresponding to the same layer number n from the equation

$$\tan \nu = l_n/R, \tag{5.3.2.2}$$

where R is the camera radius.

All the lattice parameters may be determined from separate photographs made for rotations of the crystal along different rotation axes, *i.e.* the system axis, plane and spatial diagonals (Evans & Lonsdale, 1959), without indexing the photographs. In practice, however, this method is rarely used alone and is most often applied together with other photographic methods (for example, the Weissenberg method), but it is a useful preliminary stage for other methods. In particular, the length of a unit-cell vector may be directly determined if the rotation axis coincides with this vector.

Advantages of this method are:

(*a*) simple equipment (only rotation of the crystal is required, since the film is stationary);

(*b*) immediate determination of direct-cell parameters (photographs obtained with other cameras afford information about reciprocal-lattice parameters only);

(*c*) indexing of the photographs is unnecessary.

Drawbacks of the method are:

(*a*) poor precision and accuracy of the measurement ($|\delta d|/d \approx 10^{-2}$);

(*b*) small amount of information from a single photograph (one parameter only);

(*c*) necessity of taking several photographs in the case of a lower-symmetry system if this method is the only one used.

5.3.2.3.2. *Moving-film methods*

A two-dimensional picture of a reciprocal cell from one photograph can be obtained by the methods in which rotation of the crystal is accompanied by movement of the film, as in the Weissenberg, the de Jong–Bouman, and the Buerger precession techniques. These methods give greater precision ($|\delta d|/d \approx 10^{-4}$) than the previous one (§5.3.2.3.1).

The advantages of the Weissenberg method in relation to the other two are:

(*a*) a simpler camera;

(*b*) a larger range of reciprocal-lattice points recorded on one photograph (larger range of θ angles, up to 90° for the zero layer).

On the other hand, the disadvantage, in contrast to the de Jong–Bouman and the Buerger precession methods, is that it gives deformed pictures of the reciprocal lattice. This is not a fundamental problem, especially now that computer programs that calculate lattice parameters and draw the lattice are available (Luger, 1980). In lattice-parameter measurements, both the zero-layer Weissenberg photographs and the higher-layer ones are used. The latter can be made both by the normal-beam method and by the preferable equi-inclination method. Photographs in the de Jong–Bouman and precession methods give undeformed pictures of the reciprocal lattice, but afford less information about it than do Weissenberg photographs.

5.3.2.3.3. *Combined methods*

The most effective photographic method of lattice-parameter measurement is a combination of two techniques (Buerger, 1942; Luger, 1980), which makes it possible to obtain a *three-dimensional picture* of the reciprocal lattice; for example: the rotation method with the Weissenberg (lower accuracy); or the precession (or the Weissenberg) method with the de Jong–Bouman (higher accuracy).

A suitable combination of the two methods will determine all the lattice parameters, even for monoclinic and triclinic systems, *from one crystal mounting*. This problem has been discussed and resolved by Buerger (1942, pp. 388–390), Hulme (1966), and Hebert (1978). Wölfel (1971) has constructed a special instrument for this task, being a combination of a de Jong–Bouman and a precession camera.

5.3.2.3.4. *Accurate and precise lattice-parameter determinations*

To measure with a precision and an accuracy better than is possible in routine photographic methods, additional work has to be performed. The first methods allowing precise measurement of lattice parameters were photographic powder methods (Parrish & Wilson, 1959). Special single-crystal methods with photographic recording to realize this task (earlier papers are reviewed by Woolfson, 1970, Chap. 9) combine elements of basic single-crystal methods (presented in §§5.3.2.3.1 and 5.3.2.3.2) with ideas more often met in powder methods (asymmetric film mounting). A similar treatment of some systematic errors (extrapolation) is met in both powder and single-crystal methods.

(i) The relative accuracy $\Delta I/I$ of the identity period I in the rotating-crystal method, estimated by differentiation of formula (5.3.2.1), is given by

$$\Delta I/I = -\cot \nu \Delta \nu. \tag{5.3.2.3}$$

This formula shows that the highest accuracy is obtained for ν tending to 90°. Since reflections with large values of ν are difficult to record in commonly used cameras, a special camera may be used for this task, in which a flat film is placed perpendicular to the rotation axis, or a different one, whose axis coincides with the primary beam (Umansky, 1960). The accuracy achieved with these improvements is still no better than 5 parts in 10^3.

(ii) The asymmetric film mounting proposed by Straumanis & Ieviņš (1940) in the case of powder cameras can also be used in a simple oscillating camera (Farquhar & Lipson, 1946). In particular, this idea can be realized in a precision Debye–Scherrer camera adapted to single-crystal measurements by mounting in it a goniometer head (Popović, 1974). The Straumanis mounting allows the recording of the high-angle reflections close together on the film, thus reducing the effect of film shrinkage and making it possible to measure the effective camera radius.

(iii) Sometimes, to eliminate systematic errors (uncertainty of the camera radius), the separations resulting from the wavelength differences of the $K\alpha_1$ and $K\alpha_2$ doublet are measured rather than the absolute distances on the film (Main & Woolfson, 1963; Alcock & Sheldrick, 1967). The first reference related to the zero-layer normal-beam photograph, the second to higher layer lines (in the equi-inclination method also) and oscillation photographs.

(iv) Systematic errors connected with film shrinkage can also be eliminated by means of the *ratio method*, introduced by Černohorský (1960) for powder samples and adapted by Polcarová & Zůra (1977) for single crystals. In this method, pairs of reflections that differ from one another in wavelength and/or in *hkl* indices are used and the ratio of the two diameters of the diffraction rings corresponding to these reflections is taken into account. The accuracy of the method is about 1 part in 10^4

if systematic errors due to absorption, refraction, Lp factor, temperature, changes of the camera radius, and misalignment of the sample and the goniometer are corrected. The ratio method was generalized by Horváth (1983) to the monoclinic crystal system.

(v) Graphical extrapolation, similar to that used in powder methods (Parrish & Wilson, 1959), can also be used for single crystals (Farquhar & Lipson, 1946; Weisz, Cochran & Cole, 1948), to reduce systematic errors proportional to $\sin\theta$. Least-squares refinement, on the other hand, permits a reduction of the standard deviations of the results (Main & Woolfson, 1963; Clegg, 1981). Mathematical methods of processing the data obtained from oscillation photographs, including 'eigenvalue filtering' and profile fitting (Rossmann, 1979; Reeke, 1984) have been applied to the refinement of unit-cell parameters, crystal orientation, and reflecting-range parameters needed to process oscillation photographs.

(vi) By measuring the *angle between two reflecting crystal positions*, symmetrical in relation to the primary beam [the idea used in the original Bragg spectrometer (Bragg & Bragg, 1915)], one can eliminate some sources of systematic errors. Such a spectrometer with photographic recording was used by Weisz, Cochran & Cole (1948). In spite of the great simplicity of the arrangement, the accuracy obtained was about 1 part in 10^4. The authors indicated the need for introducing counter recording to the method. 12 years later, their idea was realized by Bond (1960) (*cf.* Subsection 5.3.3.4, in particular §5.3.3.4.3).

(vii) The other way of reducing some systematic errors is to introduce a *reference crystal*. Singh & Trigunayat (1988) adapted the idea to the oscillation method. By mounting the specimen crystal and the reference crystal, properly centred and set, on two identical goniometer heads with a screw-type base, they recorded layer lines of the two crystals simultaneously. The identity period I of the crystal was then determined from the formula that results from a combination of (5.3.2.1) and (5.3.2.2) for layer lines of the two crystals (notation of the present Section):

$$I = n\lambda\left[\frac{l_n^2(I_r^2 - m^2\lambda^2)}{l_{m,r}^2 m^2\lambda^2} + 1\right]^{1/2}, \qquad (5.3.2.4)$$

in which l_n and $l_{m,r}$ are the measured distances between nth layer lines of the crystal and between mth layer lines of the specimen, respectively, and I_r is the identity period of the reference crystal. The result is thus independent of the camera radius. When the differences between l_n and $l_{m.r}$ are no greater than a few mm, the error due to film shrinkage is automatically taken care of, and the error due to a parallel shift of the axis of the cylindrical cassette in relation to the axis of rotation is negligible in practice. The other possible misalignments related to the cassette and the collimator can be readily detected beforehand by taking a complete rotation photograph.

Reference crystals are commonly used in multiple-crystal methods reviewed in Subsection 5.3.3.7.

5.3.2.3.5. *Photographic cameras for investigation of small lattice-parameter changes*

Small changes of lattice parameters caused by thermal expansion or other factors can be investigated in *multiple-exposure cameras*.

Bearden & Henins (1965) used the double-crystal spectrometer with photographic detection to examine *imperfections* and *stresses* of large crystals. The technique allowed the detection of angle deviations as small as $0.5''$. A nearly perfect calcite crystal was used as the first crystal (monochromator), the sample was the second. The device distinguished itself with very good sensitivity. The use of the long distance (200 cm) between the focus and the second crystal made possible resolution of the doublet $K\alpha_{1,2}$, and elimination of the $K\alpha_2$ radiation. An additional advantage was that the arrangement was less time-consuming, so that it was suitable for controlling the perfection of growing crystals and useful for choosing adequate samples for the wavelength measurements.

Kobayashi, Yamada & Azumi (1968) have described a special 'strainmeter' for measuring small strains of the lattice. The strain x_i along an axis normal to the i plane results in a change δd_i of the interplanar distance d_i:

$$x_i = \delta d_i/d_i = -\cot\theta_i\delta_i. \qquad (5.3.2.5)$$

The use of a large camera radius $R = 2639$ mm makes it possible to obtain both high sensitivity and high precision (2 parts in 10^6) even in the range of lower Bragg angles ($\theta \simeq 55^\circ$). The device is suitable for the investigation of defects resulting from small strains and may be used in measurements of thermal expansion.

Glazer (1972) described an automatic arrangement, based on the Weissenberg goniometer, for the photographic recording of high-angle Bragg reflections as a function of temperature, pressure, time, *etc*. A careful choice of the oscillation axis and oscillation range makes it possible to obtain a distorted but recognizable phase diagram (Fig. 5.3.2.1) within several hours. The method had been applied by Glazer & Megaw (1973) in studies of the phase transitions of $NaNbO_3$.

Popović, Šljukić & Hanic (1974) used a Weissenberg camera equipped with a thermocouple mounted on the goniometer head for precise measurement of lattice parameters and thermal expansion in the high-temperature range.

5.3.2.4. *The Kossel method and divergent-beam techniques*

5.3.2.4.1. *The principle*

Another group of methods with photographic recording has been developed in parallel with those discussed in Subsection 5.3.2.3. These are the methods in which the crystal remains stationary and the diffraction conditions are fulfilled, simultaneously for more than one set of crystallographic planes, by the use of a highly divergent beam, dispersed from a point source (Fig. 5.3.2.2). The Kossel method (Kossel, 1936, and references therein), the divergent-beam techniques initiated by Lonsdale (1947), and their numerous modifications belong to this group.

The excitation of the characteristic X-rays used in these methods can be performed by X-radiation (Lonsdale, 1947), by electron bombardment (Kossel, 1936; Gielen *et al.*, 1965; Ullrich & Schulze, 1972) or by proton irradiation (Geist & Ascheron, 1984) of a single crystal. The source of emitted X-rays may be located either *in* the sample itself (the Kossel method), *on* the surface of the sample in a layer of target material (the pseudo-Kossel method), or *outside* the sample (the divergent-beam techniques). The divergent X-ray beam diffracts from sets of crystallographic planes. The diffracted rays for each Bragg reflection form a conical surface whose semivertical angle is equal to $90^\circ - \theta$ and whose axis is normal to the Bragg plane (*i.e.* coincides with the reciprocal-lattice vector).

The conical surface of an *hkl* reflection can be described in the form (Morris, 1968; Chang, 1984):

$$x'^2 + y'^2 = z'^2\tan^2\alpha, \qquad (5.3.2.6)$$

where (x', y', z') is an orthogonal coordinate system with its origin at the vertex of the cone and with z' along the axis of the

cone and normal to the plane of interest, and α is the semivertical angle. Since α depends on the Bragg angle, it is possible to combine (5.3.2.6) with the Bragg law [equations (5.3.1.1) or (5.3.1.2)], and so with the lattice parameters. In particular, the dependence can be presented as:

$$\frac{r}{z'} = \frac{1}{\sin\theta} = \frac{2d}{n\lambda}, \qquad (5.3.2.6a)$$

where $r = (x'^2 + y'^2 + z'^2)^{1/2}$.

In another convenient coordinate system (x, y, z) common for all the cones, say with z along the direction of the incident beam, (5.3.2.6*a*) will take the form:

$$\frac{r}{c_x x + c_y y + c_z z} = \frac{2d}{n\lambda}, \qquad (5.3.2.6b)$$

where c_x, c_y, c_z are direction cosines of the angles between the z' axis and the axes x, y and z, respectively. Since the origin of the coordinate system has not been changed,

$$r = (x^2 + y^2 + z^2)^{1/2}. \qquad (5.3.2.6c)$$

The Kossel lines (Fig. 5.3.2.3) are formed at the intersections of the cones with a flat film placed parallel to the specimen surface (Fig. 5.3.2.2). When the film plane is normal to the z axis, and the focus-to-film distance is equal to Z, putting $z = Z$ in

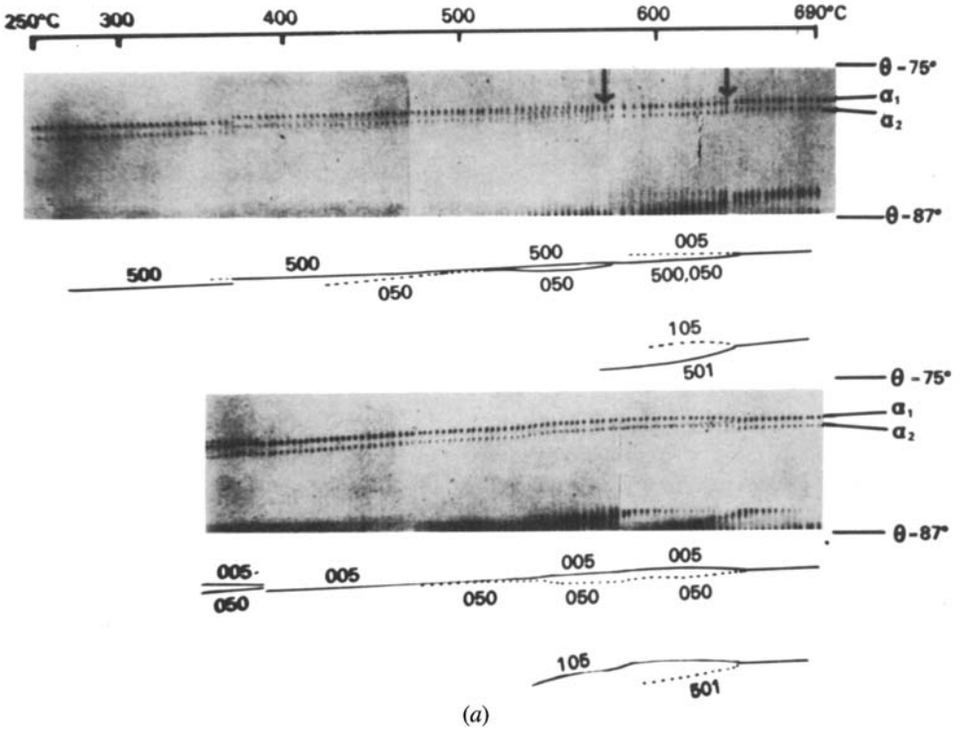

(*a*)

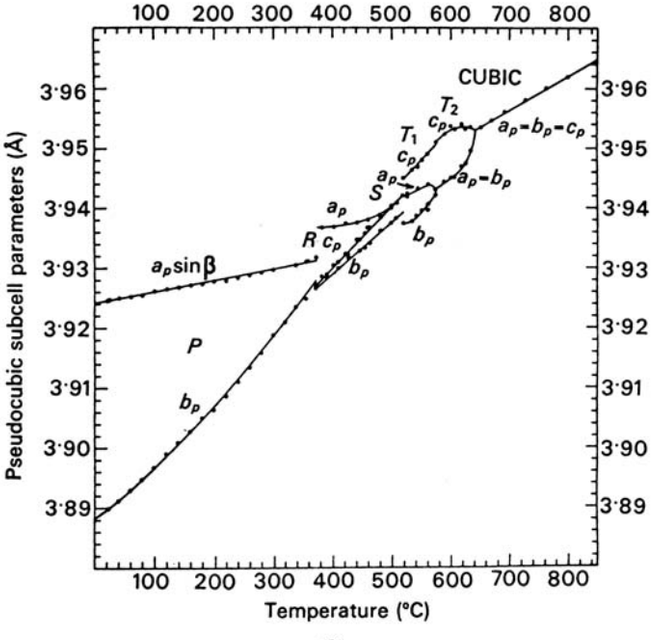

(*b*)

Fig. 5.3.2.1. (*a*) Photographic recording of lattice-parameter changes. (*b*) Corresponding diagram of the variation of lattice parameters in pseudocubic $NaNbO_3$ (Glazer & Megaw, 1973).

(5.3.2.6*b*,*c*) gives the formulae describing the conic section on the film.

A high-precision Kossel camera is described by Reichard (1969) and the generation of pseudo-Kossel patterns by the divergent-beam method has been described by Imura, Weissmann & Slade (1962), Ellis, Nanni, Shrier, Weissmann, Padawer & Hosokawa (1964), and Berg & Hall (1975).

The photographs may be in either the transmission or the back-reflection region (Fig. 5.3.2.2). The second arrangement seems to be (Lutts, 1968) more suitable for lattice-parameter determination, since the background is less intensive and the lines on the photographs have greater contrast. Both possibilities are used in practice. Photographs in the back-reflection region have been reported by Imura, Weissmann & Slade (1962), Ullrich (1967), Newman & Weissmann (1968), Newman & Shrier (1970), and Berg & Hall (1975). Examples of the use of the transmission region are given by Yakowitz (1966*a*), Reichard (1969), and Glass & Weissmann (1969).

The recommended *crystal thickness* t for work in the transmission region, according to Hanneman, Ogilvie & Modrzejewski (1962), is given by:

$$t = 1/0.2\mu_L, \qquad (5.3.2.7)$$

where μ_L is the linear absorption coefficient for $K\alpha$ radiation generated in the crystal. A more detailed study of the effect of sample thickness, as well as operating voltage, on the contrast of Kossel transmission photographs is given by Yakowitz (1966*a*).

The picture geometry does not depend, in principle, on whether the Kossel, pseudo-Kossel, or divergent-beam technique is applied. Imura (1954) has studied in detail the form of the curves of the light or deficiency type, and recorded both in the transmission and in the back-reflection region. The curves on transmission patterns can be considered to be conics; those recorded in the back-reflection region are related to ellipses, but of higher order. In general, the photograph has to be indexed before performing measurement on the film. For this purpose, the pattern may be compared with a calculated pattern (gnomonic, orthogonal, cylindrical, or stereographic projection). For lattice-parameter determination, various features of the photographs may be used, *i.e.* intersections or near-intersections of Kossel lines, their near-tangency, lens-shaped figures, and the whole lines approximated with a function.

5.3.2.4.2. *Review of methods of accurate lattice-parameter determination*

The basis of lattice-parameter determination involves measurements performed on the film. There are various methods covering most of the different geometrical features of the cones and recorded pictures. These were reviewed by Lutts (1968), Yakowitz (1966*b*, 1969) and Tixier & Waché (1970). In each case, the wavelength of the excited radiation has to be known. Often, the resolved $K\alpha_{1,2}$ doublet and/or $K\beta$ radiation is applied rather than a single (but most pronounced) $K\alpha_1$ line. The other data needed (a sufficient number of equations, the solution of which leads to lattice-parameter determination; camera geometry; crystal system; and indices) depend on the method.

Biggin & Dingley (1977) propose a classification of all the methods using a divergent beam based on the information required.

(i) All the kinds of information mentioned above are needed in the earliest method (Kossel, 1936), in which near-tangency of Kossel lines is taken into account.

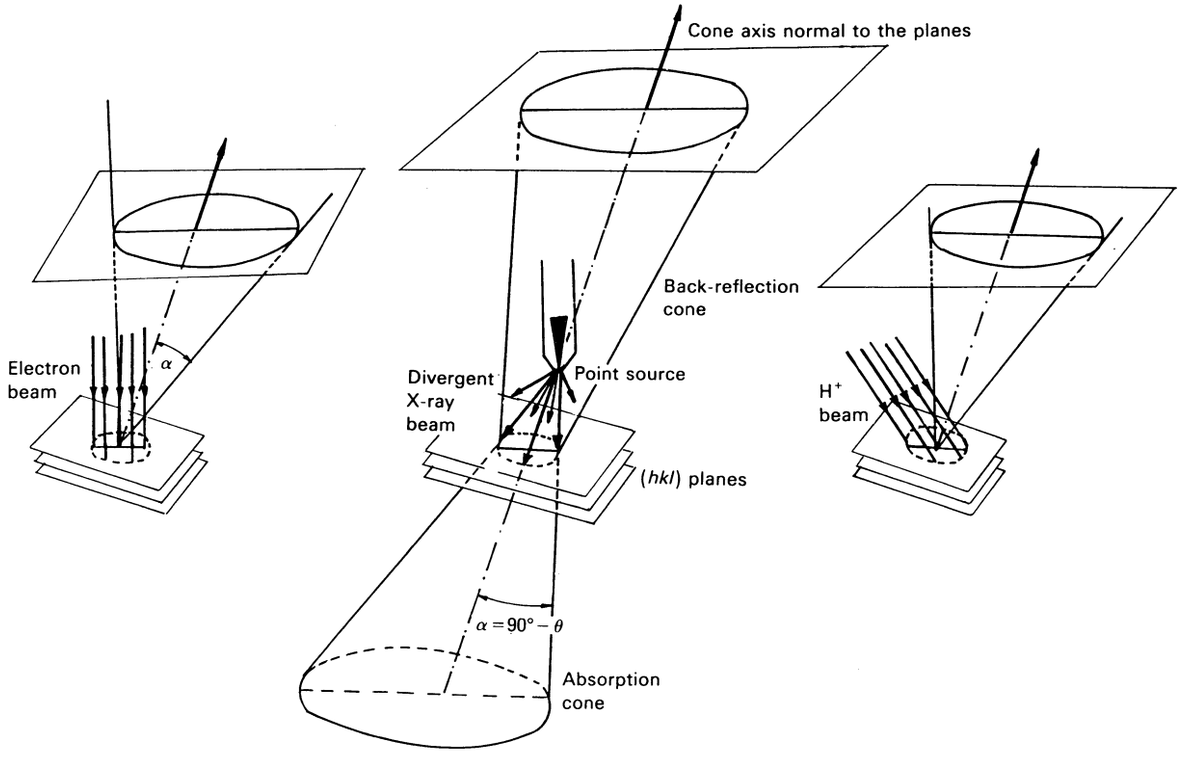

Fig. 5.3.2.2. Schematic representation of the origin of the Kossel lines. (*a*) The Kossel (1936) method. (*b*) The divergent-beam method developed by Lonsdale (1947). (*c*) The proton-induced Kossel effect (Geist & Ascheron, 1984). In (*b*), the divergent X-ray beam is directed onto the sample from a point source while in the remaining cases it is generated within a crystal by (*a*) electrons or (*c*) protons.

(ii) As has been shown in successive papers that appeared from 1947 to the early 1970's, information on camera dimensions can be eliminated if the crystallographic system is known and the photograph is indexed. Some dependence between crystal planes and, as a consequence, between lines on the photograph, is then taken into consideration. This is of great importance, since camera dimensions, in particular the distance from the focus to the centre of the photograph, are difficult to measure accurately and negatively influence the precision and accuracy of the determined lattice parameters.

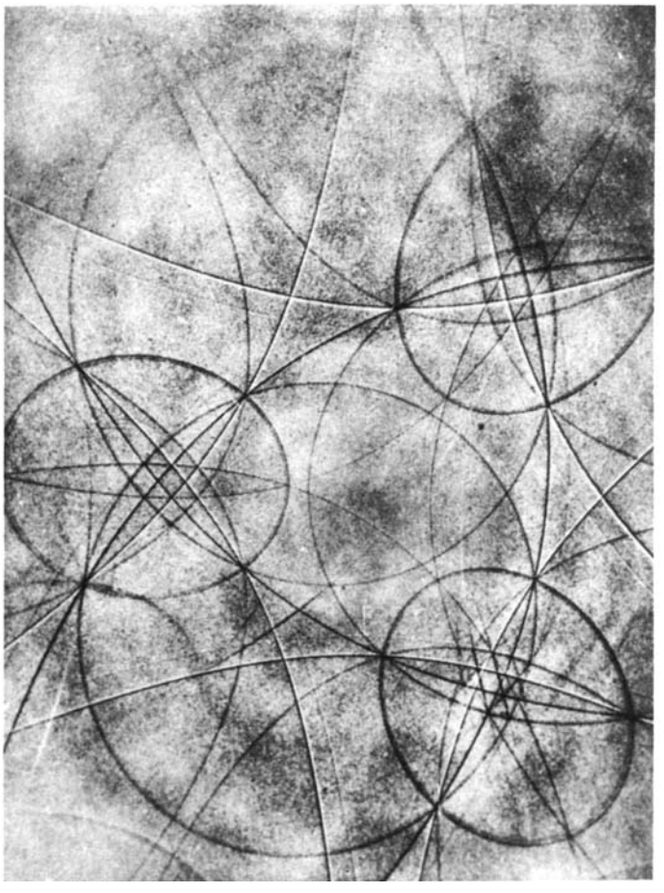

(*a*)

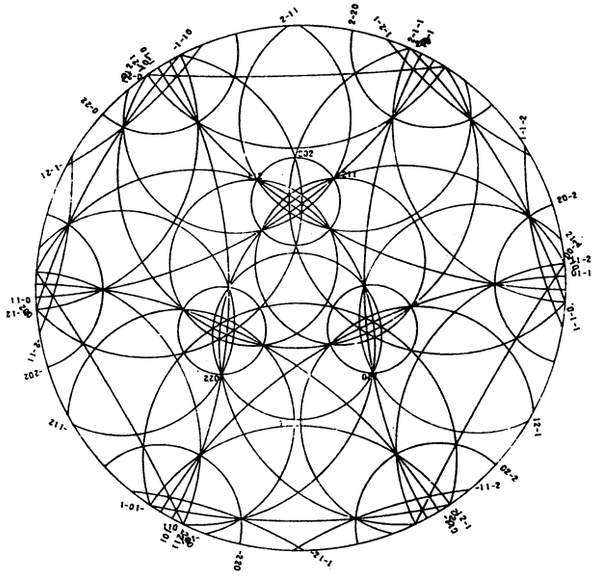

(*b*)

Fig. 5.3.2.3. (*a*) The Kossel pattern from iron and (*b*) the corresponding stereographic projection (Tixier & Waché, 1970).

The Lonsdale (1947) method is based on triple *intersections* of the Kossel lines resulting from **multiple-diffraction** effects (*cf.* Subsection 5.3.3.6), which are *dependent on the wavelength*, so first the particular wavelength has to be determined by an extrapolation. Two or three lines with known indices produced by different wavelengths ($K\alpha_1$, $K\alpha_2$, and/or $K\beta$) are used for this task (Schwartzenberger, 1959; Mackay, 1966; Isherwood & Wallace, 1971; Spooner & Wilson, 1973). Similar problems arise when near-tangency of two lines is taken into consideration (Kossel, 1936; Mackay, 1966).

With the use of reciprocal-lattice geometry, the equation of the so-called Kossel plane (Isherwood & Wallace, 1971) for a diffracting plane (*hkl*) is given by (Spooner & Wilson, 1973; Chang, 1984):

$$L_1x^* + L_2y^* + L_3z^* = \frac{1}{d}, \tag{5.3.2.8}$$

where L_1, L_2, and L_3 are direction cosines between the reciprocal vector $\mathbf{H} = h\mathbf{a}^* + k\mathbf{b}^* + l\mathbf{c}^*$ and the unit-cell vectors $\mathbf{a}^*, \mathbf{b}^*, \mathbf{c}^*$, *i.e.*

$$L_1 = \frac{ha^*}{H}, \quad L_2 = \frac{kb^*}{H}, \quad L_3 = \frac{lc^{*\prime}}{H}, \tag{5.3.2.8a}$$

where $H = |\mathbf{H}| = 1/d$, $a^* = |\mathbf{a}^*|$, $b^* = |\mathbf{b}^*|$, $c^* = |\mathbf{c}^*|$.

In the case of the triple intersection, (5.3.2.8) is satisfied simultaneously by three sets of diffracting planes, the Miller indices of those being $(h_ik_il_i)$, $i = 1, 2, 3$. From the Ewald construction, it follows that the triple point (x_0^*, y_0^*, z_0^*) must lie on the sphere of reflection:

$$x^{*2} + y^{*2} + z^{*2} = \frac{4}{\lambda_0^2}. \tag{5.3.2.8b}$$

The radius of the sphere, $2/\lambda_0$, is the modulus of the double wavevector defined by Isherwood & Wallace (1971).

For cubic crystals, where $H = (h^2 + k^2 + l^2)^{1/2}/a$, the set of equations to be solved, resulting from (5.3.2.8) and (5.3.2.8*a*), which relates to the triple point, takes the form

$$h_ix_0^* + k_iy_0^* + l_iz_0^* = (h_i^2 + k_i^2 + l_i^2)/a, \tag{5.3.2.9}$$

where $i = 1, 2, 3$.

First, coordinates x_0^*, y_0^*, z_0^* dependent on a are determined from (5.3.2.9), and next a is calculated from (5.3.2.8*b*). It should be noted that the measurements performed on the film are used here for determination of the wavelength only. As shown (theoretically and experimentally) by Brühl & Rhan (1985) for cubic lattices, positions of the lines on the film that result from the multiple-diffraction phenomenon are insensitive to lattice-parameter changes (caused by thermal expansion, for example), while positions of the primary reflections depend on actual lattice-parameter values. Practical examples of photographic multiple-diffraction methods are given by Lonsdale (1947) (see also Tixier & Waché, 1970; Chang, 1984), Isherwood & Wallace (1966), Isherwood (1968), Isherwood & Wallace (1970), Spooner & Wilson (1973), Brown, Halliwell & Isherwood (1980), and Isherwood, Brown & Halliwell (1981, 1982).

The technique, in which triple intersections of Kossel lines are analysed, can be used both for back-reflection and for transmission. In the second case, the thickness t of the crystal should be such that $\mu_L t \simeq 1$ [*cf.* equation (5.3.2.7)]. However, thicker crystals, for which $\mu_L t \gtrsim 10$, can be examined by anomalous transmission, if the degree of crystal perfection is

high (Glass & Moudy, 1974). A correction for displacement of the conics due to wafer thickness t is necessary in the case when the intersection lies along the normal to the specimen surface. One triple intersection allows the determination of the lattice parameter of a cubic crystal, but for a structure in the orthorhombic system three such intersections would be required.

Two intersecting Kossel lines sometimes form a *lens configuration* (Fig. 5.3.2.4*a*). The use of such a figure, consisting of two lenses (Fig. 5.3.2.4*b*) owing to the resolved doublet of $K\alpha_1$ and $K\alpha_2$ (or $K\beta$) radiation, makes it possible to determine lattice parameters without a knowledge of the distance between the source and the film. Lattice parameters are then calculated from the ratio L_1/L_2 of the distances L_1 and L_2 between pairs of the sections. Heise (1962) used this method for cubic crystals in the simplest case, in which the cone axes are perpendicular to the film (symmetrical method). His idea had been generalized by Gielen *et al.* (1965), who formed a theory of the lens in the case of arbitrarily situated diffracting planes and arbitrary wavelengths, but for cubic crystals only. Lutts (1968) derived suitable formulae for cubic, tetragonal, and hexagonal systems by combining the ratio L_1/L_2 with interplanar spacings and lattice parameters.

Several features of the Kossel pattern may be jointly taken into account for its interpretation and lattice-parameter determination. Hanneman, Ogilvie & Modrzejewski (1962) used the conic sections formed by $K\alpha_1$ and $K\beta$ radiation and the lens figures.

Lang & Pang (1995) observed and analysed fine streaks in the transmitted pseudo-Kossel patterns caused by both the coherent multiple diffraction and the enhanced Borrmann (anomalous) transmission. As they have found, these fine-scale features of a few arcseconds in angular width, which add markers to the broad-line Kossel patterns, may be taken into account in accurate lattice-parameter measurements.

(iii) Determination of lattice parameters by means of techniques utilizing a highly divergent beam becomes much more complicated if there is no information about indices and the *crystal system*. Such a problem arises in the case when the crystal system of the specimen is *unknown* or when the lattice is deformed. Then, a three-dimensional array of intersecting cones with a common vertex should be taken into consideration.

It is difficult to dispense with the data concerning the camera geometry. However, the distance of X-ray source from the film center may be eliminated in calculations when the *multiple-exposure technique* is used. This technique, introduced by Ellis *et al.* (1964) for back-reflection patterns, depends on recording the Kossel lines at variable but controlled distances from the focus to the film (Fig. 5.3.2.5), so that three or more positions of a cone generator can be established and, as a consequence, the cone axis and the semivertical angle are determined. The interpretation of the multiple-exposure pictures is based, in principle, on the coordinates of general points of lines rather than on their special properties.

The basic formula valid for all the methods applying the Kossel idea,

$$\mathbf{P} \cdot \mathbf{N} = \cos\alpha, \qquad (5.3.2.10)$$

where $\mathbf{P}$ is the unit vector defining the cone generator and $\mathbf{N}$ is the axial direction of a cone, can now be fully utilized, since multiple-exposure techniques make possible accurate calculations of direction cosines. Lengthy and complicated calculations resulting from measurements performed on the film may be realized by means of a computer. A suitable program is given by Fischer & Harris (1970). This technique has also been applied and developed by Slade, Weissmann, Nakajima & Hirabayashi (1964), Shrier, Kalman & Weissmann (1966), Newman & Weissmann (1968), Schneider & Weik (1968), Fischer & Harris (1970), Newman & Shrier (1970), Aristov, Shekhtman & Shmytko (1973), and Soares & Pimentel (1983) for both the back-reflection and the transmission region.

As mentioned above, the Kossel lines occurring in the back-reflection region are similar to ellipses; they can be described using an equation of the fourth degree (Newman, 1970). In general, the major axes of such ellipse-shaped figures have been

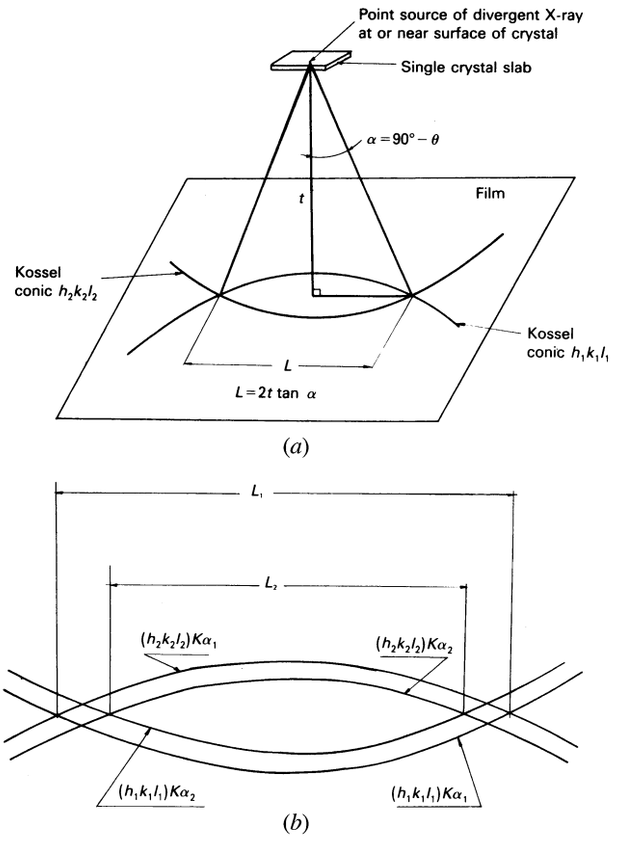

Fig. 5.3.2.4. Lens-shaped figures formed by pairs of intersecting conics. (*a*) Schematic representation of the method of Heise (1962). (*b*) The use of the $K\alpha_{1,2}$ doublet for precise and accurate lattice-parameter determination.

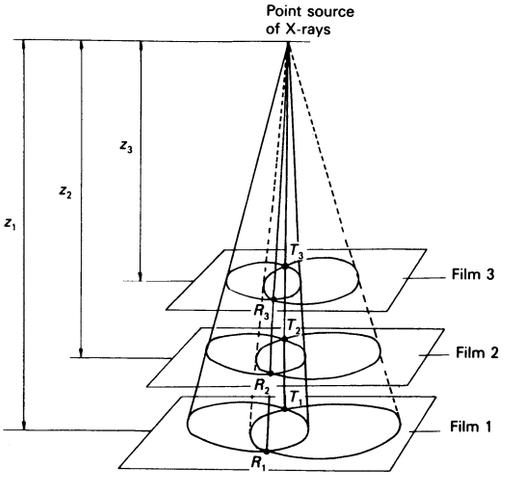

Fig. 5.3.2.5. Schematic representation of the multiple-exposure technique (after Fischer & Harris, 1970).

taken into account in lattice-parameter determination. A novelty introduced by Lider & Rozhansky (1967) was to also use the minor axes in the calculations. The essential feature of their method is the location of the X-ray source in the plane of a flat film.

(iv) The other possibility for gathering the necessary information for the recorded picture is a more detailed study of the form of the Kossel lines. Morris (1968) proposed a method based on the mathematical analysis of a cone, which makes possible the determination of lattice parameters in any crystal system, with a relative accuracy as high as 10 parts in 10^6. The necessary calculations can be made by a computer program. A conic section can usually be expressed by a general equation of the second degree (Bevis, Fearon & Rowlands, 1970; Harris & Kirkham, 1971; Morris, 1968):

$$x^2 + Ay^2 + Bxy + Cx + Dy + E = 0, \qquad (5.3.2.11)$$

which results from a combination and a transformation of (5.3.2.6*b*) and (5.3.2.6*c*). The coefficients A, B, C, D, and E, being functions of the direction cosines and of the ratio $2d/n\lambda$, can be found by the method of least squares. Methods based on *Kossel-line fitting* can be realized both in the single-exposure (Harris & Kirkham, 1971) and in the multiple-exposure technique (Aristov, Shekhtman & Shmytko, 1973; Aristov & Shmytko, 1978).

(v) From theoretical considerations based on the shape of pseudo-Kossel lines (Harris & Kirkham, 1971), it is possible to eliminate the need for information concerning camera geometry if the source and the pattern centre are accurately located. Lattice parameters of an unknown or deformed crystal can thus be determined with no information other than measurements on the film and a knowledge of the *wavelength*.

A general method for locating the X-ray source and the centre of the pattern – which permits the realization of the above idea – has been developed by Biggin & Dingley (1977). Its characteristic feature is the introduction of steel balls between the specimen and the film; these cast sharp shadows on the film by blocking the diffuse radiation. Coordinates of points along the Kossel lines as well as the shadow ellipses recorded on the film are taken into account in calculations.

5.3.2.4.3. *Accuracy and precision*

Although the precision theoretically obtainable by means of the Lonsdale (1947) method is of the order of 1 part in 10^6, this limit is unattainable in practice. The reported values are in the range of about 10^{-4}–10^{-5} Å, depending not only on the method but also on the crystal – its symmetry and perfection. The highest accuracy known by the author was achieved by Lonsdale [(1947), $\pm 5 \times 10^{-5}$ Å, for diamond], Morris [(1968), 2 parts in 10^5] and Aristov & Shmytko [(1978), $|\delta d|/d \sim 3 \times 10^{-5}$, 1–5 $\times 10^{-5}$ rad for angles between crystallographic directions].

Systematic errors due to the methods in which a divergent beam is applied have been discussed by Hanneman, Ogilvie & Modrzejewski (1962), Gielen, Yakowitz, Ganow & Ogilvie (1965), Beu (1967), Lutts (1968), and Aristov & Shmytko (1978). The main sources of systematic error are:

(i) those common to all X-ray methods, resulting from a finite depth of X-ray penetration, wavelength dispersion, refraction (Isherwood & Wallace, 1966; Isherwood, 1968), and from the real structure (substructures and mosaic blocks; and

(ii) those common to methods with photographic recording, resulting from film shrinkage and inaccurate determination of camera dimensions and distances on the film.

The errors of the second group may be to some extent removed if small differences of the length resulting from the resolved $K\alpha_{1,2}$ doublet are measured on the film rather than distances due to only one wavelength, and/or if the camera dimensions can be eliminated from the equations used in the calculations of lattice parameters (see §5.3.2.4.2). A relative misorientation between the specimen and the flat film has been analysed by Lutts (1973).

An error typical for methods realized by means of an electron microscope or an electron-beam probe may result from the thermal effects of the electron beam generating a divergent X-ray beam at the crystal surface. Uncontrolled thermal effects may also occur in the case of the Kossel method, since the sample is situated inside the X-ray tube. In the latter method, the wavelength of the radiation emitted depends on the chemical composition of the sample, since the sample plays the role of the anode of the X-ray tube.

The reported precision of the methods, limited by the finite width of the lines on the photograph, and depending also on the geometrical features taken into account, is 1 part in 10^3 to 1 part in 10^5. The highest [$\sigma(d)/d = 10^{-5}$] is reported by Hanneman, Ogilvie & Modrzejewski (1962), Gielen, Yakowitz, Ganow & Ogilvie (1965), and Lider & Rozhansky (1967). On the other hand, the lowest (1 part in 10^3), obtained by Harris & Kirkham (1971), is attributed to the method in which neither the indexing of the lines nor a knowledge of the crystallographic system or camera geometry is required.

For precision determination of lattice-parameter differences, a 'point' source (*i.e.* as small as possible) is required and the high-order Kossel lines should be used to obtain both well resolved $K\alpha_{1,2}$ doublets and 'thin' figures. The near-intersections of conic sections, applied in Lonsdale's (1947) method, the major axes of lens-shaped figures, used in Heise's (1962) method, and the small spherical polygons formed by several Kossel cones are very sensitive to lattice-parameter changes, so that these figures can be taken into account in the precise measurements reported in §5.3.2.4.4.

5.3.2.4.4. *Applications*

As was mentioned in §5.3.2.4.3, the methods in which a highly divergent beam is used are applied both to the accurate determination of the unit cell and to the precision detection of lattice-parameter changes or differences. It should be added that the Kossel method is especially suitable for small single crystals or fine-grained polycrystals, whereas the other divergent-beam techniques need larger specimens (Lutts, 1968).

Since all the methods are relatively simple (stationary specimen, stationary film, simple construction of the camera) and, on the other hand, are applicable mainly for highly symmetric systems, they proved to be particularly useful in studies of metals and semiconductors. Various applications of the Kossel method and other divergent-beam techniques for this task have been discussed by Ullrich (1967), Ullrich & Schulze (1972), and Geist & Ascheron (1984). The latter paper relates especially to semiconductors.

A task that arises both in metallurgy and in the semiconductor industry is the examination of the real structure – in particular, measurements of strains introduced by variation in temperature, pressure, mechanical stress (elastic strains) or by point defects, deviation from exact stoichiometry, irradiation damage, and phase changes (permanent strains).

Measurements of small changes in interplanar spacings of independent sets of crystal planes enable a stress–strain analysis to be made (Imura, Weissmann & Slade, 1962; Elllis *et al.*,

1964; Slade *et al.*, 1964; Newman & Weissmann, 1968; Berg & Hall, 1975). A special case of strains is an extensional deformation of the lattice in the direction of crystal growth (Isherwood, 1968).

A typical metallurgical problem is the effect of heat treatment on the microstructure of alloys. An example of the application of the Kossel method to the task is given by Shinoda, Isokawa & Umeno (1969), who reported a study of precipitation of α from β in copper–zinc alloys. The lattice parameters and thermal expansion of α-iron and its alloys were examined by Lutts & Gielen (1971). Structure defects resulting from over-pressure experiments and annealing were investigated by Potts & Pearson (1966). Irradiation effects caused by neutrons were the subject of papers of Hanneman, Ogilvie & Modrzejewski (1962), Yakowitz (1972), and Spooner & Wilson (1973); those caused by electron bombardment were reported by Ullrich (1967).

Divergent-beam techniques are considered to be a suitable tool for studying strains in epitaxic layers (Hart, 1981), since corresponding lines of the layer and substrate, observed on one photograph, can be readily identified. Relevant examples are given by Brühl (1978), Chang, Patel, Nannichi & de Prince (1979), and Chang (1979), who examined lattice mismatch in LPE heterojunction systems, and by Brown, Halliwell & Isherwood (1980), and Isherwood, Brown & Halliwell (1981, 1982), who reported characterization of distortions in hetero-epitaxic structures together with a theoretical basis (multiple diffraction) for the method.

Another task of real-structure examination is the determination of angles between crystal blocks. A method has been worked out by Aristov, Shmytko & Shulakov (1974*a*,*b*).

Divergent-beam techniques can also be used in X-ray topographic studies, realized either by means of Kossel-line scanning (Rozhansky, Lider & Lyutzau, 1966) or by line-profile analysis (Glass & Weissmann, 1969).

Schetelich & Geist (1993) used the Kossel method for lattice-parameter determination and a qualitative estimation of the crystal perfection of *quasicrystals* and showed that the fine structure of Kossel lines of quasicrystals is the same as observed for conventional crystals.

Mendelssohn & Milledge (1999) used a Dingley–Kossel camera for quick and simple computer-aided measurements of cell parameters of isotopically distinct samples of LiF over a wide temperature range of 15–375 K.

5.3.3. Methods with counter recording

5.3.3.1. *Introduction*

Although, theoretically, the limit of accuracy in all methods based on the Bragg law [equation (5.3.1.1)] is given by the accuracy of the wavelength measurement ($\delta\lambda/\lambda \sim 10^{-6}$), with photographic recording this limit is not attained. Surprisingly high accuracy may be offered by accurately applied Kossel or divergent-beam techniques. In practice, however, even in this case the accuracy achieved is poorer by an order of magnitude.

The use of Geiger–Müller, proportional, or scintillation counters together with a step-scanning motor makes it possible to record the diffraction profile in a quantitative numerical form convenient for data processing, to locate it with better accuracy and precision and, as a consequence, to obtain better accuracy and precision for the Bragg angle and thus for the lattice parameter. To make the most of this possibility, theoretical papers concerning methods of peak location, estimation of systematic and statistical errors, and optimization of the measurement were developed in parallel with constructional and experimental methods.

Methods of lattice-parameter determination with counter recording form a large and heterogeneous group. As well as measurements on two- or four-circle standard diffractometers, a separate method developed by Bond (1960) and a variety of non-dispersive (X-ray and optical interferometry) and pseudo-non-dispersive methods (two- and three-circle spectrometers, multiple-beam techniques, and combined methods) are included in this group.

5.3.3.2. *Standard diffractometers*

The determination of lattice parameters by the use of a standard diffractometer is based, as in the case of photographic methods, on (5.3.1.1) and (5.3.1.2), and the main task is to measure a sufficient number of reflections (the θ values for various *hkl* indices) for determining and solving the equations and for calculating the unknown parameters. The reflections can be chosen arbitrarily or in a special way (high θ angle, axial or non-axial reflections).

The characteristic feature of measurements performed on a diffractometer is, however, that to satisfy the Ewald condition for a given reflection the crystal and the detector are rotated or, depending on the geometry (equatorial or inclination), shifted round their axes as well. Basic and more detailed information about the geometry of diffractometers is given elsewhere (Arndt & Willis, 1966, Chap. 3; Stout & Jensen, 1968, Section 6.3; Kheiker, 1973, Chap. 4; Luger, 1980, Chap. 4; Section 2.2.6 of this volume). For calculating the *setting angles* for given *hkl* reflections, the lattice parameters (at least preliminary values) have to be known, and conversely, if the setting angles are known, it is possible to calculate or to refine lattice parameters. Therefore, not only the θ values (given by the angle 2θ of rotation of the detector about the goniometer axis) but also the values of the remaining setting angles (*i.e.* ω, φ, and χ of the crystal rotation in equatorial geometry, or μ and φ for the crystal and ν for the detector in inclination geometry) can be used for lattice-parameter determination. This problem can be treated by a matrix analysis.

5.3.3.2.1. *Four-circle diffractometer*

In the case of an automated four-circle (equatorial geometry) diffractometer, the setting angles are calculated by means of the orientation matrix $\boldsymbol{U}$, *i.e.* a matrix such that

$$\boldsymbol{A}^* = \boldsymbol{U}\boldsymbol{A}_G, \tag{5.3.3.1}$$

where

$$\boldsymbol{A}^* = \begin{bmatrix} a^* \\ b^* \\ c^* \end{bmatrix} \tag{5.3.3.1a}$$

is the reciprocal-axis system with metric

$$\boldsymbol{G}^{-1} = \begin{bmatrix} a^{*2} & a^*b^*\cos\gamma^* & a^*c^*\cos\beta^* \\ a^*b^*\cos\gamma^* & b^{*2} & b^*c^*\cos\alpha^* \\ a^*c^*\cos\beta^* & b^*c^*\cos\alpha^* & c^{*2} \end{bmatrix} \tag{5.3.3.1b}$$

and

$$\boldsymbol{A}_G = \begin{bmatrix} a_G \\ b_G \\ c_G \end{bmatrix} \tag{5.3.3.1c}$$

is the crystal-fixed orthonormal system. As can be proved (Busing & Levy, 1967; Hamilton, 1974; Luger, 1980, Section

4.1.1; Gabe, 1980), the reciprocal-cell parameters are related to the orientation matrix by the following equation:

$$\boldsymbol{A}^*\boldsymbol{A}^{*\prime} = \boldsymbol{U}\cdot\boldsymbol{U}', \tag{5.3.3.2}$$

where $\boldsymbol{A}^*\boldsymbol{A}^{*\prime} = \boldsymbol{G}^{-1}$ is given by (5.3.3.1*b*). It is thus possible to calculate the lattice parameters from the terms of the orientation matrix.

The determination of the orientation matrix is usually the first step in measurements performed on the four-circle diffractometer. This task can be accomplished when the preliminary lattice-parameter values are known, and even when they are unknown. In the first case, the setting angles of two reflections, and, in the second, of three reflections, have to be determined. The procedure (Busing & Levy, 1967; Hamilton, 1974) is usually accomplished by the software of the four-circle diffractometer. Least-squares refinement of the lattice and orientation parameters may be performed when the setting angles of several reflections have been observed (Clegg, 1984). Appropriate constraints, resulting from the presence of symmetry elements in the given crystal structure, to be introduced during the refinement, are discussed by Bolotina (1989).

In a particular case, the four-circle diffractometer can be used for lattice-parameter measurements performed in the plane perpendicular to the main goniometer axis (say, the horizontal plane), for which $\chi = 0^\circ$, so that, in practice, only 2θ and ω values are used for lattice-parameter determination (see also §5.3.3.4.1). The equations to be solved can be simplified if only axial reflections are taken into account. In an example described by Luger (1980, Section 4.2.2), the $\mathbf{b}^*$ axis of a monoclinic crystal is oriented in the direction of the main axis. Then each of the two axial lengths, a^* and c^* (see Fig. 5.3.3.1), can be obtained from only one measurement:

$$a^* = \frac{2\sin\theta}{|h|\lambda}, \tag{5.3.3.3a}$$

$$c^* = \frac{2\sin\theta}{|l|\lambda}, \tag{5.3.3.3b}$$

whereas φ values of two reflections are used to determine the β^* angle between $\mathbf{a}^*$ and $\mathbf{c}^*$ axes, since

$$\beta^* = \varphi_{h00} - \varphi_{00l}. \tag{5.3.3.3c}$$

This method is more suitable for orthogonal systems than for non-orthogonal ones, because of the difficulties in obtaining the proper orientation in the case of the monoclinic and, particularly, the triclinic system. In the latter case, the crystal has to be set three times.

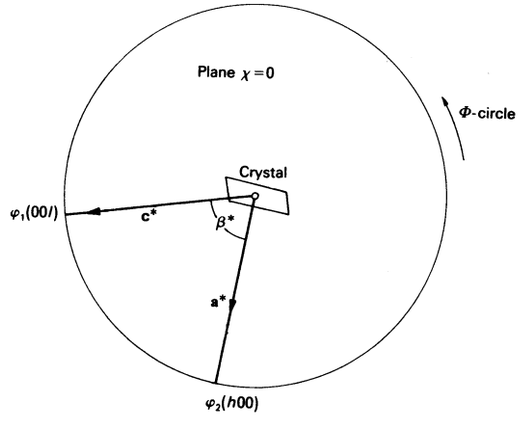

Fig. 5.3.3.1. Determination of reciprocal-lattice angles on the θ circle (after Luger, 1980).

5.3.3.2.2. *Two-circle diffractometer*

Lattice-parameter determination by the use of the two-circle (inclination) diffractometer, the so-called 'Weissenberg diffractometer', is more troublesome than by means of the four-circle one, because only two rotations [ω (or φ) of the crystal, and 2θ (or γ) of the detector] are motor-driven under computer control, while two inclination angles (μ for the crystal and ν for the detector) must be set by hand.

The problem of application of the popular two-circle (Eulerian-cradle) diffractometer for measurements similar to those presented in §5.3.3.2.1 was discussed by Clegg & Sheldrick (1984). The main idea of their paper was to introduce equations combining setting angles, obtained for selected reflections, with reciprocal-cell parameters, for calculating the latter. The authors started with zero-layer reflections for which, for a crystal mounted about the c axis,

$$\sin\theta = (x^2 + y^2)^{1/2}, \tag{5.3.3.4a}$$

$$\omega = \omega_0 + \theta - \tan^{-1}(y, x), \tag{5.3.3.4b}$$

where

$$x = \lambda(ha^* + kb^*\cos\gamma^*)/2, \tag{5.3.3.4c}$$

$$y = (\lambda kb^*\sin\gamma^*)/2, \tag{5.3.3.4d}$$

and ω_0 is a zero-point correction.

The remaining parameter c had to be determined from the inclination angle μ, measured by hand. The use of zero-layer reflections was advantageous, apart from the simplicity of the formulae (5.3.3.4*a*,*b*,*c*,*d*), because they were less affected by crystal misalignment than were upper-layer reflections. However, a zero-point correction ω_0 for ω had to be performed. For this purpose, the ω_0 value was treated as an additional parameter in off-line least-squares refinement.

As the next step, the authors introduced equations for a general crystal orientation instead of an aligned crystal (*cf.* §5.3.3.2.1) and derived equations defining the setting angles for an arbitrary reflection useful for data collection from a randomly oriented crystal if preliminary lattice-parameter values had been assumed. This made possible measurements of reflections on a range of layers; only one crystal mounting was required. The matrix formulae suitable for Eulerian-geometry diffractometers are also given by Kheiker (1973, Chap. 3, Section 9) and Gabe (1980).

In order to perform precise refinement of all six cell parameters, Clegg & Sheldrick (1984) used least squares with empirical weights:

$$W_{hkl} = 1/\sqrt{\omega_{hkl}}, \tag{5.3.3.5}$$

where ω_{hkl} is the width of the *hkl* reflection. An additional (third) motor to control the μ circle was proposed.

The authors point out that the two-circle diffractometer, owing to its simpler construction in comparison with the four-circle one, is well suited to operations that require additional attachments; for example, for low-temperature operation.

5.3.3.3. *Data processing and optimization of the experiment*

5.3.3.3.1. *Models of the diffraction profile*

Every measurement is based on a certain model of its object. By 'model' we understand here* all the systematized *a priori*

* Statisticians (Schwarzenbach, Abrahams, Flack, Gonschorek, Hahn, Huml, Marsh, Prince, Robertson, Rollett & Wilson, 1989) define model as 'conjecture about physical reality used to interpret the observations'. Based on their definition, the author proposes its operative interpretation.

knowledge concerning the given measurement, necessary for planning and performing the experiment and for estimating parameters being determined. The use of an incorrect model results in a bias, *i.e.* an additional systematic error that may appear aside from physical and geometric aberrations. Therefore, the choice of a well founded model is essential in accurate measurements.

In the case of lattice-parameter determination, the object of direct measurements is a diffraction profile, already mentioned in Subsection 5.3.1.1, and the quantity that is directly determined from the experiment is the Bragg angle θ.

The *a priori* information about the diffraction profile should define: (i) the way in which the Bragg angle θ is related to the measured profile $h(\omega)$, *i.e.* a measure of location; (ii) the mean values of the measured intensities within the profile; and (iii) their variances.

(i) In traditional photographic methods, the Bragg angle is determined from the measurement of distance on the film, where points or lines of the most intense blackening are taken into account. The blackening, which corresponds to the recorded intensity, may be estimated qualitatively ('by eye') or quantitatively, by means of a special device. In the second case, the intensity is determined as a function of the coordinates on the photograph, which, in turn, are related to the angular positions of diffracted beams. The distribution so obtained, *i.e.* the line profile or the diffraction profile, allows more precise measurements of the distances and the determination of θ angles, if a definition of the point (θ_0, h_0) of the profile $h(\theta)$, corresponding to the Bragg angle, *i.e. a measure of location*, is accepted. The analogous situation appears when the diffraction profile is recorded by means of the counter diffractometer. Then the intensities are measured by a counter, while the angular positions of the detector (2θ scan) or the sample (θ scan), or both (ω–2θ scan), are controlled by stepping motor. The device is normally combined with a computer, which facilitates the data processing.

There are various measures of location of the diffraction profile (Wilson, 1965; Thomsen & Yap, 1968). The most popular are:

(1) the centroid or the centre of gravity, defined as

$$\theta_c = \int_{\Omega_1}^{\Omega_2} \theta h(\theta)\,\mathrm{d}\theta \Big/ \int_{\Omega_1}^{\Omega_2} h(\theta)\,\mathrm{d}\theta, \qquad (5.3.3.6)$$

where Ω_1 and Ω_2 are the selected truncation limits;

(2) the median, the value θ_m that equally divides some specified portion of the line profile, *i.e.*

$$\int_{\Omega_1}^{\theta_m} h(\theta)\,\mathrm{d}\theta = \int_{\theta_m}^{\Omega_2} h(\theta)\,\mathrm{d}\theta; \qquad (5.3.3.7)$$

(3) the geometrical peak – the abscissa value θ_p for which the maximum occurs, *i.e.*

$$[\,\mathrm{d}h(\theta)/\,\mathrm{d}\theta]_{\theta=\theta_p} = 0; \qquad (5.3.3.8)$$

(4) the extrapolated peak or the midchord peak, introduced by Bearden (1933) – the point θ_{ep} of intersection of two curves, one of them approximating the midpoints of chords drawn through the profile parallel to the abscissa axis (or to the background) and the other approximating the data points (Fig. 5.3.3.2);

(5) the single midpoint of a chord θ_{mc} drawn horizontally at the defined height, αH, where H is the peak height and α is the truncation level, $0 < \alpha < 1$.

The advantages and disadvantages of these measures of location have been widely discussed (Wilson, 1965, 1967; Thomsen & Yap, 1968; Segmüller, 1970; Kirk & Caulfield, 1977; Grosswig, Jäckel & Kittner, 1986; Gałdecka, 1994), the errors, both systematic (biases) and statistical (variances), resulting from each of these definitions being taken into account. The dependence of these errors on the scanning range (truncation limits) is of great importance. Such features of the definitions as their simplicity or current usage were also considered.

The geometrical peak of the least-squares parabola, approximating the data points near the top of the profile, distinguishes itself with the best precision but rather large bias (because of the asymmetry of the profiles met in practice); the extrapolated peak – commonly used in the case of the Bond (1960) method (definition 4) – permits location of the peak with better accuracy and omitting the dispersion error (*cf.* §5.3.3.4.3.2). The centre of gravity, very useful in theoretical considerations (Wilson, 1963), is strongly dependent on the truncation limits and requires a rather large scanning range. The choice of the definition of the measure of location is the first step of lattice-parameter calculations and also of systematic and statistical error estimation.

In the papers that appeared in the mid-1950's, and which were mainly concerned with powder samples, the centre of gravity as a measure of location was more often used than the peak, probably owing to its property of additivity (the total systematic error in the Bragg angle is a sum of the partial errors related to various physical and apparatus factors) and the estimated errors were consequently referred to this point. The papers were reviewed by Wilson (1963, 1980), one of the authors, in the form of a homogeneous mathematical theory of X-ray powder diffractometry. Some of the formulae describing corrections for displacements of the centroid caused by physical and geometrical factors (collected in convenient tables) proved to be useful for single-crystal methods as well (Smakula & Kalnajs, 1955; Kheiker & Zevin, 1963). Wilson (1963) derived the general formula for calculations of the peak displacements due to various factors. As results from this, the displacements are not additive and, in the case when at least one of the partial distributions is asymmetric, the convolution of the curves [see equation (5.3.1.6)] may lead to an appreciable peak shift, if the distributions are not known. The problem has been treated by Berger (1984, 1986*a*), who used computer modelling.

In later single-crystal methods, in particular in the Bond (1960) method, the peak position of the profile was determined rather than the centroid and the respective corrections referred to the peak (§5.3.3.4.3.2). As a rule, the corrections that related to the peak position were treated as being independent. In practice, this simplifying assumption can be sufficient in measurements with moderate and even high accuracy. However, if the highest accuracy, say of 1 part in 10^7, is required, the joint effect of all the aberrations should be considered (the so-called 'cross terms' are used besides the main terms). Such considerations [Härtwig & Grosswig, 1989; *cf.* §5.3.3.4.3.2, point (7)] must be based on a well-founded physical model of the diffraction profile.

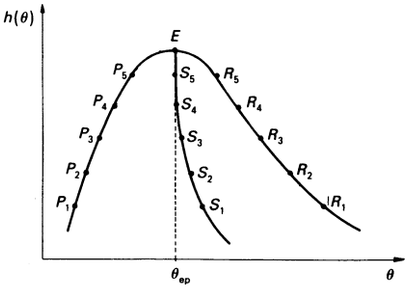

Fig. 5.3.3.2. The extrapolated-peak procedure (after Bearden, 1933).

(ii) As already mentioned in Subsection 5.3.1.1, the diffraction profile can be described as a convolution of several factors (distributions), namely the wavelength distribution, crystal profile and certain aberration profiles. To the so-obtained *net* profile [equation (5.3.1.6)], a background should be added – constant in the case of an ω scan (as in one-crystal spectrometers, for example), and more complex (but usually approximated with a straight line within a narrow angular range) in other cases. Thus, to describe accurately the distribution of the mean values of measured intensities, all individual distributions must be given.

Such complete syntheses of the diffraction profile are rarely performed, and only for the highest-accuracy absolute measurements (Härtwig, Hölzer, Förster, Goetz, Wokulska & Wolf, 1994). Since one of the basic factors of the convolution model is the wavelength distribution that characterizes a given source of radiation, its accurate determination and proper scaling in metric units is of primary importance in high-accuracy lattice-parameter measurements. At present, only a few such measurements are reported, which relate to the Cu $K\alpha$ emission line (Berger, 1986*b*; Härtwig, Hölzer, Wolf & Förster, 1993; Härtwig, Bąk-Misiuk, Berger, Brühl, Okada, Grosswig, Wokulska & Wolf, 1994) and to the Cu $K\beta$ line (the latter paper). Owing to a relatively simple analytical model proposed by Berger (1986*b*) to describe the $K\alpha_{1,2}$ doublet, the measurement results are easy to handle.

Profiles connected with individual apparatus factors (collimation, for example) can also be, in principle, described analytically, under some simplifying assumptions. Examples of such profiles are distributions related to the vertical divergence of the beam (Eastabrook, 1952) and to the horizontal (in-plane) divergence (Urbanowicz, 1981*a*). These are general enough, so can be calculated for given apparatus parameters. While performing high-accuracy measurements, however, the validity of all respective accompanying assumptions must be carefully considered (Urbanowicz, 1981*b*; Härtwig & Grosswig, 1989; Härtwig *et al.*, 1993).

In wider practice, there is a tendency towards using simpler descriptions of the diffraction profile. Often, one of the factors, apart from the spectral distribution, is dominant, and the influence of the other ones can be neglected. Berger (1986*b*), for example, neglecting small effects of both the vertical divergence and the crystal profile, obtained an analytical model of the measured Cu $K\alpha$ emission spectrum, with several adjusted parameters, and so managed to determine the pure Cu $K\alpha$ emission-spectrum profile without the necessity of calculating the deconvolution of the measured spectrum in relation to the horizontal-divergence profile.

The choice of model of the *shape* of the diffraction profile depends, of course, on the purpose for which it is applied. The simplest possible descriptions are used in low- or medium-accuracy measurements, in which first the *measured* values of Bragg angles are determined by approximation of the measured profiles with simple analytical functions (polynomials or so-called *shape functions*), the parameters of which have no physical meaning, and then all necessary corrections are calculated and subtracted from the *measured* Bragg angles – under the assumption of their additivity, mentioned in (i) – to obtain their *true* values. Another application of the simple models is just the estimation of systematic and statistical errors of the Bragg-angle determination. The choice and use of such simple models will be shown in §5.3.3.3.2.

(iii) The knowledge of variances (and covariances) of recorded counts is needed to evaluate the goodness of fit while approximating the measured profile with a given model function (appropriate criteria have been formulated by Gałdecka, 1993*a*,*b*) and to estimate the precision of the Bragg-angle determination.

Most often, one assumes that the variances of measured intensities are defined by the Poisson statistic, *i.e.*

$$\sigma^2(h) = h, \tag{5.3.3.9}$$

where h is the intensity in number of counts.

Other factors affecting the statistics of recorded counts and the validity of the assumption [equation (5.3.3.9)] have been taken into consideration by Bačkovský (1965) [see also equations (5.3.3.17) and (5.3.3.18) and the comments on these], Wilson (1965), and Gałdecka (1985). The factors are mostly errors in the angle setting and reading and also fluctuations of the primary-beam intensity, of the counting time, and of the temperature of the sample. The use of automatic scanning can cause correlations between intensities measured at different points in the profile (Gałdecka, 1985).

5.3.3.3.2. *Precision and accuracy of the Bragg-angle determination; optimization of the experiment*

The analysis of the variance $\sigma^2(\theta_0)$ of a chosen measure of location permits a combination of the precision of the Bragg-angle determination, and so of the lattice-parameter determination [equation (5.3.1.4)], with the scanning range $2\Omega = \Omega_2 - \Omega_1$ [see definition (1), §5.3.3.3.1] or truncation level α [see definition (5)], the number of measuring points n (usually $n = 2p + 1$), the parameters of the profile (number of counts H in the peak position, the half-width ω_h), and its shape. It is convenient to present the profile $h(\theta)$ in a standardized form (Thomsen & Yap, 1968) as:

$$h(\theta) = Hv[x(\theta)], \tag{5.3.3.10}$$

where

$$x(\theta) = 2\frac{\theta - \theta_0}{\omega_h} \tag{5.3.3.10a}$$

are standardized angle values and

$$v(x) = h/H \tag{5.3.3.10b}$$

is the shape function, not dependent on the parameters H and ω_h. For each measure of location [definitions (1)–(5) of §5.3.3.3.1(i)], there is the dependence:

$$\sigma^2(\theta_0) = F\frac{\omega_h^2}{I_p T}, \tag{5.3.3.11}$$

where I_p is the peak intensity, T is the total counting time, and F is a dimensionless factor that depends on the measure of location and the shape of the profile.

Since, in the case of fixed-time counting, the total counting time T is proportional to the number n of measuring points:

$$T = n\Delta t, \tag{5.3.3.12}$$

where Δt is the counting time, and since the number of counts h is proportional to the intensity I:

$$h = I\Delta t, \tag{5.3.3.13}$$

and, in particular, the number of counts H in the peak position is proportional to the peak intensity I_p:

$$H = I_p\Delta t, \tag{5.3.3.13a}$$

the dependence (5.3.3.11) can be presented as

$$\sigma^2(\theta_0) = \frac{F}{n}\frac{\omega_h^2}{H}. \tag{5.3.3.14}$$

Thus, for a given measure of location and given shape of the profile [equations (5.3.3.10), (5.3.3.10*b*)], the variance $\sigma^2(\theta_0)$ depends on the ratio ω_h^2/H of the profile parameters (ω_h, H) and decreases with an increase of the number of points, n.

In particular, the variance $\sigma^2(\theta_p)$ of the peak [definition (3), §5.3.3.3.1] of the least-squares parabola has been estimated (Wilson, 1965) as

$$\sigma^2(\theta_p) = \frac{3H}{2p\Omega^2[h''(\theta_p)]^2}, \tag{5.3.3.15}$$

where $h''(\theta_p)$ is the second derivative of $h(\theta)$ in the peak position and p is a number such that $n = 2p + 1$ ($n \approx 2p$, if p is sufficiently large).

Taking into account the standardization performed [equations (5.3.3.10), (5.3.3.10*a,b*)], equation (5.3.3.15) can be rewritten in the form:

$$\sigma^2(\theta_p) = \frac{1}{n}\,\frac{3}{4X^2[v''(0)]^2}\,\frac{\omega_h^2}{H}, \tag{5.3.3.16}$$

where X is the standardized scanning range

$$X = 2\Omega/\omega_h \tag{5.3.3.16*a*}$$

and $v''(0)$ is the second derivative of the shape function in the peak positions. By comparing (5.3.3.16) and (5.3.3.14), we find the factor F in this case to be

$$F = \frac{3}{4X^2[v''(0)]^2}. \tag{5.3.3.16*b*}$$

From (5.3.3.14) and (5.3.3.16*b*), the variance of the peak of the least-squares parabola decreases with an increase of the scanning range. On the other hand, the bias of the peak position, resulting from the asymmetry of the profile, is proportional to Ω^2 (Wilson, 1965):

$$\Delta\theta_p = 2(\Omega^2/\omega_h)[v'''(u_p)/v''(u_p)], \tag{5.3.3.16*c*}$$

where $v''(u_p)$ and $v'''(u_p)$ are the second and third derivatives of a function describing the profile at its peak position u_p. These two aspects should be taken into account in choosing the scanning range. Yet, as shown by Gałdecka (1993*b*; Section 5), (5.3.3.16*c*) may be applied to reduce the bias by extrapolating to $\Omega = 0$ the results obtained within various scanning ranges.

In the case of polynomials of higher (and even) degrees ($m = 4$, 6, 8) and $0.5 \ll X \ll 1$, the factor F can be expressed by a semi-empirical dependence (Thomsen, 1974; Gałdecka, 1993*b*):

$$F = 0.0017\, m^2\, (\tan^{-1} X)/X^3, \tag{5.3.3.16*d*}$$

but it is difficult to evaluate the bias. Therefore, as shown by Gałdecka (1993*b*), polynomials of higher degrees have no advantage over a least-squares parabola.

To minimize the bias, a reasonable shape function may be used rather than a polynomial (Gałdecka, 1993*a,b*). The function should be continuous (including its derivatives), not negative and closely related to known physical models of the diffraction profiles. Since the measured diffraction profiles are, as a rule, asymmetric, the proper selection of a description of asymmetry is of primary importance. The use of the so-called 'split functions', consisting of two 'half' functions of the same (or different) shape and different half-widths, leads to a noticeable bias, so such functions must not be used for accurate lattice-parameter determination.

The variance $\sigma^2(\theta_{\rm mc})$ of a single midpoint of a chord [definition (5), §5.3.3.3.1] has been estimated by Bačkovský (1965) as

$$\sigma^2(\theta_{\rm mc}) = \sigma^2(\theta_i) + \sigma^2(h_i)/[h'(\theta_i)]^2, \tag{5.3.3.17}$$

where $\sigma^2(\theta_i)$ and $\sigma^2(h_i)$ are the variances of the coordinates θ and h, respectively, and $h'(\theta)$ is the first derivative at the ith point. If it is assumed that $\sigma^2(\theta_i)$ is small in relation to the second component of (5.3.3.17) and if (5.3.3.9) and the standardizations (5.3.3.10), (5.3.3.10*a,b*) are taken into consideration, (5.3.3.17) can be rewritten in the form:

$$\sigma^2(\theta_{\rm mc}) = \frac{v_i}{4[v'(x_i)]^2}\,\frac{\omega_h^2}{H}, \tag{5.3.3.18}$$

where $v'(x_i)$ is the first derivative of the shape function in the ith position.

Comparison of (5.3.3.18) and (5.3.3.14), with $n = 2$, leads to

$$F = \frac{v_i}{2[v'(x_i)]^2}. \tag{5.3.3.18*a*}$$

For an arbitrary shape function $v(x)$ describing the diffraction profile, it is thus possible to find such a truncation level $\alpha = \alpha_{\rm opt}$ [§5.3.3.3.1, definition (5)], for which F is a minimum. If the shape function is the Cauchy function,

$$v = \frac{1}{1 + x^2}, \tag{5.3.3.19}$$

the optimum truncation level is $\alpha_{\rm opt} = 2/3$, and the resulting F factor, $F = F_{\rm min} = 0.84$.

In spite of a large bias introduced by the midpoint of a single chord (the difference between its position and the peak position), this measure of location is preferred by Barns (1972), because the calculations are less time-consuming than those for other points of the profile. Barns takes $\alpha = 0.5$ [$F = 1$ for the Cauchy function; equations (5.3.3.18*a*), (5.3.3.19)] and compensates the bias at this level by determining an effective value of the wavelength based on a silicon standard.

The estimators of the variance for the centroid and the median given by Wilson (1967), or estimators of both the variance and the bias of the extrapolated-peak position given by Gałdecka (1994) can also be the basis of the choice of the scanning range if these measures of location are applied.

The other possibility of affecting the precision of the measurements is to change the shape and the parameters of the profile [see equations (5.3.3.14), and (5.3.3.16*b*) or (5.3.3.18*a*)] by changing the apparatus parameters [the influence on $h_A(\theta)$, equation (5.3.1.6)], or the X-ray source profile $h_\lambda(\theta)$, or the crystal profile $h_C(\theta)$.

An example of the first possibility is the optimization of the parameters of in-plane collimation in the case when the peak of the least-squares parabola is used as the measure of the location (Urbanowicz, 1981*a*). Since both the shape and the parameters of the profile depend on the collimation parameters, the task is to choose collimator-slit dimensions to minimize the value $(\omega_h^2/H)\{1/[v''(0)]^2\}$ [*cf.* equation (5.3.3.16)]. As a result of detailed considerations, under the assumption given by (5.3.3.9), the optimum exists and is defined by the following formula:

$$d_1 = d_2 = 0.565\, L\omega_\lambda, \tag{5.3.3.20}$$

where d_1 and d_2 are the widths of the slits, L is the collimator length, and ω_λ is the half-width of the original profile $h_\lambda(\theta)$ [*cf.* equations (5.3.1.6), (5.3.1.7), and (5.3.1.8)]. Systematic errors connected with collimation have been discussed separately (Urbanowicz, 1981*b*).

The width of the original profile $h_\lambda(\theta)$ can be reduced by means of spectrally narrow sources or by the use of additional crystal(s) in multiple-crystal methods (Subsection 5.3.3.7). The latter also affects the crystal profile $h_C(\theta)$.

5.3.3.4. *One-crystal spectrometers*

5.3.3.4.1. *General characteristics*

A diffractometer in which both 2θ and ω scans are available, intended for precise and accurate lattice-parameter determination, is sometimes called a one-crystal spectrometer, by analogy with a similar device used for wavelength determination. This name has been used by Lisoivan (1982), who in his review paper described various properties and applications of such a device.

Bragg-angle determination with the one-crystal spectrometer can be performed in an asymmetric as well as in a symmetric arrangement (Arndt & Willis, 1966, pp. 262–264). In the asymmetric arrangement (Fig. 5.3.3.3*a*), the angle 2θ is the difference between two detector positions, related to the maximum intensity of the diffracted and the primary beam, respectively. Bragg-angle determination in such an arrangement is subject to several systematic errors; among these zero error, eccentricity, and absorption are of great importance. As shown by Berger (1984), the latter two errors can be eliminated when Soller slits are used.

To eliminate the zero error, a symmetric diffractometer may be used, in which each measurement of the Bragg angle is performed twice, for two equivalent diffracting positions of the sample, symmetrical in relation to the primary-beam direction (Fig. 5.3.3.3*b*). The respective positions of the counter (or counters, since sometimes two counters are used) are also symmetrical. Such an arrangement may be considered to be (Beu, 1967), in some ways, the diffractometer counterpart of the Straumanis film method (Straumanis & Ieviņš, 1940). From geometric considerations, the absolute value of the angle between the two counter positions is 4θ and the absolute value of the angle between the two sample positions, ω_1 and ω_2, is $180^\circ - 2\theta$, so that both 2θ and ω scans can be used for the Bragg-angle determination.

As was mentioned in §5.3.2.3.4(vi), the idea of calculating the θ angle from the two sample positions has been used with photographic methods (Bragg & Bragg, 1915; Weisz, Cochran & Cole, 1948). Bond (1960), in contrast, was the first to apply this to measurements on the counter diffractometer, and proved that, owing to the geometry, not only the zero error but also the eccentricity, absorption, and several other errors can be reduced.

5.3.3.4.2. *Development of methods based on an asymmetric arrangement and their applications*

Although the Bond (1960) method, based on a symmetric arrangement presented in §5.3.3.4.3, makes possible higher accuracy than that obtained by means of a standard diffractometer, an asymmetric arrangement proves to be more suitable for certain tasks connected with lattice-parameter measurement, because of its greater simplicity. The more detailed arguments for the use of such a device result from some disadvantages of the Bond method, discussed in §5.3.3.4.3.4.

One of the earliest and most often cited methods of lattice-parameter determination by means of the counter single-crystal diffractometer (in an asymmetric arrangement) is that of Smakula & Kalnajs (1955). The authors reported unit-cell determinations of eight cubic crystals. The systematic errors due to seven factors were analysed according to the formulae derived by Wilson (1950) and Eastabrook (1952) for powder samples, and valid also for single crystals. The lattice parameters computed for various diffraction angles were plotted *versus* $\cos^2\theta$; extrapolation to $2\theta = 180^\circ$ gave the lattice parameters corrected for systematic errors. Accuracy of 4 parts in 10^5, limited by the uncertainty of the X-ray wavelength, and precision of 1 part in 10^6 were achieved.

A more complete list of factors causing broadening and asymmetry of the diffraction profile, and so affecting statistical and systematic errors of lattice-parameter determination, has been given by Kheiker & Zevin (1963, Tables IV, IVa, and IVb). Since the systematic errors due to the factors causing asymmetry (specimen transparency, axial divergence, flat specimen) are, as a rule, dependent on the Bragg angle and proportional to $\cos\theta$, $\cos^2\theta$, $\cot\theta$ or $\cot^2\theta$, they can be removed or reduced – as in the method of Smakula & Kalnajs (1955) – by means of extrapolation to $\theta = 90^\circ$. The problem has also been discussed by Wilson (1963, 1980) in the case of powder diffractometry [*cf.* §5.3.3.3.1(i)]. When comparing the considerations of Kheiker & Zevin and Wilson [the list of references concerning the subject given by Kheiker & Zevin (1963) is, with few exceptions, contained in that given by Wilson (1963)], it will be noticed that some differences in the formulae result from differences in the geometry of the measurement rather than from the different nature of the samples (single crystal, powder).

As in the photographic methods, the accurate recording of the angular separation between $K\alpha$ and $K\beta$ diffraction lines can be the basis for lattice-parameter measurements with a diffractometer (Popović, 1971). The method allows one to reduce the error in the zero setting of the 2θ scale and the error due to incorrect positioning of the sample on the diffractometer, since the angular separations are independent of the zero positions of the 2θ and ω scales.

An example of a contemporary method of lattice-parameter determination is given by Berger (1984). As has been mentioned in §5.3.3.4.1, the characteristic feature of the device is the Soller slits, which limit the divergence of both primary and diffraction

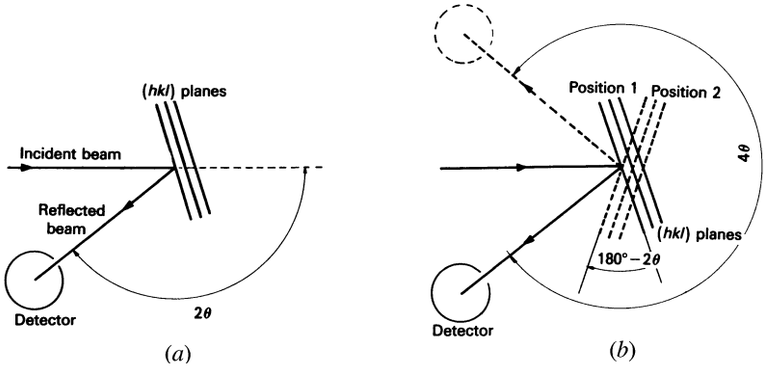

Fig. 5.3.3.3. Determination of the Bragg angle by means of the one-crystal spectrometer using (*a*) an asymmetric or (*b*) a symmetric arrangement. The zero position of the detector arms must be known in (*a*), but not in (*b*). After Arndt & Willis (1966).

beams and, at the same time, eliminate errors due to eccentricity and absorption. On the other hand, systematic errors due to refraction, vertical inclination, vertical divergence, and Soller-slit inaccuracy, as well as asymmetry of profiles and crystal imperfection, have to be analysed.

Since, in this case, the angle between the incident and the reflected beam is measured, the inclinations of both beams must be considered. As a result of the analysis [analogous to that of Burke & Tomkeieff, 1969; referred to in §5.3.3.4.3.2(4)], the following expression for the angular correction $\Delta\theta_t$ (to be added to the measured value of θ) is obtained:

$$\Delta\theta_t = \frac{\alpha\gamma}{2\sin 2\theta} + \frac{\alpha^2+\gamma^2}{4\tan 2\theta}, \qquad (5.3.3.21)$$

where α and γ are the vertical inclinations of the incident and reflected beams, respectively. The correction for vertical divergence is presented in §5.3.3.4.3.2(3).

The Soller-slit method, the accuracy and precision of which are comparable to those obtained with the Bond method, is suitable both for imperfect crystals, since only a single diffracting position of the sample is required, and for perfect samples, when an exactly defined irradiated area is required. It is applicable to absolute and to relative measurements. Examples are given by Berger, Rosner & Schikora (1989), who worked out a method of absolute lattice-parameter determination of *superlattices*; by Berger, Lehmann & Schenk (1985), who determined lattice-parameter variations in PbTe single crystals; and by Berger (1993), who examined point defects in II–VI compounds.

An original method, based on determining the Bragg angle from a two-dimensional map of the intensity distribution (around the reciprocal-lattice point) of high-angle reflections as a function of angular positions of both the specimen and the counter, was described by Kobayashi, Yamada & Nakamura (1963) and Kobayashi, Mizutani & Schmidt (1970). A finely collimated X-ray beam, with a half-width less than 3′, was used for this purpose. The accuracy of the counter setting was $\pm 0.1^\circ$, the scanning step $\Delta\theta = 0.01^\circ$. Systematic errors depending on the depth of penetration and eccentricity of the specimen were reported, and were corrected both experimentally (manifold measurements of the same planes for different diffraction ranges, and rotation of the crystal around its axis by 180°) and by means of extrapolation. The correction for refraction was introduced separately. The method was used in studies of the antiparallel 180° domains in the ferroelectric barium titanate, which were combined with optical studies.

The determination of variations in the cell parameter of GaAs as a function of homogeneity, effects of heat treatments, and surface defects has been presented by Pierron & McNeely (1969). Using a conventional diffractometer, they obtained a precision of 3 parts in 10^6 and an accuracy better than 2 parts in 10^6. The systematic errors were removed both by means of suitable corrections (Lorentz–polarization factor and refraction) and by extrapolation.

A study of the thermal expansion of α-$LiIO_3$ over a wide range of temperatures (between 20 and 520 K) in the vicinity of the phase transition has been reported by Abrahams *et al.* (1983). Lattice-parameter changes were examined by means of a standard diffractometer (CAD-4); absolute values at separate points were measured by the use of a Bond-system diffractometer.

An apparatus for the measurement of uniaxial stress based on a four-circle diffractometer has been presented by d'Amour *et al.* (1982). The stress, produced by turning a differential screw, can be measured *in situ*, *i.e.* without removing the apparatus from the diffractometer. An example of lattice-parameter measurement of Si stressed along [111] is given, in which the stress parameter ζ is calculated from intensity changes of the chosen 600 reflection.

5.3.3.4.3. *The Bond method*

5.3.3.4.3.1. *Description of the method*

By the use of the symmetric arrangement presented in §5.3.3.4.1 (Fig. 5.3.3.3*b*), it is possible to achieve very high accuracy, of about 1 part in 10^6 (Bond, 1960), and high precision (Baker, George, Bellamy & Causer, 1968) but, to make the most of this, some requirements concerning the device, the sample, the environmental conditions, the measurement itself, and the data processing have to be fulfilled; this problem will be continued below.

Bond (1960) in his notable work used a large, highly pure and perfect single crystal (zone-refined silicon) in the shape of a flat slab. The scheme of the method is given in Fig. 5.3.3.4. The crystal was mounted with the reflecting planes accurately parallel to the axis of the shaft on a graduated circle (clinometer), the angular position of which could be read accurately (to 1″). The X-ray beam travelling from the tube through a collimator (two 50 μm slits, 215 mm apart, so that the half-width of the primary beam was 0.8′) fell directly upon the crystal, set in one of the two diffracting positions. The diffracted beam was intercepted by one of two detectors [Geiger–Müller (G–M) counters], which were fixed in appropriate positions. The detectors were wide open, so that their apertures were considerably wider than the diffracted beam, which eliminated some systematic errors depending on the counter position. The crystal was rotated step by step through the reflecting position to record the diffraction profile. Next, the peak positions of both profiles were determined by the extrapolated-peak procedure [§5.3.3.3.1, definition (4)] to find the accurate positions of the sample, ω_1 and ω_2, from which the Bragg angle was calculated by use of a formula that can be written in a simple form as

$$\theta = |180^\circ - |\omega_1 - \omega_2|/2|. \qquad (5.3.3.22)$$

Before calculating the interplanar distance [equation (5.3.1.1)] or, in the simplest case, the lattice parameter directly, the systematic errors have to be discussed and evaluated. Sometimes, corrections are made to the parameters themselves rather than to the θ values. The reader is referred to §5.3.3.4.3.2, in which present knowledge is taken into account, rather than to Bond's original paper.

Bond performed measurements at room temperature (298 K) for reflections 444, 333, and 111 and, after detailed discussion of

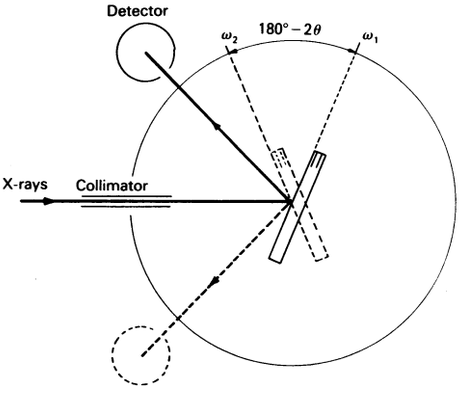

Fig. 5.3.3.4. Schematic representation of the Bond (1960) method.

errors, reported the a_0 values (in kXU), which related to these measurements (standard deviations are given in parentheses), as 5.419770 (0.000019), 5.419768 (0.000031), 5.419790 (0.000149). These values are referred to $\lambda = 1.537395$ kXU. These results were then tested by Beu, Musil & Whitney (1962) by means of the likelihood-ratio method to test the hypothesis of 'no remaining systematic errors'. They proved that the estimate for this sample of silicon is accurate within the stated precision (1 part in 390 000).

The results reported in Bond (1960) – very high accuracy and remarkable reproducibility (low standard deviation), obtained by use of a relatively simple device, which can be realized on the basis of a standard diffractometer – encourage experimenters to perform similar measurements. However, many problems arise with the adaptation of the Bond method to other kinds of samples and/or to other purposes than those described by Bond (1960) in his original paper. Both theoretical and experimental work have increased the accuracy and the precision of the method during the last 35 years.

5.3.3.4.3.2. *Systematic errors*

As mentioned above (§5.3.3.4.1), some systematic errors that affect the asymmetric diffractometer are experimentally eliminated in the Bond (1960) arrangement. According to Beu (1967), who has supplemented the list of errors given by Bond, the following systematic errors are eliminated at the $0.001^\circ\theta$ level:

(*a*) absorption, source profile, radial divergence and surface flatness; removed since the detectors are used only to measure intensities and not angular positions;

(*b*) zero, eccentricity, misalignment and diffractometer radius; eliminated since θ depends only on the difference in the crystal-angle positions and not on these geometrical factors;

(*c*) ratemeter recording does not affect the measurements since the detectors are used only for point-by-point counting;

(*d*) 2:1 tracking error is eliminated because the 2:1 tracking used in most commercial asymmetric diffractometers is not used;

(*e*) dispersion, if the peak position of the profile is determined rather than the centroid or the median, and the wavelength has been determined for the peak position also.

As well as these errors there are other systematic errors, due to both physical and apparatus factors, which should be eliminated by suitable corrections.

(1) *Lorentz–polarization error*. The Lorentz–polarization factor Lp influences the shape of the profile as follows:

$$v_1(x) = \mathrm{Lp}\, v(x), \tag{5.3.3.23}$$

where $v(x)$ and $v_1(x)$ are the shape functions [see equations (5.3.3.10), (5.3.3.10*a*,*b*)] of the undistorted and distorted profiles, respectively. It therefore produces a shift ($\Delta\theta_{\mathrm{Lp}}$) in the peak position.

The correction for the Lp factor was estimated, assuming that $v(x)$ is the Cauchy function [equation (5.3.3.19)], by Bond (1960, 1975), Segmüller (1970), and Okazaki & Ohama (1979) for two cases. For perfect crystals, when the Lp factor has the form (James, 1967, p. 59; Segmüller, 1970; Okazaki & Ohama, 1979)

$$\mathrm{Lp} = (1 + |\cos 2\theta|)/\sin 2\theta, \tag{5.3.3.24}$$

the correction is given by

$$\theta - \theta_p = (\omega_h/2)^2[\cot 2\theta_p + \sin 2\theta_p/(1 + |\cos 2\theta_p|)], \tag{5.3.3.25}$$

where ω_h is the half-width of the profile, θ_p is the Bragg angle related to the distorted profile, and θ is the corrected Bragg angle. In contrast, the following formulae are valid for mosaic crystals:

$$\mathrm{Lp} = (1 + \cos^2 2\theta)/(2 \sin 2\theta), \tag{5.3.3.26}$$

and

$$\theta - \theta_p = (\omega_h/2)^2 \cot 2\theta_p (2 + \sin^2 2\theta_p)/(2 - \sin^2 \theta_p). \tag{5.3.3.27}$$

Because of a notable difference between the values calculated from (5.3.3.25) and (5.3.3.27), the problem is to choose the formulae to be used in practice. However, the Lorentz–polarization error is usually smaller than the rest.

(2) *Refraction*. In the general case, when the crystal surface is not parallel to the reflecting planes but is rotated from the atomic planes around the measuring axis by the angle ε, the correction, which relates directly to the determined interplanar distance, has the form (Bond, 1960; Cooper, 1962; Lisoivan, 1974, 1982)

$$d = d_p\left[1 + \frac{\delta \cos^2 \varepsilon}{\sin(\theta + \varepsilon)\sin(\theta - \varepsilon)}\right], \tag{5.3.3.28}$$

where δ is unity minus the refractive index of the crystal for the X-ray wavelength used, and d_p and d are the uncorrected and corrected interplanar distances, respectively.

(3) *Errors due to axial and horizontal (in-plane) divergence*. The axial divergence of the primary beam, given by an angle $2\Delta_p$ depending on the source and collimator dimensions, causes the angle θ', formed by a separate ray of the beam with a given set of crystallographic planes, to differ from the proper Bragg angle. In general, if the plane of diffraction is not sufficiently perpendicular to the axis of rotation but lacks perpendicularity by an angle Δ, the measured Bragg angle θ' can be described, according to Bond (1960), as

$$\sin\theta' = \sec\Delta \sin\theta. \tag{5.3.3.29}$$

Let us assume that both the crystal and the collimator have been accurately adjusted so that the lack of perpendicularity results from axial divergence only. By averaging the expression (5.3.3.29) over the limits $\pm\Delta_p$, the mean value of $\sin\theta'$ can be found and, as a consequence, the following formula describing the correct d spacing can be obtained:

$$d = d'(1 + \Delta_p^2/6), \tag{5.3.3.30}$$

where d' is the apparent d spacing.

According to Berger (1984), this correction is valid only for the case of infinitely small focus, when all rays have the same intensity. Taking into consideration the shift of the centroid caused by vertical divergence when the focus emits uniformly within the axial limits $(-F, F)$, he proposes an alternative correction for θ:

$$\Delta\theta_d = \tfrac{1}{6}\tan\theta(P^2 + F^2), \tag{5.3.3.31}$$

where $2P$ is the sample height.

As tested using computer modelling (Urbanowicz, 1981*b*) and estimated analytically (Härtwig & Grosswig, 1989), the effect of the horizontal divergence on the peak position of the recorded profiles cannot be neglected, contrary to suggestions of Bond (1960). The respective systematic error is dependent on asymmetries of both the focus-tube emissivity and the spectral line, and so it is difficult to express it with a simple formula [*cf.* point (7) below]. In practice (Härtwig, Grosswig, Becker & Windisch, 1991), it proves to be the second largest error. (The first is the one caused by refraction.)

(4) *Specimen-tilt and beam-tilt error*. Since the three main sources of systematic error in diffractometer measurements, *i.e.* zero, eccentricity, and absorption, have been eliminated in the Bond method, two errors due to misalignment of the crystal and the collimator can strongly influence results of lattice-parameter

determination. They are difficult to control because of the random character; numerous authors analysing the Bond method have tried to cope with them. A review is given by Nemiroff (1982).

Bond (1960) considered the crystal-tilt error separately from the collimator tilt. However, in subsequent papers on this subject it was shown that the errors connected with the crystal tilt and the collimator tilt, *i.e.* with the angles that the normals to the crystal and collimator make, respectively, with the plane of angular measurement, are dependent and should be treated jointly.

Foreman (in Baker, George, Bellamy & Causer, 1968) derived a formula for the real value of the angle between two reflecting positions [*i.e.* ω_1 and ω_2 in equation (5.3.3.22)] when affected by both tilts. Burke & Tomkeieff (1968, 1969), in contrast, have found a dependence between the crystal tilt α and the beam tilt β and the relative error $\Delta a/a$ in lattice parameter a in the form

$$\Delta a/a = \alpha\beta/\sin\theta - (\alpha^2 + \beta^2)/2. \qquad (5.3.3.32)$$

A separate analysis is given by Gruber & Black (1970) and by Filscher & Unangst (1980).

Two approaches are used to eliminate the systematic errors considered, based on the above formula:

(i) The error resulting from the crystal tilt and the collimator tilt can be reduced experimentally. Baker, George, Bellamy & Causer (1968) have given a simple procedure that allows a collimator tilt of small but unknown magnitude to be tolerated and, at the same time, the tilt of the crystal to be adjusted to its optimum value. Burke & Tomkeieff (1968, 1969) propose a method for setting the crystal so that $\alpha = \beta$, since, as is obvious from (5.3.3.32), the error has then its minimum value; α and β have to be of the same sign. Then the influence of crystal tilt and beam tilt on the accuracy of lattice-parameter determination is negligible at the level of 1 part in 10^6.

(ii) Equation (5.3.3.32) permits calculation of the exact correction due to both crystal and collimator tilts, if the respective values of α and β are known. Halliwell (1970) proposed a method for determining the beam and the crystal tilt that requires measuring reflections from both the front and back surfaces of the crystal. In a method described by Nemiroff (1982), the two tilts are measured and adjusted independently within ± 0.5 mrad.

(5) *Errors connected with angle reading and setting*. Errors in angle reading and angle setting depend both on the class of the device and on the experimenter's technique. Some practical details are discussed by Baker, George, Bellamy & Causer (1968). Since the angles are measured by counting pulses to a stepping motor connected to a gear and worm, the errors due to angle setting and reading depend on the fidelity with which the gear follows the worm. To diminish errors affected by the gearwheel (notably eccentricity), the authors propose a closed error-loop method, which involves using each part of the gear in turn to measure the angle and averaging the results. In the diffractometer reported in the above paper, there was, originally, an angular error of about $+15''$ around the gearwheel, and this can be corrected by means of a cam so that the residual error is reduced to about $\pm 5''$.

Another example of a high-precision drive mechanism is given by Pick, Bickmann, Pofahl, Zwoll & Wenzl (1977). In the diffractometer described in their paper (see also §5.3.3.7.2), the gear was shown to follow the worm with fidelity even down to $0.01''$ steps, and a drift of $\pm 10\%$ per step was traced to insufficient stability of temperature (± 0.15 K).

(6) *Temperature correction*. An error Δd_T in the lattice parameter d owing to the uncertainty ΔT of the temperature T can be estimated from the formula (Łukaszewicz, Pietraszko, Kucharczyk, Malinowski, Stępień-Damm & Urbanowicz, 1976):

$$\Delta d_T = d\,\alpha_d\,\Delta T, \qquad (5.3.3.33)$$

if the thermal-expansion coefficient α_d in the required direction is known.

In the case of the 111 reflection of silicon, for which $\alpha_d \approx 2.33 \times 10^{-6}$, to obtain a relative accuracy (precision) of 1 part in 10^6, the temperature has to be controlled with accuracy (precision) not worse than ± 0.05 K if the temperature correction is to be neglected (Segmüller, 1970; Hubbard & Mauer, 1976; Łukaszewicz *et al.*, 1976).

(7) *Remarks*. The above list of corrections, sufficient when the Bond (1960) method is applied under the conditions similar to those described by him (large, perfect, specially cut single crystal; well collimated primary beam; large open detector window) has to be sometimes complemented in the case of different specimens and/or different measurement conditions (§5.3.3.4.3.3). When an asymmetric diffractometer is used, all the systematic errors listed in this section (see also §5.3.3.4.1) must be taken into account.

Using a complete convolution model of the diffraction profile, Härtwig & Grosswig (1989) were able to derive all known aberrations (and so respective corrections) in a rigorous, analytical way. The analytical expressions given by the authors, though based on some simplifying assumptions, are usually much more complex than the ones shown in points (1)–(6) above. Some coefficients in their equations depend on physical parameters characterizing the particular device and experiment. So, to follow the idea of Härtwig & Grosswig, one must individually consider all preliminary assumptions. As shown by the authors, to achieve the accuracy of 1 part in 10^7, all aberrations mentioned by them must be taken into account. The most important aberrations prove to be those related to refraction and to horizontal divergence.

5.3.3.4.3.3. *Development of the Bond method and its applications*

The Bond (1960) method, in its first stage, was meant for large, specially cut and set samples. In principle, only one lattice parameter can be determined in one measuring cycle. As has been shown, the method can also be adapted to other samples, with non-cubic symmetry, and to geometries of the illuminated area, different from those used by Bond. This task needs, however, some additional operations and often some additional corrections for systematic errors.

The basic application of the Bond (1960) method, because its geometry reduced several systematic errors, was to absolute lattice-parameter measurements. The method also proved useful in precise investigations of lattice-parameter changes.

Bond-system diffractometers were most often realized in practice on the basis of standard diffractometers under computer control (Baker, George, Bellamy & Causer, 1968; Segmüller, 1970; Pihl, Bieber & Schwuttke, 1973; Kucharczyk, Pietraszko & Łukaszewicz, 1993). Some were designed for special investigations, such as high-precision measurements, $\sigma(d)/d = 10^{-7}$ (Baker, George, Bellamy & Causer, 1966; Grosswig, Härtwig, Alter & Christoph, 1983; Grosswig *et al.*, 1985; Grosswig, Härtwig, Jäckel, Kittner & Melle, 1986); local measurements at chosen points of a specimen (Lisoivan & Dikovskaya, 1969; Lisoivan, 1974, 1982); examination of lattice-parameter changes over a wide temperature range (Łukaszewicz *et al.*, 1976, 1978; Okada, 1982); or the effect of high pressure on lattice parameters (Mauer, Hubbard,

Piermarini & Block, 1975; Leszczyński, Podlasin & Suski, 1993).

By introduction of synchrotron radiation to a Bond-system diffractometer (Ando *et al.*, 1989), a highly collimated and very narrow beam has been obtained, so lattice-parameter measurements can be accomplished reliably and quickly with a routinely achieved precision of 2 parts in 10^6; these can be combined with X-ray topographs made in selected areas of the sample.

(1) *Crystals with different symmetry*. Cooper (1962) used the Bond (1960) diffractometer and method for absolute measurements of lattice parameters of several crystals belonging to various orthogonal systems. Special attention was paid to preparing the samples, *i.e.* cutting and polishing, to obtain crystal surfaces parallel to the planes of interest. One sample of a given substance was sufficient to find the lattice in the case of cubic crystals but two samples were required for tetragonal and hexagonal systems, and three were necessary for the orthorhombic system. This difficulty increases when non-orthogonal lattices have to be examined. This problem was resolved by Lisoivan (1974, 1982), who used very thin single-crystal slabs, which made possible measurements both in reflection and in transmission. Lisoivan (1981, 1982), developing his first idea, derived the requirements for a precision determination of all the interaxial angles for an arbitrary system. The coplanar lattice parameters can also be determined in one crystal setting when only reflection geometry is used (Grosswig *et al.*, 1985).

Superlattices can be determined using the system proposed by Bond; a simple method for this purpose was derived by Kudo (1982).

(2) *Different sample areas*. A separate problem is to adapt the Bond method for measurement of small spherical crystals, commonly used in structure investigations. A detailed analysis of this problem is given by Hubbard & Mauer (1976), who indicate that the effect of absorption and horizontal divergence has to be taken into account if the sample dimensions are less than the cross section of the primary beam. As has been mentioned above (§§5.3.3.4.1, 5.3.3.4.3.2), these factors, as well as eccentricity and uncertainty of the zero point, could be neglected in Bond's (1960) experiment. Kheiker (1973) considered systematic errors resulting from the latter two factors when small crystals are used. He proposed a fourfold measurement of the sample position (rather than a twofold one used by Bond), in which 'both sides' of a given set of planes are taken into account, so that measurement by the Bond method is performed for two pairs of specimen positions: ω_1 and $\omega_2 = \omega_1 - 2\theta$, and $\omega_3 = 180^\circ + \omega_1$ and $\omega_4 = 180^\circ + \omega_2$. The corresponding positions of the counter are also determined and used in calculations of the Bragg angle (*cf.* §5.3.3.4.1). The mean value of the θ angle is not subject to the errors mentioned. A similar idea has been presented by Mauer *et al.* (1975).

In many practical cases, it is necessary to determine lattice parameters of thin superficial layers. One of the possibilities is to use the Bond method for this purpose. Wołcyrz, Pietraszko & Łukaszewicz (1980) used asymmetric Bragg reflections with small angles of incidence, to reduce the penetration depth of X-rays. This rather simple method permits high accuracy if proper corrections (the formulae are given by the authors) resulting from the dynamical theory of diffraction of X-rays are carefully determined. This method was used to estimate the gradient of the lattice parameter inside diffusion layers. The penetration depth was changed by rotation of the sample. Golovin, Imamov & Kondrashkina (1985) achieved a penetration depth as small as about 1 to 10 nm, using X-ray total-reflection diffraction (TRD) from the planes normal to the surface of the specimen. The sample was oriented in such a way that the conditions for total external reflection were satisfied when the X-ray beam fell on the sample at a small angle of incidence, about 0.5°.

The homogeneity of the crystal in a direction parallel to its surface may be examined by means of local measurements, described by Lisoivan & Dikovskaya (1969) and Lisoivan (1974), in which the goniometer head was specially designed so that the sample could be precisely set and displaced.

(3) *Determination of lattice-parameter changes*. Baker, George, Bellamy & Causer (1968) have shown that a carefully manufactured and adjusted Bond-system diffractometer (mentioned above) with good stability of environmental conditions (temperature, pressure, power voltage) may be a suitable tool for the investigation of lattice-parameter changes. A static method of thermal-expansion measurement is proposed, in which changes in angle of an *in situ* specimen due to changes in the lattice parameter with temperature are quickly determined. If it is assumed that the intensity and the shape of the peak have not altered with the change of conditions (*cf.* the method based on double-crystal diffractometers in §5.3.3.7.1), the change in angle can be determined by intensity measurement alone. The reported precision of the relative measurement is 1 part in 10^7. Since the shape of the profile may change with the change of conditions, the whole profile must be determined accurately and precisely, so that the whole experiment, consisting of a series of measurements, is time-consuming. The optimization problems resulting from this inconvenience have been discussed above (§5.3.3.3.2; Barns, 1972; Urbanowicz, 1981*a*,*b*).

In particular, thermal-expansion studies can detect phase transitions and the resulting changes in crystal symmetry (Kucharczyk, Pietraszko & Łukaszewicz, 1976; Kucharczyk & Niklewski, 1979; Pietraszko, Waśkowska, Olejnik & Łukaszewicz, 1979; Horváth & Kucharczyk, 1981; Pietraszko, Tomaszewski & Łukaszewicz, 1981; Keller, Kucharczyk & Küppers, 1982; Åsbrink, Wołcyrz & Hong, 1985).

Another group of applications of the Bond method is connected with single-crystal characterization problems (homogeneity, doping, stoichiometry) resulting from technological operations (epitaxy, diffusion, ion implantation) producing changes in lattice spacings, $\delta d/d = 10^{-2}$ to 10^{-5}. The examples cited below show a variety of applications.

Stępień, Auleytner & Łukaszewicz (1972) and Stępień-Damm, Kucharczyk, Urbanowicz & Łukaszewicz (1975) examined γ-irradiated $NaClO_3$. The effect of X-ray irradiation on the lattice parameter of TGS crystals in the vicinity of the phase transition was studied by Stępień-Damm, Suski, Meysner, Hilczer & Łukaszewicz (1974). Pihl, Bieber & Schwuttke (1973) dealt with ion-implanted silicon, using a Bond-system diffractometer for local measurements. The effect of silicon doping on the lattice parameters of gallium arsenide was studied by Fewster & Willoughby (1980). Crystal-perfection studies by the Bond method were reported by Grosswig, Melle, Schellenberger & Zahorowski (1983), and Wołcyrz & Łukaszewicz (1982). In the latter paper, the measurements were performed on a superficial single-crystal layer by the use of the geometry described above [paragraph (2)] (Wołcyrz, Pietraszko & Łukaszewicz, 1980). Lattice distortion in LiF single crystals was examined by Dressler, Griebner & Kittner (1987), who used the method of Grosswig *et al.* (1985) [*cf.* paragraph (1)]. The use of anomalous dispersion in studies of microdefects was considered by Holý & Härtwig (1988).

5.3.3.4.3.4. *Advantages and disadvantages of the Bond method*

The significant advantages of the Bond (1960) method, such as:

(*a*) very high accuracy;

(*b*) rather high precision;

(*c*) well elaborated analysis of errors;

(*d*) a simple arrangement, which may be realized on the basis of a standard diffractometer with computer control and, if necessary, supplemented with suitable attachment; and

(*e*) variety of applications;

make this method one of the most popular at present.

The method, however, has the following limitations:

(i) Special requirements concerning the sample are difficult to satisfy in some cases.

(ii) Problems arise with determination of all the lattice parameters of non-cubic crystals. Multiple-sample preparation or a special approach is needed in such cases.

(iii) Lattice-spacing determination from small spherical crystals requires additional corrections or fourfold measurements.

(iv) Displacement of the irradiated area on the sample surface (Wołcyrz, Pietraszko & Łukaszewicz, 1980; Berger, 1984) complicates examination of the real structure (for example, by local measurements).

(v) The method is rather time-consuming, since twofold scanning of the profile is required for determination of a single θ value.

(vi) Because two detectors, or a wide range of rotations of only one detector, are required, measurement with additional attachments is more difficult than on an asymmetric diffractometer.

Nevertheless, the geometry proposed by Bond (1960), owing to its advantages, is commonly used in precise and accurate multiple-crystal spectrometer methods (§§5.3.3.7.1, 5.3.3.7.2).

Other limitations concerning the precision and accuracy of the method are common to it and to all the 'traditional' methods (Subsection 5.3.3.5).

5.3.3.5. *Limitations of traditional methods*

As 'traditional' are considered the methods that depend on a comparison of the lattice spacings to be determined with the wavelength values of characteristic X-radiation that comes directly from laboratory (*Bremsstrahlung*) sources. The *emission lines* are *wide and asymmetric*, which limits both the accuracy and precision of lattice-parameter measurements (as discussed in Subsection 5.3.1.1). One of the limiting factors is the *uncertainty of the wavelength value*. For many years, the wavelength values determined by Bearden (1965, 1967) with an accuracy of 5 parts in 10^6 were widely used. At present, owing to remarkable progress in the measurement technique, it is possible to achieve an accuracy in wavelength of an order better, and nowadays remeasurements of some characteristic emission X-ray wavelengths are reported [*cf.* §5.3.3.3.1(iii) and Subsection 5.3.3.8]. Yet, even after reducing the uncertainty in wavelength, and after introducing all necessary corrections for systematic errors, the highest accuracy of traditional methods does not exceed 1 part in 10^6 (*cf.* Subsection 5.3.3.8).

The accuracy of an order better is possible with X-ray and optical interferometry. This *non-dispersive method (cf.* Subsection 5.3.3.8) is used for accurate lattice-spacing determination of highly perfect standard crystals; the standards are next used for both lattice-parameter determination with a double-beam comparison technique (Baker & Hart, 1975; see also §5.3.3.7.3) and for the accurate wavelength determination mentioned above.

Another problem is the limited precision attainable by traditional methods. As was discussed in Subsection 5.3.1.1, the width of the diffraction profile depends on the spectral distribution of the wavelength, (5.3.1.6), (5.3.1.7), (5.3.1.8), and cannot be less than this owing to the wavelength dispersion. However, much has been done to approach this limit and to attain the precision and accuracy of the diffraction profile location (*cf.* Subsection 5.3.3.3). The highest precision of lattice-parameter determination that it is possible to achieve with traditional methods is about 1 part in 10^7. For some problems connected with single-crystal characterization, such as the effect of irradiation, stress, defect concentration, including local measurement (topography), better precision is required.

From (5.3.1.9), the other possibility of increasing precision, besides choosing optimum parameters for the measurement and improvement of profile-location methods, is to influence the original profile $h_\lambda(\omega)$. This aim can be attained either by applying spectrally narrower X-ray sources or by reducing the width of the original profile by means of arrangements with additional crystals playing the role of monochromator and reference crystal. This second possibility is applied in double- or triple-crystal spectrometry, in multiple-beam methods, or in combined methods. These methods are called '*pseudo-non-dispersive*' methods, since the width of the diffraction profile is considerably limited in them owing to considerable limitation of the width of the original profile. A similar situation to that in *n*-crystal spectrometers, in which the beam reflected from one set of crystal planes is the source of radiation for the second (or the next) diffraction phenomena, arises in multiple-diffraction methods; this is described in Subsection 5.3.3.6.

A systematic and well illustrated review of pseudo-non-dispersive and other differential methods is given by Hart (1981), who is the author of numerous papers on this subject.

5.3.3.6. *Multiple-diffraction methods*

Multiple diffraction occurs when two or more sets of planes simultaneously satisfy the Bragg law for a single wavelength λ. The beam diffracted from one set of planes becomes the incident beam within the crystal for the next diffraction. In the reciprocal-space representation, this means that three or more reciprocal-lattice points lie simultaneously on the Ewald sphere (Fig. 5.3.3.5). These points can be detected by successive rotations of the crystal, as described below. This phenomenon, known also as

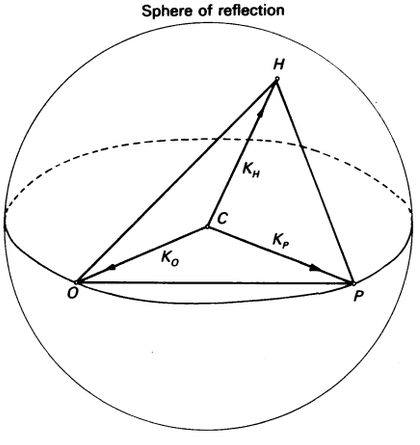

Fig. 5.3.3.5. Schematic representation of multiple diffraction in reciprocal space (after Post, 1975).

simultaneous reflection or (after Renninger, 1937) '*Umwegan-regung*', may be observed in both X-ray and neutron experiments. In the first case, it occurs both in methods with counter recording, initiated by Renninger (1937), and in methods with photographic recording in which a highly divergent beam is used (§5.3.2.4.2). The intersections of conic sections encountered in the methods developed by Kossel (1936) and Lonsdale (1947) are the cases of multiple-diffraction phenomena in photographic methods.

Simultaneous reflection, undesirable in some cases ('forbidden' reflections in measurements of intensities) can be very useful in others. Its various applications have been reviewed by Terminasov & Tuzov (1964) and Chang (1984). Only the utility of multiple diffraction in lattice-parameter determination will be discussed here.

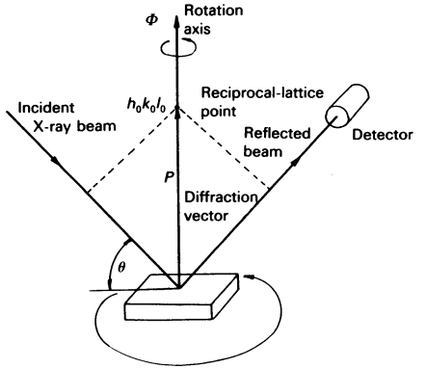

(*a*)

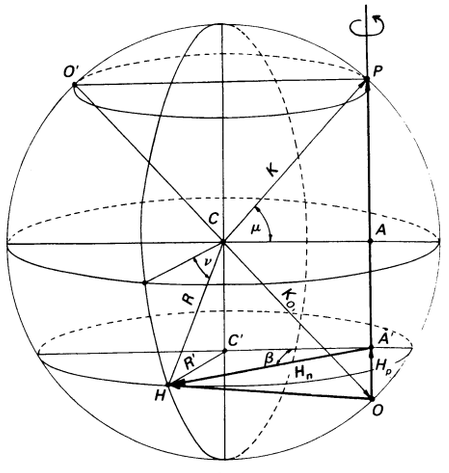

(*b*)

Fig. 5.3.3.6. Schematic representation of the multiple-diffraction method. (*a*) Experimental set-up (after Cole, Chambers & Dunn, 1962; Post, 1975). (*b*) Geometric representation in reciprocal space.

The principle of Renninger's (1937) experiment, which is also the basis of the method described by Post (1975), is shown in Fig. 5.3.3.6. The crystal in the shape of a slab is at first set in a position to diffract the primary X-ray beam. A primary reflection whose intensity is very low or which is forbidden by the space group of the crystal is usually selected. Its intensity determines the background intensity of the pattern, which should be low. The detector, with a wide-open window, is situated in the appropriate position and remains fixed throughout the experiment while the crystal is rotated around the axis perpendicular to the crystal planes (and its surface) to record successive reflections.

The multiple-diffraction pattern (an example is shown in Fig. 5.3.3.7) has next to be indexed. The principle of the method of indexing, known as the reference-vector method (Cole, Chambers & Dunn, 1962; Post, 1975; Chang, 1984), is shown in Fig. 5.3.3.6(*b*). Directions of the primary and diffracted beams are marked by vectors $\mathbf{K}_0$ and $\mathbf{K}$. The ends of the vectors lie on the Ewald sphere, the radius of which is equal to $1/\lambda$. The reciprocal vector $\mathbf{P} = h_0\mathbf{a}^* + k_0\mathbf{b}^* + l_0\mathbf{c}^*$, being the difference between the vectors $\mathbf{K}$ and $\mathbf{K}_0$, represents the first diffraction phenomenon, which is observed for setting angles equal to φ_0 and μ (usually $\mu = \theta$). Let us assume that the reciprocal vector $\mathbf{H} = h\mathbf{a}^* + k\mathbf{b}^* + l\mathbf{c}^*$, observed for setting angles $\varphi_0 + \beta$ and ν, represents the next diffraction. The vector components of $\mathbf{H}$, parallel and normal to $\mathbf{P}$, are denoted by $\mathbf{H}_p$ and $\mathbf{H}_n$, respectively. For a given wavelength, the lengths P, H, H_p, H_n of respective vectors $\mathbf{P}$, $\mathbf{H}$, $\mathbf{H}_p, \mathbf{H}_n$ are functions of lattice parameters and diffraction indices.

The task is to find the relationship between the difference β of angles of rotation (or between two values of the setting angles, β and ν) and the lengths of the reciprocal vectors. The following relations result from Fig. 5.3.3.6(*b*):

$$\cos\beta = \frac{(C'A')^2 + H_n^2 - R'^2}{2H_n(C'A')},$$
$$(C'A')^2 = R^2 - P^2/4,$$
$$H_p = P/2 - R\sin\nu,$$
$$R' = R\cos\nu.$$

Taking these into consideration, and remembering that $H^2 = H_p^2 + H_n^2$, we finally obtain

$$\cos\beta = \frac{H^2 - H_pP}{2H_n(R^2 - P^2/4)^{1/2}}. \qquad (5.3.3.34)$$

Since $\cos(-\beta) = \cos\beta$, the appearance of successive reflections does not depend on the direction of rotation. A detailed discussion of (5.3.3.34) is given by Cole, Chambers & Dunn (1962) and Chang (1984). When preliminary values of the lattice parameters are known, (5.3.3.34) can be applied for indexing multiple-diffraction patterns. A computer program (Rossmanith, 1985) can be very useful in rather complicated calculations and in the graphical representation of the multiple-diffraction

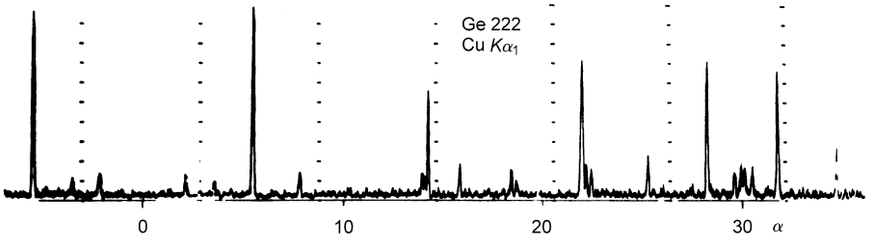

Fig. 5.3.3.7. The multiple-diffraction pattern at the 222 position in germanium (Cole, Chambers & Dunn, 1962).

pattern. Formula (5.3.3.34), since $C'A' = R\cos\mu$, can be presented in another form:

$$R = \frac{H^2 - H_p P}{2H_n \cos\mu\cos\beta}, \qquad (5.3.3.35)$$

where two setting angles, μ and β, are taken into account. When the indices are known, both (5.3.3.34) and (5.3.3.35) can be used for the determination or refinement of lattice parameters.

Another analytical method for indexing multiple-diffraction patterns, based on the determination of the Lorentz point, has been described by Kshevetsky, Mikhailyuk, Ostapovich, Polyak, Remenyuk & Fomin (1979).

Formulae (5.3.3.34) and (5.3.3.35) are valid for all crystal systems. In practice, however, the rather complicated method is used mainly for cubic crystals, and a special approach proved to be needed in order to adapt the method to other (rectangular) systems (Kshevetsky, Mikhalchenko, Stetsko & Shelud'ko, 1985). In the case of a cubic lattice, it is convenient to substitute

$$R = a/\lambda \qquad (5.3.3.35a)$$

into (5.3.3.34) and (5.3.3.35) rather than $R = 1/\lambda$ used in the general case, so that the lengths of the reciprocal vectors, being now functions of the indices only, are:

$$P = (h_0^2 + k_0^2 + l_0^2)^{1/2}, \qquad (5.3.3.35b)$$

$$H = (h^2 + k^2 + l^2)^{1/2}, \qquad (5.3.3.35c)$$

$$H_p P = \mathbf{HP} = h_0 h + k_0 k + l_0 l. \qquad (5.3.3.35d)$$

The lengths of the components of $\mathbf{H}$ can be determined from (5.3.3.35*b*,*c*,*d*) taking $H_p = H_p P/P$ and $H_n = (H^2 - H_p^2)^{1/2}$. After introducing the alterations [equation (5.3.3.35*a*) and the resulting equations (5.3.3.35*b*,*c*,*d*)], (5.3.3.35) now describes a simple dependence between the ratio a/λ, the indices, and the setting angles.

The accuracy of the lattice-parameter determination resulting from (5.3.3.35) in the cubic case can be assumed to be:

$$\frac{\Delta a}{a} = \tan\mu\,\Delta\mu + \tan\beta\,\Delta\beta; \qquad (5.3.3.36)$$

this thus depends on the values of the setting angles β, μ and their accuracies $\Delta\beta$, $\Delta\mu$. The latter depend on various systematic errors.

Since the differences between the two angular settings at which a given set of planes diffracts are measured rather than their absolute values, the systematic errors due to absorption, specimen displacement, and zero-setting are eliminated. In contrast, errors due to vertical divergence, refraction and the change of wavelength of the incident radiation (when it enters the crystal), alignment, and dynamical effects should be taken into account. In the case described by Post (1975), when a fine focus (effective size 0.4×0.5 mm) and collimation limiting the beam divergence to $2'$ were used, the vertical divergence causing the relative error in d of about 5×10^{-8} could be ignored.

The errors due to the real structure (inhomogeneity, mosaicity and internal stress) were discussed by Kshevetsky *et al.* (1979).

The accuracy possible by this method (from 1 to 4 parts in 10^6) is comparable with that obtained with the Bond (1960) method. The advantages of this method from the point of view of lattice-parameter determination are as follows:

(*a*) a large number of reflections can be measured without realigning or removing the crystal;

(*b*) all the lattice parameters can be determined and not only one, as in the Bond (1960) method;

(*c*) the narrow diffraction profiles can be located with very high accuracy and precision;

(*d*) the arrangement makes it possible to remove some systematic errors;

(*e*) the high accuracy resulting from (*a*)–(*d*), which is comparable with that obtained by means of the Bond (1960) method;

(*f*) the high precision that results from (*a*) and (*c*).

A disadvantage, on the other hand, is the complicated interpretation (indexing) of multiple-diffraction patterns, so that this method is less popular than the Bond (1960) method.

The Post (1975) method has been applied to the accurate lattice-parameter determination of germanium, silicon, and diamond single crystals (Hom, Kiszenick & Post, 1975).

5.3.3.7. *Multiple-crystal – pseudo-non-dispersive techniques*

5.3.3.7.1. *Double-crystal spectrometers*

Detailed information concerning the double-crystal spectrometer, which consists of two crystals successively diffracting the X-rays, can be found in James (1967, pp. 306–318), Compton & Allison (1935), and Azároff (1974). This device, usually used for wavelength determination, may also be applied to lattice-parameter determination, if the wavelength is accurately known. The principle of the device is shown in Fig. 5.3.3.8. The first crystal, the monochromator, diffracts the primary beam in the direction defined by the Bragg law for a given set of planes, so that the resulting beam is narrow and parallel. It can thus be considered to be both a collimator (or an additional collimator, if the primary beam has already been collimated) and a wavelength filter. The final profile $h(\theta)$, obtained as a result of the second diffraction by the specimen when the first crystal remains stationary and the second is rotated, is narrower than that which would be obtained with only one crystal. The final crystal profile $h_C(\theta)$ [*cf.* equation (5.3.1.6)] is due to both crystals, which, if it is assumed that they are cut from the same block, can be described by the autocorrelation function (Hart, 1981):

$$h_C(\theta) = K \int_{-\infty}^{\infty} R(\theta')R(\theta' - \theta)\,\mathrm{d}\theta', \qquad (5.3.3.37)$$

where $R(\theta)$ is an individual reflectivity function of one crystal and K is a coefficient of proportionality. Its half-width is 1.4 times larger than that related to only one crystal. In spite of this, the recorded profile can be as narrow as, for example, $2.6''$ (Godwod, Kowalczyk & Szmid, 1974), since the profile due to the wavelength $h_\lambda(\theta)$, modified by the first crystal, is extremely narrow. Additional advantages of the diffraction profile are: its symmetry, because $h_C(\theta)$ is symmetric as an effect of autocorreletion, and smoothness, as an effect of additional integration. The profile can thus be located with very high accuracy and precision.

When there is a small difference in the two lattice spacings, so that one has a value d and the other $d + \delta d$, if $\delta\lambda/\lambda$ is small enough, it can be assumed that the profile does not alter in shape but in its peak position [*cf.* §5.3.3.4.3.3, paragraph (3)]. If for two identical crystals this were located at θ_0, the peak position

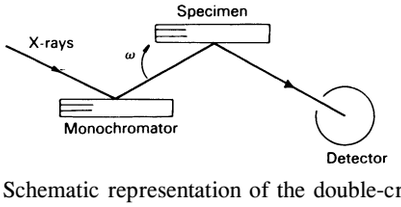

Fig. 5.3.3.8. Schematic representation of the double-crystal spectrometer.

shifts to $\theta_0 - \tan\theta\delta d/d$. The measurement of this shift rather than the absolute position of the rocking curve is the basis of all the double-crystal methods. An example of the application of a double-crystal spectrometer with photographic recording has been given in §5.3.2.3.5 (Bearden & Henins, 1965).

The basic requirements that should be fulfilled to make the most of the double-crystal spectrometer are: limitation of the primary beam by means of a collimator, parallelism of the two axes [precision as high as 1″ obtained by Godwod, Kowalczyk & Szmid (1974)], and high thermal stability (0.1 K; Godwod, Kowalczyk & Szmid, 1974). Alignment procedure, errors, and corrections valid for the double-crystal spectrometer have been considered by Bearden & Thomsen (1971).

The double-crystal diffractometer, because of the small width of the diffraction profile, is a very suitable tool for local measurements of lattice-parameter differences, for example between an epitaxic layer and its substrate. Hart & Lloyd (1975) carried out such a measurement on a standard single-axis diffractometer (APEX) to which a simple second axis, goniometer head, and detector were added (Fig. 5.3.3.9). The diffracted beam was recorded simultaneously by three detectors. A *symmetric arrangement* with two detectors, D_1 and D_2, with no layer present, makes possible the determination of the absolute value of the lattice parameter of the substrate, as in the Bond (1960) method. The third detector makes it possible to record the double-crystal rocking curve, which usually fully resolves the layer and substrate profiles. The changes in the lattice parameter between the two components can be used for determination of strain (at 1 part in 10^4).

The very important advantage of this method, from the point of view of local measurements, is that single- or double-crystal diffraction can be selected, simultaneously if needed, on exactly the same specimen area. Other examples of strain measurements by means of a double-crystal spectrometer are given by Takano & Maki (1972), who measured lattice strain due to oxygen diffusing into a silicon single crystal; by Fukahara & Takano (1977), who compared experimental rocking curves and theoretical ones computed within the frame of the dynamical theory; and Barla, Herino, Bomchil & Pfister (1984), who examined the elastic properties of silicon.

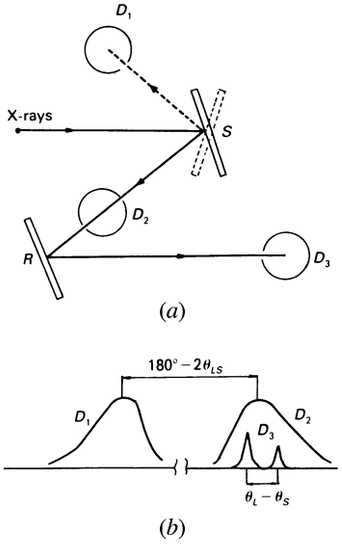

Fig. 5.3.3.9. Schematic representation of the double-crystal arrangement of Hart & Lloyd (1975) for the examination of epitaxic layers. (*a*) Experimental set-up. (*b*) Diffraction profiles recorded by detectors D_1, D_2, and D_3.

The standard double-crystal technique does not allow determination of relatively small strains, *i.e.* ones that affect the lattice parameter by, for example, less than 2–3 parts in 10^5, as in the case of (004) Si reflection and Cu $K\alpha$ radiation. To overcome this difficulty, Zolotoyabko, Sander, Komem & Kantor (1993) propose a new method that combines double-crystal X-ray diffraction with *high-frequency ultrasonic excitation*. Since ultrasound has a wavelength a little less than the X-ray excitation length, it affects the diffraction profile close to the Bragg position and so permits the detection of very small profile broadenings caused by lattice distortions. With this method, lattice distortion as small as 5 parts in 10^6 can be measured.

As has been shown in the case of the device used by Hart & Lloyd (1975), the symmetric arrangement due to Bond (1960) proves to be very useful when the double-crystal spectrometer is to be used for absolute lattice-parameter determination, since such an arrangement combines the high precision and sensitivity of a double-crystal spectrometer with the high absolute accuracy of the Bond method. Other examples of a similar idea are presented by Kurbatov, Zubenko & Umansky (1972), who report measurements of the thermal expansion of silicon; Godwod, Kowalczyk & Szmid (1974), who also discuss the theoretical basis of their arrangement; Ridou, Rousseau & Freund (1977), who examine a phase transition; Sasvári & Zsoldos (1980), and Fewster (1982). The latter two papers are concerned with epitaxic layers. A rapid method is proposed by Sasvári & Zsoldos (1980) for deconvoluting the overlapping peaks due to the layer and the substrate. A particular feature of the arrangement proposed in the first of these papers (Kurbatov, Zubenko & Umansky, 1972) is the use of a germanium-crystal monochromator with anomalous transmission, to obtain a nearly parallel primary beam (the horizontal divergence is 28″ and the vertical 14″).

The error analyses given by Godwod, Kowalczyk & Szmid (1974) and Sasvári & Zsoldos (1980) show that systematic errors due to eccentricity, absorption, and zero position are eliminated experimentally, owing to the symmetric arrangement, as in the Bond (1960) method. In contrast, the errors due to crystal tilt, refraction and the Lorentz–polarization factor [their uncertainties in lattice parameters, as evaluated by Sasvári & Zsoldos (1980), are 10^{-6} Å each], axial divergence (2×10^{-6} Å), angle reading (10^{-4} Å), and instrument correction and calculations (each to 5×10^{-5} Å) should be taken into account. The effect of absorption, discussed by Kurbatov, Zubenko & Umansky (1972), proved to be negligible. The final accuracy achieved for silicon single crystals by Godwod, Kowalczyk & Szmid (1974) is comparable with that obtained by Bond (1960).

A specific group of double-crystal arrangements is formed by those in which *white X-radiation* is used instead of characteristic. Such an arrangement makes possible very large values of the Bragg angle (larger than about 80°), which increases the accuracy, precision, and sensitivity of measurement of the lattice parameters and their change with change of temperature. This task is rather difficult to realize by means of

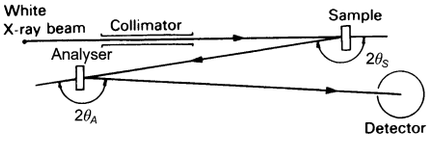

Fig. 5.3.3.10. Schematic representation of the double-crystal arrangement of Okazaki & Kawaminami (1973*a*); white incident X-rays are used.

traditional methods, in which both the wavelengths and the lattice parameters are fixed, and it is difficult to find a suitable combination of their values.

The principle of the method presented by Okazaki & Kawaminami (1973*a*) is shown in Fig. 5.3.3.10. The first crystal (the specimen to be measured) remains fixed during a single measurement, the second (the analyser) is mounted on the goniometer of an X-ray diffractometer and can be operated with either an ω or a θ–2θ scan. As diffraction phenomena appear for both the specimen and the analyser (in general of different materials) whose interplanar spacings are equal to d_s and d_A, respectively, the following relation results from Bragg's law:

$$d_s \sin\theta_s = d_A \sin\theta_A, \tag{5.3.3.38}$$

where θ_s and θ_A are the respective Bragg angles. Since d_A and θ_s are kept constant, a change in d_s as a function of temperature is determined from a change in θ_A. The relative error $\delta d/d$ resulting from (5.3.3.38) with $\theta_A \approx 90^\circ$ is

$$\frac{\delta d_s}{d_s} = \cot\theta_A \delta\theta_A = \tan(\pi/2 - \theta_A)\delta\theta_A \approx (\pi/2 - \theta_A)\delta\theta_A. \tag{5.3.3.39}$$

The method initiated by Okazaki & Kawaminami (1973*a*) has been developed by Okazaki & Ohama (1979), who constructed the special diffractometer HADOX (the positions of the specimen and the analyser were interchanged) and discussed systematic errors. Precision as high as 1 part in 10^7 was reported. Examples of the application of such an arrangement for measuring the temperature dependence of lattice parameters were given by Okazaki & Kawaminami (1973*b*) and Ohama, Sakashita & Okazaki (1979). Various versions of the HADOX diffractometer are still reported. By introducing two slits (Soejima, Tomonoga, Onitsuka & Okazaki, 1991) – one to limit the area of the specimen surface to be examined and the other to define the resolution of 2θ – it is possible to combine ω and 2θ scans and obtain a two-dimensional intensity distribution in the plane parallel to the plane of the diffractometer, and to determine the temperature dependence of lattice parameters on a selected area of the specimen (avoiding the effects of the surroundings). The HADOX diffractometer may work with both a rotating-anode high-power X-ray source (examples reported above) and a sealed-tube X-ray source. In the latter case (Irie, Koshiji & Okazaki, 1989), to increase the efficiency of the X-ray tube, the distance between the X-ray source and the first crystal has been shortened by a factor of five. As is implied by (5.3.3.39), one can increase the relative precision of the method by using the analyser angle close to $\pi/2$. This idea has been realized by Okazaki & Soejima (2001), who achieved the relative accuracy of determination of lattice-parameter changes as high as 1 part in 10^9–10^{10} by extending the Bragg angle from 78° (previous versions) to 89.99° and by elimination of systematic errors due to crystal tilt, crystal displacement, temperature effects and radiation damage.

An original method for the measurement of lateral lattice-parameter variation by means of a double-crystal arrangement with an oscillating slit was proposed by Korytár (1984). This method permitted simultaneous recording of two rocking curves from two locations on a crystal. Precision of 3 parts in 10^7 was reported. The method has been applied for the measurement of growth striations in silicon.

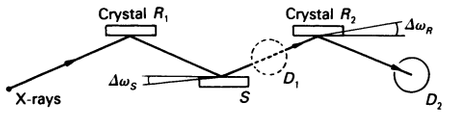

Fig. 5.3.3.11. Schematic representation of the triple-crystal spectrometer developed by Buschert (1965) (after Hart, 1981).

The main disadvantage of double-crystal spectrometers, in their basic form (Fig. 5.3.3.8), is that they cannot be used for measurements on an absolute scale. Combination of the double-crystal arrangement with the system proposed by Bond (1960) makes it possible to recover the origin of the angular scale and thus such an absolute measurement, but the reported precision is rather moderate.

There are two other ways to overcome this difficulty in pseudo-non-dispersive methods: addition either of a third crystal (more accurately, a third reflection) (§5.3.3.7.2) or of a second source (a second beam) (§5.3.3.7.3). Such arrangements require additional detectors. Combinations of both techniques are also available (§5.3.3.7.4).

5.3.3.7.2. *Triple-crystal spectrometers*

Higher precision than that obtained with the double-crystal arrangements (§5.3.3.7.1) can be achieved by means of triple-crystal diffractometers. Arrangements specially designed for the determination of lattice-parameter changes are described by Buschert (1965) and Skupov & Uspeckaya (1975), and reviewed by Hart (1981).

The principle of the triple-axis spectrometer is shown in Fig. 5.3.3.11. The arrangement consists of one standard crystal S, ultimately replaced by the sample under investigation, and two reference crystals R_1 and R_2. The principle of the measurement is as follows. First, the crystals S, R_1, and R_2 are set to their diffraction (peak) positions using two detectors D_1 and D_2. Then the standard crystal S is replaced by the sample and the new peak position is found by means of D_1 when the sample is turned from its original position to its reflecting position. The angle of rotation of the sample $\Delta\omega_s$ depends on the lattice-parameter difference Δd between the sample and the standard. The relation is given by (Hart, 1981)

$$\Delta\omega_s = -\tan\theta \Delta d/d. \tag{5.3.3.40}$$

Next, the second reference crystal R_2 is turned through the angle $\Delta\omega_R$ to its diffracting position, the intensity being controlled with the second detector D_2. From the geometry of the arrangement,

$$\Delta\omega_R = 2\Delta\omega_s. \tag{5.3.3.41}$$

Because the origin of the ω_s scale is lost during the crystal exchange, this second angle of rotation ($\Delta\omega_R$) is used to determine Δd rather than the first one ($\Delta\omega_s$), by using (5.3.3.41) and (5.3.3.40).

The diffraction profiles observed in the second detector, described by Hart (1981),

$$h(\theta)_R = \int_{-\infty}^{\infty} R^2(\theta') R(\theta' - \theta)\, \mathrm{d}\theta, \tag{5.3.3.42}$$

are not symmetric but can be as narrow as 0.1–1″, so that a precision of 2 parts in 10^8 is possible.

The main experimental problem here is to adjust the tilts of the crystals. The errors resulting both from the crystal tilts and from the vertical divergence were discussed by Skupov & Uspeckaya (1975).

Triple-crystal spectrometers are often applied as lattice-spacing comparators, when very small changes of lattice parameters ($10^{-8} \leq |\Delta d|/d \leq 10^{-6}$) are to be detected, in

particular for the examination of a correlation between lattice parameter and the dopant or impurity concentration (Baker, Tucker, Moyer & Buschert, 1968). Such an arrangement can also be a very suitable tool in deformation studies, since it allows the separation of the effect of deformation on the Bragg angle from that due to lattice-parameter change (Skupov & Uspeckaya, 1975).

The basis of the accurate lattice-parameter comparison proposed by Bowen & Tanner (1995) is the use of a high-purity silicon standard (*cf.* §5.3.3.9 below) with a well known lattice parameter. To compensate an error that may result from a slight misalignment of crystal planes in relation to the axes of the instrument, the authors recommend a twofold measurement of the diffraction-peak position of the reference crystal (for a given diffraction position and after rotating the specimen holder through 180° about the axis normal to its surface) and a similar twofold measurement of the diffraction-peak position of the sample – after replacing the reference crystal by the sample. The mean positions of the reference crystal and of the sample are used in calculations of the Bragg-angle difference and then of the unknown interplanar spacing. The method uses a standard double-crystal diffractometer fitted with a monochromator (therefore, a third crystal), which provides a well defined wavelength, and with a specimen rotation stage. The measurement is accompanied by a detailed error analysis. The accuracy of absolute lattice-parameter determination as high as a few tens of parts in 10^6, and a much greater relative sensitivity are reported.

By combining a triple-axis spectrometer with the Bond (1960) method, the device can be used for absolute measurements (Pick, Bickmann, Pofahl, Zwoll & Wenzl, 1977). The device described in the latter paper is an automatic triple-crystal diffractometer that permits intensity measurement to be made in any direction in reciprocal space in the diffraction plane with step sizes down to $0.01''$ and therefore can be used for very precise measurements [see also §5.3.3.4.3.2, paragraph (5)].

5.3.3.7.3. *Multiple-beam methods*

The other possibility of recovering the crystal-angle scale in differential measurements with a double-crystal spectrometer (*cf.* §§5.3.3.7.1, 5.3.3.7.2) is to obtain reflections from two crystal planes [for example, from (hkl) and $(\bar{h}\bar{k}\bar{l})$ planes] by means of a double-beam arrangement and to measure them simultaneously.

The second X-ray beam may come from an additional X-ray source (Hart, 1969) or may be formed from a single X-ray source by using a beam-splitting crystal (Hart, 1969, second method; Larson, 1974; Cembali, Fabri, Servidori, Zani, Basile, Cavagnero, Bergamin & Zosi, 1992). In particular, two beams with different wavelengths ($K\alpha_1, K\beta_1$) separated with a slit system can be used for this purpose (Kishino, 1973, second technique). The principle of the double-beam method is shown in Fig. 5.3.3.12. The beams are directed at the first crystal (the reference crystal) so that the Bragg condition is simultaneously fulfilled for both beams, and they then diffract from the second crystal (the specimen). As the second crystal is rotated, a double-crystal diffraction profile is recorded first in one detector and then in the other. The angle $\Delta\theta$ of crystal rotation between the two rocking curves is given by (Baker & Hart, 1975):

$$\Delta\theta = (\theta_1 - \theta_2) = \tan\theta\,\Delta d/d. \qquad (5.3.3.43)$$

This formula leads to the lattice-parameter changes Δd.

A double-beam diffractometer can be used for the examination of variations in lattice parameters of about 10 parts in 10^6 within a sample in a given direction. An example was reported by Baker, Hart, Halliwell & Heckingbottom (1976), who used Larson's (1974) arrangement for this task.

The highest reported sensitivity (1 part in 10^9) can be achieved in the double-source double-crystal X-ray spectrometer proposed by Buschert, Meyer, Stuckey Kauffman & Gotwals (1983). The device can be used for the investigation of small concentrations of dopants and defects.

The method can also be applied for the absolute determination of a lattice parameter, if that of the reference crystal is accurately known and the difference between the two parameters is sufficiently small. Baker & Hart (1975), using multiple-beam X-ray diffractometry (Hart, 1969, first technique), determined the d spacing of the 800 reflection in germanium by comparing it with the d spacing of the 355 reflection in silicon. The latter had been previously determined by optical and X-ray interferometry (Deslattes & Henins, 1973; the method is presented in Subsection 5.3.3.8).

In the case of two different wavelengths and diffraction from two different diffraction planes $(h_1k_1l_1)$ and $(h_2k_2l_2)$, the lattice parameter a_0 of a cubic crystal can be determined using the formula (Kishino, 1973)

$$a_0 = \tfrac{1}{2}\{(L\lambda_1)^2 + [(M\lambda_2 - L\lambda_1\cos\theta_{1-2})/\sin\theta_{1-2}]^2\}^{1/2}, \qquad (5.3.3.44)$$

where $L = (h_1^2 + k_1^2 + l_1^2)^{1/2}$, $M = (h_2^2 + k_2^2 + l_2^2)^{1/2}$, and θ_{1-2} is the difference between the two Bragg angles for the specimen crystal, estimated from the measurement of $\Delta\theta = |\theta_{1-2} - \theta'_{1-2}|$ if the difference θ'_{1-2} for the first (reference crystal) is known beforehand. The idea of Kishino was modified by Fukumori, Futagami & Matsunaga (1982) and Fukumori & Futagami (1988), who used the Cu $K\alpha$ doublet instead of $K\alpha_1$ and $K\beta_1$ radiation. Owing to the change, they could use only one detector (Kishino's original method needs two detectors), but a special approach is sometimes needed to resolve two peaks that relate to the components of the doublet. A similar problem of separation of two peaks (recorded by two detectors) is reported by Cembali *et al.* (1992). By introducing a computer simulation of the reflecting curves (using a convolution model), the authors managed to determine the separation with an error of $0.01''$ and to achieve a precision of some parts in 10^7. The same precision is reported by Fukumori, Imai, Hasegawa & Akashi (1997), who introduced a precise positioning device and a position-sensitive proportional counter to their instrument.

As in the other multiple-crystal methods, the most important experimental problem is accurate crystal setting. Larson (1974), as a result of detailed analysis, gave the dependence between the angular separation of two peaks and angles characterizing misalignment of the first and second crystals.

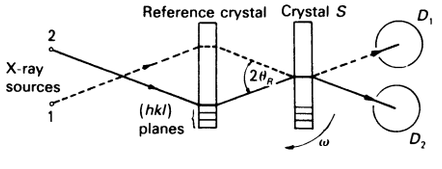

Fig. 5.3.3.12. Schematic representation of the double-beam comparator of Hart (1969).

5.3.3.7.4. *Combined methods*

The idea of multiple-beam measurement (§5.3.3.7.3) can be applied to other arrangements that combine the features of the double-beam comparator with those of the triple-crystal spectrometer; there are additional advantages in such a system.

The application of the double-beam technique makes it possible to realize a triple-reflection scheme for comparing lattice parameters on the basis of a double-axis spectrometer. The arrangement proposed by Ando, Bailey & Hart (1978), shown in Fig. 5.3.3.13, consists of a sample and a reference crystal, which are made from the same material but differ in purity (or strain, stoichiometry, vacancy concentration, *etc*). The angular difference $\Delta\theta$ in the Bragg angles of the sample and the reference crystal, θ_S and θ_R, respectively,

$$\Delta\theta = \theta_S - \theta_R, \qquad (5.3.3.45a)$$

is measured as the sample angle $\Delta\omega$ between the double-reflected peak D and the triply diffracted peak T:

$$\Delta\theta = \Delta\omega, \qquad (5.3.3.45b)$$

$$\Delta\omega = \omega_D - \omega_T. \qquad (5.3.3.45c)$$

Assuming that $\Delta\theta$ is entirely due to changes Δd in atomic spacings, the authors use the following relation for determination of the latter:

$$\Delta d/d = -\cot\theta\Delta\theta. \qquad (5.3.3.46)$$

The experimental requirements are simple and inexpensive, owing to simple shapes of both the reference crystal and the sample crystal, so that the measurement can be made quickly. By combining the two reference crystals into a single monolithic reference crystal, excellent stability, difficult to achieve with triple-axis arrangements (*cf.* §5.3.3.7.2), is obtained at the same time. The disadvantage of the method is that it covers a smaller range of lattice parameters than the other double-beam methods (Hart, 1969; Larson, 1974) described in §5.3.3.7.3. A new version of the double-crystal triple-reflection scheme (Häusermann & Hart, 1990) allows one to achieve a precision of 1 part in 10^8 in 2 min of measurement time, which includes the data analysis; 30 min are needed to change the sample. Errors due to the crystal tilt and thermal drifts are considered.

Another example of the triple-reflection scheme realized by means of the double-beam technique has been presented by Kovalchuk, Kovev & Pinsker (1975), who realized the triple-crystal arrangement on the basis of a double-crystal spectrometer by parallel mounting of the two crystals to be compared (the sample and the reference crystal) on one common axis. The advantage of this system is that Bragg angles as high as 80° are available. The device can be applied in studies of the real structure of a single crystal.

High-sensitivity ($\Delta d/d$ up to $\pm 3 \times 10^{-8}$) lattice-parameter-comparison measurement over a wide range of temperatures can be performed by means of the triple-crystal (more accurately, triple-axis) X-ray spectrometer realized by Buschert, Pace, Inzaghi & Merlini (1980). The arrangement (Fig. 5.3.3.14) consists of four crystals. The first is used for obtaining a very wide but extremely parallel exit beam, which is incident on both the standard crystal S and an unknown crystal X, placed side by side on a common axis in the cryostat. The reflected beams from S and X are recorded by partially transmitting detectors DA_2 and DB_2, so that the beams reflect from the third crystal and are detected by the counters DA_3 and DB_3. There is a small, sensitive, angle adjustment to rotate the crystal X with respect to the standard S and it is used to bring the peaks of S and X into approximate coincidence. The angular difference in the peak positions on the third axis is used for determination of lattice-parameter changes from (5.3.3.46), so that

$$\Delta\theta = \Delta\theta_3/2 - \Delta\theta_2, \qquad (5.3.3.47)$$

where $\Delta\theta_2$ and $\Delta\theta_3$ are the differences in peak positions at axes (2) and (3), respectively. The device was used, for example, to study the effect of isotope concentration on the lattice parameter of germanium perfect crystals (Buschert, Merlini, Pace, Rodriguez & Grimsditch, 1988). The measured differences in the lattice parameter, of the order of 1 part in 10^5, were compared with those evaluated theoretically, and a very good agreement was obtained.

Another variant of a multiple-beam arrangement, based on a triple-crystal spectrometer, was proposed by Kubena & Holý (1988). The authors compared the distances of lattice planes in a direction perpendicular to the surface of the sample while studying the growth striations. One well collimated and monochromated beam coming from the first crystal was directed into the sample, and then two beams – one transmitted and one diffracted in the sample – diffracted in the reference crystal. Intensities of the diffracted beams were measured by two detectors. The difference of lattice spacings of the sample and the reference crystal was determined from the difference in positions of respective peaks. The accuracy of the lattice-spacing comparison of 2 parts in 10^7 and the precision of 1 part in 10^7 were obtained.

A four-crystal six-reflection diffractometer (Fewster, 1989) was built to study crystals distorted by epitaxy and defects in nearly perfect crystals. Fig. 5.3.3.15 is a schematic diagram of this device. The two-crystal four-reflection Bartels monochromator (Bartels, 1983) defines a narrow reflectivity profile. The analyser selects the angular range diffracted from the sample. The device may be used for recording both near-perfect rocking curves from distorted crystals (when rotations of the sample and the analyser are coupled) and a diffraction-space map for studying the diffuse scattering (when the two rotations are

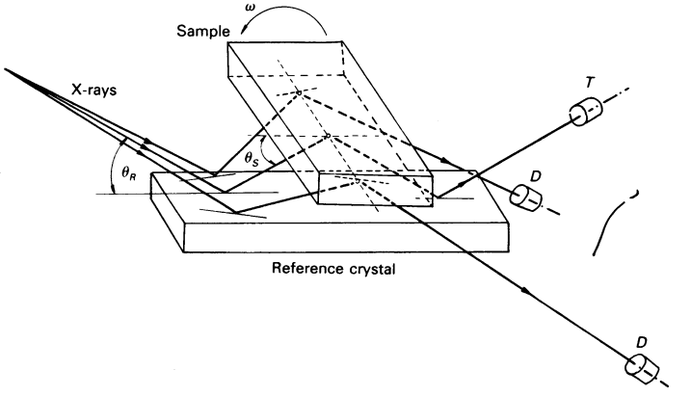

Fig. 5.3.3.13. The double-axis lattice-spacing comparator of Ando, Bailey & Hart (1978); a triple-diffracted beam is used.

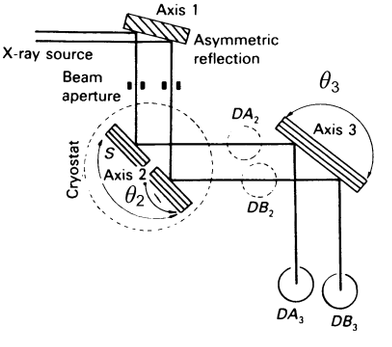

Fig. 5.3.3.14. Schematic representation of the double-beam triple-crystal spectrometer of Buschert *et al.* (1980).

uncoupled). Various applications of such high-sensitivity multiple-crystal X-ray spectrometers for reciprocal-space mapping and imaging (topography), which are outside the scope of the present paper, are reviewed by Fewster (1993, and references therein).

As was shown a few years later by Fewster & Andrew (1995), the device can also be used for absolute lattice-parameter measurements of single-crystal and polycrystalline materials with a relative accuracy of a few parts in 10^6. The authors checked the angular resolution and the sample centring of their instrument, and discussed systematic errors due to refraction, the Lorenz and polarization factor, the diffracting-plane tilt and the peak-position determination.

5.3.3.8. *Optical and X-ray interferometry – a non-dispersive technique*

The accuracy of an absolute measurement can be improved, in relation to that obtained in traditional methods (*cf.* Subsection 5.3.3.5), either if the wavelength of the radiation used in an experiment is known with better accuracy [*cf.* equation (5.3.1.3)] or if a high-quality standard single crystal is given, whose lattice spacing has been very accurately determined (Baker & Hart, 1975; mentioned in §5.3.3.7.3). The two tasks, *i.e.* very accurate determination of both lattice spacings and wavelengths in metric units, can be realized by use of combined optical and X-ray interferometry. This original concept of absolute-lattice-spacing determination directly in units of a standard light wavelength has been proposed and realized by Deslattes (1969) and Deslattes & Henins (1973).

The principle of the method is presented in Fig. 5.3.3.16. The silicon-crystal X-ray interferometer is a symmetric Laue-case type (Bonse & te Kaat, 1968). The parallel translation device consists of the stationary assembly (*a*) formed by two specially prepared crystals, and a moveable one (*b*), to which belongs the third crystal. One of the two mirrors of a high-resolution Fabry–Perot interferometer is attached to the stationary assembly and the second to the moving assembly. A stabilized He–Ne laser is used as a source of radiation, the wavelength of which has been established relative to visible standards. The first two crystals produce a standing wavefield, which is intercepted by the third crystal, so that displacement of the third crystal parallel to the diffraction vector (as suggested by the large arrow) produces alternate maxima and minima in the diffracted beams, detected by X-ray detector (*c*). Resonant transmission maxima of the optical interferometer are detected simultaneously by the photomultiplier indicated at (*d*). Analysis of the fringes (shown in Fig. 5.3.3.17) is the basis for the calculation of the lattice-spacing-to-optical-wavelength ratio (d/λ), which is given by

$$\frac{2d}{\lambda} = \frac{n}{m}\,\frac{\cos\alpha}{\cos\beta}, \qquad (5.3.3.48)$$

where n and m are the numbers of optical and X-ray diffraction fringes, respectively, and α and β are the measured angular deviations of the optical and X-ray diffraction vectors from the direction of motion. The measurements are carried out in two steps. First, the lattice parameter of silicon along the [110] crystallographic direction was measured in the metric system, independently of the X-ray wavelength used in the experiment. As the next step, a specimen of known lattice spacing, treated as a reference crystal, was used for the accurate wavelength determination of Cu $K\alpha_1$ and Mo $K\alpha_1$. Accuracy better than 1 part in 10^6 was reported (see Section 4.2.2).

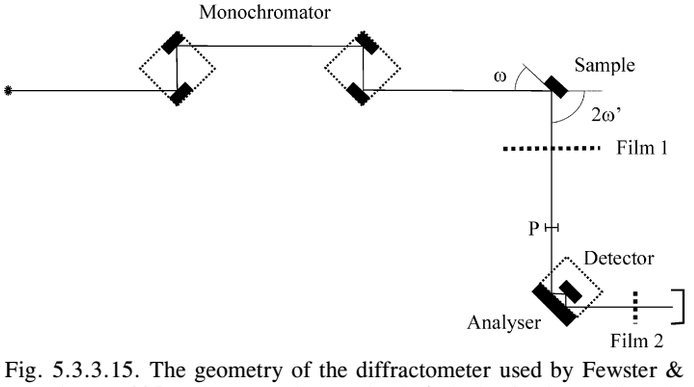

Fig. 5.3.3.15. The geometry of the diffractometer used by Fewster & Andrew (1995). The scattering angle, $2\omega'$, is the fundamental angle for determination of the interplanar spacing and P is the analyser-groove entrance.

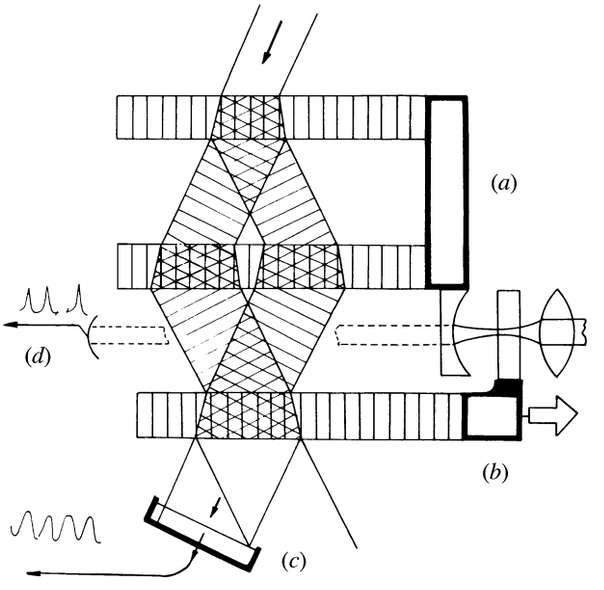

Fig. 5.3.3.16. Optical and X-ray interferometry. Schematic representation of the experimental set-up (after Deslattes & Henins, 1973; Becker *et al.*, 1981).

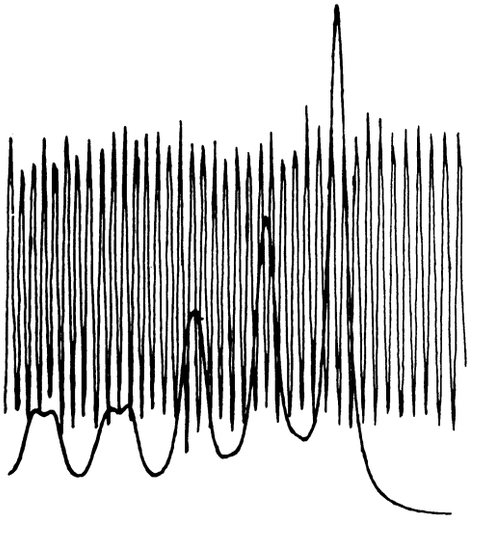

Fig. 5.3.3.17. Portion of a dual-channel recording of X-ray and optical fringes (Deslattes, 1969).

The above experiment was a turning point in accurate measurements of both wavelengths and lattice parameters. Owing to the idea of Deslattes & Henins, it became possible to determine the wavelength in nanometres rather than in troublesome XU or Å* units (*cf.* §4.2.1.1.1). However, the results obtained and the method itself needed verification and some adjustments. These were performed by another group of experimenters with a similar but different measuring device (Becker, Seyfried & Siegert, 1982, and references therein; Siegert, Becker & Seyfried, 1984).

5.3.3.9. *Lattice-parameter and wavelength standards*

An extended series of measurements performed by means of the optical and X-ray interferometry (*cf.* §5.3.3.8) led, among other things, to evaluation of the lattice spacing of a highly perfect silicon sample WASO 4.2.A (Becker *et al.*, 1981). Such silicon samples may be used as reference crystals in successive lattice-spacing comparison measurements – with a double-source double-crystal spectrometer (Windisch & Becker, 1990), for example. The latter measurements provided new excellent lattice-spacing standards (WASO 9, for example) of the well known lattice-parameter values. As shown by the authors, the differences in lattice parameters of different samples of float-zone silicon (due to oxygen or carbon content) were not greater than a few parts in 10^8. Finally, the lattice parameter of silicon, $a = 5.43102088(16)$ Å, has been accepted as the atomic scale length standard (Mohr & Taylor, 2000).

Another reference material reported is crystals of pure rhombohedral corrundum (α-Al_2O_3), *i.e.* of ruby or sapphire (Herbstein, 2000, and references therein; Shvyd'ko *et al.*, 2002).

With silicon standards, measurements or remeasurements of $K\alpha_{1,2}$ and/or $K\beta_{1,3}$ X-ray emission lines and absolute wavelength determinations of most of the 3*d* transition metals (Cr, Mn, Fe, Co, Ni and Cu) have been performed [Härtwig, Grosswig, Becker & Windisch, 1991; Hölzer, Fritsch, Deutsch, Härtwig & Förster, 1997 (see §4.2.2)].

The standard crystals may also be used for determination of such physical quantities as the Avogadro constant (Deslattes *et al.*, 1994; Deslattes, Henins, Schoonover, Caroll & Bowman, 1976). The single accurate wavelength values, on the other hand, may be used both in simple measurements of lattice parameters [based directly on the Bragg law, equation (5.3.1.1)] and for accurate scaling of the wavelength spectra, in order to use them, for example, in high-accuracy lattice-parameter measurements based on complete convolution models [*cf.* §5.3.3.3.1, point(ii)].

Unlike the X-rays emitted from an X-ray tube, for which the spectral line and the characteristic wavelength are known, there are no such characteristic features in synchrotron radiation. Therefore, special energy-selective monochromators should be applied in relative lattice-spacing measurements using synchrotron radiation. Obaidur (2002) proposes two measurement schemes, using two types of high-resolution channel-cut monolithic monochromators. The first scheme (see Fig. 5.3.3.18) is a modification of the Bond method. The second one (see Fig. 5.3.3.19) uses the simultaneous Bragg condition for the indices (5,1,3), $(\bar{5},\bar{1},\bar{3})$, (1,5,3) and $(\bar{1},\bar{5},\bar{3})$. The lattice-spacing differences in Si wafers were determined in the sub-parts in 10^6 range of 0.6 parts in 10^6 (in the first scheme) and of 0.2 parts in 10^6 (second scheme).

Recently, a new atomic scale wavelength standard was proposed by Shvyd'ko *et al.* (2000), instead of the wavelength of the Cu $K\alpha_1$ emission line or of the lattice parameter of a silicon standard. It is the wavelength, λ_M, of the ^{57}Fe Mössbauer radiation, *i.e.* of γ radiation of natural linewidth from nuclear transitions. It has been measured to the sub-parts in 10^6 accuracy: $\lambda_M = 0.86025474(16)$ Å (relative accuracy 0.19 parts in 10^6). Its advantage, in relation to the previous standards, is the high spectral sharpness of the Mössbauer radiation of 3.5×10^{-13} in relative units, which makes its wavelength λ_M extremely well defined. This standard wavelength value, which lies a little outside of scope of the present review (X-ray methods), was next used for the lattice-parameter determination of sapphire single crystals with a relative accuracy of about 0.5 parts in 10^6 (Shvyd'ko *et al.*, 2002). Fig. 5.3.3.20 is a diagram of the measurement arrangement.

5.3.4. Final remarks

Let us review the most important problems concerning accurate and precise lattice-parameter determination.

The first, commonly known, requirement for obtaining the highest accuracy and precision is the use of high-Bragg-angle reflections. The tendency to obtain, record, and use in calculation such reflections can be met in rotating-crystal cameras in which Straumanis mounting is applied (Farquhar &

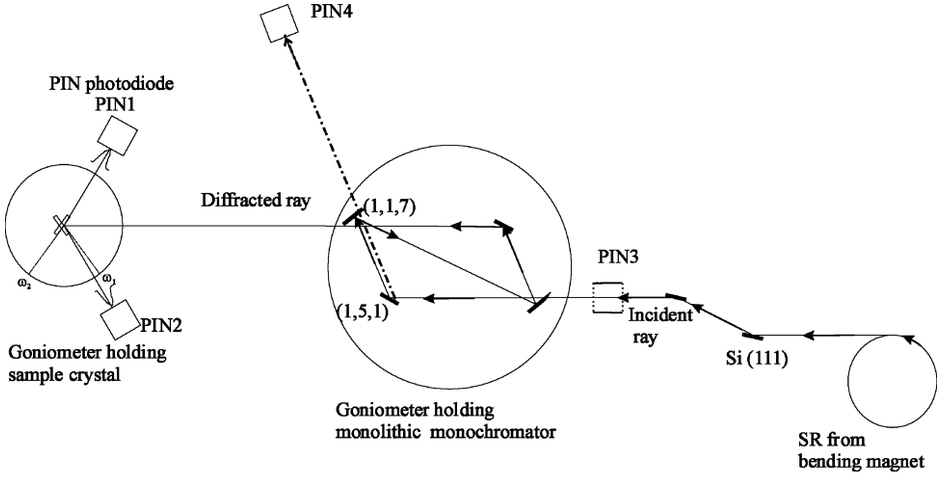

Fig. 5.3.3.18. Synchrotron radiation, SR, from the bending magnet incident on the Si(111) double-crystal monochromator and, after four reflections from the monolithic monochromator (0.1410 nm), impinges on sample Si(444). Two diffractions are recorded at the photodiode detectors, PIN1 and PIN2. The ω_1 and ω_2 values of the crystal positions are recorded using a Heiden height encoder.

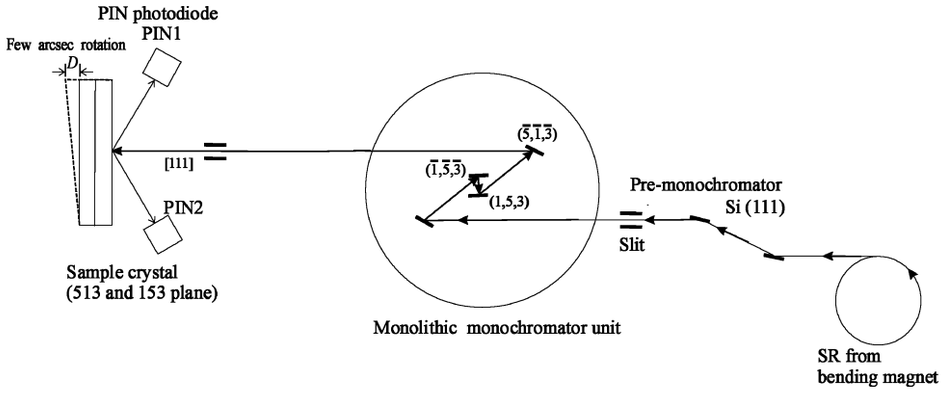

Fig. 5.3.3.19. Synchrotron radiation, SR, from the bending magnet incident on the Si(111) double-crystal monochromator and, after four reflections from the monolithic monochromator (0.1612 nm), impinges on sample Si(153). Two diffractions are recorded at the photodiode detectors, PIN1 and PIN2. The differences between the two peaks' D values are recorded using a Heiden height encoder.

Lipson, 1946; Popović, 1974), in the Weissenberg method (the use of zero-layer photographs), in multiple-exposure cameras (Glazer, 1972; Popović, Šljukić & Hanic, 1974), in standard and special diffractometers (Kobayashi, Yamada & Nakamura, 1963), in double-crystal arrangements with white X-radiation (Okazaki & Kawaminami, 1973*a*,*b*; Okazaki & Ohama, 1979; Ohama, Sakashita & Okazaki, 1979; Okazaki & Soejima, 2001), and in the triple-reflection scheme realized by means of the double-beam technique, proposed by Kovalchuk, Kovev & Pinsker (1975).

Increasing the θ value, in the case of photographic cameras or counter diffractometers, not only reduces the value of $\cot\theta$ in the formulae describing accuracy and precision, but also decreases several systematic errors proportional to $\cos\theta$, $\cos^2\theta$, $\cot\theta$ or $\cot^2\theta$ (Kheiker & Zevin, 1963; Wilson, 1963, 1980). To find the minimum total systematic error, which would occur for $\theta = 90^\circ$ (not attainable in practice), extrapolation of the results is used (Farquhar & Lipson, 1946; Weisz, Cochran & Cole, 1948; Smakula & Kalnajs, 1955; Kobayashi, Yamada & Azumi, 1968; Pierron & McNeely, 1969).

The problem of the choice of suitable reflections for the measurement, calculation, and reduction of systematic errors could be generalized. Not only are such reflections for which θ values are close to 90° desired but also those for which ν tends to 90° in rotating-crystal cameras (Umansky, 1960), high-order Kossel lines in divergent-beam techniques, axial or non-axial reflections in counter-diffractometer methods, *etc*. Zero-layer reflections in Weissenberg photographs or in two-circle

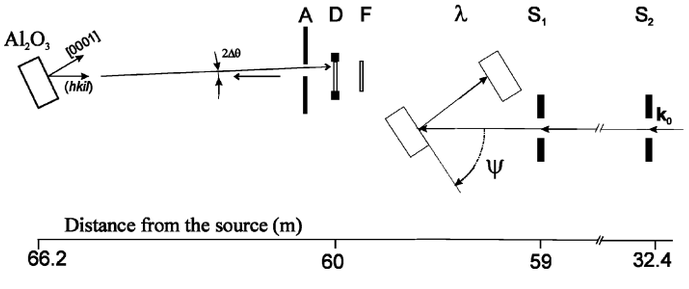

Fig. 5.3.3.20. Experimental set-up for measuring lattice parameters. X-rays after a high-heat-load monochromator (not shown) pass through the vertical slits S_1 and S_2 at a distance of 26.6 m. λ is a 'λ-meter'; F is a ^{57}Fe foil used as a source of the Mössbauer radiation of high brightness; D is a semi-transparent avalanche photodiode with 0.7 ns time resolution; Al_2O_3 is a sapphire single crystal in a furnace on a four-circle goniometer.

('Weissenberg') diffractometers are preferable to upper-layer ones, because they are less affected by crystal misalignment (Clegg & Sheldrick, 1984) and a larger range of reciprocal-lattice points can be recorded (Luger, 1980); they are not sufficient, however, for the determination of all the lattice parameters in the less-symmetric crystal systems.

Use of the orientation matrix makes possible accurate crystal setting for an arbitrary reflection and identification of recorded reflections not only in the case of the automated four-circle diffractometer or the two-circle diffractometer but also in photographic methods.

For obtaining high accuracy of lattice-parameter determination, systematic errors depending on the radiation, the crystal, and the technique should be known, evaluated, and reduced or corrected. As a rule, those systematic errors whose part in the total systematic error is the most important should be removed first. Looking at the development of the X-ray diffraction techniques, the following remarks can be made.

As far as the photographic methods are concerned, the errors due to the means of recording (film shrinkage, uncertainty of measurement of distances on the film) and camera construction (radius in the moving-crystal methods and the source-to-film distance in divergent-beam techniques) play a major role. They can be reduced to some extent by using the Straumanis mounting or the ratio method, or the resolved doublet $K\alpha_{1,2}$. Various methods have been introduced for reducing the error due to the source-to-film distance in divergent-beam techniques.

In counter-diffractometer methods, which give more accurate determinations of the Bragg angles and intensities, several instrumental and physical factors should be taken into account (Kheiker & Zevin, 1963; Wilson, 1963, 1980; Berger, 1984, 1986*a*; Härtwig & Grosswig, 1989). The effects of some can be diminished by the use of Soller slits (Berger, 1984) and the effects of most can be reduced by the Bond (1960) geometry, in its basic form or in its various modifications (Kheiker, 1973; Mauer *et al.*, 1975; Hubbard & Mauer, 1976; Wołcyrz, Pietraszko & Łukaszewicz, 1980; Kudo, 1982; Lisoivan, 1982; Grosswig *et al.*, 1985), in particular in combination with double- or triple-crystal spectrometers (Kurbatov, Zubenko & Umansky, 1972; Godwod, Kowalczyk & Szmid, 1974; Hart & Lloyd, 1975; Sasvári & Zsoldos, 1980; Fewster, 1982; Pick *et al.*, 1977; Obaidur, 2002). Another arrangement giving a partial reduction of systematic errors is that proposed by Renninger (1937) and developed by Post (1975) and Kshevetsky *et al.* (1979, 1985), in which multiple-diffraction phenomena are applied. In most one- or double-crystal asymmetric spectro-

meters, the uncertainty of the origin of the angular (ω) scale is the important problem, which can be resolved by introducing either the Bond (1960) symmetrical arrangement (combinations mentioned above) or an additional instrumental axis (or axes) for obtaining a multiple-crystal arrangement (Buschert, 1965; Skupov & Uspeckaya, 1975; Hart, 1981), or a second beam, used in multiple-beam methods (Hart, 1969; Kishino, 1973; Larson, 1974; Baker & Hart, 1975; Buschert *et al.*, 1983) or in various combined methods (Ando, Bailey & Hart, 1978; Kovalchuk, Kovev & Pinsker, 1975; Buschert *et al.*, 1980; Fewster, 1989; Shvyd'ko *et al.*, 2000; Obaidur, 2002).

The other important problem in single-crystal methods, in the case when high accuracy is desired, is the misalignment of the crystal(s) and some elements of the device. The errors due to the misalignment can be reduced to some extent experimentally, if a respective dependence is known (Baker, George, Bellamy & Causer, 1968; Burke & Tomkeieff, 1968, 1969; Bowen & Tanner, 1995), or by calculation of the exact correction (Burke & Tomkeieff, 1968, 1969; Gruber & Black, 1970; Filscher & Unangst, 1980; Larson, 1974) if the inclinations of the beam(s) and the crystal(s) can be determined (Halliwell, 1970; Nemiroff, 1982).

Along with an increase in the accuracy of the θ-angle determination, the error due to the wavelength determination becomes more important and a correction for the refraction should be introduced [the problem has been more intensively argued by Hart (1981, Section 2.3)]. Among others, measurement performed in the case of the Kossel method and divergent-beam techniques can be strongly affected by uncertainty of the wavelength, especially when the exact value of the wavelength is to be determined from the experiment. The combination of X-ray and optical interferometry (Deslattes, 1969; Deslattes & Henins, 1973; Becker *et al.*, 1981), the use of new lattice-parameter standards (Hölzer *et al.*, 1997), and new X-ray or γ-ray sources and wavelength standards (Shvyd'ko *et al.*, 2000; Obaidur, 2002) gives new possibilities for very accurate lattice-spacing measurements, up to the sub-parts in 10^6 range.

The accuracy of the method can be evaluated theoretically taking into account and estimating the errors that have not yet been eliminated. In the case of some θ-dependent errors, the maximum-likelihood method proves useful for this task (Beu, Musil & Whitney, 1962). Sometimes computer simulation is used to estimate some errors difficult to express in an analytical form (Hubbard & Mauer, 1976; Urbanowicz, 1981*b*; Berger, 1986*a*; Härtwig & Grosswig, 1989). A more objective test of the accuracy would be an inter-laboratory comparison, like that reported by Parrish (1960) many years ago. Usually, the authors introducing new methods, techniques or devices try to compare the results of their lattice-parameter determination with those obtained by other experimenters (Batchelder & Simmons, 1965, p. 2868; Hubbard, Swanson & Mauer, 1975, p. 46; Hubbard & Mauer, 1976, p. 2; Łukaszewicz *et al.*, 1976, p. 70; 1978, p. 566; Lisoivan, 1982, p. 94; Grosswig, Härtwig, Alter & Christoph, 1983, p. 506; Chang, 1984, p. 254; Härtwig, Bąk-Misiuk, Berger, Brühl, Okada, Grosswig, Wokulska & Wolf, 1994; Fewster & Andrew, 1995, p. 455; Herbstein, 2000).

In view of the new achievements in high-accuracy absolute lattice-parameter measurements, such as the results reviewed in §§5.3.3.8 and 5.3.3.9, and the accurate error analysis [Härtwig & Grosswig (1989); §5.3.3.4.3.2, point (7)], Härtwig, with his co-workers, initiated and organized an interlaboratory comparison of various 'traditional' methods and techniques, including the Bond method (*cf.* §5.3.3.4.3), the 'Soller-slit' method (§5.3.3.4.2) and the photographic multiple-diffraction (*Umweganregung*) method (§5.3.2.4.2). In all measurements performed, a common silicon standard (WASO 9, mentioned above) of accurately known lattice parameter was used as the specimen, so it was possible to check independently the validity of all corrections introduced for systematic errors. As shown by Härtwig, Bąk-Misiuk, Berger, Brühl, Okada, Grosswig, Wokulska & Wolf (1994), the agreement of their independent results was not worse than 3 parts in 10^6. The quantity defines the present-day possibilities of accurate 'dispersive' methods.

Herbstein (2000) concluded, 'there has been little improvement in claimed precision over the past 40–60 years', but his analysis relates to widely used 'dispersive' methods [including the Bond (1960) method] rather than to present-day high-precision comparison methods, which are also used for absolute measurements.

For obtaining high precision, a monochromatic and well collimated X-ray beam is desired. The first requirement can be fulfilled by using a filter or monochromator, the second can be satisfied by introducing a point source and a choice of collimation parameters, and both can be accomplished by introducing one or more additional crystals. It is not necessary for a well collimated beam to be very narrow if local measurements in selected small areas of the specimen are not the object of the experiment. The use of a large, parallel X-ray beam may be advantageous in some comparative measurements (Buschert, Pace, Inzaghi & Merlini, 1980).

Very high accuracy and high-precision measurements are, however, expensive; they need additional instrumental axes and detectors, and sometimes additional sources. Relatively simple divergent-beam techniques (photographic recording, stationary crystal) require fine X-ray sources (an electron microscope or an electron-beam probe) if high precision is to be attained.

Some authors have managed to reduce the cost of the experiment using simpler equipment. An example may be the triple-reflection scheme realized by the use of a double-axis spectrometer proposed by Ando, Bailey & Hart (1978) and Häusermann & Hart (1990). An additional advantage of the device is excellent stability.

Apart from the magnificent development of measuring techniques, an increasing role of mathematics is noticeable in contemporary papers. Matrix algebra is used for description of the crystal orientation in relation to the instrumental axes. Mathematical interpretation of the results is a very important part of the measurement, in particular in multiple-diffraction methods, both divergent-beam photographic and collimated-beam counter diffractometric. Syntheses of diffraction profiles are easily done with the aid of a computer. Algebraic and geometrical considerations make it possible to calculate proper corrections for systematic errors. Statistical methods give a tool for estimating and increasing the precision, in particular by means of least-squares refinement, and also for testing the hypothesis of 'no remaining systematic errors'. Commonly used computers are useful in numerous calculations and in controlling automatic devices.

International Tables for Crystallography (2006). Vol. C, Chapter 5.4, pp. 537–540.

5.4. Electron-diffraction methods

By A. W. S. Johnson and A. Olsen

5.4.1. Determination of cell parameters from single-crystal patterns (By A. W. S. Johnson)

5.4.1.1. *Introduction*

This article treats the recovery of cell axes and angles from (*a*) a single pattern with suitable Laue zones and (*b*) two patterns with different zone axes. It is assumed that instrument distortions, if significant, are corrected and that the patterns are free of artefacts such as twinning, double diffraction *etc.* (Edington, 1975). The treatment is valid for convergent-beam, micro and selected-area electron-diffraction patterns and accelerating voltages above approximately 30 kV. Relevant papers are by LePage (1992) and Zuo (1993), and background reading is contained in Edington (1975), Gard (1976), and Hirsch, Howie, Nicholson, Pashley & Whelan (1965).

The basic requirement in the determination of the unit cell of a crystal is to find, from one or more diffraction patterns, the basis vector set, $\mathbf{a}^*$, $\mathbf{b}^*$, $\mathbf{c}^*$, of a primitive reciprocal unit cell. The Cartesian components of these vectors form an orientation matrix

$$\boldsymbol{UB} = (\mathbf{a}^*, \mathbf{b}^*, \mathbf{c}^*),$$

which, when inverted, gives the vector components of the corresponding real-space cell. The elements of $\boldsymbol{UB}$ can be measured directly from the diffraction pattern in millimetres. Define axes x and y to be in the recording plane and z in the beam direction. A point in the diffraction pattern x, y, z is then related to the indices h, k, l by

$$\begin{pmatrix} x \\ y \\ z \end{pmatrix} = \boldsymbol{UB} \begin{pmatrix} h \\ k \\ l \end{pmatrix}.$$

Note that points with non-zero z are observed on the plane $z = 0$, see Fig. 5.4.1.1.

The metric $\boldsymbol{M}$ of $\boldsymbol{UB}^{-1}$ is used to find the unit-cell edges and angles as

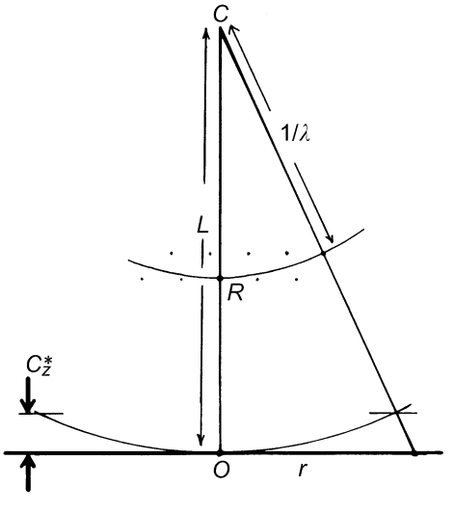

Fig. 5.4.1.1. Diffraction geometry. Crystal at *C* with the direct transmitted beam, *CRO*, intersecting the reciprocal-lattice origin at *R* and the recording plane at normal incidence at *O*. The camera length *L* is *CO* and the reciprocal of the wavelength λ is *CR*.

Table 5.4.1.1. *Unit-cell information available for photographic recording*

	Pattern type	Constants known	Information available
(1)	Zero zone	None or λ or L	d ratios and interplane angles
(2)		$L\lambda$ or L and λ	d values and interplane angles
(3)	Multiple zone	None or L	As for (1)
(4)		$L\lambda$	As for (2)
(5)		λ	Unit-cell axial ratios and angles
(6)		L and λ	Unit-cell axes and angles
(7)	Two or more zero-zone patterns*	None or L	As for (5)
(8)		$L\lambda$	As for (6)

* See text, Subsection 5.4.1.2.

$$\boldsymbol{M} = \boldsymbol{UB}^{-1} \cdot (\boldsymbol{UB}^{-1})^T,$$

where T means the transpose. Then,

$$\boldsymbol{M} = \begin{pmatrix} \mathbf{a}\cdot\mathbf{a} & \mathbf{a}\cdot\mathbf{b} & \mathbf{a}\cdot\mathbf{c} \\ \mathbf{a}\cdot\mathbf{b} & \mathbf{b}\cdot\mathbf{b} & \mathbf{b}\cdot\mathbf{c} \\ \mathbf{a}\cdot\mathbf{c} & \mathbf{b}\cdot\mathbf{c} & \mathbf{c}\cdot\mathbf{c} \end{pmatrix}$$

gives

$$a = L\lambda(\mathbf{a}\cdot\mathbf{a})^{1/2},$$
$$b = L\lambda(\mathbf{b}\cdot\mathbf{b})^{1/2},$$
$$c = L\lambda(\mathbf{c}\cdot\mathbf{c})^{1/2},$$
$$\cos\gamma = \mathbf{a}\cdot\mathbf{b}/(\mathbf{a}\cdot\mathbf{a}\,\mathbf{b}\cdot\mathbf{b})^{1/2},$$
$$\cos\beta = \mathbf{a}\cdot\mathbf{c}/(\mathbf{a}\cdot\mathbf{a}\,\mathbf{c}\cdot\mathbf{c})^{1/2},$$

and

$$\cos\alpha = \mathbf{b}\cdot\mathbf{c}/(\mathbf{b}\cdot\mathbf{b}\,\mathbf{c}\cdot\mathbf{c})^{1/2},$$

where L is the effective distance between the diffracting crystal and the recording plane and λ is the wavelength. These quantities are defined in Fig. 5.4.1.1 together with the nomenclature and geometrical relationships required in this article.

If necessary, the cell is reduced to the Bravais cell according to the procedures given in *IT* A (1983, Chapter 9.3), before calculating the metric.

In practice, there may be a difficulty in choosing a vector set that describes a *primitive* reciprocal cell. Although a record of any reasonably dense plane of reciprocal space immediately exposes two basis vectors of a cell, the third vector lies out of the plane of the diffraction pattern containing the first two vectors and may not be directly measurable. Hence, some care must be taken to ensure that the third vector chosen makes the cell

Copyright © 2006 International Union of Crystallography

primitive. This presents no difficulty in the non-zero-zone analysis given in Subsection 5.4.1.3 but needs consideration when two patterns are used as described in Subsection 5.4.1.2.

Unit-cell parameters may be partly or fully determined depending on the extent of knowledge of the effective camera length L and wavelength λ, and upon the type and number of patterns. The different situations are distinguished in Table 5.4.1.1 for photographic recording. Note that L is simply a magnification factor.

The accuracy of the non-zero-zone analysis described in Subsection 5.4.1.3 will depend on the influence of spiral, radial, and elliptical distortions. The camera length and wavelength need to be known to better than 1%.

For measurements made using microscope deflector systems, a knowledge of L may not be required depending on the location of the deflectors in the microscope column. Instead, the calibration factor of the deflectors, in suitable units, will replace L.

5.4.1.2. *Zero-zone analysis*

Two patterns are required that represent different sections through the reciprocal lattice. The angle of rotation p between these sections must be known, as well as the trace of the rotation axis in the plane of the pattern. Define the plane of the first pattern as the xy plane with the x axis, for convenience, coincident with the trace of the rotation axis. The coordinates x_0, y_0 of reflections in the first pattern are then measured. The coordinates x_1, y_1 of spots in the patterns rotated by p relative to the first pattern are then measured, care being taken to align the trace of the rotation axis with the x axis of the measuring equipment for each pattern. The coordinates of these reflections are then reduced to the coordinate system of the first pattern by the relations $x_0 = x_1$, $y_0 = y_1 \cos(p)$, $z_0 = y_1 \sin(p)$. The coordinates of all reflections measured are placed in a table that is scanned to extract the three shortest non-coplanar vectors. If the patterns come from dense, neighbouring zones, it is likely that these vectors define a primitive cell.

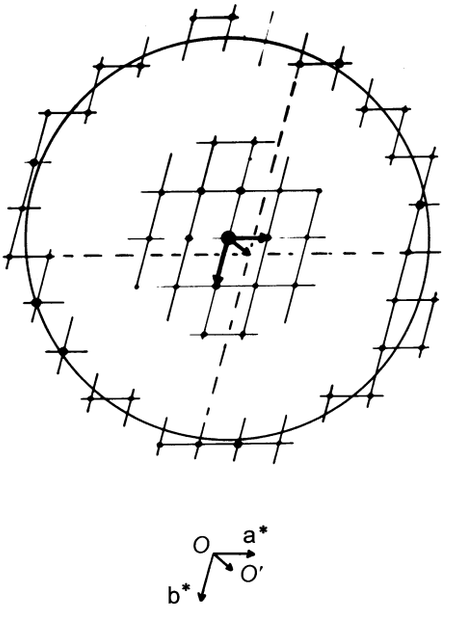

Fig. 5.4.1.2. A diffraction pattern with the crystal oriented at a zone axis. The lower diagram shows the zero-zone vectors $\mathbf{a}^*$ and $\mathbf{b}^*$, and OO', the projection on the xy plane of $\mathbf{c}^*$.

5.4.1.3. *Non-zero-zone analysis*

One pattern with well defined Laue zones taken at an arbitrary zone allows the recovery of a third vector not in the plane of the pattern. First find the components for the two shortest zero-zone vectors $\mathbf{a}^*$ and $\mathbf{b}^*$ (see Fig. 5.4.1.2). For the third vector, measure the x and y coordinates of a non-zero-zone vector. These are then transformed to components in the coordinate system defined by the two shortest vectors of the zero zone. Then the fractional part of each transformed component is taken. If the vector comes from a Laue zone of order n, these fractional parts must be divided by n. A transformation back to Cartesian coordinates gives the x and y components of the third vector $\mathbf{c}^*$, point O' in Fig. 5.4.1.2. In practice, it is best to measure a set of vectors at roughly equal angles around the zone so that an average can be taken to improve accuracy.

For certain space groups and special orientations, it is possible for half of the zero-zone reflections to be absent. If sufficient non-zero-zone vectors have been measured, two different vectors OO' should be found. New axes $(\mathbf{a}^* + \mathbf{b}^*)/2$ and $(\mathbf{a}^* - \mathbf{b}^*)/2$ must then be chosen and the x and y coordinates of $\mathbf{c}^*$ recalculated.

The z component of $\mathbf{c}^*$ is obtained (Fig. 5.4.1.1) from

$$c_z^* = L[1 - 1/(1 + r^2/L^2)^{1/2}]/n,$$

where r is the radius of the Laue circle of order n.

We now have the orientation matrix $\boldsymbol{UB}$ as

$$\boldsymbol{UB} = \begin{pmatrix} a_x^* & b_x^* & c_x^* \\ a_y^* & b_y^* & c_y^* \\ 0 & 0 & c_z^* \end{pmatrix},$$

and the measurement of the pattern is complete.

After transformation of the axes defined by $\boldsymbol{UB}$ to the Bravais axes, the inverse of the resulting $\boldsymbol{UB}_{\text{Bravais}}$ will index the pattern using

$$\begin{pmatrix} h \\ k \\ l \end{pmatrix} = \boldsymbol{UB}_{\text{Bravais}}^{-1} \begin{pmatrix} x \\ y \\ z \end{pmatrix}.$$

5.4.2. Kikuchi and HOLZ techniques (By A. Olsen)

Lattice-parameter determination based on selected-area electron-diffraction patterns requires accurate calibration of the camera constant K. This constant depends on the electron wavelength λ and the camera length L and is given by $K = \lambda L$. Because the camera constant cannot be determined with sufficient accuracy in a transmission electron microscope, a number of methods for determination of lattice parameters (or electron wavelength)

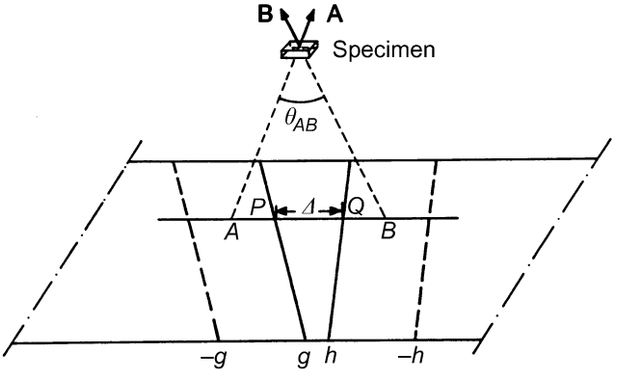

Fig. 5.4.2.1. Schematic diagram showing the geometry of a Kikuchi pattern.

have been developed based on Kikuchi or HOLZ (high-order Laue zone) lines (Uyeda, Nonoyama & Kogiso, 1965; Høier, 1969; Olsen, 1976*a*; Jones, Rackham & Steeds, 1977). In these methods, the lattice parameters can be determined, provided the electron wavelength is known (or *vice versa*) without knowing the value of K.

In the method of Uyeda *et al*. (1965), the electron wavelength can be determined from a single Kikuchi pattern provided that the lattice parameters of the crystal are known. Fig. 5.4.2.1 illustrates the geometry involved in the method. **A** and **B** are two zone axes of the specimen. The pairs of Kikuchi lines g, $-g$ and h, $-h$ belong to the zones **A** and **B**, respectively. The points P and Q are the intersections of the Kikuchi lines g and h with the line AB.

As a first approximation, the wavelength of the electrons is given by

$$\lambda = \theta_{AB}/[(1/2d_P) + (1/2d_Q) + (\Delta/D)(1/d)], \qquad (5.4.2.1)$$

where D is the measured distance between the two Kikuchi lines in either of the pairs and d is the corresponding interplanar spacing. θ_{AB} is the angle between the zone axes **A** and **B**. When the Kikuchi pattern is indexed, θ_{AB} and d can be calculated from the known lattice parameters of the specimen. d_P and d_Q are effective interplanar spacings and are given by

$$\begin{aligned} d_P &= d_g \sin\varphi_g, \\ d_Q &= d_h \sin\varphi_h; \end{aligned} \qquad (5.4.2.2)$$

d_g and d_h are the interplanar spacings corresponding to g and h, respectively. The angle φ_g (or φ_h) is the angle between the lattice plane g (or h) and the plane defined by **A** and **B**. These angles are given by

$$\begin{aligned} \sin\varphi_g &= \mathbf{g} \times (\mathbf{A} \times \mathbf{B})/(|\mathbf{g}| \cdot |\mathbf{A} \times \mathbf{B}|), \\ \sin\varphi_h &= \mathbf{h} \times (\mathbf{A} \times \mathbf{B})/(|\mathbf{g}| \cdot |\mathbf{A} \times \mathbf{B}|). \end{aligned} \qquad (5.4.2.3)$$

The values of d_P and d_Q to be used in (5.4.2.1) can be calculated from (5.4.2.2) and (5.4.2.3).

If Δ and D are measured on the photographic plate or a print of any magnification, the electron wavelength can be calculated by using (5.4.2.1). Only the ratio (Δ/D) is required for the determination of λ. The distance AB is not required. The points A and B are used only to fix the points P and Q. A and B do not need to fall inside the photographic plate when a Kikuchi pattern is symmetrical across the line AB, because in such cases P and Q can be determined from intersections of Kikuchi lines that are symmetrical with each other. The expression for λ in (5.4.2.1) is only a first approximation. More accurate expressions can be found in the paper by Uyeda *et al*. (1965).

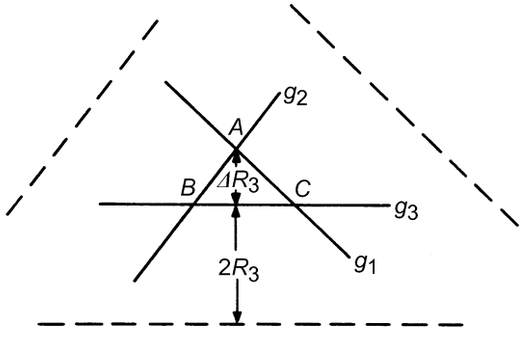

Fig. 5.4.2.2. Schematic diagram of three Kikuchi lines that nearly intersect at the same point.

A simpler and more accurate method has been developed by Høier (1969). He showed that in the cubic case it is possible to determine the ratio between the lattice parameter a and the electron wavelength λ with a relative accuracy of 0.1%. Only two quantities have to be measured on the photographic plate or a print at any magnification: the height of a triangle formed by three Kikuchi lines and one separation between a defect–excess line pair (Fig. 5.4.2.2). If three indexed Kikuchi lines g_i intersect at the same point on a photographic plate, the following equations can be derived from Bragg's law:

$$2\mathbf{g}_i\mathbf{K}_i = -|\mathbf{g}_i|^2, \quad i = 1, 2, 3. \qquad (5.4.2.4)$$

In addition, the length of **K** is equal to the electron wavelength

$$|\mathbf{K}_i| = 1/\lambda_i, \qquad (5.4.2.5)$$

where the wavelength is written λ_i for generality (for electrons, $\lambda_i = \lambda$). If the Kikuchi lines g_i do not belong to the same zone, (5.4.2.4) and (5.4.2.5) can be solved and a/λ determined.

Exact triple intersections are rare. A practical method as proposed by Høier (1969) is therefore based on three lines that nearly intersect at the same point (Fig. 5.4.2.2). The dimensions of the triangle ABC in Fig. 5.4.2.2 change with λ. Let us assume that only the wavelength in the beam giving the g_3 reflection varies. The increment $\Delta\lambda_3$ necessary to shift the line g_3 to A is then determined by

$$\lambda_3 = \lambda + \Delta\lambda_3 \sim \lambda(1 + \Delta R_3/R_3). \qquad (5.4.2.6)$$

By measuring the height in the triangle ABC and the line separation $2R_3$, the wavelength to be used in (5.4.2.5) can be calculated and the ratio a/λ determined. Care must be taken to avoid areas where the lines are displaced from kinematical positions owing to dynamical interactions.

The method of Høier (1969) for cubic crystals was later extended to lower-symmetry cases (triclinic) by Olsen (1976*a*), who also developed computer programs for least-squares refinement of the lattice parameters. The derivation of the equations for the procedure is carried out in the following in a way slightly different from that described by Olsen (1976*a*).

If three Kikuchi lines $\mathbf{g}_i(h_i, k_i, l_i)$ not belonging to the same zone intersect at the same point on the photographic plate, the direction **K** from the origin of the Ewald sphere to the intersection point of the Kikuchi lines is given by Bragg's law:

$$2\mathbf{g}_i\mathbf{K} = -|\mathbf{g}_i|^2, \quad i = 1, 2, 3. \qquad (5.4.2.7)$$

The length of the vector **K** is given by

$$|\mathbf{K}| = 1/\lambda, \qquad (5.4.2.8)$$

where λ is the electron wavelength.

Because triple intersections are rare, a practical method is therefore based on three lines that nearly intersect at the same point, as proposed by Høier (1969). In order to obtain an exact intersection, one of the lines can be changed from $\mathbf{g}_i$ to $\mathbf{g}_i + \Delta\mathbf{g}_i$, where $\Delta\mathbf{g}_i$ is a vector approximately parallel to $\mathbf{g}_i$. For this Kikuchi line (in the following assumed to be line no. 3), the Bragg condition (5.4.2.7) gives

$$2(\mathbf{g}_3 + \Delta\mathbf{g}_3)\mathbf{K} = -(\mathbf{g}_3 + \Delta\mathbf{g}_3)^2. \qquad (5.4.2.9)$$

For a pair of Kikuchi lines, the simple relation

$$2\Delta\mathbf{g}_3 = (\Delta R_3/R_3)\mathbf{g}_3 \qquad (5.4.2.10)$$

holds, where $2R_3$ is the line separation measured on the photographic plate of the centres of the two Kikuchi lines. ΔR_3 is the shift (measured on the plate) in the position of one of the lines in order to obtain an exact triple intersection.

Substitution of (5.4.2.10) into (5.4.2.9) gives

$$2\mathbf{g}_3\mathbf{K} = -|\mathbf{g}_3|^2(1 + \Delta R_3/R_3). \qquad (5.4.2.11)$$

From n measurements of intersections, the following equations are obtained:

$$h_{ji}u_j + k_{ji}v_j + l_{ji}w_j = -(1/2)(1/d_{ji})^2(1 + \delta_{i3}\Delta R_{j3}/R_{j3}), \quad i = 1, 2, 3, \quad j = 1, 2, \ldots, n, \qquad (5.4.2.12)$$

where h_{ji}, k_{ji}, l_{ji} are the indices (given in reciprocal space) of the Kikuchi lines, δ_{i3} is the Kronecker delta, u_j, v_j, w_j are the indices (given in real space) of the direction $\mathbf{K}_j$ to the intersection number $\mathbf{j}$, and d_{ji} is the interplanar spacing corresponding to the reflection h_{ji}, k_{ji}, l_{ji} and can be expressed in terms of the cell dimensions in real space. The length of the $\mathbf{K}_j$ vectors can also be expressed in terms of the lattice parameters in real space a, b, c, α, β, and γ as

$$|\mathbf{K}_j| = (u_j^2a^2 + v_j^2b^2 + w_j^2c^2 + 2u_jv_j\,ab\cos\alpha + 2u_jw_j\,ac\cos\beta + 2v_jw_j\,bc\cos\gamma)^{1/2}. \qquad (5.4.2.13)$$

Equations (5.4.2.12) can be solved with respect to u_j, v_j, w_j, and $\mathbf{K}_j$ can then be expressed in terms of the lattice parameters by substituting the expressions for u_j, v_j, w_j from (5.4.2.12) into (5.4.2.13).

If the number of intersections is greater than the number of unknown lattice parameters, a least-squares-refinement procedure can be used. This involves minimizing the function

$$Q = \sum_j (|\mathbf{K}_j| - 1/\lambda)^2. \qquad (5.4.2.14)$$

Because the expression for Q is non-linear in the lattice parameters, a refinement procedure can be used to solve the equations derived from (5.4.2.14) using the least-squares procedure. The accuracy in the lattice parameters or wavelength can be found by statistical methods. A computer program for refinement of the lattice parameters (or electron wavelength) is available (Olsen, 1976*b*). In this program, some of the lattice parameters can be held constant or kept equal during the refinement.

Methods based on measurements of distances between zone axes (poles) in the Kikuchi patterns (Thomas, 1970) are not very accurate because optical distortions make long-distance measurements inaccurate on the photographic plate or a magnified print.

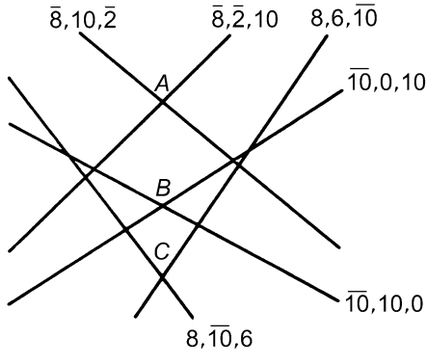

Fig. 5.4.2.3. Schematic diagram showing the indexing of the most prominent lines in the selected-area channelling pattern near the [111] zone of Si. Accelerating voltage: 25 kV.

The methods by Høier (1969) and Olsen (1976*a*) are based on 'near intersections'. Better accuracy may be obtained if the high voltage can be varied in order to obtain exact intersections. A simple method for determination of lattice parameters can be applied for crystals with symmetry as low as orthorhombic (Gjønnes & Olsen, 1984). The method is a simplified version of the Uyeda *et al*. (1965) method. If two parallel Kikuchi lines belonging to different zones overlap, then:

$$2\mathbf{g}_i\mathbf{K} = -|\mathbf{g}_i|^2, \quad i = 1, 2; \qquad (\mathbf{g}_1 \times \mathbf{g}_2)\mathbf{K} = 0, \quad |\mathbf{K}| = 1/\lambda. \qquad (5.4.2.15)$$

These equations can be solved to give the ratio between lattice parameter and electron wavelength.

A simple, rapid procedure for accelerating-voltage (or electron-wavelength) determination of a transmission electron microscope has been described by FitzGerald & Johnson (1984). In their method, it is necessary to measure the ratio of two easily found distances between points defined by the intersections of Kikuchi lines near the ⟨111⟩ zone of a silicon crystal. It is not necessary to index the Kikuchi lines, because the method is based on (*a*) a particular crystal and (*b*) an easily recognizable crystal orientation, and because the points between which distances need to be measured are specified in their paper and can be easily found. Polynominals for converting the distance measurements both to electron wavelength and to accelerating voltage are given for the range from 100 to 200 kV. A 300 K temperature change must occur (temperature coefficient of 3×10^{-6} K) before the error in the lattice parameter of silicon due to thermal expansion becomes significant.

A method for measuring small local changes in the lattice parameter of bulk specimens based on selected-area channelling patterns has been described by Walker & Booker (1982). The method utilizes the small changes in the position of high-index channelling lines due to small changes in the lattice parameters, and is based on scanning electron microscopy (SEM). The method is rapid and convenient, is suitable for bulk specimens, and can be applied to areas only a few micrometres across. The method has been used for Si and GaP and is in this case based on the intersection of pairs of $\bar{8}$,10,$\bar{2}$, $\bar{1}0$,10,0, 8,$\bar{1}0$,6 type lines (the points *A*, *B*, and *C* in Fig. 5.4.2.3). Selected-area channelling patterns from Si and GaP obtained under precisely the same conditions have the same characteristic array of lines, but with slightly different distances *AB* and *BC*. The detection limit of this method is at present 3 parts in 10^4.

When a small electron probe is used to illuminate a crystal, as in convergent-beam electron diffraction (CBED), very fine lines are often found in the diffraction discs (Steeds, 1979). These lines are called HOLZ lines. They are due to upper-layer diffraction effects and can be used in lattice-parameter determination (Rackham, Jones & Steeds, 1974; Jones, Rackham & Steeds, 1977). For highest accuracy, relatively thick crystals are required. The limitation to the accuracy is set either by the weakness of the lines or by energy losses in the specimen. Relative changes in the lattice parameters can be measured to an accuracy of 1 part in 10^4, whereas the accuracy in the absolute determination of lattice parameters is typically of an order of magnitude worse. The lattice parameters can be measured from crystal regions as small as 20 nm in diameter with an accuracy better than 1 part in 10^3. If more accurate results are desired, it is necessary to make measurements on lines that are not affected by interactions between HOLZ reflections.

5.5. Neutron methods

By B. T. M. Willis

In general, one would not expect to measure lattice parameters as precisely with neutrons as with X-rays. The main reason for this is the need to relax the resolution of the diffraction peaks observed in neutron diffraction, in order to obtain reasonable count rates. However, the high-resolution powder diffractometer D2B (on the reactor source at the Institut Laue–Langevin) and the high-resolution powder instrument HRPD (on the pulsed source at the Rutherford Appleton Laboratory) have resolutions approaching that of X-ray diffractometers. Using Rietveld refinement, lattice parameters can be determined to a precision of a few parts in 10^4 (Fischer *et al.*, 1986).

Neutron methods are better suited to the indexing of the powder pattern. This requires the accurate measurement of the d spacings of the lowest-index lines in the pattern. Whereas d spacings measured with X-rays at low values of $(\sin\theta)/\lambda$ tend to have systematic errors, this is not such a serious problem with neutrons. It is relatively straightforward, using the time-of-flight pulsed-neutron method, to measure the d spacings of the first 20–30 lines of a powder pattern to better than 0.1%.

References

5.1

Block, S. & Hubbard, C. R. (1980). Editors. *Accuracy in powder diffraction. Natl Bur. Stand. US Spec. Publ.* No. 567.

CSIRO (1988). Papers presented at the International Symposium on X-ray Powder Diffractometry, Fremantle, Australia, 20–23 August 1987. *Aust. J. Phys.* **41**(2), iv, 101–335.

Hubbard, C. R. (1983). *New standard reference materials for X-ray powder diffraction. Adv. X-ray Anal.* **26**, 45–51.

Klug, H. P. & Alexander, L. E. (1974). *X-ray diffraction procedures for polycrystalline and amorphous materials*, 2nd ed. New York: John Wiley.

Okada, Y. & Tokumaru, Y. (1984). *Precise determination of lattice parameter and thermal expansion coefficient of silicon between 300 and 1500 K. J. Appl. Phys.* **56**, 314–320.

Peiser, H. S., Rooksby, H. P. & Wilson, A. J. C. (1960). Editors. *X-ray diffraction by polycrystalline materials*, 2nd ed. London: Chapman & Hall.

Prince, E. & Stalick, J. K. (1992). Editors. *Accuracy in powder diffraction. II. NIST Spec. Publ.* No. 846.

Wilson, A. J. C. (1980). *Accuracy in methods of lattice-parameter measurement. Accuracy in powder diffraction. Natl Bur. Stand. US Spec. Publ.* No. 567.

5.2

Alexander, L. (1948). *Geometrical factors affecting the contours of X-ray spectrometer maxima. I. Factors causing asymmetry. J. Appl. Phys.* **19**, 1068–1071.

Alexander, L. (1950). *Geometrical factors affecting the contours of X-ray spectrometer maxima. II. Factors causing broadening. J. Appl. Phys.* **21**, 126–136.

Alexander, L. (1953). *The effect of vertical divergence on X-ray powder diffraction lines. Br. J. Appl. Phys.* **4**, 92–93.

Alexander, L. (1954). *The synthesis of X-ray spectrometer line profiles with application to crystallite size measurements. J. Appl. Phys.* **25**, 155–161.

Appleman, D. E. & Evans, H. T. (1973). *Indexing and least-squares refinement of powder diffraction data*. US Department of Commerce, National Technical Information Service, 5286 Port Royal Rd, Springfield, VA 22151, USA.

Barth, H. (1960). *Möglichkeit der Präzisionsgitterkonstanten-messungen mit hochmonochromatischer Röntgenstrahlung. Acta Cryst.* **13**, 830–832.

Bearden, J. A. (1964). *X-ray wavelengths*. US AEC Division of Technical Information Ext., Oak Ridge, Tennessee, USA. [The tables are reprinted more accessibly in *International tables for X-ray crystallography* (1974). Vol. IV, pp. 6–43. Birmingham: Kynoch Press. Present distributor: Kluwer Academic Publishers.]

Berkum, J. van, Sprong, G. J. M., de Keijser, Th. H., Delhez, R. & Sonneveld, E. J. (1995). *The optimum standard specimen for X-ray diffraction line-profile analysis. Powder Diffr.* **10**, 129–139.

Beu, K. E. (1964). *The evaluation of centroid lattice parameter data for tungsten by the likelihood ratio method. Acta Cryst.* **17**, 1149–1164.

Beu, K. E., Musil, F. J. & Whitney, D. R. (1962). *Precise and accurate lattice parameters by film powder methods. I. The likelihood ratio method. Acta Cryst.* **15**, 1292–1301.

Beu, K. E., Musil, F. J. & Whitney, D. R. (1963). *The likelihood ratio method for the precise and accurate determination of lattice parameters for tetragonal and hexagonal crystals. Acta Cryst.* **16**, 1241–1242.

Beu, K. E. & Whitney, D. R. (1967). *Further developments in a likelihood ratio method for the precise and accurate determination of lattice parameters. Acta Cryst.* **22**, 932–933.

Boom, G. (1966). *Accurate lattice parameters and the LPC method*. Groningen: van Denderen.

Boom, G. & Smits, D. W. (1965). *Calculation of Debye–Scherrer diffraction line profiles and their applications in precision determination of lattice parameters. Proc. K. Ned. Akad. Wet. Ser. B*, **68**, 46–52.

Bourdillon, A. J., Glazer, A. M., Hidaka, M. & Bordas, J. (1978). *High-resolution energy-dispersive diffraction using synchrotron radiation. J. Appl. Cryst.* **11**, 684–687.

Buras, B., Olsen, J. S., Gerward, L., Will, G. & Hinze, E. (1977). *X-ray energy-dispersive diffractometry using synchrotron radiation. J. Appl. Cryst.* **10**, 431–438.

Cheary, R. W. & Coelho, A. (1992). *A fundamental parameters approach to X-ray line-profile fitting. J. Appl. Cryst.* **25**, 109–121.

Cheary, R. W. & Coelho, A. (1994). *Synthesizing and fitting linear position-sensitive detector step-scanned line profiles. J. Appl. Cryst.* **27**, 673–681.

Chevallier, P., Travennier, M. & Briand, J. P. (1978). *On the natural width of the K_α x-ray [sic] line observed at the energy threshold. J. Phys. B*, **11**, L171–L179.

Copyright © 2006 International Union of Crystallography

5.2 (*cont.*)

Cohen, M. U. (1936*a*). *Elimination of systematic errors in powder photographs*. *Z. Kristallogr.* **94**, 288–298.

Cohen, M. U. (1936*b*). *Calculation of precise lattice constants for X-ray powder photographs*. *Z. Kristallogr.* **94**, 306–310.

Deslattes, R. D. & Henins, A. (1973). *X-ray to visible wavelength ratios*. *Phys. Rev. Let.* **31**, 972–975.

Deslattes, R., Henins, A. & Kessler, E. G. (1980). *Accuracy in X-ray wavelengths*. *Accuracy in powder diffraction*, edited by S. Block & C. R. Hubbard, pp. 55–71. *Natl Bur. Stand. (US) Spec. Publ.* No. 567.

Dragoo, A. L. (1986). *Standard reference materials for X-ray diffraction*. *Part I. Overview of current and future standard reference materials*. *Powder Diffr.* **1**, 294–304.

Edwards, H. J. & Toman, K. (1970). *The additivity of variances in powder diffraction profile analysis*. *J. Appl. Cryst.* **3**, 165–171.

Fawcett, T. G., Crowder, C. E., Brownell, S. J., Zhang, Y., Hubbard, C., Schreiner, W., Hamill, G. P., Huang, T. C., Sabino, E., Langford, J. I., Hamilton, R. & Louër, D. (1988). *Establishing an instrumental peak profile calibration standard for powder diffraction analyses*: *international round robin conducted by the JCPDS–ICDD and the US National Bureau of Standards*. *Powder Diffr.* **3**, 209–218.

Ferguson, I. F., Rogerson, I. F., Wolstenholme, J. F. R., Hughes, T. E. & Huyton, A. (1987). *FIRESTAR-2. A computer program for the evaluation of X-ray powder measurements and the derivation of crystal lattice parameters*. United Kingdom Atomic Energy Authority, Northern Division Report ND-R-909(S). London: HMSO, February 1987.

Fukamachi, T., Hosoya, S. & Terasaki, D. (1973). *The precision of interplanar distances measured by an energy-dispersive X-ray diffractometer*. *J. Appl. Cryst.* **6**, 117–122.

Gale, B. (1963). *The positions of Debye diffraction line peaks*. *Br. J. Appl. Phys.* **14**, 357–364.

Gale, B. (1968). *The aberrations of a focusing X-ray diffraction instrument*: *second-order theory*. *Br. J. Appl. Phys. (J. Phys. D)*, **1**, 393–408.

Giessen, B. C. & Gordon, G. E. (1968). *X-ray diffraction: new high-speed technique based on X-ray spectroscopy*. *Science*, **159**, 973–975.

Gillham, C. J. (1971). *Centroid shifts due to axial divergence and other geometrical factors in Seemann–Bohlin diffractometry*. *J. Appl. Cryst.* **4**, 498–506.

Gillham, C. J. & King, H. W. (1972). *Measurements of centroid and peak shifts due to dispersion and the Lorentz factor at very high Bragg angles*. *J. Appl. Cryst.* **5**, 23–27.

Glazer, A. M., Hidaka, M. & Bordas, J. (1978). *Energy-dispersive powder profile refinement using synchrotron radiation*. *J. Appl. Cryst.* **11**, 165–172.

Greenberg, B. (1989). *Bragg's law with refraction*. *Acta Cryst.* A**45**, 238–241.

Hart, M. (1981). *Bragg angle measurement and mapping*. *J. Cryst. Growth*, **55**, 409–427.

Hart, M., Cernik, R., Parrish, W. & Toraya, H. (1990). *Lattice-parameter determination for powders using synchrotron radiation*. *J. Appl. Cryst.* **23**, 286–291.

Hart, M., Parrish, W., Bellotto, M. & Lim, G. S. (1988). *The refractive-index correction in powder diffraction*. *Acta Cryst.* A**44**, 193–197.

Huang, T. C. (1988). *Precision peak determination in X-ray powder diffractometry*. *Aust. J. Phys.* **41**, 201–212.

Huang, T. C., Toraya, H., Blanton, T. N. & Wu, Y. (1993). *X-ray powder diffraction analysis of silver behenate, a possible low-angle diffraction standard*. *J Appl. Cryst.* **26**, 180–184.

Hubbard, C. R. (1983). *New standard reference materials for X-ray powder diffraction*. *Adv. X-ray Anal.* **26**, 45–51.

Hubbard, C. R., Swanson, H. É. & Mauer, F. A. (1975). *A silicon powder diffraction standard reference material*. *J. Appl. Cryst.* **8**, 45–48.

JCPDS–International Centre for Diffraction Data (1986). *Task group on cell parameter refinement*. *Powder Diffr.* **1**, 66–76.

Jenkins, R. & Schreiner, W. N. (1986). *Considerations in the design of goniometers for use in X-ray powder diffraction*. *Powder Diffr.* **1**, 305–319.

Kelly, E. H. (1988). *A summary of a 'round-robin' exercise comparing the output of computer programs for lattice-parameter refinement and calculations*. British Crystallographic Association.

Kogan, V. A. & Kupriyanov, M. F. (1992). *X-ray powder diffraction line profiles by Fourier synthesis*. *J. Appl. Cryst.* **25**, 16–25.

Ladell, J., Parrish, W. & Taylor, J. (1959). *Interpretation of diffractometer line profiles*. *Acta Cryst.* **12**, 561–567.

Laguitton, D. & Parrish, W. (1977). *Experimental spectral distribution versus Kramers' law for quantitative X-ray fluorescence by the fundamental parameters method*. *X-ray Spectrom.* **6**, 201–203.

Langford, J. I., Louër, D., Sonneveld, E. J. & Visser, J. W. (1986). *Applications of total pattern fitting to a study of crystallite size and strain in powder zinc oxide*. *Powder Diffr.* **1**, 211–221.

Langford, J. I., Pike, E. R. & Beu, K. E. (1964). *Precise and accurate lattice parameters by film powder methods*. *IV. Theoretical calculation of axial (vertical) divergence profiles, centroid shifts, and variances for cylindrical powder diffraction cameras*. *Acta Cryst.* **17**, 645–651.

Langford, J. I. & Wilson, A. J. C. (1962). *Counter diffractometer: the effect of specimen transparency on the intensity, position and breadth of X-ray powder diffraction lines*. *J. Sci. Instrum.* **39**, 581–585.

Louër, D. & Langford, J. I. (1988). *Peak shape and resolution in conventional diffractometry with monochromatic X-rays*. *J. Appl. Cryst.* **21**, 430–437.

Mack, M. & Parrish, W. (1967). *Seeman–Bohlin X-ray diffractometry*. *II. Comparison of aberrations and intensity with conventional diffractometer*. *Acta Cryst.* **23**, 693–700.

Mack, M. & Spielberg, N. (1958). *Statistical factors in X-ray intensity measurements*. *Spectrochim. Acta*, **12**, 169–178.

Mantler, M. & Parrish, W. (1977). *Energy dispersive X-ray diffractometry*. *Adv. X-ray Anal.* **20**, 171–186.

Mighell, A. D., Hubbard, C. R. & Stalick, J. K. (1981). *NBS∗EXAIDS83. A Fortran program for crystallographic data evaluation*. *Natl Bur. Stand. (US) Tech. Note*, No. 1141, April 1981.

Mitra, G. B., Ahmed, A. & Das Gupta, P. (1985). *Precise and accurate estimation of crystallographic parameters by maximum-likelihood and min–max methods*. *Structure and statistics in crystallography*, edited by A. J. C. Wilson, pp. 151–181. Guilderland, NY: Adenine Press.

Nakajima, T., Fukamachi, T., Terasaki, O. & Hosoya, S. (1976). *The detection of small differences in lattice constant at low temperature by an energy-dispersive X-ray diffractometer*. *J. Appl. Cryst.* **9**, 286–290.

5.2 (*cont.*)

Nelson, J. B. & Riley, D. P. (1945). *An experimental investigation of extrapolation methods in the derivation of accurate unit-cell dimensions of crystals*. *Proc. Phys. Soc. London*, **57**, 160–177, 477–495.

Okazaki, A. & Kawaminami, M. (1973). *Accurate measurement of lattice constant in a wide range of temperature: use of white X-rays and double-crystal diffractometry*. *Jpn. J. Appl. Phys.* **12**, 783–789.

Parrish, W. (1960). *Results of the IUCr precision lattice-parameter project*. *Acta Cryst.* **13**, 838–850.

Parrish, W. (1988). *Advances in synchrotron X-ray polycrystalline diffraction*. *Aust. J. Phys.* **41**, 101–112.

Parrish, W. & Hart, M. (1987). *Advantages of synchrotron radiation for polycrystalline diffractometry*. *Z. Kristallogr.* **179**, 161–173.

Parrish, W., Hart, M., Huang, T. C. & Bellotto, M. (1987). *Lattice-parameter determination using synchrotron powder data*. *Adv. X-ray Anal.* **30**, 373–382.

Parrish, W. & Huang, T. C. (1980). *Accuracy of the profile fitting method for X-ray polycrystalline diffractometry*. *Natl Bur. Stand. (US) Spec. Publ.* No. 457, pp. 95–110.

Pawley, G. S. (1981). *Unit-cell refinement from powder diffraction scans*. *J. Appl. Cryst.* **14**, 357–361.

Pike, E. R. (1957). *Counter diffractometer – the effects of vertical divergence on the displacement and breadth of powder diffraction lines*. *J. Sci. Instrum.* **34**, 355–361.

Pike, E. R. & Wilson, A. J. C. (1959). *Counter diffractometer – the theory of the use of centroids of diffraction profiles for high accuracy in the measurement of diffraction angles*. *Br. J. Appl. Phys.* **10**, 57–68.

Popović, S. (1973). *Unit-cell dimension measurements from pairs of X-ray diffraction lines*. *J. Appl. Cryst.* **6**, 122–128.

Rietveld, H. M. (1967). *Line profiles of neutron powder-diffraction peaks for structure refinement*. *Acta Cryst.* **22**, 151–152.

Rietveld, H. M. (1969). *A profile refinement method for nuclear and magnetic structures J. Appl. Cryst.* **2**, 65–71.

Sandström, A. E. (1957). *Experimental methods of X-ray spectroscopy: ordinary wavelengths*. *Handbuch der Physik*, pp. 78–245 (esp. p. 157). Berlin: Springer.

Scardi, P., Lutterotti, L. & Maistrelli, P. (1994). *Experimental determination of the instrumental broadening in Bragg–Brentano geometry*. *Powder Diffr.* **9**, 180–186.

Soller, W. (1924). *A new precision X-ray spectrometer*. *Phys. Rev.* **24**, 158–167.

Sparks, C. J. & Gedcke, D. A. (1972). *Rapid recording of powder diffraction patterns with Si(Li) X-ray energy analysis system: W and Cu targets and error analysis*. *Adv. X-ray Anal.* **15**, 240–253.

Spencer, R. C. (1931). *Additional theory of the double X-ray spectrometer*. *Phys. Rev.* **38**, 618–629.

Spencer, R. C. (1935). *The effect of the spectrometer on the width of spectral lines*. *Phys. Rev.* **48**, 473.

Spencer, R. C. (1937). *A theorem on the effect of vertical divergence*. *Phys. Rev.* **52**, 761.

Spencer, R. C. (1939). *The correction of experimental curves for the resolving power of the apparatus*. *Phys. Rev.* **55**, 239.

Spencer, R. C. (1941). *Optimum design of physical apparatus*. *Phys. Rev.* **60**, 172.

Spencer, R. C. (1949). *Discussion of ''Geometrical factors affecting X-ray spectrometer maxima''*. *J. Appl. Phys.* **20**, 413–414.

Taylor, A. & Sinclair, H. B. (1945*a*). *The influence of absorption on the shapes and positions of lines in Debye–Scherrer powder photographs*. *Proc. Phys. Soc. London*, **57**, 108–125.

Taylor, A. & Sinclair, H. B. (1945*b*). *On the determination of lattice parameters by the Debye–Scherrer method*. *Proc. Phys. Soc. London*, **57**, 126–135.

Thomsen, J. S. (1974). *High-precision X-ray spectroscopy*. *X-ray spectroscopy*, edited by L. V. Azaroff, pp. 26–132. New York: McGraw-Hill.

Thomsen, J. S. & Yap, F. Y. (1968*a*). *Effect of statistical counting errors on wavelength criteria for X-ray spectra*. *J. Res. Natl Bur. Stand. Sect. A*, **72**, 187–205.

Thomsen, J. S. & Yap, F. Y. (1968*b*). *Simplified method of computing centroids of X-ray profiles*. *Acta Cryst.* A**24**, 702–703.

Timmers, J., Delhez, R., Tuinstra, F. & Peerdeman, F. (1992). *X-ray tracing; a tool for improved accuracy in powder diffractometry*. *Accuracy in powder diffraction II. NIST Spec. Publ.* No. 846, edited by E. Prince & J. K. Stalick, p. 217.

Toraya, H. (1986). *Whole-powder-pattern fitting without reference to a structural model: application to X-ray powder diffractometer data*. *J. Appl. Cryst.* **19**, 440–447.

Toraya, H. (1988). *The deconvolution of overlapping reflections by the procedure of direct fitting*. *J. Appl. Cryst.* **21**, 192–196.

Wilkens, M. (1960). *Zur Brechungskorrektur bei Gitterkonstantmessungen an Pulverpräparaten*. *Acta Cryst.* **13**, 826–828.

Wilson, A. J. C. (1940). *On the correction of lattice spacings for refraction*. *Proc. Cambridge Philos. Soc.* **36**, 485–489.

Wilson, A. J. C. (1950). *Geiger-counter X-ray spectrometer – influence of the size and absorption coefficient of the specimen on position and shape of powder diffraction maxima*. *J. Sci. Instrum.* **27**, 321–325.

Wilson, A. J. C. (1958). *Effect of absorption on mean wavelength of X-ray emission lines*. *Proc. Phys. Soc. London*, **72**, 924–925.

Wilson, A. J. C. (1961). *A note on peak displacements in X-ray diffractometry*. *Proc. Phys. Soc. London*, **78**, 249–255.

Wilson, A. J. C. (1962). *Refraction broadening in powder diffractometer*. *Proc. Phys. Soc. London*, **80**, 303–305.

Wilson, A. J. C. (1963). *Mathematical theory of X-ray powder diffractometry*. Eindhoven: Centrex.

Wilson, A. J. C. (1965*a*). *On variance as a measure of line broadening in diffractometry. IV. The effect of physical aberrations*. *Proc. Phys. Soc. London*, **85**, 171–176.

Wilson, A. J. C. (1965*b*). *The location of peaks*. *Br. J. Appl. Phys.* **16**, 665–674.

Wilson, A. J. C. (1965*c*). *Röntgenstrahlpulverdiffractometrie. Mathematische Theorie*. Eindhoven: Centrex.

Wilson, A. J. C. (1967). *Statistical variance of line-profile parameters. Measures of intensity, location and dispersion*. *Acta Cryst.* **23**, 888–898. *Addenda and Corrigenda, ibid.*, A**24**, 478 and A**25**, 584–585.

Wilson, A. J. C. (1970*a*). *Elements of X-ray crystallography*. Reading, MA: Addison-Wesley.

Wilson, A. J. C. (1970*b*). *Limitations on the additivity of moments in line-profile analysis*. *J. Appl. Phys.* **3**, 71–73.

Wilson, A. J. C. (1971). *Some statistical considerations in the location of Mössbauer lines*. *Nucl. Instrum. Methods*, **94**, 225–227.

Wilson, A. J. C. (1973). *Note on the aberrations of a fixed-angle energy-dispersive diffractometer*. *J. Appl. Cryst.* **6**, 230–237.

5.2 (*cont.*)

Wilson, A. J. C. (1974). *Powder diffractometry. X-ray diffraction*, by L. V. Azaroff, R. Kaplow, N. Kato, R. Weiss, A. J. C. Wilson & R. A. Young, Chap. 6. New York: McGraw-Hill.

Wilson, A. J. C. (1980). *Accuracy in methods of lattice-parameter measurement. Natl Bur. Stand. (US) Spec. Publ.* No. 567, pp. 325–351.

Wilson, A. J. C. & Delf, B. W. (1961). *Effects of variations in the quantum counting efficiency of detectors on the mean wavelengths of emission lines. Proc. Phys. Soc. London*, **78**, 1256–1258.

Wilson, A. J. C. & Lipson, H. (1941). *The calibration of Debye–Scherrer X-ray powder cameras. Proc. Phys. Soc. London*, **53**, 245–250.

Wilson, A. J. C., Thomsen, J. S. & Yap, F. Y. (1965). *Minimization of the variation of parameters derived from X-ray powder diffractometer line profiles. Appl. Phys. Lett.* **7**, 163–165.

Wong-Ng, W. & Hubbard, C. R. (1987). *Standard reference materials for X-ray diffraction. Part II. Calibration using d-spacing standards. Powder Diffr.* **2**, 242–248.

Young, R. A. (1988). *Pressing the limits of Rietveld refinement. Aust. J. Phys.* **41**, 294–310.

Zevin, L. S., Umanskij, M. M., Khejker, D. M. & Pančenko, J. M. (1961). *The question of diffractometer methods of precision measurement of unit-cell parameters. Sov. Phys. Crystallogr.* **6**, 277–283.

5.3

Abrahams, S. C., Liminga, R., Marsh, P., Schrey, F., Albertsson, J., Svensson, C. & Kvick, Å. (1983). *Thermal expansivity of α-$LiIO_3$ between 20 and 520 K. J. Appl. Cryst.* **16**, 453–457.

Alcock, N. W. & Sheldrick, G. M. (1967). *The determination of accurate unit-cell dimensions from inclined Weissenberg photographs. Acta Cryst.* **23**, 35–38.

Alexander, L. (1948). *Geometrical factors affecting the contours of X-ray spectrometer maxima. I. Factors causing asymmetry. J. Appl. Phys.* **19**, 1068–1071.

Alexander, L. (1950). *Geometrical factors affecting the contours of X-ray spectrometer maxima. II. Factors causing broadening. J. Appl. Phys.* **21**, 126–136.

Alexander, L. (1954). *The synthesis of X-ray spectrometer line profiles with application to crystallite size measurements. J. Appl. Phys.* **25**, 155–161.

Alexander, L. E. & Smith, G. (1962). *Single-crystal intensity measurements with the three-circle counter diffractometer. Acta Cryst.* **15**, 983–1004.

Amorós, J. L., Buerger, M. J. & Amorós, M. C. (1975). *The Laue method*. New York: Academic Press.

d'Amour, H., Denner, W., Schulz, H. & Cardona, M. (1982). *A uniaxial stress apparatus for single-crystal X-ray diffraction on a four-circle diffractometer: Application to silicon and diamond. J. Appl. Cryst.* **15**, 148–153.

Ando, M., Bailey, D. & Hart, M. (1978). *A simple Bragg-spacing comparator. Acta Cryst.* A**34**, 484–489.

Ando, M., Hagashi, Y., Usuda, K., Yasuami, S. & Kawata, H. (1989). *A precision Bond method with SR. Rev. Sci. Instrum.* **60**, 2410–2413.

Aristov, V. V., Shekhtman, V. Sh. & Shmytko, I. M. (1973). *Precision measurement of crystallographic parameters by the X-ray divergent-beam technique*. (In Russian.) *Kristallografiya*, **18**, 706–709. (English transl: *Sov. Phys. Crystallogr.* **18**, 445–446.)

Aristov, V. V. & Shmytko, I. M. (1978). *Precision lattice parameter measurement by the X-ray divergent-beam technique. J. Appl. Cryst.* **11**, 662–668.

Aristov, V. V., Shmytko, I. M. & Shulakov, E. V. (1974*a*). *Application of the X-ray divergent-beam technique for the determination of the angles between crystal blocks. I. Reflexion from the planes parallel to the crystal surface. J. Appl. Cryst.* **7**, 409–413.

Aristov, V. V., Shmytko, I. M. & Shulakov, E. V. (1974*b*). *Application of the X-ray divergent-beam technique for the determination of the angles between crystal blocks. II. Determination of the total misorientation angle between blocks. J. Appl. Cryst.* **7**, 413–416.

Arndt, U. W. & Willis, B. T. M. (1966). *Single crystal diffractometry*. Cambridge University Press.

Åsbrink, S., Wołcyrz, M. & Hong, S.-H. (1985). *X-ray Bond-type diffractometric investigations on V_3O_5 in the temperature interval 298 to 480 K including the phase transition temperature $T_t = 428$ K. Phys. Status Solidi A*, **87**, 135–140; erratum: **89**, 415.

Azároff, L. V. (1974). *X-ray spectroscopy*, Chap. 2. New York: McGraw-Hill.

Bačkovský, J. (1965). *On the most accurate measurements of the wavelengths of X-ray spectral lines. Czech. J. Phys.* B**15**, 752–759.

Baker, J. A., Tucker, T. N., Moyer, N. E. & Buschert, R. C. (1968). *Effects of carbon on the lattice parameter of silicon. J. Appl. Phys.* **39**, 4365–4368.

Baker, J. F. C. & Hart, M. (1975). *An absolute measurement of the lattice parameter of germanium using multiple-beam X-ray diffractometry. Acta Cryst.* A**31**, 364–367.

Baker, J. F. C., Hart, M., Halliwell, M. A. G. & Heckingbottom, R. (1976). *Precise lattice parameter determination of dislocation-free gallium arsenide. I. X-ray measurements. Solid-State Electron.* **19**, 331–334.

Baker, T. W., George, J. D., Bellamy, B. A. & Causer, R. (1966). *Very high precision X-ray diffraction. Nature (London)*, **210**, 720–721.

Baker, T. W., George, J. D., Bellamy, B. A. & Causer, R. (1968). *Fully automated high-precision X-ray diffraction. Adv. X-ray Anal.* **11**, 359–375.

Barla, K., Herino, R., Bomchil, G. & Pfister, J. C. (1984). *Determination of lattice parameter and elastic properties of porous silicon by X-ray diffraction. J. Cryst. Growth,* **68**, 727–732.

Barns, R. L. (1972). *A strategy for rapid and accurate (p.p.m.) measurement of lattice parameters of single crystals by Bond's method. Adv. X-ray Anal.* **15**, 330–338.

Bartels, W. J. (1983). *Characterization of thin layers on perfect crystals with a multipurpose high-resolution X-ray diffractometer. J. Vac. Sci. Technol.* B**1**, 338–345.

Batchelder, D. N. & Simmons, R. O. (1965). *X-ray lattice constant of crystals by a rotating-camera method: Al, Ar, Au, CaF_2, Cu, Ge, Ne, Si. J. Appl. Phys.* **36**, 2864–2868.

Bearden, J. A. (1933). *The wavelengths of the silver, molybdenum, copper, iron and chromium $K\alpha_1$ lines. Phys. Rev.* **43**, 92–97.

Bearden, J. A. (1965). *Selection of W $K\alpha_1$ as the X-ray wavelength standard. Phys. Rev.* **137**, BY55–BY61.

5.3 (*cont.*)

Bearden, J. A. (1967). *X-ray wavelengths*. *Rev. Mod. Phys.* **39**, 78–124.

Bearden, J. A. & Henins, A. (1965). *Precision measurement of lattice imperfections with a photographic two-crystal method*. *Rev. Sci. Instrum.* **36**, 334–338.

Bearden, J. A., Marzolf, J. G. & Thomsen, J. S. (1968). *Crystal diffraction profiles for monochromatic radiation*. *Acta Cryst.* A**24**, 295–301.

Bearden, J. A. & Thomsen, J. S. (1971). *The double-crystal X-ray spectrometer: corrections, errors, and alignment procedure*. *J. Appl. Cryst.* **4**, 130–138.

Becker, P., Dorenwendt, K., Ebeling, G., Lauer, R., Lucas, W., Probst, R., Rademacher, H.-J., Reim, G., Seyfried, P. & Siegert, H. (1981). *Absolute measurement of the (220) lattice plane spacing in silicon crystal*. *Phys. Rev. Lett.* **46**, 1540–1543.

Becker, P., Seyfried, P. & Siegert, H. (1982). *The lattice parameter of highly pure silicon single crystals*. *Z. Phys. B*, **48**, 17–21.

Berg, H. M. & Hall, E. L. (1975). *The pseudo-Kossel technique in back reflection as a tool for measuring strains*. *Adv. X-ray Anal.* **18**, 454–465.

Berger, H. (1984). *A method for precision lattice-parameter measurement of single crystals*. *J. Appl. Cryst.* **17**, 451–455.

Berger, H. (1986*a*). *Systematic errors in precision lattice-parameter determination of single crystals caused by asymmetric line profiles*. *J. Appl. Cryst.* **19**, 34–38.

Berger, H. (1986*b*). *Study of the Kα emission spectrum of copper*. *X-ray Spectrom.* **15**, 241–243.

Berger, H. (1993). *X-ray diffraction studies on point defects in II–VI compounds*. *Cryst. Res. Technol.* **28**, 795–801.

Berger, H., Lehmann, A. & Schenk, M. (1985). *Lattice-parameter variations in PbTe single crystals*. *Cryst. Res. Technol.* **20**, 579–581.

Berger, H., Rosner, B. & Schikora, D. (1989). *Lattice parameter determination of superlattices*. *Cryst. Res. Technol.* **24**, 437–441.

Beu, K. E. (1967). *The precise and accurate determination of lattice parameters*. *Handbook of X-rays*, edited by E. F. Kaelble, Chap. 10. New York: McGraw-Hill.

Beu, K. E., Musil, F. J. & Whitney, D. R. (1962). *Precise and accurate lattice parameters by film powder methods. I. The likelihood ratio method*. *Acta Cryst.* **15**, 1292–1301.

Bevis, M., Fearon, E. O. & Rowlands, P. C. (1970). *The accurate determination of lattice parameters and crystal orientations from Kossel patterns*. *Phys. Status Solidi A*, **1**, 653–659.

Biggin, S. & Dingley, D. J. (1977). *A general method for locating the X-ray source point in Kossel diffraction*. *J. Appl. Cryst.* **10**, 376–385.

Bolotina, N. B. (1989). *Refinement of unit-cell parameters and orientation of specimen in diffractometer, taking account of symmetry of single crystal*. *Kristallografiya*, **34**, 598–601. (English transl: *Sov. Phys. Crystallogr.* **34**, 355–357.)

Bond, W. L. (1960). *Precision lattice constant determination*. *Acta Cryst.* **13**, 814–818.

Bond, W. L. (1975). *Precision lattice constant determination. Erratum*. *Acta Cryst.* A**31**, 698.

Bonse, U. & te Kaat, E. (1968). *A two-crystal X-ray interferometer*. *Z. Phys.* **214**, 16–21.

Bowen, D. K. & Tanner, B. K. (1995). *A method for the accurate comparison of lattice parameters*. *J. Appl. Cryst.* **28**, 753–760.

Bragg, W. H. & Bragg, W. L. (1915). *X-rays and crystal structure*, Chap. 2. London: G. Bell and Sons.

Brown, B. R., Halliwell, M. A. G. & Isherwood, B. J. (1980). *The characterization of distortions in heteroepitaxial structures by X-ray multiple diffraction*. *J. Microsc.* **118**, 375–381.

Brühl, H.-G. (1978). *Precision lattice parameter measurements of VPE-GaP-epitaxial layers by the 'Umweganregung' method*. *Krist. Tech.* **13**, 1247–1251.

Brühl, H.-G. & Rhan, H. (1985). *On the extension of the theory of Umweganregung with respect to the use of divergent white X-ray radiation*. *Phys. Status Solidi A*, **87**, 121–126.

Buerger, M. J. (1942). *X-ray crystallography*. London: John Wiley.

Buras, B., Olsen, J. S., Gerward, L., Will, G. & Hinze, E. (1977). *X-ray energy-dispersive diffractometry using synchrotron radiation*. *J. Appl. Cryst.* **10**, 431–438.

Burke, J. & Tomkeieff, M. V. (1968). *Specimen and beam tilt errors in Bond's method of lattice parameter determination*. *Acta Cryst.* A**24**, 683–685.

Burke, J. & Tomkeieff, M. V. (1969). *Errors in the Bond method of lattice parameter determinations. Further considerations*. *J. Appl. Cryst.* **2**, 247–248.

Buschert, R. C. (1965). *X-ray lattice parameter and linewidth studies in silicon*. *Bull. Am. Phys. Soc.* **10**, 125.

Buschert, R. C., Merlini, A. E., Pace, S., Rodriguez, S. & Grimsditch, M. H. (1988). *Effect of isotope concentration on the lattice parameter of germanium perfect crystals*. *Phys. Rev. B*, **38**, 5219–5221.

Buschert, R. C., Meyer, A. J., Stuckey Kauffman, D. & Gotwals, J. K. (1983). *A double-source double-crystal X-ray spectrometer for high-sensitivity lattice-parameter difference measurements*. *J. Appl. Cryst.* **16**, 599–605.

Buschert, R. C., Pace, S., Inzaghi, D. & Merlini, A. E. (1980). *A high-sensitivity double-beam triple-crystal spectrometer for lattice parameter and topographic measurements*. *J. Appl. Cryst.* **13**, 207–210.

Busing, W. R. & Levy, H. A. (1967). *Angle calculations for 3- and 4-circle X-ray and neutron diffractometers*. *Acta Cryst.* **22**, 457–464.

Carr, P. D., Cruickshank, D. W. J. & Harding, M. M. (1992). *The determination of unit-cell parameters from Laue diffraction patterns using their gnomonic projections*. *J. Appl. Cryst.* **25**, 294–308.

Cembali, F., Fabri, R., Servidori, M., Zani, A., Basile, G., Cavagnero, G., Bergamin, A. & Zosi, G. (1992). *Precise X-ray relative measurement of lattice parameters of silicon wafers by multiple-crystal Bragg-case diffractometry. Computer simulation of the experiment*. *J. Appl. Cryst.* **25**, 424–431.

Černohorský, M. (1960). *The ratio method for absolute measurements of lattice parameters with cylindrical cameras*. *Acta Cryst.* **13**, 823–826.

Chang, S.-L. (1979). *Direct observation of two-dimensional lattice mismatch parallel to the interfacial boundary between the LPE $Ga_{0.65}Al_{0.35}As$ layer and the GaAs substrate*. *Appl. Phys. Lett.* **34**, 239-240.

Chang, S.-L. (1984). *Multiple diffraction of X-rays in crystals*, Chap. 7.2 in particular. Berlin: Springer-Verlag.

Chang, S.-L., Patel, N. B., Nannichi, Y. & de Prince, F. C. (1979). *Determination of lattice mismatch in $Ga_{1-x}Al_xAs$ LPE layer on GaAs substrate by using a divergent X-ray source*. *J. Appl. Phys.* **50**, 2975–2976.

Clegg, W. (1981). *Least-squares refinement of unit-cell parameters from precession photographs*. *Acta Cryst.* A**37**, 437–438.

5.3 (*cont.*)

Clegg, W. (1984). *Orientation matrix refinement during four-circle diffractometer data collection*. *Acta Cryst.* A**40**, 703–704.

Clegg, W. & Sheldrick, G. M. (1984). *The refinement of unit cell parameters from two-circle diffractometer measurements*. *Z. Kristallogr.* **167**, 23–27.

Cole, H., Chambers, F. W. & Dunn, H. M. (1962). *Simultaneous diffraction: indexing Umweganregung peaks in simple cases*. *Acta Cryst.* **15**, 138–144.

Compton, A. H. & Allison, S. K. (1935). *X-rays in theory and experiment*. New York: Van Nostrand.

Cooper, A. S. (1962). *Precise lattice constants of germanium, aluminium, gallium arsenide, uranium, sulphur, quartz and sapphire*. *Acta Cryst.* **15**, 578–582.

Cruickshank, D. W. J., Carr, P. D. & Harding, M. M. (1992). *Estimation of d_{min}, λ_{min} and λ_{max} from the gnomonic projections of Laue patterns*. *J. Appl. Cryst.* **25**, 285–293.

Davis, B. L. & Johnson, L. R. (1984). *The true unit cell of ammonium hydrogen sulfate, $(NH_4)_3H(SO_4)_2$*. *J. Appl. Cryst.* **17**, 331–333.

Deslattes, R. D. (1969). *Optical and X-ray interferometry of a silicon lattice spacing*. *Appl. Phys. Lett.* **15**, 386–388.

Deslattes, R. D. & Henins, A. (1973). *X-ray to visible wavelength ratios*. *Phys. Rev. Lett.* **31**, 972–975.

Deslattes, R. D., Henins, A., Bowman, H. A., Schoonover, R. M., Caroll, C. L., Barnes, I. L., Machlan, L. A., Moore, L. J. & Shields, W. R. (1974). *Determination of the Avogadro constant*. *Phys. Rev. Lett.* **33**, 463–466.

Deslattes, R. D., Henins, A., Schoonover, R. M., Caroll, C. L. & Bowman, H. A. (1976). *Avogadro constant – correction to an earlier report*. *Phys. Rev. Lett.* **36**, 898–900.

Dressler, L., Griebner, U. & Kittner, R. (1987). *Precision measurement of lattice parameters in LiF monocrystals*. *Cryst. Res. Technol.* **22**, 1431–1435.

Eastabrook, J. N. (1952). *Effect of vertical divergence on the displacement and breadth of X-ray powder diffraction lines*. *Br. J. Appl. Phys.* **3**, 349–352.

Ellis, T., Nanni, L. F., Shrier, A., Weissmann, S., Padawer, G. E. & Hosokawa, N. (1964). *Strain and precision lattice parameter measurements by the X-ray divergent beam method. I. J. Appl. Phys.* **35**, 3364–3373.

Evans, H. T. Jr & Lonsdale, K. (1959). *Diffraction geometry*. *International tables for X-ray crystallography*, Vol. II, Chap. 4. Birmingham: Kynoch Press.

Farquhar, M. C. M. & Lipson, H. (1946). *The accurate determination of cell dimensions from single-crystal X-ray photographs*. *Proc. Phys. Soc. London*, **58**, 200–206.

Fewster, P. F. (1982). *Absolute lattice-parameter measurements of epitaxial layers*. *J. Appl. Cryst.* **15**, 275–278.

Fewster, P. F. (1989). *A high-resolution multiple-crystal multiple-reflection diffractometer*. *J. Appl. Cryst.* **22**, 64–69.

Fewster, P. F. (1993). *Structural characterisation of materials by combining X-ray diffraction space mapping and topography*. *Philips J. Res.* **47**, 235–245.

Fewster, P. F. & Andrew, N. L. (1995). *Absolute lattice-parameter measurement*. *J. Appl. Cryst.* **28**, 451–458.

Fewster, P. F. & Willoughby, A. F. W. (1980). *The effect of silicon doping on the lattice parameter of gallium arsenide grown by liquid-phase epitaxy, vapour-phase epitaxy and gradient-freeze techniques*. *J. Cryst. Growth*, **50**, 648–653.

Filscher, G. & Unangst, D. (1980). *Bond-method for precision lattice constant determination. Dependence of lattice constant error on sample adjustment and collimator tilt*. *Krist. Tech.* **15**, 955–960.

Fischer, D. G. & Harris, N. (1970). *A computer program for the calculation of lattice spacings from Kossel diffraction patterns*. *J. Appl. Cryst.* **3**, 305–313.

Fukahara, A. & Takano, Y. (1977). *Determination of strain distributions from X-ray Bragg reflexion by silicon single crystals*. *Acta Cryst.* A**33**, 137–142.

Fukumori, T. & Futagami, K. (1988). *Measurements of lattice parameters and half-widths of the rocking curve on GaAs crystal by the X-ray double-crystal method using a Cu Kα doublet*. *Jpn. J. Appl. Phys.* **27**, 442–443.

Fukumori, T., Futagami, K. & Matsunaga, K. (1982). *X-ray double-crystal method for crystal lattice parameter measurements using Cu Kα doublet*. *Jpn. J. Appl. Phys.* **21**, 1525.

Fukumori, T., Imai, K., Hasegawa, T. & Akashi, Y. (1997). *Precision lattice spacing measurement using X-ray Cu Kα doublet*. *J. Phys. Soc. Jpn*, **66**, 1976–1978.

Gabe, E. J. (1980). *Diffractometer control with minicomputers*. *Computing in crystallography*, edited by R. Diamond, S. Ramaseshan & K. Venkatesan, pp. 1.01–1.18. Bangalore: Indian Academy of Sciences.

Gałdecka, E. (1985). *The variances and covariances of measured intensities in precise lattice-constant determination by the Bond method*. *Structure & statistics in crystallography*, edited by A. J. C. Wilson, pp. 137–149. New York: Adenine Press.

Gałdecka, E. (1993*a*). *Description and peak-position determination of a single X-ray diffraction profile for high-accuracy lattice-parameter measurements by the Bond method. I. An analysis of descriptions available*. *Acta Cryst.* A**49**, 106–115.

Gałdecka, E. (1993*b*). *Description and peak-position determination of a single X-ray diffraction profile for high-accuracy lattice-parameter measurements by the Bond method. II. Testing and choice of description*. *Acta Cryst.* A**49**, 116–126.

Gałdecka, E. (1994). *The extrapolated-peak method for the peak-position determination of an X-ray diffraction profile, and the accuracy of the Bragg-angle measurements*. *Sci. Bull. Tech. Univ. Łódź Branch Bielsko-Biała*, **22**(4), 1–24.

Gamarnik, M. Ya. (1990). *Size changes of lattice parameters in ultradisperse diamond and silicon*. *Phys. Status Solidi B*, **161**, 457–462.

Geist, V. & Ascheron, C. (1984). *The proton-induced Kossel effect and its application to crystallographic studies*. *Cryst. Res. Technol.* **19**, 1231–1244.

Gielen, P., Yakowitz, H., Ganow, D. & Ogilvie, R. E. (1965). *Evaluation of Kossel microdiffraction procedures: the cubic case*. *J. Appl. Phys.* **36**, 773–782.

Glass, H. L. & Moudy, L. A. (1974). *Measurement of the lattice parameter of gadolinium gallium garnet crystals by the X-ray divergent-beam anomalous-transmission method*. *J. Appl. Cryst.* **7**, 22–24.

Glass, H. L. & Weissmann, S. (1969). *Synergy of line profile analysis and selected area topography by the X-ray divergent beam method*. *J. Appl. Cryst.* **2**, 200–209.

Glazer, A. M. (1972). *A technique for the automatic recording of phase transitions in single crystals*. *J. Appl. Cryst.* **5**, 420–423.

Glazer, A. M. & Megaw, H. D. (1973). *Studies of the lattice parameters and domains in the phase transitions of $NaNbO_3$*. *Acta Cryst.* A**29**, 489–495.

5.3 (*cont.*)

Godwod, K., Kowalczyk, R. & Szmid, Z. (1974). *Application of a precise double X-ray spectrometer for accurate lattice parameter determination*. *Phys. Status Solidi A*, **21**, 227–234.

Golovin, A. L., Imamov, R. M. & Kondrashkina, E. A. (1985). *Absolute measurements of lattice spacings in surface layers of crystals*. *Phys. Status Solidi A*, **89**, K5–K7.

Grosswig, S., Härtwig, J., Alter, U. & Christoph, A. (1983). *Precision lattice parameter determination of coloured quartz monocrystals*. *Cryst. Res. Technol.* **18**, 501–511.

Grosswig, S., Härtwig, J., Jäckel, K.-H., Kittner, R. & Melle, W. (1986). *A novel arrangement for the absolute measurement of geometric lattice parameters of monocrystals with high precision*. *Nauch. Apparat. Sci. Instrum.* **1**, 29–44.

Grosswig, S., Jäckel, K.-H. & Kittner, R. (1986). *Peak position determination of X-ray diffraction profiles in precision lattice parameter measurements according to the Bond-method with help of the polynomial approximation*. *Cryst. Res. Technol.* **21**, 133–139.

Grosswig, S., Jäckel, K.-H., Kittner, R., Dietrich, B. & Schellenberger, U. (1985). *Determination of the coplanar geometric lattice parameters of monocrystals with high precision*. *Cryst. Res. Technol.* **20**, 1093–1100.

Grosswig, S., Melle, W., Schellenberger, U. & Zahorowski, W. (1983). *High precision lattice parameter determination of KDP with different crystal perfection*. *Cryst. Res. Technol.* **18**, K28–K30.

Gruber, E. E. & Black, R. E. (1970). *Analysis of the axial misalignment error in precision lattice parameter measurement by the Bond technique*. *J. Appl. Cryst.* **3**, 354–357.

Halliwell, M. A. G. (1970). *Measurement of specimen tilt and beam tilt in the Bond method*. *J. Appl. Cryst.* **3**, 418–419.

Hamilton, W. C. (1974). *Angle settings for four-circle diffractometers*. *International tables for X-ray crystallography*, Vol. IV, pp. 274–284. Birmingham: Kynoch Press. (Present distributor: Kluwer Academic Publishers, Dordrecht.)

Hanneman, R. E., Ogilvie, R. E. & Modrzejewski, A. (1962). *Kossel line studies of irradiated nickel crystals*. *J. Appl. Phys.* **33**, 1429–1435.

Harris, N. & Kirkham, A. J. (1971). *A single-exposure method for the determination of lattice spacings and crystal orientation from Kossel diffraction patterns*. *J. Appl. Cryst.* **4**, 232–240.

Hart, M. (1969). *High precision lattice parameter measurements by multiple Bragg reflexion diffractometry*. *Proc. R. Soc. London Ser. A*, **309**, 281–296.

Hart, M. (1981). *Bragg angle measurement and mapping*. *J. Cryst. Growth*, **55**, 409–427.

Hart, M. & Lloyd, K. H. (1975). *Measurement of strain and lattice parameter in epitaxic layers*. *J. Appl. Cryst.* **8**, 42–44.

Hart, M., Parrish, W., Bellotto, M. & Lim, G. S. (1988). *The refractive-index correction in powder diffraction*. *Acta Cryst.* A**44**, 193–197.

Härtwig, J., Bąk-Misiuk, J., Berger, H., Brühl, H.-G., Okada, Y., Grosswig, S., Wokulska, K. & Wolf, J. (1994). *Comparison of lattice parameters obtained from an internal monocrystal standard*. *Phys. Status Solidi A*, **142**, 19–26.

Härtwig, J. & Grosswig, S. (1989). *Measurement of X-ray diffraction angles of perfect monocrystals with high accuracy using a single crystal diffractometer*. *Phys. Status Solidi A*, **115**, 369–382.

Härtwig, J., Grosswig, S., Becker, P. & Windisch, D. (1991). *Remeasurement of the Cu $K\alpha_1$ emission X-ray wavelength in the metrical system (present stage)*. *Phys. Status Solidi A*, **125**, 79–89.

Härtwig, J., Hölzer, G., Förster, E., Goetz, K., Wokulska, K. & Wolf, J. (1994). *Remeasurement of characteristic X-ray emission lines and their application to line profile analysis and lattice parameter determination*. *Phys. Status Solidi A*, **143**, 23–34.

Härtwig, J., Hölzer, G., Wolf, J. & Förster, E. (1993). *Remeasurement of the profile of the characteristic Cu $K\alpha$ emission line with high precision and accuracy*. *J. Appl. Cryst.* **26**, 539–548.

Häusermann, D. & Hart, M. (1990). *A fast high-accuracy lattice-parameter comparator*. *J. Appl. Cryst.* **23**, 63–69.

Hebert, H. (1978). *A simple method for obtaining triclinic cell parameters from Weissenberg photographs from one crystal setting*. *Acta Cryst.* A**34**, 946–949.

Heise, H. (1962). *Precision determination of the lattice constant by the Kossel line technique*. *J Appl. Phys.* **33**, 938–941.

Henry, N. F. M., Lipson, H. & Wooster, W. A. (1960). *The interpretation of X-ray diffraction photographs*. London: Macmillan.

Herbstein, F. H. (2000). *How precise are measurements of unit-cell dimensions from single crystals? Acta Cryst.* B**56**, 547–557.

Holý, V. & Härtwig, J. (1988). *The role of diffuse scattering on microdefects in the precise lattice parameter measurement*. *Phys. Status Solidi B*, **145**, 363–372.

Hölzer, G., Fritsch, M., Deutsch, M., Härtwig, J. & Förster, E. (1997). *$K\alpha_{1,2}$ and $K\beta_{1,3}$ X-ray emission lines of the 3d transition metals*. *Phys. Rev. A*, **56**, 4554–4568.

Hom, T., Kiszenick, W. & Post, B. (1975). *Accurate lattice constants from multiple reflection measurements. II. Lattice constants of germanium, silicon and diamond*. *J. Appl. Cryst.* **8**, 457–458.

Horváth, J. (1983). *Lattice-parameter measurements of $PbHPO_4$ single crystals by the ratio method*. *J. Appl. Cryst.* **16**, 623–628.

Horváth, J. & Kucharczyk, D. (1981). *Temperature dependence of lattice parameters of $PbHPO_4$ and $PbDPO_4$ single crystals*. *Phys. Status Solidi A*, **63**, 687–692.

Hubbard, C. R. & Mauer, F. A. (1976). *Precision and accuracy of the Bond method as applied to small spherical crystals*. *J. Appl. Cryst.* **9**, 1–8.

Hubbard, C. R., Swanson, H. E. & Mauer, F. A. (1975). *A silicon powder diffraction standard reference material*. *J. Appl. Cryst.* **8**, 45–48.

Hulme, R. (1966). *Triclinic cell parameters from one crystal setting*. *Acta Cryst.* **21**, 898–900.

Imura, T. (1954). *The study of deformation of single crystals by the divergent X-ray beams*. *Bull. Naniwa. Univ. Ser. A*, 51.

Imura, T., Weissmann, S. & Slade, J. J. Jr (1962). *A study of age-hardening of Al–3.85%Cu by the divergent X-ray beam method*. *Acta Cryst.* **15**, 786–793.

Irie, K., Koshiji, N. & Okazaki, A. (1989). *High-angle double-crystal X-ray diffractometry (HADOX): combination with a sealed-tube X-ray source*. *Jpn. J. Appl. Phys.* **28**, 1504–1506.

Isherwood, B. J. (1968). *An X-ray multiple diffraction study of yttrium iron garnet crystals*. *J. Appl. Cryst.* **1**, 299–307.

Isherwood, B. J., Brown, B. R. & Halliwell, M. A. G. (1981). *X-ray multiple diffraction as a tool for studying heteroepitaxial layers. I. Coherent, on-axis layers*. *J. Cryst. Growth*, **54**, 449–460.

5.3 (*cont.*)

Isherwood, B. J., Brown, B. R. & Halliwell, M. A. G. (1982). *X-ray multiple diffraction as a tool for studying heteroepitaxial layers. II. Coherent, off-axis layers. J. Cryst. Growth*, **60**, 33–42.

Isherwood, B. J. & Wallace, C. A. (1966). *Measurement of the lattice parameter of silicon using a double-diffraction effect. Nature (London)*, **212**, 173–175.

Isherwood, B. J. & Wallace, C. A. (1970). *An X-ray multiple diffraction study of crystals of arsenic-doped germanium. J. Appl. Cryst.* **3**, 66–71.

Isherwood, B. J. & Wallace, C. A. (1971). *The geometry of X-ray multiple diffraction in crystals. Acta Cryst.* A**27**, 119–130.

James, R. W. (1967). *The optical principles of the diffraction of X-rays*. London: Bell.

Keller, H. L., Kucharczyk, D. & Küppers, H. (1982). *The ferroelastic monoclinic low temperature modification of ammonium hydrogen oxalate hemihydrate. Z. Kristallogr.* **158**, 221–232.

Kheiker, D. M. (1973). *Rentgenowskaya diffraktometriya monokristallow*, Chaps. 3, 4, 5. Leningrad: Mashinostroyenie.

Kheiker, D. M. & Zevin, L. S. (1963). *Rentgenowskaya diffraktometriya (X-ray diffractometry)*, Chap. 4. Moscow: Fizmatgiz.

Kirk, D. & Caulfield, P. B. (1977). *Location of diffractometer profiles in X-ray stress analysis. Adv. X-ray Anal.* **20**, 283–289.

Kishino, S. (1973). *Improved techniques of lattice parameter measurements using two X-ray beams. Adv. X-ray Anal.* **16**, 367–378.

Kobayashi, J., Mizutani, I. & Schmidt, H. (1970). *X-ray study on the lattice strains of ferroelectric iron iodine boracite $Fe_3B_7O_{13}$. Phys. Rev. B*, **1**, 3801–3808.

Kobayashi, J., Yamada, N. & Azumi, I. (1968). *An X-ray method for accurate determination of lattice strain of crystals. Rev. Sci. Instrum.* **39**, 1647–1650.

Kobayashi, J., Yamada, N. & Nakamura, T. (1963). *Origin of the visibility of the antiparallel 180° domains in barium titanate. Phys. Rev. Lett.* **11**, 410–414.

Korytár, D. (1984). *Lateral lattice parameter variation measurement by means of a double crystal X-ray method with oscillating slit. Czech. J. Phys.* B**34**, 1277–1281.

Kossel, W. (1936). *Messungen am vollständigen Reflexsystem eines Kristallgitters. Ann. Phys. (Leipzig)*, **26**, 533–553.

Kovalchuk, M. V., Kovev, E. K. & Pinsker, Z. G. (1975). *The X-ray triple-crystal spectrometer and precision determination of Δd_{hkl}*. (In Russian.) *Kristallografiya*, **20**, 142–148.

Kshevetsky, S. A., Mikhailyuk, I. P., Ostapovich, M. V., Polyak, M. I., Remenyuk, P. I. & Fomin, V. G. (1979). *Application of multiple diffraction to determination of lattice parameters*. (In Russian.) *Ukr. Fiz. Zh.* **24**, 1480–1485.

Kshevetsky, S. A., Mikhalchenko, V. P., Stetsko, Yu. P. & Shelud'ko, S. A. (1985). *The lattice parameter refinement of single crystals by means of multiple-wave diffractometry*. (In Russian.) *Ukr. Fiz. Zh.* **30**, 1843–1848.

Kubena, J. & Holý, V. (1988). *Precise relative X-ray measurement of the lattice parameter of silicon crystals with growth striations. J. Appl. Cryst.* **21**, 245–251.

Kucharczyk, D. & Niklewski, T. (1979). *Accurate X-ray determination of the lattice parameters and the thermal expansion coefficients of VO_2 near the transition temperature. J. Appl. Cryst.* **12**, 370–373.

Kucharczyk, D., Pietraszko, A. & Łukaszewicz, K. (1976). *Temperature dependence of lattice parameters of $NaNO_2$ single crystals. Phys. Status Solidi A*, **37**, 287–294.

Kucharczyk, D., Pietraszko, A. & Łukaszewicz, K. (1993). *An automatic four-circle diffractometer designed for precise lattice-parameter determination. J. Appl. Cryst.* **26**, 467.

Kudo, S. (1982). *X-ray determination of incommensurate superlattices in K_2SeO_4 and $(NH_4)_2BeF_4$. Jpn. J. Appl. Phys.* **21**, 255–258.

Kurbatov, B. A., Zubenko, V. V. & Umansky, M. M. (1972). *The use of the monochromator crystal with anomalous transmission of X-rays in precise lattice parameter measurements*. (In Russian.) *Kristallografiya*, **17**, 1058–1060.

Lang, A. R. & Pang, G. (1995). *A possible new route to precise lattice-parameter measurement of perfect crystals using the divergent-X-ray-beam method. J. Appl. Cryst.* **28**, 61–64.

Larson, B. C. (1974). *High-precision measurements of lattice parameter changes in neutron-irradiated copper. J. Appl. Phys.* **45**, 514–518.

Leszczyński, M., Podlasin, S. & Suski, T. (1993). *A 10^9 Pa high-pressure cell for X-ray and optical measurements. J. Appl. Cryst.* **26**, 1–4.

Lider, V. V. & Rozhansky, V. N. (1967). *A new X-ray method of precision lattice spacing determination by divergent-beam photograph. Fiz. Tverd. Tela (Leningrad)*, **9**, 3539–3546.

Lisoivan, V. I. (1974). *Local determination of all the lattice parameters of single crystals*. (In Russian.) *Appar. Methody Rentgenovskogo Anal.* **14**, 151–157.

Lisoivan, V. I. (1981). *Experimental refinement of the angles between unit-cell axes*. (In Russian.) *Kristallografiya*, **26**, 458–463.

Lisoivan, V. I. (1982). *Measurements of unit-cell parameters on one-crystal spectrometer*. (In Russian.) Novosibirsk: Nauka.

Lisoivan, V. I. & Dikovskaya, R. R. (1969). *Local precision determination of lattice constants of a single crystal. Prib. Tech. Eksp.* No. 4, pp. 164–166; English transl: *Instrum. Exp. Tech. (USSR)*, **4**, 992–994.

Lonsdale, K. (1947). *Divergent-beam X-ray photography of crystals. Proc. R. Soc. London Ser. A*, **240**, 219–250.

Luger, P. (1980). *Modern X-ray analysis of single crystals*. In particular, Chap. 4 and Section 4.2.2. Berlin: de Gruyter.

Łukaszewicz, K., Kucharczyk, D., Malinowski, M. & Pietraszko, A. (1978). *New model of the Bond diffractometer for precise determination of lattice parameters and thermal expansion of single crystals. Krist. Tech.* **13**, 561–567.

Łukaszewicz, K., Pietraszko, A., Kucharczyk, D., Malinowski, M., Stępień-Damm, J. & Urbanowicz, E. (1976). *Precyzyjne pomiary stałych sieciowych kryształów metodą Bonda (Precision measurements of lattice constants of crystals by the Bond method)*. Wrocław: Instytut Niskich Temperatur i Badań Strukturalnych PAN.

Lutts, A. (1973). *The geometrical distortion of deficiency conic sections and its influence on lattice-parameter determinations. J. Appl. Cryst.* **6**, 428–437.

Lutts, A. & Gielen, P. (1971). *The precise determination of the lattice parameter of α-iron and some of its alloys. J. Appl. Cryst.* **4**, 242–250.

Lutts, A. H. (1968). *Determination of lattice parameters by the Kossel and divergent X-ray beam techniques. Adv. X-ray Anal.* **11**, 345–358.

Mackay, K. J. H. (1966). *Proceedings of the IVth Congress on X-ray Optics and Microanalysis*, pp. 544–554. Paris: Hermann.

5.3 (*cont.*)

Main, P. & Woolfson, M. M. (1963). *Accurate lattice parameters from Weissenberg photographs*. *Acta Cryst*. **16**, 731–733.

Mauer, F. A., Hubbard, C. R., Piermarini, G. J. & Block, S. (1975). *Measurement of anisotropic compressibilities by a single crystal diffractometer method*. *Adv. X-ray Anal*. **18**, 437–453.

Mendelssohn, M. J. & Milledge, H. J. (1999). *Divergent-beam technique used in a SEM to measure the cell parameters of isotopically distinct samples of LiF over the temperature range ~15–375 K*. *Acta Cryst*. A**55**, 204–211.

Mohr, P. J. & Taylor, B. N. (2000). *CODATA recommended values of the fundamental physical constants*. *Rev. Mod. Phys*. **72**, 351–495.

Morris, W. G. (1968). *Crystal orientation and lattice parameters from Kossel lines*. *J. Appl. Phys*. **39**, 1813–1823.

Nemiroff, M. (1982). *Precise lattice-constant determinations using measured beam and crystal tilts*. *J. Appl. Cryst*. **15**, 375–377.

Newman, B. A. (1970). *The equation of pseudo-Kossel curves*. *J. Appl. Cryst*. **3**, 191–193.

Newman, B. A. & Shrier, A. (1970). *A new method of determining interplanar spacings with the back-reflection X-ray divergent beam technique*. *J. Appl. Cryst*. **3**, 280–281.

Newman, B. A. & Weissmann, S. (1968). *Strain inhomogeneities in lightly compressed tungsten crystals*. *J. Appl. Cryst*. **1**, 139–145.

Obaidur, R. M. (2002). *Energy-selective (+,+) monolithic monochromator and relative lattice-spacing measurement of Si wafers with synchrotron radiation*. *J. Synchrotron Rad*. **9**, 28–35.

Ohama, N., Sakashita, H. & Okazaki, A. (1979). *Improvement of high-angle double-crystal X-ray diffractometry (HADOX) for measuring temperature dependence of lattice constants. II. Practice*. *J. Appl. Cryst*. **12**, 455–459.

Okada, Y. (1982). *A high-temperature attachment for precise measurement of lattice parameters by Bond's method between room temperature and 1500 K*. *J. Phys. E*, **15**, 1060–1063.

Okazaki, A. & Kawaminami, M. (1973*a*). *Accurate measurement of lattice constants in a wide range of temperature: use of white X-ray and double-crystal diffractometry*. *Jpn. J. Appl. Phys*. **12**, 783–789.

Okazaki, A. & Kawaminami, M. (1973*b*). *Lattice constant of strontium titanate at low temperatures*. *Mater. Res. Bull*. **8**, 545–550.

Okazaki, A. & Ohama, N. (1979). *Improvement of high-angle double-crystal X-ray diffractometry (HADOX) for measuring temperature dependence of lattice constants. I. Theory*. *J. Appl. Cryst*. **12**, 450–454.

Okazaki, A. & Soejima, Y. (2001). *Ultra-high-angle double-crystal X-ray diffractometry (U-HADOX) for determining a change in the lattice spacing: theory*. *Acta Cryst*. A**57**, 708–712.

Parrish, W. (1960). *Results of the IUCr precision lattice-parameter project*. *Acta Cryst*. **13**, 838-850.

Parrish, W. & Wilson, A. J. C. (1959). *Precision measurements of lattice parameters of polycrystalline specimens*. *International tables for X-ray crystallography*, Vol. II, Chap. 4.7, pp. 216–234. Birmingham: Kynoch Press.

Pick, M. A., Bickmann, K., Pofahl, E., Zwoll, K. & Wenzl, H. (1977). *A new automatic triple-crystal X-ray diffractometer for the precision measurement of intensity distribution of Bragg diffraction and Huang scattering*. *J. Appl. Cryst*. **10**, 450–457.

Pierron, E. D. & McNeely, J. B. (1969). *Precise cell parameters of semiconductor crystals and their applications*. *Adv. X-ray Anal*. **12**, 343–353.

Pietraszko, A., Tomaszewski, P. E. & Łukaszewicz, K. (1981). *X-ray and optical study of the phase transition in $LiCsSO_4$*. *Phase Transit*. **2**, 131–150.

Pietraszko, A., Waśkowska, A., Olejnik, S. & Łukaszewicz, K. (1979). *X-ray study of the phase transition in $RbHSeO_4$*. *Phase Transit*. **1**, 99–106.

Pihl, C. F., Bieber, R. L. & Schwuttke, G. H. (1973). *Precision lattice parameter studies of ion-implanted silicon*. *Phys. Status Solidi A*, **17**, 359–369.

Polcarová, M. & Zůra, J. (1977). *A method for the determination of lattice parameters on single crystals*. *Czech. J. Phys*. B**27**, 322–331.

Popović, S. (1971). *An X-ray diffraction method for lattice parameter measurements from corresponding $K\alpha$ and $K\beta$ reflexions*. *J. Appl. Cryst*. **4**, 240–241.

Popović, S. (1974). *Determination of unit-cell parameters of single crystals from rotation patterns*. *J. Appl. Cryst*. **7**, 291–292.

Popović, S., Šljukić, M. & Hanic, F. (1974). *Precise unit cell parameter and thermal expansion measurements of single crystals by X-ray diffraction*. *Phys. Status Solidi A*, **23**, 265–274.

Post, B. (1975). *Accurate lattice constants from multiple diffraction measurements. I. Geometry, techniques and systematic errors*. *J. Appl. Cryst*. **8**, 452–456.

Potts, H. R. & Pearson, G. L. (1966). *Annealing and arsenic over-pressure experiments on defects in gallium arsenide*. *J. Appl. Phys*. **37**, 2098–2103.

Reeke, G. N. J. (1984). *Eigenvalue filtering in the refinement of crystal and orientation parameters for oscillation photography*. *J. Appl. Cryst*. **17**, 238–243.

Reichard, T. E. (1969). *A high-precision Kossel camera for research and routine analytical use*. *Adv. X-ray Anal*. **12**, 188–207.

Renninger, M. (1937). *'Umweganregung', eine bisher unbeachtete Wechselwirkungserscheinung bei Raumgitterinterferezen*. *Z. Phys*. **106**, 141–176.

Ridou, C., Rousseau, M. & Freund, A. (1977). *Détermination précise des paramètres cristallins au voisinage de changement de phase cubique quadratique dans $RbCaF_3$*. *J. Phys. (Paris)*, **38**, L-359–L-363.

Rossmanith, E. (1985). *UMWEG – a computer program for calculation and graphical representation of Umweganregung patterns*. *Z. Kristallogr*. **171**, 253–254.

Rossmann, M. G. (1979). *Processing oscillation diffraction data for very large unit cells with an automatic convolution technique and profile fitting*. *J. Appl. Cryst*. **12**, 225–238.

Rozhansky, V. H., Lider, V. V. & Lyutzau, V. G. (1966). *An X-ray method for surface topography of crystal structure defects based on Kossel-line scanning*. (In Russian.) *Kristallografiya*, **11**, 701–703.

Sasvári, J. & Zsoldos, É. (1980). *Accurate lattice parameter measurements of epitaxial layers*. Invited paper at International Symposium on Industrial Applications of X-ray Spectrometry and Diffractometry, Turawa, Poland, 15–18 April 1980.

Schetelich, Ch. & Geist, V. (1993). *Observation of X-ray Kossel patterns ('Gitterquelleninterferenzen') from quasicrystals*. *Phys. Status Solidi A*, **136**, 283–289.

Schneider, J. & Weik, H. (1968). *Z. Angew. Phys*. **2**, 75–79.

Schwartzenberger, D. R. (1959). *Philos. Mag*. **4**, 1242–1246.

5.3 (*cont.*)

Schwarzenbach, D., Abrahams, S. C., Flack, H. D., Gonschorek, W., Hahn, Th., Huml, K., Marsh, R. E., Prince, E., Robertson, B. E., Rollett, J. S. & Wilson, A. J. C. (1989). *Statistical descriptors in crystallography. Report of the International Union of Crystallography Subcommittee on Statistical Descriptors. Acta Cryst.* A**45**, 63–75.

Segmüller, A. (1970). *Automated lattice parameter determination on single crystals. Adv. X-ray Anal.* **13**, 455–467.

Shinoda, G., Isokawa, K. & Umeno, M. (1969). *Kossel line microdiffraction study on precipitation of alpha from beta in copper zinc alloys. Adv. X-ray Anal.* **12**, 174–187.

Shrier, A., Kalman, Z. H. & Weissmann, S. (1966). US Government Research Report AD 631 179.

Shvyd'ko, Yu. V., Lerche, M., Jäschke, J., Lucht, M., Gerdau, E., Gerken, M., Rüter, H. D., Wille, H.-C., Becker, P., Alp, E. E., Sturhahn, W., Sutter, J. & Toellner, T. S. (2000). *γ-ray wavelength standard for atomic scales. Phys. Rev. Lett.* **85**, 495–498.

Shvyd'ko, Yu. V., Lucht, M., Gerdau, E., Lerche, M., Alp, E. E., Sturhahn, W., Sutter, J. & Toellner, T. S. (2002). *Measuring wavelengths and lattice constants with the Mössbauer wavelength standard. J. Synchrotron Rad.* **9**, 17–23.

Siegert, H., Becker, P. & Seyfried, P. (1984). *Determination of silicon unit-cell parameters by precision measurements of Bragg plane spacings. Z. Phys. B*, **56**, 273–278.

Singh, K. & Trigunayat, G. C. (1988). *Accurate determination of lattice parameters from XRD oscillation photographs. J. Appl. Cryst.* **21**, 991.

Skupov, V. D. & Uspeckaya, G. I. (1975). *The combined X-ray spectrometer for deformation measurements in single crystals.* (In Russian.) *Prib. Tekh. Eksp.* No. 2, pp. 210–213.

Slade, J. J., Weissmann, S., Nakajima, K. & Hirabayshi, M. (1964). *Stress–strain analysis of single cubic crystals and its application to the ordering of CuAu I. Paper II. J. Appl. Phys.* **35**, 3373–3385.

Smakula, A. & Kalnajs, J. (1955). *Precision determination of lattice constants with a Geiger-counter X-ray diffractometer. Phys. Rev.* **99**, 1737–1743.

Soares, D. A. W. & Pimentel, C. A. (1983). *Precision interplanar spacing measurements on boron-doped silicon. J. Appl. Cryst.* **16**, 486–492.

Soejima, Y., Tomonaga, N., Onitsuka, H. & Okazaki, A. (1991). *Two-dimensional intensity distribution in high-angle double-crystal X-ray diffractometry (HADOX). Z. Kristallogr.* **195**, 161–168.

Spooner, F. J. & Wilson, C. G. (1973). *The measurement of single-crystal lattice parameters using a double-diffraction technique. J. Appl. Cryst.* **6**, 132–135.

Stępień, J. A., Auleytner, J. & Łukaszewicz, K. (1972). *X-ray examination of the real structure of γ-irradiated $NaClO_3$ single crystals. Phys. Status Solidi A*, **10**, 631–638.

Stępień-Damm, J. A., Kucharczyk, D., Urbanowicz, E. & Łukaszewicz, K. (1975). *Effect of γ-irradiation on the thermal expansion of sodium chlorate $NaClO_3$. Bull. Acad. Pol. Sci. Ser. Sci. Chim. Geol. Geogr.* **23**, 985–988.

Stępień-Damm, J. A., Suski, T., Meysner, L., Hilczer, B. & Łukaszewicz, K. (1974). *Effect of X-ray irradiation on the lattice constant of TGS crystal in the vicinity of phase transition. Bull. Acad. Pol. Sci. Ser. Sci. Chim. Geol. Geogr.* **22**, 685–688.

Stout, G. H. & Jensen, L. H. (1968). *X-ray structure determination*. London: Macmillan.

Straumanis, M. E., Borgeaud, P. & James, W. J. (1961). *Perfection of the lattice of dislocation-free silicon, studied by the lattice-constant and density method. J. Appl. Phys.* **32**, 1382–1384.

Straumanis, M. & Ieviņš, A. (1940). *Die Präzizionsbestimmung von Gitterkonstanten nach der asymmetrischen Methode*. Berlin: Springer. [Reprinted by Edwards Brothers Inc., Ann Arbor, Michigan (1948).]

Takano, Y. & Maki, M. (1972). *X-ray measurement of lattice strain of oxygen diffused silicon. Acta Cryst.* A**28**, S171.

Terminasov, Yu. S. & Tuzov, L. V. (1964). *The double-diffraction of X-rays in crystals.* (In Russian.) *Usp. Phys. Nauk*, **83**, 223–258. (English transl: *Sov. Phys. Usp.* **7**, 734.)

Thomsen, J. S. (1974). *High-precision X-ray spectroscopy. X-ray spectroscopy*, edited by L. V. Azároff, pp. 26–132. New York: McGraw-Hill.

Thomsen, J. S. & Yap, Y. (1968). *Effect of statistical counting errors on wavelengths criteria for X-ray spectra. J. Res. Natl Bur. Stand. Sect. A*, **72**, 187–205.

Tixier, R. & Waché, C. (1970). *Kossel patterns. J. Appl. Cryst.* **3**, 466–485.

Ullrich, H.-J. (1967). *Precision lattice parameter measurements by interferences from lattice sources (Kossel lines) and divergent beam X-ray diffraction (pseudo-Kossel-lines) in back reflection. Phys. Status Solidi*, **20**, K113–K117.

Ullrich, H.-J. & Schulze, G. E. R. (1972). *Röntgenographische Mikrobeugungsuntersuchungen an kristallinen Festkörpern mittels Gitterquelleninterferezen (Kossel-Linien) und Weitwinkelinterferenzen (Pseudo-Kossel-Linien). Krist. Tech.* **7**, 207–220.

Umansky, M. M. (1960). *Apparatura rentgenostrukturnykh issledovanij*. Moscow: Fizmatgiz.

Urbanowicz, E. (1981*a*). *The influence of in-plane collimation on the precision and accuracy of lattice-constant determination by the Bond method. I. A mathematical model. Statistical errors. Acta Cryst.* A**37**, 364–368.

Urbanowicz, E. (1981*b*). *The influence of in-plane collimation on the precision and accuracy of lattice-constant determination by the Bond method. II. Verification of the mathematical model. Systematic errors. Acta Cryst.* A**37**, 369–373.

Walder, V. & Burke, J. (1971). *The elimination of specimen and beam tilt errors in the Bond method of precision lattice parameter determinations. J. Appl. Cryst.* **4**, 337–339.

Weisz, O., Cochran, W. & Cole, W. F. (1948). *The accurate determination of cell dimensions from single-crystal X-ray photographs. Acta Cryst.* **1**, 83–88.

Wilson, A. J. C. (1950). *Geiger-counter X-ray spectrometer – influence of size and absorption coefficient of specimen on position and shape of powder diffraction maxima. J. Sci. Instrum.* **27**, 321–325.

Wilson, A. J. C. (1963). *Mathematical theory of X-ray powder diffractometry*. Philips Technical Library. Eindhoven: Centrex Publishing Company.

Wilson, A. J. C. (1965). *The location of peaks. Br. J. Appl. Phys.* **16**, 665–674.

Wilson, A. J. C. (1967). *Statistical variance of line-profile parameters. Measures of intensity, location and dispersion. Acta Cryst.* **23**, 888–898. Corrigenda: A**24** (1968), 478, Addendum: A**25** (1969), 584–585.

Wilson, A. J. C. (1980). *Accuracy in methods of lattice-parameter measurement. Natl Bur. Stand. (US) Spec. Publ.* No. 567. Proceedings of Symposium on Accuracy in Powder Diffraction, NBS, Gaithersburg, MD, USA, 11–15 June 1979.

5.3 (*cont.*)

Windisch, D. & Becker, P. (1990). *Silicon lattice parameters as an absolute scale of length for high precision measurements of fundamental constants*. *Phys. Status Solidi A*, **118**, 379–388.

Wołcyrz, M. & Łukaszewicz, K. (1982). *The evaluation of crystal perfection by means of the asymmetric Bragg reflections*. *J. Appl. Cryst.* **15**, 406–411.

Wołcyrz, M., Pietraszko, A. & Łukaszewicz, K. (1980). *The application of asymmetric Bragg reflections in the Bond method of measuring lattice parameters*. *J. Appl. Cryst.* **13**, 12–16.

Wölfel, E. R. (1971). *A new film instrument for the exploration of reciprocal space*. *J. Appl. Cryst.* **4**, 297–302.

Woolfson, M. M. (1970). *An introduction to X-ray crystallography*. Cambridge University Press.

Yakowitz, H. (1966*a*). *Effect of sample thickness and operating voltage on the contrast of Kossel transmission photographs*. *J. Appl. Phys.* **37**, 4455–4458.

Yakowitz, H. (1966*b*). *Precision of cubic lattice parameter measurement by the Kossel technique*. *The electron microprobe*, edited by T. D. McKinley, K. F. J. Heinrich & D. B. Wittry, pp. 417–438. New York: John Wiley.

Yakowitz, H. (1969). *The divergent beam X-ray technique*. *Advances in electronics and electron physics*, edited by A. J. Tousimis & L. Marton, Suppl. 6, pp. 361–431. New York: Academic Press.

Yakowitz, H. (1972). *Use of divergent-beam X-ray diffraction to measure lattice expansion in LiF as a function of thermal-neutron dose up to* 6×10^{16} *nvt*. *J. Appl. Phys.* **43**, 4793–4794.

Zolotoyabko, E., Sander, B., Komem, Y. & Kantor, B. (1993). *Improved strain analysis in semiconductor crystals by X-ray diffractometry enhanced with ultrasound*. *Appl. Phys. Lett.* **63**, 1540–1542.

5.4.1

Edington, J. W. (1975). *Electron diffraction in the electron microscope*. *Monographs in practical electron microscopy in materials science*, No. 2. Eindhoven: N. V. Philips Gloeilampenfabrieken.

Gard, J. A. (1976). *Electron microscopy in mineralogy*, p. 52. Berlin: Springer.

Hirsch, P. B., Howie, A., Nicholson, R. B., Pashley, D. W. & Whelan, M. J. (1965). *Electron microscopy of thin crystals*. London: Butterworth.

International Tables for Crystallography (1983). Vol. A. Dordrecht: Kluwer Academic Publishers.

LePage, Y. (1992). *Ab initio primitive cell parameters from single convergent beam patterns: a converse route to the identificatin of microcrystals with electons*. *Miscrosc. Res. Tech.* **21**, 158–165.

Zuo, J. M. (1993). *New method of Bravais lattice determination*. *Ultramicroscopy*, **52**, 459–464.

5.4.2

FitzGerald, J. D. & Johnson, A. W. S. (1984). *A simplified method of electron microscope voltage measurement*. *Ultramicroscopy*, **12**, 231–236.

Gjønnes, J. & Olsen, A. (1984). *Analytical electron microscopy*. *JEOL News*, **22**E, 13–18.

Høier, R. (1969). *A method to determine the ratio between lattice parameter and electron wavelength from Kikuchi line intersections*. *Acta Cryst.* A**25**, 516–518.

Jones, P. M., Rackham, G. M. & Steeds, J. W. (1977). *Higher order Laue zone effects in electron diffraction and their use in lattice parameter determination*. *Proc. R. Soc. London Ser. A*, **354**, 197–222.

Olsen, A. (1976*a*). *Lattice parameter determination using Kikuchi-line intersections: application to olivine and feldspar*. *J. Appl. Cryst.* **9**, 9–13.

Olsen, A. (1976*b*). *Determination of lattice constants using Kikuchi line intersections*. Solid State Group Report Series. Institute of Physics, University of Oslo, Norway.

Rackham, G. M., Jones, P. M. & Steeds, J. W. (1974). *Upper layer diffraction effects in zone axis patterns*. Proceedings of the Eighth International Congress on Electron Microscopy, Canberra, Australia, pp. 336–337.

Steeds, J. W. (1979). *Convergent beam electron diffraction*. *Introduction to analytical electron microscopy*, edited by J. J. Hren, J. I. Goldstein & D. C. Joy, pp. 387–422. New York: Plenum.

Thomas, G. (1970). *Kikuchi electron diffraction and applications*. *Modern diffraction and imaging techniques in material science*, edited by S. Amelinckx, S. Gevers, G. Remaut & J. Van Landuyt, pp. 131–185. Amsterdam: North-Holland.

Uyeda, R., Nonoyama, M. & Kogiso, M. (1965). *Determination of the wavelength of electrons from a Kikuchi pattern*. *J. Electron Microsc.* **14**, 296–300.

Walker, A. R. & Booker, G. R. (1982). *A selected-area channelling pattern (SACP) method for measuring small local changes in lattice parameter with bulk specimens*. *Electron microscopy 1982*, Vol. 1, pp. 651–652. Hamburg: Elsevier.

5.5

Fischer, P., Zolliker, P., Meier, B. H., Ernst, R. R., Hewat, A. W., Jorgensen, J. D. & Rotella, F. J. (1986). *Structure and dynamics of terephthalic acid from 2 to 300 K*. *J. Solid State Chem.* **61**, 109–125.

International Tables for Crystallography (2006). Vol. C, Chapter 6.1, pp. 554–595.

6.1. Intensity of diffracted intensities

By P. J. Brown, A. G. Fox, E. N. Maslen, M. A. O'Keefe and B. T. M. Willis

6.1.1. X-ray scattering
(By E. N. Maslen, A. G. Fox, and M. A. O'Keefe)

6.1.1.1. *Coherent (Rayleigh) scattering*

An electromagnetic wave incident on a tightly bound electron is scattered coherently. For an incident wave of unit amplitude with the electric vector normal to the plane of the reflection $x0y$ containing the incident and diffracted beams (Fig. 6.1.1.1), the amplitude of the scattered wave at a distance r is

$$r_e/r, \tag{6.1.1.1}$$

where $r_e = (\mu_0/4\pi)(e^2/m)$ is the classical radius of the electron (2.818×10^{-15} m).

For a wave with the electric vector parallel to the plane $x0y$, the amplitude of the scattered wave is

$$\frac{r_e}{r}\cos 2\theta. \tag{6.1.1.2}$$

For unpolarized incident radiation with unit mean amplitude, the amplitude of the scattered wave is given by the Thomson formula

$$\frac{r_e}{r}\left\{\frac{1+\cos^2 2\theta}{2}\right\}^{1/2}. \tag{6.1.1.3}$$

The corresponding intensity of scattering per unit solid angle is

$$I_e = I_o r_e^2\left[\frac{1+\cos^2 2\theta}{2}\right] \tag{6.1.1.4}$$

for an unpolarized incident beam of intensity I_o.

6.1.1.2. *Incoherent (Compton) scattering*

For scattering from a free electron, the quantum nature of the radiation must be considered. Under the impact of a photon with energy hc/λ, momentum h/λ, the recoil of an electron, initially at rest, results in a change in wavelength of

$$\Delta\lambda = \frac{2h}{mc}\sin^2\theta, \tag{6.1.1.5}$$

a geometry similar to that in Fig. 6.1.1.1 being assumed. There is no fixed relationship between the phases of the incident and scattered beams – *i.e.* the scattering is incoherent. The intensity I_e predicted by the Thomson formula is modified by the correction factor $[\lambda/(\lambda+\Delta\lambda)]^3$.

6.1.1.3. *Atomic scattering factor*

For scattering by atomic electrons there are both coherent and incoherent components, with total intensity given by the Thomson formula. The phase for coherent scattering is by convention related to that of a free electron at the nucleus. There is a phase shift of π for scattering from a free electron. The scattering from an element of electron density $\rho(\mathbf{r}_j)$ has a phase difference of $i\mathbf{S}\cdot\mathbf{r}_j$, where

$$\mathbf{S} = 2\pi\mathbf{s}. \tag{6.1.1.6}$$

The total amplitude for coherent scattering from the jth electron is

$$f_j = \int \rho(\mathbf{r}_j)\exp(i\mathbf{S}\cdot\mathbf{r}_j)\,\mathrm{d}\mathbf{r}_j. \tag{6.1.1.7}$$

The intensity of coherent scattering is

$$I_{\rm coh} = I_e f_j^2. \tag{6.1.1.8}$$

The intensity of Compton scattering from that electron is

$$I_{\rm incoh} = I_e - I_{\rm coh} = I_e(1-f_j^2). \tag{6.1.1.9}$$

For an atom with atomic number Z,

$$I_{\rm coh} = I_e\left(\sum_{j=1}^{Z} f_j\right)^2 \tag{6.1.1.10}$$

and

$$I_{\rm incoh} = I_e\left(Z - f_j^2 - \sum_{j,k} f_{jk}\right), \tag{6.1.1.11}$$

where the correction term

$$f_{jk} = \int \psi_j^*\psi_k \exp(i\mathbf{S}\cdot\mathbf{r})\,\mathrm{d}\mathbf{r}, \tag{6.1.1.12}$$

owing to exchange, meets the requirements of the Pauli exclusion principle.

Atomic scattering factors for neutral atoms are listed in Table 6.1.1.1 for the range $0 < (\sin\theta)/\lambda < 6.0$ Å^{-1}. The values for hydrogen are calculated from the analytical solution to the Schrödinger equation and are effectively zero for $(\sin\theta)/\lambda > 1.5$ Å^{-1}. Those for heavier atoms are for relativistic wavefunctions, based on the calculations of Doyle & Turner (1968) using the wavefunctions of Coulthard (1967) (designated RHF in Table 6.1.1.1), or on those of Cromer & Waber (1968) using the wavefunctions of Mann (1968*a*) (designated *RHF). The latter are based on a more exact treatment of potential that allows for the finite size of the nucleus, but the effect on the scattering factors is small. The calculations of Cromer & Waber (1968) were originally made for $0 < (\sin\theta)/\lambda < 2.0$ Å^{-1}, but these have been extended to 6 Å^{-1} by Fox, O'Keefe & Tabbernor (1989); this has been done because there are increasing numbers of applications for high-angle scattering factors.

For a detailed study of the effect of changes in the electron density due to chemical bonding and lattice formation, a more general procedure is necessary, as described in Subsection 6.1.1.4. The changes due to chemical bonding are small in absolute terms, and are relatively small except in the case of hydrogen.

A more approximate treatment is adequate for many purposes. An isotropic approximation to the scattering factor for bonded hydrogen, based on an analysis of the hydrogen molecule by Stewart, Davidson & Simpson (1965), is listed in Table 6.1.1.2.

Scattering for ionic models of solids may be related to the scattering factors for the corresponding free ions. Values for

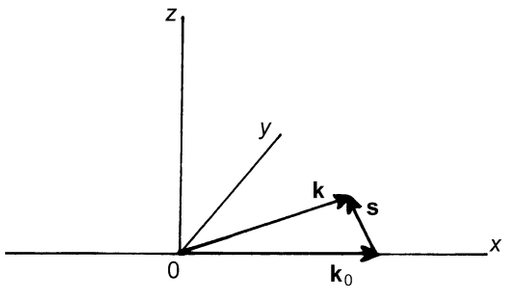

Fig. 6.1.1.1. Scattering by an electron. $\mathbf{k}_0$ and $\mathbf{k}$ are the incident and scattered wavevectors, respectively.

Copyright © 2006 International Union of Crystallography

Table 6.1.1.1. *Mean atomic scattering factors in electrons for free atoms*

Methods: E: exact; RHF, *RHF (see text): relativistic Hartree–Fock.

Element	H	He	Li	Be	B	C	N	O	F	Ne
Z	1	2	3	4	5	6	7	8	9	10
Method	E	RHF	RHF	RHF	RHF	RHF	RHF	RHF	RHF	RHF
$(\sin\theta)/\lambda$ (Å^{-1})										
0.00	1.000	2.000	3.000	4.000	5.000	6.000	7.000	8.000	9.000	10.000
0.01	0.998	1.998	2.986	3.987	4.988	5.990	6.991	7.992	8.993	9.993
0.02	0.991	1.993	2.947	3.950	4.954	5.958	6.963	7.967	8.970	9.973
0.03	0.980	1.984	2.884	3.889	4.897	5.907	6.918	7.926	8.933	9.938
0.04	0.966	1.972	2.802	3.807	4.820	5.837	6.855	7.869	8.881	9.891
0.05	0.947	1.957	2.708	3.707	4.724	5.749	6.776	7.798	8.815	9.830
0.06	0.925	1.939	2.606	3.592	4.613	5.645	6.682	7.712	8.736	9.757
0.07	0.900	1.917	2.502	3.468	4.488	5.526	6.574	7.612	8.645	9.672
0.08	0.872	1.893	2.400	3.336	4.352	5.396	6.453	7.501	8.541	9.576
0.09	0.842	1.866	2.304	3.201	4.209	5.255	6.321	7.378	8.427	9.469
0.10	0.811	1.837	2.215	3.065	4.060	5.107	6.180	7.245	8.302	9.351
0.11	0.778	1.806	2.135	2.932	3.908	4.952	6.030	7.103	8.168	9.225
0.12	0.744	1.772	2.065	2.804	3.756	4.794	5.875	6.954	8.026	9.090
0.13	0.710	1.737	2.004	2.683	3.606	4.633	5.714	6.798	7.876	8.948
0.14	0.676	1.701	1.950	2.569	3.459	4.472	5.551	6.637	7.721	8.799
0.15	0.641	1.663	1.904	2.463	3.316	4.311	5.385	6.472	7.560	8.643
0.16	0.608	1.624	1.863	2.365	3.179	4.153	5.218	6.304	7.395	8.483
0.17	0.574	1.584	1.828	2.277	3.048	3.998	5.051	6.134	7.226	8.318
0.18	0.542	1.543	1.796	2.197	2.924	3.847	4.886	5.964	7.055	8.150
0.19	0.511	1.502	1.768	2.125	2.808	3.701	4.723	5.793	6.883	7.978
0.20	0.481	1.460	1.742	2.060	2.699	3.560	4.563	5.623	6.709	7.805
0.22	0.424	1.377	1.693	1.951	2.503	3.297	4.254	5.289	6.362	7.454
0.24	0.373	1.295	1.648	1.864	2.336	3.058	3.963	4.965	6.020	7.102
0.25	0.350	1.254	1.626	1.828	2.263	2.949	3.825	4.808	5.851	6.928
0.26	0.328	1.214	1.604	1.795	2.195	2.846	3.693	4.655	5.685	6.754
0.28	0.287	1.136	1.559	1.739	2.077	2.658	3.445	4.363	5.363	6.412
0.30	0.251	1.060	1.513	1.692	1.979	2.494	3.219	4.089	5.054	6.079
0.32	0.220	0.988	1.465	1.652	1.897	2.351	3.014	3.834	4.761	5.758
0.34	0.193	0.920	1.417	1.616	1.829	2.227	2.831	3.599	4.484	5.451
0.35	0.180	0.887	1.393	1.600	1.799	2.171	2.747	3.489	4.353	5.302
0.36	0.169	0.856	1.369	1.583	1.771	2.120	2.667	3.383	4.225	5.158
0.38	0.148	0.795	1.320	1.551	1.723	2.028	2.522	3.186	3.983	4.880
0.40	0.130	0.738	1.270	1.520	1.681	1.948	2.393	3.006	3.759	4.617
0.42	0.115	0.686	1.221	1.489	1.644	1.880	2.278	2.844	3.551	4.370
0.44	0.101	0.636	1.173	1.458	1.611	1.821	2.178	2.697	3.360	4.139
0.45	0.095	0.613	1.149	1.443	1.596	1.794	2.132	2.629	3.270	4.029
0.46	0.090	0.591	1.125	1.427	1.581	1.770	2.089	2.564	3.183	3.923
0.48	0.079	0.548	1.078	1.395	1.553	1.725	2.011	2.445	3.022	3.722
0.50	0.071	0.509	1.033	1.362	1.526	1.685	1.942	2.338	2.874	3.535
0.55	0.053	0.423	0.924	1.279	1.463	1.603	1.802	2.115	2.559	3.126
0.60	0.040	0.353	0.823	1.195	1.402	1.537	1.697	1.946	2.309	2.517
0.65	0.031	0.295	0.732	1.112	1.339	1.479	1.616	1.816	2.112	2.517
0.70	0.024	0.248	0.650	1.030	1.276	1.426	1.551	1.714	1.956	2.296
0.80	0.015	0.177	0.512	0.876	1.147	1.322	1.445	1.568	1.735	1.971
0.90	0.010	0.129	0.404	0.740	1.020	1.219	1.353	1.463	1.588	1.757
1.00	0.007	0.095	0.320	0.622	0.900	1.114	1.265	1.377	1.482	1.609
1.10	0.005	0.072	0.255	0.522	0.790	1.012	1.172	1.298	1.398	1.502
1.20	0.003	0.055	0.205	0.439	0.690	0.914	1.090	1.221	1.324	1.418
1.30	0.003	0.042	0.165	0.369	0.602	0.822	1.004	1.145	1.254	1.346
1.40	0.002	0.033	0.134	0.311	0.524	0.736	0.921	1.070	1.186	1.280
1.50	0.001	0.026	0.110	0.263	0.457	0.659	0.843	0.997	1.120	1.218
1.60		0.021	0.091	0.223	0.398	0.588	0.769	0.926	1.055	1.158
1.70		0.017	0.075	0.190	0.347	0.525	0.700	0.857	0.990	1.099
1.80		0.014	0.063	0.163	0.304	0.468	0.636	0.792	0.928	1.041
1.90		0.011	0.053	0.139	0.266	0.418	0.578	0.731	0.868	0.984
2.00		0.010	0.044	0.120	0.233	0.373	0.525	0.674	0.810	0.929
2.50		0.004	0.021	0.060	0.126	0.216	0.324	0.443	0.564	0.680
3.00		0.002	0.011	0.033	0.072	0.130	0.204	0.292	0.389	0.489
3.50		0.001	0.006	0.019	0.043	0.081	0.132	0.196	0.270	0.331
4.00		0.001	0.004	0.012	0.027	0.053	0.088	0.134	0.190	0.254
5.00			0.002	0.005	0.012	0.025	0.043	0.067	0.099	0.137
6.00			0.001	0.003	0.006	0.013	0.023	0.037	0.055	0.079

Table 6.1.1.1. *Mean atomic scattering factors for free atoms (cont.)*

Element	Na	Mg	Al	Si	P	S	Cl	Ar	K	Ca
Z	11	12	13	14	15	16	17	18	19	20
Method	RHF	RHF	RHF	RHF	RHF	RHF	RHF	RHF	RHF	RHF
$(\sin\theta)/\lambda$ (Å^{-1})										
0.00	11.000	12.000	13.000	14.000	15.000	16.000	17.000	18.000	19.000	20.000
0.01	10.980	11.978	12.976	13.976	14.977	15.979	16.980	17.981	18.963	19.959
0.02	10.922	11.914	12.903	13.904	14.909	15.915	16.919	17.924	18.854	19.838
0.03	10.830	11.811	12.786	13.787	14.798	15.809	16.820	17.830	18.683	19.645
0.04	10.709	11.674	12.629	13.628	14.646	15.665	16.683	17.700	18.462	19.392
0.05	10.568	11.507	12.439	13.434	14.458	15.484	16.511	17.536	18.204	19.091
0.06	10.412	11.319	12.222	13.209	14.237	15.271	16.306	17.340	17.924	18.758
0.07	10.249	11.116	11.987	12.961	13.990	15.030	16.073	17.116	17.630	18.405
0.08	10.084	10.903	11.739	12.695	13.721	14.764	15.814	16.865	17.332	18.045
0.09	9.920	10.687	11.485	12.417	13.435	14.478	15.533	16.591	17.032	17.685
0.10	9.760	10.472	11.230	12.134	13.138	14.177	15.234	16.298	16.733	17.331
0.11	9.605	10.262	10.978	11.849	12.834	13.865	14.921	15.988	16.436	16.987
0.12	9.455	10.059	10.733	11.567	12.527	13.546	14.597	15.665	16.138	16.655
0.13	9.309	9.864	10.498	11.292	12.223	13.224	14.266	15.331	15.841	16.334
0.14	9.166	9.678	10.273	11.025	11.922	12.902	13.932	14.991	15.543	16.024
0.15	9.027	9.502	10.059	10.769	11.629	12.583	13.597	14.647	15.243	15.723
0.16	8.888	9.334	9.857	10.525	11.345	12.270	13.263	14.301	14.941	15.430
0.17	8.751	9.175	9.667	10.293	11.072	11.964	12.934	13.957	14.638	15.142
0.18	8.613	9.023	9.487	10.074	10.811	11.668	12.611	13.615	14.334	14.859
0.19	8.475	8.876	9.318	9.868	10.563	11.382	12.297	13.279	14.031	14.580
0.20	8.335	8.735	9.158	9.673	10.327	11.109	11.991	12.949	13.728	14.304
0.22	8.052	8.465	8.862	9.319	9.894	10.598	11.413	12.315	13.130	13.760
0.24	7.764	8.205	8.592	9.004	9.510	10.138	10.881	11.721	12.550	13.225
0.25	7.618	8.078	8.465	8.859	9.335	9.927	10.633	11.441	12.268	12.961
0.26	7.471	7.951	8.341	8.722	9.170	9.727	10.398	11.172	11.994	12.701
0.28	7.176	7.698	8.103	8.467	8.869	9.363	9.964	10.671	11.468	12.194
0.30	6.881	7.446	7.873	8.231	8.600	9.039	9.576	10.216	10.977	11.705
0.32	6.588	7.194	7.648	8.011	8.357	8.752	9.231	9.807	10.521	11.240
0.34	6.298	6.943	7.426	7.800	8.134	8.494	8.923	9.441	10.103	10.800
0.35	6.156	6.817	7.316	7.698	8.029	8.376	8.782	9.272	9.908	10.590
0.36	6.015	6.691	7.205	7.597	7.928	8.262	8.649	9.113	9.722	10.388
0.38	5.739	6.442	6.985	7.398	7.733	8.051	8.403	8.820	9.375	10.004
0.40	5.471	6.194	6.766	7.202	7.547	7.856	8.181	8.558	9.061	9.650
0.42	5.214	5.951	6.548	7.008	7.367	7.673	7.979	8.322	8.778	9.324
0.44	4.967	5.712	6.330	6.815	7.190	7.501	7.794	8.110	8.522	9.025
0.45	4.848	5.595	6.222	6.719	7.103	7.417	7.706	8.011	8.403	8.885
0.46	4.731	5.480	6.115	6.622	7.017	7.335	7.621	7.917	8.290	8.752
0.48	4.506	5.253	5.902	6.431	6.845	7.174	7.459	7.739	8.080	8.502
0.50	4.293	5.034	5.692	6.240	6.674	7.017	7.305	7.575	7.889	8.275
0.55	3.811	4.520	5.186	5.769	6.250	6.633	6.941	7.207	7.474	7.788
0.60	3.398	4.059	4.713	5.312	5.829	6.254	6.595	6.875	7.125	7.392
0.65	3.048	3.652	4.277	4.878	5.418	5.877	6.254	6.560	6.814	7.057
0.70	2.754	3.297	3.883	4.470	5.020	5.505	5.915	6.252	6.523	6.762
0.80	2.305	2.729	3.221	3.750	4.284	4.790	5.245	5.639	5.961	6.228
0.90	1.997	2.317	2.712	3.164	3.649	4.138	4.607	5.036	5.406	5.717
1.00	1.784	2.022	2.330	2.702	3.122	3.570	4.023	4.460	4.859	5.209
1.10	1.634	1.812	2.049	2.346	2.698	3.092	3.509	3.931	4.337	4.710
1.20	1.524	1.660	1.841	2.076	2.364	2.699	3.070	3.462	3.855	4.233
1.30	1.438	1.546	1.687	1.872	2.104	2.384	2.704	3.056	3.423	3.791
1.40	1.367	1.459	1.571	1.717	1.903	2.133	2.405	2.713	3.045	3.391
1.50	1.304	1.387	1.481	1.598	1.747	1.935	2.162	2.427	2.722	3.039
1.60	1.247	1.326	1.408	1.505	1.626	1.779	1.967	2.192	2.450	2.733
1.70	1.191	1.270	1.346	1.430	1.530	1.655	1.811	2.000	2.221	2.470
1.80	1.137	1.219	1.292	1.367	1.453	1.557	1.686	1.844	2.033	2.250
1.90	1.084	1.169	1.243	1.313	1.389	1.477	1.585	1.717	1.876	2.063
2.00	1.032	1.120	1.195	1.264	1.333	1.411	1.502	1.614	1.748	1.908
2.50	0.791	0.892	0.979	1.056	1.122	1.182	1.240	1.301	1.367	1.444
3.00	0.591	0.691	0.783	0.867	0.942	1.009	1.069	1.123	1.174	1.225
3.50	0.438	0.527	0.615	0.699	0.777	0.849	0.915	0.974	1.028	1.078
4.00	0.325	0.401	0.478	0.566	0.632	0.705	0.773	0.836	0.895	0.949
5.00	0.183	0.234	0.290	0.349	0.411	0.474	0.536	0.597	0.657	0.715
6.00	0.107	0.141	0.179	0.222	0.268	0.316	0.367	0.419	0.472	0.524

Table 6.1.1.1. *Mean atomic scattering factors for free atoms (cont.)*

Element	Sc	Ti	V	Cr	Mn	Fe	Co	Ni	Cu	Zn
Z	21	22	23	24	25	26	27	28	29	30
Method	RHF	RHF	RHF	RHF	RHF	RHF	RHF	RHF	RHF	RHF
$(\sin\theta)/\lambda$ (Å^{-1})										
0.00	21.000	22.000	23.000	24.000	25.000	26.000	27.000	28.000	29.000	30.000
0.01	20.962	21.964	22.966	23.971	24.969	25.970	26.972	27.973	28.977	29.975
0.02	20.848	21.856	22.864	23.885	24.876	25.882	26.887	27.892	28.908	29.900
0.03	20.665	21.682	22.698	23.746	24.726	25.738	26.749	27.759	28.794	29.777
0.04	20.422	21.451	22.477	23.558	24.523	25.543	26.562	27.579	28.640	29.609
0.05	20.131	21.171	22.208	23.329	24.274	25.304	26.331	27.356	28.448	29.401
0.06	19.805	20.854	21.902	23.065	23.988	25.026	26.063	27.096	28.223	29.157
0.07	19.455	20.511	21.567	22.772	23.671	24.719	25.764	26.806	27.971	28.883
0.08	19.091	20.150	21.212	22.459	23.331	24.387	25.440	26.490	27.694	28.583
0.09	18.723	19.781	20.846	22.129	22.976	24.038	25.098	26.156	27.397	28.263
0.10	18.356	19.410	20.474	21.789	22.611	23.678	24.744	25.807	27.084	27.927
0.11	17.995	19.041	20.102	21.441	22.240	23.310	24.380	25.448	26.758	27.579
0.12	17.643	18.678	19.733	21.089	21.868	22.939	24.011	25.083	26.422	27.222
0.13	17.301	18.322	19.369	20.734	21.497	22.568	23.641	24.714	26.077	26.859
0.14	16.968	17.974	19.011	20.378	21.128	22.197	23.270	24.344	25.726	26.492
0.15	16.645	17.635	18.661	20.022	20.764	21.829	22.900	23.973	25.370	26.124
0.16	16.330	17.304	18.317	19.667	20.404	21.465	22.533	23.604	25.009	25.754
0.17	16.023	16.980	17.980	19.312	20.049	21.104	22.168	23.237	24.645	25.385
0.18	15.722	16.663	17.649	18.960	19.699	20.748	21.806	22.872	24.278	25.017
0.19	15.426	16.351	17.323	18.609	19.354	20.395	21.448	22.510	23.910	24.649
0.20	15.135	16.044	17.003	18.260	19.012	20.046	21.093	22.150	23.540	24.283
0.22	14.564	15.444	16.376	17.570	18.342	19.359	20.393	21.438	22.798	23.556
0.24	14.006	14.859	15.765	16.893	17.686	18.685	19.704	20.737	22.057	22.836
0.25	13.732	14.572	15.465	16.561	17.364	18.354	19.364	20.390	21.687	22.478
0.26	13.462	14.289	15.169	16.232	17.045	18.025	19.027	20.046	21.319	22.122
0.28	12.933	13.735	14.589	15.588	16.417	17.378	18.361	19.365	20.589	21.417
0.30	12.423	13.198	14.026	14.965	15.806	16.744	17.709	18.696	19.869	20.720
0.32	11.934	12.682	13.482	14.365	15.211	16.127	17.072	18.040	19.162	20.034
0.34	11.467	12.187	12.959	13.790	14.634	15.527	16.450	17.398	18.472	19.359
0.35	11.244	11.949	12.705	13.513	14.353	15.233	16.145	17.084	18.133	19.027
0.36	11.027	11.717	12.458	13.242	14.078	14.945	15.845	16.773	17.799	18.698
0.38	10.613	11.271	11.982	12.720	13.543	14.384	15.260	16.165	17.145	18.051
0.40	10.226	10.852	11.530	12.227	13.031	13.845	14.695	15.576	16.514	17.421
0.42	9.866	10.459	11.105	11.762	12.543	13.328	14.151	15.008	15.904	16.809
0.44	9.534	10.093	10.705	11.326	12.080	12.835	13.630	14.461	15.318	16.216
0.45	9.377	9.920	10.515	11.118	11.858	12.598	13.379	14.196	15.034	15.926
0.46	9.227	9.753	10.332	10.917	11.642	12.367	13.133	13.937	14.757	15.642
0.48	8.946	9.438	9.984	10.536	11.228	11.922	12.659	13.435	14.219	15.090
0.50	8.687	9.148	9.660	10.180	10.840	11.502	12.209	12.956	13.707	14.559
0.55	8.132	8.518	8.952	9.400	9.973	10.557	11.188	11.862	12.533	13.328
0.60	7.682	8.007	8.373	8.756	9.245	9.753	10.309	10.909	11.507	12.235
0.65	7.312	7.588	7.898	8.227	8.639	9.077	9.561	10.090	10.621	11.276
0.70	6.996	7.240	7.506	7.791	8.137	8.512	8.930	9.392	9.861	10.442
0.80	6.460	6.676	6.892	7.118	7.368	7.645	7.955	8.301	8.663	9.108
0.90	5.975	6.200	6.406	6.606	6.808	7.023	7.259	7.519	7.799	8.132
1.00	5.501	5.752	5.972	6.172	6.359	6.545	6.738	6.944	7.166	7.417
1.10	5.030	5.310	5.553	5.768	5.962	6.143	6.318	6.495	6.681	6.879
1.20	4.570	4.872	5.139	5.372	5.586	5.775	5.950	6.118	6.285	6.453
1.30	4.131	4.445	4.730	4.982	5.215	5.420	5.601	5.776	5.939	6.096
1.40	3.722	4.038	4.333	4.597	4.849	5.070	5.270	5.451	5.617	5.775
1.50	3.352	3.660	3.956	4.226	4.490	4.725	4.939	5.133	5.308	5.473
1.60	3.023	3.316	3.604	3.874	4.144	4.388	4.611	4.819	5.005	5.180
1.70	2.733	3.006	3.281	3.545	3.814	4.062	4.295	4.511	4.705	4.892
1.80	2.485	2.734	2.992	3.244	3.506	3.753	3.989	4.211	4.413	4.610
1.90	2.271	2.496	2.733	2.971	3.221	3.463	3.697	3.922	4.128	4.332
2.00	2.090	2.290	2.506	2.727	2.963	3.195	3.424	3.647	3.855	4.063
2.50	1.533	1.637	1.756	1.888	2.037	2.197	2.366	2.543	2.721	2.908
3.00	1.279	1.338	1.404	1.479	1.563	1.658	1.763	1.878	2.001	2.135
3.50	1.125	1.171	1.217	1.266	1.319	1.377	1.441	1.512	1.590	1.677
4.00	0.998	1.044	1.087	1.129	1.171	1.213	1.258	1.306	1.358	1.414
5.00	0.770	0.821	0.869	0.914	0.956	0.995	1.033	1.069	1.105	1.140
6.00	0.577	0.627	0.677	0.724	0.769	0.813	0.853	0.892	0.929	0.964

Table 6.1.1.1. *Mean atomic scattering factors for free atoms (cont.)*

Element	Ga	Ge	As	Se	Br	Kr	Rb	Sr	Y	Zr
Z	31	32	33	34	35	36	37	38	39	40
Method	RHF	RHF	RHF	RHF	RHF	RHF	RHF	RHF	*RHF	*RHF
$(\sin\theta)/\lambda$ (Å^{-1})										
0.00	31.000	32.000	33.000	34.000	35.000	36.000	37.000	38.000	39.000	40.000
0.01	30.971	31.970	32.970	33.970	34.971	35.972	36.952	37.946	38.947	39.949
0.02	30.883	31.878	32.879	33.881	34.883	35.886	36.809	37.786	38.792	39.800
0.03	30.740	31.729	32.730	33.734	34.739	35.744	36.583	37.532	38.543	39.559
0.04	30.546	31.526	32.527	33.532	34.540	35.549	36.291	37.197	38.212	39.237
0.05	30.308	31.276	32.274	33.280	34.291	35.304	35.948	36.802	37.816	38.847
0.06	30.031	30.984	31.977	32.982	33.995	35.011	35.571	36.363	37.369	38.403
0.07	29.724	30.657	31.642	32.645	33.658	34.677	35.171	35.897	36.889	37.921
0.08	29.391	30.302	31.276	32.273	33.284	34.305	34.758	35.418	36.387	37.412
0.09	29.040	29.926	30.884	31.872	32.880	33.899	34.336	34.937	35.876	36.887
0.10	28.675	29.534	30.473	31.449	32.450	33.467	33.907	34.458	35.364	36.356
0.11	28.302	29.133	30.049	31.009	32.000	33.011	33.473	33.986	34.855	35.824
0.12	27.924	28.725	29.616	30.557	31.535	32.537	33.034	33.522	34.354	35.296
0.13	27.543	28.316	29.179	30.099	31.060	32.051	32.588	33.066	33.861	34.775
0.14	27.162	27.908	28.742	29.637	30.578	31.555	32.137	32.616	33.378	34.262
0.15	26.783	27.504	28.307	29.175	30.095	31.055	31.681	32.171	32.904	33.758
0.16	26.406	27.104	27.877	28.718	29.613	30.553	31.220	31.730	32.437	33.263
0.17	26.033	26.709	27.454	28.266	29.136	30.053	30.757	31.292	31.977	32.776
0.18	25.663	26.322	27.039	27.822	28.664	29.558	30.293	30.856	31.523	32.298
0.19	25.297	25.941	26.633	27.387	28.202	29.070	29.830	30.421	31.075	31.827
0.20	24.935	25.567	26.235	26.962	27.749	28.590	29.368	29.988	30.631	31.363
0.22	24.121	24.839	25.469	26.145	26.876	27.663	28.459	29.128	29.758	30.454
0.24	23.520	24.135	24.739	25.372	26.052	26.784	27.576	28.280	28.904	29.572
0.25	23.174	23.791	24.386	25.001	25.658	26.364	27.148	27.863	28.485	29.141
0.26	22.830	23.452	24.041	24.641	25.276	25.957	26.729	27.452	28.071	28.716
0.28	22.151	22.787	23.370	23.947	24.545	25.181	25.922	26.648	27.263	27.889
0.30	21.481	22.136	22.724	23.288	23.857	24.453	25.158	25.875	26.483	27.092
0.32	20.820	21.498	22.097	22.656	23.206	23.771	24.437	25.135	25.734	26.327
0.34	20.169	20.870	21.486	22.048	22.587	23.128	23.758	24.430	25.018	25.596
0.35	19.847	20.560	21.185	21.751	22.288	22.820	23.432	24.090	24.673	25.243
0.36	19.527	20.253	20.888	21.459	21.995	22.520	23.116	23.760	24.336	24.899
0.38	18.897	19.645	20.301	20.887	21.425	21.941	22.510	23.125	23.687	24.236
0.40	18.278	19.047	19.725	20.328	20.874	21.388	21.934	22.522	23.071	23.606
0.42	17.673	18.459	19.159	19.780	20.338	20.855	21.386	21.950	22.485	23.008
0.44	17.083	17.882	18.602	19.242	19.816	20.339	20.860	21.404	21.928	22.439
0.45	16.794	17.598	18.326	18.977	19.558	20.087	20.605	21.141	21.660	22.166
0.46	16.508	17.317	18.054	18.713	19.304	19.838	20.354	20.883	21.398	21.899
0.48	15.950	16.765	17.516	18.193	18.801	19.349	19.866	20.383	20.890	21.384
0.50	15.410	16.227	16.989	17.682	18.307	18.870	19.391	19.902	20.404	20.892
0.55	14.142	14.947	15.721	16.444	17.107	17.709	18.252	18.764	19.263	19.745
0.60	12.996	13.770	14.535	15.269	15.958	16.594	17.167	17.696	18.204	18.693
0.65	11.974	12.702	13.440	14.166	14.865	15.524	16.125	16.678	17.203	17.706
0.70	11.073	11.745	12.442	13.145	13.837	14.504	15.126	15.702	16.246	16.767
0.80	9.604	10.151	10.741	11.362	12.001	12.645	13.272	13.872	14.443	14.996
0.90	8.510	8.937	9.411	9.928	10.480	11.057	11.645	12.230	12.798	13.361
1.00	7.702	8.028	8.396	8.809	9.262	9.752	10.270	10.806	11.339	11.883
1.10	7.099	7.348	7.631	7.952	8.312	8.711	9.147	9.612	10.088	10.588
1.20	6.633	6.830	7.050	7.299	7.580	7.898	8.252	8.640	9.046	9.486
1.30	6.254	6.419	6.597	6.795	7.016	7.266	7.548	7.863	8.200	8.574
1.40	5.926	6.076	6.231	6.395	6.574	6.773	6.996	7.249	7.523	7.833
1.50	5.627	5.774	5.917	6.063	6.216	6.380	6.562	6.764	6.985	7.238
1.60	5.342	5.493	5.636	5.775	5.913	6.056	6.210	6.376	6.554	6.760
1.70	5.065	5.224	5.372	5.511	5.645	5.778	5.913	6.055	6.205	6.375
1.80	4.792	4.961	5.117	5.262	5.398	5.528	5.656	5.785	5.914	6.059
1.90	4.523	4.702	4.867	5.020	5.162	5.295	5.420	5.544	5.662	5.790
2.00	4.260	4.447	4.621	4.782	4.932	5.071	5.200	5.323	5.440	5.558
2.50	3.097	3.287	3.475	3.658	3.836	4.007	4.168	4.320	4.460	4.590
3.00	2.277	2.428	2.584	2.745	2.909	3.074	3.239	3.401	3.560	3.720
3.50	1.772	1.876	1.988	2.108	2.235	2.369	2.507	2.649	2.780	2.920
4.00	1.477	1.545	1.621	1.703	1.793	1.890	1.993	2.103	2.215	2.335
5.00	1.176	1.213	1.251	1.292	1.337	1.384	1.436	1.493	1.550	1.620
6.00	0.998	1.030	1.061	1.092	1.123	1.154	1.186	1.219	1.250	1.285

Table 6.1.1.1. *Mean atomic scattering factors for free atoms (cont.)*

Element	Nb	Mo	Tc	Ru	Rh	Pd	Ag	Cd	In	Sn
Z	41	42	43	44	45	46	47	48	49	50
Method	*RHF	RHF	*RHF	*RHF	*RHF	*RHF	RHF	RHF	RHF	RHF
$(\sin\theta)/\lambda$ (Å^{-1})										
0.00	41.000	42.000	43.000	44.000	45.000	46.000	47.000	48.000	49.000	50.000
0.01	40.956	41.958	42.955	43.960	44.961	45.968	46.964	47.962	48.957	49.955
0.02	40.824	41.831	42.821	43.842	44.847	45.874	46.857	47.848	48.828	49.821
0.03	40.610	41.625	42.603	43.649	44.660	45.718	46.681	47.660	48.618	49.601
0.04	40.323	41.346	42.308	43.386	44.405	45.503	46.440	47.404	48.332	49.303
0.05	39.970	41.003	41.945	43.061	44.088	45.232	46.139	47.085	47.980	48.934
0.06	39.565	40.606	41.526	42.681	43.717	44.908	45.786	46.710	47.570	48.504
0.07	39.116	40.164	41.059	42.254	43.299	44.535	45.385	46.287	47.112	48.022
0.08	38.634	39.686	40.557	41.789	42.842	44.119	44.944	45.822	46.614	47.498
0.09	38.128	39.181	40.028	41.292	42.351	43.663	44.469	45.324	46.086	46.942
0.10	37.606	38.656	39.480	40.770	41.834	43.172	43.964	44.797	45.534	46.361
0.11	37.073	38.117	38.921	40.229	41.296	42.651	43.435	44.248	44.964	45.764
0.12	36.535	37.569	38.355	39.674	40.741	42.105	42.886	43.683	44.383	45.155
0.13	35.994	37.016	37.787	39.108	40.173	41.538	42.322	43.104	43.793	44.541
0.14	35.454	36.461	37.221	38.536	39.597	40.954	41.744	42.517	43.199	43.924
0.15	34.916	35.907	36.658	37.959	39.015	40.357	41.157	41.923	42.603	43.309
0.16	34.382	35.355	36.100	37.381	38.429	39.750	40.563	41.325	42.006	42.696
0.17	33.854	34.806	35.548	36.803	37.841	39.137	39.964	40.726	41.410	42.088
0.18	33.331	34.263	35.003	36.228	37.254	38.520	39.361	40.126	40.817	41.486
0.19	32.814	33.725	34.466	35.655	36.668	37.902	38.758	39.527	40.226	40.891
0.20	32.305	33.195	33.936	35.088	36.086	37.286	38.154	38.930	39.639	40.302
0.22	31.310	32.157	32.900	33.971	34.937	36.064	36.955	37.746	38.478	39.145
0.24	30.348	31.153	31.897	32.886	33.815	34.868	35.774	36.581	37.337	38.016
0.25	29.881	30.665	31.409	32.356	33.267	34.283	35.192	36.007	36.774	37.462
0.26	29.424	30.188	30.930	31.837	32.728	33.708	34.619	35.440	36.218	36.915
0.28	28.538	29.263	29.998	30.829	31.680	32.592	33.498	34.329	35.125	35.841
0.30	27.692	28.382	29.104	29.866	30.675	31.523	32.416	33.251	34.059	34.794
0.32	26.888	27.543	28.250	28.949	29.717	30.505	31.378	32.210	33.025	33.775
0.34	26.126	26.749	27.435	28.079	28.807	29.540	30.387	31.210	32.025	32.786
0.35	25.760	26.368	27.042	27.662	28.370	29.077	29.910	30.725	31.538	32.303
0.36	25.404	25.998	26.660	27.257	27.944	28.628	29.444	30.252	31.060	31.828
0.38	24.721	25.289	25.925	26.480	27.130	27.769	28.551	29.338	30.134	30.902
0.40	24.077	24.620	25.229	25.749	26.363	26.961	27.707	28.468	29.247	30.011
0.42	23.468	23.989	24.571	25.062	25.642	26.202	26.911	27.644	28.401	29.154
0.44	22.892	23.394	23.949	24.415	24.964	25.491	26.163	26.865	27.596	28.334
0.45	22.615	23.109	23.651	24.106	24.640	25.153	25.805	26.492	27.209	27.938
0.46	22.346	22.832	23.361	23.807	24.327	24.825	25.459	26.129	26.832	27.551
0.48	21.829	22.300	22.806	23.235	23.729	24.201	24.800	25.436	26.108	26.805
0.50	21.336	21.796	22.280	22.696	23.167	23.617	24.181	24.784	25.425	26.096
0.55	20.195	20.638	21.080	21.476	21.900	22.307	22.795	23.320	23.881	24.482
0.60	19.156	19.595	20.012	20.403	20.798	21.177	21.607	22.063	22.552	23.081
0.65	18.187	18.635	19.042	19.438	19.820	20.186	20.575	20.978	21.405	21.868
0.70	17.268	17.732	18.142	18.551	18.932	19.296	19.661	20.027	20.408	20.815
0.80	15.533	16.036	16.477	16.922	17.326	17.711	18.069	18.405	18.736	19.073
0.90	13.915	14.448	14.925	15.405	15.845	16.266	16.651	17.000	17.329	17.646
1.00	12.427	12.968	13.466	13.968	14.440	14.893	15.316	15.698	16.053	16.384
1.10	11.098	11.621	12.116	12.620	13.107	13.580	14.035	14.451	14.840	15.201
1.20	9.945	10.430	10.900	11.385	11.866	12.342	12.813	13.253	13.670	14.062
1.30	8.972	9.404	9.833	10.282	10.740	11.200	11.669	12.116	12.548	12.962
1.40	8.169	8.542	8.919	9.323	9.743	10.173	10.623	11.060	11.492	11.913
1.50	7.516	7.831	8.154	8.506	8.880	9.270	9.687	10.101	10.518	10.933
1.60	6.969	7.251	7.521	7.823	8.148	8.492	8.869	9.249	9.639	10.034
1.70	6.564	6.780	7.004	7.258	7.535	7.833	8.165	8.505	8.860	9.227
1.80	6.216	6.397	6.582	6.794	7.028	7.282	7.569	7.867	8.184	8.516
1.90	5.927	6.080	6.234	6.412	6.608	6.824	7.069	7.326	7.603	7.897
2.00	5.680	5.813	5.946	6.097	6.262	6.443	6.651	6.871	7.110	7.367
2.50	4.710	4.827	4.930	5.040	5.140	5.240	5.351	5.461	5.577	5.702
3.00	3.860	3.988	4.110	4.230	4.350	4.460	4.566	4.665	4.761	4.853
3.50	3.065	3.217	3.350	3.485	3.620	3.740	3.862	3.977	4.087	4.192
4.00	2.405	2.581	2.690	2.820	2.940	3.080	3.207	3.330	3.449	3.565
5.00	1.690	1.766	1.840	1.925	2.012	2.100	2.206	2.304	2.406	2.509
6.00	1.327	1.373	1.420	1.470	1.520	1.575	1.635	1.698	1.746	1.835

Table 6.1.1.1. *Mean atomic scattering factors for free atoms (cont.)*

Element	Sb	Te	I	Xe	Cs	Ba	La	Ce	Pr	Nd
Z	51	52	53	54	55	56	57	58	59	60
Method	RHF	*RHF	RHF	RHF	RHF	RHF	*RHF	*RHF	*RHF	*RHF
$(\sin\theta)/\lambda$ (Å^{-1})										
0.00	51.000	52.000	53.000	54.000	55.000	56.000	57.000	58.000	59.000	60.000
0.01	50.955	51.954	52.955	53.956	54.932	55.925	56.926	57.928	58.929	59.931
0.02	50.819	51.818	52.820	53.821	54.732	55.703	56.708	57.715	58.722	59.728
0.03	50.596	51.594	52.597	53.601	54.417	55.350	56.360	57.375	58.392	59.404
0.04	50.293	51.288	52.292	53.297	54.008	54.888	55.900	56.924	57.956	58.977
0.05	49.915	50.906	51.911	52.917	53.527	54.345	55.351	56.385	57.439	58.468
0.06	49.474	50.458	51.460	52.467	52.996	53.743	54.736	55.779	56.861	57.899
0.07	48.977	49.951	50.950	51.954	52.430	53.106	54.076	55.127	56.242	57.288
0.08	48.434	49.395	50.387	51.388	51.839	52.450	53.388	54.446	55.599	56.651
0.09	47.856	48.800	49.781	50.775	51.229	51.786	52.687	53.750	54.943	56.000
0.10	47.250	48.174	49.142	50.125	50.603	51.122	51.982	53.047	54.281	55.342
0.11	46.625	47.526	48.476	49.447	49.963	50.460	51.278	52.345	53.617	54.680
0.12	45.988	46.863	47.793	48.747	49.309	49.802	50.580	51.646	52.952	54.017
0.13	45.344	46.193	47.099	48.033	48.645	49.146	49.888	50.952	52.288	53.354
0.14	44.699	45.519	46.400	47.311	47.971	48.492	49.202	50.263	51.623	52.689
0.15	44.056	44.848	45.702	46.588	47.291	47.839	48.523	49.579	50.957	52.022
0.16	43.419	44.182	45.008	45.868	46.606	47.186	47.849	48.901	50.289	51.353
0.17	42.789	43.526	44.323	45.155	45.921	46.533	47.182	48.227	49.620	50.682
0.18	42.168	42.879	43.648	44.453	45.237	45.882	46.519	47.557	48.950	50.009
0.19	41.556	42.245	42.987	43.763	44.559	45.232	45.862	46.892	48.280	49.334
0.20	40.955	41.623	42.340	43.088	43.888	44.586	45.212	46.233	47.610	48.660
0.22	39.783	40.419	41.091	41.788	42.578	43.309	43.932	44.933	46.278	47.317
0.24	38.652	39.267	39.904	40.557	41.320	42.064	42.686	43.663	44.967	45.989
0.25	38.100	38.709	39.333	39.967	40.713	41.456	42.078	43.042	44.323	45.336
0.26	37.556	38.163	38.776	39.393	40.121	40.859	41.481	42.432	43.688	44.690
0.28	36.495	37.102	37.702	38.294	38.982	39.702	40.321	41.244	42.448	43.428
0.30	35.465	36.079	36.675	37.251	37.904	38.598	39.212	40.104	41.256	42.210
0.32	34.464	35.090	35.690	36.259	36.881	37.546	38.153	39.014	40.113	41.040
0.34	33.491	34.131	34.741	35.310	35.909	36.545	37.145	37.975	39.022	39.920
0.35	33.016	33.663	34.279	34.850	35.440	36.063	36.659	37.474	38.496	39.379
0.36	32.547	33.202	33.824	34.399	34.981	35.593	36.185	36.985	37.982	38.851
0.38	31.631	32.299	32.936	33.520	34.094	34.685	35.270	36.040	36.989	37.830
0.40	30.745	31.424	32.075	32.671	33.241	33.818	34.397	35.139	36.042	36.854
0.42	29.888	30.575	31.238	31.847	32.419	32.986	33.562	34.277	35.137	35.922
0.44	29.063	29.753	30.427	31.047	31.624	32.187	32.760	33.451	34.269	35.029
0.45	28.663	29.352	30.030	30.656	31.236	31.798	32.370	33.051	33.849	34.596
0.46	28.270	28.959	29.640	30.271	30.854	31.415	31.988	32.658	33.437	34.171
0.48	27.511	28.194	28.877	29.517	30.107	30.670	31.243	31.893	32.635	33.347
0.50	26.784	27.458	28.141	28.785	29.382	29.948	30.523	31.154	31.862	32.553
0.55	25.113	25.748	26.412	27.054	27.661	28.238	28.817	29.409	30.040	30.683
0.60	23.646	24.226	24.851	25.470	26.072	26.652	27.231	27.791	28.358	28.960
0.65	22.366	22.885	23.459	24.038	24.619	25.189	25.759	26.289	26.803	27.367
0.70	21.253	21.711	22.228	22.758	23.303	23.851	24.401	24.901	25.370	25.899
0.80	19.424	19.783	20.193	20.618	21.072	21.547	22.031	22.469	22.867	23.325
0.90	17.958	18.262	18.599	18.943	19.310	19.701	20.106	20.481	20.824	21.214
1.00	16.696	16.986	17.293	17.591	17.900	18.224	18.561	18.881	19.182	19.513
1.10	15.537	15.841	16.150	16.438	16.722	17.008	17.300	17.583	17.854	18.139
1.20	14.429	14.759	15.090	15.390	15.676	15.953	16.227	16.491	16.745	17.003
1.30	13.355	13.712	14.072	14.396	14.700	14.988	15.265	15.526	15.776	16.024
1.40	12.321	12.698	13.082	13.432	13.759	14.067	14.362	14.633	14.888	15.138
1.50	11.341	11.726	12.125	12.494	12.845	13.175	13.489	13.776	14.042	14.303
1.60	10.431	10.811	11.214	11.592	11.956	12.305	12.636	12.939	13.218	13.493
1.70	9.602	9.966	10.360	10.736	11.104	11.461	11.807	12.123	12.414	12.704
1.80	8.861	9.201	9.576	9.940	10.303	10.661	11.009	11.333	11.631	11.932
1.90	8.208	8.518	8.868	9.212	9.558	9.907	10.253	10.576	10.878	11.185
2.00	7.642	7.921	8.239	8.556	8.881	9.213	9.550	9.868	10.166	10.473
2.50	5.836	5.980	6.142	6.315	6.502	6.704	6.917	7.117	7.333	7.567
3.00	4.945	5.040	5.132	5.229	5.332	5.440	5.550	5.663	5.800	5.930
3.50	4.295	4.390	4.478	4.566	4.651	4.735	4.820	4.910	5.000	5.090
4.00	3.678	3.780	3.891	3.991	4.087	4.178	4.270	4.360	4.445	4.525
5.00	2.615	2.722	2.828	2.935	3.041	3.146	3.240	3.340	3.435	3.530
6.00	1.909	1.990	2.067	2.150	2.237	2.325	2.410	2.490	2.580	2.670

Table 6.1.1.1. *Mean atomic scattering factors for free atoms (cont.)*

Element	Pm	Sm	Eu	Gd	Tb	Dy	Ho	Er	Tm	Yb
Z	61	62	63	64	65	66	67	68	69	70
Method	*RHF	*RHF	RHF	*RHF	*RHF	*RHF	*RHF	*RHF	*RHF	*RHF
$(\sin\theta)/\lambda$ (Å^{-1})										
0.00	61.000	62.000	63.000	64.000	65.000	66.000	67.000	68.000	69.000	70.000
0.01	60.932	61.934	62.936	63.936	64.938	65.939	66.940	67.941	68.943	69.944
0.02	60.734	61.740	62.746	63.749	64.755	65.760	66.763	67.769	68.773	69.777
0.03	60.417	61.428	62.441	63.447	64.461	65.471	66.476	67.491	68.500	69.509
0.04	59.998	61.017	62.036	63.044	64.071	65.088	66.093	67.120	68.136	69.151
0.05	59.497	60.525	61.552	62.557	63.603	64.627	65.627	66.673	67.696	68.717
0.06	58.936	59.972	61.007	62.004	63.073	64.105	65.096	66.166	67.195	68.223
0.07	58.333	59.377	60.419	61.400	62.499	63.538	64.513	65.613	66.649	67.684
0.08	57.703	58.753	59.801	60.762	61.894	62.940	63.895	65.028	66.070	67.112
0.09	57.057	58.113	59.166	60.102	61.270	62.321	63.251	64.420	65.468	66.516
0.10	56.403	57.463	58.521	59.427	60.634	61.689	62.591	63.798	64.852	65.904
0.11	55.744	56.809	57.869	58.746	59.989	61.049	61.921	63.167	64.224	65.281
0.12	55.084	56.151	57.214	58.061	59.340	60.403	61.247	62.528	63.589	64.650
0.13	54.422	55.491	56.555	57.375	58.686	59.752	60.569	61.884	62.948	64.012
0.14	53.758	54.828	55.893	56.690	58.029	59.097	59.891	61.234	62.301	63.368
0.15	53.091	54.163	55.228	56.005	57.366	58.437	59.212	60.578	61.648	62.718
0.16	52.422	53.493	54.559	55.321	56.699	57.771	58.532	59.917	60.989	62.062
0.17	51.749	52.821	53.886	54.637	56.028	57.101	57.851	59.249	60.324	61.399
0.18	51.074	52.145	53.210	53.953	55.351	56.425	57.169	58.576	59.653	60.729
0.19	50.398	51.467	52.530	53.270	54.670	55.744	56.486	57.897	58.975	60.053
0.20	49.720	50.786	51.847	52.588	53.985	55.059	55.803	57.213	58.292	59.371
0.22	48.367	49.426	50.480	51.227	52.610	53.681	54.435	55.833	56.912	57.992
0.24	47.026	48.074	49.119	49.878	51.234	52.300	53.070	54.445	55.521	56.601
0.25	46.364	47.406	48.444	49.209	50.549	51.611	52.390	53.750	54.825	55.903
0.26	45.710	46.743	47.775	48.546	49.868	50.926	51.714	53.058	54.130	55.206
0.28	44.427	45.443	46.458	47.240	48.523	49.570	50.375	51.683	52.748	53.817
0.30	43.186	44.180	45.176	45.965	47.208	48.240	49.059	50.329	51.384	52.444
0.32	41.991	42.961	43.935	44.729	45.929	46.944	47.772	49.004	50.046	51.095
0.34	40.844	41.789	42.740	43.533	44.690	45.686	46.520	47.712	48.739	49.774
0.35	40.289	41.221	42.160	42.951	44.087	45.073	45.908	47.081	48.099	49.127
0.36	39.747	40.666	41.591	42.380	43.496	44.471	45.305	46.459	47.469	48.488
0.38	38.697	39.589	40.489	41.272	42.346	43.299	44.131	45.246	46.237	47.239
0.40	37.694	38.559	39.433	40.207	41.241	42.171	42.996	44.075	45.046	46.029
0.42	36.735	37.573	38.421	39.184	40.179	41.086	41.903	42.945	43.896	44.859
0.44	35.815	36.627	37.451	38.203	39.160	40.042	40.849	41.857	42.786	43.728
0.45	35.370	36.169	36.980	37.726	38.665	39.536	40.337	41.327	42.246	43.178
0.46	34.933	35.720	36.519	37.259	38.180	39.039	39.834	40.808	41.715	42.637
0.48	34.085	34.848	35.623	36.352	37.237	38.073	38.856	39.797	40.682	41.583
0.50	33.269	34.008	34.761	35.479	36.329	37.143	37.914	38.822	39.686	40.565
0.55	31.349	32.036	32.737	33.428	34.199	34.958	35.699	36.531	37.342	38.169
0.60	29.581	30.222	30.877	31.543	32.243	32.953	33.664	34.425	35.187	35.964
0.65	27.948	28.547	29.161	29.802	30.438	31.103	31.786	32.483	33.198	33.929
0.70	26.442	27.002	27.576	28.192	28.772	29.394	30.049	30.688	31.359	32.045
0.80	23.796	24.281	24.781	25.335	25.822	26.366	26.958	27.497	28.086	28.690
0.30	21.616	22.030	22.459	22.940	23.353	23.821	24.343	24.800	25.311	25.837
1.00	19.853	20.202	20.565	20.970	21.323	21.721	22.167	22.556	22.995	23.447
1.10	18.430	18.728	19.035	19.372	19.675	20.011	20.385	20.718	21.089	21.474
1.20	17.262	17.523	17.789	18.072	18.338	18.623	18.934	19.221	19.535	19.860
1.30	16.266	16.507	16.747	16.995	17.234	17.483	17.746	17.998	18.266	18.542
1.40	15.378	15.613	15.841	16.072	16.296	16.522	16.753	16.980	17.215	17.454
1.50	14.551	14.790	15.020	15.247	15.465	15.680	15.895	16.107	16.321	16.536
1.60	13.755	14.005	14.245	14.477	14.697	14.913	15.123	15.329	15.533	15.735
1.70	12.980	13.243	13.494	13.741	13.968	14.190	14.406	14.612	14.815	15.013
1.80	12.220	12.497	12.763	13.022	13.259	13.491	13.718	13.929	14.137	14.338
1.90	11.481	11.767	12.044	12.317	12.564	12.808	13.047	13.267	13.483	13.691
2.00	10.773	11.064	11.345	11.631	11.886	12.141	12.392	12.621	12.847	13.064
2.50	7.817	8.083	8.348	8.683	8.983	9.267	9.533	9.783	10.033	10.267
3.00	6.088	6.250	6.435	6.588	6.775	6.963	7.163	7.375	7.588	7.788
3.50	5.180	5.280	5.378	5.490	5.610	5.720	5.850	5.980	6.110	6.250
4.00	4.600	4.675	4.750	4.830	4.915	5.000	5.090	5.180	5.280	5.380
5.00	3.625	3.720	3.812	3.905	3.990	4.075	4.155	4.235	4.310	4.380
6.00	2.770	2.865	2.965	3.070	3.170	3.270	3.355	3.440	3.520	3.600

Table 6.1.1.1. *Mean atomic scattering factors for free atoms (cont.)*

Element	Lu	Hf	Ta	W	Re	Os	Ir	Pt	Au	Hg
Z	71	72	73	74	75	76	77	78	79	80
Method	*RHF	*RHF	*RHF	*RHF	*RHF	*RHF	*RHF	*RHF	RHF	RHF
$(\sin\theta)/\lambda$ (Å^{-1})										
0.00	71.000	72.000	73.000	74.000	75.000	76.000	77.000	78.000	79.000	80.000
0.01	70.944	71.945	72.946	73.948	74.949	75.950	76.951	77.955	78.957	79.556
0.02	70.778	71.783	72.788	73.793	74.797	75.801	76.806	77.820	78.826	79.819
0.03	70.509	71.518	72.529	73.539	74.548	75.538	76.567	77.599	78.609	79.595
0.04	70.148	71.161	72.177	73.194	74.209	75.225	76.240	77.295	78.311	79.286
0.05	69.707	70.723	71.745	72.767	73.788	74.810	75.832	76.914	77.936	78.899
0.06	69.202	70.217	71.242	72.269	73.295	74.323	75.352	76.462	77.491	78.439
0.07	68.646	69.656	70.680	71.711	72.740	73.772	74.806	75.946	76.981	77.913
0.08	68.051	69.052	70.072	71.103	72.132	73.167	74.206	75.373	76.414	77.330
0.09	67.429	68.416	69.428	70.455	71.482	72.518	73.558	74.751	75.797	76.696
0.10	66.789	67.757	68.758	69.778	70.799	71.832	72.872	74.086	75.135	76.018
0.11	66.137	67.083	68.069	69.078	70.091	71.119	72.156	73.386	74.437	75.303
0.12	65.477	66.400	67.367	68.363	69.365	70.384	71.416	72.656	73.706	74.559
0.13	64.813	65.711	66.658	67.637	68.625	69.634	70.658	71.902	72.950	73.790
0.14	64.146	65.019	65.944	66.906	67.878	68.874	69.887	71.130	72.173	73.001
0.15	63.478	64.326	65.229	66.172	67.126	68.107	69.108	70.343	71.380	72.198
0.16	62.807	63.634	64.515	65.437	66.372	67.337	68.324	69.546	70.575	71.385
0.17	62.134	62.942	63.802	64.703	65.619	66.566	67.538	68.742	69.761	70.564
0.18	61.460	62.251	63.090	63.972	64.868	65.797	66.752	67.934	68.941	69.740
0.19	60.783	61.560	62.382	63.243	64.121	65.031	65.969	67.125	68.119	68.914
0.20	60.103	60.870	61.675	62.519	63.378	64.269	65.189	66.317	67.296	68.088
0.22	58.739	59.492	60.271	61.082	61.906	62.761	63.645	64.709	65.657	66.447
0.24	57.369	58.119	58.880	59.663	60.457	61.278	62.127	63.125	64.039	64.828
0.25	56.683	57.434	58.189	58.961	59.742	60.548	61.380	62.344	63.241	64.029
0.26	55.998	56.752	57.502	58.265	59.034	59.825	60.641	61.571	62.452	63.239
0.28	54.634	55.396	56.141	56.888	57.637	58.403	59.189	60.056	60.902	61.687
0.30	53.282	54.054	54.799	55.536	56.270	57.013	57.773	58.582	59.395	60.177
0.32	51.950	52.733	53.479	54.210	54.932	55.658	56.395	57.152	57.935	58.711
0.34	50.642	51.435	52.185	52.912	53.627	54.339	55.056	55.769	56.523	57.292
0.35	49.998	50.796	51.548	52.274	52.986	53.692	54.401	55.094	55.835	56.600
0.36	49.363	50.164	50.918	51.644	52.354	53.055	53.756	54.432	55.160	55.920
0.38	48.117	48.924	49.683	50.408	51.114	51.807	52.496	53.141	53.846	54.595
0.40	46.906	47.717	48.479	49.205	49.910	50.596	51.274	51.897	52.581	53.318
0.42	45.731	46.543	47.308	48.036	48.739	49.422	50.091	50.697	51.363	52.088
0.44	44.593	45.405	46.171	46.900	47.603	48.283	48.946	49.540	50.191	50.902
0.45	44.038	44.849	45.615	46.344	47.048	47.726	48.387	48.977	49.622	50.326
0.46	43.492	44.301	45.068	45.797	46.501	47.179	47.837	48.424	49.063	49.761
0.48	42.427	43.232	43.998	44.728	45.432	46.109	46.765	47.347	47.976	48.661
0.50	41.398	42.197	42.962	43.691	44.396	45.072	45.726	46.308	46.929	47.601
0.55	38.970	39.752	40.508	41.236	41.940	42.617	43.269	43.860	44.469	45.113
0.60	36.733	37.494	38.238	38.960	39.662	40.340	40.994	41.601	42.207	42.829
0.65	34.666	35.404	36.132	36.846	37.544	38.222	38.878	39.502	40.110	40.718
0.70	32.752	33.465	34.175	34.878	35.569	36.244	36.901	37.539	38.153	38.753
0.80	29.334	29.992	30.658	31.327	31.993	32.654	33.305	33.958	34.581	35.176
0.90	26.413	27.008	27.618	28.238	28.865	29.495	30.125	30.766	31.387	31.980
1.00	23.950	24.473	25.016	25.576	26.148	26.732	27.323	27.930	28.530	29.112
1.10	21.902	22.352	22.823	23.313	23.821	24.345	24.882	25.437	25.998	26.554
1.20	20.219	20.598	20.998	21.418	21.856	22.314	22.789	23.281	23.789	24.303
1.30	18.842	19.159	19.494	19.847	20.219	20.610	21.019	21.445	21.892	22.354
1.40	17.709	17.975	18.256	18.552	18.864	19.194	19.541	19.902	20.287	20.692
1.50	16.759	16.988	17.228	17.478	17.742	18.019	18.312	18.616	18.943	19.290
1.60	15.939	16.145	16.356	16.575	16.801	17.038	17.287	17.545	17.821	18.116
1.70	15.208	15.403	15.598	15.796	15.998	16.206	16.422	16.644	16.880	17.131
1.80	14.534	14.727	14.916	15.104	15.293	15.483	15.678	15.875	16.081	16.298
1.90	13.894	14.091	14.282	14.469	14.653	14.835	15.018	15.202	15.388	15.581
2.00	13.277	13.481	13.679	13.871	14.057	14.239	14.418	14.595	14.770	14.949
2.50	10.500	10.733	10.950	11.167	11.383	11.583	11.783	11.983	12.168	12.360
3.00	8.013	8.238	8.480	8.706	8.938	9.163	9.400	9.620	9.826	10.049
3.50	6.400	6.560	6.740	6.900	7.080	7.270	7.460	7.650	7.878	8.081
4.00	5.490	5.600	5.710	5.840	5.960	6.080	6.210	6.340	6.489	6.644
5.00	4.450	4.520	4.585	4.650	4.715	4.788	4.860	4.935	5.010	5.090
6.00	3.680	3.755	3.825	3.900	3.970	4.035	4.105	4.175	4.244	4.310

Table 6.1.1.1. *Mean atomic scattering factors for free atoms (cont.)*

Element	Tl	Pb	Bi	Po	At	Rn	Fr	Ra	Ac	Th
Z	81	82	83	84	85	86	87	88	89	90
Method	*RHF	RHF	RHF	*RHF	*RHF	RHF	*RHF	*RHF	*RHF	*RHF
$(\sin\theta)/\lambda$ (Å^{-1})										
0.00	81.000	82.000	83.000	84.000	85.000	86.000	87.000	88.000	89.000	90.000
0.01	80.950	81.949	82.947	83.944	84.944	85.945	86.922	87.915	88.915	89.916
0.02	80.799	81.792	82.784	83.778	84.776	85.777	86.694	87.664	88.664	89.669
0.03	80.553	81.536	82.518	83.506	84.502	85.502	86.332	87.263	88.260	89.269
0.04	80.217	81.186	82.154	83.134	84.125	85.123	85.854	86.734	87.723	88.735
0.05	79.798	80.750	81.700	82.669	83.654	84.649	85.286	86.104	87.077	88.085
0.06	79.305	80.237	81.167	82.121	83.098	84.087	84.647	85.397	86.346	87.344
0.07	78.748	79.656	80.563	81.501	82.466	83.448	83.955	84.638	85.553	86.533
0.08	78.134	79.018	79.901	80.819	81.770	82.742	83.222	83.845	84.719	85.672
0.09	77.473	78.332	79.189	80.086	81.020	81.979	82.457	83.030	83.859	84.779
0.10	76.773	77.607	78.438	79.312	80.226	81.169	81.666	82.202	82.985	83.867
0.11	76.042	76.851	77.657	78.506	79.398	80.322	80.852	81.368	82.105	82.946
0.12	75.284	76.071	76.852	77.677	78.545	79.448	80.018	80.528	81.225	82.025
0.13	74.507	75.274	76.032	76.831	77.674	78.554	79.167	79.685	80.348	81.107
0.14	73.715	74.464	75.202	75.976	76.794	77.648	78.303	78.839	79.474	80.196
0.15	72.912	73.645	74.365	75.117	75.908	76.737	77.430	77.990	78.605	79.294
0.16	72.101	72.822	73.527	74.257	75.023	75.826	76.550	77.138	77.739	78.400
0.17	71.285	71.997	72.689	73.400	74.143	74.920	75.667	76.285	76.879	77.516
0.18	70.467	71.172	71.855	72.549	73.269	74.021	74.785	75.431	76.023	76.642
0.19	69.648	70.349	71.026	71.706	72.405	73.133	73.907	74.578	75.172	75.777
0.20	68.830	69.530	70.203	70.871	71.553	72.258	73.035	73.728	74.326	74.922
0.22	67.205	67.907	68.578	69.232	69.885	70.552	71.320	72.043	72.654	73.242
0.24	65.600	66.310	66.987	67.634	68.269	68.907	69.653	70.389	71.014	71.602
0.25	64.807	65.523	66.204	66.852	67.481	68.109	68.841	69.576	70.208	70.798
0.26	64.022	64.743	65.430	66.080	66.706	67.325	68.043	68.775	69.412	70.005
0.28	62.478	63.210	63.909	64.567	65.193	65.802	66.491	67.210	67.855	68.454
0.30	60.970	61.712	62.425	63.093	63.725	64.332	64.996	65.696	66.345	66.951
0.32	59.503	60.253	60.977	61.658	62.301	62.912	63.556	64.235	64.884	65.497
0.34	58.079	58.833	59.566	60.260	60.915	61.535	62.167	62.826	63.473	64.091
0.35	57.383	58.138	58.875	59.575	60.236	60.862	61.489	62.140	62.785	63.405
0.36	56.698	57.453	58.193	58.899	59.566	60.198	60.823	61.466	62.110	62.731
0.38	55.362	56.116	56.859	57.573	58.253	58.898	59.520	60.151	60.792	61.416
0.40	54.072	54.820	55.563	56.283	56.974	57.631	58.256	58.879	59.517	60.143
0.42	52.826	53.567	54.306	55.029	55.728	56.397	57.026	57.646	58.282	58.910
0.44	51.625	52.356	53.089	53.811	54.515	55.194	55.829	56.448	57.084	57.713
0.45	51.041	51.766	52.495	53.215	53.921	54.604	55.242	55.862	56.497	57.127
0.46	50.467	51.187	51.910	52.629	53.335	54.021	54.663	55.284	55.919	56.550
0.48	49.352	50.058	50.771	51.483	52.189	52.879	53.527	54.151	54.787	55.419
0.50	48.276	48.969	49.669	50.373	51.075	51.767	52.420	53.048	53.684	54.317
0.55	45.753	46.411	47.077	47.752	48.435	49.119	49.777	50.413	51.050	51.684
0.60	43.442	44.069	44.700	45.343	45.997	46.659	47.310	47.948	48.580	49.211
0.65	41.313	41.914	42.517	43.127	43.750	44.384	45.017	45.646	46.268	46.889
0.70	39.337	39.921	40.501	41.085	41.678	42.281	42.891	43.504	44.110	44.716
0.80	35.755	36.322	36.879	37.430	37.980	38.533	39.095	39.664	40.229	40.795
0.90	32.561	33.127	33.680	34.220	34.751	35.277	35.804	36.335	36.863	37.391
1.00	29.687	30.252	30.805	31.344	31.872	32.389	32.900	33.408	33.912	34.413
1.10	27.109	27.662	28.208	28.744	29.271	29.787	30.292	30.790	31.283	31.770
1.20	24.824	25.350	25.875	26.397	26.915	27.426	27.926	28.418	28.906	29.387
1.30	22.827	23.313	23.804	24.298	24.794	25.291	25.779	26.263	26.744	27.219
1.40	21.110	21.546	21.992	22.446	22.909	23.379	23.845	24.312	24.779	25.244
1.50	19.652	20.034	20.429	20.836	21.256	21.689	22.123	22.564	23.008	23.454
1.60	18.424	18.754	19.097	19.453	19.826	20.215	20.608	21.014	21.427	21.846
1.70	17.394	17.674	17.969	18.277	18.602	18.944	19.295	19.660	20.036	20.421
1.80	16.524	16.764	17.017	17.281	17.562	17.859	18.165	18.488	18.823	19.170
1.90	15.780	15.989	16.207	16.435	16.677	16.934	17.199	17.481	17.776	18.083
2.00	15.131	15.317	15.510	15.711	15.922	16.143	16.377	16.623	16.880	17.149
2.50	12.530	12.724	12.896	13.060	13.230	13.386	13.550	13.700	13.860	14.020
3.00	10.270	10.482	10.690	10.900	11.090	11.282	11.460	11.640	11.815	11.980
3.50	8.290	8.495	8.704	8.910	9.120	9.329	9.530	9.730	9.930	10.130
4.00	6.800	6.973	7.145	7.320	7.500	7.686	7.878	8.070	8.255	8.440
5.00	5.175	5.260	5.351	5.440	5.540	5.650	5.755	5.870	5.933	6.118
6.00	4.374	4.441	4.505	4.567	4.630	4.702	4.768	4.840	4.910	4.982

Table 6.1.1.1. *Mean atomic scattering factors for free atoms (cont.)*

Element	Pa	U	Np	Pu	Am	Cm	Bk	Cf
Z	91	92	93	94	95	96	97	98
Method	*RHF	RHF	*RHF	*RHF	*RHF	*RHF	*RHF	*RHF
$(\sin\theta)/\lambda$ (Å^{-1})								
0.00	91.000	92.000	93.000	94.000	95.000	96.000	97.000	98.000
0.01	90.919	91.922	92.922	93.924	94.926	95.926	96.928	97.929
0.02	90.678	91.687	92.691	93.701	94.706	95.708	96.713	97.718
0.03	90.290	91.307	92.318	93.340	94.352	95.354	96.365	97.375
0.04	89.772	90.798	91.817	92.857	93.877	94.877	95.895	96.912
0.05	89.144	90.180	91.208	92.271	93.299	94.294	95.320	96.344
0.06	88.427	89.474	90.510	91.601	92.638	93.623	94.656	95.688
0.07	87.644	88.699	89.742	90.866	91.910	92.879	93.920	94.961
0.08	86.813	87.874	88.923	90.082	91.131	92.081	93.129	94.176
0.09	85.950	87.014	88.067	89.261	90.315	91.241	92.294	93.347
0.10	85.066	86.130	87.186	88.413	89.470	90.371	91.429	92.486
0.11	84.170	85.232	86.288	87.547	88.605	89.479	90.540	91.601
0.12	83.269	84.326	85.380	86.665	87.723	88.573	89.635	90.699
0.13	82.366	83.417	84.467	85.772	86.829	87.656	88.718	89.783
0.14	81.463	82.505	83.550	84.870	85.924	86.731	87.793	88.858
0.15	80.563	81.595	82.632	83.961	85.011	85.802	86.862	87.926
0.16	79.665	80.685	81.715	83.044	84.090	84.869	85.926	86.989
0.17	78.771	79.779	80.799	82.123	83.163	83.934	84.988	86.048
0.18	77.881	78.875	79.885	81.198	82.231	82.998	84.047	85.103
0.19	76.995	77.975	78.973	80.271	81.296	82.062	83.105	84.157
0.20	76.115	77.080	78.066	79.343	80.360	81.126	82.163	83.210
0.22	74.375	75.308	76.267	77.493	78.490	79.263	80.285	81.318
0.24	72.668	73.568	74.496	75.663	76.636	77.419	78.421	79.437
0.25	71.829	72.712	73.624	74.759	75.719	76.507	77.498	78.504
0.26	71.001	71.866	72.763	73.865	74.811	75.603	76.582	77.577
0.28	69.380	70.211	71.074	72.110	73.027	73.824	74.777	75.749
0.30	67.810	68.607	69.436	70.408	71.293	72.091	73.016	73.960
0.32	66.294	67.058	67.853	68.763	69.615	70.409	71.303	72.219
0.34	64.832	65.564	66.326	67.178	67.997	68.783	69.645	70.531
0.35	64.121	64.838	65.584	66.409	67.212	67.991	68.838	69.707
0.36	63.423	64.126	64.857	65.655	66.441	67.214	68.045	68.898
0.38	62.066	62.742	63.443	64.193	64.947	65.705	66.503	67.325
0.40	60.758	61.409	62.083	62.789	63.513	64.254	65.020	65.810
0.42	59.495	60.125	60.775	61.442	62.137	62.859	63.595	64.354
0.44	58.274	58.886	59.514	60.147	60.816	61.519	62.226	62.954
0.45	57.679	58.283	58.901	59.518	60.175	60.869	61.562	62.276
0.46	57.093	57.689	58.298	58.901	59.546	60.231	60.910	61.610
0.48	55.948	56.531	57.124	57.702	58.325	58.992	59.646	60.319
0.50	54.836	55.410	55.989	56.544	57.148	57.798	58.430	59.078
0.55	52.191	52.748	53.303	53.819	54.385	54.998	55.581	56.176
0.60	49.719	50.268	50.808	51.302	51.842	52.427	52.974	53.528
0.65	47.405	47.950	48.483	48.967	49.490	50.052	50.574	51.098
0.70	45.241	45.784	46.312	46.794	47.307	47.850	48.354	48.858
0.80	41.333	41.869	42.390	42.879	43.380	43.894	44.380	44.859
0.90	37.930	38.454	38.966	39.465	39.958	40.449	40.926	41.395
1.00	34.946	35.458	35.961	36.465	36.952	37.426	37.898	38.361
1.10	32.292	32.794	33.289	33.793	34.276	34.740	35.209	35.671
1.20	29.897	30.391	30.879	31.379	31.858	32.318	32.786	33.247
1.30	27.714	28.199	28.680	29.172	29.648	30.106	30.572	31.033
1.40	25.720	26.192	26.662	27.142	27.611	28.068	28.530	28.989
1.50	23.905	24.360	24.813	25.275	25.733	26.184	26.639	27.093
1.60	22.266	22.699	23.128	23.566	24.006	24.446	24.889	25.332
1.70	20.807	21.207	21.609	22.019	22.435	22.857	23.281	23.708
1.80	19.518	19.886	20.253	20.630	21.018	21.415	21.815	22.221
1.90	18.394	18.723	19.055	19.398	19.754	20.121	20.496	20.872
2.00	17.423	17.713	18.012	18.319	18.640	18.975	19.315	19.665
2.50	14.180	14.341	14.503	14.664	14.826	14.988	15.150	15.311
3.00	12.150	12.294	12.475	12.656	12.838	13.019	13.200	13.381
3.50	10.320	10.495	10.695	10.895	11.095	11.295	11.495	11.695
4.00	8.630	8.823	9.008	9.193	9.378	9.563	9.748	9.933
5.00	6.250	6.378	6.489	6.602	6.713	6.825	6.937	7.049
6.00	5.055	5.136	5.206	5.275	5.345	5.414	5.484	5.553

Table 6.1.1.2. *Spherical bonded hydrogen-atom scattering factors from Stewart, Davidson & Simpson (1965)*

$(\sin\theta)/\lambda$ (Å^{-1})	f	$(\sin\theta)/\lambda$ (Å^{-1})	f
0.0000	1.0000	0.7729	0.0254
0.0215	0.9924	0.8158	0.0208
0.0429	0.9704	0.8588	0.0171
0.0644	0.9352	0.9017	0.0140
0.0859	0.8892	0.9447	0.0116
0.1073	0.8350	0.9876	0.0096
0.1288	0.7752	1.0305	0.0080
0.1503	0.7125	1.0735	0.0066
0.1718	0.6492	1.1164	0.0056
0.1932	0.5871	1.1593	0.0047
0.2147	0.5277	1.2023	0.0040
0.2576	0.4201	1.2452	0.0035
0.3006	0.3301	1.2882	0.0031
0.3435	0.2573	1.3311	0.0027
0.3864	0.1998	1.3740	0.0025
0.4294	0.1552	1.4170	0.0022
0.4723	0.1208	1.4599	0.0020
0.5153	0.0945	1.5029	0.0018
0.5582	0.0744	1.5458	0.0016
0.6011	0.0592	1.5887	0.0015
0.6441	0.0474	1.6317	0.0013
0.6870	0.0383	1.6746	0.0011
0.7300	0.0311	1.7176	0.0010

some of the more chemically significant ions are listed in Table 6.1.1.3. For H^-, Li^+ and Be^{2+} these are based on the correlated electron calculations of Thakkar & Smith (1992). For other ions lighter than rubidium, values are based on the Hartree–Fock calculations of Cromer & Mann (1968), using the wavefunctions of Mann (1968*b*). For the heavier ions, the calculations are by Cromer & Waber (1968), based on relativistic Dirac–Slater wavefunctions, which are a good approximation to the corresponding relativistic Hartree–Fock wavefunctions. If ionic scattering factors are required for values of $(\sin\theta)/\lambda$ greater than those shown in Table 6.1.1.3, the free-atom scattering factors of Table 6.1.1.1 can be used because high-angle scattering is dominated by core electrons and is therefore very little affected by ionicity.

6.1.1.3.1. *Scattering-factor interpolation*

A general treatment of interpolation is complicated by possible difficulties resulting from singularities in tabulated functions. The interpolation of scattering factors does not involve such problems, however, and a more restricted treatment suffices.

An iterative method, applicable to a function $f(x)$ tabulated at arbitrary values $x_0, x_1, \ldots, x_n$ is due to Aitken. $f(x|x_0, x_1, \ldots, x_k)$ is the polynominal that coincides with the tabulated values at $x_0, x_1, \ldots, x_k$.

$$f(x|x_0,x_1) = \frac{1}{x_1-x_0}\begin{vmatrix} f_0\,x_0 - x \\ f_1\,x_1 - x \end{vmatrix}$$
$$f(x|x_0,x_1,x_2) = \frac{1}{x_2-x_1}\begin{vmatrix} f(x|x_0,x_1) & x_1-x \\ f(x|x_0,x_2) & x_2-x \end{vmatrix}$$
$$f(x|x_0,x_1,x_2,x_3) = \frac{1}{x_3-x_2}\begin{vmatrix} f(x|x_0,x_1,x_2) & x_2-x \\ f(x|x_0,x_1,x_3) & x_3-x \end{vmatrix}. \quad (6.1.1.13)$$

Iteration is continued until increasing k does not change the interpolated value significantly.

Another interpolation formula, due to Lagrange, is

$$f(x) = \sum_{i=0}^{n} l_i(x) f_i + R_n(x),$$

where

$$l_i(x) = \frac{\pi_n(x)}{(x-x_i)\pi_n'(x_i)}$$

and

$$R_n(x) = \pi_n(x)[x_0, x_1, \ldots, x_n, x]. \quad (6.1.1.14)$$

$\pi_n(x)$ is $(x-x_0)(x-x_1)\ldots(x-x_n)$ and $\pi_n'(x)$ is its derivative, so that

$$\pi_n'(x_k) = (x_k-x_0)(x_k-x_1)\ldots(x_k-x_{k-1}) \times (x_k-x_{k+1})\ldots(x_k-x_n)$$

while

$$[x_0,x_1] = \frac{f_0-f_1}{x_0-x_1}$$
$$[x_0,x_1,x_2] = \frac{[x_0,x_1]-[x_1,x_2]}{x_0-x_2}$$
$$[x_0,x_1\ldots x_n] = \sum_{k=0}^{n}\frac{f_k}{\pi_n'(x_k)}.$$

For the scattering factors of Tables 6.1.1.1 and 6.1.1.3, the expansion

$$f(\sin\theta/\lambda) = \sum_{i=1}^{4} a_i \exp(-b_i \sin^2\theta/\lambda^2) + c \quad (6.1.1.15)$$

has been found to be particularly effective. The coefficients listed in Table 6.1.1.4 give a close fit to the atomic scattering curves over the range $0 < (\sin\theta)/\lambda < 2.0$ Å^{-1}. Table 6.1.1.4 also contains the maximum and minimum deviations from the true curve, and the mean of the magnitude of the deviation. For 2.0 Å$^{-1} < (\sin\theta)/\lambda < 6.0$ Å^{-1}, Fox *et al.* (1989) have shown that (6.1.1.15) is highly inaccurate, and they produced a 'logarithmic polynomial' curve-fitting routine based on the equation

$$\ln\{f[(\sin\theta)/\lambda]\} = \sum_{i=0}^{3} a_i s^i \quad (6.1.1.16)$$

for these high angles. The a_i values listed in Table 6.1.1.5 give a close fit to the atomic scattering factor curves over the range $2.0 < (\sin\theta)/\lambda < 6.0$ Å^{-1}. Because f varies slowly with $(\sin\theta)/\lambda$ at these high angles, four parameters are all that is necessary for accurate fitting. Confirmation of this is given in Table 6.1.1.5 where the correlation coefficients, C, associated with each fit are also shown, and it can be seen that these are close to 1.0 in every case.

6.1.1.4. *Generalized scattering factors*

For bound atoms, it may be necessary to account for the perturbation of the electron density by interaction with other atoms, and to analyse its effect on the scattering.

The generalized scattering factor is obtained from the Fourier transform of a perturbed atomic electron-density function. The exponential factor in the transform may be written as an expansion in terms of Legendre polynomials $P_l(\cos\theta)$.†

† Special functions are as given in Abramowitz & Stegun (1964), unless defined otherwise in the text.

Table 6.1.1.3. *Mean atomic scattering factors in electrons for chemically significant ions*

Methods: C: correlated; HF: non-relativistic Hartree–Fock; RHF: relativistic Hartree–Fock; *DS: modified Dirac–Slater.

Element	H^{1-}	Li^{1+}	Be^{2+}	C_{val}	O^{1-}	F^{1-}	Na^{1+}	Mg^{2+}	Al^{3+}	Si_{val}
Z	1	3	4	6	8	9	11	12	13	14
Method	C	C	C	HF	HF	HF	RHF	RHF	HF	HF
$(\sin\theta)/\lambda$ (Å^{-1})										
0.00	2.000	2.000	2.000	6.000	9.000	10.000	10.000	10.000	10.000	14.000
0.01	1.983	1.999	1.999	5.989	8.986	9.988	9.995	9.997	9.997	13.973
0.02	1.933	1.997	1.999	5.956	8.945	9.953	9.981	9.986	9.989	13.894
0.03	1.857	1.994	1.997	5.903	8.878	9.895	9.958	9.969	9.976	13.766
0.04	1.763	1.990	1.995	5.829	8.785	9.816	9.925	9.945	9.957	13.593
0.05	1.659	1.984	1.992	5.738	8.670	9.716	9.883	9.914	9.933	13.381
0.06	1.550	1.977	1.988	5.629	8.534	9.597	9.833	9.876	9.904	13.138
0.07	1.442	1.968	1.983	5.507	8.381	9.461	9.773	9.832	9.870	12.870
0.08	1.338	1.959	1.978	5.372	8.211	9.309	9.705	9.782	9.831	12.586
0.09	1.238	1.948	1.973	5.227	8.029	9.144	9.630	9.725	9.787	12.293
0.10	1.145	1.936	1.966	5.074	7.836	8.967	9.546	9.662	9.738	11.995
0.11	1.058	1.923	1.959	4.916	7.635	8.781	9.455	9.594	9.684	11.700
0.12	0.978	1.909	1.952	4.754	7.429	8.586	9.357	9.519	9.625	11.410
0.13	0.904	1.894	1.944	4.591	7.218	8.386	9.253	9.440	9.563	11.130
0.14	0.836	1.877	1.935	4.428	7.005	8.181	9.142	9.355	9.495	10.862
0.15	0.773	1.860	1.925	4.267	6.792	7.973	9.026	9.265	9.424	10.608
0.16	0.715	1.842	1.915	4.109	6.579	7.762	8.904	9.171	9.349	10.368
0.17	0.661	1.823	1.905	3.954	6.368	7.551	8.777	9.072	9.270	10.143
0.18	0.612	1.804	1.894	3.805	6.160	7.341	8.647	8.969	9.187	9.933
0.19	0.567	1.783	1.882	3.661	5.956	7.131	8.512	8.862	9.101	9.737
0.20	0.526	1.762	1.870	3.523	5.756	6.924	8.374	8.751	9.011	9.553
0.22	0.452	1.718	1.845	3.266	5.371	6.517	8.089	8.521	8.823	9.222
0.24	0.390	1.671	1.817	3.035	5.008	6.126	7.795	8.280	8.623	8.931
0.25	0.362	1.647	1.803	2.930	4.836	5.937	7.646	8.156	8.520	8.798
0.26	0.337	1.623	1.788	2.831	4.670	5.753	7.496	8.030	8.414	8.671
0.28	0.291	1.573	1.758	2.651	4.357	5.399	7.195	7.774	8.198	8.435
0.30	0.253	1.523	1.726	2.495	4.068	5.067	6.894	7.513	7.975	8.214
0.32	0.220	1.471	1.692	2.358	3.804	4.756	6.597	7.251	7.747	8.005
0.34	0.192	1.419	1.658	2.241	3.564	4.467	6.304	6.987	7.515	7.803
0.35	0.179	1.394	1.641	2.188	3.452	4.330	6.160	6.856	7.399	7.704
0.36	0.168	1.368	1.623	2.139	3.345	4.199	6.018	6.725	7.282	7.606
0.38	0.147	1.316	1.587	2.050	3.147	3.951	5.739	6.465	7.047	7.410
0.40	0.129	1.265	1.551	1.974	2.969	3.724	5.471	6.210	6.813	7.215
0.42	0.113	1.215	1.514	1.907	2.808	3.514	5.212	5.959	6.581	7.021
0.44	0.100	1.165	1.476	1.849	2.663	3.322	4.964	5.715	6.350	6.826
0.45	0.094	1.141	1.458	1.822	2.597	3.233	4.845	5.595	6.237	6.729
0.46	0.089	1.117	1.439	1.798	2.533	3.147	4.728	5.477	6.124	6.632
0.48	0.079	1.069	1.401	1.752	2.417	2.987	4.503	5.247	5.901	6.437
0.50	0.070	1.023	1.364	1.711	2.313	2.841	4.290	5.025	5.683	6.244
0.55	0.0526	0.914	1.270	1.624	2.097	2.531	3.808	4.508	5.162	5.766
0.60	0.0401	0.814	1.179	1.552	1.934	2.288	3.395	4.046	4.681	5.303
0.65	0.0311	0.724	1.091	1.488	1.808	2.096	3.046	3.641	4.243	4.865
0.70	0.0243	0.643	1.007	1.428	1.710	1.945	2.753	3.288	3.851	4.455
0.80	0.0155	0.507	0.852	1.315	1.567	1.729	2.305	2.724	3.195	3.734
0.90	0.0102	0.400	0.717	1.204	1.463	1.585	1.997	2.315	2.693	3.150
1.00	0.0070	0.317	0.602	1.096	1.376	1.481	1.785	2.023	2.319	2.691
1.10	0.0049	0.253	0.505	0.992	1.296	1.397	1.635	1.813	2.041	2.338
1.20	0.0036	0.203	0.424	0.894	1.219	1.322	1.524	1.662	1.837	2.069
1.30	0.0026	0.164	0.357	0.802	1.143	1.252	1.438	1.548	1.685	1.867
1.40	0.0020	0.133	0.301	0.718	1.067	1.184	1.367	1.460	1.570	1.713
1.50	0.0015	0.109	0.255	0.642	0.994	1.117	1.304	1.388	1.479	1.595
1.60	0.0012	0.090	0.216				1.246	1.326		
1.70	0.0009	0.075	0.184				1.191	1.270		
1.80	0.0008	0.062	0.157				1.137	1.218		
1.90	0.0006	0.053	0.135				1.084	1.168		
2.00	0.0005	0.044	0.116				1.032	1.119		

Table 6.1.1.3. *Mean atomic scattering factors for chemically significant ions (cont.)*

Element	Si^{4+}	Cl^{1-}	K^{1+}	Ca^{2+}	Sc^{3+}	Ti^{2+}	Ti^{3+}	Ti^{4+}	V^{2+}	V^{3+}
Z	14	17	19	20	21	22	22	22	23	23
Method	HF	RHF	RHF	RHF	HF	HF	HF	HF	RHF	HF
$(\sin\theta)/\lambda$ (Å^{-1})										
0.00	10.000	18.000	18.000	18.000	18.000	20.000	19.000	18.000	21.000	20.000
0.01	9.998	17.972	17.986	17.989	17.991	19.988	18.990	17.992	20.988	19.990
0.02	9.991	17.888	17.943	17.955	17.963	19.951	18.962	17.969	20.952	19.961
0.03	9.981	17.751	17.872	17.899	17.917	19.891	18.914	17.930	20.892	19.913
0.04	9.966	17.563	17.774	17.821	17.853	19.807	18.848	17.877	20.808	19.846
0.05	9.947	17.330	17.649	17.721	17.771	19.701	18.764	17.808	20.702	19.760
0.06	9.924	17.057	17.499	17.601	17.672	19.572	18.662	17.725	20.573	19.657
0.07	9.896	16.750	17.325	17.462	17.556	19.423	18.543	17.628	20.424	19.536
0.08	9.865	16.415	17.129	17.303	17.424	19.253	18.407	17.516	20.255	19.398
0.09	9.829	16.058	16.912	17.127	17.278	19.065	18.255	17.392	20.066	19.244
0.10	9.790	15.685	16.677	16.935	17.116	18.860	18.089	17.255	19.861	19.075
0.11	9.747	15.301	16.426	16.727	16.941	18.639	17.909	17.106	19.639	18.892
0.12	9.700	14.911	16.160	16.506	16.754	18.404	17.716	16.946	19.402	18.695
0.13	9.649	14.519	15.882	16.272	16.555	18.156	17.510	16.775	19.152	18.485
0.14	9.595	14.130	15.594	16.028	16.345	17.896	17.294	16.593	18.890	18.265
0.15	9.537	13.747	15.297	15.774	16.126	17.626	17.067	16.403	18.618	18.033
0.16	9.476	13.371	14.994	15.512	15.898	17.348	16.832	16.205	18.336	17.793
0.17	9.411	13.006	14.688	15.244	15.662	17.062	16.589	15.998	18.047	17.544
0.18	9.343	12.653	14.378	14.970	15.421	16.771	16.339	15.785	17.751	17.287
0.19	9.272	12.313	14.069	14.692	15.173	16.475	16.083	15.566	17.450	17.025
0.20	9.199	11.987	13.760	14.412	14.922	16.176	15.822	15.342	17.146	16.757
0.22	9.043	11.379	13.150	13.850	14.410	15.574	15.291	14.881	16.529	16.210
0.24	8.877	10.832	12.560	13.292	13.893	14.972	14.752	14.408	15.910	15.653
0.25	8.790	10.580	12.275	13.017	13.634	14.673	14.482	14.170	15.602	15.373
0.26	8.701	10.343	11.997	12.745	13.377	14.377	14.213	13.930	15.296	15.093
0.28	8.518	9.908	11.467	12.217	12.869	13.797	13.680	13.452	14.694	14.537
0.30	8.327	9.524	10.972	11.713	12.374	13.236	13.157	12.979	14.107	13.989
0.32	8.131	9.184	10.515	11.235	11.896	12.697	12.650	12.515	13.541	13.455
0.34	7.929	8.884	10.097	10.787	11.438	12.184	12.162	12.064	12.998	12.938
0.35	7.827	8.746	9.901	10.575	11.218	11.938	11.926	11.844	12.736	12.687
0.36	7.724	8.616	9.715	10.370	11.004	11.698	11.696	11.628	12.481	12.441
0.38	7.516	8.377	9.369	9.984	10.595	11.242	11.254	11.211	11.991	11.967
0.40	7.306	8.162	9.056	9.629	10.212	10.815	10.837	10.815	11.530	11.517
0.42	7.095	7.965	8.773	9.303	9.855	10.417	10.446	10.439	11.096	11.092
0.44	6.884	7.785	8.518	9.006	9.524	10.047	10.080	10.086	10.692	10.692
0.45	6.779	7.699	8.399	8.867	9.368	9.873	9.907	9.917	10.500	10.502
0.46	6.674	7.616	8.287	8.734	9.218	9.706	9.740	9.754	10.315	10.318
0.48	6.465	7.457	8.077	8.487	8.937	9.391	9.426	9.445	9.965	9.969
0.50	6.259	7.305	7.886	8.262	8.678	9.102	9.135	9.158	9.641	9.645
0.55	5.755	6.945	7.474	7.781	8.121	8.477	8.503	8.529	8.935	8.936
0.60	5.277	6.600	7.125	7.389	7.670	7.972	7.990	8.012	8.359	8.354
0.65	4.830	6.259	6.814	7.058	7.298	7.560	7.571	7.588	7.889	7.878
0.70	4.418	5.920	6.523	6.764	6.982	7.216	7.222	7.234	7.501	7.485
0.80	3.701	5.248	5.962	6.231	6.445	6.656	6.658	6.664	6.892	6.870
0.90	3.124	4.608	5.406	5.719	5.961	6.179	6.182	6.189	6.407	6.384
1.00	2.673	4.024	4.859	5.209	5.488	5.728	5.734	5.745	5.973	5.950
1.10	2.326	3.509	4.336	4.710	5.017	5.282	5.291	5.306	5.553	5.531
1.20	2.063	3.070	3.854	4.232	4.556	4.840	4.852	4.870	5.137	5.116
1.30	1.864	2.705	3.423	3.790	4.115	4.411	4.425	4.443	4.727	4.705
1.40	1.712	2.405	3.045	3.390	3.706	4.004	4.017	4.035	4.330	4.307
1.50	1.595	2.162	2.722	3.038	3.335	3.626	3.638	3.655	3.952	3.929
1.60		1.968	2.449	2.732					3.600	
1.70		1.811	2.221	2.470					3.278	
1.80		1.686	2.033	2.250					2.989	
1.90		1.585	1.877	2.064					2.731	
2.00		1.502	1.749	1.909					2.505	

Table 6.1.1.3. *Mean atomic scattering factors for chemically significant ions (cont.)*

Element	V^{5+}	Cr^{2+}	Cr^{3+}	Mn^{2+}	Mn^{3+}	Mn^{4+}	Fe^{2+}	Fe^{3+}	Co^{2+}	Co^{3+}
Z	23	24	24	25	25	25	26	26	27	27
Method	HF	HF	HF	RHF	HF	HF	RHF	RHF	RHF	HF
$(\sin\theta)/\lambda$ (Å^{-1})										
0.00	18.000	22.000	21.000	23.000	22.000	21.000	24.000	23.000	25.000	24.000
0.01	17.993	21.988	20.990	22.988	21.990	20.992	23.989	22.991	24.989	23.990
0.02	17.974	21.952	20.961	22.953	21.961	20.968	23.954	22.962	24.954	23.962
0.03	17.941	21.892	20.913	22.894	21.913	20.927	23.895	22.914	24.897	23.914
0.04	17.895	21.808	20.845	22.812	21.846	20.871	23.814	22.848	24.818	23.848
0.05	17.837	21.702	20.759	22.707	21.760	20.799	23.711	22.763	24.716	23.764
0.06	17.766	21.574	20.655	22.581	21.656	20.712	23.587	22.660	24.593	23.661
0.07	17.682	21.425	20.534	22.433	21.534	20.610	23.441	22.539	24.450	23.541
0.08	17.587	21.256	20.395	22.266	21.395	20.493	23.276	22.401	24.287	23.404
0.09	17.480	21.067	20.240	22.080	21.240	20.363	23.091	22.247	24.104	23.250
0.10	17.362	20.861	20.069	21.875	21.070	20.218	22.889	22.078	23.904	23.081
0.11	17.234	20.638	19.884	21.654	20.884	20.061	22.669	21.893	23.687	22.896
0.12	17.095	20.400	19.685	21.418	20.684	19.891	22.435	21.695	23.455	22.698
0.13	16.946	20.148	19.474	21.167	20.472	19.710	22.185	21.483	23.207	22.486
0.14	16.789	19.884	19.250	20.904	20.247	19.517	21.923	21.258	22.946	22.261
0.15	16.622	19.609	19.016	20.629	20.011	19.315	21.648	21.023	22.673	22.024
0.16	16.448	19.324	18.772	20.344	19.765	19.102	21.363	20.776	22.389	21.777
0.17	16.266	19.030	18.519	20.050	19.509	18.881	21.068	20.521	22.095	21.520
0.18	16.078	18.729	18.258	19.748	19.246	18.652	20.765	20.256	21.791	21.253
0.19	15.883	18.423	17.991	19.440	18.975	18.415	20.455	19.984	21.481	20.978
0.20	15.683	18.112	17.718	19.126	18.697	18.172	20.140	19.705	21.164	20.696
0.22	15.268	17.481	17.157	18.488	18.127	17.669	19.494	19.130	20.514	20.114
0.24	14.839	16.845	16.585	17.841	17.543	17.149	18.838	18.538	19.850	19.513
0.25	14.620	16.527	16.297	17.517	17.247	16.884	18.508	18.238	19.516	19.207
0.26	14.399	16.210	16.008	17.193	16.951	16.617	18.178	17.937	19.180	18.899
0.28	13.955	15.584	15.431	16.551	16.357	16.079	17.520	17.331	18.510	18.280
0.30	13.509	14.972	14.862	15.920	15.768	15.540	16.871	16.727	17.845	17.659
0.32	13.067	14.378	14.303	15.304	15.187	15.005	16.234	16.130	17.191	17.043
0.34	12.631	13.805	13.759	14.707	14.619	14.477	15.614	15.543	16.550	16.435
0.35	12.417	13.528	13.494	14.417	14.341	14.217	15.312	15.254	16.236	16.135
0.36	12.205	13.257	13.234	14.132	14.068	13.961	15.014	14.970	15.927	15.838
0.38	11.792	12.734	12.730	13.581	13.536	13.458	14.436	14.414	15.324	15.258
0.40	11.392	12.238	12.248	13.055	13.024	12.972	13.881	13.877	14.743	14.694
0.42	11.010	11.770	11.790	12.556	12.536	12.504	13.352	13.361	14.186	14.151
0.44	10.644	11.330	11.357	12.083	12.072	12.057	12.848	12.868	13.653	13.629
0.45	10.469	11.121	11.150	11.857	11.848	11.841	12.606	12.630	13.396	13.376
0.46	10.298	10.918	10.950	11.638	11.632	11.630	12.370	12.398	13.146	13.129
0.48	9.970	10.533	10.567	11.219	11.216	11.225	11.919	11.953	12.664	12.652
0.50	9.662	10.174	10.210	10.827	10.826	10.843	11.494	11.531	12.207	12.200
0.55	8.973	9.386	9.419	9.954	9.956	9.982	10.542	10.581	11.176	11.171
0.60	8.396	8.737	8.764	9.229	9.223	9.252	9.737	9.772	10.293	10.286
0.65	7.915	8.205	8.224	8.626	8.615	8.641	9.063	9.092	9.546	9.534
0.70	7.515	7.766	7.779	8.128	8.111	8.132	8.501	8.523	8.917	8.900
0.80	6.888	7.091	7.095	7.365	7.341	7.352	7.640	7.651	7.948	7.921
0.90	6.399	6.578	6.580	6.808	6.779	6.785	7.023	7.026	7.257	7.224
1.00	5.968	6.143	6.145	6.360	6.330	6.334	6.546	6.548	6.739	6.703
1.10	5.556	5.738	5.742	5.963	5.933	5.938	6.144	6.145	6.320	6.283
1.20	5.147	5.341	5.348	5.585	5.555	5.562	5.775	5.778	5.951	5.913
1.30	4.741	4.949	4.958	5.213	5.183	5.193	5.419	5.423	5.605	5.566
1.40	4.344	4.564	4.573	4.846	4.815	4.826	5.068	5.074	5.268	5.228
1.50	3.965	4.191	4.202	4.487	4.454	4.467	4.722	4.729	4.936	4.895
1.60				4.140			4.384	4.392	4.609	
1.70				3.810			4.058	4.066	4.291	
1.80				3.502			3.749	3.757	3.985	
1.90				3.218			3.459	3.467	3.694	
2.00				2.960			3.192	3.199	3.421	

Table 6.1.1.3. *Mean atomic scattering factors for chemically significant ions (cont.)*

Element	Ni^{2+}	Ni^{3+}	Cu^{1+}	Cu^{2+}	Zn^{2+}	Ga^{3+}	Ge^{4+}	Br^{1-}	Rb^{1+}	Sr^{2+}
Z	28	28	29	29	30	31	32	35	37	38
Method	RHF	HF	RHF	HF	RHF	HF	HF	RHF	RHF	RHF
$(\sin\theta)/\lambda$ (Å^{-1})										
0.00	26.000	25.000	28.000	27.000	28.000	28.000	28.000	36.000	36.000	36.000
0.01	25.989	24.991	27.987	26.989	27.989	27.991	27.992	35.961	35.977	35.981
0.02	25.955	24.962	27.946	26.956	27.957	27.964	27.969	35.845	35.908	35.923
0.03	25.899	24.915	27.878	26.901	27.903	27.919	27.931	35.656	35.794	35.827
0.04	25.821	24.850	27.783	26.824	27.828	27.856	27.877	35.398	35.635	35.694
0.05	25.721	24.766	27.663	26.726	27.732	27.776	27.808	35.077	35.435	35.524
0.06	25.600	24.665	27.518	26.608	27.615	27.678	27.724	34.703	35.195	35.320
0.07	25.459	24.546	27.349	26.469	27.479	27.564	27.625	34.282	34.917	35.084
0.08	25.299	24.410	27.157	26.311	27.323	27.433	27.512	33.824	34.605	34.816
0.09	25.119	24.258	26.944	26.134	27.149	27.286	27.386	33.336	34.262	34.520
0.10	24.921	24.090	26.711	25.939	26.958	27.123	27.245	32.827	33.891	34.198
0.11	24.707	23.907	26.459	25.728	26.749	26.946	27.091	32.303	33.496	33.851
0.12	24.477	23.709	26.190	25.500	26.525	26.754	26.924	31.771	33.079	33.484
0.13	24.232	23.498	25.905	25.258	26.286	26.548	26.745	31.236	32.646	33.098
0.14	23.973	23.275	25.606	25.001	26.032	26.330	26.554	30.703	32.199	32.696
0.15	23.702	23.039	25.294	24.732	25.766	26.099	26.351	30.175	31.740	32.281
0.16	23.419	22.792	24.972	24.451	25.488	25.856	26.137	29.657	31.275	31.854
0.17	23.126	22.535	24.639	24.159	25.198	25.603	25.913	29.149	30.805	31.420
0.18	22.824	22.268	24.297	23.857	24.899	25.339	25.680	28.654	30.333	30.979
0.19	22.513	21.993	23.949	23.547	24.591	25.066	25.437	28.172	29.862	30.535
0.20	22.195	21.710	23.594	23.229	24.275	24.784	25.185	27.706	29.393	30.089
0.22	21.543	21.125	22.872	22.574	23.622	24.197	24.658	26.817	28.471	29.198
0.24	20.875	20.518	22.139	21.900	22.949	23.585	24.104	25.988	27.579	28.322
0.25	20.536	20.209	21.770	21.558	22.606	23.270	23.818	25.595	27.147	27.892
0.26	20.197	19.897	21.401	21.214	22.261	22.952	23.526	25.215	26.726	27.469
0.28	19.516	19.268	20.666	20.523	21.566	22.305	22.931	24.491	25.916	26.647
0.30	18.839	18.636	19.939	19.832	20.869	21.649	22.321	23.812	25.150	25.861
0.32	18.169	18.005	19.224	19.146	20.175	20.988	21.702	23.170	24.428	25.113
0.34	17.510	17.380	18.524	18.469	19.488	20.327	21.077	22.559	23.749	24.404
0.35	17.187	17.071	18.180	18.135	19.149	19.997	20.764	22.264	23.424	24.064
0.36	16.867	16.765	17.842	17.805	18.812	19.669	20.451	21.975	23.109	23.734
0.38	16.242	16.164	17.180	17.157	18.150	19.019	19.826	21.412	22.503	23.100
0.40	15.637	15.578	16.541	16.528	17.504	18.379	19.205	20.867	21.929	22.500
0.42	15.054	15.010	15.925	15.919	16.876	17.751	18.593	20.335	21.381	21.931
0.44	14.495	14.463	15.333	15.332	16.269	17.139	17.989	19.816	20.857	21.389
0.45	14.224	14.197	15.047	15.046	15.974	16.839	17.692	19.560	20.603	21.128
0.46	13.959	13.936	14.767	14.767	15.683	16.544	17.398	19.306	20.353	20.872
0.48	13.448	13.432	14.225	14.227	15.120	15.967	16.821	18.806	19.865	20.376
0.50	12.962	12.950	13.710	13.711	14.580	15.409	16.259	18.313	19.391	19.898
0.55	11.854	11.847	12.530	12.526	13.331	14.106	14.929	17.114	18.253	18.765
0.60	10.895	10.887	11.502	11.491	12.227	12.937	13.716	15.964	17.169	17.700
0.65	10.075	10.062	10.614	10.597	11.263	11.902	12.625	14.870	16.127	16.684
0.70	9.378	9.360	9.855	9.831	10.429	10.995	11.656	13.840	15.128	15.707
0.80	8.292	8.265	8.659	8.625	9.097	9.526	10.058	12.002	13.273	13.875
0.90	7.516	7.482	7.797	7.757	8.126	8.441	8.853	10.479	11.645	12.231
1.00	6.944	6.906	7.165	7.123	7.414	7.642	7.956	9.261	10.270	10.805
1.10	6.497	6.457	6.681	6.637	6.879	7.045	7.286	8.311	9.147	9.611
1.20	6.119	6.078	6.285	6.240	6.455	6.582	6.774	7.580	8.251	8.638
1.30	5.776	5.734	5.939	5.892	6.096	6.203	6.365	7.016	7.548	7.862
1.40	5.450	5.407	5.617	5.568	5.775	5.872	6.021	6.573	6.997	7.249
1.50	5.131	5.086	5.307	5.256	5.472	5.569	5.715	6.216	6.561	6.764
0.60	4.816		5.003		5.178			5.913	6.209	6.375
1.70	4.507		4.704		4.890			5.645	5.913	6.056
1.80	4.207		4.411		4.606			5.398	5.656	5.785
1.90	3.918		4.127		4.329			5.162	5.421	5.545
2.00	3.643		3.853		4.059			4.932	5.201	5.324

Table 6.1.1.3. *Mean atomic scattering factors for chemically significant ions (cont.)*

Element	Y^{3+}	Zr^{4+}	Nb^{3+}	Nb^{5+}	Mo^{3+}	Mo^{5+}	Mo^{6+}	Ru^{3+}	Ru^{4+}	Rh^{3+}
Z	39	40	41	41	42	42	42	44	44	45
Method	*DS	*DS	*DS	*DS	*DS	*DS	*DS	*DS	*DS	*DS
$(\sin\theta)/\lambda$ (Å^{-1})										
0.00	36.000	36.000	38.000	36.000	39.000	37.000	36.000	41.000	40.000	42.000
0.01	35.983	35.985	37.981	35.987	38.981	36.986	35.988	40.980	39.983	41.980
0.02	35.933	35.942	37.925	35.948	38.923	36.946	35.954	40.922	39.933	41.922
0.03	35.850	35.869	37.832	35.884	38.827	36.878	35.897	40.824	39.849	41.824
0.04	35.735	35.768	37.702	35.795	38.695	36.783	35.817	40.689	39.733	41.689
0.05	35.588	35.640	37.537	35.681	38.526	36.663	35.715	40.517	39.585	41.516
0.06	35.411	35.484	37.339	35.543	38.323	36.517	35.591	40.309	39.406	41.308
0.07	35.204	35.302	37.109	35.381	38.087	36.347	35.446	40.067	39.197	41.066
0.08	34.970	35.096	36.849	35.197	37.820	36.152	35.280	39.793	38.959	40.791
0.09	34.710	34.865	36.560	34.991	37.523	35.936	35.095	39.489	38.695	40.485
0.10	34.425	34.612	36.246	34.765	37.200	35.697	34.890	39.156	38.404	40.150
0.11	34.118	34.338	35.908	34.519	36.853	35.438	34.667	38.798	38.090	39.789
0.12	33.791	34.045	35.548	34.254	36.483	35.160	34.428	38.416	37.754	39.404
0.13	33.445	33.734	35.170	33.973	36.094	34.865	34.172	38.012	37.397	38.997
0.14	33.082	33.406	34.775	33.675	35.688	34.553	33.900	37.590	37.022	38.569
0.15	32.705	33.064	34.366	33.363	35.266	34.226	33.615	37.151	36.630	38.125
0.16	32.316	32.708	33.945	33.038	34.832	33.886	33.317	36.698	36.223	37.665
0.17	31.916	32.341	33.514	32.701	34.388	33.533	33.006	36.233	35.804	37.193
0.18	31.509	31.964	33.076	32.353	33.936	33.170	32.685	35.758	35.374	36.710
0.19	31.094	31.580	32.632	31.997	33.478	32.798	32.354	35.276	34.934	36.218
0.20	30.675	31.188	32.184	31.632	33.016	32.418	32.015	34.789	34.488	35.720
0.22	29.830	30.392	31.284	30.885	32.086	31.640	31.316	33.804	33.579	34.713
0.24	28.986	29.586	30.388	30.121	31.159	30.847	30.595	32.819	32.659	33.701
0.25	28.567	29.182	29.945	29.736	30.701	30.448	30.229	32.329	32.199	33.198
0.26	28.152	28.781	29.506	29.351	30.246	30.048	29.862	31.844	31.741	32.697
0.28	27.337	27.985	28.646	28.582	29.356	29.252	29.123	30.889	30.833	31.711
0.30	26.548	27.205	27.814	27.821	28.494	28.465	28.387	29.962	29.943	30.751
0.32	25.789	26.447	27.013	27.074	27.664	27.695	27.658	29.067	29.078	29.823
0.34	25.063	25.716	26.248	26.346	26.871	26.944	26.941	28.210	28.242	28.932
0.35	24.712	25.360	25.878	25.990	26.488	26.578	26.589	27.796	27.836	28.500
0.36	24.370	25.012	25.518	25.640	26.115	26.218	26.241	27.392	27.439	28.079
0.38	23.712	24.339	24.824	24.960	25.397	25.518	25.562	26.614	26.671	27.268
0.40	23.086	23.696	24.167	24.306	24.717	24.847	24.904	25.878	25.940	26.499
0.42	22.492	23.083	23.543	23.680	24.073	24.205	24.270	25.181	25.245	25.772
0.44	21.927	22.500	22.953	23.081	23.464	23.592	23.662	24.524	24.586	25.086
0.45	21.654	22.218	22.669	22.792	23.172	23.296	23.366	24.209	24.271	24.757
0.46	21.388	21.944	22.393	22.509	22.888	23.007	23.078	23.904	23.963	24.438
0.48	20.874	21.414	21.861	21.963	22.342	22.450	22.518	23.319	23.374	23.829
0.50	20.382	20.907	21.355	21.442	21.825	21.920	21.983	22.767	22.817	23.254
0.55	19.231	19.731	20.187	20.235	20.638	20.697	20.744	21.516	21.549	21.957
0.60	18.166	18.658	19.128	19.142	19.573	19.599	19.627	20.416	20.434	20.826
0.65	17.163	17.659	18.148	18.137	18.597	18.598	18.608	19.430	19.436	19.824
0.70	16.208	16.716	17.224	17.198	17.685	17.668	17.664	18.528	18.525	18.918
0.80	14.415	14.952	15.492	15.458	15.985	15.955	15.937	16.884	16.872	17.292
0.90	12.784	13.333	13.886	13.858	14.405	14.377	14.357	15.367	15.354	15.807
1.00	11.340	11.873	12.414	12.395	12.939	12.918	12.902	13.939	13.929	14.407
1.10	10.100	10.592	11.099	11.088	11.606	11.593	11.581	12.605	12.597	13.086
1.20	9.067	9.501	9.958	9.951	10.427	10.418	10.411	11.382	11.378	11.859
1.30	8.225	8.595	8.992	8.988	9.410	9.405	9.400	10.291	10.288	10.744
1.40	7.548	7.856	8.193	8.190	8.554	8.551	8.547	9.339	9.338	9.756
1.50	7.008	7.261	7.541	7.539	7.846	7.843	7.841	8.528	8.527	8.899
1.60	6.575	6.782	7.013	7.011	7.267	7.265	7.263	7.847	7.846	8.171
1.70	6.222	6.394	6.584	6.583	6.795	6.793	6.792	7.282	7.282	7.559
1.80	5.927	6.074	6.234	6.233	6.409	6.408	6.407	6.817	6.817	7.051
1.90	5.672	5.802	5.941	5.940	6.090	6.089	6.089	6.433	6.433	6.631
2.00	5.443	5.565	5.689	5.690	5.820	5.820	5.820	6.114	6.114	6.281

Table 6.1.1.3. *Mean atomic scattering factors for chemically significant ions (cont.)*

Element	Rh^{4+}	Pd^{2+}	Pd^{4+}	Ag^{1+}	Ag^{2+}	Cd^{2+}	In^{3+}	Sn^{2+}	Sn^{4+}	Sb^{3+}
Z	45	46	46	47	47	48	49	50	50	51
Method	*DS	*DS	*DS	*DS	*DS	*DS	*DS	RHF	RHF	*DS
$(\sin\theta)/\lambda$ (Å^{-1})										
0.00	41.000	44.000	42.000	46.000	45.000	46.000	46.000	48.000	46.000	48.000
0.01	40.983	43.977	41.983	45.974	44.978	45.978	45.981	47.975	45.984	47.978
0.02	40.932	43.909	41.932	45.894	44.911	45.912	45.924	47.898	45.934	47.911
0.03	40.848	43.796	41.847	45.764	44.799	45.802	45.829	47.771	45.852	47.801
0.04	40.730	43.640	41.729	45.582	44.645	45.650	45.697	47.596	45.737	47.647
0.05	40.581	43.441	41.579	45.353	44.448	45.456	45.529	47.373	45.590	47.452
0.06	40.400	43.201	41.396	45.076	44.211	45.222	45.325	47.106	45.411	47.218
0.07	40.188	42.923	41.184	44.757	43.936	44.950	45.087	46.797	45.203	46.945
0.08	39.948	42.608	40.942	44.397	43.624	44.641	44.816	46.449	44.964	46.636
0.09	39.680	42.258	40.671	43.999	43.277	44.298	44.513	46.066	44.698	46.293
0.10	39.385	41.877	40.375	43.567	42.898	43.923	44.181	45.650	44.404	45.920
0.11	39.067	41.467	40.053	43.105	42.490	43.517	43.821	45.206	44.084	45.517
0.12	38.725	41.031	39.708	42.616	42.056	43.085	43.435	44.736	43.739	45.089
0.13	38.363	40.572	39.341	42.103	41.597	42.628	43.024	44.244	43.371	44.638
0.14	37.981	40.092	38.955	41.570	41.117	42.148	42.591	43.733	42.981	44.167
0.15	37.582	39.595	38.551	41.020	40.618	41.649	42.138	43.206	42.572	43.677
0.16	37.168	39.083	38.131	40.457	40.103	41.134	41.667	42.667	42.143	43.172
0.17	36.740	38.558	37.696	39.883	39.575	40.603	41.180	42.117	41.698	42.655
0.18	36.301	38.024	37.249	39.301	39.036	40.061	40.678	41.560	41.237	42.127
0.19	35.852	37.483	36.792	38.713	38.489	39.509	40.165	40.998	40.763	41.590
0.20	35.395	36.936	36.326	38.122	37.935	38.949	39.641	40.431	40.276	41.047
0.22	34.463	35.836	35.374	36.940	36.817	37.816	38.570	39.296	39.274	39.950
0.24	33.518	34.739	34.406	35.768	35.697	36.677	37.481	38.164	38.242	38.847
0.25	33.045	34.195	33.921	35.191	35.141	36.110	36.933	37.604	37.718	38.298
0.26	32.572	33.657	33.435	34.620	34.589	35.545	36.385	37.047	37.192	37.750
0.28	31.635	32.601	32.471	33.503	33.502	34.431	35.295	35.950	36.135	36.668
0.30	30.715	31.577	31.521	32.424	32.445	33.344	34.220	34.878	35.082	35.605
0.32	29.819	30.592	30.594	31.389	31.425	32.291	33.167	33.836	34.041	34.569
0.34	28.951	29.649	29.695	30.400	30.446	31.276	32.145	32.826	33.019	33.561
0.35	28.530	29.194	29.257	29.924	29.973	30.785	31.647	32.333	32.517	33.069
0.36	28.117	28.751	28.828	29.460	29.511	30.305	31.158	31.850	32.023	32.585
0.38	27.318	27.899	27.998	28.569	28.622	29.379	30.209	30.910	31.057	31.643
0.40	26.557	27.093	27.204	27.727	27.780	28.500	29.302	30.008	30.127	30.737
0.42	25.833	26.333	26.450	26.933	26.984	27.667	28.438	29.144	29.235	29.866
0.44	25.148	25.617	25.735	26.186	26.233	26.881	27.618	28.318	28.383	29.031
0.45	24.819	25.275	25.391	25.829	25.874	26.505	27.224	27.920	27.972	28.628
0.46	24.499	24.944	25.057	25.484	25.527	26.140	26.842	27.532	27.571	28.234
0.48	23.886	24.311	24.418	24.825	24.863	25.443	26.109	26.785	26.802	27.472
0.50	23.307	23.716	23.814	24.206	24.239	24.788	25.418	26.075	26.074	26.747
0.55	21.995	22.378	22.450	22.817	22.839	23.319	23.865	24.464	24.430	25.088
0.60	20.850	21.221	21.267	21.623	21.635	22.061	22.533	23.067	23.019	23.634
0.65	19.835	20.205	20.228	20.583	20.588	20.974	21.389	21.859	21.810	22.367
0.70	18.919	19.295	19.300	19.660	19.660	20.021	20.394	20.810	20.767	21.261
0.80	17.282	17.683	17.668	18.051	18.046	18.392	18.724	19.074	19.052	19.433
0.90	15.795	16.229	16.208	16.622	16.616	16.979	17.315	17.649	17.646	17.957
1.00	14.396	14.859	14.840	15.284	15.278	15.673	16.034	16.386	16.395	16.684
1.10	13.078	13.557	13.542	14.006	14.002	14.425	14.818	15.203	15.215	15.516
1.20	11.853	12.331	12.321	12.790	12.788	13.230	13.649	14.063	14.074	14.403
1.30	10.740	11.201	11.194	11.654	11.653	12.099	12.530	12.962	12.970	13.329
1.40	9.754	10.183	10.180	10.616	10.616	11.050	11.479	11.913	11.917	12.300
1.50	8.898	9.288	9.286	9.688	9.688	10.098	10.510	10.932	10.933	11.326
1.60	8.170	8.514	8.513	8.875	8.876	9.251	9.637	10.033	10.033	10.422
1.70	7.559	7.858	7.857	8.176	8.176	8.513	8.864	9.227	9.225	9.599
1.80	7.051	7.307	7.306	7.582	7.582	7.878	8.191	8.515	8.513	8.863
1.90	6.630	6.847	6.847	7.083	7.083	7.339	7.613	7.897	7.896	8.215
2.00	6.281	6.464	6.464	6.665	6.665	6.884	7.122	7.367	7.366	7.652

Table 6.1.1.3. *Mean atomic scattering factors for chemically significant ions (cont.)*

Element	Sb^{5+}	I^{1-}	Cs^{1+}	Ba^{2+}	La^{3+}	Ce^{3+}	Ce^{4+}	Pr^{3+}	Pr^{4+}	Nd^{3+}
Z	51	53	55	56	57	58	58	59	59	60
Method	*DS	RHF	RHF	*DS	*DS	*DS	*DS	*DS	*DS	*DS
$(\sin\theta)/\lambda$ (Å^{-1})										
0.00	46.000	54.000	54.000	54.000	54.000	55.000	54.000	56.000	55.000	57.000
0.01	45.985	53.943	53.963	53.967	53.971	54.972	53.974	55.972	54.975	56.972
0.02	45.940	53.772	53.850	53.869	53.885	54.886	53.897	55.888	54.898	56.889
0.03	45.865	53.493	53.665	53.708	53.742	54.745	53.769	55.748	54.772	56.752
0.04	45.760	53.114	53.408	53.484	53.544	54.549	53.592	55.555	54.597	56.561
0.05	45.627	52.646	53.084	53.200	53.293	54.300	53.366	55.309	54.373	56.318
0.06	45.464	52.101	52.698	52.861	52.991	54.001	53.094	55.013	54.104	56.026
0.07	45.274	51.492	52.254	52.468	52.640	53.654	52.778	54.669	53.791	55.686
0.08	45.057	50.834	51.758	52.027	52.245	53.261	52.420	54.280	53.436	55.302
0.09	44.813	50.136	51.217	51.543	51.808	52.827	52.022	53.850	53.042	54.876
0.10	44.544	49.413	50.635	51.018	51.332	52.355	51.589	53.381	52.612	54.411
0.11	44.251	48.672	50.020	50.460	50.823	51.848	51.122	52.878	52.148	53.911
0.12	43.935	47.924	49.377	49.872	50.284	51.310	50.625	52.343	51.654	53.380
0.13	43.596	47.175	48.714	49.259	49.718	50.745	50.102	51.781	51.133	52.821
0.14	43.237	46.432	48.035	48.627	49.130	50.158	49.555	51.195	50.588	52.237
0.15	42.859	45.698	47.345	47.980	48.524	49.551	48.988	50.589	50.022	51.632
0.16	42.462	44.978	46.651	47.322	47.903	48.928	48.404	49.966	49.439	51.010
0.17	42.049	44.273	45.955	46.657	47.272	48.294	47.807	49.331	48.841	50.374
0.18	41.621	43.585	45.262	45.989	46.633	47.651	47.199	48.686	48.231	49.727
0.19	41.178	42.916	44.575	45.321	45.989	47.002	46.583	48.034	47.613	49.073
0.20	40.723	42.265	43.897	44.657	45.344	46.351	45.963	47.378	46.989	48.414
0.22	39.781	41.019	42.577	43.348	44.061	45.052	44.718	46.066	45.733	47.091
0.24	38.806	39.841	41.312	42.077	42.801	43.771	43.481	44.767	44.481	45.778
0.25	38.309	39.276	40.703	41.459	42.183	43.142	42.871	44.128	43.861	45.129
0.26	37.807	38.726	40.110	40.855	41.576	42.522	42.268	43.497	43.248	44.489
0.28	36.796	37.665	38.971	39.688	40.396	41.315	41.088	42.266	42.046	43.235
0.30	35.780	36.650	37.893	38.579	39.267	40.157	39.950	41.080	40.882	42.025
0.32	34.770	35.676	36.872	37.525	38.190	39.050	38.859	39.945	39.763	40.863
0.34	33.771	34.735	35.902	36.525	37.166	37.996	37.817	38.860	38.692	39.750
0.35	33.278	34.276	35.434	36.043	36.673	37.488	37.314	38.337	38.174	39.213
0.36	32.790	33.824	34.977	35.574	36.192	36.992	36.823	37.826	37.669	38.688
0.38	31.834	32.941	34.091	34.668	35.266	36.037	35.877	36.842	36.693	37.675
0.40	30.905	32.082	33.240	33.802	34.384	35.127	34.977	35.903	35.763	36.708
0.42	30.009	31.248	32.419	32.972	33.541	34.258	34.118	35.007	34.876	35.785
0.44	29.146	30.437	31.625	32.173	32.734	33.427	33.298	34.150	34.028	34.903
0.45	28.729	30.040	31.238	31.785	32.342	33.025	32.901	33.736	33.619	34.476
0.46	28.321	29.650	30.856	31.403	31.959	32.630	32.513	33.329	33.218	34.057
0.48	27.532	28.887	30.110	30.659	31.212	31.863	31.759	32.541	32.440	33.246
0.50	26.782	28.149	29.385	29.939	30.492	31.124	31.034	31.782	31.693	32.465
0.55	25.073	26.418	27.664	28.231	28.789	29.382	29.329	29.996	29.939	30.631
0.60	23.590	24.855	26.074	26.649	27.211	27.771	27.753	28.348	28.323	28.943
0.65	22.310	23.460	24.620	25.189	25.748	26.278	26.290	26.822	26.826	27.380
0.70	21.205	22.227	23.303	23.854	24.398	24.899	24.933	25.411	25.437	25.936
0.80	19.397	20.191	21.071	21.555	22.039	22.479	22.532	22.927	22.976	23.387
0.90	17.947	18.598	19.309	19.709	20.117	20.495	20.543	20.881	20.927	21.275
1.00	16.690	17.292	17.900	18.227	18.568	18.892	18.926	19.222	19.256	19.559
1.10	15.529	16.150	16.721	17.003	17.299	17.585	17.605	17.874	17.895	18.166
1.20	14.416	15.091	15.676	15.941	16.218	16.485	16.495	16.749	16.760	17.012
1.30	13.339	14.072	14.701	14.970	15.249	15.513	15.519	15.769	15.775	16.020
1.40	12.305	13.082	13.760	14.048	14.341	14.614	14.620	14.875	14.880	15.126
1.50	11.328	12.126	12.844	13.154	13.467	13.754	13.763	14.027	14.034	14.288
1.60	10.422	11.214	11.956	12.285	12.616	12.919	12.931	13.207	13.217	13.481
1.70	9.597	10.360	11.104	11.447	11.791	12.105	12.120	12.407	12.419	12.695
1.80	8.860	9.577	10.302	10.649	10.997	11.319	11.335	11.629	11.644	11.928
1.90	8.213	8.868	9.559	9.902	10.246	10.568	10.585	10.881	10.897	11.186
2.00	7.650	8.239	8.882	9.213	9.545	9.860	9.877	10.171	10.187	10.476

Table 6.1.1.3. *Mean atomic scattering factors for chemically significant ions (cont.)*

Element	Pm^{3+}	Sm^{3+}	Eu^{2+}	Eu^{3+}	Gd^{3+}	Tb^{3+}	Dy^{3+}	Ho^{3+}	Er^{3+}	Tm^{3+}
Z	61	62	63	63	64	65	66	67	68	69
Method	*DS	*DS	*DS	*DS	*DS	*DS	*DS	*DS	*DS	*DS
$(\sin\theta)/\lambda$ (Å^{-1})										
0.00	58.000	59.000	61.000	60.000	61.000	62.000	63.000	64.000	65.000	66.000
0.01	57.973	58.973	60.970	59.973	60.974	61.974	62.975	63.975	64.975	65.976
0.02	57.891	58.892	60.881	59.894	60.895	61.896	62.898	63.900	64.901	65.903
0.03	57.755	58.759	60.732	59.762	60.765	61.767	62.772	63.775	64.779	65.782
0.04	57.567	58.573	60.527	59.579	60.585	61.588	62.596	63.602	64.608	65.613
0.05	57.328	58.337	60.266	59.347	60.355	61.360	62.373	63.382	64.391	65.399
0.06	57.039	58.052	59.952	59.066	60.077	61.086	62.102	63.115	64.128	65.139
0.07	56.704	57.721	59.587	58.739	59.754	60.766	61.787	62.804	63.821	64.836
0.08	56.324	57.345	59.175	58.368	59.387	60.403	61.429	62.451	63.472	64.491
0.09	55.902	56.929	58.718	57.956	58.980	60.000	61.031	62.058	63.083	64.107
0.10	55.442	56.473	58.222	57.505	58.534	59.559	60.595	61.626	62.657	63.685
0.11	54.947	55.982	57.688	57.019	58.053	59.082	60.124	61.160	62.195	63.228
0.12	54.420	55.460	57.122	56.501	57.539	58.574	59.620	60.660	61.701	62.739
0.13	53.864	54.908	56.527	55.954	56.996	58.036	59.086	60.131	61.176	62.219
0.14	53.284	54.330	55.906	55.380	56.427	57.471	58.525	59.574	60.624	61.671
0.15	52.681	53.731	55.264	54.784	55.834	56.883	57.940	58.993	60.047	61.099
0.16	52.061	53.112	54.604	54.168	55.222	56.274	57.334	58.391	59.448	60.504
0.17	51.425	52.478	53.930	53.536	54.592	55.647	56.710	57.769	58.830	59.889
0.18	50.778	51.831	53.245	52.890	53.948	55.006	56.070	57.132	58.196	59.258
0.19	50.122	51.175	52.552	52.234	53.292	54.353	55.417	56.481	57.547	58.611
0.20	49.461	50.512	51.854	51.570	52.628	53.689	54.754	55.819	56.886	57.953
0.22	48.130	49.175	50.454	50.228	51.283	52.344	53.407	54.471	55.540	56.608
0.24	46.804	47.839	49.062	48.884	49.933	50.989	52.046	53.107	54.174	55.241
0.25	46.148	47.176	48.374	48.216	49.260	50.312	51.366	52.424	53.489	54.554
0.26	45.499	46.519	47.694	47.553	48.591	49.639	50.688	51.742	52.804	53.866
0.28	44.226	45.228	46.361	46.246	47.270	48.306	49.344	50.389	51.442	52.498
0.30	42.993	43.975	45.069	44.973	45.980	47.001	48.025	49.057	50.099	51.145
0.32	41.805	42.764	43.825	43.741	44.728	45.731	46.738	47.755	48.783	49.817
0.34	40.666	41.600	42.629	42.553	43.519	44.501	45.489	46.489	47.501	48.520
0.35	40.115	41.036	42.050	41.977	42.931	43.902	44.880	45.871	46.874	47.884
0.36	39.576	40.484	41.484	41.412	42.354	43.314	44.282	45.263	46.256	47.258
0.38	38.534	39.416	40.387	40.319	41.236	42.172	43.118	44.078	45.052	46.035
0.40	37.540	38.395	39.338	39.271	40.163	41.075	41.998	42.936	43.889	44.853
0.42	36.590	37.418	38.333	38.268	39.135	40.021	40.921	41.837	42.768	43.711
0.44	35.681	36.483	37.371	37.307	38.149	39.010	39.887	40.780	41.689	42.611
0.45	35.241	36.031	36.904	36.842	37.671	38.520	39.385	40.267	41.164	42.075
0.46	34.810	35.587	36.447	36.386	37.203	38.040	38.893	39.764	40.649	41.550
0.48	33.975	34.728	35.560	35.503	36.295	37.108	37.938	38.786	39.649	40.527
0.50	33.172	33.902	34.707	34.653	35.423	36.212	37.019	37.844	38.685	39.542
0.55	31.287	31.965	32.702	32.663	33.379	34.113	34.866	35.637	36.424	37.228
0.60	29.555	30.188	30.861	30.838	31.506	32.191	32.894	33.615	34.352	35.106
0.65	27.955	28.547	29.160	29.155	29.779	30.420	31.078	31.753	32.444	33.151
0.70	26.475	27.029	27.589	27.599	28.183	28.784	29.400	30.032	30.680	31.344
0.80	23.858	24.342	24.811	24.840	25.351	25.876	26.416	26.970	27.540	28.123
0.90	21.681	22.098	22.494	22.528	22.969	23.424	23.892	24.374	24.870	25.380
1.00	19.905	20.260	20.599	20.626	21.003	21.392	21.793	22.207	22.634	23.074
1.10	18.464	18.768	19.061	19.080	19.400	19.730	20.072	20.424	20.787	21.163
1.20	17.277	17.544	17.805	17.815	18.092	18.373	18.666	18.966	19.276	19.595
1.30	16.267	16.512	16.753	16.758	17.004	17.252	17.508	17.768	18.035	18.309
1.40	15.370	15.607	15.839	15.840	16.071	16.298	16.531	16.764	17.000	17.241
1.50	14.538	14.778	15.010	15.011	15.237	15.457	15.678	15.896	16.114	16.332
1.60	13.743	13.993	14.231	14.233	14.463	14.685	14.904	15.118	15.327	15.534
1.70	12.970	13.232	13.480	13.483	13.724	13.953	14.178	14.394	14.604	14.809
1.80	12.215	12.490	12.748	12.753	13.005	13.245	13.479	13.703	13.919	14.127
1.90	11.481	11.765	12.032	12.039	12.302	12.554	12.798	13.032	13.257	13.473
2.00	10.774	11.063	11.336	11.344	11.616	11.878	12.132	12.376	12.610	12.836

Table 6.1.1.3. *Mean atomic scattering factors for chemically significant ions (cont.)*

Element	Yb^{2+}	Yb^{3+}	Lu^{3+}	Hf^{4+}	Ta^{5+}	W^{6+}	Os^{4+}	Ir^{3+}	Ir^{4+}	Pt^{2+}
Z	70	70	71	72	73	74	76	77	77	78
Method	*DS	*DS	*DS	*DS	*DS	*DS	*DS	*DS	*DS	*DS
$(\sin\theta)/\lambda$ (Å^{-1})										
0.00	68.000	67.000	68.000	68.000	68.000	68.000	72.000	74.000	73.000	76.000
0.01	67.973	66.976	67.976	67.979	67.981	67.982	71.976	73.972	72.975	75.968
0.02	67.892	66.904	67.905	67.915	67.922	67.929	71.904	73.889	72.902	75.874
0.03	67.759	66.785	67.788	67.809	67.826	67.840	71.784	73.752	72.780	75.717
0.04	67.573	66.619	67.624	67.661	67.691	67.716	71.617	73.561	72.611	75.499
0.05	67.337	66.407	67.415	67.472	67.519	67.557	71.404	73.318	72.395	75.222
0.06	67.051	66.151	67.161	67.243	67.309	67.365	71.147	73.024	72.133	74.889
0.07	66.719	65.851	66.866	66.976	67.065	67.139	70.847	72.682	71.828	74.502
0.08	66.342	65.511	66.529	66.670	66.785	66.881	70.506	72.294	71.481	74.065
0.09	65.922	65.131	66.154	66.329	66.471	66.592	70.125	71.863	71.094	73.580
0.10	65.464	64.714	65.741	65.953	66.126	66.272	69.707	71.392	70.669	73.052
0.11	64.968	64.262	65.294	65.544	65.749	65.923	69.254	70.883	70.208	72.485
0.12	64.439	63.777	64.814	65.103	65.343	65.546	68.769	70.339	69.715	71.881
0.13	63.879	63.262	64.303	64.634	64.908	65.142	68.253	69.764	69.190	71.245
0.14	63.292	62.719	63.765	64.138	64.448	64.713	67.711	69.162	68.638	70.582
0.15	62.679	62.151	63.201	63.616	63.963	64.260	67.143	68.534	68.060	69.894
0.16	62.046	61.561	62.615	63.071	63.455	63.785	66.552	67.884	67.460	69.185
0.17	61.393	60.950	62.008	62.505	62.926	63.290	65.942	67.215	66.839	68.459
0.18	60.724	60.321	61.383	61.921	62.378	62.775	65.313	66.530	66.200	67.719
0.19	60.043	59.678	60.742	61.319	61.812	62.242	64.670	65.832	65.546	66.968
0.20	59.350	59.022	60.088	60.703	61.231	61.693	64.014	65.123	64.879	66.210
0.22	57.943	57.679	58.749	59.433	60.028	60.553	62.671	63.684	63.515	64.679
0.24	56.521	56.312	57.382	58.127	58.783	59.367	61.302	62.228	62.124	63.144
0.25	55.809	55.624	56.693	57.465	58.149	58.760	60.612	61.500	61.423	62.381
0.26	55.098	54.935	56.002	56.799	57.509	58.146	59.920	60.773	60.721	61.621
0.28	53.687	53.560	54.622	55.460	56.216	56.901	58.537	59.328	59.319	60.121
0.30	52.297	52.198	53.253	54.123	54.917	55.643	57.164	57.905	57.927	58.652
0.32	50.937	50.858	51.903	52.796	53.620	54.381	55.809	56.510	56.555	57.220
0.34	49.611	49.548	50.580	51.487	52.334	53.122	54.478	55.148	55.209	55.830
0.35	48.962	48.904	49.930	50.842	51.696	52.496	53.823	54.481	54.548	55.151
0.36	48.323	48.270	49.288	50.203	51.064	51.873	53.175	53.823	53.894	54.483
0.38	47.076	47.030	48.032	48.947	49.817	50.641	51.906	52.538	52.613	53.182
0.40	45.871	45.828	46.813	47.723	48.597	49.430	50.671	51.293	51.369	51.925
0.42	44.707	44.667	45.633	46.534	47.406	48.244	49.473	50.089	50.163	50.714
0.44	43.585	43.545	44.491	45.381	46.247	47.086	48.312	48.926	48.995	49.545
0.45	43.038	42.999	43.935	44.818	45.681	46.518	47.745	48.359	48.425	48.977
0.46	42.502	42.463	43.389	44.265	45.122	45.957	47.187	47.802	47.865	48.419
0.48	41.458	41.419	42.325	43.184	44.031	44.860	46.099	46.717	46.773	47.333
0.50	40.450	40.412	41.297	42.140	42.974	43.795	45.046	45.668	45.717	46.286
0.55	38.080	38.046	38.880	39.680	40.479	41.271	42.562	43.197	43.227	43.820
0.60	35.901	35.874	36.658	37.419	38.181	38.942	40.270	40.918	40.932	41.549
0.65	33.890	33.873	34.610	35.335	36.064	36.793	38.147	38.805	38.807	39.443
0.70	32.029	32.022	32.716	33.409	34.106	34.806	36.172	36.835	36.830	37.479
0.80	28.709	28.722	29.335	29.970	30.612	31.258	32.602	33.261	33.249	33.905
0.90	25.880	25.904	26.442	27.018	27.605	28.199	29.471	30.104	30.094	30.732
1.00	23.501	23.527	23.994	24.506	25.033	25.572	26.734	27.324	27.317	27.918
1.10	21.528	21.551	21.952	22.396	22.858	23.336	24.368	24.902	24.898	25.447
1.20	19.908	19.926	20.267	20.645	21.042	21.456	22.350	22.821	22.820	23.307
1.30	18.580	18.591	18.883	19.202	19.538	19.890	20.652	21.057	21.058	21.481
1.40	17.480	17.486	17.738	18.009	18.293	18.592	19.234	19.579	19.581	19.942
1.50	16.550	16.553	16.777	17.011	17.255	17.510	18.054	18.347	18.348	18.654
1.60	15.740	15.741	15.947	16.158	16.374	16.597	17.066	17.315	17.317	17.578
1.70	15.009	15.010	15.208	15.406	15.605	15.808	16.225	16.443	16.444	16.670
1.80	14.330	14.330	14.528	14.722	14.914	15.106	15.493	15.691	15.691	15.893
1.90	13.681	13.682	13.884	14.081	14.274	14.463	14.838	15.024	15.024	15.211
2.00	13.051	13.053	13.263	13.467	13.666	13.858	14.234	14.417	14.416	14.597

Table 6.1.1.3. *Mean atomic scattering factors for chemically significant ions (cont.)*

Element	Pt^{4+}	Au^{1+}	Au^{3+}	Hg^{1+}	Hg^{2+}	Tl^{1+}	Tl^{3+}	Pb^{2+}	Pb^{4+}	Bi^{3+}
Z	78	79	79	80	80	81	81	82	82	83
Method	*DS	*DS	*DS	*DS	*DS	*DS	*DS	*DS	*DS	*DS
$(\sin\theta)/\lambda$ (Å^{-1})										
0.00	74.000	78.000	76.000	79.000	78.000	80.000	78.000	80.000	78.000	80.000
0.01	73.975	77.964	75.972	78.962	77.968	79.961	77.975	79.966	77.975	79.969
0.02	73.901	77.855	75.888	78.850	77.875	79.845	77.891	79.864	77.899	79.878
0.03	73.778	77.676	75.750	78.664	77.719	79.653	77.753	79.695	77.774	79.727
0.04	73.606	77.428	75.557	78.406	77.503	79.388	77.560	79.461	77.599	79.516
0.05	73.387	77.113	75.311	78.080	77.229	79.052	77.314	79.164	77.376	79.249
0.06	73.123	76.736	75.015	77.689	76.897	78.650	77.017	78.807	77.106	78.926
0.07	72.814	76.299	74.669	77.238	76.512	78.186	76.670	78.392	76.790	78.550
0.08	72.462	75.807	74.276	76.731	76.076	77.665	76.276	77.924	76.430	78.124
0.09	72.070	75.264	73.839	76.173	75.591	77.093	75.836	77.406	76.028	77.651
0.10	71.639	74.676	73.361	75.570	75.062	76.474	75.355	76.843	75.586	77.134
0.11	71.173	74.046	72.843	74.925	74.492	75.814	74.833	76.238	75.106	76.577
0.12	70.673	73.380	72.290	74.245	73.884	75.119	74.275	75.597	74.590	75.983
0.13	70.141	72.683	71.705	73.535	73.243	74.394	73.683	74.922	74.041	75.355
0.14	69.581	71.958	71.089	72.798	72.571	73.644	73.060	74.220	73.461	74.698
0.15	68.995	71.211	70.448	72.041	71.874	72.873	72.409	73.493	72.853	74.014
0.16	68.386	70.446	69.783	71.266	71.153	72.085	71.733	72.745	72.220	73.308
0.17	67.756	69.665	69.097	70.477	70.413	71.286	71.035	71.981	71.563	72.581
0.18	67.107	68.874	68.395	69.679	69.658	70.477	70.319	71.204	70.885	71.839
0.19	66.443	68.075	67.678	68.874	68.889	69.663	69.586	70.417	70.190	71.083
0.20	65.766	67.271	66.949	68.065	68.111	68.847	68.841	69.623	69.479	70.317
0.22	64.380	65.658	65.466	66.445	66.536	67.214	67.320	68.023	68.020	68.764
0.24	62.968	64.054	63.965	64.836	64.952	65.597	65.776	66.425	66.527	67.199
0.25	62.256	63.260	63.213	64.040	64.162	64.797	65.001	65.631	65.772	66.416
0.26	61.543	62.472	62.462	63.251	63.376	64.005	64.226	64.841	65.015	65.636
0.28	60.119	60.923	60.969	61.698	61.821	62.448	62.685	63.284	63.501	64.090
0.30	58.707	59.413	59.499	60.184	60.296	60.931	61.163	61.759	61.995	62.569
0.32	57.315	57.947	58.058	58.714	58.810	59.458	59.670	60.275	60.509	61.081
0.34	55.951	56.529	56.653	57.290	57.367	58.031	58.214	58.833	59.052	59.631
0.35	55.281	55.839	55.965	56.596	56.663	57.335	57.502	58.128	58.336	58.922
0.36	54.619	55.161	55.288	55.914	55.972	56.651	56.800	57.436	57.629	58.223
0.38	53.323	53.841	53.967	54.586	54.625	55.318	55.432	56.085	56.247	56.858
0.40	52.065	52.571	52.689	53.306	53.327	54.032	54.110	54.781	54.908	55.538
0.42	50.847	51.348	51.457	52.073	52.079	52.792	52.837	53.523	53.614	54.263
0.44	49.669	50.172	50.269	50.885	50.879	51.596	51.613	52.309	52.367	53.033
0.45	49.095	49.600	49.691	50.308	50.296	51.015	51.018	51.719	51.762	52.435
0.46	48.531	49.040	49.124	49.742	49.725	50.444	50.435	51.140	51.167	51.847
0.48	47.431	47.950	48.021	48.640	48.615	49.332	49.304	50.013	50.014	50.704
0.50	46.370	46.899	46.958	47.578	47.548	48.261	48.217	48.927	48.905	49.602
0.55	43.871	44.432	44.464	45.085	45.050	45.742	45.677	46.377	46.318	47.018
0.60	41.573	42.163	42.175	42.795	42.764	43.429	43.364	44.040	43.969	44.653
0.65	39.447	40.062	40.060	40.679	40.656	41.294	41.241	41.888	41.822	42.481
0.70	37.470	38.103	38.093	38.709	38.696	39.311	39.275	39.895	39.844	40.473
0.80	33.885	34.534	34.518	35.131	35.133	35.718	35.714	36.293	36.278	36.857
0.90	30.713	31.352	31.338	31.944	31.952	32.523	32.538	33.096	33.108	33.657
1.00	27.905	28.513	28.504	29.090	29.100	29.659	29.679	30.227	30.249	30.784
1.10	25.440	26.000	25.996	26.549	26.557	27.097	27.114	27.648	27.669	28.194
1.20	23.305	23.807	23.806	24.315	24.319	24.828	24.839	25.349	25.364	25.871
1.30	21.482	21.921	21.923	22.378	22.379	22.846	22.850	23.325	23.332	23.811
1.40	19.945	20.322	20.325	20.723	20.722	21.139	21.138	21.568	21.568	22.009
1.50	18.658	18.978	18.981	19.324	19.322	19.686	19.682	20.062	20.058	20.453
1.60	17.580	17.853	17.856	18.148	18.146	18.460	18.454	18.784	18.778	19.124
1.70	16.672	16.907	16.909	17.160	17.157	17.426	17.420	17.705	17.697	17.997
1.80	15.894	16.101	16.102	16.320	16.319	16.550	16.546	16.790	16.784	17.043
1.90	15.211	15.401	15.401	15.597	15.596	15.800	15.797	16.010	16.005	16.229
2.00	14.596	14.777	14.777	14.958	14.958	15.143	15.141	15.332	15.329	15.527

Table 6.1.1.3. *Mean atomic scattering factors for chemically significant ions (cont.)*

Element	Bi^{5+}	Ra^{2+}	Ac^{3+}	Th^{4+}	U^{3+}	U^{4+}	U^{6+}	Np^{3+}	Np^{4+}	Np^{6+}
Z	83	88	89	90	92	92	92	93	93	93
Method	*DS	*DS	*DS	*DS	*DS	*DS	*DS	*DS	*DS	*DS
$(\sin\theta)/\lambda$ (Å^{-1})										
0.00	78.000	86.000	86.000	86.000	89.000	88.000	86.000	90.000	89.000	87.000
0.01	77.977	85.957	85.961	85.965	88.961	87.965	85.970	89.962	88.965	86.970
0.02	77.908	85.829	85.846	85.860	88.846	87.860	85.881	89.847	88.860	86.881
0.03	77.793	85.616	85.655	85.686	88.654	87.686	85.733	89.657	88.687	86.733
0.04	77.633	85.323	85.390	85.444	88.389	87.444	85.527	89.393	88.446	86.527
0.05	77.428	84.951	85.054	85.137	88.051	87.137	85.264	89.058	88.140	86.265
0.06	77.180	84.506	84.651	84.767	87.646	86.766	84.947	88.654	87.770	85.947
0.07	76.889	83.993	84.183	84.337	87.175	86.335	84.577	88.185	87.340	85.577
0.08	76.558	83.417	83.656	83.851	86.643	85.847	84.157	87.656	86.853	85.157
0.09	76.187	82.783	83.074	83.313	86.054	85.305	83.689	87.069	86.312	84.688
0.10	75.778	82.099	82.441	82.725	85.414	84.714	83.176	86.430	85.721	84.174
0.11	75.333	81.371	81.765	82.094	84.727	84.077	82.622	85.744	85.084	83.618
0.12	74.854	80.605	81.048	81.423	83.998	83.399	82.029	85.015	84.405	83.023
0.13	74.342	79.808	80.298	80.717	83.233	82.685	81.401	84.249	83.688	82.392
0.14	73.800	78.985	79.519	79.981	82.436	81.938	80.741	83.449	82.939	81.729
0.15	73.231	78.142	78.716	79.218	81.612	81.163	80.052	82.623	82.160	81.036
0.16	72.635	77.285	77.895	78.433	80.766	80.364	79.339	81.773	81.357	80.318
0.17	72.016	76.418	77.059	77.631	79.903	79.546	78.605	80.904	80.533	79.578
0.18	71.376	75.546	76.213	76.815	79.027	78.712	77.852	80.021	79.693	78.818
0.19	70.716	74.673	75.362	75.990	78.142	77.866	77.084	79.129	78.840	78.043
0.20	70.039	73.803	74.508	75.158	77.253	77.013	76.305	78.230	77.977	77.255
0.22	68.643	72.080	72.805	73.488	75.471	75.294	74.722	76.426	76.237	75.652
0.24	67.204	70.396	71.125	71.827	73.705	73.578	73.125	74.634	74.497	74.032
0.25	66.474	69.572	70.300	71.006	72.834	72.727	72.327	73.748	73.634	73.221
0.26	65.739	68.762	69.485	70.193	71.972	71.884	71.532	72.872	72.776	72.413
0.28	64.260	67.184	67.893	68.598	70.286	70.227	69.957	71.154	71.089	70.810
0.30	62.781	65.663	66.355	67.050	68.654	68.616	68.413	69.489	69.447	69.236
0.32	61.312	64.200	64.873	65.554	67.081	67.057	66.908	67.882	67.856	67.701
0.34	59.863	62.791	63.446	64.112	65.569	65.555	65.448	66.337	66.322	66.209
0.35	59.149	62.105	62.753	63.410	64.835	64.825	64.736	65.587	65.576	65.482
0.36	58.442	61.432	62.072	62.722	64.117	64.109	64.036	64.853	64.845	64.767
0.38	57.055	60.120	60.748	61.384	62.723	62.720	62.672	63.429	63.426	63.374
0.40	55.706	58.850	59.470	60.094	61.383	61.384	61.357	62.062	62.063	62.032
0.42	54.398	57.619	58.235	58.850	60.095	60.099	60.090	60.749	60.753	60.739
0.44	53.134	56.424	57.037	57.646	58.854	58.861	58.867	59.487	59.492	59.493
0.45	52.518	55.839	56.452	57.059	58.251	58.259	58.271	58.873	58.880	58.887
0.46	51.914	55.262	55.875	56.481	57.657	57.667	57.686	58.271	58.279	58.292
0.48	50.740	54.130	54.746	55.350	56.501	56.513	56.544	57.097	57.108	57.133
0.50	49.611	53.028	53.647	54.252	55.381	55.397	55.439	55.964	55.978	56.013
0.55	46.974	50.396	51.023	51.633	52.725	52.749	52.815	53.283	53.305	53.363
0.60	44.584	47.932	48.561	49.176	50.251	50.282	50.364	50.795	50.823	50.898
0.65	42.407	45.632	46.255	46.869	47.938	47.972	48.062	48.474	48.507	48.591
0.70	40.409	43.490	44.100	44.706	45.774	45.807	45.895	46.306	46.338	46.423
0.80	36.830	39.649	40.220	40.794	41.860	41.882	41.942	42.384	42.408	42.472
0.90	33.663	36.318	36.851	37.387	38.443	38.449	38.468	38.958	38.966	38.992
1.00	30.807	33.389	33.896	34.402	35.443	35.435	35.419	35.948	35.943	35.933
1.10	28.219	30.771	31.264	31.753	32.776	32.762	32.724	33.272	33.259	33.227
1.20	25.890	28.404	28.890	29.370	30.373	30.357	30.314	30.861	30.846	30.805
1.30	23.821	26.256	26.734	27.206	28.184	28.170	28.132	28.665	28.651	28.612
1.40	22.011	24.314	24.777	25.238	26.183	26.173	26.146	26.652	26.642	26.612
1.50	20.449	22.574	23.015	23.456	24.357	24.352	24.335	24.810	24.803	24.784
1.60	19.117	21.033	21.443	21.858	22.703	22.701	22.695	23.133	23.130	23.121
1.70	17.989	19.685	20.058	20.439	21.219	21.220	21.221	21.621	21.621	21.620
1.80	17.035	18.516	18.849	19.194	19.902	19.904	19.910	20.272	20.274	20.278
1.90	16.223	17.510	17.804	18.111	18.745	18.748	18.756	19.080	19.083	19.090
2.00	15.523	16.646	16.904	17.174	17.736	17.740	17.748	18.036	18.039	18.047

Table 6.1.1.3. *Mean atomic scattering factors for chemically significant ions (cont.)*

Element Z Method $(\sin\theta)/\lambda$ (Å^{-1})	Pu^{3+} 94 *DS	Pu^{4+} 94 *DS	Pu^{6+} 94 *DS
0.00	91.000	90.000	88.000
0.01	90.962	89.965	87.970
0.02	90.848	89.861	87.881
0.03	90.660	89.689	87.734
0.04	90.398	89.450	87.528
0.05	90.066	89.145	87.267
0.06	89.665	88.777	86.950
0.07	89.199	88.349	86.580
0.08	88.673	87.863	86.160
0.09	88.089	87.324	85.692
0.10	87.453	86.734	85.178
0.11	86.769	86.098	84.621
0.12	86.041	85.419	84.025
0.13	85.275	84.703	83.393
0.14	84.475	83.952	82.727
0.15	83.646	83.171	82.032
0.16	82.794	82.365	81.310
0.17	81.921	81.537	80.565
0.18	81.033	80.691	79.800
0.19	80.134	79.832	79.019
0.20	79.227	78.962	78.224
0.22	77.403	77.204	76.604
0.24	75.587	75.441	74.963
0.25	74.688	74.565	74.140
0.26	73.797	73.695	73.320
0.28	72.048	71.979	71.690
0.30	70.351	70.305	70.088
0.32	68.711	68.683	68.522
0.34	67.133	67.116	66.999
0.35	66.367	66.354	66.256
0.36	65.616	65.607	65.525
0.38	64.161	64.157	64.102
0.40	62.765	62.765	62.731
0.42	61.425	61.428	61.411
0.44	60.138	60.143	60.140
0.45	59.513	59.519	59.522
0.46	58.900	58.907	58.916
0.48	57.708	57.717	57.736
0.50	56.557	56.569	56.598
0.55	53.845	53.864	53.915
0.60	51.337	51.363	51.430
0.65	49.004	49.034	49.113
0.70	46.828	46.860	46.942
0.80	42.898	42.922	42.989
0.90	39.463	39.474	39.506
1.00	36.445	36.443	36.440
1.10	33.763	33.752	33.724
1.20	31.346	31.331	31.293
1.30	29.142	29.128	29.090
1.40	27.121	27.109	27.078
1.50	25.264	25.257	25.235
1.60	23.567	23.564	23.552
1.70	22.030	22.029	22.025
1.80	20.650	20.651	20.653
1.90	19.424	19.427	19.433
2.00	18.346	18.349	18.357

Table 6.1.1.4. *Coefficients for analytical approximation to the scattering factors of Tables 6.1.1.1 and 6.1.1.3*

		a_1	b_1	a_2	b_2	a_3	b_3	a_4	b_4	c	Maximum error	$\sin\theta/\lambda$ (Å^{-1})	Mean error
H	SDS	0.493002	10.5109	0.322912	26.1257	0.140191	3.14236	0.040810	57.7997	0.003038	0.000	0.00	0.000
H	HF	0.489918	20.6593	0.262003	7.74039	0.196767	49.5519	0.049879	2.20159	0.001305	0.000	0.17	0.000
H^{1-}	HF	0.897661	53.1368	0.565616	15.1870	0.415815	186.576	0.116973	3.56709	0.002389	0.002	0.09	0.001
He	RHF	0.873400	9.10370	0.630900	3.35680	0.311200	22.9276	0.178000	0.982100	0.006400	0.001	1.01	0.000
Li	RHF	1.12820	3.95460	0.750800	1.05240	0.617500	85.3905	0.465300	168.261	0.037700	0.005	2.00	0.001
Li^{1+}	RHF	0.696800	4.62370	0.788800	1.95570	0.341400	0.631600	0.156300	10.0953	0.016700	0.001	1.78	0.000
Be	RHF	1.59190	43.6427	1.12780	1.86230	0.539100	103.483	0.702900	0.542000	0.038500	0.003	0.56	0.001
Be^{2+}	RHF	6.26030	0.002700	0.884900	0.831300	0.799300	2.27580	0.164700	5.11460	−6.1092	0.001	1.97	0.000
B	RHF	2.05450	23.2185	1.33260	1.02100	1.09790	60.3498	0.706800	0.140300	−0.19320	0.002	0.75	0.001
C	RHF	2.31000	20.8439	1.02000	10.2075	1.58860	0.568700	0.865000	51.6512	0.215600	0.006	2.00	0.001
C_{val}	HF	2.26069	22.6907	1.56165	0.656665	1.05075	9.75618	0.839259	55.5949	0.286977	0.001	0.16	0.000
N	RHF	12.2126	0.005700	3.13220	9.89330	2.01250	28.9975	1.16630	0.582600	−11.529	0.007	0.11	0.002
O	RHF	3.04850	13.2771	2.28680	5.70110	1.54630	0.323900	0.867000	32.9089	0.250800	0.001	0.22	0.000
O^{1-}	HF	4.19160	12.8573	1.63969	4.17236	1.52673	47.0179	−20.307	−0.01404	21.9412	0.011	1.50	0.004
F	RHF	3.53920	10.2825	2.64120	4.29440	1.51700	0.261500	1.02430	26.1476	0.277600	0.001	0.01	0.000
F^{1-}	HF	3.63220	5.27756	3.51057	14.7353	1.26064	0.442258	0.940706	47.3437	0.653396	0.003	0.09	0.001
Ne	RHF	3.95530	8.40420	3.11250	3.42620	1.45460	0.230600	1.12510	21.7184	0.351500	0.002	0.25	0.001
Na	RHF	4.76260	3.28500	3.17360	8.84220	1.26740	0.313600	1.11280	129.424	0.676000	0.009	0.13	0.002
Na^{1+}	RHF	3.25650	2.66710	3.93620	6.11530	1.39980	0.200100	1.00320	14.0390	0.404000	0.001	0.70	0.000
Mg	RHF	5.42040	2.82750	2.17350	79.2611	1.22690	0.380800	2.30730	7.19370	0.858400	0.015	0.08	0.003
Mg^{2+}	RHF	3.49880	2.16760	3.83780	4.75420	1.32840	0.185000	0.849700	10.1411	0.485300	0.001	1.34	0.000
Al	RHF	6.42020	3.03870	1.90020	0.742600	1.59360	31.5472	1.96460	85.0886	1.11510	0.018	2.00	0.005
Al^{3+}	HF	4.17448	1.93816	3.38760	4.14553	1.20296	0.228753	0.528137	8.28524	0.706786	0.000	1.50	0.000
Si_v	RHF	6.29150	2.43860	3.03530	32.3337	1.98910	0.678500	1.54100	81.6937	1.14070	0.009	2.00	0.002
Si_{val}	HF	5.66269	2.66520	3.07164	38.6634	2.62446	0.916946	1.39320	93.5458	1.24707	0.001	0.53	0.001
Si^{4+}	HF	4.43918	1.64167	3.20345	3.43757	1.19453	0.214900	0.416530	6.65365	0.746297	0.000	1.50	0.000
P	RHF	6.43450	1.90670	4.17910	27.1570	1.78000	0.526000	1.49080	68.1645	1.11490	0.003	0.65	0.001
S	RHF	6.90530	1.46790	5.20340	22.2151	1.43790	0.253600	1.58630	56.1720	0.866900	0.005	0.67	0.002
Cl	RHF	11.4604	0.010400	7.19640	1.16620	6.25560	18.5194	1.64550	47.7784	−9.5574	0.007	0.78	0.003
Cl^{1-}	RHF	18.2915	0.006600	7.20840	1.17170	6.53370	19.5424	2.33860	60.4486	−16.378	0.007	0.76	0.003
Ar	RHF	7.48450	0.907200	6.77230	14.8407	0.653900	43.8983	1.64420	33.3929	1.44450	0.029	2.00	0.006
K	RHF	8.21860	12.7949	7.43980	0.774800	1.05190	213.187	0.865900	41.6841	1.42280	0.011	0.90	0.005
K^{1+}	RHF	7.95780	12.6331	7.49170	0.767400	6.35900	−0.00200	1.19150	31.9128	−4.9978	0.011	0.91	0.005
Ca	RHF	8.62660	10.4421	7.38730	0.659900	1.58990	85.7484	1.02110	178.437	1.37510	0.016	0.99	0.006
Ca^{2+}	RHF	15.6348	−0.00740	7.95180	0.608900	8.43720	10.3116	0.853700	25.9905	−14.875	0.017	2.00	0.004
Sc	RHF	9.18900	9.02130	7.36790	0.572900	1.64090	136.108	1.46800	51.3531	1.33290	0.014	1.07	0.006
Sc^{3+}	HF	13.4008	0.298540	8.02730	7.96290	1.65943	−0.28604	1.57936	16.0662	−6.6667	0.002	1.50	0.000
Ti	RHF	9.75950	7.85080	7.35580	0.500000	1.69910	35.6338	1.90210	116.105	1.28070	0.014	2.00	0.006
Ti^{2+}	HF	9.11423	7.52430	7.62174	0.457585	2.27930	19.5361	0.087899	61.6558	0.897155	0.006	1.50	0.001
Ti^{3+}	HF	17.7344	0.220610	8.73816	7.04716	5.25691	−0.15762	1.92134	15.9768	−14.652	0.001	0.00	0.000
Ti^{4+}	HF	19.5114	0.178847	8.23473	6.67018	2.01341	−0.29263	1.52080	12.9464	−13.280	0.002	1.50	0.000
V	RHF	10.2971	6.86570	7.35110	0.438500	2.07030	26.8938	2.05710	102.478	1.21990	0.014	2.00	0.005
V^{2+}	RHF	10.1060	6.88180	7.35410	0.440900	2.28840	20.3004	0.022300	115.122	1.22980	0.015	2.00	0.004
V^{3+}	HF	9.43141	6.39535	7.74190	0.383349	2.15343	15.1908	0.016865	63.9690	0.656565	0.004	1.50	0.001
V^{5+}	HF	15.6887	0.679003	8.14208	5.40135	2.03081	9.97278	−9.5760	0.940464	1.71430	0.000	0.34	0.000
Cr	RHF	10.6406	6.10380	7.35370	0.392000	3.32400	20.2626	1.49220	98.7399	1.18320	0.011	2.00	0.004
Cr^{2+}	HF	9.54034	5.66078	7.75090	0.344261	3.58274	13.3075	0.509107	32.4224	0.616898	0.002	1.50	0.000
Cr^{3+}	HF	9.68090	5.59463	7.81136	0.334393	2.87603	12.8288	0.113575	32.8761	0.518275	0.002	1.50	0.000
Mn	RHF	11.2819	5.34090	7.35730	0.343200	3.01930	17.8674	2.24410	83.7543	1.08960	0.009	2.00	0.004
Mn^{2+}	RHF	10.8061	5.27960	7.36200	0.343500	3.52680	14.3430	0.218400	41.3235	1.08740	0.009	2.00	0.002
Mn^{3+}	HF	9.84521	4.91797	7.87194	0.294393	3.56531	10.8171	0.323613	24.1281	0.393974	0.001	1.50	0.000
Mn^{4+}	HF	9.96253	4.84850	7.97057	0.283303	2.76067	10.4852	0.054447	27.5730	0.251877	0.001	1.50	0.000
Fe	RHF	11.7695	4.76110	7.35730	0.307200	3.52220	15.3535	2.30450	76.8805	1.03690	0.011	0.08	0.004
Fe^{2+}	RHF	11.0424	4.65380	7.37400	0.305300	4.13460	12.0546	0.439900	31.2809	1.00970	0.008	2.00	0.002
Fe^{3+}	RHF	11.1764	4.61470	7.38630	0.300500	3.39480	11.6729	0.072400	38.5566	0.970700	0.008	2.00	0.002
Co	RHF	12.2841	4.27910	7.34090	0.278400	4.00340	13.5359	2.34880	71.1692	1.01180	0.013	0.08	0.004
Co^{2+}	RHF	11.2296	4.12310	7.38830	0.272600	4.73930	10.2443	0.710800	25.6466	0.932400	0.006	2.00	0.001
Co^{3+}	HF	10.3380	3.90969	7.88173	0.238668	4.76795	8.35583	0.725591	18.3491	0.286667	0.000	1.50	0.000
Ni	RHF	12.8376	3.87850	7.29200	0.256500	4.44380	12.1763	2.38000	66.3421	1.0341	0.014	0.08	0.004
Ni^{2+}	RHF	11.4166	3.67660	7.40050	0.244900	5.34420	8.87300	0.977300	22.1626	0.861400	0.003	2.00	0.001
Ni^{3+}	HF	10.7806	3.54770	7.75868	0.223140	5.22746	7.64468	0.847114	16.9673	0.386044	0.000	0.57	0.000
Cu	RHF	13.3380	3.58280	7.16760	0.247000	5.61580	11.3966	1.67350	64.8126	1.19100	0.015	0.08	0.005
Cu^{1+}	RHF	11.9475	3.36690	7.35730	0.227400	6.24550	8.66250	1.55780	25.8487	0.89000	0.003	0.24	0.001
Cu^{2+}	HF	11.8168	3.37484	7.11181	0.244078	5.78135	7.98760	1.14523	19.8970	1.14431	0.001	0.26	0.000
Zn	RHF	14.0743	3.26550	7.03180	0.233300	5.16520	10.3163	2.41000	58.7097	1.30410	0.016	0.08	0.005
Zn^{2+}	RHF	11.9719	2.99460	7.38620	0.203100	6.46680	7.08260	1.39400	18.0995	0.780700	0.001	0.62	0.000
Ga	RHF	15.2354	3.06690	6.70060	0.241200	4.35910	10.7805	2.96230	61.4135	1.71890	0.025	0.08	0.008
Ga^{3+}	HF	12.6920	2.81262	6.69883	0.227890	6.06692	6.36441	1.00660	14.4122	1.53545	0.008	1.45	0.000
Ge	RHF	16.0816	2.85090	6.37470	0.251600	3.70680	11.4468	3.68300	54.7625	2.13130	0.024	0.08	0.008
Ge^{4+}	HF	12.9172	2.53718	6.70003	0.205855	6.06791	5.47913	0.859041	11.6030	1.45572	0.000	0.32	0.000

Table 6.1.1.4. *Coefficients for analytical approximation to scattering factors (cont.)*

		a_1	b_1	a_2	b_2	a_3	b_3	a_4	b_4	c	Maximum error	$\sin\theta/\lambda$ (Å^{-1})	Mean error
As	RHF	16.6723	2.63450	6.07010	0.264700	3.43130	12.9479	4.27790	47.7972	2.53100	0.019	0.09	0.008
Se	RHF	17.0006	2.40980	5.81960	0.272600	3.97310	15.2372	4.35430	43.8163	2.84090	0.016	2.00	0.006
Br	RHF	17.1789	2.17230	5.23580	16.5796	5.63770	0.260900	3.98510	41.4328	2.95570	0.012	2.00	0.004
Br^{1-}	RHF	17.1718	2.20590	6.33380	19.3345	5.57540	0.287100	3.72720	58.1535	3.17760	0.016	2.00	0.006
Kr	RHF	17.3555	1.93840	6.72860	16.5623	5.54930	0.226100	3.53750	39.3972	2.82500	0.008	2.00	0.002
Rb	RHF	17.1784	1.78880	9.64350	17.3151	5.13990	0.274800	1.52920	164.934	3.48730	0.028	0.12	0.008
Rb^{1+}	RHF	17.5816	1.71390	7.65980	14.7957	5.89810	0.160300	2.78170	31.2087	2.07820	0.002	1.99	0.001
Sr	RHF	17.5663	1.55640	9.81840	14.0988	5.42200	0.166400	2.66940	132.376	2.50640	0.021	0.13	0.005
Sr^{2+}	RHF	18.0874	1.49070	8.13730	12.6963	2.56540	24.5651	−34.193	−0.01380	41.4025	0.008	2.00	0.002
Y	*RHF	17.7760	1.40290	10.2946	12.8006	5.72629	0.125599	3.26588	104.354	1.91213	0.028	0.07	0.006
Y^{3+}	*DS	17.9268	1.35417	9.15310	11.2145	1.76795	22.6599	−33.108	−0.01319	40.2602	0.005	2.00	0.001
Zr	*RHF	17.8765	1.27618	10.9480	11.9160	5.41732	0.117622	3.65721	87.6627	2.06929	0.035	0.07	0.008
Zr^{4+}	*DS	18.1668	1.21480	10.0562	10.1483	1.01118	21.6054	−2.6479	−0.10276	9.41454	0.004	2.00	0.001
Nb	*RHF	17.6142	1.18865	12.0144	11.7660	4.04183	0.204785	3.53346	69.7957	3.75591	0.042	0.08	0.011
Nb^{3+}	*DS	19.8812	0.019175	18.0653	1.13305	11.0177	10.1621	1.94715	28.3389	−12.912	0.006	2.00	0.002
Nb^{5+}	*DS	17.9163	1.12446	13.3417	0.028781	10.7990	9.28206	0.337905	25.7228	−6.3934	0.007	2.00	0.003
Mo	RHF	3.70250	0.277200	17.2356	1.09580	12.8876	11.0040	3.74290	61.6584	4.38750	0.046	0.08	0.012
Mo^{3+}	*DS	21.1664	0.014734	18.2017	1.03031	11.7423	9.53659	2.30951	26.6307	−14.421	0.009	2.00	0.003
Mo^{5+}	*DS	21.0149	0.014345	18.0992	1.02238	11.4632	8.78809	0.740625	23.3452	−14.316	0.010	2.00	0.003
Mo^{6+}	*DS	17.8871	1.03649	11.1750	8.48061	6.57891	0.058881	0.000000	0.000000	0.344941	0.014	0.00	0.006
Tc	*RHF	19.1301	0.864132	11.0948	8.14487	4.64901	21.5707	2.71263	86.8472	5.40428	0.061	2.00	0.011
Ru	*RHF	19.2674	0.808520	12.9182	8.43467	4.86337	24.7997	1.56756	94.2928	5.37874	0.041	2.00	0.006
Ru^{3+}	*DS	18.5638	0.847329	13.2885	8.37164	9.32602	0.017662	3.00964	22.8870	−3.1892	0.013	2.00	0.004
Ru^{4+}	*DS	18.5003	0.844582	13.1787	8.12534	4.71304	0.36495	2.18535	20.8504	1.42357	0.014	2.00	0.004
Rh	*RHF	19.2957	0.751536	14.3501	8.21758	4.73425	25.8749	1.28918	98.6062	5.32800	0.021	2.00	0.004
Rh^{3+}	*DS	18.8785	0.764252	14.1259	7.84438	3.32515	21.2487	−6.1989	−0.01036	11.8678	0.014	2.00	0.004
Rh^{4+}	*DS	18.8545	0.760825	13.9806	7.62436	2.53464	19.3317	−5.6526	−0.01020	11.2835	0.014	2.00	0.003
Pd	*RHF	19.3319	0.698655	15.5017	7.98929	5.29537	25.2052	0.605844	76.8986	5.26593	0.012	1.08	0.005
Pd^{2+}	*DS	19.1701	0.696219	15.2096	7.55573	4.32234	22.5057	0.000000	0.000000	5.29160	0.011	2.00	0.004
Pd^{4+}	*DS	19.2493	0.683839	14.7900	7.14833	2.89289	17.9144	−7.9492	0.005127	13.0174	0.014	2.00	0.003
Ag	RHF	19.2808	0.644600	16.6885	7.47260	4.80450	24.6605	1.04630	99.8156	5.17900	0.016	1.14	0.007
Ag^{1+}	*DS	19.1812	0.646179	15.9719	7.19123	5.27475	21.7326	0.357534	66.1147	5.21572	0.012	1.13	0.005
Ag^{2+}	*DS	19.1643	0.645643	16.2456	7.18544	4.37090	21.4072	0.000000	0.000000	5.21404	0.011	1.14	0.005
Cd	RHF	19.2214	0.594600	17.6444	6.90890	4.46100	24.7008	1.60290	87.4825	5.06940	0.020	2.00	0.008
Cd^{2+}	*DS	19.1514	0.597922	17.2535	6.80639	4.47128	20.2521	0.000000	0.000000	5.11937	0.014	1.17	0.007
In	RHF	19.1624	0.547600	18.5596	6.37760	4.29480	25.8499	2.03960	92.8029	4.93910	0.027	2.00	0.009
In^{3+}	*DS	19.1045	0.551522	18.1108	6.32470	3.78897	17.3595	0.000000	0.000000	4.99635	0.022	2.00	0.007
Sn	RHF	19.1889	5.83030	19.1005	0.503100	4.45850	26.8909	2.46630	83.9571	4.78210	0.032	2.00	0.009
Sn^{2+}	RHF	19.1094	0.503600	19.0548	5.83780	4.56480	23.3752	0.487000	62.2061	4.78610	0.032	2.00	0.009
Sn^{4+}	RHF	18.9333	5.76400	19.7131	0.465500	3.41820	14.0049	0.019300	−0.75830	3.91820	0.016	2.00	0.004
Sb	RHF	19.6418	5.30340	19.0455	0.460700	5.03710	27.9074	2.68270	75.2825	4.59090	0.035	2.00	0.009
Sb^{3+}	*DS	18.9755	0.467196	18.9330	5.22126	5.10789	19.5902	0.288753	55.5113	4.69626	0.028	2.00	0.007
Sb^{5+}	*DS	19.8685	5.44853	19.0302	0.467973	2.41253	14.1259	0.000000	0.000000	4.69263	0.030	2.00	0.008
Te	*RHF	19.9644	4.81742	19.0138	0.420885	6.14487	28.5284	2.52390	70.8403	4.35200	0.038	2.00	0.009
I	RHF	20.1472	4.34700	18.9949	0.381400	7.51380	27.7660	2.27350	66.8776	4.07120	0.037	2.00	0.009
I^{1-}	RHF	20.2332	4.35790	18.9970	0.381500	7.80690	29.5259	2.88680	84.9304	4.07140	0.038	2.00	0.009
Xe	RHF	20.2933	3.92820	19.0298	0.344000	8.97670	26.4659	1.99000	64.2658	3.71180	0.038	2.00	0.009
Cs	RHF	20.3892	3.56900	19.1062	0.310700	10.6620	24.3879	1.49530	213.904	3.33520	0.032	2.00	0.010
Cs^{1+}	RHF	20.3524	3.55200	19.1278	0.308600	10.2821	23.7128	0.961500	59.4565	3.27910	0.037	2.00	0.009
Ba	RHF	20.3361	3.21600	19.2970	0.275600	10.8880	20.2073	2.69590	167.202	2.77310	0.032	2.00	0.009
Ba^{2+}	*DS	20.1807	3.21367	19.1136	0.283310	10.9054	20.0558	0.77634	51.7460	3.02902	0.029	2.00	0.007
La	*RHF	20.5780	2.94817	19.5990	0.244475	11.3727	18.7726	3.28719	133.124	2.14678	0.032	2.00	0.009
La^{3+}	*DS	20.2489	2.92070	19.3763	0.250698	11.6323	17.8211	0.336048	54.9453	2.40860	0.028	2.00	0.007
Ce	*RHF	21.1671	2.81219	19.7695	0.226836	11.8513	17.6083	3.33049	127.113	1.86264	0.026	2.00	0.008
Ce^{3+}	*DS	20.8036	2.77691	19.5590	0.231540	11.9369	16.5408	0.612376	43.1692	2.09013	0.023	2.00	0.005
Ce^{4+}	*DS	20.3235	2.65941	19.8186	0.218850	12.1233	15.7992	0.144583	62.2355	1.59180	0.026	2.00	0.007
Pr	*RHF	22.0440	2.77393	19.6697	0.222087	12.3856	16.7669	2.82428	143.644	2.05830	0.021	0.12	0.007
Pr^{3+}	*DS	21.3727	2.64520	19.7491	0.214299	12.1329	15.3230	0.975180	36.4065	1.77132	0.019	2.00	0.004
Pr^{4+}	*DS	20.9413	2.54467	20.0539	0.202481	12.4668	14.8137	0.296689	45.4643	1.24285	0.021	2.00	0.005
Nd	*RHF	22.6845	2.66248	19.6847	0.210628	12.7740	15.8850	2.85137	137.903	1.98486	0.024	0.13	0.007
Nd^{3+}	*DS	21.9610	2.52722	19.9339	0.199237	12.1200	14.1783	1.51031	30.8717	1.47588	0.015	2.00	0.003
Pm	*RHF	23.3405	2.56270	19.6095	0.202088	13.1235	15.1009	2.87516	132.721	2.02876	0.026	0.13	0.008
Pm^{3+}	*DS	22.5527	2.41740	20.1108	0.185769	12.0671	13.1275	2.07492	27.4491	1.19499	0.012	2.00	0.002
Sm	*RHF	24.0042	2.47274	19.4258	0.196451	13.4396	14.3996	2.89604	128.007	2.20963	0.029	0.13	0.009
Sm^{3+}	*DS	23.1504	2.31641	20.2599	0.174081	11.9202	12.1571	2.71488	24.8242	0.954586	0.009	2.00	0.002
Eu	RHF	24.6274	2.38790	19.0886	0.194200	13.7603	13.7546	2.92270	123.174	2.57450	0.031	0.14	0.010
Eu^{2+}	*DS	24.0063	2.27783	19.9504	0.173530	11.8034	11.6096	3.87243	26.5156	1.36389	0.004	2.00	0.002
Eu^{3+}	*DS	23.7497	2.22258	20.3745	0.163940	11.8509	11.3110	3.26503	22.9966	0.759344	0.006	2.00	0.001
Gd	*RHF	25.0709	2.25341	19.0798	0.181951	13.8518	12.9331	3.54545	101.398	2.41960	0.036	0.15	0.011
Gd^{3+}	*DS	24.3466	2.13553	20.4208	0.155525	11.8708	10.5782	3.71490	21.7029	0.645089	0.004	2.00	0.001

Table 6.1.1.4. *Coefficients for analytical approximation to scattering factors (cont.)*

		a_1	b_1	a_2	b_2	a_3	b_3	a_4	b_4	c	Maximum error	$\sin\theta/\lambda$ (Å^{-1})	Mean error
Tb	*RHF	25.8976	2.24256	18.2185	0.196143	14.3167	12.6648	2.95354	115.362	3.58324	0.035	0.14	0.012
Tb^{3+}	*DS	24.9559	2.05601	20.3271	0.149525	12.2471	10.0499	3.77300	21.2773	0.691967	0.005	0.00	0.001
Dy	*RHF	26.5070	2.18020	17.6383	0.202172	14.5596	12.1899	2.96577	111.874	4.29728	0.037	0.15	0.013
Dy^{3+}	*DS	25.5395	1.98040	20.2861	0.143384	11.9812	9.34972	4.50073	19.5810	0.689690	0.003	0.00	0.001
Ho	*RHF	26.9049	2.07051	17.2940	0.197940	14.5583	11.4407	3.63837	92.6566	4.56796	0.040	0.15	0.013
Ho^{3+}	*DS	26.1296	1.91072	20.0994	0.139358	11.9788	8.80018	4.93676	18.5908	0.852795	0.003	0.00	0.001
Er	*RHF	27.6563	2.07356	16.4285	0.223545	14.9779	11.3604	2.98233	105.703	5.92046	0.040	0.15	0.015
Er^{3+}	*DS	26.7220	1.84659	19.7748	0.137290	12.1506	8.36225	5.17379	17.8974	1.17613	0.003	0.00	0.001
Tm	*RHF	28.1819	2.02859	15.8851	0.238849	15.1542	10.9975	2.98706	102.961	6.75621	0.041	0.15	0.016
Tm^{3+}	*DS	27.3083	1.78711	19.3320	0.136974	12.3339	7.96778	5.38348	17.2922	1.63929	0.003	0.00	0.001
Yb	*RHF	28.6641	1.98890	15.4345	0.257119	15.3087	10.6647	2.98963	100.417	7.56672	0.042	0.15	0.016
Yb^{2+}	*DS	28.1209	1.78503	17.6817	0.159970	13.3335	8.18304	5.14657	20.3900	3.70983	0.008	0.00	0.003
Yb^{3+}	*DS	27.8917	1.73272	18.7614	0.138790	12.6072	7.64412	5.47647	16.8153	2.26001	0.003	0.00	0.002
Lu	*RHF	28.9476	1.90182	15.2208	9.98519	15.1000	0.261033	3.71601	84.3298	7.97628	0.043	0.16	0.016
Lu^{3+}	*DS	28.4628	1.68216	18.1210	0.142292	12.8429	7.33727	5.59415	16.3535	2.97573	0.004	0.14	0.002
Hf	*RHF	29.1440	1.83262	15.1726	9.59990	14.7586	0.275116	4.30013	72.0290	8.58154	0.047	0.08	0.016
Hf^{4+}	*DS	28.8131	1.59136	18.4601	0.128903	12.7285	6.76232	5.59927	14.0366	2.39699	0.002	0.00	0.001
Ta	*RHF	29.2024	1.77333	15.2293	9.37046	14.5135	0.295977	4.76492	63.3644	9.24354	0.049	0.08	0.017
Ta^{5+}	*DS	29.1587	1.50711	18.8407	0.116741	12.8268	6.31524	5.38695	12.4244	1.78555	0.002	2.00	0.001
W	*RHF	29.0818	1.72029	15.4300	9.22590	14.4327	0.321703	5.11982	57.0560	9.88750	0.051	0.09	0.017
W^{6+}	*DS	29.4936	1.42755	19.3763	0.104621	13.0544	5.93667	5.06412	11.1972	1.01074	0.001	0.00	0.000
Re	*RHF	28.7621	1.67191	15.7189	9.09227	14.5564	0.350500	5.44174	52.0861	10.4720	0.052	0.09	0.017
Os	*RHF	28.1894	1.62903	16.1550	8.97948	14.9305	0.382661	5.67589	48.1647	11.0005	0.051	0.09	0.017
Os^{4+}	*DS	30.4190	1.37113	15.2637	6.84706	14.7458	0.165191	5.06795	18.0030	6.49804	0.006	0.29	0.003
Ir	*RHF	27.3049	1.59279	16.7296	8.86553	15.6115	0.417916	5.83377	45.0011	11.4722	0.050	0.09	0.017
Ir^{3+}	*DS	30.4156	1.34323	15.8620	7.10909	13.6145	0.204633	5.82008	20.3254	8.27903	0.009	0.28	0.004
Ir^{4+}	*DS	30.7058	1.30923	15.5512	6.71983	14.2326	0.167252	5.53672	17.4911	6.96824	0.006	0.29	0.003
Pt	*RHF	27.0059	1.51293	17.7639	8.81174	15.7131	0.424593	5.78370	38.6103	11.6883	0.046	0.10	0.016
Pt^{2+}	*DS	29.8429	1.32927	16.7224	7.38979	13.2153	0.263297	6.35234	22.9426	9.85329	0.014	0.00	0.006
Pt^{4+}	*DS	30.9612	1.24813	15.9829	6.60834	13.7348	0.168640	5.92034	16.9392	7.39534	0.006	0.14	0.003
Au	RHF	16.8819	0.461100	18.5913	8.62160	25.5582	1.48260	5.86000	36.3956	12.0658	0.045	0.10	0.015
Au^{1+}	*DS	28.0109	1.35321	17.8204	7.73950	14.3359	0.356752	6.58077	26.4043	11.2299	0.023	0.12	0.009
Au^{3+}	*DS	30.6886	1.21990	16.9029	6.82872	12.7801	0.212867	6.52354	18.6590	9.09680	0.009	0.14	0.004
Hg	RHF	20.6809	0.545000	19.0417	8.44840	21.6575	1.57290	5.96760	38.3246	12.6089	0.046	0.10	0.017
Hg^{1+}	*DS	25.0853	1.39507	18.4973	7.65105	16.8883	0.443378	6.48216	28.2262	12.0205	0.027	0.12	0.011
Hg^{2+}	*DS	29.5641	1.21152	18.0600	7.05639	12.8374	0.284738	6.89912	20.7482	10.6268	0.013	0.00	0.006
Tl	*RHF	27.5446	0.655150	19.1584	8.70751	15.5380	1.96347	5.52593	45.8149	13.1746	0.059	0.09	0.021
Tl^{1+}	*DS	21.3985	1.47110	20.4723	0.517394	18.7478	7.43463	6.82847	28.8482	12.5258	0.028	0.12	0.011
Tl^{3+}	*DS	30.8695	1.10080	18.3481	6.53852	11.9328	0.219074	7.00574	17.2114	9.80270	0.008	0.01	0.004
Pb	RHF	31.0617	0.690200	13.0637	2.35760	18.4420	8.61800	5.96960	47.2579	13.4118	0.060	2.00	0.021
Pb^{2+}	*DS	21.7886	1.33660	19.5682	0.488383	19.1406	6.77270	7.01107	23.8132	12.4734	0.020	2.00	0.008
Pb^{4+}	*DS	32.1244	1.00566	18.8003	6.10926	12.0175	0.147041	6.96886	14.7140	8.08428	0.005	0.31	0.002
Bi	RHF	33.3689	0.704000	12.9510	2.92380	16.5877	8.79370	6.46920	48.0093	13.5782	0.065	2.00	0.020
Bi^{3+}	*DS	21.8053	1.23560	19.5026	6.24149	19.1053	0.469999	7.10295	20.3185	12.4711	0.015	2.00	0.006
Bi^{5+}	*DS	33.5364	0.916540	25.0946	0.39042	19.2497	5.71414	6.91555	12.8285	−6.7994	0.003	0.00	0.001
Po	*RHF	34.6726	0.700999	15.4733	3.55078	13.1138	9.55642	7.02588	47.0045	13.6770	0.066	2.00	0.018
At	*RHF	35.3163	0.685870	19.0211	3.97458	9.49887	11.3824	7.42518	45.4715	13.7108	0.062	2.00	0.015
Rn	RHF	35.5631	0.663100	21.2816	4.06910	8.00370	14.0422	7.44330	44.2473	13.6905	0.054	2.00	0.012
Fr	*RHF	35.9299	0.646453	23.0547	4.17619	12.1439	23.1052	2.11253	150.645	13.7247	0.055	2.00	0.017
Ra	*RHF	35.7630	0.616341	22.9064	3.87135	12.4739	19.9887	3.21097	142.325	13.6211	0.037	2.00	0.012
Ra^{2+}	*DS	35.2150	0.604909	21.6700	3.57670	7.91342	12.6010	7.65078	29.8436	13.5431	0.029	2.00	0.006
Ac	*RHF	35.6597	0.589092	23.1032	3.65155	12.5977	18.5990	4.08655	117.020	13.5266	0.030	0.06	0.009
Ac^{3+}	*DS	35.1736	0.579689	22.1112	3.41437	8.19216	12.9187	7.05545	25.9443	13.4637	0.021	2.00	0.004
Th	*RHF	35.5645	0.563359	23.4219	3.46204	12.7473	17.8309	4.80703	99.1722	13.4314	0.031	0.07	0.008
Th^{4+}	*DS	35.1007	0.555054	22.4418	3.24498	9.78554	13.4661	5.29444	23.9533	13.3760	0.014	2.00	0.002
Pa	*RHF	35.8847	0.547751	23.2948	3.41519	14.1891	16.9235	4.17287	105.251	13.4287	0.033	0.06	0.010
U	RHF	36.0228	0.529300	23.4128	3.32530	14.9491	16.0927	4.18800	100.613	13.3966	0.035	0.07	0.010
U^{3+}	*DS	35.5747	0.520480	22.5259	3.12293	12.2165	12.7148	5.37073	26.3394	13.3092	0.009	2.00	0.002
U^{4+}	*DS	35.3715	0.516598	22.5326	3.05053	12.0291	12.5723	4.79840	23.4582	13.2671	0.007	2.00	0.001
U^{6+}	*DS	34.8509	0.507079	22.7584	2.89030	14.0099	13.1767	1.21457	25.2017	13.1665	0.003	2.00	0.001
Np	*RHF	36.1874	0.511929	23.5964	3.25396	15.6402	15.3622	4.18550	97.4908	13.3573	0.037	0.07	0.011
Np^{3+}	*DS	35.7074	0.502322	22.6130	3.03807	12.9898	12.1449	5.43227	25.4928	13.2544	0.006	2.00	0.002
Np^{4+}	*DS	35.5103	0.498626	22.5787	2.96627	12.7766	11.9484	4.92159	22.7502	13.2116	0.005	2.00	0.001
Np^{6+}	*DS	35.0136	0.489810	22.7286	2.81099	14.3884	12.3300	1.75669	22.6581	13.1130	0.002	2.00	0.001
Pu	*RHF	36.5254	0.499384	23.8083	3.26371	16.7707	14.9455	3.47947	105.980	13.3812	0.038	0.14	0.013
Pu^{3+}	*DS	35.8400	0.484938	22.7169	2.96118	13.5807	11.5331	5.66016	24.3992	13.1991	0.005	2.00	0.001
Pu^{4+}	*DS	35.6493	0.481422	22.6460	2.89020	13.3595	11.3160	5.18831	21.8301	13.1555	0.003	2.00	0.001
Pu^{6+}	*DS	35.1736	0.473204	22.7181	2.73848	14.7635	11.5530	2.28678	20.9303	13.0582	0.001	1.36	0.001
Am	*RHF	36.6706	0.483629	24.0992	3.20647	17.3415	14.3136	3.49331	102.273	13.3592	0.040	0.07	0.013
Cm	*RHF	36.6488	0.465154	24.4096	3.08997	17.3990	13.4346	4.21665	88.4834	13.2887	0.041	0.07	0.013
Bk	*RHF	36.7881	0.451018	24.7736	3.04619	17.8919	12.8946	4.23284	86.0030	13.2754	0.042	0.07	0.014
Cf	*RHF	36.9185	0.437533	25.1995	3.00775	18.3317	12.4044	4.24391	83.7881	13.2674	0.043	0.07	0.014

Table 6.1.1.5. *Coefficients for analytical approximation to the scattering factors of Table 6.1.1.1 for the range* $2.0 < (\sin\theta)/\lambda < 6.0\ \text{Å}^{-1}$ *[equation (6.1.1.16)]*

Z	Symbol	a_0	a_1	a_2 (×10)	a_3 (×100)	C
2	He	0.52543	−3.43300	4.80070	−2.54760	1.0000
3	Li	0.89463	−2.43660	2.32500	−0.71949	1.0000
4	Be	1.25840	−1.94590	1.30460	−0.04297	1.0000
5	B	1.66720	−1.85560	1.60440	−0.65981	1.0000
6	C	1.70560	−1.56760	1.18930	−0.42715	1.0000
7	N	1.54940	−1.20190	0.51064	0.02472	1.0000
8	O	1.30530	−0.83742	−0.16738	0.47500	1.0000
9	F	1.16710	−0.63203	−0.40207	0.54352	1.0000
10	Ne	1.09310	−0.50221	−0.53648	0.60957	0.9995
11	Na	0.84558	−0.26294	−0.87884	0.76974	1.0000
12	Mg	0.71877	−0.13144	−1.20900	0.82738	1.0000
13	Al	0.67975	−0.08756	−0.95431	0.72294	1.0000
14	Si	0.70683	−0.09888	−0.98356	0.55631	1.0000
15	P	0.85532	−0.21262	−0.37390	0.20731	1.0000
16	S	1.10400	−0.40325	0.20094	−0.26058	1.0000
17	Cl	1.42320	−0.63936	0.84722	−0.76135	0.9995
18	Ar	1.82020	−0.92776	1.59220	−1.32510	0.9995
19	K	2.26550	−1.24530	2.38330	−1.91290	0.9990
20	Ca	2.71740	−1.55670	3.13170	−2.45670	0.9990
21	Sc	3.11730	−1.81380	3.71390	−2.85330	0.9990
22	Ti	3.45360	−2.01150	4.13170	−3.11710	0.9995
23	V	3.71270	−2.13920	4.34610	−3.22040	0.9995
24	Cr	3.87870	−2.19000	4.38670	−3.17520	1.0000
25	Mn	3.98550	−2.18850	4.27960	−3.02150	1.0000
26	Fe	3.99790	−2.11080	3.98170	−2.71990	1.0000
27	Co	3.95900	−1.99650	3.60630	−2.37050	1.0000
28	Ni	3.86070	−1.88690	3.12390	−1.94290	1.0000
29	Cu	3.72510	−1.65500	2.60290	−1.49760	0.9995
30	Zn	3.55950	−1.45100	2.03390	−1.02160	0.9995
31	Ga	3.37560	−1.23910	1.46160	−0.55471	0.9995
32	Ge	3.17800	−1.02230	0.89119	−0.09884	0.9995
33	As	2.97740	−0.81038	0.34861	0.32231	0.9995
34	Se	2.78340	−0.61110	−0.14731	0.69837	0.9995
35	Br	2.60610	−0.43308	−0.57381	1.00950	0.9995
36	Kr	2.44280	−0.27244	−0.95570	1.27070	0.9995
37	Rb	2.30990	−0.14328	−1.22600	1.45320	1.0000
38	Sr	2.21070	−0.04770	−1.41100	1.55410	1.0000
39	Y	2.14220	0.01935	−1.52240	1.59630	1.0000
40	Zr	2.12690	0.08618	−1.49190	1.51820	1.0000
41	Nb	2.12120	0.05381	−1.50070	1.50150	1.0000
42	Mo	2.18870	−0.00655	−1.25340	1.24010	1.0000
43	Tc	2.25730	−0.05737	−1.07450	1.06630	1.0000
44	Ru	2.37300	−0.15040	−0.77694	0.79060	0.9995
45	Rh	2.50990	−0.25906	−0.44719	0.49443	0.9995
46	Pd	2.67520	−0.39137	−0.05894	0.15404	0.9995
47	Ag	2.88690	−0.56119	0.42189	−0.25659	0.9990
48	Cd	3.08430	−0.71450	0.84482	−0.60990	0.9990
49	In	3.31400	−0.89697	1.35030	−1.03910	0.9990
50	Sn	3.49840	−1.02990	1.68990	−1.29860	0.9990
51	Sb	3.70410	−1.18270	2.08920	−1.61640	0.9990
52	Te	3.88240	−1.30980	2.41170	−1.86420	0.9990
53	I	4.08010	−1.45080	2.76730	−2.13920	0.9990
54	Xe	4.24610	−1.56330	3.04200	−2.34290	0.9990
55	Cs	4.38910	−1.65420	3.25450	−2.49220	0.9995
56	Ba	4.51070	−1.72570	3.41320	−2.59590	0.9995
57	La	4.60250	−1.77070	3.49970	−2.64050	0.9995
58	Ce	4.69060	−1.81790	3.60280	−2.70670	0.9995
59	Pr	4.72150	−1.81390	3.56480	−2.65180	0.9995
60	Nd	4.75090	−1.80800	3.51970	−2.59010	1.0000
61	Pm	4.74070	−1.76600	3.37430	−2.44210	1.0000
62	Sm	4.71700	−1.71410	3.20800	−2.28170	1.0000
63	Eu	4.66940	−1.64140	2.98580	−2.07460	1.0000
64	Gd	4.61010	−1.55750	2.73190	−1.84040	0.9995
65	Tb	4.52550	−1.45520	2.43770	−1.57950	0.9995
66	Dy	4.45230	−1.36440	2.17540	−1.34550	0.9990
67	Ho	4.37660	−1.27460	1.92540	−1.13090	0.9990
68	Er	4.29460	−1.18170	1.67060	−0.91467	0.9990
69	Tm	4.21330	−1.09060	1.42390	−0.70804	0.9990
70	Yb	4.13430	−1.00310	1.18810	−0.51120	0.9990
71	Lu	4.04230	−0.90518	0.92889	−0.29820	0.9990
72	Hf	3.95160	−0.80978	0.68951	−0.09620	0.9990
73	Ta	3.85000	−0.70599	0.41103	0.11842	0.9990
74	W	3.76510	−0.61807	0.18568	0.29787	0.9990
75	Re	3.67600	−0.52688	−0.04706	0.48180	0.9995
76	Os	3.60530	−0.45420	−0.22529	0.61700	0.9995
77	Ir	3.53130	−0.37856	−0.41174	0.75967	0.9995
78	Pt	3.47070	−0.31534	−0.56487	0.87492	0.9995
79	Au	3.41630	−0.25987	−0.69030	0.96224	0.9995
80	Hg	3.37350	−0.21428	−0.79013	1.02850	1.0000
81	Tl	3.34590	−0.18322	−0.84911	1.05970	1.0000
82	Pb	3.32330	−0.15596	−0.89878	1.08380	1.0000
83	Bi	3.31880	−0.14554	−0.90198	1.06850	1.0000
84	Po	3.32030	−0.13999	−0.89333	1.04380	1.0000
85	At	3.34250	−0.15317	−0.83350	0.97641	1.0000
86	Rn	3.37780	−0.17800	−0.74320	0.88510	1.0000
87	Fr	3.41990	−0.20823	−0.64000	0.78354	0.9995
88	Ra	3.47530	−0.25005	−0.50660	0.65836	0.9995
89	Ac	3.49020	−0.25109	−0.49651	0.64340	0.9995
90	Th	3.61060	−0.35409	−0.18926	0.36849	0.9995
91	Pa	3.68630	−0.41329	−0.01192	0.20878	0.9995
92	U	3.76650	−0.47542	0.16850	0.05060	0.9990
93	Np	3.82870	−0.51955	0.29804	−0.06566	0.9990
94	Pu	3.88970	−0.56296	0.42597	−0.18080	0.9990
95	Am	3.95060	−0.60554	0.54967	−0.29112	0.9985
96	Cm	4.01470	−0.65062	0.67922	−0.40588	0.9985
97	Bk	4.07780	−0.69476	0.80547	−0.51729	0.9985
98	Cf	4.14210	−0.73977	0.93342	−0.62981	0.9980

$$\exp(i\mathbf{S}\cdot\mathbf{r}) = \sum_{l=0}^{\infty}(2l+1)i^l j_l(Sr)P_l\left[\cos\left(\frac{\mathbf{S}\cdot\mathbf{r}}{Sr}\right)\right],$$

where j_l is a spherical Bessel function of order l and $S = |\mathbf{S}|$. The addition theorem enables this to be expressed as

$$\exp(i\mathbf{S}\cdot\mathbf{r}) = 4\pi\sum_{l=0} i^l j_l(Sr)\sum_{m=-l}^{l} Y_{lm}(\theta_S,\varphi_S)Y^*_{lm}(\theta,\varphi). \quad (6.1.1.17)$$

The $Y_{lm}(\theta,\varphi)$ are spherical (surface) harmonics

$$\begin{aligned} Y_{lm}(\theta,\varphi) &= \left[\frac{(2l+1)(l+m)!}{4\pi(l-m)!}\right]^{1/2}\frac{(-)^l e^{im\varphi}}{2^l l!(\sin\theta)^m} \\ &\quad\times\frac{\mathrm{d}^{l-m}}{\mathrm{d}(\cos\theta)^{l-m}}(\sin\theta)^{2l} \\ &= \left[\frac{(2l+1)(l-m)!}{4\pi(l+m)!}\right]^{1/2}(-)^m e^{im\varphi}P_l^m(\cos\theta) \quad m\geq 0, \end{aligned} \quad (6.1.1.18)$$

where $P_l^m(\cos\theta)$ is an associated Legendre polynomial.

With this definition of the spherical harmonics,

$$Y_{l-m} = (-)^m Y^*_{lm}. \quad (6.1.1.19)$$

Spherical harmonics with alternative phase conventions can be defined. The relationship between those in common use is given by Normand (1980). With the convention given in (6.1.1.18), the spherical harmonics up to fourth order are

$$
\begin{aligned}
Y_{00} &= (4\pi)^{-1/2} \\
Y_{1\pm1} &= \mp(3/8\pi)^{1/2} \sin\theta\, e^{\pm i\varphi} \\
Y_{10} &= (3/4\pi)^{1/2} \cos\theta \\
Y_{2\pm2} &= \left(\frac{15}{32\pi}\right)^{1/2} \sin^2\theta\, e^{\pm 2i\varphi} \\
Y_{2\pm1} &= \mp\left(\frac{15}{8\pi}\right)^{1/2} \sin\theta\cos\theta\, e^{\pm i\varphi} \\
Y_{20} &= \left(\frac{5}{16\pi}\right)^{1/2} (3\cos^2\theta - 1) \\
Y_{3\pm3} &= \mp\left(\frac{35}{64\pi}\right)^{1/2} \sin^3\theta\, e^{\pm 3i\varphi} \\
Y_{3\pm2} &= \left(\frac{105}{32\pi}\right)^{1/2} \cos\theta\sin^2\theta\, e^{\pm 2i\varphi} \\
Y_{3\pm1} &= \mp\left(\frac{21}{64\pi}\right)^{1/2} \sin\theta(4 - 5\sin^2\theta)\, e^{\pm i\varphi} \\
Y_{30} &= \left(\frac{7}{16\pi}\right)^{1/2} \cos\theta(2 - 5\sin^2\theta) \\
Y_{4\pm4} &= \left(\frac{315}{512\pi}\right)^{1/2} \sin^4\theta\, e^{\pm 4i\varphi} \\
Y_{4\pm3} &= \mp\left(\frac{315}{64\pi}\right)^{1/2} \cos\theta\sin^3\theta\, e^{\pm 3i\varphi} \\
Y_{4\pm2} &= \left(\frac{45}{128\pi}\right)^{1/2} \sin^2\theta(6 - 7\sin^2\theta)\, e^{\pm 2i\varphi} \\
Y_{4\pm1} &= \mp\left(\frac{45}{64\pi}\right)^{1/2} \cos\theta\sin\theta(4 - 7\sin^2\theta)\, e^{\pm i\varphi} \\
Y_{40} &= \left(\frac{9}{256\pi}\right)^{1/2} (3 - 30\sin^2\theta + 35\sin^4\theta).
\end{aligned}
\tag{6.1.1.20}
$$

The perturbed electron density may be written as a multipole expansion in spherical polar coordinates r, θ, φ, each term having the form

$$\rho_{lm\pm}(r) = \rho_{lm\pm}(r)\mathbf{y}(\theta, \varphi), \tag{6.1.1.21}$$

where $\mathbf{y}$ is a suitably normalized real function of the polar coordinates. A common choice is the real form of the spherical harmonics

$$Y_{lm\pm(\theta,\varphi)} = \left[\frac{(2l+1)(l-m)!}{2\pi(l+m)!(1+\delta_{0m})}\right]^{1/2} P_l^m(\cos\theta) \begin{matrix}\cos m\varphi \\ \sin m\varphi\end{matrix}, \tag{6.1.1.22}$$

where $m = 0, 1, 2, \ldots$.

These harmonics can also be expressed in terms of Cartesian components of a unit vector q_x, q_y, q_z.

The normalization in (6.1.1.17) is appropriate to wavefunctions. The physical significance of the normalization for the spherical harmonics depends on the context in which they are utilized. The implications for density functions are not the same as those for wavefunctions. A normalizing condition on the real form of the spherical harmonics that expresses the properties of the functions under integration is

$$\int |y(\theta, \varphi)|\, \mathrm{d}(\cos\theta)\, \mathrm{d}\varphi = 2 - \delta_{l0}. \tag{6.1.1.23}$$

We assume the radial function to be constant in sign, and normalized to unity. The scalar function, with $l = 0$, does not change sign. Integration over the angular coordinates gives the electron content of the scalar function. The multipole terms with $l > 0$ integrate to zero. Taking the modulus of the angular function, and then integrating, gives twice the electron transfer from the electron-deficient to the electron-enriched volume for that multipole. With this normalization, the angle-dependent factors in the expansion, in terms of the associated Legendre polynomials and in terms of direction cosines, are given in Table 6.1.1.6. For the alternative normalization such that

$$\int |y_{lmp}|^2\, \mathrm{d}(\cos\theta)\, \mathrm{d}\varphi = 1,$$

the factor multiplying the angle-dependent term is as given in (6.1.1.22).

The site symmetry of the atom restricts multipole terms to those that are invariant under the operations of the relevant point group. The restrictions for the 27 non-cubic crystallographic point groups are given in Table 6.1.1.7.

For the five cubic point groups, the functions allowed are the linear combinations of the $Y_{lmp}(\theta, \varphi)$ known as the cubic harmonics $K_{lj}(\theta, \varphi)$ (Altmann & Cracknell, 1965). These are listed in Table 6.1.1.8. The normalization constant N_{lj}^2 is given by

$$N_{lj}^2 = \int K_{lj}^2\, \mathrm{d}(\cos\theta)\, \mathrm{d}\varphi.$$

The derivation of Tables 6.1.1.7 and 6.1.1.8 is described by Kurki-Suonio (1977).

The generalized scattering factor for a particular multipole involves evaluating the Fourier transform of the density

$$\int \exp(i\mathbf{S}\cdot\mathbf{r})\rho_{lm\pm}(r)Y_{lm\pm}(\theta, \varphi)\, \mathrm{d}\mathbf{r} = f_{lm\pm}(S)Y_{lm}(\theta_S, \varphi_S),$$

where the right-hand side is obtained by substituting (6.1.1.17) and integrating over the angular coordinates for the direct-space variables. The term

$$f_{lm\pm}(S) = \int_0^\infty j_l(Sr)\rho_{lm\pm}(r)r^2\, \mathrm{d}r \tag{6.1.1.24}$$

gives the radial variation of the generalized scattering factor.

The density function $\rho_{lm\pm}(r_a)$ may be derived from atomic basis functions, which asymptotically have the form of simple exponential functions $A_n r^n \exp(-\alpha r)$. Expansions in terms of Gaussian functions $B_n r^n \exp(-\beta r^2)$ or of Laguerre functions $C_n r^l L_n^{2l+2} \exp(-\gamma r/2)$, where L is a Laguerre polynomial of order n and degree $2l+2$, are also convenient for some purposes. A_n, B_n and C_n are normalizing factors, which, when specified as

$$
\begin{gathered}
A_n = \frac{\alpha^{l+n+3}}{4\pi(l+n+2)!}, \quad B_n = \frac{2^{\beta(l+n+3)/2}}{\Gamma[(l+n+3)/2]}, \\
C_n = \frac{(-)^n n!(\gamma/2)^{2l+3}}{4\pi(2l+n+2)!},
\end{gathered}
\tag{6.1.1.25}
$$

impose the normalization condition (Stewart, 1980*a*)

$$\int_0^\infty \rho_{lm}(r_a)r_a^{l+2}\, \mathrm{d}r_a = 1. \tag{6.1.1.26}$$

With this normalization, the Fourier–Bessel transforms are, for the simple exponential,

Table 6.1.1.6. *Angle dependence of multipole functions, normalized as in equation (6.1.1.23); $\omega = \cos\theta$ and S, D, Q, O, H denote scalar, dipole, quadrupole, octupole, and hexadecapole terms, respectively*

Pole	Real spherical harmonic	Cartesian representation
S 1	$\frac{1}{4\pi}P_0^0(\omega)$	$\frac{1}{4\pi}$
D 1	$\frac{1}{\pi}P_1^1(\omega)\cos\varphi$	$\frac{1}{\pi}q_x$
D 2	$\frac{1}{\pi}P_1^1(\omega)\sin\varphi$	$\frac{1}{\pi}q_y$
D 3	$\frac{1}{\pi}P_1^0(\omega)$	$\frac{1}{\pi}q_z$
Q 1	$\frac{1}{8}P_2^2(\omega)\cos 2\varphi$	$\frac{3}{8}(q_x^2 - q_y^2)$
Q 2	$\frac{1}{8}P_2^2(\omega)\sin 2\varphi$	$\frac{3}{4}q_xq_y$
Q 3	$\frac{1}{4}P_2^1(\omega)\cos\varphi$	$\frac{3}{4}q_xq_z$
Q 4	$\frac{1}{4}P_2^1(\omega)\sin\varphi$	$\frac{3}{4}q_yq_z$
Q 5	$\frac{3\sqrt{3}}{4\pi}P_2^0(\omega)$	$\frac{9\sqrt{2}}{8\pi}(q_z^2 - \frac{1}{3})$
O 1	$\frac{4}{45\pi}P_3^3(\omega)\cos 3\varphi$	$\frac{4}{3\pi}(q_x^2 - 3q_y^2)q_x$
O 2	$\frac{4}{45\pi}P_3^3(\omega)\sin 3\varphi$	$\frac{4}{3\pi}(3q_x^2 - q_y^2)q_y$
O 3	$\frac{1}{15}P_3^2(\omega)\cos 2\varphi$	$(q_x^2 - q_y^2)q_z$
O 4	$\frac{1}{15}P_3^2(\omega)\sin 2\varphi$	$2q_xq_yq_z$
O 5	$\frac{2}{3}\left[\tan^{-1}2 + \frac{14}{5} - \frac{\pi}{4}\right]^{-1}P_3^1(\omega)\cos\varphi$	$\left[\tan^{-1}2 + \frac{14}{5} - \frac{\pi}{4}\right]^{-1}(5q_z^2 - 1)q_x$
O 6	$\frac{2}{3}\left[\tan^{-1}2 + \frac{14}{5} - \frac{\pi}{4}\right]^{-1}P_3^1(\omega)\sin\varphi$	$\left[\tan^{-1}2 + \frac{14}{5} - \frac{\pi}{4}\right]^{-1}(5q_z^2 - 1)q_y$
O 7	$\frac{20}{13\pi}P_3^0(\omega)$	$\frac{10}{13\pi}(5q_z^2 - 3)q_z$
H 1	$\frac{1}{224}P_4^4(\omega)\cos 4\varphi$	$\frac{105}{224}(q_x^4 - 6q_x^2q_y^2 + q_y^4)$
H 2	$\frac{1}{224}P_4^4(\omega)\sin 4\varphi$	$\frac{420}{224}(q_x^2 - q_y^2)q_xq_y$
H 3	$\frac{1}{84}P_4^3(\omega)\cos 3\varphi$	$\frac{105}{84}(q_x^2 - 3q_y^2)q_xq_z$
H 4	$\frac{1}{84}P_4^3(\omega)\sin 3\varphi$	$\frac{105}{84}(3q_x^2 - q_y^2)q_yq_z$
H 5	$\left(\frac{7\sqrt{7}}{272 + 56\sqrt{7}}\right)P_4^2(\omega)\cos 2\varphi$	$\frac{15}{2}\left(\frac{7\sqrt{7}}{272 + 56\sqrt{7}}\right)(7q_z^2 - 1)(q_x^2 - q_y^2)$
H 6	$\left(\frac{7\sqrt{7}}{272 + 56\sqrt{7}}\right)P_4^2(\omega)\sin 2\varphi$	$\frac{15}{2}\left(\frac{7\sqrt{7}}{272 + 56\sqrt{7}}\right)(7q_z^2 - 1)q_xq_y$
H 7	$\left(\frac{21\sqrt{7}}{256 + 14\sqrt{7}}\right)P_4^1(\omega)\cos\varphi$	$\frac{5}{2}\left(\frac{21\sqrt{7}}{256 + 14\sqrt{7}}\right)(7q_z^2 - 3)q_xq_z$
H 8	$\left(\frac{21\sqrt{7}}{256 + 14\sqrt{7}}\right)P_4^1(\omega)\sin\varphi$	$\frac{5}{2}\left(\frac{21\sqrt{7}}{256 + 14\sqrt{7}}\right)(7q_z^2 - 3)q_xq_z$
H 9	$0.55534P_4^0(\omega)$	$\frac{5}{8}(0.55534)(7q_z^4 - 6q_z^2 + \frac{3}{5})$
$^*H_{\rm cubic}$	$\frac{160}{27\sqrt{3}\pi}\left[\frac{1}{420}P_4^4(\omega)\cos 4\varphi + \frac{2}{5}P_4^0(\omega)\right]$	$\frac{160}{27\sqrt{3}\pi}(q_x^4 + q_y^4 + q_z^4 - 3/5)$

$^*H_{\rm cubic}$ is the fourth-order hexadecapole appropriate to cubic site symmetry.

$$f_{nl}(\alpha, S) = \frac{S}{(2l+1)!![1+(S/\alpha)^2]^{n+2}} \times {}_2F_1\left[\frac{l-n-1}{2}, \frac{l-n}{2}; l+\frac{3}{2}; -(S/\alpha)^2\right]; \quad (6.1.1.27)$$

for the Gaussian function,

$$g_{nl}(\beta, S) = \frac{S^1}{(2l+1)!!}\exp(-S^2/4\beta){}_1F_1\left[\frac{l-n}{2}; l+\frac{3}{2}; \frac{S^2}{4\beta}\right]; \quad (6.1.1.28)$$

and, for the Laguerre function,

$$h_{nl}(\gamma, S) = \frac{(-)^n n! 2^n S^l}{[2(l+n)+1]!![1+(2S/\gamma)^2]^{l+2}} P_n^{(l+\frac{3}{2}, l+\frac{1}{2})}(t);$$

where the Jacobi polynomial is given by

$$\begin{aligned} P_n^{(a,b)}(x) &= 2^{-n}\sum_{m=0}^{n}\binom{n+a}{m}\binom{n+b}{n-m}(x-1)^{n-m}(x+1)^m \\ &= \frac{\Gamma(a+n+1)}{n!\Gamma(a+b+n+1)} \\ &\quad \times \sum_{m=0}^{n}\binom{n}{m}\frac{\Gamma(a+b+n+m+1)}{2^m\Gamma(a+m+1)}(x-1)^m \\ &= \binom{n+a}{n}{}_2F_1\left(-n, n+a+b+1; a+1; \frac{1-x}{2}\right) \\ & \qquad\qquad a \geq -1, b \geq a \end{aligned}$$

and

$$t = \frac{[(2S/\gamma)^2 - 1]}{[(2S/\gamma)^2 + 1]}. \quad (6.1.1.29)$$

Further details are given by Stewart (1980*a*).

In the case of Slater-type orbitals, a simpler form of the radial term may be obtained *via* the recurrence relations (Avery & Watson, 1977)

$$(S^2+\alpha^2)f_{\mu+1,\nu} + (\mu+\nu)(\mu-\nu-1)f_{\mu-1,\nu} = 2\nu\alpha f_{\mu\nu}$$
$$Sf_{\mu,\nu-1} + (\mu-\nu-1)f_{\mu-1,\nu} = \alpha f_{\mu\nu}.$$

Thus, for the lower-order Slater-type functions, we obtain the values listed in Table 6.1.1.9.

Atomic wavefunctions, in the form of sets of orbital contributions using Slater-type functions, are tabulated by Clementi & Roetti (1974). Basis sets for Gaussian orbitals are described by Veillard (1968), Roos & Siegbahn (1970), Huzinaga (1971), van Duijneveldt (1971), Dunning & Jeffrey-Hay (1977), and by McLean & Chandler (1979, 1980). The application of these basis sets to molecular calculations is reviewed by Ahlrichs & Taylor (1981).

6.1.1.5. *The temperature factor*

The atoms in a solid vibrate about their equilibrium positions, with an amplitude that increases with temperature. As a result of this vibration, the amplitude for coherent scattering is modulated by the Fourier transform of the probability distribution for the vibrating atom, known as the temperature factor. The reduction in the intensity of the coherent scattering is accompanied by thermal diffuse scattering, for which the phase relationship between the incident and diffracted beams is altered by the thermal wave, or phonon.

Table 6.1.1.7. *Indices allowed by the site symmetry for the real form of the spherical harmonics $Y_{lmp(\theta,\varphi)}$; λ, μ and j are integers such that $l, m \geq 0$; $(-)^n$ implies $p = -$ for n odd and $p = +$ for n even*

Site symmetry	Coordinate axes	Indices
$\underline{1}$	Any	All (l, m, p)
$\bar{1}$	Any	$(2\lambda, m, p)$
2	$2 \parallel x$	$(l, m, (-)^{l-m})$
	$2 \parallel y$	$(l, m, (-)^l)$
	$2 \parallel z$	$(l, 2\mu, p)$
m	$m \perp x$	$(l, m, (-)^m)$
	$m \perp y$	$(l, m, +)$
	$m \perp z$	$(l, l-2j, p)$
$2/m$	$2 \parallel x, m \perp x$	$(2\lambda, m, (-)^m)$
	$2 \parallel y, m \perp y$	$(2\lambda, m, +)$
	$2 \parallel z, m \perp z$	$(2\lambda, 2\mu, p)$
222	$2 \parallel z, 2 \parallel y$	$(l, 2\mu, (-)^l)$
$mm2$	$2 \parallel x, m \perp z$	$(l, l-2j, +)$
	$2 \parallel y, m \perp z$	$(l, l-2j, (-)^l)$
	$2 \parallel z, m \perp y$	$(l, 2\mu, +)$
mmm	$m \perp z, m \perp y, m \perp z$	$(2\lambda, 2\mu, +)$
$\underline{4}$	$\underline{4} \parallel z$	$(l, 4\mu, p)$
$\bar{4}$	$\bar{4} \parallel z$	$(l, 2l-4j, p)$
$4/m$	$4 \parallel z, m \perp z$	$(2\lambda, 4\mu, p)$
422	$4 \parallel z, 2 \parallel y$	$(l, 4\mu, (-)^l)$
$4mm$	$\underline{4} \parallel z, m \perp y$	$(l, 4\mu, +)$
$\bar{4}2m$	$\bar{4} \parallel z, 2 \parallel x$	$(l, 2l-4j, (-)^l)$
	$\bar{4} \parallel z, m \perp y$	$(l, 2l-4j, +)$
$4/mmm$	$4 \parallel z, m \perp z, m \perp x$	$(2\lambda, 4\mu, +)$
$\underline{3}$	$\underline{3} \parallel z$	$(l, 3\mu, p)$
$\bar{3}$	$\bar{3} \parallel z$	$(2\lambda, 3\mu, p)$
32	$3 \parallel z, 2 \parallel y$	$(l, 3\mu, (-)^l)$
	$3 \parallel z, 2 \parallel x$	$(l, 3\mu, (-)^{l-m})$
$3m$	$3 \parallel z, m \perp y$	$(l, 3\mu, +)$
	$\underline{3} \parallel z, m \perp x$	$(l, 3\mu, (-)^m)$
$\bar{3}m$	$\bar{3} \parallel z, m \perp y$	$(2\lambda, 3\mu, +)$
	$\bar{3} \parallel z, m \perp x$	$(2\lambda, 3\mu, (-)^m)$
$\underline{6}$	$\underline{6} \parallel z$	$(l, 6\mu, p)$
$\bar{6}$	$\bar{6} \parallel z$	$(m+2j, 3\mu, p)$
$6/m$	$6 \parallel z, m \perp z$	$(2\lambda, 6\mu, p)$
622	$6 \parallel z, 2 \parallel y$	$(l, 6\mu, (-)^l)$
$6mm$	$\underline{6} \parallel z, m \perp y$	$(l, 6\mu, +)$
$\bar{6}m2$	$\bar{6} \parallel z, m \perp y$	$(m+2j, 3\mu, +)$
	$\bar{6} \parallel z, m \perp x$	$(m+2j, 3\mu, (-)^l)$
$6/mmm$	$6 \parallel z, m \perp z, m \perp y$	$(2\lambda, 6\mu, +)$

The first term in an expansion of the probability density $\rho(\mathbf{u})$ for displacement $\mathbf{u}$ about an equilibrium position at the origin is

$$\rho_o(\mathbf{u}) = \frac{\det \boldsymbol{\sigma}_\mathbf{u}^{-1/2}}{8\pi^3}\exp(-\tfrac{1}{2}\mathbf{u}^T \cdot \boldsymbol{\sigma}_\mathbf{u}^{-1} \cdot \mathbf{u}), \quad (6.1.1.30)$$

where $\boldsymbol{\sigma}_\mathbf{u}$ is the dispersion matrix describing the second moments of the displacements about the mean position. The corresponding expression for the temperature factor is

$$T_o(\mathbf{S}) = \exp(-\tfrac{1}{2}\mathbf{S}^T \cdot \boldsymbol{\sigma}_\mathbf{u} \cdot \mathbf{S}), \quad (6.1.1.31)$$

which is the Fourier transform of $\rho_o(\mathbf{u})$.

Table 6.1.1.8. *Cubic harmonics $K_{lj}(\theta, \varphi)$ for cubic site symmetries*

$K_{lj}(\theta, \varphi)$	N_{l^2j}	Site symmetry				
		23	$m3$	432	$\bar{4}3m$	$m3m$
$K_0 = Y_{00+} = 1$	4π	×	×	×	×	×
$K_3 = Y_{32-}$	$\frac{240\pi}{7}$	×			×	
$K_4 = Y_{40+} + \frac{1}{168} Y_{44+}$	$\frac{16\pi}{21}$	×	×	×	×	×
$K_{6,1} = Y_{60+} - \frac{1}{360} Y_{64+}$	$\frac{32\pi}{13}$	×	×	×	×	×
$K_{6,2} = Y_{62+} - \frac{1}{792} Y_{66+}$	$\frac{512\pi}{13} \cdot \frac{105}{11}$	×	×			
$K_7 = Y_{72-} + \frac{1}{1560} Y_{76-}$	$\frac{256\pi}{15} \cdot \frac{567}{13}$	×			×	
$K_8 = Y_{80+} + \frac{1}{5940}(Y_{84+} + \frac{1}{672} Y_{88+})$	$\frac{256\pi}{17 \cdot 33}$	×	×	×	×	×
$K_{9,1} = Y_{92-} - \frac{1}{2520} Y_{96-}$	$\frac{512\pi}{19} \cdot 165$	×			×	
$K_{9,2} = Y_{94-} - \frac{1}{4080} Y_{98-}$	$\frac{2048\pi}{19} \cdot \frac{243 \cdot 5005}{17}$	×		×		
$K_{10,1} = Y_{10,0+} - \frac{1}{5460}(Y_{10,4} + \frac{1}{4320} Y_{10,8+})$	$\frac{512\pi}{21} \cdot \frac{3}{65}$	×	×	×	×	×
$K_{10,2} = Y_{10,2+} + \frac{1}{43680}(Y_{10,6+} + \frac{1}{456} Y_{10,10+})$	$\frac{2048\pi}{21} \cdot \frac{4455}{247}$	×	×			

The mean-square displacement of the atom from its mean position in the direction of the vector $\mathbf{v}$ is given by

$$\langle \mathbf{u}^2 \rangle_{\mathbf{v}} = \mathbf{v}^T \mathbf{g}^T \boldsymbol{\sigma}_{\mathbf{u}} \mathbf{g} \mathbf{v} / (\mathbf{v}^T \mathbf{g} \mathbf{v}), \tag{6.1.1.32}$$

where g_{ij} is the covariant metric tensor with the scalar products of the unit-cell vectors $\mathbf{a}_i \cdot \mathbf{a}_j$ as components.

The thermal motion for atoms in crystals is often displayed as surfaces of constant probability density. The surface for the thermal displacement $\mathbf{u}$ is defined by

$$\mathbf{u}^T \boldsymbol{\sigma}_{\mathbf{u}}^{-1} \mathbf{u} = C^2. \tag{6.1.1.33}$$

The square of the distance from the origin to the equiprobability surface in the direction $\mathbf{v}$ is

$$C^2 \mathbf{v}^T \mathbf{g} \mathbf{v} / (\mathbf{v}^T \boldsymbol{\sigma}_{\mathbf{u}}^{-1} \mathbf{v}). \tag{6.1.1.34}$$

This is equal to (6.1.1.32) for C unity only if $\mathbf{v}$ coincides with a principal axis of the vibration ellipsoid.

The probability that a displacement falls within the ellipsoid defined by C is

$$(2/\pi)^{1/2} \int_0^C q^2 \exp(-q^2/2)\, \mathrm{d}q. \tag{6.1.1.35}$$

6.1.1.6. *The generalized temperature factor*

The Gaussian model of the probability density function (p.d.f.) $\rho_o(\mathbf{u})$ for atomic thermal motion defined in (6.1.1.30) is adequate in many cases. Where anharmonicity or curvilinear motion is important, however, more elaborate models are needed.

In the classical (high-temperature) regime, the generalized temperature factor is given by the Fourier transform of the one-particle p.d.f:

$$\rho(\mathbf{u}) = N^{-1} \exp[-V(\mathbf{u})/kT], \tag{6.1.1.36}$$

where

$$N = \int \exp[-V(\mathbf{u})/kT]\, \mathrm{d}\mathbf{u}. \tag{6.1.1.37}$$

In the cases where the potential function $V(\mathbf{u})$ is a close approximation to the Gaussian (harmonic) potential, series expansions based on a perturbation treatment of the anharmonic terms provide a satisfactory representation of the temperature factors. That is, if the deviations from the Gaussian shape are small, approximations obtained by adding higher-order corrections to the Gaussian model are satisfactory.

In an arbitrary coordinate system, the number of significant high-order tensor coefficients for the correction is large. It may be helpful to choose coordinates parallel to the principal axes for the harmonic approximation so that

$$V(\mathbf{u})/kT = 1/2 \sum_{i=1}^{3} (B_i u_i)^2, \tag{6.1.1.38}$$

in which case (6.1.1.36) may be written as

$$\rho_o(\mathbf{u}) = \frac{1}{N_0} \exp\left[-1/2 \sum_i (B_i u_i)^2 \right], \tag{6.1.1.39}$$

where

$$N_0 = \frac{B_1 B_2 B_3}{8\pi^3}. \tag{6.1.1.40}$$

The harmonic temperature factor is

$$T_o(\mathbf{S}) = \exp\left[-1/2 \sum_i (b_i S_i)^2 \right], \tag{6.1.1.41}$$

where b_i and B_i are related by the reciprocity condition

$$b_i B_i = 1. \tag{6.1.1.42}$$

Table 6.1.1.9. $f_{nl}(\alpha, S) = \int_0^\infty r^n \exp(-\alpha r) j_l(Sr)\, dr$

n \ l	1	2	3	4
0	$\frac{1}{(S^2+\alpha^2)}$	$\frac{2\alpha}{(S^2+\alpha^2)^2}$	$\frac{2(3\alpha^2-S^2)}{(S^2+\alpha^2)^3}$	$\frac{24\alpha(\alpha^2-S^2)}{(S^2+\alpha^2)^4}$
1		$\frac{2S}{(S^2+\alpha^2)^2}$	$\frac{8S\alpha}{(S^2+\alpha^2)^3}$	$\frac{8S(5\alpha^2-S^2)}{(S^2+\alpha^2)^4}$
2			$\frac{8S^2}{(S^2+\alpha^2)^3}$	$\frac{48S^2\alpha}{(S^2+\alpha^2)^4}$
3				$\frac{48S^3}{(S^2+\alpha^2)^4}$

6.1.1.6.1. *Gram–Charlier series*

In the Gram–Charlier series expansion (Kuznetsov, Stratonovich & Tikhonov, 1960), the general p.d.f. $\rho(\mathbf{u})$ is approximated by

$$\left[1 - c^j D_j + \frac{c^{jk}}{2!} D_j D_k - \ldots + (-)^p \frac{c^{jk\ldots\zeta}}{p!} D_\alpha D_\beta \ldots D_\zeta\right] \rho_o(\mathbf{u}). \tag{6.1.1.43}$$

The operator $D_\alpha D_\beta \ldots D_\zeta$ is the pth partial (covariant) derivative $\partial^p / \partial u_\alpha \partial u_\beta \ldots \partial u_\zeta$, and $c^{jk\ldots\zeta}$ is a contravariant component of the coefficient tensor. The quasi-moment coefficient tensors are symmetric for all permutations of indices. The first four have three, six, ten, and fifteen unique components for site symmetry 1. The third- and fourth-order terms describe the skewness and the kurtosis of the p.d.f., respectively.

The Gram–Charlier series may be rewritten using general multidimensional Hermite polynomial tensors, defined by

$$\begin{aligned} H_{\alpha\beta\ldots\zeta}(\mathbf{u}) &= (-)^p \exp(\tfrac{1}{2}\sigma_{jk}^{-1} u^j u^k) \\ &\quad \times D_\alpha D_\beta \ldots D_\zeta \exp(-\tfrac{1}{2}\sigma_{jk}^{-1} u^j u^k). \end{aligned} \tag{6.1.1.44}$$

For $w_j = \sigma_{jk}^{-1} u^k$, and with $\sigma_{jk}^{-1} = \sigma_{kj}^{-1}$ and $w_j w_k = w_k w_j$, the first few general Hermite polynomials may be expressed as

$$\begin{aligned} {}^0H(\mathbf{u}) &= 1 \\ {}^1H_j(\mathbf{u}) &= w_j \\ {}^2H_{jk}(\mathbf{u}) &= w_j w_k - \sigma_{jk}^{-1} \\ {}^3H_{jk}(\mathbf{u}) &= w_j w_k w_l - w_j \sigma_{kl}^{-1} - w_k \sigma_{lj}^{-1} - w_l \sigma_{jk}^{-1} \\ &= w_j w_k w_l - 3 w_{(j} \sigma_{kl)}^{-1} \\ {}^4H_{jklm}(\mathbf{u}) &= w_j w_k w_l w_m - 6 w_{(j} w_k \sigma_{lm)}^{-1} + 3 \sigma_{j(k}^{-1} \sigma_{lm)}^{-1}. \end{aligned} \tag{6.1.1.45}$$

Indices in parentheses indicate terms to be averaged over all unique permutations of those indices.

The Gram–Charlier series is then

$$\rho_o(\mathbf{u}) \left[1 + \frac{1}{3!} c^{jkl} H_{jkl}(\mathbf{u}) + \frac{1}{4!} c^{jklm} H_{jklm}(\mathbf{u}) + \ldots\right], \tag{6.1.1.46}$$

in which the mean and the dispersion of $\rho_o(\mathbf{u})$ have been chosen to make c^j and c^{jk} vanish.

The Fourier transform, after truncating at the quartic term, gives an approximation to the generalized temperature factor:

$$T(\mathbf{S}) = T_o(\mathbf{S}) \left[1 + \frac{i^3}{3!} c^{jkl} S_j S_k S_l + \frac{i^4}{4!} c^{jklm} S_j S_k S_l S_m\right], \tag{6.1.1.47}$$

i.e. the Fourier transform of the Hermite polynomial expansion about the Gaussian p.d.f. is a power-series expansion about the Gaussian temperature factor with even-order terms real and odd-order terms imaginary.

Table 6.1.1.10. *Indices nmp allowed by the site symmetry for the functions $H_n(z)\Phi_{mp}(\varphi)$; μ, ν and j are integers such that $m, n \geq 0$; $(-)^n$ implies $p = -$ for n odd and $p = +$ for n even*

Site symmetry	Coordinate axes	Indices
$\underline{1}$	Any	All (n, m, p)
$\bar{1}$	Any	$(n, n+2j, p)$
2	$2 \parallel x$	$(n, m, (-)^n)$
	$2 \parallel y$	$(n, m, (-)^{n-m})$
	$2 \parallel z$	$(n, 2\nu, p)$
m	$m \perp x$	$(n, m, (-)^m)$
	$m \perp y$	$(n, m, +)$
	$m \perp z$	$(2\mu, m, p)$
$2/m$	$2 \parallel x, m \perp x$	$(m+2j, m, (-)^m)$
	$2 \parallel y, m \perp y$	$(m+2j, m, +)$
	$2 \parallel z, m \perp z$	$(2\mu, 2\nu, p)$
222	$2 \parallel z, 2 \parallel y$	$(n, 2\nu, (-)^n)$
$mm2$	$2 \parallel x, m \perp z$	$(2\mu, m+)$
	$2 \parallel y, m \perp z$	$(2\mu, m, (-)^m)$
	$2 \parallel z, m \perp y$	$(n, 2\nu, +)$
mmm	$m \perp z, m \perp y, m \perp z$	$(2\mu, 2\nu, +)$
$\underline{4}$	$4 \parallel z$	$(n, 4\nu, p)$
$\bar{4}$	$4 \parallel z$	$(n, 2n+4j, p)$
$4/m$	$4 \parallel z, m \perp z$	$(2\mu, 4\nu, p)$
422	$4 \parallel z, 2 \parallel y$	$(n, 4\nu, (-)^n)$
$4mm$	$4 \parallel z, m \perp y$	$(n, 4\nu, +)$
$\bar{4}2m$	$\bar{4} \parallel z, 2 \parallel x$	$(n, 2n+4j, (-)^n)$
	$\bar{4} \parallel z, m \perp y$	$(n, 2n+4j, +)$
$4/mmm$	$4 \parallel z, m \perp z, m \perp x$	$(2\mu, 4\nu, +)$
$\underline{3}$	$3 \parallel z$	$(n, 3\nu, p)$
$\bar{3}$	$3 \parallel z$	$(m+2j, 3\nu, p)$
32	$3 \parallel z, 2 \parallel y$	$(n, 3\nu, (-)^{n-m})$
	$3 \parallel z, 2 \parallel x$	$(n, 3\nu, (-)^n)$
$3m$	$3 \parallel z, m \perp y$	$(n, 3\nu, +)$
	$3 \parallel z, m \perp x$	$(n, 3\nu, (-)^m)$
$\bar{3}m$	$\bar{3} \parallel z, m \perp y$	$(m+2j, 3\nu, +)$
	$\bar{3} \parallel z, m \perp x$	$(m+2j, 3\nu, (-)^m)$
$\underline{6}$	$6 \parallel z$	$(n, 6\nu, p)$
$\bar{6}$	$\bar{6} \parallel z$	$(2\mu, 3\nu, p)$
$6/m$	$6 \parallel z, m \perp z$	$(2\mu, 6\nu, p)$
622	$6 \parallel z, 2 \parallel y$	$(n, 6\nu, (-)^n)$
$6mm$	$\bar{6} \parallel z, m \perp y$	$(n, 6\nu, +)$
$\bar{6}m2$	$\bar{6} \parallel z, m \perp y$	$(2\mu, 3\nu, +)$
	$\bar{6} \parallel z, m \perp x$	$(2\mu, 3\nu, (-)^m)$
$6/mmm$	$6 \parallel z, m \perp z, m \perp y$	$(2\mu, 6\nu, +)$

Because of the symmetry of the relationship between the Fourier transform of a real function and its inverse, the functional form of the p.d.f. and that of the temperature factor can be interchanged. Exchanging the role of the Hermite polynomials and the power series from the Gram–Charlier expansion has been studied by Scheringer (1985), with the objective of obtaining the one-particle potentials more directly.

6.1.1.6.2. *Fourier-invariant expansions*

When truncated, an expression for a multipole expansion, p.d.f. or temperature factor must retain those terms essential to the accuracy required of the expansion. Some authors (*e.g.*

Table 6.1.1.11. *Indices n_x, n_y, n_z allowed for the basis functions $H_{n_x}(Ax)H_{n_y}(By)H_{n_z}(Cz)$; λ, μ, and ν are non-negative; conditions for other choices of axes are derived by cyclic permutation*

Symmetry	Coordinate axes	Allowed indices
$\underline{1}$	Any	All (n_x, n_y, n_z)
$\bar{1}$	Any	$n_x + n_y + n_z = 2\lambda$
2	$2 \parallel z$	$n_x + n_y = 2\lambda$
m	$m \perp z$	$n_z = 2\nu$
$2/m$	$2 \parallel z, m \perp z$	$n_x + n_y = 2\lambda, n_z = 2\nu$
222	$2 \parallel z, 2 \parallel y$	n_x, n_y, n_z all even or all odd
$mm2$	$2 \parallel z, m \perp y$	$n_x = 2\lambda, n_y = 2\mu$
mmm	$m \perp z, m \perp y, m \perp z$	$n_x = 2\lambda, n_y = 2\mu, n_z = 2\nu$

Stewart, 1980*b*) strongly favour classes of truncated expansion that retain symmetry properties appropriate to particular classes of transformation, such as rotation or Fourier inversion. Others, emphasizing simplicity, retain the minimum set of terms required to preserve the accuracy needed in the expansion. In either case, it is desirable for the expansion to converge rapidly, and to have a form related to physical theory.

In principle, the one-particle potential may be expanded in any complete set of functions. Harmonic oscillator functions simplify simultaneous interpretation of the probability distribution in real and reciprocal space because their form does not change under Fourier inversion (Kurki-Suonio, Merisalo & Peltonen, 1979).

If both anharmonicity and anisotropy are small, the p.d.f. may be expressed as a rapidly converging expansion in spherical polar coordinates u, θ, φ:

$$\rho(\mathbf{u}) = \rho_o(\mathbf{u})\frac{N_0}{N}\left[1 - \sum_{n,l,m,p} a_{nlmp}R_{nl}(Bu)Y_{lmp}(\theta,\varphi)\right] \quad (6.1.1.48)$$

for non-cubic and

$$\rho(\mathbf{u}) = \rho_o(\mathbf{u})\frac{N_0}{N}\left[1 - \sum_{n,l,j} a_{nlj}R_{nl}(Bu)K_{lj}(\theta,\varphi)\right] \quad (6.1.1.49)$$

for cubic site symmetry. The radial term may be written as

$$R_{nl}(x) = x^l L^{l+1/2}_{(n-l)/2}(x^2), \quad (6.1.1.50)$$

where the associated Laguerre polynomial is

$$L^{\alpha}_{k}(t) = \sum_{\nu=0}^{k}\binom{k+\alpha}{k-\alpha}\frac{(-t)^\nu}{\nu!} \quad (6.1.1.51)$$

with

$$\binom{p}{q} = \frac{\Gamma(p+1)}{[\Gamma(q+1)\Gamma(p-q+1)]} \quad (6.1.1.52)$$

and the normalizing factor

$$N = \frac{8\pi^3}{B^3}\left[1 - \sum_{\nu}(-)^\nu\frac{(2\nu+1)!}{2^{2\nu}(\nu!)^2}a_{2\nu 00+}\right]. \quad (6.1.1.53)$$

The real spherical harmonics $Y_{lmp}(\theta,\varphi)$ and the cubic harmonics $K_{lj}(\theta,\varphi)$ are as defined in Subsection 6.1.1.4. As in the case of multipole expansions, the non-zero coefficients in these expressions are limited by the site symmetry. The restrictions on the temperature factor are identical to those for the generalized scattering factor listed in Tables 6.1.1.7 and 6.1.1.8.

From the Fourier invariance of harmonic oscillator functions,

$$T(\mathbf{S}) = \frac{N_0}{N}\exp(-b^2S^2/2) \times\left[1 - \sum_{n,l,m,p} a_{nlmp}i^nR_{nl}(bS)Y_{lmp}(\theta_S,\varphi_S)\right] \quad (6.1.1.54)$$

and

$$T(\mathbf{S}) = \frac{N_0}{N}\exp(-b^2S^2/2) \times\left[1 - \sum_{n,l,j} a_{nlj}i^nR_{nl}(bS)K_{lj}(\theta_S,\varphi_S)\right] \quad (6.1.1.55)$$

for non-cubic and cubic site symmetries, respectively. θ_S and φ_S are polar coordinates in reciprocal space.

With an appropriate choice of origin, the first-order (110+) and (111±) terms vanish. The isotropic harmonic (200+) and constant (000+) terms have been removed from the summation. If coordinate axes are chosen coincident with the principal axes for the harmonic approximation, (221±) and (222−) vanish. (220+) indicates the prolateness and (222+) the non-axiality in the harmonic approximation (Kurki-Suonio, 1977). Terms with $n \geq 2$ describe the anharmonicity.

The approximations in (6.1.1.48) to (6.1.1.55) fail if the anisotropy, indicated by the size of the (220+) and (222+) terms, or the anharmonicity is large. If the anharmonicity and non-axiality are small, one can invoke Fourier-invariant expansions in cylindrical polar coordinates u_r, u_z, φ:

$$\rho(\mathbf{u}) = \rho_o(\mathbf{u})\frac{N_0}{N} \times\left[1 - \sum_{n_z,n,m,p} b_{n_znmp}H_{n_z}(B_zu_z)\mathbf{P}_{nm}(B_ru_r)\Phi_{mp}(\varphi)\right] \quad (6.1.1.56)$$

and

$$T(S) = \frac{N_0}{N}\exp[-\tfrac{1}{2}(b_r^2S_r^2 + b_z^2S_z^2)] \times\left[1 - \sum_{n_z,n,m,p} b_{n_znmp}H_{n_z}(b_zS_z)\mathbf{P}_{nm}(b_rS_r)\Phi_{mp}(\varphi_S)\right], \quad (6.1.1.57)$$

where S_r, S_z, φ_S are cylindrical coordinates for S.

$$\mathbf{P}_{nm}(x) = x^mL^m_{(n-m)/2}(x^2), \quad \Phi_{m\pm}(\varphi) = \begin{matrix}\cos m\varphi \\ \sin m\varphi\end{matrix} \quad (6.1.1.58)$$

and

$$N = \frac{8\pi^3}{B_r^2B_z}\left[1 - \sum_{\mu\nu}(-)^\nu\frac{(2\mu)!}{\mu!}b_{2\mu 2\nu 0+}\right]. \quad (6.1.1.59)$$

The indices allowed for the site symmetrical basis are as indicated in Table 6.1.1.10.

Again, the first-order (100+) and (011±) terms vanish with the appropriate choice of origin. For coordinate axes coinciding with the principal axes of the harmonic approximation, (111±) and (022−) vanish. (020+), (200+), and (000+) have been removed from the summation.

Equations (6.1.1.56) and (6.1.1.57) apply accurately to non-cubic symmetries with rotation axes higher than twofold where non-axiality vanishes. Where non-axiality is large, it is preferable to use the Cartesian Fourier invariant expansion

$$\rho(\mathbf{u}) = \frac{N_0}{N}\exp\left[-1/2\sum_i B_i^2 u_1^2\right] \times \left[1 - \sum_{n_x,n_y,n_z} c_{n_x n_y, n_z} H_{n_x}(B_x u_x) H_{n_y}(B_y u_y) H_{n_z}(B_z u_z)\right] \tag{6.1.1.60}$$

and

$$T(\mathbf{S}) = \frac{N_0}{N}\exp\left[-1/2\sum_i b_i^2 u_1^2\right] \times \left[1 - \sum_{n_x,n_y,n_z} c_{n_x n_y, n_z} H_{n_x}(b_x u_x) H_{n_y}(b_y u_y) H_{n_z}(b_z u_z)\right], \tag{6.1.1.61}$$

where

$$N = \frac{8\pi^3}{B_x B_y B_z}\left[1 - \sum_{\lambda\mu\nu} \frac{(2\lambda)!(2\mu)!(2\nu)!}{\lambda!\mu!\nu!} c_{2\lambda 2\mu 2\nu}\right]. \tag{6.1.1.62}$$

The indices allowed under the site symmetry are listed in Table 6.1.1.11.

The first-order terms vanish with suitable choice of origin. (110), (101), and (011) vanish if the coordinates coincide with the principal axes for the harmonic approximation, and (200), (020), (002), and (000) are removed from the summation. Only anharmonic terms remain.

6.1.1.6.3. *Cumulant expansion*

In a cumulant expansion (Johnson & Levy, 1974), the entire series is expressed in exponential form. The cumulant expansion about $\mathbf{S} = 0$ for the generalized temperature factor is

$$T(\mathbf{S}) = \exp\left[1 + i\kappa^j S_j + \frac{i^2}{2!}\kappa^{jk} S_j S_k + \frac{i^3}{3!}\kappa^{jkl} S_j S_k S_l + \frac{i^4}{4!}\kappa^{jklm} S_j S_k S_l S_m + \ldots\right], \tag{6.1.1.63}$$

where the coefficient tensor $\kappa^{\alpha\beta\ldots\zeta}$, a symmetric tensor of order p, is the pth-order cumulant. The inverse Fourier transform is the Edgeworth expansion around the Gaussian p.d.f. Cumulants can be expressed in terms of moments and *vice versa*. The pth moment $\mu^{\alpha\beta\ldots\zeta}$ (if it exists) of a general p.d.f., $\rho(\mathbf{x})$, is a symmetric tensor defined as

$$\mu^{\alpha\beta\ldots\zeta}(\mathbf{x}) = \int_{-\infty}^{\infty} x^\alpha x^\beta \ldots x^\zeta \rho(\mathbf{x})\,\mathrm{d}\mathbf{x}. \tag{6.1.1.64}$$

The relations between the lower-order moments and cumulants are

$$\begin{aligned}
\mu^j &= \kappa^j \\
\mu^{jk} &= \kappa^{jk} + \kappa^j\kappa^k \\
\mu^{jkl} &= \kappa^{jkl} + \kappa^j\kappa^{kl} + \kappa^k\kappa^{lj} + \kappa^l\kappa^{jk} + \kappa^j\kappa^k\kappa^l \\
&= \kappa^{jkl} + 3\kappa^{(j}\kappa^{kl)} + \kappa^j\kappa^k\kappa^l \\
\mu^{jklm} &= \kappa^{jklm} + 3\kappa^{j(k}\kappa^{lm)} + 4\kappa^{(j}\kappa^{klm)} \\
&\quad + 6\kappa^{(j}\kappa^k\kappa^{lm)} + \kappa^j\kappa^k\kappa^l\kappa^m
\end{aligned} \tag{6.1.1.65}$$

and, conversely,

$$\begin{aligned}
\kappa^j &= \mu^j \\
\kappa^{jk} &= \mu^{jk} - \mu^j\mu^k \\
\kappa^{jkl} &= \mu^{jkl} - 3\mu^{(j}\mu^{kl)} + 2\mu^j\mu^k\mu^l \\
\kappa^{jklm} &= \mu^{jklm} - 3\mu^{j(k}\mu^{lm)} - 4\mu^{(j}\mu^{klm)} \\
&\quad + 12\mu^{(j}\mu^k\mu^{lm)} - 6\mu^j\mu^k\mu^l\mu^m.
\end{aligned} \tag{6.1.1.66}$$

In the Gram–Charlier and Fourier-invariant expansions, the Fourier-transform relationship between the p.d.f. and the temperature factor to given order can be made exact. Each cumulant μ^{jkl} contributes to all higher-order quasi-moment terms and *vice versa*. Hence, a given cumulant expansion is to an extent arbitrarily truncated (Kuhs, 1983). Care is required when interpreting the coefficients (Zucker & Schulz, 1982).

On the other hand, the cumulant expansion has the advantage of yielding tractable expressions for the one-particle potential in the quantum regime (Mair, 1980*a*). In that regime, equation (6.1.1.36) for the one-particle potential is invalid, and the expressions relating $V(\mathbf{u})$ to $\rho(\mathbf{u})$ in the Gram–Charlier and Fourier-invariant expansions are cumbersome (Mair & Wilkins, 1976).

Coefficients obtained by applying least-squares methods to structure-factor equations related to the truncated cumulant expansions do not necessarily yield non-negative p.d.f.'s nor are the linear-term coefficients necessarily faithful representations of the mean. Caution must be exercised in interpreting the results.

All the methods are satisfactory in the case of rapidly converging potential series. The methods are equivalent up to λ^2 in the van Hove order parameter (Mair, 1980*b*). Difficulties are encountered with convergence of the series in the case of strong anharmonicity, in which case numerical or alternative analytical models may be necessary. If the anharmonicity is such that the difference between the expansions is significant, it may be preferable to evaluate the Fourier transforms directly, as recommended by Mackenzie & Mair (1985).

6.1.1.6.4. *Curvilinear density functions*

For groups of atoms moving on the surface of a circle or sphere, perturbation expansions in Cartesian coordinates may converge slowly. Methods of representing curvilinear density functions that are multimodal or have large amplitude are described by Press & Hüller (1973).

For atoms constrained to rotate about a single axis,

$$a(\mathbf{u}) = \frac{1}{2\pi\tau}\delta(r-\tau)\delta(z)f(\varphi), \tag{6.1.1.67}$$

where r, z, φ are cylindrical coordinates for the displacement $\mathbf{u}$. Setting

$$f(\varphi) = \sum_{m=0} c_m \exp(im\varphi) + c_m^*(-im\varphi) \tag{6.1.1.68}$$

and

$$\exp(i\mathbf{S}\cdot\mathbf{r}) = \exp(iS_z z)\exp[iS_r r\cos(\varphi_S - \varphi)] \tag{6.1.1.69}$$

and using

$$\exp[iS_r r\cos(\varphi_S - \varphi)] = \sum_{l=0}(2-\delta_{l0})i^l J_l(S_r r)\cos[l(\varphi_S - \varphi)] \tag{6.1.1.70}$$

yields

$$T(\mathbf{S}) = \sum_{l=0} i^l J_l(S_r\tau)[c_l\exp(il\varphi_S) + c_l^*\exp(-il\varphi_S)]. \tag{6.1.1.71}$$

For atoms moving on the surface and a sphere, the density function may be written

$$\rho(\mathbf{u}) = \sum_{l=0}^{\infty} \sum_{j=1}^{2l+1} a_{lj}(u) K_{lj}(\theta, \varphi), \tag{6.1.1.72}$$

where u, θ, φ are spherical polar displacement coordinates and the K_{lj} are cubic harmonics. Thus, for a rigid molecule, the density function for nuclei confined to move on a spherical shell of radius τ is

$$a_{lj}(\mathbf{u}) = c_{lj}\delta(u - \tau)/u^2. \tag{6.1.1.73}$$

Expansion of $\exp(i\mathbf{S}\cdot\mathbf{r})$ in cubic harmonics

$$\exp(i\mathbf{S}\cdot\mathbf{r}) = 4\pi \sum_{l,j} i^l j_l(Sr) K_{lj}(\theta_S, \varphi_S) K_{lj}(\theta, \varphi) \tag{6.1.1.74}$$

leads to

$$T(\mathbf{S}) = 4\pi \sum_{l,j} i^l c_{lj} j_l(S\tau) K_{lj}(\theta_S, \varphi_S). \tag{6.1.1.75}$$

Equations (6.1.1.71) and (6.1.1.75) are useful when the p.d.f.'s (6.1.1.67) and (6.1.1.72) can be approximated by a limited number of significant terms. They are readily adapted to the case of oscillations about axes of symmetry (Press & Hüller, 1973).

6.1.1.6.5. *Model-based curvilinear density functions*

For rotational oscillations, which are the curvilinear coordinate analogues of the p.d.f.'s approximating harmonic rectilinear motion, techniques for evaluating the temperature factor are described by Johnson & Levy (1974).

The p.d.f. for an atom in a group of atoms undergoing large-amplitude rotational oscillation (libration) can sometimes be approximated satisfactory by a standard p.d.f. on the circle or on the sphere. The closest analogues of the rectilinear Gaussian p.d.f. are the Brownian-diffusion p.d.f.'s defined on the closed spaces of the circle and the sphere. For statistical analysis, two other p.d.f.'s, the von Mises 'circular normal' and the Fisher 'spherical normal', are often substituted for the Brownian-diffusion density functions because of their simpler forms.

The p.d.f. for Brownian diffusion on a circle, also called the 'wrapped normal' p.d.f. (Feller, 1966; Lévy, 1938), is given by

$$\rho(\theta) = \frac{1}{(2\pi)^{1/2}\sigma} \sum_{n=-\infty}^{\infty} \exp[-(\theta - 2n\pi)^2/2\sigma^2], \tag{6.1.1.76}$$

which may be transformed (Bellman, 1961) into

$$\rho(\theta) = \frac{1}{2\pi} \sum_{m=0}^{\infty} (2 - \delta_{m0}) \exp(-m^2\sigma^2/2) \cos(m\theta). \tag{6.1.1.77}$$

The von Mises p.d.f. (Gumbel, Greenwood & Durand, 1953; Mardin, 1972; von Mises, 1918) is

$$\rho(\theta) = \frac{\exp(k_c \cos\theta)}{2\pi I_o(k_c)} = \frac{1}{2\pi} \sum_{m=0}^{\infty} (2 - \delta_{m0}) \frac{I_m(k_c)}{I_0(k_c)} \cos(m\theta). \tag{6.1.1.78}$$

$I_m(x)$ is the mth-order Bessel function of the first kind with imaginary argument. The parameter σ^2 is the variance; k_c is a measure of concentration such that when k_c is zero the probability density is uniformly distributed over the circle, and when k_c is large the density is concentrated around the modal vector at $\theta = 0$. An approximate relation between σ^2 and k_c can be obtained by equating expressions for the centres of mass of the circular Brownian diffusion and von Mises p.d.f.'s (Stephens, 1963),

$$\exp(-\sigma^2/2) = \frac{I_1(k_c)}{I_0(k_c)}. \tag{6.1.1.79}$$

For small σ^2 (large k_c), we find that

$$\sigma^2 \simeq 1/k_c. \tag{6.1.1.80}$$

Equations (6.1.1.76) to (6.1.1.78) can be generalized to describe multimodal density functions with modes (maxima) arranged symmetrically about the circle. The p.d.f. for the s-modal Brownian-diffusion p.d.f. with one of the s modes at $\theta = \theta_0$ is

$$\begin{aligned}\rho(\theta) &= \frac{1}{\sqrt{2\pi}s\sigma} \sum_{m=-\infty}^{\infty} \exp[-(\theta - \theta_0 - 2\pi m/s)^2/2\sigma^2] \\ &= \frac{1}{2\pi} \sum_{m=0}^{\infty} (2 - \delta_{m0}) \exp[-(ms\sigma)^2/2] \cos[ms(\theta - \theta_0)].\end{aligned} \tag{6.1.1.81}$$

The two-dimensional Fourier transform (Chidambaram & Brown, 1973) of the last equation in terms of the polar coordinates (S, θ) of the reciprocal-space vector $\mathbf{S}$ relative to an origin at the centre of the circle is

$$T(\mathbf{S}) = \sum_{j=0}^{\infty} (2 - \delta_{j0}) i^{js} J_{js}(Sr) \exp[-(js\sigma)^2/2] \cos js\theta_0, \tag{6.1.1.82}$$

where $J_n(x)$ is the Bessel function of the first kind of order n with real argument. Corresponding equations for the von Mises s-modal density function (Atoji, Watanabe & Lipscomb, 1953; King & Lipscomb, 1950; Mardin, 1972) are

$$\begin{aligned}\rho(\theta) &= \frac{1}{2\pi I_o(K_c)} \exp[K_c \cos s(\theta - \theta_0)] \\ &= \frac{1}{2\pi} \sum_{m=0}^{\infty} (2 - \delta_{m0}) \frac{I_m(K_c)}{I_o(K_c)} \cos ms(\theta - \theta_0)\end{aligned} \tag{6.1.1.83}$$

and

$$T(\mathbf{S}) = \sum_{j=0}^{\infty} (2 - \delta_{j0}) i^{js} J_{js}(Sr) \frac{I_j(K_c)}{I_0(K_c)} \cos js\theta_0, \tag{6.1.1.84}$$

where K_c, a measure of concentration over $1/s$th of the circle about θ_0, is substituted for the k_c parameter of the unimodal von Mises density function and K_c is related to k_c approximately by

$$I_1(k_c)/I_0(k_c) = I_s(K_c)/I_0(K_c). \tag{6.1.1.85}$$

For symmetrical Brownian diffusion on a sphere (Furry, 1957; Lévy, 1938; Mardin, 1972; Perrin, 1928), the p.d.f. in terms of the angular displacement θ from the pole is

$$\rho(\theta) = \sum_{n=0}^{\infty} \frac{2n+1}{4\pi} \exp[-n(n+1)V] P_n(\cos\theta) \sin\theta, \tag{6.1.1.86}$$

where $P_n(x)$ is the nth-order Legendre polynomial. The Fisher (1953) 'spherical normal' p.d.f. (Mardin, 1972) is a similar density function given by

$$\begin{aligned}\rho(\theta) &= \frac{k_s}{4\pi \sinh k_s} \exp(k_s \cos\theta) \sin\theta \\ &= \sum_{n=0}^{\infty} \frac{(2n+1)}{4\pi} \frac{I_{n+1/2}(k_s)}{I_{1/2}(k_s)} P_n(\cos\theta) \sin\theta.\end{aligned} \tag{6.1.1.87}$$

The parameters V (variance) and k_s are measures of concentration analogous to those for the circle and may be related (Roberts & Ursell, 1960) by an equation analogous to (6.1.1.79),

$$\exp(-V/2) = \coth k_s - \frac{1}{k_s} = \frac{I_{3/2}(k_s)}{I_{1/2}(k_s)}, \quad (6.1.1.88)$$

the small V approximation being

$$V \simeq 2/k_s. \quad (6.1.1.89)$$

Equations (6.1.1.86) and (6.1.1.87) are generalized to place the mode of the density at (r, θ', φ') by replacing $\cos\theta$ by $\cos\theta\cos\theta' + \sin\theta\sin\theta'\cos(\varphi - \varphi')$ and by replacing $P_n(\cos\theta)$ by

$$P(\cos\theta)P_n(\cos\theta') + 2\sum_{m=1}^{n}\frac{(n-m)!}{(n-m)!} \times P_n^m(\cos\theta)P_n^m(\cos\theta')\cos m(\varphi - \varphi').$$

The three-dimensional Fourier transform of the generalized form of (6.1.1.86) in terms of $\mathbf{S}$ in spherical coordinates (S, θ_S, φ_S) is

$$T(\mathbf{S}) = \sum_{q=0}^{\infty} i^q \frac{(2q+1)}{r^2}\exp[-q(q+1)V] \times \sum_{s=0}^{\infty}\frac{4}{2p+1}Y_{qs+}(\theta', \varphi')Y_{qs+}(\theta_S, \varphi_S)j_q(Sr), \quad (6.1.1.90)$$

where r is the radius of the sphere, and j_n is the nth-order spherical Bessel function of the first kind. The real spherical harmonics Y_{lmp} are normalized as in (6.1.1.22).

The Fourier transform of the generalized form of (6.1.1.87) is identical to (6.1.1.90) except that the term $\exp[-q(q+1)V]$ in (6.1.1.90) is replaced by $I_{q+1/2}(k_s)/I_{1/2}(k_s)$.

The foregoing equations describe isotropic distributions on a sphere. The p.d.f. for general anisotropic Brownian diffusion (or rotation) on a sphere is not available in a convenient form. However, some of the results of Perrin (1934) and Favro (1960) on rotational Brownian motion are applicable to thermal motion. For example, the centre of mass of a p.d.f. resulting from anisotropic diffusion on a sphere is given by equation (6.8) of Favro (1960). The following equation valid in Cartesian coordinates is obtained if the diffusion tensor $\mathbf{D}$ of Favro's equation is replaced by the substitution $\mathbf{L} = 2\mathbf{D}$

$$\langle\mathbf{x}\rangle = \exp[-\tfrac{1}{2}(\mathrm{tr}(\mathbf{L})\mathbf{I} - \mathbf{L})]\mathbf{r} = \mathbf{r} - \tfrac{1}{2}[\mathrm{tr}(\mathbf{L})\mathbf{I} - \mathbf{L}]\mathbf{r} + \tfrac{1}{8}[\mathrm{tr}(\mathbf{L})\mathbf{I} - \mathbf{L}]^2\mathbf{r} - \ldots, \quad (6.1.1.91)$$

where $\mathbf{r}$ is the vector from the centre of the sphere to the mode of the p.d.f. on the sphere and $\langle\mathbf{x}\rangle$ is the vector to the centre of mass. This equation, which is valid for all amplitudes of libration $\mathbf{L}$, can be used to describe the apparent shrinkage effect in molecules undergoing librational motion.

6.1.1.6.6. *The quasi-Gaussian approximation for curvilinear motion*

The p.d.f.'s defined by (6.1.1.77), (6.1.1.78), (6.1.1.86) and (6.1.1.87), and their Fourier transforms given in §6.1.1.6.5 may be considered 'inverted series' since zero-order terms describe uniform distributions. The inverted series converge slowly if the density is concentrated near the mode. If σ^2 in (6.1.1.76) is sufficiently small, the cyclic overlap on the circle becomes unimportant and the summation for $n \neq 0$ can be neglected. In this limiting case, the p.d.f. assumes the same form as a one-dimensional rectilinear Gaussian density function except that the variable is the angle φ. A similar relation must exist between the p.d.f. on the sphere and the two-dimensional Gaussian function. This 'quasi-Gaussian' approximation is the basis for a number of structure-factor equations for atoms with relatively small amplitude components of curvilinear motion (Dawson, 1970; Kay & Behrendt, 1963; Kendall & Stuart, 1963; Maslen, 1968; Pawley & Willis, 1970).

6.1.1.7. *Structure factor*

The amplitude of coherent scattering from the contents of one unit cell in a crystalline material is the structure factor

$$F(\mathbf{S}) = \int \rho(\mathbf{r})\exp(i\mathbf{S}\cdot\mathbf{r})\,\mathrm{d}r, \quad (6.1.1.92)$$

where the integration extends over the unit cell. If there are N atoms in the cell, this may be expressed as

$$F(\mathbf{S}) = \sum_{j=1}^{N} f_j T_j \exp(i\mathbf{S}\cdot\mathbf{r}_j), \quad (6.1.1.93)$$

where $\mathbf{r}_j$ is the mean position and T_j is the temperature factor of the jth atom. In an ideal model of the scattering process in which (6.1.1.93) is exact, f_j is the atomic scattering factor derived from (6.1.1.7). In practice, there are wavelength-dependent changes to the amplitude and phase of the atom's scattering due to dispersion or resonance. To correct for this, each scattering factor may be written

$$f = f^0 + f' + if'', \quad (6.1.1.94)$$

where f^0 is the kinematic scattering factor and f' and f'' are real and imaginary corrections for dispersion.

6.1.1.8. *Reflecting power of a crystal*

The reflecting power of a small crystal of volume ΔV, rotated at angular velocity ω through a Bragg reflection, defined as the ratio of ω times the reflected energy to the incident-beam intensity, is

$$r_e^2\left(\frac{1+\cos^2 2\theta}{2\sin 2\theta}\right)\lambda^3\frac{F(\mathbf{S})^2}{V_C^2}\Delta V, \quad (6.1.1.95)$$

where V_c is the unit-cell volume. This expression, which assumes negligible absorption, shows that the integrated intensity is proportional to the crystal volume. The maximum intensity is proportional to $(\Delta V)^2$, but the angular width of the reflecting region varies inversely as ΔV.

In the kinematic theory of diffraction, it is assumed that the crystal is comprised of small domains of perfect crystals for which the intensities are additive. In that case, (6.1.1.95) applies also to finite crystals.

6.1.2. Magnetic scattering of neutrons (By P. J. Brown)

6.1.2.1. *Glossary of symbols*

m_n	Neutron mass
m_e	Electron mass
γ	Neutron magnetic moment in nuclear magnetons (-1.91)
μ_B	Bohr magneton
μ_N	Nuclear magneton
r_e	Classical electron radius $\mu_B e^2/4\pi m_e$
$\mathbf{P}_i$	Electron momentum operator
$\mathbf{S}_e$	Electron spin operator
$\mathbf{S}_n$	Neutron spin operator
$\mathbf{M}(r)$	Magnetization density operator
$\mathbf{k}$	Scattering vector $(H/2\pi)$
$\hat{\mathbf{k}}$	A unit vector parallel to $\mathbf{k}$
$\mathbf{r}_n$	A lattice vector
$\mathbf{g}$	A reciprocal-lattice vector $(h/2\pi)$
$\boldsymbol{\tau}$	Propagation vector for a magnetic structure

$\tilde{\mathbf{s}}_n$ A unit vector parallel to the neutron spin direction
q, q' Initial and final states of the scatterer
σ, σ' Initial and final states of the neutron
E_q Energy of the state q.

6.1.2.2. *General formulae for the magnetic cross section*

The cross section for elastic magnetic scattering of neutrons is given in the Born approximation by

$$\frac{\mathrm{d}\sigma}{\mathrm{d}\Omega} = \left(\frac{m_n}{2\pi\hbar}\right)^2 \left| \left\langle q'\sigma' \middle| \int V(\mathbf{R}) \exp(i\mathbf{k}\cdot\mathbf{R})\, \mathrm{d}\mathbf{R}^3 \middle| q\sigma \right\rangle \right|^2 \times \delta(E_q - E_{q'}). \quad (6.1.2.1)$$

$V(\mathbf{R})$ is the potential of a neutron at $\mathbf{R}$ in the field of the scatterer. If the field is due to N electrons whose positions are given by $\mathbf{r}_i$, $i = 1, N$, then

$$V(\mathbf{R}) = 4\gamma\mu_B\mu_N \left\{ \sum_{i=1}^{N} \frac{(\mathbf{R}-\mathbf{R}_i)\mathbf{P}_i}{|\mathbf{R}-\mathbf{r}_i|^3} \frac{\mathbf{S}_i}{|\mathbf{R}-\mathbf{r}_i|^3} + \frac{3\mathbf{S}_i\cdot(\mathbf{R}-\mathbf{r}_i)}{|\mathbf{R}-\mathbf{r}_i|^5} + 8\pi\mathbf{S}_i\delta(\mathbf{R}-\mathbf{r}_i) \right\} \cdot \mathbf{S}_n. \quad (6.1.2.2)$$

$V(\mathbf{R})$ is more simply written in terms of a *magnetization density* operator $\mathbf{M}(\mathbf{r})$, which gives the magnetic moment per unit volume at r due to both the electron's spin and orbital motions. The potential of (6.1.2.2) can then be written (Trammell, 1953)

$$V(\mathbf{R}) = \frac{2\gamma\mu_N\mathbf{S}_n}{\pi^2} \cdot \left\{ \int_0^\infty \int_0^\infty [\hat{\mathbf{k}} \times \mathbf{M}(\mathbf{r}) \times \hat{\mathbf{k}}] \times \exp[i\mathbf{k}\cdot(\mathbf{R}-\mathbf{r})]\, \mathrm{d}\mathbf{k}^3\, \mathrm{d}\mathbf{r}^3 \right\}, \quad (6.1.2.3)$$

giving for the cross section, from (6.1.2.1),

$$\frac{\mathrm{d}\sigma}{\mathrm{d}\Omega} = (\gamma r_e)^2 \left| \left\langle q\sigma' \middle| \mathbf{S}_n \cdot \int [\hat{\mathbf{k}} \times \mathbf{M}(\mathbf{r}) \times \hat{\mathbf{k}}] \times \exp(i\mathbf{k}\cdot\mathbf{r})\, \mathrm{d}\mathbf{r}^3 \middle| q\sigma \right\rangle \right|^2. \quad (6.1.2.4)$$

The *unit-cell magnetic structure factor* $M(\mathbf{k})$ is defined as

$$M(\mathbf{k}) = \left\langle q \middle| \int_{\text{unit cell}} \mathbf{M}(r) \exp(i\mathbf{k}\cdot\mathbf{r})\, \mathrm{d}\mathbf{r}^3 \middle| q \right\rangle. \quad (6.1.2.5)$$

For periodic magnetic structures,

$$\mathbf{M}(\mathbf{r}) = \sum_{\text{lattice vectors}} \mathbf{P}(\mathbf{r}_n\cdot\tau)\cdot\mathbf{M}_u(\mathbf{r}-\mathbf{r}_n),$$

where $\mathbf{P}$ is a periodic function with a period of unity, which describes how the magnitude and direction of the magnetization density, defined within one chemical unit cell by $\mathbf{M}_u(\mathbf{r})$, propagates through the lattice. The magnetic structure factor $\mathbf{m}(\mathbf{k})$ is then given by

$$\mathbf{m}(\mathbf{k}) = (g - j\tau)\mathbf{A}(j)\cdot\mathbf{M}(\mathbf{k}), \quad (6.1.2.6)$$

where $\mathbf{A}(j)$ is the jth term in the Fourier expansion of $\mathbf{P}$ defined by

$$\mathbf{P}(\mathbf{r}\cdot\tau) = \sum_{j=-\infty}^{\infty} \mathbf{A}(j)\exp\{i(j\tau\cdot\mathbf{r})\} \quad (6.1.2.7)$$

and the scattering cross section given in terms of the magnetic interaction vector $Q(\mathbf{k})$,

$$Q(\mathbf{k}) = \hat{\mathbf{k}} \times \mathbf{m}(\mathbf{k}) \times \hat{\mathbf{k}}, \quad (6.1.2.8)$$

is

$$\frac{\mathrm{d}\sigma}{\mathrm{d}\Omega} = (\gamma r_e)^2 |\langle\sigma'|\mathbf{S}_n\cdot\mathbf{Q}(\mathbf{k})|\sigma\rangle|^2. \quad (6.1.2.9)$$

Equation (6.1.2.9) leads to two independent scattering cross sections: one for scattering of the neutron with no change in spin state ($\sigma' = \sigma$) proportional to $|\mathbf{S}_n\cdot\mathbf{Q}(\mathbf{k})|^2$, and the other to scattering with a change of neutron spin ('spin flip scattering') proportional to $|\mathbf{S}_n \times \mathbf{Q}(\mathbf{k})|^2$. The sum over all final spin states gives

$$\frac{\mathrm{d}\sigma}{\mathrm{d}\Omega} = (\gamma r_e)^2 |\mathbf{Q}(\mathbf{k})|^2. \quad (6.1.2.10)$$

6.1.2.3. *Calculation of magnetic structure factors and cross sections*

If the magnetization within the unit cell can be assigned to independent atoms so that each has a total moment μ_i aligned in the direction of the axial unit vector $\hat{\mathbf{m}}_i$, then the unit-cell structure factor can be written

$$\mathbf{M}(\mathbf{k}) = \sum_j \sum_i \mathbf{T}_j\mathbf{R}_j\cdot\hat{\mathbf{m}}_i\mu_i f_i(k)\exp[i\mathbf{k}\cdot(\mathbf{R}_j\mathbf{r}_i + \mathbf{t}_j)]. \quad (6.1.2.11)$$

$\mathbf{R}_j$ and $\mathbf{t}_j$ are the rotations and translations associated with the jth element of the space group and $\mathbf{T}_j$ is an operator that reverses all the components of moment whenever the element j includes time reversal in the magnetic space group. $f_i(k)$ is the magnetic form factor of the ith atom (see Subsection 6.1.2.3).

The vector part of the magnetic structure factor can be factored out so that

$$\mathbf{m}(\mathbf{k}) \quad \text{becomes} \quad \hat{\mathbf{m}}[m(\mathbf{k})],$$

where $m(\mathbf{k})$ is now a scalar. For collinear structures, all the atomic moments are either parallel or antiparallel to $\hat{\mathbf{m}}$, which in this case is independent of $\mathbf{k}$. The intensity of a magnetic Bragg reflection is proportional to $|\mathbf{Q}(\mathbf{k})|^2$ and

$$|\mathbf{Q}(\mathbf{k})|^2 = 1 - (\hat{\mathbf{m}}\cdot\hat{\mathbf{k}})^2|m(\mathbf{k})|^2 = \sin^2\alpha|m(\mathbf{k})|^2 = q^2|m(\mathbf{k})|^2, \quad (6.1.2.12)$$

where α is the angle between the moment direction $\hat{\mathbf{m}}$ and the scattering vector $\mathbf{k}$. The factor $1 - (\hat{\mathbf{m}}\cdot\hat{\mathbf{k}})^2$, often referred to as q^2, is the means by which the moment direction in a magnetic structure can be determined from intensity measurements. If the intensities are obtained from measurements on polycrystalline samples then the average of q^2 over all the different $\mathbf{k}$ contributing to the powder line must be taken.

$$\overline{q^2} = 1 - \frac{1}{n_g}\sum_j (\mathbf{R}_j\hat{\mathbf{k}}\cdot\hat{\mathbf{m}})^2, \quad (6.1.2.13)$$

the sum being over all n_g rotations $\mathbf{R}_j$ of the point group. $\overline{q^2}$ is given for different crystal symmetries by Shirane (1959). For uniaxial groups, the result is

$$\overline{q^2} = 1 - \tfrac{1}{2}(\sin^2\Psi\sin^2\varphi - \cos^2\Psi\cos^2\varphi), \quad (6.1.2.14)$$

where Ψ and φ are the angles between the unique axis and the scattering vector and moment direction, respectively. For cubic groups $\overline{q^2} = 2/3$ independent of the moment direction and of the direction of $\mathbf{k}$.

6.1.2.4. *The magnetic form factor*

The magnetic form factor introduced in (6.1.2.11) is determined by the distribution of magnetization within a single atom. It can be defined by

$$f(\mathbf{k}) = \frac{\langle q| \int \mathbf{M}(\mathbf{r}) \exp(i\mathbf{k}\cdot\mathbf{r})\, \mathrm{d}r^3 |q\rangle}{\langle q| \int \mathbf{M}(\mathbf{r})\, \mathrm{d}r^3 |q\rangle}, \tag{6.1.2.15}$$

where q now represents a state of an individual atom.

In the majority of cases, the magnetization of an atom or ion is due to a single open atomic shell: the d shell for transition metals, the $4f$ shell for rare earths, and the $5f$ shell for actinides. Magnetic form factors are calculated from the radial wavefunctions of the electrons in the open shells. The integrals from which the form factors are obtained are

$$\langle j_l(k)\rangle = \int_0^\infty U^2(r) j_l(kr) 4\pi r^2\, \mathrm{d}r, \tag{6.1.2.16}$$

where $U(r)$ is the radial wavefunction for the atom and $j_l(kr)$ is the lth-order spherical Bessel function. Within the dipole approximation (spherical symmetry), the magnetic form factor is given by

$$f(k) = \langle j_0(k)\rangle + (1 - 2/g)\langle j_2(k)\rangle, \tag{6.1.2.17}$$

where g is the Landé splitting factor (Lovesey, 1984). Higher approximations are needed if the orbital contribution is large and to describe departures from spherical symmetry. They involve terms in $\langle j_4\rangle\langle j_6\rangle$ *etc*. Fig. 6.1.2.1 shows the integrals $\langle j_0\rangle$, $\langle j_2\rangle$, and $\langle j_4\rangle$ for Fe^{2+} and in Fig. 6.1.2.2 the spherical spin-only form factors $\langle j_0\rangle$ for $3d$, $4d$, $4f$, and $5f$ electrons are compared. Tables of magnetic form factors are given in Section 4.4.5.

6.1.2.5. *The scattering cross section for polarized neutrons*

The cross section for scattering of neutrons with an arbitrary spin direction is obtained from (6.1.2.9) but adding also nuclear scattering given by the nuclear structure factor $F(\mathbf{k})$, which is assumed to be spin independent. In this case,

$$\frac{\mathrm{d}\sigma}{\mathrm{d}\Omega} = \langle\sigma|(\gamma r_e)\mathbf{S}_n\cdot\mathbf{Q}(\mathbf{k}) + F(\mathbf{k})|\sigma\rangle^2, \tag{6.1.2.18}$$

the scattering without change of spin direction is

$$I^{++} \propto |F'(\boldsymbol{\kappa})|^2 + |\hat{\mathbf{s}}_n\cdot\mathbf{Q}(\mathbf{k})|^2 + \hat{\mathbf{s}}_n\cdot[\mathbf{Q}^*(\mathbf{k})F'(\mathbf{k}) + \mathbf{Q}(\mathbf{k})F'^*(\mathbf{k})], \tag{6.1.2.19}$$

and, for the spin flip scattering,

$$I^{+-} \propto [\hat{\mathbf{s}}_n\times\mathbf{Q}(\mathbf{k})]\cdot[\hat{\mathbf{s}}_n\cdot\mathbf{Q}^*(\mathbf{k})] + \hat{\mathbf{s}}_n\cdot[\mathbf{Q}(\mathbf{k})\times\mathbf{Q}^*(\mathbf{k})] \tag{6.1.2.20}$$

with $F'(\mathbf{k}) = F(\mathbf{k})/(\gamma r_e)$.

The cross section I^{++} implies interference between the nuclear and the magnetic scattering when both occur for the same $\mathbf{k}$. This interference is exploited for the production of polarized neutrons, and for the determination of magnetic structure factors using polarized neutrons.

In the classical method for determining magnetic structure factors with polarized neutrons (Nathans, Shull, Shirane & Andresen, 1959), the 'flipping ratio' R, which is the ratio between the cross sections for oppositely polarized neutrons, is measured:

$$R = \frac{|F'(\mathbf{k})|^2 + 2P\hat{\mathbf{s}}_n\cdot[\mathbf{Q}(\mathbf{k})F'^*(\mathbf{k}) + \mathbf{Q}^*(\mathbf{k})F'(\mathbf{k})] + |\mathbf{Q}(\mathbf{k})|^2}{|F'(\mathbf{k})|^2 - 2Pe\hat{\mathbf{s}}_n\cdot[\mathbf{Q}(\mathbf{k})F'^*(\mathbf{k}) + \mathbf{Q}^*(\mathbf{k})F'(\mathbf{k})] + |\mathbf{Q}(\mathbf{k})|^2}. \tag{6.1.2.21}$$

In this equation, $\hat{\mathbf{s}}_n$ is a unit vector parallel to the polarization direction. P is the neutron polarization defined as

$$P = (\langle S^+\rangle - \langle S^-\rangle)/(\langle S^+\rangle + \langle S^-\rangle),$$

where $\langle S^+\rangle$ and $\langle S^-\rangle$ are the expectation values of the neutron spin parallel and antiparallel to $\hat{\mathbf{s}}_n$ averaged over all the neutrons in the beam. e is the 'flipping efficiency' defined as $e = (2f - 1)$, where f is the fraction of the neutron spins that are reversed by the flipping process. Equation (6.1.2.21) is considerably simplified when both $F(\mathbf{k})$ and $\mathbf{Q}(\mathbf{k})$ are real and the polarization direction is parallel to the magnetization direction, as in a sample

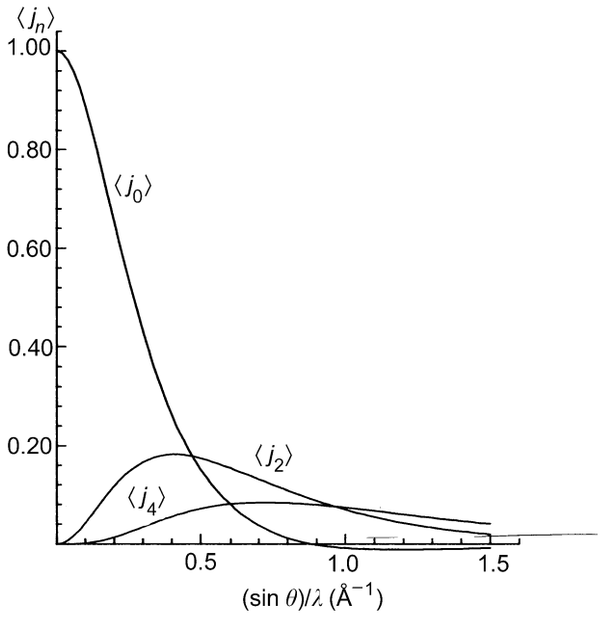

Fig. 6.1.2.1. The integrals $\langle j_0\rangle$, $\langle j_2\rangle$, and $\langle j_4\rangle$ for the Fe^{2+} ion plotted against $(\sin\theta)/\lambda$. The integrals have been calculated from wavefunctions given by Clementi & Roetti (1974).

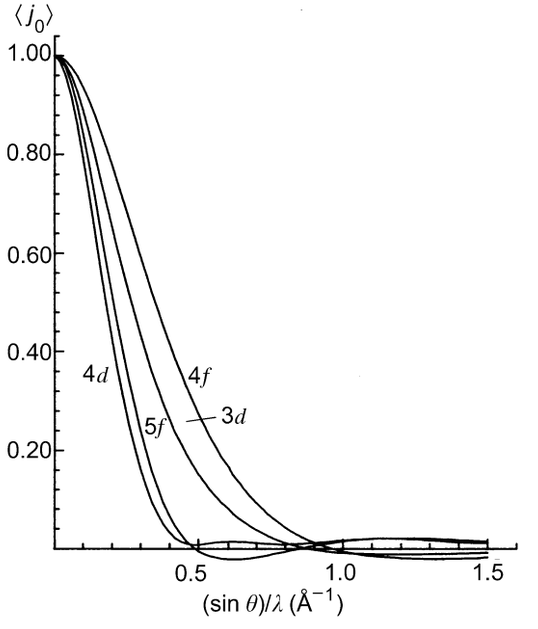

Fig. 6.1.2.2. Comparison of $3d$, $4d$, $4f$, and $5f$ form factors. The $3d$ form factor is for Co, and the $4d$ for Rh, both calculated from wavefunctions given by Clementi & Roetti (1974). The $4f$ form factor is for Gd^{3+} calculated by Freeman & Desclaux (1972) and the $5f$ is that for U^{3+} given by Desclaux & Freeman (1978).

magnetized by an external field. The 'flipping ratio' then becomes

$$R = \frac{1 + 2Py\sin^2\rho + y^2\sin^2\rho}{1 - 2Pey\sin^2\rho + y^2\sin^2\rho}, \tag{6.1.2.22}$$

with $y = (\gamma r_e)M(\mathbf{k})/F(\mathbf{k})$, ρ being the angle between the magnetization direction and the scattering vector. The solution to this equation is

$$y = \{P\sin\rho(Re+1) \pm [P^2\sin^2\rho(Re+1)^2 - (R-1)^2]^{1/2}\} \times [(R-1)\sin\rho]^{-1}; \tag{6.1.2.23}$$

the relative signs of $F(\mathbf{k})$ and $M(\mathbf{k})$ are determined by whether R is greater or less than unity. The uncertainty in the sign of the square root in (6.1.2.23) corresponds to not knowing whether $F(\mathbf{k}) > M(\mathbf{k})$ or *vice versa*.

6.1.2.6. *Rotation of the polarization of the scattered neutrons*

Whenever the neutron spin direction is not parallel to the magnetic interaction vector $\mathbf{Q}(\mathbf{k})$, the direction of polarization is changed in the scattering process. The general formulae for the scattered polarization are given by Blume (1963). The result for most cases of interest can be inferred by calculating the components of the scattered neutron's spin in the x, y, and z directions for a neutron whose spin is initially parallel to z. For simplicity, y is taken parallel to $\mathbf{k}$; x and z define a plane that contains $\mathbf{Q}(\mathbf{k})$. From (6.1.2.18),

$$\begin{aligned} S_x &= \tfrac{1}{2}\{[Q_z(\mathbf{k}) + F'(\mathbf{k})]Q_x^*(\mathbf{k}) \\ &\quad + [Q_z^*(\mathbf{k}) + F'^*(\mathbf{k})]Q_x(\mathbf{k})\}/N \\ S_y &= \frac{1}{2i}\{[Q_z(\mathbf{k}) + F'(\mathbf{k})]Q_x^*(\mathbf{k}) \\ &\quad - [Q_z^*(\mathbf{k}) + F'^*(\mathbf{k})]Q_x(\mathbf{k})\}/N \\ S_z &= \tfrac{1}{2}\{[Q_z(\mathbf{k}) + F'(\mathbf{k})][Q_z^*(\mathbf{k}) + F'^*(\mathbf{k})]\}/N \\ N &= |Q_z(\mathbf{k}) + F'(\mathbf{k})|^2 + |Q_x(\mathbf{k})|^2. \end{aligned} \tag{6.1.2.24}$$

It is clear from this set of equations that S_x and S_y are zero if $Q_x(\mathbf{k}) = 0$. Three simple cases may be taken as examples of the use of (6.1.2.24):

(*a*) A magnetic reflection from a simple antiferromagnet for which $\mathbf{Q}(\mathbf{k})$ is real, $F(k) = 0$; under these conditions,

$$\begin{aligned} S_x &= Q_x(\mathbf{k})[Q_z(\mathbf{k})]/|\mathbf{Q}(\mathbf{k})|^2 \\ S_y &= 0 \\ S_z &= \tfrac{1}{2}[Q_z(\mathbf{k})^2 - Q_x(\mathbf{k})^2]/|\mathbf{Q}(\mathbf{k})|^2, \end{aligned}$$

showing that the direction of polarization is turned through an angle 2φ in the xy plane where φ is the angle between $\mathbf{Q}(\mathbf{k})$ and the initial polarization direction.

(*b*) A satellite reflection from a magnetic structure described by a *circular helix* for which $Q_x(\mathbf{k}) = iQ_z(\mathbf{k}), F'(\mathbf{k}) = 0$; in this case,

$$\begin{aligned} S_x &= 0 \\ S_y &= Q_z^2(\mathbf{k})/|\mathbf{Q}(\mathbf{k})|^2 = \tfrac{1}{2} \\ S_z &= 0 \end{aligned}$$

and the scattered polarization is parallel to the scattering vector independent of its initial direction.

(*c*) A mixed magnetic and nuclear reflection from a Cr_2O_3-type antiferromagnet for which $\mathbf{Q}(\mathbf{k})$ is imaginary, $\mathbf{Q}(\mathbf{k}) = -\mathbf{Q}^*(\mathbf{k})$, $F(\mathbf{k})$ is real. Then,

$$\begin{aligned} S_x &= Q_x(\mathbf{k})Q_z(\mathbf{k})/[F'(\mathbf{k})^2 + |\mathbf{Q}(\mathbf{k})|^2] \\ S_y &= iF(\mathbf{k})Q_x(\mathbf{k})/[F'(\mathbf{k})^2 + |\mathbf{Q}(\mathbf{k})|^2] \\ S_z &= \tfrac{1}{2}[|Q_z(\mathbf{k}) + F'(\mathbf{k})|^2 - |Q_x(\mathbf{k})|^2] \\ &\quad \times [F'(\mathbf{k})^2 + |\mathbf{Q}(\mathbf{k})|^2]^{-1} \end{aligned}$$

so that in this case the final polarization has components along all three directions.

6.1.3. Nuclear scattering of neutrons (By B. T. M. Willis)

6.1.3.1. *Glossary of symbols*

b	Bound nuclear scattering length
b_{free}	Free nuclear scattering length
b_0	Potential scattering length
b', b''	Real and imaginary parts of resonant scattering length
b_{coh}	Coherent scattering length
$F(\mathbf{h})$	Structure factor for nuclear Bragg scattering
$2\pi\mathbf{h}$	Reciprocal-lattice vector
$\mathbf{H}$	Scattering vector ($= \mathbf{k} - \mathbf{k}_0$)
I	Nuclear spin
$\mathbf{k}$	Wavevector of scattered neutron
$\mathbf{k}_0$	Wavevector of incident neutron
M	Nuclear mass
m_n	Neutron mass
N	Number of unit cells in crystal
V	Volume of unit cell
W_j	Exponent of temperature factor $\exp(-W_j)$ of jth atom
w_+	Weight of spin state $I + \frac{1}{2}$
w_-	Weight of spin state $I - \frac{1}{2}$
σ_{coh}	Coherent scattering cross section
σ_{inc}	Incoherent scattering cross section
σ_{tot}	Total scattering cross section ($= \sigma_{\text{coh}} + \sigma_{\text{inc}}$)
$\left(\frac{\mathrm{d}\sigma}{\mathrm{d}\Omega}\right)_{\text{coh,el}}$	Differential coherent elastic scattering cross section
$\left(\frac{\mathrm{d}\sigma}{\mathrm{d}\Omega}\right)_{\text{inc,el}}$	Differential incoherent elastic scattering cross section

The nucleus is the fundamental unit involved in the scattering of neutrons by atoms. For magnetic materials, electronic scattering takes place as well (see Section 6.1.2). Apart from these two main interactions, there are a number of subsidiary ones (Shull, 1967) that are extremely weak and can be ignored in nearly all diffraction studies.

In this section, we discuss the neutron–nucleus interaction only, starting from scattering by a single nucleus, then scattering by an atom, and finally scattering by a single crystal. For a more detailed account, see Bacon (1975).

6.1.3.2. *Scattering by a single nucleus*

The nuclear forces giving rise to the scattering of neutrons have a range of 10^{-14} to 10^{-15} m. This is much smaller than the wavelength of thermal neutrons, and so (from elementary diffraction theory) the neutron wave scattered by the nucleus is spherically symmetrical. Unlike magnetic scattering, there is no 'form-factor' dependence of nuclear scattering on the scattering angle.

The incident neutron beam can be represented by the plane wave

$$\psi_0 = \exp(i\mathbf{k}_0 \cdot \mathbf{r}),$$

with $\mathbf{k}_0$ denoting the wavevector of the neutron and $\mathbf{r}$ its position relative to the nucleus. Then, for a nucleus of zero spin, the wavefunction of the scattered neutron is

$$\psi_s = -\frac{b}{r}\exp(ik_0 r).$$

b is the *bound nuclear scattering length* or *nuclear scattering amplitude*, and the negative sign ensures that b is positive for hard-sphere or potential scattering.

If the nucleus is free to recoil under the impact of the neutron, as in a gas, the scattering must be treated in the centre-of-mass system. The *free scattering length* is related to the bound scattering length b in condensed matter by

$$b_{\text{free}} = \frac{M}{m_n + M} b,$$

where M is the nuclear mass and m_n the mass of the neutron. For hydrogen, ^{1}H, the free scattering length is one half the bound scattering length, but the difference between the two rapidly diminishes for heavier nuclei.

In general, b is a complex quantity:

$$b = b_0 + b' + ib''. \qquad (6.1.3.1)$$

b_0 is the scattering length associated with potential scattering, *i.e.* scattering in which the nucleus behaves like an impenetrable sphere. b' and b'' are the real and imaginary parts of the resonance scattering that takes place with the formation of a compound nucleus (nucleus plus neutron). Resonance scattering is only significant when the excitation energy of the neutron is close to an energy level of the compound nucleus. This occurs for relatively few nuclei, *e.g.* ^{113}Cd, ^{149}Sm, ^{157}Gd, ^{176}Lu, and b then varies rapidly with wavelength (Fig. 6.1.3.1). The phenomenon of resonance scattering has been used to phase neutron reflections (Schoenborn, 1975), but one difficulty is the strong absorption arising from the imaginary component b''. For the majority of nuclei, the compound nucleus is not formed near resonance: the imaginary component is small, and the scattering length is independent of the neutron wavelength.

There is confusion in the literature regarding the appropriate signs for the real and imaginary parts of the scattering amplitude (Ramaseshan, Ramesh & Ranganath, 1975). The scattering-length curves in Fig. 6.1.3.1 have been drawn to be consistent with the structure-factor formulae in Volume A (*IT* A, 1983).

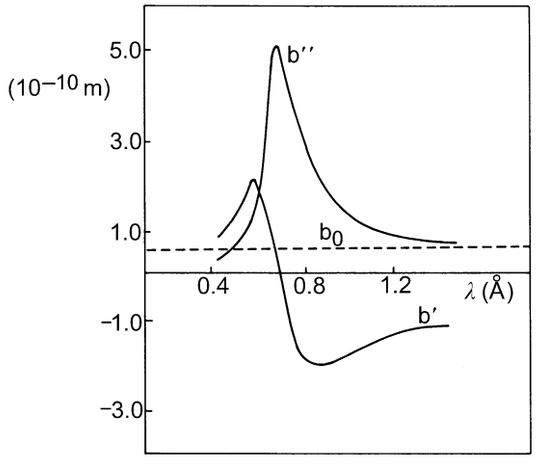

Fig. 6.1.3.1. Dependence on neutron wavelength of the coherent scattering length of ^{113}Cd. b_0 is the potential scattering component, and b' and b'' the real and imaginary components of the resonance scattering. The resonance wavelength is 0.68 Å.

Consider now the scattering from a nucleus with non-zero spin I. The neutron has spin $\frac{1}{2}$, and the spin of the combined nucleus–neutron system is either $I + \frac{1}{2}$ or $I - \frac{1}{2}$. Each spin state has its own scattering length, b_+ or b_-, and the weights of these states (for scattering unpolarized neutrons) are

$$w_+ = \frac{I+1}{2I+1} \qquad (6.1.3.2a)$$

and

$$w_- = \frac{I}{2I+1}. \qquad (6.1.3.2b)$$

Values of b_+ and b_- have been determined experimentally for just a few nuclei with non-zero spin: ^{1}H, ^{2}H, ^{23}Na, ^{59}Co, ...

6.1.3.3. *Scattering by a single atom*

For a single element containing several isotopes, each isotope has its own characteristic scattering length(s). The mean value of the scattering length of the atom is obtained by averaging (where necessary) over the two spin states of the isotope:

$$\langle b\rangle_{\text{isotope}} = w_+ b_+ + w_- b_-,$$

where the angle brackets indicate a mean and w_+ and w_- are given by (6.1.3.2); $\langle b\rangle_{\text{isotope}}$ is then averaged over all isotopes, taking into account their relative abundance. The resultant quantity, $\langle b\rangle^{\text{all}}_{\text{isotopes}}$, is known as the *coherent scattering length* of the atom, denoted b_{coh}. b_{coh} plays the same role in neutron scattering as the atomic scattering factor f in X-ray scattering. Table 4.4.4.1 lists the coherent scattering lengths for the atoms in the Periodic Table.

The coherent scattering cross section of an atom is

$$\sigma_{\text{coh}} = 4\pi b_{\text{coh}}^2.$$

It represents that part of the *total scattering cross section*, σ_{tot}, that gives interference effects with other atoms. The total cross section is

$$\sigma_{\text{tot}} = 4\pi\langle b^2\rangle^{\text{all}}_{\text{isotopes}},$$

and the *incoherent scattering cross section*, σ_{inc}, is the difference between σ_{tot} and σ_{coh}:

$$\sigma_{\text{inc}} = 4\pi\left[\langle b^2\rangle - \langle b\rangle^2\right].$$

In incoherent scattering, there is no phase relationship between the waves scattered by different atoms. σ_{inc} for hydrogen is 40 times larger than σ_{coh}, but the proportion of coherent scattering is substantially increased by deuteration. The scattering from vanadium is almost entirely incoherent, and so it is useful as a container of polycrystalline samples.

6.1.3.4. *Scattering by a single crystal*

The scattering from a single crystal can be either elastic or inelastic. An elastic process is one in which there is no exchange of energy between the neutron and the target nucleus. In an inelastic process, energy exchange occurs, giving rise to the creation or annihilation of elementary excitations such as phonons [see Section 4.1.1 of Volume B (*IT* B, 1992)]. Here we shall be concerned only with elastic Bragg scattering.

If kinematic scattering conditions are assumed, the differential cross section, $(\mathrm{d}\sigma/\mathrm{d}\Omega)_{\text{coh,el}}$, giving the probability of coherent elastic scattering by a single crystal into the solid angle $\mathrm{d}\Omega$, is

$$\left(\frac{\mathrm{d}\sigma}{\mathrm{d}\Omega}\right)_{\text{coh,el}} = N\frac{(2\pi)^3}{V}\sum_{\mathbf{h}}\left|F(\mathbf{h})\right|^2\delta(\mathbf{H}-2\pi\mathbf{h}). \qquad (6.1.3.3)$$

Here, N is the number of unit cells, each of volume V, $2\pi\mathbf{h}$ is a reciprocal-lattice vector, and $F(\mathbf{h})$ is the *nuclear structure factor* for Bragg scattering. $\mathbf{H}$ is the scattering vector

$$\mathbf{H} = \mathbf{k} - \mathbf{k}_0,$$

where $\mathbf{k}$ and $\mathbf{k}_0$ (with $k = k_0 = 2\pi/\lambda$) are the wavevectors of the scattered and incident beams, respectively, and the δ function indicates that the coherent elastic scattering is simply Bragg scattering. $F(\mathbf{h})$ is defined by

$$F(\mathbf{h}) = \sum_j b^j_{\text{coh}} \exp\bigl(i\mathbf{H}\cdot\mathbf{r}_j\bigr) \exp\bigl(-W_j\bigr),$$

in which b^j_{coh} is the coherent scattering length of the jth atom in the unit cell, $\mathbf{r}_j$ is its equilibrium position with respect to the cell origin, and $\exp\bigl(W_j\bigr)$ its Debye–Waller temperature factor.

The incoherent elastic scattering cross section is given by

$$\left(\frac{\mathrm{d}\sigma}{\mathrm{d}\Omega}\right)_{\text{inc,el}} = N\sum_j \Bigl[\bigl\langle b_j^2\bigr\rangle - \bigl\langle b_j\bigr\rangle^2\Bigr] \exp\bigl(-2W_j\bigr).$$

Apart from the influence of the Debye–Waller temperature factor, this expression shows that the incoherent scattering is distributed uniformly throughout reciprocal space.

International Tables for Crystallography (2006). Vol. C, Chapter 6.2, pp. 596–598.

6.2. Trigonometric intensity factors

By H. Lipson, J. I. Langford and H.-C. Hu

6.2.1. Expressions for intensity of diffraction

The expressions for the intensity of diffraction of X-rays contain several trigonometrical factors. The earlier series of *International Tables* (Kasper & Lonsdale, 1959, 1972) gave extensive tables of these functions, but such tables are now unnecessary, as the functions are easily computed. In fact, many crystallographers can ignore the trigonometric factors entirely, as they are built into 'black-box' data-processing programs. The formulae for single-crystal reflections (*b*) and (*c*) of Table 6.2.1.1 in the previous edition (Lipson & Langford, 1998) list only the integrated reflection power ratio (*i.e.* integrated reflection) under the strong absorption case. The revised formulae given here include both the reflection power ratio and the integrated reflection power ratio for a crystal slab of finite thickness with any values of the ratio of the absorption to the diffraction cross sections and under all possible kinds of diffraction geometry.

A conspectus of the expressions for the intensity of diffraction as recorded by various techniques, including the fundamental constants as well as the trigonometric factors, is given in Table 6.2.1.1. Details of the techniques are given elsewhere in this volume (Chapters 2.1–2.3) and in textbooks, such as those of Arndt & Willis (1966) for single-crystal diffractometry and Klug & Alexander (1974) for powder techniques. Notes on individual factors follow.

6.2.2. The polarization factor

X-rays are an electromagnetic radiation, and the amplitude with which they are scattered is proportional to the sine of the angle between the direction of the electric vector of the incident radiation and the direction of scattering. Synchrotron radiation is practically plane-polarized, with the electric vector in the plane of the ring, but the radiation from an ordinary X-ray tube is unpolarized, and it may thus be regarded as consisting of two equal parts, half with the electric vector in the plane of scattering, and half with the electric vector perpendicular to this plane. For the latter, the relevant angle is $\pi/2$, and for the former it is $(\pi/2) - 2\theta$. The intensity is proportional to the square of the amplitude, so that the polarization factor – really the non-polarization factor – is

$$\{\sin^2(\pi/2) + \sin^2[(\pi/2) - 2\theta)]\}/2 = (1 + \cos^2 2\theta)/2. \quad (6.2.2.1)$$

If the radiation has been 'monochromatized' by reflection from a crystal, it will be partially polarized, and the two parts of the beam will be of unequal intensity. The intensity of reflection then depends on the angular relations between the original, the reflected, and the scattered beams, but in the commonest arrangements all three are coplanar. The polarization factor then becomes

$$(1 + A\cos^2 2\theta)/(1 + A), \quad (6.2.2.2)$$

where

$$A = \cos^2 2\theta_M \quad (6.2.2.3)$$

and θ_M is the Bragg angle of the monochromator crystal. The expression (6.2.2.2) may be substituted for (6.2.2.1) in Table 6.2.1.1 whenever appropriate.

6.2.3. The angular-velocity factor

In experiments where the crystal is rotated or oscillated, reflection of X-rays takes place as a reciprocal-lattice point moves through the surface of the sphere of reflection. The intensity is thus proportional to the time required for the transit of the point through the surface, and so is inversely proportional to the component of the velocity perpendicular to the surface. In most experimental arrangements – the precession camera (Buerger, 1944) is an exception – the crystals move with a constant angular velocity, and the perpendicular component of the velocity varies in an easily calculable way with the 'latitude' of the reciprocal-lattice point referred to the axis of rotation. If the reciprocal-lattice point lies in the equatorial plane and the radiation is monochromatic – the most important case in practice – the angular-velocity factor is

$$\operatorname{cosec} 2\theta. \quad (6.2.3.1)$$

If the latitude of the reciprocal-lattice point is φ, a somewhat more complex calculation shows that the factor becomes

$$\operatorname{cosec}\theta(\cos^2\varphi - \sin^2\theta)^{1/2}. \quad (6.2.3.2)$$

For $\varphi = 0$, the expression (6.2.3.2) reduces to (6.2.3.1). In some texts, φ is used for the co-latitude; this and various trigonometric identities can give superficially very different appearances to (6.2.3.2).

6.2.4. The Lorentz factor

There has been some argument over the meaning to be attached to the term *Lorentz factor*, probably because Lorentz did not publish his results in the ordinary way; they appear in a note added in proof to a paper on temperature effects by Debye (1914). Ordinarily, *Lorentz factor* is used for the trigonometric part of the angular-velocity factor, or its equivalent, if the sample is stationary. (See below).

6.2.5. Special factors in the powder method

In the powder method, all rays diffracted through an angle 2θ lie on the surface of a cone, and in the absence of preferred orientation the diffracted intensity is uniformly distributed over the circumference of the cone. The amount effective in blackening film, or intercepted by the receiving slit of a diffractometer, is thus inversely proportional to the circumference of the cone, and directly proportional to the fraction of the crystallites in a position to reflect. When allowance is made for these geometrical factors, it is found that for the Debye–Scherrer and diffractometer arrangements the intensity is proportional to

$$p'' \operatorname{cosec}\theta, \quad (6.2.5.1)$$

where p'' is the multiplicity factor (the number of permutations of *hkl* leading to the same value of θ). For the flat-plate front-reflection arrangement, the variation becomes

$$p'' \cos 2\theta \operatorname{cosec}\theta. \quad (6.2.5.2)$$

Combining the polarization, angular-velocity, and special factors gives a trigonometric variation of

$$p''(1 + \cos^2 2\theta)\sec\theta \operatorname{cosec}^2\theta \quad (6.2.5.3)$$

Copyright © 2006 International Union of Crystallography

Table 6.2.1.1. *Summary of formulae for integrated powers of reflection*

(*a*) Crystal element

$$\rho = Q\delta V$$

$$Q = \frac{N^2 e^4 \lambda^3}{2m^2 c^4} \frac{1+\cos^2 2\theta}{\sin 2\theta} |F|^2 \qquad \text{for non-polarized X-rays}$$

$$Q = \frac{N^2 \lambda^3}{\sin 2\theta} |F|^2 \qquad \text{for neutrons}$$

(*b*) Reflection from a crystal slab of thickness t

$$\sigma = QW(\Delta\theta_0)$$
$$\xi = \mu/\sigma$$

1. Symmetrical Bragg geometry

$$P_H/P_0 = (\sigma t \operatorname{cosec}\theta)/(1+\sigma t \operatorname{cosec}\theta) \qquad \text{for } \mu = 0$$

$$P_H/P_0 = \{1 - \exp[-2(\xi^2+2\xi)^{1/2}\sigma t \operatorname{cosec}\theta]\}\{(\xi^2+2\xi)^{1/2} + \xi + 1 + [(\xi^2+2\xi)^{1/2} - (\xi+1)] \times \exp[-2(\xi^2+2\xi)^{1/2}\sigma t \operatorname{cosec}\theta]\}^{-1} \qquad \text{for } \mu \neq 0$$

$$\rho' = \frac{Q[1-\exp(-2\mu t \operatorname{cosec}\theta)]}{2\mu} \qquad \text{for } \mu/\sigma_0 >> 1$$

2. Asymmetrical Bragg geometry, when the reflecting planes are inclined at an angle φ to the crystal surface, and the surface normal is in the plane of the incident and reflected beams.

$$\tau = \sigma t \operatorname{cosec}(\theta+\varphi)$$
$$b = -\sin(\theta+\varphi)/\sin(\theta-\varphi)$$

angle of incidence $(\theta+\varphi)$ and angle of emergence $(\theta-\varphi)$ to the crystal surface

$$\frac{P_H}{P_0} = \frac{1-\exp[-|1+b|\operatorname{cosec}(\theta+\varphi)\sigma t]}{1-|b|\exp[-|1+b|\operatorname{cosec}(\theta+\varphi)\sigma t]} \qquad \text{for } |b|<1, \varphi<0^\circ \text{ and } \mu = 0$$

$$\frac{P_H}{P_0} = \frac{1-\exp[-|1+b|\operatorname{cosec}(\theta+\varphi)\sigma t]}{|b|-\exp[-|1+b|\operatorname{cosec}(\theta+\varphi)\sigma t]} \qquad \text{for } |b|>1, \varphi>0^\circ \text{ and } \mu = 0$$

Define $u = [(1-b)^2(\xi+1)^2 + 4b]^{1/2}$ and $v = (1-b)(\xi+1)$:

$$\frac{P_H}{P_0} = \frac{2[1-\exp(-u\tau)]}{(u+v)+(u-v)\exp(-u\tau)} \qquad \text{for } \mu \geq 0$$

$$\rho' = Q\{1-\exp[-(1-b)\mu t \operatorname{cosec}(\theta+\varphi)]\}[(1-b)\mu]^{-1} = \frac{Q}{2\mu}(1-\cot\theta\tan\varphi)\left\{1-\exp\left[-\frac{2\mu t \operatorname{cosec}(\theta+\varphi)}{1-\cot\theta\tan\varphi}\right]\right\} \qquad \text{for } \mu/\sigma_0 >> 1$$

(*c*) Transmission from a crystal slab of thickness t

1. Symmetrical Laue geometry

$$P_H/P_0 = \exp(-\xi\sigma t \sec\theta)[1-\exp(-2\sigma t\sec\theta)]/2 \qquad \text{for } \mu \geq 0$$

$$\rho' = Qt\sec\theta\exp(-\mu t\sec\theta) \qquad \text{for } \mu/\sigma_0 >> 1$$

2. Asymmetrical Laue geometry, when the reflecting planes are at $\pi/2-\varphi$ to the crystal surface, with the normal in the plane of the incident and reflected beams.

$$\tau = \sigma t \sec(\theta-\varphi)$$
$$b = \sec(\theta+\varphi)/\sec(\theta-\varphi)$$

angle of incidence $(\theta+\varphi)$ and angle of emergence $(\theta-\varphi)$ to the normal to the crystal surface

$$P_H/P_0 = (1-\tan\theta\tan\varphi)\{1-\exp[-\sec(\theta+\varphi)\sigma t - \sec(\theta-\varphi)\sigma t]\}/2 \qquad \text{for } \mu = 0$$

Define $u = [(1-b)^2(\xi+1)^2+4b]^{1/2}$ and $w = (1+b)(\xi+1)$

$$\frac{P_H}{P_0} = \{\exp[-(w-u)\tau/2] - \exp[-(w+u)\tau/2]\}/u \qquad \text{for } \mu \geq 0$$

$$\rho' = \frac{Q}{(1-b)\mu}\{\exp[-\mu t\sec(\theta+\varphi)] - \exp[-\mu t\sec(\theta-\varphi)]\} = \frac{Q}{\left[1-\frac{\sec(\theta+\varphi)}{\sec(\theta-\varphi)}\right]\mu}\{\exp[-\mu t\sec(\theta+\varphi)] - \exp[-\mu t\sec(\theta-\varphi)]\} \qquad \text{for } \mu/\sigma_0 >> 1$$

(*d*) Powder halo: no absorption correction included

$$\frac{P}{I_0} = \frac{Qp''V\cos\theta}{2} = \frac{N^2e^4\lambda^3V}{8m^2c^4}\frac{1+\cos^2 2\theta}{\sin\theta}p''|F|^2,$$

where P is the diffracted power.

(*e*) Debye–Scherrer lines on cylindrical film: no absorption correction included

$$\frac{P_l}{I_0} = \frac{Qp''lV}{8\pi r\sin\theta} = \frac{N^2e^4\lambda^3lV}{32\pi m^2c^4r}\frac{1+\cos^2 2\theta}{\sin^2\theta\cos\theta}p''|F|^2,$$

where l is the length of line measured and r is the radius of the camera. P_l is the power reflected into length l.

(*f*) Reflection from a thick block of powdered crystal of negligible transmission

$$\frac{P_l}{I_0} = \frac{Qp''l}{16\pi\mu r\sin\theta} = \frac{N^2e^4\lambda^3l}{64\pi m^2c^4\mu r}\frac{1+\cos^2 2\theta}{\sin^2\theta\cos\theta}p''|F|^2$$

(*g*) Transmission through block of powdered crystal of thickness t

$$\frac{P}{I_0} = \frac{Qp''lt}{4\pi r\sin 2\theta}\frac{\delta'}{\delta} = \frac{N^2e^4\lambda^3}{8\pi m^2c^4r}\frac{lt\delta'}{\delta}\frac{1+\cos^2 2\theta}{\sin^2 2\theta}p''|F|^2,$$

where δ', δ are the densities of the block of powder and of the crystal in bulk, respectively.

(*h*) Rotation photograph of small crystal, volume V

1. Beam normal to axis

$$\rho = \frac{QVp'}{2\pi(\cos^2\varphi - \sin^2\theta)^{1/2}} = \frac{N^2e^4\lambda^3V}{4\pi m^2c^4}\frac{1+\cos^2\theta}{\sin 2\theta}\frac{\cos\theta}{(\cos^2\varphi-\sin^2\theta)^{1/2}}p'|F|^2$$

2. Equi-inclination Weissenberg photograph

$$\rho = \frac{QV}{2\pi\xi\cos\theta}\frac{N^2e^4\lambda^3V}{4\pi m^2c^4}\frac{1+\cos^2 2\theta}{\xi\cos\theta}|F|^2$$

Absorption is neglected in both (*g*) and (*h*)

Symbols

Q	Integrated reflection from a crystal of unit volume
δV	Volume of crystal element
e, m	Electronic charge and mass

Table 6.2.1.1. *Summary of formulae for integrated powers of reflection (cont.)*

Symbols	
c	Speed of light
λ	Wavelength of radiation
μ	Linear absorption coefficient for X-rays or total attenuation coefficient for neutrons
2θ	Angle between incident and diffracted beams
φ	In (*b*) and (*c*), as defined; in (*h*), latitude of reciprocal-lattice point relative to axis of rotation
V	Volume of crystal, or of irradiated part of powder sample
N	Number of unit cells per unit volume
ξ	In (*b*) and (*c*), as defined; in (*h*), radial coordinate *xi* used in interpreting Weissenberg photographs
I_0	Energy of radiation falling normally on unit area per second
hkl	Indices of reflection
F	Structure factor of *hkl* reflection
$W(\Delta\theta_0)$	Distribution function of the mosaic blocks at angular deviation $\Delta\theta_0$ from the average reflecting plane
σ	Diffraction cross section per unit volume
σ_0	Diffraction cross section per unit volume at $\Delta\theta_0 = 0$
b	Asymmetry parameter
τ	Reduced thickness of the crystal slab
P_H/P_0	Reflection power ratio, *i.e.* the ratio of diffracted power to the incident power
ρ	Integrated reflection power ratio from a crystal element
ρ'	Integrated reflection power ratio, angular integration of reflection power ratio
p'	Multiplicity factor for single-crystal methods
p''	Multiplicity factor for powder methods

for the Debye–Scherrer and diffractometer arrangements, and

$$p''(1 + \cos^2 2\theta)\tan 2\theta \operatorname{cosec}\theta \qquad (6.2.5.4)$$

for the flat-plate front-reflection arrangement.

Nowadays, angle-dispersive experiments are normally carried out by stepping the sample and detector in small angular increments, both being stationary while the intensity at each step is recorded. The Lorentz factor for a random powder sample is then of the form $p''(\cos\theta \sin^2\theta)^{-1}$. The factor $\cos\theta$ arises from the fact that spherical shells of diffracted intensity in reciprocal space intersect the Ewald sphere at an angle that depends on θ, and the surface area of the shells increases as d^{*2}, which is emobodied in the factor $\sin^2\theta$. It turns out that this factor is equivalent to a combination of the polarization factor (6.2.2.1), the angular-velocity factor (6.2.3.1) and (6.2.5.1), and the form of (6.2.5.3) is thus unchanged.

6.2.6. Some remarks about the integrated reflection power ratio formulae for single-crystal slabs

The transfer equations for intensity may be rewritten in the form of one-dimensional power transfer equations (Hu & Fang, 1993). The P_H/P_0 in (*b*) and (*c*) for a mosaic crystal slab under symmetrical and unsymmetrical Bragg and Laue geometries are the general solutions of power transfer equations employing three dimensionless parameters b, ξ and τ. For a crystal slab with a rectangular mosaic distribution, considering multiple reflection, the integrated reflection power ratio, ρ', can be obtained by substituting σ_0 for σ in the formulae for P_H/P_0 and multiplying the result by the mosaic width. However, for crystals with other kinds of mosaic distribution, the corresponding ρ' can be obtained only by integrating the expression for $P_H(\Delta\theta_0)/P_0$ over the whole range of $\Delta\theta_0$. Formulae (1)–(3) listed in Table 6.3.3.1, *i.e.* the transmission coefficient A multiplied by Q, QA, are identical to those of (*b*) and (*c*) for the case of $\mu/\sigma_0 >> 1$, which is the integrated reflection power ratio for a crystal slab based on the kinematic approximation without consideration of multiple reflection.

The secondary extinction factor for X-ray or neutron diffraction in a mosaic crystal slab can be obtained as $\rho'/(QA)$, in which the integrated reflection power ratio with consideration of multiple reflections can be obtained as described above.

Both the transmission power ratio P_T/P_0 and the absorption power ratio P_A/P_0 can also be obtained by solving the power transfer equations. For details, see Hu (1997*a*,*b*), Werner & Arrott (1965) and Werner, Arrott, King & Kendrick (1966).

6.2.7. Other factors

The various expressions in Table 6.2.1.1 contain $|F|^2$, the square of the modulus of the structure factor. The relation of F to the atomic scattering factors, the atomic positional coordinates, and the temperature is treated in Chapter 6.1.

For the factors relevant for the precession method (Buerger, 1944), see Waser (1951*a*,*b*), Burbank (1952), and Grenville-Wells & Abrahams (1952). For the de Jong–Bouman method, see Bouman & de Jong (1938) and Buerger (1940). For the retigraph, see Mackay (1960).

International Tables for Crystallography (2006). Vol. C, Chapter 6.3, pp. 599–608.

6.3. X-ray absorption

BY E. N. MASLEN

6.3.1. Linear absorption coefficient

When a monochromatic X-ray beam of intensity I_o travels a distance T through a homogeneous isotropic material, the intensity is reduced to a value

$$I = I_o \exp(-\mu T), \tag{6.3.1.1}$$

where μ is the total linear absorption coefficient. This expression can also be applied to X-ray absorption in crystalline solids provided the absorption is insensitive to the arrangement of the atoms in the unit cell. This holds to a good approximation in most cases. If it is assumed that the absorption processes are additive,

$$\mu = \frac{1}{V_c} \sum_{n=1}^{N_n} \sigma_n, \tag{6.3.1.2}$$

where V_c is the cell volume and there are N_n contributions to absorption per cell. σ_n is the absorption cross section for the nth contribution.

Of the processes that reduce the intensity of X-rays passing through matter, described in detail by Anderson (1984), photoelectric absorption, scattering, and extinction are important for the X-ray wavelengths used in crystallography.

6.3.1.1. *True or photoelectric absorption*

In photoelectric absorption, X-ray photons disappear completely. The absorption of each photon results in the ejection from the atom of an electron that carries excess energy away as kinetic energy. The corresponding linear photoelectric absorption cross section $\sigma_{\rm ph}$ is occasionally termed the cross section for 'fluorescence'.

Excitation of an electron from a low to a higher bound state also occurs. Such an electron can be excited only if the photon energy exceeds the gap to the nearest unoccupied level. For this reason, $\sigma_{\rm ph}$ varies abruptly in the manner shown in Fig. 6.3.1.1.

The probability of ejection of an electron is largest for a photon energy just sufficient for excitation. It is small if the energy greatly exceeds that required. With increasing atomic number Z, the absorption edges shift to shorter wavelengths. The ratio of the value of $\sigma_{\rm ph}$ for λ just below and just above the edge decreases with increasing Z, especially for the K edge.

The natural width of the resulting core-vacancy state sets a lower limit to the sharpness of the absorption edge (James, 1962). In some cases, such as the K edges for certain metals, the edge is substantially less sharp than that limit (Beeman & Friedman, 1939). Natural level widths are tabulated by Krause & Oliver (1979).

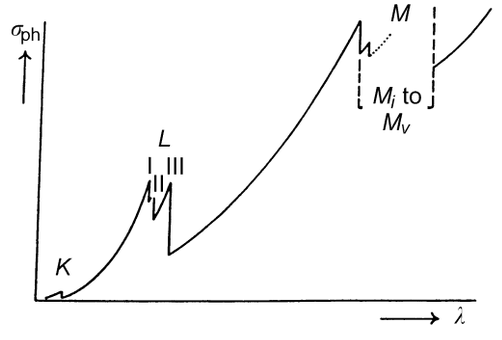

Fig. 6.3.1.1. Idealized diagram showing the variation of the photoelectric absorption coefficient $\sigma_{\rm ph}$ with wavelength λ.

The wavelength of the absorption edge for a given element shifts slightly with changes in the chemical environment of the absorbing atom. There is also fine structure in the absorption coefficient that depends, especially on the short-wavelength side, both on chemical composition and on temperature. The range of the larger effects in the fine structure is of the order of 10^{-3} Å for X-ray wavelengths of approximately 1 Å. This corresponds to a photon-energy range of tens of electron volts, whereas X-ray photon energies are of the order of 10 keV. Smaller effects in the fine structure cover a far greater range. These are observed in extended X-ray absorption fine structure (EXAFS) spectra up to 1 keV from the edge (see Section 4.2.3). However, these small terms are of limited relevance when measuring X-ray diffraction intensities.

6.3.1.2. *Scattering*

The X-ray photon is deflected from the original beam by collisions with atoms or electrons, the linear scattering cross section being $\sigma_{\rm sc}$. The total cross section

$$\sigma = \sigma_{\rm ph} + \sigma_{\rm sc} + \sigma', \tag{6.3.1.3}$$

where σ' is the combined cross section for all processes other than photoelectric absorption or scattering.

There are two types of scattering process, coherent (Rayleigh) scattering and incoherent (Compton) scattering as described in Section 6.1.1. Rayleigh scattering may be regarded as resulting from a collision between a photon and an atom as a whole. Because the effective mass of a photon is far less than that of an atom, the photon retains its original energy. In a frame with the atom at rest, the scattering is elastic – *i.e.* the photon wavelength is essentially unmodified.

Rayleigh scattering by isolated atoms increases monotonically with Z – the cross section is proportional to the square of the integral of the atomic scattering factor f. However, the photoelectric absorption cross section increases far more rapidly, so Rayleigh scattering is relatively more important for atoms with low atomic number.

The atomic Rayleigh cross sections decrease with λ. Although there are anomalies near absorption edges, these have a limited effect on σ because the Rayleigh scattering in these regions is small compared with the photoelectric cross section except for the lightest elements.

The cross section for Compton scattering depends on the state of the electrons involved in the collision, but for very short wavelengths the atomic Compton cross section is approximately proportional to the atomic number. It varies far more slowly with λ than either the photoelectric or the Rayleigh cross section.

6.3.1.3. *Extinction*

Because Rayleigh scattering is elastic, the scattering from different atoms may combine coherently, giving rise to interference, and hence to Bragg reflection from crystals.

For a crystal oriented so that there is no Bragg reflection, the interference reduces the scattered intensity far below the sum of the intensities that would be scattered by the atoms individually. For a strong Bragg reflection, on the other hand, the atomic scattering amplitudes add approximately in phase. The reduc-

Copyright © 2006 International Union of Crystallography

tion in incident-beam intensity is many times larger than the sum of the squares of the individual atomic scattering powers.

An extreme case occurs in a perfect crystal, for which total reflection is possible. There is destructive interference with the incident beam producing a marked change in the index of refraction from its normal value of

$$n = 1 - \frac{\lambda^2 e^2}{2\pi mc^2} \sum_a N_a f_a(0), \qquad (6.3.1.4)$$

where e and m are the charge and mass of the electron. $f_a(0)$ is the scattering factor in the forward direction for an atom of type a and N_a is the number of atoms of that type per unit volume.

Thus, for strong reflections in near-perfect crystals, the Rayleigh scattering is affected by both crystal texture and beam direction. This reduction of primary-beam intensity due to the Rayleigh scattering is usually included, along with other specimen-dependent factors affecting diffracted-beam intensity, in the analysis of extinction.

6.3.1.4. *Attenuation (mass absorption) coefficients*

Since the reduction of intensity depends on the quantity of matter traversed by the beam, the absorption coefficient is often expressed on a mass basis by dividing by the density ρ_m. μ/ρ_m defines the attenuation coefficient.

The determination of attenuation coefficients to high precision is possible only when contributions from all different scattering processes are analysed in detail. To a level of accuracy appropriate to most experiments, however, the coefficient can be determined from the atomic cross sections for scattering and photoelectric absorption. Ideally, absorption corrections for scattering from single crystals in the absence of extinction should be evaluated using the Rayleigh cross section for a crystal in the non-reflecting position. However, as Rayleigh scattering is a minor contribution to the total absorption except for the lighter elements, no large error is made by applying the absorption correction appropriate to an assembly of isolated atoms to a single crystal.

Likewise, μ/ρ_m is, to a good approximation, given by the sum of the attenuation coefficients for each constituent element $(\mu/\rho_m)_a$, weighted by the mass fraction g_a for that element, *i.e.*

$$\frac{\mu}{\rho_m} = \sum_a g_a(\mu/\rho_m)_a, \qquad (6.3.1.5)$$

where the sum is over the elements. The atomic cross section for attenuation is given by

$$\sigma_a = (\mu/\rho_m)_a A_a/N_A = \mu/N_a, \qquad (6.3.1.6)$$

where A_a is the atomic weight and N_a is Avogadro's number. The evaluation of the attenuation coefficients is described in Section 4.2.4.

6.3.2. Dispersion

In the wavelength regime associated with anomalous scattering, where

$$f = f^0 + f' + f'', \qquad (6.3.2.1)$$

the refractive index becomes complex, its imaginary component contributing an additional term to the absorption.

f^0 is the scattering factor for ideal elastic scattering. The dispersion corrections f' and f'' are related to the absorption since (James, 1962; Wagenfeld, 1975)

$$f''(\omega) = mc\omega\sigma(\omega)/4\pi e^2, \quad \omega = 2\pi c/\lambda \qquad (6.3.2.2)$$

$$f'(\omega) = \frac{2}{\pi} \int_0^\infty [\omega' f''(\omega')/(\omega^2 - \omega'^2)]\, \mathrm{d}\omega'. \qquad (6.3.2.3)$$

That is, the dispersion corrections are determined by the absorption cross sections. The relationships (6.3.2.2) and (6.3.2.3) can be used in measuring absorption coefficients, as described in Section 4.2.4. The dispersion terms change rapidly near the absorption edge, especially on the short-wavelength side. The changes are anisotropic, sensitive to structure and to the direction of polarization. Details are given by Templeton & Templeton (1980, 1982, 1985).

In near-perfect crystals, the changes near the absorption edge are also sensitive to temperature (Karamura & Fukamachi, 1979; Fukamachi, Karamura, Hayakawa, Nakano & Koh, 1982). The effective absorption coefficient can also be altered by the Borrmann effect (Azaroff, Kaplow, Kato, Weiss, Wilson & Young, 1974).

6.3.3. Absorption corrections

The reduction in the intensity of an X-ray reflection from a uniform beam due to absorption is given by the transmission coefficient

$$A = \frac{1}{V} \int \exp(-\mu T)\, \mathrm{d}V, \qquad (6.3.3.1)$$

where the integration is over the volume of the crystal. The absorption correction

$$A^* = 1/A. \qquad (6.3.3.2)$$

T, the path length of the X-ray beam in the crystal, is the sum of the path lengths for the incident and diffracted beams. A technique for measuring crystals for absorption measurements is described in Subsection 6.3.3.6.

Any least-squares analysis involving variation of the linear absorption coefficient, or equivalently an isotropic variation in crystal size, requires the weighted mean path length

$$\bar{T} = -A^{-1} \frac{\partial A}{\partial \mu} = \frac{1}{A^*} \frac{\partial A^*}{\delta \mu}. \qquad (6.3.3.3)$$

This path length is also required in some analyses of extinction (Zachariasen, 1968; Becker & Coppens, 1974).

6.3.3.1. *Special cases*

For special cases, the integral can be solved analytically, and in some of these the expression reduces to closed form. These are listed in Table 6.3.3.1.

6.3.3.2. *Cylinders and spheres*

For diffraction in the equatorial plane of a cylinder of radius R within the X-ray beam, the expression for the transmission coefficient reduces to

$$A = \frac{1}{A^*} = \frac{1}{\pi R^2} \int_0^R \int_0^{2\pi} \exp\Big(- \mu\{[R^2 - r^2 \sin^2(\theta + \varphi)]^{1/2} + [R^2 - r^2 \sin^2(\theta - \varphi)]^{1/2}\}\Big) \times \cosh(2\mu r \sin\theta \sin\varphi) r\, \mathrm{d}r\, \mathrm{d}\varphi. \qquad (6.3.3.4)$$

Table 6.3.3.1. *Transmission coefficients*

(1) Reflection from a crystal slab with negligible transmission; the crystal planes are inclined at an angle φ to the extended face, and the normal in the plane of the incident and diffracted beams

$$A = \frac{\sin(\theta - \varphi)}{\mu\{\sin(\theta - \varphi) + \sin(\theta + \varphi)\}}$$

(1*a*) $\varphi = 0$

$$A = 1/2\mu$$

(2) Reflection from a crystal slab of thickness t, with planes parallel to the extended face

$$A = \{1 - \exp(-2\mu t \operatorname{cosec}\theta)\}/2\mu$$

(3) Transmission through a crystal slab of thickness t; the crystal planes are at $\pi/2 - \varphi$ to the surface, with the normal in the plane of the incident and reflected beams

$$A = \frac{\exp\{-\mu t \sec(\theta + \varphi)\} - \exp\{-\mu t \sec(\theta - \varphi)\}}{\mu\left[1 - \dfrac{\sec(\theta + \varphi)}{\sec(\theta - \varphi)}\right]}$$

(3*a*) $\varphi = 0$

$$A = t \sec\theta \exp(-\mu t \sec\theta)$$

(4) Transmission through a sphere of radius R (*i.e.* for a uniform X-ray beam and $\theta = 0^\circ$)

$$A = \frac{3}{2(\mu R)^3}[1/2 - e^{-2\mu R}\{1/2 + \mu R + (\mu R)^2\}]$$

(5) Reflection from a sphere of radius R (*i.e.* for a uniform X-ray beam, and $\theta = 90^\circ$)

$$A = \frac{3}{4\mu R}\left\{1/2 - \frac{1}{16(\mu R)^2}\,[1 - (1 + 4\mu R)\,e^{-4\mu R}]\right\}$$

Values of the absorption correction A^* obtained by numerical integration by Dwiggins (1975*a*) are listed in Table 6.3.3.2.

The reduced expression for a spherical crystal of radius R is

$$\begin{aligned} A = \frac{3}{4\pi R^3} \int_0^R \int_{-1}^1 \int_0^{2\pi} \exp\Big(- \mu\{&[R^2 - r^2\cos^2\alpha \\ &- r^2\sin^2\alpha\sin^2(\theta + \varphi)]^{1/2} \\ &+ [R^2 - r^2\cos^2\alpha - r^2\sin^2\alpha\sin^2(\theta - \varphi)]^{1/2} \\ &- 2r\sin\theta\sin\alpha\sin\varphi\}\Big) r^2\,\mathrm{d}r\,\mathrm{d}(\cos\alpha)\,\mathrm{d}\varphi. \end{aligned} \tag{6.3.3.5}$$

Values of A^* obtained using numerical integration by Dwiggins (1975*b*) are listed in Table 6.3.3.3. An estimate of the accuracy of the numerical integration is given by comparison with the results for special values of θ at which equations (6.3.3.4) and (6.3.3.5) may be integrated analytically, which are included in Table 6.3.3.1. The comparison indicates a reliability for the tabulated values of better than 0.1%. Tables at finer intervals for cylinders and spheres for $\mu R < 1.0$ are given by Rouse, Cooper, York & Chakera (1970). A tabulation up to $\mu R < 5.0$ for spheres is given by Weber (1969). Interpolation for μR may be effected by the formula

$$A^*(\mu R) = \exp\left\{\sum_{m=1}^{M} K_m(\mu R)^m\right\}, \tag{6.3.3.6}$$

where the K_m are determined, for fixed θ, from the values in Tables 6.3.3.2 and 6.3.3.3.

Subsequent interpolation as a function of θ may be effected by the interpolation formula

$$A^*\{\theta\} = \sum_{n=1}^{N} L_n \sin^{2n}(\theta). \tag{6.3.3.7}$$

Interpolation is accurate to 0.1% with $N = M = 3$.

For cylinders and spheres, $\bar{T}$ may be obtained by means of the expression

$$\bar{T} = \frac{1}{A^*}\,\frac{\mathrm{d}A^*}{\mathrm{d}\mu} = R\left[\frac{1}{A^*}\,\frac{\mathrm{d}A^*}{\mathrm{d}(\mu R)}\right] \tag{6.3.3.8}$$

using the values listed in Tables 6.3.3.2 and 6.3.3.3.

Values of $(1/A^*)[\mathrm{d}A^*/\mathrm{d}(\mu R)]$ obtained by numerical integration by Flack & Vincent (1978) for spheres with $\mu R < 2.5$ are listed in Table 6.3.3.4. An equivalent table of $\mu(R/A^*)/[\mathrm{d}A^*/\mathrm{d}(\mu R)]$ for $\mu R < 4.0$ is given by Rigoult & Guidi-Morosini (1980).

Alternatively, one can differentiate the interpolation formula (6.3.3.6), yielding

$$\bar{T}(\mu R, \theta) = \frac{1}{\mu}\sum_{m=1}^{M} mK_m(\mu R)^m. \tag{6.3.3.9}$$

In this case, however, the maximum index $M = 7$ is required to obtain convergence for $\mu R \leq 2.5$. Numerical values of the coefficients K_m for cylinders and spheres evaluated by Tibballs (1982) are listed in Table 6.3.3.5.

Interpolation between the tabulated θ values is obtained from the θ interpolation formula, noting that

$$L_m = \sum_{j=1}^{7} (C^{-1})_{mj} A_j^*, \tag{6.3.3.10}$$

where

$$C_{mj} = \sin^{2m}\theta_j. \tag{6.3.3.11}$$

The elements $(C^{-1})_{mj}$ and the $K_m(\theta_j)$ for θ_j at 15° intervals in the range $0 < \theta_j < 90^\circ$ are listed in Table 6.3.3.5. Differentiating (6.3.3.7) yields

$$A^*(\mu R, \theta)\bar{T}(\mu R, \theta) = \sum_{m=0}^{M} P_m \sin^{2m}\theta, \tag{6.3.3.12}$$

where

$$P_m = R\frac{\partial L_m}{\partial(\mu R)} = \sum_{j=1}^{7}(C^{-1})_{mj} A_j^* \bar{T}_j. \tag{6.3.3.13}$$

Equation (6.3.3.12) for path lengths is the analogue of equation (6.3.3.7) for the transmission factors. It provides the basis for an interpolation formula.

In the case of a cylindrical crystal much larger than the X-ray beam, the absorption correction has been determined by Coyle (1972), in an extension of earlier work by Coyle & Schroeder (1971). The absorption correction for the case of the cylinder axis coincident with the φ axis of a Eulerian cradle, shown in Fig. 6.3.3.1, reduces to the line integral

$$\frac{1}{2\tau}\int_0^{2\tau} \exp\{-\mu[(z) + T(z)]\}\,\mathrm{d}z, \tag{6.3.3.14}$$

Table 6.3.3.2. *Values of A^* for cylinders*

μR	$\theta = 0°$	$\theta = 5°$	$\theta = 10°$	$\theta = 15°$	$\theta = 20°$	$\theta = 25°$	$\theta = 30°$	$\theta = 35°$	$\theta = 40°$	$\theta = 45°$	$\theta = 50°$	$\theta = 55°$	$\theta = 60°$	$\theta = 65°$	$\theta = 70°$	$\theta = 75°$	$\theta = 80°$	$\theta = 85°$	$\theta = 90°$
0.0	1	1	1	1	1	1	1	1	1	1	1	1	1	1	1	1	1	1	1
0.1	1.1843	1.1843	1.1842	1.1840	1.1838	1.1835	1.1832	1.1828	1.1823	1.1818	1.1813	1.1808	1.1802	1.1798	1.1793	1.1790	1.1787	1.1785	1.1785
0.2	1.4009	1.4007	1.4002	1.3995	1.3984	1.3970	1.3953	1.3934	1.3912	1.3889	1.3865	1.3841	1.3818	1.3796	1.3777	1.3761	1.3749	1.3741	1.3739
0.3	1.6548	1.6544	1.6531	1.6510	1.6481	1.6443	1.6398	1.6347	1.6290	1.6230	1.6169	1.6108	1.6049	1.5994	1.5946	1.5906	1.5876	1.5857	1.5851
0.4	1.9522	1.9513	1.9485	1.9439	1.9376	1.9296	1.9201	1.9094	1.8979	1.8857	1.8733	1.8611	1.8495	1.8388	1.8293	1.8215	1.8157	1.8121	1.8108
0.5	2.2996	2.2979	2.2926	2.2840	2.2721	2.2572	2.2398	2.2204	2.1996	2.1781	2.1564	2.1352	2.1152	2.0969	2.0809	2.0677	2.0579	2.0518	2.0497
0.6	2.7047	2.7017	2.6926	2.6775	2.6570	2.6317	2.6023	2.5701	2.5359	2.5010	2.4662	2.4327	2.4012	2.3728	2.3480	2.3277	2.3126	2.3033	2.3001
0.7	3.1762	3.1712	3.1561	3.1315	3.0982	3.0575	3.0111	2.9607	2.9081	2.8549	2.8028	2.7530	2.7068	2.6653	2.6295	2.6003	2.5786	2.5651	2.5606
0.8	3.7236	3.7157	3.6919	3.6532	3.6015	3.5392	3.4691	3.3941	3.3169	3.2400	3.1656	3.0953	3.0307	2.9732	2.9239	2.8839	2.8542	2.8359	2.8297
0.9	4.3578	4.3456	4.3093	4.2507	4.1733	4.0812	3.9792	3.8718	3.7629	3.6560	3.5538	3.4584	3.3717	3.2951	3.2299	3.1772	3.1383	3.1142	3.1061
1.0	5.0907	5.0724	5.0185	4.9323	4.8196	4.6877	4.5439	4.3948	4.2461	4.1022	3.9664	3.8413	3.7286	3.6298	3.5462	3.4790	3.4295	3.3990	3.3886
1.1	5.9356	5.9089	5.8305	5.7065	5.5466	5.3624	5.1649	4.9636	4.7660	4.5776	4.4022	4.2424	4.0998	3.9759	3.8717	3.7882	3.7269	3.6891	3.6763
1.2	6.907	6.869	6.757	6.582	6.360	6.109	5.8436	5.5782	5.3219	5.0811	4.8598	4.6604	4.4842	4.3322	4.2051	4.1038	4.0295	3.9838	3.9682
1.3	8.021	7.967	7.810	7.568	7.266	6.929	6.581	6.238	5.9125	5.6110	5.3376	5.0938	4.8805	4.6976	4.5456	4.4248	4.3365	4.2821	4.2636
1.4	9.294	9.219	9.003	8.674	8.268	7.826	7.376	6.942	6.536	6.166	5.8341	5.5413	5.2873	5.0711	4.8922	4.7506	4.6471	4.5835	4.5619
1.5	10.746	10.643	10.349	9.907	9.372	8.800	8.230	7.689	7.192	6.744	6.348	6.002	5.7036	5.4516	5.2441	5.0804	4.9609	4.8875	4.8625
1.6	12.397	12.257	11.862	11.276	10.581	9.852	9.141	8.477	7.877	7.344	6.877	6.473	6.128	5.8385	5.6007	5.4136	5.2773	5.1935	5.1650
1.7	14.267	14.080	13.555	12.788	11.897	10.982	10.106	9.304	8.589	7.963	7.420	6.955	6.561	6.231	5.961	5.7499	5.5960	5.5014	5.4691
1.8	16.379	16.131	15.441	14.450	13.323	12.189	11.125	10.168	9.327	8.600	7.976	7.446	7.000	6.628	6.326	6.089	5.9166	5.8107	5.7746
1.9	18.76	18.43	17.53	16.267	14.858	13.470	12.194	11.066	10.089	9.253	8.544	7.946	7.444	7.030	6.693	6.430	6.239	6.121	6.081
2.0	21.43	21.00	19.84	18.24	16.50	14.824	13.311	11.995	10.871	9.921	9.122	8.452	7.895	7.435	7.063	6.773	6.562	6.433	6.389
2.1	24.41	23.87	22.39	20.38	18.25	16.247	14.472	12.953	11.673	10.602	9.709	8.965	8.349	7.843	7.436	7.118	6.887	6.745	6.697
2.2	27.74	27.04	25.17	22.69	20.11	17.74	15.675	13.938	12.493	11.295	10.304	9.484	8.808	8.255	7.810	7.464	7.213	7.059	7.006
2.3	31.44	30.55	28.20	25.16	22.07	19.29	16.92	14.947	13.328	11.999	10.906	10.008	9.271	8.669	8.187	7.812	7.540	7.372	7.315
2.4	35.54	34.41	31.49	27.79	24.13	20.90	18.19	15.978	14.177	12.711	11.515	10.537	9.736	9.086	8.565	8.161	7.868	7.687	7.625
2.5	40.06	38.65	35.05	30.59	26.28	22.56	19.50	17.03	15.040	13.433	12.130	11.069	10.205	9.505	8.945	8.511	8.196	8.002	7.935

Table 6.3.3.3. *Values of A^* for spheres*

μR	$\theta = 0°$	$\theta = 5°$	$\theta = 10°$	$\theta = 15°$	$\theta = 20°$	$\theta = 25°$	$\theta = 30°$	$\theta = 35°$	$\theta = 40°$	$\theta = 45°$	$\theta = 50°$	$\theta = 55°$	$\theta = 60°$	$\theta = 65°$	$\theta = 70°$	$\theta = 75°$	$\theta = 80°$	$\theta = 85°$	$\theta = 90°$
0.0	1	1	1	1	1	1	1	1	1	1	1	1	1	1	1	1	1	1	1
0.1	1.1609	1.1609	1.1609	1.1607	1.1606	1.1603	1.1600	1.1597	1.1593	1.1589	1.1586	1.1582	1.1579	1.1575	1.1572	1.1570	1.1568	1.1567	1.1567
0.2	1.3457	1.3456	1.3452	1.3447	1.3439	1.3428	1.3415	1.3400	1.3383	1.3366	1.3348	1.3331	1.3313	1.3297	1.3282	1.3271	1.3262	1.3256	1.3254
0.3	1.5574	1.5571	1.5561	1.5546	1.5525	1.5497	1.5463	1.5426	1.5383	1.5339	1.5293	1.5248	1.5204	1.5162	1.5126	1.5096	1.5074	1.5059	1.5055
0.4	1.7994	1.7988	1.7968	1.7935	1.7891	1.7833	1.7765	1.7689	1.7604	1.7515	1.7425	1.7335	1.7249	1.7169	1.7099	1.7041	1.6997	1.6970	1.6961
0.5	2.0755	2.0743	2.0706	2.0647	2.0565	2.0462	2.0340	2.0204	2.0056	1.9901	1.9745	1.9592	1.9445	1.9311	1.9194	1.9097	1.9024	1.8979	1.8964
0.6	2.3897	2.3877	2.3816	2.3715	2.3578	2.3406	2.3206	2.2984	2.2746	2.2500	2.2255	2.2015	2.1789	2.1583	2.1403	2.1257	2.1145	2.1076	2.1063
0.7	2.7467	2.7434	2.7336	2.7177	2.6959	2.6691	2.6382	2.6042	2.5683	2.5316	2.4952	2.4602	2.4274	2.3977	2.3719	2.3508	2.3351	2.3253	2.3220
0.8	3.1511	3.1461	3.1312	3.1069	3.0740	3.0339	2.9882	2.9386	2.8869	2.8347	2.7835	2.7346	2.6892	2.6484	2.6133	2.5845	2.5632	2.5499	2.5454
0.9	3.6082	3.6009	3.5789	3.5431	3.4952	3.4374	3.3723	3.3026	3.2308	3.1592	3.0898	3.0241	2.9637	2.9098	2.8634	2.8258	2.7979	2.7805	2.7747
1.0	4.1237	4.1131	4.0815	4.0304	3.9625	3.8816	3.7917	3.6966	3.6001	3.5048	3.4135	3.3280	3.2499	3.1807	3.1216	3.0738	3.0383	3.0163	3.0090
1.1	4.7035	4.6886	4.6442	4.5729	4.4790	4.3686	4.2474	4.1211	3.9945	3.8710	3.7540	3.6455	3.5470	3.4605	3.3870	3.3276	3.2838	3.2566	3.2474
1.2	5.3542	5.3335	5.2722	5.1747	5.0476	4.9001	4.7404	4.5761	4.4137	4.2571	4.1104	3.9756	3.8542	3.7483	3.6586	3.5866	3.5334	3.5005	3.4894
1.3	6.082	6.054	5.9710	5.8399	5.6710	5.4776	5.2711	5.0617	4.8573	4.6625	4.4819	4.3175	4.1706	4.0432	3.9360	3.8500	3.7868	3.7477	3.7344
1.4	6.895	6.857	6.746	6.573	6.352	6.102	5.8400	5.5774	5.3244	5.0862	4.8676	4.6703	4.4955	4.3447	4.2183	4.1174	4.0432	3.9974	3.9819
1.5	7.801	7.750	7.604	7.377	7.092	6.775	6.447	6.123	5.8143	5.5273	5.2666	5.0333	4.8281	4.6520	4.5052	4.3883	4.3024	4.2495	4.2315
1.6	8.806	8.740	8.549	8.256	7.894	7.497	7.092	6.697	6.326	5.9849	5.6780	5.4057	5.1678	4.9647	4.7961	4.6622	4.5641	4.5036	4.4830
1.7	9.920	9.834	9.587	9.214	8.759	8.268	7.774	7.299	6.859	6.458	6.101	5.7867	5.5140	5.2823	5.0907	4.9390	4.8279	4.7595	4.7361
1.8	11.151	11.040	10.725	10.254	9.689	9.088	8.492	7.928	7.411	6.946	6.535	6.176	5.8662	5.6045	5.3888	5.2184	5.0936	5.0170	4.9908
1.9	12.507	12.366	11.967	11.380	10.685	9.957	9.246	8.583	7.982	7.447	6.978	6.572	6.224	5.9308	5.6900	5.5001	5.3613	5.2760	5.2468
2.0	13.998	13.819	13.320	12.593	11.746	10.873	10.034	9.262	8.570	7.961	7.431	6.975	6.587	6.261	5.9942	5.7842	5.6307	5.5365	5.5041
2.1	15.632	15.408	14.788	13.895	12.874	11.837	10.855	9.964	9.175	8.486	7.893	7.385	6.955	6.595	6.301	6.070	5.9017	5.7982	5.7627
2.2	17.419	17.141	16.376	15.290	14.067	12.847	11.708	10.688	9.795	9.023	8.362	7.800	7.327	6.932	6.610	6.358	6.174	6.061	6.022
2.3	19.369	19.025	18.089	16.778	15.327	13.902	12.592	11.433	10.429	9.569	8.839	8.220	7.702	7.272	6.922	6.648	6.448	6.325	6.282
2.4	21.489	21.069	19.931	18.361	16.652	15.000	13.504	12.198	11.077	10.125	9.322	8.645	8.081	7.614	7.235	6.938	6.722	6.589	6.543
2.5	23.791	23.280	21.907	20.040	18.041	16.142	14.445	12.982	11.738	10.690	9.810	9.074	8.462	7.957	7.548	7.229	6.996	6.853	6.803

Table 6.3.3.4. *Values of* $(1/A^*)(dA^*/d\mu R)$ *for spheres*

μR	$\theta = 0°$	$\theta = 5°$	$\theta = 10°$	$\theta = 15°$	$\theta = 20°$	$\theta = 25°$	$\theta = 30°$	$\theta = 35°$	$\theta = 40°$	$\theta = 45°$	$\theta = 50°$	$\theta = 55°$	$\theta = 60°$	$\theta = 65°$	$\theta = 70°$	$\theta = 75°$	$\theta = 80°$	$\theta = 85°$	$\theta = 90°$
0.0	1.5000	1.5000	1.5000	1.5000	1.5000	1.5000	1.5000	1.5000	1.5000	1.5000	1.5000	1.5000	1.5000	1.5000	1.5000	1.5000	1.5000	1.5000	1.5000
0.1	1.4845	1.4842	1.4829	1.4809	1.4782	1.4739	1.4690	1.4634	1.4569	1.4504	1.4439	1.4375	1.4309	1.4248	1.4191	1.4152	1.4117	1.4096	1.4089
0.2	1.4692	1.4682	1.4650	1.4611	1.4548	1.4472	1.4374	1.4268	1.4145	1.4019	1.3879	1.3748	1.3615	1.3491	1.3385	1.3292	1.3228	1.3180	1.3168
0.3	1.4527	1.4515	1.4476	1.4400	1.4309	1.4186	1.4044	1.3886	1.3708	1.3517	1.3327	1.3128	1.2947	1.2773	1.2624	1.2494	1.2397	1.2340	1.2321
0.4	1.4360	1.4341	1.4283	1.4190	1.4058	1.3898	1.3709	1.3492	1.3265	1.3018	1.2773	1.2531	1.2296	1.2089	1.1903	1.1748	1.1628	1.1560	1.1533
0.5	1.4186	1.4161	1.4090	1.3969	1.3803	1.3598	1.3360	1.3093	1.2812	1.2522	1.2231	1.1946	1.1678	1.1434	1.1218	1.1044	1.0910	1.0825	1.0797
0.6	1.4011	1.3980	1.3890	1.3742	1.3538	1.3289	1.3006	1.2693	1.2365	1.2033	1.1700	1.1382	1.1087	1.0816	1.0577	1.0383	1.0239	1.0147	1.0115
0.7	1.3830	1.3792	1.3683	1.3507	1.3264	1.2973	1.2643	1.2286	1.1918	1.1549	1.1184	1.0839	1.0516	1.0250	0.9978	0.9767	0.9615	0.9518	0.9484
0.8	1.3641	1.3600	1.3473	1.3262	1.2984	1.2650	1.2275	1.1879	1.1473	1.1071	1.0684	1.0314	0.9976	0.9674	0.9409	0.9195	0.9034	0.8931	0.8898
0.9	1.3451	1.3401	1.3253	1.3013	1.2696	1.2321	1.1908	1.1474	1.1038	1.0608	1.0198	0.9815	0.9465	0.9152	0.8880	0.8663	0.8495	0.8391	0.8359
1.0	1.3255	1.3198	1.3029	1.2758	1.2401	1.1987	1.1535	1.1070	1.0608	1.0157	0.9733	0.9340	0.8978	0.8661	0.8392	0.8167	0.8001	0.7897	0.7859
1.1	1.3058	1.2993	1.2800	1.2497	1.2103	1.1651	1.1165	1.0670	1.0185	0.9720	0.9286	0.8886	0.8522	0.8205	0.7931	0.7709	0.7542	0.7437	0.7400
1.2	1.2851	1.2780	1.2566	1.2228	1.1799	1.1312	1.0796	1.0278	0.9777	0.9299	0.8858	0.8455	0.8093	0.7776	0.7506	0.7285	0.7120	0.7017	0.6981
1.3	1.2645	1.2563	1.2324	1.1961	1.1494	1.0967	1.0430	0.9892	0.9377	0.8895	0.8451	0.8048	0.7691	0.7378	0.7113	0.6895	0.6733	0.6631	0.6596
1.4	1.2449	1.2349	1.2090	1.1684	1.1180	1.0628	1.0068	0.9517	0.8990	0.8504	0.8064	0.7666	0.7315	0.7009	0.6749	0.6539	0.6377	0.6278	0.6243
1.5	1.2231	1.2133	1.1845	1.1398	1.0867	1.0295	0.9711	0.9145	0.8615	0.8133	0.7696	0.7308	0.6964	0.6665	0.6414	0.6209	0.6055	0.5957	0.5922
1.6	1.2015	1.1908	1.1585	1.1118	1.0555	0.9957	0.9358	0.8782	0.8261	0.7778	0.7350	0.6970	0.6638	0.6349	0.6105	0.5907	0.5758	0.5663	0.5628
1.7	1.1806	1.1681	1.1339	1.0836	1.0244	0.9621	0.9005	0.8435	0.7912	0.7444	0.7027	0.6659	0.6334	0.6057	0.5822	0.5632	0.5484	0.5394	0.5361
1.8	1.1586	1.1456	1.1087	1.0558	0.9939	0.9294	0.8669	0.8101	0.7579	0.7121	0.6711	0.6359	0.6053	0.5787	0.5561	0.5376	0.5236	0.5148	0.5117
1.9	1.1370	1.1226	1.0835	1.0275	0.9625	0.8964	0.8341	0.7774	0.7262	0.6817	0.6420	0.6078	0.5791	0.5535	0.5321	0.5144	0.5010	0.4924	0.4892
2.0	1.1152	1.0996	1.0584	0.9982	0.9318	0.8646	0.8019	0.7457	0.6962	0.6527	0.6160	0.5830	0.5550	0.5305	0.5098	0.4927	0.4799	0.4717	0.4687
2.1	1.0932	1.0772	1.0327	0.9703	0.9014	0.8340	0.7712	0.7157	0.6678	0.6259	0.5899	0.5588	0.5322	0.5088	0.4886	0.4726	0.4603	0.4523	0.4494
2.2	1.0719	1.0543	1.0074	0.9427	0.8719	0.8039	0.7421	0.6874	0.6402	0.6003	0.5658	0.5353	0.5098	0.4884	0.4699	0.4548	0.4426	0.4347	0.4311
2.3	1.0498	1.0316	0.9822	0.9150	0.8434	0.7744	0.7133	0.6605	0.6147	0.5758	0.5433	0.5141	0.4896	0.4692	0.4518	0.4363	0.4252	0.4175	0.4149
2.4	1.0275	1.0118	0.9583	0.8889	0.8147	0.7482	0.6870	0.6340	0.5918	0.5507	0.5212	0.4937	0.4699	0.4500	0.4328	0.4187	0.4076	0.4003	0.3986
2.5	1.0108	0.9691	0.9297	0.8562	0.7904	0.7074	0.6554	0.6194	0.5618	0.5289	0.4980	0.4776	0.4554	0.4315	0.4142	0.4028	0.3921	0.3883	0.3783

Table 6.3.3.5. *Coefficients for interpolation of* A^* *and* $\bar{T}$

θ_j	0°	15°	30°	45°	60°	75°	90°	Units
K_1 (sphere)	3/2	3/2	3/2	3/2	3/2	3/2	3/2	
K_2	−7.5234	−9.4320	−15.109	−24.3812	−35.219	−44.042	−47.745	10^{-2}
K_3	−7.0935	−10.737	−18.027	−11.088	14.265	40.021	61.084	10^{-3}
K_4	−2.3096	−2.1332	−1.4693	7.4205	24.832	44.308	37.394	10^{-3}
K_5	1.8323	1.1711	4.6784	3.0970	−10.284	−27.987	−25.879	10^{-3}
K_6	−5.1259	−1.2652	−14.491	−16.740	21.910	77.007	71.458	10^{-4}
K_7	6.0265	0.7932	16.489	21.774	−22.391	−85.570	−78.812	10^{-5}
K_1 (cylinder)	$16/3\pi$	$16/3\pi$	$16/3\pi$	$16/3\pi$	$16/3\pi$	$16/3\pi$	$16/3\pi$	
K_2	−5.7832	−8.1900	−15.651	−27.048	−40.317	−51.497	−55.837	10^{-2}
K_3	−14.737	−19.551	−22.883	−27.345	−8.807	26.637	41.420	10^{-3}
K_4	5.2399	1.2934	−12.301	6.844	40.689	61.371	68.963	10^{-3}
K_5	−4.0958	−2.8349	9.6249	7.503	−11.295	−29.397	−36.556	10^{-3}
K_6	13.178	12.731	−19.881	−30.211	9.4468	60.356	80.965	10^{-4}
K_7	−14.500	−14.846	14.414	34.222	3.1492	−49.206	−70.573	10^{-5}
$(C^{-1})_{0j}$	3	0	0	0	0	0	0	All values
$(C^{-1})_{1j}$	−73	$48+24\sqrt{3}$	−24	12	−8	$48-24\sqrt{3}$	−3	multiplied
$(C^{-1})_{2j}$	518	$-496-200\sqrt{3}$	488	−268	184	$-496+200\sqrt{3}$	70	by 3
$(C^{-1})_{3j}$	−1600	$1920+560\sqrt{3}$	−2192	1536	−1136	$1920-560\sqrt{3}$	−448	to eliminate
$(C^{-1})_{4j}$	2432	$-3520-640\sqrt{3}$	4032	−3328	2752	$-3520+640\sqrt{3}$	1152	fractions
$(C^{-1})_{5j}$	−1792	$3072+256\sqrt{3}$	−3328	3072	−2816	$3072-256\sqrt{3}$	−1280	
$(C^{-1})_{6j}$	512	−1024	1024	−1024	1024	−1024	512	

where z and $T(z)$ are the path lengths for the incident and diffracted beams, respectively. τ is the radius, along the line of the incident beam, of the ellipse described by the cross section of the crystal in the plane of diffraction, shown in Fig. 6.3.3.2. The equation for the ellipse is

$$\tau = R(1 - \sin^2\theta \sin^2\chi)^{-1/2}. \qquad (6.3.3.15)$$

The outgoing elliptical radius v satisfies

$$Av^4 + Bv^2 + C = 0, \qquad (6.3.3.16)$$

where

$$\begin{aligned} A &= [1 - \sin^2\theta \sin^2\chi]^2 \\ B &= -2R^2[1 - \sin^2\theta \sin^2\chi] \\ &\quad - 2(\tau - z)^2[\cos^2\theta - \sin^2\theta \cos^2\chi] \sin^2 2\theta \sin^2\chi \\ C &= R^4 + 2R^2(\tau - z)^2 \sin^2 2\theta \sin^2\chi \cos 2\theta \\ &\quad + (\tau - z)^4 \sin^4 2\theta \sin^4\chi. \end{aligned}$$

In the case where the cylinder axis is inclined at an angle Γ to the φ axis, these equations become

$$\begin{aligned} A &= [1 - \sin^2(\theta + \beta) \sin^2\chi_1]^2 \\ B &= -2R^2[1 - \sin^2(\theta + \beta) \sin^2\chi_1] \\ &\quad - 2(\tau - z)^2[\cos^2(\theta + \beta) \\ &\quad - \sin^2(\theta + \beta) \cos^2\chi_1] \sin^2 2\theta \sin^2\chi_1 \\ C &= R^4 + 2R^2(\tau - z)^2 \sin^2 2\theta \sin^2\chi_1 \cos 2(\theta + \beta) \\ &\quad + (\tau - z)^4 \sin^4 2\theta \sin^4\chi_1, \end{aligned}$$

where

$$\tan\beta = \sin\Gamma \sin\varphi / [\sin\Gamma \cos\chi \cos\varphi + \sin\chi \cos\Gamma].$$

The roots of the quadratic equation (6.3.3.16) for v^2 are real and positive for reflection from within the crystal. The convergent path length T is given by the positive root of the triangle formula

$$T^2 - 2T(\tau - z)\cos 2\theta + (\tau - z)^2 - v^2 = 0. \qquad (6.3.3.17)$$

It should be noted that the volume of the specimen irradiated changes with the angular settings of the diffractometer. Normalization to constant volume requires that the absorption correction be multiplied by the volume-correction factor $[1 - \sin^2(\theta - \beta)\sin^2\chi_1]^{-1/2}$.

The method readily extends to the case of a cylindrical window or sheath, such as used for mounting an unstable crystal of conventional size. The correction in this case is

$$\begin{aligned} &\exp[-\mu(\tau_2 - \tau_1 + v_2 - v_1)] \\ &\quad = \exp\Big(- \mu(R_2 - R_1)\{[1 - \sin^2(\theta - \beta)\sin^2\chi_1]^{-1/2} \\ &\qquad + [1 - \sin^2(\theta + \beta)\sin^2\chi_1]^{-1/2}\}\Big), \end{aligned} \qquad (6.3.3.18)$$

where the subscripts 1 and 2 apply to the inner and outer radii, respectively.

The integral in equation (6.3.3.14) may be evaluated by Gaussian quadrature, *i.e.* by approximation as a weighted sum of the values of the function at the N zeros X_i of the Legendre polynomial of degree N in the interval $[-1, +1]$. The weights w_i for the points are tabulated by Abramowitz & Stegun (1964). Further details are given in Subsection 6.3.3.4. The emergent path lengths $T(z_1)$ and $T(z_2)$ for the case of the sheath are calculated as functions of the Gaussian variable X_i using the linear transformation

$$z_i = \tau_1 X_i + \tau_2, \quad i = 1, 2, \ldots, N. \qquad (6.3.3.19)$$

This transformation converts the Gaussian variable X into the beam coordinate z for each i of the N summation points.

6.3.3.3. *Analytical method for crystals with regular faces*

For a crystal with regular faces, (6.3.3.1) may be integrated exactly, giving the correction in analytical form. In its simplest form, the analytical method applies to specimens with no re-entrant angles. It is efficient for crystals with a small number of faces. Its accuracy does not depend on the size of the absorption coefficient. The principles can be illustrated by reference to the two-dimensional case of a triangular crystal shown in Fig. 6.3.3.3.

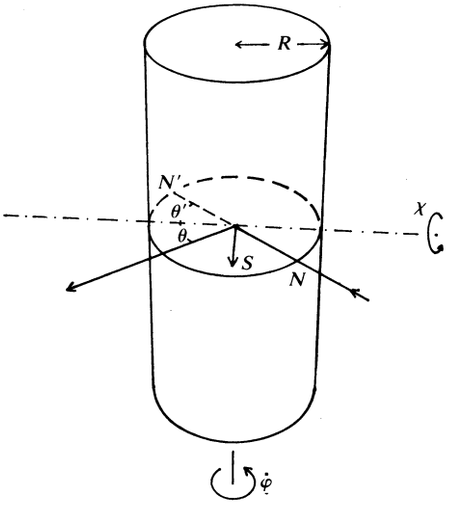

Fig. 6.3.3.1. Geometry of the Eulerian cradle with the axis of a cylindrical specimen coincident with the φ axis.

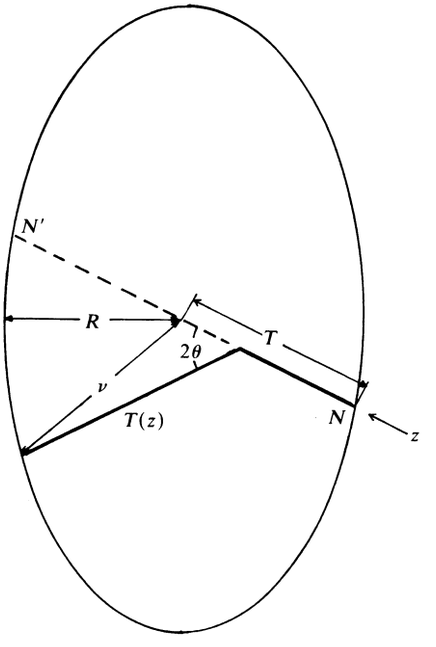

Fig. 6.3.3.2. Cross section of the plane of diffraction for a cylindrical specimen coincident with the φ axis.

The crystal is divided into polygons *ADC*, *AFD*, *CDE*, and *BEDF* as shown. The radiation incident on each polygon enters through one face of the crystal, and is either absorbed or emerges through another. Within each polygon, the loci of constant absorption are the straight lines dotted in Fig. 6.3.3.3. It is convenient to subdivide *BEDF* into the triangles *BEF* and *EDF*. By the derivation of an expression for the contribution of a triangular crystal to the scattering, including allowance for absorption, and with the sum taken over the component triangles *ADC*, *AFD*, *CDE*, *BEF*, and *EDF*, the correction for absorption can be calculated.

A three-dimensional crystal is divided into polyhedra, for each of which the radiation enters through one crystal face and leaves through another. Corners for the polyhedra are of five types, namely,

(1) Crystal vertex.

(2) An intersection of a ray through a lit vertex with an opposite face.

(3) An intersection of an incident ray through a lit (*i*) vertex with a plane of diffracted (*d*) rays through a lit (*d*) edge, and the corresponding intersection with incident and diffracted beams interchanged.

(4) An intersection of a plane of incident rays through a lit (*i*) edge with an opposite edge, and its equivalent.

(5) An intersection on a shaded face of planes of incident and diffracted rays through (*i*) and (*d*) edges.

For each vertex x, y, z, the sum of the path lengths to each of the crystal faces is calculated, and multiplied by the absorption coefficient μ to give the optical path length using the equation

$$\mu r_j = \mu(d_j - a_j x - b_j y - c_j z)/(a_j u + b_j v + c_j w),$$

where u, v, w are the direction cosines for the beam direction, and $a_j x + b_j y + c_j z = d_j$ is the equation for the crystal face. The minimum for all j is the path length to the surface.

The analytical expression for the scattering power for each polyhedron, including the effect of absorption, can be expressed in a convenient form by subdividing the polyhedra into tetrahedra. The auxiliary points define the corners of the tetrahedra.

The total diffracted intensity is proportional to the sum of contributions, one from each tetrahedron, of the form

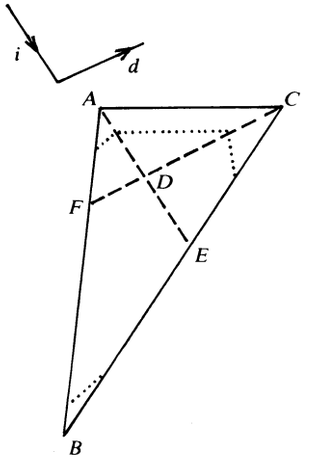

Fig. 6.3.3.3. The crystal *ABC* divided into polygons by the dashed lines *AE* and *CF* parallel to the incident (*i*) and diffracted (*d*) beams, respectively. A locus of constant absorption is shown dotted.

$$R_t = 6V_t e^{-g} H(1)$$
$$= \frac{6V_t}{(b+c)} e^{-g}\left\{\frac{h(a)-h(a+b)}{b} - \frac{h(a+b)-h(a+b+c)}{c}\right\}, \tag{6.3.3.20}$$

where

$$h(x) = \frac{1-e^{-x}}{x}. \tag{6.3.3.21}$$

V_t is the volume of the tetrahedron. For a crystal with Cartesian coordinate vertices 1, 2, 3, and 4,

$$V_t = \tfrac{1}{6}\begin{vmatrix} x_1-x_2 & x_1-x_3 & x_1-x_4 \\ y_1-y_2 & y_1-y_3 & y_1-y_4 \\ z_1-z_2 & z_1-z_3 & z_1-z_4 \end{vmatrix}. \tag{6.3.3.22}$$

The g_i are optical path lengths (*i.e.* path lengths rescaled by the absorption coefficient) ordered so that

$$g_1 < g_2 < g_3 < g_4$$

and

$$g = g_1, \quad a = g_2 - g_1, \quad b = g_3 - g_2, \quad c = g_4 - g_3. \tag{6.3.3.23}$$

The transmission factor for the crystal is the sum of the scattering powers for all the tetrahedra $\sum R_t$ divided by the volume $\sum V_t$. The equality of the total volume to the sum of the V_t values for the component tetrahedra provides a useful check on the accuracy of the calculations, since the total volume is independent of the beam directions, and must be the same for all reflections.

When any of a, b, and c are small, asymptotic forms are required for the expressions in (6.3.3.20). For $\varepsilon < 0.3 \times 10^{-2}$, and

$a < \varepsilon$ $\quad h(a) = 1 - a/2 + a^2/3!$
$\quad h(b+a) = h(b) + ah_1(b) + a^2 h_2(b)/2;$

$b < \varepsilon$ $\quad h(a+b) = h(a) + bh_1(a) + b^2 h_2(a)/2$
$\quad [h(a) - h(a+b)]/b$
$\quad = -h_1(a) - bh_2(a)/2 - b^2 h_3(a)/3!;$

$c < \varepsilon$ $\quad [h(a+b) - h(a+b+c)]/c$
$\quad = -h_1(a+b) - ch_2(a+b)/2$
$\quad -c^2 h_3(a+b)/3!;$

$b, c < \varepsilon$ $\quad H(1) = h_2(a)/2 + (2b+c)h_3(a)/3!$
$\quad + (3b^2 + 3bc + c^2)h_4(a)/4!;$

$a, c < \varepsilon$ $\quad h(a) = 1 - a/2 + a^2/3!$
$\quad [h(a+b) - h(a+b+c)]/c$
$\quad = -h_1(a+b) - ch_2(a+b)/2$
$\quad -c^2 h_3(a+b)/3!;$

$a, b < \varepsilon$ $\quad h(a+b) = 1 - (a+b)/2 + (a+b)^2/3!$
$\quad [h(a) - h(a+b)]/b$
$\quad = 1/2 - a/3 - b/3! + a^2/8 + ab/8 + b^2/4!;$

$a, b, c < \varepsilon$ $\quad H(1) = \dfrac{1}{3!} - \dfrac{a+b}{8} + (b-c)/4!$
$\quad + [(a+b+c)(4a+3b)$
$\quad + 2a^2 + ab + c^2]/5!;$

(6.3.3.24)

where the nth derivative of $h(x)$ is

$$h_n(x) = (-)^n h(x) - \{(-)^n + n h_{n-1}(x)\}/x. \qquad (6.3.3.25)$$

An alternative method of calculating the scattering power of each Howells polyhedron is based on a subdivision into slices. Within each polyhedron, the loci of constant absorption are planes, equivalent to the dotted lines for the two-dimensional example in Fig. 6.3.3.3. The loci may be determined from the path lengths of rays diffracted at each vertex of the polyhedron. The sum of the path lengths in the incident and diffracted directions is found for each vertex, and the loci determined by interpolation. The slices into which each polyhedron is divided are bounded at the upper and lower faces by planes parallel to the loci of constant absorption, such that at least one vertex of the polyhedron lies on those planes.

The volume of the slice is determined from the coordinates of the vertices on each of the opposite faces. Dummy vertices are inserted if necessary to make the number of vertices on the top and bottom faces identical. For simplicity, an axis (z) is chosen perpendicular to the upper face. This locus of constant absorption with N_v vertices x_i, y_i, z_i has an area

$$D_U = 1/2 \sum_{i=1}^{N_v} (x_i y_{i+1} - y_i x_{i+1}) = E/2. \qquad (6.3.3.26)$$

The corresponding vertices on the lower face may be written $x_i + q\Delta x_i, y_i + q\Delta y_i, z_i + q\Delta z$, with $q = 1$. The lower face has an area

$$D_L = 1/2(E + qF + q^2 G), \quad q = 1, \qquad (6.3.3.27)$$

where

$$F = \sum_{i=1}^{N_v} \Delta x_i y_{i+1} + \Delta y_{i+1} x_i - \Delta x_{i+1} y_i - \Delta y_i x_{i+1}$$

and

$$G = \sum_{i=1}^{N_v} \Delta x_i \, \Delta y_{i+1} - \Delta y_i \, \Delta x_{i+1} \qquad (6.3.3.28)$$

so that the volume of the slice is

$$V_s = 1/2(z_L - z_U)(E + F/2 + G/3). \qquad (6.3.3.29)$$

The diffracting power of an element of the slice, allowing for absorption, is $D(q)\exp(-\mu T)\,\mathrm{d}z$, where T is the total path length of the rays diffracted from this plane. Because of the definition of the Howells polyhedron, the path length

$$T = T_U + q(T_L - T_U) = T_U + q\Delta T. \qquad (6.3.3.30)$$

Thus, the total diffracting power of the slice

$$\begin{aligned} R_s &= 1/2(z_L - z_U)\exp(-\mu T_U) \\ &\quad \times \int_0^1 (E + qF + q^2 G)\exp(-\mu q \Delta T)\,\mathrm{d}q \\ &= 1/2(z_L - z_U)\exp(-\mu T_L)\left\{\frac{-E}{\mu\Delta T} - \frac{F(\mu\Delta T + 1)}{(\mu\Delta T)^2}\right. \\ &\quad \left. - G\frac{(\mu\Delta T^2 + 2\mu\Delta T + 2)}{(\mu\Delta T)^3}\right\} \\ &\quad - 1/2(z_L - z_U)\exp(-\mu T_U)\left\{\frac{-E}{\mu\Delta T} - \frac{F}{(\mu\Delta T)^2} - \frac{2G}{(\mu\Delta T)^3}\right\}. \end{aligned} \qquad (6.3.3.31)$$

The transmission factor for the Howells polyhedron is obtained by summing over the slices, and that for the whole crystal is obtained by summing over the polyhedra, *i.e.*

$$A = \sum R_s \Big/ \sum V_s, \qquad (6.3.3.32)$$

where the crystal volume is $\sum V_s$.

$\mathrm{d}A/\mathrm{d}\mu$, required in calculating $\bar{T}$ for the extinction correction, can be obtained by differentiating R_s for each slice with respect to μ, summing the derivatives for each slice, and dividing by $\sum V_s$. To reduce rounding errors in calculation, it may be desirable to rescale the crystal dimensions so that the path lengths are of the order of unity, multiplying the absorption coefficient by the inverse of the scale factor. Further details are given by Alcock, Pawley, Rourke & Levine (1972).

The number of component tetrahedra or slices, which determines the time and precision required for calculation, is a rapidly increasing function of the number of crystal faces. The method may be computationally prohibitive for crystals with complex shapes.

6.3.3.4. *Gaussian integration*

The integral in the transmission factor in equation (6.3.3.1) may be approximated by a sum over grid points spaced at intervals through the crystal volume. It is usually convenient to orient the grid parallel to the crystallographic axes. The grid is non-isometric, the points being chosen weighted by Gaussian constants to minimize the difference between the weighted sum at those points and the exact value of the integral.

Thus, an integral such as $\int_a^b f(y)\,\mathrm{d}y$ may be approximated (Stroud & Secrest, 1966) by

$$\int_a^b f(y)\,\mathrm{d}y = \frac{b-a}{2}\sum_{i=1}^{n} w_i f(y_i) + R_n, \qquad (6.3.3.33)$$

where

$$y_i = \left(\frac{b-a}{2}\right)X_i + \left(\frac{b+a}{2}\right),$$

X_i is the ith zero of the Legendre polynomial $P_n(X)$,

$$w_i = \frac{2}{(1 - X_i^2)}[P_n'(X_i)]^2, \qquad (6.3.3.34)$$

and

$$R_n = \frac{(b-a)^{2n+1}(n!)^4}{(2n+1)[(2n!)]^3}\, 2^{2n+1} f^{(2n)}(\xi), \quad -1 < \xi < 1. \qquad (6.3.3.35)$$

When applying this to the calculation of a transmission coefficient (Coppens, 1970), we commence with the a-axis grid points x_i selected such that

$$x_i = x_{\min} + (x_{\max} - x_{\min})X_i, \qquad (6.3.3.36)$$

where the X_i are the Gaussian constants.

For each x_i, a line is drawn parallel to **b** and points are then selected such that

$$y_{ij} = y_{\min}(x_i) + [y_{\max}(x_i) - y_{\min}(x_i)]\,X_j. \qquad (6.3.3.37)$$

The procedure is repeated for the c direction, yielding

$$z_{ijk} = z_{\min}(x_i, y_j) + [z_{\max}(s_i, y_j) - z_{\min}(x_i, y_j)]\,X_k. \qquad (6.3.3.38)$$

To calculate the absorption corrections, the incident and diffracted wavevectors are determined. For each grid point, the sum T_{ijk} of the path lengths for the incident and diffracted beams is evaluated. The sum that approximates the transmission coefficient is then

$$A = 1/V \sum_{i,j,k} w_i w_j w_k \exp(-\mu T_{ijk}). \qquad (6.3.3.39)$$

Gaussian constants are tabulated by Abramowitz & Stegun (1964).

Alternative schemes based on Monte Carlo and three-dimensional parabolic integration are described by de Graaff (1973, 1977).

6.3.3.5. *Empirical methods*

Some crystals do not have regular faces, or cannot be measured because these are obscured by the crystal mounting. If corrections based on measurements of the crystal shape are not feasible, absorption measurements may be estimated, either from the intensities of the same reflection at different azimuthal angles ψ (see Subsection 6.3.3.6), or from measurements of equivalent reflections, by empirical methods.

There are variants of the method related to differences in experimental technique. The principles may be illustrated by reference to the procedure for a four-circle diffractometer (Flack, 1977).

Intensities H_m are measurements for a reflection **S** at the angular positions Ω_m, 2θ, χ_m, φ_m. Corrected intensities I_m are to be derived from the measurements by means of a correction factor A_m^* such that

$$I_m = A_m^* H_m. \tag{6.3.3.40}$$

It is assumed that the correction can be written in the form of a rapidly converging Fourier series

$$A_m^* = \sum_{i,j,k,l=-\infty}^{\infty} a_{ijkl}\cos(i\Omega + j2\theta + k\chi + l\varphi) + b_{ijkl}\sin(i\Omega + j2\theta + k\chi + l\varphi). \tag{6.3.3.41}$$

The form of the geometrical terms may be simplified by taking advantage of the symmetry of the four-circle diffractometer. If it is assumed that diffraction is invariant to reversal of the incident and diffracted beams, the settings $\Omega, 2\theta, \chi, \varphi$; $\Omega, -2\theta, -\chi, \pi+\varphi$; $-\Omega, -2\theta, \pi+\chi, \varphi$; $-\Omega, 2\theta, \pi-\chi, \pi+\varphi$; $\pi+\Omega, -2\theta, \chi, \varphi$; $\pi+\Omega, 2\theta, -\chi, \pi+\varphi$; $\pi-\Omega, 2\theta, \pi+\chi, \varphi$; $\pi-\Omega, -2\theta, \pi-\chi, \pi+\varphi$ are equivalent. In shorthand notation, the series (6.3.3.41) reduces to

$$\begin{aligned} A_m^* = \sum a_{\rm cccc} + a_{\rm ccsc} + a_{\rm sccc} + a_{\rm scsc} + a_{\rm sssc} + a_{\rm sscc} \\ + a_{\rm cssc} + a_{\rm cscc} + b_{\rm cccs} + b_{\rm ccss} + b_{\rm sccs} + b_{\rm scss} \\ + b_{\rm ssss} + b_{\rm sscs} + b_{\rm csss} + b_{\rm cscs}. \end{aligned} \tag{6.3.3.42}$$

The range of indices for some terms may be restricted by noting other symmetries in the diffraction experiment. Thus, equation (6.3.3.40) will define the absorption correction for measurements of the incident-beam intensity, with $\Omega = 2\theta = 0$. Since with this geometry the correction will be invariant to rotation about the χ axis, the coefficients for the function involving $\cos(i\Omega)\cos(j2\theta)$ must vanish if the χ index, k, is non-zero. By similar reasoning with the φ axis along the incident beam, one may deduce that coefficients for $\sin(i\Omega)\cos(j2\theta)\sin(k\chi)$ will vanish unless $l = 0$.

Because for a given reflection all measurements are made at the same Bragg angle, the 2θ dependence of the correction cannot be determined by empirical methods. This factor in A is obtained from the absorption correction for a spherical crystal of equivalent radius.

Since an empirical absorption correction is defined only to within a scale factor, the scale must be specified by applying a constraint such that

$$\frac{1}{N_{\rm S}}\sum_{\rm S} A_{\rm S}^* = 1, \tag{6.3.3.43}$$

where $N_{\rm S}$ is the number of independent reflections. Equation (6.3.3.42) may be expressed in the shorthand notation

$$A_{\rm S}^* = \sum_{p=0} C_p f_{p\rm S}, \tag{6.3.3.44}$$

where C_p is the coefficient in a term such as $a_{\rm ccsc}$ or $b_{\rm ccss}$ and $f_{p\rm S}$ is the corresponding geometrical function. Labelling the constant geometrical term with a value of unity as f_0 and rearranging leads to

$$A_{\rm S}^* = 1 + \sum_{p=1} C_p\left\{f_{p\rm S} - \frac{1}{N_{\rm S}}\sum_{\rm S} f_{p\rm S}\right\} = 1 + \sum_{p=1} C_p g_{p\rm S}, \tag{6.3.3.45}$$

which defines $g_{p\rm S}$.

Equation (6.3.3.40) is now expressed as

$$I_{m\rm S} = H_{m\rm S} + H_{m\rm S}\sum_{p=1} C_p g_{p\rm S}, \tag{6.3.3.46}$$

in which the coefficients C_p are to be chosen so that the values of $I_{m\rm S}$ for each **S** are as near equal as possible. Since the values within each set will not be exactly equal, we rewrite (6.3.3.46) as

$$\Delta_{m\rm S} - H_{m\rm S} = -I_{\rm S} + H_{m\rm S}\sum_{p=1} C_p g_{p\rm S}, \tag{6.3.3.47}$$

in which the mean intensity $I_{\rm S}$ and the C_p are chosen to minimize $\sum_{{\rm S},m} w_{\rm S}^2\Delta_{m\rm S}^2$, where

$$\Delta_{m\rm S} = I_{m\rm S} - I_{\rm S}, \tag{6.3.3.48}$$

and $w_{\rm S}$ is the weight for that reflection.

If the equation to be solved

$$-w_{\rm S}H_{m\rm S} \simeq -w_{\rm S}I_m + \sum_{p=1} C_p g_{p\rm S} w_{\rm S} I_{m\rm S} \tag{6.3.3.49}$$

is written in the shorthand form

$$\boldsymbol{D} = \boldsymbol{F}\boldsymbol{C}, \tag{6.3.3.50}$$

in which $\boldsymbol{D}$ corresponds to $-w_{\rm S}H_{m\rm S}$, the I_m and C_p correspond to $\boldsymbol{C}$, with $(-w_{\rm S})$ and $w_{\rm S}g_{p\rm S}H_{m\rm S}$ corresponding to $\boldsymbol{F}$, the solution to (6.3.3.50) can be determined from the normal equations

$$\boldsymbol{C} = (\boldsymbol{F}^T\boldsymbol{F})^{-1}\boldsymbol{F}^T\boldsymbol{D}, \tag{6.3.3.51}$$

where $\boldsymbol{F}^T$ is the transpose of $\boldsymbol{F}$. This procedure suffers from the disadvantages of requiring a matrix inversion whenever the set of trial functions (*i.e.* those multiplied by the coefficients C_p) is modified. The tedious inversion of the normal equations, described by (6.3.3.51), may be replaced by a simple inversion *via* the Gram–Schmidt orthogonalizing process, *i.e.* by calculating a matrix $\boldsymbol{W}$ with mutually orthogonal columns $\boldsymbol{W}_j$ such that

$$\begin{aligned} \boldsymbol{W}_1 &= \boldsymbol{F}_1 \\ \boldsymbol{W}_j &= \boldsymbol{F}_j - \sum_{k=1}^{j-1}(\boldsymbol{F}_j\cdot\boldsymbol{W}_k)\boldsymbol{W}_k/\boldsymbol{W}_k^2. \end{aligned} \tag{6.3.3.52}$$

The minimizing of $(\boldsymbol{D}-\boldsymbol{F}\boldsymbol{C})^2$ is replaced by minimizing $(\boldsymbol{D}-\boldsymbol{W}\boldsymbol{A})^2$. Differentiating with respect to a_j yields

$$a_j = \frac{\boldsymbol{D}\cdot\boldsymbol{W}_j}{\boldsymbol{W}_j^2}. \tag{6.3.3.53}$$

If equation (6.3.3.52) is written as

$$\boldsymbol{F} = \boldsymbol{W}\boldsymbol{B},$$

where the upper triangular matrix $\boldsymbol{B}$ is

$$b_{ij} = \boldsymbol{F}_j \cdot \boldsymbol{W}_i / \boldsymbol{W}_i^2, \quad i < j; \quad b_{ij} = 1, i = j; \quad b_{ij} = 0, i > j, \tag{6.3.3.54}$$

the vector determining the coefficients is

$$\boldsymbol{C} = \boldsymbol{B}^{-1}\boldsymbol{A}, \tag{6.3.3.55}$$

in which the inversion of $\boldsymbol{B}$ is straightforward.

In difficult cases, with data affected by errors in addition to absorption, the method described may give physically unreasonable absorption corrections for some reflections. In such cases, it may help to impose the approximate constraints

$$\sum_{\mathbf{S}} w_{\mathbf{S}}^2 H_{m\mathbf{S}} \Big/ \sum_{\mathbf{S}} w_{\mathbf{S}}^2 = \sum_{\mathbf{S}} w_{\mathbf{S}}^2 I_{m\mathbf{S}} \Big/ \sum_{\mathbf{S}} w_{\mathbf{S}}^2. \tag{6.3.3.56}$$

If $m = 1, 2, \ldots, M$, this reduces to the M constraint equations

$$\sum_{p=1} C_p \left\{ \frac{\sum_{\mathbf{S}} w_{\mathbf{S}}^2 H_{m\mathbf{S}} g_{p\mathbf{S}}}{\sum_{\mathbf{S}} w_{\mathbf{S}}^2} \right\} = \sum_{p=1} C_p \left\{ \frac{\varepsilon w_m \sum_{\mathbf{S}} w_{\mathbf{S}}^2 H_{m\mathbf{S}} g_{p\mathbf{S}}}{\sum_{\mathbf{S}} w_{\mathbf{S}}^2} \right\} = 0, \tag{6.3.3.57}$$

where w_m is the square root of the weight for the weighted mean of the equivalent reflections H_m, defined as

$$H_m = \sum_{\mathbf{S}} w_{\mathbf{S}}^2 H_{m\mathbf{S}} \Big/ \sum_{\mathbf{S}} w_{\mathbf{S}}^2 \quad \text{for each } \mathbf{S}, \tag{6.3.3.58}$$

and the multiplier ε controls the strength with which the additional constraints are enforced. With the additional constraint equations, the sum of squares to be minimized, corresponding to (6.3.3.48), becomes

$$\sum_{\mathbf{S},m} w_{\mathbf{S}}^2 (I_{m\mathbf{S}} - I_m)^2 + \sum_{m} \varepsilon^2 w_m^2 (H_m - I_m)^2. \tag{6.3.3.59}$$

A closely related procedure expressing the absorption corrections as Fourier series in polar angles for the incident and diffracted beams is described by Katayama, Sakabe & Sakabe (1972). A similar method minimizing the difference between observed and calculated structure factors is described by Walker & Stuart (1983). Other experimental techniques for measuring data for empirical absorption corrections that could be analysed by the Fourier-series method are described by Kopfmann & Huber (1968), North, Phillips & Mathews (1968), Flack (1974), Stuart & Walker (1979), Lee & Ruble (1977*a*,*b*), Schwager, Bartels & Huber (1973), and Santoro & Wlodawer (1980).

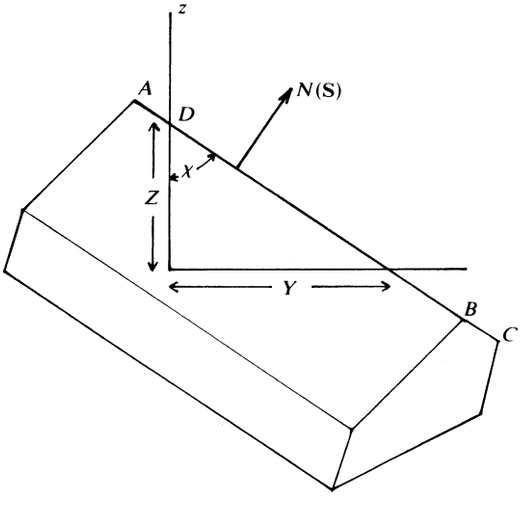

Fig. 6.3.3.4. Crystal oriented with the normal $N(\mathbf{S})$ to the face *ABCD* in the plane of view.

6.3.3.6. *Measuring crystals for absorption*

In general, A depends both on the shape of the crystal and on its orientation with respect to the incident and diffracted beams. To measure the shape of the crystal, a measuring microscope is mounted in the xy plane, and the crystal rotated about the z axis at right angles to that plane. A rotation about the z axis changes the orientation of the crystal x and y coordinates with respect to those (X and Y) for the measuring device. The x axis is directed from crystal to microscope when the angle of rotation about the z axis (φ) is zero. During rotation, each face will at some stage be oriented with its normal $N(\mathbf{S})$ perpendicular to the line of view, *i.e.* in the XY plane for instrument coordinates. If the angle of rotation at that orientation is denoted φ_N, the appearance of a typical face *ABCD* will be as indicated in Fig. 6.3.3.4.

The equation for the plane is

$$x \sin\varphi_N + y \cos\varphi_N + z \tan\chi = Y$$

or, equivalently,

$$(x \sin\varphi_N + y \cos\varphi_N) \cot\chi + z = Z.$$

For a crystal oriented on an Eulerian cradle, it is necessary to specify the orientation of the crystal, *i.e.* the angles Ω, χ, φ in which the measurements of the diffraction intensities are made. In a reflecting position, the reciprocal-lattice vector $\mathbf{S}$, which is normal to the Bragg planes, bisects the angle between the incident and diffracted beams, as shown in Fig. 6.3.3.5.

If the crystal is rotated about the reciprocal-lattice vector $\mathbf{S}$, varying the angle ψ, the crystal remains in a reflecting position. That is, there is a degree of freedom in the scattering experiment that enables the same reflection to be observed at different sets of Ω, χ, φ values. The path length varies with ψ, except for spherical crystals. In order to calculate an absorption correction, the value of ψ and its origin must be specified. For a crystal mounted on an Eulerian cradle, the bisecting position, with $\Omega = \theta$, is usually chosen as the origin for ψ.

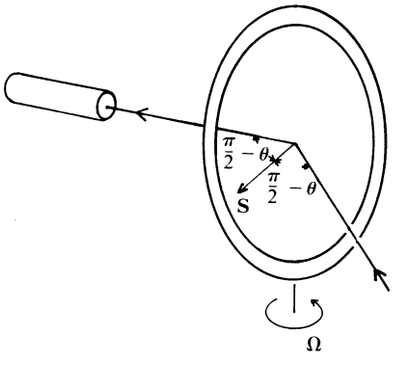

Fig. 6.3.3.5. Geometry of the Eulerian cradle in the bisecting position.

International Tables for Crystallography (2006). Vol. C, Chapter 6.4, pp. 609–616.

6.4. The flow of radiation in a real crystal

By T. M. Sabine

6.4.1. Introduction

In a diffraction experiment, a beam of radiation passes into the interior of a crystal *via* an entrance surface. When the crystal is set for Bragg reflection, a diffracted beam passes out of the crystal through the exit surface. The scattering vector is allowed to sweep over a small region around the exact Bragg position, and the total intensity scattered into a detector is recorded. This record (called the integrated intensity) contains all the information available to the crystallographer, and includes the starting point for crystal structure analysis, which is the relative magnitude of the structure factor for the reflection under examination. In order to determine the relationship between the structure factor and the observed integrated intensity, it is necessary to take into account all processes that remove intensity from the incident and diffracted beams during their passage through the crystal.

The standard theory, which is called the kinematic theory, assumes that there is no attenuation of either the incident beam or the diffracted beam during the diffraction process. The fact that this is not so in a real crystal is expressed in the following way.

$$I^{\rm obs} = EI^{\rm kin}.$$

E is equal to unity for a crystal, called the ideally imperfect crystal, which scatters in accordance with the kinematical approximation. In kinematic theory, the integrated intensity is proportional to the square of the magnitude of the structure factor, $|F|^2$. The factor E has a value very much less than unity for a perfect crystal, to which the dynamical theory of diffraction applies. In the dynamical theory, the integrated intensity is proportional to the first power of the structure-factor magnitude, $|F|$. All crystals in nature lie between these limits, either because of the microstructure of the crystal, or because of the removal of photons or neutrons by electronic or nuclear processes. A real crystal may behave as a perfect crystal for some reflections and as an imperfect crystal for others. It is the purpose of this section to give formulae by which the value of $|F|$ can be extracted from the measured intensity of a reflection from a real crystal without resorting to mechanical methods of changing its state of perfection. Those methods, such as quenching or irradiation with fast neutrons, usually introduce problems that are more difficult than those that they were designed to solve.

The formulae are constructed so that they apply at all angles of scattering, and are either analytic or rapidly convergent for ease of use in least-squares methods.

It should be noted that whenever the symbol F subsequently appears it should be interpreted as the modulus of the structure factor, which **always** *includes the Debye–Waller factor.*

In common with all published theories of extinction, the theory presented here is phenomenological, in that the assumption is made that the wavevector within the crystal does not differ from the wavevector in vacuum whatever the strength of the interaction between the incident radiation and the crystal. The results will be compared with a solution in the symmetric Bragg case in which the dynamic refractive index of the crystal has been taken into account (Sabine & Blair, 1992).

6.4.2. The model of a real crystal

Following Darwin (1922), a crystal is assumed to consist of small blocks of perfect crystal (called mosaic blocks). These blocks are separated by small-angle boundaries formed by dislocations (Read, 1953), which introduce random tilts of the blocks with respect to each other. It is necessary to divide this model into two subclasses. In the first, the introduction of tilts does not destroy the spatial correlation between atoms in different blocks that have the same relative orientation. In this model (hereafter called the correlated block model), the removal of dislocations constituting the mosaic block boundaries by, for example, thermal annealing will recover a monolithic perfect single crystal. In the second subclass, which is the original Darwin model (hereafter called the uncorrelated block model), the introduction of tilts destroys spatial coherence between blocks. The weakness of the latter model is that removal of the tilts does not recover the monolithic single crystal, but leads to a brick-wall-type structure with parallel bricks but varying thicknesses of mortar between the bricks. In practice, thermal-annealing treatments at sufficiently high temperatures always regain the single crystal.

The existence of this problem for extinction theory has been recognized (Wilkins, 1981). Theories will be given in this article for both limits. For a more complete treatment, the introduction of a mixing parameter proportional to either the dislocation density in the crystal or the physical proximity of mosaic blocks may be necessary.

For a single incident ray, only those blocks whose orientation is within the natural width for Bragg scattering from a perfect crystal will contribute to Bragg diffraction processes. For these processes, the crystal presents a sponge- or honeycomb-like aspect, since blocks that are outside the angular range for scattering do not contribute to the diffraction pattern. During the scan used for measurement of the integrated intensity, all blocks will contribute. At any angular setting, the entire volume of the crystal contributes to absorption and other non-Bragg-type interactions.

6.4.3. Primary and secondary extinction

It is customary in the literature to distinguish between primary extinction, which is extinction within a single mosaic block, and secondary extinction, which occurs when a ray reflected by one mosaic block is subsequently reflected by another block with the same orientation. In the correlated block model, no distinction is made between the two types, and the problem reduces to that of primary extinction in the crystal as a whole. The angular distribution of blocks is an indicator of the extent of diffraction coupling between blocks during the passage of a single ray through the crystal.

In the uncorrelated block model, the problem must be separated into two regimes, with the input to the secondary-extinction system being the intensities from each mosaic block after allowance for primary extinction within each mosaic block.

In all theories, it is assumed that the primary-extinction parameter (the block size) and the secondary-extinction parameter (the mosaic spread) are physically independent quantities. If the dislocations in the crystal are concentrated in the small-angle boundaries, the two parameters can be combined to give the dislocation density. Qualitatively, the lower the dislocation density the larger the block size and the smaller the mosaic spread. Cottrell (1953) has given the relationship

Copyright © 2006 International Union of Crystallography

$$\rho = \frac{\Theta}{b(D\ell)^{1/2}}, \tag{6.4.3.1}$$

where ρ is the dislocation density, Θ is the total mosaic spread in radians, b is the Burgers vector of the dislocations, ℓ is the block size and D is the size of the irradiated region.

6.4.4. Radiation flow

The radiation flow is governed by the Hamilton–Darwin (H–D) equations (Darwin, 1922; Hamilton, 1957). These equations are

$$\frac{\partial P_i}{\partial t_i} = \tau P_i + \sigma P_f, \tag{6.4.4.1}$$

$$\frac{\partial P_f}{\partial t_f} = \tau P_f + \sigma P_i. \tag{6.4.4.2}$$

Here, P_i is the radiation current density ($m^{-2}\ s^{-1}$) in the incident ($i =$ initial) beam, P_f is the current density in the diffracted ($f =$ final) beam. The distances t_i and t_f are measured along the incident and diffracted beams, respectively. The coupling constant σ is the cross section per unit volume for scattering into a single Bragg reflection, while τ, which is always negative, is the cross section per unit volume for removal of radiation from the beams by any process. In what follows, it will be assumed that absorption is the only significant process, and τ is given by $\tau = -(\sigma + \mu)$, where μ is the linear absorption coefficient (absorption cross section per unit volume). This assumption may not be true for neutron diffraction, in which incoherent scattering may have a significant role in removing radiation. In those cases, τ should include the incoherent scattering cross section per unit volume.

The H–D equations have analytical solutions in the Laue case ($2\theta = 0$) and the Bragg case ($2\theta = \pi$). The solutions at the exit surface are, respectively,

$$P_f = \frac{P_i^0}{2}\exp(-\mu D)[1 - \exp(-2\sigma D)], \tag{6.4.4.3}$$

and

$$P_f = \frac{P_i^0 \sigma \sinh(aD)}{a\cosh(aD) - \tau\sinh(aD)}, \tag{6.4.4.4}$$

with $a^2 = \tau^2 - \sigma^2$. The path length of the diffracted beam through the crystal is D. The current density at the entrance surface is P_i^0.

To find formulae for the integrated intensity, it is necessary to express σ in terms of crystallographic quantities.

6.4.5. Primary extinction

Zachariasen (1967) introduced the concept of using the kinematic result in the small-crystal limit for σ, while Sabine (1985, 1988) showed that only the Lorentzian or Fresnellian forms of the small crystal intensity distribution are appropriate for calculations of the energy flow in the case of primary extinction. Thus,

$$\sigma(\Delta k) = \frac{Q_k T}{1 + (\pi T \Delta k)^2}, \tag{6.4.5.1}$$

where $Q_k V$ is the kinematic integrated intensity on the k scale ($k = 2\sin\theta/\lambda$), $Q_k = (N_c\lambda F)^2/\sin\theta$, and T is the volume average of the thickness of the crystal normal to the diffracting plane (Wilson, 1949). To include absorption effects, which modify the diffraction profile of the small crystal, it is necessary to replace T by TC, where

$$C = \frac{\tanh(\mu D/2)}{(\mu D/2)}. \tag{6.4.5.2}$$

To determine the extinction factor, E, the explicit expression for $\sigma(\Delta k)$ [equation (6.4.5.1)] is inserted into equations (6.4.4.3) and (6.4.4.4), and integration is carried out over Δk. The limits of integration are $+\infty$ and $-\infty$. The notation E_L and E_B is used for the extinction factors at $2\theta = 0$ and $2\theta = \pi$ rad, respectively.

After integration and division by $I^{\rm kin}$, it is found that

$$E_L = \exp(-y)\{[1 - (x/2) + (x^2/4) - (5x^3/48) + (7x^4/192)]\}, \quad x \le 1, \tag{6.4.5.3}$$

$$E_L = \exp(-y)[2/(\pi x)]^{1/2}\{1 - [1/(8x)] - [3/(128x^2)] - [15/(1024x^3)]\}, \quad x > 1, \tag{6.4.5.4}$$

$$E_B = A/(1 + Bx)^{1/2}, \tag{6.4.5.5}$$

$$A = \exp(-y)\sinh y/y, \tag{6.4.5.6}$$

and

$$B = (1/y) - \exp(-y)/\sinh y = A\frac{\mathrm{d}(A^{-1})}{\mathrm{d}y}. \tag{6.4.5.7}$$

In these equations, $x = Q_k TCD$ and $y = \mu D$.

6.4.6. The finite crystal

Exact application of the formulae above requires a knowledge of the shape of the crystal or mosaic block and the angular relation between the reflecting plane and the crystal surface. These are not usually known, but it can be assumed that the average block or crystal at each value of the scattering angle (2θ) has sides of equal length parallel to the incident- and diffracted-beam directions. For this crystal,

$$T = D\sin\theta, \ D = \langle L\rangle, \tag{6.4.6.1}$$

and

$$x = N_c{}^2\lambda^2F^2\langle L\rangle^2\tanh(\mu L^*/2)/(\mu L^*/2). \tag{6.4.6.2}$$

The quantity L^* is set equal to ℓ for the mosaic block and to L for the crystal.

6.4.7. Angular variation of E

Werner (1974) has given exact solutions to the transport equations in terms of tabulated functions. However, for the simple crystal described above, a sufficiently accurate expression is

$$E(2\theta) = E_L\cos^2\theta + E_B\sin^2\theta. \tag{6.4.7.1}$$

6.4.8. The value of x

For the single mosaic block, application of the relationship $T = D\sin\theta$ leads to

$$x = (N_c\lambda F\ell)^2, \tag{6.4.8.1}$$

where ℓ is the average path length through the block. In the correlated block model, x is also a function of the tilts between blocks and the size of the crystal.

It will be assumed for the discussion that follows in this section that the mosaic blocks are cubes of side ℓ, and the distribution of tilts will be assumed to be isotropic and Gaussian, given by

$$W(\Delta) = \frac{1}{\eta\sqrt{2\pi}} \exp\left(-\frac{\Delta^2}{2\eta^2}\right), \qquad (6.4.8.2)$$

where Δ is the angular deviation of the block from the mean orientation of all blocks in the crystal, and η is the standard deviation of the distribution. (The assumption of a Gaussian distribution is not critical to the argument that follows.)

Let the crystal be a cube of side L, and let α be the probability that a ray reflected by the first block is reflected again by a subsequent block. The effective size of the crystal for Bragg scattering of a single incident ray is then

$$\langle L \rangle = \ell + (L - \ell)\alpha, \qquad (6.4.8.3)$$

while the size of the crystal for all other attenuation processes is L, since, for them, the Bragg condition does not apply. The probability of re-scattering, α, can readily be expressed in terms of crystallographic quantities. The full width at half-maximum intensity of the Darwin reflection curve is given, after conversion to the glancing-angle (θ) scale, by Zachariasen (1945) as

$$\Delta\theta = \frac{3\lambda^2 N_c F}{\pi\sqrt{2}\sin 2\theta} \text{ (radians)}. \qquad (6.4.8.4)$$

The full width at half-maximum (FWHM) of the mosaic-block distribution (6.4.8.2) is derived in the usual way, and the parameter g ($= 1/2\eta\sqrt{\pi}$) is introduced to clear (to 1%) numerical constants. Then α, which is equal to the ratio of the widths, is given by

$$\alpha = \frac{g N_c \lambda^2 F}{\sin 2\theta}. \qquad (6.4.8.5)$$

Insertion of $\langle L \rangle$ [equation (6.4.8.3)] in place of ℓ in equation (6.4.8.1) for x leads to

$$x = [N_c \lambda F \ell + g Q_\theta (L - \ell)]^2, \qquad (6.4.8.6)$$

where $Q_\theta = N_0^2 \lambda^3 F^2 / \sin 2\theta$.

6.4.9. Secondary extinction

A separate treatment of secondary extinction is required only in the uncorrelated block model, and the method given by Hamilton (1957) is used in this work. The coupling constant in the H–D equations is given by $\sigma(\Delta\theta) = Q_\theta E_p W(\Delta\theta)$, where $Q_\theta = N_c^2 \lambda^3 F^2 / \sin 2\theta$ for equatorial reflections in the neutron case, E_p is the correction for primary extinction evaluated at the angle θ, and $W(\Delta\theta)$ is the distribution function for the tilts between mosaic blocks. The choice of this function has a significant influence on the final result (Sabine, 1985), and a rectangular or triangular form is suggested.

In the following equations for the secondary-extinction factor,

$$x = E_p Q_\theta G D, \qquad (6.4.9.1)$$

and A and B are given by equations (6.4.5.6) and (6.4.5.7). The average path length through the crystal for the reflection under consideration is D and G is the integral breadth of the angular distribution of mosaic blocks. It is important to note that A should be set equal to one if the data have been corrected for absorption, and B should be set equal to one if absorption-weighted values of D are used. If D for each reflection is not known, the average dimension of the crystal may be used for all reflections.

For a rectangular function, $W(\Delta\theta) = G$, for $|\Delta\theta| \leq 1/2G$, $W(\Delta\theta) = 0$ otherwise, and the secondary-extinction factor becomes

$$E_L = \frac{\exp(-\mu D)}{2x}[1 - \exp(-2x)], \qquad (6.4.9.2)$$

$$E_B = \frac{A}{1 + Bx}. \qquad (6.4.9.3)$$

For a triangular function, $W(\Delta\theta) = G(1 - |\Delta\theta|G)$, for $|\Delta\theta| \leq 1/G$, $W(\Delta\theta) = 0$ otherwise, and the secondary-extinction factor becomes

$$E_L = \frac{\exp(-\mu D)}{x}\left\{1 - \frac{1}{2x}[1 - \exp(-2x)]\right\}, \qquad (6.4.9.4)$$

$$E_B = \frac{2A}{(Bx)^2}[Bx - \ln|1 + Bx|]. \qquad (6.4.9.5)$$

6.4.10. The extinction factor

6.4.10.1. *The correlated block model*

For this model of the real crystal, the variable x is given by equation (6.4.8.6), with ℓ and g the refinable variables. Extinction factors are then calculated from equations (6.4.5.3), (6.4.5.4), and (6.4.5.5). For a reflection at a scattering angle of 2θ from a reasonably equiaxial crystal, the appropriate extinction factor is given by (6.4.7.1) as $E(2\theta) = E_L \cos^2 2\theta + E_B \sin^2 2\theta$.

It is a meaningful procedure to refine both primary and secondary extinction in this model. The reason for the high correlation between ℓ and g that is found when other theories are applied, for example that of Becker & Coppens (1974), lies in the structure of the quantity x. In the theory presented here, x is proportional to F^2 for pure primary extinction and to Q_θ^2 for pure secondary extinction.

6.4.10.2. *The uncorrelated block model*

When this model is used, two values of x are required. These are designated x_p for primary extinction and x_s for secondary extinction. Equation (6.4.8.1) is used to obtain a value for x_p. The primary-extinction factors are then calculated from (6.4.5.3), (6.4.5.4) and (6.4.5.5), and $E_p(2\theta)$ is given by equation (6.4.7.1). In the second step, x_s is obtained from equation (6.4.9.1), and the secondary-extinction factors are calculated from either (6.4.9.2) and (6.4.9.3) or (6.4.9.4) and (6.4.9.5). The result of these calculations is then used in equation (6.4.7.1) to give $E_s(2\theta)$. It is emphasised that x_s includes the primary-extinction factor. Finally, $E(2\theta) = E_p(2\theta)E_s[E_p(2\theta), 2\theta]$.

Application of both models to the analysis of neutron diffraction data has been carried out by Kampermann, Sabine, Craven & McMullen (1995).

6.4.11. Polarization

The expressions for the extinction factor have been given, by default, for the σ-polarization state, in which the electric field vector of the incident radiation is perpendicular to the plane defined by the incident and diffracted beams. For this state, the polarization factor is unity. For the π-polarization state, in which the electric vector lies in the diffraction plane, the factor is $\cos 2\theta$. The appropriate values for the extinction factors for this state are given by multiplying F by $\cos 2\theta$ wherever F occurs.

For neutrons, which are matter waves, the polarization factor is always unity.

For an unpolarized beam from an X-ray tube, the observed integrated intensity is given by $I^{\rm obs} = \frac{1}{2} I_\theta^{\rm kin}\left(E_\sigma + E_\pi \cos^2 2\theta\right)$. In the kinematic limit, $E_\sigma = E_\pi = 1$, and the power to which $\cos 2\theta$

is raised (the polarization index n) is 2. In the pure primary-extinction limit, $E_\sigma = 1/(N_c\lambda F\ell)$, while $E_\pi = 1/(N_c\lambda F\ell\cos 2\theta)$. Hence, $n = 1$. In the pure secondary-extinction limit, $E_\sigma = 1/(gQL)$, where g is the mosaic-spread parameter, while $E_\pi = 1/(QgL\cos 2\theta)$. Hence, $n = 0$. In all real cases, n will lie between 0 and 2, and its value will reflect departures from kinematic behaviour.

6.4.12. Anisotropy

The parameters describing the microstructure of the crystal are the mosaic-block size and the angle between the mosaic blocks. These are not constrained in any way to be isotropic with respect to the crystal axes. In particular, they are not constrained by symmetry. For example, in a face-centred-cubic crystal under uniaxial stress, slip will occur on one set of {111} planes, leading to a dislocation array of non-cubic symmetry. In principle, anisotropy can be incorporated into the formal theory by allowing ℓ and g to depend on the Miller indices of the reflections. This has not been done in this work, but reference should be made to the work of Coppens & Hamilton (1970).

6.4.13. Asymptotic behaviour of the integrated intensity

From the definition of the extinction factor, the integrated intensity from a non-absorbing crystal in which the block size is sufficiently small, and the mosaic spread is sufficiently large, will approach the kinematic limit. It is instructive to examine the behaviour in the limit of large block size and low mosaic spread. The volume of the mosaic block is v and the volume of the crystal is V. The number of blocks in the crystal is V/v $(= L^3/\ell^3)$. The surface area of the block is $v^{2/3}$ and of the crystal is $V^{2/3}$. The subscripts L and B will again be used for the Laue and the Bragg case, respectively. The kinematic integrated intensity is given by

$$I^{\rm kin} = Q_\theta V = \lambda^3 N_c^2 F^2 V/\sin 2\theta. \qquad (6.4.13.1)$$

6.4.13.1. *Non-absorbing crystal, strong primary extinction*

(*a*) *Laue case*

The limiting value of E_L is $(2/\pi)^{1/2}x^{-1/2}$. Hence,

$$I_L = (4/5)N_c\lambda^2 FVv^{-1/3}/\sin 2\theta. \qquad (6.4.13.2)$$

The dynamical theory has a numerical constant of 1/2 instead of 4/5.

(*b*) *Bragg case*

The limiting value of E_B is $x^{-1/2}$. Hence,

$$I_B = N_c\lambda^2 FVv^{-1/3}/\sin 2\theta. \qquad (6.4.13.3)$$

This is in exact agreement with the dynamical theory (Ewald solution).

6.4.13.2. *Non-absorbing crystal, strong secondary extinction*

For this condition, the limiting values of the integrated intensity are $I_L = (4/5)g^{-1}V^{2/3}$, and $I_B = g^{-1}V^{2/3}$. In this limit, which was also noted by Bacon & Lowde (1948) and by Hamilton (1957), the intensity is proportional only to the mosaic spread and to the surface area of the crystal. No structural information is obtained from the experiment.

6.4.13.3. *The absorbing crystal*

Only the Bragg case for thick crystals will be considered here. The asymptotic values of A, B, and C are $1/(2\mu L^*)$, $1/(\mu L^*)$, and $2/(\mu L^*)$, respectively, so that

$$BCx = 2N_c^2\lambda^2F^2/\mu^2. \qquad (6.4.13.4)$$

For BCx small, the integrated intensity, I_B, is given by

$$I_B = (Q_\theta/2\mu)[1 - (N_cF/)2]V^{2/3}. \qquad (6.4.13.5)$$

For BCx large,

$$I_B = (1/2\sqrt{2})[1 - (\mu/2\lambda N_cF)^2]\lambda^2 N_cFV^{2/3}/\sin 2\theta. \qquad (6.4.13.6)$$

It can be shown that the parameter g (which has no relation to the parameter g used to describe the mosaic-block distribution) used by Zachariasen (1945) in discussing this case is equal to $-\mu/2NCF$. Hence, on his y scale,

$$I_B = (\pi/2\sqrt{2})[1 - g^2]. \qquad (6.4.13.7)$$

The value he obtained is $I_B = 8/3[1 - 2|g|]$, while Sabine & Blair (1992) found $I_B = 8/3[1 - 2.36|g|]$.

6.4.14. Relationship with the dynamical theory

Sabine & Blair have shown that the two classical limits for the integrated intensity in the symmetric Bragg case can be obtained from the Hamilton–Darwin equations when the dynamic refractive index of the crystal is explicitly taken into account. Their treatment is based on the following expression for $\sigma(\Delta k)$:

$$\sigma(\Delta k) = \frac{Q_k\mu DT}{\sinh(\mu D)}\left\{\frac{\sin^2(\pi\, T\Delta K) + \sinh^2(\mu D/2)}{(\pi T\Delta K)^2 + (\mu D/2)^2}\right\},$$

where ΔK refers to the scattering vector within the crystal. Use of the relation $\Delta K \cong \Delta k$ and the replacement of the Fresnellian by a Lorentzian leads to equation (6.4.5.1) with the inclusion of C (6.4.5.2). The relationship between ΔK and Δk, which is a function of the dynamic refractive index of the crystal, is derived in the original publication. Insertion of this expression into equations (6.4.4.3) and (6.4.4.4) and integration over Δk, since the diffracted beam is observed outside the crystal, leads to a dynamic extinction factor, which can be compared with the values determined from the equations given in Section 6.4.5. The integrations cannot be carried out analytically and require numerical calculation in each case.

Olekhnovich & Olekhnovich (1978, 1980) have given limited expressions for primary extinction in the parallelepiped and the cylinder based on the equations of the dynamical theory in the non-absorbing case. Comparisons with the results of the present theory are given by Sabine (1988) and Sabine, Von Dreele & Jørgensen (1988).

6.4.15. Definitions

The quantity F used in these equations is the modulus of the structure factor per unit cell. It includes the Debye–Waller factor and the scattering length of each atom. (For X-ray diffraction, the scattering length of the electron is 2.8178×10^{-15} m.) λ is the wavelength of the incident radiation. 2θ is the angle of scattering. N_c is the number of unit cells per unit volume. The path length of the diffracted beam is D, while T is the thickness of the crystal normal to the diffracting plane. In practice, when the orientation of the crystal is unknown, D can be taken equal to ℓ or L, where these are average dimensions of the mosaic block or crystal.

References

6.1.1

Abramowitz, M. & Stegun, I. A. (1964). *Handbook of mathematical functions*. National Bureau of Standards Publication AMS 55.

Ahlrichs, R. & Taylor, P. R. (1981). *The choice of Gaussian basis sets for molecular electronic structure calculations. J. Chim. Phys.* **78**, 316–323.

Altmann, S. L. & Cracknell, A. P. (1965). *Lattice harmonics. I. Cubic groups. Rev. Mod. Phys.* **37**, 19–32.

Atoji, M., Watanabe, T. & Lipscomb, W. N. (1953). *The X-ray scattering from a hindered rotator. Acta Cryst.* **6**, 62–66.

Avery, J. & Watson, K. J. (1977). *Generalized X-ray scattering factors. Simple closed-form expressions for the one-centre case with Slater-type orbitals. Acta Cryst.* A**33**, 679–680.

Bellman, R. (1961). *A brief introduction to theta functions*. New York: Holt, Reinhart and Winston.

Chidambaram, R. & Brown, G. M. (1973). *A model for a torsional oscillator in crystallographic least-squares refinement. Acta Cryst.* B**29**, 2388–2392.

Clementi, E. & Roetti, C. (1974). *Roothaan–Hartree–Fock atomic wavefunctions. Basis functions and their coefficients for ground and certain excited states of neutral and ionized atoms. At. Data Nucl. Data Tables*, **14**, 177–478.

Coulthard, M. A. (1967). *A relativistic Hartree–Fock atomic field calculation. Proc. Phys. Soc.* **91**, 44–49.

Cromer, D. T. & Mann, J. B. (1968). *X-ray scattering factors computed from numerical Hartree–Fock wave functions*. Los Alamos Scientific Laboratory Report LA-3816.

Cromer, D. T. & Waber, J. T. (1968). Unpublished work reported in *International tables for X-ray crystallography* (1974), Vol. IV, p. 71. Birmingham: Kynoch Press. (Present distributor: Kluwer Academic Publishers, Dordrecht.)

Dawson, B. (1970). *Neutron studies of nuclear charge distributions in barium fluoride and hexamethylenetetramine. Thermal neutron diffraction*, edited by B. T. M. Willis, pp. 101–123. Oxford University Press.

Doyle, P. A. & Turner, P. S. (1968). *Relativistic Hartree–Fock and electron scattering factors. Acta Cryst.* A**24**, 390–397.

Duijneveldt, F. B. van (1971). IBM Technical Report RJ-945.

Dunning, T. H. Jr & Jeffrey-Hay, P. (1977). *Gaussian basis sets for molecular calculations. Modern theoretical chemistry 3. Methods of electronic structure theory*, edited by H. F. Schaefer III, pp. 1–27. New York: Plenum.

Favro, L. D. (1960). *Theory of the rotational motion of a free rigid body. Phys. Rev.* **119**, 53–62.

Feller, W. (1966). *An introduction to probability theory and its applications*, Vol. II, Chap. 19. New York: John Wiley.

Fisher, R. (1953). *Dispersion on a sphere. Proc. R. Soc. London Ser. A*, **217**, 295–305.

Fox, A. G., O'Keefe, M. A. & Tabbernor, M. A. (1989). *Relativistic Hartree–Fock X-ray and electron atomic scattering factors at high angles. Acta Cryst.* A**45**, 786–793.

Furry, W. H. (1957). *Isotropic rotational Brownian motion. Phys. Rev.* **107**, 7–13.

Gumbel, E. J., Greenwood, J. A. & Durand, D. (1953). *The circular normal distribution: theory and tables. J. Am. Stat. Assoc.* **48**, 131–152.

Huzinaga, S. (1971). *Approximate atomic functions I, II, III*. Technical Report, University of Alberta, Edmonton, Alberta, Canada.

Johnson, C. K. & Levy, H. A. (1974). *Thermal motion of independent atoms. International tables for X-ray crystallography*. Vol. IV, pp. 317–319. Birmingham: Kynoch Press. (Present distributor: Kluwer Academic Publishers, Dordrecht.)

Kay, M. I. & Behrendt, D. R. (1963). *The structure factor for a harmonic quasi-torsional oscillator. Acta Cryst.* **16**, 157–162.

Kendall, M. G. & Stuart, A. (1963). *The advanced theory of statistics*, Vol. 1, Chaps. 2, 3 and 6. London: Griffin.

King, M. V. & Lipscomb, W. N. (1950). *The X-ray scattering from a hindered rotator. Acta Cryst.* **3**, 155–158.

Kuhs, W. F. (1983). *Statistical description of multimodal atomic probability densities. Acta Cryst.* A**39**, 149–158.

Kurki-Suonio, K. (1977). *Electron density mapping in molecules and crystals. IV. Symmetry and its implications. Isr. J. Chem.* **16**, 115–123.

Kurki-Suonio, K., Merisalo, M. & Peltonen, H. (1979). *Site symmetrized Fourier invariant treatment of anharmonic temperature factors. Phys. Scr.* **19**, 57–63.

Kuznetsov, P. I., Stratonovich, R. L. & Tikhonov, V. I. (1960). *Quasi-moment functions in the theory of random processes. Theory Probab. Appl. (USSR)*, **5**, 80–97.

Lévy, P. (1938). *C. R. Soc. Math. Fr.* p. 32. Also *Processus stochastiques et mouvement Brownian*, p. 182. Paris: Gauthier-Villars.

Mackenzie, J. K. & Mair, S. L. (1985). *Anharmonic temperature factors: the limitations of perturbation-theory expressions. Acta Cryst.* A**41**, 81–85.

McLean, A. D. & Chandler, G. S. (1979). IBM Research Report RJ-2665 (34180).

McLean, A. D. & Chandler, G. S. (1980). *Contracted basis sets for molecular calculations. I. Second row atoms, Z = 11–18. J. Chem. Phys.* **72**, 5639–5648.

Mair, S. L. (1980*a*). *Temperature dependence of the anharmonic Debye–Waller factor. J. Phys. C*, **13**, 2857–2868.

Mair, S. L. (1980*b*). *The anharmonic Debye–Waller factor in the classical limit. J. Phys. C*, **13**, 1419–1425.

Mair, S. L. & Wilkins, S. W. (1976). *Anharmonic Debye–Waller factor using quantum statistics. J. Phys. C*, **9**, 1145–1158.

Mann, J. B. (1968*a*). Unpublished work reported in *International tables for X-ray crystallography* (1974), Vol. IV, p. 71. Birmingham: Kynoch Press. (Present distributor: Kluwer Academic Publishers, Dordrecht.)

Mann, J. B. (1968*b*). Los Alamos Scientific Laboratory Report LA-3961, p. 196.

Mardin, K. V. (1972). *Statistics of directional data*. New York: Academic Press.

Maslen, E. N. (1968). *An expression for the temperature factor of a librating atom. Acta Cryst.* A**24**, 434–437.

Mises, R. von (1918). *Über die 'Ganzahligheit' der Atomgewichte und verwandte Fragen. Phys. Z.* **19**, 490–500.

Normand, J.-M. (1980). *A Lie group: rotations in quantum mechanics*, p. 461. Amsterdam: North-Holland.

Pawley, G. S. & Willis, B. T. M. (1970). *Neutron diffraction study of the atomic and molecular motion in hexamethylenetetramine. Acta Cryst.* A**26**, 263–271.

Perrin, F. (1928). *Etude mathématique du mouvement Brownien de rotation. Ann. Ecole. Norm.* Suppl. 45, pp. 1–23.

Perrin, F. (1934). *Mouvement Brownien d'un ellipsoïde (I). Dispersion diélectrique pour des molécules ellipsoïdales. J. Phys. Radium*, **5**, 497.

6.1.1 (*cont.*)

Press, W. & Hüller, A. (1973). *Analysis of orientationally disordered structures. I. Method. Acta Cryst.* A**29**, 252–256.

Roberts, P.-H. & Ursell, H. D. (1960). *Random walk on a sphere. Philos. Trans. R. Soc. London Ser. A*, **252**, 317–356.

Roos, B. & Siegbahn, P. (1970). *Gaussian basis sets for the first and second row atoms. Theor. Chim. Acta*, **17**, 209–215.

Scheringer, C. (1985). *A general expression for the anharmonic temperature factor in the isolated-atom-potential approach. Acta Cryst.* A**41**, 73–79.

Stephens, M. A. (1963). *Random walk on a circle. Biometrika*, **50**, 385–390.

Stewart, R. F. (1980*a*). *Algorithms for Fourier transforms of analytical density functions. Electron and magnetisation densities in molecules and crystals*, edited by P. Becker, pp. 439–442. New York: Plenum.

Stewart, R. F. (1980*b*). *Multipolar expansions of one-electron densities. Electron and magnetisation densities in molecules and crystals*, edited by P. Becker, pp. 405–425. New York: Plenum.

Stewart, R. F., Davidson, E. R. & Simpson, W. T. (1965). *Coherent X-ray scattering for the hydrogen atom in the hydrogen molecule. J. Chem. Phys.* **42**, 3175–3187.

Thakkar, A. J. & Smith, V. H. Jr (1992). *High-accuracy ab initio form factors for the hydride anion and isoelectronic species. Acta Cryst.* A**48**, 70–71.

Veillard, A. (1968). *Gaussian basis sets for molecular wavefunctions containing second row atoms. Theor. Chim. Acta*, **12**, 405–411.

Zucker, U. H. & Schulz, H. (1982). *Statistical approaches for the treatment of anharmonic motion in crystals. I. A comparison of the most frequently used formalisms of anharmonic thermal vibrations. Acta Cryst.* A**38**, 563–568.

6.1.2

Blume, M. (1963). *Polarization effects in the magnetic elastic scattering of slow neutrons. Phys. Rev.* **130**, 1670–1676.

Clementi, E. & Roetti, C. (1974). *Roothaan–Hartree–Fock atomic wavefunctions. Basis functions and their coefficients for ground and certain excited states of neutral and ionized atoms. At. Data Nucl. Data Tables*, **14**, 177–478.

Desclaux, J. P. & Freeman, A. J. (1978). *Dirac–Fock studies of some electronic properties of actinide ions. J. Magn. Magn. Mater.* **8**, 119–129.

Freeman, A. J. & Desclaux, J. P. (1972). *Neutron magnetic form factor of gadolinium. Int. J. Magn.* **3**, 311–317.

Lovesey, S. W. (1984). *Theory of neutron scattering from condensed matter*. Vol. 2. *Polarization effects and magnetic scattering*. The International Series of Monographs on Physics No. 72. Oxford University Press.

Nathans, R., Shull, C. G., Shirane, G. & Andresen, A. (1959). *The use of polarised neutrons in determining the magnetic scattering by iron and nickel. J. Phys. Chem. Solids*, **10**, 138–146.

Shirane, G. (1959). *A note on the magnetic intensities of powder neutron diffraction. Acta Cryst.* **12**, 282–285.

Trammell, G. T. (1953). *Magnetic scattering of neutrons from rare earth ions. Phys. Rev.* **92**, 1387–1393.

6.1.3

Bacon, G. E. (1975). *Neutron diffraction*, 3rd ed. Oxford: Clarendon Press.

International Tables for Crystallography (1983). Vol. A, edited by Th. Hahn. Dordrecht: Kluwer Academic Publishers.

International Tables for Crystallography (1992). Vol. B, edited by U. Shmueli. Dordrecht: Kluwer Academic Publishers.

Ramaseshan, S., Ramesh, T. G. & Ranganath, G. S. (1975). *A unified approach to the theory of anomalous scattering. Some novel applications of the multiple-wavelength method. Anomalous scattering*, edited by S. Ramaseshan & S. C. Abrahams, pp. 139–161. Copenhagen: Munksgaard.

Schoenborn, B. P. (1975). *Phasing of neutron protein data by anomalous dispersion. Anomalous scattering*, edited by S. Ramaseshan & S. C. Abrahams, pp. 407–421. Copenhagen: Munksgaard.

Shull, C. G. (1967). *Neutron interactions with atoms. Trans. Am. Crystallogr. Assoc.* **3**, 1–16.

6.2

Arndt, U. W. & Willis, B. T. M. (1966). *Single crystal diffractometry*. Cambridge University Press.

Bouman, J. & de Jong, W. F. (1938). *Die Intensitäten der Punkte einer photographierten reziproken Netzebene. Physica (Utrecht)*, **5**, 817–832.

Buerger, M. J. (1940). *The correction of X-ray diffraction intensities for Lorentz and polarization factors. Proc. Natl Acad. Sci. USA*, **26**, 637–642.

Buerger, M. J. (1944). *The photography of the reciprocal lattice*. American Society for X-ray and Electron Diffraction, Monograph No. 1.

Burbank, R. D. (1952). *Upper level precession photography and the Lorentz–polarization correction. Part I. Rev. Sci. Instrum.* **23**, 321–327.

Debye, P. (1914). *Interferenz von Röntgenstrahlen und Wärmebewegung. Ann. Phys. (Leipzig)*, **43**, 49–95.

Grenville-Wells, H. J. & Abrahams, S. C. (1952). *Upper level precession photography and the Lorentz–polarization correction. Part II. Rev. Sci. Instrum.* **23**, 328–331.

Hu, H.-C. (1997*a*). *A universal treatment of X-ray and neutron diffraction in crystals. I. Theory. Acta Cryst.* A**53**, 484–492.

Hu, H.-C. (1997*b*). *A universal treatment of X-ray and neutron diffraction in crystals. II. Extinction. Acta Cryst.* A**53**, 493–504.

Hu, H.-C. & Fang, Y. (1993). *Neutron diffraction in flat and bent mosaic crystals for asymmetric geometry. J. Appl. Cryst.* **26**, 251–257.

Kasper, J. S. & Lonsdale, K. (1959). *International tables for X-ray crystallography*. Vol. II. *Mathematical tables*. Birmingham: Kynoch Press.

Kasper, J. S. & Lonsdale, K. (1972). *International tables for X-ray crystallography*. Vol. II. *Mathematical tables*. Corrected reprint. Birmingham: Kynoch Press.

Klug, H. P. & Alexander, L. E. (1974). *X-ray procedures for polycrystalline and amorphous materials*. New York: John Wiley.

Mackay, A. L. (1960). *An axial retigraph. Acta Cryst.* **13**, 240–245.

Waser, J. (1951*a*). *The Lorentz factor for the Buerger precession method. Rev. Sci. Instrum.* **22**, 563–566.

Waser, J. (1951*b*). *Lorentz and polarization correction for the Buerger precession method. Rev. Sci. Instrum.* **22**, 567–568.

6.2 (*cont.*)

Werner, S. A. & Arrott, A. (1965). *Propagation of Bragg-reflected neutrons in large mosaic crystals and the efficiency of monochromators*. *Phys. Rev.* **140**, A675–A686.

Werner, S. A., Arrott, A., King, J. S. & Kendrick, H. (1966). *Propagation of Bragg-reflected neutrons in bounded mosaic crystals*. *J. Appl. Phys.* **37**, 2343–2350.

6.3

Abramowitz, M. & Stegun, I. A. (1964). *Handbook of mathematical functions*, p. 916. National Bureau of Standards Publication AMS 55.

Alcock, N. W., Pawley, G. S., Rourke, C. P. & Levine, M. R. (1972). *An improvement in the algorithm for absorption correction by the analytical method*. *Acta Cryst.* A**28**, 440–444.

Anderson, D. W. (1984). *Absorption of ionizing radiation*. Baltimore: University Park Press.

Azaroff, L. V., Kaplow, R., Kato, N., Weiss, R. J., Wilson, A. J. C. & Young, R. A. (1974). *X-ray diffraction*, pp. 282–284. New York: McGraw-Hill.

Becker, P. J. & Coppens, P. (1974). *Extinction within the limit of validity of the Darwin transfer equations. I. General formalisms for primary and secondary extinction and their application to spherical crystals*. *Acta Cryst.* A**30**, 129–147.

Beeman, W. W. & Friedman, H. (1939). *The X-ray K absorption edges of the elements Fe (26) to Ge (32)*. *Phys. Rev.* **56**, 392–405.

Coppens, P. (1970). *The evaluation of absorption and extinction in single crystal structure analysis*. *Crystallographic computing*, edited by F. R. Ahmed, S. R. Hall & C. P. Huber, pp. 255–270. Copenhagen: Munksgaard.

Coyle, B. A. (1972). *Absorption and volume corrections for a cylindrical specimen, larger than the beam, and in general orientation*. *Acta Cryst.* A**28**, 231–233.

Coyle, B. A. & Schroeder, L. W. (1971). *Absorption and volume corrections for a cylindrical sample, larger than the X-ray beam, employed in Eulerian geometry*. *Acta Cryst.* A**27**, 291–295.

Dwiggins, C. W. Jr (1975*a*). *Rapid calculation of X-ray absorption correction factors for cylinders to an accuracy of 0.1%*. *Acta Cryst.* A**31**, 146–148.

Dwiggins, C. W. Jr (1975*b*). *Rapid calculation of X-ray absorption correction factors for spheres to an accuracy of 0.05%*. *Acta Cryst.* A**31**, 395–396.

Flack, H. D. (1974). *Automatic absorption correction using intensity measurements from azimuthal scans*. *Acta Cryst.* A**30**, 569–573.

Flack, H. D. (1977). *An empirical absorption–extinction correction technique*. *Acta Cryst.* A**33**, 890–898.

Flack, H. D. & Vincent, M. G. (1978). *Absorption weighted mean path lengths for spheres*. *Acta Cryst.* A**34**, 489–491.

Fukamachi, T., Karamura, T., Hayakawa, K., Nakano, Y. & Koh, F. (1982). *Observation of effect of temperature on X-ray diffraction intensities across the In K absorption edge of InSb*. *Acta Cryst.* A**38**, 810–813.

Graaff, R. A. G. de (1973). *A Monte Carlo method for the calculation of transmission factors*. *Acta Cryst.* A**29**, 298–301.

Graaff, R. A. G. de (1977). *On the calculation of transmission factors*. *Acta Cryst.* A**33**, 859.

James, R. W. (1962). *The optical principles of the diffraction of X-rays*, pp. 135–192. Ithaca: Cornell University Press.

Karamura, T. & Fukamachi, T. (1979). *Temperature dependence of X-ray reflection intensity from an absorbing perfect crystal near an absorption edge*. *Acta Cryst.* A**35**, 831–835.

Katayama, C., Sakabe, N. & Sakabe, K. (1972). *A statistical evaluation of absorption*. *Acta Cryst.* A**28**, 293–295.

Kopfmann, G. & Huber, R. (1968). *A method of absorption correction for X-ray intensity measurements*. *Acta Cryst.* A**24**, 348–351.

Krause, M. O. & Oliver, J. H. (1979). *Natural widths of atomic K and L levels, Kα X-ray lines and several KLL Auger lines*. *J. Phys. Chem. Ref. Data*, **8**, 329–338.

Lee, B. & Ruble, J. R. (1977*a*). *A semi-empirical absorption-correction technique for symmetric crystals in single-crystal X-ray crystallography. I.* *Acta Cryst.* A**33**, 629–637.

Lee, B. & Ruble, J. R. (1977*b*). *A semi-empirical absorption-correction technique for symmetric crystals in single-crystal X-ray crystallography. II.* *Acta Cryst.* A**33**, 637–641.

North, A. C. T., Phillips, D. C. & Mathews, F. S. (1968). *A semi-empirical method of absorption correction*. *Acta Cryst.* A**24**, 351–359.

Rigoult, J. & Guidi-Morosini, C. (1980). *An accurate calculation of $\bar{T}_\mu$ for spherical crystals*. *Acta Cryst.* A**36**, 149–151.

Rouse, K. D., Cooper, M. J., York, E. J. & Chakera, A. (1970). *Absorption corrections for neutron diffraction*. *Acta Cryst.* A**26**, 682–691.

Santoro, A. & Wlodawer, A. (1980). *Absorption corrections for Weissenberg diffractometers*. *Acta Cryst.* A**36**, 442–450.

Schwager, P., Bartels, K. & Huber, R. (1973). *A simple empirical absorption-correction method for X-ray intensity data films*. *Acta Cryst.* A**29**, 291–295.

Stroud, A. H. & Secrest, D. (1966). *Gaussian quadrature formulas*. New Jersey: Prentice-Hall.

Stuart, D. & Walker, N. (1979). *An empirical method for correcting rotation-camera data for absorption and decay effects*. *Acta Cryst.* A**35**, 925–933.

Templeton, D. H. & Templeton, L. K. (1980). *Polarized X-ray absorption and double refraction in vanadyl bisacetylacetonate*. *Acta Cryst.* A**36**, 237–241.

Templeton, D. H. & Templeton, L. K. (1982). *X-ray dichroism and polarized anomalous scattering of the uranyl ion*. *Acta Cryst.* A**38**, 62–67.

Templeton, D. H. & Templeton, L. K. (1985). *Tensor optical properties of the bromate ion*. *Acta Cryst.* A**41**, 133–142.

Tibballs, J. E. (1982). *The rapid computation of mean path lengths for cylinders and spheres*. *Acta Cryst.* A**38**, 161–163.

Wagenfeld, H. (1975). *Theoretical computations of X-ray dispersion corrections*. *Anomalous scattering*, edited by S. Ramaseshan & S. C. Abrahams, pp. 13–24. Copenhagen: Munksgaard.

Walker, N. & Stuart, D. (1983). *An empirical method for correcting diffractometer data for absorption effects*. *Acta Cryst.* A**39**, 158–166.

Weber, K. (1969). *Eine neue Absorptionsfactortafel für kugelförmige Proben*. *Acta Cryst.* B**25**, 1174–1178.

Zachariasen, W. H. (1968). *Extinction and Borrmann effect in mosaic crystals*. *Acta Cryst.* A**24**, 421–424.

Bacon, G. E. & Lowde, R. D. (1948). *Secondary extinction and neutron crystallography*. *Acta Cryst*. **1**, 303–314.

Becker, P. J. & Coppens, P. (1974). *Extinction within the limit of validity of the Darwin transfer equations. I. General formalisms for primary and secondary extinction and their application to spherical crystals*. *Acta Cryst*. A**30**, 129–147.

Coppens, P. & Hamilton, W. C. (1970). *Anisotropic extinction corrections in the Zachariasen approximation*. *Acta Cryst*. A**26**, 71–83.

Cottrell, A. H. (1953). *Dislocations and plastic flow in crystals*. Oxford University Press.

Darwin, C. G. (1922). *The reflexion of X-rays from imperfect crystals*. *Philos. Mag*. **43**, 800–829.

Hamilton, W. C. (1957). *The effect of crystal shape and setting on secondary extinction*. *Acta Cryst*. **10**, 629–634.

Kampermann, S. P., Sabine, T. M., Craven, B. M. & McMullan, R. K. (1995). *Hexamethylenetetramine: extinction and thermal vibrations from neutron diffraction at six temperatures*. *Acta Cryst*. A**51**, 489–497.

Olekhnovich, N. M. & Olekhnovich, A. I. (1978). *Primary extinction for finite crystals. Square-section parallelepiped*. *Acta Cryst*. A**34**, 321–326.

Olekhnovich, N. M. & Olekhnovich, A. I. (1980). *Primary extinction for finite crystals. Cylinder*. *Acta Cryst*. A**36**, 22–27.

Read, W. T. (1953). *Dislocations in crystals*. New York: McGraw-Hill.

Sabine, T. M. (1985). *Extinction in polycrystalline materials*. *Aust. J. Phys*. **38**, 507–518.

Sabine, T. M. (1988). *A reconciliation of extinction theories*. *Acta Cryst*. A**44**, 368–373.

Sabine, T. M. & Blair, D. G. (1992). *The Ewald and Darwin limits obtained from the Hamilton–Darwin energy transfer equations*. *Acta Cryst*. A**48**, 98–103

Sabine, T. M., Von Dreele, R. B. & Jørgensen, J.-E. (1988). *Extinction in time-of-flight neutron powder diffractometry*. *Acta Cryst*. A**44**, 374–379.

Werner, S. A. (1974). *Extinction in mosaic crystals*. *J. Appl. Phys*. **45**, 3246–3254.

Wilkins, S. W. (1981). *Dynamical X-ray diffraction from imperfect crystals in the Bragg case – extinction and the asymmetric limits*. *Philos. Trans. R. Soc. London,* **299**, 275–317.

Wilson, A. J. C. (1949). *X-ray optics*. London: Methuen.

Zachariasen, W. H. (1945). *Theory of X-ray diffraction in crystals*. New York: John Wiley, Dover.

Zachariasen, W. H. (1967). *A general theory of X-ray diffraction in crystals*. *Acta Cryst*. **23**, 558–564.

International Tables for Crystallography (2006). Vol. C, Chapter 7.1, pp. 618–638.

7.1. Detectors for X-rays

BY Y. AMEMIYA, U. W. ARNDT, B. BURAS, J. CHIKAWA, L. GERWARD, J. I. LANGFORD, W. PARRISH AND P. M. DE WOLFF

7.1.1. Photographic film*

In 1962, when Volume III of *International Tables for X-ray Crystallography* was published, photographic film was the commonest detector for X-rays. Now it has been largely supplanted by the electronic devices described in other sections, but it is still much used in powder cameras and in preliminary investigation of specimens.

X-rays and other radiations cause blackening of silver halide emulsions, and their intensity can be measured accordingly. The blackening of the film is expressed in units of density:

$$D = \log_{10} (\mathscr{I}_{\text{incident}}/\mathscr{I}_{\text{transmitted}}), \qquad (7.1.1.1)$$

where $\mathscr{I}$ refers to the intensity of the ordinary light incident on the film. Measured densities must be corrected by subtracting the fog density D_F measured on a non-exposed part of the film.

Important features of the photographic process for strongly ionizing radiations such as X-rays and electrons are:

(i) For a given total exposure E the relationship between D and E is, to a close approximation, independent of the time variation of the intensity of the incident radiation. It does not matter whether the X-ray quanta arrive continuously or in short intense bursts (Mees, 1954).

(ii) The density D increases linearly with E up to $D \simeq 1$, then increases more slowly.

Photographic intensity measurements may be made either visually or by using a microdensitometer.

7.1.1.1. *Visual estimation*

Visual estimation consists of comparing the spot or line to be measured with a series of exposure-calibrated marks similar in shape to the object of measurement, and preferably made with the same specimen and incident beam. Lack of complete similarity and unfavourable background usually cause the error of such measurements to be larger than the optimum contrast threshold of the eye. For a spot area of 1 mm^2, the latter amounts to roughly 1% or 0.004 density units, a difference that can in fact be detected under favourable circumstances (low density and low background).

7.1.1.2. *Densitometry*

If the blackening is measured with a microdensitometer, an accuracy of 0.002 density units up to densities of at least 2 is easily attained. Higher precision is rarely required, as the limiting factors are graininess of the film and irregularities in the emulsion and processing. The grains in processed X-ray film are larger than those produced by visible light, and occur in clusters around each absorbed quantum. The resulting statistical fluctuations may be minimized by appropriate choice of densitometer slit dimensions and scanning speed. If the X-rays are not incident normally on double-coated film, it may be necessary to make corrections for obliquity (Whittaker, 1953; Hellner, 1954).

* Editorial condensation of the entry by P. M. de Wolff in Chapter 3.1 of Volume III.

7.1.2. Geiger counters†

Geiger-Müller counters (Geiger & Müller, 1928) are now obsolete for data collection, but are still used in portable monitors for X-rays. A cross section of a once-popular type is shown in Fig. 7.1.2.1(*a*). The cathode *C* is a cylinder made of a metal such as chrome-iron, about 2 cm in diameter and 10 cm long. The anode *A* is a tungsten wire about 0.7 mm in diameter mounted coaxially with *C* and terminated by a bead to prevent destructive electrical discharges from its tip. About 1400 V DC is applied between *C* and *A*. X-rays enter at a low-absorption end window *W*, made of mica about 0.013 mm thick or other suitable material; beryllium would now be used. The gas filling may be argon at a pressure of about 55 cm Hg or krypton at a lower pressure. A small amount of halogen (~0.4% of chlorine or bromine) helps to avoid destructive discharges. Separating the anode and the window is a dead space in which X-rays are absorbed but not detected.

The quantum-counting efficiency varies with wavelength; for Cu K and its neighbours, it is about 50% and, for Mo K, it is about 10%. For the longer wavelengths, it is limited by absorption in the window and the dead space, so it is important to keep these as thin as practicable. For the shorter wavelengths, it is limited by the transparency of the gas in the sensitive volume.

† Editorial condensation of the entry by W. Parrish in Chapter 3.1 of Volume III. Several papers on the relative advantages of various detectors are collected in Parrish (1962). Sections 7.1.2–7.1.4 have been slightly revised by J. I. Langford.

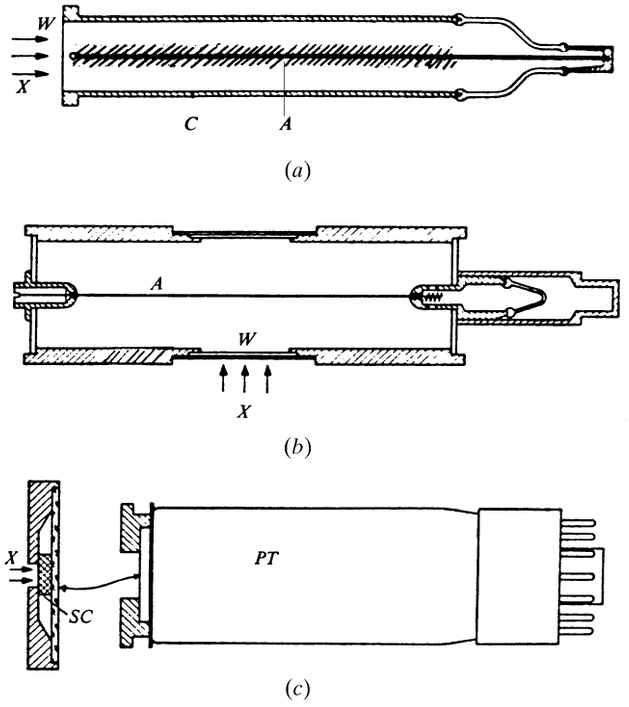

Fig. 7.1.2.1. Detectors used for diffractometry: (*a*) Geiger counter, (*b*) side-window proportional counter, (*c*) end-window scintillation counter. The arrows *X* show direction of incident X-ray beam, *W* thin window, *C* cathode, *A* anode, *SC* scintillation crystal, *PT* photomultiplier tube.

Copyright © 2006 International Union of Crystallography

The tube is not uniformly sensitive across its diameter. The maximum sensitivity is confined to the cylindrical volume shown cross-hatched in the figure. The diameter of this sensitive area depends on the gas filling and the geometry of the tube. For maximum efficiency, the X-ray beam should be directed along and close to the anode, but should not strike it. Geiger counters are not critically temperature-dependent. Linearity of response is limited by the dead-time following the discharge initiated by the absorption of a quantum and the magnification of the few hundred ions produced to some millions by their acceleration under the electric field. To produce this amplification, a certain minimum threshold voltage is required. Above this minimum, there is a plateau extending for several hundred volts within which the number of quanta detected is essentially independent of the applied voltage and the size of the pulses is essentially independent of the energy of the absorbed quantum.

Geiger counters are simple to use and show little deterioration even after prolonged use. However, since the pulses are all of about the same size, pulse-height discrimination cannot be used, and the long dead-time limits linearity of response unless special monitoring circuits are used (Eastabrook & Hughes, 1953). They have been almost completely superseded by other types of counter, described in Sections 7.1.3.–7.1.8.

7.1.3. Proportional counters (By W. Parrish)

7.1.3.1. *The detector system*

The commonest types of detector for both powder and single-crystal diffractometry are proportional counters and especially scintillation counters (Section 7.1.4). The detector system consists of the detector itself, a high-voltage power supply, a single-channel pulse-height analyser, and a scaling circuit, as shown schematically in Fig. 2.3.3.5. For position-sensitive detectors (Section 7.1.3.3) and solid-state detectors (Sections 7.1.4.2 and 7.1.5), multichannel analysers are necessary. The X-ray manufacturers and a number of electronic companies provide complete detector systems, often integrated with the computer data-collection system.

7.1.3.2. *Proportional counters*

Proportional counters are available in various sizes and gas fillings. A typical detector is a metal cylinder about 2 cm in diameter and 8–10 cm long, with central wire anode and 0.13 mm Be side window, Fig. 7.1.2.1(*b*). Some have an opposite exit window to transmit the unabsorbed beam and thus avoid fluorescence from the wall. The tube may be filled with Xe to atmospheric pressure for high absorption, and a small amount of quenching gas such as CO_2 or CH_4 is added to limit the discharge. When an X-ray quantum is absorbed, the discharge current is the sum of the Townsend avalanches of the secondary electrons and the gas amplification is about 10^4. A charge-sensitive preamplifier is generally used. Some proportional counters are filled to several atmospheres pressure to increase the gas absorption. Very thin organic film windows are used for very long wavelengths as in fluorescence spectroscopy. They may transmit moisture, and gas may migrate through them so that flow counters are used to replenish the gas. This requires careful control of the pressure to avoid changes in the counting efficiency.

7.1.3.3. *Position-sensitive detectors*

One variety of position-sensitive detector, in which the photon absorptions in different regions are counted separately, is a special type of proportional counter. The following description applies primarily to one-dimensional detectors for powder diffractometry; two-dimensional (area) detectors are treated in Section 7.1.6.

Position-sensitive detectors (PSD's) are being used in increasing number for various powder-diffraction studies. They have the great advantage of simultaneously recording a much larger region of the pattern than conventional counters. The difference in receiving apertures determines the gain in time. The position at which each quantum is detected is determined electronically by the system computer and stored in a multi-channel analyser. There is a digital addition of each incident photon address and the angular address of the diffractometer.

The PSD's are available in short straight form and as longer detectors with curvature to match the diffractometer focusing circle. The short detectors can be used in a stationary position to cover a small angular range or scanned. Göbel (1982) developed a high-speed method using a short (8° window) scanning PSD with 50 μm linear resolution in the diffractometer geometry shown in Fig. 2.3.1.12(*b*). He was able to record at speeds of a hundred or more degrees a minute, and patterns with reasonably good statistical precision in several tens of degrees a minute. This is faster than conventional energy-dispersive diffraction and has the advantage of much higher resolution.

The PSD should be selected to match best the diffraction geometry. The detector is sensitive across the 1–2 cm gas-absorption path. If the diffracted rays are not perpendicular to the window, the parallax causes broadening and loss of resolution. This becomes important in the focusing geometries and can be minimized if the diffractometer and specimen focusing circles are nearly coincident. A large loss of resolution would occur in the conventional geometry, Fig. 2.3.1.3, because only the central ray of a single reflection would be normal to the window. The problem is minimized in powder-camera geometry with a thin rod specimen, Fig. 2.3.4.1(*a*), where the entire pattern can be recorded with a long, curved PSD (Ballon, Comparat & Pouxe, 1983); see also Shishiguchi, Minato & Hashizume (1986), Lehmann, Christensen, Fjellvåg, Feidenhans'l & Nielsen (1987), Wölfel (1983), and Foster & Wölfel (1988).

7.1.3.4. *Resolution, discrimination, efficiency*

The topics of energy resolution, pulse-height discrimination, quantum-counting efficiency, and linearity are common to proportional, scintillation and solid-state counters, and are treated in Subsections 7.1.4.3.–7.1.4.5.

7.1.4. Scintillation and solid-state detectors (By W. Parrish)

7.1.4.1. *Scintillation counters*

The most frequently used detector is the scintillation counter (Parrish & Kohler, 1956). It has two elements: a fluorescent crystal and a photomultiplier tube, Fig. 7.1.2.1(*c*). For X-ray diffraction, a cleaved single-crystal plate of optically clear NaI activated with about 1% Tl in solid solution is used. The crystal is hygroscopic and is hermetically sealed in a holder with thin Be entrance window and glass back to transmit the visible-light scintillations. The size and shape of the crystal can be selected, but is usually a 2 cm diameter disc or a rectangle $20 \times 4 \times 1$ mm thick. A small thin crystal has been used to reduce the background from radioactive samples (Kohler & Parrish, 1955). A viscous mounting fluid with about the same refractive index as the glass is used to reduce light reflection and to attach it to the end of the photomultiplier tube. The crystal and

photomultiplier are mounted in a light-tight cylinder surrounded by an antimagnetic foil. The high X-ray absorption of the crystal provides a high quantum-counting efficiency.

A Cu $K\alpha$ quantum produces about 500 visible photons of average wavelength 4100 Å in the scintillation crystal (which matches the maximum spectral sensitivity of the photomultiplier), but only about 25 will be effective in the photomultiplier operation. High-speed versions with special pulse-height analysers have recently become available; they are linear to about 1% at 10^5 counts s^{-1} and can be used at rates approaching 10^6 counts s^{-1} (see Rigaku Corporation, 1990).

The detector system is as described in Subsection 7.1.3.1.

7.1.4.2. *Solid-state detectors*

The following description applies primarily to the use of solid-state detectors in powder diffractometry. Further details of their operation and their use in energy-dispersive diffractometry are treated in Section 7.1.5.

The most common form of solid-state detector consists of a lithium-drifted silicon crystal Si(Li) and liquid-nitrogen Dewar. A perfect single crystal is used with very thin gold film on the front surface for electrical contact. The first amplifier stage is a field-effect transistor (FET). The unit must be kept at liquid-nitrogen temperature at all times (even when not in use) to prevent Li diffusion and to reduce the dark current when in use. The unit is large and heavy and, if not used in a stationary position, a robust detector arm is required, which is usually counter-balanced. The crystal is made with different-size sensitive areas and the resolution is somewhat dependent on the size of the area. In the detector process, the number of free charge carriers (the electron and electron–hole pairs) generated during the X-ray absorption changes the conductivity of the crystal and is proportional to the energy of the X-ray quantum. Details of the mechanism are given in several books [see, for example, Heinrich, Newbury, Myklebust & Fiori (1981) and Russ (1984)].

Intrinsic germanium detectors have higher absorption than silicon detectors, but they have lower energy resolution and there are more interferences from escape peaks. A mercuric iodide (HgI_2) detector can be operated at room temperature and has high absorption (Nissenbaum, Levi, Burger, Schieber & Burshtein, 1984). They have poorer resolution than Si or Ge detectors but can be improved to FWHM = 200 eV at 5.9 keV by cooling to 269 K (Ames, Drummond, Iwanczyk & Dabrowski, 1983).

A small (about 16.5×10 cm), lightweight (3.2 kg) silicon detector with Peltier thermoelectric cooling is available (*e.g.* Kevex Corporation, 1990). This development has supplanted a number of the methods of collecting powder data. The elimination of the liquid-nitrogen Dewar and the compact size makes it possible to replace conventional detectors and the diffracted-beam monochromator in scanning powder diffractometry. The spectrum is displayed on a small screen and the window of the analyser can be set closely on the energy distribution obtained from a powder reflection to transmit, say, only Cu $K\alpha$. The monochromator can be eliminated for a large gain of intensity without loss of pattern resolution. The energy resolution is FWHM $\approx$ 195 eV at 5.9 keV. Elemental analysis can be performed by energy-dispersive fluorescence, and the background can be restricted to the narrow energy window selected. Bish & Chipera (1989) used it to obtain a 3–4 times increase of intensity, the same pattern resolution, and lower tails than with a graphite monochromator and scintillation counter in conventional diffractometry. The major limitation at present is the limited input intensity that can be handled. The limiting (total) count rate is about 10^4 counts s^{-1} and the detector becomes markedly nonlinear at 2×10^4 counts s^{-1}. Internal dead-time corrections can extend the range by increasing the counting times.

7.1.4.3. *Energy resolution and pulse-amplitude discrimination*

The pulse amplitudes are proportional to the energy e of the absorbed X-ray quantum so that electronic methods can be used to reduce the background from other wavelengths and sources. The rejection range is limited by the energy resolution of the detector. As noted above, the pulse amplitudes have distributions that vary around the average value A, Figs. 7.1.4.1(*a*),(*b*). The FWHM of the distribution increases linearly with increasing e (eV) and is proportional to $e^{1/2}$, *i.e.* it improves inversely with $\lambda^{1/2}$. The ratio FWHM/A (expressed in %) is a measure of the energy resolution at a given wavelength; the smaller the ratio the better the resolution. For example, as e increases from 5 to 45 keV, the FWHM approximately doubles while FWHM/e decreases from 5 to 1%. The resolution of proportional counters is about 18% for Cu $K\alpha$ and somewhat better for high-pressure gas fillings; in scintillation counters, it is about 45%. The solid-state detectors have much better resolution. The best are about 2.4% (145 eV) at 5.9 keV (which is the energy of Mn K X-rays from a radioactive ^{55}Fe source used as a standard for calibration).

The electronics include a high-voltage power supply to about 1200 V for scintillation counters and 2000–3000 V for proportional counters, and a single-channel pulse-amplitude discriminator. The latter contains pulse-shaping circuits and the amplifier, and is designed to transmit pulses whose amplitudes lie within the selected range. The lower level rejects all pulses below the selected level and the upper level rejects the higher amplitudes (Figs. 7.1.4.1*a*, *b*). The range selected is called the window and determines the pulse amplitudes that will be counted by the scaling circuit.

The multichannel analyser is generally used with solid-state detectors. It may have up to 8000 channels and sorts the pulses from the amplifier into individual channels according to their amplitudes, which are proportional to the X-ray photon energies. The pattern can be stored and displayed on a CRT screen, but nowadays a personal computer with a suitable interface card is normally used in place of the analyser. Various programs are available for peak-energy identification, spectral stripping, intensity determination, and similar data-reduction requirements. The limiting count rate that can be handled by the electronics is determined by the total number of photons striking the detector. Pulse-pileup rejectors are used to stop counting momentarily when another pulse is too close in time to allow the original pulse to return to the baseline voltage. A live-time correction extends the counting period beyond the clock time to compensate for the time the analyser is gated off. About 50 000 counts s^{-1} is the maximum rate so that the individual powder reflections have a much smaller number of pulses. If good statistical accuracy is required, the count times are, therefore, much longer than in conventional diffractometry.

For a given e, the pulse amplitudes of scintillation and proportional counters increase with increasing voltage (internal gain) and amplifier setting (external gain). The detector must be operated in the plateau region for the wavelength used (Fig. 7.1.4.1*c*). The counts are measured as a function of the voltage and/or gain, and the plateau begins where there is no further significant increase of intensity. In selecting the operating

conditions, one should avoid excessively high voltages and amplifier gains, which may cause noise pulses and unstable operation. Optimum settings can be determined by experiment and from manufacturer's instructions. The average pulse height should be set at about 20–25% of the full range of the pulse-height analyser. Lower settings move the low-energy tail into the noise, and high settings broaden the distribution and may be too wide for the window.

The pulse-amplitude distribution can be measured with a narrow (1–3 V) upper level and increasing the lower level by small equal steps. When making this calibration, it is advisable to keep the incident count rate below 10^4 counts s^{-1} to avoid nonlinearity and pulse pileup. A plot of intensity *versus* lower-level setting shows the distribution, Fig. 7.1.4.1(*a*). In some electronics, this can be done automatically and displayed on a screen. The window should be set symmetrically around the peak with the window decreasing the characteristic line intensity only a few per cent below that obtained with the lower-level set to remove only the circuit noise. The intensity change can be seen with a rate meter. Narrow windows cause a larger percentage loss of intensity than the decrease in background and, hence, the peak-to-background ratio is reduced. Asymmetric windows are sometimes used to decrease the fluorescence background.

7.1.4.4. *Quantum-counting efficiency and linearity*

The quantum-counting efficiency E of the detector, its variation with wavelength, and electronic discrimination determine the response to the X-ray spectrum. E is determined by

$$E = f_T f_A, \tag{7.1.4.1}$$

where f_T is the fraction of the incident radiation transmitted by the window (usually 0.013 mm Be) and f_A is the fraction absorbed in the detector (scintillation crystal or proportional-counter gas). E varies with wavelength as shown in Fig. 7.1.4.1(*d*). The scintillation counter has a nearly uniform E approaching 100% across the spectrum and detects the short-wavelength continuous radiation with about the same efficiency as the spectral lines. The gas-filled counters have a lower E for the short wavelengths and, therefore, may have a slightly lower inherent background; high-pressure gas counters have a higher and more uniform spectral efficiency.

The effectiveness of electronic discrimination with a scintillation counter is shown in Fig. 2.3.5.3(*c*) for 50 kV Cu target radiation. The method cannot separate the $K\alpha$-doublet components because of their small energy difference, and has little effect on the $K\beta$ peak. The results are greatly enhanced by the addition of a $K\beta$ filter, which removes most of the $K\beta$ peak and a portion of the continuous radiation below the filter absorption

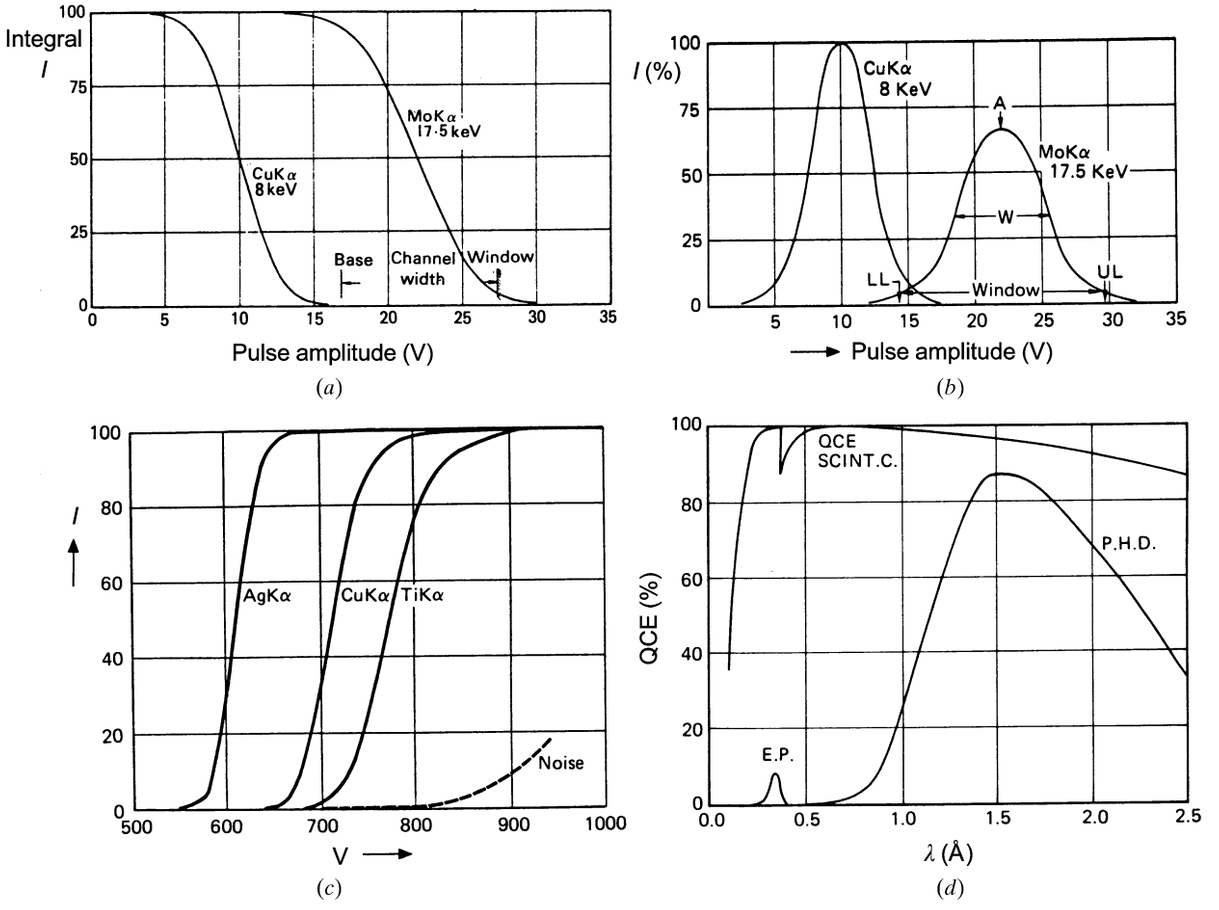

Fig. 7.1.4.1. Calculated pulse-amplitude distributions of Cu $K\alpha$ and Mo $K\alpha$ in the form of (*a*) integral curves and (*b*) differential curves. Resolution W/A for Cu $K\alpha = 50\%$. Analyser settings show window between lower level (*LL*) and upper level (*UL*). (*c*) Plateaux of scintillation counter for various wavelengths and fixed amplifier gain. Curves normalized to same intensity at highest voltage. Noise curve is plotted in counts s^{-1}. Curves can be moved to higher or lower voltages by changing amplifier gain. (*d*) Calculated quantum-counting efficiency (QCE) of scintillation counter as a function of wavelength (top curve) and its reduction when the pulse-height analyser is set for 90% Cu $K\alpha$. E.P. is escape peak at lower left.

edge, Fig. 2.3.5.3(*b*). The combination of discrimination and filter produces mainly the $K\alpha$ doublet, Fig. 2.3.5.3(*d*). Spectral analysis of the background of a non-fluorescence powder sample using this method with 50 kV Cu radiation and a scintillation counter shows it to be 50–90% characteristic radiation.

The linearity of the system is determined by the dead-time of the detector, and the resolving times of the pulse-height analyser and scaling circuit. The observed intensity n_{obs} is related to the effective dead-time of the system τ_{eff} by the relation

$$n_{true} = n_{obs}/(1 - \tau_{eff}\, n_{obs}). \qquad (7.1.4.2)$$

The value of τ_{eff} can be measured with an oscilloscope, or with the multiple-foil method in which a number of equal absorption foils (*e.g.* Al 0.025 mm or Ni 0.018 mm for Cu $K\alpha$) are inserted in the beam one or two at a time. To make certain monochromatic radiation is used, a single-crystal plate such as Si(111), which has no significant second order, and low X-ray tube voltage are employed. The linearity is determined from a regression calculation. A less accurate method is to plot n_{obs} on a log scale against the number of foils on a linear scale. Recent developments in high-speed scintillation counters have extended the linearity to the 10^5–10^6 counts s^{-1} range.

7.1.4.5. *Escape peaks*

The pulse-amplitude distribution may have two or more peaks, even when monochromatic X-rays are used (Parrish, 1966). Absorption of the incident X-rays by the counter-tube gas or scintillation crystal may cause X-ray fluorescence. If this is re-absorbed in the active volume of the counter only one pulse is produced of average amplitude A_1 proportional to the incident X-ray quantum energy e_1 (k = constant)

$$A_1 = ke_1. \qquad (7.1.4.3)$$

However, the gas or crystal has a low absorption coefficient for its own fluorescent radiation, hence, some quanta of the latter of energy e_2 may escape from the active volume of the counter, the amount depending on the geometry of the tube, gas, windows, *etc*. The average amplitude A_2 of the escape pulses is

$$A_2 = k(e_1 - e_2). \qquad (7.1.4.4)$$

Thus,

$$A_1 - A_2 = ke_2. \qquad (7.1.4.5)$$

The pulse-height analyser discriminates against pulses only on the basis of their amplitudes. When it is set to detect X-rays of energy e_0, it is also sensitive to X-rays of energy $e_0 + e_2$. For example, when using an NaI scintillation counter for Cu $K\alpha$, $e_0 = 8$ keV, and for the escape X-rays I $K\alpha$, $e_2 = 28.5$ keV. A pulse-height analyser set to detect X-rays of energy 8 keV is also sensitive to X-rays of energy 36.5 keV, because, from equations (7.1.4.3) and (7.1.4.4),

$$A_0 = k.8 = k(36.5 - 28.5) = A_2. \qquad (7.1.4.6)$$

In Figs. 2.3.5.3(*c*), (*d*) and 7.1.4.1(*d*), the escape peak E.P. shows clearly at 0.35 Å, the wavelength of 36.5 keV X-rays. There may be a number of weak escape peaks arising from the stronger powder reflections. In practice, the escape peak should not be confused with a small-angle reflection. It can be tested by reducing the X-ray tube voltage to below the absorption-edge energy of the element in the detector from which it arises.

7.1.5. Energy-dispersive detectors (By B. Buras and L. Gerward)

In white-beam energy-dispersive X-ray diffraction, the spectral distribution of the diffracted beam is measured either with a semiconductor detector (low-momentum resolution) or with a scanning-crystal monochromator (high-momentum resolution) (see Subsection 2.5.1.3). Commercially available detectors are made of lithium-drifted silicon or germanium [denoted Si(Li) and Ge(Li), respectively], or high-purity germanium (HPGe). There are, however, other materials that are good candidates for making energy-dispersive detectors.

The semiconductor detector can be regarded as the solid-state analogue of the ionization chamber. Charge carriers of opposite sign (electrons and holes) are produced by the X-ray photons. They drift in the applied electric field of the electrodes and are converted to a voltage pulse by a charge-sensitive preamplifier. The energy required for creating an electron–hole pair is 3.9 eV in silicon and 3.0 eV in germanium. The number of electron–hole pairs is proportional to the energy of the absorbed photon (the intrinsic efficiency is discussed below). There is no intrinsic gain and one has to rely on external amplification. The preamplifier employs an input field-effect transistor (FET), cooled in an integral assembly with the detector crystal in order to reduce thermal noise. Usually the detector is operated at liquid-nitrogen temperature. However, Peltier-cooled silicon detectors are available, removing the maintenance concerns of cryostat cooling. The basic counting system consists further of an amplifier, producing a near-Gaussian pulse shape, and a multichannel pulse-height analyser. It is common to use an

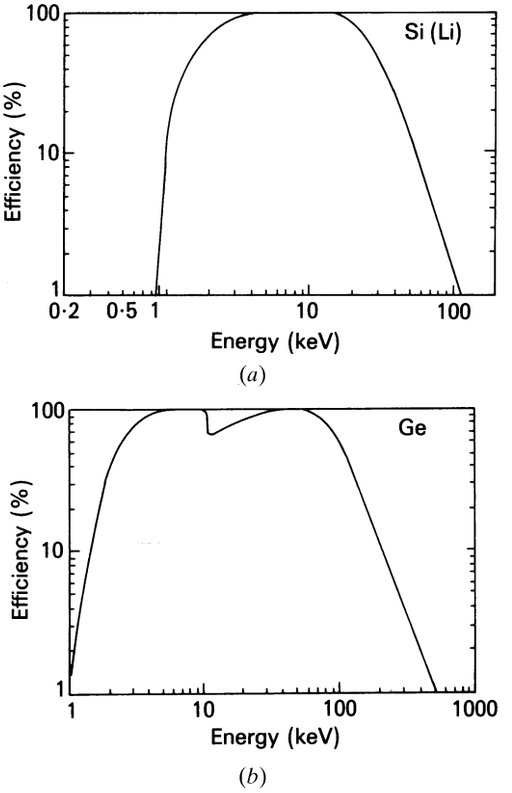

Fig. 7.1.5.1. Intrinsic efficiency of semiconductor detectors. The dimensions are selected to give typical best values of the energy resolution. (*a*) Si(Li), detector thickness 3 mm, Be-window thickness 25 μm. (*b*) HPGe, detector thickness 5 mm, Be-window thickness 50 μm.

additional circuit to reject pileup pulses that can distort the spectrum at high count rates.

The intrinsic efficiency, defined as the ratio of the number of pulses produced to the number of photons striking the detector, is close to 100% in a large energy range. Because of the penetrating power of high-energy X-rays, the efficiency declines at high energies. The low-energy limit is set mainly by the absorption in the beryllium entrance window of the detector. Fig. 7.1.5.1 shows the intrinsic efficiency for an Si(Li) detector and HPGe detector with typical crystal size and window thickness. It is seen that the useful photo-energy range is about 1–40 keV for the Si(Li) detector and 2–150 keV for the HPGe detector. Some minor complications of the HPGe detector are a dip in efficiency around the germanium K absorption edge at 11 keV and the presence of Ge $K\alpha$ and $K\beta$ escape peaks in the measured spectrum.

The energy resolution is commonly expressed as the full width at half-maximum (FWHM) of a peak in an energy spectrum. For a spectral peak with Gaussian shape, ΔE(FWHM) corresponds to 2.355 times the root mean square of the energy spread. The energy resolution, including both the detector and the associated electronics, is given by

$$\Delta E_{\rm FWHM} = \{e_n^2 + [2.355(F\varepsilon E)^{1/2}]^2\}^{1/2}, \qquad (7.1.5.1)$$

where e_n is the electronic noise contribution, F the Fano factor (about 0.1 for both silicon and germanium), and ε the energy required for creating an electron–hole pair.

The energy resolution is generally specified at 5.9 keV (Mn $K\alpha$) as a reference energy. Typical best values for a detector with 25 mm^2 area are 145 eV (2.5%) for an HPGe detector and 165 eV (2.7%) for an Si(Li) detector. The resolution is degraded for larger detector areas.

Count-rate limitations are particularly obvious in synchrotron-radiation applications, where high photon fluxes are encountered (Worgen, 1982). The count rate is limited to below 10^5 counts s^{-1}, mainly by the pulse processing system.

Cadmium telluride, mercury iodide and other wide-band-gap semiconductors could be good candidates for energy-dispersive room-temperature X-ray detectors. Until now, the best energy resolution of the Hg_2I spectrometer with both the detector and the preamplifier operating at room temperature is 295 eV (FWHM) for the 5.9 keV Mn $K\alpha$ line, corresponding to a relative resolution of 5.0%. By lowering the noise level of the preamplifier FET with cryogenic techniques, a resolution of about 200 eV (3.4%) has been achieved (Warburton, Iwanczyk, Dabrowski, Hedman, Penner-Hahn, Roe & Hodgson, 1986).

7.1.6. Position-sensitive detectors (By U. W. Arndt)

Most X-ray diffraction or scattering problems require the quantitative evaluation of a linear or of a two-dimensional pattern. Recent years have seen the development of many different types of linear and area detectors for X-diffraction purposes, that is, of position-sensitive detectors (PSD's) that allow the recording of the positions of the arrival of X-ray photons (Hendricks, 1976; Hendrix, 1982; Arndt, 1986). In addition, imaging detectors have found increasing use in related fields, such as in X-ray astronomy (Allington-Smith & Schwarz, 1984), in X-ray microscopy, in X-ray absorption spectroscopy, and in topography. Here, the emphasis is on the production of an image for direct viewing rather than on the making of quantitative intensity measurements; these applications, in general, require an ultra-high spatial resolution over a relatively small field of view and the ability to cope with very low contrast images: Imaging detectors for topography are discussed in Section 7.1.7. Lessons can also be learnt, and component parts utilized, from quantitative imaging devices developed for visible light.

Progress in these fields has been covered in the *Symposia on Photoelectronic Image Devices* held every 3 years at Imperial College London (since 1960) and in the *Wire Chamber Conferences* (since 1978) and the *London Position-Sensitive Detector Conferences* (since 1987), both reported in full in *Nuclear Instruments and Methods*. Detectors are always one of the principal subjects considered at synchrotron-radiation conferences and workshops, the highlights usually being reported in *Synchrotron Radiation News*. Detectors feature prominently in the proceedings of the *IEEE Symposia on Nuclear Science*, which appear in the *IEEE Transactions*.

Other recent reviews of X-ray detectors are by Fraser (1989), Stanton (1993), Stanton, Phillips, O'Mara, Naday & Westbrook (1993) and Sareen (1994).

The detection of X-ray photons in the energy range of interest for diffraction studies (3 to 20 keV) always involves the interaction of the photon with an inner-shell electron and its complete absorption. The processes that are of interest for the construction of PSD's are of three kinds:

(1) Photography. The characteristics of X-ray film are discussed in Section 7.1.1.

(2) The use of storage phosphors, such as europium-activated barium halide (BaFX:Eu^{2+}, X = Cl or Br) (Sonada, Takano, Miyahara & Kato, 1983; Miyahara, Takahashi, Amemiya, Kamiya & Satow, 1986), which are exposed like photographic film and then scanned with a laser beam causing photon-stimulated light emission of an intensity proportional to the original exciting X-ray intensity; this is measured with a photomultiplier. The plate is re-useable when the X-ray image has been erased. These X-ray detectors have a low background, a large dynamic range, and an adequate spatial resolution. See Section 7.1.8.

(3) Processes that involve the production of electrons. These may be the result of the ionization of a gas; they may be due to the production of electron–hole pairs in a semiconductor; they may be produced in an X-ray photocathode; finally, a phosphor may be used to convert the X-rays into visible light that then produces photoelectrons from a conventional photocathode.

At the present time, X-ray-sensitive photographic emulsions are mainly of historical interest. Storage-phosphor image plates have not only largely replaced photographic film; they have also taken over many of the applications of electronic detectors.

In the following, we are concerned only with detectors that depend on the production of electrons by incident X-rays.

In all detectors, except in semiconductor detectors, the number of primary electrons is multiplied by gas amplification, or in some device such as a microchannel plate or by some other intermediate process. In a PSD, the electron multiplication must take place with a minimum of lateral spread.

Many methods are available for deriving the position of the amplified electron stream or of the cloud of electron–ion pairs (avalanche) in an ionized gas and some of these are discussed below. However, almost any combination of photon detection, electron multiplication, and localization procedure can be used in the construction of PSD's (Fig. 7.1.6.1).

7.1.6.1. *Choice of detector*

Detectors may either be true counters in which individual detected photons are counted or they may be integrating devices that generate a signal that is a function of the rate of arrival of

photons; this signal may then be digitized for recording purposes.

The choice of a linear or of a two-dimensional, or area, PSD depends on its detection efficiency, linearity of response to incident X-ray flux, dynamic range, and spatial resolution, its uniformity of response and spatial distortion, its energy discrimination, suitability for dynamic measurements, its stability, including resistance to radiation damage, and its size and weight.

Before discussing a few of the many types of PSD individually, we shall examine these criteria in a general way. Some of them have been discussed by Gruner & Milch (1982). Table 7.1.6.1 shows the importance, on a scale of 0 to 3, of some of the factors in different fields of study. Other properties, such as stability and sensitivity, are equally important for *all* PSD's.

Table 7.1.6.1. *The importance of some detector properties for different X-ray patterns*

	Type of pattern					
Detector property	Solution	Fibre	Powder	Single crystal	Topographic	Orientation Laue
Spatial resolution	1	2	3	3	3	2
Lack of parallax	0	1	3	3	0	1
Accuracy of intensity measurement	3	3	3	3	1	1
High count rate capability	2	2	2	3	1	1
Suitability for short time slices	3	3	3	2	3	0
Suitability for short wavelengths	0	0	2	2	1	3
Energy discrimination	1	1	2	2	0	0

0 = unimportant; 3 = very important.

7.1.6.1.1. *Detection efficiency*

The detection efficiency of a detector is determined in the first instance by the fraction of the number of incident photons transmitted by any necessary window or inactive layer, multiplied by the fraction usefully absorbed in the active region of the detector. This product, which is often called the absorption efficiency or the quantum efficiency, should be somewhere between 0.5 and 1.0 since the information loss due to incident photons not absorbed in the active region cannot be retrieved by subsequent signal amplification. The *useful* efficiency is best described by the so-called detective quantum efficiency (DQE), ε (Rose, 1946; Jones, 1958). For our purposes, this can be defined as

$$\varepsilon = S^2/\sigma^2 N, \qquad (7.1.6.1)$$

where N is the number of quanta incident upon the detector and σ is the standard deviation of the analogue output signal of amplitude S. For a photon counter with an absorption efficiency q, $S = qN$, $\sigma = (qN)^{1/2}$, and $\varepsilon = q$. An analogue detector with a DQE ε thus behaves like a perfect counter that only detects a fraction ε of the incident photons.

Under favourable conditions, the DQE of analogue detectors for X-rays is in excess of 0.5, but ε varies with counting rate and is lower for detectors with a very large dynamic range, as shown below.

The DQE of CCD- and vidicon-based X-ray detectors has been discussed by Stanton, Phillips, Li & Kalata (1992*a*).

7.1.6.1.2. *Linearity of response*

The linearity of a counter depends on the counting losses, which are due to the finite dead-time of the counter and its

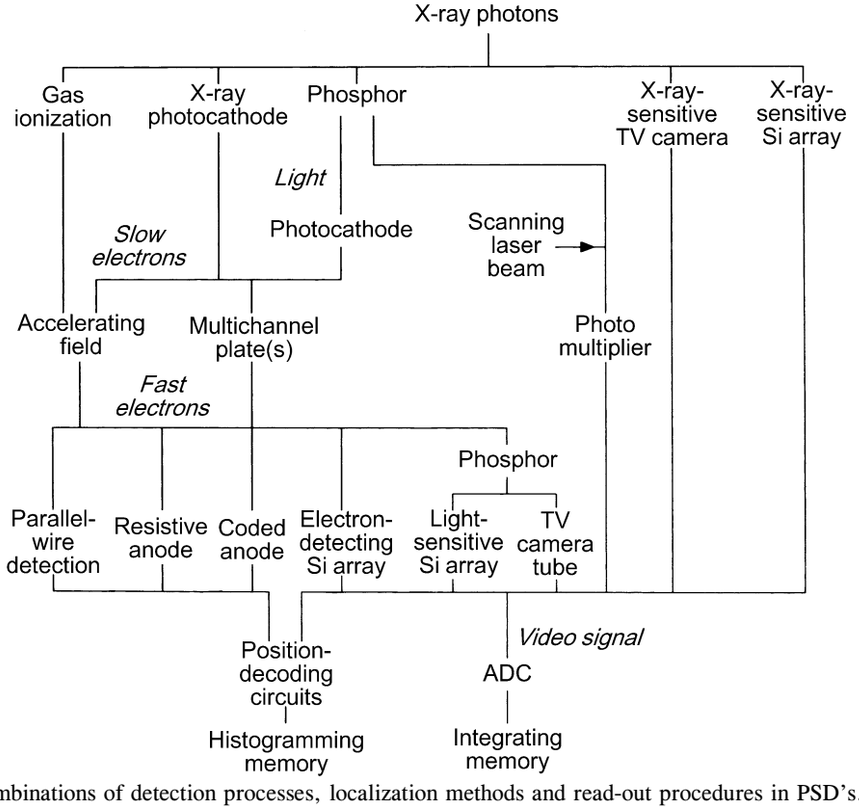

Fig. 7.1.6.1. Possible combinations of detection processes, localization methods and read-out procedures in PSD's.

processing circuits. The counting losses are affected by the time modulation, if any, of the source, as, for example, with storage rings (Arndt, 1978).

Counting losses can affect the behaviour of detectors in two different ways. In most analogue detectors and in counters with parallel read-out, each pixel behaves as an independent detector and the counting loss at any point depends only on the *local* counting rate. In other devices, such as multiwire proportional chambers with delay-line read-out (see Subsection 7.1.6.2), the whole detector becomes dead after an event anywhere in the detector and what matters is the *global* counting rate.

Fortunately, the fractional counting loss is the same for all parts of the pattern so that the *relative* intensities in a stationary pattern are not affected.

7.1.6.1.3. *Dynamic range*

The lowest practically measurable intensity is determined by the inherent background or noise of the detector. Some form of discrimination against noise pulses is usually possible with a detector that counts individual photons, but not, of course, with integrating detectors.

The maximum intensity at which a *counter* can operate is determined by the dead-time. In the case of an *integrating or analogue detector* with a variable gain, there is a trade-off between maximum intensity and DQE. Such a device can often be regarded as having an output signal with an amplitude $S = NV/M$ that is a noise-free representation of N, the number of photons detected in the integrating period of the device, where V, the maximum signal amplitude, is produced by M photons in this period. M can be varied by altering the gain of the detector. The noise can be regarded as a fixed fraction $1/r$ of the maximum amplitude V that is added to the signal. Then the DQE will be

$$\begin{aligned}\varepsilon &= S^2/\sigma^2 N \\ &= (1 + M^2/r^2 N)^{-1}. \qquad (7.1.6.2)\end{aligned}$$

This equation shows the importance of having as small a value of $1/r$ as possible; it also demonstrates that, for a given value of r, M can be increased only at the expense of a reduced DQE. This is valid for X-ray film (Arndt, Gilmore & Wonacott, 1977), for television detectors (Arndt, 1984), for the integrating gas detectors discussed in Subsection 7.1.6.2, and for many semiconductor X-ray detectors.

7.1.6.1.4. *Spatial resolution*

The spatial resolution of a PSD is determined by the number and size of resolution or picture elements (pixels) along the length or parallel to the edge of the detector. In most diffraction experiments, the size of the pattern can be scaled by altering the distance of the detector from the sample and what is important is the angular resolution of the detector when placed at a distance where it can 'see' the entire pattern. We shall see below that linear PSD's can be made with up to 2000 pixels and that area detectors are mostly limited to fewer than 512×512 pixels. The sizes of pixels range from about 10 μm for semiconductor PSD's to about 1 mm for most gas-filled detectors.

The *useful* number of pixels of a detector is determined by its point-spread function (PSF). This is the relative response as a function of distance from the centre of a point image on the detector. PSF's are not necessarily radially symmetrical and may have to be specified in at least two directions at right angles, for example along and perpendicular to the lines of a television raster scan. The width of the PSF at the 50% level determines the amount of detail visible in a directly viewed image. The accuracy of intensity measurements may depend more critically upon the width of the PSF at a lower level, since a weak spot may be immeasurable when sitting on the 'tail' of a very intense one. For various physical reasons, the PSF's of *all* PSD's, including X-ray film, have appreciable tails.

The spatial resolution of a detector is affected by parallax: when an X-ray beam is absorbed in a thick planar detector at an angle φ to the normal, the width of the resultant image is smeared out exponentially and its centroid is shifted by an amount $\sin\varphi/\mu$. For 8 keV X-rays incident at 45° on a xenon-filled counter, for example, this shift is about 4 mm for a filling pressure of 1 atm and 0.4 mm for a filling pressure of 10 atm. These figures illustrate the desirability of high-pressure xenon (Fig. 7.1.6.2) for gas-ionization detectors intended for wide-angle diffraction patterns.

7.1.6.1.5. *Uniformity of response*

All PSD's show long-range and pixel-to-pixel variations of response to larger or smaller extents. These can be corrected, in general by means of a look-up table, during data processing, but the measurements necessary for the calibration are often time-consuming. The output signals of many analogue detectors contain fixed-pattern noise that is synchronous with the read-out clock. This noise is usually removed during data processing, which in any case requires the subtraction of the background pattern.

7.1.6.1.6. *Spatial distortion*

In most detectors, there is some spatial distortion of the image. Again, the necessary calibration procedure may be time-consuming. Distortions cause point-to-point variations in pixel size, which produce response variations additional to those from other causes.

Corrections for spatial distortion and for non-uniformity of response have been discussed by Thomas (1989, 1990) and by Stanton, Phillips, Li & Kalata (1992*b*).

7.1.6.1.7. *Energy discrimination*

The amplitude of the signal due to a single photon is usually a function of the photon energy. The variance in this amplitude, or the full width at half-maximum (FWHM) of the pulse-height spectrum, for a monoenergetic input, depends on the statistics of the detection process. A sharp pulse-height-distribution (PHD) curve may permit simultaneous multi-wavelength measurements with a suitable counter, or at least afford a reduction of the background by pulse-height discrimination. In an analogue

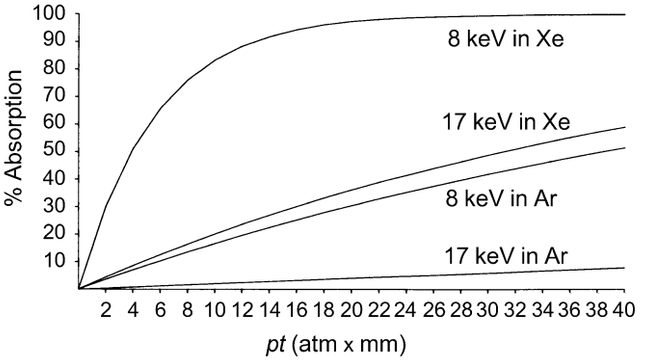

Fig. 7.1.6.2. Absorption of 8 keV and 17 keV photons in argon and xenon as a function of pressure in atm × column length in mm.

detector, the variance in the primary amplitude affects the DQE (Arndt & Gilmore, 1979).

7.1.6.1.8. *Suitability for dynamic measurements*

Many investigations, such as low-angle or fibre diffraction studies on biological materials carried out with synchrotron radiation (Boulin, Dainton, Dorrington, Elsner, Gabriel, Bordas & Koch, 1982; Huxley & Faruqi, 1983), involve the time variation of a diffraction pattern. For very short time slots, only counters can be employed; the incoming pulses must then be gated and stored in an appropriate memory (Faruqi & Bond, 1982).

Stores used for these experiments are described as histogramming memories; the contents of a given storage location are incremented by one whenever the corresponding address, which represents the position and the time of arrival of a photon, appears on the address bus (Hendricks, Seeger, Scheer & Suehiro, 1982; Hughes & Sumner, 1981).

7.1.6.1.9. *Stability*

Stability of the performance of a detector is of paramount importance. Most position-sensitive detectors are used in connection with microcomputers, which make calibration and corrections for spatial distortion, non-uniformity of response, and lack of linearity relatively easy, provided that these distortions remain constant. The long-term stability of many detectors, notably of semiconductor devices, is affected by radiation damage produced by prolonged exposure to intense irradiation.

7.1.6.1.10. *Size and weight*

The size and weight of the detector determine the ease with which the detector can be moved relative to the sample and thus the extent to which the diffractometer can be adapted to varying resolution and collimation conditions. Some detectors cannot be moved easily (Xuong, Freer, Hamlin, Nielsen & Vernon, 1978), or need very heavily engineered rotational and translational displacement devices (Phizackerley, Cork & Merritt, 1986). Others, such as spherical drift chamber multiwire proportional chambers, are designed for use at a fixed distance from the sample and may only be swung about the latter but not translated (Kahn, Fourme, Bosshard, Caudron, Santiard & Charpak, 1982).

In single-crystal diffraction patterns, the Bragg reflections may be visualized as diverging from the X-ray source while the background – fluorescence X-rays, scatter by amorphous material on the specimen crystal and its mount – diverges from the sample. Consequently, the highest reflection-to-background ratio is achieved by using a large detector at a large distance from the specimen. Of all the detectors discussed here, the image plate can most readily and economically be used to cover a large area; its present popularity is chiefly due to this property (Sakabe, 1991).

There is fairly general agreement on the specification of an ideal X-ray area detector. It should be at least 250 mm in diameter, contain at least 1000×1000 pixels, have a large dynamic range and a high detective quantum efficiency for photon energies up to 20 keV and be capable of being read-out rapidly.

Many suggestions have been made for improving the performance of existing detectors. It has become apparent, however, that the development of ideal, or even better, X-ray detectors is extremely expensive and, therefore, that their development and installation can be undertaken only in central national or international laboratories such as storage-ring synchrotron-radiation laboratories.

7.1.6.2. *Gas-filled counters*

In all gas-filled counters, whether one-, two-, or three-dimensional, the initial event is the absorption of the incoming X-ray photon in a gas molecule with the emission of a photo-, or alternatively an Auger, electron. The detection efficiency depends on the fraction of the photons absorbed in the gas and this fraction is shown in Fig. 7.1.6.2 as a function of the product of gas pressure and column length for 8 and 17 keV photons on argon and xenon. The ionization energy of noble gases is about 30 eV so that one 8 keV photon gives rise to about 270 electron–ion pairs. With adequately high collecting fields, the electrons acquire sufficient energy to produce further ionization by collision with neutral filling gas molecules; this process is often referred to as 'avalanche production' or 'gas multiplication'. The factor A by which the number of primary ion pairs is multiplied can be as great as ten to one hundred thousand. Up to a certain value of A, the total amount of ionization remains proportional to the energy of the original X-ray photon. The electrical signal generated at the anode of the counter is due very largely to the movement of the positive ions from the immediate vicinity of that electrode; at the same time, a corresponding pulse is induced on the cathode. The signal can be shaped to produce a pulse with a duration of the order of a microsecond.

In single or multiwire proportional counters, the secondary ionization (avalanche production) takes place in the highest field region, that is, within a distance of a few wire diameters of the anode wire or wires. The electrons are collected on the anode and the positive ions move towards the cathode, with very little spread of the ionization in a direction perpendicular to the field gradient, that is, parallel to the wire direction. It is thus possible to construct position-sensitive devices based on such chambers.

Proportional-counter behaviour is discussed in detail in many standard texts and review articles (Wilkinson, 1950; Price, 1964; Dyson, 1973; Rice-Evans, 1974).

The gas amplification does not have to take place in the same region of the detector as the original absorption. In so-called drift chambers, the primary ionizing event takes place in a low-field region where no avalanching takes place. The electrons drift through a grid or grids into a region where the field is sufficiently high for gas multiplication to occur. The drift field can be made cylindrical in a linear counter (Pernot, Kahn, Fourme, Leboucher, Million, Santiard & Charpak, 1982), or spherical in an area detector (Charpark, 1982; Kahn, Fourme, Bosshard, Caudron, Santiard & Charpak, 1982), centred on the point from which the X-rays diverge, that is on the specimen; the electrons then drift in a radial direction without parallax being introduced (Fig. 7.1.6.3).

In many experiments, use is made of the energy discrimination of the detector. The ratio of the full width at half-maximum to the position of the maximum of the pulse-height distribution is given by

$$w = 2.36[(F + f)/N], \qquad (7.1.6.3)$$

where N is the number of primary ion pairs produced, F is the Fano factor (Fano, 1946, 1947), which takes into account the partially stoichastic character of the gas multiplication process, and f is the avalanche factor. For proportional counters filled with typical gas mixtures (argon + methane), $F = 0.17$ and $f = 0.65$, so that for 8 keV photons $w \sim 13\%$, but, in the

so-called Penning gas mixtures (*e.g.* noble gas and ethylene), f can approach zero at a certain field strength. In a wire counter with its rapidly varying field strength, f is small only for a gas amplification of less than 50. The energy resolution for 8 keV photons could then be as low as 6%, but the pulses induced on the cathode wires of a MWPC are then too small to permit a precise localization. This problem has been overcome by using uniform-field avalanching in two regions in tandem, separated by a drift space (Schwarz & Mason, 1984, 1985). The energy information was derived after the first low-gain gas multiplication process ($A \sim 500$): a proportion of the electrons from the first avalanche then drifted into the second avalanche region which boosted the gas gain to more than 10^5, necessary to give a high spatial resolution.

In an alternative method (Charpak, 1982; Siegmund, Culhane, Mason & Sanford, 1982), the additive avalanche factor f is eliminated by deriving the energy information, not from the collected charge, but from the visible light pulse produced by the individual avalanches of each primary electron.

7.1.6.2.1. *Localization of the detected photon*

There are several methods of deriving the position of the detected photon that are applicable to both linear and area detectors.

(1) The charge produced in the avalanche can be collected on a resistive anode. In the case of linear detectors, the central wire can be given a low or a very high resistance. The latter type is most commonly made from a quartz fibre coated with carbon. The emerging pulse is detected at both ends of the wire (Borkowski & Kopp, 1968; Gabriel & Dupont, 1972). Area detectors with a resistive disc anode must have at least three read-out electrodes (Stümpel, Sanford & Goddard, 1973). With low-resistance electrodes, the position of the event can be computed by analogue circuits from the relative pulse amplitudes (Fig. 7.1.6.4*a*); a preferred method with high-resistance anodes is to measure the rise times of the output pulses that are determined by the time constant formed by the input capacity of the pulse amplifier at each output and the resistance of the path from the detection point to the output electrode (Fig. 7.1.6.4*b*).

(2) The anode or cathode can be constructed in the form of two or more interleaved resistive electrodes insulated from each other. Provided that the charge distribution covers at least one unit of the pattern, positional information can be derived by relative pulse height or by timing methods. Examples of this type of read-out are the linear backgammon (*jeu de jacquet*) counter together with its two-dimensional variant (Allemand & Thomas, 1976), the wedge-and-strip anode developed by Anger and his collaborators (Anger, 1966; Martin, Jelinsky, Lampton, Malina & Anger, 1981), and its polar coordinate analogue (Knibbeler, Hellings, Maaskamp, Ottewanger & Brongersma, 1987), for two-dimensional read-out. The method seems capable of a higher spatial resolution than any other (Schwarz & Lapington, 1985).

(3) The anode or cathode can be made from a number of sections connected to a tapped delay line (Fig. 7.1.6.4*c*). Positional information is derived from the time delay of the pulse relative to the arrival of an undelayed prompt pulse. Linear PSD's (LPSD's) with delay-line read out are usually made straight, but variants have been produced in the form of circular arcs (Wölfel, 1983; Ballon, Comparat & Pouxe, 1983).

Area detectors of this type require two parallel planes of parallel wires with the wires in the two planes at right angles to one another placed on either side of the anode, which also consists of parallel wires. The prompt pulse in such a detector, the multiwire proportional chamber (MWPC), is usually taken from the anode (Fig. 7.1.6.5). In counters without a drift space, the electron avalanche always ends up on one anode wire, and there is then a pseudo-quantization in the position measurement made at right angles to the direction of the anode wires. In drift-space detectors with a narrow anode-wire spacing, the avalanche lands on more than one wire and some interpolation is possible. In the direction parallel to the anode wires, there is never any quantization and the resolution can be better than the cathode wire spacing: Although pulses are induced on several wires, the centroid of the delayed group of pulses can be measured with precision. Delay-line read-out LPSD's have reached the highest resolution in the hands of Radeka and his group (Smith, 1984). MWPC's of this type have been used for several years (Xuong, Freer, Hamlin, Nielsen & Vernon, 1978; Bordas, Koch, Clout, Dorrington, Boulin & Gabriel, 1980; Baru, Proviz, Savinov Sidorov, Khabakhshev, Shuvalov & Yakovlev, 1978; Anisimov, Zanevskii, Ivanov, Morchan, Peshekhonov, Chan Dyk Tkhan, Chan Khyo Dao, Cheremukhina & Chernenko, 1986). They have a relatively low maximum count rate ($< 10^5$ s^{-1}) determined by the space charge due to earlier events and by the fact that position digitization takes of the order 1 μs. Limitations in the closeness of practicable wire spacing leads to a pixel size of the order of 1 mm.

(4) A faster read out is possible with MWPC's in which the positional information is derived from the centroid in amplitude of the group of induced cathode pulses (Fig. 7.1.6.4*d*). Individual amplifiers of carefully equalized gain are required for each individual wire or at least for small groups of adjacent wires (Pernot, Kahn, Fourme, Leboucher, Million, Santiard & Charpak, 1982). Counting rates in excess of 10^6 s^{-1} are then possible.

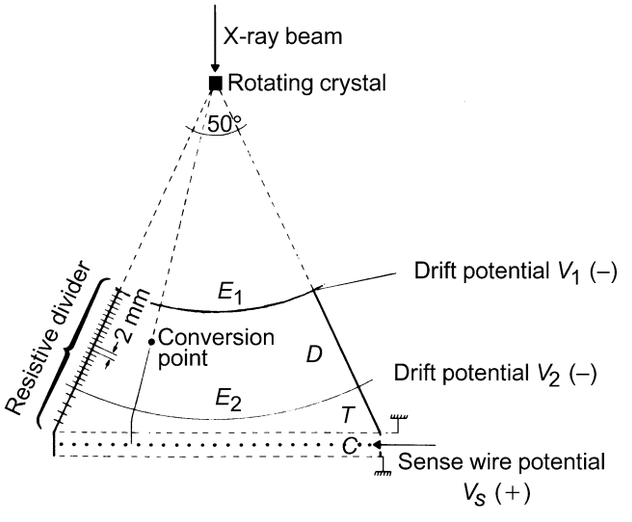

Fig. 7.1.6.3. Spherical drift chamber multiwire proportional chamber (MWPC) (Charpak, 1982; courtesy of G. Charpak).

7.1.6.2.2. *Parallel-plate counters*

In the gas-filled detectors that we have considered so far, the electric field is cylindrically symmetrical in the immediate vicinity of the wire or wires near which gas multiplication takes place and the maximum count rate is limited ultimately by the electrostatic shielding effect of the ion sheath owing to previous X-ray photons. In parallel-plate chambers, the electrodes are in the form of very fine electro-formed grids: With this structure, the pulse shape is quite different; the very sharp initial part, due to the rapidly moving electrons, can be separated, at the expense

of a loss of signal amplitude, from the slow component due to the positive ions; in addition, the shielding effect is much less pronounced. Accordingly, counting rates up to at least $10^{11}\,s^{-1}\,m^{-2}$ are possible with parallel-plate PSD's (Stümpel, Sanford & Goddard, 1973; Peisert, 1982; Hendrix, 1984).

7.1.6.2.3. *Current ionization PSD's*

For the very highest counting rates, it is necessary to abandon all methods in which individual X-ray photons are counted and instead to measure the ionization current produced by the incident X-rays on either cathode or anode. Fig. 7.1.6.6 shows the principles of a cathode read-out linear PSD. The cathode is divided into strips, each of which is connected to a capacitor and to an input terminal of a CMOS analogue multiplexer. The charge accumulated on each capacitor in a given time period is transferred to a charge-sensitive amplifier when the associated channel is selected by an addressing signal. The output voltage of the amplifier is digitized by means of an analogue-to-digital converter. The complete pattern is scanned by incrementing the addresses sequentially: The resolution is that of the strip spacing (~0.5 mm) and the principle can be extended to two dimensions (Hasegawa, Mochiki & Sekiguchi, 1981; Mochiki, Hasagawa, Sekiguchi & Yoshioka, 1981; Mochiki, 1984; Mochiki & Hasegawa, 1985). Global count rates in excess of $10^9\,s^{-1}$ are possible with this method. Lewis (1994) has published a

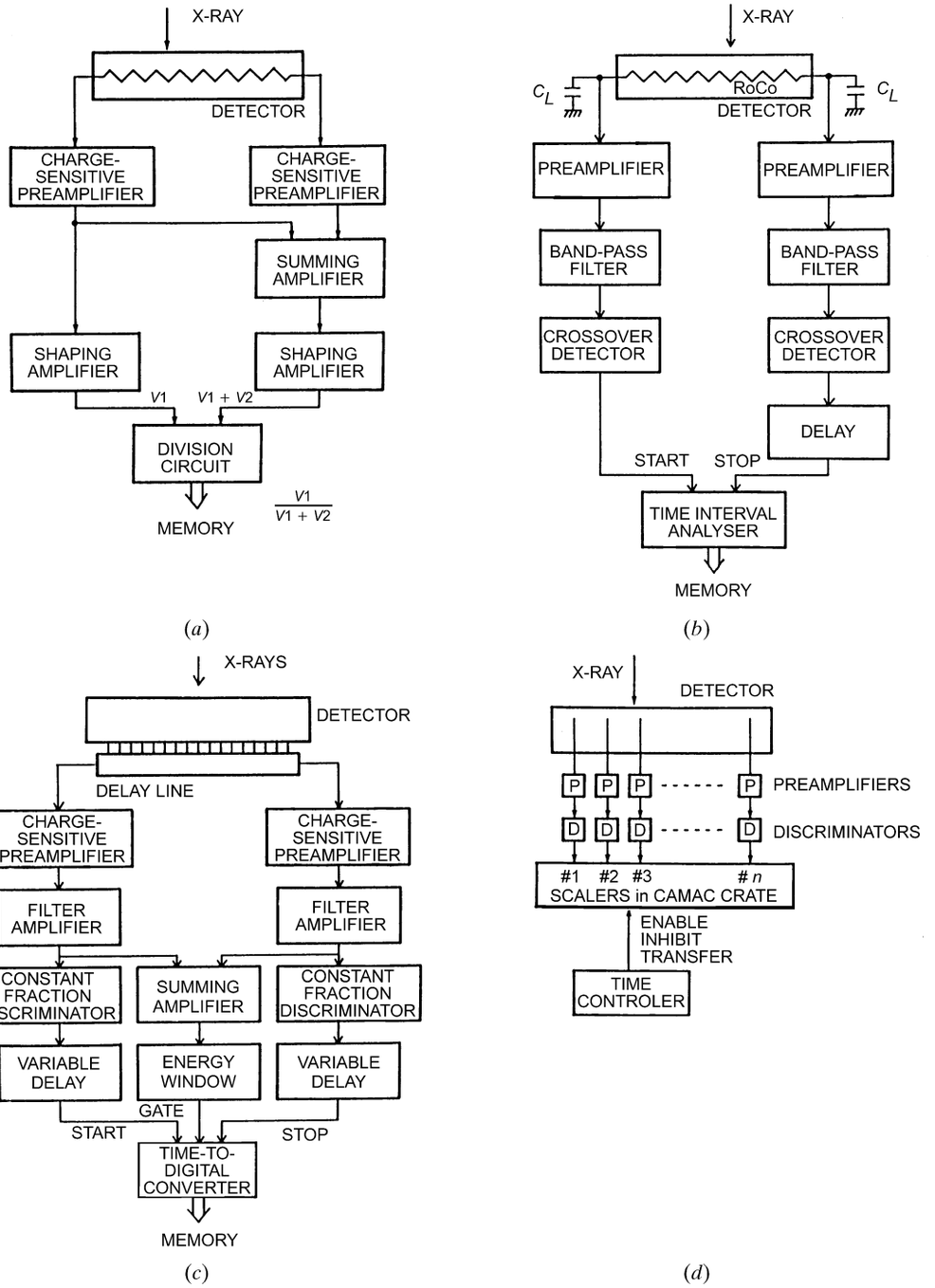

Fig. 7.1.6.4. Read-out methods for gas-filled LPSD's. (*a*) Charge division with low-resistance anode wire. (*b*) Rise-time method with high-resistance anode. (*c*) Delay-line read-out. (*d*) Amplifier-per-wire method. From Mochiki (1984); courtesy of K. Mochiki.

comprehensive survey of the present status and the future potentialities of gas-filled position-sensitive detectors.

7.1.6.3. *Semiconductor detectors*

Semiconductor detectors are essentially solid-state ionization chambers in which the incoming photon generates electron–hole pairs instead of electron–ion pairs. Semiconductor detectors are sensitive to the entire electromagnetic spectrum from visible to X-rays, and they can also detect electrons directly. There are, therefore, three possible methods of constructing semiconductor X-ray detectors, each of which has its advantages and disadvantages.

(1) They can be exposed directly to the incoming X-rays.

(2) The X-ray photons can be made to produce visible light photons that are then detected in a light sensor.

(3) The X-rays can be made to produce electrons that are detected by the semiconductor detector.

In semiconductor one- or two-dimensional PSD's, the detector and the read-out circuitry are usually integrated on the same chip. In these devices, the pixel size and position are fixed once and for all so that they are geometrically completely stable. Integrated read-out circuitry has a low input capacity and thus an extremely low read-out noise.

All semiconductor X-ray PSD's are derived from imagers for visible light, which are of two basic types: photodiode arrays (PDA's) and charge-coupled devices (CCD's) (Lowrance, 1979; Allinson, 1982; Borso, 1982; Third European Symposium on Semiconductor Detectors, 1984).

In PDA's, the detection of a photon-generated charge takes place in a depletion layer that is formed either in a suitably biased *p–n* diode or in a metal-oxide-semiconductor (MOS) capacitor. The electron–hole pairs are separated by the field associated with the depletion layer. The individual diodes store charge during the integration period; this is read out into a common video output line *via* MOS multiplexing switches. This architecture is usually adopted for linear arrays where the switches can be arranged around the periphery of the diodes with a minimum amount of dead space between them and where they can be shielded from the incident X-rays. PDA's tend to suffer from a high fixed-pattern noise due to differences in the performance of individual MOS switches.

In CCD's (Howes & Morgan, 1979), the sensing elements are always MOS capacitors suitably biased to establish charge-storage volumes. During read out, the charge is transferred in a 'bucket-brigade' fashion from one MOS capacitor to the next until it reaches the output. In linear CCD's, this output is at one end of what is essentially an analogue shift register. Most two-dimensional CCD's are frame-transfer devices: at the end of the exposure, the charge is transferred line by line to an identical array of MOS elements; while the next 'frame' is exposed in the image array, the contents of the buffer array are transferred, one line at a time, to a single-line buffer from which they are shifted out element by element. Since the transfer circuitry in CCD's is interlaced with the detector elements, they are more difficult to shield and are more subject to radiation damage.

7.1.6.3.1. *X-ray-sensitive semiconductor PSD's*

For X-ray diffraction applications, the main disadvantage of semiconductor devices is that the universal trend in their manufacture is in the direction of miniaturization, leading to a very small pixel size. Thus, imaging devices with up to 2000×2000 pixels have been produced but the pixel size is typically $\sim 10\,\mu m$ for CCD's and $\sim 20\,\mu m$ for PDA's; in most X-ray diffraction applications, it would be difficult to scale down sample and source sizes to a point where the pattern size is

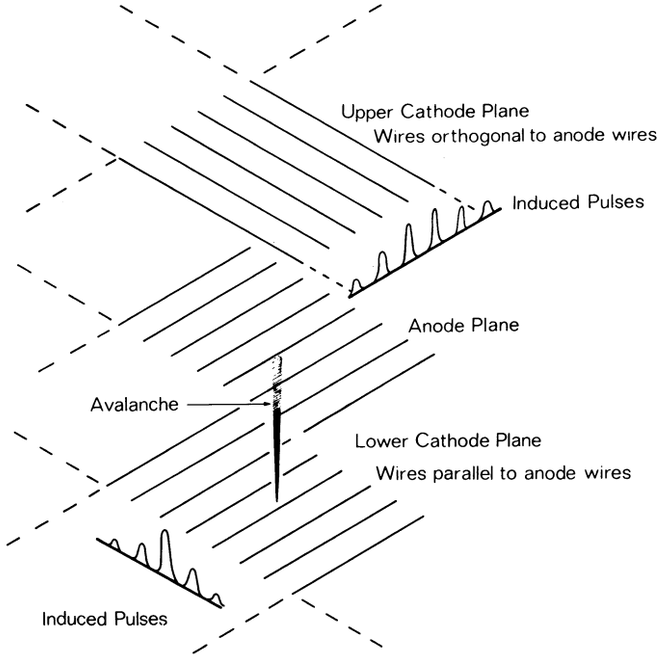

Fig. 7.1.6.5. Three-plane MWPC. Note the pseudo-quantization due to charge collection on one anode wire. The cathode wires may either be connected to a tapped delay line as in Fig. 7.1.6.4(*c*) or to individual amplifiers as in Fig. 7.1.6.4(*d*) (courtesy of A. R. Faruqi).

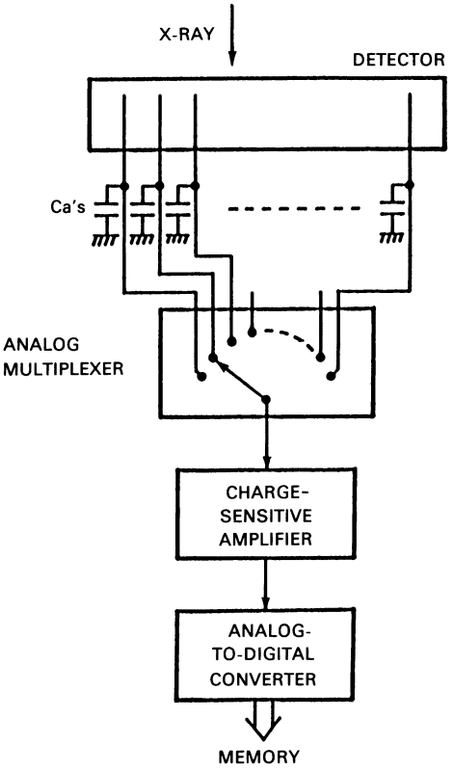

Fig. 7.1.6.6. Integrating LPSD. From Mochiki (1984); courtesy of K. Mochiki.

appropriate to a semiconductor imager, even though a 2000×2000 CCD with $27 \times 27\,\mu m$ pixels is available.

Semiconductor point counters cooled to 80 K are characterized by their very high energy resolution (better than 2% in the 8 keV region). Some counting PSD's potentially have a similar energy resolution. Two-dimensional X-ray-sensitive CCD's for X-ray astronomy research have been used as photon counters (Walton, Stern, Catura & Culhane, 1985; Lumb, Chowanietz & Wells, 1985) but they can only be used at very low counting rates. In integrating devices, the energy discrimination is lost. Silicon detectors for visible-light applications are made with depletion depths of the order of 10 μm. For the detection of 8 keV photons with more than 90% efficiency, depletion depths of 165 μm are necessary and these can be produced only from very high resistivity material (Howes & Morgan, 1979). Moreover, in commercial visible-light imagers, the depletion region is covered by circuitry or by an inactive layer that constitutes an absorbing window for X-ray detection. For the detection of X-rays or electrons, it is, therefore, customary to thin the device and to illuminate it from the back (see, for example, Meyer-Ilse, Wilhelm & Guttmann, 1993).

One-dimensional X-ray detectors utilizing PDA's, such as those made by the Reticon Corporation, have found a number of applications, especially in dispersive X-ray absorption spectroscopy (EXAFS) (Jucha, Bonin, Dartyge, Flank, Fontaine & Raoux, 1984).

A particular problem with silicon detectors is the damage caused by the incidence of X-rays or of energetic electrons. The effects can be minimized by masking all but the active part of their device and by operating it at low temperatures (Jucha *et al.*, 1984).

The use of the room-temperature semiconductor mercuric iodide in place of silicon seems promising (Patt, Delduca, Dolin & Ortale, 1986).

The X-ray diffraction applications of directly sensitive semiconductor PSD's are likely to remain limited. A previous conversion to visible light or to electrons offers the possibility of an optical or electron-optical demagnification onto the imager, as well as of avoiding some of the other problems discussed above (Deckman & Gruner, 1986).

7.1.6.3.2. *Light-sensitive semiconductor PSD's*

Standard light-sensitive semiconductor imaging devices can be used for X-ray detection if the X-rays are first converted to light by means of a phosphor. One 8 keV X-ray photon produces several hundred light photons in a good phosphor (see Table 7.1.6.2). Because of the low noise levels possible with cooled CCD's (~10 electrons r.m.s.), only 1 to 3% of these photons need to reach the device to produce a perfect X-ray detector. Unfortunately, even this is possible only with optics that do not demagnify to any considerable extent (see Subsection 7.1.6.5) and one is thus restricted to a small detector. However, CCDs are now available that can be butted along two or three edges and these make possible the construction of 'tiled' detectors that contain four or six of such CCD chips (Burke, Mountain, Harrison, Bautz, Doty, Ricker & Daniels, 1991; Fordham, Bellis, Bone & Norton, 1991; Allinson, 1994). Individual channels can be read simultaneously (Hopf & Rodricks, 1994), thus making possible a relatively rapid read out of a large number of pixels.

7.1.6.3.3. *Electron-sensitive PSD's*

In image intensifiers, an output image is produced on a phosphor screen by electrons with an energy of a few keV. A promising device with direct positional read out consists of a demagnifying intensifier in which the phosphor is replaced by a CCD. Various intensifiers have been described in which the electrons reaching the CCD have an energy of several keV so that the electron–hole generation is amplified (EBS process) (Lowrance, Zucchino, Renda & Long, 1979; Lemonnier, Richard, Piaget, Petit & Vittot, 1985). High-energy electrons are liable to cause radiation damage and similar precautions as for X-rays, such as thinning and back-illumination, are necessary. Experiments have been reported with less-damaging low-energy (200 eV) electrons produced in a microchannel plate (MCP) image intensifier (Dereniak, Roehrig, Salcido, Pommerrenig, Simms & Abrahams, 1985). Both approaches look promising but it is questionable whether a device with an X-ray phosphor input and of adequate size and resolution at an affordable price will emerge in the near future.

7.1.6.4. *Devices with an X-ray-sensitive photocathode*

Image converters and television cameras with X-ray-sensitive photocathodes have been reported. These cathodes must be thin, or they must have a low bulk density to allow the photoelectrons to escape (Bateman & Apsimon, 1979; Haubold, 1984).

Television tubes with a beryllium window and a 25 mm diameter lead oxide target are available and experimental 125 mm tubes have been described (Suzuki, Uchiyama & Ito, 1976).

X-ray-sensitive Saticon television camera tubes with an amorphous selenium–arsenic target (Chikawa, Sato & Fujimoto, 1984) have an active diameter of only 10 mm but a limiting resolution (MTF = 5%) of 6 μm. They have an absorption efficiency of 52% for Mo $K\alpha$ radiation and are used mainly for X-ray topography. Other X-ray-sensitive television camera tubes have been described by Matsushima, Koyama, Tanimoto & Tano (1987), Suzuki, Hayakawa, Usami, Hirano, Endoh & Okamura (1989) and Sato, Maruyama, Goto, Fujimoto, Shidara, Kawamura, Hirai, Sakai & Chikawa (1993). Such tubes are discussed further in Section 7.1.7.

7.1.6.5. *Television area detectors with external phosphor*

Much development has gone into quantitative measurements with area detectors in which the diffraction pattern is formed on an external phosphor fibre-optically coupled to a low-light-level television camera. Mostly the television camera embodies a demagnifying image intensifier coupled *via* demagnifying optics to a sensitive television camera tube (Arndt & Gilmore, 1979; Arndt, 1982; 1985; Arndt & In't Veld, 1988; Kalata, 1982, 1985; Gruner, Milch & Reynolds, 1982) or to a CCD or an array of CCD's (Strauss, Naday, Sherman, Kraimer & Westbrook, 1987; Strauss, Westbrook, Naday, Coleman, Westbrook, Travis, Sweet, Pflugrath & Stanton, 1990; Templer, Gruner & Eikenberry, 1988; Widom & Feng, 1989; Fuchs, Wu & Chu, 1990; Karellas, Liu, Harris & D'Orsi, 1992). Camera tubes were frequently read at commercial television rates (625 lines with a field repetition rate of 25 Hz or 525 lines with a field repetition rate of 30 Hz in Europe and in North America and Japan, respectively), leading to pixel rates of about 10 MHz. Successive images were then digitized and their sums stored in memory (see Fig. 7.1.6.7). Milch, Gruner & Reynolds (1982) developed a slow-scan method for a silicon-intensifier-target (SIT) tube. This latter method has been facilitated by the development of very large scale integration memory circuits, which have made it possible to construct economical image stores into which the camera can write at a slow rate and which can then be read at normal television rates for display purposes.

Table 7.1.6.2. *X-ray phosphors (from Arndt, 1982)*

Phosphor	Type	Bulk density	No. of photons per 8 keV quantum		Max. emission wavelength (nm)	Decay to 1% (s)
			Produced	Collected*		
ZnS (Ag)	Polycrystal	4.1	750	300	450	3×10^{-7} + slow components
Gd_2O_2S	Polycrystal	7.1	500	200	550	10^{-3}
CsI (Tl)	Monocrytal	4.5	240	62	580	10^{-6}

* These figures are for collection on a photocathode on the opposite side of a fibre-optics face plate, in the absence of a reflective coating.

CCD's are usually operated in this fashion, so that the read–out circuits can have a narrow band-width and produce an excellent signal-to-noise ratio.

For very low X-ray intensities in which the probability of the arrival of a photon per pixel per frame period is much less than one, the camera can be operated at normal frame frequencies in a digital mode. Specially designed circuits detect the charge image produced by a single X-ray photon and find the centroid of this image (Kalata, 1982); the events are 'counted' in a histogramming memory. The method is capable of some energy discrimination and has a high spatial resolution because the centroid of the image can be found to a high precision.

7.1.6.5.1. *X-ray phosphors*

The incoming X-rays are converted to light in a phosphor that is coupled to the first photocathode of the system. Both polycrystalline and monocrystalline phosphors are used for X-ray detection. The former give a higher light output but have a limited resolution; the latter tend to have a poorer light-conversion efficiency but have the best resolution. The most useful phosphors are shown in Table 7.1.6.2.

Many attempts have been made to improve the spatial resolution of phosphor screens by constructing them in the form of scintillating fibres that are optically isolated from one another so that the scintillation does not spread. This can be achieved by growing columnar scintillating crystals (Oba, Ito, Yamaguchi & Tanaka, 1988), by intagliating polycrystalline phosphors (Fouassier, Duchenois, Dietz, Guillemet & Lemonnier, 1988) and by using arrays of scintillating fibres (Bigler, Polack & Lowenthal, 1986; Ikhlef & Skowronek, 1993, 1994).

Image intensifiers designed for radiography with relatively hard radiation usually have an X-ray-transparent window – which may be up to 300 mm in diameter – and an *internal* phosphor–photocathode sandwich deposited on an X-ray-transparent substrate. Problems of compatibility of phosphor and photocathode have restricted the phosphor used, but CsI works well with multialkali photocathodes. Moy and his collaborators have constructed a large-diameter television detector in which the image intensifier has been modified by using beryllium for the window and for the sandwich substrate; this intensifier is coupled to a slow-scan CCD camera (Moy, 1994).

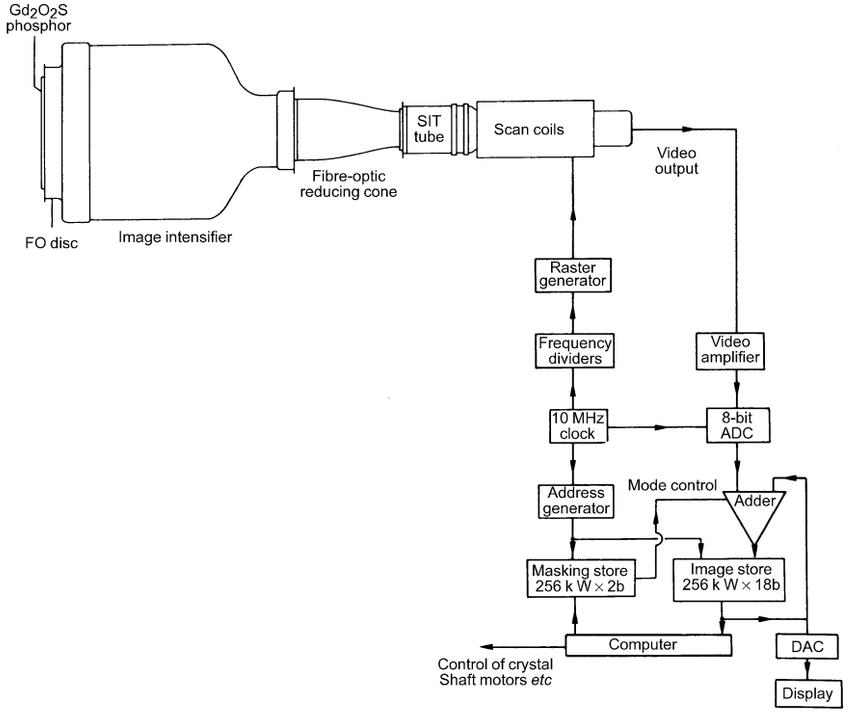

Fig. 7.1.6.7. Fast-scanning television X-ray detector (after Arndt, 1985).

7.1.6.5.2. *Light coupling*

Each incident X-ray photon should give rise to several photoelectrons from the first photocathode in order to achieve a high DQE (Arndt & Gilmore, 1979). The best photocathodes have a yield of about 0.2 electrons per light photon; only fibre-optics coupling between the phosphor and the photo-cathode can give an adequate light-collection efficiency (in excess of 80% for 1:1 imaging). With demagnifying fibre optics, the light loss is considerable for purely geometrical reasons. Fibre-optic cones, in which each individual glass fibre is conical, are available for magnification or demagnification up to about 5:1. It should be noted that image intensifiers and TV tubes with electrostatic focusing are normally made with fibre-optics face-plates and that some CCD's are also available with fibre-optics windows.

Where lens optics must be employed, it is best to use two infinity-corrected objectives of the same diameter, but not necessarily of the same focal length, back to back. In practice, the best light-collection efficiency that can be achieved at a demagnification of M is about $(2M)^{-2}$. It is for this reason that there are limitations on the maximum size of image that can be projected onto a CCD without the use of an image intensifier (but see Naday, Westbrook, Westbrook, Travis, Stanton, Phillips, O'Mara & Xie, 1994; Koch, 1994; Allinson, 1994). The function of this intensifier is to match a relatively large diameter X-ray phosphor to a small-size read-out device. As a result of the high sensitivity of CCD's, especially of slow-scan CCD's, a low photon gain in the intensifier and a low light-coupling efficiency in the coupling between intensifier and read-out device are quite adequate. It is, however, essential to couple the X-ray phosphor as efficiently as possible to the photocathode.

Roehrig *et al.* (1989) have described a design in which an image intensifier with 150 mm diameter input and output face plates is coupled by means of six demagnifying fibre-optic cones to six CCD's. Allinson (1994) has examined the need for image intensification and has shown that it is possible to construct a 150 mm square detector that has a performance approaching that of an ideal detector without using an image intensifier. Different methods of light coupling and format alteration have been discussed by Deckman & Gruner (1986).

7.1.6.5.3. *Image intensifiers*

In an image intensifier, the photoelectrons from a photocathode are made to produce a visible intensified image on an output phosphor. In so-called first-generation tubes, the intensification is produced by subjecting the electrons to accelerating voltages of up to about 15 keV: the number of visible-light photons at the output per keV of electron energy is about 80. The photon gain of the devices is typically about 100; there may be a brightness gain factor of M^2 if the electrostatic electron-optical system produces a demagnification of M. Standard first-generation image intensifiers of this type are made with input field diameters up to 80 mm, they always have fibre-optics input face plates on which X-ray phosphor may be deposited, they are stable and robust, and have a good resolution of better than 100 μm at the input. Their low gain requires the use of a low-light-level TV camera tube in the next stage (Arndt & Gilmore, 1979) or of two or more intensifiers of this type in tandem (Kalata, 1982) or of an intrinsically more sensitive slow-scan read out (Eikenberry, Gruner & Lowrance, 1986).

For military and civilian night-vision applications, first-generation image intensifiers have largely been replaced by devices embodying one or two microchannel plates (MCP's) that produce an electron gain of up to 1000 per stage (see, for example, Emberson & Holmshaw, 1972; Garfield, Wilson, Goodson & Butler, 1976). Commercial second- and third-generation intensifiers (Pollehn, 1985) are less suitable for quantitative scientific purposes than the first-generation devices: their GaAs photocathodes are less well matched to most X-ray phosphors, the gain of MCP's decreases with time, and the tubes have a slightly lower resolution than diode types of comparable diameter. Most third-generation intensifiers have plain rather than fibre-optics face plates and none appear to be available with a diameter greater than 50 mm (Airey & Morgan, 1985). Nevertheless, these high-gain intensifiers do make it possible to construct relatively cheap moderate-performance X-ray detectors using standard-sensitivity TV pick-up devices, including CCD's (Dalglish, James & Tubbenhauer, 1984), instead of the low-light-level camera tubes necessary with a lower pre-amplification.

An intensifier can, in principle, employ a variety of read-out methods, *e.g.* by substituting a resistive disc anode, a coded anode or a CCD for the output phosphor. However, the only way of employing standard modules is to couple them to a TV pick-up device.

7.1.6.5.4. *TV camera tubes*

Vacuum-tube television cameras have been largely replaced by semiconductor devices but of the former the preferred tube for use in an X-ray detector is still the silicon-intensifier-target (SIT) tube (Santilli & Conger, 1972). It has an adequate resolution for images up to 512×512 pixels and a linear transfer function (unity gamma) and its sensitivity is well matched for use with a single-stage image intensifier with a gain of 100. When cooled, this tube can be used for long exposures in an integrated slow read-out mode (Milch, Gruner & Reynolds, 1982).

When better high-gain image intensifiers become available, the preferred choice may be tubes like the Saticon (Goto, Isozaki, Shidara, Maruyama, Hirai & Fujita, 1974) whose diode gun gives them a superior resolution (Isozaki, Kumada, Okude, Oguso & Goto, 1981) and which have superior 'lag' or 'sticking' performance, that is a short 'memory' for previous high-intensity patterns to which they have been exposed (Shidara, Tanioka, Hirai & Nonaka, 1985).

7.1.6.6. *Some applications*

The use of linear and area detectors has increased markedly in recent years (Arndt, 1988). No new principles for the construction of linear devices have emerged, but more examples of each type have become commercially available.

Many more structures have been determined with area-detector diffractometers. The most commonly used gas-filled detectors at present are the delay-line read out MWPC first described by Xuong *et al.* (1978), as developed by Hamlin (1985), and a detector using a modification of the coded-anode read out due to Burns (Durbin, Burns, Moulai, Metcalf, Freymann, Blum, Anderson, Harrison & Wiley, 1986; Howard, Gilliland, Finzel, Poulos, Ohlendorf & Salemne, 1987; Derewenda & Helliwell, 1989). Corresponding instruments in the USSR and their use have been described by Anisimov, Zanevskii, Ivanov, Morchan, Peshekhonov, Chan Dyk Tkhan, Chan Khyo Dao, Cheremukhina & Chernenko (1986) and by Andrianova, Popov, Kheiker, Zanevskii, Ivanov, Peshekhonov & Chernenko (1986).

A two-dimensional photon-counting X-ray detector has been described by Collett & Podolsky (1988).

The widespread use of area-detector methods in single-crystal studies, especially for macromolecular material, has been greatly

aided by the development of complete software packages to deal with all aspects of data collection and handling. Earlier program packages (Howard, Nielson & Xuong, 1985; Pflugrath & Messerschmidt, 1987; Thomas, 1987) tended to be specific to one particular detector and its associated diffractometer. However, following the initiative of Bricogne (1987) and with financial assistance from EEC funds, a group of scientists, including most of the originators of the earlier packages, are now collaborating in writing, extending, and maintaining a comprehensive device-independent position-sensitive-detector software package.

Acknowledgements

Many helpful comments on this article by Drs A. R. Faruqi, H. E. Schwarz, and D. J. Thomas are gratefully acknowledged.

7.1.7. X-ray-sensitive TV cameras (By J. Chikawa)

High-resolution X-ray imaging systems are required for the topographic study of spatial change in crystal structures, such as that which takes place in phase transformations. From this point of view, high-resolution TV camera tubes will be described.

7.1.7.1. *Signal-to-noise ratio*

Video displays of X-ray and optical images have different features. Although X-ray photon energies are very large, the intensities available in X-ray diffraction are extremely low compared with optical images. Therefore, the photon noise resulting from the statistical fluctuation of the number of photons incident upon an image system gives a detection limit of the image.

Consider the case of defects in a crystal viewed by an imaging system: ν_p photons s^{-1} mm^{-2} are diffracted from the perfect region of a crystal, and $q\nu_p$ ($q < 1$) are absorbed by the X-ray-sensing layer of the system. An absorbed photon produces a mean number η_1 of electrons or visible photons, each of which may be rescattered to produce a mean number η_2 of electrons or photons. By repeating s such processes, the mean signal height

$$S_p = q\nu_p\eta_1\eta_2 \ldots \eta_s\delta^2 t \qquad (7.1.7.1)$$

is obtained from each square-shaped picture element $\delta \times \delta$ mm for t s. The value of δ may be taken as the limiting resolution of the system. Since $\eta_1 > 100$ owing to the large photon energy and the values of $\eta_2, \eta_3, \ldots, \eta_s$ are considered to be less than 100, the photon noise σ_p as a standard deviation of S_p is given by (Arcese, 1964)

$$\sigma_p = \eta_s\eta_{s-1} \ldots \eta_1(q\nu_p\delta^2 t)^{1/2}. \qquad (7.1.7.2)$$

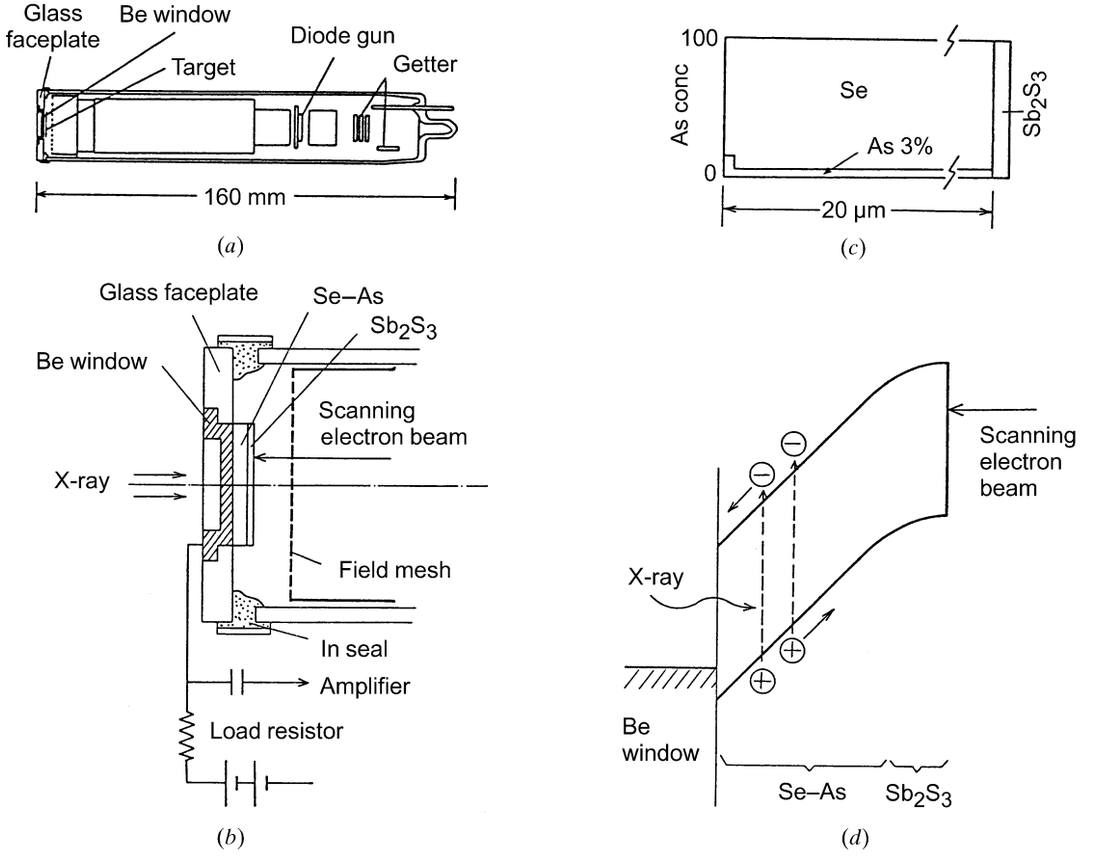

Fig. 7.1.7.1. Schematic illustration of an X-ray sensing Saticon camera tube. (*a*) Schematic representation of the tube. (*b*) Structure of the target. (*c*) Concentration (wt%) of As in the target (Se–As photoconductive layer). Since crystalline Se is metallic, As acts to stabilize the amorphous state. (*d*) Potential in the target. A blocking contact is formed between the X-ray window material and the Se–As alloy layer to prevent holes from flowing into the layer. Incident X-rays form electrons and holes in the layer, and the latter migrate toward the scanning-electron-beam side and contribute to the video signal. On the surface of the Se–As layer, Sb_2S_3 was evaporated to form another blocking contact that improves landing characteristics of the electron beam. By applying a high voltage on the layer, the holes are accelerated to produce multiplication (avalanche amplification), resulting in a great increase of the signal current.

In order to recognize the defect image in the perfect region, the signal-to-noise ratio (SNR) R_I of the image must be

$$R_I \equiv (S_d - S_p)/\sigma_p = \delta C(q\nu_p t)^{1/2} \geq \kappa, \qquad (7.1.7.3)$$

where S_d = signal height of the defect image, C = contrast of the defect image, $C = (S_d - S_p)/S_p$; and κ = threshold SNR of 1–5 (Rose, 1948).

Sensitivity is expressed by the intensity required for a certain signal height to the noise height of the imaging system and is proportional to the value of $q\eta_1 \ldots \eta_s$. As is seen from (7.1.7.3), however, the ratio of the signal to the photon noise depends only on the absorption efficiency q. For example, a 100 μm thick silicon-diode array (Rozgonyi, Haszlo & Statile, 1970) and 15 μm thick lead oxide camera tubes (Chikawa, 1974) have similar sensitivities for Mo $K\alpha$ radiation, but $q = 0.15$ and $q = 0.6$, respectively; the former obtains the sensitivity with a higher conversion efficiency ($\eta_1\eta_2 \ldots \eta_s$) of absorbed photon energy and gives a $(0.15/0.6)^{1/2} = 0.5$ times lower SNR.

It is clear from the foregoing discussion that imaging systems should be evaluated by three factors: resolution, integration time for observation, and SNR.

7.1.7.2. *Imaging system*

There are two kinds of imaging system (*e.g.* Green, 1977); one is a direct method in which X-ray input images are converted directly into video signals and the other is an indirect method in which X-ray images are first converted into visible-light images to be observed by the usual electro-optical system. In the latter, phosphor screens are widely used and the visible images can be magnified by a lens. However, the resolution is limited by the thickness of the phosphor screen that is required for a satisfactory absorption efficiency. In contrast, the direct method provides a high resolution.

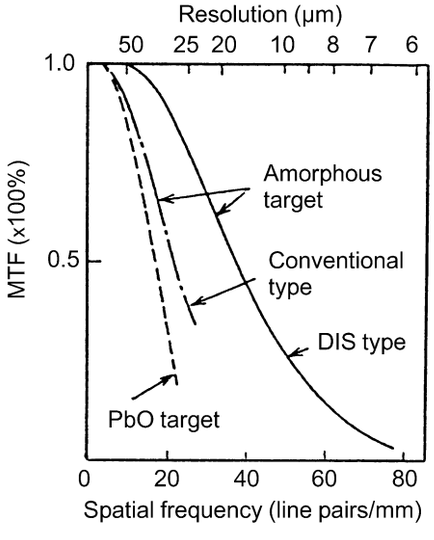

Fig. 7.1.7.2. Square-wave modulation transfer function (MTF) measured for the DIS-type, conventional-type Se–As and PbO camera tubes. This function shows the magnitude of brightness modulation in the output image obtained for an input image with a square-wave intensity distribution and is defined by

$$\mathrm{MTF} = \left(\frac{I_{o\max} - I_{o\min}}{I_{o\max} + I_{o\min}}\right)\left(\frac{I_{i\max} - I_{i\min}}{I_{i\max} + I_{i\min}}\right)^{-1},$$

where $I_{i\max}$ and $I_{i\min}$ are the maximum and minimum intensities of the input image, respectively, and $I_{o\max}$ and $I_{o\min}$ are those of the output. DIS stands for diode-operation impregnated-cathode Saticon.

Various types of indirect method are discussed in Subsections 2.7.5.2 and 7.1.6.5. Here only the direct method will be described in some detail.

A direct method using X-ray TV camera tubes has been used for real-time topography (Chikawa & Matsui, 1994). The construction and operation of an X-ray TV camera tube are similar to those of the conventional video pick-up tube, except for a beryllium window, as shown schematically in Fig. 7.1.7.1. The popular one is a vacuum glass tube which is 15 cm long and 25 mm in diameter. An X-ray sensing photoconductive layer such as Se (McMaster, Photen & Mitchell, 1967), or PbO (Chikawa, 1974) is placed on the inner surface of the window at one end of the tube and is scanned by a narrow electron beam from a cathode on the opposite end to convert image charges on the photoconductive layer into video signals. Therefore, the resolution depends upon the characteristics of the photoconductive layer and the electron-beam size on the layer.

The camera tube with a PbO photoconductive layer has absorption efficiencies of $q = 0.6$ for Mo $K\alpha$ and 0.8 for Cu $K\alpha$, using a PbO layer with a resolution-limited maximum thickness of 15 μm (Chikawa, 1974).

Dislocations in a silicon crystal were observed with the PbO camera tube and a high-power X-ray generator (tube voltage: 60 kV, current: 0.5 A) under the conditions $\nu_p =$

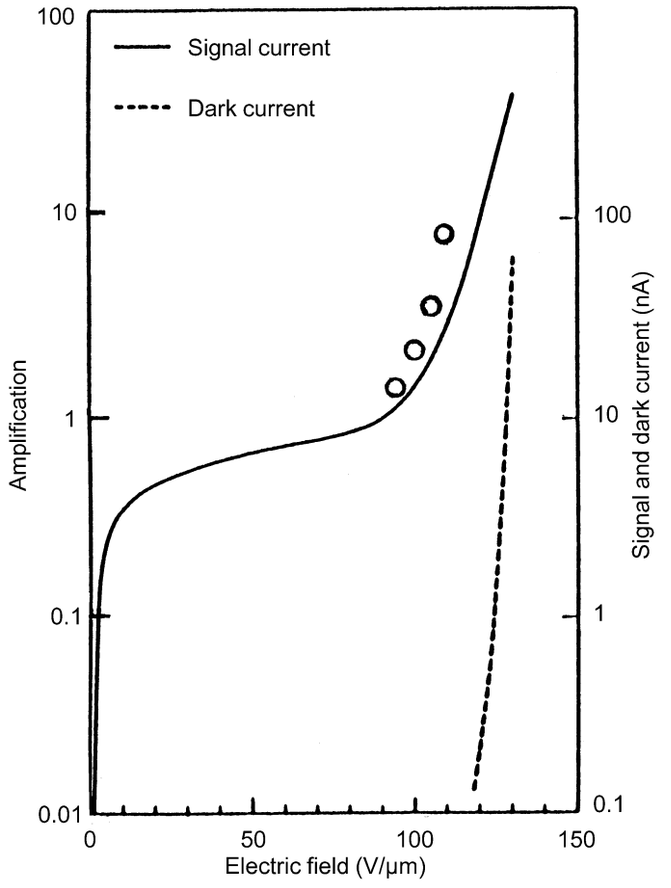

Fig. 7.1.7.3. Typical example showing dependence of the avalanche amplification on the electric field applied on the amorphous photoconductor (HARP). The solid and dashed lines show the amplification of signal current by visible light and dark current, respectively, for a 2 μm thick HARP layer. The right-hand scale shows the current (in nA). The open circles are the data for an 8 μm thick HARP layer by X-ray irradiation. Note that the thicker layer has higher amplifications owing to longer paths for running of holes.

4×10^{11} Mo $K\alpha_1$ photons s^{-1} m^{-2}, $C = 0.5$ and $\delta = 30$ μm (Chikawa, 1974) in (7.1.7.3). In order to improve the resolution further, q must be as high as possible even when ν_p is increased by 10–100 by use of synchrotron radiation, because R_I decreases with improving resolution (decreasing δ). (Note that C is not expected to increase much with improving resolution.) For example, to keep R_I at the same level as the previous case, q should be 0.7, say, for $\nu_p = 10^{13}$ photons s^{-1} m^{-2} and $\delta = 6$ μm. However, resolution and detection efficiency are, in general, mutually exclusive; the resolution of X-ray sensing photoconductive or phosphor materials is determined by the sizes of their grains and their sensitivities decrease with decreasing grain sizes. High resolution, without sacrificing detection efficiency, has been obtained with an amorphous Se–As alloy photoconductive layer, which has the advantage that no degradation of resolution occurs on increasing the layer thickness (Chikawa, Sato, Kawamura, Kuriyama, Yamashita & Goto, 1986). A layer with a thickness of 20 μm has an absorption efficiency of $q = 0.52$ for Mo $K\alpha$. The resolution of these tubes is shown with their modulation transfer functions in Fig. 7.1.7.2. The limiting resolution of 6 μm was obtained by making the scanning electron beam narrower with a diode-type electron gun have a barium-impregnated tungsten cathode (DIS type) (Chikawa, 1999). The Se–As layer shows very low lag characteristics (less than 1% after one frame).

This type of camera tube was developed primarily for TV broadcasting use and named 'Saticon' as the acronym for the components of the photoconductor, Se, As and Te. (Te enhances the sensitivity to red light.)

Such camera tubes have excellent linearity. The output signal current is proportional to the incident X-ray intensity up to 4 μA. The amplifier is always improving in signal-to-noise ratio, and, at present, the noise level of video amplifiers is ~0.2 nA; it is equivalent to an input intensity of $\sim 10^{11}$ Mo $K\alpha$ photons m^{-2} s^{-1} in the US/Japan standard scanning system (30 frames s^{-1}).

Therefore, it is important to increase conversion efficiency ($\eta_1, \eta_2, \ldots, \eta_s$). With increasing voltage applied on the photoconductive layer, the signal current is saturated (in Fig. 7.1.7.1, all the holes produced by an incident photon are collected), and then increases again further by avalanche amplification, as shown in Fig. 7.1.7.3; holes accelerated by a strong electric field cause their multiplication (Sato, Maruyama, Goto, Fujimoto, Shidara, Kawamura, Hirai, Sakai & Chikawa, 1993). It was referred to as 'HARP' (high-gain avalanche-rushing amorphous photoconductor). Together with the signal current, the dark current also increases as shown in Fig. 7.1.7.3. By allowing it to increase to the noise level of the video amplifier, an order of magnitude higher SNR can be achieved. Consequently, individual X-ray photons can be imaged as spots with a size resulting from the point-spread function, unless they are absorbed near the back surface of the photoconductive layer. For X-ray detection, a thick HARP layer should be employed with a very high applied voltage, and stable operation with avalanche amplification was confirmed for a 25 μm thick HARP layer. These pilot tubes were fabricated with a conventional electron gun and had a resolution of about 25 μm.

In general, avalanche amplification results in degradation of spatial resolution and has been used for zero-dimensional detection such as solid-state detectors. To make two-dimensional detection, isolation of each picture element is required. For the HARP, however, no appreciable degradation of resolution due to avalanche amplification was confirmed with a DIS-type tube having an 8 μm thick HARP layer by using visible light through a glass window. X-ray sensitive DIS-type tubes are now commercially available.

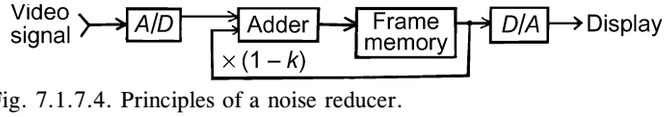

Fig. 7.1.7.4. Principles of a noise reducer.

7.1.7.3. *Image processing*

The resolution δ and integration time t should be selected appropriately according to experimental requirements (Chikawa, 1980). For example, when topographic images of a single dislocation in silicon were observed with $t = 1/30$ s by synchrotron radiation, their contrast and SNR were found to be $C = 0.5$ and $R_I = 20$ for $\delta = 30$ μm, and $C = 1$ and $R_I = 8$ for $\delta = 6$ μm. Since the SNR is desired to be 100, the integration time should be as large as possible unless images of moving objects are degraded. Digital image processing (Heynes, 1977) enables one to adjust the integration time easily. As an example, a noise reducer (McMann, Kreinik, Moore, Kaiser & Rossi, 1978; Rossi, 1978) is shown in Fig. 7.1.7.4. The video signal is sampled and digitized by the A/D converter and the digital video is sent to the adder and thence to the memory. Image information in the memory is continually sent both to the adder through the multiplier for combination with incoming data and to the display through the D/A converter. The weighting of new to old data is made by changing the factor k of the multiplier in the range $0 \leq k \leq 1$. For $k = 0$, the original input image is displayed. In the range $0 < k < 1$, a sliding summation of successive frames is displayed, and the SNR is improved by a factor of $[(1 + k)/(1 - k)]^{1/2}$. The factor k can be adjusted automatically by detecting the difference between successive frames.

Using a HARP tube, the SNR can be improved without integration of the amplifier noise by image processing, and topographs were displayed with an intensity of $\nu_p \simeq 10^9$ photons s^{-1} m^{-2} by a conventional X-ray generator.

Acquisition of extremely low intensity images, dramatic improvements in SNR *via* frame integration, and isolation and enhancement of selected-contrast ranges are possible by digital image processing (Chikawa & Kuriyama, 1991).

7.1.8. Storage phosphors (By Y. Amemiya and J. Chikawa)

A storage phosphor, called an 'imaging plate', is a two-dimensional detector having a high detective quantum efficiency (DQE) and a large dynamic range. It was developed in the early 1980's for diagnostic radiography (Sonoda, Takano, Miyahara & Kato, 1983; Kato, Miyahara & Takano, 1985). The performance characteristics of the imaging plate was quantitatively evaluated in the mid 1980's (Miyahara, Takahashi, Amemiya, Kamiya & Satow, 1986) and it was proved to be very useful also for X-ray diffraction experiments (Amemiya, Wakabayashi, Tanaka, Ueno & Miyahara, 1987; Amemiya & Miyahara, 1988). The imaging plate has replaced conventional X-ray film in many X-ray diffraction experiments.

The imaging plate (IP) is a flexible plastic plate that is coated with bunches of very small crystals (grain size about 5 μm) of photo-stimulable phosphor [previously BaFBr:Eu^{2+}, recently BaF(Br,I):Eu^{2+}] by using an organic binder. The photo-stimulable phosphor is capable of storing a fraction of the absorbed X-ray energy. When later stimulated by visible light, it emits photo-stimulated luminescence (PSL), the intensity of which is proportional to the absorbed X-ray intensity.

The mechanism of PSL is illustrated in Fig. 7.1.8.1. When the IP absorbs incoming X-rays, some of the electrons in the valence band are pumped up to the conduction band of the phosphor crystals. (This corresponds to ionization of Eu^{2+} to Eu^{3+}.) The electrons, in turn, are trapped in Br^- and F^- vacancies, which were intentionally introduced in the phosphor crystals during the manufacturing process, forming temporary colour centres, termed *F*-centres. Exposure to visible light again pumps up the trapped electrons so that they generate energy for luminescence, while returning to the valence band of the crystal. (This process corresponds to a recombination of electrons with Eu^{3+} ions, resulting in Eu^{2+} luminescence.) Because the response time of the PSL is as short as 0.8 μs, it is possible to read an X-ray image with a speed of 5–10 μs per pixel with high efficiency. The PSL is based on the allowable transition from $5d$ to $4f$ of Eu^{2+}. The wavelength of the PSL ($\lambda \simeq 390$ nm) is reasonably separated from that of the stimulating light ($\lambda = 632.8$ nm), allowing it to be collected by a conventional high-quantum-efficiency photomultiplier tube (PMT). The output of the PMT is amplified and converted to a digital image, which can be processed by a computer. The residual image on the IP can be completely erased by irradiation with visible light, to allow repeated use. The IP is easy to handle, because it is flexible, like a film, and can be kept in light before its exposure to X-rays.

The measured DQE of the IP is shown as a function of the X-ray exposure level together with that of a high-sensitivity X-ray film (Kodak DEF-5) in Fig. 7.1.8.2. The advantage of the IP over X-ray film in DQE is clearly enhanced at lower exposure levels. This arises from the fact that the background noise level of the IP is much smaller than that of X-ray film. The background noise level of the IP corresponds to the signal level of less than 3 X-ray photons/100 μm^2. This value compares favourably with the chemical 'fog' level of X-ray film, which amounts to 1000 X-ray photons per equivalent area. The background noise level of the IP depends largely on the performance of the IP read-out system, and it can be smaller than that of a single X-ray photon with a well designed IP read-out system (Amemiya, Matsushita, Nakagawa, Satow, Miyahara & Chikawa, 1988). The DQE of the IP decreases at higher exposure levels owing to 'system fluctuation noise'. Fig. 7.1.8.3 shows the fluctuation noise of the IP and X-ray film as a function of the X-ray exposure level. It is shown that the noise fluctuation at high exposure levels is governed by system fluctuation noise, which amounts to about 1%. Fig. 7.1.8.4 shows the propagation of signal and noise in the IP system. The origins of the system fluctuation noise are non-uniformity of absorption, non-uniformity of the colour-centre density, fluctuation of the laser intensity, non-uniformity of PSL collection, and fluctuation of the high-voltage supply to the PMT. Although it might be possible to reduce the total system fluctuation noise from ~1% to ~0.5%, it is very difficult to reduce it down to <0.1%. This means that the ultimate precision in intensity measurements with the IP is limited to the order of ~0.5%.

Compared to X-ray film, the dynamic range of the IP is much wider, of the order of 1:10^5 (Fig. 7.1.8.5). The response of the PSL is linear over the range from 8 to 40 000 photons/(100 μm^2), with an error rate of less than 5%. It is shown that the dynamic range of an IP is extended towards the lower exposure levels of X-ray film, but not to the higher exposure levels. The dynamic range of the IP is practically limited to four orders of magnitude by that of the PMT during the read-out. Two sets of PMT's are used in some read-out systems in order to cover the entire dynamic range of the IP.

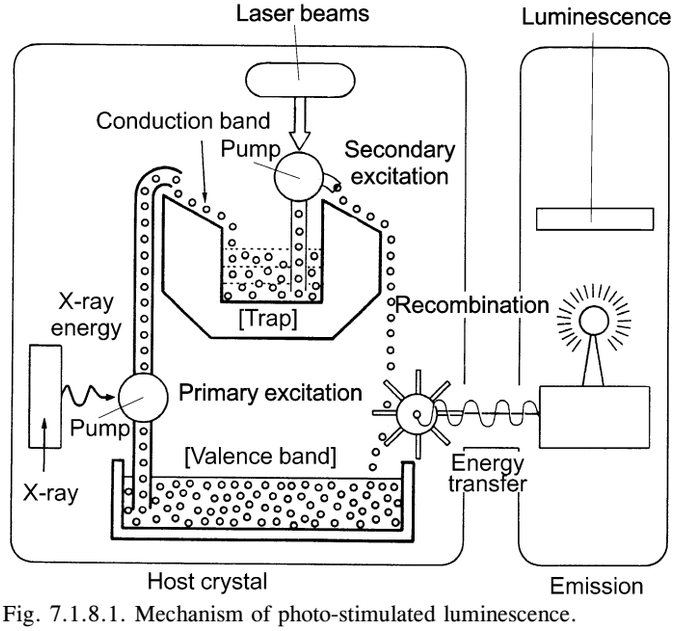

Fig. 7.1.8.1. Mechanism of photo-stimulated luminescence.

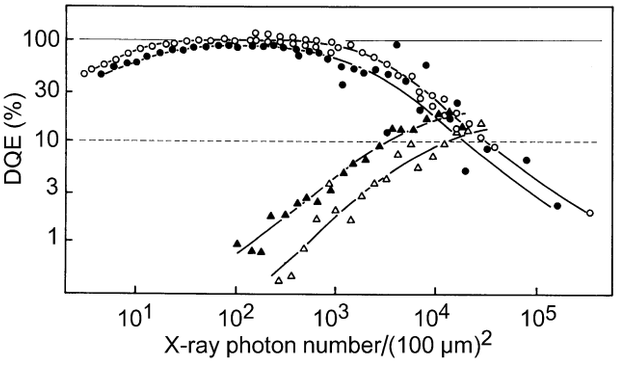

Fig. 7.1.8.2. Measured detective quantum efficiency (DQE) of the imaging plate and high-sensitivity X-ray film as a function of the exposure level. The circles correspond to the imaging plate (with the FCR 101 read-out system, Fuji Film Co. Ltd), triangles to the X-ray film (Kodak DEF-5). The filled symbols are for 8.9 keV and open symbols for 17.4 keV. The solid line indicates a noiseless counter of 100% absorption efficiency (ideal detector). The dashed line indicates a noiseless counter of 10% absorption efficiency (Amemiya & Miyahara, 1988).

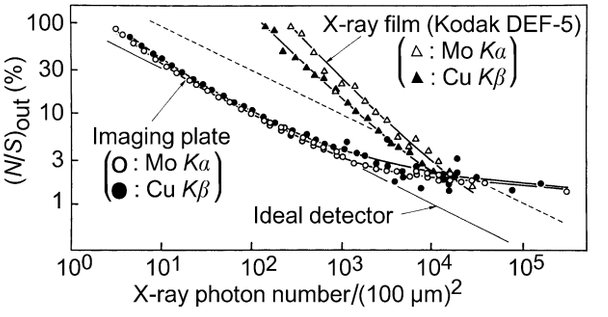

Fig. 7.1.8.3. Fluctuation noise in the signal as a function of the exposure level. The circles correspond to the imaging plate and the triangles to the X-ray film (Kodak DEF-5). The filled symbols are for 8.9 keV and the open symbols for 17.4 keV. The dashed line indicates a noiseless counter of 10% absorption efficiency (Miyahara, Takahashi, Amemiya, Kamiya & Satow, 1986).

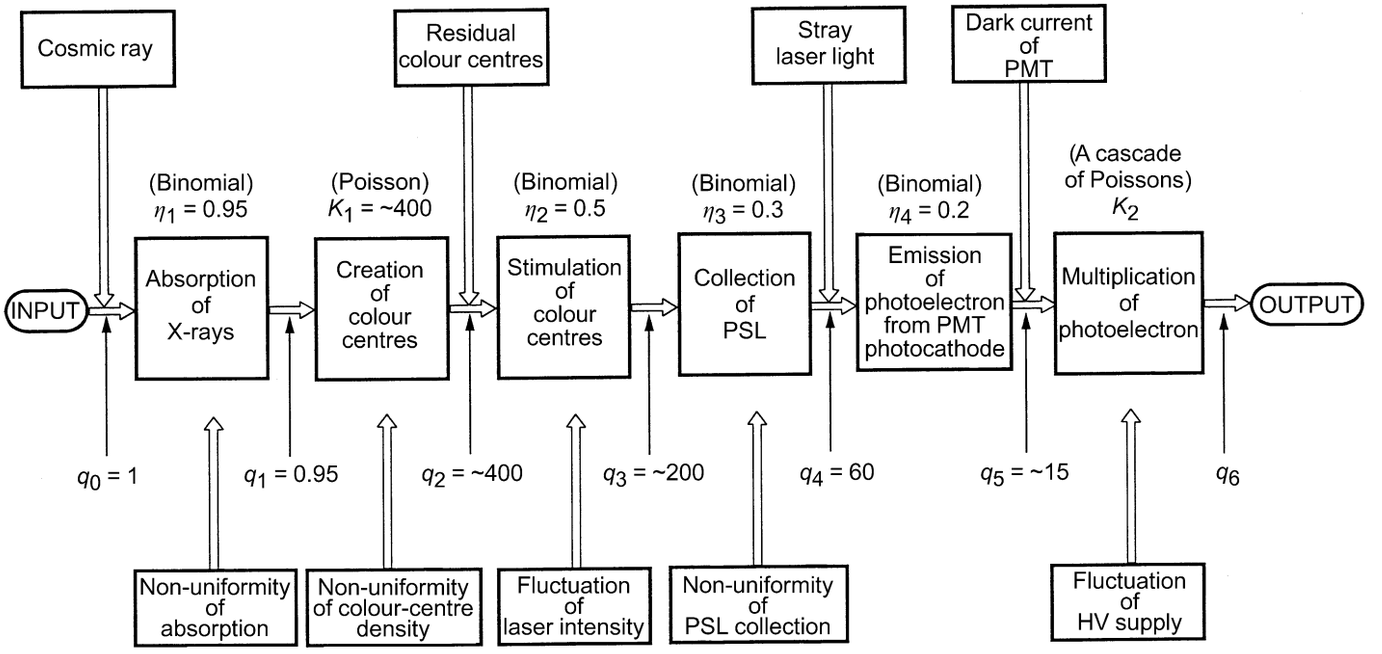

Fig. 7.1.8.4. Diagram showing a cascade of stochastic elementary processes during X-ray exposure and image read out of the imaging plate. The probability distribution of each stochastic process is described in parentheses together with the mean value. The numbers of the quanta, q_i ($i = 0, 5$), are also shown. The noise elements of the upper line contribute to the background noise, which reduces the DQE at lower exposure levels. The noise elements of the bottom line contribute to the system fluctuation noise, which reduces the DQE at higher exposure levels (Amemiya, 1995).

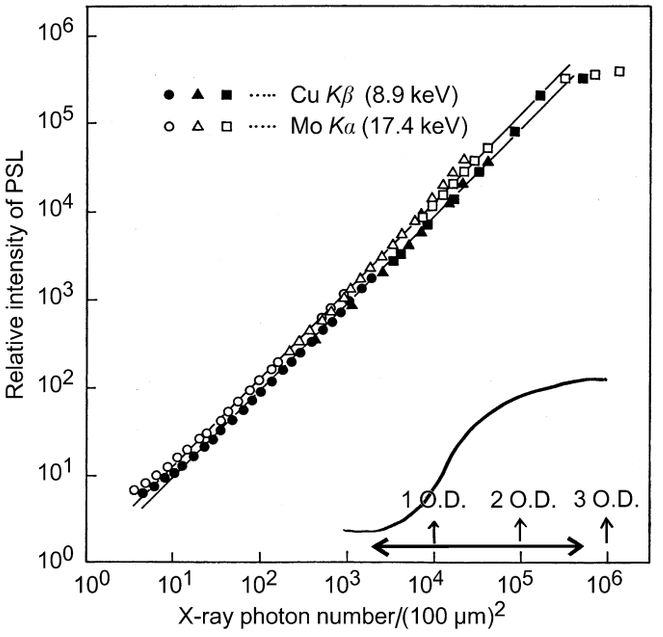

Fig. 7.1.8.5. Dynamic range of the photo-stimulated luminescence of the imaging plate. The dynamic range of typical high-sensitivity X-ray films is also shown. O.D. refers to optical density (Amemiya, 1995).

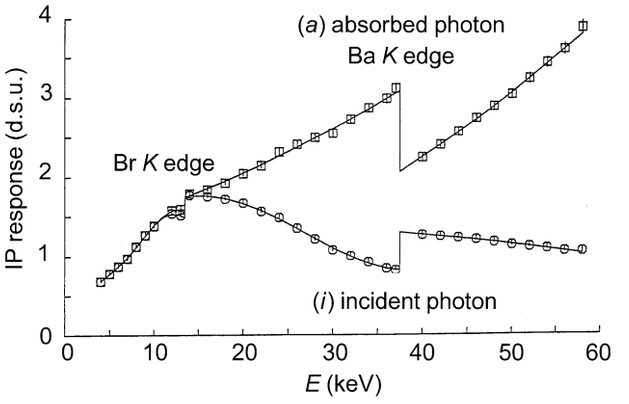

Fig. 7.1.8.6. Dependence of the IP response as a function of the energy of an X-ray photon. (*i*) is the IP response per an incident X-ray photon, and (*a*) the IP response per absorbed X-ray photon. The unit of the ordinate corresponds to the background noise level of the IP scanner (Ito & Amemiya, 1991).

The spatial resolution of the standard IP with a 100 μm laser scanning pitch is 170 μm at the full width at half-maximum (FWHM). The spatial resolution is limited by laser-light scattering in the phosphor during the read-out. A high-resolution IP that includes blue pigments in the phosphor to minimize the laser-light scattering has been developed. A spatial resolution of 43 μm is obtained at a 25 μm laser scanning pitch with the high-resolution IP with the sacrifice of 30% of the amount of PSL. The active area sizes of the available IP range from 127 × 127, 201 × 252, 201 × 400 to 800 × 400 mm.

The IP response per incident X-ray photon is shown as a function of the X-ray energy in Fig. 7.1.8.6, together with the deposited energy per absorbed X-ray photon. The abrupt decrease in the energy deposition above the barium *K*-absorption edge is due to the energy escape in the form of X-ray fluorescence. This effect is preferable because it makes the IP response curve smoother by compensating for the abrupt increase of the absorption efficiency at the absorption edge.

The image stored in the IP fades with the passage of time after exposure to X-rays. The fading rate depends on the type of IP and the temperature; it increases at higher temperature. But it does not depend on the exposure level or on the X-ray photon energy of the image. Fig. 7.1.8.7 shows the fading of an IP (type BAS III) as a function of time for two different X-ray energies at 293 K. The fading curve can be fitted well with three exponentials:

$$I(t) = A_1 \exp(-k_1 t) + A_2 \exp(-k_2 t) + A_3 \exp(-k_3 t).$$

$1/k_1$, $1/k_2$, and $1/k_3$ are 0.7, 18, and 520 h, respectively.

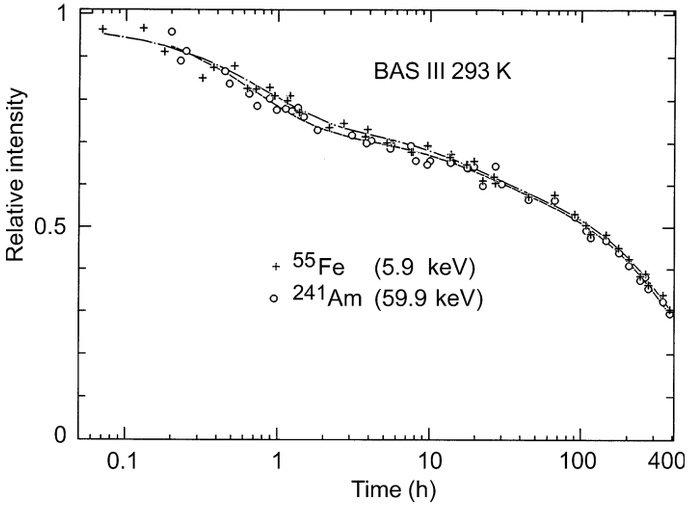

Fig. 7.1.8.7. Fading of the IP signals as a function of time with two different X-ray energies (5.9 and 59.5 keV). Temperature 293 K, type of IP: BAS III (Amemiya, 1995).

The non-uniformity of the response of the IP is about 1–2% over an active area of 250 × 200 mm. The distortion of the image is usually of the order 1%. It depends mainly on the type of IP read-out system.

Since the IP is an integrating-type detector, it is free from instantaneous count-rate limitations, which are accompanied by detectors operating in a pulse-counting mode. Therefore, the IP can make full use of a high flux of synchrotron X-radiation. Using synchrotron X-radiation, time-resolved measurements are possible by mechanically moving the IP (Amemiya, Kishimoto, Matsushita, Satow & Ando, 1989). Caution has been paid not to irradiate extremely intense X-rays (more than 10^6 photons μm^{-2}) on the IP; too intense X-rays create either non-erasable colour centres, or colour centres that are seemingly erasable but later reappear.

With minimum precautions, the IP yields reproducible results over a long period of repeated use, unlike X-ray film, whose performance is affected by slight changes in the development conditions. Various kinds of automated IP read-out systems are available, which permit on-site read-out in combination with an X-ray camera. The mechanical flexibility of the IP is also very important when it is used with a Weissenberg camera (Sakabe, 1991).

International Tables for Crystallography (2006). Vol. C, Chapter 7.2, pp. 639–643.

7.2. Detectors for electrons

By J. N. Chapman

7.2.1. Introduction

It is convenient to divide instruments used to form electron-diffraction patterns and images into two categories. In the first, all electron beams are static in the sense that neither the beams incident on nor emergent from the specimen are varied in position or orientation during the detection and recording process. Such is the case, for example, in a conventional transmission electron microscope (CTEM) where diffraction patterns and images must be recorded using a parallel or flux-density detector. By contrast, instruments in the second category employ a scanning system to vary the position or orientation of the electron beams before or after the specimen. Thus, in a scanning transmission electron microscope (STEM), diffracton patterns may be formed by rocking a beam about a point on the specimen or by positioning a stationary probe at the selected point and deflecting the beams as they emerge from the specimen. Under these conditions, the electrons are detected by a small total flux detector located on the optic axis of the instrument and the diffraction pattern (or image) is built up in a time-sequential or serial manner.

Whilst many of the properties required of total flux and flux-density detectors differ significantly, all detectors must satisfy certain criteria. A means of characterizing detectors is given in Section 7.2.2 together with a brief description of which particular features are desirable in each of the two categories. Specific detectors suitable for parallel recording are considered in Section 7.2.3, where a description is given both of their operation and of the extent to which they fulfil the criteria outlined in the preceding section. Finally, in Section 7.2.4, similar details are given for detectors suitable for serial recording purposes.

7.2.2. Characterization of detectors

Electron-diffraction patterns and images are inherently noisy due to the random arrival of electrons at the detector plane. The number of electrons N arriving in a specified time interval at the detector (or a particular detector element in the case of a flux-density detector) fluctuates in such a way that the variance of the signal σ_N^2 is equal to $\langle N\rangle$ where $\langle N\rangle$ denotes the expectation value of N. This is in accord with Poisson statistics and it follows that the signal-to-noise ratio of the incident signal $(\mathrm{SNR})_i$ may be increased indefinitely, in principle, by simply increasing the recording time until a sufficiently large number of electrons has arrived at the detector.

An ideal electron detector would be one in which the signal-to-noise ratio of the output signal was also equal to the limit imposed by Poisson statistics. Such a detector would impose no additional noise onto the signal and there would be no further loss of information. In practice, this is unattainable, and it is convenient to define a detective quantum efficiency (DQE) to provide a quantitative description of the signal degradation or information loss directly attributable to the detector. If an input signal S_i (variance σ_i^2) gives rise to an output signal S_o (variance σ_o^2), the DQE is defined as

$$\mathrm{DQE} = (\mathrm{d}S_o/\mathrm{d}S_i)^2\sigma_i^2/\sigma_o^2, \qquad (7.2.2.1)$$

where $\mathrm{d}S_o/\mathrm{d}S_i$ is the gradient of the output/input characteristic. For detectors with a linear response, (7.2.2.1) may be simplified and it is convenient to express the DQE as

$$\mathrm{DQE} = (\mathrm{SNR})_o^2/(\mathrm{SNR})_i^2, \qquad (7.2.2.2)$$

where the subscripts i and o again denote input and output. In all cases, the DQE is necessarily less than unity and factors that frequently limit the performance of detectors have been discussed in a general way as well as for specific cases by Herrmann (1984), Chapman & Morrison (1984), and Chapman, Craven & Scott (1989).

Although the DQE provides a useful quantitative figure of merit for a detector, alone it does not provide enough information to determine whether a particular detector will be suitable for a chosen application. To ascertain this, it is necessary to consider the following attributes of individual detectors:

(*a*) dynamic range;
(*b*) fraction of the dynamic range over which the detector response is (approximately) linear;
(*c*) ease of access to the output signal;
(*d*) suitability for use over a wide range of electron energies;
(*e*) speed of response;
(*f*) resolution;
(*g*) information-storage capability;
(*h*) single shot or repeated use;
(*i*) susceptibility to radiation damage;
(*j*) simplicity of construction;
(*k*) ease of use;
(*l*) cost.

For all detection and recording systems, a high DQE over a wide signal range is desirable. This is particularly so when diffraction patterns from single crystals are being studied as the intensity of diffraction spots in a single pattern can vary over many orders of magnitude. In addition, it is advantageous if an unvarying and simple relation exists between the output and input signals over the complete range of the latter. Thereafter, important attributes for parallel and serial systems can differ markedly.

Parallel detectors should have high spatial resolution and a large information-storage capacity. The latter requirement ensures that extensive and complex diffraction paterns and images may be studied at one time while the two requirements together ensure that the overall size of the detector is minimized. This is generally advantageous when optimizing overall instrumental performance. Broadly speaking, two options exist. The first is to employ a relatively complex system that may be used repeatedly and that allows easy access to a quantitative output signal, but that is inevitably expensive and complex in construction (see *e.g.* Subsection 7.2.3.3); the second is to use a simple, cheap system such as film (Subsection 7.2.3.2), which must be replaced each time a new image is to be recorded. The choice between the two options depends largely on the experiment to be undertaken and may involve such factors as whether the required information can be obtained from, for example, the symmetry or separation of spots or lines in a diffraction pattern or whether quantitative intensities across the entire field are needed. Also relevant is the delay that is acceptable between initiating a recording and obtaining the information in the form required. By contrast, the actual speed of response of the detector itself is rarely the limiting factor.

In serial electron detection systems, however, the speed of response of the detector can be crucial. The detector is generally a single undivided element with a fast enough response to ensure

Copyright © 2006 International Union of Crystallography

that recording times are sufficiently short to avoid problems arising from specimen drift or the build up of contamination during the recording. Clearly, a serial detector must also be well suited to repeated use and (reasonably) resistant to radiation damage. The output must be easily accessible and at least temporary storage must be available to allow an entire field to be examined. Although segmented detectors are sometimes used in serial detection systems (*e.g.* Burge & van Toorn, 1980), the number of individual elements is usually small and the spatial resolution of the detector is rarely a relevant consideration.

7.2.3. Parallel detectors

7.2.3.1. *Fluorescent screens*

The fluorescent screen offers the simplest means of rendering a spatially distributed electron signal visible to the eye. Screens are frequently made using ZnS powder to which small numbers of activator atoms have been added to make the wavelength at which maximum emission occurs match the maximum sensitivity of the eye. This occurs in the yellow–green region of the spectrum.

The light output from a fluorescent screen is proportional to electron current density over a wide range and, for a given current density, increases slowly with electron energy. For electrons of energy greater than ~40 keV (as are used in RHEED, CTEM, and HVEM), the output level is generally satisfactory under normal experimental conditions; however, when significantly lower electron energies are involved (as is the practice in LEED where energies are typically less than 1 keV), the electrons must be accelerated onto the screen to increase to a suitable level the number of photons emitted by each incident electron. In practice, an accelerating voltage of ~5 kV is used.

The resolution of a fluorescent screen is typically in the range 20–50 μm for powders, although significantly smaller values are achievable, particularly if single crystals are used instead. Powder phosphor screens can generally be made as large as required so that the field of view is limited by instrumental constraints rather than by any imposed by the detector itself. On removal of the electron signal, the light intensity decays in a two-stage process. The initial decrease is rapid with a time constant < 1 ms after which an afterglow lasting ~1–5 s remains. Further details of commonly used fluorescent materials have been discussed by Garlick (1966) and Reimer (1984).

Fluorescent screens may be viewed in reflection or transmission, although the optimum thickness of material (for a given incident electron energy) differs significantly in the two cases. Reflection screens are widely used simply as viewing screens and are rarely used as a component in a recording system; by contrast, transmission screens are the first stage in many systems that combine detection and recording and will appear in this context in Subsections 7.2.3.3 and 7.2.3.4.

7.2.3.2. *Photographic emulsions*

Photographic emulsions provide the most frequently used means of recording spatially distributed electron signals. They are of little use alone in that the output signal is not available until the emulsion has been developed and fixed and so are normally used in conjunction with a viewing system such as that described above. A photographic emulsion is an example of an analogue storage medium and further equipment is required (see below) if quantitative electron intensity data are to be extracted from the developed emulsion.

In most instances, the electron image or diffraction pattern is allowed to impinge directly onto a desiccated photographic emulsion stored inside the vacuum system. The probability that a silver halide grain will be rendered developable by an electron of energy ~100 keV is high and so, in practice, a single electron may relase ~10 grains. This is in contrast to what is observed when photographic emulsions are exposed to light where several quanta must be absorbed by one grain to render it developable. For this reason, there is no illumination threshold when electrons are used and the law of reciprocity is applicable over a very wide electron intensity range. Fuller details of the theory of the interaction between electrons and photographic emulsions are given by Hamilton & Marchant (1967), Valentine (1966), Farnell & Flint (1975), and Zeitler (1992).

The alternative to directly exposing film within the vacuum system to the electron beam is to convert the electron signal into an equivalent photon signal, which is then recorded outside the vacuum system. Conversion may be achieved by use of a transmission fluorescent screen, and the photon signal may be led out of the vacuum system using a fibre-optic plate (Guetter & Menzel, 1978). In this way, the need to open the vacuum system every time new films are required is eliminated, but the noise properties of the overall system are generally inferior to those achievable using direct exposure.

The relation between the density D of the developed emulsion and the exposure q (expressed as a charge/unit area) has been widely studied theoretically and experimentally over a range of electron energies (Hamilton & Marchant, 1967; Valentine, 1966). To a good approximation, the characteristic takes the form

$$D = D_s[1 - \exp(-cq)] + D_o, \qquad (7.2.3.1)$$

where D_o is the 'fog' level, D_s the saturation density, and c the speed of the emulsion (defined by the gradient of the characteristic $\mathrm{d}D/\mathrm{d}q$ at $q = 0$). Given that saturation densities up to 6 are not uncommon and the fog can be kept small, it can be seen that the variation of D with q is approximately linear to densities of ~ 1.

The DQE for a number of emulsions has been measured [for typical results see Herrmann (1984)] and, over a limited range of exposure, values between 0.7 and 0.8 may be achieved. Below and above the optimum exposure, the DQE falls. For low exposures, the effect of the background fog becomes important while saturation effects cause a fall in DQE at high exposures. These effects can be serious when, for example, diffraction patterns with a very high dynamic range are to be recorded and a number of different exposures must be used if maximum information is to be obtained.

Within bounds, the exposure at which the optimum DQE occurs can be varied by selecting different emulsions and also by varying development conditions. As faster emulsions tend to have larger grain sizes, the spatial resolution cannot be regarded as an independent or fixed parameter. For this reason, it is generally preferable when comparing different emulsions to plot the variation of DQE not with the number of electrons falling on unit area of emulsion but with the number of electrons falling on the pixel area. The latter quantity may be defined conveniently as the size of the point spread function of a single electron. Unfortunately, further complications ensue as the resolution of the emulsion depends not only on the grain size but also on the diameter of the electron diffusion cloud in the emulsion, a quantity that varies markedly with electron energy.

Using emulsions commonly employed for recording diffraction patterns and images with 100 keV electrons, a resolution of ~30 μm is typical. The film size used in electron microscopy has an area of ~50 cm^2 so that a single recording contains ~ 5×10^6 pixels. This represents a very high storage capability

and is particularly useful when recording fine detail over a wide field as occurs both in convergent-beam electron-diffraction patterns and in high-resolution images.

If quantitative electron intensity data are required, the density distribution on the emulsion must be digitized. High-precision TV cameras, flying-spot devices, drum scanners, or flat-bed scanners have all been used for this purpose. While the first named provides the data in the shortest time, flat-bed scanners offer superior precision in both intensity measurement and definition of the area from which the measurement is made, and can digitize a larger number of pixels at one time.

In summary, the extensively used photographic plate provides a cheap, convenient electron detector with a high storage capacity. It may be used under a wide range of experimental conditions and has an input/output characteristic typical of that produced when any ionizing radiation is incident on a photographic emulsion. As such, it closely resembles that obtained when X-rays are used instead of electrons. Against its advantages must be offset the inevitable delay in access to any information while the emulsion is being developed and the further delay incurred (if quantitative data are sought) while densitometry is undertaken.

7.2.3.3. *Detector systems based on an electron-tube device*

Detector and recording systems based on electron-tube devices have been reviewed in detail by Herrmann & Krahl (1984). The first stage is a transmission fluorescent screen (as described in Subsection 7.2.3.1), which converts the electron image to its photon counterpart. A fibre-optic plate may then be used to transfer the photon image to a low-light-level TV camera located outside the vacuum system. In some instances, an image intensifier is included before the TV camera to increase the intensity of the light signal being recorded. An alternative means of increasing the light signal, preferable when the energy of the incident electrons is low, is to employ a channel plate before the fluorescent screen.

Electronic systems are capable of detecting single electrons and, provided the electron current density incident on the fluorescent screen is sufficiently low, can have a DQE of ~ 0.9. The restriction to low current densities arises from the need to ensure that in a single TV frame the number of electrons arriving at any pixel is either 0 or 1. Under these conditions, truly digital images may be obtained in which the number associated with each pixel is the number of electrons that arrived at the corresponding small area of the fluorescent screen during the exposure. To achieve such an image in practice requires the accumulation of many individual TV frames (the precise number depending on the statistical accuracy required) and this is normally achieved using an image memory or frame store.

At higher electron current densities, the number of electrons arriving at each point on the fluorescent screen in a TV frame interval can be considerably greater than one. The TV output signal then varies continuously and it is impossible to determine the exact number of electrons associated with each pixel. When used in this way (the analogue mode), the maximum value of DQE is ~ 0.8.

The number of pixels in a frame is typically $\sim 3 \times 10^5$, a number appreciably lower than the storage capacity of the film commonly in use. A consequence of this is that diffraction patterns may have to be recorded at a range of camera lengths if fine detail and high-scattering-angle information are both to be observed.

The electronic detector system as described, particularly if it incorporates an intensifier, has a higher sensitivity than the naked eye. This is particularly beneficial when focusing fine structures or when working with radiation-sensitive specimens where limitations are imposed on the exposure to which the specimen may be subjected. Perhaps of even greater value, however, is the fact that the system as a whole provides storage (thus removing the need to irradiate the specimen continuously during observation) and that the storage is in a digital form. As a result, it is straightforward to interface a computer to the system and on-line processing of the stored intensity values may be undertaken readily.

A major disadvantage of the system is the cost and susceptibility to damage (if subjected to excessive intensities) of high dynamic range, low-noise electron tubes, which should be used if the highest performance is to be achieved; a further drawback for many applications is the barely adequate number of pixels/frame.

7.2.3.4. *Electronic detection systems based on solid-state devices*

Electronic detection systems resembling those described in the preceding section but with the electron tube replaced by a semiconductor array detector have been the subject of intense development recently. Initially, both charge-coupled devices (CCD) and self-scanned photodiode arrays (PDA) were explored (Herrmann, 1984), but the former have now assumed the dominant position. Early devices suffered from a barely adequate number of pixels ($\sim 10^4$) but those currently in use have between 2×10^5 and 4×10^6 pixels. As such, they frequently allow larger image fields to be explored than do standard TV systems. Furthermore, CCD-based systems offer a wide dynamic range ($>16\,000{:}1$), linearity better than 1% over the entire dynamic range, and extreme sensitivity. They display no lag or sensitivity to magnetic fields and they are not damaged by overlighting. Details of the performance of fully operational systems have been given by Krivanek, Ahn & Keeney (1987), Daberkow, Herrmann, Liu & Rau (1991), Kujawa & Krahl (1992), and Ishizuka (1993).

To achieve optimum performance, a number of precautions must be taken including modest cooling of the CCD to suppress thermally generated charge carriers. Readout speeds are long compared with TV rates so that any noise associated with this process is minimized. In practice, high-precision correlated double-sampling techniques are used for analogue-to-digital conversion to realise this end. There is also the need to compensate for fixed-pattern noise due to non-uniformities of dark current and due to the fibre plate. For these purposes, use is made of a reference image recorded when the device is simply flooded with uniform illumination. An alternative approach to reduce at least some of the fixed-pattern noise is to use a lens rather than a fibre-optic plate between the transmission fluorescent screen and the device (Fan & Ellisman, 1993). When all these precautions are taken, the resulting system has sufficient sensitivity to detect single 100 keV electrons.

From the above, it should be clear that the CCD-based system offers many advantages over the TV system if quantitative electron data (images or diffracton patterns) are required for subsequent computer analysis. However, its slower response speed means that its use is limited for alignment purposes and much *in situ* experimentation. It is advantageous, therefore, to have both systems available.

7.2.3.5. *Imaging plates*

A recent advance using a medium related to film involves the imaging plate (Mori, Katoh, Oikawa, Miyahara & Harada,

1986), which relies on the phenomenon of photostimulated luminescence. Here the active area is a coating of a photostimulable phosphor that can store energy when excited by electrons. The energy absorbed is then emitted as photons when the medium is illuminated with visible or infrared radiation and this signal is detected using a photomultiplier. The read signal is provided by a scanning He–Ne laser so that, as with the detectors in Subsections 7.2.3.3 and 7.2.3.4, information is recorded in parallel but accessed serially. Initial experiments suggest that the imaging plate offers higher sensitivity and a wider dynamic range than most film, but currently suffers from inferior spatial resolution. Recent discussion of the performance and limitations of imaging plates has been supplied by Mori, Oikawa, Katoh, Miyahara & Harada (1988) and Isoda, Saitoh, Moriguchi & Kobayashi (1991).

7.2.4. Serial detectors

7.2.4.1. *Faraday cage*

The Faraday cage is the most convenient means of determining electron-beam currents. It consists of a small electrically isolated cage with a small hole in it through which electrons enter. Provided the hole subtends a sufficiently small solid angle and the inner surface of the cage is made of a material with a low back-scattering coefficient, the probability that any electrons will re-emerge is negligible. An electrometer is normally used to measure the charge that has entered the cage.

The main use of the Faraday cage is to calibrate other detectors when absolute electron intensities are required. It also serves a very important role when the total specimen exposure in an experiment must be kept below a critical value owing to the susceptibility of the specimen to radiation damage. As electron charge is being measured, the Faraday cage may be used with electrons of any energy.

7.2.4.2. *Scintillation detectors*

One of the most widely used total flux detectors is a scintillator, the output from which is coupled into a photomultiplier by a light-pipe. In the first stage, an incident electron deposits its energy in the scintillator, producing a number of light photons with an energy deficiency of up to $\sim 20\%$ (Herrmann, 1984). By careful design of the light-pipe, an appreciable fraction of the photons will reach the photomultiplier, which should have a photocathode whose quantum yield peaks around the wavelength of the photons from the scintillator. Even though the quantum yield of the photocathode is likely to be <0.2, the number of photoelectrons emerging from the photocathode for each electron incident on the scintillator should be considerably greater than unity, provided the incident electron energy exceeds $\sim 10\,\text{keV}$. With lower-energy electrons, it is advantageous to provide an additional acceleration onto the scintillator to ensure that an adequate number of photons is generated.

Following the production of photoelectrons, considerable multiplication takes place down the dynode chain of the photomultiplier and a current pulse may easily be detected at the anode. Electron counting is therefore a possibility and to take advantage of this over as wide a current range as possible scintillators with very fast decay times (10^{-8} to 10^{-7} s) should be used. Such scintillators have the additional advantage that they may be used in systems where beam scanning is performed at TV rates.

When the rate of arrival of electrons at the detector appreciably exceeds $10^6\,\text{s}^{-1}$, it becomes increasingly difficult to distinguish the output from individual electrons and the detector must be operated in an analogue mode. Despite this, the individual electron pulse-height distributions from good scintillators are sufficiently narrow that values of DQE greater than 0.8 may be obtained (Chapman & Morrison, 1984). Scintillators meeting both speed and pulse-height distribution requirements include plastics (*e.g.* Nuclear Enterprise NE102A) and Ce-doped YAG (Schauer & Autrata, 1979). It should be noted that the materials discussed in Subsection 7.2.3.1 are generally unsuitable for fast detector systems because of their relatively long time constants and the existence of an afterglow that persists for several seconds.

To handle the large dynamic range encountered in diffraction patterns, it is advantageous to use a detector system capable of both counting the arrival of individual electrons and making analogue current measurements. Such a system, which allows signals whose magnitudes differ by a factor of 10^8 to be recorded with a high DQE in a single scan, has been described by Craven & Buggy (1984). More general advantages of detector systems based on scintillation counters are their desirable input/output characteristics, which are essentially linear, and the fact that a quantitative measure of electron intensity is directly available in a form suitable for input to a computer. Analysis of the data may thus begin as soon as its collection is completed.

The susceptibility to radiation damage of many high-efficiency scintillators, resulting in a diminution of light output with increasing use, is probably the major disadvantage of these detectors. Of importance in some instances is the fact that the entire detection system is relatively bulky and it may not always be possible to position it satisfactorily within the apparatus.

7.2.4.3. *Semiconductor detectors*

The most commonly used semiconductor detector is a silicon photodiode whose *p–n* junction is reverse biased. A fast electron incident directly on the device produces electron–hole (*e–h*) pairs and the two charge carriers are swept in opposite directions under the influence of the bias field. Thus, a charge pulse is produced and as, on average, an *e–h* pair is produced for every 3.6 eV deposited in the silicon, a 100 keV incident electron produces a pulse equivalent to $\sim 3 \times 10^4$ electrons. In practice, many devices have a contact layer on the silicon surface (which itself may be less perfect than the bulk of the material) so that some of the energy of the incident electron is lost before the sensitive volume is reached. As the energy deposited in surface layers is rarely less than 5 keV, semiconductor detectors are unsuitable for direct use with low-energy electrons.

The magnitude of the signal produced by each incident electron in a semiconductor detector is typically $\sim 10^4$ times lower than that emerging from the anode of the photomultiplier in scintillation detector systems and it is difficult to measure such small signals without adding substantial noise. A further complicating factor arises from thermally generated carriers, which can give rise to a substantial dark current from detectors of area $>1\,\text{mm}^2$. Thus, photodiode detectors cannot normally be operated in an electron-counting mode and suffer from a low DQE whenever incident electron currents are small. To optimize their performance in this range, the device should be cooled (to reduce the thermally generated signal) and the electron beam should be scanned relatively slowly so that high-gain low-noise amplifiers may be used for subsequent amplification of the signal from the photodiode. Above the low-signal threshold, the output from the photodiode varies linearly with incident electron intensity and is once again in a form suitable for direct display or for being digitized and stored.

The main advantages of semiconductor over scintillation detection systems are their robustness, cheapness, and compactness. The latter is particularly valuable for certain applications in that it allows the detector to be sited very close to the specimen even when space is very confined. This occurs, for example, when the specimen is immersed in a magnetic lens and channelling patterns from back-scattered electrons are to be recorded. A further advantage arises if images are to be formed in scanning microscopes using signals from a number of closely positioned detectors whose shapes may be quite complex. Using lithographic techniques, several detectors may be fabricated on a single silicon substrate and, provided the gains of any succeeding amplifiers are well matched, a detection system with a well defined response function results.

7.2.5. Conclusions

A wide variety of different means exists for detecting electrons. Many are almost perfect in that they add very little noise to that already present in the electron beam. However, no single detector meets all the requirements of different experiments and, before selecting a detector for a specific purpose, it is necessary to consider the relative importance of the attributes listed in Section 7.2.2. Once this is established, it should be straightforward to determine the optimum detector for the task in hand.

International Tables for Crystallography (2006). Vol. C, Chapter 7.3, pp. 644–652.

7.3. Thermal neutron detection

BY P. CONVERT AND P. CHIEUX

7.3.1. Introduction

In this chapter, we shall be concerned with the detection of neutrons having thermal and epithermal energies in the range 0.0002–10 eV (20–0.1 Å). Given the cost and the rarity of the neutron sources, it is clear that the recent trends in neutron diffractometry are more and more in the direction of designing new instruments around highly efficient and complex detection systems. These detection systems become more and more adapted to the particular requirements of the different experimental needs (counting rate, size, resolution, definition, shielding and background, TOF, *etc*.). It is therefore difficult to speak about neutron detectors and intensity measurements as such without reference to the complete spectrometers, and this should include the on-line computer.

Most neutron detectors for research experiments have been created and developed using fission reactors as neutron sources [*i.e.* with an upper limit of usable energy of 0.5 eV (0.4 Å)]. Given the relatively low intensity of reactor neutron beams, a very successful effort has been made to increase the detector efficiency and the detection area as much as possible. The recent construction of pulsed neutron sources extends the range of incident energy to at least 10 eV and generalizes the use of time-of-flight (TOF) techniques. A broad range of fully operational neutron detectors, well adapted to reactors as neutron sources, is commercially available, but this is not yet the case for pulsed sources. Probably due to the variation of intensity of the early neutron beams, it is a tradition in neutron research to monitor the incident flux with a low-efficiency detector, which in the best case has a stability of the order of 10^{-3}, *i.e.* sufficient for most experiments.

7.3.2. Neutron capture

Neutrons' lack of charge and the fact that they are only weakly absorbed by most materials require specific nuclear reactions to capture them and convert them into detectable secondary particles. Table 7.3.2.1 lists the neutron-capture reactions that are commonly used in thermal neutron detection. The incoming thermal neutron brings a negligible energy to the nuclear reaction, and the secondary charged particles or fission fragments are emitted in random directions following the conservation-of-momentum law $\sum m_i v_i = 0$. The capture or absorption cross sections for a number of nuclei of interest are plotted as a function of neutron energy in Fig. 7.3.2.1. These cross sections are commonly expressed in barns (1 barn = 10^{-28} m^2). At low energies, they are inversely proportional to neutron velocity, except in the case of Gd, which has a nuclear resonance at 0.031 eV. The total efficiency ε of neutron detection can be expressed by the equation

$$\varepsilon = \xi[1 - \exp(-N\sigma_a t)], \qquad (7.3.2.1)$$

where N is the number of absorbing nuclei per unit volume, σ_a is their energy-dependent absorption cross section, and t is the thickness of the absorbing material. The factor $1 - \exp(-N\sigma_a t)$ gives the neutron-capture efficiency, while ξ is a factor ≤ 1 that depends on the detector geometry and materials (absorption and scattering in the front window) and on the efficiency of the secondary particles.

7.3.3. Neutron detection processes

A detection process consists of a chain of events that begins with the neutron capture and ends with the macroscopic 'visualization' of the neutron by a sensor (electronic or film). The quality of a detection process will depend on the efficiency of the conversion steps and on the characteristics of the emission steps, which alternate in the process (see Table 7.3.3.1). We present below typical detection processes.

7.3.3.1. *Detection via gas converter and gas ionization: the gas detector*

The neutron capture and the trajectories of the secondary charged particles as well as the specific gas ionization along these trajectories are presented in Figs. 7.3.3.1(*a*) and (*b*). Since the gas ionization energy is about 30 eV per electron (42 eV for ^{3}He and 30 eV for CH_4), there are about 25 000 ion pairs (e^-, He^+ or e^-, CH_4^+) per captured neutron. Gases such as CH_4 or C_3H_8 are added to diminish the length of the trajectories, *i.e.* the wall effect [see Subsection 7.3.4.2(*b*)].

We give in Fig. 7.3.3.1(*c*) the proton range of an ^{3}He neutron-capture reaction in various gases (Fischer, Radeka, & Boie, 1983). A schematic drawing of a gas monodetector, which might be mounted either in axial or in radial orientation in the neutron beam, is given in Fig. 7.3.3.1(*d*).

For this type of detector, the efficiency as a function of the gas pressure, or gas-detector law, is written as

$$\varepsilon(\lambda) = \xi[1 - \exp(-bPt\lambda)],$$

with P (atm) = the detector-gas pressure at 293 K, t (cm) = the gas thickness, and λ (Å) = the detected neutron wavelength. The numerical coefficient b, obtained at 293 K from the ideal gas law, the Avogadro number N_A, and the gas absorption cross section σ_a (barns) at $\lambda_0 = 1.8$ Å, is

$$b = \frac{273}{293} \times \frac{N_A}{22\,414} \times \frac{\sigma_a}{\lambda_0}.$$

For ^{3}He, with $\sigma_a = 5333$ barns at $\lambda_0 = 1.8$ Å, $b = 0.07417$; for $^{10}BF_3$, with $\sigma_a = 3837$ barns at $\lambda_0 = 1.8$ Å, $b = 0.0533$. We give in Table 7.3.3.2 a few examples of gas-detector characteristics.

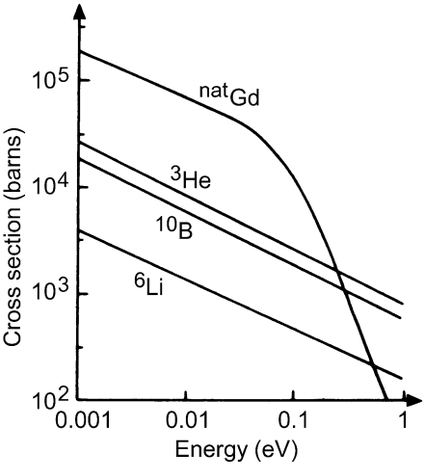

Fig. 7.3.2.1. The capture cross sections for a number of nuclei used in neutron detection. [Adapted from Convert & Forsyth (1983).]

Copyright © 2006 International Union of Crystallography

Table 7.3.2.1. *Neutron capture reactions used in neutron detection*

n = neutron, p = H^+ = proton, t = $^3H^-$ = triton, $\alpha = {}^4H^+$ = alpha, e^- = electron

Capture reaction	Cross section at 1 Å (barns)	Secondary-particle energies (MeV)
$^3He + n \rightarrow t + p$	3000	t 0.20 p 0.57
$^6Li + n \rightarrow t + \alpha$	520	t 3.74 α 2.05
$^{10}B + n \rightarrow {}^7Li^* + \alpha$ (93%) $\hookrightarrow {}^7Li + \gamma$ $\rightarrow {}^7Li + \alpha$ (7%)	2100	α 1.47 ^7Li 0.83 γ 0.48 α 1.78 ^7Li 1.01
$^{157}Gd + n \rightarrow Gd^*$ $\hookrightarrow \gamma$ + conversion electrons	74000 (^{nat}Gd: 17000)	e^- spectrum 0.07 to 0.182 γ spectrum up to 8
$^{235}U + n \rightarrow$ fission fragments	320	Fission fragments up to 80

There are two modes of operation.

In the case of *direct collection of charges*, the 25 000 electrons corresponding to one neutron capture (*primary electrons*) are collected by the anode in about 100–500 ns, and generate an input pulse in the charge preamplifier (see Section 7.3.4).

If the electrical field created by the high voltage applied to the anode exceeds a critical value, the electrons will be accelerated sufficiently to produce a cascade of ionizing collisions with the neutral molecules they encounter, the new electrons liberated in the process being called *secondary electrons*. This phenomenon, *gas multiplication*, occurs in the vicinity of the thin wire anode, since the field varies as $1/r$. The avalanche stops when all the free electrons have been collected at the anode. With proper design, the number of secondary electrons is proportional to the number of primary electrons. For cylindrical geometries, the multiplication coefficient M can be calculated (Wolf, 1974). This type of detection mode is called the proportional mode. It is very commonly used because it gives a better signal-to-noise ratio (see Section 7.3.4).

A few critical remarks about gas detectors:

(i) Some gases have a tendency to form negative ions by the attachment of a free electron to a neutral gas molecule, giving a loss of detector current. This effect is negligible for ^3He but it limits the use of $^{10}BF_3$ to about 2 atmospheres pressure, although traces of gases such as O_2 or H_2O (*e.g.* detector materials and wall outgasing) are often the reason for loss by attachment.

(ii) Pure ^3He and $^{10}BF_3$ gas detectors are practically insensitive to γ radiation. This is no longer the case when additional gases, which are necessary for ^3He, are used, although the polyatomic additives C_3H_8 and CF_4 are much better than the rare gases Kr, Xe, and Ar (Fischer, Radeka & Boie, 1983).

(iii) For various reasons (the price of ^3He and $^{10}BF_3$ and the toxicity of BF_3), neutron gas detectors are closed chambers, which must be leak-proof and insensitive to BF_3 corrosion. The wall thickness must be adapted to the inside pressure, which sometimes implies a rather thick front aluminium window (*e.g.* a 10 mm window for a 16 bar ^3He gas position-sensitive detector; aluminium is chosen for its very good transmission of neutrons, about 90% for 10 mm thickness).

7.3.3.2. *Detection via solid converter and gas ionization: the foil detector*

This mode of detection is generally used for monitors. In a typical design, a ^{10}B deposit of controlled thickness, for example $t = 0.04\,\mu m$ giving a capture efficiency of 10^{-3} at $\lambda = 1$ Å, is made on a thin aluminium plate (see Fig. 7.3.3.2). One of the two particles (α, Li) produced in the solid by the capture reaction is absorbed by the plate; the other escapes and ionizes the gas. The electrons produced are collected by the aluminium plate, itself acting as the anode, or by a separate anode wire, allowing the use of the proportional mode. The detection efficiency is proportional to the deposit thickness t, but t must be kept less than the average range r of the secondary particles in the deposit (for ^{10}B, $r_\alpha = 3.8\,\mu m$ and $r_{Li} = 1.7\,\mu m$), which limits the efficiency to a maximum value of 3–4% for $\lambda = 1$ Å. The fraction of the secondary particle energy that is lost in the deposit reduces the detector current, *i.e.* the signal-to-noise ratio, and worsens the amplitude spectrum (see Section 7.3.4).

7.3.3.3. *Detection via scintillation*

In the detection process *via* scintillation (see Table 7.3.3.1), the secondary particles produced by the neutron capture ionize and excite a number of valence-band electrons of the solid scintillator to high-energy states, from which they tend to decay with the emission of a light flash of photons detected by a photomultiplier [see Fig. 7.3.3.3(*a*)]. A number of conditions must be satisfied:

(i) The scintillation must be immediate after the neutron-capture triggering event.

(ii) The scintillation decay time must be short. It depends on materials, and is around 50–100 ns for lithium silicate glasses.

(iii) A large fraction of the energy must be converted into light (rather than heat).

(iv) The material must be transparent to its own radiation.

Most thermal neutron scintillation detectors are currently based on inorganic salt crystals or glasses doped with traces of an activating element (Eu, Ce, Ag, *etc.*) (extrinsic scintillators). (A plastic scintillator might be considered to be a solid organic solution with a neutron converter.)

The use of extrinsic scintillators (Convert & Forsyth, 1983), although less efficient energetically, permits better decoupling of the energy of the photon-emitting transition (occurring now in the activator centres) from that of the valence-band electron excitation or ionization energy. The crystal or glass is then transparent to its own emission, and the light emitted is shifted to a wavelength better adapted to the following optical treatment.

Table 7.3.3.1. *Commonly used detection processes*

	1st conversion (neutron captures)	2nd conversion	3rd conversion	Sensor
	Capture/solid $\rightarrow e^-$ $n + {}^{157}\mathrm{Gd}$			Film
Gas ionization	Capture/gas $n + {}^3\mathrm{He} \rightarrow p + t$	Gas ionization $\rightarrow e^-$ (^{3}He + add. gas)		Electronics
	Capture/solid $n + {}^{10}\mathrm{B}, {}^6\mathrm{Li}, {}^{235}\mathrm{U}$ fission products	Gas ionization $\rightarrow e^-$ (*e.g.* Ar + CO_2)		Electronics
Scintillation	Capture/solid:	Fluorescence/solid:		
	LiF + ZnS(Ag) $n + {}^6\mathrm{Li} \rightarrow \alpha + t$	LiF + ZnS(Ag) $\rightarrow \nu$		Film
	LiF + ZnS(Ag) $n + {}^6\mathrm{Li} \rightarrow \alpha + t$	LiF + ZnS(Ag) $\rightarrow \nu$	Photoelectric effect $\rightarrow e^-$	Electronics
	Ce^{3+} enriched Li glass $n + {}^6\mathrm{Li} \rightarrow \alpha + t$	Ce^{3+} enriched Li glass $\rightarrow \nu$	Photoelectric effect $\rightarrow e^-$	Electronics

ν = photon.

Table 7.3.3.2. *A few examples of gas-detector characteristics*

Detection gas	Additional gas	Gas pressure (atm)	Useful detection volume (mm × mm)	Mounting	Capture efficiency	
					$\lambda = 1$ Å	$\lambda = 2$ Å
$^{10}BF_3$		1	$L = 200$, Ø = 50	Axial Radial*	65.5% 23.4%	88.1% 41.3%
^{3}He		5	$L = 100$, Ø = 50	Axial Radial*	97.5% 84.4%	99.9% 97.5%
^{3}He		8	$L = 250$, Ø = 10	Radial*	44.7%	69.5%
^{3}He (monitor)	C_3H_8	2	100 × 40 × 40		10^{-5} to 10^{-3}	

* Value calculated for the diameter.

In order to maximize the light collected by the photomultiplier [Fig. 7.3.3.3(*b*)], a light reflector is added in front of the scintillator, and a light coupler adapts the dimensions of the scintillator to that of the photomultiplier (PM). The area of the scintillator might be very large (up to 1 m^2). The optimum thickness of a glass scintillator is about 1 to 2 mm, corresponding to a neutron detection efficiency of 40 to 97% for $\lambda = 1.8$ Å, depending on the ^{6}Li concentration (Strauss, Brenner, Chou, Schultz & Roche, 1983). In a Ce-doped Li silicate glass, the number of photons emitted per captured neutron is about 9000, giving finally about 1500 electrons at the photocathode in the optimum light-coupling configuration. The number of photons emitted per captured neutron, the number of those reaching the photocathode, and the scintillator decay time are parameters that might differ by an order of magnitude, depending on the scintillator material. However, the glass scintillator remains for the time being the best choice, since the possible gains given by other materials, in decay time or in the number of photons emitted, are always very severely offset by poor light output (*e.g.* the plastic scintillator). It is very important to maximize the number of photons per neutron reaching the photocathode, since this will help to discriminate between neutrons and γ rays [see Fig. 7.3.4.2(*e*)]. The optical coupling between the different parts of the detection system must be of very good quality.

7.3.3.4. *Films*

Films are classed as position-sensitive detectors. Two types of neutron converter are used in neutron film-detection processes. In the case of the scintillation film system, a light-sensitive film is pressed close to one or between two plastic ^{6}LiF/ZnS(Ag) scintillator screens (Thomas, 1972). In the case of the Gd-foil

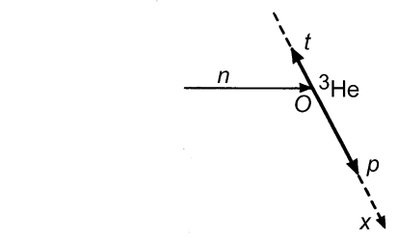

(*a*)

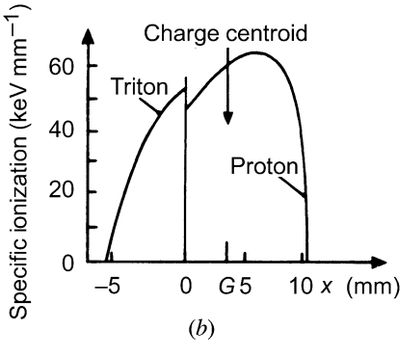

(*b*)

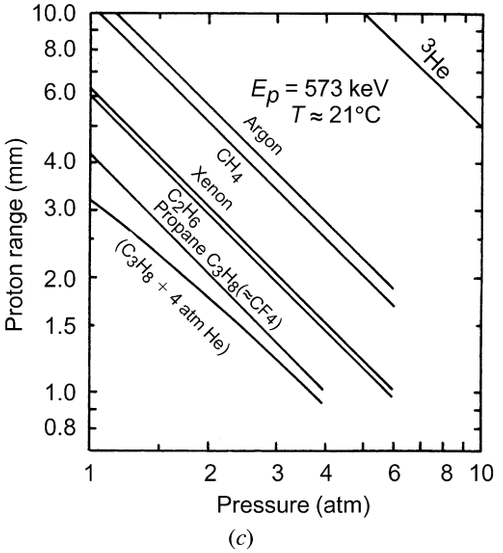

(*c*)

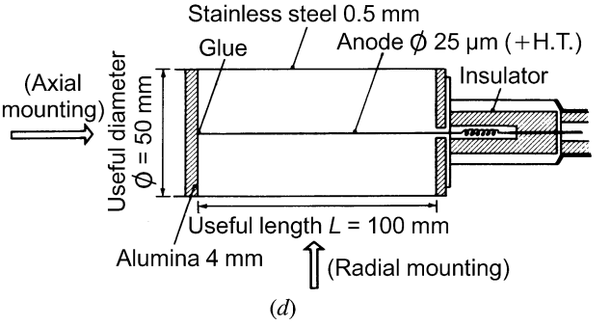

(*d*)

Fig. 7.3.3.1. (*a*) Neutron capture by an ^{3}He atom and random-direction trajectory (*Ox*) of the secondary charged particles in the gas mixture. (*b*) Calculated specific ionization along the proton and triton trajectory in a 65% ^{3}He/35% CH_4 mixture at 300 K and atmospheric pressure (Whaling, 1958). [Reproduced from Convert & Forsyth (1983).] (*c*) Range of a 0.57 MeV proton (from ^{3}He neutron capture) as a function of the pressure of various gases. [Reproduced from Convert & Forsyth (1983).] (*d*) Schematic drawing of a gas monodetector. The arrows represent the incoming beam.

converter, the conversion electrons are emitted isotropically, with a main energy peak at 72 keV, and collected by an X-ray film in close contact with the converter (Baruchel, Malgrange & Schlenker, 1983).

In addition to the advantages given by the film technique in itself (simplicity, low price, direct picture, *etc.*), neutron photographic methods give the best spatial resolution. However, the resolution is inversely related to the detector efficiency and thickness. A good compromise appears to be a thickness of 0.25 mm for a plastic scintillator [*i.e.* a capture efficiency of about 12% and a resolution of 0.1 mm for a one-screen converter at $\lambda = 1$ Å; see the size of the ionization volumes in a scintillator, Fig. 7.3.3.3(*a*)]. Here, however, as in light scattering, the optical density depends on the exposure time as well as on the incoming flux (Schwartzschild effect), which necessitates a calibration (Hohlwein, 1983). For a natural Gd-foil converter, an optimum thickness is 0.025 mm, giving a resolution of 0.020 mm. The Gd-foil film detector is one order of magnitude

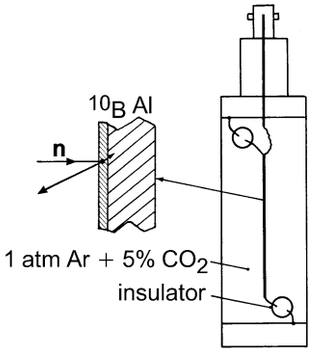

Fig. 7.3.3.2. Typical design of a ^{10}B-foil detector.

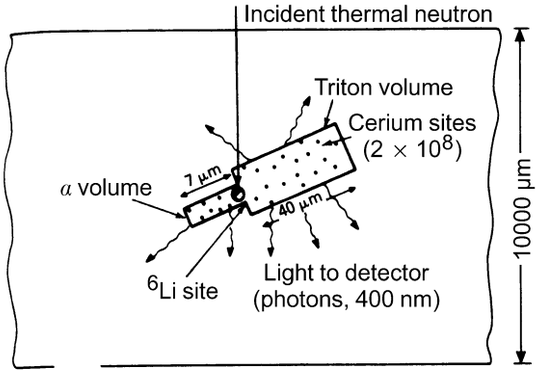

(*a*)

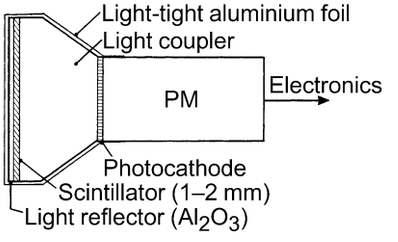

(*b*)

Fig. 7.3.3.3. (*a*) Schematic representation of the neutron capture, secondary α, and triton ionization volumes, and scintillator light emission in a cerium-doped lithium silicate glass. [Reproduced from Convert & Forsyth (1983).] (*b*) Schematic representation of a scintillation detector.

less efficient than the scintillator, but, as in electron microscopy, the optical density is nearly proportional to the exposure. This explains the use of the Gd foil in neutron-diffraction topography.

If we take into account the possible inhomogeneity of the converter and the difficulties related to the film (homogeneity, development, and photodensitometry), an accuracy of 5 to 10% is achievable in the intensity measurements under good conditions.

Owing to the differences in the processes, neutron photographic techniques are much more efficient than those for X-rays. In the case of the plastic scintillator, the gain is about 10^3, which compensates for the much lower neutron fluxes.

7.3.4. Electronic aspects of neutron detection

7.3.4.1. *The electronic chain*

Each collected burst of electrons, corresponding to one captured neutron, will be successively amplified, identified (discriminated), and transformed to a well defined signal, by a chain of electronic devices that are represented in Fig. 7.3.4.1. In the case of the gas detector, the complete electronic chain is generally contained in a grounded metallic box acting as an electrical shield. The detector is connected to this box *via* a coaxial cable as short as possible to avoid noise and parasitic capacitance. A high-voltage power supply feeds the detector anode through a filter. The charge-sensitive preamplifier contains a field-effect transistor (FET) to minimize the background noise, since, from the detector up to this stage, the electronic level is very low. At the output of the FET, the pulse corresponding to one neutron has an amplitude of about 20 mV. This pulse enters an operational amplifier with adjustable gain G, which delivers a signal of about 2 V, the analogue signal (ANA). The electronic pulse-rise time (0.5 to a few μs) is adapted to the detector electron-collecting time, *i.e.* its amplitude is roughly proportional to the number of electrons collected at the anode. The last part of the electronic chain is a discriminator with an adjustable threshold, followed by a trigger delivering a calibrated signal (*e.g.* +5/0 V), called the logic signal (LOG), which is sent to a scaler.

In the case of the scintillator, the photomultiplier ensures the conversion of light to electrons and produces a strongly amplified electronic signal that is processed through a discriminator and trigger as for the gas detector.

7.3.4.2. *Controls and adjustments of the electronics*

For the gas detector, there are basically three parameters to be adjusted, the gas-amplification coefficient M (a function of the detector high voltage), the electronic amplification gain G, and the discriminator threshold T. Since these adjustments are interactive, the high voltage is initially set at the value given by the manufacturer. The gain G is adjusted in order not to saturate the amplifier. When the electronic amplifier power supply voltage is 5 V, a typical setting of the pulse maximum amplitudes is about 3 V.

We present now the three types of operation necessary to adjust the electronics.

(*a*) *Control of the pulse shape*. The analogue pulse ANA (see Fig. 7.3.4.1) is directly observed with an oscilloscope. Depending on the construction of the electronic chain, it is important to verify if the input of the oscilloscope (or of the multichannel analyser, see below) must be adapted with a 50 Ω impedance or not. This will ensure that the amplitude of the analogue pulse and the accessible value of the voltage threshold are on the same scale (and not different by a factor of two). Fig. 7.3.4.2(*a*) shows characteristic shapes obtained when triggering the oscilloscope at, say, 0.2 V and observing a $^{10}BF_3$ gas detector either pulse by pulse or in a continuous way. This type of display allows the trained user to check the noise level, the amplitudes of the neutron pulses, the quality of the pulse shape, and the presence of any anomalous signal such as one due to flashes of parasitic electronic or electric noise (*e.g.* 50 Hz). γ rays produce fewer electrons than neutrons, so that the corresponding pulses are of a lower amplitude (by a factor of 1/5 to 1/20).

(*b*) *Control of the distribution of the pulse amplitudes*. The distribution of amplitudes of the various pulses in number of pulses per amplitude increment dN/dA is analysed and displayed using a multichannel analyser. Fig. 7.3.4.2(*b*) shows the amplitude spectrum for a $^{10}BF_3$ gas detector. The main peak at A_0 corresponds to the main neutron-capture reaction (2.3 MeV, 93%). From its FWHM, we define the detector electronic resolution $\Delta A/A_0$. The right-hand-side small peak is due to the 2.8 MeV, 7% capture reaction. The tail of amplitudes down to $4A_0/11$ corresponds to neutrons captured near the detector walls, which stop some of the secondary-particle trajectories (wall effect). The existence of a deep valley [see Fig. 7.3.4.2(*b*)] where the discriminator threshold T is placed ensures that all captured neutrons, and nothing else, are counted. The width of this valley guarantees good detection stability. Three effects might reduce this valley. Worsening of the gas quality will reduce all the pulse amplitudes (neutron and gamma), an increase in electronic noise will result in a resolution loss affecting the valley on both sides, and a high level of γ radiation will produce a pile up of the independent γ pulses, increasing their amplitude.

(*c*) *Optimization of the threshold and high-voltage values*. In order to set the threshold T at its optimum value for discrimination and stability, the total number of counts in the detector per unit time is plotted as a function of the threshold, for

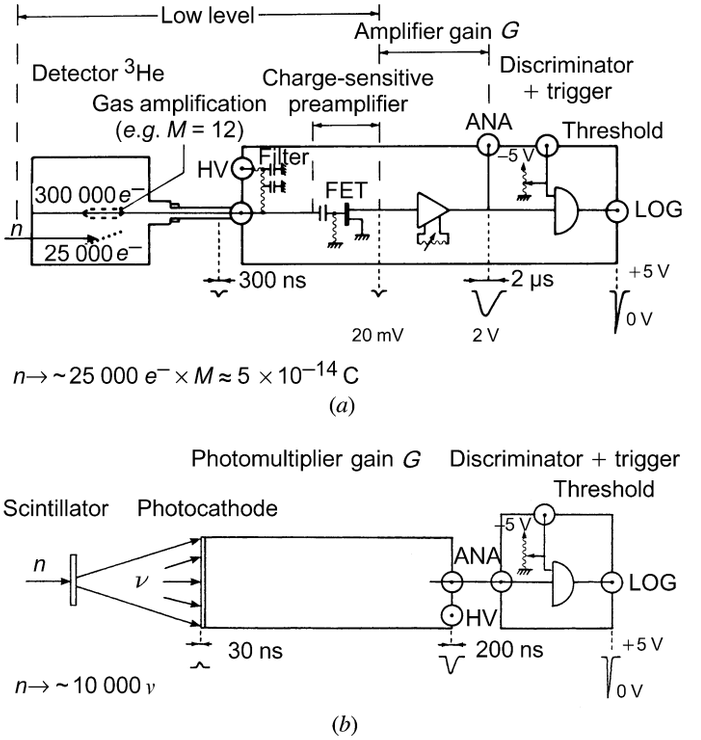

Fig. 7.3.4.1. Electronic chain following (*a*) an ^{3}He gas detector and (*b*) a scintillation detector.

a constant incident flux [see Fig. 7.3.4.2(*c*)]. On this curve, the width of the plateau and a value of the slope about 10^{-4} (in relative variation of counts per mV) give an indication of the detector quality. A good compromise is to set the threshold T at the middle of the plateau.

It is also necessary to verify that the detector high voltage, *i.e.* the gas-amplification coefficient M (see Subsection 7.3.3.1), is well adapted. With the value of the threshold T adjusted as above, the number of counts per unit time is plotted as a function of the high voltage [see Fig. 7.3.4.2(*d*)]. Typical values for the width of the plateau and its slope are 200 V and a few per cent per 100 V. If the high-voltage setting given by the manufacturer must be modified (owing to the worsening of the gas or constraints from the electronic chain, *etc.*), the complete adjustment procedure of the G and T parameters must be repeated.

The electronic adjustments and controls of types of detector other than $^{10}BF_3$ gas detectors are basically the same once the changes in the amplitude spectrum have been taken into account. We present in Fig. 7.3.4.2(*e*) the amplitude spectra for an ^{3}He gas detector with significant wall effects, for a ^{10}B solid-deposit detector with very low efficiency, and for a scintillator. The energy of the secondary particles produced in an ^{3}He gas detector is 765 keV, about three times less than in $^{10}BF_3$, reducing the signal-to-noise ratio; the relative importance of the wall effect is greater and extends to $A_0/4$. In the case of the ^{10}B deposit detector, only one of the secondary particles escapes the foil, so that we do not detect an amplitude A_0 corresponding to the full capture-reaction energy, but only that corresponding either to an average α or Li trace. The quality of the valleys depends on the t/r (foil thickness/particle range) ratio in the ^{10}B solid (see Fig. 7.3.3.2). The figure corresponds to a monitor where $t \ll r$. For the scintillator, the valley in the amplitude spectrum is not very good, even for good glasses and without γ radiation. The discrimination is therefore always much inferior to that of a gas detector. Moreover, the gain of the photomultiplier is very sensitive to the high voltage and has long-term stability problems.

7.3.5. Typical detection systems

7.3.5.1. *Single detectors*

In order to measure the scattered intensities, the single detector is mounted in a shield equipped with a collimator between sample and detector. The collimator is adapted to the sample (5 to 20′ Soller collimator for a powder diffractometer, or a hole adapted to the size of the beam diffracted by a single crystal). The sensitive area of the detector matches the size of the collimated diffracted beam. This geometry allows one to localize the scattered beam with adequate resolution and to avoid parasitic neutrons. In a powder diffraction measurement, the detector is scanned with a goniometer, each step being monitored.

7.3.5.2. *Position-sensitive detectors*

With the advantages of speed and simultaneity of data collection over broad angular ranges, position-sensitive detectors

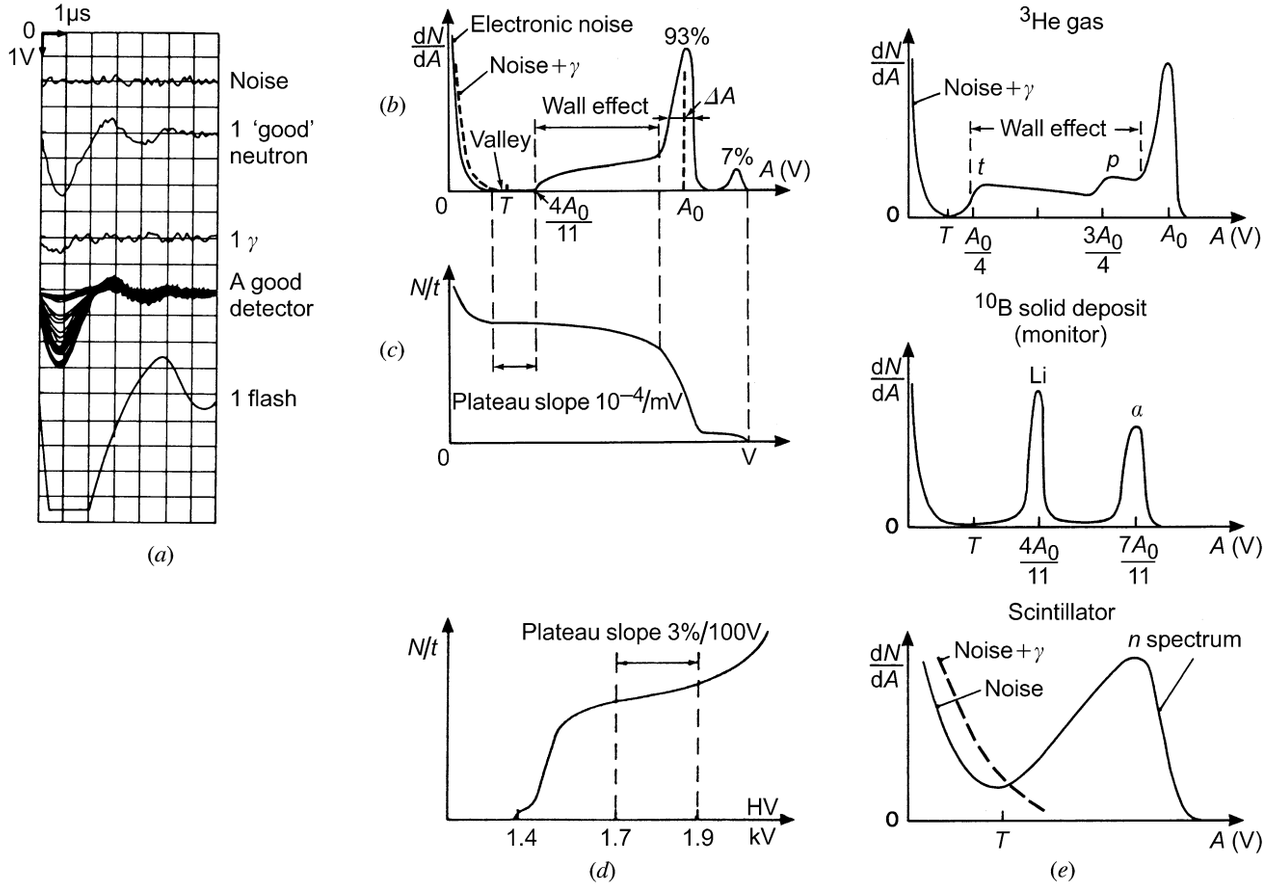

Fig. 7.3.4.2. (*a*) Characteristic $^{10}BF_3$ gas-detector analogue pulses seen on an oscilloscope. (*b*) $^{10}BF_3$ amplitude spectrum. (*c*) Plateau of a $^{10}BF_3$ detector as a function of the threshold voltage. (*d*) Typical plateau of a $^{10}BF_3$ detector in proportional mode as a function of the high voltage. (*e*) Amplitude spectra of various detectors.

(PSDs) have seen considerable development (Convert & Chieux, 1986). They are based on the fundamental detection processes described in Section 7.3.3. Their dimensions, the introduction of various systems for position encoding and decoding, and the multiplication of the number of detection chains (with necessary adjustments and controls) have produced detection systems of a complexity that can no longer be grasped by a researcher only occasionally involved in neutron-scattering experiments. The following lines give only a very crude introduction to PSDs at a descriptive level.

A PSD is always mounted in a shield that has an opening limited by the cone defined by the sample size and the detection area. Given the large opening in the shield, the PSD is very sensitive to parasitic neutrons, especially those coming from materials in the main monochromatic beam. However, if sufficient care is taken with the sample environment and beam-stop design, the signal-to-noise ratio may be as good as or even better than in a single detector. The scattering angle is determined by the angular position of the origin of the PSD, the sample-to-detector distance, and the location of the neutron capture in the PSD.

In a PSD, each individual neutron-capture reaction in the continuous converter is localized *via* an internal encoding system followed by electronic decoding. There are three types of PSD: the gas resistive wire, the gas multielectrode, and the Anger camera (scintillation).

(*a*) *Gas PSD with resistance encoding*. The simplest examples of this type of PSD are one-dimensional detectors in which the neutron-converter gas is contained in a cylindrical stainless-steel tube with a central, fine resistive wire anode. The amplitudes of the output pulses from charge-sensitive amplifiers attached to each end of the anode are then compared to derive the positional coordinate of the neutron. An alternative method of deriving the positional information is RC (resistance capacitance) encoding followed by time decoding (Borkowski & Kopp, 1975). Two-dimensional RC encoding PSDs have been developed. One of the solutions is to have a group of wires interconnected by a chain of resistors with amplifiers at the resistor chain nodes (Boie, Fischer, Inagaki, Merritt, Okuno & Radeka, 1982).

(*b*) *Gas multi-electrode PSD*. The simplest examples of this type of PSD are one-dimensional detectors with a small number of discrete electrodes, *e.g.* 64 parallel anode wires separated by 2.54 mm. Each anode wire has an amplifier. A logic system analyses the amplitudes of the output pulses corresponding to one neutron that are collected by one, two, or three neighbouring wires, and decides on which wire the neutron was detected. Large curved one-dimensional PSDs have been built on this principle, *e.g.* 800 wires covering 80°. Two-dimensional PSDs based on the same principle use a matrix system in which a neutron gives rise to two sets of signals on two orthogonal systems of electrodes (Allemand, Bourdel, Roudaut, Convert, Ibel, Jacobé, Cotton & Farnoux, 1975).

(*c*) *Neutron Anger camera*. The principle of the Anger camera is to detect an incident photon or particle with a continuous area of scintillator. The light produced is allowed to disperse before entering an array of photomultipliers (PMs) whose analogue output signals are used to derive the position of the incident neutron. In one dimension, the localization is achieved by a row of PMs (Naday & Schaefer, 1983). In two-dimensional PSDs, a close-packed array of PMs allows the location of the scintillation to be determined by calculating the X and Y centroids using a resistor-weighting scheme (Strauss, Brenner, Lynch & Morgan, 1981).

Table 7.3.5.1 gives the characteristics of some PSDs, each example being a good compromise of detector characteristics adapted to the instrument needs, powder diffraction, single-crystal diffraction, and small-angle neutron scattering (SANS). From this table, it seems that the characteristics of the various types of PSD that have been presented are nearly equivalent. The homogeneity of neutron detection over the PSD sensitive area is better than 5% in all cases. Among those PSDs, the gas PSDs, which have been installed since the early 1970s, are the most commonly used. The definite advantage of the gas multi-electrode PSD is to digitize the encoding, thus offering very good stability and reliability of the neutron localization. The resistance-encoding gas PSD has less complex electronics and permits a choice of pixel size (elementary detection area) and thereby definition. The Anger camera also offers the same flexibility in the choice of the pixel size and, because of the small thickness of the scintillator (1–2 mm), has very little parallax and is well adapted to TOF measurements. However, the γ sensitivity of the scintillators is much higher than that of the gas PSDs.

PSDs permit a simultaneous measurement of intensities over relatively large areas. As compared with the scanned single detector, this opens the way to two possibilities, either shorter counting time (*e.g.* real-time experiments) or improved statistical precision. However, the high counting rates achieved, as well as the complexity of the detection, increase the effective dead time and the occurrence of defects. The efficient use of a PSD therefore requires a detailed understanding of its operation (detection process, encoding–decoding, data storage, *etc.*) and periodic tests and calibrations.

7.3.5.3. *Banks of detectors*

When it is useful to have a large detection area without requiring spatial continuity of the detection, the solution is in the juxtaposition of several detectors. The selection of the type of detectors, the way of regrouping them, and the design of the collimation system depend on the measuring instrument. An appropriate geometry will optimize the signal-to-noise ratio and the instrumental resolution.

Banks of single detectors, up to 64 covering up to 160° in the diffraction plane with Soller collimators in front of each detector, are used for powder diffractometers in reactors [D1A and D2B, Institut Laue–Langevin (1988)]. The relative position of the detectors plus collimators and their response to the neutron intensity have to be measured and calibrated. The bank of detectors is scanned in small steps over the interval between two successive detectors in order to obtain a complete diagram over the angular range of the bank.

In a similar way, a juxtaposition of small PSDs with individual collimators is also used [D4, Institut Laue–Langevin (1988)].

In the case of spallation sources, the time-of-flight powder diffractometers are made of arrays of detectors at selected diffraction angles, to increase the detection area (Isis, 1992). Whenever it is possible, the time focusing geometry is used (Windsor, 1981). This implies a particular alignment of the detector array in order for it to become equivalent to one detector at one angle.

On the same instrument [HRPD, SANDALS, LAD (Isis, 1992)], various types of detector are used (^{3}He gas single detectors of small diameter, Li glass or Li+ZnS scintillators). For each selected diffraction angle, the choice of detector depends on the required resolution, which is better for scintillators because of their small thickness, and on other properties of the detectors (background, stability, γ discrimination), which are better for ^{3}He detectors.

Table 7.3.5.1. *Characteristics of some PSDs*

1D = one dimensional; 2D = two dimensional; *F*/ = flat; *C*/ = 1D curved; *X* = single crystal.

	Gas Resistance encoding		Gas Multi-electrode		Scintillation Anger camera	
	1D	2D	1D	2D	1D	2D
Location	*F*/ MURR (USA)	*F*/ ORNL (USA)	*F*/ ILL (France) *C*/ CENG (France)	*F*/ ILL (France) *C*/ ILL (France)	*F*/ Jülich (FRG)	*F*/ ANL (USA)
Instrument reference	Powder (1)	SANS (2)	*F*/ Liquids (3) *C*/ Powder (4)	*F*/ SANS (3,5) *C*/ *X* (3)	Powder (6)	*X* (7)
Detection area (mm)	$l = 610$ ($Ø = 25.4$)	650×650	*F*/ $l = 162.5$ ($h = 70$) *C*/ $l = 2096$ or 80° ($h = 70$)	*F*/ 640×640 *C*/ 1300×80 or $64° \times 4°$	$l = 744$ ($h = 20$)	300×300
Cell size or pixel (mm)		10×10	*F*/ 2.54 *C*/ 2.62 or 0.1°	*F*/ 5×5 *C*/ 2.54×5	0.7	0.3×0.3
Resolution (mm)	2.5	10×10	*F*/ 3.2 *C*/ 2.6	*F*/ 5×5 *C*/ 3×6.6	2.5	2.7×2.7
Efficiency (%)	70 (1.3 Å)	90 (4.75 Å)	*F*/ 90 (0.7 Å) *C*/ 52 (2.5 Å)	*F*/ 75 (11 Å) *C*/ 85 (1.5 Å)	70 (1.2 Å)	80 (1.8 Å)

MURR: Missouri University Research Reactor, Columbia, Missouri, USA.
ORNL: Oak Ridge National Laboratory, Tennessee, USA.
ILL: Institut Laue–Langevin, Grenoble, France.
ANL: Argonne National Laboratory, Argonne, Illinois, USA.
CENG: Centre d'Etudes Nucléaires de Grenoble, Grenoble, France.

References: (1) Berliner, Mildner, Sudol & Taub (1983); (2) Abele, Allin, Clay, Fowler & Kopp (1981); (3) Institut Laue–Langevin (1988); (4) Roudaut (1983); (5) Ibel (1976); (6) Schaefer, Naday & Will (1983); (7) Strauss, Brenner, Chou, Schultz & Roche (1983).

7.3.6. Characteristics of detection systems

We shall present and comment on some characteristics of detectors plus electronic chains in operational conditions.

(*a*) *Intrinsic background* (*i.e.* with the reactor or neutron source shut down). The intrinsic background level is about 6 counts h^{-1} for an ^{3}He, 3 bar (1 bar = 10^5 Pa) detector (Ø 50 mm, *L* 100 mm) in operational conditions. Of course, it is very important to protect the low-level part of the amplifier from the discriminator and trigger by separating these two stages very carefully, and from electric and electronic parasites by using good ground connections. Additional parasitic effects might be produced by (i) high-voltage flashes in the detector or in dirty or deficient plugs, (ii) microphony, and (iii) particle emission by the detector walls (*e.g.* uranium impurities in aluminium, or activation).

(*b*) γ *discrimination*. The γ discrimination of an ^{3}He detector is said to be 10^{-8}. From our own experience, we can say that a pure ^{3}He detector is insensitive to a γ dose up to 10 mGy h^{-1} (1 rem h^{-1}). However, additional gases increase the γ-detection efficiency (Fischer, Radeka & Boie, 1983). For a good scintillator, the γ discrimination is of the order of 10^{-4} (Kurz & Schelten, 1983).

(*c*) *Stability*. Under good conditions, the gas-detector stability has been verified to be better than 3×10^{-4}/day and 10^{-3}/month. The stability of operational scintillators is probably about 10^{-3}/day but it is known to drift over longer periods of time.

(*d*) *Dead time and non-linear effects due to the count rate*. The gas detector has a dead time of 1–10 μs depending on the duration of the analogue pulse, which is fixed by the detector plus adapted electronic chain. The scintillator has a dead time about 10 times shorter, *i.e.* 0.2 to 1 μs. A rule of thumb is to keep the total dead time to less than 10% of the counting time, which fixes the maximum counting rate. This limits the effects of non-linearity of the dead time as a function of the counting rate. Non-linear effects in gas detectors are complex and due to (i) the distortion of the electrostatic field near the anode by the space charge, (ii) the decrease of the high voltage at the anode produced at high counting rates by the increased ionic current passing through the high-impedance filter, and (iii) the possible shift of the zero level of the charge preamplifier.

(*e*) *TOF requirements*. In a TOF experiment, it is important to know exactly the time and place of each neutron capture. The thickness of the detector must be as small as possible in relation to the total flight path (scintillators are roughly 10 times thinner than gas detectors). The delay between the neutron capture and the logic pulse given by the amplifier gives an additional error. Again, the scintillator is about 10 times faster.

7.3.7. Corrections to the intensity measurements depending on the detection system

A good diffractometer on a reactor is supposed to give point by point for each solid-angle element $d\Omega$ an exact image of the scattered intensity. This is never perfectly achieved in practice and necessitates some corrections. In all cases, it is very important to be aware that additional background might be created when part of the shielding or of the collimator intersect the monochromatic neutron beam. We suppose for the following discussion that this effect has been corrected or avoided. The wavelength dependence of the detector response (which is needed for inelasticity corrections or TOF measurements) is generally computed from the theoretical detector law [see equation (7.3.2.1)]. At each measuring point, the collected intensity is renormalized by the integrated incident neutron flux, which is measured by the monitoring device.

In the case of TOF measurements on a spallation source, the measured intensity must also be renormalized by the wavelength spectrum of the source, obtained from the measurement of an isotropic scatterer such as vanadium.

7.3.7.1. *Single detector*

For up to 10% of dead time in the counting rate, the correction for the dead-time loss is generally considered as linear. If Δt is the electronic dead time for one neutron (1–10 μs for the gas detectors) and n the number of counts per second, the dead-time correction factor is $1/(1 - n\Delta t)$.

7.3.7.2. *Banks of detectors*

In the case of a bank of detectors used for a powder diffractometer in a reactor, one has to calibrate the relative positions of the detectors and their response to the neutron intensity by scanning the detectors through a Bragg pattern.

In the case of TOF measurements, the detector banks are installed at fixed angles. For each detector, the measured intensity depends on the detector type, size, and distance to the sample. The neutron and γ background depends moreover on the detection angle. After background corrections, the intensities measured by each detector bank are calibrated and matched using the overlaps between spectra.

7.3.7.3. *Position-sensitive detectors*

(*a*) *Calibration of the position*. For multi-electrode PSDs, the relative position of the electrodes is fixed and verified at the time of construction. In the case of other PSDs with analogue encoding, an angular calibration is made periodically with the help of a Bragg pattern, a thin neutron beam, or a cadmium mask moved across a diffuse beam incident on the PSD (Berliner, Mildner, Sudol & Taub, 1983).

(*b*) *Calibration of the PSD homogeneity*. The response function might be dependent on the position within the PSD and possibly on the intensities collected at other parts of the PSD. The homogeneity of response of a PSD, which is normally better than 5%, can be calibrated to a much higher accuracy, since the stability of the PSDs is generally very good (*e.g.* 0.1% or better for gas PSDs). In the case of a reactor, the classical method of calibration is the use of an isotropic scatterer such as vanadium. The calibration is made at angles that avoid the very small vanadium Bragg peaks (or with displacement of the PSD to several positions) and that keep a low and isotropic background. Calibration factors, sometimes called cell-efficiency coefficients α_i, are then obtained. Considering the lack of isotropy of the vanadium pattern, this method is limited to about 1% accuracy. For small PSDs, a precision of 0.1% or better is obtainable by scanning the whole PSD with a step equal to the cell spacing through any nearly isotropic pattern.

(*c*) *Particular effects due to high intensities*. The dead time of a PSD is complex. It depends on multiple parameters (the independent amplifiers and the encoding–decoding procedure). However, if there is a unique decoding logic for the whole PSD, and if this gives the highest contribution to the dead time, the ratios of the peak intensities are then conserved. In the case of strong Bragg peaks, the parasitic effect of scattering by the PSD entrance window (*e.g.* 10 mm aluminium for high-pressure gas PSDs) is detectable and can be corrected after calibration (using an intense and well localized thin beam).

International Tables for Crystallography (2006). Vol. C, Chapter 7.4, pp. 653–665.

7.4. Correction of systematic errors

By N. G. Alexandropoulos, M. J. Cooper, P. Suortti and B. T. M. Willis

7.4.1. Absorption

The positions and intensities of X-ray diffraction maxima are affected by absorption, the magnitude of the effect depending on the size and shape of the specimen. Positional effects are treated as they are encountered in the chapters on experimental techniques.

In structure determination, the effect of absorption on intensity may sometimes be negligible, if the crystal is small enough and the radiation penetrating enough. In general, however, this is not the case, and corrections must be applied. They are simplest if the crystal is of a regular geometric shape, produced either through natural growth or through grinding or cutting. Expressions for reflection from and transmission through a flat plate are given in Table 6.3.3.1, for reflection from cylinders in Table 6.3.3.2, and for reflection from spheres in Table 6.3.3.3. The calculation for a crystal bounded by arbitrary plane faces is treated in Subsection 6.3.3.3.

The values of mass absorption (attenuation) coefficients required for the calculation of corrections are given as a function of the element and of the radiation in Table 4.2.4.3.

7.4.2. Thermal diffuse scattering (By B. T. M. Willis)

7.4.2.1. *Glossary of symbols*

$\hat{e}_j$	Direction cosines of $\mathbf{e}_j(\mathbf{q})$
$\mathbf{e}_j(\mathbf{q})$	Polarization vector of normal mode $(j\mathbf{q})$
$E_j(\mathbf{q})$	Energy of mode $(j\mathbf{q})$
$E_{\rm meas}$	Total integrated intensity measured under Bragg peak
E_0	Integrated intensity from Bragg scattering
E_1	Integrated intensity from one-phonon scattering
$F(\mathbf{h})$	Structure factor
$\hbar$	Planck's constant h divided by 2π
$2\pi\mathbf{h}$	Reciprocal-lattice vector
$\mathbf{H}$	Scattering vector
j	Label for branch of dispersion relation
$\mathbf{k}_0$	Wavevector of incident radiation
$\mathbf{k}$	Wavevector of scattered radiation
k_B	Boltzmann's constant
m_n	Neutron mass
m	Mass of unit cell
N	Number of unit cells in crystal
$\mathbf{q}$	Wavevector of normal mode of vibration
q_m	Radius of scanning sphere in reciprocal space
V	Volume of unit cell
$\mathbf{v}_j$	Elastic wave velocity for branch j
$\mathbf{v}_L$	Mean velocity of elastic waves
α	TDS correction factor
2θ	Scattering angle
θ_B	Bragg angle
$\left(\frac{d\sigma}{d\Omega}\right)^{(0)}$	Differential cross section for Bragg scattering
$\left(\frac{d\sigma}{d\Omega}\right)^{(1)}$	Differential cross section for one-phonon scattering
ρ	Density of crystal
$\omega_j(\mathbf{q})$	Frequency of normal mode $(j\mathbf{q})$

Thermal diffuse scattering (TDS) is a process in which the radiation is scattered inelastically, so that the incident X-ray photon (or neutron) exchanges one or more quanta of vibrational energy with the crystal. The vibrational quantum is known as a phonon, and the TDS can be distinguished as one-phonon (first-order), two-phonon (second-order), ... scattering according to the number of phonons exchanged.

The normal modes of vibration of a crystal are characterized as either acoustic modes, for which the frequency $\omega(\mathbf{q})$ goes to zero as the wavevector $\mathbf{q}$ approaches zero, or optic modes, for which the frequency remains finite for all values of $\mathbf{q}$ [see Section 4.1.1 of *IT* B (1992)]. The one-phonon scattering by the acoustic modes rises to a maximum at the reciprocal-lattice points and so is not entirely subtracted with the background measured on either side of the reflection. This gives rise to the 'TDS error' in estimating Bragg intensities. The remaining contributions to the TDS – the two-phonon and multphonon acoustic mode scattering and all kinds of scattering by the optic modes – are largely removed with the background.

It is not easy in an X-ray experiment to separate the elastic (Bragg) and the inelastic thermal scattering by energy analysis, as the energy difference is only a few parts per million. However, this has been achieved by Dorner, Burkel, Illini & Peisl (1987) using extremely high energy resolution. The separation is also possible using Mössbauer spectroscopy. Fig. 7.4.2.1 shows the elastic and inelastic components from the 060 reflection of $LiNbO_3$ (Krec, Steiner, Pongratz & Skalicky, 1984), measured with γ-radiation from a ^{57}Co Mössbauer source. The TDS makes a substantial contribution to the measured integrated intensity; in Fig. 7.4.2.1, it is 10% of the total intensity, but it can be much larger for higher-order reflections. On the other hand, for the extremely sharp Bragg peaks obtained with synchrotron radiation, the TDS error may be reduced to negligible proportions (Bachmann, Kohler, Schulz & Weber, 1985).

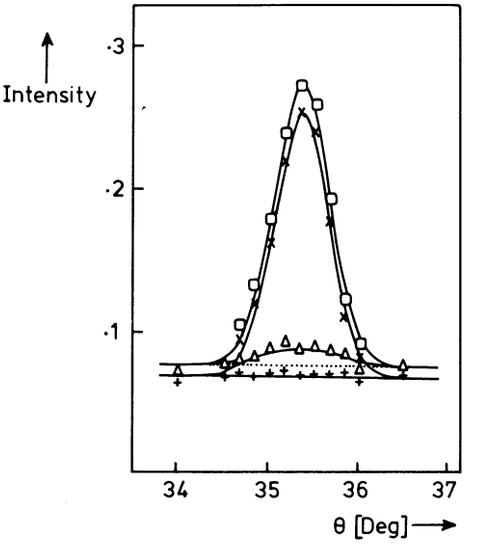

Fig. 7.4.2.1. 060 reflection of $LiNbO_3$ (Mössbauer diffraction). Inelastic (triangles), elastic (crosses), total (squares) and background (pluses) intensity (after Krec, Steiner, Pongratz & Skalicky, 1984).

Copyright © 2006 International Union of Crystallography

Let $E_{\rm meas}$ represent the *total* integrated intensity measured in a diffraction experiment, with E_0 the contribution from Bragg scattering and E_1 that from (one-phonon) TDS. Then,

$$E_{\rm meas} = E_0 + E_1 = E_0(1+\alpha), \tag{7.4.2.1}$$

where α is the ratio E_1/E_0 and is known as the 'TDS correction factor'. α can be evaluated in terms of the properties of the crystal (elastic constants, temperature) and the experimental conditions of measurement. In the following, it is implied that the intensities are measured using a single-crystal diffractometer with incident radiation of a fixed wavelength We shall treat separately the calculation of α for X-rays and for thermal neutrons.

7.4.2.2. *TDS correction factor for X-rays (single crystals)*

The differential cross section, representing the intensity per unit solid angle for Bragg scattering, is

$$\left(\frac{{\rm d}\sigma}{{\rm d}\Omega}\right)^{(0)} = \frac{N(2\pi)^3}{V}\left|F(\mathbf{h})\right|^2\delta(\mathbf{H}-2\pi\mathbf{h}),$$

where N is the number of unit cells, each of volume V, and $F(\mathbf{h})$ is the structure factor. $\mathbf{H}$ is the scattering vector, defined by

$$\mathbf{H} = \mathbf{k} - \mathbf{k}_0,$$

with $\mathbf{k}$ and $\mathbf{k}_0$ the wavevectors of the scattered and incident beams, respectively. (The scattering is elastic, so $k = k_0 = 2\pi/\lambda$, where λ is the wavelength.) $2\pi\mathbf{h}$ is the reciprocal-lattice vector and the delta function shows that the scattered intensity is restricted to the reciprocal-lattice points.

The integrated Bragg intensity is given by

$$\begin{aligned} E_0 &= \int\int\left(\frac{{\rm d}\sigma}{{\rm d}\Omega}\right)^{(0)}{\rm d}\Omega\,{\rm d}t \\ &= N\frac{(2\pi)^3}{V}\left|F(\mathbf{h})\right|^2\int\int\delta(\mathbf{H}-2\pi\mathbf{h})\,{\rm d}\Omega\,{\rm d}t, \end{aligned} \tag{7.4.2.2}$$

where the integration is over the solid angle Ω subtended by the detector at the crystal and over the time t spent in scanning the reflection. Using

$$\int\delta(\mathbf{H})\,{\rm d}\mathbf{H} = 1,$$

with ${\rm d}\mathbf{H} = H\,{\rm d}\theta$, equation (7.4.2.2) reduces to the familiar result (James, 1962)

$$E_0 = \frac{N\lambda^3\left|F(\mathbf{h})\right|^2}{V\omega_0\sin 2\theta}, \tag{7.4.2.3}$$

where ω_0 is the angular velocity of the crystal and 2θ the scattering angle.

The differential cross section for one-phonon scattering by acoustic modes of small wavevector $\mathbf{q}$ is

$$\begin{aligned} \left(\frac{{\rm d}\sigma}{{\rm d}\Omega}\right)^{(1)} &= \frac{(2\pi)^3}{V}\left|F(\mathbf{h})\right|^2 \\ &\times\sum_{j=1}^{3}\frac{\mathbf{H}\cdot\mathbf{e}_j(\mathbf{q})}{m\omega_j^2(\mathbf{q})}E_j(\mathbf{q})\delta(\mathbf{H}\pm\mathbf{q}-2\pi\mathbf{h}) \end{aligned} \tag{7.4.2.4}$$

[see Section 4.1.1 of *IT* B (1992)]. Here, $\mathbf{e}_j(\mathbf{q})$ is the polarization vector of the mode $(j\mathbf{q})$, where j is an index for labelling the acoustic branches of the dispersion relations, m is the mass of the unit cell and $E_j(\mathbf{q})$ is the mode energy. The delta function in (7.4.2.4) shows that the scattering from the mode $(j\mathbf{q})$ is confined to the points in reciprocal space displaced by $\pm\mathbf{q}$ from the reciprocal-lattice point at $\mathbf{q}=0$. The acoustic modes involved are of small wavenumber, for which the dispersion relation can be written

$$\omega_j(\mathbf{q}) = \mathbf{v}_j\left|\mathbf{q}\right|, \tag{7.4.2.5}$$

where $\mathbf{v}_j$ is the velocity of the elastic wave with polarization vector $\mathbf{e}_j(\mathbf{q})$. Substituting (7.4.2.5) into (7.4.2.4) shows that the intensity from the acoustic modes varies as $1/q^2$, and so peaks strongly at the reciprocal-lattice points to give rise to the TDS error.

Integrating the delta function in (7.4.2.4) gives the integrated one-phonon intensity

$$\begin{aligned} E_1 &= \frac{\lambda^3}{V^2\omega_0\sin 2\theta_B}H^2\left|F(\mathbf{h})\right|^2 \\ &\times\sum_q\sum_j\frac{\left[\mathbf{H}\cdot\mathbf{e}_j(\mathbf{q})\right]^2}{\rho\omega_q^2(\mathbf{q})}E_j(\mathbf{q}), \end{aligned}$$

with ρ the crystal density. The sum over the wavevectors $\mathbf{q}$ is determined by the range of $\mathbf{q}$ encompassed in the intensity scan. The density of wavevectors is uniform in reciprocal space [see Section 4.1.1 of *IT* B (1992)], and so the sum can be replaced by an integral

$$\sum_q \rightarrow \frac{NV}{(2\pi)^3}\int{\rm d}\mathbf{q}.$$

Thus, the correction factor (E_1/E_0) is given by

$$\alpha = \frac{1}{8\pi^3}\int J(\mathbf{q})\,{\rm d}\mathbf{q}, \tag{7.4.2.6}$$

where

$$J(\mathbf{q}) = \sum_j\frac{\mathbf{H}\cdot\mathbf{e}_j(\mathbf{q})^2}{\rho\omega^2(\mathbf{q})}E_j(\mathbf{q}). \tag{7.4.2.7}$$

The integral in (7.4.2.6) is over the range of measurement, and the summation in (7.4.2.7) is over the three acoustic branches. Only long-wavelength elastic waves, with a linear dispersion relation, equation (7.4.2.5), need be considered.

7.4.2.2.1. *Evaluation of* $J(\mathbf{q})$

The frequencies $\omega_j(\mathbf{q})$ and polarization vectors $\mathbf{e}_j(\mathbf{q})$ of the elastic waves in equation (7.4.2.7) can be calculated from the classical theory of Voigt (1910) [see Wooster (1962)]. If $\widehat{e}_1$, $\widehat{e}_2$, $\widehat{e}_3$ are the direction cosines of the polarization vector with respect to orthogonal axes x, y, z, then the velocity $\mathbf{v}_j$ is determined from the elastic stiffness constants c_{ijkl} by solving the following equations of motion.

$$\begin{aligned} \widehat{e}_1\left(A_{11}-\rho v_j^2\right)+\widehat{e}_2A_{12}+\widehat{e}_3A_{13} &= 0, \\ \widehat{e}_1A_{12}+\widehat{e}_2\left(A_{22}-\rho v_j^2\right)+\widehat{e}_3A_{23} &= 0, \\ \widehat{e}_1A_{13}+\widehat{e}_2A_{23}+\widehat{e}_3\left(A_{33}-\rho v_j^2\right) &= 0. \end{aligned}$$

Here, A_{km} is the km element of a 3×3 symmetric matrix $\mathbf{A}$; if $\widehat{q}_1$, $\widehat{q}_2$, $\widehat{q}_3$ are the direction cosines of the wavevector $\mathbf{q}$ with reference to x, y, z, the km element is given in terms of the elastic stiffness constants by

$$A_{km} = \sum_{l=1}^{3}\sum_{n=1}^{3}c_{klmn}\widehat{q}_l\widehat{q}_n.$$

The four indices $klmn$ can be reduced to two, replacing 11 by 1, 22 by 2, 33 by 3, 23 and 32 by 4, 31 and 13 by 5, and 12 and 21 by 6. The elements of $\mathbf{A}$ are then given explicitly by

$$
\begin{aligned}
A_{11} &= c_{11}\hat{q}_1^2 + c_{66}\hat{q}_2^2 + c_{55}\hat{q}_3^2 + 2c_{56}\hat{q}_2\hat{q}_3 \\
&\quad + 2c_{15}\hat{q}_3\hat{q}_1 + 2c_{16}\hat{q}_1\hat{q}_2, \\
A_{22} &= c_{66}\hat{q}_1^2 + c_{22}\hat{q}_2^2 + c_{44}\hat{q}_3^2 + 2c_{24}\hat{q}_2\hat{q}_3 \\
&\quad + 2c_{46}\hat{q}_3\hat{q}_1 + 2c_{26}\hat{q}_1\hat{q}_2, \\
A_{33} &= c_{55}\hat{q}_1^2 + c_{44}\hat{q}_2^2 + c_{33}\hat{q}_3^2 + 2c_{34}\hat{q}_2\hat{q}_3 \\
&\quad + 2c_{35}\hat{q}_3\hat{q}_1 + 2c_{45}\hat{q}_1\hat{q}_2, \\
A_{12} &= c_{16}\hat{q}_1^2 + c_{26}\hat{q}_2^2 + c_{45}\hat{q}_3^2 + (c_{25} + c_{46})\hat{q}_2\hat{q}_3 \\
&\quad + (c_{14} + c_{56})\hat{q}_3\hat{q}_1 + (c_{12} + c_{66})\hat{q}_1\hat{q}_2, \\
A_{13} &= c_{15}\hat{q}_1^2 + c_{46}\hat{q}_2^2 + c_{35}\hat{q}_3^2 + (c_{36} + c_{45})\hat{q}_2\hat{q}_3 \\
&\quad + (c_{13} + c_{55})\hat{q}_3\hat{q}_1 + (c_{14} + c_{56})\hat{q}_1\hat{q}_2, \\
A_{23} &= c_{56}\hat{q}_1^2 + c_{24}\hat{q}_2^2 + c_{34}\hat{q}_3^2 + (c_{23} + c_{44})\hat{q}_2\hat{q}_3 \\
&\quad + (c_{36} + c_{45})\hat{q}_3\hat{q}_1 + (c_{25} + c_{46})\hat{q}_1\hat{q}_2.
\end{aligned}
$$

The setting up of the matrix $\mathbf{A}$ is a fundamental first step in calculating the TDS correction factor. This implies a knowledge of the elastic constants, whose number ranges from three for cubic crystals to twenty one for triclinic crystals. The measurement of elastic stiffness constants is described in Section 4.1.6 of *IT* B (1992).

For each direction of propagation $\hat{\mathbf{q}}$, there are three values of ρv_j^2 $(j = 1, 2, 3)$, given by the eigenvalues of $\mathbf{A}$. The corresponding eigenvectors of $\mathbf{A}$ are the polarization vectors $\mathbf{e}_j(\mathbf{q})$. These polarization vectors are mutually perpendicular, but are not necessarily parallel or perpendicular to the propagation direction.

The function $J(\mathbf{q})$ in equation (7.4.2.7) is related to the inverse matrix $\mathbf{A}^{-1}$ by

$$J(\mathbf{q}) = \frac{k_B T}{q^2} \sum_{m=1}^{3} \sum_{n=1}^{3} \left(\mathbf{A}^{-1}\right)_{mn} H_m H_n, \tag{7.4.2.8}$$

where H_1, H_2, H_3 are the x, y, z components of the scattering vector $\mathbf{H}$, and classical equipartition of energy is assumed [$E_j(\mathbf{q}) = k_B T$]. Thus $\mathbf{A}^{-1}$ determines the anisotropy of the TDS in reciprocal space, arising from the anisotropic elastic properties of the crystal.

Isodiffusion surfaces, giving the locus in reciprocal space for which the intensity $J(\mathbf{q})$ is constant for elastic waves of a given wavelength, were first plotted by Jahn (1942). These surfaces are not spherical even for cubic crystals (unless $c_{11} - c_{12} = c_{44}$), and their shapes vary from one reciprocal-lattice point to another.

7.4.2.2.2. *Calculation of* α

Inserting (7.4.2.8) into (7.4.2.6) gives the TDS correction factor as

$$\alpha = \sum_{m=1}^{3} \sum_{n=1}^{3} T_{mn} H_m H_n, \tag{7.4.2.9}$$

where T_{mn}, an element of a 3×3 symmetric matrix $\mathbf{T}$, is defined by

$$T_{mn} = \frac{k_B T}{8\pi^3} \int \frac{\left(\mathbf{A}^{-1}\right)_{mn}}{q^2} \, \mathrm{d}\mathbf{q}. \tag{7.4.2.10}$$

Equation (7.4.2.9) can also be written in the matrix form

$$\alpha = \mathbf{H}^T \mathbf{T} \mathbf{H}, \tag{7.4.2.11}$$

with $\mathbf{H}^T = (H_1, H_2, H_3)$ representing the transpose of $\mathbf{H}$.

The components of $\mathbf{H}$ relate to orthonormal axes, whereas it is more convenient to express them in terms of Miller indices *hkl* and the axes of the reciprocal lattice. If $\mathbf{S}$ is the 3×3 matrix that transforms the scattering vector $\mathbf{H}$ from orthonormal axes to reciprocal-lattice axes, then

$$\mathbf{H} = \mathbf{S}\mathbf{h}, \tag{7.4.2.12}$$

where $\mathbf{h}^T = (h, k, l)$. The final expression for α, from (7.4.2.11) and (7.4.2.12), is

$$\alpha = \mathbf{h}^T \mathbf{S}^T \mathbf{T} \mathbf{S} \mathbf{h}. \tag{7.4.2.13}$$

This is the basic formula for the TDS correction factor.

We have assumed that the entire one-phonon TDS under the Bragg peak contributes to the measured integrated intensity, whereas some of it is removed in the background subtraction. This portion can be calculated by taking the range of integration in (7.4.2.10) as that corresponding to the region of reciprocal space covered in the background measurement.

To evaluate $\mathbf{T}$ requires the integration of the function $\mathbf{A}^{-1}$ over the scanned region in reciprocal space (see Fig. 7.4.2.2). Both the function itself and the scanned region are anisotropic about the reciprocal-lattice point, and so the TDS correction is anisotropic too, *i.e.* it depends on the direction of the diffraction vector as well as on $\sin\theta/\lambda$.

Computer programs for calculating the anisotropic TDS correction for crystals of any symmetry have been written by Rouse & Cooper (1969), Stevens (1974), Merisalo & Kurittu (1978), Helmholdt, Braam & Vos (1983), and Sakata, Stevenson & Harada (1983). To simplify the calculation, further approximations can be made, either by removing the anisotropy associated with $\mathbf{A}^{-1}$ or that associated with the scanned region. In the first case, the element T_{mn} is expressed as

$$T_{mn} = \frac{k_B T}{8\pi^3} \left\langle \left(\mathbf{A}^{-1}\right)_{mn} \right\rangle \int \frac{1}{q^2} \, \mathrm{d}q,$$

where the angle brackets indicate the average value over all directions. In the second case,

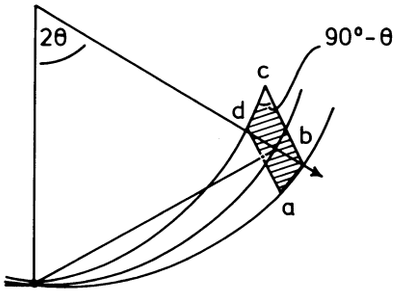

(*a*)

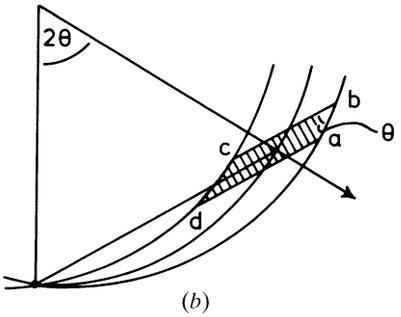

(*b*)

Fig. 7.4.2.2. Diagrams in reciprocal space illustrating the volume *abcd* swept out for (*a*) an ω scan, and (*b*) a $\theta/2\theta$, or $\omega/2\theta$, scan. The dimension of *ab* is determined by the aperture of the detector and of *bc* by the rocking angle of the crystal.

$$T_{mn} = \frac{k_B T}{8\pi^3} q_m \int\int \left(\mathbf{A}^{-1}\right)_{mn} \mathrm{d}S,$$

where q_m is the radius of the sphere that replaces the anisotropic region (Fig. 7.4.2.2) actually scanned in the experiment, and $\mathrm{d}S$ is a surface element of this sphere. q_m can be estimated by equating the volume of the sphere to the volume swept out in the scan.

If *both* approximations are employed, the correction factor is isotropic and reduces to

$$\alpha = \frac{H^2 k_B T q_m}{3\pi^2 \rho \mathbf{v}_L^2}, \qquad (7.4.2.14)$$

with $\mathbf{v}_L$ representing the mean velocity of the elastic waves, averaged over all directions of propagation and of polarization.

Experimental values of α have been measured for several crystals by γ-ray diffraction of Mössbauer radiation (Krec & Steiner, 1984). In general, there is good agreement between these values and those calculated by the numerical methods, which take into account anisotropy of the TDS. The correction factors calculated analytically from (7.4.2.14) are less satisfactory.

The principal effect of *not* correcting for TDS is to underestimate the values of the atomic displacement parameters. Writing $\exp\alpha \approx 1 + \alpha$, we see from (7.4.2.14) that the overall displacement factor is increased from B to $B + \Delta B$ when the correction is made. ΔB is given by

$$\Delta B = \frac{8 k_B T q_m}{3\pi^2 \rho \mathbf{v}_L^2}.$$

Typically, $\Delta B/B$ is 10–20%. Smaller errors occur in other parameters, but, for accurate studies of charge densities or bonding effects, a TDS correction of all integrated intensities is advisable (Helmholdt & Vos, 1977; Stevenson & Harada, 1983).

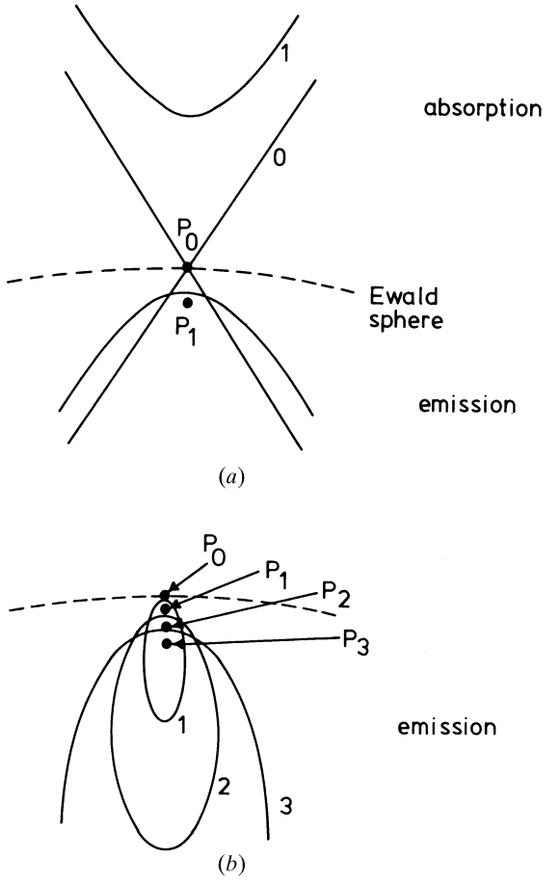

Fig. 7.4.2.3. Scattering surfaces for one-phonon scattering of neutrons: (*a*) for neutrons faster than sound ($\beta < 1$); (*b*) for neutrons slower than sound ($\beta > 1$). The scattering surface for X-rays is the Ewald sphere. P_0, P_1, *etc.* are different positions of the reciprocal-lattice point with respect to the Ewald sphere, and the scattering surfaces are numbered to correspond with the appropriate position of P.

7.4.2.3. *TDS correction factor for thermal neutrons (single crystals)*

The neutron treatment of the correction factor lies along similar lines to that for X-rays. The principal difference arises from the different topologies of the one-phonon 'scattering surfaces' for X-rays and neutrons. These surfaces represent the locus in reciprocal space of the end-points of the phonon wavevectors $\mathbf{q}$ (for fixed crystal orientation and fixed incident wavevector $\mathbf{k}_0$) when the wavevector $\mathbf{k}$ of the scattered radiation is allowed to vary. We shall not discuss the theory for pulsed neutrons, where the incident wavelength varies (see Popa & Willis, 1994).

The scattering surfaces are determined by the conservation laws for momentum transfer,

$$\mathbf{H} = \mathbf{k} - \mathbf{k}_0 = 2\pi\mathbf{h} + \mathbf{q},$$

and for energy transfer,

$$\hbar^2\left(k^2 - k_0^2\right)/2m_n = -\varepsilon\hbar\omega_j(\mathbf{q}), \qquad (7.4.2.15)$$

where m_n is the neutron mass and $\hbar\omega_j(\mathbf{q})$ is the phonon energy. ε is either $+1$ or -1, where $\varepsilon = +1$ corresponds to phonon emission (or phonon creation) in the crystal and a loss in energy of the neutrons after scattering, and $\varepsilon = -1$ corresponds to phonon absorption (or phonon annihilation) in the crystal and a gain in neutron energy. In the X-ray case, the phonon energy is negligible compared with the energy of the X-ray photon, so that (7.4.2.15) reduces to

$$k = k_0,$$

and the scattering surface is the Ewald sphere. For neutron scattering, $\hbar\omega_j(\mathbf{q})$ is comparable with the energy of a thermal neutron, and so the topology of the scattering surface is more complicated. For one-phonon scattering by long-wavelength acoustic modes with $q \ll k_0$, (7.4.2.15) reduces to

$$k = k_0 - \varepsilon\beta q,$$

where β ($= \mathbf{v}_L/\mathbf{v}_n$) is the ratio of the sound velocity in the crystal and the neutron velocity. If the Ewald sphere in the neighbourhood of a reciprocal-lattice point is replaced by its tangent plane, the scattering surface becomes a conic section with eccentricity $1/\beta$. For $\beta < 1$, the conic section is a hyperboloid of two sheets with the reciprocal-lattice point P at one focus. The phonon

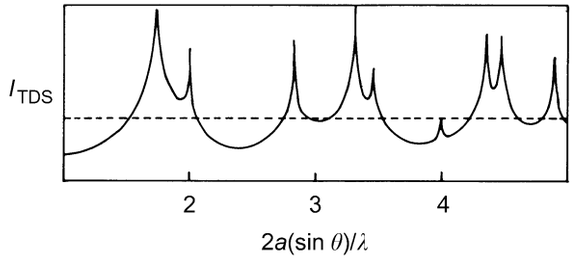

Fig. 7.4.2.4. One-phonon scattering calculated for polycrystalline nickel of lattice constant a (after Suortti, 1980).

wavevectors on one sheet correspond to scattering with phonon emission and on the other sheet to phonon absorption. For $\beta > 1$, the conic section is an ellipsoid with P at one focus. Scattering now occurs either by emission or by absorption, but not by both together (Fig. 7.4.2.3).

To evaluate the TDS correction, with **q** restricted to lie along the scattering surfaces, separate treatments are required for faster-than-sound ($\beta < 1$) and for slower-than-sound ($\beta > 1$) neutrons. The final results can be summarized as follows (Willis, 1970; Cooper, 1971):

(*a*) For faster-than-sound neutrons, the TDS rises to a maximum, just as for X-rays, and the correction factor is given by (7.4.2.13), which applies to the X-ray case. (This is a remarkable result in view of the marked difference in the one-phonon scattering surfaces for X-rays and neutrons.)

(*b*) For slower-than-sound neutrons, the correction factor depends on the velocity (wavelength) of the neutrons and is more difficult to evaluate than in (*a*). However, α will always be less than that calculated for X-rays of the same wavelength, and under certain conditions the TDS does not rise to a maximum at all so that α is then zero.

The sharp distinction between cases (*a*) and (*b*) has been confirmed experimentally using the neutron Laue technique on single-crystal silicon (Willis, Carlile & Ward, 1986).

7.4.2.4. *Correction factor for powders*

Thermal diffuse scattering in X-ray powder-diffraction patterns produces a non-uniform background that peaks sharply at the positions of the Bragg reflections, as in the single-crystal case (see Fig. 7.4.2.4). For a given value of the scattering vector, the one-phonon TDS is contributed by all those wavevectors **q** joining the reciprocal-lattice point and any point on the surface of a sphere of radius $2\sin\theta/\lambda$ with its centre at the origin of reciprocal space. These **q** vectors reach the boundary of the Brillouin zone and are not restricted to those in the neighbourhood of the reciprocal-lattice point. To calculate α properly, we require a knowledge, therefore, of the lattice dynamics of the crystal and not just its elastic properties. This is one reason why relatively little progress has been made in calculating the X-ray correction factor for powders.

7.4.3. Compton scattering
(By N. G. Alexandropoulos and M. J. Cooper)

7.4.3.1. *Introduction*

In many diffraction studies, it is necessary to correct the intensities of the Bragg peaks for a variety of inelastic scattering processes. Compton scattering is only one of the incoherent processes although the term is often used loosely to include plasmon, Raman, and resonant Raman scattering, all of which may occur in addition to the more familiar fluorescence radiation and thermal diffuse scattering. The various interactions are summarized schematically in Fig. 7.4.3.1, where the dominance of each interaction is characterized by the energy and momentum transfer and the relevant binding energy.

With the exception of thermal diffuse scattering, which is known to peak at the reciprocal-lattice points, the incoherent background varies smoothly through reciprocal space. It can be removed with a linear interpolation under the sharp Bragg peaks and without any energy analysis. On the other hand, in non-crystalline material, the elastic scattering is also diffused throughout reciprocal space; the point-by-point correction is consequently larger and without energy analysis it cannot be made empirically; it must be calculated. These calculations are imprecise except in the situations where Compton scattering is the dominant process. For this to be the case, there must be an encounter, conserving energy and momentum, between the incoming photon and an individual target electron. This in turn will occur if the energy lost by the photon, $\Delta E = E_1 - E_1$, clearly exceeds the one-electron binding energy, E_B, of the target electron. Eisenberger & Platzman (1970) have shown that this binary encounter model – alternatively known as the impulse approximation – fails as $(E_B/\Delta E)^2$.

Table 7.4.3.1. *The energy transfer, in eV, in the Compton scattering process for selected X-ray energies*

Scattering angle φ (°)	Cr $K\alpha$ 5411 eV	Cu $K\alpha$ 8040 eV	Mo $K\alpha$ 17 443 eV	Ag $K\alpha$ 22 104 eV
0	0	0	0	0
30	8	17	79	127
60	29	63	292	467
90	57	124	575	915
120	85	185	849	1344
150	105	229	1043	1648
180	112	245	1113	1757

Data calculated from equation (7.4.3.1).

The likelihood of this failure can be predicted from the Compton shift formula, which for scattering through an angle φ can be written.

$$\Delta E = E_1 - E_2 = \frac{E_1^2(1-\cos\varphi)}{mc^2[1+(E_1/mc^2)(1-\cos\varphi)]}. \qquad (7.4.3.1)$$

This energy transfer is given as a function of the scattering angle in Table 7.4.3.1 for a set of characteristic X-ray energies; it ranges from a few eV for Cr $K\alpha$ X-radiation at small angles, up to ~ 2 keV for backscattered Ag $K\alpha$ X-radiation. Clearly, in the majority of typical experiments Compton scattering will be inhibited from all but the valence electrons.

7.4.3.2. *Non-relativistic calculations of the incoherent scattering cross section*

7.4.3.2.1. *Semi-classical radiation theory*

For weak scattering, treated within the Born approximation, the incoherent scattering cross section, $(\mathrm{d}\sigma/\mathrm{d}\Omega)_{\mathrm{inc}}$, can be factorized as follows:

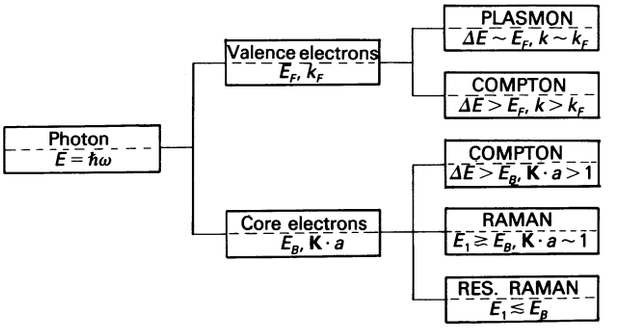

Fig. 7.4.3.1. Schematic diagram of the inelastic scattering interactions, $\Delta E = E_1 - E_2$ is the energy transferred from the photon and **K** the momentum transfer. The valence electrons are characterized by the Fermi energy, E_F, and momentum, k_F ($\hbar$ being taken as unity). The core electrons are characterized by their binding energy E_B. The dipole approximation is valid when $|\mathbf{K}|a < 1$, where a is the orbital radius of the scattering electron.

Table 7.4.3.2. *The incoherent scattering function for elements up to Z = 55*

Element	$(\sin\theta)/\lambda$ (Å^{-1})											
	0.10	0.20	0.30	0.40	0.50	0.60	0.70	0.80	0.90	1.00	1.50	2.00
1 H	0.343	0.769	0.937	0.983	0.995	0.998	0.994	0.999	1.000	1.000	1.000	1.000
2 He	0.296	0.881	1.362	1.657	1.817	1.902	1.947	1.970	1.983	1.990	1.999	2.000
3 Li	1.033	1.418	1.795	2.143	2.417	2.613	2.746	2.834	2.891	2.928	2.989	2.998
4 Be	1.170	2.121	2.471	2.744	3.005	3.237	3.429	3.579	3.693	3.777	3.954	3.989
5 B	1.147	2.531	3.190	3.499	3.732	3.948	4.146	4.320	4.469	4.590	4.895	4.973
6 C	1.039	2.604	3.643	4.184	4.478	4.690	4.878	5.051	5.208	5.348	5.781	5.930
7 N	1.08	2.858	4.097	4.792	5.182	5.437	5.635	5.809	5.968	6.113	6.630	6.860
8 O	0.977	2.799	4.293	5.257	5.828	6.175	6.411	6.596	6.755	6.901	7.462	7.764
9 F	0.880	2.691	4.347	5.552	6.339	6.832	7.151	7.376	7.552	7.703	8.288	8.648
10 Ne	0.812	2.547	4.269	5.644	6.640	7.320	7.774	8.085	8.312	8.490	9.113	9.517
11 Na	1.503	2.891	4.431	5.804	6.903	7.724	8.313	8.729	9.028	9.252	9.939	10.376
12 Mg	2.066	3.444	4.771	6.064	7.181	8.086	8.784	9.304	9.689	9.975	10.766	11.229
13 Al	2.264	4.047	5.250	6.435	7.523	8.459	9.225	9.830	10.296	10.652	11.592	12.083
14 Si	2.293	4.520	5.808	6.903	7.937	8.867	9.667	10.330	10.864	11.286	12.408	12.937
15 P	2.206	4.732	6.312	7.435	8.419	9.323	10.131	10.827	11.411	11.888	13.209	13.790
16 S	2.151	4.960	6.795	8.002	8.960	9.829	10.626	11.336	11.952	12.472	13.990	14.641
17 Cl	2.065	5.074	7.182	8.553	9.539	10.382	11.158	11.867	12.499	13.050	14.750	15.487
18 Ar	1.956	5.033	7.377	8.998	10.106	10.967	11.726	12.424	13.061	13.629	15.489	16.324
19 K	2.500	5.301	7.652	9.405	10.650	11.568	12.329	13.014	13.645	14.220	16.212	17.152
20 Ca	3.105	5.690	7.981	9.790	11.157	12.163	12.953	13.635	14.256	14.830	16.921	17.970
21 Sc	3.136	5.801	8.169	10.071	11.561	12.648	13.545	14.256	14.885	15.460	17.630	18.782
22 Ti	3.114	5.860	8.312	10.304	11.901	13.140	14.093	14.856	15.509	16.095	18.334	19.585
23 V	3.067	5.858	8.375	10.454	12.156	13.514	14.574	15.413	16.111	16.721	19.032	20.379
24 Cr	2.609	5.577	8.206	10.415	12.264	13.770	14.960	15.902	16.670	17.323	19.730	21.168
25 Mn	2.949	5.791	8.380	10.604	12.486	14.062	15.346	16.376	17.211	17.910	20.411	21.938
26 Fe	2.891	5.781	8.432	10.733	12.687	14.343	15.716	16.831	17.737	18.488	21.097	22.704
27 Co	2.832	5.764	8.469	10.844	12.867	14.596	16.050	17.249	18.229	19.039	21.777	23.462
28 Ni	2.772	5.726	8.461	10.894	12.980	14.780	16.317	17.602	18.664	19.543	22.445	24.211
29 Cu	2.348	5.455	8.310	10.778	12.942	14.847	16.494	17.885	19.043	20.002	23.107	24.957
30 Zn	2.654	5.631	8.388	10.901	13.094	15.020	16.709	18.163	19.395	20.427	23.745	25.683
31 Ga	2.791	5.939	8.599	11.082	13.290	15.233	16.947	18.445	19.734	20.831	24.370	26.400
32 Ge	2.839	6.229	8.912	11.338	13.536	15.486	17.215	18.741	20.074	21.224	24.983	27.109
33 As	2.793	6.365	9.236	11.658	13.828	15.775	17.511	19.056	20.420	21.612	25.583	27.810
34 Se	2.799	6.589	9.601	12.033	14.168	16.098	17.835	19.391	20.778	22.003	26.171	28.504
35 Br	2.771	6.748	9.940	12.440	14.552	16.456	18.185	19.747	21.149	22.399	26.747	29.190
36 Kr	2.703	6.760	10.157	12.828	14.969	16.849	18.562	20.123	21.535	22.804	27.313	29.870
37 Rb	3.225	7.062	10.431	13.206	15.410	17.282	18.974	20.526	21.940	23.221	27.871	30.543
38 Sr	3.831	7.464	10.746	13.576	15.860	17.745	19.420	20.956	22.367	23.654	28.423	31.210
39 Y	3.999	7.700	11.010	13.899	16.279	18.215	19.891	21.416	22.820	24.110	28.970	31.870
40 Zr	4.064	7.879	11.236	14.176	16.658	18.672	20.373	21.895	23.294	24.583	29.517	32.522
41 Nb	3.672	7.684	11.213	14.317	16.949	19.081	20.844	22.386	23.787	25.077	30.067	33.167
42 Mo	3.625	7.690	11.260	14.444	17.196	19.455	21.300	22.877	24.288	25.581	30.620	33.808
43 Tc	3.987	7.984	11.512	14.653	17.456	19.816	21.748	23.370	24.797	26.093	31.173	34.447
44 Ru	3.559	7.857	11.531	14.782	17.685	20.150	22.172	23.855	25.312	26.621	31.740	35.081
45 Rh	3.499	7.863	11.591	14.883	17.858	20.428	22.557	24.318	25.819	27.148	32.309	35.715
46 Pd	3.103	7.725	11.441	14.824	17.943	26.653	22.904	24.756	26.316	27.677	32.888	36.349
47 Ag	3.362	7.785	11.598	14.969	18.082	20.858	23.212	25.162	26.792	28.195	33.465	36.983
48 Cd	3.700	7.980	11.812	15.185	18.263	21.064	23.501	25.546	27.252	28.705	34.046	37.618
49 In	3.852	8.297	12.083	15.444	18.489	21.288	23.779	25.906	27.691	29.203	34.634	38.255
50 Sn	3.917	8.615	12.415	15.746	18.760	21.541	24.059	26.252	28.113	29.687	35.226	38.894
51 Sb	3.871	8.811	12.777	16.088	19.067	21.823	24.349	26.590	28.518	30.157	35.822	39.536
52 Te	3.097	9.076	13.171	16.466	19.407	22.134	25.655	26.927	28.912	30.613	36.422	40.181
53 I	3.903	9.287	13.564	16.876	19.227	22.471	24.980	27.269	29.298	31.056	37.024	40.827
54 Xe	3.841	9.340	13.892	17.307	20.175	22.833	25.324	27.619	29.680	31.488	37.628	41.477
55 Cs	4.320	9.615	14.217	17.753	20.612	23.228	25.691	27.981	30.064	31.914	38.232	42.129

$$\left(\frac{\mathrm{d}\sigma}{\mathrm{d}\Omega}\right)_{\mathrm{inc}} = \left(\frac{\mathrm{d}\sigma}{\mathrm{d}\Omega}\right)_0 S(E_1, E_2, \mathbf{K}, Z), \qquad (7.4.3.2)$$

where $(\mathrm{d}\sigma/\mathrm{d}\Omega)_0$ is the cross section characterizing the interaction, in this case it is the Thomson cross section, $(e^2/mc^2)^2\boldsymbol{\varepsilon}_1 \cdot \boldsymbol{\varepsilon}_2$; $\boldsymbol{\varepsilon}_1$ and $\boldsymbol{\varepsilon}_2$ being the initial and final state photon polarization vectors. The dynamics of the target are contained in the incoherent scattering factor $S(E_1, E_2, \mathbf{K}, Z)$, which is usually a function of the energy transfer $\Delta E = E_1 - E_2$, the momentum transfer $\mathbf{K}$, and the atomic number Z.

The electromagnetic wave perturbs the electronic system through the vector potential $\mathbf{A}$ in the Hamiltonian

$$H = \frac{e}{me}\mathbf{p}\cdot\mathbf{A} + \frac{e^2}{2me^2}\mathbf{A}\cdot\mathbf{A}. \qquad (7.4.3.3)$$

It produces photoelectric absorption through the $\mathbf{p}\cdot\mathbf{A}$ term taken in first order, Compton and Raman scattering through the $\mathbf{A}\cdot\mathbf{A}$ term and resonant Raman scattering through the $\mathbf{p}\cdot\mathbf{A}$ terms in second order.

If resonant scattering is neglected for the moment, the expression for the incoherent scattering cross section becomes

$$S = \sum_f (E_2/E_1)^2 \left| \langle \psi_f | \sum_j \exp(i\mathbf{K}\cdot\mathbf{r}_j) | \psi_i \rangle \right|^2 \delta(E_f - E_i - \Delta E), \qquad (7.4.3.4)$$

where the Born operator is summed over the j target electrons and the matrix element is summed over all final states accessible through energy conservation. In the high-energy limit of $\Delta E \gg E_B$, $S(E_1, E_2, \mathbf{K}, Z) \rightarrow Z$ but as Table 7.4.3.1 shows this condition does not hold in the X-ray regime.

The evaluation of the matrix elements in equation (7.4.3.4) was simplified by Waller & Hartree (1929) who (i) set $E_2 = E_1$ and (ii) summed over all final states irrespective of energy conservation. Closure relationships were then invoked to reduce the incoherent scattering factor to an expression in terms of form factors f_{jk}:

$$S = \sum_j [1 - |f_j(\mathbf{K})|^2] - \sum_j^{j\neq k} \sum_k |f_{jk}(\mathbf{K})|^2, \qquad (7.4.3.5)$$

where

$$f_j(\mathbf{K}) = \langle \psi_j | \exp(i\mathbf{K}\cdot\mathbf{r}_j) | \psi_j \rangle$$

and

$$f_{jk} = \langle \psi_k | \exp[i\mathbf{K}\cdot(\mathbf{r}_k - \mathbf{r}_j)] | \psi_j \rangle,$$

the latter term arising from exchange in the many-electron atom.

According to Currat, DeCicco & Weiss (1971), equation (7.4.3.5) can be improved by inserting the prefactor $(E_2/E_1)^2$, where E_2 is calculated from equation (7.4.3.1); the factor is an average for the factors inside the summation sign of equation (7.4.3.4) that were neglected by Waller & Hartree. This term has been included in a few calculations of incoherent intensities [see, for example, Bloch & Mendelsohn (1979)]. The Waller–Hartree method remains the chosen basis for the most extensive compilations of incoherent scattering factors, including those tabulated here, which were calculated by Cromer & Mann (1967) and Cromer (1969) from non-relativistic Hartree–Fock self-consistent-field wavefunctions. Table 7.4.3.2 is taken from the compilation by Hubbell, Veigele, Briggs, Brown, Cromer & Howerton (1975).

7.4.3.2.2. *Thomas–Fermi model*

This statistical model of the atomic charge density (Thomas, 1927; Fermi, 1928) considerably simplifies the calculation of coherent and incoherent scattering factors since both can be written as universal functions of $\mathbf{K}$ and Z. Numerical values were first calculated by Bewilogua (1931); more recent calculations have been made by Brown (1966) and Veigele (1967). The method is less accurate than Waller–Hartree theory, but it is a much simpler computation.

7.4.3.2.3. *Exact calculations*

The matrix elements of (7.4.3.4) can be evaluated exactly for the hydrogen atom. If one-electron wavefunctions in many-electron atoms are modelled by hydrogenic orbitals [with a suitable choice of the orbital exponent; see, for example, Slater (1937)], an analytical approach can be used, as was originally proposed by Bloch (1934).

Table 7.4.3.3. *Compton scattering of Mo Kα X-radiation through 170° from 2s electrons*

Element	$S_{\rm exact}$	$S_{\rm imp}$	$S_{\rm W-H}$
Li	0.879	0.878	0.877
B	0.879	0.878	0.877
O	0.878	0.877	0.876
Ne	0.875	0.875	0.875
Mg	0.863	0.863	0.872
Si	0.851	0.850	0.868
Ar	0.843	0.826	0.877
V	0.663	0.716	0.875
Cr	0.568	0.636	0.875

$S_{\rm exact}$ is the incoherent scattering factor calculated analytically from a hydrogenic atomic model. $S_{\rm imp}$ is the incoherent scattering factor calculated by taking the Compton profile derived in the impulse approximation and truncating it for $\Delta E < E_B$. $S_{\rm W-H}$ is the Waller–Hartree incoherent scattering factor. Data taken from Bloch & Mendelsohn (1974).

Hydrogenic calculations have been shown to predict accurate K- and L-shell photoelectric cross sections (Pratt & Tseng, 1972). The method has been applied in a limited number of cases to K-shell (Eisenberger & Platzman, 1970) and L-shell (Bloch & Mendelsohn, 1974) incoherent scattering factors, where it has served to highlight the deficiencies of the Waller–Hartree approach. In chromium, for example, at an incident energy of ~ 17 keV and a Bragg angle of 85°, the L-shell Waller–Hartree cross section is higher than the 'exact' calculation by $\sim 50\%$. A comparison of Waller–Hartree and exact results for 2s electrons, taken from Bloch & Mendelsohn (1974), is given in Table 7.4.3.3 for illustration. The discrepancy is much reduced when all electrons are considered.

In those instances where the exact method has been used as a yardstick, the comparison favours the 'relativistic integrated impulse approximation' outlined below, rather than the Waller–Hartree method.

7.4.3.3. *Relativistic treatment of incoherent scattering*

The Compton effect is a relativistic phenomenon and it is accordingly more satisfactory to start from this basis, *i.e.* the Klein & Nishina (1929) theory and the Dirac equation (see Jauch & Rohrlich, 1976). In second-order relativistic perturbation theory, there is no overt separation of $\mathbf{p}\cdot\mathbf{A}$ and $\mathbf{A}\cdot\mathbf{A}$ terms. The inclusion of electron spin produces additional terms in the Compton cross section that depend upon the polarization (Lipps & Tolhoek, 1954); they are generally small at X-ray energies. They are of increasing interest in synchrotron-based experiments where the brightness of the source and its polarization characteristics compensate for the small cross section (Blume & Gibbs, 1988).

Somewhat surprisingly, it is the spectral distribution, $\mathrm{d}^2\sigma/\mathrm{d}\Omega\,\mathrm{d}E_2$, rather than the total intensity, $\mathrm{d}\sigma/\mathrm{d}\Omega$, which is the better understood. This is a consequence of the exploitation of the Compton scattering technique to determine electron momentum density distributions through the Doppler broadening of the scattered radiation [see Cooper (1985) and Williams (1977) for reviews of the technique]. Manninen, Paakkari & Kajantie (1976) and Ribberfors (1975) have shown that the

Compton profile – the projection of the electron momentum density distribution onto the X-ray scattering vector – can be isolated from the relativistic differential scattering cross section within the impulse approximation. Several experimental and theoretical investigations have been concerned with understanding the changes in the spectral distribution when electron binding energies cannot be discounted. It has been found (*e.g.* Pattison & Schneider, 1979; Bloch & Mendelsohn, 1974) that, to a high degree of accuracy, the spectral distribution is merely truncated at energy transfers $E \leq E_B$.

This has led to the suggestion that the incoherent intensity can be obtained by integrating the spectral distributions, *i.e.* from

$$\frac{\mathrm{d}\sigma}{\mathrm{d}\Omega} = \int_{E_1 - E_B}^{\infty} \frac{\mathrm{d}^2\sigma}{\mathrm{d}\Omega\,\mathrm{d}E_2}\,\mathrm{d}E_2. \qquad (7.4.3.6)$$

Unfortunately, this requires the Compton profile of each electron shell as input [Compton line shapes have been tabulated by Biggs, Mendelsohn & Mann (1975)] for all elements.

Ribberfors (1983) and Ribberfors & Berggren (1982) have shown that this calculation can be dramatically simplified, without loss of accuracy, by crudely approximating the Compton line shape. Fig. 7.4.3.2 shows the incoherent scattering from aluminium, modelled in this way, and compared with experiment, Waller–Hartree theory, and an exact integral of the truncated impulse Compton profile.

7.4.3.4. *Plasmon, Raman, and resonant Raman scattering*

In typical X-ray experiments, as is evident from Table 7.4.3.1, the energy transfer may be so low that Compton scattering will be inhibited from all but the most loosely bound electrons. Indeed, in the situation in metals where $\mathbf{K}$, the momentum transfer, is less than $\mathbf{k}_F$ (the Fermi momentum), Compton scattering from the conduction electrons may be restricted by exclusion because of the lack of unoccupied final states [see Bushuev & Kuz'min (1977)]. Fortunately, in these uncertain circumstances, the incoherent intensities are low. In this regime, the electron gas may be excited into collective motion. For almost all solids, the plasmon excitation energy is 20–30 eV and, in the random phase approximation, the incoherent scattering factor becomes $S(\Delta E, K) \propto (K^2/w_p)\delta(\Delta E - h\omega_p)$, where ω_p is the plasma frequency.

At slightly higher energies ($\Delta E \geq E_B$), Compton scattering and Raman scattering can coexist, though the Raman component is only evident at low momentum transfer (Bushuev & Kuz'min, 1977). The resultant spectrum is often referred to as the Compton–Raman band. In semi-classical radiation theory, Raman scattering is usually differentiated from Compton scattering by dropping the requirement for momentum conservation between the photon and the individual target electron, the recoil being absorbed by the atom. The Raman band corresponds to transitions into the lowest unoccupied levels and these can be calculated within the dipole approximation as long as $|\mathbf{K}|a < 1$, where $\mathbf{K}$ is the momentum transfer and a the orbital radius of the core electron undergoing the transition. The transition probability in equation (7.4.3.4) becomes

$$\sum_f |\langle\psi_f|\mathbf{r}|\psi_i\rangle|^2 \delta(E_f - E_i - \Delta E), \qquad (7.4.3.7)$$

which implies that the near-edge structure is similar to the photoelectric absorption spectrum.

Whereas plasmon and Raman scattering are unlikely to make dramatic contributions to the total incoherent intensity, resonant Raman scattering (RRS) may, when $E_1 \leq E_B$. The excitation involves a virtual K-shell vacancy in the intermediate state and a vacancy in the L (or M or N) shell and an electron in the continuum in the final state. It has now been observed in a variety of materials [see, for example, Sparks (1974), Eisenberger, Platzman & Winick (1976), Schaupp *et al.* (1984)]. It was predicted by Gavrila & Tugulea (1975) and the theory has been treated comprehensively by Åberg & Tulkki (1985). The effect is the exact counterpart, in the inelastic spectrum, of anomalous

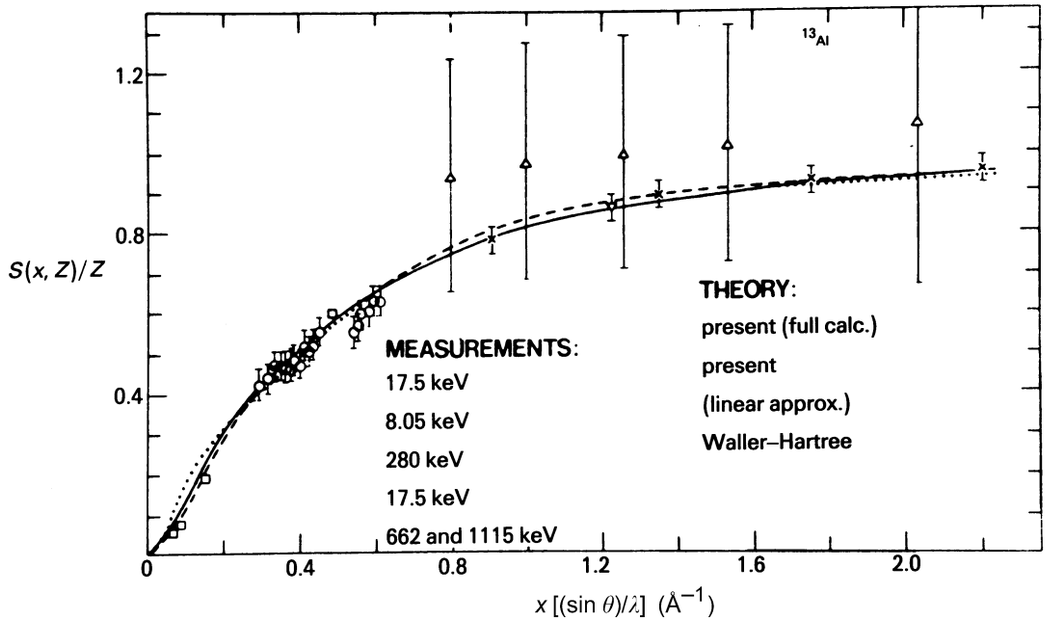

Fig. 7.4.3.2. The incoherent scattering function, $S(x, Z)/Z$, per electron for aluminium shown as a function of $x = (\sin\theta)/\lambda$. The Waller–Hartree theory (·····) is compared with the truncated impulse approximation in the tabulated Compton profiles (Biggs, Mendelsohn & Mann, 1975) cut-off at $E < E_B$ for each electron group (——). The third curve (– – –) shows the simplification introduced by Ribberfors (1983) and Ribberfors & Berggren (1982). The predictions are indistinguishable to within experimental error except at low $(\sin\theta)/\lambda$. Reference to the measurements can be found in Ribberfors & Berggren (1982).

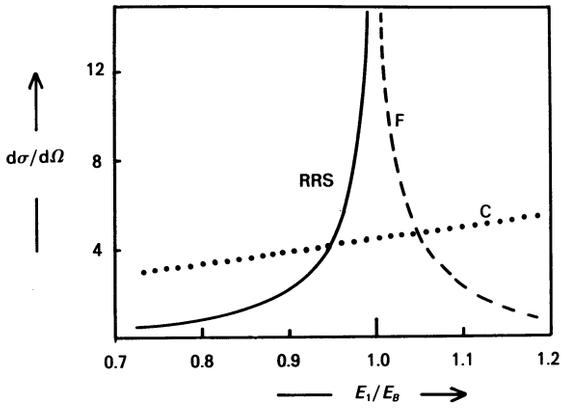

Fig. 7.4.3.3. The cross section for resonant Raman scattering (RRS) and fluorescence (F) as a function of the ratio of the incident energy, E, and the K-binding energy, E_B. The units of $d\sigma/d\Omega$ are $(e^2/mc^2)^2$ and the data are taken from Bannett & Freund (1975). For comparison, the intensity of Compton scattering (C) from copper through an angle of 30° is also shown [data taken from Hubbell *et al*. (1975)].

scattering in the elastic spectrum. It is important because, as the resonance condition is approached, the intensity will exceed that due to Compton scattering and therefore play havoc with any corrections to total intensities based solely on the latter.

Although systematic tabulations of resonance Raman scattering do not exist, Fig. 7.4.3.3, which is based on the calculations of Bannett & Freund (1975), shows how the intensity of RRS clearly exceeds that of the Compton scattering for incident energies just below the absorption edge. However, since the problems posed by anomalous scattering and X-ray fluorescence are generally appreciated, the energy range $0.9 < E_1/E_B < 1.1$ is wisely avoided by crystallographers intent upon absolute intensity measurements.

7.4.3.5. *Magnetic scattering*

Finally, and for completeness, it should be noted that the intensity of Compton scattering from a magnetic material with a net spin moment will, in principle, differ from that from a non-magnetic material. For unpolarized radiation, the effects are only discernible at photon energies greatly in excess of the electron rest mass energy, $mc^2 = 511\,\text{keV}$, but for circularly polarized radiation effects at the 1% level can be found in Compton scattering experiments carried out at $E_1 \simeq 1/10\,mc^2$ on ferromagnets such as iron. See Lipps & Tolhoek (1954) for a comprehensive description of polarization phenomena in magnetic scattering and Lovesey (1993) for an account of the scattering theory.

7.4.4. White radiation and other sources of background (By P. Suortti)

7.4.4.1. *Introduction*

By definition, the background includes everything except the signal. In an X-ray diffraction measurement, the signal is the pattern of Bragg reflections. The profiles of the reflections should be determined by the structure of the sample, and so the broadening due to the instrument should be considered as background. In the ideal angle-dispersive experiment, a well collimated beam of X-rays having a well defined energy (and a polarization, perhaps) falls on the sample, and only the radiation scattered by the sample is detected. Furthermore, the detector should be able to resolve all the components of scattering by energy, so that each scattering process could be studied separately. It is obvious that only after this kind of analysis are the Bragg reflections (plus the possible disorder scattering) unequivocally separated from the background arising from other processes. In most cases, however, this analysis is not feasible, and the reflections are separated by using certain assumptions concerning their profile, and the success of this procedure depends on the peak-to-background ratio.

The ideal situation described above is all too often not encountered, and experimenters are satisfied with too low a level of resolution. The aim of the present article is to point out the sources of the unwanted and unresolved components of the registered radiation and to suggest how these may be eliminated or resolved, so that the quality of the diffraction pattern is as high as possible. The article can cover only a few of the possible experimental situations, and only the 'almost ideal' angle-dispersive instrument is considered. It is assumed that the beam incident on the sample is monochromatized by reflection from a crystal and that the scattered radiation is registered by a low-noise quantum detector, which is the standard arrangement for modern diffractometers. Filtered radiation and photographic recording are used in certain applications, but these are excluded from the following discussion. The wavelength-dispersive or Laue methods are becoming popular at the synchrotron-radiation laboratories, and a short comment on these techniques will be included. Other sections of this volume deal with the components of scattering that are present even in the ideal experiment: thermal diffuse scattering (TDS), Compton and plasmon scattering, fluorescence and resonant Raman scattering, multiple scattering (coherent and incoherent), and disorder scattering.

The rest of the background may be termed 'parasitic' scattering, and it arises from three sources:

(1) impurities of the incident beam;
(2) impurities of the sample;
(3) surroundings of the sample.

Parasitic scattering is occasionally mentioned in the literature, but it has hardly ever been the subject of a detailed study. Therefore, the present article will discuss the general principles of the minimization of the background and then illustrate these ideas with examples. Most of the discussion will be directed to the first of the three sources of parasitic scattering, because the other two depend on the details of the experiment.

7.4.4.2. *Incident beam and sample*

An ideal diffraction experiment should be viewed as an X-ray optical system where all the parts are properly matched for the desired resolution and efficiency. The impurities of the incident beam are the wavelengths and divergent rays that do not contribute to the signal but scatter from the sample through the various processes mentioned above. The propagation of the X-ray beam through the instrument is perhaps best illustrated by the so-called phase-space analysis. The three-dimensional version, which will be used in the following, was introduced by Matsushita & Kaminaga (1980) and was elaborated further by Matsushita & Hashizume (1983). The width, divergence and wavelength range of the beam are given as a contour diagram, which originates in the X-ray source, and is modified by slits, monochromator, sample, and the detection system. The actual five-dimensional diagram is usually given as three-dimensional projections on the plane of diffraction and on the plane perpendicular to it and the beam axis, and in most cases the first projection is sufficient for an adequate description of the geometry of the experiment.

The limitations of the actual experiments are best studied through a comparison with the ideal situation. A close approximation to the ideal experimental arrangement is shown in Fig. 7.4.4.1 as a series of phase-space diagrams. The characteristic radiation from a conventional X-ray tube is almost uniformly distributed over the solid angle of 2π, and the relative width of the $K\alpha_1$ or $K\alpha_2$ emission line is typically $\Delta\lambda/\lambda = 5 \times 10^{-4}$. The acceptance and emittance windows of a flat perfect crystal are given in Fig. 7.4.4.1(*b*). The angular acceptance of the crystal (Darwin width) is typically less than 10^{-4} rad, and, if the width of the slit s or that of the crystal is small enough, none of the $K\alpha_2$ distribution falls within the window. Therefore, it is sufficient to study the size and divergence distributions of the beam in the $\lambda(K\alpha_1)$ plane only, as shown in Fig. 7.4.4.1(*c*). The beam transmitted by the flat monochromator and a slit is shown as the hatched area, and the part reflected by a small crystal by the cross-hatched area. The reflectivity curve of the crystal is probed when the crystal is rotated. In this schematic case, almost 100% of the beam contributes to the signal. The typical reflection profile shown in Fig. 7.4.4.2 reveals the details of the crystallite distribution of the sample (Suortti, 1985). The broken curve shows the calculated profile of the same reflection if the incident beam from a mosaic crystal monochromator had been used (see below).

The window of acceptance of a flat mosaic crystal is determined by the width of the mosaic distribution, which may be 100 times larger than the Darwin width of the reflection in

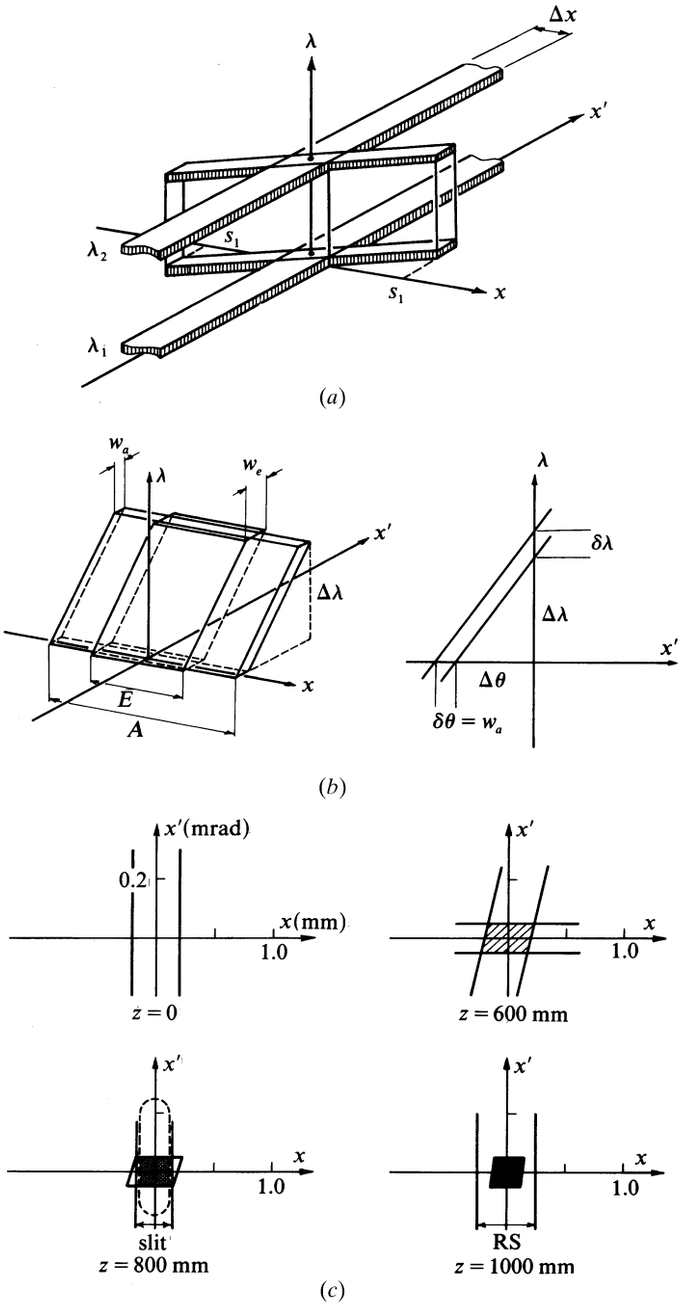

Fig. 7.4.4.1. Equatorial phase-space diagrams for a conventional X-ray source and parallel-beam geometry; x is the size and $x' = \mathrm{d}x/\mathrm{d}z$ the divergence of the X-rays. (*a*) Radiation distributions for two wavelengths, λ_1 and λ_2, at the source of width Δx, and downstream at a slit of width $\pm s_1$. (*b*) Acceptance and emittance windows of a flat perfect crystal, where the phase-space volume remains constant, $Aw_a\Delta\lambda = Ew_e\Delta\lambda$, and the (x', λ) section shows the reflection of a polychromatic beam (Laue diffraction). (*c*) Distributions for one wavelength at the source, flat perfect-crystal monochromator, sample (marked with the broken line), and the receiving slit (RS); z is the distance from the source.

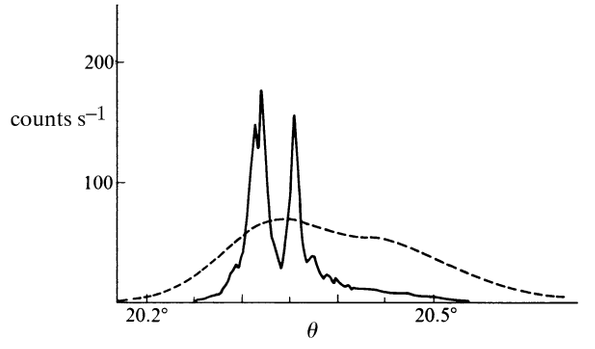

Fig. 7.4.4.2. Reflection 400 of LiH measured with a parallel beam of Mo $K\alpha_1$ radiation (solid curve). The broken curve shows the reflection as convoluted by a Gaussian instrumention function of $2\sigma = 0.1^\circ$ and $\theta(\alpha_2) - \theta(\alpha_1) = 0.13^\circ$, which values are comparable with those in Fig. 7.4.4.4.

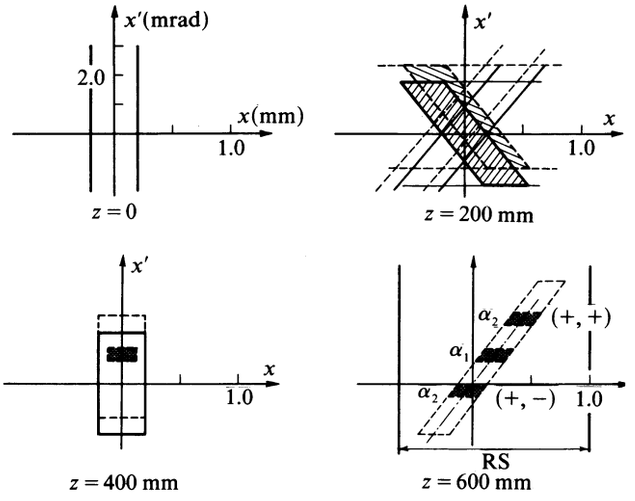

Fig. 7.4.4.3. Equatorial phase-space diagrams for two wavelengths, λ_1 (solid lines) and λ_2 (broken lines), projected on the plane $\lambda = \lambda_1$. The monochromator at $z = 200$ mm is a flat mosaic crystal, and a small sample is located at $z = 400$ mm, as shown by the shaded area. The reflected beams at the receiving slit are shown for the $(+, +)$ and $(+, -)$ configurations of the monochromator and the sample.

question. This means that a convergent beam is reflected in the same way as from a bent perfect crystal in Johann or Johansson geometry. Usually, the window is wide enough to transmit an energy band that includes both $K\alpha_1$ and $K\alpha_2$ components of the incident beam. The distributions of these components are projected on the (x, x', λ_1) plane in Fig. 7.4.4.3. The sample is placed in the (para)focus of the beam, and often the divergence of the beam is much larger than the width of the rocking curve of the sample crystal. This means that at any given time the signal comes from a small part of the beam, but the whole beam contributes to the background. The profile of the reflection is a convolution of the actual rocking curve with the divergence and wavelength distributions of the beam. The calculated profile in Fig. 7.4.4.2 demonstrates that in a typical case the profile is determined by the instrument, and the peak-to-background ratio is much worse than with a perfect-crystal monochromator.

An alternative arrangement, which has become quite popular in recent years, is one where the plane of diffraction at the monochromator is perpendicular to that at the sample. The beam is limited by slits only in the latter plane, and the wavelength varies in the perpendicular plane. An example of rocking curves measured by this kind of diffractometer is given in Fig. 7.4.4.4. The $K\alpha_1$ and $K\alpha_2$ components are seen separately plus a long tail due to continuum radiation, and the profile is that of the divergence of the beam.

In the Laue method, a well collimated beam of white radiation is reflected by a stationary crystal. The wavelength band reflected by a perfect crystal is indicated in Fig. 7.4.4.1(*b*). The mosaic blocks select a band of wavelengths from the incident beam and the wavelength deviation is related to the angular deviation by $\Delta\lambda/\lambda = \cot\theta\Delta\theta$. The angular resolution is determined by the divergences of the incident beam and the spatial resolution of the detector. The detector is not energy dispersive, so that the background arises from all scattering that reaches the detector. An estimate of the background level involves integrations over the incident spectrum at a fixed scattering angle, weighted by the cross sections of inelastic scattering and the attenuation factors. This calculation is very complicated, but at any rate the background level is far higher than that in a diffraction measurement with a monochromatic incident beam.

7.4.4.3. *Detecting system*

The detecting system is an integral part of the X-ray optics of a diffraction experiment, and it can be included in the phase-space diagrams. In single-crystal diffraction, the detecting system is usually a rectangular slit followed by a photon counter, and the slit is large enough to accept all the reflected beam. The slit can be stationary during the scan (ω scan) or follow the rotation of the sample ($\omega/2\theta$ scan). The included TDS depends on these choices, but otherwise the amount of background is proportional to the area of the receiving slit. It is obvious from a comparison between Fig. 7.4.4.1 and Fig. 7.4.4.3 that a much smaller receiving slit is sufficient in the parallel-beam geometry than in the conventional divergent-beam geometry. Mathieson (1985) has given a thorough analysis of various monochromator–sample–detector combinations and has suggested the use of a two-dimensional $\omega/2\theta$ scan with a narrow receiving slit. This provides a deconvolution of the reflection profile measured with a divergent beam, but the same result with better intensity and resolution is obtained by the parallel-beam techniques.

The above discussion has concentrated on improving the signal-to-background ratio by optimization of the diffraction geometry. This ratio can be improved substantially by an energy-dispersive detector, but, on the other hand, all detectors have some noise, which increases the background. There have been marked developments in recent years, and traditional technology has been replaced by new constructions. Much of this work has been carried out in synchrotron-radiation laboratories (for

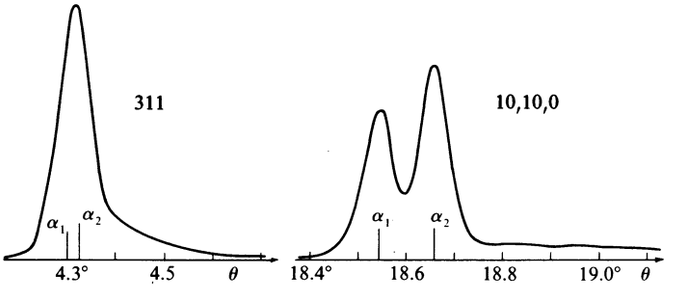

Fig. 7.4.4.4. Two reflections of beryllium acetate measured with Mo $K\alpha$. The graphite (002) monochromator reflects in the vertical plane, while the crystal reflects in the horizontal plane. The equatorial divergence of the beam is 0.8°, FWHM.

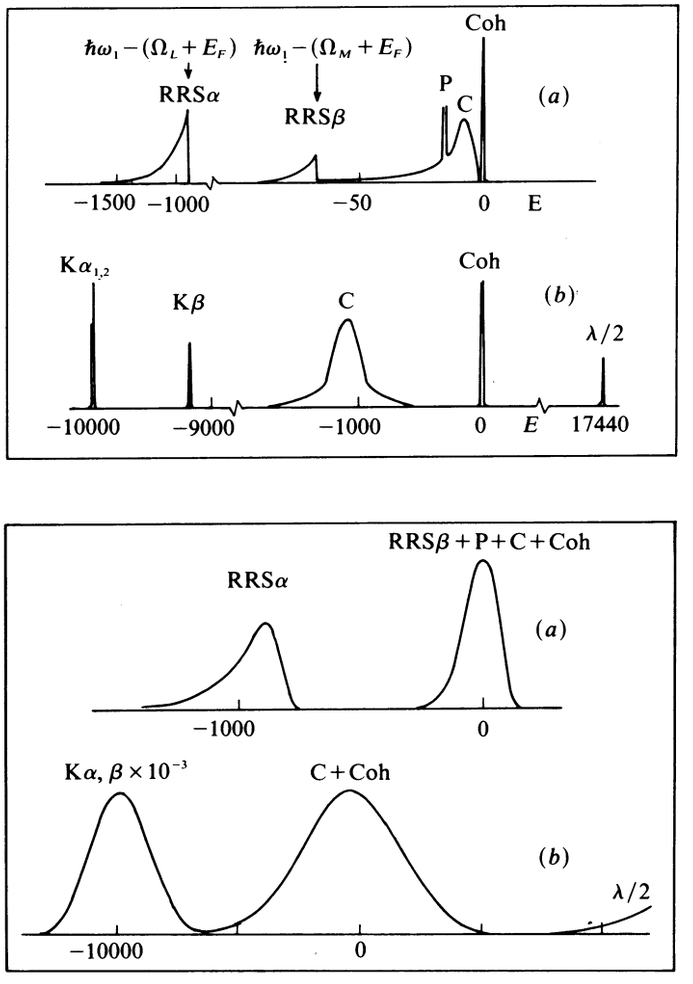

Fig. 7.4.4.5. Components of scattering at small scattering angles when the incident energy is just below the *K* absorption edge of the sample [upper part, (*a*)], and at large scattering angles when the incident energy is about twice the *K*-edge energy [upper part, (*b*)]. The abbreviations indicate resonant Raman scattering (RRS), plasmon (P) and Compton (C) scattering, coherent scattering (Coh) and sample fluorescence ($K\alpha$ and $K\beta$). The lower part shows these components as convoluted by the resolution function of the detector: (*a*) a SSD and (*b*) a scintillation counter (Suortti, 1980).

references, see Thomlinson & Williams, 1984; Brown & Lindau, 1986).

A position-sensitive detector can replace the receiving slit when a reciprocal space is scanned. TV area detectors with an X-ray-to-visible light converter and two-dimensional CCD arrays have moderate resolution and efficiency, but they work in the current mode and do not provide pulse discrimination on the basis of the photon energy. One- and two-dimensional proportional chambers have a spatial resolution of the order of 0.1 mm, and the relative energy resolution, $\Delta E/E \simeq 0.2$, is sufficient for rejection of some of the parasitic scattering.

The NaI(Tl) scintillation counter is used most frequently as the X-ray detector in crystallography. It has 100% efficiency for the commonly used wavelengths, and the energy resolution is comparable to that of a proportional counter. The detector has a long life, and the level of the low-energy noise can be reduced to about 0.1 counts s^{-1}.

The Ge and Si(Li) solid-state detectors (SSD) have an energy resolution $\Delta E/E = 0.01$ to 0.03 for the wavelengths used in crystallography. The relative Compton shift, $\Delta\lambda/\lambda$, is $(0.024\ \text{Å}/\lambda) \times (1 - \cos 2\theta)$, where 2θ is the scattering angle, so that even this component can be eliminated to some extent by a SSD. These detectors have been bulky and expensive, but new constructions that are suitable for X-ray diffraction have become available recently. The effects of the detector resolution are shown schematically in Fig. 7.4.4.5 for a scintillation counter and a SSD.

Crystal monochromators placed in front of the detector eliminate all inelastic scattering but the TDS. The monochromator must be matched with the preceding X-ray optical system, the sample included, and therefore diffracted-beam monochromators are used in powder diffraction only (see Subsection 7.4.4.4).

7.4.4.4. *Powder diffraction*

The signal-to-background ratio is much worse in powder diffraction than in single-crystal diffraction, because the background is proportional to the irradiated volume in both cases, but the powder reflection is distributed over a ring of which only the order of 1% is recorded. The phase-space diagrams of a typical measurement are shown in Fig. 7.4.4.6. The Johansson monochromator is matched to the incident beam to provide

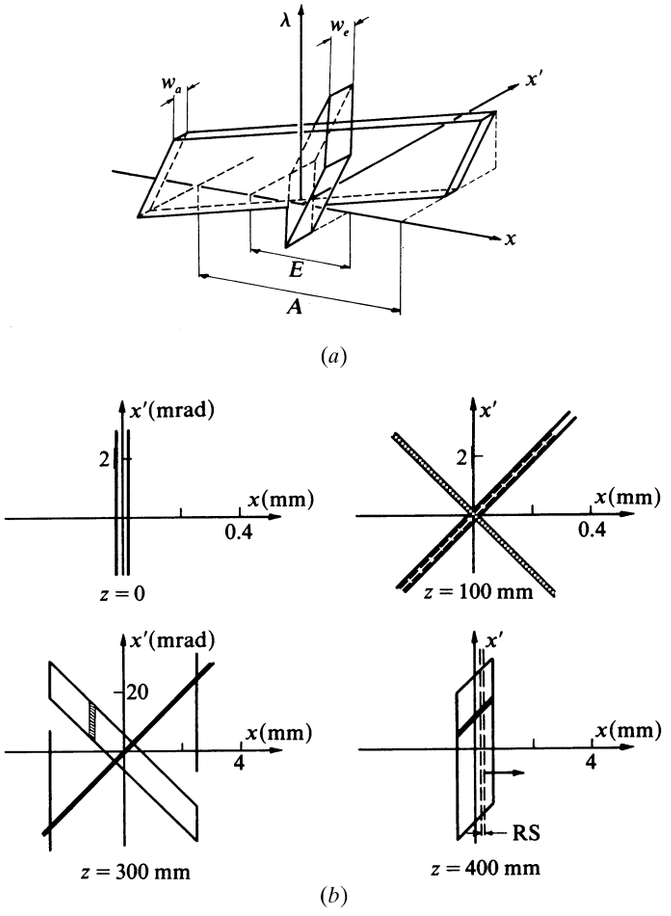

Fig. 7.4.4.6. Equatorial phase-space diagrams for powder diffraction in the Bragg–Brentano geometry. (*a*) The acceptance and emittance windows of a Johannson monochromator; (*b*) the beam in the $\lambda = \lambda_1$ plane: the exit beam from the Johansson monochromator is shown by the hatched area ($z = 100$ mm), the beam on the sample by two closely spaced lines, the reflectivity range of powder particles in a small area of the sample by the hatched area ($z = 300$ mm, note the change of scales), and the scan of the reflected beam by a slit RS by broken lines ($z = 400$ mm, at the parafocus).

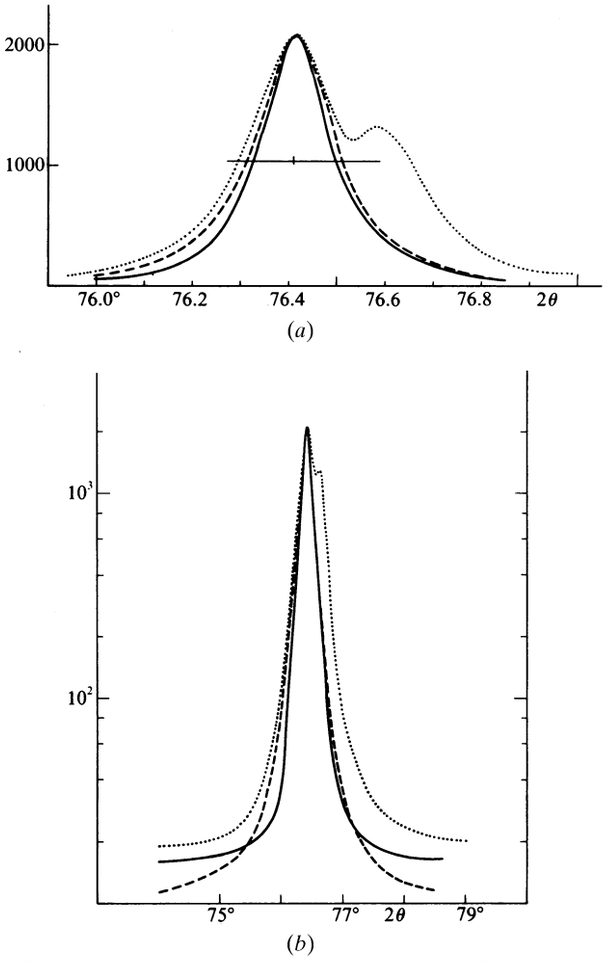

Fig. 7.4.4.7. Three measurements of the 220 reflection of Ni at $\lambda = 1.541$ Å scaled to the same peak value; (*a*) in linear scale, (*b*) in logarithmic scale. Dotted curve: graphite (00.2) Johann monochromator, conventional 0.1 mm wide X-ray source (Suortti & Jennings, 1977); solid curve: quartz (10.1) Johansson monochromator, conventional 0.05 mm wide X-ray source; broken curve: synchrotron radiation monochromatized by a (+, −) pair of Si (111) crystals, where the second crystal is sagittally bent for horizontal focusing (Suortti, Hastings & Cox, 1985). The horizontal line indicates the half-maximum value. In all cases, the effective slit width is much less than the FWHM of the reflection.

maximum flux and good energy resolution. The Bragg–Brentano geometry is parafocusing, and, if the geometrical aberrations are ignored, the reflected beam is a convolution between the angular width of the monochromator focus (as seen from the sample) and the reflectivity curve of an average crystallite of the powder sample. The profile of this function is scanned by a narrow slit, as shown in the last diagram. The slit can be followed with a Johann or Johansson monochromator that has a narrow wavelength pass-band. In this case, there is no primary-beam monochromator, so that the incident beam at the sample is that given at $z = 100$ mm. The slit RS is the 'source' for the monochromator, which focuses the beam at the detector. The obvious advantages of this arrangement are counterbalanced by certain limitations such as that the effective receiving slit is determined by the reflectivity curve of the monochromator, and this may vary over the effective area.

Examples of a powder reflection measured with different instruments and 1.5 Å radiation are given in Fig. 7.4.4.7. It should be noticed that scattering from the impurities of the sample and from the sample environment is negligible in all three cases. The width of the mosaic distribution of the 00.2 reflection of the pyrolytic graphite monochromator is 0.3°, which corresponds to a 180 eV (0.034 Å) wide transmitted beam. This is almost 10 times the separation between $K\alpha_1$ and $K\alpha_2$, and 70 times the natural width of the $K\alpha_1$ line. The width of the focal line is about 0.2 mm, or 0.07°, and is seen as broadening of the reflection profile. The quartz (10.1) monochromator reflects a band that is determined by the projected width of the X-ray source. In the present case, the band is 15 eV wide, so that the monochromator can be tuned to transmit the $K\alpha_1$ component only. The focal line is very sharp, 0.05 mm wide, and so the reflection is much narrower than in the preceding case. The third measurement was made with synchrotron radiation, and the receiving slit was replaced by a perfect-crystal analyser. The divergences of the incident and diffracted beams are about 0.1 mrad (less than 0.01°) in the plane of diffraction, so that the ideal parallel-beam geometry should prevail. However, the reflection is clearly broader than that measured with the conventional diffractometer. The reason is a wavelength gradient across the beam, which was monochromatized by a flat perfect crystal. On the other hand, the Ge (111) analyser crystal transmits elastic scattering and TDS only, and 2° away from the peak the background is 0.5% of the maximum intensity.

The above considerations may seem to have little relevance to everyday crystallographic practices. Unfortunately, many standard methods yield diffraction patterns of poor quality. The quest for maximum integrated intensity has led to designs that make reflections broad and background high. It should be realized that not the flux but the brilliance of the incident beam is important in a diffraction measurement. The other aspect is that the information should not be lost in the experiment, and a divergent wide wavelength band is quite an ignorant probe of a reflection from a single crystal.

A situation where even small departures from the ideal diffraction geometry may cause large effects is measurement at an energy just below an absorption edge. Even a small tail of the energy band of the incident beam may excite radiation that becomes the dominant component of background. Similar effects are due to the harmonic energy bands reflected by most monochromators, particularly when the continuous spectrum of synchrotron radiation is used.

Scattering from the surroundings of the sample can be eliminated almost totally by shielding and beam tunnels. The general idea of the construction should be that an optical element of the instrument 'sees' the preceding element only. Inevitably, the detector sees some of the environment of the sample. The density of air is about 1/1000 of that of a solid sample, so that 10 mm^3 of irradiated air contributes to the background as much as a spherical crystal of 0.3 mm diameter. Strong spurious peaks may arise from slit edges and entrance windows of the specimen chamber, which should never be seen by the detector. A complete measurement without the sample is always a good starting point for an experiment.

7.5. Statistical fluctuations

By A. J. C. Wilson

7.5.1. Distributions of intensities of diffraction

Intensities of diffraction have two distinct probability distributions: (1) the *a priori* probability that an arbitrarily chosen reflection of a particular substance will have a particular 'true' intensity (R in the notation used below), and (2) the probability that a 'true' R will have an observed value R_o. The distributions of the first type depend on the symmetry and composition of the material, and are treated in Chapter 2.1 of Volume B of *International Tables for Crystallography* (Shmueli, 1993). The distributions of fluctuations of the second type, variations of the values R_o observed for a particular reflection, are treated here.

The crude counts or counting rates are rarely used directly in crystallographic calculations; they are subjected to some form of data processing to provide 'intensities of reflection' I_o in a form suitable for the determination of crystal structures, electron densities, line profiles for the study of defects, *etc*. The resulting intensity for the jth reflection, $I_{o,j}$, will be directly proportional to the corresponding $R_{o,j}$; when no confusion can arise, one of the subscripts will be omitted. The value of the proportionality factor c_j in

$$I_{o,j} = c_j R_{o,j} \qquad (7.5.1.1)$$

will be different for different reflections, since they will occur at different Bragg angles, have different absorption corrections, *etc*.

7.5.2. Counting modes

Whatever the radiation, in both single-crystal and powder diffractometry, the integrated intensity of a reflection is obtained as a difference between a counting rate averaged over a volume of reciprocal space intended to include the reflected intensity and a counting rate averaged over a neighbouring volume of reciprocal space intended to include only background. If these intentions are not effectively realized, there will be a systematic error in the measured intensity, but in any case there will be statistical fluctuations in the counting rates. The two basic modes (Parrish, 1956) are fixed-time counting and fixed-count timing. In the first, counts are accumulated for a pre-determined time interval, and the variance of the observed counting rate is proportional to the true (mean) counting rate. In the second, on the other hand, the counting is continued until a pre-determined number of counts is reached, and the variance of the observed counting rate is proportional to the square of the true counting rate. Put otherwise, the relative error in the intensities goes down inversely as the square root of the intensity for fixed-time counting, whereas it is independent of the intensity for fixed-count timing. Each mode has advantages, depending on the purpose of the measurements, and numerous modifications and compromises have been proposed in order to increase the efficiency of the use of the available time. References to some of the many papers are given in Section 7.5.7.

In principle, probability distributions can be determined for any postulated counting mode. In practice, they become complicated for all but the simplest modes; this is true even for the single measurement of the total counting rate or the background counting rate, but is even more pronounced for the distribution of their difference (the reflection-only rate). For most crystallographic purposes, however, it is only necessary to know the mean (to correct for bias, if present) and the variance (for the estimation of weights in refinement processes, see Part 8) of the distribution function.

7.5.3. Fixed-time counting

In the absence of disturbing influences (mains-voltage fluctuations, unrectified or unsmoothed high-tension supplies, 'dead time' of the counter or counter circuits, *etc*.), the number of counts recorded during the predetermined time interval used in the fixed-time mode will fluctuate in accordance with the Poisson probability distribution. If the 'true' number of counts to be expected in the interval is N, the probability that the observed number will be N_o is given by

$$p(N_o) = \exp(-N)N^{N_o}/N_o!, \qquad (7.5.3.1)$$

where all quantities appearing are necessarily non-negative. Both the mean and the variance of N_o are N. If the 'true' number of counts to be expected when the diffractometer is set to receive a reflection is T, and the 'true' number when it is set to receive the immediate background is B, the 'true' intensity of the reflection is

$$R = T - B, \qquad (7.5.3.2)$$

provided that the time interval used for the reflection is equal to the time interval used for the background. In practice, the 'observed' values of T_o and B_o fluctuate with probabilities given by (7.5.3.1) with T or B replacing N, so that the observed value,

$$R_o = T_o - B_o, \qquad (7.5.3.3)$$

will also fluctuate, and can, occasionally, take on negative values. The treatment of 'measured-as-negative' intensities is discussed in Section 7.5.6.

Although the sum of two Poisson-distributed variables is also Poisson, the difference is not, and the probability of R_o given by (7.5.3.3) has been shown to be (Skellam, 1946; Wilson, 1978)

$$p(R_o) = \exp\{-(B+T)\}(T/B)^{R_o/2} I_{|R_o|}[2(BT)^{1/2}], \qquad (7.5.3.4)$$

where I_n is the hyperbolic Bessel function of the first kind. The mean and variance of R_o are $T - B$ and $T + B$, respectively. If the times used for reflection and background are not equal, but are in the ratio of $k:1$, the mean and variance of

$$R_o = T_o - kB_o \qquad (7.5.3.5)$$

are $T - kB$ and $T + k^2B$, respectively. The distribution of R_o then involves a generalized Bessel function* depending on k:

$$p(R_o) = \exp\{-(B+T)\}(T^{2-k}/B)^{R_o/2} I^k_{|R_o|}[2(BT^k)^{1/2}]; \qquad (7.5.3.6)$$

for the properties of the generalized Bessel function, see Wright (1933) and Olkha & Rathie (1971). The probability distributions (7.5.3.4) and (7.5.3.6) seem to be very close to a normal distribution with the same mean and variance for R_o near R, but the probability of moderate deviations from R is less than normal and for large deviations is greater than normal.

In applications, it is usual to work with intensities expressed as counting rates, rather than as numbers of counts, even when fixed-time counting is used. The total intensity τ expressed as a counting rate is

* The term 'generalized Bessel function' seems to have no unique meaning in mathematics. The functions given that name by Paciorek & Chapuis (1994) belong to a different group.

Copyright © 2006 International Union of Crystallography

$$\tau = T/t, \tag{7.5.3.7}$$

where t is the time devoted to the measurement, and the variance of the counting rate is

$$\sigma^2(\tau) = T/t^2 = \tau/t. \tag{7.5.3.8}$$

Similar expressions apply for the background, with B for the count, b for the time, and β for the counting rate. For the reflection count, the corresponding expressions are

$$\rho = T/t - B/b, \tag{7.5.3.9}$$

$$\sigma^2(\rho) = \tau/t + \beta/b. \tag{7.5.3.10}$$

To avoid confusion, upper-case italic letters are used for *numbers* of counts, lower-case italic for counting *times*, and the corresponding lower-case Greek letters for the corresponding counting *rates*. In accordance with common practice, however, I_j will be used for the intensity of the jth reflection, the context making it clear whether I is a number of counts or a counting rate.

7.5.4. Fixed-count timing

The probability of a time t being required to accumulate N counts when the true counting rate is ν is given by a Γ distribution (Abramowitz & Stegun, 1964, p. 255):

$$p(t)\,\mathrm{d}t = [(N-1)!]^{-1}(\nu t)^{N-1}\exp(-\nu t)\,\mathrm{d}(\nu t). \tag{7.5.4.1}$$

The ratio N/t is a slightly biased estimate of the counting rate ν; the unbiased estimate is $(N-1)/t$. The variance of this estimate is $\nu^2/(N-2)$, or, nearly enough for most purposes, $(N-1)^2/(N-2)t^2$. The differences introduced by the corrections -1 and -2 are generally negligible, but would not be so for counts as low as those proposed by Killean (1967). If such corrections are important, it should be noticed that there is an ambiguity concerning N, depending on how the timing is triggered. It may be triggered by a count that is counted, or by a count that is not counted, or may simply be begun, independently of the incidence of a count. Equation (7.5.4.1) assumes the first of these.

Equation (7.5.4.1) may be inverted to give the probability distribution of the observed counting rate ν_o instead of the probability distribution of the time t:

$$p(\nu_o)\,\mathrm{d}\nu_o = [(N-1)!]^{-1}[\nu(N-1)/\nu_o]^{N-1} \times \exp\{-(N-1)\nu/\nu_o\}\,\mathrm{d}[\nu_o/(N-1)\nu]. \tag{7.5.4.2}$$

There does not seem to be any special name for the distribution (7.5.4.2). Only its first $(N-1)$ moments exist, and the integral expressing the probability distribution of the difference of the reflection and the background rates is intractable (Wilson, 1980).

7.5.5. Complicating phenomena

7.5.5.1. *Dead time*

After a count is recorded, the detector and the counting circuits are 'dead' for a short interval, and any ionizing event occurring during that interval is not detected. This is important if the dead time is not negligible in comparison with the reciprocal of the counting rate, and corrections have to be made; these are large for Geiger counters, and may sometimes be necessary for counters of other types. The need for the correction can be eliminated by suitable monitoring (Eastabrook & Hughes, 1953); other advantages of monitoring are described in Chapter 2.3.

7.5.5.2. *Voltage fluctuations*

Mains-voltage fluctuations, unless compensated, and unsmoothed high-tension supplies may affect the sensitivity of detectors and counting circuits, and in any case cause the probability distribution of the arrival of counts to be non-Poissonian. Backlash in the diffractometer drives may be even more important in altering the observed counting rates. As de Boer (1982) says, the ideal distributions represent a Utopia that experimenters can approach but never reach. He observed erratic fluctuations in counting rates, up to ten times as big as the expected statistical fluctuations. When care is taken, the instabilities observed in practice are much less than those of the extreme cases described by de Boer. Stabilizing an X-ray source and testing its stability are discussed in Subsection 2.3.5.1.

7.5.6. Treatment of measured-as-negative (and other weak) intensities

It has been customary in crystallographic computations, but without theoretical justification, to omit all reflections with intensities less than two or three times their standard uncertainties. Hirshfeld & Rabinovich (1973) asserted that the failure to use all reflections, even those for which the subtraction of background has resulted in a negative net intensity, at their measured values will lead to a bias in the parameters resulting from a least-squares refinement. This is, however, inconsistent with the Gauss–Markov theorem (see Section 8.1.2), which shows that least-squares estimates are unbiased, independent of the weights used, if the observations are unbiased estimates of quantities predicted by a model. Giving some observations zero weight therefore cannot introduce bias. Provided the set of included observations is sufficient to give a nonsingular normal equations matrix, parameter estimates will be unbiased, but inclusion of as many well determined observations as possible will yield the most precise estimates. Requiring that the net intensity be greater than 2σ assures that the value of $|F|$ will be well determined. Furthermore, Prince & Nicholson (1985) showed that, if the net intensity, I, or $|F|^2$ is used as the observed quantity, weak reflections have very little leverage (see Section 8.4.4), and therefore omitting them cannot have a significant effect on the precision of parameter estimates.

The use of negative values of I or $|F|^2$ is also inconsistent with Bayes's theorem, which implies that a negative value cannot be an unbiased estimate of an inherently non-negative quantity. There are statistical methods for estimating the positive value of $|F|$ that led to a negative value of I. The best known approach is the Bayesian method of French & Wilson (1978), who observe that ''Instead of thanking the data for the information that certain structure factor moduli are small, we accuse them of assuming 'impossible' negative values. What we should do is combine our knowledge of the non-negativity of the true intensities with the information concerning their magnitudes contained in the data.''

7.5.7. Optimization of counting times

There have been many papers on optimizing counting times for achieving different purposes, and all optimization procedures require some knowledge of the distributions of counts or counting rates; often only the mean and variance of the distribution are required. It is also necessary to know the functional relationship between the quantity of interest and the counts (counting rates, intensities) entering into its measurement. Typically, the object is to minimize the variance of some

function of the measured intensities, say $F(I_1, I_2, \ldots, I_j, \ldots)$. General statistical theory gives the usual approximation

$$\sigma^2(F) = \sum_{i,j} \frac{\partial F}{\partial I_i}\frac{\partial F}{\partial I_j}\mathrm{cov}(I_i, I_j), \qquad (7.5.7.1)$$

where $\mathrm{cov}(I_i, I_j)$ is the covariance of I_i and I_j if $i \neq j$, and is the variance of I_j, $\sigma^2(I_j)$, if $i = j$. There is very little correlation* between successive intensity measurements in diffractometry, so that $\mathrm{cov}(I_i, I_j)$ is negligible for $i \neq j$. Equation (7.5.7.1) becomes

$$\sigma^2(F) = \sum_j \left(\frac{\partial F}{\partial I_j}\right)^2 \sigma^2(I_j). \qquad (7.5.7.2)$$

These equations are strictly accurate only if F is a linear function of the I's, a condition satisfied for the integrated intensity, but for few other quantities of interest. In most applications in diffractometry, however, the contribution of each I_j is sufficiently small in comparison with the total to make the application of equations (7.5.7.1) and (7.5.7.2) plausible. Any proportionality factors c_j (Section 7.5.1) can be absorbed into the functional relationship between F and the I_j's.

The object is to minimize $\sigma^2(F)$ by varying the time spent on each observation, subject to a fixed total time

$$T = \sum_j t_j. \qquad (7.5.7.3)$$

It is simplest to regard the total intensity and the background intensity as separate observations, so that in (7.5.7.2) the sum is over n 'background' and n 'total' observations. With I_j expressed as a counting rate, its variance is I_j/t_j [equation (7.5.3.8)], so that (7.5.7.2) becomes

$$\sigma^2(F) = \sum_j G_j^2 I_j/t_j, \qquad (7.5.7.4)$$

where for brevity G has been written for $|\partial F/\partial I|$. The variance of F will be a minimum if, for any small variations $\mathrm{d}t_j$ of the counting times t_j,

$$0 = -\sum_j G_j^2 I_j t_j^{-2}\,\mathrm{d}t_j, \qquad (7.5.7.5)$$

subject to the constancy of the total time T. There is thus the constraint

$$0 = \sum_j \mathrm{d}t_j. \qquad (7.5.7.6)$$

These equations are consistent if for all j

$$G_j^2 I_j t_j^{-2} = k^{-2}, \qquad (7.5.7.7)$$

$$t_j = k G_j I_j^{1/2}, \qquad (7.5.7.8)$$

where k is a constant determined by the total time T:

$$T = k\sum_j G_j I_j^{1/2}. \qquad (7.5.7.9)$$

The minimum variance is thus achieved if each observation is given a time proportional to the square root of its intensity. A little manipulation now gives for the desired minimum variance

$$\sigma^2_{\min}(F) = \frac{1}{T}\left[\sum_j \left(\partial F/\partial I_j\right) I_j^{1/2}\right]^2. \qquad (7.5.7.10)$$

The minimum variance is found to be a perfect square, and the standard uncertainty takes a simple form.

Here, the optimization has been treated as a modification of fixed-time counting. However, the same final expression is obtained if the optimization is treated as a modification of fixed-count timing (Wilson, Thomsen & Yap, 1965).

Space does not permit detailed discussion of the numerous papers on various aspects of optimization. If the time required to move the diffractometer from one observation position to another is appreciable, the optimization problem is affected (Shoemaker & Hamilton, 1972, and references cited therein). There is some dependence on the radiation (X-ray *versus* neutron) (Shoemaker, 1968; Werner 1972*a*,*b*). A few other papers of historical or other interest are included in the list of references, without detailed mention in the text: Grant (1973); Killean (1972, 1973); Mack & Spielberg (1958); Mackenzie & Williams (1973); Szabó (1978); Thomsen & Yap (1968); Zevin, Umanskii, Kheiker & Panchenko (1961).

* Exceptions to this statement may be important for line and area detectors, or if an interpolation function is used to estimate background. Wilson (1967) has discussed some features of the powder diffractometry case.

References

7.1.1

Hellner, E. (1954). *Intensitätsmessungen aus Aufnahmen in der Guinier-Kamera. Z. Kristallogr.* **106**, 122–145.

International Tables for X-ray Crystallography (1962). Vol. III. Birmingham: Kynoch Press.

Mees, C. E. K. (1954). *The theory of the photographic process*. New York: Macmillan.

Whittaker, E. J. W. (1953). *The Cox & Shaw factor. Acta Cryst.* **6**, 218.

7.1.2–7.1.4

Ames, L., Drummond, W., Iwanczyk, J. & Dabrowski, A. (1983). *Energy resolution measurements of mercuric iodide detectors using a cooled FET preamplifier. Adv. X-ray Anal.* **26**, 325–330.

Ballon, J., Comparat, V. & Pouxe, J. (1983). *The blade chamber: a solution for curved gaseous detectors. Nucl. Instrum. Methods*, **217**, 213–216.

Bish, D. L. & Chipera, S. J. (1989). *Comparison of a solid-state Si detector to a conventional scintillation detector–monochromator system in X-ray powder diffraction. Powder Diffr.* **4**, 137–143.

Eastabrook, J. N. & Hughes, J. W. (1953). *Elimination of dead-time corrections in monitored Geiger-counter X-ray measurements. J. Sci. Instrum.* **30**, 317–320.

Foster, B. A. & Wölfel, E. R. (1988). *Automated quantitative multiphase analysis using a focusing transmission diffractometer in conjunction with a curved position sensitive detector. Adv. X-ray Anal.* **31**, 325–330.

Geiger, H. & Müller, W. (1928). *Das Elektronenzählrohr. Z. Phys.* **29**, 839–841.

7.1.2–7.1.4 (*cont.*)

Göbel, H. E. (1982). *A Guinier diffractometer with a scanning position sensitive detector*. *Adv. X-ray Anal.* **25**, 315–324.

Heinrich, K. F. J., Newbury, D. E., Myklebust, R. L. & Fiori, C. E. (1981). Editors. *Energy dispersive X-ray spectrometry*. *US Natl Bur. Stand. Spec. Publ.* No. 604.

Kevex Corporation (1990). Brochure on equipment.

Kohler, T. R. & Parrish, W. (1955). *X-ray diffractometry of radioactive samples*. *Rev. Sci. Instrum.* **26**, 374–379.

Lehmann, M. S., Christensen, A. N., Fjellvåg, H., Feidenhans'l, R. & Nielsen, M. (1987). *Structure determination by use of pattern decomposition and the Rietveld method on synchrotron X-ray and neutron powder data; the structures of $Al_2Y_4O_9$ and I_2O_4*. *J. Appl. Cryst.* **20**, 123–129.

Nissenbaum, J., Levi, A., Burger, A., Schieber, M. & Burshtein, Z. (1984). *Supression of X-ray fluorescence background in X-ray powder diffraction by a mercuric iodide spectrometer*. *Adv. X-ray Anal.* **27**, 307–316.

Parrish, W. (1962). *Advances in X-ray diffractometry and X-ray spectrography*. Eindhoven: Centrex.

Parrish, W. (1966). *Escape peak interferences in X-ray powder diffractometry*. *Adv. X-ray Anal.* **8**, 118–133.

Parrish, W. & Kohler, T. R. (1956). *The use of counter tubes in X-ray analysis*. *Rev. Sci. Instrum.* **27**, 795–808.

Rigaku Corporation (1990). Brochure on equipment.

Russ, J. C. (1984). *Fundamentals of energy dispersive X-ray analysis*. London: Butterworth.

Shishiguchi, S., Minato, I. & Hashizume, H. (1986). *Rapid collection of X-ray powder data for pattern analysis by a cylindrical position-sensitive detector*. *J. Appl. Cryst.* **19**, 420–426.

Wölfel, E. R. (1983). *A novel curved position-sensitive proportional counter for X-ray diffractometry*. *J. Appl. Cryst.* **16**, 341–348.

7.1.5

Warburton, W. K., Iwanczyk, J. S., Dabrowski, A. J., Hedman, B., Penner-Hahn, J. E., Roe, A. L. & Hodgson, K. O. (1986). *Development of mercuric iodide detectors for XAS and XRD measurements*. *Nucl. Instrum. Methods*, A**246**, 558–560.

Worgan, J. S. (1982). *Energy-dispersive detectors for synchrotron radiation*. *Nucl. Instrum. Methods*, **201**, 85–91.

7.1.6

Airey, R. W. & Morgan, B. L. (1985). *A microchannel plate image intensifier for detection of photon-noise-limited images*. *IEE Conf. Publ. (London)*, **253**, 5–7.

Allemand, R. & Thomas, G. (1976). *New position-sensitive detectors: the 'backgammon' method*. *Nucl. Instrum. Methods*, **137**, 141–149.

Allington-Smith, J. R. & Schwarz, H. E. (1984). *Imaging photon detectors for optical astronomy, Q. J. R. Astron. Soc.* **25**, 267–289.

Allinson, N. M. (1982). *Solid-state imaging arrays for X-ray detection*. *Nucl. Instrum. Methods*, **201**, 53–64.

Allinson, N. M. (1994). *Development of non-intensified charge-coupled device area X-ray detectors*. *J. Synchrotron Rad.* **1**, 54–62.

Andrianova, M. E., Popov, A. N., Kheiker, D. M., Zanevskii, Yu. V., Ivanov, A. B., Peshekhonov, V. D. & Chernenko, S. P. (1986). *Use of coordinate X-ray diffractometer with a high-resolution chamber to obtain diffraction data for single crystals of proteins*. *Dokl. Akad. Nauk SSR,* **28**, 122–125. Translated in *Sov. Phys. Dokl. (USA)*, **31**, 358–361.

Anger, H. O. (1966). *Beam-position indentification means*. *Instrum. Soc. Am. Trans.* **5**, 311–334; US Patent 3 209 201.

Anisimov, Yu. S., Zanevskii, Yu. V., Ivanov, A. B., Morchan, V. D., Peshekhonov, V. D., Chan Dyk Tkhan, Chan Khyo Dao, Cheremukhina, G. A. & Chernenko, S. P. (1986). *Two-dimensional automated X-ray detector for diffraction experiments*. *Pribory i Tekhnika Eksperimenta*, No. 4, pp. 60–62. Translated in *Instrum. Exp. Tech.* **29**, 821–823.

Arndt, U. W. (1978). *Counting losses of detectors for X-rays from storage rings*. *J. Phys. E*, **11**, 671–673.

Arndt, U. W. (1982). *X-ray television area detectors*. *Nucl. Instrum. Methods*, **201**, 13–20.

Arndt, U. W. (1984). *Area detectors for protein crystallography at storage rings*. *Nucl. Instrum. Methods*, **222**, 252–255.

Arndt, U. W. (1985). *Television area detector diffractometers*. *Prog. Enzymol.* **114**, 472–485.

Arndt, U. W. (1986). *X-ray position-sensitive detectors*. *J. Appl. Cryst.* **19**, 145–163.

Arndt, U. W. (1988). *Position-sensitive detectors in condensed matter studies*. *Nucl. Instrum. Methods*, A**273**, 459–462.

Arndt, U. W. & Gilmore, D. J. (1979). *X-ray television area detectors for macromolecular structural studes with synchrotron radiation sources*. *J. Appl. Cryst.* **12**, 1–9.

Arndt, U. W., Gilmore, D. J. & Wonacott, A. J. (1977). *X-ray film. The rotation method in crystallography*, Chap. 14. Amsterdam: North Holland.

Arndt, U. W. & In't Veld, G. A. (1988). *Further developments of an X-ray television detector*. *Adv. Electron. Electron Phys.* **74**, 285–296.

Ballon, J., Comparat, V. & Pouxe, J. (1983). *The blade chamber: a solution for curved gaseous detectors*. *Nucl. Instrum. Methods*, **217**, 213–216.

Baru, S. E., Proviz, G. I., Savinov, G. A., Sidorov, V. A., Khabakhshev, A. G., Shuvalov, B. N. & Yakovlev, V. A. (1978). *Two-coordinate X-ray detector*. *Nucl. Instrum. Methods*, **152**, 209–212.

Bateman, J. E. & Apsimon, R. J. (1979). *A new photocathode for X-ray image intensifiers operating in the 1–50 keV region*. *Adv. Electron. Electron Phys.* **52**, 189–200.

Bigler, E., Polack, F. & Lowenthal, S. (1986). *Scintillating fibre array as an X-ray image detector*. *Proc. SPIE*, **733**, 133–137.

Bordas, J., Koch, M. J. H., Clout, P. N., Dorrington, E., Boulin, C. & Gabriel, A. (1980). *A synchrotron radiation camera and data acquisition system for time-resolved X-ray scattering studies*. *J. Phys. E*, **13**, 938–944.

Borkowski, C. J. & Kopp, M. K. (1968). *New type of position-sensitive detectors of ionizing radiation using rise-time measurement*. *Rev. Sci. Instrum.* **39**, 1515–1522.

Borso, C. S. (1982). *Optimisation of monolithic solid-state array detector for the position encoding of small-angle X-ray scattering from synchrotron sources*. *Nucl. Instrum. Methods*, **201**, 65–71.

Boulin, C., Dainton, D., Dorrington, E., Elsner, G., Gabriel, A., Bordas, J. & Koch, M. J. H. (1982). *Systems for time-resolved X-ray measurements using one-dimensional and two-dimensional detectors: requirements and practical experience*. *Nucl. Instrum. Methods*, **201**, 209–220.

Bricogne, G. (1987). *The EEC cooperative programming workshop on position-sensitive detector software. Computational aspects of protein crystal data analysis*, edited by J. R. Helliwell, P. A. Machin & M. Z. Papiz. SERC Daresbury Laboratory Report DL/SC1/R25, pp. 120–145.

7.1.6 (*cont.*)

Burke, B. E., Mountain, R. W., Harrison, D. C., Bautz, M. W., Doty, J. P., Ricker, G. R. & Daniels, P. J. (1991). *An abuttable CCD imager for visible and X-ray focal plane arrays*. *IEEE Trans. Electron Devices*, **38**, 1069–1076.

Charpak, G. (1982). *Parallax-free high-accuracy gaseous detectors for X-ray and VUV localization*. *Nucl. Instrum. Methods*, **201**, 181–192.

Chikawa, J., Sato, F. & Fujimoto, I. (1984). *High-resolution topography detector*. *Acta Cryst.* A**40**, C403.

Collett, B. & Podolsky, R. J. (1988). *2-D photon counter for X-ray imaging*. *Rev. Sci. Instrum.* **59**, 1122–1126.

Dalglish, R. L., James, V. J. & Tubbenhauer, G. A. (1984). *A 2-D X-ray diffraction pattern sensor using a solid-state area-sensitive detector*. *Nucl. Instrum. Methods*, **227**, 521–525.

Deckman, H. W. & Gruner, S. M. (1986). *Formal alterations in CCD-based electro-optic X-ray detectors*. *Nucl. Instrum. Methods*, A**246**, 527–533.

Dereniak, E. L., Roehrig, H., Salcido, M. M., Pommerrenig, D. H., Simms, R. A. & Abrahams, J. M. (1985). *Image intensifiers with electrical readout*. *IEE Conf. Publ. (London)*, **253**, 71–73.

Derewenda, Z. & Helliwell, J. R. (1989). *Calibration tests and use of Nicolet–Xentronics imaging proportional chamber mounted on a conventional source for protein crystallography*. *J. Appl. Cryst.* **22**, 123–137.

Durbin, R. M., Burns, R., Moulai, J., Metcalf, P., Freymann, D., Blum, M., Anderson, J. E., Harrison, S. C. & Wiley, D. C. (1986). *Protein, DNA and virus crystallography with a focused imaging proportional counter*. *Science*, **232**, 1127–1132.

Dyson, N. A. (1973). *X-rays in atomic & nuclear physics*. London: Longmans.

Eikenberry, E. F., Gruner, S. M. & Lowrance, J. L. (1986). *A two-dimensional X-ray detector with a slow-scan charge-coupled device readout*. *IEEE Trans. Nucl. Sci.* **33**, 542–545.

Emberson, D. L. & Holmshaw, R. T. (1972). *Some aspects of the design and performance of a small high-contrast channel image intensifier*. *Adv. Electron. Electron Phys.* **33**A, 133–144.

Fano, U. (1946). *On the theory of ionization yield of radiation in different substances*. *Phys Rev.* **70**, 44–52.

Fano, U. (1947). *Ionization yield of radiations: II. The fluctuations of the number of ions*. *Phys. Rev.* **72**, 26–29.

Faruqi, A. R. & Bond, C. C. (1982). *Multi-wire linear detector for X-ray time-resolved measurements at high counting rates*. *Nucl. Instrum. Methods*, **201**, 125–134.

Fordham, J. L. A., Bellis, J. G., Bone, D. A. & Norton, T. J. (1991). *The MIC photon-counting detector*. *Proc. SPIE*, **1449**, 87–98.

Fouassier, M., Duchenois, V., Dietz, J., Guillemet, E. & Lemonnier, M. (1988). *Image intensifier tubes with intagliated screens*. *Adv. Electron. Electron Phys.* **74**, 315–322.

Fraser, G. W. (1989). *X-ray detectors: a review*. *Proc. SPIE*, **1140**, 50–57.

Fuchs, H. F., Wu, D. Q. & Chu, B. (1990). *An area X-ray detector system based on a commercially available CCD unit*. *Rev. Sci. Instrum.* **61**, 712–716.

Gabriel, A. & Dupont, Y. (1972). *A position-sensitive proportional detector for X-ray crystallography*. *Rev. Sci. Instrum.* **43**, 1600–1602.

Garfield, B. R. C., Wilson, R. J. F., Goodson, J. H. & Butler, D. J. (1976). *Developments in proximity-focused diode image intensifiers*. *Adv. Electron. Electron Phys.* **40**A, 11–20.

Goto, N., Isozaki, Y., Shidara, K., Maruyama, E., Hirai, T. & Fujita, T. (1974). *Saticon: a new photoconductive camera tube with Se–As–Te target*. *IEEE Trans. Electron Devices*, ED-**21**, 662–666.

Gruner, S. M. & Milch, J. R. (1982). *Criteria for the evaluation of 2-dimensional X-ray detectors*. *Trans. Am. Crystallogr. Assoc.* **18**, 149–167.

Gruner, S. M., Milch, J. R. & Reynolds, G. T. (1982). *Survey of two-dimensional electro-optical X-ray detectors*. *Nucl. Instrum. Methods*, **195**, 287–297.

Hamlin, R. (1985). *Multiwire area X-ray diffractometers*. *Methods Enzymol.* **114**, 416–452.

Hasegawa, K., Mochiki, K. & Sekiguchi, A. (1981). *Integral type position-sensitive X-ray detector for high-flux diffuse scattering applications*. *IEEE Trans. Nucl. Sci. NS*-**28**, 3660–3664.

Haubold, H. G. (1984). *An integrating 2-D position-sensitive X-ray detector for high-flux diffuse scattering applications*. Communication to ESRP Working Party on Detectors.

Hendricks, R. W. (1976). *One- and two-dimensional position-sensitive X-ray and neutron detectors*. *Trans. Am. Crystallogr. Assoc.* **12**, 103–146.

Hendricks, R. W., Seeger, P. A., Scheer, J. W. & Suehiro, S. (1982). *A large-capacity high-speed multiparameter multi-channel analysis system*. *Nucl. Instrum. Methods*, **201**, 261–279.

Hendrix, J. (1982). *Position-sensitive X-ray detectors. Uses of synchrotron radiation in biology*, edited by H. B. Stuhrmann, Chap. 11. New York: Academic Press.

Hendrix, J. (1984). *The fine-grid detector: a parallel-electrode position-sensitive detector*. *IEEE Trans. Nucl. Sci.* NS-**31**, 281–284.

Hopf, R. & Rodricks, B. (1994). *A VXI-based high-speed X-ray CCD detector*. *Nucl. Instrum. Methods*, A**348**, 645–648.

Howard, A. J., Gilliland, G. L., Finzel, B. C., Poulos, T. L., Ohlendorf, D. H. & Salemne, F. R. (1987). *The use of an imaging proportional counter in macromolecular crystallography*. *J. Appl. Cryst.* **20**, 383–387.

Howard, A. J., Nielson, C. & Xuong, Ng. H. (1985). *Software for a diffractometer with multiwire area detector*. *Methods Enzymol.* **114**, 452–472.

Howes, M. J. & Morgan, D. V. (1979). Editors. *Charge-coupled devices and systems*. New York: John Wiley.

Hughes, G. & Sumner, I. (1981). *DL100 memory system*. Daresbury Laboratory Report DL/CSE/TM2.

Huxley, H. E. & Faruqi, A. R. (1983). *Time-resolved X-ray diffraction studies on vertebrate striated muscle*. *Annu. Rev. Biophys. Bioeng.* **12**, 381–417.

Ikhlef, A. & Skowronek, M. (1993). *Radiation position-sensitive detector based on plastic scintillating fibres*. *Rev. Sci. Instrum.* **61**, 2566–2569.

Ikhlef, A. & Skowronek, M. (1994). *Some emission characteristics of scintillating fibres for low-energy X- and Y-rays*. *IEEE Trans. Nucl. Sci.* NS-**41**, 408–414.

Isozaki, Y., Kumada, J., Okude, S., Oguso, C. & Goto, N. (1981). *One-inch saticon for high-definition color television cameras*. *IEEE Trans. Electron Devices*, ED-**28**, 1500–1507.

Jones, R. C. (1958). *On the quantum efficiency of photographic negatives*. *Photogr. Sci. Eng.* **2**, 57–65.

Jucha, A., Bonin, D., Dartyge, E., Flank, A. M., Fontaine, A. & Raoux, D. (1984). *Photodiode array for position-sensitive detection using high X-ray flux provided by synchrotron radiation*. *Nucl. Instrum. Methods*, **226**, 40–45.

7.1.6 (*cont.*)

Kahn, R., Fourme, R., Bosshard, R., Caudron, B., Santiard, J. C. & Charpak, G. (1982). *An X-ray diffractometer for macromolecular crystallography based on a spherical drift chamber: hardware, software and multi-wavelength data acquisition with synchrotron radiation*. *Nucl. Instrum. Methods*, **201**, 203–208.

Kalata, K. (1982). *A versatile television X-ray detector and image processing system*. *Nucl. Instrum. Methods*, **201**, 35–41.

Kalata, K. (1985). *A general-purpose computer-configurable television area detector for X-ray diffraction applications*. *Prog. Enzymol.* **114**, 486–510.

Karellas, A., Liu, H., Harris, L. J. & D'Orsi, C. J. (1992). *Operational characteristics and potential of scientific-grade CCD in X-ray imaging applications*. *Proc. SPIE*, **1655**, 85–91.

Knibbeler, C. L. C. M., Hellings, G. J. A., Maaskamp, H. J., Ottewanger, H. & Brongersma, H. H. (1987). *Novel two-dimensional positional-sensitive detection system*. *Rev. Sci. Instrum.* **58**, 125–126.

Koch, A. (1994). *Lens-coupled scintillating screen CCD X-ray area detector with a high DQE*. *Nucl. Instrum. Methods*, A**348**, 654–658.

Lemonnier, M., Richard, J. C., Piaget, C., Petit, M. & Vittot, M. (1985). *Photon-in and electron-in CCD arrays for image read-out in tubes*. *IEE Conf. Publ. (London)*, **253**, 74–76.

Lewis, R. (1994). *Multiwire gas proportional counters: decrepit antiques or classic performers? J. Synchrotron Rad.* **1**, 43–53.

Lowrance, J. L. (1979). *A review of solid-state image sensors*. *Adv. Electron. Electron Phys.* **52**, 421–429.

Lowrance, J. L., Zucchino, P., Renda, G. & Long, D. C. (1979). *ICCD development at Princeton*. *Adv. Electron. Electron Phys.* **52**, 441–452.

Lumb, D. H., Chowanietz, E. G. & Wells, A. A. (1985). *X-ray imaging with GEC/EEV CCD's*. *IEE Conf. Publ. (London)*, **253**, Suppl.

Martin, C., Jelinsky, P., Lampton, M., Malina, R. F. & Anger, H. O. (1981). *Wedge-and-strip anodes for centroid-finding position-sensitive photon and particle detectors*. *Rev. Sci. Instrum.* **52**, 1067–1074.

Matsushima, I., Koyama, K., Tanimoto, M. & Yano, Y. (1987). *Soft X-ray imaging by a commercial solid state TV camera*. *Rev. Sci. Instrum.* **58**, 600–603.

Meyer-Ilse, W., Wilhelm, T. & Guttmann, P. (1993). *Thinned back-illuminated CCD for X-ray microscopy*. *Proc. SPIE*, **1900**, 241–245.

Milch, J. R., Gruner, S. M. & Reynolds, G. T. (1982). *Area detectors capable of recording X-ray diffraction patterns at high counting rates*. *Nucl. Instrum. Methods*, **201**, 43–52.

Miyahara, J., Takahashi, K., Amemiya, Y., Kamiya, N. & Satow, Y. (1986). *A new type of X-ray area detector utilizing laser-stimulated luminescence*. *Nucl. Instrum. Methods*, A**426**, 572–578.

Mochiki, K. (1984). *Integral type position-sensitive proportional chamber*. Dissertation, Faculty of Engineering, University of Tokyo, Japan.

Mochiki, K. & Hasegawa, K. (1985). *Charge-integrating type position-sensitive proportional chamber of time-resolved measurements using intense X-ray sources*. *Nucl. Instrum. Methods*, A**234**, 593–601.

Mochiki, K., Hasegawa, K., Sekiguchi, A. A. & Yoshioka, Y. (1981). *Integral type position-sensitive proportional chamber with multiplexer read-out system for X-ray diffraction experiments*. *Adv. X-ray Anal.* **24**, 155–159.

Moy, J.-P. (1994). *A 200 mm input field 5–80 keV detector based on an X-ray image intensifier and CCD camera*. *Nucl. Instrum. Methods*, A**348**, 641–644.

Naday, I., Westbrook, E. M., Westbrook, M. L., Travis, D. J., Stanton, M., Phillips, W. C., O'Mara, D. & Xie, J. (1994). *Nucl. Instrum. Methods*, A**348**, 635–640.

Oba, K., Ito, M., Yamaguchi, M. & Tanaka, M. (1988). *A CsI(Na) scintillation plate with high spatial resolution*. *Adv. Electron. Electron Phys.* **74**, 247–255.

Patt, B. E., Delduca, A., Dolin, R. & Ortale, C. (1986). *Mercuric iodide X-ray camera*. *IEEE Trans. Nucl. Sci.* NS-**33**, 523–526.

Peisert, A. (1982). *The parallel-plate avalanche chamber as an endcap detector for time-projection chambers*. *Nucl. Instrum. Methods*, **217**, 229–235.

Pernot, P., Kahn, R., Fourme, R., Leboucher, P., Million, G., Santiard, J. C. & Charpak, G. (1982). *A high count rate one-dimensional position-sensitive detector and a data acquisition system for time-resolved X-ray scattering studies*. *Nucl. Instrum. Methods*, **201**, 145–151.

Pflugrath, J. W. & Messerschmidt, A. (1987). *FAST system software*. *Computational aspects of protein crystal data analysis*, edited by J. R. Helliwell, P. A. Machin & M. Z. Papiz. SERC Daresbury Laboratory Report DL/SC1/R25, pp. 149–161.

Phizackerley, R. P., Cork, C. W. & Merritt, E. A. (1986). *An area detector data acquisition system for protein crystallography using multiple-energy anomalous dispersion techniques*. *Nucl. Instrum. Methods*, A**246**, 579–595.

Pollehn, H. K. (1985). *Performance and reliability of third-generation image intensifiers*. *Adv. Electron. Electron Phys.* **64**A, 61–69.

Price, W. J. (1964). *Nuclear radiation detectors*. New York: McGraw-Hill.

Rice-Evans, P. (1974). *Spark, streamer, proportional and drift chambers*. London: Richelieu Press.

Roehrig, H., Dallas, W. J., Ovitt, T. W., Lamoreaux, R. D., Vercillo, R. & McNeill, K. M. (1989). *A high-resolution X-ray imaging device*. *Proc SPIE*, **1072**, 88–99.

Rose, A. (1946). *A unified approach to the performance of photographic film, television pick-up tubes and the human eye*. *J. Soc. Motion Pict. Eng.* **47**, 273–294.

Sakabe, N. (1991). *X-ray diffraction data collection system for modern protein crystallography with a Weissenberg camera and an imaging plate using synchrotron radiation*. *Nucl. Instrum. Methods*, A**303**, 448–463.

Santilli, V. J. & Conger, G. B. (1972). *TV camera with large silicon diode array targets operating in the electron-bombarded mode*. *Adv. Electron. Electron. Phys.* **33**A, 219–228.

Sareen, R. A. (1994). *Developments in X-ray detectors and associated electronics: a review of the technology and possible future trends*. *J. X-ray Sci. Technol.* **4**, 151–165.

Sato, F., Maruyama, H., Goto, K., Fujimoto, I., Shidara, K., Kawamura, T. W., Hirai, T., Sakai, H. & Chikawa, J. (1993). *Characteristics of a new high-sensitivity X-ray imaging tube for video topography*. *Jpn. J. Appl. Phys.* **32**, 2142–2146.

Schwarz, H. E. & Lapington, J. S. (1985). *Optimisation of wedge-and-strip anodes*. *IEEE Trans. Nucl. Sci.* NS-**32**, 433–437.

7.1.6 (*cont.*)

Schwarz, H. E. & Mason, I. M. (1984). *A new imaging proportional counter using a Penning gas improves energy resolution*. *Nature (London)*, **309**, 532–534.

Schwarz, H. E. & Mason, I. M. (1985). *Development of the Penning-gas imager*. *IEEE Trans. Nucl. Sci.* NS-**32**, 516–520.

Shidara, K., Tanioka, K., Hirai, T. & Nonaka, Y. (1985). *Recent improvement of Saticon target*. *IEE Conf. Publ. (London),* **253**, 29–32.

Siegmund, O. H. W., Culhane, J. L., Mason, I. M. & Sanford, P. W. (1982). *Individual electrons detected after the interaction of ionizing radiation with gases*. *Nature (London)*, **295**, 678–679.

Smith, G. (1984). *High-accuracy gaseous X-ray detectors*. *Nucl. Instrum. Methods*, **222**, 230–237.

Sonada, M., Takano, M., Miyahara, J. & Kato, H. (1983). *Computed radiography utilizing scanning laser-stimulated luminescence*. *Radiology*, **148**, 833–838.

Stanton, M. (1993). *Area detector design I*. *Nucl. Instrum. Methods*, A**325**, 550–557.

Stanton, M., Phillips, W. C., Li, Y. & Kalata, K. (1992*a*). *DQE of CCD- and vidicon-based detectors for X-ray crystallographic applications*. *J. Appl. Cryst.* **25**, 638–645.

Stanton, M., Phillips, W. C., Li, Y. & Kalata, K. (1992*b*). *Correcting spatial distortion and non-uniform response in area detectors*. *J. Appl. Cryst.* **25**, 549–558.

Stanton, M., Phillips, W. C., O'Mara, D., Naday, I. & Westbrook, E. M. (1993). *Area detector design II*. *Nucl. Instrum. Methods*, A**325**, 558–567.

Strauss, M. G., Naday, I., Sherman, I. S., Kraimer, M. R. & Westbrook, E. M. (1987). *CCD-based synchrotron X-ray detector for protein crystallography*. *IEEE Trans. Nucl. Sci.* NS-**34**, 389–395.

Strauss, M. G., Westbrook, E. M., Naday, I., Coleman, T. A., Westbrook, M. L., Travis, D. J., Sweet, R. M., Pflugrath, J. W. & Stanton, M. (1990). *A CCD-based detector for protein crystallography*. *Nucl. Instrum. Methods*, A**297**, 275–295.

Stümpel, J. W., Sanford, P. W. & Goddard, H. F. (1973). *A position-sensitive proportional counter with high spatial resolution*. *J. Phys. E*, **6**, 397–400.

Suzuki, Y., Hayakawa, K., Usami, K., Hirano, T., Endoh, T. & Okamura, Y. (1989). *X-ray sensing pick-up tube*. *Rev. Sci. Instrum.* **60**, 2299–2302.

Suzuki, Y., Uchiyama, K. & Ito, M. (1976). *A large-diameter X-ray sensitive vidicon with beryllium window*. *Adv. Electron. Electron Phys.* **40**A, 209–222.

Symposia on Photoelectronic Imaging Devices (1960, 1962, 1966, 1969, 1972, 1976, 1979, 1985). Imperial College, London. *Adv. Electron. Electron Phys.* **12** (1st, 1960), **16** (2nd, 1962), **22** (3rd, 1966), **28** (4th, 1969), **33** (5th, 1972), **40** (6th, 1976), **52** (7th, 1979), **64** (8th, 1985).

Templer, R. H., Gruner, S. M. & Eikenberry, E. F. (1988). *An image-intensified CCD area X-ray detector for use with synchrotron radiation*. *Adv. Electron. Electron Phys.* **74**, 275–283.

Third European Symposium on Semiconductor Detectors (1984). *New developments in silicon detectors*. *Nucl. Instrum. Methods*, **226**.

Thomas, D. J. (1987). *The balance between the relative capabilities of X-ray area detectors, computer and interface hardware and software packages. Computation aspects of protein crystal data analysis*, edited by J. R. Helliwell, P. A. Machin & M. Z. Papiz. SERC Daresbury Laboratory Report DL/SC1/R25, pp. 162–166.

Thomas, D. J. (1989). *Calibrating an area-detector diffractometer: imaging geometry*. *Proc. R. Soc. London Ser. A*, **425**, 129–167.

Thomas, D. J. (1990). *Calibrating an area detector diffractometer: integral response*. *Proc. R. Soc. London Ser. A*, **428**, 181–214.

Walton, D., Stern, R. A., Catura, R. C. & Culhane, J. L. (1985). *Deep-depletion CCD's for X-ray astronomy*. *SPIE Proc.* **501**.

Widom, J. & Feng, H.-P. (1989). *High-performance X-ray area detector suitable for small-angle scattering, crystallographic and kinetic studies*. *Rev. Sci. Instrum.* **60**, 3231–3238.

Wilkinson, D. H. (1950). *Ionisation Chambers & Counters*. Cambridge University Press.

Wölfel, E. R. (1983). *A novel curved position-sensitive proportional counter for X-ray diffractometry*. *J. Appl. Cryst.* **16**, 341–348.

Xuong, Ng. H., Freer, S. T., Hamlin, R., Neilsen, C. & Vernon, W. (1978). *The electronic stationary-picture method for high-speed measurement of reflection intensities from crystals with large unit cells*. *Acta Cryst.* A**34**, 289–296.

7.1.7

Arcese, A. (1964). *A note on Poisson branching processes with reference to photon–electron converters*. *Appl. Opt.* **3**, 435.

Chikawa, J. (1974). *Technique for the video display of X-ray topographic images and its application to the study of crystal growth*. *J. Cryst. Growth*, **24/25**, 61–68.

Chikawa, J. (1980). *Laboratory techniques for transmission X-ray topography. Characterization of crystal growth defects by X-ray methods*, edited by B. K. Tanner & D. K. Bowen, Chap. 15, pp. 368–400. New York: Plenum.

Chikawa, J. (1999). *Live X-ray topography and crystal growth of silicon*. *Jpn. J. Appl. Phys.* **3**, 4619–4631.

Chikawa, J. & Kuriyama, M. (1991). *Topography*. *Handbook on synchrotron radiation*, Vol. 3, edited by G. Brown & D. E. Moncton, Chap. 10, pp. 337–378. Amsterdam: Elsevier.

Chikawa, J. & Matsui, J. (1994). *Growth and evaluation of bulk crystals*. *Handbook on semiconductors*, completely revised edition, Vol. 3, edited by S. Mahajan, Chap. 1, pp. 1–71. Amsterdam: Elsevier.

Chikawa, J., Sato, F., Kawamura, T., Kuriyama, T., Yamashita, T. & Goto, N. (1986). *A high-resolution video camera tube for live X-ray topography using synchrotron radiation. X-ray instrumentation for the Photon Factory: dynamic analyses of micro structures in matter*, edited by S. Hosoya, Y. Iitaka & H. Hashizume, pp. 145–157. Tokyo: KTK Scientific Publishers.

Green, R. E. Jr (1977). *Direct display of X-ray topographic images*. *Adv. X-ray Anal.* **20**, 221–235.

Heynes, G. D. (1977). *Digital television; a glossary and bibliography*. *SMPTE J.* **86**, 6–9.

McMann, R. H., Kreinik, S., Moore, J. K., Kaiser, A. & Rossi, J. (1978). *A digital noise reducer for encoded NTSC signals*. *SMPTE J.* **87**, 129–133.

McMaster, R. C., Photen, M. L. & Mitchell, J. P. (1967). *The X-ray vidicon television image system*. *Mater. Eval.* **25**, 46–52.

Rose, A. (1948). *The sensitivity performance of the human eye on an absolute scale*. *J. Opt. Soc. Am.* **38**, 196–208.

7.1.7 (*cont.*)

Rossi, J. P. (1978). *Digital technique for reducing television noise*. *SMPTE J.* **87**, 134–140.

Rozgonyi, G. A., Haszlo, S. E. & Statile, J. L. (1970). *Instantaneous video display of X-ray topographic images with resolving capabilities better than 15*. *Appl. Phys. Lett.* **16**, 443–446.

Sato, F., Maruyama, H., Goto, K., Fujimoto, I., Shidara, K., Kawamura, T., Hirai, T., Sakai, H. & Chikawa, J. (1993). *Characteristics of a new high-sensitivity X-ray imaging tube for video topography*. *Jpn. J. Appl. Phys.* **32**, 2142–2146.

7.1.8

Amemiya, Y. (1995). *Imaging plates for use with synchrotron radiation*. *J. Synchrotron Rad.* **2**, 13–21.

Amemiya, Y., Kishimoto, S., Matsushita, T., Satow, Y. & Ando, M. (1989). *Imaging plate for time-resolved X-ray measurements*. *Rev. Sci. Instrum.* **60**, 1552–1556.

Amemiya, Y., Matsushita, T., Nakagawa, A., Satow, Y., Miyahara, J. & Chikawa, J. (1988). *Design and performance of an imaging plate system for X-ray diffraction study*. *Nucl. Instrum. Methods*, A**266**, 645–653.

Amemiya, Y. & Miyahara, J. (1988). *Imaging plate illuminates many fields*. *Nature (London)*, **336**, 89–90.

Amemiya, Y., Wakabayashi, K., Tanaka, H., Ueno, Y. & Miyahara, J. (1987). *Laster-stimulated luminescence used to measure X-ray diffraction of a contracting striated muscle*. *Science*, **237**, 164–168.

Ito, M. & Amemiya, Y. (1991). *X-ray energy dependence and uniformity of an imaging plate detector*. *Nucl. Instrum. Methods*, A**310**, 369–372.

Kato, H., Miyahara, J. & Takano, M. (1985). *New computed radiography using scanning laser stimulated luminescence*. *Neurosurg. Rev.* **8**, 53–62.

Miyahara, J., Takahashi, K., Amemiya, Y., Kamiya, K. & Satow, Y. (1986). *A new type of X-ray area detector utilizing laser stimulated luminescence*. *Nucl. Instrum. Methods*, A**246**, 572–578.

Sakabe, N. (1991). *X-ray diffraction data collection system for modern protein crystallography with a Weissenberg camera and an imaging plate using synchrotron radiation*. *Nucl. Instrum. Methods*, A**303**, 448–463.

Sonoda, M., Takano, M., Miyahara, J. & Kato, H. (1983). *Computed radiography utilizing scanning laser stimulated luminescence*. *Radiology*, **148**, 833–838.

7.2

Burge, R. E. & van Toorn, P. (1980). *Multiple images and image processing in STEM*. *Scanning Electron Microscopy/* 1980, Vol. 1, pp. 81–91. AMF O'Hare/Chicago: SEM Inc.

Chapman, J. N., Craven, A. J. & Scott, C. P. (1989). *Electron detection in the analytical electron microscope*. *Ultramicroscopy,* **28**, 108–117.

Chapman, J. N. & Morrison, G. R. (1984). *Detector systems for transmission electron microscopy*. *J. Microsc. Spectrosc. Electron.* **9**, 329–340.

Craven, A. J. & Buggy, T. W. (1984). *Correcting electron energy loss spectra for artefacts introduced by a serial data collection system*. *J. Microsc.* **136**, 227–239.

Daberkow, L., Herrmann, K.-H., Liu, L. & Rau, W. D. (1991). *Performance of electron image convertors with YAG single-crystal screen and CCD sensor*. *Ultramicroscopy*, **38**, 215–223.

Fan, G. Y. & Ellisman, M. H. (1993). *High-sensitivity lens-coupled slow-scan CCD camera for transmission electron microscopy*. *Ultramicroscopy*, **52**, 21–29.

Farnell, G. C. & Flint, R. B. (1975). *Photographic aspects of electron microscopy*. *Principles and techniques of electron microscopy*, Vol. 5, edited by M. A. Hayat, pp. 19–61. New York: Van Nostrand Rheinhold.

Garlick, G. F. J. (1966). *Cathodo- and radioluminescence*. *Luminescence of inorganic solids*, edited by P. Goldberg, Chap. 12. London: Academic Press.

Guetter, E. & Menzel, M. (1978). *An external photographic system for electron microscopes*. *Electron microscopy 1978*, Vol. 1, edited by J. M. Sturgess, pp. 92–93. Toronto: Microscopical Society of Canada.

Hamilton, J. F. & Marchant, J. C. J. (1967). *Image recording in electron microscopy*. *J. Opt. Soc. Am.* **57**, 232–239.

Herrmann, K.-H. (1984). *Detection systems*. *Quantitative electron microscopy*, edited by J. N. Chapman & A. J. Craven, Chap. 4. Edinburgh University Press.

Herrmann, K.-H. & Krahl, D. (1984). *Electronic image recording in conventional electron microscopy*. *Advances in optical and electron microscopy*, edited by R. Barer & V. E. Cosslett, Chap. 1. London: Academic Press.

Ishizuka, K. (1993). *Analysis of electron image detection efficiency of slow-scan CCD cameras*. *Ultramicroscopy*, **52**, 7–20.

Isoda, S., Saitoh, K., Moriguchi, S. & Kobayashi, T. (1991). *Utility test of image plate as a high-resolution image-recording material for radiation-sensitive specimens*. *Ultramicroscopy*, **35**, 329–338.

Krivanek, O. L., Ahn, C. C. & Keeney, R. B. (1987). *Parallel detection electron spectrometer using quadrupole lenses*. *Ultramicroscopy*, **22**, 103–115.

Kujawa, S. & Krahl, D. (1992). *Performance of a low-noise CCD camera adapted to a transmission electron microscope*. *Ultramicroscopy*, **46**, 395–403.

Mori, N., Katoh, T., Oikawa, T., Miyahara, J. & Harada, Y. (1986). *Electron microscopy 1986*, Vol. 1, edited by T. Imura, S. Maruse & T. Suzuki, pp. 29–32. Tokyo: Japanese Society of Electron Microscopy.

Mori, N., Oikawa, T., Katoh, T., Miyahara, J. & Harada, Y. (1988). *Application of the ''imaging plate'' to TEM image recording*. *Ultramicroscopy*, **25**, 195–202.

Reimer, L. (1984). *Transmission electron microscopy*, Chap. 4.6. Berlin: Springer-Verlag.

Schauer, P. & Autrata, R. (1979). *Electro-optical properties of a scintillation detector in SEM*. *J. Microsc. Spectrosc. Electron.* **4**, 633–650.

Valentine, R. C. (1966). *The response of photographic emulsions to electrons*. *Advances in optical and electron microscopy*, edited by R. Barer & V. E. Cosslett, Chap. 5. London: Academic Press.

Zeitler, E. (1992). *The photographic emulsion as analog recorder of electrons*. *Ultramicroscopy*, **46**, 405–416.

7.3

Abele, R. K., Allin, G. W., Clay, W. T., Fowler, C. E. & Kopp, M. K. (1981). *Large-area proportional counter camera for the U.S. National Small-Angle Neutron Scattering Facility*. *IEEE Trans. Nucl. Sci.* **28**(1), 811–815.

7.3 (*cont.*)

Allemand, R., Bourdel, J., Roudaut, E., Convert, P., Ibel, K., Jacobé, J., Cotton, J. P. & Farnoux, B. (1975). *Position-sensitive detectors (P.S.D.) for neutron diffraction*. *Nucl. Instrum. Methods*, **126**, 29–42.

Baruchel, J., Malgrange, C. & Schlenker, M. (1983). *Neutron diffraction topography: using position-sensitive photographic detection to investigate defects and domains in single crystals*. *Position-sensitive detection of thermal neutrons,* edited by P. Convert & J. B. Forsyth, pp. 400–406. London: Academic Press.

Berliner, R., Mildner, D. F. R., Sudol, J. & Taub, H. (1983). *Position-sensitive detectors and data collection systems at the University of Missouri Research Reactor Facility*. *Position-sensitive detection of thermal neutrons*, edited by P. Convert & J. B. Forsyth, pp. 120–128. London: Academic Press.

Boie, R. A., Fischer, J., Inagaki, Y., Merritt, F. C., Okuno, H. & Radeka, V. (1982). *Two-dimensional high precision thermal neutron detector*. *Nucl. Instrum. Methods*, **200**, 533–545.

Borkowski, C. J. & Kopp, M. K. (1975). *Design and properties of position-sensitive proportional counters using resistance-capacitance position encoding*. *Rev. Sci. Instrum.* **46**, 951–962.

Convert, P. & Chieux, P. (1986). *From BF_3 counter to PSD. An impressive and continuous increase of the data acquisition rate*. *Fifty years of neutron diffraction,* edited by G. E. Bacon, pp. 218–227. Bristol: Adam Hilger.

Convert, P. & Forsyth, J. B. (1983). *Position-sensitive detection of thermal neutrons:* Part 1, *Introduction*. *Position-sensitive detection of thermal neutrons*, pp. 1–90. London: Academic Press.

Fischer, J., Radeka, V. & Boie, R. A. (1983). *High position resolution and accuracy in ^3He two-dimensional thermal neutron PSDs*. *Position-sensitive detection of thermal neutrons*, edited by P. Convert & J. B. Forsyth, pp. 129–140. London: Academic Press.

Hohlwein, D. (1983). *Photographic methods in neutron scattering*. *Position-sensitive detection of thermal neutrons*, edited by P. Convert & J. B. Forsyth, pp. 379–390. London: Academic Press.

Ibel, K. (1976). *The neutron small-angle camera D11 at the high-flux reactor, Grenoble*. *J. Appl. Cryst.* **9**, 296–309.

Institut Laue–Langevin (1988). *Guide to neutron research facilities at the ILL*. Grenoble: Institut Laue–Langevin.

Isis (1992). *User Guide*. Didcot: Rutherford Appleton Laboratory.

Kurz, R. & Schelten, J. (1983). *Properties of various scintillators for thermal neutron detection*. *Position-sensitive detection of thermal neutrons,* edited by P. Convert & J. B. Forsyth, pp. 192–196. London: Academic Press.

Naday, I. & Schaefer, W. (1983). *A new processing method and gain stabilisation for scintillation position-sensitive detectors*. *Position-sensitive detection of thermal neutrons,* edited by P. Convert & J. B. Forsyth, pp. 197–202. London: Academic Press.

Roudaut, E. (1983). *Evolution of position-sensitive detectors for neutron diffraction experiments from 1966 to 1982 in the Nuclear Centre of Grenoble*. *Position-sensitive detection of thermal neutrons,* edited by P. Convert & J. B. Forsyth, pp. 294–301. London: Academic Press.

Schaefer, W., Naday, I. & Will, G. (1983). *Neutron powder diffractometry with the linear position-sensitive scintillation detector*. *Position-sensitive detection of thermal neutrons*, edited by P. Convert & J. B. Forsyth, pp. 209–214. London: Academic Press.

Strauss, M. G., Brenner, R., Chou, H. P., Schultz, A. J. & Roche, C. T. (1983). *Spatial resolution of neutron position scintillation detectors*. *Position-sensitive detection of thermal neutrons,* edited by P. Convert & J. B. Forsyth, pp. 175–187. London: Academic Press.

Strauss, M. G., Brenner, R., Lynch, F. J. & Morgan, C. B. (1981). *2-D position-sensitive scintillation detector for neutrons*. *IEEE Trans. Nucl. Sci.* **28**(1), 800–806.

Thomas, P. (1972). *Production of sensitive converter screens for thermal neutron diffraction patterns*. *J. Appl. Cryst.* **5**, 373–374.

Whaling, W. (1958). *The energy loss of charged particles in matter*. *Handbuch der Physik,* Vol. 34. *Corpuscles and radiation in matter II*, edited by S. Flugge, pp. 193–217. Berlin: Springer-Verlag.

Windsor, C. G. (1981). *Pulsed neutron scattering*. London: Taylor and Francis.

Wolf, R. S. (1974). *Measurement of the gas constants for various proportional counter gas mixtures*. *Nucl. Instrum. Methods*, **115**, 461–463.

7.4.2

Bachmann, R., Kohler, H., Schulz, H. & Weber, H. (1985). *Structure investigation of a CaF_2-crystal with synchrotron radiation*. *Acta Cryst.* A**41**, 35–40.

Cooper, M. J. (1971). *The evaluation of thermal diffuse scattering of neutrons for a one velocity model*. *Acta Cryst.* A**27**, 148–157.

Dorner, B., Burkel, E., Illini, Th. & Peisl, J. (1987). *First measurement of a phonon dispersion curve by inelastic X-ray scattering*. *Z. Phys. B*, **69**, 179–183.

Helmholdt, R. B., Braam, A. W. M. & Vos, A. (1983). *Improved corrections for thermal diffuse scattering*. *Acta Cryst.* A**39**, 90–94.

Helmholdt, R. B. & Vos, A. (1977). *Errors in atomic parameters and electron density distributions due to thermal diffuse scattering of X-rays*. *Acta Cryst.* A**33**, 38–45.

International Tables for Crystallography (1992). Vol. B. *Reciprocal space*, edited by U. Shmueli. Dordrecht: Kluwer.

Jahn, H. A. (1942). *Diffuse scattering of X-rays by crystals. The Faxen–Waller theory and the surfaces of isodiffusion for cubic crystals*. *Proc R. Soc. London Ser. A*, **179**, 320–340; **180**, 476–483.

James, R. W. (1962). *The optical principles of the diffraction of X-rays*. London: Bell.

Krec, K. & Steiner, W. (1984). *Investigation of a silicon single crystal by means of the diffraction of Mössbauer radiation*. *Acta Cryst.* A**40**, 459–465.

Krec, K., Steiner, W., Pongratz, P. & Skalicky, P. (1984). *Separation of elastically and inelastically scattered γ-radiation by Mössbauer diffraction*. *Acta Cryst.* A**40**, 465–468.

Merisalo, M. & Kurittu, J. (1978). *Correction of integrated Bragg intensities for anisotropic thermal scattering*. *J. Appl. Cryst.* **11**, 179–183.

Popa, N. C. & Willis, B. T. M. (1994). *Thermal diffuse scattering in time-of-flight diffractometry*. *Acta Cryst.* A**50**, 57–63.

7.4.2 (*cont.*)

Rouse, K. D. & Cooper, M. J. (1969). *The correction of measured integrated Bragg intensities for anisotropic thermal diffuse scattering*. *Acta Cryst*. A**25**, 615–621.

Sakata, M., Stevenson, A. W. & Harada, J. (1983). *G-TDSCOR: one-phonon TDS corrections for measured integrated Bragg intensities*. *J. Appl. Cryst*. **16**, 154–156.

Stevens, E. D. (1974). *Thermal diffuse scattering corrections for single-crystal integrated intensity measurements*. *Acta Cryst*. A**30**, 184–189.

Stevenson, A. W. & Harada, J. (1983). *The consequences of the neglect of TDS correction for temperature parameters*. *Acta Cryst*. A**39**, 202–207.

Suortti, P. (1980). *Powder TDS and multiple scattering*. *Accuracy in powder diffraction*, edited by S. Block & C. R. Hubbard. *Natl Bur. Stand. (US) Spec. Publ*. No. 567, pp. 8–12.

Voigt, W. (1910). *Lehrbuch der Kristallphysik*. Leipzig: Teubner.

Willis, B. T. M. (1970). *The correction of measured neutron structure factors for thermal diffuse scattering*. *Acta Cryst*. A**26**, 396–401.

Willis, B. T. M., Carlile, C. J. & Ward, R. C. (1986). *Neutron diffraction from single-crystal silicon: the dependence of the thermal diffuse scattering on the velocity of sound*. *Acta Cryst*. A**42**, 188–191.

Wooster, W. A. (1962). *Diffuse X-ray reflections from crystals*. Oxford: Clarendon Press.

7.4.3

Åberg, T. & Tulkki, J. (1985). *Inelastic X-ray scattering including resonance phenomena*. *Atomic inner shell physics*, edited by B. Crasemann, Chap. 10. New York: Plenum.

Bannett, Y. B. & Freund, I. (1975). *Resonant X-ray Raman scattering*. *Phys. Rev. Lett*. **34**, 372–376.

Bewilogua, L. (1931). *Incoherent scattering of X-rays*. *Phys. Z.* **32**, 740–744.

Biggs, F., Mendelsohn, L. B. & Mann, J. B. (1975). *Hartree Fock Compton profiles for the elements*. *At. Data Nucl. Data Tables*, **16**, 201–309.

Bloch, B. J. & Mendelsohn, L. B. (1974). *Atomic L-shell Compton profiles and incoherent scattering factors: theory*. *Phys. Rev. A*, **9**, 129–155.

Bloch, F. (1934). *Contribution to the theory of the Compton line shift*. *Phys. Rev*. **46**, 674–687.

Blume, M. & Gibbs, D. (1988). *Polarisation dependence of magnetic X-ray scattering*. *Phys. Rev. B*, **37**, 1779–1789.

Brown, W. D. (1966). *Cross-sections for coherent/incoherent X-ray scattering*. Reports D2-125136-1 and 125137-1. Boeing Co.

Bushuev, V. A. & Kuz'min, R. N. (1977). *Inelastic scattering of X-ray and synchrotron radiation in crystals, coherent effects in inelastic scattering*. *Sov. Phys. Usp*. **20**, 406–431.

Cooper, M. J. (1985). *Compton scattering and electron momentum determination*. *Rep. Prog. Phys*. **48**, 415–481.

Cromer, D. T. (1969). *Compton scattering factors for aspherical free atoms*. *J. Chem. Phys*. **50**, 4857–4859.

Cromer, D. T. & Mann, J. B. (1967). *Compton scattering factors for spherically symmetric free atoms*. *J. Chem. Phys*. **47**, 1892–1893.

Currat, R., DeCicco, P. D. & Weiss, R. J. (1971). *Impulse approximation in Compton scattering*. *Phys. Rev. B*, **4**, 4256–4261.

Eisenberger, P. & Platzman, P. M. (1970). *Compton scattering of X-rays from bound electrons*. *Phys. Rev. A*, **2**, 415–423.

Eisenberger, P., Platzman, P. M. & Winick, M. (1976). *Resonant X-ray Raman scattering studies using synchrotron radiation*. *Phys. Rev. B*, **13**, 2377–2380.

Fermi, E. (1928). *Statistical methods of investigating electrons in atoms*. *Z. Phys*. **48**, 73–79.

Gavrila, M. & Tugulea, M. N. (1975). *Compton scattering by L shell electrons*. *Rev. Roum. Phys*. **20**, 209–230.

Hubbell, J. H., Veigele, W. J., Briggs, E. A., Brown, R. T., Cromer, D. T. & Howerton, R. J. (1975). *Atomic form factors, incoherent scattering functions and photon scattering cross-sections*. *J. Phys. Chem. Ref. Data*, **4**, 471–538.

Jauch, J. M. & Rohrlich, F. (1976). *The theory of photons and electrons*. Berlin: Springer-Verlag.

Klein, O. & Nishina, Y. (1929). *Uber die Streuung von Strahlung durch freie Electronen nach der neuen relativistichers Quantendynamik von Dirac*. *Z. Phys*. **52**, 853–868.

Lipps, F. W. & Tolhoek, H. A. (1954). *Polarisation phenomena of electrons and photons I and II*. *Physica (Utrecht)*, **20**, 85–98, 395–405.

Lovesey, S. W. (1993). *Photon scattering by magnetic solids*. *Rep. Prog. Phys*. **56**, 257–326.

Manninen, S., Paakkari, T. & Kajantie, K. (1976). *Gamma ray Compton profile of aluminium*. *Philos. Mag*. **29**, 167–178.

Pattison, P. & Schneider, J. R. (1979). *Test of the relativistic 1s wavefunction in Au and Pb using experimental Compton profiles*. *J. Phys. B*, **12**, 4013–4019.

Pratt, R. H. & Tseng, H. K. (1972). *Behaviour of electron wavefunctions near the atomic nucleus and normalisation screening theory in the atomic photoeffect*. *Phys. Rev. A*, **5**, 1063–1072.

Ribberfors, R. (1975). *Relationship of the relativistic Compton cross-section to the momentum distribution of bound electron states. II. Effects of anisotropy and polarisation*. *Phys. Rev. B*, **12**, 2067–2074, 3136–3141.

Ribberfors, R. (1983). *X-ray incoherent scattering total cross-sections and energy absorption cross-sections by means of simple calculation routines*. *Phys. Rev. A*, **27**, 3061–3070.

Ribberfors, R. & Berggren, K.-F. (1982). *Incoherent X-ray scattering functions and cross sections by means of a pocket calculator*. *Phys. Rev. A*, **26**, 3325–3333.

Schaupp, D., Czerwinski, H., Smend, F., Wenskus, R., Schumacher, M., Millhouse, A. H. & Strauss, S. (1984). *Resonant Raman scattering of synchrotron X-rays by neodymium: observation of fine structure in K-L-RRS and of K-N-RRS*. *Z. Phys. A*, **319**, 1–7.

Slater, J. C. (1937). *Wavefunctions in a periodic crystal*. *Phys. Rev*. **51**, 846–851.

Sparks, C. J. (1974). *Inelastic resonance emission of X-rays: anomalous scattering associated with anomalous dispersion*. *Phys. Rev. Lett*. **33**, 262–265.

Thomas, L. H. (1927). *Calculation of atomic fields*. *Proc. Cambridge Philos. Soc*. **33**, 542–548.

Veigele, W. J. (1967). *Research of X-ray scattering cross sections: final report*. Report KN-379-67-3(R). Kaman Sciences Corp.

Waller, I. & Hartree, D. R. (1929). *Intensity of total scattering of X-rays*. *Proc. R. Soc. London Ser. A*, **124**, 119–142.

Williams, B. G. (1977). *Compton scattering*. New York: McGraw-Hill.

7.4.4

Brown, G. S. & Lindau, I. (1986). Editors, *Synchrotron radiation instrumentation*. Proceedings of the International Conference on X-ray and VUV Synchrotron Radiation Instrumentation. *Nucl. Instrum. Methods*, A**246**, 511–595.

Mathieson, A. McL. (1985). *Small-crystal X-ray diffractometry with a crystal ante-monochromator*. *Acta Cryst.* A**41**, 309–316.

Matsushita, T. & Hashizume, H. (1983). *Handbook of synchrotron radiation*, Vol. I, edited by E. E. Koch, pp. 261–314. Amsterdam: North-Holland.

Matsushita, T. & Kaminaga, U. (1980). *A systematic method of estimating the performance of X-ray optical systems for synchrotron radiation. I. Description of various optical elements in position-angle space for ideally monochromatic X-rays*. *J. Appl. Cryst.* **13**, 465–471; *II. Treatment in position–angle–wavelength space*. *J. Appl. Cryst.* **13**, 472–478.

Suortti, P. (1980). *Components of the total X-ray scattering*. *Accuracy in powder diffraction,* edited by S. Block & C. R. Hubbard, pp. 1–20. *Natl Bur. Stand. (US) Spec. Publ.* No. 567.

Suortti, P. (1985). *Parallel beam geometry for single-crystal diffraction*. *J. Appl. Cryst.* **18**, 272–274.

Suortti, P., Hastings, J. B. & Cox, D. E. (1985). *Powder diffraction with synchrotron radiation. I. Absolute measurements*. *Acta Cryst.* A**41**, 413–416.

Suortti, P. & Jennings, L. D. (1977). *Accuracy of structure factors from X-ray powder intensity measurements*. *Acta Cryst.* A**33**, 1012–1027.

Thomlinson, W. & Williams, G. P. (1984). Editors. *Synchrotron radiation instrumentation 3*. Proceedings of the Third National Conference on Synchrotron Radiation Instrumentation. *Nucl. Instrum. Methods*, **222**, 215–278.

7.5

Abramowitz, M. & Stegun, I. A. (1964). *Handbook of mathematical functions*. National Bureau of Standards Publication AMS 55.

Boer, J. L. de (1982). *Statistics of recorded counts*. *Crystallographic statistics*, edited by S. Ramaseshan, M. F. Richardson & A. J. C. Wilson, pp. 179–186. Bangalore: Indian Academy of Sciences.

Eastabrook, J. N. & Hughes, J. W. (1953). *Elimination of dead-time corrections in monitored Geiger-counter X-ray measurements*. *J. Sci. Instrum.* **30**, 317–320.

French, S. & Wilson, K. (1978). *On the treatment of negative intensity observations*. *Acta Cryst.* A**34**, 517–525.

Grant, D. F. (1973). *Single-crystal diffractometer data: the on-line control of the precision of intensity measurement*. *Acta Cryst.* A**29**, 217.

Hirshfeld, F. L. & Rabinovich, D. (1973). *Treating weak reflexions in least-squares calculations*. *Acta Cryst.* A**29**, 510–513.

Killean, R. C. G. (1967). *A note on the a priori estimation of R factors for constant-count-per-reflection diffractometer experiments*. *Acta Cryst.* **23**, 1109–1110.

Killean, R. C. G. (1972). *The a priori optimization of diffractometer data to achieve the minimum average variance in the electron density*. *Acta Cryst.* A**28**, 657–658.

Killean, R. C. G. (1973). *Optimization of scan procedure for single-crystal X-ray diffraction intensities*. *Acta Cryst.* A**29**, 216–217.

Mack, M. & Spielberg, N. (1958). *Statistical factors in X-ray intensity measurements*. *Spectrochim. Acta*, **12**, 169–178.

Mackenzie, J. K. & Williams, E. J. (1973). *The optimum distribution of counting times for determining integrated intensities with a diffractometer*. *Acta Cryst.* A**29**, 201–204.

Olkha, G. S. & Rathie, P. N. (1971). *On a generalized Bessel function and an integral transform*. *Math. Nachr.* **51**, 231–240.

Paciorek, W. A. & Chapuis, G. (1994). *Generalized Bessel functions in incommensurate structure analysis*. *Acta Cryst.* A**50**, 194–203.

Parrish, W. (1956). *X-ray intensity measurements with counter tubes*. *Philips Tech. Rev.* **17**, 206–221.

Prince, E. & Nicholson, W. L. (1985). *The influence of individual reflections on the precision of parameter estimates in least squares refinement*. *Structure & statistics in crystallography*, edited by A. J. C. Wilson, pp. 183–195. Guilderland, NY: Adenine Press.

Shmueli, U. (1993). Editor. *International tables for crystallography*. Vol. B. *Reciprocal space*. Dordrecht: Kluwer.

Shoemaker, D. P. (1968). *Optimization of counting times in computer-controlled X-ray and neutron single-crystal diffractometry*. *Acta Cryst.* A**24**, 136–142.

Shoemaker, D. P. & Hamilton, W. C. (1972). *Further remarks concerning optimization of counting times in single-crystal diffractometry: rebuttal to Killean; consideration of background counting and slewing times*. *Acta Cryst.* A**28**, 408–411.

Skellam, J. G. (1946). *The frequency distribution of the difference between two Poisson values belonging to different populations*. *J. R. Stat. Soc.* **109**, 296.

Szabó, P. (1978). *Optimization of the measuring time in diffraction intensity measurements*. *Acta Cryst.* A**34**, 551–553.

Thomsen, J. S. & Yap, F. Y. (1968). *Simplified method of computing centroids of X-ray profiles*. *Acta Cryst.* A**24**, 702–703.

Werner, S. A. (1972*a*). *Choice of scans in X-ray diffraction*. *Acta Cryst.* A**28**, 143–151.

Werner, S. A. (1972*b*). *Choice of scans in neutron diffraction*. *Acta Cryst.* A**28**, 665–669.

Wilson, A. J. C. (1967). *Statistical variance of line-profile parameters. Measures of intensity, location and dispersion*. *Acta Cryst.* **23**, 888–898.

Wilson, A. J. C. (1978). *On the probability of measuring the intensity of a reflection as negative*. *Acta Cryst.* A**34**, 474–475.

Wilson, A. J. C. (1980). *Relationship between 'observed' and 'true' intensity: effect of various counting modes*. *Acta Cryst.* A**36**, 929–936.

Wilson, A. J. C., Thomsen, J. S. & Yap, F. Y. (1965). *Minimization of the variance of parameters derived from X-ray powder diffractometer line profiles*. *Appl. Phys. Lett.* **7**, 163–165.

Wright, E. M. (1933). *On the coefficients of power series having exponential singularities*. *J. London Math. Soc.* **8**, 71–79.

Zevin, L. S., Umanskii, M. M., Kheiker, D. M. & Panchenko, Yu. M. (1961). *K voprosu o difraktometricheskikh priemah pretsizionnyh izmerenii elementarnyh yacheek*. *Kristallografiya*, **6**, 348–356.

International Tables for Crystallography (2006). Vol. C, Chapter 8.1, pp. 678–688.

8.1. Least squares

BY E. PRINCE AND P. T. BOGGS

The process of arriving at a model for a crystal structure may usefully be considered to consist of two distinct stages. The first, which may be called determination, involves the use of chemical and physical intuition, direct methods, Fourier and Patterson methods, and other techniques to arrive at an approximate model for the structure that incorporates unit-cell dimensions, space group, chemical composition, and information with respect to the immediate environment of each atom. The second stage, which we shall call refinement, involves finding the values of adjustable parameters in the model that give the best fit between the predicted diffraction intensities and those observed in an experiment, in order to extract precise information about interatomic distances and bond angles, thermal motion, site occupancies, electron distribution, and so forth. Although there are several different criteria for the best fit to data, such as maximum likelihood and maximum entropy, one of the most commonly used is the method of least squares. This chapter discusses both numerical and statistical aspects of refinement by the method of least squares. Because both aspects make extensive use of linear algebra, we begin with a summary of definitions and fundamental operations in linear algebra (Stewart, 1973; Prince, 1994) and of basic definitions and concepts in mathematical statistics (Draper & Smith, 1981; Box, Hunter & Hunter, 1978). We then discuss the principles of linear and nonlinear least squares and conclude with an extensive discussion of numerical methods used in practical implementation of the technique.

8.1.1. Definitions

8.1.1.1. *Linear algebra*

A *matrix* is an ordered, rectangular array of numbers, real or complex. Matrices will be denoted by upper-case, bold italic letters, $\boldsymbol{A}$. Their individual elements will be denoted by upper-case, italic letters with subscripts. A_{ij} denotes the element in the ith row and the jth column of $\boldsymbol{A}$. A matrix with only one row is a *row vector*; a matrix with only one column is a *column vector*. Vectors will be denoted by lower-case, bold roman letters, and their elements will be denoted by lower-case, italic letters with single subscripts. Scalar constants will usually be denoted by lower-case, Greek letters.

A matrix with the same number of rows as columns is *square*. If $A_{ij} = 0$ for all $i > j$, $\boldsymbol{A}$ is *upper triangular*. If $A_{ij} = 0$ for all $i < j$, $\boldsymbol{A}$ is *lower triangular*. If $A_{ij} = 0$ for all $i \neq j$, $\boldsymbol{A}$ is *diagonal*. If $A_{ij} = 0$ for all i and j, $\boldsymbol{A}$ is *null*. A matrix, $\boldsymbol{B}$, such that $B_{ij} = A_{ji}$ for all i and j is the *transpose* of $\boldsymbol{A}$, and is denoted by $\mathbf{A}^T$. Matrices with the same dimensions may be added and subtracted: $(\boldsymbol{A}+\boldsymbol{B})_{ij} = A_{ij} + B_{ij}$. A matrix may be multiplied by a scalar: $(\alpha\boldsymbol{A})_{ij} = \alpha A_{ij}$. Multiplication of matrices is defined by $(\boldsymbol{AB})_{ij} = \sum_{k=1}^{m} A_{ik}B_{kj}$, where m is the number of columns of $\boldsymbol{A}$ and the number of rows of $\boldsymbol{B}$ (which must be equal). Addition and multiplication of matrices obey the associative law: $(\boldsymbol{A}+\boldsymbol{B})+\boldsymbol{C} = \boldsymbol{A}+(\boldsymbol{B}+\boldsymbol{C})$; $(\boldsymbol{AB})\boldsymbol{C} = \boldsymbol{A}(\boldsymbol{BC})$. Multiplication of matrices obeys the distributive law: $\boldsymbol{A}(\boldsymbol{B}+\boldsymbol{C}) = \boldsymbol{AB}+\boldsymbol{AC}$. Addition of matrices obeys the commutative law: $\boldsymbol{A}+\boldsymbol{B} = \boldsymbol{B}+\boldsymbol{A}$, but multiplication, except in certain (important) special cases, does not: $\boldsymbol{AB} \neq \boldsymbol{BA}$. The transpose of a product is the product of the transposes of the factors in reverse order: $(\boldsymbol{AB})^T = \boldsymbol{B}^T\boldsymbol{A}^T$.

The *trace* of a square matrix is the sum of its diagonal elements. The *determinant* of an $n \times n$ square matrix, $\boldsymbol{A}$, denoted by $|\boldsymbol{A}|$, is the sum of $n!$ terms, each of which is a product of the diagonal elements of a matrix derived from $\boldsymbol{A}$ by permuting columns or rows (see Stewart, 1973). The *rank* of a matrix (not necessarily square) is the dimension of the largest square submatrix that can be formed from it, by selecting rows and columns, whose determinant is not equal to zero. A matrix has *full column rank* if its rank is equal to its number of columns. A square matrix whose diagonal elements are equal to one and whose off-diagonal elements are equal to zero is an *identity matrix*, denoted by $\boldsymbol{I}$. If $|\boldsymbol{A}| \neq 0$, $\boldsymbol{A}$ is *nonsingular*, and there exists a matrix $\boldsymbol{A}^{-1}$, the *inverse* of $\boldsymbol{A}$, such that $\boldsymbol{A}\boldsymbol{A}^{-1} = \boldsymbol{A}^{-1}\boldsymbol{A} = \boldsymbol{I}$. If $|\boldsymbol{A}| = 0$, $\boldsymbol{A}$ is *singular*, and has no inverse. The *adjoint*, or *conjugate transpose*, of $\boldsymbol{A}$ is a matrix, $A^\dagger$, such that $A^\dagger_{ij} = A^*_{ji}$, where the asterisk indicates complex conjugate. If $\boldsymbol{A}^\dagger = \boldsymbol{A}^{-1}$, $\boldsymbol{A}$ is *unitary*. If the elements of a unitary matrix are real, it is *orthogonal*. From this definition, if $\boldsymbol{A}$ is orthogonal, it follows that

$$\sum_{i=1}^{n} A_{ij}^2 = 1$$

for all j, and

$$\sum_{i=1}^{n} A_{ij}A_{ik} = 0$$

if $j \neq k$. By analogy, two column vectors, $\mathbf{x}$ and $\mathbf{y}$, are said to be orthogonal if $\mathbf{x}^T\mathbf{y} = 0$.

For any square matrix, $\boldsymbol{A}$, there exists a set of vectors, $\mathbf{x}_i$, such that $\boldsymbol{A}\mathbf{x}_i = \lambda_i\mathbf{x}_i$, where λ_i is a scalar. The values λ_i are the *eigenvalues* of $\boldsymbol{A}$, and the vectors $\mathbf{x}_i$ are the corresponding *eigenvectors*. If $\boldsymbol{A} = \boldsymbol{A}^\dagger$, $\boldsymbol{A}$ is *Hermitian*, and, if the elements are real, $\boldsymbol{A} = \boldsymbol{A}^T$, so that $\boldsymbol{A}$ is *symmetric*. It can be shown (see, for example, Stewart, 1973) that, if $\boldsymbol{A}$ is Hermitian, all eigenvalues are real, and there exists a unitary matrix, $\boldsymbol{T}$, such that $\boldsymbol{D} = \boldsymbol{T}^\dagger\boldsymbol{A}\boldsymbol{T}$ is diagonal, with the elements of $\boldsymbol{D}$ equal to the eigenvalues of $\boldsymbol{A}$, and the columns of $\boldsymbol{T}$ are the eigenvectors. An $n \times n$ symmetric matrix therefore has n mutually orthogonal eigenvectors. If the product $\mathbf{x}^T\boldsymbol{A}\mathbf{x}$ is greater than (or equal to) zero for any non-null vector, $\mathbf{x}$, $\boldsymbol{A}$ is *positive (semi)definite*. Because $\mathbf{x}$ may be, in particular, an eigenvector, all eigenvalues of a positive (semi)definite matrix are greater than (or equal to) zero. Any matrix of the form $\boldsymbol{B}^T\boldsymbol{B}$ is positive semi definite, and, if $\boldsymbol{B}$ has full column rank, $\boldsymbol{A} = \boldsymbol{B}^T\boldsymbol{B}$ is positive definite. If $\boldsymbol{A}$ is positive definite, there exists an upper triangular matrix, $\boldsymbol{R}$, or, equivalently, a lower triangular matrix, $\boldsymbol{L}$, with positive diagonal elements, such that $\boldsymbol{R}^T\boldsymbol{R} = \boldsymbol{L}\boldsymbol{L}^T = \boldsymbol{A}$. $\boldsymbol{R}$, or $\boldsymbol{L}$, is called the *Cholesky factor* of $\boldsymbol{A}$. The *magnitude*, *length* or *Euclidean norm* of a vector, $\mathbf{x}$, denoted by $\|\mathbf{x}\|$, is defined by $\|\mathbf{x}\| = (\mathbf{x}^T\mathbf{x})^{1/2}$. The *induced matrix norm* of a matrix, $\boldsymbol{B}$, denoted $\|\boldsymbol{B}\|$, is defined as the maximum value of $\|\boldsymbol{B}\mathbf{x}\|/\|\mathbf{x}\| = (\mathbf{x}^T\boldsymbol{B}^T\boldsymbol{B}\mathbf{x}/\mathbf{x}^T\mathbf{x})^{1/2}$ for $\|\mathbf{x}\| > 0$. Because $\mathbf{x}^T\boldsymbol{B}^T\boldsymbol{B}\mathbf{x}$ will have its maximum value for a fixed value of $\mathbf{x}^T\mathbf{x}$ when $\mathbf{x}$ is parallel to the eigenvector that corresponds to the largest eigenvalue of $\boldsymbol{B}^T\boldsymbol{B}$, this definition implies that $\|\boldsymbol{B}\|$ is equal to the square root of the largest eigenvalue of $\boldsymbol{B}^T\boldsymbol{B}$. The *condition number* of $\boldsymbol{B}$ is the square root of the ratio of the largest and smallest eigenvalues of $\boldsymbol{B}^T\boldsymbol{B}$. (Other definitions of norms exist, with corresponding definitions of condition number. We shall not be concerned with any of these.)

Copyright © 2006 International Union of Crystallography

We shall make extensive use of the so-called QR decomposition, which is defined as follows: For any $n \times p$ ($n \geq p$) real matrix, $\boldsymbol{Z}$, there exists an $n \times n$ orthogonal matrix, $\boldsymbol{Q}$, such that

$$\boldsymbol{Q}^T \boldsymbol{Z} = \begin{pmatrix} \boldsymbol{R} \\ \boldsymbol{O} \end{pmatrix}, \tag{8.1.1.1}$$

where $\boldsymbol{R}$ is a $p \times p$ upper triangular matrix, and $\boldsymbol{O}$ denotes an $(n-p) \times p$ null matrix. Thus, we have

$$\boldsymbol{Z} = \boldsymbol{Q} \begin{pmatrix} \boldsymbol{R} \\ \boldsymbol{O} \end{pmatrix}, \tag{8.1.1.2}$$

which is known as the QR decomposition of $\boldsymbol{Z}$. If we partition $\boldsymbol{Q}$ as $(\boldsymbol{Q}_Z, \boldsymbol{Q}_\perp)$, where $\boldsymbol{Q}_Z$ has dimensions $n \times p$, and $\boldsymbol{Q}_\perp$ has dimensions $n \times (n-p)$, (8.1.1.2) becomes

$$\boldsymbol{Z} = \boldsymbol{Q}_Z \boldsymbol{R}, \tag{8.1.1.3}$$

which is known as the QR factorization. We shall make use of the following facts. First, $\boldsymbol{R}$ is nonsingular if and only if the columns of $\boldsymbol{Z}$ are linearly independent; second, the columns of $\boldsymbol{Q}_Z$ form an orthonormal basis for the range space of $\boldsymbol{Z}$, that is, they span the same space as $\boldsymbol{Z}$; and, third, the columns of $\boldsymbol{Q}_\perp$ form an orthonormal basis for the null space of $\boldsymbol{Z}^T$, that is, $\boldsymbol{Z}^T \boldsymbol{Q}_\perp = \boldsymbol{O}$.

There are two common procedures for computing the QR factorization. The first makes use of *Householder transformations*, which are defined by

$$\boldsymbol{H} = \boldsymbol{I} - 2\mathbf{x}\mathbf{x}^T, \tag{8.1.1.4}$$

where $\mathbf{x}^T\mathbf{x} = 1$. $\boldsymbol{H}$ is symmetric, and $\boldsymbol{H}^2 = \boldsymbol{I}$, so that $\boldsymbol{H}$ is orthogonal. In three dimensions, $\boldsymbol{H}$ corresponds to a reflection in a mirror plane perpendicular to $\mathbf{x}$, because of which Stewart (1973) has suggested the alternative term *elementary reflector*. $\boldsymbol{A}$ vector $\mathbf{v}$ is transformed by $\boldsymbol{H}\mathbf{v}$ into the vector $\|\mathbf{v}\|\mathbf{e}$, where $\mathbf{e}$ represents a vector with $e_1 = 1$, and $e_i = 0$ for $i \neq 1$, if

$$\mathbf{x} = [\mathbf{v} - \|\mathbf{v}\|\mathbf{e}] \big/ \big\|[\mathbf{v} - \|\mathbf{v}\|\mathbf{e}]\big\|. \tag{8.1.1.5}$$

The factorization procedure for an $n \times p$ matrix, $\boldsymbol{A}$ (Stewart, 1973; Anderson *et al.*, 1992), takes as $\mathbf{v}$ in the first step the first column of $\boldsymbol{A}$, and forms $\boldsymbol{A}_1 = \boldsymbol{H}_1\boldsymbol{A}$, which has zeros in all elements of the first column below the diagonal. In the second step, $\mathbf{v}$ has a zero as the first element and is filled out by those elements of the second column of $\boldsymbol{A}_1$ on or below the diagonal. $\boldsymbol{A}_2 = \boldsymbol{H}_2\boldsymbol{A}_1$ then has zeros in all elements below the diagonal in the first two columns. This process is repeated $(p-2)$ more times, after which $\boldsymbol{Q} = \boldsymbol{H}_p \ldots \boldsymbol{H}_2\boldsymbol{H}_1$, and $\boldsymbol{R} = \boldsymbol{A}_p$ is upper triangular.

QR factorization by Householder transformations requires for efficiency that the entire $n \times p$ matrix be stored in memory, and requires of order np^2 operations. A procedure that requires storage of only the upper triangle makes use of *Givens rotations*, which are 2×2 matrices of the form

$$\boldsymbol{G} = \begin{pmatrix} \cos\alpha & \sin\alpha \\ -\sin\alpha & \cos\alpha \end{pmatrix}. \tag{8.1.1.6}$$

Multiplication of a $2 \times m$ matrix, $\boldsymbol{B}$, by $\boldsymbol{G}$ will put a zero in the B_{21} element if $\alpha = \arctan B_{21}/B_{11}$. The factorization of $\boldsymbol{A}$ involves reading, or computing, the rows of $\boldsymbol{A}$ one at a time. In the first step, matrix $\boldsymbol{B}_1$ consists of the first row of $\boldsymbol{R}$ and the current row of $\boldsymbol{A}$, from which the first element is eliminated. In the second step, $\boldsymbol{B}_{21}$ is the second row of $\boldsymbol{R}$ and the $(p-1)$ nonzero elements of the second row of the transformed $\boldsymbol{B}_1$. After the first p rows have been treated, each additional row of $\boldsymbol{A}$ requires $2p(p+1)$ multiplications to fill it with zeros. However, because the operation is easily vectorized, the time required may be a small proportion of the total computing time on a vector oriented computer.

8.1.1.2. *Statistics*

A *probability density function*, which will be abbreviated p.d.f., is a function, $\Phi(x)$, such that the probability of finding the random variable x in the interval $a \leq x \leq b$ is given by

$$p(a \leq x \leq b) = \int_a^b \Phi(x)\,\mathrm{d}x.$$

A p.d.f. has the properties

$$\Phi(x) \geq 0, \qquad -\infty < x < +\infty,$$

and

$$\int_{-\infty}^{+\infty} \Phi(x)\,\mathrm{d}x = 1.$$

A *cumulative distribution function*, which will be abbreviated c.d.f., is defined by

$$\Psi(x) = \int_{-\infty}^{x} \Phi(t)\,\mathrm{d}t.$$

The properties of $\Phi(x)$ imply that $0 \leq \Psi(x) \leq 1$, and $\Phi(x) = \mathrm{d}\Psi(x)/\mathrm{d}x$. The *expected value* of a function, $f(x)$, of random variable x is defined by

$$\big\langle f(x) \big\rangle = \int_{-\infty}^{+\infty} f(x)\Phi(x)\,\mathrm{d}x.$$

If $f(x) = x^n$, $\big\langle f(x) \big\rangle = \langle x^n \rangle$ is the *nth moment* of $\Phi(x)$. The first moment, often denoted by μ, is the *mean* of $\Phi(x)$. The second moment about the mean, $\big\langle (x - \langle x \rangle)^2 \big\rangle$, usually denoted by σ^2, is the *variance* of $\Phi(x)$. The positive square root of the variance is the *standard deviation*.

For a vector, $\mathbf{x}$, of random variables, $x_1, x_2, \ldots, x_n$, the *joint probability density function*, or *joint p.d.f.*, is a function, $\Phi_J(\mathbf{x})$, such that

$$\begin{aligned} &p(a_1 \leq x_1 \leq b_1;\ a_2 \leq x_2 \leq b_2; \ldots;\ a_n \leq x_n \leq b_n) \\ &\quad = \int_{a_1}^{b_1} \int_{a_2}^{b_2} \ldots \int_{a_n}^{b_n} \Phi_J(\mathbf{x})\,\mathrm{d}x_1\,\mathrm{d}x_2 \ldots \mathrm{d}x_n. \end{aligned} \tag{8.1.1.7}$$

The *marginal p.d.f.* of an element (or a subset of elements), x_i, is a function, $\Phi_M(x_i)$, such that

$$\begin{aligned} p(a_i \leq x_i \leq b_i) &= \int_{a_i}^{b_i} \Phi_M(x_i)\,\mathrm{d}x_i \\ &= \int_{-\infty}^{+\infty} \ldots \int_{a_i}^{b_i} \ldots \int_{-\infty}^{\infty} \Phi_J(\mathbf{x})\,\mathrm{d}x_1 \ldots \mathrm{d}x_i \ldots \mathrm{d}x_n. \end{aligned} \tag{8.1.1.8}$$

This is a p.d.f. for x_i alone, irrespective of the values that may be found for any other element of $\mathbf{x}$. For two random variables, x and y (either or both of which may be vectors), the *conditional p.d.f. of x given* $y = y_0$ is defined by

$$\Phi_C(x|y_0) = c\Phi_J(x, y)_{y=y_0},$$

where $c = 1/\Phi_M(y_0)$ is a *renormalizing factor*. This is a p.d.f. for x when it is known that $y = y_0$. If $\Phi_C(x|y) = \Phi_M(x)$ for all y, or, equivalently, if $\Phi_J(x, y) = \Phi_M(x)\Phi_M(y)$, the random variables x and y are said to be *statistically independent*.

Moments may be defined for multivariate p.d.f.s in a manner analogous to the one-dimensional case. The mean is a vector defined by

$$\mu_i = \langle x_i \rangle = \int x_i \Phi(\mathbf{x})\, d\mathbf{x},$$

where the volume of integration is the entire domain of $\mathbf{x}$. The *variance–covariance matrix* is defined by

$$\begin{aligned} V_{ij} &= \big\langle (x_i - \langle x_i \rangle)(x_j - \langle x_j \rangle) \big\rangle \\ &= \int (x_i - \langle x_i \rangle)(x_j - \langle x_j \rangle) \Phi_J(\mathbf{x})\, d\mathbf{x}. \end{aligned} \tag{8.1.1.9}$$

The diagonal elements of $\boldsymbol{V}$ are the variances of the marginal p.d.f.s of the elements of $\mathbf{x}$, that is, $V_{ii} = \sigma_i^2$. It can be shown that, if x_i and x_j are statistically independent, $V_{ij} = 0$ when $i \neq j$. If two vectors of random variables, $\mathbf{x}$ and $\mathbf{y}$, are related by a linear transformation, $\mathbf{x} = \boldsymbol{B}\mathbf{y}$, the means of their joint p.d.f.s are related by $\mu_x = B\mu_y$, and their variance–covariance matrices are related by $\boldsymbol{V}_\mathbf{x} = \boldsymbol{B}\boldsymbol{V}_\mathbf{y}\boldsymbol{B}^T$.

8.1.2. Principles of least squares

The method of least squares may be formulated as follows: Given a set of n observations, $y_i\ (i = 1, 2, \ldots, n)$, that are measurements of quantities that can be described by differentiable model functions, $M_i(\mathbf{x})$, where $\mathbf{x}$ is a vector of parameters, $x_j (j = 1, 2, \ldots, p)$, find the values of the parameters for which the sum

$$S = \sum_{i=1}^{n} w_i [y_i - M_i(\mathbf{x})]^2 \tag{8.1.2.1}$$

is minimum. Here, w_i represents a weight assigned to the ith observation. The values of the parameters that give the minimum value of S are called *estimates* of the parameters, and a function of the data that locates the minimum is an *estimator*. A necessary condition for S to be a minimum is for the gradient to vanish, which gives a set of simultaneous equations, the *normal equations*, of the form

$$\frac{\partial S}{\partial x_j} = -2 \sum_{i=1}^{n} w_i [y_i - M_i(\mathbf{x})] \frac{\partial M_i(\mathbf{x})}{\partial x_j} = 0. \tag{8.1.2.2}$$

The model functions, $M_i(\mathbf{x})$, are, in general, nonlinear, and there are no direct ways to solve these systems of equations. Iterative methods for solving them are discussed in Section 8.1.4. Much of the analysis of results, however, is based on the assumption that linear approximations to the model functions are good approximations in the vicinity of the minimum, and we shall therefore begin with a discussion of linear least squares.

To express linear relationships, it is convenient to use matrix notation. Let $\boldsymbol{M}(\mathbf{x})$ and $\mathbf{y}$ be column vectors whose ith elements are $M_i(\mathbf{x})$ and y_i. Similarly, let $\mathbf{b}$ be a vector and $\boldsymbol{A}$ be a matrix such that a linear approximation to the ith model function can be written

$$M_i(\mathbf{x}) = b_i + \sum_{j=1}^{p} A_{ij} x_j. \tag{8.1.2.3}$$

Equations (8.1.2.3) can be written, in matrix form,

$$\boldsymbol{M}(\mathbf{x}) = \mathbf{b} + \boldsymbol{A}\mathbf{x}, \tag{8.1.2.4}$$

and, for this linear model, (8.1.2.1) becomes

$$S = [(\mathbf{y} - \mathbf{b}) - \boldsymbol{A}\mathbf{x}]^T \boldsymbol{W} [(\mathbf{y} - \mathbf{b}) - \boldsymbol{A}\mathbf{x}], \tag{8.1.2.5}$$

where $\boldsymbol{W}$ is a diagonal matrix whose diagonal elements are $W_{ii} = w_i$. In this notation, the normal equations (8.1.2.2) can be written

$$\boldsymbol{A}^T \boldsymbol{W} \boldsymbol{A}\mathbf{x} = \boldsymbol{A}^T \boldsymbol{W} (\mathbf{y} - \mathbf{b}), \tag{8.1.2.6}$$

and their solution is

$$\hat{\mathbf{x}} = (\boldsymbol{A}^T \boldsymbol{W} \boldsymbol{A})^{-1} \boldsymbol{A}^T \boldsymbol{W} (\mathbf{y} - \mathbf{b}). \tag{8.1.2.7}$$

If $W_{ii} > 0$ for all i, and $\boldsymbol{A}$ has full column rank, then $\boldsymbol{A}^T\boldsymbol{W}\boldsymbol{A}$ will be positive definite, and S will have a unique minimum at $\mathbf{x} = \hat{\mathbf{x}}$. The matrix $\boldsymbol{H} = (\boldsymbol{A}^T\boldsymbol{W}\boldsymbol{A})^{-1}\boldsymbol{A}^T\boldsymbol{W}$ is a $p \times n$ matrix that relates the n-dimensional observation space to the p-dimensional parameter space and is known as the *least-squares estimator*; because each element of $\hat{\mathbf{x}}$ is a linear function of the observations, it is a *linear estimator*. [Note that, in actual practice, the matrix $\boldsymbol{H}$ is not actually evaluated, except, possibly, in very small problems. Rather, the linear system $\boldsymbol{A}^T\boldsymbol{W}\boldsymbol{A}\mathbf{x} = \boldsymbol{A}^T\boldsymbol{W}(\mathbf{y} - \mathbf{b})$ is solved using the methods of Section 8.1.3.]

The least-squares estimator has some special properties in statistical analysis. Suppose that the elements of $\mathbf{y}$ are experimental observations drawn at random from populations whose means are given by the model, $\boldsymbol{M}(\mathbf{x})$, for some unknown $\mathbf{x}$, which we wish to estimate. This may be written

$$\langle \mathbf{y} - \mathbf{b} \rangle = \boldsymbol{A}\mathbf{x}. \tag{8.1.2.8}$$

The expected value of the least-squares estimate is

$$\begin{aligned} \langle \hat{\mathbf{x}} \rangle &= \big\langle (\boldsymbol{A}^T\boldsymbol{W}\boldsymbol{A})^{-1}\boldsymbol{A}^T\boldsymbol{W}(\mathbf{y} - \mathbf{b}) \big\rangle \\ &= (\boldsymbol{A}^T\boldsymbol{W}\boldsymbol{A})^{-1}\boldsymbol{A}^T\boldsymbol{W}\langle \mathbf{y} - \mathbf{b} \rangle \\ &= (\boldsymbol{A}^T\boldsymbol{W}\boldsymbol{A})^{-1}\boldsymbol{A}^T\boldsymbol{W}\boldsymbol{A}\mathbf{x} \\ &= \mathbf{x}. \end{aligned} \tag{8.1.2.9}$$

If the expected value of an estimate is equal to the variable to be estimated, the estimator is said to be *unbiased*. Equation (8.1.2.9) shows that the least-squares estimator is an unbiased estimator for $\mathbf{x}$, independent of $\boldsymbol{W}$, provided only that $\mathbf{y}$ is an unbiased estimate of $\boldsymbol{M}(\mathbf{x})$, the matrix $\boldsymbol{A}^T\boldsymbol{W}\boldsymbol{A}$ is nonsingular, and the elements of $\boldsymbol{W}$ are constants independent of $\mathbf{y}$ and $\boldsymbol{M}(\mathbf{x})$. Let $\boldsymbol{V}_\mathbf{x}$ and $\boldsymbol{V}_\mathbf{y}$ be the variance–covariance matrices for the joint p.d.f.s of the elements of $\mathbf{x}$ and $\mathbf{y}$, respectively. Then, $\boldsymbol{V}_\mathbf{x} = \boldsymbol{H}\boldsymbol{V}_\mathbf{y}\boldsymbol{H}^T$. Let $\boldsymbol{G}$ be the matrix $(\boldsymbol{A}^T\boldsymbol{V}_\mathbf{y}^{-1}\boldsymbol{A})^{-1}\boldsymbol{A}^T\boldsymbol{V}^{-1}$, so that $\hat{\mathbf{x}} = \boldsymbol{G}(\mathbf{y} - \mathbf{b})$ is the particular least-squares estimate for which $\boldsymbol{W} = \boldsymbol{V}_\mathbf{y}^{-1}$. Then, $\boldsymbol{V}_\mathbf{x} = \boldsymbol{G}\boldsymbol{V}_\mathbf{y}\boldsymbol{G}^T$. If $\boldsymbol{V}_\mathbf{y}$ is positive definite, its lower triangular Cholesky factor, $\boldsymbol{L}$, exists, so that $\boldsymbol{L}\boldsymbol{L}^T = \boldsymbol{V}_\mathbf{y}$. [If $\boldsymbol{V}$ is diagonal, $\boldsymbol{L}$ is also diagonal, with $L_{ii} = (\boldsymbol{V}_\mathbf{y})_{ii}^{1/2}$.] It is readily verified that the matrix product $[(\boldsymbol{H} - \boldsymbol{G})\boldsymbol{L}][(\boldsymbol{H} - \boldsymbol{G})\boldsymbol{L}]^T = \boldsymbol{H}\boldsymbol{V}_\mathbf{y}\boldsymbol{H}^T - \boldsymbol{G}\boldsymbol{V}_\mathbf{y}\boldsymbol{G}^T$, but the diagonal elements of this product are the sums of squares of the elements of rows of $(\boldsymbol{H} - \boldsymbol{G})\boldsymbol{L}$, and are therefore greater than or equal to zero. Therefore, the diagonal elements of $\boldsymbol{V}_\mathbf{x}$, which are the variances of the marginal p.d.f.s of the elements of $\hat{\mathbf{x}}$, are minimum when $\boldsymbol{W} = \boldsymbol{V}_\mathbf{y}^{-1}$.

Thus, the least-squares estimator is unbiased for any positive-definite weight matrix, $\boldsymbol{W}$, but the variances of the elements of the vector of estimated parameters are minimized if $\boldsymbol{W} = \boldsymbol{V}_\mathbf{y}^{-1}$. [Note also that $\boldsymbol{V}_\mathbf{x} = (\boldsymbol{A}^T\boldsymbol{W}\boldsymbol{A})^{-1}$ if, *and only if*, $\boldsymbol{W} = \boldsymbol{V}_\mathbf{y}^{-1}$.] For this reason, the least-squares estimator with weights proportional to the reciprocals of the variances of the observations is referred to as the *best linear unbiased estimator* for the parameters of a model describing those observations. (These specific results are included in a more general result known as the *Gauss–Markov theorem*.)

The analysis up to this point has assumed that the model is linear, that is that the expected values of the observations can be expressed by $\langle \mathbf{y} \rangle = \mathbf{b} + \boldsymbol{A}\mathbf{x}$, where $\boldsymbol{A}$ is some matrix. In crystallography, of course, the model is highly nonlinear, and this assumption is not valid. The principles of linear least squares

can be extended to nonlinear model functions by first finding, by numerical methods, a point in parameter space, $\mathbf{x}_0$, at which the gradient vanishes and then expanding the model functions about that point in Taylor's series, retaining only the linear terms. Equation (8.1.2.4) then becomes

$$\boldsymbol{M}(\mathbf{x}) \approx \boldsymbol{M}(\mathbf{x}_0) + \boldsymbol{A}(\mathbf{x} - \mathbf{x}_0), \tag{8.1.2.10}$$

where $A_{ij} = \partial M_i(\mathbf{x})/\partial x_j$ evaluated at $\mathbf{x} = \mathbf{x}_0$. Because we have already found the least-squares solution, the estimate

$$\begin{aligned}\widehat{\mathbf{x}} &= \mathbf{x}_0 + (\boldsymbol{A}^T\boldsymbol{W}\boldsymbol{A})^{-1}\boldsymbol{A}^T\boldsymbol{W}[\mathbf{y} - \boldsymbol{M}(\mathbf{x}_0)] \\ &= \mathbf{x}_0 + \boldsymbol{H}[\mathbf{y} - \boldsymbol{M}(\mathbf{x}_0)]\end{aligned} \tag{8.1.2.11}$$

reduces to $\widehat{\mathbf{x}} = \mathbf{x}_0$. It is important, however, not to confuse $\mathbf{x}_0$, which is a convenient origin, with $\widehat{\mathbf{x}}$, which is a random variable describable by a joint p.d.f. with mean $\mathbf{x}_0$ and a variance–covariance matrix $\boldsymbol{V}_\mathbf{x} = \boldsymbol{H}\boldsymbol{V}_\mathbf{y}\boldsymbol{H}^T$, reducing to $(\boldsymbol{A}^T\boldsymbol{V}_\mathbf{y}^{-1}\boldsymbol{A})^{-1}$ when $\boldsymbol{W} = \boldsymbol{V}_\mathbf{y}^{-1}$.

This variance–covariance matrix is the one appropriate to the linear approximation given in (8.1.2.10), and it is valid (and the estimate is unbiased) only to the extent that the approximation is a good one. *A* useful criterion for an adequate approximation (Fedorov, 1972) is, for each j and k,

$$\left|\sum_{i=1}^{n} w_i\sigma_i \frac{\partial^2 M_i(\mathbf{x}_0)}{\partial x_j \partial x_k}\right| \ll \left(\left\{\sum_{i=1}^{n} w_i\left[\frac{\partial M_i(\mathbf{x}_0)}{\partial x_j}\right]^2\right\} \times \left\{\sum_{i=1}^{n} w_i\left[\frac{\partial M_i(\mathbf{x}_0)}{\partial x_k}\right]^2\right\}\right)^{1/2}, \tag{8.1.2.12}$$

where σ_i is the estimated standard deviation or *standard uncertainty* (Schwarzenbach, Abrahams, Flack, Prince & Wilson, 1995) of y_i. This criterion states that the curvature of $S(\mathbf{y}, \mathbf{x})$ in a region whose size is of order σ in observation space is small; it ensures that the effect of second-derivative terms in the normal-equations matrix on the eigenvalues and eigenvectors of the matrix is negligible. [For a further discussion and some numerical tests of alternatives, see Donaldson & Schnabel (1986).]

The process of refinement can be viewed as the construction of a conditional p.d.f. of a set of model parameters, $\mathbf{x}$, given a set of observations, $\mathbf{y}$. An important expression for this p.d.f. is derived from two equivalent expressions for the joint p.d.f. of $\mathbf{x}$ and $\mathbf{y}$:

$$\Phi_J(\mathbf{x}, \mathbf{y}) = \Phi_C(\mathbf{x}|\mathbf{y})\Phi_M(\mathbf{y}) = \Phi_C(\mathbf{y}|\mathbf{x})\Phi_M(\mathbf{x}). \tag{8.1.2.13}$$

Provided $\Phi_M(\mathbf{y}) > 0$, the conditional p.d.f. we seek can be written

$$\Phi_C(\mathbf{x}|\mathbf{y}) = \Phi_C(\mathbf{y}|\mathbf{x})\Phi_M(\mathbf{x})/\Phi_M(\mathbf{y}). \tag{8.1.2.14}$$

Here, the factor $[1/\Phi_M(\mathbf{y})]$ is the factor that is required to normalize the p.d.f. $\Phi_C(\mathbf{y}|\mathbf{x})$ is the conditional probability of observing a set of values of $\mathbf{y}$ as a function of $\mathbf{x}$. When the observations have already been made, however, this can also be considered a density function for $\mathbf{x}$ that measures the *likelihood* that those particular values of $\mathbf{y}$ would have been observed for various values of $\mathbf{x}$. It is therefore frequently written $\ell(\mathbf{x}|\mathbf{y})$, and (8.1.2.14) becomes

$$\Phi_C(\mathbf{x}|\mathbf{y}) = c\ell(\mathbf{x}|\mathbf{y})\Phi_M(\mathbf{x}), \tag{8.1.2.15}$$

where $c = [1/\Phi_M(\mathbf{y})]$ is the normalizing constant. $\Phi_M(\mathbf{x})$, the marginal p.d.f. of $\mathbf{x}$ in the absence of any additional information, incorporates all previously available information concerning $\mathbf{x}$, and is known as the *prior p.d.f.*, or, frequently, simply as the *prior* of $\mathbf{x}$. Similarly, $\Phi_C(\mathbf{x}|\mathbf{y})$ is the *posterior p.d.f.*, or the *posterior*, of $\mathbf{x}$. The relation in (8.1.2.14) and (8.1.2.15) was first stated in the eighteenth century by Thomas Bayes, and it is therefore known as Bayes's theorem (Box & Tiao, 1973). Although its validity has never been in serious question, its application has divided statisticians into two vehemently disputing camps, one of which, the frequentists, considers that Bayesian methods give nonobjective results, while the other, the Bayesians, considers that only by careful construction of a 'noninformative' prior can true objectivity be achieved (Berger & Wolpert, 1984).

Diffraction data, in general, contain no phase information, so the likelihood function for the structure factor, F, given a value of observed intensity, will have a value significantly different from zero in an annular region of the complex plane with a mean radius equal to $|F|$. Because this is insufficient information with which to determine a crystal structure, a prior p.d.f. is constructed in one (or some combination) of two ways. Either the prior knowledge that electron density is non negative is used to construct a joint p.d.f. of amplitudes and phases, given amplitudes for all reflections and phases for a few of them (direct methods), or chemical knowledge and intuition are used to construct a trial structure from which structure factors can be calculated, and the phase of $F_{\rm calc}$ is assigned to $F_{\rm obs}$. Both of these procedures can be considered to be applications of Bayes's theorem. In fact, $F_{\rm calc}$ for a refined structure can be considered a Bayesian estimate of F.

8.1.3. Implementation of linear least squares

In this section, we consider in detail numerical methods for solving linear least-squares problems, that is, the situation where (8.1.2.4) and (8.1.2.5) apply exactly.

8.1.3.1. *Use of the QR factorization*

The linear least-squares problem can be viewed geometrically as the problem of finding the point in a p-dimensional subspace, defined as the set of points that can be reached by a linear combination of the columns of $\boldsymbol{A}$, closest to a given point, $\mathbf{y}$, in an n-dimensional observation space. Since this is equivalent to finding the orthogonal projection of point $\mathbf{y}$ into that subspace, it is not surprising that an orthogonal decomposition of $\boldsymbol{A}$ helps to solve the problem. For convenience in this discussion, let us remove the weight matrix from the problem by defining the standardized design matrix by

$$\boldsymbol{Z} = \boldsymbol{U}\boldsymbol{A}, \tag{8.1.3.1}$$

where $\boldsymbol{U}$ is the upper triangular Cholesky factor of $\boldsymbol{W}$.

Consider the least-squares problem with the QR factorization of $\boldsymbol{Z}$, as given in Subsection 8.1.1.1. For $\mathbf{y}' = \boldsymbol{U}(\mathbf{y} - \mathbf{b})$, (8.1.2.5) becomes

$$\begin{aligned}S &= (\mathbf{y}' - \boldsymbol{Z}\mathbf{x})^T(\mathbf{y}' - \boldsymbol{Z}\mathbf{x}) \\ &= [\boldsymbol{Q}^T(\mathbf{y}' - \boldsymbol{Z}\mathbf{x})]^T[\boldsymbol{Q}^T(\mathbf{y}' - \boldsymbol{Z}\mathbf{x})],\end{aligned} \tag{8.1.3.2}$$

which reduces to

$$S = (\boldsymbol{Q}_Z^T\mathbf{y}' - \boldsymbol{R}\mathbf{x})^T(\boldsymbol{Q}_Z^T\mathbf{y}' - \boldsymbol{R}\mathbf{x}) + \mathbf{y}'^T\boldsymbol{Q}_\perp\boldsymbol{Q}_\perp^T\mathbf{y}'. \tag{8.1.3.3}$$

The second term in (8.1.3.3) is independent of $\mathbf{x}$, and is therefore the sum of squared residuals. The first term vanishes if

$$\boldsymbol{R}\mathbf{x} = \boldsymbol{Q}_Z^T\mathbf{y}', \tag{8.1.3.4}$$

which, because $\boldsymbol{R}$ is upper triangular, is easily solved for $\mathbf{x}$. The QR decomposition of $\boldsymbol{Z}$ therefore leads naturally to the following algorithm for solving the linear least-squares problem:

(1) compute the QR factorization of $\boldsymbol{Z}$;
(2) compute $\boldsymbol{Q}_Z^T\mathbf{y}'$;
(3) solve $\boldsymbol{R}\mathbf{x} = \boldsymbol{Q}_Z^T\mathbf{y}'$ for $\mathbf{x}$.
(4) compute the residual sum of squares by $\mathbf{y}'^T\mathbf{y}' - \mathbf{y}'\boldsymbol{Q}_Z\boldsymbol{Q}_Z^T\mathbf{y}'$.
(5) compute the variance–covariance matrix from $\boldsymbol{V}_\mathbf{x} = \boldsymbol{R}^{-1}(\boldsymbol{R}^{-1})^T$.

8.1.3.2. *The normal equations*

Let us now consider the relationship of the QR procedure for solving the linear least-squares problem to the classical method based on the normal equations. The normal equations can be derived by differentiating (8.1.3.2) and equating the result to a null vector. This yields

$$\boldsymbol{Z}^T\boldsymbol{Z}\mathbf{x} = \boldsymbol{Z}^T\mathbf{y}'. \tag{8.1.3.5}$$

The algorithm is therefore to compute the cross-product matrix, $\boldsymbol{B} = \boldsymbol{Z}^T\boldsymbol{Z}$, and the right-hand side, $\mathbf{d} = \boldsymbol{Z}^T\mathbf{y}'$, and to solve the resulting system of equations, $\boldsymbol{B}\mathbf{x} = \mathbf{d}$. This is usually accomplished by computing the Cholesky decomposition of $\boldsymbol{B}$, that is $\boldsymbol{B} = \boldsymbol{C}^T\boldsymbol{C}$, where $\boldsymbol{C}$ is upper triangular, and then solving the two triangular systems $\boldsymbol{C}^T\mathbf{v} = \mathbf{d}$ and $\boldsymbol{C}\mathbf{x} = \mathbf{v}$. Because $\boldsymbol{Z} = \boldsymbol{Q}_Z\boldsymbol{R}$, equation (8.1.3.5) becomes

$$\boldsymbol{R}^T\boldsymbol{Q}_Z^T\boldsymbol{Q}_Z\boldsymbol{R}\mathbf{x} = \boldsymbol{R}^T\boldsymbol{Q}_Z^T\mathbf{y}', \tag{8.1.3.6}$$

or

$$\boldsymbol{R}^T\boldsymbol{R}\mathbf{x} = \boldsymbol{R}^T\boldsymbol{Q}_Z^T\mathbf{y}'. \tag{8.1.3.7}$$

It is clear that $\boldsymbol{R}$ is the Cholesky factor of $\boldsymbol{Z}^T\boldsymbol{Z}$, although it is formed in a different way. This procedure requires of order $(np^2)/2$ operations to form the product $\boldsymbol{Z}^T\boldsymbol{Z}$ and $p^3/3$ operations for the Cholesky decomposition. In some situations, the extra time to compute the QR factorization is justified because of greater stability, as will be discussed below. Most other quantities of statistical interest can be computed directly from the QR factorization.

8.1.3.3. *Conditioning*

The condition number of $\boldsymbol{Z}$, which is defined (Subsection 8.1.1.1) as the square root of the ratio of the largest to the smallest eigenvalue of $\boldsymbol{Z}^T\boldsymbol{Z}$, is an indicator of the effect a small change in an element of $\boldsymbol{Z}$ will have on the elements of $(\boldsymbol{Z}^T\boldsymbol{Z})^{-1}$and of $\hat{\mathbf{x}}$. A large value of the condition number means that small errors in computing an element of $\boldsymbol{Z}$, owing possibly to truncation or roundoff in the computer, can introduce large errors into the elements of the inverse matrix. Also, when the condition number is large, the standard uncertainties of some estimated parameters will be large. A large condition number, as defined in this way, can result from either scaling or correlation or some combination of these. To illustrate this, consider the matrices

$$\boldsymbol{Z}^T\boldsymbol{Z} = \begin{pmatrix} 2+\varepsilon & 0 \\ 0 & \varepsilon \end{pmatrix}$$

and

$$\boldsymbol{Z}^T\boldsymbol{Z} = \begin{pmatrix} 1 & 1-\varepsilon \\ 1-\varepsilon & 1 \end{pmatrix},$$

where ε represents machine precision, which can be defined as the smallest number in machine representation that, when added to 1, gives a result different from 1. By the conventional definition, both of these matrices have a condition number for $\boldsymbol{Z}$ of $[(2+\varepsilon)/\varepsilon]^{1/2}$. Because numbers of order ε can be perfectly well represented, however, the first one can be inverted without loss of precision, whereas an inverse for the second would be totally meaningless. It is good practice, therefore, to factor the design matrix, $\boldsymbol{Z}$, into the form

$$\boldsymbol{Z} = \boldsymbol{T}\boldsymbol{S}, \tag{8.1.3.8}$$

where $\boldsymbol{S}$ is a $p \times p$ diagonal matrix whose elements define some kind of 'natural' unit appropriate to the parameter represented in each column of $\boldsymbol{Z}$. The ideal natural unit would be the standard uncertainty of that parameter, but this is not available until after the calculation has been completed. If correlation is not too severe, suitable values for the elements of $\boldsymbol{S}$, of the same order of magnitude as those derived from the standard uncertainty, are the column Euclidean norms, that is

$$S = \|\mathbf{z}_j\| = (\mathbf{z}_j^T\mathbf{z}_j)^{1/2}, \tag{8.1.3.9}$$

where $\mathbf{z}_j$ denotes the jth column of $\boldsymbol{Z}$. This scaling causes all diagonal elements of $\boldsymbol{Z}^T\boldsymbol{Z}$ to be equal to one, and errors in the elements of $\boldsymbol{Z}$ will have roughly equal effects.

Ill conditioning that results from correlation, as in the second example above, is more difficult to deal with. It is an indication that some linear combination of parameters, some eigenvector of the normal equations matrix, is poorly determined by the available data. Use of the QR factorization of $\boldsymbol{Z}$ to compute the Cholesky factor of $\boldsymbol{Z}^T\boldsymbol{Z}$ may be advantageous, in spite of the additional computation time, because better numerical stability is obtained in marginal situations. As a practical matter, however, it is important to recognize that an ill conditioned matrix is a symptom of a flaw in the model or in the experimental design (or both). Use can be made of the fact that, although determining the entire set of eigenvalues and eigenvectors of a large matrix is computationally an inherently difficult problem, a relatively simple algorithm, known as a *condition estimator* (Anderson *et al.*, 1992), can produce a good approximation to the eigenvector that corresponds to the smallest eigenvalue of a nearly singular matrix. This information can be used in either or both of two ways. First, without any fundamental modification to the model or the experiment, a simple, linear transformation of the parameters so that the problem eigenvector is one of the independent parameters, followed by rescaling, can resolve the numerical difficulties in computing the estimates. A common example is the situation where a phase transition results in the doubling of a unit cell, with pairs of atoms almost but not quite related by a lattice translation. A transformation that makes the estimated parameters the sums and differences of corresponding parameters in related pairs of atoms can make a dramatic improvement in the condition number. Alternatively, the problem eigenvector can be set to some value determined from theory or from some other experiment (see Section 8.3.1), or additional data can be collected that are selected to make that combination of parameters determinate.

8.1.4. Methods for nonlinear least squares

Recall (equation 8.1.2.1) that the general, nonlinear problem can be stated in the form: find the minimum of

$$S(\mathbf{x}) = \sum_{i=1}^{n} w_i[y_i - M_i(\mathbf{x})]^2, \tag{8.1.4.1}$$

where $\mathbf{x}$ is a vector of p parameters, and $\boldsymbol{M}(\mathbf{x})$ represents a set of model functions that predict the values of observations, $\mathbf{y}$. In this section, we discuss two useful ways of solving this problem and consider the relative merits of each. The first is based on iteratively linearizing the functions $M_i(\mathbf{x})$ and approximating

(8.1.4.1) by one of the form in (8.1.2.5). The second uses an unconstrained minimization algorithm, based on Newton's method, to minimize $S(\mathbf{x})$.

8.1.4.1. *The Gauss–Newton algorithm*

Let $\mathbf{x}_c$ be the current approximation to $\hat{\mathbf{x}}$, the solution to (8.1.4.1). We construct a linear approximation to $M_i(\mathbf{x})$ in the vicinity of $\mathbf{x} = \mathbf{x}_c$ by expanding it in a Taylor series through the linear terms, obtaining

$$M_i(\mathbf{x}) = M_i(\mathbf{x}_c) + \sum_{j=1}^{p} J_{ij}(\mathbf{x} - \mathbf{x}_c)_j, \tag{8.1.4.2}$$

where $\boldsymbol{J}$ is the Jacobian matrix, defined by $J_{ij} = \partial M_i(\mathbf{x})/\partial x_j$. A straightforward procedure, known as the *Gauss–Newton algorithm*, may be formally stated as follows:

(1) compute $\mathbf{d}$ as the solution of the linear system

$$\boldsymbol{J}^T\boldsymbol{W}\boldsymbol{J}\mathbf{d} = \boldsymbol{J}^T\boldsymbol{W}[\mathbf{y} - \boldsymbol{M}(\mathbf{x}_c)];$$

(2) set $\mathbf{x}_c = \mathbf{x}_c + \mathbf{d}$;

(3) if not converged (see Subsection 8.1.4.4), go to (1), else stop.

The convergence rate of the Gauss–Newton algorithm depends on the size of the residual, that is, on $S(\hat{\mathbf{x}})$. If $S(\hat{\mathbf{x}}) = 0$, then the convergence rate is quadratic; if it is small, then the rate is linear; but if $S(\hat{\mathbf{x}})$ is large, then the procedure is not locally convergent at all. Fortunately, this procedure can be altered so that it is always locally convergent, and even globally convergent, that is, convergent to a relative minimum from any starting point. There are two possibilities. First, the procedure can be modified to include a line search. This is accomplished by computing the direction $\mathbf{d}$ as above and then choosing α such that $S(\mathbf{x}_c + \alpha\mathbf{d})$ is sufficiently smaller than $S(\mathbf{x}_c)$. In order to guarantee convergence, one uses the test

$$S(\mathbf{x}_c + \alpha\mathbf{d}) < S(\mathbf{x}_c) - \alpha\gamma\mathbf{d}^T\boldsymbol{J}(\mathbf{x}_c)^T[\mathbf{y} - \boldsymbol{M}(\mathbf{x}_c)], \tag{8.1.4.3}$$

where, as actually implemented in modern codes, γ has values of the order of 10^{-4}. [In theory, a slightly stronger condition is necessary, but this is usually avoided by other means. See Dennis & Schnabel (1983) for details.] While this improves the situation dramatically, it still suffers from the deficiency that it is very slow on some problems, and it is undefined if the rank of the Jacobian, $\boldsymbol{J}(\hat{\mathbf{x}})$, is less than p. $\boldsymbol{J}(\mathbf{x})$ usually has rank p near the solution, but it may be rank deficient far away. Also, it may be 'close' to rank deficient, and give numerical difficulties (see Subsection 8.1.3.3).

8.1.4.2. *Trust-region methods – the Levenberg–Marquardt algorithm*

These remaining problems can be addressed by the utilization of a trust-region modification to the basic Gauss–Newton algorithm. For this procedure, we compute the step, $\mathbf{d}$, as the solution to the linear least-squares problem subject to the constraint that $\|\mathbf{d}\| \le \tau_c$, where τ_c is the *trust-region radius*. Here, the linearized model is modified by admitting that the linearization is only valid within a limited region around the current approximation. It is clear that, if the trust region is sufficiently large, this constrained step will in fact be unconstrained, and the step will be the same as the Gauss–Newton step. If the constraint is active, however, the step has the form

$$[\boldsymbol{J}(\mathbf{x}_c)^T\boldsymbol{W}\boldsymbol{J}(\mathbf{x}_c) + \mu\boldsymbol{I}]\mathbf{d}(\mu) = \boldsymbol{J}(\mathbf{x}_c)\boldsymbol{W}[\mathbf{y} - \boldsymbol{M}(\mathbf{x}_c)], \tag{8.1.4.4}$$

where μ is the Lagrange multiplier corresponding to the constraint (see Section 8.3.1), that is, μ is the value such that $\|\mathbf{d}(\mu)\| = \tau_c$. Formula (8.1.4.4) is known as the *Levenberg–Marquardt* equation. It can be seen from this formula that the step direction is intermediate between the Gauss–Newton direction and the direction of steepest descent, for which reason it is frequently known as ''Marquardt's compromise'' (Draper & Smith, 1981).

Efficient numerical calculation of $\mathbf{d}$ for a given value of μ is accomplished by noting that (8.1.4.4) is equivalent to the linear least-squares problem, find the minimum of

$$S = \left\| \begin{pmatrix} \boldsymbol{J}(\mathbf{x}_c) \\ \sqrt{\mu}\boldsymbol{I} \end{pmatrix}\mathbf{d} - \begin{pmatrix} [\mathbf{y} - \boldsymbol{M}(\mathbf{x}_c)] \\ \boldsymbol{O} \end{pmatrix} \right\|^2. \tag{8.1.4.5}$$

This problem can be solved by saving the QR factorization for $\mu = 0$ and updating it for various values of μ greater than 0. The actual computation of μ is accomplished by a modified Newton method applied to the constraint equation (see Dennis & Schnabel, 1983, for details). Having calculated the constrained value of $\mathbf{d}$, we set $\mathbf{x}_+ = \mathbf{x}_c + \mathbf{d}$. The algorithm is completed by specifying a procedure for updating the trust-region parameter, τ_c, after each step. This is done by comparing the actual value of $S(\mathbf{x}_+)$ with the predicted value based on the linearization. If there is good agreement between these values, τ is increased. If there is not good agreement, τ is left unchanged, and if $S(\mathbf{x}_+) > S(\mathbf{x}_c)$, the step is rejected, and τ is reduced. Global convergence can be shown under reasonable conditions, and very good computational performance has been observed in practice.

8.1.4.3. *Quasi-Newton, or secant, methods*

The second class of methods for solving the general, nonlinear least-squares problem is based on the unconstrained minimization of the function $S(\mathbf{x})$, as defined in (8.1.4.1). Newton's method for solving this problem is derived by constructing a quadratic approximation to S at the current trial point, $\mathbf{x}_c$, giving

$$S_c(\mathbf{d}) = S(\mathbf{x}_c) + \mathbf{g}(\mathbf{x}_c)^T\mathbf{d} + (1/2)\mathbf{d}^T\boldsymbol{H}(\mathbf{x}_c)\mathbf{d}, \tag{8.1.4.6}$$

from which the Newton step is obtained by minimizing S_c with respect to $\mathbf{d}$. Here, $\mathbf{g}$ represents the gradient of S and $\boldsymbol{H}$ is the Hessian matrix, the $p \times p$ symmetric matrix of second partial derivatives, $H_{jk} = \partial^2 S/\partial x_j \partial x_k$. Thus, $\mathbf{d}$ is calculated by solving the linear system

$$\boldsymbol{H}(\mathbf{x}_c)\mathbf{d} = -\mathbf{g}(\mathbf{x}_c). \tag{8.1.4.7}$$

[Note: In the literature on optimization, the notation $\nabla^2 S(\mathbf{x})$ is often used to denote the Hessian matrix of the function $S(\mathbf{x})$. This should not be confused with the Laplacian operator.] While Newton's method is locally quadratically convergent, it suffers from well known drawbacks. First, it is not globally convergent without employing some form of line search or trust region to safeguard it. Second, it requires the computation of the Hessian of S in each iteration.

The Hessian, however, has the form

$$\boldsymbol{H}(\mathbf{x}_c) = \boldsymbol{J}(\mathbf{x}_c)^T\boldsymbol{W}\boldsymbol{J}(\mathbf{x}_c) + \boldsymbol{B}(\mathbf{x}_c), \tag{8.1.4.8}$$

where $\boldsymbol{B}(\mathbf{x})$ is given by

$$B(\mathbf{x}_c)_{jk} = \sum_{i=1}^{n} w_i[y_i - M_i(\mathbf{x}_c)]\partial M_i^2(\mathbf{x}_c)/\partial x_j \partial x_k. \tag{8.1.4.9}$$

The first term of the Hessian, which is dependent only on the Jacobian, is readily available, but $\boldsymbol{B}$, even if it is available analytically, is, typically, expensive to compute. Furthermore,

in some situations, such as in the vicinity of a more symmetric model, $\boldsymbol{H}(\mathbf{x}_c)$ may not be positive definite.

In order to overcome these difficulties, various methods have been proposed to approximate $\boldsymbol{H}$ without calculating $\boldsymbol{B}$. Because these methods are based on approximations to Newton's method, they are often referred to as *quasi-Newton methods*. Two popular versions use approximations to $\boldsymbol{B}$ that are known as the Davidon–Fletcher–Powell (DFP) update and the Broyden–Fletcher–Goldfarb–Shanno (BFGS) update, with BFGS being apparently superior in practice. The basic idea of both procedures is to use values of the gradient to update an approximation to the Hessian in such a way as to preserve as much previous information as possible, while incorporating the new information obtained in the most recent step. From (8.1.4.6), the gradient of $S_c(\mathbf{d})$ is

$$\mathbf{g}(\mathbf{x}_c + \mathbf{d}) = \mathbf{g}(\mathbf{x}_c) + \boldsymbol{H}(\mathbf{x}_c)\mathbf{d}. \tag{8.1.4.10}$$

If the true function is not quadratic, or if $\boldsymbol{H}$ is only approximately known, the gradient at the point $\mathbf{x}_c + \mathbf{d}$, where $\mathbf{d}$ is the solution of (8.1.4.7), will not vanish. We make use of the value of $\mathbf{g}(\mathbf{x}_c + \mathbf{d})$ to compute a correction to $\boldsymbol{H}$ to give a Hessian that would have predicted what was actually found. That is, find an *update matrix*, $\boldsymbol{B}'$, such that

$$[\boldsymbol{H}(\mathbf{x}_c) + \boldsymbol{B}'(\mathbf{x}_c)]\mathbf{d} = \mathbf{g}(\mathbf{x}_c + \mathbf{d}) - \mathbf{g}(\mathbf{x}_c). \tag{8.1.4.11}$$

This is known as the *secant*, or *quasi-Newton*, relation. An algorithm based on the BFGS update goes as follows: Given $\mathbf{x}_c$ and $\boldsymbol{H}_c$ (usually a scaled, identity matrix is used as the initial approximation, in which case the first step is in the steepest descent direction),

(1) solve $\boldsymbol{H}_c\mathbf{d} = -\mathbf{g}(\mathbf{x}_c)$ for the direction $\mathbf{d}$;
(2) compute α such that $S(\mathbf{x}_c + \alpha\mathbf{d})$ satisfies condition (8.1.4.3);
(3) set $\mathbf{x}_c = \mathbf{x}_c + \alpha\mathbf{d}$;
(4) update $\boldsymbol{H}_c$ by $\boldsymbol{H}_c + \mathbf{g}(\mathbf{x}_c)\mathbf{g}(\mathbf{x}_c)^T/\mathbf{d}^T\mathbf{g}(\mathbf{x}_c) + \mathbf{q}\mathbf{q}^T/\alpha\mathbf{q}^T\mathbf{d}$ (see Nash & Sofer, 1995), where $\mathbf{q} = \mathbf{g}(\mathbf{x}_c + \alpha\mathbf{d}) - \mathbf{g}(\mathbf{x}_c)$;
(5) if not converged, go to (1), else stop.

If, in step (2), the additional condition is applied that $\mathbf{d}^T\mathbf{g}(\mathbf{x}_c + \alpha\mathbf{d}) = 0$, it becomes an *exact line search*. This, however, is an unnecessarily severe condition, because it can be shown that, if $\mathbf{d}^T[\mathbf{g}(\mathbf{x}_c + \alpha\mathbf{d}) - \mathbf{g}(\mathbf{x}_c)] > 0$, the approximation to the Hessian remains positive definite. The two terms in this expression are values of $\mathrm{d}S/\mathrm{d}\alpha$, and the condition states that S does not decrease more rapidly as α increases, which will always be true for some range of values of $\alpha > 0$. This algorithm is globally convergent; it *will* find a point at which the gradient vanishes, although that point may be a false minimum. It should be noted, however, that the procedure does not produce a final Hessian matrix whose inverse necessarily has any resemblance to a variance–covariance matrix. To get that it is necessary to compute $\boldsymbol{J}(\widehat{\mathbf{x}})$ and from it compute $(\boldsymbol{J}^T\boldsymbol{W}\boldsymbol{J})^{-1}$.

If a scaled, identity matrix is used as the initial approximation to $\boldsymbol{H}$, no use is made of the fact that, at least in the vicinity of the minimum, a major part of the Hessian matrix is given by $\boldsymbol{J}(\mathbf{x}_c)^T\boldsymbol{W}\boldsymbol{J}(\mathbf{x}_c)$. Thus, if there can be reasonable confidence in the general features of the model, it is useful to use $\boldsymbol{J}(\mathbf{x}_c)^T\boldsymbol{W}\boldsymbol{J}(\mathbf{x}_c)$ as the initial approximation to $\boldsymbol{H}$, in which case the first step is in the Gauss–Newton direction. The line-search provision, however, guarantees convergence, and, when n and p are both large, as in many crystallographic applications of least squares, a quasi-Newton update gives an adequate approximation to the new Hessian with a great deal less computation.

Another procedure that makes use of the fact that the linear approximation gives a major part of the Hessian constructs an approximation of the form

$$\boldsymbol{H}(\mathbf{x}) = \boldsymbol{J}(\mathbf{x})^T\boldsymbol{W}\boldsymbol{J}(\mathbf{x}) + \boldsymbol{B}(\mathbf{x}), \tag{8.1.4.12}$$

where $\boldsymbol{B}$ is generated by quasi-Newton methods. The quasi-Newton condition that must be satisfied in this case is

$$[\boldsymbol{J}(\mathbf{x}_+)^T\boldsymbol{W}\boldsymbol{J}(\mathbf{x}_+) + \boldsymbol{B}(\mathbf{x}_+)]\mathbf{d}_c = \mathbf{q}_c, \tag{8.1.4.13}$$

where $\mathbf{d}_c = \mathbf{x}_+ - \mathbf{x}_c$, and

$$\mathbf{q}_c = \boldsymbol{J}(\mathbf{x}_+)^T\boldsymbol{W}[\mathbf{y} - \boldsymbol{M}(\mathbf{x}_+)] - \boldsymbol{J}(\mathbf{x}_c)^T\boldsymbol{W}[\mathbf{y} - \boldsymbol{M}(\mathbf{x}_c)].$$

A formula based on the BFGS update (Nash & Sofer, 1995) is

$$\boldsymbol{B}(\mathbf{x}_+) = \boldsymbol{B}(\mathbf{x}_c) - \boldsymbol{G}_c\mathbf{d}_c\mathbf{d}_c^T\boldsymbol{G}_c/\mathbf{d}_c^T\boldsymbol{G}\mathbf{d}_c + \mathbf{q}_c\mathbf{q}_c^T/\mathbf{q}_c^T\mathbf{d}_c, \tag{8.1.4.14}$$

where $\boldsymbol{G}_c = \boldsymbol{J}(\mathbf{x}_+)^T\boldsymbol{W}\boldsymbol{J}(\mathbf{x}_+) + \boldsymbol{B}(\mathbf{x}_c)$. Since $\boldsymbol{J}(\mathbf{x}_+)$ and $\boldsymbol{M}(\mathbf{x}_+)$ must be computed anyway, this technique maximizes the use of information with little additional computing. The resulting approximation to the Hessian, however, may not be positive definite, and precautions must be taken to ensure convergence. In the vicinity of a correct solution, where the residuals are small, the addition of $\boldsymbol{B}$ is not likely to help much, and it can be dropped. Far from the solution, however, it can be very helpful. An implementation of this procedure has been described by Bunch, Gay & Welsch (1993); it appears to be at least as efficient as the trust region, Levenberg–Marquardt procedure, and is probably better when residuals are large.

In actual practice, it is not the Hessian matrix itself that is updated, but rather its Cholesky factor (Prince, 1994). This requires approximately the same number of operations and allows the solution of the linear system for computing $\mathbf{d}$ in a time that increases in proportion to p^2. This strategy also allows the use of the approximate Hessian in convergence checks with no significant computational overhead and no extra storage, as would be required for storing both the Hessian and its inverse.

8.1.4.4. *Stopping rules*

An iterative algorithm must contain some criterion for termination of the iteration process. This is a delicate part of all nonlinear optimization codes, and depends strongly on the scaling of the parameters. Although exceptions exist to almost all reasonable scaling rules, a basic principle is that a unit change in any variable should have approximately the same effect on the sum of squares. Thus, as discussed in Subsection 8.1.3.3 (equation 8.1.3.9), the ideal unit for each parameter is the standard uncertainty of its estimate, which can usually be adequately approximated by the reciprocal of the column norm of $\boldsymbol{J}$. In modern codes, the user has the option of supplying a diagonal scaling matrix whose elements are the reciprocals of some estimate of a typical 'significant' shift in the corresponding parameter.

In principle, the following conditions should hold when the convergence of a well scaled, least-squares procedure has reached its useful limit:

(1) $S(\mathbf{x}_c) = S(\widehat{\mathbf{x}})$;
(2) $\boldsymbol{J}(\mathbf{x}_c)^T\boldsymbol{W}[\mathbf{y} - \boldsymbol{M}(\mathbf{x}_c)] = \boldsymbol{O}$;
(3) $\mathbf{x}_c = \widehat{\mathbf{x}}$.

The actual stopping rules must be chosen relative to the algorithm used (other conditions also exist) and the particular application. It is clear, however, that, since $\widehat{\mathbf{x}}$ is not known, the last two conditions cannot be used as stated. Also, these tests are dependent on the scaling of the problem, and the variables are not related to the sizes of the quantities involved. We present tests, therefore, that are relative error tests that take into account the scaling of the variables.

The general, relative error test is stated as follows. Two scalar quantities, a and b, are said to satisfy a relative error test with respect to a tolerence T if

$$\frac{|a-b|}{|a|} \leq T. \tag{8.1.4.15}$$

Roughly speaking, if T is of the form 10^{-q} then a and b agree to q digits. Obviously, there is a problem with this test if $a = 0$ and there will be numerical difficulties if a is close to 0. Thus, in practice, (8.1.4.15) is replaced by

$$|a-b| \leq (|a|+1)T, \tag{8.1.4.16}$$

which reduces to an absolute error test as $a \to 0$. A careful examination may be required to set this tolerance correctly, but, typically, if one of the fast, stable algorithms is used, only a few more iterations are necessary to get six or eight digits if one or two are already known. Note also that the actual value depends on ε, the relative machine precision. It is fruitless to seek more digits of accuracy than are expressed in the machine representation.

A test based on condition (1) is often implemented by using the linear approximation to $\boldsymbol{M}$ or the quadratic approximation to S. Thus, using the quadratic approximation to S, we can compute the predicted reduction by

$$\Delta_{\text{pred}} = S(\mathbf{x}_c) - \mathbf{d}^T\boldsymbol{J}^T\boldsymbol{W}[\mathbf{y} - \boldsymbol{M}(\mathbf{x}_c)]. \tag{8.1.4.17}$$

Similarly, the actual reduction is

$$\Delta_{\text{act}} = S(\mathbf{x}_c) - S(\mathbf{x}_+). \tag{8.1.4.18}$$

The test then becomes $\Delta_{\text{pred}} \leq [1 + S(\mathbf{x}_c)]T$, $\Delta_{\text{act}} \leq [1 + S(\mathbf{x}_c)]T$, and $\Delta_{\text{act}} \leq 2\Delta_{\text{pred}}$. That is, we want both the predicted and actual reductions to be small and the actual reduction to agree reasonably well with the predicted reduction. A typical value for T should be 10^{-4}, although the value again depends on ε, and the user is cautioned not to make this tolerance too loose.

For a test on condition (2), we compute the cosine of the angle between the vector of residuals and the linear subspace spanned by the columns of $\mathbf{J}$,

$$\cos\zeta = \{\mathbf{d}^T\boldsymbol{J}^T\boldsymbol{W}[\mathbf{y} - \boldsymbol{M}(\mathbf{x}_+)]\}/[(\mathbf{d}^T\boldsymbol{J}^T\boldsymbol{W}\boldsymbol{J}\mathbf{d})S(\mathbf{x}_+)]^{1/2}. \tag{8.1.4.19}$$

The test is $\cos\zeta \leq T$, where, again, T should be 10^{-4} or smaller.

Test 3 above is usually only present to prevent the process from continuing when almost nothing is happening. Clearly, we do not know $\hat{\mathbf{x}}$, thus the test is typically that corresponding elements of $\mathbf{x}_+$ and $\mathbf{x}_c$ satisfy (8.1.4.16), where T is chosen to be 10^{-q}. A recommended value of q is half the number of digits carried in the computation, *e.g.* $q = 8$ for standard 64-bit (double-precision or 16 digit) calculations. Sometimes, the relative error test is of the form $|(\mathbf{x}_+)_j - (\mathbf{x}_c)_j|/\sigma_j \leq T$, where σ_j is the standard uncertainty computed from the inverse Hessian in the last iteration. Although this test has some statistical validity, it is quite expensive and usually not worth the work involved to compute.

8.1.4.5. *Recommendations*

One situation in which the Gauss–Newton algorithm behaves particularly poorly is in the vicinity of a saddle point in parameter space, where the true Hessian matrix is not positive definite. This occurs in structure refinement where a symmetric model is refined to convergence and then is replaced by a less symmetric model. The hypersurface of S will have negative curvature in a finite sized region of the parameter space for the less-symmetric model, and it is *essential* to use a safeguarded algorithm, one that incorporates a line search or a trust region, in order to get out of that region.

On the basis of this discussion, we can draw the following conclusions:

(1) In cases where the fit is poor, owing to an incomplete model or in the initial stages of refinement, methods based on the quadratic approximation to S (quasi-Newton methods) often perform better. This is particularly important when the model is close to a more symmetric configuration. These methods are more expensive per iteration and generally require more storage, but their greater stability in such problems usually justifies the cost.

(2) With small residual problems, where the model is complete and close to the solution, a safeguarded Gauss–Newton method is preferred. The trust-region implementation (Levenberg–Marquardt algorithm) has been very successful in practice.

(3) The best advice is to pick a good implementation of either method and stay with it.

8.1.5. Numerical methods for large-scale problems

Because the least-squares problems arising in crystallography are often very large, the methods we have discussed above are not always the most efficient. Some large problems have special structure that can be exploited to produce quite efficient algorithms. A particular special structure is sparsity, that is, the problems have Jacobian matrices that have a large fraction of their entries zero. Of course, not all large problems are sparse, so we shall also discuss approaches applicable to more general problems.

8.1.5.1. *Methods for sparse matrices*

We shall first discuss large, sparse, linear least-squares problems (Heath, 1984), since these techniques form the basis for nonlinear extensions. As we proceed, we shall indicate how the procedures should be modified in order to handle nonlinear problems. Recall that the problem is to find the minimum of the quadratic form $[\mathbf{y} - \boldsymbol{A}\mathbf{x}]^T\boldsymbol{W}[\mathbf{y} - \boldsymbol{A}\mathbf{x}]$, where $\mathbf{y}$ is a vector of observations, $\boldsymbol{A}\mathbf{x}$ represents a vector of the values of a set of linear model functions that predict the values of $\mathbf{y}$, and $\boldsymbol{W}$ is a positive-definite weight matrix. Again, for convenience, we make the transformation $\mathbf{y}' = \boldsymbol{U}\mathbf{y}$, where $\boldsymbol{U}$ is the upper triangular Cholesky factor of $\boldsymbol{W}$, and $\boldsymbol{Z} = \boldsymbol{U}\boldsymbol{A}$, so that the quadratic form becomes $(\mathbf{y}' - \boldsymbol{Z}\mathbf{x})^T(\mathbf{y}' - \boldsymbol{Z}\mathbf{x})$, and the minimum is the solution of the system of normal equations, $\boldsymbol{Z}^T\boldsymbol{Z}\mathbf{x} = \boldsymbol{Z}^T\mathbf{y}'$. Even if $\boldsymbol{Z}$ is sparse, it is easy to see that $\boldsymbol{H} = \boldsymbol{Z}^T\boldsymbol{Z}$ need not be sparse, because if even one row of $\boldsymbol{Z}$ has all of its elements nonzero, all elements of $\boldsymbol{H}$ will be nonzero. Therefore, the direct use of the normal equations may preclude the efficient exploitation of sparsity. But suppose $\boldsymbol{H}$ *is* sparse. The next step in solving the normal equations is to compute the Cholesky decomposition of $\boldsymbol{H}$, and it may turn out that the Cholesky factor is not sparse. For example, if $\boldsymbol{H}$ has the form

$$\boldsymbol{H} = \begin{pmatrix} x & x & x & x \\ x & x & 0 & 0 \\ x & 0 & x & 0 \\ x & 0 & 0 & x \end{pmatrix},$$

where x represents a nonzero element, then the Cholesky factor, $\boldsymbol{R}$, will not be sparse, but if

$$\boldsymbol{H} = \begin{pmatrix} x & 0 & 0 & x \\ 0 & x & 0 & x \\ 0 & 0 & x & x \\ x & x & x & x \end{pmatrix},$$

then $\boldsymbol{R}$ has the form

$$\boldsymbol{R} = \begin{pmatrix} x & 0 & 0 & x \\ 0 & x & 0 & x \\ 0 & 0 & x & x \\ 0 & 0 & 0 & x \end{pmatrix}.$$

These examples show that, although the sparsity of $\boldsymbol{R}$ is independent of the row ordering of $\boldsymbol{Z}$, the column order can have a profound effect. Procedures exist that analyse $\boldsymbol{Z}$ and select a permutation of the columns that reduces the 'fill' in $\boldsymbol{R}$. An algorithm for using the normal equations is then as follows:

(1) determine a permutation, $\boldsymbol{P}$ (an orthogonal matrix with one and only one 1 in each row and column, and all other elements zero), that tends to ensure a sparse Cholesky factor;
(2) store the elements of $\boldsymbol{R}$ in a sparse format;
(3) compute $\boldsymbol{Z}^T\boldsymbol{Z}$ and $\boldsymbol{Z}^T\mathbf{y}'$;
(4) factor $\boldsymbol{P}^T(\boldsymbol{Z}^T\boldsymbol{Z})\boldsymbol{P}$ to get $\boldsymbol{R}$;
(5) solve $\boldsymbol{R}^T\mathbf{z} = \boldsymbol{P}^T\boldsymbol{Z}^T\mathbf{y}'$;
(6) solve $\boldsymbol{R}\tilde{\mathbf{x}} = \mathbf{z}$;
(7) set $\hat{\mathbf{x}} = \boldsymbol{P}^T\tilde{\mathbf{x}}$.

This algorithm is fast, and it will produce acceptable accuracy if the condition number of $\boldsymbol{Z}$ is not too large. If extension to the nonlinear case is considered, it should be kept in mind that the first two steps need only be done once, since the sparsity pattern of the Jacobian does not, in general, change from iteration to iteration.

The QR decomposition of matrices that may be kept in memory is most often performed by the use of Householder transformations (see Subsection 8.1.1.1). For sparse matrices, or for matrices that are too large to be held in memory, this technique has several drawbacks. First, the method works by inserting zeros in the columns of $\boldsymbol{Z}$, working from left to right, but at each step it tends to fill in the columns to the right of the one currently being worked on, so that columns that are initially sparse cease to be so. Second, each Householder transformation needs to be applied to all of the remaining columns, so that the entire matrix must be retained in memory to make efficient use of this procedure.

The alternative procedure for obtaining the QR decomposition by the use of Givens rotations overcomes these problems if the entire upper triangular matrix, $\boldsymbol{R}$, can be stored in memory. Since this only requires about $p^2/2$ locations, it is usually possible. Also, it may happen that $\boldsymbol{R}$ has a sparse representation, so that even fewer locations will be needed. The algorithm based on Givens rotations is as follows:

(1) bring in the first p rows;
(2) find the QR decomposition of this $p \times p$ matrix;
(3) for $i = p + 1$ to n, do
  (*a*) bring in row i;
  (*b*) eliminate row i using $\boldsymbol{R}$ and at most p Givens rotations.

In order to specify how to use this algorithm to solve the linear least-squares problem, we must also state how to account for $\boldsymbol{Q}$. We could accumulate $\boldsymbol{Q}$ or save enough information to generate it later, but this usually requires excessive storage. The better alternatives are either to apply the steps of $\boldsymbol{Q}$ to $\mathbf{y}'$ as we proceed or to simply discard the information and solve $\boldsymbol{R}^T\boldsymbol{R}\mathbf{x} = \boldsymbol{Z}^T\mathbf{y}'$. It should be noted that the order of rows can make a significant difference. Suppose

$$\boldsymbol{Z} = \begin{pmatrix} x & 0 & 0 & 0 & 0 \\ 0 & x & 0 & 0 & 0 \\ 0 & 0 & x & 0 & 0 \\ 0 & 0 & 0 & x & 0 \\ 0 & 0 & 0 & 0 & x \\ x & 0 & 0 & 0 & 0 \\ x & 0 & 0 & 0 & 0 \\ x & 0 & 0 & 0 & 0 \\ x & x & x & x & x \end{pmatrix}.$$

The work to complete the QR decomposition is of order p^2 operations, because each element below the main diagonal can be eliminated by one Givens rotation with no fill, whereas for

$$\boldsymbol{Z} = \begin{pmatrix} x & x & x & x & x \\ x & 0 & 0 & 0 & 0 \\ x & 0 & 0 & 0 & 0 \\ x & 0 & 0 & 0 & 0 \\ x & 0 & 0 & 0 & 0 \\ 0 & x & 0 & 0 & 0 \\ 0 & 0 & x & 0 & 0 \\ 0 & 0 & 0 & x & 0 \\ 0 & 0 & 0 & 0 & x \end{pmatrix}$$

each Givens rotation fills an entire row, and the QR decomposition requires of order np^2 operations.

8.1.5.2. *Conjugate-gradient methods*

A numerical procedure that is applicable to large-scale problems that may not be sparse is called the *conjugate-gradient method*. Conjugate-gradient methods were originally designed to solve the quadratic minimization problem, find the minimum of

$$S(\mathbf{x}) = (1/2)\mathbf{x}^T\boldsymbol{H}\mathbf{x} - \mathbf{b}^T\mathbf{x}, \tag{8.1.5.1}$$

where $\boldsymbol{H}$ is a symmetric, positive-definite matrix. The gradient of S is

$$\mathbf{g}(\mathbf{x}) = \boldsymbol{H}\mathbf{x} - \mathbf{b}, \tag{8.1.5.2}$$

and its Hessian matrix is $\boldsymbol{H}$. Given an initial estimate, $\mathbf{x}_0$, the conjugate-gradient algorithm is

(1) define $\mathbf{d}_0 = -\mathbf{g}(\mathbf{x}_0)$;
(2) for $k = 0, 1, 2, ..., p - 1$, $\mathbf{d}_0$
  (*a*) $\alpha_k = -\mathbf{d}_k^T\mathbf{g}(\mathbf{x}_k)/\mathbf{d}_k^T\boldsymbol{H}\mathbf{d}_k$;
  (*b*) $\mathbf{x}_{k+1} = \mathbf{x}_k + \alpha_k\mathbf{d}_k$;
  (*c*) $\gamma_k = \mathbf{g}(\mathbf{x}_{k+1})^T\mathbf{g}(\mathbf{x}_{k+1})/\mathbf{g}(\mathbf{x}_k)^T\mathbf{g}(\mathbf{x}_k)$;
  (*d*) $\mathbf{d}_{k+1} = -\mathbf{g}(\mathbf{x}_k) + \gamma_k\mathbf{d}_k$.

This algorithm finds the exact solution for the quadratic function in not more than p steps.

This algorithm cannot be used directly for the nonlinear case because it requires $\boldsymbol{H}$ to compute α_k, and the goal is to solve the problem without computing the Hessian. To accomplish this, the exact computation of α is replaced by an actual line search, and the termination after at most p steps is replaced by a convergence test. Thus, we obtain, for a given starting value $\mathbf{x}_0$ and a general, nonquadratic function S:

(1) define $\mathbf{d}_0 = -\mathbf{g}(\mathbf{x}_0)$;
(2) set $k = 0$;
(3) do until convergence
  (*a*) $\mathbf{x}_{k+1} = \mathbf{x}_k + \alpha_k\mathbf{d}_k$, where α is chosen by a line search;
  (*b*) $\gamma_k = \mathbf{g}(\mathbf{x}_{k+1})^T\mathbf{g}(\mathbf{x}_{k+1})/\mathbf{g}(\mathbf{x}_k)^T\mathbf{g}(\mathbf{x}_k)$;
  (*c*) $\mathbf{d}_{k+1} = -\mathbf{g}(\mathbf{x}_{k+1}) + \gamma_k\mathbf{d}_k$;
  (*d*) $k = k + 1$.

Note that, as promised, $\boldsymbol{H}$ is not needed. In practice, it has been observed that the line search need not be exact, but that

periodic restarts in the steepest-descent direction are often helpful. This procedure often requires more iterations and function evaluations than methods that store approximate Hessians, but the cost per iteration is small. Thus, it is often the overall least-expensive method for large problems.

For the least-squares problem, recall that we are finding the minimum of

$$S(\mathbf{x}) = (1/2)[\mathbf{y}' - \mathbf{Z}\mathbf{x}]^T[\mathbf{y}' - \mathbf{Z}\mathbf{x}], \tag{8.1.5.3}$$

for which

$$\mathbf{g}(\mathbf{x}) = \mathbf{Z}^T(\mathbf{Z}\mathbf{x} - \mathbf{y}'). \tag{8.1.5.4}$$

By using these definitions in the conjugate-gradient algorithm, it is possible to formulate a specific algorithm for linear least squares that requires only the calculation of $\boldsymbol{Z}$ times a vector and $\boldsymbol{Z}^T$ times a vector, and never requires the calculation or factorization of $\boldsymbol{Z}^T\boldsymbol{Z}$.

In practice, such an algorithm will, due to roundoff error, sometimes require more than p iterations to reach a solution. A detailed examination of the performance of the procedure shows, however, that fewer than p iterations will be required if the eigenvalues of $\boldsymbol{Z}^T\boldsymbol{Z}$ are bunched, that is, if there are sets of multiple eigenvalues. Specifically, if the eigenvalues are bunched into k distinct sets, then the conjugate-gradient method will converge in k iterations. Thus, significant improvements can be made if the problem can be transformed to one with bunched eigenvalues. Such a transformation leads to the so-called *preconditioned conjugate-gradient method*. In order to analyse the situation, let $\boldsymbol{C}$ be a $p \times p$ matrix that transforms the variables, such that

$$\mathbf{x}' = \boldsymbol{C}\mathbf{x}. \tag{8.1.5.5}$$

Then,

$$\mathbf{y}' - \mathbf{Z}\mathbf{x} = \mathbf{y}' - \boldsymbol{Z}\boldsymbol{C}^{-1}\mathbf{x}'. \tag{8.1.5.6}$$

Therefore, $\boldsymbol{C}$ should be such that the system $\boldsymbol{C}\mathbf{x} = \mathbf{x}'$ is easy to solve, and $(\boldsymbol{Z}\boldsymbol{C}^{-1})^T\boldsymbol{Z}\boldsymbol{C}^{-1}$ has bunched eigenvalues. The ideal choice would be $\boldsymbol{C} = \boldsymbol{R}$, where $\boldsymbol{R}$ is the upper triangular factor of the QR decomposition, since $\boldsymbol{Z}\boldsymbol{R}^{-1} = \boldsymbol{Q}_{\boldsymbol{Z}}$. $\boldsymbol{Q}_{\boldsymbol{Z}}^T\boldsymbol{Q}_{\boldsymbol{Z}} = \boldsymbol{I}$ has all of its eigenvalues equal to one, and, since $\boldsymbol{R}$ is triangular, the system is easy to solve. If $\boldsymbol{R}$ were known, however, the problem would already be exactly solved, so this is not a useful alternative. Unfortunately, no universal best choice seems to exist, but one approach is to choose a sparse approximation to $\boldsymbol{R}$ by ignoring rows that cause too much fill in or by making $\boldsymbol{R}$ a diagonal matrix whose elements are the Euclidean norms of the columns of $\boldsymbol{Z}$. Bear in mind that, in the nonlinear case, an expensive computation to choose $\boldsymbol{C}$ in the first iteration may work very well in subsequent iterations with no further expense. One should be aware of the trade off between the extra work per iteration of the preconditioned-conjugate gradient method *versus* the reduction in the number of iterations. This is especially important in nonlinear problems.

The solution of large, least-squares problems is currently an active area of research, and we have certainly not given an exhaustive list of methods in this chapter. The choice of method or approach for any particular problem is dependent on many conditions. Some of these are:

(1) The size of the problem. Clearly, as computer memories continue to grow, the boundary between small and large problems also grows. Nevertheless, even if a problem can fit into memory, its sparsity structure may be exploited in order to obtain a more efficient algorithm.

(2) The number of times the problem (or similar ones) will be solved. If it is a one-shot problem (a rare occurrence), then one is usually most strongly influenced by easy-to-use, existing software. Exceptions, of course, exist where even a single solution of the problem requires extreme care.

(3) The expense of evaluating the function. With a complicated, nonlinear function like the structure-factor formula, the computational effort to determine the values of the function and its derivatives usually greatly exceeds that required to solve the linearized problem. Therefore, a full Gauss–Newton, trust-region, or quasi-Newton method may be warranted.

(4) Other structure in the problem. Rarely does a problem have a random sparsity pattern. Non-zero values usually occur in blocks or in some regular pattern for which special decomposition methods can be devised.

(5) The machine on which the problem is to be solved. We have said nothing about the existing vector and parallel processors. Suffice it to say that the most efficient procedure for a serial machine may not be the right algorithm for one of these novel machines. Appropriate numerical methods for such architectures are also being actively investigated.

8.1.6. Orthogonal distance regression

It is often useful to consider the data for a least-squares problem to be in the form (t_i, y_i), $i = 1, \ldots, n$, where the t_i are considered to be the *independent* variables and the y_i the dependent variables. The implicit assumption in ordinary least squares is that the independent variables are known exactly. It sometimes occurs, however, that these independent variables also have errors associated with them that are significant with respect to the errors in the observations y_i. In such cases, referred to as 'errors in variables' or 'measurement error models', the ordinary least-squares methodology is not appropriate and its use may give misleading results (see Fuller, 1987).

Let us define $\hat{M}(t_i, \mathbf{x})$ to be the model functions that predict the y_i. Observe that ordinary least squares minimizes the sum of the squares of the vertical distances from the observed points y_i to the curve $\hat{M}(t, \mathbf{x})$. If t_i has an error δ_i, and these errors are normally distributed, then the maximum-likelihood estimate of the parameters is found by minimizing the sum of the squares of the *weighted orthogonal distances* from the point y_i to the curve $\hat{M}(t, \mathbf{x})$. More precisely, the optimization problem to be solved is given by

$$\min_{\mathbf{x},\delta} \sum_{i=1}^{n} \left\{ \left[y_i - \hat{M}(t_i + \delta_i, \mathbf{x})\right]^T \mathbf{W}_{\mathbf{y}} \left[y_i - \hat{M}(t_i + \delta_i, \mathbf{x})\right] + \delta_i^T \mathbf{W}_{\mathbf{t}} \delta_i \right\}, \tag{8.1.6.1}$$

where $\mathbf{W}_{\mathbf{y}}$ and $\mathbf{W}_{\mathbf{t}}$ are appropriately chosen weights. Problem (8.1.6.1) is called the *orthogonal distance regression* (ODR) problem. Problem (8.1.6.1) can be solved as a least-squares problem in the combined variables $\mathbf{x}, \delta$ by the methods given above. This, however, is quite inefficient, since such a procedure would not exploit the special structure of the ODR problem. Few algorithms that exploit this structure exist; one has been given by Boggs, Byrd & Schnabel (1987), and the software, called *ODRPACK*, is by Boggs, Byrd, Donaldson & Schnabel (1989). The algorithm is based on the trust-region (Levenberg–Marquardt) method described above, but it exploits the special structure of (8.1.6.1) so that the cost of each iteration is no more expensive than the cost of a similar iteration of the corresponding

ordinary least-squares problems. For a discussion of some of the statistical properties of the resulting estimates, including a procedure for the computation of the variance–covariance matrix, see Boggs & Rogers (1990).

8.1.7. Software for least-squares calculations

Giving even general recommendations on software is a difficult task for several reasons. Clearly, the selection of methods discussed in earlier sections contains implicitly some recommendations for approaches. Among the reasons for avoiding specifics are the following:

(1) Assessing differences in performance among various codes requires a detailed knowledge of the criteria the developer of a particular code used in creating it. A program written to emphasize speed on a certain class of problems on a certain machine is impossible to compare directly with a program written to be very reliable on a wide class of problems and portable over a wide range of machines. Other measures, including ease of maintenance and modification and ease of use, and other design criteria, such as interactive *versus* batch, stand alone *versus* user-callable, automatic computation of related statistics *versus* no statistics, and so forth, make the selection of software analogous to the selection of a car.

(2) Choosing software requires detailed knowledge of the needs of the user and the resources available to the user. Considerations such as problem size, machine size, machine architecture and financial resources all enter into the decision of which software to obtain.

(3) A software recommendation made on the basis of today's knowledge ignores the fact that algorithms continue to be invented, and old algorithm continue to be rethought in the light of new developments and new machine architectures. For example, when vector processors first appeared, algorithms for sparse-matrix calculations were very poor at exploiting this capability, and it was thought that these new machines were simply not appropriate for such calculations. Now, however, recent methods for sparse matrices have achieved a high degree of vectorization. For another example, early programs for crystallographic, full-matrix, least-squares refinement spent a large fraction of the time building the normal-equations matrix. The matrix was then inverted using a procedure called Gaussian elimination, which does not exploit the fact that the matrix is positive definite. Some programs were later converted to use Cholesky decomposition, which is at least twice as fast, but many were not because the inversion process took a small fraction of the total time. Linear algebra, however, is readily adaptable to vector and parallel machines, and procedures such as QR factorization are extremely fast, while the calculation of structure factors, with its repeated evaluations of trigonometric functions, becomes the time-controlling step.

The general recommendation is to analyse carefully the needs and resources in terms of these considerations, and to seek expert assistance whenever possible. *As much as possible, avoid the temptation to write your own codes*. Despite the fact that the quality of existing software is far from uniformly high, the benefits of utilizing high-quality software generally far outweigh the costs of finding, obtaining, and installing it.

Sources of information on software have improved significantly in the past several years. Nevertheless, the task of identifying software in terms of problems that can be solved; organizing, maintaining and updating such a list; and informing the user community still remains formidable.

A current, problem-oriented system that includes both a problem classification scheme and a network tool for obtaining documentation and source code (for software in the public domain) is the *Guide to Available Mathematical Software* (GAMS). This system is maintained by the National Institute of Standards and Technology (NIST) and is continually being updated as new material is received. It gives references to software in several software repositories; the URL is http://math.nist.gov/gams.

International Tables for Crystallography (2006). Vol. C, Chapter 8.2, pp. 689–692.

8.2. Other refinement methods

By E. Prince and D. M. Collins

Chapter 8.1 discusses structure refinement by the method of least squares, which has a long history of successful use in data fitting and statistical analysis of results. It is an excellent technique to use in a wide range of practical problems, it is easy to implement, and it usually gives results that are straightforward and unambiguous. If a set of observations, y_i, is an unbiased estimate of the values of model functions, $M_i(\mathbf{x})$, a properly weighted least-squares estimate is the best, linear, unbiased estimate of the parameters, $\mathbf{x}$, provided the variances of the p.d.f.s of the populations from which the observations are drawn are finite. This assumes, however, that the model is correct and complete, an assumption whose validity may not necessarily be easily justified. Furthermore, least squares tends to perform poorly when the distribution of errors in the observations has longer tails than a normal, or Gaussian, distribution. For these reasons, a number of other procedures have been developed that attempt to retain the strengths of least squares but are less sensitive to departures from the ideal conditions that have been implicitly assumed. In this chapter, we discuss several of these methods. Two of them, maximum-likelihood methods and robust/resistant methods, are closely related to least squares. A third one uses a function that is mathematically related to the entropy function of thermodynamics and statistical mechanics, and is therefore referred to as the maximum-entropy method. For a discussion of the particular application of least squares to structure refinement with powder data that has become known as the Rietveld method (Rietveld, l969), see Chapter 8.6.

8.2.1. Maximum-likelihood methods

In Chapter 8.1, structure refinement is presented as finding the answer to the question, 'given a set of observations drawn randomly from populations whose means are given by a model, $\boldsymbol{M}(\mathbf{x})$, for some set of unknown parameters, $\mathbf{x}$, how can we best determine the means, variances and covariances of a joint probability density function that describes the probabilities that the true values of the elements of $\mathbf{x}$ lie in certain ranges?'. For a broad class of density functions for the observations, the linear estimate that is unbiased and has minimum variances for all parameters is given by the properly weighted method of least squares. The problem can also be stated in the slightly different manner, 'given a model and a set of observations, what is the *likelihood* of observing those particular values, and for what values of the parameters of the model is that likelihood a maximum?'. This set of parameters is the *maximum-likelihood estimate*.

Suppose the ith observation is drawn from a population whose p.d.f. is $\Phi_i(\Delta_i)$, where $\Delta_i = [y_i - M_i(\mathbf{x})]/s_i$, $\mathbf{x}$ is the set of 'true' values of the parameters, and s_i is a measure of scale appropriate to that observation. If the observations are independent, their joint p.d.f. is the product of the individual, marginal p.d.f.s:

$$\Phi_J(\Delta) = \prod_{i=1}^{n} \Phi_i(\Delta_i). \qquad (8.2.1.1)$$

The function $\Phi_i(\Delta_i)$ can also be viewed as a conditional p.d.f. for y_i given $M_i(\mathbf{x})$, or, equivalently, as a likelihood function for $\mathbf{x}$ given an observed value of y_i, in which case it is written $l_i(\mathbf{x}|y_i)$. Because a value actually observed logically must have a finite, positive likelihood, the density function in (8.2.1.1) and its logarithm will be maximum for the same values of $\mathbf{x}$:

$$\ln[l(\mathbf{x}|\mathbf{y})] = \sum_{i=1}^{n} \ln[l_i(\mathbf{x}|y_i)]. \qquad (8.2.1.2)$$

In the particular case where the error distribution is normal, and σ_i, the standard uncertainty of the ith observation, is known, then

$$\Phi_i(\Delta_i) = \frac{1}{\sqrt{2\pi}\sigma_i} \exp\left(-(1/2)\{[y_i - M_i(\mathbf{x})]/\sigma_i\}^2\right), \qquad (8.2.1.3)$$

and the logarithm of the likelihood function is maximum when

$$S = \sum_{i=1}^{n} \{[y - M_i(\mathbf{x})]/\sigma_i\}^2 \qquad (8.2.1.4)$$

is minimum, and the maximum-likelihood estimate and the least-squares estimate are identical.

For an error distribution that is not normal, the maximum-likelihood estimate will be different from the least-squares estimate, but it will, in general, involve finding a set of parameters for which a sum of terms like those in (8.2.1.2) is a maximum (or the sum of the negatives of such terms is a minimum). It can thus be expressed in the general form: find the minimum of the sum

$$S = \sum_{i=1}^{n} \rho(\Delta_i), \qquad (8.2.1.5)$$

where ρ is defined by $\rho(x) = -\ln[\Phi(x)]$, and $\Phi(x)$ is the p.d.f. of the error distribution appropriate to the observations. If $\rho(x) = x^2/2$, the method is least squares. If the error distribution is the Cauchy distribution, $\Phi(x) = [\pi(1 + x^2)]^{-1}$, $\rho(x) = \ln(1 + x^2)$, which increases much more slowly than x^2 as $|x|$ increases, causing large deviations to have much less influence than they do in least squares.

Although there is no need for $\rho(x)$ to be a symmetric function of x (the error distribution can be skewed), it may be assumed to have a minimum at $x = 0$, so that $\mathrm{d}\rho(x)/\mathrm{d}x = 0$. A series expansion about the origin therefore begins with the quadratic term, and

$$\rho(x) = (x^2/2)\left(1 + \sum_{k=1}^{\infty} a_k x^k\right). \qquad (8.2.1.6)$$

This procedure is thus equivalent to a variant of least squares in which the weights are functions of the deviation.

8.2.2. Robust/resistant methods

Properly weighted least squares gives the best *linear* estimate for a very broad range of distributions of random errors in the data and the maximum-likelihood estimate if that error distribution is normal or Gaussian. But the best linear estimator may nevertheless not be a very good one, and the error distribution may not be well known. It is therefore important to address the question of how good an estimation procedure may be when the conditions for which it is designed may not be satisfied. Refinement procedures may be classified according to the extent that they possess two properties known as robustness and resistance. A procedure is said to be *robust* if it works well for a broad range of error distributions and *resistant* if its results are not strongly affected by fluctuations in any small subset of the data. Because least squares is a linear estimator, the influence of any single data point on the parameter estimates increases without limit as the difference between the observation and the model increases. It therefore works poorly if the actual error

Copyright © 2006 International Union of Crystallography

distribution contains large deviations with a frequency that substantially exceeds that expected from a normal distribution. Further, it has the undesirable property that it will make the fit of a few wildly discrepant data points better by making the fit of many points a little worse. Least squares is therefore neither robust nor resistant.

Tukey (1974) has listed a number of properties a procedure should have in order to be robust and resistant. Because least squares works well when the error distribution is normal, the procedure should behave like least squares for small deviations whose distribution is similar to the normal distribution. It should de-emphasize large differences between the model and the data, and it should connect these extremes smoothly. A procedure suggested by Tukey was applied to crystal structure refinement by Nicholson, Prince, Buchanan & Tucker (1982). It corresponds to a fitting function $\rho(\Delta)$ [equation (8.2.1.5)] of the form

$$\begin{aligned} \rho(\Delta) &= \left(\Delta^2/2\right)\left(1 - \Delta^2 + \Delta^4/3\right) \qquad |\Delta| < 1, \\ \rho(\Delta) &= 1/6 \qquad\qquad\qquad\qquad\quad |\Delta| \geq 1, \end{aligned} \tag{8.2.2.1}$$

where $\Delta_i = [y_i - M_i(\mathbf{x})]/s_i$, and s is a resistant measure of scale.

In order to see what is meant by a resistant measure, consider a large sample of observations, y_i, with a normal distribution. The sample mean,

$$\overline{y} = (1/n)\sum_{i=1}^{n} y_i, \tag{8.2.2.2}$$

is an unbiased estimate of the population mean. Contamination of the sample by a small number of observations containing large, systematic errors, however, would have a large effect on the estimate. The median value of y_i is also an unbiased estimate of the population mean, but it is virtually unaffected by a few contaminating points. Similarly, the sample variance,

$$s^2 = [1/(n-1)]\sum_{i=1}^{n}(y_i - \overline{y})^2, \tag{8.2.2.3}$$

is an unbiased estimate of the population variance, but, again, it is strongly affected by a few discrepant points, whereas $[0.7413 r_q]^2$, where r_q is the *interquartile range*, the difference between the first and third quartile observations, is an estimate of the population variance that is almost unaffected by a small number of discrepant points. The median and the interquartile range are thus resistant quantities that can be used to estimate the mean and variance of a population distribution when the sample may contain points that do not belong to the population. A value of the scale parameter, s_i, for use in evaluating the quantities in (8.2.2.1), that has proved to be useful is $s_i = 9\left|\delta_m\right|\sigma_i$, where $\left|\delta_m\right|$ represents the median value of $\left|[y_i - M_i(\mathbf{x})]/\sigma_i\right|$, the *median absolute deviation*, or MAD.

Implementation of a procedure based on the function given in (8.2.2.1) involves modification of the weights used in each cycle by

$$\begin{aligned} \varphi(\Delta) &= \left(1 - \Delta^2\right)^2, \qquad |\Delta| < 1, \\ \varphi(\Delta) &= 0, \qquad\qquad\quad |\Delta| \geq 1. \end{aligned} \tag{8.2.2.4}$$

Because of this weight modification, the procedure is sometimes referred to as 'iteratively reweighted least squares'. It should be recognized, however, that the function that is minimized is more complex than a sum of squares. In a strict application of the Gauss–Newton algorithm (see Section 8.1.3) to the minimization of this function, each term in the summations to form the normal-equations matrix contains a factor $\omega(\Delta_i)$, where $\omega(\Delta) = \mathrm{d}^2\rho/\mathrm{d}\Delta^2 = 1 - 6\Delta^2 + 5\Delta^4$. This factor actually gives some data points a negative effective 'weight', because the sum is actually reduced by making the fit worse. The inverse of this normal-equations matrix is not an estimate of the variance–covariance matrix; for that the unmodified weights, equal to $1/\sigma_i^2$, must be used, but, because more discrepant points have been deliberately down weighted relative to the ideal weights, the variances are, in general, underestimated. A recommended procedure (Huber, 1973; Nicholson *et al.*, 1982) is to calculate the normal-equations matrix using the unmodified weights, invert that matrix, and premultiply by an estimate of the variance of the residuals (Section 8.4.1) using modified weights and $(n-p)$ degrees of freedom. Huber showed that this estimate is biased low, and suggests multiplication by a number, c^2, greater than one, and given by

$$c = [1 + p s_\omega^2/n\overline{\omega}^2]/\overline{\omega}, \tag{8.2.2.5}$$

where $\overline{\omega}$ is the mean value, and s_ω^2 is the variance of $\omega(\Delta_i)$ over the entire data set. The conditions under which this expression is derived are not well satisfied in the crystallographic problem, but, if n/p is large and $\overline{\omega}$ is not too much less than one, the value of c will be close to $1/\overline{\omega}$. $\overline{\omega}$ plays the role of a 'variance efficiency factor'. That is, the variances are approximately those that would be achieved with a least-squares fit to a data set with normally distributed errors that contained $n\overline{\omega}$ data points.

Robust/resistant methods have been discussed in detail by Huber (1981), Belsley, Kuh & Welsch (1980), and Hoaglin, Mosteller & Tukey (1983). An analysis by Wilson (1976) shows that a fitting procedure gives unbiased estimates if

$$\sum_{i=1}^{n}\left[\left(\frac{\partial w_i}{\partial y_{ci}}\right)\left(\frac{\mathrm{d}y_{ci}}{\mathrm{d}x}\right)\sigma_i^2\right] = 2\sum_{i=1}^{n}\left[\left(\frac{\partial w_i}{\partial y_{oi}}\right)\left(\frac{\mathrm{d}y_{ci}}{\mathrm{d}x}\right)\sigma_i^2\right], \tag{8.2.2.6}$$

where y_{oi} and y_{ci} are the observed and calculated values of y_i, respectively. Least squares is the case where all terms on both sides of the equation are equal to zero; the weights are fixed. In maximum-likelihood estimation or robust/resistant estimation, the effective weights are functions of the deviation, causing possible introduction of bias. Equation (8.2.2.6), however, suggests that the estimates will still be unbiased if the sums on both sides are zero, which will be the case if the error distribution and the weight modification function are both symmetric about $\Delta = 0$.

Note that the fact that two different weighting schemes applied to the same data lead to different values for the estimate does not necessarily imply that either value is biased. As long as the observations represent unbiased estimates of the values of the model functions, any weighting scheme gives unbiased estimates of the model parameters, although some weighting schemes will cause those estimates to be more precise than others will. Bias can be introduced if a procedure *systematically* causes fluctuations in one direction to be weighted more heavily than fluctuations in the other. For example, in the Rietveld method (Chapter 8.6), the observations are counts of quanta, which are subject to fluctuation according to the Poisson distribution, where the probability of observing k counts per unit time is given by

$$\Phi(k) = \lambda^k \exp(-\lambda)/k!. \tag{8.2.2.7}$$

The mean and the variance of this p.d.f. are both equal to λ, so that the ideal weighting should have $w_i = 1/\lambda_i$. However, λ_i is not known *a priori*, and must be estimated. The usual procedure is to take k_i as an estimate of λ_i, but this is an unbiased estimate only asymptotically for large k (Box & Tiao, 1973), and, furthermore, causes observations that have negative, random errors to be weighted more heavily than observations that have positive ones. This correlation can be removed by using, after a preliminary cycle of refinement, $M_i(\widehat{\mathbf{x}})$ as an estimate of λ_i. This

might seem to have the effect of making the weights dependent on the calculated values, so that the right-hand side of (8.2.2.6) is no longer zero, but this applies only if the weights are changed during the refinement. There is thus no conflict with the result in (8.1.2.9). In practice, in any case, many other sources of uncertainty are much more important than any possible bias that could be introduced by this effect.

8.2.3. Entropy maximization

8.2.3.1. *Introduction*

Entropy maximization, like least squares, is of interest primarily as a framework within which to find or adjust parameters of a model. Rationalization of the name 'entropy maximization' by analogy to thermodynamics is controversial, but there is formal proof (Shore & Johnson, 1980) supporting entropy maximization as the unique method of inference that satisfies basic consistency requirements (Livesey & Skilling, 1985). The proof consists of discovering the consequences of four consistency axioms, which may be stated informally as follows:

(1) the result of the inference should be unique;
(2) the result of the inference should be invariant to any transformations of coordinate system;
(3) it should not matter whether independent information is accounted for independently or jointly;
(4) it should not matter whether independent subsystems are treated separately in conditional problems or collected and treated jointly.

The term 'entropy' is used in this chapter as a name only, the name for variation functions that include the form $\varphi \ln \varphi$, where φ may represent probability or, more generally, a positive proportion. Any positive measure, either observed or derived, of the relative apportionment of a characteristic quantity among observations can serve as the proportion.

The method of entropy maximization may be formulated as follows: given a set of n observations, y_i, that are measurements of quantities that can be described by model functions, $M_i(\mathbf{x})$, where $\mathbf{x}$ is a vector of parameters, find the prior, positive proportions, $\mu_i = f(y_i)$, and the values of the parameters for which the positive proportions $\varphi = f[M_i(\mathbf{x})]$ make the sum

$$S = -\sum_{i=1}^{n} \varphi_i' \ln(\varphi_i'/\mu_i'), \tag{8.2.3.1}$$

where $\varphi_i' = \varphi_i / \sum \varphi_j$ and $\mu_i' = \mu_i / \sum \mu_j$, a maximum. S is called the *Shannon–Jaynes entropy*. For some applications (Collins, 1982), it is desirable to include in the variation function additional terms or restraints that give S the form

$$S = -\sum_{i=1}^{n} \varphi_i' \ln(\varphi_i'/\mu_i') + \lambda_1 \xi_1(\mathbf{x}, \mathbf{y}) + \lambda_2 \xi_2(\mathbf{x}, \mathbf{y}) + \ldots, \tag{8.2.3.2}$$

where the λs are undetermined multipliers, but we shall discuss here only applications where $\lambda_i = 0$ for all i, and an unrestrained entropy is maximized. A necessary condition for S to be a maximum is for the gradient to vanish. Using

$$\frac{\partial S}{\partial x_j} = \sum_{i=1}^{n} \left(\frac{\partial S}{\partial \varphi_i}\right)\left(\frac{\partial \varphi_i}{\partial x_j}\right) \tag{8.2.3.3}$$

and

$$\frac{\partial S}{\partial \varphi_i} = \sum_{k=1}^{n} \left(\frac{\partial S}{\partial \varphi_k'}\right)\left(\frac{\partial \varphi_k'}{\partial \varphi_i}\right), \tag{8.2.3.4}$$

straightforward algebraic manipulation gives equations of the form

$$\sum_{i=1}^{n} \left\{ \frac{\partial \varphi_i}{\partial x_j} - \varphi_i' \left(\sum_{k=1}^{n} \frac{\partial \varphi_k}{\partial x_j} \right) \right\} \ln\left(\frac{\varphi_i'}{\mu_i'}\right) = 0. \tag{8.2.3.5}$$

It should be noted that, although the entropy function should, in principle, have a unique stationary point corresponding to the global maximum, there are occasional circumstances, particularly with restrained problems where the undetermined multipliers are not all zero, where it may be necessary to verify that a stationary solution actually maximizes entropy.

8.2.3.2. *Some examples*

For an example of the application of the maximum-entropy method, consider (Collins, 1984) a collection of diffraction intensities in which various subsets have been measured under different conditions, such as on different films or with different crystals. All systematic corrections have been made, but it is necessary to put the different subsets onto a common scale. Assume that every subset has measurements in common with some other subset, and that no collection of subsets is isolated from the others. Let the measurement of intensity I_h in subset i be J_{hi}, and let the scale factor that puts intensity I_h on the scale of subset i be k_i. Equation (8.2.3.1) becomes

$$S = -\sum_{h=1}^{n} \sum_{i=1}^{m} (k_i I_h)' \ln\left[\frac{(k_i I_h)'}{J_{hi}'}\right], \tag{8.2.3.6}$$

where the term is zero if I_h does not appear in subset i. Because k_i and I_h are parameters of the model, equations (8.2.3.5) become

$$\sum_{i=1}^{m} k_i \ln\left[\frac{(k_i I_h)'}{J_{hi}'}\right] - \sum_{h=1}^{n} \sum_{i=1}^{m} (k_i I_h)' \left(\sum_{l=1}^{m} k_l\right) \ln\left[\frac{(k_i I_h)'}{J_{hi}'}\right] = 0, \tag{8.2.3.7a}$$

and

$$\sum_{h=1}^{n} I_h \ln\left[\frac{(k_i I_h)'}{J_{hi}'}\right] - \sum_{h=1}^{n} \sum_{i=1}^{m} (k_i I_h)' \left(\sum_{l=1}^{n} I_l\right) \ln\left[\frac{(k_i I_h)'}{J_{hi}'}\right] = 0. \tag{8.2.3.7b}$$

These simplify to

$$\ln I_h = Q - \sum_{i=1}^{m} k_i' \ln(k_i/J_{hi}) \tag{8.2.3.8a}$$

and

$$\ln k_i = Q - \sum_{h=1}^{n} I_h' \ln(I_h/J_{hi}), \tag{8.2.3.8b}$$

where

$$Q = \sum_{h=1}^{n} \sum_{i=1}^{m} (k_i I_h)' \ln[(k_i I_h)/J_{hi}]. \tag{8.2.3.8c}$$

Equations (8.2.3.8) may be solved iteratively, starting with the approximations $k_i = \sum_{h=1}^{n} J_{hi}$ and $Q = 0$.

The standard uncertainties of scale factors and intensities are not used in the solution of equations (8.2.3.8), and must be computed separately. They may be estimated on a fractional basis from the variances of estimated population means $\langle J_{hi}/I_h \rangle$ for a scale factor and $\langle J_{hi}/k_i \rangle$ for an intensity, respectively. The maximum-entropy scale factors and scaled intensities are relative, and either set may be multiplied by an arbitrary, positive constant without affecting the solution.

For another example, consider the maximum-entropy fit of a linear function to a set of independently distributed variables. Let y_i represent an observation drawn from a population with mean $a_0 + a_1 x_i$ and finite variance σ_i^2; we wish to find the maximum-entropy estimate of a_0 and a_1. Assume that the mismatch between the observation and the model is normally distributed, so that its probability density is the positive proportion

$$\varphi_i = \varphi(\Delta_i) = (2\pi\sigma_i^2)^{-1/2} \exp(-\Delta_i^2/2\sigma_i^2), \tag{8.2.3.9}$$

where $\Delta_i = y_i - (a_0 + a_1 x_i)$. The prior proportion is given by

$$\mu_i = \varphi(0) = (2\pi\sigma_i^2)^{-1/2}. \tag{8.2.3.10}$$

Letting $A_\varphi = 1/\sum \varphi_i$, equations (8.2.3.5) become

$$\sum_{i=1}^{n} \left[\varphi_i \Delta_i/\sigma_i^2 - A_\varphi \varphi_i \left(\sum_{j=1}^{n} \varphi_j \Delta_j/\sigma_j^2 \right) \right] \Delta_i^2/\sigma_i^2 = 0 \tag{8.2.3.11a}$$

and

$$\sum_{i=1}^{n} \left[\varphi_i \Delta_i x_i/\sigma_i^2 - A_\varphi \varphi_i \left(\sum_{j=1}^{n} \varphi_j \Delta_j x_j/\sigma_j^2 \right) \right] \Delta_i^2/\sigma_i^2 = 0, \tag{8.2.3.11b}$$

which simplifies to

$$\begin{pmatrix} \sum_{i=1}^{n} w_i & \sum_{i=1}^{n} w_i x_i \\ \sum_{i=1}^{n} w_i x_i & \sum_{i=1}^{n} w_i x_i^2 \end{pmatrix} \begin{pmatrix} a_0 \\ a_1 \end{pmatrix} = \begin{pmatrix} \sum_{i=1}^{n} w_i \left(y_i - \sigma_i^2 A_\varphi \sum_{j=1}^{n} \varphi_j \Delta_j/\sigma_j^2 \right) \\ \sum_{i=1}^{n} w_i \left(y_i x_i - \sigma_i^2 A_\varphi \sum_{j=1}^{n} \varphi_j \Delta_j x_j/\sigma_j^2 \right) \end{pmatrix}, \tag{8.2.3.12}$$

where w_i may be interpreted as a weight and is given by $w_i = \varphi_i \Delta_i^2/\sigma_i^4$. Equations (8.2.3.12) may be solved iteratively, starting with the approximations that the sums over j on the right-hand side are zero and $w_i = 1.0$ for all i, that is, using the solutions to the corresponding, unweighted least-squares problem. Resetting w_i after each iteration by only half the indicated amount defeats a tendency towards oscillation. Approximate standard uncertainties for the parameters, a_0 and a_1, may be computed by conventional means after setting to zero the sums over j on the right-hand side of equations (8.2.3.12). (See, however, a discussion of computing variance–covariance matrices in Section 8.1.2.) Note that w_i is small for both small and large values of $|\Delta_i|$. Thus, in contrast to the robust/resistant methods (Section 8.2.2), which de-emphasize only the large differences, this method down-weights both the small and the large differences and adjusts the parameters on the basis of the moderate-size mismatches between model and data. The procedure used in this two-dimensional, linear model can be extended to linear models, and linear approximations to nonlinear models, in any number of dimensions using methods discussed in Chapter 8.1.

The maximum-entropy method has been described (Jaynes, 1979) as being 'maximally noncommittal with respect to all other matters; it is as uniform (by the criterion of the Shannon information measure) as it can be without violating the given constraint[s]'. Least squares, because it gives minimum variance estimates of the parameters of a model, and therefore of all functions of the model including the predicted values of any additional data points, might be similarly described as 'maximally committal' with regard to the collection of more data. Least squares and maximum entropy can therefore be viewed as the extremes of a range of methods, classified according to the degree of *a priori* confidence in the correctness of the model, with the robust/resistant methods lying somewhere in between (although generally closer to least squares). Maximum-entropy methods can be used when it is desirable to avoid prejudice in favour of a model because of doubt as to the model's correctness.

International Tables for Crystallography (2006). Vol. C, Chapter 8.3, pp. 693–701.

8.3. Constraints and restraints in refinement

By E. Prince, L. W. Finger, and J. H. Konnert

In Chapter 8.1, the method of least squares is discussed as a technique for fitting a theoretical model that contains adjustable parameters to a set of observations. The discussion is very general and contains very little mention of what sorts of quantities the observations are or what the model represents. In crystallography, the model is a crystal, which is constructed from identical unit cells that contain atoms, and which diffracts X-rays, neutrons or electrons in a manner that is characteristic of the arrangement of those atoms. The sample may be either a single crystal or a polycrystalline powder, and the observations are diffracted intensities, which may be fitted directly, as in the Rietveld method for powders (see Chapter 8.6; also Rietveld, 1969), or converted to derived quantities such as integrated intensities, squared moduli of structure amplitudes, or the structure amplitudes themselves. The model generally contains a scale factor and may contain parameters describing other experimental effects, such as extinction. Each atom in the unit cell requires three parameters to describe its mean position and various parameters to describe random deviations from that position owing to thermal motion or disorder. Models that treat each atom independently, however, do not allow for the fact that a great deal more is known about a crystal initially than simply its chemical composition. Atoms have fairly definite sizes and tend to occupy sites whose surroundings conform to a rather limited set of common configurations. In this chapter, we discuss ways of using this additional information. First, we shall discuss the use of constraints to reduce the number of parameters that must be varied and account for relationships among parameters that are dictated by the laws of chemistry and physics. Then we shall discuss the use of restraints, which effectively add to the number of observations that must be fitted by the model.

8.3.1. Constrained models

The techniques of least squares are applicable for refining almost any model, but the question of the suitability of the model remains. The addition of parameters may reduce the residual disagreement, but lead to solutions that have no physical or chemical validity. Addition of constraints is one method of constricting the solutions.

8.3.1.1. *Lagrange undetermined multipliers*

The classical technique for application of constraints is the use of Lagrange undetermined multipliers, in which the set of p parameters, x_j, is augmented by $p-q$ $(q<p)$ additional unknowns, λ_k, one for each constraint relationship desired. The problem may be stated in the form: find the minimum of

$$S=\sum_{i=1}^{n} w_i[y_i-M_i(\mathbf{x})]^2, \tag{8.3.1.1a}$$

subject to the condition

$$f_k(\mathbf{x})=0 \quad (k=1,2,\ldots,p-q). \tag{8.3.1.1b}$$

This may be shown (Gill, Murray & Wright, 1981) to be equivalent to the problem: find a point at which the gradient of

$$S'=\sum_{i=1}^{n} w_i[y_i-M_i(\mathbf{x})]^2+\sum_{k=1}^{p-q}\lambda_k f_k(\mathbf{x}) \tag{8.3.1.2}$$

vanishes. Solving for the stationary point leads to a set of simultaneous equations of the form

$$\partial S'/\partial x_j=\partial S/\partial x_j+\sum_{k=1}^{p-q}\lambda_k\partial f_k(\mathbf{x})/\partial x_j=0 \tag{8.3.1.3a}$$

and

$$\partial S'/\partial\lambda_k=f_k(\mathbf{x})=0. \tag{8.3.1.3b}$$

Thus, the number of equations, and the number of unknowns, is increased from p to $2p-q$. In cases where the number of constraint relations is small, and where it may be difficult to solve the relations for some of the parameters in terms of the rest, this method yields the desired results without too much additional computation (Ralph & Finger, 1982). With the large numbers of parameters, and large numbers of constraints, that arise in many crystallographic problems, however, the use of Lagrange multipliers is computationally inefficient and cumbersome.

8.3.1.2. *Direct application of constraints*

In most cases encountered in crystallography, constraints may be applied directly, thus reducing rather than increasing the size of the normal-equations matrix. For each constraint introduced, one of the parameters becomes dependent on the remaining set, and the rank of the remaining system is reduced by one. For p parameters and $p-q$ constraints, the problem reduces to q parameters. If the Gauss–Newton algorithm is used (Section 8.1.4), the normal-equations matrix is $\boldsymbol{A}^T\boldsymbol{W}\boldsymbol{A}$, where

$$A_{ij}=\partial M_i/\partial x_j, \tag{8.3.1.4}$$

and $\boldsymbol{W}$ is a weight matrix. A constrained model, $M_i(\mathbf{z})$, maybe constructed using relations of the form

$$x_j=g_j(z_1,z_2,\ldots,z_q). \tag{8.3.1.5}$$

Applying the chain rule for differentiation, the normal-equations matrix for the constrained model is $\boldsymbol{B}^T\boldsymbol{W}\boldsymbol{B}$, where

$$B_{ik}=\partial M_i(\mathbf{x})/\partial z_k=\sum_{j=1}^{p}[\partial M_i(\mathbf{x})/\partial x_j](\partial x_j/\partial z_k). \tag{8.3.1.6}$$

This may be written in matrix form $\boldsymbol{B}=\boldsymbol{A}\boldsymbol{C}$, where $C_{jk}=\partial x_j/\partial z_k$ defines a $p\times q$ constraint matrix. The application of constraints involves (*a*) determination of the model to be used, (*b*) calculation of the elements of $\boldsymbol{C}$, and (*c*) computation of the modified normal-equations matrix.

The construction of matrix $\boldsymbol{C}$ by a procedure known as the *variable reduction method* may be presented formally as follows: Designate by $\boldsymbol{Z}$ the matrix whose elements are

$$Z_{jk}=\partial g_j(\mathbf{x})/\partial x_k, \tag{8.3.1.7}$$

and partition $\boldsymbol{Z}$ in the form $\boldsymbol{Z}=(\boldsymbol{U},\boldsymbol{V})$, where $\boldsymbol{V}$ is composed of $(p-q)$ columns of $\boldsymbol{Z}$ chosen to be linearly independent, so that $\boldsymbol{V}$ is nonsingular. [$\boldsymbol{V}$ is shown as the last $(p-q)$ columns only for convenience. Any linearly independent set may be chosen.] The rows of $\boldsymbol{Z}$ form a basis for a $(p-q)$-dimensional subspace of the p-dimensional parameter space, and we wish to construct a basis for $\mathbf{z}$, a q-dimensional subspace that is orthogonal to it, so that all shifts within *that* subspace starting at a point where the constraints are satisfied, a *feasible point*, leave the values of the constraint relations unchanged. This basis is used for the columns of $\boldsymbol{C}$, which is given by

$$\boldsymbol{C}=\begin{pmatrix}\boldsymbol{I}_q\\ -\boldsymbol{V}^{-1}\boldsymbol{U}\end{pmatrix}. \tag{8.3.1.8}$$

Copyright © 2006 International Union of Crystallography

In this formulation, the columns of $\boldsymbol{V}$ correspond to dependent parameters that are functions of the independent parameters corresponding to the columns of $\boldsymbol{U}$.

Most existing programs provide for the calculation of the structure factor, F, and its partial derivatives with respect to a conventional set of parameters, including occupancy, position, isotropic or anisotropic atomic displacement factors, and possibly higher cumulants of an atomic density function (Prince, 1994). The constrained calculation is usually performed by evaluating selected elements, $\partial x_j/\partial z_k$. Because the constraint matrix is often extremely sparse, calculation of a limited sum involving only the nonzero elements is usually computationally superior to a full matrix multiplication. After adjustment of the z's, equations (8.3.1.5) are used to update the parameters. Using this procedure, it is not necessary to express the structure factor, or its derivatives, in terms of the refined parameters. This is particularly important when the constrained model involves arbitrary molecular shapes or rigid-body thermal motions.

The need for constraints arises most frequently when the crystal structure contains atoms in special positions. Here, certain parameters will be constant or linearly related to others. If a parameter is constrained to be a constant, the corresponding row of $\boldsymbol{C}$ will contain zeros, and that column will be ignored. When parameters are linearly dependent on others, which may occur in trigonal, hexagonal, tetragonal and cubic space groups, the modification indicated in (8.3.1.6) cannot be avoided. The constraint relationships among position parameters are trivial. Levy (1956) described an algorithm for determining the constraints that pertain to second and higher cumulants in the structure-factor formula. Table 8.3.1.1 is a summary of relations that are found for anisotropic atomic displacement factors, with a listing of the space groups in which they occur. Johnson (1970) provides a table listing the number of unique coefficients for each possible site symmetry for tensors of various ranks, which is useful information for verification of constraint relationships.

Another important use of constraints applies to the occupancies of certain sites in the crystal where, for example, a molecule is disordered in two or more possible orientations or (very common in minerals) several elements are distributed among several sites. In both cases, refinement of all of the fractional occupancies tends to be extremely ill conditioned, because of high correlations between occupancies and atomic displacement parameters. The overall chemistry, however, may be known from electron microprobe (Finger, 1969) or other analytic techniques to much better precision than it is possible to determine it using diffraction data alone. The constraining equations for the occupancies of n species in m sites have the form

$$\sum_{i=1}^{m} b_i a_{ij} = p_j, \tag{8.3.1.9}$$

where b_i is the multiplicity of the ith site, a_{ij} is the fractional occupancy of the jth species in the ith site, and p is the total number of atoms of species j per unit cell. For a given crystal structure and composition, the bs and ps are known, and, furthermore, it is possible to write an additional constraint for the total occupancy of each site,

$$\sum_{j=1}^{n} a_{ij} = 1. \tag{8.3.1.10}$$

If necessary, vacancies may be included as one of the n species present. In theory, (8.3.1.9) and (8.3.1.10) could be solved for $(n-1)\times(m-1)$ unknown parameters, a_{ij}, with $m+n-1$ constraint relations, but, in practice, at most one occupancy factor per site can be refined. When constraints are applied, the correlations between occupancies and displacement factors are greatly reduced.

In the analysis of a crystal structure, it may be desirable to test various constraints on the shape or symmetry of a molecule. For example, the molecule of a particular compound may have orthorhombic symmetry in the liquid or vapour phase, but crystallize with a monoclinic or triclinic space group. Without constraints, it is impossible to determine whether the crystallization has caused changes in the molecular conformation. Residual errors in the observations will invariably lead to deviations from the original molecular geometry, but these may or may not be meaningful.

With molecular-shape constraints, it is possible to constrain the geometry to any desired conformation. The first step is to describe the molecule in a special, orthonormal coordinate system that has a well defined relationship between the coordinate axes and the symmetry elements. If this system is properly chosen, the description of the molecule is easy. The next step is to describe the transformation between this orthonormal system and the crystallographic axes. A standard, orthonormal coordinate system (Prince, 1994) can be constructed with its x axis parallel to $\mathbf{a}$ and its z axis parallel to $\mathbf{c}^*$. If the special system is translated with respect to the standard system so that they share a common origin, Eulerian angles, ω, χ, and φ, may be used to define a matrix that rotates the special coordinates into the standard system. Angle ω is defined as the clockwise rotation through which the special system must be rotated about the z axis of the standard system to bring the z axis of the special system into the x,z plane of the standard system. Similarly, angle χ is the clockwise angle through which the resulting, special system must be rotated about the y axis of the standard system to bring the z axes into coincidence, and, finally, angle φ is the clockwise angle through which the special system must be rotated about the common z axes to bring the other axes into coincidence. The overall transformation is given by

$$\boldsymbol{R} = \begin{pmatrix} \cos\varphi\cos\chi\cos\omega - \sin\varphi\sin\omega & \cos\varphi\cos\chi\sin\omega + \sin\varphi\cos\omega & -\cos\varphi\sin\chi \\ -\sin\varphi\cos\chi\cos\omega - \cos\varphi\sin\omega & -\sin\varphi\cos\chi\sin\omega + \cos\varphi\cos\omega & \sin\varphi\sin\chi \\ \sin\chi\cos\omega & \sin\chi\sin\omega & \cos\chi \end{pmatrix}. \tag{8.3.1.11}$$

The overall transformation of a vector, $\mathbf{x}'$, from the special coordinate system to the crystallographic system is given by

$$\mathbf{x} = \boldsymbol{D}^{-1}\boldsymbol{R}\mathbf{x}' + \mathbf{t}, \tag{8.3.1.12}$$

where $\mathbf{t}$ is the origin offset between the two systems and $\boldsymbol{D}$ is the upper triangular Cholesky factor (Subsection 8.1.1.1) of the metric tensor, $\mathbf{G}$, which is defined by

$$\mathbf{G} = \begin{pmatrix} \mathbf{a}\cdot\mathbf{a} & \mathbf{a}\cdot\mathbf{b} & \mathbf{a}\cdot\mathbf{c} \\ \mathbf{a}\cdot\mathbf{b} & \mathbf{b}\cdot\mathbf{b} & \mathbf{b}\cdot\mathbf{c} \\ \mathbf{a}\cdot\mathbf{c} & \mathbf{b}\cdot\mathbf{c} & \mathbf{c}\cdot\mathbf{c} \end{pmatrix}. \tag{8.3.1.13}$$

Equations (8.3.1.12) are the constraint relationships, and the refinable parameters include the adjustable parameters in the special system, the origin offset, and the three rotation angles. This set of parameters, although it is written in a very different manner, is a linear transformation of a subset of the conventional

Table 8.3.1.1. *Symmetry conditions for second-cumulant tensors*

If more than one condition is applicable for a space group, the site is identified by its Wyckoff notation following the space-group symbol. The stated conditions are valid only for the first equipoint listed for the position. For space groups with alternative choices of origin, the option with a centre of symmetry has been selected.

(*A*) Monoclinic

(1) Site symmetry m, 2, $2/m$ – four independent elements

(a) $\beta_{12} = \beta_{23} = 0$; one principal axis parallel to [010]
All groups with unique axis b

(b) $\beta_{13} = \beta_{23} = 0$; one principal axis parallel to [001]
All groups with unique axis c

(*B*) Orthorhombic

(1) Site symmetry m, 2, $2/m$ – four independent elements

(a) $\beta_{12} = \beta_{13} = 0$; one principal axis parallel to [100]
*P*222(i,j,k,l), *P*222$_1$(a,b), *C*222$_1$(a), *C*222(e,f), *F*222(e,j), *I*222(e,f), *I*2$_1$2$_1$2$_1$(a), *Pmm*2(g,h), *Pmc*2$_1$, *Pma*2(c), *Pmn*2$_1$, *Cmm*2(e), *Cmc*2$_1$, *Amm*2(d,e), *Ama*2(b), *Fmm*2(c), *Imm*2(d), *Ima*2(b), *Pmmm*(u,v), *Pnnn*(g,h), *Pccm*(i,j), *Pban*(g,h), *Pmma*(k), *Pnna*(d), *Pmna*(a,b,c,d,e,f,h), *Pbcm*(c), *Pmmn*(e), *Cmcm*(a,b,e,f), *Cmca*(a,b,d,f), *Cmmm*(n), *Cccm*(g), *Cmma*(c,d,h,i,m), *Ccca*(e), *Fmmm*(c,l,m), *Fddd*(e), *Immm*(l), *Ibam*(f), *Ibca*(c), *Imma*(a,b,f,h)

(b) $\beta_{12} = \beta_{23} = 0$; one principal axis parallel to [010]
*P*222(m,n,o,p), *P*222$_1$(c,d), *C*222$_1$(b), *C*222(g,h), *F*222(f,i), *I*222(g,h), *I*2$_1$2$_1$2$_1$(b), *Pmm*2(e,f), *Cmm*2(d), *Amm*2(c), *Abm*2(c), *Fmm*2(d), *Imm*2(c), *Pmmm*(w,x), *Pnnn*(i,j), *Pccm*(k,l), *Pban*(i,j), *Pmma*(a,b,c,d,g,h,i,j), *Pmna*(g), *Pcca*(c), *Pmmm*(f), *Pbcn*, *Pnma*, *Cmca*(e), *Cmmm*(o), *Cccm*(h), *Cmma*(e,f,j,k,n), *Ccca*(f), *Fmmm*(d,k,n), *Fddd*(f), *Immm*(m), *Ibam*(g), *Ibca*(d), *Imma*(c,d,g,i)

(c) $\beta_{13} = \beta_{23} = 0$; one principal axis parallel to [001]
*P*222(q,r,s,t), *P*2$_1$2$_1$2, *C*222(i,j,k), *F*222(g,h), *I*222(i,j), *I*2$_1$2$_1$2$_1$(c), *Pcc*2, *Pma*2(a,b), *Pnc*2, *Pba*2, *Pnn*2, *Cmm*2(c), *Ccc*2, *Abm*2(a,b), *Ama*2(a), *Aba*2, *Fmm*2(b), *Fdd*2, *Iba*2, *Ima*2(a), *Pmmm*(y,z), *Pnnn*(k,l), *Pccm*(a,b,c,d,m,n,o,p,q), *Pban*(k,l), *Pnna*(c), *Pcca*(d,e), *Pbam*, *Pccn*, *Pbcm*(d), *Pnnm*, *Cmcm*(g), *Cmmm*(e,f,m,p,q), *Cccm*(c,d,e,f,i,j,k,l), *Cmma*(l), *Ccca*(g,h), *Fmmm*(e,j,o), *Fddd*(g), *Immm*(n), *Ibam*(c,d,h,i,j), *Ibca*(e)

(2) Site symmetry *mm*2, 222, *mmm* – three independent elements

(a) $\beta_{12} = \beta_{13} = \beta_{23} = 0$ principal axes parallel to crystal axes
All space groups

(*C*) Tetragonal

(1) Site symmetry m, 2, $2/m$ – four independent elements

(a) $\beta_{12} = \beta_{13} = 0$; one principal axis parallel to [100]
*P*422(l,m,n,o), *P*4$_2$22(j,k,l,m), *I*422(h,i), *I*4$_1$22(f), *I*4$_1$*md*, *P*$\bar{4}$2*m*(i,j,k,l), *P*$\bar{4}$2*c*(g,i), *I*$\bar{4}$2*m*(f,g), *I*$\bar{4}$2*d*(d), *P*4/*mcc*(k,l), *P*4/*nbm*(k,l), *P*4/*nnc*(i,j), *P*4/*nmm*(i), *P*4$_2$/*mmc*(o,p), *P*4$_2$/*mcm*(l,m), *P*4$_2$/*nbc*(h,i), *P*4$_2$/*nnm*(i,j), *P*4$_2$/*nmc*(g), *I*4/*mmm*(n), *I*4/*mcm*(j), *I*4$_1$/*amd*(c,d,f,h), *I*4$_1$/*acd*(e)

(b) $\beta_{12} = \beta_{23} = 0$; one principal axis parallel to [010]
*P*4$_1$22(a,b), *P*4$_3$22(a,b), *P*4*mm*(e,f), *P*4$_2$*mc*, *I*4*mm*(d), *P*$\bar{4}$2*c*(h,j), *P*$\bar{4}$*m*2(j,k), *I*$\bar{4}$*m*2(i), *P*4/*mmm*(s,t)

(c) $\beta_{13} = \beta_{23} = 0$; one principal axis parallel to [001]
*P*4, *P*4$_2$, *I*4, *I*4$_1$, *P*$\bar{4}$, *I*$\bar{4}$, *P*4/*m*, *P*4$_2$/*m*, *P*4/*n*, *P*4$_2$/*n*, *I*4/*m*, *I*4$_1$/*a*, *P*422(i), *P*42$_1$2(d), *P*4$_2$22(g,h,i), *P*4$_2$2$_1$2(c,d), *I*422(f), *I*4$_1$22(c), *P*4$_2$*cm*(c), *P*4$_2$*nm*(b), *P*4*cc*, *P*4*nc*, *P*4$_2$*bc*, *I*4$_1$*cd*, *P*$\bar{4}$2*m*(m), *P*$\bar{4}$2*c*(k,l,m), *P*$\bar{4}$2$_1$*m*(d), *P*$\bar{4}$21*c*, *P*$\bar{4}$*c*2(g,h,i), *P*$\bar{4}$*b*2(e,f), *P*$\bar{4}$*n*2(e,h), *I*$\bar{4}$*c*2(f,g), *I*$\bar{4}$2*m*(h), *I*$\bar{4}$2*d*(c), *P*4/*mmm*(p,q), *P*4/*mcc*(e,i,m), *P*4/*nnc*(g), *P*4/*mbm*(i,j), *P*4/*mnc*(c,f,h), *P*4/*ncc*(e), *P*42/*mmc*(q), *P*4$_2$/*mcm*(f,k,n), *P*4$_2$/*nbc*(f,g), *P*4$_2$/*nnm*(h), *P*4$_2$/*mbc*(a,c,e,f,h), *P*4$_2$/*mnm*(c,h,i), *P*4$_2$/*ncm*(f), *I*4/*mmm*(l), *I*4/*mcm*(k), *I*4$_1$/*acd*(d)

(d) $\beta_{11} = \beta_{22}$, $\beta_{13} = -\beta_{23}$ one principal axis parallel to [110]
*P*422(j,k), *P*42$_1$2(e,f), *P*4$_1$22(c), *P*4$_1$2$_1$2, *P*4$_2$22(n,o), *P*4$_2$2$_1$2(e,f), *P*4$_3$22(c), *P*4$_3$2$_1$2, *I*422(g,j), *I*4$_1$22(d), *P*$\bar{4}$*m*2(h,i), *P*$\bar{4}$*c*2(e,f), *P*$\bar{4}$*b*2(g,h), *P*$\bar{4}$*n*2(g), *I*$\bar{4}$*m*2(g,h), *I*$\bar{4}$*c*2(e,h), *P*4/*mcc*(j), *P*4/*nbm*(e,f,i,j,m), *P*4/*nnc*(h), *P*4/*mnc*(g), *P*4$_2$/*mmc*(n), *P*4$_2$/*nbc*(j), *P*4$_2$/*nnm*(e,f,k,l,m), *P*4$_2$/*mbc*(g), *I*4/*mmm*(k), *I*4/*mcm*(e,i), *I*4$_1$/*amd*(g), *I*4$_1$/*acd*(f)

(e) $\beta_{11} = \beta_{22}$, $\beta_{13} = \beta_{23}$; one principal axis parallel to [1$\bar{1}$0]
*I*4$_1$22(e), *P*4*mm*(d), *P*4*bm*, *P*4$_2$*cm*(d), *P*4$_2$*nm*(c), *I*4*mm*(c), *I*4*cm*, *P*$\bar{4}$2*m*(n), *P*$\bar{4}$2$_1$*m*(e), *P*$\bar{4}$*n*2(f), *I*$\bar{4}$2*m*(i), *P*4/*mmm*(r), *P*4/*mbm*(k), *P*4/*nmm*(d,e,g,h,j), *P*4/*ncc*(f), *P*4$_2$/*mcm*(o), *P*4$_2$/*mnm*(j), *P*4$_2$/*nmc*(f), *P*4$_2$/*ncm*(c,d,g,h,i), *I*4/*mmm*(f,m), *I*4/*mcm*(l)

(2) Site symmetry *mm*2, 222, *mmm* – three independent elements

(a) $\beta_{12} = \beta_{13} = \beta_{23} = 0$; principal axes parallel to crystal axes
*P*422, *P*4$_2$22(a,b,c,d), *I*422(c), *P*4*mm*, *P*4$_2$*mc*, *I*4*mm*, *I*4$_1$*md*, *P*$\bar{4}$2*m*(e,f), *P*$\bar{4}$2*c*, *P*$\bar{4}$*m*2, *I*$\bar{4}$*m*2, *I*$\bar{4}$2*m*(c), *P*4/*mmm*(e,f,i,l,m,n,o), *P*4/*mcc*, *P*4/*nnc*, *P*4/*nmm*, *P*4$_2$/*mmc*, *P*4$_2$/*mcm*(e), *P*4$_2$/*nbc*(a,b), *P*4$_2$/*nnm*(c), *P*4$_2$/*nmc*, *I*4/*mmm*(c,g,i,j), *I*4$_1$/*amd*

Table 8.3.1.1. *Symmetry conditions for second-cumulant tensors (cont.)*

(*C*) Tetragonal (*cont.*)

(*b*) $\beta_{11} = \beta_{22}$, $\beta_{13} = \beta_{23} = 0$; principal axes parallel to [110], [1$\bar{1}$0] and [001]
*P*42$_1$2, *P*4$_2$22(*e*,*f*), *P*4$_2$2$_1$2, *I*422(*d*), *I*4$_1$22, *P*4*bm*, *P*4$_2$*cm*, *P*4$_2$*nm*, *I*4*cm*, *P*$\bar{4}$2*m*(*g*, *h*), *P*$\bar{4}$2$_1$*m*, *P*$\bar{4}$*c*2, *P*$\bar{4}$*b*2, *P*$\bar{4}$*n*2, *I*$\bar{4}$*c*2, *I*$\bar{4}$2*m*(*e*), *P*4/*mmm*(*j*, *k*), *P*4/*nbm*, *P*4/*mbm*, *P*4/*mnc*, *P*4/*ncc*, *P*4$_2$/*mcm*(*a*, *c*, *g*, *h*, *i*, *j*), *P*4$_2$/*nbc*(*c*), *P*4$_2$/*nnm*(*d*, *g*), *P*4$_2$/*mbc*, *P*4$_2$/*mnm*, *P*4$_2$/*ncm*, *I*4/*mmm*(*h*), *I*4/*mcm*, *I*4$_1$/*acd*

(3) Site symmetry 4, $\bar{4}$, 4/*m*, 4*mm*, $\bar{4}$2*m*, 422, 4/*mmm* – two independent elements

(*a*) $\beta_{11} = \beta_{22}$, $\beta_{12} = \beta_{13} = \beta_{23} = 0$; uniaxial with unique axis parallel to [001]
All space groups

(*D*) Trigonal (hexagonal axes) and hexagonal

(1) Site symmetry *m*, 2, 2/*m* – four independent elements

(*a*) $\beta_{13} = \beta_{23} = 0$; one principal axis parallel to [001]
*P*6, *P*6$_2$, *P*6$_4$, *P*$\bar{6}$, *P*6/*m*, *P*6$_3$/*m*, *P*622(*i*), *P*6$_2$22(*e*,*f*), *P*6$_4$22(*e*,*f*), *P*6*cc*, *P*$\bar{6}$*m*2(*l*, *m*), *P*$\bar{6}$*c*2(*k*), *P*$\bar{6}$2*m*(*j*, *k*), *P*$\bar{6}$2*c*(*h*), *P*6/*mmm*(*p*, *q*), *P*6/*mcc*(*g*, *i*, *l*), *P*6$_3$/*mcm*(*j*), *P*6$_3$/*mmc*(*j*)

(*b*) $\beta_{11} = \beta_{22}$, $\beta_{13} = -\beta_{23}$ one principal axis parallel to [110]
*P*3*m*1, *R*3*m*, *P*$\bar{3}$*m*1(*i*), *R*$\bar{3}$*m*(*h*), *P*6*mm*(*e*), *P*6$_3$*mc*, *P*$\bar{6}$*m*2(*n*)

(*c*) $\beta_{11} = \beta_{22}$, $\beta_{13} = \beta_{23}$; one principal axis parallel to [2$\bar{1}$0]
*P*312, *P*3$_1$12, *P*3$_2$12, *P*$\bar{3}$1*m*(*i*, *j*), *P*$\bar{3}$1*c*, *P*622(*l*, *m*), *P*$\bar{6}$*c*2(*j*)

(*d*) $\beta_{22} = 2\beta_{12}$, $2\beta_{13} = \beta_{23}$; one principal axis parallel to [100]
*P*321, *P*3$_1$21, *P*3$_2$21, *R*32, *P*$\bar{3}$*m*1(*e*, *f*, *g*, *h*), *P*$\bar{3}$*c*1, *R*$\bar{3}$*m*(*d*, *e*, *f*, *g*), *R*$\bar{3}$*c*, *P*622(*j*, *k*), *P*6$_1$22(*a*), *P*6$_5$22(*a*), *P*6$_2$22(*g*, *h*), *P*6$_4$22(*g*, *h*), *P*6$_3$22(*g*), *P*$\bar{6}$2*c*(*g*), *P*6/*mmm*(*o*), *P*6/*mcc*(*j*), *P*6$_3$/*mmc*(*g*, *i*, *k*)

(*e*) $\beta_{22} = 2\beta_{12}$, $\beta_{23} = 0$; one principal axis parallel to [210]
*P*31*m*, *P*$\bar{3}$1*m*(*f*, *g*, *k*), *P*6$_1$22(*b*), *P*6$_5$22(*b*), *P*6$_2$22(*i*, *j*), *P*6$_4$22(*i*, *j*), *P*6$_3$22(*h*), *P*6*mm*(*d*), *P*6$_3$*cm*, *P*$\bar{6}$2*m*(*i*), *P*6/*mmm*(*n*), *P*6/*mcc*(*k*), *P*6$_3$/*mcm*(*f*, *i*, *k*)

(2) Site symmetry *mm*2, 222, *mmm* – three independent elements

(*a*) $\beta_{22} = 2\beta_{12}$, $\beta_{13} = \beta_{23} = 0$; principal axes parallel to [100] and [001]
*P*622, *P*6$_2$22, *P*6$_4$22, *P*6*mm*, *P*$\bar{6}$2*m*, *P*6/*mmm*, *P*6/*mcc*, *P*6$_3$/*mcm*, *P*6$_3$/*mmc*

(*b*) $\beta_{11} = \beta_{22}$, $\beta_{13} = \beta_{23} = 0$; principal axes parallel to [110], [2$\bar{1}$0] and [001]
P$\bar{6}$*m*2

(3) Site symmetry 3, $\bar{3}$, 3*m*, 32, $\bar{3}$*m*, $\bar{6}$, 6, 6/*m*, $\bar{6}$*m*2, 6*mm*, 622, 6/*mmm* – two independent elements

(*a*) $\beta_{11} = \beta_{22} = 2\beta_{12}$, $\beta_{13} = \beta_{23} = 0$; unique axis parallel to **c**
All space groups

(*E*) Cubic

(1) Site symmetry *m*, 2, 2/*m* – four independent elements

(*a*) $\beta_{12} = \beta_{13} = 0$; one principal axis parallel to [100]
*P*23, *F*23, *I*23, *I*2$_1$3, *Pm*$\bar{3}$, *Pn*$\bar{3}$, *Fm*$\bar{3}$, *Fd*$\bar{3}$, *Im*$\bar{3}$, *Ia*$\bar{3}$, *P*432(*h*), *P*4$_2$32(*h*, *i*, *j*), *F*432(*i*), *F*4$_1$32(*f*), *I*432(*g*), *I*4$_1$32(*f*), *P*$\bar{4}$3*m*(*h*), *I*$\bar{4}$3*m*(*f*), *P*$\bar{4}$3*n*, *F*$\bar{4}$3*c*, *I*$\bar{4}$3*d*, *Pm*$\bar{3}$*m*(*k*, *l*), *Pn*$\bar{3}$*n*(*g*), *Pm*$\bar{3}$*n*(*k*), *Pn*$\bar{3}$*m*(*h*), *Fm*$\bar{3}$*m*(*j*), *Fm*$\bar{3}$*c*(*i*), *Fd*$\bar{3}$*c*(*f*), *Im*$\bar{3}$*m*(*j*), *Ia*$\bar{3}$*d*(*f*)

(*b*) $\beta_{11} = \beta_{22}$, $\beta_{13} = \beta_{23}$; one principal axis parallel to [1$\bar{1}$0]
P$\bar{4}$3*m*(*i*), *F*$\bar{4}$3*m*, *I*$\bar{4}$3*m*(*g*), *Pm*$\bar{3}$*m*(*m*), *Pn*$\bar{3}$*m*(*k*), *Fm*$\bar{3}$*m*(*k*), *Fd*$\bar{3}$*m*(*g*), *Im*$\bar{3}$*m*(*k*)

(*c*) $\beta_{22} = \beta_{33}$, $\beta_{12} = -\beta_{13}$; one principal axis parallel to [011]
*P*432(*i*, *j*), *P*4$_2$32(*l*), *F*432(*g*, *h*), *I*432(*h*), *P*4$_1$32, *I*4$_1$32(*g*), *Pn*$\bar{3}$*n*(*h*), *Pm*$\bar{3}$*n*(*j*), *Pn*$\bar{3}$*m*(*j*), *Fm*$\bar{3}$*c*(*h*)

(*d*) $\beta_{22} = \beta_{33}$, $\beta_{12} = \beta_{13}$; one principal axis parallel to [01$\bar{1}$]
*P*4$_2$32(*k*), *F*4$_1$32(*g*), *I*432(*i*), *P*4$_3$32, *I*4$_1$32(*h*), *Pn*$\bar{3}$*m*(*i*), *Fd*$\bar{3}$*m*(*h*, *i*), *Fd*$\bar{3}$*c*(*g*), *Im*$\bar{3}$*m*(*i*), *Ia*$\bar{3}$*d*(*g*)

(2) Site symmetry *mm*2, 222, *mmm* – three independent elements

(*a*) $\beta_{12} = \beta_{13} = \beta_{23} = 0$; principal axes parallel to crystal axes
*P*23, *I*23, *Pm*$\bar{3}$, *Pn*$\bar{3}$, *Fm*$\bar{3}$, *Im*$\bar{3}$, *P*4$_2$32(*d*), *P*$\bar{4}$3*n*, *Pm*$\bar{3}$*m*(*h*), *Pm*$\bar{3}$*n*, *Fm*$\bar{3}$*c*, *Im*$\bar{3}$*m*(*g*)

(*b*) $\beta_{22} = \beta_{33}$, $\beta_{12} = \beta_{13} = 0$; principal axes parallel to [011], [01$\bar{1}$] and [100]
*P*4$_2$32(*e*,*f*), *F*432, *I*432, *I*4$_1$32, *P*$\bar{4}$3*m*, *F*$\bar{4}$3*m*, *I*$\bar{4}$3*m*, *Pm*$\bar{3}$*m*(*i*, *j*), *Pn*$\bar{3}$*m*, *Fm*$\bar{3}$*m*, *Fd*$\bar{3}$*m*, *Im*$\bar{3}$*m*(*h*), *Ia*$\bar{3}$*d*

(3) Site symmetry 3, $\bar{3}$, 3*m*, 32, $\bar{3}$*m*, $\bar{6}$, 6, 6/*m*, $\bar{6}$*m*2, 6*mm*, 622, 6/*mmm* – two independent elements

(*a*) $\beta_{11} = \beta_{22} = \beta_{33}$, $\beta_{12} = \beta_{13} = \beta_{23}$; unique axis parallel to [111]
All space groups

(4) Site symmetry 4, $\bar{4}$, 4/*m*, 4*mm*, $\bar{4}$2*m*, 422, 4/*mmm* – two independent elements

(*a*) $\beta_{22} = \beta_{33}$, $\beta_{12} = \beta_{13} = \beta_{23} = 0$; uniaxial with unique axis parallel to [100]
All space groups

(5) Site symmetry 23, *m*3, $\bar{4}$3*m*, 432, *m*3*m* – one independent element

(*a*) $\beta_{11} = \beta_{22} = \beta_{33}$, $\beta_{12} = \beta_{13} = \beta_{23} = 0$; isotropic
All space groups

crystallographic parameters, so that statistical tests based on the F ratio or Hamilton's R ratio (Section 8.4.2; Hamilton, 1964) may be used to assess significance. Shape constraints differ from those owing to space group or chemical conditions in that the constraint equations (8.3.1.12) are not linear functions of the independent parameters. Thus, the elements of $\boldsymbol{C}$ are not constants and must therefore be evaluated in each iteration of the refinement algorithm.

Another area in which application of constraints is important arises whenever some portion of the structure undergoes thermal motion as a rigid entity. One means of determining rigid-motion parameters is to refine the conventional, anisotropic atomic displacement factors of all atoms individually and to fit a librational model to the resulting thermal factors (Schomaker & Trueblood, 1968). A problem arises with this approach because the presence of libration implies curvilinear motion in the crystallographic system, and thus the probability density function for an atom that does not lie on the axis of libration cannot be described by a Gaussian function in a rectilinear coordinate system. For neutron diffraction, where H atoms have major scattering power, the effect may be large enough to affect convergence (Prince, Dickens & Rush, 1974). Anharmonic (third-cumulant) terms could be used, but the number of parameters increases rapidly, because there are as many as ten, independent, third cumulant tensor elements per atom.

Thermal motions of rigid bodies are represented by a symmetric, translation tensor, **T**, a symmetric, libration tensor, **L**, and a nonsymmetric, screw correlation tensor, **S** (Cruickshank, 1961; Schomaker & Trueblood, 1968). Any sequence of rotations of a rigid body about a fixed point is equivalent to a single, finite rotation about some axis passing through the fixed point. This rotation can be represented (Prince, 1994) by an axial vector, $\boldsymbol{\lambda}$, where $|\lambda|$ is the magnitude of the rotation, and the direction cosines of the axis with respect to some system of orthogonal axes are given by $\alpha_i = \lambda_i/|\lambda| = \lambda_i/(\lambda_1^2 + \lambda_2^2 + \lambda_3^2)^{1/2}$. An exact expression for the displacement, **u**, of a point in the rigid body, located by a vector **r** from the centre of mass, owing to a rotation $\boldsymbol{\lambda}$ about an axis passing through the centre of mass is

$$\mathbf{u} = (\sin|\boldsymbol{\lambda}|/|\boldsymbol{\lambda}|)(\boldsymbol{\lambda}\times\mathbf{r}) + [(1-\cos|\boldsymbol{\lambda}|)/|\boldsymbol{\lambda}|^2][\boldsymbol{\lambda}\times(\boldsymbol{\lambda}\times\mathbf{r})]. \tag{8.3.1.14}$$

For small rotations, the trigonometric functions can be replaced by power-series expansions, and, because of the extremely rapid convergence of these series, (8.3.1.14) is approximated extremely well, even for values of $|\lambda|$ as large as 0.5 rad, by

$$\mathbf{u} = (1-|\boldsymbol{\lambda}|^2/6)(\boldsymbol{\lambda}\times\mathbf{r}) + [(1/2)-|\boldsymbol{\lambda}|^2/24][\boldsymbol{\lambda}\times(\boldsymbol{\lambda}\times\mathbf{r})]. \tag{8.3.1.15}$$

By expansion of the vector products, this can be written

$$u_i = \sum_{j=1}^{3}\left(A(\mathbf{r})_{ij}\lambda_j + \sum_{k=1}^{3}\left\{B(\mathbf{r})_{ijk}\lambda_j\lambda_k + \sum_{l=1}^{3}\left[C(\mathbf{r})_{ijkl}\lambda_j\lambda_k\lambda_l + \sum_{m=1}^{3}D(\mathbf{r})_{ijklm}\lambda_j\lambda_k\lambda_l\lambda_m\right]\right\}\right), \tag{8.3.1.16}$$

where the coefficients, $A(\mathbf{r})_{ij}$, $B(\mathbf{r})_{ijk}$, $C(\mathbf{r})_{ijkl}$, and $D(\mathbf{r})_{ijklm}$ are multiples of components of **r**. For example, $[\boldsymbol{\lambda}\times\mathbf{r}]_1 = \lambda_2 r_3 - \lambda_3 r_2$, so that $A(\mathbf{r})_{11} = 0$, $A(\mathbf{r})_{12} = r_3$, and $A(\mathbf{r})_{13} = -r_2$. These coefficients have been tabulated by Sygusch (1976), and expressed in Fortran source code by Prince (1994).

If the centre of mass of the rigid body also moves, the total displacement of the point at **r** is $\mathbf{v} = \mathbf{u} + \mathbf{t}$, where **t** is the displacement of the centre of mass from its equilibrium position. A discussion of the effects of rigid-body motion on diffraction intensities involves quantities like $\langle v_i\rangle$, $\langle v_i v_j\rangle$, and so forth, the ensemble averages of these quantities over many unit cells, which may be assumed to be equal to the time averages for one unit cell over a long time. The rigid-body-motion tensors are defined by $T_{ij} = \langle t_i t_j\rangle$, $L_{ij} = \langle\lambda_i\lambda_j\rangle$, and $S_{ij} = \langle\lambda_i t_j\rangle$. The distributions of t_i and λ_i can usually be assumed to be approximately Gaussian, so that fourth moments can be expressed in terms of second moments. Thus, $\langle\lambda_i\lambda_j\lambda_k\lambda_l\rangle = L_{ij}L_{kl} + L_{ik}L_{jl} + L_{il}L_{jk}$, $\langle\lambda_i\lambda_j t_k t_l\rangle = L_{ij}T_{kl} + S_{ik}S_{jl} + S_{il}S_{jk}$, and so forth. If the elements of **t** and $\boldsymbol{\lambda}$ are measured with respect to their mean positions, $\langle t_i\rangle = \langle\lambda_i\rangle = 0$. Third moments, quantities like $\langle\lambda_i\lambda_j t_k\rangle$, do not necessarily vanish, except when the rigid body is centrosymmetric, but their effects virtually always are small, and can be neglected.

A particle that is part of a librating, rigid body undergoes a curvilinear motion that results in its having a mean position that is displaced from its equilibrium position. This causes an apparent shortening of interatomic distances, which must be corrected for if accurate values of bond lengths are to be derived. The displacement, **d**, from the equilibrium position to the mean position is (Prince & Finger, 1973)

$$d_i = \langle v_i\rangle = \sum_{j=1}^{3}\sum_{k=1}^{3}\left[B(\mathbf{r})_{ijk}L_{jk} + \sum_{l=1}^{3}\sum_{m=1}^{3}D(\mathbf{r})_{ijklm}(L_{jk}L_{lm} + L_{jl}L_{km} + L_{jm}L_{kl})\right]. \tag{8.3.1.17}$$

Anisotropic atomic displacement factors, β_{ij} , B_{ij}, or U_{ij}, are related by simple, linear transformations that are functions of the unit-cell constants to the quantity $\kappa_{ij} = \langle v_i v_j\rangle - \langle v_i\rangle\langle v_j\rangle$. If the rigid body has a centre of symmetry, so that the elements of **S** vanish, this is given by

$$\kappa_{ij} = T_{ij} + \sum_{k=1}^{3}\sum_{l=1}^{3}\left(A(\mathbf{r})_{ik}A(\mathbf{r})_{jl}L_{kl} + \sum_{m=1}^{3}\sum_{n=1}^{3}\{3[A(\mathbf{r})_{ik}C(\mathbf{r})_{jlmn} + A(\mathbf{r})_{jk}C(\mathbf{r})_{ilmn}] + 2B(\mathbf{r})_{ikm}B(\mathbf{r})_{jln}\}L_{kl}L_{mn}\right). \tag{8.3.1.18}$$

Expressions including elements of **S** have been given by Sygusch (1976) and, in Fortran source code, by Prince (1994). Expressions for anisotropic atomic displacement factors in terms of **T**, **L**, and **S** that included only terms linear in the tensor elements were given by Schomaker & Trueblood (1968), who pointed out that the diagonal elements of **S** never appeared individually, but only as the differences of pairs, so that the expressions were invariant under the addition of a constant to all three elements. This 'trace of **S** singularity' was resolved by applying the additional constraint $S_{11} + S_{22} + S_{33} = 0$. As was pointed out by Sygusch (1976), the inclusion of terms that are quadratic in the tensor elements removes this indeterminacy, but the effects of the additional terms are so small that the problem remains extremely ill conditioned. In practice, therefore, these elements should still be treated as underdetermined.

Prince (1994) lists the symmetry restrictions for each type of tensor for various point groups. Although the description of thermal motion is essentially harmonic within the rigid-body system, the structure-factor formulation must include what appear to be anharmonic terms. Prince also presents computer routines that contain the relations between the elements of **T**, **L**, and **S** and the second- and third-cumulant tensor elements. As in

the case of shape constraints, the equations are nonlinear, and the elements of $\boldsymbol{C}$ must be re-evaluated in each iteration.

8.3.2. Stereochemically restrained least-squares refinement

The precision with which an approximately correct model can be refined to describe the atomic structure of a crystal depends on the ability of the model to represent the atomic distributions and on the quality of the observational data being fitted with the model. In addition, although the structure can in principle be determined by a well chosen data set only a little larger than the number of parameters to be determined (Section 8.4.4), in practice, with a nonlinear model as complex as that for a macromolecular crystal, it is necessary for the parameters defining the model to be very much over-determined by the observations. For well ordered crystals of small- and intermediate-sized molecules, it is usually possible to measure a hundred or more independent Bragg reflections for each atom in the asymmetric unit. When the model contains three position parameters and six atomic displacement parameters for each atom, the over-determinacy ratio is still greater than ten to one. In such instances, each model parameter can usually be quite well determined, and will provide an accurate representation of the average structure in the crystal, except in regions where ellipsoids are not adequate descriptions of the atomic distributions. This contrasts sharply with studies of biological macromolecules, in which positional disorder and thermal motion in large regions, if not the entire molecule, often limit the number of independent reflections in the data set to fewer than the number of parameters necessary to define the distributions of individual atoms. This problem may be overcome either by reducing the number of parameters describing the model or by increasing the number of independent observations. Both approaches utilize knowledge of stereochemistry.

A great deal of geometrical information with which an accurate model must be consistent is available at the onset of a refinement. The connectivity of the atoms is generally known, either from the approximately correct Fourier maps of the electron density obtained from a trial structure determination or from sequencing studies of the molecules. Quite tight bounds are placed on local geometry by the accumulating body of information concerning bond lengths, bond angles, group planarity, and conformational preferences in torsion angles. Additional knowledge concerns van der Waals contact potential functions and hydrogen-bonding properties, and displacement factors must also be correlated in a manner consistent with the known geometry. In Section 8.3.1, we discuss the use of constraints to introduce this stereochemical knowledge. In this section, we discuss a technique that introduces the stereochemical conditions as additional observational equations (Waser, 1963). This method differs from the other in that information is introduced in the form of distributions about mean values rather than as rigidly fixed geometries. The parameters are restrained to fall within energetically permissible bounds.

8.3.2.1. *Stereochemical constraints as observational equations*

As described in Section 8.1.2, given a set of observations, y_i, that can be described by model functions, $M_i(\mathbf{x})$, where $\mathbf{x}$ is the vector of model parameters, we seek to find $\mathbf{x}$ for which the sum

$$S = \sum_{i=1}^{n} w_i[y_i - M_i(\mathbf{x})]^2 \qquad (8.3.2.1)$$

is minimum. For restrained refinement, S is composed of several classes of observational equations, including, in addition to the ones for structure factors, equations for interatomic distances, planar groups and displacement factors.

Structure factors yield terms in the sum of the form

$$\Delta_{\rm SF} = [|F_{\rm obs}(\mathbf{h})| - |F_{\rm calc}(\mathbf{h})|]^2/\sigma^2_{\mathbf{h}}. \qquad (8.3.2.2)$$

The distances between bonded atoms and between next-nearest-neighbour atoms may be used to require bonded distances and angles to fall within acceptable ranges. This gives terms of the form

$$\Delta_d = (d_{\rm ideal} - d_{\rm model})^2/\sigma^2_d, \qquad (8.3.2.3)$$

where σ_d is the standard deviation of an empirically determined distribution of values for distances of that type. Groups of atoms may be restrained to be near a common plane by terms of the form (Schomaker, Waser, Marsh & Bergman, 1959)

$$\Delta_p = (\mathbf{m}_l \cdot \mathbf{r} - d_l)^2/\sigma^2_p, \qquad (8.3.2.4)$$

where $\mathbf{m}_l$ and d_l are parameters of the plane, σ_p is again an empirically determined standard deviation, and $\cdot$ indicates the scalar product.

If a molecule undergoes thermal oscillation, the displacement parameters of individual atoms that are stereochemically related must be correlated. These parameters may be required to be consistent with the known stereochemistry by assuming a model that gives a distribution function for the interatomic distances in terms of the individual atom parameters and then restraining the variance of that distribution function to a suitably small value. The variation with time of the distances between covalently bonded atoms can be no greater than a few hundredths of an ångström. Therefore, the thermal displacements of bonded atoms should be very similar along the bond direction, but they may be more dissimilar perpendicular to the bond. If we make the assumption that the atom with a broader distribution in a given direction is 'riding' on the atom with the narrower distribution, the variance of the interatomic distance parallel to a vector $\mathbf{v}$ making an angle $\theta(\mathbf{v}, j)$ with the direction of bond j is (Konnert & Hendrickson, 1980)

$$V_{\mathbf{v}} = \Delta^2_{\mathbf{v}} \cos^2\theta + (\Delta^4_{\mathbf{v}}/2d_0^2)(\sin^4\theta - 6\sin^2\theta\cos^2\theta) + \ldots, \qquad (8.3.2.5)$$

where d_0 is the normal distance for that type of bond, $\Delta^2_{\mathbf{v}} = (\overline{u}^2_a - \overline{u}^2_b)$, and $\overline{u}^2_a$ and $\overline{u}^2_b$ are the mean square displacements parallel to $\mathbf{v}$ of atom a and atom b, respectively. The restraint terms then have the form $V^2_{\mathbf{v}}/\sigma^2_v$. For isotropic displacement factors, these terms take the particularly simple form $(B_a - B_b)^2/\sigma^2_B$, but with the disadvantage that, when isotropic displacement parameters are used, the displacements cannot be suitably restrained along the bonds and perpendicular to the bonds simultaneously.

Several additional types of restraint term have proved useful in restraining the coordinates for the mean positions of atoms in macromolecules. Among these are terms representing nonbonded contacts, torsion angles, handedness around chiral centres, and noncrystallographic symmetry (Hendrickson & Konnert, 1980; Jack & Levitt, 1978; Hendrickson, 1985). Contacts between nonbonded atoms are important for determining the conformations of folded chain molecules. They may be described by a potential function that is strongly repulsive when the interatomic distance is less than some minimum value, but only weakly attractive, so that it can be neglected in practice, when the distance is greater than that value. This leads to terms of the form

Table 8.3.2.1. *Coordinates of atoms (in Å) in standard groups appearing in polypeptides and proteins; restraint relations may be determined from these coordinates using methods described by Hendrickson (1985)*

Main chain, links and terminal groups			
Main			
N	1.20134	0.84658	0.00000
Cα	0.00000	0.00000	0.00000
C	−1.25029	0.88107	0.00000
O	−2.18525	0.66029	−0.78409
C terminal			
N	1.20006	0.84799	0.00000
Cα	0.00000	0.00000	0.00000
C	−1.26095	0.86727	0.00000
O	−2.32397	0.27288	−0.29188
O_t	−1.15186	2.04837	0.35987
N amino terminal			
N	1.20134	0.84658	0.00000
Cα	0.00000	0.00000	0.00000
C	−1.25029	0.88107	0.00000
O	−2.18525	0.66029	−0.78409
N formyl terminal			
N	1.19423	0.82137	0.00000
Cα	0.00000	0.00000	0.00000
C	−1.24896	0.88255	0.00000
O	−2.10649	0.78632	−0.90439
O_t	2.46193	−0.77877	−0.93569
C_t	2.33913	0.39064	−0.53355
N acetyl terminal			
N	1.19423	0.82137	0.00000
Cα	0.00000	0.00000	0.00000
C	−1.24896	0.88255	0.00000
O	−2.10649	0.78632	−0.90439
O_t	2.46193	−0.77877	−0.93569
C_t1	2.33913	0.39064	−0.53355
C_t2	3.44659	1.39160	−0.63532
trans peptide link			
Cα	0.00000	0.00000	0.00000
C	0.57800	1.41700	0.00000
O	1.80400	1.60700	0.00001
N	−0.33500	2.37000	0.00000
Cα	0.00000	3.80100	0.00000
cis peptide link			
Cα	0.00000	0.00000	0.00000
C	1.30900	0.79200	0.00000
O	2.38500	0.17600	0.00000
N	1.23500	2.11000	0.00000
Cα	0.00000	2.90700	0.00000
trans proline link			
Cα	0.00000	0.00000	0.00000
C	0.57800	1.41700	0.00000
O	1.80400	1.60700	0.00001
N	−0.33500	2.37000	0.00000
Cα	0.00000	3.80100	0.00000
Cδ	−1.80000	2.19600	0.00000
cis proline link			
Cα	0.00000	0.00000	0.00000
C	1.30900	0.79200	0.00000
O	2.38500	0.17600	0.00000
N	1.23500	2.11000	0.00000
Cα	0.00000	2.90700	0.00000
Cδ	2.45500	2.93900	0.00000

Table 8.3.2.1 *(cont.)*

Side chains for amino acids			
Ala A			
Cβ	0.02022	−0.92681	1.20938
Arg R			
Cβ	−0.02207	−0.93780	1.20831
Cγ	−0.09067	−0.23808	2.55932
Cδ	−0.79074	−1.07410	3.57563
Nε	−0.76228	−0.46664	4.89930
Cζ	−1.57539	−0.83569	5.89157
Nη1	−2.60422	−1.65104	5.68019
Nη2	−1.38328	−0.33329	7.11065
Asn N			
Cβ	0.04600	−1.02794	1.12104
Cγ	−0.15292	−0.42844	2.50080
Oδ1	−0.39364	0.78048	2.63809
Nδ2	−0.06382	−1.27086	3.52863
Asp D			
Cβ	0.04600	−1.02794	1.12104
Cγ	−0.15292	−0.42844	2.50080
Oδ1	−0.39364	0.78048	2.63809
Oδ2	−0.06930	−1.21904	3.46540
Cys C			
Cβ	0.01317	−0.95892	1.18266
Sγ	−0.07941	−0.15367	2.80168
Gln Q			
Cβ	−0.01691	−0.98634	1.16423
Cγ	−0.08291	−0.32584	2.52866
Cδ	−0.20841	−1.31760	3.65937
Oε1	−0.48899	−2.49684	3.46331
Nε2	−0.00450	−0.81846	4.87646
Glu E			
Cβ	−0.06551	−0.87677	1.25157
Cγ	1.15947	−1.71468	1.59818
Cδ	1.40807	−2.90920	0.72611
Oε1	0.92644	−3.06007	−0.38343
Oε2	2.16269	−3.74330	1.27140
Gly G (no nonhydrogen atoms)			
His H			
Cβ	−0.06434	−0.96857	1.20324
Cγ	−0.52019	−0.29684	2.46369
Nδ1	0.26457	0.53405	3.22184
Cε1	−0.46699	1.05500	4.19371
Nε2	−1.69370	0.59727	4.09040
Cδ2	−1.75570	−0.25685	3.02097
Ile I			
Cβ	0.03196	−0.97649	1.23019
Cγ1	−0.83268	−2.22363	0.92046
Cγ2	−0.39832	−0.28853	2.54980
Cδ1	−0.77555	−3.32741	2.01167
Leu L			
Cβ	0.09835	−0.94411	1.20341
Cγ	−0.96072	−2.02814	1.32143
Cδ1	−0.89548	−2.98661	0.13861
Cδ2	−0.73340	−2.79002	2.62540
Lys K			
Cβ	−0.03606	−0.92129	1.21541
Cγ	1.19773	−1.81387	1.35938
Cδ	1.05466	−2.77178	2.53242
Cε	2.34215	−3.51295	2.82637
Nζ	2.16781	−4.42240	3.98733

Table 8.3.2.1 (*cont.*)

Met M			
Cβ	0.02044	−0.96506	1.17716
Cγ	−1.00916	−2.05384	1.00286
Sδ	−0.77961	−3.24454	2.37236
Cε	−2.08622	−4.42220	1.97795
Phe F			
Cβ	0.00662	−1.03603	1.11081
Cγ	0.03254	−0.49711	2.50951
Cδ1	−1.15813	−0.12084	3.13467
Cε1	−1.15720	0.38038	4.42732
Cζ	0.05385	0.51332	5.11032
Cε2	1.26137	0.11613	4.50975
Cδ2	1.23668	−0.38351	3.20288
Pro P			
Cβ	0.12372	−0.78264	1.31393
Cγ	0.89489	0.13845	2.22063
Cδ	1.87411	0.86170	1.30572
Ser S			
Cβ	−0.00255	−0.96014	1.17670
Oγ	−0.19791	−0.28358	2.40542
Thr T			
Cβ	−0.00660	−0.98712	1.23470
Oγ1	0.04119	−0.14519	2.43011
Cγ2	1.12889	−2.01366	1.21493
Trp W			
Cβ	0.02501	−0.98461	1.16268
Cγ	0.03297	−0.36560	2.51660
Cδ1	−1.03107	0.15011	3.20411
Nεl	−0.62445	0.62417	4.42903
Cε2	0.72100	0.41985	4.55667
Cζ2	1.57452	0.72329	5.60758
Cη2	2.91029	0.38415	5.45120
Cη3	3.37037	−0.23008	4.28944
Cε3	2.51952	−0.53303	3.24549
Cδ2	1.17472	−0.20516	3.37412
Tyr Y			
Cβ	0.00470	−0.95328	1.20778
Cγ	−0.18427	−0.27254	2.54372
Cδ1	0.89731	0.26132	3.25049
Cεl	0.72371	0.85064	4.50059
Cζ	−0.54776	0.88971	5.06861
Cε2	−1.63905	0.38287	4.37622
Cδ2	−1.44975	−0.19374	3.12415
Oη	−0.76405	1.40409	6.31652
Val V			
Cβ	0.05260	−0.99339	1.17429
Cγ1	−0.13288	−0.31545	2.52668
Cγ2	−0.94265	−2.12930	0.99811

$$\Delta_n = (d_{\min} - d_{\text{model}})^4/\sigma_n^4, \qquad (8.3.2.6)$$

which are included only when $d_{\text{model}} < d_{\min}$. Macromolecules usually gain flexibility by relatively unrestricted rotation about single bonds. There are, nevertheless, significant restrictions on these torsion angles, which may, therefore, be restrained by terms of the form

$$\Delta_t = (\chi_{\text{ideal}} - \chi_{\text{model}})^2/\sigma_t^2, \qquad (8.3.2.7)$$

Table 8.3.2.2. *Ideal values for distances (Å), torsion angles (°), etc. for a glycine–alanine dipeptide with a trans peptide bond; distance type 1 is a bond, type 2 a next-nearest-neighbour distance involving a bond angle*

Interatomic distances

Number				Distance	Type
1	N(1)	to	C(1)α	1.470	1
2	Cα(1)	to	C(1)	1.530	1
3	C(1)	to	O(1)	1.240	1
4	N(1)	to	C(1)	2.452	2
5	C(1)α	to	O(1)	2.414	2
6	N(2)	to	C(2)α	1.469	1
7	C(2)α	to	C(2)	1.530	1
8	C(2)	to	O(2)	1.252	1
9	N(2)	to	C(2)	2.461	2
10	C(2)α	to	O(2)	2.358	2
11	C(2)β	to	C(2)α	1.524	1
12	C(2)β	to	C(2)	2.515	2
13	C(2)β	to	N(2)	2.450	2
14	C(2)	to	O(2)$_t$	1.240	1
15	O(2)	to	O(2)$_t$	2.225	2
16	C(2)α	to	O(2)$_t$	2.377	2
17	N(2)	to	C(1)	1.320	1
18	N(2)	to	O(1)	2.271	2
19	N(2)	to	C(1)α	2.394	2
20	C(2)α	to	C(1)	2.453	2

Planar groups

1	CTRM	C(2)α	C(2)	O(2)	O(2)	
2	LINK	C(1)α	C(1)	O(1)	N(2)	C(2)α

Chiral centres

		Central atom				Chiral volume (Å^3)
1	Ala	C(2)α	N(2)	C(2)	C(2)β	2.492

Possible nonbonded contacts

Number				Distance
1	N(1)	to	O(1)	3.050
2	N(2)	to	O(2)	3.050
3	O(2)	to	C(2)β	3.350
4	N(2)	to	O(2)$_t$	3.050
5	O(2)$_t$	to	C(2)β	3.350

Torsion angles

N(1)	C(1)α	C(1)	N(2)	0.0
C(1)α	C(1)	N(2)	C(2)α	180.0
C(1)	N(2)	C(2)α	C(2)	0.0
N(2)	C(2)α	C(2)	O(2)$_t$	0.0

where χ_{ideal} and χ_{model} are dihedral angles between planar groups at opposite ends of the bond.

Interatomic distances are independent of the handedness of an enantiomorphous group. If $\mathbf{r}_c$ is the position vector of a central atom and $\mathbf{r}_1$, $\mathbf{r}_2$, and $\mathbf{r}_3$ are the positions of three atoms bonded to it, such that the four atoms are not coplanar, the *chiral volume* is defined by

$$V_c = (\mathbf{r}_1 - \mathbf{r}_c) \cdot [(\mathbf{r}_2 - \mathbf{r}_c) \times (\mathbf{r}_3 - \mathbf{r}_c)], \qquad (8.3.2.8)$$

where $\times$ indicates the vector product. The chiral volume may be either positive or negative, depending on the handedness of the group. It may be restrained by including terms of the form

$$\Delta_c = (V_{\text{ideal}} - V_{\text{model}})^2/\sigma_c^2. \qquad (8.3.2.9)$$

Table 8.3.2.1 gives ideal coordinates, in an orthonormal coordinate system measured in Å, of various groups that are

Table 8.3.2.3. *Typical values of standard deviations for use in determining weights in restrained refinement of protein structures (after Hendrickson, 1985)*

Interatomic distances		
Nearest neighbour (bond)		σ_d = 0.02 Å
Next-nearest neighbour (angle)		0.03 Å
Intraplanar distance		0.05 Å
Hydrogen bond or metal coordination		0.05 Å
Planar groups		
Deviation from plane		σ_p = 0.02 Å
Chiral centres		
Chiral volume		σ_c = 0.15 Å^3
Nonbonded contacts		
Interatomic distance		σ_n = 0.50 Å
Torsion angles		
Specified (*e.g.* helix φ and ψ)		σ_t = 15°
Planar group		3°
Staggered		15°
Thermal parameters	Anisotropic	Isotropic
Main-chain neighbour	σ_v = 0.05 Å	σ_B = 1.0 Å^2
Main-chain second neighbour	0.10 Å	1.5 Å^2
Side-chain neighbour	0.05 Å	1.5 Å^2
Side-chain second neighbour	0.10 Å	2.0 Å^2

commonly found in proteins. The ideal conformations of pairs of amino acid residues, from which the ideal values to be used in restraint terms of various types may be determined, are constructed by combining the coordinates of the individual groups. For example, consider a dipeptide composed of glycine and alanine joined by a *trans* peptide link, giving the molecule

$$\begin{array}{ccccccccc} & & & & O(1) & & C\beta(2) & O(2) & \\ & & & & \| & & | & \| & \\ N(1)\text{—}C\alpha(1)\text{—} & & C(1) & \text{—}N(2)\text{—} & & C\alpha(2) & \text{—} & C(2) & \text{—}O_t(2). \end{array}$$

The origin is placed at each of the Cα positions in turn, and interatomic distances to nearest and next-nearest neighbours are computed. Planar groups and possible nonbonded contacts are identified, and torsion angles and chiral volumes for chiral centres are computed. Table 8.3.2.2 is a summary of the restraint information for this simple molecule. In order to incorporate this information in the refinement, these ideal values are combined with suitable weights. Table 8.3.2.3 gives values of the standard deviations of the various types of constraint relation that have been found (Hendrickson, 1985) to give good results in practice.

Even for a small protein, the normal-equations matrix may contain several million elements. When stereochemical restraint relations are used, however, the matrix elements are not equally important, and many may be neglected. Convergence and stability properties can be preserved when only those elements that are different from zero for the stereochemical restraint information are retained. The number of these elements increases linearly with the number of atoms, and is typically less than 1% of the total in the matrix, so that sparse-matrix methods (Section 8.1.5) can be used. The method of conjugate gradients (Hestenes & Stiefel, 1952; Konnert, 1976; Rae, 1978) is particularly suitable for the efficient use of restrained-parameter least squares.

International Tables for Crystallography (2006). Vol. C, Chapter 8.4, pp. 702–706.

8.4. Statistical significance tests

By E. Prince and C. H. Spiegelman

In Chapter 8.1, we discussed the method of least squares and procedures for estimating the values of the adjustable parameters of a model that predicts the mean of a population from which experimental observations are drawn at random. Any model, however, will have some set of parameter values that gives the best least-squares fit. We must now address the question of whether that best fit is adequate, that is, whether it is plausible, given the precision of the data, to accept the hypothesis that the model really is a correct representation of the phenomena that have been measured in the collection of the data. In this chapter, we discuss the probability density function for the sum of squared residuals if the individual residuals are drawn from a normal distribution, the χ^2 distribution, and the conditions under which this p.d.f. may be assumed to approximate a practical case. Next, we discuss the F distribution, which is the distribution of the ratio of two independent, random variables, each of which has a χ^2 distribution, and its use in comparing the fits of constrained and unconstrained versions of a model. We also discuss a test that is useful for a more general comparison of models. Finally, we discuss the variation among data points of their effectiveness in improving the precision of parameter estimates and the application of this analysis to the optimum design of experiments.

8.4.1. The χ^2 distribution

We have seen [equation (8.1.2.1)] that the least-squares estimate is derived by finding the minimum value of a sum of terms of the form

$$R_i = w_i[y_i - M_i(\mathbf{x})]^2, \tag{8.4.1.1}$$

and, further, that the precision of the estimate is optimized if the weight, w_i, is the reciprocal of the variance of the population from which the observation is drawn, $w_i = 1/\sigma_i^2$. Using this relation, (8.4.1.1) can be written

$$R_i = \left\{\left[y_i - M_i(\mathbf{x})\right]/\sigma_i\right\}^2. \tag{8.4.1.2}$$

Each term is the square of a difference between observed and calculated values, expressed as a fraction of the standard uncertainty of the observed value. But, by definition,

$$\sigma_i^2 = \left\langle [y_i - M_i(\mathbf{x})]^2 \right\rangle, \tag{8.4.1.3}$$

where $\mathbf{x}$ has its unknown 'correct' value, so that $\langle R\rangle = 1$, and the expected value of the sum of n such terms is n. It can be shown (Draper & Smith, 1981) that each parameter estimated reduces this expected sum by one, so that, for p estimated parameters,

$$\langle S\rangle = \left\langle \sum_{i=1}^{n} \left\{\left[y_i - M_i(\widehat{\mathbf{x}})\right]/\sigma_i\right\}^2 \right\rangle = n - p, \tag{8.4.1.4}$$

where $\widehat{\mathbf{x}}$ is the least-squares estimate. The *standard uncertainty of an observation of unit weight*, also referred to as the *goodness-of-fit parameter*, is defined by

$$G = \left[\frac{S}{n-p}\right]^{1/2} = \left[\frac{\left\{\sum_{i=1}^{n} w_i\left[y_i - M_i(\widehat{\mathbf{x}})\right]^2\right\}}{n-p}\right]^{1/2}. \tag{8.4.1.5}$$

From (8.4.1.4), it follows that $\langle G\rangle = 1$ for a correct model with weights assigned in accordance with (8.4.1.2).

A value of G that is close to one, if the weights have been assigned by $w_i = 1/\sigma_i^2$, is an indicator that the model is consistent with the data. It should be noted that it is not necessarily an indicator that the model is 'correct', because it does not rule out the existence of an alternative model that fits the data as well or better. An assessment of the adequacy of the fit of a given model depends, however, on what is meant by 'close to one', which depends in turn on the spread of a probability density function for G. We saw in Chapter 8.1 that least squares with this weighting scheme would give the best, linear, unbiased estimate of the model parameters, with no restrictions on the p.d.f.s of the populations from which the observations are drawn except for the implicit assumption that the variances of these p.d.f.s are finite. To construct a p.d.f. for G, however, it is necessary to make an assumption about the shapes of the p.d.f.s for the observations. The usual assumption is that these p.d.f.s can be described by the *normal p.d.f.*,

$$\Phi_N(x, \mu, \sigma) = \frac{1}{\sqrt{2\pi}\sigma}\exp\left[\frac{(x-\mu)^2}{2\sigma^2}\right]. \tag{8.4.1.6}$$

The justification for this assumption comes from the *central-limit theorem*, which states that, under rather broad conditions, the p.d.f. of the arithmetic mean of n observations drawn from a population with mean μ and variance σ^2 tends, for large n, to a normal distribution with mean μ and variance σ^2/n. [For a discussion of the central limit theorem, see Cramér (1951).]

If we make the assumption of a normal distribution of errors and make the substitution $z = (x-\mu)/\sigma$, (8.4.1.6) becomes

$$\Phi_N(z, 0, 1) = \frac{1}{\sqrt{2\pi}}\exp\left(-\frac{z^2}{2}\right). \tag{8.4.1.7}$$

The probability that z^2 will be less than χ^2 is equal to the probability that z will lie in the interval $-\chi \le z \le \chi$, or

$$\Psi(\chi^2) = \int_0^{\chi^2} \Phi(z^2)\,\mathrm{d}z^2 = \int_{-\chi}^{+\chi} \Phi(z)\,\mathrm{d}z. \tag{8.4.1.8}$$

Letting $t = z^2/2$ and substituting in (8.4.1.7), this becomes

$$\Psi(\chi^2) = \frac{1}{\sqrt{\pi}}\int_0^{\chi^2/2} t^{-1/2}\exp(-t)\,\mathrm{d}t. \tag{8.4.1.9}$$

$\Phi(\chi^2) = \mathrm{d}\Psi(\chi^2)/\mathrm{d}\chi^2$, so that

$$\begin{array}{ll} \Phi\left(\chi^2\right) = \left(2\pi\chi^2\right)^{-1/2}\exp\left(-\chi^2/2\right), & \chi^2 > 0, \\ \Phi\left(\chi^2\right) = 0, & \chi^2 \le 0. \end{array} \tag{8.4.1.10}$$

The joint p.d.f. of the squares of two random variables, z_1 and z_2, drawn independently from the same population with a normal p.d.f. is

$$\Phi_J\left(z_1^2, z_2^2\right) = \frac{1}{2\pi z_1 z_2}\exp\left[-\frac{z_1^2 + z_2^2}{2}\right], \tag{8.4.1.11}$$

and the p.d.f. of the sum, s^2, of these two terms is the integral over the joint p.d.f. of all pairs of z_1^2 and z_2^2 that add up to s^2.

$$\Phi(s^2) = \frac{1}{2\pi}\exp\left(-\frac{s^2}{2}\right)\left[z_1^2(s^2 - z_1^2)\right]\mathrm{d}z_1^2. \tag{8.4.1.12}$$

This integral can be evaluated by use of the gamma and beta functions. The *gamma function* is defined for positive real x by

Copyright © 2006 International Union of Crystallography

Table 8.4.1.1. *Values of χ^2/ν for which the c.d.f. $\Psi(\chi^2,\nu)$ has the values given in the column headings, for various values of ν*

ν	0.5	0.9	0.95	0.99	0.995
1	0.4549	2.7055	3.8415	6.6349	7.8795
2	0.6931	2.3026	2.9957	4.6052	5.2983
3	0.7887	2.0838	2.6049	3.7816	4.2794
4	0.8392	1.9449	2.3719	3.3192	3.7151
6	0.8914	1.7741	2.0986	2.8020	3.0913
8	0.9180	1.6702	1.9384	2.5113	2.7444
10	0.9342	1.5987	1.8307	2.3209	2.5188
15	0.9559	1.4871	1.6664	2.0385	2.1868
20	0.9669	1.4206	1.5705	1.8783	1.9999
25	0.9735	1.3753	1.5061	1.7726	1.8771
30	0.9779	1.3419	1.4591	1.6964	1.7891
40	0.9834	1.2951	1.3940	1.5923	1.6692
50	0.9867	1.2633	1.3501	1.5231	1.5898
60	0.9889	1.2400	1.3180	1.4730	1.5325
80	0.9917	1.2072	1.2735	1.4041	1.4540
100	0.9933	1.1850	1.2434	1.3581	1.4017
120	0.9945	1.1686	1.2214	1.3246	1.3638
140	0.9952	1.1559	1.2044	1.2989	1.3346
160	0.9958	1.1457	1.1907	1.2783	1.3114
200	0.9967	1.1301	1.1700	1.2472	1.2763

$$\Gamma(x) = \int_0^\infty t^{x-1}\exp(-t)\,\mathrm{d}t. \qquad (8.4.1.13)$$

Although this function is continuous for all $x > 0$, its value is of interest in the context of this analysis only for x equal to positive, integral multiples of 1/2. It can be shown that $\Gamma(1/2) = \sqrt{\pi}$, $\Gamma(1) = 1$, and $\Gamma(x+1) = x\Gamma(x)$. It follows that, for a positive integer, n, $\Gamma(n) = (n-1)!$, and that $\Gamma(3/2) = \sqrt{\pi}/2$, $\Gamma(5/2) = 3\sqrt{\pi}/4$, *etc*. The *beta function* is defined by

$$B(x,y) = \int_0^1 t^{x-1}(1-t)^{y-1}\,\mathrm{d}t. \qquad (8.4.1.14)$$

It can be shown (Prince, 1994) that $B(x,y) = \Gamma(x)\Gamma(y)/\Gamma(x+y)$. Making the substitution $t = z_1^2/s^2$, (8.4.1.12) becomes

$$\begin{aligned}\Phi(s^2) &= \frac{1}{2\pi}\exp\left(-\frac{s^2}{2}\right)\int_0^1 [t(1-t)]^{-1/2}\,\mathrm{d}t \\ &= \frac{1}{2\pi}\exp\left(-\frac{s^2}{2}\right)B(1/2,1/2) \\ &= \tfrac{1}{2}\exp\left(-\frac{s^2}{2}\right), \qquad s^2 \geq 0. \end{aligned} \qquad (8.4.1.15)$$

By a similar procedure, it can be shown that, if χ^2 is the sum of ν terms, $z_1^2, z_2^2, \ldots, z_\nu^2$, where all are drawn independently from a population with the p.d.f. given in (8.4.1.10), χ^2 has the p.d.f.

$$\begin{aligned}\Phi(\chi^2,\nu) &= \frac{(\chi^2)^{\nu/2-1}}{2^{\nu/2}\Gamma(\nu/2)}\exp\left(-\frac{\chi^2}{2}\right), \qquad \chi^2 > 0, \\ \Phi(\chi^2,\nu) &= 0, \qquad \chi^2 \leq 0. \end{aligned} \qquad (8.4.1.16)$$

The parameter ν is known as the number of *degrees of freedom*, but this use of that term must not be confused with the conventional use in physics and chemistry. The p.d.f. in (8.4.1.16) is the *chi-squared distribution with ν degrees of freedom*. Table 8.4.1.1 gives the values of χ^2/ν for which the *cumulative distribution function* (*c.d.f.*) $\Psi(\chi^2,\nu)$ has various values for various choices of ν. This table is provided to enable verification of computer codes that may be used to generate more extensive tables. It was generated using a program included in the statistical library DATAPAC (Filliben, unpublished). Fortran code for this program appears in Prince (1994).

The quantity $(n-p)G$ is the sum of n terms that have mean value $(n-p)/n$. Because the process of determining the least-squares fit establishes p relations among them, however, only $(n-p)$ of the terms are independent. The number of degrees of freedom is therefore $\nu = (n-p)$, and, if the model is correct, and the terms have been properly weighted, $\chi^2 = (n-p)G^2$ has the chi-squared distribution with $(n-p)$ degrees of freedom. In crystallography, the number of degrees of freedom tends to be large, and the p.d.f. for G correspondingly sharp, so that even rather small deviations from $G^2 = 1$ should cause one or both of the hypotheses of a correct model and appropriate weights to be rejected. It is common practice to assume that the model is correct, and that the weights have correct *relative* values, that is that they have been assigned by $w_i = k/\sigma_i^2$, where k is a number different from, usually greater than, one. G is then taken to be an estimate of k, and all elements of $(\boldsymbol{A}^T\boldsymbol{W}\boldsymbol{A})^{-1}$ (Section 8.1.2) are multiplied by G^2 to get an estimated variance–covariance matrix. The range of validity of this procedure is limited at best. It is discussed further in Chapter 8.5.

8.4.2. The *F* distribution

Consider an unconstrained model with p parameters and a constrained one with q parameters, where $q < p$. We wish to decide whether the constrained model represents an adequate fit to the data, or if the additional parameters in the unconstrained model provide, in some important sense, a better fit to the data. Provided the $(p-q)$ additional columns of the design matrix, $\boldsymbol{A}$, are linearly independent of the previous q columns, the sum of squared residuals must be reduced by some finite amount by adjusting the additional parameters, but we must decide whether this improved fit would have occurred purely by chance, or whether it represents additional information.

Let s_c^2 and s_u^2 be the weighted sums of squared residuals for the constrained and unconstrained models, respectively. If the constrained and unconstrained models are equally good representations of the data, and the weights have been assigned by $w_i = 1/\sigma_i^2$, the expected values of the sums of squares are $\langle s_c^2\rangle = (n-q)$ and $\langle s_u^2\rangle = (n-p)$, and, further, they should be distributed as χ^2 with $(n-q)$ and $(n-p)$ degrees of freedom, respectively. Also, $\langle s_c^2 - s_u^2\rangle = (p-q)$, and $(s_c^2 - s_u^2)$ is distributed as χ^2 with $(p-q)$ degrees of freedom. s_c^2 and s_u^2 are not independent, but $(s_c^2 - s_u^2)$ is the squared magnitude of a vector in a $(p-q)$-dimensional subspace that is orthogonal to the $(n-p)$-dimensional space of s_u^2. Therefore, s_u^2 and $(s_c^2 - s_u^2)$ are independent, random variables, each with a χ^2 distribution. Let $\chi_1^2 = (s_c^2 - s_u^2)$, $\chi_2^2 = s_u^2$, $\nu_1 = p-q$, and $\nu_2 = n-p$. The ratio $F = (\chi_1^2/\nu_1)/(\chi_2^2/\nu_2)$ should have a value close to one, even if the weights have relative rather than absolute values, but we need a measure of how far away from one this ratio can be before we must reject the hypothesis that the two models are equally good representations of the data. The conditional p.d.f. for F, given a value of χ_2^2 , is

$$\Phi_C(F|\chi_2^2) = \frac{\left[(\nu_1/\nu_2)\chi_2^2\right]^{\nu_1/2}F^{\nu_1/2-1}}{2^{\nu_1/2}\Gamma(\nu_1/2)}\exp\left[-(\nu_1/\nu_2)\chi_2^2F/2\right], \qquad (8.4.2.1)$$

and the marginal p.d.f. for χ_2^2 is

$$\Phi_M(\chi_2^2) = \frac{(\chi_2^2)^{\nu_2/2-1}}{2^{\nu_2/2}\Gamma(\nu_2/2)}\exp(-\chi_2^2/2). \qquad (8.4.2.2)$$

Table 8.4.2.1. *Values of the F ratio for which the c.d.f. $\Psi(F,\nu_1,\nu_2)$ has the value 0.95, for various choices of ν_1 and ν_2*

ν_2 \ ν_1	1	2	4	8	15
10	4.9646	4.1028	3.4781	3.0717	2.8450
20	4.3512	3.4928	2.8661	2.4471	2.2033
30	4.1709	3.3158	2.6896	2.2662	2.0148
40	4.0847	3.2317	2.6060	2.1802	1.9245
50	4.0343	3.1826	2.5572	2.1299	1.8714
60	4.0012	3.1504	2.5252	2.0970	1.8364
80	3.9604	3.1108	2.4859	2.0564	1.7932
100	3.9361	3.0873	2.4626	2.0323	1.7675
120	3.9201	3.0718	2.4472	2.0164	1.7505
150	3.9042	3.0564	2.4320	2.0006	1.7335
200	3.8884	3.0411	2.4168	1.9849	1.7167
300	3.8726	3.0259	2.4017	1.9693	1.6998
400	3.8648	3.0183	2.3943	1.9616	1.6914
600	3.8570	3.0107	2.3868	1.9538	1.6831
1000	3.8508	3.0047	2.3808	1.9477	1.6764

The marginal p.d.f. for F is obtained by integration of the joint p.d.f.,

$$\Phi(F) = \int_0^\infty \Phi_C\left(F|\chi_2^2\right)\Phi_M\left(\chi_2^2\right)\,\mathrm{d}\chi_2^2, \tag{8.4.2.3}$$

yielding the result

$$\Phi(F,\nu_1,\nu_2) = \frac{(\nu_1/\nu_2)F^{\nu_1/2-1}}{B(\nu_1/2,\nu_2/2)\left[1+(\nu_1/\nu_2)F\right]^{(\nu_1+\nu_2)/2}}. \tag{8.4.2.4}$$

This p.d.f. is known as the *F distribution with ν_1 and ν_2 degrees of freedom*. Table 8.4.2.1 gives the values of F for which the c.d.f. $\Psi(F,\nu_1,\nu_2)$ is equal to 0.95 for various choices of ν_1 and ν_2. Fortran code for the program from which the table was generated appears in Prince (1994).

The cumulative distribution function $\Psi(F,\nu_1,\nu_2)$ gives the probability that the F ratio will be less than some value by chance if the models are equally consistent with the data. It is therefore a necessary, but not sufficient, condition for concluding that the unconstrained model gives a significantly better fit to the data that $\Psi(F,\nu_1,\nu_2)$ be greater than $1-\alpha$, where α is the desired level of significance. For example, if $\Psi(F,\nu_1,\nu_2)=0.95$, the probability is only 0.05 that a value of F this large or greater would have been observed if the two models were equally good representations of the data.

Hamilton (1964) observed that the F ratio could be expressed in terms of the crystallographic weighted R index, which is defined, for refinement on |F| (and similarly for refinement on $|F|^2$), by

$$R_w = \left[\sum w_i(|F_o|_i - |F_c|_i)^2 \Big/ \sum w_i|F_o|_i^2\right]^{1/2}. \tag{8.4.2.5}$$

Denoting by R_c and R_u the weighted R indices for the constrained and unconstrained models, respectively,

$$F = (\nu_2/\nu_1)[(R_c/R_u)^2 - 1], \tag{8.4.2.6}$$

and a c.d.f. for R_c/R_u can be readily derived from this relation. A significance test based on R_c/R_u is known as *Hamilton's R-ratio test*; it is entirely equivalent to a test on the F ratio.

8.4.3. Comparison of different models

Tests based on F or the R ratio have several limitations. One important one is that they are applicable only when the parameters of one model form a subset of the parameters of the other. Also, the F test makes no distinction between improvement in fit as a result of small improvements throughout the entire data set and a large improvement in a small number of critically sensitive data points. A test that can be used for comparing arbitrary pairs of models, and that focuses attention on those data points that are most sensitive to differences in the models, was introduced by Williams & Kloot (1953; also Himmelblau, 1970; Prince, 1982).

Table 8.4.3.1. *Values of t for which the c.d.f. $\Psi(t,\nu)$ has the values given in the column headings, for various values of ν*

ν	0.75	0.90	0.95	0.99	0.995
1	1.0000	3.0777	6.3138	31.8206	63.6570
2	0.8165	1.8856	2.9200	6.9646	9.9249
3	0.7649	1.6377	2.3534	4.5407	5.8409
4	0.7407	1.5332	2.1319	3.7469	4.6041
6	0.7176	1.4398	1.9432	3.1427	3.7074
8	0.7064	1.3968	1.8596	2.8965	3.3554
10	0.6998	1.3722	1.8125	2.7638	3.1693
12	0.6955	1.3562	1.7823	2.6810	3.0546
14	0.6924	1.3450	1.7613	2.6245	2.9769
16	0.6901	1.3368	1.7459	2.5835	2.9208
20	0.6870	1.3253	1.7247	2.5280	2.8453
25	0.6844	1.3164	1.7081	2.4851	2.7874
30	0.6828	1.3104	1.6973	2.4573	2.7500
35	0.6816	1.3062	1.6896	2.4377	2.7238
40	0.6807	1.3031	1.6839	2.4233	2.7045
50	0.6794	1.2987	1.6759	2.4033	2.6778
60	0.6786	1.2958	1.6707	2.3901	2.6603
80	0.6776	1.2922	1.6641	2.3739	2.6387
100	0.6770	1.2901	1.6602	2.3642	2.6259
120	0.6765	1.2886	1.6577	2.3578	2.6174

Consider a set of observations, y_{0i}, and two models that predict values for these observations, y_{1i} and y_{2i}, respectively. We determine the slope of the regression line $z=\lambda x$, where $z_i = \left[y_{0i} - (1/2)(y_{1i}+y_{2i})\right]/\sigma_i$, and $x_i = (y_{1i}-y_{2i})/\sigma_i$. Suppose model 1 is a perfect fit to the data, which have been measured with great precision, so that $y_{0i}=y_{1i}$ for all i. Under these conditions, $\lambda=+1/2$. Similarly, if model 2 is a perfect fit, $\lambda=-1/2$. Real experimental data, of course, are subject to random error, and $|\lambda|$ in general would be expected to be less than 1/2. A least-squares estimate of λ is

$$\widehat{\lambda} = \frac{\sum_{i=1}^n z_i x_i}{\sum_{i=1}^n x_i^2}, \tag{8.4.3.1}$$

and it has an estimated variance

$$\widehat{\sigma}_\lambda^2 = \frac{\sum_{i=1}^n z_i^2 - \widehat{\lambda}^2\sum_{i=1}^n x_i^2}{(n-1)\sum_{i=1}^n x_i^2}. \tag{8.4.3.2}$$

The hypothesis that the two models give equally good fits to the data can be tested by considering $\widehat{\lambda}$ to be an unconstrained, one-parameter fit that is to be compared with a constrained, zero-parameter fit for which $\lambda=0$. A p.d.f. for making this comparison can be derived from an F distribution with $\nu_1=1$ and $\nu_2=\nu=(n-1)$.

$$\Phi(F,1,\nu) = \frac{\Gamma[(\nu+1)/2]}{\sqrt{\pi\nu F}\,\Gamma(\nu/2)(1+F/\nu)^{(\nu+1)/2}}. \tag{8.4.3.3}$$

If we let $|t| = \sqrt{F}$, and use

$$\int_0^{F_0} \Phi(F, 1, \nu)\, \mathrm{d}F = \int_{-t_0}^{+t_0} \Phi(t, \nu)\, \mathrm{d}t, \tag{8.4.3.4}$$

we can derive a p.d.f. for t, which is

$$\Phi(t, \nu) = \frac{\Gamma[(\nu+1)/2]}{\sqrt{\pi\nu}\,\Gamma(\nu/2)[1 + t^2/\nu]^{(\nu+1)/2}}. \tag{8.4.3.5}$$

This p.d.f. is known as *Student's t distribution with ν degrees of freedom*. Setting $t = \widehat{\lambda}/\widehat{\sigma}_\lambda$, the c.d.f. $\Psi(t, \nu)$ can be used to test the alternative hypotheses $\lambda = 0$ and $\lambda = \pm 1/2$. Table 8.4.3.1 gives the values of t for which the c.d.f. $\Psi(t, \nu)$ has various values for various values of ν. Fortran code for the program from which this table was generated appears in Prince (1994).

Again, it must be understood that the results of these statistical comparisons do not imply that either model is a correct one. A statistical indication of a good fit says only that, given the model, the experimenter should not be surprised at having observed the data values that were observed. It says nothing about whether the model is plausible in terms of compatibility with the laws of physics and chemistry. Nor does it rule out the existence of other models that describe the data as well as or better than any of the models tested.

8.4.4. Influence of individual data points

When the method of least squares, or any variant of it, is used to refine a crystal structure, it is implicitly assumed that a model with adjustable parameters makes an unbiased prediction of the experimental observations for some (*a priori* unknown) set of values of those parameters. The existence of any reflection whose observed intensity is inconsistent with this assumption, that is that it differs from the predicted value by an amount that cannot be reconciled with the precision of the measurement, must cause the model to be rejected, or at least modified. In making precise estimates of the values of the unknown parameters, however, different reflections do not all carry the same amount of information (Shoemaker, 1968; Prince & Nicholson, 1985). For an obvious example, consider a space-group systematic absence. Except for possible effects of multiple diffraction or twinning, any observed intensity at a position corresponding to a systematic absence is proof that the screw axis or glide plane is not present. If no intensity is observed for any such reflection, however, any parameter values that conform to the space group are equally acceptable. It is to be expected, on the other hand, that some intensities will be extremely sensitive to small changes in some parameter, and that careful measurement of those intensities will lead to correspondingly precise estimates of the parameter values. For the purpose of precise structure refinement, it is useful to be able to identify the influential reflections.

Consider a vector of observations, $\mathbf{y}$, and a model $\boldsymbol{M}(\mathbf{x})$. The elements of $\mathbf{y}$ define an n-dimension space, and the model values, $M_i(\mathbf{x})$, define a p-dimensional subspace within it. The least-squares solution [equation (8.1.2.7)],

$$\widehat{\mathbf{x}} = (\boldsymbol{A}^T\boldsymbol{W}\boldsymbol{A})^{-1}\boldsymbol{A}^T\boldsymbol{W}(\mathbf{y} - \mathbf{y}_0), \tag{8.4.4.1}$$

is such that $\widehat{\mathbf{y}} = \boldsymbol{M}(\widehat{\mathbf{x}})$ is the closest point to $\mathbf{y}$ that corresponds to some possible value of $\mathbf{x}$. In (8.4.4.1), $\boldsymbol{W} = \boldsymbol{V}^{-1}$ is the inverse of the variance–covariance matrix for the joint p.d.f. of the elements of $\mathbf{y}$, and $\mathbf{y}_0 = \boldsymbol{M}(\mathbf{x}_0)$ is a point in the p-dimensional subspace close enough to $\boldsymbol{M}(\widehat{\mathbf{x}})$ so that the linear approximation

$$\boldsymbol{M}(\mathbf{x}) = \mathbf{y}_0 + \boldsymbol{A}(\mathbf{x} - \mathbf{x}_0) \tag{8.4.4.2}$$

[where $A_{ij} = \partial M_i(\mathbf{x})/\partial x_j$] is a good one. Let $\boldsymbol{R}$ be the Cholesky factor of $\boldsymbol{W}$, so that $\boldsymbol{W} = \boldsymbol{R}^T\boldsymbol{R}$, and let $\boldsymbol{Z} = \boldsymbol{R}\boldsymbol{A}$, $\mathbf{y}' = \mathbf{y} - \mathbf{y}_0$, and $\widehat{\mathbf{y}}' = \widehat{\mathbf{y}} - \mathbf{y}_0$. The least-squares estimate may then be written

$$\widehat{\mathbf{x}} = \mathbf{x}_0 + (\boldsymbol{Z}^T\boldsymbol{Z})^{-1}\boldsymbol{Z}^T\mathbf{y}' \tag{8.4.4.3}$$

and

$$\widehat{\mathbf{y}}' = \boldsymbol{Z}(\widehat{\mathbf{x}} - \mathbf{x}_0) = \boldsymbol{Z}(\boldsymbol{Z}^T\boldsymbol{Z})^{-1}\boldsymbol{Z}^T\mathbf{y}'. \tag{8.4.4.4}$$

Thus, the matrix $\boldsymbol{P} = \boldsymbol{Z}(\boldsymbol{Z}^T\boldsymbol{Z})\boldsymbol{Z}^T$, the *projection matrix*, is a linear relation between the observed data values and the corresponding calculated values. (Because $\widehat{\mathbf{y}}' = \boldsymbol{P}\mathbf{y}'$, the matrix $\boldsymbol{P}$ is frequently referred to in the statistical literature as the *hat matrix*.) $\boldsymbol{P}^2 = \boldsymbol{Z}(\boldsymbol{Z}^T\boldsymbol{Z})^{-1}\boldsymbol{Z}^T\boldsymbol{Z}(\boldsymbol{Z}^T\boldsymbol{Z})^{-1}\boldsymbol{Z}^T = \boldsymbol{Z}(\boldsymbol{Z}^T\boldsymbol{Z})^{-1}\boldsymbol{Z}^T = \boldsymbol{P}$, so that $\boldsymbol{P}$ is *idempotent*. $\boldsymbol{P}$ is an $n \times n$ positive semidefinite matrix with rank p, and its eigenvalues are either 1 (p times) or 0 ($n - p$ times). Its diagonal elements lie in the range $0 \le P_{ii} \le 1$, and the trace of $\boldsymbol{P}$ is p, so that the average value of P_{ii} is p/n. Furthermore,

$$P_{ii} = \sum_{j=1}^{n} P_{ij}^2. \tag{8.4.4.5}$$

A diagonal element of $\boldsymbol{P}$ is a measure of the influence that an observation has on its own calculated value. If P_{ii} is close to one, the model is forced to fit the ith data point, which puts a constraint on the value of the corresponding function of the parameters. A very small value of P_{ii}, because of (8.4.4.5), implies that all elements of the row must be small, and that observation has little influence on its own or any other calculated value. Because it is a measure of influence on the fit, P_{ii} is sometimes referred to as the *leverage* of the ith observation. Note that, because $(\boldsymbol{Z}^T\boldsymbol{Z})^{-1} = \boldsymbol{V}_{\mathbf{x}}$, the variance–covariance matrix for the elements of $\widehat{\mathbf{x}}$, $\boldsymbol{P}$ is the variance–covariance matrix for $\widehat{\mathbf{y}}$, whose elements are functions of the elements of $\widehat{\mathbf{x}}$. A large value of P_{ii} means that y_i is poorly defined by the elements of $\widehat{\mathbf{x}}$, which implies in turn that some elements of $\widehat{\mathbf{x}}$ must be precisely defined by a precise measurement of y_i'.

It is apparent that, in a real experiment, there will be appreciable variation among observations in their leverage. It can be shown (Fedorov, 1972; Prince & Nicholson, 1985) that the observations with the greatest leverage also have the largest effect on the volume of the p-dimensional confidence region for the parameter estimates. Because this volume is a rather gross measure, however, it is useful to have a measure of the influence of individual observations on individual parameters. Let $\boldsymbol{V}_n$ be the variance–covariance matrix for a refinement including n observations, and let $\mathbf{z}$ be a row vector whose elements are $z_j = [\partial M(\mathbf{x})/\partial x_j]/\sigma$ for an additional observation. $\boldsymbol{V}_{n+1}$, the variance–covariance matrix with the additional observation included, is, by definition,

$$\boldsymbol{V}_{n+1} = (\boldsymbol{Z}^T\boldsymbol{Z} + \mathbf{z}^T\mathbf{z})^{-1}, \tag{8.4.4.6}$$

which, in the linear approximation, can be shown to be

$$\boldsymbol{V}_{n+1} = \boldsymbol{V}_n - \boldsymbol{V}_n\mathbf{z}^T\mathbf{z}\boldsymbol{V}_n/(1 + \mathbf{z}\boldsymbol{V}_n\mathbf{z}^T). \tag{8.4.4.7}$$

The diagonal elements of the rank one matrix $\boldsymbol{D} = \boldsymbol{V}_n\mathbf{z}^T\mathbf{z}\boldsymbol{V}_n/(1 + \mathbf{z}\boldsymbol{V}_n\mathbf{z}^T)$ are therefore the amounts that the variances of the estimates of individual parameters will be reduced by inclusion of the additional observation.

This result depends on the elements of $\boldsymbol{Z}$ and $\mathbf{z}$ not changing significantly in the (presumably small) shift from $\widehat{\mathbf{x}}_n$ to $\widehat{\mathbf{x}}_{n+1}$. That this condition is satisfied may be verified by the following procedure. Find an approximation to $\widehat{\mathbf{x}}_{n+1}$ by a line search

along the line $\mathbf{x} = \hat{\mathbf{x}}_n + \alpha \boldsymbol{V}_{n+1}\mathbf{z}^T y'_{n+1}$, and then evaluate $\boldsymbol{B}$, a quasi-Newton update such as the BFGS update (Subsection 8.1.4.3) at that point. If $\alpha = 1$, and the gradient of the sum of squares vanishes, then the linear approximation is exact, and $\boldsymbol{B}$ is null. If

$$|B_{ij}| \ll \left[\left(\boldsymbol{Z}^T\boldsymbol{Z} + \mathbf{z}^T\mathbf{z} \right)_{ii} \left(\boldsymbol{Z}^T\boldsymbol{Z} + \mathbf{z}^T\mathbf{z} \right)_{jj} \right]^{1/2} \tag{8.4.4.8}$$

for all i and j, then (8.4.4.7) can be expected to be an excellent approximation for a nonlinear model.

International Tables for Crystallography (2006). Vol. C, Chapter 8.5, pp. 707–709.

8.5. Detection and treatment of systematic error

By E. Prince and C. H. Spiegelman

8.5.1. Accuracy

Chapter 8.4 discusses statistical tests for goodness of fit between experimental observations and the predictions of a model with adjustable parameters whose values have been estimated by least squares or some similar procedure. In addition to the estimates of parameter values, one can also make estimates of the uncertainties in those values, estimates that are usually expressed in terms of an *estimated standard deviation* or, according to recommended usage (ISO, 1993), a *standard uncertainty*. A standard deviation is a measure of *precision*, that is, a measure of the width of a confidence interval that results from random fluctuations in the measurement process. What the experimenter who collected the data wants to know about, of course, is *accuracy*, a measure of the location of a region within which nature's 'correct' value lies, as well as its width (Prince, 1994). In performing a refinement, we have assumed implicitly that the observations have been drawn at random from a population the mean of whose p.d.f. is given by a model when all of its parameters have those unknown, correct values. If this assumption is incorrect, the expected value of the estimate may no longer be near to the correct value, and the estimate contains *bias*, or *systematic error*. An accurate measurement is one that not only is precise but also has small bias. In this chapter, we shall discuss various criteria by which the results of a refinement may be judged in order to determine whether they are free of systematic error, and thus whether they may be considered accurate.

8.5.2. Lack of fit

We saw in Section 8.4.2 that the sum of squared residuals from an ideally weighted, least-squares fit to a correct model is a sum of terms that has expected value $(n-p)$ and is distributed as χ^2 with $\nu = n-p$ degrees of freedom. Further, the residuals have a distribution with zero mean. A value for the sum that exceeds $(n-p)$ by an amount that is improbably large is an indication of lack of fit, which may be due to an incorrect model for the mean or to nonideal weighting or both. {The sum, S, may be considered to be improbably large when the value of the χ^2 cumulative distribution function, $\Psi_{\chi^2}[S,(n-p)]$, is close to 1.0. A value for the sum that is substantially *less* than $(n-p)$ may also be an indication that the model contains more parameters than can be justified by the data set. Note also that a reasonable value for the sum of squared residuals does *not* prove that the model is correct. It indicates that the model adequately describes the data, but it in no way rules out the existence of alternative models that describe the data equally well.} If the sum of squares is greater than $(n-p)$, it is commonly assumed that the mean model is correct, and that the weights have appropriate relative values, although their absolute values may be too large. If $w = k^2/u_i^2$, where k is some number greater than one, and u_i is the standard uncertainty of the ith observation, the goodness-of-fit parameter,

$$G = \left\{ \sum_{i=1}^{n} w_i [y_i - M_i(\widehat{\mathbf{x}})]^2 / (n-p) \right\}^{1/2}, \qquad (8.5.2.1)$$

is taken to be an estimate of k, and all elements of the inverse of the normal-equations matrix are multiplied by k^2 to obtain the estimated variance–covariance matrix

$$\widehat{V}_{\mathbf{x}} = G^2 (\boldsymbol{A}^T \boldsymbol{W} \boldsymbol{A})^{-1}. \qquad (8.5.2.2)$$

Frequently, however, there is some other, independent estimate of the variance of the observation, σ_i^2, derived, for example, from counting statistics or from the observed scatter among symmetry-equivalent reflections. If this estimate is inconsistent with the hypothesis that all data points have been overweighted by a constant factor, then the assumption that the parameter estimates are unbiased but less precise than the original weights would indicate must be discarded. Instead, it must be assumed that the model is incorrect, or at least incomplete. A systematic error may be considered to cause the model to be incomplete, and may introduce bias into some or all of the refined parameters. (Note that in many standard statistical texts it is implicitly assumed, without so stating, that the data have already been scaled by a set of correct, relative weights. It is thus easy for the unwary reader to make the error of assuming that the practice of multiplying by the goodness-of-fit parameter is a well established procedure.)

The use of (8.5.2.2) to compute estimated variances and standard uncertainties assumes implicitly that the effect of lack of fit on parameter estimates is random, and applies equally to all parameters, even though different types of parameter may have very different mathematical relations in the model. With a model as complex as the crystallographic structure-factor formula, this assumption is certainly questionable.

Information about the nature of the model inadequacies can be obtained by examining the residuals (Belsley, Kuh & Welsch, 1980; Belsley, 1991). The standardized residuals, $R_i = [y_i - M_i(\widehat{\mathbf{x}})]/u_i'$, where $\widehat{\mathbf{x}}$ is the least-squares estimate of the parameters, should be randomly distributed, with zero mean, not only for the data set as a whole but also for subsets of the data that are chosen in a manner that depends only on the model and not on the observed values of the data. Here, u_i' is the standard uncertainty of the *residual* and is related to u_i, the standard uncertainty of the observation, by $u_i' = u_i(1-P_{ii})$, where P_{ii} is a diagonal element of the projection matrix (Section 8.4.4). A scatter plot, in which the residuals are plotted against some control variable, such as $|F_{\rm calc}|$, $\sin\theta/\lambda$, or one of the Miller indices, should reveal no general trends. The existence of any such trend may indicate a systematic effect that depends on the corresponding variable. The model may then be modified by inclusion of a factor that is proportional to that variable, and the refinement repeated. An examination of the shifts in the other parameters, and of the new row or column of the variance–covariance matrix, will then reveal which of the parameters in the unmodified model are likely to have been biased by the systematic effect. When this procedure has been followed, it is extremely important to consider carefully the nature of the additional effect and determine whether it is plausible in terms of physics and chemistry.

Another procedure for detecting systematic lack of fit makes use of the fact that, if the model is correct, and the error distribution is approximately normal, or Gaussian, the distribution of residuals will also be approximately normal. A large sample may be checked for normality by means of a quantile–quantile, or Q–Q, plot (Abrahams & Keve, 1971; Kafadar & Spiegelman, 1986). To make such a plot, the residuals are first sorted in ascending order of magnitude. If there are n points in the data set, the value of the ith sorted residual should be close to the value, x_i, for which

Copyright © 2006 International Union of Crystallography

$$\Psi(x_i) = (2i - 1)/2n, \tag{8.5.2.3}$$

where $\Psi(x)$ is the cumulative distribution function for the normal p.d.f. A plot of R_i against x_i should be a straight line with zero intercept and unit slope. A straight line with a slope greater than one suggests that the model is satisfactory, but that the variances of the data points have been systematically underestimated. Lack of fit is suggested if the curve has a higher slope near the ends, indicating that large residuals occur with greater frequency than would be predicted by the normal p.d.f.

The sorted residuals tend to be strongly correlated. A positive displacement from a smooth curve tends to be followed by another positive displacement, and a negative one by another negative one, which gives the *Q–Q* plot a wavy appearance, and it may be difficult to decide whether it is a straight line or not. Because of this, a useful alternative to the *Q–Q* plot is the conditional *Q–Q* plot (Kafadar & Spiegelman, 1986), so called because the abscissa for plotting the ith sorted residual is the mean of a conditional p.d.f. for that residual given the observed values of all the others. To construct a conditional *Q–Q* plot, first transform the distribution to a uniform p.d.f. by

$$U_i = \Psi(R_i, \mu, \sigma), \tag{8.5.2.4}$$

where μ and σ are resistant estimates (Section 8.2.2) of the mean and standard deviation of the p.d.f., such as the median and 0.75 times the interquartile range, and Ψ represents the cumulative distribution function. Letting $U_0 = 0$ and $U_{n+1} = 1$, the expected value of U_i, given all the others, is

$$\langle U_i \rangle = (U_{i-1} + U_{i+1})/2. \tag{8.5.2.5}$$

The ith abscissa for the *Q–Q* plot is then

$$x_i = \Psi^{-1}(\langle U_i \rangle, \mu, \sigma), \tag{8.5.2.6}$$

where $\Psi^{-1}(y, \mu, \sigma)$ is a *per cent point function*, or p.p.f., the value of x for which $\Psi(x, \mu, \sigma) = y$.

Q–Q plots for subsets of the data can reveal, by nonzero intercepts, that those subsets are subject to a systematic bias. Because of its property of removing short-range kinks in the curve, the conditional *Q–Q* plot can be particularly useful in this application. The values of μ and σ used for the transformation to a uniform distribution, as in (8.5.2.4), should be those determined from the entire data set.

A *Q–Q* plot will reveal data points that are in poor agreement with the model, but that do not belong to any easily identifiable subset. Because of the central limit theorem (Section 8.4.1), however, the least-squares method tends to force the distribution of the residuals toward a normal distribution, and the discrepant points may not be clearly evident. A robust/resistant procedure (see Section 8.2.2), because it reduces the influence of strongly discrepant data points, helps to separate them from the body of the data. Therefore, if a data set contains discrepant points, a *Q–Q* plot of the residuals from a robust/resistant fit will tend to have greater curvature at the extremes than one from a corresponding least-squares fit. If the discrepant data points that are thus identified have a pattern, this information may enable a systematic error to be characterized.

8.5.3. Influential data points

Section 8.4.4 discusses the influence of individual data points on the estimation of parameters and how to identify the data points that should be measured with particular care in order to make the most precise estimates of particular parameters. The same properties that cause these influential data points to be most effective in reducing the uncertainty of a parameter estimate when the model is a correct predictor for the observations also cause them to have the greatest potential for introducing bias if there is a flaw in the model or, correspondingly, if they are subject to systematic error. Reviews of procedures for studying the effects of influential data points and outliers have been given by Beckman & Cook (1983), by Chatterjee & Hadi (1986), and by Belsley (1991).

The effects of possible systematic error can be studied by identifying influential data points and then observing the effects of deleting them one by one from the refinement. The deletion of a data point should affect the standard uncertainty of an estimate, but should not cause a shift in its mean that is more than a small multiple of the resulting standard uncertainty. As in Section 8.4.4, we define the design matrix, $\boldsymbol{A}$, by

$$A_{ij} = \partial M_i(\mathbf{x})/\partial x_j, \tag{8.5.3.1}$$

where $M_i(\mathbf{x})$ is the model function for the ith data point, and $\mathbf{x}$ is a vector of adjustable parameters. Let $\boldsymbol{R}$ be the upper triangular Cholesky factor of the weight matrix, so that $\boldsymbol{W} = \boldsymbol{R}^T\boldsymbol{R}$, and define the weighted design matrix by $\boldsymbol{Z} = \boldsymbol{RA}$ and the weighted vector of observations by $\mathbf{y}' = \boldsymbol{R}\mathbf{y}$. The least-squares estimate of $\mathbf{x}$ is then

$$\widehat{\mathbf{x}} = (\boldsymbol{Z}^T\boldsymbol{Z})^{-1}\boldsymbol{Z}^T\mathbf{y}', \tag{8.5.3.2}$$

and the vector of predicted values is

$$\widehat{\mathbf{y}}' = \boldsymbol{Z}(\boldsymbol{Z}^T\boldsymbol{Z})^{-1}\boldsymbol{Z}^T\mathbf{y}' = \boldsymbol{P}\mathbf{y}', \tag{8.5.3.3}$$

where $\boldsymbol{P}$ is the projection, or hat, matrix. A diagonal element, P_{ii}, of $\boldsymbol{P}$ is a measure of the leverage, that is of the relative influence, of the ith data point, and therefore of the sensitivity of the estimates of the elements of $\mathbf{x}$ to an error in the measurement of that data point. P_{ii} lies in the range $0 \leq P_{ii} \leq 1$, and it has average value p/n, so that data points with values of P_{ii} greater than $2p/n$ can be considered particularly influential.

Let $\boldsymbol{H} = \boldsymbol{Z}^T\boldsymbol{Z}$ be the normal-equations matrix, let $\boldsymbol{V} = \boldsymbol{H}^{-1}$ be the estimated variance–covariance matrix, and let $\mathbf{q} = \boldsymbol{Z}^T\mathbf{y}'$, so that $\widehat{\mathbf{x}} = \boldsymbol{V}\mathbf{q}$. Let $\mathbf{z}_i$ be the ith row of $\boldsymbol{Z}$, and denote by $\boldsymbol{Z}^{(i)}$, $\boldsymbol{H}^{(i)}$, $\boldsymbol{V}^{(i)}$, $\mathbf{q}^{(i)}$, and $\widehat{\mathbf{x}}^{(i)}$ the respective matrices and vectors computed with the ith data point deleted from the data set. We wish to find large values of $|\widehat{x}_j - \widehat{x}_j^{(i)}|/[V_{jj}^{(i)}]^{1/2}$, so we need to compute $\boldsymbol{V}^{(i)}$ and $\mathbf{x}^{(i)}$. With a derivation similar to that for (8.4.4.7), it can be shown (Fedorov, 1972; Prince & Nicholson, 1985) that

$$\boldsymbol{V}^{(i)} = \boldsymbol{V} + \frac{\boldsymbol{V}\mathbf{z}_i^T\mathbf{z}_i\boldsymbol{V}}{(1 - \mathbf{z}_i\boldsymbol{V}\mathbf{z}_i^T)} = \boldsymbol{V} + \frac{\boldsymbol{V}\mathbf{z}_i^T\mathbf{z}_i\boldsymbol{V}}{(1 - P_{ii})}. \tag{8.5.3.4}$$

Note that, if $P_{ii} = 1$, all elements of $\boldsymbol{V}^{(i)}$ become infinite, implying that $\boldsymbol{H}^{(i)}$ is singular. Thus, if such a data point is deleted, the solution is no longer determinate. Now,

$$\widehat{\mathbf{x}}^{(i)} = \boldsymbol{V}^{(i)}\mathbf{q}^{(i)} \tag{8.5.3.5}$$

and

$$\mathbf{q}^{(i)} = \mathbf{q} - y_i'\mathbf{z}_i^T, \tag{8.5.3.6}$$

so that, when $\boldsymbol{V}$ and $\widehat{\mathbf{x}}$ have been computed once, it is a straightforward and inexpensive additional computation to determine whether any parameter has been strongly influenced, and therefore potentially biased, by the inclusion of any data point in the refinement. If there is any reason to be concerned about possible systematic error, the leverage of every data point included in the refinement should be computed, and the effects of deletion of all of those with leverage greater than $2p/n$ should be observed.

8.5.4. Plausibility of results

A study of residuals to detect a pattern of discrepancies will reveal the presence of systematic error, or model inadequacy, only if different subsets of the data are affected differently. Some sources of bias, however, have noticeable effects throughout the data set, and missing parameters may mimic others that have been included, thus introducing bias without any apparent lack of fit. To cite an obvious example, determination of unit-cell dimensions requires an accurate value of the wavelength of the radiation being used. If this value is incorrect, inferred values of the cell constants may be reproduced repeatedly with great precision, but all will be subject to a systematic bias that has no effect on the quality of the fit. Even though the structure of the residuals in such a case reveals little about possible systematic error, it is still possible to detect it by critical examination of the estimated parameters.

Even before any data have been collected in preparation for the determination of a crystal structure, a great deal is known about certain details. It is known that the crystal is composed of atoms of certain elements that are present in certain proportions. It is known that pairs of atoms of various elements cannot be less than a certain distance apart, and, further, that adjacent atoms tend to be separated by distances that fall within a rather narrow range. It is known that thermal vibration amplitudes are likely to be larger in directions normal to interatomic vectors than parallel to them, although, particularly in the case of hydrogen bonds, there may be an apparent amplitude parallel to a vector because of atomic disorder. Even when there is a particularly unusual feature in a structure, most of the structure will conform to commonly observed patterns. Thus, if a refined crystal structure overall has reasonable features, such as interatomic distances that are appropriate to oxidation state and coordination number and displacement ellipsoids that make sense, one or two unusual features may be accepted with confidence. On the other hand, if there is wide variation in the lengths of chemically similar bonds, or if the eigenvectors of the thermal motion tensors point in odd directions relative to the interatomic vectors, there must be a presumption that systematic errors have been compensated for by biased estimates of parameters.

A particular problem arises when there is a question of the presence or absence of symmetry, such as a choice between two space groups, one of which possesses a centre of symmetry or a mirror plane, or a case where a symmetric molecule occupies a position whose environment has a less-symmetric point group. If symmetry constraints are relaxed, the model can always be refined to a lower sum of squared residuals. (For a discussion of numerical problems that occur in the vicinity of a symmetric configuration, see Section 8.1.3.) The problem comes from the fact that the removal of the symmetry element almost always introduces too many additional parameters. Statistical tests are then quite likely to indicate that the lower-symmetry model gives a significantly better fit, but consideration of internal consistency and chemical or physical plausibility is likely to suggest that much systematic error has been absorbed by the additional parameters. The proper procedure is to devise a model with noncrystallographic constraints (see Section 8.3.2) that expresses what is, for chemical or physical reasons, known or probable. To do so may require great patience and perseverence.

International Tables for Crystallography (2006). Vol. C, Chapter 8.6, pp. 710–712.

8.6. The Rietveld method

By A. Albinati and B. T. M. Willis

In the Rietveld method of analysing powder diffraction data, the crystal structure is refined by fitting the entire profile of the diffraction pattern to a calculated profile. There is no intermediate step of extracting structure factors, and so patterns containing many overlapping Bragg peaks can be analysed. The method was applied originally by Rietveld (1967, 1969) to the refinement of neutron intensities recorded at a fixed wavelength. Subsequently, it has been used successfully for analysing powder data from all four categories of experimental technique, with neutrons or X-rays as the primary radiation and with scattered intensities measured at a fixed wavelength (and variable scattering angle) or at a fixed scattering angle (and variable wavelength).

Powder refinements are usually less satisfactory than those on single-crystal data, as the three-dimensional information of the reciprocal lattice is compressed into one dimension in the powder pattern. Nevertheless, a large number of successful refinements by the Rietveld method has been reported; reviews have been given by Taylor (1985), Hewat (1986), Cheetham & Wilkinson (1992), Young (1993), Harris & Tremayne (1996), Masciocchi & Sironi (1997), Harris *et al.* (2001) and David *et al.* (2002). Here we shall discuss only the basic principles of the refinement procedure.

8.6.1. Basic theory

The model of the structure is refined by least-squares minimization of the residual

$$M = \sum_{i=1}^{N} w_i \left[y_i(\text{obs.}) - y_i(\text{calc.}) \right]^2. \qquad (8.6.1.1)$$

y_i(obs.) is the intensity measured at a point i in the diffraction pattern corrected for the background intensity b_i, w_i is its weight, and y_i(calc.) is the calculated intensity. If the background at each point is assumed to be zero, and if the only source of error in measuring the intensities is that from counting statistics, the weight is given by

$$w_i = \left[y_i(\text{obs.}) \right]^{-1}.$$

The summation in (8.6.1.1) runs over all N data points. The number of data points can be arbitrarily increased by reducing the interval between adjacent steps. However, this does not necessarily imply an improvement in the standard uncertainties (s.u.'s; see Section 8.1.2) of the structural parameters (see Subsection 8.6.2.5), which are dependent on the number of linearly independent columns in the design matrix [equation (8.1.2.3)]. The number of independent observations in a powder pattern is determined by the extent of overlapping of adjacent reflections. An intuitive argument for estimating this number has been proposed by Altomare *et al.* (1995) and a more rigorous statistical estimate has been described by Sivia (2000). The strategy for choosing the number of steps and apportioning the available counting time has been discussed by McCusker *et al.* (1999) and references therein. The relation between counting statistics and the s.u.'s has been discussed by Baharie & Pawley (1983) and by Scott (1983).

The calculated intensity is evaluated using the equation

$$y_i(\text{calc.}) = s \sum_{k=k_1}^{k_2} m_k L_k \left| F_k \right|^2 G_{ik}, \qquad (8.6.1.2)$$

where s is a scale factor, m_k is the multiplicity factor for the kth reflection, L_k is the Lorentz–polarization factor, F_k is the structure factor and G_{ik} is the 'peak-shape function' (PSF). The summation in (8.6.1.2) is over all nearby reflections, k_1 to k_2, contributing to a given data point i.

A fundamental problem of the Rietveld method is the formulation of a suitable peak-shape function. For X-rays, a mixture of Gaussian and Lorentzian components is sometimes used (see Subsection 8.6.2.2). For neutrons, it is easier to find a suitable analytical function, and this is, perhaps, the main reason for the initial success of neutron Rietveld analysis. For a neutron diffractometer operating at a fixed wavelength and moderate resolution, the PSF is approximately a Gaussian of the form

$$G_{ik} = \frac{2}{H_k} \sqrt{\frac{\ln 2}{\pi}} \exp\left[-\frac{4 \ln 2 \, (2\theta_i - 2\theta_k)^2}{H_k^2} \right], \qquad (8.6.1.3)$$

where H_k is the full width at half-maximum (FWHM) of the peak, $2\theta_i$ is the scattering angle at the ith point, and θ_k is the Bragg angle for reflection k.

The angular dependence of the FWHM for a Gaussian peak-shape function can be written in the form

$$H_k^2 = U \tan^2 \theta_k + V \tan \theta_k + W,$$

where U, V and W are half-width parameters independent of θ_k (Caglioti, Paoletti & Ricci, 1958). To allow for intrinsic sample broadening and instrumental resolution, U, V and W are treated as adjustable variables in the least-squares refinement. The tails of a Gaussian peak decrease rapidly with distance from the maximum, and the intensity at one-and-a-half times the FWHM from the peak is only about 0.2% of the intensity at the peak. Thus, no large error is introduced by assuming that the peak extends over a range of approximately $\pm 1.5 H_k$ and is cut off outside this range. The FWHM for the Lorentzian (see Subsection 8.6.2.2) can be modelled by the relation

$$H_k = X \tan \theta_k + Y / \cos \theta_k.$$

The Lorentzian function extends over a much wider range than the Gaussian. A more flexible approach to this line-broadening problem is described by McCusker *et al.* (1999).

The least-squares parameters are of two types. The first contains the usual structural parameters: for example, fractional coordinates of each atom in the asymmetric unit and the corresponding isotropic or anisotropic displacement parameters. The second type represents 'profile parameters' which are not encountered in a least-squares refinement of single-crystal data. These include the half-width parameters and the dimensions of the unit cell. Further parameters may be added to both groups allowing for the modelling of the background and for the asymmetry of the reflections. The maximum number of parameters that can be safely included in a Rietveld refinement is largely determined by the quality of the diffraction pattern, but intrinsic line broadening will set an upper limit to this number (Hewat, 1986).

The following indicators are used to estimate the agreement with the model during the course of the refinement.

Copyright © 2006 International Union of Crystallography

Profile R factor:

$$R_P = \frac{\sum_i \left| y_i(\text{obs.}) - y_i(\text{calc.}) \right|}{\sum_i y_i(\text{obs.})}.$$

Weighted profile R factor:

$$R_{wP} = \left[\frac{\sum_i w_i \left| y_i(\text{obs.}) - y_i(\text{calc.}) \right|^2}{\sum_i w_i y_i^2(\text{obs.})} \right]^{1/2}.$$

Bragg R factor:

$$R_I = \frac{\sum_k \left| I_k(\text{obs.}) - I_k(\text{calc.}) \right|}{\sum_k I_k(\text{obs.})}.$$

Expected R factor:

$$R_E = \left[\frac{\mathcal{N} - P}{\sum_i w_i y_i^2(\text{obs.})} \right]^{1/2}.$$

I_k is the integrated intensity of the kth reflection, $\mathcal{N}$ is the number of independent observations, and P is the number of refined parameters. The most important indicators are R_{wP} and R_E. The ratio R_{wP}/R_E is the so-called 'goodness-of-fit', χ^2: in a successful refinement χ^2 should approach unity. The Bragg R factor is useful, since it depends on the fit of the structural parameters and not on the profile parameters.

8.6.2. Problems with the Rietveld method

One should be aware of certain problems that may give rise to failure in a Rietveld refinement.

8.6.2.1. *Indexing*

The first step in refinement is the indexing of the pattern. As the Rietveld method is often applied to the refinement of data for which the unit-cell parameters and space group are already known, there is then little difficulty in indexing the pattern, provided that there are a few well resolved lines. Without this knowledge, the indexing requires, as a starting point, the measurement of the d values of low-angle diffraction lines to high accuracy. According to Shirley (1980): 'Powder indexing works beautifully on good data, but with poor data it usually will not work at all'. The indexing of powder patterns and associated problems are discussed by Shirley (1980), Pawley (1981), Cheetham (1993) and Werner (2002).

8.6.2.2. *Peak-shape function (PSF)*

The appropriate function to use varies with the nature of the experimental technique. In addition to the Gaussian PSF in (8.6.1.3), functions commonly used for angle-dispersive data are (Young & Wiles, 1982):

$$G_{ik} = \frac{2}{\pi H_k} \left[1 + 4 \left(\frac{\Delta 2\theta_{ik}}{H_k} \right)^2 \right]^{-1} \quad \text{(Lorentzian)}$$

$$G_{ik} = \frac{2\eta}{\pi H_k} \left[1 + 4 \left(\frac{\Delta 2\theta_{ik}}{H_k} \right)^2 \right]^{-1} + (1 - \eta) \frac{2\sqrt{\ln 2}}{\sqrt{\pi} H_k} \exp \left[-4 \ln 2 \left(\frac{\Delta 2\theta_{ik}}{H_k} \right)^2 \right] \quad \text{(pseudo-Voigt)}$$

$$G_{ik} = \frac{2\Gamma(n)\left(2^{1/n} - 1\right)}{\pi H_k \Gamma\left(n - \frac{1}{2}\right)} \left[1 + 4\left(2^{1/n} - 1\right) \left(\frac{\Delta 2\theta_{ik}}{H_k} \right)^2 \right]^{-n} \quad \text{(Pearson VII)}$$

where $\Delta 2\theta_{ik} = 2\theta_i - 2\theta_k$. η is a parameter that defines the fraction of Lorentzian character in the pseudo-Voigt profile. $\Gamma(n)$ is the gamma function: when $n = 1$, Pearson VII becomes a Lorentzian, and when $n = \infty$, it becomes a Gaussian.

The tails of a Gaussian distribution fall off too rapidly to account for particle size broadening. The peak shape is then better described by a convolution of Gaussian and Lorentzian functions [*i.e.* Voigt function: see Ahtee, Nurmela & Suortti (1984) and David & Matthewman (1985)]. A pulsed neutron source gives an asymmetrical line shape arising from the fast rise and slow decay of the neutron pulse: this shape can be approximated by a pair of exponential functions convoluted with a Gaussian (Albinati & Willis, 1982; Von Dreele, Jorgensen & Windsor, 1982).

The pattern from an X-ray powder diffractometer gives peak shapes that cannot be fitted by a simple analytical function. Will, Parrish & Huang (1983) use the sum of several Lorentzians to express the shape of each diffraction peak, while Hepp & Baerlocher (1988) describe a numerical method of determining the PSF. Pearson VII functions have also been successfully used for X-ray data (Immirzi, 1980). A modified Lorentzian function has been employed for interpreting data from a Guinier focusing camera (Malmros & Thomas, 1977). PSFs for instruments employing X-ray synchrotron radiation can be represented by a Gaussian (Parrish & Huang, 1980) or a pseudo-Voigt function (Hastings, Thomlinson & Cox, 1984).

8.6.2.3. *Background*

The background may be determined by measuring regions of the pattern that are free from Bragg peaks. This procedure assumes that the background varies smoothly with $\sin\theta/\lambda$, whereas this is not the case in the presence of disorder or thermal diffuse scattering (TDS), which rises to a maximum at the Bragg positions. An alternative approach is to include a background function in the refinement model (Richardson, 1993). If the background is not accounted for satisfactorily, the temperature factors may be incorrect or even negative. The various procedures for estimating the background for X-ray, synchrotron, constant-wavelength and TOF neutron powder patterns are reviewed by McCusker *et al.* (1999).

In neutron diffraction, the main contribution to the background from hydrogen-containing samples is due to incoherent scattering. Deuterating the sample is essential in order to substantially reduce this background.

8.6.2.4. *Preferred orientation and texture*

Preferred orientation is a formidable problem which can drastically affect the measured intensities. A simple correction formula for plate-like morphology was given by Rietveld (1969). Ahtee, Unonius, Nurmela & Suortti (1989) have shown how the effects of preferred orientation can be included in the refinement by expanding the orientation distribution in spherical harmonics. Quantitative texture analysis based on spherical harmonics has been implemented in the Rietveld refinement code by Von Dreele (1997). A general model of the texture has also been described by Popa (1992). It may be possible to remove or reduce the effect of preferred orientation by mixing the sample with a suitable diluent.

An additional problem is caused by particle size and strain broadening, which are not smooth functions of the diffraction angle. These effects can be taken into account by phenomenological models (*e.g.* Dinnebier *et al.*, 1999; Pratapa, O'Connor & Hunter, 2002) or by an analytical approach such as that of Popa & Balzar (2002).

The determination of the elastic stresses and strains in polycrystals can be determined from diffraction line shifts using Rietveld refinement (Popa & Balzar, 2001).

8.6.2.5. *Statistical validity*

Sakata & Cooper (1979) criticized the Rietveld method on the grounds that different residuals

$$y_i(\text{obs.}) - y_i(\text{calc.})$$

related to the same Bragg peak are correlated with one another, and they asserted that this correlation leads to an uncertainty in the standard uncertainties of the structural parameters. Prince (1981) has challenged this conclusion and stated that the s.u.'s given by the Rietveld procedure are correct if the crystallographic model adequately fits the data. However, even if the s.u.'s are correct, they are measures of precision rather than accuracy, and attempts to assess accuracy are hampered by lack of information concerning correlations between systematic errors (Prince, 1985, 1993).

8.7. Analysis of charge and spin densities

By P. Coppens, Z. Su and P. J. Becker

8.7.1. Outline of this chapter

Knowledge of the electron distribution is crucial for our understanding of chemical and physical phenomena. It has been assumed in many calculations (*e.g.* Thomas, 1926; Fermi, 1928; and others), and formally proven for non-degenerate systems (Hohenberg & Kohn, 1964) that the electronic energy is a functional of the electron density. Thus, the experimental measurement of electron densities is important for our understanding of the properties of atoms, molecules and solids. One of the main methods to achieve this goal is the use of scattering techniques, including elastic X-ray scattering, Compton scattering of X-rays, magnetic scattering of neutrons and X-rays, and electron diffraction.

Meaningful information can only be obtained with data of the utmost accuracy, which excludes most routinely collected crystallographic data sets. The present chapter will review the basic concepts and expressions used in the interpretation of accurate data in terms of the charge and spin distributions of the electrons. The structure-factor formalism has been treated in Chapter 1.2 of Volume B (*IT*B, 1992).

8.7.2. Electron densities and the *n*-particle wavefunction

A wavefunction $\psi(1, 2, 3, \ldots, n)$ for a system of n electrons is a function of the $3n$ space and n spin coordinates of the electrons. The wavefunction must be antisymmetric with respect to the interchange of any two electrons. The most general density function is the n-particle density matrix, of dimension $4n \times 4n$, defined as

$$\Gamma^n(1, 2, \ldots, n; 1', 2', \ldots, n') = \psi(1, 2, \ldots, n)\psi^*(1', 2', \ldots, n'). \quad (8.7.2.1)$$

In this expression, each index represents both the continuous space coordinates and the discontinuous spin coordinates of each of the n particles. Thus, the n-particle density matrix is a representation of the state in a $6n$-dimensional coordinate space, and the n-dimensional (discontinuous) spin state.

The *pth reduced density matrix* can be derived from (8.7.2.1) by integration over the space and spin coordinates of $n - p$ particles,

$$\Gamma^p(1, 2, \ldots, p; 1', 2', \ldots, p') = \binom{n}{p} \int \Gamma^n(1, 2, \ldots, p, p+1, \ldots, n; 1', 2', \ldots, p', p+1, \ldots, n)\, \mathrm{d}(p+1) \ldots \mathrm{d}n. \quad (8.7.2.2)$$

According to a basic postulate of quantum mechanics, physical properties are represented by their expectation values $\langle F \rangle$ obtained from the corresponding *operator equation*,

$$\langle F \rangle = \langle \psi | \widehat{F} | \psi \rangle / \langle \psi | \psi \rangle, \quad (8.7.2.3)$$

where $\widehat{F}$ is a (Hermitian) operator. As almost all operators of interest are one- or two-particle operators, the one- and two-particle matrices $\Gamma^1(1\ ;1')$ and $\Gamma^2(1, 2\ ;1', 2')$ are of prime interest. The charge density, or *one-electron density*, can be obtained from $\Gamma^1(1; 1')$ by setting $1' = 1$ and integrating over the spin coordinates, *i.e.*

$$\rho(\mathbf{r}) = n \int \Gamma^1(1, 1)\, \mathrm{d}s_1 = n \int \psi(1, 2, \ldots, n)\psi^*(1, 2, \ldots, n)\, \mathrm{d}s_1\, \mathrm{d}2 \ldots \mathrm{d}n. \quad (8.7.2.4)$$

An electron density $\rho(\mathbf{r})$ that can be represented by an antisymmetric N-electron wave function and is derivable from that wave function through (8.7.2.4) is called N-representable. As in any real system, the particles will undergo vibrations, so (8.7.2.4) must be modified to allow for the continuous change in the configuration of the nuclei. The commonly used Born–Oppenheimer approximation assumes that the electrons rearrange instantaneously in the field of the oscillating nuclei, which leads to the separation

$$\psi = \psi_e(\mathbf{r}, \mathbf{R}) \cdot \psi_N(\mathbf{R}), \quad (8.7.2.5)$$

where $\mathbf{r}$ and $\mathbf{R}$ represent the electronic and nuclear coordinates, respectively, and ψ_e is the electronic wavefunction, which is a function of both the electronic and nuclear coordinates. The time-averaged, one-electron density $\langle \rho(\mathbf{r}) \rangle$, which is accessible experimentally through the elastic X-ray scattering experiment, is obtained from the static density by integration over all nuclear configurations:

$$\langle \rho(\mathbf{r}) \rangle = \int \rho(\mathbf{r}, \mathbf{R}) P(\mathbf{R})\, \mathrm{d}\mathbf{R}, \quad (8.7.2.6)$$

where $P(\mathbf{R})$ is the normalized probability distribution function of the nuclear configuration $\mathbf{R}$. The total X-ray scattering can be derived from the two-particle matrix $\Gamma(1, 2, 1', 2')$ through use of the two-particle scattering operator. The total X-ray scattering includes the inelastic incoherent Compton scattering, which is related to the momentum density $\pi(\mathbf{p})$.

The wavefunction in momentum space, defined by the coordinates $\widehat{\mathbf{J}} = \widehat{p}_j, s_j$ of the jth particle (here the caret indicates momentum-space coordinates), is given by the Dirac–Fourier transform of ψ,

$$\widehat{\psi}(\widehat{1}, \widehat{2}, \ldots, \widehat{n}) = (2\pi\hbar)^{-3n/2} \int \psi(1, 2, \ldots, n) \times \exp\left(-i/\hbar \sum_j \mathbf{p}_j \cdot \mathbf{r}_j\right) \mathrm{d}\mathbf{r}_1\, \mathrm{d}\mathbf{r}_2 \ldots \mathrm{d}\mathbf{r}_n, \quad (8.7.2.7)$$

leading, in analogy to (8.7.2.2), to the one-electron density matrix

$$\pi^1(\widehat{1}, \widehat{1}') = n \int \psi(\widehat{1}, \widehat{2}, \ldots, \widehat{n})\psi^*(\widehat{1}, \widehat{2}, \ldots, \widehat{n})\, \mathrm{d}\widehat{2} \ldots \mathrm{d}\widehat{n}, \quad (8.7.2.8)$$

and the *momentum density*

$$\pi(p) = \int \pi^1(\widehat{1}, \widehat{1})\, \mathrm{d}s_1. \quad (8.7.2.9)$$

The *spin density distribution* of the electrons, $s(\mathbf{r})$, can be obtained from $\Gamma^1(1, 1')$ by use of the operator for the z component of the spin angular momentum. If

$$s(\mathbf{r}, \mathbf{r}') = (2M)^{-1} \int s_z(1)\Gamma(1, 1')\, \mathrm{d}s_1, \quad s(\mathbf{r}) = s(\mathbf{r}, \mathbf{r}), \quad (8.7.2.10)$$

where M, the total magnetization, is the eigenvalue of the operator

$$S_z = \sum_i s_z(i).$$

Copyright © 2006 International Union of Crystallography

8.7.3. Charge densities

8.7.3.1. *Introduction*

The charge density is related to the elastic X-ray scattering amplitude $F(\mathbf{S})$ by the expression

$$\langle \rho(\mathbf{r}) \rangle = \int F(\mathbf{S}) \exp(-2\pi i \mathbf{S} \cdot \mathbf{r}) \, \mathrm{d}\mathbf{S}, \tag{8.7.3.1}$$

or, for scattering by a periodic lattice,

$$\langle \rho(\mathbf{r}) \rangle = \frac{1}{V} \sum_{\mathbf{h}} F(\mathbf{h}) \exp(-2\pi i \mathbf{h} \cdot \mathbf{r}).$$

As $F(\mathbf{h})$ is in general complex, the Fourier transform (8.7.3.1) requires calculation of the phases from a model for the charge distribution. In the centrosymmetric case, the free-atom model is in general adequate for calculation of the signs of $F(\mathbf{h})$. However, for non-centrosymmetric structures in which phases are continuously variable, it is necessary to incorporate deviations from the free-atom density in the model to obtain estimates of the experimental phases.

Since the total density is dominated by the core distribution, differences between the total density $\rho(\mathbf{r})$ and reference densities are important. The reference densities represent hypothetical states without chemical bonding or with only partial chemical bonding. Deviations from spherical, free-atom symmetry are obtained when the reference state is the *promolecule*, the superposition of free-space spherical atoms centred at the nuclear positions. This difference function is referred to as the *deformation* density (or standard deformation density)

$$\Delta\rho(\mathbf{r}) = \rho(\mathbf{r}) - \rho_p(\mathbf{r}), \tag{8.7.3.2}$$

where $\rho_p(\mathbf{r})$ is the promolecule density. In analogy to (8.7.3.1), the deformation density may be obtained from

$$\langle \Delta\rho(\mathbf{r}) \rangle = \frac{1}{V} \sum \left[F_{\mathrm{obs}}(\mathbf{h}) - F_{\mathrm{calc,free\ atom}}(\mathbf{h}) \right] \exp(-2\pi i \mathbf{h} \cdot \mathbf{r}), \tag{8.7.3.3}$$

where F_{obs} and F_{calc} are in general complex.

Several other different density functions analogous to (8.7.3.3), summarized in Table 8.7.3.1, may be defined. Particularly useful for the analysis of effects of chemical bonding is the fragment deformation density, in which a chemical fragment is subtracted from the total density of a molecule. The fragment density is calculated theoretically and thermally smeared before subtraction from an experimental density. 'Prepared' atoms rather than spherical atoms may be used as a reference state to emphasize the electron-density shift due to covalent bond formation.

Table 8.7.3.1. *Definition of difference density functions*

$$\Delta\rho = \frac{2}{V} \left\{ \sum_{0}^{1/2} (A_1 - A_2) \cos 2\pi \mathbf{h} \cdot \mathbf{r} + \sum_{0}^{1/2} (B_1 - B_2) \sin 2\pi \mathbf{h} \cdot \mathbf{r} \right\}$$

with $F = A + iB$.

(*a*) Residual map	A_1, B_1 from observations calculated with model phases. A_2, B_2 from refinement model.
(*b*) $X - X$ deformation map	A_1, B_1 from observation, with model phases. A_2, B_2 from high-order refinement, free-atom model, or other reference state.
(*c*) $X - N$ deformation map [as (*b*) but]	A_2, B_2 calculated with neutron parameters.
(*d*) $X - (X + N)$ deformation map [as (*b*) but]	A_2, B_2 calculated with parameters from joint refinement of X-ray neutron data.
(*e*) $X - X$, $X - N$, $X - (X + N)$ valence map	As (*b*), (*c*), (*d*) with A_1, B_1 calculated with core-electron contribution only.
(*f*) Dynamic model map	A_1, B_1 from model. A_2, B_2 with parameters from model refinement and free-atom functions.
(*g*) Static model map	$\rho_{\mathrm{model}} - \rho_{\mathrm{free\ atom}}$, where ρ_{model} is sum of static model density functions.

8.7.3.2. *Modelling of the charge density*

The electron density $\rho(\mathbf{r})$ in the structure-factor expression

$$F_{\mathrm{calc}}(\mathbf{h}) \int_{\text{unit cell}} \rho(\mathbf{r}) \exp(2\pi i \mathbf{h} \cdot \mathbf{r}) \, \mathrm{d}\mathbf{r} \tag{8.7.3.4a}$$

can be approximated by a sum of non-normalized density functions $g_i(\mathbf{r})$ with scattering factor $f_i(\mathbf{h})$ centred at $\mathbf{r}_i$,

$$\rho(\mathbf{r}) = \sum_i g_i(\mathbf{r}) * \delta(\mathbf{r} - \mathbf{r}_i). \tag{8.7.3.5}$$

Substitution in (8.7.3.4*a*) gives

$$F(\mathbf{h}) = \sum_i f_i(\mathbf{h}) \exp(2\pi i \mathbf{h} \cdot \mathbf{r}_i). \tag{8.7.3.4b}$$

When $g_i(\mathbf{r})$ is the spherically averaged, free-atom density, (8.7.3.4*b*) represents the free-atom model. A distinction is often made between *atom-centred* models, in which all functions $g(\mathbf{r})$ are centred at the nuclear positions, and models in which additional functions are centred at other locations, such as in bonds or lone-pair regions.

A simple, atom-centred model with spherical functions $g(\mathbf{r})$ is defined by

$$\rho_{\mathrm{atom}}(\mathbf{r}) = P_{\mathrm{core}} \rho_{\mathrm{core}}(\mathbf{r}) + \kappa^3 P_{\mathrm{valence}} \rho_{\mathrm{valence}}(\kappa \mathbf{r}). \tag{8.7.3.6}$$

This 'kappa model' allows for charge transfer between atomic valence shells through the population parameter P_{valence}, and for a change in nuclear screening with electron population, through the parameter κ, which represents an expansion ($\kappa < 1$), or a contraction ($\kappa > 1$) of the radial density distribution.

The atom-centred, spherical harmonic expansion of the electronic part of the charge distribution is defined by

$$\rho_{\mathrm{atom}}(\mathbf{r}) = P_{\mathrm{c}} \rho_{\mathrm{core}}(\mathbf{r}) + P_{\mathrm{v}} \kappa^3 \rho_{\mathrm{valence}}(\kappa r) + \sum_{l=0}^{l(\max)} \kappa'^3 R_l(\kappa' \zeta r) \sum_{m=0}^{l} \sum_{p} P_{lmp} d_{lmp}(\theta, \varphi), \tag{8.7.3.7}$$

where $p = \pm$ when m is larger than 0, and $R_l(\kappa' \zeta r)$ is a radial function.

The real spherical harmonic functions d_{lmp} and their Fourier transforms have been described in *International Tables for Crystallography*, Volume B, Chapter 1.2 (Coppens, 1992). They differ from the functions y_{lmp} by the normalization condition, defined as $\int |d_{lmp}| \, \mathrm{d}\Omega = 2 - \delta_{l0}$. The real spherical harmonic functions are often referred to as *multipoles*, since each

represents the component of the charge distribution $\rho(\mathbf{r})$ that gives a non-zero contribution to the integral for the electrostatic multipole moment q_{lmp},

$$q_{lmp} = -\int \rho_{\rm atom}(\mathbf{r}) r^l c_{lmp}\, \mathrm{d}\mathbf{r}, \qquad (8.7.3.8)$$

where the functions c_{lmp} are the Cartesian representations of the real spherical harmonics (Coppens, 1992).

More general models include non-atom centred functions. If the wavefunction ψ in (8.7.2.4) is an antisymmetrized product of molecular orbitals ψ_i, expressed in terms of a linear combination of atomic orbitals χ_μ, $\psi_i = \sum_\mu c_{i\mu}\chi_\mu$ (LCAO formalism), the integration (8.7.2.4) leads to

$$\rho(\mathbf{r}) = \sum_\mu \sum_\nu P_{\mu\nu}\chi_\mu(\mathbf{r}-\mathbf{R}_\mu)\chi_\nu(\mathbf{r}-\mathbf{R}_\nu), \qquad (8.7.3.9)$$

with $\mathbf{R}_\mu$ and $\mathbf{R}_\nu$ defining the centres of χ_μ and χ_ν, respectively, $P_{\mu\nu} = \sum_i n_i c_{i\mu} c_{i\nu}$, and the sum is over all molecular orbitals with occupancy n_i. Expression (8.7.3.9) contains products of atomic orbitals, which may have significant values for orbitals centred on adjacent atoms. In the 'charge-cloud' model (Hellner, 1977), these products are approximated by bond-centred, Gaussian-shaped density functions. Such functions can often be projected efficiently into the one-centre terms of the spherical harmonic multipole model, so that large correlations occur if both spherical harmonics and bond-centred functions are adjusted independently in a least-squares refinement.

According to (8.7.2.4) and (8.7.3.9), the population of the two-centre terms is related to the one-centre occupancies. A molecular-orbital based model, which implicitly incorporates such relations, has been used to describe local bonding between transition-metal and ligand atoms (Becker & Coppens, 1985).

8.7.3.3. *Physical constraints*

There are several physical constraints that an electron-density model must satisfy. With the exception of the electroneutrality constraint, they depend strongly on the electron density close to the nucleus, which is poorly determined by the diffraction experiment.

8.7.3.3.1. *Electroneutrality constraint*

Since a crystal is neutral, the total electron population must equal the sum of the nuclear charges of the constituent atoms. A constraint procedure for linear least squares that does not increase the size of the least-squares matrix has been described by Hamilton (1964). If the starting point is a neutral crystal, the constraint equation becomes

$$\sum \Delta P_i S_i = 0, \qquad (8.7.3.10)$$

where $S_i = \int g(\mathbf{r})\, \mathrm{d}\mathbf{r}$, g being a general density function, and the ΔP_i are the shifts in the population parameters. For the multipole model, only the monopolar functions integrate to a non-zero value. For normalized monopole functions, this gives

$$\sum_{\rm monopoles} \Delta P_i = 0. \qquad (8.7.3.11)$$

If the shifts without constraints are given by the vector $\mathbf{y}$ and the constrained shifts by $\mathbf{y}_c$, the Hamilton constraint is expressed as

$$\mathbf{y}_c^T = \mathbf{y}^T - \mathbf{y}^T \boldsymbol{Q}^T (\boldsymbol{Q}\boldsymbol{A}^{-1}\boldsymbol{Q}^T)^{-1}\boldsymbol{Q}\boldsymbol{A}^{-1}, \qquad (8.7.3.12)$$

where the superscript T indicates transposition, $\boldsymbol{A}$ is the least-squares matrix of the products of derivatives, and $\boldsymbol{Q}$ is a row vector of the values of S_i for elements representing density functions and zeros otherwise.

Expression (8.7.3.12) cannot be applied if the unconstrained refinement corresponds to a singular matrix. This would be the case if all population parameters, including those of the core functions, were to be refined together with the scale factor. In this case, a new set of independent parameters must be defined, as described in Chapter 8.1 on least-squares refinements. Alternatively, one may set the scale factor to one and rescale the population parameters to neutrality after completion of the refinement. This will in general give a non-integral electron population for the core functions. The proper interpretation of such a result is that a core-like function is an appropriate component of the density basis set representing the valence electrons.

8.7.3.3.2. *Cusp constraint*

The electron density at a nucleus i with nuclear charge Z_i must satisfy the electron–nuclear cusp condition given by

$$\lim_{\mathbf{r}_i \to 0} \left(\frac{\partial}{\partial \mathbf{r}_i} + 2Z_i \right) \rho_{0i}(\mathbf{r}_i) = 0, \qquad (8.7.3.13)$$

where $\rho_{0i}(\mathbf{r}_i) = (1/4\pi)\int \rho(\mathbf{r})\, \mathrm{d}\Omega_i$ is the spherical component of the expansion of the density around nucleus i.

Only 1s-type functions have non-zero electron density at the nucleus and contribute to (8.7.3.13). For the hydrogen-like atom or ion described by a single exponent radial function $R(r) = N\exp(-\zeta r)$, (8.7.3.13) gives $\zeta = 2Z/a_0$, where Z is the nuclear charge, and a_0 is the Bohr unit. Thus, a modification of ζ for 1s functions, as implied by (8.7.3.6) and (8.7.3.7) if applied to H atoms, leads to a violation of the cusp constraint. In practice, the electron density at the nucleus is not determined by a limited resolution diffraction experiment; the single exponent function $R(r)$ is fitted to the electron density away from, rather than at the nucleus.

8.7.3.3.3. *Radial constraint*

Poisson's electrostatic equation gives a relation between the gradient of the electric field $\nabla^2\Phi(\mathbf{r})$ and the electron density at $\mathbf{r}$.

$$\nabla^2\Phi(\mathbf{r}) = -4\pi\rho(\mathbf{r}). \qquad (8.7.3.14)$$

As noted by Stewart (1977), this equation imposes a constraint on the radial functions $R(r)$. For $R_l(r) = N_l r^{n(l)}\exp(-\zeta_l r)$, the condition $n(l) \geq l$ must be obeyed for $R_l r^{-l}$ to be finite at $r = 0$, which satisfies the requirement of the non-divergence of the electric field ∇V, its gradient $\nabla^2 V$, the gradient of the field gradient $\nabla^3 V$, *etc.*

8.7.3.3.4. *Hellmann–Feynman constraint*

According to the electrostatic Hellmann–Feynman theorem, which follows from the Born–Oppenheimer approximation and the condition that the forces on the nuclei must vanish when the nuclear configuration is in equilibrium, the nuclear repulsions are balanced by the electron–nucleus attractions (Levine, 1983). The balance of forces is often achieved by a very sharp polarization of the electron density very close to the nuclei (Hirshfeld & Rzotkiewicz, 1974), which may be represented in the X-ray model by the introduction of dipolar functions with large values of ζ. The Hellmann–Feynman constraint offers the possibility for obtaining information on such functions even though they may contribute only marginally to the observed X-ray scattering (Hirshfeld, 1984).

As the Hellmann–Feynman constraint applies to the static density, its application presumes a proper deconvolution of the thermal motion and the electron density in the scattering model.

8.7.3.4. *Electrostatic moments and the potential due to a charge distribution*

8.7.3.4.1. *Moments of a charge distribution**

Use of the expectation value expression

$$\langle O\rangle = \int \widehat{O}\rho(\mathbf{r})\,\mathrm{d}\mathbf{r}, \tag{8.7.3.15}$$

with the operator $\widehat{O} = \widehat{\gamma} r_{\alpha_1} r_{\alpha_2} r_{\alpha_3} \ldots r_{\alpha_l} = r_{\alpha_1} r_{\alpha_2} r_{\alpha_3} \ldots r_{\alpha_l}$ gives for the electrostatic moments of a charge distribution $\rho(\mathbf{r})$

$$\mu_{\alpha_1\alpha_2\alpha_3\ldots\alpha_l} = \int \rho(\mathbf{r}) r_{\alpha_1} r_{\alpha_2} r_{\alpha_3} \ldots r_{\alpha_l}\,\mathrm{d}\mathbf{r}, \tag{8.7.3.16}$$

in which the r_α are the three components of the vector $\mathbf{r}$ ($\alpha_i = 1, 2, 3$), and the integral is over the complete volume of the distribution.

For $l = 0$, (8.7.3.16) represents the integral over the charge distribution, which is the total charge, a scalar function described as the *monopole*. The higher moments are, in ascending order of l, the *dipole*, a vector, the *quadrupole*, a second-rank tensor, and the *octupole*, a third-rank tensor. Successively higher moments are named the *hexadecapole* ($l = 4$), the *tricontadipole* ($l = 5$), and the *hexacontatetrapole* ($l = 6$). An alternative, traceless, definition is often used for moments with $l \geq 2$. In the traceless definition, the quadrupole moment, $\Theta_{\alpha\beta}$, is given by

$$\Theta_{\alpha\beta} = \tfrac{1}{2}\int \rho(\mathbf{r})\left[3r_\alpha r_\beta - r^2\delta_{\alpha\beta}\right]\mathrm{d}r, \tag{8.7.3.17}$$

where $\delta_{\alpha\beta}$ is the Kronecker delta function. The term $\int \rho(\mathbf{r}) r^2\,\mathrm{d}r$, which is subtracted from the diagonal elements of the tensor, corresponds to the spherically averaged second moment of the distribution.

Expression (8.7.3.17) is a special case of the following general expression for the lth-rank traceless tensor elements.

$$M^{(l)}_{\alpha_1\alpha_2\ldots\alpha_l} = \frac{(-1)^l}{l!}\int \rho(\mathbf{r}) r^{2l+1} \frac{\partial^l}{\partial r_{\alpha_1}\partial r_{\alpha_2}\ldots\partial r_{\alpha_l}}\left(\frac{1}{r}\right)\mathrm{d}\mathbf{r}. \tag{8.7.3.18}$$

Though the traceless moments can be derived from the unabridged moments, the converse is not the case because the information on the spherically averaged moments is no longer present in the traceless moments. The general relations between the traceless moments and the unabridged moments follow from (8.7.3.18). For the quadrupole moments, we obtain with (8.7.3.17)

$$\begin{aligned}\Theta_{xx} &= \tfrac{3}{2}\mu_{xx} - \tfrac{1}{2}\left(\mu_{xx} + \mu_{yy} + \mu_{zz}\right)\\ &= \mu_{xx} - \tfrac{1}{2}\left(\mu_{yy} + \mu_{zz}\right),\end{aligned}$$

and

$$\Theta_{xy} = \tfrac{3}{2}\mu_{xy}. \tag{8.7.3.19}$$

Expressions for the other elements are obtained by simple permutation of the indices.

For a site of point symmetry 1, the electrostatic moment $\mu_{\alpha_1\alpha_2\alpha_3\ldots\alpha_l}$ of order l has $(l+1)(l+2)/2$ unique elements. In the traceless definition, not all elements are independent. Because the trace of the tensor has been set to zero, only $2l+1$ *independent* components remain. For the quadrupole there are 5 *independent* components of the form (8.7.3.19).

In a different form, the traceless moment operators can be written as the Cartesian spherical harmonics c_{lmp} (*IT*B, 1992) multiplied by r^l, which defines the *spherical* electrostatic moments

$$\Theta_{lmp} = \int \rho(\mathbf{r}) c_{lmp} r^l\,\mathrm{d}r. \tag{8.7.3.20}$$

The expressions for c_{lmp} are listed in Volume B of *International Tables for Crystallography* (*IT*B, 1992); for the $l = 2$ moment, the c_{lmp} have the well known form $3z^2 - 1$, xz, yz, $(x^2 - y^2)/2$, and xy, where x, y and z are the components of a unit vector from the origin to the point being described. The spherical electrostatic moments have $(2l+1)$ components, which equals the number of independent components in the traceless definition (8.7.3.18), as it should. The linear relationships are

$$\begin{aligned}\Theta_{zz} &= (1/2)\Theta_{20},\\ \Theta_{xx} &= (1/2)\left[3\Theta_{22+} - (1/2)\Theta_{20}\right],\\ \Theta_{yy} &= (1/2)\left[-3\Theta_{22+} - (1/2)\Theta_{20}\right],\\ \Theta_{xz} &= (3/2)\Theta_{21+},\\ \Theta_{yz} &= (3/2)\Theta_{21-},\\ \Theta_{xy} &= (3/2)\Theta_{22-}.\end{aligned} \tag{8.7.3.21}$$

8.7.3.4.1.1. *Moments as a function of the atomic multipole expansion*

In the multipole model [expression (8.7.3.7)], the charge density is a sum of atom-centred density functions, and the moments of a whole distribution can be written as a sum over the atomic moments plus a contribution due to the shift to a common origin. An atomic moment is obtained by integration over the charge distributions $\rho_{\mathrm{total},i}(\mathbf{r}) = \rho_{\mathrm{nuclear},i} - \rho_{e,i}$ of atom i,

$$\mu_{\alpha_1\alpha_2\alpha_3\ldots\alpha_l} = \int \rho_{\mathrm{total},i}(\mathbf{r}) r_{\alpha_1} r_{\alpha_2} r_{\alpha_3} \ldots r_{\alpha_l}\,\mathrm{d}r, \tag{8.7.3.22}$$

where the electronic part of the atomic charge distribution is defined by the multipole expansion

$$\begin{aligned}\rho_{e,i}(\mathbf{r}) = {} & P_{i,c}\rho_{\mathrm{core}}(r) + P_{i,v}\kappa_i^3\rho_{i,\mathrm{valence}}(\kappa_i r)\\ & + \sum_{l=0}^{l_{\max}} \kappa_i'^3 R_{i,l}\left(\kappa_i' r\right)\sum_{m=0}^{l}\sum_{p} P_{i,lmp} d_{lmp}(\theta,\varphi),\end{aligned} \tag{8.7.3.23}$$

where $p = \pm$ when $m > 0$, and $R_l(\kappa_i' r)$ is a radial function.

We get for the jth moment of the valence density

$$\begin{aligned}\mu^j &= \mu_{\alpha_1\alpha_2\alpha_3\ldots\alpha_j}\\ &= -\int\left[P_{i,v}\kappa_i^3\rho_{i,\mathrm{valence}}(\kappa_i r) + \sum_{l=0}^{l_{\max}}\kappa_i'^3 R_{i,l}\left(\kappa_i' r\right)\right.\\ &\quad\left.\times\sum_{m=0}^{l}\sum_{p} P_{i,lmp} d_{lmp}(\theta,\varphi)\right] r_{\alpha_1} r_{\alpha_2}\ldots r_{\alpha_j}\,\mathrm{d}\mathbf{r},\end{aligned} \tag{8.7.3.24}$$

in which the minus sign arises because of the negative charge of the electrons.

We will use the symbol $\widehat{O}$ for the moment operators. We get

$$\mu^j = -\kappa_i'^3\int \widehat{O}_j \sum_{l=1}^{l_{\max}}\left[\sum_{m=0}^{l}\sum_{p} P_{lmp} d_{lmp} R_l\right]\mathrm{d}\mathbf{r}, \tag{8.7.3.25}$$

where, as before, $p = \pm$. The requirement that the integrand be totally symmetric means that only the dipolar terms in the multipole expansion contribute to the dipole moment. If we use the traceless definition of the higher moments, or the equivalent definition of the moments in terms of the spherical harmonic functions, only the quadupolar terms of the multipole expansion will contribute to the quadrupole moment; more generally, in the traceless definition *the lth-order multipoles are the sole contributors to the lth moments*. In terms of the spherical moments, we get

* An excellent review of experimental results has appeared in the literature (Spackman, 1992).

$$\Theta_{lmp} = -P_{lmp} \int \widehat{O}_{lmp}\left[d_{lmp} R_l\right] \mathrm{d}\mathbf{r}. \tag{8.7.3.26}$$

Substitution with $R_l = \{(\kappa'\zeta)^{n(l)+3}/[n(l)+2]!\} r^{n(l)} \exp(-\zeta r)$ and $\widehat{O}_{lmp} = c_{lmp} r^l$ and subsequent integration over r gives

$$\Theta_{lmp} = -P_{lmp} \frac{1}{(\kappa'\zeta)^l} \frac{[n(l)+l+2]!}{[n(l)+2]!} \frac{1}{D_{lm} M_{lm}} \int y_{lmp}^2 \sin\theta \, \mathrm{d}\theta \, \mathrm{d}\varphi, \tag{8.7.3.27}$$

where the definitions

$$d_{lmp} = L_{lm} c_{lmp} = \left(\frac{L_{lm}}{M_{lm}}\right) y_{lmp} \quad \text{and} \quad c_{lmp} = \left(\frac{1}{M_{lm}}\right) y_{lmp} \tag{8.7.3.28}$$

have been used (*IT*B, 1992). Since the y_{lmp} functions are wavefunction normalized, we obtain

$$\Theta_{lmp} = -P_{lmp} \frac{1}{(\kappa'\zeta)^l} \frac{[n(l)+l+2]!}{[n(l)+2]!} \frac{L_{lm}}{(M_{lm})^2}. \tag{8.7.3.29}$$

Application to dipolar terms with $n(l) = 2$, $L_{lm} = 1/\pi$ and $M_{lm} = (3/4\pi)^{1/2}$ gives the x component of the atomic dipole moment as

$$\mu_x = -\int P_{11+} d_{11+} R_1 x \, \mathrm{d}\mathbf{r} = -\frac{20}{3\kappa'\zeta} P_{11+}. \tag{8.7.3.30}$$

For the atomic quadrupole moments in the spherical definition, we obtain directly, using $n(l) = 2$, $l = 2$ in (8.7.3.29),

$$\Theta_{20} = -\frac{30}{(\kappa'\zeta)^2} \frac{L_{20}}{(M_{20})^2} P_{20} = -\frac{36\sqrt{3}}{(\kappa'\zeta)^2} P_{20}, \tag{8.7.3.31}$$

and, for the other elements,

$$\Theta_{2mp} = -\frac{30}{(\kappa'\zeta)^2} \frac{L_{2m}}{(M_{2m})^2} P_{2mp} = -\frac{6\pi}{(\kappa'\zeta)^2} P_{2mp}. \tag{8.7.3.32}$$

As the traceless quadrupole moments are linear combinations of the spherical quadrupole moments, the corresponding expressions follow directly from (8.7.3.31), (8.7.3.32) and (8.7.3.21). We obtain with $n(2) = 2$

$$\begin{aligned}
\Theta_{zz} &= -\frac{18\sqrt{3}}{(\kappa'\zeta)^2} P_{20}, \\
\Theta_{yy} &= +\frac{9}{(\kappa'\zeta)^2}\left(\sqrt{3} P_{20} + \pi P_{22+}\right), \\
\Theta_{xx} &= \frac{9}{(\kappa'\zeta)^2}\left(\sqrt{3} P_{20} - \pi P_{22+}\right),
\end{aligned}$$

and

$$\Theta_{xz} = -\frac{9\pi}{(\kappa'\zeta)^2} P_{21+}, \tag{8.7.3.33}$$

and analogously for the other off-diagonal elements.

8.7.3.4.1.2. *Molecular moments based on the deformation density*

The moments derived from the total density $\rho(\mathbf{r})$ and from the deformation density $\Delta\rho(\mathbf{r})$ are not identical. To illustrate the relation for the diagonal elements of the second-moment tensor, we rewrite the xx element as

$$\begin{aligned}
\mu_{xx}\left(\rho_{\text{total}}\right) &= \int \rho x^2 \, \mathrm{d}\mathbf{r} \\
&= \int \rho_{\text{promolecule}} x^2 \, \mathrm{d}\mathbf{r} + \int \Delta\rho x^2 \, \mathrm{d}\mathbf{r}.
\end{aligned} \tag{8.7.3.34}$$

The promolecule is the sum over spherical atom densities, or

$$\begin{aligned}
\int \rho_{\text{promolecule}} x^2 \, \mathrm{d}\mathbf{r} &= \int \sum_i \rho_{\text{spherical atom},i} x^2 \, \mathrm{d}\mathbf{r} \\
&= \sum_i \int \rho_{\text{spherical atom},i} x^2 \, \mathrm{d}\mathbf{r}.
\end{aligned} \tag{8.7.3.35}$$

If $\mathbf{R}_i = (X_i, Y_i, Z_i)$ is the position vector for atom i, each single-atom contribution can be rewritten as

$$\begin{aligned}
\mu_{i,xx,\text{spherical atom}} &= \int \rho_{i,\text{spherical atom}} x^2 \, \mathrm{d}\mathbf{r} \\
&= \int \rho_{i,\text{spherical atom}} (x - X_i)^2 \, \mathrm{d}\mathbf{r} \\
&\quad + X_i \int \rho_{i,\text{spherical atom}} 2(x - X_i) \, \mathrm{d}\mathbf{r} \\
&\quad + X_i^2 \int \rho_{i,\text{spherical atom}} \, \mathrm{d}\mathbf{r}.
\end{aligned} \tag{8.7.3.36}$$

Since the last two integrals are proportional to the atomic dipole moment and its net charge, respectively, they will be zero for neutral spherical atoms. Substitution in (8.7.3.35) gives, with $\left\langle (x - X)_i^2 \right\rangle = \frac{1}{3}\left\langle r_i^2 \right\rangle$, and $\left\langle r_i^2 \right\rangle = \int \rho_i(r) r^2 \, \mathrm{d}\mathbf{r}$,

$$\int \rho_{\text{promolecule}} x^2 \, \mathrm{d}\mathbf{r} = \tfrac{1}{3} \sum_{\text{atoms}} \left\langle r^2 \right\rangle_{\text{spherical atom}}, \tag{8.7.3.37}$$

and, by substitution in (8.7.3.34),

$$\mu_{xx}\left(\rho_{\text{tot}}\right) = \mu_{xx}(\Delta\rho) + \tfrac{1}{3} \sum_{\text{atoms}} \left\langle r^2 \right\rangle_{\text{spherical atom}}, \tag{8.7.3.38a}$$

with

$$\mu_{xx}(\Delta\rho) = \sum_i \left(\int \Delta\rho_i x^2 \, \mathrm{d}\mathbf{r} + 2X_i \mu_i + X_i^2 q_i \right), \tag{8.7.3.38b}$$

in which μ_i and q_i are the atomic dipole moment and the charge on atom i, respectively.

The last term in (8.7.3.38*a*) can be derived rapidly from analytical expressions for the atomic wavefunctions. Results for Hartree–Fock wavefunctions have been tabulated by Boyd (1977). Since the off-diagonal elements of the second-moment tensor vanish for the spherical atom, the second term in (8.7.3.38*a*) disappears, and the off-diagonal elements are identical for the total and deformation densities.

The relation between the second moments $\mu_{\alpha\beta}$ and the traceless moments $\Theta_{\alpha\beta}$ of the deformation density can be illustrated as follows. From (8.7.3.17), we may write

$$\Theta_{\alpha\beta}(\Delta\rho) = \tfrac{3}{2} \mu_{\alpha\beta}(\Delta\rho) - \tfrac{1}{2} \delta_{\alpha\beta} \int \Delta\rho \, r^2 \, \mathrm{d}\mathbf{r}. \tag{8.7.3.39}$$

Only the spherical density terms contribute to the integral on the right. Assuming for the moment that the spherical deformation is represented by the valence-shell distortion (*i.e.* neglect of the second monopole in the aspherical atom expansion), we have, with density functions ρ normalized to 1, for each atom

$$(\Delta\rho)_{\text{spherical}} = \kappa^3 P_{\text{valence}} \rho_{\text{valence}}(\kappa r) - P^0_{\text{valence}} \rho_{\text{valence}}(r) \tag{8.7.3.40}$$

and

$$\begin{aligned}
\int \Delta\rho \, r^2 \, \mathrm{d}\mathbf{r} &= \int \sum_i \left[\kappa_i^3 P_{\text{valence},i} \rho_{\text{valence},i}(\kappa_i r) \right. \\
&\quad \left. - P^0_{\text{valence},i} \rho_{\text{valence},i}(r) \right] r^2 \, \mathrm{d}\mathbf{r} \\
&= \sum_i \left(P_{\text{valence},i}/\kappa_i^2 - P^0_{\text{valence}} \right) \left\langle r_i^2 \right\rangle_{\text{spherical valence shell}} \\
&\quad + R_i^2 \left(P_{\text{valence},i} - P^0_{\text{valence},i} \right),
\end{aligned} \tag{8.7.3.41}$$

which, on substitution in (8.7.3.39), gives the required relation.

8.7.3.4.1.3. *The effect of an origin shift on the outer moments*

In general, the multipole moments depend on the choice of origin. This can be seen as follows. Substitution of $\mathbf{r}'_\alpha = \mathbf{r}_\alpha - \mathbf{R}_\alpha$ in (8.7.3.16) corresponds to a shift of origin by $\mathbf{R}_\alpha$, or $\mathbf{X}$, $\mathbf{Y}$, $\mathbf{Z}$ in the original coordinate system. In three dimensions, we get, for the first moment, the charge q,

$$q' = q, \tag{8.7.3.42}$$

and for the transformed first and second moments

$$\begin{aligned}
&\mu'_x = \mu_x - q\mathbf{X};\ \ \mu'_y = \mu_y - q\mathbf{Y};\ \ \mu'_z = \mu_z - q\mathbf{Z};\\
&\mu'_{\alpha\alpha} = \mu_{\alpha\alpha} - 2\mu_\alpha R_\alpha + qR_\alpha^2;\\
&\mu'_{\alpha\beta} = \mu_{\alpha\beta} - \mu_\alpha R_\beta - \mu_\beta R_\alpha + qR_\alpha R_\beta.
\end{aligned} \tag{8.7.3.43}$$

For the traceless quadrupole moments, the corresponding equations are obtained by substitution of $\mathbf{r}'_\alpha = \mathbf{r}_\alpha - \mathbf{R}_\alpha$ and $\mathbf{r}' = \mathbf{r} - \mathbf{R}$ into (8.7.3.17), which gives

$$\begin{aligned}
\Theta'_{\alpha\beta} = \Theta_{\alpha\beta} &+ \tfrac{1}{2}\left(3\mathbf{R}_\alpha\mathbf{R}_\beta - \mathbf{R}^2\delta_{\alpha\beta}\right)q\\
&- \tfrac{3}{2}\left(\mathbf{R}_\beta\mu_\alpha + \mathbf{R}_\alpha\mu_\beta\right) + \sum_\gamma\left(\mathbf{R}_\gamma\mu_\gamma\right)\delta_{\alpha\beta}.
\end{aligned} \tag{8.7.3.44}$$

Similar expressions for the higher moments are reported in the literature (Buckingham, 1970).

We note that *the first non-vanishing moment is origin-independent*. Thus, the dipole moment of a neutral molecule, but not that of an ion, is independent of origin; the quadrupole moment of a molecule without charge and dipole moment is not dependent on the choice of origin and so on. The molecular electric moments are commonly reported with respect to the centre of mass.

8.7.3.4.1.4. *Total moments as a sum over the pseudoatom moments*

The moments of a molecule or of a molecular fragment are obtained from the sum over the atomic moments, plus a contribution due to the shift to a common origin for all but the monopoles. If individual atomic coordinate systems are used, as is common if chemical constraints are applied in the least-squares refinement, they must be rotated to have a common orientation. Expressions for coordinate system rotations have been given by Cromer, Larson & Stewart (1976) and by Su & Coppens (1994*a*).

The transformation to a common coordinate origin requires use of the origin-shift expressions (8.7.3.42)–(8.7.3.44), with, for an atom at $\mathbf{r}_i$, $\mathbf{R} = -\mathbf{r}_i$. The first three moments summed over the atoms i located at $\mathbf{r}_i$ become

$$q_{\text{total}} = \sum q_i, \tag{8.7.3.45}$$

$$\mu_{\text{total}} = \sum_i \mu_i + \sum \mathbf{r}_i q_i, \tag{8.7.3.46}$$

and

$$\mu_{\alpha\beta,\text{total}} = \sum_i\left(\mu_{\alpha\beta i} + r'_{\beta i}\mu_\alpha + r'_{\alpha i}\mu_\beta + r'_{\alpha i}r'_{\beta i}q_i\right) \tag{8.7.3.47}$$

with $\alpha, \beta = x, y, z$; and expressions equivalent to (8.7.3.44) for the traceless components $\Theta_{\alpha\beta}$.

8.7.3.4.1.5. *Electrostatic moments of a subvolume of space by Fourier summation*

Expression (8.7.3.16) for the outer moment of a distribution within a volume element V_T may be written as

$$\mu_{\alpha_1\alpha_2\ldots\alpha_l} = \int_{V_T} \rho(\mathbf{r})\widehat{\gamma}_{\alpha_1\alpha_2\alpha_3\ldots\alpha_l}\,\mathrm{d}\mathbf{r}, \tag{8.7.3.16}$$

with $\widehat{\gamma}_{\alpha_1\alpha_2\alpha_3\ldots\alpha_l} = r_{\alpha_1}r_{\alpha_2}r_{\alpha_3}\ldots r_{\alpha_l}$, and integration over the volume V_T.

Replacement of $\rho(\mathbf{r})$ by the Fourier summation over the structure factors gives

$$\begin{aligned}
\mu^l_{(V_T)} &= \frac{1}{V}\int_{V_T}\widehat{\gamma}_l\sum F(\mathbf{h})\exp(-2\pi i\mathbf{h}\cdot\mathbf{r})\,\mathrm{d}\mathbf{r}\\
&= \frac{1}{V}\sum F(\mathbf{h})\int_{V_T}\widehat{\gamma}_l\exp(-2\pi i\mathbf{h}\cdot\mathbf{r})\,\mathrm{d}\mathbf{r},
\end{aligned} \tag{8.7.3.48}$$

where $\widehat{\gamma}_l$ is the product of l coordinates according to (8.7.3.16), and μ^l represents the moment of the static distribution if the $F(\mathbf{h})$ are the structure factors on an absolute scale after deconvolution of thermal motion. Otherwise, the moment of the thermally averaged density is obtained.

The integral $\int_{V_T}\widehat{\gamma}_l\exp(-2\pi i\mathbf{h}\cdot\mathbf{r})\,\mathrm{d}\mathbf{r}$ is defined as the *shape transform* S of the volume V_T.

$$\mu^l(V_T) = \frac{1}{V}\sum F(\mathbf{h})S_{V_T}(\widehat{\gamma}_l, \mathbf{h}).$$

For regularly shaped volumes, the integral can be evaluated analytically. A volume of complex shape may be subdivided into integrable subvolumes such as parallelepipeds. By choosing the subvolumes sufficiently small, a desired boundary surface can be closely approximated.

If the origin of each subvolume is located at $\mathbf{r}_i$, relative to a coordinate system origin at P, the total electronic moment relative to this origin is given by

$$\mu^l\left(\sum_i V_{T,i}\right) = \frac{1}{V}\sum_{\mathbf{h}} F(\mathbf{h})S_{V_T}(\widehat{\gamma}_l, \mathbf{h})\sum_i \exp(-2\pi i\mathbf{h}\cdot\mathbf{r}_i). \tag{8.7.3.49}$$

Expressions for S_{V_T} for $l \leq 2$ and a subvolume parallelepipedal shape are given in Table 8.7.3.2. Since the spherical order Bessel functions $j_n(x)$ that appear in the expressions generally decrease with increasing x, the moments are strongly dependent on the low-order reflections in a data set. An example is the shape transform for the dipole moment. Relative to an origin O,

$$S(\widehat{\gamma}_1, \mathbf{h}) = \int_{V_t}\mathbf{r}_0\exp(-2\pi i\mathbf{h}\cdot\mathbf{r}_0)\,\mathrm{d}\mathbf{r}.$$

A shift of origin by $-\mathbf{r}_i$ leads to

$$\begin{aligned}
\mu^{1'}(V_T) &= \frac{1}{V}\sum F(\mathbf{h})\left[S_{V_T}(\widehat{\gamma}_1, \mathbf{h}) + \mathbf{r}_1\int\exp(-2\pi i\mathbf{h}\cdot r_0)\,\mathrm{d}\mathbf{r}\right]\\
&\quad\times\exp(-2\pi i\mathbf{h}\cdot\mathbf{r}_1)\\
&= \mu^1(V_T) + \mathbf{r}_1 q,
\end{aligned}$$

in agreement with (8.7.3.46).

8.7.3.4.2. *The electrostatic potential*

8.7.3.4.2.1. *The electrostatic potential and its derivatives*

The electrostatic potential $\Phi(\mathbf{r}')$ due to the electronic charge distribution is given by the Coulomb equation,

$$\Phi(\mathbf{r}') = -k\int\frac{\rho(\mathbf{r})}{|\mathbf{r} - \mathbf{r}'|}\,\mathrm{d}\mathbf{r}, \tag{8.7.3.50}$$

where the constant k is dependent on the units selected, and will here be taken equal to 1. For an assembly of positive point nuclei and a continuous distribution of negative electronic charge, we obtain

$$\Phi(\mathbf{r}') = \sum_M\frac{Z_M}{|\mathbf{R}_M - \mathbf{r}'|} - \int\frac{\rho(\mathbf{r})}{|\mathbf{r} - \mathbf{r}'|}\,\mathrm{d}\mathbf{r}, \tag{8.7.3.51}$$

in which Z_M is the charge of nucleus M located at $\mathbf{R}_M$.

The *electric field* **E** at a point in space is the gradient of the electrostatic potential at that point.

$$\mathbf{E}(\mathbf{r}) = -\nabla\Phi(\mathbf{r}) = -\mathbf{i}\frac{\partial\Phi(\mathbf{r})}{\partial x} - \mathbf{j}\frac{\partial\Phi(\mathbf{r})}{\partial y} - \mathbf{k}\frac{\partial\Phi(\mathbf{r})}{\partial z}. \quad (8.7.3.52)$$

As **E** is the negative gradient vector of the potential, the electric force is directed 'downhill' and proportional to the slope of the potential function. The explicit expression for **E** is obtained by differentiation of the operator $|\mathbf{r}-\mathbf{r}'|^{-1}$ in (8.7.3.50) towards x, y, z and subsequent addition of the vector components. For the negative slope of the potential in the x direction, one obtains

$$\mathbf{E}_x(\mathbf{r}') = \int \frac{\rho_{\text{total}}(\mathbf{r})}{|\mathbf{r}'-\mathbf{r}|^2}\frac{(\mathbf{r}'-\mathbf{r})_x}{|\mathbf{r}'-\mathbf{r}|}\,\mathrm{d}\mathbf{r} = \int \frac{\rho_{\text{total}}(\mathbf{r})}{|\mathbf{r}'-\mathbf{r}|^3}(\mathbf{r}'-\mathbf{r})_x\,\mathrm{d}\mathbf{r}, \quad (8.7.3.53)$$

which gives, after addition of the components,

$$\mathbf{E}(\mathbf{r}') = -\nabla\Phi(\mathbf{r}') = \int \frac{\rho_t(\mathbf{r})(\mathbf{r}'-\mathbf{r})}{|\mathbf{r}-\mathbf{r}'|^3}\,\mathrm{d}\mathbf{r}. \quad (8.7.3.54)$$

The electric field gradient (EFG) is the tensor product of the gradient operator $\nabla = \mathbf{i}\frac{\partial}{\partial x} + \mathbf{j}\frac{\partial}{\partial y} + \mathbf{k}\frac{\partial}{\partial z}$ and the electric field vector **E**;

$$\nabla\mathbf{E} = \nabla : \mathbf{E} = -\nabla : \nabla\Phi. \quad (8.7.3.55)$$

It follows that in a Cartesian system the EFG tensor is a symmetric tensor with elements

$$\nabla\mathbf{E}_{\alpha\beta} = -\frac{\partial^2\Phi}{\partial r_\alpha \partial r_\beta}. \quad (8.7.3.56)$$

The EFG tensor elements can be obtained by differentiation of the operator in (8.7.3.53) for $\mathbf{E}_\alpha$ to each of the three directions β. In this way, the traceless result

$$\begin{aligned}\nabla\mathbf{E}_{\alpha\beta}(\mathbf{r}') &= \frac{\partial\mathbf{E}_\alpha}{\partial(r_\beta - r'_\beta)} \\ &= -\int \frac{1}{|\mathbf{r}-\mathbf{r}'|^5}\Big\{3(r_\alpha - r'_\alpha)(r_\beta - r'_\beta) \\ &\quad - |\mathbf{r}-\mathbf{r}'|^2\delta_{\alpha\beta}\Big\}\rho_{\text{total}}(\mathbf{r})\,\mathrm{d}\mathbf{r} \end{aligned} \quad (8.7.3.57)$$

is obtained. We note that according to (8.7.3.57) the electric field gradient can equally well be interpreted as the tensor of the traceless quadrupole moments of the distribution $-2\rho_{\text{total}}(\mathbf{r})/|\mathbf{r}-\mathbf{r}'|^5$ [see equation (8.7.3.17)].

Definition (8.7.3.56) and result (8.7.3.57) differ in that (8.7.3.56) does not correspond to a zero-trace tensor. The situation is analogous to the two definitions of the second moments, discussed above, and is illustrated as follows. The trace of the tensor defined by (8.7.3.56) is given by

$$-\nabla^2\Phi = -\nabla\cdot\nabla\Phi = -\left(\frac{\partial^2\Phi}{\partial x^2} + \frac{\partial^2\Phi}{\partial y^2} + \frac{\partial^2\Phi}{\partial z^2}\right). \quad (8.7.3.58)$$

Poisson's equation relates the divergence of the gradient of the potential $\Phi(\mathbf{r})$ to the electron density at that point:

$$\nabla^2\Phi(\mathbf{r}) = -4\pi\big[-\rho_e(\mathbf{r})\big] = 4\pi\rho_e(\mathbf{r}). \quad (8.7.3.59)$$

Thus, the EFG as defined by (8.7.3.56) is not traceless, unless the electron density at **r** is zero.

The potential and its derivatives are sometimes referred to as *inner moments* of the charge distribution, since the operators in (8.7.3.50), (8.7.3.52) and (8.7.3.54) contain the negative power of the position vector. In the same terminology, the electrostatic moments discussed in §8.7.3.4.1 are described as the *outer* moments.

Table 8.7.3.2. *Expressions for the shape factors S for a parallelepiped with edges δ_x, δ_y, and δ_z (from Moss & Coppens, 1981)*

j_0 and j_1 are the zero- and first-order spherical Bessel functions: $j_0(x) = \sin x/x$, $j_1(x) = \sin x/x^2 - \cos x/x$; V_T is volume of integration.

$\hat{y}$	Property	$S[\hat{y}(\mathbf{r}), \mathbf{h}]$
1	Charge	$V_T j_0(2\pi h_x\delta_x) j_0(2\pi h_y\delta_y) j_0(2\pi h_z\delta_z)$
r_α	Dipole μ_α	$-iV_T\delta_\alpha j_1(2\pi h_\alpha\delta_\alpha)$ $\times j_0(2\pi h_\beta\delta_\beta) j_0(2\pi h_\gamma\delta_\gamma)$
$r_\alpha r_\beta$	Second moment $\mu_{\alpha\beta}$ off-diagonal	$-V_T\delta_\alpha\delta_\beta j_1(2\pi h_\alpha\delta_\alpha)$ $\times j_1(2\pi h_\beta\delta_\beta) j_0(2\pi h_\gamma\delta_\gamma)$
$r_\alpha r_\alpha$	Second moment $\mu_{\alpha\alpha}$ diagonal	$-V_T\delta_\alpha^2\left\{\frac{j_1(2\pi h_\alpha\delta_\alpha)}{\pi h_\alpha\delta_\alpha} - j_0(2\pi h_\alpha\delta_\alpha)\right\}$ $\times j_0(2\pi h_\beta\delta_\beta) j_0(2\pi h_\gamma\delta_\gamma)$

It is of interest to evaluate the electric field gradient at the atomic nuclei, which for several types of nuclei can be measured accurately by nuclear quadrupole resonance and Mössbauer spectroscopy. The contribution of the atomic valence shell centred on the nucleus can be obtained by substitution of the multipolar expansion (8.7.3.7) in (8.7.3.57). The quadrupolar ($l = 2$) terms in the expansion contribute to the integral. For the radial function $R_l = \{\zeta^{n(l)+3}/[n(l)+2]!\}r^{n(l)}\exp(-\zeta r)$ with $n(l) = 2$, the following expressions are obtained:

$$\begin{aligned}\nabla\mathbf{E}_{11} &= +(3/5)\Big(\pi P_{22+} - \sqrt{3}P_{20}\Big)Q_r, \\ \nabla\mathbf{E}_{22} &= -(3/5)\Big(\pi P_{22+} + \sqrt{3}P_{20}\Big)Q_r, \\ \nabla\mathbf{E}_{33} &= +(6/5)\Big(\sqrt{3}P_{20}\Big)Q_r, \\ \nabla\mathbf{E}_{12} &= +(3/5)(\pi P_{22-})Q_r, \\ \nabla\mathbf{E}_{13} &= +(3/5)\big(\pi P_{21+}\big)Q_r, \\ \nabla\mathbf{E}_{23} &= +(3/5)(\pi P_{21-})Q_r, \end{aligned} \quad (8.7.3.60)$$

with

$$\begin{aligned} Q_r &= \big\langle r^3\big\rangle_{3\,\mathrm{d}} \\ &= \int_0^\infty [R(r)/r]\,\mathrm{d}r \\ &= (\kappa'\zeta)^3/[n_2(n_2+1)(n_2+2)] \\ &= (\kappa'\zeta)^3/120, \end{aligned}$$

in the case that $n_2 = 4$ (Stevens, DeLucia & Coppens, 1980).

The contributions of neighbouring atoms can be subdivided into point-charge, point-multipole, and penetration terms, as discussed by Epstein & Swanton (1982) and Su & Coppens (1992, 1994*b*), where appropriate expressions are given. Such contributions are in particular important when short interatomic distances are involved. For transition-metal atoms in coordination complexes, the contribution of neighbouring atoms is typically much smaller than the valence contribution.

8.7.3.4.2.2. *Electrostatic potential outside a charge distribution*

Hirshfelder, Curtiss & Bird (1954) and Buckingham (1959) have given an expression for the potential at a point $\mathbf{r}_i$ outside a charge distribution:

$$\Phi(\mathbf{r}_i) = \frac{q}{r_i} + \frac{\mu_\alpha r_\alpha}{r_i^3} + \tfrac{1}{2}\left[3r_\alpha r_\beta - r^2\delta_{\alpha\beta}\right]\frac{\Theta_{\alpha\beta}}{r_i^5} + \left[5r_\alpha r_\beta r\gamma - r^2\left(r_\alpha\delta_{\beta\gamma} + r_\beta\delta_{\gamma\alpha} + r_\gamma\delta_{\alpha\beta}\right)\right]\frac{\Omega_{\alpha\beta\gamma}}{5r_i^7} + \ldots, \tag{8.7.3.61}$$

where summation over repeated indices is implied. The outer moments q, μ_α, $\Phi_{\alpha\beta}$ and $\Omega_{\alpha\beta\gamma}$ in (8.7.3.61) must include the nuclear contributions, but, for a point outside the distribution, the spherical neutral-atom densities and the nuclear contributions cancel, so that the potential outside the charge distribution can be calculated from the deformation density.

The summation in (8.7.3.61) is slowly converging if the charge distribution is represented by a single set of moments. When dealing with experimental charge densities, a multicentre expansion is available from the analysis, and (8.7.3.61) can be replaced by a summation over the distributed moments centred at the nuclear positions, in which case r_i measures the distance from a centre of the expansion to the field point. The result is equivalent to more general expressions given by Su & Coppens (1992), which, for very large values of r_i, reduce to the sum over atomic terms, each expressed as (8.7.3.61). The interaction between two charge distributions, A and B, is given by

$$E_{AB} = \int \Phi_A(\mathbf{r})\rho_B(\mathbf{r})\,\mathrm{d}\mathbf{r},$$

where ρ_B includes the nuclear charge distribution.

8.7.3.4.2.3. *Evaluation of the electrostatic functions in direct space*

The electrostatic properties of a well defined group of atoms can be derived directly from the multipole population coefficients. This method allows the 'lifting' of a molecule out of the crystal, and therefore the examination of the electrostatic quantities at the periphery of the molecule, the region of interest for intermolecular interactions. The difficulty related to the origin term, encountered in the reciprocal-space methods, is absent in the direct-space analysis.

In order to express the functions as a sum over atomic contributions, we rewrite (8.7.3.51), (8.7.3.54) and (8.7.3.57) for the electrostatic properties at point P as a sum over atomic contributions.

$$\Phi(\mathbf{R}_p) = \sum_{M\neq P}\frac{Z_M}{|\mathbf{R}_{MP}|} - \sum_M\int\frac{\rho_{e,M}(\mathbf{r}_M)}{|\mathbf{r}_p|}\,\mathrm{d}\mathbf{r}_M, \tag{8.7.3.62}$$

$$\mathbf{E}(\mathbf{R}_p) = -\sum_{M\neq P}\frac{Z_{MP}\mathbf{R}_{MP}}{|\mathbf{R}_{MP}|^3} + \sum_M\int\frac{\mathbf{r}_p\rho_{e,M}(\mathbf{r}_M)}{|\mathbf{r}_p|^3}\,\mathrm{d}\mathbf{r}_M, \tag{8.7.3.63}$$

$$\nabla\mathbf{E}_{\alpha\beta}(\mathbf{R}_p) = -\sum_{M\neq P}\frac{Z_M(3R_\alpha R_\beta - \delta_{\alpha\beta}|R_{MP}|^2)}{|R_{MP}|^5} + \sum_M\int\frac{\rho_{e,M}(\mathbf{r}_M)(3r_\alpha r_\beta - \delta_{\alpha\beta}|\mathbf{r}_p|^2)}{|\mathbf{r}_p|^5}\,\mathrm{d}\mathbf{r}_M, \tag{8.7.3.64}$$

in which the exclusion of $M = P$ only applies when the point P coincides with a nucleus, and therefore only occurs for the central contributions. Z_M and $\mathbf{R}_M$ are the nuclear charge and the position vector of atom M, respectively, while $\mathbf{r}_P$ and $\mathbf{r}_M$ are, respectively, the vectors from P and from the nucleus M to a point $\mathbf{r}$, such that $\mathbf{r}_P = \mathbf{r} - \mathbf{R}_P$, and $\mathbf{r}_M = \mathbf{r} - \mathbf{R}_M = \mathbf{r}_P + \mathbf{R}_P - \mathbf{R}_M = \mathbf{r}_P - \mathbf{R}_{MP}$. The subscript M in the second, electronic part of the expressions refers to density functions centred on atom M.

Expressions for the evaluation of (8.7.3.62)–(8.7.3.64) from the charge-density parameters of the multipole expansion have been given by Su & Coppens (1992). They employ the Fourier convolution theorem, used by Epstein & Swanton (1982) to evaluate the electric field gradient at the atomic nuclei. A direct-space method based on the Laplace expansion of $1/|\mathbf{R}_p - \mathbf{r}|$ was reported by Bentley (1981).

8.7.3.4.3. *Electrostatic functions of crystals by modified Fourier summation*

Expression (8.7.3.49) is an example of derivation of electrostatic properties by direct Fourier summations of the structure factors. The electrostatic potential and its derivatives may be obtained in an analogous manner.

In order to obtain the electrostatic properties of the total charge distribution, it is convenient to define the 'total' structure factor $F_{\text{total}}(\mathbf{h})$ including the nuclear contribution,

$$F_{\text{total}}(\mathbf{h}) = F_N(\mathbf{h}) - F(\mathbf{h}),$$

where $F_N(\mathbf{h}) = \sum_j Z_j\exp(2\pi i\mathbf{h}\cdot\mathbf{R}_j)$, the summation being over all atoms j with nuclear charge Z_j, located at R_j. If $\Phi(\mathbf{h})$ is defined as the Fourier transform of the direct-space potential, we have

$$\Phi(\mathbf{r}) = \int\Phi(\mathbf{h})\exp(-2\pi i\mathbf{h}\cdot\mathbf{r})\,\mathrm{d}\mathbf{h}$$

and

$$\nabla^2\Phi(\mathbf{r}) = -4\pi^2\int h^2\Phi(\mathbf{h})\exp(-2\pi i\mathbf{h}\cdot\mathbf{r})\,\mathrm{d}\mathbf{h},$$

which equals $-4\pi\rho_{\text{total}}$ according to the Poisson equation (8.7.3.59). One obtains with

$$\rho_{\text{total}}(\mathbf{r}) = \int F_{\text{total}}(\mathbf{h})\exp(-2\pi i\mathbf{h}\cdot\mathbf{r})\,\mathrm{d}\mathbf{h},$$
$$\Phi(\mathbf{h}) = +F_{\text{total}}(\mathbf{h})/\pi h^2, \tag{8.7.3.65}$$

and, by inverse Fourier transformation of (8.7.3.65),

$$\Phi(\mathbf{r}) = \frac{1}{\pi V}\sum F_{\text{total}}(\mathbf{h})/h^2\exp(-2\pi i\mathbf{h}\cdot\mathbf{r}) \tag{8.7.3.66}$$

(Bertaut, 1978; Stewart, 1979). Furthermore, the electric field due to the electrons is given by

$$\mathbf{E}(\mathbf{r}) = -\nabla_r\Phi(\mathbf{r}) = -\nabla\int\Phi(\mathbf{h})\exp(-2\pi i\mathbf{h}\cdot\mathbf{r})\,\mathrm{d}\mathbf{h} = 2\pi i\int\mathbf{h}\Phi(\mathbf{h})\exp(-2\pi i\mathbf{h}\cdot\mathbf{r})\,\mathrm{d}\mathbf{h}.$$

Thus, with (8.7.3.65),

$$\mathbf{E}(\mathbf{r}) = \frac{2i}{V}\sum\left[F_{\text{total}}(\mathbf{h})/h^2\right]\mathbf{h}\exp(-2\pi i\mathbf{h}\cdot\mathbf{r}), \tag{8.7.3.67a}$$

which implies

$$\mathbf{E}(\mathbf{h}) = \frac{2i}{h^2}\mathbf{h}F_{\text{total}}(\mathbf{h}).$$

Similarly, the $\mathbf{h}$ Fourier component of the electric field gradient tensor with trace $4\pi\rho(\mathbf{r})$ is

$$[\nabla:\mathbf{E}](\mathbf{h}) = +4\pi^2\mathbf{h}:\mathbf{h}\Phi(\mathbf{h}) = +4\pi\mathbf{h}:\mathbf{h}F_{\text{total}}(\mathbf{h})/h^2, \tag{8.7.3.67b}$$

where $\mathbf{i}:\mathbf{k}$ represents the tensor product of two vectors. This leads to the expression for the electric field gradient in direct space,

$$[\nabla:\mathbf{E}](\mathbf{r}) = \frac{4\pi}{V}\sum \mathbf{h}:\mathbf{h}F_{\text{total}}(\mathbf{h})/h^2 \exp(-2\pi i\mathbf{h}\cdot\mathbf{r}). \quad (8.7.3.68)$$

(The elements of $\mathbf{h}:\mathbf{h}$ are the products h_ih_j.)

The components of $\mathbf{E}$ and the elements of the electric field gradient defined by (8.7.3.67*a*) and (8.7.3.68) are with respect to the reciprocal-lattice coordinate system. Proper transforms are required to get the values in other coordinate systems. Furthermore, to get the traceless $\nabla\mathbf{E}$ tensor, the quantity $-(4\pi/3)\rho_e(\mathbf{r}) = -(4\pi/3V)\sum F(\mathbf{h})\exp(-2\pi i\mathbf{h}\cdot\mathbf{r})$ must be subtracted from each of the diagonal elements $\nabla\mathbf{E}_{ii}$.

The Coulombic self-electronic energy of the crystal can be obtained from

$$\begin{aligned} E_{\text{Coulombic, electronic}} &= \tfrac{1}{2}\int\int \frac{\rho_e(\mathbf{r})\rho_e(\mathbf{r}')}{|\mathbf{r}-\mathbf{r}'|}\,\mathrm{d}\mathbf{r}\,\mathrm{d}\mathbf{r}', \\ &= \tfrac{1}{2}\int \Phi_e(\mathbf{r})\rho(\mathbf{r})\,\mathrm{d}\mathbf{r}. \end{aligned}$$

Since $\int \Phi(\mathbf{r})\rho(\mathbf{r})\,\mathrm{d}\mathbf{r} = \int \Phi(\mathbf{h})F(\mathbf{h})\,\mathrm{d}\mathbf{h}$ (Parseval's rule), the summation can be performed in reciprocal space,

$$E_{\text{Coulombic, electronic}} = \frac{1}{2\pi V}\sum F^2(\mathbf{h})/h^2, \quad (8.7.3.69a)$$

and, for the total Coulombic energy,

$$E_{\text{Coulombic, total}} = \frac{1}{2\pi V}\sum F^2_{\text{total}}(\mathbf{h})/h^2, \quad (8.7.3.69b)$$

where the integral has been replaced by a summation.

The summations are rapidly convergent, but suffer from having a singularity at $\mathbf{h}=0$ (Dahl & Avery, 1984; Becker & Coppens, 1990). The contribution from this term to the potential cannot be ignored if different structures are compared. The term at $\mathbf{h}=0$ gives a constant contribution to the potential, which, however, has no effect on the energy of a neutral system. For polar crystals, an additional term occurs in (8.7.3.69*a*, *b*), which is a function of the dipole moment D of the unit cell (Becker, 1990),

$$E_{\text{Coulombic, total}} = \frac{1}{2\pi V}\sum F^2_{\text{total}}(\mathbf{h})/h^2 + \frac{2\pi}{3V}D^2. \quad (8.7.3.69c)$$

To obtain the total energy of the static crystal, electron exchange and correlation as well as electron kinetic energy contributions must be added.

8.7.3.4.4. *The total energy of a crystal as a function of the electron density*

One can write the total energy of a system as

$$E = e_c[\rho] + T + E_{xc}, \quad (8.7.3.70)$$

where T is the kinetic energy, E_{xc} represents the exchange and electron correlation contributions, and $E_c[\rho]$, the Coulomb energy, discussed in the previous section, is given by

$$E_c = \tfrac{1}{2}\sum_{i\neq j}\frac{Z_iZ_j}{R_{ij}} - \sum_i Z_i\Phi(\mathbf{R}_i) + \tfrac{1}{2}\int\int\frac{\rho(\mathbf{r})\rho(\mathbf{r}')}{|\mathbf{r}-\mathbf{r}'|}\,\mathrm{d}\mathbf{r}\,\mathrm{d}\mathbf{r}', \quad (8.7.3.71)$$

where Z_i is the nuclear charge for an atom at position $\mathbf{R}_i$, and $\mathbf{R}_{ij} = \mathbf{R}_j - \mathbf{R}_i$.

Because of the theorem of Hohenberg & Kohn (1964), E is a unique functional of the electron density ρ, so that $T + E_{xc}$ must be a functional of ρ. Approximate density functionals are discussed extensively in the literature (Dahl & Avery, 1984) and are at the centre of active research in the study of electronic structure of various materials. Given an approximate functional, one can estimate non-Coulombic contributions to the energy from the charge density $\rho(\mathbf{r})$.

In the simplest example, the functionals are those applicable to an electronic gas with slow spatial variations (the 'nearly free electron gas'). In this approximation, the kinetic energy T is given by

$$T = c_k\int \rho t[\rho]\,\mathrm{d}^3\mathbf{r}, \quad (8.7.3.72)$$

with $c_k = (3/10)(2\pi^2)^{2/3}$; and the function $t[\rho] = \rho^{2/3}$. The exchange-correlation energy is also a functional of ρ,

$$E_{xc} = -c_x\int \rho e_{xc}[\rho]\,\mathrm{d}^3\mathbf{r},$$

with $c_x = (3/4)(3/\pi)^{1/3}$ and $e_{xc}[\rho] = \rho^{1/3}$.

Any attempt to minimize the energy with respect to ρ in this framework leads to very poor results. However, cohesive energies can be described quite well, assuming that the change in electron density due to cohesive forces is slowly varying in space.

An example is the system AB, with closed-shell subsystems A and B. Let ρ_A and ρ_B be the densities for individual A and B subsystems. The interaction energy is written as

$$\begin{aligned} \Delta E = {} & E_c[\rho] - E_c[\rho_A] - E_c[\rho_B] \\ & + c_k\int \mathrm{d}\mathbf{r}\{\rho t[\rho] - \rho_A t[\rho_A] - \rho_B t[\rho_B]\} \\ & - c_x\int \mathrm{d}\mathbf{r}\{\rho e_{xc}[\rho] - \rho_A e_{xc}[\rho_A] - \rho_B e_{xc}[\rho_B]\}. \end{aligned} \quad (8.7.3.73)$$

This model is known as the Gordon–Kim (1972) model and leads to a qualitatively valid description of potential energy surfaces between closed-shell subsystems. Unlike pure Coulombic models, this density functional model can lead to an equilibrium geometry. It has the advantage of depending only on the charge density ρ.

8.7.3.5. *Quantitative comparison with theory*

Frequently, the purpose of a charge density analysis is comparison with theory at various levels of sophistication. Though the charge density is a detailed function, the features of which can be compared at several points of interest in space, it is by no means the only level at which comparison can be made. The following sequence represents a progression of functions that are increasingly related to the experimental measurement.

$$\begin{array}{lll} & & \text{electrostatic properties} \\ & & \uparrow \\ \psi(1,2,\ldots,n) \rightarrow \Gamma^1(1,1) & \rightarrow \rho(\mathbf{r}) \rightarrow & \langle\rho(\mathbf{r})\rangle \rightarrow F(\mathbf{h}) \rightarrow I(\mathbf{h}) \\ & \downarrow & \\ & \Delta\rho(\mathbf{r}) \rightarrow & \langle\Delta\rho(\mathbf{r})\rangle, \end{array} \quad (8.7.3.74)$$

where the angle brackets refer to the thermally averaged functions.

The experimental information may be reduced in the opposite sequence:

Table 8.7.3.3. *The matrix M^{-1} relating d-orbital occupancies P_{ij} to multipole populations P_{lm} (from Holladay, Leung & Coppens, 1983)*

d-orbital populations	Multipole populations					
	P_{00}	P_{20}	P_{22+}	P_{40}	P_{42+}	P_{44+}
P_z^2	0.200	1.039	0.00	1.396	0.00	0.00
P_{xz}	0.200	0.520	0.942	−0.931	1.108	0.00
P_{yz}	0.200	0.520	−0.942	−0.931	−1.108	0.00
$P_{x^2-y^2}$	0.200	−0.039	0.00	0.233	0.00	1.571
P_{xy}	0.200	−1.039	0.00	0.233	0.00	−1.571

Mixing terms

	P_{21}	P_{21-}	P_{22+}	P_{22-}	P_{41+}	P_{41-}	P_{42+}	P_{42-}	P_{43+}	P_{43-}	P_{44-}
$P_{z^2/xz}$	1.088	0.00	0.00	0.00	2.751	0.00	0.00	0.00	0.00	0.00	0.00
$P_{z^2/yz}$	0.00	1.088	0.00	0.00	0.00	2.751	0.00	0.00	0.00	0.0	0.00
P_{z^2/x^2-y^2}	0.00	0.00	−2.177	0.00	0.00	0.00	1.919	0.00	0.00	0.0	0.00
$P_{z^2/xy}$	0.00	0.00	0.00	−2.177	0.00	0.00	0.00	1.919	0.00	0.0	0.00
$P_{xz/yz}$	0.00	0.00	0.00	1.885	0.00	0.00	0.00	2.216	0.00	0.0	0.00
P_{xz/x^2-y^2}	1.885	0.00	0.00	0.00	−0.794	0.00	0.00	0.00	2.094	0.0	0.00
$P_{xz/xy}$	0.00	1.885	0.00	0.00	0.00	−0.794	0.00	0.00	0.00	2.094	0.00
P_{yz/x^2-y^2}	0.00	−1.885	0.00	0.00	0.00	0.794	0.00	0.00	0.00	2.094	0.00
$P_{yz/xy}$	1.885	0.00	0.00	0.00	−0.794	0.00	0.00	0.00	−2.094	0.00	0.00
$P_{x^2-y^2/xy}$	0.00	0.00	0.00	0.00	0.00	0.00	0.00	0.00	0.00	0.00	3.142

$$\begin{array}{ccccccc} \text{electrostatic properties} & & & & & & \\ \uparrow & & & & & & \\ \rho(\mathbf{r}) & \leftarrow & \langle\rho(\mathbf{r})\rangle & \leftarrow & F(\mathbf{h}) & \leftarrow & I(\mathbf{h}) \\ \downarrow & & \downarrow & & & & \\ \Delta\rho(\mathbf{r}) & \leftarrow & \langle\Delta\rho(\mathbf{r})\rangle. & & & & \end{array} \tag{8.7.3.75}$$

The crucial step in each sequence is the thermal averaging (top sequence) or the deconvolution of thermal motion (bottom sequence), which in principle requires detailed knowledge of both the internal (molecular) and the external (lattice) modes of the crystal. Even within the generally accepted Born–Oppenheimer approximation, this is a formidable task, which can be simplified for molecular crystals by the assumption that the thermal smearing is dominated by the larger-amplitude external modes. The procedure (8.7.3.65) requires an adequate thermal-motion model in the structure-factor formalism applied to the experimental structure amplitudes. The commonly used models may include anharmonicity, as described in Volume B, Chapter 1.2 (*IT*B, 1992), but assume that a density function centred on an atom can be assigned the thermal motion of that atom, which may be a poor approximation for the more diffuse functions.

The missing link in scheme (8.7.3.75) is the sequence $\psi \leftarrow \Gamma^1(1,1) \leftarrow \rho(\mathbf{r})$. In order to describe the wavefunction analytically, a basis set is required. The number of coefficients in the wavefunction is minimized by the use of a minimal basis for the molecular orbitals, but calculations in general lead to poor-quality electron densities.

If the additional approximation is made that the wavefunction is a single Slater determinant, the idempotency condition can be used in the derivation of the wavefunction from the electron density. A simplified two-valence-electron two-orbital system has been treated in this manner (Massa, Goldberg, Frishberg, Boehme & La Placa, 1985), and further developments may be expected.

A special case occurs if the overlap between the orbitals on an atom and its neighbours is very small. In this case, a direct relation can be derived between the populations of a minimal basis set of valence orbitals and the multipole coefficients, as described in the following sections.

8.7.3.6. *Occupancies of transition-metal valence orbitals from multipole coefficients*

In general, the atom-centred density model functions describe both the valence and the two-centre overlap density. In the case of transition metals, the latter is often small, so that to a good approximation the atomic density can be expressed in terms of an atomic orbital basis set d_i, as well as in terms of the multipolar expansion. Thus,

$$\begin{aligned} \rho_d &= \sum_{i=1}^{5}\sum_{j\geq i}^{5} P_{ij} d_i d_j, \\ &= \sum_{l=0}^{4} \kappa'^3 \left\{ R_l(\kappa' r) \sum_{m=0}^{l}\sum_{p} P_{lmp} d_{lmp} \right\}, \end{aligned} \tag{8.7.3.76}$$

in which d_{lmp} are the density functions.

The orbital products $d_i d_j$ can be expressed as linear combinations of spherical harmonic functions, with coefficients listed in Volume B, Chapter 1.2 (*IT*B, 1992), which leads to relations between the P_{ij} and P_{lmp}. In matrix notation,

$$\mathbf{P}_{lmp} = \boldsymbol{M}\mathbf{P}_{ij}, \tag{8.7.3.77}$$

where $\mathbf{P}_{lmp}$ is a vector containing the coefficients of the 15 spherical harmonic functions with $l = 0$, 2, or 4 that are generated by the products of d orbitals. The matrix $\boldsymbol{M}$ is also a function of the ratio of orbital and density-function normalization coefficients, given in Volume B, Chapter 1.2 (*IT*B, 1992).

Table 8.7.3.4. *Orbital–multipole relations for square-planar complexes (point group D_{4h})*

		P_{00}	P_{20}	P_{40}	P_{44+}
P_{20}	a_{1g}	0.200	1.039	1.396	0.00
P_{21+}	e_g	0.200	0.520	−0.931	0.00
P_{21-}		0.200	0.520	−0.931	0.00
P_{22+}	b_{1g}	0.200	−1.039	0.233	1.570
P_{22}	b_{2g}	0.200	−1.039	0.233	−1.570

The d-orbital occupancies can be derived from the experimental multipole populations by the inverse expression,

$$\mathbf{P}_{ij} = \boldsymbol{M}^{-1}\mathbf{P}_{lmp} \tag{8.7.3.78}$$

(Holladay, Leung & Coppens, 1983).

The matrix $\boldsymbol{M}^{-1}$ is given in Table 8.7.3.3. Point-group-specific expressions can be derived by omission of symmetry-forbidden terms. Matrices for point group $4/mmm$ (square planar) and for trigonal point groups ($\bar{3}$, $\bar{3}$, 32, $3m$, $\bar{3}m$) are listed in Tables 8.7.3.4 and 8.7.3.5, respectively. Point groups with and without vertical mirror planes are distinguished by the occurrence of both d_{lm+} and d_{lm-} functions in the latter case, and only d_{lm+} in the former, with m being restricted to n, the order of the rotation axis. The d_{ln-} functions can be eliminated by rotation of the coordinate system around a vertical axis through an angle ψ_0 given by $\psi_0 = (1/n)\arctan(P_{ln-}/P_{ln+})$.

8.7.3.7. *Thermal smearing of theoretical densities*

8.7.3.7.1. *General considerations*

In the Born–Oppenheimer approximation, the electrons rearrange instantaneously to the minimum-energy state for each nuclear configuration. This approximation is generally valid, except when very low lying excited electronic states exist. The thermally smeared electron density is then given by

$$\langle\rho(\mathbf{r})\rangle = \int \rho(\mathbf{r},\mathbf{R})P(\mathbf{R})\,\mathrm{d}(\mathbf{R}), \tag{8.7.3.79}$$

where $\mathbf{R}$ represents the $3N$ nuclear space coordinates and $P(\mathbf{R})$ is the probability of the configuration $\mathbf{R}$. Evaluation of (8.7.3.79) is possible if the vibrational spectrum is known, but requires a large number of quantum-mechanical calculations at points along the vibrational path. A further approximation is the convolution approximation, which assumes that the charge density near each nucleus can be convoluted with the vibrational motion of that nucleus,

$$\langle\rho(\mathbf{r})\rangle = \sum_n \int \rho_n(\mathbf{r}-\mathbf{u}-\mathbf{R}_n)P_n(\mathbf{u})\,\mathrm{d}\mathbf{u}, \tag{8.7.3.80}$$

where ρ_n stands for the density of the nth pseudo-atom. The convolution approximation thus requires decomposition of the density into atomic fragments. It is related to the thermal-motion formalisms commonly used, and requires that two-centre terms in the theoretical electron density be either projected into the atom-centred density functions, or assigned the thermal motion of a point between the two centres. In the LCAO approximation (8.7.3.9), the two-centre terms are represented by

$$\rho_{\mu\nu}(\mathbf{r}) = P_{\mu\nu}\chi_\mu(\mathbf{r}-\mathbf{R}_\mu)\chi_\nu(\mathbf{r}-\mathbf{R}_\nu), \tag{8.7.3.81}$$

where χ_μ and χ_ν are basis functions centred at $\mathbf{R}_\mu$ and $\mathbf{R}_\nu$, respectively. As the motion of a point between the two vibrating atoms depends on their relative phase, further assumptions must be made. The simplest is to assume a gradual variation of the thermal motion along the bond, which gives at a point $\mathbf{r}_i$ on the internuclear vector of length $R_{\mu\nu}$

$$U_{ij}(\mathbf{r}_i) = \left[U_{ij}(\mathbf{R}_\mu)\left|\mathbf{R}_\mu - \mathbf{r}_i\right| + U_{ij}(\mathbf{R}_\nu)\left|\mathbf{R}_\nu - \mathbf{r}_i\right|\right]/R_{\mu\nu}. \tag{8.7.3.82}$$

This expression may be used to assign thermal parameters to a bond-centred function.

Table 8.7.3.5. *Orbital–multipole relations for trigonal complexes*

	P_{00}	P_{2-}	P_{40}	P_{43+}	P_{43-}
(*a*) In terms of d orbitals					
P_{20}	0.200	1.039	1.396	0.00	0.00
P_{21+}	0.200	0.520	−0.931	0.00	0.00
P_{21-}	0.200	0.520	−0.931	0.00	0.00
P_{22+}	0.200	−1.039	0.233	0.00	0.00
P_{22-}	0.200	−1.039	0.233	0.00	0.00
$P_{21+/22+}$	0.00	0.00	0.00	2.094	0.00
$P_{21+/22-}$	0.00	0.00	0.00	0.00	2.094
$P_{21-/22+}$	0.00	0.00	0.00	0.00	2.094
$P_{21-/22-}$	0.00	0.00	0.00	−2.094	0.00
(*b*) In terms of symmetry-adapted orbitals*†					
$P_1(a_{1g})$	0.200	1.039	1.396	0.00	
$P_2(e_g)$	0.400	−1.039	−0.310	−1.975	
$P_3(e'_g)$	0.400	0.00	−1.087	1.975	
$P_4(e_{g^+}e'_g + e_{g^-}e'_{g^-})$	0.00	−2.942	2.193	1.397	

* The electron density in terms of the symmetry-adapted orbitals is given by:

$$\rho_{3d} = P_1 a_{1g}^2 + \tfrac{1}{2}P_2(e_{g^+}^2 - e_{g^-}^2) + \tfrac{1}{2}P_4(e_{g^+}e'_g + e_{g^-}e'_{g^-}),$$

with: $a_{1g} = d_{z^2}$; $e_{g^+} = \sqrt{(2/3)}d_{x^2-y^2} - \sqrt{(1/3)}d_{xz}$; $e_{g^-} = \sqrt{(2/3)}d_{xy} + \sqrt{(1/3)}d_{yz}$; $e'_{g^+} = \sqrt{(1/3)}d_{x^2-y^2} + \sqrt{(2/3)}d_{xz}$; and $e'_{g^-} = \sqrt{(1/3)}d_{xy} - \sqrt{(2/3)}d_{yz}$. † The signs given here imply a positive e'_g lobe in the positive xz quadrant. Care should be exercised in defining the coordinate system if this lobe is to point towards a ligand atom.

8.7.3.7.2. *Reciprocal-space averaging over external vibrations*

Thermal averaging of the electron density is considerably simplified for modes in which adjacent atoms move in phase. In molecular crystals, such modes correspond to rigid-body vibrations and librations of the molecule as a whole. Their frequencies are low because of the weakness of intermolecular interactions. Rigid-body motions therefore tend to dominate thermal motion, in particular at temperatures for which kT ($k = 0.7\ \mathrm{cm}^{-1}$) is large compared with the spacing of the vibrational energy levels of the external modes (internal modes are typically not excited to any extent at or below room temperature).

For a translational displacement ($\mathbf{u}$), the dynamic density is given by

$$\rho_{\mathrm{dyn}}(\mathbf{r}) = \int \rho(\mathbf{r}-\mathbf{u})P(\mathbf{u})\,\mathrm{d}\mathbf{u}, \tag{8.7.3.83}$$

with $\rho(\mathbf{r})$ defined by (8.7.3.81) (Stevens, Rees & Coppens, 1977). In the harmonic approximation, $P(\mathbf{u})$ is a normalized three-dimensional Gaussian probability function, the exponents

of which may be obtained by rigid-body analysis of the experimental data. In general, for a translational displacement (**u**) and a librational oscillation (ω),

$$\rho_{\rm dyn}(\mathbf{r}) = \left(\sum P_{\mu\nu}\chi_\mu\chi_\nu\right) * P(\mathbf{u},\omega). \tag{8.7.3.84}$$

If correlation between **u** and ω can be ignored (neglect of the screw tensor **S**), $P(\mathbf{u},\omega) = P(\mathbf{u})P(\omega)$, and both types of modes can be treated independently. For the translations

$$\begin{aligned}\langle\rho\rangle_{\rm trans} &= \sum P_{\mu\nu}\left\{\chi_\mu(\mathbf{r})\chi_\nu(\mathbf{r}) * P(\mathbf{u})\right\}\\ &= \sum P_{\mu\nu}F^{-1}\left\{f_{\mu\nu}(\mathbf{h})\cdot T_{\rm tr}(\mathbf{h})\right\},\end{aligned} \tag{8.7.3.85}$$

where F^{-1} is the inverse Fourier transform operator, and $T_{\rm tr}(\mathbf{h})$ is the translational temperature factor.

If $\boldsymbol{R}$ is an orthogonal rotation matrix corresponding to a rotation ω, we obtain for the librations

$$\begin{aligned}\langle\rho\rangle_{\rm libr} &= \sum P_{\mu\nu}\left\{\chi_\mu(\boldsymbol{R}\mathbf{r})\chi_\nu(\boldsymbol{R}\mathbf{r}) * P(\omega)\right\}\\ &= \sum P_{\mu\nu}F^{-1}\left\{\left\langle f_{\mu\nu}(\boldsymbol{R}\mathbf{h})\right\rangle\right\},\end{aligned} \tag{8.7.3.86}$$

in which $f(\mathbf{h})$ has been averaged over the distribution of orientations of **h** with respect to the molecule;

$$\left\langle f_{\mu\nu}(\mathbf{h})\right\rangle = \int f_{\mu\nu}(\boldsymbol{R}\mathbf{h})P(\omega)\,{\rm d}\omega. \tag{8.7.3.87}$$

Evaluation of (8.7.3.85) and (8.7.3.86) is most readily performed if the basis functions ψ have a Gaussian-type radial dependence, or are expressed as a linear combination of Gaussian radial functions.

For Gaussian products of *s* orbitals, the molecular scattering factor of the product $\psi_\mu\psi_\nu = N_\mu\exp[-\alpha_\mu(\mathbf{r}-\mathbf{r}_A)^2]\times N_\nu\exp[-\alpha_\nu(\mathbf{r}-\mathbf{r}_B)^2]$, where N_μ and N_ν are the normalization factors of the orbitals μ and ν centred on atoms *A* and *B*, is given by

$$\begin{aligned}f^{s,s}_{\rm stat}(\mathbf{h}) = N_\mu N_\nu &\exp\left(-\frac{\alpha_\mu\alpha_\nu}{\alpha_\mu+\alpha_\nu}\left|\mathbf{r}_A-\mathbf{r}_B\right|^2\right)\left(\frac{\pi}{\alpha_\mu+\alpha_\nu}\right)^{3/2}\\ &\times\exp\left(\frac{-\pi^2|h|^2}{\alpha_\mu+\alpha_\nu}\right)\exp(2\pi i\mathbf{h}\cdot\mathbf{r}_c),\end{aligned} \tag{8.7.3.88}$$

where the centre of density $\mathbf{r}_c$ is defined by $\mathbf{r}_c = (\alpha_\mu\mathbf{r}_A+\alpha_\nu\mathbf{r}_B)/(\alpha_\mu+\alpha_\nu)$.

For the translational modes, the temperature-factor exponent $-2\pi^2\sum_i\sum_j U_{ij}h_ih_j$ is simply added to the Gaussian exponent in (8.7.3.88) to give

$$\exp\left(-\frac{\pi^2|h|^2}{\alpha_\mu+\alpha_\nu}\right) - 2\pi^2\sum_i\sum_j U_{ij}h_ih_j.$$

For librations, we may write

$$\boldsymbol{R}\mathbf{r} = \mathbf{r} + \mathbf{u}_{\rm lib}$$

As $(\boldsymbol{R}\mathbf{h})\cdot\mathbf{r} = \mathbf{h}\cdot\boldsymbol{R}^T\mathbf{r} = \mathbf{h}\cdot\mathbf{r} - (\boldsymbol{R}\mathbf{h})\cdot\mathbf{u}_{\rm lib}$, for a function centred at **r**,

$$\begin{aligned}\left\langle\exp(2\pi\mathbf{h}\cdot\mathbf{r}_c)\right\rangle &= \sum\exp\left[2\pi i(\boldsymbol{R}\mathbf{h})\cdot\mathbf{r}_c\right]P(\delta)\,{\rm d}\omega\\ &= \exp(2\pi\mathbf{h}\cdot\mathbf{r}_c)\int\exp\left[-2\pi i(\boldsymbol{R}\mathbf{h})\cdot\mathbf{u}^c_{\rm lib}\right]P(\omega)\,{\rm d}\omega,\end{aligned} \tag{8.7.3.89}$$

which shows that for *ss* orbital products the librational temperature factor can be factored out, or

$$f^{s,s}_{\rm dyn} = f^{s,s}_{\rm stat}\int\exp\left[-2\pi i(\boldsymbol{R}\mathbf{h})\cdot\mathbf{u}^c_{\rm lib}\right]P(\omega)\,{\rm d}\omega. \tag{8.7.3.90}$$

Expressions for $P(\omega)$ are described elsewhere (Pawley & Willis, 1970).

For general Cartesian Gaussian basis functions of the type

$$\psi(\mathbf{r}) = (x-x_A)^m(y-y_A)^n(z-z_A)^p\exp(-\alpha|\mathbf{r}-\mathbf{r}_A|^2), \tag{8.7.3.91}$$

the scattering factors are more complicated (Miller & Krauss, 1967; Stevens, Rees & Coppens, 1977), and the librational temperature factor can no longer be factored out. However, it may be shown that, to a first approximation, (8.7.3.90) can again be used. This 'pseudotranslation' approximation corresponds to a neglect of the change in orientation (but not of position) of the two-centre density function and is adequate for moderate vibrational amplitudes.

Thermally smeared density functions are obtained from the averaged reciprocal-space function by performing the inverse Fourier transform with phase factors depending on the position coordinates of each orbital product

$$\langle\rho\rangle = \frac{1}{V}\sum P_{\mu\nu}\sum_{\mathbf{h}} f_{\mu\nu}(\mathbf{h})\exp\left[-2\pi i\mathbf{h}\cdot(\mathbf{r}-\mathbf{r}_c)\right], \tag{8.7.3.92}$$

where the orbital product $\chi_\mu\chi_\nu$ is centred at $\mathbf{r}_c$. If the summation is truncated at the experimental limit of $(\sin\theta)/\lambda$, both thermal vibrations and truncation effects are properly introduced in the theoretical densities.

8.7.3.8. *Uncertainties in experimental electron densities*

It is often important to obtain an estimate of the uncertainty in the deformation densities in Table 8.7.3.1. If it is assumed that the density of the static atoms or fragments that are subtracted out are precisely known, three sources of uncertainty affect the deformation densities: (1) the uncertainties in the experimental structure factors; (2) the uncertainties in the positional and thermal parameters of the density functions that influence $\rho_{\rm calc}$; and (3) the uncertainty in the scale factor *k*.

If we assume that the uncertainties in the observed structure factors are not correlated with the uncertainties in the refined parameters, the variance of the electron density is given by

$$\begin{aligned}\sigma^2(\Delta\rho) = \sigma^2\left(\rho'_{\rm obs}\right) + \sigma^2\left(\rho_{\rm calc}\right) + \left(\rho'_{\rm obs}\right)^2\frac{\sigma^2(k)}{k^2}\\ + \sum_p\frac{\delta\rho_{\rm calc}}{\delta u_p}\sigma\left(u_p\right)\rho'_{\rm obs}\frac{\sigma(k)}{k}\gamma\left(u_p,k\right),\end{aligned} \tag{8.7.3.93}$$

where $\rho'_{\rm obs} = \rho_{\rm obs}/k$, u_p is a positional or thermal parameter, and the $\gamma(u_p,k)$ are correlation coefficients between the scale factor and the other parameters (Rees, 1976, 1978; Stevens & Coppens, 1976).

Similarly, for the covariance between the deformation densities at points *A* and *B*,

$$\begin{aligned}{\rm cov}(\Delta\rho_A,\Delta\rho_B) = {\rm cov}\left(\rho_{{\rm obs},A},\rho_{{\rm obs},B}\right)/k^2\\ + {\rm cov}\left(\rho_{{\rm calc},A},\rho_{{\rm calc},B}\right)\\ + \rho_{{\rm obs},A}\rho_{{\rm obs},B}[\sigma(k)/k]^2,\end{aligned} \tag{8.7.3.94}$$

where it is implied that the second term includes the effect of the scale factor/parameter correlation.

Following Rees (1976), we may derive a simplified expression for the covariance valid for the space group $P\bar{1}$. Since the structure factors are not correlated with each other,

$$\operatorname{cov}\left(\rho_{\mathrm{obs},A}, \rho_{\mathrm{obs},B}\right) \simeq \sum \frac{\partial \rho_{\mathrm{obs},A}}{\partial F_{\mathrm{obs}}(\mathbf{h})} \frac{\partial \rho_{\mathrm{obs},B}}{\partial F_{\mathrm{obs}}(\mathbf{h})} \sigma^2\left[F_{\mathrm{obs}}(\mathbf{h})\right]$$
$$\simeq \frac{2}{V^2} \sum_{1/2} \sigma^2(F_{\mathrm{obs}}) \left[\cos 2\pi(\mathbf{r}_A + \mathbf{r}_B)\cdot\mathbf{h} + \cos 2\pi(\mathbf{r}_A - \mathbf{r}_B)\cdot\mathbf{h}\right], \quad (8.7.3.95)$$

where the latter equality is specific for $P\bar{1}$, and $\sum_{1/2}$ indicates summation over a hemisphere in reciprocal space. In general, the second term rapidly averages to zero as $h_{\max}$ increases, while the first term may be replaced by its average

$$\left\langle \cos 2\pi(\mathbf{r}_A - \mathbf{r}_B)\cdot\mathbf{h} \right\rangle = 3(\sin u - u\cos u)/u^3 \equiv \mathrm{C}(u), \quad (8.7.3.96)$$

with $u = 2\pi|\mathbf{r}_A - \mathbf{r}_B|h_{\max}$, or $\operatorname{cov}(\rho_{\mathrm{obs},A}\rho_{\mathrm{obs},B}) \simeq (2/V^2)C(u) \times \sum_{1/2}\sigma^2(F_0)$ and $\sigma^2(\rho_{\mathrm{obs}}) \simeq (2/V^2)\sum_{1/2}\sigma^2(F_0)$, a relation derived earlier by Cruickshank (1949). A discussion of the applicability of this expression in other centrosymmetric space groups is given by Rees (1976).

8.7.3.9. *Uncertainties in derived functions*

The electrostatic moments are functions of the scale factor, the positional parameters x, y and z of the atoms, and their charge-density parameters κ and P_{lmp}. The standard uncertainties in the derived moments are therefore dependent on the variances and covariances of these parameters.

If $\boldsymbol{M}_p$ represents the $m \times m$ variance–covariance matrix of the parameters p_j, and $\boldsymbol{T}$ is an $n \times m$ matrix defined by $\partial\mu^l/\partial p_j$ for the lth moment with n independent elements, the variances and covariances of the elements of m^l are obtained from

$$\boldsymbol{M}_\mu = \boldsymbol{T}\boldsymbol{M}_p\boldsymbol{T}^T. \quad (8.7.3.96a)$$

If a moment of an assembly of pseudo-atoms is evaluated, the elements of $\boldsymbol{T}$ include the effects of coordinate rotations required to transfer atomic moments into a common coordinate system.

A frequently occurring case of interest is the evaluation of the magnitude of a molecular dipole moment and its standard deviation. Defining

$$y = \mu^2 = \boldsymbol{\mu}\boldsymbol{G}\boldsymbol{\mu}^T, \quad (8.7.3.96b)$$

where $\boldsymbol{\mu}$ is the dipole-moment vector and $\boldsymbol{G}$ is the direct-space metric tensor of the appropriate coordinate system. If $\boldsymbol{Y}$ is the 1×3 matrix of the derivatives $\partial y/\partial\mu_i$,

$$\sigma^2(y) = \boldsymbol{Y}\boldsymbol{M}_\mu\boldsymbol{Y}^T, \quad (8.7.3.96c)$$

where $\boldsymbol{M}_\mu$ is defined by (8.7.3.96*a*). The standard uncertainty in μ may be obtained from $\sigma(\mu) = \sigma(y)/2\mu$. Significant contributions often result from uncertainties in the positional and charge-density parameters of the H atoms.

8.7.4. Spin densities

8.7.4.1. *Introduction*

Magnetism and magnetic ordering are among the central problems in condensed-matter research. One of the main issues in macroscopic studies of magnetism is a description of the magnetization density $\boldsymbol{\mu}$ as a function of temperature and applied field: phase diagrams can be explained from such studies.

Diffraction techniques allow determination of the same information, but at a microscopic level. Let $\mathbf{m}(\mathbf{r})$ be the microscopic magnetization density, a function of the position $\mathbf{r}$ in the unit cell (for crystalline materials). Macroscopic and microscopic magnetization densities are related by the simple expression

$$\boldsymbol{\mu} = \frac{1}{V}\int_{\mathrm{cell}} \mathbf{m}(\mathbf{r})\,\mathrm{d}\mathbf{r}, \quad (8.7.4.1)$$

where V is the volume of the unit cell, $\mathbf{m}(\mathbf{r})$ is the sum of two contributions: $\mathbf{m}_s(\mathbf{r})$ originating from the spins of the electrons, and $\mathbf{m}_L(\mathbf{r})$ originating from their orbital motion.

$$\mathbf{m}(\mathbf{r}) = \mathbf{m}_s(\mathbf{r}) + \mathbf{m}_L(\mathbf{r}). \quad (8.7.4.2)$$

8.7.4.2. *Magnetization densities from neutron magnetic elastic scattering*

The scattering process is discussed in Section 6.1.3 and only the features that are essential to the present chapter will be summarized here.

For neutrons, the nuclear structure factor $F_N(\mathbf{h})$ is given by

$$F_N(\mathbf{h}) = \sum_j b_j T_j \exp(2\pi i\mathbf{h}\cdot\mathbf{R}_j). \quad (8.7.4.3)$$

b_j, T_j, $\mathbf{R}_j$ are the coherent scattering length, the temperature factor, and the equilibrium position of the jth atom in the unit cell.

Let $\boldsymbol{\sigma}$ be the spin of the neutron (in units of $\hbar/2$). There is a dipolar interaction of the neutron spin with the electron spins and the currents associated with their motion. The magnetic structure factor can be written as the scalar product of the neutron spin and an 'interaction vector' $\mathbf{Q}(\mathbf{h})$:

$$F_M(\mathbf{h}) = \boldsymbol{\sigma}\cdot\mathbf{Q}(\mathbf{h}). \quad (8.7.4.4)$$

$\mathbf{Q}(\mathbf{h})$ is the sum of a spin and an orbital term: $\mathbf{Q}_s$ and $\mathbf{Q}_L$, respectively. If $r_0 = \gamma r_e \sim 0.54 \times 10^{-12}$ cm, where γ is the gyromagnetic factor ($=1.913$) of the neutron and r_e the classical Thomson radius of the electron, the spin term is given by

$$\mathbf{Q}_s(\mathbf{h}) = r_0\hat{\mathbf{h}} \times \mathbf{M}_s(\mathbf{h}) \times \hat{\mathbf{h}}, \quad (8.7.4.5)$$

$\hat{\mathbf{h}}$ being the unit vector along $\mathbf{h}$, while $\mathbf{M}_s(\mathbf{h})$ is defined as

$$\mathbf{M}_s(\mathbf{h}) = \left\langle \sum_j \boldsymbol{\sigma}_j \exp(2\pi i\mathbf{h}\cdot\mathbf{r}_j) \right\rangle, \quad (8.7.4.6)$$

where $\boldsymbol{\sigma}_j$ is the spin of the electron at position $\mathbf{r}_j$, and angle brackets denote the ensemble average over the scattering sample. $\mathbf{M}_s(\mathbf{h})$ is the Fourier transform of the spin-magnetization density $\mathbf{m}_s(\mathbf{r})$, given by

$$\mathbf{m}_s(\mathbf{r}) = \left\langle \sum_j \boldsymbol{\sigma}_j \delta(\mathbf{r} - \mathbf{r}_j) \right\rangle. \quad (8.7.4.7)$$

This is the spin-density vector field in units of $2\mu_B$.

The orbital part of $\mathbf{Q}(\mathbf{h})$ is given by

$$\mathbf{Q}_L(\mathbf{h}) = -\frac{ir_0}{2\pi h}\hat{\mathbf{h}} \times \left\langle \sum_j \mathbf{p}_j \exp(2\pi i\mathbf{h}\cdot\mathbf{r}_j) \right\rangle, \quad (8.7.4.8)$$

where $\mathbf{p}_j$ is the momentum of the electrons. If the current density vector field is defined by

$$\mathbf{j}(\mathbf{r}) = -\frac{e}{2m}\left\langle \sum_j \left\{\mathbf{p}_j\delta(\mathbf{r} - \mathbf{r}_j) + \delta(\mathbf{r} - \mathbf{r}_j)\mathbf{p}_j\right\} \right\rangle, \quad (8.7.4.9)$$

$\mathbf{Q}_L(\mathbf{h})$ can be expressed as

$$\mathbf{Q}_L(\mathbf{h}) = -\frac{ir_0}{2\pi h}\hat{\mathbf{h}} \times \mathbf{J}(\mathbf{h}), \quad (8.7.4.10)$$

where $\mathbf{J}(\mathbf{h})$ is the Fourier transform of the current density $\mathbf{j}(\mathbf{r})$.

The electrodynamic properties of $\mathbf{j}(\mathbf{r})$ allow it to be written as the sum of a rotational and a nonrotational part:

$$\mathbf{j}(\mathbf{r}) = \nabla\psi + \nabla \times [\mathbf{m}_L(\mathbf{r})], \tag{8.7.4.11}$$

where $\nabla\psi$ is a 'conduction' component and $\mathbf{m}_L(\mathbf{r})$ is an 'orbital-magnetization' density vector field.

Substitution of the Fourier transform of (8.7.4.11) into (8.7.4.10) leads in analogy to (8.7.4.5) to

$$\mathbf{Q}_L(\mathbf{h}) = r_0 \hat{\mathbf{h}} \times \mathbf{M}_L(\mathbf{h}) \times \hat{\mathbf{h}}, \tag{8.7.4.12}$$

where $\mathbf{M}_L(\mathbf{h})$ is the Fourier transform of $\mathbf{m}_L(\mathbf{r})$. The rotational component $\nabla\psi$ of $\mathbf{j}(\mathbf{r})$ does not contribute to the neutron scattering process. It is therefore possible to write $\mathbf{Q}(\mathbf{h})$ as

$$\mathbf{Q}(\mathbf{h}) = r_0 \hat{\mathbf{h}} \times \mathbf{M}(\mathbf{h}) \times \hat{\mathbf{h}}, \tag{8.7.4.13}$$

with

$$\mathbf{M}(\mathbf{h}) = \mathbf{M}_s(\mathbf{h}) + \mathbf{M}_L(\mathbf{h}) \tag{8.7.4.14}$$

being the Fourier transform of the 'total' magnetization density vector field, and

$$\mathbf{m}(\mathbf{r}) = \mathbf{m}_s(\mathbf{r}) + \mathbf{m}_L(\mathbf{r}). \tag{8.7.4.15}$$

As $\mathbf{Q}(\mathbf{h})$ is the projection of $\mathbf{M}(\mathbf{h})$ onto the plane perpendicular to $\mathbf{h}$, there is no magnetic scattering when $\mathbf{M}$ is parallel to $\mathbf{h}$. It is clear from (8.7.4.13) that $\mathbf{M}(\mathbf{h})$ can be defined to any vector field $\mathbf{V}(\mathbf{h})$ parallel to $\mathbf{h}$, *i.e.* such that $\mathbf{h} \times \mathbf{V}(\mathbf{h}) = 0$.

This means that in real space $\mathbf{m}(\mathbf{r})$ is defined to any vector field $\mathbf{v}(\mathbf{r})$ such that $\nabla \times \mathbf{v}(\mathbf{r}) = 0$. Therefore, $\mathbf{m}(\mathbf{r})$ is defined to an arbitrary gradient.

As a result, magnetic neutron scattering cannot lead to a uniquely defined orbital magnetization density. However, the definition (8.7.4.7) for the spin component is unambiguous.

However, the integrated magnetic moment $\boldsymbol{\mu}$ is determined unambiguously and must thus be identical to the magnetic moment defined from the principles of quantum mechanics, as discussed in §8.7.4.5.1.3.

Before discussing the analysis of magnetic neutron scattering in terms of spin-density distributions, it is necessary to give a brief description of the quantum-mechanical aspects of magnetization densities.

8.7.4.3. *Magnetization densities and spin densities*

8.7.4.3.1. *Spin-only density at zero temperature*

Let us consider first an isolated open-shell system, whose orbital momentum is quenched: it is a spin-only magnetism case. Let $\hat{\mathbf{m}}_s$ be the spin-magnetization-density operator (in units of $2\mu_B$):

$$\hat{\mathbf{m}}_s = \sum_j \hat{\boldsymbol{\sigma}}_j \, \delta(\mathbf{r} - \mathbf{r}_j). \tag{8.7.4.16}$$

$\mathbf{r}_j$ and $\hat{\boldsymbol{\sigma}}_j$ are, respectively, the position and the spin operator (in $\hbar$ units) of the jth electron. This definition is consistent with (8.7.4.7).

The system is assumed to be at zero temperature, under an applied field, the quantization axis being Oz. The ground state is an eigenstate of $\hat{\mathbf{S}}^2$ and $\hat{S}_z$, where $\hat{\mathbf{S}}$ is the total spin:

$$\hat{\mathbf{S}} = \sum_j \hat{\boldsymbol{\sigma}}_j. \tag{8.7.4.17}$$

Let S and M_s be the eigenvalues of $\hat{\mathbf{S}}^2$ and $\hat{S}_z$. (M_s will in general be fixed by Hund's rule: $M_S = S$.)

$$2M_S = [n_\uparrow - n_\downarrow], \tag{8.7.4.18}$$

where $n_\uparrow$ and $n_\downarrow$ are the numbers of electrons with ($\uparrow$: $+\frac{1}{2}$) and ($\downarrow$: $-\frac{1}{2}$) spin, respectively.

The spin-magnetization density is along $\mathbf{z}$, and is given by

$$m_{Sz}(\mathbf{r}) = \left\langle \psi_{SM_S} \left| \sum_j \hat{\boldsymbol{\sigma}}_{jz} \, \delta(\mathbf{r} - \mathbf{r}_j) \right| \psi_{SM_S} \right\rangle. \tag{8.7.4.19}$$

$m_{Sz}(\mathbf{r})$ is proportional to the normalized spin density that was defined for a pure state in (8.7.2.10).

$$m_{Sz}(\mathbf{r}) = M_S s(\mathbf{r}). \tag{8.7.4.20}$$

If $\rho_\uparrow(\mathbf{r})$ and $\rho_\downarrow(\mathbf{r})$ are the charge densities of electrons of a given spin, the normalized spin density is defined as

$$s(\mathbf{r}) = [\rho_\uparrow(\mathbf{r}) - \rho_\downarrow(\mathbf{r})] \frac{1}{[n_\uparrow - n_\downarrow]}, \tag{8.7.4.21}$$

compared with the total charge density $\rho(\mathbf{r})$ given by

$$\rho(\mathbf{r}) = \rho_\uparrow(\mathbf{r}) + \rho_\downarrow(\mathbf{r}). \tag{8.7.4.22}$$

A strong complementarity is thus expected from joint studies of $\rho(\mathbf{r})$ and $s(\mathbf{r})$.

In the particular case of an independent electron model,

$$\rho_\alpha(\mathbf{r}) = \sum_{i=1}^{N_\alpha} |\varphi_{i\alpha}(\mathbf{r})|^2 \quad (\alpha = \uparrow, \downarrow), \tag{8.7.4.23}$$

where $\varphi_{i\alpha}(\mathbf{r})$ is an occupied orbital for a given spin state of the electron.

If the ground state is described by a correlated electron model (mixture of different configurations), the one-particle reduced density matrix can still be analysed in terms of its eigenvectors $\psi_{i\alpha}$ and eigenvalues $n_{i\alpha}$ (natural spin orbitals and natural occupancies), as described by the expression

$$\rho_\alpha(\mathbf{r}) = \sum_{i=1}^{\infty} n_{i\alpha} |\psi_{i\alpha}(\mathbf{r})|^2, \tag{8.7.4.24}$$

where $\langle \psi_{i\alpha} | \psi_{j\beta} \rangle = \delta_{ij}\delta_{\alpha\beta}$, since the natural spin orbitals form an orthonormal set, and

$$n_{i\alpha} \leq 1 \quad \sum_{i=1}^{\infty} n_{i\alpha} = n_\alpha. \tag{8.7.4.25}$$

As the quantization axis is arbitrary, (8.7.4.20) can be generalized to

$$\mathbf{m}_s(\mathbf{r}) = \hat{\mathbf{S}} s(\mathbf{r}). \tag{8.7.4.26}$$

Equation (8.7.4.26) expresses the proportionality of the spin-magnetization density to the normalized spin density function.

8.7.4.3.2. *Thermally averaged spin-only magnetization density*

The system is now assumed to be at a given temperature T. S remains a good quantum number, but all (SM_S) states ($M_S = -S, \ldots, S$) are now populated according to Boltzmann statistics. We are interested in the thermal equilibrium spin-magnetization density:

$$\mathbf{m}_s(\mathbf{r}) = \sum_{M_S=-S}^{+S} p(M_S) \langle \psi_{SM_S} | \hat{\mathbf{m}}_s | \psi_{SM_S} \rangle, \tag{8.7.4.27}$$

where $p(M_S)$ is the population of the M_S state. The operator $\hat{\mathbf{m}}_s$ fulfils the requirements to satisfy the Wigner–Eckart theorem (Condon & Shortley, 1935), which states that, within the S manifold, all matrix elements of $\hat{\mathbf{m}}_s$ are proportional to $\hat{\mathbf{S}}$. The consequence of this remarkable property is that

$$\langle\psi_{SM_S}|\hat{\mathbf{m}}_s|\psi_{SM_S}\rangle = \langle\psi_{SM_S}|\hat{\mathbf{S}}|\psi_{SM_S}\rangle f_S(\mathbf{r}), \tag{8.7.4.28}$$

where $f_S(\mathbf{r})$ is a function that depends on S, but not on M_S. Comparison with (8.7.4.26) shows that $f_S(\mathbf{r})$ is the normalized spin-density function $s(\mathbf{r})$, which therefore is an invariant for the S manifold [$s(\mathbf{r})$ is calculated as the normalized spin density for any M_S]. Expression (8.7.4.27) can thus be written as

$$\mathbf{m}_s(\mathbf{r}) = \langle\mathbf{S}\rangle s(\mathbf{r}), \tag{8.7.4.29}$$

where $\langle\mathbf{S}\rangle$ is the expected value for the total spin, at a given temperature and under a given external field. As $s(\mathbf{r})$ is normalized, the total moment of the system is

$$\boldsymbol{\mu}_S = \langle\mathbf{S}\rangle.$$

The behaviour of $\langle\mathbf{S}\rangle$ is governed by the usual laws of magnetism: it can be measured by macroscopic techniques. In paramagnetic species, it will vary as T^{-1} to a first approximation; unless the system is studied at very low temperatures, the value of $\langle\mathbf{S}\rangle$ will be very small. The dependence of $\langle\mathbf{S}\rangle$ on temperature and orienting field is crucial.

Finally, (8.7.4.29) has to be averaged over vibrational modes. Except for the case where there is strong magneto-vibrational interaction, only $s(\mathbf{r})$ is affected by thermal atomic motion. This effect can be described in terms similar to those used for the charge density (Subsection 8.7.3.7).

The expression (8.7.4.29) is very important and shows that the microscopic spin-magnetization density carries two types of information: the nature of spin ordering in the system, described by $\langle\mathbf{S}\rangle$, and the delocalized nature of the electronic ground state, represented by $s(\mathbf{r})$.

8.7.4.3.3. *Spin density for an assembly of localized systems*

A complex magnetic system can generally be described as an ensemble of well defined interacting open-shell subsystems (ions or radicals), where each subsystem has a spin $\hat{\mathbf{S}}_n$, and S_n^2 is assumed to be a good quantum number. The magnetic interaction occurs essentially through exchange mechanisms that can be described by the Heisenberg Hamiltonian:

$$\mathcal{H} = -\sum_{n<m} J_{nm}\,\hat{\mathbf{S}}_n \cdot \hat{\mathbf{S}}_m - \sum_n \mathbf{B}_0 \cdot \mathbf{S}_n, \tag{8.7.4.30}$$

where J_{nm} is the exchange coupling between two subsystems, and $\mathbf{B}_0$ an applied external field (magneto-crystalline anisotropic effects may have to be added). Expression (8.7.4.30) is the basis for the understanding of magnetic ordering and phase diagrams. The interactions lead to a local field $\mathbf{B}_n$, which is the effective orienting field for the spin $\mathbf{S}_n$.

The expression for the spin-magnetization density is

$$\mathbf{m}_s(\mathbf{r}) = \sum_n \langle\mathbf{S}_n\rangle s_n(\mathbf{r}). \tag{8.7.4.31}$$

The relative arrangement of $\langle\mathbf{S}_n\rangle$ describes the magnetic structure; $s_n(\mathbf{r})$ is the normalized spin density of the nth subsystem.

In some metallic systems, at least part of the unpaired electron system cannot be described within a localized model: a band-structure description has to be used (Lovesey, 1984). This is the case for transition metals like Ni, where the spin-magnetization density is written as the sum of a localized part [described by (8.7.4.31)] and a delocalized part [described by (8.7.4.29)].

8.7.4.3.4. *Orbital magnetization density*

We must now address the case where the orbital moment is not quenched. In that case, there is some spin-orbit coupling, and the description of the magnetization density becomes less straightforward.

The magnetic moment due to the angular momentum $\mathbf{l}_j$ of the electron is $\frac{1}{2}\mathbf{l}_j$ (in units of $2\mu_B$). As $\mathbf{l}_j$ does not commute with the position $\mathbf{r}_j$, orbital magnetization density is defined as

$$\mathbf{m}_L(\mathbf{r}) = \tfrac{1}{4}\left\langle \sum_j \{\mathbf{l}_j\,\delta(\mathbf{r}-\mathbf{r}_j) + \delta(\mathbf{r}-\mathbf{r}_j)\mathbf{l}_k\} \right\rangle. \tag{8.7.4.32}$$

If $\mathbf{L}$ is the total orbital moment,

$$\mathbf{L} = \sum_j \mathbf{l}_j. \tag{8.7.4.33}$$

Only open shells contribute to the orbital moment. But, in general, neither $\mathbf{L}^2$ nor $\mathbf{L}_z$ are constants of motion. There is, however, an important exception, when open-shell electrons can be described as localized around atomic centres. This is the case for most rare-earth compounds, for which the 4*f* electrons are too close to the nuclei to lead to a significant interatomic overlap. It can also be a first approximation for the *d* electrons in transition-metal ions. Spin-orbit coupling will be present, and thus only $\mathbf{L}^2$ will be a constant of motion. One may define the total angular momentum

$$\mathbf{J} = \mathbf{L} + \mathbf{S} \tag{8.7.4.34}$$

and $\{J^2, L^2, S^2, J_z\}$ become the four constants of motion.

Within the J manifold of the ground state, $\mathbf{m}_s(\mathbf{r})$ and $\mathbf{m}_L(\mathbf{r})$ do not, in general, fulfil the conditions for the Wigner–Eckart theorem (Condon & Shortley, 1935), which leads to a very complex description of $\mathbf{m}(\mathbf{r})$ in practical cases.

However, the Wigner–Eckart theorem can be applied to the magnetic moments themselves, leading to

$$\mathbf{L} + 2\mathbf{S} = g\mathbf{J}, \tag{8.7.4.35}$$

with the Lande factor

$$g = 1 + \frac{J(J+1) - L(L+1) + S(S+1)}{2J(J+1)} \tag{8.7.4.36}$$

and, equivalently,

$$\begin{aligned} \mathbf{S} &= (g-1)\mathbf{J} \\ \mathbf{L} &= (2-g)\mathbf{J}. \end{aligned} \tag{8.7.4.37}$$

The influence of spin–orbit coupling on the scattering will be discussed in Subsection 8.7.4.5.

8.7.4.4. *Probing spin densities by neutron elastic scattering*

8.7.4.4.1. *Introduction*

The magnetic structure factor $F_M(\mathbf{h})$ [equation (8.7.4.4)] depends on the spin state of the neutron. Let $\boldsymbol{\lambda}$ be the unit vector defining a quantization axis for the neutron, which can be either parallel ($\uparrow$) or antiparallel ($\downarrow$) to $\boldsymbol{\sigma}$. If $I_{\sigma\sigma'}$ stands for the cross section where the incident neutron has the polarization σ and the scattered neutron the polarization σ', one obtains the following basic expressions:

$$\begin{aligned} I_{\uparrow\uparrow} &= |F_n + \boldsymbol{\lambda}\cdot\mathbf{Q}|^2 \\ I_{\downarrow\downarrow} &= |F_n - \boldsymbol{\lambda}\cdot\mathbf{Q}|^2 \\ I_{\uparrow\downarrow} &= I_{\downarrow\uparrow} = |\boldsymbol{\lambda}\times\mathbf{Q}|^2. \end{aligned} \tag{8.7.4.38}$$

If no analysis of the spin state of the scattered beam is made, the two measurable cross sections are

$$I_\uparrow = I_{\uparrow\uparrow} + I_{\uparrow\downarrow}$$
$$I_\downarrow = I_{\downarrow\downarrow} + I_{\downarrow\uparrow}, \qquad (8.7.4.39)$$

which depend only on the polarization of the incident neutron.

8.7.4.4.2. *Unpolarized neutron scattering*

If the incident neutron beam is not polarized, the scattering cross section is given by

$$I = \tfrac{1}{2}[I_\uparrow + I_\downarrow] = |F_N|^2 + |\mathbf{Q}|^2. \qquad (8.7.4.40)$$

Magnetic and nuclear contributions are simply additive. With $x = Q/F_N$, one obtains

$$I = |F_N|^2[1 + |x|^2]. \qquad (8.7.4.41)$$

Owing to its definition, $|x|$ can be of the order of 1 if and only if the atomic moments are ordered close to saturation (as in the ferro- or antiferromagnets). In many situations of structural and chemical interest, $|x|$ is small.

If, for example, $|x| \sim 0.05$, the magnetic contribution in (8.7.4.41) is only 0.002 of the total intensity. Weak magnetic effects, such as occur for instance in paramagnets, are thus hardly detectable with unpolarized neutron scattering.

However, if the magnetic structure does not have the same periodicity as the crystalline structure, magnetic components in (8.7.4.40) occur at scattering vectors for which the nuclear contribution is zero. In this case, the unpolarized technique is of unique interest. Most phase diagrams involving antiferromagnetic or helimagnetic order and modulations of such ordering are obtained by this method.

8.7.4.4.3. *Polarized neutron scattering*

It is generally possible to polarize the incident beam by using as a monochromator a ferromagnetic alloy, for which at a given Bragg angle $I_\downarrow(\text{monochromator}) = 0$, because of a cancellation of nuclear and magnetic scattering components. The scattered-beam intensity is thus $I_\uparrow$. By using a radio-frequency (r.f.) coil tuned to the Larmor frequency of the neutron, the neutron spin can be flipped into the ($\downarrow$) state for which the scattered beam intensity is $I_\downarrow$. This allows measurement of the 'flipping ratio' $R(\mathbf{h})$:

$$R(\mathbf{h}) = \frac{I_\uparrow(\mathbf{h})}{I_\downarrow(\mathbf{h})}. \qquad (8.7.4.42)$$

As the two measurements are made under similar conditions, most systematic effects are eliminated by this technique, which is only applicable to cases where both F_N and F_M occur at the same scattering vectors. This excludes any antiferromagnetic type of ordering.

The experimental set-up is discussed by Forsyth (1980).

8.7.4.4.4. *Polarized neutron scattering of centrosymmetric crystals*

If $\boldsymbol{\lambda}$ is assumed to be in the vertical Oz direction, $\mathbf{M}(\mathbf{h})$ will in most situations be aligned along Oz by an external orienting field. If α is the angle between $\mathbf{M}$ and $\mathbf{h}$, and

$$x = \frac{r_0 M(\mathbf{h})}{F_N(\mathbf{h})}, \qquad (8.7.4.43)$$

with F_N expressed in the same units as r_0, one obtains, for centrosymmetric crystals,

$$R = \frac{1 + 2x\sin^2\alpha + x^2\sin^2\alpha}{1 - 2x\sin^2\alpha + x^2\sin^2\alpha}. \qquad (8.7.4.44)$$

If $x \ll 1$,

$$R \sim 1 + 4x\sin^2\alpha. \qquad (8.7.4.45)$$

For $x \sim 0.05$ and $\alpha = \pi/2$, R now departs from 1 by as much as 20%, which proves the enormous advantage of polarized neutron scattering in the case of low magnetism.

Equation (8.7.4.44) can be inverted, and x and its sign can be obtained directly from the observation. However, in order to obtain $M(\mathbf{h})$, the nuclear structure factor $F_N(\mathbf{h})$ must be known, either from nuclear scattering or from a calculation. All systematic errors that affect $F_N(\mathbf{h})$ are transferred to $M(\mathbf{h})$.

For two reasons, it is not in general feasible to access all reciprocal-lattice vectors. First, in order to have reasonable statistical accuracy, only reflections for which both $I_\uparrow$ and $I_\downarrow$ are large enough are measured; *i.e.* reflections having a strong nuclear structure factor. Secondly, $\sin\alpha$ should be as close to 1 as possible, which may prevent one from accessing all directions in reciprocal space. If $\mathbf{M}$ is oriented along the vertical axis, the simplest experiment consists of recording reflections with $\mathbf{h}$ in the horizontal plane, which leads to a projection of $\mathbf{m}(\mathbf{r})$ in real space. When possible, the sample is rotated so that other planes in the reciprocal space can be recorded.

Finally, if $\alpha = \pi/2$, $I_{\uparrow\downarrow}$ vanishes, and neutron spin is conserved in the experiment.

8.7.4.4.5. *Polarized neutron scattering in the noncentrosymmetric case*

If the space group is noncentrosymmetric, both F_N and M have a phase, φ_N and φ_M, respectively.

If for simplicity one assumes $\alpha = \pi/2$, and, defining $\delta = \varphi_M - \varphi_N$,

$$R = \frac{1 + |x|^2 + 2|x|\cos\delta}{1 + |x|^2 - 2|x|\cos\delta}, \qquad (8.7.4.46)$$

which shows that $|x|$ and δ cannot both be obtained from the experiment.

The noncentrosymmetric case can only be solved by a careful modelling of the magnetic structure factor as described in Subsection 8.7.4.5.

In practice, neither the polarization of the incident beam nor the efficiency of the r.f. flipping coil is perfect. This leads to a modification in the expression for the flipping ratios [see Section 6.1.3 or Forsyth (1980)].

8.7.4.4.6. *Effect of extinction*

Since most measurements correspond to strong nuclear structure factors, extinction severely affects the observed data. To a first approximation, one may assume that both $I_{\uparrow\uparrow}$ and $I_{\downarrow\downarrow}$ will be affected by this process, though the spin-flip processes $I_{\uparrow\downarrow}$ and $I_{\downarrow\uparrow}$ are not. If $y_{\uparrow\uparrow}$ and $y_{\downarrow\downarrow}$ are the associated extinction factors, the observed flipping ratio is

$$R_{\text{obs}} \sim \frac{I_{\uparrow\uparrow}y_{\uparrow\uparrow} + I_{\uparrow\downarrow}}{I_{\downarrow\downarrow}y_{\downarrow\downarrow} + I_{\uparrow\downarrow}}, \qquad (8.7.4.47)$$

where the expressions for $y_{\uparrow\uparrow,\downarrow\downarrow}$ are given elsewhere (Bonnet, Delapalme, Becker & Fuess, 1976).

It should be emphasized that, even in the case of small magnetic structure factors, extinction remains a serious problem since, even though $y_{\uparrow\uparrow}$ and $y_{\downarrow\downarrow}$ may be very close to each other,

so are $I_{\uparrow\uparrow}$ and $I_{\downarrow\downarrow}$. An incorrect treatment of extinction may entirely bias the estimate of x.

8.7.4.4.7. *Error analysis*

In the most general case, it is not possible to obtain x, and thus $M(\mathbf{h})$ directly from R. Moreover, it is unlikely that all Bragg spots within the reflection sphere could be measured. Modelling of $\mathbf{M}(\mathbf{h})$ is thus of crucial importance. The analysis of data must proceed through a least-squares routine fitting $R_{\rm calc}$ to $R_{\rm obs}$, minimizing the error function

$$\varepsilon = \sum_{\substack{\mathbf{h}\\ \text{observed}}} \frac{1}{\sigma^2(R)} [R_{\rm obs}(\mathbf{h}) - R_{\rm calc}(\mathbf{h})]^2, \tag{8.7.4.48}$$

where $R_{\rm calc}$ corresponds to a model and $\sigma^2(R)$ is the standard uncertainty for R.

If the same counting time for $I_\uparrow$ and for $I_\downarrow$ is assumed, only the counting statistical error may be considered important in the estimate of R, as most systematic effects cancel. In the simple case where $\alpha = \pi/2$, and the structure is centrosymmetric, a straightforward calculation leads to

$$\frac{\sigma^2(x)}{x^2} = \frac{\sigma^2(R)}{R^2} \frac{R}{(R-1)^2}; \tag{8.7.4.49}$$

with

$$\frac{\sigma^2(R)}{R^2} \sim \frac{1}{I_\uparrow} + \frac{1}{I_\downarrow}, \tag{8.7.4.50}$$

one obtains the result

$$\frac{\sigma^2(x)}{x^2} = \tfrac{1}{8} \frac{(F_N^2 + M^2)}{(F_N M)^2}. \tag{8.7.4.51}$$

In the common case where $x \ll 1$, this reduces to

$$\frac{\sigma^2(x)}{x^2} \sim \tfrac{1}{8} \frac{1}{M^2} = \frac{1}{8F_N^2} \frac{1}{x^2}. \tag{8.7.4.52}$$

In addition to this estimate, care should be taken of extinction effects.

The real interest is in $M(\mathbf{h})$, rather than x:

$$\frac{\sigma^2(M)}{M^2} = \frac{\sigma^2(x)}{x^2} + \frac{\sigma^2(F_N)}{F_N^2}. \tag{8.7.4.53}$$

If F_N is obtained by a nuclear neutron scattering experiment,

$$\sigma^2(F_N) \sim a + bF_N^2,$$

where a accounts for counting statistics and b for systematic effects.

The first term in (8.7.4.53) is the leading one in many situations. Any systematic error in F_N can have a dramatic effect on the estimate of $M(\mathbf{h})$.

8.7.4.5. *Modelling the spin density*

In this subsection, the case of spin-only magnetization is considered. The modelling of $\mathbf{m}_s(\mathbf{r})$ is very similar to that of the charge density.

8.7.4.5.1. *Atom-centred expansion*

We first consider the case where spins are localized on atoms or ions, as it is to a first approximation for compounds involving transition-metal atoms. The magnetization density is expanded as

$$\mathbf{m}_S(\mathbf{r}) = \sum_j \langle \mathbf{S}_j \rangle \, \langle s_j(\mathbf{r} - \mathbf{R}_j) \rangle, \tag{8.7.4.54}$$

where $\langle \mathbf{S}_j \rangle$ is the spin at site j, and $\langle s_j \rangle$ the thermally averaged normalized spin density $f_j(\mathbf{h})$, the Fourier transform of $s_j(\mathbf{r})$, is known as the 'magnetic form factor'. Thus,

$$\mathbf{M}(\mathbf{h}) = \sum_j \langle \mathbf{S}_j \rangle \, f_j(\mathbf{h}) \, T_j \exp(2\pi \mathbf{h} \cdot \mathbf{R}_j), \tag{8.7.4.55}$$

where T_j and $\mathbf{R}_j$ are the Debye–Waller factor and the equilibrium position of the jth site, respectively.

Most measurements are performed at temperatures low enough to ensure a fair description of T_j at the harmonic level (Coppens, 1992). T_j represents the vibrational relaxation of the open-shell electrons and may, in some situations, be different from the Debye–Waller factor of the total charge density, though at present no experimental evidence to this effect is available.

8.7.4.5.1.1. *Spherical-atom model*

In the crudest model, $s_j(\mathbf{r})$ is approximated by its spherical average. If the magnetic electrons have a wavefunction radial dependence represented by the radial function $U(r)$, the magnetic form factor is given by

$$f(h) = \int_0^\infty U^2(r) 4\pi r^2 \, \mathrm{d}r j_0(2\pi hr) = \langle j_0 \rangle, \tag{8.7.4.56}$$

where j_0 is the zero-order spherical Bessel function. For free atoms and ions, these form factors can be found in *IT* IV (1974).

One of the important features of magnetic neutron scattering is the fact that, to a first approximation, closed shells do not contribute to the form factor. Thus, it is a unique probe of the electronic structure of heavy elements, for which theoretical calculations even at the atomic level are questionable. Relativistic effects are important. Theoretical relativistic form factors can be used (Freeman & Desclaux, 1972; Desclaux & Freeman, 1978). It is also possible to parametrize the radial behaviour of U. A single contraction-expansion model [κ refinement, expression (8.7.3.6)] is easy to incorporate.

8.7.4.5.1.2. *Crystal-field approximation*

Crystal-field effects are generally of major importance in spin magnetism and are responsible for the spin state of the ions, and thus for the ground-state configuration of the system. Thus, they have to be incorporated in the model.

Taking the case of a transition-metal compound, and neglecting small contributions that may arise from spin polarization in the closed shells (see Subsections 8.7.4.9 and 8.7.4.10), the normalized spin density can be written by analogy with (8.7.3.76) as

$$s(\mathbf{r}) = \sum_{i=1}^{5} \sum_{j \geq i}^{5} D_{ij} \, d_i(\mathbf{r}) d_j(\mathbf{r}), \tag{8.7.4.57}$$

where D_{ij} is the normalized spin population matrix. If $\rho_{d\uparrow}$ and $\rho_{d\downarrow}$ are the densities of a given spin,

$$s(\mathbf{r}) = \frac{\rho_{d\uparrow} - \rho_{d\downarrow}}{n_\uparrow - n_\downarrow}, \tag{8.7.4.58}$$

the d-type charge density is

$$\rho_d(\mathbf{r}) = \rho_{d\uparrow} + \rho_{d\downarrow} \tag{8.7.4.59}$$

and is expanded in a similar way to $s(\mathbf{r})$ [see (8.7.3.76)],

$$\rho_d(\mathbf{r}) = \sum_i \sum_{j \geq i} P_{ij} d_i d_j; \tag{8.7.4.60}$$

writing

$$\rho_{d\sigma} = \sum P_{ij}^{\sigma} d_i d_j \tag{8.7.4.61}$$

with $\sigma = \uparrow$ and $\downarrow$, one obtains

$$\begin{aligned} P_{ij} &= P_{ij}^{\uparrow} + P_{ij}^{\downarrow} \\ D_{ij} &= (P_{ij}^{\uparrow} - P_{ij}^{\downarrow})/(n_{\uparrow} - n_{\downarrow}). \end{aligned} \tag{8.7.4.62}$$

Similarly to $\rho_d(\mathbf{r})$, $s(r)$ can be expanded as

$$s(\mathbf{r}) = U^2(r) \sum_{l=0}^{4} \sum_{m=0}^{l} \sum_{p} D_{lmp}\, y_{lmp}(\theta, \varphi), \tag{8.7.4.63}$$

where $U(r)$ describes the radial dependence. Spin polarization leads to a further modification of this expression. Since the numbers of electrons of a given spin are different, the exchange interaction is different for the two spin states, and a spin-dependent effective screening occurs. This leads to

$$\rho_{d\sigma}(\mathbf{r}) = \kappa_{\sigma}^3 U^2(\kappa_{\sigma} r) \sum_{lmp} P_{lmp}^{\sigma}\, y_{lmp}, \tag{8.7.4.64}$$

with $\sigma = \uparrow$ or $\downarrow$, where two κ parameters are needed.

The complementarity between charge and spin density in the crystal field approximation is obvious. At this particular level of approximation, expansions are exact and it is possible to estimate d-orbital populations for each spin state.

8.7.4.5.1.3. *Scaling of the spin density*

The magnetic structure factor is scaled to $F_N(\mathbf{h})$. Whether the nuclear structure factors are calculated from refined structural parameters or obtained directly from a measurement, their scale factor is not rigorously fixed.

As a result, it is not possible to obtain absolute values of the effective spins $\langle \mathbf{S}_n \rangle$ from a magnetic neutron scattering experiment. It is necessary to scale them through the sum rule

$$\sum_{n} \langle \mathbf{S}_n \rangle = \boldsymbol{\mu}, \tag{8.7.4.65}$$

where $\boldsymbol{\mu}$ is the macroscopic magnetization of the sample.

The practical consequences of this constraint for a refinement are similar to the electroneutrality constraint in charge-density analysis (§8.7.3.3.1).

8.7.4.5.2. *General multipolar expansion*

In this subsection, the localized magnetism picture is assumed to be valid. However, each subunit can now be a complex ion or a radical. Covalent interactions must be incorporated.

If $\chi_{\mu}(\mathbf{r})$ are atomic basis functions, the spin density $s(\mathbf{r})$ can always be written as

$$s(\mathbf{r}) = \sum_{\mu} \sum_{\nu} D_{\mu\nu} \chi_{\mu}(\mathbf{r} - \mathbf{R}_{\mu}) \chi_{\nu}(\mathbf{r} - \mathbf{R}_{\nu}), \tag{8.7.4.66}$$

an expansion that is similar to (8.7.3.9) for the charge density.

To a first approximation, only the basis functions that are required to describe the open shell have to be incorporated, which makes the expansion simple and more flexible than for the charge density.

As for the charge density, it is possible to project (8.7.4.66) onto the various sites of the ion or molecule by a multipolar expansion:

$$\begin{aligned} s(\mathbf{r}) &\sim \sum_{j} s_j(\mathbf{r} - \mathbf{R}_j) * P_j(\mathbf{R}_j), \\ s_j(\mathbf{r}) &= \sum_{j} \kappa_j^3 R_{lj}(\kappa_j r) \sum_{m} \sum_{p} D_{jlmp}\, y_{lmp}. \end{aligned} \tag{8.7.4.67}$$

$P(\mathbf{R}_j)$ is the vibrational p.d.f. of the jth atom, which implies use of the convolution approximation.

The monopolar terms D_{j00} give an estimate of the amount of spin transferred from a central metal ion to the ligands, or of the way spins are shared among the atoms in a radical.

The constraint (8.7.4.65) becomes

$$\sum_{n} \langle \mathbf{S}_n \rangle \sum_{j} D_{j00}^{(n)} = \boldsymbol{\mu}, \tag{8.7.4.68}$$

where (n) refers to the various subunits in the unit cell. Expansion (8.7.4.67) is the key for solving noncentrosymmetric magnetic structure (Boucherle, Gillon, Maruani & Schweizer, 1982).

8.7.4.5.3. *Other types of model*

One may wish to take advantage of the fact that, to a good approximation, only a few molecular orbitals are involved in $s(\mathbf{r})$. In an independent particle model, one expands the relevant orbitals in terms of atomic basis functions (LCAO):

$$\varphi_{i\sigma} = \sum_{\mu} c_{i\mu}^{\sigma} \chi_{\mu}^{\sigma}(\mathbf{r} - \mathbf{R}_{\mu}) \tag{8.7.4.69}$$

with $\sigma = \uparrow$ or $\downarrow$, and the spin density is expanded according to (8.7.4.21) and (8.7.4.23). Fourier transform of two centre-term products is required. Details can be found in Forsyth (1980) and Tofield (1975).

In the case of extended solids, expansion (8.7.4.69) must refer to the total crystal, and therefore incorporate translational symmetry (Brown, 1986).

Finally, in the simple systems such as transition metals, like Ni, there is a d–s type of interaction, leading to some contribution to the spin density from delocalized electrons (Mook, 1966). If s_l and s_d are the localized and delocalized parts of the density, respectively,

$$s(\mathbf{r}) = a s_l(\mathbf{r}) + [1 - a] s_d(\mathbf{r}), \tag{8.7.4.70}$$

where a is the fraction of localized spins. $s_d(\mathbf{r})$ can be modelled as being either constant or a function with a very small number of Fourier adjustable coefficients.

8.7.4.6. *Orbital contribution to the magnetic scattering*

$Q_L(\mathbf{h})$ is given by (8.7.4.10) and (8.7.4.12). Since $\nabla\psi$ in (8.7.4.11) does not play any role in the scattering cross section, we can use the restriction

$$\mathbf{j}(\mathbf{r}) = \nabla \times \mathbf{m}_L(\mathbf{r}), \tag{8.7.4.71}$$

where $\mathbf{m}_L(\mathbf{r})$ is defined to an arbitrary gradient. It is possible to constrain $\mathbf{m}_L(\mathbf{r})$ to have the form

$$\mathbf{m}_L(\mathbf{r}) = \hat{\mathbf{r}} \times \mathbf{v}(\mathbf{r}),$$

since any radial component could be considered as the radial component of a gradient. With spherical coordinates, (8.7.4.71) becomes

$$\mathbf{j} = -\frac{1}{r} \frac{\partial}{\partial r} [r\mathbf{v}],$$

which can be integrated as

$$\mathbf{r} \times \mathbf{v} = -\int_{r}^{\infty} y \hat{\mathbf{r}} \times \mathbf{j}(y\hat{\mathbf{r}})\, \mathrm{d}y;$$

one finally obtains

$$\mathbf{m}_L(\mathbf{r}) = \frac{1}{r} \int_{y=r}^{y=\infty} \hat{\mathbf{r}} y \times \mathbf{j}(\hat{\mathbf{r}} y)\, \mathrm{d}y. \tag{8.7.4.72}$$

With $f(x)$ defined by

$$f(x) = -\frac{1}{x^2}\int_0^{ix} tl^t\,\mathrm{d}t, \qquad (8.7.4.73)$$

the expression for $\mathbf{M}_L(\mathbf{h})$ is obtained by Fourier transformation of (8.7.4.72):

$$M_L(\mathbf{h}) = \tfrac{1}{2}\int \mathbf{r}\times\mathbf{j}(\mathbf{r}) f(\mathbf{h}\cdot\mathbf{r})\,\mathrm{d}\mathbf{r},$$

which leads to

$$\mathbf{M}_L(\mathbf{h}) = \tfrac{1}{4}\left\langle \sum_j \left\{ \mathbf{l}_j f(2\pi\mathbf{h}\cdot\mathbf{r}_j) + f(2\pi\mathbf{h}\cdot\mathbf{r}_j)\mathbf{l}_j \right\} \right\rangle \qquad (8.7.4.74)$$

by using the definition (8.7.4.9) of $\mathbf{j}$.

This expression clearly shows the connection between orbital magnetism and the orbital angular momentum of the electrons. It is of general validity, whatever the origin of orbital magnetism.

Since $f(0) = 1$,

$$\mathbf{M}_L(0) = \tfrac{1}{2}\langle\mathbf{L}\rangle, \qquad (8.7.4.75)$$

as expected.

8.7.4.6.1. *The dipolar approximation*

The simplest approximation involves decomposing $\mathbf{j}(\mathbf{r})$ into atomic contributions:

$$\mathbf{j}(\mathbf{r}) = \sum_n \mathbf{j}_n(\mathbf{r}-\mathbf{R}_n). \qquad (8.7.4.76)$$

One obtains

$$\mathbf{M}_L = \sum_n \mathbf{M}_{L,n}(\mathbf{h}) \exp(2\pi i\mathbf{h}\cdot\mathbf{R}_n). \qquad (8.7.4.77)$$

$\mathbf{M}_{L,n}(\mathbf{h})$ is the atomic magnetic orbital structure factor.

We notice that $f(2\pi\mathbf{h}\cdot\mathbf{r})$ as defined in (8.7.4.73) can be expanded as

$$f(2\pi\mathbf{h}\cdot\mathbf{r}) = 4\pi\sum_l\sum_m (i)^l \gamma_l(2\pi hr)\, Y_{lm}(\hat{r})\, Y^*_{lm}(\hat{h}), \qquad (8.7.4.78)$$

where

$$\gamma_l(x) = \frac{2}{x^2}\int_0^x tj_l(t)\,\mathrm{d}t. \qquad (8.7.4.79)$$

j_l is a spherical Bessel function of order l, and Y_{lm} are the complex spherical harmonic functions.

If one considers only the spherically symmetric term in (8.7.4.78), one obtains the 'dipolar approximation', which gives

$$\mathbf{M}^D_{L,n} = \tfrac{1}{2}\langle\mathbf{L}_n\rangle\langle\gamma_{0n}\rangle, \qquad (8.7.4.80)$$

with

$$\langle\gamma_{0n}\rangle = \int_0^\infty 4\pi r^2 U_n^2(r)\gamma_0(2\pi hr)\,\mathrm{d}r,$$

and

$$\gamma_0(x) = \frac{2}{x^2}(1-\cos x). \qquad (8.7.4.81)$$

$U_n(r)$ is the radial function of the atomic electrons whose orbital momentum is unquenched. Thus, in the dipolar approximation, the atomic orbital scattering is proportional to the effective orbital angular momentum and therefore to the orbital part of the magnetic dipole moment of the atom.

Within the same level of approximation, the spin structure factor is

$$\mathbf{M}_S = \sum_n \mathbf{M}_{S,n}(\mathbf{h}) \exp(2\pi i\mathbf{h}\cdot\mathbf{R}_n), \qquad (8.7.4.82)$$

with

$$\mathbf{M}_{S,n}(\mathbf{h}) = \langle\mathbf{S}_\mathbf{n}\rangle\langle j_{0n}\rangle,$$

and

$$\langle j_{0n}\rangle = \int_0^\infty 4\pi r^2 U_n^2(r) j_0(2\pi hr)\,\mathrm{d}r.$$

Finally, the atomic contribution to the total magnetic structure factor is

$$\mathbf{M}^D_n = \langle\mathbf{S}_n\rangle\langle j_{0n}\rangle + \tfrac{1}{2}\langle\mathbf{L}_n\rangle\langle\gamma_{0n}\rangle. \qquad (8.7.4.83)$$

If $\langle\mathbf{J}_n\rangle$ is the total angular momentum of atom n and g_n its gyromagnetic ratio, (8.7.4.35)–(8.7.4.37) lead to:

$$\mathbf{M}^D_n = \langle\mathbf{J}_n\rangle\left\{[g_n-1]\langle j_{0n}\rangle + \frac{2-g_n}{2}\langle\gamma_{0n}\rangle\right\}. \qquad (8.7.4.84a)$$

Another approach, which is applicable only to the atomic case, is often used, which is based on Racah's algebra (Marshall & Lovesey, 1971). At the dipolar approximation level, it leads to a slightly different result, according to which $\langle\gamma_{0n}\rangle$ is replaced by

$$\langle\gamma_{0n}\rangle \sim \langle j_{0n}\rangle + \langle j_{2n}\rangle. \qquad (8.7.4.85)$$

The two results are very close for small $\mathbf{h}$ where the dipolar approximation is correct. With (8.7.4.35)–(8.7.4.37), (8.7.4.84*a*) can also be written as

$$\mathbf{M}^D_n = \mathbf{M}^D_{S,n} + \langle\mathbf{S}_n\rangle\frac{2-g_n}{2(g_n-1)}\langle\gamma_{0n}\rangle, \qquad (8.7.4.84b)$$

where the second term is the 'orbital correction'. Its magnitude clearly depends on the difference between g_n and 2, which is small in 3*d* elements but can become important for rare earths.

8.7.4.6.2. *Beyond the dipolar approximation*

Expressions (8.7.4.74) and (8.7.4.78) are valid in any situation where orbital scattering occurs. They can in principle be used to estimate from the diffraction experiment the contribution of a few configurations that interact due to the $\mathbf{L}\cdot\mathbf{S}$ operator. In delocalized situations, (8.7.4.74) is the most suitable approach, while Racah's algebra can only be applied to one-centre cases.

8.7.4.6.3. *Electronic structure of rare-earth elements*

When covalency is small, the major aims are the determination of the ground state of the rare-earth ion, and the amount of delocalized magnetization density *via* the conduction electrons.

The ground state $|\psi\rangle$ of the ion is written as

$$|\psi\rangle = \sum_M a_M|JM\rangle, \qquad (8.7.4.86)$$

which is well suited for the Johnston (1966) and Marshall–Lovesey (1971) formulation in terms of general angular-momentum algebra. A multipolar expansion of spin and orbital components of the structure factor enables a determination of the expansion coefficient a_M (Schweizer, 1980).

8.7.4.7. *Properties derivable from spin densities*

The derivation of electrostatic properties from the charge density was treated in Subsection 8.7.3.4. Magnetostatic properties can be derived from the spin-magnetization density $\mathbf{m}_s(\mathbf{r})$ using parallel expressions.

8.7.4.7.1. *Vector fields*

The vector potential field is defined as

$$\mathbf{A}(\mathbf{r}) = \int \frac{\mathbf{m}_s(\mathbf{r}') \times (\mathbf{r} - \mathbf{r}')}{|\mathbf{r} - \mathbf{r}'|^3} \, \mathrm{d}\mathbf{r}'. \quad (8.7.4.87)$$

In the case of a crystal, it can be expanded in Fourier series:

$$\mathbf{A}(\mathbf{r}) = \frac{2i}{V} \sum_{\mathbf{h}} \left\{ \frac{\mathbf{M}_S(\mathbf{h}) \times \mathbf{h}}{h^2} \right\} \exp(-2\pi i \mathbf{h} \cdot \mathbf{r}); \quad (8.7.4.88)$$

the magnetic field is simply

$$\begin{aligned} \mathbf{B}(\mathbf{r}) &= \boldsymbol{\nabla} \times \mathbf{A}(\mathbf{r}) \\ &= -\frac{4\pi}{V} \sum_{\mathbf{h}} \left[\frac{\mathbf{h} \times \mathbf{M}_S(\mathbf{h}) \times \mathbf{h}}{h^2} \right] \exp(-2\pi i \mathbf{h} \cdot \mathbf{r}). \end{aligned} \quad (8.7.4.89)$$

One notices that there is no convergence problem for the $\mathbf{h} = 0$ term in the $\mathbf{B}(\mathbf{r})$ expansion.

The magnetostatic energy, *i.e.* the amount of energy that is required to obtain the magnetization $\mathbf{m}_s$, is

$$\begin{aligned} E_{ms} &= -\tfrac{1}{2} \int_{\text{cell}} \mathbf{m}_s(\mathbf{r}) \cdot \mathbf{B}(\mathbf{r}) \, \mathrm{d}r \\ &= \frac{2\pi}{V} \sum_{\mathbf{h}} \frac{[\mathbf{M}_s(-\mathbf{h}) \times \mathbf{h}] \cdot [\mathbf{M}_S(\mathbf{h}) \times \mathbf{h}]}{h^2}. \end{aligned} \quad (8.7.4.90)$$

It is often interesting to look at the magnetostatics of a given subunit: for instance, in the case of paramagnetic species.

For example, the vector potential outside the magnetized system can be obtained in a similar way to the electrostatic potential (8.7.3.30):

$$\mathbf{A}(\mathbf{r}') = \int \frac{[\boldsymbol{\nabla} \times \mathbf{m}_S(\mathbf{r})]}{|\mathbf{r} - \mathbf{r}'|} \, \mathrm{d}\mathbf{r}. \quad (8.7.4.91)$$

If $r' \gg r$, $1/|\mathbf{r} - \mathbf{r}'|$ can be easily expanded in powers of $1/r'$, and $\mathbf{A}(\mathbf{r}')$ can thus be obtained in powers of $1/r'$. If $\mathbf{m}_s(\mathbf{r}) = \langle \mathbf{S} \rangle s(\mathbf{r})$,

$$\mathbf{A}(\mathbf{r}') = \langle \mathbf{S} \rangle \times \int \frac{\boldsymbol{\nabla} s(\mathbf{r})}{|\mathbf{r} - \mathbf{r}'|} \, \mathrm{d}\mathbf{r}. \quad (8.7.4.92)$$

8.7.4.7.2. *Moments of the magnetization density*

Among the various properties that are derivable from the delocalized spin density function, the dipole coupling tensor is of particular importance:

$$D_{nij}(\mathbf{R}_n) = \int s(\mathbf{r}) \frac{[3 r_{ni} r_{nj} - r_n^2 \delta_{ij}]}{r_n^5} \, \mathrm{d}\mathbf{r}, \quad (8.7.4.93)$$

where $\mathbf{R}_n$ is a nuclear position and $\mathbf{r}_n = \mathbf{r} - \mathbf{R}_n$. This dipolar tensor is involved directly in the hyperfine interaction between a nucleus with spin $\mathbf{I}_n$ and an electronic system with spin $\mathbf{s}$, through the interaction energy

$$\sum_{i,j} I_{ni} D_{nij} S_j. \quad (8.7.4.94)$$

This tensor is measurable by electron spin resonance for either crystals or paramagnetic species trapped in matrices. The complementarity with scattering is thus of strong importance (Gillon, Becker & Ellinger, 1983).

Computational aspects are the same as in the electric field gradient calculation, $\rho(\mathbf{r})$ being simply replaced by $s(\mathbf{r})$ (see Subsection 8.7.3.4).

8.7.4.8. *Comparison between theory and experiment*

Since it is a measure of the imbalance between the densities associated with the two spin states of the electron, the spin-density function is a probe that is very sensitive to the exchange forces in the system. In an independent-particle model (Hartree–Fock approximation), the exchange mean field potential involves exchange between orbitals with the same spin. Therefore, if the numbers of ↑ and ↓ spins are different, one expects $V_{\text{exch}}\uparrow$ to be different from $V_{\text{exch}}\downarrow$. The main consequence of this is the necessity to solve two different Fock equations, one for each spin state. This is known as the spin-polarization effect: starting from a paired orbital, a slight spatial decoupling arises from this effect, and closed shells do have a participation in the spin density.

It can be shown that this effect is hardly visible in the charge density, but is enhanced in the spin density.

Spin densities are a very good probe for calculations involving this spin-polarization effect: The unrestricted Hartree–Fock approximation (Gillon, Becker & Ellinger, 1983).

From a common spin-restricted approach, spin polarization can be accounted for by a mixture of Slater determinants (configuration interaction), where the configuration interaction is only among electrons with the same spin. There is also a correlation among electrons with different spins, which is more difficult to describe theoretically. There seems to be evidence for such effects from comparison of experimental and theoretical spin densities in radicals (Delley, Becker & Gillon, 1984), where the unrestricted Hartree–Fock approximation is not sufficient to reproduce experimental facts. In such cases, local-spin-density functional theory has revealed itself very satisfactorily. It seems to offer the most efficient way to include correlation effects in spin-density functions.

As noted earlier, analysis of the spin-density function depends more on modelling than that of the charge density. Therefore, in general, 'experimental' spin densities at static densities and the problem of theoretical averaging is minor here. Since spin density involves essentially outer-electron states, resolution in reciprocal space is less important, except for analysis of the polarization of the core electrons.

8.7.4.9. *Combined charge- and spin-density analysis*

Combined charge- and spin-density analysis requires performing X-ray and neutron diffraction experiments at the same temperature. Magnetic neutron experiments are often only feasible around 4 K, and such conditions are more difficult to achieve by X-ray diffraction. Even if the two experiments are to be performed at different temperatures, it is often difficult to identify compounds suitable for both experiments.

Owing to the common parametrization of $\rho(\mathbf{r})$ and $s(\mathbf{r})$, a combined least-squares-refinement procedure can be implemented, leading to a description of $\rho_\uparrow(\mathbf{r})$ and $\rho_\downarrow(\mathbf{r})$, the spin-dependent electron densities. Covalency parameters are obtainable together with spin polarization effects in the closed shells, by allowing $\rho_\uparrow$ and $\rho_\downarrow$ to have different radial behaviour.

Spin-polarization effects would be difficult to model from the spin density alone. But the arbitrariness of the modelling is strongly reduced if both ρ and s are analysed at the same time (Becker & Coppens, 1985; Coppens, Koritszansky & Becker, 1986).

8.7.4.10. *Magnetic X-ray scattering separation between spin and orbital magnetism*

8.7.4.10.1. *Introduction*

In addition to the usual Thomson scattering (charge scattering), there is a magnetic contribution to the X-ray amplitude (de Bergevin & Brunel, 1981; Blume, 1985; Brunel & de Bergvin, 1981; Blume & Gibbs, 1988). In units of the chemical radius r_e of the electron, the total scattering amplitude is

$$A_x = F_C + F_M, \tag{8.7.4.95}$$

where F_C is the charge contribution, and F_M the magnetic part.

Let $\hat{\boldsymbol{\varepsilon}}$ and $\hat{\boldsymbol{\varepsilon}}'$ be the unit vectors along the electric field in the incident and diffracted direction, respectively. $\mathbf{k}$ and $\mathbf{k}'$ denote the wavevectors for the incident and diffracted beams. With these notations,

$$F_C = F(\mathbf{h})\,\hat{\boldsymbol{\varepsilon}} \cdot \hat{\boldsymbol{\varepsilon}}', \tag{8.7.4.96}$$

where $F(\mathbf{h})$ is the usual structure factor, which was discussed in Section 8.7.3 [see also Coppens (1992)].

$$F_M = -i\,\frac{h\omega}{mc^2}\,\{\mathbf{M}_L(\mathbf{h}) \cdot \mathbf{A} + \mathbf{M}_S(\mathbf{h}) \cdot \mathbf{B}\}. \tag{8.7.4.97}$$

$\mathbf{M}_L$ and $\mathbf{M}_S$ are the orbital and spin-magnetization vectors in reciprocal space, and $\mathbf{A}$ and $\mathbf{B}$ are vectors that depend in a rather complicated way on the polarization and the scattering geometry:

$$\begin{aligned}\mathbf{A} &= 4\sin^2\theta\,\hat{\boldsymbol{\varepsilon}} \times \hat{\boldsymbol{\varepsilon}}' - (\hat{\mathbf{k}} + \hat{\boldsymbol{\varepsilon}})(\hat{\mathbf{k}} \cdot \hat{\boldsymbol{\varepsilon}}') + (\hat{\mathbf{k}}' \times \hat{\boldsymbol{\varepsilon}}')(\hat{\mathbf{k}}' \cdot \hat{\boldsymbol{\varepsilon}})\\ \mathbf{B} &= \hat{\boldsymbol{\varepsilon}}' \times \hat{\boldsymbol{\varepsilon}} + (\mathbf{k}' + \boldsymbol{\varepsilon}')(\mathbf{k} \cdot \boldsymbol{\varepsilon}) - (\hat{\mathbf{k}} \times \hat{\boldsymbol{\varepsilon}})(\hat{\mathbf{k}} \cdot \hat{\boldsymbol{\varepsilon}}')\\ &\quad - (\hat{\mathbf{k}}' \times \hat{\boldsymbol{\varepsilon}}') \times (\hat{\mathbf{k}} \times \hat{\boldsymbol{\varepsilon}}).\end{aligned} \tag{8.7.4.98}$$

For comparison, the magnetic neutron scattering amplitude can be written in the form

$$F_M^{\text{neutron}} = [\mathbf{M}_L(\mathbf{h}) + M_S(\mathbf{h})] \cdot \mathbf{C}, \tag{8.7.4.99}$$

with $\mathbf{C} = \hat{\mathbf{h}} \times \boldsymbol{\sigma} \times \hat{\mathbf{h}}$.

From (8.7.4.99), it is clear that spin and orbital contributions cannot be separated by neutron scattering. In contrast, the polarization dependencies of $\mathbf{M}_L$ and $\mathbf{M}_S$ are different in the X-ray case. Therefore, owing to the well defined polarization of synchrotron radiation, it is in principle possible to separate experimentally spin and orbital magnetization.

However, the prefactor $(h\omega/mc^2) \sim 10^{-2}$ makes the magnetic contributions weak relative to charge scattering. Moreover, F_C is roughly proportional to the total number of electrons, and F_M to the number of unpaired electrons. As a result, one expects $|F_M/F_C|$ to be about 10^{-3}.

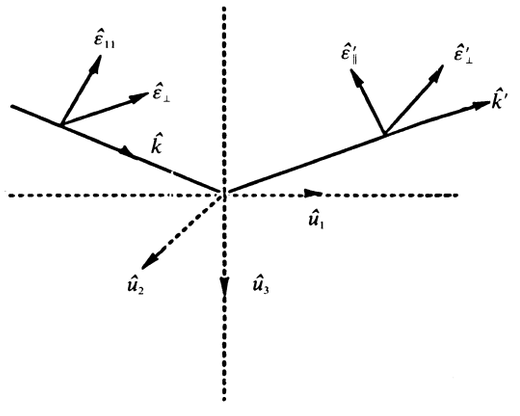

Fig. 8.7.4.1. Some geometrical definitions.

It should also be pointed out that F_M is in quadrature with F_C. In many situations, the total X-ray intensity is therefore

$$I_x = |F_C|^2 + |F_M|^2.$$

Thus, under these conditions, the magnetic effect is typically 10^{-6} times the X-ray intensity.

Magnetic contributions can be detected if magnetic and charge scattering occur at different positions (antiferromagnetic type of ordering). Furthermore, Blume (1985) has pointed out that the photon counting rate for $|F_M|^2$ at synchrotron sources is of the same order as the neutron rate at high-flux reactors.

Finally, situations where the 'interference' $F_C F_M$ term is present in the intensity are very interesting, since the magnetic contribution becomes 10^{-3} times the charge scattering.

The polarization dependence will now be discussed in more detail.

8.7.4.10.2. *Magnetic X-ray structure factor as a function of photon polarization*

Some geometrical definitions are summarized in Fig. 8.7.4.1, where parallel ($\parallel$) and perpendicular ($\perp$) polarizations will be chosen in order to describe the electric field of the incident and diffracted beams. In this two-dimensional basis, vectors $\mathbf{A}$ and $\mathbf{B}$ of (8.7.4.98) can be written as (2×2) matrices:

$$\mathbf{A} = \sin^2\theta \begin{pmatrix} 0 & -(\hat{\mathbf{k}} + \hat{\mathbf{k}}') \\ (\hat{\mathbf{k}} + \hat{\mathbf{k}}') & 2(\hat{\mathbf{k}} \times \hat{\mathbf{k}}') \end{pmatrix} \begin{matrix} \perp \\ \parallel \end{matrix}$$
$$\begin{matrix} i \rightarrow & \perp & \parallel & \uparrow f \end{matrix}$$

(i and f refer to the incident and diffracted beams, respectively);

$$\mathbf{B} = \begin{pmatrix} \hat{\mathbf{k}} \times \hat{\mathbf{k}}' & -2\hat{\mathbf{k}}'\sin^2\theta \\ 2\hat{\mathbf{k}}\sin^2\theta & \hat{\mathbf{k}} \times \hat{\mathbf{k}}' \end{pmatrix}. \tag{8.7.4.100}$$

By comparison, for the Thomson scattering,

$$\hat{\boldsymbol{\varepsilon}} \cdot \hat{\boldsymbol{\varepsilon}}' = \begin{pmatrix} 1 & 0 \\ 0 & \cos 2\theta \end{pmatrix}. \tag{8.7.4.101}$$

The major difference with Thomson scattering is the occurrence of off-diagonal terms, which correspond to scattering processes with a change of polarization. We obtain for the structure factors A_{if}:

$$\begin{aligned} A_{\perp\perp} &= F - i\,\frac{\hbar\omega}{mc^2}(\hat{\mathbf{k}} \times \hat{\mathbf{k}}') \cdot \mathbf{M}_S\\ A_{\perp\parallel} &= -2i\,\frac{\hbar\omega}{mc^2}\sin^2\theta\{(\hat{\mathbf{k}} + \hat{\mathbf{k}}') \cdot \mathbf{M}_L + \hat{\mathbf{k}}' \cdot \mathbf{M}_S\}\\ A_{\parallel\perp} &= 2i\,\frac{\hbar\omega}{mc^2}\sin 2\theta\{(\hat{\mathbf{k}} + \hat{\mathbf{k}}') \cdot \mathbf{M}_L + \hat{\mathbf{k}}' \cdot \mathbf{M}_S\}\\ A_{\parallel\parallel} &= F\cos^2\theta - i\,\frac{\hbar\omega}{mc^2}(\hat{\mathbf{k}} \times \hat{\mathbf{k}}') \cdot \{4\sin^2\theta\,\mathbf{M}_L\mathbf{M}_S\}. \end{aligned} \tag{8.7.4.102}$$

For a linear polarization, the measured intensity in the absence of diffracted-beam polarization analysis is

$$I_\alpha = |A_{\perp\perp}\cos\alpha + A_{\parallel\perp}\sin\alpha|^2 + |A_{\perp\parallel}\cos\alpha + A_{\parallel\parallel}\sin\alpha|^2, \tag{8.7.4.103}$$

where α is the angle between $\mathbf{E}$ and $\hat{\boldsymbol{\varepsilon}}$. In the centrosymmetric system, without anomalous scattering, no interference term occurs in (8.7.4.103). However, if anomalous scattering is present, $F = F' + iF''$, and terms involving $F''M_S$ or $F''M_L$ appear in the intensity expression.

The radiation emitted in the plane of the electron or positron orbit is linearly polarized. The experimental geometry is

generally such that $(\hat{\mathbf{k}}, \hat{\mathbf{k}}')$ is a vertical plane. Therefore, the polarization of the incident beam is along $\hat{\boldsymbol{\varepsilon}}$ ($\alpha = 0$). If a diffracted-beam analyser passes only $\parallel$ components of the diffracted beam, one can measure $|A_{\perp\parallel}|^2$, and thus eliminate the charge scattering.

For non-polarized radiation (with a rotating anode, for example), the intensity is

$$I = \tfrac{1}{2}[|A_{\parallel\parallel}|^2 + |A_{\parallel\perp}|^2 + |A_{\perp\parallel}|^2 + |A_{\perp\perp}|^2]. \qquad (8.7.4.104)$$

The radiation emitted out of the plane of the orbit contains an increasing amount of circularly polarized radiation. There also exist experimental devices that can produce circularly polarized radiation. For such incident radiation,

$$E_\parallel = \pm iE_\perp \qquad (8.7.4.105)$$

for left- or right-polarized photons. If $\mathbf{E}'$ is the field for the diffracted photons,

$$\begin{aligned} E'_\perp &= A_{\perp\perp} + iA_{\parallel\perp} \\ E'_\parallel &= A_{\parallel\perp} + iA_{\parallel\parallel}. \end{aligned} \qquad (8.7.4.106)$$

In this case, 'mixed-polarization' contributions are in phase with F, leading to a strong interference between charge and magnetic scattering.

The case of radiation with a general type of polarization is more difficult to analyse. The most elegant formulation involves Stokes vectors to represent the state of polarization of the incident and scattered radiation (see Blume & Gibbs, 1988).

Acknowledgements

Support of this work by the National Science Foundation (CHE8711736 and CHE9615586) is gratefully acknowledged.

International Tables for Crystallography (2006). Vol. C, Chapter 8.8, pp. 735–743.

8.8. Accurate structure-factor determination with electron diffraction

BY J. GJØNNES

Several techniques have been developed for accurate determination of structure factors with electrons, mostly based on convergent-beam electron diffraction (CBED) and interpreted by dynamical scattering theory. Intensities are measured as one- or two-dimensional rocking curves, or as special intensity features in the CBED patterns, *e.g.* critical voltages. The main application of these methods so far has been to strong inner reflections from simple structures in relation to bonding effects, occupation numbers or ordering. Low-order reflections in electron diffraction are particularly sensitive to details in the distribution of valence electrons, through the difference $Z - f^X$ in the expression for the atomic scattering amplitude

$$f^{\rm el}(2\theta) = \frac{2}{a_H}\,\frac{Z - f^X}{(2\pi q)^2}, \tag{8.8.1}$$

where $a_H = \hbar^2/m_0e^2$ is the first Bohr radius; the diffraction variable $q = 2\sin\theta/\lambda$, and f^X is the X-ray scattering factor for atomic number Z. A further advantage is that these methods can provide absolute measurement of structure factors, *i.e.* without a scaling procedure. The limitation to inner reflections may be overcome by measurement of intensities integrated across Kossel-line features in CBED patterns (Vincent, Bird & Steeds, 1984; Gjønnes & Bøe, 1994; Tsuda & Tanaka, 1995; Tomokiyo & Kuroiwa, 1990).

As distinct from the X-ray case where scattering from one electron is a convenient unit, commonly agreed upon for the atomic scattering factor as well as for the amplitude of the structure factor, there are several units and definitions possible in electron diffraction; see Cowley (1992), Spence & Zuo (1992). The *scattering amplitude* associated with the unit cell may have the same unit as the atomic scattering factor, *i.e. length*. The *structure factor* (or *Fourier potential*) is usually defined as the Fourier component, U_g, of the scattering potential that appears in the wave equation, and is expressed either in volts, as an SI unit, or in reciprocal-length squared. The latter unit follows from the common way of writing the Schrödinger equation in scattering theory, *viz*

$$\{\nabla_r^2 + 4\pi^2k^2 + 4\pi^2U(r)\}\Psi(r) = 0, \tag{8.8.2}$$

with the factor $4\pi^2$ introduced in order to conform with crystallographic conventions for reciprocal vectors and wave vectors. In this notation, the structure factor or Fourier potential may appear in units of (length)$^{-2}$:

$$U_g = \frac{m}{m_0}\,\frac{1}{\Omega_\pi}\sum_j f^{\rm el}(2\theta)\exp[-M_g^j]\exp[2\pi i\mathbf{g}\cdot\mathbf{r}_j], \tag{8.8.3}$$

where Ω is the volume of the unit cell, m is the relativistic electron mass corresponding to the accelerating voltage and $\exp[-M]$ the Debye–Waller factor. The translation to volts is given by $U_g(\text{volts}) = 0.00665U_g(\text{Å}^{-2})$. Results are usually quoted for the rest mass m_0, but in scattering calculations the factor m/m_0 must be included. For comparison with theoretical calculations of charge distributions, the electron results are usually transformed to X-ray scattering factors. The structure factor associated with forward scattering has a special meaning, quite different from the X-ray case where F_0^X is a measure of the number of electrons. In electron diffraction, U_0 is the mean inner potential – a measure of the average screening of the nuclear charges, or the average extent of the electron clouds. For spherical neutral atoms, we obtain from (1) in the limit $q \to 0$

$$f^{\rm el}(0) = \frac{2}{3a_H}\sum\langle r_j^2\rangle, \tag{8.8.4}$$

where the sum is over atomic electrons. For ions, this will diverge, but a limit can still be found by adding contributions from positive and negative ions, in which case the measured inner potential will depend upon the direction of the incident beam. U_0 can be measured by interference experiments, *e.g.* by a biprism. For a review of experiments, see Spence (1993) and Saldin & Spence (1994).

Experimental determinations of structure factors U_g have been based on various techniques: thickness fringes in bright-field or dark-field electron micrographs, Kikuchi patterns, and, in recent years, especially by convergent-beam diffraction. The intensity distribution within the CBED discs can be recorded photographically, with image plates, or by a CCD camera connected to a YAG screen in the microscope – preferably with an energy filter, which will improve the signal-to-noise ratio and facilitate background subtraction (Burgess, Preston, Bolton, Zaluzec & Humphreys, 1994). Alternatives to the parallel recording in CBED may be to scan the pattern over the slit in an EELS system – or in a modified PEELS as described by Holmestad, Krivanek, Høier, Marthinsen & Spence (1993).

Because of dynamical interactions between beams, the scattered intensity will depend upon several structure factors. Refinement of structure factors must therefore be based on extensive calculations. These are usually performed in the Bloch-wave representation, which is the most convenient theoretical basis (in contrast to higher-resolution imaging, where multislice dynamical calculations are commonly used). The diffracted intensity as a function of the thickness t and the diffraction condition, defined by the components k_x, k_y of the incident wave vector, can be expressed as

$$\begin{aligned} I_g(t, k_x, k_y) = {} & \sum_i |C_0^iC_g|^2\exp[-2\pi\mu^i t] \\ & + \sum_{i\neq j}\sum C_0^{i*}C_g^iC_0^jC_g^{j*}\exp[2\pi i(\gamma^i - \gamma^j)t] \\ & \times \exp[-\pi(\mu^i + u^j)t], \end{aligned} \tag{8.8.5}$$

where the Bloch-wave coefficients C_h^j are eigenvectors, and the *Anpassungen* γ^j are eigenvalues obtained by the diagonalization. The absorption coefficients μ^j for the Bloch waves j can be calculated from the imaginary potential $U'(r)$ by a perturbation procedure or by non-Hermitian diagonalization (Bird, 1990). $U'(r)$ describes the spatial variation within the unit cell of the diffuse scattering power, derived mainly from thermal scattering (Yoshioka & Kainuma, 1962). Calculations are usually based on an Einstein model (Radi, 1970; Bird & King, 1990).

The CBED patterns are used in measurement strategies based on different beam configurations, Fig. 8.8.1, *viz* (*a*) two-beam-like intensity profiles in systematic rows; (*b*) three- or four-beam cases in non-systematic configurations; (*c*) patterns in dense zones with strong many-beam dynamical interactions. The one- or two-dimensional intensity distributions are fitted to theoretical calculations by a least-squares procedure with low-order structure factors and certain experimental parameters as free variables.

Copyright © 2006 International Union of Crystallography

Systematic row. Measurement of *s*-fringe profiles in CBED discs from strong inner reflections in systematic rows was tried by MacGillavry (1940) and developed into a method for structure-factor determination by Goodman & Lehmpfuhl (1967) and later authors. At present, this may be the commonest method for refinement of low-order structure factors from CBED. A detailed account is given in the book by Spence & Zuo (1992) and in Spence (1993). Strong non-systematic interactions should be avoided. The intensity profiles can often be approximated by the two-beam expression

$$I_g(s_g) = \frac{(U_g/k)^2}{s^2 + (U_g/k)^2} \sin^2\left[\pi t \sqrt{s_g^2 + (U_g/k)^2}\,\right], \qquad (8.8.6)$$

especially when U_g is substituted by an 'effective potential' which may be defined by the corresponding gap at the dispersion surface, *viz* $U_g^{\rm eff} = k(\gamma^i - \gamma^j)_{\rm min} = k/\xi^{ij}$, where ξ^{ij} is an extinction distance. The outer part of the profile (large s_g) depends mainly on the thickness, whereas the inner part is sensitive to the product tU_g. Different perturbation expressions have been proposed for the effective potential. The Bethe potential

$$U_g^{\rm eff} = U_g - \sum_h \frac{U_h U_{g-h}}{2ks_h} \qquad (8.8.7)$$

is often used, *e.g.* in the early steps of the refinement procedure (Gjønnes, Gjønnes, Zuo & Spence, 1988), and especially in order to treat weak beams beyond the typically 60–80 beams included in the Bloch-wave diagonalization (Zuo, 1993). Procedures and computer programs adapted to least-squares refinement of structure factors from energy-filtered line profiles are described by Spence (1993), Zuo (1993) and Deininger, Necker & Mayer (1994). The refinement will usually include experimental parameters (thickness, beam orientations) as well as elastic and absorptive parts of a few low-order structure factors for each profile – but not high-order structure factors and thermal parameters, which are assumed. Low-order structure factors for a number of simple substances have been determined. Errors in the best results, referred to as X-ray structure amplitudes, are of the order of 0.1% – which may be a tenth of the bonding effect in covalent compounds. See, for example, the recent study of the intermetallic compound TiAl and a variant doped with 5% Mn (Holmestad, Weickenmeier, Zuo, Spence & Horita, 1993), where the charge-density deformation distribution

$$\Delta\rho(\mathbf{r}) = \frac{1}{\Omega} \sum_g [F_g^X(\text{crystal}) - F_g^X(\text{free atom})] \exp[2\pi i \mathbf{g}\cdot\mathbf{r}] \qquad (8.8.8)$$

was constructed from nine-low-order structure factors.

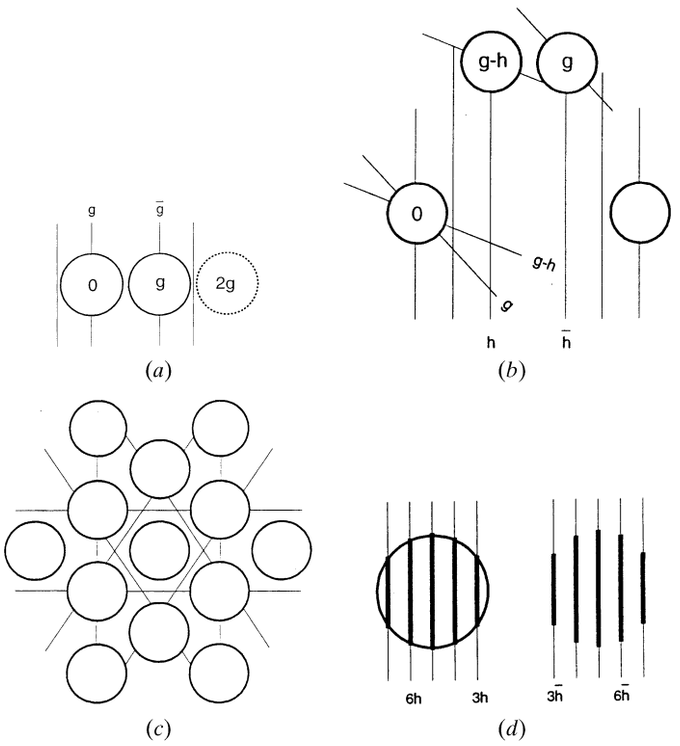

Fig. 8.8.1. Schematic representations of four convergent-beam configurations used for structure-factor determination: (*a*) intensity profile of a low-order reflection, *g*; (*b*) non-systematic three- or four-beam configuration with a strong coupling reflection, *h*; (*c*) symmetric many-beam configuration in a dense zone; (*d*) integrated intensity measurement of high-order reflections using a wide aperture (Taftø & Metzger, 1985).

Three– and four-beam, non-systematic cases. Several magnitudes can be extracted from Kikuchi or CBED patterns in such configurations, see *e.g.* Gjønnes & Høier (1971). In the non-systematic critical-voltage method, the condition for extinction of line contrast is measured; in the IKL (intersecting Kikuchi line) method, one measures the separation between line segments of the split line appearing at the intersection with a strong Kikuchi band. The precision of these methods, originally developed for Kikuchi patterns, was increased considerably when CBED was used instead (Matsuhata, Tomokiyo, Watanabe & Eguchi, 1982; Taftø & Gjønnes, 1985).

A further improvement is expected when the intensity distribution over the whole CBED discs is recorded and fitted to dynamical calculations. This has been explored recently by Høier, Bakken, Marthinsen & Holmestad (1993); the addition of non-systematic reflections in a parallel row can be seen as an extension of the systematic row configuration above. The experience so far is that the three- and four-beam configurations are very sensitive to structure-factor phases, but may not yield as accurate values for structure amplitudes as those obtained from the line profiles in the systematic row.

Zone axis CBED. Convergent-beam patterns around the axis of a dense zone contain extensive multiple-beam dynamical interaction. Bird & Saunders (1992) claim that this leads to high sensitivity as well as a high number of structure factors that can be determined from one CBED pattern. Their results from refinement of structure amplitudes in f.c.c., diamond and sphalerite structures may confirm this. From filtered intensities measured with a CCD camera, Saunders, Bird, Midgley & Vincent (1994) determined structure factors for silicon up to 331 from one pattern in the [110] zone. The point-spread function for the detector was deconvoluted from the raw data. Thickness, background level and a scaling factor were included in the refinement from a grid of 21×21 intensities in each disc. Starting values were neutral atom scattering factors, absorptive scattering amplitude calculated from TDS and a preliminary thickness determination. 121 beams were included in the diagonalization, a further 270 beams by perturbation.

Critical voltage and intersecting-Kikuchi-line (IKL) method. The above methods, based on line scans or two-dimensional intensity distributions in CBED discs, rely on extensive

calculations of dynamical scattering at a number of incident-beam directions. In calculations of the critical-voltage effect (Watanabe, Uyeda & Fukuhara, 1969; Gjønnes & Høier, 1971; Matsuhata & Steeds, 1987; Matsuhata & Gjønnes, 1994), which corresponds to an accidental degeneracy of Bloch waves, only one beam direction is considered. The condition for the associated vanishing contrast (or contrast reversal) of a Kikuchi or Kossel line is determined from CBED patterns taken at a series of voltages and compared with the Bloch-wave calculations for the particular direction. This is a very sensitive method – with the disadvantage that only a relation between structure factors is obtained. In the original experiment by Watanabe, Uyeda & Fukuhara (1969), the relation between the structure factors for a strong first-order reflection and its second order was determined from measurement of the disappearance voltage for the second-order line, *cf.* formula (4.3.7.8). This second-order critical voltage depends on high-voltage microscopy – and a strong first-order reflection. A number of metals and simple alloy phases have been studied with this method in recent years by Fox and co-workers, see the review by Fox & Fisher (1988) and Fox & Tabbernor (1991). The extension to non-systematic cases in the normal accelerating-voltage range was first shown by Gjønnes & Høier (1971). In principle, the Bloch-wave degeneracy will appear at a certain combination of excitation errors for any non-systematic three-beam configuration in centrosymmetric crystals. The difficulty is to find conditions that can be measured with sufficient precision. Matsuhata & Gjønnes (1994) analysed a number of non-systematic critical voltages in symmetrical configurations and showed how they can be measured in the range below 2–300 kV for simple structures. From rutile-type SnO_2, Matsuhata, Gjønnes & Taftø (1994) measured four critical voltages, which were analysed in terms of ionicity; structure factors were determined for two low-order reflections. The calculations are simpler and less time consuming than for the intensity profiles, but also more dependent on known high-order structure factors and temperature factors. An alternative to the measurement of a critical voltage is to measure the position in the pattern where the degeneracy occurs – as in the IKL method (Gjønnes & Høier, 1971; Taftø & Gjønnes, 1985; Matsumura, Tomokiyo & Oki, 1989; Wang & Peng, 1994).

Phases and absorption in multiple-beam cases. Centrosymmetry was assumed in the original derivations of the accidental Bloch-wave degeneracy leading to the critical-voltage effect. In non-centrosymmetrical crystals, we can find degeneracies related to other symmetry elements, *i.e.* mirror planes or rotation axes or 'pseudocritical voltages' when the deviation from centrosymmetry is small (Matsuhata & Gjønnes, 1994). For larger deviations, the position of minimum contrast can be used to determine structure-factor phase invariants, based again on the Bethe approximation. Høier & Marthinsen (1983) give the expression

$$|U_g^{\rm eff}| = |U_g|\sqrt{\left\{1 - \left|\frac{U_h U_{g-h}}{U_h}\right| \frac{\cos\varphi}{2ks_g}\right\}^2 + \left|\frac{U_h U_{g-h}}{U_g 2ks_h}\right|^2 \sin^2\varphi}, \tag{8.8.9}$$

where the phase invariant $\varphi = \varphi_h + \varphi_{g-h} + \varphi_{-g}$. Subsequent studies, *e.g.* Zuo, Høier & Spence (1989), showed this three-beam effect to be very sensitive to the phase invariant. From CBED profile measurements, Zuo, Spence, Downs & Mayer (1993) determined the structure-factor phase of the 00.2 reflection in Be with the remarkable precision of 0.1°. Bird (1990) pointed out that the treatment of the absorptive part needs special attention in non-centrosymmetrical crystals.

Thickness fringes. Thickness fringes were used for structure-factor determination at an early stage, *e.g.* Ando, Ichimiya & Uyeda (1974). The analogous effect in the diffraction pattern is the measurement of a split reflection from a wedge, which is an interesting visualization of Bloch waves; see Lehmpfuhl (1974). Today these techniques may appear to have mainly historical interest, although thickness fringes can be an alternative for determination of Bloch-wave absorption parameters μ^j and thereby the imaginary Fourier potentials.

Comparison, evaluation and extension to integrated intensities. The convergent-beam electron-diffraction methods for determination of structure factors from small unit cells have been developed to high precision during the last 5–10 years. Least-squares fit of one- and two-dimensional intensity distributions within CBED discs appears today as the most sensitive method for determination of the lowest-order components of the charge distribution in organic structures with small unit cells. The accuracy may be as good as or better than the best X-ray methods – with the important provision that other structure parameters, high-order structure factors and Debye–Waller factors, are known to sufficient accuracy. Measurements of special features, *e.g.* critical voltages, offer an important supplement with less extensive computation efforts. Applications have been mainly to simple structures with atoms in special positions and refinement of low-order structure factors only. It should be noted that the deformation density $\Delta\rho$ may have significant components beyond the low-order structure factors that are usually determined by CBED methods – and in a range where $f^X < Z/2$ and X-rays thus inherently more sensitive to charge redistribution.

The extension of precise measurements to more reflections and to larger unit cells with position parameters is thus seen as a main challenge – which may be attacked along different avenues. Higher-order reflection profiles are narrower, less dynamic in character and not so suitable for the profile fitting described above. An alternative is to measure integrated intensities across Kossel-line segments, as has been done in several beam configurations. Vincent *et al.* (1984) measured integrated intensities of HOLZ-line segments, *i.e.* with the central CBED disc around the zone axis. Holmestad, Weickenmeier, Zuo, Spence & Horita (1993) measured selected HOLZ reflections in less-dense zones for determination of Debye–Waller factors. Taftø & Metzger (1985) showed the sensitivity of high-order lines in a dense systematic row to atomic coordinates. This wide-angle CBED technique has been applied to coordinate refinement in intermetallic compounds (Ma, Rømming, Lebech, Gjønnes & Taftø, 1992). Gjønnes & Bøe (1994) measured intensities of a range of reflections in the $00l$ row from the superconductors $YBa_2Cu_3O_7$ and a Co-substituted variant. Since the high-order lines are narrow, it is possible to measure relative intensities from a number of reflections in one exposure. Assuming a two-beam-like shape, the integral may be related to the gap at the dispersion surface, according to the Blackman formula (Blackman, 1939)

$$\int I_g^{\rm two\ beam}(s_g, t)\,{\rm d}s_g = (A_g/t)\int_0^{A_g} J_0(x)\,{\rm d}x, \tag{8.8.10}$$

where $A_g = U_g^{\rm eff} t$, and J_0 is the Bessel function of zero order. For a small gap, the intensity is proportional to $|U^{\rm eff}|^2$. By many-beam calculations, Gjønnes & Bøe (1994) showed the integrated intensities to be less sensitive to dynamical interactions along the row than that indicated from the Bethe potentials, and that relative intensities are fairly independent of thickness. Coordinate refinement based on intensities from a few high-order Kossel-line segments appear to produce accuracies roughly one order of magnitude poorer than good single-crystal X-ray determination. This may suggest that if some form of three-dimensional intensity data could be collected in electron diffraction the same level of accuracies as with X-rays may be attainable – which, however, remains to be seen.

References

8.1

Anderson, E., Bai, Z., Bischof, C., Demmel, J., Dongarra, J., Du Croz, J., Greenbaum, A., Hammarling, S., McKenney, A., Ostrouchov, S. & Sorenson, D. (1992). *LAPACK user's guide*, 2nd ed. Philadelphia: SIAM Publications.

Berger, J. O. & Wolpert, R. L. (1984). *The likelihood principle*. Hayward, CA: Institute of Mathematical Statistics.

Boggs, P. T., Byrd, R. H., Donaldson, J. R. & Schnabel, R. B. (1989). *ODRPACK – software for weighted orthogonal distance regression. ACM Trans. Math. Softw.* **15**, 348–364.

Boggs, P. T., Byrd, R. H. & Schnabel, R. B. (1987). *A stable and efficient algorithm for nonlinear orthogonal distance regression. SIAM J. Sci. Stat. Comput.* **8**, 1052–1078.

Boggs, P. T. & Rogers, J. E. (1990). *Orthogonal distance regression. Contemporary mathematics: statistical analysis of measurement error models and applications*. Providence, RI: AMS.

Box, G. E. P., Hunter, W. G. & Hunter, J. S. (1978). *Statistics for experimenters: an introduction to design, data analysis and model building*. New York: John Wiley.

Box, G. E. P. & Tiao, G. C. (1973). *Bayesian inference in statistical analysis*. Reading, MA: Addison-Wesley.

Bunch, D. S., Gay, D. M. & Welsch, R. E. (1993). *Algorithm 717: subroutines for maximum likelihood and quasi-likelihood estimation of parameters in nonlinear regression models. ACM Trans. Math. Softw.* **19**, 109–130.

Dennis, J. E. & Schnabel, R. B. (1983). *Numerical methods for unconstrained optimization and nonlinear equations*. Englewood Cliffs, NJ: Prentice Hall.

Donaldson, J. R. & Schnabel, R. B. (1986). *Computational experience with confidence regions and confidence intervals for nonlinear least squares. Computer science and statistics. Proceedings of the Seventeenth Symposium on the Interface*, edited by D. M. Allen, pp. 83–91. New York: North-Holland.

Draper, N. & Smith, H. (1981). *Applied regression analysis*. New York: John Wiley.

Fedorov, V. V. (1972). *Theory of optimal experiments*, translated by W. J. Studden & E. M. Klimko. New York: Academic Press.

Fuller, W. A. (1987). *Measurement error models*. New York: John Wiley & Sons.

Heath, M. T. (1984). *Numerical methods for large, sparse, linear least squares problems. SIAM J. Sci. Stat. Comput.* **5**, 497–513.

Nash, S. & Sofer, A. (1995). *Linear and nonlinear programming*. New York: McGraw-Hill.

Prince, E. (1994). *Mathematical techniques in crystallography and materials science*, 2nd ed. Berlin: Springer.

Schwarzenbach, D., Abrahams, S. C., Flack, H. D., Prince, E. & Wilson, A. J. C. (1995). *Statistical descriptors in crystallography. II. Report of a Working Group on Expression of Uncertainty in Measurement. Acta Cryst.* A**51**, 565–569.

Stewart, G. W. (1973). *Introduction to matrix computations*. New York: Academic Press.

8.2

Belsley, D. A., Kuh, E. & Welsch, R. E. (1980). *Regression diagnostics*. New York: John Wiley.

Box, G. E. P. & Tiao, G. C. (1973). *Bayesian inference in statistical analysis*. Reading, MA: Addison-Wesley.

Collins, D. M. (1982). *Electron density images from imperfect data by iterative entropy maximization. Nature (London)*, **298**, 49–51.

Collins, D. M. (1984). *Scaling by entropy maximization. Acta Cryst.* A**40**, 705–708.

Hoaglin, D. C., Mosteller, M. & Tukey, J. W. (1983). *Understanding robust and exploratory data analysis*. New York: John Wiley.

Huber, P. J. (1973). *Robust regression: asymptotics, conjectures and Monte Carlo. Ann. Stat.* **1**, 799–821.

Huber, P. J. (1981). *Robust statistics*. New York: John Wiley.

Jaynes, E. T. (1979). *Where do we stand on maximum entropy? The maximum entropy formalism,* edited by R. D. Liven & M. Tribus, pp. 44–49. Cambridge, MA: Massachusetts Institute of Technology.

Livesey, A. K. & Skilling, J. (1985). *Maximum entropy theory. Acta Cryst.* A**41**, 113–122.

Nicholson, W. L., Prince, E., Buchanan, J. & Tucker, P. (1982). *A robust/resistant technique for crystal structure refinement. Crystallographic statistics: progress and problems,* edited by S. Rameseshan, M. F. Richardson & A. J. C. Wilson, pp. 220–263. Bangalore: Indian Academy of Sciences.

Rietveld, H. M. (1969). *A profile refinement method for nuclear and magnetic structures. J. Appl. Cryst.* **2**, 65–71.

Shore, J. E. & Johnson, R. W. (1980). *Axiomatic derivation of the principle of maximum entropy and the principle of minimum cross-entropy. IEEE Trans. Inf. Theory*, IT-**26**, 26–37; correction: IT-**29**, 942–943.

Tukey, J. W. (1974). *Introduction to today's data analysis. Critical evaluation of chemical and physical structural information,* edited by D. R. Lide & M. A. Paul, pp. 3–14. Washington: National Academy of Sciences.

Wilson, A. J. C. (1976). *Statistical bias in least-squares refinement. Acta Cryst.* A**32**, 994–996.

8.3

Cruickshank, D. W. J. (1961). *Coordinate errors due to rotational oscillations of molecules*. *Acta Cryst*. **14**, 896–897.

Finger, L. W. (1969). *The crystal structure and cation distribution of a grunerite*. *Mineral. Soc. Am. Spec. Pap*. **2**, 95–100.

Gill, P. E., Murray, W. & Wright, M. M. (1981). *Practical optimization*. New York: Academic Press.

Hamilton, W. C. (1964). *Statistics in physical science: estimation, hypothesis testing and least squares*. New York: Ronald Press.

Hendrickson, W. A. (1985). *Stereochemically restrained refinement of macromolecular structures*. *Methods in enzymology*, Vol. 115. *Diffraction methods for biological macromolecules, Part B*, edited by H. W. Wyckoff, C. H. W. Hirs & S. N. Timasheff, pp. 252–270. New York: Academic Press.

Hendrickson, W. A. & Konnert, J. H. (1980). *Incorporation of stereochemical information into crystallographic refinement*. *Computing in crystallography*, edited by R. Diamond, S. Ramaseshan & D. Venkatesan, pp. 13.01–13.26. Bangalore: Indian Academy of Sciences.

Hestenes, M. & Stiefel, E. (1952). *Methods of conjugate gradients for solving linear systems*. *J. Res. Natl Bur. Stand*. **49**, 409–436.

Jack, A. & Levitt, M. (1978). *Refinement of large structures by simultaneous minimization of energy and R factor*. *Acta Cryst*. A**34**, 931–935.

Johnson, C. K. (1970). *Generalized treatments for thermal motion*. *Thermal neutron diffraction*, edited by B. T. M. Willis, pp. 132–160. Oxford University Press.

Konnert, J. H. (1976). *A restrained-parameter structure-factor least-squares refinement procedure for large asymmetric units*. *Acta Cryst*. A**32**, 614–617.

Konnert, J. H. & Hendrickson, W. A. (1980). *A restrained-parameter thermal-factor refinement procedure*. *Acta Cryst*. A**36**, 344–350.

Levy, H. A. (1956). *Symmetry relations among coefficients of anisotropic temperature factors*. *Acta Cryst*. **9**, 679.

Prince, E. (1994). *Mathematical techniques in crystallography and materials science*, 2nd ed. Berlin/Heidelberg/New York/London/Paris/Tokyo/Hong Kong/Barcelona/Budapest: Spring-Verlag.

Prince, E., Dickens, B. & Rush, J. J. (1974). *A study of one-dimensional hindered rotation in NH_3OHClO_4*. *Acta Cryst*. B**30**, 1167–1172.

Prince, E. & Finger, L. W. (1973). *Use of constraints on thermal motion in structure refinement of molecules with librating side groups*. *Acta Cryst*. B**29**, 179–183.

Rae, A. D. (1978). *An optimized conjugate gradient solution for least-squares equations*. *Acta Cryst*. A**34**, 578–582.

Ralph, R. L. & Finger, L. W. (1982). *A computer program for refinement of crystal orientation matrix and lattice constants from diffractometer data with lattice symmetry constraints*. *J. Appl. Cryst*. **15**, 537–539.

Rietveld, H. M. (1969). *A profile refinement method for nuclear and magnetic structures*. *J. Appl. Cryst*. **2**, 65–71.

Schomaker, V. & Trueblood, K. N. (1968). *On the rigid-body motion of molecules in crystals*. *Acta Cryst*. B**24**, 63–76.

Schomaker, V., Waser, J., Marsh, R. E. & Bergman, G. (1959). *To fit a plane or a line to a set of points by least squares*. *Acta Cryst*. **12**, 600–604.

Sygusch, J. (1976). *Constrained thermal motion refinement for a rigid molecule with librating side groups*. *Acta Cryst*. B**32**, 3295–3298.

Waser, J. (1963). *Least-squares refinement with subsidiary conditions*. *Acta Cryst*. **16**, 1091–1094.

8.4

Cramér, H. (1951). *Mathematical methods of statistics*. Princeton, NJ: Princeton University Press.

Draper, N. & Smith, H. (1981). *Applied regression analysis*. New York: John Wiley.

Fedorov, V. V. (1972). *Theory of optimal experiments*, translated by W. J. Studden & E. M. Klimko. New York: Academic Press.

Hamilton, W. C. (1964). *Statistics in physical science: estimation, hypothesis testing and least squares*. New York: Ronald Press.

Himmelblau, D. M. (1970). *Process analysis by statistical methods*. New York: John Wiley.

Prince, E. (1982). *Comparison of the fits of two models to the same data set*. *Acta Cryst*. B**38**, 1099–1100.

Prince, E. (1994). *Mathematical techniques in crystallography and materials science,* 2nd ed. Berlin/Heidelberg/New York/London/Paris/Tokyo/Hong Kong/Barcelona/Budapest: Springer-Verlag.

Prince, E. & Nicholson, W. L. (1985). *Influence of individual reflections on the precision of parameter estimates in least squares refinement*. *Structure and statistics in crystallography*, edited by A. J. C. Wilson, pp. 183–195. Guilderland, NY: Adenine Press.

Shoemaker, D. P. (1968). *Optimization of counting time in computer controlled X-ray and neutron single-crystal diffractometry*. *Acta Cryst*. A**24**, 136–142.

Williams, E. J. & Kloot, N. H. (1953). *Interpolation in a series of correlated observations*. *Aust. J. Appl. Sci*. **4**, 1–17.

8.5

Abrahams, S. C. & Keve, E. T. (1971). *Normal probability plot analysis of error in measured and derived quantities and standard deviations*. *Acta Cryst*. A**27**, 157–165.

Beckman, R. J. & Cook, R. D. (1983). *Outlier.....s*. *Technometrics*, **25**, 119–149.

Belsley, D. A. (1991). *Conditioning diagnostics*. New York: John Wiley & Sons.

Belsley, D. A., Kuh, E. & Welsch, R. E. (1980). *Regression diagnostics*. New York: John Wiley & Sons.

Chatterjee, S. & Hadi, A. S. (1986). *Influential observations, high leverage points, and outliers in linear regression*. *Stat. Sci*. **1**, 379–393.

Fedorov, V. V. (1972). *Theory of optimal experiments*, translated by W. J. Studden & E. M. Klimko. New York: Academic Press.

ISO (1993). *Guide to the expression of uncertainty in measurement*. Geneva: International Organization for Standardization.

Kafadar, K. & Spiegelman, C. H. (1986). *An alternative to ordinary Q–Q plots: conditional Q–Q plots*. *Comput. Stat. Data Anal*. **4**, 167–184.

Prince, E. (1994). *Mathematical techniques in crystallography and materials science*, 2nd ed. Berlin/Heidelberg/New York/London/Paris/Tokyo/Hong Kong/Barcelona/Budapest: Springer-Verlag.

8.5 (*cont.*)

Prince, E. & Nicholson, W. L. (1985). *Influence of individual reflections on the precision of parameter estimates in least squares refinement. Structure and statistics in crystallography*, edited by A. J. C. Wilson, pp. 183–195. Guilderland, NY: Adenine Press.

8.6

Ahtee, M., Nurmela, M. & Suortti, P. (1989). *A Voigtian as profile shape function in Rietveld refinement. J. Appl. Cryst.* **17**, 352–357.

Ahtee, M., Unonius, L., Nurmela, M. & Suortti, P. (1984). *Correction for preferred orientation in Rietveld refinement. J. Appl. Cryst.* **22**, 261–268.

Albinati, A. & Willis, B. T. M. (1982). *The Rietveld method in neutron and X-ray powder diffraction. J. Appl. Cryst.* **15**, 361–374.

Altomare, A., Cascarano, G., Giacovazzo, C., Guagliardi, A., Moliterni, A. G., Burla, M. C. & Polidori, G. (1995). *On the number of statistically independent observations in powder diffraction. J. Appl. Cryst.* **15**, 361–374.

Baharie, E. & Pawley, G. S. (1983). *Counting statistics and powder diffraction scan refinements. J. Appl. Cryst.* **16**, 404–406.

Caglioti, G., Paoletti, A. & Ricci, F. P. (1958). *Choice of collimators for a crystal spectrometer for neutron diffraction. Nucl. Instrum. Methods*, **3**, 223–228.

Cheetham, A. K. (1993). *Ab initio structure solution with powder diffraction data. The Rietveld method. IUCr Monographs on Crystallography*, No. 5, edited by R. A. Young, pp. 276–292. Oxford University Press.

Cheetham, A. K. & Wikinson, A. P. (1992). *Synchrotron X-ray and neutron diffraction studies in solid state chemistry. Angew. Chem. Int. Ed. Engl.* **31**, 1557–1570.

David, W. I. F. & Matthewman, J. C. (1985). *Profile refinement of powder diffraction patterns using the Voigt function. J. Appl. Cryst.* **18**, 461–466.

David, W. I. F., Shankland, K., McCusker, L. B. & Baerlocher, Ch. (2002). Editors. *Structure determination from powder diffraction data. IUCr Monographs on Crystallography*, No. 13. Oxford University Press.

Dinnebier, R. E., Von Dreele, R. B., Stephens, P. W., Jelonek, S. & Sieber, J. (1999). *Structure of sodium para-hydroxybenzoate by powder diffraction: application of a phenomenological model of anisotropic peak width. J. Appl. Cryst.* **32**, 761–769.

Harris, K. D. M. & Tremayne, M. (1996). *Crystal structure determination from powder diffraction data. Chem. Mater.* **8**, 2554–2570.

Harris, K. D. M., Tremayne, M. & Kavinki, B. M. (2001). *Contemporary advances in the use of powder X-ray diffraction for structure determination. Angew. Chem. Int. Ed.* **40**, 1626–1651.

Hastings, J. B., Thomlinson, W. & Cox, D. E. (1984). *Synchrotron X-ray powder diffraction. J. Appl. Cryst.* **17**, 85–95.

Hepp, A. & Baerlocher, Ch. (1988). *Learned peak-shape functions for powder diffraction data. Aust. J. Phys.* **41**, 229–236.

Hewat, A. W. (1986). *High-resolution neutron and synchrotron powder diffraction. Chem. Scr.* **26**A, 119–130.

Immirzi, A. (1980). *Constrained powder profile refinement based on generalized coordinates. Application to X-ray data of isotactic polypropylene. Acta Cryst.* B**36**, 2378–2385.

Malmros, G. & Thomas, J. O. (1977). *Least-squares structure refinement based on profile analysis of powder film intensity data measured on an automatic microdensitometer. J. Appl. Cryst.* **10**, 7–11.

Masciocchi, N. & Sironi, A. (1997). *The contribution of powder diffraction methods to structural coordination chemistry. J. Chem. Soc. Dalton Trans.* pp. 4643–4650.

McCusker, L. B., Von Dreele, R. B., Cox, D. E., Louer, D. & Scardi, P. (1999). *Rietveld refinement guidelines. J. Appl. Cryst.* **32**, 36–50.

Parrish, W. & Huang, T. C. (1980). *Accuracy of the profile fitting method for X-ray polycrystalline diffractrometry. Natl Bur. Stand. (US) Spec. Publ.* No. 567, pp. 95–110.

Pawley, G. S. (1981). *Unit cell refinement from powder diffraction scans. J. Appl Cryst.* **14**, 357–361.

Popa, N. C. (1992). *Texture in Rietveld refinement. J. Appl Cryst.* **25**, 611–616.

Popa, N. C. & Balzar, D. (2001). *Elastic strain and stress determination by Rietveld refinement: generalized treatment for textured polycrystals for all Laue classes. J. Appl. Cryst.* **34**, 187–195.

Popa, N. C. & Balzar, D. (2002). *An analytical approximation for a size-broadened profile given by the lognormal and gamma distributions. J. Appl. Cryst.* **35**, 338–346.

Pratapa, S., O'Connor, B. & Hunter, B. (2002). *A comparative study of single-line and Rietveld strain-size evaluation procedures using MgO ceramics. J. Appl. Cryst.* **35**, 155–162.

Prince, E. (1981). *Comparison of profile and and integrated-intensity methods in powder refinement. J. Appl. Cryst.* **14**, 157–159.

Prince, E. (1985). *Precision and accuracy in structure refinement by the Rietveld method. Structure and statistics in crystallography*, edited by A. J. C. Wilson. New York: Adenine Press.

Prince, E. (1993). *Mathematical aspects of Rietveld refinement. The Rietveld method. IUCr Monographs on Crystallography,* No. 5, edited by R. A. Young, pp. 43–54. Oxford University Press.

Richardson, J. W. (1993) *Background modelling in Rietveld analysis. The Rietveld method. IUCr Monographs on Crystallography*, No. 5, edited by R. A. Young, pp. 102–110. Oxford University Press.

Rietveld, H. M. (1967). *Line profiles of neutron powder diffraction peaks for structure refinement. Acta Cryst.* **22**, 151–152.

Rietveld, H. M. (1969). *A profile refinement method for nuclear and magnetic structures. J. Appl. Cryst.* **2**, 65–71.

Sakata, M. & Cooper, M. J. (1979). *An analysis of the Rietveld profile refinement method. J. Appl. Cryst.* **12**, 554–563.

Scott, H. G. (1983). *The estimation of standard deviations in powder diffraction refinement. J. Appl. Cryst.* **16**, 589–610.

Shirley, R. (1980). *Data accuracy for powder indexing. Natl Bur. Stand (US) Spec. Publ.* No. 567, pp. 361–382.

Sivia, D. S. (2000). *The number of good reflections in a powder pattern. J. Appl. Cryst.* **33**, 1295–1301.

Taylor, J. C. (1985). *Technique and performance of powder diffraction in crystal structure studies. Aust. J. Phys.* **38**, 519–538.

8.6 (*cont.*)

Von Dreele, R. B. (1997). *Quantitative texture analysis by Rietveld refinement*. *J. Appl. Cryst.* **30**, 517–525.

Von Dreele, R. B., Jorgensen, J. D. & Windsor, C. G. (1982). *Rietveld refinement with spallation neutron powder diffraction data*. *J. Appl Cryst.* **15**, 581–589.

Werner, P. E. (2002). *Autoindexing. Structure determination from powder diffraction data. IUCr Monographs on Crystallography*, No. 13, edited by W. I. F. David, K. Shankland, L. B. McCusker & Ch. Baerlocher, pp. 118–135. Oxford University Press.

Will, G., Parrish, W. & Huang, T. C. (1983). *Crystal structure refinement by profile fitting and least-squares analysis of powder diffractometer data*. *J. Appl Cryst.* **16**, 611–622.

Young, R. A. (1993). Editor. *The Rietveld method. IUCr Monographs on Crystallography,* No. 5. Oxford University Press.

Young, R. A. & Wiles, D. B. (1982). *Profile shape functions in Rietveld refinements*. *J. Appl. Cryst.* **15**, 430–438.

8.7

Becker, P. (1990). *Electrostatic properties from X-ray structure factors*. Unpublished results.

Becker, P. & Coppens, P. (1985). *About the simultaneous interpretation of charge and spin density data*. *Acta Cryst.* A**41**, 177–182.

Becker, P. & Coppens, P. (1990). *About the Coulombic potential in crystals*. *Acta Cryst.* A**46**, 254–258.

Bentley, J. (1981). In *Chemical Applications of Atomic and Molecular Electrostatic Potentials*, edited by P. Politzer & D. G. Truhlar. New York/London: Plenum Press.

Bergevin, F. de & Brunel, M. (1981). *Diffraction of X-rays by magnetic materials. I. General formulae and measurements on ferro- and ferrimagnetic compounds*. *Acta Cryst.* A**37**, 314–324.

Bertaut, E. F. (1978). *Electrostatic potentials, fields and gradients*. *J. Phys. Chem. Solids*, **39**, 97–102.

Blume, M. (1985). *Magnetic scattering of X-rays*. *J. Appl. Phys.* **57**, 3615–3618.

Blume, M. & Gibbs, D. (1988). *Polarization dependence of magnetic X-ray scattering*. *Phys. Rev. B*, **37**, 1779–1789.

Bonnet, M., Delapalme, A., Becker, P. & Fuess, H. (1976). *Polarized neutron diffraction – a tool for testing extinction models: application to yttrium iron garnet*. *Acta Cryst.* A**32**, 945–953.

Boucherle, J. X., Gillon, B., Maruani, J. & Schweizer, J. (1982). *Spin densities in centrally unsymmetric structures*. *J. Phys.* (*Paris*) *Colloq.* **7**, 227–230.

Boyd, R. J. (1977). *The radial density function for the neutral atoms from helium to xenon*. *Can. J. Phys.* **55**, 452–455.

Brown, P. J. (1986). *Interpretation of magnetization density measurements in concentrated magnetic systems: exploitation of the crystal translational symmetry*. *Chem. Scr.* **26**, 433–439.

Brunel, M. & de Bergevin, F. (1981). *Diffraction of X-rays by magnetic materials. II. Measurements on antiferromagnetic* Fe_2O_3. *Acta Cryst.* A**37**, 324–331.

Buckingham, A. D. (1959). *Molecular quadrupole moments*. *Q. Rev. Chem. Soc.* **13**, 183–214.

Buckingham, A. D. (1970). *Physical chemistry. An advanced treatise*, Vol. 4. *Molecular properties*, edited by D. Henderson, pp. 349–386. New York: Academic Press.

Condon, E. U. & Shortley, G. H. (1935). *The theory of atomic spectra*. Cambridge University Press.

Coppens, P. (1992). *The structure factor. International tables for crystallography*, Vol. B, edited by U. Shmueli, ch. 1.2. Dordrecht: Kluwer Academic Publishers.

Coppens, P., Koritsanszky, T. & Becker, P. (1986). *Transition metal complexes: what can we learn by combining experimental spin and charge densities? Chem. Scr.* **26**, 463–467.

Cromer, D. T., Larson, A. C. & Stewart, R. F. (1976). *Crystal structure refinements with generalized scattering factors*. *J. Chem. Phys.* **65**, 336–349.

Cruickshank, D. W. J. (1949). *The accuracy of electron density maps in X-ray analysis with special reference to dibenzyl*. *Acta Cryst.* **2**, 65–82.

Dahl, J. P. & Avery, J. (1984). *Local density approximations in quantum chemsitry and solid state physics*. New York/London: Plenum.

Delley, B., Becker, P. & Gillon, B. (1984). *Local spin-density theory of free radicals: nitroxides*. *J. Chem. Phys.* **80**, 4286–4289.

Desclaux, J. P. & Freeman, A. J. (1978). *J. Magn. Magn. Mater.* **8**, 119–129.

Epstein, J. & Swanton, D. J. (1982). *Electric field gradients in imidazole at 103K from X-ray diffraction*. *J. Chem. Phys.* **77**, 1048–1060.

Fermi, E. (1928). *Eine statitische Methode zur Bestimmung einiger Eigenschaften des Atoms und ihre Anwendung auf die Theorie des periodischen Systems der Elemente*. *Z. Phys.* **48**, 73–79.

Forsyth, J. B. (1980). In *Electron and magnetization densities in molecules and solids*, edited by P. Becker. New York/London: Plenum.

Freeman, A. J. & Desclaux, J. P. (1972). *Neutron magnetic form factor of gadolinium*. *Int. J. Magn.* **3**, 311–317.

Gillon, B., Becker, P. & Ellinger, Y. (1983). *Theoretical spin density in nitroxides. The effect of alkyl substitutions*. *Mol. Phys.* **48**, 763–774.

Gordon, R. G. & Kim, Y. S. (1972). *Theory for the forces between closed-shell atoms and molecules*. *J. Chem. Phys.* **56**, 3122–3133.

Hamilton, W. C. (1964). *Statistical methods in physical sciences*. New York: Ronald Press.

Hellner, E. (1977). *A simple refinement of density distributions of bonding electrons*. *Acta Cryst.* B**33**, 3813–3816.

Hirshfeld, F. L. (1984). *Hellmann–Feynman constraint on charge densities, an experimental test*. *Acta Cryst.* B**40**, 613–615.

Hirshfeld, F. L. & Rzotkiewicz, S. (1974). *Electrostatic binding in the first-row AH and* A_2 *diatomic molecules*. *Mol. Phys.* **27**, 1319–1343.

Hirshfelder, J. O., Curtis, C. F. & Bird, R. B. (1954). *Molecular theory of gases and liquids*. New York: John Wiley.

Hohenberg, P. & Kohn, W. (1964). *Inhomogeneous electron gas*. *Phys. Rev. B*, **136**, 864–867.

Holladay, A., Leung, P. C. & Coppens, P. (1983). *Generalized relation between d-orbital occupancies of transition-metal atoms and electron-density multipole population parameters from X-ray diffraction data*. *Acta Cryst.* A**39**, 377–387.

International Tables for Crystallography (1992). Vol. B, edited by U. Shmueli. Dordrecht: Kluwer Academic Publishers.

International Tables for X-ray Crystallography (1974). Vol. IV. Birmingham: Kynoch Press. (Present distributor: Kluwer Academic Publishers, Dordrecht.)

Johnston, D. F. (1966). *Theory of the electron contribution to the scattering of neutrons by magnetic ions in crystals*. *Proc. Phys. Soc. London*, **88**, 37–52.

Levine, I. L. (1983). *Quantum chemistry*, 3rd ed. Boston/London/Sydney: Allyn and Bacon Inc.

Lovesey, S. W. (1984). *Theory of neutron scattering from condensed matter*. Oxford: Clarendon Press.

Marshall, W. & Lovesey, S. W. (1971). *Theory of thermal neutron scattering*. Oxford University Press.

Massa, L., Goldberg, M., Frishberg, C., Boehme, R. F. & La Placa, S. J. (1985). *Wave functions derived by quantum modeling of the electron density from coherent X-ray diffraction: beryllium metal*. *Phys. Rev. Lett.* **55**, 622–625.

Miller, K. J. & Krauss, M. (1967). *Born inelastic differential cross sections in H_2*. *J. Chem. Phys.* **47**, 3754–3762.

Mook, H. A. (1966). *Magnetic moment distribution of Ni metal*. *Phys. Rev.* **148**, 495–501.

Moss, G. & Coppens, P. (1981). *Pseudomolecular electrostatic potentials from X-ray diffraction data*. In *Molecular electrostatic potentials in chemistry and biochemistry*, edited by P. Politzer & D. Truhlar. New York: Plenum.

Pawley, G. S. & Willis, B. T. M. (1970). *Temperature factor of an atom in a rigid vibrating molecule. II. Anisotropic thermal motion*. *Acta Cryst.* A**36**, 260–262.

Rees, B. (1976). *Variance and covariance in experimental electron density studies, and the use of chemical equivalence*. *Acta Cryst.* A**32**, 483–488.

Rees, B. (1978). *Errors in deformation-density and valence-density maps: the scale-factor contribution*. *Acta Cryst.* A**34**, 254–256.

Schweizer, J. (1980). In *Electron and magnetization densities in molecules and crystals*, edited by P. Becker. New York: Plenum.

Spackman, M. A. (1992). *Molecular electric moments from X-ray diffraction data*. *Chem. Rev.* **92**, 1769.

Stevens, E. D. & Coppens, P. (1976). *A priori estimates of the errors in experimental electron densities*. *Acta Cryst.* A**32**, 915–917.

Stevens, E. D., DeLucia, M. L. & Coppens, P. (1980). *Experimental observation of the effect of crystal field splitting on the electron density distribution of iron pyrite*. *Inorg. Chem.* **19**, 813–820.

Stevens, E. D., Rees, B. & Coppens, P. (1977). *Calculation of dynamic electron distributions from static molecular wave functions*. *Acta Cryst.* A**33**, 333–338.

Stewart, R. F. (1977). *One-electron density functions and many-centered finite multipole expansions*. *Isr. J. Chem.* **16**, 124–131.

Stewart, R. F. (1979) *On the mapping of electrostatic properties from Bragg diffraction data*. *Chem. Phys. Lett.* **65**, 335–342.

Su, Z. & Coppens, P. (1992). *On the mapping of electrostatic properties from the multipole description of the charge density*. *Acta Cryst.* A**48**, 188–197.

Su, Z. & Coppens, P. (1994*a*). *Rotation of real spherical harmonics*. *Acta Cryst.* A**50**, 636–643.

Su, Z. & Coppens, P. (1994*b*). *On the evaluation of integrals useful for calculating the electrostatic potential and its derivatives from pseudo-atoms*. *J. Appl. Cryst.* **27**, 89–91.

Thomas, L. H. (1926). *Proc. Cambridge Philos. Soc.* **23**, 542–548.

Tofield, B. C. (1975). *Structure and bonding*, Vol. 21. Berlin: Springer-Verlag.

Ando, Y., Ichimiya, A. & Uyeda, R. (1974). *A determination of values and signs of the 111 and 222 structure factors of silicon*. *Acta Cryst.* A**30**, 600–601.

Bird, D. M. (1990). *Absorption in high-energy electron diffraction from non-centrosymmetric crystals*. *Acta Cryst.* A**46**, 208–214.

Bird, D. M. & King, Q. A. (1990). *Absorption form factors for high-energy electron diffraction*. *Acta Cryst.* A**46**, 202–208.

Bird, D. M. & Saunders, M. (1992). *Sensitivity and accuracy of CBED pattern matching*. *Ultramicroscopy*, **45**, 241–252.

Blackman, M. (1939). *Intensities of electron diffraction rings*. *Proc. R. Soc. London Ser A*, **173**, 68–82.

Burgess, W. G., Preston, A. R., Botton, G. A., Zaluzec, N. J. & Humphreys, C. J. (1994). *Benefits of energy filtering for advanced convergent beam electron diffraction patterns*. *Ultramicroscopy*, **55**, 276–283.

Cowley, J. M. (1992). *Electron diffraction techniques*, Vol. 1. Oxford University Press.

Deininger, C., Necker, G. & Mayer, J. (1994). *Determination of structure factors, lattice strains and accelerating voltage by energy-filtered electron diffraction*. *Ultramicroscopy*, **54**, 15–30.

Fox, A. G. & Fisher, R. M. (1988). *A summary of low-angle X-ray atomic scattering factors measured by the critical voltage effect in high energy electron diffraction*. *Aust. J. Phys.* **41**, 461–468.

Fox, A. G. & Tabbernor, M. A. (1991). *The bonding charge density of β' NiAl*. *Acta Metall.* **39**, 669–678.

Gjønnes, J. & Høier, R. (1971). *The application of non-systematic many-beam dynamic effects to structure-factor determination*. *Acta Cryst.* A**27**, 313–316.

Gjønnes, K. & Bøe, N. (1994). *Refinement of temperature factors and charge distributions in $YBa_2Cu_3O_7$ and $YBa_2(Cu,Co)_3O_7$ from CBED intensities*. *Micron Microsc. Acta*, **25**, 29–44.

Gjønnes, K., Gjønnes, J., Zuo, J. & Spence, J. C. H. (1988). *Two-beam features in electron diffraction patterns – application to refinement of low-order structure factors in GaAs*. *Acta Cryst.* A**44**, 810–820.

Goodman, P. & Lehmpfuhl, G. (1967). *Electron diffraction study of MgO h00 systematic interactions*. *Acta Cryst.* **22**, 14–24.

Høier, R., Bakken, L. N., Marthinsen, K. & Holmestad, R. (1993). *Structure factor determination in non-centrosymmetrical crystals by a two-dimensional CBED-based multi-parameter refinement method*. *Ultramicroscopy*, **49**, 159–170.

Høier, R. & Marthinsen, K. (1983). *Effective structure factors in many-beam X-ray diffraction – use of the second Bethe approximation*. *Acta Cryst.* A**39**, 854–860.

Holmestad, R., Krivanek, O. L., Høier, R., Marthinsen, K. & Spence, J. C. H. (1993). *Commercial spectrometer modifications for energy filtering of diffraction patterns and images*. *Ultramicroscopy*, **52**, 454–458.

Holmestad, R., Weickenmeier, A. L., Zuo, J. M., Spence, J. C. H. & Horita, Z. (1993). *Debye–Waller factor measurement in TiAl from HOLZ reflections*. *Electron Microscopy and Analysis 1993*, pp. 141–144. Bristol: IOP Publishing.

Lehmpfuhl, G. (1974). *Dynamical interaction of electron waves in a perfect single crystal*. *Z. Naturforsch. Teil A*, **27**, 424–433.

8.8 (*cont.*)

Ma, Y., Rømming, C., Lebech, B., Gjønnes, J. & Taftø, J. (1992). *Structure refinement of Al_3Zr using single-crystal X-ray diffraction, powder neutron diffraction and CBED. Acta Cryst.* B**48**, 11–16.

MacGillavry, C. H. (1940). *Dynamical theory of electron diffraction. Physica (Utrecht)*, **7**, 329–343.

Matsuhata, H. & Gjønnes, J. (1994). *Bloch-wave degeneracies and non-systematic critical voltage: a method for structure-factor determination. Acta Cryst.* A**50**, 107–115.

Matsuhata, H., Gjønnes, J. & Taftø, J. (1994). *A study of the structure factors in rutile-type SnO_2 by higher-energy electron diffraction. Acta Cryst.* A**50**, 115–123.

Matsuhata, H. & Steeds, J. W. (1987). *Observation of accidental Bloch-wave degeneracies of zone-axis critical voltage. Philos Mag.* B**55**, 39–54.

Matsuhata, H., Tomokiyo, Y., Watanabe, H. & Eguchi, T. (1982). *Determination of structure factors of Cu and Cu_3Au by the intersecting Kikuchi line method. Acta Cryst.* B**40**, 544–549.

Matsumura, S., Tomokiyo, Y. & Oki, K. (1989). *Study of temperature factors in cubic crystal by high-voltage electron diffraction. J. Eletron Microsc. Tech.* **12**, 262–271.

Radi, G. (1970). *Complex lattice potential in electron diffraction calculated for a number of crystals. Acta Cryst.* A**26**, 41–56.

Saldin, D. K. & Spence, J. C. H. (1994). *On the measurement of inner potential in high- and low-energy electron diffraction. Ultramicroscopy*, **55**, 397–406.

Saunders, M., Bird, D. M., Midgley, P. A. & Vincent, R. (1994). *Structure factor refinement by zone-axis CBED pattern matching*. 13th International Congress on Electron Microscopy, Paris, 17–22 July 1994. Vol. 1, pp. 847–848.

Spence, J. C. H. (1993). *On the accurate measurement of structure-factor amplitudes and phases by electron diffraction. Acta Cryst.* A**49**, 231–260.

Spence, J. C. H. & Zuo, J. M. (1992). *Electron microdiffraction*. New York: Plenum.

Taftø, J. & Gjønnes, J. (1985). *The intersecting Kikuchi line method: critical voltage at any voltage. Ultramicroscopy*, **17**, 329–334.

Taftø, J. & Metzger, T. H. (1985). *Large-angle convergent beam electron diffraction: a simple technique for the study of structures with application to U_2D. J. Appl. Cryst.* **6**, 110–113.

Tomokiyo, Y. & Kuroiwa, T. (1990). *Determination of static displacements of atoms by means of large-angle convergent-beam electron diffraction. Proceedings of XII International Congress on Electron Microscopy*, Vol. 2, pp. 526–527. San Francisco Press.

Tsuda, K. & Tanaka, M. (1995). *Refinement of crystal structure parameters using convergent-beam electron diffraction: the low-temperature phase of $SrTiO_3$. Acta Cryst.* A**51**, 7–19.

Vincent, R., Bird, D. M. & Steeds, J. W. (1984). *Structure of AuGeAs determined by convergent beam electron diffraction. II. Refinement of structural parameters Philos. Mag.* A**50**, 765–786.

Wang, S. Q. & Peng, L. M. (1994). *LACBED determination of structure factors and alloy composition of GeSi/Si SLS. Ultramicroscopy*, **55**, 57–74.

Watanabe, D., Uyeda, R. & Fukuhara, A. (1969). *Determination of the atomic form factor by high-voltage electron diffraction. Acta Cryst.* A**25**, 138–140.

Yoshioka, H. & Kainuma, Y. (1962). *The effect of thermal vibration on electron diffraction. J. Phys. Soc. Jpn.* Suppl. B**2**, 134–136.

Zuo, J. M. (1993). *Automated structure-factor refinement from convergent-beam electron diffraction patterns. Acta Cryst.* A**49**, 429–435.

Zuo, J. M., Høier, R. & Spence, J. C. H. (1989). *Three-beam and many-beam theory in electron diffraction and its use for structure-factor phase determination in non-centrosymmetrical crystal structures. Acta Cryst.* A**45**, 839–851.

Zuo, J. M., Spence, J. C. H., Downs, J. & Mayer, J. (1993). *Measurement of individual structure-factor phases with tenth-degree accuracy: the 00.2 reflection in BeO studied by electron and X-ray diffraction. Acta Cryst.* A**49**, 422–429.

International Tables for Crystallography (2006). Vol. C, Chapter 9.1, pp. 746–751.

9.1. Sphere packings and packings of ellipsoids

By E. Koch and W. Fischer

9.1.1. Sphere packings and packings of circles

9.1.1.1. *Definitions*

For the characterization of many crystal structures, geometrical aspects have proved to be a useful tool. Among these, sphere-packing considerations stand out in particular.

A *sphere packing* in the most general sense is an infinite, three-periodic set of non-intersecting spheres (*i.e.* a set of non-intersecting spheres with space-group symmetry) with the property that any pair of spheres is connected by a chain of spheres with mutual contact. If all spheres are symmetry-equivalent, the sphere packing is called *homogeneous*, otherwise it is called *heterogeneous*.

A homogeneous sphere packing may be represented uniquely by the set of symmetry-equivalent points that are the centres of the spheres [point configuration, *cf. IT*A (1983, Chapter 14.1)]. This point configuration is distinguished by equal shortest distances giving rise to a connected graph. As all spheres of a homogeneous sphere packing must be equal in size, their common radius can be calculated as half this shortest distance.

A heterogeneous sphere packing consists of at least two symmetry-distinct subsets of spheres, the centres of which form a respective number of point configurations. The radii of symmetrically distinct spheres can be either equal or different. In the first case, the heterogeneous sphere packing may be represented by its set of sphere centres, quite similar to a homogeneous one. In the case of different sphere radii, however, the knowledge of at least some of the radii is additionally necessary.

As there exists an infinite number of both homogeneous and heterogeneous sphere packings, it is convenient to classify the sphere packings into types: two sphere packings belong to the same *type* if there exists a biunique mapping that brings the spheres of one packing onto the spheres of the other packing and that preserves all contact relations between spheres.

The number of types of homogeneous sphere packings is finite whereas the number of types of heterogeneous sphere packings is infinite.

All definitions and properties mentioned so far may be transferred from sets of spheres in three-dimensional space to sets of circles in two-dimensional space, giving rise to *heterogeneous* and *homogeneous packings of circles*.

A characteristic property of types of homogeneous sphere (circle) packings is the number k of contacts per sphere (circle): $3 \leq k \leq 12$ for sphere packings and $3 \leq k \leq 6$ for packings of circles.

A sphere (circle) packing is called *stable* [close, *cf. IT*II (1972, Chapter 7.1)] if no sphere (circle) can be moved without moving neighbouring spheres (circles) at the same time. As a consequence, a stable sphere (circle) packing has at least four (three) contacts per sphere (circle), and not all these contacts must fall in one hemisphere (semicircle).

The *density* of a homogeneous sphere (circle) packing is defined as the fraction of volume (area) occupied by spheres (circles). It may be calculated as

$$\rho = \tfrac{4}{3}\pi \frac{nr^3}{V}$$

for sphere packings, and as

$$\rho = \pi \frac{nr^2}{A}$$

for packings of circles. Here, r is the radius of the spheres (circles), n the number of spheres (circles) per unit cell, V the unit-cell volume, and A the unit-cell area.

Geometric properties of different sphere (circle) packings of the same type may be different. Such properties are, *e.g.*, the density and the property of being a stable packing.

9.1.1.2. *Homogeneous packings of circles*

The homogeneous packings of circles in the plane may be classified into 11 types (*cf.* Niggli, 1927, 1928; Haag, 1929, 1937; Sinogowitz, 1939; Fischer, 1968; Koch & Fischer, 1978). These correspond to the 11 types of planar nets with equivalent vertices derived by Shubnikov (1916). If, in addition, symmetry is used for classification, the number of distinct cases becomes larger (31 cases according to Sinogowitz, 1939).

Table 9.1.1.1 gives a summary of the 11 types. In column 1, the type of circle packing is designated by a modified Schläfli symbol that characterizes the polygons meeting at one vertex of a corresponding Shubnikov net. The contact number k is given in column 2. The next column displays the highest possible symmetry for each type of circle packing. The corresponding parameter values are listed in column 4. The appropriate shortest distances d between circle centres and densities ρ are given in columns 5 and 6, respectively.

With three exceptions (3^6, $3^4 6$, 46.12), all types include circle packings that are not similar in the mathematical sense and that differ, therefore, in their geometrical properties. The highest possible symmetry for a type of homogeneous circle packing corresponds necessarily to the lowest possible density ρ of that type. Therefore, homogeneous circle packings of type 3.12^2 with symmetry *p6mm* are the least dense. The highest possible density is achieved by the circle packings with contact number 6 referring to triangular nets with hexagonal symmetry.

All circle packings described in Table 9.1.1.1 are stable in the sense defined above. Only circle packings of types 3.12^2 and 48^2 may be unstable.

9.1.1.3. *Homogeneous sphere packings*

The number of homogeneous sphere-packing types is not known so far. Sinogowitz (1943) systematically derived sphere packings with non-cubic symmetry from planar sets of spheres, but he did not compare sphere packings with different symmetry and classify them into types. Fischer calculated the parameter conditions for all cubic (Fischer, 1973, 1974) and all tetragonal (Fischer, 1991*a*,*b*, 1993) sphere packings. 199 types of homogeneous sphere packings with cubic symmetry and 394 types with tetragonal symmetry exist in all. 12 of these types are common to both systems. In a similar way, Zobetz (1983) calculated the sphere-packing conditions for Wyckoff position $R\bar{3}m$ 6(*c*). Using a different approach, Koch & Fischer (1995) derived all types of homogeneous sphere packings with contact number $k = 3$. Because of the unique correspondence of each homogeneous sphere packing to a graph, studies on three-dimensional nets also give contributions to the knowledge on sphere-packing types. In particular, papers by Wells (1977, 1979, 1983), O'Keeffe (1991, 1992), O'Keeffe & Brese (1992) and Treacy, Randall, Rao, Perry & Chadi (1997) contain some information on sphere packings with $k = 3$ and $k = 4$.

Copyright © 2006 International Union of Crystallography

Table 9.1.1.1. *Types of circle packings in the plane*

Type	k	Symmetry			Parameters	Distance d	Density
3^6	6	*p6mm*	1(*a*)	0, 0		a	0.9069
3^2434	5	*p4gm*	4(*c*)	$x, x+\frac{1}{2}$	$x=\frac{1}{4}\sqrt{3}-\frac{1}{4}$	$\frac{1}{2}(\sqrt{6}-\sqrt{2})a$	0.8418
3^34^2	5	*c2mm*	4(*d*)	x, 0	$x=1-\frac{1}{2}\sqrt{3}$; $b/a=2-\sqrt{3}$	b	0.8418
3^46	5	*p6*	6(*d*)	x, y	$x=\frac{3}{7}$; $y=\frac{1}{7}$	$\frac{1}{7}\sqrt{7}a$	0.7773
4^4	4	*p4mm*	1(*a*)	0, 0		a	0.7854
3464	4	*p6mm*	6(*e*)	$x, \bar{x}$	$x=\frac{1}{2}-\frac{1}{6}\sqrt{3}$	$\frac{1}{2}(\sqrt{3}-1)a$	0.7290
3636	4	*p6mm*	3(*c*)	$\frac{1}{2}$, 0		$\frac{1}{2}a$	0.6802
6^3	3	*p6mm*	2(*b*)	$\frac{1}{3}, \frac{2}{3}$		$\frac{1}{3}\sqrt{3}a$	0.6046
48^2	3	*p4mm*	4(*d*)	x, 0	$x=1-\frac{1}{2}\sqrt{2}$	$(\sqrt{2}-1)a$	0.5390
46.12	3	*p6mm*	12(*f*)	x, y	$x=\frac{1}{6}\sqrt{3}+\frac{1}{6}$; $y=\frac{1}{6}\sqrt{3}-\frac{1}{6}$	$(\frac{1}{2}-\frac{1}{6}\sqrt{3})a$	0.4860
3.12^2	3	*p6mm*	6(*c*)	$x, \bar{x}$	$x=1-\frac{1}{3}\sqrt{3}$	$(2-\sqrt{3})a$	0.3907

Table 9.1.1.2 shows examples for sphere packings with high contact numbers and high densities in the upper part and with small contact numbers and low densities in the lower part. Column 1 gives reference numbers to designate the types in the following. Column 2 displays the contact numbers k. The highest possible symmetry for each type is described in column 3. Coordinates and metrical parameters referring to the most regular sphere packings of each type are listed in column 4; the respective shortest distances d between sphere centres are given in column 5. For a sphere packing that can be subdivided into plane nets of spheres with mutual contact, the direction and the type of these nets are shown in column 6. Column 7 contains stacking information: the contact numbers to the nets above and below, and the number of layers per translation period in the direction perpendicular to the layers. The last column displays the density with respect to the parameters of column 4. For all cases, this value gives the minimal density for that type of sphere packing.

The densest homogeneous sphere packings known so far may be derived from the densest packings of circles (3^6 in Table 9.1.1.1). Such sphere packings can always be subdivided into parallel plane layers of spheres with six contacts per sphere within each layer and with three contacts to each of the neighbouring layers above and below (*cf.* Fig. 9.1.1.1). Consequently, the contact number k becomes 12. As there exist two stacking possibilities for each layer with respect to the previous layer, infinitely many stacking sequences can be derived in principle, but only two refer to homogeneous sphere packings. If for each layer the two neighbouring layers are stacked directly upon each other, a sphere packing of a two-layer type with hexagonal symmetry (type 1) results. It is called *hexagonal closest packing* (abbreviated h.c.p.). If for all layers the neighbouring layers are never stacked directly upon each other, a sphere packing of a three-layer type with cubic symmetry (type 2) is formed. It is designated *cubic closest packing* (c.c.p.). In spite of these terms, for a long time it was only known that the cubic closest packings are the densest ones that correspond to lattices (Minkowski, 1904). Only recently, Hsiang (1993) published a proof that there does not exist any packing of spheres of equal size with a higher density, but the completeness of this proof is still doubted (*cf. e.g.* Hales, 1994).

Independently of the stacking sequences, closest packings of spheres contain ideal octahedral and ideal tetrahedral voids. The number of octahedra per unit cell equals the respective number of spheres, whereas the number of tetrahedral voids is twice as large. The distances between the centres and the vertices of these voids are $\sqrt{2}d/2$ and $\sqrt{6}d/4$, respectively. Within a cubic closest packing, faces are shared only between octahedral and tetrahedral voids. Each edge is common to two octahedra and two tetrahedra. In contrast, piles of face-sharing octahedra are formed within a hexagonal closest packing, whereas the tetrahedra are arranged as pairs with one face in common. The other faces are shared between octahedra and tetrahedra. Again, each edge belongs to two octahedra and two tetrahedra.

Densest layers of spheres may also be stacked such that each sphere is in contact with two spheres of the previous layers (*cf.* Fig. 9.1.1.2). Such a stacking results in contact number 10. Again, infinitely many periodic stacking sequences are possible, but only four give rise to homogeneous sphere packings [types 9, 10, 11: *cf.* Hellner (1986); type 12: *cf.* O'Keeffe (1988)]. In the most symmetrical forms of these four cases, each sphere is located exactly above or below the middle of two neighbouring spheres of the adjacent layers. This kind of stacking gives rise to distorted tetrahedral voids only. The number of tetrahedra per unit cell is six times the number of spheres. Two kinds of differently distorted tetrahedra exist in the ratio 1:2. The two-layer type 9 corresponds to a tetragonal body-centred lattice with specialized axial ratio.

Furthermore, densest layers of spheres may be stacked in a mixed sequence with three contacts per sphere to one neighbouring layer and two contacts to the other layer. This kind of stacking results in five types of homogeneous sphere packings (3 to 7) with contact number 11.

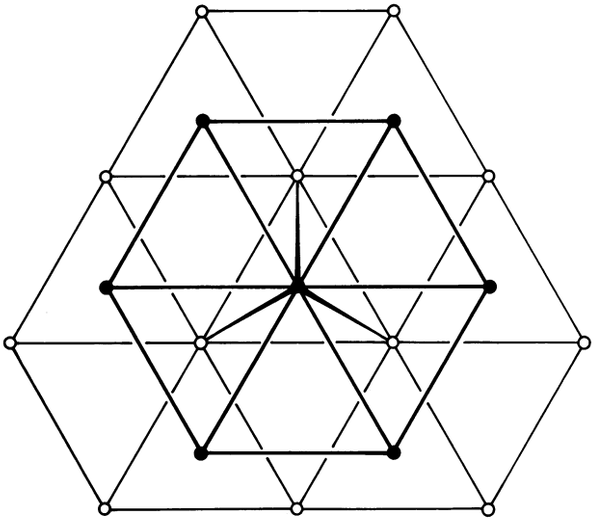

Fig. 9.1.1.1. Two triangular nets representing two densest packed layers of spheres. The layers are stacked in such a way that each sphere is in contact with three spheres of the other layer.

Table 9.1.1.2. *Examples for sphere packings with high contact numbers and high densities and with low contact numbers and low densities*

Type	k	Symmetry			Parameters	Distance d	Net	Stacking	Density
1	12	$P6_3/mmc$	$2(c)$	$\frac{1}{3},\frac{2}{3},\frac{1}{4}$	$c/a=\frac{2}{3}\sqrt{6}$	a	(001) 3^6	3, 3 2	0.7405
2	12	$Fm\bar{3}m$	$4(a)$	$0,0,0$	–	$\frac{1}{2}\sqrt{2}a$	{111} 3^6 {001} 4^4	3, 3 3 4, 4 2	
3	11	$Cmca$	$8(f)$	$0,y,z$	$y=\frac{1}{6}, z=\frac{3}{2}\sqrt{2}-2$ $b/a=\sqrt{3}, c/a=\frac{2}{3}\sqrt{6}+\sqrt{3}$	a	(001) 3^6	3, 2 4	0.7187
4	11	$P3_121$	$6(c)$	x,y,z	$x=\frac{1}{2}, y=\frac{5}{6}, z=\sqrt{2}-\frac{4}{3}$ $c/a=\sqrt{6}+\frac{3}{2}\sqrt{3}$	a	(001) 3^6	3, 2 6	
5	11	$Fdd2$	$16(b)$	x,y,z	$x=\frac{1}{6}, y=\frac{3}{4}\sqrt{2}-1, z=0$ $b/a=\frac{4}{3}\sqrt{2}+2, c/a=\frac{1}{3}\sqrt{3}$	c	(010) 3^6	3, 2 8	
6	11	$P6_522$	$12(c)$	x,y,z	$x=\frac{1}{6}, y=\frac{1}{3}, z=\frac{1}{2}\sqrt{2}-\frac{2}{3}$ $c/a=2\sqrt{6}+3\sqrt{3}$	a	(001) 3^6	3, 2 12	
7	11	$C2/m$	$4(i)$	$x,0,z$	$x=\frac{1}{2}\sqrt{2}-\frac{1}{2}, z=3\sqrt{2}-4$ $b/a=\frac{1}{3}\sqrt{3}, c/a=\frac{1}{6}\sqrt{6}+\frac{1}{3}\sqrt{3}$ $\cos\beta=\frac{1}{6}\sqrt{6}-\frac{1}{3}\sqrt{3}$	b	(001) 3^6	3, 2 12	
8	11	$P4_2/mnm$	$4(f)$	$x,x,0$	$x=\frac{1}{2}\sqrt{2}-\frac{1}{2}, c/a=2-\sqrt{2}$	c	–	–	0.7187
9	10	$I4/mmm$	$2(a)$	$0,0,0$	$c/a=\frac{1}{3}\sqrt{6}$	c	{110} 3^6	2, 2 2	0.6981
10	10	$P6_222$	$3(c)$	$\frac{1}{2},0,0$	$c/a=\frac{3}{2}\sqrt{3}$	a	(001) 3^6	2, 2 3	
11	10	$Fddd$	$8(a)$	$0,0,0$	$b/a=\sqrt{3}, c/a=2\sqrt{3}$	a	(001) 3^6	2, 2 4	
12	10	$Fddd$	$16(g)$	$\frac{1}{8},\frac{1}{8},z$	$z=\frac{5}{16}, b/a=\sqrt{3}, c/a=4\sqrt{3}$	a	(001) 3^6	2, 2 8	
13	10	$Cmcm$	$4(c)$	$0,y,\frac{1}{4}$	$y=\frac{3}{10}, b/a=\frac{1}{3}\sqrt{15}, c/a=\frac{2}{5}\sqrt{10}$	$\frac{1}{3}\sqrt{6}a$	(001) 4^4	3, 3 2	0.6981
14	10	$Pnma$	$4(c)$	$x.\frac{1}{4},z$	$x=\frac{7}{20}, z-\frac{7}{8}, b/a=\frac{4}{5}, c/a=\frac{2}{15}\sqrt{15}$	c	(010) 4^4	3, 3 2	
15	10	$P6_3/mmc$	$4(f)$	$\frac{1}{3},\frac{2}{3},z$	$z=\frac{3}{4}-\frac{1}{4}\sqrt{6}, c/a=\frac{2}{3}\sqrt{6}+2$	a	(001) 3^6	3, 1 4	0.6657
16	10	$R\bar{3}m$	$6(c)$	$0,0,z$	$z=\frac{1}{2}-\frac{1}{6}\sqrt{6}, c/a=\sqrt{6}+3$	a	(001) 3^6	3, 1 6	
17	10	$Cmcm$	$4(c)$	$0,y,\frac{1}{4}$	$y=\frac{3}{4}-\frac{1}{4}\sqrt{6}$, $c/a=1, b/a=\sqrt{3}+\sqrt{2}$	a	(010) 4^4	4, 2 4	0.6657
18	10	$I4_1/amd$	$8(e)$	$0,0,z$	$z=\frac{1}{2}-\frac{1}{8}\sqrt{6}, c/a=2\sqrt{3}+2\sqrt{2}$	a	(001) 4^4	4, 2 8	
19	10	$I4/m$	$8(h)$	$x,y,0$	$x=\frac{6}{17}-\frac{1}{17}\sqrt{2}, y=\frac{7}{17}-\frac{4}{17}\sqrt{2}$ $c/a=(\frac{14}{17}-\frac{8}{17}\sqrt{2})^{1/2}$	c	–	–	0.6619
20	10	$R\bar{3}$	$18(f)$	x,y,z	$x=\frac{3}{7}, y=\frac{1}{7}, z=0, c/a=\frac{1}{7}\sqrt{42}$	$\frac{1}{7}\sqrt{7}a$	(001) 3^46	3, 2 3	0.6347
21	4	$Fd\bar{3}m$	$32(e)$	x,x,x	$x=\frac{3}{8}-\frac{1}{8}\sqrt{6}$	$(\frac{3}{4}\sqrt{2}-\frac{1}{2}\sqrt{3})a$	–	–	0.1235
22	4	$Im\bar{3}m$	$48(j)$	$0,y,z$	$y=\frac{4}{7}-\frac{3}{28}\sqrt{2}, z=\frac{5}{14}-\frac{1}{28}\sqrt{2}$	$(\frac{3}{14}\sqrt{2}-\frac{1}{7})a$	–	–	0.1033
23	4	$I4_132$	$48(i)$	x,y,z	$x=y=\frac{1}{8}\sqrt{2}, z=0$	$(\frac{1}{2}-\frac{1}{4}\sqrt{2})a$	–	–	0.0789
24	3	$I4_132$	$24(h)$	$\frac{1}{8},y,\frac{1}{4}-y$	$y=\frac{1}{4}\sqrt{3}-\frac{3}{8}$	$(\frac{1}{2}\sqrt{6}-\frac{3}{4}\sqrt{2})a$	–	–	0.0555

Two other types of homogeneous sphere packings (15 and 16) with contact number $k = 10$ also refer to densest layers of spheres. In these cases, each sphere has three contacts to one neighbouring layer and one contact to the other layer that is stacked directly above or below the original layer.

Cubic closest packings may also be regarded as built up from square layers 4^4 stacked in such a way that each sphere has four neighbouring spheres in the same layer and four neighbours each from the layers above and below (*cf.* Fig. 9.1.1.3). If square layers are stacked such that each sphere has contact to four spheres of one neighbouring layer and to two spheres of the other layer (*cf.* Fig. 9.1.1.4), sphere packings with contact number 10 result. In total, two types of homogeneous packings (17 and 18) with this kind of stacking exist. Sphere packings of type 9 may also be decomposed into 4^4 layers parallel to (101) or (011) in a five-layer sequence. These nets are made up from parallel rhombi and stacked such that each sphere has contact with three other spheres from the layer above and from the layer below. If such layers are stacked in a two-layer sequence, sphere packings of type 13 with symmetry *Cmcm* result (O'Keeffe, 1998). Sphere packings of type 14 are also build up from 4^4 layers, but here the rhombi occur in two different orientations (O'Keeffe, 1998). Sphere packings with high contact numbers may also be derived by stacking of other layers. Type 20, for example, refers to 3^46 layers where each sphere is in contact with three spheres of one neighbouring net and two spheres of the other one (Sowa & Koch, 1999). Such a sphere packing may alternatively be derived from the cubic closest packing by omitting systematically 1/7 of the spheres in each of the 3^6 nets.

Sphere packings of types 8 and 19 (*cf.* Figs. 9.1.1.5 and 9.1.1.6) cannot be built up from plane layers of spheres in contact although their contact numbers are also high.

Table 9.1.1.2 contains complete information on homogeneous sphere packings with $k = 10$, 11, and 12 and with cubic or tetragonal symmetry.

The least dense (most open) homogeneous sphere packings known so far have already been described by Heesch & Laves (1933). Sphere packings of that type (24) cannot be stable because their contact number is 3 (*cf.* Fig. 9.1.1.7). As discussed

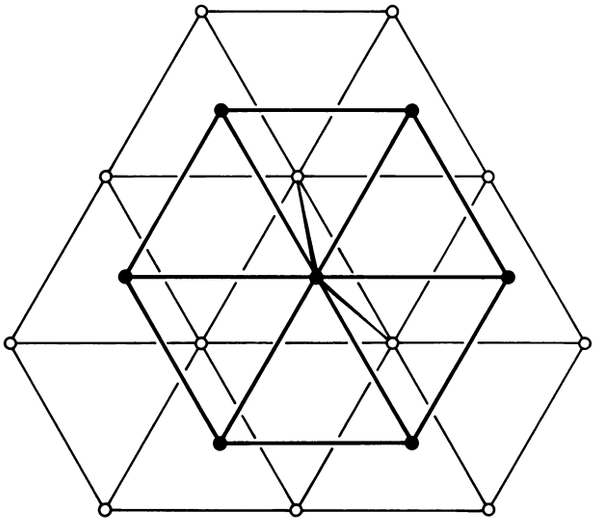

Fig. 9.1.1.2. Two triangular nets representing two densest packed layers of spheres. The layers are stacked in such a way that each sphere is in contact with two spheres of the other layer.

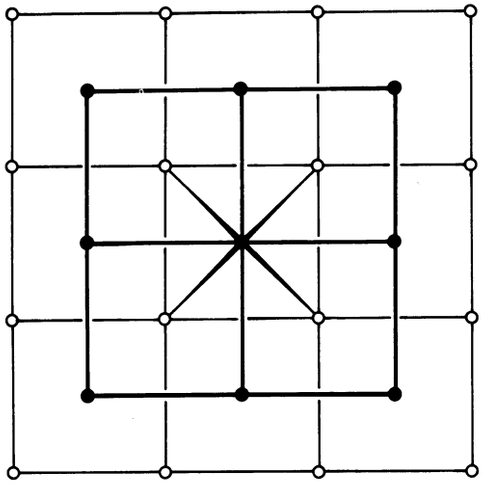

Fig. 9.1.1.3. Two square nets representing two layers of spheres stacked in such a way that each sphere is in contact with four spheres of the other layer.

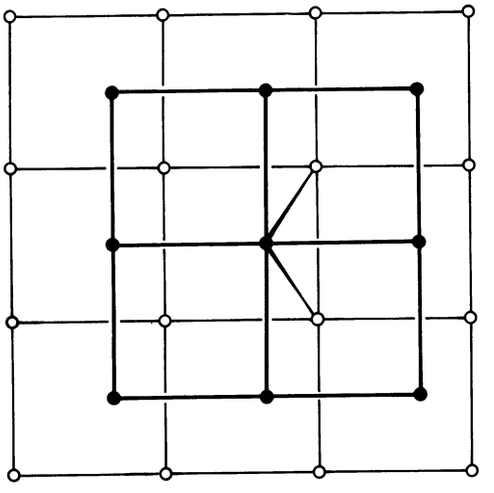

Fig. 9.1.1.4. Two square nets representing two layers of spheres stacked in such a way that each sphere is in contact with two spheres of the other layer.

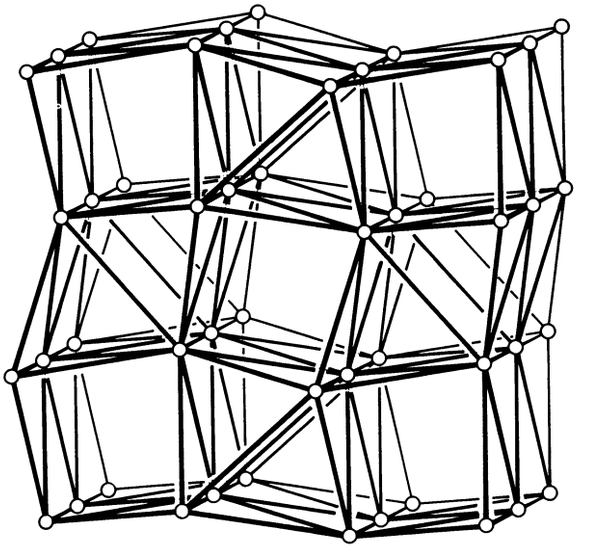

Fig. 9.1.1.5. Sphere packing of type 8 (Table 9.1.1.2) represented by a graph: $k = 11$, $P4_2/mnm$, $4(f)$, $xx0$.

by Fischer (1976), it is very probable that no homogeneous sphere packings with lower density exist; those discussed by Melmore (1942*a*,*b*) with $\rho = 0.042$ and $\rho = 0.045$ are heterogeneous ones. Recently, Koch & Fischer (1995) proved that the Heesch–Laves packing is the least dense homogeneous sphere packing with three contacts per sphere.

The least dense sphere packings with contact number 4 derived so far are described as type 23. All sphere packings of this type are similar in the geometrical sense and are not stable. In contrast, the sphere packings of type 22 are stable. Sphere packings of type 21 (Heesch & Laves, 1933), which have been supposed to be the most open stable ones (*cf.* Hilbert & Cohn-Vossen, 1932, 1952), have a slightly higher density.

On the basis of the material known at that time, Slack (1983) tried to develop empirical formulae for the minimal and the maximal density of circle packings and sphere packings depending on the contact number. A paper by O'Keeffe (1991) on four-connnected nets pays special attention to the densest and the least dense sphere packings with four contacts per sphere.

9.1.1.4. *Applications*

Sphere packings have been used for the description of inorganic crystal structures in different ways and by several authors (*e.g.* Brunner, 1971; Figueiredo & Lima-de-Faria, 1978; Frank & Kasper, 1958; Hellner, 1965; Hellner, Koch & Reinhardt, 1981; Koch, 1984, 1985; Laves, 1930, 1932; Lima-de-Faria, 1965; Lima-de-Faria & Figueiredo, 1969*a*,*b*; Loeb, 1958; Morris & Loeb, 1960; Niggli, 1927; Smirnova, 1956*a*,*b*, 1958*a*,*b*, 1959*a*,*b*,*c*, 1964; Sowa, 1988, 1997).

In the simplest case, the structure of an element may be described as a sphere packing if all atoms are interrelated by equal or almost equal shortest distances. This does not imply that the atoms really have to be considered as hard spheres of that size. Often such sphere packings are homogeneous ones with a high contact number k (*e.g.* Cu, Mg with $k = 12$; Pa with $k = 10$; W with $k = 8$). Low values of k (*e.g.* diamond with $k = 4$, white tin with $k = 6$) and heterogeneous sphere packings (La with $k = 12$) have also been observed for structures of elements.

Crystal structures consisting of different atoms may be related to sphere packings in different ways:

(1) The structure as a whole may be considered as a heterogeneous sphere packing. In that case, contacts at least between different spheres are present (*e.g.* CsCl, NaCl, CaF_2). In addition, contacts between equal atoms may exist (I—I contacts in CsI) or may even be necessary (CdI_2). In general, a type of heterogeneous sphere packing is compatible with a certain range of radius ratios (*cf.* alkali halides). In special cases, a heterogeneous sphere packing may be derived from a homogeneous one by subgroup degradation (*e.g.* NaCl, CsCl, PtCu).

(2) Part of the crystal structure, *e.g.* the anions or the more frequent kind of atoms, may be considered as a sphere packing whereas the other atoms are located within the voids of that sphere packing. For this approach, the atoms corresponding to the sphere packing need not necessarily be in contact (*cf.* *e.g.* the Cl—Cl distances in NaCl and LiCl). Voids within sphere packings have been discussed in particular in connection with closest packings (*e.g.* Cl in NaCl, O in Li_2O, S in ZnS, O in olivine), but numerous examples for non-closest packings are known in addition (*e.g.* B in CaB_6 with $k = 5$; O in rutile with $k = 11$, type 8 in Table 9.1.1.2; Si in α-$ThSi_2$ with $k = 3$). Sphere packings and their voids form the basis for Hellner's framework concept (*cf.* *e.g.* Hellner *et al.*, 1981). Voids may be calculated systematically as vertices of Dirichlet domains (*cf.* Hellner *et al.*, 1981; Koch, 1984). The tendency to form regular voids of the appropriate size for the cations may counteract the tendency to form an ideal sphere packing of the anions. Examples are spinel and garnet (*cf.* Hellner, Gerlich, Koch & Fischer, 1979).

(3) Frequently, the cations within a crystal structure are also distributed according to a sphere packing. This is explicable because the repulsion between the cations also favours an arrangement with equal but maximal shortest distances (*cf.* Brunner, 1971). In this sense, many crystal structures may be

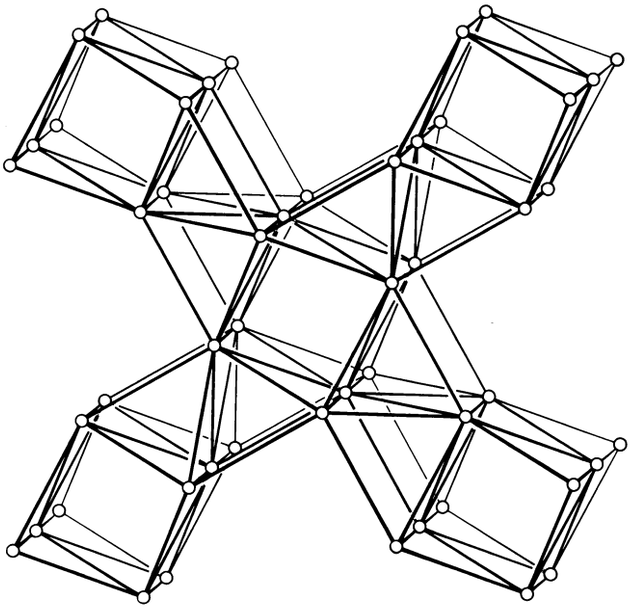

Fig. 9.1.1.6. Sphere packing of type 19 (Table 9.1.1.2) represented by a graph: $k = 10$, $I4/m$, 8(*h*), *xy*0.

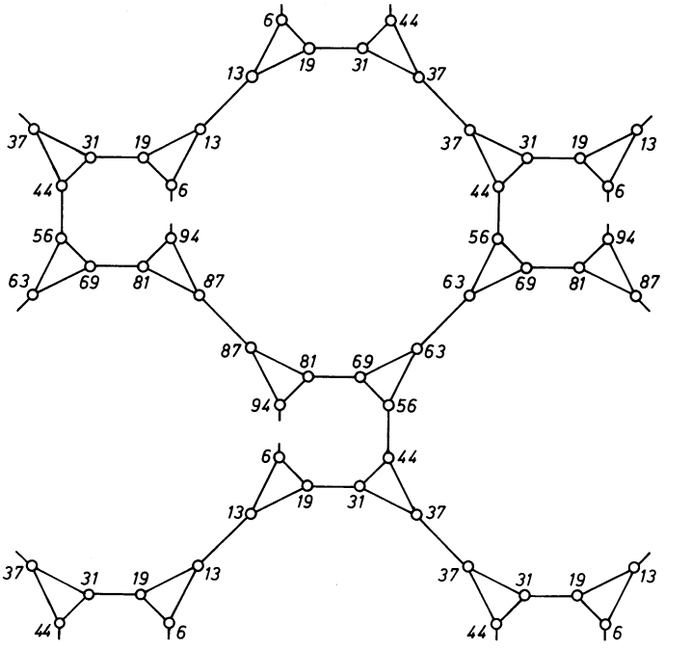

Fig. 9.1.1.7. Least dense sphere packing known so far (type 24 of Table 9.1.1.2) represented by a graph: $k = 3$, $I4_132$, 24(*h*), $\frac{1}{8}, y, \frac{1}{4} - y$. *z* coordinates given in multiples of 1/100.

described as sets of several sphere packings (one for each kind of atom) that are fitted into each other (*e.g.* NaCl, CaF_2, CaB_6, α-$ThSi_2$, rutile, Cu_2O, $CaTiO_3$).

Because of their importance for problems in digital communication (error-correcting codes) and in number theory (solving of diophantine equations), densest sphere packings in higher dimensions are of mathematical interest (*cf.* Conway & Sloane, 1988).

9.1.1.5. *Interpenetrating sphere packings*

Special homogeneous or heterogeneous sets of spheres may be subdivided into a small number i of subsets such that each subset, regarded by itself, forms a sphere packing and that spheres of different subsets do not have mutual contact. Sets of spheres with these properties are called *interpenetrating sphere packings*.

The cubic Laves phases are a well known example for heterogeneous interpenetrating sphere packings. The Mg atoms in $MgCu_2$ [$Fd\bar{3}m$, 8(a)], for example, correspond to a sphere packing with shortest distances $d_1 = \sqrt{3}a/4$ and contact number $k = 4$ whereas the copper atoms [16(d)] refer to another sphere packing with shortest distances $d_2 = \sqrt{2}a/4$ and $k = 6$. The shortest distances between centres of different spheres are $d_3 = \sqrt{11}a/8 > (d_1 + d_2)/2$.

The crystal structure of Cu_2O gives an example of a different kind. If one takes into account the size of the atoms, sphere contacts can only be expected between different spheres. As a consequence, the heterogeneous set of spheres disintegrates into two heterogeneous but congruent subsets with no mutual contact.

In the case of homogeneous interpenetrating sphere packings, all i subsets have to be symmetry-equivalent. Then the symmetry of each subset is a subgroup of index i of the original space group. Homogeneous interpenetrating sphere packings with cubic symmetry have been derived completely by Fischer & Koch (1976). They may be classified into 39 types. For 33 of the 39 types, the number i of subsets is 2; i is 3, 4, and 8 for 1, 3, and 2 types, respectively.

Remarkable are those homogeneous interpenetrating sphere packings that are built up from sphere packings of type 24 (Table 9.1.1.2), *i.e.* that type with the least dense sphere packing. Combinations of 2, 4, or 8 such sphere packings result in altogether 8 different types of interpenetrating sphere packings (Fischer, 1976). The P atoms in the crystal structure of Th_3P_4 give an example for such interpenetrating sphere packings built up from two congruent subsets (Koch, 1984).

Complete results for other crystal systems are not available. With tetragonal symmetry, interpenetrating sphere packings are known, built up from 2, 3, or 5 congruent subsets (Fischer, 1970). Analogous interpenetration patterns are formed by hydrogen bonds within certain molecular structures (Ermer, 1988; Ermer & Eling, 1988).

Interpenetrating sphere packings may be brought in relation to interpenetrating labyrinths as formed by periodic minimal surfaces or by periodic zero-potential surfaces without self-intersection (*cf. e.g.* Andersson, Hyde & von Schnering, 1984; Fischer & Koch, 1987, 1996; von Schnering & Nesper, 1987).

9.1.2. Packings of ellipses and ellipsoids

The problem of deriving packings of ellipses in two-dimensional space or of ellipsoids in three-dimensional space may be regarded as a generalization of the problem of deriving circle packings and sphere packings. It is much more complicated, however, because a circle or sphere is fully determined by its centre and its radius, whereas the knowledge of the centre, the lengths of the two semiaxes, and the direction of one of them is needed to construct an ellipse. For an ellipsoid, the knowledge of its centre, the length of its three semiaxes, and the directions of two of them is necessary. Accordingly, the point configuration corresponding to the ellipsoid centres does not define the ellipsoid packing and not even its type.

Nowacki (1948) derived 54 homogeneous 'essentially different packings of ellipses'. In contrast to the definition of types of sphere (circle) packings (Section 9.1.1), Nowacki distinguished between similar packings with different plane-group symmetry, *i.e.* between packings that may differ in the orientation of their ellipses. Under an equivalent classification, Grünbaum & Shephard (1987) derived 57 different cases of ellipse packings, thus correcting and completing Nowacki's list. Each of these 57 cases corresponds uniquely to one of the 11 types of circle packings if one takes into account only the contact relations between ellipses and circles. In eight cases, each ellipse has six contacts. Two of these cases can be derived from the densest packing of circles by affine transformations and, therefore, have the same density, namely $\rho = 0.9069$, irrespective of the shape of the ellipses (Matsumoto & Nowacki, 1966). Presumably for the other six cases this density can only be reached (but not exceeded) if the ellipses become circles. A corresponding proof is in progress (Matsumoto, 1968; Tanemura & Matsumoto, 1992; Matsumoto & Tanemura, 1995).

Very little systematic work seems to be carried out on homogeneous or heterogeneous packings of ellipsoids. Matsumoto & Nowacki (1966) derived packings of ellipsoids with contact numbers 12 and high densities by affine deformation of cubic and hexagonal closest packings of spheres. They postulate (without proof) the following: Densest packings of ellipsoids have the same contact number and density as closest packings of spheres and can be derived always from closest sphere packings by affine transformations. If this assumption is true, densest packings of ellipsoids would necessarily consist of parallel ellipsoids only.

Packings of ellipsoids seemed to be useful for the interpretation of the arrangements of organic molecules in crystals. The studies of Kitaigorodsky (1946, 1961, 1973), however, showed that molecular crystals may rather be regarded as dense packings of molecules with irregular shape.

Heterogeneous packings of ellipsoids may possibly be adequate for the geometrical interpretation of some intermetallic compounds like cubic $MgCu_2$ (*cf.* Subsection 9.1.1.4) or Cr_3Si. The ellipsoids enable the use of different 'atomic radii' with respect to neighbouring atoms of the same kind or of different kinds. In $MgCu_2$, for example, the magnesium atoms have cubic site symmetry $\bar{4}3m$ [$Fd\bar{3}m$, 8(a)] and therefore can only be represented by spheres. The Cu atoms [16(d)] with site symmetry $.\bar{3}m$, however, may be represented by flattened ellipsoids of revolution.

International Tables for Crystallography (2006). Vol. C, Chapter 9.2, pp. 752–773.

9.2. Layer stacking

BY S. ĎUROVIČ, P. KRISHNA AND D. PANDEY

9.2.1. Layer stacking in close-packed structures (By D. Pandey and P. Krishna)

The crystal structures of a large number of materials can be described in terms of stacking of layers of atoms. This chapter provides a brief account of layer stacking in materials with structures based on the geometrical principle of close packing of equal spheres.

9.2.1.1. *Close packing of equal spheres*

9.2.1.1.1. *Close-packed layer*

In a close-packed layer of spheres, each sphere is in contact with six other spheres as shown in Fig. 9.2.1.1. This is the highest number of nearest neighbours for a layer of identical spheres and therefore yields the highest packing density. A single close-packed layer of spheres has two-, three- and sixfold axes of rotation normal to its plane. This is depicted in Fig. 9.2.1.2(*a*), where the size of the spheres is reduced for clarity. There are three symmetry planes with indices $(1\bar{2}.0)$, $(\bar{2}1.0)$, and (11.0) defined with respect to the smallest two-dimensional hexagonal unit cell shown in Fig. 9.2.1.2(*b*). The point-group symmetry of this layer is 6*mm* and it has a hexagonal lattice. As such, a layer with such an arrangement of spheres is often called a hexagonal close-packed layer. We shall designate the positions of spheres in the layer shown in Fig. 9.2.1.1 by the letter '*A*'. This *A* layer has two types of triangular interstices, one with the apex angle up (△) and the other with the apex angle down (▽). All interstices of one kind are related by the same hexagonal lattice as that for the *A* layer. Let the positions of layers with centres of spheres above the centres of the △ and ▽ interstices be designated as '*B*' and '*C*', respectively. In the cell of the *A* layer shown in Fig. 9.2.1.1 ($a = b =$ diameter of the sphere and $\gamma = 120°$), the three positions *A*, *B*, and *C* on projection have coordinates (0, 0), $(\frac{1}{3}, \frac{2}{3})$, and $(\frac{2}{3}, \frac{1}{3})$, respectively.

9.2.1.1.2. *Close-packed structures*

A three-dimensional close-packed structure results from stacking the hexagonal close-packed layers in the *A*, *B*, or *C* position with the restriction that no two successive layers are in identical positions. Thus, any sequence of the letters *A*, *B*, and *C*, with no two successive letters alike, represents a possible manner of stacking the hexagonal close-packed layers. There are thus infinite possibilities for close-packed layer stackings. The identity period *n* of these layer stackings is determined by the number of layers after which the stacking sequence starts repeating itself. Since there are two possible positions for a new layer on the top of the preceding layer, the total number of possible layer stackings with a repeat period of *n* is 2^{n-1}.

In all the close-packed layer stackings, each sphere is surrounded by 12 other spheres. However, it is touched by all 12 spheres only if the axial ratio h/a is $\sqrt{2/3}$, where *h* is the separation between two close-packed layers and *a* is the diameter of the spheres (Verma & Krishna, 1966). Deviations from the ideal value of the axial ratio are common, especially in hexagonal metals (Cottrell, 1967). The arrangement of spheres described above provides the highest packing density of 0.7405 in the ideal case for an infinite lattice (Azaroff, 1960). There are, however, other arrangements of a finite number of equal spheres that have a higher packing density (Boerdijk, 1952).

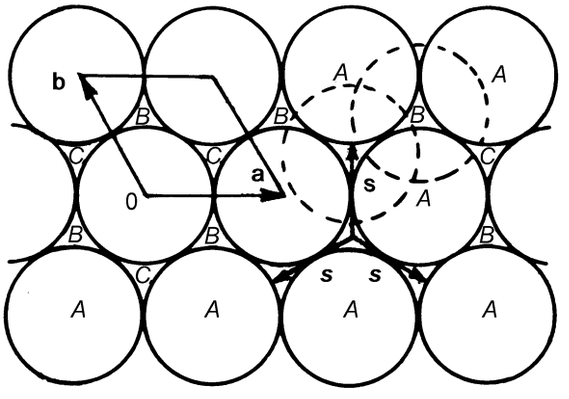

Fig. 9.2.1.1. The close packing of equal spheres in a plane.

9.2.1.1.3. *Notations for close-packed structures*

In the Ramsdell notation, close-packed structures are designated as *nX*, where *n* is the identity period and *X* stands for the lattice type, which, as shown later, can be hexagonal (*H*), rhombohedral (*R*), or in one special case cubic (*C*) (Ramsdell, 1947).

In the Zhdanov notation, use is made of the stacking offset vector **s** and its opposite −**s**, which cause, respectively, a

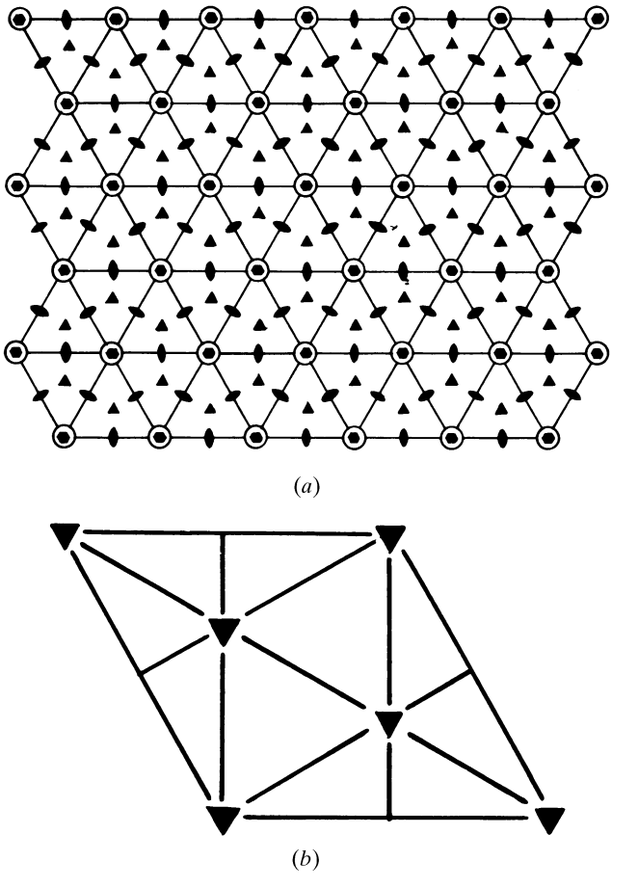

(*a*)

(*b*)

Fig. 9.2.1.2. (*a*) Symmetry axes of a single close-packed layer of spheres and (*b*) the minimum symmetry of a three-dimensional close packing of spheres.

Copyright © 2006 International Union of Crystallography

Table 9.2.1.1. *Common close-packed metallic structures*

Stacking sequence	Identity period	Ramsdell notation	Zhdanov notation	Jagodzinski notation	Prototype
$AB, A\ldots$	2	2*H*	11	*h*	Mg
$ABC, A\ldots$	3	3*C*	∞	*c*	Cu
$ABCB, A\ldots$	4	4*H*	22	*hc*	La
$ABCBCACAB, A\ldots$	9	9*R*	21	*hhc*	Sm

cyclic ($A \rightarrow B \rightarrow C \rightarrow A$) or anticyclic ($A \rightarrow C \rightarrow B \rightarrow A$) shift of layers in the same plane. The vector **s** can be either (1/3)[1$\bar{1}$00], (1/3)[01$\bar{1}$0], or (1/3)[$\bar{1}$010]. Zhdanov (1945) suggested summing the number of consecutive offsets of each kind and designating them by numeral figures. Successive numbers in the Zhdanov symbol have opposite signs. The rhombohedral stackings have three identical sets of Zhdanov symbols in an identity period. It is usually sufficient to write only one set.

Yet another notation advanced, amongst others, by Jagodzinski (1949*a*) makes use of configurational symbols for each layer. A layer is designated by the symbol *h* or *c* according as its neighbouring layers are alike or different. Letter '*k*' in place of '*c*' is also used in the literature.

Some of the common close-packed structures observed in metals are listed in Table 9.2.1.1 in terms of all the notations.

9.2.1.2. *Structure of compounds based on close-packed layer stackings*

Frequently, the positions of one kind of atom or ion in inorganic compounds, such as SiC, ZnS, CdI_2, and GaSe, correspond approximately to those of equal spheres in a close packing, with the other atoms being distributed in the voids. All such structures will also be referred to as close-packed structures though they may not be ideally close packed. In the close-packed compounds, the size and coordination number of the smaller atom/ion may require that its close-packed neighbours in the neighbouring layers do not touch each other.

9.2.1.2.1. *Voids in close packing*

Three-dimensional close packings of spheres have two kinds of voids (Azaroff, 1960):

(i) If the triangular interstices in a close-packed layer have spheres directly over them, the resulting voids are called tetrahedral voids because the four spheres surrounding the void are arranged at the corners of a regular tetrahedron (Figs. 9.2.1.3*a*,*b*). If *R* denotes the radius of the four spheres surrounding a tetrahedral void, the radius of the sphere that would just fit into this void is given by 0.225*R* (Verma & Krishna, 1966). The centre of the tetrahedral void is located at a distance 3*h*/4 from the centre of the sphere on top of it.

(ii) If the triangular interstices pointing up in one close-packed layer are covered by triangular interstices pointing down in the adjacent layer, the resulting voids are called octahedral voids (Figs. 9.2.1.3*c*,*d*) since the six spheres surrounding each such void lie at the corners of a regular octahedron. The radius of the sphere that would just fit into an octahedral void is given by 0.414*R* (Verma & Krishna, 1966). The centre of this void is located half way between the two layers of spheres.

While there are twice as many tetrahedral voids as the spheres in close packing, the number of octahedral voids is equal to the number of spheres (Krishna & Pandey, 1981).

9.2.1.2.2. *Structures of SiC and ZnS*

SiC has a binary tetrahedral structure in which Si and C layers are stacked alternately, each carbon layer occupying half the tetrahedral voids between successive close-packed silicon layers. One can regard the structure as consisting of two identical interpenetrating close packings, one of Si and the other of C, with the latter displaced relative to the former along the stacking axis through one fourth of the layer spacing. Since the positions of C atoms are fixed relative to the positions of layers of Si atoms, it is customary to use the letters *A*, *B*, and *C* as representing Si–C double layers in the close packing. To be more exact, the three kinds of layers need to be written as $A\alpha$, $B\beta$, and $C\gamma$ where Roman and Greek letters denote the positions of Si and C atoms, respectively. Fig. 9.2.1.4 depicts the structure of SiC-6*H*, which is the most common modification.

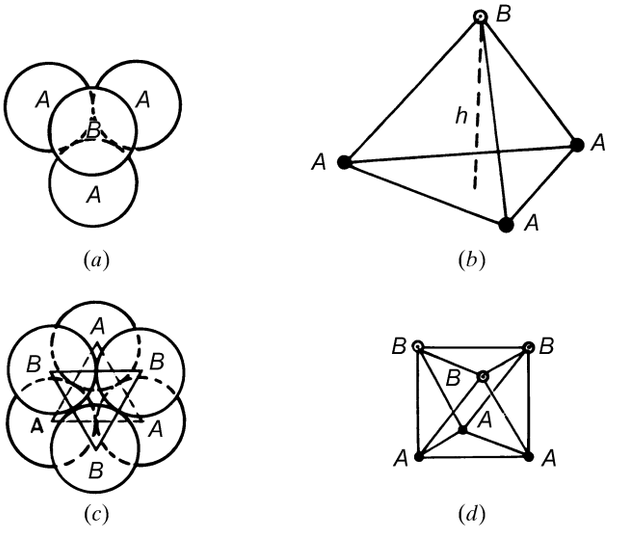

Fig. 9.2.1.3. Voids in a close packing: (*a*) tetrahedral void; (*b*) tetrahedron formed by the centres of spheres; (*c*) octahedral void; (*d*) octahedron formed by the centres of spheres.

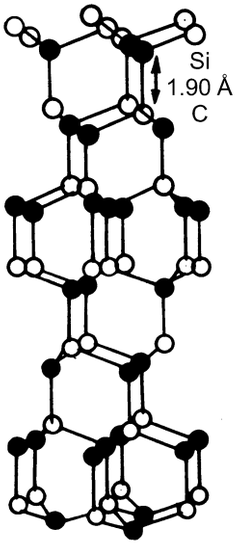

Fig. 9.2.1.4. Tetrahedral arrangement of Si and C atoms in the SiC-6*H* structure.

Table 9.2.1.2. *List of SiC polytypes with known structures in order of increasing periodicity (after Pandey & Krishna, 1982a)*

Polytype	Structure (Zhdanov sequence)	Polytype	Structure (Zhdanov sequence)
$2H$	11	$57H$	$(23)_9 3333$
$3C$	∞	$57R$	$(33)_2 34$
$4H$	22	$69R_1$	$(33)_3 32$
$6H$	33	$69R_2$	33322334
$8H$	44	$75R_2$	$(32)_3(23)_2$
$10H$	3322	$81H$	$(33)_5 35(33)_6 34$
$14H$	$(22)_2 33$	$84R$	$(33)_3(32)_2$
$15R$	23	$87R$	$(33)_4 32$
$16H_1$	$(33)_2 22$	$90R$	$(23)_4 3322$
$18H$	$(22)_3 33$	$93R$	$(33)_4 34$
$19H$	$(23)_3 22$	$96R_1$	$(33)_3 3434$
$20H$	$(22)_3 44$	$99R$	$(33)_4 3222$
$21H$	333534	$105R$	$(33)_5 32$
$21H_2$	$(33)_2 63$	$111R$	$(33)_5 34$
$21R$	34	$120R$	$(22)_5 23222333$
$24R$	35	$123R$	$(33)_6 32$
$27H$	$(33)_2(23)_3$	$126R$	$(33)_2 2353433223$
$27R$	2223	$129R$	$(33)_6 34$
$33R$	3332	$125R$	$32(33)_2 23(33)_3 23$
$33H$	$(33)_2 353334$	$141R$	$(33)_7 32$
$34H$	$(33)_4 2332$	$147R$	$(3332)_4 32$
$36H_1$	$(33)_2 32(33)_2 34$	$150R_1$	$(23)_3 32(23)_3 322332$
$36H_2$	$(33)_4 3234$	$150R_2$	$(23)_2(3223)_4$
$39H$	$(33)_2 32(33)_3(32)_2$	$159R$	$(33)_8 32$
$39R$	3334	$168R$	$(23)_{10} 33$
$40H$	$(33)_5 2332$	$174R$	$(33)_6 6(33)_5 4$
$45R$	$(23)_2 32$	$189R$	$(34)_8 43$
$51R_1$	$(33)_2 32$	$267R$	$(23)_{17} 22$
$51R_2$	$(22)_3 23$	$273R$	$(23)_{17} 33$
$54H$	$(33)_6 323334$	$393R$	$(33)_{21} 32$

A large number of crystallographically different modifications of SiC, called polytypes, has been discovered in commercial crystals grown above 2273 K (Verma & Krishna, 1966; Pandey & Krishna, 1982*a*). Table 9.2.1.2 lists those polytypes whose structures have been worked out. All these polytypes have $a = b = 3.078$ Å and $c = n \times 2.518$ Å, where n is the number of Si–C double layers in the hexagonal cell. The $3C$ and $2H$ modifications, which normally result below 2273 K, are known to undergo solid-state structural transformation to $6H$ (Jagodzinski, 1972; Krishna & Marshall, 1971*a*,*b*) through a non-random insertion of stacking faults (Pandey, Lele & Krishna, 1980*a*,*b*,*c*; Kabra, Pandey & Lele, 1986). The lattice parameters and the average thickness of the Si–C double layers vary slightly with the structure, as is evident from the h/a ratios of 0.8205 (Adamsky & Merz, 1959), 0.8179, and 0.8165 (Taylor & Jones, 1960) for the $2H$, $6H$, and $3C$ structures, respectively. Even in the same structure, crystal-structure refinement has revealed variation in the thickness of Si–C double layers depending on their environment (de Mesquita, 1967).

The structure of ZnS is analogous to that of SiC. Like the latter, ZnS crystals grown from the vapour phase also display a large variety of polytype structures (Steinberger, 1983). ZnS crystals that occur as minerals usually correspond to the wurtzite ($/AB/\ldots$) and the sphalerite ($/ABC/\ldots$) modifications. The structural transformation between the $2H$ and $3C$ structures of ZnS is known to be martensitic in nature (Sebastian, Pandey & Krishna, 1982; Pandey & Lele, 1986*b*). The h/a ratio for ZnS-$2H$ is 0.818, which is somewhat different from the ideal value (Verma & Krishna, 1966). The structure of the stackings in polytypic AgI is analogous to those in SiC and ZnS (Prager, 1983).

9.2.1.2.3. *Structure of CdI_2*

The structure of cadmium iodide consists of a close packing of the I ions with the Cd ions distributed amongst half the octahedral voids. Thus, the Cd and I layers are not stacked alternately; there is one Cd layer after every two I layers as shown in Fig. 9.2.1.5. The structure actually consists of molecular sheets (called minimal sandwiches) with a layer of Cd ions sandwiched between two close-packed layers of I ions. The bonding within the minimal sandwich is ionic in character and is much stronger than the bonding between successive sandwiches, which is of van der Waals type. The importance of polarization energy for the stability of such structures has recently been emphasized by Bertaut (1978). It is because of the weak van der Waals bonding between the successive minimal sandwiches that the material possesses the easy cleavage characteristic of a layer structure. In describing the layer stackings in the CdI_2 structure, it is customary to use Roman letters to denote the I positions and Greek letters for the Cd positions. The two most common modifications of CdI_2 are $4H$ and $2H$ with layer stackings $A\gamma B\,C\alpha B\ldots$ and $A\gamma B\,A\gamma B$, respectively. In addition, this material also displays a number of polytype modifications of large repeat periods (Trigunayat & Verma, 1976; Pandey & Krishna, 1982*a*). From the structure of CdI_2, it follows that the identity period of all such modifications must consist of an even number of I layers. The h/a ratio in all these modifications of CdI_2 is 0.805, which is very different from the ideal value (Verma & Krishna, 1966). The structure of PbI_2, which also displays a large number of polytypes, is analogous to CdI_2 with one important difference. Here, the distances between two I layers with and without an intervening Pb layer are quite different (Trigunayat & Verma, 1976).

9.2.1.2.4. *Structure of GaSe*

The crystal structure of GaSe consists of four-layered slabs, each of which contains two close-packed layers of Ga (denoted by symbols A, B, C) and Se (denoted by symbols α, β, γ) each in the sequence Se–Ga–Ga–Se (Terhell, 1983). The Se atoms sit on the corners of a trigonal prism while each Ga atom is tetrahedrally coordinated by three Se and one Ga atoms. If the Se layers are of A type, then the stacking sequence of the four

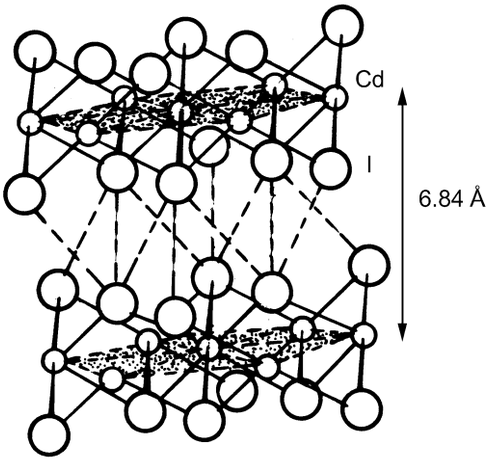

Fig. 9.2.1.5. The layer structure of CdI_2: small circles represent Cd ions and larger ones I ions (after Wells, 1945).

layers in the slab can be written as $A\beta\beta A$ or $A\gamma\gamma A$. There are thus six possible sequences for the unit slab. These unit slabs can be stacked in the manner described for equal spheres. Thus, for example, the $2H$ structure can have three different layer stackings: $/A\beta\beta A\,B\gamma\gamma B/\ldots$, $/A\beta\beta A\,B\alpha\alpha B/\ldots$ and $/A\beta\beta A\,C\beta\beta C/$. Periodicities containing up to 21 unit slabs have been reported for GaSe (see Terhell, 1983). The bonding between the layers of a slab is predominantly covalent while that between two adjacent slabs is of the van der Waals type, which imparts cleavage characteristics to this material.

9.2.1.3. *Symmetry of close-packed layer stackings of equal spheres*

It can be seen from Fig. 9.2.1.2(*a*) that a stacking of two or more layers in the close-packed manner still possesses all three symmetry planes but the twofold axes disappear while the sixfold axes coincide with the threefold axes (Verma & Krishna, 1966). The lowest symmetry of a completely arbitrary periodic stacking sequence of close-packed layers is shown in Fig. 9.2.1.2(*b*). Structures resulting from such stackings therefore belong to the trigonal system. Even though a pure sixfold axis of rotation is not possible, close-packed structures belonging to the hexagonal system can result by virtue of at least one of the three symmetry axes parallel to [00.1] being a 6_3 axis (Verma & Krishna, 1966). This is possible if the layers in the unit cell are stacked in special ways. For example, a $6H$ stacking sequence $/ABCACB/\ldots$ has a 6_3 axis through 0, 0. It follows that, for an nH structure belonging to the hexagonal system, n must be even. A packing nH/nR with n odd will therefore necessarily belong to the trigonal system and can have either a hexagonal or a rhombohedral lattice (Verma & Krishna, 1966).

Other symmetries that can arise by restricting the arbitrariness of the stacking sequence in the identity period are: (i) a centre of symmetry at the centre of either the spheres or the octahedral voids; and (ii) a mirror plane perpendicular to [00.1]. Since there must be two centres of symmetry in the unit cell, the centrosymmetric arrangements may possess both centres either at sphere centres/octahedral void centres or one centre each at the centres of spheres and octahedral voids (Patterson & Kasper, 1959).

9.2.1.4. *Possible lattice types*

Close packings of equal spheres can belong to the trigonal, hexagonal, or cubic crystal systems. Structures belonging to the hexagonal system necessarily have a hexagonal lattice, *i.e.* a lattice in which we can choose a primitive unit cell with $a = b \neq c$, $\alpha = \beta = 90^\circ$, and $\gamma = 120^\circ$. In the primitive unit cell of the hexagonal close-packed structure $/AB/\ldots$ shown in Fig. 9.2.1.6, there are two spheres associated with each lattice point, one at 0, 0, 0 and the other at $\frac{1}{3}, \frac{2}{3}, \frac{1}{2}$. Structures belonging to the trigonal system can have either a hexagonal or a rhombohedral lattice. By a rhombohedral lattice is meant a lattice in which we can choose a primitive unit cell with $a = b = c$, $\alpha = \beta = \gamma \neq 90^\circ$. Both types of lattice can be referred to either hexagonal or rhombohedral axes, the unit cell being non-primitive when a hexagonal lattice is referred to rhombohedral axes and *vice versa* (Buerger, 1953). In close-packed structures, it is generally convenient to refer both hexagonal and rhombohedral lattices to hexagonal axes. Fig. 9.2.1.7 shows a rhombohedral lattice in which the primitive cell is defined by the rhombohedral axes a_1, a_2, a_3; but a non-primitive hexagonal unit cell can be chosen by adopting the axes A_1, A_2, C. The latter has lattice points at $0, 0, 0$; $\frac{2}{3}, \frac{1}{3}, \frac{1}{3}$; and $\frac{1}{3}, \frac{2}{3}, \frac{2}{3}$. If this rhombohedral lattice is rotated through 60° around [00.1], the hexagonal unit cell will then be centred at $\frac{1}{3}, \frac{2}{3}, \frac{1}{3}$ and $\frac{2}{3}, \frac{1}{3}, \frac{2}{3}$. These two settings are crystallographically equivalent for close packing of equal spheres. They represent twin arrangements when both occur in the same crystal. The hexagonal unit cell of an nR structure is made up of three elementary stacking sequences of $n/3$ layers that are related to each other either by an anticyclic shift of layers $A \rightarrow C \rightarrow B \rightarrow A$ (obverse setting) or by a cyclic shift of layers $A \rightarrow B \rightarrow C \rightarrow A$ (reverse setting) in the direction of z increasing (Verma & Krishna, 1966). Evidently, n must be a multiple of 3 for nR structures.

In the special case of the close packing $/ABC/\ldots$ [with the ideal axial ratio of $\sqrt{(2/3)}$], the primitive rhombohedral unit cell has $\alpha = \beta = \gamma = 60^\circ$, which enhances the symmetry and enables the choice of a face-centred cubic unit cell. The relationship between the face-centred cubic and the rhombohedral unit cell is shown in Fig. 9.2.1.8. The threefold axis of the rhombohedral unit cell coincides with one of the ⟨111⟩ directions of the cubic unit cell. The close-packed layers are thus parallel to the {111} planes in the cubic close packing.

9.2.1.5. *Possible space groups*

It was shown by Belov (1947) that consistent combinations of the possible symmetry elements in close packing of equal spheres can give rise to eight possible space groups: $P3m1$, $P\bar{3}m1$,

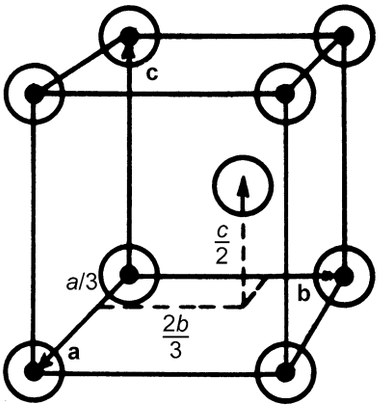

Fig. 9.2.1.6. The primitive unit cell of the $2H$ close packing.

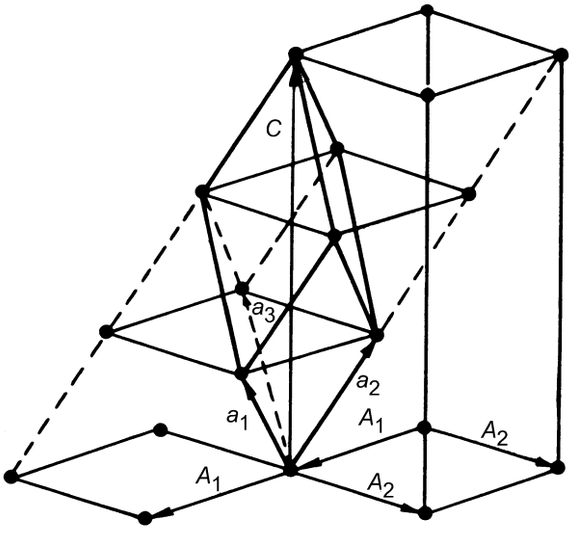

Fig. 9.2.1.7. A rhombohedral lattice (a_1, a_2, a_3) referred to hexagonal axes (A_1, A_2, C) (after Buerger, 1953).

$P\bar{6}m2$, $P6_3mc$, $P6_3/mmc$, $R3m$, $R\bar{3}m$, and $Fm3m$. The last space group corresponds to the special case of cubic close packing $/ABC/\ldots$. The tetrahedral arrangement of Si and C in SiC does not permit either a centre of symmetry ($\bar{1}$) or a plane of symmetry (m) perpendicular to [00.1]. SiC structures can therefore have only four possible space groups $P3m1$, $R3m1$, $P6_3mc$, and $F\bar{4}3m$. CdI_2 structures can have a centre of symmetry on octahedral voids, but cannot have a symmetry plane perpendicular to [00.1]. CdI_2 can therefore have five possible space groups: $P3m1$, $P\bar{3}m$, $R3m$, $R\bar{3}m$, and $P6_3mc$. Cubic symmetry is not possible in CdI_2 on account of the presence of Cd atoms, the sequence $/A\gamma BC\beta AB\alpha C/$ representing a 6R structure.

9.2.1.6. *Crystallographic uses of Zhdanov symbols*

From the Zhdanov symbols of a close-packed structure, it is possible to derive information about the symmetry and lattice type (Verma & Krishna, 1966). Let n_+ and n_- be the number of positive and negative numerals in the Zhdanov sequence of a given structure. The lattice is rhombohedral if $n_+ - n_- = \pm 1 \bmod 3$, otherwise it is hexagonal. The + sign corresponds to the reverse setting and − to the obverse setting of the rhombohedral lattice. Since this criterion is sufficient for the identification of a rhombohedral structure, the practice of writing three units of identical Zhdanov symbols has been abandoned in recent years (Pandey & Krishna, 1982*a*). Thus the 15R polytype of SiC is written as (23) rather than $(23)_3$.

As described in detail by Verma & Krishna (1966), if the Zhdanov symbol consists of an odd set of numbers repeated twice, *e.g.* (22), (33), (221221) *etc.*, the structure can be shown to possess a 6_3 axis. For the centre of symmetry at the centre of a sphere or an octahedral void, the Zhdanov symbol will consist of a symmetrical arrangement of numbers of like signs surrounding a single even or odd Zhdanov number, respectively. Thus, the structures (2)32(4)23 and (3)32(5)23 have centres of symmetry of the two types in the numbers within parentheses. For structures with a symmetry plane perpendicular to [00.1], the Zhdanov symbols consist of a symmetrical arrangement of a set of numbers of opposite signs about the space between two succession numbers. Thus, a stacking |522|225| has mirror planes at positions indicated by the vertical lines.

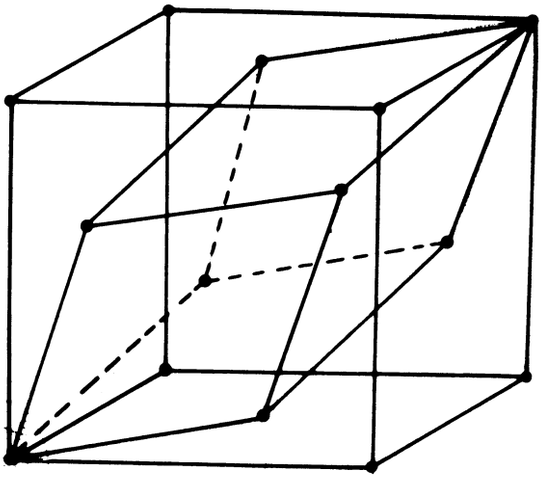

Fig. 9.2.1.8. The relationship between the f.c.c. and the primitive rhombohedral unit cell of the c.c.p. structure.

The use of abridged symbols to describe crystal structures has sometimes led to confusion in deciding the crystallographic equivalence of two polytype structures. For example, the structures (13) and (31) are identical for SiC but not for CdI_2 (Jain & Trigunayat, 1977*a*,*b*).

9.2.1.7. *Structure determination of close-packed layer stackings*

9.2.1.7.1. *General considerations*

The different layer stackings (polytypes) of the same material have identical a and b parameters of the direct lattice. The a^*b^* reciprocal-lattice net is therefore also the same and is shown in Fig. 9.2.1.9. The reciprocal lattices of these polytypes differ only along the c^* axis, which is perpendicular to the layers. It is evident from Fig. 9.2.1.9 that for each reciprocal-lattice row parallel to $\mathbf{c}^*$ there are five others with the same value of the radial coordinate ξ. For example, the rows 10.l, 01.l, $\bar{1}1.l$, $\bar{1}0.l$, $0\bar{1}.l$, and $1\bar{1}.l$ all have $\xi = |\mathbf{a}^*|$. Owing to symmetry considerations, it is sufficient to record any one of them on X-ray diffraction photographs. The reciprocal-lattice rows $hk.l$ can be classified into two categories according as $h - k = 0 \bmod 3$ or $\pm 1 \bmod 3$. Since the atoms in an nH or nR structure lie on three symmetry axes $A : [00.1]_{00}$, $B : [00.1]_{\frac{1}{3},-\frac{1}{3}}$, and $C : [00.1]_{-\frac{1}{3},\frac{1}{3}}$, the structure factor F_{hkl} can be split into three parts:

$$F_{hkl} = P + Q\exp[2\pi i(h-k)/3] + R\exp[-2\pi i(h-k)/3],$$

where $P = \sum_{z_A} \exp(2\pi i l z_A/n)$, $Q = \sum_{z_B} \exp(2\pi i l z_B/n)$, $R = \sum_{z_C} \exp(2\pi i l z_C/n)$, and z_A/n, z_B/n, z_C/n are the z coordinates of atoms at A, B, and C sites, respectively. For $h - k = 0 \bmod 3$,

$$F_{hkl} = P + Q + R = \sum_{z=0}^{n=-1} \exp(2\pi i l z/n),$$

which is zero except when $l = 0, n, 2n, \ldots$. Hence, the reflections 00.l, 11.l, 30.l, *etc.*, for which $h - k = 0 \bmod 3$, will be extinguished except when $l = 0, n, 2n, \ldots$. Thus, only those $hk.l$ reciprocal-lattice rows for which $h - k \neq 0 \bmod 3$ carry information about the stacking sequence and contain in general reflections with $l = 0, 1, 2, \ldots, n-1$, *etc.* It is sufficient to record any one such row, usually the 10.l row with $\xi = |\mathbf{a}^*|$, on an oscillation, Weissenberg, or precession photograph to obtain information about the lattice type, identity period, space group, and hence the complete structure (Verma & Krishna, 1966).

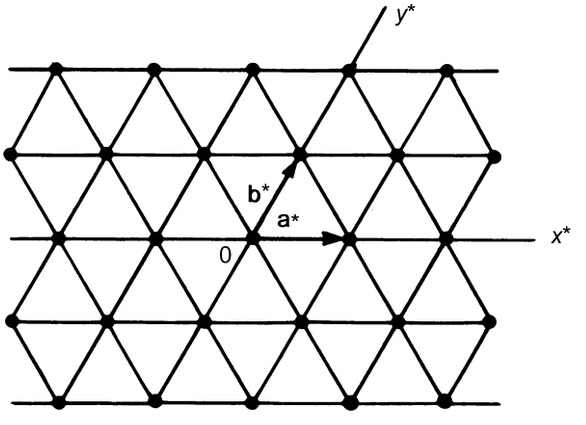

Fig. 9.2.1.9. The $\mathbf{a}^*$–$\mathbf{b}^*$ reciprocal-lattice net for close-packed layer stackings.

9.2.1.7.2. *Determination of the lattice type*

When the structure has a hexagonal lattice, the positions of spots are symmetrical about the zero layer line on the *c*-axis oscillation photograph. However, the intensities of the reflections on the two sides of the zero layer line are the same only if the structure possesses a 6_3 axis, and not for the trigonal system. An apparent mirror symmetry perpendicular to the *c* axis results from the combination of the 6_3 axis with the centre of symmetry introduced by X-ray diffraction. For a structure with a rhombohedral lattice, the positions of X-ray diffraction spots are not symmetrical about the zero layer line because the hexagonal unit cell is non-primitive causing the reflections *hkl* to be absent when $-h + k + l \neq 3n$ ($\pm n = 0, 1, 2, \ldots$). For the 10.*l* row, this means that the permitted reflections will have $l = 3n + 1$, which implies above the zero layer line $10.\bar{1}$, $10.\bar{4}$, $10.\bar{7}$, *etc*. reflections and below the zero layer line $10.\bar{2}$, $10.\bar{5}$, $10.\bar{8}$, *etc*. The zero layer line will therefore divide the distance between the nearest spots on either side (namely 10.1 and $10.\bar{2}$) approximately in the ratio 1:2. This enables a quick identification of a rhombohedral lattice. It is also possible to identify rhombohedral lattices by the appearance of an apparent 'doubling' of spots along the Bernal row lines on a rotation photograph. This is because of the threefold symmetry which makes reciprocal-lattice rows such as 10.*l*, $\bar{1}1.l$, and $01.\bar{l}$ identical with each other but different from the other identical set, 01.*l*, $\bar{1}0.l$, and $1\bar{1}.l$. The extinction condition for the second set requires $l = 3n - 1$, *i.e.* $l = 2, 5, 8$, and $\bar{1}, \bar{4}, \bar{7}$, *etc.*, which is different from that for the first set. Consequently, on the rotation photograph, reciprocal-lattice rows with $\xi = |\mathbf{a}^*|$ will have spots for $l = 3n \pm 1$ causing the apparent 'doubling'.

In crystals of layer structures, such as CdI_2, where *a*-axis oscillation photographs are normally taken, the identification of the rhombohedral lattice is performed by checking for the non-coincidence of the diffraction spots with those for the 2*H* or 4*H* structures. In an alternative method, one compares the positions of spots in two rows of the type 10.*l* and 20.*l*. This can conveniently be done by taking a Weissenberg photograph (Chadha, 1977).

9.2.1.7.3. *Determination of the identity period*

The number of layers, *n*, in the hexagonal unit cell can be found by determining the *c* parameter from the *c*-axis rotation or oscillation photographs and dividing this by the layer spacing *h* for that compound which can be found from reflections with $h - k = 0 \bmod 3$. The density of reciprocal-lattice points along rows parallel to $\mathbf{c}^*$ depends on the periodicity along the *c* axis. The larger the identity period along **c**, the more closely spaced are the diffraction spots along $\mathbf{c}^*$. In situations where there are not many structural extinctions, *n* can be determined by counting the number of spacings after which the sequence of relative intensities begins to repeat along the 10.*l* row of spots on an oscillation or Weissenberg photograph (Krishna & Verma, 1963). If the structure contains a random stacking disorder of close-packed layers (stacking faults), this will effectively make the **c** parameter infinite ($\mathbf{c}^* \rightarrow 0$) and lead to the production of characteristic continuous diffuse streaks along reciprocal-lattice rows parallel to $\mathbf{c}^*$ for reflections with $h - k \neq 0 \bmod 3$ (Wilson, 1942). It is therefore difficult to distinguish by X-ray diffraction between structures of very large unresolvable periodicities and those with random stacking faults. Lattice resolution in the electron microscope has been used in recent years to identify such structures (Dubey, Singh & Van Tendeloo, 1977). A better resolution of diffraction spots along the 10.*l* reciprocal-lattice row can be obtained by using the Laue method. Standard charts for rapid identification of SiC polytypes from Laue films are available in the literature (Mitchell, 1953). Identity periods as large as 594 layers have been resolved by this method (Honjo, Miyake & Tomita, 1950). Synchrotron radiation has been used for taking Laue photographs of ZnS polytypes (Steinberger, Bordas & Kalman, 1977).

9.2.1.7.4. *Determination of the stacking sequence of layers*

For an *nH* or 3*nR* polytype, the *n* close-packed layers in the unit cell can be stacked in 2^{n-1} possible ways, all of which cannot be considered for ultimate intensity calculations. A variety of considerations has therefore been used for restricting the number of trial structures. To begin with, symmetry and space-group considerations discussed in Subsection 9.2.1.4 and 9.2.1.5 can considerably reduce the number of trial structures.

When the short-period structures act as 'basic structures' for the generation of long-period polytypes, the number of trial structures is considerably reduced since the crystallographic unit cells of the latter will contain several units of the small-period structures with faults between or at the end of such units. The basic structure of an unknown polytype can be guessed by noting the intensities of 10.*l* reflections that are maximum near the positions corresponding to the basic structure. If the unknown polytype belongs to a well known structure series, such as $(33)_n32$ and $(33)_n34$ based on SiC-6*H*, empirical rules framed by Mitchell (1953) and Krishna & Verma (1962) can allow the direct identification of the layer-stacking sequence without elaborate intensity calculations.

It is possible to restrict the number of probable structures for an unknown polytype on the basis of the faulted matrix model of polytypism for the origin of polytype structures (for details see Pandey & Krishna, 1983). The most probable series of structures as predicted on the basis of this model for SiC contains the numbers 2, 3, 4, 5 and 6 in their Zhdanov sequence (Pandey & Krishna, 1975, 1976*a*). For CdI_2 and PbI_2 polytypes, the possible Zhdanov numbers are 1, 2 and 3 (Pandey & Krishna, 1983; Pandey, 1985). On the basis of the faulted matrix model, it is not only possible to restrict the numbers occurring in the Zhdanov sequence but also to restrict drastically the number of trial structures for a new polytype.

Structure determination of ZnS polytypes is more difficult since they are not based on any simple polytype and any number can appear in the Zhadanov sequence. It has been observed that the birefringence of polytype structures in ZnS varies linearly with the percentage hexagonality (Brafman & Steinberger, 1966), which in turn is related to the number of reversals in the stacking sequence, *i.e.* the number of numbers in the Zhdanov sequence. This drastically reduces the number of trial structures for ZnS (Brafman, Alexander & Steinberger, 1967).

Singh and his co-workers have successfully used lattice imaging in conjunction with X-ray diffraction for determining the structures of long-period polytypes of SiC that are not based on a simple basic structure. After recording X-ray diffraction patterns, single crystals of these polytypes were crushed to yield electron-beam-transparent flakes. The one- and two-dimensional lattice images were used to propose the possible structures for the polytypes. Usually this approach leads to a very few possibilities and the correct structure is easily determined by comparing the observed and calculated X-ray intensities for the proposed structures (Dubey & Singh, 1978; Rai, Singh, Dubey & Singh, 1986).

Direct methods for the structure determination of polytypes from X-ray data have also been suggested by several workers (Tokonami & Hosoya, 1965; Dornberger-Schiff & Farkas-

Jahnke, 1970; Farkas-Jahnke & Dornberger-Schiff, 1969) and have been reviewed by Farkas-Jahnke (1983). These have been used to derive the structures of ZnS, SiC, and $TiS_{1.7}$ polytypes. These methods are extremely sensitive to experimental errors in the intensities.

9.2.1.8. *Stacking faults in close-packed structures*

The two alternative positions for the stacking of successive close-packed layers give rise to the possibility of occurrence of faults where the stacking rule is broken without violating the law of close packing. Such faults are frequently observed in crystals of polytypic materials as well as close-packed martensites of cobalt, noble-metal-based and certain iron-based alloys (Andrade, Chandrasekaran & Delaey 1984; Kabra, Pandey & Lele, 1988*a*; Nishiyama, 1978; Pandey, 1988).

The classical method of classifying stacking faults in 2*H* and 3*C* structures as growth and deformation types, depending on whether the fault has resulted as an accident during growth or by shear through the vector **s**, leads to considerable ambiguities since the same fault configuration can result from more than one physical process. For a detailed account of the limitations of the notations based on the process of formation, the reader is referred to the articles by Pandey (1984*a*) and Pandey & Krishna (1982*b*).

Frank (1951) has classified stacking faults as intrinsic or extrinsic purely on geometrical considerations. In intrinsic faults, the perfect stacking sequence on each side of the fault extends right up to the contact plane of the two crystal halves while in extrinsic faults the contact plane does not belong to the stacking sequence on either side of it. In intrinsic faults, the contact plane may be an atomic or non-atomic plane whereas in extrinsic faults the contact plane is always an atomic plane. Instead of contact plane, one can use the concept of fault plane defined with respect to the initial stacking sequence. This system of classification is preferable to that based on the process of formation. However, the terms intrinsic and extrinsic have been used in the literature in a very restricted sense by associating these with the precipitation of vacancies and interstitials, respectively (see, for example, Weertman & Weertman, 1984). While the precipitation of vacancies may lead to intrinsic fault configuration, this is by no means the only process by which intrinsic faults can result. For example, there are geometrically 18 possible intrinsic fault configurations in the 6*H* (33) structure (Pandey & Krishna, 1975) but only two of these can result from the precipitation of vacancies. Similarly, layer-displacement faults involved in SiC transformations are extrinsic type but do not result from the precipitation of interstitials (see Pandey, Lele & Krishna, 1980*a*,*b*,*c*; Kabra, Pandey & Lele, 1986). It is therefore desirable not to associate the geometrical notation of Frank with any particular process of formation.

The intrinsic–extrinsic scheme of classification of faults when used in conjunction with the concept of assigning subscripts to different close-packed layers (Prasad & Lele, 1971; Pandey & Krishna, 1976*b*) can provide a very compact and unique way of representing intrinsic fault configurations even in long-period structures (Pandey, 1984*b*). We shall briefly explain this notation in relation to one hexagonal (6*H*) and one rhombohedral (9*R*) structure.

In the 6*H* (*ABCACB*, ... or *hkkhkk*) structure, six kinds of layers that can be assigned subscripts 0, 1, 2, 3, 4, and 5 need to be distinguished (Pandey, 1984*b*). Choosing the 0-type layer in '*h*' configuration such that the layer next to it is related through the shift vector $+\mathbf{s}$ (which causes cyclic $A \rightarrow B \rightarrow C \rightarrow A$ shift), the perfect 6*H* structure can be written as

$$\begin{array}{cccccccccccc} & h & k & k & h & k & k & h & k & k & h & k & k & \\ \ldots & A_0 & B_1 & C_2 & A_3 & C_4 & B_5 & A_0 & B_1 & C_2 & A_3 & C_4 & B_5 & \ldots. \\ & +\mathbf{s} & +\mathbf{s} & +\mathbf{s} & -\mathbf{s} & -\mathbf{s} & -\mathbf{s} & +\mathbf{s} & +\mathbf{s} & +\mathbf{s} & -\mathbf{s} & -\mathbf{s} & & \end{array}$$

There are six crystallographically equivalent ways of writing this structure with the first layer in position *A*: (i) $A_0B_1C_2A_3C_4B_5$; (ii) $A_1B_2C_3B_4A_5C_0$; (iii) $A_2B_3A_4C_5B_0C_1$; (iv) $A_3C_4B_5A_0B_1C_2$; (v) $A_4C_5B_0C_1A_2B_3$; and (vi) $A_5C_0A_1B_2C_3B_4$. Similarly, there are six ways of writing the 6*H* structure with the starting layer in position *B* or *C*. Since an intrinsic fault marks the beginning of a fresh 6*H* sequence, there can be 36 possible intrinsic fault configurations in the 6*H* (*ABCACB*, ...) structure. All these intrinsic fault configurations can be described by symbols like $I_{r,s}$, where *r* and *s* stand for the subscript of the layer on the left- and right-hand sides of the fault plane while *I* represents intrinsic. Knowing the two symbols (*r* and *s*), one can write down the complete *ABC* stacking sequence. It may be noted that, of the 36 possible intrinsic fault configurations, only 14 are crystallographically indistinguishable (for details, see Pandey, 1984*b*). This notation can be used for any hexagonal polytype and requires only the identification of various layer types in the structure. For rhombohedral polytypes, one must consider the layer types in both the obverse and the reverse settings. For example, six layer types need to be distinguished in the 9*R* (*hhk*) structure:

Obverse:

$$\begin{array}{cccccccccc} & h & h & k & h & h & k & h & h & k & \\ \ldots & A_0 & B_1 & A_2 & C_0 & A_1 & C_2 & B_0 & C_1 & B_2 & \ldots; \\ & +\mathbf{s} & -\mathbf{s} & -\mathbf{s} & +\mathbf{s} & -\mathbf{s} & -\mathbf{s} & +\mathbf{s} & -\mathbf{s} & & \end{array}$$

Table 9.2.1.3. *Intrinsic fault configurations in the 6H* $(A_0B_1C_2A_3C_4B_5, \ldots)$ *structure*

Fault configuration *ABC* sequence	Subscript notation
$\ldots A\,B\,C\,A\,C\,B\,A_0 \mid C_0\,A\,B\,C\,B\,A\,C \ldots$	$I_{0,0}$
$\ldots A\,B\,C\,A\,C\,B\,A_0 \mid C_1\,A\,B\,A\,C\,B\,C \ldots$	$I_{0,1}$
$\ldots A\,B\,C\,A\,C\,B\,A_0 \mid C_2\,A\,C\,B\,A\,B\,C \ldots$	$I_{0,2}$
$\ldots A\,B\,C\,A\,C\,B\,A_0 \mid C_3\,B\,A\,C\,A\,B\,C \ldots$	$I_{0,3}$
$\ldots A\,B\,C\,A\,C\,B\,A_0 \mid C_4\,B\,A\,B\,C\,A\,C \ldots$	$I_{0,4}$
$\ldots A\,B\,C\,A\,C\,B\,A_0 \mid C_5\,B\,C\,A\,B\,A\,C \ldots$	$I_{0,5}$
$\ldots A\,B\,C\,A\,C\,B\,A\,B_1 \mid A_0\,B\,C\,A\,C\,B\,A \ldots$	$I_{1,0}$
$\ldots A\,B\,C\,A\,C\,B\,A\,B_1 \mid A_1\,B\,C\,B\,A\,C\,A \ldots$	$I_{1,1}$
$\ldots A\,B\,C\,A\,C\,B\,A\,B_1 \mid A_2\,B\,A\,C\,B\,C\,A \ldots$	$I_{1,2}$
$\ldots A\,B\,C\,A\,C\,B\,A\,B_1 \mid A_3\,C\,B\,A\,B\,C\,A \ldots$	$I_{1,3}$
$\ldots A\,B\,C\,A\,C\,B\,A\,B_1 \mid A_4\,C\,B\,C\,A\,B\,A \ldots$	$I_{1,4}$
$\ldots A\,B\,C\,A\,C\,B\,A\,B_1 \mid A_5\,C\,A\,B\,C\,B\,A \ldots$	$I_{1,5}$
$\ldots A\,B\,C\,A\,C\,B\,A\,B\,C_2 \mid B_0\,C\,A\,B\,A\,C\,B \ldots$	$I_{2,0}$
$\ldots A\,B\,C\,A\,C\,B\,A\,B\,C_2 \mid B_1\,C\,A\,C\,B\,A\,B \ldots$	$I_{2,1}$
$\ldots A\,B\,C\,A\,C\,B\,A\,B\,C_2 \mid B_2\,C\,B\,A\,C\,A\,B \ldots$	$I_{2,2}$
$\ldots A\,B\,C\,A\,C\,B\,A\,B\,C_2 \mid B_3\,A\,C\,B\,C\,A\,B \ldots$	$I_{2,3}$
$\ldots A\,B\,C\,A\,C\,B\,A\,B\,C_2 \mid B_4\,A\,C\,A\,B\,C\,B \ldots$	$I_{2,4}$
$\ldots A\,B\,C\,A\,C\,B\,A\,B\,C_2 \mid B_5\,A\,B\,C\,A\,C\,B \ldots$	$I_{2,5}$

Notes:

(1) Dotted vertical lines represent the location of the fault plane with respect to the initial stacking sequence on the left-hand side.

(2) $I_{0,1}$ and $I_{2,3}$, $I_{0,2}$ and $I_{1,3}$, $I_{1,1}$ and $I_{2,2}$, and $I_{1,4}$ and $I_{2,5}$ are crystallographically equivalent.

Table 9.2.1.4. *Intrinsic fault configurations in the 9R ($A_0B_1A_2C_0A_1C_2B_0C_1B_2, \ldots$) structure*

Fault configuration *ABC* sequence	Subscript notation
$\ldots A\ B\ A\ C\ A\ C\ B\ C\ B\ A_0 \mid C_0\ A\ C\ B\ C\ B\ A\ B\ A \ldots$	$I_{0,0}$
$\ldots A\ B\ A\ C\ A\ C\ B\ C\ B\ A_0 \mid C_1\ B\ A\ B\ A\ C\ A\ C\ B \ldots$	$I_{0,1}$
$\ldots A\ B\ A\ C\ A\ C\ B\ C\ B\ A_0 \mid C_2\ B\ C\ B\ A\ B\ A\ C\ A \ldots$	$I_{0,2}$
$\ldots A\ B\ A\ C\ A\ C\ B\ C\ B\ A_0 \mid C_{\bar{0}}\ B\ C\ A\ C\ A\ B\ A\ B \ldots$	$I_{0,\bar{0}}$
$\ldots A\ B\ A\ C\ A\ C\ B\ C\ B\ A_0 \mid C_{\bar{1}}\ A\ B\ A\ B\ C\ B\ C\ A \ldots$	$I_{0,\bar{1}}$
$\ldots A\ B\ A\ C\ A\ C\ B\ C\ B\ A_0 \mid C_{\bar{2}}\ A\ C\ A\ B\ A\ B\ C\ B \ldots$	$I_{0,\bar{2}}$
$\ldots A\ B\ A\ C\ A\ C\ B\ C\ B\ A\ B_1 \mid C_0\ A\ C\ B\ C\ B\ A\ B\ A \ldots$	$I_{1,0}$
$\ldots A\ B\ A\ C\ A\ C\ B\ C\ B\ A\ B_1 \mid C_1\ B\ A\ B\ A\ C\ A\ C\ B \ldots$	$I_{1,1}$
$\ldots A\ B\ A\ C\ A\ C\ B\ C\ B\ A\ B_1 \mid C_2\ B\ C\ B\ A\ B\ A\ C\ A \ldots$	$I_{1,2}$
$\ldots A\ B\ A\ C\ A\ C\ B\ C\ B\ A\ B_1 \mid C_{\bar{0}}\ B\ C\ A\ C\ A\ B\ A\ B \ldots$	$I_{1,\bar{0}}$
$\ldots A\ B\ A\ C\ A\ C\ B\ C\ B\ A\ B_1 \mid C_{\bar{1}}\ A\ B\ A\ B\ C\ B\ C\ A \ldots$	$I_{1,\bar{1}}$
$\ldots A\ B\ A\ C\ A\ C\ B\ C\ B\ A\ B_1 \mid C_{\bar{2}}\ A\ C\ A\ B\ A\ B\ C\ B \ldots$	$I_{1,\bar{2}}$
$\ldots A\ B\ A\ C\ A\ C\ B\ C\ B\ A\ B\ A_2 \mid B_0\ C\ B\ A\ B\ A\ C\ A\ C \ldots$	$I_{2,0}$
$\ldots A\ B\ A\ C\ A\ C\ B\ C\ B\ A\ B\ A_2 \mid B_1\ A\ C\ A\ C\ B\ C\ B\ A \ldots$	$I_{2,1}$
$\ldots A\ B\ A\ C\ A\ C\ B\ C\ B\ A\ B\ A_2 \mid B_2\ A\ B\ A\ C\ A\ C\ B\ C \ldots$	$I_{2,2}$
$\ldots A\ B\ A\ C\ A\ C\ B\ C\ B\ A\ B\ A_2 \mid B_{\bar{0}}\ A\ B\ C\ B\ C\ A\ C\ A \ldots$	$I_{2,\bar{0}}$
$\ldots A\ B\ A\ C\ A\ C\ B\ C\ B\ A\ B\ A_2 \mid B_{\bar{1}}\ C\ A\ C\ A\ B\ A\ B\ C \ldots$	$I_{2,\bar{1}}$
$\ldots A\ B\ A\ C\ A\ C\ B\ C\ B\ A\ B\ A_2 \mid B_{\bar{2}}\ C\ B\ C\ A\ C\ A\ B\ A \ldots$	$I_{2,\bar{2}}$

Note: $I_{0,\bar{0}}$ and $I_{1,\bar{1}}$, $I_{0,\bar{1}}$ and $I_{1,\bar{2}}$, $I_{0,\bar{2}}$ and $I_{2,\bar{1}}$, and $I_{1,2}$ and $I_{2,0}$ are crystallographically equivalent.

Reverse:

$$\begin{array}{cccccccccc} & h & h & k & h & h & k & h & h & k & \\ \ldots & A_{\bar{0}} & C_{\bar{1}} & A_{\bar{2}} & B_{\bar{0}} & A_{\bar{1}} & B_{\bar{2}} & C_{\bar{0}} & B_{\bar{1}} & C_{\bar{2}} & \ldots. \\ & -\mathbf{s} & +\mathbf{s} & +\mathbf{s} & -\mathbf{s} & +\mathbf{s} & +\mathbf{s} & -\mathbf{s} & +\mathbf{s} & & \end{array}$$

In the obverse setting, we choose the origin layer (0 type) in the *h* configuration such that the next layer is cyclically shifted whereas in the reverse setting the origin layer ($\bar{0}$ type) in the *h* configuration is related to the next layer through an anticyclic shift. Tables 9.2.1.3 and 9.2.1.4 list the crystallographically unique intrinsic fault configurations in the 6*H* and 9*R* structures.

9.2.1.8.1. *Structure determination of one-dimensionally disordered crystals*

Statistical distribution of stacking faults in close-packed structures introduces disorder along the stacking axis of the close-packed layers. As a result, one observes on a single-crystal diffraction pattern not only normal Bragg scattering near the nodes of the reciprocal lattice of the average structure but also continuous diffuse scattering between the nodes owing to the incomplete destructive interference of scattered rays. Just like the extra polytype reflections, the diffuse streaks are also confined to only those rows for which $h - k \neq 0 \bmod 3$. A complete description of the real structure of such one-dimensionally disordered polytypes requires knowledge of the average structure as well as a statistical specification of the fluctuations due to stacking faults in the electron-density distribution of the average structure. This cannot be accomplished by the usual consideration of the normal Bragg reflections alone but requires a careful analysis of the diffuse intensity distribution as well (Pandey, Kabra & Lele, 1986).

The first step in the structure determination of one-dimensionally disordered structures is the specification of the geometry of stacking faults and their distribution, both of which require postulation of the physical processes responsible for their formation. An entirely random distribution of faults may result during the layer-by-layer growth of a crystal (Wilson, 1942) or during plastic deformation (Paterson, 1952). On the other hand, when faults bring about the change in the stacking sequence of layers during solid-state transformations, their distribution is non-random (Pandey, Lele & Krishna, 1980*a*,*b*,*c*; Pandey & Lele, 1986*a*,*b*; Kabra, Pandey & Lele, 1986). Unlike growth faults, which are accidentally introduced in a sequential fashion from one end of the stack of layers to the other during the actual crystal growth, stacking faults involved in solid-state transformations are introduced in a random space and time sequence (Kabra, Pandey & Lele, 1988*b*). Since the pioneering work of Wilson (1942), several different techniques have been advanced for the calculation of intensity distributions along diffuse streaks making use of Markovian chains, random walk, stochastic matrices, and the Paterson function for random and non-random distributions of stacking faults on the assumption that these are introduced in a sequential fashion (Hendricks & Teller, 1942; Jagodzinski 1949*a*,*b*; Kakinoki & Komura, 1954; Johnson, 1963; Prasad & Lele, 1971; Cowley, 1976; Pandey, Lele & Krishna, 1980*a*,*b*). The limitations of these methods for situations where non-randomly distributed faults are introduced in the random space and time sequence have led to the use of Monte Carlo techniques for the numerical calculation of pair correlations whose Fourier transforms directly yield the intensity distributions (Kabra & Pandey, 1988).

The correctness of the proposed model for disorder can be verified by comparing the theoretically calculated intensity distributions with those experimentally observed. This step is in principle analogous to the comparison of the observed Bragg intensities with those calculated for a proposed structure in the structure determination of regularly ordered layer stackings. This comparison cannot, however, be performed in a straightforward manner for one-dimensionally disordered crystals due to special problems in the measurement of diffuse intensities using a single-crystal diffractometer, stemming from incident-beam divergence, finite size of the detector slit, and multiple scattering. The problems due to incident-beam divergence in the measurement of the diffuse intensity distributions were first

pointed out by Pandey & Krishna (1977) and suitable correction factors have recently been derived by Pandey, Prasad, Lele & Gauthier (1987). A satisfactory solution to the problem of structure determination of one-dimensionally disordered stackings must await proper understanding of all other factors that may influence the true diffraction profiles.

9.2.2. Layer stacking in general polytypic structures (By S. Ďurovič)

9.2.2.1. *The notion of polytypism*

The common property of the structures described in Section 9.2.1 was the stacking ambiguity of adjacent layer-like structural units. This has been explained by the geometrical properties of close packing of equal spheres, and the different modifications thus obtained have been called *polytypes*.

This phenomenon was first recognized by Baumhauer (1912, 1915) as a result of his investigations of many SiC single crystals by optical goniometry. Among these, he discovered three *types* and his observations were formulated in five statements:

(1) all three types originate simultaneously in the same melt and seemingly also under the same, or nearly the same, conditions;

(2) they can be related in a simple way to the same axial ratio (each within an individual primary series);

(3) any two types (I and II, II and III) have certain faces in common but, except the basal face, there is no face occurring simultaneously in all three types;

(4) the crystals belonging to different, but also to all three, types often form intergrowths with parallel axes;

(5) any of the three types exhibits a typical X-ray diffraction pattern and thus also an individual molecular or atomic structure.

Baumhauer recognized the special role of these *types* within modifications of the same substance and called this phenomenon *polytypism* – a special case of polymorphism. The later determination of the crystal structures of Baumhauer's three types indicated that his results can be interpreted by a family of structures consisting of identical layers with hexagonal symmetry and differing only in their stacking mode.

The stipulation that the individual polytypes grow from the same system and under (nearly) the same conditions influenced for years the investigation of polytypes because it logically led to the question of their growth mechanism.

In the following years, many new polytypic substances have been found. Their crystal structures revealed that polytypism is restricted neither to close packings nor to heterodesmic 'layered structures' (*e.g.* CdI_2 or GaSe; *cf.* homodesmic SiC or ZnS; see §§9.2.1.2.2 to 9.2.1.2.4), and that the reasons for a stacking ambiguity lie in the crystal chemistry – in all cases the geometric nearest-neighbour relations between adjacent layers are preserved. The preservation of the bulk chemical composition was not questioned.

Some discomfort has arisen from refinements of the structures of various phyllosilicates. Here especially the micas exhibit a large variety of isomorphous replacements and it turns out that a certain chemical composition stabilizes certain polytypes, excludes others, and that the layers constituting polytypic structures need not be of the same kind. But subsequently the opinion prevailed that the sequence of individual kinds of layers in polytypes of the same family should remain the same and that the relative positions of adjacent layers cannot be completely random (*e.g.* Zvyagin, 1988). The postulates declared mixed-layer and turbostratic structures as non-polytypic. All this led to certain controversies about the notion of polytypism. While Thompson (1981) regards polytypes as 'arising through different ways of stacking structurally compatible tabular units ... [provided that this] ... should not alter the chemistry of the crystal as a whole', Angel (1986) demands that 'polytypism arises from different modes of stacking of one or more structurally compatible modules', dropping thus any chemical constraints and allowing also for rod- and block-like modules.

The present official definition (Guinier *et al.*, 1984) reads:

> ''An element or compound is *polytypic* if it occurs in several different structural modifications, each of which may be regarded as built up by stacking layers of (nearly) identical structure and composition, and if the modifications differ only in their stacking sequence. Polytypism is a special case of polymorphism: the two-dimensional translations within the layers are (essentially) preserved whereas the lattice spacings normal to the layers vary between polytypes and are indicative of the stacking period. No such restrictions apply to polymorphism.
>
> *Comment*: The above definition is designed to be sufficiently general to make polytypism a useful concept. There is increasing evidence that some polytypic structures are characterized either by small deviations from stoichiometry or by small amounts of impurities. (In the case of certain minerals like clays, micas and ferrites, deviations in composition up to 0.25 atoms per formula unit are permitted within the same polytypic series: two layer structures that differ by more than this amount should not be called polytypic.) Likewise, layers in different polytypic structures may exhibit slight structural differences and may not be isomorphic in the strict crystallographic sense.
>
> The *Ad-Hoc* Committee is aware that the definition of polytypism above is probably too wide since it includes, for example, the turbostratic form of graphite as well as mixed-layer phyllosilicates. However, the sequence and stacking of layers in a polytype are always subject to well-defined limitations. On the other hand, a more general definition of polytypism that includes 'rod' and 'block' polytypes may become necessary in the future.''

This definition was elaborated as a compromise between members of the IUCr *Ad-Hoc* Committee on the Nomenclature of Disordered, Modulated and Polytype Structures. It is a slightly modified definition proposed by the IMA/IUCr Joint Committee on Nomenclature (Bailey *et al.*, 1977), which was the target of Angel's (1986) objections.

The official definition has indeed its shortcomings, but not so much in its restrictiveness concerning the chemical composition and structural rigidity of layers, because this can be overcome by a proper degree of abstraction (see below). More critical is the fact that it is not 'geometric' enough. It specifies neither the 'layers' (except for their two-dimensional periodicity), nor the limitations concerning their sequence and stacking mode, and it does not state the conditions under which a polytype belongs to a family.

Very impressive evidence that even polytypes that are in keeping with the first Baumhauer's statement may not have exactly the same composition and the structure of their constituting layers *cannot* be identical has been provided by studies on SiC carried out at the Leningrad Electrotechnical Institute (Sorokin, Tairov, Tsvetkov & Chernov, 1982; Tsvetkov, 1982). They indicate also that each periodic polytype is *sensu stricto* an individual polymorph. Therefore, it appears that the question whether some *real* polytypes belong to the same

family depends mainly on the idealization and/or abstraction level, *relevant to a concrete purpose*.

This very idealization and/or abstraction process caused the term *polytype* to become also an *abstract notion* meaning a *structural type* with relevant geometrical properties,* belonging to an abstract family whose members consist of layers with identical structure and keep identical bulk composition. Such an abstract notion lies at the root of all systemization and classification schemes of polytypes.

A still higher degree of abstraction has been achieved by Dornberger-Schiff (1964, 1966, 1979) who abstracted from chemical composition completely and investigated the manifestation of crystallochemical reasons for polytypism in the *symmetry of layers* and *symmetry relations between layers*. Her theory of OD (order–disorder) structures is thus a theory of symmetry of polytypes, playing here a role similar to that of group theory in traditional crystallography. In the next section, a brief account of basic terms, definitions, and logical constructions of OD theory will be given, together with its contribution to a geometrical definition of polytypism.

9.2.2.2. *Symmetry aspects of polytypism*

9.2.2.2.1. *Close packing of spheres*

Polytypism of structures based on close packing of equal spheres (note this idealization) is explained by the fact that the spheres of any layer can be placed *either* in all the voids ∇ of the preceding layer, *or* in all the voids $\triangle$ – not in both because of steric hindrance (Section 9.2.1, Fig. 9.2.1.1).

A closer look reveals that the two voids are *geometrically* (but not translationally) *equivalent*. This implies that the two possible pairs of adjacent layers, say *AB* and *AC*, are geometrically equivalent too – this equivalence is brought about *e.g.* by a reflection in any plane perpendicular to the layers and passing through the centres of mutually contacting spheres *A*: such a reflection transforms the layer *A* into itself, and *B* into *C*, and *vice versa*. Another important point is that the symmetry proper of any layer is described by the layer group $P(6/m)mm$,† and that the relative position of any two adjacent layers is such that only some of the 24 symmetry operations of that layer group remain valid for the pair. It is easy to see that 12 out of the total of 24 transformations do not change the z coordinate of any starting point, and that these operations constitute a subgroup of the index [2]. These are the so-called τ *operations*. The remaining 12 operations change any z into $-z$, thus turning the layer upside down; they constitute a coset. The latter are called ρ *operations*. Out of the 12 τ operations, only 6 are valid for the layer pair. One says that only these 6 operations have a *continuation* in the adjacent layer. Let us denote the general multiplicity of the group of τ operations of a single layer by N, and that of the subgroup of these operations with a continuation in the adjacent layer by F: then the number Z of positions of the adjacent layer leading to geometrically equivalent layer pairs is given by $Z = N/F$ (Dornberger-Schiff, 1964, pp. 32 ff.); in our case, $Z = 12/6 = 2$ (Fig. 9.2.2.1). This is the so-called *NFZ relation*, valid with only minor alterations for all categories of OD structures (§9.2.2.2.7). It follows that all conceivable structures based on close packing of equal spheres are built on the same symmetry principle: they consist of equivalent layers (*i.e.* layers of the same kind) and of equivalent layer pairs, and, in keeping with these stipulations, any layer can be stacked onto its predecessor in two ways. Keeping in mind that the layer pairs that are geometrically equivalent are also energetically equivalent, and neglecting in the first approximation the interactions between a given layer and the next-but-one layer, we infer that all structures built according to these principles are also energetically equivalent and thus equally likely to appear.

It is important to realize that the above symmetry considerations hold not only for close packing of spheres but also for *any conceivable structure* consisting of two-dimensionally periodic layers with symmetry $P(6/m)mm$ and containing pairs of adjacent layers with symmetry $P(3)m1$. Moreover, the OD theory sets a quantitative stipulation for the relation between any two adjacent layers: they have to remain *geometrically equivalent* in any polytype belonging to a family. This is far more exact than the description: 'the stacking of layers is such that it preserves the nearest-neighbour relationships'.

9.2.2.2.2. *Polytype families and OD groupoid families*

All polytypes of a substance built on the same *structural principle* are said to belong to the same *family*. All polytypic structures, even of different substances, built according to the same *symmetry principle* also belong to a family, but different from the previous one since it includes structures of various polytype families, *e.g.* SiC, ZnS, AgI, which differ in their composition, lattice dimensions, *etc*. Such a family has been called an *OD groupoid family*; its members differ only in the relative distribution of *coincidence operations** describing the respective symmetries, irrespective of the crystallochemical content. These coincidence operations can be *total* or *partial* (local) and their set constitutes a groupoid (Dornberger-Schiff, 1964, pp. 16 ff.; Fichtner, 1965, 1977). Any polytype (abstract) belonging to such a family has its own stacking of layers, and its symmetry can be described by the appropriate individual groupoid. Strictly speaking, these groupoids are the members of an OD groupoid family. Let us recall that any space group

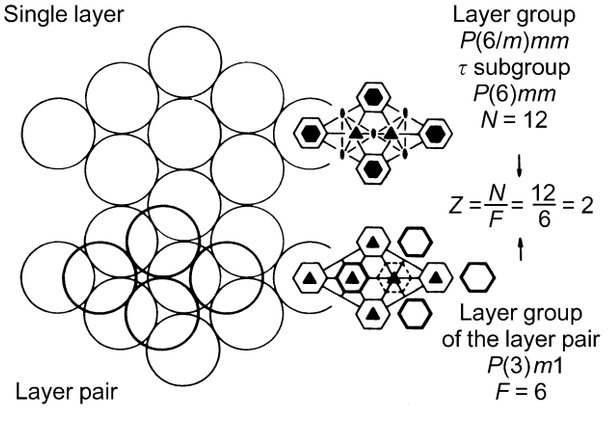

Fig. 9.2.2.1. Symmetry interpretation of close packings of equal spheres. The layer group of a single layer, the subgroup of its τ operations, and the number of asymmetric units N per unit mesh of the former, are given at the top right. The τ operations that have a continuation for the pair of adjacent layers, the layer group of the pair, and the value of F are indicated at the bottom right.

* This is an interesting example of how a development in a scientific discipline influences semantics: *e.g.* when speaking of a 6*H* polytype of SiC, one has very often in mind a characteristic sequence of Si–C layers rather than deviations from stoichiometry, presence and distribution of foreign atoms, distortion of coordination tetrahedra, *etc*.

† The direction in which there is no periodicity is indicated by parentheses (Dornberger-Schiff, 1959).

* A coincidence operation is a space transformation (called also *isometric mapping*, *isometry*, or *motion*), which preserves distances between any two points of the given object.

consists of total coincidence operations only, which therefore become the symmetry operations for the entire structure.

9.2.2.2.3. *MDO polytypes*

Any family of polytypes theoretically contains an infinite number of periodic (Ross, Takeda & Wones, 1966; Mogami, Nomura, Miyamoto, Takeda & Sadanaga, 1978; McLarnan, 1981*a*,*b*,*c*) and non-periodic structures. The periodic polytypes, in turn, can again be subdivided into two groups, the 'privileged' polytypes and the remaining ones, and it depends on the approach as to how this is done. Experimentalists single out those polytypes that occur most frequently, and call them *basic*. Theorists try to predict basic polytypes, *e.g.* by means of geometrical and/or crystallochemical considerations. Such polytypes have been called *simple, standard*, or *regular*. Sometimes the agreement is very good, sometimes not. The OD theory pays special attention to those polytypes in which *all layer triples, quadruples, etc.*, are geometrically equivalent or, at least, which contain the smallest possible number of *kinds* of these units. They have been called polytypes with *maximum degree of order*, or *MDO polytypes*. The general philosophy behind the MDO polytypes is simple: all interatomic bonding forces decrease rapidly with increasing distance. Therefore, the forces between atoms of adjacent layers are decisive for the build-up of a polytype. Since the pairs of adjacent layers remain geometrically equivalent in all polytypes of a given family, these polytypes are in the first approximation also energetically equivalent. However, if the longer-range interactions are also considered, then it becomes evident that layer triples such as *ABA* and *ABC* in close-packed structures are, in general, energetically non-equivalent because they are also geometrically non-equivalent. Even though these forces are much weaker than those between adjacent layers, they may not be negligible and, therefore, under given crystallization conditions either one or the other kind of triples becomes energetically more favourable. It will occur again and again in the polytype thus formed, and not intermixed with the other kind. Such structures are – as a rule – sensitive to conditions of crystallization, and small fluctuations of these may reverse the energetical preferences, creating stacking faults and twinnings. This is why many polytypic substances exhibit non-periodicity.

As regards the close packing of spheres, the well known cubic and hexagonal polytypes *ABCABC*... and *ABAB*..., respectively, are MDO polytypes; the first contains only the triples *ABC*, the second only the triples *ABA*. Evidently, the MDO philosophy holds for a layer-by-layer rather than for a spiral growth mechanism. Since the symmetry principle of polytypic structures may differ considerably from that of close packing of equal spheres, the OD theory contains exact algorithms for the derivation of MDO polytypes in any category (Dornberger-Schiff, 1982; Dornberger-Schiff & Grell, 1982*a*).

9.2.2.2.4. *Some geometrical properties of OD structures*

As already pointed out, all relevant geometrical properties of a polytype family can be deduced from its symmetry principle. Let us thus consider a hypothetical simple family in which we shall disregard any concrete atomic arrangements and use geometrical figures with the appropriate symmetry instead.

Three periodic polytypes are shown in Fig. 9.2.2.2 (left-hand side). Any member of this family consists of equivalent layers perpendicular to the plane of the drawing, with symmetry $P(1)m1$. The symmetry of layers is indicated by isosceles triangles with a mirror plane [*.m.*]. All pairs of adjacent layers are also equivalent, no matter whether a layer is shifted by $+b/4$ or $-b/4$ relative to its predecessor, since the reflection across [*.m.*] transforms any given layer into itself and the adjacent layer from one possible position into the other. These two positions follow also from the *NFZ* relation: $N = 2$, $F = 1$ [the layer group of the pair of adjacent layers is $P(1)11$] and thus $Z = 2$.

The layers are all equivalent and accordingly there must also be two coincidence operations transforming any layer into the adjacent one. The first operation is evidently the translation, the second is the glide reflection. If any of these becomes total for the remaining part of the structure, we obtain a polytype with all layer triples equivalent, *i.e.* a MDO polytype. The polytype (*a*) (Fig. 9.2.2.2) is one of them: the translation $\mathbf{t} = \mathbf{a}_0 + \mathbf{b}/4$ is the total operation ($|\mathbf{a}_0|$ is the distance between adjacent layers). It has basis vectors $\mathbf{a}_1 = \mathbf{a}_0 + \mathbf{b}/4$, $\mathbf{b}_1 = \mathbf{b}$, $\mathbf{c}_1 = \mathbf{c}$, space group $P111$, Ramsdell symbol $1A$,* Hägg symbol $|+|$. This polytype also has its enantiomorphous counterpart with Hägg symbol $|-|$. In the other polytype (*b*) (Fig. 9.2.2.2), the glide reflection is the total operation. The basis vectors of the polytype are

* According to Guinier *et al.* (1984), triclinic polytypes should be designated *A* (anorthic) in their Ramsdell symbols.

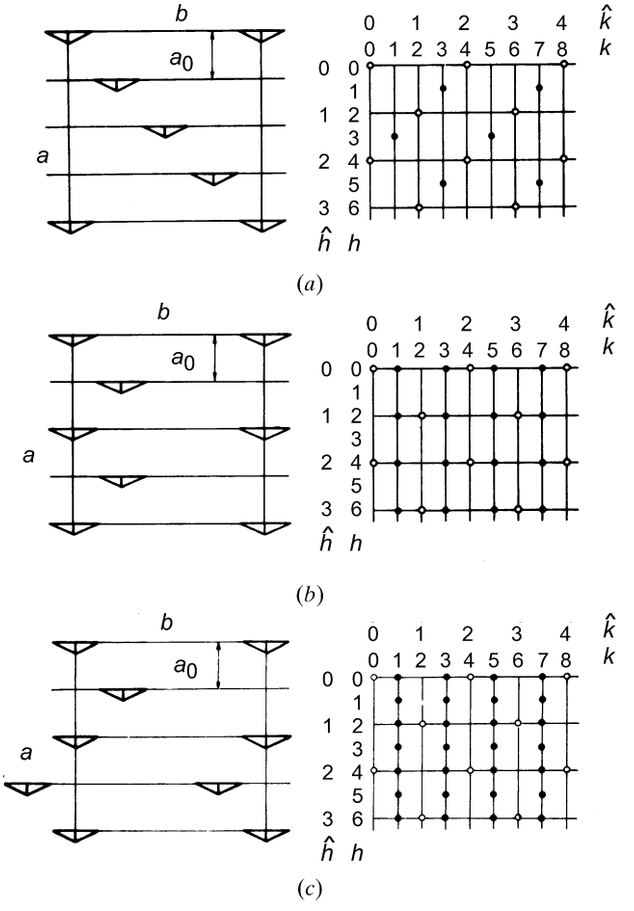

Fig. 9.2.2.2. Schematic representation of three structures belonging to the OD groupoid family $P(1)m1|1$, $y = 0.25$ (left). The layers are perpendicular to the plane of the drawing and their constituent atomic configurations are represented by isosceles triangles with symmetry [*.m.*]. All structures are related to a common orthogonal four-layer cell with $\mathbf{a} = 4\mathbf{a}_0$. The $hk0$ nets in reciprocal space corresponding to these structures are shown on the right and the diffraction indices refer also to the common cell. Family diffractions common to all members of this family ($k = 2\hat{k}$) and the characteristic diffractions for individual polytypes ($k = 2k + 1$) are indicated by open and solid circles, respectively.

$\mathbf{a}_2 = 2\mathbf{a}_0$, $\mathbf{b}_2 = \mathbf{b}$, $\mathbf{c}_2 = \mathbf{c}$, space group $P1a1$, Ramsdell symbol $2M$, Hägg symbol $|+-|$. The equivalence of all layer triples in either of these polytypes is evident. The third polytype (*c*) (Fig. 9.2.2.2) is not a MDO polytype because it contains two kinds of layer triples, whereas it is possible to construct a polytype of this family containing only a selection of these. The polytype is again monoclinic with basis vectors $\mathbf{a}_3 = 4\mathbf{a}_0$, $\mathbf{b}_3 = \mathbf{b}$, $\mathbf{c}_3 = \mathbf{c}$, space group $P1a1$, Ramsdell symbol $4M$, and Hägg symbol $|+--+|$.

Evidently, the partial mirror plane is crucial for the polytypism of this family. And yet the space group of none of its periodic members can contain it – simply because it can never become total. The space-group symbols thus leave some of the most important properties of periodic polytypes unnoticed. Moreover, the atomic coordinates of different polytypes expressed in terms of the respective lattice geometries cannot be immediately compared. And, finally, for non-periodic members of a family, a space-group symbol cannot be written at all. This is why the OD theory gives a *special symbol* indicating the symmetry proper of individual layers (λ symmetry) as well as the coincidence operations transforming a layer into the adjacent one (σ symmetry). The symbol of the OD groupoid family of our hypothetical example thus consists of two lines (Dornberger-Schiff, 1964, pp. 41 ff.; Fichtner, 1979*a*,*b*):

$$\begin{array}{llll} P(1) & m & 1 & \lambda \text{ symmetry} \\ \{(1) & a_2 & 1\} & \sigma \text{ symmetry,} \end{array}$$

where the unusual subscript 2 indicates that the glide reflection transforms the given layer into the subsequent one.

It is possible to write such a symbol for any OD groupoid family for equivalent layers, and thus also for the close packing of spheres. However, keeping in mind that the number of asymmetric units here is 24 (λ symmetry), one has to indicate also 24 σ operations, which is instructive but unwieldy. This is why Fichtner (1980) proposed simplified one-line symbols, containing full λ symmetry and only the rotational part of *any one* of the σ operations plus its translational components. Accordingly, the symbol of our hypothetical family reads: $P(1)m1|1,\ y = 0.25$; for the family of close packings of equal spheres: $P(6/m)mm|1,\ x = 2/3,\ y = 1/3$ (the layers are in both cases translationally equivalent and the rotational part of a translation is the identity).

An OD groupoid family symbol should not be confused with a *polytype symbol*, which gives information about the structure of an individual polytype (Dornberger-Schiff, Ďurovič & Zvyagin, 1982; Guinier *et al.*, 1984).

9.2.2.2.5. *Diffraction pattern – structure analysis*

Let us now consider schematic diffraction patterns of the three structures on the right-hand side of Fig. 9.2.2.2. It can be seen that, while being in general different, they contain a common subset of diffractions with $k = 2\hat{k}$ – these, normalized to a constant number of layers, have the same distribution of intensities and monoclinic symmetry. This follows from the fact that they correspond to the so-called *superposition structure* with basis vectors $\mathbf{A} = 2\mathbf{a}_0$, $\mathbf{B} = \mathbf{b}/2$, $\mathbf{C} = \mathbf{c}$, and space group $C1m1$. It is a fictitious structure that can be obtained from any of the structures in Fig. 9.2.2.2 as a normalized sum of the structure in its given position and in a position shifted by $b/2$, thus

$$\hat{\rho}(xyz) = \tfrac{1}{2}[\rho(xyz) + \rho(x, y + 1/2, z)].$$

Evidently, this holds for all members of the family, including the non-periodic ones. In general, the superposition structure is obtained by simultaneous realization of all Z possible positions of all OD layers in any member of the family (Dornberger-Schiff, 1964, p. 54). As a consequence, its symmetry can be obtained by completing any of the family groupoids to a group (Fichtner, 1977). This structure is by definition periodic and *common to all members* of the family. Thus, the corresponding diffractions are also always sharp, common, and characteristic for the family. They are called *family diffractions*.

Diffractions with $k = 2\hat{k} + 1$ are characteristic for individual members of the family. They are sharp for periodic polytypes but appear as diffuse streaks for non-periodic ones. Owing to the C centring of the superposition structure, only diffractions with $\hat{h} + \hat{k} = 2n$ are present. It follows that $0\hat{k}\hat{l}$ diffractions are present only for $\hat{k} = 2n$, which, in an indexing referring to the actual **b** vector reads: $0kl$ present only for $k = 4n$. This is an example of non-space-group absences exhibited by many polytypic structures. They can be used for the determination of the OD groupoid family (Dornberger-Schiff & Fichtner, 1972).

There is no routine method for the determination of the structural principle of an OD structure. It is easiest when one has at one's disposal many different (at least two) periodic polytypes of the same family with structures solved by current methods. It is then possible to compare these structures, determine equivalent regions in them (Grell, 1984), and analyse partial symmetries. This results in an OD interpretation of the substance and a description of its polytypism.

Sometimes it is possible to arrive at an OD interpretation from one periodic structure, but this necessitates experience in the recognition of the partial symmetry and prediction of potential polytypism (Merlino, Orlandi, Perchiazzi, Basso & Palenzona, 1989).

The determination of the structural principle is complex if only disordered polytypes occur. Then – as a rule – the superposition structure is solved first by current methods. The actual structure of layers and relations between them can then be determined from the intensity distribution along diffuse streaks (for more details and references see Jagodzinski, 1964; Sedlacek, Kuban & Backhaus, 1987; Müller & Conradi, 1986). High-resolution electron microscopy can also be successfully applied – see Subsection 9.2.2.4.

9.2.2.2.6. *The vicinity condition*

A polytype family contains periodic as well as non-periodic members. The latter are as important as the former, since the very fact that they can be non-periodic carries important crystallochemical information. Non-periodic polytypes do not comply with the classical definition of crystals, but we believe that this definition should be generalized to include rather than exclude non-periodic polytypes from the world of crystals (Dornberger-Schiff & Grell, 1982*b*). The OD theory places them, together with the periodic ones, in the hierarchy of the so-called *VC structures*. The reason for this is that all periodic structures, even the non-polytypic ones, can be thought of as consisting of *disjunct*, two-dimensionally periodic slabs, the *VC layers*, which are stacked together according to three rules called the *vicinity condition* (VC) (Dornberger-Schiff, 1964, pp. 29 ff., 1979; Dornberger-Schiff & Fichtner, 1972):

(α) VC layers are either geometrically equivalent or, if not, they are relatively few in kind;

(β) translation groups of all VC layers are either identical or they have a common subgroup;

(γ) equivalent sides of equivalent layers are faced by equivalent sides of adjacent layers so that the resulting pairs are equivalent [for a more detailed specification and explanation see Dornberger-Schiff (1979)].

If the stacking of VC layers is unambiguous, traditional three-dimensionally periodic structures result (*fully ordered structures*). *OD structures* are VC structures in which the stacking of VC layers is ambiguous at every layer boundary ($Z > 1$). The corresponding VC layers then become *OD layers*. OD layers are, in general, not identical with crystallochemical layers; they may contain half-atoms at their boundaries. In this context, they are analogous with unit cells in traditional crystallography, which may also contain parts of atoms at their boundaries. However, *the choice of OD layers is not absolute*: it depends on the polytypism, either actually observed or reasonably anticipated, on the degree of symmetry idealization, and other circumstances (Grell, 1984).

9.2.2.2.7. *Categories of OD structures*

Any OD layer is two-dimensionally periodic. Thus, a unit mesh can be chosen according to the conventional rules for the corresponding layer group; the corresponding vectors or their linear combinations (Zvyagin & Fichtner, 1986) yield the basis vectors parallel to the layer plane and thus also their lengths as units for fractional atomic coordinates. But, in general, there is no periodicity in the direction perpendicular to the layer plane and it is thus necessary to define the corresponding unit length in some other way. This depends on the symmetry principle of the family in question – or, more narrowly, on the *category* to which this family belongs.

OD structures can be built of *equivalent layers* or contain *layers of several kinds*. The rule (γ) of the VC implies that a projection of any OD structure – periodic or not – on the stacking direction is periodic. This period, called *repeat unit*, is the required unit length.

9.2.2.2.7.1. *OD structures of equivalent layers*

If the OD layers are equivalent then they are either all polar or all non-polar in the stacking direction. Any two adjacent polar layers can be related either by τ operations only, or by ρ operations only. For non-polar layers, the σ operations are both τ and ρ. Accordingly, there are *three categories* of OD structures of equivalent layers. They are shown schematically in Fig. 9.2.2.3; the character of the corresponding λ and σ operations is as follows (Dornberger-Schiff, 1964, pp. 24 ff.):

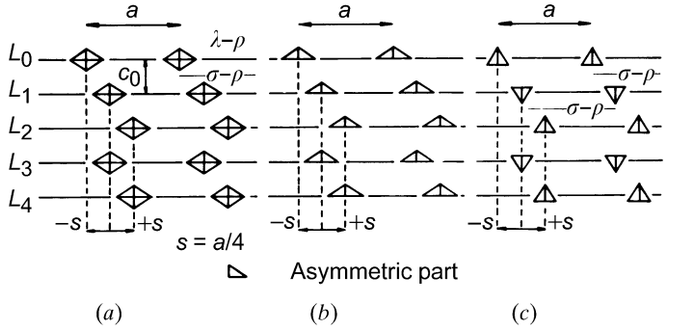

Fig. 9.2.2.3. Schematic examples of the three categories of OD structures consisting of equivalent layers (perpendicular to the plane of the drawing): (*a*) category I – OD layers non-polar in the stacking direction; (*b*) category II – polar OD layers, all with the same sense of polarity; (*c*) category III – polar OD layers with regularly alternating sense of polarity. The position of ρ planes is indicated.

	category I	category II	category III
λ operations	τ and ρ	τ	τ
σ operations	τ and ρ	τ	ρ

Category II is the simplest: the OD layers are polar and all with the same sense of polarity (they are τ-equivalent); our hypothetical example given in §9.2.2.2.4 belongs to this category. The layers can thus exhibit only one of the 17 polar layer groups. The projection of any vector between two τ-equivalent points in two adjacent layers on the stacking direction (perpendicular to the layer planes) is the repeat unit and it is denoted by $\mathbf{c}_0$, $\mathbf{a}_0$, or $\mathbf{b}_0$ depending on whether the basis vectors in the layer plane are **ab**, **bc**, or **ca**, respectively. The choice of origin in the stacking direction is arbitrary but preferably so that the z coordinates of atoms within a layer are positive. Examples are SiC, ZnS, and AgI.

OD layers in category I are non-polar and they can thus exhibit any of the 63 non-polar layer groups. Inspection of Fig. 9.2.2.3(*a*) reveals that the symmetry elements representing the λ–ρ operations (*i.e.* the operations turning a layer upside down) can lie only in one plane called the *layer plane*. Similarly, the symmetry elements representing the σ–ρ operations (*i.e.* the operations converting a layer into the adjacent one) also lie in one plane, located exactly halfway between two nearest layer planes. These two kinds of planes are called ρ planes. The distance between two nearest layer planes is the repeat unit c_0. Examples are close packing of equal spheres, GaSe, α-wollastonite (Yamanaka & Mori, 1981), β-wollastonite (Ito, Sadanaga, Takéuchi & Tokonami, 1969), $K_3[M(CN)_6]$ (Jagner, 1985), and many others.

The OD structures belonging to the above two categories contain pairs of adjacent layers, all equivalent. This does not apply for structures of category III, which consist of polar layers that are converted into their neighbours by ρ operations. It is evident (Fig. 9.2.2.3*c*) that two kinds of pairs of adjacent layers are needed to build any such structure. It follows that only even-numbered layers can be mutually τ-equivalent and the same holds for odd-numbered layers. There are only σ–ρ planes in these structures, and again they

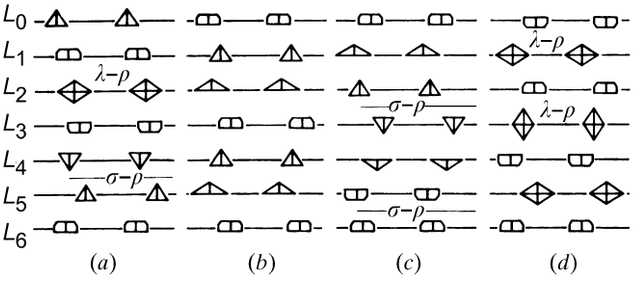

Fig. 9.2.2.4. Schematic examples of the four categories of OD structures consisting of more than one kind of layer (perpendicular to the plane of the drawing). Equivalent OD layers are represented by equivalent symbolic figures. (*a*) Category I – three kinds of OD layers: one kind (L_{2+5n}) is non-polar, the remaining two are polar. One and only one kind of non-polar layer is possible in this category. (*b*) Category II – three kinds of polar OD layers; their triples are polar and retain their sense of polarity in the stacking direction. (*c*) Category III – three kinds of polar OD layers; their triples are polar and regularly change their sense of polarity in the stacking direction. (*d*) Category IV – three kinds of OD layers: two kinds are non-polar (L_{1+4n} and L_{3+4n}), one kind is polar. Two and only two kinds of non-polar layers are possible in this category. The position of ρ planes is indicated.

are of two kinds; the origin can be placed in either of them. c_0 is the distance between two nearest ρ planes of the same kind, and slabs of this thickness contain two OD layers. There are three examples for this category known to date: foshagite (Gard & Taylor, 1960), γ-$Hg_3S_2Cl_2$ (Ďurovič, 1968), and 2,2-aziridinedicarboxamide (Fichtner & Grell, 1984).

9.2.2.2.7.2. *OD structures with more than one kind of layer*

If an OD structure consists of $N > 1$ kinds of OD layers, then it can be shown (Dornberger-Schiff, 1964, pp. 64 ff.) that it can fall into one of *four categories*, according to the polarity or non-polarity of its constituent layers and their sequence. These are shown schematically in Fig. 9.2.2.4; the character of the corresponding λ and σ operations is

	category I	category II	category III	category IV
λ operations	τ and ρ (one set) τ ($N-1$ sets)	τ (N sets)	τ (N sets)	τ and ρ (two sets) τ ($N-2$ sets)
σ operations	ρ (one set)	none	ρ (two sets)	none.

Here also category II is the simplest. The structures consist of N kinds of cyclically recurring polar layers whose sense of polarity remains unchanged (Fig. 9.2.2.4*b*). The choice of origin in the stacking direction is arbitrary; c_0 is the projection on this direction of the shortest vector between two τ-equivalent points – a slab of this thickness contains all N OD layers of different kinds. Examples are the structures of the serpentine–kaolin group.

Structures of category III also consist of polar layers but, in contrast to category II, the N-tuples containing all N different OD layers each alternate regularly the sense of their polarity in the stacking direction. Accordingly (Fig. 9.2.2.4*c*), there are two kinds of σ–ρ planes and two kinds of pairs of equivalent adjacent layers in these structures. The origin can be placed in either of the two ρ planes. c_0 is the distance between the nearest two equivalent ρ planes; a slab with this thickness contains $2 \times N$ non-equivalent OD layers. No representative of this category is known to date.

The structures of category I contain one, and only one, kind of non-polar layer, the remaining $N-1$ kinds are polar and alternate in their sense of polarity along the stacking direction (Fig. 9.2.2.4*a*). Again, there are two kinds of ρ planes here, but one is a λ–ρ plane (the layer plane of the non-polar OD layer), the other is a σ–ρ plane. These structures thus contain only one kind of pair of equivalent adjacent layers. The origin is placed in the λ–ρ plane. c_0 is the distance between the nearest two equivalent ρ planes and a slab with this thickness contains $2 \times (N-1)$ non-equivalent polar OD layers plus one entire non-polar layer. Examples are the MX_2 compounds (CdI_2, MoS_2, *etc*.) and the talc–pyrophyllite group.

The structures of category IV contain two, and only two, kinds of non-polar layers. The remaining $N-2$ kinds are polar and alternate in their sense of polarity along the stacking direction (Fig. 9.2.2.4*d*). Both kinds of ρ planes are λ–ρ planes, identical with the layer planes of the non-polar OD layers; the origin can be placed in any one of them. c_0 is chosen as in categories I and III. A slab with this thickness contains $2 \times (N-2)$ non-equivalent polar layers plus the two non-polar layers. Examples are micas, chlorites, vermiculites, *etc*.

OD structures containing $N > 1$ kinds of layers need special symbols for their OD groupoid families (Grell & Dornberger-Schiff, 1982).

A slab of thickness c_0 containing the N non-equivalent polar OD layers in the sequence as they appear in a given structure of category II represents completely its composition. In the remaining three categories, a slab with thickness $c_0/2$, the polar part of the structure contained between two adjacent ρ planes, suffices. Such slabs are higher structural units for OD structures of more than one kind of layer and have been called *OD packets*. An OD packet is thus defined as the smallest continuous part of an OD structure that is periodic in two dimensions and which represents its composition completely (Ďurovič, 1974*a*).

The hierarchy of VC structures is shown in Fig. 9.2.2.5.

9.2.2.2.8. *Desymmetrization of OD structures*

If a fully ordered structure is refined, using the space group determined from the systematic absences in its diffraction pattern and then by using some of its subgroups, serious discrepancies are only rarely encountered. Space groups thus characterize the general symmetry pattern quite well, even in real crystals. However, experience with refined periodic polytypic structures has revealed that there are always significant deviations from the OD symmetry and, moreover, even the atomic coordinates within OD layers in different polytypes of the same family may differ from one another. The OD symmetry thus appears as only an approximation to the actual symmetry pattern of polytypes. This phenomenon was called *desymmetrization* of OD structures (Ďurovič, 1974*b*, 1979).

When trying to understand this phenomenon, let us recall the structure of rock salt. Its symmetry $Fm\bar{3}m$ is an expression of the energetically most favourable relative position of Na^+ and Cl^- ions in this structure – the right angles $\alpha\beta\gamma$ follow from the symmetry. Since the whole structure is cubic, we cannot expect that the environment of any building unit, *e.g.* of any octahedron $NaCl_6$, would exercise on it an influence that would decrease its symmetry; the symmetries of these units and of the whole structure are not 'antagonistic'.

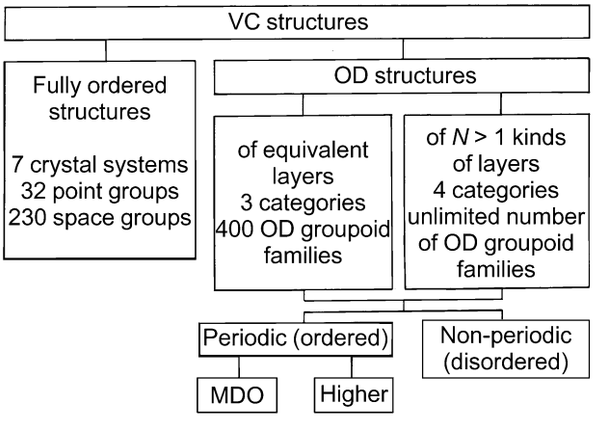

Fig. 9.2.2.5. Hierarchy of VC structures indicating the position of OD structures within it.

Not so in OD structures, where any OD layer is by definition situated in a disturbing environment because its symmetry does not conform to that of the entire structure. 'Antagonistic' relations between these symmetries are most drastic in pure MDO structures because of the regular sequence of layers. The partial symmetry operations become irrelevant and the OD groupoid degenerates into the corresponding space group.

The more disordered an OD structure is, the smaller become the disturbing effects that the environment exercises on an OD layer. These can be, at least statistically, neutralized by random positions of neighbouring layers so that partial symmetry operations can retain their relevance throughout the structure. This can be expressed in the form of a paradox: the less periodic an OD structure is, the more symmetric it appears.

Despite desymmetrization, the OD theory remains a geometrical theory that can handle properly the *general symmetry pattern* of polytypes (which group theory cannot). It establishes a *symmetry norm* with which deviations observed in real polytypes can be compared. Owing to the high abstraction power of OD considerations, systematics of entire families of polytypes at various degree-of-idealization levels can be worked out, yielding thus a common point of view for their treatment.

9.2.2.2.9. *Concluding remarks*

Although very general physical principles (OD philosophy, MDO philosophy) underlie the OD theory, it is mainly a geometrical theory, suitable for a *description* of the symmetry of polytypes and their families rather than for an *explanation* of polytypism. It thus does not compete with crystal chemistry, but cooperates with it, in analogy with traditional crystallography, where group theory does not compete with crystal chemistry.

When speaking of polytypes, one should always be aware, whether one has in mind a concrete *real* polytype – more or less in Baumhauer's sense – or an *abstract* polytype as a structural type (Subsection 9.2.2.1).

A substance can, in general, exist in the form of various polymorphs and/or polytypes of one or several families. Since polytypes of the same family differ only slightly in their crystal energy (Verma & Krishna, 1966), an entire family can be considered as an energetic analogue to one polymorph. As a rule, polytypes belonging to different families of the same substance do not co-exist. $Al(OH)_3$ may serve as an example for two different families: the bayerite family, in which the adjacent planes of OH groups are stacked according to the principle of close packing (Zvyagin *et al.*, 1979), and the gibbsite–nordstrandite family in which these groups coincide in the normal projection.* Another example is the phyllosilicates (§9.2.2.3.1). The compound $Hg_3S_2Cl_2$, on the other hand, is known to yield two polymorphs α and β (Carlson, 1967; Frueh & Gray, 1968) and one OD family of γ structures (Ďurovič, 1968).

As far as the definition of *layer polytypism* is concerned, OD theory can contribute specifications about the layers themselves and the geometrical rules for their stacking within a family (all incorporated in the vicinity condition). A possible definition might then read:

Polytypism is a special case of polymorphism, such that the individual polymorphs (called *polytypes*) may be regarded as arising through different modes of stacking layer-like structural units. The layers and their stackings are limited by the *vicinity condition*. All polytypes built on the same structural principle belong to a *family*; this depends on the degree of a structural and/or compositional *idealization*.

Geometrical theories concerning rod and block polytypism have not yet been elaborated, the main reason is the difficulty of formulating properly the vicinity condition (Sedlacek, Grell & Dornberger-Schiff, private communications). But such structures are known. Examples are the structures of tobermorite (Hamid, 1981) and of manganese(III) hydrogenbis(orthophosphite) dihydrate (Císařová, Novák & Petříček, 1982). Both structures can be thought of as consisting of a three-dimensionally periodic framework of certain atoms into which one-dimensionally periodic chains and aperiodic finite configurations of the remaining atoms, respectively, 'fit' in two equivalent ways.

9.2.2.3. *Examples of some polytypic structures*

The three examples below illustrate the three main methods of analysis of polytypism indicated in §9.2.2.2.5.

9.2.2.3.1. *Hydrous phyllosilicates*

The basic concepts were introduced by Pauling (1930*a*,*b*) and confirmed later by the determination of concrete crystal structures. A *crystallochemical analysis* of these became the basis for generalizations and systemizations. The aim was the understanding of geometrical reasons for the polytypism of these substances as well as the development of identification routines through the derivation of basic polytypes (§9.2.2.2.3). Smith & Yoder (1956) succeeded first in deriving the six basic polytypes in the mica family.

Since the 1950's, two main schools have developed: in the USA, represented mainly by Brindley, Bailey, and their co-workers (for details and references see Bailey, 1980, 1988*a*; Brindley, 1980), and in the former USSR, represented by Zvyagin and his co-workers (for details and references see Zvyagin, 1964, 1967; Zvyagin *et al.*, 1979). Both these schools based their systemizations on idealized structural models corresponding to the ideas of Pauling, with *hexagonal* symmetry of tetrahedral sheets (see later). The US school uses indicative symbols (Guinier *et al.*, 1984) for the designation of individual polytypes, and single-crystal as well as powder X-ray diffraction methods for their identification, whereas the USSR school uses unitary descriptive symbols for polytypes of all mineral groups and mainly electron diffraction on oblique textures for identification purposes. For the derivation of basic polytypes, both schools use crystallochemical considerations; symmetry principles are applied tacitly rather than explicitly.

In contrast to crystal structures based on close packings, where all relevant details of individual (even multilayer) polytypes can be recognized in the $(11\bar{2}0)$ section, the structures of hydrous phyllosilicates are rather complex. For their representation, Figueiredo (1979) used the concept of *condensed models*.

Since 1970, the OD school has also made its contribution. In a series of articles, basic types of hydrous phyllosilicates have been interpreted as OD structures of $N > 1$ kinds of layers: the serpentine–kaolin group (Dornberger-Schiff & Ďurovič, 1975*a*,*b*), Mg-vermiculite (Weiss & Ďurovič, 1980), the mica group (Dornberger-Schiff, Backhaus & Ďurovič, 1982; Backhaus & Ďurovič, 1984; Ďurovič, Weiss & Backhaus, 1984; Weiss & Wiewióra, 1986), the talc–pyrophyllite group (Ďurovič & Weiss, 1983; Weiss & Ďurovič, 1985*a*), and the chlorite group (Ďurovič, Dornberger-Schiff & Weiss, 1983;

* Sandwiches with composition $Al(OH)_3$ (similar to those in CdI_2) are the same in both families, but their stacking mode is different. This and similar situations in other substances might have been the reason for distinguishing between 'polytype diversity' and 'OD diversity' (Zvyagin, 1988).

Weiss & Ďurovič, 1983). The papers published before 1983 use the Pauling model; the later papers are based on the model of Radoslovich (1961) with *trigonal* symmetry of tetrahedral sheets. In all cases, MDO polytypes (§9.2.2.2.3) have been derived systematically: their sets partially overlap with basic polytypes presented by the US or the USSR schools. The OD models allowed the use of unitary descriptive symbols for individual polytypes from which all the relevant symmetries can be determined (Ďurovič & Dornberger-Schiff, 1981) as well as of extended indicative Ramsdell symbols (Weiss & Ďurovič, 1985*b*). The results, including principles for identification of polytypes, have been summarized by Ďurovič (1981).

The main features of polytypes of basic types of hydrous phyllosilicates, of their diffraction patterns and principles for their identification, are given in the following.

9.2.2.3.1.1. *General geometry*

Tetrahedral and octahedral sheets are the fundamental, *two-dimensionally periodic* structural units, common to all hydrous phyllosilicates. Any *tetrahedral sheet* consists of $(Si,Al,Fe^{3+},Ti^{4+})O_4$ tetrahedra joined by their three basal O atoms to form a network with symmetry $P(3)1m$ (Fig. 9.2.2.6*a*). The atomic coordinates can be related either to a hexagonal axial system with a primitive unit mesh and basis vectors $\mathbf{a}_1$, $\mathbf{a}_2$, or to an orthohexagonal system with a *c*-centred unit mesh and basis vectors $\mathbf{a}$, $\mathbf{b}$ ($b = \sqrt{3}a$). Any *octahedral sheet* consists of $M(O,OH)_6$ octahedra with shared edges (Fig. 9.2.2.6*b*), and with cations *M* most frequently Mg^{2+}, Al^{3+}, Fe^{2+}, Fe^{3+}, but also Li^{+}, Mn^{2+} ($r_M <\sim 0.9$ Å), *etc*. There are three octahedral sites per unit mesh $\mathbf{a}_1, \mathbf{a}_2$. Crystallochemical classification distinguishes between two extreme cases: *trioctahedral* (all three octahedral sites are occupied) and *dioctahedral* (one site is – even statistically – empty). This classification is based on a bulk chemical composition. A classification from the symmetry point of view distinguishes between three cases: *homo-octahedral* [all three octahedral sites are occupied by the same kind of crystallochemical entity, *i.e.* either by the same kind of ion or by a statistical average of different kinds of ions including voids; symmetry of such a sheet is $H(\bar{3})12/m$];* *meso-octahedral* [two octahedral sites are occupied by the same kind of crystallochemical entity, the third by a different one, in an ordered way; symmetry $P(\bar{3})12/m$)]; and *hetero-octahedral* [each octahedral site is occupied by a different crystallochemical entity in an ordered way; symmetry $P(3)12$]. The prefixes homo-, meso-, hetero- can be combined with the prefixes tri-, di-, or used alone (Ďurovič, 1994).

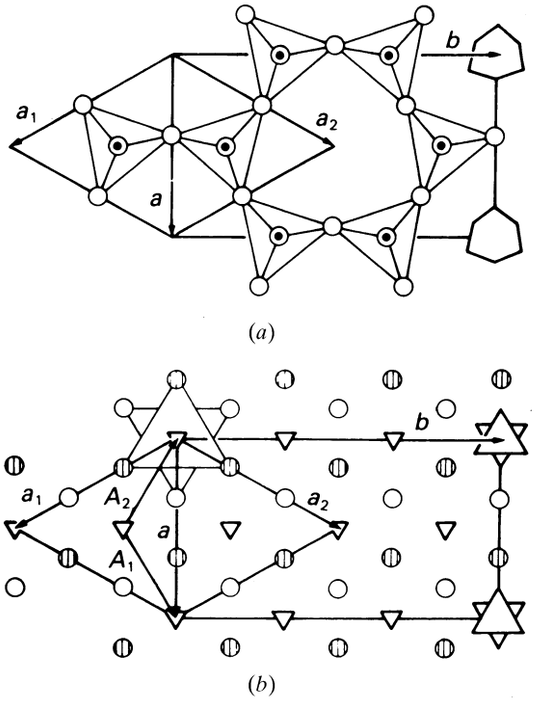

Fig. 9.2.2.6. (*a*) Tetrahedral sheet in a normal projection. Open circles: basal oxygen atoms, circles with black dots: apical oxygen atoms and tetrahedral cations. Hexagonal and orthohexagonal basis vectors and symbolic figures (ditrigons) for pictorial representation of these sheets are also shown. (*b*) Octahedral sheet. Open and shaded circles belong to the lower and the upper oxygen atomic planes, respectively; small triangles denote octahedral sites. Triangular stars on the right are the symbolic figures for pictorial representation of these sheets: the two triangles correspond to the lower and upper basis of any octahedron, respectively.

A tetrahedral sheet (*Tet*) can be combined with an octahedral sheet (*Oc*) either by a shared plane of apical O atoms (in all groups of hydrous phyllosilicates, Fig. 9.2.2.7*a*), or by hydrogen bonds (in the serpentine–kaolin group and in the chlorite group, Fig.9.2.2.7*b*). Two tetrahedral sheets can either form a pair anchored by interlayer cations (in the mica group, Fig. 9.2.2.8*a*) or an unanchored pair (in the talc–pyrophyllite group, Fig. 9.2.2.8*b*).

The ambiguity in the stacking occurs at the centres between adjacent *Tet* and *Oc* and between adjacent *Tet* in the talc–pyrophyllite group. From the solved and refined crystal structures it follows that the displacement of (the origin of) one sheet relative to (the origin of) the adjacent one can only be one (or simultaneously three – for homo-octahedral sheets) of the nine vectors shown in Fig. 9.2.2.9.

The number of possible positions of one sheet relative to the adjacent one can be determined by the corresponding *NFZ* relations (§9.2.2.2.1). As an example, the contact (*Tet*; *Oc*) by shared apical O atoms, and the contacts (*Oc*; *Tet*) by hydrogen

* A hexagonally centred unit mesh $\mathbf{a}_1, \mathbf{a}_2$ instead of a primitive mesh $\mathbf{A}_1, \mathbf{A}_2$ is used (Fig. 9.2.2.6*b*).

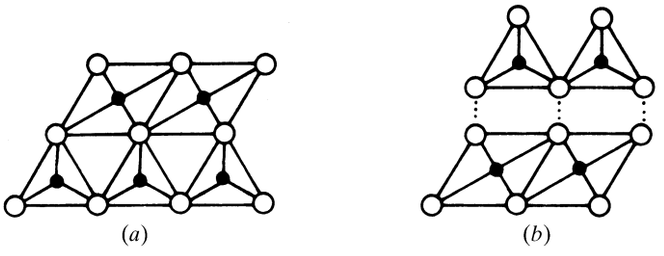

Fig. 9.2.2.7. Two possible combinations of one tetrahedral and one octahedral sheet (*a*) by shared apical O atoms, (*b*) by hydrogen bonds (side projection).

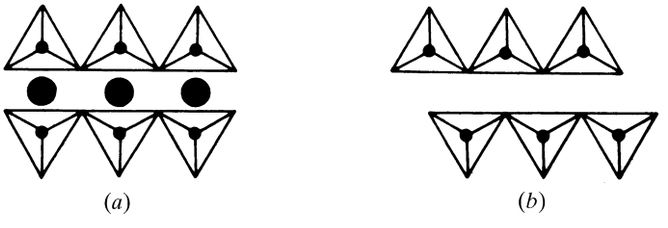

Fig. 9.2.2.8. Combination of two adjacent tetrahedral sheets (*a*) in the mica group, (*b*) in the talc–pyrophyllite group (side projection).

bonds, for a homo-octahedral case, are illustrated in Figs. 9.2.2.10(*a*) and 9.2.2.10(*b*),(*c*), respectively. The two kinds of sheets are represented by the corresponding symbolic figures indicated in Fig. 9.2.2.6. For Fig. 9.2.2.10(*a*): the symmetry of *Tet* is $P(3)1m$, thus $N = 6$; the symmetry of *Oc* is $H(\bar{3})12/m$ and its position relative to *Tet* is such that the symmetry of the pair is $P(3)1m$, thus $F = 6$ and $Z = 1$: this stacking is unambiguous.* But, if the sequence of these two sheets is reversed, $Z = 3$, because $N_{Oc} = 18$ (*h* centring of *Oc*). For Figs. 9.2.2.10(*b*) and (*c*), $Z = 3$. Similar relations can be derived for meso- and hetero-octahedral sheets as well as for the pair (*Tet*; *Tet*) in the talc–pyrophyllite group.

A detailed geometrical analysis shows that the possible positions are always related by vectors $\pm\mathbf{b}/3$. This, together with the trigonal symmetry of the individual sheets, leads to the fact that any superposition structure (§9.2.2.2.5) is trigonal (also rhombohedral) or hexagonal, and the set of diffractions with $k_{\rm ort} \equiv 0 \pmod 3$ has this symmetry too. This is important for the analysis of diffraction patterns.

Some characteristic features of basic types of hydrous phyllosilicates are as follows:

The serpentine–kaolin group: The general structural principle is shown in Fig. 9.2.2.11. The structures belong to category II (§9.2.2.2.7.2). In the homo-octahedral family, there are 12 non-equivalent (16 non-congruent) MDO polytypes (any two polytypes belonging to an enantiomorphous pair are equivalent but not congruent); in the meso-octahedral family, there are 36 non-equivalent (52 non-congruent) MDO polytypes. These sets are identical with the sets of *standard* or *regular* polytypes derived by Bailey (for references see Bailey, 1980) (trioctahedral) and by Zvyagin (1967) (dioctahedral and trioctahedral). The individual polytypes can be ranged into four groups (subfamilies, which are individual OD groupoid families), each with a characteristic superposition structure.

The mica group: The general structural principle is shown in Fig. 9.2.2.12. The structures belong to category IV. There are 6 non-equivalent (8 non-congruent) homo-octahedral MDO polytypes, 14 (22) meso-octahedral, and 36 (60) hetero-octahedral MDO polytypes. The homo-octahedral MDO polytypes are identical with those derived by Smith & Yoder (1956); meso-octahedral MDO polytypes include also those with non-centrosymmetric 2:1 layers (*Tet*; *Oc*; *Tet*); some of these have also been derived by Zvyagin *et al.* (1979). The individual polytypes can be ranged into two groups (subfamilies). For complex polytypes and growth mechanisms, see Baronnet (1975, 1986).

The talc–pyrophyllite group: The general structural principle is shown in Fig. 9.2.2.13. The structures belong to category I. There are 10 (12) MDO polytypes in the talc family (homo-octahedral) and 22 (30) MDO polytypes in the pyrophyllite family (meso-octahedral); some of these have been derived also by Zvyagin *et al.* (1979). The structures can be ranged into two

* If the symmetry of *Tet* is $P(6)mm$ (in the Pauling model), $Z = 2$. This case is common in the literature. However, with the trigonal symmetry of *Tet*, these two possibilities would correspond to Franzini (1969) types *A* and *B*, which are not geometrically equivalent.

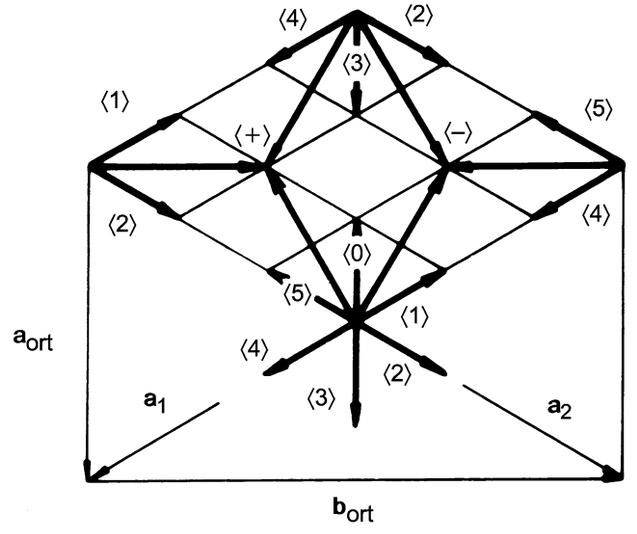

Fig. 9.2.2.9. The nine possible displacements in the structures of polytypes of phyllosilicates. The individual vectors are designated by their conventional numerical characters and the signs +,−. The zero displacement ⟨∗⟩ is not indicated. The relations of these vectors to the basis vectors $\mathbf{a}_1, \mathbf{a}_2$ or $\mathbf{a}, \mathbf{b}$ are evident.

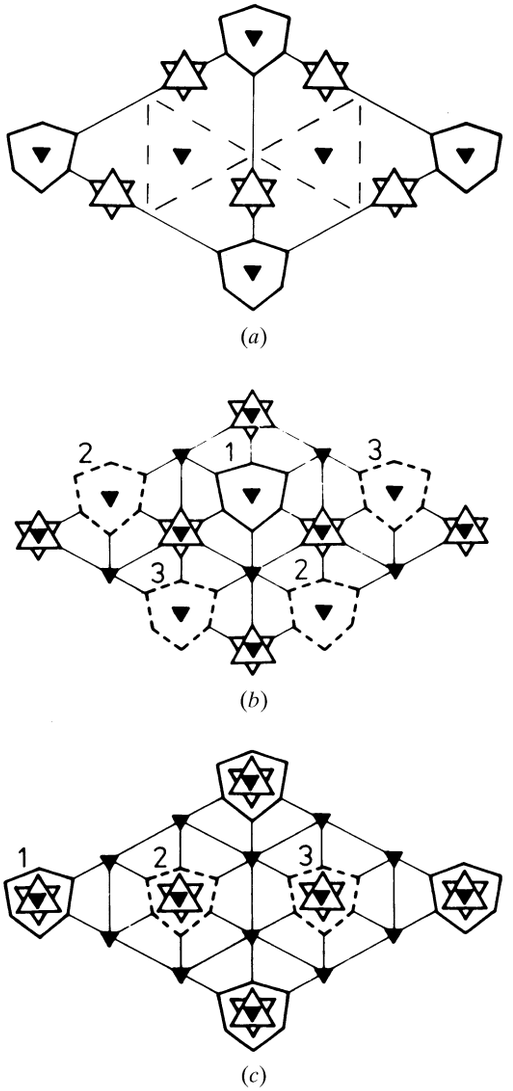

Fig. 9.2.2.10. The *NFZ* relations (*a*) for the pair tetrahedral sheet–homo-octahedral sheet (with shared apical O atoms), (*b*), (*c*) for the pair homo-octahedral sheet–tetrahedral sheet (by hydrogen bonds). The sheets are represented by their symbolic figures; some relevant symmetry elements are also indicated. One of the possible positions (labelled 1) is drawn by full, the other two (2, 3) by broken lines.

groups (subfamilies). For more details, see also Evans & Guggenheim (1988).

The chlorite–vermiculite group: There are two kinds of octahedral sheets in these structures: the *Oc* sandwiched between two *Tet* and the *interlayer* (Fig. 9.2.2.14). The structures belong to category IV. Any *Oc* can be independently homo-, meso-, or hetero-octahedral, and thus, theoretically, there are nine families here. Although vermiculites have a crystal chemistry different from chlorites, they can be, from the symmetry point of view, treated together. There are 20 (24) homo-homo-octahedral, 44 (60) homo-meso-octahedral and 164 (256) meso-meso-octahedral MDO polytypes (the first prefix refers to the 2:1 layer, the second to the interlayer); the other families have not yet been treated. Some of these polytypes have also been derived by other authors (for references, see Bailey, 1980; Zvyagin *et al.*, 1979).

In order to preserve a unitary system, some monoclinic polytypes necessitate a 'third' setting, with the *a* axis unique. These should not be transformed into the standard second setting.

9.2.2.3.1.2. *Diffraction pattern and identification of individual polytypes*

Owing to the trigonal symmetry of the basic structural units and their stacking mode, the single-crystal diffraction pattern of hydrous phyllosilicates has a hexagonal *geometry* and it can be referred to hexagonal or orthohexagonal reciprocal vectors $\mathbf{a}_1^*$, $\mathbf{a}_2^*$ or $\mathbf{a}^*$, $\mathbf{b}^*$, respectively (Figs. 9.2.2.15 and 9.2.2.16). It contains three types of diffractions:

(1) Diffractions 00*l* (or 000*l*), always sharp and common to all polytypes of a family including all its subfamilies. They are indicative of the mineral group, but useless for the identification of polytypes.

(2) The remaining diffractions with $k_{\rm ort} \equiv 0 \pmod 3$, always sharp and common to all polytypes of the same subfamily.

(3) All other diffractions: sharp only for periodic polytypes, otherwise present on diffuse rods parallel to $\mathbf{c}^*$. These are characteristic of individual polytypes. Diffractions 0*kl* – if sharp – are common to all polytypes of the family with the same *bc* projection.

From descriptive geometry, it is known that two orthogonal projections suffice to characterize unambiguously any structure and, therefore, the superposition structure (which implicitly contains the *ac* projection) together with the *bc* projection suffice for an unambiguous characterization of any polytype. It also follows that the diffractions with $k \equiv 0 \pmod 3$ together with the 0*kl* diffractions with $k \not\equiv 0 \pmod 3$ suffice for its determination (except for homometric structures) (Ďurovič, 1981).

From the trigonal or hexagonal symmetry of any superposition structure and from Friedel's law, it follows that the reciprocal rows 20*l*, 13*l*, $\bar{1}3l$, $\bar{2}0l$, $\bar{1}\bar{3}l$, and $1\bar{3}l$ (Fig. 9.2.2.16) carry the same information. Therefore, for identification purposes, it suffices to calculate the distribution of intensities along the reciprocal rows 20*l* (superposition structure – subfamily) and 02*l* (*bc* projection) for all MDO polytypes. Experience shows (Weiss & Ďurovič, 1980) that a mere visual comparison of calculated and observed intensities along these two rows suffices for an unambiguous identification of a MDO polytype. A similar scheme has been presented by Bailey (1988*b*).

The above considerations are based on the ideal Radoslovich model. Diffraction patterns of real structures may exhibit deviations owing to the distortion of the ideal lattice geometry and/or symmetry of the structure.

9.2.2.3.2. *Stibivanite Sb_2VO_5*

The crystal structure of this mineral has been determined by Szymański (1980). It turned out to be identical with that of the compound of the same composition synthesized earlier (Darriet, Bovin & Galy, 1976). The structure is monoclinic with space group $C12/c1$, lattice parameters $a = 17.989\ (6)$, $b = 4.7924\ (7)$, $c = 5.500\ (2)$ Å, $\beta = 95.13\ (3)^\circ$.

Structural units are formed of SbO_2–O–VO–O–SbO_2 extended along **a**, with adjacent units bonded along **c** through Sb—O—Sb and V—O—V bonds. Ribbons are thus formed with no bonding along **b**, and only the Sb—O interactions [2.561 (4) Å] along **a** (Fig. 9.2.2.17). This accounts for the excellent acicular cleavage.

Merlino *et al.* (1989) recognized in this structure sheets of VO_5 square pyramids (*Pyr*) parallel to **bc**, with layer symmetry $P(2/m)2/c2_1/m$ alternating with sheets containing chains of distorted SbO_3 tetrahedron-like pyramids (*Tet*) with layer symmetry $P(1)2_1/c1$ (Fig. 9.2.2.18). Owing to the higher symmetry of *Pyr*, they concluded that there may also exist an alternative attachment of *Tet* to *Pyr*, such that the triples (*Tet*; *Pyr*; *Tet*) will exhibit the layer symmetry $Pmc2_1$, and they will be arranged so that another polytype 2*O* with symmetry $P2_1/m2_1/c2_1/n$ (Fig. 9.2.2.19) is formed [in the original 2*M* polytype, the triples (*Tet*; *Pyr*; *Tet*) have the layer symmetry $P(1)2/c1$]. A mineral with such a structure, with lattice parameters $a = 17.916\ (3)$, $b = 4.700\ (1)$, $c = 5.509\ (1)$ Å, has actually been found.

The polytypism of stibivanite is reflected in its OD character: the two kinds of sheets *Pyr* and *Tet* correspond to two kinds of non-polar layers: their relative position is given by the family symbol:

$$\begin{array}{ll} P(1)2_1/c1 & P(m)cm \\ [1/4, -0.0733\ldots] & \text{category IV,} \end{array}$$

the *NFZ* relations being

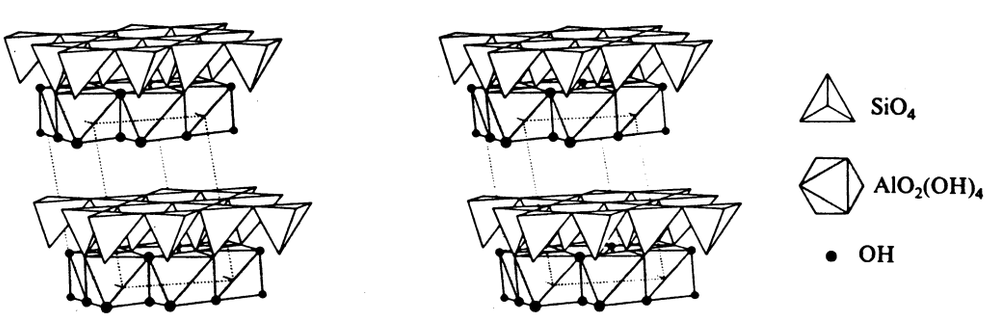

Fig. 9.2.2.11. Stereopair showing the sequence of sheets in the structures of the serpentine–kaolin group (kaolinite-1*A*, courtesy Zoltai & Stout, 1985).

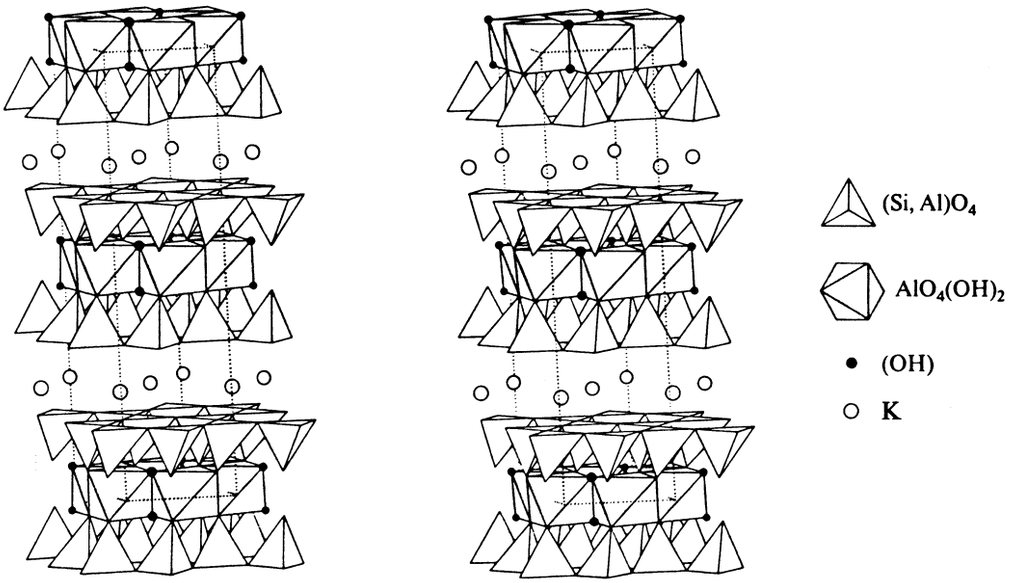

Fig. 9.2.2.12. Stereopair showing the sequence of sheets in the structures of the mica group (muscovite-2M_1, courtesy of Zoltai & Stout, 1985).

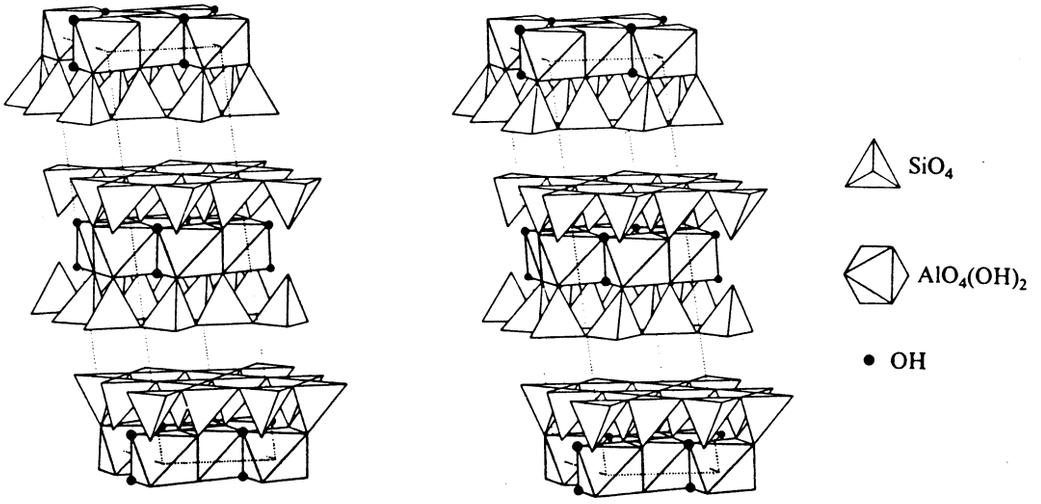

Fig. 9.2.2.13. Stereopair showing the sequence of sheets in the structures of the talc-pyrophyllite group (pyrophyllite-2M, courtesy of Zoltai & Stout, 1985).

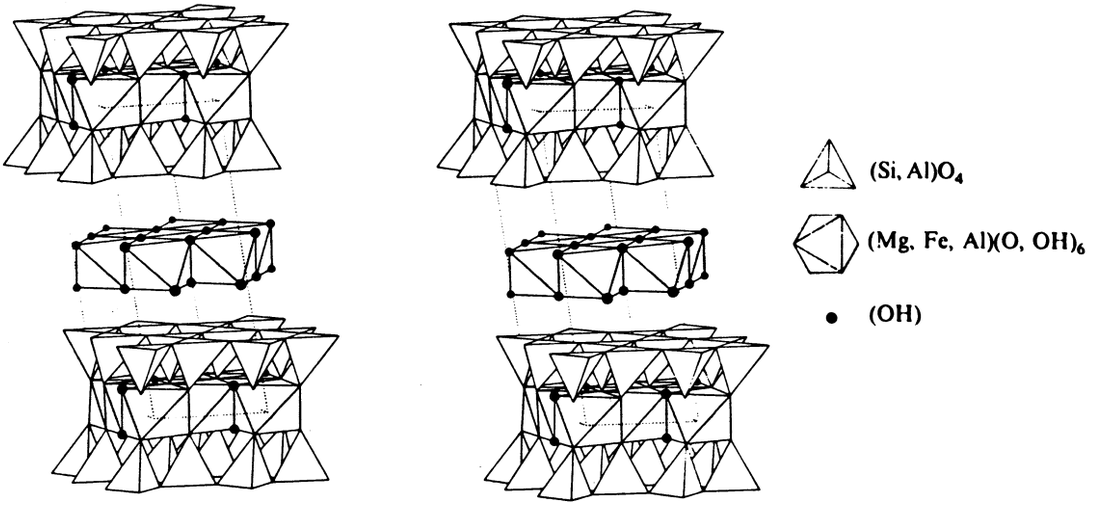

Fig. 9.2.2.14. Stereopair showing the sequence of sheets in the structures of the chlorite–vermiculite group (chlorite-1M, courtesy of Zoltai & Stout, 1985).

OD layer	layer group	subgroup of λ–τ oper.	N	F	Z
L_{2n+1}	$P(2/m)\,2/c\,2_1/m$	$P(2)cm$	4		1
			↘		↗
				2	
			↗		↘
L_{2n}	$P(1)\,2_1/c\,1$	$P(1)c1$	2		2.

Both polytypes are slightly desymmetrized. Since the shift between the origins of *Pyr* and *Tet* is irrational, stibivanite has no superposition structure and thus the diffraction patterns of its polytypes have no common set of family diffractions. Another remarkable point is that the recognition of these structures as OD structures of *layers* has nothing to do with their system of chemical bonds (see above).

9.2.2.3.3. γ-$Hg_3S_2Cl_2$

Among about 40 investigated crystals synthesized by Carlson (1967), not one was periodic. All diffraction patterns exhibited a common set of family diffractions, but the distribution of intensities along diffuse streaks varied from crystal to crystal (Ďurovič, 1968). The maxima on these streaks indicated in some cases a simultaneous presence of domains of three periodic polytypes – one system of diffuse maxima was always present and it was referred to a rectangular cell with $a = 9,328\,(5)$, $b = 16.28\,(1)$, $c = 9.081\,(6)$ Å with monoclinic symmetry. All crystals were more or less twinned, sometimes simulating orthorhombic symmetry in their diffraction patterns.

The superposition structure with $\mathbf{A} = \mathbf{a}$, $\mathbf{B} = \mathbf{b}/2$, $\mathbf{C} = 2\mathbf{c}$ and space group *Pbmm* was solved first. Here, a comparison of the family diffractions with the diffraction pattern of the α modification (Frueh & Gray, 1968) proved decisive. It turned out that only one kind of Hg atom contributed with half weight to the superposition structure. This means that only these atoms repeat in the actual structure with periods $\mathbf{b} = 2\mathbf{B}$ and $\mathbf{c} = 2\mathbf{C}$. All other atoms (in the first approximation) repeat with the periods of the superposition structure and thus do not contribute to the diffuse streaks.

The symmetry of the superposition structures is compatible with the OD groupoid family determined from systematic absences:

$A(2)$	m	m	
$\{(b_{1/2})$	$2_{1/2}$	$2\}$	
$\{(b_{1/2})$	$2_{1/2}$	$2\}$	category III,

where the subscripts 1/2 indicate translational components of $b/4$ (Dornberger-Schiff, 1964, pp. 41 ff.).

The solution of the structural principle thus necessitated only the correct location of the 'disordered' Hg atom in one of two

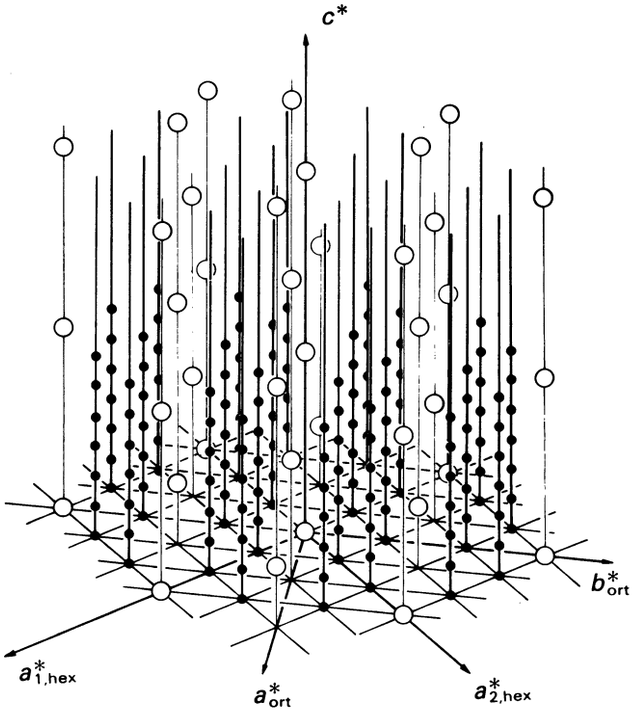

Fig. 9.2.2.15. Clinographic projection of the general scheme of a single-crystal diffraction pattern of hydrous phyllosilicates. Family diffractions are indicated by open circles and correspond in this case to a rhombohedral superposition structure. Only the part with $l \geq 0$ is shown.

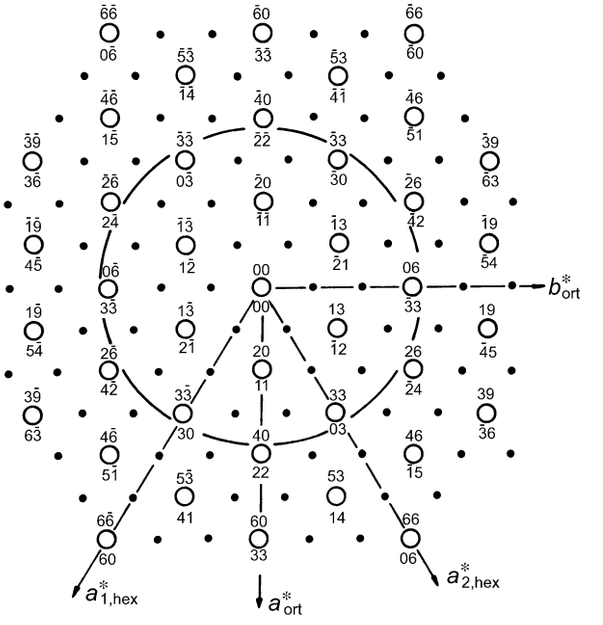

Fig. 9.2.2.16. Normal projection of the general scheme of a single-crystal diffraction pattern of hydrous phyllosilicates. Rows of family diffractions are indicated by open circles; the h, k indices refer to hexagonal (below) and orthogonal (above) axial systems.

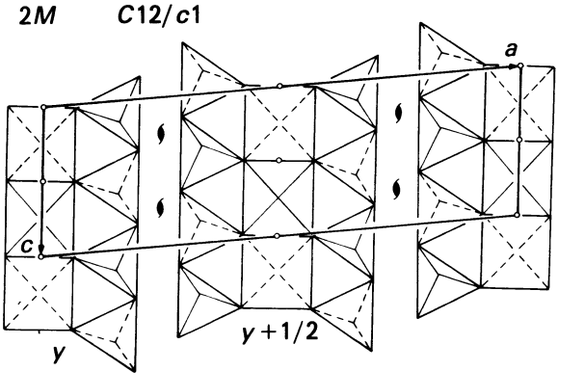

Fig. 9.2.2.17. The structure of stibivanite-2M. The unit cell is outlined and some relevant symmetry operations are indicated (after Merlino *et al.*, 1989).

possible positions indicated by the superposition structure. An analysis of the Fourier transform relevant to the above OD groupoid family showed that the Patterson function calculated with coefficients $|\Lambda(hkl)|^2 = |F(hkl)|^2 + |F(\bar{h}kl)|^2$ shows interatomic vectors *within* any single OD layer, and it turned out that even a first generalized projection of the function yields the necessary 'yes/no' answer.

The structural principle is shown in Fig. 9.2.2.20.

There are two MDO polytypes in this family. Both are monoclinic (*c* axis unique) and consist of equivalent triples of OD layers. The first, MDO_1, is periodic after two layers and has symmetry $A2/m$. The second, MDO_2, is periodic after four layers, has symmetry $F2/m$ and basis vectors $2\mathbf{a}, \mathbf{b}, \mathbf{c}$. Domains of MDO_1 were present in all crystals (the system of diffuse maxima, mentioned above), but some of them also contained small proportions of MDO_2.

Later, single crystals of pure periodic MDO_1 were also found in specimens prepared hydrothermally (Rabenau, private communication). The results of a structure analysis confirmed the previous results but indicated desymmetrization (Ďurovič, 1979). The atomic coordinates deviated significantly from the ideal OD model; the monoclinic angle became 90.5°. Even the family diffractions, which in the disordered crystals exhibited an orthorhombic symmetry, deviated significantly from it in their positions and intensities.

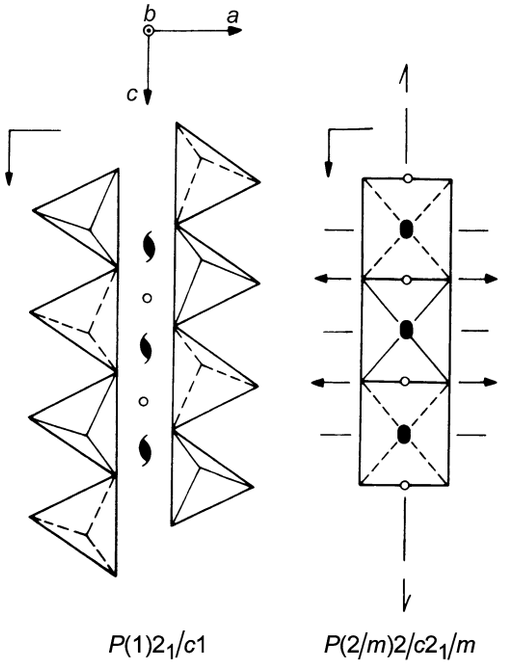

Fig. 9.2.2.18. The two kinds of OD layers in the stibivanite family (after Merlino *et al.*, 1989).

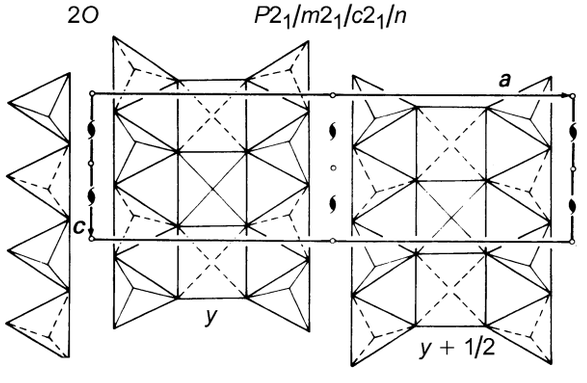

Fig. 9.2.2.19. The structure of stibivanite-2*O* (after Merlino *et al.*, 1989).

9.2.2.3.4. *Remarks for authors*

When encountering a polytypic substance showing disorder, many investigators try to find in their specimens a periodic single crystal suitable for a structure analysis by current methods. So far, no objections. But a common failing is that they often neglect to publish a detailed account of the disorder phenomena observed on their diffraction photographs: presence or absence of diffuse streaks, their position in reciprocal space, positions of diffuse maxima, suspicious twinning, non-space-group absences, higher symmetry of certain subsets of diffractions, *etc*. These data should always be published, even if the author does not interpret them: otherwise they will inevitably be lost. Similarly, preliminary diffraction photographs (even of poor quality) showing these phenomena and the crystals themselves should be preserved – they may be useful for someone in the future.

9.2.2.4. *List of some polytypic structures*

A few examples of some less-common polytypic structures published up to 1994 are listed below:

Minerals: McGillite (Iijima, 1982), tridymite (Wennemer & Thompson, 1984), pyrosmalite (Takéuchi, Ozawa & Takahata, 1983), zirconolite (White, Segall, Hutchison & Barry, 1984), Ti-biotite (Zhukhlistov, Zvyagin & Pavlishin, 1990), diamond (Phelps, Howard & Smith, 1993), scholzite (Taxer, 1992), fiedlerite (Merlino, Pasero & Perchiazzi, 1994), penkvilskite (Merlino, Pasero, Artioli & Khomyakov, 1994), lengebachite – non-commensurate structure (Makovický, Leonardsen & Moelo, 1994).

Inorganic compounds: Borates with general formula $RAl_3(BO_3)_4$, where R = Y, Nd, Gd (Belokoneva & Timchenko,

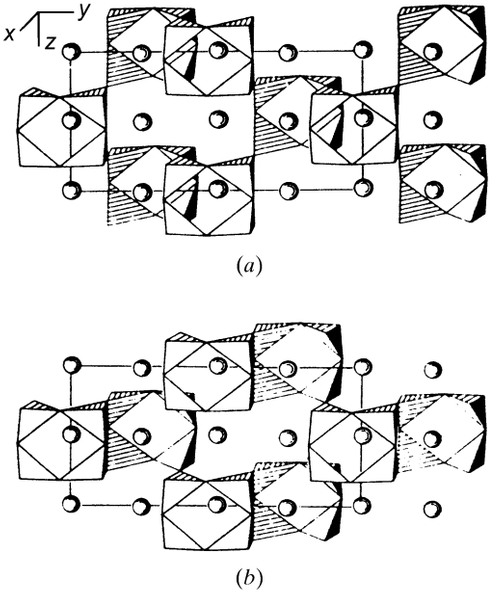

Fig. 9.2.2.20. The structural principle of γ-$Hg_3S_2Cl_2$. The shared corners of the pyramids are occupied by the Hg atoms; unshared corners are occupied by the S atoms. A pair of layers, but only the Cl atoms at their common boundary, are drawn. The two geometrically equivalent arrangements (*a*) and (*b*) are shown.

1983), $BaCrO_3$ (Chamberland, 1983), hexacyanocomplexes of transition metals (Jagner, 1985), chromium iron carbides (Kowalski, 1985), $Fe_{1-x}S$ (Kuban, 1985), hexagonal copper(I) ferrite (Effenberger, 1991), $PbS \cdot 18TiS_2$ – a modulated structure (van Smaalen & de Boer, 1992), α-$LiNH_4SO_4$ (Tomaszewski, 1992), fullerene C_{60} (de Boer, van Smaalen, Petříček, Dušek, Verheijen & Meijer, 1994).

Organic compounds: Oxalates (Fichtner-Schmittler, 1979), primetine (Jarchow & Schmalle, 1985), 2-hydroxy-4-methoxy-2*H*-1,4-benzoxazin-3-one, $C_9H_9NO_4$ (Kutschabsky, Kretschmer, Schrauber, Dathe & Schneider, 1986), carbamazepine dihydrate (Reck & Dietz, 1986), piroxicam (Reck, Dietz, Laban, Günther, Bannier & Höhne, 1988), *E*-octadecanoic acid (Kaneko, Sakashita, Kobayashi, Kitagawa, Matsuura & Suzuki, 1994).

Metals, intermetallic compounds and alloys: Alloys are treated in a monograph by Nikolin (1984); a lecture note by Amelinckx (1986) gives details of high-resolution electron microscopy and examples of the investigation of some alloys but also of other polytypic structures. Special papers: Li metal (Schwarz & Blaschko, 1990), $Zr(FeCr)_2$ Laves phases (Burany & Northwood, 1991), doped Co–W and Co–Mo alloys (Nikolin, Babkevich, Izdkovskaya & Petrova, 1993).

Further data are given in articles by Bailey *et al*. (1977), Dornberger-Schiff (1979), Zvyagin (1988), Baronnet (1992) and Zorkii & Nesterova (1993).

High-resolution electron microscopy (HREM) applied in the structure analysis of (also disordered) polytypic substances: orientite (Mellini, Merlino & Pasero, 1986), ardennite (Pasero & Reinecke, 1991), pseudowollastonite (Ingrin, 1993), laurionite and paralaurionite (Merlino, Pasero & Perchiazzi, 1993), perovskites in the system $La_4Ti_3O_{12}$–$LaTiO_3$ (Bontchev, Darriet, Darriet, Weill, Van Tendeloo & Amelinckx, 1993), baumhauerite (Pring & Graeser, 1994), bementite (Heinrich, Eggleton & Guggenheim, 1994), parsettensite (Eggleton & Guggenheim, 1994).

9.3. Typical interatomic distances: metals and alloys

BY J. L. C. DAAMS, J. R. RODGERS, AND P. VILLARS

Following the discovery of X-ray diffraction, atomic radii have been discussed and tabulated many times. Teatum, Gschneider & Waber (1960, 1968) derived empirical metallic radii for 12-coordinated atoms; their values were taken, wherever possible, from the elements and adjusted to 12-coordination. These radii have been found to be the most generally useful set for metallic phases and are given in Fig. 9.3.1(*a*). Although metallic bonding exists only in very few cases, as will be discussed later, it was common to assume that in intermetallics we have a purely metallic bonding character. In general, the bonding situation is much more complex; it is a mixture of metallic, ionic, and covalent bonding. At the present time, it is not possible to predict which bonding situation is formed for a given element–element combination. This rather complex bonding situation in intermetallics has been found to exist in the 3000+ structure types that have been compiled in *Pearson's Handbook* (Villars & Calvert, 1991) and in CRYSTMET (Rodgers & Villars, 1988). For comparison, the covalent radii according to Pauling and the ionic radii of Kordes (1939*a*,*b*, 1940, 1960) are given in Figs. 9.3.1(*b*) and (*c*), respectively (Samsonov, 1968).

Pearson (1979), and also Villars & Girgis (1982), reported a linear dependence between the interatomic distance d_{AB} and the (concentration-weighted) mean metallic radii $\overline{R}$ for compounds crystallizing in over 100 different intermetallic structure types. For demonstration purposes, it is not necessary to make the rather complicated calculation given by Villars & Girgis (1982); instead, Daams (1995) showed this linear dependence by plotting the mean radii of the atoms concerned *versus* half of the mean shortest interatomic distances between these atoms. As an example, for compounds crystallizing in the *hP*3 AlB_2 structure type, we have two atoms in the asymmetric unit, and half of the shortest interatomic distance between these atoms (d_{AB}) is $\frac{1}{2}\left[\frac{1}{3}a^2 + \frac{1}{4}c^2\right]^{1/2}$. For binary compounds, the mean radius ($\overline{R}$) is the mean of the metallic radii (Teatum, Gschneider & Waber, 1960, 1968) of the atoms involved. For ternary compounds, we first calculated the mean radius of the atoms mixing on the same position, weighted for their mixing concentration, and then calculated the mean radius of the atoms in the structure. In Fig. 9.3.2(*a*), this linear dependence is plotted for the binary compounds crystallizing in *hP*3 AlB_2, and it shows that there is a 1:1 dependence, meaning that the mean radius of the atoms involved equals the available space in the structure. The next two examples show that there is not always a 1:1 dependence, but that this linear dependence varies from structure type to structure type, with each of them combining their particular groups of atoms. Fig. 9.3.2(*b*) shows this linear dependence for the binary 2:1 compounds crystallizing in the *oP*12 Co_2Si type. We see that in general the mean radii of the atoms are more than half of the shortest interatomic distances, although a linear relationship still exists. The opposite is observed for compounds crystallizing in the *tP*6 Cu_2Sb (see Fig. 9.3.2*c*), where in general the mean radii are smaller than half the shortest distances. These differences can be understood if we look at the combinations of elements crystallizing in these structure types. In *tP*6 Cu_2Sb, we have mainly combinations of rare earths with a *p* element, giving rise to a covalent bonding character with, as a result, smaller radii. In *oP*12 Co_2Si, there is no such preference, so we have predominantly a metallic bonding character. Such linear dependencies for each structure type are more precise than those obtained by using Pauling's (1947) general equation for bond numbers, $R_{(1)} - R_{(n)} = 0.30 \log n$, where $R_{(1)}$ is the single-

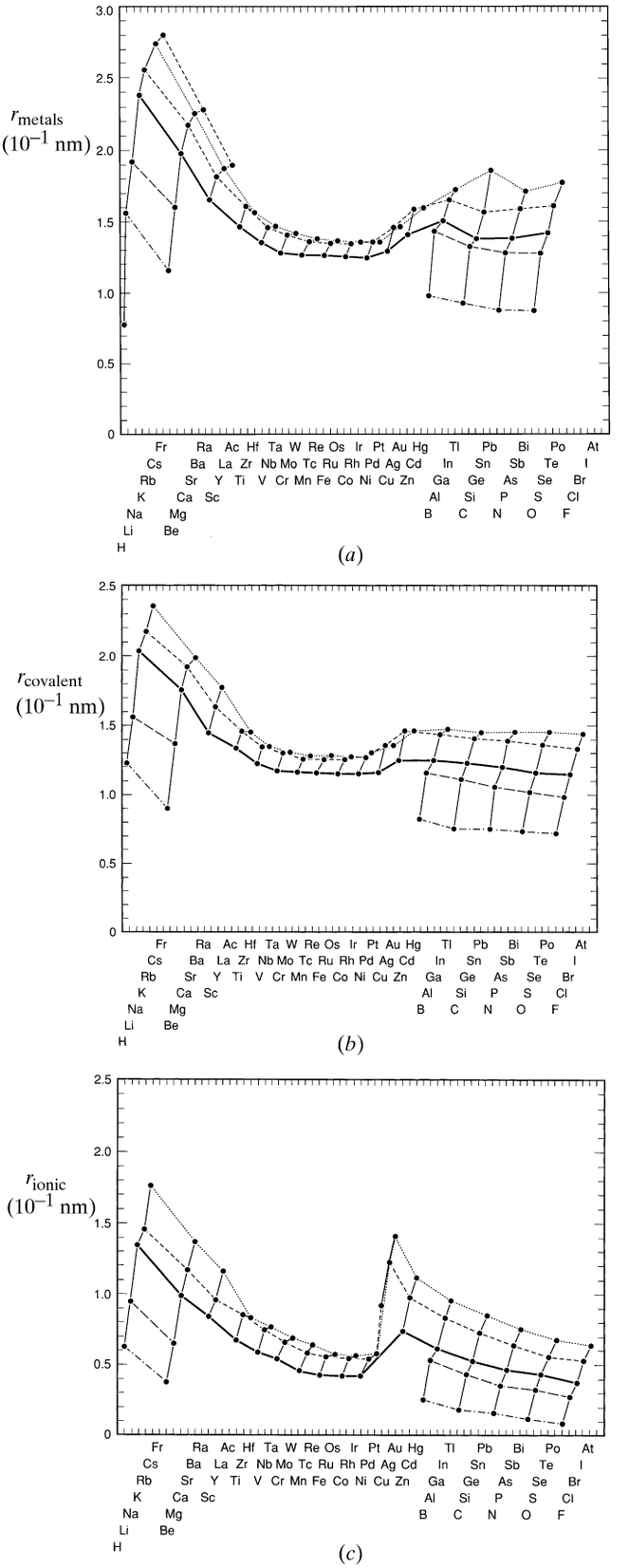

Fig. 9.3.1. (*a*) The radii for CN = 12 after Teatum *et al*. (1960, 1968). (*b*) The covalent radii according to Pauling. (*c*) The ionic radii according to Kordes (Samsonov, 1968).

Copyright © 2006 International Union of Crystallography

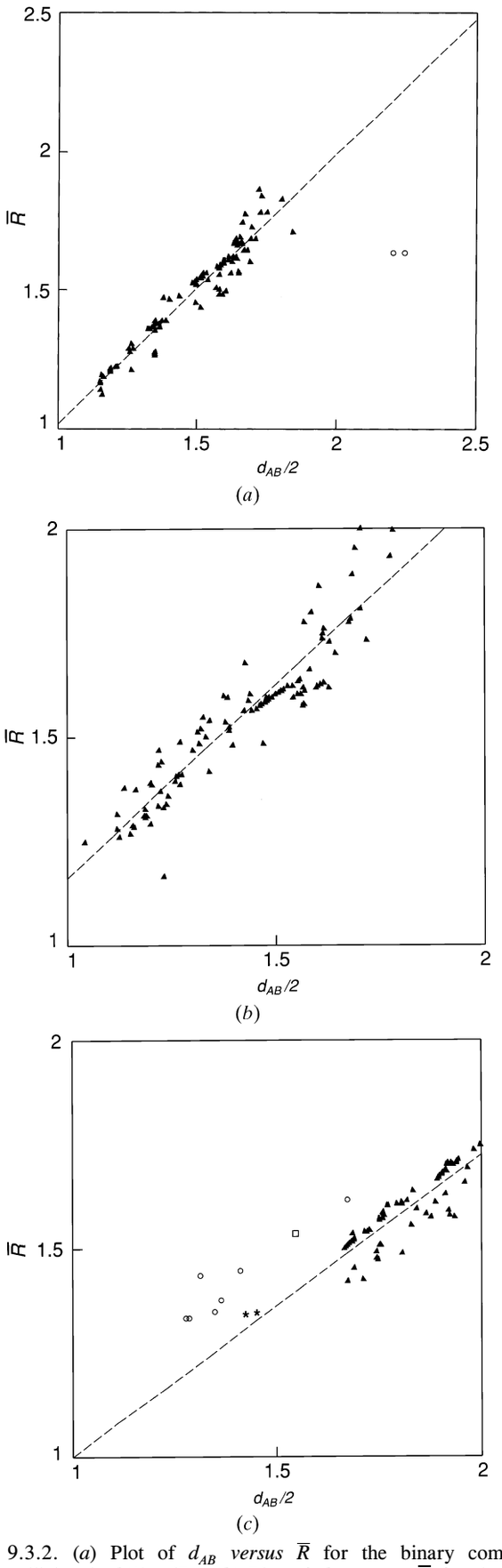

Fig. 9.3.2. (*a*) Plot of d_{AB} *versus* $\overline{R}$ for the binary compounds crystallizing in *hP*3 AlB_2. (*b*) Plot of d_{AB} *versus* $\overline{R}$ for the binary compounds crystallizing in *oP*12 Co_2Sb. (*c*) Plot of d_{AB} *versus* $\overline{R}$ for the binary compounds crystallizing in *tP*6 Cu_2Sb.

bond radius, and $n = V/12$, with V being the elemental valence, to adjust the radii to coordination numbers other than 12. The adjustment of the radii to the coordination numbers of the structure type of concern is a first approximation adjustment to the structure type. The broken lines in Figs. 9.3.2(*a*)–(*c*) are the results of a least-squares analysis.

Much more information about the short-range atomic arrangement, and a deeper insight into the geometry within a structure type, is obtained by looking at the coordination polyhedra (atomic environments AE) instead of looking only at the interatomic distances. These coordination polyhedra or AE not only give geometrical information about an atom and its neighbours but also give the correct coordination number. An AE is determined by using Brunner & Schwarzenbach's (1971) method, in which all interatomic distances between an atom and its neighbours are plotted in a next-neighbour histogram (NNH), as shown in Fig. 9.3.3(*a*). In most cases, a clear maximum gap is revealed. All atoms to the left of the maximum gap belong to the AE of the central atom; the coordination polyhedron constructed with these atoms is depicted in Fig. 9.3.3(*b*).

In cases where no maximum gap is found, Daams, Villars & van Vucht (1992) used the maximum convex rule. The maximum convex volume is defined as the maximum volume around only one central atom enclosed by convex faces with all the coordinating atoms lying at the intersection of at least three faces. Systematic studies of all intermetallic structure types

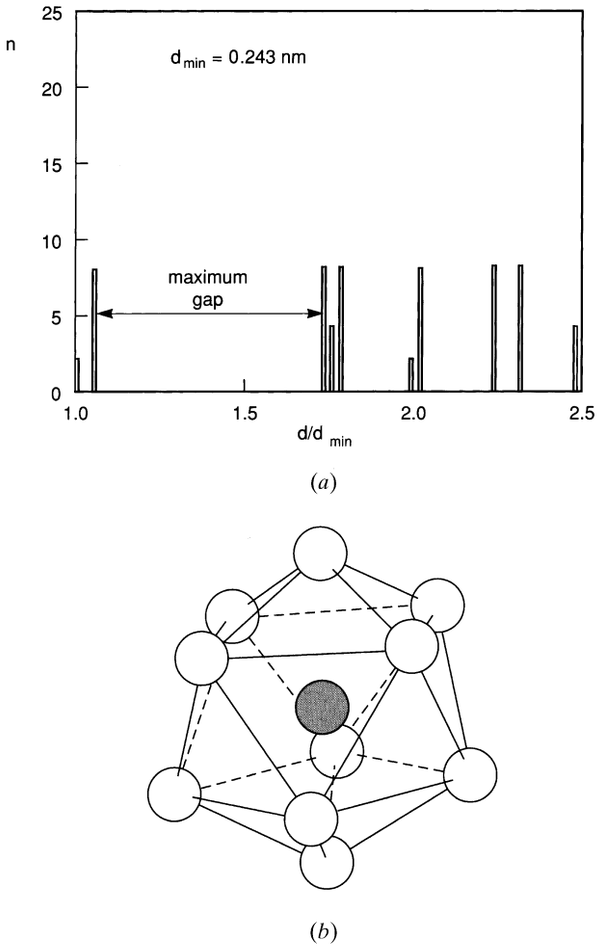

Fig. 9.3.3. (*a*) A typical example of a next-neighbour histogram (NNH) and (*b*) the atomic environment (AE) coordination polyhedron belonging to this NNH.

belonging to the cubic, rhombohedral, hexagonal, and tetragonal crystal systems (Daams & Villars, 1993, 1994, 1997) revealed that 23 AEs, defined as atomic environment types (AETs), are favoured. These 23 most frequently occurring AETs are shown in Fig. 9.3.4(*a*). In Fig. 9.3.4(*b*), the AETs are plotted *versus* the number of point sets investigated. Heavily preferred are the tetrahedron (CN4), the octahedron (CN6), the equatorial tricapped trigonal prism (CN9), the icosahedron (CN12), the cubo-octahedron (CN12), and the CN14 Kasper polyhedron as AEs in intermetallic compounds. We also conclude from the observed AEs that the metallic radii that were published by Teatum *et al*. (1960) are in general not valid for intermetallic compounds. The assumption that the atoms have CN = 12 is probably never met in actual compounds. The above-mentioned

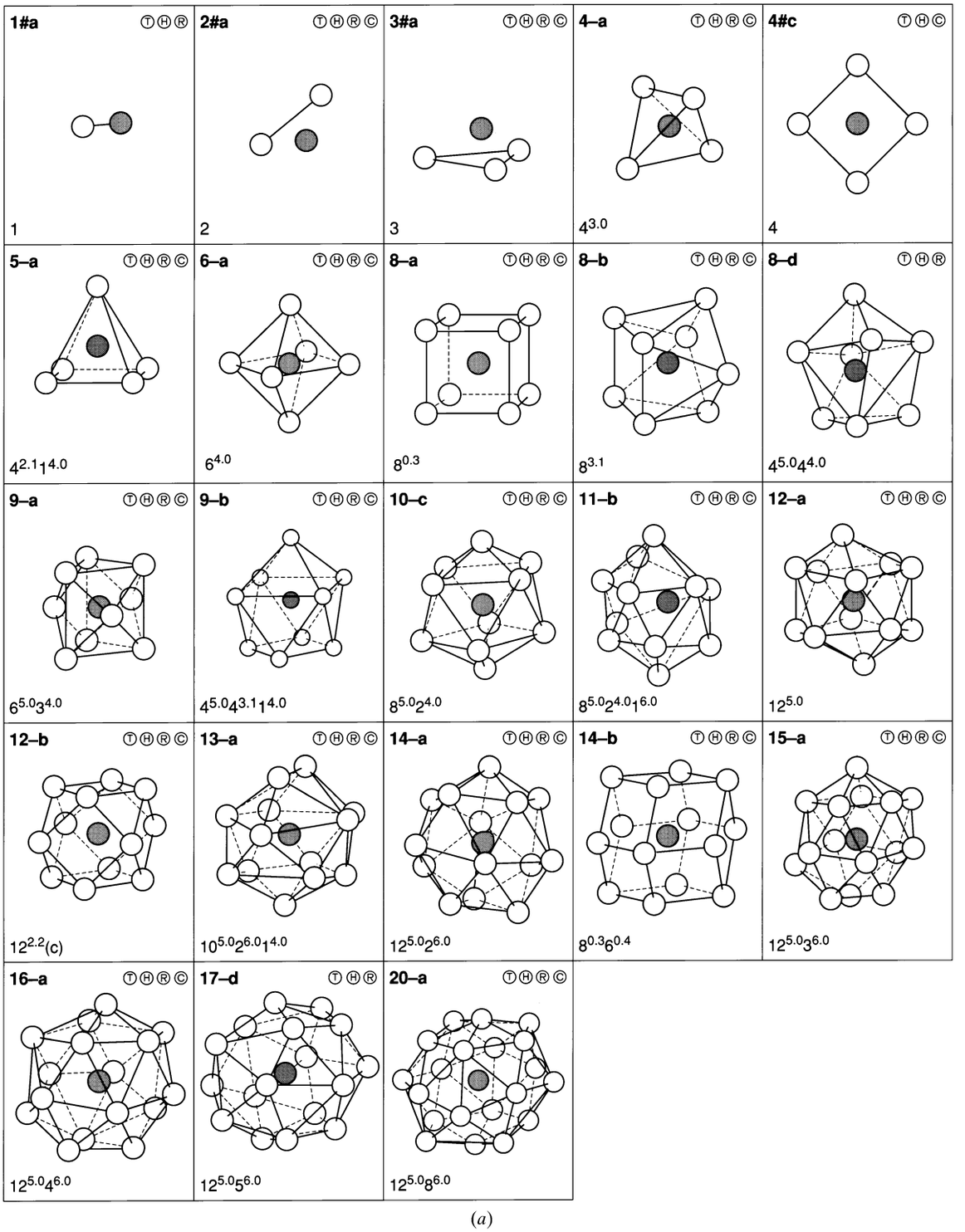

(*a*)

Fig. 9.3.4. (*a*) The 23 most frequently occurring atomic environment types (AET) with their polyhedron code (lower left corner of each box). In the upper left corner of each box, the assigned labels are given, consisting of the coordination number followed by a letter (*a*, *b*, ...). At the top right-hand corner, the crystal systems in which the AET occur are marked. (*b*) A frequency plot of the 23 most frequently occurring AETs *versus* the number of point sets.

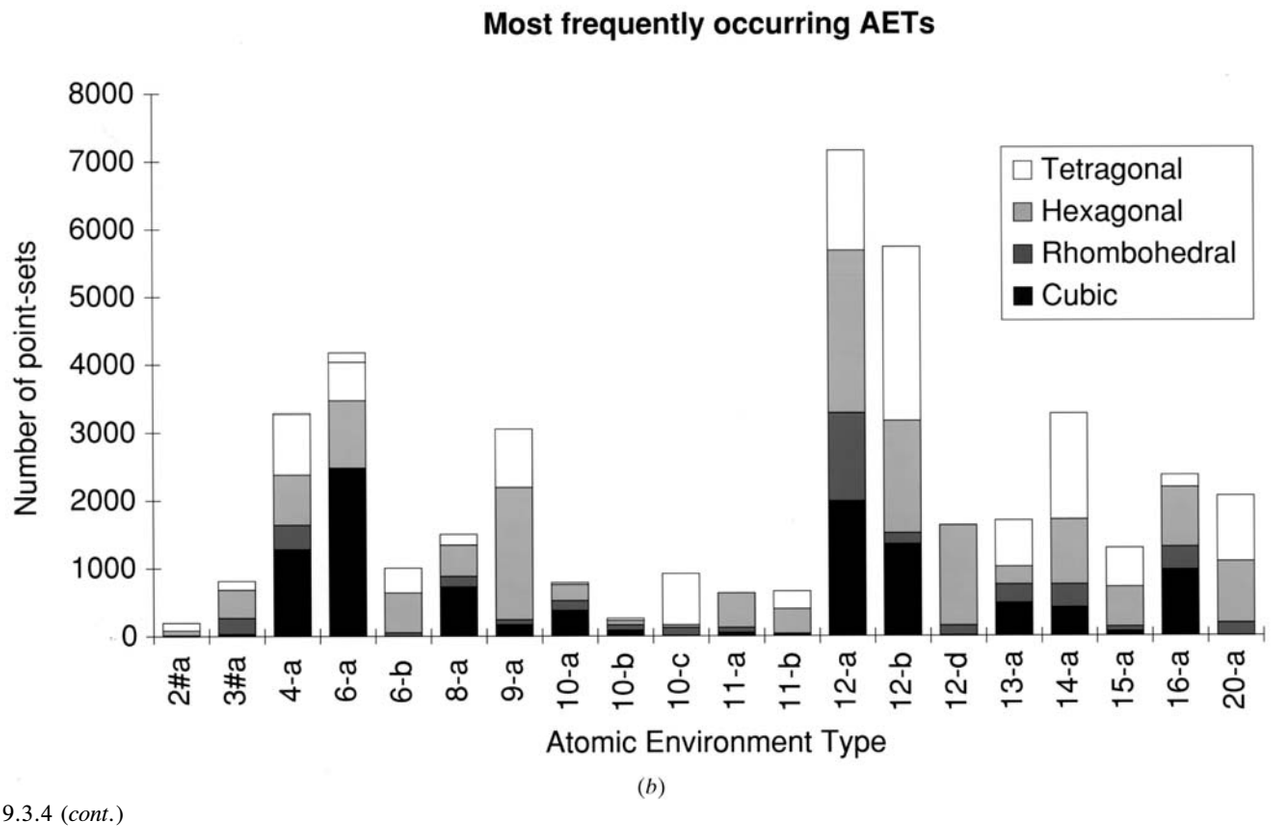

(*b*)

Fig. 9.3.4 (*cont.*)

systematic analysis shows that we have in general, especially for real intermetallic compounds, low coordination numbers, CN < 9, for the *p* elements, CN numbers between 9 and 14 for the *d* elements, and CN > 12 for the *s* and *f* elements. In structure types where we have covalent or ionic bonding, we observe much lower coordination numbers. For example, the atoms of the compounds crystallizing in *cF*8 ClNa have CN $= 6$, and they have the octahedron as an AE.

9.3.1. Glossary

Intermetallic compound: Intermetallic compounds are binary, ternary, quaternary, *etc*. compounds containing the chemical elements other than oxygen, the halides, and the noble gases. Also excluded are compounds containing typical inorganic groups like –NH, $-NH_2$, $-N_2$, *etc*. This definition was used for *Pearson's Handbook* (Villars & Calvert, 1991), the *Atlas of Crystal Structure Types* (Daams, Villars & van Vucht, 1991) and the CRYSTMET database (Rodgers & Villars, 1988). This definition therefore also includes sulfides, selenides, carbides, and nitrides, which most material scientists would not consider to be intermetallic compounds, but, because of their structural similarity, they have been included.

Structure type (or prototype): Based on space-group theory, a crystal structure is completely determined by the following data:
chemical formula;
crystal system and unit-cell dimension(s);
space group;
occupation number and coordination of the occupied point sets.

Crystal structure types are named by the first intermetallic compound found to be unique in respect of the third and fourth items and are represented by the Pearson symbol followed by the formula of the prototype, *e.g*. *hP*3 AlB_2. The first two letters of the Pearson symbol are identical to the Bravais-lattice type, and the digits give the number of atoms per unit cell.

International Tables for Crystallography (2006). Vol. C, Chapter 9.4, pp. 778–789.

9.4. Typical interatomic distances: inorganic compounds

BY G. BERGERHOFF AND K. BRANDENBURG

9.4.1. Introduction

In inorganic compounds, the intrinsic interatomic distances vary over a wide range, depending on atomic size, oxidation state, coordination number, bonding type, conditions of state, *etc*. The experimental values depend also on the conditions of measurement and possibly the defect structure of the sample in question.

To a first approximation, interatomic distances can be calculated from the sum of ionic radii taken from various tables. Mean values from experimental values from a limited number of structures determined up to 1960 are listed in *International Tables for X-ray Crystallography* (*IT* III, 1962). Today, databases allow all experimental results determined up to the present to be summarized and subjected to statistical analyses. For the Inorganic Crystal Structure Database (ICSD) (Bergerhoff & Brown, 1987), this analysis has been performed starting with 24 496 structure determinations in the 1990 version for all combinations of ions and atoms. For 8329 combinations, at least one distance inside the range 0 to 500 pm could be calculated. The statistical procedure is described in the following Section, and the results are given in Tables 9.4.1.1 to 9.4.1.12 for many pairs for which more than two distances had been determined. For more detailed discussions, and other ion pairs, the CD-ROM version of the ICSD is recommended. With the command 'check distances' in the *CVIS* program for the ICSD, the general distance distribution of a combination of elements can be compared with the distance distribution in a specific phase. Extreme values can be traced to their origin.

9.4.2. The retrieval system

By means of the retrieval system *CRYSTIN* (Sievers & Hundt, 1987), sets of structures were selected and combined; these contained:

(i) one ion in a specific oxidation state (if appropriate);
(ii) the other ion of the pair in a specific oxidation state (if appropriate);
(iii) structures determined at room temperature;
(iv) structures determined at normal pressure;
(v) no disordered structures;
(vi) no solid solutions;
(vii) no defect structures;
(viii) structures for which atomic coordinates were given;
(ix) only structures with $R < 6\%$ when there were many determinations.

For the M structures so defined, n interatomic distances were calculated for the atoms and ions in question. In so doing, all symmetrically equivalent and non-equivalent distances were taken into account. From these, a frequency distribution was calculated automatically. All distances d were collected into ranges of 2 pm. In (9.4.2.1)–(9.4.2.2), $n(d)$ is the number of distances in the range with midpoint d, d_1 is the midpoint of the lowest range, and d_2 is the midpoint of the highest range selected for the calculation of the mean. The choice of d_1 and d_2 is discussed in Section 9.4.3. The mean and the standard uncertainty (s.u.) of one set of distances were calculated by means of the equations

$$N = \sum_{d_1}^{d_2} n(d), \tag{9.4.2.1}$$

$$\text{mean} = \mu = N^{-1} \sum_{d_1}^{d_2} dn(d), \tag{9.4.2.2}$$

$$\text{s.u.} = \left(N^{-1} \sum_{d_1}^{d_2} (d - \mu)^2 n(d) \right)^{1/2}. \tag{9.4.2.3}$$

9.4.3. Interpretation of frequency distributions

It is obvious that the results have to be interpreted carefully when they are applied to crystal-structure discussions. In performing the analysis, the frequency distribution was inspected for each pair of ions. If all values were distributed around a single maximum, then d_1 and d_2 were set equal to zero and 500 pm, respectively. If there were two or more maxima, one was carefully selected and d_1 and d_2 were set to the left and right in such a way that the frequency was zero at both limits. In combinations with oxygen, so many distances were available for the most probable maximum that the program could select d_1 and d_2 automatically.

Maxima outside the selected range may come from errors in data or distances to ions in the second coordination sphere [*e.g.* Mg^{2+}—Cl^- in $Mg(H_2O)_6Cl_2$]. Generally, different oxidation states give rise to different maxima, which therefore have been tabulated separately (*e.g.* Cr^{2+}, Cr^{3+}, Cr^{4+}, Cr^{5+}, Cr^{6+} in combination with O^{2-}). In some typical cases, oxidation states cannot be clearly defined. Then the oxidation states have been omitted (*e.g.* Os—F, Rh—Br, N—S). Nevertheless, sometimes one oxidation state can be separated (*e.g.* W—Cl and W^{6+}—Cl^{1-}). Atomic distances between equally charged ions will be contact distances and vary over a wide range (*e.g.* O^{2-}—O^{2-} distances within SO_4^{2-} ions and between such ions).

Copyright © 2006 International Union of Crystallography

Table 9.4.1.1. *Atomic distances between halogens and main-group elements in their preferred oxidation states*

Atom pair	N	Mean	s.u.	d_1	Smallest 5%	First quartile	Median	Third quartile	d_2
Li^+—F^-	108	193.0	14.2	150.0	166.4	184.6	195.0	202.7	250.0
Na^+—F^-	265	230.8	19.7	0.0	211.5	222.7	227.8	236.7	500.0
K^+—F^-	354	269.3	19.5	180.0	241.8	258.5	267.0	282.3	340.0
Rb^+—F^-	158	294.2	17.5	250.0	268.6	280.8	292.9	309.2	350.0
Cs^+—F^-	230	311.3	13.6	260.0	290.1	303.0	312.8	319.6	360.0
Li^+—Cl^-	30	246.1	11.1	210.0	223.0	240.3	247.0	255.0	300.0
Na^+—Cl^-	100	282.7	11.5	250.0	267.5	273.4	280.5	290.8	330.0
K^+—Cl^-	191	318.8	16.1	270.0	296.4	308.7	316.8	328.4	370.0
Rb^+—Cl^-	135	336.4	14.8	290.0	319.5	325.1	333.2	348.9	390.0
Cs^+—Cl^-	216	356.9	17.9	290.0	333.6	344.8	357.7	367.7	420.0
Li^+—Br^-	9	282.3	27.7	0.0	246.9	266.5	275.0	287.5	500.0
Na^+—Br^-	15	303.8	18.5	270.0	281.5	294.8	298.2	312.5	360.0
K^+—Br^-	72	331.8	26.4	0.0	289.2	314.0	332.0	342.7	500.0
Rb^+—Br^-	48	349.2	16.1	300.0	325.4	337.0	348.7	360.5	400.0
Cs^+—Br^-	64	372.2	15.3	350.0	352.4	360.0	368.3	385.0	430.0
Li^+—I^-	7	307.9	26.0	270.0	274.7	283.5	303.0	326.5	370.0
Na^+—I^-	7	342.1	24.5	0.0	320.7	322.8	325.0	372.2	500.0
K^+—I^-	24	363.6	29.2	0.0	334.4	344.0	364.0	374.0	500.0
Rb^+—I^-	29	372.0	16.3	320.0	340.9	362.8	373.0	381.2	430.0
Cs^+—I^-	63	393.4	13.8	350.0	374.8	381.9	391.7	404.8	450.0
Be^{2+}—F^-	78	150.6	6.3	120.0	140.6	148.2	152.2	153.9	200.0
Mg^{2+}—F^-	96	198.8	9.2	150.0	188.2	195.1	200.7	203.3	250.0
Ca^{2+}—F^-	127	230.9	16.9	0.0	216.2	223.8	228.7	236.2	500.0
Sr^{2+}—F^-	35	246.5	9.6	0.0	227.8	241.5	246.2	250.2	500.0
Ba^{2+}—F^-	94	266.6	9.3	0.0	256.7	259.9	264.6	269.3	500.0
Be^{2+}—Cl^-	2	200.0	1.4	0.0	198.2	199.0	200.0	201.0	500.0
Mg^{2+}—Cl^-	16	250.9	11.9	210.0	229.6	246.7	249.0	258.0	300.0
Ca^{2+}—Cl^-	55	286.2	15.1	260.0	271.8	275.1	280.8	293.2	350.0
Sr^{2+}—Cl^-	42	302.4	6.7	0.0	294.2	301.6	303.0	304.8	500.0
Ba^{2+}—Cl^-	64	316.3	12.2	270.0	298.8	308.7	314.8	324.0	370.0
Ca^{2+}—Br^-	10	300.6	18.9	250.0	259.0	290.5	308.0	311.0	350.0
Sr^{2+}—Br^-	30	305.4	15.5	0.0	279.0	291.0	311.0	315.0	500.0
Ba^{2+}—Br^-	17	331.9	13.2	0.0	307.7	320.5	337.0	340.8	500.0
Ca^{2+}—I^-	4	324.5	11.8	300.0	312.4	314.0	322.0	324.0	360.0
Sr^{2+}—I^-	20	305.7	20.6	250.0	278.0	284.7	312.7	322.0	350.0
Ba^{2+}—I^-	8	348.2	9.7	0.0	336.4	338.0	346.0	357.0	500.0
B^{3+}—F^-	39	136.6	7.1	110.0	125.9	133.8	136.8	139.1	180.0
Al^{3+}—F^-	121	180.6	7.5	150.0	170.1	176.6	179.3	184.6	230.0
Ga^{3+}—F^-	17	191.2	6.0	0.0	183.7	186.8	189.7	193.9	500.0
In^{3+}—F^-	24	204.0	9.1	0.0	192.4	202.0	204.6	206.7	500.0
Tl^{3+}—F–	14	203.0	6.7	0.0	189.4	199.0	203.3	208.5	500.0
B^{3+}—Cl^-	8	175.8	16.9	140.0	142.8	173.0	176.0	178.0	220.0
Al^{3+}—Cl^-	50	211.1	7.2	190.0	204.3	209.8	211.1	212.4	270.0
Ga^{3+}—Cl^-	12	212.8	4.4	0.0	204.6	211.0	213.3	216.0	500.0
In^{3+}—Cl^-	20	248.7	10.7	220.0	238.0	241.2	246.0	253.0	300.0
Tl^{3+}—Cl^-	19	248.2	6.9	200.0	233.9	243.5	249.0	253.2	300.0
B^{3+}—Br^-	3	197.7	13.6	150.0	186.3	187.5	193.0	212.5	250.0
Al^{3+}—Br^-	4	226.5	5.7	0.0	222.2	223.0	224.0	226.0	500.0
Ga^{3+}—Br^-	4	230.0	3.5	0.0	224.4	226.0	231.0	232.0	500.0
In^{3+}—Br^-	11	262.6	11.9	0.0	248.6	250.8	261.0	274.2	500.0
Tl^{3+}—Br^-	13	253.3	6.0	0.0	245.3	250.2	253.0	255.8	500.0
B^{3+}—I^-	2	240.0	41.0	200.0	210.2	211.0	212.0	269.0	300.0
Al^{3+}—I^-	3	248.3	2.3	220.0	246.1	246.8	247.5	250.5	280.0
Ga^{3+}—I^-	2	253.0	0.0	0.0	252.1	252.5	253.0	253.5	500.0
In^{3+}—I^-	7	275.9	10.3	250.0	264.4	265.8	275.0	280.5	320.0

Table 9.4.1.1. *Atomic distances between halogens and main-group elements (cont.)*

Atom pair	*N*	Mean	s.u.	d_1	Smallest 5%	First quartile	Median	Third quartile	d_2
Ge^{4+}—F^-	20	176.7	3.9	150.0	168.0	176.0	177.1	178.4	210.0
Sn^{4+}—F^-	24	195.8	6.4	0.0	184.4	194.6	196.3	198.0	500.0
Pb^{4+}—F^-	9	209.7	7.2	0.0	196.9	206.5	210.5	212.8	500.0
C^{4+}—Cl^-	6	163.0	21.8	120.0	120.6	157.0	174.0	175.5	200.0
Sn^{4+}—Cl^-	46	238.7	5.7	0.0	230.1	235.0	240.4	242.7	500.0
Pb^{4+}—Cl^-	9	249.0	2.0	0.0	244.9	248.4	249.0	249.6	500.0
Sn^{4+}—Br^-	5	251.0	9.7	0.0	236.5	244.5	255.0	258.8	500.0
Ge^{4+}—I^-	3	254.3	4.6	0.0	248.3	249.5	256.5	257.2	500.0
Sn^{4+}—I^-	10	263.4	20.9	0.0	209.0	263.5	265.0	269.0	500.0
Pb^{4+}—I^-	2	310.0	1.4	0.0	308.2	309.0	310.0	311.0	500.0
P^{5+}—F^-	40	155.6	6.4	130.0	144.0	151.3	156.8	159.3	200.0
As^{5+}—F^-	89	164.6	6.7	130.0	155.4	160.9	165.5	168.4	200.0
Sb^{5+}—F^-	81	182.6	6.5	150.0	174.1	179.2	182.7	184.7	230.0
Bi^{5+}—F^-	9	192.1	11.3	0.0	178.4	188.2	189.7	195.5	500.0
P^{5+}—Cl^-	52	193.2	3.6	170.0	187.2	190.6	193.3	195.4	210.0
Sb^{5+}—Cl^-	66	233.1	6.6	200.0	220.6	229.8	233.8	236.4	270.0
P^{5+}—Br^-	12	211.2	5.1	0.0	201.2	208.0	213.0	214.7	500.0
Sb^{5+}—Br^-	6	254.0	2.1	250.0	250.6	252.5	254.0	255.5	270.0
S^{6+}—F^-	25	151.1	4.2	140.0	141.2	150.1	152.1	153.7	160.0
Te^{6+}—F^-	9	176.1	6.9	0.0	160.9	174.5	179.0	180.5	500.0
S^{6+}—Cl^-	10	197.6	5.7	170.0	185.0	195.5	197.3	201.0	220.0
I^{7+}—F^-	6	179.7	4.7	0.0	170.6	179.0	180.7	181.7	500.0

Table 9.4.1.2. *Atomic distances between halogens and main-group elements in their special oxidation states*

Atom pair	*N*	Mean	s.u.	d_1	Smallest 5%	First quartile	Median	Third quartile	d_2
Tl^+—F^-	36	282.6	19.0	250.0	259.8	267.1	273.0	297.3	350.0
Tl^+—Cl^-	38	326.2	19.0	0.0	291.8	316.3	326.0	339.0	500.0
Tl^+—Br^-	17	335.0	9.1	0.0	309.7	332.5	336.5	341.8	500.0
Tl^+—I^-	28	347.6	9.4	0.0	333.4	340.0	346.7	356.0	500.0
C^{2+}—F^-	17	131.2	2.4	110.0	126.8	130.1	131.3	132.7	160.0
Sn^{2+}—F^-	38	205.6	8.8	170.0	189.8	200.2	205.7	209.4	250.0
Pb^{2+}—F^-	49	247.5	10.3	160.0	227.4	239.5	250.5	256.5	290.0
Ge^{2+}—Cl^-	7	227.3	10.4	0.0	210.7	215.5	231.0	235.2	500.0
Sn^{2+}—Cl^-	26	253.3	9.0	220.0	236.6	250.2	253.0	257.8	290.0
Pb^{2+}—Cl^-	69	297.9	19.2	0.0	274.5	285.2	293.5	311.9	500.0
Sn^{2+}—Br^-	12	287.8	28.4	0.0	253.2	264.0	280.0	314.0	500.0
Pb^{2+}—Br^-	31	296.0	14.0	250.0	275.1	288.4	294.8	302.2	350.0
Ge^{2+}—I^-	3	283.0	8.0	260.0	274.3	275.5	283.0	290.5	310.0
Sn^{2+}—I^-	17	316.4	17.6	0.0	295.7	303.6	307.5	330.8	500.0
Pb^{2+}—I^-	32	322.7	18.4	270.0	296.6	316.0	320.0	338.0	380.0
N^{3-}—F^-	218	275.1	23.6	170.0	233.8	266.2	278.1	289.9	350.0
N^{2-}—F^-	26	270.2	29.6	0.0	212.6	260.5	268.0	277.0	500.0
P^{3+}—F^-	7	153.6	3.8	140.0	148.4	149.8	153.5	156.5	170.0
As^{3+}—F^-	6	165.0	5.1	150.0	156.6	162.5	164.0	169.0	200.0
Sb^{3+}—F^-	73	193.4	5.5	170.0	186.6	190.9	192.7	194.5	240.0
Bi^{3+}—F^-	21	235.7	18.8	0.0	218.1	222.1	226.5	253.5	500.0

Table 9.4.1.2. *Atomic distances between halogens and main-group elements (cont.)*

Atom pair	N	Mean	s.u.	d_1	Smallest 5%	First quartile	Median	Third quartile	d_2
N^{3-}—Cl^-	349	323.0	24.4	250.0	279.6	311.1	325.0	335.2	410.0
N^{2-}—Cl^-	28	305.9	18.4	250.0	274.8	290.0	306.0	319.5	350.0
As^{3+}—Cl^-	7	211.6	7.5	200.0	202.7	205.5	209.5	216.5	250.0
Sb^{3+}—Cl^-	36	272.1	43.6	0.0	205.6	235.3	262.0	306.0	500.0
Bi^{3+}—Cl^-	39	292.8	34.0	0.0	246.9	265.5	304.2	318.5	500.0
N^{3-}—Br^-	113	342.8	24.4	280.0	297.6	324.8	343.9	353.6	420.0
As^{3+}—Br^-	4	232.0	4.8	200.0	224.4	226.0	234.0	235.0	260.0
Sb^{3+}—Br^-	14	283.3	23.3	0.0	245.4	271.0	278.0	293.5	500.0
Bi^{3+}—Br^-	26	307.7	28.3	250.0	270.1	279.0	316.4	321.0	370.0
N^{3-}—I^-	61	366.8	25.2	290.0	326.0	360.5	368.8	377.5	440.0
P^{2+}—I^-	4	244.5	3.8	0.0	238.4	240.0	246.0	247.0	500.0
As^{3+}—I^-	6	268.3	9.6	250.0	254.6	261.0	268.0	278.5	300.0
Sb^{3+}—I–	28	307.2	27.4	0.0	274.4	288.0	304.5	312.0	500.0
Bi^{3+}—I^-	18	322.6	25.3	0.0	283.8	305.0	316.0	350.5	500.0
S^{4+}—F^-	8	152.2	7.6	130.0	136.8	150.0	152.0	157.0	180.0
Te^{4+}—F^-	17	187.1	6.5	160.0	178.9	182.2	186.5	191.5	230.0
S^{4+}—Cl^-	13	200.8	7.0	190.0	194.3	195.6	197.2	207.5	240.0
Se^{4+}—Cl^-	16	217.8	25.3	150.0	153.6	210.0	215.0	239.5	300.0
Te^{4+}—Cl^-	23	241.9	15.0	190.0	224.1	229.8	247.5	252.2	290.0
Se^{4+}—Br^-	6	245.3	13.7	0.0	224.6	231.0	252.0	255.0	500.0
Te^{4+}—Br^-	16	268.0	14.7	0.0	243.6	267.0	268.7	269.6	500.0
Te^{4+}—I^-	13	282.4	12.5	0.0	265.3	272.5	279.0	293.4	500.0
Br^{3+}—F^-	6	178.0	9.6	0.0	168.3	169.5	172.0	188.5	500.0
I^{5+}—F^-	9	185.4	10.3	0.0	168.9	180.2	183.0	195.5	500.0
I^+—F^-	5	326.6	31.5	0.0	278.5	310.5	341.0	345.5	500.0
Br^+—Cl^-	9	290.1	4.6	0.0	282.9	286.5	290.5	293.5	500.0

Table 9.4.1.3. *Atomic distances between halogens and transition metals*

Atom pair	N	Mean	s.u.	d_1	Smallest 5%	First quartile	Median	Third quartile	d_2
Sc^{3+}—F^-	17	206.8	13.5	0.0	193.7	200.2	204.5	207.4	500.0
Ti^{3+}—F^-	10	191.8	4.4	0.0	186.5	188.5	191.0	193.5	500.0
Ti^{4+}—F^-	37	190.1	11.2	0.0	177.7	184.9	188.8	191.4	500.0
V^{4+}—F^-	14	183.3	11.1	0.0	160.7	179.0	188.0	191.0	500.0
V^{5+}—F^-	13	183.6	9.1	0.0	165.3	178.5	186.3	189.5	500.0
Cr^{2+}—F^-	10	201.2	5.2	0.0	195.0	197.5	199.3	207.0	500.0
Cr^{3+}—F^-	68	192.6	12.1	0.0	184.1	187.5	190.9	195.1	500.0
Cr^{4+}—F^-	13	183.0	7.5	0.0	167.3	180.5	185.5	188.5	500.0
Cr^{6+}—F^-	3	163.0	5.3	140.0	156.3	157.5	165.0	166.5	200.0
Fe^{2+}—F^-	40	204.4	8.7	160.0	188.0	199.2	204.3	208.0	250.0
Fe^{3+}—F^-	103	189.7	6.5	150.0	180.8	187.4	190.7	192.7	240.0
Co^{2+}—F^-	28	200.9	8.0	180.0	193.4	196.7	200.0	203.2	250.0
Co^{3+}—F^-	12	189.2	2.6	160.0	183.2	188.0	189.5	191.0	220.0
Ni^{2+}—F^-	66	196.5	6.2	170.0	188.9	193.0	195.9	199.4	250.0
Ni^{3+}—F^-	8	186.0	3.2	0.0	178.8	185.0	186.7	188.0	500.0
Ni^{4+}—F^-	7	176.7	4.1	0.0	170.4	171.8	178.3	179.5	500.0
Cu^{2+}—F^-	82	195.6	12.8	160.0	184.6	188.3	191.6	197.0	250.0
Cu^{3+}—F^-	7	185.9	7.8	0.0	172.7	182.5	183.7	194.2	500.0
Zn^{2+}—F^-	48	197.2	11.2	150.0	178.8	194.0	198.4	202.7	250.0

Table 9.4.1.3. *Atomic distances between halogens and transition metals (cont.)*

Atom pair	N	Mean	s.u.	d_1	Smallest 5%	First quartile	Median	Third quartile	d_2
Sc^{3+}—Cl^-	9	255.7	6.9	0.0	240.9	254.2	255.7	257.8	500.0
Ti^{3+}—Cl^-	6	244.0	6.3	0.0	232.6	241.0	246.0	247.5	500.0
Ti^{4+}—Cl^-	16	225.0	17.0	170.0	181.6	219.0	224.0	234.7	270.0
V^{2+}—Cl^-	8	250.0	2.8	0.0	246.3	247.3	250.0	252.7	500.0
V^{3+}—Cl^-	10	235.6	4.6	0.0	227.0	233.0	236.0	237.7	500.0
V^{4+}—Cl^-	4	227.5	7.7	0.0	216.4	218.0	228.0	232.0	500.0
V^{5+}—Cl^-	5	221.0	5.8	200.0	212.5	218.5	221.0	223.5	250.0
Cr^{2+}—Cl^-	30	246.7	15.2	220.0	236.2	239.0	241.2	247.0	320.0
Cr^{3+}—Cl^-	17	231.6	4.8	200.0	217.7	229.5	232.5	233.9	270.0
Cr^{6+}—Cl^-	3	218.3	1.2	200.0	216.3	217.5	218.5	219.2	250.0
Fe^{2+}—Cl^-	29	244.9	10.2	200.0	222.4	243.2	247.8	251.2	280.0
Fe^{3+}—Cl^-	39	227.1	9.8	200.0	216.2	217.9	226.5	235.2	280.0
Co^{2+}—Cl^-	39	237.6	12.4	200.0	220.5	225.2	244.1	247.3	280.0
Co^{3+}—Cl^-	10	228.4	30.5	150.0	167.0	225.0	228.0	231.0	310.0
Ni^{2+}—Cl^-	12	238.3	6.1	200.0	221.2	237.0	240.0	242.0	280.0
Cu^{+}—Cl^-	38	245.5	25.5	210.0	217.3	229.0	235.2	270.5	320.0
Cu^{2+}—Cl^-	51	228.1	5.1	200.0	217.1	225.9	228.7	230.4	240.0
Zn^{2+}—Cl^-	54	227.5	9.1	200.0	218.4	222.7	225.0	230.1	280.0
Ti^{4+}—Br^-	3	249.0	18.0	0.0	230.3	231.5	249.0	266.5	500.0
V^{2+}—Br^-	5	259.8	6.3	0.0	248.5	260.2	261.5	263.5	500.0
V^{3+}—Br^-	5	250.6	2.6	0.0	246.5	248.5	251.0	252.8	500.0
Cr^{2+}—Br^-	7	247.3	8.0	0.0	238.7	240.8	243.0	255.2	500.0
Cr^{3+}—Br^-	7	244.1	4.7	210.0	238.7	240.8	243.0	246.5	290.0
Mn^{2+}—Br^-	12	261.2	11.2	220.0	235.2	259.0	265.0	268.0	320.0
Fe^{2+}—Br^-	7	247.9	10.9	220.0	232.7	235.5	249.0	258.5	290.0
Fe^{3+}—Br^-	4	239.0	13.4	220.0	230.4	232.0	233.0	234.0	290.0
Co^{2+}—Br^-	8	253.0	7.9	0.0	238.8	248.7	250.0	260.7	500.0
Ni^{2+}—Br^-	3	257.7	7.0	0.0	250.3	251.5	257.0	264.5	500.0
Cu^{+}—Br^-	22	260.8	20.1	210.0	236.2	246.5	253.0	277.5	310.0
Cu^{2+}—Br–	18	260.3	23.3	210.0	231.8	244.5	251.0	287.5	310.0
Zn^{2+}—Br^-	17	235.0	14.5	200.0	203.7	234.5	236.9	237.9	300.0
V^{2+}—I^-	4	287.0	7.3	0.0	278.4	280.0	284.0	292.0	500.0
Cr^{2+}—I^-	20	261.2	31.6	0.0	190.0	242.0	275.0	278.5	500.0
Mn^{2+}—I^-	10	287.2	6.4	0.0	275.0	281.0	290.0	291.7	500.0
Fe^{2+}—I^-	3	268.3	15.0	240.0	250.3	251.5	276.5	277.2	300.0
Ni^{2+}—I^-	4	295.5	11.0	250.0	278.4	280.0	300.7	301.3	310.0
Cu^{+}—I^-	36	268.7	16.9	0.0	248.8	258.0	264.4	272.0	500.0
Zn^{2+}—I^-	5	264.6	17.2	240.0	252.5	256.2	257.5	261.5	310.0
Y^{3+}—F^-	34	226.7	18.9	0.0	199.4	217.0	224.7	235.0	500.0
Zr^{4+}—F^-	66	203.1	10.1	0.0	191.5	199.0	201.5	205.4	500.0
Nb^{3+}—F^-	6	195.0	2.2	0.0	190.6	194.3	195.3	196.5	500.0
Nb^{4+}—F^-	5	201.8	3.6	0.0	196.5	198.5	203.0	204.8	500.0
Nb^{5+}—F^-	52	191.0	12.7	150.0	159.2	184.5	192.0	199.5	240.0
Mo^{3+}—F^-	11	204.1	6.3	0.0	195.1	202.3	203.4	204.8	500.0
Mo^{5+}—F^-	8	185.5	10.1	160.0	172.4	174.0	185.0	186.0	230.0
Mo^{6+}—F^-	17	190.1	12.5	150.0	169.7	180.5	190.5	193.8	250.0
Ru^{5+}—F^-	7	182.1	9.0	0.0	166.7	176.8	183.0	190.2	500.0
Rh^{3+}—F^-	14	196.3	4.8	170.0	181.4	195.5	198.0	199.0	220.0
Pd^{2+}—F^-	9	206.8	11.6	0.0	192.4	194.5	211.0	216.8	500.0
Pd^{4+}—F^-	10	186.6	1.0	0.0	167.0	184.5	187.0	189.5	500.0
Ag^{+}—F^-	9	250.3	24.8	200.0	220.9	226.5	247.0	275.5	300.0
Ag^{2+}—F^-	12	205.5	4.8	180.0	195.2	204.0	206.4	207.6	240.0
Cd^{2+}—F^-	23	222.1	14.4	180.0	200.3	215.5	221.7	232.2	270.0

Table 9.4.1.3. *Atomic distances between halogens and transition metals (cont.)*

Atom pair	N	Mean	s.u.	d_1	Smallest 5%	First quartile	Median	Third quartile	d_2
Y^{3+}—Cl^-	10	274.0	23.4	220.0	227.0	259.0	278.0	285.5	330.0
Zr^{3+}—Cl^-	9	250.6	6.8	0.0	232.9	250.8	252.3	253.8	500.0
Zr^{4+}—Cl^-	9	240.1	6.7	0.0	230.4	232.5	244.2	245.4	500.0
Nb—Cl^-	9	245.4	11.2	0.0	228.9	238.5	243.0	258.5	500.0
Nb^{5+}—Cl^-	13	232.8	18.1	200.0	215.3	224.2	227.0	231.5	300.0
Mo^{2+}—Cl^-	11	240.8	6.2	0.0	227.1	238.5	240.5	244.5	500.0
Mo^{3+}—Cl^-	11	240.1	2.1	0.0	236.6	238.5	240.2	241.6	500.0
Mo^{4+}—Cl^-	3	224.3	5.8	0.0	220.1	220.8	221.5	230.5	500.0
Mo^{5+}—Cl^-	7	230.7	5.8	0.0	222.7	226.8	229.0	236.5	500.0
Mo^{6+}—Cl^-	12	229.3	4.7	210.0	221.2	225.3	230.0	233.3	260.0
Ru^{2+}—Cl^-	11	233.9	6.1	200.0	219.1	231.2	235.0	238.2	260.0
Ru^{3+}—Cl^-	15	234.7	5.4	220.0	230.4	231.9	233.4	235.5	270.0
Ru^{4+}—Cl^-	8	234.0	3.0	220.0	230.3	231.3	234.0	236.0	260.0
Rh^{3+}—Cl^-	9	232.3	2.8	210.0	228.4	230.2	231.7	234.8	260.0
Pd^{2+}—Cl^-	15	230.7	2.9	210.0	227.5	228.9	230.2	231.4	260.0
Pd^{4+}—Cl^-	3	210.3	16.3	0.0	198.3	199.5	203.0	228.5	500.0
Ag^+—Cl^-	16	261.9	13.5	0.0	237.6	250.0	262.0	271.0	500.0
Cd^{2+}—Cl^-	58	258.0	8.5	220.0	241.9	252.1	258.5	263.0	300.0
Zr^{3+}—Br^-	4	266.5	1.0	0.0	264.4	266.0	266.7	267.3	500.0
Nb^{5+}—Br^-	7	253.3	7.8	230.0	240.7	250.8	252.5	256.5	290.0
Mo—Br^-	12	257.7	14.0	0.0	229.2	254.5	256.0	260.0	500.0
Rh—Br^-	3	245.7	4.2	0.0	240.3	241.5	247.0	248.5	500.0
Ag—Br^-	6	267.7	17.8	0.0	254.6	258.5	260.0	267.0	500.0
Cd^{2+}—Br^-	16	274.0	12.1	250.0	253.6	264.0	276.7	284.0	310.0
Zr—I^-	21	287.1	1.7	250.0	284.0	286.2	287.1	288.0	320.0
Zr^{4+}—I^-	5	284.6	14.2	0.0	268.2	269.2	294.3	295.2	500.0
Nb—I^-	13	277.3	16.3	0.0	241.3	265.2	281.5	283.8	500.0
Nb^{5+}—I^-	4	274.5	8.7	0.0	262.4	264.0	274.0	280.0	500.0
Mo—I^-	4	270.0	12.7	0.0	250.4	252.0	276.0	277.0	500.0
Ru—I^-	3	269.7	2.3	250.0	266.3	267.5	270.5	271.2	300.0
Ag^+—I^-	61	283.1	11.6	250.0	267.0	278.2	281.2	284.9	330.0
Cd^{2+}—I^-	30	293.5	11.0	260.0	273.0	291.0	297.6	299.1	340.0
La^{3+}—F^-	30	240.9	5.8	0.0	234.3	237.4	240.6	242.2	500.0
Hf^{4+}—F^-	9	209.9	10.4	0.0	198.4	202.2	205.0	217.2	500.0
Ta^{5+}—F^-	29	190.6	5.5	160.0	178.9	188.4	191.2	194.6	220.0
W^{6+}—F^-	13	183.5	11.8	150.0	163.3	177.2	179.2	192.8	230.0
Re—F^-	18	187.6	14.9	150.0	163.8	179.0	182.0	195.0	240.0
Os—F^-	10	182.8	14.9	0.0	157.0	171.0	184.0	194.5	500.0
Pt^{4+}—F^-	12	189.0	6.8	0.0	169.2	188.6	189.4	192.0	500.0
Au^{3+}—F^-	7	196.1	3.8	180.0	190.4	191.8	198.2	199.1	220.0
Hg—F^-	19	278.1	26.8	0.0	215.9	271.8	282.3	287.5	500.0
Hg^{2+}—F^-	25	242.7	23.8	0.0	204.5	223.5	243.0	261.9	500.0
La^{3+}—Cl^-	21	293.1	16.1	0.0	256.0	294.2	297.0	302.4	500.0
Ta^{5+}—Cl^-	4	227.5	2.5	210.0	224.4	226.0	227.0	228.0	260.0
W—Cl^-	9	234.1	6.5	210.0	224.9	228.5	233.0	240.5	260.0
W^{6+}—Cl^-	8	219.2	11.1	190.0	202.8	208.0	224.0	228.0	270.0
Re—Cl^-	46	231.6	8.7	200.0	218.3	227.0	231.1	235.4	280.0
Os—Cl^-	14	239.3	6.8	200.0	226.7	236.2	238.0	243.8	280.0
Ir—Cl^-	11	235.4	7.4	200.0	223.1	230.8	234.5	240.5	270.0
Pt^{2+}—Cl^-	26	231.5	3.4	200.0	226.6	229.5	231.0	232.8	270.0
Pt^{4+}—Cl^-	31	231.9	7.0	0.0	225.1	230.2	232.1	234.2	500.0
Au^+—Cl^-	14	241.1	16.6	0.0	225.4	229.7	233.0	249.0	500.0
Au^{3+}—Cl^-	35	232.1	12.8	200.0	219.5	226.1	227.7	234.5	300.0
Hg^+—Cl^-	7	255.0	9.5	230.0	242.7	250.5	251.7	258.5	300.0
Hg^{2+}—Cl^-	68	250.5	25.5	200.0	223.4	231.0	238.0	276.7	310.0

Table 9.4.1.3. *Atomic distances between halogens and transition metals (cont.)*

Atom pair	N	Mean	s.u.	d_1	Smallest 5%	First quartile	Median	Third quartile	d_2
La^{3+}—Br^-	3	310.3	34.1	0.0	270.3	271.5	329.0	330.5	500.0
W^{6+}—Br^-	5	245.0	10.7	0.0	230.5	242.5	244.5	245.8	500.0
Re^{3+}—Br^-	4	237.5	6.6	0.0	232.2	233.0	234.0	238.0	500.0
Os^{4+}—Br^-	3	246.3	6.4	0.0	238.3	239.5	249.0	250.5	500.0
Ir^{3+}—Br^-	4	244.0	3.8	0.0	240.2	241.0	242.0	246.0	500.0
Pt^{2+}—Br^-	9	246.3	6.6	0.0	240.9	242.8	244.5	246.8	500.0
Pt^{4+}—Br^-	8	242.5	10.6	200.0	216.8	243.0	246.0	248.0	270.0
Pt—Br	22	247.4	7.9	230.0	240.2	243.2	246.0	248.5	290.0
Au^{3+}—Br^-	10	243.0	2.7	0.0	239.0	241.0	242.7	245.0	500.0
Hg^{+}—Br^-	5	263.0	14.3	0.0	240.5	256.5	269.0	271.5	500.0
Hg^{2+}—Br^-	27	268.8	25.9	230.0	238.7	247.5	257.0	294.5	330.0
Os—I	8	275.8	4.8	0.0	272.2	273.0	274.0	276.0	500.0
Pt^{4+}—I^-	10	266.2	2.1	0.0	262.5	264.5	266.5	267.8	500.0
Pt—I	24	265.4	3.9	0.0	258.4	263.0	265.2	268.0	500.0
Au^{+}—I^-	4	258.5	3.0	0.0	254.4	256.0	258.0	261.0	500.0
Au^{3+}—I^-	3	265.0	3.5	0.0	262.1	262.8	263.5	268.5	500.0
Hg^{2+}—I^-	40	284.2	27.3	0.0	258.0	267.3	273.6	281.0	500.0

Table 9.4.1.4. *Atomic distances between halogens and lanthanoids*

Atom pair	N	Mean	s.u.	d_1	Smallest 5%	First quartile	Median	Third quartile	d_2
Ce^{3+}—F^-	16	239.0	7.4	0.0	225.6	236.0	237.6	240.0	500.0
Ce^{4+}—F^-	4	216.5	14.9	0.0	198.4	200.0	214.0	220.0	500.0
Nd^{3+}—F^-	8	242.8	21.3	0.0	222.8	232.0	237.0	242.0	500.0
Sm^{3+}—F^-	6	232.0	8.2	0.0	220.6	223.0	234.0	237.5	500.0
Gd^{3+}—F^-	5	226.6	3.3	0.0	220.5	226.2	227.5	228.8	500.0
Tb^{3+}—F^-	3	229.0	7.2	0.0	220.3	221.5	231.0	234.5	500.0
Ho^{3+}—F^-	7	222.4	13.0	0.0	196.7	215.5	227.0	229.2	500.0
Er^{3+}—F^-	10	216.0	1.0	0.0	197.0	212.5	216.0	217.7	500.0
Yb^{3+}—F^-	16	217.2	7.2	0.0	208.5	211.0	218.0	222.0	500.0
Lu^{3+}—F^-	5	210.2	15.3	0.0	186.5	204.5	213.0	219.5	500.0
Pr^{3+}—Cl^-	18	286.2	12.1	0.0	253.8	277.0	289.0	291.0	500.0
Nd^{3+}—Cl^-	12	294.5	25.2	0.0	253.2	274.0	289.0	310.0	500.0
Eu^{3+}—Cl^-	5	285.4	12.4	0.0	276.2	277.2	282.5	283.8	500.0
Gd^{3+}—Cl^-	13	278.8	10.2	0.0	266.4	272.5	277.2	283.2	500.0
Gd—Cl	24	274.4	1.0	0.0	261.2	267.0	273.0	280.0	500.0
Tb^{3+}—Cl^-	4	271.0	5.4	0.0	266.4	268.0	269.0	270.0	500.0
Yb^{2+}—Cl^-	8	277.2	9.0	0.0	270.3	271.3	274.0	278.0	500.0
Nd^{3+}—Br^-	6	307.0	13.1	0.0	294.3	295.5	300.0	322.5	500.0
Gd^{3+}—Br^-	4	290.5	15.9	0.0	268.4	270.0	292.0	296.0	500.0
Eu^{2+}—I^-	4	330.5	11.0	0.0	324.1	324.7	325.3	326.0	500.0

Table 9.4.1.5. *Atomic distances between halogens and actinoids*

Atom pair	N	Mean	s.u.	d_1	Smallest 5%	First quartile	Median	Third quartile	d_2
Th^{4+}—F^-	26	233.3	10.4	0.0	219.3	226.8	231.3	237.0	500.0
Pa^{5+}—F^-	4	216.5	3.4	0.0	212.4	214.0	216.0	218.0	500.0
U^{4+}—F^-	35	232.1	12.7	0.0	216.8	222.5	228.3	241.2	500.0
U^{5+}—F^-	16	204.4	10.4	0.0	192.5	196.0	203.0	208.0	500.0
U^{6+}—F^-	25	211.8	21.4	170.0	180.2	187.6	220.3	223.9	280.0
Np^{4+}—F^-	8	215.8	17.8	0.0	172.8	218.0	220.0	222.0	500.0
Pu^{3+}—F^-	4	241.5	6.4	0.0	234.4	236.0	238.0	247.0	500.0
Th^{4+}—Cl^-	15	292.9	19.4	0.0	245.5	279.5	302.4	303.3	500.0
U^{4+}—Cl^-	14	268.1	17.7	0.0	241.4	261.0	264.7	267.5	500.0
U^{5+}—Cl^-	5	250.6	11.7	0.0	242.2	243.2	247.0	249.5	500.0
U^{6+}—Cl^-	17	264.6	20.1	0.0	229.7	246.5	273.0	275.9	500.0
Pu^{3+}—Cl^-	6	281.0	19.9	0.0	252.6	270.5	272.0	293.0	500.0
Am^{3+}—Cl^-	4	281.5	24.0	0.0	250.4	252.0	280.0	288.0	500.0
Th^{4+}—Cl^-	15	292.9	19.4	0.0	245.5	279.5	302.4	303.3	500.0
Th^{4+}—Br^-	5	288.6	26.7	0.0	256.5	282.5	285.0	287.5	500.0
U^{4+}—Br^-	5	281.0	24.2	0.0	260.5	270.5	273.0	277.5	500.0
Pu^{3+}—Br^-	4	309.0	8.2	0.0	302.4	304.0	306.0	308.0	500.0
U^{3+}—I^-	4	320.5	7.2	0.0	314.4	316.0	318.0	320.0	500.0

Table 9.4.1.6. *Atomic distances between oxygen and main-group elements in their preferred oxidation states*

Atom pair	N	Mean	s.u.	d_1	Smallest 5%	First quartile	Median	Third quartile	d_2
Li^+—O^{2-}	745	194.9	10.2	164.0	178.4	188.4	193.9	203.0	218.0
Na^+—O^{2-}	1914	233.6	10.8	196.0	214.9	227.6	233.7	239.4	268.0
K^+—O^{2-}	1434	276.4	13.0	254.0	259.3	267.4	273.8	282.6	326.0
Rb^+—O^{2-}	330	288.7	12.1	258.0	269.5	280.7	288.4	295.2	322.0
Cs^+—O^{2-}	290	305.2	12.4	270.0	280.5	297.5	306.3	314.1	328.0
Be^{2+}—O^{2-}	195	161.1	5.1	146.0	152.8	157.6	161.1	164.1	178.0
Mg^{2+}—O^{2-}	1121	201.6	9.0	166.0	185.2	197.6	202.8	206.6	228.0
Ca^{2+}—O^{2-}	1624	233.0	12.4	184.0	209.8	228.1	233.2	238.6	286.0
Sr^{2+}—O^{2-}	372	248.7	11.4	212.0	226.8	242.9	250.5	256.9	270.0
Ba^{2+}—O^{2-}	1012	273.8	14.6	222.0	246.9	265.4	274.9	283.0	312.0
B^{3+}—O^{2-}	407	134.3	3.6	116.0	127.1	132.8	134.8	136.6	142.0
Al^{3+}—O^{2-}	914	161.8	4.5	138.0	154.1	160.0	162.4	164.4	170.0
Ga^{3+}—O^{2-}	111	180.3	3.5	170.0	175.0	177.7	180.3	183.0	188.0
In^{3+}—O^{2-}	153	208.2	8.8	184.0	189.6	203.9	209.1	213.2	230.0
Tl^{3+}—O^{2-}	23	214.2	4.4	206.0	187.6	210.8	214.2	217.5	224.0
C^{4+}—O^{2-}	413	125.3	4.9	104.0	115.9	123.5	126.0	128.3	142.0
Si^{4+}—O^{2-}	2679	159.6	5.3	126.0	150.6	157.8	160.0	162.4	180.0
Ge^{4+}—O^{2-}	329	172.1	7.7	144.0	160.3	169.3	172.1	175.0	194.0
Sn^{4+}—O^{2-}	170	202.8	6.4	188.0	191.7	198.1	204.0	206.2	222.0
Pb^{4+}—O^{2-}	56	211.9	5.0	200.0	201.2	207.5	213.7	215.4	222.0
N^{5+}—O^{2-}	301	120.7	4.0	106.0	112.3	118.9	121.5	123.4	132.0
P^{5+}—O^{2-}	1391	149.6	4.7	122.0	142.3	147.3	150.1	152.4	172.0
As^{5+}—O^{2-}	251	166.0	3.9	150.0	159.4	164.4	166.3	167.7	182.0
Sb^{5+}—O^{2-}	161	197.7	7.1	184.0	188.0	193.2	196.7	200.0	220.0
Bi^{5+}—O^{2-}	6	229.0	0.0	228.0	226.5	227.2	228.2	229.1	230.0
S^{6+}—O^{2-}	998	144.3	5.5	118.0	135.6	142.5	144.7	146.6	178.0
Se^{6+}—O^{2-}	86	160.8	3.2	152.0	154.3	159.6	161.3	162.9	168.0
Te^{6+}—O^{2-}	113	189.2	4.1	176.0	182.2	186.8	190.0	191.5	200.0
Cl^{7+}—O^{2-}	89	139.5	5.5	122.0	128.3	136.8	140.9	143.1	150.0
Br^{7+}—O^{2-}	3	160.3	1.2	158.0	158.3	159.5	160.5	161.2	162.0
I^{7+}—O^{2-}	39	180.3	4.7	170.0	171.6	177.4	180.4	183.6	190.0

Table 9.4.1.7. *Atomic distances between oxygen and main-group elements in their special oxidation states*

Atom pair	N	Mean	s.u.	d_1	Smallest 5%	First quartile	Median	Third quartile	d_2
Tl^{+}—O^{2-}	101	265.4	12.9	240.0	244.2	254.2	268.6	275.7	286.0
C^{2+}—O^{2-}	308	110.5	4.5	88.0	102.7	108.8	111.2	112.9	124.0
Sn^{2+}—O^{2-}	14	201.1	2.3	196.0	196.7	200.2	201.3	202.8	206.0
Pb^{2+}—O^{2-}	367	233.2	16.1	190.0	208.1	222.5	232.0	244.2	268.0
N^{2+}—O^{2-}	23	115.3	3.5	108.0	110.3	112.8	114.3	117.6	124.0
N^{3+}—O^{2-}	166	119.9	5.4	102.0	109.5	116.7	121.5	123.9	130.0
N^{4+}—O^{2-}	5	119.0	0.0	118.0	117.8	118.2	118.8	119.4	120.0
P^{+}—O^{2-}	12	149.7	2.3	146.0	145.9	148.0	149.2	152.0	154.0
P^{3+}—O^{2-}	43	149.9	2.1	142.0	146.1	148.7	149.8	151.3	154.0
P^{4+}—O^{2-}	10	151.6	1.0	150.0	149.6	150.3	151.2	152.3	154.0
As^{3+}—O^{2-}	61	175.1	4.6	164.0	166.1	172.2	175.6	178.4	186.0
Sb^{3+}—O^{2-}	101	195.7	5.4	184.0	186.4	192.5	195.3	199.6	208.0
Bi^{3+}—O^{2-}	122	227.0	5.4	216.0	218.0	222.7	227.7	231.1	238.0
S^{2+}—O^{2-}	9	145.7	2.2	140.0	140.9	144.5	146.5	147.2	148.0
S^{4+}—O^{2-}	110	146.3	5.5	130.0	136.2	142.6	147.1	151.0	154.0
S^{5+}—O^{2-}	38	145.4	2.7	142.0	141.5	143.8	144.9	145.8	156.0
Se^{4+}—O^{2-}	125	166.5	3.1	154.0	160.8	164.9	166.5	168.5	176.0
Te^{4+}—O^{2-}	124	186.4	4.0	174.0	179.3	184.2	185.9	189.1	198.0
Cl^{3+}—O^{2-}	8	156.2	1.5	154.0	154.2	155.0	156.0	157.3	160.0
Cl^{5+}—O^{2-}	23	145.5	3.9	136.0	139.1	143.2	146.8	148.6	150.0
Br^{5+}—O^{2-}	11	164.5	0.9	162.0	166.0	164.2	164.6	165.3	166.0
Xe^{6+}—O^{2-}	4	172.5	1.9	170.0	170.2	171.0	172.0	174.0	176.0

Table 9.4.1.8. *Atomic distances between oxygen and transition elements in their preferred and special oxidation states*

Atom pair	N	Mean	s.u.	d_1	Smallest 5%	First quartile	Median	Third quartile	d_2
Y^{3+}—O^{2-}	208	228.7	7.6	212.0	217.4	222.3	228.0	235.5	244.0
Ti^{2+}—O^{2-}	7	206.4	2.2	202.0	202.7	204.8	206.5	208.2	210.0
Ti^{3+}—O^{2-}	79	200.4	4.0	188.0	192.0	197.9	201.7	203.1	208.0
Ti^{4+}—O^{2-}	661	188.7	10.2	156.0	169.9	182.2	190.3	196.1	212.0
V^{2+}—O^{2-}	10	206.6	3.4	202.0	213.8	204.2	205.5	209.0	214.0
V^{3+}—O^{2-}	112	198.0	3.7	188.0	191.7	196.1	197.7	199.8	210.0
V^{4+}—O^{2-}	93	165.8	8.8	150.0	156.2	159.3	163.3	171.8	190.0
V^{5+}—O^{2-}	328	165.1	8.5	142.0	152.8	160.5	164.2	168.8	196.0
Cr^{2+}—O^{2-}	13	203.8	2.8	198.0	196.3	201.5	203.7	206.4	208.0
Cr^{3+}—O^{2-}	215	196.4	4.0	186.0	190.2	194.0	196.3	198.6	208.0
Cr^{4+}—O^{2-}	4	167.5	1.0	166.0	166.1	166.7	167.3	168.0	170.0
Cr^{5+}—O^{2-}	3	169.0	0.0	168.0	164.3	165.5	167.0	168.5	170.0
Cr^{6+}—O^{2-}	164	159.9	5.0	144.0	150.8	157.2	159.6	163.1	172.0
Mn^{2+}—O^{2-}	507	210.0	10.4	178.0	193.1	204.1	209.8	215.6	240.0
Mn^{3+}—O^{2-}	151	191.5	6.1	176.0	181.2	187.6	191.1	195.9	208.0
Mn^{4+}—O^{2-}	74	191.5	6.1	180.0	182.9	187.3	190.5	194.6	208.0
Mn^{7+}—O^{2-}	9	158.8	1.6	156.0	154.8	157.1	158.8	159.9	162.0
Fe^{2+}—O^{2-}	640	203.6	9.3	172.0	187.3	198.5	203.8	209.3	236.0
Fe^{3+}—O^{2-}	900	192.9	9.1	164.0	176.9	187.4	193.4	198.7	224.0
Co^{2+}—O^{2-}	263	202.1	7.1	188.0	190.5	196.6	202.6	206.9	222.0
Co^{3+}—O^{2-}	118	191.8	4.9	176.0	183.9	189.2	191.3	193.9	206.0
Ni^{2+}—O^{2-}	282	200.3	7.9	176.0	185.1	195.9	202.4	205.3	218.0
Cu^{2+}—O^{2-}	614	193.5	7.3	164.0	180.7	190.2	193.7	196.5	220.0
Zn^{2+}—O^{2-}	432	198.1	8.0	182.0	186.7	192.4	196.6	203.2	228.0

Table 9.4.1.8. *Atomic distances between oxygen and transition elements (cont.)*

Atom pair	N	Mean	s.u.	d_1	Smallest 5%	First quartile	Median	Third quartile	d_2
Sc^{3+}—O^{2-}	151	205.1	5.2	188.0	196.6	201.6	205.7	208.4	222.0
Zr^{4+}—O^{2-}	268	203.4	7.3	176.0	188.6	201.1	204.4	207.4	222.0
Nb^{4+}—O^{2-}	7	189.9	1.1	188.0	185.9	187.5	189.4	190.8	192.0
Nb^{5+}—O^{2-}	416	186.6	9.4	166.0	171.4	179.1	186.3	194.8	208.0
Mo^{3+}—O^{2-}	6	207.0	1.8	204.0	200.9	204.5	207.0	208.5	210.0
Mo^{4+}—O^{2-}	34	192.1	5.7	182.0	182.0	185.8	194.8	196.9	200.0
Mo^{5+}—O^{2-}	26	165.8	3.7	158.0	160.3	163.2	165.6	167.6	176.0
Mo^{6+}—O^{2-}	357	171.5	8.3	146.0	158.9	167.6	170.7	174.8	202.0
Tc^{7+}—O^{2-}	4	171.0	0.0	170.0	169.1	169.8	170.5	171.2	172.0
Ru^{2+}—O^{2-}	3	263.0	0.0	262.0	261.6	262.1	262.7	263.4	264.0
Pd^{2+}—O^{2-}	31	201.0	2.7	194.0	196.6	199.1	200.9	202.9	208.0
Ag^{2+}—O^{2-}	6	205.3	2.3	202.0	202.3	203.5	205.0	207.0	210.0
Cd^{2+}—O^{2-}	276	221.9	10.8	184.0	200.8	217.1	222.5	227.8	254.0
La^{3+}—O^{2-}	317	244.1	9.2	222.0	230.1	237.7	243.1	249.9	268.0
Hf^{4+}—O^{2-}	11	202.8	1.7	198.0	201.1	202.2	203.0	203.8	206.0
Ta^{4+}—O^{2-}	5	193.0	1.4	190.0	190.5	192.2	193.0	193.8	196.0
Ta^{5+}—O^{2-}	262	191.7	7.6	168.0	177.7	186.5	193.5	196.8	210.0
W^{5+}—O^{2-}	12	189.5	3.1	184.0	179.0	187.0	189.3	192.5	194.0
W^{6+}—O^{2-}	355	180.0	11.3	150.0	161.8	171.8	178.9	190.0	206.0
Re^{5+}—O^{2-}	21	207.5	3.2	202.0	204.0	204.9	206.5	209.5	216.0
Re^{6+}—O^{2-}	3	163.0	0.0	162.0	161.8	162.2	162.8	163.4	164.0
Re^{7+}—O^{2-}	34	175.1	5.3	166.0	168.3	171.2	173.8	178.5	188.0
Os^{6+}—O^{2-}	3	175.0	0.0	174.0	173.6	174.1	174.8	175.4	176.0
Os^{8+}—O^{2-}	12	173.2	2.2	168.0	170.6	172.0	173.2	174.7	178.0
Ir^{3+}—O^{2-}	5	196.6	1.7	194.0	194.2	195.2	196.5	197.8	200.0
Ir^{4+}—O^{2-}	7	193.9	3.2	190.0	188.3	190.3	193.0	196.5	200.0
Pt^{2+}—O^{2-}	20	199.3	3.5	192.0	194.0	196.0	200.0	202.0	206.0
Pt^{4+}—O^{2-}	56	201.6	4.5	194.0	193.1	198.9	201.2	203.8	214.0
Au^{3+}—O^{2-}	9	198.3	1.0	196.0	195.7	197.3	198.5	199.2	200.0
Hg^{2+}—O^{2-}	94	209.3	11.0	192.0	194.9	202.6	205.7	214.5	236.0

Table 9.4.1.9. *Atomic distances between oxygen and lanthanoids*

Atom pair	N	Mean	s.u.	d_1	Smallest 5%	First quartile	Median	Third quartile	d_2
La^{3+}—O^{2-}	317	244.1	9.2	222.0	230.1	237.7	243.1	249.9	268.0
Ce^{3+}—O^{2-}	75	239.2	7.5	220.0	225.5	234.5	238.2	246.1	254.0
Ce^{4+}—O^{2-}	49	234.1	4.9	222.0	224.5	234.0	235.1	236.7	242.0
Pr^{3+}—O^{2-}	57	239.1	4.8	230.0	232.2	235.7	238.8	241.8	252.0
Nd^{3+}—O^{2-}	185	235.4	6.4	218.0	224.1	232.0	235.5	239.3	250.0
Sm^{3+}—O^{2-}	45	228.8	4.2	218.0	221.2	225.5	229.3	232.6	236.0
Eu^{3+}—O^{2-}	47	231.4	5.4	220.0	222.7	227.2	231.8	235.6	242.0
Gd^{3+}—O^{2-}	78	228.2	5.7	216.0	219.4	223.9	227.6	231.9	240.0
Tb^{3+}—O^{2-}	36	229.4	5.7	216.0	218.8	225.0	230.9	233.3	238.0
Dy^{3+}—O^{2-}	39	226.9	5.6	214.0	216.9	222.5	228.1	231.1	236.0
Ho^{3+}—O^{2-}	48	227.6	5.4	218.0	220.2	223.3	226.7	231.3	242.0
Er^{3+}—O^{2-}	69	224.6	5.4	212.0	214.4	220.9	224.6	228.8	236.0
Tm^{3+}—O^{2-}	24	223.3	4.9	214.0	216.5	220.0	223.3	226.0	234.0
Yb^{3+}—O^{2-}	78	221.8	4.4	210.0	214.5	218.9	221.4	224.9	234.0
Lu^{3+}—O^{2-}	35	220.4	7.3	208.0	210.1	213.8	220.5	226.2	234.0

9.4.1.10. *Atomic distances between oxygen and actinoids*

Atom pair	N	Mean	s.u.	d_1	Smallest 5%	First quartile	Median	Third quartile	d_2
Th^{4+}—O^{2-}	90	237.7	5.8	220.0	225.0	235.5	238.8	241.4	248.0
Pa^{5+}—O^{2-}	21	233.7	3.0	226.0	228.1	231.6	233.8	235.9	240.0
U^{6+}—O^{2-}	290	181.3	9.6	156.0	168.3	175.4	178.8	188.8	206.0
Np^{6+}—O^{2-}	2	173.0	0.0	172.0	171.6	172.1	172.8	173.4	174.0
Pu^{3+}—O^{2-}	6	235.0	0.0	234.0	233.3	233.8	234.6	235.3	236.0
Am^{3+}—O^{2-}	4	236.5	1.9	234.0	234.2	235.0	236.0	238.0	240.0

Table 9.4.1.11. *Atomic distances in sulfides and thiometallates*

Atom pair	N	Mean	s.u.	d_1	Smallest 5%	First quartile	Median	Third quartile	d_2
Li^{+}—S^{2-}	19	251.0	20.7	200.0	209.9	242.5	249.0	262.2	350.0
Na^{+}—S^{2-}	93	295.2	33.6	0.0	269.6	280.1	287.2	299.1	500.0
K^{+}—S^{2-}	82	325.0	13.3	300.0	308.0	316.1	323.5	331.1	380.0
Rb^{+}—S^{2-}	26	338.2	12.8	300.0	318.6	329.5	338.0	345.0	400.0
Cs^{+}—S^{2-}	51	358.8	11.7	300.0	341.1	349.5	359.7	368.9	400.0
Mg^{2+}—S^{2-}	9	249.4	10.0	200.0	234.9	240.5	253.0	258.5	300.0
Ca^{2+}—S^{2-}	21	283.8	12.7	0.0	260.1	274.5	285.0	293.5	500.0
Sr^{2+}—S^{2-}	13	300.8	6.0	270.0	292.6	296.6	300.3	305.5	350.0
Ba^{2+}—S^{2-}	86	317.3	13.6	250.0	300.4	309.8	315.0	326.5	370.0
B—S	10	180.2	8.3	150.0	161.0	178.3	180.0	183.7	250.0
Al^{3+}—S^{2-}	20	225.7	8.9	180.0	210.0	221.3	223.6	230.0	300.0
Ga^{3+}—S^{2-}	61	223.3	5.6	0.0	212.1	220.8	223.7	226.2	500.0
In^{3+}—S^{2-}	66	247.0	12.1	0.0	220.6	241.2	247.4	255.3	500.0
Tl^{+}—S^{2-}	67	305.4	16.5	0.0	278.4	294.8	306.2	316.1	500.0
C—S	19	170.6	11.8	140.0	143.9	164.8	173.0	179.2	210.0
Si^{4+}—S^{2-}	25	210.9	8.2	180.0	202.5	208.8	211.0	213.5	250.0
Ge^{4+}—S^{2-}	44	215.9	9.2	0.0	208.4	214.2	218.3	219.9	500.0
Sn^{2+}—S^{2-}	38	263.1	20.7	0.0	231.8	251.0	261.3	271.5	500.0
Sn^{4+}—S^{2-}	63	248.4	18.9	0.0	231.4	235.9	243.5	256.8	500.0
Pb^{2+}—S^{2-}	111	274.4	28.5	0.0	231.1	269.9	279.7	289.1	500.0
N—S	65	154.1	9.9	100.0	138.2	149.6	154.8	157.9	210.0
P—S	67	201.8	6.6	150.0	189.6	197.6	201.9	207.4	250.0
As^{5+}—S^{2-}	16	214.6	6.9	150.0	193.6	214.0	215.0	216.0	250.0
As—S	97	221.5	16.1	150.0	191.9	217.2	222.4	225.6	310.0
Sb^{3+}—S^{2-}	114	244.1	12.6	200.0	227.4	239.3	242.7	247.2	310.0
Sb^{5+}—S^{2-}	9	233.4	4.1	200.0	226.9	232.1	233.2	235.5	280.0
Bi^{3+}—S^{2-}	77	263.1	12.7	240.0	248.4	255.7	260.1	267.1	320.0
Sc^{3+}—S^{2-}	18	254.9	5.9	0.0	244.9	251.5	255.3	257.8	500.0
Ti^{4+}—S^{2-}	22	242.5	9.4	0.0	224.2	239.5	242.6	245.0	500.0
V^{5+}—S^{2-}	9	218.3	7.6	0.0	208.9	212.5	218.5	220.8	500.0
Cr^{3+}—S^{2-}	32	240.1	5.5	200.0	233.2	236.0	240.3	243.2	300.0
Mn^{2+}—S^{2-}	35	246.1	11.8	0.0	227.5	237.9	243.0	256.2	500.0
Fe—S	117	230.4	13.6	180.0	212.4	220.1	229.1	239.2	280.0
Co^{3+}—S^{2-}	8	226.0	2.4	222.0	222.4	224.0	226.0	228.0	230.0
Co^{2+}—S^{2-}	6	234.7	2.0	232.0	230.4	232.0	234.0	236.5	238.0
Co^{0}—S^{0}	18	214.9	2.0	210.0	211.4	213.4	214.9	216.2	220.0
Ni—S	64	229.4	13.5	190.0	213.1	218.5	228.0	238.0	280.0
Cu—S	221	226.0	8.1	190.0	211.4	222.3	226.4	230.8	270.0
Zn^{2+}—S^{2-}	37	232.8	8.1	200.0	214.9	230.8	233.4	235.3	270.0

Table 9.4.1.11. *Atomic distances in sulfides and thiometallates (cont.)*

Atom pair	N	Mean	s.u.	d_1	Smallest 5%	First quartile	Median	Third quartile	d_2
Y^{3+}—S^{2-}	3	275.0	6.0	0.0	268.3	269.5	275.0	280.5	500.0
Zr^{4+}—S^{2-}	10	257.2	7.1	0.0	248.5	252.5	256.0	260.5	500.0
Nb—S	28	242.8	11.0	210.0	215.4	240.0	247.0	249.1	280.0
Mo—S	76	236.4	9.6	180.0	217.1	235.0	239.2	241.1	280.0
Ru—S	9	236.3	7.8	200.0	218.9	234.2	236.5	241.5	270.0
Rh—S	4	223.5	15.4	0.0	200.4	202.0	228.0	232.0	500.0
Pd—S	29	232.7	4.2	0.0	225.4	229.2	233.2	236.2	500.0
Ag^{+}—S^{2-}	102	252.7	15.2	220.0	227.4	244.1	250.0	259.0	320.0
Cd^{2+}—S^{2-}	37	254.4	10.6	200.0	241.7	245.6	252.6	263.5	300.0
La^{3+}—S^{2-}	43	292.8	15.7	250.0	264.1	285.8	290.3	301.7	350.0
Hf—S	5	259.4	7.7	0.0	250.5	252.5	259.0	265.5	500.0
Ta—S	40	242.6	7.8	200.0	224.0	239.1	242.4	247.0	300.0
W—S	6	250.3	13.6	200.0	238.6	240.5	242.0	253.5	300.0
Re—S	15	233.4	12.1	0.0	199.5	233.5	237.0	238.2	500.0
Os—S	29	237.7	3.4	0.0	229.4	235.8	237.9	240.2	500.0
Pt—S	14	224.7	19.6	0.0	189.4	223.0	232.0	237.0	500.0
Au—S	7	234.1	19.5	200.0	216.7	226.8	229.0	231.2	300.0
Hg^{2+}—S^{2-}	63	244.5	11.1	200.0	229.1	238.4	244.1	251.5	300.0
Ce—S	31	290.5	9.5	0.0	278.3	283.4	288.2	298.2	500.0
Pr—S	7	288.4	15.7	0.0	270.7	275.5	287.0	308.2	500.0
Nd—S	12	286.8	7.8	0.0	276.4	278.0	287.0	294.7	500.0
Sm—S	15	276.9	13.7	0.0	233.5	276.8	281.2	284.5	500.0
Eu—S	26	292.5	9.4	0.0	275.3	285.0	294.0	299.2	500.0
Gd—S	5	289.0	27.1	0.0	274.2	274.8	275.7	283.5	500.0
Ho—S	8	263.8	7.6	0.0	246.8	261.0	267.0	268.7	500.0
Er—S	15	261.7	28.3	0.0	193.5	258.8	266.2	272.5	500.0
Yb—S	22	271.3	9.5	0.0	258.2	265.5	270.5	273.7	500.0
Lu—S	11	267.4	4.8	0.0	260.5	264.5	266.5	270.5	500.0
Th—S	15	283.9	11.0	0.0	259.5	278.8	285.5	290.5	500.0
U—S	46	277.8	9.1	0.0	264.6	274.3	276.4	279.1	500.0
Np—S	2	277.0	19.8	0.0	262.2	263.0	264.0	291.0	500.0
Pu—S	6	293.3	10.3	0.0	276.6	289.0	293.0	301.0	500.0

Table 9.4.1.12. *Contact distances between some negatively charged elements*

Atom pair	N	Mean	s.u.	d_1	Smallest 5%	First quartile	Median	Third quartile	d_2
O^{2-}—O^{2-}	14849	254.5	37.9	0.0	205.4	240.0	255.4	271.0	500.0
S^{2-}—S^{2-}	1414	343.1	42.8	0.0	279.7	325.9	342.6	364.0	500.0
Se^{2-}—Se^{2-}	314	360.5	46.3	0.0	245.4	339.6	363.2	388.2	500.0
Te^{2-}—Te^{2-}	135	392.5	51.2	0.0	281.5	373.8	401.5	425.6	500.0
F^{-}—F^{-}	2096	256.8	37.2	0.0	211.0	243.2	257.5	270.3	500.0
Cl^{-}—Cl^{-}	1667	341.3	41.6	0.0	301.7	326.1	341.2	359.7	500.0
Br^{-}—Br^{-}	534	364.3	47.5	0.0	314.4	350.5	367.5	384.9	500.0
I^{-}—I^{-}	489	396.4	46.9	0.0	313.6	384.6	402.8	419.8	500.0
O^{2-}—F^{-}	723	269.1	28.4	0.0	233.0	255.5	268.2	280.4	500.0
O^{2-}—Cl^{-}	827	313.5	35.3	0.0	267.3	302.9	314.4	328.3	500.0
O^{2-}—Br^{-}	230	332.0	32.9	0.0	293.5	319.4	331.7	344.3	500.0
O^{2-}—I^{-}	109	353.6	44.4	0.0	288.9	345.6	359.4	374.5	500.0
S^{2-}—F^{-}	27	294.3	61.7	0.0	160.7	259.8	299.0	334.2	500.0
S^{2-}—Cl^{-}	53	349.3	38.8	0.0	279.3	330.6	347.7	373.5	500.0
S^{2-}—Br^{-}	26	353.0	35.2	0.0	310.6	344.5	351.0	373.5	500.0
S^{2-}—I^{-}	42	357.9	54.9	0.0	306.1	360.7	368.0	375.0	500.0

International Tables for Crystallography (2006). Vol. C, Chapter 9.5, pp. 790–811.

9.5. Typical interatomic distances: organic compounds

BY F. H. ALLEN, D. G. WATSON, L. BRAMMER, A. G. ORPEN AND R. TAYLOR

9.5.1. Introduction

The determination of molecular geometry is of vital importance to our understanding of chemical structure and bonding. The majority of experimental data have come from X-ray and neutron diffraction, microwave spectroscopy, and electron diffraction. Over the years, compilations of results from these techniques have appeared sporadically. The first major compilation was Chemical Society Special Publication No. 11: *Tables of Interatomic Distances and Configuration in Molecules and Ions* (Sutton, 1958). This volume summarized results obtained by diffraction and spectroscopic methods prior to 1956; a supplementary volume (Sutton, 1965) extended this coverage to 1959. Summary tables of bond lengths between carbon and other elements were also published in Volume III of *International Tables for X-ray Crystallography* (Kennard, 1962). Some years later, the Cambridge Crystallographic Data Centre (Allen, Bellard, Brice, Cartwright, Doubleday, Higgs, Hummelink, Hummelink-Peters, Kennard, Motherwell, Rodgers & Watson, 1979) produced an atlas-style compendium of all organic, organometallic and metal-complex crystal structures published in the period 1960–1965 (Kennard, Watson, Allen, Isaacs, Motherwell, Pettersen & Town, 1972). More recently, a survey of geometries determined by spectroscopic methods (Harmony, Laurie, Kuczkowski, Schwendemann, Ramsay, Lovas, Lafferty & Maki, 1979) has extended coverage in this area to mid-1977.

The production of further comprehensive compendia of X-ray and neutron diffraction results has been precluded by the steep rise in the number of published crystal structures, as illustrated by Fig. 9.5.1.1. Printed compilations have been effectively superseded by computerized databases. In particular, the Cambridge Structural Database now (1991) contains bibliographic, chemical, and numerical results for some 86 000 organo-carbon crystal structures. This machine-readable file fulfils the function of a comprehensive structure-by-structure compendium of molecular geometries. However, the amount of data now held in the CSD is so large that there is also a need for concise, printed tabulations of average molecular dimensions.

The only tables of average geometry in general use are those contained in Sutton (1958, 1965) which list mean bond lengths for a variety of atom pairs and functional groups. Since these early tables were based on data obtained before 1960, we have used the CSD to prepare a new table of average bond lengths in organic compounds. Table 9.5.1.1 given here specifically lists average lengths for bonds involving the elements H, B, C, N, O, F, Si, P, S, Cl, As, Se, Br, Te, and I. Mean values are presented for 682 different bond types involving these elements.

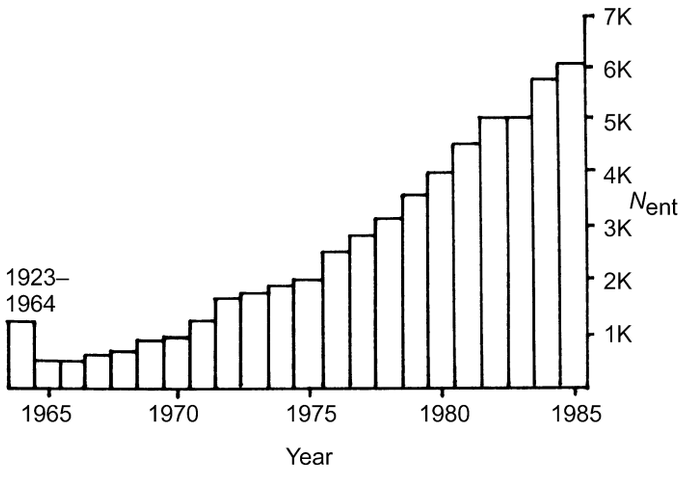

Fig. 9.5.1.1. Growth of the Cambridge Structural Database 1965–1985 as number of entries (N_{ent}) published in a given year.

9.5.2. Methodology

9.5.2.1. *Selection of crystallographic data*

All results given in Table 9.5.1.1 are based on X-ray and neutron diffraction results retrieved from the September 1985 version of the CSD. Neutron diffraction data only were used to derive mean bond lengths involving H atoms. This version of the CSD contained results for 49 854 single-crystal diffraction studies of organo-carbon compounds; 10 324 of these satisfied the acceptance criteria listed below and were used in the averaging procedures:

(i) Structure is 'organic', *i.e.* belongs to the CSD chemical classes 1–65 or 70 (*Cambridge Crystallographic Data Centre User Manual*, 1978).

(ii) Atomic coordinates for the structure have been published and are available in the CSD.

(iii) Structure was determined from diffractometer data.

(iv) Structure does not contain unresolved numeric data errors from the original publication (such errors are usually typographical and are normally resolved by consultation with the authors).

(v) Structure was not reported to be disordered.

(vi) Only structures of higher precision were included on the basis of *either* (*a*) the crystallographic *R* factor was ≤ 0.07 and the reported mean estimated standard deviation (e.s.d.) of the C—C bond lengths was ≤ 0.010 Å (corresponds to AS flag = 1 or 2 in the CSD), *or* (*b*) the crystallographic *R* factor ≤ 0.05 and the mean e.s.d. for C—C bonds was not available in the database (AS = 0 in the CSD).

(vii) Where the structure of a given compound had been determined more than once within the limits of (i)–(vi), then only the most precise determination was used.

9.5.2.2. *Program system*

All calculations were performed on the University of Cambridge IBM 3081 D using the programs *BIBSER*, *CONNSER*, *RETRIEVE*, *GEOM*78, and *PLUTO*78 (Allen *et al.*, 1979). A stand-alone program was written to implement the selection criteria, whilst a new program (*STATS*) was written to perform the statistical calculations described below. It was also necessary to modify *CONNSER* to improve the precision with which it locates chemical substructures. In particular, the program was altered to permit the location of atoms with specified coordination numbers. This was essential in the case of carbon so that atoms with coordination numbers 2, 3 and 4 (equivalent to formal hybridization states sp^1, sp^2, sp^3) could be distinguished easily and reliably. Considerable care was taken to ensure that the correct molecular fragment was located by *GEOM*78 in the generation of geometrical tabulations. This often involved the explicit specification of H atoms in fragments, and the extensive use of geometrical tests on valence and torsion angles. Considerable use was also made of chemical structural diagrams, which are available in the Cambridge in-house version

Copyright © 2006 International Union of Crystallography

of the CSD for some 81% of all entries. Chemical diagrams proved useful, for example, in identifying the various coordination environments commonly adopted by atoms such as As, B, P, *etc*.

9.5.2.3. *Classification of bonds*

The classification of bonds used in Table 9.5.1.1 is based on common functional groups, rings and ring systems, coordination spheres, *etc*. It is designed: (i) to appear logical, useful and reasonably self-explanatory to chemists, crystallographers, and others who may use the table; (ii) to permit a meaningful average value to be cited for each bond length. With reference to (ii), it was considered that a sample of bond lengths could be averaged meaningfully if: (*a*) the sample was unimodally distributed; (*b*) the sample standard deviation (σ) was reasonably small, ideally less than *ca* 0.02 Å; (*c*) there were no conspicuous outlying observations – those that occurred at $> 4\sigma$ from the mean were automatically eliminated from the sample by *STATS*, other outliers were inspected carefully; (*d*) there were no compelling chemical reasons for further subdivision of the sample.

9.5.2.4. *Statistics*

Where there are less than four independent observations of a given bond length, then each individual observation is given explicitly in the table. In all other cases, the following statistics were generated by the program *STATS*.

(i) The unweighted sample mean, d, where

$$d = \sum_{i=1}^{n} d_i/n$$

and d_i is the ith observation of the bond length in a total sample of n observations. Recent work (Taylor & Kennard, 1983, 1985, 1986) has shown that the unweighted mean is an acceptable (even preferable) alternative to the weighted mean, where the ith observation is assigned a weight equal to $1/\sigma^2(d_i)$. This is especially true (Taylor & Kennard, 1985) where structures have been pre-screened on the basis of precision.

(ii) The sample median, m. This has the property that half of the observations in the sample exceed m, and half fall short of it.

(iii) The sample standard deviation, denoted here as σ, where:

$$\sigma = \sum_{i=1}^{n} [(d_i - d)^2/(n-1)]^{1/2}.$$

(iv) The lower quartile for the sample, q_l. This has the property that 25% of the observations are less than q_l and 75% exceed it.

(v) The upper quartile for the sample, q_u. This has the property that 25% of the observations exceed q_u, and 75% fall short of it.

(vi) The number (n) of observations in the sample.

The statistics given in the final table correspond to distributions for which the automatic 4σ cut-off (see above) had been applied, and any manual removal of additional outliers (an infrequent operation) has been performed. In practice, a very small percentage of observations was excluded by these methods. The major effect of removing outliers is to improve the sample standard deviation, as shown in Fig. 9.5.2.1 in which a single observation is deleted.

The statistics chosen for tabulation effectively describe the distribution of bond lengths in each case. For a symmetrical, normal distribution: the mean (d) will be approximately equal to the median (m); the lower and upper quartiles (q_l, q_u) will be approximately symmetric about the median: $m - q_l \simeq q_u - m$, and 95% of the observations may be expected to lie within $\pm 2\sigma$ of the mean value. For a skewed distribution, d and m may differ appreciably and q_l and q_u will be asymmetric with respect to m. When a bond-length distribution is negatively skewed as in Fig. 9.5.2.2, *i.e.* very short values are more common than very long values, then it may be due to thermal-motion effects; the distances used to prepare the table were not corrected for thermal libration.

In a number of cases, the initial bond-length distribution was clearly bimodal, as in Fig. 9.5.2.3(*a*). All cases of bimodality were resolved on chemical grounds before inclusion in the table, on the basis of hybridization, conformation-dependent conjugation interactions, *etc*. For example, the histogram of Fig. 9.5.2.3(*a*) was resolved into the two discrete unimodal distributions of Figs. 9.5.2.3(*b*), (*c*), which correspond to planar N(sp^2), pyramidal N(sp^3), respectively. The mean valence angle at N was used as the discriminator, with a range of 108–114° for N(sp^3) and $\geq 117.5°$ for N(sp^2).

9.5.3. Content and arrangement of the table

The upper triangular matrix of Fig. 9.5.3.1(*a*) shows the 120 possible element-pair combinations that can be formed from the 15 elements As, B, Br, C, Cl, F, H, I, N, O, P, S, Se, Si, Te.

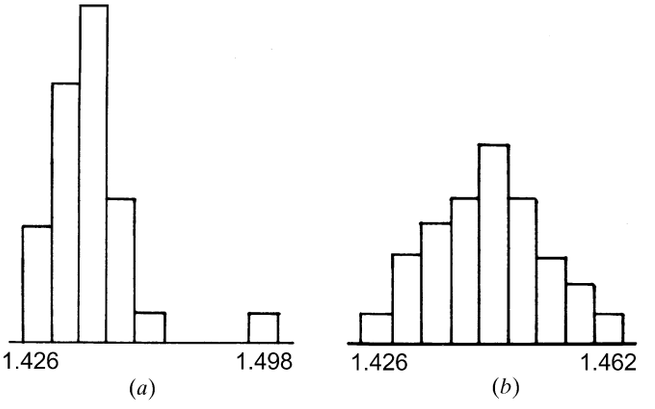

Fig. 9.5.2.1. Effect of the removal of outliers (contributors that are $> 4\sigma$ from the mean) for the C—C bond in C_{ar}—C≡N fragments. Relevant statistics (see text) are:

	d	m	σ	q_l	q_u	n
(*a*) before	1.445	1.444	0.012	1.436	1.448	32
(*b*) after	1.455	1.444	0.008	1.436	1.448	31.

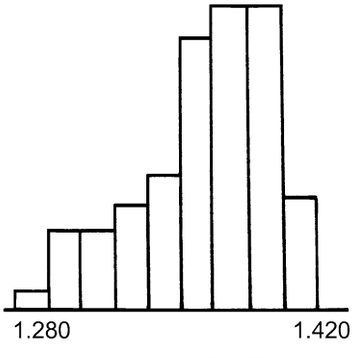

Fig. 9.5.2.2. Skewed distribution of B—F bond lengths in BF_4^- ions: $d = 1.365$, $m = 1.372$, $\sigma = 0.029$, $q_l = 1.352$, $q_u = 1.390$ for 84 observations. Note that $d \neq m$ and that q_l, q_u are asymmetrically disposed about the mean d.

Fig. 9.5.3.1(*a*) contains the number of discrete average bond lengths given in the table for each element pair. 682 average values are cited for 65 element pairs, of which 511 (75%) involve carbon. Bond-length values from individual structures are given for a further 30 element pairs indicated by an asterisk in Fig. 9.5.3.1(*a*). Individual structures are identified by their CSD reference code (*e.g.* BOGSUL), and short-form literature references, ordered alphabetically by reference code, are given in Appendix 2. For eight element pairs, the acceptance criterion (vi) was relaxed to include all available structures, irrespective of precision. These entries are denoted by a dagger in the table. No bonds were found for 25 element pairs within the subset of CSD used in this study.

Each entry in Table 9.5.1.1 contains nine columns, of which six record the statistics of the bond-length distribution described above. The content of the remaining three columns: 'Bond', 'Structure', 'Note', are now described.

9.5.3.1. *Ordering of entries: the 'Bond' column*

For an element pair X—Y, the primary ordering is alphabetic by element symbols according to the rows of Fig. 9.5.3.1(*a*); *i.e.* X changes slowest, Y fastest. The complete sequence runs from As—As to Te—Te with bonds involving carbon in the natural position: As—C...C—C...C—Te. Within a given X—Y pair, a secondary ordering is based on the coordination numbers (j) of X and Y, and on the nature of the bond between them. The bond definition is of the form $X(j)$—$Y(j)$, with j decreasing fastest for Y, slowest for X, and with all single bonds preceding any multiple bonds. For carbon, the formal hybridization state replaces (but is equivalent to) the coordination number and it is for this element that the ordering rules are most clearly required. The ordering of the most populous C—C, C—N, C—O sections is illustrated in Fig. 9.5.3.1(*b*). The 13 possible C—C combinations follow the sequence Csp^3—Csp^3, Csp^3—Csp^2, Csp^3—C_{ar}, Csp^3—Csp^1, Csp^2—Csp^2, Csp^2—C_{ar}, Csp^2—Csp^1, C_{ar}—C_{ar}, C_{ar}—Csp^1, Csp^1—Csp^1, Csp^2=Csp^2, C_{ar}⋯C_{ar}, Csp^1≡Csp^1. The symbol C_{ar} represents aryl carbon in six-membered rings, which is treated separately from Csp^2 throughout the table. The symbol ⋯ is used to indicate a delocalized double or aromatic bond according to context.

9.5.3.2. *Definition of 'Substructure'*

The chemical environment of each bond is normally defined by a linear formulation of the substructure. The target bond is set in bold type, *e.g.* C_{ar}—**C**≡**N** (aryl cyanides); C—**C**H_2—**O**—C_{ar} (primary alkyl aryl ethers); (C—O)$_2$—**P**(⋯**O**)$_2$ (phosphate diesters). Occasionally, the chemical name of a functional group or ring system is used to define bond environment, *e.g.* in naphthalene, C2—C3; in imidazole, N1—C2. To avoid any possible ambiguity in these cases, we include numbered chemical diagrams in Fig. 9.5.3.2.

	As	B	Br	C	Cl	F	H	I	N	O	P	S	Se	Si	Te
As	1	*	*	6	1	1	0	*	2	2	+	2	+	+	+
B	2	2	5	2	2	0	*	4	2	1	4	0	0	0	
Br	1	5	+	0	0	*	*	1	*	+	*	*	*		
C	175	16	13	10	2	97	119	12	40	3	6	2			
Cl	*	0	0	*	*	1	2	1	*	2	1				
F	0	0	0	1	0	2	2	0	3	*					
H	0	0	2	3	0	0	0	0	0						
I	1	*	1	+	*	0	0	1							
N	15	18	15	8	*	6	*								
O	4	20	9	*	5	2									
P	2	3	1	1	*										
S	5	1	1	2											
Se	1	0	+												
Si	1	0													
Te	*														

(*a*)

	C—C							C—N				C—O	
	Csp^3	Csp^2	C_{ar}	Csp^1	Csp^2	C_{ar}	Csp^1	N(4)	N(3)	N(2)	N(1)	O(2)	O(1)
Csp^3—	27	30	6	4	-	-	-	5	22	2	-	60	-
Csp^2—	24	14	2	-	-	-	-	28	1	-	17	-	
C_{ar}—	2	2	-	-	-	1	9	2	-	4	-		
Csp^1—	1	-	-	-	-	-	-	-	-	-			
Csp^2=	34	-	-	-	1	8	-	-	38				
C_{ar}⋯	24	-	-	3	9	-	-	-					
Csp^1≡	5	-	-	1	5	-	-						

(*b*)

Fig. 9.5.3.1. (*a*) Distribution of mean bond-length values reported in the table by element pair. An asterisk indicates a bonded pair represented by less than four contributors in the original data set. A '+' indicates bonded pairs located when restrictions on R factor and reported e.s.d. limits were lifted (see text). (*b*) Distribution of mean bond-length values reported in the table for C—C, C—O, C—N.

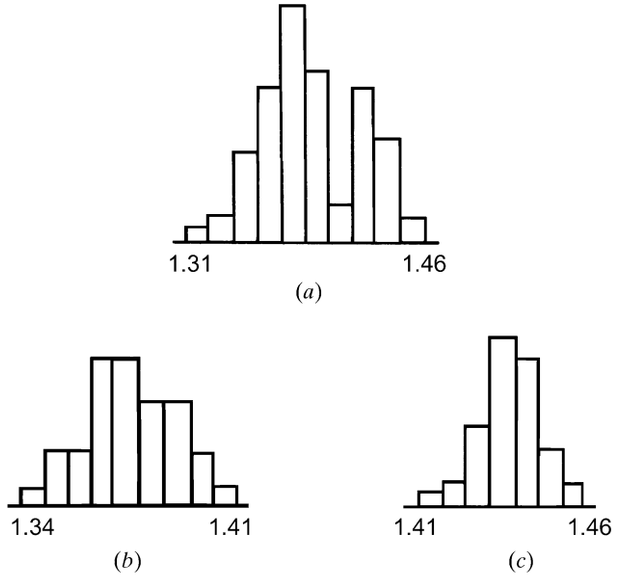

Fig. 9.5.2.3. Resolution of the bimodal distribution of C—N bond lengths in C_{ar}—N(Csp^3)$_2$ fragments: (*a*) complete distribution; (*b*) distribution for planar N, mean valence angle at $N > 117.6°$; (*c*) distribution for pyramidal N, mean valence angle at N in the range 108–114°.

A combination of chemical name and linear formulation is often employed to increase the precision of the definition, *e.g.* $\mathbf{N}H_2—\mathbf{C}=O$ in acyclic amides; $C=\mathbf{C}—\mathbf{C}(=O)—\mathbf{C}=O$ in benzoquinone. Finally, for very simple ions, the accepted conventional representation is deemed to be sufficient, *e.g.* in NO_3^-, SO_4^{2-}, *etc.*

The chemical definition of substructure may be followed by brief qualifying information, concerning substitution, conformational restrictions, *etc.* For example: $C sp^3—C sp^3$: in cyclobutane (any substituent); $X—\mathbf{C}—\mathbf{F}_3$ (X = C, H, N, O); $\mathbf{C}_{ar}—\mathbf{N}H—C sp^3$ ($N sp^3$: pyramidal). Where the generic symbol X is unqualified, it denotes any element type, including hydrogen. If the qualifying information is too extensive, then it will be given as a table footnote (see below).

The 'Substructure' column is designed to convey as much unambiguous information as possible within a small space. For $C sp^3$, we have employed the short forms C* and $C^{\#}$. C* indicates $C sp^3$ whose bonds, additional to those specified in the linear formulation, are to C or H atoms only. C*—OH would then represent the group of alcohols $CH_3—OH$, $—C—CH_2—OH$, $—C_2—CH—OH$ and $—C_3—C—OH$. C* is frequently used to restrict the secondary environment of a given bond to avoid the perturbing influence of, *e.g.*, electronegative substituents. The symbol $C^{\#}$ is merely a space-saving device to indicate any $C sp^3$ atom and includes C* as a subset.

9.5.3.3. *Use of the 'Note' column*

The 'Note' column refers to the footnotes collected in Appendix 1. These record additional information as follows: (*a*) additional details concerning the chemical definition of substructures, *e.g.* the omission of three- and four-membered rings; (*b*) statements of geometrical constraints used in obtaining the cited average, *e.g.* definition of planarity or pyramidality at

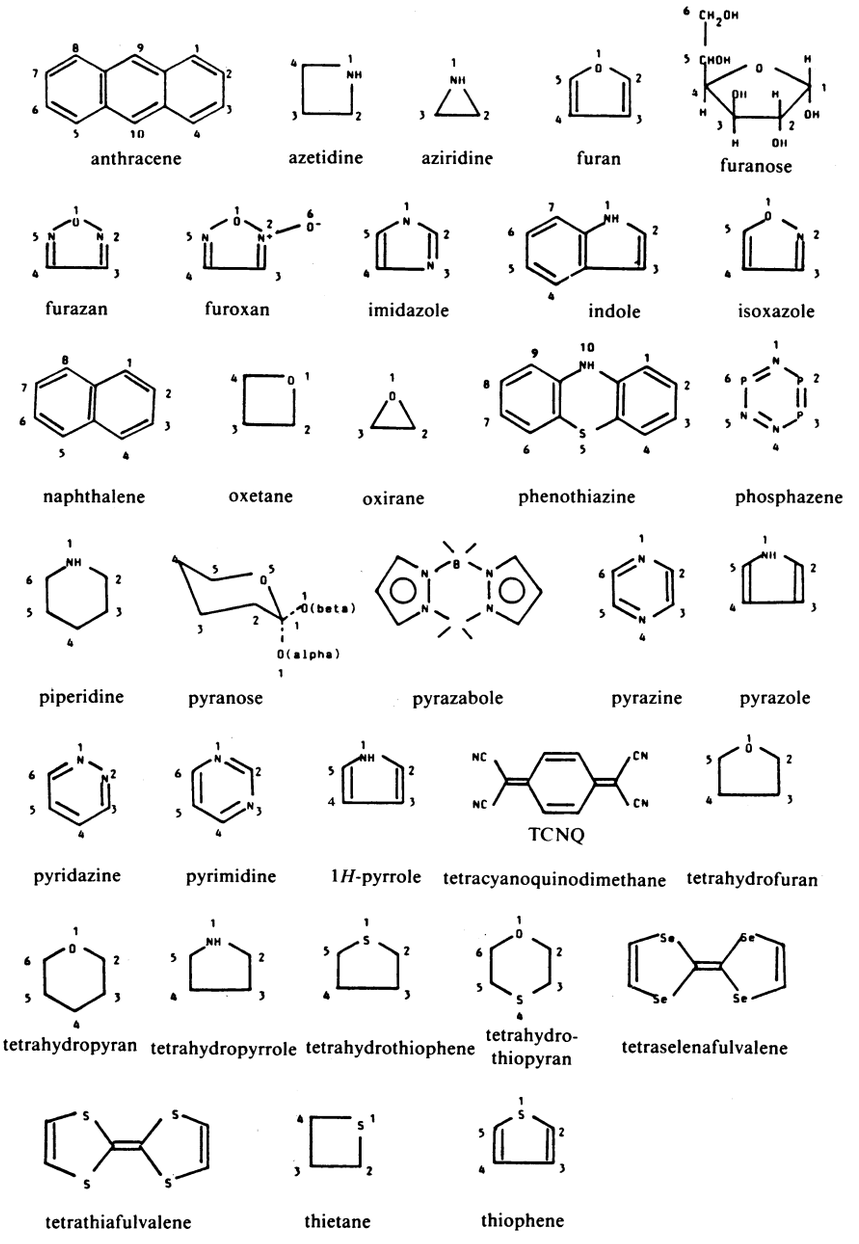

Fig. 9.5.3.2. Alphabetized index of ring systems referred to in the table; the numbering scheme used in assembling the bond-length data is given where necessary.

N, torsional constraints in conjugated systems; (*c*) any peculiarities of a particular bond-length distribution, *e.g.* sample dominated by C* = methyl; (*d*) references to previously published surveys of crystallographic results relevant to the substructure in question. We do not claim that these references are in any way comprehensive and we would be grateful to authors for notification (to FHA) of any omissions. This will serve to improve the content of any future version of the table.

9.5.4. Discussion

It should be remembered that this table has been derived from the organic section of CSD. We are aware that a number of organic bond types which occur very frequently in organometallics and metal complexes (*e.g.* C⋯C in cyclopentadienyl, C—P in triphenylphosphine, *etc.*) are either absent or poorly represented in this work. These omissions are rectified in Chapter 9.6. We also note that certain bond types listed here (*e.g.* As—O, Si—O, Si—N, *etc.*) will occur with greater frequency in inorganic compounds. The interested reader is referred to the Inorganic Crystal Structure Database (Bergerhof, Hundt, Sievers & Brown, 1983) for a machine-readable compendium of more relevant structural data.

The tabulation given here represents the first stage in a major project designed to obtain the average geometries of function groups, rigid rings, and the low-energy conformations of flexible rings. Details of mean bond lengths, valence angles, and conformational preferences in a wide range of substructures will form the basis of a machine-readable 'fragment library' for use in molecular modelling and other areas of research. The systematic survey will be extended to derive information about distances, angles, directionality, and environmental dependence of hydrogen bonds and non-bonded interactions.

APPENDIX 1
Notes to Table 9.5.1.1

(1) Sample dominated by B—CH_3. For longer bonds in B^-—CH_3, see LITMEB10 [B(4)—CH_3 = 1.621–1.644 Å].
(2) $p(\pi)$—$p(\pi)$ bonding with Bsp^2 and Nsp^2 coplanar (τBN = 0 ± 15°) predominates. See G. Schmidt, R. Boese & D. Bläser [*Z. Naturforsch. Teil B* (1982), **37**, 1230–1233].
(3) 84 observations range from 1.38 to 1.62 Å and individual values depend on substituents on B and O. For a discussion of borinic acid adducts, see S. J. Rettig & J. Trotter [*Can. J. Chem.* (1982), **60**, 2957–2964].
(4) See M. Kaftory (1983). [In *The chemistry of functional groups*. Supplement D: *The chemistry of halides, pseudo-halides and azides*, Part 2, Chap. 24, edited by S. Patai & Z. Rappoport. New York: John Wiley.]
(5) Bonds that are endocyclic or exocyclic to any three- or four-membered rings have been omitted from all averages in this section.
(6) The overall average given here is for Csp^3—Csp^3 bonds which carry only C or H substituents. The value cited reflects the relative abundance of each 'substitution' group. The 'mean of means' for the nine subgroups is 1.538 (σ = 0.022) Å.
(7) See (*a*) F. H. Allen [*Acta Cryst.* (1980), B**36**, 81—96] and (*b*) F. H. Allen [*Acta Cryst.* (1981), B**37**, 890–900].
(8) See F. H. Allen [*Acta Cryst.* (1984), B**40**, 64–72].
(9) See F. H. Allen [*Tetrahedron* (1982), **38**, 2843–2853].
(10) See F. H. Allen [*Tetrahedron* (1982), **38**, 645–655].
(11) Cyclopropanones and cyclobutanones excluded.
(12) See W. B. Schweizer & J. D. Dunitz [*Helv. Chim. Acta* (1982), **65**, 1547–1554].
(13) See L. Norskov-Lauritsen, H.-B. Bürgi, P. Hoffmann & H. R. Schmidt [*Helv. Chim. Acta* (1985), **68**, 76–82].
(14) See P. Chakrabarti & J. D. Dunitz [*Helv. Chim. Acta* (1982), **65**, 1555–1562].
(15) See J. L. Hencher (1978). [In *The chemistry of the C≡C triple bond*, Chap. 2, edited by S. Patai. New York: John Wiley.]
(16) Conjugated: torsion angles about central C—C single bond is 0 ± 20° (*cis*) or 180 ± 20° (*trans*).
(17) Unconjugated: torsion angle about central C—C single bond is 20–160°.
(18) Other conjugative substituents excluded.
(19) TCNQ is tetracyanoquinodimethane (see diagrams).
(20) No difference detected between C2⋯C3 and C3⋯C4 bonds.
(21) Derived from neutron diffraction results only.
(22) Nsp^3: pyramidal; mean valence angle at N is in the range 108–114°.
(23) Nsp^2: planar; mean valence angle at N is ≥ 117.5°.
(24) Cyclic and acyclic peptides.
(25) See R. H. Blessing [*J. Am. Chem. Soc.* (1983), **105**, 2776–2783].
(26) See L. Lebioda [*Acta Cryst.* (1980), B**36**, 271–275].
(27) n = 3 or 4; *i.e.* tri- or tetrasubstituted ureas.
(28) Overall value also includes structures with mean valence angle at N in the range 115–118°.
(29) See F. H. Allen & A. J. Kirby [*J. Am. Chem. Soc.* (1984), **106**, 6197–6200].
(30) See A. J. Kirby (1983). [*The anomeric effect and related stereoelectronic effects at oxygen*. Berlin: Springer.]
(31) See B. Fuchs, L. Schleifer & E. Tartakovsky [*Nouv. J. Chim.* (1984), **8**, 275–278].
(32) See S. C. Nyburg & C. H. Faerman [*J. Mol. Struct.* (1986), **140**, 347–349].
(33) Sample dominated by P—CH_3 and P—CH_2—C.
(34) Sample dominated by C* = methyl.
(35) See A. Kálmán, M. Czugler & G. Argay [*Acta Cryst.* (1981), B**37**, 868–877].
(36) Bimodal distribution resolved into 22 'short' bonds and 5 longer outliers.
(37) All 24 observations come from BUDTEZ.
(38) 'Long' O—H bonds in centrosymmetric O···H···O H-bonded dimers are excluded.
(39) N—N bond length also dependent on torsion angle about N—N bond and on nature of substituent C atoms – these effects are ignored here.
(40) N pyramidal has average angle at N in the range 100–113.5°; N planar has average angle ≥ 117.5°.
(41) See R. R. Holmes & J. A. Deiters [*J. Am. Chem. Soc.* (1977), **99**, 3318–3326].
(42) No detectable variation in S=O bond length with type of C substituent.

APPENDIX 2
Short-form references to individual CSD entries cited by reference code in Table 9.5.1.1

REFCODE	Journal	Vol.	Page	Year
ACBZPO01	*J. Am. Chem. Soc.*	97	6729	1975
ACLTEP	*J. Organomet. Chem.*	184	417	1980
ASAZOC	*Dokl. Akad. Nauk SSSR*	249	120	1979
BALXOB	*J. Am. Chem. Soc.*	103	4587	1981

BAPPAJ	*Inorg. Chem.*	20	3071	1981	CMBIDZ	*J. Org. Chem.*	44	1447	1979
BARRIV	*Acta Chem. Scand. Ser. A*	35	433	1981	CODDEE	*Z. Naturforsch. Teil B*	39	1257	1984
BAWFUA	*Cryst. Struct. Commun.*	10	1345	1981	CODDII	*Z. Naturforsch. Teil B*	39	1257	1984
BAWGAH	*Cryst. Struct. Commun.*	10	1353	1981	COFVOI	*Z. Naturforsch. Teil B*	39	1027	1984
BECTAE	*J. Org. Chem.*	46	5048	1981	COJCUZ	*Chem. Ber.*	117	2686	1984
BELNIP	*Z. Naturforsch. Teil B*	37	299	1982	COSDIX	*Z. Naturforsch. Teil B*	39	1344	1984
BEMLIO	*Chem. Ber.*	115	1126	1982	COZPIQ	*Chem. Ber.*	117	2063	1984
BEPZEB	*Cryst. Struct. Commun.*	11	175	1982	COZVIW	*Z. Anorg. Allg. Chem.*	515	7	1984
BETJOZ	*J. Am. Chem. Soc.*	104	1683	1982	CTCNSE	*J. Am. Chem. Soc.*	102	5430	1980
BETUTE10	*Acta Chem. Scand. Ser. A*	30	719	1976	CUCPIZ	*J. Am. Chem. Soc.*	106	7529	1984
BIBLAZ	*Zh. Strukt. Khim.*	22	118-4	1981	CUDLOC	*J. Cryst. Spectrosc.*	15	53	1985
BICGEZ	*Z. Anorg. Allg. Chem.*	486	90	1982	CUDLUI	*J. Cryst. Spectrosc.*	15	53	1985
BIHXIZ	*J. Chem. Soc. Chem. Commun.*		982	1982	CUGBAH	*Acta Cryst. Sect. C*	41	476	1985
BIRGUE10	*Z. Naturforsch. Teil B*	38	20	1983	CXMSEO	*Acta Cryst. Sect. B*	29	595	1973
BIRHAL10	*Z. Naturforsch. Teil B*	37	1410	1982	DGLYSE	*Acta Cryst. Sect. B*	31	1785	1975
BIZJAV	*J Organomet. Chem.*	238	C1	1982	DMESIP01	*Acta Cryst. Sect. C*	40	895	1984
BOGPOC	*Z. Naturforsch. Teil B*	37	1402	1982	DSEMOR10	*J. Chem. Soc. Dalton Trans.*		628	1980
BOGSUL	*Z. Naturforsch. Teil B*	37	1230	1982	DTHIBR10	*Inorg. Chem.*	10	697	1971
BOJLER	*Z. Anorg. Allg. Chem.*	493	53	1982	EPHTEA	*Inorg. Chem.*	19	2487	1980
BOJPUL	*Acta Chem. Scand. Ser. A*	36	829	1982	ESEARS	*J. Chem. Soc. C*		1511	1971
BOPFER	*Chem. Ber.*	116	146	1983	ETEARS	*J. Chem. Soc. C*		1511	1971
BOPFIV	*Chem. Ber.*	116	146	1983	FMESIB	*J. Organomet. Chem.*	197	275	1980
BOVMEE	*Acta Cryst. Sect. B*	38	1048	1982	FPHTEL	*J. Chem. Soc. Dalton Trans.*		2306	1980
BQUINI	*Acta Cryst. Sect. B*	35	1930	1979	FPSULF10	*J. Am. Chem. Soc.*	104	1683	1982
BTUPTE	*Acta Chem. Scand. Ser. A*	29	738	1975	HCLENE10	*Acta Cryst. Sect. B*	38	3139	1982
BUDTEZ	*Z. Naturforsch. Teil B*	38	454	1983	HMTITI	*Acta Cryst. Sect. B*	31	1505	1975
BUPSIB10	*Z. Anorg. Allg. Chem.*	474	31	1981	HMTNTI	*Z. Anorg. Allg. Chem.*	409	237	1974
BUSHAY	*Z. Naturforsch. Teil B*	38	692	1983	HXPASC	*J. Chem. Soc. Dalton Trans.*		1381	1975
BUTHAZ10	*Inorg. Chem.*	23	2582	1984	IBZDAC11	*J. Chem. Soc. Dalton Trans.*		854	1979
BUTSUE	*J. Chem. Soc. Chem. Commun.*		862	1983	IFORAM	*Monatsh. Chem.*	105	621	1974
BUWZUO	*Acta Chem. Scand. Ser. A*	37	219	1983	IODMAM	*Acta Cryst. Sect. B*	33	3209	1977
BZPRIB	*Z. Naturforsch. Teil B*	36	922	1981	IPMUDS	*Acta Cryst. Sect. B*	29	2128	1973
BZTPPI	*Inorg. Chem.*	17	894	1978	ISUREA10	*Acta Cryst. Sect. B*	28	643	1972
CAHJOK	*Inorg. Chem.*	22	1809	1983	LITMEB10	*J. Am. Chem. Soc.*	97	6401	1975
CAJMAB	*Chem. Z.*	107	169	1983	MESIAD	*Z. Naturforsch. Teil B*	35	789	1980
CANLUY	*Tetrahedron Lett.*	24	4337	1983	METAMM	*Acta Cryst.*	17	1336	1964
CASSAQ	*J. Struct. Chem.*	2	101-2	1983	MNPSIL	*J. Am. Chem. Soc.*	91	4134	1969
CASTOF10	*Acta Cryst. Sect. C*	40	1879	1984	MODIAZ	*J. Heterocycl. Chem.*	17	1217	1980
CASYOK	*J. Struct. Chem.*	2	107-2	1983	MOPHTE	*Acta Chem. Scand. Ser. A*	34	333	1980
CECHEX	*Z. Anorg. Allg. Chem.*	508	61	1984	MORTRS10	*J. Chem. Soc. Dalton Trans.*		628	1980
CECXEN	*J. Struct. Chem.*	2	207-3	1983	NAPSEZ10	*J. Am. Chem. Soc.*	102	5070	1980
CEDCUJ	*J. Org. Chem.*	48	5149	1983	NBBZAM	*Z. Naturforsch. Teil B*	32	1416	1977
CEHKAB	*Z. Naturforsch. Teil B*	39	139	1984	OPIMAS	*Aust. J. Chem.*	30	2417	1977
CELDOM	*Acta Cryst. Sect. C*	40	556	1984	OPNTEC10	*J. Chem. Soc. Dalton Trans.*		251	1982
CESSAU	*Acta Cryst. Sect. C*	40	653	1984	PHASCL	*Acta Cryst. Sect. B*	37	1357	1981
CETTAW	*Chem. Ber.*	117	1089	1984	PHASOC01	*Aust. J. Chem.*	28	15	1975
CETUTE	*Acta Chem. Scand. Ser. A*	29	763	1975	PNPOSI	*J. Am. Chem. Soc.*	90	5102	1968
CEYLUN	*Isv. Akad. Nauk SSR Ser. Khim.*		2744	1983	SEBZQI	*J. Chem. Soc. Chem. Commun.*		325	1977
CIFZUM	*Acta Chem. Scand. Ser. A*	38	289	1984	SPSEBU	*Acta Chem. Scand. Ser. A*	33	403	1979
CIHRAM	*Angew. Chem. Int. Ed. Engl.*	23	302	1984	TEACBR	*Cryst. Struct. Commun.*	3	753	1974
CILRUK	*J. Chem. Soc. Chem. Commun.*		1023	1984	THINBR	*J. Am. Chem. Soc.*	92	4002	1970
CILSAR	*J. Chem. Soc. Chem. Commun.*		1021	1984	TMPBTI	*Acta Cryst. Sect. B*	31	1116	1975
CIMHIP	*Acta Cryst. Sect. C*	40	1458	1984	TPASSN	*J. Chem. Soc. Dalton Trans.*		514	1977
CINTEY	*Dokl. Acak. Nauk SSSR*	274	615	1984	TPASTB	*Cryst. Struct. Commun.*	5	39	1976
CIPBUY	*J. Struct. Chem.*	2	281-4	1983	TPHOSI	*Z. Naturforsch. Teil B*	34	1064	1979
CISMUM	*Z. Naturforsch. Teil B*	39	485	1984	TTEBPZ	*Z. Naturforsch. Teil B*	34	256	1979
CISTED	*Z. Anorg. Allg. Chem.*	511	95	1984	ZCMXSP	*Cryst. Struct. Commun.*	6	93	1977
CIWYIQ	*Inorg. Chem.*	23	1946	1984					
CIYFOF	*Inorg. Chem.*	23	1790	1984					

Pages of the form *n-m* indicate page *n* of issue *m*.

Table 9.5.1.1. *Average lengths (Å) for bonds involving the elements H, B, C, N, O, F, Si, P, S, Cl, As, Se, Br, Te, and I*

Bond	Substructure	*d*	*m*	σ	q_l	q_u	*n*	Note
As(3)—As(3)	X_2—**As**—**As**—X_2	2.459	2.457	0.011	2.456	2.466	8	
As—B	see CUDLOC (2.065), CUDLUI (2.041)							
As—Br	see CODDEE, CODDII (2.346–3.203)							
As(4)—C	X_3—**As**—**C**H_3 $(X)_2$(C, O, S=)**As**—**C**sp^3 **As**—**C**$_{ar}$ in Ph_4As^+ $(X)_2$(C, O, S=)**As**—**C**$_{ar}$	1.903 1.927 1.905 1.922	1.907 1.929 1.909 1.927	0.016 0.017 0.012 0.016	1.893 1.921 1.897 1.908	1.916 1.937 1.912 1.934	12 16 108 36	
As(3)—C	X_2—**As**—**C**sp^3 X_2—**As**—**C**$_{ar}$	1.963 1.956	1.965 1.956	0.017 0.015	1.948 1.944	1.978 1.964	6 41	
As(3)—Cl	X_2—**As**—**Cl**	2.268	2.256	0.039	2.247	2.281	10	
As(6)—F	in **AsF**$_6^-$	1.678	1.676	0.020	1.659	1.695	36	
As(3)—I	see OPIMAS (2.579, 2.590)							
As(3)—N(3)	X_2—**As**—**N**—X_2	1.858	1.858	0.029	1.839	1.873	19	
As(4)=N(2)	see TPASSN (1.837)							
As(4)—O	$(X)_2$(O=)**As**—**O**H	1.710	1.712	0.017	1.695	1.726	6	
As(3)—O	see ASAZOC, PHASOC01 (1.787–1.845)							
As(4)=O	X_3—**As**=**O**	1.661	1.661	0.016	1.652	1.667	9	
As(3)—P(3)	see BELNIP (2.350, 2.362)							†
As(3)=P(3)	see BUTHAZ10 (2.124)							†
As(3)—S	X_2—**As**—**S**	2.275	2.266	0.032	2.247	2.298	14	
As(4)=S	X_3—**As**=**S**	2.083	2.082	0.004	2.080	2.086	9	
As(3)—Se(2)	see COSDIX, ESEARS (2.355–2.401)							†
As(3)—Si(4)	see BICGEZ, MESIAD (2.351–2.365)							†
As(3)—Te(2)	see ETEARS (2.571, 2.576)							†
B(*n*)—B(*n*)	*n* = 5–7 in boron cages	1.775	1.773	0.031	1.763	1.786	688	
B(4)—B(4)	see CETTAW (2.041)							
B(4)—B(3)	see COFVOI (1.698)							
B(3)—B(3)	X_2—**B**—**B**—X_2	1.701	1.700	0.014	1.691	1.712	8	
B(6)—Br		1.967	1.971	0.014	1.954	1.979	7	†
B(4)—Br		2.017	2.008	0.031	1.990	2.044	15	†
B(*n*)—C	*n* = 5–7: **B**—**C** in cages *n* = 3–4: **B**—**C**sp^3 not cages *n* = 4: **B**—**C**$_{ar}$ **B**$^-$—**C**$_{ar}$ in Ph_4B^- *n* = 3: **B**—**C**$_{ar}$	1.716 1.597 1.606 1.643 1.556	1.717 1.599 1.607 1.643 1.552	0.020 0.022 0.012 0.006 0.015	1.707 1.585 1.596 1.641 1.546	1.728 1.611 1.615 1.645 1.566	96 29 41 16 24	*1*
B(*n*)—Cl	**B**(5)—**Cl** and **B**(3)—**Cl** **B**(4)—**Cl**	1.751 1.833	1.751 1.833	0.011 0.013	1.743 1.821	1.761 1.843	14 22	
B(4)—F	**B**—**F** (B neutral) **B**$^-$—**F** in BF_4^-	1.366 1.365	1.368 1.372	0.017 0.029	1.356 1.352	1.375 1.390	25 84	

Table 9.5.1.1. *Average lengths (cont.)*

Bond	Substructure	*d*	*m*	σ	q_l	q_u	*n*	Note
B(4)—I	see TMPBTI (2.220, 2.253)							
B(4)—N(3)	X_3—**B**—**N**(=C)(*X*) in pyrazaboles	1.611 1.549	1.617 1.552	0.013 0.015	1.601 1.536	1.625 1.560	8 10	
B(3)—N(3)	X_2—**B**—**N**—C_2: all coplanar for τ(BN) > 30° see BOGSUL, BUSHAY, CILRUK (1.434–1.530) S_2—**B**—**N**—X_2	1.404 1.447	1.404 1.443	0.014 0.013	1.389 1.435	1.408 1.470	40 14	*2*
B(4)—O	**B**—**O** in BO_4^- for neutral **B**—**O** see Note 3	1.468	1.468	0.022	1.453	1.479	24	*3*
B(3)—O(2)	X_2—**B**—**O**—*X*	1.367	1.367	0.024	1.349	1.382	35	
B(*n*)—P	*n* = 4: **B**—**P** *n* = 3: see BUPSIB10 (1.892, 1.893)	1.922	1.927	0.027	1.900	1.954	10	
B(4)—S	**B**(4)—**S**(3) **B**(4)—**S**(2)	1.930 1.896	1.927 1.896	0.009 0.004	1.925 1.893	1.934 1.899	10 6	
B(3)—S	N—**B**—S_2 (=*X*—)(N—)**B**—**S**	1.806 1.851	1.806 1.854	0.010 0.013	1.799 1.842	1.816 1.859	28 10	
Br—Br	see BEPZEB, TPASTB	2.542	2.548	0.015	2.526	2.551	4	
Br—C	**Br**—**C*** **Br**—C*sp*^{3} (cyclopropane) **Br**—C*sp*^{2} **Br**—C_{ar} (mono-Br + *m*,*p*-Br_2) **Br**—C_{ar} (*o*-Br_2)	1.966 1.910 1.883 1.899 1.875	1.967 1.910 1.881 1.899 1.872	0.029 0.010 0.015 0.012 0.011	1.951 1.900 1.874 1.892 1.864	1.983 1.914 1.894 1.906 1.884	100 8 31 119 8	*4* *4* *4* *4*
$^-$Br(2)—Cl	see TEACBR (2.362–2.402)							†
Br—I	see DTHIBR10 (2.646), TPHOSI (2.695)							
Br—N	see NBBZAM (1.843)							
Br—O	see CIYFOF	1.581	1.581	0.007	1.574	1.587	4	
Br—P	see CISTED (2.366)							
Br—S(2)	see BEMLIO (2.206)							†
Br—S(3)	see CIWYIQ (2.435, 2.453)							†
Br—S(3)$^+$	see THINBR (2.321)							†
Br—Se	see CIFZUM (2.508, 2.619)							
Br—Si	see BIZJAV (2.284)							
Br—Te	In $\mathbf{Br_6Te}^{2-}$ see CUGBAH (2.692–2.716) **Br**—**Te**(4) see BETUTE10 (3.079, 3.015) **Br**—**Te**(3) see BTUPTE (2.835)							
C*sp*^{3}—C*sp*^{3}	C$^\#$—**C**H_2—**C**H_3 ($C^\#$)$_2$—**C**H—**C**H_3 ($C^\#$)$_3$—**C**—**C**H_3 C$^\#$—**C**H_2—**C**H_2—C$^\#$ ($C^\#$)$_2$—**C**H—**C**H_2—C$^\#$ ($C^\#$)$_3$—**C**—**C**H_2—C$^\#$ ($C^\#$)$_2$—**C**H—**C**H—($C^\#$)$_2$ ($C^\#$)$_3$—**C**—**C**H—($C^\#$)$_2$ ($C^\#$)$_3$—**C**—**C**—($C^\#$)$_3$ **C***—**C*** (overall)	1.513 1.524 1.534 1.524 1.531 1.538 1.542 1.556 1.588 1.530	1.514 1.526 1.534 1.524 1.531 1.539 1.542 1.556 1.580 1.530	0.014 0.015 0.011 0.014 0.012 0.010 0.011 0.011 0.025 0.015	1.507 1.518 1.527 1.516 1.524 1.533 1.536 1.549 1.566 1.521	1.523 1.534 1.541 1.532 1.538 1.544 1.549 1.562 1.610 1.539	192 226 825 2459 1217 330 321 215 21 5777	*5, 6*

Table 9.5.1.1. *Average lengths (cont.)*

Bond	Substructure	d	m	σ	q_l	q_u	n	Note
Csp^3—Csp^3 (*cont.*)	in cyclopropane (any substituent)	1.510	1.509	0.026	1.497	1.523	888	*7*
	in cyclobutane (any substituent)	1.554	1.553	0.021	1.540	1.567	679	*8*
	in cyclopentane (C,H substituents)	1.543	1.543	0.018	1.532	1.554	1641	
	in cyclohexane (C,H substituents)	1.535	1.535	0.016	1.525	1.545	2814	
	cyclopropyl—C* (exocyclic)	1.518	1.518	0.019	1.505	1.531	366	*7*
	cyclobutyl—C* (exocyclic)	1.529	1.529	0.016	1.519	1.539	376	*8*
	cyclopentyl—C* (exocyclic)	1.540	1.541	0.017	1.527	1.549	956	
	cyclohexyl—C* (exocyclic)	1.539	1.538	0.016	1.529	1.549	2682	
	in cyclobutene (any substituent)	1.573	1.574	0.017	1.566	1.586	25	*8*
	in cyclopentene (C,H substituents)	1.541	1.539	0.015	1.532	1.549	208	
	in cyclohexene (C,H substituents)	1.541	1.541	0.020	1.528	1.554	586	
	in oxirane (epoxide)	1.466	1.466	0.015	1.458	1.474	249	*9*
	in aziridine	1.480	1.481	0.021	1.465	1.496	67	*9*
	in oxetane	1.541	1.541	0.019	1.527	1.557	16	
	in azetidine	1.548	1.543	0.018	1.536	1.558	22	
	oxiranyl—C* (exocyclic)	1.509	1.507	0.018	1.497	1.519	333	*9*
	aziridinyl—C* (exocyclic)	1.512	1.512	0.018	1.496	1.526	13	*9*
Csp^3—Csp^2	**C**H_3—**C**=C	1.503	1.504	0.011	1.497	1.509	215	
	C$^{\#}$—**C**H_2—**C**=C	1.502	1.502	0.013	1.494	1.510	483	
	(C$^{\#}$)$_2$—**C**H—**C**=C	1.510	1.510	0.014	1.501	1.518	564	
	(C$^{\#}$)$_3$—**C**—**C**=C	1.522	1.522	0.016	1.511	1.533	193	
	C*—**C**=C (overall)	1.507	1.507	0.015	1.499	1.517	1456	*5*
	C*—**C**=C (endocylic):							
	in cyclopropene	1.509	1.508	0.016	1.500	1.516	20	*10*
	in cyclobutene	1.513	1.512	0.018	1.500	1.525	50	*8*
	in cyclopentene	1.512	1.512	0.014	1.502	1.521	208	
	in cyclohexene	1.506	1.505	0.016	1.495	1.516	391	
	in cyclopentadiene	1.502	1.503	0.019	1.490	1.515	18	
	in cyclohexa-1,3-diene	1.504	1.504	0.017	1.491	1.517	56	
	C*—**C**≡C (exocyclic):							
	cyclopropenyl—C*	1.478	1.475	0.012	1.470	1.485	7	*10*
	cyclobutenyl—C*	1.489	1.483	0.015	1.479	1.496	11	*8*
	cyclopentenyl—C*	1.504	1.506	0.012	1.495	1.512	115	
	cyclohexenyl—C*	1.511	1.511	0.013	1.502	1.519	292	
	C*—**C**H=O in aldehydes	1.510	1.510	0.008	1.501	1.518	7	
	(**C***)$_2$—**C**=O in ketones	1.511	1.511	0.015	1.501	1.521	952	*11*
	in cyclobutanone	1.529	1.530	0.016	1.514	1.545	18	
	in cyclopentanone	1.514	1.514	0.016	1.505	1.523	312	
	acyclic and 6+ rings	1.509	1.509	0.016	1.499	1.519	626	
	C*—**C**OOH in carboxylic acids	1.502	1.502	0.014	1.495	1.510	176	
	C*—**C**OO$^-$ in carboxylate anions	1.520	1.521	0.011	1.516	1.528	57	
	C*—**C**(=O)(—OC*) in acyclic esters	1.497	1.496	0.018	1.484	1.509	553	*12*
	in β-lactones	1.519	1.519	0.020	1.500	1.538	4	*13*
	in γ-lactones	1.512	1.512	0.015	1.501	1.521	110	*12*
	in δ-lactones	1.504	1.502	0.013	1.495	1.517	27	*12*
	cyclopropyl (**C**)—**C**=O in ketones, acids, and esters	1.486	1.485	0.018	1.474	1.497	105	*7*
	C*—**C**(=O)(—NH_2) in acyclic amides	1.514	1.512	0.016	1.506	1.526	32	*14*
	C*—**C**(=O)(—NHC*) in acyclic amides	1.506	1.505	0.012	1.498	1.515	78	*14*
	C*—**C**(=O)[—N(C*)$_2$] in acyclic amides	1.505	1.505	0.011	1.496	1.517	15	*14*
Csp^3—C$_{ar}$	**C**H_3—**C**$_{ar}$	1.506	1.507	0.011	1.501	1.513	454	
	C$^{\#}$—**C**H_2—**C**$_{ar}$	1.510	1.510	0.009	1.505	1.516	674	
	(C$^{\#}$)$_2$—**C**—**C**$_{ar}$	1.515	1.515	0.011	1.508	1.522	363	
	(C$^{\#}$)$_3$—**C**—**C**$_{ar}$	1.527	1.530	0.016	1.517	1.539	308	
	C*—**C**$_{ar}$ (overall)	1.513	1.513	0.014	1.505	1.521	1813	
	cylopropyl (**C**)—**C**$_{ar}$	1.490	1.490	0.015	1.479	1.503	90	*7*

Table 9.5.1.1. *Average lengths (cont.)*

Bond	Substructure	d	m	σ	q_l	q_u	n	Note
Csp^3—Csp^1	**C***—**C**≡C	1.466	1.465	0.010	1.460	1.469	21	*15*
	C$^{\#}$—**C**≡C	1.472	1.472	0.012	1.464	1.481	88	*15*
	C*—**C**≡N	1.470	1.469	0.013	1.463	1.479	106	*7(b)*
	cyclopropyl (**C**)—**C**≡N	1.444	1.447	0.010	1.436	1.451	38	*7*
Csp^2—Csp^2	C=**C**—**C**=C (conjugated)	1.455	1.455	0.011	1.447	1.463	30	*16, 18*
	(unconjugated)	1.478	1.476	0.012	1.470	1.479	8	*17, 18*
	(overall)	1.460	1.460	0.015	1.450	1.470	38	
	C=**C**—**C**=**C**—**C**=C	1.443	1.445	0.013	1.431	1.454	29	*18*
	C=**C**—**C**=C (endocyclic in TCNQ)	1.432	1.433	0.012	1.424	1.441	280	*19*
	C=**C**—**C**(=O)(—C*) (conjugated)	1.464	1.462	0.018	1.453	1.476	211	*16, 18*
	(unconjugated)	1.484	1.486	0.017	1.475	1.497	14	*17, 18*
	(overall)	1.465	1.462	0.018	1.453	1.478	226	
	C=**C**—**C**(=O)—**C**=C:							
	in benzoquinone (C,H substituents only)	1.478	1.476	0.011	1.469	1.488	28	
	in benzoquinone (any substituent)	1.478	1.478	0.031	1.464	1.498	172	
	non-quinonoid	1.456	1.455	0.012	1.447	1.464	28	
	C—**C**—COOH	1.475	1.476	0.015	1.461	1.488	22	
	C=**C**—COOC*	1.488	1.489	0.014	1.478	1.497	113	
	C=**C**—COO$^-$	1.502	1.499	0.017	1.488	1.510	11	
	HOO**C**—COOH	1.538	1.537	0.007	1.535	1.541	9	
	HOO**C**—COO$^-$	1.549	1.552	0.009	1.546	1.553	13	
	$^-$OO**C**—COO$^-$	1.564	1.559	0.022	1.554	1.568	9	
	formal Csp^2—Csp^2 single bond in selected, non-fused heterocycles:							
	in 1*H*-pyrrole (C3—C4)	1.412	1.410	0.016	1.401	1.427	29	
	in furan (C3—C4)	1.423	1.423	0.016	1.412	1.433	62	
	in thiophene (C3—C4)	1.424	1.425	0.015	1.415	1.433	40	
	in pyrazole (C3—C4)	1.410	1.412	0.016	1.400	1.418	20	
	in isoxazole (C3—C4)	1.425	1.425	0.016	1.413	1.438	9	
	in furazan (C3—C4)	1.428	1.427	0.007	1.422	1.435	6	
	in furoxan (C3—C4)	1.417	1.417	0.006	1.412	1.422	14	
Csp^2—C$_{ar}$	C=**C**—**C**$_{ar}$ (conjugated)	1.470	1.470	0.015	1.463	1.480	37	*16, 18*
	(unconjugated)	1.488	1.490	0.012	1.480	1.496	87	*17, 18*
	(overall)	1.483	1.483	0.015	1.472	1.494	124	
	cyclopropenyl (C=**C**)—**C**$_{ar}$	1.447	1.448	0.006	1.441	1.452	8	*10*
	C$_{ar}$—**C**(=O)—C*	1.488	1.489	0.016	1.478	1.500	84	
	C$_{ar}$—**C**(=O)—**C**$_{ar}$	1.480	1.481	0.017	1.468	1.494	58	
	C$_{ar}$—COOH	1.484	1.485	0.014	1.474	1.491	75	
	C$_{ar}$—**C**(=O)(—OC*)	1.487	1.487	0.012	1.480	1.494	218	
	C$_{ar}$—COO$^-$	1.504	1.509	0.014	1.495	1.512	26	
	C$_{ar}$—**C**(=O)—NH$_2$	1.500	1.503	0.020	1.498	1.510	19	
	C$_{ar}$—**C**=N—C$^{\#}$ (conjugated)	1.476	1.478	0.014	1.466	1.486	27	*16*
	(unconjugated)	1.491	1.490	0.008	1.485	1.496	48	*17*
	(overall)	1.485	1.487	0.013	1.481	1.493	75	
	in indole (C3—C3a)	1.434	1.434	0.011	1.428	1.439	40	
Csp^2—Csp^1	C=**C**—**C**≡C	1.431	1.427	0.014	1.425	1.441	11	*7(b)*
	C=**C**—**C**≡N in TCNQ	1.427	1.427	0.010	1.420	1.433	280	*19*
C$_{ar}$—C$_{ar}$	in biphenyls (*ortho* substituent all H)	1.487	1.488	0.007	1.484	1.493	30	
	(≥ 1 non-H *ortho* substituent)	1.490	1.491	0.010	1.486	1.495	212	
C$_{ar}$—Csp^1	**C**$_{ar}$—**C**≡C	1.434	1.436	0.006	1.430	1.437	37	
	C$_{ar}$—**C**≡N	1.443	1.444	0.008	1.436	1.448	31	
Csp^1—Csp^1	C≡**C**—**C**≡C	1.377	1.378	0.012	1.374	1.384	21	
Csp^2=Csp^2	C*—**C**H=**C**H$_2$	1.299	1.300	0.027	1.280	1.311	42	
	(C*)$_2$—**C**=**C**H$_2$	1.321	1.321	0.013	1.313	1.328	77	
	C*—**C**H=**C**H—C* (*cis*)	1.317	1.318	0.013	1.310	1.232	106	
	(*trans*)	1.312	1.311	0.011	1.304	1.320	19	
	(overall)	1.316	1.317	0.015	1.309	1.323	127	

Table 9.5.1.1. *Average lengths (cont.)*

Bond	Substructure	*d*	*m*	σ	q_l	q_u	*n*	Note
Csp^2=Csp^2 (*cont.*)	(C*)$_2$—**C**=**C**H—C*	1.326	1.328	0.011	1.319	1.334	168	
	(C*)$_2$—**C**=**C**—(C*)$_2$	1.331	1.330	0.009	1.326	1.334	89	
	(C*,H)$_2$—**C**=**C**—(C*,H)$_2$ (overall)	1.322	1.323	0.014	1.315	1.331	493	*5*
	in cyclopropene (any substituent)	1.294	1.288	0.017	1.284	1.302	10	*10*
	in cyclobutene (any substituent)	1.335	1.335	0.019	1.324	1.347	25	*8*
	in cyclopentene (C,H substituents)	1.323	1.324	0.013	1.314	1.331	104	
	in cyclohexene (C,H substituents)	1.326	1.325	0.012	1.318	1.334	196	
	C=**C**=**C** (allenes, any substituents)	1.307	1.307	0.005	1.303	1.310	18	
	C=**C**—**C**=**C** (C,H substituents, conjugated)	1.330	1.330	0.014	1.322	1.338	76	*16*
	C=**C**—**C**=**C**—**C**=**C** (C,H substituents, conjugated)	1.345	1.345	0.012	1.337	1.350	58	*16*
	C=**C**—C$_{ar}$ (C,H substituents, conjugated)	1.339	1.340	0.011	1.334	1.346	124	*16*
	C=**C** in cyclopenta-1,3-diene (any substituent)	1.341	1.341	0.017	1.328	1.356	18	
	C=**C** in cyclohexa-1,3-diene (any substituent)	1.332	1.332	0.013	1.323	1.341	56	
	in **C**=**C**—C=O (C,H substituent, conjugated)	1.340	1.340	0.013	1.332	1.348	211	*16, 18*
	(C,H substituent, unconjugated)	1.331	1.330	0.008	1.326	1.339	14	*17, 18*
	(C,H substituent, overall)	1.340	1.339	0.013	1.332	1.348	226	
	in cyclohexa-2,5-dien-1-ones	1.329	1.327	0.011	1.321	1.335	28	
	in *p*-benzoquinones (C*,H substituents)	1.333	1.337	0.011	1.325	1.338	14	
	(any substituent)	1.349	1.339	0.030	1.330	1.364	86	
	in TCNQ (endocyclic)	1.352	1.353	0.010	1.345	1.358	142	*19*
	(exocyclic)	1.392	1.391	0.017	1.379	1.405	139	*19*
	C=**C**—OH in enol tautomers	1.362	1.360	0.020	1.349	1.370	54	
	in heterocycles (any substituent)							
	1*H*-pyrrole (C2—C3, C4—C5)	1.375	1.377	0.018	1.361	1.388	58	
	furan (C2—C3, C4—C5)	1.341	1.342	0.021	1.329	1.351	125	
	thiophene (C2—C3, C4—C5)	1.362	1.359	0.025	1.346	1.377	60	
	pyrazole (C4—C5)	1.369	1.372	0.019	1.362	1.383	20	
	imidazole (C4—C5)	1.360	1.361	0.014	1.352	1.367	44	
	isoxazole (C4—C5)	1.341	1.336	0.012	1.331	1.355	9	
	indole (C2—C3)	1.364	1.363	0.012	1.355	1.371	40	
C$_{ar}$ ⋯ C$_{ar}$	in phenyl rings with C*,H substituents only:							
	H—**C**⋯**C**—H	1.380	1.381	0.013	1.372	1.388	2191	
	C*—**C**⋯**C**—H	1.387	1.388	0.010	1.382	1.393	891	
	C*—**C**⋯**C**—C*	1.397	1.397	0.009	1.392	1.403	182	
	C⋯**C** (overall)	1.384	1.384	0.013	1.375	1.391	3264	
	F—**C** ⋯ **C**—F	1.372	1.374	0.011	1.366	1.380	84	*4*
	Cl—**C** ⋯ **C**—Cl	1.388	1.389	0.014	1.380	1.398	152	*4*
	in napthalene (D_{2h}) C1—C2	1.364	1.364	0.014	1.356	1.373	440	
	(any substituent) C2—C3	1.406	1.406	0.014	1.397	1.415	218	
	C1—C8a	1.420	1.419	0.012	1.412	1.426	440	
	C4a—C8a	1.422	1.424	0.011	1.417	1.429	109	
	in anthracene (D_{2h}) C1—C2	1.356	1.356	0.009	1.350	1.360	56	
	(any substituent) C2—C3	1.410	1.410	0.010	1.401	1.416	34	
	C1—C9a	1.430	1.430	0.006	1.426	1.434	56	
	C4a—C9a	1.435	1.436	0.007	1.429	1.440	34	
	C9—C9a	1.400	1.402	0.009	1.395	1.406	68	
	in pyridine (C,H substituent)	1.379	1.381	0.012	1.371	1.387	276	*20*
	(any substituents)	1.380	1.380	0.015	1.371	1.389	537	*20*
	in pyridinium cation:							
	(N^+—H; C,H substituents on C) C2—C3	1.373	1.375	0.012	1.368	1.380	30	
	C3—C4	1.379	1.380	0.011	1.371	1.388	30	
	(N^+—*X*; C,H substituents on C) C2—C3	1.373	1.372	0.019	1.362	1.382	151	
	C3—C4	1.383	1.385	0.019	1.372	1.394	151	
	in pyrazine (H substituent on C)	1.379	1.377	0.010	1.370	1.388	10	
	(any substituent on C)	1.405	1.405	0.024	1.388	1.420	60	
	in pyrimidine (C,H substituents on C)	1.387	1.389	0.018	1.379	1.400	28	

Table 9.5.1.1. *Average lengths (cont.)*

Bond	Substructure	*d*	*m*	σ	q_l	q_u	*n*	Note
Csp^1≡Csp^1	*X*—**C**≡**C**—*X*	1.183	1.183	0.014	1.174	1.193	119	*15*
	C,H—**C**≡**C**—C,H	1.181	1.181	0.014	1.173	1.192	104	*15*
	in **C**≡**C**—C(sp^2, ar)	1.189	1.193	0.010	1.181	1.195	38	*15*
	in **C**≡**C**—**C**≡**C**	1.192	1.192	0.010	1.187	1.197	42	*15*
	in **C**H≡**C**—C#	1.174	1.174	0.011	1.167	1.180	42	*15*
Csp^3—Cl	Omitting 1,2-dichlorides:							
	C—**C**H_2—**Cl**	1.790	1.790	0.007	1.783	1.795	13	*4*
	C_2—**C**H—**Cl**	1.803	1.802	0.003	1.800	1.807	8	*4*
	C_3—**C**—**Cl**	1.849	1.856	0.011	1.837	1.858	5	*4*
	X—**C**H_2—**Cl** (*X* = C,H,N,O)	1.790	1.791	0.011	1.783	1.797	37	*4*
	X_2—**C**H—**Cl** (*X* = C,H,N,O)	1.805	1.803	0.014	1.800	1.812	26	*4*
	X_3—**C**—**Cl** (*X* = C,H,N,O)	1.843	1.838	0.014	1.835	1.858	7	*4*
	X_2—**C**—**Cl**$_2$ (*X* = C,H,N,O)	1.779	1.776	0.015	1.769	1.790	18	*4*
	X—**C**—**Cl**$_3$ (*X* = C,H,N,O)	1.768	1.765	0.011	1.761	1.776	33	*4*
	Cl—CH(—C)—**C**H(—C)—**Cl**	1.793	1.793	0.013	1.786	1.800	66	*4*
	Cl—**C**(—C_2)—**C**(—C_2)—**Cl**	1.762	1.760	0.010	1.757	1.765	54	*4*
	cyclopropyl—Cl	1.755	1.756	0.011	1.749	1.763	64	
Csp^2—Cl	C=**C**—**Cl** (C,H,N,O substituents on C)	1.734	1.729	0.019	1.719	1.748	63	*4*
	C=**C**—**Cl**$_2$ (C,H,N,O substituents on C)	1.720	1.716	0.013	1.708	1.729	20	*4*
	Cl—**C**=**C**—**Cl**	1.713	1.711	0.011	1.705	1.720	80	*4*
C_{ar}—Cl	**C**$_{ar}$—**Cl** (mono-Cl + *m,p*-Cl_2)	1.739	1.741	0.010	1.734	1.745	340	*4*
	C$_{ar}$—**Cl** (*o*-Cl_2)	1.720	1.720	0.010	1.713	1.717	364	*4*
Csp^1—Cl	see HCLENE10 (1.634, 1.646)							
Csp^3—F	Omitting 1,2-difluorides:							
	C—**C**H_2—**F** and C_2—**C**H—**F**	1.399	1.399	0.017	1.389	1.408	25	*4*
	C_3—**C**—**F**	1.428	1.431	0.009	1.421	1.435	11	*4*
	(C*,H)$_2$—**C**—**F**$_2$	1.349	1.347	0.012	1.342	1.356	58	*4*
	C*—**C**—**F**$_3$	1.336	1.334	0.007	1.330	1.344	12	*4*
	F—**C***—**C***—**F**	1.371	1.374	0.007	1.362	1.375	26	*4*
	X_3—**C**—**F** (*X* = C,H,N,O)	1.386	1.389	0.033	1.373	1.408	70	*4*
	X_2—**C**—**F**$_2$ (*X* = C,H,N,O)	1.351	1.349	0.013	1.342	1.356	58	*4*
	X—**C**—**F**$_3$ (*X* = C,H,N,O)	1.322	1.323	0.015	1.314	1.332	309	*4*
	F—**C**(—*X*)$_2$—**C**(—*X*)$_2$—**F** (*X* = C,H,N,O)	1.373	1.374	0.009	1.362	1.377	30	*4*
	F—**C**(—*X*)$_2$—NO_2 (*X* = any substituent)	1.320	1.319	0.009	1.312	1.327	18	
Csp^2—F	C=**C**—**F** (C,H,N,O substituents on C)	1.340	1.340	0.013	1.334	1.346	34	*4*
C_{ar}—F	**C**$_{ar}$—**F** (mono-F + *m,p*-F_2)	1.363	1.362	0.008	1.357	1.368	38	*4*
	C$_{ar}$—**F** (*o*-F_2)	1.340	1.340	0.009	1.336	1.344	167	*4*
Csp^3—H	C—**C**—**H**$_3$ (methyl)	1.059	1.061	0.030	1.039	1.083	83	*21*
	C_2—**C**—**H**$_2$ (primary)	1.092	1.095	0.013	1.088	1.099	100	*21*
	C_3—**C**—**H** (secondary)	1.099	1.097	0.004	1.095	1.103	14	*21*
	$C_{2,3}$—**C**—**H** (primary and secondary)	1.093	1.095	0.012	1.089	1.100	118	*21*
	X—**C**—**H**$_3$ (methyl)	1.066	1.074	0.028	1.049	1.087	160	*21*
	X_2—**C**—**H**$_2$ (primary)	1.092	1.095	0.012	1.088	1.099	230	*21*
	X_3—**C**—**H** (secondary)	1.099	1.099	0.007	1.095	1.103	117	*21*
	$X_{2,3}$—**C**—**H** (primary and secondary)	1.094	1.096	0.011	1.091	1.100	348	*21*
Csp^2—H	C—C=**C**—**H**	1.077	1.079	0.012	1.074	1.085	14	*21*
C_{ar}—H	**C**$_{ar}$—**H**	1.083	1.083	0.011	1.080	1.087	218	*21*
Csp^3—I	**C***—**I**	2.162	2.159	0.015	2.149	2.179	15	*4*
C_{ar}—I	**C**$_{ar}$—**I**	2.095	2.095	0.015	2.089	2.104	51	*4*
Csp^3—N(4)	**C***—**N**H_3^+	1.488	1.488	0.013	1.482	1.495	298	
	(C*)$_2$—**N**H_2^+	1.494	1.493	0.016	1.484	1.503	249	
	(C*)$_3$—**N**H^+	1.502	1.502	0.015	1.491	1.512	509	
	(C*)$_4$—**N**$^+$	1.510	1.509	0.020	1.496	1.523	319	
	C*—**N**$^+$ (overall)	1.499	1.498	0.018	1.488	1.510	1370	

Table 9.5.1.1. *Average lengths (cont.)*

Bond	Substructure	*d*	*m*	σ	q_l	q_u	*n*	Note
Csp^3—N(3)	**C***—**N**$^+$ in N-substituted pyridinium	1.485	1.484	0.009	1.477	1.490	32	
	C*—**N**H$_2$ (Nsp^3: pyramidal)	1.469	1.470	0.010	1.462	1.474	19	*22*
	(**C***)$_2$—**N**H (Nsp^3: pyramidal)	1.469	1.467	0.012	1.461	1.477	152	*5, 22*
	(**C***)$_3$—**N** (Nsp^3: pyramidal)	1.469	1.468	0.014	1.460	1.476	1042	*5, 22*
	C*—**N**sp^3 (overall)	1.469	1.468	0.014	1.460	1.476	1201	
	Csp^3—**N**sp^3 in aziridine	1.472	1.471	0.016	1.464	1.482	134	
	in azetidine	1.484	1.481	0.018	1.472	1.495	21	
	in tetrahydropyrrole	1.475	1.473	0.016	1.464	1.483	66	
	in piperidine	1.473	1.473	0.013	1.460	1.479	240	
	Csp^3—Nsp^2 (N planar) in:							*23*
	acyclic amides **C***—**N**H—C=O	1.454	1.451	0.011	1.446	1.461	78	*14*
	β-lactams **C***—**N**(—*X*)—C=O (*endo*)	1.464	1.465	0.012	1.458	1.475	23	*13*
	γ-lactams **C***—**N**H—C=O (*endo*)	1.457	1.458	0.011	1.449	1.465	20	*13*
	C*—**N**(—C*)—C=O (*endo*)	1.462	1.461	0.010	1.453	1.466	15	*13*
	C*—**N**(—**C***)—C=O (*exo*)	1.458	1.456	0.014	1.448	1.465	15	*13*
	δ-lactams **C***—**N**H—C=O (*endo*)	1.478	1.472	0.016	1.467	1.491	6	*14*
	C*—**N**(—C*)—C=O (*endo*)	1.479	1.476	0.007	1.475	1.482	15	*14*
	C*—**N**(—**C***)—C=O (*exo*)	1.468	1.471	0.009	1.462	1.477	15	*14*
	nitro compounds (1,2-dinitro omitted):							
	C—**C**H$_2$—**N**O$_2$	1.485	1.483	0.020	1.478	1.502	8	
	C$_2$—**C**H—**N**O$_2$	1.509	1.509	0.011	1.502	1.511	12	
	C$_3$—**C**—**N**O$_2$	1.533	1.533	0.013	1.530	1.539	17	
	C$_2$—**C**—(**N**O$_2$)$_2$	1.537	1.536	0.016	1.525	1.550	19	
	1,2-dinitro: **N**O$_2$—**C***—**C***—**N**O$_2$	1.552	1.550	0.023	1.536	1.572	32	
Csp^3—N(2)	**C**$^{\#}$—**N**=N	1.493	1.493	0.020	1.477	1.506	54	
	C*—**N**=C—C$_{ar}$	1.465	1.468	0.011	1.461	1.472	75	
Csp^2—N(3)	C=**C**—**N**H$_2$ Nsp^2 planar	1.336	1.344	0.017	1.317	1.348	10	*23*
	C=**C**—**N**H—C$^{\#}$ Nsp^2 planar	1.339	1.340	0.016	1.327	1.351	17	*23*
	C=**C**—**N**—(C$^{\#}$)$_2$ Nsp^2 planar	1.355	1.358	0.014	1.341	1.363	22	*23*
	Nsp^3 pyramidal	1.416	1.418	0.018	1.397	1.432	18	*22*
	Csp^2—Nsp^2 (N planar) in:							*23*
	acyclic amides **N**H$_2$—**C**=O	1.325	1.323	0.009	1.318	1.331	32	*14*
	acyclic amides C*—**N**H—**C**=O	1.334	1.333	0.011	1.326	1.343	78	*14*
	acyclic amides (C*)$_2$—**N**—**C**=O	1.346	1.342	0.011	1.339	1.356	5	*14*
	β-lactams C*—**N**H—**C**=O	1.385	1.388	0.019	1.374	1.396	23	*13*
	γ-lactams C*—**N**H—**C**=O	1.331	1.331	0.011	1.326	1.337	20	*13*
	γ-lactams C*—**N**(—C*)—**C**=O	1.347	1.344	0.014	1.335	1.359	15	*13*
	δ-lactams C*—**N**H—**C**=O	1.334	1.334	0.006	1.330	1.339	6	*14*
	δ-lactams C*—**N**(—C*)—**C**=O	1.352	1.353	0.010	1.344	1.356	15	*14*
	peptides C$^{\#}$—**N**(—*X*)—**C**(—C$^{\#}$)(=O)	1.333	1.334	0.013	1.326	1.340	380	*24*
	ureas (**N**H$_2$)$_2$—**C**=O	1.334	1.334	0.008	1.329	1.339	48	*25,26*
	ureas (C$^{\#}$—**N**H)$_2$—**C**=O	1.347	1.345	0.010	1.341	1.354	26	*25*
	ureas [(C$^{\#}$)$_n$—**N**]$_2$—**C**=O	1.363	1.359	0.014	1.354	1.370	40	*25, 27*
	thioureas (*X*$_2$**N**)$_2$—**C**=S	1.346	1.343	0.023	1.328	1.361	192	
	imides [C$^{\#}$—**C**(=O)]$_2$—**N**H	1.376	1.377	0.012	1.369	1.383	64	
	[C$^{\#}$—**C**(=O)]$_2$—**N**—C$^{\#}$	1.389	1.383	0.017	1.376	1.404	38	
	[Csp^2—**C**(=O)]$_2$—**N**—C$^{\#}$	1.396	1.396	0.010	1.389	1.403	46	
	[Csp^2—**C**(=O)]$_2$—**N**—Csp^2	1.409	1.406	0.020	1.391	1.419	28	
	guanidinium [**C**—(**N**H$_2$)$_3$]$^+$ (unsubstituted)	1.321	1.320	0.008	1.314	1.327	39	
	(any substituent)	1.328	1.325	0.015	1.317	1.333	140	
	in heterocyclic systems (any substituent):							
	1*H*-pyrrole (N1—C2, N1—C5)	1.372	1.374	0.016	1.363	1.384	58	
	indole (N1—C2)	1.370	1.370	0.012	1.364	1.377	40	
	pyrazole (N1—C5)	1.357	1.359	0.012	1.347	1.365	20	
	imidazole (N1—C2)	1.349	1.349	0.018	1.338	1.358	44	
	imidazole (N1—C5)	1.370	1.370	0.010	1.365	1.377	44	
Csp^2—N(2)	in imidazole (N3—C4)	1.376	1.377	0.011	1.369	1.384	44	
C$_{ar}$—N(4)	**C**$_{ar}$—**N**$^+$(C,H)$_3$	1.465	1.466	0.007	1.461	1.470	23	

Table 9.5.1.1. *Average lengths (cont.)*

Bond	Substructure	d	m	σ	q_l	q_u	n	Note
C_{ar}—N(3)	$\mathbf{C}_{ar}$—$\mathbf{NH}_2$ (Nsp^2: planar)	1.355	1.360	0.020	1.340	1.372	33	*23*
	(Nsp^3: pyramidal)	1.394	1.396	0.011	1.385	1.403	25	*22*
	(overall)	1.375	1.377	0.025	1.363	1.394	98	*28*
	$\mathbf{C}_{ar}$—$\mathbf{NH}$—$\mathbf{C}^{\#}$ (Nsp^2: planar)	1.353	1.353	0.007	1.347	1.359	16	*23*
	(Nsp^3: pyramidal)	1.419	1.423	0.017	1.412	1.432	8	*22*
	(overall)	1.380	1.364	0.032	1.353	1.412	31	*28*
	$\mathbf{C}_{ar}$—$\mathbf{N}$—$(\mathbf{C}^{\#})_2$ (Nsp^2: planar)	1.371	1.370	0.016	1.363	1.382	41	*23*
	(Nsp^3: pyramidal)	1.426	1.425	0.011	1.421	1.431	22	*22*
	(overall)	1.390	1.385	0.030	1.366	1.420	69	*28*
	in indole (N1—C7a)	1.372	1.372	0.007	1.367	1.376	40	
	$\mathbf{C}_{ar}$—$\mathbf{NO}_2$	1.468	1.469	0.014	1.460	1.476	556	
C_{ar}—N(2)	$\mathbf{C}_{ar}$—$\mathbf{N}$=N	1.431	1.435	0.020	1.422	1.442	26	
Csp^2=N(3)	in furoxan ($^+$N2=C3)	1.316	1.316	0.009	1.311	1.324	14	
Csp^2=N(2)	C_{ar}—$\mathbf{C}$=$\mathbf{N}$—$C^{\#}$	1.279	1.279	0.008	1.275	1.285	75	
	$(C,H)_2$—$\mathbf{C}$=$\mathbf{N}$—OH in oximes	1.281	1.280	0.013	1.273	1.288	67	
	S—$\mathbf{C}$=$\mathbf{N}$—X	1.302	1.302	0.021	1.285	1.319	36	
	in pyrazole (N2=C3)	1.329	1.331	0.014	1.315	1.339	20	
	in imidazole (C2=N3)	1.313	1.314	0.011	1.307	1.319	44	
	in isoxazole (N2=C3)	1.314	1.315	0.009	1.305	1.320	9	
	in furazan (N2=C3, C4=N5)	1.298	1.299	0.006	1.294	1.303	12	
	in furoxan (C4=N5)	1.304	1.306	0.008	1.300	1.308	14	
C_{ar} ⋯ N(3)	$\mathbf{C}$⋯$\mathbf{N}^+$—H (pyrimidinium)	1.335	1.334	0.015	1.325	1.342	30	
	$\mathbf{C}$⋯$\mathbf{N}^+$—C* (pyrimidinium)	1.346	1.346	0.010	1.340	1.352	64	
	$\mathbf{C}$⋯$\mathbf{N}^+$—O^- (pyrimidinium)	1.362	1.359	0.013	1.353	1.369	56	
C_{ar} ⋯ N(2)	$\mathbf{C}$⋯$\mathbf{N}$ (pyridine)	1.337	1.338	0.012	1.300	1.344	269	
	$\mathbf{C}$⋯$\mathbf{N}$ (pyrazine)	1.336	1.335	0.022	1.319	1.347	120	
	$\mathbf{C}$⋯$\mathbf{N}$⋯$\mathbf{C}$ (pyrimidine)	1.339	1.338	0.015	1.333	1.342	28	
	$\mathbf{N}$⋯$\mathbf{C}$⋯$\mathbf{N}$ (pyrimidine)	1.333	1.335	0.013	1.326	1.337	28	
	$\mathbf{C}$⋯$\mathbf{N}$ (pyrimidine) (overall)	1.336	1.337	0.014	1.331	1.339	56	
	in any six-membered N-containing aromatic ring:							
	H—$\mathbf{C}$⋯$\mathbf{N}$⋯$\mathbf{C}$—H	1.334	1.334	0.014	1.327	1.341	146	
	H—$\mathbf{C}$⋯$\mathbf{N}$⋯$\mathbf{C}$—C*	1.339	1.341	0.013	1.336	1.345	38	
	C*—$\mathbf{C}$⋯$\mathbf{N}$⋯$\mathbf{C}$—C*	1.345	1.345	0.008	1.342	1.348	24	
	$\mathbf{C}$⋯$\mathbf{N}$⋯$\mathbf{C}$ (overall)	1.336	1.337	0.014	1.329	1.344	204	
Csp^1≡N(2)	*X*—$\mathbf{N}^+$≡$\mathbf{C}^-$ (isocyanide)	1.144	1.147	0.006	1.140	1.148	6	
Csp^1≡N(1)	C*—$\mathbf{C}$≡$\mathbf{N}$	1.136	1.137	0.010	1.131	1.142	140	
	C=C—$\mathbf{C}$≡$\mathbf{N}$ in TCNQ	1.144	1.144	0.008	1.139	1.149	284	*19*
	C_{ar}—$\mathbf{C}$≡$\mathbf{N}$	1.138	1.138	0.007	1.133	1.143	31	
	X—S—$\mathbf{C}$≡$\mathbf{N}$	1.144	1.141	0.012	1.138	1.151	10	
	$(S—\mathbf{C}≡\mathbf{N})^-$	1.155	1.156	0.012	1.147	1.165	14	
Csp^3—O(2)	in alcohols:							
	$\mathbf{C}H_3$—$\mathbf{O}$H	1.413	1.414	0.018	1.395	1.425	17	
	C—$\mathbf{C}H_2$—$\mathbf{O}$H	1.426	1.426	0.011	1.420	1.431	75	
	C_2—$\mathbf{C}$H—$\mathbf{O}$H	1.432	1.431	0.011	1.425	1.439	266	
	C_3—$\mathbf{C}$—$\mathbf{O}$H	1.440	1.440	0.012	1.432	1.449	106	
	$\mathbf{C}$*—$\mathbf{O}$H (overall)	1.432	1.431	0.013	1.424	1.441	464	
	in dialkyl ethers:							*29*
	$\mathbf{C}H_3$—$\mathbf{O}$—C*	1.416	1.418	0.016	1.405	1.426	110	
	C—$\mathbf{C}H_2$—$\mathbf{O}$—C*	1.426	1.424	0.011	1.418	1.435	34	
	C_2—$\mathbf{C}$H—$\mathbf{O}$—C*	1.429	1.430	0.010	1.420	1.437	53	
	C_3—$\mathbf{C}$—$\mathbf{O}$—C*	1.452	1.450	0.011	1.445	1.458	39	
	$\mathbf{C}$*—$\mathbf{O}$—$\mathbf{C}$* (overall)	1.426	1.425	0.019	1.414	1.437	236	*5*
	in aryl alkyl ethers:							*29*
	$\mathbf{C}H_3$—$\mathbf{O}$—C_{ar}	1.424	1.424	0.012	1.417	1.431	616	
	C—$\mathbf{C}H_2$—$\mathbf{O}$—C_{ar}	1.431	1.430	0.013	1.422	1.438	188	

Table 9.5.1.1. *Average lengths (cont.)*

Bond	Substructure	*d*	*m*	σ	q_l	q_u	*n*	Note
Csp^2—O(2) (*cont.*)	in aryl alkyl ethers (*cont.*)							
	C_2—**C**H—**O**—C_{ar}	1.447	1.446	0.020	1.435	1.466	58	
	C_3—**C**—**O**—C_{ar}	1.470	1.469	0.018	1.456	1.483	55	
	C*—**O**—C_{ar} (overall)	1.429	1.427	0.018	1.419	1.436	917	
	in alkyl esters of carboxylic acids:							*12, 29*
	CH_3—**O**—C(=O)—C*	1.448	1.449	0.010	1.442	1.455	200	
	C—CH_2—**O**—C(=O)—C*	1.452	1.453	0.009	1.445	1.458	32	
	C_2—**C**H—**O**—C(=O)—C*	1.460	1.460	0.010	1.454	1.465	78	
	C_3—**C**—**O**—C(=O)—C*	1.477	1.475	0.008	1.472	1.484	6	
	C*—**O**—C(=O)—C* (overall)	1.450	1.451	0.014	1.442	1.459	314	
	in alkyl esters of α, β-unsaturated acids:							
	C*—**O**—C(=O)—C=C (overall)	1.453	1.452	0.013	1.444	1.459	112	
	in alkyl esters of benzoic acid							
	C*—**O**—C(=O)—C(phenyl) (overall)	1.454	1.454	0.012	1.446	1.463	219	
	in ring systems:							
	oxirane (epoxide) (any substituent)	1.446	1.446	0.014	1.438	1.456	498	*9*
	oxetane (any substituent)	1.463	1.460	0.015	1.451	1.474	16	
	tetrahydrofuran (C,H substituents)	1.442	1.441	0.017	1.430	1.451	154	
	tetrahydropyran (C,H substituents)	1.441	1.442	0.015	1.431	1.451	22	
	β-lactones: **C***—**O**—C(=O)	1.492	1.494	0.010	1.481	1.501	4	*16*
	γ-lactones: **C***—**O**—C(=O)	1.464	1.464	0.012	1.455	1.473	110	*12*
	δ-lactones: **C***—**O**—C(=O)	1.461	1.464	0.017	1.452	1.473	27	*12*
	O—C—O systems in *gem*-diols, and pyranose and furanose sugars:							*30, 31*
	HO—**C***—**O**H	1.397	1.401	0.012	1.388	1.405	18	
	C_5—O_5—C_1—O_1H in pyranoses:							
	O_1 axial (α): C_5—O_5	1.439	1.440	0.008	1.432	1.445	29	
	O_5—C_1	1.427	1.426	0.012	1.421	1.432	29	
	C_1—O_1	1.403	1.400	0.012	1.391	1.412	29	
	O_1 equatorial (β): C_5—O_5	1.435	1.436	0.008	1.429	1.440	17	
	O_5—C_1	1.430	1.431	0.010	1.424	1.436	17	
	C_1—O_1	1.393	1.393	0.007	1.386	1.399	17	
	$\alpha + \beta$ (overall): C_5—O_5	1.439	1.440	0.008	1.432	1.446	60	
	O_5—C_1	1.430	1.429	0.012	1.421	1.436	60	
	C_1—O_1	1.401	1.399	0.011	1.392	1.407	60	
	C_4—O_4—C_1—O_1H in furanoses:							
	(overall values) C_4—O_4	1.442	1.446	0.012	1.436	1.449	18	
	(overall values) O_4—C_1	1.432	1.432	0.012	1.421	1.443	18	
	(overall values) C_1—O_1	1.404	1.405	0.013	1.397	1.409	18	
	C_5—O_5—C_1—O_1—**C*** in pyranoses:							
	O_1 axial (α): C_5—O_5	1.439	1.438	0.010	1.433	1.446	67	
	O_5—C_1	1.417	1.417	0.009	1.410	1.424	67	
	C_1—O_1	1.409	1.409	0.014	1.401	1.417	67	
	O_1—C*	1.435	1.435	0.013	1.427	1.443	67	
	O_1 equatorial (β): C_5—O_5	1.434	1.435	0.006	1.429	1.439	39	
	O_5—C_1	1.424	1.424	0.008	1.418	1.431	39	
	C_1—O_1	1.390	1.390	0.011	1.381	1.400	39	
	O_1—C*	1.437	1.438	0.013	1.428	1.445	39	
	$\alpha + \beta$ (overall): C_5—O_5	1.436	1.436	0.009	1.431	1.442	126	
	O_5—C_1	1.419	1.419	0.011	1.412	1.426	126	
	C_1—O_1	1.402	1.403	0.016	1.391	1.413	126	
	O_1—C*	1.436	1.436	0.013	1.428	1.445	126	
	C_4—O_4—C_1—O_1—**C*** in furanoses:							
	(overall values) C_4—O_4	1.443	1.445	0.013	1.429	1.453	23	
	(overall values) O_4—C_1	1.421	1.418	0.012	1.413	1.431	23	
	(overall values) C_1—O_1	1.410	1.409	0.014	1.401	1.420	23	
	(overall values) O_1—C*	1.439	1.437	0.014	1.429	1.449	23	
	Miscellaneous:							
	C$^{\#}$—**O**—SiX_3	1.416	1.416	0.017	1.405	1.428	29	
	C*—**O**—SO_2—C	1.465	1.461	0.014	1.454	1.475	33	

Table 9.5.1.1. *Average lengths (cont.)*

Bond	Substructure	d	m	σ	q_l	q_u	n	Note
Csp^2—O(2) (*cont.*)	in enols: C=**C**—**O**H	1.333	1.331	0.017	1.324	1.342	53	
	in enol esters: C=**C**—**O**—C*	1.354	1.353	0.016	1.341	1.363	40	
	in acids: C*—**C**(=O)—**O**H	1.308	1.311	0.019	1.298	1.320	174	
	C=C—**C**(=O)—**O**H	1.293	1.295	0.019	1.279	1.307	22	
	C_{ar}—**C**(=O)—**O**H	1.305	1.311	0.020	1.291	1.317	75	
	in esters: C*—**C**(=O)—**O**—C*	1.336	1.337	0.014	1.328	1.346	551	*12, 29*
	C=C—**C**(=O)—**O**—C*	1.332	1.331	0.011	1.324	1.339	112	
	C_{ar}—**C**(=O)—**O**—C*	1.337	1.335	0.013	1.329	1.344	219	*12*
	C*—**C**(=O)—**O**—C=C	1.362	1.359	0.018	1.351	1.374	26	
	C*—**C**(=O)—**O**—C=C	1.407	1.405	0.017	1.394	1.420	26	
	C*—**C**(=O)—**O**—C_{ar}	1.360	1.359	0.011	1.355	1.367	40	*12*
	in anhydrides: O=**C**—**O**—**C**=O	1.386	1.386	0.011	1.379	1.393	70	
	in ring systems:							
	furan (O1—C2, O1—C5)	1.368	1.369	0.015	1.359	1.377	125	
	isoxazole (O1—C5)	1.354	1.354	0.010	1.345	1.360	9	
	β-lactones: C*—**C**(=O)—**O**—C*	1.359	1.359	0.013	1.348	1.371	4	*13*
	γ-lactones: C*—**C**(=O)—**O**—C*	1.350	1.349	0.012	1.342	1.359	110	*12*
	δ-lactones: C*—**C**(=O)—**O**—C*	1.339	1.339	0.016	1.332	1.347	27	*12*
C_{ar}—O(2)	in phenols: $\mathbf{C}_{ar}$—**O**H	1.362	1.364	0.015	1.353	1.373	511	
	in aryl alkyl ethers: $\mathbf{C}_{ar}$—**O**—C*	1.370	1.370	0.011	1.363	1.377	920	*29, 32*
	in diaryl ethers: $\mathbf{C}_{ar}$—**O**—$\mathbf{C}_{ar}$	1.384	1.381	0.014	1.375	1.391	132	
	in esters: $\mathbf{C}_{ar}$—**O**—C(=O)—C*	1.401	1.401	0.010	1.394	1.408	40	*12*
Csp^2=O(1)	in aldehydes and ketones:							
	C*—**C**H=**O**	1.192	1.912	0.005	1.188	1.197	7	
	$(C^*)_2$—**C**=**O**	1.210	1.210	0.008	1.206	1.215	474	*5*
	$(C^{\#})_2$—**C**=**O** in cyclobutanones	1.198	1.198	0.007	1.194	1.204	12	
	in cyclopentanones	1.208	1.208	0.007	1.203	1.212	155	
	in cyclohexanones	1.211	1.211	0.009	1.207	1.216	312	
	C=C—**C**=**O**	1.222	1.222	0.010	1.216	1.229	225	
	$(C{=}C)_2$—**C**=**O**	1.233	1.229	0.010	1.226	1.242	28	
	C_{ar}—**C**=**O**	1.221	1.218	0.014	1.212	1.229	85	
	$(C_{ar})_2$—**C**=**O**	1.230	1.226	0.015	1.220	1.238	66	
	C=**O** in benzoquinones	1.222	1.220	0.013	1.211	1.231	86	
	delocalized double bonds in carboxylate anions:							
	H—**C**$\cdots$$\mathbf{O}_2^-$ (formate)	1.242	1.243	0.012	1.234	1.252	24	
	C*—**C**$\cdots$$\mathbf{O}_2^-$	1.254	1.253	0.010	1.247	1.261	114	
	C=C—**C**$\cdots$$\mathbf{O}_2^-$	1.250	1.248	0.017	1.238	1.261	52	
	C_{ar}—**C**$\cdots$$\mathbf{O}_2^-$	1.255	1.253	0.010	1.249	1.262	22	
	HOOC—**C**$\cdots$$\mathbf{O}_2^-$ (hydrogen oxalate)	1.243	1.247	0.015	1.232	1.256	26	
	$^-\mathbf{O}_2\cdots$**C**—**C**$\cdots$$\mathbf{O}_2^-$ (oxalate)	1.251	1.251	0.007	1.248	1.254	18	
	in carboxylic acids (X—COOH):							
	C*—**C**(=**O**)—OH	1.214	1.214	0.019	1.203	1.224	175	
	C=C—**C**(=**O**)—OH	1.229	1.226	0.017	1.218	1.237	22	
	C_{ar}—**C**(=**O**)—OH	1.226	1.223	0.020	1.211	1.241	75	
	in esters:							
	C*—**C**(=**O**)—O—C*	1.196	1.196	0.010	1.190	1.202	551	*12*
	C=C—**C**(=**O**)—O—C*	1.199	1.198	0.009	1.193	1.203	113	
	C_{ar}—**C**(=**O**)—O—C*	1.202	1.201	0.009	1.196	1.207	218	*12*
	C*—**C**(=**O**)—O—C=C	1.190	1.190	0.014	1.184	1.198	26	
	C*—**C**(=**O**)—O—C_{ar}	1.187	1.188	0.011	1.181	1.195	40	*12*
	in anhydrides: **O**=**C**—O—**C**=**O**	1.187	1.187	0.010	1.184	1.193	70	
	in β-lactones: C*—**C**(=**O**)—O—C*	1.193	1.193	0.006	1.187	1.198	4	*13*
	γ-lactones: C*—**C**(=**O**)—O—C*	1.201	1.202	0.009	1.196	1.206	109	*12*
	δ-lactones: C*—**C**(=**O**)—O—C*	1.205	1.207	0.008	1.201	1.209	27	*12*
	in amides:							
	NH_2—**C**(—C*)=**O**	1.234	1.233	0.012	1.225	1.243	32	*14*
	(C*—)(C*,H—)N—**C**(—C*)=**O**	1.231	1.231	0.012	1.224	1.238	378	*14*
	β-lactams: C*—NH—**C**=**O**	1.198	1.200	0.012	1.193	1.204	23	*13*

Table 9.5.1.1. *Average lengths (cont.)*

Bond	Substructure	*d*	*m*	σ	q_l	q_u	*n*	Note
Csp^2═O(1) (*cont.*)	in amides (*cont.*)							
	γ-lactams: C*—NH—**C═O**	1.235	1.235	0.008	1.232	1.240	20	*13*
	γ-lactams: C*—N(—C*)—**C═O**	1.225	1.226	0.011	1.217	1.233	15	*13*
	δ-lactams: C*—NH—**C═O**	1.240	1.241	0.003	1.237	1.243	6	*14*
	δ-lactams: O*—N(—C*)—**C═O**	1.233	1.233	0.007	1.229	1.239	15	*14*
	in ureas:							
	$(NH_2)_2$—**C═O**	1.256	1.256	0.007	1.249	1.261	24	*25, 26*
	$(C^{\#}—NH)_2$—**C═O**	1.241	1.237	0.011	1.235	1.245	13	*25*
	$[(C^{\#})_n—N]_2$—**C═O**	1.230	1.230	0.007	1.224	1.234	20	*25, 27*
Csp^3—P(4)	C_3—**P^+**—**C***	1.800	1.802	0.015	1.790	1.812	35	*33*
	C_2—**P**(═O)—**CH_3**	1.791	1.790	0.006	1786	1.795	10	
	C_2—**P**(═O)—**CH_2**—C	1.806	1.806	0.009	1.801	1.813	45	
	C_2—**P**(═O)—**CH**—C_2	1.821	1.821	0.009	1.815	1.828	15	
	C_2—**P**(═O)—**C**—C_3	1.841	1.842	0.008	1.835	1.847	14	
	C_2—**P**(═O)—**C*** (overall)	1.813	1.811	0.017	1.800	1.822	84	
Csp^3—P(3)	C_2—**P**—**C***	1.855	1.857	0.019	1.840	1.870	23	
C_{ar}—P(4)	C_3—**P^+**—**C_{ar}**	1.793	1.792	0.011	1.786	1.800	276	
	C_2—**P**(═O)—**C_{ar}**	1.801	1.802	0.011	1.796	1.807	98	
	Ph_3—**P**═N^+═**P**—**Ph_3**	1.795	1.795	0.008	1.789	1.800	197	
C_{ar}—P(3)	C_2—**P**—**C_{ar}**	1.836	1.837	0.010	1.830	1.844	102	
	$(N⋯)_2$**P**—**C_{ar}** (P⋯N aromatic)	1.795	1.793	0.011	1.788	1.803	43	
Csp^3—S(4)	**C***—**SO_2**—C (C* = CH_3 excluded)	1.786	1.782	0.018	1.774	1.797	75	
	C*—**SO_2**—C (overall)	1.779	1.778	0.020	1.764	1.790	94	
	C*—**SO_2**—O—*X*	1.745	1.744	0.009	1.738	1.754	7	*34*
	C*—**SO_2**—N—X_2	1.758	1.736	0.018	1.746	1.773	17	*34*
Csp^3—S(3)	**C***—**S**(═O)—C (C* = CH_3 excluded)	1.818	1.814	0.024	1.802	1.829	69	
	C*—**S**(═O)—C (overall)	1.809	1.806	0.025	1.793	1.820	88	
	CH_3—**S^+**—X_2	1.786	1.787	0.007	1.779	1.792	21	
	C*—**S^+**—X_2 (C* = CH_3 excluded)	1.823	1.820	0.016	1.812	1.834	18	
	C*—**S^+**—C_2 (overall)	1.804	1.794	0.025	1.788	1.820	41	
Csp^3—S(2)	**C***—**SH**	1.808	1.805	0.010	1.800	1.819	6	
	CH_3—**S**—C*	1.789	1.787	0.008	1.784	1.794	9	
	C—**CH_2**—**S**—C*	1.817	1.816	0.013	1.808	1.824	92	
	C_2—**CH**—**S**—C*	1.819	1.819	0.011	1.811	1.825	32	
	C_3—**C**—**S**—C*	1.856	1.860	0.011	1.854	1.863	26	
	C*—**S**—**C*** (overall)	1.819	1.817	0.019	1.809	1.827	242	
	in thiirane	1.834	1.835	0.025	1.810	1.858	4	*9*
	in thietane: see ZCMXSP (1.817, 1.844)							
	in tetrahydrothiophene	1.827	1.826	0.018	1.811	1.837	20	
	in tetrahydrothiopyran	1.823	1.821	0.014	1.812	1.832	24	
	C—**CH_2**—**S**—S—*X*	1.823	1.820	0.014	1.813	1.832	41	
	C_3—**C**—**S**—S—*X*	1.863	1.865	0.015	1.848	1.878	11	
	C*—**S**—S—*X* (overall)	1.833	1.828	0.022	1.818	1.848	59	
Csp^2—S(2)	C═**C**—**S**—C*	1.751	1.755	0.017	1.740	1.764	61	
	C═**C**—**S**—C═C (in tetrathiafulvalene)	1.741	1.741	0.011	1.733	1.750	88	
	C═**C**—**S**—C═C (in thiophene)	1.712	1.712	0.013	1.703	1.722	60	
	O═**C**—**S**—$C^{\#}$	1.762	1.759	0.018	1.747	1.778	20	
C_{ar}—S(4)	**C_{ar}**—**SO_2**—C	1.763	1.764	0.009	1.756	1.769	96	
	C_{ar}—**SO_2**—O—*X*	1.752	1.750	0.008	1.749	1.756	27	
	C_{ar}—**SO_2**—N—X_2	1.758	1.759	0.013	1.749	1.765	106	*35*
C_{ar}—S(3)	**C_{ar}**—**S**(═O)—C	1.790	1.790	0.010	1.783	1.798	41	
	C_{ar}—**S^+**—X_2	1.778	1.779	0.010	1.771	1.787	10	
C_{ar}—S(2)	**C_{ar}**—**S**—C*	1.773	1.774	0.009	1.765	1.779	44	
	C_{ar}—**S**—**C_{ar}**	1.768	1.767	0.010	1.762	1.774	158	

Table 9.5.1.1. *Average lengths (cont.)*

Bond	Substructure	*d*	*m*	σ	q_l	q_u	*n*	Note
C_{ar}—S(2) (*cont.*)	$\mathbf{C}_{ar}$—**S**—$\mathbf{C}_{ar}$ (in phenothiazine) $\mathbf{C}_{ar}$—**S**—S—*X*	1.764 1.777	1.764 1.777	0.008 0.012	1.760 1.767	1.769 1.785	48 47	
C*sp*^{1}—S(2)	N≡**C**—**S**—*X*	1.679	1.683	0.026	1.645	1.698	10	
C*sp*^{1}—S(1)	(N≡**C**—**S**)$^-$	1.630	1.630	0.014	1.619	1.641	14	
C*sp*^{2}=S(1)	(C*)$_2$—**C**=**S**: see IPMUDS (1.599) (C_{ar})$_2$—**C**=**S**: see CELDOM (1.611) (*X*)$_2$—**C**=**S** (*X* = C,N,O,S) X_2N—**C**(=**S**)—S—*X* (X_2N)$_2$—**C**=**S** (thioureas) N—**C**(⋯**S**)$_2$	 1.671 1.660 1.681 1.720	 1.675 1.660 1.684 1.721	 0.024 0.016 0.020 0.012	 1.656 1.648 1.669 1.709	 1.689 1.674 1.693 1.731	 245 38 96 20	
C*sp*^{3}—Se	$\mathbf{C}^{\#}$—**Se**	1.970	1.967	0.032	1.948	1.998	21	
C*sp*^{2}—Se(2)	C=**C**—**Se**—**C**=C (in tetraselenafulvalene)	1.893	1.895	0.013	1.882	1.902	32	
C_{ar}—Se(3)	$\mathbf{Ph}_3$—$\mathbf{Se}^+$	1.930	1.929	0.006	1.924	1.936	13	
C*sp*^{3}—Si(5)	$\mathbf{C}^{\#}$—$\mathbf{Si}^-$—X_4	1.874	1.876	0.015	1.859	1.884	9	
C*sp*^{3}—Si(4)	$\mathbf{C}H_3$—**Si**—X_3 **C***—**Si**—X_3 (C* = CH_3 excluded) **C***—**Si**—X_2 (overall)	1.857 1.888 1.863	1.857 1.887 1.861	0.018 0.023 0.024	1.848 1.872 1.850	1.869 1.905 1.875	552 124 681	
C_{ar}—Si(4)	$\mathbf{C}_{ar}$—**Si**—X_3	1.868	1.868	0.014	1.857	1.878	178	
C*sp*^{1}—Si(4)	C≡**C**—**Si**—X_3	1.837	1.840	0.012	1.824	1.849	8	
C*sp*^{3}—Te	$\mathbf{C}^{\#}$—**Te**	2.158	2.159	0.030	2.128	2.177	13	
C_{ar}—Te	$\mathbf{C}_{ar}$—**Te**	2.116	2.115	0.020	2.104	2.130	72	
C*sp*^{2}=Te	see CEDCUJ (2.044)							
Cl—Cl	see PHASCL (2.306, 2.227)							
Cl—I	see CMBIDZ (2.563), HXPASC (2.541, 2.513), METAMM (2.552), BQUINI (2.416, 2.718)							
Cl—N	see BECTAE (1.743–1.757), BOGPOC (1.705)							
Cl—O(1)	in ClO_4^-	1.414	1.419	0.026	1.403	1.431	252	
Cl—P	(N⋯)$_2$**P**—**Cl** (N⋯P aromatic) **Cl**—**P** (overall)	1.997 2.008	1.994 2.001	0.015 0.035	1.989 1.986	2.004 2.028	46 111	
Cl—S	**Cl**—**S** (overall) see also longer bonds in CILSAR (2.283), BIHXIZ (2.357), CANLUY (2.749)	2.072	1.079	0.023	2.047	2.091	6	
Cl—Se	See BIRGUE10, BIRHAL10, CTCNSE (2.234–2.851)							
Cl—Si(4)	**Cl**—**Si**—X_3 (monochloro) $\mathbf{Cl}_2$—**Si**—X_2 and $\mathbf{Cl}_3$—**Si**—*X*	2.072 2.020	2.075 2.012	0.009 0.015	2.066 2.007	2.078 2.036	5 5	
Cl—Te	Cl—Te in range 2.34–2.60 see also longer bonds in BARRIV, BOJPUL, CETUTE, EPHTEA, OPNTEC10 (2.73–2.94)	2.520	2.515	0.034	2.493	2.537	22	*36*
F—N(3)	**F**—**N**—C_2 and $\mathbf{F}_2$—**N**—C	1.406	1.404	0.016	1.395	1.416	9	
F—P(6)	in hexafluorophosphate, PF_6^-	1.579	1.587	0.025	1.563	1.598	72	
P—P(3)	(N⋯)$_2$**P**—**F** (N⋯P aromatic)	1.495	1.497	0.016	1.481	1.510	10	

Table 9.5.1.1. *Average lengths (cont.)*

Bond	Substructure	*d*	*m*	σ	q_l	q_u	*n*	Note
F—S	43 observations in range 1.409–1.770 in a wide variety of environments							
	F—**S**(6) in $\mathbf{F_2}$—$\mathbf{SO_2}$—C_2 (see FPSULF10, BETJOZ)	1.640	1.646	0.011	1.626	1.649	6	
	F—**S**(4) in $\mathbf{F_2}$—**S**(=O)—N (see BUDTEZ)	1.527	1.528	0.004	1.524	1.530	24	*37*
F—Si(6)	in SiF_6^{2-}	1.694	1.701	0.013	1.677	1.703	6	
F—Si(5)	**F**—$\mathbf{Si}^-$—X_4	1.636	1.639	0.035	1.602	1.657	10	
F—Si(4)	**F**—**Si**—X_3	1.588	1.587	0.014	1.581	1.599	24	
F—Te	see CUCPIZ [F—Te(6) = 1.942, 1.937], FPHTEL [F—Te(4) = 2.006]							
H—N(4)	X_3—$\mathbf{N}^+$—**H**	1.033	1.036	0.022	1.026	1.045	87	*21*
H—N(3)	X_2—**N**—**H**	1.009	1.010	0.019	0.997	1.023	95	*21*
H—O(2)	in alcohols C*—**O**—**H**	0.967	0.969	0.010	0.959	0.974	63	*21*
	$C^{\#}$—**O**—**H**	0.967	0.970	0.010	0.959	0.974	73	*21*
	in acids O=C—**O**—**H**	1.015	1.017	0.017	1.001	1.031	16	*21, 38*
I—I	in I_3^-	2.917	2.918	0.011	2.907	2.927	6	
I—N	see BZPRIB, CMBIDZ, HMTITI, HMTNTI, IFORAM, IODMAM (2.042–2.475)							
I—O	X—**I**—**O** (see BZPRIB, CAJMAB, IBZDAC11)	2.144	2.144	0.028	2.127	2.164	6	
	for IO_6^- see BOVMEE (1.829–1.912)							
I—P(3)	see CEHKAB (2.490–2.493)							†
I—S	see DTHIBR10 (2.687), ISUREA10 (2.629), BZTPPI (3.251)							
I—Te(4)	**I**—**Te**—X_3	2.926	2.928	0.026	2.902	2.944	8	
N(4)—N(3)	X_3—$\mathbf{N}^+$—$\mathbf{N}^0$—X_2 (N^0 planar)	1.414	1.414	0.005	1.412	1.418	13	
N(3)—N(3)	(C)(C,H)—$\mathbf{N}_a$—$\mathbf{N}_b$—(C)(C,H)							*5, 39*
	N_a, N_b pyramidal	1.454	1.452	0.021	1.444	1.457	44	*40*
	N_a pyramidal, N_b planar	1.420	1.420	0.015	1.407	1.433	68	*40*
	N_a, N_b planar	1.401	1.401	0.018	1.384	1.418	40	*40*
	overall	1.425	1.425	0.027	1.407	1.443	139	
N(3)—N(2)	in pyrazole (**N**1—**N**2)	1.366	1.366	0.019	1.350	1.375	20	
	in pyridazinium ($\mathbf{N1}^+$⋯**N**2)	1.350	1.349	0.010	1.345	1.361	7	
N(2)⋯N(2)	**N**⋯**N** (aromatic) in pyridazine							
	with C,H as *ortho* substituents	1.304	1.300	0.019	1.287	1.326	6	
	with N,Cl as *ortho* substituents	1.368	1.373	0.011	1.362	1.375	9	
N(2)=N(2)	$C^{\#}$—**N**=**N**—$C^{\#}$ (*cis*)	1.245	1.244	0.009	1.239	1.252	21	
	(*trans*)	1.222	1.222	0.006	1.218	1.227	6	
	(overall)	1.240	1.241	0.012	1.230	1.251	27	
	C_{ar}—**N**=**N**—C_{ar}	1.255	1.253	0.016	1.247	1.262	13	
	X—**N**=**N**=N (azides)	1.216	1.226	0.028	1.202	1.237	19	
N(2)=N(1)	X—N=**N**=**N** (azides)	1.124	1.128	0.015	1.114	1.137	19	
N(3)—O(2)	$(C,H)_2$—**N**—**O**H (Nsp^2: planar)	1.396	1.394	0.012	1.390	1.401	28	
	C_2—**N**—**O**—C (Nsp^3: pyramidal)	1.463	1.465	0.012	1.457	1.468	22	
	C_2—**N**—**O**—C (Nsp^2: planar)	1.397	1.394	0.011	1.388	1.409	12	
	in furoxan (N2—O1)	1.438	1.436	0.009	1.430	1.447	14	
N(3)—O(1)	$(C⋯)_2\mathbf{N}^+$—$\mathbf{O}^-$ in pyridine *N*-oxides	1.304	1.299	0.015	1.291	1.316	11	
	in furoxan ($^+$N2—O6$^-$)	1.234	1.234	0.008	1.228	1.240	14	

Table 9.5.1.1. *Average lengths (cont.)*

Bond	Substructure	*d*	*m*	σ	q_l	q_u	*n*	Note
N(2)—O(2)	in oximes:							
	$(C^{\#})_2$—C═**N**—**O**H	1.416	1.418	0.006	1.416	1.420	7	
	(H)(Csp^2)—C═**N**—**O**H	1.390	1.390	0.011	1.380	1.401	20	
	($C^{\#}$)(Csp^2)—C═**N**—**O**H	1.402	1.403	0.010	1.393	1.410	18	
	(Csp^2)$_2$—C═**N**—**O**H	1.378	1.377	0.017	1.365	1.393	16	
	$(C,H)_2$—C═**N**—**O**H (overall)	1.394	1.395	0.018	1.379	1.408	67	
	in furazan (O1—N2, O1—N5)	1.385	1.383	0.013	1.378	1.392	12	
	in furoxan (O1—N5)	1.380	1.380	0.011	1.370	1.388	14	
	in isoxazole (O1—N2)	1.425	1.425	0.010	1.417	1.434	9	
N(3)═O(1)	in nitrate ions $\mathbf{NO_3^-}$	1.239	1.240	0.020	1.227	1.251	105	
	in nitro groups:							
	C*—$\mathbf{NO_2}$	1.212	1.214	0.012	1.206	1.221	84	
	$C^{\#}$—$\mathbf{NO_2}$	1.210	1.210	0.011	1.203	1.218	251	
	C_{ar}—$\mathbf{NO_2}$	1.217	1.218	0.011	1.211	1.215	1116	
	C—$\mathbf{NO_2}$ (overall)	1.218	1.219	0.013	1.210	1.226	1733	
N(3)—P(4)	X_2—**P**(═*X*)—**N**X_2 Nsp^2: planar	1.652	1.651	0.024	1.634	1.670	205	
	Nsp^3: pyramidal	1.683	1.683	0.005	1.680	1.686	6	
	(overall)	1.662	1.662	0.029	1.639	1.682	358	
	subsets of this group are:							
	O_2—**P**(═S)—**N**X_2	1.628	1.624	0.015	1.615	1.634	9	
	C—**P**(═S)—$(\mathbf{N}X_2)_2$	1.691	1.694	0.018	1.678	1.703	28	
	O—**P**(═S)—$(\mathbf{N}X_2)_2$	1.652	1.654	0.014	1.642	1.664	28	
	P(═O)—$(\mathbf{N}X_2)_3$	1.663	1.668	0.026	1.640	1.679	78	
N(3)—P(3)	—**N***X*—**P**(—*X*)—**N***X*—**P**(—*X*)— (P_2N_2 ring)	1.730	1.721	0.017	1.716	1.748	20	
	—**N***X*—**P**(═S)—**N***X*—**P**(═S)— (P_2N_2 ring)	1.697	1.697	0.015	1.690	1.703	44	
	in P-substituted phosphazenes:							
	$(N{\equiv})_2$**P**—**N** (amino)	1.637	1.638	0.014	1.625	1.651	16	
	(aziridinyl)	1.672	1.674	0.010	1.665	1.676	15	
N(2)═P(4)	Ph_3—**P**═$\mathbf{N^+}$═**P**—Ph_3	1.571	1.573	0.013	1.563	1.580	66	
	Ph_3—**P**═**N**—C,S	1.599	1.597	0.018	1.580	1.615	7	
N(2)≡P(3)	**N**≡**P** aromatic in phosphazenes	1.582	1.582	0.019	1.571	1.594	126	
	in **P**≡**N**≡S	1.604	1.606	0.009	1.594	1.612	36	
N(3)—S(4)	C—$\mathbf{SO_2}$—$\mathbf{NH_2}$	1.600	1.601	0.012	1.591	1.610	14	*35*
	C—$\mathbf{SO_2}$—**N**H—$C^{\#}$	1.633	1.633	0.019	1.615	1.652	47	*35*
	C—$\mathbf{SO_2}$—**N**—$(C^{\#})_2$	1.642	1.641	0.024	1.623	1.659	38	*35*
N(3)—S(2)	C—**S**—**N**X_2 Nsp^2: planar	1.710	1.707	0.019	1.698	1.722	22	*23*
	(for Nsp^3 pyramidal see MODIAZ: 1.765)							
	X—**S**—**N**X_2 Nsp^2: planar	1.707	1.705	0.012	1.699	1.715	30	*23*
N(2)—S(2)	C═**N**—**S**—*X*	1.656	1.663	0.027	1.632	1.677	36	
N(2)≡S(2)	**N**≡**S** aromatic in P≡**N**≡**S**	1.560	1.558	0.011	1.554	1.563	37	
N(2)═S(2)	**N**═**S** in **N**═**S**═**N** and **N**═**S**═S	1.541	1.546	0.022	1.521	1.558	37	
N(3)—Se	see COJCUZ (1.830), DSEMOR10 (1.846, 1.852), MORTRS10 (1.841)							
N(2)—Se	see SEBZQI (1.805), NAPSEZ10 (1.809, 1.820)							
N(2)═Se	see CISMUM (1.790, 1.791)							
N(3)—Si(5)	see DMESIP01, BOJLER, CASSAQ, CASYOK, CECXEN, CINTEY, CIPBUY, FMESIB, MNPSIL, PNPOSI (1.973–2.344)							
N(3)—Si(4)	X_3—**Si**—**N**X_2 (overall)	1.748	1.746	0.022	1.735	1.757	170	
	subsets of this group are:							
	X_3—**Si**—**N**H*X*	1.714	1.719	0.014	1.702	1.727	16	

Table 9.5.1.1. *Average lengths (cont.)*

Bond	Substructure	*d*	*m*	σ	q_l	q_u	*n*	Note
N(3)—Si(4) (*cont.*)	X_3—**Si**—**N**X—**Si**—X_3 acyclic	1.743	1.744	0.016	1.731	1.755	45	
	N—**Si**—**N** in four-membered rings	1.742	1.742	0.009	1.735	1.748	53	
	N—**Si**—**N** in five-membered rings	1.741	1.742	0.019	1.726	1.749	33	
N(2)—Si(4)	X_3—**Si**—**N**$^-$—**Si**—X_3	1.711	1.712	0.019	1.693	1.729	15	
N—Te	see ACLTEP (2.402), BIBLAZ (1.980), CESSAU (2.023)							
O(2)—O(2)	C*—**O**—**O**—C*,H τ(OO) = 70–85°	1.464	1.464	0.009	1.458	1.472	12	
	τ(OO) approx. 180°	1.482	1.480	0.005	1.478	1.486	5	
	(overall)	1.469	1.471	0.012	1.461	1.478	17	
	O=C—**O**—**O**—C=O see ACBZPO01 (1.446), CEYLUN (1.452), CIMHIP (1.454)							
	Si—**O**—**O**—Si	1.496	1.499	0.005	1.490	1.499	10	
O(2)—P(5)	X—**P**—(**O**X)$_4$							*41*
	trigonal bipyramidal: axial	1.689	1.685	0.024	1.675	1.712	20	
	equatorial	1.619	1.622	0.024	1.604	1.628	20	
	square pyramidal	1.662	1.661	0.020	1.649	1.673	28	
O(2)—P(4)	C—**O**—**P**(⋯O)$_3^{2-}$	1.621	1.622	0.007	1.615	1.628	12	
	(H—**O**)$_2$—**P**(⋯O)$_2^-$	1.560	1.561	0.009	1.555	1.566	16	
	(C—**O**)$_2$—**P**(⋯O)$_2^-$	1.608	1.607	0.013	1.599	1.615	16	
	(C$^\#$—**O**)$_3$—**P**=O	1.558	1.554	0.011	1.550	1.564	30	
	(C$_{ar}$—**O**)$_3$—**P**=O	1.587	1.588	0.014	1.572	1.599	19	
	X—**O**—**P**(=O)—(C,N)$_2$	1.590	1.585	0.016	1.577	1.601	33	
	(X—**O**)$_2$—**P**(=O)—(C,N)	1.571	1.572	0.013	1.563	1.579	70	
O(2)—P(3)	(N⋯)$_2$**P**—**O**—C (N⋯P aromatic)	1.573	1.573	0.011	1.563	1.584	16	
O(1)=P(4)	C—O—**P**(⋯**O**)$_3^{2-}$ (delocalized)	1.513	1.512	0.008	1.508	1.518	42	
	(H—O)$_2$—**P**(⋯**O**)$_2^-$ (delocalized)	1.503	1.503	0.005	1.499	1.508	16	
	(C—O)$_2$—**P**(⋯**O**)$_2^-$ (delocalized)	1.483	1.485	0.008	1.474	1.490	16	
	(C—O)$_3$—**P**=**O**	1.449	1.448	0.007	1.446	1.452	18	
	C$_3$—**P**=**O**	1.489	1.486	0.010	1.481	1.496	72	
	N$_3$—**P**=**O**	1.461	1.462	0.014	1.449	1.470	26	
	(C)$_2$(N)—**P**=**O**	1.487	1.489	0.007	1.479	1.493	5	
	(C,N)$_2$(O)—**P**=**O**	1.467	1.465	0.007	1.462	1.472	33	
	(C,N)(O)$_2$—**P**=**O**	1.457	1.458	0.009	1.454	1.462	35	
O(2)—S(4)	C—**O**—**S**O$_2$—C	1.577	1.576	0.015	1.566	1.584	41	
	C—**O**—**S**O$_2$—CH$_3$	1.569	1.569	0.013	1.556	1.582	7	
	C—**O**—**S**O$_2$—C$_{ar}$	1.580	1.578	0.015	1.571	1.588	27	
O(1)=S(4)	C—**S**O$_2$—C	1.436	1.437	0.010	1.431	1.442	316	*42*
	X—**S**O$_2$—NX_2	1.428	1.428	0.010	1.422	1.434	326	
	C—**S**O$_2$—N—(C,H)$_2$	1.430	1.430	0.009	1.425	1.435	206	
	C—**S**O$_2$—O—C	1.423	1.423	0.008	1.418	1.428	82	
	in **S**O$_4^{2-}$	1.472	1.473	0.013	1.463	1.481	104	
O(1)=S(3)	C—**S**(=**O**)—C	1.497	1.498	0.013	1.489	1.505	90	*5*
O—Se	see BAPPAJ, BIRGUE10, BIRHAL10, CXMSEO, DGLYSE, SPSEBU (1.597 for O=Se to 1.974 for O—Se)							
O(2)—Si(5)	(X—**O**)$_3$—**Si**—(N)(C)	1.663	1.658	0.023	1.650	1.665	21	
O(2)—Si(4)	X_3—**Si**—**O**—X (overall)	1.631	1.630	0.022	1.617	1.646	191	
	subsets of this group are:							
	X_3—**Si**—**O**—C$^\#$	1.645	1.647	0.012	1.634	1.652	29	
	X_3—**Si**—**O**—Si—X_3	1.622	1.625	0.014	1.614	1.631	70	
	X_3—**Si**—**O**—**O**—**Si**—X_3	1.680	1.676	0.008	1.673	1.688	10	
O(2)—Te(6)	(X—**O**)$_6$—**Te**	1.927	1.927	0.020	1.908	1.942	16	
O(2)—Te(4)	(X—**O**)$_2$—**Te**—X_2	2.133	2.136	0.054	2.078	2.177	12	

Table 9.5.1.1. *Average lengths (cont.)*

Bond	Substructure	d	m	σ	q_l	q_u	n	Note
P(4)—P(4)	X_3—**P**—**P**—X_3	2.256	2.259	0.025	2.243	2.277	6	
P(4)—P(3)	see CECHEX (2.197), COZPIQ (2.249)							
P(3)—P(3)	X_2—**P**—**P**—X_2	2.214	2.210	0.022	2.200	2.224	41	
P(4)═P(4)	see BUTSUE (2.054)							
P(3)═P(3)	see BALXOB (2.034)							
P(4)═S(1)	C_3—**P**═**S** $(N,O)_2(C)$—**P**═**S** $(N,O)_3$—**P**═**S**	1.954 1.922 1.913	1.952 1.924 1.914	0.005 0.014 0.014	1.950 1.913 1.906	1.957 1.927 1.921	13 26 50	
P(4)═Se(1)	X_3—**P**═**Se**	2.093	2.099	0.019	2.075	2.108	12	
P(3)—Si(4)	X_2—**P**—**Si**—X_3: 3- and 4-rings excluded (see BOPFER, BOPFIV, CASTOF10, COZVIW: 2.201–2.317)	2.264	2.260	0.019	2.249	2.283	22	
P(4)═Te(1)	see MOPHTE (2.356), TTEBPZ (2.327)							
S(2)—S(2)	C—**S**—**S**—C τ (SS) = 75–105° τ (SS) = 0–20° (overall) in polysulfide chain —**S**—**S**—**S**—	2.031 2.070 2.048 2.051	2.029 2.068 2.045 2.050	0.015 0.022 0.026 0.022	2.021 2.057 2.028 2.037	2.038 2.077 2.068 2.065	46 28 99 126	
S(2)—S(1)	X—N═**S**—**S**	1.897	1.896	0.012	1.887	1.908	5	
S—Se(4)	see BUWZUO (2.264, 2.269)							
S—Se(2)	X—**Se**—**S** (any)	2.193	2.195	0.015	2.174	2.207	9	
S(2)—Si(4)	X_3—**Si**—**S**—X	2.145	2.138	0.020	2.130	2.158	19	
S(2)—Te	X—**S**—**Te** (any) X═**S**—**Te** (any)	2.405 2.682	2.406 2.686	0.022 0.035	2.383 2.673	2.424 2.694	10 28	
Se(2)—Se(2)	X—**Se**—**Se**—X	2.340	2.340	0.024	2.315	2.361	15	
Se(2)—Te(2)	see BAWFUA, BAWGAH (2.524–2.561)							†
Si(4)—Si(4)	X_3—**Si**—**Si**—X_3 three-membered rings excluded: see CIHRAM (2.511)	2.359	2.359	0.012	2.349	2.366	42	
Te—Te	see CAHJOK (2.751, 2.704)							

† See opening paragraph of Section 9.5.3. For numbered footnotes, see Appendix 1.

International Tables for Crystallography (2006). Vol. C, Chapter 9.6, pp. 812–896.

9.6. Typical interatomic distances: organometallic compounds and coordination complexes of the *d*- and *f*-block metals

By A. G. Orpen, L. Brammer, F. H. Allen, D. G. Watson, and R. Taylor

9.6.1. Introduction

The determination of molecular geometry is of vital importance to our understanding of chemical structure and bonding. The majority of experimental data have come from X-ray and neutron diffraction, microwave spectroscopy, and electron diffraction. Over the years, compilations of results from these techniques have appeared sporadically. The first major compilation was Chemical Society Special Publication No. 11: *Tables of Interatomic Distances and Configuration in Molecules and Ions* (Sutton, 1958). This volume summarized results obtained by diffraction and spectroscopic methods prior to 1956; a supplementary volume (Sutton, 1965) extended this coverage to 1959. Summary tables of bond lengths between carbon and other elements were also published in Volume III of *International Tables for X-ray Crystallography* (Kennard, 1962). Some years later, the Cambridge Crystallographic Data Centre (Allen, Bellard, Brice, Cartwright, Doubleday, Higgs, Hummelink, Hummelink-Peters, Kennard, Motherwell, Rodgers & Watson, 1979) produced an atlas-style compendium of all organic, organometallic and metal-complex crystal structures published in the period 1960–1965 (Kennard, Watson, Allen, Isaacs, Motherwell, Pettersen & Town, 1972). More recently, a survey of geometries determined by spectroscopic methods (Harmony, Laurie, Kuczkowski, Schwendemann, Ramsay, Lovas, Lafferty & Maki, 1979) has extended coverage in this area to mid-1977. A notable compendium of structural data, without geometric information, was given in *Comprehensive Organometallic Chemistry* (Bruce, 1981), covering all complexes with metal–carbon bonds. The BIDICS (Brown, Brown & Hawthorne, 1982) series, which finished in 1981, provided for some years a full coverage of metal complexes giving both bibliographic and geometric information. There have also been valuable annual summaries, without geometric information, on the structures of organometallic compounds determined by diffraction methods (Russell, 1988).

The production of further comprehensive compendia of X-ray and neutron diffraction results has been precluded by the steep rise in the number of published crystal structures, as illustrated by Fig. 9.6.1.1. Print compilations have been effectively superseded by computerized databases. In particular, the Cambridge Structural Database now contains bibliographic, chemical, and numerical results for some 86 000 organo-carbon crystal structures. This machine-readable file fulfils the function of a comprehensive structure-by-structure compendium of molecular geometries. However, the amount of data now held in the CSD is so large that there is also a need for concise, printed tabulations of average molecular dimensions.

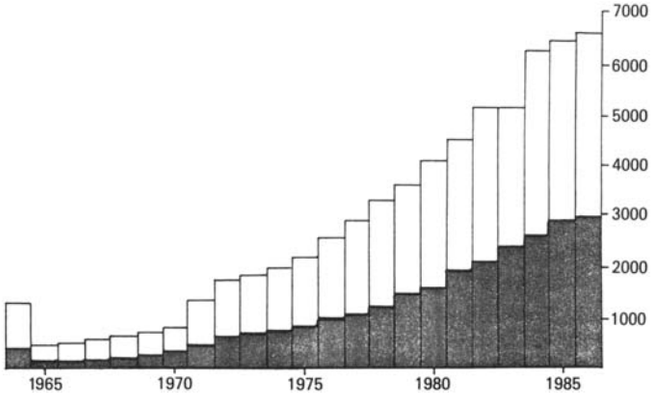

Fig. 9.6.1.1. Growth of the Cambridge Structural Database as number of entries (N_{ent}) added annually. The structures containing *d*- or *f*-block metals are indicated by shading.

The only tables of average geometry in general use are those contained in the Chemical Society Special Publications of 1958 and 1965 (Sutton, 1958, 1965), which list mean bond lengths for a variety of atom pairs and functional groups. Since these early tables were based on data obtained before 1960, we have used the CSD to prepare a new table of average bond lengths in organic compounds (see Chapter 9.5) and in metal complexes. The table given here (Table 9.6.3.3) specifically lists average lengths for metal–ligand distances, together with intra-ligand distances, involving bonds between the *d*- and *f*-block metals (Sc–Zn, Y–Cd, La–Hg, Ce–Lu, Th–U) and atoms H, B, C, N, O, F, Si, P, S Cl, As, Se, Br, Te, and I of ligands. Mean values are presented for 324 different bond types involving such metal–ligand bonds.

9.6.2. Methodology

9.6.2.1. *Selection of crystallographic data*

All results given in Table 9.6.3.3 are based on X-ray and neutron diffraction results retrieved from the September 1985 version of the CSD. Neutron diffraction data only were used to derive mean bond lengths involving hydrogen atoms. This version of the CSD contained results for 49 854 single-crystal diffraction studies of organo-carbon compounds; 9802 of these satisfied the acceptance criteria listed below and were used in the averaging procedures:

(i) Structure contains a *d*- or *f*-block metal.

(ii) Atomic coordinates for the structure have been published and are available in the CSD.

(iii) Structure was determined from diffractometer data.

(iv) Structure does not contain unresolved numeric data errors from the original publication (such errors are usually typographical and are normally resolved by consultation with the authors).

(v) Only structures of higher precision were included on the basis that *either* (*a*) the crystallographic *R* factor was ≤ 0.07 and the reported mean estimated standard deviation (e.s.d.) of the C—C bond lengths was ≤ 0.030 Å (corresponds to AS flag = 1, 2 or 3 in the CSD), *or* (*b*) the crystallographic *R* factor ≤ 0.05 and the mean e.s.d. for C—C bonds was not available in the database (AS = 0 in the CSD).

(vi) Where the structure of a given compound had been determined more than once within the limits of (i)–(v), then only the most precise determination was used.

The structures used in Table 9.6.3.3 do not include compounds whose structure precludes them from the CSD (*i.e.* not containing 'organic' carbon). In practice, structures including at least one C—H bond are taken to contain 'organic' carbon. Thus, the entry for Cr—CO distances has a contribution from $[NEt_4][Cr(\mu\text{-H})(CO)_{10}]$ but *not* from $K[Cr(\mu\text{-H})(CO)_{10}]$ or $[Cr(CO)_6]$.

Copyright © 2006 International Union of Crystallography

9.6.2.2. *Program system*

All calculations were performed on a University of Bristol VAX 11/750 computer. Programs *BIBSER*, *CONNSER*, *RETRIEVE* (Allen *et al.*, 1979) and *GEOSTAT* (Murray-Rust & Raftery, 1985*a*,*b*), as locally modified, were used. A stand-alone program was written to implement the selection criteria, whilst a new program (*STATS*) was used for statistical calculations described below. It was also necessary to modify *CONNSER* to improve the precision with which it locates chemical substructures. In particular, the program was altered to permit the location of atoms with specified coordination numbers. This was essential in the case of carbon so that atoms with coordination numbers 2, 3, and 4 (equivalent to formal hybridization state sp^1, sp^2, sp^3) could be distinguished easily and reliably. Considerable care was taken to ensure that the correct molecular fragment was located by *GEOSTAT* in the generation of geometrical tabulations. Searches were conducted for all metals together and statistics for individual metal elements and subdivision of the entry for a given metal carried out subsequently. An important modification to *GEOSTAT* allowed for calculation of metal-atom coordination number with due allowance for multihapto ligands and μ_2 ligands. Thus, η^5-C_5H_5, η^6-C_6H_6, and other η^5 and η^6 ligands were assigned to occupy 3 coordination sites, η^3 and η^4 ligands such as allyls and dienes to occupy 2 coordination sites, and η^2 ligands such as alkenes 1 site, and so on. The approach taken in dealing with (μ_2) bridging ligands was that when a metal–metal bond is bridged by one atom of a ligand [*e.g.* as in Cl, CO, OMe *etc.* as in (*a*), (*b*) below] then only the non-metal atom is counted as occupying a coordination site. For the relatively rare case of bridging polyhapto ligands (in which the bridging atoms are linked by direct bonds), the assignment follows logically, thus, μ_2-η^2,η^2-alkyne, see (*c*) below, occupies one site on each metal. Bridging ligands that do not have one atom bonded to both metals [*e.g.* acetate in (*d*) below] contribute to metal coordination numbers as do terminal ligands. In examples (*a*)–(*d*) below, the metal atoms therefore have coordination numbers as follows: (*a*), Rh 4; (*b*), Fe 6; (*c*), Co 4; (*d*), Rh 6. For cases where coordination number is very difficult to assign, notably where a metal atom is bonded to more than one other metal atom as in metal cluster complexes, no assignment was attempted.

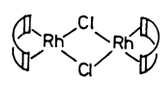

(*a*)

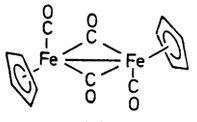

(*b*)

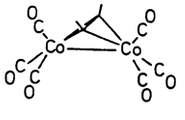

(*c*)

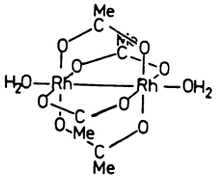

(*d*)

The non-location of hydrogen atoms presents major difficulties, both in the determination of coordination numbers for metal atoms, and for correct identification of ligands (*e.g.* to distinguish methoxide from methanol). Care was therefore taken to exclude cases where any ambiguity existed [*e.g.* no data taken for M—(OCH_3) and M—O(H)CH_3 distances when both are present in a structure in which hydrogen-atom positions were not reported].

9.6.2.3. *Classification of bonds*

The classification of metal–ligand bonds in Table 9.6.3.3 is based on the ligating contacting atom. Thus, all metal–boron distances appear in sections 2.1–2.3 of Table 9.6.3.3, all metal–carbon distances in sections 3.1–3.22, and so on. Where intra-ligand interatomic distances (*e.g.* P—C distances in tertiary phosphines) are given in Table 9.6.3.3, they are averaged over all metals and precede the individual metal–ligand interatomic distances for that ligand.

Table 9.6.3.3 is designated: (i) to appear logical, useful, and reasonably self-explanatory to chemists, crystallographers, and others who may use it; (ii) to permit a meaningful average value to be cited for each bond length. With reference to (ii), it was considered that a sample of bond lengths could be averaged meaningfully if: (*a*) the sample was unimodally distributed; (*b*) the sample standard deviation (σ) was reasonably small, ideally less than *ca* 0.04 Å; (*c*) there were no conspicuous outlying observations – those that occurred at $> 4\sigma$ from the mean were automatically eliminated from the sample by *STATS*, other outliers were inspected carefully; (*d*) there were no compelling chemical reasons for further subdivision of the sample. It should be noted that Table 9.6.3.3 is not intended to be complete in covering all possible ligands. The purpose of the table is to provide information on the interatomic distances for ligands of the greatest *chemical* importance, notably for those that are simple and/or common.

9.6.2.4. *Statistics*

Where there are less than four independent observations of a given bond length, then each individual observation is given explicitly in Table 9.6.3.3. In all other cases, the following statistics were generated by the program *STATS*.

(i) The unweighted sample mean, d, where

$$d = \sum_{i=1}^{n} d_i/n$$

and d_i is the ith observation of the bond length in a total sample of n observations. Recent work (Taylor & Kennard, 1983, 1985, 1986) has shown that the unweighted mean is an acceptable (even preferable) alternative to the weighted mean, where the ith observation is assigned a weight equal to $1/\mathrm{var}(d_i)$. This is especially true where structures have been pre-screened on the basis of precision.

(ii) The sample median, m. This has the property that half of the observations in the sample exceed m, and half fall short of it.

(iii) The sample standard deviation, σ, where

$$\sigma = \left[\sum_{i=1}^{n}(d_i - d)^2/(n-1)\right]^{1/2}.$$

(iv) The lower quartile for the sample, q_l. This has the property that 25% of the observations are less than q_l and 75% exceed it.

(v) The upper quartile for the sample, q_u. This has the property that 25% of the observations exceed q_u and 75% fall short of it.

(vi) The number (n) of observations in the sample.

The statistics given in Table 9.6.3.3 correspond to distributions for which the automatic 4σ cut-off (see above) had been applied, and any manual removal of additional outliers (an infrequent operation) had been performed. In practice, a very small percentage of observations were excluded by these methods. The major effect of removing outliers is to improve

the sample standard deviation, as shown in Fig. 9.6.2.1(*b*) in which four (out of 366) observations are deleted.

The statistics chosen for tabulation effectively describe the distribution of bond lengths in each case. For a symmetrical, normal distribution, the mean (d) will be approximately equal to the median (m), the lower and upper quartiles (q_l, q_u) will be approximately symmetric about the median $m - q_l \simeq q_u - m$, and 95% of the observations may be expected to lie within $\pm 2\sigma$ of the mean value. For a skewed distribution, d and m may differ appreciably and q_l and q_u will be asymmetric with respect to m. When a bond-length distribution is negatively skewed, *i.e.* very short values are more common than very long values, then it may be due to thermal-motion effects; the distances used to prepare the table were not corrected for thermal libration.

In a number of cases, the initial bond-length distribution was clearly not unimodal as in Fig. 9.6.2.1(*a*). Where possible, such distributions were resolved into their unimodal components (as in Fig. 9.6.2.1*c*) on chemical or structural criteria. The case illustrated in Fig. 9.6.2.1, for Cu—Cl bonds, is one of the most spectacular examples, owing to the dramatic consequences of oxidation state and coordination number (and Jahn–Teller effects) on the structures of copper complexes.

9.6.3. Content and arrangement of table of interatomic distances

Table 9.6.3.1 indicates how the interatomic distances covered in Table 9.6.3.3 are subdivided. Metal–ligand distances are grouped according to the ligand contact atom, which leads to ordering by atomic number of that contact atom. For a given contact atom (H, B, C, *etc.*), the ligands are grouped by type as listed in Table 9.6.3.1. The class of ligand is identified numerically (*e.g.* alkoxides are class 5.3, alcohols class 5.23, ethers 5.24, *etc.*). Particular ligands are identified by a third number (*e.g.* methoxide is ligand 5.3.1). Finally, alternative bonding modes for a particular ligand are denoted by a fourth number [*e.g.* terminal alkoxides 5.3.1.1, bridging (μ_2) alkoxides 5.3.1.2]. In general, the bonding modes are arranged in the sequence $\eta^1, \eta^2, \ldots, \eta^n$, μ_2, μ_3, *etc.*, where η^n implies n atoms of the ligand are bonded to metal atoms, and μ_m that m metal atoms are bonded to the ligand. Thus, acetates are represented by entries headed 5.5.2.1 (η^1), 5.5.2.2 (chelating, η^2) and 5.5.2.3 (bridging, μ_2). For each ligand, the metal–ligand bonds then follow a sequence of ascending atomic

Table 9.6.3.1. *Ligand index*

Contact atom	Ligand class	Ligand class identifier
Hydrogen	hydride	1.1
	tetrahydroborate (BH_4^-)	1.2
Boron	borohydrides	2.1
	boranes/carbaboranes	2.2
	boroles, borylenes, other heteroboracycles	2.3
Carbon	carbide (C)	3.1
	carbyne/alkylidyne (C*R*)	3.2
	vinylidene/alkenylidene (CCR_2)	3.3
	acetylide/alkynyl (CCR)	3.4
	cyano (CN)	3.5
	isocyanides (CN*R*)	3.6
	carbon monoxide (CO)	3.7
	thiocarbonyl (CS)	3.8
	carbene/alkylidene (CR_2)	3.9
	vinyl/alkenyl (CRCR_2)	3.10
	aryl (C_6R_5)	3.11
	acyl [C(O)*R*]	3.12
	alkyl (CR_3)	3.13
	η-alkenes (C_2R_4, allenes, *etc.*)	3.14
	alkynes (*R*CCR)	3.15
	η^3 ligands (allyls, *etc.*)	3.16
	η^4 ligands (conjugated dienes, *etc.*)	3.17
	η^5 ligands (dienyls, *etc.*)	3.18
	η^6 ligands (arenes, *etc.*)	3.19
	η^7, η^8 ligands	3.20
	carbaboranes, boroles	3.21
	miscellaneous (CO_2, CS_2, *etc.*)	3.22
Nitrogen	nitride (N)	4.1
	nitrene/imide (N*R*)	4.2
	methyleneamido (N=CR_2)	4.3
	nitriles (NC*R*)	4.4
	isocyanate, isothiocyanate (NCO, NCS)	4.5
	dinitrogen (N_2)	4.6
	diazonium (N_2R), diazoalkanes (N_2CR_2)	4.7
	azide (N_3)	4.8
	nitrosyl, thionitrosyl (NO, NS)	4.9
	amide (NR_2)	4.10

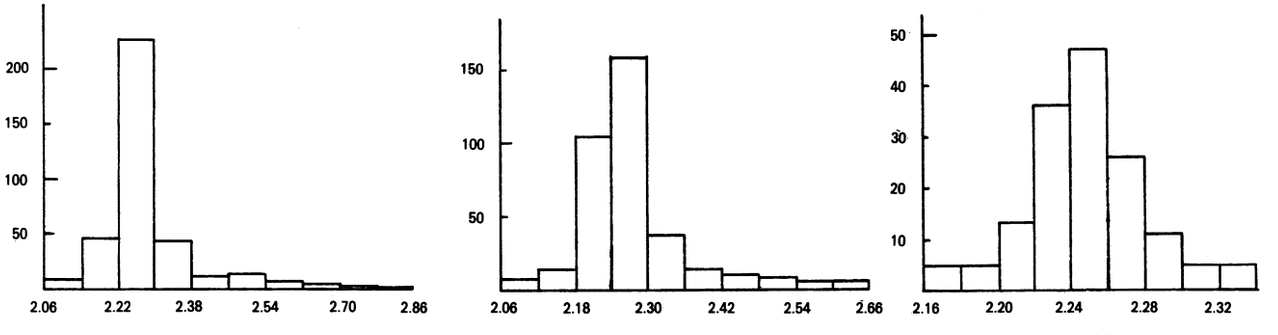

(*a*) (*b*) (*c*)

Fig. 9.6.2.1. Effects of outlier removal and subdivision based on coordination number and oxidation state. Cu—Cl: (*a*) all data; (*b*) all data without outliers [$> 4\sigma$ (sample) from mean]; (*c*) all data for which Cu is 4-coordinate, Cu^{II}.

	d	m	σ	q_1	q_u	N
(*a*)	2.282	2.255	0.105	2.233	2.296	366
(*b*)	2.276	2.254	0.092	2.232	2.292	362
(*c*)	2.248	2.246	0.032	2.233	2.263	153

Table 9.6.3.1. *Ligand index* (*cont.*)

Contact atom	Ligand class	Ligand class identifier
Nitrogen (*cont.*)	amidinate [*R*NC(*R*)N*R*]	4.11
	Schiff bases	4.12
	phthalocyanines, porphyrins, pyrroles	4.13
	pyrazolate, imidazolate and derivatives	4.14
	pyridine, polypryidyls (bpy, *o*-phen)	4.15
	pyrazines, pyridazines, pyrimidines	4.16
	other N_2 ligands (N*R*N*R*$_2$, NN*R*$_2$, N*R*N*R*)	4.17
	triazenido (*R*NNN*R*)	4.18
	hydrazones and related species (N*R*$_2$N=C*R*)	4.19
	oximes	4.20
	N-nitrite (NO_2)	4.21
	amine (N*R*$_3$)	4.22
	borazines	4.23
Oxygen	oxo (O)	5.1
	hydroxy (OH)	5.2
	alkoxy, aryloxy, *etc*. (O*R*)	5.3
	O-ketones (OC*R*$_2$), urea	5.4
	carboxylates (O_2C*R*)	5.5
	oxalate (O_2CCO_2)	5.6
	acetylacetonates [*R*C(O)C*R*C(O)C*R*]	5.7
	α, β-diones (*e.g*. *o*-quinones)	5.8
	carbonate (CO_3^{2-})	5.9
	N-oxides (*e.g*. pyridine *N*-oxide)	5.10
	nitrate (NO_3^-)	5.11
	O-nitrite (NO_2^-)	5.12
	dioxygen, peroxides	5.13
	phosphine oxides (OP*R*$_3$)	5.14
	phosphate (PO_4^{3-})	5.15
	other P—O anions	5.16
	O-dialkyl sulfoxides (OS*R*$_2$)	5.17
	sulfate (SO_4^{2-})	5.18
	other S—O anions (sulfonates, *etc*.)	5.19
	O-SO_2	5.20
	other oxyanions (*e.g*. ClO_4^-)	5.21
	aqua	5.22
	alcohols (*R*OH)	5.23
	ethers (*ROR*′)	5.24
	miscellaneous (η^2-acyl, η^2-CO_2, μ-NCO)	5.25
Fluorine	fluoride (F)	6.1
	fluoroanions (BF_4^-, PF_6^-)	6.2
Silicon	miscellaneous	7.1
Phosphorus	phosphorus (P)	8.1
	phosphinidenes (P*R*)	8.2
	phosphides (P*R*$_2$)	8.3
	oligo-phosphorus ligands (P_3, P*R*$_2$P*R*$_2$, P*R*P*R*, *etc*.)	8.4
	phosphines (P*R*$_3$)	8.5
	diphosphines (*e.g*. diphos)	8.6
	phosphites [P(O*R*)$_3$]	8.7
	aminophosphines, cyclotriphosphazenyl, misc. P—N ligands	8.8
Sulfur	sulfides (S)	9.1
	thiolates (S*R*)	9.2

Table 9.6.3.1. *Ligand index (cont.)*

Contact atom	Ligand class	Ligand class identifier
Sulfur (*cont.*)	*S*-thiocyanate (SCN)	9.3
	thioketones, thiourea (S=C*R*$_2$)	9.4
	thiocarboxylates (S_2C*R*$^-$)	9.5
	thiocarbamates (S_2CN*R*$_2^-$)	9.6
	xanthates (S_2CO*R*$^-$), dithiocarbonates	9.7
	trithiocarbonate (CS_3^{2-}), thioxanthates	9.8
	α, β-dithiones	9.9
	phosphine sulfides	9.10
	dithiophosphinates (S_2P*R*$_2^-$)	9.11
	polysulfur ligands (S_2, SS*R*, *etc*.)	9.12
	thioethers (S*R*$_2$)	9.13
	S-SO_2, *S*-SO_3, *etc*.	9.14
	disulfides (*R*SS*R*)	9.15
	S-dialkyl sulfoxides (*R*$_2$SO)	9.16
	miscellaneous (η^2-CS_2)	9.17
Chlorine	chloride (Cl)	10.1
Arsenic	arsines (As*R*$_3$)	11.1
	miscellaneous	11.2
Selenium	miscellaneous	12.1
Bromine	bromide (Br)	13.1
Tellurium	miscellaneous	14.1
Iodine	iodide (I)	15.1

number of the metal. For a given metal, the first line of an entry in Table 9.6.3.3 gives statistics covering all appropriate occurrences of metal–ligand distances. Further lines give statistics for metal–ligand distances for subdivision based largely on chemical criteria (*e.g*. metal oxidation state or coordination number). Cases where one atom of a ligand bridges two or more metal atoms were included only when the metal atoms were all of the same type and, unless specified, only when the metal–ligand distances were symmetrical (range for distances ≤ 0.1 Å).

In many instances, the number of structures having interatomic distances involving a given metal for a particular ligand is too small (< 4) for statistics to be quoted. In these cases, individual structures, and the distances in them, are given. These structures are identified by their CSD reference code (*e.g*. BOZMIN); short-form literature references, ordered alphabetically by reference code, are in Appendix 2.

Each line of Table 9.6.3.3 contains nine columns of which six record the statistics of the bond-length distribution described above. The content of the remaining three columns: Bond, Substructure, and Note, are described below.

9.6.3.1. *The 'Bond' column*

This specifies the atom pair to which the line refers. Therefore, in the case of triethylphosphine complexes (section 8.5.2), there are 18 lines, in which the bond column contains P—C, followed by 17 entries for Ti—P through to Au—P, indicating statistics for both intraligand and metal–ligand atom pairs.

9.6.3.2. *Definition of 'Substructure'*

This column provides details of any subdivision of particular metal–ligand bonds that has been applied. Thus, for terminal

iron–chlorine bonds (in section 10.1.1.1), the second and third lines of the Fe—Cl entry refer to complexes in which the iron atom is four-coordinate and in oxidation state II and III, respectively. In some cases, subdivision has been carried out on the basis of ligand substituents in those cases where a well defined subdistribution was observed. For clarity, in a number of cases the ligand structure and numbering scheme are illustrated in Fig. 9.6.3.1. The reader will be aware that formal oxidation

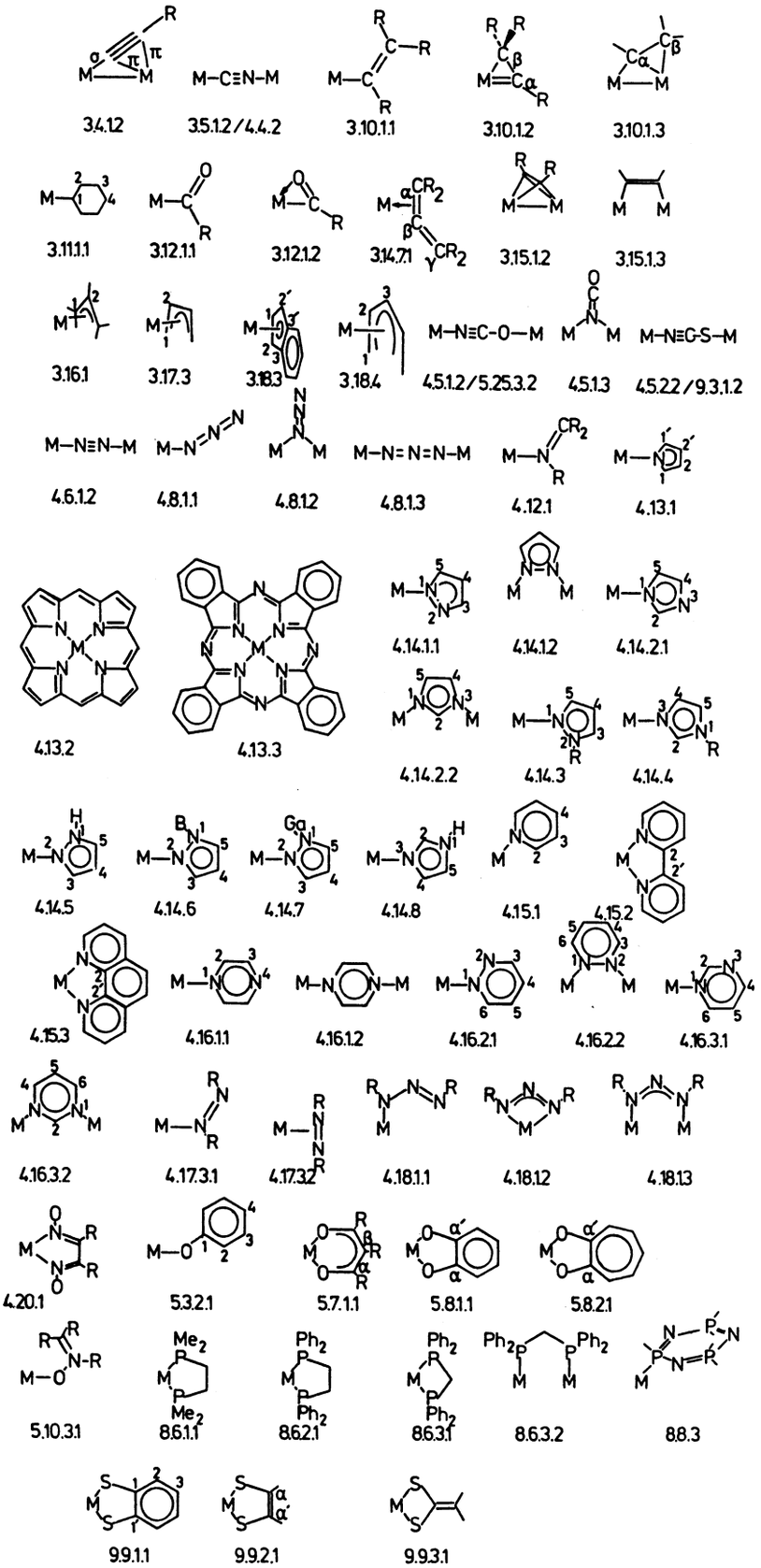

Fig. 9.6.3.1. Diagrams of ligands in Table 9.6.3.3, showing table entry number and ligand atom labelling.

Table 9.6.3.2. *Numbers of entries in Table 9.6.3.3*

Numbers of entries for which < 4 examples are known are given first, followed by numbers of entries for which statistics are quoted (*i.e.* those with > 4 examples).

	Ligand atoms														
	H	B	C	N	O	F	Si	P	S	Cl	As	Se	Br	Te	I
Ligand class / Metal *†	5	4	66	71	79	4	1	32	49	3	2	1	3	1	3
Sc[1]		1, 0	0, 1		0, 4										
Ti[2,3]		2, 0	6, 8	14, 5	4, 15	1, 0		1, 2	4, 3	1, 2	1, 0		1, 0		
V[4,5,6]		2, 0	8, 8	6, 5	10, 10	0, 1		3, 3	2, 6	0, 2	1, 0				1, 0
Cr[7]	1, 0	1, 2	9, 15	12, 13	5, 19	0, 1		9, 5	1, 7	1, 1	0, 2	1, 0	2, 0	1, 0	1, 0
Mn		0, 3	15, 12	14, 13	14, 10	1, 0	1, 0	5, 6	7, 4	0, 2	0, 2	1, 0	1, 1	0, 1	1, 1
Fe	0, 2	1, 2	10, 33	13, 19	14, 12		0, 1	6, 13	7, 16	0, 2	0, 2	0, 1	2, 0	0, 1	1, 1
Co[8]	2, 0	0, 4	11, 27	5, 28	18, 22			6, 10	7, 11	1, 2	0, 2		0, 1		0, 1
Ni[9,10]	0, 1	2, 1	7, 20	9, 23	9, 18	1, 0		6, 8	12, 13	0, 2	1, 1	0, 1	0, 2		1, 1
Cu[11,12]	1, 0	3, 0	1, 11	7, 35	18, 31	3, 0		3, 3	7, 12	0, 3	0, 1	1, 0	0, 3		0, 3
Zn	1, 0	2, 0	3, 2	7, 16	14, 10				7, 3	0, 2			0, 1		0, 1
Y[1]		1, 0	0, 1		2, 6					0, 1					
Zr[13]		1, 0	6, 8	10, 1	5, 7	0, 1		1, 1	4, 0	0, 2		1, 0			1, 0
Nb[14]			4, 6	3, 5	2, 9	0, 1		2, 0	1, 6	1, 2	0, 1				
Mo[15,16]	1, 1	1, 0	11, 25	17, 26	7, 28	1, 1	1, 0	5, 11	3, 20	1, 2	0, 2	1, 0	0, 2	1, 0	0, 2
Tc[17,18]			0, 1	5, 5	3, 5			1, 2	1, 2	1, 1	0, 1		2, 0		
Ru	0, 1	2, 1	12, 25	19, 9	11, 8		0, 1	2, 13	4, 4	0, 2	0, 2		0, 2		1, 1
Rh	2, 1	0, 2	11, 25	12, 18	11, 14		1, 0	5, 13	6, 7	0, 2	1, 1	0, 1	0, 2		0, 2
Pd		0, 1	9, 15	14, 13	6, 6			8, 7	4, 10	1, 2	1, 1		0, 1		1, 1
Ag		1, 0	4, 2	8, 6	8, 2	1, 0		2, 3	4, 6	2, 1		1, 0	1, 0		1, 2
Cd[19]				3, 14	12, 10			2, 0	6, 4	0, 3			1, 2		0, 1
La§				1, 1	4, 7				1, 0	1, 0					
Ce§			0, 2	0, 1	4, 4				0, 1	1, 0					
Pr§			1, 1	1, 0	2, 5					2, 0					
Nd§				2, 2	7, 5					1, 0					
Sm§			0, 1	2, 1	8, 6										
Eu§			0, 1	0, 1	3, 6										
Gd§			0, 1	1, 0	2, 4										
Tb§					1, 0										
Dy§				2, 1	1, 2				0, 1						
Ho§					0, 1										
Er§			0, 1	1, 1	4, 4					1, 0					
Tm§									0, 1						
Yb§			0, 2	2, 2	3, 2					2, 0					1, 0
Lu§			1, 2	1, 0	0, 1				0, 1						
Hf[13]			2, 4	1, 0	2, 2			0, 2		1, 0					
Ta[23]	1, 0		5, 7	4, 1	4, 2			2, 2	2, 4	0, 2			1, 0		
W[24,159]	0, 2	1, 1	9, 20	10, 7	4, 12	1, 0	1, 0	4, 6	7, 5	1, 2	1, 0	1, 0	0, 1		1, 1
Re	0, 2	0, 1	10, 13	9, 9	11, 12	1, 0	0, 1	4, 5	4, 3	0, 2	0, 1	1, 0	0, 2		0, 2
Os	0, 2	2, 0	12, 11	9, 7	6, 6		1, 0	4, 6	3, 3	0, 2	1, 0	1, 0	1, 0		0, 1
Ir	1, 1	1, 1	11, 12	12, 4	3, 4	1, 0	1, 0	5, 9	5, 5	0, 2		1, 0	0, 2		0, 2
Pt	2, 0	0, 1	4, 25	11, 13	8, 10	1, 0	0, 1	6, 13	8, 11	0, 2	0, 1	1, 0	0, 2	1, 0	0, 2
Au[25]		0, 1	4, 3	6, 0	4, 0			5, 3	7, 3	0, 1			0, 1		1, 0
Hg[26]		1, 0	8, 3	10, 5	11, 2		0, 1	3, 2	2, 6	1, 2		1, 0	0, 2	0, 1	0, 2
Th§	1, 0		1, 2	0, 3	5, 8			1, 0	0, 1	0, 1					
U§		0, 1	1, 5	7, 5	16, 18	1, 2		1, 0	1, 1	0, 2			0, 1		

* No entries for Pm, Pa, and Ac. † Superscripts refer to entries in Appendix 1. § See references 1, 20–23 in Appendix 1.

state is not always well defined, where no assignment was possible then this is indicated by (−) rather than the roman numeral used elsewhere. Finally, cases where the ligand oxidation state is variable are identified (*e.g.* for O_2, *o*-quinones *etc*.) by references to the footnotes at the end of Table 9.6.3.3.

9.6.3.3. *Use of the 'Note' column*

The 'Note' column refers to the footnotes collected in Appendix 1. These record additional information as follows: (*a*) notable features of the distribution of distances, *e.g.* likely bias due to dominance by one structure of substructure, skewness, bimodality (subdivisions of the entry usually follow, which remove these features whenever possible); (*b*) further details of the chemical substructure, such as the exclusion of structures with particular *trans* ligands; (*c*) details of exclusion criteria used for a given entry or group of entries, such as the constraint that the two *M*—Cl distances, in bridging (μ_2) chloride complexes, differ by <0.1 Å (section 10.1.1.2); (*d*)

references to previously published surveys of crystallographic results relevant to the entry in question. We do not claim that these entries are in any way comprehensive and we would be grateful to authors for notification (to AGO) of any omissions. This will serve to improve the content of any future version of Table 9.6.3.3.

9.6.3.4. *Locating an entry in Table 9.6.3.3*

Table 9.6.3.2 provides a 'guide' to the contents of Table 9.6.3.3. The number of entries for which individual examples of *M*—ligand distances are quoted, and the number of entries for which statistics are given in Table 9.6.3.3 are listed for each metal. Inspection of Table 9.6.3.2 shows which element pairs have no bond lengths recorded in Table 9.6.3.3. Thus, while there are no cobalt–fluorine distances in Table 9.6.3.3, there are 6 classes of cobalt–phosphorus distances for which there are examples quoted and 10 for which statistics are given.

Let us say one wished to find typical lengths for cobalt–triethylphosphine (Co—PEt_3) bonds. Table 9.6.3.1 shows that PEt_3, a tertiary phosphine, falls under ligand class 8.5. In Table 9.6.3.3, the section dealing with such ligands starts with 8.5.1 (trimethylphosphine) followed by 8.5.2 (triethylphosphine). Under this section, we find that Co—PEt_3 bonds average 2.208 Å in length (with sample standard deviation $\sigma = 0.039$ Å), and in cobaltacarbaboranes the average is 2.224 Å, and for (η-$C_5H_5CoL_2$) species the average is 2.147 Å.

Polydentate ligands with different elements able to act as contact atoms present particular difficulty. The convention we have adopted is to place the individual *M*—*L* interatomic distances under separate entries according to the contact element. Thus, thiocyanate (SCN) appears in ligand class 4.4.5 when *N*-bonded (*i.e.* isothiocyanate *M*—NCS) *and* in ligand class 9.3 when *S*-bonded (*M*—SCN). When bridging with *both* S and N bonded to metals (as in *M*—NCS—*M'*), then the *M*—N distances (as well as *all* intraligand distances) will be under ligand class 4.5 and *M'*—S distances under ligand class 9.3. Thus, in such cases the intraligand dimensions will accompany the metal–ligand distances in the first ligand class (*i.e.* the lower-numbered class).

9.6.4. Discussion

Table 9.6.3.3 has been derived from the CSD, and, as a result, does not contain every precisely determined metal–ligand interatomic distance. For example, there are many ammine (*M*—NH_3), carbonyl (*M*—CO), halide (*M*—Cl *etc.*), and aqua (*M*—OH_2) complexes that do not fall within the scope of the CSD. For such bond types, and other metal–non-metal bond-length information, the interested reader is referred to the Inorganic Crystal Structure Database (Bergerhoff, Hundt, Sievers & Brown, 1983).

The tabulation given here is a first attempt to obtain average dimensions for (*d*- and *f*-block) metal–ligand and intraligand bonds. Inspection of Table 9.6.3.3 shows that, in general, the sample standard deviations of metal–contact-atom interatomic distances are typically larger than those of the intraligand distances [*e.g.* for Fe—PPh_3 complexes (section 8.5.3), Fe—P mean 2.237, σ 0.038 Å, *cf.* P—C mean 1.834, σ 0.011 Å]. There are several factors that cause this phenomenon. Firstly, in many (but not all) cases no account has been taken of substituent effects at the metal, such as the *trans* influence of other ligands. In contrast, the substituent pattern at the ligand is usually well defined; therefore, the chemical causes for variation in the metal–ligand and intraligand distances are different. Secondly, it is likely that metal–ligand bonds are softer, *i.e.* have lower force constants, than the intraligand bonds, leading to a broader distribution of distances whatever the *cause* of variation. Finally, it should be noted that a substantial contribution to the standard deviation of both metal–ligand and intraligand distances comes from *random* errors arising most importantly from the rather poor location of light (B, C, N, O, F) atoms in the presence of 5*d*, 4*f*, and 5*f* metals (La–U). For example, C—O bond lengths

(*continued on page 884*)

Table 9.6.3.3. *Interatomic distances* (Å)

Bond	Substructure (coordination number, oxidation state, comment)	*d*	*m*	σ	q_l	q_u	*n*	Note
1.1.1.1 Hydrides (terminal)								*27*
Fe–H	all BASLIQ10	1.609	1.610	0.004	1.605	1.612	6	
Zn–H	see MAEMAZ11 (1.617)							
Mo–H	see HCYPMO02 (1.684)							
Rh–H	see CONFEQ01 (1.578, 1.583)							
Ta–H	see TACPTH (1.769, 1.774, 1.776)							
W–H	all IPPHWH01	1.732	1.734	0.010	1.725	1.740	6	
Re–H	(8), (-)	1.684	1.681	0.015	1.676	1.697	12	
Os–H	all THMPOS01	1.659	1.656	0.017	1.646	1.677	4	
Ir–H	all DETSOK	1.603	1.607	0.021	1.582	1.623	5	
Pt–H	see CAKNEH01 (1.610)							
1.1.1.2 Hydrides (μ_2-H)								*27*
Cr–H	see KCPTCR01 (1.725, 1.723)							
Fe–H	all HMYCFE01	1.670	1.670	0.001	1.669	1.672	4	
Mo–H	(6,7), (II,III)	1.842	1.843	0.023	1.819	1.864	4	
Ru–H	(*), (-)	1.782	1.776	0.019	1.773	1.791	22	
Rh–H	(4,*), (I)	1.775	1.768	0.040	1.738	1.811	8	
W–H	(6), (0)	1.900	1.897	0.028	1.876	1.926	5	
Re–H	(8,*), (I,IV)	1.832	1.832	0.039	1.793	1.870	16	
Os–H	(*), (-)	1.817	1.824	0.029	1.798	1.837	34	
Ir–H	see CUSGAY (1.821, 1.847)							
Pt–H	see CAKNEH01 (range 1.656–2.049)							
1.1.1.3 Hydrides (μ_3-H)								*27*
Co–H	see HMPCIC01 (1.728, 1.731, 1.742)							
Ni–H	all TCPNIH11	1.691	1.684	0.022	1.673	1.715	9	
Rh–H	see HMPCRH11(1.847, 1.855, 1.873)							

Table 9.6.3.3. *Interatomic distances (Å) (cont.)*

Bond	Substructure (coordination number, oxidation state, comment)	*d*	*m*	σ	q_l	q_u	*n*	Note
1.2.1.1 BH_4 [M–(μ_2-H)–B]								*28*
Cu–H	see TMPCUB01 (1.698)							
1.2.1.2 BH_4 [M–(μ_2-H)$_2$–BH_2]								
Co–H	see BEGBIY01 (1.707, 1.740)							
Th–H	see MCHFHB10 (2.069, 2.120)							
2.1.1 Borohydrides [M(–H–)BH_2R]								*28*
Sc–B	see BOVCAQ (2.528)							
Ti–B	see CPCLBT (2.178)							
Cr–B	see BOSKUP (2.294)							
Co–B	(–), (I): (η^2-BH_4, μ_2-η^1, $\eta^{1'}$-BH_4)	2.218	2.224	0.030	2.199	2.241	6	
Ni–B	see YBAENI (3.088)							
Cu–B	see BOLJAN (2.441), CICFID (2.204, 2.232), PHRLCU (2.079), TMPCUB01 (2.517)							
Zn–B	see CAPFOO (2.219), NBCZNB10 (2.252, 2.253)							
Y–B	see BUWBAW (2.478, 2.836), HBTHFY (2.574, 2.680)							
Zr–B	see CANFAY (2.335)							
Mo–B	see HBMPMO (2.468)							
Ru–B	see CIZBOC (2.237)							
Os–B	see COCKOU (2.300)							
U–B	(–), (III,IV): all	2.569	2.510	0.136	2.494	2.644	16	
	(–), (IV): [(μ-H)$_3$BR]	2.493	2.498	0.040	2.459	2.515	11	
2.2.1 Boranes/carbaboranes (not H-bridged) (see also 3.21.1)								*29*
Ti–B	see CEXTII (2.355, 2.375, 2.383)							
V–B	see BUPLAZ10 (2.246, 2.322, 2.333)							
Cr–B		2.228	2.252	0.054	2.178	2.266	9	
Mn–P		2.255	2.231	0.058	2.213	2.306	9	
Fe–B		2.140	2.135	0.066	2.103	2.179	111	
Co–B		2.086	2.082	0.073	2.036	2.124	270	
Ni–B		2.106	2.108	0.049	2.071	2.142	41	
Cu–B	see BOTPCU (2.209, 2.237), TPCUBF (2.273)							
Ru–B	:all	2.263	2.234	0.167	2.041	2.377	16	*30*
	:short <2.10	2.035	2.033	0.012	2.026	2.046	5	
	:long >2.25	2.367	2.355	0.067	2.318	2.399	11	
Rh–B		2.224	2.219	0.061	2.188	2.252	55	
Pd–B		2.237	2.244	0.041	2.197	2.260	10	
Ag–B	see TPACUB (2.352, 2.420, 2.522)							
W–B		2.403	2.393	0.036	2.381	2.416	7	
Re–B		2.292	2.287	0.056	2.239	2.349	6	
Os–B	see BUVROZ (2.147, 2.184, 2.283)							
Ir–B		2.236	2.205	0.083	2.183	2.287	29	
Pt–B		2.243	2.244	0.062	2.213	2.283	94	
Au–B		2.238	2.228	0.034	2.206	2.256	11	
Hg–B	see COBHGA (2.201, 2.286), TPMCDB10 (2.204, 2.498, 2.521)							
2.2.2 Boranes/carbaboranes [M(–H–)B] (hydrogen located)								*29*
Mn–B		2.228	2.222	0.025	2.208	2.254	4	
Fe–B	see TPCUBF (2.115)							
Co–B		2.100	2.086	0.032	2.079	2.125	15	
Cu–B	see TPCUBF (2.164)							
Zn–B	see CEXSAZ (2.264, 2.274)							
Ru–B	see COKTIF (2.327, 2.462)							
Rh–B		2.342	2.330	0.040	2.311	2.384	4	
W–B	see COVROU (2.413)							
Ir–B	see BELJEH (2.290, 2.281), CTPIRB (2.250), TPICBO (2.452, 2.480)							
2.3.1 Boracycles (see also 3.21.2 and 4.23.1)								*31–33*
V–B	see BOKXEE (2.369)							
Cr–B	excluding BRNOCR (2.566)	2.340	2.349	0.026	2.312	2.360	7	
Mn–B		2.291	2.282	0.047	2.252	2.299	7	
Fe–B		2.227	2.185	0.097	2.163	2.279	13	
Co–B		2.123	2.097	0.076	2.073	2.189	12	
Ni–B	see CIDBOG (2.411), CPBORN (2.175), FMBCNI (2.260), SIBONI (2.226), VIBONI (2.500, 2.550)							
3.1.1.1 Carbide (μ_4-C)								*34, 35*
Hg–C	see FAHGME (2.042)							
3.1.1.2 Carbide (μ_5-C)								*34, 35*
Ru–C		2.049	2.043	0.057	2.004	2.084	40	
Os–C		2.060	2.056	0.059	2.004	2.108	35	
3.1.1.3 Carbide (μ_6-C)								*34, 35*
Ru–C		2.060	2.063	0.023	2.040	2.076	60	
Rh–C	see CBACRC (2.122, 2.132, 2.125)							

Table 9.6.3.3. *Interatomic distances (Å) (cont.)*

Bond	Substructure (coordination number, oxidation state, comment)	*d*	*m*	σ	q_l	q_u	*n*	Note
3.2.1.1 Carbyne/alkylidyne (terminal C*R*, *R* = any C)								*36, 37*
C–C		1.468	1.475	0.031	1.436	1.495	18	
Cr–C	(6), (-)	1.702	1.710	0.029	1.679	1.720	5	*38*
Mo–C	see BENFEF (1.799)							
Ta–C	see BESPIY (1.850), TABYCP10 (1.849)							
W–C	(5,6), (IV,VI)	1.815	1.821	0.041	1.777	1.840	9	
Re–C	see CECROR (1.742)							
3.2.1.2 Carbynes/alkylidynes (μ_2-C*R*, *R* = any C, H)								*39*
C–C		1.480	1.478	0.030	1.452	1.510	4	
Ru–C	see VCPRUB10 (1.933, 1.941), CIFXOE (1.936)							
W–C		1.955	1.947	0.021	1.940	1.973	6	
3.2.1.3 Carbynes/alkylidynes (μ_3-C*R*, *R* = any C, H)								
C–C		1.510	1.505	0.025	1.494	1.526	21	
Fe–C		1.928	1.933	0.024	1.910	1.939	15	
Co–C		1.896	1.895	0.035	1.874	1.920	27	
Mo–C		2.059	2.056	0.019	2.042	2.075	11	
Ru–C		2.084	2.089	0.027	2.067	2.102	6	
Rh–C	all *R* = H	1.964	1.970	0.020	1.945	1.980	7	
Os–C	all COTPOQ01	2.101	2.102	0.004	2.097	2.105	6	
3.2.2.1 Amino carbynes (terminal CNR_2)								
(*M*)C–N		1.322	1.334	0.053	1.271	1.368	5	
N–C		1.469	1.470	0.027	1.441	1.485	8	
Cr–C	see BAMCOH (1.750), SNCOCR (1.743)							
Mo–C	see BITKIY (1.797)							
W–C	see CAVREW (1.776, 1.747)							
3.2.3.1 Thiocarbynes (terminal CS*R*)								
C–S	(1.712, 1.713)							
Mo–C	see CAWSAU (1.801)							
W–C	see TPCPTW (1.810)							
3.3.1.1 Vinylidenes/alkenylidenes (terminal CCR_2)								*40*
C=C		1.318	1.312	0.032	1.295	1.329	7	
Fe–C	see COPMID (1.780, 1.799)							
Mo–C	see BUJFIV (1.918), CVMOMP10 (1.833)							
Ru–C	see BOJJUF (1.845)							
Rh–C	see CAYMAQ (1.820)							
W–C	see CEFVUE (1.983)							
3.3.1.2 Vinylidenes/alkenylidenes (μ_2-CCR_2)								
C=C		1.317	1.315	0.023	1.305	1.326	7	
Mn–C	see EYCCMN (1.971, 1.978)							
Fe–C	see CHPECI (1.969, 1.955)							
Co–C		1.885	1.885	0.021	1.864	1.904	4	
Ru–C	see VCPRUA10 (2.025, 2.034)							
Rh–C	see BECVOU (1.987, 1.989)							
Os–C	see BEXJUJ (2.096, 2.102)							
3.4.1.1 Acetylides/alkynyls (terminal CC*R*)								
C≡C		1.188	1.188	0.017	1.178	1.202	16	
C–C		1.456	1.451	0.030	1.436	1.465	16	
V–C	see CIJLUC (2.074)							
Fe–C	see CPFPEY (1.920)							
Rh–C	see BIMTEW (1.939)							
Pd–C	see EYPIPD (1.953)							
W–C	see BONSUS (2.134)							
Ir–C	see CEFPEI (2.041)							
Pt–C	(4,6), (II,IV)	1.992	2.000	0.032	1.985	2.009	8	*41*
Hg–C	see PEYHGP (2.047, 2.031)							
3.4.1.2 Acetylides/alkynyls (μ_2-CC*R*)†								*42*
C–C		1.231	1.232	0.026	1.206	1.256	4	
Fe–Cσ	see ACYPCI (1.890)							
–Cπ	(2.117, 2.283)							

Table 9.6.3.3. *Interatomic distances (Å) (cont.)*

Bond	Substructure (coordination number, oxidation state, comment)	*d*	*m*	σ	q_l	q_u	*n*	Note
3.4.1.2 Acetylides/alkynyls (μ_2-CC*R*)† (*cont.*)								
Ru–Cσ	see BAYCOS (2.047), BOBTOB (2.044)							
–Cπ	(2.323, 2.423); (2.285, 2.508)							
Pt–Cσ	see MSIPEP (1.964)							
–Cπ	(2.141, 2.468)							
3.5.1.1 Cyano (terminal CN)								*43*
C–N		1.146	1.146	0.014	1.138	1.154	168	
V–C	see CIRSAX (2.067), CIRSEB (2.088)							
Cr–C	(6), (-): all	2.058	2.063	0.024	2.031	2.080	8	*7*
Mn–C	see CAZJAO10 (1.996, 1.989)							
Fe–C	(5,6), (0,II,III): all	1.937	1.935	0.023	1.923	1.950	33	
Co–C	(5,6), (-): all	1.896	1.900	0.019	1.883	1.907	50	*8*
Ni–C	(4,5), (-): all	1.883	1.868	0.076	1.852	1.873	30	
	excluding 2 > 2.1	1.864	1.868	0.021	1.851	1.872	28	
Cu–C	(3,5), (-): all	2.003	1.975	0.101	1.924	2.098	5	*12*
Zn–C	(4), (-): all	2.000	1.997	0.012	1.991	2.013	4	
Mo–C	(6,7,8), (-): all	2.167	2.166	0.021	2.155	2.184	21	*15, 44*
Ru–C	see BEPJIP (2.025)							
Pd–C	see BEJHUT (1.997)							
Ag–C	see COLSEB (2.093)							
Pt–C	(4,5), (II): all	1.943	1.931	0.031	1.916	1.977	5	
Au–C	see CIGCOK (2.003)							
Hg–C	see BINRAR (2.187, 2.174), CAHRUY (2.100)							
3.5.1.2 Cyano (μ_2-CN)† (see also 4.4.2)								
C–N		1.143	1.147	0.016	1.132	1.153	21	
Cr–C	see CYCRTF (1.999, 1.972, 1.965)							
Mn–C	see CAZJAO10 (1.995)							
Fe–C	(6), (III)	1.948	1.942	0.025	1.928	1.972	6	
Ni–C	(4), (II)	1.859	1.853	0.017	1.847	1.877	4	
Cu–C	(4), (I)	1.951	1.965	0.030	1.914	1.974	6	*12*
Pd–C	see BUSRIQ (2.011)							
3.6.1.1 Isocyanides (terminal CN*R*, *R* = any C)								*45, 46*
C–N		1.149	1.147	0.016	1.139	1.157	220	
V–C	see CIRSAX (2.003), CLBCNV (2.189)							
Cr–C	(6,7), (0-III): *R* = Ph, ^{t}Bu, Bz	1.996	2.003	0.038	1.969	2.014	21	*7*
Mn–C	(6), (-): *R* = Ph, ^{t}Bu, Me	1.927	1.924	0.028	1.900	1.947	15	
Fe–C	(5,6,*), (0-II): all	1.862	1.867	0.048	1.819	1.901	12	
	(6), (II): all	1.874	1.874	0.043	1.832	1.901	7	
Co–C	see BISJOC (1.851, 1.846, 1.866)							
Ni–C	(3,4), (0): *R* = ^{t}Bu	1.853	1.854	0.021	1.838	1.870	6	
Cu–C	(3,4), (I): *R* = ^{t}Bu, *p*-Tol, cyh	1.896	1.895	0.009	1.890	1.905	7	
Nb–C	(7,8), (-): *R* = ^{t}Bu	2.241	2.237	0.036	2.208	2.270	6	
Mo–C	(5-8), (0-IV)	2.107	2.115	0.040	2.089	2.135	61	*15*
	(5-8), (II)	2.111	2.115	0.032	2.094	2.131	56	
	(5-7), (II): *R* = ^{t}Bu	2.108	2.115	0.030	2.089	2.125	36	
Ru–C	(6,*), (-)	1.986	1.997	0.040	1.941	2.014	7	
Rh–C	(4-6), (-)	1.968	1.969	0.036	1.955	1.983	21	
	(4), (-)	1.956	1.962	0.031	1.947	1.975	13	
Pd–C	(3-5), (-)	1.985	1.974	0.036	1.958	2.020	18	*47*
	(4), (-)	1.978	1.972	0.035	1.955	1.994	15	
Ag–C	see BUXGAC (2.162, 2.136)							
Pr–C	see CXINPR10 (2.654)							
W–C	(7), (II): *R* = ^{t}Bu	2.102	2.105	0.035	2.070	2.125	11	
Re–C	(6,7), (I-II)	2.002	2.008	0.022	1.980	2.018	12	
Os–C	see CIRJAO (1.983, 2.004), HOSTBC10 (2.032)							
Ir–C	see MCPEIR (1.945), MICPIR10 (1.986)							
Pt–C	(4,5,*), (-)	1.936	1.924	0.059	1.896	1.968	13	
	(4,5), (-)	1.944	1.966	0.036	1.912	1.968	7	
3.6.1.2 Isocyanides (μ_2-CN*R*)								
C–N		1.221	1.227	0.038	1.196	1.241	15	
Fe–C		1.941	1.941	0.025	1.920	1.948	12	
Ni–C	all MINCNI	1.881	1.880	0.022	1.861	1.903	4	
Os–C	see HYBIOS (2.072, 2.039)							
Pt–C	all BIDCAS	2.100	2.086	0.070	2.038	2.170	12	
3.7.1.1 Carbon monoxide (terminal CO)								*48*
C–O		1.145	1.143	0.020	1.132	1.156	10022	

Table 9.6.3.3. *Interatomic distances (Å) (cont.)*

Bond	Substructure (coordination number, oxidation state, comment)	*d*	*m*	σ	q_l	q_u	*n*	Note
3.7.1.1 Carbon monoxide (terminal CO) (*cont.*)								
Ti–C		2.003	1.997	0.030	1.980	2.030	5	*49*
V–C		1.946	1.946	0.037	1.924	1.974	60	
Cr–C		1.866	1.867	0.037	1.835	1.895	925	*38*
Mn–C		1.808	1.805	0.034	1.784	1.833	789	
Fe–C		1.782	1.784	0.030	1.765	1.801	2572	*50*
Co–C		1.780	1.781	0.034	1.758	1.801	662	
Ni–C		1.771	1.776	0.029	1.750	1.794	34	*51*
Cu–C		1.787	1.782	0.019	1.776	1.807	18	*12*
Zr–C	see CCPZRA (2.187)							*49*
Nb–C		2.073	2.073	0.028	2.056	2.092	26	
Mo–C		1.978	1.973	0.041	1.947	2.007	748	*15*
Tc–C		1.884	1.883	0.021	1.866	1.904	4	*17*
Ru–C		1.896	1.896	0.036	1.873	1.919	1453	
Rh–C		1.847	1.846	0.040	1.821	1.869	238	
Ta–C	see BISZIM (2.036), BUVGII (2.083), CPMPTA (2.008)							
W–C		2.002	2.007	0.043	1.971	2.034	508	*24*
Re–C		1.936	1.933	0.050	1.898	1.978	370	
Os–C		1.902	1.903	0.036	1.880	1.927	1443	
Ir–C		1.870	1.876	0.042	1.839	1.898	148	
Pt–C		1.853	1.854	0.056	1.821	1.878	29	
3.7.1.2 Carbon monoxide (μ_2-CO)								*52*
C–O		1.171	1.171	0.022	1.159	1.183	279	
Mn–C	(all)	1.940	1.930	0.021	1.926	1.955	8	
	(M–C–M < 70°)	1.929	1.928	0.005	1.924	1.933	6	
Fe–C	(all)	1.941	1.925	0.041	1.914	1.971	104	
	(M–C–M < 80°)	1.985	1.995	0.037	1.953	2.018	20	
	(80° < M–C–M < 86°)	1.930	1.921	0.034	1.908	1.946	80	
Co–C		1.914	1.919	0.046	1.883	1.947	114	
Ni–C		1.882	1.880	0.021	1.870	1.892	14	
Cu–C		1.861	1.862	0.015	1.854	1.872	6	
Mo–C	(all)	2.127	2.091	0.095	2.045	2.237	6	
	(Mo=Mo only)	2.068	2.064	0.027	2.045	2.095	4	
Ru–C	(all)	2.072	2.055	0.047	2.038	2.099	66	
	(non-clusters)	2.040	2.039	0.021	2.026	2.055	20	
	(clusters)	2.086	2.087	0.048	2.043	2.114	46	
Rh–C	(all)	2.040	2.037	0.055	1.994	2.076	180	
	(M–C–M < 85°)	2.057	2.058	0.059	2.000	2.111	106	
	(85° < M–C–M < 95°)	2.018	2.029	0.037	1.984	2.046	68	
	(M–C–M > 115°)	1.983	1.982	0.007	1.977	1.990	4	
Pd–C	(all)	2.004	1.997	0.039	1.979	2.015	14	
Re–C	(all BAWTOI)	2.073	2.072	0.009	2.063	2.080	6	
Os–C		2.081	2.063	0.057	2.042	2.122	6	
Ir–C		2.065	2.072	0.039	2.026	2.093	30	
Pt–C		2.044	2.039	0.032	2.018	2.063	6	
3.7.1.3 Carbon monoxide (μ_3-CO)								*42*
C–O		1.190	1.191	0.038	1.173	1.202	33	
Fe–C		2.002	1.990	0.037	1.980	1.997	15	
Co–C		1.950	1.949	0.032	1.937	1.962	15	
Ni–C	see TCPDNI01 (1.931, 1.932)							
Ru–C		2.171	2.169	0.020	2.153	2.193	8	
Rh–C	see POSHRH10 (2.205, 2.155, 2.238)							
Pd–C	see BUJYIO (2.190, 2.078, 2.157)							
3.8.1.1 CS (terminal)								
C–S		1.563	1.570	0.030	1.536	1.587	5	
Cr–C	see BUGRIE (1.778), MBZCRC (1.797), TLCSCR (1.751)							
Mn–C	see ICPNMN (1.803)							
Fe–C	see BEPDEF (1.662)							
3.8.1.2 CS (μ_2-CS)								
C–S	(1.597, 1.606, 1.618)							
Fe–C	all CPTCFF	1.886	1.889	0.007	1.878	1.891	4	
3.9.1.1 Carbene/alkylidene (terminal CH_2)								*36*
Re–C	see CAHZUG (1.898)							
Os–C	see CAMTEP (1.924)							
3.9.1.2 Carbenes/alkylidenes (μ_2-CR_2, R = any C, H)								*39, 53*
Mn–C	see BANGIG10 (2.026), MYCCMN10 (2.018, 2.019)							

Table 9.6.3.3. *Interatomic distances (Å) (cont.)*

Bond	Substructure (coordination number, oxidation state, comment)	*d*	*m*	σ	q_l	q_u	*n*	Note
3.9.1.2 Carbenes/alkylidenes (μ_2-CR_2, R = any C, H) (*cont.*)								
Fe–C		2.006	1.990	0.045	1.974	2.052	6	
Co–C		1.934	1.925	0.025	1.909	1.961	7	
Ru–C		2.085	2.095	0.056	2.076	2.112	12	
Rh–C		2.048	2.059	0.033	2.017	2.075	15	
W–C	excluding BIJJAF (2.127, 2.436)	2.298	2.296	0.035	2.266	2.331	4	
Re–C	all CEHFEA	2.141	2.132	0.030	2.119	2.171	4	
Os–C	excluding CODCON (1.922, 1.909)	2.160	2.155	0.041	2.136	2.192	20	
Au–C		2.112	2.102	0.026	2.095	2.139	4	
3.9.2.1 Carbenes/alkylidenes (terminal CHR)								
C–C		1.490	1.493	0.027	1.462	1.513	14	
Ta–C	(5,6,8), (V): all	1.963	1.938	0.065	1.932	2.030	7	*54, 55*
W–C	(5-7), (IV,VI)	1.953	1.942	0.086	1.871	2.041	5	*38, 55*
Re–C	see BOBYAS (1.949), CECROR (1.873)							
3.9.3.1 Carbenes/alkylidenes (terminal CR_2)								
C–C	[R = C(sp^3)]	1.503	1.509	0.024	1.500	1.519	12	
Mn–C	see CERJIS (1.853), MCBCMN (1.864, 1.871)							
Fe–C	see CPCFEA10 (1.978)							
W–C	see DPCBWC (2.132, 2.154)							*38, 55*
Ir–C	see PYBPIR (1.998)							
3.9.4.1 Alkoxy carbenes [terminal CR(OR), R = any C]								
(M)C–O		1.318	1.314	0.023	1.300	1.338	18	
(M)C–C		1.501	1.503	0.032	1.479	1.524	18	
O–C		1.466	1.459	0.024	1.452	1.484	18	
Cr–C	(6), (-)	2.012	2.006	0.029	1.988	2.039	5	*38, 55*
Mn–C	see BOCWAR (1.848), MNXCMN (1.890), NPMCMN (1.950)							*55*
Co–C	see PGECBC (1.912)							
Mo–C	see BEBTUX (2.087)							
W–C	(6), (-)	2.161	2.161	0.014	2.148	2.175	4	
Re–C	see CMNCBR (2.098)							
Os–C	see BODGUW10 (1.981)							
Pt–C	see CIPTMN (1.889), EOBCPT10 (1.920)							
3.10.1.1 Vinyls (σ-CRCR_2)†								*41*
C=C		1.345	1.344	0.024	1.333	1.357	98	
Ti–C	(8), (IV)	2.215	2.239	0.042	2.171	2.243	7	
Cr–C	all MPEYCR10	2.035	2.033	0.009	2.027	2.045	4	
Mn–C	see BIZJEZ (1.985), CECCIW (2.009), MASBCM (2.027)							
Fe–C	(5,6), (II)	1.991	1.997	0.039	1.954	2.030	10	
Co–C	(6), (-)	1.934	1.932	0.019	1.914	1.946	8	
Ni–C	(4,5), (-)	1.892	1.900	0.017	1.874	1.903	4	
Zr–C	see CPPHZR (2.249, 2.265)							
Mo–C	(7), (-)	2.204	2.223	0.049	2.151	2.247	5	
Ru–C	see CNBRUB (2.073), CXFMPR (2.082), PCFMRU10 (2.034)							
Rh–C		2.040	2.060	0.054	1.986	2.085	5	
Pd–C	(4), (II)	2.000	2.006	0.024	1.989	2.011	16	*47*
Hf–C	see CPTPHF (2.190, 2.219)							
W–C	see BEDGAS (2.202), COPMEZ (2.275), MCTCEW (2.194)							
Os–C	see CIRNOG (2.052)							
Ir–C	(5,6), (-)	2.071	2.073	0.044	2.036	2.103	6	
Pt–C	(4,5), (-)	2.024	2.022	0.037	1.991	2.058	17	*41*
Au–C	see BULPED (2.039, 2.045)							
3.10.1.2 Vinyls (η^2-CRCR_2)†								
C_α–C_β		1.408	1.407	0.013	1.418	1.442	8	
Mo–C_α		1.936	1.937	0.020	1.917	1.954	4	
–C_β		2.292	2.293	0.027	2.265	2.316	4	
W–C_α		1.918	1.907	0.030	1.898	1.949	4	
–C_β		2.251	2.249	0.078	2.181	2.324	4	
3.10.1.3 Vinyls (μ_2-η^1, η^2-CRCR_2)†								*39*
C_α–C_β		1.408	1.407	0.022	1.395	1.421	43	
Mn^1–C_α	see BOWYOB (2.058, 2.053)							
Mn^2–C_α	(2.086, 2.102)							
–C_β	(2.263, 2.263)							
Fe^1–C_α		1.996	2.004	0.036	2.000	2.009	8	
Fe^2–C_α		2.102	2.095	0.039	2.079	2.111	8	

Table 9.6.3.3. *Interatomic distances (Å) (cont.)*

Bond	Substructure (coordination number, oxidation state, comment)	*d*	*m*	*σ*	q_l	q_u	*n*	Note
3.10.1.3 Vinyls (μ_2-η^1, η^2-$CRCR_2$)† *(cont.)*								
Fe^2–C_β		2.219	2.197	0.046	2.183	2.260	8	
Co^1–C_α	see BOCCOC (1.973, 1.968), BULYOW (1.981)							
Co^2–C_α	(2.009, 2.011), (1.995)							
–C_β	(2.132, 2.115), (2.127)							
Mo^1–C_α	see BEDDAP (2.151, 2.140), CAMKIK (2.141)							
Mo^2–C_α	(2.181, 2.181), (2.232)							
–C_β	(2.301, 2.301), (2.446)							
Ru^1–C_α		2.079	2.075	0.043	2.060	2.089	13	
Ru^2–C_α		2.221	2.227	0.057	2.191	2.260	13	
–C_β		2.276	2.276	0.042	2.247	2.284	13	
Rh^1–C_α	see BATNIT (2.045), FMPENR (2.025, 2.028)							
Rh^2–C_α	(2.100), (2.058, 2.102)							
–C_β	(2.222), (2.139, 2.205)							
W^1–C_α	(6,7), (O,II,IV): all	2.158	2.145	0.043	2.128	2.203	6	
W^2–C_α	(6), (IV): excluding 2.266, 2.124	2.412	2.412	0.034	2.380	2.445	4	
–C_β	(6), (II,IV): excluding 1 at 2.220	2.458	2.470	0.047	2.410	2.500	5	
Re^1–C_α	see COTFAS (2.170, 2.098)							
Re^2–C_α	(2.359, 2.255)							
–C_β	(2.352, 2.307)							
Os^2–$^1C_\alpha$	see CHVINO (2.108), HPETOS (2.154), UCHXOS (2.170)							
Os^2–C_α	(2.273), (2.151), (2.188)							
–C_β	(2.362), (2.300), (2.311)							
3.11.1.1 σ-Aryls (η^1-Ar)†								
C^1–C^2		1.396	1.396	0.021	1.381	1.409	398	
C^2–C^3		1.393	1.392	0.022	1.379	1.406	398	
C^3–C^4		1.378	1.379	0.025	1.364	1.395	399	
Ti–C	see PFPBTI (2.135), PSIBTI (2.161)							
V–C	(4, 6), (II,III)	2.114	2.115	0.012	2.102	2.124	4	
Cr–C	(5,6), (II,III)	2.075	2.072	0.019	2.061	2.089	10	*38*
Mn–C	(6), (I)	2.064	2.059	0.021	2.044	2.083	6	
Fe–C	(4,6), (I,II)	2.031	2.022	0.062	1.985	2.065	6	
	(6), (I,II)	2.008	2.021	0.021	1.974	2.030	5	
Co–C	see DMDECO01 (1.995), ETPSCO10 (1.997), TOPFCO10 (1.931)							
Ni–C	(4,5), (II,III)	1.917	1.929	0.038	1.893	1.942	18	
Cu–C	see CODJIO (2.020)							
Mo–C	(4,5,7), (0,II,IV): all	2.193	2.176	0.054	2.164	2.195	11	*38*
	(4,5), (II,IV)	2.172	2.169	0.016	2.160	2.187	9	
Ru–C	(5,6), (II)	2.092	2.121	0.057	2.013	2.136	7	
Rh–C	(5,6), (II,III)	2.011	2.000	0.026	1.990	2.037	9	
Pd–C	(4,*), (II): all	1.981	1.987	0.032	1.965	2.002	28	*47*
Lu–C	see CILCUV (2.425, 2.427, 2.455)							
Ta–C	(5), (V)	2.199	2.173	0.073	2.147	2.276	4	
Re–C	see PHTPRE (2.024, 2.029)							
Os–C	(6,*), (-)	2.090	2.092	0.032	2.058	2.120	4	
Ir–C	(4-6,*), (I,III): all	2.070	2.067	0.038	2.043	2.092	17	
	(6), (III)	2.053	2.049	0.024	2.037	2.071	10	
Pt–C	(4-6), (I,II,IV): all	2.049	2.061	0.046	2.033	2.079	35	*41*
	(4), (I,II)	2.055	2.062	0.039	2.043	2.079	28	
Au–C	(2-4,*), (I,III): all	2.059	2.062	0.024	2.052	2.073	22	
	(2,3), (I)	2.053	2.050	0.009	2.045	2.062	5	
	(4), (III)	2.062	2.068	0.031	2.055	2.081	13	
Hg–C	(2-4,*), (II): all	2.086	2.088	0.040	2.054	2.120	24	
	(2,3), (II)	2.053	2.057	0.027	2.040	2.075	12	
	(*), (-): all BIPHHG	2.120	2.119	0.014	2.115	2.126	12	
3.12.1.1 Acyls [η^1-C(O)R]†								
C=O		1.210	1.209	0.023	1.195	1.218	60	
Mn–C	see PNMNCP (2.012), PYRMNC (2.076)							
Fe–C	(6), (II)	1.997	2.004	0.033	1.967	2.028	18	
Co–C	see BOBSUG (1.915), OXCOCP10 (2.055)							
Ni–C	(4,5), (II)	1.850	1.870	0.059	1.788	1.893	4	
Mo–C	see BOLCIO10 (2.049), MABUMO10 (2.168)							
Ru–C	see BEWMAR (2.091)							
Rh–C	(5,6), (III): all	1.995	1.996	0.031	1.969	2.006	10	
Pd–C	(4), (II): all	1.982	1.992	0.029	1.951	2.002	4	
Re–C	(6), (I)	2.190	2.183	0.027	2.175	2.214	7	
Os–C	see BUYMAJ (2.161)							
Ir–C	see NRBIRB (1.971), POIRID (2.067)							
Pt–C	(4), (II)	1.991	2.000	0.025	1.969	2.008	7	

Table 9.6.3.3. *Interatomic distances (Å) (cont.)*

Bond	Substructure (coordination number, oxidation state, comment)	*d*	*m*	σ	q_l	q_u	*n*	Note
3.12.1.2	Acyls [η^2-C(O)*R*]† (see also 5.25.1)							
C=O		1.240	1.238	0.014	1.227	1.248	10	
Zr–C	see BOPSII (2.181, 2.186)							
Mo–C		2.014	2.020	0.011	2.003	2.023	6	
W–C	see BUSYIX (2.030), COSSOS (2.000)							
3.13.1.1	Methyl (terminal CH_3)							
Ti–C	see BASMOX (1.969), INDMTI (2.206)							
Cr–C	see CAMVER (2.168)							
Mn–C	(6), (IV): all CAJHOK	2.095	2.105	0.030	2.068	2.124	4	
Fe–C	see BNTLFE (2.080), CEDMON (2.065), CMZTFE (2.077)							*50*
Co–C	(6), (III)	2.014	2.014	0.023	1.993	2.032	16	
Ni–C	see BAPKEI (2.035), PEAMNI (2.023)							*56*
Zr–C	IV, (4-6,8)	2.292	2.279	0.049	2.257	2.346	8	
Nb–C	see CPSNBA (2.346), CPSNBB (2.327)							*54*
Mo–C	(5-7), (II-IV,VI): all	2.254	2.282	0.065	2.189	2.296	15	
Ru–C	(5,6), (II)	2.179	2.156	0.045	2.143	2.226	5	
Rh–C	(5,6), (II,III)	2.092	2.101	0.027	2.064	2.113	4	
Hf–C	(8), (IV)	2.275	2.267	0.049	2.233	2.325	4	
Ta–C	(6,7), (III,V)	2.217	2.215	0.035	2.181	2.247	7	*54*
W–C	(4-6), (II,III,VI)	2.189	2.187	0.039	2.166	2.213	13	
Re–C	(5,6), (I,III)	2.173	2.188	0.051	2.123	2.201	8	
Ir–C	see BEJBEX (2.218), CODPIR10 (2.133)							
Pt–C	(4-6), (II,IV): all	2.083	2.077	0.045	2.047	2.117	58	*41*
	(4,5), (II)	2.107	2.115	0.044	2.069	2.136	30	
	(6), (IV)	2.057	2.056	0.028	2.038	2.077	28	
Au–C	(4), (III)	2.066	2.045	0.045	2.030	2.118	18	*57*
Hg–C	(2-4), (II)	2.072	2.071	0.026	2.056	2.092	29	
Th–C	see COSZOZ (2.567)							
3.13.2.1	Primary alkyls [CH_2R, $R = C(sp^3)$]							
C–C		1.521	1.528	0.033	1.512	1.540	90	
Ti–C	see BILWIC (2.138, 2.152), BOYZOE (2.210)							
Mn–C	(4,6), (I,II)	2.176	2.173	0.024	2.154	2.199	5	
Fe–C	(6), (II)	2.091	2.082	0.030	2.071	2.102	8	
Co–C	(6), (II,III)	2.039	2.037	0.032	2.018	2.061	14	
Ni–C	see ACTPEN (1.970), BENIIB (1.973), DIPNIP (1.948)							*56*
Zn–C	see PMCZNE (1.964)							
Nb–C	see CPETNB (2.316), ONBCBU (2.322)							*54*
Mo–C	(4-8), (II-IV,VI): all	2.250	2.252	0.061	2.208	2.272	12	
	(4-8), (III,IV,VI)	2.230	2.234	0.042	2.195	2.269	10	
Ru–C	(4), (III): all CIBGEZ	2.036	2.033	0.010	2.029	2.045	6	
Rh–C	see CIDJEE (2.094), PBUDRI10 (2.098, 2.107)							
Pd–C	see BIHLOT01 (2.051), HIMPDA (2.009, 2.023)							
Ta–C	(5,7), (V)	2.225	2.208	0.056	2.183	2.289	6	*54*
W–C	see COPXIO (2.141, 2.126), DMPMPW10 (2.257)							
Re–C	see COMPRH (2.285), ETDYRE (2.296)							
Os–C	see BOTTAF (2.220, 2.219), BUYNEO (2.203)							
Pt–C	(4-6), (II,IV)	2.062	2.065	0.031	2.039	2.085	14	*41*
Hg–C	see CIRMAR (2.125)							
3.13.3.1	Primary alkyl [CH_2R, $R = C(sp^2)$]							
C–C		1.477	1.478	0.028	1.464	1.496	108	
Ti–C	see CEYCOY (2.203, 2.204)							
Cr–C	see BELTUH (2.101)							
Mn–C	see ACPMNA (2.209), BUFLET (2.199), CABYUZ (2.127)							
Fe–C	(5,6), (0,II)	2.131	2.133	0.038	2.098	2.155	9	
Co–C	(5,6), (-)	2.061	2.085	0.061	2.001	2.109	5	
Ni–C	see IPRNIP (1.977)							*56*
Zn–C	see CLPDZN (2.030)							
Zr–C	(8), (IV)	2.320	2.306	0.034	2.298	2.355	4	
Nb–C	(8), (IV,V)	2.289	2.291	0.024	2.271	2.306	14	*54*
Mo–C	(4-6), (II,III,VI)	2.211	2.214	0.027	2.187	2.233	9	
Ru–C	see CALHIG (2.200)							
Rh–C	see CIHYOH (2.103)							
Pd–C	(4,5,*), (II,-)	2.050	2.044	0.042	2.019	2.071	20	
Hf–C	see CEYCUE (2.274, 2.284)							
Ta–C	see CBZYTA (2.304), CPBZTB (2.188, 2.233)							*54*
W–C	(5-8), (II,III,V): all	2.238	2.185	0.090	2.163	2.328	9	
Re–C	see BUVSOA (2.203), BZHREC (2.284)							
Os–C	see BUYMAJ (2.217)							
Ir–C	see BIYJIC (2.127), CIYKAW (2.167), POIRID (2.133)							
Pt–C	(4,5), (II)	2.067	2.081	0.033	2.032	2.089	4	*41*

Table 9.6.3.3. *Interatomic distances (Å) (cont.)*

Bond	Substructure (coordination number, oxidation state, comment)	*d*	*m*	σ	q_l	q_u	*n*	Note
3.13.3.1	Primary alkyl [CH_2R, $R = C(sp^2)$] (*cont.*)							
Hg–C	see CHGACA (2.107), DBEZHG (2.064)							
Th–C	all CEKGEE	2.554	2.555	0.022	2.535	2.570	7	
U–C	(6,10), (IV)	2.509	2.521	0.039	2.468	2.539	4	
3.13.4.1	Secondary alkyls [terminal CHR_2, $R = C(sp^3)$]							
C–C		1.532	1.534	0.033	1.510	1.554	72	
Fe–C	see BULLFE (2.168), CAGKEA (2.060), MEDOFE10 (2.079)							
Co–C	(6), (III)	2.086	2.090	0.028	2.058	2.111	4	
Ni–C	see CONBIQ (1.929)							*56*
Zr–C	see CALNUY (2.381)							
Ru–C	(5,6), (II)	2.145	2.153	0.032	2.112	2.171	4	
Rh–C	see HBUPRH (2.083)							
Pd–C	(4,5), (II)	2.035	2.041	0.036	2.003	2.051	9	
Ir–C	(5,6), (III)	2.107	2.107	0.035	2.074	2.141	7	
Pt–C	(4,5), (II)	2.078	2.073	0.038	2.046	2.116	4	*41*
Hg–C	see CHGALD (2.085)							
3.13.5.1	Secondary alkyls {CHR_2, $R_2 \neq [C(sp^3)_2]$}							
C–C	$R = C(sp^2)$	1.474	1.475	0.023	1.461	1.485	82	
	$R = C(sp^3)$	1.532	1.527	0.022	1.518	1.545	40	
Ti–C	see TCYPTI10 (2.332)							
Fe–C	(5,6), (-)	2.131	2.138	0.027	2.110	2.151	16	
Co–C	(6), (-)	2.075	2.086	0.029	2.052	2.093	5	
Zr–C	see PDPMZR10 (2.379, 2.396)							
Mo–C	see BIRLIX (2.405)							
Ru–C	see BDMFRU (2.180), CTERUC (2.138)							
Rh–C	see BIGHAA (2.192), CASDIJ (2.154)							
Pd–C	(4,5), (II)	2.083	2.092	0.040	2.052	2.106	11	
Re–C	(6), (I)	2.311	2.335	0.065	2.243	2.356	4	
Os–C	see BUYNEO (2.221), CINKAL (2.215), EYPCOS (2.185)							
Ir–C	see CAYGAK (2.420)							
Pt–C	(4,5), (II)	2.113	2.120	0.036	2.082	2.141	9	***41***
Au–C	see BAJZAN (2.146), CEPYIF (2.175)							***57***
Hg–C	see BAVMUG (2.122), TPHGDI10 (2.292)							
3.13.6.1	Tertiary alkyls (terminal CR_3, R = any C)							
C–C		1.501	1.502	0.045	1.468	1.534	84	*109*
Fe–C	(5,6), (II)	2.127	2.128	0.027	2.098	2.153	6	
Co–C	see COJBOS (2.154)							
Zn–C	see COPLEY (2.050)							
Mo–C	see CYPRMO (2.414)							
Pd–C	(4), (II)	2.147	2.150	0.040	2.140	2.174	8	
Pt–C	(4), (II)	2.148	2.139	0.028	2.133	2.162	9	*41*
Au–C	see BENNOX (2.213), BUJXAF (2.197)							*57*
3.13.7.1	Trifluoromethyl (terminal CF_3)							
C–F		1.347	1.343	0.030	1.329	1.355	22	
Pt–C	(4,5), (II)	2.098	2.087	0.057	2.056	2.146	5	
3.14.1	η^2-Ethene (C_2H_4)							
C=C		1.392	1.390	0.044	1.363	1.415	43	
Co–C	(5), (I)	2.035	2.033	0.012	2.025	2.048	4	
Ni–C	(3,4), (0)	1.985	1.978	0.025	1.970	1.989	18	
Cu–C	(3,4), (I)	2.010	2.011	0.011	2.001	2.019	6	*12*
Nb–C	see CPETNB (2.278, 2.320)							*54*
Ru–C	(6), (II)	2.198	2.204	0.022	2.174	2.215	4	
Rh–C	(4,5), (I)	2.129	2.135	0.033	2.091	2.160	12	
Ta–C	see NPNTAB (2.228, 2.285)							*54*
W–C	(5,6), (-)	2.205	2.185	0.043	2.176	2.246	8	
Ir–C	see CETPIR (2.124, 2.111)							
Pt–C	(3,4,*), (0,II)	2.172	2.176	0.042	2.143	2.193	28	*41, 58*
3.14.2	η^2-Alkenes (CH_2CHR, R = any C)							*59*
C=C		1.383	1.383	0.033	1.361	1.404	44	
Fe–C	(5), (0)	2.090	2.088	0.012	2.079	2.102	4	*58, 60*
Co–C	(5), (I)	2.084	2.085	0.034	2.052	2.115	4	
Ni–C	(4,5), (II)	2.035	2.039	0.053	1.984	2.082	4	*9, 58, 61*
Cu–C	(3,*), (I)	2.060	2.061	0.025	2.046	2.080	6	*12*
Mo–C	(6), (0,II)	2.282	2.271	0.027	2.265	2.310	4	

Table 9.6.3.3. *Interatomic distances (Å) (cont.)*

Bond	Substructure (coordination number, oxidation state, comment)	*d*	*m*	σ	q_l	q_u	*n*	Note
3.14.2 η^2-Alkenes (CH_2CHR, R = any C) (*cont.*)								
Ru–C	(5,6), (-)	2.198	2.190	0.034	2.171	2.232	4	
Rh–C	(4,6), (I,-)	2.172	2.164	0.058	2.118	2.216	10	
	(4), (I)	2.150	2.141	0.040	2.117	2.194	8	
Pd–C	(4,5), (II)	2.189	2.179	0.040	2.151	2.233	12	
Ag–C	(3-5), (I)	2.535	2.542	0.050	2.486	2.582	6	
W–C	(6), (0): all	2.386	2.410	0.080	2.302	2.454	10	*30*
	: short < 2.35 (*trans* to C=C)	2.299	2.298	0.010	2.290	2.308	4	
	: long > 2.40 (*trans* to CO)	2.443	2.434	0.036	2.412	2.484	6	
Ir–C	see COPNIR (2.179, 2.162)							
Pt–C	(4), (II)	2.179	2.173	0.051	2.139	2.205	22	*41*
3.14.3 η-Alkenes (CH_2CR_2, R = any C)								
C=C		1.387	1.396	0.029	1.354	1.413	8	
Fe–C	(5), (0)	2.124	2.119	0.065	2.072	2.188	6	*60*
Ru–C	see BOVLUT (2.168, 2.203)							
Pd–C	see CARJOU (2.187, 2.107)							
Ag–C	all CIXYAJ	2.421	2.419	0.081	2.345	2.499	4	
3.14.4 η^2-Alkenes ($CHRCHR$, R = any C)								
C=C		1.391	1.389	0.032	1.372	1.407	280	*62*
V–C	see EFMCPV (2.213, 2.186)							
Cr–C	see MOBOCO10 (2.248, 2.300)							
Mn–C	see CPTOMN (2.193, 2.203)							
Fe–C	(5,6), (0,II): all	2.134	2.143	0.063	2.079	2.183	22	
	: R electron withdrawing	2.067	2.072	0.022	2.041	2.087	8	
	: R = alkyl	2.172	2.169	0.041	2.144	2.195	14	
Co–C	all NBPCCO	2.138	2.137	0.005	2.134	2.144	4	
Ni–C	(3-5), (0,II): all	2.057	2.054	0.050	2.000	2.095	17	*9, 58, 61*
	: R electron withdrawing	1.991	1.997	0.015	1.979	2.000	5	
	: 1,5-cod	2.084	2.089	0.028	2.052	2.107	12	
Cu–C	(3,4,*), (I): all	2.079	2.079	0.033	2.063	2.089	20	*12*
Mo–C	(6), (0,II) : all	2.369	2.347	0.083	2.298	2.446	28	
	: *trans* to CO	2.468	2.463	0.039	2.428	2.499	10	
	: not *trans* to CO	2.314	2.310	0.034	2.284	2.346	18	
Ru–C	: all	2.223	2.196	0.076	2.172	2.251	64	*63*
	: nbd, 1,5-cod only	2.191	2.187	0.036	2.167	2.206	49	
Rh–C	(4-6,*), (I-III): all	2.157	2.143	0.049	2.123	2.188	206	
	: nbd, 1,5-cod only	2.156	2.143	0.047	2.122	2.189	184	
Pd–C	(4), (II)	2.214	2.208	0.037	2.194	2.221	30	
Ag–C	see BUZMUE (2.705, 2.611)							
W–C	(6), (-)	2.430	2.430	0.033	2.400	2.457	6	
Re–C	see BAXLER (2.275)							
Os–C	: all R electron withdrawing	2.167	2.176	0.033	2.133	2.193	4	
Ir–C	(4-6,*), (I,III): all	2.170	2.160	0.061	2.124	2.200	94	
	: 1,5-cod only	2.163	2.160	0.051	2.124	2.186	76	
Pt–C	(4,5,*), (0,II) : all	2.209	2.223	0.056	2.173	2.252	52	*41, 58*
	: 1,5-cod only	2.230	2.236	0.039	2.193	2.254	40	
3.14.5 η^2-Alkenes ($CHRCR_2$, R = any C)								
C=C		1.411	1.403	0.025	1.392	1.427	12	
Mo–C	see OCTCMO10 (2.211, 2.227)							
Ru–C	see CXFMPR (2.171, 2.184)							
Rh–C	(4,5), (I)	2.130	2.121	0.023	2.111	2.155	14	
Ir–C	all COTFEW	2.148	2.150	0.020	2.130	2.165	4	
Pt–C	see COTFPT (2.059, 2.072)							*41, 58*
3.14.6 η^2-Alkenes (CR_2CR_2, R = any C)								
C=C		1.436	1.438	0.044	1.415	1.454	15	
Fe–C	: all	2.144	2.085	0.127	2.048	2.269	8	
	: excluding *trans* to CO	2.079	2.058	0.045	2.045	2.121	6	
Co–C	see EXPHCO (2.084, 2.134)							
Mo–C	see CPOMOA (2.231, 2.234)							
Rh–C	(4,5), (I)	2.175	2.173	0.025	2.153	2.199	4	
Pd–C	(4), (II)	2.248	2.258	0.055	2.191	2.296	4	
Ag–C	see BUGGAL (2.472, 2.632)							
Ir–C	see IRCNIR (2.098, 2.130)							
Pt–C		2.130	2.128	0.026	2.106	2.156	4	*41, 58*
Hg–C	see BODYEY (2.556, 2.577)							
3.14.7.1 η^2-Allenes (R_2CCCR_2)†								
C_α=C_β	(coordinated)	1.403	1.403	0.028	1.375	1.431	5	
C_β=C_γ	(free)	1.319	1.321	0.010	1.311	1.327	5	

Table 9.6.3.3. *Interatomic distances (Å) (cont.)*

Bond	Substructure (coordination number, oxidation state, comment)	*d*	*m*	*σ*	q_l	q_u	*n*	Note
3.14.7.1	η^2-Allenes (R_2CCCR_2)† (*cont.*)							
Fe–C_α	see FPCYTP10 (1.982)							
–C_β	(1.897)							
Rh–C_α	see MARHAA10 (2.177, 2.178)							
–C_β	(2.032, 2.027)							
Pd–C_α	see ALETPD (2.118)							
–C_β	(2.068)							
Pt–C_α	see MALLPT (2.107)							*41*
–C_β	(2.049)							
3.15.1.1	Alkynes (η^2-C_2R_2, R = any C)							*64*
C≡C	all	1.285	1.287	0.030	1.269	1.299	73	
	2*e* donor	1.269	1.271	0.034	1.242	1.284	23	
	3*e* donor	1.285	1.292	0.024	1.268	1.299	15	
	4*e* donor	1.304	1.309	0.027	1.280	1.321	15	
V–C	see CPFVLV (2.076)							
Cr–C	all PHACCS	1.960	1.960	0.009	1.952	1.969	6	
Mn–C	see HDYCMN (1.239)							
Co–C	see ACNCOB20 (1.977, 1.981), BETCUY10 (1.847, 1.856)							
Cu–C	(3), (I): R = $SiMe_3$, H	2.019	2.020	0.029	1.994	2.043	5	*12*
Nb–C	(6,8), (III): R = Ph	2.082	2.054	0.061	2.041	2.148	8	*54*
Mo–C	varying electron donation (2-4*e*): all	2.078	2.072	0.050	2.043	2.143	40	*65*
	2*e* donor	2.129	2.131	0.031	2.099	2.148	12	
	3*e* donor	2.071	2.066	0.033	2.053	2.082	12	
	4*e* donor	2.027	2.035	0.028	1.997	2.049	12	
Rh–C	: R = Ph, CF_3	2.041	2.045	0.015	2.030	2.051	6	
Pd–C	see FMEACA10 (2.040, 2.053)							
Ta–C		2.059	2.064	0.024	2.032	2.079	6	*54*
W–C	varying electron donation (2-4*e*): all	2.060	2.059	0.036	2.034	2.083	36	*65*
	2*e* donor	2.080	2.076	0.041	2.059	2.104	14	
	3*e* donor	2.066	2.066	0.016	2.053	2.078	12	
	4*e* donor	2.025	2.022	0.014	2.013	2.036	10	
Re–C		2.043	2.042	0.022	2.029	2.063	6	
Ir–C		2.083	2.083	0.041	2.044	2.122	4	
Pt–C		2.025	2.029	0.016	2.020	2.037	18	*41*
3.15.1.2	Alkynes (μ_2-η^2, $\eta^{2'}$-C_2R_2)†							*64*
C≡C		1.353	1.355	0.031	1.337	1.365	29	
Co–C		1.954	1.940	0.033	1.930	1.966	47	
Ni–C	all FLCPNI	1.910	1.909	0.011	1.901	1.921	4	*61*
Mo–C		2.171	2.178	0.050	2.137	2.199	32	
Rh–C	all CFBYRH	2.054	2.056	0.029	2.026	2.081	4	
Ta–C	see ACTHTA (2.217, 2.418)							
W–C	all: (show twisting from $C_{2v} \rightarrow C_2$)	2.122	2.099	0.102	2.050	2.214	12	
	excluding CAMLAD	2.117	2.099	0.059	2.086	2.158	8	
3.15.1.3	Alkynes (μ_2-η^1, $\eta^{1'}$-C_2R_2)†							*64*
C≡C		1.315	1.316	0.024	1.301	1.340	14	
Co–C	see CAHHAU (2.066)							
Ru–C		2.084	2.091	0.016	2.068	2.094	4	
Rh–C		2.021	2.001	0.041	1.992	2.064	6	
Ir–C		2.112	2.109	0.041	2.082	2.156	8	
Pt–C		2.059	2.056	0.009	2.051	2.068	5	*41*
3.16.1	η^3-Allyls ($R_2C.CR.CR_2$)†							
C^1–C^2		1.404	1.404	0.035	1.388	1.421	375	
V–C^1	all ALCPPV	2.349	2.352	0.013	2.342	2.357	6	
–C^2	(2.222, 2.228, 2.245)							
Cr–C^1	see CAMWOC (2.171, 2.247)							
–C^2	(2.193)							
Mn–C^1	(6), (I)	2.223	2.227	0.018	2.205	2.233	8	
–C^2		2.120	2.120	0.004	2.116	2.124	4	
Fe–C^1	(5,6), (0-II)	2.155	2.155	0.044	2.135	2.181	70	*60*
–C^2		2.068	2.070	0.033	2.048	2.092	36	
Co–C^1		2.082	2.083	0.029	2.054	2.112	17	
–C^2		2.000	2.007	0.021	1.985	2.015	9	
Ni–C^1	(4,5), (-)	2.044	2.031	0.057	2.005	2.075	34	*66*
–C^2		1.962	1.967	0.040	1.937	1.995	17	
Zr–C^1	(7), (II)	2.472	2.469	0.028	2.444	2.498	8	
–C^2		2.470	2.476	0.019	2.450	2.485	4	
Mo–C^1	(6,7), (-): most (7), (II)	2.353	2.352	0.057	2.321	2.375	73	
–C^2		2.244	2.234	0.048	2.214	2.274	37	

Table 9.6.3.3. *Interatomic distances (Å) (cont.)*

Bond	Substructure (coordination number, oxidation state, comment)	*d*	*m*	σ	q_l	q_u	*n*	Note
3.16.1 η^3-Allyls ($R_2C.CR.CR_2$)† (*cont.*)								
Ru–C^1	(5,6), (-): most (6), (II)	2.254	2.247	0.058	2.209	2.293	27	
–C^2		2.168	2.174	0.041	2.130	2.197	14	
Rh–C^1	(4-6), (I,III)	2.191	2.193	0.048	2.151	2.233	24	
–C^2		2.148	2.138	0.041	2.122	2.159	12	
Pd–C^1	: most (4), (II)	2.142	2.133	0.041	2.115	2.172	62	
–C^2		2.118	2.116	0.034	2.100	2.143	31	
W–C^1	(7), (II)	2.303	2.303	0.053	2.256	2.339	16	
–C^2		2.240	2.229	0.061	2.182	2.293	8	
Ir–C^1	(5,6), (I,III): all	2.212	2.188	0.048	2.175	2.268	8	
–C^2		2.168	2.165	0.059	2.113	2.225	4	
–C^1	(5), (I)	2.174	2.176	0.006	2.167	2.179	4	
–C^2	(2,100, 2.152)							
–C^1	(6), (III)	2.249	2.260	0.039	2.208	2.279	4	
–C^2	(2.241, 2.178)							
Pt–C^1	(4), (II)	2.194	2.191	0.044	2.159	2.242	10	*41*
–C^2		2.170	2.184	0.034	2.138	2.194	5	
U–C^1	(7,9), (IV)	2.670	2.663	0.038	2.640	2.701	10	
–C^2		2.748	2.781	0.070	2.674	2.806	5	
3.17.1 η^4-Cyclobutadiene (C_4H_4)								
C–C		1.423	1.434	0.035	1.409	1.441	16	
Fe–C		2.027	2.031	0.026	2.020	2.039	12	
–centroid	(1.759, 1.757, 1.763)							
Co–C		1.990	1.974	0.034	1.965	2.024	6	
–centroid	(1.682, 1.748)							
3.17.2 η^4-Cyclobutadienes (C_4R_4, $R_4 \neq H_4$)								
C–C		1.462	1.464	0.019	1.455	1.472	136	
Mn–C	all BUKGET	2.107	2.109	0.019	2.088	2.124	4	
–centroid	(1.837)							
Fe–C	(5), (0)	2.044	2.039	0.025	2.024	2.066	12	*50*
–centroid	(1.760, 1.766, 1.779)							
Co–C	(5), (I)	1.989	1.987	0.026	1.975	2.003	51	
–centroid		1.704	1.694	0.037	1.689	1.706	13	
Ni–C	(4,5), most (II)	2.027	2.025	0.036	2.001	2.060	16	*67*
–centroid		1.742	1.740	0.018	1.727	1.761	4	
Mo–C	(6), (0,I)	2.280	2.270	0.041	2.249	2.299	16	
–centroid		2.032	2.033	0.036	1.998	2.065	4	
–C	(6), (0)	2.308	2.298	0.040	2.276	2.338	8	
–centroid	(2.060, 2.066)							
–C	(6), (I)	2.253	2.252	0.018	2.240	2.269	8	
–centroid	(1.995, 2.006)							
Ru–C	(5,6), (0,II)	2.224	2.184	0.086	2.168	2.312	8	
–centroid	(2.006, 1.926)							
–C	(5), (0): all COCLEL	2.261	2.256	0.116	2.159	2.368	4	
–C	(6), (II): all CIMVID	2.188	2.184	0.015	2.176	2.204	4	
Rh–C	(5), (I)	2.114	2.105	0.025	2.102	2.120	8	
–centroid	(1.850, 1.829)							
Pd–C	(4,5), (II)	2.148	2.135	0.065	2.106	2.160	16	
–centroid		1.887	1.873	0.042	1.857	1.932	4	
–C	(5), (II)	2.130	2.135	0.027	2.106	2.145	12	
Pt–C	all CBFPPT10	2.219	2.214	0.096	2.129	2.314	4	
–centroid	(1.963)							
3.17.3 η^4-1,3-Butadienes ($R_2C.CR.CR.CR_2$)†								*68*
C^1–C^2		1.420	1.420	0.021	1.409	1.433	213	
C^2–C^2		1.405	1.404	0.023	1.392	1.416	108	
Cr–C^1		2.332	2.349	0.046	2.277	2.370	6	
–C^2		2.147	2.134	0.043	2.110	2.200	6	
Mn–C^1	(5), (0)	2.134	2.135	0.007	2.128	2.141	8	
–C^2		2.080	2.071	0.025	2.066	2.106	8	
Fe–C^1		2.130	2.128	0.029	2.111	2.148	113	*60*
–C^2		2.059	2.058	0.018	2.050	2.068	113	
Co–C^1	(5,6), (0,I)	2.089	2.102	0.045	2.061	2.125	12	
–C^2		2.015	2.003	0.033	1.994	2.018	12	
–C^1	excluding $2 < 2.015$	2.105	2.106	0.025	2.095	2.132	10	
–C^2	excluding $2 > 2.075$	2.001	1.998	0.012	1.993	2.013	10	
Ni–C^1	see BUJFUH (2.360, 2.106)							
–C^2	(2.074, 2.018)							
Zr–C^1	(7,8), (-): all	2.402	2.323	0.162	2.305	2.526	14	*69*
–C^2		2.522	2.549	0.120	2.397	2.582	14	
–C^1	structures with $Zr–C^1 < Zr–C^2$	2.314	2.311	0.021	2.298	2.326	10	

Table 9.6.3.3. *Interatomic distances (Å) (cont.)*

Bond	Substructure (coordination number, oxidation state, comment)	*d*	*m*	*σ*	q_l	q_u	*n*	Note
3.17.3 η^4-1,3-Butadienes ($R_2C.CR.CR.CR_2$)† *(cont.)*								
Zr–C^2		2.582	2.563	0.078	2.542	2.624	10	
Mo–C^1	(5-7), (-)	2.356	2.364	0.052	2.331	2.378	20	
–C^2		2.280	2.280	0.038	2.251	2.309	20	
Ru–C^1	(5,6), (0,II)	2.254	2.246	0.060	2.223	2.267	17	
–C^2		2.181	2.173	0.050	2.155	2.194	17	
–C^1	excluding 2 > 2.385	2.236	2.233	0.033	2.218	2.265	15	
–C^2	excluding 2 > 2.29	2.165	2.169	0.025	2.155	2.180	15	
Rh–C^1		2.214	2.224	0.047	2.165	2.252	4	
–C^2		2.177	2.198	0.043	2.134	2.199	4	
Hf–C^1	(6), (0): all	2.369	2.368	0.019	2.350	2.387	8	*69*
–C^2		2.400	2.400	0.006	2.395	2.407	8	
W–C^1	see HPMXCW10 (2.453, 2.460)							
–C^2	(2.335, 2.263)							
Re–C^1	see BIBJEB (2.310, 2.277)							
–C^2	(2.276, 2.258)							
Os–C^1	see OXBUDC10 (2.243, 2.300)							
–C^2	(2.198, 2.240)							
Ir–C^1	see BUHIPI (2.277, 2.162); CBUTIR (2.186)							
–C^2	(2.141, 2.202) (2.153)							
3.17.4 η^4-1,5-Cyclooctadiene (1,5-cod)								*62*
	(see 3.14.4)							
3.17.5 η^4-Norbornadiene (nbd)								*62*
	(see 3.14.4)							
3.18.1 η^5-Cyclopentadienyl (C_5H_5)								
C–C		1.397	1.398	0.028	1.380	1.415	6804	
Sc–C	all TCYPSC10	2.494	2.499	0.023	2.473	2.513	10	
–centroid	(2.189, 2.194)							
Ti–C		2.374	2.375	0.031	2.354	2.396	832	
–centroid		2.062	2.061	0.026	2.044	2.082	170	
V–C		2.281	2.281	0.026	2.260	2.301	226	
–centroid		1.952	1.950	0.020	1.938	1.970	46	
Cr–C		2.225	2.226	0.033	2.197	2.250	295	
–centroid		1.876	1.882	0.029	1.847	1.898	61	
Mn–C	: all	2.166	2.149	0.094	2.127	2.164	321	*30*
–centroid	: all	1.824	1.786	0.132	1.775	1.798	67	*30*
–C	(-), (-): low spin	2.143	2.146	0.026	2.125	2.161	300	
–centroid	: low spin	1.783	1.784	0.018	1.774	1.794	61	
–C	: Mn^{II}, high spin	2.511	2.499	0.052	2.479	2.541	20	
–centroid		2.237	2.229	0.051	2.196	2.262	6	
Fe–C		2.080	2.088	0.035	2.052	2.106	1309	*60*
–centroid		1.706	1.721	0.039	1.662	1.735	265	
Co–C		2.068	2.066	0.031	2.045	2.089	740	
–centroid		1.696	1.692	0.029	1.676	1.716	152	
Ni–C		2.116	2.113	0.033	2.093	2.138	315	*70*
–centroid		1.748	1.750	0.025	1.734	1.762	65	
Cu–C	all TPCYCU	2.211	2.205	0.018	2.195	2.231	5	
–centroid	(1.864)							
Zn–C		2.348	2.332	0.080	2.299	2.440	15	
–centroid		2.044	2.038	0.027	2.021	2.072	4	
Y–C		2.649	2.646	0.040	2.626	2.668	75	
–centroid		2.382	2.379	0.041	2.356	2.386	15	
Zr–C		2.529	2.529	0.031	2.510	2.546	649	*71*
–centroid		2.236	2.233	0.023	2.220	2.251	132	
–C	excluding BOYLUW	2.528	2.528	0.026	2.510	2.545	638	
–centroid	excluding BOYLUW	2.235	2.232	0.022	2.220	2.250	131	
Nb–C		2.408	2.406	0.037	2.385	2.435	353	*54*
–centroid		2.093	2.093	0.029	2.075	2.110	71	
Mo–C		2.336	2.338	0.042	2.304	2.368	1363	
–centroid		2.011	2.010	0.033	1.992	2.026	278	
Ru–C		2.236	2.240	0.041	2.204	2.267	284	
–centroid		1.892	1.898	0.042	1.857	1.929	58	
Rh–C		2.239	2.236	0.037	2.218	2.264	256	
–centroid		1.895	1.898	0.032	1.879	1.914	53	
Pd–C	all BUPTEL	2.344	2.350	0.050	2.303	2.381	5	
–centroid	(2.015)							
Pr–C	all CXINPR10	2.778	2.765	0.026	2.760	2.801	15	*1, 21*
–centroid	(2.526, 2.527, 2.526)							
Gd–C	all CPTHGD10	2.738	2.744	0.025	2.722	2.747	15	*1, 21*
–centroid	(2.472, 2.490, 2.494)							

Table 9.6.3.3. *Interatomic distances (Å) (cont.)*

Bond	Substructure (coordination number, oxidation state, comment)	*d*	*m*	σ	q_l	q_u	*n*	Note
3.18.1 η^5-Cyclopentadienyl (C_5H_5) *(cont.)*								
Er–C	all BOBWAQ	2.667	2.665	0.005	2.663	2.671	5	*1, 21*
–centroid	(2.391)							
Yb–C	(8, 10), (-)	2.657	2.642	0.047	2.621	2.693	25	*1, 21*
–centroid		2.383	2.383	0.043	2.340	2.426	5	
Lu–C	all OHCPLU	2.600	2.599	0.018	2.584	2.615	10	*1, 21*
–centroid	(2.309, 2.316)							
Hf–C		2.505	2.507	0.020	2.494	2.520	60	*71*
–centroid		2.208	2.211	0.015	2.195	2.220	12	
Ta–C		2.392	2.395	0.036	2.373	2.411	60	*54*
–centroid		2.072	2.068	0.031	2.040	2.101	12	
W–C		2.337	2.337	0.042	2.307	2.364	566	
–centroid		2.005	2.007	0.035	1.985	2.026	114	
Re–C	(6–8), (-)	2.296	2.293	0.039	2.270	2.327	103	
–centroid		1.959	1.958	0.026	1.946	1.980	21	
Os–C	(6), (-)	2.235	2.233	0.032	2.220	2.262	10	
–centroid	(1.916, 1.856)							
Ir–C		2.263	2.273	0.030	2.244	2.281	35	
–centroid		1.922	1.917	0.012	1.913	1.936	7	
U–C		2.759	2.765	0.031	2.740	2.776	63	
–centroid		2.493	2.491	0.015	2.483	2.506	13	
3.18.2 η^5-Pentamethylcyclopentadienyl (C_5Me_5)								
C–C(ring)		1.417	1.418	0.024	1.404	1.433	1164	
C–C(Me)		1.512	1.509	0.025	1.497	1.523	1239	
Ti–C		2.403	2.394	0.028	2.384	2.418	61	
–centroid		2.086	2.071	0.027	2.064	2.116	13	
V–C		2.334	2.339	0.054	2.283	2.357	30	
–centroid		2.009	2.010	0.047	1.979	2.051	6	
Cr–C		2.209	2.204	0.017	2.197	2.232	10	
–centroid	(1.847, 1.858)							
Mn–C		2.146	2.147	0.027	2.126	2.158	25	
–centroid		1.777	1.777	0.027	1.755	1.800	5	
Fe–C		2.116	2.115	0.026	2.095	2.136	25	
–centroid		1.739	1.730	0.026	1.715	1.766	5	
Co–C		2.098	2.099	0.035	2.078	2.118	155	
–centroid		1.717	1.722	0.035	1.705	1.735	31	
Ni–C	all BINFUZ	2.102	2.120	0.027	2.073	2.122	5	
–centroid	(1.725)							
Cu–C	all BUPWOY10	2.271	2.271	0.051	2.223	2.319	5	
–centroid	(1.920)							
Zr–C		2.545	2.545	0.031	2.522	2.562	55	
–centroid		2.244	2.244	0.023	2.232	2.253	11	
Mo–C		2.365	2.364	0.047	2.328	2.407	78	
–centroid		2.034	2.032	0.029	2.010	2.058	16	
Ru–C	all COPKEX	2.268	2.269	0.012	2.258	2.279	5	
–centroid	(1.917)							
Rh–C		2.217	2.217	0.057	2.168	2.254	367	
–centroid		1.856	1.870	0.060	1.795	1.908	75	
Pd–C	all BUSHEC	2.341	2.351	0.073	2.280	2.397	5	
–centroid	(2.003)							
Sm–C	(8), (II,III): all	2.809	2.808	0.063	2.745	2.864	40	*1, 30, 60*
–centroid		2.537	2.535	0.067	2.472	2.601	8	
–C	(8), (II): all CALCEX	2.864	2.863	0.030	2.836	2.889	20	
–centroid		2.599	2.601	0.006	2.593	2.604	4	
–C	(8), (III): all BUFNOF	2.754	2.747	0.031	2.727	2.786	20	
–centroid		2.475	2.475	0.005	2.470	2.479	4	
Eu–C	all CIFCAV	2.815	2.808	0.019	2.799	2.834	5	*1, 60*
–centroid	(2.550)							
Yb–C	: all	2.608	2.597	0.052	2.576	2.631	127	*1, 60*
–centroid		2.320	2.324	0.053	2.283	2.340	27	
–C	excluding BIKTIY	2.597	2.592	0.035	2.574	2.619	117	
–centroid		2.308	2.303	0.033	2.283	2.335	25	
Lu–C	all CIXTUY	2.710	2.731	0.090	2.623	2.780	10	*1, 60*
–centroid	(2.360, 2.493)							
Ta–C		2.439	2.435	0.039	2.404	2.469	53	*54*
–centroid		2.122	2.118	0.029	2.095	2.137	11	
Re–C		2.297	2.289	0.041	2.266	2.336	30	
–centroid		1.956	1.976	0.034	1.913	1.979	6	
Os–C	all BIJKOU	2.244	2.218	0.043	2.211	2.291	5	
–centroid	(1.887)							
Ir–C	(6,7), (III,V): all	2.158	2.157	0.043	2.139	2.185	56	
–centroid		1.792	1.783	0.049	1.760	1.808	12	
–C	(6), (III)	2.151	2.155	0.024	2.134	2.170	46	
–centroid		1.773	1.778	0.025	1.753	1.791	10	

Table 9.6.3.3. *Interatomic distances (Å) (cont.)*

Bond	Substructure (coordination number, oxidation state, comment)	*d*	*m*	σ	q_l	q_u	*n*	Note
3.18.2 η^5-Pentamethylcyclopentadienyl (C_5Me_5) *(cont.)*								
Ir–C	(7), (V): all CECKOK	2.245	2.249	0.018	2.227	2.258	10	
–centroid	(1.875, 1.893)							
Th–C		2.817	2.822	0.026	2.793	2.838	15	
–centroid	(2.536, 2.547, 2.573)							
U–C		2.752	2.752	0.033	2.724	2.776	58	
–centroid		2.479	2.484	0.022	2.460	2.493	12	
3.18.3 η^5-Indenyl (C_9H_7)†								
C^1–C^2		1.407	1.410	0.028	1.400	1.421	34	
C^2–C^3		1.444	1.449	0.020	1.428	1.458	34	
C^3–$C^{3'}$		1.432	1.427	0.017	1.420	1.441	17	
Cr–C^1	see BABFOZ (2.176)							
–C^2	(2.184, 2.197)							
–C^3	(2.288, 2.301)							
–centroid	(1.869)							
Mo–C^1	(6), (-) (2.341, 2.346, 2.350)							
–C^2		2.341	2.354	0.065	2.278	2.392	6	
–C^3		2.409	2.430	0.041	2.370	2.439	6	
–centroid	(2.051, 2.034, 2.025)							
Rh–C^1	(5,6), (-)	2.223	2.221	0.019	2.213	2.236	9	
–C^2		2.226	2.224	0.034	2.200	2.243	18	
–C^3		2.399	2.401	0.051	2.364	2.426	18	
–centroid		1.948	1.954	0.037	1.921	1.961	9	
Ce–C^1	all INDCEP (2.748, 2.757, 2.782)							*60*
–C^2		2.805	2.794	0.043	2.766	2.849	6	
–C^3		2.961	2.964	0.036	2.933	2.988	6	
–centroid	(2.587, 2.591, 2.606)							
U–C^1	see CAFNOM (2.709)							
–C^2	(2.710, 2.720)							
–C^3	(2.769, 2.813)							
–centroid	(2.455)							
3.18.4 η^5-Dienyls (C_5H_7 and derivatives)†								*72, 73*
C^1–C^2		1.408	1.403	0.026	1.391	1.422	24	
C^2–C^3		1.415	1.414	0.021	1.399	1.427	24	
V–C^1	all COGXOL	2.179	2.180	0.017	2.162	2.195	**4**	
–C^2		2.231	2.233	0.011	2.219	2.240	**4**	
–C^3	(2.236, 2.236)							
Cr–C^1	see COGXUR (2.159, 2.174)							
Cr–C^2	(2.147, 2.177)							
Cr–C^3	(2.166)							
Mn–C^1	see OAZPMN10 (2.209, 2.298)							
–C^2	(2.137, 2.143)							
–C^3	(2.146)							
Fe–C^1	all MEPEFE10	2.108	2.109	0.016	2.094	2.122	4	
–C^2		2.073	2.072	0.015	2.060	2.088	4	
–C^3	(2.081, 2.086)							
Co–C^1	(5), (I)	2.135	2.136	0.010	2.125	2.143	4	
–C^2		2.078	2.075	0.015	2.066	2.094	4	
–C^3	(2.060, 2.087)							
Zr–C^1	see HMPEZR (2.432, 2.446)							
–C^2	(2.428, 2.438)							
–C^3	(2.469)							
Ru–C^1	(6), (II)	2.169	2.171	0.016	2.154	2.181	6	
–C^2		2.168	2.167	0.028	2.149	2.194	6	
–C^3	(2.177, 2.257, 2.258)							
3.19.1 η^6-Benzene (C_6H_6)								*74*
C–C		1.399	1.398	0.023	1.385	1.413	105	
Ti–C	all BELGOO10	2.228	2.225	0.009	2.220	2.236	12	
–centroid	(1.736, 1.742)							
Cr–C	(6), (0,I)	2.180	2.176	0.044	2.147	2.219	20	
–centroid		1.676	1.691	0.056	1.618	1.725	5	
Fe–C	all BUVLEJ	2.059	2.063	0.025	2.035	2.077	12	
–centroid	(1.542, 1.548)							
Co–C	see BNZCTC (2.123)							
–centroid	(1.603)							
Mo–C	(7), (II)	2.279	2.273	0.051	2.247	2.315	18	
–centroid	(1.767, 1.805, 1.819)							
Ru–C	(6), (-): all	2.187	2.168	0.042	2.154	2.227	21	
–centroid		1.674	1.659	0.043	1.644	1.720	4	
Re–C	(5,6), (-)	2.217	2.214	0.034	2.186	2.249	30	

Table 9.6.3.3. *Interatomic distances (Å) (cont.)*

Bond	Substructure (coordination number, oxidation state, comment)	*d*	*m*	σ	q_l	q_u	*n*	Note
3.19.1 η^6-Benzene (C_6H_6) (*cont.*)								
Re–centroid		1.725	1.725	0.026	1.703	1.747	5	
Os–C	(6), (-)	2.166	2.165	0.055	2.135	2.191	30	
–centroid		1.657	1.635	0.057	1.620	1.705	5	
3.19.2 η^6-Arenes (C_6R_6, R = any C, H)								*74*
C–C	(intra-ring)	1.411	1.411	0.021	1.398	1.423	818	
Ti–C	(6,7), (0,II): all	2.330	2.247	0.125	2.240	2.479	18	*30*
Ti–C	(6), (0)	2.245	2.244	0.010	2.238	2.248	12	
–centroid	(1.742, 1.744)							
–C	(7), (II)	2.498	2.502	0.037	2.465	2.530	6	
–centroid	(2.055)							
V–C	all DFBENV	2.192	2.192	0.010	2.181	2.203	6	
–centroid	(1.692)							
Cr–C	(6), (0,I)	2.216	2.216	0.045	2.196	2.239	412	
–centroid		1.710	1.718	0.046	1.699	1.733	73	
Fe–C	(5,6), (0,II)	2.101	2.097	0.036	2.078	2.114	82	
–centroid		1.563	1.549	0.032	1.539	1.586	14	
Co–C	(5,6), (I,II)	2.167	2.131	0.060	2.122	2.228	13	
–centroid	(1.602, 1.766, 1.628)							
Ni–C	(5), (II)	2.209	2.216	0.041	2.170	2.238	10	*75*
–centroid	(1.713, 1.699)							
Zr–C	all CLZRAL	2.590	2.592	0.030	2.558	2.619	9	
–centroid	(2.164, 2.178)							
Nb–C		2.404	2.457	0.096	2.283	2.479	28	*30*
–centroid		1.939	1.938	0.005	1.935	1.944	5	
–C	long > 2.425	2.473	2.474	0.016	2.459	2.484	18	
–C	short < 2.352	2.280	2.282	0.019	2.264	2.289	10	
Mo–C	(6,7), (0-III)	2.320	2.322	0.057	2.274	2.370	93	
–centroid		1.841	1.838	0.061	1.794	1.904	16	
Ru–C	(5,6), (0,II)	2.247	2.235	0.051	2.212	2.264	78	
–centroid		1.745	1.727	0.059	1.697	1.767	13	
–C	(5,6), (0,II): excluding BENLOV	2.238	2.230	0.040	2.210	2.258	72	
–centroid		1.733	1.727	0.042	1.695	1.757	12	
Rh–C	(5,6), (-)	2.327	2.315	0.052	2.291	2.363	22	
–centroid		1.845	1.864	0.051	1.793	1.878	4	
Hf–C	all SNTLHF	2.481	2.493	0.041	2.433	2.519	6	
–centroid	(2.041)							
W–C	(6,7), (0,II)	2.291	2.293	0.038	2.269	2.309	46	
–centroid		1.803	1.805	0.043	1.768	1.821	8	
Re–C	all CIZNUU	2.327	2.328	0.005	2.323	2.331	6	
–centroid	(1.863)							
Os–C	(4,6), (-)	2.213	2.198	0.053	2.181	2.230	18	
–centroid	(1.638, 1.718, 1.719)							
3.20.1 η^7-Tropylium (C_7H_7) and derivatives								
C–C		1.408	1.409	0.022	1.393	1.418	126	
Ti–C	(7), (-)	2.228	2.236	0.020	2.204	2.242	21	
centroid	(1.484, 1.544, 1.569)							
Cr–C	(7), (-)	2.220	2.210	0.043	2.189	2.241	14	
–centroid	(1.445, 1.571)							
Mo–C	(7), (-)	2.280	2.278	0.032	2.256	2.300	105	
–centroid		1.607	1.596	0.035	1.577	1.649	15	
3.20.2 η^8-Cyclooctatetraene (C_8H_8) and derivatives								
C–C		1.397	1.399	0.027	1.385	1.409	114	
Ti–C	(7), (III,IV)	2.349	2.373	0.043	2.319	2.384	32	
–centroid		1.471	1.490	0.063	1.409	1.524	5	
–C	(7), (III)	2.368	2.378	0.027	2.338	2.388	24	*30*
–centroid		1.495	1.504	0.040	1.453	1.527	4	
–C	short < 2.35	2.329	2.328	0.009	2.321	2.336	7	
–C	long > 2.37	2.384	2.383	0.009	2.378	2.391	17	
–C	(7), (IV): all CEXTII	2.291	2.293	0.023	2.270	2.311	8	
–centroid	(1.377)							
V–C	all BUPLAZ10	2.282	2.281	0.039	2.257	2.293	8	
–centroid	(1.376)							
Zr–C	(7), (II,IV)	2.461	2.459	0.017	2.449	2.474	16	
–centroid	(1.685, 1.650)							
Ce–C	all COCTCE	2.710	2.709	0.015	2.700	2.720	8	*1*
–centroid	(2.007)							
Th–C	(8), (IV)	2.712	2.710	0.016	2.701	2.724	16	
–centroid	(2.029, 2.003)							
U–C	(8), (IV)	2.653	2.648	0.019	2.637	2.667	48	
–centroid		1.917	1.919	0.005	1.913	1.921	5	

Table 9.6.3.3. *Interatomic distances (Å) (cont.)*

Bond	Substructure (coordination number, oxidation state, comment)	*d*	*m*	σ	q_l	q_u	*n*	Note
3.21.1 Carbaboranes (see also 2.2.1)								*29*
Ti–C	see CEXTII (2.265, 2.340)							
V–C	see BUPLAZ10 (2.191, 2.269)							
Cr–C		2.197	2.188	0.065	2.140	2.265	6	
Mn–C	see PMCMNB (2.043, 2.047)							
Fe–C		2.073	2.069	0.070	2.041	2.108	62	
Co–C		2.046	2.049	0.055	2.013	2.078	76	
Ni–C		2.087	2.071	0.071	2.045	2.145	15	
Ru–C	see RUCABO (2.097, 2.185)							
Rh–C		2.239	2.237	0.065	2.187	2.287	26	
Pd–C	see BICPDB (2.599), MPPDBN (2.414, 2.492)							
W–C		2.420	2.431	0.044	2.374	2.455	4	
Re–C	see CSCREC (2.310, 2.316)							
Pt–C	(range 2.142–2.768)	2.441	2.447	0.199	2.277	2.591	12	
Hg–C		2.101	2.106	0.013	2.089	2.110	5	
3.21.2 Borylenes *etc.* (see also 2.3.1)								*31–33*
V–C	see BOKXEE (2.297)							
Mn–C		2.197	2.188	0.037	2.167	2.234	10	
Fe–C		2.118	2.098	0.050	2.086	2.150	16	
Co–C		2.062	2.031	0.061	2.025	2.091	19	
Ni–C	:all	2.120	2.091	0.085	2.053	2.193	9	
	:excluding FMBCNI	2.080	2.076	0.036	2.044	2.144	7	
3.22.1 η^2-CO_2 (see also 5.25.2)								
(None)								
3.22.2 η^2-CS_2 (see also 9.17.1)								
C=S	(coordinated)	1.665	1.671	0.018	1.656	1.676	6	
C=S	(free)	1.613	1.616	0.006	1.607	1.618	6	
V–C	see CPCDSV (2.075, 2.089)							
Fe–C	see SPHFEC10 (1.983)							
Co–C	see TPHCOA (1.882)							
Ni–C	see COGWOK (1.858)							
Nb–C	see CPSNBA (2.206)							
4.1.1.1 Nitride (terminal N)								*76*
Cr–N	see BOZYIY (1.562)							
Mn–N	see ZEGGUN (1.512)							
Mo–N	(5,6), (VI)	1.636	1.636	0.006	1.630	1.641	4	*77*
Tc–N	see BAGWAH (1.604), CETKUH (1.629)							
Re–N	(5,6), (V): see BOCLOU (1.660), NEPPRE (1.788), NETPRE (1.602), NREDTC10 (1.656)							
4.1.1.2 Nitride (μ-N)								*78*
Mo–N (μ_2)	see BUPZIV (1.662, 2.150; 1.643, 2.167)							
Ru–N (μ_2)	see CEPBII (1.742)							
W–N (μ_2)	see CAWGAI (1.740, 2.661)							
Mo–N (μ_3)	see BAXFEL (range 1.900–1.979)							
Ru–N (μ_4)	see BITRAX (1.913, 1.943, 2.103, 2.114)							
Rh–N (μ_6)	see BOZBOH (range 2.124–2.137)							
4.2.1.1 Nitrenes/imides (terminal N*R*, *R* = any C)								*79*
N–C		1.415	1.394	0.047	1.387	1.457	51	
V–N	see CIZTEK (1.730)							
Nb–N	see CAHJIE (1.783), COBLIO (1.733)							
Mo–N	(5-7), (V,VI):	1.729	1.728	0.019	1.719	1.733	20	
	: excluding 1 with Mo–N–C 139.4°	1.726	1.728	0.013	1.718	1.732	19	
Ta–N	see BEHHIF (1.765), COBDUS (1.762)							
W–N	(4-6), (V,VI)	1.738	1.739	0.026	1.725	1.754	13	
Re–N	(6), (V-VII)	1.701	1.694	0.019	1.688	1.709	9	
Os–N	see ADOOSA (1.697), ADOOSB (1.706, 1.720)							
U–N	see CESVUR (2.063)							
4.2.1.2 Nitrenes/imides (μ_2-N*R*)								
N–C	*R* = C(sp^2)	1.392	1.395	0.021	1.374	1.409	7	
	R = ^{t}Bu	1.483	1.484	0.007	1.475	1.488	4	
Ti–N	see BIJJUZ10 (1.920), BUIMWB (1.921, 1.926)							
Zr–N	see TBIAZR (2.060, 2.071)							
Nb–N	all BENRAN	2.043	2.042	0.011	2.033	2.053	4	
Mo–N	(6), (-): excluding BUMEMO (1.819, 2.322)	1.970	1.973	0.010	1.958	1.978	6	
W–N	see BUIMWA (1.841, 2.288), CACRIH (1.891, 2.312)							

Table 9.6.3.3. *Interatomic distances (Å) (cont.)*

Bond	Substructure (coordination number, oxidation state, comment)	*d*	*m*	σ	q_l	q_u	*n*	Note
4.3.1.1	Alkylideneamido (N=CR_2, linear)							*80*
N–C	(1.258, 1.275, 1.259)							
Zr–N	see CEFSIP (2.013)							
Mo–N	see BUDZEF (1.878), CPBUMO (1.892)							
4.4.1	Nitriles (NCR, R = any C)							
N–C		1.133	1.134	0.020	1.121	1.144	102	
Ti–N	see ECYFTI (2.245)							
V–N	see ACNCVO (2.097), BZTCOV (2.124), COPHAV (2.107)							
Fe–N	(5,6), (II,III): all	2.029	1.976	0.153	1.928	2.161	7	
	(5,6), (II): low spin	1.946	1.966	0.041	1.905	1.977	5	
Co–N	(4,5), (0,I): all	1.971	1.951	0.068	1.920	2.041	4	
Ni–N	see BCETPN (2.082), CARWAT (2.109), EFUMNI (1.873)							
Cu–N	(4-6,*), (I,II): all	2.121	2.005	0.249	1.968	2.321	11	
	(4,*), (I,II)	1.983	1.975	0.042	1.960	2.036	8	
Nb–N	(6), (IV,V): all	2.322	2.303	0.083	2.254	2.414	8	*81*
	(6), (IV,V)	2.282	2.292	0.042	2.238	2.315	6	*44*
Mo–N	(5-7), (II,VI)	2.147	2.144	0.041	2.125	2.177	9	*44*
Tc–N	see CETKUH (2.492)							
Ru–N	(5,6,*), (0,II,IV): all	2.090	2.108	0.037	2.052	2.118	5	
Rh–N	(4-6), (I,II)	2.139	2.152	0.091	2.052	2.232	11	*30*
	(4,5), (I)	2.050	2.052	0.006	2.045	2.056	5	
	(6), (II)	2.214	2.225	0.043	2.166	2.252	6	*82*
Pd–N	see CAKNIL10 (2.063)							
Cd–N	see CDCYAC (2.372)							
Re–N	(6), (I,II): all	2.107	2.125	0.040	2.065	2.137	13	
Os–N	(6,*), (-): all	2.098	2.096	0.028	2.084	2.124	10	
Ir–N	see BESSEX (2.054), CEYBEN (2.044), IRTCPP10 (2.024)							
Pt–N	(4,5), (I,II): all	2.003	1.982	0.048	1.978	2.036	8	
	(4), (II)	1.980	1.979	0.019	1.971	1.990	6	
U–N	see CIHLIO (2.604, 2.580)							
4.4.2	Cyano (μ_2-CN)† (see also 3.5.1.2)							
Cr–N	see CYCRTF (1.975, 1.975, 1.994)							
Mn–N	see CAZJAO10 (2.165), CAZJES10 (2.186)							
Cu–N	(4-6), (II): all	2.051	2.001	0.135	1.956	2.103	11	
	: excluding 2 > 2.3	1.994	1.995	0.052	1.955	2.022	9	
Pd–N	see BUSRIQ (2.067)							
Cd–N	(4,6), (II)	2.361	2.352	0.042	2.327	2.403	4	
4.5.1.1	Isocyanate (terminal NCO) (see also 5.25.3.1)							*83*
N–C		1.141	1.148	0.020	1.125	1.156	16	
C–O		1.202	1.197	0.016	1.189	1.215	16	
Ti–N	see CPTICN10 (2.007, 2.018)							
Cr–N	see CPNOCC10 (1.980)							
Mn–N	see CENRES (1.919, 1.934), TRENCM (2.051)							
Co–N	see CNTPCP (1.949), CYZNIC10 (2.055)							
Cu–N	(4-6,*), (II): all	1.935	1.926	0.049	1.897	1.954	8	
4.5.1.2	Isocyanate (μ_2-NCO) (see also 5.25.3.2)†							
N–C	(1.152, 1.154)							
C–O	(1.182, 1.216)							
Cu–N	see CNPRCV (1.946,), ICNPCU10 (1.952)							
4.5.1.3	Isocyanate (μ_2-*N,N*-NCO)							
N–C	(1.168)							
C–O	(1.173)							
Cu–N	see COVYIV (2.266, 2.023)							
4.5.2.1	*N*-Isothiocyanates (terminal NCS) (see also 9.3.1.1)							*84*
N–C		1.149	1.150	0.017	1.141	1.159	230	
C–S		1.620	1.619	0.022	1.608	1.632	231	
Ti–N	see CPITTI (2.021)							
Cr–N	(6), (III): excluding CEFMAB (2.250)	1.999	1.998	0.016	1.984	2.012	12	*85*
Mn–N	(5-7), (II,III)	2.166	2.167	0.051	2.128	2.196	13	
	(6), (II): Mn–N–C > 152°	2.141	2.146	0.027	2.107	2.167	7	
Fe–N	(5-7), (II,III): all	2.063	2.095	0.084	1.982	2.133	12	
	(6,7), (high spin II)	2.108	2.106	0.031	2.088	2.139	7	
Co–N	(4-6), (II,III)	2.000	1.992	0.076	1.927	2.072	42	*30*
	(4), (II)	1.956	1.957	0.010	1.948	1.964	8	

Table 9.6.3.3. *Interatomic distances (Å) (cont.)*

Bond	Substructure (coordination number, oxidation state, comment)	*d*	*m*	σ	q_l	q_u	*n*	Note
4.5.2.1	*N*-Isothiocyanates (terminal NCS) (see also 9.3.1.1) (*cont.*)							
	(5), (II)	2.034	2.028	0.050	2.004	2.064	6	
	(6), (II)	2.073	2.075	0.029	2.064	2.099	15	
	(6), (III): excluding ITDASC (2.117)	1.911	1.910	0.015	1.900	1.922	12	
Ni–N	(4-6), (II): all	2.035	2.064	0.079	2.026	2.077	44	*30*
	(4)	1.855	1.835	0.046	1.827	1.886	6	
	(6)	2.064	2.068	0.027	2.054	2.079	36	
Cu–N	(4-6), (II): all	2.045	1.970	0.165	1.945	2.101	25	*86*
	(5), (II): (Cu–N–C >152°)	2.013	1.968	0.102	1.946	2.073	21	*86*
Zn–N	(4-6), (II): all	1.988	1.945	0.081	1.923	2.083	8	*30*
	(4), (II)	1.931	1.929	0.013	1.919	1.945	5	
Zr–N	see TCBPZR (2.183)							
Nb–N	(6,8), (IV,V)	2.132	2.130	0.035	2.100	2.166	4	
Mo–N	(6,7), (V,VI)	2.148	2.166	0.077	2.065	2.183	11	*81, 87*
Tc–N	(6), (II, III, V)	2.049	2.046	0.011	2.043	2.057	6	
Pd–N	(4), (II)	2.023	2.025	0.028	2.011	2.043	9	
Cd–N	(5,6), (II)	2.245	2.241	0.047	2.212	2.259	7	
Dy–N	see CIKTOF (2.433)							
Re–N	(6), (III,V)	2.024	2.018	0.023	2.009	2.038	7	
Pt–N	see PEYEPP (2.025)							
Th–N	(8), (IV)	2.496	2.496	0.024	2.474	2.513	9	
U–N	(8,9,11), (IV)	2.439	2.448	0.046	2.407	2.467	18	
4.5.2.2	Isothiocyanates (μ_2-NCS) (see also 9.3.1.2)†							
N–C		1.144	1.149	0.020	1.129	1.160	24	
C–S		1.642	1.643	0.017	1.632	1.650	24	
Mn–N	see TCMNET10 (2.143)							
Co–N	(6), (II)	2.111	2.118	0.020	2.091	2.128	5	
Ni–N	see TCYENI10 (2.031)							
Cu–N	(4,5), (II): excluding COHHIQ (2.205)	1.962	1.951	0.031	1.939	1.999	6	
Ag–N	see CENSUJ (2.281), CENTAQ (2.332)							
Cd–N	(5,6), (II)	2.287	2.294	0.019	2.267	2.300	4	
Pt–N	see TPPTCP01 (1.966)							
Hg–N	see TCHXPH10 (2.517), TCPPHG10 (2.405, 2.735)							
4.6.1.1	Dinitrogen (η^1-N_2)							*88*
N–N		1.100	1.110	0.048	1.074	1.124	18	
Cr–N	see CAVMOB (1.957)							
Fe–N	see PHSNFE (1.866)							
Co–N	see CARKIP (1.814), PPHCHN10 (1.783, 1.832)							
Zr–N	see MCPNZR (2.187, 2.188)							
Mo–N	(6), (0,I)	2.013	1.996	0.056	1.971	2.072	4	*89*
Ru–N	see ENAZPU10 (1.893)							
Rh–N	see HNBPRH10 (1.970)							
W–N	see BUYBUS (2.038)							
Re–N	see BIBJAX (1.956), BUKMID (2.055), CNMPRE (1.966)							*90*
Os–N	see CAJCEV (1.909)							
4.6.1.2	Dinitrogen (μ_2-η^1, $\eta^{1'}$-N_2)†							
N–N	excluding BEJGAY (1.282), IMNPTA10 (1.298)	1.155	1.155	0.020	1.137	1.174	5	
Ti–N	(7), (II): all NPMCTI	2.017	2.014	0.012	2.007	2.029	4	
Fe–N	see BALWUG (1.877)							
Zr–N	see MCPNZR (2.087, 2.075)							
Mo–N	see NMSPEM (2.042)							
Ta–N	see BEJGAY (1.796), IMNPTA10 (1.837)							
4.7.1	Diazoniums/Diazenido (η^1-NNR)							*80*
N–N		1.219	1.224	0.032	1.210	1.236	14	
N–C		1.428	1.427	0.024	1.414	1.438	14	
Mn–N	see FTLAMN (1.696)							
Mo–N	(6,7), (0-VI): all Mo–N–N > 160°, N–N–C < 130°	1.806	1.816	0.028	1.778	1.832	8	
Ru–N	see CTZPRU (1.795)							
Rh–N	see CPZRHF10 (1.961)							
W–N	see CPCMZW (1.850)							
Os–N	see HPZPOS (1.867)							
Ir–N	see PAZMPI (1.834)							

Table 9.6.3.3. *Interatomic distances (Å) (cont.)*

Bond	Substructure (coordination number, oxidation state, comment)	*d*	*m*	σ	q_l	q_u	*n*	Note
4.7.2 Diazoalkanes (η^1-NNCR_2)								
N–N	all bent N–N–C	1.319	1.312	0.027	1.300	1.346	8	
N–C		1.309	1.311	0.015	1.294	1.320	8	
Mn–N	see AZMLMN (1.796)							
Mo–N	see BAMTAK10 (1.759, 1.782), CIYBAN (1.797)							
W–N	see AZPPBW10 (1.723), BCAZWB (1.784), CIXJIC (1.776)							
Ir–N	see PCLPIR (1.825)							
4.8.1.1 Azido (η^1-N_3)†								*84*
(*M*)N–N		1.180	1.183	0.020	1.175	1.193	37	
N–N		1.149	1.150	0.020	1.141	1.163	37	
Ti–N	see AZCPTI (2.025)							
Mn–N	see MNACAZ30 (2.244)							
Co–N	(5,6), (I,III)	1.991	1.967	0.047	1.952	2.030	7	
Cu–N	(4–6), (I,II): all	2.012	1.969	0.088	1.962	2.040	15	
	(4–6), (II): excluding 3 > 2.16	1.966	1.964	0.024	1.948	1.980	11	
Mo–N	(5,6), (II,VI): all	2.095	2.062	0.078	2.026	2.175	10	*30*
	(5,6), (VI)	2.037	2.036	0.025	2.019	2.054	6	
	(6), (II): all BUNZOZ	2.182	2.175	0.021	2.167	2.203	4	
Ru–N	see ENAZPU10 (2.122)							
Pd–N	see AZENPD10 (2.077), BEJJAB (2.044)							
U–N	see BOPTEF (2.382)							
4.8.1.2 Azido (μ_2-N^1,N^1-N_3)†								
N^1–N^2		1.210	1.202	0.025	1.195	1.220	11	
N^2–N^3	excluding 2 > 1.25	1.135	1.136	0.015	1.127	1.146	9	
Cu–N	(4–6), (II): excluding 1 > 2.4	2.014	2.018	0.040	1.986	2.034	15	
Zr–N	see BAXFOV (2.202, 2.204)							
Rh–N	see AFMZRH (2.133, 2.105)							
4.8.1.3 Azido (μ_2-N^1,N^3-N_3)†								
N–N		1.173	1.171	0.015	1.167	1.183	8	
Ni–N	see ZTANPB (2.196, 2.069)							
Cu–N	see BUVNIP (2.456, 1.979), MDNCAZ10 (2.252, 1.985), TTZZCU10 (2.013, 1.994)							
4.9.1.1 Nitrosyl (terminal NO)								*78, 80*
N–O	all	1.172	1.173	0.036	1.155	1.194	211	*91*
	M–N–O >150°	1.176	1.175	0.030	1.156	1.194	197	
	M–N–O <140°	1.114	1.125	0.057	1.064	1.164	10	
V–N	see BEYFEQ (1.809), BIVGAO (1.760)							
Cr–N	(4,6,7): (Cr–N–O 166–180°)	1.684	1.680	0.022	1.675	1.694	16	
Mn–N	(5,6): (Mn–N–O 164–180°)	1.651	1.648	0.013	1.641	1.659	14	
Fe–N	(4–6,*): (Fe–N–O 144–180°)	1.671	1.666	0.028	1.650	1.681	51	*92*
	: (Fe–N–O >155°)	1.669	1.666	0.023	1.650	1.680	50	
Co–N	(4–6): (Co–N–O 124–180°)	1.697	1.667	0.084	1.640	1.805	22	*8, 30, 92*
	: (Co–N–O >158°)	1.646	1.649	0.030	1.617	1.669	15	
	(Co–N–O <133°) excluding BUBBAB (1.705)	1.822	1.815	0.020	1.806	1.842	6	
Ni–N	(3,4): (Ni–N–O 161–180°)	1.628	1.629	0.024	1.612	1.649	11	
Mo–N	(5–8): (Mo–N–O 166–180°)	1.787	1.779	0.041	1.760	1.804	44	
Ru–N	(4–6): (Ru–N–O 143–180°)	1.751	1.752	0.038	1.732	1.766	12	
	(Ru–N–O >168°) excluding RUNCPP10 (1.839)	1.743	1.751	0.027	1.727	1.763	11	
Rh–N	see NSDPRH10 (1.801)							
W–N	(5–7): (W–N–O 168–180°)	1.792	1.800	0.034	1.770	1.822	7	
Re–N	(4,6): (Re–N–O 170–180°)	1.749	1.780	0.026	1.734	1.766	16	
Os–N	(4–6): (Os–N–O 133–180°)	1.751	1.748	0.067	1.732	1.776	7	*92*
	Os–N–O >174°: excluding NSOSPP10 (1.859)	1.733	1.743	0.051	1.708	1.771	6	
Ir–N	(4,5): (Ir–N–O 124–180°)	1.780	1.757	0.106	1.688	1.872	8	*92*
	(Ir–N–O >163°) excluding CNOPIR (1.972), ICNPIR (1.900)	1.720	1.713	0.046	1.678	1.765	6	
4.9.1.2 Nitrosyl (μ_2-NO)								*78*
N–O		1.210	1.208	0.025	1.195	1.218	19	
Cr–N	see BRNOCR (1.892, 1.924)							
Mn–N		1.855	1.858	0.007	1.850	1.860	18	
Fe–N	see MENTFE (1.818)							
Co–N		1.817	1.821	0.012	1.804	1.826	4	
Ru–N	all BISKOD	1.918	1.919	0.005	1.913	1.922	4	
Rh–N	see COBGIJ (1.952)							
Os–N		2.042	2.040	0.029	2.014	2.073	6	

Table 9.6.3.3. *Interatomic distances (Å) (cont.)*

Bond	Substructure (coordination number, oxidation state, comment)	*d*	*m*	σ	q_l	q_u	*n*	Note
4.9.1.3 Nitrosyl (μ_3-NO)								*78*
N–O	(1.247)							
Mn–N	see TCPMNN10 (1.933, 1.917, 1.939)							
4.9.2.1 Thionitrosyl (terminal NS)								*80, 93*
N–S		1.518	1.509	0.022	1.504	1.541	4	
Cr–N	see CTNSCR10 (1.693)							
Ru–N	see COGHEL (1.729)							
Os–N	see CESNET (1.779), CIBKED (1.730)							
4.10.1.1 NH_2								
(None)								
4.10.2.1 Primary amides (NH*R*)								*94*
N–C		1.434	1.429	0.035	1.404	1.470	4	
Mo–N	see ADASMO (2.058), MPBMOE10 (1.955, 1.964)							
Os–N	see BOSRUW (1.896)							
4.10.3.1 Secondary amides [NR_2, $R = C(sp^3)$]								*94*
N–C		1.464	1.463	0.017	1.455	1.472	162	
Ti–N	(4,5), (IV): all	1.939	1.943	0.016	1.928	1.947	11	
Zr–N	see TBIAZR (2.058, 2.062)							
Mo–N	(4,5), (III): (mainly Mo_2)	1.955	1.952	0.020	1.945	1.967	44	
Tc–N	see CEWZIN10 (1.908, 1.916)							
Ta–N	(5,6), (V)	1.964	1.963	0.017	1.954	1.978	12	
W–N	(4), (III,VI)	1.952	1.955	0.015	1.937	1.967	7	
U–N	(4,5), (IV)	2.206	2.212	0.033	2.172	2.235	4	
4.10.3.2 Amides (μ_2-NR_2)								
N–C	all C(sp^3)	1.479	1.482	0.036	1.470	1.493	10	
Ti–N	see BUNKEA (2.147, 2.191)							
Cu–N	see CIDBAS (1.901, 1.907)							
Mo–N	see PAIDMO (2.178, 2.250)							
Au–N	see CASPIV (2.142, 2.139)							
U–N	see URDEAM10 (2.456, 2.571)							
4.11.1.1 Amidinates [η^1-*R*NC(*R*)N*R*]								
(None)								
4.11.1.2 Amidinates [chelating, η^2-*R*NC(*R*)N*R*]								*84*
N–C		1.315	1.311	0.021	1.300	1.324	12	
Mo–N	(7), (II)	2.171	2.177	0.021	2.148	2.188	10	
Re–N	see BIYWUB (2.215, 2.217)							
4.11.1.3 Amidinates [bridging, μ_2-η^1, $\eta^{1'}$-*R*NC(*R*)N*R*]								
N–C		1.340	1.336	0.022	1.323	1.352	22	
Cr–N	all MBZACR	2.032	2.031	0.009	2.024	2.041	4	
Mo–N	(5), (II)	2.149	2.151	0.016	2.134	2.161	12	
Re–N	all PBARTC	2.077	2.076	0.015	2.063	2.092	4	
4.12.1 Schiff bases (η^1-*R*N=CR_2)†								*95*
N=C		1.287	1.286	0.021	1.275	1.300	768	
N–C		1.471	1.473	0.022	1.461	1.485	765	
Ti–N	see ESALTJ (2.136, 2.139)							
V–N	(5,6), (IV): all	2.047	2.041	0.024	2.036	2.054	7	
Cr–N	(5,6), (0,I,III): all	2.079	2.028	0.073	2.018	2.152	9	
	(5,6), (0)	2.153	2.152	0.032	2.123	2.182	4	
	(6), (I,III)	2.019	2.019	0.006	2.014	2.025	5	
Mn–N	(6,7), (II,III): all	2.163	2.116	0.143	2.051	2.292	10	*96, 97*
Fe–N	(5-7), (0,II,III): all	2.038	1.992	0.103	1.942	2.109	78	*30*
	(5), (0): all	1.953	1.932	0.039	1.926	1.997	6	
	(5,6), (II): all	2.044	2.031	0.098	1.950	2.119	32	*30*
	: low spin	1.958	1.954	0.021	1.938	1.977	16	
	: high spin	2.131	2.115	0.057	2.086	2.162	16	
	(5,6), (III): all	2.022	1.991	0.086	1.937	2.108	36	*30*
	: low spin	1.949	1.944	0.024	1.931	1.973	20	
	: high spin	2.113	2.108	0.029	2.094	2.123	16	
	(7), (II)	2.258	2.260	0.014	2.244	2.270	4	

Table 9.6.3.3. *Interatomic distances (Å) (cont.)*

Bond	Substructure (coordination number, oxidation state, comment)	*d*	*m*	σ	q_l	q_u	*n*	Note
4.12.1 Schiff bases (η^1-$RN{=}CR_2$)† *(cont.)*								
Co–N	(4–6), (I–III): all	1.943	1.917	0.084	1.891	1.946	142	*30*
	(4), (II)	1.907	1.876	0.065	1.871	1.921	25	*86*
	(5,6), (II)	2.015	2.036	0.109	1.897	2.128	44	*30*
	: short (<1.95)	1.897	1.894	0.023	1.881	1.916	18	
	: long (>1.99)	2.097	2.115	0.054	2.048	2.140	26	
	(5,6), (III): all	1.914	1.917	0.021	1.897	1.931	71	
Ni–N	(4–6,*), (0,II,IV): all	1.929	1.906	0.080	1.860	2.000	136	
	(4), (0): all	1.924	1.924	0.006	1.922	1.930	7	
	(4), (II)	1.888	1.871	0.048	1.855	1.917	77	*86*
	(5), (II): all	1.922	1.889	0.084	1.853	2.031	16	*30*
	: short (<1.925)	1.869	1.859	0.028	1.843	1.898	11	
	: long (>2.025)	2.038	2.039	0.010	2.029	2.048	5	
	6, (II): all	2.051	2.055	0.034	2.022	2.075	27	
	6, (IV)	1.872	1.872	0.004	1.869	1.876	4	
Cu–N	(3–6,*), (I,II): all	1.969	1.964	0.053	1.936	1.990	227	*86*
	(3,4), (I)	2.005	1.989	0.073	1.947	2.075	18	
	(4), (II)	1.954	1.947	0.043	1.921	1.977	97	
	(5), (II)	1.966	1.965	0.039	1.936	1.986	88	
	(6), (II): all	2.010	2.005	0.049	1.966	2.049	14	
Zn–N	(4–6,*), (II): all	2.122	2.120	0.049	2.114	2.167	11	
Zr–N	all SAZPZR	2.428	2.435	0.021	2.406	2.443	4	
Mo–N	(5–7), (0–VI): all	2.189	2.181	0.065	2.131	2.237	31	
	(6), (0)	2.244	2.254	0.042	2.203	2.274	6	
	(7), (II)	2.216	2.221	0.028	2.204	2.233	10	
	(–), (V,VI): excluding 2>2.30	2.124	2.130	0.013	2.113	2.133	12	
Tc–N	(5,6), (V)	2.034	2.023	0.029	2.002	2.066	7	
Ru–N	see BAVSIA (2.190), COGXRU (2.138)							
Rh–N	(4,6), (I,III): all	2.053	2.039	0.046	2.013	2.103	8	
	(6), (III)	2.023	2.026	0.019	2.005	2.039	5	
Pd–N	(4,5,*), (II): all	2.037	2.032	0.040	2.017	2.046	26	
Ag–N	(4–6), (I,II): all	2.403	2.429	0.112	2.311	2.447	9	
Cd–N	see BEHMOQ (2.399, 2.457)							
La–N	all EPAILA	2.714	2.721	0.025	2.688	2.734	4	
Ce–N	(8), (IV)	2.615	2.614	0.025	2.608	2.638	8	
W–N	see ALBCIW (2.219)							
Re–N	(6), (V)	2.121	2.122	0.023	2.099	2.143	6	
Os–N	[all μ-N(R)=C(R) clusters]	2.145	2.150	0.025	2.125	2.161	18	
Ir–N	see SCLIRA10 (2.098)							
Pt–N	see BISIPT (2.171, 2.176), BZHXDB (2.021, 1.995)							
Au–N	see MEAZAU (1.976, 1.980)							
Hg–N	see BOCWEV (2.158)							
Th–N	(8), (IV): all	2.641	2.654	0.022	2.618	2.659	5	
U–N	(7), (VI): excluding COKPIB (2.710)	2.572	2.568	0.012	2.565	2.586	6	
4.13.1 Pyrroles†								
N–C^1		1.375	1.376	0.022	1.363	1.388	168	
C^1–C^2		1.429	1.434	0.039	1.399	1.453	168	
C^2–$C^{2'}$		1.368	1.371	0.025	1.350	1.384	83	
Ti–N	see CPYRTI10 (2.067, 2.100)							
Mn–N	(6), (–): all	2.126	2.141	0.041	2.095	2.148	5	
Fe–N	(5,6), (II,III): all	2.020	1.995	0.075	1.948	2.107	8	
	(5,6), (III)	1.969	1.985	0.031	1.936	1.995	5	
Co–N	(5), (II)	2.044	2.063	0.033	2.009	2.065	6	
Ni–N	(4), (II)	1.906	1.897	0.030	1.877	1.937	18	
Cu–N	(4,5), (II)	1.908	1.899	0.023	1.890	1.929	13	
Zn–N	(4,5), (II)	1.999	1.990	0.040	1.975	2.004	13	
	(4), (II)	1.980	1.976	0.009	1.974	1.990	10	
Zr–N	see CYPRZR10 (2.167, 2.170)							
Mo–N	see BOXHUR (2.151)							
Tc–N	see TPPTCC (2.161)							
Rh–N	(4,*), (I,II)	2.067	2.065	0.017	2.052	2.083	4	
Pd–N	see BESFOU (2.010, 2.071)							
Hf–N	see CESJOZ (2.164, 2.178)							
Pt–N	see CAFFIY (2.045)							
Hg–N	see FMTPHG (2.016), TAMPHG (2.325)							
U–N	see CIMINU10 (2.490, 2.527, 2.533)							
4.13.2 Porphinates†								*98*
N–C		1.380	1.379	0.011	1.373	1.385	564	
Ti–N	(5), (IV)	2.112	2.115	0.016	2.098	2.124	8	
V–N	(5,6), (II,IV)	2.085	2.098	0.027	2.051	2.104	6	
Cr–N	(4,5), (II,V)	2.037	2.036	0.005	2.033	2.042	6	

Table 9.6.3.3. *Interatomic distances (Å) (cont.)*

Bond	Substructure (coordination number, oxidation state, comment)	*d*	*m*	σ	q_l	q_u	*n*	Note
4.13.2 Porphinates† (*cont.*)								
Mn–N	(4–6), (II-IV): all	2.024	2.013	0.046	1.998	2.030	34	
	(4-6), (II)	2.057	2.029	0.053	2.009	2.124	14	
	(5,6), (III,IV)	2.001	2.002	0.020	1.992	2.016	20	
Fe–N	(4-6), (II,III): all	2.031	2.038	0.036	1.995	2.062	88	*30,98,99*
	(4-6), (II)	2.009	2.000	0.035	1.987	2.006	22	
	(4-6), (III)	2.034	2.050	0.034	1.999	2.067	66	
	(4-6), (II,III): short (<2.014)	1.995	1.995	0.009	1.991	2.003	41	
	(4-6), (II,III): long (>2.022)	2.063	2.062	0.017	2.051	2.074	47	
Co–N	(4-6), (II,III): all	1.969	1.983	0.022	1.947	1.988	19	
Ni–N	(4), (II)	1.943	1.949	0.014	1.931	1.954	16	
Cu–N	(4), (II)	1.991	1.992	0.009	1.985	1.996	6	
Zn–N	(4,5), (II)	2.068	2.063	0.024	2.058	2.074	18	
Nb–N	(6,7), (V)	2.234	2.239	0.037	2.209	2.247	16	
Mo–N	(5,6), (II,IV): excluding OTPHMO	2.086	2.090	0.017	2.075	2.097	28	*44*
Ru–N	(5,6), (II,III)	2.047	2.047	0.007	2.043	2.055	24	
Rh–N	(5,6), (III)	2.034	2.031	0.010	2.026	2.042	6	
Cd–N	all PHPNCD	2.145	2.150	0.029	2.115	2.169	4	
Pt–N	see CEZKEX (2.005)							
4.13.3 Phthalocyanines†								
N–C		1.380	1.381	0.011	1.379	1.389	70	
Ti–N	(5), (IV): all BITSAY	2.066	2.064	0.013	2.055	2.080	4	
V–N	(5), (IV): all VPHTHC	2.026	2.029	0.013	2.012	2.037	4	
Mn–N	see MNPHCY03 (1.938, 1.939)							
Fe–N	(4,6), (II)	1.934	1.931	0.009	1.927	1.941	6	
Co–N	(4,6), (II)	1.921	1.915	0.017	1.910	1.938	4	
Ni–N	see NIPHTI (1.887)							
Zn–N	see PTHCZN (1.978, 1.980)							
Nb–N	(6), (IV): all BEJTIT	2.144	2.144	0.015	2.129	2.159	4	
Nd–N	all CIZGIB02	2.471	2.471	0.009	2.463	2.479	4	
Os–N	(6), (II): all PCPCOS	2.016	2.015	0.041	1.980	2.055	4	
4.14.1.1 **Pyrazol**ates (η^1-$C_3R_3N_2$)†								
N^1–N^2	(1.361, 1.369, 1.367)							
N^1–C^5	(1.347, 1.350, 1.345)							
N^2–C^3	(1.340, 1.332, 1.327)							
C^3–C^4	(1.376, 1.386, 1.383)							
C^4–C^5	(1.384, 1.368, 1.373)							
Mo–N	see CAFLEA (2.157, 2.166)							
Ir–N	see BIXBUF10 (2.080)							
4.14.1.2 Pyrazolates (μ_2-η^1, $\eta^{1'}$-$C_3R_3N_2$)†								
N–N		1.367	1.368	0.014	1.360	1.375	34	
N–C		1.345	1.345	0.020	1.338	1.350	68	
C–C		1.378	1.377	0.017	1.370	1.385	68	
Ti–N	see PZCPTI (2.205, 2.183)							
Fe–N	all DMPZFE	2.005	2.007	0.004	2.001	2.009	4	
Co–N	all DMPZCO	1.988	1.988	0.007	1.982	1.995	4	
Ni–N	(3,4), (0-II)	1.957	1.971	0.044	1.917	1.997	16	
Cu–N	(3,5), (I,II)	1.929	1.934	0.035	1.892	1.958	8	
Rh–N	(4-6), (I,III): all	2.080	2.084	0.017	2.065	2.094	24	
Pd–N	all PZALPD10	2.073	2.071	0.006	2.069	2.079	4	
Ir–N	(4,5), (I,II)	2.070	2.078	0.022	2.053	2.091	7	
4.14.2.1 Imidazolates (η^1-$C_3R_3N_2$)†								
N^1–C^2		1.344	1.345	0.023	1.329	1.360	21	
N^1–C^5		1.376	1.369	0.026	1.355	1.398	21	
C^2–N^3		1.336	1.338	0.017	1.322	1.346	21	
N^3–C^4		1.356	1.355	0.024	1.340	1.372	21	
C^4–C^5		1.380	1.382	0.021	1.373	1.393	21	
Co–N	see ACNTCC (2.005), CTENCO20 (1.956)							
Cu–N	(4,5), (II): all	1.994	1.992	0.024	1.980	2.009	6	
Pd–N	see ADBPPD (2.015)							
Ag–N	see IMDZAG (2.074, 2.098)							
Ir–N	see CEXZIO (2.321, 2.116), CEXZOU (2.081), CEYBEN (2.081)	2.035	2.030	0.035	2.005	2.070	4	
Pt–N	(4), (II)							
Hg–N	see ADMEHH (2.070), CIRMAR (2.081)							
4.14.2.2 Imidazolates (μ_2-η^1, $\eta^{1'}$-$C_3N_2R_3$)†								
N^1–N^2		1.332	1.332	0.012	1.325	1.341	49	
N^1–C^5		1.372	1.373	0.016	1.363	1.381	49	

Table 9.6.3.3. *Interatomic distances (Å) (cont.)*

Bond	Substructure (coordination number, oxidation state, comment)	*d*	*m*	σ	q_l	q_u	*n*	Note
4.14.2.2	Imidazolates (μ_2-η^1, $\eta^{1'}$-$C_3N_2R_3$)† (*cont.*)							
C^4–C^5		1.358	1.354	0.015	1.348	1.368	25	
Mn–N	all IMIDZA	2.154	2.114	0.078	2.099	2.250	6	*30*
Fe–N	(4,6), (II)	2.065	2.043	0.070	2.012	2.137	8	
Cu–N	(4-6), (II): excluding BIMTCU (2.323)	1.966	1.967	0.022	1.957	1.979	19	
Zn–N	see IMZZNN (1.986, 1.993)							
Rh–N	(4,5), (-)	2.104	2.104	0.034	2.071	2.138	8	
Ir–N	see CEYBEN (2.087, 2.094)							
Hg–N	(2,3), (II)	2.086	2.084	0.008	2.079	2.094	4	
4.14.3	*N*-Alkylpyrazoles†							
N^1–N^2		1.360	1.360	0.015	1.350	1.368	53	
N^1–C^5		1.331	1.333	0.015	1.324	1.340	53	
N^2–C^3		1.349	1.350	0.012	1.342	1.358	53	
C^3–C^4		1.356	1.358	0.020	1.344	1.371	53	
C^4–C^5		1.387	1.387	0.015	1.377	1.396	53	
N^2–C(*R*)		1.452	1.452	0.023	1.439	1.469	53	
Cr–N	all CEYBIR	2.101	2.097	0.023	2.082	2.128	6	
Co–N	see DPPTCC (2.021, 2.036)							
Ni–N	(5,6), (II)	2.057	2.047	0.031	2.034	2.089	4	
Cu–N	(2,4,5,*), (I,II): all	1.973	1.979	0.072	1.927	1.994	19	
	(2), (I)	1.876	1.878	0.009	1.867	1.884	4	
	(4), (I)	1.991	1.990	0.039	1.963	2.030	8	
	(4,5), (II): excluding BENDED (2.173)	1.985	1.985	0.007	1.979	1.992	5	
Mo–N	see CAFLAW (2.123)							
Rh–N	see COSTIN (2.102, 2.111)							
Pd–N	(4), (II)	2.026	2.031	0.018	2.007	2.040	4	
Ag–N	see PMPZAG10 (2.243)							
Pt–N	(4,6), (II,IV): all	2.189	2.210	0.064	2.121	2.236	4	
Au–N	see BOFCEE (2.130, 2.141)							
Th–N	all FAPZTH10	2.637	2.633	0.017	2.624	2.655	4	
U–N	all UHXAPY10	2.574	2.582	0.024	2.549	2.593	4	
4.14.4	*N*-Alkylimidazoles†							
N^1–C^2		1.346	1.344	0.014	1.337	1.353	103	
C^2–N^3		1.320	1.320	0.017	1.310	1.328	104	
N^3–C^4		1.382	1.380	0.016	1.370	1.393	104	
N^1–C^5		1.369	1.369	0.015	1.361	1.380	104	
C^4–C^5		1.359	1.362	0.023	1.342	1.375	104	
N^1–C(R)		1.468	1.468	0.020	1.458	1.480	104	
Mn–N	see MNTPPI10 (2.191)							
Fe–N	(6), (II): excluding BERTAT (2.021)	2.199	2.191	0.018	2.183	2.218	5	
Co–N	(4-6), (II,III): all	2.058	2.036	0.065	2.015	2.096	21	*8*
	(4), (II)	2.019	2.016	0.008	2.013	2.026	6	
	(5,6), (II)	2.100	2.096	0.067	2.031	2.161	10	
	(6), (III)	2.021	2.042	0.053	1.970	2.062	5	
Ni–N	see CESKIU (2.102, 2.110)							
Cu–N	(4-6), (I,II): all	2.022	2.004	0.051	1.995	2.046	33	
	(4), (II)	1.974	1.970	0.019	1.959	1.995	7	
	(5), (II)	2.040	2.007	0.061	1.996	2.092	16	
	(6), (II)	2.023	2.022	0.021	2.006	2.041	9	
Zn–N	see CEPGUZ (2.083), MADCZB10 (2.040)							
Mo–N	see COFZEC (2.141, 2.273)							
Ru–N	see BAKDUM (2.094)							
Rh–N	see RACCAF (2.316)							
Pd–N	see COHCUX (1.988), ENGUPD (2.013), TCMIPD10 (2.011)							
Ag–N	(2,3), (I)	2.141	2.139	0.016	2.126	2.155	8	
Cd–N	see BEGNAC (2.358)							
Pt–N	(4), (II): all	2.017	2.015	0.014	2.008	2.027	20	
Hg–N	see BEJGIG (2.132), CAGSIM (2.125), MEGUHG (2.087)							
4.14.5	Pyrazole†							
N^1–N^2		1.352	1.353	0.015	1.345	1.356	43	
N^2–C^3		1.329	1.329	0.009	1.325	1.336	42	
N^1–C^5		1.339	1.338	0.010	1.333	1.345	43	
C^4–C^5		1.357	1.357	0.019	1.350	1.367	43	
C^3–C^4		1.388	1.387	0.017	1.376	1.396	43	
Mn–N	(6), (I,II): all	2.209	2.240	0.071	2.168	2.249	6	
	(6), (II)	2.237	2.243	0.021	2.219	2.252	5	
Fe–N	see MEPZFE (2.068)							
Co–N	see FMPZCO (2.032, 2.040, 2.042)							
Ni–N	(6), (II): excluding PYRZNI (1.905, 1.908)	2.102	2.098	0.016	2.089	2.118	4	

Table 9.6.3.3. *Interatomic distances (Å) (cont.)*

Bond	Substructure (coordination number, oxidation state, comment)	*d*	*m*	σ	q_l	q_u	*n*	Note
4.14.5 Pyrazole† (*cont.*)								
Cu–N	(5,6), (II)	1.988	1.995	0.030	1.964	2.011	12	
Zn–N	see CIRVOO (2.016, 2.017)							
Mo–N	(6,7), (0,II,III): all	2.193	2.174	0.059	2.142	2.251	6	
Ru–N	see CIZBES (2.211)							
Rh–N	(4,6), (I,III)	2.102	2.100	0.016	2.088	2.118	4	
Pd–N	see BABTUT (2.101)							
Pt–N	see CEZMUP (2.027)							
4.14.6 Pyrazolylborates†								
N^1–N^2		1.366	1.366	0.012	1.360	1.372	210	
N^2–N^3		1.339	1.339	0.014	1.329	1.347	211	
N^1–C^5		1.347	1.347	0.011	1.340	1.354	209	
C^4–C^5		1.366	1.368	0.016	1.360	1.375	211	
C^3–C^4		1.383	1.382	0.015	1.373	1.391	210	
N^1–B		1.546	1.543	0.019	1.535	1.555	211	
Cr–N	(4), (II)	2.061	2.060	0.006	2.057	2.067	4	
Fe–N	(6,7), (II,III): all	2.129	2.147	0.055	2.102	2.169	22	
Co–N	(4,6), (II,III): all	1.948	1.951	0.048	1.916	1.979	6	*30*
Ni–N	all PYZBNI [excluding PPZBNI (1.891)]	2.092	2.090	0.007	2.087	2.099	6	
Cu–N	(2-6), (I,II): all	2.035	2.002	0.134	1.949	2.052	29	*86*
	(2-5), (I)	2.001	1.987	0.075	1.946	2.041	23	
	(3), (I)	1.936	1.941	0.028	1.913	1.958	5	
Zr–N	see CEFHEA (2.387, 2.438, 2.430)							
Mo–N	(5-7), (0-VI): all	2.218	2.219	0.042	2.188	2.245	90	
Tc–N	see CHBPTC (2.088, 2.089, 2.259)							
Ru–N	see PZRBZRU10 (2.101, 2.112)							
Rh–N	(4-6), (I,III): all	2.098	2.083	0.043	2.071	2.123	12	
Ag–N	see PRZBAG (2.194, 2.412)							
Yb–N	all BORVIN	2.469	2.453	0.074	2.405	2.530	8	
Ta–N	see CEXHUI (2.227, 2.273, 2.294)							
W–N	(6), (-)	2.215	2.213	0.028	2.200	2.218	9	
Pt–N	(4,5), (II)	2.098	2.121	0.050	2.054	2.129	9	
Au–N	see CEPMAL (2.119, 2.127)							
4.14.7 Pyrazolylgallates†								
N^1–N^2		1.370	1.368	0.009	1.362	1.377	40	
N^2–C^3		1.336	1.339	0.014	1.334	1.344	40	
N^1–C^5		1.344	1.344	0.011	1.339	1.352	40	
C^4–C^5		1.363	1.364	0.017	1.355	1.372	40	
C^3–C^4		1.380	1.381	0.012	1.373	1.386	40	
N^1–Ga		1.966	1.975	0.029	1.942	1.989	40	
Mn–N	see BATZIF (2.077), BEWVEE (2.076, 2.080)							
Fe–N	see MEPGFE (2.107)							
Ni–N	(4-6), (0-II): all	1.986	1.981	0.075	1.920	2.068	11	
	(4), (0-II)	1.932	1.922	0.038	1.898	1.976	6	
Cu–N	(4), (I,II)	1.982	1.979	0.026	1.960	2.006	5	
Mo–N	(5-7), (0-II): all	2.252	2.264	0.048	2.221	2.288	13	
	(7), (-)	2.267	2.270	0.033	2.237	2.289	11	
Rh–N	(4,6), (I,II)	2.168	2.173	0.038	2.168	2.188	7	
4.14.8 Imidazole†								
N^3–C^2		1.324	1.324	0.012	1.316	1.330	194	
N^3–C^4		1.381	1.380	0.015	1.372	1.391	197	
C^2–N^1		1.340	1.339	0.014	1.332	1.347	196	
N^1–C^5		1.369	1.366	0.018	1.358	1.379	196	
C^4–C^5		1.361	1.356	0.021	1.347	1.373	197	
Cr–N	see BOPPIF10 (2.062, 2.050), LDHPCR10 (2.057)							
Mn–N	(5,6), (I,II): all	2.237	2.248	0.057	2.196	2.276	10	
	(5,6), (II)	2.251	2.266	0.042	2.205	2.279	9	
Fe–N	(4,6), (-): all	2.157	2.152	0.091	2.107	2.235	7	
Co–N	(4-6), (II,III): all	2.010	2.013	0.077	1.930	2.089	22	*8*
	(4), (II)	2.022	2.019	0.011	2.013	2.034	4	
	(5,6), (II)	2.103	2.097	0.028	2.088	2.112	7	
	(6), (III)	1.946	1.930	0.036	1.916	1.958	11	
Ni–N	(4,6), (II): all	2.103	2.099	0.024	2.082	2.128	30	
Cu–N	(3-6), (I,II): excluding IMZCUN (2.593)	1.988	1.981	0.050	1.961	2.008	82	
	(4), (II)	1.982	1.981	0.024	1.963	2.001	19	
	(5), (II): all	1.984	1.975	0.038	1.961	1.997	35	*86*
	(5), (II): excluding 2 > 2.07	1.976	1.974	0.020	1.961	1.994	33	
	(6), (II): excluding 3 > 2.13	1.996	2.009	0.038	1.954	2.029	23	
Zn–N	(4-6), (II)	2.043	2.056	0.044	1.997	2.076	21	
	(4), (II)	2.023	2.010	0.033	1.995	2.056	11	

Table 9.6.3.3. *Interatomic distances (Å) (cont.)*

Bond	Substructure (coordination number, oxidation state, comment)	d	m	σ	q_l	q_u	n	Note
4.14.8 Imidazole† (*cont.*)								
Zn–N	(6), (II)	2.084	2.076	0.027	2.066	2.098	8	
Mo–N	see MOSHIS10 (2.238, 2.245)							
Ru–N	see BAKDOG (2.087)							
Pd–N	see BOLRID (2.005), HISTPD (2.029)							
Ag–N	see ADAGPC (2.154), AGIMHN01 (2.118, 2.132)							
Cd–N	(6,8), (II)	2.302	2.290	0.054	2.255	2.349	11	
Os–N	see CASVIB (2.153)							
Ir–N	see CEYBEN (2.081)							
4.15.1 Pyridine†								
N–C^2		1.341	1.339	0.018	1.331	1.348	612	
C^2–C^3		1.382	1.380	0.020	1.371	1.393	613	
C^3–C^4		1.372	1.372	0.021	1.360	1.384	610	
Ti–N	see ESALTJ (2.279)							
V–N	see TPYCLV (2.188)							
Cr–N	(6), (-)	2.178	2.158	0.076	2.147	2.171	11	*100*
	(6), (-)	2.146	2.158	0.030	2.122	2.168	9	*85*
Mn–N	see BANVUH10 (2.018), COTGEX (2.377), FACMNB (2.086, 2.109)							
Fe–N	(5,6), (0,II,III): all	2.224	2.242	0.102	2.148	2.270	14	*87, 96*
Co–N	(4–6), (II,III): all	2.082	2.066	0.084	2.004	2.172	50	*8*
	(6), (III): excluding CORHOG (2.214)	2.034	2.040	0.044	1.992	2.071	29	
	(6), (II): excluding BACREC10 (1.953, 1.963)	2.185	2.183	0.037	2.170	2.214	15	
Ni–N	(4,6), (-): all	2.111	2.116	0.059	2.085	2.150	33	
	(6), (-)	2.122	2.117	0.042	2.096	2.152	31	
Cu–N	(-), (-) : all	2.070	2.046	0.072	2.033	2.061	32	*86*
	(4), (-)	2.024	2.023	0.019	2.007	2.043	4	
	(5), (-)	2.113	2.060	0.105	2.024	2.183	11	
	(6), (-)	2.054	2.046	0.032	2.039	2.055	16	
Zn–N	(4–6), (-)	2.095	2.081	0.063	2.051	2.149	16	
	(4), (-)	2.064	2.064	0.057	2.027	2.115	6	
	(5), (-)	2.116	2.121	0.069	2.046	2.178	6	
	(6), (-)	2.111	2.099	0.058	2.063	2.173	4	
Mo–N	(5–7), (-): all	2.300	2.279	0.078	2.252	2.336	25	*15, 100*
	: excluding HPHOMO10 (2.446)	2.282	2.278	0.046	2.249	2.329	23	*85*
Ru–N	(6), (I–III): all	2.124	2.108	0.049	2.095	2.138	28	*100*
		2.114	2.107	0.031	2.094	2.121	26	*85*
Rh–N	(6), (II–III): all	2.119	2.066	0.090	2.056	2.222	13	*30, 100*
		2.063	2.062	0.016	2.050	2.075	9	*85*
Pd–N	(4), (-)	2.089	2.085	0.061	2.033	2.149	4	
Ag–N	(-), (-)	2.299	2.322	0.056	2.228	2.331	7	
Cd–N	(6,7), (-)	2.381	2.368	0.042	2.355	2.413	5	
Ta–N	see PCTATL10 (2.423)							
W–N	(5,6): all	2.284	2.283	0.098	2.201	2.323	11	
	: excluding CAKTUD (2.528)	2.260	2.263	0.059	2.196	2.322	10	
Re–N	(5,6), (IV–VII): all	2.235	2.176	0.114	2.142	2.339	13	*87*
Os–N	(6), (-): all	2.165	2.169	0.053	2.106	2.217	6	
Ir–N	see PCHIRH10 (2.140), PHPCIR10 (2.176)							
Pt–N	(4,6), (-): all	2.085	2.061	0.078	2.036	2.125	11	
	(4), (-)	2.050	2.045	0.048	2.014	2.091	8	
Hg–N	excluding ETACHG (2.656)	2.164	2.146	0.054	2.127	2.198	6	*26*
4.15.2 2,2′-Bipyridyl (chelating, η^2-bpy)†								
N–C		1.352	1.351	0.017	1.343	1.359	329	
C^2–$C^{2'}$		1.471	1.474	0.021	1.462	1.481	166	
V–N	(5,6), (-): all	2.186	2.151	0.075	2.126	2.280	12	*30*
	: short (<2.2)	2.137	2.133	0.028	2.114	2.153	8	
Cr–N	(6), (III): all	2.085	2.076	0.037	2.059	2.088	20	*30*
Mn–N	see BPYMNA (2.291, 2.311), TNBPMN (2.087, 1.996)							
Fe–N	(5,6), (0,II,III): all	2.008	1.964	0.089	1.958	2.123	23	*30*
	(5,6), (II,III): low spin	1.961	1.962	0.012	1.954	1.967	16	
	(6), (III): high spin	2.151	2.153	0.024	2.123	2.172	6	
Co–N	(6), (II,III): all	2.098	2.129	0.093	2.072	2.147	10	*8, 30*
	(6), (II)	2.141	2.133	0.023	2.126	2.152	8	
Ni–N	(4,5,6), (-): all	1.956	1.948	0.044	1.934	1.960	12	*9*
	(4)	1.944	1.939	0.033	1.921	1.959	9	
Cu–N	(4,5,6), (-): all	2.031	2.007	0.057	1.991	2.071	108	*12, 86*
	(4), (II)	2.002	1.997	0.025	1.986	2.018	12	
	(5), (-)	2.038	2.010	0.062	1.992	2.081	70	*86*
	(6), (-)	2.024	2.003	0.053	1.990	2.053	22	*86*
Zn–N	(-), (-): all	2.088	2.090	0.034	2.056	2.117	4	
Zr–N	see TCBPZR (2.412)							
Nb–N	see TCBPNB (2.319)							

Table 9.6.3.3. *Interatomic distances (Å) (cont.)*

Bond	Substructure (coordination number, oxidation state, comment)	*d*	*m*	σ	q_l	q_u	*n*	Note
4.15.2 2,2′-Bipyridyl (chelating, η^2-bpy)† (*cont.*)								
Mo–N	(5,6,7), (-): all	2.260	2.251	0.074	2.210	2.314	32	*15*
Ru–N	(6), (-): all	2.064	2.063	0.028	2.044	2.087	34	
Rh–N	see BIHJORH10 (2.020, 2.029)							
Pd–N	(3,4,6), (0,II,IV): all	2.088	2.086	0.087	2.014	2.169	8	
Ag–N	see BPYAGN (2.179, 2.153)							
Cd–N	(6), (-): all	2.369	2.367	0.033	2.339	2.396	14	
Re–N	see DPCLRE10 (2.245)							
Os–N	see CIXLIE (2.071, 2.112)							
Ir–N	(6), (-)	2.071	2.049	0.042	2.039	2.115	20	
Pt–N	see BIBFUN (2.107, 2.103), BPYCPT (2.001)							
Hg–N	(5,6,7), (-): all	2.307	2.293	0.057	2.276	2.358	8	
U–N	(9), (-): all	2.627	2.623	0.018	2.612	2.646	4	
4.15.3 Phenanthroline (chelating, η^2-*o*-phen)†								
N–C		1.361	1.360	0.014	1.353	1.367	157	
C^2–$C^{2'}$		1.428	1.429	0.017	1.419	1.439	84	
Ti–N	see PNOLTI (2.147, 2.223)							
Cr–N	see BUWYIB (2.055, 2.057)							
Mn–N	(6), (I,II): all	2.106	2.069	0.070	2.055	2.190	6	
	(6), (I)	2.062	2.052	0.013	2.055	2.075	4	
Fe–N	(6), (II): all	2.059	1.982	0.122	1.968	2.182	25	
	: tris-phen only	1.969	1.970	0.015	1.958	1.979	15	
Co–N	(6), (I-III): all	2.027	1.998	0.096	1.943	2.133	16	*30*
	(6), (I,II)	2.141	2.137	0.020	2.124	2.156	6	
	(6), (III)	1.958	1.947	0.033	1.938	1.992	10	
Ni–N	(4-6), (II): all	2.053	2.063	0.047	2.009	2.092	16	*9*
	(4), (II)	1.989	1.985	0.011	1.982	2.001	4	
	(5), (II)	2.034	2.033	0.011	2.024	2.045	4	
	(6), (II)	2.093	2.092	0.015	2.080	2.104	8	
Cu–N	(4-6), (I,II): all	2.059	2.023	0.069	2.009	2.087	51	*12, 86*
	(4), (I)	2.083	2.078	0.040	2.056	2.122	14	
	(5), (II): excluding 3 > 2.21	2.021	2.015	0.027	2.009	2.021	18	
	(6), (II): short (<2.05)	2.008	2.005	0.016	1.998	2.012	10	
	: long (>2.09)	2.129	2.124	0.025	2.111	2.149	5	
Zn–N	(4), (II)	2.063	2.063	0.007	2.057	2.069	4	
Nb–N	see OPENBO10 (2.280, 2.332)							
Mo–N	(5,6), (0,IV,VI):	2.276	2.273	0.076	2.205	2.351	4	
Ru–N	see MPTBRH (2.083, 2.092)							
Rh–N	(6), (III): all CELLAG	1.934	1.933	0.009	1.925	1.934	4	
Cd–N	(6,*), (II)	2.369	2.368	0.018	2.354	2.384	5	
Ir–N	see CAYGAK (2.085, 2.122)							
Pt–N	see BOVLED (2.165, 2.175), CNPLPT (2.053, 2.762; 2.063, 2.007)							
Hg–N	(4,6,8), (II): all	2.486	2.408	0.147	2.391	2.669	11	*30*
4.16.1.1 Pyrazines (η^1-$C_4R_4N_2$)†								
N^1–C^2		1.340	1.336	0.016	1.330	1.344	36	
C^2–C^3		1.390	1.387	0.022	1.376	1.403	37	
C^3–N^4		1.334	1.334	0.018	1.325	1.342	38	
Cr–N	see ACPCRB (2.315)							
Fe–N	see PYZTCI (2.031)							
Co–N	(6), (II): all	2.145	2.125	0.054	2.104	2.190	6	
Cu–N	(5,6), (II): excluding PYZCUA01 (2.167)	2.011	2.004	0.041	1.975	2.053	4	
Zn–N	see AZNPYD (2.145)							
Ru–N	see CABYIN (2.129, 2.152), PYZRUA (2.006)							
Rh–N	see PRNRHC (2.363)							
Ir–N	see CLPZIR (2.018)							
4.16.1.2 Pyrazines (μ_2-$C_4R_4N_2$)†								
N–C		1.337	1.333	0.022	1.326	1.345	18	
C–C		1.383	1.380	0.015	1.369	1.398	9	
Cu–N	(4,5), (II)	2.024	2.016	0.021	2.009	2.046	4	
Rh–N	see BUZZAX (2.100)							
Pd–N	see BENDAZ (2.051)							
Yb–N	see CPPYYB01 (2.614)							
Hg–N	see PAZHGN (2.263)							
4.16.2.1 Pyridazines (η^1-$C_4R_4N_2$)†								
N^1–N^2		1.334	1.334	0.006	1.328	1.340	4	
N^1–C^6		1.325	1.327	0.007	1.318	1.330	4	
N^2–C^3		1.335	1.334	0.005	1.329	1.337	4	
C^3–C^4		1.374	1.377	0.026	1.349	1.397	4	
C^4–C^5		1.347	1.351	0.012	1.334	1.356	4	

Table 9.6.3.3. *Interatomic distances (Å) (cont.)*

Bond	Substructure (coordination number, oxidation state, comment)	*d*	*m*	σ	q_l	q_u	*n*	Note
4.16.2.1	Pyridazines (η^1-$C_4R_4N_2$)† (*cont.*)							
C^5–C^6		1.388	1.387	0.017	1.373	1.405	4	
Fe–N	see TAZCFE (2.013)							
Cu–N	see BEJNIN (2.052, 2.071), PYAZCU10 (2.122)							
4.16.2.2	Pyridazines (μ_2-$C_4R_4N_2$)†							
N^1–N^2		1.352	1.357	0.028	1.333	1.373	14	
N^1–C^6		1.319	1.316	0.020	1.303	1.335	28	
C^3–C^4		1.417	1.415	0.027	1.392	1.442	28	
C^4–C^5		1.373	1.380	0.038	1.337	1.406	14	
Fe–N	see DAZHCF (1.955, 1.956)							
Ni–N	see HPCXNI (2.075, 2.060)							
Cu–N	(4-6,*), (II): all	2.015	2.013	0.029	1.988	2.039	22	
Ru–N	see DAZRUC10 (2.132, 2.136)							
4.16.3.1	Pyrimidines (η^1-$C_4R_4N_2$)†							
N^1–C^2		1.360	1.361	0.026	1.346	1.377	95	
N^1–C^6		1.361	1.357	0.022	1.349	1.374	95	
N^3–C^2		1.345	1.342	0.033	1.321	1.374	95	
N^3–C^4		1.359	1.356	0.024	1.341	1.377	95	
C^4–C^5		1.372	1.375	0.030	1.351	1.395	95	
C^5–C^6		1.401	1.397	0.029	1.378	1.422	95	
Co–N	(4,II) or (6,III): excluding CICYAO (2.158)	1.981	1.981	0.006	1.976	1.987	4	
Ni–N	see URCLNI (2.144)							
Cu–N	(3-6), (I,II): excluding CLPRCV	2.006	1.992	0.047	1.981	2.020	19	
	(4-6), (II)	1.999	1.992	0.027	1.981	2.016	16	
Zn–N	(4,6), (II): all	2.065	2.065	0.013	2.056	2.074	6	
Mo–N	(5,6), (II,V): all	2.203	2.183	0.058	2.158	2.243	10	
	(5), (II)	2.178	2.173	0.026	2.157	2.198	8	
Pd–N	see BUCBUW (2.086), DCMCPD (2.031)							
Ag–N	(2-5), (I): all	2.188	2.188	0.026	2.167	2.209	5	
Cd–N	(4-6,8), (II): all	2.295	2.295	0.065	2.239	2.324	7	
	(4-6), (II)	2.275	2.289	0.042	2.232	2.304	6	
W–N	(5,8), (II,IV): all	2.161	2.163	0.010	2.156	2.169	8	
Pt–N	(4,5), (II): all	2.033	2.033	0.015	2.024	2.044	26	
Hg–N	(2,5), (II): all	2.117	2.100	0.033	2.092	2.151	5	
4.16.3.2	Pyrimidines (μ_2-$C_4R_4N_2$)†							
N^1–C^2		1.349	1.351	0.019	1.328	1.367	6	
N^1–C^6		1.330	1.322	0.024	1.310	1.353	6	
C^4–C^5		1.378	1.375	0.044	1.354	1.406	6	
Ti–N	see PMDTTI10 (2.174, 2.239)							
Cu–N	see COPFOC (2.007, 2.011)							
Ag–N	see SULPMS (2.205, 2.460)							
4.17.1	Hydrazido(1−)(η^1-N*R*NR_2)							*80*
N–N	(1.318, 1.388)							
Re–N	see CEXKAR (1.949)							
Ir–N	see NPHZIR (1.912)							
4.17.2	Hydrazido(2−)(η^1-NNR_2, R = C, H)							*80*
N–N		1.300	1.293	0.032	1.282	1.324	16	
Fe–N	see CESTOJ (1.811)							
Mo–N	(5,6), (II,IV,VI)	1.768	1.764	0.024	1.748	1.794	9	*77*
W–N	(6,7), (IV,V)	1.751	1.752	0.014	1.738	1.763	5	
Re–N	see BILMUE (1.937)							
4.17.3.1	Diazenes (η^1-*R*NN*R*)†							
N–N	(1.235, 1.240, 1.131)							
Pd–N	see DCAZPD (2.023, 2.023)							
Au–N	see AZTLAW (2.151)							
4.17.3.2	Diazenes (η^2-*R*NN*R*)†							
N–N	(1.340)							
Ti–N	see AZBCTI10 (1.965, 1.971)							
4.17.4.1	Hydrazines (η^1-NR_2NR_2)							
N–N		1.424	1.421	0.020	1.411	1.433	81	

Table 9.6.3.3. *Interatomic distances (Å) (cont.)*

Bond	Substructure (coordination number, oxidation state, comment)	*d*	*m*	*σ*	q_l	q_u	*n*	Note
4.17.4.1 Hydrazines (η^1-NR_2NR_2) (*cont.*)								
Mn–N	see PHYZMN (2.345)							
Fe–N	see BEPZIF (2.273, 2.276)							
Co–N	(5,6), (II,III): all	2.105	2.173	0.115	1.980	2.208	7	*30*
	(5,6), (II)	2.196	2.194	0.024	2.175	2.220	4	
Ni–N	(4,6), (II): all	2.100	2.119	0.064	2.093	2.133	21	
	(6), (II)	2.118	2.120	0.027	2.101	2.133	19	
Cu–N	(4-6), (I,II): all	2.019	2.011	0.033	2.004	2.033	15	
Zn–N	(6), (II)	2.158	2.167	0.022	2.130	2.175	7	
Ru–N	see DMHERU01 (2.166, 2.279, 2.203)							
Rh–N	(6), (III)	2.118	2.115	0.023	2.098	2.136	10	
Cd–N	(6), (II)	2.451	2.469	0.070	2.367	2.502	6	
Sm–N	see ISNHSM (2.628, 2.651, 2.719)							
Dy–N	see CECLIF10 (2.570)							
Er–N	all CECLEB10	2.540	2.537	0.010	2.533	2.550	4	
4.17.4.2 Hydrazines (μ_2-NR_2NR_2)								
N–N	(1.423)							
Fe–N	see HZBTFE (2.245)							
4.18.1.1 Triazenido (terminal, η^1-*R*NNN*R*)†								*84, 101*
(*M*)N–N	(1.336, 1.333, 1.339)							
N–N	(1.286, 1.282, 1.274)							
Pd–N	see CTAZPD10 (2.033)							
Pt–N	see PAZPPT10 (2.084, 2.089)							
4.18.1.2 Triazenido (chelating, η^2-*R*NNN*R*)†								*101*
N–N		1.308	1.313	0.024	1.298	1.322	6	
Mo–N	see TLTZMO (2.232, 2.270)							
Ru–N	see TAZRUP10 (2.149, 2.179)							
Hg–N	see MNAZHG (2.313, 2.434)							
4.18.1.3 Triazenido (μ-η^1, $\eta^{1'}$-*R*NNN*R*)								*101*
N–N		1.308	1.303	0.020	1.295	1.318	46	
Cu–N	all CUDPTZ10	2.019	2.008	0.044	1.980	2.061	8	
Zn–N	all BISPAU	2.002	2.003	0.012	1.992	2.013	6	
Mo–N	(5), (III): (asymmetric)	2.212	2.210	0.056	2.159	2.261	6	
Rh–N	(5), (-)	2.117	2.117	0.022	2.095	2.138	8	
Pd–N	(5), (II)	2.078	2.079	0.042	2.034	2.123	16	
W–N	see MOPAZW (2.107, 2.096)							
4.19.1.1 Hydrazones and related ligands (η^1-NR_2N=CR_2)								
N–N		1.382	1.380	0.021	1.367	1.397	137	
N=C		1.294	1.293	0.017	1.281	1.308	137	
Cr–N	(7), (III): see COHTOI (2.196, 2.259), DAPSCR10 (2.023, 2.397)							
Mn–N	(5-7), (II)	2.293	2.289	0.030	2.274	2.316	12	
Fe–N	(6,7), (II,III): all	2.100	2.124	0.126	1.957	2.202	14	*96*
Co–N	(5-7), (I,II)	2.171	2.169	0.049	2.148	2.198	30	
Ni–N	(5-7,*), (II): all	2.102	2.095	0.060	2.071	2.126	38	
	(6), (II)	2.092	2.093	0.049	2.065	2.111	32	
Cu–N	(4-6), (II): excluding 2 > 2.40	1.986	1.982	0.047	1.938	2.036	20	
Zn–N	(4,6,7), (II): all	2.232	2.234	0.069	2.187	2.293	6	
	(6,7), (II)	2.255	2.247	0.043	2.216	2.299	5	
Mo–N	see CLOSMO (2.194)							
Pd–N	(4), (II)	2.043	2.030	0.031	2.020	2.068	6	
Yb–N	see PCPHYB (2.534)							
Pt–N	see BHZEPT (2.221), COPGAP (2.249), HAPZPT10 (2.166)							
4.20.1 *vic*-Dioximes [chelating, η^2-N(O)C*R*C*R*N(O)]†								
N–C		1.299	1.299	0.014	1.291	1.308	548	
N–O		1.356	1.352	0.026	1.339	1.369	550	
C–C		1.467	1.466	0.019	1.456	1.482	268	
Fe–N	(6), (II)	1.901	1.901	0.018	1.886	1.918	4	
Co–N	(4,6), (II,III): all	1.893	1.889	0.030	1.882	1.897	363	*102*
	(6), (II): excluding FLDXCO10 (2.12-2.15)	1.903	1.897	0.026	1.887	1.928	12	
	(6), (III)	1.890	1.888	0.014	1.881	1.896	332	
Ni–N	(4,6), (II): all	1.939	1.872	0.103	1.864	2.067	45	*9, 30*
	(4), (II)	1.869	1.868	0.013	1.860	1.872	30	
	(6), (II)	2.079	2.082	0.035	2.054	2.105	15	

Table 9.6.3.3. *Interatomic distances (Å) (cont.)*

Bond	Substructure (coordination number, oxidation state, comment)	*d*	*m*	σ	q_l	q_u	*n*	Note
4.20.1 *vic*-Dioximes [chelating, η^2-N(O)C*R*C*R*N(O)]† (*cont.*)								
Cu–N	(4-6), (I,II): all	2.012	1.992	0.072	1.961	2.034	38	*30*
	(4,5), (I)	2.135	2.137	0.022	2.110	2.156	10	
	(4-6), (II)	1.974	1.980	0.027	1.951	1.998	28	
Rh–N	(6), (III)	2.009	1.998	0.034	1.988	2.023	34	
Pd–N	(4,5,*), (II)	1.991	1.983	0.023	1.973	2.002	28	
Pt–N	(4,6,*), (II,IV)	1.994	1.991	0.019	1.980	2.010	38	
4.21.1 *N*-Nitrite (η^1-NO_2) (see also 5.12.1)								*103, 104*
N–O		1.221	1.227	0.027	1.212	1.236	172	*91*
Cr–N	see HMTZCR (2.203)							
Co–N	(6), (III): excluding BISHUG (2.105)	1.932	1.932	0.023	1.920	1.943	67	
Ni–N	(4,6), (0,II): all	2.118	2.125	0.071	2.084	2.153	6	*9*
	(6), (II)	2.143	2.129	0.043	2.118	2.174	5	
Cu–N	see PMPDCU (2.052)							
Ru–N	see BUPMOO (2.099)							
Pd–N	(4), (II)	2.020	2.020	0.021	2.001	2.035	6	
Pt–N	(4,6), (II-IV): all	2.132	2.171	0.076	2.038	2.188	6	
	(6), (III,IV)	2.181	2.179	0.013	2.169	2.195	4	
4.22.1 Ammonia (NH_3)								*105*
Cr–N	(6), (III)	2.069	2.069	0.008	2.063	2.076	5	
Co–N	(6), (III)	1.965	1.963	0.021	1.953	1.974	119	
Ni–N	(4,6), (II): all	2.074	2.115	0.093	1.941	2.141	7	*30*
	(6), (II)	2.128	2.130	0.019	2.109	2.146	5	
Cu–N	(4-6), (II)	1.987	1.988	0.017	1.977	1.996	11	
Zn–N	see CAXPUM (2.036, 2.051)							
Mo–N	see MEKTMO (2.217)							
Ru–N	(6), (II,III): all	2.126	2.123	0.024	2.109	2.145	37	
	(6), (II)	2.151	2.150	0.012	2.142	2.162	14	
	(6), (III)	2.110	2.111	0.016	2.104	2.122	19	
Rh–N	(4,6), (I,III): all	2.114	2.120	0.018	2.111	2.124	7	
	(4), (I)	2.120	2.121	0.007	2.113	2.126	6	
Pd–N	see APDPZC (2.026, 2.038)							
Re–N	see ATCTPR (2.253)							
Os–N	see TCTPOS (2.136)							
Pt–N	(4-6,*), (II-IV): all	2.050	2.048	0.021	2.036	2.059	102	
	(4), (II)	2.049	2.046	0.017	2.035	2.060	40	
	(6), (III, IV)	2.050	2.051	0.009	2.045	2.056	25	
	(5), (II)	2.052	2.053	0.023	2.038	2.069	23	
	(*), (-)	2.032	2.036	0.013	2.019	2.045	12	
4.22.2 Primary amines [NH_2R, $R = C(sp^3)$]								
N–C		1.484	1.484	0.019	1.474	1.494	1577	
Cr–N	(6), (III)	2.078	2.080	0.021	2.068	2.089	138	
Mn–N	(5), (II)	2.198	2.199	0.007	2.192	2.204	6	
Fe–N	(6,II): all picolylamine	2.067	2.030	0.070	2.019	2.084	15	*30*
	(6,II): excluding FEPICA	2.035	2.027	0.027	2.012	2.063	12	
Co–N	(4-6), (II,III): all	1.966	1.964	0.025	1.952	1.977	716	
	(6), (III)	1.965	1.964	0.021	1.952	1.976	710	
Ni–N	(4-6,*), (-): all	2.074	2.089	0.064	2.071	2.115	130	*30*
	(4), (II): excluding BIHFAZ, NETNIP02	1.917	1.918	0.008	1.912	1.922	16	
	(4), (II): only BIHFAZ, NETNIP02	2.084	2.086	0.008	2.075	2.091	6	
	(6), (II)	2.097	2.096	0.024	2.078	2.117	99	
Cu–N	(4-6,*), (-): all	2.019	2.013	0.039	1.996	2.030	274	*12, 86*
	(4), (II)	2.011	2.009	0.026	1.995	2.025	61	
	(5), (-)	2.024	2.014	0.040	1.998	2.033	132	*86*
	(6), (II): excluding 3 > 2.150	2.014	2.016	0.023	1.997	2.029	62	
Zn–N	(4-6), (II): all	2.114	2.102	0.065	2.063	2.152	51	
	(5), (II)	2.064	2.063	0.034	2.043	2.074	18	
	(6), (II)	2.152	2.139	0.054	2.103	2.206	30	
Mo–N	(6-8), (II,IV-VI): all	2.290	2.271	0.067	2.237	2.355	13	*30*
	(6-8), (II,IV,V)	2.243	2.251	0.030	2.224	2.267	8	
	(6), (VI)	2.364	2.362	0.023	2.343	2.387	5	
Tc–N	(6), (V)	2.171	2.173	0.026	2.144	2.191	6	
Ru–N	(6), (II,IV): all	2.123	2.120	0.025	2.108	2.141	27	
Rh–N	(6), (III)	2.061	2.062	0.009	2.053	2.068	12	*85*
Pd–N	(4,5), (II): all	2.037	2.041	0.022	2.027	2.050	42	
Ag–N	see AGENPC10 (2.169, 2.171)							
Cd–N	(6), (II)	2.291	2.292	0.013	2.279	2.298	13	
Nd–N	all BILSIY	2.628	2.627	0.020	2.613	2.638	6	
W–N	see BOWLUU (2.407), CACRIH (2.213)							
Re–N	(6), (V)	2.164	2.161	0.018	2.149	2.179	8	
Os–N	(6), (IV,VI)	2.128	2.114	0.037	2.109	2.155	5	

Table 9.6.3.3. *Interatomic distances (Å) (cont.)*

Bond	Substructure (coordination number, oxidation state, comment)	*d*	*m*	σ	q_l	q_u	*n*	Note
4.22.2	Primary amines [NH_2R, $R = C(sp^3)$] (*cont.*)							
Pt–N	(4-6,*), (II,IV): all	2.049	2.048	0.030	2.034	2.065	107	
	(4), (II)	2.043	2.046	0.026	2.033	2.061	65	
	(6), (II,IV)	2.069	2.065	0.034	2.047	2.079	27	
Au–N	see ENSPAU (2.119, 2.134)							
Hg–N	see COKDUB (range 2.179-2.416)							
4.22.3	Primary amines [NH_2R,$R = C(sp^2)$]							
N–C		1.437	1.440	0.025	1.429	1.449	43	
Co–N	(5,6), (II,III): all	2.012	2.009	0.051	1.977	2.042	13	
	(5,6), (II)	2.016	2.014	0.009	2.008	2.025	4	
	(6), (III)	2.010	2.001	0.062	1.947	2.066	9	
Ni–N	see MAQUNI10 (2.057, 2.063)							
Cu–N	(4-6,*), (II): excluding BZBCUA (2.216)	2.036	2.027	0.028	2.012	2.066	5	*12*
Zn–N	(4-6), (II)	2.095	2.085	0.053	2.049	2.150	4	
Mo–N	see ABTCMO (2.001, 2.009)							
Ru–N	see CANBRU (2.213)							
Rh–N	see BAYJAM (2.155), PRNRHD (2.324)							
Pd–N	see SULPDC10 (2.055)							
Cd–N	(5-7), (II)	2.402	2.423	0.039	2.359	2.435	9	
Nd–N	see BABNAT (2.743)							
Re–N	see ACANRE (2.246)							
Pt–N	see BATLPT10 (2.103), XAXASP (2.074)							
4.22.4	Secondary amines [NHR_2, $R = C(sp^3)$]							
N–C		1.488	1.487	0.021	1.476	1.499	1718	
Ti–N	see BUNKIE (2.284, 2.301)							
V–N	see CAGSAE (2.328), CINKUF (2.150, 2.160, 2.328)							
Cr–N	(6), (0,II,III): all	2.090	2.086	0.033	2.071	2.100	40	
	(6), (II,III)	2.085	2.085	0.021	2.070	2.093	38	
Fe–N	(6,7), (II,III): all	2.158	2.164	0.078	2.133	2.181	44	
	(6), (III)	2.142	2.157	0.062	2.125	2.179	40	
	(7), (II)	2.316	2.306	0.042	2.283	2.360	4	
Co–N	(6), (II,III): all	1.976	1.970	0.050	1.949	1.991	229	
	(6), (II)	2.168	2.161	0.031	2.152	2.176	9	
	(6), (III)	1.968	1.967	0.030	1.947	1.986	216	
Ni–N	(4-6), (II): all	2.042	2.067	0.086	1.954	2.108	204	*30*
	(4), (II)	1.930	1.930	0.028	1.916	1.953	60	
	(6), (II)	2.097	2.098	0.042	2.072	2.121	124	
Cu–N	(4-6,*), (II): all	2.034	2.026	0.056	2.008	2.048	166	*12, 86*
	(4), (II)	2.030	2.025	0.034	2.008	2.049	17	
	(5), (II): all	2.043	2.029	0.067	2.010	2.055	97	*86*
	: excluding 5 > 2.23	2.029	2.027	0.032	2.008	2.049	92	
	6, (II): all	2.022	2.022	0.027	2.002	2.048	35	
Zn–N	(4-6), (II): all	2.143	2.162	0.079	2.066	2.214	17	
	(4), (II): all MAMPZN	2.039	2.039	0.006	2.032	2.045	4	
	(5), (II): all	2.188	2.200	0.051	2.155	2.219	10	
Mo–N	(5-8), (0,II-VI)	2.271	2.259	0.054	2.219	2.329	32	*81, 87*
Tc–N	all BAPPIR	2.126	2.125	0.011	2.115	2.137	4	
Ru–N	(6), (II,III): all	2.127	2.085	0.085	2.071	2.238	10	*30*
	(6), (III)	2.075	2.083	0.018	2.064	2.085	7	
Rh–N	(4,6), (I,III): all	2.116	2.094	0.084	2.044	2.201	14	*30*
	(4), (I)	2.202	2.202	0.036	2.163	2.236	6	
	(6), (III)	2.051	2.051	0.032	2.019	2.084	8	
Pd–N	(4,6),(II,IV): all	2.043	2.053	0.035	2.007	2.060	28	
	(4), (II)	2.041	2.047	0.036	2.003	2.059	25	
Ag–N	(5,6), (I): excluding TZTDAG01 (2.159, 2.162)	2.483	2.476	0.054	2.443	2.536	10	
Cd–N	(4-7), (II): all	2.318	2.329	0.051	2.267	2.370	10	
W–N	see CAPSOB (2.333, 2.338)							
Re–N	(6), (I)	2.248	2.250	0.021	2.230	2.268	6	
Pt–N	(4,6), (II,IV): all	2.054	2.046	0.052	2.020	2.075	31	
	(4), (II)	2.060	2.052	0.059	2.003	2.122	21	
	(6), (IV)	2.049	2.048	0.013	2.036	2.063	8	
Hg–N	see BUPSUA (2.275, 2.439), HGTXZO (2.724)							
U–N	see SDAPOU20 (2.589)							
4.22.5	Secondary amines [NHR_2, $R_2 \neq C(sp^3)_2$]							
N–C	$R = C(sp^2)$	1.452	1.452	0.021	1.436	1.468	14	
	$R = C(sp^3)$	1.488	1.484	0.015	1.497	1.478	14	
Ni–N	(4,6), (II): all	2.070	2.090	0.084	2.018	2.143	10	
	(6), (II)	2.105	2.091	0.045	2.066	2.156	8	
Zn–N	see CAKGAW (2.213, 2.214)							
Mo–N	see BESJOY (2.357, 2.379)							

Table 9.6.3.3. *Interatomic distances (Å) (cont.)*

Bond	Substructure (coordination number, oxidation state, comment)	*d*	*m*	σ	q_l	q_u	*n*	Note
4.22.6 Tertiary amines (NR_3, R = any C)								
N–C		1.487	1.487	0.021	1.475	1.500	2246	
Ti–N	(6), (IV)	2.296	2.294	0.025	2.273	2.317	6	
V–N	(6,7), (III-V)	2.277	2.279	0.056	2.262	2.294	12	
Cr–N	(5,6), (0,II,III): all	2.152	2.138	0.106	2.066	2.209	20	
	(6), (0)	2.207	2.209	0.016	2.192	2.221	4	
	(6), (III): excluding BILDIJ (2.355)	2.093	2.089	0.044	2.046	2.138	13	
Mn–N	(4-6), (I-III): all	2.306	2.338	0.120	2.197	2.384	9	
	(5,6), (II)	2.393	2.354	0.076	2.341	2.465	5	
Fe–N	(5-7), (II,III): all	2.215	2.199	0.112	2.090	2.317	36	
	(5), (II): all	2.155	2.162	0.079	2.080	2.191	11	*96*
	(5-7), (III): all	2.241	2.292	0.115	2.099	2.319	25	*30, 96*
	(5-7), (III): Fe–N < 2.18	2.101	2.089	0.031	2.085	2.105	9	
	(5-7), II: Fe–N > 2.26	2.321	2.316	0.044	2.294	2.338	16	
Co–N	(4-6), (I-III): all	2.080	2.040	0.135	1.961	2.199	91	*86*
	(4), (II)	2.075	2.068	0.026	2.062	2.102	7	
	(6), (II)	2.216	2.218	0.039	2.187	2.237	25	
	(6), (III)	1.961	1.960	0.027	1.938	1.977	43	
Ni–N	(4-6), (0-III): all	2.112	2.115	0.109	2.062	2.177	95	
	(4), (II)	1.957	1.973	0.048	1.894	1.996	11	
	(6), (II)	2.144	2.147	0.057	2.101	2.177	59	
	(6), (III): all CEXHAO	1.924	1.926	0.012	1.912	1.939	7	
Cu–N	(4-6,*), (I,II): all	2.098	2.071	0.093	2.045	2.112	260	*12, 86*
	(4), (I)	2.139	2.135	0.053	2.099	2.178	44	
	(4), (II)	2.057	2.055	0.039	2.045	2.073	35	
	(5)	2.099	2.067	0.112	2.043	2.095	125	*86*
	(6): all	2.091	2.049	0.095	2.034	2.105	43	*30, 86*
	(6): short (<2.12)	2.046	2.042	0.028	2.021	2.062	34	
	(6): long (>2.19)	2.260	2.244	0.056	2.213	2.299	9	
Zn–N	(4-6), (II): excluding CMPORZ (2.530)	2.159	2.147	0.071	2.105	2.197	24	
	(4)	2.111	2.106	0.031	2.086	2.143	11	
	(5)	2.234	2.205	0.059	2.191	2.300	6	
	(6): all	2.171	2.147	0.068	2.110	2.244	7	
Mo–N	(5,6,*) (II-IV): all	2.372	2.387	0.094	2.273	2.450	33	
	(*), (IV): clusters only	2.252	2.255	0.016	2.242	2.265	6	
	(6), (II)	2.398	2.410	0.054	2.344	2.447	6	
	(6), (IV)	2.419	2.409	0.046	2.382	2.462	5	
	(6), (VI)	2.430	2.428	0.078	2.354	2.514	6	*81*
Tc–N	(6), (-)	2.196	2.200	0.029	2.170	2.220	5	
Ru–N	see CIYTUZ01 (2.306)							
Rh–N	(6), (I,III): all	2.087	2.083	0.066	2.032	2.152	9	
	(6), (III)	2.050	2.052	0.040	2.020	2.086	6	
Pd–N	(4,5,*), (-): all	2.111	2.098	0.052	2.097	2.147	66	
	(4), (-)	2.110	2.093	0.053	2.077	2.145	61	*81*
Ag–N	(3,4,*), (I)	2.372	2.380	0.031	2.342	2.406	9	
Cd–N	(5-8), (II)	2.437	2.428	0.074	2.379	2.499	18	
La–N	see HETALA11 (2.804, 2.835)							
Pr–N	see BIFYUK (2.696, 2.731)							
Nd–N	see BILSIY (2.701, 2.717)							
Sm–N	(9,10), (III)	2.715	2.716	0.059	2.659	2.771	4	
Eu–N	(7,9), (-): excluding CEXHUL (2.899)	2.606	2.627	0.062	2.540	2.651	4	
Gd–N	see BIFZEV (2.625, 2.677)							
Dy–N	(8,9), (-)	2.602	2.596	0.031	2.577	2.634	4	
Er–N	see HENAEB (2.523, 2.561)							
Yb–N	(8,9), (-)	2.571	2.555	0.054	2.529	2.628	4	
Lu–N	see CILCUV (2.588, 2.478, 2.468)							
W–N	see CEPLUE (2.492, 2.325)							
Re–N	see BOTFOF (2.326), COLWAB (2.242, 2.269)							
Os–N	see CHDQOS (2.231)							
Ir–N	(4,6), (I,II): all	2.095	2.078	0.049	2.066	2.134	5	
	(6), (III)	2.074	2.077	0.013	2.061	2.085	4	
Pt–N	(4-6), (II): all	2.137	2.116	0.083	2.082	2.146	18	*86*
	(4), (II)	2.108	2.116	0.035	2.078	2.126	13	
Hg–N	see CEFCUL (2.888)							
U–N	see EMASOU10 (2.692)							
4.23.1 Borazines (see also 2.3.1)								
V–N	see BOKXEE (2.218)							
Cr–N	see BRNOCR (2.067, 2.069), BUZPIV (2.205, 2.211), EMABOB (2.133, 2.159)							
Fe–N	see BEHLOP (2.090), BEMLAG10 (2.008), BUCZOO (2.012)							
Ni–N	see CIDBOG (2.495)							
5.1.1.1 Oxo (terminal O)								*106*
V–O	(5-7), (-)	1.607	1.606	0.026	1.588	1.622	79	*107*

Table 9.6.3.3. *Interatomic distances (Å) (cont.)*

Bond	Substructure (coordination number, oxidation state, comment)	*d*	*m*	σ	q_l	q_u	*n*	Note
5.1.1.1 Oxo (terminal O) (*cont.*)								
Cr–O	(4,5), (-)	1.616	1.598	0.041	1.590	1.651	11	*7*
Nb–O	(5-7), (-)	1.720	1.731	0.030	1.695	1.745	17	
Mo–O	(4-7), (-)	1.693	1.694	0.021	1.678	1.707	346	*77, 108*
Tc–O	(5-6), (-): all	1.676	1.660	0.051	1.632	1.743	14	*30*
	(5,6), (-): not *trans* to O	1.647	1.652	0.022	1.626	1.664	10	*44*
	(6), (V): *trans* to O	1.749	1.751	0.006	1.743	1.754	4	
W–O	(-), (-)	1.692	1.697	0.020	1.674	1.706	22	
Re–O	(4-6), (-)	1.709	1.709	0.032	1.695	1.723	54	*90*
Os–O	(4-6), (-)	1.718	1.722	0.022	1.711	1.732	17	*110*
U–O	(6-8), (-)	1.763	1.762	0.026	1.748	1.776	161	
5.1.1.2 Oxo (μ_2-O)								*106*
Ti–O	(5-8), (-)	1.820	1.824	0.028	1.794	1.841	44	
V–O	see BIGVAO (1.697, 1.884; 1.694, 1.874), BUPCEU (1.763, 1.875)							
Cr–O	see CEYBIR (1.812, 1.818), HMTCRC10 (1.764)							
Fe–O	(4-7), (-)	1.794	1.779	0.065	1.770	1.791	22	
	: excluding CEFVOY	1.775	1.774	0.017	1.769	1.787	20	
Zr–O	(4,8), (IV)	1.957	1.958	0.008	1.950	1.964	11	
Nb–O	(6-8), (IV,V)	1.946	1.926	0.036	1.913	1.983	21	
Mo–O	(5-7,*), (-): excluding CABHIW	1.924	1.927	0.028	1.910	1.941	239	
Tc–O	(6), (-)	1.914	1.914	0.008	1.907	1.923	6	
Hf–O	see OXMCHF (1.941)							
Ta–O	(6,7), (V)	1.924	1.923	0.027	1.900	1.951	4	
W–O	(5,6,*), (-)	1.916	1.920	0.023	1.899	1.933	64	
Re–O	(6), (II-VII)	1.926	1.920	0.026	1.907	1.945	16	
Os–O	(5,6), (IV,VI)	1.859	1.830	0.061	1.811	1.922	5	*87*
U–O	see PAUELI10 (2.161, 2.197)							
5.1.1.3 Oxo (μ_3-O)								
Ti–O	all CPTIOO	1.972	1.971	0.006	1.968	1.977	20	
V–O		1.946	1.985	0.061	1.872	1.995	20	*30*
Cr–O		1.937	1.936	0.008	1.933	1.944	13	
Mn–O	see OACPMN (1.942)							
Fe–O	all COCNAJ	1.929	1.956	0.056	1.863	1.968	6	
Co–O	see OXCFOR (2.039, 2.055, 2.114)							
Nb–O		2.062	2.039	0.046	2.027	2.118	12	*30*
Mo–O		2.015	2.003	0.035	1.990	2.048	47	
Ru–O	see BAHPEF (2.056, 2.067, 2.114)							
Rh–O		1.959	1.965	0.040	1.920	1.996	6	
W–O		1.994	1.999	0.019	1.981	2.007	28	
U–O	see BIHCUQ (2.229, 2.231, 2.243)							
5.2.1.1 Hydroxy (terminal OH)								
Cr–O	[including H · · · O(H)-Cr]	1.929	1.926	0.013	1.919	1.936	6	
Co–O	see CHXPCO (1.895), HGXIMC (2.190)							
Zn–O	see ACBZNM (2.268)							
Mo–O		1.988	1.976	0.043	1.957	2.032	4	
Re–O	see BAXJOZ (1.795)							
Pt–O		2.006	2.002	0.017	1.992	2.023	9	
5.2.1.2 Hydroxy (μ_2-OH)								
V–O	see CINKUF (1.955, 1.968)							
Cr–O	(6), (II,III)	1.959	1.960	0.023	1.946	1.972	55	
Fe–O	(5,6,*), (III): dominated by COCNAJ	1.967	1.965	0.039	1.951	1.989	34	
Co–O	(6), (III)	1.905	1.908	0.019	1.895	1.924	11	
Cu–O	(4,5,*), (II)	1.918	1.913	0.029	1.897	1.931	55	*111*
Zr–O	see COSROR (2.091, 2.167)							
Mo–O	(6-8), (III,IV)	2.061	2.081	0.068	2.040	2.098	10	*87*
Ru–O	(6,*), (II,III)	2.093	2.112	0.049	2.031	2.132	13	*87*
Rh–O	(6), (III)	2.110	2.108	0.046	2.090	2.135	10	
Yb–O	see PCPHYB (2.188, 2.216)							
Ta–O	see BUCLUG (2.024, 2.041)							
Re–O	(6), (I,VII)	2.100	2.070	0.054	2.060	2.165	6	*87*
	(6), (VII)	2.065	2.065	0.006	2.059	2.070	4	
Os–O	see CIRNUM (2.120, 2.133)							
Ir–O	all BAHVAH	2.120	2.119	0.004	2.117	2.125	4	
Pt–O	all HEPPTB	2.130	2.130	0.041	2.094	2.167	4	
U–O	see BUFFUD (2.336, 2.346)							
5.2.1.3 Hydroxy (μ_3-OH)								
Ni–O	all TACNIH10	2.087	2.091	0.011	2.079	2.096	7	
Cu–O	(*), (II)	1.995	1.988	0.033	1.969	2.024	10	
Zn–O	see ACBZNM (1.990, 2.089, 2.096)							
Mo–O	all CHPMOC	2.100	2.074	0.067	2.055	2.172	12	*30*
Ru–O	(*), (-)	2.146	2.141	0.028	2.123	2.173	4	

Table 9.6.3.3. *Interatomic distances (Å) (cont.)*

Bond	Substructure (coordination number, oxidation state, comment)	*d*	*m*	σ	q_l	q_u	*n*	Note
5.2.1.3 Hydroxy (μ_3-OH) (*cont.*)								
W–O	all DPEPOW	2.211	2.229	0.048	2.161	2.247	12	
Re–O	see BALZUJ (2.210)							
5.3.1.1 Alkoxy [terminal O-C(sp^3)]								
O–C		1.426	1.427	0.030	1.411	1.443	287	
Ti–O	(6-8), (IV)	1.847	1.855	0.055	1.812	1.883	6	
V–O	see PRXHQV (1.774)							
Cr–O	(4,5), (III,IV)	1.816	1.824	0.045	1.773	1.855	5	
Mn–O	see BOPWAE (1.838)							
Fe–O	see LIBCRC (1.806, 1.829), MPORFE10 (1.815)							
Co–O	(6), (-): dominated by (III)	1.921	1.931	0.026	1.897	1.939	9	
Ni–O	see BIBSAG (1.853), FMPHNI (1.840, 1.842)							
Cu–O	(4,5), (II): excluding 1 > 2.46	1.899	1.908	0.025	1.875	1.917	17	
Zr–O	(7,8), (IV)	1.924	1.921	0.020	1.905	1.944	5	
Nb–O	(6), (V)	1.869	1.877	0.048	1.818	1.910	15	
Mo–O	(4-6,*), (-)	1.911	1.908	0.046	1.885	1.935	114	*15*
Tc–O	see ASMETE (1.963, 1.936)							
Rh–O	see INDRHA (2.081), INDRHB (2.013)							
Ce–O	see FLMECE (2.196, 2.203, 2.230)							
W–O		1.900	1.901	0.044	1.868	1.934	85	
Re–O	(6), (V,VI)	1.890	1.886	0.028	1.869	1.901	8	
Os–O	(5,6), (VI)	1.914	1.896	0.047	1.873	1.970	8	
Pt–O	(4,6), (II,IV)	2.028	2.029	0.031	2.000	2.056	4	
U–O	(7,8), (IV,VI)	2.122	2.121	0.084	2.047	2.199	4	
5.3.1.2 Alkoxy [μ_2-OC(sp^2)]								
O–C		1.433	1.429	0.029	1.410	1.455	42	
Cr–O	(6), (I,II)	1.980	1.980	0.026	1.957	2.005	4	
Fe–O	see BIGPOW (1.998, 1.948)							
Cu–O	(4,5,*), (II)	1.929	1.934	0.018	1.918	1.944	20	*111*
Zn–O		1.958	1.969	0.027	1.929	1.975	4	
Zr–O	all BUXLEL	2.156	2.158	0.026	2.130	2.180	6	
Nb–O	all NBPMOX	2.149	2.151	0.023	2.127	2.170	4	
Mo–O		2.094	2.105	0.054	2.032	2.154	12	
Rh–O	see BUHTON (2.051, 2.063)							
Pd–O	all BIJPAL	1.996	1.999	0.010	1.985	2.004	4	
W–O		2.081	2.087	0.057	2.029	2.114	16	
Re–O	all MXOXRE10	2.113	2.109	0.021	2.095	2.135	4	
Pt–O	see MODIPT (2.040, 2.161)							
5.3.1.3 Alkoxy [μ_3-OC(sp^3)]								
O–C		1.445	1.441	0.026	1.429	1.459	49	
Fe–O	see BOWCAR10 (1.985, 1.989, 1.941)							
Co–O	(-), (II, III): all (many asymmetric)	2.044	2.091	0.104	1.911	2.135	20	*30*
	(-), (III): all are <1.93	1.899	1.903	0.019	1.886	1.911	6	
	(-), (II): all are >2.02	2.106	2.101	0.042	2.082	2.143	14	
Ni–O		2.066	2.062	0.035	2.032	2.084	18	
Cu–O	(-), (I,II): all	2.147	1.986	0.260	1.959	2.422	68	*30*
	(-), (II): short (<2.12)	1.968	1.963	0.026	1.954	1.977	41	
	(-), (II): long (>2.22)	2.518	2.540	0.116	2.428	2.596	21	
Zn–O	all BOYTOY	2.017	2.064	0.017	2.056	2.086	12	
Mo–O		2.186	2.166	0.049	2.154	2.221	13	*111*
Ru–O	see IPVRUB (2.127, 2.145, 2.210)							
W–O	see HXETOW10 (2.174, 2.201, 2.160)							
5.3.2.1 Aryloxy (terminal OAr)†								
O–C^1		1.321	1.318	0.022	1.307	1.333	442	
C^1–C^2		1.410	1.411	0.018	1.399	1.422	888	
C^2–C^3		1.394	1.393	0.026	1.375	1.411	890	
C^3–C^4		1.381	1.379	0.024	1.367	1.394	890	
Ti–O	(5,6,8), (III,IV): all	1.873	1.898	0.064	1.828	1.920	9	
V–O	(5,6), (IV,V): all	1.917	1.925	0.043	1.906	1.945	13	
Cr–O	(6), (III)	1.921	1.924	0.007	1.914	1.926	6	
Mn–O	(6), (III)	1.914	1.896	0.064	1.866	1.953	8	
Fe–O	(4-6,*), (II,III)	1.913	1.905	0.043	1.882	1.937	66	
Co–O	(4-6), (I-III): all	1.907	1.896	0.051	1.873	1.919	93	*86*
	(4), (II)	1.867	1.860	0.028	1.847	1.880	22	
	(5), (II)	1.923	1.925	0.039	1.879	1.953	15	
	(6), (II)	1.977	1.995	0.062	1.906	2.030	17	*30*
	(6), (III)	1.894	1.895	0.014	1.886	1.903	34	

Table 9.6.3.3. *Interatomic distances (Å) (cont.)*

Bond	Substructure (coordination number, oxidation state, comment)	*d*	*m*	σ	q_l	q_u	*n*	Note
5.3.2.1 Aryloxy (terminal OAr)† (*cont.*)								
Ni–O	(4-6), (II): all	1.915	1.865	0.085	1.847	2.006	37	*30*
	(4), (II)	1.865	1.856	0.049	1.824	1.888	16	
	(5), (II): excluding 2 > 1.97	1.848	1.849	0.007	1.842	1.853	8	
	(6), (II)	2.023	2.023	0.021	2.005	2.045	11	
Cu–O	(2-6), (I,II): all	1.908	1.898	0.039	1.887	1.927	89	*111*
	(4), (II)	1.893	1.892	0.015	1.884	1.900	48	
	(5), (II)	1.920	1.918	0.034	1.892	1.940	25	
	(6), (II)	1.940	1.943	0.022	1.928	1.957	12	
Zn–O	see CPZHZN (1.953), MPZHZN (1.957), SALEZN (1.937)							
Y–O	all BIRJUH	2.298	2.297	0.013	2.287	2.310	4	
Zr–O	(8), (IV)	2.074	2.086	0.033	2.030	2.099	7	
Mo–O	(4-6), (II-VI)	1.964	1.956	0.080	1.915	1.974	29	*15*
	(4-6), (III,IV)	1.927	1.926	0.026	1.902	1.954	11	
Tc–O	see CEPHUA (1.987), COKZAD (1.949)							
Ru–O	see CESNAP (2.080, 2.129)							
Rh–O	(4,6), (I,III)	2.035	2.035	0.010	2.024	2.041	7	
Pd–O	(4), (II)	2.016	1.992	0.041	1.984	2.056	12	
Ce–O	all CEZYUB	2.215	2.219	0.021	2.194	2.233	4	
Ta–O	see BUNKAW (1.909), COLVII (1.836)							
W–O	(5-7), (II,V,VI): all	1.955	1.936	0.063	1.919	1.962	18	
	(5,6) (V,VI)	1.935	1.931	0.031	1.916	1.956	16	
Re–O	(6), (III-V)	1.971	1.975	0.021	1.951	1.992	8	
Os–O	(6), (II)	1.988	1.987	0.016	1.973	2.005	5	
Ir–O	see MICPIR10 (2.062, 2.050), SCLIRA10 (2.004)							
Pt–O	(4), (II)	1.996	2.003	0.020	1.978	2.010	5	
Th–O	(8,9), (IV)	2.321	2.335	0.026	2.301	2.344	7	
U–O	(7,8), (VI)	2.235	2.234	0.023	2.213	2.238	7	
5.3.2.2 Alkoxy/aryloxy [μ_2-OC(sp^2)]								
O–C		1.330	1.331	0.029	1.315	1.344	68	
Ti–O	see CIGVET (2.041, 2.080), CLPHTI (1.911, 2.121)							
V–O	see BUVNUB (1.963, 2.269)							
Fe–O	(5,6), (I,III)	2.009	2.003	0.048	1.965	2.057	6	
Co–O	(6), (II)	2.077	2.085	0.062	2.016	2.130	14	
Ni–O	(4,6), (II): all	2.003	2.010	0.072	1.982	2.054	14	
	(6), (II)	2.031	2.039	0.041	1.988	2.061	12	
Cu–O	(3-6,*), (I,II): all	2.021	1.977	0.145	1.923	2.069	78	*30*
	(4-6,*), (II): short (<2.14)	1.956	1.949	0.055	1.916	1.985	58	
	: long (>2.26)	2.357	2.348	0.067	2.299	2.413	10	
Mo–O	see BCATMO (2.038, 2.324), PXTCMO10 (2.048, 2.052)							
Ru–O	see CIYTUZ01 (2.203, 2.211)							
Cd–O	see PYXCDC (2.306, 2.317)							
Re–O	see PHCORE (2.152, 2.149)							
Hg–O	see PHGMQU (2.161, 2.790)							
U–O	all BIHCUQ	2.522	2.531	0.033	2.497	2.548	6	
5.4.1 Ketones (terminal, η^1-OCR_2, R = any C)								
O–C		1.264	1.264	0.022	1.252	1.272	24	
V–O	see DPKEVB (2.081)							
Fe–O	see MEOBFE (1.997)							
Ru–O	see ACSNRU (2.194)							
Cd–O	(7), (II): all CIHNEM	2.283	2.285	0.009	2.276	2.289	6	
Er–O	(7), (III): all MPYOER10	2.280	2.299	0.044	2.252	2.321	7	
Re–O	see PXBURE (2.159)							
Ir–O	see CEXLUM (2.234, 2.220)							
U–O	(6,7), (VI)	2.336	2.341	0.059	2.228	2.396	6	
5.4.2 Urea [terminal, η^1-OC(NH_2)$_2$]								*112*
O–C		1.266	1.266	0.014	1.254	1.277	52	
C–N		1.330	1.328	0.016	1.319	1.342	103	
Sc–O	(8), (III): all URSCNI	2.105	2.099	0.021	2.089	2.126	4	
Ti–O	see TIUREA01 (2.014)							
Cr–O	(6), (III): all $Cr[OC(NH_2)_2]_6^{3+}$	1.971	1.973	0.007	1.964	1.976	8	
Mn–O	see BOPWEI (1.985)							
Co–O	(6), (II)	2.091	2.094	0.010	2.081	2.099	4	
Cu–O	(6), (II)	2.127	2.130	0.022	2.105	2.148	5	*82*
Zn–O	see UREAZN (2.147, 2.073, 2.091)							
Mo–O	see BOHYEC (2.135)							
Pr–O	see ACURLB (2.479, 2.504)							
Nd–O	see CEFHOK (2.472, 2.500)							
U–O	(7), (VI)	2.356	2.360	0.034	2.332	2.382	21	

Table 9.6.3.3. *Interatomic distances (Å) (cont.)*

Bond	Substructure (coordination number, oxidation state, comment)	*d*	*m*	σ	q_l	q_u	*n*	Note
5.5.1.1 Formate (η^1-O_2CH)								
(*M*)O–C		1.257	1.260	0.022	1.249	1.270	22	
C–O		1.234	1.230	0.021	1.220	1.250	22	
Fe–O	see FEFRMT (2.167)							
Ni–O	see CESGAI10 (1.936)							
Cu–O		1.966	1.956	0.030	1.949	1.988	5	
Zn–O	see AQNCZN (2.089)							
Y–O		2.343	2.364	0.046	2.296	2.370	7	
Cd–O	see AFNICD (2.284)							
U–O		2.352	2.328	0.052	2.309	2.408	5	
5.5.1.2 Formate (η^2-O_2CH)								
O–C	(1.253, 1.261, 1.188)							
Cu–O	see CAXMIX (2.352)							
Y–O	see CAVYON (2.414, 2.425)							
5.5.1.3 Formate (μ_2-O_2CH)								
O–C		1.262	1.263	0.014	1.251	1.272	47	
Cr–O	(6), (II)	2.021	2.023	0.005	2.015	2.026	8	
Co–O	see COKCIQ (1.912)							
Mo–O	(5,6), (II): all	2.121	2.123	0.013	2.106	2.132	12	
Ru–O	(6,*), (0,II/III): all	2.042	2.026	0.046	2.021	2.033	14	
	(6), (II/III)	2.024	2.023	0.007	2.020	2.030	12	
Rh–O	see BIHJOR10 (2.040, 2.049)							
Re–O	(6, III) all CLFORE10	2.041	2.053	0.026	2.012	2.058	6	
Os–O	all BIYXAI	2.167	2.166	0.008	2.159	2.174	4	
5.5.2.1 Acetate (terminal, η^1-O_2CMe)								
(*M*)O–C		1.264	1.263	0.028	1.252	1.280	46	
C–O		1.236	1.237	0.031	1.229	1.250	46	
C–C		1.512	1.510	0.026	1.499	1.523	46	
Cr–O	see ACETCR (2.306)							
Fe–O	see CIRDAI (1.898)							
Co–O	(4-6), (II)	1.990	1.970	0.059	1.947	2.049	10	*8*
Ni–O	see ACATEN (2.063, 2.080), NIAQAC03 (2.072)							
Cu–O	(4-6), (II)	1.957	1.957	0.015	1.949	1.966	10	*12*
Zn–O	(4), (II)	1.966	1.967	0.019	1.947	1.984	4	
Mo–O	see PNPMOA (2.208)							
Rh–O	see CESYAA (2.342)							
Pd–O	see AMXPPD (2.115), SFSTPD (2.164)							
Ag–O	see CELJEI (2.686)							
Cd–O	see ETNTCD (2.281)							
W–O	(6,7), (0,IV): all	2.124	2.125	0.100	2.030	2.214	6	*30*
Os–O	see BOWLII (2.018, 2.032)							
Au–O	see CILYAX (2.063)							
Hg–O	see ACHPHG (2.454, 2.410), PHHGAC01 (2.083)							
5.5.2.2 Acetate (chelating, η^2-O_2CMe)								*113*
O–C		1.257	1.263	0.024	1.244	1.270	66	
C–C		1.496	1.497	0.025	1.480	1.514	34	
Co–O	see BIHYEW (2.086, 2.109)							
Cu–O	(6), (II)	2.306	2.259	0.208	2.172	2.477	6	*12*
Ru–O	see ACMPRU, ACTFIR, MPRUAC (in range 2.173–2.279)							
Rh–O	see AZBRHA10 (2.240, 2.219), BOXNEH (2.235, 2.162)							
Cd–O	see ACCDSC10, CDACET (in range 2.303–2.544)							
Pr–O	see ACURLB (2.538, 2.536)							
Nd–O	see CEFHOK (2.527, 2.516)							
Sm–O	see BEDZAL (2.513, 2.421)							
Gd–O	see ACAQGD (in range 2.427–2.484)							
Re–O	see ACTPRE (2.233, 2.197)							
Os–O	see BOWLII (2.169, 2.127)							
Hg–O	see ETACHG, TBPAHG10 (in range 2.244–2.666)							
U–O	(7,8), (VI): all	2.467	2.465	0.025	2.452	2.484	20	
5.5.2.3 Acetate (μ_2-O_2CMe)								
O–C		1.263	1.263	0.019	1.255	1.273	373	
C–C		1.509	1.507	0.023	1.495	1.524	187	
Cr–O	(5,6), (II): all Cr≡Cr	2.010	2.007	0.014	2.001	2.021	26	*7*
Co–O		1.927	1.926	0.014	1.915	1.941	6	*8*
Ni–O	see BAPHAB (2.033, 2.052)							

Table 9.6.3.3. *Interatomic distances (Å) (cont.)*

Bond	Substructure (coordination number, oxidation state, comment)	*d*	*m*	σ	q_l	q_u	*n*	Note
5.5.2.3	Acetate (μ_2-O_2CMe) (*cont.*)							
Cu–O	(6), (II)	1.971	1.970	0.013	1.963	1.980	38	*12*
Mo–O	(5-7), (II-IV)	2.110	2.110	0.021	2.096	2.122	97	
Tc–O	(5,6), (II,III)	2.068	2.066	0.009	2.060	2.072	10	
Ru–O	(6), (II,III)	2.036	2.020	0.033	2.013	2.062	22	
Rh–O	(5,6), (I-III)	2.038	2.035	0.025	2.026	2.046	97	*83, 86*
Pd–O	(5,6), (I,II)	2.095	2.106	0.051	2.050	2.127	18	
W–O	(6,7), (II-IV)	2.092	2.089	0.029	2.072	2.111	22	
Re–O	(5,6), (III)	2.025	2.025	0.009	2.015	2.031	10	
Os–O	see CESXUT, COHNUI (in range 2.005-2.223)							
Pt–O	(6), (II): all	2.087	2.117	0.081	2.004	2.161	18	*30*
	: long (>2.075)	2.155	2.160	0.026	2.141	2.175	10	
	: short (<2.025)	2.003	2.003	0.016	1.993	2.016	8	
5.5.3.1	Alkylcarboxylates [terminal, η^1-$O_2CC(sp^3)$]							
(*M*)O–C		1.278	1.279	0.021	1.266	1.291	769	
C–O		1.234	1.233	0.017	1.224	1.244	768	
C–C		1.521	1.521	0.019	1.510	1.532	768	
Ti–O	(6), (IV)	2.000	1.983	0.043	1.967	2.015	15	
V–O	(6,7), (III-V): all	2.019	2.006	0.042	1.991	2.035	36	
	(6), (IV,V): excluding BUPCIY	2.002	2.003	0.017	1.990	2.010	23	
Cr–O	(5,6), (III,V): all	1.963	1.963	0.019	1.952	1.975	52	*8*
	(6), (III)	1.965	1.965	0.016	1.954	1.975	50	
Mn–O	(6), (I-III): all	2.059	2.040	0.121	1.913	2.165	35	
	(6), (II)	2.161	2.164	0.022	2.146	2.180	15	
	(6), (III): all	1.974	1.913	0.114	1.903	2.013	17	*86*
	: excluding 2>2.23	1.937	1.909	0.050	1.902	1.998	15	*86*
Fe–O	(6,7), (II,III): all	2.033	2.038	0.069	1.974	2.094	40	
	(6), (III)	2.018	2.012	0.057	1.971	2.048	15	
	(7), (III)	2.041	2.046	0.068	1.976	2.099	22	
Co–O	(4-6), (II,III): all	1.938	1.911	0.071	1.896	1.942	195	*8,86*
	(4), (II)	1.966	1.955	0.022	1.948	1.989	10	
	(6), (II)	2.088	2.075	0.050	2.062	2.097	26	
	(6), (III)	1.906	1.904	0.019	1.894	1.918	153	
Ni–O	(4-6), (II,III): all	2.051	2.055	0.056	2.038	2.087	72	
	(6), (II)	2.065	2.059	0.034	2.044	2.089	66	
Cu–O	(4-6), (II,III): all	2.015	1.961	0.145	1.946	1.982	123	***86, 114***
	(4), (II)	1.948	1.947	0.026	1.931	1.964	25	
	(5), (II): all	1.991	1.957	0.108	1.947	1.976	44	*86*
	: excluding 4>2.2	1.960	1.952	0.036	1.945	1.973	40	
	(6), (II): all	2.074	1.977	0.184	1.957	2.205	51	*30*
	: short (<2.14)	1.962	1.967	0.024	1.947	1.978	36	
	: long (>2.2)	2.342	2.351	0.106	2.303	2.401	15	
Zn–O	(4-6), (II): all	2.038	2.050	0.059	1.978	2.079	29	
	(4), (II)	1.946	1.952	0.022	1.923	1.963	4	
	(5), (II)	2.018	1.997	0.059	1.967	2.080	8	
	(6), (II)	2.070	2.071	0.034	2.048	2.092	17	
Nb–O	see CNBPAC (2.161)							
Mo–O	(5-8), (0-VI): all	2.130	2.118	0.063	2.093	2.151	38	
Tc–O	(6), (-): all	2.050	2.025	0.070	2.011	2.063	8	*86*
	: excluding PCLTCA10 (2.215)	2.027	2.019	0.023	2.009	2.036	7	
Ru–O	(6), (II)	2.091	2.095	0.014	2.086	2.102	8	
Rh–O	(6), (III)	2.023	2.027	0.018	2.003	2.038	9	
Pd–O	(4,5), (II)	2.023	2.019	0.024	2.006	2.029	16	
Cd–O	(6,7), (II)	2.372	2.358	0.048	2.338	2.389	8	
La–O	(10), (III)	2.503	2.497	0.019	2.486	2.526	6	
Ce–O	(9), (III)	2.483	2.480	0.021	2.472	2.489	7	
Pr–O	(9), (III): all BIFYUK	2.458	2.447	0.027	2.441	2.484	4	
Nd–O	see ODACND (2.428)							
Sm–O	(9), (III): all NSMEDT02	2.421	2.421	0.021	2.400	2.441	4	
Eu–O	(9), (III)	2.394	2.395	0.096	2.317	2.470	5	
Gd–O	(9), (III): all BIFZEV	2.399	2.395	0.022	2.381	2.421	4	
Dy–O	(8,9), (III)	2.363	2.365	0.064	2.295	2.415	8	
Er–O	see HENAEB (2.240, 2.262, 2.265)							
Yb–O	(8,9), (III)	2.286	2.282	0.035	2.252	2.308	10	
W–O	see CIFNIO (2.132)							
Os–O	see BABWAC (2.038), FATBOS10 (2.207)							
Ir–O	(6), (III)	2.066	2.055	0.032	2.042	2.093	6	
Pt–O	(4,6), (II,IV)	2.031	2.014	0.040	2.003	2.045	13	
Hg–O	see FAHGME10 (2.064), PHGTFA (2.121)							
Th–O	(9,10), (IV)	2 402	2.402	0.012	2.393	2.413	5	
U–O	(7), (VI)	2.356	2.359	0.032	2.325	2.366	7	
5.5.3.2	Alkylcarboxylates [chelating, η^2-$O_2CC(sp^3)$]							
O–C		1.256	1.256	0.013	1.246	1.263	44	

Table 9.6.3.3. *Interatomic distances (Å) (cont.)*

Bond	Substructure (coordination number, oxidation state, comment)	*d*	*m*	σ	q_l	q_u	*n*	Note
5.5.3.2 Alkylcarboxylates [chelating, η^2-$O_2CC(sp^3)$] (*cont.*)								
C–C		1.516	1.521	0.024	1.501	1.529	22	
Ti–O	(8), (IV)	2.163	2.163	0.005	2.161	2.166	6	
Co–O	see BIYHOG (2.145, 2.223)							
Cu–O	see CEJPEM (2.528, 2.037)							
Zn–O	(6), (II)	2.205	2.191	0.072	2.162	2.244	6	
Mo–O	see FAMPMO (2.296, 2.338)							
Cd–O	see ABPENC (2.262, 2.716), BAYDIO (2.378, 2.350)							
Nd–O	see BODZEZ (2.535, 2.510)							
Sm–O	see BOTWUC (2.495, 2.455; 2.495, 2.585)							
U–O	see BIMAOU10 (2.526, 2.578)							
5.5.3.3 Alkylcarboxylates [μ_2-$O_2CC(sp^3)$]								
O–C		1.258	1.257	0.020	1.246	1.270	434	
C–C		1.519	1.519	0.026	1.504	1.536	222	
Cr–O	(6), (II)	2.018	2.017	0.003	2.015	2.021	5	
Cu–O	(6), (-)	1.966	1.968	0.014	1.956	1.975	95	
Nb–O	all CIPNEU	2.151	2.145	0.014	2.141	2.163	10	
Mo–O	(5,6,*), (-)	2.114	2.114	0.018	2.104	2.128	126	
Ru–O	(6), (-)	2.134	2.132	0.009	2.128	2.142	8	
Rh–O	(6), (-)	2.035	2.034	0.010	2.029	2.041	90	*115*
Pd–O	all BXCAPD	2.040	2.039	0.022	2.021	2.061	4	
Cd–O	all CIFGON	2.266	2.259	0.020	2.251	2.289	8	
Nd–O	all CIGRAL	2.422	2.422	0.018	2.406	2.439	4	
W–O	(5,6,*)	2.092	2.091	0.016	2.082	2.103	66	
Re–O	see OCPPRE (2.093, 2.097)							
Os–O	(6), (III)	2.014	2.015	0.010	2.007	2.021	8	
5.5.4.1 Carboxylates [η^1-$O_2CC(sp^2)$]								
(*M*)O–C		1.277	1.277	0.017	1.266	1.288	74	
C–O		1.234	1.239	0.015	1.227	1.247	73	
C–C(sp^2)		1.508	1.507	0.014	1.499	1.513	74	
V–O	see BIGFAY01 (1.896, 1.912)							
Cr–O	see CAKCIA (1.946, 1.958)							
Mn–O	see ABZAMN (2.187), ZEGPEG (2.111)							
Co–O	see BELLEJ (2.130), CEBDIW (2.102), CUCOES (1.996), FSCUCO (1.941, 1.954)							
Ni–O	(4,6), (II): all	2.049	2.053	0.084	1.984	2.123	14	
	(6), (II): mononuclear	2.100	2.118	0.044	2.053	2.135	9	
Cu–O	(4-6,*), (II): all	1.992	1.947	0.170	1.930	1.967	38	*86*
	(4), (II)	1.927	1.934	0.032	1.896	1.951	13	
	(5), (II)	1.953	1.950	0.027	1.937	1.967	17	
	(6), (II): excluding 3 > 2.45	1.964	1.954	0.041	1.931	2.007	4	
Zn–O	(4,6), (II)	2.033	2.010	0.053	1.989	2.090	5	
Cd–O	see CITDEO (2.253)							
Sm–O	see COSLEB (2.273), SALASM10 (2.488)							
Er–O	see COSLIF (2.198)							
Au–O	see CIYMEC (2.073, 2.074)							
5.5.4.2 Carboxylates [chelating, η^2-$O_2CC(sp^2)$]								
O–C		1.266	1.265	0.019	1.253	1.278	39	
C–C		1.481	1.482	0.022	1.474	1.493	20	
Ti–O	all BUCBEG	2.148	2.150	0.009	2.138	2.155	4	
Cu–O	see MESACV (1.976, 2.596)							
Ru–O	see BAWZUU (2.118), BZCPRU (2.166, 2.130)							
Cd–O	(7), (II): excluding CDMALD	2.409	2.427	0.058	2.351	2.445	10	
La–O	see ALANIC (2.568, 2.646)							
Nd–O	see BABNAT (2.529, 2.517), COSLAX (2.559, 2.512)							
Sm–O	see COSLEB (2.467, 2.521), SMNICD (2.486, 2.567)							
Dy–O	see AMAQDY (2.353, 2.517; 2.418, 2.502)							
U–O	see BAWRIA (2.452, 2.543)							
5.5.4.3 Carboxylates [μ_2-$O_2CC(sp^2)$]								
O–C		1.267	1.267	0.018	1.252	1.280	97	
C–C		1.493	1.492	0.024	1.476	1.508	49	
Co–C	(6), (II): excluding PYMCXC	2.037	2.030	0.021	2.020	2.056	8	*8*
Cu–O	(4-6,*), (I,II)	1.972	1.972	0.016	1.964	1.979	28	
Zn–O	see ACBZNM (1.979, 2.018)							
Mo–O	(5,6), (II,III)	2.110	2.107	0.017	2.099	2.119	22	
Rh–O	(6), (II)	2.038	2.036	0.011	2.027	2.050	16	
W–O	(5), (II)	2.079	2.079	0.012	2.070	2.087	12	
Re–O	(5,6), (II)	2.015	2.016	0.010	2.006	2.025	8	

Table 9.6.3.3. *Interatomic distances (Å) (cont.)*

Bond	Substructure (coordination number, oxidation state, comment)	*d*	*m*	σ	q_l	q_u	*n*	Note
5.5.5.1 Carbamates (chelating, η^2-O_2CNR_2)								
O–C		1.297	1.298	0.002	1.296	1.299	4	
C–N	(1.298, 1.319)							
N–C		1.462	1.457	0.011	1.456	1.473	4	
Ta–O	all BOBXUL	2.131	2.131	0.018	2.114	2.147	4	
5.5.6.1 *O*-Thiocarbamates [terminal, η^1-OC(S)NR_2] (see also 9.6.2.1)								
(None)								
5.5.6.2 Thiocarbamates (chelating, η^2-OSCNR_2) (see also 9.6.2.2)								
O–S		1.274	1.274	0.010	1.267	1.281	15	
S–C		1.728	1.731	0.009	1.725	1.733	15	
C–N		1.336	1.338	0.014	1.325	1.345	15	
N–C	excluding 1 > 1.6	1.478	1.474	0.027	1.461	1.496	29	
Ti–O	see EMTCTJ (2.088, 2.077, 2.075)							
Co–O	see TMTCPC (2.157)							
Zr–O	see BUWMAH (2.249), EMTCZR (2.180, 2.200)							
U–O		2.408	2.402	0.040	2.381	2.439	5	
5.5.7.1 *O*-Thiocarboxylates [terminal, η^1-OC(S)R] (see also 9.5.2.1)								
(None)								
5.5.7.2 Thiocarboxylates (chelating, η^2-OSCR) (see also 9.5.2.2)								
O–C		1.236	1.246	0.035	1.234	1.255	9	
S–C		1.705	1.702	0.012	1.698	1.716	9	
C–C		1.521	1.522	0.025	1.501	1.531	9	
Ni–O	(6), (II)	2.142	2.135	0.035	2.119	2.171	9	
5.5.7.3 Thiocarboxylates (μ_2-OSCR) (see also 9.5.2.3)								
O–C		1.255	1.255	0.025	1.239	1.267	15	
S–C		1.694	1.696	0.018	1.681	1.703	15	
C–C		1.510	1.501	0.028	1.487	1.535	15	
Mn–O	(7), (II)	2.315	2.313	0.036	2.283	2.342	8	
Rh–O	see TACDRH10 (2.099, 2.114)							
Ag–O	see CEFMIJ (2.510)							
Eu–O	all BOTVIP10	2.511	2.508	0.032	2.483	2.541	4	
5.6.1.1 Oxalate [chelating, $\eta^2(O_2C)_2$]								
(*M*)O–C		1.279	1.279	0.015	1.269	1.288	222	
C–C		1.546	1.546	0.018	1.536	1.556	111	
C–O		1.224	1.224	0.015	1.216	1.234	222	
Ti–O	(6-8), (III,IV): all	2.041	2.031	0.054	1.992	2.086	30	*81*
V–O	(5,6), (IV,V): all	2.083	2.036	0.090	2.015	2.164	18	*81, 86*
	: short (<2.1)	2.020	2.022	0.021	2.006	2.036	11	*44*
Cr–O	(6), (III)	1.969	1.975	0.019	1.959	1.981	24	
Mn–O	(6), (III): all ZZZCCG10	2.000	2.018	0.077	1.911	2.074	6	
Co–O	(6), (III)	1.911	1.912	0.011	1.903	1.920	22	
Cu–O	(4-6), (II)	1.951	1.949	0.018	1.934	1.964	29	
Y–O	(8), (III): all CIBZAO	2.335	2.340	0.018	2.329	2.344	6	
Zr–O	(8), (IV)	2.202	2.195	0.034	2.183	2.219	10	
Mo–O	(6,7,*), (-)	2.119	2.101	0.038	2.092	2.140	22	
Rh–O	(6), (III): all CAZCIP	2.021	2.021	0.015	2.006	2.037	6	
Nd–O	all CICBOF	2.474	2.457	0.042	2.448	2.518	4	
Gd–O	all CICBUL	2.429	2.406	0.055	2.395	2.485	4	
Er–O	(8), (III): all CIBYOB	2.333	2.336	0.011	2.321	2.342	6	
Hf–O	(8), (IV): all KOXHFP10	2.190	2.184	0.022	2.171	2.211	8	
Re–O	(6), (IV): all KXOXRE	2.063	2.060	0.029	2.038	2.085	8	
Pt–O	(*), (-)	2.003	1.999	0.014	1.990	2.019	8	
U–O	(7,10), (IV,VI)	2.412	2.428	0.031	2.373	2.436	10	
5.7.1.1 Acetylacetonates [chelating, η^2-*R*C(O)C*R*C(O)*R*]†								
O–C_α		1.270	1.270	0.019	1.258	1.280	484	
C_α–C_β		1.387	1.387	0.020	1.377	1.397	488	
C_α–*R*		1.518	1.514	0.025	1.501	1.533	489	
Sc–O	(6), (III): all ACACSC	2.070	2.068	0.010	2.061	2.080	6	
Ti–O	(6), (IV)	1.979	1.964	0.052	1.941	2.032	12	*81*
V–O	(5,6), (III,IV)	1.981	1.984	0.015	1.966	1.993	8	*107*
Cr–O	(6), (III)	1.959	1.961	0.008	1.954	1.965	39	*7*
Mn–O	(5,6), (II,III)	2.034	2.026	0.119	1.915	2.145	20	*30*

Table 9.6.3.3. *Interatomic distances (Å) (cont.)*

Bond	Substructure (coordination number, oxidation state, comment)	*d*	*m*	σ	q_l	q_u	*n*	Note
5.7.1.1	Acetylacetonates [chelating, η^2-*R*C(O)C*R*C(O)*R*]† (*cont.*)							
Mn–O	(6), (II)	2.158	2.149	0.021	2.144	2.180	8	
	(5,6), (II): all	1.952	1.924	0.075	1.910	1.940	12	
	: excluding 2 > 2.1	1.921	1.916	0.013	1.910	1.933	10	
Fe–O	(6), (II,III)	2.002	1.999	0.024	1.980	2.025	8	
Co–O	(6), (II,III)	1.939	1.894	0.074	1.884	2.012	64	*86, 87*
	(6), (II)	2.033	2.034	0.035	2.003	2.062	23	
	(6), (III)	1.887	1.887	0.013	1.879	1.892	41	
Ni–O	(4,6), (II): all	1.999	2.015	0.050	1.969	2.035	10	*9*
	(6), (II)	2.020	2.021	0.023	2.000	2.044	8	
Cu–O	(4-6), (II): all	1.961	1.947	0.068	1.920	1.980	42	*86, 116*
	(4,5), (II): excluding 1 > 2.1	1.931	1.922	0.032	1.906	1.953	22	
Zn–O	see ZNACAT10 (2.002, 1.971)							
Y–O	all CYSFAC10	2.324	2.318	0.017	2.311	2.341	4	
Zr–O	(8,9), (IV)	2.164	2.161	0.066	2.108	2.228	16	*109, 116*
	(8), (IV)	2.123	2.118	0.041	2.084	2.160	10	
	(9), (IV)	2.232	2.238	0.033	2.205	2.254	6	
Nb–O	(8), (IV): all PIVMNB10	2.132	2.133	0.009	2.125	2.142	8	
Mo–O	(5-7), (II-V): all	2.096	2.077	0.052	2.068	2.110	24	*81*
		2.087	2.075	0.034	2.068	2.105	23	*44*
Tc–O	all TCACTC01	2.015	2.013	0.006	2.010	2.021	4	
Ru–O	all BISKOD	2.031	2.036	0.011	2.019	2.041	8	
Rh–O	(4-6,*), (I,III)	2.041	2.046	0.032	2.014	2.061	32	
Pd–O	(4), (II)	2.049	2.061	0.051	2.002	2.092	49	*30, 109*
		2.007	1.995	0.048	1.973	2.024	18	
		2.073	2.077	0.035	2.059	2.096	31	
Cd–O	see CAYJAN (2.223, 2.274)							
La–O	all AQACAL	2.472	2.480	0.024	2.453	2.489	6	
Pr–O	all CAZGUF	2.443	2.459	0.032	2.425	2.460	6	
Sm–O	all CAZHAM	2.392	2.401	0.027	2.380	2.407	6	
Eu–O	(7,8), (III)	2.348	2.354	0.024	2.325	2.364	24	
Er–O	(6,8), (III)	2.285	2.295	0.073	2.221	2.351	10	*116*
	(6), (III)	2.212	2.214	0.046	2.167	2.255	4	
	(8), (III)	2.333	2.331	0.038	2.301	2.368	6	
Re–O	all PASACR	2.007	2.009	0.009	1.997	2.015	4	
Ir–O	(4,6), (I,III)	2.064	2.041	0.063	2.021	2.099	6	
Pt–O	(4,6), (II,IV)	2.042	2.052	0.039	1.996	2.067	10	
Th–O	all TACTHB	2.402	2.405	0.019	2.391	2.416	8	
U–O	(7), (VI)	2.387	2.375	0.031	2.362	2.414	26	
5.8.1.1	*o*-Quinones (chelating, η^2-*o*-$O_2C_6R_4$)†							*117*
O–C_α	all	1.323	1.339	0.037	1.291	1.348	132	*30*
		1.270	1.274	0.022	1.252	1.287	38	*118, 119*
		1.343	1.345	0.011	1.338	1.350	93	*120*
C_α–$C_{\alpha'}$	all	1.423	1.413	0.042	1.402	1.429	66	
		1.439	1.438	0.014	1.429	1.452	12	*118, 119*
	μ-chloranilates	1.529	1.530	0.009	1.522	1.536	7	
		1.404	1.404	0.017	1.400	1.415	47	*120*
Ti–O	(6), (IV)	1.978	1.980	0.048	1.940	2.009	12	*120*
V–O	(5,6), (III,IV)	1.973	1.966	0.036	1.942	1.999	18	*118, 119*
Cr–O	(6), (0,III)	1.962	1.952	0.023	1.944	1.986	14	*118, 119*
Mn–O	(6), (IV)	1.880	1.872	0.034	1.853	1.916	4	
Fe–O	(6), (III)	2.026	2.024	0.023	2.011	2.037	20	*119, 120*
Ni–O	(6), (II)	2.068	2.063	0.043	2.027	2.107	6	*118, 119*
Cu–O	see BAKPUY (1.945, 2.454), PMECAC (1.955, 2.196)							
Mo–O	(6,*), (-): excluding PHQUMO	1.992	1.955	0.062	1.940	2.050	18	*8, 120*
Rh–O	(5), (I,III)	2.031	2.037	0.026	2.003	2.051	4	
Pd–O	see TCATPD (2.030, 2.039)							
Ce–O	see CECATI (2.357, 2.362)							
Pr–O	all CAZZAE	2.488	2.490	0.016	2.471	2.501	6	
Hf–O	see HFCATH (2.194, 2.220)							
Ir–O	see BRNPIR (2.008, 1.905)							
Pt–O	see CINREW (2.017, 1.994)							
Th–O	see CATETH (2.418, 2.421)							
U–O	see SCATUR (2.362, 2.389)							
5.8.2.1	*o*-Tropolonates (chelating, η^2-*o*-$O_2C_7R_5$)†							
O–C_α		1.286	1.286	0.016	1.274	1.299	26	
C_α–$C_{\alpha'}$		1.464	1.465	0.009	1.459	1.469	14	
Sc–O	(6,8), (III)	2.189	2.179	0.064	2.163	2.209	7	
Co–O	see COTROP (2.050, 2.068), COTROQ (1.888, 1.885, 1.882)							*87*
Cu–O	see CUTROP01 (1.913, 1.914)							
Rh–O	see TROPRH (2.034, 2.081)							
Th–O	(9), (IV): all TROPTH	2.450	2.444	0.018	2.438	2.463	8	
U–O	see TROPUE (2.393, 2.373)							

Table 9.6.3.3. *Interatomic distances (Å) (cont.)*

Bond	Substructure (coordination number, oxidation state, comment)	*d*	*m*	*σ*	q_l	q_u	*n*	Note
5.9.1.1 Carbonate (chelating, η^2-CO_3)								*121*
(*M*)O–C		1.300	1.301	0.031	1.297	1.324	16	
C–O		1.237	1.237	0.022	1.215	1.261	8	
Co–O	(6), (III): excluding CAIMCO	1.905	1.906	0.015	1.893	1.916	6	
Zr–O	see COMPEZ (2.198)							
Pt–O	see BUPPUX (2.059)							
U–O	all BANDAV	2.428	2.431	0.021	2.407	2.446	4	
5.9.1.2 Carbonate (μ_2-CO_3)								*121*
(*M*)O–C		1.264	1.256	0.027	1.252	1.288	9	
C–O		1.278	1.283	0.027	1.250	1.300	4	
Cu–O	(5), (II)	1.991	1.978	0.036	1.972	2.038	7	
Pt–O	see CIXHEW (2.085)							
5.9.1.3 Alkyl carbonates (μ-O_2COR)								
O–C		1.272	1.273	0.019	1.254	1.289	4	
C–O(*R*)	(1.294, 1.328)							
Mo–O	(all BCBXMO)	2.127	2.127	0.015	2.113	2.141	4	
5.10.1.1 Amine oxides (η^1-ONR_3)								
O–N	(1.409, 1.408)							
Cu–O	see AQOXCU (1.948)							
Re–O	see BUTTOZ (2.149)							
5.10.2.1 Pyridine *N*-oxides (terminal, C_5R_5NO)								
O–N		1.335	1.333	0.017	1.324	1.345	49	
N–C		1.352	1.347	0.022	1.340	1.362	96	
Mn–O	see BIVWIM (2.155)							
Fe–O	see FEHPYO (2.111)							
Co–O	(6), (II)	2.086	2.090	0.035	2.050	2.119	5	
Ni–O	(6), (II)	2.054	2.049	0.022	2.036	2.076	4	
Cu–O	(4–6), (II): all	2.066	1.976	0.171	1.949	2.115	18	*86*
	(4–6), (II): short (<2.10)	1.987	1.958	0.067	1.946	2.077	14	
Zn–O	(5,6), (II)	2.076	2.076	0.031	2.049	2.103	4	
Cd–O	see CITDEO (2.329)							
Th–O	(9), (IV)	2.422	2.419	0.040	2.392	2.438	10	
U–O	(7), (VI)	2.329	2.331	0.017	2.311	2.344	4	
5.10.3.1 Hydroxamates [η^1-$ON(=CR_2)R$]†								
O–N		1.365	1.366	0.017	1.350	1.377	54	
N=C		1.315	1.311	0.018	1.303	1.322	55	
N–C		1.456	1.462	0.017	1.442	1.469	55	
Cr–O	see CRMTBH (1.965, 1.967, 1.976)							
Mn–O	see MNMTBH (1.959, 1.941, 2.132)							
Fe–O	(6), (III)	1.981	1.985	0.023	1.957	2.001	12	
Co–O	see COMTBH (1.937, 1.925, 1.943)							
Mo–O	(5,6), (VI)	2.047	2.025	0.053	2.010	2.065	15	
Rh–O	see BIWLAU (2.037)							
Hf–O	(8), (IV)	2.132	2.130	0.023	2.117	2.143	8	
Pt–O	see CACMIC (2.059)							
Th–O	(8), (IV)	2.352	2.342	0.023	2.336	2.373	5	
U–O	see CIBHAW (2.418, 2.379)							
5.11.1.1 Nitrate (terminal, η^1-NO_3)								*104*
(*M*)O–N		1.267	1.266	0.030	1.250	1.260	64	
N–O		1.227	1.229	0.023	1.216	1.240	127	
Ti–O	see BASSAP (2.059, 2.086)							
Mn–O	see MALCDB (2.251), TNBPMN (1.865)							
Fe–O	see CNOFEA (1.973)							
Co–O	(5,7), (II)	2.103	2.102	0.029	2.080	2.127	5	
Ni–O	(6), (II)	2.082	2.061	0.055	2.040	2.135	5	
Cu–O	(4-6,*), (II)	2.285	2.284	0.259	2.027	2.532	26	
	(4,5), (II): short (<2.055)	1.996	1.996	0.037	1.964	2.037	9	
Zn–O	see CATKOX (2.179)							
Rh–O	(6), (III)	2.117	2.124	0.037	2.078	2.148	4	
Pd–O	see CAYXAB (1.995, 1.989)							
Ag–O	see MCYTAG10 (2.469), NTPAAG (2.259)							
Cd–O	(6,7), (II)	2.385	2.402	0.056	2.317	2.437	6	
Nd–O	see BAWDIM10 (2.525)							

Table 9.6.3.3. *Interatomic distances (Å) (cont.)*

Bond	Substructure (coordination number, oxidation state, comment)	d	m	σ	q_l	q_u	n	Note
5.11.1.1	Nitrate (terminal, η^1-NO_3) (*cont.*)							
Pt–O	(4,6), (II,III)	2.143	2.168	0.063	2.098	2.174	5	
Hg–O	see PYHGAN10 (2.702, 2.723)							
5.11.1.2	Nitrate (chelating, η^2-NO_3)							
(M)O–N								*104*
N–O		1.255	1.259	0.027	1.239	1.273	290	
		1.217	1.218	0.016	1.207	1.226	147	
Sc–O	all URSCNI	2.351	2.336	0.061	2.303	2.415	4	
Ti–O	all BEYGAN	2.146	2.145	0.036	2.113	2.179	4	
Mn–O	see TNBPMN (2.102, 2.386; 2.225, 2.183)							
Fe–O	see CALGAX (2.323, 2.019)							
Co–O	(6,7), (II): many asymmetric	2.212	2.200	0.131	2.108	2.297	18	
Ni–O	(6), (II)	2.166	2.156	0.052	2.132	2.210	12	
Cu–O	(5,6,*), (II): all	2.298	2.416	0.276	1.993	2.554	44	*12, 30*
	: short (<2.05)	1.993	1.992	0.021	1.985	2.007	18	
	: long (>2.17)	2.509	2.532	0.132	2.455	2.575	26	
Zn–O	see CATKOX (2.228, 2.253), CEMWEW (2.301, 2.500)							
Zr–O	(8,9), (IV)	2.310	2.302	0.043	2.277	2.320	10	
Rh–O	see NCPRHB (2.188, 2.184)							
Ag–O	(4,5), (I): many asymmetric	2.555	2.552	0.102	2.462	2.658	6	
Cd–O	(6–8), (II): many asymmetric	2.460	2.408	0.159	2.342	2.596	18	
La–O	(11,12), (III)	2.664	2.665	0.051	2.627	2.686	36	
Ce–O	(10,11), (III,IV)	2.629	2.641	0.096	2.551	2.699	10	*45, 87*
Nd–O	(10–12), (III)	2.584	2.576	0.063	2.549	2.613	32	
Sm–O	all SMHXAZ10	2.543	2.528	0.055	2.503	2.578	12	
Eu–O	(10,11), (III)	2.504	2.498	0.050	2.477	2.513	12	
Gd–O	(9,10), (III)	2.483	2.490	0.047	2.446	2.520	10	
Hg–O	(5,6,8), (II)	2.558	2.675	0.270	2.245	2.771	12	
Th–O	(12), (IV)	2.586	2.572	0.040	2.560	2.598	16	*122*
U–O	(8), (VI)	2.528	2.527	0.027	2.509	2.538	24	*122*
5.11.1.3	Nitrate (μ_2-NO_3)							
(M)O–N								*104*
N–O		1.257	1.258	0.023	1.240	1.279	12	
		1.229	1.227	0.017	1.215	1.241	6	
Cu–O	see CERCUX (2.790, 2.534), COLDOW (2.331, 2.421), NTPHCU (2.335, 1.995)							
Ag–O	see CIXYAJ (2.381, 2.481)							*12*
Hg–O	see BIPYHG (2.705, 2.535)							
5.12.1.1	*O*-Nitrite (terminal, η^1-ONO) (see also 4.21.1)							
(M)O–N								*103, 104*
N–O		1.293	1.293	0.028	1.265	1.312	6	
		1.196	1.197	0.035	1.174	1.223	7	
Cr–O	see NTPYCR (1.963)							
Co–O	see EINICI (1.915)							
Ni–O	see HPNONI (2.112), NMEDNI10 (2.114)							
Cu–O	see BPNICU (2.074), CEZNIE (1.969)							*9*
Zn–O	see BEKPUC (2.220)							
5.12.1.2	*O*-Nitrite (η^2-O_2N) (see also 4.21.1)							
O–N								*103, 104*
		1.247	1.249	0.019	1.235	1.258	29	
Ni–O	(6), (II)	2.151	2.143	0.020	2.136	2.173	6	
Cu–O	(6), (II): all	2.272	2.277	0.217	2.057	2.466	10	*30*
	: short (<2.25)	2.081	2.072	0.083	2.007	2.160	5	
	: long (>2.35)	2.463	2.462	0.090	2.388	2.539	5	
Zn–O	(6), (II): all	2.221	2.251	0.145	2.072	2.331	13	*30*
	: short (<2.1)	2.063	2.072	0.024	2.046	2.077	5	
	: long (>2.2)	2.319	2.298	0.085	2.254	2.356	8	
5.13.1	Dioxygen (terminal, η^1-O_2)							
O–O	(1.301, 1.276, 1.283)							*123, 124* *118*
Co–O	see FSMICO (1.881), MESOCO (1.888), OAMSCO (1.885)							*8*
5.13.2	Dioxygen (η^2-O_2)							
O–O								*123–125*
		1.460	1.463	0.026	1.442	1.472	44	*120*
Ti–O	(5,6), (IV)	1.852	1.850	0.024	1.832	1.867	10	*120, 126*
V–O	(5,6), (IV-V)	1.895	1.884	0.034	1.868	1.913	22	*86, 120*
Co–O	see MPASCO (1.862, 1.868)							*8*
Nb–O	(5,6), (V)	1.980	1.980	0.017	1.969	1.985	8	*120*
Mo–O	(5,6), (VI)	1.932	1.929	0.019	1.915	1.951	36	*77, 120*
Rh–O	(5), (I)	2.034	2.026	0.033	2.009	2.067	4	

Table 9.6.3.3. *Interatomic distances (Å) (cont.)*

Bond	Substructure (coordination number, oxidation state, comment)	*d*	*m*	σ	q_l	q_u	*n*	Note
5.13.2 Dioxygen (η^2-O_2) (*cont.*)								
Ir–O	(5), (I)	2.058	2.057	0.020	2.039	2.078	4	
U–O	see BANDAV (2.219, 2.250)							
5.13.3 Dioxygen (μ_2-O_2)								*125*
O–O		1.482	1.487	0.019	1.463	1.496	4	*120*
Co–O		1.894	1.889	0.018	1.882	1.908	5	*120*
5.13.4 Peroxy (OO*R*)								*125*
O–O	excluding CEMMIQ (1.215)	1.467	1.465	0.023	1.445	1.489	5	
V–O(η^2)	see CAMXOD (1.872, 1.999)							
Co–O(η^1)	see CUMPCO (1.897), SCQUCO (1.854)							*8*
Pt–O(η^1)	see BOVLED (2.032), BULTEH (2.051), CEMMIQ (1.989)							
5.14.1.1 Tertiary phosphine oxide (terminal OPR_3)								
O–P		1.506	1.505	0.018	1.496	1.522	28	
P–C		1.791	1.794	0.026	1.777	1.807	87	
Mn–O	see CONTEE (2.084, 2.147)							
Co–O	see BIRXIJ (1.990), CLTPOC01 (1.940)							
Cu–O	(4,*), (II)	1.947	1.948	0.013	1.934	1.959	5	
Zn–O	see BIJWEW (1.966), CLPOZN (1.983)							
Nb–O	see COJYEF (2.135)							
Rh–O	see CXPORH (2.049)							
Ce–O	see NTPOCE (2.215, 2.222)							
W–O	see CXPHOW (2.163, 2.175), PMYPCW (2.198)							
Re–O	see CADMAV (2.092)							
U–O	(6-8), (IV,VI): excluding CAMCUO	2.279	2.265	0.049	2.243	2.321	10	
5.15.1.1 Phosphate (chelating, η^2-PO_4)								
(None)								*104*
5.15.1.2 Hydrogenphosphate (μ_2-PO_4H)								
Mo–O	see PYMOPH (2.001, 2.007)							
Pt–O	see CAJFAU (1.987–2.020)							
5.15.1.3 Alkylphosphates (PO_4R)								
(*M*)O–P		1.519	1.521	0.016	1.511	1.534	8	
Co–O		1.963	1.964	0.033	1.931	1.994	4	*8*
Cd–O		2.238	2.252	0.046	2.189	2.273	4	
5.16.1.1 Dialkylphosphinates (η^1-O_2PR_2)								*104*
(*M*)O–P	(1.506)							
P–O	(1.508)							
P–C	(1.834, 1.778)							
Mn–O	see AMPMNC (2.140)							
5.16.1.2 Dialkylphosphinates (μ_2-O_2PR_2)								
O–P		1.509	1.512	0.013	1.505	1.519	23	
P–O		1.798	1.801	0.017	1.788	1.808	24	
Mn–O	all AMMPMN	2.163	2.155	0.037	2.133	2.204	4	
Cu–O	(4,5), (II)	1.919	1.918	0.010	1.914	1.923	14	
Zn–O	see BISCEL (1.926)							
Re–O	all DPINRE	2.167	2.153	0.034	2.147	2.202	4	
5.17.1.1 *O*-Dialkyl sulfoxide (terminal, η^1-OSR_2) (see also 9.16.1)								*127*
O–S		1.525	1.520	0.021	1.516	1.621	40	
S–C		1.787	1.788	0.020	1.775	1.799	77	
Fe–O	(6), (III)	2.016	2.012	0.013	2.006	2.029	5	
Cu–O	see CEBREG (2.525), TMSCCU (1.945, 1.950)							
Mo–O	(6), (-)	2.256	2.258	0.082	2.202	2.335	12	*87*
Ru–O	see BESXRU (2.051), CDMSOR (2.142)							
Rh–O	see BEGFEY (2.234, 2.262), MSORHB (2.240)							*82*
Cd–O	see BEGNAC (2.291)							
Eu–O	see MTXPVE (2.404)							
Re–O	see ACMRHD (2.302)							
Pt–O	see BINJEN (2.126)							
Hg–O	see DMSOHG (2.318, 2.320; 2.377, 2.576)							
Th–O	see CPHSTH (2.459, 2.460)							
U–O	see BOZDID (2.432), CEMCUS (2.317), FDMSON (2.352)							

Table 9.6.3.3. *Interatomic distances (Å) (cont.)*

Bond	Substructure (coordination number, oxidation state, comment)	*d*	*m*	σ	q_l	q_u	*n*	Note
5.18.1.1 Sulfate (terminal, η^1-SO_4)								*104*
(*M*)O–S		1.479	1.479	0.022	1.459	1.501	9	
S–O		1.465	1.463	0.025	1.457	1.482	27	
Mn–O	see AQSUMN (2.129)							
Cu–O	(5), (II): short; see AXEXAC (1.948), PYRCUD (1.909), TIMCUS (2.015)							
	(5,6), (II): long; see AENCUS (2.492), DAPRCX (2.496)							
Th–O	see BOHPUJ (2.378)							
U–O	see BEMPOY10 (2.377), TURURS01 (2.408)							
5.18.1.2 Sulfate (chelating, η^2-SO_4)								
(None)								
5.18.1.3 Sulfate (μ_2-SO_4)								
(*M*)O–S		1.507	1.500	0.031	1.476	1.538	10	
S–O		1.457	1.459	0.023	1.437	1.478	10	
Fe–O	see CNOFEB (1.983)							
Cu–O	see HETXCU (2.441)							
Cd–O		2.407	2.391	0.087	2.333	2.497	4	
Pt–O	all BINJEN	2.010	2.009	0.010	2.005	2.015	4	
5.18.1.4 Sulfate (μ_3-SO_4)								
(*M*)O–S		1.486	1.492	0.014	1.475	1.492	9	
Co–O	see EFASCO01 (2.005)							
Cu–O	see COLDUC (2.168, 2.060, 2.346)							
U–O	see URSDUR03 (2.374, 2.389)							
5.19.1.1 Alkyl sulfonates (terminal, η^1-OSO_2R)								
(*M*)O–S		1.453	1.450	0.015	1.443	1.456	8	
S–O		1.446	1.449	0.021	1.432	1.464	16	
S–C		1.785	1.780	0.022	1.767	1.806	8	
Fe–O	see CAWTAV (2.007)							
Cu–O	(6), (II)	2.358	2.356	0.022	2.338	2.380	4	
Pd–O	see FMSEPD (2.272)							
Au–O	see MAUFMS (2.201)							
5.19.1.2 Alkyl sulfonates [chelating, η^2-$O_2S(O)R$]								
(None)								
5.19.1.3 Alkyl sulfonates [μ-$O_2S(O)R$]								
(*M*)O–S		1.452	1.452	0.013	1.440	1.465	8	
S–O		1.452	1.452	0.010	1.443	1.462	4	
S–C		1.784	1.780	0.034	1.754	1.819	4	
Cu–O(μ_3)	see CAWJAL (2.068, 2.049), COMMAS (2.060, 2.385)							
Cd–O(μ_2)	see CAMSOB (2.404, 2.412)							
U–O(μ_2)	see URMSUL (2.363, 2.399)							
5.19.2.1 Alkyl sulfites (terminal, η^1-SO_2R)								
O–S	(1.501, 1.533)							
Fe–O	see FEBUTS10 (2.004)							
Cu–O	see PYSLCU (1.957)							
5.20.1 *O*-Sulfur dioxide (η^1-OSO) (see also 9.14.1)								*104*
O–S	(1.448)							
S–O	(1.410)							
Mn–O	see CONTEE (2.282)							
5.21.1.1 Perchlorate (terminal, η^1-ClO_4)								*128*
(*M*)O-Cl		1.430	1.437	0.026	1.409	1.447	33	
Cl–O		1.407	1.414	0.031	1.393	1.429	99	
Co–O	see PNENCO10 (2.360)							
Ni–O	see ZEGGET (2.221, 2.235)							
Cu–O	(4-6), (I,II)	2.496	2.517	0.119	2.425	2.568	26	*91*
	(5,6), (II)	2.508	2.532	0.115	2.485	2.570	24	*91*
La–O	see APXLAP (2.494)							
Sm–O	see HBHOSM (2.364)							
Hg–O	see OTPCHG (2.726), TTHPHG (2.757)							

Table 9.6.3.3. *Interatomic distances (Å) (cont.)*

Bond	Substructure (coordination number, oxidation state, comment)	*d*	*m*	σ	q_l	q_u	*n*	Note
5.21.1.2 Perchlorate (η^2-ClO_4)								
(*M*)O–Cl		1.437	1.450	0.029	1.406	1.462	5	
Cl–O		1.397	1.401	0.030	1.475	1.418	5	
Ag–O	see CAMROX (2.291, 2.754)							
La–O	see APXLAP (2.683, 2.291)							
Sm–O	see HBHOSM (2.642)							
5.21.1.3 Perchlorate (μ_2-ClO_4)								
(*M*)O–Cl		1.400	1.417	0.055	1.359	1.436	6	
Cu–O	see BAMCIB10 (2.541, 2.569), OXMCUA (2.552, 2.428)							
Ag–O	see BUZMUE (2.581, 2.342)							
5.22.1 Aqua (terminal OH_2)								
Ti–O	(6-8), (III-IV)	2.066	2.063	0.052	2.024	2.122	8	
V–O	(6), (-): all	2.129	2.063	0.131	2.013	2.250	14	*30*
	: short (<2.1)	2.024	2.025	0.030	1.996	2.047	8	*44*
	: long (>2.2) (*trans* to O)	2.268	2.260	0.048	2.228	2.317	6	*129*
Cr–O	(6,7), (-): all	1.997	1.979	0.070	1.955	2.007	33	*86*
	: excluding 5>2.06	1.997	1.986	0.052	1.966	2.008	28	*85*
	: excluding Cr^{II}	1.987	1.982	0.036	1.965	2.003	26	
Mn–O	(6,7), (-): all	2.189	2.183	0.040	2.162	2.216	88	*130*
Fe–O	(6,7), (-): all	2.085	2.108	0.066	2.043	2.135	29	
	excluding MAZCOC	2.099	2.109	0.046	2.054	2.136	27	
Co–O	(4-7), (-): all	2.085	2.090	0.064	2.059	2.123	121	
	excluding TAZOCO	2.081	2.090	0.055	2.058	2.122	119	*91*
Ni–O	(6,7), (-): all	2.079	2.078	0.038	2.050	2.105	126	*9*
Cu–O	(4-6), (-): all	2.186	2.208	0.215	1.965	2.355	219	*30*
	(4), (II)	1.942	1.946	0.016	1.931	1.954	10	
	(5), (-): all	2.209	2.257	0.187	2.000	2.344	116	
	: short (<2.08)	1.986	1.974	0.038	1.961	2.010	41	
	: long (>2.14)	2.331	2.316	0.103	2.259	2.372	75	
	(6), (-): all	2.189	2.125	0.246	1.960	2.408	87	*30*
	: short (<2.01)	1.963	1.960	0.019	1.950	1.973	42	
	: long (>2.12)	2.399	2.399	0.154	2.275	2.520	45	
Zn–O	(4-7), (-): all	2.090	2.092	0.061	2.051	2.137	56	
	(4), (-)	2.006	2.001	0.017	1.994	2.020	5	
	(5), (-)	2.078	2.091	0.079	2.007	2.159	7	
	(6), (-)	2.097	2.093	0.049	2.059	2.145	40	
Y–O	(7-9)	2.398	2.412	0.068	2.335	2.440	9	
Nb–O	(6-8), (-): all	2.248	2.188	0.137	2.158	2.368	6	
		2.167	2.177	0.030	2.135	2.189	4	*44*
Mo–O	(-), (-): all	2.201	2.187	0.094	2.146	2.263	37	*85*
	(*), (-): (clusters)	2.142	2.151	0.052	2.109	2.176	21	*131*
Tc–O	see CEPHOU (2.282)							
Ru–O	(6), (-)	2.074	2.066	0.051	2.031	2.119	12	*85*
Rh–O	(4-6), (I-III): all	2.190	2.178	0.096	2.108	2.296	14	
		2.105	2.108	0.035	2.100	2.129	7	*85*
		2.274	2.295	0.045	2.227	2.309	7	*82*
Pd–O	see BQAPPD (2.200)							
Ag–O	see CERFAG (2.334), COVBIY (2.367)							
Cd–O	(5-8), (-)	2.318	2.299	0.065	2.272	2.345	73	*86*
La–O	(8-10), (-)	2.556	2.564	0.062	2.511	2.610	17	
Ce–O	(9,11), (-)	2.565	2.601	0.063	2.467	2.6 5	5	
Pr–O	(8,9), (-)	2.518	2.519	0.038	2.482	2.537	13	
Nd–O	(7,11), (-)	2.533	2.528	0.058	2.478	2.582	25	
Sm–O	(8,9), (-)	2.459	2.447	0.050	2.420	2.477	24	*86*
Eu–O	(9), (-)	2.441	2.412	0.055	2.400	2.486	8	
Gd–O	(9), (-)	2.443	2.418	0.074	2.392	2.526	13	
Tb–O	see ZZZARD01 (2.382, 2.527)							
Dy–O	(8,9), (-)	2.409	2.374	0.074	2.356	2.469	12	
Ho–O	(7-9), (-)	2.407	2.392	0.069	2.354	2.477	10	
Er–O	(7-9), (-)	2.404	2.372	0.083	2.352	2.427	15	
Yb–O	(8,9), (-)	2.353	2.342	0.066	2.311	2.388	12	
Lu–O	(9), (-): all	2.404	2.408	0.116	2.298	2.507	4	
W–O	(-), (-): all	2.115	2.106	0.065	2.072	2.148	14	
		2.101	2.092	0.045	2.072	2.142	13	*44*
Re–O	(6), (-): all	2.199	2.214	0.091	2.106	2.276	4	
Os–O	see CIBKED (2.166)							
Au–O	see MAUFMS (2.157)							
Hg–O	(4,6), (-): all	2.690	2.680	0.083	2.612	2.773	5	
Th–O	(9,10), (-): all	2.483	2.483	0.032	2.452	2.513	4	
U–O	(7,8), (-): all	2.455	2.464	0.047	2.430	2.478	15	

Table 9.6.3.3. *Interatomic distances (Å) (cont.)*

Bond	Substructure (coordination number, oxidation state, comment)	*d*	*m*	σ	q_l	q_u	*n*	Note
5.22.2 Aqua (μ_2-OH_2)								
Mn–O	see MNPROP (2.223, 2.369)							
Co–O	(6), (II,III)	2.151	2.156	0.021	2.132	2.167	5	
Ni–O	(6), (II)	2.102	2.103	0.030	2.072	2.133	8	
Cu–O	see AXEXAC (2.300, 2.487), CESYII (2.755)							
Zn–O	see CITKIZ (2.100, 2.326)							
Ru–O	see COCXOH (2.159, 2.168)							
Ag–O	see BUGFUE (2.437, 2.451)							
U–O	see AQOURI (2.354, 2.375)							
5.23.1 Alkyl alcohols [*R*OH, $R = C(sp^3)$]								
O–C		1.436	1.435	0.022	1.425	1.448	196	
V–O	see CIJDAA (1.918, 2.233)							
Mn–O	(4,6), (II,III): all	2.223	2.202	0.055	2.184	2.248	19	
	: excluding 1 > 2.39	2.213	2.201	0.035	2.182	2.246	18	
Fe–O	(6), (II,III)	2.133	2.157	0.052	2.078	2.175	5	
Co–O	(5,6), (II,III): all	2.089	2.085	0.091	2.068	2.108	28	
	(6), (III)	1.951	1.953	0.017	1.934	1.967	4	
	(6), (II)	2.098	2.086	0.042	2.076	2.108	23	
Ni–O	(4,6,*), (II): all	2.101	2.093	0.073	2.065	2.140	31	
	(6), (II)	2.099	2.089	0.043	2.071	2.128	25	
Cu–O	(4-6), (I,II): all	2.162	2.039	0.206	1.991	2.375	61	*30*
	(4), (II)	1.973	1.977	0.027	1.948	1.996	8	
	(5,6), (II): short (<2.07)	2.003	2.000	0.031	1.978	2.029	24	
	(5,6), (II): long (>2.16)	2.384	2.404	0.102	2.290	2.474	26	
Zn–O	(5,6), (II)	2.122	2.105	0.041	2.085	2.166	10	
Mo–O	(5,6), (V,VI)	2.326	2.326	0.035	2.308	2.358	6	
Rh–O	(4,6), (I,II): all	2.259	2.273	0.047	2.223	2.296	6	
	(6), (II): all $Rh_2(O_2CR)_4.L_2$	2.276	2.277	0.023	2.255	2.296	5	
La–O	(9-11), (III)	2.574	2.579	0.025	2.547	2.595	6	
Pr–O	(8,9), (III)	2.539	2.533	0.033	2.513	2.568	5	
Nd–O	see BAWDIM10 (2.480, 2.547)							
Eu–O	see CEYRON (2.433, 2.470)							
Er–O	see BUHVOP (2.468), HENAEB (2.240)							
Yb–O	see GEIAYB10 (2.386, 2.420)							
Hg–O	see TESTHG (2.487)							
Th–O	see BURPEJ (2.579)							
U–O	(6,7), (VI)	2.439	2.460	0.052	2.387	2.481	5	
5.23.2 Alkyl, aryl alcohols [ArOH, *R*OH, $R = C(sp^2)$]								
O–C		1.378	1.365	0.034	1.361	1.397	9	
Fe–O	see CAYGOY (2.317)							
Co–O	see APIMCO (2.154), BAVJOX10 (1.937, 1.937)							
Ni–O	see APIMNI (2.102)							
Cu–O	see CAXYOP (2.600)							
Mo–O	see CETGIR (2.601, 2.645)							
Sm–O	see SALASM10 (2.434)							
5.24.1 Tetrahydrofuran (thf)								
O–C		1.453	1.453	0.025	1.438	1.466	167	
Ti–O	(7-8), (II-IV): all	2.205	2.219	0.069	2.166	2.257	8	
V–O	(6), (II-IV): all	2.128	2.132	0.063	2.070	2.153	14	
	excluding BUXTAP	2.115	2.131	0.042	2.070	2.151	13	
Cr–O	(6), (0-III): all	2.125	2.084	0.137	2.002	2.279	6	
		2.042	2.023	0.058	2.000	2.104	4	*85*
Mn–O	see CLTIMN (2.227), HFURMN (2.100)							
Fe–O	see PTHFFE (2.352)							
Ni–O	see BECXIQ (1.964)							
Y–O	(9,10), (III)	2.405	2.413	0.054	2.350	2.457	5	
Zr–O	see COTZRH (2.446), COTZRF (2.274)							
Mo–O	(6), (II-VI): all	2.430	2.432	0.148	2.307	2.570	6	*30*
Cd–O	see PHPNCD (2.643)							
La–O	see CEYPEB (2.555, 2.509, 2.490)							
Ce–O	see COCTCE (2.577, 2.588)							
Sm–O	(8), (II): all CALCEX	2.634	2.628	0.018	2.620	2.652	4	
Eu–O	see CIFCAV (2.602, 2.641)							
Gd–O	see CPTHGD10 (2.494)							
Er–O	see BOBWAQ (2.351, 2.365, 2.452)							
Yb–O	see CPFYBA10 (2.412), CPYBHF (2.525)							
Ta–O	see ACTHTA (2.282), BEHHIF (2.379), BEJGAY (2.308)							
Re–O	see BOJSUO (2.486, 2.469)							
Hg–O	see BIYPAA (2.645)							
Th–O	see COCTFT10 (2.573, 2.525)							
U–O	(8-10), (III,IV)	2.471	2.470	0.045	2.439	2.494	6	

Table 9.6.3.3. *Interatomic distances (Å) (cont.)*

Bond	Substructure (coordination number, oxidation state, comment)	*d*	*m*	σ	q_l	q_u	*n*	Note
5.24.2 Ethers [OR_2, $R = C(sp^3)$]								
O–C		1.432	1.434	0.033	1.415	1.450	383	
Ti–O	all TCXNTI	2.134	2.124	0.026	2.118	2.161	4	
Cr–O	(5), (II): excluding FACCRE (2.244)	2.133	2.132	0.007	2.128	2.138	6	
Mn–O	(8), (II): predominantly ODMNBR	2.319	2.325	0.051	2.274	2.369	6	
Co–O	(6,7), (II)	2.230	2.207	0.092	2.142	2.327	20	*8,30*
Ni–O	(6), (II)	2.147	2.151	0.063	2.089	2.187	14	
Cu–O	(6,7), (II)	2.431	2.404	0.187	2.299	2.608	22	
Zn–O	see CEPMOZ (2.093)							
Y–O	see BUWBAW (2.385)							
Mo–O	(5,6), (II,V): excluding CETGEN	2.263	2.269	0.027	2.242	2.285	6	
Ag–O	all CIJWIB	2.575	2.575	0.015	2.561	2.588	4	
Cd–O	(6-8,*), (II)	2.569	2.541	0.120	2.466	2.697	11	
La–O	(10-12), (III)	2.685	2.693	0.053	2.641	2.730	42	*20*
Nd–O	(10,12), (III)	2.665	2.646	0.076	2.600	2.719	11	
Sm–O	(9,10), (III)	2.504	2.503	0.046	2.473	2.537	14	
Eu–O	(6,10,11), (II,III)	2.618	2.638	0.088	2.529	2.680	9	
	(10,11), (III)	2.596	2.601	0.080	2.508	2.665	7	
Ta–O	see BUBKUE (2.462, 2.166, 2.411, 2.176)							
Hg–O	see CESZOP (2.825), HGTXZO (2.909, 2.935)							
U–O	see BAMVUG (2.602, 2.586)							
5.24.3 Ethers {OR_2, $R_2 \neq [C(sp^3)]_2$}								
O–C(sp^2)		1.390	1.389	0.014	1.380	1.400	51	
O–C(sp^3)		1.444	1.446	0.020	1.429	1.455	51	
V–O	see BUCTOI (2.196, 2.219, 2.229)							
Cr–O	(5), (II): all Cr≡Cr	2.131	2.131	0.009	2.127	2.135	7	
Co–O	see BXZPCO (2.325)							
Ni–O	(6), (II)	2.176	2.175	0.052	2.141	2.201	11	
Cu–O	(6,7), (II)	2.393	2.371	0.096	2.310	2.472	8	
Mo–O	all DMXPMO10	2.269	2.269	0.019	2.252	2.287	4	
Ru–O	see CEFNOQ (2.472), CPASRU (2.257, 2.299)							
Pd–O	see BUWJUY (2.236)							
Cd–O	see CATKUD (2.614, 2.731)							
La–O	(10), (III)	2.697	2.699	0.031	2.679	2.729	8	*22*
Sm–O	see HBHOSM (2.417, 2.437, 2.591)							*22*
5.25.1 η^2Acyl [η^2-C(O)R] (see also 3.12.1.2)								
Zr–O	see BOPSII (2.249, 2.251)							
Mo–O		2.267	2.289	0.050	2.214	2.300	6	
W–O	see BUSYIX (2.223), COSSOS (2.167)							
5.25.2 η^2-CO_2 (see also 3.22.1)								
(None)								
5.25.3.1 *O*-Isocyanate (terminal -OCN) (see also 4.5.1.1)								
(None)								
5.25.3.2 Isocyanate (μ_2-NCO) (see also 4.5.1.2)†								
Cu–O	see CNPRCV (2.607), ICNPCU10 (2.663)							
5.25.4 Borates (all types)								*132*
O–B	(1.437, 1.405, 1.431)							
Ni–O	see CECWEM (2.038, 2.056, 2.057)							
O–B	(1.527, 1.547)							
Mo–O	see BAXHEN (2.129, 2.145)							
6.1.1.1 Fluoro (terminal F)								
Ti–F	see FPOTIP (1.853, 1.887)							
V–F	(5,6), (IV,V): all	1.856	1.876	0.059	1.790	1.908	8	
Cr–F	(6), (III)	1.870	1.872	0.027	1.847	1.892	5	
Mn–F	see TMAFMN (1.809, 1.867)							
Ni–F	see FACTNI (2.081, 2.093)							
Cu–F	see BIPTAV (1.935)							
Zr–F	(7,8), (-): all	2.043	2.051	0.037	2.024	2.063	22	*133*
Nb–F	(6), (V): all	1.957	1.941	0.069	1.906	1.982	11	
		1.940	1.936	0.041	1.903	1.980	10	*44*
Mo–F	see AFXPCM (2.058), TCMOFM (1.922, 1.845)							
W–F	see CPBXOG (2.081)							
Re–F	see COLWAB (2.036)							
Pt–F	see TEPPTB (2.043)							
U–F	(7,10), (-): all	2.240	2.268	0.077	2.178	2.289	5	
	(7), (-)	2.274	2.276	0.020	2.254	2.293	4	

Table 9.6.3.3. *Interatomic distances (Å) (cont.)*

Bond	Substructure (coordination number, oxidation state, comment)	*d*	*m*	σ	q_l	q_u	*n*	Note
6.1.1.2 Fluoro (μ_2-F)								*134*
Cu–F	see CASYEA (1.927, 1.919)							
Mo–F	(6), (VI): all	2.168	2.147	0.046	2.134	2.212	6	
Ag–F	see BIWVEI (2.548, 2.550)							
U–F	(7,10), (IV,VI): all	2.316	2.325	0.041	2.273	2.350	4	
6.2.1 BF_4 (terminal, η^1)								
(*M*)F–B	all	1.366	1.357	0.044	1.330	1.391	6	
	excluding 1 > 1.43	1.349	1.357	0.019	1.330	1.365	5	
B–F	all	1.331	1.347	0.058	1.305	1.378	18	
	excluding 4 < 1.25	1.360	1.357	0.023	1.337	1.378	14	
Cu–F	see BUWWOF10 (2.560)							
Ir–F	see BEVYIK (2.272)							
U–F	see CISZOT (2.420, 2.403)							
6.2.2 PF_6 (terminal, η^1)								
(None)								
7.1 Silicon ligands (all types)								*135*
Mn–Si	see BOTGAS (2.351), CATSUL (2.254), DPSCMN (2.402), MSISMN (2.564)							
Fe–Si	: SiR_3, SiX_3, SiX_2, SiR_3, *etc.*: all	2.329	2.348	0.066	2.264	2.367	15	
	: Si with halide substituents	2.263	2.258	0.014	2.251	2.280	6	
	: without halide substituents	2.374	2.363	0.045	2.349	2.411	9	
Mo–Si	see FBSIMO (2.603, 2.608)							
Ru–Si	: SiX_3, SiR_3, μ-SiR_2	2.423	2.439	0.057	2.365	2.463	9	
	: excluding SiX_3	2.447	2.451	0.037	2.414	2.465	7	
Rh–Si	see CONFEQ01 (2.379)							
W–Si	see ESITCO (2.586)							
Re–Si	all ESICRE, HETSRE	2.543	2.547	0.007	2.536	2.549	5	
Os–Si	see BEGKAZ (2.400, 2.421), CAFCUH (2.429)							
Ir–Si	see HTSIXI10 (2.398, 2.417)							
Pt–Si	SiR_3, μ-SiR_2	2.336	2.318	0.060	2.313	2.382	7	
Hg–Si	(6), (II): SiR_3	2.533	2.544	0.026	2.506	2.549	4	
8.1.1 Phosphorus (μ_n-P)								
Co–P	(μ_3-P): all CPCOPT	2.233	2.218	0.022	2.216	2.256	7	
Ru–P	(μ_5-P): see BUTKUW range 2.327–2.263							
Rh–P	(μ_8): all BEAMRH	2.425	2.421	0.026	2.402	2.451	8	
8.2.1.1 Phosphinidenes (terminal, η^1-P*R*)								
(None)								
8.2.1.2 Phosphinidenes (μ_2-P*R*)								*136*
P–C	(1.897)							
Cr–P	see CIHXIA (2.288, 2.315)							
8.2.1.3 Phosphinidenes (μ_3-P*R*)								*136*
P–C	predominantly *R* = Ph	1.808	1.809	0.013	1.799	1.816	23	
Fe–P	(*), (-)	2.204	2.204	0.030	2.179	2.223	42	
Co–P	see COTSEJ (2.156, 2.163, 2.170)							
Ru–P	(*), (-)	2.302	2.292	0.039	2.277	2.327	21	
Ir–P	see BUNMEC (2.255, 2.279, 2.285)							
8.2.1.4 Phosphinidenes (μ_4-P*R*)								*136*
P–C	*R* = aryl	1.812	1.817	0.018	1.801	1.825	16	
	R = Me: all BUZRAP	1.862	1.863	0.007	1.855	1.867	4	
Fe–P	(*), (-)	2.261	2.254	0.051	2.235	2.287	52	
Co–P	all PPCOC01	2.240	2.240	0.014	2.229	2.245	8	
Ru–P	asymmetrics included	2.408	2.353	0.089	2.343	2.483	12	
Rh–P		2.388	2.397	0.032	2.358	2.415	8	
8.3.1.1 Phosphino (η^1-terminal PR_2, *R* = alkyl)								
P–C		1.865	1.865	0.012	1.861	1.877	20	
Fe–P	see CPFMPI10 (2.265)							
Mo–P	all CEHTUE	2.274	2.276	0.007	2.267	2.279	4	
Hf–P	(5,8), (IV): planar at P	2.500	2.496	0.025	2.478	2.526	4	
	: not planar at P, see CAKSOW (2.682)							
8.3.1.2 Phosphino (μ_2-PR_2)								
P–C	all but *R* = ^{t}Bu; mostly *R* = Ph	1.831	1.830	0.016	1.821	1.839	264	

Table 9.6.3.3. *Interatomic distances (Å) (cont.)*

Bond	Substructure (coordination number, oxidation state, comment)	*d*	*m*	σ	q_l	q_u	*n*	Note
8.3.1.2 Phosphino (μ_2-PR_2) *(cont.)*								
P–C	R = ^{t}Bu	1.909	1.919	0.020	1.899	1.921	25	
V–P	all DMPCOV	2.357	2.357	0.005	2.352	2.361	6	
Cr–P	all MPCRCO	2.318	2.318	0.001	2.317	2.319	4	
Mn–P	(5,6), (0,I)	2.289	2.282	0.039	2.260	2.290	12	
Fe–P	(4-6,*), (-)	2.222	2.217	0.030	2.204	2.233	67	
Co–P	(4,5,*), (-)	2.189	2.188	0.036	2.160	2.224	44	
Ni–P	(3,4), (-)	2.189	2.185	0.039	2.161	2.228	15	
Cu–P	see PHPECU01 (2.357, 2.370)							
Mo–P	(6,7), (-)	2.390	2.381	0.030	2.364	2.419	12	
Ru–P	(5,*), (-)	2.333	2.327	0.041	2.310	2.355	62	
Rh–P	(4,*), (-)	2.307	2.299	0.037	2.285	2.327	22	
Os–P	(5,6,*), (-)	2.379	2.391	0.051	2.341	2.415	8	
Ir–P	all CEFVIS	2.355	2.358	0.046	2.312	2.395	4	
Pt–P	(4,*), (-)	2.282	2.281	0.037	2.256	2.312	24	
8.3.2.1 Phospha-vinyls (η^1-PR=CR_2)								
P=C	(1.679, 1.651, 1.661)							
P–C	(1.822, 1.818, 1.793)							
Cr–P	see MESTCR (2.356)							
Pt–P	see BESHAI (2.218), BEXLEV (2.199)							
8.3.3 Diaminophosphino [P(NR_2)$_2$]								
P–N		1.615	1.624	0.028	1.598	1.632	8	
Fe–P	all CINLAM	2.106	2.124	0.061	2.041	2.152	4	
8.4.1 P–P bonded ligands (η^1-P–P single bond)								*137*
P–P		2.211	2.205	0.034	2.193	2.220	54	
Cr–P	(6), (0)	2.385	2.383	0.036	2.361	2.403	11	
Mn–P	see COGSIA (2.355, 2.369), PDMNC (2.215)							
Fe–P	(4,5), (-)	2.235	2.221	0.027	2.217	2.263	10	
Ni–P	see PSNIMO (2.221)							
Mo–P	(6), (0)	2.511	2.512	0.045	2.463	2.534	11	
Rh–P	see BUYKIP (2.285, 2.302)							
W–P	see BAVKAK (2.573), CIPGAJ (2.535)							
Re–P	see BTPCRE10 (2.478, 2.539)							
Ir–P	see CAYLAP (2.423, 2.433)							
Hg–P	see TMDPHG (2.490)							
8.4.2 P_3 (η^3-P_3)								*137*
P–P		2.135	2.137	0.016	2.122	2.149	18	
Co–P	(5), (-)	2.311	2.309	0.011	2.302	2.321	4	
Ni–P	see CAFSOR (2.308, 2.309, 2.309)							*9*
Rh–P	see PPMERH (2.418)							
Pd–P	(5), (-)	2.452	2.450	0.045	2.411	2.497	6	
Ir–P	see PPMEIR (2.436)							
Pt–P	see BUSLEG (2.430, 2.433, 2.437)							
8.4.3 P–P bonded ligands (η^1-P=P double bond)								*137, 138*
P=P		2.038	2.039	0.014	2.023	2.052	5	
Cr–P	see CEGHAX (2.360), CIKPUH (2.315)							
Fe–P	see BUPJAX (2.226), CAYFAJ (2.232), CEMXIB (2.215)							
8.4.4 P–P bonded ligands (η^2-P=P double bond)								*137, 138*
P=P		2.150	2.146	0.027	2.128	2.176	4	
Fe–P	see CEGHEB (2.346, 2.361)							
Ni–P	see EPMSPN11 (2.234, 2.259)							
Mo–P	see CPPYMO10 (2.536, 2.550)							
Pd–P	see BIHGOO (2.366)							
8.5.1 Trimethylphosphine (PMe_3)								*137*
P–C		1.824	1.824	0.023	1.811	1.837	1243	
V–P		2.510	2.509	0.010	2.502	2.520	4	
Cr–P		2.389	2.370	0.069	2.328	2.460	5	*87*
Mn–P	(4-7), (-): all	2.455	2.453	0.164	2.293	2.619	8	*38*
	(5,6), (-)	2.304	2.295	0.027	2.285	2.332	4	
	(4,7), (-)	2.605	2.605	0.042	2.566	2.645	4	
Fe–P	(5,6), (-): all	2.246	2.248	0.042	2.223	2.268	20	

Table 9.6.3.3. *Interatomic distances (Å) (cont.)*

Bond	Substructure (coordination number, oxidation state, comment)	*d*	*m*	σ	q_l	q_u	*n*	Note
8.5.1 Trimethylphosphine (PMe_3) *(cont.)*								
Fe–P	(5), (-)	2.230	2.228	0.037	2.215	2.252	11	
	(6), (-)	2.265	2.255	0.042	2.239	2.296	9	
Co–P	(4-6,*), (-): all	2.217	2.212	0.043	2.183	2.241	38	*12, 139*
	(4,5,6), (-)	2.209	2.208	0.036	2.181	2.238	35	*140*
Ni–P	(3-5), (-): all	2.204	2.202	0.031	2.188	2.216	37	*9, 51*
	(3), (-)	2.182	2.170	0.060	2.138	2.233	5	
	(4), (-)	2.200	2.200	0.020	2.184	2.208	20	
	(5), (-)	2.220	2.215	0.024	2.204	2.245	12	
Zr–P	see COPVIM (2.692)							
Mo–P	(5-7), (-): all	2.462	2.455	0.046	2.429	2.487	46	*38*
	(5), (-)	2.530	2.535	0.031	2.497	2.546	9	
	(6), (-)	2.459	2.457	0.031	2.432	2.481	16	
	(7), (-)	2.435	2.435	0.027	2.425	2.457	21	
Ru–P	all	2.307	2.307	0.050	2.271	2.335	65	
	excluding MEPRUA, MPMYRU	2.298	2.303	0.037	2.268	2.329	58	
Rh–P	(4-6), (-): all	2.266	2.259	0.036	2.248	2.297	22	
	(4), (-)	2.284	2.296	0.037	2.256	2.308	12	
	(6), (-)	2.249	2.250	0.017	2.247	2.260	9	
Pd–P		2.287	2.281	0.018	2.273	2.305	6	
Ta–P	(5-8), (-): all	2.589	2.588	0.044	2.555	2.625	32	
	(5), (-)	2.564	2.565	0.027	2.535	2.591	13	
	(6), (-)	2.611	2.614	0.048	2.593	2.648	12	
	(8), (-)	2.611	2.627	0.047	2.563	2.651	5	
W–P	excluding CIPDIO and PHIMDW	2.485	2.496	0.039	2.456	2.509	40	*38, 139*
Re–P	all	2.369	2.374	0.065	2.324	2.407	29	
	excluding CACWOS, MEORHC, NOMPRE	2.348	2.335	0.050	2.321	2.383	24	
Os–P		2.328	2.323	0.029	2.297	2.359	15	
Ir–P		2.323	2.329	0.028	2.309	2.341	30	*139*
Pt–P		2.295	2.306	0.036	2.265	2.321	36	*91, 142*
8.5.2 Triethylphosphine (PEt_3)								
P–C		1.832	1.831	0.021	1.820	1.843	557	
Ti–P	see BOZMIM (2.585)							
Cr–P		2.374	2.372	0.061	2.319	2.433	6	*38, 81*
Mn–P	see COLDIQ (2.568), TEPPMN01 (2.253)							
Fe–P	see BDODFE (2.220), CATGEJ (2.234)							
Co–P	all	2.208	2.225	0.039	2.181	2.236	18	
	cobaltacarboranes	2.224	2.226	0.021	2.215	2.241	11	
	$CpML_2$	2.147	2.139	0.024	2.128	2.172	4	
Ni–P	(3,4), (-): all	2.196	2.189	0.036	2.173	2.233	10	*9, 51*
	(3)	2.169	2.176	0.023	2.145	2.187	4	
	(4)	2.214	2.222	0.031	2.183	2.238	6	
Mo–P		2.507	2.513	0.042	2.477	2.545	9	*38*
Ru–P		2.356	2.355	0.006	2.351	2.362	4	
Rh–P		2.338	2.346	0.029	2.316	2.360	13	
Pd–P		2.315	2.321	0.022	2.294	2.336	18	*139*
Ta–P	see BEHHIF (2.667)							
W–P		2.537	2.539	0.015	2.522	2.551	4	*38*
Re–P	see CEVHOA (2.479)							
Os–P	see HETPOS (2.412)							
Ir–P	(6), (-)	2.334	2.332	0.013	2.325	2.341	6	*139*
Pt–P	(-), (-): all, mostly (4,5)	2.296	2.298	0.047	2.259	2.326	100	*139, 142*
	(4,5), (-)	2.288	2.293	0.041	2.255	2.321	92	*139*
	(6), (-)	2.385	2.396	0.036	2.336	2.410	7	*139*
Au–P	see AGLPAU (2.259), CIMGEK (2.328), COSMOM (2.278)							
8.5.3 Triphenylphosphine (PPh_3)								
P–C		1.828	1.828	0.014	1.819	1.837	2239	
V–P	see ALCPPV (2.486, 2.485), CPHSVB (2.472)							
Cr–P	see CEDHUO (2.315), HETCRB10 (2.321), MBZCRP (2.338)							*38*
Mn–P		2.305	2.304	0.044	2.277	2.340	9	
Fe–P		2.237	2.233	0.038	2.213	2.274	31	
Co–P	all	2.243	2.211	0.096	2.174	2.283	52	*8*
	(-), (0): clusters excluded	2.227	2.228	0.016	2.211	2.243	4	
	(6), (III)	2.392	2.397	0.046	2.362	2.423	9	
	(4,5,6), (I,III)	2.202	2.199	0.038	2.174	2.230	33	
Ni–P		2.225	2.208	0.069	2.159	2.309	21	*9, 30, 51*
	short <2.25	2.187	2.197	0.035	2.154	2.221	15	
	long >2.30	2.321	2.320	0.012	2.312	2.331	6	
Cu–P		2.252	2.256	0.044	2.226	2.273	53	*12*
Mo–P		2.524	2.528	0.042	2.511	2.560	15	*38*
Tc–P	see CETKUH (2.494, 2.525), TCACTC (2.433)							
Ru–P	(4-6,*), (-): all	2.370	2.367	0.044	2.337	2.408	59	

Table 9.6.3.3. *Interatomic distances (Å) (cont.)*

Bond	Substructure (coordination number, oxidation state, comment)	*d*	*m*	σ	q_l	q_u	*n*	Note
8.5.3 Triphenylphosphine (PPh_3) (*cont.*)								
Ru–P	(4), (-)	2.342	2.341	0.009	2.334	2.351	4	
	(5), (-)	2.372	2.382	0.040	2.343	2.395	13	
	(6), (-)	2.370	2.367	0.049	2.332	2.419	30	
	(*), (-)	2.379	2.377	0.041	2.362	2.408	12	
Rh–P	(4-6, *), (-): all	2.314	2.324	0.050	2.282	2.344	85	*100*
	(4), (-)	2.302	2.321	0.053	2.248	2.334	44	
	(5), (-)	2.331	2.335	0.048	2.288	2.370	20	
	(6), (-)	2.321	2.331	0.041	2.288	2.346	18	
Pd–P	excluding TTPPDB (2.458)	2.308	2.320	0.038	2.281	2.337	51	*91*
Ag–P		2.419	2.414	0.046	2.388	2.455	27	
Cd–P	see CIFGON (2.524)							
W–P		2.535	2.558	0.069	2.479	2.590	6	*38, 100*
Re–P	all	2.432	2.427	0.048	2.398	2.472	41	
	(-), (I-III)	2.411	2.413	0.036	2.381	2.433	29	
	(-), (IV,V,VII)	2.484	2.487	0.027	2.472	2.505	12	
Os–P		2.388	2.385	0.037	2.361	2.416	42	
Ir–P	(4-6,*), (-): all	2.345	2.341	0.039	2.319	2.374	91	*143*
	(4), (-)	2.328	2.325	0.025	2.314	2.344	36	
	(5), (-)	2.350	2.348	0.037	2.330	2.378	33	
	(6), (-)	2.365	2.378	0.048	2.328	2.408	20	
Pt–P	(-), (-): all	2.294	2.298	0.032	2.273	2.313	151	*142*
	(3), (-)	2.280	2.279	0.023	2.267	2.298	29	
	(4), (-)	2.298	2.302	0.032	2.287	2.317	99	
Au–P	(2-4,*), (-): all	2.303	2.295	0.043	2.281	2.312	62	*144*
	(2), (-)	2.272	2.278	0.025	2.255	2.291	15	
	(4), (-)	2.377	2.398	0.055	2.347	2.411	8	
	(*), (-)	2.297	2.298	0.020	2.288	2.308	34	
Hg–P		2.453	2.457	0.034	2.429	2.483	8	*26*
8.5.4 Triisopropylphosphine (P^iPr_3)								
P–C		1.863	1.863	0.015	1.855	1.872	93	
Rh–P		2.309	2.300	0.047	2.274	2.355	22	
Pd–P	see BUPTEL (2.242), BUSHEC (2.275)							
W–P	see CEJDEA (2.487, 2.503)							*38*
Ir–P	see APRPIR (2.270), BUHIPI (2.300, 2.322)							
Pt–P	see BUPPUX (2.261)							
Au–P	see CEPYIF (2.266)							*142*
8.5.5 Tri-*n*-propylphosphine (P^nPr_3)								
P–C		1.827	1.829	0.028	1.817	1.847	27	
Pd–P	see CEKGOO (2.248, 2.248)							
Pt–P		2.245	2.257	0.024	2.219	2.265	5	*142*
Hg–P	see CIPTAW (2.425, 2.410)							*145*
8.5.6 Tri-*tert*-butylphosphine (P^tBu_3)								
P–C		1.926	1.922	0.026	1.907	1.936	54	
Fe–P	see TBPCFE (2.363)							
Ni–P	see BPBRNI10 (2.494)							
Cu–P	see BOZRAJ (2.228, 2.228)							
Ru–P		2.574	2.476	0.057	2.521	2.624	4	
Rh–P	see BUPCRH (2.427, 2.433)							
Pt–P		2.275	2.267	0.027	2.262	2.276	7	*142*
Hg–P	see TBPAHG10 (2.370)							*26*
8.5.7 Tricyclohexylphosphine [P-(*cyclo*-$C_6H_{11})_3$]								
P–C		1.856	1.855	0.017	1.846	1.867	144	
Mn–P	see COBSOB (2.362)							
Co–P	see BECTIM (2.463)							
Ni–P		2.211	2.226	0.036	2.172	2.242	5	*51*
Cu–P	see CCHXPC (2.183), CHPCUP (2.262)							
Ru–P	see BOMMEV (2.419), CAVVEA (2.424, 2.420)							
Rh–P	see CIDHEC (2.256)							
Pd–P	see FMEACA10 (2.359, 2.363)							
Ir–P	see PCHIRH10 (2.287, 2.291, 2.281)							
Pt–P		2.323	2.327	0.034	2.306	2.343	23	*142*
Hg–P		2.413	2.412	0.034	2.379	2.444	7	*26*
8.5.8 Methyldiphenylphosphine (PPh_2Me)								
P–C(Ph)		1.823	1.822	0.013	1.813	1.833	112	
P–C(Me)		1.827	1.827	0.016	1.815	1.840	56	

Table 9.6.3.3. *Interatomic distances (Å) (cont.)*

Bond	Substructure (coordination number, oxidation state, comment)	*d*	*m*	σ	q_l	q_u	*n*	Note
8.5.8 Methyldiphenylphosphine (PPh_2Me) (*cont.*)								
V–P	see CAPFOO (2.459, 2.529)							
Mn–P	see CABZAG (2.684), COLNAS (2.612)							
Fe–P	see BOPPAX10 (2.260, 2.276)							
Co–P	see CNCOPP10 (2.254, 2.257)							
Ni–P	see MPFPNI (2.206)							*51*
Cu–P		2.266	2.260	0.018	2.250	2.285	5	
Mo–P		2.487	2.483	0.079	2.419	2.561	4	*38, 85*
Ru–P		2.396	2.418	0.060	2.333	2.438	4	
Ag–P		2.438	2.445	0.031	2.406	2.464	4	
Re–P	see CAJGEZ (2.373, 2.397, 2.414)							
Os–P	see CEVFUE10 (2.315)							
Ir–P		2.334	2.322	0.035	2.315	2.365	10	
Pt–P	all	2.300	2.309	0.034	2.270	2.238	17	*142*
	(*trans* to P, CO)	2.317	2.320	0.018	2.299	2.332	13	
	(*trans* to Cl, S*R*)	2.246	2.246	0.002	2.244	2.248	4	
Au–P		2.331	2.303	0.081	2.275	2.416	4	
8.5.9 Dimethyl(phenyl)phosphine ($PPhMe_2$)								
P–C(Ph)		1.826	1.826	0.017	1.815	1.836	252	
P–C(Me)		1.825	1.824	0.021	1.813	1.837	502	
V–P	see BOBZUN (2.523)							
Fe–P		2.259	2.268	0.021	2.237	2.272	4	
Co–P	see BISNEW (2.161), CAHZAM (2.191), PCOPIM10 (2.230)							
Ni–P		2.227	2.223	0.037	2.188	2.261	11	*9, 51*
Nb–P	see CIDBEW (2.697, 2.702)							
Mo–P	all	2.499	2.501	0.038	2.474	2.532	25	*38*
	trans to P, or good σ-donors	2.532	2.532	0.017	2.520	2.544	12	
	trans to weak σ-donors	2.468	2.475	0.022	2.457	2.479	13	
Tc–P	all	2.437	2.463	0.054	2.416	2.478	7	
	all CTMPTC	2.455	2.466	0.028	2.421	2.479	6	
Ru–P		2.342	2.346	0.046	2.316	2.365	20	
Rh–P	all	2.325	2.327	0.055	2.283	2.383	14	*30, 81, 146*
	long >2.35	2.373	2.383	0.020	2.352	2.388	7	*146*
	short <2.31	2.278	2.285	0.029	2.267	2.296	7	
Pd–P	all	2.293	2.275	0.052	2.247	2.350	12	*30, 81*
	long >2.32	2.348	2.352	0.014	2.335	2.359	5	*147*
	short <2.30	2.253	2.258	0.022	2.227	2.265	7	
Cd–P	see MPPCDC (2.560)							
Ta–P	CPMPTA (2.633, 2.649)							
W–P		2.523	2.528	0.033	2.499	2.548	22	*38*
Re–P		2.393	2.393	0.057	2.353	2.435	31	
Os–P		2.326	2.329	0.030	2.297	2.349	38	
Ir–P		2.319	2.313	0.038	2.286	2.347	27	
Pt–P		2.299	2.303	0.037	2.281	2.323	54	*142*
Au–P	see MPAUSN (2.310, 2.318)							
8.5.10 Trifluorophosphine (PF_3)								*148*
P–F		1.542	1.542	0.020	1.529	2.551	39	
Ti–P	all CPFPTI10	2.344	2.344	0.003	2.342	2.347	4	
Cr–P	(6), (0)	2.143	2.140	0.016	2.129	2.159	4	
Rh–P	all PACPRH10	2.219	2.220	0.007	2.213	2.226	4	
Pt–P	see CEPFPP (2.142)							
8.6.1.1 1,2-Bis(dimethylphosphino)ethane (chelating, η^2-dmpe)†								
P–C(Me)		1.824	1.824	0.019	1.813	1.833	160	
P–C(CH_2)		1.841	1.842	0.021	1.827	1.851	80	
C–C		1.514	1.516	0.024	1.497	1.533	38	
Ti–P		2.604	2.608	0.049	2.570	2.637	8	
Mn–P	(-), (I), see also Mn^{II} in COLNEW (2.674)	2.211	2.212	0.004	2.207	2.215	4	
Co–P	see BOHGAG (2.264, 2.248), CADHOE (2.205)							
Ni–P	see COFVIC (2.155, 2.179)							
Zr–P		2.797	2.796	0.049	2.752	2.850	6	
Mo–P	see CITCIR (2.541), NMSPEM (2.409, 2.395)							
Ru–P		2.296	2.297	0.017	2.280	2.311	4	
Pd–P	see CAWLIV (2.304)							
Hf–P		2.687	2.688	0.010	2.678	2.696	4	
Ta–P		2.591	2.602	0.047	2.532	2.629	14	
W–P		2.469	2.470	0.024	2.447	2.491	4	
Ir–P		2.343	2.342	0.005	2.340	2.348	4	
Pt–P	see COMSUS (2.262, 2.270)							
Th–P	see CEKGEE (3.156, 3.152)							
U–P	see CEKGII (3.020, 3.010)							

Table 9.6.3.3. *Interatomic distances (Å) (cont.)*

Bond	Substructure (coordination number, oxidation state, comment)	*d*	*m*	σ	q_l	q_u	*n*	Note
8.6.2.1 1,2-Bis(diphenylphosphino)ethane (chelating, η^2-dppe/diphos)†								
P–C(Ph)		1.827	1.826	0.016	1.816	1.838	287	
P–C(CH_2)		1.845	1.844	0.016	1.835	1.855	143	
C–C		1.527	1.527	0.028	1.513	1.541	72	
V–P	(7), (I)	2.458	2.460	0.025	2.434	2.481	4	
Fe–P	(5,6), (0,II)	2.199	2.201	0.016	2.185	2.210	8	
Co–P	(4,5), (0,III)	2.235	2.239	0.017	2.217	2.248	4	*8*
Ni–P	(5), (II,III)	2.212	2.209	0.021	2.194	2.232	4	*9*
Cu–P	(4), (I)	2.304	2.302	0.011	2.295	2.316	4	
Mo–P	(6,7), (0,II,IV)	2.524	2.530	0.048	2.493	2.556	16	*38*
Tc–P	(6), (II,III)	2.475	2.469	0.033	2.443	2.507	4	
Rh–P	(4,5), (I)	2.294	2.293	0.061	2.232	2.355	8	
Pd–P	(3,4), (0,II)	2.260	2.255	0.029	2.235	2.293	8	
W–P	(5,6), (II)	2.530	2.529	0.021	2.513	2.542	20	*38*
Re–P	excluding CAFZUE	2.428	2.440	0.035	2.403	2.453	10	*81*
Ir–P	(5,6), (I,III)	2.353	2.349	0.036	2.327	2.375	22	
Pt–P	(4,5,*), (0,II)	2.278	2.274	0.033	2.256	2.302	18	
Au–P	(4), (I)	2.400	2.397	0.013	2.389	2.416	8	
8.6.3.1 Bis(diphenylphosphino)methane (chelating-dppm)†								
P–C(Ph)		1.818	1.817	0.013	1.809	1.830	58	
P–C(CH_2)		1.848	1.846	0.014	1.837	1.858	29	
Fe–P	(5,6), (0,II)	2.214	2.217	0.013	2.201	2.215	4	
Nb–P	see CEGGUQ (2.664, 2.660)							
Mo–P	see CEDXEO (2.527, 2.549)							
Ru–P	see CEZXAG (2.341, 2.367)							
Rh–P	(5,6), (I,III)	2.336	2.329	0.024	2.322	2.354	8	
Pd–P	(4), (II)	2.258	2.257	0.020	2.239	2.278	4	
Os–P	all CEZWOT	2.320	2.322	0.022	2.299	2.339	4	
Pt–P	see CACLUN (2.249, 2.335)							
Au–P	see CACPIF (2.360)							
8.6.3.2 Bis(diphenylphosphino)methane (μ_2-dppm)†								
P–C(Ph)		1.822	1.822	0.015	1.813	1.831	174	
P–C(CH_2)		1.836	1.837	0.015	1.825	1.848	87	
Co–P	see BOHBIJ (2.176, 2.178)							
Mo–P	see CIKKAI (2.509, 2.510)							
Ru–P	(*), (-)	2.320	2.317	0.012	2.314	2.329	6	
Rh–P	(4-6,*), (-)	2.321	2.319	0.035	2.307	2.345	42	
Pd–P	see BOGFOS (2.324, 2.359)							
Ag–P	(4,5), (-)	2.427	2.425	0.026	2.406	2.454	6	
Re–P	(6), (-)	2.500	2.501	0.028	2.474	2.524	4	
Os–P	see CEMTIX (2.443, 2.452)							
Ir–P	see BUNMEC (2.310, 2.324), CTDPIR (2.319)							
Pt–P	(4,5), (-)	2.309	2.305	0.021	2.297	2.327	16	
Au–P	see PPEAUC (2.284, 2.325)							
8.7.1 Trimethylphosphite [$P(OMe)_3$]								
P–O		1.595	1.595	0.019	1.582	1.608	311	
O–C		1.432	1.436	0.027	1.419	1.446	311	*91*
Cr–P	see CROPPH10 (2.269)							*38*
Mn–P		2.216	2.219	0.043	2.175	2.240	7	*149*
Fe–P		2.151	2.152	0.017	2.145	2.159	14	*149*
Co–P		2.156	2.153	0.042	2.124	2.174	19	*149*
Ni–P		2.189	2.187	0.020	2.171	2.208	4	*8, 149*
Mo–P		2.400	2.395	0.053	2.358	2.425	28	*38, 149*
Ru–P	all	2.291	2.284	0.043	2.273	2.345	16	*81*
	not *trans* to $P(OMe)_3$	2.267	2.279	0.025	2.239	2.285	11	
	trans to $P(OMe)_3$	2.346	2.346	0.002	2.344	2.347	5	
Rh–P	see BPHPRH10 (2.178)							
Pd–P	see COWGEA (2.281, 2.277)							
Ag–P	see MPNDAG (2.409)							
W–P	see CANHAA (2.453)							*38*
Os–P		2.283	2.283	0.002	2.281	2.285	4	
Ir–P		2.272	2.274	0.022	2.257	2.291	9	
8.7.2 Triphenylphosphite [$P(OPh)_3$]								
P–O		1.600	1.602	0.011	1.593	1.610	45	
O–C		1.404	1.403	0.019	1.394	1.414	45	
Cr–P	see POTCDR (2.251)							
Mn–P	see COLZEI (2.198, 2.202, 2.207)							*38*

Table 9.6.3.3. *Interatomic distances (Å) (cont.)*

Bond	Substructure (coordination number, oxidation state, comment)	*d*	*m*	σ	q_l	q_u	*n*	Note
8.7.2 Triphenylphosphite [$P(OPh)_3$] *(cont.)*								
Rh–P	(4,5,*), (-): all	2.195	2.188	0.047	2.155	2.241	8	*85*
	(4,5), (-)	2.172	2.184	0.023	2.145	2.189	6	*85*
Pd–P	see DTCPPD10 (2.323)							
8.8.1 Aminophosphines and μ-phosphides [$P(NR_2)R'_2$ *etc.*]								
P–N		1.678	1.676	0.026	1.658	1.696	104	
Cr–P	see BUJNOJ (2.322)							
Mn–P	(6,7), (I,III)	2.331	2.330	0.028	2.310	2.354	5	
Fe–P	(5,6), (0,II)	2.183	2.192	0.049	2.128	2.212	11	
Co–P	(5,6), (0,I,III)	2.128	2.102	0.053	2.089	2.158	18	
Mo–P	(6), (0,I)	2.402	2.385	0.053	2.355	2.461	18	
Ag–P	see CEMSUI (2.394, 2.396)							
W–P	see BEGYAN (2.497), BUDBEH (2.437)							
Os–P	see BUPYOA (2.375, 2.399), BUPYUG (2.441)							
Pt–P	all BIYVIO	2.252	2.252	0.015	2.238	2.266	4	
8.8.2 Iminoaminophosphines [$P(NR)NR_2$]								
P=N		1.540	1.551	0.022	1.516	1.556	6	
P–N		1.669	1.674	0.015	1.655	1.678	6	
Cr–P	see PCBASC (2.304, 2.321)							
Re–P	see CECGUM (2.477)							
Pt–P	(3,4), (0)	2.248	2.246	0.021	2.228	2.268	4	
8.8.3 Cyclotriphosphazenyl† and related ligands								
P–N		1.644	1.642	0.014	1.636	1.656	13	
Cr–P	see COLPIC (2.349)							
Fe–P	(6), (II)	2.232	2.236	0.042	2.190	2.273	6	
Mo–P	see COLPOI (2.512)							
9.1.1.1 Sulfur (terminal S)								*150*
V–S	see BAWBUW01 (2.060)							
Mo–S	(4-6,*), (IV-VI)	2.131	2.133	0.022	2.112	2.151	28	
Ta–S	see CIFMAF (2.204), STAETC (2.181)							
W–S	(4,*), (VI)	2.153	2.158	0.013	2.142	2.162	9	
9.1.1.2 Sulfur (μ_2-S)								
V–S	(6,*), (-)	2.234	2.230	0.019	2.219	2.248	10	
Cr–S	all SCPDCC	2.074	2.074	0.003	2.071	2.077	4	
Fe–S	(4,*), (-)	2.225	2.224	0.019	2.210	2.241	50	*90*
Ni–S	see PMENIB20 (2.035)							
Nb–S	(6-8), (III,IV): all	2.479	2.523	0.129	2.343	2.579	18	
	(6), (III,IV)	2.324	2.338	0.029	2.290	2.343	6	
	(7,8), (III,IV)	2.557	2.556	0.075	2.522	2.631	12	
Mo–S	(4-7,*), (-)	2.317	2.320	0.022	2.306	2.328	102	
Rh–S	see TPPMRH10 (2.368)							
W–S	(6), (IV,V)	2.324	2.319	0.022	2.308	2.342	5	
Re–S	see COJDUA (2.375, 2.387)							
Ir–S	see CTDPIR (2.462)							
Au–S	see BITYIM (2.157, 2.161)							
9.1.1.3 Sulfur (μ_3-S)								
Cr–S		2.299	2.308	0.035	2.253	2.328	17	
Fe–S		2.281	2.282	0.035	2.261	2.306	237	*99*
Co–S		2.223	2.230	0.047	2.173	2.264	11	
Ni–S	all BIYCUH	2.201	2.203	0.007	2.195	2.207	6	
Cu–S	all CIHRIU	2.163	2.161	0.007	2.157	2.166	12	
Mo–S	excluding BALJIH, CEFYAN	2.352	2.347	0.019	2.340	2.356	51	
Ru–S	see BUPVUD (2.354, 2.366, 2.350)							
Rh–S	all CEGCIA	2.351	2.352	0.006	2.347	2.356	12	
Os–S		2.428	2.428	0.037	2.406	2.451	60	
Pt–S	see CIXRUW (2.357, 2.369, 2.372)							
9.2.1.1 Alkyl thiolates [terminal, S*R*, $R = C(sp^3)$]								
S–C		1.829	1.829	0.026	1.816	1.846	213	
Ti–S	see BIPFUB10 (2.404), CIRHUG (2.333)							
V–S	(5,6), (III,IV)	2.378	2.377	0.007	2.371	2.385	13	
Cr–S	see LDHPCR10 (2.332), MCENCR (2.337), SCYSCR (2.417)							
Mn–S	(4,5), (II,III): all	2.366	2.339	0.054	2.322	2.432	11	*30*
	(4), (II): all CEMSIW	2.433	2.434	0.008	2.425	2.440	4	
	(5), (III)	2.328	2.323	0.011	2.319	2.339	7	
Fe–S	(4-6,*), (-)	2.271	2.269	0.028	2.251	2.296	72	*99*

Table 9.6.3.3. *Interatomic distances (Å) (cont.)*

Bond	Substructure (coordination number, oxidation state, comment)	*d*	*m*	σ	q_l	q_u	*n*	Note
9.2.1.1	Alkyl thiolates [terminal, S*R*, *R* = C(sp^3)] (*cont.*)							
Co–S	(4,6,*), (II,III)	2.254	2.249	0.025	2.233	2.271	18	*8*
Ni–S	(4), (II)	2.187	2.186	0.007	2.181	2.192	8	
Zn–S	see AMETZN (2.295)							
Mo–S	(4-6,8,*), (II-VI)	2.401	2.408	0.050	2.366	2.424	66	
Tc–S	(5,6), (III,V)	2.302	2.302	0.015	2.286	2.314	8	
Cd–S	see ABPENC (2.444)							
Ir–S	see BEPZEB (2.512), COCKAG (2.411)							
Pt–S	(4), (II)	2.320	2.317	0.015	2.308	2.335	5	
Au–S	see AGLPAU (2.293)							
Hg–S	(2-4), (II)	2.402	2.403	0.065	2.339	2.464	4	
9.2.1.2	Alkyl thiolates [μ_2-S*R*, *R* = C(sp^3)]							
S–C		1.840	1.837	0.028	1.822	1.858	194	
V–S	(6,7), (III): all	2.438	2.418	0.052	2.393	2.493	24	*30*
	: short (<2.44)	2.401	2.401	0.019	2.386	2.418	15	
	: long (>2.48)	2.500	2.493	0.016	2.489	2.513	9	
Cr–S	(6,*), (-)	2.342	2.349	0.022	2.332	2.356	23	
Mn–S	see BUFPUN01 (2.346, 2.631), MCETMN (2.242 2.270)							
Fe–S	(4-6,*), (-): all	2.298	2.289	0.059	2.255	2.349	109	
	: excluding 5 > 2.41	2.291	2.280	0.049	2.251	2.325	104	
Co–S	(4,6,*), (-)	2.294	2.298	0.037	2.280	2.315	20	*8*
Ni–S	(4,*), (-)	2.201	2.199	0.024	2.183	2.227	16	
Cu–S	all CEDNOO	2.278	2.277	0.020	2.265	2.291	12	*12*
Zn–S	see MCECZN (2.284, 2.343)							
Nb–S	all BAGBUG	2.555	2.556	0.017	2.548	2.566	8	
Mo–S	(5-7), (-)	2.460	2.455	0.047	2.419	2.490	60	
Ru–S	(*), (-)	2.400	2.400	0.063	2.336	2.457	8	
Pd–S	(4,*), (-)	2.328	2.329	0.007	2.321	2.332	16	
Cd–S	see CAHGUN (2.528, 2.622)							
W–S	(6,7), (-): excluding asymmetrics	2.466	2.464	0.051	2.421	2.478	14	*151*
Os–S	(5,*), (-)	2.414	2.411	0.011	2.405	2.421	10	
Ir–S	(4,5,*), (-)	2.413	2.397	0.050	2.375	2.443	32	
Pt–S	(4), (II)	2.337	2.343	0.046	2.292	2.379	8	
Hg–S	(2-4,*), (-): excluding asymmetrics	2.494	2.454	0.115	2.407	2.598	8	*151*
9.2.1.3	Thiolates (μ_3-S*R*)							
S–C(sp^3)	(secondary, tertiary)	1.871	1.864	0.020	1.853	1.890	11	
S–C(sp^2)		1.769	1.765	0.011	1.762	1.780	9	
Fe–S	(*), (-): all	2.177	2.148	0.051	2.137	2.224	29	*30*
	: short (<2.16)	2.137	2.139	0.012	2.126	2.146	17	
	: long (>2.21)	2.233	2.224	0.022	2.219	2.243	12	
Ru–S	see CHPRUS10 (2.272, 2.273, 2.275)							
Ag S		2.641	2.625	0.118	2.572	2.688	24	
Ir–S	see BAMDOI10 (2.339, 2.342, 2.467)							
9.2.2.1	Aryl thiolates (terminal, SAr)							
S–C		1.761	1.762	0.020	1.748	1.773	127	
Mn–S	all CEMSES	2.376	2.377	0.006	2.370	2.382	4	
Fe–S	(4-6,*), (-)	2.302	2.298	0.027	2.283	2.318	45	
Co–S	(4-6), (-)	2.247	2.255	0.019	2.245	2.258	7	*8*
Ni–S	(4), (-)	2.215	2.217	0.017	2.195	2.230	6	
Cu–S	(3-5), (I,II)	2.292	2.271	0.111	2.184	2.425	6	*12*
	(3), (I): (2.170, 2.188)							
	(4), (II): (2.263, 2.278)							
	(5), (II): (2.425, 2.425)							
Zr–S	see OCBTZR (2.542)							
Mo–S	(5,6,*), (-): all	2.408	2.412	0.056	2.376	2.429	31	
	(5,6), (-): all	2.402	2.411	0.044	2.374	2.427	30	
Tc–S	see BUMCER (2.340, 2.353, 2.358)							
Ru–S	(4,5), (IV): all	2.238	2.214	0.067	2.204	2.258	6	
	: excluding 1 of 2.373	2.210	2.211	0.010	2.202	2.219	5	
Cd–S	see MERQCD10 (2.425, 2.446)							
W–S	see BILRET (2.425)							
Os–S	see CAJCEV (2.507)							
Ir–S	(6), (III)	2.382	2.378	0.032	2.354	2.414	4	
Pt–S	see BATPER (2.365), CFTPVP (2.304), MTPAPT (2.308)							
Hg–S	(3,4), (II)	2.413	2.369	0.088	2.362	2.527	7	
	(3,4), (II): excluding 2 > 2.52	2.362	2.365	0.012	2.352	2.370	5	
9.2.2.2	Aryl thiolates (μ_2-SAr)							
S–C		1.782	1.783	0.018	1.775	1.791	66	
Mn–S	all CEMSES	2.462	2.459	0.016	2.448	2.478	10	

Table 9.6.3.3. *Interatomic distances (Å) (cont.)*

Bond	Substructure (coordination number, oxidation state, comment)	*d*	*m*	σ	q_l	q_u	*n*	Note
9.2.2.2 Aryl thiolates (μ_2-SAr) (*cont.*)								
Fe–S	(4,5), (-)	2.318	2.331	0.052	2.263	2.370	26	*151*
Co–S	(4,6), (-)	2.312	2.318	0.029	2.310	2.329	14	*8, 151*
Cu–S	all CBZTET10	2.288	2.285	0.026	2.264	2.304	12	
Zn–S	(4), (II)	2.351	2.352	0.021	2.338	2.364	16	
Mo–S	(7), (II,III)	2.513	2.534	0.044	2.456	2.548	12	
Rh–S	(4,5), (I,II)	2.352	2.361	0.038	2.307	2.382	12	
Pd–S	(4), (II)	2.294	2.296	0.084	2.200	2.379	6	*151*
Ag–S	(3,*), (I)	2.454	2.454	0.047	2.408	2.501	8	*151*
W–S	(6,*), (-)	2.484	2.479	0.048	2.447	2.494	14	
Ir–S	all HPSCIR	2.407	2.406	0.009	2.399	2.415	4	
9.3.1.1 *S*-Isothiocyanate (terminal, η^1-SCN) (see also 4.5.2.1)								
S–C		1.660	1.660	0.024	1.646	1.676	36	
C–N		1.140	1.139	0.020	1.131	1.150	36	
Cu–S	see CIKJUB (2.733), STETCU (2.606)							
Rh–S	see ACOXRH (2.374, 2.385)							*12*
Pd–S	(4), (II)	2.351	2.362	0.029	2.329	2.374	9	
Ag–S	(4,5), (I)	2.564	2.546	0.043	2.531	2.613	6	
Pt–S	(4), (II)	2.322	2.322	0.007	2.314	2.328	4	
Au–S	see BACVOQ10 (2.791), BEHYUI (2.469)							
Hg–S	(3,4), (II)	2.493	2.472	0.043	2.461	2.513	11	*26*
9.3.1.2 *S*-Isothiocyanate (μ-SCN)† (see also 4.5.2.2)								
Mn–S	see TCMNET10 (2.691)							
Ni–S	see TCYENI10 (2.570)							
Cu–S	(5), (II): excluding CEVLAQ (2.323), COHHIQ (2.412)	2.808	2.792	0.059	2.760	2.865	5	*12*
Ag–S	see CENSUJ (2.474), CENTAQ (2.496)							
Cd–S	(5,6), (II)	2.679	2.663	0.090	2.602	2.772	4	
Pt–S	see TPPTCP01 (2.408)							
Hg–S		2.550	2.536	0.053	2.508	2.592	8	*26*
9.4.1 Thioketones (terminal, η^1-S=CR_2)								
S–C	(1.657, 1.603)							
Mn–S	see BEHGAW (2.193)							
Os–S	see CAFJUO (2.349)							
9.4.2 Thiourea [terminal, η^1-S=C$(NH_2)_2$]								
S–C		1.725	1.721	0.019	1.714	1.732	40	
C–N		1.322	1.324	0.016	1.315	1.332	80	
Fe–S	all TDCURF	2.588	2.588	0.024	2.567	2.608	4	
Co–S	see BEXTON (2.300), BOVGAU (2.281, 2.300), CTHUCO10 (2.502, 2.553)							
Ni–S	see TIOUNB (2.494, 2.503, 2.520)							*9*
Cu–S	(3-6), (I,II): excluding 1 at 2.943	2.295	2.296	0.052	2.245	2.333	14	*12*
	(3,4), (I)	2.287	2.296	0.045	2.240	2.331	12	
Pd–S	all THUPDC	2.334	2.336	0.013	2.320	2.345	4	
Ag–S	(3,4), (I)	2.493	2.484	0.048	2.454	2.536	6	
Re–S	see OACTUR (2.340, 2.355), OATURE (2.311)							
9.5.1.1 Dithiocarboxylates (terminal, η^1-S_2CR) (None)								
9.5.1.2 Dithiocarboxylates (chelating, η^2-S_2CR, R = any C)								
S–C		1.685	1.684	0.015	1.674	1.696	44	
C–C		1.483	1.479	0.025	1.461	1.505	22	
Ti–S	all CSACTI	2.526	2.526	0.032	2.503	2.550	6	
Mn–S	see BESBIK10 (2.344, 2.376)							
Ni–S	see PTCDNI20 (2.213, 2.216)							
Cu–S	see PHTHCU01 (2.400, 2.422)							*9*
Mo–S	(5-8), (II,IV,V): all	2.505	2.493	0.071	2.464	2.529	24	
	: excluding 2 > 2.69 Å	2.486	2.485	0.035	2.464	2.518	22	*44*
Pd–S	all PDTHBA10	2.328	2.325	0.009	2.322	2.335	6	
W–S	see CONKEV (2.471, 2.473)							
Re–S	see BESBOQ10 (2.488, 2.503)							
Pt–S	see CERDAE (2.321, 2.322)							
9.5.1.3 Dithiocarboxylates (μ_2-S_2CR, R = any C)								
S–C		1.678	1.678	0.016	1.667	1.686	38	
C–C		1.517	1.516	0.022	1.503	1.537	20	
Ni–S	all DTPANI10	2.214	2.210	0.010	2.208	2.225	4	*9*
Mo–S	(5), (II)	2.464	2.465	0.008	2.458	2.470	12	
Pd–S	(*), (II)	2.325	2.325	0.010	2.319	2.330	10	
Pt–S	(5,6), (II)	2.319	2.319	0.009	2.310	2.326	12	

Table 9.6.3.3. *Interatomic distances (Å) (cont.)*

Bond	Substructure (coordination number, oxidation state, comment)	*d*	*m*	σ	q_l	q_u	*n*	Note
9.5.2.1 *S*-Thiocarboxylates [terminal, η^1-SC(O)*R*] (see also 5.5.7.1)								
(None)								
9.5.2.2 Thiocarboxylates (η^2-SOC*R*) (see also 5.5.7.2)								
Ni–S	(6), (II)	2.453	2.452	0.016	2.444	2.456	9	
9.5.2.3 Thiocarboxylates (μ_2-SOC*R*) (see also 5.5.7.3)								
Ni–S	(4), (II)	2.178	2.176	0.010	2.172	2.181	8	
Cu–S	all BEFJIF10	2.274	2.271	0.010	2.268	2.284	4	
Rh–S	see TACDRH10 (2.256, 2.262)							
Ag–S	see CEFMIJ (2.513)							
9.6.1.1 Dithiocarbamates (terminal, η^1-S_2CNR_2, *R* = any C)								
(*M*)S–C		1.748	1.747	0.022	1.730	1.771	6	
C–S		1.674	1.676	0.013	1.661	1.684	6	
C–N		1.343	1.345	0.011	1.334	1.352	6	
N–C(*R*)		1.467	1.468	0.018	1.453	1.482	12	
Zn–S	see TMTCZN10 (2.299, 2.312)							
W–S	see CIXKAV (2.496)							
Pt–S	see IBTCPT (2.335)							*24*
Au–S	see AUDETC (2.333, 2.347)							
9.6.1.2 Dithiocarbamates (chelating, η^2-S_2CNR_2, *R* = any C)								
S–C		1.714	1.715	0.018	1.704	1.726	539	
C–N		1.324	1.322	0.021	1.313	1.334	269	
N–*R*		1.473	1.475	0.030	1.462	1.487	537	
V–S	all ETCOXV	2.402	2.405	0.010	2.391	2.409	4	
Cr–S	(6,7), (II,III)	2.416	2.407	0.026	2.396	2.441	24	
Mn–S	all MORTMN, MOTCMN	2.459	2.465	0.078	2.385	2.529	12	*130*
Fe–S	(5,6), (0,II,IV): mostly (III), all	2.354	2.336	0.060	2.307	2.422	112	*30*
	: <2.375 (mostly low spin)	2.319	2.313	0.026	2.299	2.340	78	
	: >2.390	2.436	2.434	0.020	2.428	2.449	34	
Co–S	(5,6), (III)	2.267	2.270	0.013	2.255	2.277	32	
Ni–S	(4,6), (II): excluding BDTCBR (2.261)	2.207	2.206	0.017	2.196	2.218	18	
Cu–S	**(4,5)**, (II,III)	2.250	2.222	0.044	2.214	2.286	14	*12, 152*
Zn–S	**(4,5)**, (II)	2.436	2.452	0.056	2.406	2.466	16	
Zr–S	**see** BOVYUG (2.635, 2.724)							
Nb–S	**all** CAHJIE	2.602	2.586	0.054	2.565	2.632	6	
Mo–S	(5-7), (II-IV): all	2.513	2.507	0.059	2.478	2.530	164	
	: excluding asymmetry >0.10	2.504	2.504	0.043	2.478	2.527	144	*44, 153*
Tc–S	(5,7), (II,III,V)	2.457	2.476	0.043	2.405	2.490	14	
Ru–S	(6,7), (II-IV)	2.379	2.392	0.039	2.345	2.400	20	
Rh–S	all MOTCRH	2.370	2.374	0.014	2.353	2.382	6	
Pd–S	(4), (II)	2.323	2.319	0.031	2.315	2.323	18	
Cd–S	all BEGNUW	2.711	2.717	0.037	2.679	2.740	6	
Ta–S	all STAETC	2.577	2.559	0.056	2.538	2.613	6	
W–S	(6,7), (II,V)	2.526	2.531	0.031	2.496	2.550	6	*24*
Re–S	(5-7), (III-V)	2.442	2.441	0.040	2.410	2.474	20	
Os–S	(6,7), (III,IV)	2.410	2.417	0.021	2.405	2.424	20	
Ir–S	all EDTCIR	2.367	2.365	0.003	2.365	2.370	4	
Pt–S	see BOFJIP (2.347, 2.299)							
Au–S	(4,5), (III)	2.349	2.336	0.033	2.330	2.381	12	
Hg–S	see HGETCB10 (2.399, 2.965)							
9.6.2.1 *S*-Thiocarbamates [terminal, η^1-SC(O)NR_2]								
(None)								
9.6.2.2 Thiocarbamates (chelating, η^2-SOCNR_2) (see also 5.5.6.2)								
Ti–S	see EMTCTJ (2.477, 2.477, 2.489)							
Co–S	see TMTCPC (2.584)							
Zr–S	see BUWMAH (2.641), EMTCZR (2.669, 2.689)							
U–S		2.869	2.870	0.005	2.865	2.874	5	
9.7.1.1 Xanthates (terminal, η^1-S_2CR)								*154*
C–S(Ni)	(1.720)							
C=S(free)	(1.651)							
C–O(Me)	(1.334)							
Ni–S	see BIMMOZ (2.195)							
9.7.1.2 Xanthates (chelating, η^2-S_2CO*R*)								*154*
S–C		1.676	1.677	0.018	1.664	1.688	32	
C–O		1.329	1.327	0.014	1.317	1.339	16	

Table 9.6.3.3. *Interatomic distances (Å) (cont.)*

Bond	Substructure (coordination number, oxidation state, comment)	*d*	*m*	σ	q_l	q_u	*n*	Note
9.7.1.2 Xanthates (chelating, η^2-S_2COR) *(cont.)*								
V–S	all BIRYOO10	2.503	2.482	0.059	2.471	2.492	12	
Co–S	see CADHOE (2.254, 2.290)							
Ni–S	(4,6), (0,II)	2.407	2.418	0.056	2.346	2.455	8	
Zn–S	see EXAPYZ (2.294, 2.747)							
Mo–S	(5), (III)	2.517	2.516	0.009	2.508	2.525	4	
Pd–S	see TXPCPD (2.328, 2.332)							
Cd–S	see EXPNCD (2.647, 2.743)							
9.7.1.3 Xanthates (μ_2-S_2COR)								
C–S		1.690	1.689	0.006	1.686	1.697	4	
C–O	(1.330, 1.317)							
Cd–S		2.567	2.570	0.026	2.541	2.589	4	
9.7.2.1 Dithiocarbonate [terminal, η^1-SC(O)S]								
(None)								
9.7.2.2 Dithiocarbonate (chelating, η^2-S_2CO)								
S–C		1.728	1.722	0.033	1.711	1.737	9	
C–O		1.242	1.249	0.029	1.215	1.266	5	
Co–S	see BELTIV10 (2.259, 2.250)							
Rh–S	all MPTCRH	2.374	2.374	0.010	2.365	2.382	4	
Pd–S	see BEMLUA (2.318)							
Pt–S	see TCTPPU (2.340, 2.325)							
9.7.2.3 Dithiocarbonates (μ_2-S_2CO)								
S–C		1.684	1.683	0.006	1.678	1.690	4	
C–O	(1.336, 1.333)							
Mo–S	all EDTCMO	2.478	2.478	0.002	2.475	2.480	4	
9.8.1.1 Trithiocarbonate (terminal, η^1-CS_3)								
(None)								
9.8.1.2 Trithiocarbonate (chelating, η^2-CS_3)								
Fe(S)–C	(1.719, 1.720)							
C–S	(1.666)							
Fe–S	see BULZIR (2.325, 2.335)							
9.8.1.3 Trithiocarbonate (μ-η^1, $\eta^{1\prime}$-CS_3)								
(None)								
9.8.2.1 Thioxanthates (η^1-S_2CSR)								
(None)								
9.8.2.2 Thioxanthates (chelating, η^2-S_2CSR)								
(*M*)S–C		1.692	1.692	0.012	1.684	1.700	40	
C–S*R*		1.718	1.719	0.013	1.712	1.724	20	
Cr–S	all ETXACR10	2.400	2.398	0.008	2.395	2.408	12	
Fe–S	see ESEXFE10 (2.344, 2.333)							
Co–S	(6), (III)	2.272	2.271	0.007	2.264	2.277	14	
Ni–S	see BZTCDN (2.207, 2.211)							
Cu–S	see TPTHCC (2.451, 2.439)							
Mo–S	see IPTXMO (2.438, 2.454)							
Pd–S	all TETCPD	2.338	2.334	0.008	2.333	2.348	6	
9.8.2.3 Thioxanthates (μ_2-S_2CSR)								
(*M*)S–C		1.684	1.681	0.010	1.677	1.694	4	
C–S*R*	(1.749, 1.743)							
Fe–S	(6), (III)	2.281	2.285	0.011	2.269	2.288	4	
9.9.1.1 *o*-Dithioquinones (chelating, η^2-$C_6R_4S_2$)†								*155*
$S–C^1$		1.751	1.750	0.018	1.738	1.765	42	
$C^1–C^{1\prime}$		1.398	1.399	0.020	1.387	1.414	23	
$C^1–C^2$		1.403	1.401	0.017	1.391	1.412	42	
$C^2–C^3$		1.378	1.378	0.026	1.360	1.394	42	
$C^3–C^{3\prime}$		1.378	1.382	0.023	1.358	1.398	23	
Ti–S	see BTCPTI (2.411, 2.418)							
Fe–S	(4,5), (-)	2.223	2.227	0.012	2.211	2.232	8	
Co–S	(4,5), (-)	2.131	2.115	0.028	2.111	2.167	6	

Table 9.6.3.3. *Interatomic distances (Å) (cont.)*

Bond	Substructure (coordination number, oxidation state, comment)	*d*	*m*	*σ*	q_l	q_u	*n*	Note
9.9.1.1	*o*-Dithioquinones (chelating, η^2-$C_6R_4S_2$)† (*cont.*)							
Zr–S	see BZDTZR10 (2.537, 2.538, 2.554)							
Nb–S	all BZDTNB10	2.441	2.439	0.011	2.432	2.452	6	
Mo–S	(6,7), (-)	2.357	2.360	0.018	2.342	2.371	5	
Cd–S	all CADPEC	2.508	2.506	0.017	2.493	2.526	4	
Ta–S	all PABZTA	2.428	2.424	0.036	2.396	2.463	4	
Au–S	all BAMHUS	2.311	2.312	0.009	2.302	2.319	4	
9.9.2.1	α,β-Dithiones/dithiolates {chelating, η^2-[S=C(*R*)]$_2$}†							*155*
S–C_α		1.725	1.725	0.019	1.711	1.738	106	
C_α–$C_{\alpha'}$		1.352	1.356	0.024	1.337	1.367	55	
Ti–S	see CPMNTI (2.439, 2.455)							
Fe–S	(5), (-)	2.171	2.166	0.027	2.150	2.178	16	
Co–S	all PAPMCO10	2.229	2.230	0.020	2.211	2.248	4	*8*
Ni–S	(4), (-)	2.148	2.142	0.019	2.134	2.163	34	*9*
Cu–S	(4), (-)	2.258	2.258	0.013	2.250	2.264	10	
Mo–S	(6), (-)	2.387	2.391	0.011	2.377	2.397	9	
Ru–S	see TPRUET21 (2.282, 2.320)							
Rh–S	(5), (-)	2.308	2.318	0.027	2.280	2.327	4	
W–S	see ASCETU (2.364, 2.368, 2.382)							
Re–S	all REPETD10	2.324	2.328	0.011	2.318	2.332	6	
Pt–S	(4), (-)	2.258	2.257	0.010	2.249	2.269	14	
Au–S	(4), (-)	2.301	2.305	0.012	2.289	2.311	4	
9.9.3.1	α,α-Alkenedithiolates (chelating, η^2-$S_2C{=}CR_2$)†							*155*
S–C		1.734	1.736	0.023	1.715	1.749	11	
C=C		1.358	1.365	0.018	1.352	1.367	6	
Fe–S	see DEDTFE10 (2.288, 2.301, 2.305)							
Ni–S	see ANIDED10 (2.193, 2.196)							
Cu–S	see KCUDED10 (2.189, 2.199)							
9.10.1.1	Tertiary phosphine sulfides (η^1-SPR_3)							
S–P		2.000	1.996	0.021	1.986	2.012	11	
P–C		1.805	1.806	0.017	1.799	1.817	33	
Mn–S	see BOFMOY (2.410)							
Ni–S	see BOPFOB (2.194)							
Cu–S	(3,4), (I,II)	2.280	2.302	0.044	2.236	2.313	5	
Mo–S	see OXCPSM10 (2.460)							
Pd–S	see COSWUC (2.334), EPPTPD (2.350)							
Au–S	see ZEGNOP (2.324)							
9.11.1.1	Dithiophosphinates (chelating, η^2-S_2PR_2)							
S–P		2.007	2.012	0.016	1.997	2.020	73	
P–C		1.828	1.832	0.025	1.809	1.848	73	
Ti–S	all ETPSTI	2.473	2.472	0.034	2.440	2.507	8	
Ni–S	all DMDTPN10	2.237	2.237	0.004	2.234	2.241	4	*9*
Zn–S	(4), (II)	2.422	2.446	0.052	2.369	2.452	4	
Mo–S	all BAVLAL11	2.535	2.538	0.033	2.504	2.565	4	
Ce–S	all BIYYOX	2.990	3.003	0.033	2.956	3.012	4	
Dy–S	all DCHPDY10	2.741	2.744	0.007	2.732	2.746	6	
Tm–S	all BIYYUD	2.870	2.851	0.084	2.794	2.948	8	
Lu–S	all DCHPLU10	2.692	2.695	0.007	2.684	2.697	6	
Th–S	(8), (IV)	2.908	2.911	0.017	2.900	2.921	12	
U–S	(7), (VI)	2.873	2.868	0.023	2.854	2.895	18	
9.11.1.2	Dithiophosphinates (μ_2-η^1, $\eta^{1'}$-S_2PR_2)							
S–P		2.015	2.019	0.009	2.005	2.023	6	
P–C		1.810	1.810	0.007	1.803	1.818	6	
Zn–S	see BEDBUH (2.306, 2.321)							
Mo–S	all BUXMIQ	2.530	2.530	0.005	2.525	2.534	4	
9.12.1	Disulfide (η^2-S_2)							*150, 156*
S–S		2.053	2.054	0.026	2.036	2.072	18	
V–S	see BONCIQ01 (2.393)							
Nb–S	(8), (V)	2.498	2.493	0.050	2.450	2.538	6	
Mo–S	(4,5,7), (IV-VI)	2.412	2.408	0.027	2.389	2.441	22	
Re–S	see CECGOG (2.410)							
Ir–S	see SPPEIR (2.389, 2.422)							
U–S	see BEFBIX (2.711)							

Table 9.6.3.3. *Interatomic distances (Å) (cont.)*

Bond	Substructure (coordination number, oxidation state, comment)	*d*	*m*	σ	q_l	q_u	*n*	Note
9.12.2	Polysulfur ligands (η^1-SS*Z*, *Z* = any atom)							*150, 156*
S–S		2.053	2.047	0.038	2.026	2.072	46	
Ti–S	(8), (IV)	2.432	2.434	0.017	2.416	2.448	4	
V–S	(6,8), (IV): all	2.348	2.316	0.086	2.277	2.453	6	
	(6), (IV): only μ-S_2	2.294	2.299	0.026	2.268	2.316	4	
Fe–S	(6), (II,III)	2.192	2.187	0.067	2.129	2.259	5	
Ni–S	(4,*), (-)	2.137	2.125	0.027	2.122	2.158	5	
Zn–S	see TPCUMZ (2.317)							
Mo–S	(5,7), (IV,VI)	2.415	2.397	0.060	2.372	2.472	10	
W–S	see CAFFEU (2.506), CPDYSW10 (2.419, 2.420)							
Re–S	all COJDOU	2.257	2.259	0.017	2.240	2.271	4	
Os–S	see PSTOSA (2.443)							
Pt–S	(4), (II)	2.316	2.336	0.053	2.260	2.351	4	
9.13.1.1	Dialkyl thioethers [terminal, SR_2, $R = C(sp^3)$]							*158*
S–C		1.817	1.817	0.019	1.807	1.827	570	
Cr–S	(6), (0)	2.397	2.418	0.043	2.348	2.428	8	
Mn–S	see PSMNPC10 (2.310)							
Fe–S	(5,6), (0,II): excluding CIJYOJ	2.301	2.304	0.028	2.278	2.328	8	
Co–S	(6), (II,III): all	2.316	2.263	0.106	2.243	2.456	40	*8, 30*
	(6), (II)	2.483	2.479	0.030	2.461	2.508	11	
	(6), (III)	2.253	2.250	0.019	2.240	2.269	29	
Ni–S	(4-6), (I,II): excluding PTOCNI10	2.376	2.397	0.092	2.369	2.433	30	
	(6), (II)	2.416	2.399	0.037	2.391	2.440	22	
Cu–S	(3-6), (I,II): all	2.364	2.343	0.082	2.318	2.385	89	*86*
	(3,4), (I)	2.313	2.301	0.047	2.271	2.348	18	
	(4-6), (II): excluding 3 > 2.65	2.364	2.347	0.053	2.323	2.390	68	
Zn–S	see TAZTDG (2.601)							
Nb–S	(6), (III-V)	2.700	2.716	0.046	2.649	2.738	6	
Mo–S	(5-7), (0,II-IV): all	2.541	2.536	0.064	2.484	2.569	22	
	: excluding 2 > 2.700	2.525	2.533	0.039	2.484	2.560	20	
Ru–S	see BIGLAE (2.262, 2.333)							
Rh–S	(5,6,*), (0-II): all	2.430	2.415	0.064	2.406	2.481	7	
Pd–S	(4,5), (II)	2.283	2.275	0.030	2.262	2.307	21	
Ag–S	(3-6,*), (I): all	2.669	2.624	0.164	2.558	2.803	18	
Cd–S	see TDACCD10 (2.669)							
La–S	see APXLAP (3.032, 3.045)							
Ta–S	(6), (III)	2.657	2.634	0.067	2.619	2.706	5	
W–S	see CPHMOC (2.560), ESCTHW20 (2.570)							*159*
Ir–S	(6), (III)	2.353	2.361	0.032	2.325	2.376	5	
Pt–S	(4), (II)	2.244	2.242	0.012	2.233	2.256	4	
	(6), (IV)	2.470	2.473	0.009	2.461	2.478	4	
Au–S	see CIBLUU (2.275)							
Hg–S	(4,5), (II)	2.624	2.618	0.054	2.577	2.672	6	*26*
9.13.1.2	Dialkyl thioethers [μ_2-SR_2, $R = C(sp^3)$]							
S–C		1.830	1.826	0.032	1.810	1.850	24	
Fe–S	see OCHTPI (2.141, 2.206)							
Cu–S	see DTHCUC (2.314, 2.336)							
Mo–S	(6), (II,III)	2.376	2.390	0.039	2.335	2.404	4	
Ag–S	(3,5,6), (I)	2.534	2.537	0.031	2.504	2.561	6	
Ta–S	(6), (III)	2.390	2.390	0.007	2.384	2.396	5	
Ir–S	see CETSIR (2.327, 2.343)							
9.13.2.1	Thioethers [terminal, SR_2, $R_2 \neq C(sp^3)_2$]							
S–C(sp^2)		1.778	1.778	0.020	1.758	1.788	55	
S–C(sp^3)		1.826	1.823	0.020	1.811	1.837	39	
Cr–S	(6), (0)	2.384	2.384	0.014	2.370	2.391	11	
Mn–S	see BATZIF (2.389), CECCIW (2.434)							
Fe–S	(6), (II)	2.249	2.250	0.054	2.196	2.300	4	
Co–S	see BEMNIQ (2.468, 2.502)							
Ni–S	see BOSNEC (2.431, 2.473), BTZDNI (2.162, 2.165), DAPSMO (2.534)							
Cu–S	(4-6), (I,II)	2.418	2.438	0.069	2.347	2.470	4	
Mo–S	see FMBTMO (2.552)							
Rh–S	see CETMRH (2.312), HMTNRH (2.273)							
Pd–S	(4), (II)	2.295	2.292	0.008	2.290	2.302	5	
Cd–S	see CEZWEJ (2.738)							
Ta–S	see CIFMAF (2.706, 2.836)							
W–S	see MCTCEW (2.441), MEPOSW (2.555)							
Pt–S	(4), (II)	2.265	2.262	0.024	2.245	2.289	4	
Hg–S	see BAVKIS (3.124, 3.131)							

Table 9.6.3.3. *Interatomic distances (Å) (cont.)*

Bond	Substructure (coordination number, oxidation state, comment)	*d*	*m*	σ	q_l	q_u	*n*	Note
9.14.1.1	*S*-SO_2 (terminal, η^1) (see also 5.20.1)							*104, 160*
S–O		1.421	1.428	0.041	1.389	1.454	16	
Fe–S	see BOGPIW (2.109)							
Ni–S	see SXPMNI01 (2.012)							*9*
Rh–S	see CPSXER (2.096), CSTPRH (2.450)							
Pt–S	(3,4), (0)	2.380	2.379	0.068	2.316	2.446	4	
9.14.1.2	*S*-SO_2 (μ_2)							*160*
S–O		1.458	1.457	0.021	1.438	1.476	19	
Fe–S	(6), (I)	2.253	2.258	0.032	2.222	2.280	4	
Rh–S	see CACFUH (2.249, 2.235), SOCPRH (2.252)							
Pt–S	(*), (0)	2.274	2.275	0.056	2.251	2.292	12	
9.14.2	*S*-SO_3 (η^1)							*104*
S–O		1.477	1.479	0.012	1.471	1.485	33	
Co–S	(6), (III)	2.230	2.227	0.024	2.206	2.252	9	*8*
Au–S	see ENSPAU (2.301, 2.308)							
9.14.3	*S*-SO_3R (η^1)							
S–O	(1.445, 1.448)							
S–O(*R*)	(1.619)							
Pt–S	see MSTPPT (2.305)							
9.15.1.1	η^1-*RSSR*							
S–S		2.050	2.040	0.025	2.032	2.079	7	
Co–S	see BINHUB (2.262), DSENCO (2.272)							
Ni–S	see BPESNI (2.455), PMISNI (2.470)							
Cu–S	see PYDSCU10 (2.396, 2.438)							
Ag–S	see CONSON (2.533)							
9.15.1.2	μ-η^1, $\eta^{1\prime}$-*RSSR*							
S–S	(2.063, 2.065)							
Cu–S	see BIGLUY (2.332, 2.338)							
Ag–S	see CONSON (2.503, 2.638)							
9.16.1	*S*-Dialkyl sulfoxides [terminal, η^1-S(O)R_2] (see 5.17.1.1)							*127*
S–O		1.469	1.468	0.013	1.459	1.476	43	
S–C	most *R* = primary alkyl	1.785	1.781	0.023	1.774	1.797	88	
Cr–S	see PCTXCR (2.331)							
Fe–S	see SPCNFE (2.307)							
Ru–S	(6), (II)	2.288	2.263	0.051	2.257	2.339	8	
Rh–S	(6), (II,III): all	2.315	2.290	0.067	2.284	2.329	7	
	(6), (III)	2.293	2.288	0.032	2.273	2.326	6	*85*
Pd–S	see PDDMSX10 (2.299)							
Pt–S	(4), (II)	2.223	2.219	0.033	2.199	2.232	26	
9.17.1	CS_2 (terminal, η^2) (see also 3.22.2)							
V–S	see CPCDSV (2.432, 2.444)							
Fe–S	see SPHFEC10 (2.333)							
Co–S	see TPHCOA (2.206)							
Ni–S	see COGWOK (2.195)							
Nb–S	see CPSNBA (2.503)							
10.1.1.1	Chlorine (terminal)							
Ti–Cl	(-), (-): all	2.305	2.311	0.058	2.262	2.352	98	
	(6), (not III)	2.281	2.294	0.048	2.247	2.316	60	
	(7), (-)	2.313	2.320	0.046	2.269	2.361	8	
	(8), (not III)	2.362	2.363	0.018	2.352	2.369	24	
V–Cl	(-), (-): all	2.294	2.297	0.074	2.223	2.333	31	
	(5), (-)	2.224	2.218	0.041	2.187	2.265	9	
	(6), (not II)	2.297	2.318	0.047	2.261	2.319	17	*30*
Cr–Cl	(6), (-): all	2.335	2.318	0.055	2.303	2.370	9	
	(6), (-)	2.309	2.316	0.018	2.299	2.319	7	*147*
Mn–Cl	(-), (-): all	2.445	2.465	0.087	2.361	2.518	33	
	(5), (-): excluding MEIMMN	2.346	2.351	0.014	2.337	2.358	7	
	(6), (II)	2.516	2.495	0.048	2.478	2.560	15	
Fe–Cl	(-), (-): all	2.262	2.246	0.070	2.205	2.311	119	
	(4), (II)	2.301	2.303	0.028	2.275	2.327	15	
	(4), (III)	2.195	2.192	0.016	2.184	2.207	39	

Table 9.6.3.3. *Interatomic distances (Å) (cont.)*

Bond	Substructure (coordination number, oxidation state, comment)	*d*	*m*	σ	q_l	q_u	*n*	Note
10.1.1.1	Chlorine (terminal) (*cont.*)							
Fe–Cl	(5), (III)	2.235	2.224	0.028	2.214	2.252	10	
	(6), (II)	2.384	2.363	0.053	2.342	2.435	9	
	(6), (III)	2.308	2.310	0.036	2.292	2.330	22	
Co–Cl	(-), (-): all	2.272	2.259	0.048	2.244	2.281	191	*86*
	(4), (-)	2.254	2.256	0.026	2.232	2.271	96	
	(6), (II)	2.414	2.417	0.057	2.348	2.468	11	
	(6), (III): excluding 3 > 2.36	2.260	2.256	0.019	2.248	2.274	70	
Ni–Cl	(-), (-): all	2.339	2.314	0.117	2.243	2.426	63	
	(4), (II)	2.217	2.206	0.044	2.183	2.252	18	
	(5), (II)	2.308	2.306	0.019	2.302	2.314	11	
	(6), (II)	2.441	2.428	0.053	2.406	2.467	26	
Cu–Cl	(-), (-): all	2.276	2.254	0.092	2.232	2.292	362	*12*
	(2), (I)	2.090	2.090	0.010	2.080	2.099	6	
	(3), (I)	2.179	2.156	0.044	2.140	2.220	15	
	(4), (I)	2.361	2.351	0.065	2.321	2.406	11	
	(4), (II)	2.248	2.246	0.032	2.233	2.263	153	
	(5), (II): all	2.323	2.276	0.123	2.240	2.362	145	*86*
	: short (<2.4)	2.269	2.260	0.048	2.233	2.296	116	
	: long (>2.4)	2.537	2.515	0.091	2.467	2.618	29	
	(6), (II): all	2.354	2.284	0.188	2.256	2.327	17	
	: short (<2.4)	2.274	2.280	0.035	2.242	2.298	14	
Zn–Cl	(-), (-): all	2.255	2.256	0.035	2.231	2.276	183	
	(4), (-)	2.253	2.256	0.033	2.229	2.276	173	
	(5), (-)	2.257	2.255	0.033	2.232	2.286	8	
Zr–Cl	(-), (-): all	2.470	2.449	0.061	2.429	2.522	31	
	(6), (-)	2.426	2.425	0.027	2.410	2.453	8	
	(8), (-)	2.464	2.447	0.037	2.440	2.492	13	
	(9), (-)	2.561	2.559	0.008	2.555	2.570	6	
Nb–Cl	(-), (-): all	2.395	2.401	0.053	2.351	2.429	94	
	(6), (-)	2.374	2.382	0.041	2.339	2.405	65	
	(7), (-)	2.415	2.416	0.069	2.348	2.481	5	
	(8), (-)	2.457	2.463	0.036	2.429	2.483	19	
Mo–Cl	(-), (-): all	2.410	2.404	0.072	2.368	2.445	193	
	(5), (-)	2.409	2.414	0.043	2.394	2.444	28	
	(6), (-)	2.389	2.388	0.053	2.356	2.419	112	*44, 85*
	(7), (-)	2.481	2.474	0.049	2.440	2.524	14	
Tc–Cl	(5,6), (-): all	2.359	2.328	0.077	2.318	2.359	29	*86*
	(-), (not III): *trans* to PR_3	2.323	2.325	0.018	2.317	2.333	23	*44, 85*
Ru–Cl	(-), (-): all	2.416	2.416	0.049	2.386	2.441	115	
	(6), (-)	2.409	2.415	0.040	2.385	2.434	102	*44, 161*
	(5), (-)	2.434	2.455	0.051	2.371	2.483	7	
Rh–Cl	(-), (-): all	2.377	2.364	0.052	2.342	2.391	139	*86*
	(4), (-)	2.369	2.370	0.026	2.353	2.387	40	
	(5), (-)	2.400	2.388	0.053	2.363	2.437	23	
	(6), (-)	2.374	2.354	0.060	2.335	2.393	76	*86*
Pd–Cl	(-), (-): all	2.331	2.312	0.067	2.298	2.356	248	
	(4), (-)	2.326	2.312	0.043	2.298	2.354	224	
	(5), (-): excluding 2 > 2.8	2.345	2.320	0.045	2.316	2.376	13	
Ag–Cl	see AGSURE10 (2.854), CMURAG (2.650), PMBPAG10 (2.502)							
Cd–Cl	(-), (-): all	2.499	2.471	0.085	2.443	2.550	45	*145*
	(4), (-)	2.448	2.451	0.023	2.436	2.458	18	
	(6), (-): all	2.556	2.550	0.085	2.495	2.591	22	
	(6), (-): excluding 2 > 2.7	2.536	2.546	0.055	2.494	2.581	20	
La–Cl	see CERKUF (2.751)							
Ce–Cl	see CLCAME01 (2.594, 2.605, 2.619)							
Pr–Cl	see TPYRPR (2.877)							
Nd–Cl	see BIDNEH (2.871), BOKPEW (2.666, 2.670)							
Er–Cl	see BOBWAQ (2.613, 2.620)							
Yb–Cl	see BAWLAM (2.593), BAWLEQ (2.594, 2.596)							
Hf–Cl	see BIHWUK (2.365), CTMSIC (2.436)							
Ta–Cl	(-), (-): all	2.399	2.388	0.068	2.355	2.440	119	
	(6), (-)	2.383	2.375	0.055	2.349	2.418	83	
	(7), (-)	2.428	2.404	0.067	2.380	2.445	15	
	(7), (-): excluding 2 > 2.5	2.406	2.398	0.034	2.378	2.439	13	*30*
	(8), (-):	2.463	2.497	0.088	2.383	2.541	17	
	(8), (-): excluding 4 < 2.4 from COWSOW	2.505	2.510	0.046	2.462	2.544	13	
W–Cl	(-), (-): all	2.408	2.395	0.059	2.370	2.433	124	
	(5), (-)	2.390	2.393	0.030	2.374	2.409	19	
	(6), (-)	2.392	2.388	0.045	2.364	2.422	80	
	(7), (-)	2.472	2.453	0.056	2.428	2.529	12	
Re–Cl	(-), (-): all	2.389	2.380	0.062	2.355	2.411	116	*86*
	(5), (-)	2.368	2.378	0.026	2.355	2.387	14	
	(6), (-): excluding 3 long >2.49	2.380	2.378	0.042	2.355	2.409	90	*85, 162*
Os–Cl	(5,6), (-): all	2.368	2.361	0.077	2.307	2.411	54	
	(6), (-)	2.357	2.357	0.053	2.307	2.389	50	*44, 85*

Table 9.6.3.3. *Interatomic distances (Å) (cont.)*

Bond	Substructure (coordination number, oxidation state, comment)	*d*	*m*	σ	q_l	q_u	*n*	Note
10.1.1.1	Chlorine (terminal) (*cont.*)							
Ir–Cl	(-), (-): all	2.390	2.370	0.051	2.355	2.429	83	
	(4), (-)	2.389	2.381	0.055	2.355	2.418	11	
	(5), (-)	2.380	2.368	0.038	2.356	2.416	7	
	(6), (-): all	2.391	2.370	0.052	2.353	2.439	65	*30*
	: short (<2.4)	2.361	2.359	0.020	2.349	2.372	46	
	: long (>2.4)	2.463	2.465	0.028	2.440	2.470	19	
Pt–Cl	(-), (-): all	2.324	2.310	0.038	2.297	2.348	354	*41, 86*
	(4), (-)	2.323	2.308	0.038	2.297	2.349	293	*86*
	(5), (-)	2.330	2.321	0.048	2.303	2.346	15	
	(6), (-)	2.326	2.316	0.036	2.306	2.327	42	
Au–Cl	(-), (-): all	2.301	2.276	0.094	2.271	2.287	54	*86, 144*
	(4), (not I, II)	2.276	2.276	0.010	2.270	2.284	36	
Hg–Cl	(-), (-): all	2.423	2.391	0.120	2.328	2.480	101	*86, 26*
	(2), (-)	2.330	2.332	0.018	2.317	2.350	11	
	(3), (-)	2.292	2.289	0.016	2.281	2.305	5	
	(4), (-): all	2.447	2.440	0.121	2.349	2.521	68	
	: excluding 3 > 2.76	2.430	2.437	0.091	2.348	2.480	65	
Th–Cl	(7,8), (-): all	2.728	2.752	0.039	2.690	2.756	8	
U–Cl	(-), (-): all	2.646	2.653	0.046	2.625	2.671	61	
	(6), (-): all	2.644	2.656	0.045	2.625	2.621	40	
	: excluding 2 < 2.254	2.653	2.656	0.023	2.630	2.671	38	
	(8), (-)	2.642	2.651	0.028	2.614	2.659	14	
10.1.1.2	Chlorine (μ_2-Cl)							*134*
Ti–Cl	(6-8), (III,IV): all	2.520	2.536	0.039	2.486	2.545	24	
	(6,7), (IV)	2.459	2.465	0.017	2.438	2.473	6	
	(7,8), (III)	2.541	2.540	0.014	2.532	2.548	18	
V–Cl	(6), (II): all CANZUM	2.476	2.474	0.006	2.472	2.482	6	
Cr–Cl	see CATSEV (2.372, 2.377)							
Mn–Cl	(5-6), (I,II): all	2.539	2.555	0.066	2.512	2.575	18	
	(6), (II)	2.559	2.559	0.046	2.532	2.583	14	
Fe–Cl	(5,*), (-)	2.306	2.289	0.027	2.288	2.341	6	
Co–Cl	(6), (II)	2.397	2.403	0.026	2.370	2.417	4	
Ni–Cl	(4-6), (II): all	2.372	2.404	0.093	2.242	2.426	36	*9*
	(5,6), (II)	2.426	2.410	0.051	2.384	2.459	20	*86*
	(5,6), (II)	2.402	2.402	0.025	2.382	2.422	14	*151*
	(4), (II)	2.238	2.236	0.005	2.235	2.239	10	
Cu–Cl	(3-6,*), (I,II): all	2.337	2.313	0.098	2.280	2.359	66	*12*
	(3), (I)	2.275	2.276	0.021	2.263	2.280	12	
	(4), (I)	2.364	2.360	0.065	2.307	2.411	10	
	(4), (II)	2.343	2.347	0.039	2.303	2.383	8	
	(5), (II): all	2.367	2.315	0.137	2.296	2.519	26	*30*
	: short (<2.34)	2.284	2.306	0.058	2.276	2.315	18	
	: long (>2.50)	2.554	2.554	0.041	2.519	2.574	8	
Zn–Cl	(4), (II)	2.364	2.359	0.019	2.351	2.372	6	
Y–Cl	(8,9), (III)	2.710	2.699	0.042	2.678	2.754	4	
Zr–Cl	(6,8), (III,IV)	2.588	2.576	0.053	2.541	2.638	6	
Nb–Cl	(6-8), (II-IV)	2.531	2.512	0.048	2.503	2.567	26	
Mo–Cl	(6,7), (II-V)	2.486	2.486	0.040	2.473	2.509	40	*85*
Tc–Cl	see OXPTCC (2.679)							
Ru–Cl	(6,*), (II-IV)	2.428	2.427	0.056	2.377	2.486	12	*85*
Rh–Cl	(4-6,*), (I-III): all	2.444	2.417	0.064	2.393	2.478	34	
	(4), (-)	2.408	2.406	0.025	2.391	2.414	18	
	(5), (I)	2.578	2.584	0.030	2.546	2.603	4	
	(6), (-)	2.470	2.476	0.042	2.457	2.500	16	
Pd–Cl	(4,5), (II): all	2.419	2.416	0.065	2.382	2.463	50	
	(4), (II): all	2.404	2.407	0.058	2.342	2.438	42	
	: Pd–Cl–Pd > 85°	2.432	2.425	0.063	2.389	2.472	14	
	: Pd–Cl–Pd <85°	2.390	2.401	0.051	2.332	2.429	28	
Ag–Cl	see BEBGEU (2.618, 2.639)							
Cd–Cl	(6,*), (-)	2.629	2.628	0.043	2.602	2.653	52	
Pr–Cl	see BAMZUK (2.805, 2.821)							
Yb–Cl	see MCPYBC (2.627, 2.647)							
Ta–Cl	(6,8), (-): all	2.513	2.510	0.049	2.477	2.553	26	
	: Ta–Cl–Ta < 70°	2.501	2.500	0.040	2.475	2.543	22	
	: Ta–Cl–Ta > 90°	2.584	2.573	0.037	2.556	2.624	4	
W–Cl	(6), (II,III,V): all	2.514	2.549	0.097	2.393	2.598	6	
Re–Cl	(6,*), (I,III,IV): all	2.456	2.426	0.060	2.399	2.515	35	*30, 85*
	(*), (-)	2.409	2.415	0.016	2.393	2.422	12	
	(6), (-): all	2.481	2.509	0.059	2.439	2.517	23	
	: Re–Cl–Re > 83°	2.514	2.515	0.012	2.502	2.525	17	
	: Re–Cl–Re < 70°	2.385	2.391	0.026	2.359	2.405	6	
Os–Cl	(6), (-): all	2.430	2.431	0.023	2.410	2.450	4	
Ir–Cl	(6), (III): all	2.442	2.428	0.060	2.392	2.455	12	
Pt–Cl	(4,6), (-): all	2.455	2.496	0.073	2.401	2.506	12	

Table 9.6.3.3. *Interatomic distances (Å) (cont.)*

Bond	Substructure (coordination number, oxidation state, comment)	*d*	*m*	σ	q_l	q_u	*n*	Note
10.1.1.2	Chlorine (μ_2-Cl) (*cont.*)							
Pt–Cl	(4), (-)	2.363	2.359	0.050	2.320	2.410	4	
	(6), (-)	2.501	2.501	0.010	2.495	2.506	8	
Hg–C	(4-6), (II): all	2.757	2.728	0.122	2.686	2.780	20	
	: excluding TAMHGC	2.723	2.719	0.062	2.681	2.762	18	
U–Cl	(8), (-): all PMCPUC10	2.900	2.905	0.014	2.882	2.912	6	
10.1.1.3	Chlorine (μ_3-Cl)							
Ti–Cl	see COTTIC10 (2.557, 2.609)							
Co–Cl	see EFASCO01 (2.479)							
Cu–Cl	(4 *), (I,II): all asymmetric	2.476	2.464	0.139	2.369	2.527	24	*12*
Nb–Cl	see BUVCAW10 (2.524, 2.945, 2.817)							
Mo–Cl	see CIKHOT (2.484, 2.490, 2.513)							
Pd–Cl	see CEHMOR (2.520, 2.520, 2.525)							
Ag–Cl	(4), (I)	2.653	2.642	0.073	2.600	2.724	12	
Cd–Cl	(6), (II)	2.740	2.738	0.057	2.700	2.783	9	
W–Cl	see TMPHWE (2.462, 2.465, 2.476)							
Hg–Cl	see CEGNAD (2.519, 2.937, 3.115), METHGD (2.715, 2.922, 3.065)							
11.1.1	Arsines (AsR_3, R = any C)							*137*
As–C		1.943	1.943	0.021	1.931	1.955	405	
Ti–As	see CIRHUG (2.692, 2.690), PASETI (2.677)							
Cr–As	(6), (0)	2.460	2.467	0.040	2.417	2.494	4	*38*
Mn–As	(6), (0,I)	2.400	2.405	0.013	2.387	2.410	6	
Fe–As	(5,6,*), (0,II)	2.352	2.339	0.043	2.328	2.362	8	
Co–As	(5,6,*), (-)	2.323	2.326	0.021	2.307	2.337	16	*8*
Ni–As	(4-6), (-): excluding CMASNI	2.333	2.340	0.035	2.309	2.356	11	*9*
Cu–As	(4,*), (I)	2.367	2.369	0.016	2.362	2.380	8	
Nb–As	(8), (IV,V)	2.741	2.739	0.008	2.735	2.750	5	
Mo–As	(6,7), (II)	2.582	2.583	0.036	2.546	2.618	8	
Tc–As	all DASTCA10	2.512	2.511	0.005	2.508	2.517	4	
Ru–As	(5,6,*), (-)	2.446	2.450	0.031	2.415	2.475	12	
Rh–As	(4-6), (I,III): all	2.416	2.400	0.039	2.394	2.427	12	
	(4-6), (I)	2.400	2.399	0.015	2.392	2.409	10	
Pd–As	(4,6), (II,IV)	2.386	2.387	0.052	2.339	2.441	12	
	(4), (II)	2.372	2.376	0.046	2.334	2.401	10	
Re–As	all PASMRE	2.575	2.573	0.006	2.570	2.582	4	
Pt–As	(3-5), (0,II)	2.366	2.387	0.058	2.318	2.402	11	
11.2	Arsenic ligands (all types except AsR_3)							
V–As	see BAJZER (2.536)							
Cr–As	(6), (-): μ_3-As, μ-AsR_2, μ-AsR, η^1-As_2R_2, η^1-As_2R_4	2.431	2.417	0.050	2.386	2.480	23	*38*
Mn–As	(6), (-): μ_3-As, μ-AsR_2, *etc.*	2.375	2.319	0.126	2.247	2.508	11	*30*
	: short (<2.32)	2.269	2.250	0.039	2.240	2.319	6	
	: long (>2.46) (μ-AsR_2)	2.502	2.508	0.029	2.476	2.525	5	
Fe–As	(4-6,*), (-): η^1-As_4O_5, μ_3-AsR, μ_2-AsR_2 *etc.*	2.349	2.326	0.057	2.315	2.377	38	
	: μ_2-AsR_2, μ_3-AsR only	2.341	2.327	0.041	2.315	2.376	31	
Co–As	(4-6,*), (-): μ-AsR_2, $(OAsR_2)_2$, As_2 *etc.*	2.316	2.308	0.050	2.270	2.368	24	
Ni–As	see CADYAH (2.262), IATCNI (2.736)							
Mo–As	(6,7,*), (-): μ-AsR_2, μ_3-As, μ-As_2, μ-As_5	2.582	2.563	0.092	2.546	2.664	30	
Ru–As	(*), (-): μ-AsR_2	2.420	2.418	0.029	2.394	2.447	6	
Rh–As	see COSTEJ (2.470, 2.490)							
Pd–As	see COWGEA (2.447, 2.478)							
W–As	see BEBREF (2.549, 2.558), BIGHAA (2.351)							
Os–As	see BAHHOH (2.481, 2.483)							
12.1	Selenium ligands (all types)							*158, 163*
Cr–Se	see BAMCOH (2.562), BELFUT (2.453)							
Mn–Se	see BUJBIR (2.356, 2.358, 2.486, 2.481)							
Fe–Se	(-), (-): μ- and μ_3-Se; μ-SeR	2.393	2.399	0.038	2.359	2.424	13	
Ni–Se	(4,6), (II,IV): chelating SeR *etc*; excluding TMRNSN (2.678)	2.351	2.357	0.040	2.319	2.387	12	
Cu–Se	see APROCU (3.109)							
Zr–Se	see COMYUY (2.639, 2.670)							
Mo–Se	see TFMESM (2.491)							
Rh–Se	all CEGCOG	2.457	2.457	0.002	2.455	2.460	4	
Ag–Se	see CONSUT (2.581, 2.616, 2.711)							
W–Se	see COLFEO (2.635, 2.637) SNSCRB (2.735)							
Re–Se	see BIZZAL (2.572, 2.585)							
Os–Se	see SECPOS (2.541, 2.553)							
Ir–Se	see BOHDUX (2.529, 2.539)							
Pt–Se	see BESSAT (2.443, 2.461), BIHSAM (2.400, 2.376), BSEMEP (2.598, 2.590)							
Hg–Se	see BEGPUY (2.624, 2.615), CICLOP (2.637), DPSEHG01 (2.653, 2.918), MSEUHG (2.477)							

Table 9.6.3.3. *Interatomic distances (Å) (cont.)*

Bond	Substructure (coordination number, oxidation state, comment)	*d*	*m*	σ	q_l	q_u	*n*	Note
13.1.1.1 Bromine (terminal)								
Cr–Br	see TBCBFE (2.577)							
Mn–Br	(-), (-): all	2.588	2.548	0.094	2.534	2.685	8	
	(6), (not II)	2.541	2.539	0.010	2.534	2.551	4	
Fe–Br	see BAVHEL (2.494), BPEPFE (2.368), BTPPFE (2.348)							
Co–Br	(-), (-): all	2.416	2.390	0.086	2.383	2.401	14	
	(4), (-)	2.384	2.388	0.017	2.381	2.390	7	
	(6), (not II)	2.389	2.394	0.015	2.374	2.399	5	
Ni–Br	(-), (-): all	2.410	2.372	0.098	2.339	2.458	47	
	(4), (not I)	2.341	2.343	0.029	2.309	2.368	23	
	(5), (-): all	2.428	2.391	0.101	2.353	2.458	12	
	: short (<2.5)	2.389	2.380	0.044	2.348	2.427	10	
	(6)	2.554	2.548	0.028	2.536	2.572	9	
Cu–Br	(-), (-): all	2.412	2.400	0.109	2.357	2.428	60	*12*
	(3), (I)	2.298	2.284	0.028	2.280	2.325	6	
	(4), (-)	2.393	2.387	0.042	2.356	2.425	22	
	(5), (-): all	2.465	2.419	0.121	2.392	2.480	29	
	: short (<2.46)	2.407	2.401	0.023	2.390	2.423	22	
	: long (>2.50)	2.648	2.598	0.124	2.547	2.732	7	
Zn–Br	(-), (-): all	2.390	2.395	0.029	2.360	2.417	17	
	(4), (-)	2.386	2.393	0.028	2.357	2.399	15	
Mo–Br	(-), (-): all	2.616	2.595	0.071	2.568	2.654	32	
	(6), (-)	2.603	2.587	0.042	2.574	2.625	13	*85*
	(7), (-)	2.651	2.655	0.049	2.625	2.676	9	
Tc–Br	see CAKGIE (2.440)							
Ru–Br	(6), (II): all	2.521	2.538	0.035	2.477	2.547	6	
Rh–Br	(-), (-): all	2.530	2.526	0.039	2.500	2.564	13	
	(6), (-)	2.536	2.529	0.033	2.521	2.562	10	
Pd–Br	(4), (-): all	2.458	2.434	0.061	2.412	2.538	11	
	(4), (not I): all	2.450	2.433	0.057	2.410	2.469	10	
	: excluding 2 > 2.53	2.424	2.430	0.018	2.406	2.439	8	
Ag–Br	see BTCMAN (2.450)							
Cd–Br	(-), (-): all	2.611	2.582	0.064	2.569	2.659	6	
	(4), (-)	2.588	2.576	0.032	2.567	2.622	4	
Ta–Br	see BOBXOF (2.604)							
W–Br	(6,7), (-): all	2.619	2.611	0.042	2.590	2.644	8	
Re–Br	(5-7), (-): all	2.573	2.603	0.065	2.493	2.627	15	
	(6,7), (-)	2.606	2.613	0.039	2.563	2.629	11	
Os–Br	see BRFOSA10 (2.627), CIRJAO (2.558), COVVUE (2.545)							
Ir–Br	(5,6), (-): all	2.580	2.593	0.054	2.518	2.633	8	
Pt–Br	(-), (-): all	2.460	2.437	0.054	2.421	2.503	22	
	(4), (II): all	2.438	2.426	0.040	2.417	2.446	14	
	: excluding 2 > 2.5	2.424	2.423	0.018	2.414	2.434	12	
Au–Br	(-), (-): all	2.413	2.407	0.028	2.387	2.435	9	
	(3,4), (-)	2.417	2.411	0.028	2.390	2.438	8	
Hg–Br	(-), (-): all	2.539	2.519	0.089	2.499	2.549	14	
	(4), (-): all	2.555	2.529	0.089	2.508	2.560	11	
	: excluding 2 > 2.70	2.517	2.509	0.028	2.493	2.540	9	
U–Br	(6), (-): all	2.797	2.800	0.030	2.770	2.828	13	
13.1.1.2 Bromine (μ_2-Br)								*134*
Ti–Br	see BMCPTI (2.705, 2.722)							
Cr–Br	see BIWBEO (2.575, 2.607)							
Mn–Br	see TMAMNB01 (2.698, 2.711)							
Fe–Br	see BVINBF (2.443, 2.463)							
Ni–Br	(5), (II)	2.494	2.483	0.047	2.460	2.519	6	*9*
Cu–Br	(-), (-): all	2.494	2.471	0.061	2.451	2.548	20	*12*
	(3,4), (I)	2.483	2.469	0.057	2.451	2.487	12	
Mo–Br	(6), (-)	2.667	2.641	0.047	2.636	2.724	6	
Tc–Br	see CAWBAD (2.843)							
Ru–Br	(-), (-)	2.572	2.576	0.031	2.537	2.599	6	*85*
Rh–Br	(6), (III)	2.594	2.582	0.029	2.573	2.630	6	
Cd–Br	(-), (-)	2.776	2.753	0.055	2.730	2.843	6	
Re–Br	(-), (-)	2.651	2.659	0.027	2.635	2.670	20	
Ir–Br	(6), (III): all PMCBRI	2.570	2.570	0.006	2.565	2.576	4	
Pt–Br	(6), (IV): all BSEMEP	2.629	2.630	0.007	2.622	2.635	4	
Hg–Br	(4), (II): all $[Hg_2Br_6]^{2-}$	2.762	2.754	0.047	2.720	2.810	4	
13.1.1.3 Bromine (μ_3-Br)								
Cu–Br	(4,*), (I): all	2.543	2.544	0.066	2.491	2.599	13	*12*
Cd–Br	see CAHGOH (2.925, 2.971, 3.005)							
14.1 Tellurium (all ligand types)								*158, 163, 164*
Cr–Te	see COSSAE (2.801, 2.813)							
Mn–Te	(-), (-): μ_2- and μ_3-Te	2.486	2.474	0.027	2.464	2.515	5	
Fe–Te	(-), (-): μ-Te*R*, μ_3-Te	2.560	2.551	0.056	2.538	2.576	13	

Table 9.6.3.3. *Interatomic distances (Å) (cont.)*

Bond	Substructure (coordination number, oxidation state, comment)	*d*	*m*	σ	q_l	q_u	*n*	Note
14.1	Tellurium (all ligand types) (*cont.*)							
Mo–Te	see HTEMOA (2.791)							
Pt–Te	see CEXNAU (2.575)							
Hg–Te	(-), (-): Ph_2Te, PhTe	2.732	2.717	0.055	2.687	2.786	5	
15.1.1.1	Iodine (terminal)							
V–I	see BIVGAO (2.653)							
Cr–I	see CPAINC (2.669), CPCBCR (2.781)							
Mn–I	see ICPNMN (2.645)							
Fe–I	(-), (-): all	2.593	2.599	0.050	2.548	2.632	10	
	(6), (II)	2.623	2.624	0.027	2.599	2.645	5	
Co–I	(-), (-): all	2.640	2.611	0.094	2.563	2.743	8	
	: not (6), (II)	2.593	2.575	0.042	2.559	2.644	6	
Ni–I	(-), (-): all	2.673	2.626	0.150	2.545	2.804	22	
	(4), (-)	2.514	2.516	0.026	2.489	2.538	5	
	(5), (II): all	2.706	2.658	0.151	2.605	2.834	11	*30*
	: short <2.67	2.608	2.609	0.047	2.550	2.658	7	
	: long >2.83	2.877	2.848	0.099	2.804	2.980	4	
	(6), (II)	2.810	2.821	0.087	2.724	2.885	4	
Cu–I	(-), (-): all	2.594	2.563	0.077	2.528	2.664	12	
	(3), (I): not CENFAC01	2.534	2.531	0.026	2.511	2.561	6	*12*
	(5), (II)	2.682	2.674	0.043	2.647	2.725	4	
Zn–I	(-), (-): all	2.574	2.561	0.036	2.549	2.599	12	
	(4), (-)	2.564	2.556	0.024	2.547	2.578	10	
Zr–I	see COPVIM (2.897), COPVOS (2.869)							
Mo–I	(-), (-): all	2.867	2.848	0.135	2.777	2.878	35	*30*
	(6), (-)	2.797	2.773	0.065	2.758	2.866	12	*85*
	(7), (-)	2.855	2.858	0.027	2.823	2.873	11	
	(8), (-)	2.841	2.848	0.039	2.809	2.870	5	
Ru–I	(6,7), (II,IV): all	2.744	2.743	0.028	2.719	2.770	6	
	(6), (II)	2.742	2.732	0.031	2.716	2.774	5	
Rh–I	(-), (-): all	2.715	2.701	0.071	2.663	2.766	12	
Pd–I	(-), (-): all	2.624	2.602	0.040	2.593	2.658	15	
	(4), (not I)	2.612	2.601	0.027	2.593	2.641	13	
Ag–I	see BEVMAQ (2.828)							
Cd–I	(-), (-): all	2.750	2.714	0.082	2.705	2.794	12	*30*
	(4), (-)	2.704	2.708	0.014	2.691	2.714	8	
Yb–I	see BAWKUF (3.027)							
W–I	(6,7), (-): all	2.840	2.869	0.063	2.802	2.878	7	
	(7), (II)	2.864	2.876	0.036	2.836	2.888	5	
Re–I	(4-6), (-): all	2.718	2.764	0.079	2.625	2.786	13	*30*
	(5), (-)	2.630	2.621	0.020	2.617	2.647	5	
	(6), (-)	2.784	2.772	0.021	2.765	2.806	7	
Os–I	(-), (-): all	2.774	2.760	0.055	2.733	2.817	6	
	(6), (II)	2.758	2.760	0.035	2.724	2.790	4	
Ir–I	(-), (-): all	2.729	2.691	0.089	2.681	2.752	10	*86*
	(6), (III)	2.685	2.687	0.008	2.679	2.691	5	
Pt–I	(-), (-): all	2.658	2.651	0.082	2.606	2.668	28	*86*
	(4), (II)	2.622	2.604	0.050	2.581	2.666	11	
	(6), (IV): excluding COTDOE (2.843)	2.652	2.654	0.020	2.647	2.667	15	
Au–I	see BESBEG (2.536, 2.551), CIYMIG (2.857), IFPPAU (2.599)							
Hg–I	(-), (-): all	2.702	2.691	0.059	2.669	2.743	20	
	(4), (-)	2.708	2.695	0.050	2.674	2.743	16	
15.1.1.2	Iodine (μ_2-I)							*134*
Mn–I	(6), (I): all COGSIA	2.719	2.725	0.014	2.705	2.726	4	
Fe–I	see PCRNIB (2.591, 2.605)							
Ni–I	see EAPZNI (2.755, 2.760)							
Cu–I	(-), (-): all	2.675	2.660	0.107	2.602	2.703	28	*12*
	(3,4), (-): all	2.647	2.660	0.051	2.591	2.688	25	
	(3), (-)	2.578	2.577	0.012	2.567	2.589	4	
	(4), (-)	2.661	2.660	0.044	2.642	2.692	21	
Mo–I		2.830	2.818	0.056	2.797	2.860	10	
Ru–I	see IPHPRU (2.685, 2.711)							
Rh–I	(6), (III)	2.730	2.734	0.014	2.715	2.741	4	
Pd–I	see CODJAG (2.665, 2.723)							
Ag–I	(4), (I)	2.907	2.914	0.019	2.887	2.918	4	
W–I	see BURFOJ (2.831, 2.862)							
Re–I	(-), (I)	2.817	2.816	0.015	2.804	2.830	6	
Ir–I	(6), (III)	2.710	2.712	0.005	2.706	2.713	6	
Pt–I	(4), (II): all CODHIM	2.559	2.560	0.003	2.556	2.561	4	*85*
Hg–I	(4), (II)	2.927	2.931	0.039	2.891	2.957	6	
15.1.1.3	Iodine (μ_3-I)							
Cu–I	(-), (I): all	2.690	2.694	0.052	2.663	2.726	95	*12*
Ag–I	(-), (I): all	2.905	2.886	0.074	2.841	2.976	17	

in carbonyl complexes (section 3.7.1) of the individual 3*d* metals show sample standard deviations (σ) in the range 0.011–0.024 Å, while the 5*d* metals have σ in the range 0.023–0.035 Å. This last effect is somewhat reduced by the screening on the AS flag, as described above. While other contributions to the variance in interatomic distances undoubtedly play a part, readers should be aware of these various factors when making use of the averages and other statistics of Table 9.6.3.3. In the longer term, as more structures are determined, it will become possible to derive more precise averages by further subdivision of the distributions represented in Table 9.6.3.3.

APPENDIX 1

Footnotes, notes, and references to Tables 9.6.3.2 and 9.6.3.3

* Cluster complexes, no coordination number assigned.
† See Fig. 9.6.3.1.

(1) T. J. Marks & R. D. Ernst (1982). *Comprehensive organometallic chemistry*, Vol. 3, pp. 173–270. London: Pergamon Press.
(2) D. Cozak & M. Melník (1986). *Coord. Chem. Rev.* **74**, 53–99.
(3) M. Melník & D. Cozak (1986). *Rev. Inorg. Chem.* **8**, 221–286.
(4) C. E. Holloway & M. Melník (1985). *Rev. Inorg. Chem.* **7**, 75–160.
(5) C. E. Holloway & M. Melník (1986). *Rev. Inorg. Chem.* **8**, 287–335.
(6) C. E. Holloway & M. Melník (1986). *J. Organomet. Chem.* **304**, 41–82.
(7) L. F. Larkworthy, K. B. Nolan & P. O'Brien (1987). *Comprehensive coordination chemistry*, Vol. 3, pp. 699–969. London: Pergamon Press.
(8) D. A. Buckingham & C. R. Clark (1987). *Comprehensive coordination chemistry*, Vol. 4, pp. 635–900. London: Pergamon Press.
(9) L. Sacconi, F. Mani & A. Bencini (1987). *Comprehensive coordination chemistry*, Vol. 5, pp. 1–347. London: Pergamon Press.
(10) K. Nag & A. Chakravorty (1980). *Coord. Chem. Rev.* **33**, 87–147.
(11) B. J. Hathaway (1984). *Struct. Bonding (Berlin)*, **57**, 55–118.
(12) B. J. Hathaway (1987). *Comprehensive coordination chemistry*, Vol. 5, pp. 553–774. London: Pergamon Press.
(13) C. E. Holloway, I. M. Walker & M. Melník (1986). *Rev. Inorg. Chem.* **8**, 170–220.
(14) C. E. Holloway & M. Melník (1985). *Rev. Inorg. Chem.* **7**, 161–250.
(15) S. W. Kirtley (1982). *Comprehensive organometallic chemistry*, Vol. 3, pp. 1079–1148. London: Pergamon Press.
(16) M. Melník & P. Sharrock (1985). *Coord. Chem. Rev.* **65**, 49–85.
(17) G. Bandoli, U. Mazzi, E. Roncari & E. Deutsch (1982). *Coord. Chem. Rev.* **44**, 191–227.
(18) M. Melník & J. E. Van Lier (1986). *Coord. Chem. Rev.* **77**, 275–324.
(19) D. G. Tuck (1979). *Rev. Inorg. Chem.* **1**, 209–243.
(20) F. A. Hart (1987). *Comprehensive coordination chemistry*, Vol. 3, pp. 1059–1127. London: Pergamon Press.
(21) K. N. Raymonds & C. W. Eigenbrot Jr (1980). *Acc. Chem. Res.* **13**, 276–283.
(22) J.-C. G. Bünzli & D. Wessner (1984). *Coord. Chem. Rev.* **60**, 191–253.
(23) C. E. Holloway & M. Melník (1985). *Rev. Inorg. Chem.* **7**, 1–74.
(24) S. W. Kirtley (1982). *Comprehensive organometallic chemistry*, Vol. 3, pp. 1255–1319. London: Pergamon Press.
(25) M. Melník & R. V. Parrish (1986). *Coord. Chem. Rev.* **70**, 157–257.
(26) K. Brodersen & H. U. Hummel (1987). *Comprehensive coordination chemistry*, Vol. 5, pp. 1047–1097. London: Pergamon Press.
(27) R. G. Teller & R. Bau (1981). *Struct. Bonding (Berlin)*, **44**, 1–82.
(28) K. B. Gilbert, S. K. Boocock & S. G. Shore (1982). *Comprehensive organometallic chemistry*, Vol. 6, pp. 879–945. London: Pergamon Press.
(29) R. N. Grimes (1982). *Comprehensive organometallic chemistry*, Vol. 1, pp. 459–542. London: Pergamon Press.
(30) Distribution is bimodal.
(31) G. E. Herberich (1982). *Comprehensive organometallic chemistry*, Vol. 1, pp. 381–410. London: Pergamon Press.
(32) W. Siebert (1980). *Adv. Organomet. Chem.* **18**, 301–340.
(33) G. E. Herberich & H. Ohst (1985). *Adv. Organomet. Chem.* **25**, 199–236.
(34) J. S. Bradley (1982). *Adv. Organomet. Chem.* **22**, 1–58.
(35) M. Tachikawa & E. L. Muetterties (1981). *Prog. Inorg. Chem.* **28**, 203–238.
(36) M. A. Gallop & W. R. Roper (1985). *Adv. Organomet. Chem.* **25**, 121–198.
(37) H. P. Kim & R. J. Angelici (1987). *Adv. Organomet. Chem.* **27**, 51–111.
(38) S. W. Kirtley (1982). *Comprehensive organometallic chemistry*, Vol. 3, pp. 783–951. London: Pergamon Press.
(39) J. Holton, M. F. Lappert, R. Pearce & P. I. W. Yarrow (1983). *Chem. Rev.* **83**, 135–201.
(40) M. I. Bruce & A. G. Swincer (1982). *Adv. Organomet. Chem.* **22**, 59–128.
(41) F. R. Hartley (1982). *Comprehensive organometallic chemistry*, Vol. 6, pp. 471–762. London: Pergamon Press.
(42) E. Sappa, A. Tiripicchio & P. Braunstein (1985). *Coord. Chem. Rev.* **65**, 219–284.
(43) Distances for M–C–N $\geq 173°$ only.
(44) Distances for ligands *trans* to oxo excluded.
(45) Y. Yamamoto (1980). *Coord. Chem. Rev.* **32**, 193–233.
(46) E. Singleton & H. E. Oosthuizen (1982). *Adv. Organomet. Chem.* **22**, 209–310.
(47) P. M. Maitlis, P. Espinet & M. J. H. Russell (1982). *Comprehensive organometallic chemistry*, Vol. 6, pp. 279–349. London: Pergamon Press.
(48) Distances for M–C–O $\geq 173°$ only.
(49) D. J. Sikova, D. W. Macomber & M. D. Rausch (1985). *Adv. Organomet. Chem.* **25**, 317–379.
(50) M. D. Johnson (1982). *Comprehensive organometallic chemistry*, Vol. 4, pp. 331–376. London: Pergamon Press.
(51) P. W. Jolly (1982). *Comprehensive organometallic chemistry*, Vol. 6, pp. 15–36. London: Pergamon Press.
(52) R. Colton & M. J. McCormick (1980). *Coord. Chem. Rev.* **31**, 1–52.
(53) W. A. Herrmann (1982). *Adv. Organomet. Chem.* **20**, 159–263.

APPENDIX 1 (*cont.*)

(54) J. A. Labinger (1982). *Comprehensive organometallic chemistry*, Vol. 3, pp. 705–782. London: Pergamon Press.
(55) U. Schubert (1984). *Coord. Chem. Rev.* **55**, 261–286.
(56) P. W. Jolly (1982). *Comprehensive organometallic chemistry*, Vol. 6, pp. 37–100. London: Pergamon Press.
(57) G. K. Anderson (1982). *Adv. Organomet. Chem.* **20**, 39–114.
(58) D. M. P. Mingos (1982). *Comprehensive organometallic chemistry*, Vol. 3, pp. 1–88. London: Pergamon Press.
(59) S. J. Bryan, P. G. Huggett, K. Wade, J. A. Daniels & J. R. Jennings (1982). *Coord. Chem. Rev.* **44**, 149–189.
(60) A. J. Deeming (1982). *Comprehensive organometallic chemistry*, Vol. 4, pp. 377–512. London: Pergamon Press.
(61) P. W. Jolly (1982). *Comprehensive organometallic chemistry*, Vol. 6, pp. 101–143. London: Pergamon Press.
(62) I. Omae (1983). *Coord. Chem. Rev.* **51**, 1–39.
(63) Distribution is positively skewed.
(64) E. Sappa, A. Tiripicchio & P. Braunstein (1983). *Chem. Rev.* **83**, 203–239.
(65) J. L. Templeton, P. B. Winston, & B. C. Ward (1981). *J. Am. Chem. Soc.* **103**, 7713–7721.
(66) P. W. Jolly (1982). *Comprehensive organometallic chemistry*, Vol. 6, pp. 145–182. London: Pergamon Press.
(67) P. W. Jolly (1982). *Comprehensive organometallic chemistry*, Vol. 6, pp. 183–187. London: Pergamon Press.
(68) H. Yasuda, K. Tatsumi & A. Nakamura (1985). *Acc. Chem. Res.* **18**, 120–126.
(69) G. Erker, C. Krüger & G. Müller (1984). *Adv. Organomet. Chem.* **24**, 1–39.
(70) P. W. Jolly (1982). *Comprehensive organometallic chemistry*, Vol. 6, pp. 189–228. London: Pergamon Press.
(71) D. J. Cardin, M. F. Lappert, C. L. Raston & P. I. Riley (1982). *Comprehensive organometallic chemistry*, Vol. 3, pp. 559–633. London: Pergamon Press.
(72) R. D. Ernst (1984). *Struct. Bonding (Berlin)*, **57**, 1–53; R. D. Ernst (1985). *Acc. Chem. Res.* **18**, 56–62.
(73) P. Powell (1986). *Adv. Organomet. Chem.* **26**, 125–164.
(74) E. L. Muetterties, J. R. Bleeke, E. J. Wucherer & T. A. Albright (1982). *Chem. Rev.* **82**, 499–525.
(75) P. W. Jolly (1982). *Comprehensive organometallic chemistry*, Vol. 6, pp. 229–231. London: Pergamon Press.
(76) D. J. Gulliver & W. Levason (1982). *Coord. Chem. Rev.* **46**, 1–127.
(77) E. I. Steifel (1987). *Comprehensive coordination chemistry*, Vol. 3, pp. 1375–1420. London: Pergamon Press.
(78) W. L. Gladfelter (1984). *Adv. Organomet. Chem.* **24**, 41–86.
(79) W. A. Nugent & B. L. Haymore (1980). *Coord. Chem. Rev.* **31**, 123–175.
(80) B. F. G. Johnson, B. L. Haymore & J. R. Dilworth (1987). *Comprehensive coordination chemistry*, Vol. 2, pp. 99–159. London: Pergamon Press.
(81) Distribution may be affected by unresolved *trans*-influence effects.
(82) Distances for ligands in the axial site in $M_2(\mu\text{-}O_2CR)_4$ adducts only.
(83) F. H. Jardine (1987). *Comprehensive coordination chemistry*, Vol. 4, pp. 901-1096. London: Pergamon Press.
(84) K. Vrieze & G. Van Koten (1987). *Comprehensive coordination chemistry*, Vol. 2, pp. 189–244. London: Pergamon Press.
(85) Distances for ligand in the axial site in $M_2(\mu\text{-}O_2CR)_4$ adducts excluded.
(86) Distribution is positively skewed.
(87) Unresolved metal oxidation state effects present in this distribution.
(88) P. Pelikán & R. Boča (1984). *Coord. Chem. Rev.* **55**, 55–112.
(89) G. J. Leigh & R. L. Richards (1987). *Comprehensive coordination chemistry*, Vol. 3, pp. 1265–1299. London: Pergamon Press.
(90) K. A. Connor & R. A. Walton (1987) *Comprehensive coordination chemistry*, Vol. 4, pp. 125–213. London: Pergamon Press.
(91) Distribution is negatively skewed.
(92) Distribution may be distorted by unresolved bond-angle dependence within ligand.
(93) H. W. Roesky & K. K. Pandey (1983). *Adv. Inorg. Chem. Radiochem.* **26**, 337–356.
(94) M. H. Chisholm & I. P. Rothwell (1987). *Comprehensive coordination chemistry*, Vol. 2, pp. 170–176. London: Pergamon Press.
(95) M. Calligaris & L. Randaccio (1987). *Comprehensive coordination chemistry*, Vol. 2, pp. 715–738. London: Pergamon Press.
(96) Distribution may be distorted by unresolved metal spin state effects.
(97) B. Chiswell, E. D. Mackenzie & L. F. Lindoy (1987). *Comprehensive coordination chemistry*, Vol. 4, pp. 1–122. London: Pergamon Press.
(98) T. Mashiko & D. Dolphin (1987). *Comprehensive coordination chemistry*, Vol. 2, pp. 813–898. London: Pergamon Press.
(99) S. M. Nelson (1987). *Comprehensive coordination chemistry*, Vol. 4, pp. 217–276. London: Pergamon Press.
(100) Distribution includes distances for ligands in axial site in $M_2(O_2CR)_4$ adducts.
(101) D. S. Moore & S. D. Robinson (1986). *Adv. Inorg. Chem. Radiochem.* **30**, 1–68.
(102) R. W. Kemmit & D. R. Russell (1982). *Comprehensive organometallic chemistry*, Vol. 5, pp. 1–276. London: Pergamon Press.
(103) M. A. Hitchiman & G. L. Rowbottom (1982). *Coord. Chem. Rev.* **42**, 55–132.
(104) B. J. Hathaway (1987). *Comprehensive coordination chemistry*, Vol. 2, pp. 413–434. London: Pergamon Press.
(105) D. A. House (1987). *Comprehensive coordination chemistry*, Vol. 2, pp. 23–72. London: Pergamon Press.
(106) F. Bottomley & L. Sutin (1988). *Adv. Organomet. Chem.* **28**, 339–396.
(107) L. V. Boas & J. C. Pessoa (1987). *Comprehensive coordination chemistry*, Vol. 3, pp. 453–583. London: Pergamon Press.
(108) C. D. Garner & J. M. Charnock (1987). *Comprehensive coordination chemistry*, Vol. 3, pp. 1329–1374. London: Pergamon Press.
(109) Distribution may be affected by unresolved ligand substituent effects.

APPENDIX 1 (*cont.*)

(110) W. P. Griffith (1987). *Comprehensive coordination chemistry*, Vol. 4, pp. 519–633. London: Pergamon Press.
(111) M. Melník (1982). *Coord. Chem. Rev.* **42**, 259–293.
(112) T. Theophanides & P. D. Harvey (1987). *Coord. Chem. Rev.* **76**, 237–264.
(113) G. B. Deacon & R. J. Phillips (1980). *Coord. Chem. Rev.* **33**, 227–250.
(114) M. Melník (1981). *Coord. Chem. Rev.* **36**, 1–44.
(115) E. B. Boyar & S. D. Robinson (1983). *Coord. Chem. Rev.* **50**, 109–208.
(116) Distribution may be affected by unresolved metal coordination number effects.
(117) C. G. Pierpont & R. M. Buchanan (1981). *Coord. Chem. Rev.* **38**, 45–87.
(118) Distances for mono-anionic ligand.
(119) Distances for neutral ligand.
(120) Distances for di-anionic ligand.
(121) D. A. Palmer & R. Van Eldik (1983). *Chem. Rev.* **83**, 651–731.
(122) U. Casellato, P. A. Vigato & M. Vidali (1981). *Coord. Chem. Rev.* **36**, 183–265.
(123) R. Boca (1983). *Coord. Chem. Rev.* **50**, 1–72.
(124) M. H. Gubelmann & A. F. Williams (1983). *Struct. Bonding (Berlin)*, **55**, 1–65.
(125) H. A. O. Hill & D. G. Tew (1987). *Comprehensive coordination chemistry*, Vol. 2, pp. 315–333. London: Pergamon Press.
(126) C. A. McAuliffe & D. S. Barratt (1987). *Comprehensive coordination chemistry*, Vol. 3, pp. 323–361. London: Pergamon Press.
(127) J. A. Davies (1981). *Adv. Inorg. Chem. Radiochem.* **24**, 115–187.
(128) N. M. N. Gowda, S. B. Naikar & G. K. N. Reddy (1984). *Adv. Inorg. Chem. Radiochem.* **28**, 255–299.
(129) Distances for ligands *trans* to oxo *only*.
(130) B. Chiswell, E. D. Mackenzie & L. F. Lindoy (1987). *Comprehensive coordination chemistry*, Vol. 4, pp. 1–112. London: Pergamon Press.
(131) Distances for cluster complexes only.
(132) J. B. Farmer (1982). *Adv. Inorg. Chem. Radiochem.* **25**, 187–237.
(133) R. C. Fay (1987). *Comprehensive coordination chemistry*, Vol. 3, pp. 363–451. London: Pergamon Press.
(134) A. J. Edwards (1987). *Comprehensive coordination chemistry*, Vol. 2, pp. 675–688. London: Pergamon Press.
(135) P. G. Harrison & T. Kikabbai (1987). *Comprehensive coordination chemistry*, Vol. 2, pp. 15–21. London: Pergamon Press; K. M. McKay & B. K. Nicholson (1982). *Comprehensive organometallic chemistry*, Vol. 6, pp. 1043–1114. London: Pergamon Press; B. J. Aylett (1982). *Adv. Inorg. Chem. Radiochem.* **25**, 1–133.
(136) G. Huttner & K. Evertz (1986). *Acc. Chem. Res.* **19**, 406–413.
(137) C. A. McAuliffe (1987). *Comprehensive coordination chemistry*, Vol. 2, pp. 986–1066. London: Pergamon Press.
(138) A. H. Cowley & N. C. Norman (1986). *Prog. Inorg. Chem.* **34**, 1–63.
(139) Distances for structures in which the three P–C bond lengths vary by <0.1 Å *only*.
(140) Distances excluded for ligands in the axial site of an octahedral complex containing a planar N_4 or N_2O_2 macrocyclic ligand (see 141).
(141) P. D. Smith, B. R. James & D. H. Dolphin (1981). *Coord. Chem. Rev.* **39**, 31–75.
(142) D. M. Roundhill (1987). *Comprehensive coordination chemistry*, Vol. 5, pp. 351–531. London: Pergamon Press.
(143) As for (139) but variation <0.07 Å *only*.
(144) R. J. Puddephatt (1987). *Comprehensive coordination chemistry*, Vol. 5, pp. 861–923. London: Pergamon Press.
(145) R. J. Lancashire (1987). *Comprehensive coordination chemistry*, Vol. 5, pp. 775–859. London: Pergamon Press.
(146) As for (139), but variation <0.15 Å *only*.
(147) Distances for ligands *trans* to $\equiv CR$ excluded.
(148) J. F. Nixon (1985). *Adv. Inorg. Chem. Radiochem.* **29**, 41–141.
(149) As for (139), but variation <0.1 Å in both P–O and O–C lengths.
(150) A. Müller & E. Diemann (1987). *Comprehensive coordination chemistry*, Vol. 2, pp. 515–550. London: Pergamon Press.
(151) Distances excluded for cases where the *M–L* lengths within a bridge differ by >0.1 Å.
(152) W. Levason & M. D. Spicer (1987). *Coord. Chem. Rev.* **76**, 45–120.
(153) Distances for ligands *trans* to $=NR$ excluded.
(154) G. Winter (1980). *Rev. Inorg. Chem.* **2**, 253–342.
(155) R. Eisenberg (1970). *Prog. Inorg. Chem.* **12**, 295–369.
(156) A. Müller, W. Jaegermann & J. H. Enemark (1982). *Coord. Chem. Rev.* **46**, 245–280.
(157) A. Müller & E. Diemann (1987). *Adv. Inorg. Chem. Radiochem.* **31**, 89–122.
(158) S. G. Murray & F. R. Hartley (1981). *Chem. Rev.* **81**, 365–414.
(159) Z. Dori (1981). *Prog. Inorg. Chem.* **28**, 239–307.
(160) R. R. Ryan, G. J. Kubas, D. C. Moody & P. G. Eller (1981). *Struct. Bonding (Berlin)*, **46**, 47–100.
(161) Distances for ligands *trans* to hydride excluded.
(162) Distances for ligands *trans* to $\equiv N$ excluded.
(163) F. J. Berry (1987). *Comprehensive coordination chemistry*, Vol. 2, pp. 661–674. London: Pergamon Press.
(164) H. J. Gysling (1982). *Coord. Chem. Rev.* **42**, 133–244.

APPENDIX 2
Short-form references to individual CSD entries cited in Table 9.6.3.3

REFCODE	JOURNAL	Vol.	Page	Year
ABPENC	*Inorg. Chem.*	16	177	1977
ABTCMO	*Inorg. Chem.*	17	1981	1978
ABZAMN	*Zh. Strukt. Khim.*	19	1120	1978
ACACSC	*Inorg. Chem.*	12	927	1973
ACANRE	*J. Organomet. Chem.*	140	309	1977
ACAQGD	*J. Chem. Soc. Dalton Trans.*		454	1980
ACATEN	*Finn. Chem. Lett.*		246	1977
ACBZNM	*Bull. Chem. Soc. Jpn*	49	595	1976
ACCDSC10	*Dokl. Akad. Nauk. SSSR*	250	852	1980
ACETCR	*Inorg. Chem.*	17	2004	1978
ACHPHG	*J. Chem. Res.*	360	4101	1979
ACMPRU	*J. Chem. Soc. Dalton Trans.*		2184	1976
ACMRHD	*J. Chem. Soc. Dalton Trans.*		409	1979
ACNOB20	*J. Am. Chem. Soc.*	105	4662	1983
ACNCVO	*Acta Cryst. Sect. B*	31	1833	1975
ACNTCC	*J. Am. Chem. Soc.*	100	5756	1978
ACOXRH	*Latv. PSR Zinat. Akad. Vestis*		48	1980
ACPCRB	*Inorg. Chem.*	19	328	1980

APPENDIX 2 (*cont.*)

ACPMNA	*J. Organomet. Chem.*	204	79	1981
ACSNRU	*J. Chem. Soc. Dalton Trans.*		76	1978
ACTFIR	*J. Chem. Soc. Dalton Trans.*		2556	1975
ACTHTA	*Inorg. Chem.*	19	2354	1980
ACTPEN	*J. Am. Chem. Soc.*	96	4820	1974
ACTPRE	*J. Organomet. Chem.*	112	297	1976
ACURLB	*Dokl. Akad. Nauk. SSSR*	248	1337	1979
ACYPCI	*Inorg. Chem.*	16	1593	1977
ADAGPC	*Inorg. Chem.*	16	2469	1977
ADASMO	*Inorg. Chem.*	19	777	1980
ADBPPD	*Inorg. Chem.*	18	176	1979
ADMEHH	*Can. J. Chem.*	59	1311	1981
ADOOSA	*J. Am. Chem. Soc.*	101	7265	1979
ADOOSB	*J. Am. Chem. Soc.*	101	7265	1979
AENCUS	*Cryst. Struct. Commun.*	7	565	1978
AFMZRH	*J. Chem. Soc. Dalton Trans.*		371	1979
AFNICD	*Koord. Khim.*	7	461	1981
AFXPCM	*J. Chem. Soc. Dalton Trans.*		1966	1977
AGENPC10	*Acta Chem. Scand. Ser. A*	32	555	1978
AGIMHN01	*Acta Chem. Scand.*	25	1758	1971
AGLPAU	*Cryst. Struct. Commun.*	9	679	1980
AGSURE10	*Inorg. Chem.*	7	1351	1968
ALANIC	*J. Am. Chem. Soc.*	94	1858	1972
ALBCIW	*Cryst. Struct. Commun.*	6	253	1977
ALCPPV	*J. Organomet. Chem.*	121	189	1976
ALETPD	*J. Organomet. Chem.*	65	427	1974
AMAQDY	*Koord. Khim.*	7	445	1981
AMETZN	*Acta Cryst. Sect. B*	34	2859	1978
AMMPMN	*Acta Cryst. Sect. B*	33	2648	1977
AMPMNC	*Acta Cryst. Sect. B*	33	2763	1977
AMXPPD	*Acta Cryst. Sect. B*	35	2411	1979
ANIDED10	*Inorg. Chem.*	15	1853	1976
APDPZC	*Acta Cryst. Sect. B*	30	1370	1974
APIMCO	*Koord. Khim.*	5	762	1979
APIMNI	*Koord. Khim.*	5	762	1979
APROCU	*Finn. Chem. Lett.*		71	1978
APRPIR	*Cryst. Struct. Commun.*	3	721	1974
APXLAP	*J. Chem. Soc. Dalton Trans.*		376	1980
AQACAL	*Inorg. Chem.*	7	2295	1968
AQNCZN	*Koord. Khim.*	5	1889	1979
AQOURI	*Inorg. Chem.*	19	1067	1980
AQOXCU	*Acta Cryst. Sect. B*	36	1650	1980
AQSUMN	*Acta Cryst. Sect. B*	37	1214	1981
ASCETU	*Inorg. Chem.*	12	2140	1973
ASMETE	*Inorg. Chem.*	20	1617	1981
ATCTPR	*Z. Anorg. Allg. Chem.*	456	163	1979
AUDETC	*Cryst. Struct. Commun.*	2	81	1973
AXEXAC	*Inorg. Chem.*	18	3015	1979
AZBCTI10	*Gazz. Chim. Ital.*	110	423	1980
AZBRHA10	*J. Chem. Soc. Dalton Trans.*		2138	1972
AZCPTI	*Acta Cryst. Sect. B*	33	578	1977
AZENPD10	*J. Chem. Soc. Dalton Trans.*		725	1976
AZMLMN	*Chem. Ber.*	114	276	1981
AZNPYD	*Acta Cryst. Sect. B*	30	628	1974
AZPPBW10	*J. Chem. Soc. Dalton Trans.*		1150	1980
AZTLAW	*Gazz. Chim. Ital.*	108	627	1978
BABFOZ	*Acta Cryst. Sect. B*	37	1656	1981
BABNAT	*Zh. Strukt. Khim.*	22	113-3	1981
BABTUT	*Inorg. Chem.*	20	1545	1981
BABWAC	*Inorg. Chem.*	20	2023	1981
BACREC10	*Acta Cryst. Sect. B*	38	1738	1982
BACVOQ10	*Acta Cryst. Sect. B*	38	2047	1982
BAGBUG	*J. Organomet. Chem.*	206	C33	1981
BAGWAH	*J. Chem. Soc. Dalton Trans.*		1798	1981
BAHHOH	*J. Chem. Soc. Dalton Trans.*		1879	1981
BAHPEF	*Nouv. J. Chim.*	5	423	1981
BAHVAH	*J. Chem. Soc. Dalton Trans.*		1997	1981
BAJZAN	*J. Organomet. Chem.*	220	125	1981
BAJZER	*J. Organomet. Chem.*	220	45	1981
BAKDOG	*J. Am. Chem. Soc.*	103	5747	1981
BAKDUM	*J. Am. Chem. Soc.*	103	5747	1981
BAKPUY	*Proc. Natl Sci. Counc. B, ROC*	5	139	1981
BALJIH	*J. Am. Chem. Soc.*	103	1927	1981
BALWUG	*Chem. Ber.*	114	2754	1981
BALZUJ	*Acta Cryst. Sect. B*	37	2062	1981
BAMCIB10	*J. Am. Chem. Soc.*	106	2328	1984
BAMCOH	*Chem. Ber.*	114	3220	1981
BAMDOI10	*Nouv. J. Chim.*	7	545	1983
BAMHUS	*Inorg. Chem.*	20	2872	1981
BAMTAK10	*Inorg. Chem.*	23	2303	1984
BAMVUG	*Inorg. Chem.*	20	2869	1981
BAMZUK	*J. Chem. Soc. Chem. Commun.*		1190	1981
BANDAV	*Zh. Neorg. Khim.*	26	718	1981
BANGIG10	*Inorg. Chem.*	21	3741	1982
BANVUH10	*J. Am. Chem. Soc.*	106	2041	1984
BAPHAB	*Inorg. Chem.*	20	2390	1981
BAPKEI	*Inorg. Chem.*	20	2372	1981
BAPPIR	*Inorg. Chem.*	20	2386	1981
BASLIQ10	*Inorg. Chem.*	23	2823	1984
BASMOX	*J. Am. Chem. Soc.*	103	4255	1981
BASSAP	*Z. Anorg. Allg. Chem.*	479	113	1981
BATLPT10	*J. Chem. Soc. A*		1873	1970
BATNIT	*J. Chem. Soc. Dalton Trans.*		2321	1981
BATPER	*J. Chem. Soc. Dalton Trans.*		2471	1981
BATZIF	*Can. J. Chem.*	59	2391	1981
BAVHEL	*Cryst. Struct. Commun.*	10	1523	1981
BAVJOX10	*J. Am. Chem. Soc.*	105	4671	1983
BAVKAK	*Cryst. Struct. Commun.*	10	1259	1981
BAVKIS	*Inorg. Chem.*	20	3819	1981
BAVLAL11	*Z. Naturforsch. Teil B*	37	1437	1982
BAVMUG	*Acta Cryst. Sect. B*	37	2223	1981
BAVSIA	*Inorg. Chem.*	20	3598	1981
BAWBUW01	*Inorg. Chem.*	20	3571	1981
BAWDIM10	*Chem. Lett.*		1501	1981
BAWKUF	*Inorg. Chem.*	20	3271	1981
BAWLAM	*Inorg. Chem.*	20	3271	1981
BAWLEQ	*Inorg. Chem.*	20	3271	1981
BAWRIA	*Acta Cryst. Sect. B*	38	105	1982
BAWTOI	*J. Chem. Soc. Chem. Commun.*		27	1982
BAWZUU	*Cryst. Struct. Commun.*	10	1227	1981
BAXFEL	*J. Chem. Soc. Chem. Commun.*		75	1982
BAXFOV	*Z. Anorg. Allg. Chem.*	482	113	1981
BAXHEN	*Inorg. Chem.*	20	3890	1981
BAXJOZ	*Acta Cryst. Sect. B*	38	96	1982
BAXLER	*J. Organomet. Chem.*	218	C39	1981
BAYCOS	*J. Chem. Soc. Chem. Commun.*		750	1979
BAYDIO	*Acta Cryst. Sect. B*	38	262	1982
BAYJAM	*Sci. Sin.*	24	1111	1981
BCATMO	*Inorg. Chem.*	18	1616	1979
BCAZWB	*J. Chem. Soc. Chem. Commun.*		879	1980
BCBXMO	*J. Am. Chem. Soc.*	100	1727	1978
BCETPN	*J. Am. Chem. Soc.*	99	8102	1977
BDMFRU	*J. Organomet. Chem.*	117	171	1976
BDODFE	*J. Am. Chem. Soc.*	97	5739	1975
BDTCBR	*J. Am. Chem. Soc.*	95	774	1973
BEAMRH	*Inorg. Chem.*	18	129	1979
BEBGEU	*J. Chem. Soc. Dalton Trans.*		207	1982
BEBHIZ	*J. Chem. Soc. Dalton Trans.*		25	1982
BEBHUL	*J. Chem. Soc. Dalton Trans.*		25	1982
BEBREF	*Z. Naturforsch. Teil B*	36	1580	1981
BEBTUX	*J. Chem. Soc. Chem. Commun.*		215	1982
BECTIM	*J. Chem. Soc. Dalton Trans.*		129	1982
BECVOU	*J. Chem. Soc. Dalton Trans.*		319	1982
BECXIQ	*J. Organomet. Chem.*	222	343	1981
BEDBUH	*J. Am. Chem. Soc.*	103	7398	1981
BEDDAP	*J. Chem. Soc. Dalton Trans.*		187	1982
BEDGAS	*J. Organomet. Chem.*	226	C1	1982
BEDZAL	*Zh. Strukt. Khim.*	22	120-5	1981
BEFBIX	*Inorg. Chem.*	21	237	1982
BEFJIF10	*J. Am. Chem. Soc.*	106	3727	1984
BEGBIY01	*Inorg. Chem.*	21	192	1982
BEGFEY	*Inorg. Chem.*	21	431	1982
BEGKAZ	*Inorg. Chem.*	20	4361	1981
BEGNAC	*Acta Cryst. Sect. B*	38	942	1982
BEGNUW	*J. Chem. Soc. Dalton Trans.*		493	1982
BEGPUY	*J. Chem. Soc. Dalton Trans.*		607	1982
BEGYAN	*J. Chem. Soc. Chem. Commun.*		287	1982
BEHGAW	*J. Organomet. Chem.*	221	183	1981
BEHHIF	*Inorg. Chem.*	21	223	1982
BEHLOP	*Chem. Ber.*	115	738	1982
BEHMOQ	*J. Chem. Soc. Dalton Trans.*		407	1982
BEHYUI	*Acta Cryst. Sect. B*	38	1318	1982
BEJBEX	*J. Am. Chem. Soc.*	104	922	1982
BEJGAY	*Inorg. Chem.*	21	218	1982
BEJGIG	*Inorg. Chem.*	20	4293	1981
BEJHUT	*Inorg. Chim. Acta*	57	29	1982
BEJJAB	*Inorg. Chim. Acta*	57	29	1982
BEJNIN	*Acta Cryst. Sect. B*	38	1165	1982
BEJTIT	*Acta Cryst. Sect. B*	38	1288	1982

APPENDIX 2 (*cont.*)

BEKPUC	*Aust. J. Chem.*	34	2061	1981
BELFUT	*Z. Naturforsch. Teil B*	37	13	1982
BELGOO10	*Khim. Fiz.*		1459	1983
BELJEH	*J. Chem. Soc. Dalton Trans.*		713	1982
BELLEJ	*Zh. Strukt. Khim.*	22	124-6	1981
BELTIV10	*Inorg. Chem.*	21	4166	1982
BELTUH	*Organometallics*	1	302	1982
BEMLAG10	*Chem. Ber.*	115	3830	1982
BEMLUA	*Chem. Ber.*	115	1004	1982
BEMNIQ	*Z. Naturforsch. Teil B*	37	341	1982
BEMPOY10	*Koord. Khim.*	7	1880	1981
BENDAZ	*J. Am. Chem. Soc.*	104	994	1982
BENDED	*Inorg. Chem.*	21	1014	1982
BENFEF	*J. Chem. Soc. Chem. Commun.*		493	1982
BENIIB	*J. Organomet. Chem.*	169	219	1979
BENLOV	*Inorg. Chem.*	21	987	1982
BENNOX	*J. Organomet. Chem.*	221	375	1981
BENRAN	*J. Organomet. Chem.*	228	153	1982
BEPDEF	*Inorg. Chem.*	21	1208	1982
BEPJIP	*Koord. Khim.*	8	111	1982
BEPZEB	*Cryst. Struct. Commun.*	11	175	1982
BEPZIF	*Cryst. Struct. Commun.*	11	169	1982
BERTAT	*Cryst. Struct. Commun.*	11	305	1982
BESBEG	*Z. Anorg. Allg. Chem.*	485	81	1982
BESBIK10	*Z. Naturforsch. Teil B*	38	747	1983
BESBOQ10	*Z. Naturforsch. Teil B*	38	747	1983
BESFOU	*J. Am. Chem. Soc.*	104	1272	1982
BESHAI	*J. Am. Chem. Soc.*	104	1756	1982
BESJOY	*Inorg. Chem.*	21	917	1982
BESPIY	*J. Am. Chem. Soc.*	104	1710	1982
BESSAT	*J. Am. Chem. Soc.*	104	1290	1982
BESSEX	*J. Am. Chem. Soc.*	104	1426	1982
BESXRU	*Inorg. Chem.*	15	2270	1976
BETCUY10	*J. Am. Chem. Soc.*	105	4662	1983
BEVMAQ	*Acta Cryst. Sect. B*	38	1603	1982
BEVYIK	*Chem. Ber.*	115	2271	1982
BEWMAR	*J. Chem. Soc. Dalton Trans.*		1013	1982
BEWVEE	*Can. J. Chem.*	59	3123	1981
BEXJUJ	*J. Chem. Soc. Dalton Trans.*		899	1982
BEXLEV	*Polyhedron*	1	89	1982
BEXTON	*Bull. Soc. Chim. Belg.*	91	171	1982
BEYFEQ	*J. Organomet. Chem.*	232	229	1982
BEYGAN	*J. Organomet. Chem.*	232	41	1982
BHZEPT	*J. Chem. Soc. Dalton Trans.*		2386	1976
BIBFUN	*J. Am. Chem. Soc.*	104	2147	1982
BIBJAX	*Polyhedron*	1	37	1982
BIBJEB	*Polyhedron*	1	37	1982
BIBSAG	*Cryst. Struct. Commun.*	11	733	1982
BICPDB	*J. Chem. Soc. Dalton Trans.*		2263	1975
BIDCAS	*J. Am. Chem. Soc.*	104	2329	1982
BIDNEH	*Koord. Khim.*	8	402	1982
BIFYUK	*Acta Cryst. Sect. B*	38	2155	1982
BIFZEV	*Acta Cryst. Sect. B*	38	2155	1982
BIGFAY01	*J. Am. Chem. Soc.*	104	2165	1982
BIGHAA	*Chem. Ber.*	115	2035	1982
BIGLAE	*J. Chem. Soc. Dalton Trans.*		1465	1982
BIGLUY	*J. Chem. Soc. Dalton Trans.*		1401	1982
BIPOW	*Inorg. Chem.*	21	2444	1982
BIGVAO	*Inorg. Chim. Acta*	52	169	1981
BIHCUQ	*Inorg. Chem.*	21	2350	1982
BIHFAZ	*Inorg. Chem.*	21	2257	1982
BIHGOO	*J. Chem. Soc. Chem. Commun.*		932	1982
BIHJOR10	*Koord. Khim.*	10	844	1984
BIHLOT01	*Inorg. Chem.*	21	3284	1982
BIHSAM	*Inorg. Chem.*	21	2624	1982
BIHWUK	*J. Chem. Soc. Chem. Commun.*		805	1982
BIHYEW	*Am. Cryst. Assoc. Ser. 2*	10	16	1982
BIJJAF	*J. Chem. Soc. Chem. Commun.*		1006	1982
BIJJUZ10	*J. Am. Chem. Soc.*	105	7295	1983
BIJKOU	*J. Am. Chem. Soc.*	104	3722	1982
BIJPAL	*Inorg. Chem.*	21	3090	1982
BIJWEW	*Inorg. Chem.*	21	3173	1982
BIKTIY	*Inorg. Chem.*	21	2647	1982
BILDIJ	*Organometallics*	1	38	1982
BILMUE	*Inorg. Chem.*	21	2578	1982
BILRET	*J. Chem. Soc. Chem. Commun.*		1025	1982
BILSIY	*Inorg. Chem.*	21	2867	1982
BILWIC	*J. Am. Chem. Soc.*	103	7358	1981
BIMAOU10	*Acta. Cryst. Sect. B*	30	2659	1974
BIMMOZ	*Bull. Chem. Soc. Jpn*	55	2083	1982
BIMTCU	*Inorg. Chem.*	18	141	1979
BIMTEW	*J. Organomet. Chem.*	235	105	1982
BINFUZ	*J. Am. Chem. Soc.*	104	4278	1982
BINHUB	*Inorg. Chem.*	21	3186	1982
BINJEN	*Inorg. Chem.*	21	2889	1982
BINRAR	*Acta Cryst. Sect. B*	38	2468	1982
BIPFUB10	*Acta Cryst. Sect. C*	39	42	1983
BIPHHG	*Cryst. Struct. Commun.*	10	613	1981
BIPTAV	*Inorg. Chim. Acta*	52	205	1981
BIPYHG	*Cryst. Struct. Commun.*	7	165	1978
BIRJUH	*Kristallografiya*	27	489	1982
BIRLIX	*Chem. Ber.*	115	3049	1982
BIRXIJ	*Cryst. Struct. Commun.*	11	847	1982
BIRYOO10	*Z. Anorg. Allg. Chem.*	498	85	1983
BISCEL	*Inorg. Chim. Acta*	59	225	1982
BISHUG	*Cryst. Struct. Commun.*	11	1163	1982
BISIPT	*J. Chem. Soc. Dalton. Trans.*		1294	1979
BISJOC	*Cryst. Struct. Commun.*	11	1049	1982
BISKOD	*Acta Cryst. Sect. B*	38	2674	1982
BISNEW	*Chem. Ber.*	115	3224	1982
BISPAU	*Acta Chem. Scand. Ser. A*	35	739	1981
BISZIM	*Cryst. Struct. Commun.*	11	861	1982
BITKIY	*Chem. Ber.*	115	3152	1982
BITRAX	*J. Chem. Soc. Chem. Commun.*		1081	1982
BITSAY	*Z. Kristallogr.*	159	173	1982
BITYIM	*Z. Naturforsch. Teil B*	37	944	1982
BIVGAO	*J. Chem. Soc. Chem. Commun.*		1039	1982
BIVWIM	*Acta Chem. Scand. Ser. A*	36	767	1982
BIWBEO	*J. Organomet. Chem.*	229	169	1982
BIWLAU	*Inorg. Chim. Acta*	60	141	1982
BIWVEI	*Inorg. Chim. Acta*	61	195	1982
BIXBUF10	*J. Organomet. Chem.*	269	91	1984
BIYCUH	*Angew. Chem. Int. Ed. Engl.*	21	705	1982
BIYHOG	*Inorg. Chem.*	21	3270	1982
BIYJIC	*J. Am. Chem. Soc.*	104	3773	1982
BIYPAA	*Acta Cryst. Sect. B*	38	2886	1982
BIYVIO	*J. Organomet. Chem.*	220	251	1981
BIYWUB	*Inorg. Chim. Acta*	61	255	1982
BIYXAI	*Inorg. Chem.*	21	3295	1982
BIYYOX	*J. Chem. Soc. Dalton Trans.*		1809	**1982**
BIYYUD	*J. Chem. Soc. Dalton Trans.*		1809	**1982**
BIZJEZ	*J. Organomet. Chem.*	238	223	**1982**
BIZZAL	*J. Chem. Soc. Dalton Trans.*		2065	**1982**
BMCPTI	*Inorg. Chem.*	16	1645	1977
BMTCFE	*J. Chem. Soc. Chem. Commun.*		506	1978
BNTLFE	*Acta Cryst. Sect. B*	36	1950	1980
BNZCTC	*J. Organomet. Chem.*	73	103	1974
BOBSUG	*J. Am. Chem. Soc.*	104	5250	1982
BOBTOB	*Organometallics*	1	1013	1982
BOBWAQ	*Organometallics*	1	998	1982
BOBXOF	*J. Am. Chem. Soc.*	104	4879	1982
BOBXUL	*J. Am. Chem. Soc.*	104	4879	1982
BOBYAS	*J. Am. Chem. Soc.*	104	4865	1982
BOBZUN	*J. Chem. Soc. Chem. Commun.*		1421	1982
BOCCOC	*Inorg. Chem.*	17	1995	1978
BOCLOU	*Acta Cryst. Sect. B*	38	3081	1982
BOCWAR	*Organometallics*	1	1085	1982
BOCWEV	*Organometallics*	1	1066	1982
BODGUW10	*J. Am. Chem. Soc.*	106	5926	1984
BODYEY	*J. Am. Chem. Soc.*	104	5515	1982
BODZEZ	*Bull. Chem. Soc. Jpn*	55	2840	1982
BOFCEE	*J. Chem. Soc. Dalton Trans.*		1795	1982
BOFJIP	*J. Chem. Soc. Dalton Trans.*		2343	1982
BOFMOY	*Z. Naturforsch. Teil B*	37	1289	1982
BOGFOS	*J. Chem. Soc. Chem. Commun.*		5	1983
BOGPIW	*Z. Naturforsch. Teil B*	37	1234	1982
BOHBIJ	*Inorg. Chem.*	21	3811	1982
BOHDUX	*Inorg. Chem.*	21	3666	1982
BOHGAG	*Acta Cryst. Sect. C*	39	49	1983
BOHPUJ	*J. Chem. Soc. Dalton Trans.*		1	1983
BOHYEC	*Ko Hsueh Tung Pao*	27	728	1982
BOJJUF	*J. Chem. Soc. Dalton Trans.*		2203	1982
BOJSUO	*Z. Anorg. Allg. Chem.*	491	73	1982
BOKPEW	*J. Chem. Soc. Chem. Commun.*		69	1983
BOKXEE	*Chem. Ber.*	115	3830	1982
BOLCIO10	*J. Am. Chem. Soc.*	106	3214	1984
BOLJAN	*Inorg. Chem.*	21	4096	1982
BOLRID	*Acta Cryst. Sect. C*	39	188	1983
BOMMEV	*Cryst. Struct. Commun.*	11	1655	1982

APPENDIX 2 (*cont.*)

BONCIQ01	*Organometallics*	2	350	1983
BONSUS	*Z. Naturforsch. Teil B*	38	67	1983
BOPFOB	*Chem. Ber.*	116	46	1983
BOPPAX10	*J. Am. Chem. Soc.*	105	4826	1983
BOPPIF10	*Acta Cryst. Sect. C*	40	1322	1984
BOPSII	*J. Am. Chem. Soc.*	104	6360	1982
BOPTEF	*Acta Cryst. Sect. C*	39	181	1983
BOPWAE	*Inorg. Chem.*	21	4301	1982
BOPWEI	*Inorg. Chem.*	21	3903	1982
BORVIN	*Inorg. Chem.*	21	4050	1982
BOSKUP	*J. Am. Chem. Soc.*	104	6961	1982
BOSNEC	*Inorg. Chem.*	21	3923	1982
BOSRUW	*J. Am. Chem. Soc.*	104	6161	1982
BOTFOF	*Koord. Khim.*	8	1700	1982
BOTGAS	*J. Am. Chem. Soc.*	104	7378	1982
BOTPCU	*J. Chem. Soc. Dalton Trans.*		37	1977
BOTTAF	*J. Am. Chem. Soc.*	104	7325	1982
BOTVIP10	*Inorg. Chim. Acta.*	87	129	1984
BOTWUC	*Zh. Strukt. Khim.*	23	135-3	1982
BOVCAQ	*J. Chem. Soc. Chem. Commun.*		206	1983
BOVGAU	*Koord. Khim.*	8	1527	1982
BOVLED	*J. Chem. Soc. Chem. Commun.*		267	1983
BOVLUT	*J. Chem. Soc. Chem. Commun.*		222	1983
BOVYUG	*Inorg. Chem.*	22	759	1983
BOWCAR10	*J. Chem. Soc. Dalton Trans.*		1557	1983
BOWLII	*Polyhedron*	1	840	1982
BOWLUU	*Polyhedron*	1	561	1982
BOWYOB	*J. Chem. Soc. Dalton Trans.*		205	1983
BOXHUR	*Polyhedron*	1	617	1982
BOXNEH	*Inorg. Chem.*	22	45	1983
BOYLUW	*J. Struct. Chem.*	1	73-1	1982
BOYTOY	*Organometallics*	1	1074	1982
BOYZOE	*J. Chem. Soc. Chem. Commun.*		356	1983
BOZBOH	*J. Chem. Soc. Dalton Trans.*		253	1983
BOZDID	*Koord. Khim.*	8	1561	1982
BOZMIM	*J. Am. Chem. Soc.*	105	416	1983
BOZNEJ	*Inorg. Chem.*	22	171	1983
BOZRAJ	*Inorg. Chem.*	22	395	1983
BOZYIY	*Inorg. Chem.*	22	884	1983
BPBRNI10	*Cryst. Struct. Commun.*	11	1713	1982
BPEPFE	*Inorg. Chem.*	17	810	1978
BPESNI	*Inorg. Chem.*	14	1773	1975
BPHPRH10	*Acta Cryst. Sect. B*	30	738	1974
BPNICU	*Acta Cryst. Sect. B*	33	1669	1977
BPYAGN	*Cryst. Struct. Commun.*	2	279	1973
BPYCPT	*J. Chem. Soc. Dalton Trans.*		1002	1974
BPYMNA	*Inorg. Chim. Acta*	53	L197	1981
BQAPPD	*J. Chem. Soc. Dalton Trans.*		1490	1978
BRFOSA10	*J. Organomet. Chem.*	249	149	1983
BRNOCR	*Inorg. Chem.*	19	3626	1980
BRNPIR	*Inorg. Chem.*	19	1803	1980
BSEMEP	*J. Chem. Soc. Chem. Commun.*		713	1979
BTCMAN	*J. Cryst. Mol. Struct.*	1	155	1971
BTCPTI	*Z. Anorg. Allg. Chem.*	390	195	1972
BTPCRE10	*J. Chem. Soc. Dalton Trans.*		1189	1978
BTPPFE	*Aust. J. Chem.*	30	2655	1977
BTZDNI	*J. Chem. Soc. Dalton Trans.*		2382	1976
BUBBAB	*Inorg. Chem.*	22	371	1983
BUBKUE	*J. Chem. Soc. Chem. Commun.*		420	1983
BUCBEG	*Inorg. Chem.*	22	628	1983
BUCBUW	*J. Am. Chem. Soc.*	105	976	1983
BUCLUG	*Inorg. Chem.*	22	868	1983
BUCTOI	*Inorg. Chem.*	22	560	1983
BUCZOO	*Chem. Ber.*	116	951	1983
BUDBEH	*Z. Naturforsch. Teil B*	38	417	1983
BUDTEZ	*Z. Naturforsch. Teil B*	38	454	1983
BUDZEF	*J. Organomet. Chem.*	247	39	1983
BUFFUD	*Acta Cryst. Sect. C*	39	573	1983
BUFLET	*Chem. Ber.*	116	1070	1983
BUFNOF	*J. Am. Chem. Soc.*	105	1401	1983
BUFPUN01	*Inorg. Chem.*	22	4091	1983
BUGFUE	*J. Chem. Soc. Dalton Trans.*		799	1983
BUGGAL	*J. Chem. Soc. Dalton Trans.*		799	1983
BUGRIE	*J. Chem. Soc. Chem. Commun.*		634	1983
BUHIPI	*Gazz. Chim. Ital.*	105	529	1975
BUHTON	*Bull. Chem. Soc. Jpn*	56	657	1983
BUHVOP	*Acta Cryst. Sect. C*	39	540	1983
BUIMWA	*J. Am. Chem. Soc.*	103	357	1981
BUIMWB	*J. Am. Chem. Soc.*	103	357	1981
BUJBIR	*Angew. Chem. Int. Ed. Engl.*	22	314	1983
BUJFIV	*J. Chem. Soc. Chem. Commun.*		673	1983
BUJFUH	*J. Chem. Soc. Chem. Commun.*		648	1983
BUJNOJ	*Phosphorus Sulfur*	14	161	1983
BUJXAF	*J. Chem. Soc. Dalton Trans.*		809	1983
BIJYIO	*Organometallics*	1	1709	1982
BUKGET	*Organometallics*	1	1567	1982
BUKMID	*Polyhedron*	1	441	1982
BULLFE	*Chem. Ber.*	105	3936	1972
BULPED	*J. Chem. Soc. Dalton Trans.*		1131	1983
BULTEH	*J. Chem. Soc. Dalton Trans.*		911	1983
BULYOW	*Inorg. Chim. Acta*	71	141	1983
BULZIR	*Inorg. Chim. Acta*	70	29	1983
BUMCER	*Aust. J. Chem.*	35	2413	1982
BUMEMO	*J. Am. Chem. Soc.*	102	1759	1980
BUNKAW	*Organometallics*	1	1538	1982
BUNKEA	*J. Am. Chem. Soc.*	105	2927	1983
BUNKIE	*J. Am. Chem. Soc.*	105	2927	1983
BUNMEC	*J. Chem. Soc. Dalton Trans.*		1479	1983
BUNZOZ	*Inorg. Chem.*	22	1221	1983
BUPCEU	*Inorg. Chem.*	22	1168	1983
BUPCIY	*Inorg. Chem.*	22	1168	1983
BUPCRH	*Chem. Ber.*	110	1020	1977
BUPJAX	*J. Am. Chem. Soc.*	105	2085	1983
BUPLAZ10	*Organometallics*	3	599	1984
BUPMOO	*Acta Cryst. Sect. C*	39	838	1983
BUPPUX	*Acta Cryst. Sect. C*	39	858	1983
BUPSUA	*Inorg. Chim. Acta*	69	29	1983
BUPTEL	*J. Organomet. Chem.*	250	517	1983
BUPVUD	*J. Organomet. Chem.*	249	273	1983
BUPWOY10	*J. Chem. Soc. Dalton Trans.*		1555	1984
BUPYOA	*J. Organomet. Chem.*	248	171	1983
BUPYUG	*J. Organomet. Chem.*	248	171	1983
BUPZIV	*Z. Anorg. Allg. Chem.*	495	127	1982
BURFOJ	*J. Organomet. Chem.*	249	127	1983
BURPEJ	*Inorg. Chim. Acta*	69	77	1983
BUSHEC	*Z. Naturforsch. Teil B*	38	733	1983
BUSLEG	*J. Organomet. Chem.*	250	183	1983
BUSRIQ	*J. Chem. Soc. Dalton Trans.*		1305	1983
BUSYIX	*J. Chem. Soc. Dalton Trans.*		1003	1983
BUTKUW	*Inorg. Chem.*	22	1409	1983
BUTTOZ	*Organometallics*	2	515	1983
BUVCAW10	*Z. Anorg. Allg. Chem.*	514	25	1984
BUVGII	*Inorg. Chem.*	22	1865	1983
BUVLEJ	*Organometallics*	2	506	1983
BUVNIP	*J. Cryst. Spectrosc.*	13	303	1983
BUVNUB	*J. Am. Chem. Soc.*	105	2680	1983
BUVROZ	*J. Chem. Soc. Chem. Commun.*		951	1983
BUVSOA	*Organometallics*	1	1204	1982
BUWBAW	*Zh. Strukt. Khim.*	24	66-2	1983
BUWJUY	*J. Organomet. Chem.*	250	537	1983
BUWMAH	*Organometallics*	2	44	1983
BUWWOF01	*J. Chem. Soc. Dalton Trans.*		2333	1983
BUWYIB	*Bull. Chem. Soc. Jpn*	56	1982	1983
BUXGAC	*Inorg. Chem.*	22	1603	1983
BUXLEL	*J. Am. Chem. Soc.*	105	3353	1983
BUXMIQ	*Inorg. Chem.*	22	1306	1983
BUXTAP	*Inorg. Chem.*	22	1825	1983
BUYBUS	*Polyhedron*	2	185	1983
BUYKIP	*J. Am. Chem. Soc.*	105	4487	1983
BUYMAJ	*J. Am. Chem. Soc.*	105	4104	1983
BUYNEO	*J. Am. Chem. Soc.*	105	4092	1983
BUZMUE	*J. Organomet. Chem.*	251	413	1983
BUZPIV	*Chem. Ber.*	116	2994	1983
BUZRAP	*Chem. Ber.*	116	2765	1983
BUZYAW	*J. Organomet. Chem.*	252	71	1983
BUZZAX	*J. Organomet. Chem.*	252	231	1983
BVINBF	*Isr. J. Chem.*	10	201	1972
BXCAPD	*J. Am. Chem. Soc.*	102	1047	1980
BXZPCO	*Inorg. Chem.*	16	1665	1977
BZBCUA	*Zh. Strukt. Khim.*	20	89	1979
BZCPRU	*Cryst. Struct. Commun.*	7	583	1978
BZDTNB10	*Inorg. Chem.*	15	1589	1976
BZDTZR10	*Inorg. Chem.*	15	1595	1976
BZHREC	*Chem. Ber.*	111	3740	1978
BZHXDB	*Inorg. Chem.*	20	890	1981
BZTCDN	*J. Am. Chem. Soc.*	95	8566	1973
BZTCOV	*Acta Cryst. Sect. B*	36	304	1980
CABHIW	*J. Struct. Chem.*	2	29	1983
CABYIN	*J. Chem. Soc. Dalton Trans.*		1571	1983

APPENDIX 2 (*cont.*)

CABYUZ	*J. Chem. Soc. Dalton Trans.*		2025	1983
CABZAG	*J. Chem. Soc. Dalton Trans.*		2025	1983
CACFUH	*J. Chem. Soc. Chem. Commun.*		963	1981
CACLUN	*J. Chem. Soc. Dalton Trans.*		2091	1983
CACMIC	*J. Chem. Soc. Dalton Trans.*		2011	1983
CACPIF	*J. Chem. Soc. Dalton Trans.*		1679	1983
CACRIH	*Polyhedron*	2	843	1983
CACWOS	*Organometallics*	2	535	1983
CADHOE	*Acta Cryst. Sect. C*	39	997	1983
CADMAV	*Z. Anorg. Allg. Chem.*	502	35	1983
CADPEC	*Can. J. Chem.*	61	1146	1983
CADYAH	*Angew. Chem. Int. Ed. Engl.*	22	503	1983
CAFCUH	*Organometallics*	2	935	1983
CAFFEU	*Organometallics*	2	938	1983
CAFFIY	*Organometallics*	2	938	1983
CAFJUO	*Acta Cryst. Sect. C*	39	1197	1983
CAFLAW	*J. Organomet. Chem.*	253	53	1983
CAFLEA	*J. Organomet. Chem.*	253	53	1983
CAFNOM	*Acta Cryst. Sect. C*	39	1041	1983
CAFSOR	*Acta Cryst. Sect. C*	39	1210	1983
CAFZUE	*J. Organomet. Chem.*	248	C26	1983
CAGKEA	*Organometallics*	2	558	1983
CAGSAE	*Acta Cryst. Sect. C*	39	1367	1983
CAGSIM	*J. Chem. Soc. Dalton Trans.*		1873	1983
CAHGOH	*Inorg. Chem.*	22	1897	1983
CAHGUN	*Inorg. Chem.*	22	1794	1983
CAHHAU	*Inorg. Chem.*	22	1791	1983
CAHJIE	*Inorg. Chem.*	22	1744	1983
CAHRUY	*J. Chem. Soc. Dalton Trans.*		2117	1983
CAHZAM	*J. Am. Chem. Soc.*	105	5834	1983
CAHZUG	*J. Am. Chem. Soc.*	105	5804	1983
CAIMCO	*J. Chem. Soc. A*		2558	1970
CAJCEV	*Transition Met. Chem.*	8	127	1983
CAJFAU	*Inorg. Chem.*	22	1887	1983
CAJGEZ	*J. Am. Chem. Soc.*	105	5137	1983
CAJHOK	*J. Chem. Soc. Chem. Commun.*		1163	1983
CAKCIA	*Inorg. Chem.*	22	1739	1983
CAKGAW	*J. Chem. Soc. Dalton Trans.*		1789	1983
CAKGIE	*Inorg. Chem.*	22	1695	1983
CAKNEH01	*Inorg. Chem.*	23	122	1984
CAKNIL10	*Inorg. Chim. Acta*	75	199	1983
CAKSOW	*Organometallics*	2	1049	1983
CAKTUD	*J. Am. Chem. Soc.*	105	4955	1983
CALCEX	*J. Am. Chem. Soc.*	103	6507	1981
CALGAX	*Inorg. Chem.*	20	3904	1981
CALHIG	*J. Chem. Soc. Chem. Commun.*		1177	1983
CALNUY	*J. Chem. Soc. Chem. Commun.*		1283	1983
CAMCUO	*Inorg. Chim. Acta*	75	103	1983
CAMKIK	*Organometallics*	2	1172	1983
CAMLAD	*Organometallics*	2	1167	1983
CAMROX	*Inorg. Chem.*	22	2356	1983
CAMSOB	*Rev. Chim. Minér.*	16	555	1979
CAMTEP	*J. Am. Chem. Soc.*	105	5939	1983
CAMVER	*J. Am. Chem. Soc.*	105	5954	1983
CAMWOC	*Angew. Chem. Int. Ed. Engl.*	22	498	1983
CAMXOD	*Nouv. J. Chim.*	7	467	1983
CANBRU	*J. Organomet. Chem.*	72	247	1974
CANFAY	*Inorg. Chem.*	22	2351	1983
CANHAA	*J. Organomet. Chem.*	255	231	1984
CANZUM	*J. Chem. Soc. Chem. Commun.*		1377	1983
CAPFOO	*J. Am. Chem. Soc.*	105	6163	1983
CAPSOB	*Inorg. Chim. Acta*	75	173	1983
CARJOU	*Organometallics*	2	1369	1983
CARKIP	*Organometallics*	2	1437	1983
CARWAT	*J. Chem. Soc. Chem. Commun.*		1358	1983
CASDIJ	*Z. Naturforsch. Teil B*	38	1454	1983
CASPIV	*Z. Anorg. Allg. Chem.*	504	7	1983
CASVIB	*J. Organomet. Chem.*	256	349	1983
CASYEA	*J. Chem. Soc. Chem. Commun.*		1366	1983
CATETH	*J. Am. Chem. Soc.*	100	7882	1978
CATGEJ	*J. Organomet. Chem.*	256	111	1983
CATKOX	*J. Chem. Soc. Chem. Commun.*		1351	1983
CATKUD	*J. Chem. Soc. Chem. Commun.*		1351	1983
CATMIT	*Inorg. Chem.*	22	2736	1983
CATSEV	*Z. Naturforsch. Teil B*	38	1406	1983
CATSUL	*Z. Naturforsch. Teil B*	38	1488	1983
CAVMOB	*J. Chem. Soc. Chem. Commun.*		1490	1983
CAVREW	*J. Am. Chem. Soc.*	105	6162	1983
CAVVEA	*J. Chem. Soc. Dalton Trans.*		2375	1983
CAVYON	*Koord. Khim.*	9	986	1983
CAWBAD	*Koord. Khim.*	9	1114	1983
CAWGAI	*Inorg. Chem.*	22	2903	1983
CAWJAL	*Inorg. Chem.*	22	2892	1983
CAWLIV	*Angew. Chem. Int. Ed. Engl.*	22	774	1983
CAWSUO	*Inorg. Chem.*	22	3361	1983
CAWTAV	*Inorg. Chem.*	22	3355	1983
CAXMIX	*Acta Cryst. Sect. C*	39	1643	1983
CAXPUM	*Acta Cryst. Sect. C*	39	1620	1983
CAXYOP	*Inorg. Chim. Acta*	80	57	1983
CAYFAJ	*J. Am. Chem. Soc.*	105	7460	1983
CAYGAK	*J. Organomet. Chem.*	258	357	1983
CAYGOY	*J. Am. Chem. Soc.*	105	7280	1983
CAYJAN	*Can. J. Chem.*	61	2141	1983
CAYLAP	*Angew. Chem. Int. Ed. Engl.*	22	790	1983
CAYMAQ	*Angew. Chem. Int. Ed. Engl.*	22	414	1983
CAYXAB	*Inorg. Chim. Acta*	73	261	1983
CAZCIP	*J. Sci. Hiroshima Univ. A*	47	1	1983
CAZGUF	*Jilin Daxue Ziran Kex. Xue*		103-2	1983
CAZHAM	*Jilin Daxue Ziran Kex. Xue*		103-2	1983
CAZJAO10	*Z. Naturforsch. Teil B*	39	880	1984
CAZJES10	*Z. Naturforsch. Teil B*	39	880	1984
CAZZAE	*Inorg. Chem.*	22	3090	1983
CBACRC	*J. Chem. Soc. Dalton Trans.*		52	1980
CBFPPT10	*Inorg. Chem.*	12	1663	1973
CBUTIR	*Cryst. Struct. Commun.*	2	527	1973
CBZTET10	*Polyhedron*	2	1031	1983
CBZYTA	*J. Am. Chem. Soc.*	100	3793	1978
CCHXPC	*Inorg. Chem.*	18	166	1979
CCPZRA	*Inorg. Chem.*	19	3812	1980
CDACET	*J. Chem. Soc. Dalton Trans.*		956	1972
CDCYAC	*J. Chem. Soc. Dalton Trans.*		285	1974
CDMALD	*J. Chem. Soc. Dalton Trans.*		674	1974
CDMSOR	*J. Chem. Soc. Dalton Trans.*		2480	1975
CEBDIW	*Acta Chem. Scand. Ser. A*	37	697	1983
CEBREG	*Finn. Chem. Lett.*		120	1983
CECATI	*Inorg. Chem.*	18	1611	1979
CECCIW	*Angew. Chem. Int. Ed. Engl.*	22	996	1983
CECGOG	*Angew. Chem. Int. Ed. Engl.*	22	1000	1983
CECGUM	*Angew. Chem. Int. Ed. Engl.*	22	984	1983
CECKOK	*Organometallics*	2	1458	1983
CECLEB10	*Koord. Khim.*	10	123	1984
CECLIF10	*Koord. Khim.*	10	1128	1984
CECROR	*Organometallics*	2	1505	1983
CECWEM	*Z. Kristallogr.*	164	237	1983
CEDHUO	*J. Chem. Soc. Commun.*		175	1984
CEDMON	*Organometallics*	2	1595	1983
CEDNOO	*Polyhedron*	2	1031	1983
CEDXEO	*Inorg. Chem.*	22	3424	1983
CEFCUL	*Inorg. Chem.*	22	3480	1983
CEFHEA	*Organometallics*	2	1763	1983
CEFHOK	*Kristallografiya*	28	886	1983
CEFMAB	*Polyhedron*	2	1317	1983
CEFMIJ	*Polyhedron*	2	1201	1983
CEFNOQ	*S. Afr. J. Chem.*	36	97	1983
CEFPEI	*Organometallics*	2	1889	1983
CEFSIP	*Angew. Chem. Int. Ed. Engl.*	23	68	1984
CEFVIS	*J. Chem. Soc. Chem. Commun.*		282	1984
CEFVOY	*J. Am. Chem. Soc.*	106	329	1984
CEFVUE	*J. Am. Chem. Soc.*	105	7789	1983
CEFYAN	*Inorg. Chem.*	22	3671	1983
CEGCIA	*J. Chem. Soc. Dalton Trans.*		55	1984
CEGCOG	*J. Chem. Soc. Dalton Trans.*		55	1984
CEGGUQ	*Inorg. Chem.*	22	3654	1983
CEGHAX	*J. Am. Chem. Soc.*	105	7750	1983
CEGHEB	*J. Am. Chem. Soc.*	105	7750	1983
CEGNAD	*Z. Kristallogr.*	164	259	1983
CEHFEA	*J. Chem. Soc. Chem. Commun.*		240	1984
CEHMOR	*J. Am. Chem. Soc.*	106	410	1984
CEHTUE	*J. Am. Chem. Soc.*	105	6763	1983
CEHXAO	*Inorg. Chem.*	22	3489	1983
CEJDEA	*J. Am. Chem. Soc.*	106	451	1984
CEJPEM	*Acta Cryst. Sect. C*	40	82	1984
CEKGEE	*Organometallics*	3	293	1984
CEKGII	*Organometallics*	3	293	1984
CEKGOO	*Acta Cryst. Sect. C*	40	409	1984
CELJEI	*Acta Cryst. Sect. C*	40	354	1984
CELLAG	*Acta Cryst. Sect. C*	40	359	1984
CEMCUS	*Inorg. Chim. Acta*	72	141	1983
CEMMIQ	*Inorg. Chem.*	22	3706	1983

APPENDIX 2 (*cont.*)

CEMSES	*Inorg. Chem.*	22	4091	1983
CEMSIW	*Inorg. Chem.*	22	4091	1983
CEMSUI	*Inorg. Chem.*	23	88	1984
CEMTIX	*Inorg. Chem.*	23	99	1984
CEMWEW	*Inorg. Chem.*	22	3911	1983
CEMXIB	*J. Am. Chem. Soc.*	105	7751	1983
CENFAC01	*J. Chem. Soc. Dalton Trans.*		1917	1983
CENRES	*Inorg. Chem.*	22	3776	1983
CENSUJ	*J. Chem. Soc. Dalton Trans.*		229	1984
CENTAQ	*J. Chem. Soc. Dalton Trans.*		229	1984
CEPBII	*J. Chem. Soc. Chem. Commun.*		434	1984
CEPFPP	*J. Chem. Soc. Dalton Trans.*		2043	1977
CEPGUZ	*J. Inorg. Biochem.*	19	237	1983
CEPHOU	*Inorg. Chem.*	23	227	1984
CEPHUA	*Inorg. Chem.*	23	227	1984
CEPLUE	*J. Chem. Soc. Chem. Commun.*		485	1984
CEPMAL	*Aust. J. Chem.*	36	1107	1983
CEPMOZ	*J. Am. Chem. Soc.*	96	5427	1974
CEPYIF	*J. Organomet. Chem.*	262	123	1984
CERCUX	*Acta Cryst. Sect. C*	40	616	1984
CERDAE	*Acta Cryst. Sect. C*	40	619	1984
CERFAG	*Acta Cryst. Sect. C*	40	635	1984
CERFEK	*Acta Cryst. Sect. C*	40	635	1984
CERJIS	*J. Organomet. Chem.*	264	327	1984
CERKUF	*J. Chem. Soc. Chem. Commun.*		425	1984
CESGAI10	*Organometallics*	3	1003	1984
CESJOZ	*J. Cryst. Spectrosc.*	14	21	1984
CESKIU	*J. Cryst. Spectrosc.*	14	143	1984
CESNAP	*J. Chem. Soc. Dalton Trans.*		735	1984
CESNET	*J. Chem. Soc. Dalton Trans.*		719	1984
CESTOJ	*J. Am. Chem. Soc.*	106	1699	1984
CESVUR	*J. Am. Chem. Soc.*	106	1853	1984
CESXUT	*J. Chem. Soc. Chem. Commun.*		501	1984
CESYAA	*J. Chem. Soc. Chem. Commun.*		501	1984
CESYII	*Inorg. Chem.*	22	3251	1983
CESZOP	*Can. J. Chem.*	62	332	1984
CESZUV	*Can. J. Chem.*	62	332	1984
CETGEN	*Inorg. Chim. Acta*	70	159	1983
CETGIR	*Inorg. Chim. Acta*	70	159	1983
CETKUH	*J. Chem. Soc. Dalton Trans.*		833	1984
CETMRH	*Inorg. Chem.*	18	2438	1979
CETPIR	*J. Organomet. Chem.*	90	101	1975
CETSIR	*Acta Cryst. Sect. B*	36	1206	1980
CEVFUE10	*J. Am. Chem. Soc.*	106	5934	1984
CEVHOA	*J. Am. Chem. Soc.*	106	1323	1984
CEVLAQ	*J. Chem. Soc. Dalton Trans.*		785	1984
CEWZIN10	*Acta Cryst. Sect. C*	40	1544	1984
CEXHUI	*Inorg. Chem.*	23	349	1984
CEXKAR	*Inorg. Chem.*	23	363	1984
CEXKUL	*Inorg. Chem.*	23	359	1984
CEXLUM	*Inorg. Chem.*	23	354	1984
CEXNAU	*Organometallics*	3	596	1984
CEXSAZ	*Inorg. Chem.*	23	511	1984
CEXTII	*Organometallics*	3	599	1984
CEXZIO	*Inorg. Chem.*	23	343	1984
CEXZOU	*Inorg. Chem.*	23	343	1984
CEYBEN	*Inorg. Chem.*	23	338	1984
CEYBIR	*Inorg. Chem.*	23	409	1984
CEYCOY	*J. Chem. Soc. Dalton Trans.*		399	1984
CEYCUE	*J. Chem. Soc. Dalton Trans.*		399	1984
CEYPEB	*J. Organomet. Chem.*	266	45	1984
CEYRON	*Acta Cryst. Sect. C*	40	795	1984
CEZKEX	*Acta Cryst. Sect. C*	40	751	1984
CEZMUP	*Acta Cryst. Sect. C*	40	746	1984
CEZNIE	*Inorg. Chim. Acta*	85	L19	1984
CEZWEJ	*Inorg. Chim. Acta*	84	57	1984
CEZWOT	*Inorg. Chim. Acta*	84	179	1984
CEZXAG	*Inorg. Chim. Acta*	84	179	1984
CEZYUB	*Inorg. Chim. Acta*	84	187	1984
CFBYRH	*Acta Cryst. Sect. B*	35	2321	1979
CFTPVP	*J. Organomet. Chem.*	150	157	1978
CHBPTC	*J. Am. Chem. Soc.*	101	4581	1979
CHDQOS	*J. Chem. Soc. Chem. Commun.*		853	1978
CHGACA	*Acta Cryst. Sect. B*	35	1239	1979
CHGALD	*J. Chem. Soc. Dalton Trans.*		1573	1978
CHPCUP	*Can. J. Chem.*	53	1949	1975
CHPECI	*J. Organomet. Chem.*	149	345	1978
CHPMOC	*Acta Cryst. Sect. B*	34	2439	1978
CHPRUS10	*J. Chem. Soc. Dalton Trans.*		2220	1981
CHVINO	*Acta Cryst. Sect. B*	34	2466	1978
CHXPCO	*Aust. J. Chem.*	31	47	1978
CIBGEZ	*J. Chem. Soc. Chem. Commun.*		799	1984
CIBHAW	*Inorg. Chim. Acta*	81	47	1984
CIBKED	*Z. Naturforsch. Teil B*	39	590	1984
CIBLUU	*Z. Naturforsch. Teil B*	39	538	1984
CIBYOB	*Inorg. Chim. Acta*	82	167	1984
CIBZAO	*Inorg. Chim. Acta*	82	167	1984
CICBOF	*Inorg. Chim. Acta*	82	161	1984
CICBUL	*Inorg. Chim. Acta*	82	161	1984
CICFID	*Inorg. Chim. Acta*	81	147	1984
CICLOP	*Z. Naturforsch. Teil B*	39	582	1984
CICYAO	*Acta Cryst.*	40	935	1984
CIDBAS	*Inorg. Chem.*	23	936	1984
CIDBEW	*Inorg. Chem.*	23	945	1984
CIDBOG	*Chem. Ber.*	117	1052	1984
CIDHEC	*J. Am. Chem. Soc.*	106	2990	1984
CIDJEE	*J. Am. Chem. Soc.*	106	2965	1984
CIFCAV	*J. Chem. Soc. Chem. Commun.*		710	1984
CIFGON	*Inorg. Chem.*	23	914	1984
CIFMAF	*J. Chem. Soc. Dalton Trans.*		845	1984
CIFNIO	*Inorg. Chem.*	23	938	1984
CIFXOE	*J. Chem. Soc. Chem. Commun.*		841	1984
CIGCOK	*Angew. Chem. Int. Ed. Engl.*	23	377	1984
CIGRAL	*Inorg. Chim. Acta*	92	151	1984
CIGVET	*Inorg. Chem.*	23	1009	1984
CIHLIO	*Acta Cryst. Sect. C*	40	1186	1984
CIHNEM	*Acta Cryst. Sect. C*	40	1161	1984
CIHRIU	*Angew. Chem. Int. Ed. Engl.*	23	311	1984
CIHXIA	*J. Organomet. Chem.*	263	C33	1984
CIHYOH	*J. Am. Chem. Soc.*	106	3054	1984
CIJDAA	*J. Struct. Chem.*	3	57	1984
CIJLUC	*J. Organomet. Chem.*	265	249	1984
CIJWIB	*Angew. Chem. Int. Ed. Engl.*	23	376	1984
CIJYOJ	*Acta Cryst. Sect. C*	40	1172	1984
CIKHOT	*J. Struct. Chem.*	3	13	1984
CIKJUB	*J. Am. Chem. Soc.*	106	2579	1984
CIKKAI	*J. Am. Chem. Soc.*	106	2583	1984
CIKPUH	*Angew. Chem. Int. Ed. Engl.*	22	977	1983
CIKTOF	*Inorg. Chim. Acta.*	84	221	1984
CILCUV	*Organometallics*	3	939	1984
CILYAX	*Acta Cryst. Sect. C*	40	1320	1984
CIMGEK	*Acta Cryst. Sect. C*	40	1357	1984
CIMINU10	*J. Am. Chem. Soc.*	97	4519	1975
CIMVID	*J. Chem. Soc. Chem. Commun.*		1141	1984
CINKAL	*J. Chem. Soc. Chem. Commun.*		1000	1984
CINKUF	*Inorg. Chem.*	23	1387	1984
CINLAM	*J. Organomet. Chem.*	265	C19	1984
CINREW	*Koord. Khim.*	10	850	1984
CIPDIO	*J. Am. Chem. Soc.*	106	3356	1984
CIPGAJ	*Acta Cryst. Sect. C*	40	1552	1984
CIPNEU	*J. Am. Chem. Soc.*	106	3527	1984
CIPTAW	*Inorg. Chim. Acta*	83	75	1984
CIPTMN	*J. Chem. Soc. Dalton Trans.*		1625	1980
CIRDAI	*Polyhedron*	3	651	1984
CIRHUG	*Polyhedron*	3	505	1984
CIRJAO	*Polyhedron*	3	385	1984
CIRMAR	*Acta Cryst. Sect. C*	40	1533	1984
CIRNOG	*J. Chem. Soc. Dalton Trans.*		2039	1984
CIRNUM	*J. Chem. Soc. Dalton Trans.*		2039	1984
CIRSAX	*Inorg. Chem.*	23	1739	1984
CIRSEB	*Inorg. Chem.*	23	1739	1984
CIRVOO	*Acta Cryst. Sect. C*	40	1562	1984
CISZOT	*J. Chem. Soc. Chem. Commun.*		1082	1984
CITCIR	*J. Am. Chem. Soc.*	106	3371	1984
CITDEO	*Polyhedron*	3	303	1984
CITKIZ	*Aust. J. Chem.*	36	2175	1983
CIXHEW	*Inorg. Chem.*	23	2271	1984
CIXJIC	*J. Chem. Soc. Dalton Trans.*		1675	1984
CIXKAV	*Inorg. Chem.*	23	2286	1984
CIXLIE	*J. Am. Chem. Soc.*	106	4460	1984
CIXRUW	*Can. J. Chem.*	62	696	1984
CIXTUY	*Angew. Chem. Int. Ed. Engl.*	23	522	1984
CIXYAJ	*Teor. Eksp. Khim.*	19	685	1983
CIYBAN	*Inorg. Chem.*	23	2303	1984
CIYKAW	*Organometallics*	3	1223	1984
CIYMEC	*Organometallics*	3	1312	1984
CIYMIG	*Organometallics*	3	1310	1984
CIYTUZ01	*Organometallics*	3	1158	1984
CIZBES	*J. Chem. Soc. Chem. Commun.*		1317	1984

APPENDIX 2 (*cont.*)

CIZBOC	*J. Chem. Soc. Dalton Trans.*		1731	1984
CIZGIB02	*Kristallografiya*	29	455	1984
CIZNUU	*J. Chem. Soc. Dalton Trans.*		1059	1984
CIZTEK	*J. Organomet. Chem.*	270	C49	1984
CLBCNV	*Inorg. Chem.*	19	3379	1980
CLCAME01	*Zh. Neorg. Khim.*	28	597	1983
CLFORE10	*Koord. Khim.*	6	963	1980
CLOSMO	*Transition Met. Chem.*	5	172	1980
CLPDZN	*Bull. Chem. Soc. Jpn*	53	1101	1980
CLPHTI	*Inorg. Chem.*	5	1782	1966
CLPOZN	*Acta Cryst. Sect. B*	36	2409	1980
CLPRCV	*Acta Cryst. Sect. B*	37	945	1981
CLPZIR	*J. Inorg. Nucl. Chem.*	35	4103	1973
CLTIMN	*Inorg. Chem.*	17	1848	1978
CLTPOC01	To be published			1980
CLZRAL	*J. Organomet. Chem.*	208	327	1981
CMASNI	*Inorg. Chim. Acta*	40	171	1980
CMNCBR	*J. Am. Chem. Soc.*	97	3053	1975
CMPORZ	*J. Am. Chem. Soc.*	100	3025	1978
CMURAG	*J. Cryst. Mol. Struct.*	2	125	1972
CMZTFE	*J. Am. Chem. Soc.*	96	7826	1974
CNBPAC	*J. Organomet. Chem.*	165	39	1979
CNBRUB	*J. Chem. Soc. Chem. Commun.*		271	1981
CNCOPP10	*Inorg. Chem.*	12	1304	1973
CNMPRE	*Inorg. Chem.*	10	578	1971
CNOFEA	*Koord. Khim.*	7	949	1981
CNOFEB	*Koord. Khim.*	7	949	1981
CNOPIR	*Inorg. Chem.*	7	2345	1968
CNPLPT	*J. Chem. Soc. Dalton Trans.*		973	1980
CNPRCV	*J. Cryst. Mol. Struct.*	10	61	1980
CNTPCP	*J. Chem. Soc. Dalton Trans.*		1932	1980
COBDUS	*J. Chem. Soc. Dalton Trans.*		1069	1984
COBGIJ	*J. Chem. Soc. Dalton Trans.*		1659	1984
COBHGA	*Inorg. Chem.*	20	863	1981
COBLIO	*J. Am. Chem. Soc.*	106	4749	1984
COBSOB	*J. Organomet. Chem.*	272	C17	1984
COBXOG	*J. Chem. Soc. Chem. Commun.*		1400	1984
COCKAG	*Inorg. Chem.*	23	2207	1984
COCKOU	*J. Chem. Soc. Chem. Commun.*		1362	1984
COCLEL	*J. Chem. Soc. Chem. Commun.*		1351	1984
COCNAJ	*Angew. Chem. Int. Ed. Engl.*	23	77	1984
COCPOZ	*Acta Cryst. Sect. C*	40	1699	1984
COCTCE	*Inorg. Chem.*	11	171	1972
COCTFT10	*Inorg. Chem.*	19	2560	1980
COCXOH	*J. Organomet. Chem.*	272	C62	1984
COCZEZ	*Inorg. Chim. Acta*	86	101	1984
CODCON	*J. Chem. Soc. Chem. Commun.*		1402	1984
CODHIM	*J. Cryst. Spectrosc.*	14	383	1984
CODJAG	*Organometallics*	3	1414	1984
CODJIO	*Organometallics*	3	1444	1984
CODPIR10	*Inorg. Chem.*	12	260	1973
COFVIC	*Z. Naturforsch. Teil B*	39	1076	1984
COFZEC	*Inorg. Chim. Acta*	86	L65	1984
COGHEL	*J. Chem. Soc. Dalton Trans.*		2081	1984
COGSIA	*Gazz. Chim. Ital.*	113	761	1983
COGWOK	*Inorg. Chem.*	23	2838	1984
COGXOL	*Inorg. Chem.*	23	2732	1984
COGXRU	*Inorg. Chem.*	19	3343	1980
COGXUR	*Inorg. Chem.*	23	2732	1984
COHCUX	*Aust. J. Chem.*	37	1395	1984
COHHIQ	*Inorg. Chem.*	23	2803	1984
COHNUI	*Inorg. Chim. Acta*	87	115	1984
COHTOI	*J. Chem. Soc. Chem. Commun.*		1425	1984
COJBOS	*J. Chem. Soc. Chem. Commun.*		1508	1984
COJDOU	*Z. Naturforsch. Teil B*	39	1199	1984
COJDUA	*Z. Naturforsch. Teil B*	39	1199	1984
COJYEF	*Koord. Khim.*	10	1116	1984
COKCIO	*Acta Cryst. Sect. C*	40	1820	1984
COKDUB	*Acta Cryst. Sect. C*	40	1836	1984
COKPIB	*Inorg. Chim. Acta*	95	147	1984
COKTIF	*J. Chem. Soc. Chem. Commun.*		1398	1984
COKZAD	*Inorg. Chim. Acta*	95	217	1984
COLDIQ	*Angew. Chem. Int. Ed. Engl.*	23	721	1984
COLDOW	*Inorg. Chem.*	23	2459	1984
COLDUC	*Inorg. Chem.*	23	2459	1984
COLFEO	*Angew. Chem. Int. Ed. Engl.*	23	726	1984
COLNAS	*J. Am. Chem. Soc.*	106	2033	1984
COLNEW	*J. Am. Chem. Soc.*	106	2033	1984
COLPIC	*J. Am. Chem. Soc.*	106	5561	1984
COLPOI	*J. Am. Chem. Soc.*	106	5561	1984
COLSEB	*Inorg. Chem.*	23	2519	1984
COLVII	*Inorg. Chem.*	23	2575	1984
COLWAB	*Aust. J. Chem.*	37	35	1984
COLZEI	*Angew. Chem. Int. Ed. Engl.*	23	735	1984
COMMAS	*J. Organomet. Chem.*	276	287	1984
COMPEZ	*Koord. Khim.*	10	1266	1984
COMPRH	*Z. Naturforsch. Teil B*	35	1104	1980
COMSUS	*J. Chem. Soc. Chem. Commun.*		1689	1984
COMTBH	*Inorg. Chem.*	18	3037	1979
COMYUY	*Organometallics*	3	1495	1984
CONBIQ	*J. Organomet. Chem.*	276	99	1984
CONFEQ01	*J. Am. Chem. Soc.*	106	5458	1984
CONKEV	*J. Chem. Soc. Dalton Trans.*		1343	1984
CONSON	*J. Chem. Soc. Dalton Trans.*		1781	1984
CONSUT	*J. Chem. Soc. Dalton Trans.*		1781	1984
CONTEE	*J. Chem. Soc. Chem. Commun.*		1283	1984
COPFOC	*Acta Cryst. Sect. C*	40	2030	1984
COPGAP	*Acta Cryst. Sect. C*	40	2035	1984
COPHAV	*Acta Cryst. Sect. B*	36	304	1980
COPKEX	*J. Chem. Soc. Chem. Commun.*		16	1985
COPLEY	*J. Am. Chem. Soc.*	106	5729	1984
COPMEZ	*J. Organomet. Chem.*	273	C29	1984
COPMID	*J. Organomet. Chem.*	273	C39	1984
COPNIR	*J. Organomet. Chem.*	197	95	1980
COPVIM	*J. Am. Chem. Soc.*	106	5178	1984
COPVOS	*J. Am. Chem. Soc.*	106	5178	1984
COPXIO	*J. Am. Chem. Soc.*	106	6305	1984
CORHOG	*J. Am. Chem. Soc.*	106	4478	1984
COSLAX	*Bull. Chem. Soc. Jpn*	57	1809	1984
COSLEB	*Bull. Chem. Soc. Jpn*	57	1809	1984
COSLIF	*Bull. Chem. Soc. Jpn*	57	1809	1984
COSMOM	*J. Chem. Soc. Chem. Commun.*		1710	1984
COSROR	*J. Organomet. Chem.*	275	63	1984
COSSAE	*J. Organomet. Chem.*	273	221	1984
COSSOS	*Angew. Chem. Int. Ed. Engl.*	23	640	1984
COSTEJ	*Angew. Chem. Int. Ed. Engl.*	23	626	1984
COSTIN	*J. Organomet. Chem.*	276	79	1984
COSWUC	*Acta Cryst. Sect. C*	41	27	1985
COSZOZ	*J. Am. Chem. Soc.*	106	6841	1984
COTDOE	*J. Organomet. Chem.*	270	365	1984
COTFAS	*J. Organomet. Chem.*	273	333	1984
COTFEW	*J. Organomet. Chem.*	273	111	1984
COTFPT	*J. Chem. Soc. Dalton Trans.*		2095	1980
COTGEX	*Inorg. Chem.*	23	2867	1984
COTPOQ01	*Acta Cryst. Sect. B*	40	606	1984
COTROP	*J. Chem. Soc. Dalton Trans.*		1898	1975
COTROQ	*Aust. J. Chem.*	32	1219	1979
COTSEJ	*Angew. Chem. Int. Ed. Engl.*	23	160	1984
COTTIC10	*J. Organomet. Chem.*	92	329	1975
COTZRF	*J. Organomet. Chem.*	42	129	1972
COTZRH10	*Inorg. Chem.*	14	3053	1975
COVBIY	*Inorg. Chem.*	23	2853	1984
COVROU	*J. Chem. Soc. Chem. Commun.*		1585	1984
COVVUE	*J. Organomet. Chem.*	273	361	1984
COVYIV	*J. Chem. Soc. Chem. Commun.*		178	1985
COWGEA	*Angew. Chem. Int. Ed. Engl.*	23	740	1984
COWSOW	*Acta Cryst. Sect. C*	41	55	1985
CPAINC	*J. Chem. Soc. Dalton Trans.*		83	1979
CPASRU	*Inorg. Chem.*	18	2658	1979
CPBORN	*Z. Naturforsch. Teil B*	33	1410	1978
CPBUMO	*J. Chem. Soc. Dalton Trans.*		2629	1973
CPBZTB	*J. Am. Chem. Soc.*	102	6744	1980
CPCBCR	*Chem. Ber.*	112	1320	1979
CPCDSV	*J. Chem. Soc. Dalton Trans.*		1612	1979
CPCFEA10	*Inorg. Chem.*	21	1321	1982
CPCLBT	*Zh. Strukt. Khim.*	17	1073	1976
CPCMZW	*Inorg. Chem.*	18	2423	1979
CPCOPT	*J. Am. Chem. Soc.*	95	2175	1973
CPDYSW10	*J. Cryst. Mol. Struct.*	2	135	1972
CPETNB	*J. Am. Chem. Soc.*	96	5420	1974
CPFMPI10	*J. Chem. Soc. Dalton Trans.*		291	1975
CPFPEY	*J. Chem. Soc. Dalton Trans.*		2025	1974
CPFPTI10	*J. Am. Chem. Soc.*	105	416	1983
CPFVLV	*J. Organomet. Chem.*	197	217	1980
CPFYBA10	*Inorg. Chem.*	19	2999	1980
CPHMOC	*J. Organomet. Chem.*	212	77	1981
CPHSTH	*Acta Cryst. Sect. B*	36	292	1980
CPHSVB	*Inorg. Chem.*	19	2755	1980
CPITTI	*Acta Cryst. Sect. B*	32	909	1976

APPENDIX 2 (*cont.*)

CPMNTI	*Acta Cryst. Sect. B*	32	909	1976
CPMPTA	*J. Chem. Soc. Dalton Trans.*		793	1981
CPNOCC10	*J. Chem. Soc. A*		605	1970
CPOMOA	*J. Am. Chem. Soc.*	103	1269	1981
CPPHZR	*J. Organomet. Chem.*	204	67	1981
CPPYMO10	*Acta Cryst. Sect. B*	33	2608	1977
CPPYYB01	*Inorg. Chem.*	16	2710	1977
CPSENI	*Inorg. Chim. Acta*	39	111	1980
CPSNBA	*Acta Cryst. Sect. B*	36	2986	1980
CPSNBB	*Acta Cryst. Sect. B*	36	2986	1980
CPSXER	*Inorg. Chem.*	15	797	1976
CPTCFF	*J. Organomet. Chem.*	179	187	1979
CPTHGD10	*J. Organomet. Chem.*	192	65	1980
CPTICN10	*J. Chem. Soc. Dalton Trans.*		152	1979
CPTIOO	*J. Am. Chem. Soc.*	99	5829	1977
CPTOMN	*J. Chem. Soc. Chem. Commun.*		404	1977
CPTPHF	*J. Am. Chem. Soc.*	98	2454	1976
CPYBHF	*J. Chem. Soc. Chem. Commun.*		810	1980
CPYRTI10	*Inorg. Chem.*	19	2368	1980
CPZHZN	*J. Chem. Soc. Dalton Trans.*		447	1976
CPZRHF10	*Inorg. Chem.*	14	352	1975
CRMTBH	*Inorg. Chem.*	18	3037	1979
CROPPH10	*Inorg. Chem.*	21	657	1982
CSACTI	*Cryst. Struct. Commun.*	9	469	1980
CSCREC	*Inorg. Chem.*	5	1189	1966
CSTPRH	*Inorg. Chem.*	8	1921	1969
CTAZPD10	*Inorg. Chem.*	15	2428	1976
CTDPIR	*Inorg. Chem.*	19	2733	1980
CTENCO20	*Acta Cryst. Sect. B*	31	85	1975
CTERUC	*J. Am. Chem. Soc.*	90	5412	1968
CTHUCO10	*Inorg. Chem.*	8	2367	1969
CTMPTC	*J. Chem. Soc. Dalton Trans.*		125	1976
CTMSIC	*J. Chem. Soc. Dalton Trans.*		2010	1980
CTNSCR10	*Inorg. Chem.*	18	3548	1979
CTPIRB	*J. Chem. Soc. Dalton Trans.*		117	1979
CTZPRU	*Inorg. Chem.*	12	1676	1973
CUCOES	*Bull. Chem. Soc. Jpn*	51	2920	1978
CUDPTZ10	*Aust. J. Chem.*	28	2377	1975
CUMPCO	*J. Organomet. Chem.*	113	57	1976
CUSGAY	*Inorg. Chem.*	23	4758	1984
CUTROP01	*Acta Cryst. Sect. B*	34	3071	1978
CVMOMP10	*Inorg. Chem.*	13	1667	1974
CXFMPR	*J. Chem. Soc. Dalton Trans.*		390	1976
CXINPR10	*J. Organomet. Chem.*	120	361	1976
CXPHOW	*Acta Cryst. Sect. B*	34	762	1978
CXPORH	*J. Organomet. Chem.*	71	125	1974
CYCRTF	*J. Organomet. Chem.*	131	65	1977
CYPRMO	*Inorg. Chem.*	14	98	1975
CYPRZR10	*Inorg. Chem.*	19	2368	1980
CYSFAC10	*Inorg. Chem.*	7	1770	1968
CYZNIC10	*Koord. Khim.*	5	585	1979
DAESCO	*Acta Chem. Scand. Ser. A*	32	501	1978
DAPRCX	*Finn. Chem. Lett.*		58	1978
DAPSCR10	*Inorg. Chem.*	15	1814	1976
DAPSMO	*Aust. J. Chem.*	32	1199	1979
DASTCA10	*Acta Cryst. Sect. B*	36	1662	1980
DAZHCF	*J. Am. Chem. Soc.*	99	3293	1977
DAZRUC10	*J. Am. Chem. Soc.*	99	6588	1977
DBEZHG	*Acta Cryst. Sect. B*	35	746	1979
DCAZPD	*Inorg. Chem.*	14	2475	1975
DCHPDY10	*J. Chem. Soc. Dalton Trans.*		1300	1980
DCHPLU10	*J. Chem. Soc. Dalton Trans.*		1300	1980
DCMCPD	*Inorg. Chem.*	16	2403	1977
DEDTFE10	*Inorg. Chem.*	16	2691	1977
DETSOK	*J. Am. Chem. Soc.*	107	7212	1985
DFBENV	*Inorg. Chem.*	15	2976	1976
DIPNIP	*Z. Naturforsch. Teil B*	34	1289	1979
DMDECO01	*Acta Cryst. Sect. B*	35	2547	1979
DMDTPN10	*Acta Cryst. Sect. B*	25	1939	1969
DMHERU01	*J. Chem. Soc. Dalton Trans.*		1040	1978
DMPCOV	*Chem. Ber.*	111	3472	1978
DMPMPW10	*Inorg. Chem.*	18	2454	1979
DMPZCO	*Can. J. Chem.*	57	3119	1979
DMPZFE	*Can. J. Chem.*	57	3119	1979
DMSOHG	*Acta Chem. Scand. Ser. A*	32	95	1978
DMXPMO10	*Inorg. Chem.*	17	2087	1978
DPCBWC	*J. Am. Chem. Soc.*	99	2127	1977
DPCLRE10	*Koord. Khim.*	3	1060	1977
DPEPOW	*J. Organomet. Chem.*	34	353	1972
DPINRE	*Chem. Ber.*	111	2067	1978
DPKEVB	*Inorg. Chem.*	20	1173	1981
DPPTCC	*Acta Cryst. Sect. B*	36	159	1980
DPSCMN	*J. Am. Chem. Soc.*	95	783	1973
DPSEHG01	*Z. Naturforsch. Teil B*	33	1227	1978
DSENCO	*Inorg. Chem.*	19	2545	1980
DTCPPD10	*J. Chem. Soc. Dalton Trans.*		572	1976
DTHCUC	*J. Chem. Soc. Dalton Trans.*		416	1978
DTPANI10	*J. Chem. Soc. Dalton Trans.*		2315	1977
EAPZNI	*Can. J. Chem.*	57	3099	1979
ECYFTI	*J. Coord. Chem.*	4	71	1974
EDTCIR	*J. Chem. Soc. Dalton Trans.*		32	1976
EDTCMO	*Inorg. Chem.*	12	2179	1973
EFASCO01	*Acta Cryst. Sect. B*	38	2541	1982
EFMCPV	*Inorg. Chem.*	18	2282	1979
EFUMNI	*J. Organomet. Chem.*	110	129	1976
EINICI	*Inorg. Chem.*	18	1109	1979
EMABOB	*J. Organomet. Chem.*	191	15	1980
EMASOU10	*J. Inorg. Nucl. Chem.*	36	1999	1974
EMTCTJ	*J. Am. Chem. Soc.*	101	5268	1979
EMTCZR	*Inorg. Chem.*	17	2120	1978
ENAZPU10	*Inorg. Chem.*	9	2768	1970
ENGUPD	*Can. J. Chem.*	58	381	1980
ENSPAU	*Acta Cryst. Sect. B*	31	370	1975
EOBCPT10	*J. Chem. Soc. Dalton Trans.*		684	1979
EPAILA	*J. Chem. Soc. Chem. Commun.*		774	1979
EPMSPN11	*Acta Cryst. Sect. B*	38	748	1982
EPPTPD	*Acta Cryst. Sect. B*	31	2691	1975
ESALTJ	*J. Chem. Soc. Dalton Trans.*		545	1978
ESCTHW20	*J. Chem. Soc. Dalton Trans.*		506	1981
ESEXFE10	*Inorg. Chem.*	9	2775	1970
ESICRE	*Inorg. Chem.*	16	2321	1977
ESITCO	*J. Am. Chem. Soc.*	93	7156	1971
ETACHG	*Aust. J. Chem.*	32	311	1979
ETCOXV	*J. Chem. Soc. Dalton Trans.*		26	1976
ETDYRE	*Chem. Ber.*	114	867	1981
ETNTCD	*Koord. Khim.*	6	1606	1980
ETPSCO10	*Chem. Ber.*	116	1441	1983
ETPSTI	*Z. Anorg. Allg. Chem.*	472	133	1981
ETXACR10	*Acta Cryst. Sect. B*	30	2788	1974
EXAPYZ	*Aust. J. Chem.*	29	731	1976
EXPHCO	*J. Organomet. Chem.*	150	279	1978
EXPNCD	*Aust. J. Chem.*	29	739	1976
EYCCMN	*Inorg. Chem.*	18	3483	1979
EYPCOS	*Inorg. Chem.*	18	156	1979
EYPIPD	*J. Organomet. Chem.*	129	273	1977
FACCRE	*Inorg. Chem.*	17	176	1978
FACMNB	*Inorg. Chem.*	20	1287	1981
FACTNI	*Acta Cryst. Sect. B*	37	240	1981
FAHGME	*J. Chem. Soc. Chem. Commun.*		646	1974
FAHGME10	*Cryst. Struct. Commun.*	11	565	1982
FAMPMO	*J. Am. Chem. Soc.*	102	1558	1980
FAPZTH10	*Inorg. Chem.*	15	1827	1976
FATBOS10	*J. Organomet. Chem.*	259	215	1983
FBSIMO	*Inorg. Chem.*	20	199	1981
FDMSON	*J. Chem. Soc. Dalton Trans.*		2171	1975
FEBUTS10	*Inorg. Chem.*	9	2430	1970
FEFRMT	*Acta Cryst. Sect. B*	36	3107	1980
FEHPYO	*Aust. J. Chem.*	31	713	1978
FEPICA	*Inorg. Chem.*	19	658	1980
FLCPNI	*J. Fluorine Chem.*	16	339	1980
FLDXCO10	*J. Chem. Soc. Dalton Trans.*		337	1982
FLMECE	*Inorg. Chem.*	19	3553	1980
FMBCNI	*J. Chem. Soc. Dalton Trans.*		2466	1975
FMBTMO	*J. Chem. Soc. Chem. Commun.*		410	1979
FMEACA10	*J. Organomet. Chem.*	220	239	1981
FMPENR	*Acta Cryst. Sect. B*	33	319	1977
FMPHNI	*Inorg. Chem.*	17	3478	1978
FMPZCO	*Cryst. Struct. Commun.*	5	441	1976
FMSEPD	*Inorg. Chem.*	18	1129	1979
FMTPHG	*Acta Cryst. Sect. B*	35	1770	1979
FPCYTP10	*Koord. Khim.*	2	278	1976
FPOTIP	*Helv. Chim. Acta*	55	2990	1972
FSCUCO	*Inorg. Chem.*	19	2945	1980
FSMICO	*J. Am. Chem. Soc.*	98	5153	1976
FTLAMN	*Inorg. Chem.*	19	2740	1980
GEIAYB10	*Koord. Khim.*	9	1131	1983
HAPZPT10	*J. Am. Chem. Soc.*	99	5277	1977
HBHOSM	*J. Chem. Soc. Dalton Trans.*		1983	1979
HBMPMO	*J. Chem. Soc. Dalton Trans.*		467	1980

APPENDIX 2 (*cont.*)

HBTHFY	*Inorg. Chem.*	17	844	1978
HBUPRH	*J. Chem. Soc. Chem. Commun.*		498	1979
HCYPMO02	*Inorg. Chem.*	16	3303	1977
HDYCMN	*J. Chem. Soc. Dalton Trans.*		1630	1979
HENAEB	*Zh. Neorg. Khim.*	25	1999	1980
HEPPTB	*Can. J. Chem.*	56	1773	1978
HETALA11	*Koord. Khim.*	8	1688	1982
HETCRB10	*J. Am. Chem. Soc.*	103	6073	1981
HETPOS	*J. Chem. Soc. Chem. Commun.*		801	1981
HETSRE	*Inorg. Chem.*	16	2325	1977
HETXCU	*Inorg. Chem.*	17	3034	1978
HFCATH	*Inorg. Chem.*	18	1611	1979
HFURMN	*J. Organomet. Chem.*	197	357	1980
HGETCB10	*Acta Cryst. Sect. B*	29	2115	1973
HGTXZO	*Acta Cryst. Sect. B*	35	1702	1979
HGXIMC	*J. Chem. Soc. Dalton Trans.*		96	1976
HIMPDA	*J. Chem. Soc. Dalton Trans.*		1992	1980
HISTPD	*Acta Cryst. Sect. B*	32	2472	1976
HMPCIC01	*J. Am. Chem. Soc.*	100	3071	1978
HMPEZR	*J. Am. Chem. Soc.*	102	4941	1980
HMTCRC10	*Acta Cryst. Sect. B*	31	423	1975
HMTNRH	*Cryst. Struct. Commun.*	8	1011	1979
HMTZCR	*Inorg. Chem.*	16	1055	1977
HMYCFE01	*J. Am. Chem. Soc.*	103	1485	1981
HNBPRH10	*Inorg. Chem.*	15	2462	1976
HOSTBC10	*Inorg. Chem.*	18	1909	1979
HPCXNI	*Inorg. Chem.*	16	1127	1977
HPETOS	*J. Chem. Soc. Dalton Trans.*		788	1981
HPHOMO10	*Acta Cryst. Sect. B*	28	1278	1972
HPMCRH11	*Inorg. Chem.*	23	1828	1984
HPMXCW10	*Z. Anorg. Allg. Chem.*	455	43	1979
HPNONI	*Acta Cryst. Sect. B*	36	1944	1980
HPSCIR	*Acta Cryst. Sect. B*	32	1513	1976
HPZPOS	*Inorg. Chem.*	14	2617	1975
HTEMOA	*Z. Anorg. Allg. Chem.*	473	91	1981
HTSIXI10	*J. Organomet. Chem.*	164	371	1979
HXETOW10	*J. Am. Chem. Soc.*	103	6093	1981
HYBIOS	*Inorg. Chem.*	18	2255	1979
HZBTFE	*Z. Naturforsch. Teil B*	33	1341	1978
IATCNI	*Rec. J. R. Neth. Chem. Soc.*	99	65	1980
IBTCPT	*Inorg. Chem.*	17	394	1978
ICNPCU10	*Acta Cryst. Sect. B*	38	2145	1982
ICNPIR	*Inorg. Chem.*	8	1282	1969
ICPNMN	*Acta Cryst. Sect. B*	36	1933	1980
IFPPAU	*J. Chem. Soc. Dalton Trans.*		1481	1972
IMDZAG	*J. Chem. Soc. Dalton Trans.*		1682	1980
IMIDZA	*Z. Anorg. Allg. Chem.*	464	187	1980
IMNPTA10	*Inorg. Chem.*	20	2899	1981
IMZCUN	*J. Chem. Soc. Dalton Trans.*		263	1975
IMZZNN	*J. Am. Chem. Soc.*	100	6063	1978
INDCEP	*Acta Cryst. Sect. B*	35	457	1979
INDMTI	*Inorg. Chem.*	14	1757	1975
INDRHA	*J. Chem. Soc. Dalton Trans.*		400	1981
INDRHB	*J. Chem. Soc. Dalton Trans.*		400	1981
IPHPRU	*J. Chem. Soc. Dalton Trans.*		366	1977
IPPHWH01	*Inorg. Chem.*	23	4103	1984
IPRNIP	*Tetrahedron Lett.*		1457	1972
IPTXMO	*Inorg. Chem.*	17	414	1978
IPVRUB	*J. Chem. Soc. Chem. Commun.*		476	1981
IRCNIR	*Inorg. Chem.*	19	3168	1980
IRTCPP10	*J. Am. Chem. Soc.*	93	2391	1971
ISNHSM	*Inorg. Chem.*	18	2045	1979
ITDASC	*Inorg. Chem.*	14	624	1975
KCPTCR01	*Inorg. Chem.*	20	158	1981
KCUDED10	*Inorg. Chem.*	15	1853	1976
KOXHFP10	*Acta Cryst. Sect. B*	33	3126	1977
KXOXRE	*Acta Cryst. Sect. B*	31	1594	1975
LDHPCR10	*J. Chem. Soc. Dalton Trans.*		1604	1977
LIBCRC	*J. Chem. Soc. Dalton Trans.*		1863	1980
MABUMO10	*J. Organomet. Chem.*	129	91	1977
MADCZB10	*Acta Cryst. Sect. B*	32	1687	1976
MAEMAZ11	*Acta Cryst. Sect. B*	36	2950	1980
MALCDB	*Koord. Khim.*	6	793	1980
MALLPT	*J. Organomet. Chem.*	90	111	1975
MAMPZN	*Acta Cryst. Sect. B*	33	1310	1977
MAQUNI10	*J. Chem. Soc. Dalton Trans.*		2494	1975
MARHAA10	*J. Chem. Soc. A*		817	1971
MASBCM	*J. Chem. Soc. Dalton Trans.*		783	1974
MAUFMS	*Inorg. Chem.*	16	2138	1977
MAZCOC	*J. Am. Chem. Soc.*	103	1431	1981
MBZACR	*Inorg. Chem.*	18	3566	1979
MBZCRC	*J. Organomet. Chem.*	94	409	1975
MBZCRP	*J. Organomet. Chem.*	101	209	1975
MCBCMN	*J. Organomet. Chem.*	139	C68	1977
MCECZN	*J. Am. Chem. Soc.*	95	1170	1973
MCENCR	*Inorg. Chem.*	12	2690	1973
MCETMN	*J. Chem. Soc. Dalton Trans.*		1077	1977
MCHFHB10	*J. Am. Chem. Soc.*	100	2709	1978
MCPEIR	*Inorg. Chem.*	15	58	1976
MCPNZR	*J. Am. Chem. Soc.*	98	8351	1976
MCPYBC	*Inorg. Chem.*	14	1376	1975
MCTCEW	*J. Chem. Soc. Chem. Commun.*		30	1979
MCYTAG10	*Inorg. Chem.*	18	240	1979
MDNCAZ10	*Inorg. Chem.*	17	444	1978
MEAZAU	*Inorg. Chem.*	20	853	1981
MEDOFE10	*J. Org. Chem.*	46	3630	1981
MEGUHG	*J. Chem. Soc. Dalton Trans.*		1693	1980
MEIMMN	*Acta Cryst. Sect. B*	32	687	1976
MEKTMO	*Acta Cryst. Sect. B*	31	297	1975
MENTFE	*J. Am. Chem. Soc.*	96	6519	1974
MEOBFE	*J. Organomet. Chem.*	208	353	1981
MEORHC	*J. Chem. Soc. Dalton Trans.*		2467	1980
MEPEFE10	*Organometallics*	2	1220	1983
MEPGFE	*Can. J. Chem.*	57	3113	1979
MEPOSW	*J. Am. Chem. Soc.*	103	817	1981
MEPRUA	*J. Chem. Soc. Dalton Trans.*		1771	1980
MEPZFE	*Inorg. Chem.*	19	3655	1980
MERQCD10	*Latv. PSR Zinat. Akad. Vestis. Kim. Sec.*		259	1979
MESACV	*Acta Cryst. Sect. B*	34	1842	1978
MESOCO	*Inorg. Chem.*	15	2758	1976
MESTCR	*J. Organomet. Chem.*	210	211	1981
METHGD	*Aust. J. Chem.*	32	1165	1979
MICPIR10	*J. Chem. Soc. Dalton Trans.*		1119	1978
MICCNI	*J. Coord. Chem.*	1	275	1971
MNACAZ30	*Inorg. Chem.*	14	722	1975
MNAZHG	*Transition Met. Chem.*	6	86	1981
MNMTBH	*Inorg. Chem.*	18	**3037**	**1979**
MNPHCY03	*Acta Cryst. Sect. B*	36	**2963**	**1980**
MNPROP	*Acta Cryst. Sect. B*	33	**2964**	**1977**
MNTPPI10	*J. Am. Chem. Soc.*	99	2557	**1977**
MNXCMN	*J. Organomet. Chem.*	146	39	1978
MOBOCO10	*J. Chem. Soc. Dalton Trans.*		1876	1974
MODIPT	*Inorg. Chem.*	20	633	1981
MOPAZW	*Inorg. Chem.*	19	1450	1980
MORTMN	*J. Am. Chem. Soc.*	98	5159	1976
MOSHIS10	*J. Chem. Soc. Dalton Trans.*		1077	1975
MOTCMN	*J. Chem. Soc. Dalton Trans.*		2517	1975
MOTCRH	*J. Chem. Soc. Dalton Trans.*		2517	1975
MPASCO	*Can. J. Chem.*	55	438	1977
MPAUSN	*Acta Cryst. Sect. B*	34	278	1978
MPBMOE10	*J. Chem. Soc. Dalton Trans.*		429	1982
MPCRCO	*Chem. Ber.*	111	3472	1978
MPEYCR10	*J. Chem. Soc. Dalton Trans.*		671	1983
MPFPNI	*J. Chem. Soc. Dalton Trans.*		670	1972
MPMYRU	*J. Am. Chem. Soc.*	101	4128	1979
MPNDAG	*Inorg. Chem.*	14	632	1975
MPORFE10	*Inorg. Chem.*	22	2982	1983
MPPCDC	*Inorg. Chim. Acta*	38	191	1980
MPPDBN	*J. Chem. Soc. Chem. Commun.*		322	1978
MPRUAC	*S. Afr. J. Chem.*	31	155	1978
MPTBRH	*J. Chem. Soc. Dalton Trans.*		804	1980
MPTCRH	*J. Chem. Soc. Dalton Trans.*		1713	1976
MPYOER10	*Cryst. Struct. Commun.*	10	703	1981
MPZHZN	*J. Chem. Soc. Dalton Trans.*		447	1976
MSEUHG	*J. Organomet. Chem.*	172	201	1979
MSIPEP	*J. Chem. Soc. Dalton Trans.*		1749	1979
MSISMN	*I. Organomet. Chem.*	47	403	1973
MSORHB	*Inorg. Chem.*	19	2347	1980
MSTPPT	*Transition Met. Chem.*	4	147	1979
MTPAPT	*Acta Cryst. Sect. B*	27	73	1971
MTXPVE	*J. Am. Chem. Soc.*	95	6046	1973
MXOXRE10	*J. Chem. Soc. Dalton Trans.*		2467	1980
MYCCMN10	*Inorg. Chem.*	21	645	1982
NBCZNB10	*Koord. Khim.*	5	1103	1979
NBPCCO	*Acta Cryst. Sect. B*	34	1978	1978
NBPMOX	*Inorg. Chem.*	15	1196	1976
NCPRHB	*J. Organomet. Chem.*	192	235	1980
NEPPRE	*Inorg. Chem.*	6	197	1967

APPENDIX 2 (*cont.*)

NETNIP02	*Inorg. Chem.*	21	1729	1982
NETPRE	*Inorg. Chem.*	6	204	1967
NIAQAC03	*Kristallografiya*	25	287	1980
NIPHTI	*J. Am. Chem. Soc.*	102	6702	1980
NMEDNI10	*Aust. J. Chem.*	34	2047	1981
NMSPEM	*Acta Cryst. Sect. B*	30	2778	1974
NOMPRE	*J. Am. Chem. Soc.*	102	6154	1980
NPHZIR	*Inorg. Chem.*	16	2462	1977
NPMCMN	*Chem. Ber.*	105	1230	1972
NPMCTI	*J. Am. Chem. Soc.*	98	8358	1976
NPNTAB	*J. Am. Chem. Soc.*	103	169	1981
NRBIRB	*Inorg. Chem.*	19	3755	1980
NREDTC10	*J. Chem. Soc. Dalton Trans.*		1079	1972
NSDPRH10	*Inorg. Chem.*	16	2473	1977
NSMEDT02	*Acta Cryst. Sect. C*	40	1687	1984
NSOSPP10	*J. Chem. Soc. Dalton Trans.*		463	1975
NTPAAG	*Z. Kristallogr.*	152	253	1980
NTPHCU	*J. Chem. Soc. Dalton Trans.*		1993	1975
NTPOCE	*Inorg. Chem.*	10	115	1971
NTPYCR	*Inorg. Chim. Acta*	22	81	1977
OACPMN	*J. Chem. Soc. Chem. Commun.*		62	1978
OACTUR	*Acta Cryst. Sect. B*	32	2707	1976
OAMSCO	*Inorg. Chem.*	18	125	1979
OATURE	*Acta Cryst. Sect. B*	33	944	1977
OAZPMN10	*Acta Cryst. Sect. B*	30	1635	1974
OCBTZR	*J. Organomet. Chem.*	166	179	1979
OCHTPI	*J. Am. Chem. Soc.*	96	5070	1974
OCPPRE	*Inorg. Chem.*	7	1784	1968
OCTCMO10	*J. Chem. Soc. Dalton Trans.*		187	1982
ODACND	*Acta Chem. Scand.*	24	3257	1970
ODMNBR	*Inorg. Chem.*	19	1801	1980
OHCPLU	*J. Chem. Soc. Chem. Commun.*		706	1981
ONBCBU	*Koord. Khim.*	3	1600	1977
OPENBO10	*Acta Cryst. Sect. B*	27	1582	1971
OTPCHG	*Can. J. Chem.*	57	2217	1979
OTPHMO	*Inorg. Chem.*	19	2061	1980
OXBUDC10	*Inorg. Chem.*	17	1976	1978
OXCFOR	*Transition Met. Chem.*	1	151	1976
OXCOCP10	*Chem. Ber.*	112	1731	1979
OXCPSM10	*J. Chem. Soc. Dalton Trans.*		1350	1978
OXMCHF	*Inorg. Chem.*	15	2284	1976
OXMCUA	*Inorg. Chem.*	20	537	1981
OXPTCC	*J. Am. Chem. Soc.*	102	1570	1980
PABZTA	*Inorg. Chem.*	14	1358	1975
PACPRH10	*Inorg. Chem.*	15	97	1976
PAIDMO	*Inorg. Chem.*	18	1634	1979
PAPMCO10	*Inorg. Chem.*	9	2211	1970
PASACR	*Acta Cryst. Sect. B*	35	951	1979
PASETI	*Inorg. Chim. Acta*	50	125	1981
PASMRE	*Aust. J. Chem.*	28	1201	1975
PAUELI10	*Inorg. Chem.*	16	1090	1977
PAZHGN	*Z. Anorg. Allg. Chem.*	409	1	1974
PAZMPI	*J. Am. Chem. Soc.*	98	7608	1976
PAZPPT10	*Inorg. Chem.*	15	2794	1976
PBARTC	*Inorg. Chem.*	14	2027	1975
PBUDRI10	*Inorg. Chem.*	19	3590	1980
PCBASC	*J. Organomet. Chem.*	142	195	1977
PCFMRU10	*J. Cryst. Mol. Struct.*	5	163	1975
PCHIRH10	*Inorg. Chem.*	21	1307	1982
PCLPIR	*Inorg. Chem.*	19	1231	1980
PCLTCA10	*Inorg. Chem.*	21	1941	1982
PCOPIM10	*J. Organomet. Chem.*	172	251	1979
PCPCOS	*Inorg. Chem.*	19	134	1980
PCPHYB	*Inorg. Chem.*	15	2226	1976
PCRNIB	*Z. Anorg. Allg. Chem.*	475	109	1981
PCTATL10	*Inorg. Chem.*	19	2352	1980
PCTXCR	*Cryst. Struct. Commun.*	6	835	1977
PDDMSX10	*Acta Cryst.*	23	788	1967
PDPMNC	*Z. Naturforsch. Teil B*	31	1166	1976
PDPMZR10	*J. Am. Chem. Soc.*	99	6645	1977
PDTHBA10	*J. Chem. Soc. Dalton Trans.*		2250	1975
PEAMNI	*Inorg. Chem.*	16	1669	1977
PEYEPP	*J. Organomet. Chem.*	117	91	1976
PEYHGP	*Acta Cryst. Sect. B*	34	3382	1978
PFPBTI	*Inorg. Chem.*	17	3257	1978
PGECBC	*J. Organomet. Chem.*	179	215	1979
PHACCS	*Koord. Khim.*	6	1407	1980
PHCORE	*J. Organomet. Chem.*	188	367	1980
PHGMQU	*Aust. J. Chem.*	31	537	1978
PHGTFA	*Izv. Jugosl. Cent. Krist. Ser. A*	11	32	1976
PHHGAC01	*Croat. Chem. Acta*	57	145	1984
PHIMDW	*J. Chem. Soc. Chem. Commun.*		103	1981
PHPCIR10	*S. Afr. J. Chem.*	36	85	1983
PHPECU01	*J. Organomet. Chem.*	159	441	1978
PHPNCD	*J. Chem. Soc. Chem. Commun.*		492	1980
PHQUMO	*Inorg. Chem.*	16	2970	1977
PHRLCU	*Acta Cryst. Sect. B*	36	2407	1980
PHSNFE	*J. Organomet. Chem.*	205	193	1981
PHTHCU01	*Cryst. Struct. Commun.*	11	1495	1982
PHTPRE	*J. Chem. Soc. Chem. Commun.*		825	1978
PHYZMN	*Koord. Khim.*	5	909	1979
PIVMNB10	*J. Am. Chem. Soc.*	97	2712	1975
PMBPAG10	*Inorg. Chem.*	22	2356	1983
PMCBTI	*Inorg. Chem.*	18	1215	1979
PMCMNB	*Inorg. Chem.*	12	2262	1973
PMCPUC10	*Organometallics*	1	170	1982
PMCZNE	*Inorg. Chem.*	17	388	1978
PMDTTI10	*Inorg. Chem.*	18	3069	1979
PMECAC	*Inorg. Chem.*	16	2367	1977
PMENIB20	*Inorg. Chem.*	17	632	1978
PMISNI	*Inorg. Chem.*	13	2529	1974
PMPDCU	*Acta Cryst. Sect. B*	35	3058	1979
PMPZAG10	*Acta Cryst. Sect. B*	35	177	1979
PMYPCW	*Inorg. Chem.*	12	2923	1973
PNENCO10	*Inorg. Chem.*	15	2989	1976
PNMNCP	*J. Am. Chem. Soc.*	100	6766	1978
PNOLTI	*J. Am. Chem. Soc.*	102	5969	1980
PNPMOA	*J. Am. Chem. Soc.*	103	398	1981
POIRID	*Transition Met. Chem.*	5	222	1980
POSHRH10	*J. Chem. Soc. Dalton Trans.*		515	1981
POTCDR	*Inorg. Chem.*	11	161	1972
PPCOCO01	*J. Organomet. Chem.*	193	247	1980
PPEAUC	*Chem. Ber.*	110	2751	1977
PPHCHN10	*Inorg. Chem.*	8	2719	1969
PPMEIR	*Inorg. Chim. Acta*	37	L543	1979
PPMERH	*Inorg. Chim. Acta*	37	L543	1979
PPZBNI	*Inorg. Chim. Acta*	17	121	1976
PRNRHC	*Inorg. Chem.*	20	600	1981
PRNRHD	*Inorg. Chem.*	20	600	1981
PRXHQV	*Inorg. Chem.*	12	1758	1973
PRZBAG	*J. Chem. Soc. Dalton Trans.*		956	1981
PSIBTI	*Inorg. Chem.*	17	3257	1978
PSMNPC10	*Inorg. Chem.*	14	1138	1975
PSNIMO	*Acta Cryst. Sect. B*	37	439	1981
PSTOSA	*J. Am. Chem. Soc.*	102	6346	1980
PTCDNI20	*J. Am. Chem. Soc.*	94	7323	1972
PTHCZN	*J. Am. Chem. Soc.*	99	1101	1977
PTHFFE	*J. Am. Chem. Soc.*	102	2302	1980
PTOCNI10	*J. Chem. Soc. Dalton Trans.*		575	1984
PXBURE	*Can. J. Chem.*	51	1116	1973
PXTCMO10	*J. Chem. Soc. Dalton Trans.*		356	1977
PYAZCU10	*Acta Cryst. Sect. B*	28	1052	1972
PYBPIR	*J. Chem. Soc. Chem. Commun.*		589	1977
PYDSCU10	*J. Am. Chem. Soc.*	98	7569	1976
PYHGAN10	*Cryst. Struct. Commun.*	5	149	1976
PYMCXC	*Z. Anorg. Allg. Chem.*	432	203	1977
PYMOPH	*Inorg. Chem.*	18	3562	1979
PYRCUD	*J. Chem. Soc. Chem. Commun.*		906	1980
PYRMNC	*J. Am. Chem. Soc.*	98	1166	1976
PYRZNI	*Koord. Khim.*	6	1891	1980
PYSLCU	*Inorg. Chem.*	16	310	1977
PYXCDC	*J. Inorg. Nucl. Chem.*	40	1259	1978
PYZBNI	*Cryst. Struct. Commun.*	8	965	1979
PYZCUA01	*Acta Cryst. Sect. B*	31	762	1975
PYZRUA	*Inorg. Chem.*	20	1522	1981
PYZTCI	*J. Am. Chem. Soc.*	96	3438	1974
PZALPD10	*J. Cryst. Mol. Struct.*	7	137	1977
PZBZRU10	*Inorg. Chem.*	14	3046	1975
PZCPTI	*Inorg. Chem.*	17	2074	1978
RACCAF	*J. Chem. Soc. Chem. Commun.*		186	1980
REPETD10	*Inorg. Chem.*	5	411	1966
RUCABO	*J. Am. Chem. Soc.*	102	5782	1980
RUNCPP10	*Helv. Chim. Acta*	62	2159	1979
SALASM10	*Inorg. Chem.*	16	289	1977
SALEZN	*Chem. Pharm. Bull.*	27	424	1979
SAZPZR	*Inorg. Chem.*	18	2908	1979
SCATUR	*J. Am. Chem. Soc.*	100	7882	1978
SCLIRA10	*Inorg. Chem.*	20	2691	1981
SCPDCC	*Inorg. Chem.*	18	3542	1979

APPENDIX 2 (*cont.*)

SCQUCO	*J. Chem. Soc. Dalton Trans.*		1504	1981
SCYSCR	*Inorg. Chem.*	16	1494	1977
SDAPOU20	*Acta Cryst. Sect. B*	35	3091	1979
SECPOS	*J. Am. Chem. Soc.*	101	6577	1979
SFSTPD	*Koord. Khim.*	6	1115	1980
SIBONI	*J. Organomet. Chem.*	191	27	1980
SMHXAZ10	*Inorg. Chem.*	18	3044	1979
SMNICD	*J. Am. Chem. Soc.*	94	1858	1972
SNCOCR	*Cryst. Struct. Commun.*	9	383	1980
SNSCRB	*J. Organomet. Chem.*	216	245	1981
SNTLHF	*J. Chem. Soc. Chem. Commun.*		117	1981
SOCPRH	*Chem. Ber.*	114	716	1981
SPCNFE	*J. Chem. Soc. Dalton Trans.*		1965	1980
SPHFEC10	*Inorg. Chem.*	17	2568	1978
SPPEIR	*J. Am. Chem. Soc.*	94	3413	1972
STAETC	*Inorg. Chem.*	17	1410	1978
STETCU	*Inorg. Chem.*	8	2763	1969
SULPDC10	*Acta Cryst. Sect. B*	32	669	1976
SULPMS	*Inorg. Chem.*	15	1807	1976
SXPMNI01	*Inorg. Chem.*	15	2768	1976
TABYCP10	*Inorg. Chem.*	18	171	1979
TACDRH10	*Zh. Neorg. Khim.*	23	1044	1978
TACNIH10	*Acta Chem. Scand. Ser. A*	31	501	1977
TACPTH	*J. Am. Chem. Soc.*	99	1775	1977
TACTHB	*Acta Cryst. Sect. B*	34	3770	1978
TAMHGC	*Cryst. Struct. Commun.*	6	157	1977
TAMPHG	*J. Am. Chem. Soc.*	101	7729	1979
TAZCFE	*Isr. J. Chem.*	15	165	1977
TAZOCO10	*Inorg. Chem.*	16	271	1977
TAZRUP10	*Inorg. Chem.*	15	2788	1976
TAZTDG	*J. Chem. Soc. Dalton Trans.*		144	1975
TBARHC	*Inorg. Chem.*	10	566	1971
TBCBFE	*Chem. Ber.*	111	3530	1978
TBIAZR	*Inorg. Chem.*	18	2030	1979
TBPAHG10	*J. Chem. Soc. Dalton Trans.*		253	1978
TBPCFE	*J. Organomet. Chem.*	107	241	1976
TCACTC	*J. Chem. Soc. Dalton Trans.*		1837	1977
TCACTC01	*Acta Cryst. Sect. B*	34	3359	1978
TCATPD	*Inorg. Chem.*	14	343	1975
TCBPNB	*Inorg. Chem.*	15	309	1976
TCBPZR	*Inorg. Chem.*	15	309	1976
TCHXPH10	*J. Chem. Soc. Dalton Trans.*		1845	1977
TCMIPD10	*Acta Cryst. Sect. C*	39	186	1983
TCMNET10	*Phys. Rev. B*	19	306	1979
TCMOFM	*Transition Met. Chem.*	1	2	1975
TCPDNI01	*J. Am. Chem. Soc.*	103	1942	1981
TCPMNN10	*Inorg. Chem.*	13	1037	1974
TCPNIH11	*J. Am. Chem. Soc.*	101	5631	1979
TCPPHG01	*Can. J. Chem.*	57	2555	1979
TCTPOS	*Inorg. Chem.*	8	1078	1969
TCTPPU	*Inorg. Chem.*	17	394	1978
TCXNTI	*J. Chem. Soc. Dalton Trans.*		1176	1978
TCYENI10	*Finn. Chem. Lett.*		71	1977
TCYPSC10	*J. Am. Chem. Soc.*	95	1488	1973
TCYPTI10	*J. Am. Chem. Soc.*	93	3592	1971
TDACCD10	*Acta Cryst. Sect. B*	31	2531	1975
TDCURF	*Transition Met. Chem.*	4	82	1979
TEPPMN01	*Cryst. Struct. Commun.*	10	1263	1981
TEPPTB	*J. Chem. Soc. Dalton Trans.*		1737	1980
TESTHG	*Acta Cryst. Sect. B*	24	935	1968
TETCPD	*J. Am. Chem. Soc.*	95	8566	1973
TFMESM	*J. Chem. Soc. A*		2285	1971
THMPOS01	*J. Am. Chem. Soc.*	99	7557	1977
THUPDC	*Bull. Chem. Soc. Jpn*	33	861	1960
TIMCUS	*Acta Chem. Scand. Ser. A*	28	578	1974
TIOUNB	*Inorg. Chem.*	8	424	1969
TIUREA01	*Inorg. Chem.*	9	1111	1970
TLCSCR	*Cryst. Struct. Commun.*	9	821	1980
TLTZMO	*Inorg. Chem.*	20	171	1981
TMAFMN	*J. Chem. Soc. Dalton Trans.*		1512	1979
TMANB01	*Acta Cryst. Sect. B*	34	1970	1978
TMDPHG	*Cryst. Struct. Commun.*	6	359	1977
TMENSN	*Finn. Chem. Lett.*		75	1977
TMPCUB01	*J. Am. Chem. Soc.*	103	5165	1981
TMPHWE	*J. Am. Chem. Soc.*	102	1431	1980
TMSCCU	*Inorg. Chem.*	18	761	1979
TMTCPC	*Inorg. Chem.*	13	1674	1974
TMTCZN10	*J. Chem. Soc. Dalton Trans.*		1945	1980
TNBPMN	*Can. J. Chem.*	50	3332	1972
TOPFCO10	*Inorg. Chem.*	19	1221	1980
TPACUB	*J. Chem. Soc. Chem. Commun.*		192	1980
TPCPTW	*J. Am. Chem. Soc.*	101	7618	1979
TPCUBF	*J. Am. Chem. Soc.*	101	754	1979
TPCUMZ	*J. Am. Chem. Soc.*	94	7323	1972
TPCYCU	*J. Am. Chem. Soc.*	92	2353	1970
TPHCOA	*Inorg. Chem.*	19	2968	1980
TPHGDI10	*Acta Cryst. Sect. B*	34	2300	1978
TPICBO	*J. Chem. Soc. Chem. Commun.*		80	1980
TPMCDB10	*J. Chem. Soc. Dalton Trans.*		619	1979
TPPMRH10	*Inorg. Chem.*	19	2726	1980
TPPTCC	*J. Am. Chem. Soc.*	97	3952	1975
TPPTCP01	*J. Chem. Soc. A*		2770	1970
TPRUET21	*J. Cryst. Mol. Struct.*	4	43	1974
TPTHCC	*Acta Cryst. Sect. B*	33	619	1977
TPYCLV	*Cryst. Struct. Commun.*	2	421	1973
TPYRPR	*Inorg. Chem.*	10	1463	1971
TRENCM	*Inorg. Chem.*	17	457	1978
TROPRH	*Inorg. Chim. Acta*	42	105	1980
TROPTH	*J. Am. Chem. Soc.*	92	3626	1970
TROPUE	*J. Cryst. Mol. Struct.*	3	221	1973
TTHPHG	*J. Chem. Soc. Chem. Commun.*		140	1979
TTPPDB	*Zh. Strukt. Khim.*	17	135	1976
TTZZCU10	*J. Am. Chem. Soc.*	106	93	1984
TUNCPF10	*Acta Cryst. Sect. B*	30	**1357**	**1974**
TURURS01	*Inorg. Chem.*	19	**776**	**1980**
TXPCPD	*Inorg. Chem.*	17	**22**	**1978**
TZTDAG01	*Inorg. Chem.*	17	**49**	**1978**
UCHXOS	*J. Chem. Soc. Dalton Trans.*		562	1979
UHXAPY10	*Inorg. Chem.*	15	1827	1976
URCLNI	*Acta Cryst. Sect. B*	36	2251	1980
URDEAM10	*Inorg. Chem.*	15	2498	1976
UREAZN	*Cryst. Struct. Commun.*	1	257	1972
URMSUL	*Acta Cryst. Sect. B*	34	2302	1978
URSCNI	*Kristallografiya*	23	1196	1978
URSDUR03	*Inorg. Chem.*	22	1557	1983
VCPRUA10	*J. Chem. Soc. Dalton Trans.*		2661	1983
VCPRUB10	*J. Chem. Soc. Dalton Trans.*		2661	1983
VIBONI	*J. Organomet. Chem.*	215	255	1981
VPHTHC	*J. Chem. Soc. Dalton Trans.*		2300	1980
XAXASP	*Cryst. Struct. Commun.*	7	219	1978
YBAENI	*Inorg. Chem.*	16	1623	1977
ZEGCET	*J. Chem. Soc. Dalton Trans.*		1531	1982
ZEGGUN	*Inorg. Chem.*	22	888	1983
ZEGNOP	*J. Am. Chem. Soc.*	106	801	1984
ZEGPEG	*Inorg. Chim. Acta*	82	35	1984
ZNACAT10	*Acta Cryst. Sect. B*	24	904	1968
ZTANPB	*Inorg. Chem.*	14	604	1975
ZZZARD01	*Acta Cryst. Sect. C*	40	781	1984
ZZZCCG10	*Acta Cryst. Sect. B*	36	1938	1980

International Tables for Crystallography (2006). Vol. C, Chapter 9.7, pp. 897–906.

9.7. The space-group distribution of molecular organic structures

By A. J. C. Wilson, V. L. Karen, and A. Mighell

9.7.1. *A priori* classifications of space groups

The space group $P2_1/c$ accounts for about 1/3 of all known molecular organic structures, whereas the space group $P2/m$ has no certain example. Why? Ultimately, the space group of a crystal of a particular substance is determined by the minimum (or a local minimum) of the thermodynamic potential (Gibbs free energy) of the van der Waals and other forces, but a very simple model goes a long way towards 'explaining' the relative frequency of the various space groups within a crystal class or larger grouping. Nowacki (1943) discussed the basic idea that space-group frequency is determined by packing considerations, and had earlier (1942) given statistics for the structures known at the time. Nowacki's statistics were used by Kitajgorodskij* (1945), and recent writers tend to cite Kitajgorodskij as having originated the idea. Kitajgorodskij pointed out that the most frequent space groups are those that permit the close packing of triaxial ellipsoids. Later, Kitajgorodskij (1955) showed that the same space groups allowed close packing of objects of any reasonable shape, 'close packing' meaning packing with 12-point contact. Wilson (1988, 1990, 1993*d*) used the complementary idea that space groups are rare when they contain symmetry elements – notably mirror planes and rotation axes – that prevent the molecules from freely choosing their positions within the unit cell. A twofold axis excludes molecular centres from a column of diameter equal to some molecular diameter (say M), a mirror plane from a layer of thickness M, and a centre of symmetry from a sphere of diameter M. The volumes excluded by screw axes and glide planes are small in comparison.

9.7.1.1. *Kitajgorodskij's categories*

In his book† *Organicheskaya Kristallokhimiya*, Kitajgorodskij (1955) treated the triclinic, monoclinic and orthorhombic space groups in considerable detail, analysing the possibility of (*a*) forming close-packed layers (six-point contact), and (*b*) close stacking of the layers. On this basis, he divided the layers and the space groups into four categories each. For the layers they are:

(1) *Coordination close-packed layers*. A coordination close-packed layer is one in which molecules of arbitrary shape and symmetry can be packed with six-point coordination.
(2) *Closest-packed layers*. A closest-packed layer is one in which one can select the orientation of molecules of given shape and symmetry so as to produce a cell of minimal dimensions.
(3) *Limitingly close-packed layers*. A limitingly close-packed layer for a given symmetry is a closest-packed layer in which a molecule retains inherent symmetry; in other words, in which it occupies a special position.
(4) *Permissible layers*. A permissible layer is coordination close packed but *neither* closest packed *nor* limitingly close packed.

The categories of space groups are:

(1) Closest-packed space groups are those that permit the closest stacking of closest-packed layers – the packing can be made no denser by varying the cell parameters and the orientation of the molecules. Closest stackings can be made by a monoclinic displacement (a translation making an arbitrary angle with the layer plane), a centre of symmetry, a glide plane, or a screw axis.
(2) Limitingly close-packed space groups are those that contain limitingly close-packed layers stacked as closely as possible.
(3) Permissible space groups fall into three subcategories: (*a*) Those containing closest-packed layers that can be closely stacked if the layer relief is suitable; this group contains layers stacked by centring (C, I, F) or by diad axes. (*b*) Those containing limitingly close-packed layers that can be most closely stacked if the layer relief is suitable. (*c*) Those containing permissible layers stacked in the densest fashion.
(4) Impossible space groups fall into two subcategories: (*a*) Those containing any layers (even closest-packed layers) that are related by mirror planes and translations normal to the layer plane. (*b*) Those containing permissible coordination close-packed layers not stacked in the densest possible way.

Kitajgorodskij expected the frequency of space groups to decrease in the order (1) > (2) > (3) > (4). In particular, 'permissible space groups should be found but rarely, as exceptions'. The categorization is summarized in Table 9.7.1.1, based on Table 8 of Kitajgorodskij (1955).

Kitajgorodskij's categorization proved very successful in broad outline, but Wilson's (1993*b*,*c*) detailed statistics revealed about a dozen anomalous space-group types. The anomalies were of two kinds. The first was the frequent occurrence of molecules in general positions in space groups in which Kitajgorodskij expected molecules to use inherent symmetry in special positions. Wilson (1993*a*) pointed out that in such cases structural dimers* can be formed, with two molecules in general positions related by the required symmetry elements – both enantiomers would be required if the element were $\overline{1}$ or m. Such space groups could therefore be added to Kitajgorodskij's table, in the column for 'molecular symmetry 1'. The second kind of anomaly was the fairly frequent occurrence of structures with the 'impossible' space groups Pc and $P2/c$. These could be transferred from 'impossible' to 'permissible', subgroup (*a*), by the same packing argument that Kitajgorodskij had used for $P1$. These and a few other reclassifications are indicated in Table 9.7.1.1, the new entries being enclosed in square brackets for distinction. Where the change is a transfer to a higher category, the original position of the space group is indicated in round brackets.

9.7.1.2. *Symmorphism and antimorphism*

Wilson (1993*d*) classified the space groups by degree of symmorphism. A fully symmorphic space group contains only the 'syntropic' symmetry elements

$$2,\ 3,\ 4,\ 6;\ \overline{2} = m,\ \overline{3} = 3 + \overline{1},\ \overline{4},\ \overline{6} = 3/m$$

and a fully antimorphic space group contains only the 'antitropic' elements

* Names in Cyrillic characters are transliterated in many ways in non-Russian languages. In this chapter, 'Kitajgorodskij' is used thoughout the text, but the source transliteration is retained in the list of references. Similar complications arise with other names in Cyrillic characters.

† The US translation (Kitajgorodskij, 1961) differs from the original in several respects. Only relevant differences are noted in this chapter.

* Empirically, only dimers involving a centre of symmetry or a diad axis are important in the systems under consideration. In principle, n-mers involving any point-group symmetry could be formed.

Copyright © 2006 International Union of Crystallography

Table 9.7.1.1. *Kitajgorodskij's categorization of the triclinic, monoclinic and orthorhombic space groups, as modified by Wilson (1993a)*

Wilson's additions are enclosed in square brackets [···] and the original positions of space groups transferred by him by round brackets (···). Space groups not listed belong to the 'impossible' category.

Molecular symmetry	1	$\bar{1}$	2	*m*	2/*m*	222	*mm*	*mmm*
Closest packed	$P\bar{1}$ $P2_1$ $P2_1/c$ [$C2/c$] $P2_12_12_1$ $Pca2_1$ $Pna2_1$ [*Pbca*]	$P\bar{1}$ $P2_1/c$ $C2/c$ *Pbca*	[$C2/c$]					
Limitingly close packed	[$P2_12_12$]		($C2/c$) $P2_12_12$		$C2/m$	$C222$ $F222$ $I222$		
				$Pmc2_1$ $Cmc2_1$			$Fmm2$	
	[*Pbcn*]		*Pbcn*	*Pnma*			*Pmma*, *Pmmn*	
					Cmca	*Ccca* *		*Cmmm* *Fmmm* *Immm*
Permissible	*P*1 *C*2 [*Pc*]		*C*2					
	Cc [$P2/c$] ($P2_12_12$) [$C222_1$]		 [$P2/c$] [$C222_1$]	*Cm* $P2_1/m$ $Pmn2_1$	*Pbam*			
			*Aba*2 [*Fdd*2]	*Ama*2 *Ima*2				
	(*Pbca*) [*Pccn*]	*Pccn*		*Pbcm*†				

*Kitajgorodskij (1961) includes *Pnnm* at this position, but this is inconsistent with the text of either the Russian or the English version.
†Kitajgorodskij (1961) correctly includes *Pbcm* at this position.

$$2_1,\ 3_{1,2},\ 4_{1,3},\ 6_{1,5};\ \text{any glide plane.}$$

The remaining symmetry elements

$$1,\ \bar{1};\ 4_2;\ \bar{4};\ 6_{2,4} = 2 + 3_{1,2};\ 6_3 = 2_1 + 3$$

are 'atropic'. The two triclinic space groups, *P*1 and $P\bar{1}$, contain only 'atropic' elements, and are thus not classified by these criteria. The rest are divided into five groups, in accordance with the balance of symmetry elements within the unit cell. For the 71 non-triclinic space groups symmorphic in the strict sense (Wilson, 1993*d*; Subsection 1.4.2.1), the classification gives:

(1) Fully symmorphic (only syntropic elements): 14.
(2) Tending to symmorphism (mainly syntropic elements): 28.
(3) Equally balanced (equal numbers of syntropic and antitropic elements): 20.
(4) Tending to antimorphism (mainly antitropic elements): 9.
(5) Fully antimorphic (only antitropic elements): 0.

The distribution of the 230 space groups (11 enantiomorphic couples merged) by arithmetic crystal class and degree of symmorphism is given in Table 9.7.1.2.

A few points about the symmorphic groups are worth noting. The 14 'fully symmorphic' space groups are those that (i) have primitive cells and (ii) have no secondary or tertiary axes (three each monoclinic, orthorhombic, tetragonal, hexagonal; two trigonal; no cubic). Secondary axes, even though syntropic in the conventional space-group notation, generate additional antitropic axes in accordance with the principles set out by Bertaut (1995, Chap. 4.1). These additional axes are not indicated in the 'full' Hermann–Mauguin space-group symbol, but should appear in the 'extended' symbol (Bertaut, 1995, Table 4.3.1‡). As a result of the additional axes, 21 symmorphic space groups with primitive cells are shifted to the 'tending to symmorphism' column (five tetragonal, six trigonal, five hexagonal, five cubic). Lattice centring has a similar or greater effect; the 36 centred symmorphic space groups are spread over the three columns 'tending to symmorphism' (seven), 'equally balanced' (20) and 'tending to antimorphism' (nine).

‡ Table 4.3.1 is not strictly consistent in its treatment of the 'extended' symbols. Tetragonal space groups are extended in full detail, but the extension of orthorhombic space groups is minimal.

Table 9.7.1.2. *Space groups arranged by arithmetic crystal class and degree of symmorphism (Wilson, 1993d), as frequented by homomolecular structures with one molecule in the general position (in superscript numerals; according to Belsky, Zorkaya & Zorky, 1995)*

(*a*) Triclinic, monoclinic and orthorhombic systems. The triclinic space groups are a special case, with 'degree of symmorphism' undefined, and they are not assigned to any particular column. For *, † see Subsection 9.7.4.1.

Arithmetic crystal class	Fully symmorphic	Tending to symmorphism	Equally balanced	Tending to antimorphism	Fully antimorphic
$1P$			$*P1\dagger^{(90)}$		
$\bar{1}P$			$*P\bar{1}\dagger^{(1796)}$		
$2P$	$*P2^{(0)}$	...	...	...	$P2_1\dagger^{(1327)}$
$2C$	...	...	$*C2\dagger^{(109)}$	...	...
mP	$*Pm^{(0)}$	...	...	...	$Pc\ddagger^{(58)}$
mC	...	...	$*Cm^{(0)}$	...	$Cc\dagger^{(144)}$
$2/mP$	$*P2/m^{(0)}$	...	$P2_1/m^{(0)}$	...	$P2_1/c\dagger^{(5951)}$
			$P2/c^{(11)}$		
$2/mC$	...	...	$*C2/m^{(0)}$	$C2/c\ddagger^{(587)}$	...
$222P$	$*P222^{(0)}$	$P222_1^{(0)}$	...	$P2_12_12^{(30)}$	$P2_12_12_1\ddagger^{(2795)}$
$222C$	...	$*C222^{(0)}$	...	$C222_1\ddagger^{(11)}$	...
$222F$	...	...	$*F222^{(0)}$	...	...
$222I$	...	...	$*I222^{(0)}$	...	...
			$I2_12_12_1\ddagger^{(0)}$		
$mm2P$	$*Pmm2^{(0)}$	$Pma2^{(0)}$	...	$Pmc2_1^{(0)}$	$Pca2_1^{(153)}$
				$Pcc2^{(1)}$	$Pna2_1\ddagger^{(367)}$
				$Pnc2^{(1)}$	
				$Pmn2_1^{(0)}$	
				$Pba2^{(1)}$	
				$Pnn2^{(1)}$	
$mm2C$	...	$*Cmm2^{(0)}$	...	$Cmc2_1\dagger^{(0)}$	...
				$Ccc2^{(0)}$	
$2mmC$	...	$*Amm2^{(0)}$	...	$Abm2^{(0)}$	...
				$Ama2^{(0)}$	
				$Aba2\dagger^{(11)}$	
$mm2F$			$*Fmm2^{(0)}$	$Fdd2\dagger^{(35)}$	
$mm2I$	...	...	$*Imm2^{(0)}$	$Iba2\dagger^{(14)}$	
				$Ima2^{(0)}$	
$mmmP$	$*Pmmm^{(0)}$	$Pccm^{(0)}$	$Pnnn^{(0)}$	$Pnna^{(1)}$	$Pbca\dagger^{(827)}$
		$Pmma^{(0)}$	$Pban^{(0)}$	$Pcca^{(3)}$	
			$Pmna^{(0)}$	$Pbam^{(0)}$	
			$Pmmn^{(0)}$	$Pccn^{(37)}$	
				$Pbcm^{(0)}$	
				$Pnnm^{(0)}$	
				$Pbcn^{(60)}$	
				$Pnma^{(0)}$	
$mmmC$	...	$*Cmmm^{(0)}$	$Cmma^{(0)}$	$Cmcm^{(0)}$	...
				$Cmca^{(0)}$	
				$Cccm^{(0)}$	
				$Ccca\dagger^{(0)}$	
$mmmF$	...	...	$*Fmmm^{(0)}$	$Fddd\dagger^{(2)}$	...
$mmmI$	...	...	$*Immm^{(0)}$	$Ibam^{(0)}$	
				$Ibca^{(0)}$	
				$Imma^{(0)}$	

From the nature of the definitions, no symmorphic space group can be 'fully antimorphic'. The 14 groups under the latter heading consist of (i) 12 space groups with no special positions (Subsection 9.7.4.1), and (ii) two space groups whose only special positions have symmetry $\bar{1}$ (Subsection 9.7.4.2). On these criteria, the two triclinic groups excluded from discussion would fall naturally into the column 'fully antimorphic'. The remaining space groups have no obvious outstanding characteristics. Most of them fall under the heading 'tending to antimorphism', though there are some in each of the columns 'tending to symmorphism' and 'equally balanced'.

9.7.1.3. *Comparison of Kitajgorodskij's and Wilson's classifications*

Since both Kitajgorodskij's and Wilson's classifications were made with a view to 'explaining' the empirically observed frequencies of space groups – though neither makes any use of

Table 9.7.1.2. *Space groups arranged by arithmetic crystal class and degree of symmorphism (cont.)*

(*b*) Tetragonal space groups. For *, † see Subsection 9.7.4.1.

Arithmetic crystal class	Fully symmorphic	Tending to symmorphism	Equally balanced	Tending to antimorphism	Fully antimorphic
$4P$	$*P4^{(0)}$	$P4_2^{(1)}$	...	...	$P4_{1,3}\dagger^{(40)}$
$4I$	...	...	$I4_1\dagger^{(3)}$	$*I4^{(3)}$	...
$\bar{4}P$	$*P\bar{4}\dagger^{(0)}$	...	...	...	...
$\bar{4}I$	...	...	$*I\bar{4}\dagger^{(7)}$	...	...
$4/mP$	$*P4/m^{(0)}$	$P4_2/m^{(0)}\ P4/n^{(1)}$	$P4_2/n\dagger^{(20)}$	...	...
$4/mI$	...	...	...	$*I4/m^{(0)}\ I4_1/a\dagger^{(29)}$	...
$422P$	...	$*P422^{(0)}$	$P42_12^{(0)}$	$P4_{1,3}2_12\dagger^{(49)}$	...
		$P4_222^{(0)}$	$P4_{1,3}22^{(1)}$	$P4_22_12^{(1)}$	
$422I$	...	...	$I4_122\dagger^{(0)}$	$*I422^{(0)}$	...
$4mmP$	...	$*P4mm^{(0)}$	$P4bm^{(0)}$	$P4_2cm^{(0)}$	...
				$P4_2nm^{(0)}$	
				$P4cc^{(0)}$	
				$P4nc^{(0)}$	
				$P4_2mc^{(0)}$	
				$P4_2bc\dagger^{(1)}$	
$4mmI$	...	...	...	$*I4mm^{(0)}$	...
				$I4cm^{(0)}$	
				$I4_1md^{(0)}$	
				$I4_1cd\dagger^{(5)}$	
$\bar{4}2mP$	...	$*P\bar{4}2m^{(0)}$	$P\bar{4}2c^{(0)}$	$P\bar{4}2_1c\dagger^{(12)}$	...
			$P\bar{4}2_1m^{(0)}$		
$\bar{4}m2P$	...	$*P\bar{4}m2^{(0)}$	$P\bar{4}c2^{(0)}$	...	...
			$P\bar{4}b2^{(0)}$		
			$P\bar{4}n2^{(0)}$		
$\bar{4}m2I$	...	...	$*I\bar{4}m2^{(0)}$	$I\bar{4}c2\dagger^{(0)}$	...
$\bar{4}2mI$	...	...	$*I\bar{4}2m^{(0)}$	$I\bar{4}2d\dagger^{(0)}$	...
$4/mmmP$	...	$*P4/mmm^{(0)}$	$P4/mcc^{(0)}$	$P4/nbm^{(0)}$	...
		$P4_2/mmc^{(0)}$	$P4/nmm^{(0)}$	$P4/nnc^{(0)}$	
		$P4_2/mcm^{(0)}$		$P4/mbm^{(0)}$	
				$P4/mnc^{(0)}$	
				$P4/ncc^{(0)}$	
				$P4_2/nbc^{(0)}$	
				$P4_2/nnm^{(0)}$	
				$P4_2/mbc^{(0)}$	
				$P4_2/mnm^{(0)}$	
				$P4_2/nmc^{(0)}$	
				$P4_2/ncm^{(0)}$	
$4/mmmI$	...	$*I4/mmm^{(0)}$	...	$I4/mcm^{(0)}$	
				$I4_1/amd^{(0)}$	
				$I4_1/acd\dagger^{(0)}$	

empirical frequencies – it would be expected that there should be considerable correlation between them. All 'closest-packed' space groups are also 'fully antimorphic', and most of the 'limitingly close packed' and 'permissible' are 'tending to antimorphism'; a few requiring high molecular symmetry (222, *mm*2, *mmm*) and a couple of others are 'equally balanced'. Two 'fully antimorphic' groups, *Pc* and *Cc*, are merely 'permissible'. All 'fully symmorphic' space groups are 'impossible'.

9.7.1.4. *Relation to structural classes*

Structural classes (Belsky & Zorky, 1977, and papers cited there and below) are not an *a priori* classification of space groups but are a classification of structures within a space-group type in accordance with the number and kind of Wyckoff positions occupied by the molecules. As a considerable knowledge of the structures is required before their structural classes can be assigned, they form an *a posteriori* classification, and will be described (Section 9.7.5 below) after the empirical frequencies of space groups have been discussed.

9.7.2. Special positions of given symmetry

As noted by Kitajgorodskij, in many crystal structures molecules with inherent symmetry may occupy Wyckoff special positions, so that molecular and crystallographic symmetry elements coincide, and this may affect the relative frequencies of occurrence of structures with particular space groups. Tables of the frequency of occurrence of space groups have been published by many authors, from Nowacki (1942) onwards. Some typical recent papers are Brock & Dunitz (1994), Donohue (1985), Mighell, Himes & Rodgers (1983), Padmaya, Ramakumar & Viswamitra (1990), Wilson (1988, 1990,

Table 9.7.1.2. *Space groups arranged by arithmetic crystal class and degree of symmorphism (cont.)*

(*c*) Trigonal space groups. For *, † see Subsection 9.7.4.1.

Arithmetic crystal class	Fully symmorphic	Tending to symmorphism	Equally balanced	Tending to antimorphism	Fully antimorphic
$3P$	$*P3^{(0)}$	...	...	...	$P3_{1,2}\dagger^{(33)}$
$3R$	...	...	...	$*R3\dagger^{(11)}$	...
$\bar{3}P$	$*P\bar{3}\dagger^{(1)}$	...	...	...	...
$\bar{3}R$	...	...	...	$*R\bar{3}\dagger^{(30)}$	...
$312P$ $321P$	...	$*P312^{(0)}$ $*P321^{(0)}$	...	$P3_{1,2}12\dagger^{(0)}$ $P3_{1,2}21\dagger^{(10)}$	...
$32R$	...	...	...	$*R32\dagger^{(0)}$	...
$3m1P$ $31mP$	...	$*P3m1^{(0)}$ $*P31m^{(0)}$	...	$P3c1\dagger^{(0)}$ $P31c\dagger^{(0)}$	...
$3mR$	...	...	...	$*R3m^{(0)}$ $R3c\dagger^{(7)}$	...
$\bar{3}m1P$ $\bar{3}1mP$	...	$*P\bar{3}m1^{(0)}$ $*P\bar{3}1m^{(0)}$	...	$P\bar{3}c1\dagger^{(0)}$ $P\bar{3}1c\dagger^{(0)}$	...
$\bar{3}mR$	...	...	...	$*R\bar{3}m^{(0)}$ $R\bar{3}c\dagger^{(0)}$	...

(*d*) Hexagonal space groups. For *, † see Subsection 9.7.4.1.

Arithmetic crystal class	Fully symmorphic	Tending to symmorphism	Equally balanced	Tending to antimorphism	Fully antimorphic
$6P$	$*P6^{(0)}$	...	$P6_{2,4}^{(1)}$ $P6_3^{(0)}$	...	$P6_{1,5}\dagger^{(22)}$
$\bar{6}P$	$*P\bar{6}\dagger^{(0)}$	...	...	...	...
$6/mP$	$*P6/m^{(0)}$	...	$P6_3/m\dagger^{(0)}$	...	...
$622P$	...	$*P622^{(0)}$ $P6_{2,4}22^{(0)}$	...	$P6_322^{(1)}$ $P6_{1,5}22\dagger^{(2)}$	...
$6mmP$	...	$*P6mm^{(0)}$	...	$P6cc^{(0)}$	...
				$P6_3cm^{(0)}$ $P6_3mc^{(0)}$	
$\bar{6}m2P$ $\bar{6}2mP$	...	$*P\bar{6}m2^{(0)}$ $*P\bar{6}2m^{(0)}$	...	$P\bar{6}c2\dagger^{(0)}$ $P\bar{6}2c\dagger^{(0)}$	
$6/mmmP$	...	$*P6/mmm^{(0)}$	...	$P6/mcc\dagger^{(0)}$	...
				$P6_3/mcm^{(0)}$ $P6_3/mmc^{(0)}$	

(*e*) Cubic space groups. For *, †, see Subsection 9.7.4.1. No examples with one molecule in general position were found, so the frequencies are omitted.

Arithmetic crystal class	Fully symmorphic	Tending to symmorphism	Equally balanced	Tending to antimorphism	Antimorphic except for 3
$23P$	...	$*P23$	...	...	$P2_13\dagger$
$23F$	...	...	$*F23\dagger$	...	...
$23I$	...	...	$*I23$ $I2_13\dagger$	...	...
$m\bar{3}P$	...	$*Pm\bar{3}$	$Pn\bar{3}$	...	$Pa\bar{3}\dagger$
$m\bar{3}F$	...	...	$*Fm\bar{3}$	$Fd\bar{3}\dagger$	...
$m\bar{3}I$	...	...	$*Im\bar{3}$	$Ia\bar{3}\dagger$	...
$432P$	...	$*P432$	...	$P4_232\dagger$ $P4_{1,3}32\dagger$	...
$432F$	...	...	$*F432$	$F4_132\dagger$	...
$432I$	...	...	$*I432$	$I4_132\dagger$	...
$\bar{4}3mP$	...	$*P\bar{4}3m$	...	$P\bar{4}3n\dagger$	...
$\bar{4}3mF$	...	...	$*F\bar{4}3m$	$F\bar{4}3c\dagger$	...
$\bar{4}3mI$	...	...	$*I\bar{4}3m$	$I\bar{4}3d\dagger$	...
$m\bar{3}mP$	...	$*Pm\bar{3}m$	$Pm\bar{3}n$ $Pn\bar{3}m$	$Pn\bar{3}\dagger$	...
$m\bar{3}mF$	...	$*Fm\bar{3}m$	...	$Fm\bar{3}c$ $Fd\bar{3}m$	$Fd\bar{3}c\dagger$
$m\bar{3}mI$	...	$*Im\bar{3}m$	...	$Ia\bar{3}d\dagger$	...

1993*b*,*c*), but many of them hardly go beyond recognizing the fact that structures frequently made use of molecular symmetry – Wilson (1988) explicitly chose to ignore it. The early work of Belsky, Zorky and their colleagues did not attract much attention outside Russian-speaking areas. Recently, however, there has been a spate of interest (Wilson, 1991, 1993*b*,*c*,*d*; Brock & Dunitz, 1994; Belsky, Zorkaya & Zorky, 1995). Earlier lack of results is partly due to the fact that the Cambridge Structural Database (Section 9.7.3) did not provide a search program that would distinguish between occupation of a general position and multiple occupation of special positions of the required symmetry (Wilson, 1993*d*, Section 3). Belsky, Zorkaya & Zorky (1995) were able to make this distinction, and their paper is the source of many of the statistics quoted without special citation here.

It would be interesting to know which space groups possess positions with the symmetry of each of the 32 point groups 1, $\bar{1}$, 2, m, $2/m$, ..., $m\bar{3}m$. Volume A of *International Tables for Crystallography* (Hahn, 1995) enumerates the symmetry of all the special positions of a given space group, but does not readily

answer the reverse question: which space groups contain special positions of given point group $\mathcal{G}$? Some general points may be noted.

(i) Special positions of symmetry $\mathcal{G}$ will be found in the symmorphic, but not other, space groups of the geometric class $\mathcal{G}$. Thus, for example, there are special positions of symmetry *mmm* in *Pmmm*, *Cmmm*, *Fmmm*, *Immm*, but not in any other space group in the geometric class *mmm*.

(ii) A 'family tree' of point groups is given in Fig. 10.3.2 of Volume A of *International Tables for Crystallography* (Hahn, 1995). Special positions of symmetry $\mathcal{G}$ may be sought in space groups of the geometric classes linked to $\mathcal{G}$ by a line (possibly zigzag) having a generally upwards direction. Thus, to take the same example, special positions of symmetry *mmm* are found in certain space groups of $4/mmm$ ($P4/mmm$, $P4/mbm$, $4_2/mmc$, $P4_2/mcm$, $P4_2/mmm$, $I4/mmm$, $I4/mcm$), in $\bar{6}/mmm$ ($P\bar{6}/mmm$), in $m\bar{3}$ ($Pm\bar{3}$, $Im\bar{3}$), and in $m\bar{3}m$ ($Pm\bar{3}m$, $Fm\bar{3}m$).

(iii) Obviously, the higher up the tree the symmetry $\mathcal{G}$ is, the fewer will be the space groups in which it can occur – special positions of symmetry $m\bar{3}m$ can occur only in the three symmorphic space groups of the corresponding geometric class. The lower symmetries (2, m, $\bar{1}$, $\bar{3}$), with nothing below them but 1, can be traced upwards along many branches, and so can occur in many space groups, but not all are equally favoured. Special positions of symmetry 2 can be sought in all higher geometric classes except $\bar{6}$, $3m$, and $\bar{3}$, but those of symmetry 3 could occur only in the classes of the trigonal, hexagonal, and cubic systems. An approximate count* (Table 9.7.2.1) shows that special positions of symmetry 2 occur in 167 space groups, of m in 99, of $\bar{1}$ in 38, and of 3 in 57. The only other special positions with space-group frequencies of this order are $2/m$ (39), 222 (30), and *mm* (57).

9.7.3. Empirical space-group frequencies

Empirical space-group frequencies are based on two major collections of structural data for organic substances, in Cambridge and Moscow, respectively.

The Cambridge Structural Database (Allen *et al.*, 1991) contains assignments of space groups for a variety of different types of organic compounds. The file can be computer searched in many ways; it is easy, for example, to trace all structures having a particular space group, or those having a particular space group and a particular number of formula units per unit cell. For the present purpose, a selection has to be made, omitting space groups not substantiated by a full structure determination or dubious because of disorder in the crystal. The packing considerations discussed in previous paragraphs would not apply to crystals in which the intermolecular binding was ionic rather than van der Waals or the like, so that space groups of ionic structures (for example salts of organic acids) are also rejected. Unfortunately, as it is implemented at present (early 1995), it is not possible to search for structures with molecules occupying general positions or specified special positions, so that, in particular, the frequency data of Wilson (1993*d*) are inflated by the inability to distinguish between single occupation of a general position and multiple occupation of special positions.

The file compiled by V. A. Belsky at the L. Ya. Karpov Institute of Physical Chemistry in Moscow is the source of the data used by Belsky, Zorkaya & Zorky (1995). This file differs in objective from the Cambridge file; the latter includes all reasonably established organic structures short of proteins and high polymers, whereas the former concentrates on structures containing only a single type of molecule ('homomolecular structures'). It thus contains appreciably fewer entries than the Cambridge file, even if structures of the types mentioned in the previous paragraph are excluded from the latter. The Moscow file is, of course, the primary source for the data of Belsky, Zorkaya & Zorky (1995), in which the occupation of general and special positions is explicitly presented.

9.7.4. Use of molecular symmetry

It has long been recognized that in many crystal structures molecules with inherent symmetry occupy Wyckoff special positions, so that molecular and crystallographic symmetry elements coincide, but until recently systematic data have been lacking. Now the occurrence of molecules of particular symmetry in structures of various space-group types can be traced in the data of Belsky, Zorkaya & Zorky (1995), and will be discussed briefly.

9.7.4.1. *Positions with symmetry 1*

The empirical results for 'homomolecular structures' with one molecule in the general position are given in Table 9.7.1.2. The classification by arithmetic crystal class and degree of symmorphism follows Wilson (1993*d*); the numerical data are taken from Belsky, Zorkaya & Zorky (1995). Space groups symmorphic in the technical sense (Wilson, 1993*d*) are prefixed by an asterisk (∗), and in each arithmetic crystal class the space group most nearly antimorphic is followed by an obelus (†). The number of known structures having precisely one molecule in the general Wyckoff position is given as a superscript in brackets. It will be noticed immediately that structures with space groups 'fully symmorphic' or 'tending to symmorphism' are extremely rare. Most have no examples; three ($P4_2$, $P4/n$ and $P\bar{3}$) are credited with a single example each. The frequency of space groups increases rapidly with increasing antimorphism. In the monoclinic system, the 'fully symmorphic' space group $P2/m$ has no examples with one molecule in the general position, the 'equally balanced' $P2/c$ has 11 examples, the 'tending to antimorphism' $C2/c$ has 587, and the 'fully antimorphic' $P2_1/c$ has 5951. Other systems have fewer examples, but the trend is the same; the really popular space groups are the 'fully antimorphic' plus $P1$ and $P\bar{1}$.

All space groups, of course, possess general positions of symmetry 1, and the data in Table 9.7.2.1 show that 116 of them exhibit structures of some kind, and that 57 exhibit structures in which one or more general positions are used. 13 space groups ($P1$, $P2_1$, Pc, Cc, $P2_12_12_1$, $Pca2_1$, $Pna2_1$, $P4_{1,3}$, $P3_{1,2}$, $P6_{1,5}$) have no positions with symmetry higher than 1. These space groups contain no syntropic symmetry elements, and all are relatively popular.

9.7.4.2. *Positions with symmetry $\bar{1}$*

Many space groups are centrosymmetric (all those in the geometric classes $\bar{1}$, $2/m$, *mmm*, $4/m$, $4/mmm$, $\bar{3}$, $\bar{3}m$, $6/m$, $6/mmm$, $m\bar{3}$, $m\bar{3}m$), but comparatively few of them possess special positions of symmetry $\bar{1}$, as the centres of symmetry are often encumbered by other symmetry elements. All centres of symmetry in $P\bar{1}$, $P2_1/c$ and *Pbca* are free, as are some of those in $P\bar{3}$ and $R\bar{3}$. When the encumbrance is an antitropic symmetry element, the special position can still be occupied by a molecule of symmetry $\bar{1}$ only, but when the encumbrance is syntropic or atropic the position cannot accommodate such a molecule. Table

* Such counts are tedious and subject to error, but the table should be correct within a few units.

Table 9.7.2.1. *Statistics of the use of Wyckoff positions of specified symmetry $\mathcal{G}$ in the homomolecular organic crystals, based on the data by Belsky, Zorkaya & Zorky (1995)*

$\mathcal{G}$	Space groups with positions of symmetry $\mathcal{G}$	Space groups actually occurring	Space groups using such positions
1	230	116	57
2	167	79	38
m	99	42	25
$\bar{1}$	38	28	10
3	57	18	7
4	24	6	4
$\bar{4}$	29	17	8
222	50	15	5
$mm2$	57	18	5
$2/m$	39	21	6
6	5	1	0
$\bar{6}$	8	3	1
32	22	5	1
$3m$	22	8	5
$\bar{3}$	14	7	4
422	9	1	1
$\bar{4}2m, \bar{4}m2$	19	5	3
$4mm$	8	3	0
$4/m$	7	2	1
mmm	16	3	2
23	12	3	2
622	2	1	0
$\bar{6}2m, \bar{6}m2$	5	1	1
$6mm$	2	0	0
$6/m$	2	1	0
$\bar{3}m$	8	3	1
$4/mmm$	4	2	1
432	5	0	0
$\bar{4}3m$	6	2	1
$m\bar{3}$	5	2	1
$6/mmm$	1	0	0
$m\bar{3}m$	3	2	2

9.7.2.1 indicates that there are 38 space groups with special positions of symmetry $\bar{1}$, that 28 of them have examples of structures of some kind, and that ten have structures in which the centre of symmetry is actually used by a molecule.

The three space groups with no special positions except those of symmetry $\bar{1}$ are very popular, whether or not the centre of symmetry is actually used by the molecule. The single criterion 'no special positions except possibly free centres of symmetry' thus selects the space groups favoured by structures in which inherent molecular symmetry is not used.

9.7.4.3. *Other symmetries*

Table 9.7.2.1 gives statistics for the number of space groups possessing Wyckoff positions of symmetry $\mathcal{G}$, where $\mathcal{G}$ is one of the 32 point groups, the number exhibiting structures of some kind, and the number in which the special position of symmetry $\mathcal{G}$ is actually used. It has to be remembered that this table represents the state of knowledge in 1994, that there may be small errors in the counts in the second column, and that new structures will gradually increase the numbers in the third and fourth columns. Nevertheless, some trends are clear. The arrangement of the point groups is in ascending order of their 'order' (Hahn, 1995, p. 781), and all numbers show a general decrease with increasing order. When molecular symmetry is used, the favourite is the diad axis 2, closely followed by the mirror plane m, with the centre of symmetry $\bar{1}$, the triad axis 3 and the tetrad inversion axis $\bar{4}$ trailing. It must also be remembered that these data are for numbers of *space groups*, not numbers of *structures*.

9.7.4.4. *Positions with the full symmetry of the geometric class*

The symmorphic space groups are in a one-to-one correspondence with the arithmetic crystal classes, and each has at least one Wyckoff position with the full symmetry of the geometric crystal class. It would thus be possible for each symmorphic space group to accommodate molecules with the full symmetry of the point group corresponding to the geometric crystal class. With the obvious exceptions of $P1$ and $P\bar{1}$, there seem to be no symmorphic space groups with primitive cells and one molecule only in the cell that do so, but the data of Belsky, Zorkaya &

Zorky (1995) show that about half the possibilities are realized in symmorphic space groups with centred cells. The situation is set out in Table 9.7.4.1.

Although about half the point groups are not represented in symmorphic space groups with one molecule in the appropriate special position, it is interesting to look for molecules of these symmetries in space groups of higher symmetry. A few are in fact to be found in non-symmorphic space groups, but seven point groups have no established examples.

9.7.5. Structural classes

As developed so far (Belsky, Zorkaya & Zorky, 1995), structural classes relate primarily to homomolecular structures – structures in which all molecules are the same. Nevertheless, they are important in a study of the space-group distribution of molecular organic structures, as structures belonging to the same space-group type but to different structural classes are found to have very different frequencies. The germ of the idea is implicit in Kitajgorodskij's subdivision of his four categories by molecular symmetry.

In its general form, the symbol of a structural class has the form

$$\mathcal{SG}, Z = n[(x)^a, (y)^b, \ldots],$$

where $\mathcal{SG}$ is the standard space-group symbol, n is the number of molecules in the unit cell, $x, y, \ldots$ are the symbols of the point-group symmetries of the Wyckoff positions occupied, and $a, b, \ldots$ are the numbers of occupied Wyckoff positions of those symmetries. An example will make this clearer. There is a structural class

$$P\bar{4}m2, Z = 32[(mm)^4, m^4, 1].$$

This indicates that the space group is $P\bar{4}m2$ and that there are 32 molecules in the unit cell occupying four positions of symmetry *mm*, four of symmetry *m*, and one general position. On consulting the multiplicity of the special positions for this space group in Volume A of *International tables for crystallography* (Hahn, 1995), one finds that the 32 molecule total is accounted for as $(4 \times 2) + (4 \times 4) + (1 \times 8)$. If (as is usually the case) the square brackets are unnecessary, they are omitted, as in

$$P\bar{4}n2, Z = 2(222) \text{ and } P4/nnc, Z = 4(4).$$

Occasionally, two distinguishable structural classes will lead to the same symbol. As yet, Belsky, Zorkaya & Zorky prefer to deal with this problem on an *ad hoc* basis, rather than by attempting to devise any general rules.

Belsky, Zorkaya & Zorky divide the structural classes into six groups, in accordance with the number of examples found. The groups are 'anomalous' (up to five examples, 199 structural classes); 'rare' (up to 19 examples, 55 classes); 'small' (up to 49 examples, 24 classes); 'big' (13 classes); 'giant' (eight classes); and 'supergiant' (six classes). The last three are not explicitly defined, but examination of the tables shows that the dividing line between 'big' and 'giant' is about 250, and between 'giant' and 'supergiant' is about 750. All these statistics, of course, are subject to modification as the number of known structures increases.

9.7.6. A statistical model

Wilson (1988, 1990, 1991) has discussed the factors that, on statistical analysis, appear to govern the relative frequency of occurrence of the space groups of molecular organic crystals. In its developed form (Wilson, 1990), the statistical model postulated that, within an arithmetic crystal class (see Chapter 1.4), the number of examples, N_{sg}, of a space-group type would depend exponentially on the numbers of symmetry elements within the unit cell, thus:

$$N_{sg} = A \exp\left\{ -\sum_j B_j [e_j]_{sg} \right\}. \qquad (9.7.6.1)$$

In this equation, A is a normalizing constant depending on the arithmetic crystal class, $[e_j]_{sg}$ is the number of symmetry elements of type e_j within the unit cell in the space group, and B_j is a parameter depending on the arithmetic crystal class and the symmetry element e_j; A and B_j are independent of the space group. Empirically, B_j has a positive sign for the syntropic symmetry elements (k and $\bar{k}$, where $n = 2, 3, 4, 6$) and a negative sign for $\bar{1}$ and the antitropic symmetry elements (glide planes and screw axes). Often, however, laws of 'conservation of symmetry elements', of the type

$$[2] + [2_1] = c, \qquad (9.7.6.2)$$

or in general

$$\sum_j [e_j] = c, \qquad (9.7.6.3)$$

where c is a constant for the crystal class, eliminate a separate dependence on one or more of the e_j's (Wilson, 1990). Often a cohort larger than an arithmetic crystal class can be used, with arithmetic crystal class included as an additional factor.* With this adjustment, the model can be used for such cohorts as geometric crystal class or even crystal system, giving fits within the usual crystallographic range ($R_2 \lesssim 0.05$), but, for some classes (in particular *mmm*), statistical tests based on the scaled deviance indicated residual systematic error (Wilson, 1980). This was traced (Wilson, 1991) to the failure of an explicit postulate: 'The second possibility is that the distribution is seriously affected by molecular symmetry. Some molecules possess inherent symmetry ..., and this symmetry could coincide with the corresponding crystallographic symmetry element, again increasing the variance and/or bias of the number of examples per space group. ... The comparative rarity of utilization of molecular symmetry suggests that it can be ignored in an exploratory statistical survey ...' (abbreviated from Wilson, 1988). This procedure was perhaps reasonable in a first 'exploratory' survey, and in fact agreement in the usual crystallographic range ($R_2 \lesssim 0.05$) was achieved (Wilson, 1988, 1990). However, the scaled deviance indicated that systematic errors still remained (Wilson, 1980), and the discrepancy was traced to the use of molecular symmetry in many structures (Wilson, 1990, 1992). If such structures are eliminated, R_2 falls to trivial values, and the agreement between observed and calculated frequencies becomes too good to be interesting.

9.7.7. Molecular packing

9.7.7.1. *Relation to sphere packing*

The effect of molecular symmetry cannot be ignored in overall statistical surveys as well as in structure prediction. However, in most structures, the molecular symmetry is low or it is not used

* Statistical modelling programs distinguish between variates and factors. The values of variates are ordinary numbers; [2], [*m*], ... are variates. Factors are qualitative. In the immediate context, 'arithmetic crystal class' is a factor, but other categories, such as metal-organic compound, polypeptide, structural class (Belsky & Zorky, 1977), ..., could be included if desired. The programs allow appropriately for both variates and factors; see Baker & Nelder (1978, Sections 1.2.1, 8.5.2, 22.1 and 22.2.1).

Table 9.7.4.1. *Occurrence of molecules with specified point group in centred symmorphic and other space groups, based on the statistics by Belsky, Zorkaya & Zorky (1995)*

There is no entry in the 'other space group' column if examples are found in the centred symmorphic group.

Point group	Symmorphic space group	Other space group	Frequency
2	$C2$	...	18
m	Cm	...	6
$2/m$	$C2/m$	...	20
222	None	$Ccca$	4
	...	$Fddd$	2
	...	$P\bar{4}n2$	2
	...	$P4/ncc$	1
	...	$I4_1/acd$	3
$mm2$	$Fmm2$	...	2
mmm	None	$P4_2/mnm$	6
	...	$Im\bar{3}$	1
4	$I4$	...	1
$\bar{4}$	None	$P4/n$	1
	...	$P4_2/n$	3
	...	$I4_1/a$	12
	...	$P\bar{4}2_1c$	17
	...	$I\bar{4}2d$	1
	...	$I4_1/acd$	1
$4/m$	$I4/m$	...	1
422	None	$P4/nnc$	1
$4mm$	None	None	None
$\bar{4}2m$	$I\bar{4}2m$	...	3
$4/mmm$	$I4/mmm$	...	1
3	$R3$	...	8
$\bar{3}$	$R\bar{3}$	...	6
32	None	$R\bar{3}c$	5
$3m$	$R3m$	...	10
$\bar{3}m$	$R\bar{3}m$	...	2
6	None	None	None
$\bar{6}$	None	$P6_3/m$	12
$6/m$	None	None	None
622	None	None	None
$6mm$	None	None	None
$\bar{6}m2$	None	$P6_3/mmc$	1
$6/mmm$	None	None	None
23	None	$F\bar{4}3c$	1
$m\bar{3}$	$Fm\bar{3}$	...	2
432	None	None	None
$\bar{4}3m$	$I\bar{4}3m$	...	4
$m\bar{3}m$	$Fm\bar{3}m$	...	9
	$Im\bar{3}m$	...	2

in the packing. In about 90% of crystalline compounds, the molecules crystallize in low-symmetry space groups, so that a given molecule has a 12-point contact with neighbouring molecules. As 12 corresponds to the number of nearest neighbours in cubic and hexagonal closest packing of spheres, the periodic assembly of most molecular structures can be regarded as the closest packing of distorted spheres, where symmetry ensures the interlocking of complex shapes (Gavezzotti, 1994).

For the relatively infrequent cases where high molecular symmetry is reflected in high crystal symmetry, the packing of molecules can be derived from the appropriate, though not necessarily the densest, packing of spheres. For example, ten-point, eight-point and six-point molecular contacts can be achieved, respectively, by tetragonal close packing ($I4/mmm$), by I-centred cubic packing ($Im\bar{3}m$), and by primitive cubic packing ($Pm\bar{3}m$). For a review and some derivations of the densest packing of equal spheres, see Chapter 9.1 and Patterson & Kasper (1959), Coutanceau Clarke (1972), and Smith (1973); and for packing of clusters of unequal spheres, see Williams (1987).

With spheres having infinite point symmetry $\mathcal{K}_{\infty h}$, every sphere can be located on syntropic symmetry elements at special positions with high symmetry up to the symmetry of the lattice. The lattice translations, pertinent to the fully symmorphic space group, are then able to generate the entire crystal structure. When spheres are deformed, symmetry is removed and the non-lattice translations involved with antimorphic space groups

(which must be subgroups of the sphere-packing groups) become necessary to ensure space filling with the repetitive patterns of complex molecular shapes. In a similar manner, other objects with infinite elements of symmetry (*e.g.* rods; Lidin, Jacob & Andersson, 1995) can be subjected to a rigorous analysis of close packing.

9.7.7.2. *The hydrogen bond and the definition of the packing units*

The variously shaped molecular packing units of organic crystal structures are not necessarily identical with the individual molecule. The molecule (of a shape defined by chemical bonds on the inside and van der Waals forces on the outside) can be subjected to clustering under formation of intermolecular hydrogen bonds. Although far weaker than the chemical bond, hydrogen bonds are strong enough to alter the shape of the packing units of the crystal structure significantly. This may have far-reaching consequences for the adopted packing and symmetry. An extreme example is represented by the clustering of H_2O molecules, where two hydrogen bonds and two regular O—H bonds create a $\bar{4}3m$ point symmetry at each O atom, and a highly symmetrical structure emerges with an infinite bond network, similar to that in quartz, SiO_2. From the point of view of an individual H_2O molecule, the structure is very open. In contrast, a pseudo-close-packed structure of crystalline water, assuming an effective H_2O radius of 1.38 Å, would have specific density of 1.8 g cm^{-3}.

Analogous principles apply to organic structures with hydrogen bonding. CH_3OH, for example, forms hydrogen-bonded zigzag chains in its crystal structure. Obviously, the shape of the hydrogen-bonded cluster of molecules depends on the number and orientations of the hydrogen bonds relative to the size and shape of the molecule, causing three-dimensional, planar and linear 'polymers', or the formation of dimers and trimers. As in the example of water, this introduces additional symmetry elements and decreases the degree of space filling.

There is a general rule that ensures that this phenomenon is widespread. The principle of maximum hydrogen bonding states that all the H atoms in the active (polar) groups of a molecule are employed in hydrogen-bond formation (Evans, 1964). Therefore, as the O···HO and O···HN hydrogen bonds are both energetic and common, they are also of the greatest importance in this respect. Although most pronounced in smaller molecules, the symmetry-altering influence of hydrogen bonding also applies to relatively large molecules with a lower proportion of hydrogen bonding as, for example, in long-chain carboxylic acids that are linked in pairs. In large molecules with many active groups, however, the hydrogen bonds merely become the new delimiters of the shape of the individual molecule. The perils of the symmetry-statistical treatments of the hydrogen-bonded structures are well recognized and, for some purposes, the strategy adopted is to exclude such systems from the statistical pool (Filippini & Gavezzotti, 1992).

9.7.8. *A priori* predictions of molecular crystal structures

As physical properties of a molecular compound are a function of the spatial arrangement of molecules, an important goal of the structural chemist is to predict the space group and crystal structure from the molecular shape. On the basis of the observation that many structures of organic compounds are formed on the principle of periodic close packing of variously shaped molecules, it seems that such prediction would be a more or less straightforward computational task. However, the task of predicting the crystal structure of a specific molecular solid is complicated owing to the occurrence of hydrogen bonding (Subsection 9.7.7.2) and the widespread phenomenon of polymorphism (Gavezzotti, 1994). With only subtle differences in their Gibbs free energies, the occurrence of the structural modifications can be influenced by various non-equilibrium factors during crystallization.

In spite of the above problems, experience has shown that prediction algorithms can often be used to generate several reasonable structures for any given molecule and that in many cases the correct structure is among them. There are two general strategies that have been adapted for structure prediction. In the first one, developed by Kitajgorodskij (1955, 1973), the molecular shape is physically constructed from models of atoms having van der Waals radii, resulting in the calot model. The physical calot model is then used for an analogue calculation of the space filling using a mechanical instrument that relates the molecules in three-dimensional space so that the projection of one molecule fits into the voids of other molecules. When the unit-cell dimensions are known, the entire crystal structure can be derived in this way. In the second approach, the same yet abstract 'fused sphere model' is analysed for its symmetry by what can be called a 'morphic' (as opposed to metric) transformation by the methods of molecular topology (Mezey, 1993). The abstract topological molecular shapes can in principle be treated more rigorously and are computable into probable crystal structures.

Such *a priori* predictions of molecular structures are still in a relatively early stage of development. Several recent studies are indicative of the current progress in the field. For layered structures, good predictions can be obtained using construction techniques, symmetry probabilities, and potential energy functions (Scaringe, 1991). An algorithm for the generation of crystal structures by the optimization of packing potential energy over several possible space groups has been devised by Gavezzotti (1991, 1994). In a third approach, energy minimization without symmetry constraints is used for determining molecular crystal structures (Gibson & Scheraga, 1995).

In spite of recent progress, the conceptual link between the molecular and crystal structures still relies to a large extent on the chemical intuition of scientists. The space-group statistics have played a critical role, as they provide the researcher with a summary of what happens in nature. It is likely that the prediction process can be enhanced by calculating statistics of the space-group frequencies and symmetry for molecules that are the most closely related to the shape or chemistry of the molecule under study. As such statistical subsets are often significantly different from the overall statistics, they may prove more valuable in the *a priori* prediction of the crystal structure for a specific molecule. The space-group frequencies and symmetry statistics remain one of the important strings in this link.

International Tables for Crystallography (2006). Vol. C, Chapter 9.8, pp. 907–955.

9.8. Incommensurate and commensurate modulated structures

By T. Janssen, A. Janner, A. Looijenga-Vos, and P. M. de Wolff

9.8.1. Introduction

9.8.1.1. *Modulated crystal structures*

Lattice periodicity is a fundamental concept in crystallography. This property is widely considered as essential for the characterization of the concept of a crystal. In recent decades, however, more and more long-range-ordered condensed-matter phases have been observed in nature that do not have lattice periodicity, but nevertheless only differ from normal crystal phases in very subtle and not easy to observe structural and physical properties.

It is convenient to extend the concept of a crystal in such a way that it includes these ordered phases as well. If properly applied, crystallographic symmetry concepts are then still valid and of relevance for structural (and physical) investigation. Instead of limiting the validity of crystallographic notions, these developments show how rich the crystallographic ordering can be.

Incommensurate crystals are characterized by Bragg reflection peaks in the diffraction pattern that are well separated but do not belong to a lattice and cannot be indexed by three integer indices. This means that the description in terms of three-dimensional point and space groups, as given in *IT* A (1992), breaks down. It is possible, however, to generalize the crystallographic concepts on which the usual description is based. The ensuing symmetry groups and their equivalence classes are different from those of three-dimensional crystallography. The main properties of these new groups and the specific problems posed by their application to incommensurate crystal structures form the subject of the following sections.

The tables presented here, and their explanation, have been restricted to cover mainly the simplest case: *modulated crystal structures* (in particular, those with a single modulation wave). Nevertheless, most of the basic concepts also apply for the other classes of incommensurate crystal structures.

A modulation is here considered to be a periodic deformation of a 'basic structure' having space-group symmetry. If the periodicity of the modulation does not belong to the periodicities of the basic structure, the modulated crystal structure is called incommensurate.

That description is based on the observation in the diffraction pattern of modulated structures of main reflections, situated on a reciprocal lattice, and additional reflections, generally of weaker intensity, called satellites.

As far as we know, the first indications that complex crystal structures could exist not having normal lattice periodicity came, at the end of the 19th century, from studies of the morphology of the mineral calaverite. It was found that the faces of this compound do not obey the law of rational indices (Smith, 1903; Goldschmidt, Palache & Peacock, 1931). Donnay (1935) showed that faces that could not be indexed correspond to additional reflections in the X-ray diffraction pattern. From the experience with manufacturing of optical gratings, it was already known that periodic perturbation gives rise to additional diffraction spots. Dehlinger (1927) used this theory of '*Gittergeister*' (lattice ghosts) to explain line broadening in Debye–Scherrer diagrams of metals and alloys. Preston (1938) called the '*Gittergeister*' he found in diffraction from an aluminium–copper alloy 'satellites'. Periodic displacement (modulation) waves were considered by Daniel & Lipson (1943) as the origin of satellites in a copper–iron–nickel alloy. Complex magnetic ordering giving rise to satellites was found in magnetic crystals (Herpin, Meriel & Villain, 1960; Koehler, Cable, Wollan & Wilkinson, 1962). In the early 1970's, the importance of the irrationality was realized and the term 'incommensurate phase' was introduced for modulated crystal phases with wavevectors that have irrational components. Such phases were found in insulators as well (Tanisaki, 1961, 1963; Brouns, Visser & de Wolff, 1964). The remarkable morphological properties of calaverite could also be related to the existence of an incommensurate modulation (Dam, Janner & Donnay, 1985). Structures that are well ordered, show sharp incommensurate spots in the diffraction pattern, but cannot be described as a modulation of a lattice periodic system, were also discovered, indicating that incommensurability is not restricted to modulated crystals. Examples are the composite (or intergrowth) crystals (Jellinek, 1972) and, more recently, quasicrystals (Shechtman, Blech, Gratias & Cahn, 1984). The latter not only lack three-dimensional lattice periodicity, but also show non-crystallographic symmetry elements, such as five-, eight- or twelvefold axes. For a review, see Janssen & Janner (1987).

We denote a basis for the lattice of main reflections by $\mathbf{a}^*$, $\mathbf{b}^*$, $\mathbf{c}^*$. The satellites are separated from the main reflections by vectors that are integral linear combinations of some basic modulation vectors denoted by $\mathbf{q}_j$ $(j = 1, 2, \ldots, d)$. Accordingly, the positions of the Bragg reflections are given by

$$\mathbf{H} = h\mathbf{a}^* + k\mathbf{b}^* + l\mathbf{c}^* + m_1\mathbf{q}_1 + m_2\mathbf{q}_2 + \ldots + m_d\mathbf{q}_\mathbf{d}. \quad (9.8.1.1)$$

If the modulation is incommensurate, the set of all positions (9.8.1.1) does not form a lattice. Mathematically, it has the structure of a Z-module, and its elements are three-dimensional vectors (of the reciprocal space). Accordingly, we call it a (reciprocal) *vector module*.

The modulation that gives rise to the satellites can be:

(i) a displacive modulation, consisting of a periodic displacement from the atomic positions of the basic structure;

(ii) an occupation modulation, in which the atomic positions of the basic structure are occupied with a periodic probability function.

Mixed forms also occur. Other modulation phenomena found are, for example, out-of-phase structures and translation interface modulated structures. The satellite reflections of modulated structures for the various types of modulation were systematically studied by Korekawa (1967).

For an incommensurate structure, at least one component of a basic modulation wavevector $\mathbf{q}_j$ with respect to the lattice of main reflections is irrational. As argued later, even in the case of a commensurate modulation, *i.e.* when all components of these modulation wavevectors are rational, it is sometimes convenient to adopt the description of equation (9.8.1.1) and to apply the formalism developed for the incommensurate crystal case.

The modulated crystal case presented above is only the simplest one giving rise to incommensurate crystal structures. Another class is represented by the so-called *composite* or *intergrowth crystal structures*. Here the basic structure consists of two or more subsystems each with its own space-group symmetry (neglecting mutual interaction) such that, in general, the corresponding lattices are incommensurate. This means that these lattices are not sublattices of a common one. Actually, a mutual interaction is in general present giving rise to periodic deviations, *i.e.* to modulations. These crystals are different from the previous ones, in the sense that they show more than one set of main reflections. In the case of an intergrowth crystal, the

Copyright © 2006 International Union of Crystallography

Bragg reflections can be labelled by a finite set of integral indices as well and the Fourier wavevectors form a vector module as defined above. The difference from the previous case is that the basic structure itself is incommensurate, even if one disregards modulation.

A third class of incommensurate crystals found in nature is represented by the *quasicrystals* (examples of which are the icosahedral phases). In that case also, the basic structure is incommensurate, the difference from the previous case being that the splitting in subsystems of main reflections and/or in main reflections and satellites is not a natural one, even in the lowest approximation.

It is justified to assume that crystal phases allow for an even wider range of ordered structures than those mentioned above. Nevertheless, all the cases studied so far allow a common approach based on higher-dimensional crystallography, *i.e.* on crystallographic properties one obtains after embedding the crystal structure in a higher-dimensional Euclidean space.

To present that approach in its full generality would require a too abstract language. On the other hand, restriction to the simplest case of a modulated crystal would give rise to misleading views. It what follows, the basic ideas are formulated as simply as possible, but still within a general point of view. Their application and the illustrative examples are mainly restricted to the modulated crystal case. The tables presented here, even if applicable to more general cases, cover essentially the one-dimensional modulated case [$d = 1$ in equation (9.8.1.1)].

9.8.1.2. *The basic ideas of higher-dimensional crystallography*

Incommensurate modulated crystals are systems that do not obey the classical requirements for crystals. Nevertheless, their long-range order is as perfect as that of ordinary crystals. In the diffraction pattern they also show sharp, well separated spots, and in the morphology flat faces. Dendritic crystallization with typical point-group symmetry is observed in both commensurate and incommensurate materials. Therefore, we shall consider both as crystalline phases and generalize for that reason the concept of a crystal. The positions of the Bragg diffraction peaks given in (9.8.1.1) are a special case. In general, they are elements of a vector module M^* and can be written as

$$\mathbf{H} = \sum_{i=1}^{n} h_i \mathbf{a}_i^*, \quad \text{integers } h_i. \tag{9.8.1.2}$$

This leads to the following *definition of crystal*.

An *ideal crystal* is considered to be a matter distribution having Fourier wavevectors expressible as an integral linear combination of a finite number (say n) of them and such that its diffraction pattern is characterized by a discrete set of resolved Bragg peaks, which can be indexed accordingly by a set of n integers $h_1, h_2, \ldots, h_n$.

Implicit in this definition is the possibility of neglecting diffraction intensities below a given threshold, allowing one to identify and to label individual Bragg peaks even when n is larger than the dimension m of the crystal, which is usually three. Actually, for incommensurate crystals, the unresolved Bragg peaks of arbitrarily small intensities form a dense set, because they may come arbitrarily close to each other.

Here some typical examples are indicated. In the *normal crystal* case, $n = m = 3$ and $\mathbf{a}_1^*, \mathbf{a}_2^*, \mathbf{a}_3^*$ are conventionally denoted by $\mathbf{a}^*, \mathbf{b}^*, \mathbf{c}^*$ and the indices h_1, h_2, h_3 by h, k, l.

In the case of a one-dimensionally *modulated crystal*, which can be described as a periodic plane wave deformation of a normal crystal (defining the basic structure), one has $n = 4$. Conventionally, $\mathbf{a}_1^*$, $\mathbf{a}_2^*$, $\mathbf{a}_3^*$ are chosen to be $\mathbf{a}^*$, $\mathbf{b}^*$, and $\mathbf{c}^*$ generating the positions of the main reflections, whereas $\mathbf{a}_4^* = \mathbf{q}$ is the wavevector of the modulation. The corresponding indices are usually denoted by h, k, l and m. Also, crystals having two- and three-dimensional modulation are known: in those cases, $n = 5$ and $n = 6$, respectively.

In the case of a *composite crystal*, one can identify two or more subsystems, each with its own space-group symmetry. As an example, consider the case where two subsystems share $\mathbf{a}^*$ and $\mathbf{b}^*$ of their reciprocal-lattice basis, whereas they differ in periodicity along the c axis and have, respectively, $\mathbf{c}_1^*$ and $\mathbf{c}_2^*$ as third basis vector. Then again, $n = 4$ and $\mathbf{a}_1^*, \ldots, \mathbf{a}_4^*$ can be chosen as $\mathbf{a}^*$, $\mathbf{b}^*$, $\mathbf{c}_1^*$, and $\mathbf{c}_2^*$. The indices can be denoted by h, k, l_1, l_2. In general, the subsystems interact, giving rise to modulations and possibly (but not necessarily) to a larger value of n. In addition to the main reflections from the undistorted subsystems, satellite reflections then occur.

In the case of a *quasicrystal*, the Bragg reflections require more than three indices, but they do not arise from structurally different subsystems having lattice periodicity. So, for the icosahedral phase of AlMn alloy, $n = 6$, and one can take for $\mathbf{a}_1^*$, $\mathbf{a}_2^*$, $\mathbf{a}_3^*$ a cubic basis $\mathbf{a}^*$, $\mathbf{b}^*$, and $\mathbf{c}^*$ and for $\mathbf{a}_4^*$, $\mathbf{a}_5^*$, $\mathbf{a}_6^*$ then $\tau\mathbf{a}^*$, $\tau\mathbf{b}^*$, and $\tau\mathbf{c}^*$, respectively, with τ the golden number $[1 + \sqrt{5}]/2$.

The *Laue point group* P_L of a crystal is the point symmetry group of its diffraction pattern. This subgroup of the orthogonal group $O(3)$ is of finite order. The finite order of the group follows from the discreteness of the (resolved) Bragg peak positions, implying a finite number only of peaks of the same intensity lying at a given distance from the origin.

Under a symmetry rotation R, the indices of each reflection are transformed into those of the reflection at the rotated position. Therefore, a symmetry rotation is represented by an $n \times n$ non-singular matrix $\Gamma(R)$ with integral entries. Accordingly, a Laue point group admits an n-dimensional faithful integral representation $\Gamma(P_L)$. Because any finite group of matrices is equivalent with a group of orthogonal matrices of the same dimension, it follows that:

(1) P_L is isomorphic to an n-dimensional crystallographic point group;

(2) there exists a lattice basis $a_{s1}^*, \ldots, a_{sn}^*$ of a Euclidean n-dimensional (reciprocal) space, which projects on the Fourier wavevectors $\mathbf{a}_1^*, \ldots, \mathbf{a}_n^*$;

(3) the three-dimensional Fourier components $\hat{\rho}(h_1, \ldots, h_n)$ of the crystal density function $\rho(\mathbf{r})$ can be attached to corresponding points of an n-dimensional reciprocal lattice and considered as the Fourier components of a density function $\rho_s(r_s)$ having lattice periodicity in that higher-dimensional space (r_s is an n-dimensional position vector).

Such a procedure is called the *superspace embedding* of the crystal.

Note that this procedure only involves a reinterpretation of the structural data (expressed in terms of Fourier coefficients): the structural information in the n-dimensional space is exactly the same as that in the three-dimensional description.

The *symmetry group* of a crystal is then defined as the Euclidean symmetry group of the crystal structure embedded in the superspace.

Accordingly, the symmetry of a crystal whose diffraction pattern is labelled by n integral indices is an n-dimensional space group.

The *equivalence relation* of these symmetry groups follows from the requirement of invariance of the equivalence class with respect to the various possible choices of bases and embeddings. Because of that, the equivalence relation is not simply the one valid for n-dimensional crystallography.

In the case of modulated crystals, such an equivalence relation has been worked out explicitly, giving rise to the concept of the $(3+d)$-dimensional *superspace group*.

The concepts of point group, lattice holohedry, Bravais classes, systems of non-primitive translations, and so on, then follow from the general properties of n-dimensional space groups together with the (appropriate) equivalence relations.

A glossary of symbols is given in Appendix A and a list of definitions in Appendix B.

9.8.1.3. *The simple case of a displacively modulated crystal*

9.8.1.3.1. *The diffraction pattern*

To introduce what follows, the simple case of a displacively modulated crystal structure is considered. The point-atom approximation is adopted and the modulation is supposed to be a sinusoidal plane wave.

This means that the structure can be described in terms of atomic positions of a *basic structure* with three-dimensional space-group symmetry, periodically displaced according to the modulation wave. Writing for the position of the jth particle in the unit cell of the basic structure given by the lattice vector $\mathbf{n}$:

$$\mathbf{r}_0(\mathbf{n}, j) = \mathbf{n} + \mathbf{r}_j, \tag{9.8.1.3}$$

the position of the same particle in the modulated structure is given by

$$\mathbf{r}(\mathbf{n}, j) = \mathbf{n} + \mathbf{r}_j + \mathbf{U}_j \sin[2\pi\mathbf{q}\cdot(\mathbf{n}+\mathbf{r}_j) + \varphi_j], \tag{9.8.1.4}$$

where $\mathbf{q}$ is the wavevector of the modulation and $\mathbf{U}_j$ is the polarization vector for the jth particle's modulation. (This is not the most general sinusoidal modulation, because different components $U_{j\alpha}$ may have different phases $\varphi_{j\alpha}, \alpha = 1, 2, 3$.) In general, the symmetry of the modulated structure is different from that of the basic structure and the only translations that leave the modulated structure invariant are those lattice translations $\mathbf{m}$ of the basic structure satisfying the condition $\mathbf{q}\cdot\mathbf{m} =$ integer. If the components α, β, and γ of the wavevector $\mathbf{q}$ with respect to the basis $\mathbf{a}^*, \mathbf{b}^*, \mathbf{c}^*$ are all rational numbers, there is a full lattice of such translations, the structure then is a *superstructure* of the original one and has space-group symmetry. If at least one of the α, β, and γ is irrational, the structure does not have three-dimensional lattice translation symmetry. Nevertheless, the crystal structure is by no means disordered: it is fully determined by the basic structure and the modulation wave(s).

The crystalline order is reflected in the structure factor, which is given by the expression

$$\begin{aligned} S_{\mathbf{H}} &= \sum_{\mathbf{n},j} f_j \exp[2\pi i \mathbf{H}\cdot\mathbf{r}(\mathbf{n}, j)] \\ &= \sum_{\mathbf{n},j} f_j \exp[2\pi i \mathbf{H}\cdot(\mathbf{n}+\mathbf{r}_j)] \\ &\quad \times \exp\{2\pi i \mathbf{H}\cdot\mathbf{U}_j \sin[2\pi\mathbf{q}\cdot(\mathbf{n}+\mathbf{r}_j)+\varphi_j]\}, \end{aligned} \tag{9.8.1.5}$$

where f_j is the atomic scattering factor (which still, in general, depends on $\mathbf{H}$). Using the Jacobi–Anger relation, one can rewrite (9.8.1.5) as

$$\begin{aligned} S_{\mathbf{H}} &= \sum_{\mathbf{n}} \sum_{j} \sum_{m=-\infty}^{\infty} \exp[2\pi i(\mathbf{H} - m\mathbf{q})\cdot(\mathbf{n}+\mathbf{r}_j)] \\ &\quad \times f_j \exp(-im\varphi_j) J_{-m}(2\pi\mathbf{H}\cdot\mathbf{U}_j), \end{aligned} \tag{9.8.1.6}$$

where $J_m(x)$ is the mth-order Bessel function. The summation over $\mathbf{n}$ results in a sum of δ functions on the positions of the reciprocal lattice:

$$\Delta(\mathbf{H} - m\mathbf{q}) = \sum_{h,k,l} \delta(\mathbf{H} - m\mathbf{q} - h\mathbf{a}^* - k\mathbf{b}^* - l\mathbf{c}^*).$$

Consequently, the structure factor $S_{\mathbf{H}}$ vanishes unless there are integers h, k, l, and m such that

$$\mathbf{H} = h\mathbf{a}^* + k\mathbf{b}^* + l\mathbf{c}^* + m\mathbf{q}. \tag{9.8.1.7}$$

If $\mathbf{q}$ is incommensurate, *i.e.* if there is no integer N such that $N\mathbf{q}$ belongs to the reciprocal lattice spanned by $\mathbf{a}^*, \mathbf{b}^*, \mathbf{c}^*$, one needs more than three integers (in the present case four) for indexing $\mathbf{H}$. This is characteristic for incommensurate crystal phases.

In the diffraction pattern of such a modulated phase, one distinguishes between main reflections (for which $m = 0$) and satellites (for which $m \neq 0$). The intensities of the satellites fall off rapidly for large m so that the observed diffraction spots remain separated, although vectors of the form (9.8.1.7) may come arbitrarily close to each other.

In the commensurate case also, there are main reflections and satellites, but, since here there is an integer N such that $N\mathbf{q}$ belongs to the reciprocal lattice, one may restrict the values of m in (9.8.1.7) to the range from 0 to $N-1$.

9.8.1.3.2. *The symmetry*

There is more than one way for expressing the long-range order present in an incommensurate crystal in terms of symmetry. One natural way is to adopt the point of view that the measuring process limits the precision in the determination of a modulation wavevector. Accordingly, one can try an *approximation* of the modulation wavevector $\mathbf{q}$ *by a commensurate one*: an irrational number can be approximated arbitrarily well by a rational one.

There are two main disadvantages in this approach. Firstly, a good approximation implies, in general, a large unit cell for the corresponding superstructure, which involves a large number of parameters. Secondly, the space group one finds may depend essentially on the rational approximation adopted. Consider, for example, an orthorhombic basic structure with space group $Pcm2_1$ and modulation with wavevector $\mathbf{q} = \gamma\mathbf{c}^*$, polarization along the b direction and positions of the particles given by

$$\mathbf{r}(\mathbf{n}, j) = \mathbf{n} + \mathbf{r}_j + \mathbf{U}\sin[2\pi\mathbf{q}\cdot(\mathbf{n}+\mathbf{r}_j)], \tag{9.8.1.8}$$

where for convenience the polarization has been taken as independent of j. Under the glide reflection $\{m_x|(m+\frac{1}{2})\mathbf{c}\}$ (integer m) present in the basic structure, the transformed positions are

$$\begin{aligned} \mathbf{r}'(\mathbf{n}, j) &= \mathbf{r} + \mathbf{U}\sin\{2\pi[\mathbf{q}\cdot\mathbf{r} - \gamma(m+\tfrac{1}{2})]\}, \\ &\qquad \text{with } \mathbf{r} = \mathbf{n} + \mathbf{r}_j. \end{aligned} \tag{9.8.1.9}$$

Consider the rational approximation of γ given by P/Q, with P and Q relatively prime integers. Then such a glide transformation as given above is (for certain values of m) a symmetry of the modulated structure only if P is even and Q odd, because only in that case does the equation $P(m+\frac{1}{2}) = lQ$ have a solution for integers l and m. Analogously, the mirror m_y only occurs as a glide plane if P/Q is odd/even, whereas the screw axis along the z axis requires the case odd/odd. Hence, if, for example, one approximates the same irrational number successively by 5/12, 7/17 or 8/19, one finds different symmetry groups. Furthermore, in all the cases, the point group is monoclinic and the information contained in the orthorhombic point-group symmetry of the main reflections is lost.

These difficulties are avoided if one embeds the modulated crystal according to the basic ideas expressed in the previous section. Conceptually, it corresponds (de Wolff, 1974, 1977;

Janner & Janssen, 1977) to *enlarging the class of symmetry transformations* admitted, from Euclidean in three dimensions to Euclidean in n dimensions (here $n = 4$). A four-dimensional Euclidean operation transforms the three-dimensional structure but does not leave distances invariant in general. To illustrate this phenomenon, consider the effect of a lattice translation of the basic structure on the modulation: it gives rise to a shift of the phase. Combining such a translation with an appropriate (compensating) shift of the phase, one obtains a transformation that leaves the basic structure *and* the modulation invariant. Such a transformation corresponds precisely to a lattice translation in four dimensions for the embedded crystal structure. In the real space, however, a shift of the phase is not an admitted Euclidean transformation as it does not leave invariant the distance between the particles, so that the combination of lattice translation and (compensating) phase shift also is not admitted as such, even if for an incommensurate modulation it simply corresponds to a relabelling of the atoms leaving the global structure invariant.

From what has been said, it should be apparent that the four-dimensional embedding of the modulated structure according to the superspace approach can also be obtained directly by considering as additional coordinate the phase t of the modulation. The positions in three dimensions are then the intersection of the lines of the atomic positions (parametrized by t) with the hyperplane $t = 0$. For the modulated structure of (9.8.1.4), these lines are given by

$$(\mathbf{n} + \mathbf{r}_j + \mathbf{U}_j \sin\{2\pi[\mathbf{q}\cdot(\mathbf{n}+\mathbf{r}_j)+t]+\varphi_j\}, t) \quad \text{any real } t, \qquad (9.8.1.10a)$$

and for a more general, not necessarily sinusoidal, modulation by

$$(\mathbf{n} + \mathbf{r}_j + \mathbf{u}_j\{\mathbf{q}\cdot[\mathbf{n}+\mathbf{r}_j]+t\}, t), \qquad (9.8.1.10b)$$

where $\mathbf{u}_j(x)$ is a periodic vector function: $\mathbf{u}_j(x+1) = \mathbf{u}_j(x)$. A general point in four-dimensional space is $r_s = (\mathbf{r}, t)$ with $\mathbf{r} = (x, y, z)$.

The notation adopted here for the $(3+1)$-dimensional embedding of the modulated structure is a shorthand notation intended to stress the double role of the variable t as a parameter in the three-dimensional description of the structure and as a coordinate in the $(3+1)$-dimensional embedding. In the latter case, it implicitly assumes the choice of a fourth basis vector $\mathbf{d}$ perpendicular to the physical space of the crystal, so that the following four-dimensional vector notations are considered to be equivalent:

$$r_s = (\mathbf{r}, \mathbf{t}) = (\mathbf{r}, t\mathbf{d}) = (\mathbf{r}, t).$$

The pattern of lines (9.8.1.10a, b) has lattice periodicity. Indeed, it is invariant under the shift $t \to t+1$ and, for every lattice translation $\mathbf{n}$ from the basic structure, there is a compensating phase shift: the pattern is left invariant under the combination of the translation $\mathbf{n}$ and the phase shift $t \to t - \mathbf{q}\cdot\mathbf{n}$. Therefore, (9.8.1.10$a, b$) is invariant under translations from a four-dimensional lattice with basis

$$a_{s1} = (\mathbf{a}, -\mathbf{q}\cdot\mathbf{a}), \quad a_{s2} = (\mathbf{b}, -\mathbf{q}\cdot\mathbf{b}), \quad a_{s3} = (\mathbf{c}, -\mathbf{q}\cdot\mathbf{c}), \quad a_{s4} = (0, 1). \qquad (9.8.1.11)$$

In accordance with the equivalent descriptions given for r_s, equivalent descriptions for a_{s4} are $a_{s4} = (0, 1) = (0, \mathbf{d})$ with dual basis vector $a^*_{s4} = (\mathbf{q}, 1) = (\mathbf{q}, \mathbf{d}^*)$, where $\mathbf{d}^*$ is reciprocal to $\mathbf{d}$ in the fourth direction. With respect to the axes (9.8.1.11), a general point in four dimensions can be written as

$$r_s = \sum_{i=1}^{4} x_i a_{si} = (\mathbf{r}, r_I),$$

with

$$\mathbf{r} = x_1\mathbf{a} + x_2\mathbf{b} + x_3\mathbf{c}, \quad \text{and} \quad r_I = t = x_4 - \mathbf{q}\cdot\mathbf{r}. \qquad (9.8.1.12)$$

Some, or sometimes all, transformations of the space group of the basic structure give rise to a symmetry transformation for the modulated structure when combined with an appropriate phase shift, possibly together with an inversion of the phase. If $\{R|\mathbf{v}\}$ is an element of the space group of the basic structure, Δ is a phase shift and $\varepsilon = \pm 1$, then the point $(\mathbf{r}, t)$ is transformed to $(R\mathbf{r} + \mathbf{v}, \varepsilon t + \Delta)$. The pattern (9.8.1.10$b$) is left invariant by $(\{R|\mathbf{v}\}, \{\varepsilon|\Delta\})$ if

$$(R\mathbf{n} + R\mathbf{r}_j + \mathbf{v} + R\mathbf{u}_j[\mathbf{q}\cdot(\mathbf{n}+\mathbf{r}_j) + \varepsilon t - \varepsilon\Delta], t) = (\mathbf{n}' + \mathbf{r}_{j'} + \mathbf{u}_{j'}[\mathbf{q}\cdot(\mathbf{n}'+\mathbf{r}_{j'}) + t], t). \qquad (9.8.1.13)$$

The position $\mathbf{n}' + \mathbf{r}_{j'}$ is the transform of $\mathbf{n} + \mathbf{r}_j$ in the basic structure and therefore also belongs to the basic structure.

One can conclude that the pattern has as symmetry transformations all elements $(\{R|\mathbf{v}\}, \{\varepsilon|\Delta\})$ satisfying (9.8.1.13). These form a space group in four dimensions.

The reciprocal to the basis (9.8.1.11) is

$$a^*_{s1} = (\mathbf{a}^*, 0), \quad a^*_{s2} = (\mathbf{b}^*, 0), \quad a^*_{s3} = (\mathbf{c}^*, 0), \quad a^*_{s4} = (\mathbf{q}, 1). \qquad (9.8.1.14)$$

A general reciprocal-lattice vector is now

$$H_s = \sum_{i=1}^{4} h_i a^*_{si} = (h_1\mathbf{a}^* + h_2\mathbf{b}^* + h_3\mathbf{c}^* + h_4\mathbf{q}, h_4).$$

The projection of this reciprocal-lattice vector is of the form (9.8.1.7), as it should be. Moreover, the projection of the four-dimensional Fourier transform on the hyperplane $t = 0$ is exactly the Fourier transform of the structure in this hyperplane. If, as a consequence of the four-dimensional space-group symmetry, the four-dimensional diffraction pattern shows systematic extinctions, the same extinctions are present in the diffraction pattern of the three-dimensional structure.

There are also other ways to describe the symmetry relations of incommensurate modulated structures. One is based on representation theory. This method has in particular been used when the modulation occurs as a consequence of a soft mode. Then the irreducible representation of the space group to which the soft mode belongs gives information on the modulation function as well. Heine & McConnell have treated the symmetry with a method related to the Landau theory of phase transitions (Heine & McConnell, 1981; McConnell & Heine, 1984). Perez-Mato *et al.* have given a formulation in terms of three-dimensional structures parametrized by what are here the additional coordinates (Perez-Mato, Madariaga & Tello, 1984, 1986; Perez-Mato, Madariaga, Zuñiga & Garcia Arribas, 1987). Other treatments of the problem can be found in Koptsik (1978), Lifshitz (1996), and de Wolff (1984).

9.8.1.4. *Basic symmetry considerations*

9.8.1.4.1. *Bravais classes of vector modules*

For a modulated crystal structure with a one-dimensional modulation, the positions of the diffraction spots are given by vectors

$$\mathbf{H} = \sum_{i=1}^{3} h_i \mathbf{a}^*_i + m\mathbf{q}. \qquad (9.8.1.15)$$

This set of vectors is a vector module M^*. The vectors $\mathbf{a}_1^*, \mathbf{a}_2^*, \mathbf{a}_3^*$ form a basis of the reciprocal lattice Λ^* of the basic structure and $\mathbf{q}$ is the modulation wavevector. The choice of the basis of Λ^* has the usual freedom, the wavevector $\mathbf{q}$ is only determined up to a sign and up to a reciprocal-lattice vector of the basic structure.

A vector module M^* has point-group symmetry K, which is the subgroup of all elements R of $O(3)$ leaving it invariant.

In the case of an incommensurate one-dimensional modulation, M^* is generated by the lattice Λ^* of main reflections and the modulation wavevector $\mathbf{q}$. It then follows that K is characterized by the following properties:

(1) It leaves Λ^* invariant. (Only in this way are main reflections transformed into main reflections and satellites into satellites.)

(2) Any element R of K then transforms $\mathbf{q}$ into $\pm\mathbf{q}$ (modulo reciprocal-lattice vectors of Λ^*).

An element R of K then transforms the basic vectors $\mathbf{a}_1^*, \mathbf{a}_2^*, \mathbf{a}_3^*$, $\mathbf{q}$ into ones of the form (9.8.1.15). If one denotes, as in (9.8.1.2), $\mathbf{q}$ by $\mathbf{a}_4^*$, this implies

$$R\mathbf{a}_i^* = \sum_{j=1}^{4} \Gamma^*(R)_{ji}\mathbf{a}_j^*, \quad i = 1, \ldots, 4, \tag{9.8.1.16}$$

with $\Gamma^*(R)$ a 4×4 matrix with integral entries. In the case of an incommensurate modulated crystal structure, only two vectors with the same length as $\mathbf{q}$ are $\mathbf{q}$ and $-\mathbf{q}$. As Λ^* is left invariant, it follows that for a one-dimensionally modulated structure $\Gamma^*(R)$ has the form

$$\Gamma^*(R) = \begin{pmatrix} \Gamma_E^*(R) & \Gamma_M^*(R) \\ 0 & \varepsilon(R) \end{pmatrix}, \quad \text{where } \varepsilon(R) = \pm 1. \tag{9.8.1.17}$$

This matrix represents the orthogonal transformation R when referred to the basis vectors $\mathbf{a}_i^*$ $(i = 1, 2, 3, 4)$ of the vector module M^*. As in the case of lattices, two vector modules of modulated crystals are equivalent if they have bases (*i.e.* a basis for the reciprocal lattice Λ^* of the basic structure together with a modulation wavevector $\mathbf{q}$) such that the set of matrices $\Gamma^*(K)$ representing their symmetry is the same for both vector modules. Equivalent vector modules form a *Bravais class*.

Again, as in the case of three-dimensional lattices, it is sometimes convenient to consider a vector module that includes as subset the one spanned by all diffraction spots as in (9.8.1.15). Within such a larger vector module, the actual diffraction peaks then obey *centring conditions*. For a vector module associated with a modulated structure, centring may involve main reflections (the basic structure then has a centred lattice), or satellites, or both. For example, if in a structure with primitive orthorhombic basic structure the modulation wavevector is given by $\alpha\mathbf{a}_1^* + \frac{1}{2}\mathbf{a}_2^*$, one may describe the diffraction spots by means of the non-primitive lattice basis $\mathbf{a}_1^*, \frac{1}{2}\mathbf{a}_2^*, \mathbf{a}_3^*$ and by the modulation wavevector $\alpha\mathbf{a}_1^*$.

Crystallographic point groups are denoted generally by the same letter K.

9.8.1.4.2. *Description in four dimensions*

The matrices $\Gamma^*(R)$ form a faithful integral representation of the three-dimensional point group K. It is also possible to consider them as four-dimensional orthogonal transformations leaving a lattice with basis vectors (9.8.1.14) invariant. Indeed, one can consider the vectors (9.8.1.15) as *projections* of four-dimensional lattice vectors $H_s = (\mathbf{H}, H_I)$, which can be written as

$$H_s = \sum_{i=1}^{4} h_i a_{si}^*, \tag{9.8.1.18}$$

where [*cf.* (9.8.1.14)] m has now been replaced by h_4 and

$$a_{si}^* = (\mathbf{a}_i^*, 0), \quad i = 1, 2, 3; \quad a_{s4}^* = (\mathbf{q}, 1). \tag{9.8.1.19}$$

As will be explained in Section 9.8.4, these vectors span the four-dimensional reciprocal lattice for a periodic structure having as three-dimensional intersection (say defined by the hyperplane $t = 0$) the modulated crystal structure (a specific example has been given in Subsection 9.8.1.3). In direct space, the point group K_s in four dimensions with elements R_s of $O(4)$ then acts on the corresponding dual basis vectors (9.8.1.11) of the four-dimensional *direct lattice* as

$$R_s a_{si} = \sum_{j=1}^{4} \Gamma(R)_{ji} a_{sj} \quad (i = 1, 2, 3, 4), \tag{9.8.1.20a}$$

where $\Gamma(R)$ is the transpose of the matrix $\Gamma^*(R^{-1})$ appearing in (9.8.1.17) and therefore for incommensurate one-dimensionally modulated structures it has the form

$$\Gamma(R) = \begin{pmatrix} \Gamma_E(R) & 0 \\ \Gamma_M(R) & \varepsilon(R) \end{pmatrix}. \tag{9.8.1.20b}$$

9.8.1.4.3. *Four-dimensional crystallography*

Let us summarize the results obtained in the previous paragraph. The matrices $\Gamma(R)$ form a faithful integral representation of the three-dimensional point group K with a four-dimensional carrier space V_s. It is a reducible representation having as invariant subspaces the physical three-dimensional space, denoted by V (or sometimes also by V_E), and the additional one-dimensional space, denoted by V_I. In V, the four-dimensional point-group transformation acts as R (sometimes also denoted by R_E), in V_I it acts as one of the two one-dimensional point-group transformations: the identity or the inversion. Therefore, the space V_s can be made Euclidean with $\Gamma(R)$ defining a four-dimensional point-group transformation R_s, which is an element of a crystallographic subgroup K_s of $O(4)$. The four-dimensional point-group transformations are of the form (R, ε), with $\varepsilon = \pm 1$ and they act on the four-dimensional lattice basis as

$$(R, \varepsilon)a_{si} = \sum_{j=1}^{4} \Gamma(R)_{ji} a_{sj}, \quad i = 1, \ldots, 4, \tag{9.8.1.21}$$

where ε stands for $\varepsilon(R)$ as in (9.8.1.20*b*). So the point-group symmetry operations are crystallographic and given by pairs of a three-dimensional crystallographic point-group transformation and a one-dimensional $\varepsilon = \pm 1$, respectively. The case $\varepsilon = -1$ corresponds to an *inversion of the phase of the modulation function*.

As in the three-dimensional case, one can define equivalence classes among those four-dimensional point groups.

Two point groups K_s and K_s' belong to the same *geometric crystal class* if their three-dimensional (external) parts (forming the point group K_E and K_E', respectively) are in the same three-dimensional crystal class [*i.e.* are conjugated subgroups of $O(3)$] and their one-dimensional internal parts (forming the point groups K_I and K_I', respectively) are equal. The latter condition implies that corresponding point-group elements have the same value of ε.

Such a geometric crystal class can then be denoted by the symbol of the three-dimensional crystal class together with the values of ε that correspond to the generators.

Also, the notion of *arithmetic equivalence* can be generalized to these four-dimensional point groups, as they admit the same faithful integral representation $\Gamma(K)$ given above. This means

that two such groups are arithmetically equivalent if there is a basis transformation for the reciprocal-vector module, which transforms main reflections into main reflections and satellites into satellites and which transforms one of the matrix groups into the other. The arithmetic classes are determined by the arithmetic equivalence class of the three-dimensional group K_E [*i.e.* by $\Gamma_E(K)$] and by the components of the modulation wavevector with respect to the corresponding reciprocal-lattice basis. This is because the elements ε are fixed by the relation

$$R\mathbf{q} \equiv \varepsilon\mathbf{q} \text{ (modulo reciprocal-lattice vectors of the basic structure).} \qquad (9.8.1.22)$$

Note that these $(3+1)$-dimensional equivalence classes are not simply those one obtains in four-dimensional crystallography, as the relation between the higher-dimensional space V_s and the three-dimensional physical space V plays a fundamental role.

The embedded structures in four dimensions have lattice periodicity. So the symmetry groups are four-dimensional space groups, called *superspace groups*. The new name has been introduced because of the privileged role played by the three-dimensional subspace V. A superspace-group element g_s consists of a point-group transformation (R, ε) and a translation $(\mathbf{v}, \Delta)$. The action of such an element on the four-dimensional space is then given by

$$g_s r_s = \{(R, \varepsilon)|(\mathbf{v}, \Delta)\}(\mathbf{r}, t) = (R\mathbf{r} + \mathbf{v}, \varepsilon t + \Delta). \qquad (9.8.1.23)$$

It is important to realize that a superspace-group symmetry of an embedded crystal induces three-dimensional transformations leaving the original modulated structure invariant. Corresponding to (9.8.1.23), one obtains the following relations [*cf.* (9.8.1.13)]:

$$\boldsymbol{u}_{j'}[\mathbf{q}\cdot(\mathbf{n}' + \mathbf{r}_{j'})] = R\mathbf{u}_j[\mathbf{q}\cdot(\mathbf{n} + \mathbf{r}_j) - \varepsilon\Delta] \qquad (9.8.1.24)$$

with

$$\mathbf{n}' + \mathbf{r}_{j'} = R(\mathbf{n} + \mathbf{r}_j) + \mathbf{v}.$$

These are purely three-dimensional symmetry relations, but of course not Euclidean ones.

In three-dimensional Euclidean space, the types of space-group transformation are translations, rotations, rotoinversions, reflections, central inversion, screw rotations, and glide planes. Only the latter two transformations have intrinsic non-primitive translations. For superspace groups, the types of transformation are determined by the point-group transformations. By an appropriate choice of the basis in V_s, each of the latter can be brought into the form

$$\begin{pmatrix} \cos\varphi & -\sin\varphi & 0 & 0 \\ \sin\varphi & \cos\varphi & 0 & 0 \\ 0 & 0 & \delta & 0 \\ 0 & 0 & 0 & \varepsilon \end{pmatrix}; \quad \varepsilon, \delta = \pm 1. \qquad (9.8.1.25)$$

By a choice of origin, each translational part can be reduced to its intrinsic part, which in combination with the point-group element (R, ε) gives one of the transformations in V indicated above together with the inversion, or the identity, or a shift in V_I. So, for phase inversion (when $\varepsilon = -1$), the intrinsic shift in V_I vanishes. When $\varepsilon = +1$, the intrinsic shift in V_I is given by τ. It will be shown in Subsection 9.8.3.3 that the value of τ is one of

$$0, \frac{1}{2}, \frac{\pm 1}{3}, \frac{\pm 1}{4}, \frac{\pm 1}{6}. \qquad (9.8.1.26)$$

Therefore, a superspace-group element can be denoted by a symbol that consists of a symbol for the three-dimensional part following the conventions given in Volume A of *International Tables for Crystallography*, a symbol that determines ε, and one for the corresponding intrinsic internal translation τ.

9.8.1.4.4. *Generalized nomenclature*

In Section 9.8.4, the theory is extended to structures containing d modulations, with $d \geq 1$. In this case, each point-group transformation in internal space is given by R_I and the associated internal translation by the (d-dimensional) vector $\mathbf{v}_I$. Thus,

$$g_s = \{(R, R_I)|(\mathbf{v}, \mathbf{v}_I)\}.$$

The transformations R and R_I are represented by the matrices $\Gamma_E(R)$ and $\Gamma_I(R)$, respectively. In the following discussion, this nomenclature (but with v_I rather than $\mathbf{v}_I$) is sometimes also applied for the $(3+1)$-dimensional case. The usual formulae are obtained by replacing R_I by ε and v_I by Δ.

9.8.1.4.5. *Four-dimensional space groups*

Four-dimensional space groups were obtained in the $(3+1)$-reducible case by Fast & Janssen (1969) and in the general case by Brown, Bülow, Neubüser, Wondratschek & Zassenhaus (1978). The groups were determined on the basis of algorithms developed by Zassenhaus (1948), Janssen, Janner & Ascher (1969), Brown (1969), and Fast & Janssen (1971). In the book by Brown, Bülow, Neubüser, Wondratschek & Zassenhaus, quoted above, a mathematical characterization of the basic crystallographic concepts is given together with corresponding tables for the dimensions one, two, three, and four. One finds there, in particular, a full list of four–dimensional space groups. The list by Fast & Janssen is restricted to space groups with $(3+1)$-reducible point groups. The four-dimensional groups in the work of Brown *et al.* are labelled by numbers. For these same groups, alternative symbols have been developed by Weigel, Phan, Veysseyre and Grebille generalizing the principles of the notation adopted by *International Tables for Crystallography*, Volume A, for the three-dimensional space groups (Weigel, Phan & Veysseyre, 1987; Veysseyre & Weigel, 1989; Grebille, Weigel, Veysseyre & Phan, 1990).

The difference in the listing of four-dimensional crystallographic groups one finds in Brown *et al.* and in Weigel *et al.* with respect to that in the present tables is not simply a matter of notation. In the first place, here only those groups appear that can occur as symmetry groups of one-dimensional incommensurate modulated phases (there are 371 such space groups). Furthermore, as already mentioned, a finer equivalence relation has been considered that reflects the freedom one has in embedding a three-dimensional modulated structure in a four-dimensional Euclidean space. Instead of 371, one then obtains 775 inequivalent groups for which the name superspace group has been introduced. A $(3+1)$-dimensional superspace group is thus a four-dimensional space group having some additional properties. In Section 9.8.4, the precise definitions are given.

In the commensurate one-dimensionally modulated case, 3833 four-dimensional space groups may occur, out of which 320 already belong to the previous 371. The corresponding additional $(3+1)$-dimensional superspace groups are also present in the listing by Fast & Janssen (1969) and have been considered again (and applied to structure determination) by van Smaalen (1987). The Bravais classes for the commensurate $(3+1)$-dimensional case are given in Table 9.8.3.2(*b*).

The relation between modulated crystals and the superspace groups is treated in a textbook by Opechowski (1986). That between the superspace-group symbols of the present tables and those of Weigel *et al.* is discussed in Grebille *et al.* (1990).

Note that no new names have been introduced for the underlying crystallographic concepts like Bravais classes, geometric and arithmetic crystal classes, even if in those cases also the equivalence relation is not simply that of four-dimensional Euclidean crystallography, an explicit distinction always being possible by specifying the dimension as $(3+1)$ instead of four.

9.8.1.5. *Occupation modulation*

Another type of modulation, the occupation modulation, can be treated in a way similar to the displacive modulation. As an example consider an alloy where the positions of the basic structure have space-group symmetry, but are statistically occupied by either of two types of atoms. Suppose that the position $\mathbf{r}$ is occupied by an atom of type A with probability $p(\mathbf{r})$ and by one of type B with probability $1-p(\mathbf{r})$ and that p is periodic. The probability of finding an A atom at site $\mathbf{n}+\mathbf{r}_j$ is

$$P_A(\mathbf{n}+\mathbf{r}_j) = p_j[\mathbf{q}\cdot(\mathbf{n}+\mathbf{r}_j)], \tag{9.8.1.27}$$

with $p_j(x) = p_j(x+1)$. In this case, the structure factor becomes

$$S_{\mathbf{H}} = \sum_{\mathbf{n}}\sum_{j}\left[\left(f_A p_j[\mathbf{q}\cdot(\mathbf{n}+\mathbf{r}_j)] + f_B\{1-p_j[\mathbf{q}\cdot(\mathbf{n}+\mathbf{r}_j)]\}\right) \times \exp[2\pi i\mathbf{H}\cdot(\mathbf{n}+\mathbf{r}_j)]\right], \tag{9.8.1.28}$$

where f_A and f_B are the atomic scattering factors. Because of the periodicity, one has

$$p_j(x) = \sum_m w_{jm}\exp(2\pi i m x). \tag{9.8.1.29}$$

Hence,

$$S_{\mathbf{H}} = \sum_j\left\{f_B\Delta(\mathbf{H})\exp(2\pi i\mathbf{H}\cdot\mathbf{r}_j) + (f_A - f_B)\sum_m \Delta(\mathbf{H}+m\mathbf{q})w_{jm} \times \exp[2\pi i(\mathbf{H}+m\mathbf{q})\cdot\mathbf{r}_j]\right\}, \tag{9.8.1.30}$$

where $\Delta(\mathbf{H})$ is the sum of δ functions over the reciprocal lattice of the basic structure:

$$\Delta(\mathbf{H}) = \sum_{h_1h_2h_3}\delta\left(\mathbf{H} - \sum_{i=1}^{3} h_i\mathbf{a}_i^*\right).$$

Consequently, the diffraction peaks occur at positions $\mathbf{H}$ given by (9.8.1.7). For a simple sinusoidal modulation [$m=\pm1$ in (9.8.1.29)], there are only main reflections and first-order satellites ($m=\pm1$). One may introduce an additional coordinate t and generalize (9.8.1.27) to

$$P_A(\mathbf{n}+\mathbf{r}_j, t) = p_j[\mathbf{q}\cdot(\mathbf{n}+\mathbf{r}_j)+t], \tag{9.8.1.31}$$

which has $(3+1)$-dimensional space-group symmetry. Generalization to more complex modulation cases is then straightforward.

9.8.2. Outline for a superspace-group determination

In the case of a modulated structure, the diffraction pattern consists of main reflections and satellites. The main reflections span a reciprocal lattice generated by $\mathbf{a}_1^*, \mathbf{a}_2^*, \mathbf{a}_3^*$. Considerations are here restricted for simplicity to the one-dimensional modulated case, *i.e.* to the $n=4$ case. Extension to the more general $n=3+d$ case is conceptually not difficult and does not modify the general procedure outlined here.

(1) *The first step* is the determination of the *Laue group* P_L of the diffraction pattern: it is the point group in three dimensions that transforms every diffraction peak into a peak of the same intensity.†

As P_L leaves invariant the subset of main reflections, this Laue group belongs to one of the 11 Laue symmetry classes. Accordingly, the Laue group determines a three-dimensional holohedral point group which determines a crystallographic system.

(2) *The second step* consists of choosing a basis according to the conventions of *IT* A for the main reflections and choosing a modulation wavevector.

From the centring extinctions, one can deduce to which Bravais class the main reflections belong. This is one of the 14 three-dimensional Bravais classes. Notice that the cubic Bravais classes do not occur because a one-dimensional (incommensurate) modulation is incompatible with cubic symmetry. For this same reason, only the nine non-cubic Laue-symmetry classes occur in the one-dimensional incommensurate case.

The main reflections are indexed by $hkl0$ and the satellite reflections by $hklm$. The Fourier wavevector of a general reflection $hklm$ is given by

$$\mathbf{H} = h\mathbf{a}^* + k\mathbf{b}^* + l\mathbf{c}^* + m\mathbf{q}. \tag{9.8.2.1}$$

Note that this step involves a choice because the system of satellite reflections is only defined modulo the main reflections. When a satellite is in the vicinity of a main reflection, it is reasonable to assign it to that reflection. But one has, especially when deciding whether or not situations are equivalent, to be aware of the fact that each satellite may be assigned to an arbitrary main reflection. It is even possible to assign a satellite to an extinct main reflection. One takes by preference the $\mathbf{q}$ vector along a symmetry axis or in a mirror plane. According to equation (9.8.2.1), the fourth basis vector $\mathbf{a}_4^*$ is equal to the chosen $\mathbf{q}$, the modulation wavevector.

(3) In the *third step*, one determines the space group of the *average structure* (from the main reflections).

The average structure is unique but possibly involves split atoms. The space group of the average structure is often the symmetry group of the undistorted phase. That helps to make a good choice for the basic structure and also gives an insight as to how the satellite reflections split from the main reflections at the phase transition.

(4) *Step four* is the identification of the $(3+1)$-dimensional Bravais lattice type. In superspace also, centring gives rise to *centring extinctions*, and that corresponds to making the choice of a *conventional unit cell* in $(3+1)$ dimensions.

The previous three steps establish $\mathbf{a}^*$, $\mathbf{b}^*$, $\mathbf{c}^*$, the three-dimensional Bravais class and $\mathbf{q} = \alpha\mathbf{a}^* + \beta\mathbf{b}^* + \gamma\mathbf{c}^*$, where the components α, β, and γ are given with respect to the three-dimensional conventional basis.

$$\alpha = \mathbf{q}\cdot\mathbf{a}, \quad \beta = \mathbf{q}\cdot\mathbf{b}, \quad \gamma = \mathbf{q}\cdot\mathbf{c}. \tag{9.8.2.2}$$

The $(3+1)$-dimensional Bravais class is fixed by that three-dimensional Bravais class and the components α, β, γ of $\mathbf{q}$.

Just as for three-dimensional lattices, a conventional cell can be chosen for $(3+1)$-dimensional lattices. To this end, the

† Except for deviations from Friedel's law caused by dispersion; see *IT* B (1993, p. 241, Subsection 2.3.4.1).

vector $\mathbf{q}$ must be considered. The vector $\mathbf{q}$ can be split into an invariant (or irrational) and a rational component according to:

$$\mathbf{q} = \mathbf{q}^i + \mathbf{q}^r \quad \text{with} \quad \mathbf{q}^i = \frac{1}{N}\sum_R \varepsilon(R)(R\mathbf{q}), \tag{9.8.2.3}$$

where summation is over the elements R of the Laue group P_L, N is the order of P_L, and $\varepsilon = \pm 1$ follows from the property (valid in the one-dimensional modulated case):

$$R\mathbf{q} = \varepsilon\mathbf{q} \text{ (modulo main-reflection vectors).} \tag{9.8.2.4}$$

If the splitting (9.8.2.3) results in $\mathbf{q}^r = 0$, there is no problem. For $\mathbf{q}^r \neq 0$ we choose $\mathbf{q}^i$ as the new modulation wavevector. This may cause satellites to be assigned to extinct main reflections, or even to 'main reflections' with non-integer indices. In this case, it is desirable to choose a new basis $\mathbf{a}_c^*, \mathbf{b}_c^*, \mathbf{c}_c^*$ such that all reflections can be written as

$$H\mathbf{a}_c^* + K\mathbf{b}_c^* + L\mathbf{c}_c^* + m\mathbf{q}^i \tag{9.8.2.5}$$

with H, K, L, and m integer numbers. The basis obtained is the conventional basis for the M^* module and corresponds to the choice of a conventional cell for the $(3+1)$-dimensional Bravais lattice.

Observed (possible) centring conditions for the reflections can be applied to determine the $(3+1)$-dimensional Bravais class.

Example 1. As an example, consider a C-centred orthorhombic lattice with modulation wavevector $\mathbf{q} = (\alpha 0 \tfrac{1}{2})$, or $\mathbf{q}^i = (\alpha 00)$ and $\mathbf{q}^r = (00\tfrac{1}{2})$. The general reflection condition is: $hklm$, $h + k =$ even. A reflection

$$h\mathbf{a}^* + k\mathbf{b}^* + l\mathbf{c}^* + m(\alpha\mathbf{a}^* + \tfrac{1}{2}\mathbf{c}^*) \tag{9.8.2.6}$$

can be described on a conventional basis with $\mathbf{a}_c^* = \mathbf{a}^*$, $\mathbf{b}_c^* = \mathbf{b}^*$, $\mathbf{c}_c^* = \mathbf{c}^*/2$ as

$$H\mathbf{a}_c^* + K\mathbf{b}_c^* + L\mathbf{c}_c^* + m\alpha\mathbf{a}_c^*. \tag{9.8.2.7}$$

Because $H = h$, $K = k$, $L/2 = l + m/2$, and h, k and l are integers with $h + k$ even, one has the conditions $H + K =$ even and $L + m =$ even. The adopted conventional basis has centring $(\frac{1}{2}\frac{1}{2}00, 00\frac{1}{2}\frac{1}{2}, \frac{1}{2}\frac{1}{2}\frac{1}{2}\frac{1}{2})$. The conditions $H + K =$ even and $L + m =$ even become, after interchange of H and L, $K + L =$ even and $H + m =$ even, which according to Table 9.8.3.6 gives $mmmA(\frac{1}{2}0\gamma)$. Changing back to the original setting gives the Bravais class $mmmC(\alpha 0\frac{1}{2})$.

Example 2. As a second example, consider a C-centred orthorhombic lattice of main reflections. Suppose that an arbitrary reflection is given by

$$H\mathbf{a}^* + K\mathbf{b}^* + L\mathbf{c}^* + m\gamma\mathbf{c}^* \tag{9.8.2.8}$$

with respect to the conventional basis $\mathbf{a}^*, \mathbf{b}^*, \mathbf{c}^*$ of the C-centred lattice and that the general reflection condition is

$$H + K + m = \text{even}. \tag{9.8.2.9}$$

This is in agreement with the C-centring condition $H + K =$ even for the main reflections. Equation (9.8.2.9) implies a centring $(\frac{1}{2}\frac{1}{2}0\frac{1}{2})$ of the $(3+1)$-dimensional lattice Σ. Its conventional basis corresponding to (9.8.2.8) is

$$(\mathbf{a}, 0), (\mathbf{b}, 0), (\mathbf{c}, -\gamma), (0, 1). \tag{9.8.2.10}$$

Because of the centring translation $[(\mathbf{a} + \mathbf{b})/2, 1/2]$, a primitive basis of Σ is

$$\left(\frac{\mathbf{a}+\mathbf{b}}{2}, -1/2\right), \left(\frac{\mathbf{a}-\mathbf{b}}{2}, -1/2\right), (\mathbf{c}, -\gamma), (0, 1), \tag{9.8.2.11}$$

which corresponds, according to (9.8.1.11), to a choice $\mathbf{q} = \mathbf{a}^* + \gamma\mathbf{c}^*$. In terms of this modulation vector, an arbitrary reflection (9.8.2.8) can be described as

$$h\mathbf{a}^* + k\mathbf{b}^* + l\mathbf{c}^* + m(\mathbf{a}^* + \gamma\mathbf{c}^*). \tag{9.8.2.12}$$

Because $H = h + m$, $K = k$, and $L = l$, the reflection condition (9.8.2.9) now becomes $h + k =$ even, again in agreement with the fact that the lattice of main reflections is C-centred.

(5) *Step five*: one lists all point groups (more precisely, the arithmetic crystal classes) compatible with the external Bravais class (*i.e.* the three-dimensional one), the components of the modulation vector $\mathbf{q}$ with respect to the conventional basis of this class, and the observed general extinctions. These groups are listed in Table 9.8.3.3.

The external part of the $(3+1)$-dimensional point group does not need to be the same as the point group of the average structure: it can never be larger, but is possibly a subgroup only.

(6) *Step six* consists of finding the superspace groups compatible with the previously derived results and with the special extinctions observed in the diffraction pattern.

For each arithmetic point group, the non-equivalent superspace groups are listed in Table 9.8.3.5.

Example 3. Continue with example 2 of step 4. The external Bravais class of the modulated crystal is $mmmC$ and $q = (10\gamma)$. Consider the two cases of special reflection conditions.

(1) The observed condition is: $00Lm, m = 2n$. Then there is only one superspace group that obeys this condition: No. 21.4 with symbol $C222(10\gamma)00s$ in Table 9.8.3.5. [See Subsection 9.8.3.3 for explanation of symbols; note that $C222$ denotes the external part of the $(3+1)$-dimensional space group.]

(2) There is no special reflection condition. Possible superspace groups are:

$C222(10\gamma)$, No. 21.3,	$Cmm2(10\gamma)$, No. 35.4,
$C2mm(10\gamma)$, No. 38.3,	$Cmmm(10\gamma)$, No. 65.4.

In this second case, there are thus four possible superspace groups, three without and one with inversion symmetry. The difficulty stems from the fact that (in the absence of anomalous dispersion) the Laue group always has an inversion centre. Just as in three-dimensional crystallography, the ambiguity can only be solved by a complete determination of the structure, or by non-diffraction methods.

In the determination of modulated structures, one generally starts with the assumption that the external part of the $(3+1)$-dimensional point group is equal to the point group of the basic structure. This is, however, not necessarily true. The former may be a subgroup of the latter. Especially when the basic structure contains atoms at special positions, the point-group symmetry may be lowered by the modulation.

(7) *Step seven* concerns the restrictions imposed on/by the displacive or occupation modulation waves. For each occupied special Wyckoff position of the basic structure, one has to verify the validity of the restrictions imposed by the elements of the superspace group on the modulation as expressed in equation (9.8.1.24).

During the structure determination, one should check for each Wyckoff position which is occupied by an atom of the basic

structure, whether the assumed displacive or occupation modulations obey the site symmetry of the Wyckoff position considered. An atom at a special position transforms into itself by the site symmetry of the position. For such a symmetry transformation, $j' = j$, $\mathbf{v} = 0$, and thus $\Delta(\varepsilon = 1) = \tau$, $\Delta(\varepsilon = -1) = 0$ (*cf.* Subsection 9.8.3.3). In the modulated structure, the site symmetry is preserved only if, for each of its symmetry operations, the appropriate relation is obeyed by the modulations [*cf.* (9.8.1.24)].

For displacive modulations, the conditions are

$$\begin{aligned} \mathbf{u}_j(\mathbf{q}\cdot\mathbf{r}) &= R\mathbf{u}_j(\mathbf{q}\cdot\mathbf{r}-\tau) \quad \text{for } \varepsilon = 1, \\ \mathbf{u}_j(\mathbf{q}\cdot\mathbf{r}) &= R\mathbf{u}_j(\mathbf{q}\cdot\mathbf{r}) \quad \text{for } \varepsilon = -1 \end{aligned} \tag{9.8.2.13}$$

and, for occupation modulation,

$$\begin{aligned} p_j(\mathbf{q}\cdot\mathbf{r}) &= p_j(\mathbf{q}\cdot\mathbf{r}-\tau) \quad \text{for } \varepsilon = 1, \\ p_j(\mathbf{q}\cdot\mathbf{r}) &= p_j(\mathbf{q}\cdot\mathbf{r}) \quad \text{for } \varepsilon = -1. \end{aligned} \tag{9.8.2.14}$$

Example 4. Assume, as for the case discussed above, that the basic structure has the space group *Cmmm*. Can the superspace group be *Cmmm*(10γ)? In this superspace group, $\tau = 0$ for all symmetry operations with $\varepsilon = 1$. Displacive modulations at special positions must thus obey $\mathbf{u}_j(\mathbf{q}\cdot\mathbf{r}) = R\mathbf{u}_j(\mathbf{q}\cdot\mathbf{r})$ for the superspace group to be correct. For an atom at special position *mmm*, this is not possible for all site symmetry operations unless $\mathbf{u}_j = 0$. Suppose that the structure model contains a displacive modulation polarized along **a** for that atom. The allowed site symmetry is then lowered to 2*mm*, and as a consequence the superspace group is *C*2*mm*(10γ) rather than *Cmmm*(10γ).

9.8.3. Introduction to the tables

In what follows, the tables dealing with the $(3+1)$-dimensional case will be presented. The explanations can easily be applied to the $(2+d)$-dimensional case also [Tables 9.8.3.1(*a*), (*b*) and 9.8.3.4(*a*), (*b*)].

9.8.3.1. *Tables of Bravais lattices*

The $(3+1)$-dimensional lattice Σ^* is determined by the three-dimensional vectors $\mathbf{a}^*, \mathbf{b}^*, \mathbf{c}^*$ and the modulation vector **q**. The former three vectors give by duality **a**, **b**, and **c**, the external components of lattice basis vectors, and the products $-\mathbf{q}\cdot\mathbf{a} = -\alpha$, $-\mathbf{q}\cdot\mathbf{b} = -\beta$, and $-\mathbf{q}\cdot\mathbf{c} = -\gamma$ the corresponding internal components. Therefore, it is sufficient to give the arithmetic crystal class of the group $\Gamma_E(K)$ and the components σ_j ($\sigma_1 = \alpha$, $\sigma_2 = \beta$, and $\sigma_3 = \gamma$) of the modulation vector **q** with respect to a conventional basis $\mathbf{a}^*, \mathbf{b}^*, \mathbf{c}^*$. The arithmetic crystal class is denoted by a modification of the symbol of the three-dimensional symmorphic space group of this class (see Chapter 1.4) plus an indication for the row matrix σ (having entries σ_j). In this way, one obtains the so-called one-line symbols used in Tables 9.8.3.1(*a*), (*b*) and 9.8.3.2(*a*), (*b*).

As an example, the symbol $2/mB(0\frac{1}{2}\gamma)$ denotes a Bravais class for which the main reflections belong to a *B*-centred monoclinic lattice (unique axis **c**) and the satellite positions are generated by the point-group transforms of $\frac{1}{2}\mathbf{b}^* + \gamma\mathbf{c}^*$. Then the matrix σ becomes $\sigma = (0\frac{1}{2}\gamma)$. It has as irrational part $\sigma^i = (00\gamma)$ and as rational part $\sigma^r = (0\frac{1}{2}0)$. The external part of the $(3+1)$-dimensional point group of the Bravais lattice is $2/m$. By use of the relation [*cf.* (9.8.2.4)]

$$R\mathbf{q}^i = \varepsilon\mathbf{q}^i, \quad R\mathbf{q}^r \equiv \varepsilon\mathbf{q}^r \text{ (modulo } \mathbf{b}^*), \tag{9.8.3.1}$$

Table 9.8.3.1(*a*). $(2+1)$-*Dimensional Bravais classes for incommensurate structures*

The holohedral point group K_s is given in terms of its external and internal parts, K_E and K_I, respectively. The reflections are given by $h\mathbf{a}^* + k\mathbf{b}^* + m\mathbf{q}$ where **q** is the modulation wavevector. If the rational part $\mathbf{q}^r$ is not zero, there is a corresponding centring translation in three-dimensional space. The conventional basis $(\mathbf{a}_c^*, \mathbf{b}_c^*, \mathbf{q}^i)$ given for the vector module M^* is shown such that $\mathbf{q}^r = 0$. The basis vectors are given by components with respect to the conventional basis $\mathbf{a}^*, \mathbf{b}^*$ of the lattice Λ^* of main reflections.

No.	Symbol	K_E	K_I	**q**	Conventional basis	Centring
Oblique						
1	$2p(\alpha\beta)$	2	$\bar{1}$	$(\alpha\beta)$	(10), (01), $(\alpha\beta)$	
Rectangular						
2	$mmp(0\beta)$	mm	$1\bar{1}$	(0β)	(10), (01), (0β)	
3	$mmp(\frac{1}{2}\beta)$	mm	$1\bar{1}$	$(\frac{1}{2}\beta)$	$(\frac{1}{2}0)$, (01), (0β)	$\frac{1}{2}0\frac{1}{2}$
4	$mmc(0\beta)$	mm	$1\bar{1}$	(0β)	(10), (01), (0β)	$\frac{1}{2}\frac{1}{2}0$

we see that the operations 2 and m are associated with the internal space transformations $\varepsilon = 1$ and $\varepsilon = -1$, respectively. This is denoted by the one-line symbol $(2/m, 1\bar{1})$ for the $(3+1)$-dimensional point group of the Bravais lattice. In direct space, the symmetry operation $\{R, \varepsilon(R)\}$ is represented by the matrix $\Gamma(R)$ which transforms the components $v_j, j = 1, \ldots, 4$, of a vector v_s to:

$$v_j' = \sum_{k=1}^{4} \Gamma(R)_{jk} v_k.$$

The operations (2, 1) and $(m, \bar{1})$ are represented by the matrices:

$$\Gamma(2) = \begin{pmatrix} -1 & 0 & 0 & 0 \\ 0 & -1 & 0 & 0 \\ 0 & 0 & 1 & 0 \\ 0 & -1 & 0 & 1 \end{pmatrix}; \quad \Gamma(m) = \begin{pmatrix} 1 & 0 & 0 & 0 \\ 0 & 1 & 0 & 0 \\ 0 & 0 & -1 & 0 \\ 0 & 1 & 0 & -1 \end{pmatrix}. \tag{9.8.3.2}$$

The 3×3 part $\Gamma_E(R)$ of each matrix is obtained by considering the action of R on the external part **v** of v_s. The 1×1 part $\Gamma_I(R)$ is the value of the ε associated with R and the remaining part $\Gamma_M(R)$ follows from the relation

$$\Gamma_M(R) = -\Gamma_I(R)\sigma^r + \sigma^r\Gamma_E(R). \tag{9.8.3.3}$$

Bravais classes can be denoted in an alternative way by two-line symbols. In the two-line symbol, the Bravais class is given by specifying the arithmetic crystal class of the external symmetry by the symbol of its symmorphic space group, the associated elements $\Gamma_I(R) = \varepsilon$ by putting their symbol under the corresponding symbols of $\Gamma_E(R)$, and by the rational part σ^r indicated by a prefix. In the following table, this prefix is given for the components of $\mathbf{q}^r$ that play a role in the classification.

P	(000)	R	$(\frac{1}{3}, \frac{1}{3}, 0)$		
A	$(\frac{1}{2}, 0, 0)$	B	$(0, \frac{1}{2}, 0)$	C	$(0, 0, \frac{1}{2})$
L	(1, 0, 0)	M	(0, 1, 0)	N	(0, 0, 1)
U	$(0, \frac{1}{2}, \frac{1}{2})$	V	$(\frac{1}{2}, 0, \frac{1}{2})$	W	$(\frac{1}{2}, \frac{1}{2}, 0)$.

Note that the integers appearing here are not equivalent to zero because they express components with respect to a conventional lattice basis (and not a primitive one). For the Bravais class

Table 9.8.3.1(*b*). (2 + 2)-*Dimensional Bravais classes for incommensurate structures*

The holohedral point group K_s is given in terms of its external and internal parts, K_E and K_I, respectively. The basis of the vector module M^* contains two modulation wavevectors and the reflections are given by $h\mathbf{a}^* + k\mathbf{b}^* + m_1\mathbf{q}_1 + m_2\mathbf{q}_2$. If $\mathbf{q}_1^r$or $\mathbf{q}_2^r$ are not zero, there are corresponding centring translations in four-dimensional space. The conventional basis ($\mathbf{a}_c^*$, $\mathbf{b}_c^*$, $\mathbf{q}_1^i$, $\mathbf{q}_2^i$) for the vector module M^* is chosen such that $\mathbf{q}_1^r = \mathbf{q}_2^r = 0$. The basis vectors are indicated by their components with respect to the conventional basis $\mathbf{a}^*$, $\mathbf{b}^*$ of the lattice Λ^* of main reflections.

No.	Symbol	K_E	K_I	$\mathbf{q}_1$	$\mathbf{q}_2$	Conventional basis	Centring
Oblique							
1	$2p(\alpha\beta, \lambda\mu)$	2	2	$(\alpha\beta)$	$(\lambda\mu)$	(10), (01), $(\alpha\beta)$, $(\lambda\mu)$	
Rectangular							
2	$mmp(0\beta, 0\mu)$	mm	12	(0β)	(0μ)	(10), (01), (0β), (0μ)	
3	$mmp(\frac{1}{2}\beta, 0\mu)$	mm	12	$(\frac{1}{2}\beta)$	(0μ)	$(\frac{1}{2}0)$, (01), (0β), (0μ)	$\frac{1}{2}0\frac{1}{2}0$
4	$mmp(\alpha 0, 0\mu)$	mm	mm	$(\alpha 0)$	(0μ)	(10), (01), $(\alpha 0)$, (0μ)	
5	$mmp(\alpha\frac{1}{2}, 0\mu)$	mm	mm	$(\alpha\frac{1}{2})$	(0μ)	(10), $(0\frac{1}{2})$, $(\alpha 0)$, (0μ)	$0\frac{1}{2}\frac{1}{2}0$
6	$mmp(\alpha\frac{1}{2}, \frac{1}{2}\mu)$	mm	mm	$(\alpha\frac{1}{2})$	$(\frac{1}{2}\mu)$	$(\frac{1}{2}0)$, $(0\frac{1}{2})$, $(\alpha 0)$, (0μ)	$\frac{1}{2}00\frac{1}{2}$, $0\frac{1}{2}\frac{1}{2}0$
7	$mmp(\alpha\beta)$	mm	mm	$(\alpha\beta)$	$(\alpha\bar{\beta})$	(10), (01), $(\alpha 0)$, (0β)	$00\frac{1}{2}\frac{1}{2}$
8	$mmc(0\beta, 0\mu)$	mm	12	(0β)	(0μ)	(10), (01), (0β), (0μ)	$\frac{1}{2}\frac{1}{2}00$
9	$mmc(\alpha 0, 0\mu)$	mm	mm	$(\alpha 0)$	(0μ)	(10), (01), $(\alpha 0)$, (0μ)	$\frac{1}{2}\frac{1}{2}00$
10	$mmc(\alpha\beta)$	mm	mm	$(\alpha\beta)$	$(\alpha\bar{\beta})$	(10), (01), $(\alpha 0)$, (0β)	$\frac{1}{2}\frac{1}{2}00$, $00\frac{1}{2}\frac{1}{2}$
Square							
11	$4p(\alpha\beta)$	4	4	$(\alpha\beta)$	$(\bar{\beta}\alpha)$	(10), (01), $(\alpha\beta)$, $(\bar{\beta}\alpha)$	
12	$4mp(\alpha 0)$	$4m$	$4m$	$(\alpha 0)$	(0α)	(10), (01), $(\alpha 0)$, (0α)	
13	$4mp(\alpha\frac{1}{2})$	$4m$	$4m$	$(\alpha\frac{1}{2})$	$(\frac{1}{2}\alpha)$	$(\frac{1}{2}\frac{1}{2})$, $(\frac{\bar{1}}{2}\frac{1}{2})$, $(\gamma\gamma)$, $(\delta\bar{\delta})$ $\gamma = (2\alpha+1)/4$, $\delta = (2\alpha-1)/4$	$\frac{1}{2}\frac{1}{2}00$, $00\frac{1}{2}\frac{1}{2}$
14	$4mp(\alpha\alpha)$	$4\dot{m}$	$4\ddot{m}$	$(\alpha\alpha)$	$(\bar{\alpha}\alpha)$	(10), (01), $(\alpha\alpha)$, $(\bar{\alpha}\alpha)$	
Hexagonal							
15	$6p(\alpha\beta)$	6	6	$(\alpha\beta)$	$(\bar{\beta}\alpha+\beta)$	(10), (01), $(\alpha\beta)$, $(\bar{\beta}\alpha+\beta)$	
16	$6mp(\alpha 0)$	$6m$	$6m$	$(\alpha 0)$	(0α)	(10), (01), $(\alpha 0)$, (0α)	
17	$6mp(\alpha\alpha)$	$6\dot{m}$	$6\ddot{m}$	$(\alpha\alpha)$	$(\bar{\alpha}2\alpha)$	(10), (01), $(\alpha\alpha)$, $(\bar{\alpha}2\alpha)$	

mentioned above, the two-line symbol is $B_{1\ \bar{1}}^{2/mB}$. This symbol has the advantage that the internal transformation (the value of ε) is explicitly given for the corresponding generators. It has, however, certain typographical drawbacks. It is rare for the printer to put the symbol together in the correct manner: $B_{1\ \bar{1}}^{2/mB}$.

In Tables 9.8.3.1(*a*), (*b*) and 9.8.3.2(*a*), (*b*) the symbols for the (2 + *d*)- and (3 + 1)-dimensional Bravais classes are given in the one-line form. It is, however, easy to derive from each one-line symbol the corresponding two-line symbol because the bottom line for the two-line symbol appears in the tables as the internal part of the point-group symbol.

The number of symbols in the bottom line of the two-line symbol should be equal to that of the generators given in the top line. A symbol '1' is used in the bottom line if the corresponding R_I is the unit transformation. If necessary, a mirror perpendicular to a crystal axis is indicated by $\dot{m}$ and one that is not by $\ddot{m}$. This situation only occurs for $d \geq 2$. So the (2 + 2)-dimensional class P_{4m}^{4mp} is actually $P_{4\dot{m}}^{4\dot{m}p}$ and is different from the class $P_{4\ddot{m}}^{4\ddot{m}p}$. In a one-line symbol, their difference is apparent, the first being $4mp(\alpha 0)$, whereas the second is $4mp(\alpha\alpha)$.

9.8.3.2. *Table for geometric and arithmetic crystal classes*

In Table 9.8.3.3, the geometric and the arithmetic crystal classes of (3 + 1)-dimensional superspace are given.

The symbols for *geometric crystal classes* indicate the pairs $[R, \varepsilon(R)]$ of the generators of the point group. This is done by giving the crystal class for the point group K_E and the symbols for the corresponding elements of K_I. So, for example, the geometric crystal class belonging to the holohedral point group of the Bravais class $2/mB(0\frac{1}{2}\gamma)$, mentioned above, is $(2/m, \bar{1}\bar{1})$.

The notation for the *arithmetic crystal classes* is similar to that for the Bravais classes. In the tables, their one-line symbols are given. They consist of the (modified) symbol of the three-dimensional symmorphic space group and, in parentheses, the appropriate components of the modulation wavevector. The three arithmetic crystal classes implying a lattice belonging to the Bravais class $2/mB(0\frac{1}{2}\gamma)$ are $2B(0\frac{1}{2}\gamma)$, $mB(0\frac{1}{2}\gamma)$, and $2/mB(0\frac{1}{2}\gamma)$. The corresponding geometric crystal classes are $(2, \bar{1})$, $(m, \bar{1})$, and $(2/m, \bar{1}\bar{1})$.

9.8.3.3. *Tables of superspace groups*

9.8.3.3.1. *Symmetry elements*

The transformations g_s belonging to a (3 + 1)-dimensional superspace group consist of a point-group transformation R_s given by the integral matrix $\Gamma(R)$ and of the associated translation. So the superspace group is determined by the arithmetic crystal class of its point group and the corresponding translational components. The symbol for the arithmetic crystal

Table 9.8.3.2(*a*). (3 + 1)-*Dimensional Bravais classes for incommensurate structures*

The holohedral point group K_s is given in terms of its external and internal parts, K_E and K_I, respectively. The reflections are given by $h\mathbf{a}^* + k\mathbf{b}^* + l\mathbf{c}^* + m\mathbf{q}$, where $\mathbf{q}$ is the modulation wavevector. If the rational part $\mathbf{q}^r$ is not zero, there is a corresponding centring translation in four-dimensional space. A conventional basis ($\mathbf{a}_c^*$, $\mathbf{b}_c^*$, $\mathbf{c}_c^*$, $\mathbf{q}^i$) for the vector module M^* is then chosen such that $\mathbf{q}^r = 0$. The basis vectors are indicated by their components with respect to the conventional basis $\mathbf{a}^*$, $\mathbf{b}^*$ $\mathbf{c}^*$ of the lattice Λ^* of main reflections. The Bravais classes can also be found in Janssen (1969) and Brown *et al.* (1978). The notation of the Bravais classes there is here given in the columns Ref. *a* and Ref. *b*, respectively.

No.	Symbol	K_E	K_I	$\mathbf{q}$	Conventional basis	Centring translation(s)	Ref. *a*	Ref. *b*
Triclinic								
1	$\bar{1}P(\alpha\beta\gamma)$	$\bar{1}$	$\bar{1}$	$(\alpha\beta\gamma)$	(100), (010), (001), $(\alpha\beta\gamma)$		I *P*	I/I
Monoclinic								
2	$2/mP(\alpha\beta 0)$	$2/m$	$\bar{1}1$	$(\alpha\beta 0)$	(100), (010), (001), $(\alpha\beta 0)$		II *P*	II/I
3	$2/mP(\alpha\beta\frac{1}{2})$	$2/m$	$\bar{1}1$	$(\alpha\beta\frac{1}{2})$	(100), (010), $(00\frac{1}{2})$, $(\alpha\beta 0)$	$00\frac{1}{2}\frac{1}{2}$	II *I*	II/II
4	$2/mB(\alpha\beta 0)$	$2/m$	$\bar{1}1$	$(\alpha\beta 0)$	(100), (010), (001), $(\alpha\beta 0)$	$\frac{1}{2}0\frac{1}{2}0$	II *I*	II/II
5	$2/mP(00\gamma)$	$2/m$	$1\bar{1}$	(00γ)	(100), (010), (001), (00γ)		III *P*	III/I
6	$2/mP(\frac{1}{2}0\gamma)$	$2/m$	$1\bar{1}$	$(\frac{1}{2}0\gamma)$	$(\frac{1}{2}00)$, (010), (001), (00γ)	$\frac{1}{2}00\frac{1}{2}$	III *I*	III/II
7	$2/mB(00\gamma)$	$2/m$	$1\bar{1}$	(00γ)	(100), (010), (001), (00γ)	$\frac{1}{2}0\frac{1}{2}0$	III *I*	III/II
8	$2/mB(0\frac{1}{2}\gamma)$	$2/m$	$1\bar{1}$	$(0\frac{1}{2}\gamma)$	(100), $(0\frac{1}{2}0)$, (001), (00γ)	$\frac{1}{2}0\frac{1}{2}0$, $0\frac{1}{2}0\frac{1}{2}$	III *G*	III/III
Orthorhombic								
9	$mmmP(00\gamma)$	mmm	$11\bar{1}$	(00γ)	(100), (010), (001), (00γ)		IV *P*	IV/I
10	$mmmP(0\frac{1}{2}\gamma)$	mmm	$11\bar{1}$	$(0\frac{1}{2}\gamma)$	(100), $(0\frac{1}{2}0)$, (001), (00γ)	$0\frac{1}{2}0\frac{1}{2}$	IV *B*	IV/III
11	$mmmP(\frac{1}{2}\frac{1}{2}\gamma)$	mmm	$11\bar{1}$	$(\frac{1}{2}\frac{1}{2}\gamma)$	$(\frac{1}{2}00)$, $(0\frac{1}{2}0)$, (001), (00γ)	$\frac{1}{2}00\frac{1}{2}$, $0\frac{1}{2}0\frac{1}{2}$	IV *F*	IV/VI
12	$mmmI(00\gamma)$	mmm	$11\bar{1}$	(00γ)	(100), (010), (001), (00γ)	$\frac{1}{2}\frac{1}{2}\frac{1}{2}0$	IV *I*	IV/IV
13	$mmmC(00\gamma)$	mmm	$11\bar{1}$	(00γ)	(100), (010), (001), (00γ)	$\frac{1}{2}\frac{1}{2}00$	IV *C*	IV/II
14	$mmmC(10\gamma)$	mmm	$11\bar{1}$	(10γ)	(100), (010), (001), (00γ)	$\frac{1}{2}\frac{1}{2}0\frac{1}{2}$	IV *I*	IV/IV
15	$mmmA(00\gamma)$	mmm	$11\bar{1}$	(00γ)	(100), (010), (001), (00γ)	$0\frac{1}{2}\frac{1}{2}0$	IV *B*	IV/III
16	$mmmA(\frac{1}{2}0\gamma)$	mmm	$11\bar{1}$	$(\frac{1}{2}0\gamma)$	$(\frac{1}{2}00)$, (010), (001), (00γ)	$0\frac{1}{2}\frac{1}{2}0$, $\frac{1}{2}00\frac{1}{2}$	IV *G*	IV/V
17	$mmmF(00\gamma)$	mmm	$11\bar{1}$	(00γ)	(100), (010), (001), (00γ)	$\frac{1}{2}\frac{1}{2}00$, $\frac{1}{2}0\frac{1}{2}0$	IV *F*	IV/VI
18	$mmmF(10\gamma)$	mmm	$11\bar{1}$	(10γ)	(100), (010), (001), (00γ)	$\frac{1}{2}\frac{1}{2}0\frac{1}{2}$, $\frac{1}{2}0\frac{1}{2}\frac{1}{2}$	IV *G*	IV/V
Tetragonal								
19	$4/mmmP(00\gamma)$	$4/mmm$	$1\bar{1}11$	(00γ)	(100), (010), (001), (00γ)		VII *P*	VI/I
20	$4/mmmP(\frac{1}{2}\frac{1}{2}\gamma)$	$4/mmm$	$1\bar{1}11$	$(\frac{1}{2}\frac{1}{2}\gamma)$	$(\frac{1}{2}\frac{1}{2}0)$, $(\bar{\frac{1}{2}}\frac{1}{2}0)$, (001), (00γ)	$\frac{1}{2}\frac{1}{2}0\frac{1}{2}$	VII *I*	VI/II
21	$4/mmmI(00\gamma)$	$4/mmm$	$1\bar{1}11$	(00γ)	(100), (010), (001), (00γ)	$\frac{1}{2}\frac{1}{2}\frac{1}{2}0$	VII *I*	VI/II
Trigonal								
22	$\bar{3}mR(00\gamma)$	$\bar{3}m$	$\bar{1}1$	(00γ)	(100), (010), (001), (00γ)	$\frac{1}{3}\frac{2}{3}\frac{2}{3}0$	VI *P*	VII/I
23	$\bar{3}1mP(\frac{1}{3}\frac{1}{3}\gamma)$	$\bar{3}1m$	$\bar{1}11$	$(\frac{1}{3}\frac{1}{3}\gamma)$	$(\frac{1}{3}\frac{1}{3}0)$, $(\bar{\frac{1}{3}}\frac{2}{3}0)$, (001), (00γ)	$\frac{1}{3}\frac{2}{3}0\frac{2}{3}$	VI *P*	VII/I
Hexagonal								
24	$6/mmmP(00\gamma)$	$6/mmm$	$1\bar{1}11$	(00γ)	(100), (010), (001), (00γ)		V *P*	VII/II

class has been discussed in Subsection 9.8.3.2. Given a point-group transformation R_s, the associated translation is determined up to a lattice translation. As in three dimensions, the translational part generally depends on the choice of origin. To avoid this arbitrariness, one decomposes that translation into a component (called intrinsic) independent of the origin, and a remainder. The (3 + 1)-dimensional translation v_s associated with the point-group transformation R_s is given by

$$v_s = \sum_{i=1}^{3+1} v_i a_{is}. \qquad (9.8.3.4)$$

Its origin-invariant part v_s^o is given by

$$v_s^o = \sum_{j=1}^{4} v_j^o a_{sj} \quad \text{with} \quad v_j^o = \frac{1}{n}\sum_{m=1}^{n}\sum_{k=1}^{4} \Gamma(R^m)_{jk} v_k, \qquad (9.8.3.5)$$

where n is now the order of the point-group transformation R so that R^n is the identity. As customary also in three-dimensional crystallography, one indicates in the space-group symbol the invariant components v_j^o. Notice that this means that there is an origin for R_s in (3 + 1)-dimensional superspace such that the translation associated with R_s has these components. This origin, however, may not be the same for different transformations R_s, as is known in three-dimensional crystallography.

(*continued on page* 920)

Table 9.8.3.2(*b*). (3 + 1)-*Dimensional Bravais classes for commensurate structures*

The holohedral point group K_s is given in terms of its external and internal parts, K_E and K_I, respectively. The reflections are given by $h\mathbf{a}^* + k\mathbf{b}^* + l\mathbf{c}^* + m\mathbf{q}$, where $\mathbf{q}$ is the modulation wavevector. Here $\mathbf{q}$ is a commensurate vector having rational components with respect to $\mathbf{a}^*, \mathbf{b}^*, \mathbf{c}^*$. The rank of the vector module M^* is three. Therefore, there are three basis vectors for M^*. They are given by their components with respect to the conventional basis $\mathbf{a}^*, \mathbf{b}^*, \mathbf{c}^*$ of the lattice of main reflections. If they do not coincide with the primitive basis vectors of the lattice Λ^* of main reflections, there is a centring in four-dimensional space. The notation of the Bravais classes in Janssen (1969) is here given in the column Ref. *a*. Notice that for a commensurate one-dimensional modulation cubic symmetry is also possible.

No.	Symbol	K_E	K_I	$\mathbf{q}$	Conventional basis	Centring translation(s)	Ref. *a*
Triclinic							
1	$\bar{1}P(000)$	$\bar{1}1$	$1\bar{1}$	(000)	(100), (010), (001)		II *P*
2	$\bar{1}P(\frac{1}{2}\frac{1}{2}\frac{1}{2})$	$\bar{1}1$	$1\bar{1}$	$(\frac{1}{2}\frac{1}{2}\frac{1}{2})$	$(\bar{1}\frac{1}{2}\frac{1}{2})$, $(\frac{1}{2}\bar{1}\frac{1}{2})$, $(\frac{1}{2}\frac{1}{2}\bar{1})$	$\frac{1}{2}\frac{1}{2}\frac{1}{2}\frac{1}{2}$	II *I*
Monoclinic							
3	$2/mP(000)$	$2/m1$	$11\bar{1}$	(000)	(100), (010), (001)		IV *P*
4	$2/mP(\frac{1}{2}\frac{1}{2}0)$	$2/m1$	$11\bar{1}$	$(\frac{1}{2}\frac{1}{2}0)$	$(\frac{1}{2}\frac{1}{2}0)$, $(\bar{\frac{1}{2}}\frac{1}{2}0)$, (001)	$\frac{1}{2}\frac{1}{2}0\frac{1}{2}$	IV *B*
5	$2/mP(00\frac{1}{2})$	$2/m1$	$11\bar{1}$	$(00\frac{1}{2})$	(100), (010), $(00\frac{1}{2})$	$00\frac{1}{2}\frac{1}{2}$	IV *C*
6	$2/mP(\frac{1}{2}\frac{1}{2}\frac{1}{2})$	$2/m1$	$11\bar{1}$	$(\frac{1}{2}\frac{1}{2}\frac{1}{2})$	$(\frac{1}{2}\frac{1}{2}0)$, $(\bar{\frac{1}{2}}\frac{1}{2}0)$, $(00\frac{1}{2})$	$\frac{1}{2}\frac{1}{2}0\frac{1}{2}$, $00\frac{1}{2}\frac{1}{2}$	IV *F*
7	$2/mB(000)$	$2/m1$	$11\bar{1}$	(000)	(100), (010), (001)	$\frac{1}{2}0\frac{1}{2}0$	IV *B*
8	$2/mB(100)$	$2/m1$	$11\bar{1}$	(100)	(100), (010), (001)	$\frac{1}{2}0\frac{1}{2}\frac{1}{2}$	IV *I*
9	$2/mB(0\frac{1}{2}0)$	$2/m1$	$11\bar{1}$	$(0\frac{1}{2}0)$	(100), $(0\frac{1}{2}0)$, (001)	$\frac{1}{2}0\frac{1}{2}0$, $0\frac{1}{2}0\frac{1}{2}$	IV *G*
Orthorhombic							
10	$mmmP(000)$	$mmm1$	$111\bar{1}$	(000)	(100), (010), (001)		VIII *P*
11	$mmmP(00\frac{1}{2})$	$mmm1$	$111\bar{1}$	$(00\frac{1}{2})$	(100), (010), $(00\frac{1}{2})$	$00\frac{1}{2}\frac{1}{2}$	VIII *A*
12	$mmmP(0\frac{1}{2}\frac{1}{2})$	$mmm1$	$111\bar{1}$	$(0\frac{1}{2}\frac{1}{2})$	(100), $(0\frac{1}{2}0)$, $(00\frac{1}{2})$	$0\frac{1}{2}0\frac{1}{2}$, $00\frac{1}{2}\frac{1}{2}$	VIII *F*
13	$mmmP(\frac{1}{2}\frac{1}{2}\frac{1}{2})$	$mmm1$	$111\bar{1}$	$(\frac{1}{2}\frac{1}{2}\frac{1}{2})$	$(\frac{1}{2}00)$, $(0\frac{1}{2}0)$, $(00\frac{1}{2})$	$\frac{1}{2}00\frac{1}{2}$, $0\frac{1}{2}0\frac{1}{2}$, $00\frac{1}{2}\frac{1}{2}$	VIII *S*
14	$mmmI(000)$	$mmm1$	$111\bar{1}$	(000)	(100), (010), (001)	$\frac{1}{2}\frac{1}{2}\frac{1}{2}0$	VIII *E*
15	$mmmI(111)$	$mmm1$	$111\bar{1}$	(111)	(100), (010), (001)	$\frac{1}{2}\frac{1}{2}\frac{1}{2}\frac{1}{2}$	VIII *I*
16	$mmmI(\frac{1}{2}\frac{1}{2}\frac{1}{2})$	mmm	$\bar{1}\bar{1}\bar{1}$	$(\frac{1}{2}\frac{1}{2}\frac{1}{2})$	$(\frac{1}{2}00)$, $(0\frac{1}{2}0)$, $(00\frac{1}{2})$	$\frac{1}{4}\frac{1}{4}\frac{1}{4}\frac{1}{4}$, $\frac{\bar{1}}{4}\frac{1}{4}\frac{1}{4}\frac{\bar{1}}{4}$, $\frac{1}{4}\frac{\bar{1}}{4}\frac{\bar{1}}{4}\frac{1}{4}$, $\frac{1}{4}\frac{1}{4}\frac{\bar{1}}{4}\frac{\bar{1}}{4}$	VIII *K*
17	$mmmF(000)$	$mmm1$	$111\bar{1}$	(000)	(100), (010), (001)	$\frac{1}{2}\frac{1}{2}00$, $\frac{1}{2}0\frac{1}{2}0$	VIII *F*
18	$mmmF(001)$	$mmm1$	$111\bar{1}$	(001)	(100), (010), (001)	$\frac{1}{2}\frac{1}{2}00$, $\frac{1}{2}0\frac{\bar{1}}{2}\frac{1}{2}$	VIII *H*
19	$mmmC(000)$	$mmm1$	$111\bar{1}$	(000)	(100), (010), (001)	$\frac{1}{2}\frac{1}{2}00$	VIII *A*
20	$mmmC(100)$	$mmm1$	$111\bar{1}$	(100)	(100), (010), (001)	$\frac{1}{2}\frac{1}{2}0\frac{1}{2}$	VIII *E*
21	$mmmC(00\frac{1}{2})$	$mmm1$	$111\bar{1}$	$(00\frac{1}{2})$	(100), (010), $(00\frac{1}{2})$	$\frac{1}{2}\frac{1}{2}00$, $00\frac{1}{2}\frac{1}{2}$	VIII *G*
22	$mmmC(10\frac{1}{2})$	$mmm1$	$111\bar{1}$	$(10\frac{1}{2})$	(100), (010), $(00\frac{1}{2})$	$\frac{1}{2}\frac{1}{2}0\frac{1}{2}$, $\frac{1}{2}\frac{1}{2}\frac{1}{2}0$	VIII *H*
Tetragonal							
23	$4/mmmP(000)$	$4/mmm1$	$1111\bar{1}$	(000)	(100), (010), (001)		XII *P*
24	$4/mmmP(00\frac{1}{2})$	$4/mmm1$	$1111\bar{1}$	$(00\frac{1}{2})$	(100), (010), $(00\frac{1}{2})$	$00\frac{1}{2}\frac{1}{2}$	XII *A*
25	$4/mmmP(\frac{1}{2}\frac{1}{2}0)$	$4/mmm1$	$1111\bar{1}$	$(\frac{1}{2}\frac{1}{2}0)$	$(\frac{1}{2}\frac{1}{2}0)$, $(\bar{\frac{1}{2}}\frac{1}{2}0)$, (001)	$\frac{1}{2}\frac{1}{2}0\frac{1}{2}$	XII *E*
26	$4/mmmP(\frac{1}{2}\frac{1}{2}\frac{1}{2})$	$4/mmm1$	$1111\bar{1}$	$(\frac{1}{2}\frac{1}{2}\frac{1}{2})$	$(\frac{1}{2}\frac{1}{2}0)$, $(\bar{\frac{1}{2}}\frac{1}{2}0)$, $(00\frac{1}{2})$	$\frac{1}{2}\frac{1}{2}0\frac{1}{2}$, $00\frac{1}{2}\frac{1}{2}$	XII *H*
27	$4/mmmI(000)$	$4/mmm1$	$1111\bar{1}$	(000)	(100), (010), (001)	$\frac{1}{2}\frac{1}{2}\frac{1}{2}0$	XII *E*
28	$4/mmmI(111)$	$4/mmm1$	$1111\bar{1}$	(111)	(100), (010), (001)	$\frac{1}{2}\frac{1}{2}\frac{1}{2}\frac{1}{2}$	XII *I*
29	$4/mmmI(\frac{1}{2}\frac{1}{2}\frac{1}{2})$	$4/mmm$	$\bar{1}\bar{1}\bar{1}1$	$(\frac{1}{2}\frac{1}{2}\frac{1}{2})$	(100), (010), (001)		XII *N*
Trigonal							
30	$\bar{3}m1R(000)$	$\bar{3}m1$	$11\bar{1}$	(000)	(100), (010), (001)	$\frac{2}{3}\frac{1}{3}\frac{1}{3}0$	X *R*
31	$\bar{3}m1R(00\frac{1}{2})$	$\bar{3}m1$	$11\bar{1}$	$(00\frac{1}{2})$	(100), (010), $(00\frac{1}{2})$	$00\frac{1}{2}\frac{1}{2}$, $\frac{2}{3}\frac{1}{3}\frac{1}{6}\frac{1}{6}$	X *RI*
Hexagonal							
32	$6/mmmP(000)$	$6/mmm1$	$1111\bar{1}$	(000)	(100), (010), (001)		X *P*
33	$6/mmmP(00\frac{1}{2})$	$6/mmm1$	$1111\bar{1}$	$(00\frac{1}{2})$	(100), (010), $(00\frac{1}{2})$	$00\frac{1}{2}\frac{1}{2}$	X *A*
34	$6/mmmP(\frac{1}{3}\frac{1}{3}0)$	$6/mmm$	$\bar{1}11\bar{1}$	$(\frac{1}{3}\frac{1}{3}0)$	$(\frac{1}{3}\frac{1}{3}0)$, $(\bar{\frac{1}{3}}\frac{2}{3}0)$, (001)	$\frac{1}{3}\frac{2}{3}0\frac{2}{3}$	X *R*
35	$6/mmmP(\frac{1}{3}\frac{1}{3}\frac{1}{2})$	$6/mmm$	$\bar{1}11\bar{1}$	$(\frac{1}{3}\frac{1}{3}\frac{1}{2})$	$(\frac{1}{3}\frac{1}{3}0)$, $(\bar{\frac{1}{3}}\frac{2}{3}0)$, $(00\frac{1}{2})$	$\frac{1}{3}\frac{2}{3}0\frac{2}{3}$, $00\frac{1}{2}\frac{1}{2}$	X *RI*
Cubic							
36	$m3mP(000)$	$m\bar{3}m1$	$111\bar{1}$	(000)	(100), (010), (001)		XIV *P*
37	$m3mP(\frac{1}{2}\frac{1}{2}\frac{1}{2})$	$m\bar{3}m1$	$111\bar{1}$	$(\frac{1}{2}\frac{1}{2}\frac{1}{2})$	$(\frac{1}{2}00)$, $(0\frac{1}{2}0)$, $(00\frac{1}{2})$	$\frac{1}{2}00\frac{1}{2}$, $0\frac{1}{2}0\frac{1}{2}$, $00\frac{1}{2}\frac{1}{2}$	XIV *S*
38	$m3mI(000)$	$m\bar{3}m1$	$111\bar{1}$	(000)	(100), (010), (001)	$\frac{1}{2}\frac{1}{2}\frac{1}{2}0$	XIV *V*
39	$m3mI(111)$	$m\bar{3}m1$	$111\bar{1}$	(111)	(100), (010), (001)	$\frac{1}{2}\frac{1}{2}\frac{1}{2}\frac{1}{2}$	XIV *I*
40	$m3mI(\frac{1}{2}\frac{1}{2}\frac{1}{2})$	$m\bar{3}m$	$\bar{1}\bar{1}1$	$(\frac{1}{2}\frac{1}{2}\frac{1}{2})$	$(\frac{1}{2}00)$, $(0\frac{1}{2}0)$, $(00\frac{1}{2})$	$\frac{1}{4}\frac{1}{4}\frac{1}{4}\frac{1}{4}$, $\frac{\bar{1}}{4}\frac{1}{4}\frac{1}{4}\frac{\bar{1}}{4}$, $\frac{1}{4}\frac{1}{4}\frac{\bar{1}}{4}\frac{\bar{1}}{4}$	XIV *K*
41	$m3mF(000)$	$m\bar{3}m1$	$111\bar{1}$	(000)	(100), (010), (001)	$\frac{1}{2}\frac{1}{2}00$, $\frac{1}{2}0\frac{1}{2}0$	XIV *F*

Table 9.8.3.3. *(3 + 1)-Dimensional point groups and arithmetic crystal classes*

The four-dimensional point group K_s has external part K_E, which belongs to a three-dimensional system. Depending on the Bravais class of the four-dimensional lattice left invariant by K_s, this point group gives rise to an integral 4×4 matrix group $\Gamma(K)$ which belongs to one of the arithmetic crystal classes given in the last column.

System	Point group		External Bravais class	Arithmetic crystal class(es)
	K_E	K_s		
Triclinic	1	$(1, 1)$	$\bar{1}P$	$1P(\alpha\beta\gamma)$
	$\bar{1}$	$(\bar{1}, \bar{1})$	$\bar{1}P$	$\bar{1}P(\alpha\beta\gamma)$
Monoclinic	2	$(2, \bar{1})$	$2/mP$	$2P(\alpha\beta0), 2P(\alpha\beta\frac{1}{2})$
			$2/mB$	$2B(\alpha\beta0)$
		$(2, 1)$	$2/mP$	$2P(00\gamma), 2P(\frac{1}{2}0\gamma)$
			$2/mB$	$2B(00\gamma), 2B(0\frac{1}{2}\gamma)$
	m	$(m, 1)$	$2/mP$	$mP(\alpha\beta0), mP(\alpha\beta\frac{1}{2})$
			$2/mB$	$mB(\alpha\beta0)$
		$(m, \bar{1})$	$2/mP$	$mP(00\gamma), mP(\frac{1}{2}0\gamma)$
			$2/mB$	$mB(00\gamma), mB(0\frac{1}{2}\gamma)$
	$2/m$	$(2/m, \bar{1}1)$	$2/mP$	$2/mP(\alpha\beta0), 2/mP(\alpha\beta\frac{1}{2})$
			$2/mB$	$2/mB(\alpha\beta0)$
		$(2/m, 1\bar{1})$	$2/mP$	$2/mP(00\gamma), 2/mP(\frac{1}{2}0\gamma)$
			$2/mB$	$2/mB(00\gamma), 2/mB(0\frac{1}{2}\gamma)$
Orthorhombic	222	$(222, \bar{1}\bar{1}1)$	$mmmP$	$222P(00\gamma), 222P(0\frac{1}{2}\gamma), 222P(\frac{1}{2}\frac{1}{2}\gamma)$
			$mmmI$	$222I(00\gamma)$
			$mmmF$	$222F(00\gamma), 222F(10\gamma)$
			$mmmC$	$222C(00\gamma), 222C(10\gamma)$
		$(222, 1\bar{1}\bar{1})$	$mmmC$	$222C(\alpha00), 222C(\alpha0\frac{1}{2})$
	$mm2$	$(mm2, 111)$	$mmmP$	$mm2P(00\gamma), mm2P(0\frac{1}{2}\gamma), mm2P(\frac{1}{2}\frac{1}{2}\gamma)$
			$mmmI$	$mm2I(00\gamma)$
			$mmmF$	$mm2F(00\gamma), mm2F(10\gamma)$
			$mmmC$	$mm2C(00\gamma), mm2C(10\gamma)$
		$(2mm, 111)$	$mmmC$	$2mmC(\alpha00), 2mmC(\alpha0\frac{1}{2})$
		$(2mm, \bar{1}1\bar{1})$	$mmmP$	$2mmP(00\gamma), 2mmP(0\frac{1}{2}\gamma), 2mmP(\frac{1}{2}\frac{1}{2}\gamma)$
			$mmmI$	$2mmI(00\gamma)$
			$mmmF$	$2mmF(00\gamma), 2mmF(10\gamma)$
			$mmmC$	$2mmC(00\gamma), 2mmC(10\gamma)$
		$(mm2, \bar{1}1\bar{1})$	$mmmC$	$mm2C(\alpha00), mm2C(\alpha0\frac{1}{2})$
		$(m2m, 1\bar{1}\bar{1})$	$mmmP$	$m2mP(0\frac{1}{2}\gamma)$
		$(m2m, \bar{1}\bar{1}1)$	$mmmC$	$m2mC(\alpha00), m2mC(\alpha0\frac{1}{2})$
	mmm	$(mmm, 11\bar{1})$	$mmmP$	$mmmP(00\gamma), mmmP(0\frac{1}{2}\gamma), mmmP(\frac{1}{2}\frac{1}{2}\gamma)$
			$mmmI$	$mmmI(00\gamma)$
			$mmmF$	$mmmF(00\gamma), mmmF(10\gamma)$
			$mmmC$	$mmmC(00\gamma), mmmC(10\gamma)$
		$(mmm, \bar{1}11)$	$mmmC$	$mmmC(\alpha00), mmmC(\alpha0\frac{1}{2})$
Tetragonal	4	$(4, 1)$	$4/mmmP$	$4P(00\gamma), 4P(\frac{1}{2}\frac{1}{2}\gamma)$
			$4/mmmI$	$4I(00\gamma)$
	$\bar{4}$	$(\bar{4}, \bar{1})$	$4/mmmP$	$\bar{4}P(00\gamma), \bar{4}P(\frac{1}{2}\frac{1}{2}\gamma)$
			$4/mmmI$	$\bar{4}I(00\gamma)$
	$4/m$	$(4/m, 1\bar{1})$	$4/mmmP$	$4/mP(00\gamma), 4/mP(\frac{1}{2}\frac{1}{2}\gamma)$
			$4/mmmI$	$4/mI(00\gamma)$
	422	$(422, 1\bar{1}\bar{1})$	$4/mmmP$	$422P(00\gamma), 422P(\frac{1}{2}\frac{1}{2}\gamma)$
			$4/mmmI$	$422I(00\gamma)$
	$4mm$	$(4mm, 111)$	$4/mmmP$	$4mmP(00\gamma), 4mmP(\frac{1}{2}\frac{1}{2}\gamma)$
			$4/mmmI$	$4mmI(00\gamma)$
	$\bar{4}2m$	$(\bar{4}2m, \bar{1}\bar{1}1)$	$4/mmmP$	$\bar{4}2mP(00\gamma), \bar{4}2mP(\frac{1}{2}\frac{1}{2}\gamma)$
			$4/mmmI$	$\bar{4}2mI(00\gamma)$
	$\bar{4}m2$	$(\bar{4}m2, \bar{1}1\bar{1})$	$4/mmmP$	$\bar{4}m2P(00\gamma), \bar{4}m2P(\frac{1}{2}\frac{1}{2}\gamma)$
			$4/mmmI$	$\bar{4}m2I(00\gamma)$
	$4/mmm$	$(4/mmm, 1\bar{1}11)$	$4/mmmP$	$4/mmmP(00\gamma), 4/mmmP(\frac{1}{2}\frac{1}{2}\gamma)$
			$4/mmmI$	$4/mmmI(00\gamma)$
Trigonal	3	$(3, 1)$	$\bar{3}mR$	$3R(00\gamma)$
			$6/mmmP$	$3P(00\gamma), 3P(\frac{1}{3}\frac{1}{3}\gamma)$
	$\bar{3}$	$(\bar{3}, \bar{1})$	$\bar{3}mR$	$\bar{3}R(00\gamma)$
			$6/mmmP$	$\bar{3}P(00\gamma), \bar{3}P(\frac{1}{3}\frac{1}{3}\gamma)$
	32	$(32, 1\bar{1})$	$\bar{3}mR$	$32R(00\gamma)$
			$6/mmmP$	$312P(00\gamma), 312P(\frac{1}{3}\frac{1}{3}\gamma), 321P(00\gamma)$

Table 9.8.3.3. $(3+1)$-*Dimensional point groups and arithmetic crystal classes (cont.)*

System	Point group K_E	Point group K_s	External Bravais class	Arithmetic crystal class(es)
Trigonal (*cont.*)	$3m$	$(3m, 11)$	$\bar{3}mR$	$3mR(00\gamma)$
			$6/mmmP$	$3m1P(00\gamma)$, $31mP(00\gamma)$, $31mP(\frac{1}{3}\frac{1}{3}\gamma)$
	$\bar{3}m$	$(\bar{3}m, \bar{1}1)$	$\bar{3}mR$	$\bar{3}mR(00\gamma)$
			$6/mmmP$	$\bar{3}1mP(00\gamma)$, $\bar{3}1mP(\frac{1}{3}\frac{1}{3}\gamma)$, $\bar{3}m1P(00\gamma)$
Hexagonal	6	$(6, 1)$	$6/mmmP$	$6P(00\gamma)$
	$\bar{6}$	$(\bar{6}, \bar{1})$	$6/mmmP$	$\bar{6}P(00\gamma)$
	$6/m$	$(6/m, 1\bar{1})$	$6/mmmP$	$6/mP(00\gamma)$
	622	$(622, 1\bar{1}\bar{1})$	$6/mmmP$	$622P(00\gamma)$
	$6mm$	$(6mm, 111)$	$6/mmmP$	$6mmP(00\gamma)$
	$\bar{6}m2$	$(\bar{6}m2, \bar{1}1\bar{1})$	$6/mmmP$	$\bar{6}m2P(00\gamma)$
	$\bar{6}2m$	$(\bar{6}2m, \bar{1}\bar{1}1)$	$6/mmmP$	$\bar{6}2mP(00\gamma)$
	$6/mmm$	$(6/mmm, 1\bar{1}11)$	$6/mmmP$	$6/mmmP(00\gamma)$

Written in components, the non-primitive translation υ_s associated with the point-group element (R, R_I) is $(\mathbf{v}, \upsilon_I)$, where υ_I can be written as $\delta - \mathbf{q}\cdot\mathbf{v}$. In accordance with (9.8.1.12), δ is defined as υ_4. The origin-invariant part υ_s^o of υ_s is

$$\upsilon_s^o = (\mathbf{v}^o, \upsilon_I^o) = \frac{1}{n}\sum_{m=1}^{n}(R^m\mathbf{v}, R_I^m\upsilon_I) = (\mathbf{v}^o, \tau - \mathbf{q}\cdot\mathbf{v}^o), \quad (9.8.3.6)$$

where

$$\tau = \upsilon_4^o = \upsilon_I^o + \mathbf{q}\cdot\mathbf{v}^o.$$

The internal transformation $R_I(R) = \varepsilon(R) = \varepsilon$ is either $+1$ or -1. When $\varepsilon = -1$ it follows from (9.8.3.6) that $\upsilon_I^o = 0$. For $\varepsilon = +1$, one has $\upsilon_I^o = \upsilon_I$. Because in that case

$$\mathbf{q}\cdot\mathbf{v}^o = \frac{1}{n}\sum_{m=1}^{n}\mathbf{q}\cdot R^m\mathbf{v} = \mathbf{q}^i\cdot\mathbf{v}, \quad (9.8.3.7)$$

it follows that

$$\tau = \upsilon_I + \mathbf{q}\cdot\mathbf{v}^o = \delta - \mathbf{q}\cdot\mathbf{v} + \mathbf{q}\cdot\mathbf{v}^o = \delta - \mathbf{q}^r\cdot\mathbf{v}. \quad (9.8.3.8)$$

For R_s of order n, R_s^n is the identity and the associated translation is a lattice translation. The ensuing values for τ are $0, \frac{1}{2}, \pm\frac{1}{3}, \pm\frac{1}{4}$ or $\pm\frac{1}{6}$ (modulo integers). This remains true also in the case of a centred basis. The symbol of the $(3+1)$-dimensional space-group element is determined by the invariant part of its three-dimensional translation and τ. Again, that information can be given in terms of either a one-line or a two-line symbol.

In the one-line symbol, one finds: the symbol according to *International Tables for Crystallography*, Volume A, for the space group generated by the elements $\{R|\mathbf{v}\}$, in parentheses the components of the modulation vector $\mathbf{q}$ followed by the values of τ, one for each generator appearing in the three-dimensional space-group symbol. A letter symbolizes the value of τ according to

τ	0	$\frac{1}{2}$	$\pm\frac{1}{3}$	$\pm\frac{1}{4}$	$\pm\frac{1}{6}$
symbol	0	s	t	q	h

(9.8.3.9)

As an example, consider the superspace group

$$P2_1/m(\alpha\beta0)0s.$$

The external components $\{R|\mathbf{v}\}$ of the elements of this group form the three-dimensional space group $P2_1/m$. The modulation wavevector is $\alpha\mathbf{a}^* + \beta\mathbf{b}^*$ with respect to a conventional basis of the monoclinic lattice with unique axis $\mathbf{c}$. Therefore, the point group is $(2/m, \bar{1}1)$. The point-group element $(2, \bar{1})$ has associated a non-primitive translation with invariant part $(\frac{1}{2}\mathbf{c}, 0) = (00\frac{1}{2}0)$ and the point-group generator $(m, 1)$ one with $(\mathbf{0}, \frac{1}{2}) = (000\frac{1}{2})$.

Table 9.8.3.4(a). $(2+1)$-*Dimensional superspace groups*

The number labelling the superspace group is denoted by $n.m$, where n is the number attached to the two-dimensional basic space group and m numbers the various superspace groups having the same basic space group. The symbol of the basic space group, the symbol for the three-dimensional point group, the number of the three-dimensional Bravais class to which the superspace group belongs (Table 9.8.3.1a) and the superspace-group symbol are also given.

No.	Basic space group	Point group K_s	Bravais class No.	Group symbol
Oblique				
1.1	$p1$	$(1, \underline{1})$	1	$p1(\alpha\beta)$
2.1	$p2$	$(2, \bar{1})$	1	$p2(\alpha\beta)$
Rectangular				
3.1	pm	$(m, 1)$	2	$pm1(0\beta)$
3.2			2	$pm1(0\beta)s0$
3.3			3	$pm1(\frac{1}{2}\beta)$
3.4		$(m, \bar{1})$	2	$p1m(0\beta)$
3.5			3	$p1m(\frac{1}{2}\beta)$
4.1	pg	$(m, 1)$	2	$pg1(0\beta)$
4.2			3	$pg1(\frac{1}{2}\beta)$
4.3		$(m, \bar{1})$	2	$p1g(0\beta)$
5.1	cm	$(m, 1)$	4	$cm1(0\beta)$
5.2			4	$cm1(0\beta)s0$
5.3		$(m, \bar{1})$	4	$c1m(0\beta)$
6.1	pmm	$(mm, 1\bar{1})$	2	$pmm(0\beta)$
6.2			2	$pmm(0\beta)s0$
6.3			3	$pmm(\frac{1}{2}\beta)$
7.1	pmg	$(mm, 1\bar{1})$	2	$pmg(0\beta)$
7.2			2	$pgm(0\beta)$
7.3			3	$pgm(\frac{1}{2}\beta)$
8.1	pgg	$(mm, 1\bar{1})$	2	$pgg(0\beta)$
9.1	cmm	$(mm, 1\bar{1})$	4	$cmm(0\beta)$
9.2			4	$cmm(0\beta)s0$

Table 9.8.3.4(*b*). (2 + 2)-*Dimensional superspace groups*

The number labelling the superspace group is denoted by *n.m*, where *n* is the number attached to the two-dimensional basic space group and *m* numbers the various superspace groups having the same basic space group. The symbol of the basic space group, the symbol for the four-dimensional point group, the number of the four-dimensional Bravais class to which the superspace group belongs (Table 9.8.3.1*b*) and the superspace-group symbol are also given.

No.	Basic space group	Point group K_s	Bravais classs No.	Group symbol
Oblique				
1.1	*p*1	(1, 1)	1	$p1(\alpha\beta, \lambda\mu)$
2.1	*p*2	(2, 2)	1	$p2(\alpha\beta, \lambda\mu)$
Rectangular				
3.1	*pm*	(*m*, 1)	2	$pm1(0\beta, 0\mu)$
3.2			2	$pm1(0\beta, 0\mu)s0, 0$
3.3			3	$pm1(\frac{1}{2}\beta, 0\mu)$
3.4			3	$pm1(\frac{1}{2}\beta, 0\mu)s0, 0$
3.5		(*m*, 2)	2	$p1m(0\beta, 0\mu)$
3.6			3	$p1m(\frac{1}{2}\beta, 0\mu)$
3.7		(*m*, *m*)	4	$pm1(\alpha 0, 0\mu)$
3.8			4	$pm1(\alpha 0, 0\mu)0s, 0$
3.9			5	$pm1(\alpha\frac{1}{2}, 0\mu)$
3.10			5	$pm1(\alpha\frac{1}{2}, 0\mu)0s, 0$
3.11			5	$p1m(\alpha\frac{1}{2}, 0\mu)$
3.12			5	$p1m(\alpha\frac{1}{2}, 0\mu)0, s0$
3.13			6	$pm1(\alpha\frac{1}{2}, \frac{1}{2}\mu)$
3.14			7	$pm1(\alpha\beta)$
4.1	*pg*	(*m*, 1)	2	$pg1(0\beta, 0\mu)$
4.2			3	$pg1(\frac{1}{2}\beta, 0\mu)$
4.3		(*m*, 2)	2	$p1g(0\beta, 0\mu)$
4.4		(*m*, *m*)	4	$pg1(\alpha 0, 0\mu)$
4.5			7	$pg1(\alpha\frac{1}{2}, \frac{1}{2}\mu)$
5.1	*cm*	(*m*, 1)	8	$cm1(0\beta, 0\mu)$
5.2			8	$cm1(0\beta, 0\mu)s0, 0$
5.3		(*m*, 2)	8	$c1m(0\beta, 0\mu)$
5.4		(*m*, *m*)	9	$cm1(\alpha 0, 0\mu)$
5.5			9	$cm1(\alpha 0, 0\mu)0s, 0$
5.6			10	$cm(\alpha\beta)$
6.1	*pmm*	(*mm*, 12)	2	$pmm(0\beta, 0\mu)$
6.2			2	$pmm(0\beta, 0\mu)s0, 0$
6.3			3	$pmm(\frac{1}{2}\beta, 0\mu)$
6.4			3	$pmm(\frac{1}{2}\beta, 0\mu)s0, 0$
6.5		(*mm*, *mm*)	4	$pmm(\alpha 0, 0\mu)$
6.6			4	$pmm(\alpha 0, 0\mu)0s, 0$
6.7			4	$pmm(\alpha 0, 0\mu)0s, s0$
6.8			5	$pmm(\alpha\frac{1}{2}, 0\mu)$
6.9			5	$pmm(\alpha\frac{1}{2}, 0\mu)0s, 0$
6.10			6	$pmm(\alpha\frac{1}{2}, \frac{1}{2}\mu)$
6.11			7	$pmm(\alpha\beta)$
7.1	*pmg*	(*mm*, 12)	2	$pmg(0\beta, 0\mu)$
7.2			2	$pmg(0\beta, 0\mu)0s, 0$
7.3			2	$pgm(0\beta, 0\mu)$
7.4			3	$pgm(\frac{1}{2}\beta, 0\mu)$
7.5		(*mm*, *mm*)	4	$pgm(\alpha 0, 0\mu)$
7.6			4	$pgm(\alpha 0, 0\mu)0, s0$
7.7			5	$pmg(\alpha\frac{1}{2}, 0\mu)$
7.8			5	$pmg(\alpha\frac{1}{2}, 0\mu)0s, 0$
7.9			7	$pgm(\alpha\beta)$
8.1	*pgg*	(*mm*, 12)	2	$pgg(0\beta, 0\mu)$
8.2		(*mm*, *mm*)	4	$pgg(\alpha 0, 0\mu)$
8.3			7	$pgg(\alpha\beta)$
9.1	*cmm*	(*mm*, 12)	8	$cmm(0\beta, 0\mu)$
9.2			8	$cmm(0\beta, 0\mu)0s, 0$
9.3		(*mm*, *mm*)	9	$cmm(\alpha 0, 0\mu)$

Table 9.8.3.4(*b*). (2 + 2)-*Dimensional superspace groups (cont.)*

No.	Basic space group	Point group K_s	Bravais class No.	Group symbol
Rectangular (*cont.*)				
9.4			9	$cmm(\alpha 0, 0\mu)0s, 0$
9.5			9	$cmm(\alpha 0, 0\mu)0s, s0$
9.6			10	$cmm(\alpha\beta)$
Tetragonal				
10.1	*p*4	(4, 4)	11	$p4(\alpha\beta)$
11.1	*p*4*m*	(4*m*, 4*m*)	12	$p4m(\alpha 0)$
11.2			12	$p4m(\alpha 0)0, 0s$
11.3			13	$p4m(\alpha\frac{1}{2})$
11.4		(4$\dot{m}$, 4$\ddot{m}$)	14	$p4m(\alpha\alpha)$
11.5			14	$p4m(\alpha\alpha)0, 0s$
12.1	*p*4*g*	(4*m*, 4*m*)	12	$p4g(\alpha 0)$
12.2			12	$p4g(\alpha 0)0, 0s$
12.3		(4$\dot{m}$, 4$\ddot{m}$)	14	$p4g(\alpha\alpha)$
12.4			14	$p4g(\alpha\alpha)0, 0s$
Hexagonal				
13.1	*p*3	(3, 3)	15	$p3(\alpha\beta)$
14.1	*p*3*m*1	(3*m*, 3*m*)	16	$p3m1(\alpha 0)$
14.2		(3$\dot{m}$, 3$\ddot{m}$)	17	$p3m1(\alpha\alpha)$
15.1	*p*31*m*	(3*m*, 3*m*)	16	$p31m(\alpha 0)$
16.1	*p*6	(6, 6)	15	$p6(\alpha\beta)$
17.1	*p*6*m*	(6*m*, 6*m*)	16	$p6m(\alpha 0)$
17.2		(6$\dot{m}$, 6$\ddot{m}$)	17	$p6m(\alpha\alpha)$

In the two-line symbol, one finds in the upper line the symbol for the three-dimensional space group, in the bottom line the value of τ for the case $\varepsilon = +1$ and the symbol '$\bar{1}$' when $\varepsilon = -1$. The rational part of $\mathbf{q}$ is indicated by means of the appropriate prefix. In the case considered, $\mathbf{q}^r = 000$. So the prefix is *P* and the same superspace group is denoted in a two-line symbol as

$$P^{P2_1/m}_{\bar{1}\ s}\ .$$

In Table 9.8.3.5, the (3 + 1)-dimensional space groups are given by one-line symbols. These are so-called short symbols. Sometimes, a full symbol is required. Then, for the example given above one has $P112_1/m(\alpha\beta 0)000s$ and $P^{P112_1/m}_{111\ s}$, respectively. Note that in the short one-line symbol for $\tau = 0$ superspace groups (where the non-primitive translations can be transformed to zero by a choice of the origin) the zeros for the translational part are omitted. Not so, of course, in the full symbol. For example, short symbol $P2_1/m(\alpha\beta 0)$ and full symbol $P112_1/m(\alpha\beta 0)0000$. Table 9.8.3.5 is an adapted version of the tables given by de Wolff, Janssen & Janner (1981) and corrected by Yamamoto, Janssen, Janner & de Wolff (1985).

9.8.3.3.2. *Reflection conditions*

The indexing of diffraction vectors is a matter of choice of basis. When the basis chosen is not a primitive one, the indices have to satisfy certain conditions known as *centring conditions*. This holds for the main reflections (centring in ordinary space) as well as for satellites (centring in superspace). These centring conditions for reflections have been discussed in Subsection 9.8.2.1.

In addition to these general reflection conditions, there may be special reflection conditions related to the existence of non-

(*continued on page* 934)

Table 9.8.3.5. (3 + 1)-*Dimensional superspace groups*

The number labelling the superspace group is denoted by *n.m*, where *n* is the number attached to the three-dimensional basic space group and *m* numbers the various superspace groups having the same basic space group. The symbol of the basic space group, the symbol for the four-dimensional point group K_s, the number of the four-dimensional Bravais class to which the superspace group belongs (Table 9.8.3.2*a*), and the superspace-group symbol are also given. The superspace-group symbol is indicated in the short notation, *i.e.* for the basic group one uses the short symbol from *International Tables for Crystallography*, Volume A, and then the values of τ are given for each of the generators in this symbol, unless all these values are zero. Then, instead of writing a number of zeros, one omits them all. Finally, the special reflection conditions due to non-primitive translations are given, for *hklm* if $\mathbf{q}^r = 0$ and for *HKLm* otherwise. Recall the *HKLm* are the indices with respect to a conventional basis $\mathbf{a}_c^*, \mathbf{b}_c^*, \mathbf{c}_c^*, \mathbf{q}^i$ as in Table 9.8.3.2(*a*). The reflection conditions due to centring translations are given in Table 9.8.3.6.

No.	Basic space group	Point group K_s	Bravais class No.	Group symbol	Special reflection conditions
1.1	$P1$	$(1, 1)$	1	$P1(\alpha\beta\gamma)$	
2.1	$P\bar{1}$	$(\bar{1}, \bar{1})$	1	$P\bar{1}(\alpha\beta\gamma)$	
3.1	$P2$	$(2, \bar{1})$	2	$P2(\alpha\beta 0)$	
3.2		$(2, \bar{1})$	3	$P2(\alpha\beta\frac{1}{2})$	
3.3		$(2, 1)$	5	$P2(00\gamma)$	
3.4		$(2, 1)$	5	$P2(00\gamma)s$	$00lm$: $m = 2n$
3.5		$(2, 1)$	6	$P2(\frac{1}{2}0\gamma)$	
4.1	$P2_1$	$(2, \bar{1})$	2	$P2_1(\alpha\beta 0)$	$00l0$: $l = 2n$
4.2		$(2, 1)$	5	$P2_1(00\gamma)$	$00lm$: $l = 2n$
4.3		$(2, 1)$	6	$P2_1(\frac{1}{2}0\gamma)$	$00Lm$: $L = 2n$
5.1	$B2$	$(2, \bar{1})$	4	$B2(\alpha\beta 0)$	
5.2		$(2, 1)$	7	$B2(00\gamma)$	
5.3		$(2, 1)$	7	$B2(00\gamma)s$	$00lm$: $m = 2n$
5.4		$(2, 1)$	8	$B2(0\frac{1}{2}\gamma)$	
6.1	Pm	$(m, 1)$	2	$Pm(\alpha\beta 0)$	
6.2		$(m, 1)$	2	$Pm(\alpha\beta 0)s$	$hk0m$: $m = 2n$
6.3		$(m, \bar{1})$	3	$Pm(\alpha\beta\frac{1}{2})$	
6.4		$(m, \bar{1})$	5	$Pm(00\gamma)$	
6.5		$(m, \bar{1})$	6	$Pm(\frac{1}{2}0\gamma)$	
7.1	Pb	$(m, 1)$	2	$Pb(\alpha\beta 0)$	$hk0m$: $k = 2n$
7.2		$(m, 1)$	3	$Pb(\alpha\beta\frac{1}{2})$	$HK0m$: $K = 2n$
7.3		$(m, \bar{1})$	5	$Pb(00\gamma)$	$hk00$: $k = 2n$
7.4		$(m, \bar{1})$	6	$Pb(\frac{1}{2}0\gamma)$	$HK00$: $K = 2n$
8.1	Bm	$(m, 1)$	4	$Bm(\alpha\beta 0)$	
8.2		$(m, 1)$	4	$Bm(\alpha\beta 0)s$	$hk0m$: $m = 2n$
8.3		$(m, \bar{1})$	7	$Bm(00\gamma)$	
8.4		$(m, \bar{1})$	8	$Bm(0\frac{1}{2}\gamma)$	
9.1	Bb	$(m, 1)$	4	$Bb(\alpha\beta 0)$	$hk0m$: $k = 2n$
9.2		$(m, \bar{1})$	7	$Bb(00\gamma)$	$hk00$: $k = 2n$
10.1	$P2/m$	$(2/m, \bar{1}1)$	2	$P2/m(\alpha\beta 0)$	
10.2		$(2/m, \bar{1}1)$	2	$P2/m(\alpha\beta 0)0s$	$hk0m$: $m = 2n$
10.3		$(2/m, \bar{1}1)$	3	$P2/m(\alpha\beta\frac{1}{2})$	
10.4		$(2/m, 1\bar{1})$	5	$P2/m(00\gamma)$	
10.5		$(2/m, 1\bar{1})$	5	$P2/m(00\gamma)s0$	$00lm$: $m = 2n$
10.6		$(2/m, 1\bar{1})$	6	$P2/m(\frac{1}{2}0\gamma)$	
11.1	$P2_1/m$	$(2/m, \bar{1}1)$	2	$P2_1/m(\alpha\beta 0)$	$00l0$: $l = 2n$
11.2		$(2/m, \bar{1}1)$	2	$P2_1/m(\alpha\beta 0)0s$	$00l0$: $l = 2n$; $hk0m$: $m = 2n$
11.3		$(2/m, 1\bar{1})$	5	$P2_1/m(00\gamma)$	$00lm$: $l = 2n$
11.4		$(2/m, 1\bar{1})$	6	$P2_1/m(\frac{1}{2}0\gamma)$	$00Lm$: $L = 2n$
12.1	$B2/m$	$(2/m, \bar{1}1)$	4	$B2/m(\alpha\beta 0)$	
12.2		$(2/m, \bar{1}1)$	4	$B2/m(\alpha\beta 0)0s$	$hk0m$: $m = 2n$
12.3		$(2/m, 1\bar{1})$	7	$B2/m(00\gamma)$	
12.4		$(2/m, 1\bar{1})$	7	$B2/m(00\gamma)s0$	$00lm$: $m = 2n$
12.5		$(2/m, 1\bar{1})$	8	$B2/m(\frac{1}{2}0\gamma)$	
13.1	$P2/b$	$(2/m, \bar{1}1)$	2	$P2/b(\alpha\beta 0)$	$hk0m$: $k = 2n$
13.2		$(2/m, \bar{1}1)$	3	$P2/b(\alpha\beta\frac{1}{2})$	$HK0m$: $m = 2n$
13.3		$(2/m, 1\bar{1})$	5	$P2/b(00\gamma)$	$hk00$: $k = 2n$
13.4		$(2/m, 1\bar{1})$	5	$P2/b(00\gamma)s0$	$00lm$: $m = 2n$; $hk00$: $k = 2n$
13.5		$(2/m, 1\bar{1})$	6	$P2/b(\frac{1}{2}0\gamma)$	$HK00$: $K = 2n$
14.1	$P2_1/b$	$(2/m, \bar{1}1)$	2	$P2_1/b(\alpha\beta 0)$	$00l0$: $l = 2n$; $hk0m$: $k = 2n$
14.2		$(2/m, 1\bar{1})$	5	$P2_1/b(00\gamma)$	$00lm$: $l = 2n$; $hk00$: $k = 2n$
14.3		$(2/m, 1\bar{1})$	6	$P2_1/b(\frac{1}{2}0\gamma)$	$00Lm$: $L = 2n$; $HK00$: $K = 2n$
15.1	$B2/b$	$(2/m, \bar{1}1)$	4	$B2/b(\alpha\beta 0)$	$hk0m$: $k = 2n$
15.2		$(2/m, 1\bar{1})$	7	$B2/b(00\gamma)$	$hk00$: $k = 2n$
15.3		$(2/m, 1\bar{1})$	7	$B2/b(00\gamma)s0$	$00lm$: $m = 2n$; $hk00$: $k = 2n$

Table 9.8.3.5. (3 + 1)-*Dimensional superspace groups (cont.)*

No.	Basic space group	Point group K_s	Bravais class No.	Group symbol	Special reflection conditions
16.1	$P222$	$(222, \bar{1}\bar{1}1)$	9	$P222(00\gamma)$	
16.2			9	$P222(00\gamma)00s$	$00lm$: $m=2n$
16.3			10	$P222(0\frac{1}{2}\gamma)$	
16.4			11	$P222(\frac{11}{22}\gamma)$	
17.1	$P222_1$	$(222, \bar{1}\bar{1}1)$	9	$P222_1(00\gamma)$	$00lm$: $l=2n$
17.2			10	$P222_1(0\frac{1}{2}\gamma)$	$00Lm$: $L=2n$
17.3			11	$P222_1(\frac{11}{22}\gamma)$	$00Lm$: $L=2n$
17.4			9	$P2_122(00\gamma)$	$h000$: $h=2n$
17.5			9	$P2_122(00\gamma)00s$	$h000$: $h=2n$; $00lm$: $m=2n$
17.6			10	$P2_122(0\frac{1}{2}\gamma)$	$H000$: $H=2n$
18.1	$P2_12_12$	$(222, \bar{1}\bar{1}1)$	9	$P2_12_12(00\gamma)$	$h000$: $h=2n$; $0k00$: $k=2n$
18.2			9	$P2_12_12(00\gamma)00s$	$h000$: $h=2n$; $0k00$: $k=2n$; $00lm$: $m=2n$
18.3			9	$P2_122_1(00\gamma)$	$h000$: $h=2n$; $00lm$: $l=2n$
18.4			10	$P2_122_1(0\frac{1}{2}\gamma)$	$H000$: $H=2n$; $00Lm$: $L=2n$
19.1	$P2_12_12_1$	$(222, \bar{1}\bar{1}1)$	9	$P2_12_12_1(00\gamma)$	$h000$: $h=2n$; $0k00$: $k=2n$; $00lm$: $l=2n$
20.1	$C222_1$	$(222, \bar{1}\bar{1}1)$	13	$C222_1(00\gamma)$	$00lm$: $l=2n$
20.2			14	$C222_1(10\gamma)$	$00Lm$: $L=2n$
20.3			15	$A2_122(00\gamma)$	$h000$: $h=2n$
20.4			15	$A2_122(00\gamma)00s$	$h000$: $h=2n$; $00lm$: $m=2n$
21.1	$C222$	$(222, \bar{1}\bar{1}1)$	13	$C222(00\gamma)$	
21.2			13	$C222(00\gamma)00s$	$00lm$: $m=2n$
21.3			14	$C222(10\gamma)$	
21.4			14	$C222(10\gamma)00s$	$00Lm$: $m=2n$
21.5			15	$A222(00\gamma)$	
21.6			15	$A222(00\gamma)00s$	$00lm$: $m=2n$
21.7			16	$A222(\frac{1}{2}0\gamma)$	
22.1	$F222$	$(222, \bar{1}\bar{1}1)$	17	$F222(00\gamma)$	
22.2			17	$F222(00\gamma)00s$	$00lm$: $m=2n$
22.3			18	$F222(10\gamma)$	
23.1	$I222$	$(222, \bar{1}\bar{1}1)$	12	$I222(00\gamma)$	
23.2			12	$I222(00\gamma)00s$	$00lm$: $m=2n$
24.1	$I2_12_12_1$	$(222, \bar{1}\bar{1}1)$	12	$I2_12_12_1(00\gamma)$	$h000$: $h=2n$; $0k00$: $k=2n$; $00lm$: $l=2n$
24.2			12	$I2_12_12_1(00\gamma)00s$	$h000$: $h=2n$; $0k00$: $k=2n$; $00lm$: $l+m=2n$
25.1	$Pmm2$	$(mm2, 111)$	9	$Pmm2(00\gamma)$	
25.2			9	$Pmm2(00\gamma)s0s$	$0klm$: $m=2n$
25.3			9	$Pmm2(00\gamma)ss0$	$0klm$: $m=2n$; $h0lm$: $m=2n$
25.4			10	$Pmm2(0\frac{1}{2}\gamma)$	
25.5			10	$Pmm2(0\frac{1}{2}\gamma)s0s$	$0KLm$: $m=2n$
25.6			11	$Pmm2(\frac{1}{2}\frac{1}{2}\gamma)$	
25.7		$(m2m, 1\bar{1}\bar{1})$	10	$Pm2m(0\frac{1}{2}\gamma)$	
25.8			10	$Pm2m(0\frac{1}{2}\gamma)s00$	$0KLm$: $m=2n$
25.9		$(2mm, \bar{1}1\bar{1})$	9	$P2mm(00\gamma)$	
25.10			9	$P2mm(00\gamma)0s0$	$h0lm$: $m=2n$
25.11			10	$P2mm(0\frac{1}{2}\gamma)$	
25.12			11	$P2mm(\frac{1}{2}\frac{1}{2}\gamma)$	
26.1	$Pmc2_1$	$(mm2, 111)$	9	$Pmc2_1(00\gamma)$	$h0lm$: $l=2n$
26.2			9	$Pmc2_1(00\gamma)s0s$	$0klm$: $m=2n$; $h0lm$: $l=2n$
26.3			10	$Pmc2_1(0\frac{1}{2}\gamma)$	$H0Lm$: $L=2n$
26.4			10	$Pmc2_1(0\frac{1}{2}\gamma)s0s$	$0KLm$: $m=2n$; $H0Lm$: $L=2n$
26.5			10	$Pcm2_1(0\frac{1}{2}\gamma)$	$0KLm$: $L=2n$
26.6			11	$Pmc2_1(\frac{1}{2}\frac{1}{2}\gamma)$	$H0Lm$: $L=2n$
26.7		$(2mm, \bar{1}1\bar{1})$	9	$P2_1am(00\gamma)$	$h0lm$: $h=2n$
26.8			9	$P2_1am(00\gamma)0s0$	$h0lm$: $h+m=2n$
26.9			9	$P2_1ma(00\gamma)$	$hk00$: $h=2n$
26.10			9	$P2_1ma(00\gamma)0s0$	$h0lm$: $m=2n$; $hk00$: $h=2n$
26.11			10	$P2_1am(0\frac{1}{2}\gamma)$	$H0Lm$: $H=2n$
26.12			10	$P2_1ma(0\frac{1}{2}\gamma)$	$HK00$: $H=2n$
27.1	$Pcc2$	$(mm2, 111)$	9	$Pcc2(00\gamma)$	$0klm$: $l=2n$; $h0lm$: $l=2n$
27.2			9	$Pcc2(00\gamma)s0s$	$0klm$: $l+m=2n$; $h0lm$: $l=2n$
27.3			10	$Pcc2(0\frac{1}{2}\gamma)$	$0KLm$: $L=2n$; $H0Lm$: $L=2n$
27.4			11	$Pcc2(\frac{1}{2}\frac{1}{2}\gamma)$	$0KLm$: $L=2n$; $H0Lm$: $L=2n$
27.5		$(2mm, \bar{1}1\bar{1})$	9	$P2aa(00\gamma)$	$h0lm$: $h=2n$; $hk00$: $h=2n$
27.6			9	$P2aa(00\gamma)0s0$	$h0lm$: $h+m=2n$; $hk00$: $h=2n$
27.7			10	$P2aa(0\frac{1}{2}\gamma)$	$H0Lm$: $H=2n$; $HK00$: $H=2n$
28.1	$Pma2$	$(mm2, 111)$	9	$Pma2(00\gamma)$	$h0lm$: $h=2n$
28.2			9	$Pma2(00\gamma)s0s$	$0klm$: $m=2n$; $h0lm$: $h=2n$

Table 9.8.3.5. (3 + 1)-*Dimensional superspace groups (cont.)*

No.	Basic space group	Point group K_s	Bravais class No.	Group symbol	Special reflection conditions
28.3			9	$Pma2(00\gamma)ss0$	$0klm$: $m=2n$; $h0lm$: $h+m=2n$
28.4			9	$Pma2(00\gamma)0ss$	$h0lm$: $h+m=2n$
28.5			10	$Pma2(0\frac{1}{2}\gamma)$	$H0Lm$: $H=2n$
28.6			10	$Pma2(0\frac{1}{2}\gamma)s0s$	$0KLm$: $m=2n$; $H0Lm$: $H=2n$
28.7		$(m2m, 1\bar{1}\bar{1})$	10	$Pm2a(0\frac{1}{2}\gamma)$	$HK00$: $H=2n$
28.8			10	$Pm2a(0\frac{1}{2}\gamma)s00$	$0KLm$: $m=2n$; $HK00$: $H=2n$
28.9			10	$Pc2m(0\frac{1}{2}\gamma)$	$0KLm$: $L=2n$
28.10		$(2mm, \bar{1}1\bar{1})$	9	$P2cm(00\gamma)$	$h0lm$: $l=2n$
28.11			9	$P2mb(00\gamma)$	$hk00$: $k=2n$
28.12			9	$P2mb(00\gamma)0s0$	$h0lm$: $m=2n$; $hk00$: $k=2n$
28.13			10	$P2cm(0\frac{1}{2}\gamma)$	$H0Lm$: $L=2n$
28.14			11	$P2cm(\frac{1}{2}\frac{1}{2}\gamma)$	$H0Lm$: $L=2n$
29.1	$Pca2_1$	$(mm2, 111)$	9	$Pca2_1(00\gamma)$	$0klm$: $l=2n$; $h0lm$: $h=2n$
29.2			9	$Pca2_1(00\gamma)0ss$	$0klm$: $l=2n$; $h0lm$: $h+m=2n$
29.3			10	$Pca2_1(0\frac{1}{2}\gamma)$	$0KLm$: $L=2n$; $H0Lm$: $H=2n$
29.4		$(2mm, \bar{1}1\bar{1})$	9	$P2_1ca(00\gamma)$	$hk00$: $h=2n$; $h0lm$: $l=2n$
29.5			9	$P2_1ab(00\gamma)$	$h0lm$: $h=2n$; $hk00$: $k=2n$
29.6			9	$P2_1ab(00\gamma)0s0$	$h0lm$: $h+m=2n$; $hk00$: $k=2n$
29.7			10	$P2_1ca(0\frac{1}{2}\gamma)$	$H0Lm$: $L=2n$; $HK00$: $H=2n$
30.1	$Pcn2$	$(mm2, 111)$	9	$Pcn2(00\gamma)$	$0klm$: $l=2n$; $h0lm$: $h+l=2n$
30.2			9	$Pcn2(00\gamma)s0s$	$0klm$: $l+m=2n$; $h0lm$: $h+l=2n$
30.3			10	$Pcn2(0\frac{1}{2}\gamma)$	$0KLm$: $L=2n$; $H0Lm$: $H+L=2n$
30.4		$(2mm, \bar{1}1\bar{1})$	9	$P2na(00\gamma)$	$h0lm$: $h+l=2n$; $hk00$: $h=2n$
30.5			9	$P2an(00\gamma)$	$h0lm$: $h=2n$; $hk00$: $h+k=2n$
30.6			9	$P2an(00\gamma)0s0$	$h0lm$: $h+m=2n$; $hk00$: $h+k=2n$
30.7			10	$P2na(0\frac{1}{2}\gamma)$	$H0Lm$: $H+L=2n$; $HK00$: $H=2n$
30.8			11	$P2an(\frac{1}{2}\frac{1}{2}\gamma)0q0$	$H0Lm$: $2H+m=4n$; $HK00$: $H+K=2n$
31.1	$Pmn2_1$	$(mm2, 111)$	9	$Pmn2_1(00\gamma)$	$h0lm$: $h+l=2n$
31.2			9	$Pmn2_1(00\gamma)s0s$	$0klm$: $m=2n$; $h0lm$: $h+l=2n$
31.3			10	$Pmn2_1(0\frac{1}{2}\gamma)$	$H0Lm$: $H+L=2n$
31.4			10	$Pmn2_1(0\frac{1}{2}\gamma)s0s$	$0KLm$: $m=2n$; $H0Lm$: $H+L=2n$
31.5		$(2mm, \bar{1}1\bar{1})$	9	$P2_1nm(00\gamma)$	$h0lm$: $h+l=2n$
31.6			9	$P2_1mn(00\gamma)$	$hk00$: $h+k=2n$
31.7			9	$P2_1mn(00\gamma)0s0$	$hk00$: $h+k=2n$; $h0lm$: $m=2n$
31.8			10	$P2_1nm(0\frac{1}{2}\gamma)$	$H0Lm$: $H+L=2n$
32.1	$Pba2$	$(mm2, 111)$	9	$Pba2(00\gamma)$	$0klm$: $k=2n$; $h0lm$: $h=2n$
32.2			9	$Pba2(00\gamma)s0s$	$0klm$: $k+m=2n$; $h0lm$: $h=2n$
32.3			9	$Pba2(00\gamma)ss0$	$0klm$: $k+m=2n$; $h0lm$: $h+m=2n$
32.4			11	$Pba2(\frac{1}{2}\frac{1}{2}\gamma)qq0$	$0KLm$: $2K+m=4n$; $H0Lm$: $2H+m=4n$
32.5		$(m2m, 1\bar{1}\bar{1})$	10	$Pc2a(0\frac{1}{2}\gamma)$	$0KLm$: $L=2n$; $HK00$: $H=2n$
32.6		$(2mm, \bar{1}1\bar{1})$	9	$P2cb(00\gamma)$	$h0lm$: $l=2n$; $hk00$: $k=2n$
33.1	$Pbn2_1$	$(mm2, 111)$	9	$Pbn2_1(00\gamma)$	$0klm$: $k=2n$; $h0lm$: $h+l=2n$
33.2			9	$Pbn2_1(00\gamma)s0s$	$0klm$: $k+m=2n$; $h0lm$: $h+l=2n$
33.3			11	$Pbn2_1(\frac{1}{2}\frac{1}{2}\gamma)qq0$	$0KLm$: $2K+m=4n$; $H0Lm$: $2H+2L+m=4n$
33.4		$(2mm, \bar{1}1\bar{1})$	9	$P2_1nb(00\gamma)$	$h0lm$: $h+l=2n$; $hk00$: $k=2n$
33.5			9	$P2_1cn(00\gamma)$	$h0lm$: $l=2n$; $hk00$: $h+k=2n$
34.1	$Pnn2$	$(mm2, 111)$	9	$Pnn2(00\gamma)$	$0klm$: $k+l=2n$; $h0lm$: $h+l=2n$
34.2			9	$Pnn2(00\gamma)s0s$	$0klm$: $k+l+m=2n$; $h0lm$: $h+l=2n$
34.3			11	$Pnn2(\frac{1}{2}\frac{1}{2}\gamma)qq0$	$0KLm$: $2K+2L+m=4n$; $H0Lm$: $2H+2L+m=4n$
34.4		$(2mm, \bar{1}1\bar{1})$	9	$P2nn(00\gamma)$	$h0lm$: $h+l=2n$; $hk00$: $h+k=2n$
34.5			11	$P2nn(\frac{1}{2}\frac{1}{2}\gamma)0q0$	$H0Lm$: $2H+2L+m=4n$; $HK00$: $H+K=2n$
35.1	$Cmm2$	$(mm2, 111)$	13	$Cmm2(00\gamma)$	
35.2			13	$Cmm2(00\gamma)s0s$	$0klm$: $m=2n$
35.3			13	$Cmm2(00\gamma)ss0$	$0klm$: $m=2n$; $h0lm$: $m=2n$
35.4			14	$Cmm2(10\gamma)$	
35.5			14	$Cmm2(10\gamma)s0s$	$0KLm$: $m=2n$
35.6			14	$Cmm2(10\gamma)ss0$	$0KLm$: $m=2n$; $H0Lm$: $m=2n$
35.7		$(2mm, \bar{1}1\bar{1})$	15	$A2mm(00\gamma)$	
35.8			15	$A2mm(00\gamma)0s0$	$h0lm$: $m=2n$
35.9			16	$A2mm(\frac{1}{2}0\gamma)$	
35.10			16	$A2mm(\frac{1}{2}0\gamma)0s0$	$H0Lm$: $m=2n$
36.1	$Cmc2_1$	$(mm2, 111)$	13	$Cmc2_1(00\gamma)$	
36.2			13	$Cmc2_1(00\gamma)s0s$	$0klm$: $m=2n$; $h0lm$: $l=2n$
36.3			14	$Cmc2_1(10\gamma)$	$H0Lm$: $L=2n$
36.4			14	$Cmc2_1(10\gamma)s0s$	$0KLm$: $m=2n$; $H0Lm$: $L=2n$
36.5		$(2mm, \bar{1}1\bar{1})$	15	$A2_1am(00\gamma)$	$h0lm$: $h=2n$

Table 9.8.3.5. (3 + 1)-*Dimensional superspace groups (cont.)*

No.	Basic space group	Point group K_s	Bravais class No.	Group symbol	Special reflection conditions
36.6			15	$A2_1am(00\gamma)0s0$	$h0lm$: $h+m=2n$
36.7			15	$A2_1ma(00\gamma)$	$hk00$: $h=2n$
36.8			15	$A2_1ma(00\gamma)0s0$	$h0lm$: $m=2n$; $hk00$: $h=2n$
37.1	$Ccc2$	($mm2$, 111)	13	$Ccc2(00\gamma)$	$0klm$: $l=2n$; $h0lm$: $l=2n$
37.2			13	$Ccc2(00\gamma)s0s$	$0klm$: $l+m=2n$; $h0lm$: $l=2n$
37.3			14	$Ccc2(10\gamma)$	$0KLm$: $L=2n$; $H0Lm$: $L=2n$
37.4			14	$Ccc2(10\gamma)s0s$	$0KLm$: $L+m=2n$; $H0Lm$: $L=2n$
37.5		($2mm$, $\bar{1}1\bar{1}$)	15	$A2aa(00\gamma)$	$h0lm$: $h=2n$; $hk00$: $h=2n$
37.6			15	$A2aa(00\gamma)0s0$	$h0lm$: $h+m=2n$; $hk00$: $h=2n$
38.1	$C2mm$	($2mm$, $\bar{1}1\bar{1}$)	13	$C2mm(00\gamma)$	
38.2			13	$C2mm(00\gamma)0s0$	$h0lm$: $m=2n$
38.3			14	$C2mm(10\gamma)$	
38.4			14	$C2mm(10\gamma)0s0$	$H0Lm$: $m=2n$
38.5		($mm2$, 111)	15	$Amm2(00\gamma)$	
38.6			15	$Amm2(00\gamma)s0s$	$0klm$: $m=2n$
38.7			15	$Amm2(00\gamma)ss0$	$0klm$: $m=2n$; $h0lm$: $m=2n$
38.8			15	$Amm2(00\gamma)0ss$	$h0lm$: $m=2n$
38.9			16	$Amm2(\frac{1}{2}0\gamma)$	
38.10			16	$Amm2(\frac{1}{2}0\gamma)0ss$	$H0Lm$: $m=2n$
38.11		($m2m$, $1\bar{1}\bar{1}$)	15	$Am2m(00\gamma)$	
38.12			15	$Am2m(00\gamma)s00$	$0klm$: $m=2n$
38.13			16	$Am2m(\frac{1}{2}0\gamma)$	
39.1	$C2mb$	($2mm$, $\bar{1}1\bar{1}$)	13	$C2mb(00\gamma)$	$hk00$: $k=2n$
39.2			13	$C2mb(00\gamma)0s0$	$h0lm$: $m=2n$; $hk00$: $k=2n$
39.3			14	$C2mb(10\gamma)$	$HK00$: $K=2n$
39.4			14	$C2mb(10\gamma)0s0$	$H0Lm$: $m=2n$; $HK00$: $K=2n$
39.5		($mm2$, 111)	15	$Abm2(00\gamma)$	$0klm$: $k=2n$
39.6			15	$Abm2(00\gamma)s0s$	$0klm$: $k+m=2n$
39.7			15	$Abm2(00\gamma)ss0$	$0klm$: $k+m=2n$; $h0lm$: $m=2n$
39.8			15	$Abm2(00\gamma)0ss$	$0klm$: $k=2n$; $h0lm$: $m=2n$
39.9			16	$Abm2(\frac{1}{2}0\gamma)$	$0KLm$: $K=2n$
39.10			16	$Abm2(\frac{1}{2}0\gamma)0ss$	$0KLm$: $K+m=2n$
39.11		($m2m$, $1\bar{1}\bar{1}$)	15	$Ac2m(00\gamma)$	$0klm$: $l=2n$
39.12			15	$Ac2m(00\gamma)s00$	$0klm$: $l+m=2n$
39.13			16	$Ac2m(\frac{1}{2}0\gamma)$	$0KLm$: $L=2n$
40.1	$C2cm$	($2mm$, $\bar{1}1\bar{1}$)	13	$C2cm(00\gamma)$	$h0lm$: $l=2n$
40.2			14	$C2cm(10\gamma)$	$H0Lm$: $L=2n$
40.3		($mm2$, 111)	15	$Ama2(00\gamma)$	$h0lm$: $h=2n$
40.4			15	$Ama2(00\gamma)s0s$	$0klm$: $m=2n$; $h0lm$: $h=2n$
40.5			15	$Ama2(00\gamma)ss0$	$0klm$: $m=2n$; $h0lm$: $h+m=2n$
40.6			15	$Ama2(00\gamma)0ss$	$h0lm$: $h+m=2n$
40.7		($m2m$, $1\bar{1}\bar{1}$)	15	$Am2a(00\gamma)$	$hk00$: $h=2n$
40.8			15	$Am2a(00\gamma)s00$	$0klm$: $m=2n$; $hk00$: $h=2n$
41.1	$C2cb$	($2mm$, $\bar{1}1\bar{1}$)	13	$C2cb(00\gamma)$	$h0lm$: $l=2n$; $hk00$: $k=2n$
41.2			14	$C2cb(10\gamma)$	$H0Lm$: $L=2n$; $HK00$: $K=2n$
41.3		($mm2$, 111)	15	$Aba2(00\gamma)$	$0klm$: $k=2n$; $h0lm$: $h=2n$
41.4			15	$Aba2(00\gamma)s0s$	$0klm$: $k+m=2n$; $h0lm$: $h=2n$
41.5			15	$Aba2(00\gamma)ss0$	$0klm$: $k+m=2n$; $h0lm$: $h+m=2n$
41.6			15	$Aba2(00\gamma)0ss$	$0klm$: $k=2n$; $h0lm$: $h+m=2n$
41.7		($m2m$, $1\bar{1}\bar{1}$)	15	$Ac2a(00\gamma)$	$0klm$: $l=2n$; $hk00$: $h=2n$
41.8			15	$Ac2a(00\gamma)s00$	$0klm$: $l+m=2n$; $hk00$: $h=2n$
42.1	$Fmm2$	($mm2$, 111)	17	$Fmm2(00\gamma)$	
42.2			17	$Fmm2(00\gamma)s0s$	$0klm$: $m=2n$
42.3			17	$Fmm2(00\gamma)ss0$	$0klm$: $m=2n$; $h0lm$: $m=2n$
42.4			18	$Fmm2(10\gamma)$	
42.5			18	$Fmm2(10\gamma)s0s$	$0KLm$: $m=2n$
42.6			18	$Fmm2(10\gamma)ss0$	$0KLm$: $m=2n$; $H0Lm$: $m=2n$
42.7		($2mm$, $\bar{1}1\bar{1}$)	17	$F2mm(00\gamma)$	
42.8			17	$F2mm(00\gamma)0s0$	$h0lm$: $m=2n$
42.9			18	$F2mm(10\gamma)$	
42.10			18	$F2mm(10\gamma)0s0$	$H0Lm$: $m=2n$
43.1	$Fdd2$	($mm2$, 111)	17	$Fdd2(00\gamma)$	$0klm$: $k+l=4n$
43.2			17	$Fdd2(00\gamma)s0s$	$0klm$: $k+l+2m=4n$; $h0lm$: $h+l=4n$
43.3		($2mm$, $\bar{1}1\bar{1}$)	17	$F2dd(00\gamma)$	$h0lm$: $h+l=4n$
44.1	$Imm2$	($mm2$, 111)	12	$Imm2(00\gamma)$	
44.2			12	$Imm2(00\gamma)s0s$	$0klm$: $m=2n$

Table 9.8.3.5. (3 + 1)-*Dimensional superspace groups (cont.)*

No.	Basic space group	Point group K_s	Bravais class No.	Group symbol	Special reflection conditions
44.3			12	$Imm2(00\gamma)ss0$	$0klm$: $m=2n$; $h0lm$: $m=2n$
44.4		$(2mm, \bar{1}1\bar{1})$	12	$I2mm(00\gamma)$	
44.5			12	$I2mm(00\gamma)0s0$	$h0lm$: $m=2n$
45.1	$Iba2$	$(mm2, 111)$	12	$Iba2(00\gamma)$	$0klm$: $k=2n$; $h0lm$: $h=2n$
45.2			12	$Iba2(00\gamma)s0s$	$0klm$: $k+m=2n$; $h0lm$: $h=2n$
45.3			12	$Iba2(00\gamma)ss0$	$0klm$: $k+m=2n$; $h0lm$: $h+m=2n$
45.4		$(2mm, \bar{1}1\bar{1})$	12	$I2cb(00\gamma)$	$h0lm$: $l=2n$; $hk00$: $k=2n$
45.5			12	$I2cb(00\gamma)0s0$	$h0lm$: $l+m=2n$; $hk00$: $k=2n$
46.1	$Ima2$	$(mm2, 111)$	12	$Ima2(00\gamma)$	$h0lm$: $h=2n$
46.2			12	$Ima2(00\gamma)s0s$	$0klm$: $m=2n$; $h0lm$: $h=2n$
46.3			12	$Ima2(00\gamma)ss0$	$0klm$: $m=2n$; $h0lm$: $h+m=2n$
46.4			12	$Ima2(00\gamma)0ss$	$h0lm$: $h+m=2n$
46.5		$(2mm, \bar{1}1\bar{1})$	12	$I2mb(00\gamma)$	$hk00$: $k=2n$
46.6			12	$I2mb(00\gamma)0s0$	$h0lm$: $m=2n$; $hk00$: $k=2n$
46.7			12	$I2cm(00\gamma)$	$h0lm$: $l=2n$
46.8			12	$I2cm(00\gamma)0s0$	$h0lm$: $l+m=2n$
47.1	$Pmmm$	$(mmm, 11\bar{1})$	9	$Pmmm(00\gamma)$	
47.2			9	$Pmmm(00\gamma)s00$	$0klm$: $m=2n$
47.3			9	$Pmmm(00\gamma)ss0$	$0klm$: $m=2n$; $h0lm$: $m=2n$
47.4			10	$Pmmm(0\frac{1}{2}\gamma)$	
47.5			10	$Pmmm(0\frac{1}{2}\gamma)s00$	$0KLm$: $m=2n$
47.6			11	$Pmmm(\frac{1}{2}\frac{1}{2}\gamma)$	
48.1	$Pnnn$	$(mmm, 11\bar{1})$	9	$Pnnn(00\gamma)$	$0klm$: $k+l=2n$; $h0lm$: $h+l=2n$; $hk00$: $h+k=2n$
48.2			9	$Pnnn(00\gamma)s00$	$0klm$: $k+l+m=2n$; $h0lm$: $h+l=2n$; $hk00$: $h+k=2n$
48.3			11	$Pnnn(\frac{1}{2}\frac{1}{2}\gamma)qq0$	$0KLm$: $2K+2L+m=4n$; $H0Lm$: $2H+2L+m=2n$; $HK00$: $H+K=2n$
49.1	$Pccm$	$(mmm, 11\bar{1})$	9	$Pccm(00\gamma)$	$0klm$: $l=2n$; $h0lm$: $l=2n$
49.2			9	$Pccm(00\gamma)s00$	$0klm$: $l+m=2n$; $h0lm$: $l=2n$
49.3			9	$Pmaa(00\gamma)$	$h0lm$: $h=2n$; $hk00$: $h=2n$
49.4			9	$Pmaa(00\gamma)s00$	$0klm$: $m=2n$; $h0lm$: $h=2n$; $hk00$: $h=2n$
49.5			9	$Pmaa(00\gamma)ss0$	$0klm$: $m=2n$; $h0lm$: $h+m=2n$; $hk00$: $h=2n$
49.6			9	$Pmaa(00\gamma)0s0$	$h0lm$: $h+m=2n$; $hk00$: $h=2n$
49.7			10	$Pccm(0\frac{1}{2}\gamma)$	$0KLm$: $L=2n$; $H0Lm$: $L=2n$
49.8			10	$Pmaa(0\frac{1}{2}\gamma)$	$H0Lm$: $H=2n$; $HK00$: $H=2n$
49.9			10	$Pmaa(0\frac{1}{2}\gamma)s00$	$0KLm$: $m=2n$; $H0Lm$: $H=2n$; $HK00$: $H=2n$
49.10			11	$Pccm(\frac{1}{2}\frac{1}{2}\gamma)$	$0KLm$: $L=2n$; $H0Lm$: $L=2n$
50.1	$Pban$	$(mmm, 11\bar{1})$	9	$Pban(00\gamma)$	$0klm$: $k=2n$; $h0lm$: $h=2n$
50.2			9	$Pban(00\gamma)s00$	$0klm$: $k+m=2n$; $h0lm$: $h=2n$
50.3			9	$Pban(00\gamma)ss0$	$0klm$: $k+m=2n$; $h0lm$: $h+m=2n$
50.4			9	$Pcna(00\gamma)$	$0klm$: $l=2n$; $h0lm$: $h+l=2n$; $hk00$: $h=2n$
50.5			9	$Pcna(00\gamma)s00$	$0klm$: $l+m=2n$; $h0lm$: $h+l=2n$; $hk00$: $h=2n$
50.6			10	$Pcna(0\frac{1}{2}\gamma)$	$0KLm$: $L=2n$; $H0Lm$: $H+L=2n$; $HK00$: $H=2n$
50.7			11	$Pban(\frac{1}{2}\frac{1}{2}\gamma)qq0$	$0KLm$: $2K+m=4n$; $H0Lm$: $2H+m=4n$; $HK00$: $H+K=2n$
51.1	$Pmma$	$(mmm, 11\bar{1})$	9	$Pmma(00\gamma)$	$hk00$: $h=2n$
51.2			9	$Pmma(00\gamma)s00$	$0klm$: $m=2n$; $hk00$: $h=2n$
51.3			9	$Pmma(00\gamma)ss0$	$0klm$: $m=2n$; $h0lm$: $m=2n$; $hk00$: $h=2n$
51.4			9	$Pmma(00\gamma)0s0$	$h0lm$: $m=2n$; $hk00$: $h=2n$
51.5			9	$Pmam(00\gamma)$	$h0lm$: $h=2n$
51.6			9	$Pmam(00\gamma)s00$	$0klm$: $m=2n$; $h0lm$: $h=2n$
51.7			9	$Pmam(00\gamma)ss0$	$0klm$: $m=2n$; $h0lm$: $h+m=2n$
51.8			9	$Pmam(00\gamma)0s0$	$h0lm$: $h+m=2n$
51.9			9	$Pmcm(00\gamma)$	$h0lm$: $l=2n$
51.10			9	$Pmcm(00\gamma)s00$	$0klm$: $m=2n$; $h0lm$: $l=2n$
51.11			10	$Pmma(0\frac{1}{2}\gamma)$	$HK00$: $H=2n$
51.12			10	$Pmma(0\frac{1}{2}\gamma)s00$	$0KLm$: $m=2n$; $HK00$: $H=2n$
51.13			10	$Pmam(0\frac{1}{2}\gamma)$	$H0Lm$: $H=2n$
51.14			10	$Pmam(0\frac{1}{2}\gamma)s00$	$0KLm$: $m=2n$; $H0Lm$: $H=2n$
51.15			10	$Pmcm(0\frac{1}{2}\gamma)$	$H0Lm$: $L=2n$
51.16			10	$Pmcm(0\frac{1}{2}\gamma)s00$	$0KLm$: $m=2n$; $H0Lm$: $L=2n$
51.17			10	$Pcmm(0\frac{1}{2}\gamma)$	$0KLm$: $L=2n$
51.18			11	$Pcmm(\frac{1}{2}\frac{1}{2}\gamma)$	$0KLm$: $L=2n$
52.1	$Pnna$	$(mmm, 11\bar{1})$	9	$Pnna(00\gamma)$	$0klm$: $k+l=2n$; $h0lm$: $h+l=2n$; $hk00$: $h=2n$
52.2			9	$Pnna(00\gamma)s00$	$0klm$: $k+l+m=2n$; $h0lm$: $h+l=2n$; $hk00$: $h=2n$
52.3			9	$Pbnn(00\gamma)$	$0klm$: $k=2n$; $h0lm$: $h+l=2n$; $hk00$: $h+k=2n$

Table 9.8.3.5. (3 + 1)-*Dimensional superspace groups (cont.)*

No.	Basic space group	Point group K_s	Bravais class No.	Group symbol	Special reflection conditions
52.4			9	*Pbnn*(00γ)*s*00	0*klm*: $k+m=2n$; *h*0*lm*: $h+l=2n$; *hk*00: $h+k=2n$
52.5			9	*Pcnn*(00γ)	0*klm*: $l=2n$; *h*0*lm*: $h+l=2n$; *hk*00: $h+k=2n$
52.6			9	*Pcnn*(00γ)*s*00	0*klm*: $l+m=2n$; *h*0*lm*: $h+l=2n$; *hk*00: $h+k=2n$
52.7			11	*Pbnn*($\frac{1}{2}\frac{1}{2}\gamma$)*qq*0	0*KLm*: $2K+m=4n$; *H*0*Lm*: $2H+2L+m=4n$; *HK*00: $H+K=2n$
53.1	*Pmna*	(*mmm*, 11$\bar{1}$)	9	*Pmna*(00γ)	*h*0*lm*: $h+l=2n$; *hk*00: $h=2n$
53.2			9	*Pmna*(00γ)*s*00	0*klm*: $m=2n$; *h*0*lm*: $h+l=2n$; *hk*00: $h=2n$
53.3			9	*Pcnm*(00γ)	0*klm*: $l=2n$; *h*0*lm*: $h+l=2n$
53.4			9	*Pcnm*(00γ)*s*00	0*klm*: $l+m=2n$; *h*0*lm*: $h+l=2n$
53.5			9	*Pbmn*(00γ)	0*klm*: $k=2n$; *hk*00: $h+k=2n$
53.6			9	*Pbmn*(00γ)*s*00	0*klm*: $k+m=2n$; *hk*00: $h+k=2n$
53.7			9	*Pbmn*(00γ)*ss*0	0*klm*: $k+m=2n$; *h*0*lm*: $m=2n$; *hk*00: $h+k=2n$
53.8			9	*Pbmn*(00γ)0*s*0	0*klm*: $k=2m$; *h*0*lm*: $m=2n$; *hk*00: $h+k=2n$
53.9			10	*Pmna*($0\frac{1}{2}\gamma$)	*H*0*Lm*: $H+L=2n$; *HK*00: $H=2n$
53.10			10	*Pmna*($0\frac{1}{2}\gamma$)*s*00	0*KLm*: $m=2n$; *H*0*Lm*: $H+L=2n$; *HK*00: $H=2n$
53.11			10	*Pcnm*($0\frac{1}{2}\gamma$)	0*KLm*: $L=2n$; *H*0*Lm*: $H+L=2n$
54.1	*Pcca*	(*mmm*, 11$\bar{1}$)	9	*Pcca*(00γ)	0*klm*: $l=2n$; *h*0*lm*: $l=2n$; *hk*00: $h=2n$
54.2			9	*Pcca*(00γ)*s*00	0*klm*: $l+m=2n$; *h*0*lm*: $l=2n$; *hk*00: $h=2n$
54.3			9	*Pcaa*(00γ)	0*klm*: $l=2n$; *h*0*lm*: $h=2n$; *hk*00: $h=2n$
54.4			9	*Pcaa*(00γ)0*s*0	0*klm*: $l=2n$; *h*0*lm*: $h+m=2n$; *hk*00: $h=2n$
54.5			9	*Pbab*(00γ)	0*klm*: $k=2n$; *h*0*lm*: $h=2n$; *hk*00: $k=2n$
54.6			9	*Pbab*(00γ)*s*00	0*klm*: $k+m=2n$; *h*0*lm*: $h=2n$; *hk*00: $k=2n$
54.7			9	*Pbab*(00γ)*ss*0	0*klm*: $k+m=2n$; *h*0*lm*: $h+m=2n$; *hk*00: $k=2n$
54.8			9	*Pbab*(00γ)0*s*0	0*klm*: $k=2n$; *h*0*lm*: $h+m=2n$; *hk*00: $k=2n$
54.9			10	*Pcca*($0\frac{1}{2}\gamma$)	0*KLm*: $L=2n$; *H*0*Lm*: $L=2n$; *HK*00: $H=2n$
54.10			10	*Pcaa*($0\frac{1}{2}\gamma$)	0*KLm*: $L=2n$; *H*0*Lm*: $H=2n$; *HK*00: $H=2n$
55.1	*Pbam*	(*mmm*, 11$\bar{1}$)	9	*Pbam*(00γ)	0*klm*: $k=2n$; *h*0*lm*: $h=2n$
55.2			9	*Pbam*(00γ)*s*00	0*klm*: $k+m=2n$; *h*0*lm*: $h=2n$
55.3			9	*Pbam*(00γ)*ss*0	0*klm*: $k+m=2n$; *h*0*lm*: $h+m=2n$
55.4			9	*Pcma*(00γ)	0*klm*: $l=2n$; *hk*00: $h=2n$
55.5			9	*Pcma*(00γ)0*s*0	0*klm*: $l=2n$; *h*0*lm*: $m=2n$; *hk*00: $h=2n$
55.6			10	*Pcma*($0\frac{1}{2}\gamma$)	0*KLm*: $L=2n$; *HK*00: $H=2n$
56.1	*Pccn*	(*mmm*, 11$\bar{1}$)	9	*Pccn*(00γ)	0*klm*: $l=2n$; *h*0*lm*: $l=2n$; *hk*00: $h+k=2n$
56.2			9	*Pccn*(00γ)*s*00	0*klm*: $l+m=2n$; *h*0*lm*: $l=2n$; *hk*00: $h+k=2n$
56.3			9	*Pbnb*(00γ)	0*klm*: $k=2n$; *h*0*lm*: $h+l=2n$; *hk*00: $k=2n$
56.4			9	*Pbnb*(00γ)*s*00	0*klm*: $k+m=2n$; *h*0*lm*: $h+l=2n$; *hk*00: $k=2n$
57.1	*Pcam*	(*mmm*, 11$\bar{1}$)	9	*Pcam*(00γ)	0*klm*: $l=2n$; *h*0*lm*: $h=2n$
57.2			9	*Pcam*(00γ)0*s*0	0*klm*: $l=2n$; *h*0*lm*: $h+m=2n$
57.3			9	*Pmca*(00γ)	*h*0*lm*: $l=2n$; *hk*00: $h=2n$
57.4			9	*Pmca*(00γ)*s*00	0*klm*: $m=2n$; *h*0*lm*: $l=2n$; *hk*00: $h=2n$
57.5			9	*Pbma*(00γ)	0*klm*: $k=2n$; *hk*00: $h=2n$
57.6			9	*Pbma*(00γ)*s*00	0*klm*: $k+m=2n$; *hk*00: $h=2n$
57.7			9	*Pbma*(00γ)*ss*0	0*klm*: $k+m=2n$; *h*0*lm*: $m=2n$; *hk*00: $h=2n$
57.8			9	*Pbma*(00γ)0*s*0	0*klm*: $k=2n$; *h*0*lm*: $m=2n$; *hk*00: $h=2n$
57.9			10	*Pcam*($0\frac{1}{2}\gamma$)	0*KLm*: $L=2n$; *H*0*Lm*: $H=2n$
57.10			10	*Pmca*($0\frac{1}{2}\gamma$)	*H*0*Lm*: $L=2n$; *HK*00: $H=2n$
57.11			10	*Pmca*($0\frac{1}{2}\gamma$)*s*00	0*KLm*: $m=2n$; *H*0*Lm*: $L=2n$; *HK*00: $H=2n$
58.1	*Pnnm*	(*mmm*, 11$\bar{1}$)	9	*Pnnm*(00γ)	0*klm*: $k+l=2n$; *h*0*lm*: $h+l=2n$
58.2			9	*Pnnm*(00γ)*s*00	0*klm*: $k+l+m=2n$; *h*0*lm*: $h+l=2n$
58.3			9	*Pmnn*(00γ)	*h*0*lm*: $h+l=2n$; *hk*00: $h+k=2n$
58.4			9	*Pmnn*(00γ)*s*00	0*klm*: $m=2n$; *h*0*lm*: $h+l=2n$; *hk*00: $h+k=2n$
59.1	*Pmmn*	(*mmm*, 11$\bar{1}$)	9	*Pmmn*(00γ)	*hk*00: $h+k=2n$
59.2			9	*Pmmn*(00γ)*s*00	0*klm*: $m=2n$; *hk*00: $h+k=2n$
59.3			9	*Pmmn*(00γ)*ss*0	0*klm*: $m=2n$; *h*0*lm*: $m=2n$; *hk*00: $h+k=2n$
59.4			9	*Pmnm*(00γ)	*h*0*lm*: $h+l=2n$
59.5			9	*Pmnm*(00γ)*s*00	0*klm*: $m=2n$; *h*0*lm*: $h+l=2n$
59.6			10	*Pmnm*($0\frac{1}{2}\gamma$)	*H*0*Lm*: $H+L=2n$
59.7			10	*Pmnm*($0\frac{1}{2}\gamma$)*s*00	0*KLm*: $m=2n$; *H*0*Lm*: $H+L=2n$
60.1	*Pbcn*	(*mmm*, 11$\bar{1}$)	9	*Pbcn*(00γ)	0*klm*: $k=2n$; *h*0*lm*: $l=2n$; *hk*00: $h+k=2n$
60.2			9	*Pbcn*(00γ)*s*00	0*klm*: $k+m=2n$; *h*0*lm*: $l=2n$; *hk*00: $h+k=2n$
60.3			9	*Pnca*(00γ)	0*klm*: $k+l=2n$; *h*0*lm*: $l=2n$; *hk*00: $h=2n$
60.4			9	*Pnca*(00γ)*s*00	0*klm*: $k+l+m=2n$; *h*0*lm*: $l=2n$; *hk*00: $h=2n$
60.5			9	*Pbna*(00γ)	0*klm*: $k=2n$; *h*0*lm*: $h+l=2n$; *hk*00: $h=2n$
60.6			9	*Pbna*(00γ)*s*00	0*klm*: $k+m=2n$; *h*0*lm*: $h+l=2n$; *hk*00: $h=2n$
61.1	*Pbca*	(*mmm*, 11$\bar{1}$)	9	*Pbca*(00γ)	0*klm*: $k=2n$; *h*0*lm*: $l=2n$; *hk*00: $h=2n$
61.2			9	*Pbca*(00γ)*s*00	0*klm*: $k+m=2n$; *h*0*lm*: $l=2n$; *hk*00: $h=2n$

Table 9.8.3.5. (3 + 1)-*Dimensional superspace groups (cont.)*

No.	Basic space group	Point group K_s	Bravais class No.	Group symbol	Special reflection conditions
62.1	*Pnma*	(*mmm*, 11$\bar{1}$)	9	*Pnma*(00γ)	0*klm*: $k+l=2n$; *hk*00: $h=2n$
62.2			9	*Pnma*(00γ)0*s*0	0*klm*: $k+l=2n$; *h*0*lm*: $m=2n$; *hk*00: $h=2n$
62.3			9	*Pbnm*(00γ)	0*klm*: $k=2n$; *h*0*lm*: $h+l=2n$
62.4			9	*Pbnm*(00γ)*s*00	0*klm*: $k+m=2n$; *h*0*lm*: $h+l=2n$
62.5			9	*Pmcn*(00γ)	*h*0*lm*: $l=2n$; *hk*00: $h+k=2n$
62.6			9	*Pmcn*(00γ)*s*00	0*klm*: $m=2n$; *h*0*lm*: $l=2n$; *hk*00: $h+k=2n$
63.1	*Cmcm*	(*mmm*, 11$\bar{1}$)	13	*Cmcm*(00γ)	*h*0*lm*: $l=2n$
63.2			13	*Cmcm*(00γ)*s*00	0*klm*: $m=2n$; *h*0*lm*: $l=2n$
63.3			14	*Cmcm*(10γ)	*H*0*Lm*: $L=2n$
63.4			14	*Cmcm*(10γ)*s*00	0*KLm*: $m=2n$; *H*0*Lm*: $L=2n$
63.5			15	*Amam*(00γ)	*h*0*lm*: $h=2n$
63.6			15	*Amam*(00γ)*s*00	0*klm*: $m=2n$; *h*0*lm*: $h=2n$
63.7			15	*Amam*(00γ)*ss*0	0*klm*: $m=2n$; *h*0*lm*: $h+m=2n$
63.8			15	*Amam*(00γ)0*s*0	*h*0*lm*: $h+m=2n$
63.9			15	*Amma*(00γ)	*hk*00: $h=2n$
63.10			15	*Amma*(00γ)*s*00	0*klm*: $m=2n$; *hk*00: $h=2n$
63.11			15	*Amma*(00γ)*ss*0	0*klm*: $m=2n$; *h*0*lm*: $m=2n$; *hk*00: $h=2n$
63.12			15	*Amma*(00γ)0*s*0	*h*0*lm*: $m=2n$; *hk*00: $h=2n$
64.1	*Cmca*	(*mmm*, 11$\bar{1}$)	13	*Cmca*(00γ)	*h*0*lm*: $l=2n$; *hk*00: $h=2n$
64.2			13	*Cmca*(00γ)*s*00	0*klm*: $m=2n$; *h*0*lm*: $l=2n$; *hk*00: $h=2n$
64.3			14	*Cmca*(10γ)	*H*0*Lm*: $L=2n$; *HK*00: $H=2n$
64.4			14	*Cmca*(10γ)*s*00	0*KLm*: $m=2n$; *H*0*Lm*: $L=2n$; *HK*00: $H=2n$
64.5			15	*Abma*(00γ)	0*klm*: $k=2n$; *hk*00: $h=2n$
64.6			15	*Abma*(00γ)*s*00	0*klm*: $k+m=2n$; *hk*00: $h=2n$
64.7			15	*Abma*(00γ)*ss*0	0*klm*: $k+m=2n$; *h*0*lm*: $m=2n$; *hk*00: $h=2n$
64.8			15	*Abma*(00γ)0*s*0	0*klm*: $k=2n$; *h*0*lm*: $m=2n$; *hk*00: $h=2n$
64.9			15	*Acam*(00γ)	0*klm*: $l=2n$; *h*0*lm*: $h=2n$
64.10			15	*Acam*(00γ)*s*00	0*klm*: $l+m=2n$; *h*0*lm*: $h=2n$
64.11			15	*Acam*(00γ)*ss*0	0*klm*: $l+m=2n$; *h*0*lm*: $h+m=2n$
64.12			15	*Acam*(00γ)0*s*0	0*klm*: $l=2n$; *h*0*lm*: $h+m=2n$
65.1	*Cmmm*	(*mmm*, 11$\bar{1}$)	13	*Cmmm*(00γ)	
65.2			13	*Cmmm*(00γ)*s*00	0*klm*: $m=2n$
65.3			13	*Cmmm*(00γ)*ss*0	0*klm*: $m=2n$; *h*0*lm*: $m=2n$
65.4			14	*Cmmm*(10γ)	
65.5			14	*Cmmm*(10γ)*s*00	0*KLm*: $m=2n$
65.6			14	*Cmmm*(10γ)*ss*0	0*KLm*: $m=2n$; *H*0*Lm*: $m=2n$
65.7			15	*Ammm*(00γ)	
65.8			15	*Ammm*(00γ)*s*00	0*klm*: $m=2n$
65.9			15	*Ammm*(00γ)*ss*0	0*klm*: $m=2n$; *h*0*lm*: $m=2n$
65.10			15	*Ammm*(00γ)0*s*0	*h*0*lm*: $m=2n$
65.11			16	*Ammm*($\frac{1}{2}$0γ)	
65.12			16	*Ammm*($\frac{1}{2}$0γ)0*s*0	*H*0*Lm*: $m=2n$
66.1	*Cccm*	(*mmm*, 11$\bar{1}$)	13	*Cccm*(00γ)	0*klm*: $l=2n$; *h*0*lm*: $l=2n$
66.2			13	*Cccm*(00γ)*s*00	0*klm*: $l+m=2n$; *h*0*lm*: $l=2n$
66.3			14	*Cccm*(10γ)	0*KLm*: $L=2n$; *H*0*Lm*: $L=2n$
66.4			14	*Cccm*(10γ)*s*00	0*KLm*: $L+m=2n$; *H*0*Lm*: $L=2n$
66.5			15	*Amaa*(00γ)	*h*0*lm*: $h=2n$; *hk*00: $h=2n$
66.6			15	*Amaa*(00γ)*s*00	0*klm*: $m=2n$; *h*0*lm*: $h=2n$; *hk*00: $h=2n$
66.7			15	*Amaa*(00γ)*ss*0	0*klm*: $m=2n$; *h*0*lm*: $h+m=2n$; *hk*00: $h=2n$
66.8			15	*Amaa*(00γ)0*s*0	*h*0*lm*: $h+m=2n$; *hk*00: $h=2n$
67.1	*Cmma*	(*mmm*, 11$\bar{1}$)	13	*Cmma*(00γ)	*hk*00: $h=2n$
67.2			13	*Cmma*(00γ)*s*00	0*klm*: $m=2n$; *hk*00: $h=2n$
67.3			13	*Cmma*(00γ)*ss*0	0*klm*: $m=2n$; *h*0*lm*: $m=2n$; *hk*00: $h=2n$
67.4			14	*Cmma*(10γ)	*HK*00: $H=2n$
67.5			14	*Cmma*(10γ)*s*00	0*KLm*: $m=2n$; *HK*00: $H=2n$
67.6			14	*Cmma*(10γ)*ss*0	0*KLm*: $m=2n$; *H*0*Lm*: $m=2n$; *HK*00: $H=2n$
67.7			15	*Acmm*(00γ)	0*klm*: $l=2n$
67.8			15	*Acmm*(00γ)*s*00	0*klm*: $l+m=2n$
67.9			15	*Acmm*(00γ)*ss*0	0*klm*: $l+m=2n$; *h*0*lm*: $m=2n$
67.10			15	*Acmm*(00γ)0*s*0	0*klm*: $l=2n$; *h*0*lm*: $m=2n$
67.11			16	*Acmm*($\frac{1}{2}$0γ)	0*KLm*: $L=2n$
67.12			16	*Acmm*($\frac{1}{2}$0γ)0*s*0	0*KLm*: $L=2n$; *H*0*Lm*: $m=2n$
68.1	*Ccca*	(*mmm*, 11$\bar{1}$)	13	*Ccca*(00γ)	0*klm*: $l=2n$; *h*0*lm*: $l=2n$; *hk*00: $h=2n$
68.2			13	*Ccca*(00γ)*s*00	0*klm*: $l+m=2n$; *h*0*lm*: $l=2n$; *hk*00: $h=2n$
68.3			14	*Ccca*(10γ)	0*KLm*: $L=2n$; *H*0*Lm*: $L=2n$; *HK*00: $H=2n$
68.4			14	*Ccca*(10γ)*s*00	0*KLm*: $L+m=2n$; *H*0*Lm*: $L=2n$; *HK*00: $H=2n$

Table 9.8.3.5. (3 + 1)-*Dimensional superspace groups (cont.)*

No.	Basic space group	Point group K_s	Bravais class No.	Group symbol	Special reflection conditions
68.5			15	$Acaa(00\gamma)$	$0klm$: $l=2n$; $h0lm$: $h=2n$; $hk00$: $h=2n$
68.6			15	$Acaa(00\gamma)s00$	$0klm$: $l+m=2n$; $h0lm$: $h=2n$; $hk00$: $h=2n$
68.7			15	$Acaa(00\gamma)ss0$	$0klm$: $l+m=2n$; $h0lm$: $h+m=2n$; $hk00$: $h=2n$
68.8			15	$Acaa(00\gamma)0s0$	$0klm$: $l=2n$; $h0lm$: $h+m=2n$; $hk00$: $h=2n$
69.1	$Fmmm$	$(mmm, 11\bar{1})$	17	$Fmmm(00\gamma)$	
69.2			17	$Fmmm(00\gamma)s00$	$0klm$: $m=2n$
69.3			17	$Fmmm(00\gamma)ss0$	$0klm$: $m=2n$; $h0lm$: $m=2n$
69.4			18	$Fmmm(10\gamma)$	
69.5			18	$Fmmm(10\gamma)s00$	$0KLm$: $m=2n$
69.6			18	$Fmmm(10\gamma)ss0$	$0KLm$: $m=2n$; $H0Lm$: $m=2n$
70.1	$Fddd$	$(mmm, 11\bar{1})$	17	$Fddd(00\gamma)$	$0klm$: $k+l=4n$; $h0lm$: $h+l=4n$; $hk00$: $h+k=4n$
70.2			17	$Fddd(00\gamma)s00$	$0klm$: $k+l+2m=4n$; $h0lm$: $h+l=4n$; $hk00$: $h+k=4n$
71.1	$Immm$	$(mmm, 11\bar{1})$	12	$Immm(00\gamma)$	
71.2			12	$Immm(00\gamma)s00$	$0klm$: $m=2n$
71.3			12	$Immm(00\gamma)ss0$	$0klm$: $m=2n$; $h0lm$: $m=2n$
72.1	$Ibam$	$(mmm, 11\bar{1})$	12	$Ibam(00\gamma)$	$0klm$: $k=2n$; $h0lm$: $h=2n$
72.2			12	$Ibam(00\gamma)s00$	$0klm$: $k+m=2n$; $h0lm$: $h=2n$
72.3			12	$Ibam(00\gamma)ss0$	$0klm$: $k+m=2n$; $h0lm$: $h+m=2n$
72.4			12	$Imcb(00\gamma)$	$h0lm$: $l=2n$; $hk00$: $k=2n$
72.5			12	$Imcb(00\gamma)s00$	$0klm$: $m=2n$; $h0lm$: $l=2n$; $hk00$: $k=2n$
72.6			12	$Imcb(00\gamma)ss0$	$0klm$: $m=2n$; $h0lm$: $l+m=2n$; $hk00$: $k=2n$
72.7			12	$Imcb(00\gamma)0s0$	$h0lm$: $l+m=2n$; $hk00$: $k=2n$
73.1	$Ibca$	$(mmm, 11\bar{1})$	12	$Ibca(00\gamma)$	$0klm$: $k=2n$; $h0lm$: $l=2n$; $hk00$: $h=2n$
73.2			12	$Ibca(00\gamma)s00$	$0klm$: $k+m=2n$; $h0lm$: $l=2n$; $hk00$: $h=2n$
73.3			12	$Ibca(00\gamma)ss0$	$0klm$: $k+m=2n$; $h0lm$: $l+m=2n$; $hk00$: $h=2n$
74.1	$Imma$	$(mmm, 11\bar{1})$	12	$Imma(00\gamma)$	$hk00$: $h=2n$
74.2			12	$Imma(00\gamma)s00$	$0klm$: $m=2n$; $hk00$: $h=2n$
74.3			12	$Imma(00\gamma)ss0$	$0klm$: $m=2n$; $h0lm$: $m=2n$; $hk00$: $h=2n$
74.4			12	$Icmm(00\gamma)$	$0klm$: $l=2n$
74.5			12	$Icmm(00\gamma)s00$	$0klm$: $l+m=2n$
74.6			12	$Icmm(00\gamma)ss0$	$0klm$: $l+m=2n$; $h0lm$: $m=2n$
74.7			12	$Icmm(00\gamma)0s0$	$0klm$: $l=2n$; $h0lm$: $m=2n$
75.1	$P4$	(4, 1)	19	$P4(00\gamma)$	
75.2			19	$P4(00\gamma)q$	$00lm$: $m=4n$
75.3			19	$P4(00\gamma)s$	$00lm$: $m=2n$
75.4			20	$P4(\frac{1}{2}\frac{1}{2}\gamma)$	
75.5			20	$P4(\frac{1}{2}\frac{1}{2}\gamma)q$	$00Lm$: $m=4n$
76.1	$P4_1$	(4, 1)	19	$P4_1(00\gamma)$	$00lm$: $l=4n$
76.2			20	$P4_1(\frac{1}{2}\frac{1}{2}\gamma)$	$00Lm$: $L=4n$
77.1	$P4_2$	(4, 1)	19	$P4_2(00\gamma)$	$00lm$: $l=2n$
77.2			19	$P4_2(00\gamma)q$	$00lm$: $2l+m=4n$
77.3			20	$P4_2(\frac{1}{2}\frac{1}{2}\gamma)$	$00Lm$: $L=2n$
77.4			20	$P4_2(\frac{1}{2}\frac{1}{2}\gamma)q$	$00Lm$: $2L+m=4n$
78.1	$P4_3$	(4, 1)	19	$P4_3(00\gamma)$	$00lm$: $l=4n$
78.2			20	$P4_3(\frac{1}{2}\frac{1}{2}\gamma)$	$00Lm$: $L=4n$
79.1	$I4$	(4, 1)	21	$I4(00\gamma)$	
79.2			21	$I4(00\gamma)q$	$00lm$: $m=4n$
79.3			21	$I4(00\gamma)s$	$00lm$: $m=2n$
80.1	$I4_1$	(4, 1)	21	$I4_1(00\gamma)$	$00lm$: $l=4n$
80.2			21	$I4_1(00\gamma)q$	$00lm$: $l+m=4n$
81.1	$P\bar{4}$	$(\bar{4}, \bar{1})$	19	$P\bar{4}(00\gamma)$	
81.2			20	$P\bar{4}(\frac{1}{2}\frac{1}{2}\gamma)$	
82.1	$I\bar{4}$	$(\bar{4}, \bar{1})$	21	$I\bar{4}(00\gamma)$	
83.1	$P4/m$	$(4/m, 1\bar{1})$	19	$P4/m(00\gamma)$	
83.2			19	$P4/m(00\gamma)s0$	$00lm$: $m=2n$
83.3			20	$P4/m(\frac{1}{2}\frac{1}{2}\gamma)$	
84.1	$P4_2/m$	$(4/m, 1\bar{1})$	19	$P4_2/m(00\gamma)$	$00lm$: $l=2n$
84.2			20	$P4_2/m(\frac{1}{2}\frac{1}{2}\gamma)$	$00Lm$: $L=2n$
85.1	$P4/n$	$(4/m, 1\bar{1})$	19	$P4/n(00\gamma)$	$hk00$: $h+k=2n$
85.2			19	$P4/n(00\gamma)s0$	$00lm$: $m=2n$; $hk00$: $h+k=2n$
85.3			20	$P4/n(\frac{1}{2}\frac{1}{2}\gamma)q0$	$00Lm$: $m=4n$; $HK00$: $H=2n$, $K=2n$
86.1	$P4_2/n$	$(4/m, 1\bar{1})$	19	$P4_2/n(00\gamma)$	$00lm$: $l=2n$; $hk00$: $h+k=2n$
86.2			20	$P4_2/n(\frac{1}{2}\frac{1}{2}\gamma)q0$	$00Lm$: $2L+m=4n$; $HK00$: $H=2n$, $K=2n$
87.1	$I4/m$	$(4/m, 1\bar{1})$	21	$I4/m(00\gamma)$	

Table 9.8.3.5. (3 + 1)-*Dimensional superspace groups (cont.)*

No.	Basic space group	Point group K_s	Bravais class No.	Group symbol	Special reflection conditions
87.2			21	$I4/m(00\gamma)s0$	$00lm$: $m=2n$
88.1	$I4_1/a$	$(4/m, 1\bar{1})$	21	$I4_1/a(00\gamma)$	$00lm$: $l=4n$; $hk00$: $h=2n$
89.1	$P422$	$(422, 1\bar{1}\bar{1})$	19	$P422(00\gamma)$	
89.2			19	$P422(00\gamma)q00$	$00lm$: $m=4n$
89.3			19	$P422(00\gamma)s00$	$00lm$: $m=2n$
89.4			20	$P422(\frac{1}{2}\frac{1}{2}\gamma)$	
89.5			20	$P422(\frac{1}{2}\frac{1}{2}\gamma)q00$	$00Lm$: $m=4n$
90.1	$P42_12$	$(422, 1\bar{1}\bar{1})$	19	$P42_12(00\gamma)$	$h000$: $h=2n$
90.2			19	$P42_12(00\gamma)q00$	$00lm$: $m=4n$; $h000$: $h=2n$
90.3			19	$P42_12(00\gamma)s00$	$00lm$: $m=2n$; $h000$: $h=2n$
91.1	$P4_122$	$(422, 1\bar{1}\bar{1})$	19	$P4_122(00\gamma)$	$00lm$: $l=4n$
91.2			20	$P4_122(\frac{1}{2}\frac{1}{2}\gamma)$	$00Lm$: $L=4n$
92.1	$P4_12_12$	$(422, 1\bar{1}\bar{1})$	19	$P4_12_12(00\gamma)$	$00lm$: $l=4n$; $h000$: $h=2n$
93.1	$P4_222$	$(422, 1\bar{1}\bar{1})$	19	$P4_222(00\gamma)$	$00lm$: $l=2n$
93.2			19	$P4_222(00\gamma)q00$	$00lm$: $2l+m=4n$
93.3			20	$P4_222(\frac{1}{2}\frac{1}{2}\gamma)$	$00Lm$: $L=2n$
93.4			20	$P4_222(\frac{1}{2}\frac{1}{2}\gamma)q00$	$00Lm$: $2L+m=4n$
94.1	$P4_22_12$	$(422, 1\bar{1}\bar{1})$	19	$P4_22_12(00\gamma)$	$00lm$: $l=2n$; $h000$: $h=2n$
94.2			19	$P4_22_12(00\gamma)q00$	$00lm$: $2l+m=4n$; $h000$: $h=2n$
95.1	$P4_322$	$(422, 1\bar{1}\bar{1})$	19	$P4_322(00\gamma)$	$00lm$: $l=4n$
95.2			20	$P4_322(\frac{1}{2}\frac{1}{2}\gamma)$	$00Lm$: $L=4n$
96.1	$P4_32_12$	$(422, 1\bar{1}\bar{1})$	19	$P4_32_12(00\gamma)$	$00lm$: $l=4n$; $h000$: $h=2n$
97.1	$I422$	$(422, 1\bar{1}\bar{1})$	21	$I422(00\gamma)$	
97.2			21	$I422(00\gamma)q00$	$00lm$: $m=4n$
97.3			21	$I422(00\gamma)s00$	$00lm$: $m=2n$
98.1	$I4_122$	$(422, 1\bar{1}\bar{1})$	21	$I4_122(00\gamma)$	$00lm$: $l=4n$
98.2			21	$I4_122(00\gamma)q00$	$00lm$: $l+m=4n$
99.1	$P4mm$	$(4mm, 111)$	19	$P4mm(00\gamma)$	
99.2			19	$P4mm(00\gamma)ss0$	$00lm$: $m=2n$; $0klm$: $m=2n$
99.3			19	$P4mm(00\gamma)0ss$	$0klm$: $m=2n$; $hhlm$: $m=2n$
99.4			19	$P4mm(00\gamma)s0s$	$00lm$: $m=2n$; $hhlm$: $m=2n$
99.5			20	$P4mm(\frac{1}{2}\frac{1}{2}\gamma)$	
99.6			20	$P4mm(\frac{1}{2}\frac{1}{2}\gamma)0ss$	$0KLm$: $m=2n$; $HHLm$: $m=2n$
100.1	$P4bm$	$(4mm, 111)$	19	$P4bm(00\gamma)$	$0klm$: $k=2n$
100.2			19	$P4bm(00\gamma)ss0$	$00lm$: $m=2n$; $0klm$: $m=2n$
100.3			19	$P4bm(00\gamma)0ss$	$0klm$: $k+m=2n$; $hhlm$: $m=2n$
100.4			19	$P4bm(00\gamma)s0s$	$00lm$: $m=2n$; $0klm$: $k=2n$; $hhlm$: $m=2n$
100.5			20	$P4bm(\frac{1}{2}\frac{1}{2}\gamma)qq0$	$00Lm$: $m=4n$; $KKLm$: $2K+m=4n$
100.6			20	$P4bm(\frac{1}{2}\frac{1}{2}\gamma)qqs$	$00Lm$: $m=4n$; $KKLm$: $2K+m=4n$; $H0Lm$: $m=2n$
101.1	$P4_2cm$	$(4mm, 111)$	19	$P4_2cm(00\gamma)$	$00lm$: $l=2n$; $0klm$: $l=2n$
101.2			19	$P4_2cm(00\gamma)0ss$	$00lm$: $l=2n$; $0klm$: $l+m=2n$; $hhlm$: $m=2n$
101.3			20	$P4_2cm(\frac{1}{2}\frac{1}{2}\gamma)$	$00Lm$: $L=2n$; $HHLm$: $L=2n$
101.4			20	$P4_2cm(\frac{1}{2}\frac{1}{2}\gamma)0ss$	$00Lm$: $L=2n$; $HHLm$: $L+m=2n$; $H0Lm$: $m=2n$
102.1	$P4_2nm$	$(4mm, 111)$	19	$P4_2nm(00\gamma)$	$00lm$: $l=2n$; $0klm$: $k+l=2n$
102.2			19	$P4_2nm(00\gamma)0ss$	$00lm$: $l=2n$; $0klm$: $k+l+m=2n$; $hhlm$: $m=2n$
102.3			20	$P4_2nm(\frac{1}{2}\frac{1}{2}\gamma)qq0$	$00Lm$: $2L+m=4n$; $HHLm$: $2H+2L+m=4n$
102.4			20	$P4_2nm(\frac{1}{2}\frac{1}{2}\gamma)qqs$	$00Lm$: $2L+m=4n$; $HHLm$: $2H+2L+m=4n$; $H0Lm$: $m=2n$
103.1	$P4cc$	$(4mm, 111)$	19	$P4cc(00\gamma)$	$0klm$: $l=2n$; $hhlm$: $l=2n$
103.2			19	$P4cc(00\gamma)ss0$	$00lm$: $m=2n$; $0klm$: $l+m=2n$; $hhlm$: $l=2n$
103.3			20	$P4cc(\frac{1}{2}\frac{1}{2}\gamma)$	$HHLm$: $L=2n$; $H0Lm$: $L=2n$
104.1	$P4nc$	$(4mm, 111)$	19	$P4nc(00\gamma)$	$0klm$: $k+l=2n$; $hhlm$: $l=2n$
104.2			19	$P4nc(00\gamma)ss0$	$00lm$: $m=2n$; $0klm$: $k+l+m=2n$; $hhlm$: $l=2n$
104.3			20	$P4nc(\frac{1}{2}\frac{1}{2}\gamma)qq0$	$00Lm$: $m=4n$; $HHLm$: $2H+2L+m=4n$; $H0Lm$: $L=2n$
105.1	$P4_2mc$	$(4mm, 111)$	19	$P4_2mc(00\gamma)$	$00lm$: $l=2n$; $hhlm$: $l=2n$
105.2			19	$P4_2mc(00\gamma)ss0$	$00lm$: $l+m=2n$; $0klm$: $m=2n$; $hhlm$: $l=2n$
105.3			20	$P4_2mc(\frac{1}{2}\frac{1}{2}\gamma)$	$00Lm$: $L=2n$; $H0Lm$: $L=2n$
106.1	$P4_2bc$	$(4mm, 111)$	19	$P4_2bc(00\gamma)$	$00lm$: $l=2n$; $0klm$: $k=2n$; $hhlm$: $l=2n$
106.2			19	$P4_2bc(00\gamma)ss0$	$00lm$: $l+m=2n$; $0klm$: $k+m=2n$; $hhlm$: $l=2n$
106.3			20	$P4_2bc(\frac{1}{2}\frac{1}{2}\gamma)qq0$	$00Lm$: $2L+m=4n$; $HHLm$: $2H+m=4n$; $H0Lm$: $L=2n$
107.1	$I4mm$	$(4mm, 111)$	21	$I4mm(00\gamma)$	
107.2			21	$I4mm(00\gamma)ss0$	$00lm$: $m=2n$; $0klm$: $m=2n$
107.3			21	$I4mm(00\gamma)0ss$	$0klm$: $m=2n$; $hhlm$: $m=2n$

Table 9.8.3.5. (3 + 1)-*Dimensional superspace groups (cont.)*

No.	Basic space group	Point group K_s	Bravais class No.	Group symbol	Special reflection conditions
107.4			21	$I4mm(00\gamma)s0s$	$00lm$: $m=2n$; $hhlm$: $m=2n$
108.1	$I4cm$	$(4mm, 111)$	21	$I4cm(00\gamma)$	$0klm$: $l=2n$
108.2			21	$I4cm(00\gamma)ss0$	$00lm$: $m=2n$; $0klm$: $l+m=2n$
108.3			21	$I4cm(00\gamma)0ss$	$0klm$: $l+m=2n$; $hhlm$: $m=2n$
108.4			21	$I4cm(00\gamma)s0s$	$00lm$: $m=2n$; $0klm$: $l=2n$; $hhlm$: $m=2n$
109.1	$I4_1md$	$(4mm, 111)$	21	$I4_1md(00\gamma)$	$00lm$: $l=4n$; $hhlm$: $2h+l=4n$
109.2			21	$I4_1md(00\gamma)ss0$	$00lm$: $l+2m=4n$; $0klm$: $m=2n$; $hhlm$: $2h+l=4n$
110.1	$I4_1cd$	$(4mm, 111)$	21	$I4_1cd(00\gamma)$	$00lm$: $l=4n$; $0klm$: $l=2n$; $hhlm$: $2h+l=4n$
110.2			21	$I4_1cd(00\gamma)ss0$	$00lm$: $l+2m=4n$; $0klm$: $l+m=2n$; $hhlm$: $2h+l=4n$
111.1	$P\bar{4}2m$	$(\bar{4}2m, \bar{1}\bar{1}1)$	19	$P\bar{4}2m(00\gamma)$	
111.2			19	$P\bar{4}2m(00\gamma)00s$	$hhlm$: $m=2n$
111.3			20	$P\bar{4}2m(\frac{1}{2}\frac{1}{2}\gamma)$	
111.4			20	$P\bar{4}2m(\frac{1}{2}\frac{1}{2}\gamma)00s$	$H0Lm$: $m=2n$
112.1	$P\bar{4}2c$	$(\bar{4}2m, \bar{1}\bar{1}1)$	19	$P\bar{4}2c(00\gamma)$	$hhlm$: $l=2n$
112.2			20	$P\bar{4}2c(\frac{1}{2}\frac{1}{2}\gamma)$	$H0Lm$: $L=2n$
113.1	$P\bar{4}2_1m$	$(\bar{4}2m, \bar{1}\bar{1}1)$	19	$P\bar{4}2_1m(00\gamma)$	$h000$: $h=2n$
113.2			19	$P\bar{4}2_1m(00\gamma)00s$	$h000$: $h=2n$; $hhlm$: $m=2n$
114.1	$P\bar{4}2_1c$	$(\bar{4}2m, \bar{1}\bar{1}1)$	19	$P\bar{4}2_1c(00\gamma)$	$h000$: $h=2n$; $hhlm$: $l=2n$
115.1	$P\bar{4}m2$	$(\bar{4}m2, \bar{1}1\bar{1})$	19	$P\bar{4}m2(00\gamma)$	
115.2			19	$P\bar{4}m2(00\gamma)0s0$	$0klm$: $m=2n$
115.3			20	$P\bar{4}m2(\frac{1}{2}\frac{1}{2}\gamma)$	
116.1	$P\bar{4}c2$	$(\bar{4}m2, \bar{1}1\bar{1})$	19	$P\bar{4}c2(00\gamma)$	$0klm$: $l=2n$
116.2			20	$P\bar{4}c2(\frac{1}{2}\frac{1}{2}\gamma)$	$HHLm$: $L=2n$
117.1	$P\bar{4}b2$	$(\bar{4}m2, \bar{1}1\bar{1})$	19	$P\bar{4}b2(00\gamma)$	$0klm$: $k=2n$
117.2			19	$P\bar{4}b2(00\gamma)0s0$	$0klm$: $k+m=2n$
117.3			20	$P\bar{4}b2(\frac{1}{2}\frac{1}{2}\gamma)0q0$	$HHLm$: $2H+m=4n$
118.1	$P\bar{4}n2$	$(\bar{4}m2, \bar{1}1\bar{1})$	19	$P\bar{4}n2(00\gamma)$	$0klm$: $k+l=2n$
118.2			20	$P\bar{4}n2(\frac{1}{2}\frac{1}{2}\gamma)0q0$	$HHLm$: $2H+2L+m=4n$
119.1	$I\bar{4}m2$	$(\bar{4}m2, \bar{1}1\bar{1})$	21	$I\bar{4}m2(00\gamma)$	
119.2			21	$I\bar{4}m2(00\gamma)0s0$	$0klm$: $m=2n$
120.1	$I\bar{4}c2$	$(\bar{4}m2, \bar{1}1\bar{1})$	21	$I\bar{4}c2(00\gamma)$	$0klm$: $l=2n$
120.2			21	$I\bar{4}c2(00\gamma)0s0$	$0klm$: $l+m=2n$
121.1	$I\bar{4}2m$	$(\bar{4}2m, \bar{1}\bar{1}1)$	21	$I\bar{4}2m(00\gamma)$	
121.2			21	$I\bar{4}2m(00\gamma)00s$	$hhlm$: $m=2n$
122.1	$I\bar{4}2d$	$(\bar{4}2m, \bar{1}\bar{1}1)$	21	$I\bar{4}2d(00\gamma)$	$hhlm$: $2h+l=4n$
123.1	$P4/mmm$	$(4/mmm, 1\bar{1}11)$	19	$P4/mmm(00\gamma)$	
123.2			19	$P4/mmm(00\gamma)s0s0$	$00lm$: $m=2n$; $0klm$: $m=2n$
123.3			19	$P4/mmm(00\gamma)00ss$	$0klm$: $m=2n$; $hhlm$: $m=2n$
123.4			19	$P4/mmm(00\gamma)s00s$	$00lm$: $m=2n$; $hhlm$: $m=2n$
123.5			20	$P4/mmm(\frac{1}{2}\frac{1}{2}\gamma)$	
123.6			20	$P4/mmm(\frac{1}{2}\frac{1}{2}\gamma)00ss$	$HHLm$: $m=2n$; $H0Lm$: $m=2n$
124.1	$P4/mcc$	$(4/mmm, 1\bar{1}11)$	19	$P4/mcc(00\gamma)$	$0klm$: $l=2n$; $hhlm$: $l=2n$
124.2			19	$P4/mcc(00\gamma)s0s0$	$00lm$: $m=2n$; $0klm$: $l+m=2n$; $hhlm$: $l=2n$
124.3			20	$P4/mcc(\frac{1}{2}\frac{1}{2}\gamma)$	$HHLm$: $L=2n$; $H0Lm$: $L=2n$
125.1	$P4/nbm$	$(4/mmm, 1\bar{1}11)$	19	$P4/nbm(00\gamma)$	$hk00$: $h+k=2n$; $0klm$: $k=2n$
125.2			19	$P4/nbm(00\gamma)s0s0$	$00lm$: $m=2n$; $hk00$: $h+k=2n$; $0klm$: $k+m=2n$
125.3			19	$P4/nbm(00\gamma)00ss$	$hk00$: $h+k=2n$; $0klm$: $k+m=2n$; $hhlm$: $m=2n$
125.4			19	$P4/nbm(00\gamma)s00s$	$00lm$: $m=2n$; $hk00$: $h+k=2n$; $0klm$: $k=2n$; $hhlm$: $m=2n$
125.5			20	$P4/nbm(\frac{1}{2}\frac{1}{2}\gamma)q0q0$	$00Lm$: $m=4n$; $HK00$: $H=2n$, $K=2n$; $HHLm$: $2H+m=4n$
125.6			20	$P4/nbm(\frac{1}{2}\frac{1}{2}\gamma)q0qs$	$00Lm$: $m=4n$; $HK00$: $H=2n$, $K=2n$; $HHLm$: $2H+m=4n$; $H0Lm$: $m=2n$
126.1	$P4/nnc$	$(4/mmm, 1\bar{1}11)$	19	$P4/nnc(00\gamma)$	$hk00$: $h+k=2n$; $h0lm$: $h+l=2n$; $hhlm$: $l=2n$
126.2			19	$P4/nnc(00\gamma)s0s0$	$00lm$: $m=2n$; $hk00$: $h+k=2n$; $h0lm$: $h+l+m=2n$; $hhlm$: $l=2n$
126.3			20	$P4/nnc(\frac{1}{2}\frac{1}{2}\gamma)q0q0$	$00Lm$: $m=4n$; $HK00$: $H=2n$, $K=2n$; $HHLm$: $2H+2L+m=4n$; $H0Lm$: $L=2n$
127.1	$P4/mbm$	$(4/mmm, 1\bar{1}11)$	19	$P4/mbm(00\gamma)$	$0klm$: $k=2n$
127.2			19	$P4/mbm(00\gamma)s0s0$	$00lm$: $m=2n$; $0klm$: $k+m=2n$
127.3			19	$P4/mbm(00\gamma)00ss$	$0klm$: $k+m=2n$; $hhlm$: $m=2n$
127.4			19	$P4/mbm(00\gamma)s00s$	$00lm$: $m=2n$; $0klm$: $k=2n$; $hhlm$: $m=2n$
128.1	$P4/mnc$	$(4/mmm, 1\bar{1}11)$	19	$P4/mnc(00\gamma)$	$0klm$: $k+l=2n$; $hhlm$: $l=2n$
128.2			19	$P4/mnc(00\gamma)s0s0$	$00lm$: $m=2n$; $0klm$: $k+l+m=2n$; $hhlm$: $l=2n$
129.1	$P4/nmm$	$(4/mmm, 1\bar{1}11)$	19	$P4/nmm(00\gamma)$	$hk00$: $h+k=2n$

Table 9.8.3.5. (3 + 1)-*Dimensional superspace groups (cont.)*

No.	Basic space group	Point group K_s	Bravais class No.	Group symbol	Special reflection conditions
129.2			19	$P4/nmm(00\gamma)s0s0$	$00lm$: $m=2n$; $hk00$: $h+k=2n$; $0klm$: $m=2n$
129.3			19	$P4/nmm(00\gamma)00ss$	$hk00$: $h+k=2n$; $0klm$: $m=2n$; $hhlm$: $m=2n$
129.4			19	$P4/nmm(00\gamma)s00s$	$00lm$: $m=2n$; $hk00$: $h+k=2n$; $hhlm$: $m=2n$
130.1	$P4/ncc$	$(4/mmm, 1\bar{1}11)$	19	$P4/ncc(00\gamma)$	$hk00$: $h+k=2n$; $0klm$: $l=2n$; $hhlm$: $l=2n$
130.2			19	$P4/ncc(00\gamma)s0s0$	$00lm$: $m=2n$; $hk00$: $h+k=2n$; $0klm$: $l+m=2n$; $hhlm$: $l=2n$
131.1	$P4_2/mmc$	$(4/mmm, 1\bar{1}11)$	19	$P4_2/mmc(00\gamma)$	$00lm$: $l=2n$; $hhlm$: $l=2n$
131.2			19	$P4_2/mmc(00\gamma)s0s0$	$00lm$: $l+m=2n$; $0klm$: $m=2n$; $hhlm$: $l=2n$
131.3			20	$P4_2/mmc(\frac{1}{2}\frac{1}{2}\gamma)$	$00Lm$: $L=2n$; $H0Lm$: $L=2n$
132.1	$P4_2/mcm$	$(4/mmm, 1\bar{1}11)$	19	$P4_2/mcm(00\gamma)$	$00lm$: $l=2n$; $0klm$: $l=2n$
132.2			19	$P4_2/mcm(00\gamma)00ss$	$00lm$: $l=2n$; $0klm$: $l+m=2n$; $hhlm$: $m=2n$
132.3			20	$P4_2/mcm(\frac{1}{2}\frac{1}{2}\gamma)$	$00Lm$: $L=2n$; $HHLm$: $L=2n$
132.4			20	$P4_2/mcm(\frac{1}{2}\frac{1}{2}\gamma)00ss$	$00Lm$: $L=2n$; $HHLm$: $L+m=2n$; $H0Lm$: $m=2n$
133.1	$P4_2/nbc$	$(4/mmm, 1\bar{1}11)$	19	$P4_2/nbc(00\gamma)$	$00lm$: $l=2n$; $hk00$: $h+k=2n$; $0klm$: $k=2n$; $hhlm$: $l=2n$
133.2			19	$P4_2/nbc(00\gamma)s0s0$	$00lm$: $l+m=2n$; $hk00$: $h+k=2n$; $0klm$: $k+m=2n$; $hhlm$: $l=2n$
133.3			20	$P4_2/nbc(\frac{11}{22}\gamma)q0q0$	$00Lm$: $2L+m=4n$; $HK00$: $H=2n$, $K=2n$; $HHLm$: $2H+m=4n$; $H0Lm$: $L=2n$
134.1	$P4_2/nnm$	$(4/mmm, 1\bar{1}11)$	19	$P4_2/nnm(00\gamma)$	$00lm$: $l=2n$; $hk00$: $h+k=2n$; $0klm$: $k+l=2n$
134.2			19	$P4_2/nnm(00\gamma)00ss$	$00lm$: $l=2n$; $hk00$: $h+k=2n$; $0klm$: $k+l+m=2n$; $hhlm$: $m=2n$
134.3			20	$P4_2/nnm(\frac{1}{2}\frac{1}{2}\gamma)q0q0$	$00Lm$: $2L+m=4n$; $HK00$: $H=2n$, $K=2n$; $HHLm$: $2H+2L+m=4n$
134.4			20	$P4_2/nnm(\frac{1}{2}\frac{1}{2}\gamma)q0qs$	$00Lm$: $2L+m=4n$; $HK00$: $H+K=2n$; $HHLm$: $2H+2L+m=4n$; $H0Lm$: $m=2n$
135.1	$P4_2/mbc$	$(4/mmm, 1\bar{1}11)$	19	$P4_2/mbc(00\gamma)$	$00lm$: $l=2n$; $0klm$: $k=2n$; $hhlm$: $l=2n$
135.2			19	$P4_2/mbc(00\gamma)s0s0$	$00lm$: $l+m=2n$; $0klm$: $k+m=2n$; $hhlm$: $l=2n$
136.1	$P4_2/mnm$	$(4/mmm, 1\bar{1}11)$	19	$P4_2/mnm(00\gamma)$	$00lm$: $l=2n$; $0klm$: $k+l=2n$
136.2			19	$P4_2/mnm(00\gamma)00ss$	$00lm$: $l=2n$; $0klm$: $k+l+m=2n$; $hhlm$: $m=2n$
137.1	$P4_2/nmc$	$(4/mmm, 1\bar{1}11)$	19	$P4_2/nmc(00\gamma)$	$00lm$: $l=2n$; $hk00$: $h+k=2n$; $hhlm$: $l=2n$
137.2			19	$P4_2/nmc(00\gamma)s0s0$	$00lm$: $l+m=2n$; $hk00$: $h+k=2n$; $0klm$: $m=2n$; $hhlm$: $l=2n$
138.1	$P4_2/ncm$	$(4/mmm, 1\bar{1}11)$	19	$P4_2/ncm(00\gamma)$	$00lm$: $l=2n$; $hk00$: $h+k=2n$; $0klm$: $l=2n$
138.2			19	$P4_2/ncm(00\gamma)00ss$	$00lm$: $l=2n$; $hk00$: $h+k=2n$; $0klm$: $l+m=2n$; $hhlm$: $m=2n$
139.1	$I4/mmm$	$(4/mmm, 1\bar{1}11)$	21	$I4/mmm(00\gamma)$	
139.2			21	$I4/mmm(00\gamma)s0s0$	$00lm$: $m=2n$; $0klm$: $m=2n$
139.3			21	$I4/mmm(00\gamma)00ss$	$0klm$: $m=2n$; $hhlm$: $m=2n$
139.4			21	$I4/mmm(00\gamma)s00s$	$00lm$: $m=2n$; $hhlm$: $m=2n$
140.1	$I4/mcm$	$(4/mmm, 1\bar{1}11)$	21	$I4/mcm(00\gamma)$	$0klm$: $l=2n$
140.2			21	$I4/mcm(00\gamma)s0s0$	$00lm$: $m=2n$; $0klm$: $l+m=2n$
140.3			21	$I4/mcm(00\gamma)00ss$	$0klm$: $l+m=2n$; $hhlm$: $m=2n$
140.4			21	$I4/mcm(00\gamma)s00s$	$00lm$: $m=2n$; $0klm$: $l=2n$; $hhlm$: $m=2n$
141.1	$I4_1/amd$	$(4/mmm, 1\bar{1}11)$	21	$I4_1/amd(00\gamma)$	$00lm$: $l=4n$; $hk00$: $h=2n$; $hhlm$: $2h+l=4n$
141.2			21	$I4_1/amd(00\gamma)s0s0$	$00lm$: $l+2m=4n$; $hk00$: $h=2n$; $0klm$: $m=2n$; $hhlm$: $2h+l=4n$
142.1	$I4_1/acd$	$(4/mmm, 1\bar{1}11)$	21	$I4_1/acd(00\gamma)$	$00lm$: $l=4n$; $hk00$: $h=2n$; $0klm$: $l=2n$; $hhlm$: $2h+l=4n$
142.2			21	$I4_1/acd(00\gamma)s0s0$	$00lm$: $l+2m=4n$; $hk00$: $h=2n$; $0klm$: $l+m=2n$; $hhlm$: $2h+l=4n$
143.1	$P3$	$(3, 1)$	23	$P3(\frac{1}{3}\frac{1}{3}\gamma)$	
143.2			24	$P3(00\gamma)$	
143.3			24	$P3(00\gamma)t$	$00lm$: $m=3n$
144.1	$P3_1$	$(3, 1)$	23	$P3_1(\frac{1}{3}\frac{1}{3}\gamma)$	$00Lm$: $L=3n$
144.2			24	$P3_1(00\gamma)$	$00lm$: $l=3n$
145.1	$P3_2$	$(3, 1)$	23	$P3_2(\frac{1}{3}\frac{1}{3}\gamma)$	$00Lm$: $L=3n$
145.2			24	$P3_2(00\gamma)$	$00lm$: $l=3n$
146.1	$R3$	$(3, 1)$	22	$R3(00\gamma)$	
146.2			22	$R3(00\gamma)t$	$00lm$: $m=3n$
147.1	$P\bar{3}$	$(\bar{3}, \bar{1})$	23	$P\bar{3}(\frac{1}{3}\frac{1}{3}\gamma)$	
147.2			24	$P\bar{3}(00\gamma)$	
148.1	$R\bar{3}$	$(\bar{3}, \bar{1})$	22	$R\bar{3}(00\gamma)$	
149.1	$P312$	$(312, 11\bar{1})$	23	$P312(\frac{1}{3}\frac{1}{3}\gamma)$	
149.2			24	$P312(00\gamma)$	

Table 9.8.3.5. $(3+1)$-*Dimensional superspace groups (cont.)*

No.	Basic space group	Point group K_s	Bravais class No.	Group symbol	Special reflection conditions
149.3			24	$P312(00\gamma)t00$	$00lm$: $m=3n$
150.1	$P321$	$(321, 1\bar{1}1)$	24	$P321(00\gamma)$	
150.2			24	$P321(00\gamma)t00$	$00lm$: $m=3n$
151.1	$P3_112$	$(312, 11\bar{1})$	23	$P3_112(\frac{1}{3}\frac{1}{3}\gamma)$	$00Lm$: $L=3n$
151.2			24	$P3_112(00\gamma)$	$00lm$: $l=3n$
152.1	$P3_121$	$(321, 1\bar{1}1)$	24	$P3_121(00\gamma)$	$00lm$: $l=3n$
153.1	$P3_212$	$(312, 11\bar{1})$	23	$P3_212(\frac{1}{3}\frac{1}{3}\gamma)$	
153.2			24	$P3_212(00\gamma)$	$00lm$: $l=3n$
154.1	$P3_221$	$(321, 1\bar{1}1)$	24	$P3_221(00\gamma)$	$00lm$: $l=3n$
155.1	$R32$	$(32, 1\bar{1})$	22	$R32(00\gamma)$	
155.2			22	$R32(00\gamma)t0$	$00lm$: $m=3n$
156.1	$P3m1$	$(3m1, 111)$	24	$P3m1(00\gamma)$	
156.2			24	$P3m1(00\gamma)0s0$	$0klm$: $m=2n$
157.1	$P31m$	$(31m, 111)$	23	$P31m(\frac{1}{3}\frac{1}{3}\gamma)$	
157.2			23	$P31m(\frac{1}{3}\frac{1}{3}\gamma)00s$	$H\bar{H}Lm$: $m=2n$
157.3			24	$P31m(00\gamma)$	
157.4			24	$P31m(00\gamma)00s$	$hhlm$: $m=2n$
158.1	$P3c1$	$(3m1, 111)$	24	$P3c1(00\gamma)$	$0klm$: $l=2n$
159.1	$P31c$	$(31m, 111)$	23	$P31c(\frac{1}{3}\frac{1}{3}\gamma)$	$H\bar{H}Lm$: $L=2n$
159.2			24	$P31c(00\gamma)$	$hhlm$: $l=2n$
160.1	$R3m$	$(3m, 11)$	22	$R3m(00\gamma)$	
160.2			22	$R3m(00\gamma)0s$	$hhlm$: $m=2n$
161.1	$R3c$	$(3m, 11)$	22	$R3c(00\gamma)$	$hhlm$: $l=2n$
162.1	$P\bar{3}1m$	$(\bar{3}1m, \bar{1}11)$	23	$P\bar{3}1m(\frac{1}{3}\frac{1}{3}\gamma)$	
162.2			23	$P\bar{3}1m(\frac{1}{3}\frac{1}{3}\gamma)00s$	$H\bar{H}Lm$: $m=2n$
162.3			24	$P\bar{3}1m(00\gamma)$	
162.4			24	$P\bar{3}1m(00\gamma)00s$	$hhlm$: $m=2n$
163.1	$P\bar{3}1c$	$(\bar{3}1m, \bar{1}11)$	23	$P\bar{3}1c(\frac{1}{3}\frac{1}{3}\gamma)$	$H\bar{H}Lm$: $L=2n$
163.2			24	$P\bar{3}1c(00\gamma)$	$hhlm$: $l=2n$
164.1	$P\bar{3}m1$	$(\bar{3}m1, \bar{1}11)$	24	$P\bar{3}m1(00\gamma)$	
164.2			24	$P\bar{3}m1(00\gamma)0s0$	$0klm$: $m=2n$
165.1	$P\bar{3}c1$	$(\bar{3}m1, \bar{1}11)$	24	$P\bar{3}c1(00\gamma)$	$0klm$: $l=2n$
166.1	$R\bar{3}m$	$(\bar{3}m, \bar{1}1)$	22	$R\bar{3}m(00\gamma)$	
166.2			22	$R\bar{3}m(00\gamma)0s$	$hhlm$: $m=2n$
167.1	$R\bar{3}c$	$(\bar{3}m, \bar{1}1)$	22	$R\bar{3}c(00\gamma)$	$hhlm$: $l=2n$
168.1	$P6$	$(6, 1)$	24	$P6(00\gamma)$	
168.2			24	$P6(00\gamma)h$	$00lm$: $m=6n$
168.3			24	$P6(00\gamma)t$	$00lm$: $m=3n$
168.4			24	$P6(00\gamma)s$	$00lm$: $m=2n$
169.1	$P6_1$	$(6, 1)$	24	$P6_1(00\gamma)$	$00lm$: $l=6n$
170.1	$P6_5$	$(6, 1)$	24	$P6_5(00\gamma)$	$00lm$: $l=6n$
171.1	$P6_2$	$(6, 1)$	24	$P6_2(00\gamma)$	$00lm$: $l=3n$
171.2			24	$P6_2(00\gamma)h$	$00lm$: $2l+m=6n$
172.1	$P6_4$	$(6, 1)$	24	$P6_4(00\gamma)$	$00lm$: $l=3n$
172.2			24	$P6_4(00\gamma)h$	$00lm$: $2l+m=6n$
173.1	$P6_3$	$(6, 1)$	24	$P6_3(00\gamma)$	$00lm$: $l=2n$
173.2			24	$P6_3(00\gamma)h$	$00lm$: $3l+m=6n$
174.1	$P\bar{6}$	$(\bar{6}, \bar{1})$	24	$P\bar{6}(00\gamma)$	
175.1	$P6/m$	$(6/m, 1\bar{1})$	24	$P6/m(00\gamma)$	
175.2			24	$P6/m(00\gamma)s0$	$00lm$: $m=2n$
176.1	$P6_3/m$	$(6/m, 1\bar{1})$	24	$P6_3/m(00\gamma)$	$00lm$: $l=2n$
177.1	$P622$	$(622, 1\bar{1}\bar{1})$	24	$P622(00\gamma)$	
177.2			24	$P622(00\gamma)h00$	$00lm$: $m=6n$
177.3			24	$P622(00\gamma)t00$	$00lm$: $m=3n$
177.4			24	$P622(00\gamma)s00$	$00lm$: $m=2n$
178.1	$P6_122$	$(622, 1\bar{1}\bar{1})$	24	$P6_122(00\gamma)$	$00lm$: $l=6n$
179.1	$P6_522$	$(622, 1\bar{1}\bar{1})$	24	$P6_522(00\gamma)$	$00lm$: $l=6n$
180.1	$P6_222$	$(622, 1\bar{1}\bar{1})$	24	$P6_222(00\gamma)$	$00lm$: $l=3n$
180.2			24	$P6_222(00\gamma)h00$	$00lm$: $2l+m=6n$
181.1	$P6_422$	$(622, 1\bar{1}\bar{1})$	24	$P6_422(00\gamma)$	$00lm$: $l=3n$
181.2			24	$P6_422(00\gamma)h00$	$00lm$: $2l+m=6n$
182.1	$P6_322$	$(622, 1\bar{1}\bar{1})$	24	$P6_322(00\gamma)$	
182.2			24	$P6_322(00\gamma)h00$	$00lm$: $3l+m=6n$
183.1	$P6mm$	$(6mm, 111)$	24	$P6mm(00\gamma)$	
183.2			24	$P6mm(00\gamma)ss0$	$00lm$: $m=2n$; $0klm$: $m=2n$

Table 9.8.3.5. $(3+1)$-*Dimensional superspace groups (cont.)*

No.	Basic space group	Point group K_s	Bravais class No.	Group symbol	Special reflection conditions
183.3			24	$P6mm(00\gamma)0ss$	$0klm$: $m=2n$; $hhlm$: $m=2n$
183.4			24	$P6mm(00\gamma)s0s$	$00lm$: $m=2n$; $hhlm$: $m=2n$
184.1	$P6cc$	$(6mm, 111)$	24	$P6cc(00\gamma)$	$0klm$: $l=2n$; $hhlm$: $l=2n$
184.2			24	$P6cc(00\gamma)s0s$	$00lm$: $m=2n$; $0klm$: $l=2n$; $hhlm$: $l+m=2n$
185.1	$P6_3cm$	$(6mm, 111)$	24	$P6_3cm(00\gamma)$	$00lm$: $l=2n$; $0klm$: $l=2n$
185.2			24	$P6_3cm(00\gamma)0ss$	$00lm$: $l=2n$; $0klm$: $l+m=2n$; $hhlm$: $m=2n$
186.1	$P6_3mc$	$(6mm, 111)$	24	$P6_3mc(00\gamma)$	$00lm$: $l=2n$; $hhlm$: $l=2n$
186.2			24	$P6_3mc(00\gamma)0ss$	$00lm$: $l=2n$; $0klm$: $m=2n$; $hhlm$: $l+m=2n$
187.1	$P\bar{6}m2$	$(\bar{6}m2, \bar{1}1\bar{1})$	24	$P\bar{6}m2(00\gamma)$	
187.2			24	$P\bar{6}m2(00\gamma)0s0$	$0klm$: $m=2n$
188.1	$P\bar{6}c2$	$(\bar{6}m2, \bar{1}1\bar{1})$	24	$P\bar{6}c2(00\gamma)$	$0klm$: $l=2n$
189.1	$P\bar{6}2m$	$(\bar{6}2m, \bar{1}\bar{1}1)$	24	$P\bar{6}2m(00\gamma)$	
189.2			24	$P\bar{6}2m(00\gamma)00s$	$hhlm$: $m=2n$
190.1	$P\bar{6}2c$	$(\bar{6}2m, \bar{1}\bar{1}1)$	24	$P\bar{6}2c(00\gamma)$	$hhlm$: $l=2n$
191.1	$P6/mmm$	$(6/mmm, 1\bar{1}11)$	24	$P6/mmm(00\gamma)$	
191.2			24	$P6/mmm(00\gamma)s0s0$	$00lm$: $m=2n$; $0klm$: $m=2n$
191.3			24	$P6/mmm(00\gamma)00ss$	$0klm$: $m=2n$; $hhlm$: $m=2n$
191.4			24	$P6/mmm(00\gamma)s00s$	$00lm$: $m=2n$; $hhlm$: $m=2n$
192.1	$P6/mcc$	$(6/mmm, 1\bar{1}11)$	24	$P6/mcc(00\gamma)$	$0klm$: $l=2n$; $hhlm$: $l=2n$
192.2			24	$P6/mcc(00\gamma)s00s$	$00lm$: $m=2n$; $0klm$: $l=2n$; $hhlm$: $l+m=2n$
193.1	$P6_3/mcm$	$(6/mmm, 1\bar{1}11)$	24	$P6_3/mcm(00\gamma)$	$00lm$: $l=2n$; $0klm$: $l=2n$
193.2			24	$P6_3/mcm(00\gamma)00ss$	$00lm$: $l=2n$; $0klm$: $l+m=2n$; $hhlm$: $m=2n$
194.1	$P6_3/mmc$	$(6/mmm, 1\bar{1}11)$	24	$P6_3/mmc(00\gamma)$	$00lm$: $l=2n$; $hhlm$: $l=2n$
194.2			24	$P6_3/mmc(00\gamma)00ss$	$00lm$: $l=2n$; $0klm$: $m=2n$; $hhlm$: $l+m=2n$

primitive translations in the $(3+1)$-dimensional space group, just as is the case for glide planes and screw axes in three dimensions.

Special reflection conditions can be derived from transformation properties of the structure factor under symmetry operations. Transforming the geometric structure factor by an element $g_s = (\{R|\mathbf{v}\}, \{R_I|\upsilon_I\})$, one obtains

$$S_{\mathbf{H}} = S_{R^{-1}\mathbf{H}} \exp[-2\pi i(\mathbf{H}\cdot\mathbf{v} + H_I\cdot\upsilon_I)]. \qquad (9.8.3.10)$$

Therefore, if $R\mathbf{H}=\mathbf{H}$, the corresponding structure factor vanishes unless $\mathbf{H}\cdot\mathbf{v} + H_I\cdot\upsilon_I$ is an integer.

The form of such a reflection condition in terms of allowed or forbidden sets of indices depends on the basis chosen. When a lattice basis is chosen, one has

$$H_s = (\mathbf{H}, H_I) = \sum_{i=1}^{4} h_i \mathbf{a}_{si}^*, \qquad (9.8.3.11)$$

$$\upsilon_s = (\mathbf{v}, \upsilon_I) + \sum_{i=1}^{4} \upsilon_i \mathbf{a}_{si}. \qquad (9.8.3.12)$$

Then the reflection condition becomes

$$H_s\cdot\upsilon_s = \sum_{i=1}^{4} h_i\upsilon_i = \text{integer} \quad \text{for } R\mathbf{H}=\mathbf{H}. \qquad (9.8.3.13)$$

In terms of external and internal shift components, the reflection condition can be written as

$$H_s\cdot\upsilon_s = \mathbf{H}\cdot\mathbf{v} + H_I\cdot\upsilon_I = \mathbf{H}\cdot\mathbf{v} + m\upsilon_I = \text{integer for } R\mathbf{H}=\mathbf{H}. \qquad (9.8.3.14)$$

With $\mathbf{H} = \mathbf{K} + m\mathbf{q}$ and $\upsilon_I = \delta - \mathbf{q}\cdot\mathbf{v}$, (9.8.3.14) gives

$$\mathbf{K}\cdot\mathbf{v} + m\delta = \text{integer} \quad \text{for } R\mathbf{H}=\mathbf{H}. \qquad (9.8.3.15)$$

For $\mathbf{v} = \upsilon_1\mathbf{a} + \upsilon_2\mathbf{b} + \upsilon_3\mathbf{c}$ and $\mathbf{K} = h\mathbf{a}^* + k\mathbf{b}^* + l\mathbf{c}^*$, (9.8.3.15) takes the form (9.8.3.13):

$$h\upsilon_1 + k\upsilon_2 + l\upsilon_3 + m\delta = \text{integer} \quad \text{for } R\mathbf{H}=\mathbf{H}. \qquad (9.8.3.16)$$

When the modulation wavevector has a rational part, one can choose another basis (Subsection 9.8.2.1) such that $\mathbf{K}' = \mathbf{K} + m\mathbf{q}^r$ has integer coefficients:

$$\mathbf{H} = \mathbf{K}' + m\mathbf{q}^i = H\mathbf{a}_c^* + K\mathbf{b}_c^* + L\mathbf{c}_c^* + m\mathbf{q}^i.$$

Then, (9.8.3.15) with $\tau = \delta - \mathbf{q}^r\cdot\mathbf{v}$ becomes

$$\mathbf{K}'\cdot\mathbf{v} + m\tau = \text{integer} \quad \text{for } R\mathbf{H}=\mathbf{H} \qquad (9.8.3.17)$$

and (9.8.3.16) transforms into

$$H\upsilon_1' + K\upsilon_2' + L\upsilon_3' + m\tau = \text{integer} \quad \text{for } R\mathbf{H}=\mathbf{H}, \qquad (9.8.3.18)$$

in which υ_1', υ_2', and υ_3' are the components of $\mathbf{v}$ with respect to the basis $\mathbf{a}_c$, $\mathbf{b}_c$, and $\mathbf{c}_c$.

As an example, consider a $(3+1)$-dimensional space-group transformation with R a mirror perpendicular to the x axis, $\varepsilon = 1$, $\mathbf{v} = \frac{1}{2}\mathbf{b}$, and $\tau = \frac{1}{4}$ with $\mathbf{b}$ orthogonal to $\mathbf{a}$. The modulation wavevector is supposed to be $(\frac{1}{2}\frac{1}{2}\gamma)$. Then $\delta = \frac{1}{4} + \mathbf{q}^r\cdot\mathbf{v} = \frac{1}{2}$. The vectors $\mathbf{H}$ left invariant by R satisfy the relation $2h + m = 0$. For such a vector, the reflection condition becomes

$$\mathbf{K}\cdot\mathbf{v} + m\delta = \tfrac{1}{2}\mathbf{K}\cdot\mathbf{b} + \tfrac{1}{2}m = \frac{k+m}{2} = \text{integer}, \quad \text{or } k+m=2n.$$

For the basis $\frac{1}{2}(\mathbf{a}^* + \mathbf{b}^*)$, $\frac{1}{2}(\mathbf{a}^* - \mathbf{b}^*)$, $\mathbf{c}^*$, the rational part of the wavevector vanishes. The indices with respect to this basis are $H = h + k + m$, $K = h - k$, $L = l$ and m. The condition now becomes

$$\mathbf{K}'\cdot\mathbf{v} + m\tau = \frac{H - K + m}{4} = \text{integer},$$

$$\text{or} \quad H - K + m = 4n, \quad \text{for } K = -H.$$

Of course, both calculations give the same result: $k+m=2n$ for $h, k, l, -2h$ and $H - K + m = 4n$ for $H, -H, L, m$.

Table 9.8.3.6 *Centring reflection conditions for* $(3+1)$*-dimensional Bravais classes*

The centring reflection conditions are given for the 24 Bravais classes, belonging to six systems (with number and symbol according to Table 9.8.3.2*a*). If $\mathbf{q}^i = \mathbf{q}$ these are the usual conditions for *hklm*, the indices of the reflections expressed with respect to $\mathbf{a}^*$, $\mathbf{b}^*$, $\mathbf{c}^*$, $\mathbf{q}$. Otherwise the conditions are for indices *HKLm* with respect to a conventional basis $\mathbf{a}_c^*$, $\mathbf{b}_c^*$, $\mathbf{c}_c^*$, $\mathbf{q}^i$ of the vector module M^*. The relation between indices *HKLm* and *hklm* is given in the fourth column. Planar monoclinic and axial monoclinic mean a monoclinic lattice of main reflections and with the (irrational part of the) modulation wavevector in the mirror plane, or along the unique axis, respectively.

System	$\mathbf{q}^i$ vector	Reflection conditions	Relation of indices	Bravais class	
				No.	Symbol
Triclinic	$(\alpha\beta\gamma)$			1	$\bar{1}P(\alpha\beta\gamma)$
Planar monoclinic	$(\alpha\beta 0)$	$L+m=2n$ $h+l=2n$	$L=2l+m$	2 3 4	$2/mP(\alpha\beta 0)$ $2/mP(\alpha\beta\frac{1}{2})$ $2/mB(\alpha\beta 0)$
Axial monoclinic	(00γ)	$H+m=2n$ $h+l=2n$ $H+L=2n,\ K+m=2n'$	$H=2h+m$ $K=2k+m$	5 6 7 8	$2/mP(00\gamma)$ $2/mP(\frac{1}{2}0\gamma)$ $2/mB(00\gamma)$ $2/mB(0\frac{1}{2}\gamma)$
Orthorhombic	(00γ)	$K+m=2n$ $K+m=2n,\ H+m=2n'$ $h+k+l=2n$ $h+k=2n$ $H+K+m=2n$ $k+l=2n$ $H+m=2n,\ K+L=2n'$ $h+k=2n,\ h+l=2n'$ $H+K+m=2n,$ $K+L=2n'$	$K=2k+m$ $K=2k+m,\ H=2h+m$ $H=h+m$ $H=2h+m$ $H=h+m$	9 10 11 12 13 14 15 16 17 18	$mmmP(00\gamma)$ $mmmP(0\frac{1}{2}\gamma)$ $mmmP(\frac{1}{2}\frac{1}{2}\gamma)$ $mmmI(00\gamma)$ $mmmC(00\gamma)$ $mmmC(10\gamma)$ $mmmA(00\gamma)$ $mmmA(\frac{1}{2}0\gamma)$ $mmmF(00\gamma)$ $mmmF(10\gamma)$
Tetragonal	(00γ)	$H+K+m=2n$ $h+k+l=2n$	$H=h+k+m,\ K=k-h$	19 20 21	$4/mmmP(00\gamma)$ $4/mmmP(\frac{1}{2}\frac{1}{2}\gamma)$ $4/mmmI(00\gamma)$
Hexagonal/Trigonal	(00γ)	$h-k-l=3n$ $H-K-m=3n$	$H=2h+k+m,\ K=k-h$	22 23 24	$\bar{3}mR(00\gamma)$ $\bar{3}1mP(\frac{1}{3}\frac{1}{3}\gamma)$ $6/mmmP(00\gamma)$

The special reflection conditions for the elements occurring in $(3+1)$-dimensional space groups are given in Table 9.8.3.5.

9.8.3.4. *Guide to the use of the tables*

In the tables, Bravais classes, point groups, and space groups are given for three-dimensional incommensurate modulated crystals with a modulation of dimension one and for two-dimensional crystals (*e.g.* surfaces) with one- and two-dimensional modulation (Janssen, Janner & de Wolff, 1980). In the following, we discuss briefly the information given. Examples of their use can be found in Subsection 9.8.3.5.

To determine the symmetry of the modulated phase, one first determines its average structure, which is obtained from the main reflections. Since this structure has three-dimensional space-group symmetry, this analysis is performed in the usual way.

The diffraction pattern of the three-dimensional modulated phase can be indexed by $3+1$ integers. The Bravais class is determined by the symmetry of the vector module spanned by the $3+1$ basis vectors. The crystallographic system of the pattern is equal to or lower than that implied by the main reflections. One chooses a conventional basis ($\mathbf{q}^r = 0$) for the vector module, and finds the Bravais class from the general reflection conditions using Table 9.8.3.6. The relation between indices *hklm* with respect to the basis $\mathbf{a}^*$, $\mathbf{b}^*$, $\mathbf{c}^*$, and $\mathbf{q}$ and *HKLm* with respect to the conventional basis $\mathbf{a}_c^*$, $\mathbf{b}_c^*$, $\mathbf{c}_c^*$, and $\mathbf{q}^i$ is also given there.

Table 9.8.3.2(*a*) gives the number labelling the $(3+1)$-dimensional Bravais class, its symbol, its external and internal point group, and the modulation wavevector. Moreover, the superspace conventional basis (for which the rational part $\mathbf{q}^r$ vanishes) and the corresponding $(3+1)$-dimensional centring are given. Because the four-dimensional lattices belong to Euclidean Bravais classes, the corresponding class is also given in the notation of Janssen (1969) and Brown *et al.* (1978).

The point group of the modulated structure is a subgroup of the holohedry of its lattice Λ. In Table 9.8.3.3, for each system the $(3+1)$-dimensional point groups are given. Each system contains one or more Bravais classes. Each geometric crystal class contains one or more arithmetic crystal classes. The $(3+1)$-dimensional arithmetic classes belonging to a given geometric crystal class are also listed in Table 9.8.3.3.

Starting from the space group of the average structure, one can determine the $(3+1)$-dimensional superspace group. In Table 9.8.3.5, the full list of these $(3+1)$-dimensional superspace groups is given for the incommensurate case and are ordered according to their basic space group. They have a number *n.m* where *n* is the number of the basic space group one

finds in *International Tables for Crystallography*, Volume A. The various $(3+1)$-dimensional superspace groups for each basic group are distinguished by the number m. Furthermore, the symbol of the basic space group, the point group, and the symbol for the corresponding superspace group are given. In the last column, the special reflection conditions are listed for typical symmetry elements. These may help in the structure analysis. The $(2+d)$-dimensional superspace groups, relevant for modulated surface structures, are given in Tables 9.8.3.4(*a*) and (*b*).

9.8.3.5. *Examples*

(*A*) Na_2CO_3

Na_2CO_3 has a phase transition at about 753 K from the hexagonal to the monoclinic phase. At about 633 K, one vibration mode becomes unstable and below the transition temperature $T_i = 633$ K there is a modulated γ-phase (de Wolff & Tuinstra, 1986). At low temperature (128 K), a transition to a commensurate phase has been reported.

The main reflections in the modulated phase belong to a monoclinic lattice, and the satellites to a modulation with wavevector $\mathbf{q} = \alpha\mathbf{a}^* + \gamma\mathbf{c}^*$, b axis unique. The dimension of the modulation is one. The main reflections satisfy the condition

$$hkl0, h + k = \text{even}.$$

Therefore, the lattice of the average structure is C-centred monoclinic. For the satellites, the same general condition holds ($hklm, h + k = \text{even}$). From Table 9.8.3.6, one sees after a change of axes that the Bravais class of the modulated structure is

$$\text{No. } 4\text{: } 2/mC(\alpha 0\gamma).$$

Table 9.8.3.2(*a*) shows that the point group of the vector module is $2/m(\bar{1}1)$. The point group of the modulated structure is equal to or a subgroup of this one.

The space group of the average structure determined from the main reflections is $C2/m$ (No. 12 in *International Tables for Crystallography*, Volume A). The superspace group may then be determined from the special reflection condition

$$h0lm, m = \text{even}$$

using Table 9.8.3.5. There are five superspace groups with basic group No. 12. Among them there are two in Bravais class 4. The reflection condition mentioned leads to the group

$$\text{No. } 12.2 = C2/m(\alpha 0\gamma)0s = P^{C2/m}_{\bar{1}\ s}.$$

In principle, the superspace group could be a subgroup of this, but, since the transition normal–incommensurate is of second order, Landau theory predicts that the basic space group is the symmetry group of the unmodulated monoclinic phase, which is $C2/m$.

(*B*) $ThBr_4$

Thorium tetrabromide has an incommensurately modulated phase below $T_i = 95$ K (Currat, Bernard & Delamoye, 1986). Above that temperature, the structure has space group $I4_1/amd$ (No. 141 in *International Tables for Crystallography*, Volume A). At T_i, a mode becomes unstable and a modulated β-phase sets in with modulation wavevector $\gamma\mathbf{c}^*$. The dimension of the modulation is one, consequently.

The main reflections belong to a tetragonal lattice. The general reflection condition is

$$hklm, h + k + l \text{ even}.$$

Looking at Table 9.8.3.6, one finds the Bravais class to be No. $21 = I4/mmm(00\gamma)$. Table 9.8.3.2(*a*) gives $4/mmm(\bar{1}\bar{1}11)$ for the point group of the vector module.

For the determination of the symmetry group of the modulated structure, one has the special reflection conditions

$$hk00, h \text{ even}; \quad hhl0, 2h + l = 4n; \quad (00l0, l = 4n)$$
$$0klm \text{ (and } h0lm\text{) absent for } m = 1.$$

Higher-order satellites have not been observed. The main reflections lead to the basic group $I4_1/amd$. If one generalizes the reflection condition observed for $0klm$ to $0klm$, $m = \text{even}$, the superspace group is found from Table 9.8.3.5 under the groups $141.x$ as

$$\text{No. } 141.2 = I4_1/amd(00\gamma)s0s0 = P^{I4_1/amd}_{s\ \bar{1}s1}.$$

(*C*) PAMC

Bis(*n*-propylammonium) tetrachloromanganate (PAMC) has several phase transitions. Above about 395 K, it is orthorhombic with space group *Abma*. At T_i, this β-phase goes over into the incommensurately modulated γ-phase (Depmeier, 1986; Kind & Muralt, 1986). The wavevector of the modulation is $\alpha\mathbf{a}^* + \mathbf{c}^*$. Therefore, the dimension of the modulation is one. Interchanging the a and c axes, one sees from Table 9.8.3.2(*a*) that the Bravais class is No. $14 = mmmC(10\gamma)$. In this new setting, the conventional basis of the vector module is $\mathbf{a}^*$, $\mathbf{b}^*$, $\mathbf{c}^*$, and $\gamma\mathbf{c}^*$ and the general reflection condition becomes

$$HKLm, H + K + m = \text{even}.$$

Therefore, if one considers the vector module as the projection of a four-dimensional lattice, the reflection condition corresponds to a $(\frac{1}{2}\frac{1}{2}0\frac{1}{2})$ centring in four dimensions.

The point group of the vector module is $mmm(11\bar{1})$. The basic space group being *Abma* (or *Ccmb* in the new setting), the superspace group follows from Table 9.8.3.5 as

$$\text{No. } 64.3 = Ccmb(10\gamma) = L^{Ccmb}_{11\bar{1}}$$

or, in the original setting

$$\text{No. } 64.3 = Abma(\alpha 01) = N^{Abma}_{\bar{1}11}.$$

No. 64.4 can be excluded because the reflections do not show the special reflection condition $0KLm$, $m = \text{even}$.

9.8.3.6. *Ambiguities in the notation*

The invariant part v_s^o of the translation part v_s of a $(3+1)$-dimensional superspace-group element is uniquely determined by (9.8.3.5). This does not imply that for each element of the point group there is a translation for which the invariant part is unique up to lattice vectors. The reason is that, for a given element R of the point group and given origin, v_s may be changed when R is combined with a three-dimensional lattice translation $w_s = (\mathbf{w}, 0)$. This situation is well known in ordinary three-dimensional crystallography. For example, the twofold rotation $(x, y, z) \rightarrow (-x, z, y)$ in the space group $P4_132$ has according to Volume A of *International Tables for Crystallography* a translation part $(\frac{1}{4}, \frac{3}{4}, \frac{1}{4})$. Its invariant part is $(0, \frac{1}{2}, \frac{1}{2})$. However, when the translation part is equivalently taken as $(\frac{1}{4}, \frac{3}{4}, -\frac{3}{4})$, the invariant part vanishes. Therefore, in the symbol for that space group, the corresponding generator is given as the rotation '2' and not as the screw axis '2_1'.

The same situation may occur in $3+1$ dimensions. This can be seen very clearly from the definition of τ [equation (9.8.3.8)]. Since $\mathbf{v}$ is only determined modulo a lattice vector, one may add to it a lattice vector that has a non-vanishing product with $\mathbf{q}^r$.

This results in a change for τ. For example, the $(3+1)$-dimensional space group $Pmmm(\frac{1}{2}0\gamma)000 = A^{Pmmm}_{1\,1\,\bar{1}}$ has a mirror perpendicular to the a axis with associated value $\tau = 0$. The parallel mirror at a distance $a/2$ has $\mathbf{v} = \mathbf{a}$ and consequently $\tau = \frac{1}{2}$. Hence, the symbols $Pmmm(\frac{1}{2}0\gamma)000$ and $Pmmm(\frac{1}{2}0\gamma)s00$ indicate the same group. This non-uniqueness in the symbol, however, does not have serious practical consequences.

Another source of ambiguity is the fact that the assignment of a satellite to a main reflection is not unique. For example, the reflection conditions for the group $I2cb(00\gamma)0s0 = P^{I2cb}_{\bar{1}s\bar{1}}$ are $h+k+l =$ even because of the centring and $l+m =$ even and $h+m =$ even for $h0lm$ because of the two glide planes perpendicular to the b axis. When one takes for the modulation vector $\mathbf{q} = \gamma'\mathbf{c}^* = (1-\gamma)\mathbf{c}^*$, the new indices are h, k, l', and m' with $l' = l+m$ and $m' = -m$. Then the reflection conditions become $l' =$ even and $h+m =$ even for $h0l'm'$. The first of these conditions implies the symbol $I2cb(00\gamma)000 = P^{I2cb}_{\bar{1}\,1\,\bar{1}}$ for the group considered. This, however, is the symbol for the nonequivalent group with condition $h =$ even for $h0lm$. This difficulty may be avoided by sometimes using a non-standard setting of the three-dimensional space group (see Yamamoto *et al.*, 1985). In this case, the setting $I2ab$ instead of $I2cb$ avoids the problem.

9.8.4. Theoretical foundation

9.8.4.1. *Lattices and metric*

A periodic crystal structure is defined in a three-dimensional Euclidean space V and is invariant with respect to translations $\mathbf{n}$ which are integral linear combinations of three fundamental ones $\mathbf{a}_1, \mathbf{a}_2, \mathbf{a}_3$:

$$\mathbf{n} = \sum_{i=1}^{3} n_i \mathbf{a}_i, \quad n_i \text{ integers.} \tag{9.8.4.1}$$

These translations are linearly independent and span a lattice Λ. The *dimension* of Λ is the dimension of the space spanned by $\mathbf{a}_1, \mathbf{a}_2, \mathbf{a}_3$ and the *rank* is the (smallest) number of free generators of those integral linear combinations. In the present case, both are equal to three. Accordingly,

$$\{\Lambda\} = V \quad \text{and} \quad \Lambda \approx Z^3. \tag{9.8.4.2}$$

The elements of Z^3 are triples of integers that correspond to the coordinates of the lattice points. The Bragg reflection peaks of such a crystal structure are at the positions of a reciprocal lattice Λ^*, also of dimension and rank equal to three. Furthermore, the Fourier wavevectors $\mathbf{H}$ belong to Λ^* (after identification of lattice vectors with lattice points):

$$\mathbf{H} = \sum_{i=1}^{3} h_i \mathbf{a}_i^*, \quad h_i \text{ integers} \tag{9.8.4.3}$$

where $\{\mathbf{a}_i^*\}$ is the reciprocal basis

$$\mathbf{a}_i \cdot \mathbf{a}_k^* = \delta_{ik}.$$

The two corresponding metric tensors g and g^*,

$$g_{ik} = \mathbf{a}_i \cdot \mathbf{a}_k \quad \text{and} \quad g_{ik}^* = \mathbf{a}_i^* \cdot \mathbf{a}_k^*, \tag{9.8.4.4}$$

are positive definite and dual:

$$\sum_{k=1}^{3} g_{ik} g_{kj}^* = \delta_{ij}.$$

We now consider crystal structures defined in the same three-dimensional Euclidean space V with Fourier wavevectors that are integral linear combinations of $n = (3+d)$ fundamental ones $\mathbf{a}_1^*, \ldots, \mathbf{a}_n^*$:

$$\mathbf{H} = \sum_{i=1}^{n} h_i \mathbf{a}_i^*, \quad h_i \text{ integers.} \tag{9.8.4.5}$$

The components $(h_1, \ldots, h_n)$ are the indices labelling the corresponding Bragg reflection peaks.

A crystal is *incommensurate* when $d > 0$ and the vectors $\mathbf{a}_i^*$ linearly independent over the rational numbers. In that case, the crystal does not have lattice periodicity and is said to be *aperiodic*. The above description can still be convenient, even in the case that the vectors $\mathbf{a}_i^*$ are not independent over the rationals: one or more of them is then expressed as rational linear combinations of the others. A typical example is that of a superstructure arising from the (commensurate) modulation of a basic structure with lattice periodicity.

Let us denote by M^* the set of all integral linear combinations of the vectors $\mathbf{a}_1^*, \ldots, \mathbf{a}_n^*$. These are said to form a *basis*. It is a set of free Abelian generators, therefore the *rank* of M^* is n. The *dimension* of M^* is the dimension of the Euclidean space spanned by M^*

$$\{M^*\} = V \quad \text{and} \quad M^* \approx Z^n. \tag{9.8.4.6}$$

The elements of Z^n are precisely the set of indices introduced above. Mathematically speaking, M^* has the structure of a (free Abelian) module. Its elements are vectors. So we call M^* a *vector module*. This nomenclature is intended as a *generic* characterization. When a series of structures is considered with different values of the components of the last d vectors with respect to the first three, the generic values of these components are irrational, but accidentally they may become rational as well. This situation typically arises when considering crystal structures under continuous variation of parameters like temperature, pressure or chemical composition. In the case of an ordinary crystal, rank and dimension are equal, the crystal structure is *periodic*, and the vector module becomes a (reciprocal) lattice.

Lattices and vector modules are, mathematically speaking, free Z modules. For such a module, there exists a dual one that is also free and of the same rank. In the periodic crystal case, that duality can be expressed by a scalar product, but for an aperiodic crystal this is no longer possible. It is possible to keep the metrical duality by enlarging the space and considering the vector module M^* as the projection of an n-dimensional (reciprocal) lattice Σ^* in an n-dimensional Euclidean space V_s.

$$M^* \to \Sigma^*, \quad \{\Sigma^*\} = V_s \quad \text{and} \quad \Sigma^* \approx Z^n, \tag{9.8.4.7}$$

with the orthogonal projection π_E of V_s onto V defined by

$$M^* = \pi_E \Sigma^*. \tag{9.8.4.8}$$

This corresponds to attaching to the diffraction peak with indices $(h_1, \ldots, h_n)$ the point of an n-dimensional reciprocal lattice having the same set of coordinates. The orthocomplement of V in V_s is called internal space and denoted by V_I. The embedding is uniquely defined by the relations

$$a_{si}^* = (\mathbf{a}_i^*, \mathbf{a}_{Ii}^*), \quad i = 1, \ldots, n, \tag{9.8.4.9}$$

where $\{a_{si}^*\}$ is a basis of Σ^* and $\{\mathbf{a}_i^*\}$ a basis of M^*. The vectors $\mathbf{a}_{Ii}^*$ span V_I.

The crystal density ρ in V can also be embedded as ρ_s in V_s by identifying the Fourier coefficients $\hat{\rho}$ at points of M^* and of Σ^* having correspondingly the same components.

$$\hat{\rho}_s(h_1, \ldots, h_n) \equiv \hat{\rho}(h_1, \ldots, h_n). \tag{9.8.4.10}$$

Then ρ_s is invariant with respect to translations of the lattice Σ with basis

$$a_{si} = (\mathbf{a}_i, \mathbf{a}_{Ii}) \tag{9.8.4.11}$$

dual to (9.8.4.9). In the commensurate case, this correspondence requires that the given superstructure be considered as the limit of an incommensurate crystal [for which the embedding (9.8.4.10) is a one-to-one relation].

As discussed below, point-group symmetries R of the diffraction pattern, when expressed in terms of transformation of the set of indices, define n-dimensional integral matrices that can be considered as being n-dimensional orthogonal transformations R_s in V_s, leaving invariant the Euclidean metric tensors:

$$g_{sik} = a_{si} \cdot a_{sk} \quad \text{and} \quad g^*_{sik} = a^*_{si} \cdot a^*_{sk}. \tag{9.8.4.12}$$

The crystal classes considered in the tables suppose the existence of main reflections defining a three-dimensional reciprocal lattice. For that case, the embedding can be specialized by making the choice

$$\begin{aligned} a^*_{si} &= (\mathbf{a}^*_i, 0) \qquad i = 1, 2, 3, \\ a^*_{s(3+j)} &= (\mathbf{a}^*_{3+j}, \mathbf{d}^*_j) \qquad j = 1, 2, \ldots, d = n - 3, \end{aligned} \tag{9.8.4.13}$$

and, correspondingly,

$$\begin{aligned} a_{si} &= (\mathbf{a}_i, \mathbf{a}_{Ii}) \qquad i = 1, 2, 3, \\ a_{s(3+j)} &= (0, \mathbf{d}_j) \qquad j = 1, 2, \ldots, d, \end{aligned} \tag{9.8.4.14}$$

with $\mathbf{d}^*_i \cdot \mathbf{d}_k = \delta_{ik}$ and $\mathbf{a}^*_i \cdot \mathbf{a}_k = \delta_{ik}$. These are called *standard lattice bases*.

9.8.4.2. *Point groups*

9.8.4.2.1. *Laue class*

Definition 1. The *Laue point group* P_L of the diffraction pattern is the point group in three dimensions that transforms every diffraction peak into a peak of the same intensity.†

Because all diffraction vectors are of the form (9.8.4.5), the action of an element R of the Laue group is given by

$$R\mathbf{a}^*_i = \sum_{j=1}^{3+d} \Gamma^*(R)_{ji}\mathbf{a}^*_j, \quad i = 1, \ldots, 3 + d. \tag{9.8.4.15}$$

The $(3 + d) \times (3 + d)$ matrices $\Gamma^*(R)$ form a finite group of integral matrices $\Gamma^*(K)$ for K equal to P_L or to one of its subgroups. A well known theorem in algebra states that then there is a basis in $3 + d$ dimensions such that the matrices $\Gamma^*(R)$ on that basis are orthogonal and represent $(3 + d)$-dimensional orthogonal transformations R_s. The corresponding group is a $(3 + d)$-dimensional crystallographic group denoted by K_s. Because R is already an orthogonal transformation on V, R_s is reducible and can be expressed as a pair (R, R_I) of orthogonal transformations, in 3 and d dimensions, respectively. The basis on which (R, R_I) acts according to $\Gamma^*(R)$ is denoted by $\{(\mathbf{a}^*_i, \mathbf{a}^*_{Ii})\}$. It spans a lattice Σ^* that is the reciprocal of the lattice Σ with basis elements $(\mathbf{a}_i, \mathbf{a}_{Ii})$. The pairs (R, R_I), sometimes also noted (R_E, R_I), leave Σ invariant:

$$(R, R_I)(\mathbf{a}_i, \mathbf{a}_{Ii}) \equiv (R\mathbf{a}_i, R_I\mathbf{a}_{Ii}) = \sum_{j=1}^{3+d} \Gamma(R)_{ji}(\mathbf{a}_j, \mathbf{a}_{Ij}), \tag{9.8.4.16}$$

where $\Gamma(R)$ is the transpose of $\Gamma^*(R^{-1})$.

In many cases, one can distinguish a lattice of main reflections, the remaining reflections being called satellites. The main reflections are generally more intense. Therefore, main reflections are transformed into main reflections by elements of the Laue group. On a standard lattice basis (9.8.4.13), the matrices $\Gamma(R)$ take the special form

$$\Gamma(R) = \begin{pmatrix} \Gamma_E(R) & 0 \\ \Gamma_M(R) & \Gamma_I(R) \end{pmatrix}. \tag{9.8.4.17}$$

The transformation of main reflections and satellites is then given by $\Gamma^*(R)$ as in (9.8.4.15), the relation with $\Gamma(R)$ being (as already said)

$$\Gamma^*(R) = \tilde{\Gamma}(R^{-1}),$$

where the tilde indicates transposition. Accordingly, on a standard basis one has

$$\Gamma^*(R) = \begin{pmatrix} \Gamma^*_E(R) & \Gamma^*_M(R) \\ 0 & \Gamma^*_I(R) \end{pmatrix}. \tag{9.8.4.18}$$

The set of matrices $\Gamma_E(R)$ for R elements of K forms a crystallographic point group in three dimensions, denoted K_E, having elements R of $O(3)$, and the corresponding set of matrices $\Gamma_I(R)$ forms one in d dimensions denoted by K_I with elements R_I of $O(d)$.

For a modulated crystal, one can choose the $\mathbf{a}^*_i$ $(i = 1, 2, 3)$ of a standard basis. These span the (reciprocal) lattice of the basic structure. One can then express the additional vectors $\mathbf{a}^*_{3+j}$ (which are modulation wavevectors) in terms of the basis of the lattice of main reflections:

$$\mathbf{a}^*_{3+j} = \sum_{i=1}^{3} \sigma_{ji}\mathbf{a}^*_i, \quad j = 1, 2, \ldots, d. \tag{9.8.4.19}$$

The three components of the jth row of the $(d \times 3)$-dimensional matrix σ are just the three components of the jth modulation wavevector $\mathbf{q}_j = \mathbf{a}^*_{3+j}$ with respect to the basis $\mathbf{a}^*_1, \mathbf{a}^*_2, \mathbf{a}^*_3$. It is easy to show that the internal components $\mathbf{a}_{Ii}$ $(i = 1, 2, 3)$ of the corresponding dual standard basis can be expressed as

$$\mathbf{a}_{Ii} = -\sum_{j=1}^{d} \sigma_{ji}\mathbf{d}_j, \quad i = 1, 2, 3. \tag{9.8.4.20}$$

This follows directly from (9.8.4.19) and the definition of the reciprocal standard basis (9.8.4.13). From (9.8.4.16) and (9.8.4.17), a simple relation can be deduced between σ and the three constituents $\Gamma_E(R)$, $\Gamma_I(R)$, and $\Gamma_M(R)$ of the matrix $\Gamma(R)$:

$$-\Gamma_I(R)\sigma + \sigma\Gamma_E(R) = \Gamma_M(R). \tag{9.8.4.21}$$

Notice that the elements of $\Gamma_M(R)$ are integers, whereas σ has, in general, irrational entries. This requires that the irrational part of σ gives zero when inserted in the left-hand side of equation (9.8.4.21). It is therefore possible to decompose formally σ into parts σ^i and σ^r as follows.

$$\sigma = \sigma^i + \sigma^r, \quad \text{with} \quad \sigma^i \equiv \frac{1}{N}\sum_R \Gamma_I(R)\sigma\Gamma_E(R)^{-1}, \tag{9.8.4.22}$$

where the sum is over all elements of the Laue group of order N. It follows from this definition that

$$\Gamma_I(R)\sigma^i\Gamma_E(R)^{-1} = \sigma^i. \tag{9.8.4.23}$$

This implies

$$\Gamma_M(R) = -\Gamma_I(R)\sigma^r + \sigma^r\Gamma_E(R). \tag{9.8.4.24}$$

The matrix σ^r has rational entries and is called the rational part of σ. The part σ^i is called the irrational (or invariant) part.

The above equations simplify for the case $d = 1$. The elements $\sigma_{1i} = \sigma_i$ are the three components of the wavevector $\mathbf{q}$, the row matrix $\sigma\Gamma_E(R)$ has the components of $R^{-1}\mathbf{q}$ and $\Gamma_I(R) = \varepsilon = \pm 1$

† See footnote on p. 913.

since, for $d = 1$, $\mathbf{q}$ can only be transformed into $\pm\mathbf{q}$. One has the corresponding relations

$$\mathbf{q} = \mathbf{q}^i + \mathbf{q}^r, \quad \text{with} \quad \mathbf{q}^i \equiv \frac{1}{N}\sum_R \varepsilon R\mathbf{q}, \tag{9.8.4.25}$$

and

$$R\mathbf{q} \equiv \varepsilon\mathbf{q} \text{ (modulo reciprocal lattice } \Lambda^*); \quad R\mathbf{q}^i = \varepsilon\mathbf{q}^i. \tag{9.8.4.26}$$

The reciprocal-lattice vector that gives the difference between $R\mathbf{q}$ and $\varepsilon\mathbf{q}$ has as components the elements of the row matrix $\Gamma_M(R)$.

9.8.4.2.2. *Geometric and arithmetic crystal classes*

According to the previous section, in the case of modulated structures a standard basis can be chosen (for M^* and correspondingly for Σ^*). According to equation (9.8.4.15), for each three-dimensional point-group operation R that leaves the diffraction pattern invariant, there is a point-group transformation R_E in the external space (the physical one, so that $R_E = R$) and a point-group transformation R_I in the internal space, such that the pair (R, R_I) is a $(3+d)$-dimensional orthogonal transformation R_s leaving a $(3+d)$-dimensional lattice Σ invariant. For incommensurate crystals, this internal transformation is unique and follows from the transformation by R of the modulation wavevectors [see equations (9.8.4.15) and (9.8.4.18) for the $\mathbf{a}^*_{3+j}$ basis vectors]: there is exactly one R_I for each R. This is so because in the incommensurate case the correspondence between M^* and Σ^* is uniquely fixed by the embedding rule (9.8.4.10) (see Subsection 9.8.4.1). Because the matrices $\Gamma(R)$ and the corresponding transformations in the $(3+d)$-dimensional space form a group, this implies that there is a mapping from the group K_E of elements R_E to the group K_I of elements R_I that transforms products into products, *i.e.* is a group homomorphism. A point group K_s of the $(3+d)$-dimensional lattice constructed for an incommensurate crystal, therefore, consists of a three-dimensional crystallographic point group K_E, a d-dimensional crystallographic point group K_I, and a homomorphism from K_E to K_I.

Definition 2. Two $(3+d)$-dimensional point groups K_s and K'_s are *geometrically equivalent* if they are connected by a pair of orthogonal transformations (T_E, T_I) in V_E and V_I, respectively, such that for every R_s from the first group there is an element R'_s of the second group such that $R_E T_E = T_E R'_E$ and $R_I T_I = T_I R'_I$.

A point group determines a set of groups of matrices, one for each standard basis of each lattice left invariant.

Definition 3. Two groups of matrices are *arithmetically equivalent* if they are obtained from each other by a transformation from one standard basis to another standard basis.

The arithmetic equivalence class of a $(3+d)$-dimensional point group is fully determined by a three-dimensional point group and a standard basis for the vector module M^* because of relation (9.8.4.15).

In three dimensions, there are 32 geometrically non-equivalent point groups and 73 arithmetically non-equivalent point groups. In one dimension, these numbers are both equal to two. Therefore, one finds all $(3+1)$-dimensional point groups of incommensurately modulated structures by considering all triples of one of the 32 (or 73) point groups, for each one of the two one-dimensional point groups and all homomorphisms from the first to the second.

Analogously, in $(3+d)$ dimensions, one takes one of the 32 (73) groups, one of the d-dimensional groups, and all homomorphisms from the first to the second. If one takes all triples of a three-dimensional group, a d-dimensional group, and a homomorphism from the first to the second, one finds, in general, groups that are equivalent. The equivalent ones still have to be eliminated in order to arrive at a list of non-equivalent groups.

9.8.4.3. *Systems and Bravais classes*

9.8.4.3.1. *Holohedry*

The Laue group of the diffraction pattern is a three-dimensional point group that leaves the positions (and the intensities)† of the diffraction spots as a set invariant, thus the vector module M^* also. As discussed in Subsection 9.8.4.2, each of the elements of the Laue group can be combined with an orthogonal transformation in the internal space. The resulting point group in $3+d$ dimensions leaves the lattice Σ^* invariant for which the vector module M^* is the projection. Conversely, if one has a point group that leaves the $(3+d)$-dimensional lattice invariant, its three-dimensional (external) part with elements $R_E = R$ leaves the vector module invariant.

Definition 4. The holohedry of the lattice Σ^* is the subgroup of the direct product $O(3) \times O(d)$, *i.e.* the group of all pairs of orthogonal transformations $R_s = (R, R_I)$ that leave the lattice invariant.

This choice is possible because the point groups are reducible, *i.e.* leave the subspaces V and V_I of the direct sum space V_s invariant. In the case of an incommensurate crystal, the projection of Σ^* on M^* is one-to-one as one can see as follows. The vector

$$H_s = \sum_{i=1}^{3} h_i(\mathbf{a}_i^*, 0) + \sum_{j=1}^{d} m_j(\mathbf{q}_j, \mathbf{d}_j^*) \tag{9.8.4.27}$$

of Σ^* is projected on $\mathbf{H} = \sum_i h_i\mathbf{a}_i^* + \sum_j m_j\mathbf{q}_j$. The vectors projected on the null vector satisfy, therefore, the relation $\sum_i h_i\mathbf{a}_i^* + \sum_j m_j\mathbf{q}_j = 0$. For an incommensurate phase, the basis vectors are rationally independent, which means that $h_i = 0$ and $m_j = 0$ for any i and j. Consequently, precisely one vector of Σ^* is projected on each given vector of M^*.

Suppose now $R = 1$. This transformation leaves the component of every vector belonging to Σ^* in V invariant. If R_I is the corresponding orthogonal transformation in V_I of an element R_s of the point group, a vector with component $\mathbf{H}_I$ is transformed into a vector with component H'_I. Since a given $\mathbf{H}$ is the component of only one vector of Σ^*, this implies $\mathbf{H}_I = \mathbf{H}'_I$. Consequently, R_I is also the identity transformation. Therefore, for incommensurate modulated phases, there are no point-group elements with $R = R_E = 1$ and $R_I \neq 1$. For commensurate crystal structures embedded in the superspace, this is different: point-group elements with internal component different from the identity associated with an external component equal to unity can occur.

For modulated crystal structures, the holohedral point group can be expressed with respect to a lattice basis of standard form

† See footnote on p. 913.

(9.8.4.13). It is then faithfully represented by integral matrices that are of the form indicated in (9.8.4.17) and (9.8.4.18).

9.8.4.3.2. *Crystallographic systems*

Definition 5. A *crystallographic system* is a set of lattices having geometrically equivalent holohedral point groups.

In this way, a given holohedral point group (and even each crystallographic point group) belongs to exactly one system. Two lattices belong to the same system if there are orthonormal bases in V and in V_I, respectively, such that the holohedral point groups of the two lattices are represented by the same set of matrices.

9.8.4.3.3. *Bravais classes*

Definition 6. Two lattices belong to the same *Bravais class* if their holohedral point groups are arithmetically equivalent.

This means that each of them admits a lattice basis of standard form such that their holohedral point group is represented by the same set of integral matrices.

9.8.4.4. *Superspace groups*

9.8.4.4.1. *Symmetry elements*

The elements of a $(3+d)$-dimensional superspace group are pairs of Euclidean transformations in 3 and d dimensions, respectively:

$$g_s = (\{R|\mathbf{v}\}, \{R_I|\mathbf{v}_I\}) \in E(3) \times E(d), \tag{9.8.4.28}$$

i.e. are elements of the direct product of the corresponding Euclidean groups. The elements $\{R|\mathbf{v}\}$ form a three-dimensional space group, but the same does not hold for the elements $\{R_I|\mathbf{v}_I\}$ of $E(d)$. This is because the internal translations $\mathbf{v}_I$ also contain the 'compensating' transformations associated with the corresponding translation $\mathbf{v}$ in V [see (9.8.4.32)]. In other words, a basis of the lattice Σ does not simply split into one basis for V and one for V_I.

As for elements of a three-dimensional space group, the translational component $\upsilon_s = (\mathbf{v}, \mathbf{v}_I)$ of the element g_s can be decomposed into an intrinsic part υ_s^o and an origin-dependent part υ_s^a:

$$(\upsilon, \upsilon_I) = (\mathbf{v}^o, \mathbf{v}_I^o) + (\mathbf{v}^a, \mathbf{v}_I^a),$$

with

$$(\mathbf{v}^o, \mathbf{v}_I^o) = \frac{1}{n}\sum_{m=1}^{n} (R^m\mathbf{v}, R_I^m\mathbf{v}_I), \tag{9.8.4.29}$$

where n denotes the order of the element R. In particular, for $d = 1$ the intrinsic part $\mathbf{v}_I^o$ of $\mathbf{v}_I$ is equal to $\mathbf{v}_I$ if $R_I = \varepsilon = +1$ and vanishes if $\varepsilon = -1$. The latter means that for $d = 1$ there is always an origin in the internal space such that the internal shift $\mathbf{v}_I$ can be chosen to be zero for an element with $\varepsilon = -1$.

The internal part of the intrinsic translation can itself be decomposed into two parts. One part stems from the presence of a translation in the external space. The lattice of the $(3+d)$-dimensional space group has basis vectors

$$(\mathbf{a}_i, \mathbf{a}_{Ii}), (0, \mathbf{d}_j), \quad i = 1, 2, 3, \quad j = 1, \ldots, d. \tag{9.8.4.30}$$

The internal part of the first three basis vectors is

$$\mathbf{a}_{Ii} = -\Delta\mathbf{a}_i = -\sum_{j=1}^{d} \sigma_{ji}\mathbf{d}_j \tag{9.8.4.31}$$

according to equation (9.8.4.20). The three-dimensional translation $\mathbf{v} = \sum_i \upsilon_i\mathbf{a}_i$ then entails a d-dimensional translation $-\Delta\mathbf{v}$ in V_I given by

$$\Delta\mathbf{v} = \Delta\left(\sum_{i=1}^{3} \upsilon_i\mathbf{a}_i\right) = \sum_{i=1}^{3} \upsilon_i\Delta\mathbf{a}_i. \tag{9.8.4.32}$$

These are the so-called compensating translations. Hence, the internal translation $\mathbf{v}_I$ can be decomposed as

$$\mathbf{v}_I = -\Delta\mathbf{v} + \boldsymbol{\delta}, \tag{9.8.4.33}$$

where $\boldsymbol{\delta} = \sum_{j=1}^{d} \upsilon_{3+j}\mathbf{d}_j$.

This decomposition, however, does still depend on the origin. Consider the case $d = 1$. Then an origin shift $\mathbf{s}$ in the three-dimensional space changes the translation $\mathbf{v}$ to $\mathbf{v} + (1-R)\mathbf{s}$ and its internal part $-\Delta\mathbf{v} = -\mathbf{q}\cdot\mathbf{v}$ to $-\mathbf{q}\cdot\mathbf{v} - \mathbf{q}\cdot(1-R)\mathbf{s}$. This implies that for the case that $\varepsilon = 1$ the part δ changes to $\delta + \mathbf{q}\cdot(1-R)\mathbf{s} = \delta + \mathbf{q}^r\cdot(1-R)\mathbf{s}$, because $\mathbf{q}^i$ is invariant under R. Therefore, δ changes, in general. The internal translation

$$\tau = \delta - \mathbf{q}^r\cdot\mathbf{v}, \tag{9.8.4.34}$$

however, is invariant under an origin shift in V.

Definition 7. *Equivalent superspace groups*. Two superspace groups are equivalent if they are isomorphic and have point groups that are arithmetically equivalent.

Another definition leading to the same partition of equivalent superspace groups considers equivalency with respect to affine transformations among bases of standard form.

This means that two equivalent superspace groups admit standard bases such that the two space groups are represented by the same set of $(4+d)$-dimensional affine transformation matrices. We recall that an n-dimensional Euclidean transformation $g_s = \{R_s|v_s\}$ if referred to a basis of the space can be represented isomorphically by an $(n+1)$-dimensional matrix, of the form

$$A(g_s) = \begin{pmatrix} R_s & v_s \\ 0 & 1 \end{pmatrix} \tag{9.8.4.35}$$

with R_s an $n \times n$ matrix and v_s an n-dimensional column matrix, all with real entries.

9.8.4.4.2. *Equivalent positions and modulation relations*

A $(3+d)$-dimensional space group that leaves a function invariant maps points in $(3+d)$-space to points where the function has the same value. The atomic positions of a modulated crystal represent such a pattern, and the superspace group leaving the crystal invariant leads to a partition into equivalent atomic positions. These relations can be formulated either in $(3+d)$-dimensional space or, equally well, in three-dimensional space. As a simple case, we first consider a crystal with a one-dimensional occupation modulation: this implies $d = 1$. Again, as in §9.8.1.3.2, we omit to indicate the basis vectors $\mathbf{d}_1$ and $\mathbf{d}_1^*$ and give only the corresponding components.

An element of the $(3+1)$-dimensional superspace group is a pair

$$g_s = (\{R|\mathbf{v}\}, \{\varepsilon|\upsilon_I\}) \tag{9.8.4.36}$$

of Euclidean transformations in V and V_I, respectively. This element maps a point located at $r_s = (\mathbf{r}, t)$ to one at $(R\mathbf{r} + \mathbf{v}, \varepsilon t + \upsilon_I)$. Suppose the probability for the position $\mathbf{n} + \mathbf{r}_j$ to be occupied by an atom of species A is given by

$$P_A(\mathbf{n}, j, t) = p_j[\mathbf{q}\cdot(\mathbf{n} + \mathbf{r}_j) + t], \tag{9.8.4.37}$$

where $p_j(x) = p_j(x+1)$. By g_s, the position $\mathbf{n}+\mathbf{r}_j$ is transformed to the equivalent position $\mathbf{n}'+\mathbf{r}_{j'} = R\mathbf{n}+R\mathbf{r}_j+\mathbf{v}$. As the crystal is left invariant by the superspace group, the occupation probability on equivalent points has to be the same:

$$P_A(\mathbf{n}', j', t) = P_A[\mathbf{n}, j, \varepsilon(t-\upsilon_I)]. \tag{9.8.4.38}$$

This implies that for the structure in the three-dimensional space one has the relation

$$P_A(\mathbf{n}', j', 0) = P_A(\mathbf{n}, j, -\varepsilon\upsilon_I). \tag{9.8.4.39}$$

In terms of the modulation function p_j this means

$$p_{j'}[\mathbf{q}\cdot(\mathbf{n}'+\mathbf{r}_{j'})] = p_j[\mathbf{q}\cdot(\mathbf{n}+\mathbf{r}_j)-\varepsilon\upsilon_I]. \tag{9.8.4.40}$$

In the same way, one derives the following property of the modulation function:

$$p_{j'}(x) = p_j[\varepsilon(x-\delta)+\mathbf{K}\cdot(\mathbf{r}_{j'}-\mathbf{v})], \quad \text{where } R\mathbf{q} = \varepsilon\mathbf{q}+\mathbf{K}. \tag{9.8.4.41}$$

Analogously, for a displacive modulation, the position $\mathbf{n}+\mathbf{r}_j$ with displacement $\mathbf{u}_j(t_o)$, where $t_o = \mathbf{q}\cdot(\mathbf{n}+\mathbf{r}_j)$, is transformed to $\mathbf{n}'+\mathbf{r}_{j'}$ with displacement

$$\mathbf{u}_{j'}(t_o') = R\mathbf{u}_j(t_o-\varepsilon\upsilon_I). \tag{9.8.4.42}$$

To be invariant, the displacement function has to satisfy the relation

$$\mathbf{u}_{j'}(x) = R\mathbf{u}_j[\varepsilon x-\varepsilon\delta+\mathbf{K}\cdot(\mathbf{r}_{j'}-\mathbf{v})], \quad \text{where } R\mathbf{q} = \varepsilon\mathbf{q}+\mathbf{K}. \tag{9.8.4.43}$$

The expressions for $d > 1$ are straightforward generalizations of these.

9.8.4.4.3. *Structure factor*

The scattering from a set of atoms at positions $\mathbf{r}_n$ is described in the kinematic approximation by the structure factor:

$$S_{\mathbf{H}} = \sum_n f_n(\mathbf{H})\exp(2\pi i\mathbf{H}\cdot\mathbf{r}_n), \tag{9.8.4.44}$$

where $f_n(\mathbf{H})$ is the atomic scattering factor. For an incommensurate crystal phase, this structure factor $S_{\mathbf{H}}$ is equal to the structure factor S_{H_s} of the crystal structure embedded in $3+d$ dimensions, where $\mathbf{H}$ is the projection of H_s on V_E. This structure factor is expressed by a sum of the products of atomic scattering factors f_n and phase factors $\exp(2\pi i H_s\cdot r_{sn})$ over all particles in the unit cell of the higher-dimensional lattice. For an incommensurate phase, the number of particles in such a unit cell is infinite: for a given atom in space, the embedded positions form a dense set on lines or hypersurfaces of the higher-dimensional space. Disregarding pathological cases, the sum may be replaced by an integral. Including the possibility of an occupation modulation, the structure factor becomes (up to a normalization factor)

$$S_{\mathbf{H}} = \sum_A \sum_j \int_\Omega \mathrm{d}\mathbf{t}\, f_A(\mathbf{H})P_{Aj}(\mathbf{t}) \times \exp\{2\pi i(\mathbf{H},\mathbf{H}_I)\cdot[\mathbf{r}_j+\mathbf{u}_j(\mathbf{t}),\mathbf{t}]\}, \tag{9.8.4.45}$$

where the first sum is over the different species, the second over the positions in the unit cell of the basic structure, the integral over a unit cell of the lattice spanned by $\mathbf{d}_1,\ldots,\mathbf{d}_d$ in V_I; f_A is the atomic scattering factor of species A, $P_{Aj}(\mathbf{t})$ is the probability of atom j being of species A when the internal position is $\mathbf{t}$.

In particular, for a given atomic species, without occupational modulation and a sinusoidal one-dimensional displacive modulation

$$P_j(t) = 1; \quad \mathbf{u}_j(t) = \mathbf{U}_j\sin[2\pi(\mathbf{q}\cdot\mathbf{r}_j+t+\varphi_j)]. \tag{9.8.4.46}$$

According to (9.8.4.45), the structure factor is

$$S_{\mathbf{H}} = \sum_j \int_0^1 \mathrm{d}t f_j(\mathbf{H})\exp(2\pi i\mathbf{H}\cdot\mathbf{r}_j)\exp(2\pi imt) \times \exp[2\pi i\mathbf{H}\cdot\mathbf{U}_j\sin 2\pi(\mathbf{q}\cdot\mathbf{r}_j+t+\varphi_j)]. \tag{9.8.4.47}$$

For a diffraction vector $\mathbf{H} = \mathbf{K}+m\mathbf{q}$, this reduces to

$$S_{\mathbf{H}} = \sum_j f_j(\mathbf{H})\exp(2\pi i\mathbf{K}\cdot\mathbf{r}_j)J_{-m}(2\pi\mathbf{H}\cdot\mathbf{U}_j) \times \exp(-2\pi im\varphi_j). \tag{9.8.4.48}$$

For a general one-dimensional modulation with occupation modulation function $p_j(t)$ and displacement function $\mathbf{u}_j(t)$, the structure factor becomes

$$S_{\mathbf{H}} = \sum_j \int_0^1 \mathrm{d}t\, f_j(\mathbf{H})p_j(\mathbf{q}\cdot\mathbf{r}_j+t+\psi_j)\exp[2\pi i(\mathbf{H}\cdot\mathbf{r}_j+mt)] \times \exp[2\pi i\mathbf{H}\cdot\mathbf{u}_j(\mathbf{q}\cdot\mathbf{r}_j+t+\varphi_j)]. \tag{9.8.4.49}$$

Because of the periodicity of $p_j(t)$ and $\mathbf{u}_j(t)$, one can expand the Fourier series:

$$p_j(\mathbf{q}\cdot\mathbf{r}_j+t+\psi_j)\exp[2\pi i\mathbf{H}\cdot\mathbf{u}_j(\mathbf{q}\cdot\mathbf{r}_j+t+\varphi_j)] = \sum_k C_{j,k}(\mathbf{H})\exp[2\pi ik(\mathbf{q}\cdot\mathbf{r}_j+t)], \tag{9.8.4.50}$$

and consequently the structure factor becomes

$$S_{\mathbf{H}} = \sum_j f_j(\mathbf{H})\exp(2\pi i\mathbf{K}\cdot\mathbf{r}_j)C_{j,-m}(\mathbf{H}), \quad \text{where } \mathbf{H} = \mathbf{K}+m\mathbf{q}. \tag{9.8.4.51}$$

The diffraction from incommensurate crystal structures has been treated by de Wolff (1974), Yamamoto (1982*a*,*b*), Paciorek & Kucharczyk (1985), Petricek, Coppens & Becker (1985), Petříček & Coppens (1988), Perez-Mato *et al*. (1986, 1987), and Steurer (1987).

9.8.5. Generalizations

9.8.5.1. *Incommensurate composite crystal structures*

The basic structure of a modulated crystal does not always have space-group symmetry. Consider, for example, composite crystals (also called intergrowth crystals). Disregarding modulations, one can describe these crystals as composed of a finite number of subsystems, each with its own space-group symmetry. The lattices of these subsystems can be mutually incommensurate. In that case, the overall symmetry is not a space group, the composite crystal is incommensurate and so also is its basic structure. The superspace approach can also be applied to such crystals. Let the subsystems be labelled by an index ν. For the subsystem ν, we denote the lattice by Λ_ν with basis vectors $\mathbf{a}_{\nu i}$ $(i=1,2,3)$, its reciprocal lattice by Λ_ν^* with basis vectors $\mathbf{a}_{\nu i}^*$ $(i=1,2,3)$, and the space group by G_ν. The atomic positions of the basic structure are given by

$$\mathbf{n}_\nu+\mathbf{r}_{\nu j}, \tag{9.8.5.1}$$

where $\mathbf{n}_\nu$ is a lattice vector belonging to Λ_ν. In the special case that the subsystems are mutually commensurate, there are three basis vectors $\mathbf{a}^*, \mathbf{b}^*, \mathbf{c}^*$ such that all vectors $\mathbf{a}_{\nu i}^*$ are integral linear combinations of them. In general, however, more than three basis vectors are needed, but never more than three times the number of subsystems. Suppose that the vectors $\mathbf{a}_i^*$ $(i=1,\ldots,n)$

form a basis set such that every $\mathbf{a}^*_{\nu i}$ can be expressed as an integral linear combination of them:

$$\mathbf{a}^*_{\nu i} = \sum_{k=1}^{n} Z^{\nu}_{ik}\mathbf{a}^*_k, \quad Z^{\nu}_{ik} \text{ integers}, \tag{9.8.5.2}$$

with $n = 3 + d_o$ and $d_o > 0$. Then the vectors of the diffraction pattern of the unmodulated system are again of the form (9.8.4.5) and generate a vector module M^*_o of dimension three and rank $(3 + d_o)$, which can be considered as projection of a $(3 + d_o)$-dimensional lattice Σ^*_o.

We now assume that one can choose $\mathbf{a}^*_{li} = 0$ for $i = 1, 2, 3$ and we denote $\mathbf{a}^*_{l3+j}$ by $\mathbf{d}^*_j$. This corresponds to assuming the existence of a subset of Bragg reflections at the positions of a three-dimensional reciprocal lattice Λ^*. Then there is a standard basis for the lattice Σ_o, which is the reciprocal of Σ^*_o, given by

$$(\mathbf{a}_i, \mathbf{a}_{li}), \quad (0, \mathbf{d}_j), \quad i = 1, 2, 3, \quad j = 1, \ldots, d_o. \tag{9.8.5.3}$$

In order to find the $(3 + d_o)$-dimensional periodic structure for which this composite crystal is the three-dimensional intersection, one associates with a translation $\mathbf{t}$ in the internal space V_I three-dimensional independent shifts, one for each subsystem. These shifts of the subsystems replace the phase shifts adopted for the modulated structures: V_I is now the space of the variable relative positions of the subsystems. Again, a translation in the superspace can give rise to a non-Euclidean transformation in the three-dimensional space of the crystal, because of the variation in the relative positions among subsystems. Each subsystem, however, is rigidly translated. For the basis vectors $\mathbf{d}_j$, the shift of the subsystem ν is defined in terms of projection operators π_ν:

$$\pi_\nu \mathbf{d}_j = \sum_{i=1}^{3} Z^{\nu}_{i3+j}\mathbf{a}_{\nu i}, \quad j = 1, \ldots, d_o. \tag{9.8.5.4}$$

Then an arbitrary translation $\mathbf{t} = \sum_j t_j \mathbf{d}_j$ in V_I displaces the subsystem ν over a vector $\sum_j t_j(\pi_\nu \mathbf{d}_j)$. A translation $(\mathbf{a}, \mathbf{a}_I + \mathbf{d})$ belonging to the $(3 + d_o)$-dimensional lattice Σ_o induces for the subsystem ν in ordinary space a relative translation over vector $\mathbf{a} + \pi_\nu(\mathbf{a}_I + \mathbf{d})$. The statement is that this translation is a vector of the lattice Λ_ν and leaves therefore the subsystem ν invariant. So the lattice translations belonging to Σ_o form a group of symmetry operations for the composite crystal as a whole.

The proof is as follows. If $\mathbf{k}$ belongs to Λ^*_ν, the vector $(\mathbf{k}, \mathbf{k}_I)$ belongs to Σ^*_o. In particular, for $\mathbf{k} = \mathbf{a}^*_{\nu i}$, one has, because of (9.8.5.2) and (9.8.5.4),

$$\mathbf{a}^*_{\nu i} \cdot \pi_\nu \mathbf{d}_j = Z^{\nu}_{i3+j}, \quad j = 1, \ldots, d_o, \tag{9.8.5.5}$$

and

$$\mathbf{k}_I = \sum_{j=1}^{d_o} Z^{\nu}_{i3+j}\mathbf{d}^*_j \quad \text{and therefore} \quad \mathbf{k}_I \cdot \mathbf{d}_j = Z^{\nu}_{i3+j}.$$

Note that one has $\mathbf{k}_I \cdot \mathbf{t} = \mathbf{k} \cdot \pi_\nu \mathbf{t}$, for any $\mathbf{t}$ from V_I as π_ν is a linear operator. Because of the linearity, this holds for every $\mathbf{k}$ from Λ^*_ν as well. Since $(\mathbf{k}, \mathbf{k}_I)$ belongs to Σ^*_o and $(\mathbf{a}, \mathbf{a}_I + \mathbf{d})$ to Σ_o, one has for their inner product:

$$\mathbf{k} \cdot \mathbf{a} + \mathbf{k}_I \cdot \mathbf{a}_I + \mathbf{k}_I \cdot \mathbf{d} = \mathbf{k} \cdot (\mathbf{a} + \pi_\nu \mathbf{a}_I + \pi_\nu \mathbf{d}) \equiv 0 \pmod 1,$$

which implies that $\mathbf{a} + \pi_\nu \mathbf{a}_I + \pi_\nu \mathbf{d}$ is an element of Λ_ν.

In conclusion, one may state that the composite structure is the intersection with the ordinary space ($\mathbf{t} = 0$) of a pattern having atomic position vectors given by

$$(\mathbf{n}_\nu + \mathbf{r}_{\nu j} - \pi_\nu \mathbf{t}, \mathbf{t}) \quad \text{for any } \mathbf{t} \text{ of } V_I. \tag{9.8.5.6}$$

Such a pattern is invariant under the $(3 + d_o)$-dimensional lattice Σ_o. Again, orthogonal transformations R of $O(3)$ leaving the vector module M^*_o invariant can be extended to orthogonal transformation R_s of $O(3) \times O(d_o)$ allowing a Euclidean structure to be given to the superspace. One can then consider the superspace-group symmetry of the basic structure defined by atomic positions as in (9.8.5.6). A superspace-group element g_s as in (9.8.4.28) induces (in three-dimensional space) for the subsystem ν the transformation

$$g_s : \mathbf{n}_\nu + \mathbf{r}_{\nu j} \to R\mathbf{n}_\nu + R\mathbf{r}_{\nu j} + \mathbf{v} + R\pi_\nu R_I^{-1}\mathbf{v}_I, \tag{9.8.5.7}$$

changing the position $\mathbf{n}_\nu + \mathbf{r}_{\nu j}$ into an equivalent one of the composite structure, not necessarily, however, within the same subsystem ν.

Finally, the composite structure can also be modulated. For the case of a one-dimensional modulation of each subsystem ν, the positions are

$$\mathbf{n}_\nu + \mathbf{r}_{\nu j} + \mathbf{u}_{\nu j}[\mathbf{q}_\nu \cdot (\mathbf{n}_\nu + \mathbf{r}_{\nu j})]. \tag{9.8.5.8}$$

Possibly the modulation vectors can also be expressed as integral linear combinations of the $\mathbf{a}^*_i$ $(i = 1, \ldots, 3 + d_o)$. Then, the dimension of V_I is again d_o. In general, however, one has to consider $(d - d_o)$ additional vectors, in order to ensure the validity of (9.8.4.5), now for $n = 3 + d$. We can then write

$$\mathbf{q}_\nu = \sum_{j=1}^{3+d} Q^{\nu}_j \mathbf{a}^*_j, \quad Q^{\nu}_j \text{ integers}. \tag{9.8.5.9}$$

The peaks of the diffraction pattern are at positions defined by a vector module M^*, which can be considered as the projection of a $(3 + d)$-dimensional lattice Σ^*, the reciprocal of which leaves invariant the pattern of the modulated atomic positions in the superspace given by

$$\{\mathbf{n}_\nu + r_{\nu j} - \pi_\nu \mathbf{t} + \mathbf{u}_{\nu j}[\mathbf{q}_\nu \cdot (\mathbf{n}_\nu + \mathbf{r}_{\nu j} - \pi_\nu \mathbf{t}) + \mathbf{q}_{I\nu} \cdot \mathbf{t}], \mathbf{t}\}, \quad \text{for any } \mathbf{t} \text{ of } V_I \tag{9.8.5.10}$$

with $\pi_\nu \mathbf{d}_j = 0$ for $j > d_o$, where $\mathbf{q}_{I\nu}$ is the internal part of the $(3 + d)$-dimensional vector that projects on $\mathbf{q}_\nu$. Their symmetry is a $(3 + d)$-dimensional superspace group G_s. The transformation induced in the modulated composite crystal by an element under g_s of G_s is now readily written down. For the case $d = d_o = 1$ and $g_s = (\{R|\mathbf{v}\}, \{\varepsilon|\Delta\})$, the position $\mathbf{n}_\nu + \mathbf{r}_{\nu j}$ is transformed into

$$R(\mathbf{n}_\nu + \mathbf{r}_{\nu j}) + \mathbf{v} + \varepsilon R\pi_\nu \Delta \mathbf{d}_1, \tag{9.8.5.11}$$

and the modulation $\mathbf{u}_{\nu j}[\mathbf{q}_\nu \cdot (\mathbf{n}_\nu + \mathbf{r}_{\nu j})]$ into

$$R\mathbf{u}_{\nu j}[\mathbf{q}_\nu \cdot (\mathbf{n}_\nu + \mathbf{r}_{\nu j} + \varepsilon\pi_\nu \Delta \mathbf{d}_1) - \varepsilon \mathbf{q}_{I\nu} \cdot \Delta \mathbf{d}_1].$$

This shows how the superspace-group approach can be applied to a composite (modulated) structure. Note that composite systems do not necessarily have an invariant set of (main) reflections at lattice positions.

9.8.5.2. *The incommensurate versus the commensurate case*

As said earlier, it sometimes makes sense also to use the description as developed for incommensurate crystal phases for a (commensurate) superstructure. In fact, very often the modulation wavevector also shows, in addition to continuously varying (incommensurate) values, several rational values at various phase transitions of a given crystal or in different compounds of a given structural family. In these cases, there is three-dimensional space-group symmetry. Generally, the space groups of the various phases are different. The description as used for incommensurate phases then gives the possibility of a more unified characterization for the symmetry of related modulated crystal phases. In fact, the theory of higher-dimensional space groups for modulated structures is largely independent of the

assumption of irrationality. Only some of the statements need to be adapted. The most important change is that there is no longer a one-to-one correspondence between the points of the reciprocal lattice Σ^* and its projection on V defining the positions of the Bragg peaks. Furthermore, the projection of the lattice Σ on the space V_I forms a discrete set. The latter means the following. For an incommensurate modulation, the incommensurate structure, which is the intersection of a periodic structure with the hyperplane $\mathbf{r}_I = 0$, is also the intersection of the same periodic structure with a hyperplane $\mathbf{r}_I = \text{constant}$, where this constant is of the form

$$\sum_{i=1}^{3} h_i \mathbf{a}_{Ii} + \sum_{j=1}^{d} m_j \mathbf{a}_{I3+j}. \qquad (9.8.5.12)$$

Because for an incommensurate structure these vectors form a dense set in V_I, the phase of the modulation function with respect to the basic structure is not determined. For a commensurate modulation, however, the points (9.8.5.12) form a discrete set, even belong to a lattice, and the phase (or the phases) of the modulation are determined within vectors of this lattice. Notice that the grid of this lattice becomes finer as the denominators in the rational components become larger.

When G_s is a $(3+d)$-dimensional superspace group, its elements, in general, do not leave the ordinary space V invariant. The subgroup of all elements that do leave V invariant, when restricted to V, is a group of distance-preserving transformations in three dimensions and thus a subgroup of $E(3)$, the three-dimensional Euclidean group. In general, this subgroup is not a three-dimensional space group. It is so when the modulation wavevectors all have rational components only, *i.e.* when σ is a matrix with rational entries. Because the phase of the modulation function is now determined (within a given rational number smaller than 1), the space group depends in general on this phase.

As an example, consider a one-dimensional modulation of a basic structure with orthorhombic space group *Pcmn*. Suppose that the modulation wavevector is $\gamma\mathbf{c}^*$. Then the mirror $R = m_z$ perpendicular to the c axis is combined with $R_I = \varepsilon = -1$. Suppose, furthermore, that the glide reflection perpendicular to the a axis and the b mirror are both combined with a phase shift $\frac{1}{2}$. In terms of the coordinates x, y, z with respect to the a, b and c axes, and internal coordinate t, the generators of the $(3+1)$-dimensional superspace group $Pcmn(00\gamma)ss0$ act as

$$(x, y, z, t) \to (x + k, y + l, z + m, t - \gamma m + n), \quad k, l, m, n \text{ integers}, \qquad (9.8.5.13a)$$

$$(x, y, z, t) \to (-x + k + \tfrac{1}{2}, y + l, z + \tfrac{1}{2} + m, t - \gamma/2 - \gamma m + \tfrac{1}{2} + n), \qquad (9.8.5.13b)$$

$$(x, y, z, t) \to (x + k, -y + l + \tfrac{1}{2}, z + m, t - \gamma m + \tfrac{1}{2} + n), \qquad (9.8.5.13c)$$

$$(x, y, z, t) \to (x + \tfrac{1}{2} + k, y + \tfrac{1}{2} + l, -z + \tfrac{1}{2} + m, -t - \gamma/2 - \gamma m + n). \qquad (9.8.5.13d)$$

Note that these positions are referred to a split basis (*i.e.* of basis vectors lying either in V or in V_I) and not to a basis of the lattice Σ. When the superstructure is the intersection of a periodic structure with the plane at $t = t_o$, its three-dimensional space group follows from equation (9.8.5.13) by the requirement $t' = t_o$. When γ has the rational value r/s with r and s relatively prime, the conditions for each of the generators to give an element of the three-dimensional space group are, respectively:

$$-rm + sn = 0 \qquad (9.8.5.14a)$$

$$-2rm + 2sn = r - s \qquad (9.8.5.14b)$$

$$-2rm + 2sn = -s \qquad (9.8.5.14c)$$

$$-2rm + 2sn = 4st, \qquad (9.8.5.14d)$$

for m, n, r, s integers and t real. These conditions are never satisfied simultaneously. It depends on the parity of both r and s which element occurs, and for the elements with $\varepsilon = -1$ it also depends on the value of the 'phase' t, or more precisely on the product $\tau = 4st$. The translation group is determined by the first condition as in (9.8.5.14*a*). Its generators are

$$\mathbf{a}, \mathbf{b}, \text{ and } s\mathbf{c},$$

where the last vector is the external part of the lattice vector $s(\mathbf{c}, -r/s) + r(0, 1)$. The other space-group elements can be derived in the same way. The possible space groups are:

$\gamma = r/s$	τ even integer	τ odd integer	otherwise
r even, s odd	$11\frac{2_1}{n}$	$2_12_12_1$	112_1
r odd, s even	$1\frac{2_1}{c}1$	2_1cn	1c1
r odd, s odd	$\frac{2_1}{c}11$	$c2_1n$	$c11$

In general, the three-dimensional space groups compatible with a given $(3+d)$-dimensional superspace group can be determined using analogous equations.

As one can see from the table above, the orthorhombic $(3+d)$-dimensional superspace group leads in several cases to monoclinic three-dimensional space groups. The lattice of main reflections, however, still has orthorhombic point-group symmetry. Description in the conventional way by means of three-dimensional groups then neglects some of the structural features present. Even if the orthorhombic symmetry is slightly broken, the orthorhombic basic structure is a better characterization than a monoclinic one. Note that in that case the superspace-group symmetry is also only an approximation.

When the denominators of the wavevector components become small, additional symmetry operations become possible. Because the one-to-one correspondence between Σ^* and M^* is no longer present, there may occur symmetry elements with trivial action in V but with nontrivial transformation in V_I. For $d = 1$, these possibilities have been enumerated. The corresponding Bravais classes are given in Table 9.8.3.2(*b*).

APPENDIX *A*
Glossary of symbols

M^* Vector module in m-dimensional reciprocal space ($m = 1, 2, 3$; normally $m = 3$), isomorphic to Z^n with $n \geq m$. The dimension of M^* is m, its rank n.

$\mathbf{a}_i^*$ ($i = 1, \ldots, n$.) Basis of a vector module M^* of rank n; if $n = 4$ and $\mathbf{q}$ is modulation wavevector (the $n = 4$ case is restricted in what follows to modulated crystals), the basis of M^* is chosen as $\mathbf{a}^*, \mathbf{b}^*, \mathbf{c}^*, \mathbf{q}$, with $\mathbf{a}^*, \mathbf{b}^*, \mathbf{c}^*$ a basis of the lattice of main reflections.

Λ^* Lattice of main reflections, m-dimensional reciprocal lattice.

$\mathbf{a}^*, \mathbf{b}^*, \mathbf{c}^*$ (Conventional) basis of Λ^* for $m = 3$.

Λ Direct m-dimensional lattice, dual to Λ^*.

V_s Superspace; Euclidean space of dimension $n = m + d$; $V_s = V \oplus V_I$.

V Physical (or external) space of dimension m ($m = 1, 2$ or 3), also indicated by V_E.

V_I Internal (or additional) space of dimension d.

Σ^* Reciprocal lattice in n-dimensional space, whose orthogonal projection on V is M^*.

Σ Lattice in n-dimensional superspace for which Σ^* is the reciprocal one.

a^*_{si} Lattice basis of Σ^* in V_s ($i = 1, \ldots, n$);
if $n = 4$, this basis can be chosen as $\{(\mathbf{a}^*, 0), (\mathbf{b}^*, 0), (\mathbf{c}^*, 0), (\mathbf{q}, 1)\}$ and is called standard. An equivalent notation is $(\mathbf{q}, 1) = (\mathbf{q}, \mathbf{d}^*)$;
for $n = 3 + d$, the general form of a standard basis is $(\mathbf{a}^*, 0)$, $(\mathbf{b}^*, 0)$, $(\mathbf{c}^*, 0)$, $(\mathbf{q}_1, \mathbf{d}^*_1), \ldots, (\mathbf{q}_j, \mathbf{d}^*_j), \ldots, (\mathbf{q}_d, \mathbf{d}^*_d)$.

a_{si} ($i = 1, \ldots, n$.) Lattice basis of Σ in V_s dual to $\{a^*_{si}\}$;
if $n = 4$, the standard basis is $(\mathbf{a}, -\mathbf{q}\cdot\mathbf{a}), (\mathbf{b}, -\mathbf{q}\cdot\mathbf{b}), (\mathbf{c}, -\mathbf{q}\cdot\mathbf{c}), (0, 1) = (0, \mathbf{d})$;
for $n = 3 + d$, a standard basis is dual to the standard one given above.

$\mathbf{q}_j$ Modulation wavevector(s) $\mathbf{q}_j = \sum_{i=1}^{3} \sigma_{ji}\mathbf{a}^*_i$;
if $n = 4$, $\mathbf{q} = \sum_{i=1}^{3} \sigma_i \mathbf{a}^*_i = \alpha\mathbf{a}^* + \beta\mathbf{b}^* + \gamma\mathbf{c}^*$;
$\sigma = (\alpha, \beta, \gamma)$;
if $n = 4$, $\mathbf{q} = \mathbf{q}^i + \mathbf{q}^r$, with $\mathbf{q}^i = (1/N)\sum_{R \text{ in } K} \varepsilon(R) R\mathbf{q}$, where $\varepsilon(R) = R_I$, and N is the order of K.

$\mathbf{H}$ Bragg reflections: $\mathbf{H} = \sum_{i=1}^{n} h_i \mathbf{a}^*_i = (h_1, h_2, \ldots, h_n)$;
if $n = 4$, $\mathbf{H} = \sum_{i=1}^{4} h_i \mathbf{a}^*_i = h\mathbf{a}^* + k\mathbf{b}^* + l\mathbf{c}^* + m\mathbf{q} = (h, k, l, m)$.

H_s Embedding of $\mathbf{H}$ in V_s: for $\mathbf{H} = (h_1, \ldots, h_n) = \sum_{i=1}^{n} h_i \mathbf{a}^*_i$, one has correspondingly $H_s = (\mathbf{H}, \mathbf{H}_I) = \sum_{i=1}^{n} h_i a^*_{si}$.

P_L Laue point group.

$O(m)$ Orthogonal group in m dimensions.

R Orthogonal point-group transformation, element of $O(m)$.

K Point group, crystallographic subgroup of $O(m)$.

R_s Superspace point-group element: $R_s = (R_E, R_I) = (R, R_I)$ element of $O(m) \times O(d)$ with $R_E = R$ external, and R_I internal part of R_s, respectively;
if $n = 4$, superspace point-group element: $[R, \varepsilon(R)]$ with $\varepsilon(R) = \pm 1$, also written (R, ε).

K_s Point group, crystallographic subgroup of $O(m) \times O(d)$.

K_E External part of K_s, crystallographic point group, subgroup of $O(m)$ with as elements the external part transformations of K_s.

K_I Internal part of K_s, crystallographic point group, subgroup of $O(d)$ with as elements the internal part transformations of K_s.

$\mathbf{r}_o(\mathbf{n}, j)$ Atomic positions in the basic structure: $\mathbf{r}_o(\mathbf{n}, j) = \mathbf{n} + \mathbf{r}_j$ with $\mathbf{n} \in \Lambda$.

$\mathbf{r}(\mathbf{n}, j)$ Atomic positions in the displacively modulated structure;
($d = 1$): $\mathbf{r}(\mathbf{n}, j) = \mathbf{r}_o(\mathbf{n}, j) + \mathbf{u}_j[\mathbf{q}\cdot\mathbf{r}(\mathbf{n}, j) + \varphi_j]$. In general, however, different phases $\varphi_{j\alpha}$ may occur for different components $u_{j\alpha}$ along the crystallographic axes.

$\mathbf{u}_j(x)$ Modulation function for displacive modulation with $\mathbf{u}_j(x + 1) = \mathbf{u}_j(x)$.

$p_j(x)$ Modulation function for occupation modulation with $p_j(x + 1) = p_j(x)$.

g Euclidean transformation in m dimensions; $g = \{R|\mathbf{v}\}$ element of the space group G with rotational part R and translational part $\mathbf{v}$.

$\mathbf{v}^o$ Intrinsic translation part (origin independent).

g_s Superspace group transformation ($d = 1$):
$g_s = \{(R, \varepsilon)|(\mathbf{v}, \Delta)\} = (\{R|\mathbf{v}\}, \{\varepsilon|\Delta\}) = \{R_s|\upsilon_s\}$
element of the superspace group G_s.
In the $(3 + d)$-dimensional case:
$g_s = \{(R, R_I)|(\mathbf{v}, \mathbf{v}_I)\} = (\{R|\mathbf{v}\}, \{R_I|\mathbf{v}_I\})$.

υ_I Internal shift ($d = 1$): $\upsilon_I = \Delta = \delta - \mathbf{q}\cdot\mathbf{v}$.

τ Intrinsic internal shift ($d = 1$): $\tau = \delta - \mathbf{q}^r\cdot\mathbf{v}$.

$\Gamma^*(R)$ Point-group transformation R with respect to a basis of M^* and at the same time superspace point-group transformation R_s with respect to a corresponding basis of Σ^*.

$\Gamma(R)$ Superspace point-group transformation with respect to a lattice basis of Σ dual to that of Σ^* leading to $\Gamma^*(R)$. The mutual relation is then $\Gamma^*(R) = \tilde{\Gamma}(R^{-1})$ with the tilde denoting transposition.

$\Gamma_E(R)$, $\Gamma_I(R)$, $\Gamma_M(R)$: external, internal, and mixed blocks of $\Gamma(R)$, respectively.

$\Gamma^*_E(R)$, $\Gamma^*_I(R)$, $\Gamma^*_M(R)$: external, internal, and mixed blocks of $\Gamma^*(R)$, respectively.

$S_{\mathbf{H}}$ Structure factor:

$$S_{\mathbf{H}} = \sum_{\mathbf{n}} \sum_{j} f_j(\mathbf{H}) \exp[2\pi i \mathbf{H}\cdot\mathbf{r}(\mathbf{n}, j)].$$

$f_j(\mathbf{H})$ Atomic scattering factor for atom j.

APPENDIX *B*
Basic definitions

In the following, we give a short definition of the most important notions appearing in the theory and of the equivalence relations used in the tables. The latter are especially adapted to the case of modulated crystal phases.

[i] *Vector module*. A set of all integral linear combinations of a finite number of vectors. The *dimension* of the vector module is the dimension (m) of the space V (also indicated as V_E and called external) generated by it over the real numbers. Its *rank* (n) is the minimal number of rationally independent vectors that generate the vector module. If this rank is equal to the dimension, the vector module is also a lattice. In general, a vector module of rank n and dimension m is the orthogonal projection on the m-dimensional space V of an n-dimensional lattice. We shall restrict ourselves mainly to the case $m = 3$ and $n = 4$, but the following definitions are valid for modulated phases of arbitrary dimension and rank. The *dimension of the modulation* (d) is $n - m$. The modulation phases span a d-dimensional space V_I (called internal or additional).

[ii] *Superspace*. V_s is an n-dimensional Euclidean space that is the direct sum of an m-dimensional *external* space V (of the crystal) and a d-dimensional *internal* space V_I (for the additional degrees of freedom). V is sometimes denoted by V_E.

[iii] *Split basis*. For the space $V_s = V \oplus V_I$, this is a basis with m basis vectors in V and $d = n - m$ basis vectors in V_I.

[iv] *Standard basis*. For the $(m + d)$-dimensional space $V_s = V \oplus V_I$, a standard basis in direct space is one having the last d basis vectors lying in V_I (d = dimension of V_I = dimension of the modulation). A standard basis in

reciprocal space (V^* identified with V) is one with the first m basis vectors lying in V (m = dimension of V).

[v] *Conventional basis*. For a lattice Λ in three dimensions, it is a basis such that (i) the lattice generated by it is contained in Λ as a sublattice and (ii) there is the standard relationship between the basis vectors (*e.g.* for a cubic lattice a conventional basis consists of three mutually perpendicular vectors of equal length).

The lattice Λ is obtained from the lattice spanned by the conventional basis by adding (a small number of) *centring vectors*. [For example, the b.c.c. lattice is obtained from the conventional cubic lattice by centring the unit cell with $(\frac{1}{2}\frac{1}{2}\frac{1}{2})$.] The reciprocal basis for the conventional basis is a conventional basis for the reciprocal lattice Λ^*.

In the $(m+d)$-dimensional superspace, a conventional basis for the lattice Σ satisfies the same conditions (i) and (ii) as formulated above for the three-dimensional case. In addition, however, one requires that the basis is standard and such that the non-vanishing external components satisfy the relations of an ($m = 3$) conventional basis and that the corresponding internal components only involve the irrational components of the modulation vector(s) (for $d = 1$ the basis is such that $\mathbf{q}^r = 0$, thus $\mathbf{q}^i = \mathbf{q}$). Again a conventional basis for Σ^* is dual to the same for Σ.

[vi] *Holohedry*. The holohedry of a vector module is the group of orthogonal transformations of the same dimension that leaves the vector module invariant. The holohedry of an $(m+d)$-dimensional lattice is the subgroup of $O(m) \times O(d)$ that leaves the lattice invariant.

[vii] *Point group*. An $(m+d)$-dimensional crystallograhic point group $K_s = (K_E, K_I)$ is a subgroup of $O(m) \times O(d)$. With respect to a standard lattice basis its elements $R_s = (R, R_I)$ are of the form

$$\Gamma(R) = \begin{pmatrix} \Gamma_E(R) & 0 \\ \Gamma_M(R) & \Gamma_I(R) \end{pmatrix},$$

where all the entries are integers and R is an element of an m-dimensional point group K, which is actually the same as K_E. For an incommensurate modulated crystal, K_s and K are isomorphic groups. If $d = 1$, $\Gamma_I(R) = \varepsilon = \pm 1$.

[viii] *Geometric crystal class*. Two point groups $K_s = (K_E, K_I)$ and $K_s' = (K_E', K_I')$ of pairs (R_E, R_I) of orthogonal transformations [R_E belongs to $O(m)$ and R_I to $O(d)$] are geometrically equivalent if and only if there are orthogonal transformations T_E and T_I of $O(m)$ and $O(d)$, respectively, such that $R_E' = T_E \cdot R_E \cdot T_E^{-1}$ and $R_I' = T_I \cdot R_I \cdot T_I^{-1}$ for some group isomorphism $(R_E, R_I) \rightarrow (R_E', R_I')$. For $d = 1$, that condition takes a simpler form because $R_I = \varepsilon = \pm 1$.

[ix] *Arithmetic crystal class*. A group of integral matrices $\Gamma^*(R)$ [for $R \in K$ of $O(m)$] is determined on a basis $\{\mathbf{a}_i^*; i = 1, \ldots, n\} = \mathbf{a}^*, \mathbf{b}^*, \mathbf{c}^*, \mathbf{q}_1, \ldots, \mathbf{q}_d$ of a vector module in reciprocal space by an m-dimensional point group K (here $m = 3$). For modulated crystals, the transformations in direct space are given by matrices $\Gamma(R) =$ transpose of $\Gamma^*(R^{-1})$ which are of the form (9.8.4.17). Two groups $\Gamma'(K')$ and $\Gamma(K)$ are arithmetically equivalent if and only if there is an $(m+d)$-dimensional matrix S of the form

$$S = \begin{pmatrix} S_E & 0 \\ S_M & S_I \end{pmatrix}$$

with integral entries and determinant ± 1 such that $\Gamma'(K') = S\Gamma(K) \cdot S^{-1}$. Here S_E is $m \times m$ and S_I is $d \times d$ dimensional. An alternative formulation is: the matrix groups $\Gamma(K)$ and $\Gamma'(K')$ determined as in equation (9.8.1.16) or in equation (9.8.1.21) are arithmetically equivalent if

(*a*) the groups K and K' are geometrically equivalent m-dimensional point groups [the corresponding $(m+d)$-dimensional point groups K_s and K_s' are then also geometrically equivalent];

(*b*) there are vector module bases $\mathbf{a}^*, \ldots, \mathbf{q}_d$ and $\mathbf{a}^{*\prime}, \ldots, \mathbf{q}_d'$ such that K on the first basis gives the same group of matrices as K' on the second basis.

[x] *Bravais class*. Two vector modules are in the same Bravais class if the groups of matrices determined by their holohedries are arithmetically equivalent. Two $(m+d)$-dimensional lattices are in the same Bravais class if their holohedries are arithmetically equivalent. In both cases, one can find bases for the two structures such that the holohedries take the same matrix form. In the $(m+d)$-dimensional case, the lattice bases both have to be standard.

[xi] *Superspace group*. An $(m+d)$-dimensional superspace group is an n-dimensional space group ($n = m + d$) such that it has a d-dimensional lattice of internal translations. (This latter property reflects the periodicity of the modulation.) It is determined on a standard lattice basis by the matrices $\Gamma(R)$ of the point-group transformations and by the components $\upsilon_i(R)$ ($i = 1, \ldots, m+d$) of the translation parts of its elements. The matrices $\Gamma(R)$ represent at the same time the elements R of the m-dimensional point group K and the corresponding elements R_s of the $(n+d)$-dimensional point groups K_s. Two $(m+d)$-dimensional superspace groups are equivalent if there is an origin and a standard lattice basis for each group such that the collection $\{\Gamma(K), \upsilon_s(K)\}$ is the same for both groups. [In previous formulae, $\upsilon_s(R)$ is often simply indicated as υ_s.]

References

9.1

Andersson, S., Hyde, S. T. & von Schnering, H. G. (1984). *The intrinsic curvature of solids*. *Z. Kristallogr.* **168**, 1–17.

Brunner, G. O. (1971). *An unconventional view of the closest sphere packings*. *Acta Cryst.* A**27**, 388–390.

Conway, J. H. & Sloane, N. J. A. (1988). *Sphere packings, lattices and groups*. New York: Springer.

Ermer, O. (1988). *Fivefold-diamond structure of adamantane-1,3,5,7-tetracarboxylic acid*. *J. Am. Chem. Soc.* **110**, 3747–3754.

Ermer, O. & Eling, A. (1988). *Verzerrte Dreifach-Diamantstruktur von 3,3-Bis(carboxymethyl)glutarsäure (''Methantetraessigsäure'')*. *Angew. Chem.* **100**, 856–860.

Figueiredo, M. O. & Lima-de-Faria, J. (1978). *Condensed models of structures based on loose packings*. *Z. Kristallogr.* **148**, 7–19.

9.1 (*cont*)

Fischer, W. (1968). *Kreispackungsbedingungen in der Ebene*. *Acta Cryst*. A**24**, 67–81.

Fischer, W. (1970). *Homogene Kugelpackungen und ihre Existenzbedingungen in Raumgruppen tetragonaler Symmetrie*. Habilitationsschrift, Philipps-Universität Marburg, Germany.

Fischer, W. (1973). *Existenzbedingungen homogener Kugelpackungen zu kubischen Gitterkomplexen mit weniger als drei Freiheitsgraden*. *Z. Kristallogr*. **138**, 129–146.

Fischer, W. (1974). *Existenzbedingungen homogener Kugelpackungen zu Gitterkomplexen mit drei Freiheitsgraden*. *Z. Kristallogr*. **140**, 50–74.

Fischer, W. (1976). *Eigenschaften der Heesch–Laves-Packung und ihres Kugelpackungstyps*. *Z. Kristallogr*. **143**, 140–155.

Fischer, W. (1991*a*). *Tetragonal sphere packings. I. Lattice complexes with zero or one degree of freedom*. *Z. Kristallogr*. **194**, 67–85.

Fischer, W. (1991*b*). *Tetragonal sphere packings. II. Lattice complexes with two degrees of freedom*. *Z. Kristallogr*. **194**, 87–110.

Fischer, W. (1993). *Tetragonal sphere packings. III. Lattice complexes with three degrees of freedom*. *Z. Kristallogr*. **205**, 9–26.

Fischer, W. & Koch, E. (1976). *Durchdringungen von Kugelpackungen mit kubischer Symmetrie*. *Acta Cryst*. A**32**, 225–232.

Fischer, W. & Koch, E. (1987). *On 3-periodic minimal surfaces*. *Z. Kristallogr*. **179**, 31–52.

Fischer, W. & Koch, E. (1996). *Spanning minimal surfaces*. *Philos. Trans. R. Soc. London Ser. A*, **354**, 2105–2142.

Frank, F. C. & Kasper, J. S. (1958). *Complex alloy structures regarded as sphere packings. I. Definitions and basic principles*. *Acta Cryst*. **11**, 184–194.

Grünbaum, B. & Shephard, G. C. (1987). *Tilings and patterns*. New York: Freeman.

Haag, F. (1929). *Die Kreispackungen von Niggli*. *Z. Kristallogr*. **70**, 353–366.

Haag, F. (1937). *Die Polygone der Ebenenteilungen*. *Z. Kristallogr*. **96**, 78–80.

Hales, T. C. (1994). *The status of the Kepler conjecture*. *Math. Intelligencer*, **16**, 47–58.

Heesch, H. & Laves, F. (1933). *Über dünne Kugelpackungen*. *Z. Kristallogr*. **85**, 443–453.

Hellner, E. (1965). *Descriptive symbols for crystal-structure types and homeotypes based on lattice complexes*. *Acta Cryst*. **19**, 703–712.

Hellner, E. (1986). *Einführung in eine anorganische Strukturchemie*. *Z. Kristallogr*. **175**, 227–248.

Hellner, E., Gerlich, R., Koch, E. & Fischer, W. (1979). *The oxygen framework in garnet and its occurrence in the structures of* $Na_3Al_2Li_3F_{12}$, $Ca_3Al_2(OH)_{12}$, $RhBi_4$ *and* Hg_3TeO_6. *Physik Daten – Physics Data,* **16**(1), 1–40.

Hellner, E., Koch, E. & Reinhardt, A. (1981). *The homogeneous framework of the cubic crystal structures*. *Physik Daten – Physics Data*, **16**(2), 1–67.

Hilbert, D. & Cohn-Vossen, S. (1932). *Anschauliche Geometrie*. Berlin: Springer.

Hilbert, D. & Cohn-Vossen, S. (1952). *Geometry and the imagination*. New York: Chelsea.

Hsiang, W. Y. (1993). *On the sphere packing problem and the proof of Kepler's conjecture*. *Int. J. Math*. **4**, 739–831.

International Tables for Crystallography (1983). Vol. A. Dordrecht: Kluwer Academic Publishers.

International Tables for X-ray Crystallography (1972). Vol. II, 3rd ed. Birmingham: Kynoch Press.

Kitaigorodsky, A. I. (1946). *Arrangement of molecules in organic crystals*. Thesis, Moscow, Russia. [In Russian.]

Kitaigorodsky, A. I. (1961). *Organic chemical crystallography*. New York: Consultants Bureau. [Russian text published by Press of the Academy of Sciences of the USSR, Moscow, 1955.]

Kitaigorodsky, A. I. (1973). *Molecular crystals and molecules*. New York/London: Academic Press.

Koch, E. (1984). *A geometrical classification of cubic point configurations*. *Z. Kristallogr*. **166**, 23–52.

Koch, E. (1985). *The geometrical characteristics of the* α-$ThSi_2$ *structure type and of its parameter field*. *Z. Kristallogr*. **173**, 205–224.

Koch, E. & Fischer, W. (1978). *Types of sphere packings for crystallographic point groups, rod groups and layer groups*. *Z. Kristallogr*. **148**, 107–152.

Koch, E. & Fischer, W. (1995). *Sphere packings with three contacts per sphere and the problem of the least dense sphere packing*. *Z. Kristallogr*. **210**, 407–414.

Laves, F. (1930). *Die Bauzusammenhänge innerhalb der Kristallstrukturen*. *Z. Kristallogr*. **73**, 202–265.

Laves, F. (1932). *Zur Klassifikation der Silikate*. *Z. Kristallogr*. **82**, 1–14.

Lima-de-Faria, J. (1965). *Systematic derivation of inorganic close-packed structures: AX and* AX_2 *compounds, sequence of equal layers*. *Z. Kristallogr*. **122**, 359–374.

Lima-de-Faria, J. & Figueiredo, M. O. (1969*a*). *A table relating simple inorganic close-packed structure types*. *Z. Kristallogr*. **130**, 41–53.

Lima-de-Faria, J. & Figueiredo, M. O. (1969*b*). *Systematic derivation of inorganic basic structure types:* X_mY_n *and* A_mX_n *compounds, X and Y in cubic or hexagonal close packing, A in octahedral voids*. *Z. Kristallogr*. **130**, 54–67.

Loeb, A. (1958). *A binary algebra describing crystal structures with closely-packed anions*. *Acta Cryst*. **11**, 469–476.

Matsumoto, T. (1968). *Proof that the pgg packing of ellipses has never the maximum density*. *Z. Kristallogr*. **126**, 170–174.

Matsumoto, T. & Nowacki, W. (1966). *On densest packings of ellipsoids*. *Z. Kristallogr*. **123**, 401–421.

Matsumoto, T. & Tanemura, M. (1995). *Density of the p3 packing of ellipses*. *Z. Kristallogr*. **210**, 585–596.

Melmore, S. (1942*a*). *Open packing of spheres*. *Nature (London)*, **149**, 412.

Melmore, S. (1942*b*). *Open packing of spheres*. *Nature (London),* **149**, 669.

Minkowski, M. (1904). *Dichteste gitterförmige Lagerung kongruenter Körper*. *Nachr. Ges. Wiss. Göttingen Math. Phys. Kl*. p. 311.

Morris, I. L. & Loeb, A. (1960). *A binary algebra describing crystal structures with closely packed anions. Part II: a common system of reference for cubic and hexagonal structures*. *Acta Cryst*. **13**, 434–443.

Niggli, P. (1927). *Die topologische Strukturanalyse I. Z. Kristalllogr*. **65**, 391–415.

Niggli, P. (1928). *Die topologische Strukturanalyse II. Z. Kristallogr*. **68**, 404–466.

Nowacki, W. (1948). *Symmetrie und physikalisch–chemische Eigenschaften kristallisierter Verbindungen. V. Über Ellipsenpackungen in der Kristallebene*. *Schweiz. Mineral. Petrogr. Mitt*. **28**, 502–508.

O'Keeffe, M. (1991). *Dense and rare four-connected nets*. *Z. Kristallogr*. **196**, 21–37.

O'Keeffe, M. (1992). *Uninodal 4-connected 3D nets. II. Nets with 3-rings. Acta Cryst.* A**48**, 670–673.

O'Keeffe, M. (1998). *Sphere packings and space filling by congruent simple polyhdra. Acta Cryst.* A**54**, 320–329.

O'Keeffe, M. & Brese, N. E. (1992). *Uninodal 4-connected 3D nets. I. Nets without 3- or 4-rings. Acta Cryst.* A**48**, 663–669.

Schnering, H. G. von & Nesper, R. (1987). *Die natürliche Anpassung von chemischen Strukturen an gekrümmte Flächen. Angew. Chem.* **99**, 1097–1119.

Shubnikov, A. V. (1916). *On the structure of crystals. Izv. Akad. Nauk SSSR Ser.* 6, **10**, 755–799.

Sinogowitz, U. (1939). *Die Kreislagen und Packungen kongruenter Kreise in der Ebene. Z. Kristallogr.* **100**, 461–508.

Sinogowitz, U. (1943). *Herleitung aller homogenen nicht kubischen Kugelpackungen. Z. Kristallogr.* **105**, 23–52.

Slack, G. A. (1983). *The most-dense and least-dense packings of circles and spheres. Z. Kristallogr.* **165**, 1–22.

Smirnova, N. L. (1956*a*). *Structure types with atomic close packing: possible structure types for the composition AB_3. Sov. Phys. Crystallogr.* **1**, 128–131.

Smirnova, N. L. (1956*b*). *Structure types with closest atomic packing: possible structure types for the AB_4 composition. Sov. Phys. Crystallogr.* **1**, 399–401.

Smirnova, N. L. (1958*a*). *Structural types for close packing of atoms. III. Possible structures for the composition AB_6. Sov. Phys. Crystallogr.* **3**, 232–234.

Smirnova, N. L. (1958*b*). *On structural types with closest atomic packing. Possible structural types with the composition AB_{12}. Sov. Phys. Crystallogr.* **3**, 362–364.

Smirnova, N. L. (1959*a*). *The superstructures possible in close-packed structures. Sov. Phys. Crystallogr.* **4**, 10–16.

Smirnova, N. L. (1959*b*). *Possible superstructures in a simple cubic structure. Sov. Phys. Crystallogr.* **4**, 17–20.

Smirnova, N. L. (1959*c*). *Possible arrangement of atoms in the octahedral voids in the hexagonal close-packed structure. Sov. Phys. Crystallogr.* **4**, 734–737.

Smirnova, N. L. (1964). *Possible superstructures in the n-th layer of closest packing. B atoms have 4 or 2; or 4 or 1 nearest A atoms. Sov. Phys. Crystallogr.* **9**, 206–208.

Sowa, H. (1988). *Changes of the oxygen packing of low quartz and ReO_3-structure under high pressure. Z. Kristallogr.* **184**, 257–268.

Sowa, H. (1997). *Pressure-induced $Fm\bar{3}m \rightarrow R\bar{3}$ phase transition in $NaSbF_6$. Acta Cryst.* B**53**, 25–31.

Sowa, H. & Koch, E. (1999). *Sphere configurations with symmetry $R\bar{3}m$ 18(*h*).m. Z. Kristallogr. Submitted.*

Tanemura, M. & Matsumoto, T. (1992). *On the density of the p31m packing of ellipses. Z. Kristallogr.* **198**, 89–99.

Treacy, M. M. J., Randall, K. H., Rao, S., Perry, J. A. & Chadi, D. J. (1997). *Enumeration of periodic tetrahedral frameworks. Z. Kristallogr.* **212**, 768–791.

Wells, A. F. (1977). *Three-dimensional nets and polyhedra*. New York: John Wiley & Sons.

Wells, A. F. (1979). *Further studies of three-dimensional nets*. ACA Monograph No. 8.

Wells, A. F. (1983). *Six new three-dimensional 3-connected nets $4.n^2$. Acta Cryst.* B**39**, 652–654.

Zobetz, E. (1983). *Über Kugellagerungen, Wirkungsbereichsteilungen und Koordinationszahlen von Punktkonfigurationen mit trigonaler Symmetrie $R\bar{3}m$. Z. Kristallogr.* **163**, 167–180.

Adamsky, R. F. & Merz, K. M. (1959). *Synthesis and crystallography of the wurtzite form of silicon carbide. Z. Kristallogr.* **111**, 350–361.

Andrade, M., Chandrasekaran, M. & Delaey, L. (1984). *The basal plane stacking faults in 18R martensite of copper base alloys. Acta Metall.* **32**, 1809–1816.

Azaroff, L. V. (1960). *Introduction to solids*. London: McGraw-Hill.

Belov, N. V. (1947). *The structure of ionic crystals and metal phases*. Moscow: Izd. Akad. Nauk SSSR. [In Russian.]

Bertaut, E. F. (1978). *The equivalent charge concept and its application to the electrostatic energy of charges and multipoles. J. Phys. (Paris)*, **39**, 1331–1348.

Boerdijk, A. H. (1952). *Some remarks concerning close-packing of equal spheres. Philips Res. Rep.* **7**, 303–313.

Brafman, O., Alexander, E. & Steinberger, I. T. (1967). *Five new zinc sulphide polytypes: 10L(82); 14L (5423); 24L $(53)_3$; 26L (17 423) and 28L (9559). Acta Cryst.* **22**, 347–252.

Brafman, O. & Steinberger, I. T. (1966). *Optical band gap and birefringence of ZnS polytypes. Phys. Rev.* **143**, 501–505.

Buerger, M. J. (1953). *X-ray crystallography*. New York: John Wiley.

Chadha, G. K. (1977). *Identification of the rhombohedral lattice in CdI_2 crystals. Acta Cryst.* A**33**, 341.

Cottrell, A. (1967). *An introduction to metallurgy*. London: Edward Arnold.

Cowley, J. M. (1976). *Diffraction by crystals with planar faults. I. General theory. Acta Cryst.* A**32**, 83–87.

Dornberger-Schiff, K. & Farkas-Jahnke, M. (1970). *A direct method for the determination of polytype structures. I. Theoretical basis. Acta Cryst.* A**26**, 24–34.

Dubey, M. & Singh, G. (1978). *Use of lattice imaging in the electron microscope in the structure determination of the 126R polytype of SiC. Acta Cryst.* A**34**, 116–120.

Dubey, M., Singh, G. & Van Tendeloo, G. (1977). *X-ray diffraction and transmission electron microscopy study of extremely large-period polytypes in SiC. Acta Cryst.* A**33**, 276–279.

Farkas-Jahnke, M. (1983). *Structure determination of polytypes. Crystal growth and characterization of polytype structures*, edited by P. Krishna, pp. 163–211. Oxford: Pergamon Press.

Farkas-Jahnke, M. & Dornberger-Schiff, K. (1969). *A direct method for the determination of polytype structures. II. Determination of a 66R structure. Acta Cryst.* A**25**, 35–41.

Frank, F. C. (1951). *Crystal dislocation – elementary concepts and definitions. Philos. Mag.* **42**, 809–819.

Hendricks, S. & Teller, E. (1942). *X-ray interference in partially ordered layer lattices. J. Chem. Phys.* **10**, 147–167.

Honjo, G., Miyake, S. & Tomita, T. (1950). *Silicon carbide of 594 layers. Acta Cryst.* **3**, 396–397.

Jagodzinski, H. (1949*a*). *Eindimensionale Fehlordnung in Kristallen und ihr Einfluss auf die Rontgeninterferenzen. I. Berechnung des Fehlordnungsgrades aus den Rontgenintensitaten. Acta Cryst.* **2**, 201–207.

Jagodzinski, H. (1949*b*). *Eindimensionale Fehlordnung in Kristallen und ihr Einfluss auf die Rontgeninterferenzen.II. Berechnung de fehlgeordneten dichtesten Kugelpackungen mit Wechselwirkungen der Reichweite 3. Acta Cryst.* **2**, 208–214.

Jagodzinski, H. (1972). *Transition from cubic to hexagonal silicon carbide as a solid state reaction. Sov. Phys. Crystallogr.* **16**, 1081–1090.

9.2.1 (*cont.*)

Jain, P. C. & Trigunayat, G. C. (1977*a*). *On centrosymmetric space groups in close-packed MX_2-type structures*. *Acta Cryst.* A**33**, 255–256.

Jain, P. C. & Trigunayat, G. C. (1977*b*). *Resolution of ambiguities in Zhdanov notation: actual examples of homometric structures*. *Acta Cryst.* A**33**, 257–260.

Johnson, C. A. (1963). *Diffraction by FCC crystals containing extrinsic stacking faults*. *Acta Cryst.* **16**, 490–497.

Kabra, V. K. & Pandey, D. (1988). *Long range ordered phases without short range correlations*. *Phys. Rev. Lett.* **61**, 1493–1496.

Kabra, V. K., Pandey, D. & Lele, S. (1986). *On a diffraction approach for the study of the mechanism of 3C to 6H transformation in SiC*. *J. Mater. Sci.* **21**, 1654–1666.

Kabra, V. K., Pandey, D. & Lele, S. (1988*a*). *On the characterization of basal plane stacking faults in the N9R and N18R martensites*. *Acta Metall.* **36**, 725–734.

Kabra, V. K., Pandey, D. & Lele, S. (1988*b*). *On the calculation of diffracted intensities from SiC crystals undergoing 2H to 6H transformation by the layer displacement mechanism*. *J. Appl. Cryst.* **21**, 935–942.

Kakinoki, J. & Komura, Y. (1954). *Intensity of X-ray diffraction by a one-dimensionally disordered crystal. III. The close-packed structure*. *J. Phys. Soc. Jpn,* **9**, 177–183.

Krishna, P. & Marshall, R. C. (1971*a*). *The structure, perfection and annealing behaviour of SiC needles grown by a VLS mechanism*. *J. Cryst. Growth*, **9**, 319–325.

Krishna, P. & Marshall, R. C. (1971*b*). *Direct transformation from the 2H to 6H structure in single crystal SiC*. *J. Cryst. Growth*, **11**, 147–150.

Krishna, P. & Pandey, D. (1981). *Close-packed structures*. Teaching Pamphlet of the International Union of Crystallography. University College Cardiff Press.

Krishna, P. & Verma, A. R. (1962). *An X-ray diffraction study of silicon carbide structure types $[(33)_n34]_3R$*. *Z. Kristallogr.* **117**, 1–15.

Krishna, P. & Verma, A. R. (1963). *Anomalies in silicon carbide polytypes*. *Proc. R. Soc. London Ser. A*, **272**, 490–502.

Mesquita, A. H. G. de (1967). *Refinement of the crystal structure of SiC type 6H*. *Acta Cryst.* **23**, 610–617.

Mitchell, R. S. (1953). *Application of the Laue photograph to the study of polytypism and syntaxic coalescence in silicon carbide*. *Am. Mineral.* **38**, 60–67.

Nishiyama, Z. (1978). *Martensitic transformation*. New York: Academic Press.

Pandey, D. (1984*a*). *Stacking faults in close-packed structures: notations and definitions*. Deposited with the British Library Document Supply Centre as Supplementary Publication No. SUP 39176 (23 pp.). Copies may be obtained through The Managing Editor, International Union of Crystallography, 5 Abbey Square, Chester CH1 2HU, England.

Pandey, D. (1984*b*). *A geometrical notation for stacking faults in close-packed structures*. *Acta Cryst.* B**40**, 567–569.

Pandey, D. (1985). *Origin of polytype structures in CdI_2: application of faulted matrix model revisited*. *J. Cryst. Growth,* **71**, 346–352.

Pandey, D. (1988). *Role of stacking faults in solid state transformations*. *Bull. Mater. Sci.* **10**, 117–132.

Pandey, D., Kabra, V. K. & Lele, S. (1986). *Structure determination of one-dimensionally disordered polytypes*. *Bull. Minéral.* **109**, 49–67.

Pandey, D. & Krishna, P. (1975). *On the spiral growth of polytype structures in SiC from a faulted matrix. I. Polytypes based on the 6H structure*. *Mater. Sci. Eng.* **20**, 243–249.

Pandey, D. & Krishna, P. (1976*a*). *On the spiral growth of polytype structures in SiC from a faulted matrix. II. Polytypes based on the 4H and 15R structures*. *Mater. Sci. Eng.* **26**, 53–63.

Pandey, D. & Krishna, P. (1976*b*). *X-ray diffraction from a 6H structure containing intrinsic faults*. *Acta Cryst.* A**32**, 488–492.

Pandey, D. & Krishna, P. (1977). *X-ray diffraction study of stacking faults in single crystal of 2H SiC*. *J. Phys. D*, **10**, 2057–2068.

Pandey, D. & Krishna, P. (1982*a*). *Polytypism in close-packed structures*. *Current topics in materials science,* Vol. IX, edited by E. Kaldis, pp. 415–491. Amsterdam: North-Holland.

Pandey, D. & Krishna, P. (1982*b*). *X-ray diffraction study of periodic and random faulting in close-packed structures*. *Synthesis, crystal growth and characterization of materials*, edited by K. Lal, pp. 261–285. Amsterdam: North-Holland.

Pandey, D. & Krishna, P. (1983). *The origin of polytype structures*. *Crystal growth and characterization of polytype structures*, edited by P. Krishna, pp. 213–257. Oxford: Pergamon Press.

Pandey, D. & Lele, S. (1986*a*). *On the study of the FCC–HCP martensitic transformation using a diffraction approach. I. FCC→HCP transformation*. *Acta Metall.* **34**, 405–413.

Pandey, D. & Lele, S. (1986*b*). *On the study of the FCC–HCP martensitic transformation using a diffraction approach. II. HCP→FCC transformation*. *Acta Metall.* **34**, 415–424.

Pandey, D., Lele, S. & Krishna, P. (1980*a*). *X-ray diffraction from one-dimensionally disordered 2H crystals undergoing solid state transformation to the 6H structure. I. The layer displacement mechanism*. *Proc. R. Soc. London Ser. A*, **369**, 435–449.

Pandey, D., Lele, S. & Krishna, P. (1980*b*). *X-ray diffraction from one-dimensionally disordered 2H crystals undergoing solid state transformation to the 6H structure. II. The deformation mechanism*. *Proc. R. Soc. London Ser. A*, **369**, 451–461.

Pandey, D., Lele, S. & Krishna, P. (1980*c*). *X-ray diffraction from one-dimensionally disordered 2H crystals undergoing solid state transformation to the 6H structure. III. Comparison with experimental observations on SiC*. *Proc. R. Soc. London Ser. A*, **369**, 463–477.

Pandey, D., Prasad, L., Lele, S. & Gauthier, J. P. (1987). *Measurement of the intensity of directionally diffuse streaks on a 4-circle diffractometer: divergence correction factors for bisecting setting*. *J. Appl. Cryst.* **20**, 84–89.

Paterson, M. S. (1952). *X-ray diffraction by face-centred cubic crystals with deformation faults*. *J. Appl. Phys.* **23**, 805–811.

Patterson, A. L. & Kasper, J. S. (1959). *Close-packing*. *International tables for X-ray crystallography*, Vol. II, edited by J. S. Kasper & K. Lonsdale, pp. 342–354. Birmingham: Kynoch Press.

Prager, P. R. (1983). *Growth and characterization of AgI polytypes*. *Crystal growth and characterization of polytype structures*, edited by P. Krishna, pp. 451–491. Oxford: Pergamon Press.

Prasad, B. & Lele, S. (1971). *X-ray diffraction from double hexagonal close-packed crystals with stacking faults*. *Acta Cryst.* A**27**, 54–64.

Rai, R. S., Singh, S. R., Dubey, M. & Singh, G. (1986). *Lattice imaging studies on structure and disorder in SiC polytypes*. *Bull. Minéral.* **109**, 509–527.

9.2.1 (*cont.*)

Ramsdell, L. S. (1947). *Studies on silicon carbide. Am. Mineral.* **32**, 64–82.

Sebastian, M. T., Pandey, D. & Krishna, P. (1982). *X-ray diffraction study of the 2H to 3C solid state transformation of vapour grown single crystals of ZnS. Phys. Status Solidi A*, **71**, 633–640.

Steinberger, I. T. (1983). *Polytypism in zinc sulphide. Crystal growth and characterization of polytype structures*, edited by P. Krishna, pp. 7–53. Oxford: Pergamon Press.

Steinberger, I. T., Bordas, J. & Kalman, Z. H. (1977). *Microscopic structure studies of ZnS crystals using synchrotron radiation. Philos. Mag.* **35**, 1257–1267.

Taylor, A. & Jones, R. M. (1960). *The crystal structure and thermal expansion of cubic and hexagonal silicon carbide. Silicon carbide – a high temperature semiconductor*, edited by J. R. O'Connor & J. Smiltens, pp. 147–154. Oxford: Pergamon Press.

Terhell, J. C. J. M. (1983). *Polytypism in the III–VI layer compounds. Crystal growth and characterization of polytype structures*, edited by P. Krishna, pp. 55–109. Oxford: Pergamon Press.

Tokonami, M. & Hosoya, S. (1965). *A systematic method for unravelling a periodic vector set. Acta Cryst.* **18**, 908–916.

Trigunayat, G. C. & Verma, A. R. (1976). *Polytypism and stacking faults in crystals with layer structure. Crystallography and crystal chemistry of materials with layered structures*, edited by F. Levy, pp. 269–340. Dordrecht: Reidel.

Verma, A. R. & Krishna, P. (1966). *Polymorphism and polytypism in crystals*. New York: John Wiley.

Weertman, J. & Weertman, J. R. (1984). *Elementary dislocation theory*. New York: Macmillan.

Wells, A. F. (1945). *Structural inorganic chemistry*. Oxford: Clarendon Press.

Wilson, A. J. C. (1942). *Imperfection in the structure of cobalt. II. Mathematical treatment of proposed structure. Proc. R. Soc. London Ser. A*, **180**, 277–285.

Zhdanov, G. S. (1945). *The numerical symbol of close-packing of spheres and its application in the theory of close-packings. C. R. Dokl. Acad. Sci. URSS,* **48**, 43.

9.2.2

Amelinckx, S. (1986). *High-resolution electron microscopy in materials science. Examining the submicron world*, edited by R. Feder, J. W. McGowan & M. Shinozaki, pp. 71–132. New York: Plenum.

Angel, R. J. (1986). *Polytypes and polytypism. Z. Kristallogr.* **176**, 193–204.

Backhaus, K.-O. & Ďurovič, S. (1984). *Polytypism in micas. I. MDO polytypes and their derivation. Clays Clay Miner.* **32**, 453–464.

Bailey, S. W. (1980). *Structures of layer silicates. Crystal structures of clay minerals and their X-ray identification*, edited by G. M. Brindley & G. Brown, pp. 1–123. London: Mineralogical Society.

Bailey, S. W. (1988*a*) Editor. *Hydrous phyllosilicates* (*Reviews in mineralogy*, Vol. 19). Washington, DC: Mineralogical Society of America.

Bailey, S. W. (1988*b*). *X-ray diffraction indentification of the polytypes of mica, serpentine, and chlorite. Clays Clay Miner.* **36**, 193–213.

Bailey, S. W., Frank-Kamenetskii, V. A., Goldsztaub, S., Kato, A., Pabst, A., Schulz, H., Taylor, H. F. W., Fleischer, M. & Wilson, A. J. C. (1977). *Report of the International Mineralogical Association (IMA)–International Union of Crystallography (IUCr) Joint Committee on Nomenclature. Acta Cryst.* A**33**, 681–684.

Baronnet, A. (1975). *Growth spirals and complex polytypism in micas. I. Polytypic structure generation. Acta Cryst.* A**31**, 345–355.

Baronnet, A. (1986). *Growth spirals and complex polytypism in micas. II. Occurrence frequencies in synthetic species. Bull Minéral.* **109**, 489–508.

Baronnet, A. (1992). *Polytypism and stacking disorder. Reviews in mineralogy*, Vol. 27, pp. 231–288. Washington DC: Mineralogical Society of America.

Baumhauer, H. (1912). *Über die Kristalle des Carborundums. Z. Kristallogr.* **50**, 33–39.

Baumhauer, H. (1915). *Über die verschiedenen Modificationen des Carborundums und die Erscheinung der Polytypie. Z. Kristallogr.* **55**, 249–259.

Belokoneva, E. L. & Timchenko, T. I. (1983). *Polytypic relations in the structures of borates with a general formula* $RAl_3(BO_3)_4$ *(R = Y, Nd, Gd). Kristallografiya,* **28**, 1118–1123. [In Russian.]

Boer, J. L. de, van Smaalen, S., Petříček, V., Dušek, M., Verheijen, M. A. & Meijer, G. (1994). *Hexagonal close-packed C-60. Chem. Phys. Lett.* **219**, 469–472.

Bontchev, R., Darriet, B., Darriet, J., Weill, F., Van Tendeloo, G. & Amelinckx, S. (1993). *New cation deficient perovskite-like oxides in the system* $La_4Ti_3O_{12}$–$LaTiO_3$. *Eur. J. Solid State Inorg. Chem.* **30**, 521–537.

Brindley, G. W. (1980). *Order–disorder in clay mineral stuctures. Crystal structures of clay minerals and their X-ray identification*, edited by G. W. Brindley & G. Brown, pp. 125–195. London: Mineralogical Society.

Burany, X. M. & Northwood, D. O. (1991). *Polytypic structures in close-packed* $Zr(FeCr)_2$ *Laves phases. J. Less-Common Met.* **170**, 27–35.

Carlson, E. H. (1967). *The growth of HgS and* $Hg_3S_2Cl_2$ *single crystals by a vapour phase method. J. Cryst. Growth*, **1**, 271–277.

Chamberland, B. L. (1983). *Crystal structure of the 6H* $BaCrO_3$ *polytype. J. Solid State Chem.* **48**, 318–322.

Císařová, I., Novák, C. & Petříček, V. (1982). *The structure of twinned manganese(III) hydrogenbis(orthophosphite) dihydrate. Acta Cryst.* B**38**, 1687–1689.

Darriet, B., Bovin, J.-O. & Galy, J. (1976). *Un nouveau composé de l'antimoine III:* $VOSb_2O_4$. *Influence stéréochimique de la paire non lié E, relations structurales, mécanismes de la réaction chimique. J. Solid State Chem.* **19**, 205–212.

Dornberger-Schiff, K. (1959). *On the nomenclature of the 80 plane groups in three dimensions. Acta Cryst.* **12**, 173.

Dornberger-Schiff, K. (1964). *Grundzüge einer Theorie von OD-Strukturen aus Schichten. Abh. Dtsch. Akad. Wiss. Berlin. Kl. Chem.* **3**.

Dornberger-Schiff, K. (1966). *Lehrgang über OD-Strukturen*. Berlin: Akademie Verlag.

Dornberger-Schiff, K. (1979). *OD structures – a game and a bit more. Krist. Tech.* **14**, 1027–1045.

Dornberger-Schiff, K. (1982). *Geometrical properties of MDO polytypes and procedures for their derivation. I. General concept and applications to polytype families consisting of OD layers all of the same kind. Acta Cryst.* A**38**, 483–491.

9.2.2 (*cont.*)

Dornberger-Schiff, K., Backhaus, K.-O. & Ďurovič, S. (1982). *Polytypism of micas: OD interpretation, stacking symbols, symmetry relations. Clays Clay Miner.* **30**, 364–374.

Dornberger-Schiff, K. & Ďurovič, S. (1975*a*). *OD interpretation of kaolinite-type structures. I. Symmetry of kaolinite packets and their stacking possibilities. Clays Clay Miner.* **23**, 219–229.

Dornberger-Schiff, K. & Ďurovič, S. (1975*b*). *OD interpretation of kaolinite-type structures. II. The regular polytypes (MDO polytypes) and their derivation. Clays Clay Miner.* **23**, 231–246.

Dornberger-Schiff, K., Ďurovič, S. & Zvyagin, B. B. (1982). *Proposal for general principles for the construction of fully descriptive polytype symbols. Cryst. Res. Technol.* **17**, 1449–1457.

Dornberger-Schiff, K. & Fichtner, K. (1972). *On the symmetry of OD structures consisting of equivalent layers. Krist. Tech.* **7**, 1035–1056.

Dornberger-Schiff, K. & Grell, H. (1982*a*). *Geometrical properties of MDO polytypes and procedures for their derivation. II. OD families containing OD layers of M > 1 kinds and their MDO polytypes. Acta Cryst.* A**38**, 491–498.

Dornberger-Schiff, K. & Grell, H. (1982*b*). *On the notions: crystal, OD crystal and MDO crystal. Kristallografiya*, **27**, 126–133. [In Russian.]

Ďurovič, S. (1968). *The crystal structure of γ-$Hg_3S_2Cl_2$. Acta Cryst.* B**24**, 1661–1670.

Ďurovič, S. (1974*a*). *Notion of 'packets' in the theory of OD structures of M > 1 kinds of layers. Examples: kaolinites and MoS_2. Acta Cryst.* B**30**, 76–78.

Ďurovič, S. (1974*b*). *Die Kristallstruktur des $K_4[Si_8O_{18}]$: Eine desymmetrisierte OD-Struktur. Acta Cryst.* B**30**, 2214–2217.

Ďurovič, S. (1979). *Desymmetrization of OD structures. Krist. Tech.* **14**, 1047–1053.

Ďurovič, S. (1981). *OD-Charakter, Polytypie und Identifikation von Schichtsilikaten. Fortschr. Mineral.* **59**, 191–226.

Ďurovič, S. (1994). *Classification of phyllosilicates according to the symmetry of their octahedral sheets. Ceramics-Silikáty*, **38**, 81–84.

Ďurovič, S. & Dornberger-Schiff, K. (1981). *New fully descriptive polytype symbols for the basic types of clay minerals. 8th Conference on Clay Mineralogy and Petrology, Teplice, Czechoslovakia,* 1979, edited by S. Konta, pp. 19–25. Praha: Charles University.

Ďurovič, S., Dornberger-Schiff, K. & Weiss, Z. (1983). *Chlorite polytypism. I. OD interpretation and polytype symbolism of chlorite structures. Acta Cryst.* B**39**, 547–552.

Ďurovič, S. & Weiss, Z. (1983). *Polytypism of pyrophyllite and talc. Part I. OD interpretation and MDO polytypes. Silikáty*, **27**, 1–18.

Ďurovič, S., Weiss, Z. & Backhaus, K.-O. (1984). *Polytypism of micas. II. Classification and abundance of MDO polytypes. Clays Clay Miner.* **32**, 464–474.

Effenberger, H. (1991). *Structures of hexagonal copper(I) ferrite. Acta Cryst.* C**47**, 2644–2646.

Eggleton, R. A. & Guggenheim, S. (1994). *The use of electron optical methods to determine the crystal structure of a modulated phyllosilicate: parsettensite. Am. Mineral.* **79**, 426–437.

Evans, B. W. & Guggenheim, S. (1988). *Talc, pyrophyllite, and related minerals. Reviews in mineralogy*, Vol. 19, edited by S. W. Bailey, pp. 225–294. Washington, DC: Mineralogical Society of America.

Fichtner, K. (1965). *Zur Existenz von Gruppoiden verschiedener Ordnungsgrade bei OD-Strukturen aus gleichartigen Schichten. Wiss. Z. Tech. Univ. Dresden,* **14**, 1–13.

Fichtner, K. (1977). *Zur Symmetriebeschreibung von OD-Kristallen durch Brandtsche und Ehresmannsche Gruppoide. Beitr. Algebra Geom.* **6**, 71–79.

Fichtner, K. (1979*a*). *On the description of symmetry of OD structures (I). OD groupoid family, parameters, stacking. Krist. Tech.* **14**, 1073–1078.

Fichtner, K. (1979*b*). *On the description of symmetry of OD structures (II). The parameters. Krist. Tech.* **14**, 1453–1461.

Fichtner, K. (1980). *On the description of symmetry of OD structures (III). Short symbols for OD groupoid families. Krist. Tech.* **15**, 295–300.

Fichtner, K. & Grell, H. (1984). *Polytypism, twinning and disorder in 2,2-aziridinedicarboxamide. Acta Cryst.* B**40**, 434–436.

Fichtner-Schmittler, H. (1979). *On some features of X-ray powder patterns of OD structures. Krist. Tech.* **14**, 1079–1088.

Figueiredo, M. O. D. (1979). *Características de empilhamento e modelos condensados das micas e filossilicatos afins*. Lisboa: Junta de Investigacoes Científicas do Ultramar.

Franzini, M. (1969). *The A and B mica layers and the crystal structure of sheet silicates. Contrib. Mineral. Petrol.* **21**, 203–224.

Frueh, A. J. & Gray, N. (1968). *Confirmation and refinement of the structure of $Hg_3S_2Cl_2$. Acta Cryst.* B**24**, 156.

Gard, J. A. & Taylor, H. F. W. (1960). *The crystal structure of foshagite. Acta Cryst.* **13**, 785–793.

Grell, H. (1984). *How to choose OD layers. Acta Cryst.* A**40**, 95–99.

Grell, H. & Dornberger-Schiff, K. (1982). *Symbols for OD groupoid families referring to OD structures (polytypes) consisting of more than one kind of layer. Acta Cryst.* A**38**, 49–54.

Guinier, A., Bokij, G. B., Boll-Dornberger, K., Cowley, J. M., Ďurovič, S., Jagodzinski, H., Krishna, P., de Wolff, P. M., Zvyagin, B. B., Cox, D. E., Goodman, P., Hahn, Th., Kuchitsu, K. & Abrahams, S. C. (1984). *Nomenclature of polytype structures. Report of the International Union of Crysallography Ad-Hoc Committee on the Nomenclature of Disordered, Modulated and Polytype Structures. Acta Cryst.* A**40**, 399–404.

Hamid, S. A. (1981). *The crystal structure of the 11 Å natural tobermorite $Ca_{2.25}[Si_3O_{7.5}(OH)_{1.5}]\cdot 1H_2O$. Z. Kristallogr.* **154**, 189–198.

Heinrich, A. R., Eggleton, R. A. & Guggenheim, S. (1994). *Structure and polytypism of bementite, a modulated layer silicate. Am. Mineral.* **79**, 91–106.

Iijima, S. (1982). *High-resolution electron microscopy of mcGillite. II. Polytypism and disorder. Acta Cryst.* A**38**, 695–702.

Ingrin, J. (1993). *TEM imaging of polytypism in pseudowollastonite. Phys. Chem. Miner.* **20**, 56–62.

Ito, T., Sadanaga, R., Takéuchi, Y. & Tokonami, M. (1969). *The existence of partial mirrors in wollastonite. Proc. Jpn Acad.* **45**, 913-918.

Jagner, S. (1985). *On the origin of the order–disorder structures (polytypes) of some transition metal hexacyano complexes. Acta Chem. Scand.* **139**, 717–724.

Jagodzinski, H. (1964). *Allgemeine Gesichtspunkte für die Deutung diffuser Interferenzen von fehlgeordneten Kristallen. Advances in structure research by diffraction methods*, Vol. I, edited by R. Brill, pp. 167–198. Braunschweig: Vieweg, and New York/London: Interscience.

9.2.2 (*cont.*)

Jarchow, O. & Schmalle, H. W. (1985). *Fehlordnung, Polytypie und Struktur von Primetin: 5,8-Dihydroxy-2-phenylchromen-4-on*. *Z. Kristallogr.* **173**, 225–236.

Kaneko, F., Sakashita, H., Kobayashi, M., Kitagawa, Y., Matsuura, U. & Suzuki, M. (1994). *Double-layered polytypic structure of the E form of octadecanoic acid, $C_{18}H_{36}O_2$*. *Acta Cryst.* C**50**, 247–250.

Kowalski, M. (1985). *Polytypic structures of chromium iron [$(Cr,Fe)_7C_3$] carbides*. *J. Appl. Cryst.* **18**, 430–435.

Kuban, R.-J. (1985). *Polytypes of the system $Fe_{1-x}S$*. *Cryst. Res. Technol.* **20**, 1649–1656.

Kutschabsky, L., Kretschmer, R.-G., Schrauber, H., Dathe, W. & Schneider, G. (1986). *Structure of the OD disordered 2-hydroxy-4-methoxy-2H-1,4-benzoxazin-3-one, $C_9H_9NO_4$*. *Cryst. Res. Technol.* **21**, 1521–1529.

McLarnan, T. J. (1981*a*). *Mathematic tools for counting polytypes*. *Z. Kristallogr.* **155**, 227–245.

McLarnan, T. J. (1981*b*). *The number of polytypes of sheet silicates*. *Z. Kristallogr.* **155**, 247–268.

McLarnan, T. J. (1981*c*). *The number of polytypes in close packings and related structures*. *Z. Kristallogr.* **155**, 269–291.

Makovický, E., Leonardsen, E. & Moelo, Y. (1994). *The crystallography of lengenbachite, a mineral with the non-commensurate layer structure*. *N. Jahrb. Mineral. Abh.* **166**, 169–191.

Mellini, M., Merlino, S. & Pasero, M. (1986). *X-ray and HRTEM structure analysis of orientite*. *Am. Mineral.* **71**, 176–187.

Merlino, S., Orlandi, P., Perchiazzi, N., Basso, R. & Palenzona, A. (1989). *Polytypism in stibivanite*. *Can. Mineral.* **27**, 625–632.

Merlino, S., Pasero, M., Artioli, G. & Khomyakov, A. P. (1994). *Penkvilskite, a new kind of silicate structure – OD character, X-ray single-crystal (1M), and powder Rietveld (2O) refinements of 2 MDO polytypes*. *Am. Mineral* **79**, 1185–1193.

Merlino, S., Pasero, M. & Perchiazzi, N. (1993). *Crystal structure of paralaurionite and its OD relationship with laurionite*. *Mineral. Mag.* **57**, 323–328.

Merlino, S., Pasero, M. & Perchiazzi, N. (1994). *Fiedlerite – revised chemical formula ($Pb_3Cl_4F(OH)\cdot H_2O$), OD description and crystal-structure refinement of the 2 MDO polytypes*. *Mineral Mag.* **58**, 69–78.

Mogami, K., Nomura, K., Miyamoto, M., Takeda, H. & Sadanaga, R. (1978). *On the number of distinct polytypes of mica and SiC with a prime layer-number*. *Can. Mineral.* **16**, 427–435.

Müller, U. & Conradi, E. (1986). *Fehlordnung bei Verbindungen MX_3 mit Schichtenstruktur. I. Berechnung des Intensitätsverlaufs auf den Streifen der diffusen Röntgenstreuung*. *Z. Kristallogr.* **176**, 233–261.

Nikolin, B. I. (1984). *Multi-layer structures and polytypism in metallic alloys*. *Kiev: Naukova dumka*. [In Russian.]

Nikolin, B. I., Babkevich, A. Yu., Izdkovskaya, T. V. & Petrova, S. N. (1993). *Effect of heat-treatment on the crystalline structure of martensite in iron-doped, nickel-doped, manganese-doped and silicon-doped Co–W and Co–Mo alloys*. *Acta Metall.* **41**, 513–515.

Pasero, M. & Reinecke, T. (1991). *Crystal-chemistry, HRTEM analysis and polytypic behavior of ardennite*. *Eur. J. Mineral.* **3**, 819–830.

Pauling, L. (1930*a*). *Structure of micas and related minerals*. *Proc. Natl Acad. Sci. USA*, **16**, 123–129.

Pauling, L. (1930*b*). *Structure of the chlorites*. *Proc. Natl Acad. Sci. USA*, **16**, 578–582.

Phelps, A. W., Howard, W. & Smith, D. K. (1993). *Space groups of the diamond polytypes*. *J. Mater. Res.* **8**, 2835–2839.

Pring, A. & Graeser, S. (1994). *Polytypism in baumhauerite*. *Am. Mineral.* **79**, 302–307.

Radoslovich, E. W. (1961). *Surface symmetry and cell dimensions of layer-lattice silicates*. *Nature (London)*, **191**, 67–68.

Reck, G. & Dietz, G. (1986). *The order–disorder structure of carbamazepine dihydrate: 5H-dibenz[b,f]azepine-5-carboxamide dihydrate, $C_{15}H_{12}N_2O\cdot 2H_2O$*. *Cryst. Res. Technol.* **21**, 1463–1468.

Reck, G., Dietz, G., Laban, G., Günther, W., Bannier, G. & Höhne, E. (1988). *X-ray studies on piroxicam modifications*. *Pharmazie*, **43**, 477–481.

Ross, M., Takeda, H. & Wones, D. R. (1966). *Mica polytypes: systematic description and identification*. *Science*, **151**, 191–193.

Schwarz, W. & Blaschko, O. (1990). *Polytype structures of lithium at low-temperatures*. *Phys. Rev. Lett.* **65**, 3144–3147.

Sedlacek, P., Kuban, R.-J. & Backhaus, K.-O. (1987). *Structure determination of polytypes*. *Cryst. Res. Technol.* **22**, 793–798 (I), 923–928 (II).

Smaalen, S. van & de Boer, J. L. (1992). *Structure of polytype of the inorganic misfit-layer compound $(PbS)1.18TiS_2$*. *Phys. Rev B*, **46**, 2750–2757.

Smith, J. V. & Yoder, H. S. (1956). *Experimental and theoretical studies of the mica polymorphs*. *Mineral. Mag.* **31**, 209–235.

Sorokin, N. D., Tairov, Yu. M., Tsvetkov, V. F. & Chernov, M. A. (1982). *The laws governing the changes of some properties of different silicon carbide polytypes*. *Dokl. Akad. Nauk SSSR,* **262**, 1380–1383. [In Russian]. See also *Kristallografiya*, **28**, 910–914.

Szymański, J. T. (1980). *A redetermination of the structure of Sb_2VO_5, stibivanite, a new mineral*. *Can. Mineral.* **18**, 333–337.

Takéuchi, Y., Ozawa, T. & Takahata, T. (1983). *The pyrosmalite group of minerals. III. Derivation of polytypes*. *Can. Mineral.* **21**, 19–27.

Taxer, K. (1992). *Order–disorder and polymorphism of the compound with the composition of scholzite, $CaZn_2[PO_4]_2\cdot 2H_2O$*. *Z. Kristallogr.* **198**, 239–255.

Thompson, J. B (1981). *Polytypism in complex crystals: contrasts between mica and classical polytypes. Structure and bonding in crystals II*, edited by M. O'Keefe & A. Navrotsky, pp. 168–196. New York/London/Toronto/Sydney/San Francisco: Academic Press.

Tomaszewski, P. E. (1992). *Polytypism of α-$LiNH_4SO_4$ crystals*. *Solid State Commun.* **81**, 333–335.

Tsvetkov, V. F. (1982). *Problems and prospects of growing large silicon carbide single crystals*. *Izv. Leningr. Elektrotekh. Inst.* **302**, 14–19. [In Russian.]

Verma, A. J. & Krishna, P. (1966). *Polymorphism and polytypism in crystals*. New York: John Wiley.

Weiss, Z. & Ďurovič, S. (1980). *OD interpretation of Mg-vermiculite. Symbolism and X-ray identification of its polytypes*. *Acta Cryst.* A**36**, 633–640.

Weiss, Z. & Ďurovič, S. (1983). *Chlorite polytypism. II. Classification and X-ray identification of trioctahedral polytypes*. *Acta Cryst.* B**39**, 552–557.

Weiss, Z. & Ďurovič, S. (1985*a*). *Polytypism of pyrophyllite and talc. Part II. Classification and X-ray identification of MDO polytypes*. *Silikáty,* **28**, 289–309.

9.2.2 (*cont.*)

Weiss, Z. & Ďurovič, S. (1985*b*). *A unified classification and X-ray identification of polytypes of 2:1 phyllosilicates. 5th Meeting of the European Clay Groups, Prague*, 1983, edited by J. Konta, pp. 579–584. Praha: Charles University.

Weiss, Z. & Wiewióra, A. (1986). *Polytypism in micas. III. X-ray diffraction identification. Clays Clay Miner.* **34**, 53–68.

Wennemer, M. & Thompson, A. B. (1984). *Tridymite polymorphs and polytypes. Schweiz. Mineral. Petrogr. Mitt.* **64**, 335–353.

White, T. J., Segall, R. L., Hutchison, J. L. & Barry, J. C. (1984). *Polytypic behaviour of zirconolite. Proc. R. Soc. London Ser. A*, **392**, 343–358.

Yamanaka, T. & Mori, H. (1981). *The crystal structure and polytypes of α-$CaSiO_3$ (pseudowollastonite). Acta Cryst.* B**37**, 1010–1017.

Zhukhlistov, A. P., Zvyagin, B. B. & Pavlishin, V. I. (1990). *The polytype 4M of the Ti-biotite displayed on an oblique-texture electron-diffraction pattern. Kristallografiya,* **35**, 406–413. [In Russian.]

Zoltai, T. & Stout, J. H. (1985). *Mineralogy: concepts and principles*. Minneapolis, Minnesota: Burgess.

Zorkii, P. M. & Nesterova, Ya. M. (1993). *Interlayered polytypism in organic crystals. Zh. Fiz. Khim.* **67**, 217–220. [In Russian.]

Zvyagin, B. B. (1964). *Electron diffraction analysis of clay minerals*. Moskva: Nauka. [In Russian.]

Zvyagin, B. B. (1967). *Electron diffraction analysis of clay minerals*. New York: Plenum.

Zvyagin, B. B. (1988). *Polytypism in crystal structures. Comput. Math. Appl.* **16**, 569–591.

Zvyagin, B. B. & Fichtner, K. (1986). *Geometrical conditions for the formation of polytypes with a supercell in the basis plane. Bull. Minéral.* **109**, 45–47.

Zvyagin, B. B., Vrublevskaya, Z. V., Zhoukhlistov, A. P., Sidorenko, O. V., Soboleva, S. V. & Fedotov, A. F. (1979). *High-voltage electron diffraction in the investigation of layered minerals*. Moskva: Nauka [In Russian.]

9.3

Brunner, G. O. & Schwarzenbach, D. (1971). *Zur Abgrenzung der Koordinationsphäre und Ermittlung det Koordinationszahl in Kristallstrukturen. Z. Kristallogr.* **133**, 127–133.

Daams, J. L. C. (1995). *Atomic environments in some related intermetallic structure types. Intermetallic compounds, principles and practice*, edited by J. H. Westbrook & R. L. Fleischer, Vol. 1, pp. 363–383. New York: John Wiley.

Daams, J. L. C. & Villars, P. (1993). *Atomic-environment classification of the rhombohedral ''intermetallic'' structure types. J. Alloys Compd.* **197**, 243–269.

Daams, J. L. C. & Villars, P. (1994). *Atomic-environment classification of the hexagonal ''intermetallic'' structure types. J. Alloys Compd.* **215**, 1–34.

Daams, J. L. C. & Villars, P. (1997). *Atomic enironment classification of the tetragonal ''intermetallic'' structure types. J. Alloys Compd.* **252**, 110–142.

Daams, J. L. C., Villars, P. & van Vucht, J. H. N. (1991). *Atlas of crystal structure types for intermetallic phases*. Materials Park, OH: ASM International.

Daams, J. L. C., Villars, P. & van Vucht, J. H. N. (1992). *Atomic-environment classification of the cubic ''intermetallic'' structure types. J. Alloys Compd.* **182**, 1–33.

Kordes, E. (1939*a*). *Die Ermittlung von Atomabständen aus der Lichtbrechnung. I. Mitteilung. Über eine einfache Beziehung zwischen Ionenrefraktion, Ionenradius und Ordnungszahl der Elemente. Z. Phys. Chem. B*, **44**, 249–260.

Kordes, E. (1939*b*) *Die Ermittlung von Atomabständen aus der Lichtbrechnung. II. Mitteilung. Z. Phys. Chem. B*, **44**, 327–343.

Kordes, E. (1940). *Ionenradien und periodisches System. II. Mitteilung. Berechnung der Ionenradien mit Hilfe atomphysicher Grössen. Z. Phys. Chem.* **48**, 91–107.

Kordes, E. (1960). *Direkte Berechnung der Ionenradien allein aus den Ionen-abständen. Naturwissenschaften*, **47**, 463.

Pauling, L. (1947). *The nature of the interatomic forces in metals. II. Atomic radii and interatomic distances in metals. J. Am. Chem. Soc.* **69**, 542–553.

Pearson, W. B. (1979). *The stability of metallic phases and structures: phases with the AlB_2 and related structures. Proc. R. Soc. London Ser. A*, **365**, 523–535.

Rodgers, J. R. & Villars, P. (1988). *Computer evaluation of crystallographic data*. In *Proceedings of the 11th International CODATA Conference, Karlsruhe, FRG*, edited by P. S. Glaeser. New York: Hemisphere Publishing Corp.

Samsonov, G. V. (1968). Editor. *Handbook of physicochemical properties of elements*, p. 98. New York/Washington: IFI/Plenum Data Corporation.

Teatum, E. T., Gschneider, K. Jr & Waber, J. T. (1960). *Compilation of calculated data useful in predicting metallurgical behaviour of the elements in binary alloy systems*. USAEC Report LA–2345, 225 pp. Washington, DC: United States Atomic Energy Commission.

Teatum, E. T., Gschneider, K. Jr & Waber, J. T. (1968). *Compilation of calculated data useful in predicting metallurgical behaviour of the elements in binary alloy systems*. USAEC Report LA–4003, 206 pp. [Supercedes Report LA-2345 (1960).] Washington, DC: United States Atomic Energy Commission.

Villars, P. & Calvert, L. D. (1991). *Pearson's handbook of crystallographic data for intermetallic phases*, 2nd ed. Materials Park, OH: ASM International.

Villars, P. & Girgis, K. (1982). *Regelmäßigkeiten in binären intermetallischen Verbindungen. Z. Metallkd.* **73**, 455–462.

9.4

Bergerhoff, G. & Brown, I. D. (1987). *Inorganic crystal structure database*. In *Crystallographic databases*, edited by F. H. Allen, G. Bergerhoff & R. Sievers, pp. 77–95. Bonn/Cambridge/Chester: International Union of Crystallography.

International Tables for X-ray Crystallography (1962). Vol. III, pp. 257–274. Birmingham: Kynoch Press.

Sievers, R. & Hundt, R. (1987). *Crystallographic information system CRYSTIN*. In *Crystallographic databases*, edited by F. H. Allen, G. Bergerhoff & R. Sievers, pp. 210–221. Bonn/Cambridge/Chester: International Union of Crystallography.

9.5

Allen, F. H., Bellard, S., Brice, M. D., Cartwright, B. A., Doubleday, A., Higgs, H., Hummelink, T., Hummelink-Peters, B. G., Kennard, O., Motherwell, W. D. S., Rodgers, J. R. & Watson, D. G. (1979). *The Cambridge Crystallographic Data Centre: computer-based search, retrieval, analysis and display of information. Acta Cryst.* B**35**, 2331–2339.

9.5 (*cont.*)

Bergerhoff, G., Hundt, R., Sievers, R. & Brown, I. D. (1983). *The Inorganic Crystal Structure Database*. *J. Chem. Inf. Comput. Sci.* **23**, 66–70.

Cambridge Crystallographic Data Centre User Manual (1978). 2nd ed. Cambridge University, England.

Harmony, M. D., Laurie, V. W., Kuczkowski, R. L., Schwendemann, R. H., Ramsay, D. A., Lovas, F. J., Lafferty, W. J. & Maki, A. G. (1979). *Molecular structures of gas-phase polyatomic molecules determined by spectroscopic methods*. *J. Phys. Chem. Ref. Data*, **8**, 619–721.

Kennard, O. (1962). *Tables of bond lengths between carbon and other elements*. *International tables for X-ray crystallography*, Vol. III, Section 4.2, pp. 275–276. Birmingham: Kynoch Press.

Kennard, O., Watson, D. G., Allen, F. H., Isaacs, N. W., Motherwell, W. D. S., Pettersen, R. C. & Town, W. G. (1972). *Molecular structures and dimensions*, Vol. A1. *Interatomic distances 1960–65*. Utrecht: Oosthoek.

Sutton, L. E. (1958). *Tables of interatomic distances and configuration in molecules and ions*. Spec. Publ. No. 11. London: The Chemical Society.

Sutton, L. E. (1965). *Tables of interatomic distances and configuration in molecules and ions*. Spec. Publ. No. 18. London: The Chemical Society.

Taylor, R. & Kennard, O. (1983). *The estimation of average molecular dimensions from crystallographic data*. *Acta Cryst.* B**39**, 517–525.

Taylor, R. & Kennard, O. (1985). *The estimation of average molecular dimensions. 2. Hypothesis testing with weighted and unweighted means*. *Acta Cryst.* A**41**, 85–89.

Taylor, R. & Kennard, O. (1986). *Cambridge Crystallographic Data Centre. 7. Estimating average molecular dimensions from the Cambridge Structural Database*. *J. Chem. Inf. Comput. Sci.* **26**, 28–32.

9.6

Allen, F. H., Bellard, S., Brice, M. D., Cartwright, B. A., Doubleday, A., Higgs, H., Hummelink, T., Hummelink-Peters, B. G., Kennard, O., Motherwell, W. D. S., Rodgers, J. R. & Watson, D. G. (1979). *The Cambridge Crystallographic Data Centre*: *computer-based search, retrieval, analysis and display of information*. *Acta Cryst.* B**35**, 2331–2339.

Bergerhoff, G., Hundt, R., Sievers, R. & Brown, I. D. (1983). *The Inorganic Crystal Structure Database*. *J. Chem. Inf. Comput. Sci.* **23**, 66–70.

Brown, I. D., Brown, M. C. & Hawthorne, F. C. (1982). *BIDICS-1981, Bond index to the determinations of inorganic crystal structures*. Institute for Materials Research, Hamilton, Ontario, Canada.

Bruce, M. I. (1981). *Comprehensive organometallic chemistry*, Vol. 9, pp. 1209–1520. London; Pergamon Press.

Cambridge Crystallographic Data Centre User Manual (1978). 2nd ed. Cambridge University, England.

Harmony, M. D., Laurie, R. W., Kuczkowski, R. L., Schwendemann, R. H., Ramsay, D. A., Lovas, F. J., Lafferty, W. J. & Maki, A. G. (1979). *Molecular structures of gas-phase polyatomic molecules determined by spectroscopic methods*. *J. Phys. Chem. Ref. Data*, **8**, 619–721.

Kennard, O. (1962). *Tables of bond lengths between carbon and other elements*. *International tables for X-ray crystallography*, Vol. III, pp. 275–276. Birmingham: Kynoch Press.

Kennard, O., Watson, D. G., Allen, F. H., Isaacs, N. W., Motherwell, W. D. S., Pettersen, R. C. & Town, W. G. (1972). *Molecular structures and dimensions*, Vol. A1. *Interatomic distances, 1960–65*. Utrecht: Oosthoek.

Murray-Rust, P. & Raftery, J. (1985*a*). *J. Mol. Graphics*, **3**, 50–59.

Murray-Rust, P. & Raftery, J. (1985*b*). *J. Mol. Graphics*, **3**, 60–68.

Russell, D. R. (1988). *Specialist periodical reports, organometallic chemistry*, pp. 427–525. London: Royal Society of Chemistry.

Sutton, L. E. (1958). *Tables of interatomic distances and configuration in molecules and ions*. Spec. Publ. No. 11. London: Chemical Society.

Sutton, L. E. (1965). *Tables of interatomic distances and configuration in molecules and ions*. Spec. Publ. No. 18. London: Chemical Society.

Taylor, R. & Kennard, O. (1983). *The estimation of average molecular dimensions from crystallographic data*. *Acta Cryst.* B**39**, 517–525.

Taylor, R. & Kennard, O. (1985). *The estimation of average molecular dimensions. 2. Hypothesis testing with weighted and unweighted means*. *Acta Cryst.* A**41**, 85–89.

Taylor, R. & Kennard, O. (1986). *Cambridge Crystallographic Data Centre. 7. Estimating average molecular dimensions from the Cambridge Structural Database*. *J. Chem. Inf. Comput. Sci.* **26**, 28–32.

9.7

Allen, F. H., Davies, J. E., Galloy, J. J., Johnson, O., Kennard, O., Macrae, C. F., Mitchell, E. M., Smith, J. M. & Watson, D. G. (1991). *The development of versions 3 and 4 of the Cambridge Structural Database system*. *J. Chem. Inf. Comput. Sci.* **31**, 187–204.

Baker, R. J. & Nelder, J. A. (1978). *The GLIM System*. Release 3. Oxford: Numerical Algorithms Group.

Belsky, V. K., Zorkaya, O. N. & Zorky, P. M. (1995). *Structural classes and space groups of organic homomolecular crystals: new statistical data*. *Acta Cryst.* A**51**, 473–481.

Belsky, V. K. & Zorky, P. M. (1977). *Distribution of homomolecular crystals by chiral types and structural classes*. *Acta Cryst.* A**33**, 1004–1006.

Bertaut, E. F. (1995). *International tables for crystallography*, Vol. A, fourth, revised edition, Chap. 4.1. Dordrecht: Kluwer Academic Publishers.

Brock, C. P. & Dunitz, J. D. (1994). *Towards a grammar of crystal packing*. *Chem. Mater.* **6**, 1118–1127.

Coutanceau Clarke, J. A. R. (1972). *New periodic close packings of identical spheres*. *Nature (London)*, **240**, 408–410.

Donohue, J. (1985). *Revised space-group frequencies for organic compounds*. *Acta Cryst.* A**41**, 203–204.

Evans, R. C. (1964). *An introduction to crystal chemistry*. Cambridge University Press.

Filippini, G. & Gavezzotti, A. (1992). *A quantitative analysis of the relative importance of symmetry operators in organic molecular crystals*. *Acta Cryst.* B**48**, 230–234.

Gavezzotti, A. (1991). *Generation of possible crystal structures from the molecular structure for low-polarity organic compounds*. *J. Am. Chem. Soc.* **113**, 4622–4629.

9.7 (*cont.*)

Gavezzotti, A. (1994). *Molecular packing and correlations between molecular and crystal properties. Structure correlation* , Vol. 2, edited by H.-B. Bürgi & J. D. Dunitz, Chap. 12, pp. 509–542. Weinheim/New York/Basel/Cambridge/Tokyo: VCH Publishers.

Gibson, K. D. & Scheraga, H. A. (1995). *Crystal packings without symmetry constraints. 1. Test of a new algorithm for determining crystal structures by energy minimization. J. Phys. Chem.* **99**, 3752–3764.

Hahn, Th. (1995). Editor. *International tables for crystallography* , Vol. A, *Space-group symmetry*, fourth, revised edition. Dordrecht: Kluwer Academic Publishers.

Kitaigorodskii, A. I. (1961). *Organic chemical crystallography*. New York: Consultants Bureau.

Kitaigorodsky, A. I. (1945). *The close-packing of molecules in crystals of organic compounds. J. Phys. (Moscow)*, **9**, 351–352.

Kitaigorodsky, A. I. (1973). *Molecular crystals and molecules*. New York: Academic Press.

Kitajgorodskij, A. I. (1955). *Organicheskaya Kristallokhimiya*. Moscow: Academy of Science.

Lidin, S., Jacob, M. & Andersson, S. (1995). *A mathematical analysis of rod packings. J. Solid State Chem.* **114**, 36–41.

Mezey, P. G. (1993). *Shape in chemistry, an introduction into molecular shape and topology*. New York/Weinheim/Cambridge: VCH Publishers.

Mighell, A. D., Himes, V. L. & Rodgers, J. R. (1983). *Space-group frequencies for organic compounds. Acta Cryst.* A**39**, 737–740.

Nowacki, W. (1942). *Symmetrie und physikalisch-chemische Eigenschaften krystallisierter Verbindungen. I. Die Verteilung der Kristallstrukturen über die 219 Raumgruppen. Helv. Chim. Acta*, **25**, 863–878.

Nowacki, W. (1943). *Symmetrie und physikalisch-chemische Eigenschaften kristallisierter Verbindungen. II. Die allgemeinen Bauprinzipien organischer Verbindungen. Helv. Chim. Acta*, **26**, 459–462.

Padmaya, N., Ramakumar, S. & Viswamitra, M. A. (1990). *Space-group frequencies of proteins and of organic compounds with more than one formula unit in the asymmetric unit. Acta Cryst.* A**46**, 725–730.

Patterson, A. L. & Kasper, J. S. (1959). *Close packing. International tables for X-ray crystallography*, Vol. II, *Mathematical tables*, pp. 342–354. Birmingham: Kynoch Press.

Scaringe, R. P. (1991). *A theoretical technique for layer structure prediction. Electron crystallography of organic molecules*, edited by J. R. Fryer & D. L. Dorset, pp. 85–113. Dordrecht: Kluwer Academic Publishers.

Smith, A. J. (1973). *Periodic close packings of identical spheres. Nature (London) Phys. Sci.* **246**(149), 10–11.

Williams, D. E. G. (1987). *Close packing of spheres. J. Chem. Phys.* **87**, 4207–4210.

Wilson, A. J. C. (1980). *Testing the hypothesis 'no remaining systematic error' in parameter determination. Acta Cryst.* A**36**, 937–944.

Wilson, A. J. C. (1988). *Space groups rare for organic structures. I. Triclinic, monoclinic and orthorhombic crystal classes. Acta Cryst.* A**44**, 715–724.

Wilson, A. J. C. (1990). *Space groups rare for organic structures. II. Analysis by arithmetic crystal class. Acta Cryst.* A**46**, 742–754.

Wilson, A. J. C. (1991). *Space groups rare for molecular organic structures: the arithmetic crystal class mmmP. Z. Kristallogr.* **197**, 85–88.

Wilson, A. J. C. (1992). *International tables for crystallography*, Vol. C, *Mathematical, physical and chemical tables*, edited by A. J. C. Wilson, Chap. 9.7. Dordrecht: Kluwer Academic Publishers.

Wilson, A. J. C. (1993*a*). *Kitajgorodskij's categories. Acta Cryst.* A**49**, 210–212.

Wilson, A. J. C. (1993*b*). *Kitajgorodskij and space-group popularity. Acta Chim. Acad. Sci. Hung.* **130**, 183–196.

Wilson, A. J. C. (1993*c*). *Symmetry of organic crystalline compounds in the works of Kitajgorodskij. Kristallografiya*, **38**, 153–163. [In Russian.]

Wilson, A. J. C. (1993*d*). *Space groups rare for organic structures. III. Symmorphism and inherent molecular symmetry. Acta Cryst.* A**49**, 795–806.

9.8

Brouns, E., Visser, J. W. & de Wolff, P. M. (1964). *An anomaly in the crystal structure of Na_2CO_3. Acta Cryst.* **17**, 614

Brown, H. (1969). *An algorithm for the determination of space groups. Math. Comput.* **23**, 499–514.

Brown, H., Bülow, H., Neubüser, J., Wondratschek, H. & Zassenhaus, H. (1978). *Crystallographic groups of four-dimensional space*. New York: John Wiley.

Currat, R., Bernard, L. & Delamoye, P. (1986). *Incommensurate phase in β-$ThBr_4$. Incommensurate phases in dielectrics*, edited by R. Blinc & A. P. Levanyuk, pp. 161–203. Amsterdam: North-Holland.

Dam, B., Janner, A. & Donnay, J. D. H. (1985). *Incommensurate morphology of calaverite crystals. Phys. Rev. Lett.* **55**, 2301–2304.

Daniel, V. & Lipson, H. (1943). *An X-ray study of the dissociation of an alloy of copper, iron and nickel. Proc. R. Soc. London*, **181**, 368–377.

Dehlinger, U. (1927). *Über die Verbreiterung der Debyelinien bei kaltbearbeiteten Metallen. Z. Kristallogr.* **65**, 615–631.

Depmeier, W. (1986). *Incommensurate phases in PAMC: where are we now? Ferroelectrics*, **66**, 109–123.

Donnay, J. D. H. (1935). *Morphologie des cristaux de calaverite. Ann. Soc. Geol. Belg.* B**55**, 222-230.

Fast, G. & Janssen, T. (1969). *Non-equivalent four-dimensional generalized magnetic space–time groups*. Report 6–68, KU Nijmegen, The Netherlands.

Fast, G. & Janssen, T. (1971). *Determination of n-dimensional space groups by means of an electronic computer. J. Comput. Phys.* **7**, 1–11.

Goldschmidt, V., Palache, Ch. & Peacock, M. (1931). *Über Calaverit. Neues Jahrb. Mineral.* **63**, 1–58.

Grebille, D., Weigel, D., Veysseyre, R. & Phan, T. (1990). *Crystallography, geometry and physics in higher dimensions. VII. The different types of symbols of the 371 mono-incommensurate superspace groups. Acta Cryst.* A**46**, 234–240.

Heine, V. & McConnell, J. D. C. (1981). *Origin of modulated incommensurate phases in insulators. Phys. Rev. Lett.* **46**, 1092–1095.

Heine, V. & McConnell, J. D. C. (1984). *The origin of incommensurate structures in insulators. J. Phys. C*, **17**, 1199–1220.

Herpin, A., Meriel, P. & Villain, J. (1960). *Antiferromagnétisme hélicoïdal. J. Phys. Radium*, **21**, 67.

9.8 (*cont.*)

International Tables for Crystallography (1992). Vol. A, edited by Th. Hahn. Dordrecht: Kluwer Academic Publishers.

International Tables for Crystallography (1993). Vol. B, edited by U. Shmueli. Dordrecht: Kluwer Academic Publishers.

Janner, A. & Janssen, T. (1977). *Symmetry of periodically distorted crystals. Phys. Rev. B*, **15**, 643–658.

Janner, A., Janssen, T. & de Wolff, P. M. (1983). *Bravais classes for incommensurate crystal phases. Acta Cryst.* A**39**, 658–666; *Wyckoff positions used for the classification of Bravais classes of modulated crystals*, 667–670; *Determination of the Bravais class for a number of incommensurate crystals*, 671–678.

Janssen, T. (1969). *Crystallographic groups in space and time. III. Four-dimensional Euclidean crystal classes. Physica (Utrecht)*, **42**, 71–92.

Janssen, T. & Janner, A. (1987). *Incommensurability in crystals. Adv. Phys.* **36**, 519–624.

Janssen, T., Janner, A. & Ascher, E. (1969). *Crystallographic groups in space and time. I. General definitions and basic properties. Physica (Utrecht),* **41**, 541–565; *Crystallographic groups in space and time. II. Central extensions*, **42**, 41–70.

Janssen, T., Janner, A. & de Wolff, P. M. (1980). *Symmetry of incommensurate surface layers. Proceeding of Colloquium on Group-Theoretical Methods in Physics, Zvenigorod*, edited by M. Markov, pp. 155–166. Moscow: Nauka.

Jellinek, F. (1972). *Structural transitions of some transition-metal chalcogenides. Proceedings 5th Materials Research Symposium, Washington. NBS Publ.* No. 364, pp. 625–635.

Kind, R. & Muralt, P. (1986). *Unique incommensurate–commensurate phase transitions in a layer structure perovskite. Incommensurate phases in dielectrics*, edited by R. Blinc & A. P. Levanyuk, pp. 301–317. Amsterdam: North-Holland.

Koehler, W. C., Cable, J. W., Wollan, E. O. & Wilkinson, M. K. (1962). *Neutron diffraction study of magnetic ordering in thulium. J. Appl. Phys.* **33**, 1124–1125.

Koptsik, V. A. (1978). *The theory of symmetry of space modulated structures. Ferroelectrics*, **21**, 499.

Korekawa, M. (1967). *Theorie der Satellitenreflexe*. Habilitationsschrift der Ludwig-Maximilian Universität München, Germany.

Lifshitz, R. (1996). *The symmetry of quasiperiodic crystals. Physica (Utrecht)*, A**232**, 633–647.

McConnell, J. D. C. & Heine, V. (1984). *An aid to the structural analysis of incommensurate phases. Acta Cryst.* A**40**, 473–482.

Opechowski, W. (1986). *Crystallographic and metacrystallographic groups*. Amsterdam: North-Holland.

Paciorek, W. A. & Kucharczyk, D. (1985). *Structure factor calculations in refinement of a modulated crystal structure. Acta Cryst.* A**41**, 462–466.

Perez-Mato, J. M., Madariaga, G. & Tello, M. J. (1984). *Superspace transformation properties of incommensurate irreducible distortions. Modulated structure materials*, edited by T. Tsakalakos, pp. 151–159. Dordrecht: Nijhoff.

Perez-Mato, J. M., Madariaga, G. & Tello, M. J. (1986). *Diffraction symmetry of incommensurate structures. J. Phys. C*, **19**, 2613–2622.

Perez-Mato, J. M., Madariaga, G., Zuñiga, F. J. & Garcia Arribas, A. (1987). *On the structure and symmetry of incommensurate phases. A practical formulation. Acta Cryst.* A**43**, 216–226.

Petříček, V. & Coppens, P. (1988). *Structure analysis of modulated molecular crystals. III. Scattering formalism and symmetry considerations: extension to higher-dimensional space groups. Acta Cryst.* A**44**, 235–239.

Petricek, V., Coppens, P. & Becker, P. (1985). *Structure analysis of displacively modulated molecular crystals. Acta Cryst.* A**41**, 478–483.

Preston, G. D. (1938). *The diffraction of X-rays by age-hardening aluminium alloys. Proc. R. Soc. London*, **167**, 526–538.

Shechtman, D., Blech, I., Gratias, D. & Cahn, J. W. (1984). *Metallic phase with long-range orientational order and no translation symmetry. Phys. Rev. Lett.* **53**, 1951–1953.

Smaalen, S. van (1987). *Superspace-group description of short-period commensurately modulated crystals. Acta Cryst.* A**43**, 202–207.

Smith, G. F. H. (1903). *Über das bemerkenswerthe Problem der Entwickelung der Kristallformen des Calaverit. Z. Kristallogr.* **37**, 209–234.

Steurer, W. (1987). *(3+1)-dimensional Patterson and Fourier methods for the determination of one-dimensionally modulated structures. Acta Cryst.* A**43**, 36–42.

Tanisaki, S. (1961). *Microdomain structure in paraelectric phase of $NaNO_2$. J. Phys. Soc. Jpn,* **16**, 579.

Tanisaki, S. (1963). *X-ray study on the ferroelectric phase transition of $NaNO_2$. J. Phys. Soc. Jpn*, **18**, 1181.

Veysseyre, R. & Weigel, D. (1989). *Crystallography, geometry and physics in higher dimensions. V. Polar and mono-incommensurate point groups in the four-dimensional space $\mathbb{E}^4$. Acta Cryst.* A**45**, 187–193.

Weigel, D., Phan, T. & Veysseyre, R. (1987). *Crystallography, geometry and physics in higher dimensions. III. Geometrical symbols for the 227 crystallographic point groups in four-dimensional space. Acta Cryst.* A**43**, 294–304.

Wolff, P. M. de (1974). *The pseudo-symmetry of modulated crystal structures. Acta Cryst.* A**30**, 777–785.

Wolff, P. M. de (1977). *Symmetry considerations for displacively modulated structures. Acta Cryst.* A**33**, 493–497.

Wolff, P. M. de (1984). *Dualistic interpretation of the symmetry of incommensurate structures. Acta Cryst.* A**40**, 34–42.

Wolff, P. M. de, Janssen, T. & Janner, A. (1981). *The superspace groups for incommensurate crystal structures with a one-dimensional modulation. Acta Cryst.* A**37**, 625–636.

Wolff, P. M. de & Tuinstra, F. (1986). *The incommensurate phase of Na_2CO_3. Incommensurate phases in dielectrics*, edited by R. Blinc & A. P. Levanyuk, pp. 253–281. Amsterdam: North-Holland.

Yamamoto, A. (1982*a*). *A computer program for the refinement of modulated structures*. Report NIRIM, Ibaraki, Japan.

Yamamoto, A. (1982*b*). *Structure factor of modulated crystal structures. Acta Cryst.* A**38**, 87–92.

Yamamoto, A., Janssen, T., Janner, A. & de Wolff, P. M. (1985). *A note on the superspace groups for one-dimensionally modulated structures. Acta Cryst.* A**41**, 528–530.

Zassenhaus, H. (1948). *Über einen Algorithmus zur Bestimmung der Raumgruppen. Commun. Helv. Math.* **21**, 117–141.

10.1. Introduction

By D. C. Creagh and S. Martinez-Carrera

WARNING. In this section, the main objectives of protection from ionizing radiation will be discussed and such information as may be necessary for the interpretation of legal documents relating to radiation protection will be given. The material contained herein is drawn from a wide variety of sources but principally from Vol. 26 of the International Commission on Radiological Protection (1977) (ICRP, 1977) and Part 4 (AS-2243/4) of the Standards Association of Australia (1979).

It must be stressed that the recommendations made here have no legal force, nor indeed do either ICRP-26 or AS-2243/4. The precise legal requirements will be stipulated in government legislation and by the regulations pertaining to the laboratory in which the researcher is working.

Notwithstanding the legal requirements, a moral requirement exists for the operator of a laboratory involved in research with ionizing radiation to be aware of the dangers involved, and to take such steps as are necessary to ensure that both he* and his workers are fully educated in the protective measures to be taken to preserve their own safety.

In Vol. III of *International Tables for X-ray Crystallography*, Cook & Oosterkamp (1968) restricted their discussions, in the main, to the effects of X-rays and neutrons. However, with the increasing use of Mössbauer and other γ-ray techniques in crystallography and the development of nuclear magnetic resonance techniques involving the orientation of (radioactive) nuclei (NMRON), the scope of this chapter will be necessarily more general than that of *IT* III (1968).

Finally, since this chapter can have only an advisory nature and the final arbiter is the legislation of the state and local authority concerned, a list of countries that are known to have legislation concerning radiation protection is given in Table 10.3.1. Also shown in the table is the law under which control is effected and the authority responsible under the act for the implementation of radiation safety procedures. This list results from the return of questionnaires sent to all countries and is believed to be correct as of 1 October 1997.

10.1.1. Definitions

10.1.1.1. *Ionizing radiation*

Ionizing radiation is defined as radiation that by its nature and energy has the capacity to interact with and remove electrons from (*i.e.* ionize) the atoms of substances through which the radiation passes. Sufficiently energetic radiations may cause permanent changes in the nuclei of the atoms of the substance. Radiation may be propagated in the form of electromagnetic radiation (X-rays and γ-rays) or particles (β and α particles, neutrons, protons, and other nuclear particles).

In the list of definitions that follows SI units will be used. The relation between these SI units and the earlier system of units is given in Table 10.1.1.

10.1.1.2. *Absorbed dose*

The energy per unit mass imparted to matter by ionizing radiation at the place of interest [SI unit = gray (Gy)].

Table 10.1.1. *The relationship between SI and the earlier system of units*

Quantity	SI	Earlier
Absorbed dose [gray (Gy = J kg^{-1})]	1 J kg^{-1} 0.01 J kg^{-1}	100 rad 1 rad
Activity [becquerel (Bq = s^{-1})]	1 Bq 3.7 × 10^{10} Bq	2.7 × 10^{11} Ci 1 Ci
Dose equivalent [sievert (Sv = J kg^{-1})]	1 Sv 0.01 Sv	100 rem 1 rem
Exposure	1 C kg^{-1} 2.58 × 10^{-4} C kg^{-1}	3876 R 1 R

10.1.1.3. *Activity*

The number of nuclear transformations per unit time occurring in a radionuclide.

10.1.1.4. *Adequate protection*

Protection against ionizing radiations such that the radiation doses received by an individual from internal or external sources, or both, are as low as reasonably achievable and do not exceed the maximum levels given in Table 10.1.2.

10.1.1.5. *Background (radiation)*

Ionizing radiation other than that to be measured, but which contributes to the quantity being measured.

10.1.1.6. *Becquerel (Bq)*

The SI unit of activity 1 Bq corresponds to one nuclear transformation per second. It replaces the curie (Ci).

10.1.1.7. *Designated radiation area*

An area where the occupational exposure of personnel to radiation or radioactive material is under the supervision of a designated radiation safety officer.

10.1.1.8. *Dose equivalent*

Product of absorbed dose and quality factor (Subsection 10.1.1.24). This enables the dose received by individuals to be expressed on a scale common to all ionizing radiations. Where the term 'dose' is used without qualification it is implied that 'dose equivalent' is meant.

10.1.1.9. *Exposure of X-ray or γ-radiation*

A measure of the radiation at a certain place based on its ability to produce ionization in air. [SI unit = coulomb kg^{-1}. It replaces the röntgen (R).]

10.1.1.10. *External radiation*

Ionizing radiation received by the body from sources outside the body.

*In what follows, 'he', 'his' and similar pronouns are to be interpreted in a non-gender-specific manner.

Copyright © 2006 International Union of Crystallography

10.1.1.11. *Glove box*

A closed box having polymer gloves and viewing ports that is used to enclose completely radioactive materials whilst being manipulated.

10.1.1.12. *Gray (Gy)*

The SI unit of absorbed dose. [SI unit = 1 J kg^{-1}. It replaces the rad.]

10.1.1.13. *Half life*

The period of time in which half the nuclei in a given sample of a particular radionuclide undergo decay.

10.1.1.14. *Internal radiation*

Radiation received from the body from sources within the body.

10.1.1.15. *Irradiating apparatus*

Apparatus capable of producing ionizing radiation.

10.1.1.16. *Leakage radiation*

All radiation except the useful beam coming from within a protective housing.

10.1.1.17. *Licensable quantity*

The amount of any radionuclide or mixture thereof that is permitted under statutory regulations.

10.1.1.18. *Maximum permissible concentration*

The concentration of a radionuclide in the air when breathed or water when ingested that would result in an individual receiving the maximum permissible dose (to the whole body or to a specific organ depending on the radionuclide in question).

10.1.1.19. *Natural background*

Ionizing radiation received by the body from natural sources (cosmic radiation or naturally occurring radionuclides).

10.1.1.20. *Non-stochastic effects*

Effects on a biological system in which the severity of the effect varies with the dose and for which a threshold is likely to occur.

10.1.1.21. *Nuclide*

A species of atom characterized by the number of protons and neutrons in its nucleus.

10.1.1.22. *Occupied area*

An area that may be occupied by personnel and where a radiation hazard may exist.

10.1.1.23. *Protective housing*

A housing of an X-ray tube or of a sealed source intended to reduce the leakage radiation to a specified level.

10.1.1.24. *Quality factor (QF)*

A non-dimensional factor used to reduce the biological effects of radiation to a common scale (see Table 10.1.3).

10.1.1.25. *Radiation laboratory*

A laboratory in which irradiating apparatus or sealed radioactive sources are used or stored. It does not contain any unsealed radioactive material.

10.1.1.26. *Radioactive contamination*

The contamination of any material, surface or environment, or of a person by radioactive material.

10.1.1.27. *Radioactive material*

Any substance that consists of, or contains any, radionuclide provided that the activity of such material is greater than 0.1 Bq kg^{-1}.

10.1.1.28. *Radioisotope laboratory*

A laboratory in which unsealed radioactive material is used or stored. It does not contain any irradiating apparatus.

10.1.1.29. *Radiological hazard*

The potential danger to health arising from exposure to ionizing radiation.

10.1.1.30. *Radiological laboratory*

A laboratory in which unsealed radioactive material and/or sealed radioactive material or irradiating apparatus is used or stored.

10.1.1.31. *Radionuclide*

Species of atom that undergoes spontaneous nuclear transformation with consequent emission of corpuscular and/or electromagnetic radiations.

10.1.1.32. *Radiotoxicity*

The toxicity attributable to ionizing radiation emitted by a radionuclide (and its decay products). It is related to both radioactivity and chemical effects.

10.1.1.33. *Sealed source*

Any radioactive material firmly bonded within metals and sealed in a capsule or similar container of adequate mechanical strength so as to prevent dispersion of the active material into its surroundings under foreseeable conditions of use and wear.

10.1.1.34. *Sievert (Sv)*

The SI unit for dose equivalent.

10.1.1.35. *Stochastic effects*

Effects on a biological system in which the probability of an effect occurring rather than its severity is regarded as a function of dose without threshold.

10.1.1.36. *Unsealed source*

A source that is not a sealed source and that can produce contamination under normal conditions.

Table 10.1.2. *Maximum primary-dose limit per quarter [based on National Health and Medical Research Council (1977), as amended]*

Note: The annual MPD is typically twice the quarterly MPD

Part of body	MPD (i) (workers)	MPD (ii) (public)
Gonads, bone marrow, whole body	**30 mSv** (3 rem)	**2.5 mSv** (2.5 rem)
Skin, bone, thyroid	**150 mSv** (15 rem)	**15 mSv** (1.5 rem)
Hands, forearms, feet, ankles	**400 mSv** (40 rem)	**35 mSv** (3.5 rem)
Organs (including eye lens)	**80 mSv** (8 rem)	**7.5 mSv** (0.75 rem)
Abdomen of female of reproductive age	**13 mSv** (1.3 rem)	**1 mSv** (0.1 rem)
Foetus between diagnosis of and completion of a pregnancy	**10 mSv** (1 rem)	

Note: The maximum primary dose limits as set here are advisory only, and ultimately one should strive to achieve an MPD limit as low as reasonably achievable (often referred to by the acronym ALARA), economic and social factors being taken into account.

10.1.1.37. *Useful beam*

That part of the primary and secondary radiation that passes through the aperture, cone, or other device for collimating a beam of ionizing radiation.

10.1.2. Objectives of radiation protection

Radiation protection is concerned with the protection of individuals, their offspring, and society as a whole, at the same time allowing for the participation in activities for which radiation exposure might take place. There are two aspects of these deleterious effects: the somatic effects which become manifest in the individuals themselves, and the hereditary effects which become manifest in their descendants.

For the dose range involved in radiation protection, hereditary processes are regarded as being stochastic (thresholdless) processes. Some somatic effects are stochastic, and carcinogenesis is considered to be the chief risk at low doses and therefore a significant problem in radiation protection.

Non-stochastic processes are specific to particular tissues, *e.g.* damage to the cataract of the eye lens, non-malignant damage to the skin, damage to the bone marrow causing depletion of the red-cell count, and gonadal cell damage which impairs fertility. For these changes, the severity of the effect depends on the dose received and a clear threshold exists below which no detrimental effect has been found to occur.

A balance has to be achieved between the risk of damage to individuals and the benefits to society in the use of the ionizing radiation in experiments. Bearing this in mind:

Table 10.1.3. *Quality factors (QF)*

Type of radiation	QF
X-rays, γ-rays, and electrons	1
Neutrons, protons, singly charged particles of rest mass not greater than one atomic mass unit of unknown energy	10
α particles and multiply charged particules	20

1 Sv = (dose in grays) × QF.

(i) no practice ought to be adopted unless its introduction produces a positive net benefit;

(ii) all exposures should be kept as low as reasonably achievable under the existing economic and social circumstances;

(iii) the dose equivalent to individuals should not exceed the limits indicated in Table 10.1.2.

10.1.3. Responsibilities

10.1.3.1. *General*

In laboratories using ionizing radiations, a clearly defined chain of responsibility has to be established with the employer accepting the responsibility for the provision of services and equipment for the implementation of radiation-protection procedures under whatever legal or administrative procedures are valid for the country in question.

10.1.3.2. *The radiation safety officer*

The radiation safety officer (RSO) is responsible for the controlled areas within a given establishment. He (or she) is responsible to his employer for the implementation of a radiation-protection programme. His duties will vary according to the legislation and administrative arrangements applicable to his institution but will include, *inter alia*:

(i) giving advice on working practices to management and employees;

(ii) monitoring and surveying all controlled areas;

(iii) maintaining all equipment for monitoring radiation levels, including personal radiation monitoring devices;

(iv) keeping records of radiation levels in controlled areas, dosages to employees, stocks and locations of all radioactive materials and irradiating apparatus;

(v) keeping in safe custody all radioactive materials;

(vi) arranging the safe disposal of all radioactive waste;

(vii) preparing the local rules concerning accident safety and emergencies;

(viii) recording and reporting to the appropriate authorities all breaches of the radiation-protection rules.

10.1.3.3. *The worker*

In English common law, the employer is responsible for the actions of his employees but this does not absolve personnel from a duty of care to their fellows. Ultimately, the responsibility for radiation protection lies with the worker concerned. He (or she) should:

(i) ensure that he has an appropriate radiation dosimetry device and wears it;

(ii) inform the RSO whenever he is to work with radioactive materials or irradiating devices;

(iii) report to the RSO all known or suspected unsafe situations;

(iv) be aware of the directionality of scattered beams, particularly in the case of X-rays scattered from extended single crystals;

(v) be familiar with the relevant codes of practice as laid down in legislation and local instructions.

10.1.3.4. *Primary-dose limits*

Two classes of people are envisaged

(i) persons exposed to ionizing radiation in the course of the pursuance of their duties,

(ii) members of the general public.

In Table 10.1.2, the *maximum primary dose* (MPD) for those in class (i) and class (ii) is tabulated. SI units are shown in bold type, and the earlier units are shown in parentheses in light type.

Planned special exposures are permissible in emergency circumstances provided that in any single exposure twice the annual dose limit is not exceeded, and in a lifetime five times the limit.

Also, to allow for the different biological effectiveness of different types of radiation, the *quality factor* listed in Table 10.1.3 is applied to determine the dose.

References

Brodsky, A. (1982). Editor. *Handbook of radiation measurement and protection*, Vols I and II. Florida: CRC Press.

Cook, J. E. & Oosterkamp, P. W. J. (1968). *Protection against radiation injury*. *International tables for X-ray crystallography*, Vol. III, Chap 6, pp. 333–338. Birmingham: Kynoch Press.

International Commission on Radiological Protection (1977). *Recommendations of the International Commission on Radiological Protection* (adopted 17 January 1977). ICRP Publication 26. Oxford: Pergamon Press.

International Tables for X-ray Crystallography (1968). Vol. III. Birmingham: Kynoch Press.

National Heath and Medical Research Council (1977). *Revised radiation protection standards for individuals exposed to ionizing radiation* (as amended). ACT: NHMRC (Australia).

Standards Association of Australia (1979). *Safety in Laboratories*. Part 4. *Ionizing radiations*. AS-2243/4. Sydney: Standards Association of Australia.

Stott, A. M. B. (1983). *Radiation protection*. *Nuclear power and technology,* Vol. 3, edited by W. Marshall, pp. 50–77. Oxford: Clarendon Press.

Other publications containing relevant material

Information relevant to this part may be obtained from the sources listed below.

Recommendations of the International X-ray and Radiation Protection Commission (1931). *Br. J. Radiol.* **4**, 485.

International Commission on Radiological Protection, Clifton Avenue, Sutton, Surrey SM2 5PU, England.

International Commission on Radiation Units and Measurements, 7910 Woodmont Avenue, Suite 1016, Washington, DC 20013, USA.

International Atomic Energy Agency, Wagramerstrasse 5, PO Box 100, A-1400 Vienna, Austria.

World Health Organization, CH-1211 Genève 27, Switzerland.

National Health and Medical Research Council of Australia, PO Box 100, Woden, ACT 2606, Australia.

International Labour Organization, 4 route des Morillons, CH-1211 Genève 22, Switzerland.

OECD Nuclear Energy Agency, 38 Bd Suchet, F-75016 Paris, France.

National Committee on Radiation Protection and Measurement, C/- National Institute of Standards and Technology, Gaithersburg, MD 20899, USA.

Her Majesty's Stationery Office, PO Box 598, London SE1 9NH, England.

National Radiological Protection Board, Chilton, Didcot, Oxford OX11 0RQ, England.

Food and Drug Administration, 5600 Fishers Lane, Rockville, MD 20857, USA.

Hospital Physicists Association, 47 Belgrave Square, London SW1X 8QX, England.

National Competent Authorities Responsible for Approvals and Authorizations in Respect of the Transport of Radioactive Material (1997). List No. 28. International Atomic Energy Agency, Vienna.

International Tables for Crystallography (2006). Vol. C, Chapter 10.2, pp. 962–963.

10.2. Protection from ionizing radiation

By D. C. Creagh and S. Martinez-Carrera

10.2.1. General

Because of the diversity of apparatus for the generation of ionizing radiations and the significant differences that exist between laboratories within and between countries, it is not possible to give other than general guidelines as to the preventative measures to be taken.

It will be assumed here that the most likely sources of exposure will be X-ray generators and radioisotopes used in the manufacture of specimens for Mössbauer and NMRON use, for example. The basis for this assumption is the belief that establishments maintaining neutron and particle accelerator sources will have local regulations more stringent than those of the country in which they exist – certainly more stringent than those suggested in ICRP-26. They will also have a radiation protection officer who will discharge a list of duties similar to those stated in Subsection 10.1.3.2.

10.2.2. Sealed sources and radiation-producing apparatus

The types of source and apparatus covered in this section include: (1) sealed sources, such as those used for radiography, and for X-ray scattering experiments; (2) apparatus that produces ionizing radiations, such as X-ray generators and particle accelerators; (3) apparatus that produces ionizing radiation incidentally, such as electron microscopes, cathode-ray oscilloscopes, and high-voltage electronic rectifiers.

10.2.2.1. *Enclosed installations*

Most modern equipment is produced in such a form as to meet the prevailing radiation-protection regulations of the country in which it is sold, and care must be taken that safety circuits provided by the manufacturer are not defeated by staff members undertaking setting-up procedures. Such safety devices might cause visual or audible signals to be given and turn off power to the irradiating device.

Many early X-ray generators, electron microscopes, *etc*. have by modern standards inadequate radiation-protection facilities. Where practicable, therefore, special enclosures should be fabricated to house the apparatus producing the ionizing radiation. These should be designed such that:

(i) no person should have access to the interior during irradiation;

(ii) access should be prevented during irradiation by the provision of fail-safe interlocks that turn off the irradiating source;

(iii) no person should be able to remain in an enclosure during irradiation;

(iv) a means of rapid exit should be available to an individual should by chance he (she) be within a enclosure when irradiation commences;

(v) the source can be turned off from within the enclosure;

(vi) during operation the dose equivalent at any accessible surface outside the enclosure shall not exceed 25 mSv (2.5 rem) per hour;

(vii) when not in use, sealed sources should be capable of being housed, by remote control, within suitable shielding inside the enclosure;

(viii) all interlocks should be fail-safe enabling isolation of the source in the event of the loss of electrical power.

10.2.2.2. *Open installations*

An open installation because of operational requirements cannot have many of the safeguards suggested in Subsection 10.2.2.1. It is essential that extreme caution be exerted by the operators of such installations. They should bear in mind the following facts:

(i) almost all radiation injuries in X-ray diffraction laboratories are to the fingers of the operators and occur when setting up monochromators close to the radiation source. Necrosis of the skin occurs within seconds under these circumstances.

(ii) The beams scattered from single crystals are highly directional and very intense. Finding and monitoring these beams is usually difficult, and normal radiation monitors tend to underestimate the dose.

10.2.2.3. *Sealed sources*

Sealed sources ought to be manipulated only by remote means such as forceps and long tongs. Shielding should be close to the source to minimize the risk of scattered radiation reaching other workers.

Sealed sources should be registered by the RSO according to nature and activity. He (or she) is also responsible for their physical integrity and for regular examinations to detect corrosion or other damage.

Note that high-activity neutron sources can activate their immediate housings and give rise to additional radiation hazards.

10.2.2.4. *X-ray diffraction and X-ray analysis apparatus*

X-ray-generating devices such as sealed tubes and rotating-anode generators produce intense beams of small cross section and are capable of giving severe radiation burns within a second or so of exposure. Great care is necessary when working close to the exit port of these devices.

Apertures in the housing enclosing the X-ray source should be covered by a shutter when the source is not being used. Interlocking devices should exist to prevent the emission of X-rays when:

(i) the shutter is open without the analysing components and the beam stops being in place;

(ii) the analysing device is not properly in its position in relation to the housing.

Housings, shutters, shielded enclosures, and beam stops should be constructed such that the dose equivalent at any accessible point 0.05 m from their surface does not exceed 25 mSv for all practical operating conditions of the source.

Warning lights and illuminated signs should be fitted, interlocked such that they are lit when a shutter is open.

10.2.2.5. *Particle accelerators*

The codification of rules for the safe operation of high-energy particle accelerators is not simple because the various ionizing radiations produced by them require different protective procedures.

Particle accelerators ought to be operated in an enclosure from a remote control room in which the dose equivalent rate does not exceed 25 mSv h^{-1}. A lower dose rate (2.5 mSv h^{-1}) is required in adjacent areas used by non-radiation workers.

Copyright © 2006 International Union of Crystallography

The probability of mixed radiations (*e.g.* X-rays and neutrons) co-existing makes servicing hazardous and all maintenance should be performed under the supervision of the RSO.

10.2.3. Ionizing-radiation protection – unsealed radioactive materials

The most common controlled situation in which unsealed radioactive materials is used is in the construction of samples for use in Mössbauer experiments, NMRON experiments, and radioactive tracer experiments. Uncontrolled situations can occur, for example, whenever maintenance is being carried out on particle accelerators and neutron generators where radioactivity might be induced in the materials being handled by the particle beams. Great care should be taken to avoid the radioactive material being taken into the body by inhalation, ingestion or absorption through the skin or a wound.

Factors that influence the manner in which unsealed radioactive materials are handled include: its radiotoxicity, its volatility, the external radiation level, the nature of the work, and the design of the equipment and ultimately the design of the laboratory.

The decision concerning the manner of handling unsealed radioactive materials is the responsibility of the RSO and the safe implementaion is that of the worker.

A great many rules exist concerning the handling of this material, but in the final analysis the worker should:

(i) think the problem through, rehearsing his actions where possible;

(ii) use his common sense by minimizing the risk of breathing, eating or absorbing on his skin the radioactive material. In particular, eating, drinking or smoking in radioactive environments is to be avoided;

(iii) exercise caution and wear the appropriate protective clothing at all times;

(iv) be fully cognisant of the rules and regulations pertinent to the laboratory in which he is working. It is the duty of the RSO to ensure that this is so;

(v) ensure that he carries the appropriate radiation monitor and the RSO records his levels of exposure regularly;

(vi) have ready access to handbooks and textbooks on radiation safety, *e.g.* Brodsky (1982) and Stott (1983).

References

Brodsky, A. (1982). Editor. *Handbook of radiation measurement and protection*, Vols I and II. Florida: CRC Press.

Cook, J. E. & Oosterkamp, P. W. J. (1968). *Protection against radiation injury*. *International tables for X-ray crystallography*, Vol. III, Chap 6, pp. 333–338. Birmingham: Kynoch Press.

International Commission on Radiological Protection (1977). *Recommendations of the International Commission on Radiological Protection* (adopted 17 January 1977). ICRP Publication 26. Oxford: Pergamon Press.

International Tables for X-ray Crystallography (1968). Vol. III. Birmingham: Kynoch Press.

National Heath and Medical Research Council (1977). *Revised radiation protection standards for individuals exposed to ionizing radiation* (as amended). ACT: NHMRC (Australia).

Standards Association of Australia (1979). *Safety in Laboratories*. Part 4. *Ionizing radiations*. AS-2243/4. Sydney: Standards Association of Australia.

Stott, A. M. B. (1983). *Radiation protection*. *Nuclear power and technology,* Vol. 3, edited by W. Marshall, pp. 50–77. Oxford: Clarendon Press.

Other publications containing relevant material

Information relevant to this part may be obtained from the sources listed below.

Recommendations of the International X-ray and Radiation Protection Commission (1931). *Br. J. Radiol.* **4**, 485.

International Commission on Radiological Protection, Clifton Avenue, Sutton, Surrey SM2 5PU, England.

International Commission on Radiation Units and Measurements, 7910 Woodmont Avenue, Suite 1016, Washington, DC 20013, USA.

International Atomic Energy Agency, Wagramerstrasse 5, PO Box 100, A-1400 Vienna, Austria.

World Health Organization, CH-1211 Genève 27, Switzerland.

National Health and Medical Research Council of Australia, PO Box 100, Woden, ACT 2606, Australia.

International Labour Organization, 4 route des Morillons, CH-1211 Genève 22, Switzerland.

OECD Nuclear Energy Agency, 38 Bd Suchet, F-75016 Paris, France.

National Committee on Radiation Protection and Measurement, C/- National Institute of Standards and Technology, Gaithersburg, MD 20899, USA.

Her Majesty's Stationery Office, PO Box 598, London SE1 9NH, England.

National Radiological Protection Board, Chilton, Didcot, Oxford OX11 0RQ, England.

Food and Drug Administration, 5600 Fishers Lane, Rockville, MD 20857, USA.

Hospital Physicists Association, 47 Belgrave Square, London SW1X 8QX, England.

National Competent Authorities Responsible for Approvals and Authorizations in Respect of the Transport of Radioactive Material (1997). List No. 28. International Atomic Energy Agency, Vienna.

10.3. Responsible bodies

By D. C. Creagh and S. Martinez-Carrera

It has been stressed that the foregoing information is of an advisory nature only and that it has no legal force. Countries that have responded to the questionnaire on radiation safety produced by the Commission on Crystallographic Apparatus by 1 October 1997 are shown in Table 10.3.1. *It is to the regulatory authorities designated in Table 10.3.1 that questions on radiation safety should be referred.*

Table 10.3.1. *Regulatory authorities*

Country	Legislation	Proclaimed	Responsible authority
Argentina	—	—	Ministereo de Educacion, Conseuo Nacional de Investigacion Científica y Técnica.
Australia	Code of Practice for Protection Against Ionizing Radiation Emitted from X-ray Analaysis Equipment	1/6/84	National Health and Medical Research Council, PO Box 100, Woden, ACT 2606. Note: Each state and territory has its own specific regulations.
Austria	Strahlen Schutzgesetz (Radiation Protection Law)	11/6/69	Federal Ministry for Health and Environment Protection, Stubenring 1, A-1010 Wien.
Belgium	Protection of the Population Against the Hazards of Ionizing Radiations	29/3/58	Service de Protection Contrôles Radiations Ionisantes.
	Royal Decrees	12/3/94	Ministère de la Santé Publique, Cité Administrative de l'Etat, Quartier Vesale 2/3, B-1010 Bruxelles.
Brazil	Normas Bãsicas de Radioproteção (Basic Norms of Radiation Protection)	19/9/73	Comissão National de Energia Nuclear, Rua General Severiano, 90-Botafogo, 22.290, Rio de Janeiro.
Canada	Radiation Emitting Devices Regulations (1981)	—	Radiation and Protection Bureau, Health and Welfare (Canada), Ottawa, Ontario K1A 0K9.
Chile	Decree Concerning Radiological Protection (1976)	—	Comisión Nacional de Investigacion, Cientifica y Tecnologica, Cassilia 308, Santiago.
China	—	—	National Environmental Protection Agency, 115 Nanxiaouie, Xizhemen, Beijing 100035.
Cyprus	—	—	Senior Medical Physicist, Nicosia General Hospital, Nicosia.
Czech Republic	Act of the Ministry of Health of the Czech Republic	30/6/72	State Office for Nuclear Security, Sleszka 9, 12029 Praha 2.
	Czechoslovak State Norm No. 341725	24/7/68	
Denmark	Order Concerning X-ray Analytical Equipment	15/4/30	National Institute of Radiation Hygiene, 378 Fredrikssundsvej, DK-2700 Brønshøj, Copenhagen.
Egypt	—	—	Atomic Energy Authority, 101 Kasr El-Eini Street, Cairo.
Finland	Radiation Protection Act	26/4/57	Finnish Centre for Radiation and Protection, PO Box 14, FIN-00881 Helsinki.

Copyright © 2006 International Union of Crystallography

Table 10.3.1. *Regulatory authorities (cont.)*

Country	Legislation	Proclaimed	Responsible authority
France	—	—	Ministère de la Santé Publique, 31 rue de l'Ecluse, BP 35, 78110 Levesinet.
			CEA, 31–33 rue de la Fédération, 75752 Paris CEDEX 15.
Germany	Gesetz über die friedliche Verwendung der Kernenergie und den Schutz gegen ihre Gefahren (Atomgesetz)	23/12/59	Bundesministerium für Verkehr, Referat A 13, Robert-Schumann Platz, D-53175 Bonn.
	Verordnung über den Schutz vor Schäden durch Ionisierende Strahlen (Strahlenschutz Verordnung)	13/10/78	
	Verordnung über den Schutz vor Schäden durch Röntgenstrahlen (Röntgen Verordnung)	8/1/87	
Greece	Protection from Ionizing Radiation	18/1/74	Greek Atomic Energy Commission, 153 10 Aghia paraskevi-Attiki, PO Box 60228.
Hungary	Act 1/1980	1/6/80	National Atomic Energy Commission, 1374 Budapest Pf 365.
India	Atomic Energy Act of 1962	1962	Indian Atomic Energy Regulatory Board, 4th Floor, Vikram Sarabhai Bkavan Anushaktinagar, Bombay 400 094.
Ireland	Order No. 166, Nuclear Energy Act of 1971	1971	Nuclear Energy Board, 20–22 Lr Hatch Street, Dublin 2.
	Sealed Sources SI No. 17	1972	
	Unsealed Sources SI No. 249	1972	
Israel	Occupational Radiation Protection Regulation of 1981	1981	The Licensing Division, Israeli Atomic Energy Commission, PO Box 7061, Tel Aviv 61070.
	Employment of Women	1980	
Italy	Legislative Act No. 185	13/2/64	Nuclear Safety and Health Protection Directorate, ENEA, Via Vitaliano, Brancati 48, 00144 Rome-EUR.
Japan	The Atomic Energy Basic Law; Law concerning Prevention from Radiation Hazards due to Radioisotopes *etc*.	—	Radiation Council, 2-2-1 Kasumigaseki, Chiyoda-ku, Tokyo.
Korea, South	The Atomic Energy Law	11/3/58	Atomic Energy Bureau, Ministry of Science and Technology, The Second Integrated Government Building, Gwacheon, Kyunggi-D, 427 760.
New Zealand	Radiation Protectin Act	1965	National Radiation Laboratory, Department of Health, PO Box 25-099, Christchurch.
Norway	Act Relating to the Use of X-rays, Radium, *etc*.	18/6/38	National Institute of Radiation Hygiene, PO Box 55, N-1345 Østeras.
Pakistan	Pakistan Nuclear Safety and Radiation Protection Ordinance No. IV of 1984	26/1/84	Pakistan Atomic Energy Commission, Directorate of Nuclear Safety and Radiation Protection, PO Box 1912, Islamabad.

Table 10.3.1. *Regulatory authorities (cont.)*

Country	Legislation	Proclaimed	Responsible authority
Peru	—	—	Insituto Peruano de Energia Nuclear, Direccion de Seguridad Nuclear y Proteccion Radiologica, Direccion Av. Canada No. 1470, Lima 41.
Portugal	Normas Cerais parra Protecção das Pessons contra as Radiações Ionizantes	25/11/61	Ministerio da Suude, Direccao-Geral da saude, Almeda D. Alfonso Henriques, 45, P-1056, Lisboa Codex.
Russian Federation	—	—	Ministry for Atomic Energy, Committee on Safety, Ecology, and Emergency Situations, ul. B. Ordynka 24/26, 101000 Moscow.
Singapore	The Radiation Protection Act 19B and Regulations 1974	1/9/74	Radiation Protection Inspectorate, Department of Scientific Services, Outram Road, Singapore 0316.
Slovak Republic	Act of the Ministry of Health of the Slovak Socialist Republic No. 65	12/9/72	Ministry of Health of the Slovak Republic, Limbová 2, SK-83341 Bratislava.
	Czechoslovak State Norm No. 451725	24/7/68	
Spain	Ley Reguladora de la Energia Nuclear	29/4/64	Consejo de Seguridad Nuclear, Paseo de La Castellana 135, Madrid.
	Reglamento Sobre Instalaciones Nucleares y Radiactivas	21/7/72	
	Reglamento s. Protection-Sanitaria contra Radiaciones Ionizantes	8/10/82	
South Africa	—	—	Deparment of Health and Welfare, Civitas Building, Cnr Andrew Struken St, Pretoria 0001 (Private Bag X63).
Sweden	Act Concerning Protection Against Radiation	14/3/58	Swedish Radiation Protection Institute, S-17116 Stockholm.
Switzerland	Federal Order (1980)	—	Office Fédéral de la Santé Publique, Division of Radiation Protection, CH-3003 Berne.
Turkey	Radiological Health and Safety	1967	Turkish Atomic Energy Authority, Radiological Health and Safety Department, Karantil Sk. No. 67, Bakanliklar-Ankara.
United Kingdom	Health and Safety at Work Act	1974	Health and Safety Executive, Rose Court, 2 Southwark Bridge, London SE1 9HS.
	Ionizing Radiation Regulations	1/1/86	
United States of America	Atomic Energy Act of 1954	1954	Nuclear Regulatory Commission, Matomic Building, 1717th Street NW, Washington, DC 20555.
	Executive Order 10831		Department of Energy, Forestal Building, 1000 Independence Avenue SW, Washington, DC 20585.

References

Brodsky, A. (1982). Editor. *Handbook of radiation measurement and protection*, Vols I and II. Florida: CRC Press.

Cook, J. E. & Oosterkamp, P. W. J. (1968). *Protection against radiation injury*. *International tables for X-ray crystallography*, Vol. III, Chap 6, pp. 333–338. Birmingham: Kynoch Press.

International Commission on Radiological Protection (1977). *Recommendations of the International Commission on Radiological Protection* (adopted 17 January 1977). ICRP Publication 26. Oxford: Pergamon Press.

International Tables for X-ray Crystallography (1968). Vol. III. Birmingham: Kynoch Press.

National Heath and Medical Research Council (1977). *Revised radiation protection standards for individuals exposed to ionizing radiation* (as amended). ACT: NHMRC (Australia).

Standards Association of Australia (1979). *Safety in Laboratories*. Part 4. *Ionizing radiations*. AS-2243/4. Sydney: Standards Association of Australia.

Stott, A. M. B. (1983). *Radiation protection*. *Nuclear power and technology,* Vol. 3, edited by W. Marshall, pp. 50–77. Oxford: Clarendon Press.

Other publications containing relevant material

Information relevant to this part may be obtained from the sources listed below.

Recommendations of the International X-ray and Radiation Protection Commission (1931). *Br. J. Radiol.* **4**, 485.

International Commission on Radiological Protection, Clifton Avenue, Sutton, Surrey SM2 5PU, England.

International Commission on Radiation Units and Measurements, 7910 Woodmont Avenue, Suite 1016, Washington, DC 20013, USA.

International Atomic Energy Agency, Wagramerstrasse 5, PO Box 100, A-1400 Vienna, Austria.

World Health Organization, CH-1211 Genève 27, Switzerland.

National Health and Medical Research Council of Australia, PO Box 100, Woden, ACT 2606, Australia.

International Labour Organization, 4 route des Morillons, CH-1211 Genève 22, Switzerland.

OECD Nuclear Energy Agency, 38 Bd Suchet, F-75016 Paris, France.

National Committee on Radiation Protection and Measurement, C/- National Institute of Standards and Technology, Gaithersburg, MD 20899, USA.

Her Majesty's Stationery Office, PO Box 598, London SE1 9NH, England.

National Radiological Protection Board, Chilton, Didcot, Oxford OX11 0RQ, England.

Food and Drug Administration, 5600 Fishers Lane, Rockville, MD 20857, USA.

Hospital Physicists Association, 47 Belgrave Square, London SW1X 8QX, England.

National Competent Authorities Responsible for Approvals and Authorizations in Respect of the Transport of Radioactive Material (1997). List No. 28. International Atomic Energy Agency, Vienna.

Author Index

Entries refer to part, chapter or section numbers

Abele, R. K., 7.3
Åberg, T., 7.4.3
Abragam, A., 2.6.2
Abrahams, J. M., 7.1.6
Abrahams, K., 4.4.2
Abrahams, S. C., 1.4, 4.2.2, 4.2.6, 5.3, 6.2, 8.1, 8.5, 9.2.2
Abramowitz, M., 6.1.1, 6.3, 7.5
Achiwa, N., 2.9
Ackermann, I., 4.3.7
Adams, L. H., 3.2
Adamsky, R. F., 9.2.1
Adlhart, W., 3.4
Agamalyan, M. M., 4.4.2
Agarwal, B. K., 4.2.6
Ahahama, Y., 4.2.5
Ahlrichs, R., 6.1.1
Ahmed, A., 5.2
Ahn, C. C., 4.3.4, 7.2
Ahtee, M., 2.3, 8.6
Airey, R. W., 7.1.6
Akashi, Y., 5.3
Akhiezer, A. I., 4.2.6
Akiyoshi, T., 2.9
Alani, R., 3.5
Albers, R. C., 4.2.3
Albertsson, J., 5.3
Albinati, A., 8.6
Alcock, N. W., 5.3, 6.3
Aldred, P. J. E., 4.2.6
Alefeld, B., 2.6.2, 4.4.2
Aleksandrov, K. S., 3.1
Alexander, E., 9.2.1
Alexander, H., 4.3.8
Alexander, L., 5.2, 5.3
Alexander, L. E., 2.3, 3.4, 5.1, 5.3, 6.2
Alexander, T. K., 4.4.2
Alexandropoulos, N. G., 7.4.3
Alkire, R. W., 3.4
Allemand, R., 2.4.2, 7.1.6, 7.3
Allen, F. H., 9.5, 9.6, 9.7
Allen, J. P., 3.1
Allen, S., 3.4
Allen, S. J. M., 4.2.4
Allewell, N. M., 3.4
Allin, G. W., 7.3
Allington-Smith, J. R., 7.1.6
Allinson, N. M., 2.7, 7.1.6
Allison, S. K., 2.3, 2.7, 4.2.1, 5.3
Allsopp, D. W. E., 2.7
Alp, E. E., 5.3
Alstrup, I., 4.2.3, 4.2.6
Alstrup, O., 2.5.1
Altarelli, M., 4.3.4
Alter, U., 5.3
Altmann, S. L., 6.1.1
Altomare, A., 8.6
Alvarez, L. W., 4.2.3, 4.4.2
Amadori, R., 4.4.2
Amelinckx, S., 3.5, 4.3.8, 9.2.2
Amemiya, Y., 7.1.6, 7.1.8
Ames, L., 7.1.4
Ammon, H. L., 3.1
Amorós, J. L., 2.2, 5.3
Amorós, M. C., 2.2, 5.3
d'Amour, H., 5.3
Anderegg, J. W., 2.6.1
Anderson, C. A. F., 2.3
Anderson, D., 2.2, 3.4
Anderson, D. W., 6.3
Anderson, E., 8.1
Anderson, I., 4.4.2
Anderson, I. S., 4.4.2
Anderson, J. E., 7.1.6
Anderson, R., 2.4.1
Anderson, W. F., 3.1
Andersson, B., 4.3.7
Andersson, S., 9.1, 9.7
Ando, M., 2.2, 2.7, 2.8, 5.3, 7.1.8
Ando, T., 4.3.3
Ando, Y., 4.3.7, 8.8
Andrade, M., 9.2.1
Andresen, A., 6.1.2
Andrew, N. L., 5.3
Andrews, S. J., 2.2, 2.3
Andrianova, M. E., 7.1.6
Andrus, J., 2.7
Angel, R. J., 9.2.2
Anger, H. O., 7.1.6
Anisimov, Yu. S., 7.1.6
Ankner, J. F., 2.9, 4.4.2
Ansara, I., 2.6.2
Anstis, G. R., 4.3.8
d'Anterroches, C., 4.3.8
Aoki, K., 3.4
Aoki, Y., 4.3.7
Appleman, D. E., 5.2
Apsimon, R. J., 7.1.6
Arai, T., 2.3
Arakali, S. V., 3.1
Arcese, A., 7.1.7
Archer, B. T., 4.3.3
Archer, J. M., 3.4
Argos, P., 3.4
Argoud, R., 3.4
Aristov, V. V., 4.2.6, 5.3
Armstrong, R. W., 2.7
Arndt, U. W., 2.2, 2.7, 3.4, 4.2.1, 4.2.2, 5.3, 6.2, 7.1.6
Arnesen, S. P., 4.3.3
Arnold, E., 3.4
Arnold, H., 3.4
Arnold, P., 2.5.2
Arrott, A., 6.2
Arrott, A. S., 2.8
Arsenin, V. Ya., 2.6.1
Artioli, G., 9.2.2
Artymiuk, P., 2.2
Arvedson, M., 4.3.3
Åsbrink, S., 5.3
Ascher, E., 9.8
Ascheron, C., 5.3
Ateiner, J., 2.3
Atoji, M., 6.1.1
Attfield, J. P., 2.3
Auleytner, J., 5.3
Austerman, S. B., 2.7
Authier, A., 2.7
Autrata, R., 7.2
Averbach, B. L., 2.3
Avery, J., 6.1.1, 8.7
Avilov, A. S., 2.4.1, 4.3.5
Axe, J. D., 4.4.2, 4.4.3
Axelrod, H. J., 3.1
Axelsson, U., 4.2.2
Ayers, G. L., 2.3
Azaroff, L. V., 2.3, 4.2.3, 5.3, 6.3, 9.2.1
Azumi, I., 5.3

Bąk-Misiuk, J., 5.3
Babkevich, A. Yu., 9.2.2
Bacchella, C. L., 2.6.2
Bach, H., 3.5
Bachmann, R., 2.3, 7.4.2
Backhaus, K.-O., 9.2.2
Bačkovský, J., 5.3
Bacon, G. E., 2.6.2, 3.6, 4.4.2, 4.4.4, 6.1.3, 6.4
Bacon, J. R., 2.6.1
Badurek, G., 4.4.2
Baerlocher, Ch., 2.3, 8.6
Bagchi, S. N., 2.6.1
Baharie, E., 8.6
Bai, Z., 8.1
Baigarin, K. A., 4.2.1
Baik, D. H., 4.2.2
Bailey, D., 5.3
Bailey, I., 2.4.2
Bailey, R. L., 4.2.1
Bailey, S. W., 9.2.2
Baker, J. A., 5.3
Baker, J. F. C., 5.3
Baker, R. F., 4.3.4
Baker, R. J., 9.7
Baker, S. M., 2.9
Baker, T. W., 2.3, 5.3
Bakken, L. N., 4.3.7, 8.8
Balaic, D. X., 4.2.5
Baldock, P., 3.1
Ballon, J., 7.1.3, 7.1.6
Balzar, D., 8.6
Band, I. M., 4.2.4
Banerjee, D., 3.5
Bannett, Y. B., 7.4.3
Bannier, G., 9.2.2
Baptista, G. B., 4.2.4
Barber, D. J., 3.5
Barclay, A. N., 3.4
Barla, K., 5.3
Barna, S. L., 2.7
Barnea, Z., 4.2.5
Barnes, I. L., 5.3
Barnes, P., 3.4
Barns, R. L., 5.3
Baronnet, A., 9.2.2
Barraud, J., 2.3
Barreau, G. H., 4.2.2
Barrett, C. S., 2.3, 2.7, 4.3.5
Barrientos, J., 4.3.3
Barry, J. C., 9.2.2
Bartell, L. S., 4.3.3
Bartels, K., 3.4, 6.3
Bartels, K. S., 3.4
Bartels, W. J., 5.3
Barth, H., 2.7, 5.2
Bartl, H., 3.4
Bartunik, H. D., 3.4
Baru, S. E., 7.1.6
Baruchel, J., 2.8, 7.3
Basile, G., 4.2.2, 5.3
Basinski, Z. S., 4.3.6.2
Basso, R., 9.2.2
Batchelder, D. N., 5.3
Bateman, J. E., 7.1.6
Bateman, O., 3.4
Bates, D. R., 3.4
Bates, F. S., 2.6.2
Batson, P. E., 4.3.4
Battagliarin, M., 2.3
Batterman, B. W., 2.7
Baumhauer, H., 9.2.2
Bauspiess, W., 2.7
Bautz, M. W., 7.1.6
Bayvel, L. P., 2.6.1
Bearden, J. A., 2.3, 4.2.2, 5.2, 5.3
Beaumont, J. H., 2.3, 2.7, 4.2.5
Becherer, G., 2.6.1
Becker, J., 4.4.2
Becker, P., 4.2.2, 5.3, 8.7, 9.8
Becker, P. J., 6.3, 6.4, 8.7
Beckman, R. J., 8.5
Bednarski, S., 4.4.2
Bedzyk, M. J., 4.2.3
Beeman, W. W., 2.6.1, 6.3
Begg, G. S., 3.4
Begum, R., 4.2.6
Behlke, J., 2.6.1
Behrendt, D. R., 6.1.1
Bellamy, B. A., 2.3, 5.3
Bellard, S., 9.5, 9.6
Bellis, J. G., 7.1.6
Bellman, R., 6.1.1
Bellotto, M., 2.3, 5.2, 5.3
Belokoneva, E. L., 9.2.2
Belov, N. V., 1.4, 9.2.1
Belsky, V. K., 9.7
Belsley, D. A., 8.2, 8.5
Benedetti, A., 2.3
Beni, G., 4.2.3
Bennett, C. L., 3.4
Benoit, H., 2.6.2
Bentley, J., 8.7
Berendsen, H. J. C., 3.1
Berestetsky, V. B., 4.2.6
Berg, H. M., 5.3
Berg, W. F., 2.7
Bergamin, A., 4.2.2, 5.3
Berger, H., 5.3
Berger, J. O., 8.1
Berger, S. D., 4.3.4
Bergerhoff, G., 9.4, 9.5, 9.6
Bergevin, F. de, 4.2.5, 8.7
Berggren, K.-F., 7.4.3
Bergman, G., 8.3
Bergstrom, J. C., 4.2.1
Bergstrom, P. M. Jr, 4.2.6
Berk, N. F., 2.9
Berkum, J. van, 5.2
Berliner, R., 7.3
Berman, H., 3.2, 3.3
Berman, L. E., 4.2.5
Bernal, J. D., 2.2, 3.2, 4.3.5

Bernard, L., 9.8
Bernard, Y., 3.1
Berndtsson, A., 4.2.2
Berneron, M., 4.4.2
Bernstein, S., 4.4.2
Berry, B. S., 2.3
Bertaut, E. F., 1.4, 8.7, 9.2.1, 9.7
Bertin, E. P., 4.2.3
Berzina, T. S., 2.9
Besson, J. M., 2.5.1
Beth, H. A., 4.3.3
Bethe, H., 4.3.4
Bethe, H. A., 2.4.1, 4.3.1
Beu, K. E., 5.2, 5.3
Bevis, M., 5.3
Bewilogua, L., 7.4.3
Beyer, H., 4.2.2
Bhat, H. L., 3.4
Bhatt, V. P., 3.4
Bianconi, A., 4.2.3, 4.3.4
Bickmann, K., 5.3
Bieber, R. L., 5.3
Bienenstock, A., 4.2.1, 4.2.3, 4.2.6
Biggin, S., 5.3
Biggs, F., 4.3.3, 7.4.3
Bigler, E., 7.1.6
Bijvoet, J. M., 2.2, 4.2.6
Bilderback, D. H., 2.2, 4.2.5
Binnig, G., 4.3.8
Bird, D. M., 4.3.2, 4.3.7, 8.8
Bird, R. B., 8.7
Birks, L. S., 2.3
Birnbaum, H. R., 4.2.3
Bischof, C., 8.1
Bish, D. L., 2.3, 7.1.4
Bishop, A. C., 3.1
Bjerrum Møller, H., 4.4.3
Black, D. R., 3.4
Black, R. E., 5.3
Blackman, M., 2.4.1, 4.3.1, 8.8
Blair, D. G., 6.4
Blake, A. J., 2.3
Blake, R. G., 4.3.7
Blakeslee, D. M., 3.1
Blanc, Y., 4.4.2
Blanton, T. N., 5.2
Blaschko, O., 9.2.2
Bläser, D., 3.4
Blech, I., 9.8
Bleeksma, J., 2.3
Bloch, B. J., 7.4.3
Bloch, F., 4.4.2, 7.4.3
Block, S., 2.3, 5.1, 5.3
Blow, D. M., 3.1, 3.4
Blum, M., 7.1.6
Blume, M., 4.2.6, 6.1.2, 7.4.3, 8.7
Blundell, S. A., 4.2.2
Blundell, T. L., 2.2, 3.1
Bøe, N., 4.3.7, 8.8
Boehli, T., 4.2.1
Boehme, R. F., 8.7
Boer, D. K. G. de, 2.9
Boer, J. L. de, 7.5, 9.2.2
Boerdijk, A. H., 9.2.1
Boersch, H., 4.3.4
Boese, R., 3.4
Boettinger, W. J., 2.7
Boeuf, A., 2.8
Boggs, P. T., 8.1
Böhlen, K. van, 3.4
Bohlin, H., 2.3
Boie, R. A., 7.3
Bojarski, Z., 2.3
Bokij, G. B., 9.2.2
Bołd, T., 2.3
Boll-Dornberger, K., 9.2.2
Bolling, E. D., 4.4.2
Bolotina, N. B., 5.3
Bomchil, G., 5.3
Bond, C. C., 7.1.6
Bond, W. L., 2.7, 5.3
Bone, D. A., 7.1.6
Bonelle, J. P., 4.2.3
Bongaarts, P. J. M., 4.4.2
Bonham, R. A., 4.3.3
Böni, P., 4.4.2
Bonin, D., 7.1.6
Bonnet, M., 8.7
Bonnet, R., 3.4
Bonse, M., 2.6.2
Bonse, U., 2.2, 2.3, 2.6.1, 2.7, 4.1, 4.2.2, 4.2.5, 4.2.6, 4.4.2, 5.3
Bontchev, R., 9.2.2
Booker, G. R., 5.4.2
Boom, G., 5.2
Boothroyd, A. T., 2.6.2
Borchert, G. L., 4.2.2
Bordas, J., 2.5.1, 4.1, 5.2, 7.1.6, 9.2.1
Bordet, J., 2.4.2
Bordet, P., 3.1
Borg, I. Y., 2.3
Borgeaud, P., 5.3
Borkowski, C. J., 7.1.6, 7.3
Börner, H. G., 4.2.2
Borovilova, N. V., 4.4.2
Borso, C. S., 7.1.6
Bosshard, R., 3.4, 7.1.6
Böttger, G., 4.4.2
Botton, G. A., 8.8
Boucherle, J. X., 8.7
Bouchiat, M. A., 4.4.2
Bouldin, C. E., 4.2.3
Boulin, C., 7.1.6
Bouman, J., 6.2
Bouquiere, J. P., 3.4
Bourdel, J., 7.3
Bourdillon, A. J., 2.5.1, 4.3.4, 5.2
Bourke, P., 4.2.1
Bourret, A., 4.3.8
Bovin, J.-O., 9.2.2
Bowen, D. K., 2.7, 4.1, 4.2.3, 5.3
Bowen, T. S., 4.2.1
Bowman, H. A., 5.3
Box, G. E. P., 8.1, 8.2
Boyarskaya, R. V., 4.3.5
Boyd, R. J., 8.7
Boyers, D. G., 4.2.1
Braam, A. W. M., 7.4.2
Bracewell, R., 2.6.1
Brádler, J., 2.7
Brady, R. L., 3.1, 3.4
Brafman, O., 9.2.1
Bragg, W. H., 2.2, 2.3, 5.3
Bragg, W. L., 2.2, 2.6.2, 5.3
Braillon, P., 3.5
Brammer, L., 9.5, 9.6
Brandenburg, K., 9.4
Breitenstein, M., 4.3.3
Brenner, R., 7.3
Brentano, J. C. M., 2.3
Brese, N. E., 9.1
Bretherton, L., 3.4
Briand, J. P., 5.2
Brice, M. D., 9.5, 9.6
Bricogne, G., 4.3.7, 7.1.6
Briggs, E. A., 4.2.4, 4.2.6, 7.4.3
Brindley, G. W., 9.2.2
Brister, K. E., 4.2.5
Britton, D., 3.1
Brock, C. P., 9.7
Brockhouse, B. N., 4.4.2
Brockway, L. O., 4.3.3
Brodsky, A., , 4.2.5
Brongersma, H. H., 7.1.6
Brooks, I., 2.2
Bross, H., 4.3.4
Brouns, E., 9.8
Brown, A. S., 4.2.5
Brown, B. R., 5.3
Brown, D., 4.2.1
Brown, D. B., 2.3
Brown, G. E., 4.2.6
Brown, G. M., 6.1.1
Brown, G. S., 4.2.3, 7.4.4
Brown, H., 1.4, 9.8
Brown, I. D., 9.4, 9.5, 9.6
Brown, L. M., 4.3.4, 4.3.8
Brown, M. C., 9.6
Brown, N. E., 3.4
Brown, P. J., 4.4.5, 6.1.2, 8.7
Brown, R. T., 4.2.4, 4.2.6, 7.4.3
Brown, W. D., 7.4.3
Brownell, S. J., 2.3, 5.2
Brownell, W. E., 2.3
Bruce, M. I., 9.6
Brühl, H.-G., 5.3
Brumberger, H., 2.6.1
Brunegger, A., 4.3.4
Brunel, M., 8.7
Brunner, G. O., 9.1, 9.3
Brydson, R., 4.3.4
Brysk, H., 4.2.6
Bubenzer, A., 4.3.4
Buchanan, D., 2.3
Buchanan, J., 8.2
Buckingham, A. D., 8.7
Budinger, T. F., 4.3.8
Budnick, J. L., 4.4.2
Bueche, A. M., 2.6.1
Buerger, M. J., 1.4, 2.2, 2.3, 3.4, 5.3, 6.2, 9.2.1
Buffat, P., 4.4.2
Buggy, T. W., 4.3.4, 7.2
Bührer, W., 4.4.2
Bulkin, B. J., 4.1
Bülow, H., 9.8
Bülow, R., 1.4
Bunch, D. S., 8.1
Bunge, A. V., 4.3.3
Bunge, C., 4.3.3
Bunge, C. F., 4.3.3
Bunge, H.-J., 4.3.5
Bunkenburg, J., 4.2.1
Bunker, B., 4.2.3
Bunker, G., 4.2.3
Bunn, C. W., 3.1
Bunyan, P. J., 4.3.3
Burany, X. M., 9.2.2
Buras, B., 2.5.1, 2.5.2, 4.2.1, 4.2.6, 5.2, 5.3, 7.1.5
Burbank, R. D., 6.2
Burch, T. J., 4.4.2
Burdette, H. E., 2.7, 3.4
Burek, A. J., 4.2.1
Burge, R. E., 7.2
Burger, A., 7.1.4
Burgers, W. G., 2.2
Burgess, W. G., 8.8
Burgy, M. T., 4.4.2
Burke, B. E., 7.1.6
Burke, J., 5.3
Burkel, E., 7.4.2
Burla, M. C., 8.6
Burley, S. K., 3.1
Burns, R., 7.1.6
Burr, A. F., 2.3, 4.2.2
Burshtein, Z., 7.1.4
Bursill, L. A., 4.3.8
Buschert, R. C., 5.3
Buseck, P., 4.3.4
Buseck, P. R., 4.3.8
Bushnell-Wye, G., 2.3
Bushuev, V. A., 7.4.3
Busing, W. R., 3.4, 5.3
Butler, D. J., 7.1.6
Butler, E. P., 3.5
Butler, M., 2.3
Butler, R. D., 3.3
Buttiker, M., 2.9
Buxton, B. F., 4.3.7
Bychkova, V. E., 2.6.1
Byer, R. L., 4.2.1
Byrd, R. H., 8.1

Caballero, A., 4.2.3
Cable, J. W., 9.8
Caglioti, G., 2.3, 2.4.2, 4.4.3, 8.6
Cahn, J. W., 9.8
Cahn, R. W., 1.3
Calas, G., 4.2.3, 4.3.4
Calvert, L. D., 2.3, 9.3
Campbell, J. E., 3.4
Campos, C., 3.4
Camps, R. A., 4.3.8
Capasso, S., 3.1
Capel, M. S., 2.6.2
Capellmann, H., 4.4.2
Caplan, H. S., 4.2.1
Cardona, M., 4.2.2, 5.3
Cardoso, L. P., 3.4
Carlile, C. J., 2.4.2, 4.4.2, 7.4.2
Carlson, E. H., 9.2.2
Caroll, C. L., 5.3
Carpenter, J. M., 4.4.1
Carr, M. J., 2.4.1
Carr, P. D., 2.2, 3.4, 5.3
Carter, C. B., 4.3.8
Carter, C. W., 3.1
Carter, C. W. Jr, 3.1
Cartwright, B. A., 9.5, 9.6
Carver, T. R., 4.4.2
Cascarano, G., 8.6
Cascio, D., 3.4
Case, A. L., 2.8
Caspar, D. L. D., 4.4.2
Cassetta, A., 2.2

Castaing, R., 4.2.1, 4.3.4
Castelli, C. M., 2.7
Caticha-Ellis, S., 3.4
Catti, M., 1.3
Catura, R. C., 7.1.6
Cauchois, Y., 4.2.2
Caudron, B., 7.1.6
Caulfield, P. B., 5.3
Causer, R., 2.3, 5.3
Cavagnero, G., 4.2.2, 5.3
Cembali, F., 5.3
Cernik, R., 5.2
Cernik, R. J., 2.3
Černohorský, M., 5.3
Cerva, H., 2.7
Ceska, T. A., 3.1
Chadha, G. K., 9.2.1
Chadi, D. J., 9.1
Chaimdi, M., 3.4
Chakera, A., 6.3
Chamberland, B. L., 9.2.2
Chambers, F. W., 5.3
Chambers, W. F., 2.4.1
Chan Dyk Tkhan, 7.1.6
Chance, B., 4.2.3
Chandler, G. S., 6.1.1
Chandrasekaran, M., 9.2.1
Chandrashekar, G. V., 3.1
Chang, S.-L., 5.3
Chan Khyo Dao, 7.1.6
Chantler, C. T., 4.2.6
Chapman, J. N., 7.2
Chapuis, G., 4.2.6, 7.5
Charpak, G., 2.2, 7.1.6
Chatterjee, S., 8.5
Chau, K., 4.3.8
Chayen, N. E., 3.1
Cheary, R. W., 5.2
Cheetham, A. K., 2.3, 8.6
Cheetham, G. M. T., 2.3, 3.1
Chen, C. H., 4.3.4
Chen, H., 4.2.3, 4.4.2
Chen, S. H., 2.6.1, 2.6.2
Chen, S.-H., 2.9
Chen-Mayer, H. H., 4.4.2
Cheng, T. Z., 4.3.8
Cheremukhina, G. A., 7.1.6
Chernenko, S. P., 7.1.6
Chernov, M. A., 9.2.2
Cherns, D., 4.3.8
Chesser, N. J., 4.4.2, 4.4.3
Cheung, S., 4.4.2
Chevallier, P., 5.2
Chidambaram, R., 6.1.1
Chieux, P., 7.3
Chikawa, J., 7.1.6, 7.1.7, 7.1.8
Chikawa, J.-I., 2.7
Chipera, S. J., 7.1.4
Chipman, D. R., 4.2.3
Chirino, A. J., 3.1
Chou, H. P., 7.3
Chowanietz, E. G., 7.1.6
Christ, J., 4.4.2
Christen, D. K., 2.6.2
Christensen, A. N., 2.3, 7.1.3
Christoph, A., 5.3
Chu, B., 7.1.6
Chung, S. J., 1.3
Chupp, T. E., 4.4.2
Chwaszczewska, J., 2.5.1
Císařová, I., 9.2.2
Cisney, E., 2.3
Citrin, P. H., 4.1, 4.2.3
Clark, G. F., 2.7
Clark, S. M., 2.5.1, 3.4
Clay, R. E., 4.2.1
Clay, W. T., 7.3
Cleemann, J. C., 2.6.1
Clegg, W., 3.4, 5.3
Clementi, E., 4.4.5, 6.1.1, 6.1.2
Clifton, I. J., 3.4
Cline, J. P., 2.3
Clout, P. N., 7.1.6
Cochran, W., 5.3
Cockayne, D. J. H., 4.3.8
Cocking, S. J., 4.4.2
Cody, V., 3.1
Coelho, A., 5.2
Coene, W., 4.3.8
Coene, W. M. J., 4.3.8
Coffman, D., 4.3.3
Cohen, E. R., 4.2.1, 4.2.2, 4.2.3
Cohen, G. G., 2.7
Cohen, J. B., 2.3
Cohen, M. U., 5.2
Cohn-Vossen, S., 9.1
Cole, H., 2.7, 4.2.6, 5.3
Cole, W. F., 5.3
Colegrove, F. D., 4.4.2
Coleman, T. A., 7.1.6
Collett, B., 7.1.6
Colliex, C., 4.3.4
Collins, C. B., 4.2.1
Collins, D. M., 8.2
Colwell, J. F., 4.4.2
Comparat, V., 7.1.3, 7.1.6
Compton, A. H., 2.3, 2.7, 4.2.1, 5.3
Condon, E. U., 8.7
Conger, G. B., 7.1.6
Conolly, M. L., 3.4
Conradi, E., 9.2.2
Constenoble, M. L., 2.3
Conturie, Y., 4.2.1
Convert, P., 2.4.2, 7.3
Conway, J. H., 9.1
Cook, J. E.,
Cook, R. D., 8.5
Cookson, D. J., 4.2.6
Cooper, A. S., 5.3
Cooper, C. W., 2.6.1
Cooper, M. J., 4.2.3, 4.4.3, 6.3, 7.4.2, 7.4.3, 8.6
Copley, J. R. D., 4.4.2
Coppens, P., 2.2, 3.4, 6.3, 6.4, 8.7, 9.8
Cork, C., 2.2
Cork, C. W., 7.1.6
Cosier, J., 3.4
Cosslet, V. E., 4.2.3
Cosslett, V. E., 4.2.1
Cotton, J. P., 2.4.2, 7.3
Cottrell, A., 9.2.1
Cottrell, A. H., 6.4
Couderchon, G., 4.4.2
Coulter, K. P., 4.4.2
Coulthard, M. A., 4.3.1, 6.1.1
Coustham, J., 2.6.2
Coutanceau Clarke, J. A. R., 9.7
Cowley, J. M., 2.4.1, 4.1, 4.3.1, 4.3.2, 4.3.6.1, 4.3.7, 4.3.8, 8.8, 9.2.1, 9.2.2
Cowley, R. A., 4.4.3
Cox, A. R., 3.5
Cox, D. E., 2.3, 2.5.1, 4.2.6, 7.4.4, 8.6, 9.2.2
Cox, H. L. Jr, 4.3.3
Cox, M. J., 3.1
Coyle, B. A., 6.3
Cracknell, A. P., 6.1.1
Crain, J., 2.3
Cramér, H., 8.4
Craven, A. J., 4.3.4, 7.2
Craven, B. M., 6.4
Crawford, F. S., 4.2.3
Crawford, R. K., 2.9
Craxton, R. S., 4.2.1
Creagh, D. C., 4.2.3, 4.2.4, 4.2.5, 4.2.6, 10
Cressey, G., 2.3
Crewe, A. V., 4.3.4, 4.3.8
Crichton, R. R., 2.6.1, 2.6.2
Croce, P., 2.9
Cromer, D. T., 4.2.4, 4.2.6, 4.3.1, 6.1.1, 7.4.3, 8.7
Cross, J. O., 4.2.3
Crowder, C. E., 2.3, 5.2
Crowfoot, D., 3.2
Crozier, E. D., 4.2.3
Crozier, P. A., 4.3.4
Cruickshank, D. W. J., 2.2, 3.4, 5.3, 8.3, 8.7
Cudney, B., 3.1
Culhane, J. L., 7.1.6
Cullen, E. E., 4.2.4
Cullity, B. D., 2.3
Currat, R., 4.4.2, 7.4.3, 9.8
Curtis, C. F., 8.7
Cusack, S., 2.6.2
Cusatis, C., 4.2.6
Cuttitta, F., 3.2
Czerwinski, H., 7.4.3

Daams, J. L. C., 9.3
Dabbs, J. W. T., 4.4.2
Daberkow, I., 4.3.8
Daberkow, L., 7.2
Dabrowski, A., 7.1.4
Dabrowski, A. J., 7.1.5
Dahl, J. P., 8.7
Dainton, D., 7.1.6
Dalglish, R. L., 7.1.6
Dallas, W. J., 7.1.6
Dallé, D., 3.4
Dam, B., 9.8
Damaschun, G., 2.6.1
Damaschun, H., 2.6.1
Dana, E. S., 3.5
Daniel, V., 9.8
Daniels, J., 4.3.4
Daniels, P. J., 7.1.6
D'Antonio, P., 3.1
Danz, H., 3.4
D'Aprile, F., 3.4
Darriet, B., 9.2.2
Darriet, J., 9.2.2
Dartyge, E., 7.1.6
Darwin, C. G., 6.4
Das Gupta, P., 5.2
Dash, J. G., 4.4.2
Dathe, W., 9.2.2
D'Auria, S., 3.1
Davanloo, F., 4.2.1
David, W. I. F., 2.3, 2.5.2, 8.6
Davidson, E. R., 6.1.1
Davidson, J. B., 2.8
Davies, J. E., 9.7
Davies, N. C., 3.5
Davies, S. T., 2.7, 4.2.3
Davis, B. L., 2.3, 5.3
Dawson, B., 6.1.1
Day, M. W., 3.1
Deacon, A., 2.2
Debye, P., 2.3, 2.6.1, 6.2
DeCicco, P. D., 7.4.3
Deckman, H. W., 7.1.6
Degoy, S., 3.1
Dehlinger, U., 9.8
Deininger, C., 8.8
Delaey, L., 9.2.1
Delamoye, P., 9.8
De Lange, P. W., 4.4.2
Delapalme, A., 2.5.2, 4.4.2, 8.7
Delduca, A., 7.1.6
Delettrez, J., 4.2.1
Delf, B. W., 4.2.5, 5.2
Del Grande, N. K., 4.2.3, 4.2.4
Delhez, R., 2.3, 5.2
Dellby, N., 4.3.7, 4.3.8
Delley, B., 8.7
Deltour, J., 2.3
DeLucia, M. L., 8.7
De Marco, J. J., 4.2.4
Demasi, D., 3.1
Demierre, C., 2.2
Demmel, J., 8.1
Denesyuk, A. I., 2.6.1
Denley, D., 4.2.3
Denne, W. A., 3.4
Denner, W., 5.3
Dennis, J. E., 8.1
Dent Glasser, L. S., 3.4
Depmeier, W., 9.8
Dereniak, E. L., 7.1.6
Derewenda, Z., 7.1.6
Desai, C. F., 3.4
Descamps, J., 4.2.1
Desclaux, J. P., 4.2.2, 4.4.5, 6.1.2, 8.7
Deslattes, R., 5.2
Deslattes, R. D., 4.2.1, 4.2.2, 5.2, 5.3
Desseaux, J., 4.3.8
DeTitta, G. T., 3.1
Deutsch, M., 2.3, 4.2.2, 4.2.6, 5.3
Dewan, J. C., 3.4
Dexpert, H., 4.2.3
Dexter, D. L., 2.3
D'Eye, R. W. M., 3.4
Dickens, B., 8.3
Dideberg, O., 3.4
Dietrich, B., 5.3
Dietz, G., 9.2.2
Dietz, J., 7.1.6
DiGiovanni, H. J., 2.3
Dikovskaya, R. R., 5.3
Diller, T. C., 3.1
Dimitrov, D. P., 2.6.1
Dingley, D. J., 5.3
Dinnebier, R. E., 8.6
Di Nova, K., 4.2.1
Dischler, B., 4.3.4
Disko, M. M., 4.3.4

Divadeenam, M., 4.4.4
Dixon, N. E., 3.1
Dobrzynski, L., 4.4.2
Dobson, P. J., 4.3.8
Dodson, G. G., 3.4
Doi, K., 2.8
Dolin, R., 7.1.6
Doll, C., 4.4.2
Dollase, W. A., 2.3
Dolling, G., 4.4.2
Donaldson, J. R., 8.1
Dongarra, J., 8.1
Doniach, S., 2.6.1, 4.2.3
Donnay, G., 1.3
Donnay, J. D. H., 1.3, 1.4, 9.8
Dönni, A., 4.4.2
Donohue, J., 9.7
Dorenwendt, K., 4.2.2, 5.3
Dornberger-Schiff, K., 3.4, 9.2.1, 9.2.2
Dorner, B., 4.4.3, 7.4.2
Dorrington, E., 7.1.6
Dorset, D. L., 3.5, 4.3.7, 4.3.8
D'Orsi, C. J., 7.1.6
Doscher, M. S., 3.4
Doty, J. P., 7.1.6
Doubleday, A., 9.5, 9.6
Downing, K. H., 4.3.8
Downing, R. G., 4.4.2
Downs, J., 4.3.7, 8.8
Doyle, P. A., 4.2.4, 4.3.1, 4.3.2, 6.1.1
Drabkin, G. M., 4.4.2
Dragoo, A. L., 5.2
Draper, N., 8.1, 8.4
Dreier, P., 4.2.3, 4.2.6
Drenth, J., 3.1
Dressler, L., 5.3
Drits, V. A., 2.4.1, 4.3.5
Drum, C. M., 3.5
Drummond, W., 7.1.4
Duarte, P. W. E. P., 4.2.4
Dubey, M., 9.2.1
Duchenois, V., 7.1.6
Du Croz, J., 8.1
Ducruix, A., 3.1
Dudarev, S. L., 4.3.2
Dudley, M., 2.8
Duijneveldt, F. B. van, 6.1.1
Duisenberg, A. J. M., 3.4
Duke, P. J., 4.2.1
Düker, H., 4.3.8
Dumas, P., 3.4
Du Mond, J. W. M., 2.3, 2.7
Dunitz, J. D., 9.7
Dunn, H. M., 5.3
Dunning, T. H. Jr, 6.1.1
Dupont, Y., 7.1.6
Duppich, J., 4.4.2
Durand, D., 6.1.1
Durbin, R., 2.2
Durbin, R. M., 7.1.6
Durham, J. P., 4.3.4
Durham, P. J., 4.2.3
Ďurovič, S., 9.2.2
Dürr, J., 4.2.3
Dušek, M., 9.2.2
Dvoryankina, G. G., 2.4.1
Dwiggins, C. W. Jr, 6.3
Dyson, N. A., 2.3, 4.2.1, 7.1.6
Early, J. G., 3.4
Eastabrook, J. N., 5.3, 7.1.2, 7.5
Ebeling, G., 4.2.2, 5.3
Eberhardt, W., 4.1
Ebert, M., 4.4.2
Ebisawa, T., 2.9, 4.4.2
Eckert, J., 4.4.3
Eddy, M. M., 2.3
Edington, J. W., 3.5, 5.4.1
Edwards, H. J., 2.3, 5.2
Edwards, S. L., 3.4
Edwards, T. H., 2.3
Effenberger, H., 9.2.2
Egelstaff, P. A., 4.4.2
Egerton, R. F., 4.3.4
Eggleton, R. A., 9.2.2
Egidy, T. V., 4.2.2
Egorov, A. I., 4.4.2
Eguchi, T., 4.3.7, 8.8
Ehrenberg, W., 4.2.1
Eichelle, G., 3.1
Eigner, W.-D., 2.6.1
Eikenberry, E. F., 2.7, 7.1.6
Eiselé, J.-L., 3.1
Eisenberg, H., 2.6.2
Eisenberger, P., 2.2, 4.1, 4.2.3, 7.4.3
Eklund, H., 3.4
El Korashy, A., 3.4
Elder, M., 3.4
Eling, A., 9.1
Ellinger, Y., 8.7
Ellis, T., 5.3
Ellisman, M. H., 7.2
Elsenhans, O., 4.4.2
Elsner, G., 7.1.6
Emberson, D. L., 7.1.6
Emmerich, C., 2.2
Endesfelder, A., 4.3.3
Endoh, H., 4.3.8
Endoh, T., 7.1.6
Eng, P. J., 4.2.5
Enge, H. A., 4.3.4
Engel, D. H., 4.2.6
Engel, P., 1.4
Engel, W., 4.3.4
Engelman, D. M., 2.6.2
Englander, M., 2.8
Engstrom, P., 4.2.5
Enzo, S., 2.3
Epstein, J., 4.3.3, 8.7
Erickson, J. W., 3.4
Ermer, O., 9.1
Ernst, R. R., 5.5
Ertl, G., 4.1
Escoffier, A., 4.4.2
Esquivel, R. O., 4.3.3
Esteva, J. M., 4.3.4
Evans, B. W., 9.2.2
Evans, E. H., 3.4
Evans, H. T., 2.2, 5.2
Evans, H. T. Jr, 5.3
Evans, J. C., 3.4
Evans, R. C., 2.3, 9.7
Evans, R. G., 3.5
Ewing, F., 3.1
Ewins, C., 3.5
Eyres, B. L., 3.5

Faber, W., 4.4.2
Fabian, D. J., 4.2.2
Fabri, R., 5.3
Fagherazzi, A., 2.3
Fagherazzi, G., 2.3
Fåk, B., 2.8
Fan, G. Y., 4.3.7, 7.2
Fan, H. F., 4.3.8
Fang, Y., 6.2
Fankuchen, I., 2.3
Fano, U., 4.3.4, 7.1.6
Farabaugh, E. N., 3.5
Farge, Y., 4.2.1
Farkas-Jahnke, M., 9.2.1
Farnell, G. C., 7.2
Farnoux, B., 2.4.2, 7.3
Farquhar, M. C. M., 5.3
Faruqi, A. R., 7.1.6
Fast, G., 9.8
Favro, L. D., 6.1.1
Fawcett, T. G., 2.3, 5.2
Fearon, E. O., 5.3
Feder, R., 2.3
Fedorov, B. A., 2.6.1
Fedorov, V. V., 8.1, 8.4, 8.5
Fedotov, A. F., 4.3.5, 9.2.2
Feher, G., 3.1
Feidenhans'l, R., 2.3, 7.1.3
Feigin, L. A., 2.6.1, 2.9
Fejes, P. L., 4.3.4, 4.3.8
Felcher, G. P., 2.9
Feldman, C., 4.1
Feller, W., 6.1.1
Feng, H.-P., 7.1.6
Ferguson, I. F., 5.2
Fermi, E., 4.2.6, 7.4.3, 8.7
Ferraris, G., 1.3, 4.3.5
Ferré-D'Amaré, A. R., 3.1
Festenberg, C. V., 4.3.4
Fewster, P. F., 5.3
Fichtner, K., 9.2.2
Fichtner-Schmittler, H., 9.2.2
Fields, P. M., 4.3.8
Figueiredo, M. O., 9.1
Figueiredo, M. O. D., 9.2.2
Filhol, A., 3.4
Filippini, G., 9.7
Filscher, G., 5.3
Finger, L. W., 2.3, 2.5.1, 3.4, 8.3
Fink, J., 4.3.4
Fink, M., 4.3.3
Finlayson, H., 4.2.2
Finney, J. L., 3.4
Finzel, B. C., 7.1.6
Fiori, C. E., 7.1.4
Fiorito, R. B., 4.2.1
Fischer, D. G., 5.3
Fischer, D. W., 4.3.4
Fischer, J., 3.4, 7.3
Fischer, K., 2.7, 4.2.6
Fischer, K. F., 1.4
Fischer, P., 4.4.2, 5.5
Fischer, S., 4.4.2
Fischer, W., 1.4, 9.1
Fisher, R., 6.1.1
Fisher, R. G., 3.1
Fisher, R. M., 4.3.7, 8.8
FitzGerald, J. D., 4.3.8, 5.4.2
Fitzsimmons, M., 2.9
Fjellvåg, H., 2.3, 7.1.3
Flack, H. D., 1.3, 4.2.2, 5.3, 6.3, 8.1
Flank, A. M., 7.1.6
Fleischer, M., 9.2.2
Flint, R. B., 7.2
Flower, H. M., 3.5
Fock, V., 4.2.6
Foit, F. F. Jr, 3.4
Foltyn, T., 4.4.2
Fomin, V. G., 5.3
Fontaine, A., 7.1.6
Fontecilla-Camps, J. C., 3.1
Ford, W. E., 3.5
Fordham, J. L. A., 7.1.6
Förster, E., 4.2.2, 5.3
Forsyth, J. B., 4.4.2, 4.4.5, 7.3, 8.7
Forsyth, J. M., 4.1, 4.2.1
Forsythe, E., 3.1
Forte, M., 4.4.2
Foster, B. A., 7.1.3
Fouassier, M., 7.1.6
Fourme, R., 2.2, 3.4, 4.2.1, 7.1.6
Fourmond, M., 2.6.2
Fournet, G., 2.6.1, 2.6.2
Fournier, T., 3.1
Fowler, C. E., 7.3
Fox, A. G., 4.3.1, 4.3.2, 4.3.7, 6.1.1, 8.8
Fraaije, J. G. E. M., 3.1
Fraase Storm, G. M., 3.4
Frahm, A., 4.2.3
Frank, F. C., 9.1, 9.2.1
Frank, J., 4.3.8
Frankel, R. D., 4.1, 4.2.1
Frank-Kamenetskii, V. A., 9.2.2
Franklin, K. R., 2.3
Franzini, M., 9.2.2
Fraser, G. W., 7.1.6
Frauenfelder, H., 3.4
Freeborn, B. R., 2.6.2
Freeborn, W. P., 2.3
Freeman, A. J., 4.4.5, 6.1.2, 8.7
Freeman, F. F., 4.4.2
Freer, S. T., 7.1.6
French, S., 7.5
Freund, A., 4.2.6, 5.3
Freund, A. K., 4.2.5, 4.4.2
Freund, I., 7.4.3
Frevel, L. K., 2.3, 2.4.1
Frey, F., 3.4, 4.4.2
Freymann, D., 7.1.6
Fricke, H., 4.2.3
Friedli, H. P., 4.4.2
Friedman, H., 6.3
Friedrich, H., 4.4.2
Friedrich, W., 2.1, 2.2
Frishberg, C., 8.7
Fritsch, E., 4.3.4
Fritsch, M., 4.2.2, 5.3
Frolova, K. E., 4.3.5
Frolow, F., 3.4
Frueh, A. J., 9.2.2
Fryer, J. R., 3.5, 4.3.8
Fu, Z. Q., 4.3.8
Fuchs, H. F., 7.1.6
Fuchs, R., 4.3.4
Fuess, H., 3.4, 4.4.2, 8.7
Fuggle, J. C., 4.2.2, 4.3.4
Fujii, K., 4.2.2
Fujii, Y., 4.4.3
Fujikawa, B. K., 4.2.4, 4.2.6

Fujimoto, I., 2.7, 7.1.6, 7.1.7
Fujimoto, Z., 4.2.2
Fujita, T., 7.1.6
Fujiwara, K., 4.3.1
Fujiwara, M., 4.2.3
Fujiyoshi, Y., 4.3.7, 4.3.8
Fukahara, A., 5.3
Fukamachi, T., 2.5.1, 5.2, 6.3
Fukuhara, A., 4.3.7, 4.3.8, 8.8
Fukumachi, T., 4.2.5
Fukumori, T., 5.3
Fuller, W. A., 8.1
Fuoss, P. H., 4.2.3, 4.2.6
Furry, W. H., 6.1.1
Futagami, K., 5.3

Gabe, E. J., 5.3
Gabel, K., 4.2.5
Gabor, D., 4.3.8
Gabriel, A., 7.1.6
Gähler, R., 4.4.2
Gainsford, G. J., 2.3
Gałdecka, E., 5.3
Gale, B., 5.2
Gallo, R., 3.4
Galloy, J. J., 9.7
Galy, J., 9.2.2
Gamarnik, M. Ya., 5.3
Gamblin, S. J., 3.4
Gandolfi, G., 2.3
Ganow, D., 5.3
Garavito, R. M., 3.1
Garcia Arribas, A., 9.8
García-Ruiz, J. M., 3.1
Gard, J. A., 5.4.1, 9.2.2
Garfield, B. R. C., 7.1.6
Garlick, G. F. J., 7.2
Garman, E. F., 3.4
Garrett, R., 4.2.5
Garrett, R. F., 4.2.5
Garroff, S., 2.9
Gasgnier, M., 4.3.4
Gaultier, J.-P., 4.3.5
Gauthier, J. P., 9.2.1
Gavezzotti, A., 9.7
Gavin, R. M. Jr, 4.3.3
Gavrila, M., 4.2.6, 7.4.3
Gay, D. M., 8.1
Gearhart, R. A., 4.2.1
Gedcke, D. A., 5.2
Geiger, H., 7.1.2
Geiger, J., 4.3.3, 4.3.4
Geist, V., 5.3
George, B., 2.6.2
George, J. D., 2.3, 5.3
Gerber, C., 4.3.8
Gerdau, E., 5.3
Gerken, M., 5.3
Gerlich, R., 9.1
Gernat, C., 2.6.1
Gerold, V., 2.7
Gerstenberg, H., 4.2.3
Gerstenberg, H. M., 4.2.3, 4.2.4
Gerward, L., 2.5.1, 2.5.2, 4.2.3, 4.2.4, 4.2.6, 5.2, 5.3
Ghose, S., 3.4
Giacovazzo, C., 8.6
Gibbons, P. C., 4.3.4
Gibbs, D., 2.9, 7.4.3, 8.7
Gibson, K. D., 9.7
Giegé, R., 3.1
Gielen, P., 5.3
Giessen, B. C., 2.3, 2.5.1, 5.2
Giles, C., 4.2.5
Gill, P. E., 8.3
Gillham, C. J., 2.3, 5.2
Gilliland, G. L., 3.1, 7.1.6
Gillon, B., 8.7
Gilmore, C. J., 4.3.7, 4.3.8
Gilmore, D. J., 7.1.6
Girgis, K., 9.3
Gjønnes, J., 4.3.3, 4.3.7, 5.4.2, 8.8
Gjønnes, K., 4.3.7, 8.8
Glaeser, R. M., 4.3.7, 4.3.8
Glass, H. L., 5.3
Glatter, O., 2.6.1, 2.6.2
Glättli, H., 2.6.2, 4.4.4
Glauber, R., 4.3.3
Glazer, A. M., 2.5.1, 3.4, 5.2, 5.3
Glazer, J., 4.3.7
Glinka, C. J., 4.4.2
Glover, I., 3.4
Glusker, J. P., 2.2
Gobel, H., 4.2.6
Göbel, H. E., 2.3, 7.1.3
Gobert, G., 4.4.2
Goddard, H. F., 7.1.6
Goddard, P. A., 2.7
Godwin, R. P., 4.2.1
Godwod, K., 5.3
Goetz, K., 4.2.2, 5.3
Golay, M. J. E., 2.3
Goldberg, M., 4.2.1, 8.7
Goldman, L. M., 4.2.1
Goldman, M., 4.4.4
Goldschmidt, V., 9.8
Goldsmith, C. C., 2.3
Goldsztaub, S., 4.2.1, 9.2.2
Golob, P., 4.3.4
Golovin, A. L., 5.3
Golub, R., 4.4.2
Gonschorek, W., 5.3
Gonzalez, A., 3.4
Goodhew, P. J., 3.5
Goodisman, J., 2.6.1
Goodman, P., 2.4.1, 4.3.6.1, 4.3.7, 8.8, 9.2.2
Goodson, J. H., 7.1.6
Goral, K., 2.6.1
Gorceix, O., 4.2.2
Gordon, G. E., 2.3, 2.5.1, 5.2
Gordon, R. G., 8.7
Gorshkov, A. I., 4.3.5
Goto, K., 2.7, 7.1.6, 7.1.7
Goto, N., 7.1.6, 7.1.7
Gottschalk, H., 4.3.8
Gotwals, J. K., 5.3
Goulon, J., 4.2.5
Graaff, R. A. G. de, 6.3
Graafsma, H., 3.4
Graeff, W., 2.7
Graeser, S., 9.2.2
Graf, W., 4.4.2
Grant, B. K., 2.3
Grant, D. F., 7.5
Grant, G. A., 3.5
Grant, I., 4.3.1, 4.3.2
Grasselli, J. G., 4.1
Gratias, D., 9.8
Graubner, H., 3.2
Gray, N., 9.2.2
Grebille, D., 9.8
Greegor, R. B., 4.3.4
Green, M., 2.3, 4.2.1
Green, R. E. Jr, 2.7, 7.1.7
Greenbaum, A., 8.1
Greenberg, B., 5.2
Greene, G. C., 4.4.2
Greene, G. L., 4.2.2
Greenhough, T. J., 2.2, 3.4
Greenwood, J. A., 6.1.1
Grell, H., 9.2.2
Grenville-Wells, H. J., 6.2
Greville, T. N. E., 2.6.1
Grey, D., 4.2.5
Griebner, U., 5.3
Griffith, J. P., 3.4
Grigson, C. W. B., 2.4.1
Grimmer, H., 1.3, 4.4.2
Grimsditch, M. H., 5.3
Grimvall, G., 4.2.6
Grinton, G. R., 4.3.8
Gritsaenko, G. S., 4.3.5
Gronsky, R., 4.3.8
Grossi, F., 4.2.5
Grossman, T., 4.4.2
Grosso, J. S., 2.3
Grosswig, S., 5.3
Groves, G. W., 3.5
Grubel, G., 4.2.5
Gruber, E. E., 5.3
Grünbaum, B., 9.1
Gruner, S. M., 2.7, 7.1.6
Grunes, L. A., 4.3.4
Gschneider, K. Jr, 9.3
Guagliardi, A., 8.6
Gubbens, A. J., 4.3.7
Gudat, W., 4.3.4
Guetter, E., 7.2
Guggenheim, S., 9.2.2
Guidi-Morosini, C., 6.3
Guigay, J. P., 2.8
Guillemet, E., 7.1.6
Guinet, P., 4.4.2
Guinier, A., 2.3, 2.6.1, 2.6.2, 2.7, 4.3.5, 9.2.2
Gumbel, E. J., 6.1.1
Günther, W., 9.2.2
Guo, C.-L., 4.2.1
Guo, S. Y., 3.2
Gupta, S. K., 3.5
Gurman, S. J., 4.2.3
Guttmann, P., 7.1.6
Guyot, P., 2.6.2
Gyax, F. N., 4.1

Hausermann, D., 4.2.5
Haag, F., 9.1
Haas, J., 2.6.1, 2.6.2
Habash, J., 2.2, 3.4
Hadi, A. S., 8.5
Haendler, H. M., 3.4
Haga, K., 4.2.3
Hagashi, Y., 5.3
Hagemann, H. J., 4.3.4
Hagen, W., 2.7
Hägg, G., 2.2
Hahn, Th., 1.3, 1.4, 5.3, 9.2.2, 9.7
Haider, M., 4.3.8
Hails, J. E., 2.2
Hainisch, B., 2.6.1
Hajdu, J., 3.4
Hale, K. F., 3.5
Hales, T. C., 9.1
Halfon, Y., 3.4
Hall, E. L., 5.3
Hall, M. M. Jr., 2.3
Halliwell, M. A. G., 5.3
Hamacher, E. A., 2.3
Hamelin, B., 4.4.2
Hamid, S. A., 9.2.2
Hamill, G. P., 2.3, 5.2
Hamilton, J. F., 7.2
Hamilton, L. D., 2.6.1
Hamilton, R., 2.3, 5.2
Hamilton, W., 2.9
Hamilton, W. A., 2.9
Hamilton, W. C., 2.2, 5.3, 6.4, 7.5, 8.3, 8.4, 8.7
Hamley, I. W., 2.9
Hamlin, R., 2.2, 3.4, 7.1.6
Hammarling, S., 8.1
Hanawalt, J. D., 2.3
Hanfland, M., 4.2.5
Hanic, F., 5.3
Hann, R. A., 3.5
Hanneman, R. E., 5.3
Hansen, N. K., 4.1
Hansen, P. G., 4.2.2
Hanson, H. P., 4.3.3
Hanson, I. R., 3.4
Harada, J., 4.2.5, 7.4.2
Harada, Y., 4.3.7, 7.2
Harding, M. M., 2.2, 2.3, 3.1, 3.4, 5.3
Hardman, K. D., 3.4
Harlos, K., 3.1
Harmon, H. E., 4.4.2
Harmony, M. D., 9.5, 9.6
Harper, R. G., 3.5
Harris, J. L., 4.2.1
Harris, K. D. M., 8.6
Harris, L. J., 7.1.6
Harris, N., 5.3
Harrison, D. C., 7.1.6
Harrison, S. C., 2.2, 7.1.6
Harrison, W. T. A., 2.3
Hart, M., 2.2, 2.3, 2.5.1, 2.6.1, 2.6.2, 2.7, 4.2.2, 4.2.5, 4.2.6, 4.4.2, 5.2, 5.3
Hartl, W. A. M., 4.3.4
Hartmann, H., 3.4
Hartmann, W., 2.7
Hartmann-Lotsch, I., 4.2.6
Hartree, D. R., 4.2.6, 7.4.3
Hartshorne, N. H., 3.1, 3.3
Härtwig, J., 4.2.2, 5.3
Haruta, K., 2.7
Hasegawa, K., 7.1.6
Hasegawa, T., 5.3
Hashimoto, H., 2.7, 4.2.6, 4.3.8
Hashizume, H., 2.2, 2.3, 2.7, 4.2.5, 7.1.3, 7.4.4
Hasnain, S. S., 4.2.3
Hastings, J. B., 2.2, 2.3, 4.2.3, 4.2.6, 7.4.4, 8.6
Hastings, T. J., 3.4
Haszlo, S. E., 7.1.7
Hatton, P. D., 2.3
Hattori, S., 4.2.6
Haubold, H. G., 7.1.6

Haumann, J., 2.9
Hauptmann, H., 3.2
Häusermann, D., 2.5.1, 5.3
Hautecler, S., 4.4.2
Hawkes, D. J., 4.2.4
Hawthorne, F. C., 9.6
Hayakawa, K., 2.7, 6.3, 7.1.6
Hayes, C., 4.4.2
Hayter, J. B., 2.6.2, 2.9, 4.4.2
Hazen, R. M., 2.5.1, 3.4
Heal, K. M., 3.4
Heald, A., 4.2.3
Heath, M. T., 8.1
Heathman, S. P., 4.4.2
Hebert, H., 5.3
Heckingbottom, R., 5.3
Hedman, B., 7.1.5
Heesch, H., 9.1
Hehn, R., 4.4.2
Heidorn, D. B., 2.6.1
Heigl, A., 3.2
Heil, W., 4.4.2
Heine, S., 2.6.1
Heine, V., 4.3.4, 9.8
Heinrich, A. R., 9.2.2
Heinrich, K. F. J., 4.2.4, 7.1.4
Heise, H., 5.3
Heisenberg, W., 4.3.3
Hellings, G. J. A., 7.1.6
Helliwell, J. R., 2.1, 2.2, 2.3, 3.1, 3.4, 4.2.1, 4.2.3, 4.2.6, 7.1.6
Helliwell, M., 3.1
Hellkötter, H., 4.2.6
Hellner, E., 7.1.1, 8.7, 9.1
Helmholdt, R. B., 7.4.2
Hemley, R. J., 2.5.1
Henderson, R., 4.3.8
Henderson, R. J., 4.3.7
Hendricks, R. W., 2.6.1, 7.1.6
Hendricks, S., 9.2.1
Hendrickson, W. A., 3.2, 4.2.6, 8.3
Hendrix, J., 2.6.1, 7.1.6
Henins, A., 4.2.2, 5.2, 5.3
Henke, B. L., 4.2.4, 4.2.6
Hennig, M., 3.1
Henning, A., 4.2.6
Henriksen, K., 3.4
Henry, L., 4.3.4
Henry, N. F. M., 2.2, 3.1, 5.3
Hensler, D. H., 2.3
Heo, N. H., 3.4
Hepp, A., 2.3, 8.6
Herbstein, F. H., 5.3
Herino, R., 5.3
Herpin, A., 9.8
Herrman, K., 4.3.8
Herrmann, K.-H., 4.3.4, 7.2
Hertz, G., 4.2.3
Hestenes, M., 8.3
Heuss, K. L., 3.4
Hewat, A. W., 2.4.2, 5.5, 8.6
Hewett, C. A., 2.3
Hewitt, R., 4.2.3
Hey, P. D., 2.4.2, 4.4.2
Heynes, G. D., 7.1.7
Hezemans, A. M. F., 3.1
Hickling, N., 3.2
Hida, M., 4.2.3
Hidaka, M., 2.5.1, 5.2
Higashi, T., 2.2, 3.4
Higgins, S. A., 4.4.3
Higgs, H., 9.5, 9.6
Hiismäki, P., 4.4.2
Hikaru, T., 4.2.3
Hilbert, D., 9.1
Hilczer, B., 5.3
Hildebrandt, G., 2.7
Hilderbrandt, R. L., 4.3.3
Hill, R. J., 2.3
Hilleke, R. O., 2.9
Hillier, J., 4.3.4
Hilton, M. R., 4.3.7
Himes, V. L., 2.4.1, 9.7
Himmelblau, D. M., 8.4
Hines, W. A., 4.4.2
Hinze, E., 5.2, 5.3
Hirabayashi, M., 4.2.3
Hirabayshi, M., 5.3
Hiraga, K., 4.3.8
Hirai, T., 2.7, 7.1.6, 7.1.7
Hirano, T., 7.1.6
Hirota, F., 4.3.3
Hirs, C. H. W., 2.2
Hirsch, P. B., 2.3, 3.5, 4.3.6.2, 4.3.8, 5.4.1
Hirshfeld, F. L., 7.5, 8.7
Hirshfelder, J. O., 8.7
Hirvonen, J.-P., 2.9
Hitchcock, A. P., 4.3.4
Hjelm, R. P., 2.6.2
Ho, A. H., 4.2.1
Ho, M. M., 4.3.7
Hoaglin, D. C., 8.2
Hobbs, L. W., 3.5
Hock, R., 4.4.2
Hodeau, J. L., 3.1
Hodges, C. H., 4.3.4
Hodgson, K. O., 2.6.1, 4.2.3, 4.2.6, 7.1.5
Hoerni, J. A., 4.3.3
Hofer, F., 4.3.4
Hofer, M., 2.6.1
Hoff, R. W., 4.2.2
Hoffmann, H., 2.6.1, 2.6.2
Hoffmann, R., 4.3.4
Hofmann, A., 4.2.1
Hofmann, D., 4.4.2
Hofmann, E. G., 2.3
Høghøj, P., 4.4.2
Hohberger, H. I., 4.3.4
Hohenberg, P., 8.7
Hohlwein, D., 3.4, 7.3
Höhne, E., 9.2.2
Høier, R., 4.3.7, 5.4.2, 8.8
Holden, N. E., 4.4.4
Holladay, A., 8.7
Holland, F. M., 3.5
Holmes, K. C., 2.6.1, 3.4
Holmestad, R., 4.3.7, 8.8
Holmshaw, R. T., 7.1.6
Holt, S. A., 4.2.5
Holý, V., 2.9, 5.3
Holzapfel, W. B., 2.5.1
Hölzer, G., 4.2.2, 5.3
Hom, T., 5.3
Honess, A. P., 3.5
Hong, S.-H., 5.3
Honjo, G., 2.4.1, 9.2.1
Honkimaki, V., 4.2.1
Hönl, H., 4.2.6
d'Hooghe, P., 4.4.2
Hope, H., 3.4
Hopf, R., 7.1.6
Hoppe, W., 2.6.2
Horisberger, M., 4.4.2
Horita, Z., 4.3.7, 8.8
Horiuchi, S., 4.3.8
Hornstra, J., 3.4
Horota, F., 4.3.3
Horstmann, M., 2.4.1
Horváth, J., 5.3
Hosemann, R., 2.6.1, 2.7
Hosokawa, N., 5.3
Hosoya, S., 2.5.1, 2.8, 4.2.6, 5.2, 9.2.1
Hossfeld, F., 2.6.1, 2.6.2, 4.4.2
Hovmöller, S., 3.4, 4.3.7
Howard, A., 2.2
Howard, A. J., 7.1.6
Howard, C. J., 2.4.2
Howard, S. A., 2.3
Howard, W., 9.2.2
Howerton, R. J., 4.2.4, 4.2.6, 7.4.3
Howes, M. J., 7.1.6
Howie, A., 3.5, 4.3.6.2, 4.3.7, 4.3.8, 5.4.1
Hoya, H., 3.4
Hoylaerts, M., 2.6.1
Hsiang, W. Y., 9.1
Hsu, B. T., 3.1
Hu, H.-C., 6.2
Huang, D. X., 4.3.8
Huang, T. C., 2.3, 5.2, 8.6
Hubbard, C., 2.3, 5.2
Hubbard, C. R., 2.3, 5.1, 5.2, 5.3
Hubbard, K. M., 2.9
Hubbard, S. T., 2.6.1
Hubbell, J. H., 4.2.3, 4.2.4, 4.2.6, 7.4.3
Huber, H., 3.4
Huber, P. J., 8.2
Huber, R., 6.3
Huffman, F. N., 4.2.2
Huggins, F. G., 2.3
Hughes, D. J., 4.4.2
Hughes, G., 7.1.6
Hughes, J. W., 7.1.2, 7.5
Hughes, T. E., 5.2
Huke, K., 4.2.1
Hull, A. W., 2.3
Hüller, A., 6.1.1
Hulme, R., 5.3
Hulubei, H., 4.2.2
Humblot, H., 4.4.2
Huml, K., 5.3
Hummelink, T., 9.5, 9.6
Hummelink-Peters, B. G., 9.5, 9.6
Humphreys, C. J., 4.3.6.2, 8.8
Hundt, R., 9.4, 9.5, 9.6
Hunter, B., 8.6
Hunter, J. S., 8.1
Hunter, W. G., 8.1
Hustache, R., 2.8
Hutchings, M. T., 4.4.6
Hutchinson, J. L., 4.3.8
Hutchison, J. L., 9.2.2
Huxham, M., 3.5
Huxley, H. E., 7.1.6
d'Huysser, A., 4.2.3
Huyton, A., 5.2
Huzinaga, S., 6.1.1
Hwang, S. R., 4.4.2
Hyde, S. T., 9.1
Hyman, A., 3.5
Hyogah, H., 4.2.6

I'anson, K. J., 2.6.1
Ibach, H., 4.3.4
Ibel, K., 2.4.2, 2.6.1, 2.6.2, 4.4.2, 7.3
Ibers, J. A., 4.3.1
Ichimiya, A., 4.3.7, 8.8
Ieviņš, A., 5.3
Ihara, H., 4.2.3
Ihringer, J., 3.4
Iijima, S., 4.3.8, 9.2.2
Iijima, T., 4.3.3
Ikeda, S., 4.2.3
Ikhlef, A., 7.1.6
Illini, Th., 7.4.2
Imada, K., 3.4
Imai, K., 5.3
Imamov, R. M., 2.4.1, 5.3
Immirzi, A., 8.6
Imura, T., 5.3
Inagaki, Y., 7.3
Inagami, T., 3.4
Incoccia, L., 4.2.3
Indelicato, P., 4.2.2
Ingrin, J., 9.2.2
Inkinen, O., 2.3
Inokuti, M., 4.3.4
In't Veld, G. A., 7.1.6
Inzaghi, D., 5.3
Irie, K., 5.3
Isaacs, N. W., 3.4, 9.5, 9.6
Isaacson, M., 4.3.4
Isaacson, M. S., 4.3.4
Isherwood, B. J., 5.3
Ishida, K., 4.2.6
Ishigaki, A., 2.5.1
Ishiguro, T., 4.2.3
Ishikawa, T., 2.7, 4.2.5, 4.2.6
Ishimura, T., 4.2.1, 4.2.3
Ishizawa, N., 3.4
Ishizuka, K., 4.3.8, 7.2
Isoda, S., 7.2
Isokawa, K., 5.3
Isozaki, Y., 7.1.6
Israel, H., 4.2.6
Israel, H. I., 4.2.4
Ito, M., 2.7, 7.1.6, 7.1.8
Ito, T., 9.2.2
Ivanov, A. B., 7.1.6
Iwai, S., 3.4
Iwanczyk, J., 7.1.4
Iwanczyk, J. S., 7.1.5
Iwasaki, N., 4.2.6
Izdkovskaya, T. V., 9.2.2

Jack, A., 8.3
Jäckel, K.-H., 5.3
Jackson, D. F., 4.2.4
Jacob, M., 9.7
Jacobé, J., 2.4.2, 7.3
Jacobs, L., 2.7, 4.2.2
Jacobs, S., 4.2.1
Jacobson, R. A., 3.4
Jacrot, B., 2.6.2
Jagner, S., 9.2.2

Jagodzinski, H., 2.3, 3.4, 9.2.1, 9.2.2
Jahn, H. A., 7.4.2
Jain, P. C., 9.2.1
James, R. W., 4.2.6, 5.3, 6.3, 7.4.2
James, V. J., 7.1.6
James, W. J., 5.3
Jancarik, J., 3.1
Jänig, G. R., 2.6.1
Janin, J., 3.1
Janner, A., 9.8
Janot, C., 2.6.2
Jansen, J., 3.5
Jansonius, J. N., 3.1
Janssen, R. W., 4.3.4
Janssen, T., 9.8
Jap, B. K., 4.3.7, 4.3.8
Jarchow, O., 9.2.2
Järvinen, M., 2.3
Jäschke, J., 5.3
Jauch, J. M., 7.4.3
Jauch, W., 2.5.2
Jaynes, E. T., 8.2
Jeffery, J. W., 2.2, 3.1, 3.4
Jeffrey-Hay, P., 6.1.1
Jeitschko, W., 2.3
Jelinsky, P., 7.1.6
Jelley, E. E., 3.3
Jellinek, F., 9.8
Jelonek, S., 8.6
Jenkins, R., 2.3, 4.2.1, 5.2
Jennings, L. D., 4.2.3, 4.2.5, 7.4.4
Jensen, L. H., 2.2, 3.1, 3.4, 5.3
Jensen, T., 2.5.1
Jephcoat, A. P., 2.5.1
Jepsen, O., 4.3.4
Jesson, D. E., 4.3.8
Jiang, S.-S., 2.7
Johann, H. H., 2.3
Johansson, T., 2.3
Johnson, A. L., 4.3.4
Johnson, A. W. S., 4.3.8, 5.4.1, 5.4.2
Johnson, C. A., 9.2.1
Johnson, C. K., 6.1.1, 8.3
Johnson, D., 4.3.4
Johnson, D. E., 4.3.4
Johnson, D. W., 4.3.4
Johnson, G. G. Jr, 2.4.1
Johnson, J. E., 3.4
Johnson, K. H., 4.3.4
Johnson, L. N., 2.2, 3.1, 3.4
Johnson, L. R., 5.3
Johnson, M. W., 2.5.2
Johnson, O., 9.7
Johnson, R. W., 8.2
Johnson, W. R., 4.2.2
Johnston, D. F., 8.7
Johnston, J., 3.2
Jones, A., 3.4
Jones, A. R., 2.6.1
Jones, E. Y., 3.4
Jones, P. M., 4.3.6.2, 5.4.2
Jones, R. C., 7.1.6
Jones, R. M., 9.2.1
Jong, W. F. de, 6.2
Jonson, B., 4.2.2
Jorde, C., 2.6.1
Jorgensen, J. D., 2.5.2, 5.5, 8.6
Jørgensen, J.-E., 6.4
Jostsons, A., 4.3.7
Jouffrey, B., 4.3.4
Joy, D. C., 4.2.3, 4.3.4
Jucha, A., 7.1.6
Jurnak, F., 3.1

Kaat, E. de, 5.3
Kabra, V. K., 9.2.1
Kabsch, W., 3.4
Kaesberg, P., 2.6.1
Kaesberg, P. J., 2.6.1
Kafadar, K., 8.5
Kahn, R., 2.2, 3.4, 7.1.6
Kahovec, L., 2.6.1
Kainuma, Y., 8.8
Kaiser, A., 7.1.7
Kaiser, W., 4.4.2
Kajantie, K., 7.4.3
Kakinoki, J., 9.2.1
Kakudo, M., 4.3.5
Kakuta, N., 4.3.3
Kalata, K., 7.1.6
Kalenik, J., 3.1
Kalinin, Y. G., 4.2.1
Kalman, Z. H., 2.5.1, 5.3, 9.2.1
Kalnajs, J., 5.3
Kalus, J., 2.6.1, 2.6.2
Kamada, K., 2.8
Kambe, K., 4.3.4, 4.3.7, 4.3.8
Kaminaga, U., 7.4.4
Kamino, N., 4.2.3
Kamiya, K., 7.1.8
Kamiya, N., 7.1.6
Kammerer, O. F., 4.4.2
Kampermann, S. P., 6.4
Kane, P. P., 4.2.4, 4.2.6
Kaneko, F., 9.2.2
Kantor, B., 5.3
Kaplow, R., 2.3, 6.3
Kappler, E., 2.7
Karamura, T., 6.3
Karellas, A., 7.1.6
Karen, V. L., 9.7
Kariuki, B. M., 2.3, 3.1
Karle, I. L., 4.3.3
Karle, J., 4.2.6, 4.3.3
Karlsson, R., 3.1
Karnatak, R. C., 4.3.4
Karplus, M., 3.4
Kasai, N., 4.3.5
Kasman, Ya. A., 4.4.2
Kasper, J. S., 6.2, 9.1, 9.2.1, 9.7
Katayama, C., 6.3
Kato, A., 9.2.2
Kato, H., 7.1.6, 7.1.8
Kato, N., 2.7, 6.3
Katoh, H., 4.2.6
Katoh, T., 7.2
Katsube, Y., 3.4
Kaucic, V., 3.1
Kaufmann, E. N., 4.1
Kavinki, B. M., 8.6
Kawaminami, M., 5.2, 5.3
Kawamura, T., 2.7, 4.2.5, 7.1.7
Kawamura, T. W., 7.1.6
Kawasaki, M., 4.3.8
Kawasaki, T., 4.2.1
Kawata, H., 5.3
Kay, M. I., 6.1.1
Keast, D. J., 3.5
Keeney, R. B., 4.3.4, 7.2
Keijser, Th. H. de, 2.3, 5.2
Keil, P., 4.3.4
Kellar, J. N., 2.3
Keller, H. L., 5.3
Kelley, D. M., 3.4
Kelley, M. H., 4.3.3
Kelly, A., 3.5
Kelly, E. H., 5.2
Kelly, P. M., 4.3.7
Kendall, M. G., 6.1.1
Kendrick, H., 6.2
Kennard, C. H. L., 3.4
Kennard, O., 9.5, 9.6, 9.7
Kephart, J. O., 4.2.1
Kessler, E., 4.2.2
Kessler, E. G., 4.2.2, 5.2
Kessler, E. G. Jr, 4.2.2
Kessler, J., 4.3.3
Ketkar, S. N., 4.3.3
Keve, E. T., 8.5
Khabakhshev, A. G., 7.1.6
Kharitonov, Yu. I., 4.2.4
Kheiker, D. M., 5.3, 7.1.6, 7.5
Khejker, D. M., 5.2
Khomyakov, A. P., 9.2.2
Kihara, H., 4.3.7
Kihn, Y., 4.3.4
Kikuta, S., 2.7, 4.2.5
Killat, U., 4.3.4
Killean, R. C. G., 7.5
Kim, S., 3.4
Kim, S.-H., 3.1
Kim, Y. K., 4.2.2
Kim, Y. S., 8.7
Kimura, M., 4.3.3
Kimura, T., 4.2.3
Kincaid, B. M., 2.2, 4.1, 4.2.3
Kind, R., 9.8
King, H. E. Jr, 2.3
King, H. W., 2.3, 5.2
King, J. S., 6.2
King, M. V., 3.4, 6.1.1
King, Q. A., 4.3.2, 8.8
Kirfel, A., 4.2.6
Kirisits, M. J., 3.1
Kirk, D., 5.3
Kirkham, A. J., 5.3
Kirkland, A., 4.3.8
Kirkpatrick, H., 2.3
Kirkpatrick, H. B., 3.5
Kirkpatrick, P., 4.2.1
Kirste, R. G., 2.6.1, 2.6.2
Kishimoto, S., 7.1.8
Kishino, S., 2.7, 5.3
Kisker, E., 4.3.4
Kissel, L., 4.2.4, 4.2.6
Kiszenick, W., 5.3
Kitagawa, Y., 9.2.2
Kitaigorodskii, A. I., 9.7
Kitaigorodsky, A. I., 9.1, 9.7
Kitajgorodskij, A. I., 9.7
Kitano, T., 2.7
Kittner, R., 5.3
Kjeldgaard, M., 2.6.2
Klapper, H., 1.3
Kleb, R., 2.9
Klein, A. G., 4.4.4
Klein, O., 7.4.3
Klemperer, O., 4.3.4
Kliewer, K., 4.3.4
Klimanek, P., 4.4.2
Kloos, G., 2.3
Kloot, N. H., 8.4
Klug, A., 4.1
Klug, H. P., 2.3, 3.4, 5.1, 6.2
Knibbeler, C. L. C. M., 7.1.6
Knipping, P., 2.1, 2.2
Knoll, W., 2.6.2
Knop, W., 2.6.2
Knop, W. E., 1.4
Knox, J. R., 3.4
Ko, T.-S., 3.4
Kobayakawa, M., 4.2.1
Kobayashi, J., 5.3
Kobayashi, K., 4.2.6, 4.3.8
Kobayashi, M., 9.2.2
Kobayashi, T., 4.3.8, 7.2
Kobayashi, Y., 4.2.6
Koch, A., 7.1.6
Koch, B., 4.2.4
Koch, E., 1.1, 1.2, 1.3, 9.1
Koch, E. E., 4.2.1
Koch, M., 4.4.2
Koch, M. H. J., 2.6.1, 2.6.2
Koch, M. J. H., 7.1.6
Koehler, W. C., 9.8
Koester, L., 4.4.4
Kogan, V. A., 5.2
Kogiso, M., 4.3.7, 5.4.2
Koh, F., 6.3
Kohl, D. A., 4.3.3
Kohl, H., 4.3.2
Kohler, H., 2.3, 7.4.2
Kohler, T. R., 7.1.4
Kohn, W., 4.2.6, 8.7
Kohra, K., 2.2, 2.7, 4.2.3, 4.2.5
Koidl, P., 4.3.4
Koike, H., 4.3.8
Kolpakov, A. V., 4.1
Komarov, F. F., 4.2.5
Komem, Y., 5.3
Komoda, T., 4.3.8
Komura, Y., 9.2.1
Konaka, S., 4.3.3
Kondrashkina, E. A., 5.3
Konnert, J. H., 3.1, 8.3
Kopfmann, G., 6.3
Kopp, M., 7.1.6
Kopp, M. K., 7.3
Koptsik, V. A., 1.4, 9.8
Kordes, E., 9.3
Korekawa, M., 9.8
Koritsanszky, T., 8.7
Korneev, D. A., 4.4.2
Korolev, V. D., 4.2.1
Korytár, D., 5.3
Koshiji, N., 5.3
Kossel, W., 5.3
Kostarev, A. L., 4.2.3
Kosten, K., 3.4
Kostorz, G., 2.6.2
Kostroun, V. O., 2.7
Kosugi, N., 4.3.4
Kottke, T., 3.4
Kovalchuk, M. V., 5.3
Kovev, E. K., 5.3
Kowalczyk, R., 5.3
Kowalski, M., 9.2.2
Koyama, K., 7.1.6
Kozaki, S., 2.3, 4.2.1, 4.2.6
Kraft, S., 4.2.2

Krahl, D., 4.3.4, 4.3.7, 7.2
Kraimer, M. R., 7.1.6
Kramers, H. A., 4.2.1
Kranold, R., 2.6.1
Kratky, C., 3.4
Kratky, O., 2.6.1, 2.6.2
Krause, M. O., 6.3
Krauss, M., 8.7
Krec, K., 7.4.2
Kreinik, S., 7.1.7
Kretschmer, R.-G., 9.2.2
Krigbaum, W. R., 2.6.1
Krijgsman, P. C. J., 2.6.2
Krinari, G., 4.3.5
Krinary, G. A., 4.3.5
Krishna, P., 9.2.1, 9.2.2
Krivanek, O. L., 4.3.4, 4.3.7, 4.3.8, 7.2, 8.8
Kröber, R., 2.6.1
Kroeger, K. S., 3.4
Kröger, E. Z., 4.3.4
Kroll, N. M., 4.2.2
Kronig, R. de L., 4.2.3
Kroon, J., 3.1
Kruger, E., 4.4.2
Kruit, P., 4.3.4
Krumpolc, M., 2.6.2
Kshevetsky, S. A., 5.3
Kuban, R.-J., 9.2.2
Kubena, J., 2.9, 5.3
Kucharczyk, D., 5.3, 9.8
Kuchitsu, K., 9.2.2
Kuczkowski, R. L., 9.5, 9.6
Kudo, S., 5.3
Kudriashov, V. A., 4.4.2
Kuetgens, U., 4.2.2
Kugasov, A. G., 4.4.2
Kügler, F. R., 2.6.1
Kuh, E., 8.2, 8.5
Kühl, W., 2.7
Kühlbrandt, W., 4.3.7
Kuhn, K., 4.2.1
Kuhs, W. F., 6.1.1
Kujawa, S., 7.2
Kulda, J., 4.4.2
Kulenkampff, H., 4.2.1
Kulipanov, G. N., 4.2.1
Kulpe, S., 3.4
Kumachov, M. A., 4.2.1
Kumada, J., 7.1.6
Kumakov, M. A., 4.2.5
Kumaraswamy, S., 3.4
Kumosinski, T. F., 2.6.1
Kündig, W., 4.1
Kundrot, C. E., 3.2, 3.4
Kuntz, I. D. Jr, 3.4
Kunz, A. B., 4.3.4
Kunz, C., 4.1, 4.2.1, 4.3.4
Kunze, G., 2.3
Küppers, H., 5.3
Küppers, J., 4.1
Kupriyanov, M. F., 5.2
Kurbatov, B. A., 5.3
Kurittu, J., 7.4.2
Kuriyama, M., 2.7, 7.1.7
Kuriyama, T., 7.1.7
Kuriyan, J., 3.4
Kurki-Suonio, K., 6.1.1
Kuroda, H., 4.2.3, 4.3.4
Kuroda, K., 2.8
Kuroiwa, T., 8.8
Kurz, R., 7.3
Kusev, S. V., 4.2.1
Küster, A., 3.4
Kutschabsky, L., 9.2.2
Kutzler, F. W., 4.2.3
Kuyatt, C. E., 4.2.2, 4.3.4
Kuz'min, R. N., 4.1, 7.4.3
Kuznetsov, P. I., 6.1.1
Kvick, Å., 5.3
Kwong, P. D., 3.2

Laan, G. van der, 4.3.4
Laban, G., 9.2.2
Labergerie, D., 4.2.5
Labzowsky, L., 4.2.2
Laclare, J. L., 4.2.1
Ladd, M. F. C., 3.1
Ladell, J., 2.3, 5.2
Ladner, J. E., 3.1
Lafferty, W. J., 9.5, 9.6
Lagasse, A., 3.5
Laggner, P., 2.6.1
Lagomarsino, S., 2.8
Laguitton, D., 5.2
Lähteenmäki, I., 2.5.1
Laine, E., 2.5.1
Lairson, B. M., 2.2
Lambert, N., 2.6.1
Lamoreaux, R. D., 7.1.6
Lampton, M., 7.1.6
Landau, L., 4.3.4
Lander, G., 4.4.1
Landre, J. K., 2.7
Lang, A. R., 2.3, 2.7, 5.3
Lang, W., 4.2.2
Lange, B. A., 3.4
Lange, G., 3.4
Langer, J. A., 2.6.2
Langford, J. I., 2.3, 5.2, 6.2, 7.1.2
Langridge, R., 2.6.1
Lanz, H. Jr, 3.2
Lapington, J. S., 7.1.6
La Placa, S. J., 8.7
LaRock, J. G., 4.4.2
Larsen, E. S. Jr, 3.3
Larsen, F. K., 3.4
Larsen, P. K., 4.3.8
Larson, A. C., 3.4, 8.7
Larson, B. C., 5.3
Lartigue, C., 4.4.2
Laue, M. von, 2.1, 2.2
Lauer, R., 4.2.2, 5.3
Laugier, J., 3.4
Laurie, V. W., 9.5, 9.6
Laves, F., 9.1
Lawrance, J. L., 2.7
Lea, K., 4.2.1
Lea, K. R., 4.2.6
Leapman, R. D., 4.2.3, 4.3.4
Lebech, B., 2.5.2, 4.3.7, 8.8
Leber, M. L., 4.3.7
Leboucher, P., 7.1.6
Lebugle, A., 4.2.2
Leciejewicz, J., 2.5.2
Leduc, M., 4.4.2
Lee, B., 6.3
Lee, J. S., 4.3.3
Lee, P., 4.2.4, 4.2.6
Lee, P. A., 4.1, 4.2.3
Lefaucheux, F., 3.1
LeGalley, D. P., 2.3
Legrand, E., 4.4.2
Lehmann, A., 5.3
Lehmann, M. S., 2.3, 3.4, 7.1.3
Lehmpfuhl, G., 4.3.7, 4.3.8, 8.8
Leifer, K., 4.4.2
Leising, G., 4.3.4
Lele, S., 9.2.1
Lemonnier, M., 2.2, 7.1.6
Lengeler, B., 4.2.3, 4.2.6
Lenglet, M., 4.2.3
Leon, R., 4.2.5
Leonardsen, E., 9.2.2
Leopold, H., 2.6.1
LePage, Y., 1.3, 5.4.1
Le Peltier, F., 4.2.3
Lerche, M., 5.3
Lereboures, B., 4.2.3
Leroux, J., 4.2.4
Leszczyński, M., 3.4, 5.3
Leung, P. C., 8.7
Levi, A., 7.1.4
Levine, I. L., 8.7
Levine, M. R., 6.3
Levinger, J. S., 4.2.4
Levitt, M., 8.3
Levy, H. A., 3.4, 5.3, 6.1.1, 8.3
Lévy, P., 6.1.1
Lewis, M. H., 3.5
Lewis, O., 4.2.1
Lewis, R., 7.1.6
Lewis, S. J., 3.4
Lewit-Bentley, A., 3.1
Ley, L., 4.2.2
Li, F. H., 4.3.8
Li, J. Q., 4.3.8
Li, Q., 4.2.1
Li, Y., 7.1.6
Liang, K. S., 2.3
Liberman, D., 4.2.4, 4.2.6
Liberman, D. A., 4.2.6
Lichte, H., 4.3.8
Lider, V. V., 5.3
Lidin, S., 9.7
Liebhafsky, H. A., 4.2.4
Liesen, D., 4.2.2
Lietzke, R., 2.6.2
Lifchitz, E., 4.3.4
Lifshitz, R., 9.8
Lim, G., 2.3
Lim, G. S., 5.2, 5.3
Lima-de-Faria, J., 9.1
Liminga, R., 5.3
Lindau, I., 4.2.4, 7.4.4
Lindegaard-Andersen, A., 2.5.1
Lindemann, R., 2.3
Linderstrom-Lang, K., 3.2
Lindgren, I., 4.2.2
Lindhard, J., 4.3.4
Lindley, P., 3.4
Lindley, P. F., 3.1, 3.2, 3.4
Lindner, P., 2.6.2
Lindner, T., 4.3.4
Lindroth, E., 4.2.2
Lindstrom, R. M., 4.4.2
Lippman, R., 3.4
Lipps, F. W., 7.4.3
Lipscomb, W. N., 6.1.1
Lipson, H., 2.2, 2.3, 5.2, 5.3, 6.2, 9.8
Lischka, K., 2.9
Lisher, E. J., 4.4.5
Lisoivan, V. I., 5.3
Liss, K.-D., 4.4.2
Litrenta, T., 4.4.2
Liu, H., 7.1.6
Liu, J. W., 4.3.3
Liu, L., 4.3.8, 7.2
Livesey, A. K., 8.2
Livingood, J. J., 4.3.4
Lloyd, K. H., 5.3
Lobashov, V. M., 4.4.2
Löchner, U., 3.4
Loeb, A., 9.1
Long, D. C., 7.1.6
Long, N., 4.3.8
Lonsdale, K., 2.2, 5.3, 6.2
Lontie, R., 2.6.1
Looijenga-Vos, A., 9.8
Loopstra, B. O., 2.4.2
Lorber, B., 3.1
Lorenz, G., 3.4
Lotsch, H., 4.2.6
Lotz, B., 3.5
Louër, D., 2.3, 5.2, 8.6
Lourie, B., 2.2
Lovas, F. J., 9.5, 9.6
Love, G., 4.2.1
Lovesey, S. W., 4.1, 6.1.2, 7.4.3, 8.7
Lovey, F. C., 4.3.8
Low, B. W., 3.2
Lowde, R. D., 2.5.2, 4.4.2, 6.4
Lowe, B. M., 2.3
Lowenthal, S., 7.1.6
Lowitzsch, K., 2.3
Lowrance, J. L., 7.1.6
Lucas, W., 4.2.2, 5.3
Lucht, M., 5.3
Luft, J., 3.1
Luft, J. R., 3.1
Luger, P., 3.4, 5.3
Łukaszewicz, K., 5.3
Lukehart, C. M., 2.5.2
Lum, G. K., 4.2.2
Lumb, D. H., 7.1.6
Lund, L., 4.2.1
Luo, M., 3.4
Lushchikov, V. I., 4.4.2
Lutterotti, L., 5.2
Lutts, A., 5.3
Lutts, A. H., 5.3
Lutz, H. D., 2.3
Luzzati, V., 2.6.1, 2.6.2
Lynch, D. F., 4.3.6.1, 4.3.8
Lynch, F. J., 7.3
Lynch, J., 4.2.3, 4.3.8
Lynn, J. E., 4.4.4
Lytle, F. W., 4.2.3, 4.3.4
Lyutzau, V. G., 5.3

Ma, H., 4.3.4
Ma, Y., 4.2.3, 4.3.7, 8.8
Maaskamp, H. J., 7.1.6
MacGillavry, C. H., 3.1, 4.2.4, 4.3.1, 8.8
Machado, W. G., 2.7
Machin, K. J., 3.4
Machin, P. A., 3.4
Machlan, L. A., 5.3
Mack, B., 2.4.2
Mack, B. J., 4.4.2

Mack, M., 2.3, 5.2, 7.5
Mackay, A. L., 1.4, 3.4, 6.2
Mackay, K. J. H., 5.3
Mackenzie, J. K., 6.1.1, 7.5
Macrae, C. F., 9.7
Madar, R., 4.4.2
Madariaga, G., 9.8
Madsen, I. C., 2.3
Maeda, H., 4.2.3
Maeder, D. L., 3.1
Magerl, A., 4.4.2
Magorrian, B. G., 2.7
Maher, D., 4.2.3
Maher, D. M., 4.3.4
Mai, Z.-H., 2.7
Maier-Leibnitz, H., 4.4.2
Main, P., 5.3
Mair, S. L., 4.2.6, 6.1.1
Maistrelli, P., 5.2
Majkrzak, C. F., 2.9, 4.4.2
Makarova, I. P., 3.1
Makepeace, A. P. W., 2.7
Maki, A. G., 9.5, 9.6
Maki, M., 5.3
Makita, Y., 4.3.8
Makovický, E., 9.2.2
Makowski, I., 3.4
Malgrange, C., 2.8, 7.3
Malik, S. S., 2.9
Malina, R. F., 7.1.6
Malinowski, A., 2.6.2
Malinowski, M., 3.4, 5.3
Mallett, J. H., 4.2.3, 4.2.4
Malmros, G., 2.3, 8.6
Malzfeldt, W., 4.2.6
Mamy, J., 4.3.5
Mana, G., 4.2.2
Mann, J. B., 4.2.4, 4.3.1, 4.3.3, 6.1.1, 7.4.3
Mannami, M., 4.3.8
Manne, R., 4.2.1
Manninen, S., 7.4.3
Manoubi, T., 4.3.4
Mantler, M., 5.2
Manzke, R., 4.3.4
Mao, H. K., 2.5.1
Marchant, J. C. J., 7.2
Marcus, M., 4.2.3
Mardin, K. V., 6.1.1
Mardix, S., 2.7
Maréschal, J., 4.4.2
Marezio, M., 3.1
Marks, L., 4.3.8
Marmeggi, J. C., 2.5.2
Marr, G. V., 4.2.1
Marsh, D. J., 3.4
Marsh, P., 5.3
Marsh, R. E., 5.3, 8.3
Marshall, R. C., 9.2.1
Marshall, W., 4.1, 8.7
Martens, G., 4.2.3
Mårtensson, N., 4.2.2
Marthinsen, K., 4.3.7, 8.8
Martin, C., 7.1.6
Martinez-Carrera, S., 10
Martini, M., 4.2.3
Maruani, J., 8.7
Maruyama, E., 7.1.6
Maruyama, H., 2.7, 7.1.6, 7.1.7
Maruyama, X. K., 4.2.1
Marvin, D. A., 2.6.1
Marx, D., 4.4.2
Marxreiter, J., 3.4
Marzolf, J. G., 4.2.2, 5.3
Masaki, N., 2.8
Masciocchi, N., 2.3, 8.6
Maslen, E. N., 4.2.6, 6.1.1, 6.3
Maslen, V. M., 4.3.4
Mason, B., 3.2
Mason, I. M., 7.1.6
Massa, L., 8.7
Massalski, T. B., 2.3, 4.3.5
Massey, H. S. W., 4.3.3, 4.3.4
Masuda, K., 4.2.1
Materlik, G., 2.2, 2.7, 4.2.3, 4.2.6
Mateu, L., 2.6.2
Mathews, F. S. 3.4, 6.3
Mathias, H. G., 3.4
Mathieson, A. McL., 7.4.4
Matsuhata, H., 4.3.7, 8.8
Matsui, J., 2.7, 7.1.7
Matsumoto, T., 9.1
Matsumura, S., 8.8
Matsunaga, K., 5.3
Matsushima, I., 7.1.6
Matsushita, T., 2.2, 2.7, 4.2.3, 4.2.5, 7.1.8, 7.4.4
Matsuura, U., 9.2.2
Matthewman, J. C., 8.6
Matthews, B. W., 3.1, 3.2, 3.4
Matthews, D., 2.2
Matthews, G. D., 4.2.2
Matzfeld, W., 4.2.3
Mauer, F. A., 5.2, 5.3
Maurice, J. L., 4.3.4
Mawhorter, R. J., 4.3.3
Max, N., 3.4
May, C., 4.4.2
May, R. P., 2.6.2
May, W., 2.5.1
Mayer, J., 4.3.7, 8.8
Mayer, J. W., 4.1
Mayers, D. F., 4.3.4
Mazzarella, L., 3.1
McCallum, B., 4.3.8
McClelland, J. J., 4.3.3
McConnell, C. H., 3.5
McConnell, J. D. C., 9.8
McCourt, M. P., 4.3.8
McCrory, L. R., 4.2.1
McCusker, L., 2.3, 8.6
McDermott, G., 3.1
McKeever, B., 3.4
McKenney, A., 8.1
McKie, C., 2.2
McKie, D., 2.2
McKinstry, H. A., 3.4
McLarnan, T. J., 9.2.2
McLaughlin, P. J., 3.4
McLean, A. D., 4.3.3, 6.1.1
McLean, R. S., 4.3.3
McMahon, M., 4.2.5
McMahon, M. I., 2.3, 2.5.1
McMann, R. H., 7.1.7
McMaster, R. C., 7.1.7
McMaster, W. H., 4.2.3, 4.2.4
McMeeking, R., 2.3
McMullan, D., 4.3.4
McMullan, R. K., 6.4
McMurdie, H. F., 3.4
McNeely, J. B., 5.3
McNeill, K. M., 7.1.6
McPherson, A., 3.1, 3.4
McSweeney, S., 2.2
Meardon, B. H., 4.4.2
Medarde, M., 4.4.2
Mees, C. E. K., 7.1.1
Megaw, H. D., 5.3
Mei, R., 4.2.3
Meier, B. H., 5.5
Meier, F., 2.7
Meier, J., 4.4.4
Meier, P. F., 4.1
Meieran, E. S., 2.7
Meijer, G., 9.2.2
Meisheng, H., 4.3.8
Meister, H., 4.4.2
Melgaard, D. K., 2.4.1
Melkanov, M. A., 4.3.3
Melle, W., 5.3
Mellema, J. E., 2.6.2
Mellini, M., 9.2.2
Melmore, S., 9.1
Mendelsohn, L. B., 4.3.3, 7.4.3
Mendelssohn, M. J., 5.3
Menke, H., 2.6.1
Menotti, A. H., 4.4.2
Menter, J. W., 4.3.8
Menzel, M., 7.2
Meriel, P., 2.6.2, 9.8
Méring, J., 4.3.5
Merisalo, M., 2.3, 6.1.1, 7.4.2
Merlini, A. E., 5.3
Merlino, S., 9.2.2
Merritt, E. A., 7.1.6
Merritt, F. C., 7.3
Merwin, H. E., 3.3
Merz, K. M., 9.2.1
Merzbacher, E., 2.9
Mesquita, A. H. G. de, 9.2.1
Messerschmidt, A., 3.4, 7.1.6
Metcalf, P., 7.1.6
Metchnik, V., 4.2.1
Metherell, A. J. F., 4.3.4
Metoki, N., 2.9
Metzger, T. H., 4.3.7, 8.8
Meuth, H., 4.2.3
Meyer, A. J., 5.3
Meyer, C. E., 4.3.7
Meyer, G., 2.4.1
Meyer, H., 4.3.3
Meyer-Ilse, W., 7.1.6
Meyrowitz, R., 3.2, 3.3
Meysner, L., 5.3
Mezei, F., 4.4.2
Mezey, P. G., 9.7
Michalowicz, A., 2.8
Midgley, H. G., 3.2
Midgley, P. A., 4.3.7, 8.8
Mighell, A. D., 2.4.1, 5.2, 9.7
Mihama, K., 2.4.1
Mikhailyuk, I. P., 5.3
Mikhalchenko, V. P., 5.3
Mikke, K., 2.5.2
Mikol, V., 3.1
Milch, J. R., 7.1.6
Mildner, D. F. R., 4.4.2, 7.3
Miles, M. J., 2.6.1
Milledge, H. J., 4.2.4, 5.3
Miller, A., 2.6.2
Miller, B., 4.3.3
Miller, B. R., 4.3.3
Miller, K. J., 8.7
Miller, P. H., 4.4.2
Millhouse, A. H., 7.4.3
Million, G., 7.1.6
Mills, D. L., 4.3.4
Milne, A. D., 2.7
Minakawa, N., 2.8
Minato, I., 2.3, 3.4, 7.1.3
Miner, B. A., 4.3.4
Mingos, D. M. P., 2.3
Minkowski, M., 9.1
Misemer, D. K., 4.2.3
Mises, R. von, 6.1.1
Misselwitz, R., 2.6.1
Mitchell, E. M., 9.7
Mitchell, J. P., 7.1.7
Mitchell, P. W., 4.4.3
Mitchell, R. S., 9.2.1
Mitra, G. B., 5.2
Mitsunaga, T., 4.2.3
Mittelbach, P., 2.6.1
Mittemeijer, E. J., 2.3
Miyahara, J., 7.1.6, 7.1.8, 7.2
Miyake, S., 9.2.1
Miyamoto, M., 9.2.2
Miyata, T., 3.4
Miyoshi, A., 2.7
Mizusaki, T., 4.3.7
Mizutani, I., 5.3
Mochiki, K., 7.1.6
Modrzejewski, A., 5.3
Moelo, Y., 9.2.2
Moews, P. C., 3.4
Moffat, K., 2.2, 3.4
Mogami, K., 9.2.2
Mohr, P. J., 4.2.2, 5.3
Moliterni, A. G., 8.6
Möllenstedt, G., 4.3.8
Monaco, H. L., 3.1
Montenegro, E. C., 4.2.4
Moodie, A. F., 4.3.1, 4.3.6.1, 4.3.8
Moody, P. C. E., 3.4
Mook, H. A., 4.4.2, 8.7
Moon, K. J., 2.7
Mooney, P. E., 4.3.7, 4.3.8
Mooney, T., 4.2.2
Mooney, T. M., 4.2.2
Moore, J. K., 7.1.7
Moore, L. J., 5.3
Moore, M., 2.7
Moore, P. B., 2.6.1, 2.6.2
Moran, M. J., 4.2.1
Moras, D., 3.4
Morawe, C., 2.9
Morchan, V. D., 7.1.6
Moreno, A., 3.1
Moret, R., 3.4
Moretto, R., 3.4
Morgan, B. L., 7.1.6
Morgan, C. B., 7.3
Morgan, D. V., 7.1.6
Morgenroth, W., 4.2.6
Mori, H., 9.2.2
Mori, N., 4.3.7, 4.3.8, 7.2
Moriguchi, S., 7.2
Morikawa, K., 4.3.7
Moring-Claesson, O., 2.6.1
Morosin, B., 3.4
Morris, I. L., 9.1
Morris, M. C., 2.3, 3.4

Morris, P. L., 3.5
Morris, R. E., 2.3
Morris, V. J., 2.6.1
Morris, W. G., 5.3
Morrison, G. R., 7.2
Morse, P. M., 4.3.3
Mort, K., 4.2.3
Mortensen, K., 2.6.2
Mortier, W. J., 2.3
Mory, C., 4.3.4
Moss, G., 8.7
Mosteller, M., 8.2
Motherwell, W. D. S., 9.5, 9.6
Motohashi, H., 2.8
Mott, N. F., 4.3.4
Mott, N. I., 4.3.3
Moudy, L. A., 5.3
Moulai, J., 7.1.6
Mountain, R. W., 7.1.6
Mountfield, M. J., 3.5
Mourou, X., 4.2.1
Moy, J.-P., 7.1.6
Moyer, N. E., 5.3
Mücklich, F., 4.4.2
Mughabghab, S. F., 4.4.4
Mughier, J., 3.5
Müller, A., 4.2.1
Muller, J., 3.4
Müller, J. E., 4.2.3, 4.3.4
Müller, J. J., 2.6.1
Müller, K., 2.6.1
Müller, U., 9.2.2
Müller, W., 7.1.2
Müller-Heinzerling, T., 4.3.4
Munshi, S. K., 3.4
Muralt, P., 9.8
Muramatsu, T., 4.3.3
Murata, T., 4.2.3
Murray, W., 8.3
Murray-Rust, P., 9.6
Murshudov, G. N., 3.4
Mursic, Z., 4.4.2
Murthy, M. R. N., 3.4
Musil, F. J., 5.2, 5.3
Mustre de Leon, J., 4.2.3
Myklebust, R. L., 7.1.4
Myles, D., 3.4

Naday, I., 7.1.6, 7.3
Naday, Y., 4.3.4
Nagakura, S., 4.3.8
Nagel, D. J., 4.2.1
Naiki, T., 4.3.8
Najmudin, S., 3.4
Nakagawa, A., 7.1.8
Nakajima, K., 5.3
Nakajima, T., 5.2
Nakamura, T., 5.3
Nakamura, Y., 4.3.8
Nakano, Y., 4.2.5, 6.3
Nakayama, K., 2.7, 4.2.2
Nanni, L. F., 5.3
Nannichi, Y., 5.3
Napier, J. G., 4.3.7
Narayana, S. V. L., 3.4
Nash, S., 8.1
Nastasi, M., 2.9
Nathans, R., 4.4.2, 4.4.3, 6.1.2
Natoli, C. R., 4.2.3
Naukkarinen, K., 2.7
Nave, C., 2.6.1, 3.4
Navrotsky, A., 3.4
Nazarenko, V. A., 4.4.2
Necker, G., 8.8
Neder, R. B., 3.4
Neilsen, C., 7.1.6
Nelder, J. A., 9.7
Nellist, P., 4.3.8
Nelmes, R. J., 2.3, 2.5.1
Nelms, A. T., 4.2.6
Nelson, J. B., 5.2
Nemiroff, M., 5.3
Nesper, R., 9.1
Nesterova, Ya. M., 9.2.2
Neubüser, J., 1.4, 9.8
Neuling, H. W., 2.5.1
Nevot, L., 2.9
Newbury, D. E., 7.1.4
Newkirk, J. B., 2.7
Newman, B. A., 5.3
Newsam, J. M., 2.3
Newville, M., 4.2.3
Ng, E. W., 4.3.3
Nichols, M. C., 2.3
Nicholson, J. R. S., 2.7
Nicholson, R. B., 3.5, 4.3.6.2, 4.3.8, 5.4.1
Nicholson, W. L., 7.5, 8.2, 8.4, 8.5
Nicol, J. M., 2.3
Niculescu, V., 4.4.2
Nielsen, C., 2.2, 3.4
Nielsen, M., 2.3, 4.4.3, 7.1.3
Nielson, C., 7.1.6
Nielson, M., 4.4.3
Nieman, H. F., 3.4
Niemann, W., 4.2.3, 4.2.6
Nierhaus, K. H., 2.6.2
Niggli, P., 9.1
Niimura, N., 2.5.1
Niinikoski, T. O., 2.6.2
Niklewski, T., 5.3
Nikolin, B. I., 9.2.2
Ninio, J., 2.6.1
Nishina, Y., 7.4.3
Nishiyama, Z., 9.2.1
Nissenbaum, J., 7.1.4
Nittono, O., 2.7
Nixon, W. C., 4.2.1
Nomura, K., 9.2.2
Nomura, M., 4.2.3
Nonaka, Y., 7.1.6
Nonoyama, M., 5.4.2
Nordfors, B., 4.2.3
Norman, D., 4.2.3
Normand, J.-M., 6.1.1
North, A. C. T., 3.4, 6.3
Northwood, D. O., 9.2.2
Norton, T. J., 7.1.6
Nothnagel, A., 2.6.1
Novák, C., 9.2.2
Nowacki, W., 9.1, 9.7
Nowotny, V., 2.6.2
Nugent, K. A., 4.2.5
Numerov, B. V., 4.3.3
Nunes, A. C., 4.4.2
Nunez, V., 2.9, 4.4.2
Nurmela, M., 2.3, 8.6
Nyholm, R., 4.2.2

Oba, K., 2.7, 7.1.6
Obaidur, R. M., 5.3
Obashi, M., 4.2.3
Oberthür, R. C., 2.6.1, 2.6.2
O'Connor, B., 8.6
Ogawa, T., 4.2.6
Ogilvie, R. E., 2.3, 5.3
Oguso, C., 7.1.6
Ohama, N., 5.3
O'Hara, S., 2.7
Ohkawa, T., 4.2.6
Ohlendorf, D. H., 7.1.6
Ohlidal, I., 2.9
Ohshima, K.-I., 3.4
Ohta, T., 4.2.3
Ohtaka, K., 4.2.4
Ohtsuki, Y. H., 4.2.4
Oikawa, T., 4.3.7, 4.3.8, 7.2
Okada, Y., 5.1, 5.3
Okamoto, S., 2.9
Okamura, Y., 7.1.6
Okazaki, A., 3.4, 5.2, 5.3
O'Keefe, M. A., 4.3.1, 4.3.2, 4.3.8, 6.1.1
O'Keeffe, M., 9.1
Oki, K., 8.8
O'Mara, D., 7.1.6
Okorokov, A. I., 4.4.2
Okude, S., 7.1.6
Okuno, H., 7.3
Oldfield, T. J., 3.1
Olejnik, S., 5.3
Olekhnovich, A. I., 6.4
Olekhnovich, N. M., 6.4
Oliver, J. H., 6.3
Olkha, G. S., 7.5
Olsen, A., 4.3.7, 4.3.8, 5.4.2
Olsen, J. S., 2.5.1, 5.2, 5.3
Olthoff-Münter, K., 2.7
Omote, K., 2.3
Onitsuka, H., 5.3
Oosterkamp, P. W. J., Oosterkamp, W. J., 4.2.1
Op de Beeck, M., 4.3.8
Opechowski, W., 1.4, 9.8
Oppenheimer, I., 4.2.6
Orchowski, A., 4.3.8
Orlandi, P., 9.2.2
Orpen, A. G., 9.5, 9.6
Ortale, C., 7.1.6
Ortiz, C., 2.3
Oshima, K., 4.2.5
Ostapovich, M. V., 5.3
Ostrouchov, S., 8.1
Ostrowski, G., 2.9
Otten, E. W., 4.4.2
Ottewanger, H., 7.1.6
Otto, A., 4.3.4
Otto, J. W., 2.5.1
Øverbø, I., 4.2.3, 4.2.4
Ovitt, T. W., 7.1.6
Oyanagi, H., 4.2.3, 4.2.5
Ozawa, S., 4.3.8
Ozawa, T., 9.2.2

Paakkari, T., 7.4.3
Pabst, A., 9.2.2
Pace, S., 5.3
Paciorek, W. A., 7.5, 9.8
Padawer, G. ,E., 5.3
Padmaya, N., 9.7
Pahl, R., 4.2.5
Palache, Ch., 9.8
Palenzona, A., 9.2.2
Palmer, R. A., 3.1
Palmer, S. B., 2.8
Panchenko, J. M., 5.2
Panchenko, Yu. M., 7.5
Pandey, D., 9.2.1
Pang, G., 5.3
Pangborn, W. A., 3.1
Pannhorst, V., 2.4.1
Panson, A. Y., 4.3.4
Pantos, E., 4.2.3
Paoletti, A., 2.3, 2.4.2, 4.4.3, 8.6
Paolini, F. R., 2.3
Papatzacos, P., 4.2.3
Papiz, M. Z., 2.3, 3.4
Parak, F., 3.4
Paretzkin, B., 3.4
Parfait, J., 2.6.1
Parfait, R., 2.6.2
Parker, N. W., 4.3.4
Parmon, V. S., 2.4.1
Parratt, L. G., 2.3, 4.2.2, 4.2.3
Parrish, W., 2.3, 2.5.1, 5.2, 5.3, 7.1.2, 7.1.3, 7.1.4, 7.5, 8.6
Parsons, D. F., 4.1
Parthé, E., 2.3
Pasemann, M., 4.3.8
Pasero, M., 9.2.2
Pashley, D. W., 3.5, 4.3.6.2, 4.3.8, 5.4.1
Passell, L., 4.4.2
Patel, N. B., 5.3
Patel, S., 3.1
Paterson, M. S., 9.2.1
Patt, B. E., 7.1.6
Patterson, A. L., 9.2.1, 9.7
Pattison, P., 7.4.3
Pätzold, H., 4.3.7
Paul, R. L., 4.4.2
Pauling, L., 9.2.2, 9.3
Paulus, M., 3.5
Pavlishin, V. I., 9.2.2
Pavlov, M. Yu., 2.6.2
Pawley, G. S., 2.3, 5.2, 6.1.1, 6.3, 8.6, 8.7
Peacock, M., 9.8
Pearce-Percy, H. T., 4.3.4
Pearl, L. H., 3.1
Pearlman, S., 2.3
Pearson, G. L., 5.3
Pearson, W. B., 9.3
Pease, D. M., 4.2.3
Pedersen, J. S., 2.6.2, 2.9
Peele, A. G., 4.2.5
Peerdeman, A. F., 4.2.6
Peerdeman, F., 5.2
Peierls, R. E., 4.2.6
Peiser, H. S., 2.3, 5.1
Peisert, A., 7.1.6
Peisl, J., 7.4.2
Peixoto, E. M. A., 4.3.3
Peltonen, H., 6.1.1
Pendry, J. B., 4.2.3, 4.3.4, 4.3.6.2
Penfold, J., 2.6.2, 2.9, 4.4.2
Peng, L.-M., 4.3.1, 4.3.2, 8.8
Pennartz, P. U., 3.4
Penner-Hahn, J. E., 4.2.3, 7.1.5
Penneycook, S. J., 3.5
Pennock, G. M., 3.5
Pennycook, S. J., 4.3.8

Perchiazzi, N., 9.2.2
Perez, J. P., 4.3.4
Perez-Mato, J. M., 9.8
Perez-Mendez, V., 2.2
Perfettii, P., 4.2.3
Perlman, M. L., 4.2.3
Pernot, P., 7.1.6
Perrier de la Bathie, R., 2.8, 4.4.2
Perrin, F., 6.1.1
Perry, J. A., 9.1
Persson, E., 4.2.6
Persson, H., 4.2.2
Perutz, M. F., 2.6.2
Peshekhonov, V. D., 7.1.6
Pesonen, A., 2.3
Pessen, H., 2.6.1
Peterson, R. C., 3.4
Petiau, J., 4.2.3, 4.3.4
Petit, M., 7.1.6
Petri, E., 4.3.4
Petricek, V., 9.2.2, 9.8
Petroff, J. F., 2.7, 2.8
Petrova, S. N., 9.2.2
Petsko, G. A., 3.4
Pettersen, R. C., 9.5, 9.6
Petzow, G., 4.4.2
Pfeiffer, H. G., 4.2.4
Pfister, J. C., 5.3
Pflüger, J., 4.3.4
Pflugrath, J., 3.4
Pflugrath, J. W., 7.1.6
Phan, T., 9.8
Phelps, A. W., 9.2.2
Philipp, H. R., 4.3.4
Philips, J. C., 4.2.6
Phillips, D. C., 2.2, 3.4, 6.3
Phillips, F. C., 3.1
Phillips, G. N. Jr, 3.4
Phillips, W. C., 2.3, 4.2.1, 7.1.6
Phizackerley, R. P., 7.1.6
Photen, M. L., 7.1.7
Piaget, C., 7.1.6
Pick, M. A., 5.3
Pickart, S. J., 4.4.2
Pickford, M. G., 3.4
Picot, D., 3.1
Picraux, S. T., 4.1
Piermarini, G. J., 5.3
Pierron, E. D., 5.3
Piestrup, M. A., 4.2.1
Pietraszko, A., 5.3
Pihl, C. F., 5.3
Pike, E. R., 2.3, 5.2
Piltz, R. O., 2.3
Pilz, I., 2.6.1
Pimentel, C. A., 5.3
Pincus, C. I., 4.2.1
Pinot, M., 2.6.2
Pinsker, Z. G., 2.4.1, 2.7, 4.3.5, 5.3
Pirenne, M. H., 4.2.4
Pirouz, P., 4.3.8
Plançon, A., 4.3.5
Platzman, P. M., 7.4.3
Plechaty, E. F., 4.2.4
Plies, E., 4.3.4
Plotnikov, V. P., 4.3.5
Plotz, W., 2.9
Plummer, E. W., 4.1
Podlasin, S., 3.4, 5.3
Podolsky, R. J., 7.1.6
Pofahl, E., 5.3
Polack, F., 7.1.6
Polcarová, M., 5.3
Polidori, G., 8.6
Polizzi, S., 2.3
Pollehn, H. K., 7.1.6
Polyak, M. I., 5.3
Pommerrenig, D. H., 7.1.6
Pongratz, P., 7.4.2
Ponomarev, I. Yu., 4.4.2
Poole, M. W., 4.2.1
Popa, N. C., 7.4.2, 8.6
Popov, A. N., 7.1.6
Popović, S., 5.2, 5.3
Porat, Z., 3.5
Porod, G., 2.6.1, 2.6.2
Porsev, G. D., 4.4.2
Porteus, I. O., 4.2.3
Posselt, D., 2.6.2
Post, B., 5.3
Post, J. E., 2.3
Potts, H. R., 5.3
Poulos, T. L., 7.1.6
Pound, A., 3.2
Pouxe, J., 7.1.3, 7.1.6
Powell, B. M., 3.4
Powell, C. J., 4.2.2, 4.3.4
Powell, H. R., 2.3
Powers, L. S., 4.2.3
Prager, P. R., 9.2.1
Prandl, W., 3.4
Prasad, B., 9.2.1
Prasad, L., 9.2.1
Pratapa, S., 8.6
Pratt, R. H., 4.2.4, 4.2.6, 7.4.3
Press, W., 6.1.1
Preston, A. R., 8.8
Preston, G. D., 9.8
Preston, K. D., 2.3
Prewitt, C. T., 2.3, 3.4
Price, P. F., 4.2.6
Price, W. J., 7.1.6
Prince, E., 2.3, 4.2.2, 5.1, 5.3, 7.5, 8.1, 8.2, 8.3, 8.4, 8.5, 8.6
Prince, F. C. de, 5.3
Pring, A., 9.2.2
Prins, J. A., 2.6.1
Probst, R., 4.2.2, 5.3
Prout, C. K., 2.3
Proviz, G. I., 7.1.6
Provost, K., 3.1
Przybylska, M., 3.1, 3.4
Ptitsyn, O. B., 2.6.1
Pulay, P., 4.3.3
Pürschel, H. V., 2.6.1
Pusey, M., 3.1
Puxley, D. C., 3.4
Pynn, R., 2.9, 4.4.2, 4.4.3
Pyrros, N. P., 2.3

Quayle, J. A., 2.7
Queisser, H.-J., 2.7

Rabe, P., 2.7, 4.2.3, 4.2.6
Rabinovich, D., 2.2, 7.5
Rabukhin, V. B., 3.2
Rachinger, W. A., 2.3
Rackham, G. M., 4.3.6.2, 5.4.2
Radeka, V., 7.3
Rademacher, H.-J., 4.2.2, 5.3
Radi, G., 8.8
Radoslovich, E. W., 9.2.2
Rae, A. D., 8.3
Rae, W. N., 3.2
Raether, H., 4.3.4
Raftery, J., 9.6
Rai, R. S., 9.2.1
Raia, C. A., 3.1
Raiko, V. I., 4.2.1
Raj, K., 4.4.2
Ralph, R. L., 8.3
Ramachandran, G. N., 2.7
Ramakrishnan, V., 2.6.2
Ramakumar, S., 9.7
Ramaseshan, S., 4.2.6, 6.1.3
Ramesh, R., 4.3.7
Ramesh, T. G., 6.1.3
Ramsay, D. A., 9.5, 9.6
Ramsdell, L. S., 9.2.1
Randall, K. H., 9.1
Ranganath, G. S., 6.1.3
Rao, C. N., 4.3.4
Rao, Ch. P., 3.4
Rao, S., 9.1
Raoux, D., 7.1.6
Rask, J. H., 4.3.4
Rasmussen, B. F., 3.4
Rasmussen, S. E., 3.4
Rathie, P. N., 7.5
Rau, W., 4.3.8
Rau, W. D., 4.3.8, 7.2
Rauch, H., 2.7, 4.4.2, 4.4.4
Ravel, B., 4.2.3
Ravn, H. L., 4.2.2
Rayment, I., 3.4
Raynal, J., 4.3.3
Read, M. H., 2.3
Read, W. T., 6.4
Reck, G., 9.2.2
Redinbo, M. R., 3.1
Reed, M., 4.2.1
Reed, R. E., 4.4.2
Reed, S. J. B., 2.3, 4.2.1
Reeke, G. N. J., 5.3
Rees, A. L. G., 2.4.1
Rees, B., 8.7
Rees, D. C., 3.1
Rehr, J. J., 4.2.3
Reichard, T. E., 5.3
Reider, M., 3.4
Reifsnider, K., 2.7
Reilly, J., 3.2
Reim, G., 4.2.2, 5.3
Reimer, L., 4.3.4, 7.2
Reinecke, T., 9.2.2
Reinhardt, A., 9.1
Rem, P. C., 4.4.2
Remaut, G., 3.5
Remenyuk, P. I., 5.3
Remington, S. J., 3.1
Ren, G., 4.3.2
Renault, A., 4.3.8
Renda, G., 7.1.6
Rendle, D. F., 2.3
Rennekamp. R., 4.3.4
Renninger, M., 2.3, 2.7, 5.3
Resouche, E., 4.4.2
Reverchon, F., 3.5
Reynolds, G. T., 7.1.6
Reynolds, R. A., 3.1
Reynolds, R. C., 2.3
Rez, D., 4.3.1, 4.3.2
Rez, P., 4.3.1, 4.3.2, 4.3.4
Rhan, H., 5.3
Ribberfors, R., 7.4.3
Ricci, F. P., 2.3, 2.4.2, 4.4.3, 8.6
Rice, S. B., 4.3.8
Rice-Evans, P., 7.1.6
Richard, J. C., 7.1.6
Richards, F. M., 3.2, 3.4
Richardson, J. W., 8.6
Richardson, M. C., 4.2.1
Richardson, M. C. M., 4.2.5
Richter, D., 4.4.2
Ricker, G. R., 7.1.6
Ridou, C., 5.3
Rieck, C. D., 4.2.2
Riekel, C., 3.1
Ries-Kautt, M., 3.1
Rietveld, H. M., 2.3, 2.4.2, 5.2, 8.2, 8.3, 8.6
Rieubland, J. M., 2.6.2
Rieubland, M., 2.6.2
Riggs, P. J., 4.2.3
Riglet, P., 2.7
Rigoult, J., 6.3
Rijlart, A., 2.6.2
Rijllart, A., 2.6.2
Riley, D. P., 5.2
Rindby, A., 4.2.5
Ringe, D., 3.4
Ringe-Ponzi, D., 3.4
Rink, W. J., 3.4
Rinn, H. W., 2.3
Ripp, R., 3.4
Riquet, J. P., 3.4
Risler, J. L., 3.4
Riste, T., 4.4.2
Ritchie, R. H., 4.3.4
Ritland, H. N., 2.6.1
Ritsko, J. J., 4.3.4
Ritter, R., 4.4.2
Rizkallah, P. J., 3.1
Robert, M. C., 3.1
Roberts, K. J., 2.7, 3.4
Roberts, L. D., 4.4.2
Roberts, P.-H., 6.1.1
Robertson, B. E., 5.3
Robin, J., 4.2.1
Robinson, R. A., 4.4.3
Roche, C. T., 7.3
Rode, A. V., 4.2.5
Rodeau, J.-L., 3.1
Rodenburg, J., 4.3.8
Rodgers, J. R., 9.3, 9.5, 9.6, 9.7
Rodricks, B., 7.1.6
Rodrigues, A. R. D., 2.3, 2.7, 4.2.5
Rodriguez, S., 5.3
Roe, A. L., 7.1.5
Roe, S. M., 3.4
Roehrig, H., 7.1.6
Roetti, C., 4.4.5, 6.1.1, 6.1.2
Rogers, D. W., 3.4
Rogers, J. E., 8.1
Rogerson, I. F., 5.2
Rohe, D., 4.4.2
Rohrer, H., 4.3.8
Rohrlich, F., 7.4.3
Rollett, J. S., 5.3
Rømming, C., 4.3.7, 8.8

Rooksby, H. P., 2.3, 5.1
Rooms, G., 4.4.2
Roos, B., 6.1.1
Roppert, J., 2.6.1
Rose, A., 7.1.6, 7.1.7
Rose, H., 4.3.4
Rosier, D. J. de, 4.1
Rosner, B., 5.3
Ross, A. W., 4.3.3
Ross, M., 9.2.2
Ross, P. A., 2.3
Rossbach, M., 4.4.2
Rossi, F. A., 3.4
Rossi, J., 7.1.7
Rossi, J. P., 7.1.7
Rossi, M., 3.1
Rossmanith, E., 5.3
Rossmann, M. G., 2.2, 3.4, 5.3
Rossouw, C. J., 4.3.4
Rotella, F. J., 2.5.2, 5.5
Rouault, M., 4.3.3
Roubeau, A., 2.6.2
Roudaut, E., 2.4.2, 7.3
Rourke, C. P., 6.3
Rouse, K. D., 6.3, 7.4.2
Rousseau, M., 5.3
Rousseaux, F., 2.2, 4.3.5
Roux, M., 4.3.3
Rowe, J. M., 4.4.2, 4.4.3
Rowlands, P. C., 5.3
Roy, S. C., 4.2.4, 4.2.6
Rozgonyi, G. A., 7.1.7
Rozhanski, V. N., 4.3.8
Rozhansky, V. H., 5.3
Rozhansky, V. N., 5.3
Rubin, H., 2.3
Rubinstein, I., 3.5
Ruble, J. R., 6.3
Ruckpaul, K., 2.6.1
Rudakov, L. I., 4.2.1
Rudman, R., 3.4
Rule, D. W., 4.2.1
Rullhausen, P., 4.2.4, 4.2.6
Rumpf, A., 2.7
Runov, V. V., 4.4.2
Ruoff, A. L., 2.5.1
Rush, J. J., 8.3
Russ, J. C., 7.1.4
Russell, D. R., 9.6
Russell, T. P., 2.9
Rustichelli, F., 2.8, 4.4.2
Rüter, H. D., 5.3
Rzotkiewicz, S., 8.7

Sabine, T. M., 6.4
Sabino, E., 2.3, 5.2
Sadanaga, R., 9.2.2
Sadaoui, N., 3.1
Sadler, D. M., 2.6.1
Sagar, R. P., 4.3.3
Sagerman, G., 3.4
Sah, R. E., 4.3.4
Saito, M., 4.2.3
Saitoh, K., 7.2
Sakabe, K., 6.3
Sakabe, N., 2.2, 4.2.5, 6.3, 7.1.6, 7.1.8
Sakai, H., 2.7, 7.1.6, 7.1.7
Sakamaki, T., 3.4
Sakashita, H., 5.3, 9.2.2
Sakata, M., 7.4.2, 8.6
Sakurai, H., 4.2.1
Sakurai, K., 4.2.1
Salcido, M. M., 7.1.6
Saldin, D. K., 4.3.4, 8.8
Salemne, F. R., 7.1.6
Saloman, E. B., 4.2.3, 4.2.4
Salomonson, S., 4.2.2
Salva-Ghilarducci, A., 2.6.2
Samotoin, N. D., 4.3.5
Samsonov, G. V., 9.3
Sander, B., 5.3
Sandström, A. E., 5.2
Sanford, P. W., 7.1.6
Sankey, O. F., 4.3.4
Sano, H., 4.2.4
Santiard, J. C., 2.2, 7.1.6
Santilli, V. J., 7.1.6
Santoro, A., 6.3
Sapirstein, J., 4.2.2
Sareen, R. A., 7.1.6
Sarikaya, M., 4.3.7
Sarma, R., 3.4
Sasaki, A., 4.2.3
Sasaki, H., 4.3.3
Sasvári, J., 5.3
Sato, F., 2.7, 7.1.6, 7.1.7
Sato, M., 3.4
Sato, S., 4.2.6
Sato-Sorensen, Y., 3.4
Satow, Y., 7.1.6, 7.1.8
Sauder, W. C., 4.2.2
Sauer, H., 4.3.4
Sauli, F., 2.2
Saunders, M., 4.3.7, 8.8
Sauvage, M., 2.7, 2.8
Savage, H. F. J., 3.4
Savinov, G. A., 7.1.6
Savitzky, A., 2.3
Sawada, M., 4.2.1, 4.2.3
Sawada, T., 4.3.3
Sawatsky, G. A., 4.3.4
Saxton, W., 4.3.8
Saxton, W. O., 4.3.8
Sayers, D. E., 4.2.3, 4.3.4
Sazaki, T., 4.3.4
Sbitnev, V. I., 4.4.2
Scarborough, G. A., 3.1
Scardi, P., 5.2, 8.6
Scaringe, R. P., 9.7
Schaefer, W., 7.3
Schaerpf, O., 4.4.2
Schäfer, L., 4.3.3
Schalt, W., 4.4.2
Schärpf, O., 2.6.2, 4.4.2
Schattschneider, P., 4.3.4
Schauer, P., 7.2
Schaupp, D., 4.2.4, 4.2.6, 7.4.3
Schearer, L. D., 4.4.2
Schebetov, A. F., 4.4.2
Scheckenhofer, H., 2.9
Schedler, E., 4.4.2
Schedrin, B. M., 2.6.1
Scheer, J. W., 7.1.6
Scheerer, B., 4.3.4
Scheetz, B. E., 2.3
Schefer, J., 4.4.2
Scheinfein, M., 4.3.4
Schellenberger, U., 5.3
Schelten, J., 2.6.1, 2.6.2, 4.4.2, 7.3
Schenk, M., 5.3
Scheraga, H. A., 9.7
Scheringer, C., 6.1.1
Scherm, R., 2.8, 4.4.2
Scherm, R. H., 4.4.2
Scherrer, P., 2.3
Scherzer, O., 4.3.8
Schetelich, Ch., 5.3
Schick, B., 3.1
Schieber, M., 7.1.4
Schikora, D., 5.3
Schildkamp, W., 2.2
Schiller, C., 3.4
Schindler, D. G., 2.6.2
Schink, H.-J., 2.6.2
Schirber, J. E., 3.4
Schirmer, A., 4.4.2
Schiske, P., 4.3.8
Schlenker, M., 2.8, 7.3
Schlenoff, J. B., 3.4
Schlesier, B., 3.1
Schmalle, H. W., 9.2.2
Schmatz, W., 4.4.2
Schmetzer, K., 2.3
Schmider, H., 4.3.3
Schmidt, H., 5.3
Schmidt, K., 2.6.2
Schmidt, L., 4.2.1
Schmidt, V. V., 4.2.3
Schnabel, R. B., 8.1
Schnatterly, S. E., 4.3.4
Schneider, D. K., 2.6.2
Schneider, G., 9.2.2
Schneider, J., 3.4, 5.3
Schneider, J. R., 2.5.2, 4.1, 7.4.3
Schnering, H. G. von, 9.1
Schnopper, H. W., 4.2.3
Schoenborn, B. P., 2.6.2, 4.4.2, 6.1.3
Schomacher, V., 4.3.3
Schomaker, V., 4.3.3, 8.3
Schoonover, R. M., 5.3
Schrauber, H., 2.6.1, 9.2.2
Schreiner, W., 2.3, 5.2
Schreiner, W. N., 2.3, 5.2
Schrey, F., 5.3
Schreyer, A., 2.9
Schröder, B., 4.3.4
Schröder, W., 2.2, 2.7
Schroeder, L. W., 6.3
Schubert, P., 3.4
Schultz, A. J., 2.5.2, 7.3
Schultz, H., 2.3
Schulz, H., 3.4, 5.3, 6.1.1, 7.4.2, 9.2.2
Schulz, L. G., 2.7
Schulze, G. E. R., 3.2, 5.3
Schulze, H., 2.6.2
Schumacher, M., 4.2.4, 4.2.6, 7.4.3
Schurz, J., 2.6.1
Schuster, M., 4.2.6
Schutt, C. E., 2.2
Schwager, P., 3.4, 6.3
Schwahn, D., 2.6.2
Schwartz, L. S., 2.3
Schwartzenberger, D. R., 5.3
Schwarz, H. E., 7.1.6
Schwarz, W., 9.2.2
Schwarzenbach, D., 4.2.2, 5.3, 8.1, 9.3
Schweig, A., 4.3.3
Schweizer, J., 4.4.2, 8.7
Schwendemann, R. H., 9.5, 9.6
Schweppe, J., 4.2.2
Schweppe, J. E., 4.2.2
Schwinger, J., 4.2.1
Schwitz, W., 4.2.2
Schwuttke, G. H., 2.7, 5.3
Scofield, J., 4.2.6
Scofield, J. H., 4.2.3, 4.2.4
Scott, C. P., 7.2
Scott, H. G., 8.6
Scott, V. D., 4.2.1
Scuderi, J., 3.4
Sears, V. F., 2.9, 4.2.3, 4.4.2, 4.4.4
Seary, A. J., 4.2.3
Sebastian, M. T., 9.2.1
Sébilleau, F., 2.3
Secrest, D., 6.3
Sedlacek, P., 9.2.2
Seebold, R. E., 2.3
Seeds, W. E., 2.6.1
Seegar, P. A., 4.4.4
Seeger, A., 4.4.2
Seeger, P. A., 7.1.6
Seemann, H., 2.3
Segall, R. L., 9.2.2
Segmüller, A., 2.3, 5.3
Seip, H. M., 4.3.3
Seip, R., 4.3.3
Seka, W., 4.2.1
Seki, R., 4.2.2
Sekiguchi, A., 7.1.6
Sekiguchi, A. A., 7.1.6
Self, P. G., 4.3.8
Selsmark, B., 2.5.1
Semiletov, S. A., 2.4.1
Senemaud, C., 4.2.1, 4.2.2
Senzaki, K., 4.2.3
Serdyuk, I. N., 2.6.2
Serebrov, A. P., 4.4.2
Serughetti, J., 3.5
Servidori, M., 5.3
Sette, F., 4.3.4
Sevely, J., 4.3.4
Sevillano, E., 4.2.3
Seyfried, P., 4.2.2, 5.3
Seymann, E., 4.4.4
Shaham, H., 3.4
Sham, L. S., 4.2.6
Shankland, K., 4.3.7, 8.6
Shannon, C. E., 2.6.1
Shapiro, F. L., 4.4.2
Shapiro, S. M., 4.4.2
Sharov, V. A., 4.4.2
Shaw Stewart, P. D., 3.1
Shaw, A., 3.1
Shechtman, D., 9.8
Shekhtman, V. Sh., 5.3
Sheldon, J., 3.4
Sheldrick, G. M., 5.3
Shelud'ko, S. A., 5.3
Shenoy, G. K., 4.1
Shephard, G. C., 9.1
Sherman, I. S., 4.3.4, 7.1.6
Sherwood, J. N., 2.7, 2.8
Sheu, E. Y., 2.6.1, 2.6.2
Shibata, S., 4.3.3
Shidara, K., 2.7, 7.1.6, 7.1.7
Shields, W. R., 5.3
Shiles, E., 4.3.4

Shimakura, H., 4.2.6
Shimambukuro, R. L., 4.2.4, 4.2.6
Shindo, D., 4.3.8
Shinoda, G., 5.3
Shiraiwa, T., 4.2.3
Shiraiwa, Y., 4.2.1
Shirane, G., 4.4.2, 4.4.3, 6.1.2
Shirley, R., 8.6
Shishiguchi, S., 2.3, 7.1.3
Shmueli, U., 7.5
Shmytko, I. M., 4.2.6, 5.3
Shoemaker, D. P., 7.5, 8.4
Shoji, T., 2.3
Shore, J. E., 8.2
Shortley, G. H., 8.7
Shrier, A., 5.3
Shubnikov, A. V., 9.1
Shulakov, E. V., 4.2.6, 5.3
Shull, C. G., 2.8, 6.1.2, 6.1.3
Shulman, R. G., 4.2.3
Shulman, S., 2.6.1
Shuman, H., 4.3.4
Shuvalov, B. N., 7.1.6
Shvarts, D., 4.2.1
Shvyd'ko, Yu. V., 5.3
Sica, F., 3.1
Siddons, D. P., 2.3, 2.7, 4.2.6
Siddons, P., 4.2.6
Sidorenko, O. V., 4.3.5, 9.2.2
Sidorov, V. A., 7.1.6
Sieber, J., 8.6
Siegbahn, M., 4.2.1
Siegbahn, P., 6.1.1
Siegel, R. W., 4.1
Siegert, H., 4.2.2, 5.3
Siegmund, O. H. W., 7.1.6
Siegmund, W., 4.2.5
Siemensmeyer, K., 4.4.2
Sievers, R., 9.4, 9.5, 9.6
Silcox, J., 4.3.4
Sillers, I.-Y., 2.6.2
Sillou, D., 2.8
Silzer, R. M., 4.2.1
Simmons, R. O., 5.3
Simms, R. A., 7.1.6
Simon, J. P., 2.6.2
Simons, A. L., 4.2.3
Simpson, J. A., 4.3.4
Simpson, K., 2.6.2
Simpson, W. T., 6.1.1
Sinclair, H. B., 5.2
Sinfelt, J. H., 4.2.3
Singh, G., 9.2.1
Singh, K., 5.3
Singh, S. R., 9.2.1
Sinha, S. K., 2.9
Sinogowitz, U., 9.1
Sirianni, A. F., 2.3
Sironi, A., 8.6
Sirota, E. B., 2.9
Sirota, M. I., 2.4.1
Sivia, D. S., 8.6
Skalicky, P., 7.4.2
Skellam, J. G., 7.5
Skilling, J., 8.2
Skopik, D. M., 4.2.1
Skowronek, M., 7.1.6
Skupov, V. D., 5.3
Skuratowski, I. Ya., 4.2.1
Slack, G. A., 9.1
Slade, J. J., 5.3
Slade, J. J. Jr, 5.3
Slater, J. C., 7.4.3
Sleight, A. W., 2.3
Sleight, J., 4.2.1
Slingsby, S., 3.4
Šljukić, M., 5.3
Sloane, N. J. A., 9.1
Sluis, P. van der, 3.1
Smaalen, S. van, 9.2.2, 9.8
Smakula, A., 5.3
Smend, F., 4.2.4, 4.2.6, 7.4.3
Smirnov, V. V., 4.3.8
Smirnova, N. L., 9.1
Smith, A. J., 9.7
Smith, D., 4.3.3
Smith, D. G. W., 2.3
Smith, D. J., 3.5, 4.3.7, 4.3.8
Smith, D. K., 2.3, 9.2.2
Smith, D. T., 3.4
Smith, D. Y., 4.2.6, 4.3.4
Smith, G., 5.3, 7.1.6
Smith, G. F. H., 9.8
Smith, G. S., 2.3, 2.9
Smith, H., 8.1, 8.4
Smith, J. M., 9.7
Smith, J. V., 9.2.2
Smith, S. T., 2.3
Smith, S. Y., 4.3.4
Smith, T. B., 4.4.2
Smith, V. H., 4.3.3
Smith, V. H. Jr, 4.3.3, 6.1.1
Smits, D. W., 5.2
Snavely, M. K., 4.1
Snell, E., 2.2
Snigirev, A., 4.2.5
Snigireva, I., 4.2.5
Snyder, D., 4.2.1
Snyder, R. L., 2.3
Soares, D. A. W., 5.3
Soboleva, S. V., 4.3.5, 9.2.2
Söchtig, J., 4.4.2
Soejima, Y., 3.4, 5.3
Sofer, A., 8.1
Soff, G., 4.2.2
Soller, W., 2.3, 5.2
Somiya, S., 2.3
Somlyo, A. P., 4.3.4
Sommers, H. S., 4.4.2
Sonada, M., 7.1.6
Sonneveld, E. J., 2.3, 5.2
Sonoda, M., 7.1.8
Sorenson, D., 8.1
Sorenson, L. B., 4.2.3
Sorenson, L. O., 4.2.6
Soriano, T. M. B., 3.1
Sorokin, N. D., 9.2.2
Soures, J. M., 4.2.1
Sowa, H., 9.1
Spackman, M. A., 8.7
Spangfort, M. D., 3.1
Spargo, A. E. C., 4.3.7, 4.3.8
Sparks, C. J., 5.2, 7.4.3
Sparks, R. A., 2.3, 3.4
Sparrow, T. G., 4.3.4
Spear, W. E., 4.2.1
Spehr, R., 4.3.4
Speier, W., 4.3.4
Spence, A. J., 4.3.8
Spence, J. C. H., 4.3.4, 4.3.7, 4.3.8, 8.8
Spencer, R. C., 5.2
Spiegelman, C. H., 8.4, 8.5
Spielberg, N., 2.3, 5.2, 7.5
Spooner, F. J., 5.3
Springer, T., 2.6.2, 4.4.2
Sprong, G. J. M., 5.2
Squire, G. D., 3.4
Srinivasan, K., 2.5.2
Stępień, J. A., 5.3
Stępień-Damm, J., 5.3
Stępień-Damm, J. A., 5.3
Stalick, J. K., 2.3, 2.4.1, 5.1, 5.2
Stalke, D., 3.4
Stanglmeier, F., 4.2.6
Stanley, H. B., 2.9
Stanton, M., 7.1.6
Stasiecki, P., 2.6.1
Statile, J. L., 7.1.7
Staub, U., 4.4.2
Stearns, D. G., 4.2.6
Stedman, R., 4.4.3
Steeds, J. W., 4.3.6.2, 4.3.7, 5.4.2, 8.8
Steeple, H., 2.3
Stegun, I. A., 6.1.1, 6.3, 7.5
Steichele, E., 2.5.2, 4.4.2
Steigemann, W., 3.4
Steinberger, I. T., 9.2.1
Steinberger, J., 4.4.2
Steiner, M., 4.4.2
Steiner, W., 7.4.2
Steinhauser, K. A., 2.9
Steinmeyer, P. A., 2.3
Steinsvoll, O., 4.4.2, 4.4.3
Stemple, N. R., 4.2.6
Stephens, M. A., 6.1.1
Stephens, P. W., 4.2.5, 8.6
Stephenson, S. T., 4.2.1
Stern, E. A., 4.2.1, 4.2.3, 4.3.4
Stern, R. A., 7.1.6
Steryl, A., 2.9
Stetsko, Yu. P., 5.3
Steurer, W., 9.8
Stevels, A. L. N., 2.7
Stevens, E. D., 7.4.2, 8.7
Stevenson, A. W., 7.4.2
Stevenson, M. L., 4.2.3
Stewart, G. W., 8.1
Stewart, R. F., 4.3.3, 6.1.1, 8.7
Stibius-Jensen, M., 4.2.3, 4.2.6
Stiefel, E., 8.3
Stipcich, S., 4.2.3
Stirling, W. G., 4.4.2
Stobbs, W. M., 4.3.8
Stock, A. M., 3.4
Stock, S. R., 4.2.3
Stohr, J., 4.2.3, 4.3.4
Stølevik, V., 4.3.3
Storm, A. R., 4.2.3
Storm, E., 4.2.4, 4.2.6
Stott, A. M. B.,
Stout, C. D., 3.1
Stout, G. H., 2.2, 3.1, 3.4, 5.3
Stout, J. H., 9.2.2
Strack, R., 4.2.5
Stragier, H., 4.2.3
Stratonovich, R. L., 6.1.1
Straumanis, M., 5.3
Straumanis, M. E., 2.3, 5.3
Strauss, M. G., 4.3.4, 7.1.6, 7.3
Strauss, S., 7.4.3
Strinskii, A. N., 4.2.1
Strobel, P., 3.1
Stroud, A. H., 6.3
Stuart, A., 3.1, 3.3, 6.1.1
Stuart, D., 6.3
Stuart, D. I., 3.4
Stubbings, S. J., 3.4
Stuckey Kauffman, D., 5.3
Stuesser, N., 4.4.2
Stuhrmann, H., 4.2.1
Stuhrmann, H. B., 2.6.1, 2.6.2
Stümpel, J., 4.2.2
Stümpel, J. W., 7.1.6
Stura, E. A., 3.1
Sturhahn, W., 5.3
Sturkey, L., 2.4.1
Sturm, K., 4.3.4
Sturm, M., 4.2.6
Su, L. S., 4.3.3
Su, Z., 8.7
Suck, D., 3.4
Sudol, J., 7.3
Suehiro, S., 7.1.6
Sueno, S., 3.4
Suh, I.-H., 3.4
Suh, J.-M., 3.4
Sukharev, Y., 4.3.7
Suller, V. P., 4.2.1
Sullivan, J. D., 3.2
Sumner, I., 7.1.6
Suortti, P., 2.3, 4.2.1, 4.2.4, 4.2.6, 7.4.2, 7.4.4, 8.6
Surin, B. P., 3.1
Surkau, R., 4.4.2
Suski, T., 3.4, 5.3
Sussieck-Fornefeld, C., 2.3
Sussini, J., 4.2.5
Sutter, J., 5.3
Sutton, L. E., 9.5, 9.6
Suzuki, M., 9.2.2
Suzuki, S., 2.7
Suzuki, T., 4.3.8
Suzuki, Y., 7.1.6
Svensson, C., 5.3
Svensson, L. A., 3.1
Svergun, D. I., 2.6.1
Swann, P. R., 3.5, 4.3.4
Swanson, D. K., 3.4
Swanson, H. E., 5.2, 5.3
Swanton, D. J., 8.7
Swapp, S. M., 3.4
Sweet, R. M., 3.1, 7.1.6
Swoboda, M., 4.3.7
Swyt, C. R., 4.3.4
Sygusch, J., 8.3
Syromyatnikov, F. V., 3.2
Szabó, P., 7.5
Szarras, S., 2.5.1
Szmid, Z., 2.5.1, 5.3
Szymański, J. T., 9.2.2

Tabbernor, M. A., 4.3.1, 4.3.2, 4.3.7, 6.1.1, 8.8
Taft, E. A., 4.3.4
Taftø, J., 4.3.4, 4.3.7, 8.8
Tairov, Yu. M., 9.2.2
Takahashi, H., 4.3.7
Takahashi, K., 7.1.6, 7.1.8
Takahata, T., 9.2.2
Takama, T., 4.2.6
Takano, M., 7.1.6, 7.1.8

Takano, Y., 5.3
Takayanagi, K., 4.3.8
Takeda, H., 9.2.2
Takeda, T., 4.2.3, 4.4.2
Takéuchi, Y., 9.2.2
Tanaka, H., 7.1.8
Tanaka, M., 4.2.2, 4.3.7, 7.1.6, 8.8
Tanaka, N., 3.4
Tanaka, T. J., 4.2.4, 4.2.6
Tanemura, M., 9.1
Tanimoto, M., 7.1.6
Tanioka, K., 7.1.6
Tanisaki, S., 9.8
Tanner, B. K., 2.7, 4.1, 5.3
Tanoue, H., 4.2.3
Tao, K., 2.3
Taran, Yu. V., 4.4.2
Tardieu, A., 2.6.2
Tarling, S. E., 3.4
Tasset, F., 4.4.2
Tate, M. W., 2.7
Taub, H., 7.3
Taupin, D., 2.3
Tavard, C., 4.3.3
Taxer, K., 9.2.2
Taylor, A., 2.3, 4.2.1, 5.2, 9.2.1
Taylor, B. N., 4.2.1, 4.2.2, 4.2.3, 5.3
Taylor, H. F. W., 9.2.2
Taylor, J., 2.3, 5.2
Taylor, J. C., 8.6
Taylor, P. R., 6.1.1
Taylor, R., 9.5, 9.6
Tazzari, S., 4.2.1, 4.2.6
Tchoubar, C., 4.3.5
Tchoubar, D., 4.3.5
Teatum, E. T., 9.3
Teeter, M. M., 3.4
Teller, E., 9.2.1
Teller, R. G., 2.5.2
Tello, M. J., 9.8
Templer, R. H., 7.1.6
Templeton, D. H., 4.2.3, 4.2.6, 6.3
Templeton, L. K., 4.2.3, 4.2.6, 6.3
Tence, M., 4.3.4
Teng, T. Y., 3.4
Tennevin, J., 2.7
Teo, B. K., 4.2.3, 4.3.4
Terada, N., 4.2.3
Terasaki, D., 5.2
Terasaki, O., 2.5.1, 4.3.7, 5.2
Terhell, J. C. J. M., 9.2.1
Terminasov, Yu. S., 5.3
Termonia, Y., 2.3
Teuchert, W., 4.4.2
Thakkar, A. J., 4.3.3, 6.1.1
Thaller, C., 3.1
Thatcher, D. R., 3.1
Theisen, R., 4.2.4
Theobald-Dietrich, A., 3.1
Thiel, D. J., 4.2.5
Thierry, J. C., 3.4
Thiessen, M. J., 3.1
Thinh, T. P., 4.2.4
Thole, B. T., 4.3.4
Thomas, D. J., 7.1.6
Thomas, G., 3.5, 5.4.2, 7.1.6
Thomas, J. M., 4.3.4
Thomas, J. O., 8.6
Thomas, L. H., 4.2.6, 7.4.3, 8.7
Thomas, P., 7.3
Thomas, R. K., 2.9
Thomlinson, W., 2.3, 7.4.4, 8.6
Thompson, A. B., 9.2.2
Thompson, A. W., 2.2, 3.4
Thompson, D. J., 4.2.1
Thompson, J. B, 9.2.2
Thompson, P., 2.3
Thompson, T. E., 3.2
Thomsen, J. S., 4.2.2, 5.2, 5.3, 7.5
Thuesen, G., 4.2.3, 4.2.6
Thut, R., 4.4.2
Tiao, G. C., 8.1, 8.2
Tibballs, J. E., 6.3
Tighe, N. J., 3.5
Tikhonov, A. N., 2.6.1
Tikhonov, V. I., 6.1.1
Tilton, R. F., 3.4
Tilton, R. F. Jr, 3.4
Timasheff, S. N., 2.2, 2.6.1
Timchenko, T. I., 9.2.2
Timmers, J., 5.2
Timmins, P. A., 2.6.2
Tindle, G. L., 4.4.3
Tipson, R. S., 3.1
Tissen, J. T. W. M., 3.1
Tivol, W. F., 4.3.8
Tixier, R., 5.3
Toby, B. H., 2.3
Tode, G. E., 3.4
Toellner, T. S., 5.3
Tofield, B. C., 8.7
Tohji, K., 4.2.1
Tokonami, M., 9.2.1, 9.2.2
Tokumaru, Y., 5.1
Tokumoto, M., 4.2.3
Tolhoek, H. A., 7.4.3
Toman, K., 5.2
Tomaszewski, P. E., 5.3, 9.2.2
Tomimitsu, H., 2.8
Tomita, T., 9.2.1
Tomkeieff, M. V., 5.3
Tomlin, S. G., 4.2.1
Tomokiyo, Y., 4.3.7, 8.8
Tomonaga, N., 5.3
Tonomura, A., 4.3.8
Toorn, P. van, 7.2
Toraya, H., 2.3, 5.2
Tossel, J. A., 4.3.4
Tournarie, M., 2.3
Town, W. G., 9.5, 9.6
Toyoshima, N., 3.4
Trail, J., 4.2.1
Trammell, G. T., 6.1.2
Trautmann, N., 4.4.2
Travennier, M., 5.2
Travis, D. J., 7.1.6
Treacy, M. M. J., 4.3.8, 9.1
Trebbia, P., 4.3.4
Tremayne, M., 8.6
Treverton, J. A., 3.5
Trewhella, J., 2.6.1
Trigunayat, G. C., 5.3, 9.2.1
Tripathi, A. N., 4.3.3
Troitsky, V. I., 2.9
Trost, A., 2.3
Trueblood, K. N., 2.2, 8.3
Trzhaskovskaya, M. B., 4.2.4
Tse, T., 4.2.5
Tseng, H. K., 7.4.3
Tsernoglou, D., 3.4
Tsu, Y., 4.2.3
Tsuda, K., 4.3.7, 8.8
Tsuji, M., 4.3.8
Tsukimura, K., 3.4
Tsuno, K., 4.3.8
Tsutsumi, K., 4.2.3
Tsvetkov, V. F., 9.2.2
Tsypursky, S. I., 2.4.1
Tu, H. Y., 3.1
Tubbenhauer, G. A., 7.1.6
Tucker, P., 8.2
Tucker, T. N., 5.3
Tugulea, M. N., 7.4.3
Tuinstra, F., 3.4, 5.2, 9.8
Tukey, J. W., 8.2
Tulkki, J., 7.4.3
Tung, M., 3.1
Tuomi, T., 2.7
Turberfield, K. C., 2.5.2
Turchin, V. F., 4.4.2
Turkenburg, J. P., 3.4
Turner, J. N., 4.3.8
Turner, P. S., 2.4.1, 4.2.4, 4.3.1, 4.3.2, 6.1.1
Tutton, A. E., 3.2
Tuzov, L. V., 5.3
Tzafaras, N., 3.4

Uchiyama, K., 7.1.6
Udagawa, Y., 4.2.1, 4.2.3
Uehling, E. A., 4.2.2
Ueno, Y., 7.1.8
Ugarte, D., 4.3.4
Ullrich, H.-J., 5.3
Ullrich, J. B., 4.4.2
Umanskii, M. M., 7.5
Umanskij, M. M., 5.2
Umansky, M. M., 5.3
Umeno, M., 5.3
Umezawa, K., 4.2.6
Unangst, D., 5.3
Uno, R., 2.5.1
Unonius, L., 2.3, 8.6
Unwin, P. N. T., 4.3.7, 4.3.8
Urbanowicz, E., 5.3
Ursell, H. D., 6.1.1
Usami, K., 7.1.6
Usha, R., 3.4
Uspeckaya, G. I., 5.3
Usuda, K., 5.3
Utlaut, M., 4.3.4
Uyeda, N., 4.3.8
Uyeda, R., 2.7, 4.3.7, 5.4.2, 8.8

Vacquier, V. D., 3.1
Vainshtein, B. K., 2.2, 2.4.1, 4.3.5
Vajda, I., 2.3
Valentine, R. C., 7.2
Valvoda, V., 4.1
Van Bommel, A. J., 4.2.6
Van Dyck, D., 4.3.8
Van Landuyt, J., 4.3.8
Van Mellaert, L., 2.7
Vanoni, F., 4.4.2
Vansteelandt, L., 4.4.2
Van Tendeloo, G., 4.3.8, 9.2.1, 9.2.2
Varghese, J. N., 4.2.5
Varnum, C. M., 4.4.2
Vaughan, D. J., 4.3.4
Veeraraghavan, V. G., 2.3
Veigele, W. J., 4.2.4, 4.2.6, 7.4.3
Veillard, A., 6.1.1
Venghaus, H., 4.3.4
Vercillo, R., 7.1.6
Vergamini, P. J., 3.4
Verheijen, M. A., 9.2.2
Verin, I. A., 3.1
Verma, A. J., 9.2.2
Verma, A. R., 9.2.1
Vernon, W., 2.2, 7.1.6
Vettier, C., 4.2.5
Veysseyre, R., 9.8
Via, G. H., 4.2.3
Victoreen, J. A., 4.2.4
Villain, F., 4.2.3
Villain, J., 9.8
Villars, P., 9.3
Vincent, M. G., 6.3
Vincent, R., 4.3.7, 8.8
Vincze, L., 4.2.5
Vineyard, G. H., 2.3
Visser, J. W., 2.3, 5.2, 9.8
Viswamitra, M. A., 9.7
Vittone, E., 4.2.2
Vittot, M., 7.1.6
Vogels, A. B. P., 2.3
Vogt, T., 4.4.2
Voigt, W., 7.4.2
Voigt-Martin, I. G., 4.3.7
Vollath, D., 4.2.4
Volz, K., 2.2
Von Dreele, R. B., 6.4, 8.6
Von Festenberg, C., 4.3.4
Voronin, L. A., 2.6.1
Vos, A., 7.4.2
Voss, R., 4.3.7, 4.3.8
Vossers, H., 3.4
Vriend, G., 3.4
Vrublevskaya, Z. V., 4.3.5, 9.2.2
Vucht, J. H. N. van, 9.3
Vvedensky, D. D., 4.3.4

Waarzak, I., 3.1
Waber, J. T., 4.2.4, 4.2.6, 4.3.1, 6.1.1, 9.3
Waché, C., 5.3
Wachtel, E., 2.6.2
Wada, N., 4.2.3
Waddington, W. G., 4.3.8
Wade, R. H., 4.3.8
Wagenfeld, H., 4.2.6, 6.3
Wagner, C. N. J., 2.3
Wagner, R., 2.6.2
Wagner, V., 4.4.2
Wagshul, M. E., 4.4.2
Wait, E., 3.4
Wakabayashi, K., 7.1.8
Wakita, H., 4.2.3
Walder, V., 5.3
Walker, A. R., 5.4.2
Walker, G. A., 2.3
Walker, N., 6.3
Wall, J., 4.3.8
Wall, M. E., 2.7
Wallace, C. A., 2.7, 5.3
Waller, I., 4.2.6, 7.4.3

Walls, M. G., 4.3.4
Walter, G., 2.6.1
Walters, K., 4.4.2
Walton, D., 7.1.6
Wang, D. N., 4.3.7
Wang, J., 4.3.3
Wang, M. S., 4.2.6
Wang, S. Q., 8.8
Warble, C. E., 4.3.8
Warburton, W. K., 4.2.3, 7.1.5
Ward, K. B., 3.1
Ward, R. C., 7.4.2
Ward, R. C. C., 2.7
Ware, N. G., 2.3
Warren, B. E., 2.3, 4.2.5, 4.3.5
Warrington, D. H., 1.3
Waschkowski, W., 4.4.4
Waser, J., 6.2, 8.3
Washburn, J., 3.5
Waśkowska, A., 5.3
Wassermann, G., 2.3
Watanabe, D., 4.3.7, 8.8
Watanabe, H., 4.3.7, 8.8
Watanabe, T., 4.2.3, 6.1.1
Watenpaugh, K. D., 3.4
Watkin, D. J., 2.3
Watson, D. G., 9.5, 9.6, 9.7
Watson, D. L., 2.7
Watson, K. J., 6.1.1
Watson, L. M., 4.2.2
Weaver, L. H., 3.1
Weaver, W., 2.6.1
Weber, H., 7.4.2
Weber, H.-P., 2.3
Weber, K., 6.3
Weber, P. C., 3.1
Weber, W., 4.2.6
Weckerman, B., 4.4.2
Weertman, J., 9.2.1
Weertman, J. R., 9.2.1
Wehenkel, C., 4.3.4
Weibel, E., 4.3.8
Weickenmeier, A., 4.3.2
Weickenmeier, A. L., 4.3.7, 8.8
Weigel, D., 9.8
Weik, H., 5.3
Weill, F., 9.2.2
Weill, G., 2.5.1
Weininger, M. S., 3.4
Weinstock, B., 4.3.3
Weisenberger, P., 4.2.3
Weisgerber, S., 2.2
Weiss, R. J., 6.3, 7.4.3
Weiss, Z., 9.2.2
Weissenberg, K., 2.2
Weissmann, S., 5.3
Weisz, O., 5.3
Welberry, T. R., 3.4
Wellenstein, H., 4.3.3
Wells, A. A., 7.1.6
Wells, A. F., 9.1, 9.2.1
Wells, M., 4.4.5
Welsch, R. E., 8.1, 8.2, 8.5
Welsh, R. C. J., 4.4.2
Weng, X. D., 4.3.4
Wenk, H. R., 4.3.8
Wennemer, M., 9.2.2
Wenskus, R., 7.4.3
Wenzl, H., 5.3
Werner, K., 4.4.2
Werner, P. E., 2.3, 8.6
Werner, S., 2.8
Werner, S. A., 4.4.3, 4.4.4, 6.2, 6.4, 7.5
Wertheim, G., 2.3
Wery, J. P., 3.4
West, D. R. F., 3.5
West, J. M., 3.5
West, K., 2.3
Westbrook, E. M., 3.2, 7.1.6
Westbrook, M. L., 7.1.6
Whaling, W., 7.3
Whatmore, R. W., 2.7
Whelan, M. J., 3.5, 4.3.2, 4.3.6.2, 4.3.8, 5.4.1
White, E. T., 3.2
White, T. J., 9.2.2
Whitfield, H., 4.3.7
Whitney, D. R., 5.2, 5.3
Whittaker, E. J. W., 7.1.1
Whittemore, W. L., 4.4.2
Wichmann, E. H., 4.2.2
Wick, G. C., 4.4.2
Wicks, B. J., 3.5
Widom, J., 7.1.6
Wiedmann, L., 4.2.1
Wiegand, C. E., 4.2.2
Wien, W., 4.3.4
Wiesler, D. G., 2.9
Wiewióra, A., 9.2.2
Wiewiorosky, J., 2.3
Wignall, G. D., 2.6.2
Wikinson, A. P., 8.6
Wiles, D. B., 2.3, 8.6
Wiley, D. C., 7.1.6
Wilhelm, T., 7.1.6
Wilkens, M., 5.2
Wilker, C. N., 4.3.4
Wilkins, J. W., 4.3.4
Wilkins, M. H. F., 2.6.1
Wilkins, S. W., 4.2.5, 6.1.1, 6.4
Wilkinson, A. P., 2.3
Wilkinson, C., 2.2
Wilkinson, D. H., 7.1.6
Wilkinson, M. K., 9.8
Will, G., 2.3, 5.2, 5.3, 7.3, 8.6
Wille, H.-C., 5.3
Wille, P., 4.4.2
Williams W. G., 4.4.2
Williams, B. G., 4.3.4, 7.4.3
Williams, D. B., 4.3.8
Williams, D. E. G., 9.7
Williams, E. J., 7.5, 8.4
Williams, G. P., 7.4.4
Williams, J. C., 3.5
Williams, J. M., 2.5.2
Williams, R., 3.4
Williams, W. G., 4.4.2
Williamson, G. K., 3.5
Willis, B. T. M., 2.2, 2.3, 2.5.2, 3.6, 4.4.6, 5.3, 5.5, 6.1.1, 6.1.3, 6.2, 7.4.2, 8.6, 8.7
Willoughby, A. F. W., 5.3
Willson, P. D., 2.3
Wilson, A. J. C., 1.4, 2.3, 2.4.2, 2.5.1, 3.3, 4.2.2, 4.3.5, 5.1, 5.2, 5.3, 6.3, 6.4, 7.5, 8.1, 8.2, 9.2.1, 9.2.2, 9.7
Wilson, A. R., 4.3.8
Wilson, C. G., 5.3
Wilson, E., 3.1
Wilson, H. R., 2.6.1
Wilson, K., 7.5
Wilson, R. J. F., 7.1.6
Wilson, R. R., 4.2.1
Wilson, S. A., 2.8
Winchell, P. G., 2.3
Windisch, D., 5.3
Windsor, C. G., 2.5.2, 4.1, 4.4.6, 7.3, 8.6
Winick, H., 4.2.1, 4.2.3
Winick, M., 7.4.3
Winkler, F. K., 2.2
Winslow, E. H., 4.2.4
Wippler, C., 2.6.2
Witters, R., 2.6.1
Wittmann, H. G., 3.4
Wittmann, J. C., 3.5
Wittono, G., 4.2.6
Witz, J., 2.2, 2.6.2
Wlodawer, A., 2.2, 6.3
Woicik, J. C., 4.2.3
Wokulska, K., 4.2.2, 5.3
Wołcyrz, M., 5.3
Wolf, B. de, 2.6.2
Wolf, J., 4.2.2, 5.3
Wolf, R. S., 7.3
Wölfel, E. R., 2.3, 5.3, 7.1.3, 7.1.6
Wolff, P. M. de, 1.4, 2.3, 7.1.1, 9.2.2, 9.8
Wollan, E. O., 9.8
Wolpert, R. L., 8.1
Wolstenholme, J. F. R., 5.2
Wonacott, A. J., 2.2, 3.4, 7.1.6
Wondratschek, H., 1.4, 9.8
Wones, D. R., 9.2.2
Wong, T. C., 4.3.3
Wong-Ng, W., 3.4, 5.2
Wood, G. J., 4.3.8
Wood, I. G., 3.4
Wood, R. A., 3.4
Woodruff, D. P., 4.2.3
Woodward, J. B., 4.2.6
Woolfson, M. M., 2.2, 5.3
Wooster, W. A., 2.2, 5.3, 7.4.2
Worcester, D. L., 2.6.1
Worgan, J. S., 7.1.5
Worlton, T. G., 2.5.2
Worthmann, W., 2.6.1, 2.6.2
Wright, A. F., 3.4, 4.4.2
Wright, D. J., 2.6.1
Wright, E. M., 7.5
Wright, M. M., 8.3
Wroblewski, T., 3.4
Wroe, H., 4.4.2
Wu, C. C., 2.7
Wu, D. Q., 7.1.6
Wu, Y., 5.2
Wu, Y.-Q., 4.2.1
Wulff, P., 3.2
Wunderlich, J. A., 3.2
Wurmbach, P., 2.6.2
Wyckoff, H. W., 2.2, 3.4

Xiao, Q. F., 4.4.2
Xie, J., 7.1.6
Xie, S.-D., 4.3.3
Xuong, Ng. H., 2.2, 3.4, 7.1.6

Yaakobi, B., 4.2.1
Yabuki, S., 2.6.2
Yagi, K., 4.3.8
Yakovlev, V. A., 7.1.6
Yakowitz, H., 5.3
Yamada, N., 5.3
Yamada, S., 2.9
Yamagishi, H., 4.3.7
Yamaguchi, M., 2.7, 7.1.6
Yamaguchi, T., 4.2.3
Yamamoto, A., 9.8
Yamamoto, M., 3.4
Yamanaka, T., 9.2.2
Yamashita, T., 7.1.7
Yamazaki, H., 3.4
Yan, D. H., 4.3.7
Yano, Y., 7.1.6
Yao, T., 4.2.1, 4.2.3
Yap, F. Y., 4.2.2, 5.2, 7.5
Yap, Y., 5.3
Yasuami, S., 5.3
Yates, A. C., 4.3.3
Yeates, T. O., 3.1
Yeh, J. J., 4.2.4
Yin, Y., 3.1
Yocum, C. F., 4.2.3
Yoder, H. S., 9.2.2
Yonath, A., 3.4
York, E. J., 6.3
Yoshida, N., 4.2.3
Yoshimatsu, M., 2.3, 4.2.1
Yoshimura, M., 2.3
Yoshioka, H., 8.8
Yoshioka, Y., 7.1.6
Young, A. C. M., 3.4
Young, H. D., 4.4.4
Young, R. A., 2.3, 4.2.5, 5.2, 6.3, 8.6
Yvon, K., 2.3

Zaanen, J., 4.3.4
Zabel, H., 2.9
Zabidarov, E. I., 4.4.2
Zaccai, G., 2.6.2
Zach, J., 4.3.8
Zachariasen, W. H., 4.2.6, 4.4.2, 6.3, 6.4
Zagari, A., 3.1
Zagofsky, A., 2.3
Zahorowski, W., 5.3
Zakharov, N. D., 4.3.8
Zaloga, G., 3.4
Zaluzec, N. J., 4.3.4, 8.8
Zanchi, G., 4.3.4
Zanevskii, Yu. V., 7.1.6
Zani, A., 5.3
Zarka, A., 2.8
Zassenhaus, H., 1.4, 9.8
Zeedijk, H. B., 3.5
Zeidler, T., 2.9
Zeisler, R., 4.4.2
Zeissler, C. J., 4.4.2
Zeitler, E., 3.5, 4.3.4, 7.2
Zemany, P. D., 4.2.4
Zemlin, F., 3.5
Zeppenfeld, K., 4.3.4
Zeppezauer, E. S., 3.4
Zeppezauer, M., 3.4
Zerby, C. D., 4.2.6
Zernicke, F., 2.6.1
Zevin, L. S., 5.2, 5.3, 7.5
Zeyen, C. M. E., 4.4.2
Zha, C. S., 2.5.1

Zhang, X.-J., 3.4
Zhang, Y., 2.3, 5.2
Zhao, Z. X., 4.3.8
Zhdanov, G. S., 4.1, 9.2.1
Zhou, X.-L., 2.9
Zhoukhlistov, A. P., 9.2.2
Zhu, J., 4.3.4
Zhukhlistov, A. P., 4.3.5, 9.2.2
Zimmermann, J., 4.2.1
Zimmermann, S., 4.3.4
Zinke, M., 2.6.1
Zipper, P., 2.6.1
Zirwer, D., 2.6.1
Zittlau, W., 4.3.3
Zobel, D., 3.4
Zobetz, E., 9.1
Zocco, T. G., 2.9
Zolensky, M. E., 2.3
Zolliker, P., 5.5
Zolotoyabko, E., 5.3
Zoltai, T., 9.2.2
Zorkaya, O. N., 9.7
Zorkii, P. M., 9.2.2
Zorky, P. M., 9.7
Zosi, G., 4.2.2, 5.3
Zou, X. D., 4.3.7
Zsoldos, É., 5.3
Zubenko, V. V., 5.3
Zucchino, P., 7.1.6
Zucker, U. H., 6.1.1
Zuñiga, F. J., 9.8
Zuo, J., 8.8
Zuo, J. M., 4.3.7, 4.3.8, 5.4.1, 8.8
Zůra, J., 5.3
Zurek, S., 3.4
Zvyagin, B. B., 3.5, 4.3.5, 9.2.2
Zwoll, K., 5.3

Subject Index

Abbe refractometer, 160
Abbe theory, 420
Abelian module, 937
Aberrations (see also Systematic errors)
  centroid displacements, 494
  coefficients, 426
  geometrical, 46, 83, 86, 493
  in powder diffractometry, 46, 48, 50
  line-profile breadths, 494
  of an energy-dispersive diffractometer, 497
  physical, 46, 85, 86, 493, 494
  refraction, 492
  transparency, 49
Absolute calibration of SANS data, 108
Absolute intensity in SANS, 108
Absolute measurements, 505
  of lattice spacings, 505, 526, 529–533
Absorbed dose, definition of, 958
Absorption, 599, 609, 653
  air, 73
  anomalous, 416
  coefficients, 213, 218
  coefficients for Bloch waves, 735
  coefficients for neutrons, 461
  coefficients, linear, 599
  coefficients, mass, 600
  cross sections, macroscopic, 461
  edges, 191, 202, 205, 206, 209, 599
  edges, wavelengths of, 205–211
  effects, 261
  efficiency, 623
  factor, 51
  function, 261
  in XED, 86
  length, 188
  minimization by suitable mounting of single crystals, 163
  of generated X-rays in target, 191
  photoelectric, 599
  systematic error, 528
  systematic error, elimination, 521–524, 528–529
  X-ray, 599–608
Absorption corrections, 170, 600–608
  neutron diffraction, 177
Accelerating voltage
  fluctuations, 424
  of a transmission electron microscope, determination, 539
Accessible range of *d*'s, 38
Accuracy, 490, 492, 707
  factors determining, 501
Accuracy of lattice-parameter (lattice-spacing) determination, 505, 507, 526, 533–536
  evaluation, 534
  (methods of) increasing, 532–536
  relative, 505
Acoustic modes, 653, 654
Activity, definition of, 958
Adequate protection, definition of, 958
Adhesives for mounting specimens, 163
Aggregation effects in SANS, 107
Air absorption, 73
Air and window transmission, 73
Air scattering, 74, 665
ALCHEMI (atom location by channelling enhanced microanalysis), 411
Alignment and angular calibration, 46
Aluminium
  dielectric coefficients, 402
  effective number density, 411
  film, 393
Ambiguities in modulated structure notation, 936
Amorphous material, diffraction from, 24
Analyser, 530
  perfect-crystal, 665
Analysis of charge density, 713–734
Analysis of spin density, 713–734
Analytical extrapolation of lattice parameters, 493
Anatase, high-energy resolution spectra, 408
Anger camera for neutrons, 650
Angle definition, use of peak or centroid for, 63
Angle-dispersive diffractometry, 491, 495–496
Angle-reading error, 524
Angle-setting error, 524
Angles between crystal blocks, determination, 516
Angles in direct and reciprocal space, 4
Angles of reciprocal cell, determination, 517
Angular distribution of reflections in Laue diffraction, 29
Angular momentum, 727
  orbital, 731
Angular setting errors (precession), 35
Angular-velocity factors, 596
Anharmonicity, 585, 722
Anisotropic mosaic crystals, 432
Anisotropic temperature factors, 697
Anisotropic thermal diffuse scattering correction, 654
Anode current/voltage relationship in electrochemical thinning, 175
Anomalous absorption, 416
Anomalous dispersion (scattering) (see also Dispersion), 21, 188, 241, 733
  not anomalous, 241
Anomalous transmission, 116
Anti-equi-inclination setting, 31
Antiferromagnetic order, 728
Antiferromagnetism, 140
Antiferromagnets, 728
Antimorphism, 897
Antiscatter slits, 45
Aperiodic lattice, 921, 928, 937
Approximations
  Born, 591
  Born–Oppenheimer, 713, 722, 723
  commensurate, 909
  convolution, 723
  crystal-field, 729
  dipolar, 731
  first Born, 389
  Glauber, 391
  harmonic, 723
  Hartree–Fock, 732
  impulse, 657
  kinematical, 260
  LCAO, 723
  Moliere high-energy, 260
  no-upper-layer-line, 415
  phase-grating, 260
  projected charge-density, 423
Approximations
  quasi-Gaussian, 590
  two-beam, 260
  weak-phase-object, 423
Archimedes method for density measurement, 158
Area-detector diffractometry, 36, 170
Area detectors,
  geometric effects, 41
  non-uniformity of response, 41
  television, 630
Arithmetic crystal classes, 15, 897, 898, 911, 917, 939, 945
  (3+1)-dimensional, 917
  as classification of space groups, 15
  classification by size, 20
  derivation of, 15
  four-dimensional, 15
  notation for, 15
  one-dimensional, 15, 16
  three-dimensional, 15–20
  two-dimensional, 15, 16
  uses of, 15
Arithmetic equivalence, 911, 939
Arithmetic point groups, 914
Arithmetically equivalent point groups, 939
Arrangements giving partial reduction of systematic errors, 515, 514, 521–523, 526, 528–531
Associated Legendre polynomials, 581
Astigmatism, 421, 424
Asymmetric Bragg reflections, 526
Asymmetric (Straumanis) film mounting, 509
Asymmetry
  factor, 118
  of peaks, 67
Asymptotic behaviour of SANS curves, 110
Atom-centred expansion, 729
Atom-centred models, 714
Atom-centred spherical harmonic approximation, 714
Atom location by channelling enhanced microanalysis (ALCHEMI), 411
Atomic beams, 189
Atomic dipole moment, 716
Atomic environment types, 776
Atomic form factor, 242
Atomic orbital basis, 722
Atomic quadrupole moment, 717
Atomic scattering factors, 188, 242, 259
  analytical approximation for (tables), 578–581
  for electrons (tables), 263–281
  free atoms (tables), 555–564
  generalized, 565
  ions (tables), 566–577
Atomic volumes, 774
Attenuation coefficients, 213, 230, 600
Auger shifts, 204, 205
Automation, computer-controlled, 63
Avalanche multiplication, 619, 634
Avalanche production, 626
Average structure, 913
Avogadro constant, determination of, 534
Axial divergence, 46, 50, 53, 494, 497
Axial-divergence error, 494, 523
  correction for, 523
Axial holography, 427

Axial lengths, determination of, 532
Axial reflections, 517

Back reflection, 512–515
Backgammon (*jeu de jacquet*) counter, 627
Background, 68, 661
  in SANS, 108, 109
Background counting rates, 667
Background radiation, definition of, 958
Backlash in diffractometer drives, 47, 503, 667
Balanced filters, 74, 78, 79, 238
Bandwidth, 197
Basic polytypes, 763, 766, 767
Basic structural features, 745–944
Basic structure, 909
Basis
  conventional, 944
  crystallographic, conventional, 3
  crystallographic, non-primitive, 3
  crystallographic, primitive, 2
  primitive reciprocal, 2
  standard, 944
  vectors, 944
Bayerite family, 766
Bayes's theorem, 681
Beam centring, 45
Beam conditions, 120
Beam divergence, 45, 425, 498
Beam-splitting crystal, 531
Beam tilt (see also Misalignment), 524
Becquerel, definition of, 958
Bending magnets, 198
Bent crystals, 77
Berg–Barrett method, 114
Beryllium, cross section for neutrons, 439
Beryllium acetate, 663
Bessel function, 589, 666
  spherical, 460, 581, 592
Best linear unbiased estimator, 680
Best overall fit, 493
Beta function, 703
Bethe approximation, 736
Bethe ridge, 411
Bethe theory for inelastic scattering, 406–408
Bias, 689, 707, 709
  of midpoint of a chord, 520
  of peak, 520
Bijvoet-pair intensity ratios, 251
Bijvoet-pair techniques, 251
Binding effects, 391
Biological macromolecules, SANS, 105
Birefringence, 153
  of polytypes, 757
Black-body radiation in X-ray region, 198–199
Blackman curve, 81
Blind region, 34
Bloch standing waves, 411
Bloch-wave method, 259, 415–416, 426, 735
Block collimation, 99
Block polytypism, 760, 766
Boltzmann statistics, 726
Bond angles, 698
Bond lengths, 698, 813
Bond method, 498, 507, 508, 522–526, 529, 531, 534, 535–536
  for small spherical crystals, 525
  in multiple-crystal spectrometers, 529–531
  systematic errors, 523–524
Bond-system diffractometers, 522, 524
Bonding electrons, distribution of, 425
Bonds, classification of, 791, 813
Bonse–Hart camera, 100
Bonse–Hart interferometer, 121
Born approximation, 591
  first, 389
Born–Oppenheimer approximation, 713, 722, 723
Born series, 259
Borrmann effect, 113, 116, 600
Borrmann triangle, 116
Bound nuclear scattering lengths, 593
Boundaries, low-angle, 114
Bragg angle, 187
  accuracy of, 505–506, 516
  determination, 506, 519, 521
  errors, 491, 494
  from a diffraction profile, 519–521
  from a photograph, 519
  from a two-dimensional map of intensity, 522
  measurement of, 505, 518
  operational definitions, 491
Bragg–Brentano (Parrish) angle-dispersive diffractometers, 44, 495, 664
Bragg cut-off, 438
Bragg law, 505
Bragg optics, 432
Bragg reflection, 3, 432
  magnetic, 591
Bravais classes, 910, 913, 940, 945
  (2+1)-dimensional, 915
  (2+2)-dimensional, 916
  (3+1)-dimensional, 917–918
  one-line symbols, 915, 920
  two-line symbols, 915, 920
Bravais lattice, 3, 15, 913
Brazil twins, 11
Bremsstrahlung, 37, 191
  for XED, 84
Brilliance, synchrotron radiation, 197
Brillouin zone, 657
Broadening function, 710
Brownian diffusion, 589
Broyden–Fletcher–Goldfarb–Shano update, 684

Cadmium iodide, 754, 756
Cadmium telluride detector, 623
Calculated powder patterns, 60
Calculation of the twin element, 14
Cambridge Structural Database, 790, 812
Camera methods for lattice-parameter determination, 491, 497
Camera radius
  extremely large, 510
  uncertainty, elimination, 510
Camera tubes
  high-resolution TV, 633
  lead oxide, 634
Cameras
  back-reflection, 71
  Bonse–Hart, 100
  cylindrical, 70
  Debye–Scherrer, 42, 70
  ellipsoidal mirror in SANS, 106
  flat-film, 71
  for recording lattice-parameter changes, 510
  Gandolfi, 71
  Guinier focusing, 44, 68, 70
  Kossel, 512
  Kratky, 99
Cameras
  mirror, 106
  miscellaneous, 70
  pinhole, in SANS, 106
  pinhole, in SAXS, 100
  powder, 69–71
  small-angle, 99
  systems for synchrotron radiation, 100
Capillary tubes for mounting specimens, 162
Carcinogenesis, 960
Cast films, 176
Castaing & Henry filter, 397
Categories of OD structures, 764
Cauchy curves, 67
Cauchy distribution, 689
Causality, principle of, 246
CBED (convergent-beam electron diffraction), 416, 540, 735
CBED disc, 417
Cell dimensions, incorrect assignment, 170
Cellulose film containers, 162, 163
Central-limit theorem, 702
Centre of gravity (centroid), 518
  additivity, 518
  variance, 518
Centred lattices, 3
Centred unit cells, 3
Centring conditions, 921
Centring lattice vectors, 3
Centring reflection conditions, 921
  for (3+1)-dimensional Bravais classes, 935
Centroid of a reflection, 492
Centroid of wavelength distribution, 494
Ceramics, preparation of specimens, 171
Cerenkov radiation, 401
Cerium oxide (intensity standard), 500, 503
Channel-cut monochromators, 77, 121
Channelling, 189
Characteristic function, 90
Characteristic line spectrum, 191, 202
Characteristic radiation, efficiency of production, 192
Characteristic X-rays, excitation of, 510
Characterization of detectors, 639
Charge, 187
Charge-cloud model, 715
Charge-coupled devices, 629
Charge densities, analysis of, 713–734
Chemical
  analysis, 154
  etchants for thin section preparation, 173
  etching, 173
  polishing, 174
  properties, 154
  thinning, 175
Chi-squared (χ^2) distributions, 702, 703
Chiral volumes, 700
Chlorite group, 765, 769
Chlorite–vermiculite group, 769–770
Choice of reflections, 535
Cholesky decomposition, 681, 685
Cholesky factor, 678, 681, 694, 708
Choppers, 443
Chromatic aberration constant, 423, 424
Chromium oxide (intensity standard), 500, 503
Circle packings, 746–747, 752
Classification
  of bonds, 791, 813
  of experimental techniques, 24
  of space groups, 15
Cleavage, 153

Close-packed structures, 752, 761, 897
interstices in, 753
lattices possible, 755
notations for, 753–754, 756
polytypes, 754–756
space groups possible, 755
spheres, 747, 752
stacking faults in, 758–760
structure determination of, 756–758
symmetry of layers, 753
symmetry of stacking, 755
voids in, 753
Cobalt martensites, stacking faults in, 758
Coherent inelastic scattering, 177
Coherent multiple scattering, 661
Coherent (Rayleigh) scattering, 554
Coherent scattering cross sections, 594
Coherent scattering lengths, 594
Cohesive energy, 721
Coincidence operations, 761
Cold neutrons, 105
Collimation, 37
block, 99
in-plane, 522
of neutrons, 105, 431
systematic errors connected with, 523–524
Collimators
misalignment (tilt), 523–524
misalignment (tilt), error, 524
Soller, 82, 443
Collinear structures, 591
Colour groups, 21
Column approximation, 414
Combined aberrations, 50
Combined methods, spectrometers for, 531
Commensurate approximation, 909
Commensurate modulated structures, 907–944
Comparison measurements of lattice parameters, 508
Compensating transformations, 940
Compensating translations, 940
Composite crystal structures, 907, 941
Composition surfaces, 10
Compton scattering, 90, 213, 242, 554, 599, 657–661, 663, 713
non-relativistic approximations, 657–659
relativistic treatment, 659–660
Compton shift formula, 657
Compton wavelength, 260
Computer-controlled automation, 63
Computer graphics for powder patterns, 69
Computer programs
CRYSTIN, 778
data processing, 596
Computer simulation in estimation of error, 536
Computing methods for electron diffraction, 425
Concentration effects, 97
elimination of, 98
Condensed models, 766
Condition number, 678, 682
Conditional probability density function, 679
Conditional Q–Q plot, 708
Conditioning, 684
Cone-axis photography, 35
Confidence level, 64
Conic section, 515
Conical surface of an *hkl* reflection, 510
Conjugate-gradient methods, 686
Conservation laws, 657
Constrained models, 693
Constraints in refinement, 693, 693–701
Contact number, 747, 749
Continuous spectrum, 192
Contrast
diffraction, 113, 735
extinction, 113
first-fringe, 116
match-point, 107
orientation, 113
variation in SANS, 107
variation in SAXS, 97
variation, inverse, 108
variation, spin, 108
Conventional basis, 3, 945
Conventional unit cell, 913
Conventional X-ray sources, 37
Convergent-beam electron diffraction (CBED), 80, 416, 417, 540, 735
Convolution, 66, 505, 518, 534
Convolution equations, 67
Convolution of rocking curves, 663
Convolution range, 66
Convolution square-root technique, 103
Coordination complexes, typical interatomic distances, 812–896
Coordination number, 774
Core-electron spectroscopy, 404
Core-loss spectroscopy, 404
Correction factor
for absorption and extinction, 612
for powders, 657
Correction of systematic error, 653
Correlated and uncorrelated mosaic blocks, 610
Correlation coefficients, 724
Correlation energy, 391
Correlation function, 90
Correlation length, 93
Correlations between recorded intensities, 519
Corundum
etching, 173
intensity standard, 500, 503
Coulombic self-electronic energy, 721
Counters
backgammon (*jeu de jacquet*), 627
gas-filled, 626
Geiger–Müller, 522
parallel-plate, 627
Counting losses, 625
Counting modes, 666
Counting rates, 666–668
background, 667
erratic fluctuations, 666
reflection only, 666
total, 666
Counting statistics, 64, 666–668
Critical-voltage effect, 416, 736
Critical wavelength, 196
Cross sections
differential scattering, 260
dispersion corrections, 221
elastic differential scattering, 262
ionization, 407
of a rod-like particle, 93
PDDF of, 102,
plasmon, 399
scattering and absorption, 439, 444
Cryoprotectants, 166,
Crystal(s)
analysers, 56
datum orientation, 33
definition of, 908
displacively modulated, 909
edges, 3
ideal, 908
ideally imperfect, 113
ideally perfect, 113
intergrowth, 941
misalignment (tilt), 424
misalignment (tilt), error, 524
modulated, 908
monochromators, 76, 662
mosaicity, 170
normal, 908
orientation matrix, 33
real, 419
reflecting power, 590
rocking curves, 34, 37, 40
rocking widths, 33
selection, 148, 151
slippage within capillary, 165
systems, 6
Crystal classes
arithmetic, 15, 911, 945
geometric, 15, 911, 913
Crystal-field approximation, 729
Crystal-lattice vector and crystal setting, 168
Crystal profile, 505
Crystal-size analysis, 81
Crystal structure
determination by HREM, 419
images, 422
Crystal systems
cubic, 9, 19
hexagonal, 7, 15, 19
monoclinic, 6, 16
oblique, 15
orthorhombic, 6, 16
rectangular, 15
rhombohedral, 8
square, 15
tetragonal, 7, 17
triclinic, 6
trigonal, 7, 18
Crystal thickness
determination by electron diffraction, 416, 419
in transmission geometry, 512, 513
Crystalline solids, 259
Crystallite-size effects, 62
Crystallization, 148
Crystallographic system, 940
Cubic closest packing, 747
Cubic crystal system, 9, 19
Cubic harmonics, 585
Cumulant expansion, 588
Cumulative distribution function, 679
Current density, 725
Current ionization position-sensitive detectors, 628
Curvature, lattice, 114
Curvilinear density functions, 588–590
Cusp constraint, 715
Cyclic twins, 10
Cylinder
elliptic, 92
homogeneous, 96
inhomogeneous, 96
Cylindrical camera, 70

Cylindrical collimators, 432
Cylindrical detector recording, 32
Cylindrical powder cameras, 70
Cylindrical powder specimens, 57
Cylindrical sample
  2θ scan, 57
  for neutron diffraction, 177

d orbital occupancies, 722
Darwin width, 662
DAS (differential anomalous X-ray scattering) technique, 218
Data evaluation, 100
Data processing
  program for intensity factors, 596
  single-crystal methods, 505, 517, 536
Databases
  inorganic structures, 778
  organic structures, organometallic structures and coordination complexes, 790, 812
  powder diffraction, 81
Datum orientation of the crystal, 33
Dauphiné twins, 11
Davidon–Fletcher–Powell update, 684
de Broglie's law, 186
Dead-time, 619, 624, 666
Debye formula, 104
Debye–Scherrer camera, 70, 162
  aberrations in, 498
Debye–Scherrer–Hull method, 42
Debye–Waller factor, 415, 729, 735
Deconvolution
  in SANS, 107, 111
  techniques, 393
Defect types, electron diffraction, 424
Defects, 419
  images, 426
  lattice, 113
  study of, 506, 531
  viewed by an imaging system, 633
Deformation density, 714
Deformation map
  $X - N$, 714
  $X - X$, 714
  $X - (X+N)$, 714
Degrees of freedom, 703
Delay-line read-out, 627
Delbrück scattering, 242
Dense systems in SANS, 112
Densitometry, 618
Density, 154
Density functionals, 721
Density measurement
  Archimedes method, 158
  flotation, 158
  gradient tube (column), 156
  immersion microbalance, 158
  penetration or swelling of solid, 156
  pycnometry, 158
  vibrating-string method, 158
  volumenometry, 158
Depth-profiling analysis, 58
Derivative lattice, 11
Designated radiation area, definition of, 958
Desymmetrization of OD structures, 765
Detection
  efficiency, 624
  limits, 410
  of systematic error, 498–499, 707–709
  quantum efficiency, 639
  systems, 397, 663
Detection processes (neutrons), 644–652
  electronic aspects, 648–649
  films, 646
  gas ionization, 644–646
  neutron capture, 644
  scintillation, 645–646
Detection systems (neutrons), 649–651
  Anger camera, 650
  corrections, 652
  gas position-sensitive, 650
  position-sensitive, 649–651
  single detectors, 649
Detective quantum efficiency (DQE), 624, 639
Detector recording
  cylindrical, 32
  plane, 32
  V-shaped, 32
Detector-response correction in SANS, 109
Detectors
  background from, 663
  characterization, 639
  energy-dispersive, 622, 663
  for electrons, 639
  for neutrons, 644, 649
  gas-filled, 82
  imaging, 623
  in X-ray spectrometers, 522, 529–531
  multiwire, 82
  position-sensitive, 82, 87, 100, 113, 664
  resolution of, 82
  scintillation, 642, 664
  semiconductor, 622–623, 629, 642
  single-wire, 82
  solid-state, 82, 664
  with wide-open window, 522, 527
Detectors for X-rays, 618–638
  Geiger counters, 618
  photographic film, 498, 618
  proportional counters, 619
  scintillation counters, 619
  solid-state detectors, 620
Diagram levels, 191
Diamagnetism, 154
Dielectric coefficients, 401
Dielectric description, 399
Difference densities, 714
Differential anomalous X-ray scattering (DAS) technique, 218
Differential methods, 527
Differential scattering cross section, 260
Diffraction
  contrast, 113, 735
  coordinates, 31
  geometry, practical realization, 36
  grazing-incidence, 58
  imaging, 124
  intensities, 596
  spot size and shape, 37, 39
  topography, 113, 124
Diffraction absorption fine structure (DAFS), 254
Diffraction profile, 48, 528, 530
  asymmetry of, 521
  broadening of, 521
  double-crystal, 528
  (in) standardized (form), 519
  location of, 518
  narrow, 528, 530
  parameters of, 528
  shape of, 521
  symmetric, 528
Diffractometers
  alignment, 46
  area-detector, 36, 170
  background scattering with, 664
  Bragg–Brentano, 495
  double-crystal in SANS, 106
  for powder diffraction, 42
  four-circle, 170, 516
  gears, 503
  inclination, 517
  kappa, 36
  neutron powder, 82, 652
  neutron powder, high-resolution, 541
  operation control, 64
  Seemann–Bohlin, 492, 495
  three-circle, 170
Diffractometry, 36
  angle-dispersive, 491, 495–496
  energy-dispersive, 491
Diffuse scattering, 261
Diffusion, Brownian, 589
Digital image processing, 635
Dimension of a lattice, 945
Dioctahedral sheet, 767
Dipolar approximation, 731
Dipole, 716
Dipole moment
  atomic, 717
  molecular, 724
Dirac–Fock, 205
Direct and reciprocal lattices, 2
Direct crystallization, 174
Direct image, 115
Direct lattice, 412, 911
Direct-lattice parameters, 505
Direct method, X-ray detectors, 634
Direct structure analysis, 103
Direction angles of a crystal face, 4
Disc specimens, 171
Disc thinning method, 174
Dislocations, 114
Dispersion, 21, 75, 590, 600
Dispersion corrections, 241–258
  for XED, 86
  tables of, 255–257
  theory of, 243
Dispersion surfaces, 416, 417, 736
Displacive modulation, 907
Distance distribution functions, 104
Divergent-beam techniques, 510–516
  classification, 512
Dopant concentration, study of, 531
Dose equivalent, definition of, 958
Double-beam
  comparator, 531
  diffractometer, 531
  spectrometer, 531
  technique, 531
Double-crystal diffraction profile, 528
Double-crystal diffractometer in SANS, 106
Double-crystal monochromator (at synchrotron), 39
Double-crystal spectrometers, 528–530
  combined with double-beam technique, 531
  with photographic recording, 510, 529
  with symmetric (Bond) arrangement, 529
  with white X-radiation, 529
Double-crystal topography, 117
Double-oscillation method, 168
DQE (detective quantum efficiency), 624
Drift chambers, 626

Drude model, 400
Du Mond diagram, 117
Duane–Hunt limit, 192
Dynamic measurements, 626
Dynamic *R* factor, 427
Dynamic range, 624
Dynamical diffraction, 80
  Bloch-wave method, 41
  calculations, 261
  many-beam, 80
  multislice method, 414
Dynamical wave amplitudes, 414

Eccentricity error, 524
  elimination, 521–523, 529
EELS (electron energy-loss spectroscopy), 219, 391–412, 428
Effect on lattice parameters
  of electric field, 508
  of irradiation, 525
  of pressure, 508
  of temperature, 507, 510, 516, 522, 524, 529
Effective misorientation, 119
Efficiency of the production of characteristic radiation, 192
Eigenvalue filtering, 510
Eigenvalues, 678
Eigenvectors, 678
Elastic constants, 654
Elastic differential scattering cross section, 262
Elastic scattering, 416
  factors, 262
  neutron, 727
Elastic specular neutron diffraction, 126
Elastic stiffness constants, 654
Elastic wave, velocity of, 654
Electric field gradient, 719
Electrical properties, 154
Electrochemical thinning, 175
Electromagnetic waves, 186
Electron beam, misalignment, 424
Electron binding energies, 203
Electron density, 90, 713
  experimental, errors in, 724
  thermally smeared, 723
Electron diffraction, 259
  absorption effects, 188, 261
  boundary conditions, 259
  computing methods, 425
  convergent-beam, 80, 735
  crystal thickness, 188, 419
  detectors for, 639–643
  determination of crystal thickness, 416, 419
  HOLZ technique, 538
  interaction constant, 259
  intensities, 416
  Kikuchi technique, 538
  lattice-parameter determination, 537
  measurement of structure factors, 416
  oriented texture patterns, 412–414
  pattern analysis, 537
  pattern indexing, 537
  patterns, 80, 390
  potential field, 259
  preparation of specimens, 171
  propagation function, 259
  reciprocal-space representation, 412
  relativistic values, 259
Electron diffraction
  scattering factors, 188, 259
  selected-area, 80, 538
  structure factors, 416
  transmission function, 259
  useful parameters as a function of accelerating voltage, 281
Electron diffractometry, 413
Electron distributions, 713
Electron energy-loss near-edge structure (ELNES), 408
Electron energy-loss spectrometry
  Castaing & Henry filter, 397
  crystallographic information from, 397
  parallel detection, 397
  Wien filter, 396
Electron energy-loss spectroscopy (EELS), 219, 391–412, 428
  aberrations in, 396
  analysers for, 395
  detection systems, 397
  monochromators for, 395
  non-characteristic background, 394
  spectrometers for, 394–397
  types of excitation in, 393
Electron holography, 426, 427
Electron inelastic scattering, 378
Electron kinetic energy, 721
Electron microscopy, 80, 419
  preparation of specimens, 171
Electron multiplication
  in position-sensitive detectors, 622–623
  in proportional counters, 623
Electron paramagnetic resonance, 190
Electron scattering
  amplitudes, 259
  inelastic, 391
Electron spin, interaction with neutron spin, 725–726
Electron transitions, 261
Electron-transparent specimens, 171
Electron-tube device for measurement of intensities, 642
Electron wavelength of a transmission electron microscope, determination, 540
Electroneutrality constraint, 715
Electronic detectors, 639
Electronic instability, 424
Electrons
  properties, 187
  scattering factors, 262
  wavelength, 424
Electropolishing, 174
Electrostatic moments, 716, 717, 718
Electrostatic potential, 186, 718
Electrostatic properties, 721
Elimination of concentration effects, 98
Ellipse and ellipsoid packing, 751–752
Ellipsoid, 92
Ellipsoid of revolution, 94
Ellipsoidal-mirror SANS camera, 106
Elliptic cylinder, 92
ELNES (electron energy-loss near-edge structure), 408
Emission lines, 202, 203, 204, 206, 209
Emission-spectrum profile, 519
Empirical correction factor for preferred orientation, 61
Empirical metallic radii, 774
Enantiomorphous pairs of space groups, 20
Energy discrimination, 625
Energy-dispersive
  analysis, 428
  detectors, 625, 641, 663
  diffraction, 58, 619
  diffractometer, aberrations of, 497
  methods, in lattice-spacing determination, 496, 507
  neutron diffraction, 87
  techniques, 496
  X-ray diffraction, 84, 619
Energy-filtered lattice images, 428
Energy-flow triangle, 115
Energy-flow vector, 119
Energy-loss spectrometer, 395
Energy of radiation, 187
Energy resolution, 396, 619, 620, 622
Enhanced symmetry, 13
Entrance slit, 45
Entropy maximization, 691
Epitaxic formation, 176
Epitaxic layers, study of, 516, 529
Epitaxy, 153
EPR (electron paramagnetic resonance), 190
Equatorial divergence, 497
Equatorial geometry, 516
Equi-inclination setting, 31
Equivalent origins, 15
Equivalent superspace groups, 940
Erratic fluctuations in counting rates, 667
Errors (see also Aberrations, Systematic errors)
  and aberrations in lattice-parameter measurements, 490
  and uncertainties in wavelength, 493
  in angle reading, 524
  in angle setting, 524
  in experimental electron density, 725
  of the Bragg angle, 491
Escape peaks, 622
Estimated standard deviation, 707
  of an observation of unit weight, 702
Estimates, 680
Etch figures, 153
Etching
  chemical, 173
  corundum, 173
  ion sources, 173
  sputter, 173
Euclidean norm, 678
Eulerian angles, 694
Eulerian-cradle diffractometer, 517
Eulerian-geometry diffractometer, 517
Evaporated thin films, 173
Ewald sphere, 26, 526, 656
EXAFS (extended X-ray absorption fine structure), 24, 189, 213–220, 254, 409
Exchange-correlation energy, 721
Excitation errors, 414
Excitation of characteristic X-rays, 510
EXELFS (extended electron fine structure), 409
Exit beam, extremely parallel, 532
Expectation values, 679
Experimental techniques
  classification of, 24
  for crystal structure analysis, 25
Exposure of radiation, definition of, 958
Extended electron fine structure (EXELFS), 409
Extended solids, 730

Extended X-ray absorption fine structure [(E)XAFS], 24, 189, 213–220, 254, 409
  facilities for, 219
External space, 944
External standard, 499
External vibrations, 723
Extinction, 113, 599, 728
  contrast, 113
  correction factor for, 612
  correction, neutron diffraction, 177
  correction, XED, 86
  distance, 736
  length, 187
  primary, 609, 610
  secondary, 609, 611
  symbol, 13
Extrapolated (midchord) peak, 518
Extrapolation in lattice-parameter determination, 505, 510, 521–522, 535
  analytical, 493–494
  graphical, 493

F distribution, 702
Face normals, 5
Face or cleavage plane of a crystal, 4
Factors determining accuracy, 501
Family diffractions, 765
Fano factor, 626
Fano plots, 408
Faraday cage, 642
Faster-than-sound neutrons, 657
Faults in polytypes, 758–760
Feasible point, 693
Fermi chopper, 443
Fermi level, 398
  germanium, 406
  heavy metals, 406
  sulfur, 406
  transition elements, 406
Fermi pseudopotential, 444
Ferrimagnetism, 154
Ferroelectricity, 154
Ferromagnetism, 154
Ferromagnets, 728
Fibre optics, 632
Fibre texture, 414
Fibres, diffraction from, 24
Film
  aluminium, 393
  for neutrons, 646
  germanium, 394
Film shrinkage, 498
  error, elimination of, 509
Filters, 38, 76
  balanced, 74, 78, 238
  Castaing & Henry, 397
  for common target elements, 79
  for neutrons, 438
  for X-rays, 236
  graphite, 82
  optimum-thickness, 238
  polarizing, 438, 440
  single, 78
  thickness, 78
  wavelength change by, 239
  Wien, 396
  with scintillation counters, 621
Fine-grained substances, oriented texture patterns, 412
First-fringe contrast, 116
First-order Laue zone (FOLZ), 417, 418
First/second derivatives, 65
Fixed-count timing, 667
Fixed-time counting, 666
Flat-cone setting, 31
Flat crystal, 77
Flat-crystal monochromator, 39
Flat-film camera for Laue patterns, 70
Flat particles, 95
  cross-sectional inhomogeneity, 96
  molecular weight, 93
Flat-specimen aberration, 47, 48
Flipping coil, radio-frequency, 728
Flipping ratios, 592, 728
Flotation, 158
Fluctuations
  in particle orientation, 61–62, 492
  in recording counts, 492, 666
Fluorescence radiation, 657
Fluorescence scattering, 661
Fluorescence spectroscopy, 619
Fluorescence techniques, 218
Fluorescent screens, 640
Fluorophlogopite reflection angles, 503
Focal-line width, 48
Focusing diffractometer geometries, 43
Focusing geometry, 83
Focusing monochromator, 82
Focusing, neutron scattering, 443
Focusing powder camera, 70
Fog density, 618
Fog level, 640
Foil detector, 645
FOLZ (first-order Laue zone), 417, 418
Forbidden reflections, 527
Form factors, magnetic, 454, 591
Four-circle diffractometer, 516
Four-dimensional crystal classes, 16
Fourier imaging, *n*-beam, 422
Fourier integral, 89
Fourier-invariant expansions, 586
Fourier potential, 735
Fourier series, 89
Fourier transformation, 89
  indirect, 111
  techniques, 393
Free-electron gas
  Drude model, 400–401
  Lorentz model, 400
Free-radical scavengers to improve crystal lifetime, 166
Free scattering length, 594
Frequency of space groups, 15
Fresnel diffraction theory, 259
Friedel-pair intensity ratios, 251
Friedel-pair techniques, 251
Friedel's law, 913
Fringe patterns, stacking-fault, 116
Fringe period, 419
Fringe visibility, 421
Full symbols for superspace groups, 921

Gallium selenide, 754
Gamma function, 702
Gamma rays, 187
Gas amplification, 626–627
Gas detector for neutrons, 644
Gas-filled counters, 82, 626
Gas multi-electrode position-sensitive detectors for neutrons, 650
Gas multiplication, 626
Gauss–Markov theorem, 680
Gauss–Newton algorithm, 683, 690, 693
Gaussian curves, 66, 711
Gaussian fits to X-ray scattering factors, 261
Gaussian radial functions, 724
Geiger counter, 618
Gelatine capsules, 163
Generalized Bessel function, 666
Generation of X-rays, 191
Generator stability, 72
Geometric crystal classes, 15, 911, 945
Geometrical aberrations, 41, 493
  for XED, 86
Geometrical analysis of oriented texture patterns, 412
Geometrical instrument parameters, 44
Geometrical peak, 518
Geometry of SANS, 106
Germanium, Fermi level, 406
Germanium film, 394
Gibbs instability, 415
Gibbsite–nordstrandite family, 766
Gittergeister (lattice ghosts), 907
Givens rotations, 679
Glauber approximation, 391
Globular particles, 93
Glove box, definition of, 959
Gnomonic transformations, 29
Gold, dielectric coefficients, 401
Goodness-of-fit parameters, 702, 707
Gordon–Kim model, 721
Gradient tube (column)
  cavities, problem of, 156
  Ficoll gradient, 157
  inclusions, problem of, 156
  shallow gradient, 157
Gram–Charlier series expansion, 586
Graphical extrapolation of lattice parameters, 493
Graphite
  dielectric functions, 403
  monochromator, 37, 38, 51, 620
Gray, definition of, 959
Grazing-incidence diffraction, 58
Grigson scanning method, 81
Growth striations, study of, 530
Growth twins, 10
Guinier and Tennevin technique, 119
Guinier approximation, 92, 110
Guinier camera, 162
Guinier focusing, 70

Half-life, definition of, 959
Half-width, 506, 519, 522, 526, 528
  (methods of) reducing, 526
  minimum, 506
  of wavelength distribution, 506
Hamilton's *R*-factor ratio test, 704
Hankel transform, 102
Hard-sphere interference model, 98
Hard X-rays, 187
Hardness, 153
Harmonics, cubic, 585
Hartree–Fock
  approximation, 732
  model, 243
  self-consistent field, 659
  wavefunctions, 460
Hat matrix, 705
Heat capacity, 154
Heavy metals, Fermi level, 406
HEED (high-energy electron diffraction), 412

Helimagnetic order, 728
Hellmann–Feynman constraint, 715
Hermite polynomial tensors, 586
Hessian matrix, 684
Heterogeneous packing, 746
Hetero-octahedral sheet, 767
Hexacontatetrapole, 716
Hexadecapole, 716
Hexagonal
  closest packing, 747, 752
  crystal system, 7, 15, 19
High-angle annular dark-field (HAADF) images, 428
High-angle Bragg reflections in lattice-parameter determination, 509, 522, 529, 532
High-energy electron diffraction (HEED), 412
High-order Laue zone (HOLZ), 418, 424, 538, 539
High-pressure structural studies, 87
High-purity germanium detector, 622
High-resolution electron microscopy (HREM), 261, 419, 773
High-resolution energy-dispersive diffraction, 58
High-resolution experiments, 97
High-resolution powder diffractometers
  D2B at Institut Laue–Langevin, 541
  HRPD at Rutherford Appleton Laboratory, 541
High-sensitivity lattice-parameter comparison, 531–532
High-tension supplies, unsmoothed, 667
Higher-dimensional crystallography, 908
Histogramming memories, 626
Hohenberg and Kohn theorem, 721
Hollow cylinders, 92
Hollow particles, 96
Holographic reconstructions, 427
Holohedry, 12, 939, 945
HOLZ (high-order Laue zone), 418, 424, 538, 539
Homogeneous cylinder, 96
Homogeneous packing, 746
Homogeneous particles, 93
Homogeneous triaxial bodies, 92
Homometric mapping, 751
Homo-octahedral sheet, 767
Horizontal divergence, error, 525
Horizontal Soller slits, 56
Householder transformations, 679, 686
HREM (high-resolution electron microscopy), 261, 419, 773
Hydrogen-atom scattering factors, 565
Hydrogen bonding, 906
Hyperbolic Bessel function, 666
Hyperfine interaction, 732
Hyper-resolution, 427
Hypothesis testing (no remaining systematic errors), 523

ICDD Powder Diffraction File, 81
Icosahedral viruses, SANS, 111
Ideal crystals, 908
Ideally imperfect crystals, 113
Ideally perfect crystals, 113
Idempotency conditions, 722
Idempotent, 705
Identity period, 752
Identity period determination, 508
  accuracy of, 510
Ill-conditioned least-squares problems, 101
Image intensifiers, 122, 632, 635
Image processing, 427, 635
Imaging detectors, 623
Imaging plates, 426, 635, 641
Immersion microbalance, 158
Impulse approximation, 657
Incidence aperture, 53
Incident-beam monochromatization, 120
Incident-beam monochromator, 53
Inclination diffractometer, 517
Inclination of plane of specimen, 494
Incoherent elastic scattering cross section, 595
Incoherent multiple scattering, 108, 661
Incoherent scattering, 177, 554
  Compton, 90
  cross section, 594
  functions (Table 7.4.3.2), 658
  level, 109
Incommensurate modulated structures, 907–944
Index of refraction, 600
Indexing powder patterns, 541
Indirect method, X-ray detectors, 634
Indirect transformation method, 101
Indium antimonide, dielectric coefficients, 401
Induced matrix norm, 678
Inelastic coherent scattering, 109
Inelastic crystal excitations, 425
Inelastic scattering, 378, 416, 657
  Bethe theory, 406–408
  electrons, 391
  neutrons, 391
Inelastic scattering factors for electrons (Table 4.3.3.2), 378–388
Inelastically scattered electrons, 81
Influential data points, 705, 708
Information resolution limit, 424
Infrared radiation, 187
Inhomogeneities in matter, 105
Inhomogeneous cylinders, 96
Inhomogeneous particles, 96
Inner moments, 718
Inner surface area, 109
Inorganic compounds
  silicates, 766–769
  typical interatomic distances, 778–789
Inorganic Crystal Structure Database, 778
Insertion devices, 197
Instrument parameters, geometrical, 44
Instrumental broadening and aberrations, 47, 101
Integrated intensity
  for XED and powder samples, 85
  formulae for, 600
  of a reflection, 668
Integrated reflections, 114
Intensity, 519
  distribution, two-dimensional map, 522
  of characteristic lines, 191
  of diffracted intensities, 554–595
  standards, 500
  statistics, 519
  variation with take-off angle, 74
Intensity factors, 596
  angular velocity, 596
  data-processing programs for, 596
  in single-crystal methods, 596–598
  polarization, 596
  trigonometric, 596–598
Interatomic distances, 778–896
  in inorganic compounds, 778–789
  in metals, 774–777
  in organic compounds, 790–811
  programs for calculating, 778
Interaxial angles, determination, 525
Interband transition, 401
Interference model, hard sphere, 98
Interferometers
    Bonse & Hart, 121
    Fabry–Perot, 533
Interferometry, combined optical and X-ray, 533–534
Intergrowth crystal structures, 907
Interlaboratory comparison, 536
Internal
  space, 912, 937, 944
  standard, 499
  translation, 912
Interparticle interference, 97, 98
Interpenetrating packing, 751
Interplanar spacing determination
  accuracy of, 505
  precision of, 505
Interquartile range, 690
Intersecting-Kikuchi-line method, 736
Interstices in close-packed structures, 753
Intramolecular multiple scattering, 392
Intrinsic background (neutrons), 651
Intrinsic component, 917
Intrinsic efficiency, 622
Intrinsic part of a space group, 940
Inverse contrast variation, 108
Inversion twins, 10, 12
Ion-beam thinning, 171–173
Ion-implanted silicon, 525
Ion sources for etching, 173
Ionic radii, 778
Ionicity, degree of, 425
Ionization cross sections, 407
Ionizing radiation
  definition of, 958
  protection from, 962–963
Irradiated area
  displacement of, 526
  exactly defined, 522
Irradiated specimen length, 45
Irradiation, study of effects of, 516, 525
Isometric point groups (crystal classes), 939
Isotopic replacement, triple, 111
IUPAC notation, X-ray diagram levels, 191

Jagodzinski notation, silicon carbide, 754
Johann monochromator, 664
Johansson monochromator, 664
Joint probability density function, 679

$K\alpha$ doublet, 62, 510, 512–515
$K\alpha_1$ and $K\beta_1$ wavelengths in lattice-spacing determination, 521
$K\alpha_2$ radiation, elimination, 510
$K\beta$ line in lattice-spacing determination, 507
Kaolinite, 769
Kappa diffractometer (definition), 37
Kappa model, 714
Kikuchi lines, 419
Kikuchi patterns, 735
Kikuchi techniques, 538
Kinematic image, 115
Kinematic theory, 590
Kinematical approximation, 80, 260, 262

Kinetic energy, 721
Kitajgorodskij's categories, 897
Knife-edge calibration, 498
Kossel
  camera, 512
  cone, 510, 514
  lines, 510–515
  lines, intersections of, 512–513
  method, 510–516
  pattern, 512–514, 735
  plane, 513
Kramer's constant, 192
Kramers–Kronig transform, 245
Kratky cameras, 99

Label triangulation, 111
Labelling, 97
  isotopic, 108
Lagrange polynomials, 111
Lagrange undetermined multipliers, 693
Lambda curves (Laue), 39
Lambda symmetry (operations), 763
Lamellar particles, 97
Lamellar textures, 412
Lanthanum hexaboride, instrumental sample, 501
Large-scale problems, 685
Larmor frequency, 728
Laser, He–Ne, 533
Laser plasma X-ray sources, 189
Latex particles, 107
Lattice(s)
  aperiodic, 937
  Bravais, 3, 15, 913
  centred, 3
  curvature, 114
  defects, 113
  derivative, 11
  dimension, 937
  direct, 911
  direct and reciprocal, 2
  for close-packed structures, 755
  holohedry, 939
  point, 2
  rank, 937
  twin, 10
  vector, 2
  vector centring, 3
  vector, reciprocal, 2
Lattice bases, standard, 938
Lattice-fringe images, 421
Lattice ghosts (*Gittergeister*), 907
Lattice-parameter changes, study of, 507, 510, 522, 525, 529–530
Lattice-parameter determination, 490–541
  aberrations in, 493
  absolute, 505, 525, 529–532
  for rectangular systems, 528
  from one crystal mounting, 509, 510
  from separate photographs, 509
  HOLZ techniques, 538, 540
  inter-laboratory comparison, 536
  Kikuchi techniques, 538–540
  least-squares methods, 498
  local, 525, 529, 532
  neutron diffraction, 541
  of cubic lattice, 528
  of deformed lattice, 513–515
  of imperfect crystal, 522
  of large flat slab, 507, 522, 524, 527
  of perfect crystal, 522
Lattice-parameter determination
  of polycrystals (Kossel method), 515
  of single crystals, 505–536
  of small spherical crystals, 507, 525
  of standard crystal, 507
  powder diffraction, 491, 506, 509, 518, 521
  precision, 505, 509, 515, 526, 530, 536
  preliminary, 507
  relative, 505
  sensitivity of, 505, 507, 532
  standards, 499
  systematic errors in, 493, 498
  wavelength problems, 492
Lattice-parameter determination methods
  camera, 497, 507
  diffractometer, 495–496, 516–517
  electron diffraction, 537–540
  energy-dispersive, 496–497
  neutron diffraction, 541
  non-dispersive, 506, 509, 526, 533–534
  polycrystalline X-ray, 491–504
  pseudo-non-dispersive, 506, 526, 528
  single-crystal X-ray, 505–536
  synchrotron, 495
  whole-pattern, 496
  X-ray, 534
Lattice-parameter differences, determination of, 507, 522, 525, 528–531
Lattice-parameter measurements
  accuracy of, 490
  discrepancy for silicon, 490
  possible effect of filter, 239
Lattice parameters
  of silicon, 490, 499
  of silver, 499
  of tungsten, 499
Lattice-spacing comparators, 530
Laue class, 13, 938
Laue diffraction
  multiplicity distribution, 27
  neutron single-crystal, 87
Laue geometry, 26, 38
Laue method, 663
Laue patterns, 27, 124
  flat-film camera for recording, 70
Laue photography combined with powder diffraction, 506
Laue point group, 908, 913, 938
Laue sphere, 26
Layer-line screen (precession), 34
Layer-line screen (Weissenberg), 35
Layer lines, 414
Layer polytypism, 760, 766
Layer silicates, 414
Layer stacking, 752–773
  in polytypes, 760–773
LCAO (linear combination of atomic orbitals) approximation, 715, 723
Lead oxide camera tubes, 634
Leakage radiation, definition of, 959
Least-dense sphere packings, 748, 749
Least-squares calculations, 678–688
  estimator, 680
  nonlinear, 682
  software for, 688
Least-squares refinement, 504, 505, 510, 517
  problems, 101
LEED (low-energy electron diffraction), 24
Legendre polynomial, 565
  associated, 581
Lens configuration, 514
Lens-shaped figures, 512–514
Levenberg–Marquardt algorithm, 683
Leverage, 705, 708
Libration (rotational oscillation), 589
Libration tensor, 697
Librational model, 697
Librational temperature factor, 723, 724
Licensable quantity, definition of, 959
Likelihood, 689
Likelihood-ratio method, 523
Limited projection topographs, 116
Limiting resolution of X-ray detectors, 634
Line focus, 194
Line profile, 518
  calculated by convolution, 662
Linear algebra, 678
Linear attenuation coefficient, 213
Linear combination of atomic orbitals (LCAO) approximation, 715, 723
Linear estimator, 680
Linearity, 621
Linearity of response, 619
Lithium-drifted germanium detector, 622
Lithium-drifted silicon detector, 622
Live X-ray topographs, 122
Local measurements (topography), 516, 525–527, 529
Location of diffraction profile, 518
Long-period polytypes, 757
Lorentz factor, 497, 596, 710
Lorentz model, 400
Lorentz–polarization factor, errors, 60, 523, 596
  correction for, 523
Lorentzian curves, 66
Lorentzian functions, 711
Lorentzian profiles, 67, 400
Low-angle boundaries, 114
Low-angle reflections, confusion with escape peaks, 622
Low-energy electron diffraction (LEED), 24
Low-Q scattering, 105
Lower quartile, 813
Luminescence, photostimulated, 635

Macromolecules, biological, use of SANS, 105
Macroscopic absorption cross section, 461
Magnetic
  Bragg reflection, 591
  domains, 124
  form factors, 454, 592
  interaction vector, 591
  orbital structure factor, 731
  ordering, 725
  space group, 591
Magnetic properties, 154
  of the neutron, 108
Magnetic scattering
  of neutrons, 590
  of neutrons, elastic, 591
  X-ray, 733
Magnetic structure factors, 591, 726, 727
  unit-cell, 591
  X-ray, 733
Magnetism, 725
Magnetization density, 591, 725
Magnetostatic energy, 731
Magnetostatic properties, 731
Magnets, bending, 197
Main reflections, 907

Mains-voltage fluctuations, 667
Many-beam dynamical diffraction, 80
Marginal probability density function, 679
Mass absorption coefficients, 213, 600
Mass attenuation coefficients, 213–214
  tables of, 230–236
Mathematical interpretation in single-crystal methods, 536
Mathematical theory of powder diffractometry, 518
Matrix diagonalization, 425
Matrix formulae for two-circle diffractometer, 517
Maximum degree of order (MDO) polytypes, 762, 767, 768, 769, 770, 772
Maximum dimension of a particle, 93, 102
Maximum-entropy method, 428, 689
Maximum-likelihood estimate, 689
Maximum-likelihood methods, 691
Maximum oscillation angle, 33
Maximum primary dose (MPD), 960
MDO (maximum degree of order) polytypes, 762, 767, 768, 769, 770, 772
Mean, 679, 813
Mean-square broadening, 493
Measured-as-negative intensities, 667
Measured profile, 505
  as a convolution, 503
Measurements of lattice parameters
  absolute, 505
  relative, 505
Mechanical (deformation, glide) twins, 10
Mechanical properties, 153
Mechanical twins, 10
Median, 520
  absolute deviation, 690
  variance of, 520
Melt-grown crystals, 114
Melting point, 154
Membrane proteins, 24
Mercury iodide detector, 623
Mercury sulfide chloride, γ-$Hg_3S_2Cl_2$, 771, 772
Merohedral point groups, 12
Meso-octahedral sheet, 767
Metallic radii, empirical, 774
Metals
  preparation of specimens, 173
  texture studies, 414
  typical interatomic distances, 774–777
Methyl methacrylate resin containers, 162
Metric tensor, 694
Mezei flipper, 442
Mica containers, 162
Mica group, 765, 768–770
Microanalysis, 54
  quantitative, 410
Microdensitometer, 618
Microdiffractometers, 491
Microdiffractometry, 53
Microfocus sources, 71
Microrefractometer, 160
Microtome, 171
Microwaves, 190
Midchord peak, 518
Midpoint of a single chord, 518
  bias, 520
  variance, 520
Miller formulae, 5
Miller indices, 5, 11
Mimetic twinning, 153
Mirror cameras, 106
Mirrors, 37
  for neutrons, 436
  reflection devices, 435
Misalignment, 506, 531, 535–536
  diffraction, 424
  of electron beam, 424
Misorientation functions, 414
Misorientation matrices, 33
Mixed-layer structures, 760
Model calculations in SAXS, 103
Model fitting in SANS, 111
Modelling of space-group frequencies, 897
Moderators for neutrons, 431
Modulated crystal structures, 907–944
  examples, 936
  types defined, 907
Modulation
  displacive, 907
  occupation, 907, 913
  relations, 941
Modulation transfer function (MTF), 634
Moiré topography, 121
Molecular beams, 189
Molecular biology, isotopic composition in SANS, 107
Molecular dipole moment, 725
Molecular geometry, 812
Molecular organic structures
  packing in, 897
  space-group distribution of, 905
Molecular packing, 904
Molecular scattering factors, 390
Molecular weight, 93
Moliere high-energy approximation, 260
Moment, 679
Moments of a charge distribution, 716
Momentum density distributions, 659, 713
Momentum space, 713
Monitor methods, 72
Monitoring circuits, 619
Monochromatic radiation, θ–2θ scan, 55
Monochromatic still exposure, 30
Monochromator-scan method for diffraction, 85
Monochromators, 37, 43, 46, 51, 76, 99, 120, 395, 528, 662
  alignment, 46
  angular calibration, 46
  channel-cut, 77, 121, 239
  common types, 77
  comparison of, 433
  crystal, 76
  different diffraction geometries, 43
  diffracted beam, 44, 46
  double-reflection, 239
  focusing, 82
  for neutrons, 432–435
  for X-rays, 236
  graphite, 38, 239, 620, 664–665
  incident-beam, 53
  Johann, 664
  Johansson, 664
  mosaic crystals, 432, 662
  multi-reflection, 239
  perfect-crystal, 39, 443, 663
  pyrolytic graphite, 46, 72
  quartz, 661
  scanning-crystal, 622
  single-reflection, 239
Monoclinic crystal system, 6, 16
Monodisperse systems, 91
Monopole, 716
Morphological properties, 153
Morphology, and mounting of single crystals, 164
Morse approximation, 389
Mosaic-crystal monochromator, 662
Mosaic spread, 432
Mosaicity, 443
  neutron diffraction, 433
Moseley's law, 76
Mössbauer radiation, 656
Mössbauer spectroscopy, 189, 719
Mott–Bethe formula, 261
Mounting of specimens, 163
  biological macromolecule single crystals, 165
  polycrystalline specimens, 162
  single crystals, 164
  small organic and inorganic single crystals, 164
Moving splines, 111
Multichannel pulse-height analyser, 496
Multi-component complex, label triangulation, 111
Multidetector, 82
Multilayer materials, 171
Multilayer polarizers, 436
Multiple-beam methods, 531
Multiple-crystal techniques, 528–532
Multiple diffraction, 513
Multiple-diffraction methods, 526–528
  with counter recording, 526–528
  with photographic recording, 513
Multiple-diffraction pattern, 527
  indexing, 527
Multiple-exposure techniques, 514
Multiple-order reflections (Laue), 27
Multiple scattering, 661
  deconvolution techniques, 391
  incoherent, 661
  intramolecular, 392
  neutron diffraction, 177
  Poisson distribution, 393
  problems associated with, 392
Multiple twins, 10
Multiplicity distribution in Laue diffraction, 27
Multiplicity factor, 596
Multipole expansions, 103, 714, 716, 730
Multipole functions, angle dependence, 583
Multipole model, 716
Multi-reflection devices, 121
Multislice method, 414–416, 425
  programs for, 415
Multiwire detectors, 82
Multiwire proportional chamber (MWPC), 627
Muons, 189
Muskovite, 771

n-beam Fourier imaging, 422
n-particle density matrix, 713
n-particle wavefunction, 713
Natural background, definition of, 959
Near-edge fine structures, 408
Neighbours, nearest (direct) and next-nearest (indirect), 775
Net planes, 4
Neutron Anger camera, 650
Neutron-beam definition, 431
Neutron-capture reactions, 644–645

Neutron diffraction, 26
  cross section (tables), 445–461
  energy-dispersive, 87
  Laue, 87
  powder, 82
  preparation of specimens, 177
  scattering lengths (tables), 445–461
  time-of-flight, 87
  time-of-flight, powder, 88
  white-beam, 87
Neutron polarization, 592
Neutron powder data, 68
  Rietveld analysis of, 710–712
Neutron resonance spin echo (NRSE), 443
Neutron scattering, 591–595
  elastic, 728
  focusing, 443
  form factors, 454–461
  inelastic, in spectroscopy of solids, 391
  magnetic, 591, 726
  monochromators, 443
  nuclear, 593
  polarized, 728
  resolution functions, 443
  scattering factors, 454–461
  Soller collimators, 443
  spectrometers, 444
Neutron sources
  pulsed spallation, 189
  reactors, 430
  spallation, 87, 430
Neutron spin, 444
  interaction with electron spin, 725–726
Neutrons
  absorption coefficients (Table 4.4.6.1), 461
  cold, 105
  faster-than-sound, 657
  films for, 646
  filters, 438
  guide tubes, 432, 435
  moderated, 430
  monochromators, 432
  polarized, 108, 592
  properties, 187
  reflectivity, 126, 433
  reflectometry, 126
  scattering-length densities, 441
  slower-than-sound, 657
  topography, 124
Next-nearest (indirect) neighbours, 775
NFZ relation, 761
NIST (National Institute of Standards and Technology) silicon standard, 495
NMR (nuclear magnetic resonance), 154, 190
No-upper-layer-line approximation, 415
Nodal reflections, 27
Noise reducer for image processing, 635
Non-crystalline samples, diffraction from, 24
Non-crystallographic symmetry elements, 907
Non-dispersive methods (techniques), 506, 526, 533–534
Non-linear least squares, 683
Non-periodic systems, 89
Non-stochastic effects, 959
Non-systematic interactions, 81
Non-uniformity of response, area detectors, 41
Normal attenuation, 214
Normal-beam equatorial geometry, 36
Normal-beam rotation method, 31
Normal crystal, 908
Normal equations, 680, 682
Normal modes of vibration, 653
Normal probability distribution function, 66, 702
Normalized spin density, 727
Notations for close-packed structures, 753, 758
Nuclear magnetic resonance (NMR), 154, 190
Nuclear reactors, 430
Nuclear scattering
  amplitude, 594
  length, bound, 594
  of neutrons, 593
Nuclear structure factors, 595, 725, 732
Nuclear Thomson scattering, 242
Numbers of reciprocal-lattice points within resolution sphere, 28
Numerical approximations to $f(s)$, 261
Numerical methods, 685

Objective-lens defocus, 421
Oblate ellipsoid of revolution, 94
Oblique crystal system, 15
Oblique-texture electron difraction patterns, 412
Obliquity, 41
Occupation modulation, 907, 913
Octahedral sheet, 767
Octupole, 716
OD (order–disorder)
  diffraction pattern, 763
  groupoid families, 761, 763, 765, 773
  layers, 764
  packets, 765
  repeat unit, 764
  structures, 761, 764
  structures, desymmetrization of, 765
  theory, 761
One-crystal spectrometers, 521–526
  asymmetric (arrangement), 521–522
  symmetric (arrangement), 521–526
One-dimensional crystal classes, 15, 16
One-line symbols for Bravais classes, 915, 920
One-particle reduced density matrix, 726
Open shell electrons, 727
Operations in polytypes, 762–763
Optic modes, 653
Optical
  activity, 153
  antipodes, 153
  diffractograms, 427
  interferometry, 533–534
  properties, 153, 160
  reflectivity, graphite, 403
  wavelength as a standard, 533
Optimization (of measurement), 517–520, 526–528, 532–534, 667
Optimum design of experiments, 74, 702
Orbital angular momentum, 731
Orbital magnetism, 731
Orbital moment, 727
Orbital momentum, 726
Orbitals, Slater-type, 584
Order–disorder (OD)
  diffraction pattern, 763
  groupoid families, 761, 763, 765, 773
  layers, 764
  packets, 765
  repeat unit, 764
  structures, 761, 764
  structures, desymmetrization of, 765
  theory, 761
Organic compounds
  preparation of specimens for electron diffraction and electron microscopy, 176
  space-group distribution of molecular, 905
  typical interatomic distances, 790–811
Organometallic compounds
  label triangulation, 111
  typical interatomic distances, 812–896
Orientated solidification, 176
Orientation contrast, 113
Orientation matrix, 516, 535, 537
  determination, 517
  four-circle diffractometer, 516–517
Orientation of crystals, 134
Orientation of the lattice relative to the point group, 15
Oriented texture patterns, 412
Origin of angular scale
  recovery of, 530
  uncertainty of, 530, 536
Original profile, 505, 520
  half-width of, 506, 520
Origins, equivalent, 15
Orthorhombic crystal system, 6, 16
Oscillation angle, maximum, 33
Oscillation photographs processing, 510
Outer moments, 718–720
Outlier removal, 813

Packing
  contact number in, 746–747, 752
  density of, 746
  heterogeneous, defined, 746
  homogeneous, defined, 746
  interpenetrating, 751
  of circles, 746–747, 752
  of ellipses and ellipsoids, 751–752
  of layers, 752–773
  of spheres, 746–751, 752, 904
  stable, 747, 750
  types, tables of, 747–748
  voids in, 750
Pair-distance distribution function (PDDF), 90
Pair-production cross sections, 213
Parafocusing, 47
Parallax, 41, 624
Parallel-beam geometry, 54, 663
Parallel detection, 397
Parallel-plate counters, 627
Parallel recording, 639
Paramagnetism, 154
Paramagnets, 728
Parasitic scattering, 661
Partial coincidence operations, 761
Partial structure factors in SANS, 112
Partial wave phase shifts, 389
Partially stimulated reflections (partials), 34, 39
Particle(s), 186
  latex, 107
  mass in SANS, 110
  maximum dimension, 102
  parameters of, 91
  shape in SANS, 110
  shape in SAXS, 93
Particle orientation, fluctuations, 492
Particle size, 62, 89, 162
  distribution, 111
Patterson synthesis, 21
Pauli principle, 412
Pauling model of hydrous phyllosilicates, 767

PCD (projected charge-density) approximation, 423
PDDF (pair-distance distribution function), 90
Peak
  asymmetry, 67
  displacements, 518
  height, 518
  of a reflection, 492
  satellite, 75
  search, 65
  shift, 518
  variance, 520
Peak flux, 431
Peak-shape function, 710–711
Peak-to-background ratio, 65, 661
  with scintillation counters, 622
Pearson VII function, 67, 711
Pendellösung, 250
Penetration depth, 58
  of X-rays, methods of reducing, 525
Peptides, standard coordinates, 699
Per cent point function, 708
Perfect-crystal analysers, 665
Perfect-crystal monochromators, 444, 663
Perfect single crystals, 510, 519
Persistence length, 93
Petrographic sections, 171
Phase analysis, electron diffraction, 412
Phase diagrams, determination of, 510
Phase-grating approximation, 260
Phase identification, 42, 81
  from electron-diffraction patterns, 81
Phase-space analysis, 661
Phase-space diagrams, 661
Phase transitions, study of, 509, 522, 525, 529
Phonon absorption, 656
Phonons, 261, 653
Phosphor screens, 634
Phosphoric acid as etchant, 173
Phosphors, 630
  storage, 635
Photoabsorption measurements, 406
Photoconductive layer
  amorphous Se–As alloy, 635
  lead oxide, 634
  X-ray-sensing, 634
Photo-effect data, theoretical, 221
Photoelectric absorption, 599
Photographic emulsions, 640
Photographic film
  graininess, 640
  properties of, 640
  shrinkage, 498
Photographic methods
  electron diffraction powder pattern, 81
  single-crystal, 508–516
  single-crystal, classification of, 508
Photographs
  cone-axis, 36
  setting (precession), 35
  upper-layer (precession), 35
  upper-layer (Weissenberg), 35
  zero-layer (precession), 35
  zero-layer (Weissenberg), 34
Photomultiplier tube, 619
Photon energy, 84
Photon-induced X-ray analysis, 189
Photon interaction cross sections, tables of, 223–229
Photon noise, 633
Photon scattering cross section, 213
Photons, 186
Photostimulated luminescence, 635
Phyllosilicates, 413, 766–771
Physical aberrations, 493, 493
  for XED, 86
Physical constraints, 715
Physical properties, relation to crystal structure, 151–153
Picture elements (pixels), 634
Piezoelectricity, 154
Pinhole cameras
  in SANS, 106
  in SAXS, 100
PIX (proton-induced X-ray analysis), 189
Pixels (picture elements), 634
Planck's law, 186
Plane detector recording, 32
Plane-wave topography, 121
Plasmas, 191
Plasmon(s), 261, 403
  cross section, 399
  dispersion, 398
  energies in metals, 397
  excitation energy, 660
  lifetime, 399
  scattering, 657, 661
Plasticity, 153
Pleochroism, 153
Point group(s), 939
  arithmetic, 913
  arithmetically equivalent, 939
  definition of, 945
  equivalence class, 939
  geometrically equivalent, 939
  Laue, 908, 913
  merohedral, 12
  orientation of the lattice relative to, 15
  reducible, 940
Point lattice, 2
Point row, 3
Point-spread factor, 40
Point-spread function (PSF), 625
Poisson distribution, 393, 666, 690
  difference of two, 666
  sum of two, 666
Poisson statistics, 519
Poisson's electrostatic equation, 719
Polarization, 193
  dependence, 732
  incident neutron, 727
  index, 611
  neutron, 592
  rotation of, 593
  vector, 654
Polarization factor, 51, 596
  for XED, 85
Polarized neutron scattering, 728
Polarized neutrons, 108, 592
Polarized radiation, circularly, 734
Polarizers, multilayer, 435
Polarizing
  filters, 438
  microscope, 154
  mirrors, 440
  neutron guides, 431
Polishing, 174
Polycrystalline samples for neutron diffraction, 177
Polydisperse systems, 89, 99
Polymers
  isotopic composition in SANS, 107
  preparation of specimens for electron diffraction and electron microscopy, 176
  texture studies, 414
Polypeptides, restraints in refining, 699–700
Polysynthetic twins, 10
Polytypes, 754–756, 760–773
  basic, 762
  families, 761
  faults in, 758–760
  layer stacking in, 760–773
  long-period, 757
  maximum degree of order (MDO), 762
  mixed-layer structures, 761
  regular, 762
  rod, 760, 766
  simple, 762
  standard, 762
  turbostratic structures, 761
Polytypism
  definition, 760
  layer, 766
  oriented texture patterns, 412
  rod, 760, 766
Position-sensitive detectors, 82, 87, 100, 113, 619, 623–633, 664
  choice of detectors, 623
  detection efficiency, 623–624
  detector properties, 623–625
  for neutrons, 649, 652
  localization of detected photon, 627
  photographic film, 623
  size and weight, 626
  software packages, 633
  storage phosphors, 634, 635–638
Positron annihilation spectroscopy (PAS), 189
Positrons, 189
Posterior probability density function, 681
Potential scattering, 594
Powder cameras, 70
Powder diffraction, 42, 664
  advantages of synchrotron, 54
  combined with Laue photography, 506
  electron techniques, 80
  methods, basic, 55
  neutron techniques, 82
  special factors in, 596
  standards, 498–499
  tilted-beam techniques, 80
Powder diffraction data, Rietveld analysis of, 710–712
Powder diffractometry, mathematical theory of, 518
Powder methods compared with single-crystal methods, 506
Powder-pattern geometry, 80
Powder-pattern indexing, 541
Powder-pattern intensities, 80
Powder patterns
  calculation of, 60
  computer graphics for, 69
Powders, correction factor for, 657
Poynting vector, 119
Precautions against radiation injury, 958–967
Precession geometry, 35
  setting, 168
Precision, 490, 492, 497, 501, 707
  of parameter estimates, 702

Precision of lattice-spacing determination, 505
  and profile shape, 517–519
  (methods of) increasing, 518, 533–534
  relative, 505
Preferred orientation, 60, 80, 162, 712
  empirical correction factor, 61
  minimization of, 60
Preparation
  of crystals, 153
  of specimens for electron diffraction and electron microscopy, 171
  of specimens for neutron diffraction, 177
Pressure, effect on lattice parameters, study of, 508
Primary dose limits, 960
Primary extinction, 609, 610
Primitive
  crystallographic basis, 2
  reciprocal basis, 2
  unit cell, 2
Principle of causality, 246
Prior probability density function, 681
Probability density function, 681
Probability distribution function (p.d.f.), 707
Profile fitting, 65, 492, 710
  computer procedures, 491
  functions, 66, 710
  in oscillation photographs, 510
Profile parameters, 710
Projected charge-density (PCD) approximation, 423
Projection matrix, 705, 706
Projection topograph, 115
Prolate ellipsoid of revolution, 94
Promolecule, 714
Promolecule density, 714
Propagation function, 415
Proportional counters, 619
Protection from ionizing radiation, 962–963
Proteins
  label triangulation, 111
  restraints in refining, 699–701
Proton-induced X-ray analysis (PIX), 189
Pseudo-atom moments, 718
Pseudo-non-dispersive methods, 506, 526, 528–533
Pseudo-Voigt function, 67, 711
Pulse-amplitude discrimination, 73, 620
Pulse-amplitude distributions, 621
Pulse-height analyser, 622
Pulse-height discrimination, 619
Pulse-height distribution, 626
Pulsed neutron source, 711
Pulsed (spallation) neutron source, 87, 189, 430–431
Pycnometry, 158
Pyroelectricity, 154
Pyrolytic graphite, 43, 77, 438, 665
  cross section for neutrons, 439
Pyrophyllite, 768

Q–Q (quantile–quantile) plot, 707, 708
QED corrections, 204, 205
QR decomposition, 679
Quadrupole, 716
Quadrupole moment, 717
Quality factor (QF), definition of, 959
Quanta, 186
Quantile–quantile plot, 707, 708
Quantitative microanalysis, 410
Quantum counting efficiency, 621
Quantum efficiency, 624
Quartz monochromator, 664
Quartz twins, 11
Quasi-Gaussian approximation, 590
Quasi-Newton methods, 683
Quasicrystals, 908

R factors, 68, 710–711
  dynamical, 427
  weighted, 68
Racah's algebra, 731
Radial constraint, 715
Radial distribution function, 97
Radiation damage, 166, 417, 626, 630
Radiation injury
  definition of terms, 958–960
  possible sources, 962–963
  precautions against, 958–967
  regulatory authorities, 964–966
  responsibilities, 960–961
Radiation protection, 957, 962
Radiation safety officer, 960
Radiations used in crystallography
  electromagnetic waves, 186
  particles, 186, 259
Radioactive samples, 619
Radioactive sources, 189
Radio-frequency flipping coil, 728
Radionuclides, 75, 196
  definition of, 959
Radiotoxicity, definition of, 959
Radius of gyration, 91
  of the cross section, 92
  of the thickness, 92
Radoslovich model, 769
Raman effect, 153
Raman scattering, 657, 660
  resonant, 657, 660, 661
Raman spectroscopy, 189
Ramsdell notation, 752
Rank of a lattice, 937
Rate-meter measurements, 63
Ratio method
  for powder samples, 509
  for single crystals, 509
Ratio of lattice spacing to optical wavelength, 533
Rational twin axis, 10
Rayleigh criterion, 427
Rayleigh scattering, 214, 242, 554, 599
Rayleigh scattering data, theoretical, 221
RBS (Rutherford backscattering), 189
Reactors, 430
Real crystals, 419
Real solids, 401
Real structure
  determination, 516, 531
  errors due to, 528
Receiving slit, 45
  aperture, 53
  width, 48
Reciprocal cell
  picture of, three-dimensional, 509
  picture of, two-dimensional, 509
  picture of, undeformed, 509
Reciprocal lattice, 412
  angles, determination, 517
  geometry, 513
  layer lines and crystal setting, 168
  parameters, determination, 517
Reciprocal lattice
  point, 415
  vector, 3
Recording counts, fluctuations of, 492
Recording range, 52
Rectangular crystal system, 15
Reducible point groups, 939
Reference crystal(s), 531–532
Reference sample in SANS, 109
Refinement
  least-squares, 503, 505, 510, 517
  of structural parameters, 677
  problems, least-squares, 101
  Rietveld, 56, 82, 541
  Rietveld, using XED, 86
Reflecting power of a crystal, 590
Reflection
  angles, 499
  conditions, for a twinned crystal, 13
  conditions, special, 921
  of light, 153
Reflection electron microscopy (REM), 428
Reflection high-energy electron diffraction (RHEED), 428
Reflection-only counting rates, 666
Reflection specimen, θ–2θ scan, 44, 53
Reflection topographs, 113, 114
Reflection twins, 10, 12
Reflections
  integrated, 114
  main, 907
  multiple-order (Laue), 27
  nodal, 29
  satellite, 907
  single-order (Laue), 27
Reflectivity function, 528
Refraction, 527
  correction for, 492, 505, 523, 536
  effects, 81
Refractive index, 81, 154, 160, 189, 599–600
  immersion media for measurement of, 160
Regular polytypes, 762
Regulatory authorities, 964
Relative measurements of lattice spacing, 505
Relative molecular mass in SANS, 110
Relativistic corrections, 390
Relativistic effects, 186, 260, 262
REM (reflection electron microscopy), 428
Remanent systematic error, testing for, 498
Repeated twins, 10
Residual, 707
Residual map, 714
Resolution
  in XED, 85
  sphere, 27
Resolution errors
  detector element, 106
  gravity, 106
  in SANS, 106
  slit, 106
  wavelength, 106
Resolution functions in neutron scattering, 443
Resonance scattering, 594
Resonant Raman scattering, 657, 660, 661
Restraints in refinement, 691, 693–701
RHEED (reflection high-energy electron diffraction), 428
Rho operations, 763
Rhombohedral crystal system, 8
Ribosomes, scattering curves from, 111

Rietveld method, 56, 82, 422, 493, 496, 541, 690, 710
  background, 711
  indexing, 711
  peak-shape function, 710–711
  preferred orientation, 712
  problems with, 711
  using XED, 86
Rigid-motion parameters, 697
Robust/resistant methods, 689
Rock minerals, preparation of specimens, 171
Rocking curves, 37, 39, 188, 662
  double-crystal, 529
Rod-like particles, 94
  molecular weight, 93
  radial inhomogeneity, 96
Rod polytypes, 760, 766
Rotating-anode tubes, 71, 189, 194
Rotation diagrams, 414
Rotation geometry setting with moving-crystal methods, 168
Rotation method, 29
  normal beam, 31
Rotation of polarization, 593
Rotation/oscillation geometry, 31
Rotation twins, 10, 12
Rotational oscillation (libration), 589
Rutherford backscattering (RBS), 189
Rutile, intensity standard, 503

Sample mean, 813
Sample median, 813
Sample standard deviation, 813
SANS (small-angle neutron scattering), 105, 110
Satellite
  peaks, 75
  reflections, 907
Saticon television camera tubes, 630
SAXS (small-angle X-ray scattering), 89
Sayre's equation, 428
Scale factor, estimation of, 691
Scanning-crystal monochromator, 622
Scanning electron microscopy (SEM), 540
Scanning range, 519–520
Scanning transmission electron microscope (STEM), 427
Scanning tunnelling microscope, 428
Scattering
  coherent multiple, 661
  Compton, 242, 554, 599, 661
  Delbrück, 242
  diffuse, 261
  elastic, 416
  electron, 259
  fluorescence, 661
  inelastic, 416, 657
  low-Q, 105
  magnetic, 730
  magnetic X-ray, 730
  multiple, 661
  multiple, deconvolution techniques, 393
  multiple, incoherent, 661
  multiple, intramolecular, 392
  multiple, neutron diffraction, 177
  multiple, Poisson distribution, 393
  multiple, problems associated with, 392
  neutrons, magnetic, 591
  neutrons, nuclear, 593
  nuclear and magnetic, 435
  parasitic, 661
Scattering
  plasmon, 657, 661
  potential, 594
  Raman, 657
  Rayleigh, 242, 554, 599
  resonance, 594
  resonant Raman, 657, 660, 661
  spin-flip, 591
  thermal diffuse, 416, 653, 655, 657, 661
  Thomson, 733
Scattering amplitudes, 389
  for electrons, 263–281
  nuclear, 594
Scattering cross sections
  coherent, 594
  Compton, 213
  elastic, 213
  elastic differential, 262
  incoherent, 594
  incoherent elastic, 595
  inelastic, 213
  magnetic, 593
  nuclear, 591
  pair-production, 213
  Rayleigh, 213
  total, 213, 594
  total (tables), 223–229
Scattering factors
  atomic, 554, 566
  complex, 188, 262
  electron, 188, 259
  for electrons, molecular, 390
  for electrons, partial wave (Table 4.3.3.1), 286–377
  for neutral atoms, 263
  free atoms, 555
  generalized, 565
  hydrogen-atom, 565
  interpolation, 565
  magnetic, 461
  parameterization, 262, 461
  X-ray, Gaussian fits, 261
  X-ray incoherent, 389
Scattering functions, 89
  incoherent (Table 7.4.3.2), 658
Scattering intensities
  calculation of, 104
  neutron, 105
Scattering-length densities, 105
  match-point, 107
Scattering lengths, 444
  bound nuclear, 594
  coherent, 594
  density, 105
  density, match-point, 107
  for neutrons, 188, 444
  free, 594
  total, 91
Scattering surfaces, 656
Scattering vector, 3, 90
Scherzer focus, 422, 423, 424, 426
Schrödinger wave equation, 186, 415, 735
Scintillation detectors, 619, 642, 664
Screen menu (CRT) for diffractometer-operation control, 64
Screenless rotation technique for large-molecule data collection, 169
Screw correlation tensor, 697
Secant methods, 683
Secondary extinction, 609, 611
Section topograph, 115
Seemann–Bohlin diffractometers, 495
Seemann–Bohlin geometry, 43
Seemann–Bohlin method, 52
  advantages, 53
Selected-area channelling patterns, 540
Selected-area diffraction patterns, 428
Selected-area electron diffraction, 80, 538
Selection of crystals, 151
Self-centring slit, 45
Self-consistent field (Hartree–Fock) method, 243
SEM (scanning electron microscopy), 540
Semiconductor crystals, 428
Semiconductor detectors, 629, 642
Sensitivity (of lattice-spacing determination)
  increasing, 505
  (methods of) highest, 531
Separation plots, structural, 774
Serial recording, 639
Serpentine–kaolin group, 766–769
Setting
  θ–2θ, 47
  anti-equi-inclination, 31
  azimuthal, 168
  equi-inclination, 31
  flat cone, 31
  Guinier, 39
  photograph (precession), 35
  precession geometry, 168
  rotation geometry, 168
  stationary crystal, 168
Setting angles in standard diffractometers, 516
Shadowing, 189
Shannon–Jaynes entropy, 691
Shape function, 520, 523
Shape of profile
  affected by collimation, 520
  and precision, 519–521
Shape transform, 718
Sheets
  dioctahedral, 767
  hetero-octahedral, 767
  homo-octahedral, 767
  meso-octahedral, 767
  octahedral, 767
  tetrahedral, 768
  trioctahedral, 767
Short symbols for superspace groups, 921
Siegbahn notation, 191
Sievert, definition of, 959
Sigma symmetry (operations), 763
Signal-to-noise ratio, 633, 645
Significance tests, 702
Silicates (phyllosilicates), 766–771
Silicon, lattice parameter of, 490, 495, 499
Silver, lattice parameter of, 499
Silver behenate reflection angles, 503
Simple polytypes, 762
Simulations in SAXS, 103
Simultaneous reflection, 526
Single crystal
  characterization, 525
  Laue diffraction, neutron, 87
  monochromators (at synchrotron), 39
  topography, 114
  XED methods, 87
Single-crystal methods
  compared with powder methods, 506
  photographic, 508–516
  with counter recording, 516–533

Single-crystal X-ray techniques, 26, 505–536
  classification of, 25
Single filters, 78
Single-order reflections (Laue), 27
Single-particle scattering, 110
Single-wire detectors, 82
Skewness, 586
Slater determinant, 722
Slater-type orbitals, 584
Slits
  antiscatter, 45
  design, 45
  self-centring, 45
Slower-than-sound neutrons, 657
Small-angle approximation, 80
Small-angle cameras, 99
Small-angle neutron scattering (SANS), 105, 110
Small-angle X-ray scattering (SAXS), 89
Small angles of incidence, 525
Small particles
  essential, 56
  line broadening from, 62
Small spherical crystals, lattice-parameter determination of, 507, 525
Solid-state detectors, 82, 620, 642, 664
Solid-state effects, 400
Solid-state valence-band theory, 415
Soller collimators, 82, 432, 443
Soller slits, 46, 56, 82, 494, 521–522
Solutions, diffraction from, 24
Somatic effects, 960
Sound velocity, 656
Source intensity distribution and size, 73
Sources of X-radiation, 507
Space-group frequencies
  statistical modelling of, 897–906
  tables, 905
Space groups
  and arithmetic crystal class, 15–20
  arranged by arithmetic crystal class, 16
  classification of, 15, 897
  closest-packed, 897
  distribution of molecular organic structures, 897
  enantiomorphous pairs, 20
  for close-packed structures, 755
  frequency of, 15
  impossible, 897
  limitingly close-packed, 897
  magnetic, 591
  one-line symbol, 920
  permissible, 897
  symmetry, 695
  two-line symbol, 921
Spallation neutron sources, 87, 189, 430–431
Spark erosion, 174
Sparse matrices, 685
Sparse matrix methods, 701
Spatial distortions, 41, 625, 633
Spatial non-uniformity, 633
Special reflection conditions, 921
  for (3+1)-dimensional space groups, 934
Specific heat, 154
Specific isotopic labelling, 107
Specific surface, 93
Specimen
  aberrations, 48
  absorption, 497, 498
  displacement, 494, 498, 499
  displacement error, correction, 528
Specimen
  factors, 60
  fluorescence, 43, 78
  focusing circle, 44
  irradiated length, 45
  mounting, 162
  orientation, 44
  preparation, 171, 177, 503
  surface displacement, 48, 499, 503
  transparency, 494, 497, 499
  transparency aberration, 50
Specimen-tilt and beam-tilt error correction, 524
Spectral breadth, 189
Spectral brightness, 197
Spectral profiles, 48
Spectral purity, 72
Spectrometers, 395
  asymmetric, 521–522
  combined (techniques), 531
  double-beam, 531
  double-crystal, 510, 528–530
  one-crystal, 521–526
  stability of, 532
  symmetric, 521–526, 529–531
  time-of-flight, 444
  triple-axis, 444, 531–532
  triple-crystal, 531–532
Spectroscopy
  electron energy-loss, 391
  infrared, 189
  Raman, 189
Sphalerite, 754
Sphere(s), 92, 94
  close-packing, 746, 752, 761
  hollow, 92
  of reflection (Laue sphere), 26
  packing, 747
Spherical aberration, 421
Spherical Bessel function, 460, 565, 592
Spherical harmonic approximation, atom-centred, 714
Spherical harmonic functions, 581, 714, 722
Spherical harmonic multipole model, 715
Spherical symmetry, 103
Spherically symmetric particles, 96
Spin
  flipper, 442
  of neutrons, 443
  polarization, 388
Spin-contrast variation, 108
Spin density
  analysis of, 713–734
  errors, 729
Spin-flip processes, 728
Spin-flip scattering, 591
Spin-magnetization densities, 725, 727, 731
Spin-orbit coupling, 727
Spin-orientation devices, 442
Spin-polarization effect, 732
Spin structure factor, 731
Spin-turn coil (flipper), 442
Split basis, 944
Spot size and shape, 37, 39
Sputter etching, 173
Sputtered thin films, 173
Square crystal system, 15
Square-root technique, convolution, 103
Square-wave modulation transfer function, 634
Stability of spectrometers, 532
Stability of X-ray sources, 72
Stable packing, 746, 750
Stacking faults, 754, 762
  fringe patterns, 116
Stacking sequence, determination of, 757
Standard basis, 944
Standard crystal, 507, 531–532
  lattice-parameter determination of, 507
Standard deviation, 679
Standard lattice bases, 938
Standard polytypes, 762
Standard reference materials, 498
Standard specimens, 501
Standard uncertainty, 681, 707
Standards
  intensity, 500
  powder-diffraction, 498–499
Static model map, 714
Stationary-crystal method, 168
Stationary-phase focus, 422
Statistical errors of lattice-parameter determination, 505, 519, 523
Statistical fluctuations, 69, 492, 666
Statistical modelling, 904
Statistical significance tests, 702–705
Statistical validity
  in general, 702–705
  of Rietveld method, 712
Statistics, 679
  of recorded counts, 519
  Poisson, 519
STEM (scanning transmission electron microscope), 427
Step size and count time, 64
Stereochemical constraints, 698
Stereographic projection of Kossel pattern, 513
Stereographic transformation, 29
Stibivanite, 769–772
Still exposure, monochromatic, 31
Still photographs for initial crystal setting, 169
Stochastic effects, 959
Stopping rules, 684
Storage phosphors, 623, 635
Storage rings, 196
  synchrotron-radiation sources, 199
Strain, measurement of, 510, 516, 529
Strainmeter, 510
Straumanis film mounting, 509
Stress
  internal, 528
  study of, 510, 516, 522
Strip-chart recordings, 63
Stroboscopic X-ray topography, 120
Structural classes, 904
Structural separation plots, 774
Structure amplitude, complex, 261
Structure analysis
  direct, 103
  electron diffraction, 413
Structure determination of close-packed stackings, 756–758
Structure factor(s), 590, 941
  determination, 735
  magnetic, 725, 728, 730
  magnetic orbital, 731
  magnetic, unit-cell, 591
  magnetic X-ray, 733
  measurement by electron diffraction, 416
  nuclear, 595, 725, 730
  partial, 112
  SANS, 112

Structure factor(s)
spin, 731
X-ray, 737
Structure imaging, electron diffraction, 424
Structure prediction, 897
Structure refinement, 426
Student's t distribution, 704
Subfamilies, 769
Sub-grains, 114
Sublimed films, 176
Sulfur, Fermi level, 406
Superficial layers (see also Epitaxic layers), study of, 525
Superlattices, determination of, 525
Supermirrors, 435
Superposition structure, 763
Superspace, 944
embedding, 908
Superspace groups, 909, 912, 916, 940, 945
(2+1)-dimensional (table), 920
(2+2)-dimensional (table), 921
(3+1)-dimensional (table), 922–934
equivalent, 940
full symbols, 921
short symbols, 921
symbols for, 921
Superstructure, 919
Surface diffraction, 24
Surface of a particle, 93
Surface plasmons, 403
Surface-roughness scattering, 108, 128
Surface structure, 428
Symmetric arrangement in single-crystal methods, 509, 521–526, 529–531
Symmetry
conditions for second cumulant tensors, 695–696
elements, non-crystallographic, 907
enhanced, 13
group, 908
of Patterson synthesis, 21
spherical, 103
Symmorphism, 15, 897
Synchrotron radiation, 54, 99, 114, 119, 187, 191, 596, 623, 653, 665, 711
camera systems for, 100
determination of wavelength, 495
facilities (for EXAFS), 219
for XED, 84
sources, 38, 198, 495
special applications, 189
spectrum, 197
Synchrotron X-ray topography, 120
Systematic errors (see also Aberrations), 490, 492, 501, 653–665, 707
background, 661–665
connected with collimation, 523–524
detection and treatment, 498–499, 707–709
estimation of, 535
in counter-diffractometer methods, 518, 535
in divergent-beam methods, 515
in photographic methods, 508, 515, 535
in single-crystal spectrometers, 521, 522, 523
in the Bond method, 523–525
of wavelength determination, 535
plasmon scattering, 660
Raman scattering, 660–661
reduced experimentally, 512, 515, 521, 526, 528–530
Systematic errors (see also Aberrations)
reduced by detailed analysis of Kossel patterns, 512–515
reduced by extrapolation, 505, 535
reduced by least-squares refinement, 517
remanent, 408
specimen displacement, 517, 531
testing for, 498–499
thermal diffuse scattering, 653–657
white radiation, 661–665
Systematic interactions, 81

Take-off angle, 74
Talc–pyrophyllite group, 768–770
Tangent formula, 428
Tau operations, 764
Television area detectors, 630
Television camera tubes, 632
TEM (transmission electron microscopy), 171, 428, 540
Temperature correction, 524
Temperature dependence of lattice parameters, study of, 507, 530
Temperature factor(s), 586
anisotropic, 697
generalized, 586
librational, 724
Tensors, symmetry of, 695–696
Tetragonal crystal system, 7, 17
Tetrahedral sheet, 767
Texture
axis, 412
basis, 412
fibre, 413
lamellar, 412
patterns, 412
Theoretical photo-effect data, 221
Theoretical Rayleigh scattering data, 221
Thermal diffuse scattering, 415, 653, 656, 661, 711
correction, anisotropic, 655
correction factor, 654
correction factor for thermal neutrons, 656
error, 653
Thermal effects, error connected with, 515
Thermal expansion, 154
study of, 510, 516, 522, 525, 529
Thermal neutron detection, 644–652
detection process, 644–648
detection systems, 649–651
electronic aspects, 648
via gas ionization, 645
via scintillation, 645
Thermal smearing, 723
Thermodynamic properties, 154
Thickness
distance distribution function of, 103
fringes, 735
of crystal (sample), 512, 513
of lamellar particles, 93
Thin films and thinning, 173
Thin sections, 171, 174
Thinning solution, 175
Thomas–Fermi method, 659
Thomas–Fermi model, 243
Thomson formula, 90
Thomson scattering, 733
by a free electron, 242
Three-axis spectrometers, 444
Three-beam fringes, 422
Three-dimensional crystal classes, 15–20

Tilt(s)
of beam, 524
of crystals, 530
Tilt-series reconstruction method, 427
Time-averaged flux, 431
Time-constant errors, 492
Time-of-flight neutron diffraction, 87, 431
Time-of-flight SANS, 106
Time-of-flight spectrometers, 444
Time reversal, 591
Topography, 113–123, 516, 525–527
detectors suitable for, 634
Topotaxy, 154
Total coincidence operations, 761
Total counting rates, 666
Total external reflection, 525
Total scattering cross section, 594
Total scattering lengths, 91
Townsend avalanches, 619
Trace of S singularity, 697
Transformation(s)
compensating, 940
gnomonic, 29
stereographic, 29
twins, 10
Transition elements, Fermi level, 406
Transition-radiation X-rays, 192
Translation, internal, 912
Translation tensor, 697
Translations, compensating, 940
Transmission coefficients, 601
Transmission electron microscopy (TEM), 428, 540
preparation of specimens, 171
Transmission factor for XED, 86
Transmission function, 414, 432
Transmission geometry, 512, 513, 525
crystal thickness for, 512, 513
Transmission method, advantage of, 52
Transmission specimen, θ–2θ scan, 49
Transmission topographs, 113, 114, 124
Transparency aberration, 49
Traverse topograph, 115
Triaxial bodies, homogeneous, 92
Triclinic crystal system, 6
Tricontadipole, 716
Trigonal crystal system, 7, 18
Trigonometric intensity factors, 596
Trimercury dichloride disulfide, 766, 771–772
Trioctahedral sheet, 767
Triple-axis spectrometers, 444, 531–532
Triple-crystal spectrometers, 531–532
Triple isotopic replacement, 111
Triple-reflection scheme, 532
Truncation level, 518
optimum, 520
Trust-region methods, 683
Tungsten
lattice parameter of, 499
reflection angles, 499, 502
Turbostratic structures, 760
TV cameras, X-ray-sensitive, 633
Twin(s)
axis, 10, 11
axis, rational, 10
boundary, 10
Brazil, 11
centre, 10
centred lattice, 11
components, 10

Twin(s)
cyclic, 10
Dauphiné, 11
element, 10, 14
growth, 10
index, 11
interface, 10
inversion, 10, 12
lattices, 10
law, 10
mechanical (deformation, glide), 10
mimetic, 153
multiple, 10
operation, 10
plane, 10, 11
polysynthetic, 10
primitive lattice, 11
quartz, 11
reflection, 10, 12
repeated, 10
rotation, 10, 12
simulated Laue class of, 13
transformation, 10
Twinned crystal, reflection conditions, 13
Twinning, 10
by merohedry, 12
by pseudomerohedry, 12
in polytypes, 762
reciprocal-space implications, 12
Two-beam approximation, 80, 260
Two-circle diffractometers, 517
matrix formulae, 517
Two-dimensional crystal classes, 15, 16
Two-line symbols for Bravais classes, 915, 920

Ultramicrotomy, 171
Ultraviolet radiation, 187, 189
Umweganregung, 527
Undulators, 197
Uniformity of response, 625
Unit cell
conventional, 913
conventional or centred, 2
magnetic structure factor, 591
primitive, 2
volume, 2
Unsmoothed high-tension supplies, 667
Upper-layer photographs (precession), 35
Upper-layer photographs (Weissenberg), 35
Upper quartile, 813

V-shaped detector recording, 32
Valence map, $X-X$, $X-N$, and $X-(X+N)$, 714
Vanadium, scattering from, 594
Variable reduction method, 693
Variance, 679
of centroid, 520
of measure of location, 519
of median, 520
of peak, 520
of single midpoint of chord, 520
Variance–covariance matrices, 680, 692, 707
Variances of measured intensities (recorded counts), 519
Variations in cell parameters, 522
VC (vicinity condition), 763
VC layers, 765
VC structures, 765
Vector(s)
basis, 944
energy-flow, 119
lattice, 2
module, 907, 937, 944
Poynting, 119
reciprocal-lattice, 3
scattering, 3
Velocity of sound, 656
Velocity of the elastic wave, 654
Vermiculites, 765
Vertical divergence, 82
Vertical inclination
correction for, 522
of incident beam, 522
of reflected beam, 522
Vibrating-string method for density measurement, 158
Vibration, normal modes, 653
Vicinity condition (VC), 763
Viruses, SANS, 106, 111
Visual estimation, 618
Voids in close-packed structures, 753
Voigt function, 67, 711
Volume
of a homogeneous particle, 92
plasmons, 398
Volumenometry, 158
Voronoi polyhedron, 774

Waller–Hartree method, 659
Wave amplitudes, dynamical, 414
Wavefunction, 186
Wavelength calibration, 55
Wavelength determination, 506, 528, 533
accuracy of, 526
errors in, 541
Wavelength filter, 528
Wavelength normalization (Laue), 39
Wavelength problems, 492
Wavelength selection, 75
easy, 55
Wavelength shifts, 197
Wavelengths
γ-rays, 187
determination, 533
distribution, 506
errors, 492
synchrotron radiation, 187
uncertainty, 536
X-rays, 187, 191, 200, 201, 206, 209
Wavevector, 186
Weak-peak measurement, 65
Weak-phase-object (WPO) approximation, 423, 427
Weighted R factors, 68
Weissenberg camera, setting of single crystals, 168
Weissenberg diffractometer, 517
Weissenberg geometry, 34
White-beam energy-dispersive X-ray diffraction, 622
White-beam neutron diffraction, 87, 124
White radiation, 661
in double-crystal spectrometer, 529
in lattice-parameter determination, 507, 508, 529
streaks and crystal setting, 169
topography, 119
Whole-powder-pattern fitting, 68
Wien filter, 396
Wigglers, 197
Wigner–Eckart theorem, 727
Window thinning method, 174
WPO (weak-phase-object) approximation, 423, 427
Wurtzite, 754
Wyckoff positions, 914

XAFS (extended X-ray absorption fine structure), 24, 189, 213–220, 254, 409
as a short-range-order phenomenon, 214
data analysis, 217
XANES (X-ray absorption near-edge structure), 214–220, 258, 403
XED (X-ray energy-dispersive diffraction), 84
XPS (X-ray photoemission spectroscopy), 189
X-ray absorption, 599–612
X-ray absorption coefficients, 220
absolute measurement of, 214
data analysis of EXAFS, 217–218
experimental techniques, 214
X-ray absorption near-edge structure (XANES), 214–220, 258, 401
X-ray absorption spectra, 213–241
X-ray attenuation coefficients, 220
X-ray background over a spot, 34
X-ray beam
extremely parallel, 532
highly divergent, 507, 508, 510–516
in single-crystal techniques, 507
well collimated, 507, 508, 536
X-ray diffraction
detectors for, 618–638
texture patterns, 412
X-ray dispersion corrrections, 241
X-ray energies, 236
X-ray energy-dispersive diffraction (XED), 84
X-ray generators, 72
X-ray imaging systems, 633
X-ray incoherent scattering factors, 389
X-ray interferometry, 201
combined with optical interferometry, 533–534
X-ray levels, 191
X-ray microanalysis, 82
X-ray microscopy, 189
X-ray optics, 37
X-ray phosphors, 631
X-ray photoemission spectroscopy (XPS), 189
X-ray powder techniques, 42–79, 492–503
aberrations in, 47–50
energy-dispersive, 58
filters, 78–79
focusing geometries, 43
history, 42–43
literature, 42–43
microdiffractometry, 53–54
monochromators in, 43, 76–78
parallel-beam geometries, 54
Seemann–Bohlin geometry, 43, 52–53
Soller slits in, 50, 56
specimen fluorescence in, 43
zero position, 46
X-ray scattering, 554–590
magnetic, 733
X-ray-sensitive TV cameras, 633
X-ray source(s), 191
conventional, 37
in the sample, 510
laser plasma, 189

X-ray source(s)
  on the sample, 510
  outside the sample, 510
  radioactive, 195
  synchrotron, 38, 196
  X-ray tube, 193
X-ray spectra, 71, 74
  Bremsstrahlung, 191
X-ray spectrometers
  Bragg, 510
  double-crystal, 528
  symmetric, 510, 521, 529
  triple-crystal, 530
X-ray techniques, single-crystal, 26
X-ray topography, 115, 516, 525–527
X-ray tubes, 71–74, 193
  loading, 195
  power dissipation in, 195
X-ray wavelengths, 187, 191, 200–212, 221
  conversion factors, 191
  in single-crystal methods, 506
X-rays
  hard, 187
  properties, 187
  soft, 187
  special applications, 189

Z-module, 907
Zebra patterns, 119
Zeeman polarizers, 442
Zero-angle calibration, 494
Zero-error elimination, 517, 521, 523, 529
Zero-layer photographs (precession), 35
Zero-layer photographs (Weissenberg), 34
Zero line, 415
Zero-order Laue zone (ZOLZ), 418
Zero plane, 415
Zero-point correction, 517
Zero setting, 528
Zhdanov notation, 752
Zinc oxide (intensity standard), 503
Zinc sulfide, 754
ZOLZ (zero-order Laue zone), 418
Zone axis, 3, 10
Zone equation, 4